

SYMPOSIUM BI01

Early Career Development—Insights from Academia and Industry
November 28 - December 6, 2022

Symposium Organizers

Isabel Gessner, Miltenyi Biotec
Katherine A. Mazzio, Helmholtz-Zentrum Berlin für Materialien und Energie
Shayandev Sinha, Intel Corporation
Qing Tu, Texas A&M University

* Invited Paper
+ Distinguished Invited

SESSION BI01.01: Career Pathways I
Session Chair: Isabel Gessner
Monday Morning, November 28, 2022
Hynes, Level 1, Room 105

10:30 AM *BI01.01.01

What You Want to Do vs What You Can Do [Jina Ko](#); University of Pennsylvania, United States

Growing up, I did not have any professors or scientists around me. I did not know how to become a professor and I never thought about it as my future career. I majored in Bioengineering and French Studies and I was still very naive when I was about to graduate. I did not know too much about different directions that I can take after graduation. For me, there were two options to choose from - either going to industry or continuing being a student - and it was a very easy decision to make. I will be working for 30+ years anyway so why not spend a little more time in academia as a graduate student? Then, the next question was Master's vs. PhD, which was also very easy to answer. If you pursue PhD, Master's degree is included so why not just do PhD right away? That's how I began my life as a PhD student.

I met the best possible advisor during my PhD and everyday was full of joy working with him on great science. I learned so much and I enjoyed the whole process. However, it was not enough to think about becoming a professor because there were always some challenging moments. Many of my research articles were rejected after multiple rounds of review process. Very precious samples that I collected for many weeks turned out to be degraded during that time. We built a microchip that achieved high diagnostic performance, which turned out to be due to some errors and we had to re-do the whole process after fixing the errors. Every time I faced these challenges, it was very frustrating and science was really hard. However, I never wanted to give up on anything and my advisor was always highly supportive, which made me successfully complete my PhD.

At the end of my PhD, there were another two options to choose from - either going to industry or pursuing postdoc - and I decided to do both. I worked in a company as an intern for three months and then I started my postdoc. I wanted to experience both paths so that I can really find out what I like and what I do not like. And I liked both working in a company and in a postdoc lab. From both experiences, I realized that I really enjoy ups and downs and that dynamic situations brought me more joy. This is why I wanted to stay in academia but I was not sure if I would become a good professor. And my PhD advisor told me that I should do what I want to do and don't think too much about if I can do it. And here I am.

Finding a good fit seems like a success to both securing a position and being happy in that position afterwards. It's always helpful to know someone in a department who is excited about your research and can endorse you during the recruitment process. High impact papers are good to have but they do not seem to matter once you pass the first round of screening interviews. Showing your fit, passion, and niche will make people excited about your case and want to have you as a colleague. A life as an assistant professor has been very fun and rewarding. I love working with students and colleagues. It gets very busy with meetings, grant writing, research, and conferences but they are all enjoyable since you are the one who make decisions, not someone else.

11:00 AM *BI01.01.02

Turning Academic Research into Building a Start-Up [Martin Wilkovitsch](#)^{1,2}; ¹TU Wien, Austria; ²Velaex Technologies, Austria

After graduating from university, finding early career perspectives in academia or industry can be a challenging task, especially if the actual deep desire is to found an own company. Often, scientists are deterred by this process as there are no clear guidelines that can be followed to guarantee success of a startup company.

Based on the research during my PhD as a chemist at TU Wien I embraced the opportunity and have taken the first steps toward building my own business in the field of life sciences. 'Velaex Technologies' is a young biotech startup currently incubated in the i²ncubator of the Innovation Incubation Center of TU Wien with the mission to "Bringing Chemistry to Life".

The focus is to overcome the poor selectivity of conventional cancer chemotherapeutics by improving the site-specificity and especially the safety of those drugs. The basic underlying principle is to precisely deliver and activate drugs **only** at the site of disease by exploiting controllable, ultra-fast *in vivo* chemical reactions. Based on unique molecular designs, our team developed superior chemical tools that outperform current state-of-the-art technologies by several orders of magnitude thereby elevating the standards for the field. With *Velaex Technologies* we aim to provide methods to 'preprogram' the movement of compounds within living systems and thus enable drug targeting strategies with unprecedented efficiency, selectivity, and safety, paving the way to high-precision therapeutics.

As a deep-biotech startup at the interface of chemistry and biology, still with a very strong connection to academia, we are looking forward to discussing

our recent experiences of how to turn an academic research project into starting a business and launching a future startup / spin-off company. We will share our challenges along the way (including finding adequate funding support, mentoring/advisory strategies, building a team,...) especially addressing students, postdocs and other young professionals who envision founding a startup company in the future.

11:30 AM *BI01.01.03

Transitioning from Academia to Industry—How I Found my Way, How I Stayed Engaged and Why I (Still) Love my Job! [Jonathan A. Fauerbach](#); Miltenyi Biotec, Germany

Should I pursue the academic path and become a Postdoc or even a Professor? Where will I do that and what is my chance of success and survival? What about becoming independent as an Entrepreneur? What is needed for a start-up? How will I be able to bring my ideas and vision to life and convince others to invest on it? What about the industrial market? Should I “sell” my soul? How can I apply? What are the differences? Who can help me trying to figure this out? What is the role of networking? Where can I found support?

These questions and many more were some of the ones I faced when making a career choice and transitioning from academia to industry in 2016.

Throughout my (rollercoaster of) life I have moved from South-America, to North-America to Europe. I worked in Analytical Chemistry, Organic Chemistry, Protein Biophysical, Biochemistry and Cellular Biology labs and teams. I went from Academia, Entrepreneurship to Industry. I completed my Masters and PhD in Chemistry and most recently an Executive MBA. Worked my way from student, to Postdoc, to Group Leader to Manager. And managed to form a family, have two children and provide for us all.

My goal with this talk is to simply share my story, discuss and reflect on the process I went through, overcoming uncertainty and fears, debunking myths and biases, and ultimately offer tools, tips and resources to empower everyone who is at the crossroads of career paths.

Yes! You can do this. You can find your way. It will be awesome!

Keywords: career path, job application, work-life balance

SESSION BI01.02: Mentoring and Work-Life Balance
Session Chairs: Katherine A. Mazzio and Shayandev Sinha
Monday Afternoon, November 28, 2022
Hynes, Level 1, Room 105

1:30 PM *BI01.02.01

Balancing Work and Life While Pursuing an Academic Career [Rachel S. Goldman](#); University of Michigan, United States

As a second generation academician, I learned at a young age that if you love what you do (for a living), your work is your hobby, your collaborators are your close friends, and your students are part of your extended family. Through persistence and luck, I have been fortunate to live this dream in my adult life. In this presentation, I will discuss strategies for pursuing a fulfilling academic career, drawing upon my experiences at the University of Michigan.

2:00 PM BI01.02.02

Creating a Culture of Success Through Holistic Mentoring [Yvonne Kavanagh](#); South East Technological University, Ireland

To have a successful career it is important that leadership skills and resilience are developed as part of the academic journey of a student. This is facilitated and supported by the faculty who supervise research students. Successful careers must be framed in a changing environment where a graduate has choices and teasing out these by exposing the student to many environments is promoted.

As a research supervisor, an important part of the role is the development of successful confident researchers who can be the leaders of tomorrow in either academia or industry. These skills require development through various pathways. In addition to the role as a research leader developing timelines with project and publication milestones, the supervisory role has the capability of being a mentor who supports a holistic approach to leadership development. Being a mentor provides a platform for informal support which guides the student through various stages of their research by supporting and developing other skills. In this area it is important that there is a structure in place which can be replicated for all research students to enable them to reach their full potential.

This talk will focus on some strategies to support research students develop holistic leadership skills.

The approach includes strategies on:

- Supporting minorities in materials engineering
- Engaging students in exchange programmes
- Developing leadership skills through outreach management
- Providing leadership opportunities in various areas.
- Supporting well being and resilience.

2:15 PM *BI01.02.03

How (Not) to Run an Academic Research Group—Insights on Mentoring and Work-Life Balance [Alexandra Zevalkink](#); Michigan State University, United States

Running a research group and mentoring students is not something that we are explicitly trained to do during our graduate studies. At best, we spend five plus years observing how our Ph.D. or postdoc advisors do it, making a long mental list of what to do (and what definitely NOT to do) along the way. As a non-expert on this subject, my goal is to help you avoid some of the many pitfalls that I encountered, by telling you what worked and what didn't work for me. I'll discuss the realities of work-life balance, and the implications of being both “mom” and “professor”. Effective time management skills are certainly a critical requirement for reaching a semblance of equilibrium. However, even with the best laid plans, there are inevitably gaps between how I *plan* to spend my time (e.g., revising and submitting a manuscript) and how I *actually* spend my time (e.g., zoom meetings while entertaining a sick toddler who had to stay home from daycare). I'll discuss how my group management and mentoring approach has evolved over the past six years of my career thanks to trial-and-error and a good deal of “mentoring up” from my endlessly-patient students, and I'll share the toolkit that I've developed in an effort to foster a

diverse, self-driven, collegial, and growth-oriented research group.

2:45 PM BREAK

SESSION BI01.03: Grant Writing and Publishing

Session Chair: Shayandev Sinha

Monday Afternoon, November 28, 2022

Hynes, Level 1, Room 105

3:15 PM *BI01.03.02

The Art and Science of Writing and Publishing Impactful Papers [Gopal R. Rao](#)^{1,2}; ¹Materials Research Society, United States; ²MRS Bulletin, United States

The importance of publishing one's research cannot be understated, for scientists in general, but for early career researchers in particular. Publishing papers is part of the scientific research endeavor to communicate our results and move science forward. However, it is important to publish in the right journal and in the right format. The quality of the science is of course foremost when considering a publication, however, the quality of writing and ease of communication are critical for acceptance of papers as well as for subsequent citations. This talk will overview the scientific scholarly publication process, including the process of writing up your research, deciding the journal and format, composing an outstanding manuscript, submitting the paper, and navigating the publications process including managing reviews. There are many nuances to writing and publishing scientific papers, and this presentation will cover several of them.

3:45 PM *BI01.03.03

NSF's Division of Materials Research—Opportunities and Requirements [Birgit Schwenzer](#); National Science Foundation, United States

The National Science Foundation is well-known for supporting innovative and transformative research. Just as importantly though, significant emphasis is placed on training the next generation of STEM researchers and educators as well as increasing diversity, inclusion and equity in STEM as part of the grants awarded. Every single proposal contains a broader impacts section to address these or other aspects, justifying how the proposed research benefits society.

The Division of Materials Research (DMR) supports fundamental materials research through its eight Topical Materials Research Programs (TMRPs): Biomaterials, Ceramics, Condensed Matter and Materials Theory, Condensed Matter Physics, Electronic and Photonic Materials, Metals and Metallic Nanostructures, Polymers, and Solid State and Materials Chemistry. Additionally, there are regularly opportunities to submit proposal for centers and center-type activities. This presentation addresses opportunities to engage with DMR either as a principal investigator on a proposal or as a reviewer.

SESSION BI01.04: Career Pathways II

Session Chairs: Isabel Gessner and Katherine A. Mazzio

Tuesday Morning, November 29, 2022

Hynes, Level 1, Room 105

10:00 AM *BI01.04.02

Being Intentional about the Industry-To-Academia Transition and Other Thoughts on Preparing for an Academic Career [Aaron D. Franklin](#); Duke University, United States

Ask ten professors their opinions about the pros and cons of a post-doctoral transition from industry to academia and you're likely to get ten different answers. Given this variance in perspective, are there any commonalities regarding how to make the transition to a faculty position as successful as possible? In my opinion, there are and I will offer these best practices in this talk. The points I share are based on my experience in transitioning to academia after spending six years on the research staff at IBM. My perspective has been further developed by my observation of faculty recruiting these past 8+ years as a professor at Duke. There are certain things a person can do while in a PhD-level industry position to improve their preparation for, and future opportunities in, a faculty position. Most of these recommended steps must be intentional, meaning they will not often develop naturally in the regular course of working in industry. They include seeking mentoring opportunities, building a teaching portfolio, and maintaining a track-record of innovation. Importantly, these points are also completely relevant to those working in other areas (e.g., government labs) or even PhD students still determining the best first steps to take in their career. There's no perfect recipe for attracting and succeeding in a faculty position, but being intentional in your preparation can certainly help your chances for success!

SESSION BI01.05: Scientific Leadership and Education

Session Chair: Shayandev Sinha

Tuesday Afternoon, November 29, 2022

Hynes, Level 1, Room 105

1:30 PM *BI01.05.01

Inclusive Practices in the Classroom, Laboratory and Workplace [Rebecca J. Anthony](#); Michigan State University, United States

Changing the climate for underrepresented minorities in Materials Science and Engineering, and other STEM fields, is one issue at the forefront of broadening participation in these areas. The solution to effecting this change is not a sweeping singular event, but instead a mobilization of each member of

the community to take action towards diversity, equity, and inclusion (DEI). Across academic and industrial professions, there is an increasing emphasis on a potential job candidate's DEI efforts – with many job applications as well as promotion packets requiring a statement on the candidate's activities and interests around DEI. But for many, deciding what exactly one's interests are – and how to promote DEI in classroom, research lab, and professional settings, can feel daunting to say the least. Additionally, sometimes it can be difficult to envision the change that is needed to reach an improved climate for underrepresented groups. However, small steps taken in all of these settings can go a long way in improving the climate for everyone, and by recognizing these small actions, we can not only learn about how to promote DEI in our own professions but also gain perspective on the activities that can make a big impact, but also suit our personalities and interests.

In this presentation, I will share some ideas for best practices to create an inclusive learning, research, and work environment and how those practices can become structured parts of our professional lives. I will also outline the vision of what an inclusive, diverse, and equitable Materials Science and Engineering workplace and educational space could look like – and how to selectively participate in achieving this vision by leveraging your strengths and interests towards activities that have demonstrated impact in promoting DEI.

2:00 PM BI01.05.02

Embedding Scientific Training in Course-Based Research for Undergraduates—An Example of a Lab Bundle for Clean Energy Research Yiliang Luan; Binghamton University, The State University of New York, United States

Research Experience for Undergraduates (REU) is popular as students can get diverse research experience over the summer. However, course-based research for undergraduates is rare but provides more than just research experience. In such courses, scientific training is usually embedded in individual practical labs for different training purposes, but these discrete contents make it hard for students to utilize their accumulated knowledge in their further research. To resolve this issue, a bundle of successive and interconnected labs enclosed with scientific training based on the study of perovskite quantum dots (PQDs) will be presented as an example. Determination of photoluminescence quantum yield is first set for the practice of basic lab skills such as transfer, measurement, and dilution. Supersaturation synthesis of CsPbBr₃ PQDs is adopted followingly due to its simplicity. Microwave synthesis of CsPbBr₃ PQDs is used as a transition before the students move to the more complicated hot-injection method. These successive labs are enclosed with scientific research principles such as methods screening, interpretation of method in literature into a practical procedure, impact from the ambient environment, viable controls, and united data analysis. Additionally, these labs are carried out in different teaching modes, including peer-mentor leading, instructor facilitating, and fully independent, which could occur when students start research in a new lab. Eventually, the students not only have sufficient hands-on experience but also can understand the principles of experimental designs and processes. This successive and interconnected lab bundle demonstrates a way to embed the scientific training in the course-based research, which achieves the goals of accumulating research experience, practicing lab skills, and understanding the scientific principles simultaneously at the initial research stage for undergraduates.

2:15 PM BI01.05.03

Innovation Fellowship—Novel Postdoctoral Training to Build a Pipeline of Innovation-Minded Professionals and Promote Commercialization in Academic Units Anastasia Visheratina¹, Dylan Neale¹, Kaylee Steen¹, Elizabeth H. Peters¹, Nadine Wong² and Joerg Lahann¹; ¹University of Michigan–Ann Arbor, United States; ²Duke University, United States

The Biointerfaces Institute (BI) at the University of Michigan (U-M) is rooted in the mission to advance biomedical discoveries by disrupting the status quo of isolated science and fostering cross-disciplinary technological breakthroughs in nanotechnology, advanced materials, cell engineering, and neural engineering. By co-locating 28 research groups from twelve departments across the U-M schools of Engineering, Dentistry, Medicine, and Pharmacy, forward-thinking collaborations lead to healthcare breakthroughs and advanced learning. To further accelerate the path from basic research to real-world health outcomes, the BI has created a novel postdoctoral fellowship to train the next generation of scientists in commercialization and translation. The Innovation Fellowship provides a blueprint for biomedical research units to train and mentor individuals in a systematic manner that encourages out-of-the-box thinking, experiential learning that supports commercialization efforts, and enhances the network of innovation leaders.

The Innovation Fellowship focuses on five main objectives, with the help of its strategic partners, to develop the Fellows' professional competencies in translation and commercialization. Fellows will receive (1) Innovation & Entrepreneurship Training, (2) Networking and Mentorship, (3) Professional Development Opportunities, and engage in (4) Technology Assessment and (5) Facilitate Project Development at all stages of the commercialization pipeline. In January 2022, BI launched the first of its kind Innovation Fellowship with Dr. Dylan Neale and Dr. Anastasia Visheratina as the inaugural cohort Fellows. During the term, fellows are trained to become a champion of innovation and translation at BI, advance BI's commercialization resources, and collaborate with BI research groups to uncover new projects with commercialization potential. They also engage with stakeholders to understand the opportunities and challenges of potential innovations as well as work with BI teams to advance projects.

Collectively, the Innovation Fellowship is creating a new pipeline of scientifically trained individuals and developing them as commercialization thought leaders to advance precision medicine, detect diseases earlier, restore body function, and improve drug delivery. In my talk, I will give a thorough overview of the Innovation Fellowship, our results, and its influence on my career development.

2:30 PM BI01.05.04

A Framework for Infusing Data Science and Computation into Engineering Curricula Wesley Reinhart, R. A. Kimel, Ryan Solnosky and Rebecca Napolitano; The Pennsylvania State University, United States

While data science, data analytics, and machine learning topics continue to grow in popularity with engineering students and employers, so does the gap between practical skills needed in the modern computing environment and fundamental concepts taught in traditional engineering curricula (i.e., mathematical, computational, and statistical foundations). Despite the known benefits of contextualizing data science education to domain-specific knowledge, it remains a significant challenge for faculty without formal training in data science to develop curriculum to support the integration of data-science-related topics with existing curricula. The National Academies have also cited challenges in (i) recruiting and retaining faculty to teach integrated introductory courses in data science and (ii) encouraging industry partnerships to keep the education and training of the workforce well matched to the needs of the industry. Thus, a framework for teaching data science to engineers which considers domain-specific knowledge, ethical problem solving, transferability to new faculty and new institutions, and which encourages industry partnerships is needed.

In this talk, we will describe our current progress and future plans for an ongoing collaborative project between six universities and colleges as a part of the NSF Data Science Corps program. The objectives of this project are to facilitate data science education and workforce development for engineering and related topics, provide opportunities for students to participate in practical learning experiences, and expand and diversify the data science talent pool. To this end, our team is curating curriculum and datasets which will be made available to undergraduate instructors nationwide. These resources are intended to include everything that engineering faculty would need to port any part of this data science education framework into their own courses, reducing the barrier to implementation. Furthermore, they will be developed in collaboration with industry contributors to enable workforce development and build closer relationships between educators and employers of the next generation of engineers.

2:45 PM BI01.05.05

Biomolecular Electronics Experiments Using Nanoscience and Biophysics from an Undergrad Perspective Aderlyn M. Castillo, Keshani G. Pattiya Arachchillage, Subrata Chandra and Juan M. Artes Vivancos; University of Massachusetts Lowell, United States

The scanning tunneling microscope (STM) was the first artifact capable of non-destructively imaging matter with an atomic-scale resolution. Over 30 years ago, Gerd Binnig and Heinrich Rohrer shared the Nobel Prize for Physics for inventing the first STM¹. Beyond topographic imaging, STM offers the possibility of spectroscopic measurements with high resolution (atomic in many cases). This opened the door to single-molecule electrical measurements². The scientific community was astounded when the electronic conductance of individual molecules bound between electrodes could be measured reliably³ using the scanning tunneling microscope break junction (STMBJ) method. The STMBJ method is a powerful technique for creating single-molecule junctions and studying charge transport in biomolecules. In this method, the current is measured while the STM tip is brought into contact with the sample and retracted from the substrate surface several times⁴. The current recorded (I) can be related to conductance (G) by $G = I/V$, with V being the voltage, and conductance histograms can be constructed by acquiring thousands of curves to determine an individual molecule's conductance⁵. On the other hand, the current-time method provides less yield and is used to study the spontaneous formation of molecular junctions⁴. STM has applications in a variety of other disciplines, including biophysics⁶ and biomedicine⁵. From the biophysics perspective, it can be used to detect biomolecular interactions electrically⁷. On the other side, from the biomedicine perspective, it could be used to detect detrimental diseases such as cancer and COVID and its variants⁵. In this contribution/Herein, we show an overview of the STMBJ method applied to the study of biomaterials and individual biomolecules⁶ from an undergraduate perspective, in the context of the immersive scholars UML summer challenge. The results include high-resolution STM substrate imaging in air and buffered solution and preliminary trials on molecules and biomolecules. These results, potential problems, and alternative solutions open the doors to further develop STM, automatizing and miniaturizing it to make it a widespread user-friendly nanotechnology tool.

References

1. Binnig, Gerd, and Heinrich Rohrer, "Scanning tunneling microscopy." *Surface science* 126.1-3. (1983): 236-244.
2. Mzoughi T. Salem Press Encyclopedia of Science, 2022, 6p, 89317201. Scanning Tunneling Microscopy And Atomic Force Microscopy.
3. Nichols RJ. STM studies of electron transfer through single molecules at electrode-electrolyte interfaces. *Electrochimica Acta*. 2021;387. doi:10.1016/j.electacta.2021.138497
4. Lee W, Reddy P. Creation of stable molecular junctions with a custom-designed scanning tunneling microscope. *Nanotechnology*. 2011;22(48):485703. doi:10.1088/0957-4484/22/48/485703
5. *J. Mater. Chem. B*, 2021,9, 6994-7006. RNA Biomolecular Electronics: towards new tools for biophysics and biomedicine.
6. Chandra, S., Arachchillage, K. G. G., Kliuchnikov, E., Maksudov, F., Ayoub, S., Barsegov, V., & Artes Vivancos, J. M. (2022). Single-Molecule conductance of double-stranded RNA oligonucleotides. *Nanoscale*, 14(7), 2572-2577.
7. Chandra, S., Arachchillage, K. G. G., Kliuchnikov, E., Maksudov, F., Castillo, A., Barsegov, V., & Artes Vivancos, J. M. (2022). Base-mediated electrical conductance through individual single-stranded RNA molecules. In preparation.

SESSION BI01.06: Virtual Session
Session Chairs: Isabel Gessner and Shayandeve Sinha
Tuesday Afternoon, December 6, 2022
BI01-virtual

1:30 PM *BI01.06.02

A Perspective from an Early Career Scientist Working in a National Lab Wanyi Nie; Los Alamos National Laboratory, United States

At the end of the PhD training, it is time to decide the future career path. It can be confusing and a challenging time. Here I will share my path after graduating from Wake Forest University, and pursuing my research career at Los Alamos National Laboratory. I started as a postdoc research associate and then converted to a staff scientist. After my conversion, I have obtained significant experiences about maintaining a research group, raising funding, mentoring students and postdocs. In particular, I will discuss my experience and what I've learnt from the grant applications. Further, I will share my experience conducting research, mentoring postdoc and students in a national laboratory environment.

2:00 PM BI01.06.03

Developing Entrepreneurial Mindset in Engineering Students Through a Scaffolded Group Project Designing a Research Proposal Russell K. Pirllo; University of Dayton, United States

Entrepreneurial Mindset (EM) encompasses recognizing and identifying opportunities and applying one's skillset to create value and impact by solving societal problems. The Kern Entrepreneurial Engineering Network (KEEN) promotes a framework for entrepreneurial-minded learning (EML) comprised of three student learning outcomes that contribute to an EM, curiosity, connections, and creating value (the 3 C's). We present a collection of learning modules comprising a semester-long scaffolded approach to developing curiosity and creating value by identifying and addressing technical gaps through a group project writing an engineering research proposal. These modules were designed for and implemented in upper-level undergraduate and graduate-level biomedical engineering courses with the goal of developing all the three C's with emphasis on connections and creating value.

The collection of modules and course project accounted for half the effort in the course, and each module built upon the prior exercises and integrated core course content as well as a self-directed literature search. Project groups included 4-5 students from multiple majors within the undergraduate level. Modules included 'formative exercises' on sub-field exploration, strategic focus, needs finding, value/impact evaluation via quad-chart, technical gap identification, graphical organization of thought through technical approach and instrument diagrams, risk assessment and mitigation, proposal presentations, and a written proposal.

The impact of the modules was evaluated with a pre and post 5-point Likert scale survey. Based on multiple prior instruments evaluating EM, questions addressed students' self-perception of ability in ideation, open-mindedness, altruism, problem-solving, engaging stakeholders, value creation, ability to learn, analyzing market conditions, managing complex tasks, ability to anticipate technological developments, and intrinsic curiosity. Wilcoxon signed-rank statistical analysis revealed significant improvements ($p < 0.05$) in students' perception of their ability to manage complex tasks, cope with failure, lead a team to work on a project, actively seek as much information as they can in a new situation, and anticipate technical developments. Strategies to evaluate the effectiveness of individual assignments to impact specific outcomes will be discussed, including recommendations on question types and using Learning Management System (LMS) metrics in combination with assessment instruments. Finally, the work demonstrates how to leverage research experience in the classroom to train students for careers in academia or industry.

2:15 PM *BI01.06.04

On a Personal Journey from an Industrial Research Lab to Academia [Jihui Yang](#); University of Washington, United States

I am the Vice Dean of College of Engineering and Kyocera Chair Professor in the Materials Science and Engineering Department of the University of Washington (UW). My research interests include Electrochemical Energy Storage, Solid State Energy Conversion, Electrocatalysis, and Transport Properties of Two-dimensional Materials.

In my current role as the principal research administrator, I develop and facilitate faculty-led research, and I focus on integrating research to meet the college's educational goals. More precisely, I am responsible for ensuring ethical, creative, and efficient research conduct. Prior to joining the U.W in the Fall of 2011, I was a Technical Fellow and Lab Group Manager at General Motors Research and Development Center, where I started working as an intern in 1995.

My talk will recount my professional and personal journey from being an intern, scientist, lab manager, faculty member, and how these roles best prepared me for my current role as a university administrator. Therefore, I will share back stories, projects that I worked on, challenges I overcame, the lessons that I learned, and how I have found great satisfaction throughout my journey. Above all else, I would like to share my personal experiences with individuals that wish to make a change within their respective fields.

2:45 PM DISCUSSION TIME

SYMPOSIUM CH01

Understanding Dynamic Processes of Materials Synthesis, Self-Assembly and Processing via In Situ Techniques
November 28 - December 7, 2022

Symposium Organizers

Qian Chen, University of Illinois at Urbana-Champaign
Yu Han, King Abdullah University of Science and Technology
Barnaby Levin, Direct Electron LP
Dongsheng Li, Pacific Northwest National Laboratory

Symposium Support

Bronze
King Abdullah University of Science and Technology
MilliporeSigma

* Invited Paper
+ Distinguished Invited

SESSION CH01.01: Characterization Self-Assembly Process and Its Controlling Factors I
Session Chairs: James De Yoreo and Dongsheng Li
Monday Morning, November 28, 2022
Hynes, Level 1, Room 102

10:30 AM +CH01.01.01

An *In Situ* Look at Interfacial Controls on Crystallization and Self-Assembly in Inorganic and Biomolecular Systems [James J. De Yoreo](#)^{1,2}; ¹Pacific Northwest National Laboratory, United States; ²University of Washington, United States

Interfaces play a critical role in solution-based phenomena, such as ion segregation, mineral nucleation, and biomolecular and colloidal self-assembly. The interface alters the distribution of water and ions from that of the bulk, introduces an interfacial free energy that largely determines the free energy barrier for nucleation, and creates an entropic repulsion that acts like a volume exclusion force to drive colloidal assembly. The origin and characteristic length scales of these phenomena are inherently atomic-to-molecular but are manifest in ensemble dynamics and outcomes. Moreover, processes like nucleation and self-assembly arise from fluctuations, making the events that must be probed transient in nature. Consequently, in situ imaging techniques that can capture structure and its evolution, particularly at high speed, are required to build a quantitative picture of such processes. Here I use examples from and in situ TEM, high-speed AFM and fast force mapping studies of interfacial structure, nucleation, and assembly in inorganic and biomolecular systems to elucidate the mechanisms by which interfaces direct these processes, leading to unique pathways, materials and morphologies. The results reveal the importance of surface charge, chemical gradients, colloidal forces, molecular mobility, and solvent organization near interfaces in determining how ordered materials emerge from the solution.

11:00 AM CH01.01.02

Understanding of Non-Classical Crystal Growth via Particle Assembly via *In Situ* Liquid Cell TEM [Dongsheng Li](#); Pacific Northwest National Laboratory, United States

The nanoparticle assembly into structures of superlattices and crystals attracts great attention due to their unique optical, thermoelectric, magnetic, energy storage, and catalytic properties. Understanding of mechanisms of particle assembly and interaction between active species can help to establish conditions to control the assembly process and structures of superlattices and crystals, which are closely tied to the physical and chemical properties. However, little is known about the driving forces and controlling factors during the process of particle self-assembly. In this work, we analyzed dynamic information of the process and investigated the Van der Waals force, steric hindrance, Brownian force, and the hydrodynamic force, based on measured particle positions and velocities by directly observing the process of particle self-assembly and tracking individual particles as a function of time via *in situ* TEM. We studied the crystal surface interactions as a function of pH, electrolyte type, and concentration. We further studied the crystal growth process via particle-oriented attachment, a special type of particle assembly. The results of this work enable the control of particle assembly and the resulting structures and the design of materials with tailored properties.

11:15 AM CH01.01.03

Nanostructural Transformation of Photo-Crosslinking Peptides Visualized by *In Situ* Liquid-Phase Transmission Electron Microscopy Junho Hwang and Eunji Lee; Gwangju Institute of Science and Technology, Korea (the Republic of)

Peptide self-assembling nanostructures based on diphenylalanine (FF) can have organized beta-sheet secondary structures that can result in the formation of spheres, cylinders, and tubes depending on the strong interaction of phenyl groups between adjacent derivatives. Due to the structural stability and biocompatibility of FF, it has been widely used in biological applications such as drug delivery and tissue regeneration, and its biological significance has motivated numerous research fields including self-assembly and functional biomaterials with mechanical, piezoelectric, and semiconductor properties. Up to now, the conventional bulk solution characterization approaches have been used for the majority of studies on the kinetics, dynamics, and phase transitions of FF assemblies, however, these technologies lack a direct understanding of the dynamics and morphology. In this study, short peptides were modified using a tyrosine-mediated crosslink to adopt the characteristic of the resilin of the dragonfly, vinegar fly, and beetle that photooxidation-reduction can occur and alter the antiparallel structure to generate 1D nanostructure. In this context, protein-mimetic structural evolution was investigated. Through the use of liquid-phase transmission electron microscope (LP-TEM) imaging, the structural conversion of 1D to 3D structures by peptide cross-linking was demonstrated. This result suggests that because of their packing sensitivity and geometrical limitations, the nature-protein motion should be studied to acquire insights for developing peptide-based materials. Furthermore, the observation of the assembly and dynamics of FFs in real-time with LP-TEM would enable us to understand the paths for assembly and phase transformations.

11:30 AM CH01.01.04

Real-Time Study of Surface-Guided Nanowire Growth by *In Situ* SEM Ernesto Joselevich; Weizmann Institute, Israel

The large-scale assembly of NWs with controlled orientation on surfaces remains one challenge toward their integration into practical devices. During the last decade, we have reported the growth of perfectly aligned, millimeter-long, horizontal NWs of GaN, ZnO, ZnSe, ZnTe, CdSe, CdS, CsPbBr₃ and other materials, with controlled crystallographic orientations on different planes of sapphire, SiC, quartz, and spinel. The growth directions and crystallographic orientation of the NWs are controlled by their epitaxial relationship with the substrate, as well as by a graphoepitaxial effect that guides their growth along surface steps and grooves. We demonstrated the massively parallel "self-integration" of NWs into circuits via guided growth and the production of optoelectronic nanosystems, including photodetectors, photodiodes and photovoltaic cells. This talk will focus on our systematic studies aimed at understanding the mechanism of guided nanowire growth based on both *in situ* and *ex situ* kinetic studies. *Ex situ* studies reveal the role of dimensionality in guided growth being controlled by the surface-diffusion of adatoms over the substrate. *In situ* SEM studies yield beautiful movies of guided nanowires growing in real time, and reveal intricate details of the guided growth mechanism.

SESSION CH01.02: Characterization Self-Assembly Process and Its Controlling Factors II

Session Chairs: Judy Cha and Frances Ross

Monday Afternoon, November 28, 2022

Hynes, Level 1, Room 102

1:45 PM *CH01.02.01

Multi-Modal *In Situ* Characterizations for Phase Transformations of Nanomaterials Judy Cha^{1,2}; ¹Yale University, United States; ²Cornell University, United States

Understanding the dynamic processes of materials synthesis and phase transformation is indispensable for most applications as these processes determine the microstructure and thus the properties of materials. *In situ* techniques can uniquely capture short-lived transient states and time-dependent changes in structure-property relations during the synthesis and phase transformation, thus providing important information and opportunities to engineer the dynamic processes and ultimately material properties.

In this talk, I will discuss several examples of nanoscale phase transformations and syntheses in which the changes in structure and properties were systematically and directly probed by *in situ* TEM (cooling, liquid synthesis, heating, and electrical biasing), *in situ* Raman spectroscopy, and *in situ* electron transport measurements. These examples will include discovery of metastable and transient intermediate phases during synthesis of metal and metal oxide nanostructures, emergence of new electronic phases via intercalation of metal ions in two-dimensional materials, effects of heterointerface and nanoscale confinement on the thermodynamics of phase transformations in various two-dimensional and quantum materials. In each example, unexpected nanoscale effects and the unique advantages of *in situ* techniques to capture the nanoscale effects will be highlighted. In particular, the importance of multi-modal *in situ* characterization approach will be emphasized, which is necessary to establish structure-property relationships during these dynamic processes.

2:15 PM CH01.02.02

Synthesis of Alkyne-Bearing Nanoparticles by SET CRP Polymerisation Induced Self-Assembly Daniela V. Tomasino¹, Ruairi Brannigan² and Andreas Heise¹; ¹Royal College of Surgeon in Ireland, Ireland; ²Dublin City University, Ireland

Polymerization-induced self-assembly (PISA) has emerged as a straightforward methodology for the *in situ* preparation of nano-objects with tuneable shape and dimensions.^{1,2} Copper catalysed alkyne-azide cycloaddition (CuAAC) is a robust synthetic method with the aim of binding two molecular blocks together through heteroatom linkages (C-X-C).³ The integration of the two techniques creates a facile strategy for the design of versatile nanoparticles. In this work, the combination of PISA and CuAAC allowed for the preparation and post-functionalization of NPs due to the incorporation of a propargylic

moiety within the hydrophilic shell of the NPs. The NPs were prepared *via* aqueous dispersion single electron transfer living radical polymerization induced self-assembly (SET-LR-PISA). Poly(ethylene glycol methyl ether methacrylate)-*statistical*-poly(propargyl methacrylate) [P(PEGMA)]₁₈₋₅-P(PgM)₅] was obtained by conventional atom-transfer copolymerization (ATRP). The hydrophilic macroinitiator was then chain extended with 2-hydroxypropyl methacrylate (HPMA) *via* SET-LRP, which induced self-assembly, yielding [P(PEGMA)]₁₈₋₅-P(PgM)₅-*b*-[PHPMA] NPs. Fixing the mean molecular weight of [P(PEGMA)]₁₈₋₅-P(PgM)₅] to 6.2 kDa and varying HPMA DP, monomer conversion of the system was investigated *via* ¹H NMR and the stability was improved thanks to the addition of tetrabutyl ammonium salt during the reaction. The final diblock copolymer structure was analysed *via* ¹H NMR, GPC. The remaining copper concentration in the final product was assessed by inductively coupled plasma mass spectroscopy (ICP MS) analysis. After having characterized the NPs in terms of size and shape *via* dynamic light scattering (DLS) and transmission-electron microscopy (TEM), the corona was functionalized with various compounds *i.e.* fluorescein azide, methoxypolyethylen glycol azide, mannosyl derivatives; demonstrating that the system provides a unique platform for the preparation of biorelevant modifiable materials through ATRP type polymerisation.

1. Karagoz, B.; Esser, L.; Duong, H. T.; Basuki, J. S.; Boyer, C.; Davis, T. P. *Polym Chem.* 2004, 5 (2), 350-355
2. Blanz, A.; Ryan, A. J.; Armes, S. P. *Macromolecules* 2012, 45 (12), 5099-5107
3. Kolb, H. C.; Finn, M. G.; Sharpless, K. B. *Angew Chem Int Ed Engl* 2001, 40 (11), 2004-2021

2:30 PM CH01.02.03

Modification of Molecular Assemblies of Azobenzene Derivatives by Electrical Stimuli Sylvie Godey¹, Hugo Therssen¹, David Guérin¹, Yannick Dappe², Thierry Melin¹ and Stéphane Lenfant¹; ¹IEMN-CNRS, France; ²SPEC, France

In recent years, molecular switches such as azobenzene adsorbed on metal surfaces have attracted considerable attention due to their potential use in nanotechnology, information storage or molecular electronics [1,2,3]. In particular, the 3,3',5,5'-tetra-tert-butylazobenzene (TBA) molecule is a promising candidate for such studies, due to the four lateral tert-butyl-groups which act as "spacer leg" to reduce the electronic coupling between the active part of the molecule (azobenzene) and the metal surface. This azobenzene derivative switches reversibly between the two isomeric states (*trans*-TBA and *cis*-TBA). This isomerization has already been demonstrated by scanning-tunneling microscopy (STM) using either the electric field induced by the STM tip [4] or by exposure to UV or blue light [5].

Here we report another effect of electric field for one-monolayer TBA coverage on Au(111), both characterized by STM and non-contact AFM (nc-AFM) with sub-molecular resolution using stiff (length extensionalv resonator) probes. These studies enable to observe and characterize an in-situ modification of the formed TBA self-assembly under electrical stimuli.

After the TBA evaporation, molecules are organized on the Au(111) surface in the *trans* isomer with four lobes corresponding to the 4 "legs", with an apparent height of 0.25 ± 0.02 nm. STM imaging at 77K reveals domains only visible in negative polarity; by scanning these TBA assemblies at -2V, bright spots appear with an apparent height of 0.36 ± 0.05 nm confirmed by nc-AFM. These spots are usually associated to the *cis*-TBA induced by the *trans*-TBA to *cis*-TBA isomerization under the presence of an electric field [4]. For domains imaged with both polarities in STM, an in-plane rotation of TBA network is observed in STM and nc-AFM after scanning at negative polarity (-1V). The origin of this in-situ in-plane rotation will be discussed. These results show how crucial are the intramolecular and molecular-substrate forces control and understanding in the perspective of molecular electronics.

- [1] Huang, X. H.; Li, T., *Journal of Materials Chemistry C* 2020, 8 (3), 821-848.
- [2] Molecular Switches 2nd. B.L. Feringa, W. R. B., Ed. Wiley-VCH, Weinheim, Germany; 2011.
- [3] Thomas, L., Arbouch, I., Guérin, D., Wallart, X., Van Dyck, C., Mélin, T., Cornil, J., Vuillaume, D., Lenfant, S., *Nanoscale* 2021 13, 14, 6977-6990.
- [4] Alemani, M.; Peters, M. V.; Hecht, S.; Rieder, K.-H.; Moresco, F.; Grill, L., *E JACS* 2006, 128 (45), 14446-14447.
- [5] Comstock, M. J.; Levy, N.; Cho, J.; Berbil-Bautista, L.; Crommie, M. F.; Poulsen, D. A.; Frechet, J. M. J., *APL* 2008, 92 (12), 123107-3

2:45 PM CH01.02.04

Interfacial Dynamics of Cu-Cu₂O Nanocatalysts Unveiled Through *In Situ* Electrochemical Polymer Liquid Cell Electron Microscopy Jiawei Wan^{1,2}, Qiubo Zhang¹, Sophia Betzler¹, Junyi Shangguan^{1,2}, Qi Zheng¹, Xianhu Sun¹, Xinxing Peng¹, Xin Chen^{1,2}, Rohan Dhall¹, Karen Bustillo¹ and Haimei Zheng^{1,2}; ¹Lawrence Berkeley National Laboratory, United States; ²University of California, Berkeley, United States

The catalyst-electrolyte interfaces provide active sites which are fundamental for electrocatalysis. However, measuring structural dynamics of these delicate interfaces at atomic level remains challenging due to the limited experimental capabilities. Here, we report in situ electrochemical transmission electron microscopy (TEM) imaging of the interfacial evolutions of Cu-Cu₂O core-shell nanowires during electrochemical carbon dioxide reduction reaction (CO₂RR) using our newly developed polymer liquid cell. Our direct observations reveal that the catalyst-electrolyte interfacial interaction leads to several structural scenarios during CO₂RR, including Cu mass loss, Cu₂O shell fragmentation, and reshaping and growth of Cu nanoparticles. We find the competitive advantage of Cu-electrolyte interface is responsible for stabilizing Cu^I species, and the abundant grain boundaries with disordered intermediate structures contribute to high catalytic efficiency. Our study offers insights into catalyst-electrolyte interfacial evolutions during CO₂ electroreduction, and it suggests opportunity to study diverse electrochemical processes at the atomic resolution.

3:00 PM BREAK

3:30 PM *CH01.02.05

Patterning and Self Assembly on 2D Materials Visualized Using *In Situ* Electron Microscopy Frances M. Ross; Massachusetts Institute of Technology, United States

The fascinating characteristics of two-dimensional (2D) materials offer prospects for understanding new physical phenomena and developing innovative functional devices. *In situ* electron microscopy can play a critical role by providing the ability to pattern 2D materials as well as to image during deposition onto their surfaces. We first discuss *in situ* irradiation as a tool to drive local transformations in 2D materials, exploring in particular a rearrangement of the 2D magnet CrSBr that changes the layer orientation, aiming to modulate properties such as magnetic texture. We then explore *in situ* imaging of deposition onto 2D surfaces as a means to understand the growth mechanisms involved and the resulting morphology and defects of the deposited layer. In these experiments, controlled environment and atomic level precision offer unique benefits. The rapid advances in *in situ* TEM instrumentation therefore promise exciting future opportunities to understand and use nanoscale materials reactions to create complex structures based on 2D materials.

4:00 PM CH01.02.07

Light-Patterned Electrochemical Microbubbles for Large-Scale Precision Assembly of Nanocolloids Hyungmok Joh¹, Zhichao Ma², Peer Fischer³ and Donglei (Emma) Fan¹; ¹The University of Texas at Austin, United States; ²Max Planck Institute for Intelligent Systems, Germany; ³University of Stuttgart, Germany

Microbubbles in aqueous suspensions have enabled a variety of applications ranging from pumping, mixing, drug delivery, to nanoparticle assembly. However, as far as we know, it remains a formidable challenge to create arrays of bubbles and we are not aware of a method that permits custom patterns of bubbles to be dynamically formed and refreshed. In this work, we report a novel approach to achieve custom 'on demand' bubble patterns via an opto-electrochemical technique. It permits us to achieve controlled bubble sizes in the range from a few to ~140 micrometers. Entire patterns can be formed in ~1 second, including lattices, rings, squares, and arbitrary 2D images. The required minimum light intensity (532 nm) of ~0.1 W / cm² is similar to that of sun light, several orders of magnitudes lower than those of optothermal/optoelectronic printing methods, which makes the reported technique parallel and scalable. Interestingly, the bubble patterns can be used to assemble structures from nanocolloids. For a demonstration, we show that nanocolloids can be arranged into different patterns on substrates with light-addressed electrochemical microbubbles across a dimension of millimeters and at an accuracy of less than 1 μ m. This forms a new printing technique that is quite general and that enables fast and non-contact particle assembly and manipulation. We expect that it will find application in nanomanufacturing, single-cell biotechnology, and in arranging optoelectronic building blocks.

4:15 PM CH01.02.08

Insights into the Kinetics and Self-Assembly Order of Hybrid Small-Molecule Organic Semiconductor / Quantum Dot Blends During Blade Coating Daniel Toolan¹, Michael P. Weir², Richard Jones³ and Anthony J. Ryan¹; ¹Department of Chemistry, The University of Sheffield, United Kingdom; ²The University of Nottingham, United Kingdom; ³The University of Manchester, United Kingdom

Hybrid organic-inorganic nanocomposite films formed from blends of small-molecule organic semiconductors and colloidal quantum dots are attractive candidates for high efficiency, low-cost solar energy harvesting devices. Understanding and controlling the self-assembly of the resulting hybrid material is crucial in optimising device performance, not only at a lab-scale but for large-scale, high-throughput printing and coating methods. This talk will show how *in situ* grazing incidence X-ray scattering (GIXS) gives direct insights into how small-molecule organic semiconductors and colloidal quantum dots self-assemble during blade coating. Results show that for two blends separated only by a small difference in the structure of the small molecule forming the organic phase, crystallisation may proceed down two distinct routes. It either occurs spontaneously or is mediated by the formation of quantum dot aggregates. Irrespective of the initial crystallisation route, the small-molecule crystallisation acts to exclude the quantum dot inclusions from the growing crystalline matrix phase. These results provide important fundamental understanding of structure formation in nanocomposite films of organic small molecules and colloidal quantum dots prepared via solution processing routes. This work highlights the fundamental difference to structural evolution which can be made by seemingly small changes in system composition. It provides routes for the structural design and optimisation of solution-processed hybrid nanocomposites that are compatible with the large scale deposition manufacturing techniques that are crucial in driving their wider adoption in energy harvesting applications.

SESSION CH01.03: Crystal Nucleation and Growth I
Session Chairs: Jungwon Park and Haimei Zheng
Tuesday Morning, November 29, 2022
Hynes, Level 1, Room 102

8:00 AM CH01.03.01

Self-Assembly of Polystyrene on Graphene Nanoplatelets Surfaces Yu-Chung Lin¹, Tavan Bhatia², Haaris Alam³, Ruijia Zhang⁴, Gavin Onghai⁵ and Miriam Rafailovich¹; ¹SUNY Stony Brook University, United States; ²Staples High School, United States; ³Portola High School, United States; ⁴Ed W. Clark High School, United States; ⁵Earl L. Vandermeulen High School, United States

Polymer nanocomposites (PNCs) with a reinforced filler, are significant in engineering applications to enhance functional properties. The key parameter that influenced the final performance is the dispersion of the fillers, the shape of the fillers, and polymer-fillers interfacial properties. Thus, it is crucial to investigate the dynamics of the polymer nanocomposites in the melts to understand the behavior of the PNCs. Here, we are trying to design a polymer blend nanocomposite with a better affinity polymer to the Graphene nanoplatelets (GNPs) and a lower affinity polymer to GNPs to create a percolation pathway.

We probed the relative affinity for GNP in PS and PMMA. Affinity for the nanoparticle inclusion is evidenced by adsorption of the polymer chains which decreases the internal tracer diffusion coefficient. Following the method developed by Hu et al for-silicate clays, we performed the following experiments to determine the impact on the internal chain mobility.[1] We made the following four sets of bilayer samples to measure the tracer diffusion coefficient; PS on PS/dPS, PS on dPS/GNP, PS/GNP on dPS/PS, and PS/GNP on dPS/GNPs, where in all cases the DPS and GNP concentrations were 20 and 2 weight percent, respectively. All the samples were annealed at 150°C for 24 hours then the concentration of deuterium, carbon, hydrogen, and Si ions within the sample were profiled using time-of-flight Secondary Ion Mass Spectrometry (TOF-SIMS). The tracer diffusion coefficients for the four types of samples were, 2.8 x10⁻¹⁷cm²/s, 6 x10⁻¹⁸cm²/s, 3.8 x10⁻¹⁷cm²/s, and 1.1 x 10⁻¹⁷cm²/s, respectively. From the data we see that the largest decrease in the coefficient occurred when the GNP was in both upper and lower layers, indicating adsorption of the PS chains to the GNP. A similar study will be performed for PMMA/dPMMA. It is interesting to note that the diffusion coefficient was higher than the control when dPS was migrating towards an HPS layer containing GNP, while the coefficient was lower than the control when the GNP and the DPS were in the same layer. We, therefore, hypothesized that in addition to the adsorption of GNP to PS, preferential adsorption existed between dPS and GNP relative to the PS GNP interaction. This was further investigated by measuring the contact angle between dPS or PS and a graphene-coated Si surface. From the contact angle and the known surface tension, we obtain work of adhesion of 40.42 mN/m and 60.71 mN/m confirming the higher interfacial energy. DFT calculations were performed by placing PS molecules onto graphene surfaces where the energy for different conformations was calculated. In each case, attractive interactions were obtained confirming the diffusion results. Comparing the dPS to HPS calculations we obtain a measurable difference -0.022 eV for fully adsorbed dPS molecules in agreement with the difference in the work of adhesion measured. Comparing the outcome of this study with that of ref 1, we find that the relative difference in attraction between HPS and dPS has to be considered in the interpretation of the results, and dPS cannot use an indiscriminate tracer molecule.

1 Hu, X. S.; Zhang, W. H.; Si, M. Y.; Gelfer, M.; Hsiao, B.; Rafailovich, M.; Sokolov, J.; Zaitsev, V.; Schwarz, S., Dynamics of polymers in organosilicate nanocomposites. *Macromolecules* 2003, 36 (3), 823-829

8:15 AM CH01.03.02

Controlled Synthesis of Targeted Nanoparticles Using *In Situ* X-Ray Synchrotron Techniques with Inline UV-Vis Measurements and Machine Learning Assisted Predictions Sanjit Ghose¹, Matthew Greenberg², ChengHung Lin¹ and Ai Kagawa¹; ¹Brookhaven National Laboratory, United States; ²Bard College, United States

Metal halide perovskites quantum dots (QDs) have recently attracted attention for use in a wide variety of optoelectronic applications, including solar cells

and light emitting diodes, due to their ease of synthesis, strong light absorption, and chemical tunability. The chemical synthesis of these materials enables precise control over the size, shape, and composition. Despite substantial progress in the synthesis of QDs over the past three decades, issues with scalability and batch-to-batch variation persist. These issues are a symptom of the complexity of crystal nucleation, limited understanding of the QDs formation mechanisms, and poor control over the rapid kinetics of formation. To address these issues, we developed a continuous flow reactor with automated input parameter control during the reaction process. The solution is monitored *in situ* to measure the reactants and intermediates along each stage of the nucleation and growth processes. The ability to rapidly canvas the input parameter space and collect *in situ* Synchrotron X-ray and photophysical data generates large data sets to identify the effects of reaction conditions on reaction outcomes. The data was analyzed to obtain corresponding time resolved structure, morphological information, and photophysical properties. Subsequently, using Artificial Intelligence (AI) & Machine Learning (ML) algorithms to understand the underpinning mechanisms, we identify variables that control the outcome of the colloidal synthesis, and achieve the targeted structure of the PQDs. In this case, we studied sub-sec snap shots of nanocrystal pre-nucleation, nucleation, and growth processes of room temperature flow synthesis of CsPbX₃ (X= Br, Cl, I) at NSLS-II synchrotron X-ray beamlines. This approach enables precise control over the synthesis outcome and enhances the speed of targeted Quantum materials discovery.

8:30 AM +CH01.03.03

***In Situ* Transmission Electron Microscopy Imaging of Nanomaterials Growth and Transformations** [Haimei Zheng](#); Lawrence Berkeley National Laboratory, United States

An understanding of nanoscale materials transformations is significant for the synthesis and applications of nanostructured materials. At the atomic level, heterogeneity and fluctuations may play a governing role in the growth and transformation processes. The recent development of high-resolution liquid cell transmission electron microscopy (TEM) has enabled breakthroughs in our ability to follow the atomic level structural, morphological, or chemical changes of materials. Thus, it has provided an unprecedented opportunity to resolve the growth and transformation mechanisms of materials that cannot be predicted based on thermodynamic equilibrium. I will show our recent development of high resolution liquid cell TEM for imaging of nanoscale materials growth and transformations. With the high resolution liquid cell TEM, we have been able to study the defect-mediated ripening of Cd-CdCl₂ core-shell nanoparticles (CSN). Ripening was found to start by dissolution of the nanoparticle with an incomplete CdCl₂ shell, and that the Cd core that was exposed to the solution dissolved first. The growth of an Cd-CdCl₂ CSN was achieved by generating crack defects in the shell, followed by ion diffusion through the cracks. The healing of crack defects led to a highly crystalline CSN at the end. The formation and annihilation of crack defects in the shell, accompanied by disordering and crystallization of the shell structure, mediated the ripening of CSN in the solution. I will also show our in-situ high resolution liquid cell TEM study of the nucleation of CdS nanoclusters. The growth of semiconductor nanocrystals is classical in colloidal nanocrystal synthesis, and it has been studied for many years. However, this is the first time that we were able to achieve direct observe the growth of semiconductor nanocrystals. Many fascinating dynamic phenomena were achieved, and they provide critical insights on their nucleation and growth mechanisms.

9:00 AM CH01.03.04

Effects of Crystallization on the Conductance of HfO_x ReRAM by *In Situ* TEM Method Baoming Wang¹, [Alexandre Foucher](#)¹, Thomas Defferriere¹, Teodor Todorov², Martin Frank², Franco Stellari², Takashi Ando², John Rozen², Harry Tuller¹ and Frances M. Ross¹; ¹Massachusetts Institute of Technology, United States; ²IBM Thomas J Watson Research Center, United States

HfO_x is broadly explored as a favored material for resistive RAM (ReRAM) device applications. The microstructure, composition and phase of HfO_x all play fundamental roles in the switching mechanisms and stochasticity governing resistive RAM operations, and understanding the relation between the atomistic properties and final device behavior remains challenging. To guide the design of HfO_x-based ReRAM devices, we applied scanning transmission electron microscopy techniques to investigate the structure-property-behavior relationship during operation *in situ*. We developed a process to fabricate lamella devices that showed switching behavior consistent with the macroscopic state-of-the-art HfO_x ReRAM devices from which they had been cut. We then observed the compositional and structural changes taking place during switching of the device and correlated those with the electrical characteristics. We found that crystallization and grain growth occurs during repeated switching, and that the formation of crystalline regions correlates with increases in conductance. Using electron energy loss spectroscopy, we found that the grains formed during switching are more oxygen-depleted than the original amorphous phase. This hints at the role of oxygen vacancies in the conductance of these ReRAM devices. We also showed that other methods of forming crystalline regions, particularly electron beam irradiation, produce structures that are similar to the original amorphous phase or even more oxygen abundant, and do not contribute to increases in conductance. The combination of operando testing and structural and spectroscopic observation yields unique and detailed information on the processes that control switching. From the comparison of the different crystallization mechanisms, we discuss how the microstructure may be controlled to improve the cycling performance of the devices.

9:15 AM CH01.03.05

Multilayer Growth in Ternary InGaAs Nanowires Revealed by *In Situ* Transmission Electron Microscopy [Robin Sjökvist](#), Marcus Tornberg, Mikelis Marnauza, Daniel Jacobsson and Kimberly Dick; Lund University, Sweden

In Situ transmission electron microscopy (TEM) has proven itself to be an important and powerful tool for unraveling many different aspects of III-V semiconductor nanowire growth, including growth dynamics¹⁻³ and compositional relationships.^{4,5} Recently, the *In Situ* TEM investigations have shown the possibility of having more than one biatomic layer nucleate and grow simultaneously at the growth front of binary compound nanowires growing in the vapor liquid solid (VLS) mode.^{6,7} The classical view has been that liquid nanoparticle mediated growth only allows the nucleation and growth of singular layers, separated by incubation periods. The discovery of multiple nucleation events and subsequent growth of multilayers contradicts this previous assumption. The finding is important, since the possibility of multiple nucleations will change the way continuous growth is viewed, and unravels more details about the delicate energy balance at the growth front. Therefore, in order to gain a deeper understanding of the nanowire growth process, and to give new insight into axial nanowire growth, the multilayer growth mode must be further investigated.

In this study, the growth of Au-seeded InGaAs nanowires were investigated using environmental TEM, revealing the occurrence of multilayers in ternary nanowires *In Situ*. The experiments were carried out in a Hitachi HF3300S environmental transmission electron microscope with an open cell configuration, integrated with a metal-organic chemical vapor deposition (MOCVD) system. The MOCVD system was used to supply the metal-organic and hydride precursors for the growth near a resistively heated, partially electron transparent micro-electro-mechanical system (MEMS) chip. Pre-deposited Au nanoparticles on the MEMS chip collected the growth material and initiated the growth of the nanowires. The growth was observed and recorded using a Gatan OneView IS camera, and compositional analysis was carried out through X-ray energy dispersive spectroscopy.

We show that multilayer growth is more prominent in InGaAs than for the binary cases previously shown, and that when multilayer growth occurs, the stacks of layers growing simultaneously can reach much larger sizes.⁷ The multilayer stacks are observed in conjunction with defects in the material, such as crystallographic twins and small compositional changes, but also at sharper compositional heterostructures. Importantly, material transport is observed between the simultaneously growing layers, indicating that the final composition of the segment could be affected. We have also observed multilayer growth as an intermediate step to kinking, a process where the nanowire changes growth direction, which is often unwanted. Since composition and

uncontrolled kinking of the nanowire greatly affects its properties and performance, the discoveries are important for device applications. This shows why multilayer growth needs to be further explored, so that it can be controlled and accounted for in future nanowire growth.

References:

1. Maliakkal, C. B. *et al.* Independent Control of Nucleation and Layer Growth in Nanowires. *ACS Nano* **14**, 3868–3875 (2020).
2. Tornberg, M. *et al.* Kinetics of Au–Ga Droplet Mediated Decomposition of GaAs Nanowires. *Nano Lett.* **19**, 3498–3504 (2019).
3. Harmand, J. C. *et al.* Atomic Step Flow on a Nanofacet. *Phys. Rev. Lett.* **121**, 166101 (2018).
4. Maliakkal, C. B. *et al.* In situ analysis of catalyst composition during gold catalyzed GaAs nanowire growth. *Nat. Commun.* **10**, 4577 (2019).
5. Sjökvist, R. *et al.* Compositional Correlation between the Nanoparticle and the Growing Au-Assisted InxGa1–xAs Nanowire. *J. Phys. Chem. Lett.* **12**, 7590–7595 (2021).
6. Tornberg, M. *et al.* Direct Observations of Twin Formation Dynamics in Binary Semiconductors. *ACS Nanosci. Au* **2**, 49–56 (2022).
7. Gamalski, A. D. *et al.* Atomic Resolution in Situ Imaging of a Double-Bilayer Multistep Growth Mode in Gallium Nitride Nanowires. *Nano Lett.* **16**, 2283–2288 (2016).

9:30 AM CH01.03.06

In Situ Monitoring of 2D Nanocrystal Nucleation and Growth Kinetics by Using Time-Resolved Liquid Interface Grazing Incidence X-Ray Scattering Techniques [Ziyi Zhang](#) and Xudong Wang; University of Wisconsin - Madison, United States

The design and synthesis of high-quality two-dimensional (2D) materials with desired morphology are essential for property control. One critical challenge that impedes the understanding and control of 2D crystal nucleation and growth is the inability of direct observation of the nanocrystal evolution process with high enough time resolution. Here, we demonstrated an in situ X-ray scattering approach that directly reveals 2D nanocrystal nucleation and growth at the air-water interface.¹ A few-nm thick wurtzite ZnO nanosheets (NSs) were grown through the ionic layer epitaxy (ILE) method with the guidance of an ionic surfactant monolayer at the air-water interface. Fast monitoring of both in-plane and out-of-plane crystal structures were achieved with a time resolution of only a few minutes by applying grazing incidence X-ray diffraction (GID) and grazing incidence X-ray off-specular scattering (GIXOS) techniques, allowing direct observation of the 2D crystal nucleation and growth processes with a unit-cell resolution. We discovered an obvious lattice deformation in the first two surface layers, which is different from the inner bulk phase. This discovery of surface strain in ILE may open a new route toward strain-induced physical property tuning of 2D nanomaterials by surfactant engineering. Our results also uncovered a lateral to vertical growth kinetics switch phenomenon in the ZnO nanosheet growth. This switch represents the 2D to three-dimensional (3D) crystal structure evolution, which governs the size and thickness of nanosheets, respectively. This phenomenon evidences the significance of the surfactant monolayer in ILE NS growth and can guide 2D nanocrystal synthesis with rationally controlled size and thickness. In addition, we show the impacts of different synthesis parameters on the NS growth behavior. Higher surfactant density enhanced the effects of the electrical double layer extending the lateral growth period, and higher Zn²⁺ concentration accelerated the 2D crystal growth, which is both favorable for large NS morphology formation. These results provide fundamental insights into the surfactant templated 2D growth mechanism in the ILE NS synthesis. The successful in situ diffraction characterization expands the toolbox and opens a new pathway to reveal the fast crystal nucleation and growth kinetics at the liquid interfaces by using time-resolved grazing incidence X-ray scattering techniques.

REFERENCE

1. Zhang, Z. *et al.* Nucleation Kinetics and Structure Evolution of Quasi-Two-Dimensional ZnO at the Air-Water Interface: An In Situ Time-Resolved Grazing Incidence X-ray Scattering Study. *Nano Letters* **22**(7), 3040-3046, doi:10.1021/acs.nanolett.2c00300 (2022).

9:45 AM CH01.03.07

Optimization of Growth and Properties of Unintentionally Doped Single Crystalline Ga₂O₃ Using Pulsed Laser Deposition [Kishor Upadhyaya](#)¹, [Naga Krishnakanth Katturi](#)¹, [Katharina Lorenz](#)² and [Iman S. Roqan](#)¹; ¹King Abdullah University of Science and Technology, Saudi Arabia; ²Instituto Superior Técnico, Campus Tecnológico e Nuclear, Portugal

Although pulsed laser deposition (PLD) is one of the most cost-effective techniques for growing epitaxial thin films, its use for obtaining single-crystal β -Ga₂O₃ is still challenging. In this work, we report on the systematic investigation of the effect of PLD growth conditions on the structural and optical properties of β -Ga₂O₃ thin films grown on different substrates, such as sapphire, Si, p-GaN and Ga₂O₃. X-ray diffraction (XRD) analyses show that the films grown on sapphire and p-GaN exhibit a single crystalline structure along the [-201] direction, while the films grown on Si substrate are polycrystalline in nature with [400] direction as the dominant peak. Increase in the substrate temperature and the number of laser pulses results in a considerable peak shift in θ -scans irrespective of the substrate used, indicating presence of strain in the film. The XRD rocking curves are investigated to evaluate the crystal quality with respect to the type of substrate and growth conditions. While Field Emission Scanning Electron Microscope (FESEM) images reveal variations in the morphology, High Resolution Transmission Electron Microscope (HRTEM) characterizations show different structural defects that affect the material quality, the extent of which is observed to depend on the growth conditions and the substrate type. Atomic force microscopy (AFM) analyses further reveal that the surface roughness changes as the temperature increases from 800°C to 850°C, as well as due to the increase in the number of laser pulses. For the optimized samples, optical characterizations show a typical Ga₂O₃ absorption curve, while a defect band emission is weak. However, the energy gap of the samples widens as the growth temperature and the number of laser pulses are increased. Raman spectroscopy analyses shows the effect of defects and strain on the material quality. Post-annealing under different conditions is carried out, and structural as well as optical characterizations reveal enhancement in the film properties. The results obtained in this study will assist in the optimization of β -Ga₂O₃ properties, which is essential for its use in optoelectronic and high-power device applications.

10:00 AM BREAK

10:30 AM *CH01.03.08

Nucleation, Growth and Shape Transformation of Nanoparticles by In Situ TEM [Jungwon Park](#); Seoul National University, Korea (the Republic of)

Molecular or atomistic mechanistic understanding of nucleation, growth, and structural transformations of materials have not achieved enough at the nanoscale or below. It is mainly because of a lack of appropriate analytical methods that can obtain in-situ structural information with a spatial resolution at such small length scale along with sub-msec temporal resolution. The in situ, both in liquid phase and dry state, transmission electron microscopy (TEM) offers an opportunity to directly observe diverse classes of chemical reactions. In liquid phase TEM, there are two-types of liquid cell that are widely used: silicon nitride window liquid cell and graphene liquid cell. The former allows real time observation in relatively low spatial resolution but it is possible to incorporate electrical biasing or heating conditions into imaging. The latter suggests an opportunity for high-resolution in situ imaging of materials reactions occurring in thin liquid media. Here we present applications of in situ TEM to study nucleation, crystallization, and shape transformation of diverse types of nanoparticles. We reveal that the early stage of crystal growth is driven by reversible transition between disordered and ordered phases before crystalline phase is stable above a certain size. It is also frequently observed that different types of non-classical pathway, including two-step

nucleation, amorphous-to-crystalline transition, and coalescence of clusters, are heavily involved in different conditions of crystallization of materials. We also present a new development using liquid phase TEM to investigate 3D atomic structures of nanoparticles directly in the colloidal synthesis batch.

11:00 AM CH01.03.09

Exploring the Dynamics of the III-Sb Nanowires During *In Situ* Growth Mikelis Marnauza, Robin Sjökvist, Marcus Tornberg, Daniel Jacobsson and Kimberly Dick; Lund University, Sweden

Group III-Sb semiconductor nanowires (GaSb, InSb, AlSb and their combinations) are an important material system for potential uses in applications such as quantum electronics, optoelectronics and sensing. This is due to their excellent electrical properties, including high carrier mobility and narrow band gap.¹ Among the III-Sb materials perhaps the most notable examples are InSb and GaSb nanowires which display the highest electron and hole mobilities among III-V nanowires, respectively.²

Despite the superior properties of this material system little research has been conducted into it when compared to other group III-V materials, such as group III-As. To a large extent this is caused by the complex growth conditions of antimonides, as elemental antimony exhibits low vapour pressure and surfactant effect.³ The investigation of this material system is further complicated by the difficulty of growing III-Sb nanowires directly from single crystal substrates often resulting in the need to use III-As/III-Sb heterostructures.^{1,4} In these heterostructured nanowires several dynamic effects can take place when switching from the III-As to the III-Sb segment such as unwanted radial expansion, change in crystal structure and facet change. Therefore, exploring the III-Sb growth parameter space has become unrealistic using conventional growth methods like metal organic chemical vapour deposition (MOCVD) which notoriously does not allow examination of the growth dynamics.

In this work, we have investigated the III-Sb nanowire growth process by growing these nanowires in-situ using an open cell Hitachi HF-3300S environmental transmission electron microscope combined with an MOCVD system.⁵ To facilitate nanowire growth, metal-organics and hydrides were used as precursors and introduced near a SiN_x micro-electro-mechanical system (MEMS) heating chip covered with pre-deposited Au nanoparticles. To analyse nanowires during growth we employed X-Ray Electron Dispersive Spectroscopy (XEDS) measurements in combination with atomically resolved high-resolution transmission electron microscopy (HRTEM) imaging and videos.

We focus on the III-As/III-Sb heterostructure formation; wherein we have investigated droplet composition during growth, changes in nanowire morphology, and the connection between droplet composition and growth dynamics. Special attention is directed towards the GaAs/GaSb heterostructures where we have demonstrated that radial expansion of the GaSb segment can be minimized by fine-tuning of TMGa flow. Additionally we demonstrate that both excess TMGa and TMSb supply in the vapour phase can lead to kinking of the nanowires.

Results of this study have given insight into the connection between droplet composition and nanowire diameter during III-As/III-Sb heterostructure formation. This knowledge could ultimately be used in fabricating smaller diameter nanowire heterostructures ex-situ, important for device applications.

References:

- (1) Mattias Borg, B.; Wernersson, L.-E. Synthesis and Properties of Antimonide Nanowires. *Nanotechnology* **2013**, *24* (20), 202001. <https://doi.org/10.1088/0957-4484/24/20/202001>.
- (2) Ghalamestani, S. G.; Ek, M.; Dick, K. A. Realization of Single and Double Axial InSb – GaSb Heterostructure Nanowires *Phys. Status Solidi*. **2014**, *273* (3), 269–273. <https://doi.org/10.1002/psr.201308331>.
- (3) Ghalamestani, S. G.; Lehmann, S.; Dick, K. A. Can Antimonide-Based Nanowires Form Wurtzite Crystal Structure? *Nanoscale*. **2016**, *2778*–2786. <https://doi.org/10.1039/c5nr07362f>.
- (4) Yip, S.; Shen, L.; Ho, J. C. Recent Advances in III-Sb Nanowires: From Synthesis to Applications. *Nanotechnology* **2019**, *30* (20). <https://doi.org/10.1088/1361-6528/aafccc>.
- (5) Tornberg, M.; Maliakkal, C. B.; Jacobsson, D.; Wallenberg, R.; Dick, K. A. Enabling In Situ Studies of Metal-Organic Chemical Vapor Deposition in a Transmission Electron Microscope. *Microsc. Microanal.* **2022**, 1–9. <https://doi.org/10.1017/s1431927622000769>.

11:15 AM CH01.03.10

***In Situ* Investigation of Crystallization Pathway of Solution-Processed Magnesium-Alloyed Zinc Tin Oxide Thin Films** Baran Demir and Rebecca L. Peterson; University of Michigan, United States

Multi-cation metal oxides are a key material class for applications in solar cells, electronics and sensing technologies, as well as batteries and fuel cells. For successful use in these applications, it is crucial to control the material crystallinity. Crystalline metal oxides are valuable for gas sensing applications, where improvement in sensing qualities is linked to the material's crystal structure and quality. Amorphous-phase metal oxides are commercially used for dielectrics in CMOS and as semiconductors in the display backplane industry due to their excellent electrical properties. In particular, zinc oxide alloys exhibit a wide, direct bandgap in the UV. Here, we choose as a base material amorphous zinc tin oxide, an n-type semiconductor with mobility of about 22 cm²V⁻¹s⁻¹ and a bandgap of about 3.0 eV [1,2]. By alloying this material with magnesium, we aim to further increase its bandgap and improve the insulating property of this quaternary alloy. To obtain these improvements, we need to understand and control its crystallization.

Therefore, in this work, we use *in situ* heating grazing incident x-ray diffraction (GIXRD) to examine the effects of magnesium alloying on crystallization of zinc tin oxide (ZTO) thin films. Four ZTO films - one unalloyed and three alloyed with Mg - are deposited on Si/SiO₂ substrates using solution processing. The Mg metal ratio, [Mg]/([Mg]+[Zn]+[Sn]), was 2.5%, 7.5%, 20% for the three alloyed samples. All films were x-ray amorphous after the deposition process. In order to investigate the crystallization pathways and the effect of Mg incorporation, films were slowly annealed up to and beyond their crystallization temperatures. The evolution of crystalline phases was observed by *in situ* heating during x-ray diffraction using Rigaku SmartLab. XRD data was collected from 500°C to 750°C using 20°C increments to extract crystallization temperatures. The data for higher temperatures was collected from 550°C to 1050°C using 100°C increments by using new samples. Heating time of 1 hour was set between each increment.

All of the films have a Zn-to-Sn metal ratio of 7:3 which is close to the stoichiometric ratio in inverse spinel Zn₇SnO₄. For this stoichiometry, the inverse spinel is expected to be the most stable phase. However, our *in situ* XRD shows that the unalloyed film crystallizes predominantly in an orthorhombic structure around 650°C. Similar results have been seen in low-dimensional ZTO structures obtained by solution processing or hydrothermal synthesis [3,4]. At temperatures above 750°C, the unalloyed film begins to show spinel peaks, and this matches the theoretical thermodynamic stability calculations of ZTO systems [5]. When Mg is introduced into the system, a mixed phase film containing inverse spinel and orthorhombic phases forms at temperatures below 750°C. As the Mg percentage increases to 20%, the orthorhombic x-ray peaks completely vanish and the thin film crystallizes into a single spinel phase. This is expected, as spinel is the stable phase for the Mg_{2-x}Zn_xSnO₄ system. After a slow cooling process down to 50°C, the spinel peaks disappear from the unalloyed ZTO thin film, whereas they remain for the 20% Mg-incorporated sample. To summarize, ZTO without Mg first crystallizes into an orthorhombic structure before converting toward the spinel phase at higher temperature, whereas Mg incorporation into ZTO strongly promotes the formation of spinel-phase crystals, over orthorhombic. By tailoring the Mg content, the crystal structure and crystallization dynamics can be controlled to obtain the desired materials properties and function.

[1] Y. Son *et al.*, *J. Mater. Chem. C* **5**, (2017).

- [2] C. Allemang *et al.*, *Adv. Electron. Mater.* **6**, 2000195 (2020).
[3] A. Rovisco *et al.*, *ACS Appl. Nano Mater.* **1**, 3986–3997 (2018).
[4] Y. Chen *et al.*, *Nanotechnology* **23**, 415501 (2012).
[5] J. Lee *et al.*, *Journal of Materials Chemistry C* **1**, 6364 (2013).

11:30 AM CH01.03.11

A Kinetic Isotope Effect in the Formation of Lanthanide Phosphate Nanocrystals Gal Schwartz¹, Uri Hananel¹, Liat Avram², Amir Goldbourt¹ and Gil Markovich¹; ¹Tel Aviv University, Israel; ²Weizmann Institute of Science, Israel

Studies of kinetic isotope effects in various reactions have been useful for elucidating reaction mechanisms, and it is believed that the same may apply for crystal formation kinetics. We present a kinetic study of the formation of europium-doped terbium phosphate nanocrystals under acidic conditions, including a strong H/D isotope effect. The nanocrystal growth process could be quantitatively followed through monitoring of the europium luminescence intensity, combined with ³¹P NMR kinetics measurements. Such lanthanide-based nanocrystals may serve as an excellent model system for further studying and gaining a deeper understanding of crystal nucleation and growth processes. We conclude that the observed delayed nucleation occurs due to initial formation of pre-nucleation clusters or polymers of the lanthanide and phosphate ions, which undergo a phase transformation to crystal nuclei and further grow by cluster attachment.

<https://pubs.acs.org/articlesonrequest/AOR-YDYQEM32KMCHKRAQSJWS>

SESSION CH01.04: Crystal Nucleation and Growth II
Session Chairs: Peter Crozier and Andrej Kuznetsov
Tuesday Afternoon, November 29, 2022
Hynes, Level 1, Room 102

1:30 PM *CH01.04.01

Probing Nanoparticle Optical Properties and Responses with *In Situ* Electron Microscopy Piyush Haluai, Yifan Wang, Martha McCartney and Peter A. Crozier; Arizona State University, United States

The interaction of materials with photons is critical to many technologies including opto-electronic devices, photovoltaics and photocatalysis. The optical response is determined by the real and imaginary parts of the dielectric function which can in turn be impacted by the ambient conditions such as temperature, gas/liquid environment as well as structural factors such as point defects and interfaces. To explore the optical response of materials at the nanometer level, we have developed *in situ* optical illumination systems for transmission electron microscopy (TEM) [1-3]. The system is installed in an FEI Titan environmental TEM and is compatible with both heating, cooling and gas ambients. Materials can be thermally processed in a variety of different gases and illuminated with light. Optical properties and responses can be probed *in situ* with monochromated electron energy-loss spectroscopy (EELS) and electron holography.

In semiconducting devices, separation of electron-hole pairs generated via photon absorption is often facilitated by selective charge transport across heterostructure interfaces. The efficiency of the charge transfer process will depend on materials' thermodynamics and kinetic factors regulated by interface characteristics (such as Schottky barriers). We have been exploring the variation in the charge state of supported metal nanoparticle photocatalysts using *in situ* electron microscopy. Specifically, we have investigated the effect of visible light absorption in Ni supported on Rh-doped strontium titanate particles [4]. During illumination, electrons generated from photon absorption may transfer to the metal nanoparticle changing its charge state. Electron holography allows us to detect phase shifts in the fast electron wavefunction associated with photon illumination.

The optical properties of oxides are strongly affected by the concentration of point defects such as oxygen vacancies and dopants. In dielectric materials, photonic or guided light modes may be present which depend on both the nanoparticles shape, size, and refractive index [5]. For many non-stoichiometric oxides such as CeO₂, the oxygen vacancy concentration can be affected by the temperature and oxygen partial pressure. We are investigating the variation in photonic modes with changes in temperature and gas environment. The change in the photonic modes might be associated with changes in density and oxygen vacancy concentration leading to corresponding variations in the refractive index [6]. The sensitivity of photonic modes to small changes in the optical properties of materials is being explored.

1. B. K. Miller and P. A. Crozier, *Microscopy and Microanalysis* 2013. **19** Issue 2 Pages 461-469
2. Q. Liu *et al.*, *Microscopy and Microanalysis* 2016 Vol. 22 Issue S3 Pages 730-731
3. Q. Liu *et al.*, arXiv preprint arXiv:2104.02006 2021
4. P. Haluai and P.A. Crozier *Microscopy and Microanalysis* 2022 28 (S1), 1880-1882.
5. Q. Liu *et al.*, *Physical Review B* 2019 Vol. 99 Issue 16 Pages 165102, DOI: 10.1103/PhysRevB.99.165102
6. Y. Wang *et al.*, *Microscopy and Microanalysis* 28 (S1), 1972-1974
7. We gratefully acknowledge support of DOE grant BES DE-SC0004954, the use of ASU's John M. Cowley Center for High Resolution Electron Microscopy.

2:00 PM CH01.04.02

Synthesis and Incorporation of Buffer Components into the Framework of Bioinspired Polyserotonin Keuna Jeon^{1,2}, Justin Asuncion^{1,2}, Alexander Corbett^{1,2}, Tiange Yuan², Meera Patel^{1,2}, Nisha Andoy², Oleksandr Voznyy^{1,2} and Ruby Sullan^{1,2}; ¹University of Toronto, Canada; ²University of Toronto at Scarborough, Canada

Polyserotonin is a new class of bioinspired nanomaterial with recently demonstrated therapeutic potential in biomedical applications and surface coatings. It is therefore important to establish a robust and rapid method of synthesizing polyserotonin nanoparticles (PSeNP) and films for *in vivo* utilization. Since the formation of PSeNP is based-catalyzed, we report the influence of solution pH, in the presence of different base systems, on the kinetics of PSeNP formation and physico-chemical properties of the resulting polyserotonin. We show that the rate of formation and the size of PSeNP depend on both the nature of the base and the initial pH of the reaction. In addition, we show that buffer components are incorporated into the polymer matrix. While we observe no difference in elasticity of PSeNP synthesized in different buffers, the nanoscale properties of polyserotonin films revealed dissimilarities in surface functional groups influenced by solvent molecules. This presents a significant advance in the polyserotonin synthesis and provides a facile approach in tuning the size and surface functionality of PSe nanomaterial to suit various applications. Furthermore, we show that similar to serotonin, PSeNP also exhibits free-radical scavenging property. Our results demonstrate that PSeNP has the potential to become a key player in the advancement of nanotechnology-mediated antioxidative therapy.

2:15 PM CH01.04.03

Study of Ultra-Thin ALD Grown Gallium Oxide Films by *In Situ* Ellipsometry with Unambiguous Thickness and Optical Property Determination Florian Maudet¹, Sourish Banerjee¹, Hanno Kröncke¹, Sven Wiesner¹, Veeresh Deshpande¹ and Catherine Dubourdieu^{1,2}; ¹Helmholtz-Zentrum Berlin für Materialien und Energie, Germany; ²Freie Universität Berlin, Germany

Atomic layer deposition (ALD) of metal oxide is a chemical vapor deposition method that relies on the cyclic self-limited deposition of a metal precursor molecule followed by an oxidizing reactant specie. To study the growth process, spectroscopic ellipsometry is one of the favored *In Situ* characterization as it can be used in a non-UHV environment, and it has a high surface sensitivity. This method can be applied to monitor the evolution of the thickness and of the complex dielectric permittivity of the film. However, as ultrathin films are considered, the relative contributions of the dielectric permittivity and thickness cannot be disambiguated from a model as it is usually done for thicker films. To solve this issue, a fixed dielectric constant is usually considered and only the thickness evolution is studied. However, this is fundamentally incorrect. Each of the four steps during one ALD cycle is indeed specific to a different chemical reaction/mechanism happening on the surface. The optical properties of the precursor molecule absorbed on the surface or of a sub-monolayer film are different from those of a dense layer. Furthermore, a change in the optical properties of the film will be interpreted as a thickness evolution. Here, we present a method to unambiguously determine the thickness and optical properties of the growing oxide in an *in situ* measurement. We apply this method to analyze the evolution of the optical properties in the first stages of the growth of gallium oxide deposited by plasma enhanced ALD. Trimethyl gallium and O₂ plasma are used as a precursor and oxidizing agent respectively. We determine the change in thickness as a function of time for each step of an ALD cycle with a relatively high sampling rate (100 ms). The role of the O₂ plasma exposure time on the growth and optical properties of the films is analyzed and correlated to their electrical properties. The study of the optical properties reveals that a “bulk-like” gallium oxide film is obtained after ~35 PEALD cycles corresponding to a thickness of 2.35 nm. The bandgap of the growing thin film is at first much larger (5.41 eV) than its bulk counterpart (4.97 eV) and then progressively decreases with increasing number of cycles, tending towards the bulk value. Quantum confinement occurring at reduced dimensions is at the origin of the increased band gap value.

2:30 PM CH01.04.05

***In Situ* Imaging of CDW Phase Transition in Two-Dimensional Rare-Earth Tellurides Using 4D-STEM** Saif Siddique¹, James L. Hart¹, Ratnadwip Singha², Leslie Schoop² and Judy Cha¹; ¹Cornell University, United States; ²Princeton University, United States

Rare earth tellurides of the form RTe₃ (where R is a rare-earth element) are quasi-two-dimensional materials, with an orthorhombic crystal structure having two consecutive square-planar Te sheets separated by corrugated R-Te slabs. Peierls instability in the square Te sheets results in charge density wave (CDW) ordering in these materials.¹ The physics involving CDW order in RTe₃ is interesting because of its interplay with other quantum states hosted by this class of materials, such as superconductivity and spin-density waves. A recent report shows the existence of axial Higgs mode in this system which in turn show the unconventional nature of the CDW states and complexity of the associated order parameter.² To gain an understanding of the changes in the local structure and to track the complex order parameter across the CDW phase transition, we use 4D-STEM (scanning transmission electron microscopy) for a nanoscale structural characterization. Previous works show the dependence of CDW transition temperature (T_{CDW}) on the thickness of the 2D flakes, which are attributed to the lattice compression/expansion of the inner Te sheets.³ However, this was never confirmed by atomic-scale imaging. A continuously variable temperature cryogenic TEM specimen holder (developed by HennyZ Co.) is used to image the sample using 4D-STEM, which gives both real- and reciprocal-space information, allowing us to track the CDW phase transition as a function of temperature and nanoscale confinements.

1. Siddique, S. *et al.* Emerging two-dimensional tellurides. *Mater. Today* **51**, 402–426 (2021).

2. Wang, Y. *et al.* Axial Higgs mode detected by quantum pathway interference in RTe₃. *Nature* 1–6 (2022) doi:10.1038/s41586-022-04746-6.

3. Chen, Y. *et al.* Raman spectra and dimensional effect on the charge density wave transition in GdTe₃. *Appl. Phys. Lett.* **115**, 151905 (2019).

2:45 PM BREAK

3:15 PM *CH01.04.06

Self-Organized Lateral Polymorphic Regrowth in Ion Irradiated Gallium Oxide Andrej Kuznetsov; University of Oslo, Norway

Gallium oxide is an ultra-wide bandgap semiconductor exhibiting a number of unique properties and promising applications for power electronics and optoelectronics. Importantly, gallium oxide can be crystallized in a range of different polymorphs having different structures and, consequently, different physical properties, which can be potentially exploited in the devices. However, gaining control over the polymorphic transitions in a technologically viable way is a challenge. Very recently, a novel method to form such polymorph films was discovered, specifically applying paradoxical idea of the disorder-induced ordering in ion beam irradiated samples [1]. The present talk reviews the data from Ref [1] and extends the description with not yet published data. In particular, including a spectacular ex-situ and in-situ observations of the lateral solid state polymorph regrowth at the interfaces between different polymorphs as well as reporting on the functionalities of the gallium oxide polymorph films and interfaces. Altogether, these novel data pave the way for a new synthesis technology of the metastable polymorph heterostructures and regularly shaped interfaces in device components not achievable by conventional deposition methods.

References

[1] A. Azarov, C. Baziotti, V. Venkatachalapathy, P. Vajeeston, E. Monakhov, and A. Kuznetsov, *Phys. Rev. Lett.* **128** (2022) 015704

3:45 PM CH01.04.07

***In Situ* Studies of Crystalline Polymer Formations via Topochemical Reactions** Chongqing Yang¹, Rebecca S. Khoo^{1,2}, He Li¹, Christopher Anderson^{1,2}, Christopher G. Jones³, Carolin M. Sutter-Fella¹, Jian Zhang¹, Hosea M. Nelson³ and Yi Liu¹; ¹Lawrence Berkeley National Laboratory, United States; ²University of California, Berkeley, United States; ³California Institute of Technology, United States

To address the negative environmental influence associated with the fabrication of synthetic polymers, the development of eco-friendly and sustainable chemistries has been crucial but challenging. Distinct from the conventional solution-based polymer growth, topochemical polymerization (TCP) offers a ‘green’ way for scalable fabrication of high fidelity polymers without the need of catalysts, auxiliaries, or solvents. With crystallinity embedded during the synthesis, it is also one of the few ways to produce single crystalline polymers suitable for atomic structure determination. However, only a handful of TCP reactions have been reported to date, and it is still challenging to expand new chemistries in this area, due to the difficulty in controlling the reactivity in crystalline solids. Moreover, most of the polymers from TCP reactions have low solubility which renders their characterization and application challenging. In this work, we present that an azaquinodimethane (AQM) family has shown great topochemical reactivity in the forms of single crystals, polycrystalline powders, and thin films under visible light irradiation or heat. The resultant crystalline polymer structures were successfully resolved by single crystal X-ray diffraction (for large crystals), or cryo-EM based microelectron diffraction with 1 Å resolution (for microcrystals). The high efficiency of solid-state polymerization was evidenced by the ultrahigh molecular weight ($M_w > 10^6$ g/mol) of a soluble TCP polymer bearing pendent 3,5-dihexyloxyphenyl groups.

Moreover, the solid-state reactivity of AQMs also shows remarkable functional group tolerance, allowing the introduction of different side groups without decreasing the polymerization efficiency. Notably, the intensity of the absorption peaks of monomers in the range of 400-500 nm undergoes a characteristic decrease upon polymerization. This spectroscopic change provides a distinctive optical feature to track the polymerization process via in-situ UV/vis characterization with a time resolution of 0.1 s. Kinetic studies of AQM polymerization showed a relatively small activation energy of $\sim 19.7 \text{ kcal K}^{-1} \text{ mol}^{-1}$, providing key quantitative information of the easily accessible and fast polymerization process. Further kinetic details were obtained from the temperature-dependent polymerization of AQMs bearing different conjugated aromatic units or chiral sidechains, allowing fundamental understanding of a structure-reactivity relationship of such AQMs. Such insight paves the way for the future design and synthesis of functional polymers in an environmentally friendly way.

References

Dou, L.; Zheng, Y.; Shen, X.; Wu, G.; Fields, K.; Hsu, W.-C.; Zhou, H.; Yang, Y.; Wudl, F., *Science* **2014**, 343, 272.
Hema, K.; Ravi, A.; Raju, C.; Pathan, J. R.; Rai, R.; Sureshan, K. M., *Chem. Soc. Rev.* **2021**, 50, 4062.
Anderson, C. L.; Li, H.; Jones, C. G.; Teat, S. J.; Settineri, N. S.; Dailing, E. A.; Liang, J.; Mao, H.; Yang, C.; Klivansky, L. M.; Li, X.; Reimer, J. A.; Nelson, H. M.; Liu, Y., *Nat. Commun.* **2021**, 12, 6818.

4:00 PM CH01.04.08

Characterisation of Nucleation and Growth of Mineral Phases Colin Freeman, Emma Armstrong, Vittoria Fantauzzo, Stephen Yeandel and John Harding; University of Sheffield, United Kingdom

There remains strong interest in the formation of inorganic molecular salts including CaCO_3 , CaSO_4 and KNO_3 . These materials are ubiquitous as they are found in nature within geological and biological settings but are also used extensively within industry. They are challenging to study due to the range of speciation and phases that can form out of solution and the strong influence of supersaturation, concentration and interfaces. Computational methods remain a powerful tool for characterising the formation of materials. We can use these techniques to test our fundamental understanding such as classical nucleation theory and step-based growth models. Computational approaches can also provide a detailed atomic scale view of the processes taking place during nucleation and growth which are often beyond the lengthscales of experimental techniques.

We present a set of classical atomic scale simulations on inorganic molecular salts. We demonstrate the use of a new methodology to produce interfacial free energies of these materials which allows us to predict phase formation and morphologies of the crystals to compare with experiment and test the applicability of classical nucleation theory to the formation of these phases. We further explore phase growth by utilising constant chemical potential reservoirs to link simulations to more realistic solution concentrations. We discuss the further potential impact of computational methods in exploring material synthesis.

4:15 PM CH01.04.09

Controlling Crystallisation Using Surface Topography Thomas Dunn, Phillip Lee, Stuart Micklethwaite, Alexander Kulak, Liam Hunter, Zabeada Aslam, Johanna Galloway, Yi-Yeoun Kim and Fiona Meldrum; University of Leeds, United Kingdom

The use of heterogeneous nucleants to trigger crystallisation provides a means of controlling the size/structure of the crystals produced, where they form, and the induction time. However, with the exception of structural matching, there is little rationale for the identification of effective nucleants for many crystals. In this work, we explore the potential of using surface topography to direct crystal nucleation, where evidence is scattered across the literature that nucleation is promoted in features such as pits, pores and scratches. Substrates patterned with natural surface cracks are created in this study. These cracks spontaneously form in brittle materials whose surfaces are under strain. The cracked substrates are then coated with a thin film of a noble metal and chemically functionalised to optimise the surface chemistry. Controlling both the topography and surface chemistry of these substrates is shown to be highly effective in directing the nucleation of a range of substances including various inorganic and organic crystals. The origin and universality of this phenomenon is explored to determine how the topography and chemistry of a surface can promote the nucleation of a specific crystal. Controlling surface topography is therefore a valuable and frequently overlooked tool in controlling nucleation and can be used in the design of effective nucleants.

4:30 PM CH01.04.10

In Situ Study of (1) Aqueous Room-Temperature Synthesis of Crystalline Nano-Ceria and (2) Nano-Zirconia—Transformation from Amorphous to Crystalline Phase(s) Siu Chan; Columbia University, United States

In-situ studies are presented: (i) Ultra-Small-Angle X-ray Scattering (USAXS) of the formation and growth of nano-ceria ($n\text{-CeO}_2$) (ii) Wide Angle X-Ray Diffraction (WAXRD) of the amorphous-to-cubic crystallization of nano- ZrO_2 in a reducing environment. In the first study, in situ monitoring of characteristics from 1 nm as a function of the temperature allowed for the identification of the nucleation and growth of ceria nano-crystals. Monitoring flow rate, temperature and pH of the suspension have permitted real-time studies of the nano-ceria crystalline synthesis from homogeneous solution over many hours. Incubation times for each temperature and minimum critical nucleus-size of 6 nm have been identified which yield the interfacial energy of $n\text{-CeO}_2$ in the aqueous solution. Activation energy for growth has been measured to be $\sim 0.5 \text{ eV}$. In the second study, pair distribution function and reverse Monte Carlo simulation were applied to provide details of the local structure during the crystallization. The local structure of the amorphous phase bears resemblance to the short-range arrangement of cubic ZrO_2 . The amorphous-to-cubic (a-c) crystallization of nano- ZrO_2 in a reducing environment was studied. A reverse Monte Carlo (RMC) simulation provided details of the local structure during the crystallization process as well as partial Pair Distribution Function's (PDF's) of Zr-Zr and Zr-O during the crystallization. The number of Zr's next-nearest neighbors of Zr remains 12, whereas the number of O's as nearest neighbors of Zr increases from 6.7 to 7.3 as the amorphous evolves into a cubic structure, suggesting the persistence of a high concentration of oxygen vacancies. The simulated atomic local structure of the amorphous phase bears resemblance to the short-range arrangement of cubic ZrO_2 , consistent with the results of X-ray Absorption Near Edge Spectroscopy (XANES) at Zr L_{II} and L_{III} . The amorphous-to-crystalline phase transformation is affected by the environment. Under an oxidizing condition, the amorphous phase crystallizes directly to tetragonal and subsequently to monoclinic zirconia.

1 *J. Appl. Cryst.*, (2008), 41, pp 918–929 DOI:10.1107/S0021889808023078
2 *Chem. Mater.*, (2007), 19 (13), pp 3118–3126 DOI: 10.1021/cm061739w

8:30 AM *CH01.05.01

Towards the Detection of Spin Charge Accumulation at a Metal/Insulator Interface Using High Energy Resolution STEM-EELS Khalil El Hajraoui^{1,2}, Vlado Lazarov², Quentin Ramasse^{1,3} and Demie Kepaptsoglou^{1,2}; ¹SuperSTEM Laboratory, United Kingdom; ²University of York, United Kingdom; ³University of Leeds, United Kingdom

Magnonics is an emergent field within spintronics utilising the ability to generate and propagate controllably a spin-wave (or magnon) in nm-sized magnetic structures, with a view to build a new generation of devices for data processing and storage. It was also recently demonstrated that magnons can be utilised to convert spin to charge (or charge to spin) currents, a critical step for integration of spin and charge devices. However, despite recent progress in the field, many challenges hinder further practical development due, among other factors, to a lack of experimental methodologies to probe these processes directly at the nanoscale, and in particular in the vicinity of interfaces, thus limiting our fundamental understanding of these phenomena. State-of-the-art monochromated electron energy loss spectroscopy (EELS) in the scanning transmission electron microscope (STEM), which offers the ability to map materials and atomic structures with an angstrom size electron beam and an energy resolution for EELS under 5meV, was proposed to be a leading candidate technique to attempt the detection of magnons at the nanoscale, perhaps down to the atomic scale, thanks to a recently developed theoretical calculation framework and preliminary experimental investigations [1]. Here, we report on progress in designing experiments building on these initial steps using in-situ STEM-EELS. The prototypical spin-to-charge conversion system considered for this proof of principle attempt consists of Yttrium Iron Garnet (YIG)/platinum (Pt) bilayer, a widely used materials combination where a magnon created by a thermal gradient creates spin accumulation at the YIG/Pt interface, which subsequently diffuses into the nonmagnetic Pt, and via inverse spin Hall effect (ISHE) creates a voltage signal in the Pt layer [2]. We aim to correlate the atomic structure to the spin-to-charge conversion properties in a working device using in-situ heating STEM-EELS, making use of custom-made silicon nitride (Si₃N₄) membranes where a focused ion beam (FIB) lamella extracted from the YIG/Pt device is electrically connected to a specific heater geometry allowing local Joule heating to create the required gradient of temperature along it. Plasmon energy expansion thermometry, a nanoscale temperature mapping EELS technique is used to monitor the temperature at the metal contact as well as the temperature gradient along the FIB lamella, while HR-EELS signal at the interface is correlated to the local structural and chemical environment.

[1] K. Lyon et al., Phys. Rev. B, 104, 214418 (2021)

[2] A. Hoffmann et al., IEEE Trans. Magn. 49, 5172 (2013)

9:00 AM CH01.05.02

Contribution of Carbon Nanopores Towards the Improved Performance of Ionic Liquid-Based EDLCs at Sub-Zero Temperatures Vladimir Pavlenko^{1,2}; ¹Al-Farabi Kazakh National University, Kazakhstan; ²Nazarbayev University, Kazakhstan

During the presentation an important role of nanopores investigated in electric double-layer capacitors (EDLCs) operating from 24 °C down to -50 °C by using carbons with hierarchical porosity will be discussed. Home-made carbons were prepared using different precursors as the carbon source, while a binary mixture of imidazolium-based fluorinated ionic liquids was used as a solvent-free electrolyte. It will be shown that short-range graphene layers produced with 8-nm silica nanoparticles lead to the creation of transport channels which better accommodate ions. We explain these findings per coulombic interactions among the ions and between the pore wall and the ionic species under confinement and electrochemical polarization conditions. Further, it will be shown that a microporous carbon performs better than hierarchical carbons at room temperature; however, owing to the large fraction of mesopores, the latter exhibit far higher capacitance down to -50 °C. While the ordering of ions in confinement is more critical at room temperature and dictated by the micropores, low temperature performance of supercapacitors is determined by the mesopores that provide channels for facile ion movement and keep the bulk ionic liquid-like properties.

9:15 AM CH01.05.04

Hydrogen Network in a Tetrapeptide Crystal Characterized by X-Ray Diffraction and Raman Spectroscopy Kazunori Motai¹, Masaki Kawano¹, Takehiko Mori¹, Yuji Mochizuki² and Yuhei Hayamizu¹; ¹Tokyo Institute of Technology, Japan; ²Rikkyo University, Japan

In recent years, much attention has been paid to research aimed at elucidating the self-assembly mechanism of dipeptides, the smallest constituent unit of living organisms [1]. Attempts have been made to develop enzyme-inspired peptide-based supramolecular catalysts and to apply them to green piezoelectric materials that meet the requirements of biocompatible ultra-sensitivity, flexibility, and durability. In understanding their functionality, hydrogen bonds play should be investigated due to their important role in stabilizing the steric structure of proteins and in expressing their functions. The strength of hydrogen bonds has been investigated by single-crystal structural analysis and spectroscopic techniques. Nakamoto et al. found a linear relationship between the stretching vibrational modes of hydrogen bonds and the interatomic distance[2]. Elena et al. have combined angle-resolved Raman measurements and single-crystal structure analysis to investigate the thermal behavior of amino acid derivative crystals[3]. However, these studies were limited to relatively small molecular compounds such as amino acids. In this study, the hydrogen bonding network in peptide crystals was investigated using the tetrapeptide FEFE as a model system. Single-crystal X-ray structure analysis revealed that the crystal structure of FEFE has branched hydrogen bonds. Raman spectroscopy showed that the vibrational frequencies of the amide bonds correlate linearly with their interatomic distances. On the other hand, the lattice expansion-dependent vibrational frequency shift is significantly smaller than in previous studies. Our fragment molecular orbital (FMO) calculations revealed that branched hydrogen bonds affect the strength of hydrogen bonds differently from the Nakamoto diagram.

Branched hydrogen bonds in proteins have been studied using both experimental approaches and computational analysis[4][5]. Our findings differ from previous works investigating amino acids or other small organic molecules and made a connection with natural proteins as a model system of peptides. We believe that this study opens a way for discussing the effects of branched-type hydrogen bonds in various peptide crystals.

[reference]

[1] C. Yuan, W. Ji, R. Xing, J. Li, E. Gazit, X. Yan, Nat. Rev. Chem. 2019, 3, 567–588.

[2] K. Nakamoto, M. Margoshes, R. E. Rundle, J. Am. Chem. Soc. 1955, 77, 6480–6486.

[3] B. A. Zakharov, B. A. Kolesov, E. V. Boldyreva, Phys. Chem. Chem. Phys. 2011, 13, 13106–13116.

[4] E. S. Brielle, I. T. Arkin, J. Am. Chem. Soc. 2020, 142, 14150–14157.

[5] E. S. Feldblum, I. T. Arkin, Proc. Natl. Acad. Sci. U. S. A. 2014, 111, 4085–4090.

9:30 AM CH01.05.07

In Situ Nanoscale Characterization of Electrical and Magnetic Properties of 3D Nanostructures by Combination of AFM, SEM and FIB Christian H. Schwalb¹, Hajo Frerichs¹, Lukas Stühn¹, Sebastian Seibert¹, Marion Wolff¹, Michele Brugger-Hatzl², Lukas Seewald², Robert Winkler² and Harald Plank²; ¹Quantum Design Microscopy GmbH, Germany; ²Graz University of Technology, Austria

Combining different analytical methods into one instrument is of great importance for the simultaneous acquisition of complementary information. Especially the in-situ combination of scanning electron microscopy (SEM) and atomic force microscopy (AFM) enables completely new insights in the micro and nano-world. In this work, we present the unique in-situ combination of scanning electron and ion microscopy (SEM/FIB) and atomic force

microscopy (AFM) for nanoscale characterization [1-2].

We will present a variety of case studies to highlight the advantages of interactive correlative in-situ nanoscale characterization for different materials and nanostructures. We show results for *in-situ* electrical characterization by conductive AFM for 2D materials as well as electrostatic force microscopy (EFM) of piezoceramic films that enables the precise analysis of grain boundary potential barriers in semiconducting BaTiO₃-based ceramics [3]. The grain boundaries were located by BSE-SEM and afterwards measured with in-situ EFM. The barriers were shown to be significantly thinner and more pronounced as the amount of SiO₂ was increased from 0 to 5 mol%. These results can be directly correlated with electron backscatter diffraction (EBSD) measurements in order to link the AFM and SEM data to the crystallographic microstructure.

In addition, we will present results for the in-situ characterization of magnetic nanostructures by combination of SEM and high-vacuum magnetic force microscopy (MFM). For the in-situ MFM measurements we use specialized magnetic cantilever probes that are fabricated using electron beam-induced deposition (EBID) for high-aspect ratio magnetic tips that surpass standard magnetic cantilever tips in lateral and magnetic resolution. The SEM enables to identify the grain boundaries on multilayer thin-film samples or stainless steel in order to measure the magnetic properties directly via MFM with nanometer resolution.

[1] D. Yablon, et al., *Microscopy and Analysis*, **31** (2), 14-18 (2017)

[2] S.H. Andany, et al., *Beilstein J. Nanotechnol.*, **11**, 1272-1279 (2020)

[3] J.M. Prohning, J. Hütner, K. Reichmann, S. Bigl, *Scripta Materialia*, **214**, 114646 (2022)

9:45 AM BREAK

10:15 AM *CH01.05.08

Atomic-Resolution Electron Microscopy of Catalyst Dynamics Fu-Rong Chen¹, Dirk Van Dyck², Christian Kisielowski³, Lars Hansen⁴, Martin Ek Rosén⁵, Christian D. Damsgaard^{6,6}, Joerg R. Jinschek^{6,6} and Stig Helveg⁶; ¹Hong Kong City University, Hong Kong; ²University of Antwerp, Belgium; ³Lawrence Berkeley National Laboratory, United States; ⁴Topsoe A/S, Denmark; ⁵Lund University, Sweden; ⁶Technical University of Denmark, Denmark

Electron microscopy has become a powerful tool in catalysis science. Advances in electron optics and detection have enabled visualizations of catalytic nanomaterials with three-dimensional atomic-resolution and, the advent of gas and liquid cells has enabled *in situ* observations of catalysts immersed in chemical reaction environments as well as *operando* studies through concurrent measurements of catalytic functionality [1]. These developments open up for unprecedented new insights into the labile behavior of catalysts and provide mechanistic and kinetic information on atomic processes unfolding during catalysis. However, the atomic-resolution electron microscopy observations are often intricately modulated by dynamic processes induced by the electron beam, which are difficult to predict but imperative to characterize, quantify and suppress [2]. In this contribution, we outline progress in electron microscopy that advances the chemical relevance of atomic-scale visualizations and present electron microscopy research that aims discerning inherent and induced atom-dynamic processes in catalytic nanomaterials [3-5].

[1] S. Helveg, *J. Catal.* **328**, 102 (2015). [2] S. Helveg, C. Kisielowski, J.R. Jinschek, P. Specht, G. Yuan, H. Frei, *Micron* **68**, 176 (2014). [3] M. Ek, Q.M. Ramasse, L. Arnarson, P.G. Moses, S. Helveg, *Nat. Commun.* **8**, 305 (2017). [4] M. Ek, L. Arnarson, P.G. Moses, S.B. Rasmussen, M. Skoglundh, E. Olsson, S. Helveg, *Nanoscale* **13**, 7266 (2021). [5] F.-R. Chen, D. Van Dyck, C. Kisielowski, L.P. Hansen, B. Barton, S. Helveg, *Nat. Commun.* **12**, 5007 (2021).

10:45 AM CH01.05.09

Controlling the Surface Reactivity of Hybrid Ti₃CNT_x MXene via *In Situ* Electrocatalysis Ekenedilichukwu Uwadiunor and Abdoulaye Djire; Texas A&M University, United States

Two-dimensional (2D) carbide and nitride MXenes possess properties that are desirable for a broad range of electrocatalytic applications including hydrogen evolution reaction (HER). These properties include high surface area, hydrophilicity, heterogeneity of redox-active transition metals, and tunable surface functionalities allowing for low HER overpotentials. MXenes are prepared from their MAX precursors by etching of the Al layers, using partial etching we synthesize a hybrid Ti₃CN capable of surface modifications using in situ electrochemistry. In this presentation, we report on the cathodic etching and -O/-OH functionalization of hybrid Ti₃CN upon the application of an external potential for improved HER performance and show that the active sites for HER on this MXene catalyst are located primarily on the -O- and -OH functional groups. The overpotential for the hybrid Ti₃CN improves by 350 mV upon in-situ -O functionalization and reaches -0.46 V vs. RHE at a current density of 10 mA cm⁻². Structural and electrochemical characterization results showed that the functionalized hybrid Ti₃CNT_x MXene catalyst is structurally and electrochemically stable. Further insights into the mechanism of simultaneous in situ etching and functionalization were provided by in-situ spectroelectrochemical techniques and the results will be presented. Ultimately, these findings provide a novel path forward to controlling the surface reactivity of MXenes using in-situ functionalization and electrochemical exfoliation.

11:00 AM DISCUSSION TIME

11:15 AM CH01.05.11

Visualization of Ferroelectric Domains with Picosecond Time and Nanometer Length Resolution Burak GuzelTURK; Argonne National Laboratory, United States

Engineering domains and domain walls in ferroelectric materials is at the heart of realizing novel nanoelectronic and photonic devices. To this end, electric fields, light, strain and doping have been employed to manipulate domains at the atomic scale. Control of the domain structures with light pulses particularly presents strong potential to engineer electronic and optoelectronic functionalities in these materials in an all-optical fashion. Nevertheless, non-equilibrium photoexcited states in such complex materials could not be resolved in space and time with the desired resolution, i.e., picoseconds and nanometers, due to limitations in available characterization techniques. In this work, we develop a novel characterization approach to visualize nanoscale domain structures in photoexcited ferroelectric thin films over picosecond time with nanometer length scales via time-resolved nanoprobe X-ray diffraction imaging (TR-NXRD) at the Advanced Photon Source. Using this approach, we investigate stripe-domain bismuth ferrite (BFO) thin films that exhibit periodic 71 degree domain walls. Surprisingly, we find that the domain pattern transiently melts following an intense above bandgap laser pulse as revealed by strongly bleached domain pattern contrast. The washout of the domain pattern immediately after the photoexcitation arises due to weakening of the in-plane ferroelectric polarization linked with a large out-of-plane photostriction and rhombohedral-to-tetragonal phase transformation which overall destabilize the domain walls. Furthermore, we find that the dynamic domain evolution is fully reversible as the domain pattern reappears after 10 ns following the excitation laser pulse. Reappearance of the domains is consistent with the fact that the domain structure is pinned by the mechanical boundary conditions between the substrate and the thin film. Overall, we unveil a novel way to manipulate stripe domains in BFO thin film at sub-nanosecond timescales by visualizing via TR-NXRD. This technique is further applicable to a broad range of materials to visualize non-equilibrium dynamics across nanoscale spatial heterogeneities critical to uncovering hidden structure-property relationships overlooked before due to the absence of methods that can simultaneous access high spatial and temporal resolution.

11:30 AM CH01.05.12

Real-Time Studies of Filament Evolution in Metal-Filament-Based Resistive Switching Devices Using *In Situ* Transmission Electron Microscopy
Saurabh Pandey and Robert Hull; Rensselaer Polytechnic Institute, United States

Hardware implementation of neuromorphic computing requires the development of artificial synapses that exhibit low power and repeatable and reliable switching into multiple resistance states. Filamentary resistive switching devices are a strong candidate for these artificial synapses, but they are limited by their state resistance dispersion. The state resistances of these devices are determined by the morphology of conducting filament(s) bridging the anode and cathode in these devices. It is therefore imperative to understand the entire filament evolution process in real-time to identify the factors that can influence the final filament morphology. For this purpose, we have developed an in-situ TEM electrical biasing methodology to study filament evolution during the electroforming of Cu/SiO₂/Cu devices at nanometer-scale spatial resolution and sub-second temporal resolution.

To image the real-time filament evolution at electrode-dielectric interfaces and within the dielectric, we have designed and fabricated devices with ~100 nm laterally separated electrodes. We use electron-beam lithography and lift-off to pattern 50 nm thick Copper electrodes onto 50 nm silicon nitride support film substrates to ensure electron transparency. We use ~10 nm of Titanium as an adhesion layer between Copper and Silicon Nitride and another ~10 nm of Titanium as a diffusion barrier between Copper and Silicon dioxide. We deposit ~65 nm Silicon dioxide thin film by RF sputtering of SiO₂ target at 200 W and 3 mtorr Argon pressure to conformally fill the electrode gap. We utilize a Gatan in-situ TEM electrical biasing holder and a Keithley voltage source/pico-ammeter to perform a stepped voltage ramp and simultaneous imaging and current measurement during the electroforming of the devices.

We find that the as-fabricated device has high resistance (>1 GΩ). During the voltage sweep, Copper clusters ~5 nm in size initially appear non-uniformly across the anode-dielectric interface. With increasing voltage, more clusters are formed in the dielectric close to the previous clusters along the direction of the electric field. The resulting filaments grow further along the electric field with increasing voltage until clusters are formed at the cathode-dielectric interface and the filament(s) are established. This coincides with a sudden reduction in the resistance (to ~200 MΩs) of the device at ~50-60 V bias. The shape and size of individual previously formed clusters also change with time and voltage with some clusters decreasing in size and ultimately disappearing and others increasing in size and merging with other clusters as the filament evolution process progresses. The device resistance increases back to the as-fabricated level (> 1 GΩ) upon the removal of applied bias. The device regains the low resistance state (~200 MΩs) at comparatively low voltage (~20 V) indicating the existence of threshold switching in the device.

Through this work, we are able to provide insight into the filament evolution process at the cluster-by-cluster and filament-by-filament level. This work also lays the framework for our future work on the study of SiO₂ density and composition on filament evolution in these devices.

This work was supported by the NYSTAR Focus Center at RPI, contract #C150117, and made extensive use of cleanroom and characterization facilities in the Center for Materials, Devices, and Integrated Systems (CMDIS) at Rensselaer Polytechnic Institute.

SESSION CH01.06: Characterization of Catalytical, Electrical and Mechanical Properties II

Session Chairs: Qian Chen and Michele Conroy

Wednesday Afternoon, November 30, 2022

Hynes, Level 1, Room 102

1:30 PM *CH01.06.01

Investigating the Ferroelasticity Governing the Dynamics of Improper Ferroelectric Domain Walls by *In Situ* Biasing 4D-STEM Michele S. Conroy¹, Steven Zeltmann^{2,3}, Sinead M. Griffin³, Jim Ciston³, Benjamin Savitzky³, Roger Whatmore¹ and Colin Ophus²; ¹Imperial College London, United Kingdom; ²University California Berkeley, United States; ³Lawrence Berkeley National Laboratory, United States

Dynamic conducting ferroelectric domain walls overturn the classical idea that our electronic circuits need to consist of fixed components of hardware.[1] Domain wall topologies in ferroelectrics are an emerging research focus in nano-electronics and potential quantum technologies.[2, 3] However, due to the high energetic cost of creating charged walls in conventional ferroelectrics they are not stable long term. Improper ferroelectrics circumvent this issue as their driving force is not a polar instability, but rather the critical dynamics of symmetry-breaking of the non-polar primary mode. With these benefits there has been a recent surge in improper ferroelectric topology research.[4]

We focus our studies on the improper ferroelectric boracite material system, known for their stable conducting and insulating domain walls and anomalous motion associated with negative capacitance.[5, 6] Boracite is an improper ferroelectric material where the primary order parameter is the physical quantity spontaneous shear strain. As a ferroelastic material the conductivity of the charged walls is governed by the shear strain direction of the neighbouring domains. Thus, traditional atomic resolution STEM polarity mapping will not give a true picture of the ferroelectric properties. In order to understand the mechanism of the wall movement and the fundamental physics governing their formation, strain analysis was completed using four-dimensional scanning transmission electron microscopy (4D-STEM)[7, 8] strain mapping. This strain analysis was then compared to the atomic resolution STEM imaging and polarity mapping.[9]

The dynamic nature of the topologies was first investigated by utilising the applied electric field of the STEM probe.[10] We show long-ranged re-ordering of shear strain during wall motion that is not present when the walls are stationary, and the complexity of the domain walls' local strain as they move through defects such as twin boundaries. Additionally we used an in-situ biasing holder set up in a parallel contact mode to compare to our previous device level work on negative capacitance measurements.[5] When mobile, the insulating domain walls have a very distinct local change in both strain and symmetry compared to the conducting walls. Finally, we explore the motion of higher order topology junctions such as vertices and vortices. Theoretical calculations confirm the shear strain to polarization vector relationship and charged topology energetics. We will present the benefits of 4D-STEM characterization for wall topologies governed by ferroelasticity, over the use of segmented detectors, where differential phase contrast mapping cannot detangle the strain and polar signals. The opportunities time-resolved 4D-STEM characterization methods can bring to the field of ferroelastic governed polar topology physics will be discussed in detail.

References:

[1] G Catalan, J Seidel, R Ramesh and JF Scott, *Reviews of Modern Physics* **84** (2012) 10.1103/RevModPhys.84.119

[2] JPV McConville, et al. *Advanced Functional Materials* **30** (2020) 10.1002/adfm.202000109

[3] D Meier and SM Selbach, *Nature Reviews Materials* (2021) 10.1038/s41578-021-00375-z

[4] D Meier, et al., *Nature Materials* **11** (2012) 10.1038/nmat3249

[5] JGM Guy, et al., *Advanced Materials* **33** (2021) 10.1002/adma.202008068

[6] RGP McQuaid, et al., *Nature Communications* **8** (2017) 10.1038/ncomms15105

[7] C Ophus, *Microscopy and Microanalysis* **25** (2019) 10.1017/S1431927619000497

[8] BH Savitzky, et al., *Microscopy and Microanalysis* **27** (2020) 10.1017/S1431927621000477

[9] E O'Connell, et al., (2021) arXiv:2110.00112

[10] M Conroy, et al., *Microscopy and Microanalysis*, **26** (2020) 10.1017/S1431927620023594

2:00 PM CH01.06.02

Atomic-Scale Insights into Hydrogen Absorption and Desorption in Palladium Nanocrystals Sophia Betzler^{1,2}, Daewon Lee^{1,2}, Mark Asta^{1,2} and Haimei Zheng^{1,2}; ¹Lawrence Berkeley National Laboratory, United States; ²University of California, United States

Hydrogen-induced phase transformations in palladium (Pd) is a topic that has attracted significant interest for many years. The palladium hydride (PdH_x) system consists of a hydrogen-poor α phase and a hydrogen-rich β phase. The α to β transformation involves the large Pd lattice expansion and thus causes specific interfacial structures to accommodate the lattice mismatch strain. Although the bulk PdH_x phase transformations are well-understood, the phase transformations of Pd nanocrystals have recently started to be explained due to advances in in-situ characterization techniques. In-situ environmental transmission electron microscopy (ETEM) and X-ray imaging demonstrated the corner nucleation and propagation of the β phase during absorption of Pd nanocrystals. However, there have been no direct atomic-scale insights into the phase boundaries during the dynamic hydrogen-induced phase transformations in Pd nanocrystals.

In this work, we use the in-situ liquid cell TEM to visualize the hydrogen-induced phase transformations in Pd nanocrystals at the atomic level. We synthesize Pd nanocubes and load them with an aqueous solution into a liquid cell. H₂ gas is generated by the electron-beam radiolysis of water in liquid cells. We image the hydrogen-induced phase transformations in individual Pd nanocubes at the atomic level. During the H₂ absorption, a unique interface is formed. The interface boundary is broadened, and there is a lattice tilt within the boundary. No dislocation is observed. However, during the H₂ desorption, the atomically sharp interface is found with dislocations identified at the interface. We also systematically study the particle size effects on hydrogen-induced phase transformations in Pd nanocubes. Variations in the interfaces suggesting differences in lattice strain relaxation mechanisms are revealed. This research expands our fundamental understanding of the solute-induced phase transformations, and assists the future design of advanced materials for hydrogen storage or other applications.

Acknowledgement: This work was supported by the U.S. Department of Energy, Office of Science, Office of Basic Energy Sciences (BES), Materials Sciences and Engineering Division under Contract No. DE-AC02-05-CH11231 within the in-situ TEM program (KC22ZH). Work at the Molecular Foundry of Lawrence Berkeley National Laboratory (LBNL) was supported by the U.S. Department of Energy under Contract No. DE-AC02-05CH11231. S.B.B. acknowledges financial support from the Alexander-von-Humboldt Association. D.L. acknowledges the Kwanjeong Study Abroad Scholarship from the KEF (Kwanjeong Educational Foundation) (KEF-2019).

2:15 PM OPEN DISCUSSION

2:30 PM BREAK

3:30 PM *CH01.06.04

In Situ Observation of Crystallization Processes Using LC-TEM with the Support of Machine Learning Yuki Kimura; Institute of Low Temperature Science, Japan

We have observed the crystallization processes of hen egg-white lysozyme protein [1] and the aggregation processes of amyloid- β protein [2], which is considered to cause Alzheimer's disease, by liquid-cell transmission electron microscopy (LC-TEM). In these observations, it is necessary to examine the issues of water radiolysis and electron damage to the sample due to electron irradiation. For example, in the crystallization experiment of lysozyme protein, the dependence of crystal growth rate on electron dose was observed. Therefore, we determined the threshold electron dose rate at which the crystal growth rate measured under an optical microscope was maintained, and made observations at lower electron dose rate than the threshold. Fortunately, the electron dose rate was not so small, 320 electron nm⁻² s⁻¹, and therefore, there were no significant problem with observation at low magnifications. However, for observation at a high magnification or when the sample is more sensitive to electron beams, it is necessary to lower the electron dose rate, resulting in a dark image for observation. Although post-processing can brighten the image and increase contrast, we must make decisions about observation and experimental conditions during in-situ observation based on the dark image. We have therefore developed an algorithm of machine learning to enable image sharpening through real-time image processing during in-situ observation [3].

Another challenge for in situ experiments of crystallization is the detection of particles; in a typical in situ TEM, it is difficult to save all images during the experiment. Therefore, using the look back function provided in the TEM camera, recording is started when the phenomenon is confirmed to have occurred, starting with the image from a few seconds earlier. However, because the human eye has difficulty noticing slow phenomena, it may not be possible to record the initial process at the time we notice it. Therefore, we developed a machine-learning algorithm to detect the initial stage of the phenomenon by real-time image processing. This has made it possible to detect nanoparticles generated from solution through nucleation as quickly as possible [4].

By modifying an algorithm for particle detection, we used machine learning to analyze the relationship between the nucleation of nanoparticles from solution and the dissolution process [5]. In aqueous solution, clustering of ions and degradation of clusters are taking place, and we hypothesized that this is recorded as fluctuations in the TEM images. Therefore, we attempted to predict the formation of nanoparticles by machine learning using images taken several images before the time when the particles were formed. By changing the time period for learning, it may be possible to determine how many seconds before the nanoparticles form, clustering is occurring. Also, if particles undergo the same structure as clustering when they dissolve, machine learning should falsely detect the formation of new particles at the moment they dissolve. I will introduce our latest results of in-situ observation of crystallization with a support of machine learning.

[1] T. Yamazaki, Y. Kimura, P. G. Vekilov, E. Furukawa, M. Shirai, H. Matsumoto, A. E. S. Van Driessche, K. Tsukamoto, *Proc. Natl. Acad. Sci. USA*, **114** (2017) 2154.

[2] K. Nakajima, T. Yamazaki, Y. Kimura, M. So, Y. Goto, H. Ogi, *J. Phys. Chem. Lett.*, **11** (2020) 6176.

[3] H. Katsuno, Y. Kimura, T. Yamazaki, I. Takigawa, *Microscopy and Microanalysis*, **28** (2022) 138-144.

[4] H. Katsuno, Y. Kimura, T. Yamazaki, I. Takigawa, *Frontiers in Chemistry*, **10** (2022) 818230.

[5] Y. Kimura, H. Katsuno, T. Yamazaki, *Faraday Discussions*, (2022) in press. DOI: 10.1039/D1FD00125F

4:00 PM CH01.06.05

Nanoscale Operando Experiments in Environmental Transmission Electron Microscopy for Solid Oxide Fuel Cell Devices Quentin Jeangros¹, Matthieu Bugnet², Thierry Epicier³, Cédric Frantz¹, Stefan Diethelm¹, Dario Montinaro⁴, Elizaveta Tyukalova⁵, Yevheniy Pivak⁶, Jan Van Herle¹, Aïcha

Hessler-Wyser¹ and Martial Duchamp^{5,7}; ¹Ecole Polytechnique Fédérale de Lausanne, Switzerland; ²Univ Lyon, CNRS, INSA Lyon, UCBL, MATEIS, UMR 5510, France; ³Univ Lyon, Université Claude Bernard Lyon 1, CNRS, IRCÉLYON, France; ⁴SOLIDpower SpA, Switzerland; ⁵Nanyang Technological University, Singapore; ⁶DENSsolutions, Netherlands; ⁷MajuLab, International Joint Research Unit, UMI 3654, Univ Côte d'Azur, National University of Singapore, Nanyang Technological University, Singapore

Solid oxide fuel cells (SOFC) are a class of solid-state electrochemical conversion devices that produce electricity directly by oxidizing a fuel gas. They consist in an anode-cathode duet separated by a solid electrolyte, i.e., a material conducting oxygen ions. The anode is fed with hydrogen or other fuels whereas the cathode is in contact with air, meaning oxygen. Overall, a SOFC operates thanks to the combined action of two external stimuli: a gaseous environment and temperature. Owing to the recent advances in *in situ* and *operando* transmission electron microscopy (TEM), we have set up an experiment to operate a SOFC inside an environmental TEM to identify how the device microstructure determines its electrical properties. To do so, an elementary anode-electrolyte-cathode sandwich was prepared by focused ion beam (FIB) and mounted on a heating and biasing microelectromechanical (MEMS)-based specimen holder (DENSsolutions) and inserted in an Environmental TEM (FEI Titan ETEM), as shown in Fig. 1. Standard SOFC materials were investigated: the cathode was strontium-doped lanthanum manganite (LSM) co-sintered with yttria-stabilized zirconia (YSZ), the electrolyte was YSZ, and the anode a cermet of NiO co-sintered with YSZ. NiO was first reduced to Ni, leaving pores in the structure due to the volume loss and hence enabling the penetration of the fuel to the triple phase boundaries Ni/YSZ/porosity at the anode side. For practical reasons, we used a single chamber configuration to trigger the operation the cell: the anode and cathode were exposed simultaneously to the oxidant and reducing gases. Due to a difference in the catalytic activity between the electrodes, O₂ should reduce at the cathode, while H₂ should oxidize at the anode, thus leading to a voltage difference between the two terminals.

The reduction of NiO was first performed under a forming gas N₂:H₂ in the ratio 20:1 under 15 mbar up to 750°C (N₂ was constantly used as a mixing gas for safety reasons due to the need of mixing O₂ and H₂ in the single-chamber configuration). The O₂ to H₂ ratio was then increased to trigger the operation of the cell. A small quantity of O₂ was introduced into the microscope, leading to a total pressure of about 16 mbar at 600°C. At this point, the variation of voltage between the anode and cathode was correlated to the gas composition and the anode microstructure (see Fig. 2). The latter was analyzed by means of conventional and high-resolution imaging, diffraction, and EELS (electron energy-loss spectroscopy). The system was cycled several times by decreasing and re-increasing the O₂ concentration in the gas flow, and correlations between microstructure, gas composition, and cell voltage were established, as it will be discussed at the conference. Results were further confirmed by macroscopic *ex situ* tests in an oven using the same materials [1]. The operation of a SOFC in a single chamber configuration was demonstrated using *operando* ETEM. Such *operando* experiments open numerous perspectives to investigate the root cause of failure pathways affecting SOFCs, like poisoning of active sites or coarsening of the Ni catalyst [2].

[1] Q. Jeangros, M. Bugnet, T. Epicier, C. Frantz, S. Diethelm, E. Tyukalova, G. Pivak, J. Van herle, A. Hessler-Wyser, M. Duchamp, under review (submitted 2021/10/12).

[2] The authors acknowledge the French microscopy network METSA for funding and the consortium Lyon-St-Etienne de microscopie for ETEM access. The FIB preparation was performed at the facilities for analysis, characterization, testing and simulations (FACTS, Nanyang Technological University). Additional support was provided by the INSTANT project (France-Singapore MERLION program 2019-2021) and the start-up grant M4081924 at Nanyang Technological University.

4:15 PM CH01.06.06

Reversible Conversion Between Schottky and Ohmic Contact of Zinc Oxide Microwire-Based Device Hue T. Tran, Yugyeong Je, Hyunjeong Jeong and Sang Wook Lee; Ewha Womans University, Korea (the Republic of)

In this study, electromechanical responses of individual ZnO microwires were observed under optical microscopy. In situ electrical measurements and the mechanical manipulation of ZnO microwires were carried out using a homemade micro-manipulation system. Here, the energy barrier height is tuned by inducing piezoelectric polarization charges at the local metal-semiconductor interface when a mechanical deformation was applied to ZnO microwire. As a result, the metal-semiconductor local contact can be transformed from Schottky to Ohmic and vice versa. This work demonstrates a method for controlling the electrical properties of ZnO nanowires to achieve reversible tuning between the Schottky contact and Ohmic contact on one device, which could be potential in developing multifunctional and Ohmic/Schottky-based sensors, switches, rectifiers, and other functional electronic devices.

4:30 PM CH01.06.07

Catalytic Nanoparticles with Propelled Motion Observed Under Liquid Cell TEM Zhiheng Lyu¹, Lehan Yao¹, Chang Qian¹, Zhisheng Wang² and Qian Chen¹; ¹University of Illinois at Urbana-Champaign, United States; ²The University of Hong Kong, China

Nanomotors have attracted increasing attention in recent years due to their wide applications in a variety of fields such as drug delivery, self-assembly, and active sensors. However, due to the small size of nanoparticles, their motions are hard to be tracked by conventional optical microscopes with a resolution of hundreds of nanometers. This challenge, on the other hand, can be overcome with the development of liquid cell TEM, which enables the characterization and tracking of nanoparticles with high spatial (down to a few nanometers or even below) and temporal resolution. In this work, we introduce, for the first time, the propelled motion of nanoparticles characterized in the liquid cell TEM driven by catalytic reactions. Pt nanoparticles with asymmetric shapes were chosen as the model system, which reacted with a chemical fuel in an aqueous solution and generated a local concentration gradient around the nanoparticle that served as the driving force. Compared with the same concentration of inert salt, more Pt nanoparticles with propelled and directional motion were observed in chemical fuels, further confirming the existence of catalytic reactions and thus driving force. The symmetry of nanoparticles was also found to play an important role in their movements, with faster motion observed in asymmetric nanoparticles relative to the symmetric ones. We hope this work could provide real-time observation and mechanistic understanding of the propelled motion of nanoparticles driven by catalytic reactions using liquid cell TEM, stimulating more efforts into the design of nanomotors and characterization of their motions with advanced techniques.

4:45 PM CH01.06.08

In Depth Investigations of Graphene Oxide Reduction via *In Situ* TEM Measurements Raul Arenal^{1,2,3}, Mario Pelaez-Fernandez^{1,2}, Simon Hettler^{1,2}, Ana Benito⁴ and Wolfgang Maser⁴; ¹Instituto de Nanociencia y Materiales de Aragon (INMA), CSIC-Universidad de Zaragoza, Spain; ²Universidad de Zaragoza, Spain; ³ARAID Foundation, Spain; ⁴CSIC, Spain

Graphene oxide (GO) strongly attracts research interest due to its use as precursor material for graphene-based material and its high flexibility in terms of functional modification offering promising applications in numerous fields [1-5]. Despite the efforts for investigating its atomic structure, which is critical for knowing its properties, several aspects remain unknown in particular the behavior of the physi-/chemi-sorbed and of the oxygen functional groups (OFGs) during GO reduction. Thus, here we present two different approaches for studying, in depth, the GO reduction via in-situ TEM investigations: thermal reduction and Joule heating. For achieving these comprehensive studies [7,8], we have performed high-resolution TEM (HRTEM) imaging and electron energy-loss spectroscopy (EELS) measurements and coupled (for the second of these studies) with electrical conductivity measurements. In both studies we have identified the transformations of different oxygen functional groups, the desorption of physisorbed and chemisorbed water and the

graphitization of the GO flakes. These in-depth analyses provide a detailed roadmap of the behavior of GO during its reduction. All these findings improve the knowledge of this complex and heterogeneous material, which is crucial for the study of their physical and chemical properties and its future applications.

- [1] G. Eda, & M. Chhowalla, *Advanced materials*, 22, 2392 (2010).
- [2] K.P. Loh, Q. Bao, G. Eda, M. Chhowalla, *Nature chemistry* 2, 1015 (2010).
- [3] D.J. Nuñez, et al., *Chem. Science* (2016).
- [4] D. D'Angelo, et al. *J. Phys. Chem. C*, 121, 5408 (2017).
- [5] C. Backes, et al., *2D Mat.* 7, 022001 (2020).
- [6] M. Pelaez-Fernandez, A. Bermejo-Solis, A.M. Benito, W. Maser, R. Arenal, *Carbon* 78, 477 (2021).
- [7] S. Hettler, D. Sebastian, M. Pelaez-Fdez, A. Benito, W. Maser, R. Arenal, *2D Mat.* 8, 031001 (2021).
- [8] RA acknowledges funding from the EU H2020 program "Graphene Flagship" (Grant Agreement 881603) and EU H2020 program "ESTEEM3" (Grant Agreement 823717). MICINN (project grants PID2019-104739GB-I00/AEI/10.13039/501100011033 and PID2019-104272RB-C51/AEI/10.13039/501100011033) and Government of Aragon (projects DGA E13_20R and T03-20R) are also acknowledged.

SESSION CH01.07: Poster Session
Session Chairs: Yuki Kimura and Barnaby Levin
Wednesday Afternoon, November 30, 2022
8:00 PM - 10:00 PM
Hynes, Level 1, Hall A

CH01.07.02

***In Situ* Growth of Gamma-Cyclodextrin-Based Metal Organic Frameworks on Poly(ethylene terephthalate) Fibers** Fatemeh Mashhadi Abolghasem and JR Kim; Korea Institute of Industrial Technology, Korea (the Republic of)

Metal organic frameworks (MOFs) are highly porous materials with large surface areas of 1000–10,000 m²/g, which are much higher than those of zeolites and activated carbons. However, when MOFs are used alone in toxic gas removal systems, they are difficult to handle because they are very fragile and often break down into nanosized particles, which have low stability and tend to form agglomerates. Thus, MOFs are often used in composites, where they are embedded in a polymeric matrix, or attached to a matrix surface. A common limitation of MOF fibrous composites is the low binding strength of the MOFs to the substrate. When MOF crystals are coated on a substrate surface, they are often only weakly adhered to the surface and easily fall off. In addition, when MOFs are incorporated into a polymeric matrix, their cavities can be blocked, resulting in a decrease in the surface area and porosity. The growth of self-supported MOFs onto the surfaces of substrates may solve this problem. Specifically, fibrous substrates can provide mechanical support and reduce MOF aggregation, leading to good performance for gas adsorption. Moreover, MOF growth on fibrous substrates enables more than one type of MOF to be incorporated to simultaneously provide multiple functions.

Cyclodextrin-based MOFs (CD-MOFs) are synthesized from the enzymatic degradation of starch and have received much attention toward the green synthesis of MOFs. CD-MOFs have truncated cone-shaped crystals with an external hydrophilic surface owing to the hydroxyl groups and internal hydrophobic cavity covered by glycosidic oxygens and C–H units. The presence of –OCO– binding groups only in the CD primary and secondary faces is advantageous for fabricating biocompatible and non-toxic MOFs. CD-MOFs are versatile because of the free primary hydroxyl groups present in CD that bind with reactive functional groups for the reversible formation of carbonic acid. These features have led to their applications into gas capture, adsorption, and removal of air pollutants <!--[[endif]]-->

In this study, an effective strategy was introduced for *in situ* growth of cyclodextrin-based metal organic frameworks (CD-MOFs) through the vapor diffusion method combined with O₂ plasma treatment. A structure of self-supported γ -CD-MOF on poly(ethylene terephthalate) (PET) fibers was developed, and the effect of the *in situ* growth time on its properties was evaluated. The growth rate of γ -CD-MOFs on PET fibers (CD-MOFs–PET) was determined over 136 h, and 24 h growth of CD-MOFs–PET showed the highest surface area and CD-MOFs growth without deformation for air-filter applications. The CD-MOF crystals grown on PET fibers had an average side length of 818 nm. The specific surface area of the CD-MOFs–PET grown with 24 h growth time was 142.88 m²/g, which was almost 235 times higher than that of the pristine showed a high efficiency of SO₂ gas adsorption performance up to 95% removal using a real-time gas monitoring system. The reusability of CD-MOFs–PET recovered most of its adsorption ability (85–95%) after vacuum oven drying. This study intends to provide an informative discussion of the applicability of textile-based CD-MOFs and the development of reusable filters for the removal of SO₂.

CH01.07.03

***In Situ* X-Ray Scattering of Atypical Nucleation and Kinetics of Strongly Coupled Nanocrystal Superlattice Self-Assembly** Vivian R. Wall, Christian P. Tanner and Naomi S. Ginsberg; UC Berkeley, United States

Self-assembly of colloidal nanocrystals (NCs) into long-range ordered arrays represents an appealing strategy toward the bottom-up design of hierarchically organized functional and multifunctional materials. These superlattices (SLs) are typically assembled from NCs with long, insulating organic ligands that inhibit strong electronic coupling. Recently, our team has developed a novel method to self-assemble metallic and high dielectric semiconductor NCs with short, multivalent, inorganic chalcogenometallate (ChM) ligands into strongly electronically coupled ordered SLs in ChM electrolytic environments. We are gaining a deeper understanding of the nucleation, kinetics, and phase diagram associated with this self-assembly process as a function of the system and environment composition, in order to better control assembly of these high dielectric semiconductor NCs and extend this method of assembly to semiconductor NCs with more typical, lower dielectric constants. To do so, we employ *in situ* small angle X-ray scattering (SAXS) to non-perturbatively probe the structure of PbS NC colloid, liquid, and SL phases as a function of time during self-assembly with millisecond time resolution. From fitting *in situ* SAXS patterns, we calculate the densities of different phases and thereby quantitatively map experimental phase diagrams for the first time. By identifying and exploring different regions of the phase diagram, we have also observed both classical one-step SL nucleation and non-classical two-step SL nucleation, where a liquid of NCs nucleates from colloidal NCs first, and crystallization into a SL occurs from within the liquid phase. This more complex nucleation process has been observed in protein crystallization and predicted for inorganic NC systems, but had not yet been shown experimentally. We have further explored the non-classical nature of this system by quantitatively comparing rates of assembly to classical nucleation theory, as well as by studying NC diffusion and cluster density fluctuations that lead to nucleation, in order to better control the nucleation process and final ordered configurations. The kinetic and dynamic lessons from these novel *in situ* experiments will help us push forward the goal of assembling strongly coupled SL materials from semiconducting NCs.

CH01.07.04

Photo-Responsive Chiral Supramolecular Polymers Based on C₃-Symmetric Triphenylene Triimides [Namhee Kim](#) and Byeong-Su Kim; Yonsei University, Korea (the Republic of)

A new type of C₃-symmetric triphenylene triimides (TTI) bearing different oligo(ethylene glycol) side chains via imide linkages is developed in this study. By exploiting this unique TTI molecule as a building block, a supramolecular polymerization is explored on the basis of π - π stacking and hydrophilic/hydrophobic interaction depending on the type of solvents and rates of heating/cooling process. The molecular chirality of TTI monomer triggers the formation of a preferential helicity in fibrous structures. The stacking type of supramolecular polymerization is highly dependent on the presence of the point chirality of side chains, as evidenced by a collection of spectroscopic analyses including UV/vis and CD spectroscopy together with AFM, TEM, and WAXS. Interestingly, while the fibrous structure in assembled state is maintained due to the intermolecular interaction, the self-assembly does not occur in monomeric state due to the formation of radical anion of imide groups under UV irradiation. This study is anticipated to provide a new direction in the control of the supramolecular chiral assembly.

CH01.07.05

Lateral Particle Migration in Shear-Thinning Fluid Observed with Versatile Dual-View Optical Microscopy [Daewkon Jin](#) and Jumin Kim; Ajou University, Korea (the Republic of)

Microfluidics-based technologies have been extensively used to count and sort particles, as well as synthesize functional micro- and nanoparticles. Until now, the dynamics of microparticles or the synthesis process in the microchannel have been observed with conventional optical microscopes equipped with a vertically aligned objective lens. Therefore, there are limitations to the observation of particle dynamics or polymer photopolymerization, which requires direct observation in both the depth and width directions of the microchannel simultaneously. However, existing methods employing holography or micromirrors have the disadvantage of requiring costly optical setups or complicated channel fabrication techniques.

In this work, we demonstrate that it is possible to build up a system capable of simultaneously capturing images in the width and depth directions of a poly(dimethyl siloxane) (PDMS)-based microchannel by installing two objective lenses in the vertical and horizontal directions together with two cameras that are controlled with a trigger. We also showed that by coating the channel side-wall with PDMS and stacking it with a glass slide, the scattered reflection of light caused by the roughness of the channel side-wall as a result of the inevitable channel cutting procedure can be minimized. Using this method, we demonstrated that our system can be used to investigate the three-dimensional distribution of particles in non-Newtonian viscoelastic fluids with shear-thinning viscosities. We expect that our method will be widely used to understand the particle dynamics in numerous solution-based processes employing viscoelastic fluids where the particle distribution is strongly affected by medium viscoelasticity. In addition, we anticipate that this system will contribute to the understanding of the particle synthesis procedures of stop-flow lithography which has been widely used to fabricate non-spherical particles in microchannels.

CH01.07.06

Composite Crystallization of Two Active Pharmaceutical Ingredients Using Polymer-Directed Crystallization Mechanism [Juhee Lim](#) and Jonghwi Lee; Chung-Ang University, Korea (the Republic of)

Particle engineering of pharmaceutical and food ingredients by crystallization is important and widely used to meet the complex requirements. By adding a small amount of polymer during crystallization, various properties such as bioavailability, crystal stability, and drug release control can be controlled, and many advantages such as high efficiency and cost reduction can be obtained. This polymer-directed crystallization can trigger crystal formation through a route of non-classical crystallization, which is mediated by the physical adsorption of long-chain molecules. We hypothesized that by polymer-induced crystallization, one polymer could connect crystals of two different drug molecules. Composite drug crystals can obtain advantages such as improved processability and stability, reduced number of drug tablets, and reduced price by making two drugs into one tablet. The two drugs used in this study are the antihypertensive drugs Valsartan (VAL) and Amlodipine besylate (AMB). The polymer dissolved in the solution is adsorbed on the surfaces of the nuclei, and the crystals form an assembly of crystals. OM and SEM showed two different types of crystals. Additionally, crystallinity changes were observed through birefringence observation. The melting point measurements by differential scanning calorimetry showed that the melting point of the two drugs were significantly changed in the composite crystal, indicating significant change in the interaction between the drugs and polymer. Powder X-ray diffraction showed that the crystal form changed according to the composition ratio of the drug. The proton nuclear magnetic resonance confirmed the composition ratio of the obtained crystals, and as a result, it was indicated that the precipitated ratio was like the added ratio. This novel complex crystal manufacturing method may provide new opportunities for convenient production of complex formulations and improved processability and stability.

CH01.07.07

Simulations and Experiments on the Synthesis of 2D Nanomaterials by Resistive Heating of Metallic Wires [Beatriz Rodríguez Fernández](#), Pedro Hidalgo and Bianchi Mendez; Complutense University of Madrid, Spain

Two dimensional materials are synthesized from different techniques like *chemical vapor deposition* or *physical vapor deposition* among others. Thermal oxidation growth has the advantage of its simplicity, but most of the reported synthesis of oxide low dimensional structures by this method, required growth times in the range of hours. A more rapid method of metal oxide structures synthesis, also based on thermal oxidation of metals, is the direct resistive heating of a metallic wires by the flow of an electric current in ambient conditions. The high current density applied during the Joule heating favors the diffusion processes involved in the growth, been considered the underlying mechanism the electromigration processes. Applying external electric fields with different orientations to the current flow during treatments, we are able to inhibit or enhance the ions diffusion and, therefore, the formation of structures.

In this work, we report a simple and effective method to obtain nano- and microstructures in a very fast way with promising applications. Simultaneous COMSOL simulations have been carried out to verify the experimental result. A detailed analysis of the behavior of the current density, potential difference and thermal gradient is presented in order to understand what is happening in the material during the flow of the electric current and how the growth originates on the surface of the wire. Simulations have also been carried out for treatments with electric field application with the purpose of comprehend how the electric field interacts with the material during Joule heating. In summary, the results obtained shed some light to better understand how electromigration processes take part in the formation of the structures. This study encourages in-situ measurements during the growth process by direct resistive heating of a metallic wire, which could also be extrapolated to a wide range of materials.

CH01.07.08

Standard Methodology for Investigating Thermal Robustness of Porous Materials Satyanarayana Bonakala, [Anas I. Abutaha](#), Elumalai Palani, Ayman Samara, Said Mansour and Fadwa El Mellouhi; Qatar Environment and Energy Research Institute (QEERI), Hamad Bin Khalifa University (HBKU), Qatar

With the pressing need of having reliable materials for carbon dioxide capture, metal-organic frameworks (MOFs) have shown promising performance due

to their flexibility sign and tunable functionality by applying reticular chemistry principles. One of the main characteristics of practical MOFs is to design thermally robust candidates for sustainable functionality. Here, we introduce a comprehensive methodology for examining the thermal stability of MOFs by combining theoretical calculations and affordable experimental methods to fully describe its performance under thermal variations. We choose the prototypical MOF, HKUST-1, to assess the methodology by performing density functional theory and classical molecular dynamics simulations and validating with experiments such as in-situ powder X-ray diffraction, differential scanning calorimetry, and thermogravimetric analysis. HKUST-1 shows thermal robustness until a temperature of 240 C at different atmospheric gases with a reversible breathing trend with temperature. This methodology is affordable as it uses minimal experimental testing and can be applied to any MOF materials to explore its suitability for practical applications.

CH01.07.10

In Situ UV-vis Spectroscopic Investigation of Feroxyhite Nanomaterial Synthesis by DC Atmospheric Microplasma Yucheng Lan¹, Grace Farrell¹, Gregory Severn² and Willie Rockward¹; ¹Morgan State University, United States; ²University of San Diego, United States

Feroxyhite nanomaterials were synthesized in aqueous solutions by DC atmospheric microplasma at room temperature. The chemical reaction during the plasma synthesis was in-situ investigated by UV-vis spectroscopy. Specially, the time-dependent and location-dependent crystallographic quality of the products was detected from the UV-vis spectra, including the bandgap of the nanomaterials and concentration. The effects of voltage, electric strength, and polarity were investigated too. The synthesized nanomaterials were characterized by X-ray powder diffraction, Raman scattering, and electron microscopy too. The mechanism of the plasma synthesis was discussed. Work supported by DOE grant DE-FE0031906 and NSF nos. PHY-1804240, and PHY-2108298, 2108636.

CH01.07.12

Chemical Vapor Deposition as a Novel Method for Synthesizing Two-Dimensional Conductive Metal-Organic Frameworks Thin Films Myeonggeun Choe and Hee Cheul Choi; Postech, Korea (the Republic of)

We demonstrated the synthesis of a conductive two-dimensional metal-organic framework (MOF) thin film with a single-step all-gas-phase chemical vapor deposition (CVD) method. The large-area thin film of the synthesized $\text{Cu}_3(\text{HHB})_2$ ($\text{Cu}_3(\text{C}_6\text{O}_6)_2$, HHB = hexahydroxybenzene) has a new phase of the structure and highly crystalline edge-on orientation. The $\text{Cu}_3(\text{HHB})_2$ thin film microdevices were fabricated by e-beam lithography (EBL), and showed an electrical conductivity value of 110.6 S/cm. Synthesis of conductive MOF thin films by the all-gas-phase CVD method is essential because it contributes to basic research on physical properties and brings them closer to the utilization of conductive MOFs in practical applications.

CH01.07.13

Rotation of Graphene on Cu(111) Surface During Chemical Vapor Deposition and Controlling the Stacking Angle of Bilayer Graphene Hyeeyeon Cho and Hee Cheul Choi; Pohang University of Science and Technology, Korea (the Republic of)

Control of stacking angle (θ_s) of bilayer graphene (BLG) is an essential task for the understanding and applications of BLG whose properties largely depend on θ_s . Up to date, BLG is frequently obtained by a layer-by-layer stacking of individual single-layer graphene manually, which is inferior to the potential alternative by chemical vapor deposition (CVD) method in the view of chemical purity. In this presentation, we introduce graphene rotation on Cu(111) surface during the CVD process and its application to obtaining AB-stacked BLG ($\theta_s = 0^\circ$) and 30° -twisted-BLG by edge state engineering of the second layer of BLG. It was found that the graphene could be rotated because of the population changes of BLG, as evidenced by population variation of AB-stacked and 30° -twisted BLG. Since the rotation of graphene is largely affected by the edge state of graphene, it is important to tune the edge state of graphene by growth temperature. Changes in programmed growth temperatures lead to block or accelerate the rotation of BLG and resulted in highly selective growth of AB-stacked or 30° -twisted BLG can be achieved. Both experimental and calculation studies on the unprecedented graphene rotation phenomenon on Cu(111) surface during CVD will be discussed in detail.

CH01.07.14

Strain Modulation of Crystallinity, Orientation and Piezoelectric Properties of Poly(vinylidene)—Poly(methyl methacrylate) Blends Michał Wyskiel¹, Kamal K. Meena², Konrad Schneider², Krzysztof Janus¹ and Adam Kiersnowski¹; ¹Wroclaw University of Science and Technology, Poland; ²Leibniz Institute for Polymer Research Dresden, Germany

Technologically-relevant semicrystalline, electroactive polymers such as poly(vinylidene fluoride) (PVDF) have attracted a lot of attention because of their potential applications in sensors and energy harvesting units. From a viewpoint of basic research, crystallization and crystal phase transitions of PVDF provided an interesting topic to study formation of different crystal polymorphs under the influence of external stimuli such as electric field and mechanical stress. Over four decades of experimental studies on PVDF provided a solid knowledge on relationships between nucleation, crystallization rate, and solid-state recrystallization, which underpinned market development of several high-tech companies in 21st century.

Imparting piezoelectricity to PVDF requires uniaxially, homogeneously and permanently oriented dipole moments of $\text{CH}_2\text{-CF}_2$ monomer units in polar crystal polymorphs. There are several technologically-proven strategies to render PVDF piezoelectric. One of the strategies is based on blending of PVDF with poly(methyl methacrylate) (PMMA) and deformation of the blends under the external electric field. PVDF and PMMA are thermodynamically miscible above upper critical solubility temperature. Generally, PMMA reduces the overall crystallinity of PVDF by “trapping” PVDF macromolecules in the PMMA bulk. The “trapping” reduces the crystallization rate. Therefore melt crystallization of PVDF in the PVDF:PMMA blends requires extended annealing at crystallization temperature or slow cooling of the melt. Quenching the molten PVDF:PMMA blends makes them amorphous whereas an appropriate thermal treatment of the fully amorphous blends can cause a preferential formation of polar crystals. Mechanical stress enhances the latter process and causes the crystals to orient along the deformation axis. However, the mechanism of formation of polar crystals after phase separation as well as recrystallization of non-polar polymorphs raise controversies. So does the role of a strain in the case of the blends.

Our study was aimed, therefore, at explaining the role of PMMA on formation of polar polymorphs of PVDF, i.e. the β and γ crystal phases. Our experiments were also supposed to shed light on mechanism of transforming of the isotropic non-polar PVDF polymorph (the α -phase) into oriented polar crystals during deformation in a viscoelastic state. The experimental approach included real-time, in-situ mapping of crystal structure development in the blends of PVDF with four different ratios of PMMA during their uniaxial deformation. PVDF crystal structure was monitored with time-resolved wide angle X-ray diffraction (WAXD) with 30-microns spatial resolution to precisely address the role of local strain on crystal orientation and phase composition. Small-angle X-ray scattering experiments were performed to supplement the WAXD data with variation of the lamellar structure of PVDF upon deformation. Additionally, the ex-situ Fourier transform infrared spectroscopy (FTIR) was used to refine the conclusions from WAXD. The studies performed with the high-spatial resolution enabled finding correlations between the local strain, orientation and the phase composition of the blends, including the γ to β ratios in different samples as a function of blend composition and local strain. In the contribution, we present static phase composition maps of samples under deformation and the evolution of the maps upon varying the strain. We also discuss correlation between Hermans orientation factors and phase compositions. The work can be considered as a fundamental contribution for development of the polymer blends for sensing and energy harvesting applications.

Acknowledgement

WAXS and SAXS experiments were performed at the P03 Beamline at PETRA III/German Electron Synchrotron (DESY) Hamburg, Germany. The work was supported by National Science Centre Poland (NCN) through the grant UMO-2017/25/B/ST5/02869

CH01.07.15

Colorimetric Strain Sensor Using High Refractive Index Iron Oxide Core-Shell Particles Seamin Park, Jungmin Kim and Youngseok Kim; Korea Electronics Technology Institute, Korea (the Republic of)

Three-dimensional photonic crystals have properties that can be useful for detecting physical deformations. Compared with 3D polymer photonic crystals with weak color and high viewing angle dependence, inorganic core-shell particles promise high color purity and reflectivity. In this study, iron oxide particles (130-160nm) having a high refractive index were prepared through hydrothermal synthesis and then silica was coated with the Stober method. Homogeneously synthesized inorganic particles can be arranged into highly ordered hybrid films using melt shear techniques. Inorganic particle core materials featuring smart soft/hard shell polymers enhance photonic crystal film preparation and provide convenient access to novel photonic materials as sensing platforms.

CH01.07.16

Micro-Encapsulation of Photonic Ink Containing Charge-Stabilized Superparamagnetic Iron Oxide Nanoparticles in Non-Polar Medium Jungmin Kim^{1,2}, Wonmok Lee² and Youngseok Kim¹; ¹Korea Electronics Technology Institute, Korea (the Republic of); ²Sejong University, Korea (the Republic of)

Color-tunable surfaces are of great interest in industries such as displays, automobiles, and interiors of buildings. In this study, monodisperse superparamagnetic iron oxide nanoparticles (SPIONs) were used to prepare photonic inks with high color purity and vivid colors due to light absorption. It was then encapsulated and implemented in the form of a stable film. A photonic crystal colloidal array was prepared by stabilizing the charge of Fe₃O₄@SiO₂ core-shell particles (130-160nm) using a charge control agent in a non-polar medium, and color conversion properties were observed. In addition, through a complex coacervation process, the SPION dispersion was processed into a double-layer microcapsule containing gelatin and polysaccharides to secure stability and color tunability by magnetic and electric fields. These microcapsules exhibited excellent mechanical strength enough to be applied to replica molding and photocuring, thus exhibiting long-term stability while maintaining flexibility and color tunability.

CH01.07.17

Advanced Characterization of Precipitates in Additively Manufactured AA 7075 Aluminium Alloy Irena Paulin¹, Črtomir Donik¹, Stefan Zaefferer², Christian Bross² and Matjaz Godcic¹; ¹Institute of Metals and Technology, Slovenia; ²Max-Planck-Institut für Eisenforschung, Germany

High strength Al alloys, e.g. for aerospace applications, obtain most of their strength from hardening by coherent precipitation, e.g. η' and η phases. These precipitates are formed in a sequence of solution annealing and ageing treatments. During this process care must be taken to avoid formation of large incoherent particles, e.g. S-phase. The related mechanisms and processes are well-understood for conventionally produced materials which usually consist of a deformation process which supports the dissolution of precipitates and following annealing. For additive manufacturing (AM) by 3D printing, which in principle is a very promising method to produce morphologically complicated parts, unfortunately, a deformation step does not exist and the process-inherent heat treatment is most inconvenient for precipitation control. Furthermore, as remarked in a recent publication in nature materials, the large solidification interval of high strength Al alloys makes them rather prone to hot cracking during or after printing. Nevertheless, printing of these alloys is of great interest for technological applications but also in the general sense of understanding how to extend the 3D metal printing process to more demanding materials. Also, the 3D printing process may hold advantages for high strength Al alloys as it is known from other alloys that a large number of dislocations are formed which may act as nucleation sites for coherent precipitation.

A parameter assessment has been carried out on the 3D printing process to obtain crack free printing of these alloys. We envisage a number of parameters to check, namely the temperature of the base plate, the laser power/density and the printing atmosphere. The aim of the study is to better understand (and subsequently control) the precipitation process in AM-produced material. Solution and ageing treatments will then be designed to influence and potentially optimize the microstructures. Most of the microstructure characterization work was done by electron microscopy, particularly using the outstanding features of controlled electron channelling contrast imaging (eCCEI). This technique allows direct and high resolution observation of defects (dislocations and grain boundaries) on bulk samples.

CH01.07.18

Solid-Liquid Contact Charge Separation and its Consequences Pravash Bista¹, Xiaomei Li¹ and Stefan A. Weber^{1,2}; ¹Max Plank Institute for Polymer Research, Germany; ²Johannes Gutenberg University, Germany

Understanding the effects and origins of slide electrification, i.e., the spontaneous charge separation in sliding drops [1-4], is of great importance in energy harvesting and wetting. We explored the consequences of spontaneous charge separation in drop motion [3]. We found that the electrostatic force on the sliding drop can be up to almost 50% of the total force. This finding shows that self-induced electrostatics should be considered while studying the drop motion. To understand the molecular processes behind slide electrification, we recently proposed a physical model to describe the dynamics in charge separation as successive water drops slide down a neutral hydrophobic surface. We describe this effect using a three-phase contact line voltage that changes or adapts when the surface is in contact with water. This deeper understanding can open the way for surface engineering to achieve desired wetting properties.

[1] Yatsuzuka, K., Mizuno, Y., & Asano, K. (1994). Electrification phenomena of pure water droplets dripping and sliding on a polymer surface. *Journal of electrostatics*, 32(2), 157-171.

[2] Stetten, A. Z., Golovko, D. S., Weber, S. A., & Butt, H. J. (2019). Slide electrification: charging of surfaces by moving water drops. *Soft Matter*, 15(43), 8667-8679.

[3] Li, X., Bista, P., Stetten, A. Z., Bonart, H., Schür, M. T., Hardt, S., ... & Butt, H. J. (2022). Spontaneous charging affects the motion of sliding drops. *Nature Physics*, 1-7.

[4] Bista, P., Stetten, A. Z., Wong, W. S., Butt, H. J., & Weber, S. A. (2022). Adaptive two capacitor model to describe slide electrification in moving water drops. *arXiv preprint arXiv:2202.03948*.

CH01.07.19

Adaptive Two Capacitor Model to Describe Slide Electrification in Moving Water Drops Pravash Bista¹, Amy Stetten¹, William S. Wong¹, Hans-Jürgen Butt¹ and Stefan A. Weber^{1,2}; ¹Max Plank Institute for Polymer Research, Germany; ²Johannes Gutenberg University, Germany

Triboelectric charging between solid surfaces is a well-known phenomenon. It is less obvious that a similar charge separation process can be observed in water drops moving on a hydrophobic surface [1-4]. In so-called slide electrification experiments, neutral water drops slide over a neutral hydrophobic surface, accumulating and leaving behind a net charge [2]. The accumulated drop charge for successive sliding drops decreases and eventually reaches a steady state. On hydrophobic/hydrophilic mixed surfaces, we could even observe a polarity flip in the drop charge upon decreasing the drop rate. To rationalize the charge separation process, we propose an electric circuit model based on capacitors and a voltage generated at the moving three-phase contact line. By introducing a voltage adaptation upon water contact, we can successfully describe drop charge experiments on many surfaces, including the drop-rate-dependent polarity flips. The characteristic adaptation times hint toward molecular processes affecting the solid-liquid charge separation. Thus, our adaptive two-capacitor model enables new insights into the molecular details of the charge separation mechanism.

[1] Yatsuzuka, K., Mizuno, Y., & Asano, K. (1994). Electrification phenomena of pure water droplets dripping and sliding on a polymer surface. *Journal of electrostatics*, 32(2), 157-171.

[2] Stetten, A. Z., Golovko, D. S., Weber, S. A., & Butt, H. J. (2019). Slide electrification: charging of surfaces by moving water drops. *Soft Matter*, 15(43), 8667-8679.

[3] Li, X., Bista, P., Stetten, A. Z., Bonart, H., Schür, M. T., Hardt, S., ... & Butt, H. J. (2022). Spontaneous charging affects the motion of sliding drops. *Nature Physics*, 1-7.

[4] Bista, P., Stetten, A. Z., Wong, W. S., Butt, H. J., & Weber, S. A. (2022). Adaptive two capacitor model to describe slide electrification in moving water drops. *arXiv preprint arXiv:2202.03948*.

CH01.07.21

Chiroptical Neuromorphic Phototransistor Based on Self-Assembled Supramolecular Nanostructure of Diketopyrrolopyrrole-Based π -Conjugated Organogelator [Hanna Lee](#)^{1,2}, Changsoon Choi¹, Hyemi Han¹, Seung Ho Song¹, Do Kyung Hwang¹, Jeong Ho Cho² and Jung Ah Lim¹;

¹Korea Institute of Science and Technology, Korea (the Republic of); ²Yonsei University, Korea (the Republic of)

Chiral optoelectronic has gathered significant attention in various applications of quantum computation, optical spintronics, bio-sensing, 3D imaging, and encryption. To realize chiral optoelectronics technology, the development of chiroptical optoelectronic devices, which can provide distinguishable electrical signals according to the handedness of circularly polarized (CP) light (i.e., right- or left-circular polarization) is essential. From a viewpoint of materials, chiral π -conjugated molecules of whose chiroptical properties can be effectively controlled by programmable molecular design are one of the key materials to impart the chiroptical activity of the optoelectronic device. So far, many demonstrations of chiroptical π -conjugated molecules and their supramolecular structures have been intensively demonstrated, however, the development of chiroptical optoelectronic devices based on chiral π -conjugated molecules or their supramolecular structure is rarely reported.

In this work, we propose a chiroptical hybrid phototransistor based on the supramolecular nanohelix of a π -conjugated molecule for neuromorphic imaging technology. To provide highly strong chiroptical activity to the transistor, diketopyrrolopyrrole-based donor-acceptor type organogelator (DPP-organogelator) was newly synthesized. Supramolecular nanohelix structure of DPP-organogelator was successfully fabricated under optimized self-assembly conditions and exhibited strong and stable chiroptical properties. The suggested chiroptical hybrid phototransistor based on the DPP-organogelator nanohelix distinguishably detected the circularly polarized light with the different circular polarization directions. Especially, the device exhibited the frequency-dependent plasticity behavior in the photocurrent. Based on this, we successfully developed unique chiroptical imaging sensors showing enhanced contrast in the images obtained under cp light with different polarization directions.

CH01.07.22

Optimization of Balloon Surface Morphology Using Breath Figure Method to Enhance Stent Retention Force [Han C. Lee](#)^{1,2}, Woojin Kim¹, Dong Yun Choi¹ and Gyu M. Kim²; ¹Korea Institute of Industrial Technology, Korea (the Republic of); ²Kyungpook National University, Korea (the Republic of)

Recently, the need for multifunctional medical balloons is increasing for stent delivery, drug delivery, and biosensing applications. To meet this demand, researches were conducted to apply coronary intervention by increasing the drug loading efficiency, which was done by increasing the specific surface area through texturing on the surface of the balloon. In addition, studies have been conducted to apply micro/nanoscale structures to enteroscopy procedures by increasing the frictional force in the human body. Among the various applications of medical balloons, stent delivery is the most commonly used balloon worldwide. Recently, bioabsorbable vascular stents (BVS) have been continuously developed as an improvement of the drug-eluting stent (DES) and bare-metal stents (BMS).

However, despite these advantages, the BVS sometimes dislodges from the balloon in an undesirable place during its delivery to the lesion. This is owing to the phenomenon of using slippery materials, such as Nylon12 and PEBA, to withstand the high-pressure expansion force (more than 20 ATM) of the medical balloon. Despite the issue of stent delivery, research and development related to this issue are insufficient.

In this study, we present a balloon with the porous surface that can increase stent retention strength. A porous film was formed using a thermoplastic polyurethane with high adhesion, and this was applied to the balloon surface. In particular, we focused on increasing the contact area with the stent strut through the 3D porous structure when the stent is crimped on the balloon.

To form a 3D-porous structure, the breath figure method (BFM), a type of self-assembly, is used along with the dip-coating method. Our system is templateless, porogenless, and simple to configure. BFM is a process that self-arranges the condensed droplets on the triple interface of air, water, and solvent using the Marangoni and capillary effects as driving forces.

When the film is in liquid state, that is, before being solidified, the droplets condense on the interface and either float or sink depending on Y_w (surface tension of water), Y_s (surface tension of solution), $Y_{w/s}$ (interfacial tension between water and solution). Accordingly, monolayer or multilayer coating structures can be formed. In this study, we control Y_s with the concentration of the polymer solution and mixing ratio (chloroform + pentane) to control the cross-sectional structure of the coating layer according to the variable surface tension over a wide range. In addition, Y_w is controlled as the concentration of the aqueous solution containing the surfactant F-127 or NaCl. As a result, the decrease in Y_w shows a tendency to create a hemispherical monolayer structure on the surface of the coating layer, and we can observe that this phenomenon is caused by water droplets floating on the liquid interface. On the other hand, when Y_w increases, spherical pores are generated in a multilayered structure, because water droplets sink into the polymer solution before the film solidifies. When only Y_s decreases, spherical pores are created, and it is confirmed that they are formed as monolayers. However, as Y_s increases, hemispherical pores are formed as monolayers. These results indicate that the viscosity of the polymer solution during the BFM process is related to the shape of the structure. Consequently, when the stent dislodgement test is performed, the maximum **retention** force is observed as the porosity of the structure increases.

CH01.07.24

Novel Coating-Plus-Irrigation Strategy on Ni-Rich Layered Cathode for Lithium-Ion Batteries [Moonsu Yoon](#)¹, Jaephil Cho² and Ju Li¹;

¹Massachusetts Institute of Technology, United States; ²Ulsan National Institute of Science and Technology, Korea (the Republic of)

Engineered polycrystalline electrodes are critical to the cycling stability and safety of lithium-ion batteries, yet it is challenging to construct high-quality coatings at both the primary- and secondary-particle levels. Herein, This work applies reactive wetting phenomena to protect electrode particles and their grain boundaries (GBs). We report a novel “coating-plus-irrigation” strategy on an industrially important Ni-rich layered cathode $\text{LiNi}_{0.8}\text{Co}_{0.1}\text{Mn}_{0.1}\text{O}_2$ (NCM). Cobalt boride is electronically conductive, and the nanolayers that forms in between grains also conducts Li^+ , forming a mixed ionic and electronic conductor (MIEC) network. The cobalt boride coating demonstrates 100% surface coverage of secondary oxide particles (proved by X-ray photoelectron spectroscopy over extended sample area over mm^2 , unlike typical literature “proof” using transmission electron microscope over nm^2 local area) as well as facile infusion into all grain boundaries between its primary particles. This is extraordinary considering everything happens at room temperature, without high-temperature alteration to the crystalline bulk of the primary particles, but with drastic changes in the GBs as they are infiltrated by MIEC nanochannels. Thus, the MIEC network protects the secondary particle from cracking and exposing fresh surfaces to the electrolyte, which greatly enhances the cycle stability, especially at high rates. Cobalt boride is used industrially as structural metal coating to improve corrosion and wear resistance, thus it does not easily chip or fracture at nanoscale, making it a mechanically tough MIEC at nanoscale, which can deform to accommodate the anisotropic deformation of the primary particles with lithiation/delithiation. Such facile kinetics and resulting irrigation network are enabled by the huge chemical driving force from the strong hybridized interfacial bonding from our first-principles calculations. It not only ensures ultra-uniform conformal coating/irrigation, but also de-activates labile surface oxygen of the cathodes. As a result, our strategy offers superior electrochemical performance of high-loading (10.5 mg cm^{-2} , $\sim 2.05 \text{ mAh cm}^{-2}$) and high-electrode-density (3.20 g cm^{-3}) cathodes under high-rate (up to $1,540 \text{ mA g}^{-1}$, $\sim 7 \text{ C}$) and high-temperature ($45 \text{ }^\circ\text{C}$) conditions, by simultaneous suppression of the correlated microstructural degradation (stress-corrosion cracking, SCC problem) and side reactions of Ni-rich layered cathodes as well as the cross-over effect on lithium metal anodes (all of them are fully supported by extensive, direct experimental evidences). It also improves the safety according to differential scanning calorimetry, where the exothermal decomposition takes place at higher temperature with less heat generation, which offers a strong proof of the chemical passivation effect we proposed.

CH01.07.26

Electric-Field-Mediated In-Sensor Alignment of Antibody’s Orientation to Enhance the Antibody–Antigen Binding for Ultra-High Sensitivity of Sensor [Hye Jin Kim](#)^{1,2}; ¹Seoul National University, Korea (the Republic of); ²Institute for Basic Science (IBS), Korea (the Republic of)

Applying an electric field (E -field) during antibody immobilization aligns the orientation of the antibody on the biosensor surface, thereby enhancing the binding probability between the antibody and antigen and maximizing the sensitivity of the biosensor. In this study, a biosensor with enhanced antibody-antigen binding probability was developed using the alignment of polar antibodies (immunoglobulin G [IgG]) under an E -field applied inside the interdigitated electrodes. The optimal alignment condition was first theoretically calculated and then experimentally confirmed by comparing the impedance change before and after the alignment of IgG (a purified anti- β -amyloid antibody). With the optimized condition, the impedance change of the biosensor was maximized owing to the alignment of IgG orientation on the sensor surface; the detection sensitivity of the antigen amyloid-beta 1-42 was also maximized. The E -field-based in-sensor alignment of antibodies is an easy and effective method for enhancing biosensor sensitivity.

CH01.07.27

Grafting Superhydrophobic Moieties on Cellulose Nanofibers via Ionic Bonding [Zhuolun Jiang](#); The Chinese University of Hong Kong, Hong Kong

Magnesium stearate (MS) as a derivative product of stearic acid (SA) biomass was chosen as the superhydrophobic agent for in-situ modification of citric acid (CA) crosslinked and alkaline treated cellulose nanofibers (CNFs). MS is a common food additive and possesses high thermal stability ($T_m = 200 \text{ }^\circ\text{C}$, $T_d = 359 \text{ }^\circ\text{C}$).¹ Our approach is taking advantage of ionic bonding and the ion exchange interaction to induce the self-assembly between MS and CA-CNF⁻ K^+ to prepare the highly hydrophobic and rough CNF substrates, thus obtaining a superhydrophobic biomass-based surface with controlled superhydrophobicity, roughness and self-cleaning function via a simple and green way.²

Through vacuum filtration and air drying processes, a MS-CA-CNF disk with distinctly different roughness on each side was prepared, of which the appearance is similar to that of the biowax-mineral hybrid modified paper substrate.³ Side A is rough, with spherical particles of diameter from 200 to 500 nm and Side B is smooth. Water contact angle test reveals the high hydrophobic Side A (150°) and hydrophilic Side B. The quite high WCA of Side A can be explained by its low surface energy and high roughness. X-ray diffraction (XRD) has been used to analyze the crystalline structure of crystalline structures of both sides. Side A displays a similar crystalline diffraction peak to MS while Side B exhibits more similar crystalline pattern to CNFs. Based on this, surface of Side A is speculated to be mainly composed of stearic chains. SEM energy dispersive spectrum (SEM EDS) characterization has specified the distribution and concentration of Mg on Side A and Side B and strongly supported above speculation. The wt% of C, O, Mg elements on both surfaces has been calculated. Quite low concentration of Mg was detected on Side A and Side B. Side A possesses a remarkably higher concentration of C and much lower concentration of O compared with Side B, which may be due to the tight aggregation of stearic chains on Side A. The distribution of Mg on the cross-section of MS-CA-CNF disk has also been tested. The concentration of Mg near the rough surface Side A is much higher than other locations, indicating that Mg^{2+} may act as the linkers between stearic chains and CA-CNF⁻ so that MS is able to sit stably on CA-CNF⁻. Based on this, a mechanism has been proposed to explain the self-assembly phenomenon of this disk. Due to the very low surface energy of stearic chains and the ionic binding role of Mg^{2+} , MS will highly self-assemble and be stably attached to CA-CNF⁻. As a result, the white layer is mainly composed of stearic chains while Mg^{2+} acts as the bridge between stearic chain and CA-CNF⁻. Due to the preferential evaporation of ethanol (EtOH) and better affinity between MS and EtOH, MS will move toward the surface while EtOH is evaporating. The evaporation-induced self-assembly mechanism was once used to explain the different aggregation pattern of zein on bacterial cellulose membrane. The synergetic effect of ionic bonding and solvent effect can assist the self-assembly of MS-CA-CNF and explain the distinctly different water barrier property on each side of disk.

References

1. M. He, M. Xu and L. Zhang, Controllable Stearic Acid Crystal Induced High Hydrophobicity on Cellulose Film Surface. *ACS Appl. Mater. Interfaces* 2013, 5 (3), 585-591.
2. T. S. G. Raja and K. Jeyasubramanian, Tuning the Superhydrophobicity of Magnesium Stearate Decorated ZnO Porous Structures for Self-Cleaning Urinary Coatings. *Appl. Surf. Sci.* 2017, 423, 293-304.
3. J. Wan, P. Wang, X. Qian, M. Zhang, S. Song, M. Wang, Q. Guo and J. Shen, Bioinspired Paper-Based Nanocomposites Enabled by Biowax–Mineral Hybrids and Proteins. *ACS Sustainable Chem. Eng.* 2020, 8, 9906-9919.

CH01.07.28

Crystalline-Amorphous Nanocomposites Strengthened and Toughened with Hierarchical and Interconnected Nanostructure [Liqiang Wang](#); City University of Hong Kong, Hong Kong

Amorphous-nanocrystalline dual phase structure were proved to be an effective way for overcoming the strength-ductility trade-off and break the limitation of reverse Hall-Petch effect. Here, we proposed a new strategy to develop a hierarchical and interconnected amorphous-crystalline dual-phase nanocomposite by the nanoscale elements interdiffusion and partition. The nanocomposite consists of three-dimensional continuous crystalline phase (Cr-

Co-Ni-Al) embedded in amorphous network (Al-Ni-Co or Al-O). This unique microstructure can achieve ultrahigh yield strength of ~3.6 GPa with a large homogeneous deformation over 60% strain, effectively suppressing the plasticity instability occurred in conventional nanocrystalline alloy. In situ Transmission Electron Microscopy studies reveal that exceptional strength-ductility combination results from the pronounced dislocation nucleation-movement-annihilation activities promoted by 3D nano-architected dual-phase interface, the homogenous plasticity flow of nano-sized amorphous phase, and deformation-induced devitrification induced self-toughening effect. This strategy breaks through the composites design limitations of conventional nanolaminates and provides a paradigm to develop high-strength and high-ductility dual phase nanocomposites with hierarchical microstructure.

CH01.07.30

Unraveling Acid Etching-Induced Anisotropic Morphology Evolution of ZnO Nanorods by *In Situ* Liquid Cell TEM [Fangyuan Liu](#) and Pu-Xian Gao; University of Connecticut, United States

Wet chemical etching of metals, semiconductors, and insulators is a significant technique that enables surface cleaning, micromachining, shaping and engineering of various structural and functional surface and bulk features [1-3]. However, the microscale shape and size evolution of ionic semiconductors such as zinc oxide during the anisotropic wet etching process is less understood owing to the challenge of complex etching mechanism and limited resolution for visualization of the etching process in acidic liquid medium [4]. In this work, via *in situ* liquid cell transmission electron microscopy (LC-TEM), we directly observe the shape transformation of ZnO nanorod to pencil-shaped nanostructure during the hydrochloride (HCl) acid etching process. Time-lapse LC-TEM images revealed a dynamic etching process along the nanorod tip front. Specifically, the nano-pencil tip shrinks with a slower rate along [000-1] than that along <10-10> directions, with a rapid cyclic tip dissolution and removal in the acid due to accelerating etching rates along various crystal directions. Thus, the base region of the original nano-pencil tip is revealed as a new tip followed by the repeating of the nano-pencil tip angle shrinking step. The high index surfaces, such as {10-1*m*} (*m*=0, 1, 2, 3) and {2-1-1*n*} (*n*=0, 1, 2, 3), are found to preferentially expose in different ratios, as attributed to selective Cl⁻ passivation on Zn-terminated surfaces. The surface energetics calculation suggests the preferential Cl⁻ passivation over the {10-11} and (0001) surfaces of lower energy than others, leading to preferential surface exposures. These investigations shed light on the understanding of anisotropic wet chemical etching of wurtzite-type semiconductor crystals and the design of new functional materials.

References:

1. Cai ZX, et al. Tailored Catalytic Nanoframes from Metal-Organic Frameworks by Anisotropic Surface Modification and Etching for the Hydrogen Evolution Reaction. *Angew. Chem. Int. Ed.* **60**, 4747-4755 (2021).
2. Kyeremateng NA, Brousse T, Pech D. Microsupercapacitors as miniaturized energy-storage components for on-chip electronics. *Nat. Nanotechnol.* **12**, 7-15 (2017).
3. Ye X, et al. Single-particle mapping of nonequilibrium nanocrystal transformations. *Science* **354**, 874-877 (2016).
4. Sun M, Tian J, Chen Q. The studies on wet chemical etching via *in situ* liquid cell TEM. *Ultramicroscopy* **231**, 113271 (2021).

SESSION CH01.08: Studies of Dynamics and Kinetics of Materials Synthesis and Processing I

Session Chairs: Koji Harano and Barnaby Levin

Thursday Morning, December 1, 2022

Hynes, Level 1, Room 102

8:00 AM *CH01.08.01

Optimal Sampling Strategies for Controlled Dose *In Situ* and High Resolution Scanning Transmission Electron Microscopy (STEM) Nigel Browning^{1,2}, Alex W. Robinson¹, Daniel Nicholls¹, Jack Wells¹, Amirafshar Moshaghpour^{1,3}, Angus Kirkland^{3,4} and Beata Layla Mehdi¹; ¹University of Liverpool, United Kingdom; ²Sivananthan Laboratories, United States; ³Rosalind Franklin Institute, United Kingdom; ⁴University of Oxford, United Kingdom

For many imaging and microanalysis experiments using state-of-the-art aberration corrected scanning transmission electron microscopy (STEM), the resolution and precision of the final result is primarily determined by the tolerance of the sample to the applied electron beam dose. In the case of *in-situ* experiments, where the goal is to image a chemical or structural process as it evolves, the effect of the beam dose can be harder to unravel, as a change in structure/chemistry is the expectation of the experiment – when you are looking for a change in a complex experiment and do actually see one, it is natural to expect that the change you see is exactly the one you were looking for. However, if the dose is not controlled, the kinetics of the observations can be dramatically changed by the beam, leading to a different structure/chemistry than would be expected from an *ex-situ* experiment under similar reaction conditions. Recent results at the University of Liverpool have shown that the optimal solution for dose control in any form of transmission electron microscopy (TEM) is to form the image from discrete locations of a small electron beam separated by as far as possible in space and time. Instead of forming the image with an extended beam (as with TEM) or from a regular raster pattern (as in conventional STEM) this condition is satisfied ideally by moving the STEM probe over the area of the image using large jumps between the acquisition pixels. This form of STEM imaging presents numerous challenges to the stability of the microscope, but these stability issues can be routinely overcome using either a form of random walk scanning, a calibrated random scanning or a mixture of conventional scanning and rapid beam blanking. The larger than standard jumps between pixel acquisition locations in this methodology creates problems with image interpretation, as the gaps between locations of acquisition are missing information. Fortunately, we can use Inpainting (a form of compressive sensing) to retrieve the missing information and retrieve the full image of the sample. In this presentation, we will discuss the methodology behind the use of sub-sampling and Inpainting, with particular reference to the speed and efficiency of the reconstruction method and the potential for future real-time imaging. In addition, the use of simulations to provide a starting point for image interpretation and the use of deep learning approaches to allow the microscope to adapt its own imaging conditions to the sample being studied, will also be discussed. Finally, this complete integrated artificial intelligence work flow for image acquisition and processing ideally lends itself to integrated image analytics that can be used, for example, to quantify feature sizes and their rate of change directly from the sub-sampled datasets.

8:30 AM CH01.08.02

In Situ Evolution of Density During Sintering of Ultra-High-Molecular-Weight Polyethylene [Ying Zhou](#)¹, Takuya Ohnishi² and Alan J. Lesser¹; ¹University of Massachusetts, Amherst, United States; ²Tosoh Corporation, Japan

Ultra-high-molecular-weight polyethylene (UHMWPE) nascent powders have been commercially processed by sintering for decades even though key aspects the mechanisms and kinetics of this process are not fully understood. Herein, the density evolution during each stage of the sintering process is presented from resulting *in-situ* measurements and other characterization methods.

Results show that the α -transition plays a significant role in the early stages of the sintering process. Under no pressure, a large change in the apparent

volume occurs before melting. In contrast, significant densification of the nascent powder is observed to occur as the powder is heated through the α -transition. The volume change during the melt explosion is presented and kinetics of the density change that occurs in the non-equilibrium melt is shown for different process pressures and temperatures. From the in-situ measurements, five distinct processes are identified. These include; room temperature densification, further densification during heating through the α -transition, the melt-explosion, isothermal evolution of the non-equilibrium melt, and the subsequent recrystallization during pressure cooling.

The in-situ measurements are complemented by other characterization techniques to describe how different physical and engineering properties change with process conditions and molecular parameters.

8:45 AM CH01.08.03

The Demand for *In Situ* Metrology in Microgravity R&D—Redefining Dynamic Processes and Technology Innovation [Rose M. Hernandez](#); International Space Station National Laboratory, United States

R&D in space provides a unique opportunity to benefit life by advancing science and technology in ways not possible in unit gravity conditions. For a decade, research on the International Space Station (ISS) has unveiled alternate outcomes of physicochemical phenomena from those known to occur on Earth. For instance, it is well established that the microgravity environment nearly eliminates density-driven segregation in dynamic processes that can result in nucleation processes with better monodispersity, more uniform structures, and homogenous materials leading to superior properties. Similarly, buoyancy-driven convection is negligible in microgravity making diffusion the predominant transport process. All the above affects interfacial energies and dynamics resulting in different surface energies, surface tension, heat and mass transport rates, crystallization kinetics, multiphase system dynamics, fluid dynamics, etc.; yielding novel materials structures and scientific possibilities.

Analytical capabilities are key to understanding and controlling the dynamics of materials synthesis and assembly that result in some of the most advanced science and products developed in space. In this account, the ISS National Laboratory presents examples of technological breakthroughs that were realized by in-situ characterization, data analysis and process optimization on orbit. From industrial applications such as advanced optical systems and additive manufacturing to biomedical applications like protein crystal growth and tissue engineering, the need for in-situ characterization and in-situ process metrology has become essential for the success and acceleration of projects flown to station. Moreover, capabilities to enable in-situ surface and microanalysis, chemical analysis, spectroscopy, and other advanced imaging techniques are discussed.

9:00 AM CH01.08.05

EXAFS-Based Nanothermometry of Inductively Heated Nanocrystals [Daniel J. Rosen](#)¹, [Shengsong Yang](#)¹, [Emanuele Marino](#)¹, [Zhiqiao Jiang](#)^{1,2} and [Christopher B. Murray](#)¹; ¹University of Pennsylvania, United States; ²Stanford University, United States

The ability to heat nanocrystalline materials through magnetic induction has been used in the fields of catalysis, biomedical sciences, and polymer degradation. However, the working temperature to which the inductively coupled material rises is still poorly understood. We use extended X-ray absorption fine structure spectroscopy (EXAFS) in conjunction with thermal imaging to improve the understanding of heating in inductively coupled systems. After extraction of the Debye–Waller factor from the spectroscopy, we obtain the temperature of inductively heated nanocrystals from the correlated Debye model. We combine carbon-supported iron oxide nanocrystals as induction heating agents with platinum nanocrystals as thermal probes. By testing these nanocrystal species as both unattached nanocrystals and heterodimers, we have shown that nanostructured systems show a significant temperature difference of up to 73.60 °C when compared to their local support environment. This result has implications for inductively heated catalysis, magnetic hyperthermia for targeted cell death, and polymer synthesis.

9:15 AM CH01.08.06

In Operando Correlated Studies in Energy Materials via Combined AFM/ToF-SIMS Platform [Anton V. Ievlev](#); Oak Ridge National Laboratory, United States

The performance of energy storage and conversion devices, including batteries, fuel cells, and photovoltaics, is defined by the delicate interplay of electrical response and charge carrier migration at the nanoscale. Although physical behavior and macroscopic functional response is well established, intrinsic chemical phenomena associated with ionic motion or localized electrochemical reactions can dramatically alter behavior and restrict utility of these materials. Over the last decade, advancements in development of novel characterization tools such as atomic force microscopy (AFM) have revolutionized our understanding of the electrical and mechanical response of materials; however, *dynamic* electrochemical behavior and ion migration remain poorly understood. Recently time-of-flight secondary ion mass spectrometry (ToF-SIMS) has proven to be effective tool for characterization of static chemical states in energy materials. However, its application to study of dynamic electrochemical processes still requires development. Here we introduce approach based on combined AFM/ToF-SIMS platform for correlated studies of the dynamic chemical phenomena on the nanoscale in operando conditions. Being used for characterization of the perovskite materials it allowed direct observation of the ionic migration within the device in externally applied electric fields, which is important for fundamental understanding of the material functionality. Similarly, this approach allowed to study relaxation processes of the chemical phenomena in ferroelectric materials as a function of sample temperature. Altogether, developed approach enables direct characterization of interplay between chemical and functional response in energy materials and aids in the development and optimization of novel devices.

This research was conducted at the Center for Nanophase Materials Sciences, which is a DOE Office of Science User Facility and using instrumentation within ORNL's Materials Characterization Core provided by UT-Battelle, LLC under Contract No. DE-AC05-00OR22725 with the U.S. Department of Energy.

9:30 AM CH01.08.07

Selective Reduction of Ni/Co Metal Nanoparticles from Spinel Oxides [Scott T. Misture](#); Alfred University, United States

In-situ techniques offer insights into reaction mechanisms and microstructure development that may be missed entirely when studying complex materials systems. Nickel/cobalt aluminate spinel is an interesting case study, where reducing atmospheres extract reducible cations from the MAl_2O_4 spinel starting phase. The spinel materials are chemically highly tailorable, and selectively reduced materials are useful as catalysts for fuel reforming, for example. The microstructures, however, are of critical importance. Here we present a study employing *in-situ* scanning electron microscopy as the primary tool for tracking the processes dynamically. In-situ neutron powder diffraction, Raman spectroscopy, and S/TEM complement the FEGSEM data. The talk will show how we track first the evolution of the faceting of the base oxide particles, then sintering of particles, and finally Ni/Co exsolution and resorption – as functions of temperature and oxygen partial pressure. Reduction of the metal nanoparticles from the oxide yields surface sockets and the time/temperature profiles determine the self-organization of the metal particles on the oxide surfaces, as well as the particle sintering. We find that rapid mass transport occurs on the surface, enabling the metal nanoparticles to diffuse along the surface and coalesce. Using catalysis measurements, we show that the oxide surfaces are in fact oxygen deficient, allowing rapid near-surface oxygen ion transport and that simple control over the reduction reactions yields optimized catalysis behavior. We consider possible mechanisms that enable rapid diffusion of particles on these unique oxide surfaces.

9:45 AM BREAK

10:15 AM *CH01.08.08

Cinematic Molecular Science Explored by High-Speed Electron Microscopic Video Imaging [Koji Harano](#); National Institute for Materials Science, Japan

Single-molecule atomic-resolution time-resolved electron microscopy (SMART-EM) with a high-speed, high-resolution transmission electron microscope has ushered in the era of "cinematic molecular science", in which the dynamic behavior of organic and inorganic molecules can be studied through real-time video images [1, 2]. High speed imaging without increase of electron dose results in very low electron dose per frame, which often causes a very low signal to noise ratio. We have established a method to improve the image quality optimized for SMART-EM by applying the Chambolle Total Variation (CTV) denoising, which enables tracking of molecular motion with sub-millisecond temporal resolution and sub-angstrom localization precision [3]. Herein we demonstrate in-situ observation of a nanomechanical shuttling motion of a single molecule [4], and cascade reactions of nanocarbons [5,6], as applications of the high-speed SMART-EM. We also introduce a new molecular model, atomic-number-correlated (ZC) molecular model, designed for spreading the microscopic molecular imaging to chemists who are still unfamiliar to electron microscopy [7].

References

- [1] E Keinan, *AsiaChem* **2** (2021), p. 96.
- [2] E Nakamura, *Acc. Chem. Res.* **50** (2017), p. 1281.
- [3] J Stuckner et al., *Microsc. Microanal.* **26** (2020), p. 667.
- [4] T Shimizu et al., *Bull. Chem. Soc. Jpn.* **93** (2020), p. 1079.
- [5] T Shimizu et al. *J. Am. Chem. Soc.* **144** (2022), p 9797.
- [6] D Liu et al. *Proc. Natl. Acad. Sci. U.S.A.* **119** (2022) e2200290119.
- [7] J Xing et al. *Proc. Natl. Acad. Sci. U.S.A.* **119** (2022) e2114432119.

10:45 AM OPEN DISCUSSION

11:00 AM CH01.08.11

X-Ray Tomoscopy Reveals the Dynamics of Ice Templating Paul H. Kamm^{1,2}, Kaiyang Yin^{3,4}, Tillmann R. Neu^{1,2}, Christian M. Schlepütz⁵, Francisco Garcia-Moreno^{1,2} and Ulrike G. Wegst^{4,6}; ¹Helmholtz-Zentrum Berlin für Materialien und Energie, Germany; ²Technische Universität Berlin, Germany; ³University of Freiburg, Germany; ⁴Northeastern University, United States; ⁵Swiss Light Source, Switzerland; ⁶Dartmouth College, United States

Still little understood are the complex dynamics of microstructure formation by ice-templating that occur when aqueous solutions or slurries are directionally solidified (freeze cast) into cellular solids. With synchrotron-based, time-resolved X-ray tomography, also termed X-ray tomoscopy, it is now possible to study in situ under well-defined experimental conditions the anisotropic, partially faceted growth of ice crystals in aqueous polymer solutions. Obtaining one full tomogram per second for ~270 s with a spatial resolution of 6 μm it is possible to capture with minimal X-ray absorption the freezing front that typically progresses at 5–30 μm/s. These time and length scales render X-ray tomoscopy ideally suited to quantify in 3D otherwise elusive ice crystal growth phenomena that determine the performance-defining hierarchical architecture of freeze-cast materials, which consists, on the one hand, of a complex pore morphology and, on the other, of ridges, and 'jellyfish'- and 'tentacle'-like features, which decorate the cell walls.

11:15 AM CH01.08.12

In Situ Pyroelectric Heat Detection for Elucidating Atomic Layer Deposition Thermodynamics and Kinetics Ashley Bielinski and Alex Martinson; Argonne National Laboratory, United States

The detailed mechanisms, kinetics, thermodynamics, and complexities of even the most well-studied atomic layer deposition (ALD) reactions remain insufficiently resolved experimentally to test present computational hypotheses. We design, implement, calibrate, and electrically model a pyroelectric thin film calorimeter to enable quantitative ALD reaction heat detection. With a thermal and temporal resolution down to 0.1 μJ/cm² and 50 ns, this sensitive and ultrafast probe is poised to improve our fundamental understanding of numerous ALD reaction mechanisms through quantitative comparison to first-principles computation predictions. We offer new insight into the thermodynamics and kinetics of the trimethylaluminum (TMA) and H₂O ALD half reactions. The half-reactions produce heat greater than that predicted by computational models based on crystalline Al₂O₃ substrates and closely aligned with the heat predicted by standard heats of formation. Comparing the experimental heat with published computational literature and additional first principles modeling highlights the need to refine our models and mechanistic understanding of even the most ubiquitous ALD reactions.

SESSION CH01.09: Studies of Dynamics and Kinetics of Materials Synthesis and Processing II

Session Chairs: Andrew Lupini and Utkur Mirsaidov

Thursday Afternoon, December 1, 2022

Hynes, Level 1, Room 102

1:45 PM *CH01.09.01

Atomic Scale Dopant Control [Andrew Lupini](#)¹, Ondrej Dyck¹, Mina Yoon¹, Sergei V. Kalinin² and Stephen Jesse¹; ¹Oak Ridge National Laboratory, United States; ²The University of Tennessee, Knoxville, United States

The ability to construct new materials starting from the scale of single atoms could potentially enable new materials and technologies. However, this process involves two separate challenges: How to see where the atoms are, and then how to control where they go. The scanning transmission electron microscope (STEM) provides an answer to the first challenge, with the Z-contrast imaging mode able to reveal the structure and bonding of a variety of materials. Perhaps even more excitingly, the STEM might also provide an answer to the second challenge of how to control the position of the atoms. Working in a high-vacuum system, the atomic-scale probe size obtained in an aberration-corrected STEM allows single atoms to be manipulated in and on a variety of materials, with examples including heavy dopant atoms inside silicon crystals, and a variety of different atoms in graphene. Recent work has highlighted the potential for this technique [1], elucidated the underlying mechanisms [2], and extended the range of elements that can be used [3]. Nevertheless, numerous challenges remain, such as: How do we find the ideal conditions? How do we control the supply of dopants? And to what extent can the atoms be positioned where we want them? [4]

- [1] B. Hudak, et al. Directed Atom-by-Atom Assembly of Dopants in Silicon, ACS Nano 12(6) (2018) DOI:10.1021/acsnano.8b02001
- [2] A. Markevich, et al, Mechanism of Electron-Beam Manipulation of Single-Dopant Atoms in Silicon, J. Phys. Chem. C (2021), 125, 29, 16041–16048 DOI:10.1021/acs.jpcc.1c03549
- [3] O. Dyck, et al. Doping transition-metal atoms in graphene for atomic-scale tailoring of electronic, magnetic, and quantum topological properties, Carbon, 173, (2021), <https://doi.org/10.1016/j.carbon.2020.11.015>.
- [4] This material is based upon work supported by the U.S. Department of Energy, Office of Science, Basic Energy Sciences, Materials Sciences and Engineering Division and was performed at the Oak Ridge National Laboratory's Center for Nanophase Materials Sciences (CNMS), a U.S. Department of Energy, Office of Science User Facility.

2:15 PM CH01.09.02

Colloidal Templating and Layered Extrusion Assemblies—Unconventional Shapes and Folding Objects [Rigoberto C. Advincula](#)^{1,2,3}; ¹The University of Tennessee, Knoxville, United States; ²Case Western Reserve University, United States; ³Oak Ridge National Laboratory, United States

The preparation of new polymers and colloidal nanomaterials requires hierarchical levels of ordering and structuring: from molecular to macroscopic. The tools and methods are available for evincing order requiring design principles that start from non-covalent interactions all the way to object patterns that can be manipulated by non-lithographic methods. This talk will highlight the templating and assembly methods in: 1) colloidal nanosphere lithography used by our group to produce systems that include: conjugated polymers, electropolymerized molecularly imprinted sensors, electronanopatterning, and polymer brush lithography. 2) Polymer layered systems based on melt extrusion roll-to-roll process, 3) Hard-soft matter bilayers based on reactive ion etching of "origami" like structures. We also demonstrate the importance of surface-sensitive spectroscopic and microscopic analytical tools applied rationally to highlight evidence of order and function. The ability to synthesize and fabricate layered ordered systems results in new material stimuli-responsive properties.

2:30 PM CH01.09.04

Imaging the Conversion of Metal Oxide Nanoparticles into Bimetallic Hollow Nanostructures Through Galvanic Replacement and Etching Reactions [Wenhui Wang](#) and Utkur Mirsaidov; National University of Singapore, Singapore

Hollow nanomaterials with controlled chemical composition and morphology are an important class of materials used in many applications, such as catalysis, energy storage, and biomedicine, because of their low mass density, high surface area, and reduced diffusion length for mass and charge transport. Various approaches have been explored for the synthesis of hollow NPs as electrocatalysts with improved activity and selectivity, among which, the GR reaction is frequently adopted due to their effectiveness and low-temperature. However, the mechanism behind the chemical conversion from a template NP to a hollow nanostructure through GR may be more complex than that expected from straightforward electrochemical dissolution. In fact, the hollowing process usually accompanied by dealloying, kirkendall diffusion or etching reactions. For example, it has been reported that the transition of Ag nanocube to a hollow Au structure through GR reaction with HAuCl₄ solution is due to the nucleation and propagation of voids within the nanocubes, suggesting that kirkendall effect couples to GR in the reaction between Ag and Au. Apart from metal NPs, metal oxide NPs are also widely used in synthesizing bimetallic hollow nanostructures, while the conversion dynamics and underlying mechanisms are less investigated comparing to that of metal NP templates. Due to the versatile composition and earth abundance of metal oxide NPs, it is vital to understand the GR process on a metal oxide template NP through which hollow nanostructure is achieved.

Metallic shell growth and template removal through which metal oxide NPs are converted into bimetallic hollow nanostructures by GR and etching reactions are complex chemical processes with various short-lived intermediate states. Moreover, the morphological and compositional evolution of a bimetallic hollow nanostructure in catalytic relevant conditions involve with intricate regional surface reactions at nanoscale. The key questions remain unresolved are as follows. (1) Which surface sites, such as corners, edges, and facets of the metal oxide template, are the most susceptible to GR reaction? (2) How do the shells form and NPs become hollow? (3) How does the reaction conditions control the etching pathways? (4) How does the structure of the bimetallic hollow nanostructures change in catalytic reaction conditions? Capturing the transient stages of these processes and addressing these questions requires an approach that enables direct visualization of these nanoscale processes as they take place.

Here, we use liquid-phase TEM imaging to resolve the details of the GR and etching reactions through which spherical and cubic Cu₂O NP templates are converted into bimetallic PdCu hollow nanostructures. We chose to synthesis PdCu NPs because they are promising candidate for CO₂ reduction reactions which converts CO₂ to value-added industrial chemicals or fuels. Furthermore, we chose Cu₂O as a template material because it has suitable redox potential to that of Pd for the GR reaction taking place. In our study, the conversion reactions are initiated by flowing the H₂PdCl₄ solution into a liquid cell through a fluidic channel. We imaged the conversion process using ultralow electron flux imaging conditions to minimize the effects associated with the electron beam. Our in situ TEM observations show that Cu₂O NPs are converted into hollow PdCu nanostructures through uniform growth of PdCu shell together with anisotropic etching of template NP. Moreover, the thermodynamic and kinetic etching pathways of Cu₂O NP are controlled by the concentrations of the etchant. Furthermore, we extended our study to test the stability of these PdCu hollow nanostructures under conditions relevant to CO₂ reduction reactions. We reveal that Cu dissolve from the skeleton of the hollow nanostructure and redeposition onto the surface of the NP and electrode, which may lead to a low faraday efficiency for hydrocarbon products.

2:45 PM BREAK

3:15 PM *CH01.09.05

Cryogenic STEM Imaging and Spectroscopy for Energy and Quantum Materials [Miaofang Chi](#); Oak Ridge National Laboratory, United States

Many energy and quantum materials require characterizations to be performed at a low temperature. Recent advancements in cryogenic scanning transmission electron microscopy (Cryo-STEM) are opening new opportunities for related research areas. For example, exotic states in quantum materials usually only occur at low temperatures. Newly developed liquid nitrogen cooling cryogenic stages with desirable stability at both base and variable temperatures enable us to elucidate phase transformations of quantum materials in real space at the atomic scale. Electron beam damage in an electron microscope is often a considerable limitation in analyzing energy materials such as soft or superionics at the atomic scale. *Cooling the specimens* to a low temperature *may* help to reduce the beam damage. However, energy conversion and storage materials often contain loosely bonded ions, soft structures, or organic components. Multiple beam damage mechanisms are involved in during electron-matter interactions. Robust atomic scale microscopy analysis becomes challenging. In this talk, I will give several examples to demonstrate how cryo-STEM enables energy and quantum materials research. I will also discuss other critical experimental parameters to be considered during high resolution analysis in order to minimize beam damage. Data analysis and acquisition methods that help to reduce electron dose will also be introduced.

3:45 PM CH01.09.07

In Operando X-Ray Diffraction Investigation of Reduced Graphene Oxide in Aqueous Solution [Maria del Pilar Bernicola Garcia](#)¹, Elena del Corro¹ and Jose A. Garrido^{1,2}; ¹Catalan Institute of Nanoscience and Nanotechnology, Spain; ²Institución Catalana de Investigación y Estudios Avanzados, Spain

In the recent years, reduced graphene oxide (rGO) has been studied in many different fields due to its remarkable physicochemical properties. In the healthcare applications field, rGO films have been widely studied because of their biocompatibility and biochemical sensing capabilities [1]. Also, rGO can be engineered to prepare films exhibiting large electroactive surface area, large electrochemical potential window, and high electrical conductivity. Regarding these properties, a fundamental understanding of key aspects of the films processing, such as the evolution of the functional groups during the reduction process of rGO and the role of ionic diffusion, is extremely relevant due to their impact on the stability and the final performance of rGO-based devices.

In this work, by combining ex-situ and in-operando electrochemical and spectroscopic techniques, we investigate the solid-liquid interaction between rGO-based nanoporous electrodes and the environment. We aim to reveal those events happening during electrochemical processes, involving ionic intercalation, charge adsorption and functional groups evolution, that may have an impact on the chemical and structural properties of resulting rGO. X-ray photoelectron spectroscopy (XPS), Raman spectroscopy and contact angle are ex-situ techniques used to follow the evolution of functional groups upon the reduction degree of GO/rGO at different stages (before and after electrochemical treatments) [2]. The number of functional groups are related with the hydrophobicity and conductivity of rGO, and these properties are linked with the electrochemical properties of the material. Ex-situ electrochemical techniques such cyclic voltammetry (CV), charge-discharge techniques and potentiostatic electrochemical impedance spectroscopy (PEIS) are used to evaluate electrochemical properties such as specific capacitance, ion diffusion, electrochemical potential window and charge transfer resistance at different potentials. Mentioned techniques gives us information of the electrode at different stages but information related the chemical mechanisms involved in the electrochemical processes would remain missing. In-operando techniques are an emergency tool that contributes to have a better understanding of the mechanism that take place during the electrochemical treatments.

In this study, we develop a home-made spectro-electrochemical cell for in-operando X-ray diffraction spectroscopy (XRD) which allows us to follow the chemical and structural changes of the rGO material in aqueous solution during different electrochemical processes. With this in-operando technique, we aim to study the ionic intercalation process, the changes on the interlayer distance and its dependence with the applied potential. Such knowledge help us to understand the mechanism that leads to achieve a highly capacitive material. This work aims at expanding the current understanding of the properties of rGO-based nanoporous thin films for their potential use as electrode material in healthcare applications.

[1] Apollo, N. V., Maturana, M.I., Tong, W., Nayagam, D., Shivdasani, M.N., Foroughi, J., Wallace, G., Praver, S., Ibbotson, M.R. (2015) Soft, flexible freestanding neural stimulation and recording electrodes fabricated from reduced graphene oxide, *Adv. Funct. Mater.*, 25, 3551-3559.

[2] Huang, H., Kanishka, K., De Silva, H., Kumara, G. R. A., Yoshimura, M., (2018) Structural Evolution of Hydrothermally Derived Reduced Graphene Oxide, *Sci. Rep* 8, 6849

4:00 PM CH01.09.08

3D Reconstruction of the Alloying Process of AuAg Nanoparticles by Small Angle X-Ray Scattering Siyu Wu¹, Xiaobing Zuo² and Yugang Sun¹;

¹Temple University, United States; ²Argonne National Laboratory, United States

The element distribution pattern in a bimetallic nanoparticle system is usually varying during the synthesis, post-processing, and catalysis reactions under operando conditions. The structural complexity of the nanoparticle system brings significant difficulty in determining the relationship between the structures and their physical and chemical properties. Small angle x-ray scattering (SAXS) can be used to characterize size, morphology, and density of a nanoparticle system under operando conditions. We applied SAXS on monodispersed core-shell AuAg nanoparticle system to monitor the growth of Au layers on Ag nanoparticles and the following alloying process when the nanoparticles are heated. The nanoparticle density distribution change caused by the diffusion of Au and Ag atoms is reconstructed by DENsity from Solution Scattering (DENSS) algorithm with a sub-nanometer resolution. The time-resolved series of 3D images enables the quantitative study of the 3D evolution of size, morphology, composition, and element distribution of the alloying AuAg nanoparticle system. The density contrast SAXS imaging protocol established in this work provides a transformative way to "see inside" nanoparticle structure other than the traditional electron microscopic methods.

4:15 PM CH01.09.09

Time-Resolved Study of Phase and Mechanical Developments of Martensitic α' Phase in Ti-6Al-4V Under Laser Processing via Synchrotron X-Ray Diffraction Seunghee Oh¹, Joseph Aroh¹, Nicholas Lamprinakos¹, Andrew Chuang², Robert M. Suter¹ and Anthony D. Rollett¹; ¹Carnegie Mellon University, United States; ²Argonne National Laboratory, United States

Laser powder bed fusion (LPBF) is one of the most actively studied additive manufacturing (AM) processes. Based on laser melting with sub-millimeter tracks in a metal powder bed, it can build complex and precise parts. The processing involves rapid heating and cooling of the material, which induces unusual microstructural evolution.

Ti-6Al-4V (Ti64) has been extensively studied as an AM alloy because of its unique combination of excellent properties in weldability, strength, density, corrosion resistance, and biocompatibility. This $\alpha+\beta$ type Ti alloy involves a solid-state phase transformation of β and α around 980 degrees Celsius. Under fast cooling conditions, the high-temperature phase, β , is known to undergo a martensitic transformation, which results in $\alpha'+\alpha+\beta$ or α' microstructures. The as-printed LPBF Ti64 is typically composed of the martensitic phase, α' , because the laser-based processing is accompanied by rapid cooling. It has been reported that the fractions of β and α' strongly affect the ductility and strength of Ti64. Therefore, the resultant microstructures associated with laser processing are important predictors of the material properties of the printed parts. However, the microstructural evolution depends sensitively on the process conditions, and little is known about the transformation of the β phase because of its high reaction temperatures. Moreover, the extremely fast process in a small processing volume makes it more challenging to characterize the development during laser processing.

In this study, an *in situ* synchrotron X-ray diffraction experiment with high temporal and spatial resolution was utilized to observe the rapid phase evolution in melt pools developed by laser melting. Based on the transmission mode setup, the high-energy monochromatic X-ray beam passed through a sample under laser processing, during which the diffracted x-rays were collected on an area detector. The samples were prepared from as-printed Ti64 fabricated in an LPBF system (EOS M290) and sliced into thin plates of thickness 0.4 mm. Metallography provided substantial information that confirmed the results obtained from the X-ray diffraction measurements.

The analysis confirmed that the prepared samples from the as-printed Ti64 are fully martensitic with no β phase present. The dynamic acquisition of 2D diffraction images showed how the martensitic phase evolved before and after the laser melting. The multiple *in situ* measurements at different locations of the melt pool showed how the phase configuration developed in the fully resolidified region and heat-affected zone (HAZ). The variation in the lattice spacing with azimuth (*i.e.*, direction sampled by the diffraction) implied an anisotropic mechanical response in the laser processed regions, which were investigated both qualitatively and quantitatively. The changes in the lattice parameter of β and α' during the martensitic transformation indicated how α' evolves with respect to the depth below the surface of the melt pool and how the phase evolution correlated with that of the macro-strain. From the changes in the diffraction profile, it was found that pre-existing micro-strain in the martensitic α' relaxed in the HAZ as a result of the laser processing. The estimated temperature profiles based on thermal expansion facilitated comparisons with expectations from equilibrium phase relationships. The developments of the phase composition and residual strain under laser processing were investigated, which is expected to provide valuable information for

optimizing the laser processing of Ti64.

SESSION CH01.10: Virtual Session I: In Situ Investigation of Dynamics of Materials Synthesis and Processing I
Session Chairs: See Wee Chee and Barnaby Levin
Wednesday Morning, December 7, 2022
CH01-virtual

10:30 AM *CH01.10.01

Electrocatalyst Transformations Under Reaction Conditions—Insights from *Operando* Transmission Electron Microscopy of Well-Controlled Pre-Catalysts See Wee Chee; Fritz Haber Institute of the Max Planck Society, Germany

The conversion of base molecules found in our environment (e.g., H₂O, CO₂) into the valuable chemicals and fuels needed by our modern society via electrocatalysis is currently an active area of research due to its potential for green energy applications. However, for many of these technologies, the search for optimal catalysts is still a laborious process because we lack a robust understanding of the relationship between a catalyst's structure and its catalytic function. It is important to note that the catalytic performance is not solely determined by the starting catalyst (or pre-catalyst) structure, the dynamic catalyst structure that exists under reaction conditions also plays a key role. Moreover, probing this dynamic structure is not straightforward because it may not be retained when we examine the catalysts after reaction in the absence of the electrolyte and applied potential. Here, I will present work from my group studying the dynamical transformations that take place in Cu-based catalysts for the electrochemical reduction of carbon dioxide using *operando* electrochemical cell transmission electron microscopy (EC-TEM). To elucidate the impact of these transformations on catalytic performance, we adopted highly tuneable catalyst synthesis strategies that generate near-identical electrocatalysts for both EC-TEM and benchtop electrochemical and product selectivity measurement setups. Our *in situ* observations indicate that the application of a reductive potential generally leads to drastic structural changes, such as catalyst detachment, fragmentation, and re-deposition, within minutes. I will also discuss how these effects correlate with changes in catalyst activity and selectivity, thereby providing insights that can inform the design of better electrocatalysts.

11:00 AM CH01.10.02

Identification and Characterization for Spherulization in Methylammonium-Guanidinium Lead Iodide Perovskite Material—A Structural and Morphological Investigation of Microstructural Evolution Monika Mukul¹, Selvaraj Kaliaperumal², Mamta Rani¹ and Surya Kant Tripathi³; ¹DAV University, India; ²CSIR-National Chemical Laboratory, India; ³Panjab University, India

Hybrid organic-inorganic perovskite materials (HOIP) have gained tremendous popularity in the past decade for their unique optoelectronic properties for photovoltaic applications. This report presents comprehensive structural and morphological analysis which infuses new insights into the evolution of polycrystalline self-assembled spherulitic microstructures with different hierarchical architectures in HOIP material which are hitherto unattempted. X-ray diffraction (XRD) analysis confirms the formation of guanidinium (GUAI)-rich MAI-GUAI-PbI₂-DMF pure intermediate phase of the dendritic perovskite spherulites and transformation to stable α -tetragonal or quasi-cubic perovskite converted phase of Ma_{0.75}Gua_{0.25}PbI₃ material composition with calculated crystal structure parameters; a=b=6.31074 Å and c=6.33810 Å, $\alpha=\beta=\gamma=90^\circ$ and a cell volume of 252.418 Å³ via slow crystallization in extreme humidity levels of 92±4% and temperature 24.5±1.5°C. This work also shed light on microstructural heterogeneity of these materials in their intermediate phase. The Field Emission Scanning Electron Microscope (FESEM) analysis unravels the fundamental microstructure of embryonic spherulitic nuclei in perovskites; lamellar arrangements, categorize the mature perovskite spherulitic microislands (PSMs); transcrystalline layers (TCL), spherulite bridges, nucleation of hole, impingement behavior, coupled-PSMs, and defects such as pits and spherulitic microcracks. The inner-core and outer area of all the freshly prepared spherulitic forms are evaluated to range between 203.6-380.5 μm² and 974.4-1900.0 μm² respectively. To assess the stability of this spherulitic perovskite and understand its phase transformation, XRD and FESEM study has been done after 10 days. New zero-dimensional (0-D) orthorhombic Pmmm(47) polymorph with blood-cell like morphology have been observed in the wheat sheave branches of the aged perovskite sample. Optical microscopic images also confirms the wheat-sheaf like morphology. The UV-Visible results have shown the absorbance peak of 3-D quasi-cubic perovskite phase around 788 nm. Energy-dispersive X-ray analysis (EDX) confirms the stoichiometric homogeneity of intermediate phase with similar value of C, Pb and I atomic ratios from different regions of the thin-film. As from the viewpoint of crystallography and performance, the individual perovskite grains may display very different properties. Thus findings of this work not only enhances the understanding on organic-inorganic spherulitic microstructures but also an attempt to evident the polymeric aspect of HOIPs, intermediate phase, and phase transformation that can serve to improve the morphology and phase stability for higher device performance of HOIPs.

11:15 AM CH01.10.03

Deducing Electric-Field Mediated Peptide Materials Design Julia Robbins, Tiffany Ji and Subhasish Chatterjee; Kean University, United States

Self-assembly of gene-encoded peptide motifs offers a bioinspired strategy for developing the design of functional nanomaterials. The current work illustrates contrasting effects of the electric field in the formation of peptide-based supramolecular materials. We have applied both atomistic and coarse-grained molecular dynamics simulations; our results highlight how the applied electric field can modulate the interaction between the hydrophobic and hydrophilic components of amphiphilic peptides, leading to the formation of dynamic soft materials.

11:30 AM CH01.10.04

Dislocation-Induced Stop-and-Go Kinetics of Interfacial Transformations Xianhu Sun¹, Dongxiang Wu¹, Lianfeng Zou¹, Stephen House², Xiaobo Chen¹, Meng Li², Dmitri Zakharov³, Judith C. Yang² and Guangwen Zhou¹; ¹SUNY at Binghamton, United States; ²University of Pittsburgh, United States; ³Brookhaven National Laboratory, United States

Engineering materials are typically based on multiphase microstructures produced either through the control of phase equilibria or by the fabrication of different materials as in thin-film processing. In both processes, the microstructure relaxes toward equilibrium by mismatch dislocations (or geometric misfit dislocations) across the heterophase interfaces. Fundamental understanding of mismatch dislocations and their dynamic coupling to phase transformations has been a longstanding topic of study. Unfortunately, directly probing misfit dislocation dynamics has been a major challenge due to their buried nature and the difficulty of direct experimental measurements at the atomic scale. Transmission electron microscopy (TEM) is one of the few tools capable of accessing buried interfaces and has demonstrated its versatility and atomic-scale precision in elucidating the location and configuration of misfit dislocations. However, directly probing the dynamic action of mismatch dislocations during phase transformations is challenging because it requires not only a capability to atomically capture the fast evolution of interfaces but also to apply stimuli to drive the interface transformation. Using the example of Cu₂O→Cu interfacial transformation, we demonstrate the unique role of mismatch dislocations in modulating oxide/metal interfacial transformations in an

intermittent manner, by which the lateral flow of interfacial ledges is pinned at the core of mismatch dislocations until the dislocation climbs to the new oxide/metal interface location¹. Together with atomistic calculations, we identify that the pinning effect is associated with the non-local transport of metal atoms to fill vacancies at the dislocation core. These results provide mechanistic insight into solid-solid interfacial transformations and have significant implications in utilizing structural defects at buried interfaces to modulate mass transport and transformation kinetics.

Reference:

¹X.H. Sun, D.X. Wu, L.F. Zou, S.D. House, X.B. Chen, M. Li, D.N. Zakharov, J.C. Yang, G.W. Zhou, "Misfit-dislocation induced stop-and-go kinetics of interfacial transformations", Nature (in press, DOI: 10.1038/s41586-022-04880-1)

11:45 AM CH01.10.05

Laser-Induced Photo-Thermal Reduction—Mechanism & Applications Ehud Greenberg, Nina Armon, Eitan Edri and Hagay Shpaisman; Bar-Ilan University, Israel

Assembly of materials into microstructures under laser guidance is attracting wide attention. The ability to pattern various materials and to form 2D and 3D structures with micron/sub-micron resolution and less energy and material waste compared with standard top-down methods make laser-based printing promising for many applications in sensing, medical devices, and microelectronics. Assembly from liquids provides smaller feature size than powders and has advantages over other states of matter in terms of the relatively simple setup, easy handling, and recycling. However, the simplicity of the setup conceals a variety of underlying mechanisms, which cannot be identified simply according to the starting or resulting materials.

Here, we shed light on one of the mechanisms through systematic analysis of photo-thermal reaction products forming iron oxide and silver at different interfaces. Examination of the nanostructure of deposits on a substrate using high-resolution transmission electron microscopy and selected area diffraction pattern analysis reveals a combination of both amorphous and crystalline moieties. We found that focusing the laser inside the solution leads to exclusive formation of crystalline products, while focusing on the liquid/air interface leads to formation of amorphous products due to kinetic considerations. Ring-shaped microstructures observed on the substrate indicate that microbubbles are involved in the deposition. Our findings suggest that crystalline nanoparticles formed in solution are pinned to the base of the microbubbles. These stationary deposits absorb the laser light, resulting in extensive local heating, which leads to a fast thermal-reaction of the metal ions that are added as amorphous nanostructures. The presence of both crystalline and amorphous nanostructures therefore results from two different mechanisms. Finally, we demonstrate how microfluidics could be utilized to enhance the capabilities of multi-layered laser micro-printing by quickly switching between precursors. The concepts presented here could provide new opportunities for fabrication of multi-layered micro-electronic devices and sensors.

12:00 PM CH01.10.06

Comprehension of the Behavior of Rectifier Diodes Through the *In Situ* Study of the Electrically Induced Phenomena on the Active Si Component Sara Román-Sánchez¹, Aida Serrano¹, Alberto Moure¹, Jesús López-Sánchez¹, Juan Rubio-Zuazo², Adolfo del Campo¹ and José Francisco Fernández¹;

¹Institute of Ceramics and Glass, Spain; ²European Synchrotron Radiation Facility, France

Nowadays, there are numerous advanced characterization techniques that offer great versatility in the field of materials. Concretely, confocal Raman microscopy (CRM) or techniques based on synchrotron radiation, such as single-crystal X-ray diffraction (SCD) are of major relevance for carrying out studies in solids. These non-destructive techniques allow exhaustive *in situ* structural analysis at the local scale of several materials, without the need for very specific sample preparation, and achieving high spatial resolution.

Located *in situ* structural studies are of great utility in the semiconductor-based technology field. One of the main limiting factors of these devices is the modifications that may take place on their structure as a consequence of the high electrical current that flows through them when they are in operation. Press-fit rectifier diodes are an application example of Si-based electronic devices, which have a great interest in the automotive industry. Thanks to their ability to allow the current to flow in one direction only and blocked it in the opposite one, they are often employed to transform the alternating current produced by the alternator into a direct current, in order to make it suitable for the power supply of the vehicle. *At in operando* conditions, diodes endure electrical current in the order of tens of A, which leads to the overheating of the device by the Joule effect at temperatures about 250 °C. This fact may pose a problem, not only because of the thermal degradation of the devices but because of the appearance of structural damage associated with their multicomponent nature. Rectifier diodes are commonly composed of several materials: a silicon semiconductor wafer where the rectifier technology is located, joined to a copper heat-sink and to an epoxy region, whose function is to provide mechanical and electrical protection. Their thermal response is different for each one, leading to the appearance of mechanical stress as a consequence of the mismatch of the thermal expansion coefficients. In addition, other structural variations that the electric current may induce on the active Si, which can influence the behavior of the diode, such as carrier dynamics, may also take place on the devices at *in operando* conditions.

In order to optimize the performance of the diodes, it is essential to know their behavior and the different phenomena occurring during their operation. For that, in this work, an *in-situ* characterization has been carried out using different techniques. First, a preliminary study of the thermal response of the whole diode by infrared thermography revealed the inhomogeneous heating of the device. Then, the structural modifications that the active semiconductor undergoes were evaluated by confocal Raman microscopy and X-ray diffraction in synchrotron (ESRF, Grenoble). Results have allowed discerning the influence of the heating phenomenon caused by the Joule effect from other non-purely thermal phenomena, characteristic of these devices, as well as to identify the presence of different regions located in the Si, whose differences are based on the stress and doping scheme of this component. Experiments were carried out in diodes with different technologies (Schottky, MOS and PN) and proceeding from different providers (different designs), intending to evaluate the influence of different parameters. The study was useful to comprehend the phenomenology induced on the active Si region of rectifier diodes in working conditions in order to increase their useful life by reducing their failure rate.

12:15 PM CH01.10.07

Investigating Iron Corrosion with *In Situ* Liquid TEM Surabhi Agrawal, Mobbassar Hassan Sk, Richard Langford and Stuart Clarke; University of Cambridge, United Kingdom

Corrosion is the environmental degradation of metallic structures over time due to an electrochemical reaction on the surface. Whilst it starts at the surface, it can often get deep into the structure locally, leading to catastrophic structural failures. Understanding corrosion process at the most fundamental level is of great scientific and commercial interest, as it underpins novel and efficient corrosion mitigation approaches and reliable prediction models. Despite the importance of early stages of the phenomena, earlier works have been largely limited to speculation based on ex-situ studies of iron and steel pieces, which are unable to capture many subtle sub-stages of the process. Moreover, removal of samples from the native state necessarily results in quenching/transformation before characterisation. It is important to understand the nucleation stage of the dynamic process under 'real conditions', through *in-situ* techniques. Here, we demonstrate the use of liquid TEM to study iron corrosion in sodium chloride solution, using a commercially available liquid holder. Two silicon nitride chips is assembled with a spacer in-between, and clamped in a metal holder. Microfluidic connections allow liquid flow, and the spacer sets the liquid layer thickness in the beam path. The sample is a thin film of iron (30-50 nm) deposited, via electron beam evaporation, on one of the silicon nitride membrane chips, before assembly. The sample is imaged in a FEI Philips Tecnai 20 LaB6 TEM. A combination of bright and dark field imaging, and selected area electron diffraction is employed to capture the early reaction stages.

</div> <div> We address the two key processes – iron dissolution in solution and iron oxide nucleation process. The nature of the nucleation process (homogenous or heterogeneous), corrosion precursor (amorphous or crystallinity) and its evolution is investigated. We find that nucleation initiates on the metal surface, with preferential growth along the grain-boundaries of the iron film (quantified). We also identify the early-stage nuclei to be crystalline, characterised by its diffraction pattern. On the basis of our findings, we present a primary mechanism for nucleation of iron oxides on a reactive iron surface.</div> </div>

12:30 PM CH01.10.08

Microfluidic Supported Emulsion Polymerization and *In Situ* Assemblies for Synthesis of Size and Shape-Tunable Soft Polymer Nanoparticles [Nikunj Kumar Visaveliya](#); The City College of New York, United States

Polymer particles are promising nanoscale materials for a wide range of applications in the field of biomedicine, sensing, and labeling. Controlled structural aspects of the polymer nanoparticles such as size, shape, surface topology, morphology, internal softness, interior cross-linking, and core composition determine their impact on the cargo loading capacity and controlled/sustained release, the possibility of endocytosis, and degradability during their biomedical application. The designed interfacial features, on the other side, such as stimuli-responsive surfaces, wrinkling, surface porosity, shell-layer swellability, layer-by-layer surface functionalization, surface charge, surface roughness, and textures regulate nanoparticles' interfacial interactions, controlled assembly, movement and collision, and compatibility with the surroundings like a solvent and biological environments. These characteristics define polymer nanoparticles' overall properties/functions based on homogeneity, stability, interfacial tension, and minimization of the surface energy barrier. If nanoparticles are not uniform in their size or shape, the resultant outcome may be significantly lower directly related to the concept of the structure-function relationship. Therefore, a key requirement is to produce well-defined and uniform polymer nanoparticles with controlled characteristics. However, because polymers are amorphous (or semi-crystalline), flexible, and soft materials, controlling their structural/interfacial features through the single-step process is a challenge. The microfluidic reaction strategy can provide the platform for homogeneous mixing of reactants and the production of uniform particles with controlled assemblies. Here, the state-of-the-art fundamental characteristics of the polymer nanoparticles are presented through experimental results. We have applied a semi-microfluidic approach where initial emulsification has been formed inside the microfluidic channel and the completion of polymerization together with their in-situ assemblies realized externally. In the case of utilizing molecular surfactants, the spherical polymer nanoparticles between the size range of 50 nm and 500 nm were obtained. Besides, we observed that the application of polyionic polyelectrolytes was the key driving force for initiating the in-situ assemblies of the growing polymer nanoparticles during polymerization to form the anisotropic structures. In this way, we created the library of the shape-controlled polymer nanoparticles in the form of ellipsoidal, dumbbell, elongated chain-like, branched-shape, and flower-shaped polymer nanoparticles.

12:45 PM DISCUSSION TIME

SESSION CH01.11: Virtual Session II: In Situ Investigation of Dynamics of Materials Synthesis and Processing II
Session Chairs: See Wee Chee and Barnaby Levin
Wednesday Afternoon, December 7, 2022
CH01-virtual

9:00 PM *CH01.11.01

Direct Nanoscale Observation of Thermally Driven Grain Boundary Migration Associated with Their Triple Junction Motion [Utkur Mirsaidov](#); National University of Singapore, Singapore

Thermally activated grain structure evolution in polycrystalline materials has been an important research area due to its scientific and technological significance, since many physical properties of materials are highly dependent on the structure and density of grain boundaries (GBs). GBs and their intersections known as triple junctions (TJs) are the major elements of a complex network in polycrystalline materials, and while the motion of GBs has been extensively studied for decades, the effect of TJs on the grain growth kinetics only recently started to receive due attention. Moreover, many critical details of coupled GB-TJ evolution can only be described at the atomic scale, where direct real-time experimental observations are still lacking. We chose to use cobalt (Co) for its technological importance and two-phase nature, as it normally contains both *fcc* and *hcp* grains. Using *in situ* transmission electron microscopy (TEM), we captured the thermally activated grain growth in a natural nanocrystalline Co film at both the mesoscale and the atomic scale. We found that discrete TJ motion governs the grain size evolution dynamics by initiating or delaying GB migration, whereby TJ displacements are correlated with dynamic dihedral angles and the grain area modification. We linked the changes in mesoscale GB shape with atomic-scale disconnection dynamics, showing how the normal GB migration occurs through a lateral motion of disconnections emitted at TJs. Overall, this study provides experimental evidence for the critical role of disconnection dynamics for the coupled motion of TJs and GBs in a general nanocrystalline metal film.

9:30 PM CH01.11.03

Rapid Hierarchical Nanostructures of Lamellar Block Copolymer Thin Films via Microwave Annealing [Ugur Aslan](#); University of Houston, United States

Block copolymers (BCP) have been long investigated to achieve periodic nanostructures on silicon substrates which have a wide range of applications from the semiconductor industry to nanoelectronics. The nano periodicity of BCP in different shapes such as cylinders, lamella, spheres, and gyroids, is achieved by self-assembly by manipulating BCP composition and temperature. While these structures can be achieved by thermal annealing (TA), it is a slow process. In contrast, microwave is a fast, effective and intriguing energy source, and a desirable method for heating various materials. We obtain hierarchically ordered lamellar BCP nanostructures in thin films by short-time microwave annealing on boron-doped silicon substrates, chosen for its high microwave absorption. We investigate the fast ordering kinetics of BCP films in as little as 10s compared to hours in TA, with respect to domain spacings (L_0) formation in parallel lamellar BCP morphology, as measured by island and hole formation characteristics on the film surface. An exciting feature is that $\frac{1}{2} L_0$ plateau form around the holes within a short time of microwave annealing, that is not typically observed in TA. These $\frac{1}{2} L_0$ relief structures transition to $1 L_0$ when further subjected to extended TA. Lastly, we compared the domain spacing and average hole diameters evolution of microwave annealing of the BCP films with that of TA. We conclude that microwave annealing can be effectively used to obtain parallel, both non-traditional $\frac{1}{2} L_0$ and traditional L_0 lamellar relief topography structures, in very short times, making it suitable for industrial processing.

9:45 PM CH01.11.04

Experimental Investigation of Powder Electrical Characteristics and Smoke Behavior in Electron Beam Additive Manufacturing Using AlSi10Mg and 64Ti Powder [Takayuki Ishii](#), Hao Wang, Kenta Aoyagi and Akihiko Chiba; Institute for Materials Research Tohoku University, Japan

Powder bed fusion using an electron beam (PBF-EB) is expected to be applied for medical equipment and aerospace since PBF-EB process can produce object with little thermal strain and contaminant because of high temperature vacuum process. However, when powders are charged up due to electron beam scanning on powder bed, powders are often spread out because of electrostatic force between powders. This phenomenon is called as smoke phenomenon and is problem in PBF-EB process. The physical origin of smoke phenomenon is empirically considered to be charge-up, but it is not known in detail what kinds of factor affect occurrence of smoke phenomenon. In order to clarify the mechanism of smoke phenomenon, we have investigated powder properties and conducted experimental smoke test using AlSi10Mg and 64Ti powder.

In the confirmation of the physical properties of the powder, the electrical characteristics of the powder were investigated using the electrochemical impedance measurement that has been conducted in the previous studies, and the time constant of the powder was analyzed by waveform analysis. The Coulomb repulsion between powders was calculated using the time constant, and it was assumed that smoke is generated when the Coulomb repulsion is larger than the weight of one powder particle, and smoke is not generated when the Coulomb repulsion is smaller than the weight of one powder particle. We predicted the possibility of smoke generation during the building process on this assumption. By comparing the prediction by calculation with the presence or absence of smoke generation (smoke test) by experiment, the mechanism of smoke phenomenon was considered. In 64Ti, there was a good match between the prediction of smoke generation and the results of the smoke test, proving that the smoke mechanism is due to the Coulomb repulsion. However, in AlSi10Mg, the prediction of smoke generation and the result of the smoke test did not match, suggesting that factors other than the Coulomb repulsion are involved as the smoke mechanism. As factors other than the Coulomb repulsion, the permeability of the electron beam and the temperature rise of the powder due to the electron beam were considered, but none of them can completely explain the mechanism of smoke generation. It was found that detailed discussion on the mechanism is needed in the further study. In conclusion, it is necessary to consider not only the electrical factor due to the Coulomb repulsion but also other complex factors in the mechanism of smoke generation.

10:00 PM CH01.11.05

The Influence of Polymer Binder on Melting Process and Mechanical Properties in a Novel Laser Deposition Method Using Metal Paste Weicheng Heng^{1,2}, Kenta Aoyagi¹ and Akihiko Chiba¹; ¹Institute for Materials Research, Tohoku University, Japan; ²Graduate School of Engineering, Tohoku University, Japan

Additive manufacturing has been widely applied in many industrial fields including medical, automobile, and aerospace due to the capability on processing products with complex topology design. However, in metal material processing field, the two conventional additive manufacturing methods, powder bed fusion using a laser beam (PBF-LB) and directed energy deposition (DED) still have their own weakness. The lower metal powder utilization rate in PBF-LB and the requirement of support structure for overhanging parts in DED not only increase the production cost, but also cause the waste of raw materials. In order to increase the metal powder utilization rate by reducing the material waste and the economic cost in powder recycle process, a new additive manufacturing method using a laser beam as a heat source has been developed in this research. In this method, metallic paste coated on a base plate is melted by a laser beam, which not only keeps the layer-by-layer processing feature of additive manufacturing, but also reduces the waste of powder by only supplying powder on processing area. Due to the stratification phenomena of the metal powder-organic solvent mixture, the polymer is added in the paste as binder to adjust viscosity. Since polymer has much lower melting point than metal and decomposes at high temperature, it is necessary to reveal the influence of polymer on microstructure and properties of built parts.

In this study, the influence of binder on melting process was investigated via single bead experiment with in-situ observation by high-speed camera. With the increase of binder content under same process condition, the size of spatters became smaller and the amount of spatters obviously increase. Lower brightness of spatter was observed in the scanning process of the sample with higher binder content.

The observation of printed samples and the evaluation of the surface quality were achieved via optical microscope. Comparing with no-binder samples, with-binder samples have smoother edges of melting track and lower roughness surface. Moreover, the same conclusion with high-speed imaging can be drawn from the analysis on the spatter size distribution: the spatter of high binder content sample has a more concentrated distribution on lower diameter. Some of the spatter generated from the sample with high binder content is hard to be distinguished from raw powder. The melting depth and the hump height were evaluated through the observation of cross section via scanning electron microscope. Lower melting depth and hump height were observed with the increase of binder content. The decomposition of binder is considered as the main reason for these changes.

In the observation on the microstructure of with-binder and pure metal samples, the with-binder sample has finer grain than pure metal sample. The microhardness was evaluated by nanoindentation method to investigate the influence of polymer binder on mechanical properties. The results showed that with-binder sample has higher hardness but lower elastic modulus than pure metal samples. The EPMA analysis revealed that the with-binder samples have more carbon content than pure metal samples, which is considered as the main reason of the difference on their microhardness.

10:15 PM CH01.11.08

Spherical Confinement, Packing and 3D Electron Microscopy—Structuring and Understanding Hierarchical Matter Da Wang^{1,2}, Ernest van der Wee¹, Tonnishtha Dasgupta¹, Michiel Hermes¹, Thomas Altantzis², Daniele Zanaga², Yaoting Wu³, Daniel Arenas Esteban², Ajinkya Anil Kadu², Luis Liz-Marzan⁴, Christopher B. Murray³, Marjolein Dijkstra¹, Sara Bals² and Alfons van Blaaderen¹; ¹Soft Condensed Matter, Debye Institute for Nanomaterials Science, Utrecht University, Netherlands; ²Electron Microscopy for Materials Science (EMAT), University of Antwerp, Belgium; ³Department of Chemistry, University of Pennsylvania, Philadelphia, PA, United States; ⁴CIC biomaGUNE, Basque Research and Technology Alliance (BRTA), 20014 Donostia-San Sebastián, Spain, Spain

The synthesis of monodisperse colloidal particles with controllable size, shape, composition, interaction which act as “artificial atoms” has progressed significantly in the past decades. Studies on the self-assembly of multicomponent colloidal particles with controllable size, component and properties provides insight into the fundamental understanding of formation of hierarchical matter on multiple length scales and bring new opportunities for structuring functional materials with collective and synergistic properties on mesoscale. Here, we will demonstrate that slow drying emulsion droplets containing colloidal particles is a robust way to make hierarchical superstructures, the so-called supraparticles [1] (particles made of particles), which can be applied as building blocks for further step self-assembly. We show that both single component and binary sized colloids interacting with a hard interaction potential self-assembly in a spherical confinement leads to equilibrium phases with icosahedral symmetry when supraparticles are composed of 100,000 particles, which are different from bulk stable structures [1,2]. Intriguingly, an excess of one species in the binary colloidal mixture negates the spherical confinement effect, leading to a bulk-like crystal with a spherical geometry [3]. Moreover, the interplay between the flat facets, sharp corners of convex-shaped hard colloidal particles and spherical confinement can be used to tune both positional- and orientational order of the building blocks in 3D [4]. Quantitative electron tomography allows us to track both positions and orientations of colloidal building blocks at a single particle scale [1-4]. By integrating experiments and computer simulations, we can understand the underlying driving force for the formation of supraparticles. Going one step further, we will outlook the possibility of characterizing 3D structures of colloidal self-assemblies in a realistic condition, which is expected to be beneficial for structure analysis of beam-sensitive materials.

References

- [1] B. de Nijs, S. Dussi, F. Smalenburg, J. D. Meeldijk, D. J. Groenendijk, L. Filion, A. Imhof, A. van Blaaderen and M. Dijkstra, *Nat. Mater.*, 14, 50 (2015).
- [2] D. Wang, T. Dasgupta, E. B. van der Wee, D. Zanaga, T. Altantzis, Y. Wu, G. M. Coli, C. B. Murray, S. Bals, M. Dijkstra and A. van Blaaderen, *Nat. Phys.*, 17, 128 (2021).
- [3] D. Wang, E. B. van der Wee, D. Zanaga, T. Altantzis, Y. Wu, T. Dasgupta, M. Dijkstra, C. B. Murray, S. Bals, and A. van Blaaderen, *Nat. Commun.*, 12, 3980 (2021).
- [4] D. Wang, M. Hermes, R. Kotni, Y. Wu, N. Tasios, Y. Liu, B. de Dijs, E. B. van der Wee, C. B. Murray, M. Dijkstra and A. van Blaaderen, *Nat. Commun.*, 9, 2228 (2018).

10:30 PM DISCUSSION TIME

SYMPOSIUM CH02

Frontiers of Imaging and Spectroscopy in Transmission Electron Microscopy
November 28 - December 6, 2022

Symposium Organizers

Miaofang Chi, Oak Ridge National Laboratory
Ryo Ishikawa, The University of Tokyo
Robert Klie, University of Illinois at Chicago
Quentin Ramasse, SuperSTEM Laboratory

Symposium Support

Bronze
Gatan
JEOL USA Inc.
Protochips Inc
Thermo Fisher Scientific

* Invited Paper
+ Distinguished Invited

SESSION CH02.01: Electron Energy-Loss Spectroscopy
Session Chairs: Quentin Ramasse and Arashdeep Thind
Monday Morning, November 28, 2022
Hynes, Level 1, Room 101

10:30 AM *CH02.01.01

Nanoscale Imaging of Interfacial Phonon Modes and Dynamics by Electron Microscopy [Xiaoqing Pan](#); University of California, Irvine, United States

Crystal defects and interfaces affect the thermal and heat-transport properties of materials by scattering phonons and modifying phonon spectra. Spatially resolved vibrational mapping of nanostructures and defects is indispensable to the development and understanding of thermal nanodevices, modulation of thermal transport and novel nanostructured thermoelectric materials. Through the engineering of complex structures, such as alloys, nanostructures and superlattice interfaces, one can significantly alter the propagation of phonons and suppress material thermal conductivity while maintaining electrical conductivity. There have been no correlative experiments that spatially track the modulation of phonon properties in and around individual defects and nanostructures due to spatial resolution limitations of conventional optical phonon detection techniques. In this talk, we demonstrate that space- and angle-resolved vibrational spectroscopy in a transmission electron microscope makes it possible to map the vibrational spectra of a single interface and a quantum dot. We detect a red shift of several millielectronvolts in the energy of acoustic vibration modes near a single stacking fault in cubic silicon carbide, together with substantial changes in their intensity, and find that these changes are confined to within a few nanometres of the stacking fault.[1] At a high-quality epitaxial Si-Ge interface, localized interfacial phonon modes at ~ 48 meV.[2] Simulations show that the interfacial phonon modes have an obvious contribution to the total thermal interface conductance. By tracking the variation of the Si optical mode in a phonon map from a single SiGe quantum dot, the nanoscale modification of the composition-induced red shift is observed.[3] We also develop a novel technique to differentially map phonon momenta, providing direct evidence that the interplay between diffuse and specular reflection largely depends on the detailed atomistic structure. Our work unveils the non-equilibrium phonon dynamics at nanoscale interfaces and can be used to study actual nanodevices and aid in the understanding of heat dissipation near nanoscale hotspots, which is crucial for future high-performance nanoelectronics.

References:

- [1] X. Yan *et al.*, *Nature* **589** (2021), p. 65–69.

[2] C. A. Gadre, X. Yan *et al.*, *Nature* **606** (2022), p. 292–297.

[3] Z. Cheng, R. Li, X. Yan *et al.*, *Nat. Commun.* **12** (2021), p. 6901.

[4] This work was supported by the Department of Energy, Office of Basic Energy Sciences, Division of Materials Sciences and Engineering (DE-SC0014430), and partially by the NSF under grant number DMR-2034738. The authors acknowledge the use of facilities and instrumentation at the UC Irvine Materials Research Institute (IMRI) supported in part by the National Science Foundation through the Materials Research Science and Engineering Center program (DMR-2011967).

11:00 AM CH02.01.02

Prospect of π^* Orbital Mapping in Graphene Using Electron Energy-Loss Spectroscopy [Mathieu Bugnet](#)^{1,2,3}, Manuel Ederer⁴, Vlado Lazarov⁵, Lian Li⁶, Quentin Ramasse^{1,2,2}, Stefan Loeffler⁴ and Demie Kepaptsoglou^{1,5}; ¹SuperSTEM Laboratory, United Kingdom; ²University of Leeds, United Kingdom; ³Univ Lyon, CNRS, INSA Lyon, UCBL, MATEIS, UMR 5510, France; ⁴TU Wien, Austria; ⁵University of York, United Kingdom; ⁶University of West Virginia, United States

Electronic states are paramount to most physical and chemical properties of materials. For instance, electronic orbitals are responsible for chemical bonding between atoms of a crystal. Their experimental observation at defects and interfaces would help understanding material properties better and developing nanostructures with novel functionalities. Nevertheless, the visualization of orbitals in real space at the atomic scale is extremely elusive, and is mostly determined by surface microscopy tools, thus only with surface sensitivity. However, using electron energy-loss spectroscopy (EELS) in the scanning transmission electron microscope (STEM) allows to probe electronic transitions from core levels to momentum- and site-projected empty states, *i.e.*, orbitals, in the bulk of the crystal, as demonstrated in rutile [1].

In this work [2], the capability to map individual electronic states in the TEM is explored from a combined experimental-theoretical approach in epitaxially-grown graphene layers, whose inherent 2-dimensionality presents surfaces as structural discontinuities. Core-level EELS spectra were recorded in a Nion HERMES scanning transmission electron microscope, equipped with a high-energy-resolution monochromator, a C_s aberration corrector up to the fifth order, and operated at 60 kV. The experimental signals are interpreted on the basis of inelastic channelling calculations (ICCs) of the energy filtered maps [3].

The extent of the π^* ($1s \rightarrow 2p_z$) and σ^* ($1s \rightarrow 2p_{x,y}$) state distributions is determined in epitaxial graphene layers observed in side-view, in a 25-nm-thick TEM lamella. Despite higher intensity of the π^* fine structures relative to the σ^* in between the graphene layers, the absolute π^* intensity is higher on the C planes, and as a result π^* states appear essentially localized on the graphene layers. However, the π^*/σ^* ratio map shows intensity maxima in between graphene layers, as highlighted by the π^*/σ^* and HAADF intensity profiles. All maps are well reproduced by ICCs, as exemplified by the remarkable overlap of experimental and calculated π^*/σ^* intensity profiles. ICCs also enable an evaluation of the effect of thickness on the orbital contrast. The π^* map of an extremely (unrealistically) thin specimen (0.43 nm) displays lobes outside the C planes, and additional intensity is also expected on the C columns. For larger and more realistic thicknesses up to the experimental value of ~ 25 nm, the π^* intensity becomes progressively more important on the C planes than outside, in agreement with experiments. This work highlights the current potential of core-level EELS towards the direct visualization of electronic orbitals in a wide range of materials, which is of interest to better understand chemical bonding among many other properties at interfaces and defects in solids [4].

[1] S. Löffler, *et al.*, *Ultramicroscopy* **177**, 26 (2017).

[2] M. Bugnet, *et al.*, *Physical Review Letters* **128**, 116401 (2022).

[3] S. Löffler, *et al.*, *Ultramicroscopy* **131**, 39 (2013).

[4] The electron microscopy work was supported by the EPSRC (UK). SuperSTEM Laboratory is the EPSRC National Research Facility for Advanced Electron Microscopy. MB is grateful to the SuperSTEM Laboratory for microscope access, and to the School of Chemical and Process Engineering at the University of Leeds for a visiting associate professorship and financial support. ME and SL acknowledge funding from the Austrian Science Fund (FWF) under grant nr. I4309-N36.

11:15 AM CH02.01.03

EELS Studies of the Tuning and Robustness of Plasmonic Response in High Aspect Ratio Gold Nanostructures [Raul Arena](#)^{1,2,3}, Mario Pelaez-Fernandez^{1,2}, Bruno Majerus⁴, Romain Dufour⁴, Daniel Funes⁵, Jean-Luc Duvail⁵ and Luc Henrard⁴; ¹Instituto de Nanociencia y Materiales de Aragon (INMA), CSIC-Universidad de Zaragoza, Spain; ²Universidad de Zaragoza, Spain; ³ARAID Foundation, Spain; ⁴Universite de Namur, Belgium; ⁵IMN - Universite de Nantes, France

For the past couple of decades, plasmonics [1] has been on the spotlight of research, mainly for its varied applications [2,3]. Within this field, the study and tuning of localized surface plasmon resonances (LSPRs) in metallic nanowires has been of importance due to their application versatility; ranging from photonics to electronics, sensors [4], or even chemical analysis through surface-enhanced light spectroscopies [5]. Additionally, recent works have shown it is possible to modify the morphology of these nanowires by means of laser irradiation, hence providing a new realm of high aspect-ratio nanostructures with potential new properties [6].

Low-loss electron energy loss spectroscopy (EELS) is a very fitting technique regarding the study of plasmonic resonances in these novel nanostructures, combining a nanometric spatial resolution and a very accurate spectral resolution. In this way, the monochromated EELS studies shown in this work, combined with state-of-the-art discrete dipole approximation (DDA) modelling, show how the plasmonic response of high aspect ratio gold 1D nanostructures can be tuned by means of coupled and non-coupled nanoparticles attached to the tips of gold nanowires, as well as a proof of concept as to how this technique can be used to understand coupling in these nanostructures [7,8]. Specifically, these studies have been carried out on gold nanowires and nanostructures consisting of nanoparticles of various sizes joint to them, producing high aspect-ratio half-dumbbells and dumbbells. The investigation of the surface plasmon resonances has been developed through a non-negative matrix (NMF) decomposition of EELS spectrum images. This high aspect-ratio gold nanostructures sustain Fabry-Perot-like surface plasmon responses from infrared to visible. We show that these resonances can be tuned by means of laser irradiation, where low energy modes stay unperturbed. All these analyses serve as experimental proof of the selective tuning (or robustness) of the plasmonic modes in a specific spectral range, which is of critical interest regarding applications for sensing devices and nano-sources, as well as optical remote control.

[1] M. L. Brongersma, *Science*. **440**, 10–12 (2012).

[2] S. Pillai, M. A. Green, *Solar Energy Materials and Solar Cells*. **94**, 1481–1486 (2010).

[3] F. de Angelis *et al.*, *Nature Nanotechnology*. **5**, 67–72 (2010).

[4] K. M. Mayer, J. H. Hafner, *ACS Chemical Reviews*. **111**, 3828–3857 (2011).

[5] M. Moskovits, *Journal of Raman Spectroscopy*. **36**, 485–496 (2005).

[6] S.V. Makarov *et al.*, *Laser and Photonics Reviews*. **11**, 1–25 (2017).

[7] M. Pelaez-Fernandez, B. Majerus, D. Funes-Hernando, R. Dufour, J.-L. Duvail, L. Henrard, R. Arenal, submitted to *Nanophotonics*.

[8] This work was supported by the Spanish MICINN (project grant PID2019-104739GB-I00/AEI/10.13039/501100011033), the Government of Aragon

(project DGA E13_20R) and European Union H2020 programs Marie Skłodowska-Curie “Enabling Excellence” (642742) and “ESTEEM3” (823717).

11:30 AM *CH02.01.04

Phonon Vibrations Probed Using the Electron Microscope Rebecca J. Nicholls; University of Oxford, United Kingdom

Recent advances in hardware mean we can now probe phonon vibrations in an electron microscope, giving us access to spectra with previously unprecedented spatial resolution and having the benefit of atomically resolved chemical analysis within the same instrument. Interpreting the spectra containing the signal from phonon vibrations is not always trivial, and simulation can be a vital part of maximising the information extracted from the data. There are several different theoretical approaches to simulating spectra, and this presentation will focus on modelling spectra from first principles. I will first discuss why spectra obtained in different experimental geometries (impact and aloof modes) require different theoretical approaches. I will then show how first principles calculations can be used to describe spectra taken in the aloof regime from molecular crystals and that it is possible to distinguish between different crystal polymorphs of the same molecule.

SESSION CH02.02: Ultrafast Electron Microscopy

Session Chairs: Ryo Ishikawa and Robert Klie

Monday Afternoon, November 28, 2022

Hynes, Level 1, Room 101

1:30 PM *CH02.02.01

Ultrafast Pulsed-Beam Transmission Electron Microscopy David J. Flannigan^{1,2}; ¹University of Minnesota, United States; ²Minnesota Institute for Ultrafast Science, United States

Fundamental non-equilibrium chemical, biological, and materials phenomena originate from ultrafast atomic-scale processes, such as electron transfer, bond formation and breaking, and electron-phonon coupling. [Here, ultrafast is defined as spanning femtosecond (fs) to nanosecond timescales.] As noted in the description of this symposium, TEM spatial and energy resolutions are presently more than sufficient for visualizing atoms and resolving low-energy phonon spectra. Arguably then, the final frontier in TEM dimensional resolution is time. Indeed, while millisecond atomic-scale dynamics have been resolved with fast detectors, and nanosecond nanoscale processes have long been studied with laser-based and laser-free pulsed beams, conducting fs atomic-scale studies with TEM has been far more challenging. Nevertheless, significant progress has been made since the seminal work of the late Ahmed Zewail and his group at Caltech, where they first coupled a fs laser oscillator to a modified commercial 120 kV TEM equipped with a conventional thermionic Wehnelt electron gun [1]. This was a watershed moment, motivating the establishment of other 4D ultrafast electron microscopy (UEM) labs and inspiring the development of other methods and uses of fs-precision pulsed electron beams, such as photon-induced near-field electron microscopy (PINEM) and the mitigation of specimen radiation damage [2,3]. Here, in addition to providing an overview of the current status of the field, I will describe the main challenges to imaging dynamics with combined Å-fs spatiotemporal resolution, the general dearth of quantitative information on UEM instrument limits, and the frontiers being pushed to overcome these challenges and limitations. I will also describe how my group has successfully used UEM to directly image ultrafast defect-modulated phonon dynamics and to resolve non-equilibrium topological phenomena, with implications for quantum information transfer and topological phononics [4-7]. I will conclude by sharing my perspective on the current opportunities yet to be fully exploited and the exciting new directions beginning to emerge [8].

[1] V. A. Lobastov, R. Srinivasan, and A. H. Zewail, Proc. Natl. Acad. Sci. U.S.A. **102**, 7069 (2005). <https://doi.org/10.1073/pnas.0502607102>

[2] B. Barwick, D. J. Flannigan, and A. H. Zewail, Nature **462**, 902 (2009). <https://doi.org/10.1038/nature08662>

[3] E. J. VandenBussche and D. J. Flannigan, Nano Lett. **19**, 6687 (2019). <https://doi.org/10.1021/acs.nanolett.9b03074>

[4] Y. Zhang and D. J. Flannigan, Nano Lett. **21**, 7332 (2021). <https://doi.org/10.1021/acs.nanolett.1c02524>

[5] S. A. Reisbick, *et al.*, J. Phys. Chem. Lett. **12**, 6439 (2021). <https://doi.org/10.1021/acs.jpcclett.1c01673>

[6] É. Dumur, *et al.*, npj Quant. Info. **7**, 173 (2021). <https://doi.org/10.1038/s41534-021-00511-1>

[7] B. Peng, *et al.*, Sci. Adv. **6**, eabd1618 (2020). <https://doi.org/10.1126/sciadv.abd1618>

[8] This material is based on work supported by the U.S. Department of Energy, Office of Science, Office of Basic Energy Sciences under Award No. DE-SC0018204. This material is based upon work supported by the National Science Foundation under Grant No. DMR-1654318. This work was partially supported by the National Science Foundation through the University of Minnesota MRSEC under Award Number DMR-2011401.

2:00 PM CH02.02.02

Understanding Phonon Coupling in Heterostructure Systems Using Ultrafast Electron Microscopy Thomas E. Gage, Haihua Liu and Ilke Arslan; Argonne National Laboratory, United States

Understanding the transition of optical excitation to full thermal equilibrium in heterostructure systems is of fundamental scientific interest and technological importance. Optically excited nanoparticles initially relax via electron-phonon lattice coupling. Phonons in the nanoparticles will further relax by coupling to the substrate. By choosing a suitable pump wavelength, without exciting the phonon mode of the substrate, a nanoparticle can act as a localized phonon generator. Selecting a graphite nanoparticle on a crystalline silicon substrate, we employ ultrafast electron microscopy (UEM) to visualize the coupling of the optically excited nanoparticle phonon mode to the crystalline silicon substrate with nanometer spatial resolution and one picosecond temporal resolution [1]. Here, using a 515nm/300fs optical pump pulse, we observe intensity oscillations in bright-field UEM mode arising from phonon vibrations of 77GHz in 200nm graphite nanoparticles, which begin at approximately time zero. After a delay on the order of tens of picoseconds, phonon oscillations appear in the silicon substrate propagating radially away from the graphite particles. By utilizing UEM, we explore the parameter space of the optical pump pulse and materials system studying the resulting dynamics observed in both the nanoparticles and substrate to gain a better understanding of the phonon coupling process.

[1] Cremons, D., Plemmons, D. & Flannigan, D. Femtosecond electron imaging of defect-modulated phonon dynamics. Nat Commun **7**, 11230 (2016).

Work performed at the Center for Nanoscale Materials, a U.S. Department of Energy Office of Science User Facility, was supported by the U.S. DOE, Office of Basic Energy Sciences, under Contract No. DE-AC02-06CH11357.

2:15 PM *CH02.02.03

Development of Ultrafast Scanning Transmission Electron Microscopy with Pixelated Detector Takahiro Shimojima¹, Asuka Nakamura¹ and Kyoko

Ishizaka^{1,2}; ¹RIKEN CEMS, Japan; ²The University of Tokyo, Japan

A promising way to improve the time resolution of the electron microscopy is the application of the ultrafast optical pump-probe technique[1]. Previous ultrafast TEM[2-4] and STEM[5] studies reported the morphological changes of the nanostructures with the time resolution being independent of the camera response time (ms). While these results opened a door to investigate ultrafast phenomena in nanoscale materials, it has been difficult to map out the physical quantities.

Here, by combining the ultrafast STEM with the pixelated detector, we improved the time resolution of the differential phase contrast and convergent beam electron diffraction STEM imagings [6]. These methods provide the ultrafast nanoscale movies of physical quantities in nano-materials, such as crystal lattice deformation, magnetization vector and electric field. We demonstrate the observations of the photo-induced acoustic phonon propagation with an accuracy of 4 ps and 8 nm [7], and ultrafast demagnetization under zero magnetic field with 10 ns and 400 nm resolution, by utilizing these methods.

[1] B. Barwick, et al., *Science* **322**, 1227 (2008).

[2] D. R. Cremons, D. A. Plemmons and D. J. Flannigan *Nat. Commun.* **7**, 11230 (2016).

[3] A. Nakamura, T. Shimojima et al., *Nano Lett.* **20**, 4932 (2020).

[4] T. Shimojima et al., *Sci. Adv.* **7**, eabg1322 (2021).

[5] V. Ortalan and A. H. Zewail, *J. Am. Chem. Soc.*, **133**, 10732 (2011).

[6] T. Shimojima, A. Nakamura and K. Ishizaka, Submitted.

[7] A. Nakamura, T. Shimojima and K. Ishizaka, *Faraday Discuss.*, 2022, Advance Article DOI: 10.1039/d2fd00062h

2:45 PM BREAK

SESSION CH02.03: Three-Dimensional TEM Imaging

Session Chairs: Ryo Ishikawa and Robert Klie

Monday Afternoon, November 28, 2022

Hynes, Level 1, Room 101

3:15 PM *CH02.03.01

Real-Space Observations of Three-Dimensional Topological Spin Textures and Their Dynamics Xiuzhen Yu¹, Yizhou Liu¹, Kostatian Iakoubovskii¹, Fehmi Yasin¹, Licong Peng¹, Kiyomi Nakajima¹, Kosuke Karube¹, Naoya Kanazawa², Taka-hisa Arima², Yasujiro Taguchi¹, Naoto Nagaosa¹ and Yoshinori Tokura¹; ¹RIKEN, Japan; ²University of Tokyo, Japan

Nanometer-scale electron spin textures, such as two-dimensional (2D) magnetic skyrmions (Sks) and anti-Sks with integer topological indices, attract much attention in condensed matter physics [1-2]. In addition to such 2D textures appearing in cubic chiral-lattice magnets, 3D spin textures, such as Sk strings carrying (anti)monopole (spin hedgehog) (point defects) [3-4] have been observed by X-ray magnetic circular dichroism for mapping the 3D scalar field of Sk strings in a Heusler magnet [5]. The more complicated 3D spin textures, like hopfion and its bundle, have also been theoretically predicted in the chiral-lattice magnets [6] but remain to be experimentally confirmed. Accordingly, there is a demand to develop 3D magnetic imaging with a high spatial resolution to map the vector field in 3D topological objects for identifying tiny defects or nodes. In the present study, we have modified tomographic transmission electron microscopy (TomoTEM) at Lorentz mode (field-free mode) and demonstrated the complete operation of the 3D Lorentz TEM imaging procedure. Furthermore, we simplified the reconstruction routine to map the 3D vector field in magnetic objects, allowing us to process data analyses quickly. Using the 3D TomoLorentz TEM, the 3D spin textures of Sk strings, antiSk, and spin hedgehog have been demonstrated [7]. In addition, the fractional hopfions with non-integer topological indices and their fascinating dynamical phenomena have been revealed under in-plane magnetic fields and pulsed electric currents in a chiral-lattice magnet FeGe [8].

*This work was supported in part by Grants-In-Aid for Scientific Research (A) (Grant No. 19H00660) from the Japan Society for the Promotion of Science (JSPS) and the Japan Science and Technology Agency (JST) CREST program (Grant No. JPMJCR1874, JPMJCR20T1), Japan.

[1] Y. Tokura, and N. Kanazawa, *Chem. Rev.* **121**, 2857 (2021).

[2] N. Nagaosa, and Y. Tokura, *Nat. Nanotechnol.* **8**, 899 (2013).

[3] P. Milde, et al. *Science* **340**, 1076 (2013).

[4] X.Z. Yu, et al. *Nano Lett.* **20**, 7313 (2020).

[5] Seki, S. et al. *Nat. Mater.* **21**, 181 (2022).

[7] X.Z. Yu, et al. submitted (2022), DOI: 10.21203/rs.3.rs-1231859/v1

[8] X.Z. Yu, Yizhou Liu, et al. in preparation.

3:45 PM CH02.03.02

Measuring 3D Chemistry with Fused Multi-Modal Electron Tomography Jonathan Schwartz¹, Jacob Pietryga^{1,2}, Jason Manassa¹, Yiwen Qian³, Zichao Di Wendy⁴, Yi Jiang⁴, Alyssa Fielitz⁵, Junsu Gu⁵, Peter Ercius³, Jeffery Fessler¹, Steve Rozeveld⁵, Ting Xu³ and Robert Hovden¹; ¹University of Michigan, United States; ²Northwestern University, United States; ³University of California, Berkeley, United States; ⁴Argonne National Laboratory, United States; ⁵Dow, United States

In principle, electron tomography used in combination with energy dispersive X-ray (EDX) or electron energy loss (EELS) spectroscopy can characterize complex three-dimensional (3D) material chemistry at the nanoscale [1,2]. However in practice, chemical tomography using core excitation spectroscopy demands high electron doses that almost always exceed the specimen limits (e.g. $> 10^7$ e/Å²). At best, researchers must choose between measuring 3D structure with high-angle annular dark-field (HAADF) tomography or characterizing chemistry along a single viewing direction. Recent developments in multi-modal data fusion paved new opportunities by substantially reducing the dose requirements for high-resolution chemical imaging [3]. In alignment with the principles of fused multi-modal electron microscopy, we report extending its algorithmic framework into the third dimension.

Here we introduce fused multi-modal electron tomography, a technique that offers high SNR and high-resolution recovery of material chemistry in 3D by leveraging correlated information encoded within both elastic scattering (HAADF) and inelastic scattering (EDX / EELS) signals. Although sparse chemical measurements are severely underdetermined in Fourier space, fusing this data with higher HAADF sampling fills in missing information, improving resolution and reconstruction quality.

We experimentally demonstrate chemical tomography at nanometer resolution using fused multi-modal electron tomography on Cu-SiC nanoparticles. Despite the noisy EDX maps, the recovered chemical tomograms quality is substantially improved over traditional tomography as ~4 nm Cu nanoparticles over a 250 nm field of view is clearly visible. We further illustrate fused multi-modal electron tomography on Au-Fe₃O₄ nanoparticles in a carbon support using core-loss EELS maps. Using the fused multi-modal reconstructions the distribution of the Au and Fe₃O₄ nanoparticles are clearly distinguished in 3D. These results demonstrate fused multi-modal tomography provides direct observation of 3D chemical structure at the nanoscale with high resolution and SNR.

References:

- [1] M. Weyland & P. Midgley *Microsc. Microanal.* **9**, 542 (2003).
- [2] A. Yurtsever, M. Weyland & D. Muller *Appl. Phys. Lett.* **89** (2006).
- [3] J. Schwartz, *et. al. npj Computational Materials* **8**, 16 (2022).

4:00 PM CH02.03.03

Data-Mining of *In Situ* TEM Experiments on CoCrFeMnNi Alloys—4D Reconstruction of Dislocation Dynamics and Sampling of the Energy Landscape Chen Zhang¹, Hengxu Song¹, Daniela Oliveros², Anna Fraczkiewicz², Marc Legros² and Stefan Sandfeld^{1,4}; ¹Forschungszentrum Jülich, Germany; ²CEMES-CNRS, France; ³École des Mines de Saint Étienne, France; ⁴RWTH Aachen University, Germany

During *In Situ* transmission electron microscopy (TEM) straining experiments of high entropy alloys (HEA), pinning points frequently hinder the motion of dislocations. They lead to abrupt changes in the curvature of moving dislocations in the middle of in situ samples. Because their nature remains a key question in HEA, we propose a data-mining strategy for extracting quantitative information from the real-time dynamics of dislocation lines to retrieve the local strength of these obstacles.

An experiment on equimolar CoCrFeMnNi HEA (Cantor alloy) demonstrates the capabilities of our data-mining approach. We show how the 3D dislocation structure can be reconstructed and the force variation along the lines retrieved automatically. A novel coarse-graining method is employed to statistically extract quantitative information on the nature, dispersion and strength of pinning points, along with their evolution upon deformation. This subsequently provides new ideas for understanding deformation mechanisms in high-entropy alloys.

SESSION CH02.04: High-Resolution Analysis
Session Chairs: Francisco Lagunas and Colin Ophus
Tuesday Morning, November 29, 2022
Hynes, Level 1, Room 101

8:30 AM *CH02.04.01

Giant Optical Anisotropy from Tiny Atomic Displacements Resolved Using Theory and Microscopy Rohan Mishra; Washington University in St. Louis, United States

Hexagonal perovskite sulfides of the form $A_{1+x}BS_3$ (A, B = metals) have a quasi-one-dimensional crystal structure with face-shared (BS_6) octahedral chains. Giant optical anisotropy has been reported in one such compound, BaTiS₃. Replacing, Ba²⁺ with isoivalent Sr²⁺ to form SrTiS₃ results in further enhancement of the optical anisotropy. Furthermore, Sr_{1+x}TiS₃ is observed to display periodic structural modulations, where the periodicity x can be modulated by changing the synthesis conditions. However, the origins of giant optical anisotropy in these compounds and their connection with structural modulations remain unresolved. Here, we combine density-functional theory calculations with atomic-scale characterization using STEM to reveal that subtle periodic modulations in Sr_{1+x}TiS₃ structures and sub-Ångström displacements in BaTiS₃ enables their record-breaking optical anisotropy. Acknowledgements: This work was supported by ARO through the MURI program with award number W911NF-21-1-0327, and NSF through DMR-2122070 and DMR-2122071.

<!--[endif]-->

9:00 AM CH02.04.02

Electronic Structure Engineering Through Atomic-Scale Strain Control in Complex Oxide Heterostructures Peter A. Van Aken; Max Planck Institute for Solid State Research, Germany

In complex oxide systems, the coupling of local atomic configurations and electronic degrees of freedom play a fundamental role in understanding exotic phenomena such as formation of charge ordering, metal-insulator transition and colossal magnetoresistance. Atomic-scale thin film syntheses enable to disentangle these competing interactions and tune novel ground states of materials, which do not exist in bulk crystals. Modifying strain by depositing epitaxial thin films on substrates with different lattice spacing results in a precise control of the local physical behavior. Scanning transmission electron microscopy (STEM) combined with electron energy-loss spectroscopy (EELS) not only provides information on the local atomic structure, but also on the site-specific chemical composition and electronic structure of materials and interfaces. Such direct real-space observations are important to unveil the microscopic origins of macroscopic properties in complex oxides and are essential for possible applications in relevant electronic and spintronic devices.

Here, I demonstrate how strain locally alters physical properties in two different complex oxide systems using STEM-EELS. I will first describe our observation of epitaxial LiV₂O₄ thin films grown on SrTiO₃ and MgO substrates. I find that the V-3d electrons redistribute in the lattice and become confined or delocalize depending on the epitaxial strain, hereby generating ordered or disordered patterns. I reveal two competing behaviors of the thin films on the two different substrates, a metallic charge-disordered phase on SrTiO₃ and an insulating charge-ordered phase on MgO. These findings evidence that charge fluctuations can freeze into an insulating “charge-glass”-like state, when epitaxial strain is applied, which relieves the frustration in LiV₂O₄.

The second part focuses on La_{0.5}Sr_{0.5}MnO₃-La₂CuO₄ heterostructures grown on three different substrates, SrTiO₃, (LaAlO₃)_{0.3}-(Sr₂AlTaO₆)_{0.7} and LaSrAlO₄ [1]. I find that charge rearrangements in these systems give rise to two different magnetic phases, an interfacial antiferromagnetic layer and an enhanced ferromagnetic metallic region away from the interfaces. Furthermore, the epitaxial strain controls the magnitude of charge redistribution and

further influences the macroscopic electronic and magnetic structures in these heterostructures differently from the strain affects reported on single-phase films. These results provide a route for understanding, controlling and designing local novel phases in complex oxides heterostructures [2].

References:

- [1] Y.-M. Wu, Y. Suyolcu, G. Kim, G. Christiani, Y. Wang, B. Keimer, G. Logvenov, P.A. van Aken: Atomic-Scale Tuning of the Charge Distribution by Strain Engineering in Oxide Heterostructures, ACS Nano 15 (2021) 16228-16235.
- [2] This project has received funding from the European Union's Horizon 2020 research and innovation programme under grant agreement No. 823717 – ESTEEM3.

9:15 AM CH02.04.03

Atomistic Segregation Behaviors of Ti in Al₂O₃ Grain Boundaries Chuchu Yang¹, Bin Feng¹, Naoya Shibata^{1,2} and Yuichi Ikuhara^{1,2}; ¹The University of Tokyo, Japan; ²Japan Fine Ceramics Center, Japan

Grain boundaries (GBs) have a great influence on the properties of polycrystalline Al₂O₃. Doping foreign elements has been known as one of the most popular strategies to alter the GB behaviors and hence material performances in Al₂O₃. Among various dopants for polycrystalline Al₂O₃, titanium (Ti) can strongly affect the resultant properties, such as conductivity [1], GB diffusivity [2] and creep resistance [3]. Although the structure-property relationships in the Al₂O₃ GBs have been widely studied [4], mechanisms of dopant segregation in the GBs are still under investigation. For instance, it is unclear how the GB structures affect the segregation of a certain element and how the dopant segregation affects GB electronic band structures. With the aid of the state-of-the-art scanning transmission electron microscopy (STEM), it becomes possible to uncover atomic segregation sites in doped GBs. In this study, we investigated the atomistic segregation behaviors of Ti dopants in two Al₂O₃ model GBs ($\Sigma 7\{4-510\}$ and $\Sigma 7\{2-310\}$) and the effect of Ti dopants on the GB bandgaps, using STEM, energy dispersive X-ray spectroscopy (EDS) and valence electron energy-loss spectroscopy (VEELS). Bicrystal-based model experiments were performed for the analysis of atomic structures, which enable us to find out the decisive factors governing the GB segregation. Our results indicate that the preferential segregation of Ti at specific atom sites in GBs was mainly driven by the ionic size mismatch between Ti³⁺ and Al³⁺. Furthermore, VEELS measurements showed that Ti doping has introduced the extra impurity state in Al₂O₃ GB bandgaps.

References

- [1] H. Unno, et al. J. Electron Microsc. 59 (2010) S107.
- [2] H. Yoshida, et al. Mater. Trans. 50 (2009) 1032.
- [3] H. Yoshida, et al. Acta Mater. 50 (2002) 2955.
- [4] J. P. Buban, et al. Science 311 (2006) 212.

9:30 AM CH02.04.04

Co-Segregation of Aliovalent Dopants at α -Al₂O₃ $\Sigma 13$ Grain Boundary Toshihiro Futazuka¹, Ryo Ishikawa¹, Naoya Shibata^{1,2} and Yuichi Ikuhara^{1,2}; ¹The University of Tokyo, Japan; ²JFCC, Japan

Impurity doping at grain boundary (GB) is a major strategy to control the properties of polycrystalline materials. The isovalent impurity with a low solubility limit is usually segregated to the specific sites at the GB core and forms the periodic GB structure [1]. However, the segregation behavior of aliovalent impurities is still unclear. Aliovalent impurities should form charged defects that will be compensated by the other charged defects, and therefore segregation behavior would be complex [2]. In this study, we investigated the segregation mechanism of counterbalancing charged defects of Ca_{Al}¹⁻ and Si_{Al}¹⁺, which are typical sintering additives for Al₂O₃, at α -Al₂O₃ $\Sigma 13$ GB by scanning transmission electron microscopy (STEM) combined with systematic density functional theory (DFT) calculations.

Atomic-resolution annular dark/bright-field (ADF/ABF) STEM observations revealed that the atomic structure of Ca/Si-doped GB is significantly transformed from that in the pristine $\Sigma 13$ GB. The energy dispersive x-ray spectroscopy (EDS) in STEM revealed that both Ca and Si are periodically segregated to the specific sites at the GB core. To understand the origin of this GB structural transformation, we first reconstructed the framework GB structure by referring to the ABF-STEM image. The GB energy of the framework structure is 4.17 J m⁻², which is much higher than that of the stable $\Sigma 13$ GB structure (2.40 J m⁻²). This result suggests that the framework structure may be stabilized by the co-segregation of Ca and Si. To determine the stable segregation sites of Ca_{Al}¹⁻ and Si_{Al}¹⁺, the segregation energies of Ca_{Al}¹⁻ and Si_{Al}¹⁺ are evaluated for all Al sites within 10 Å from the GB core. These atomic sites with minimum segregation energies agree with the Ca/Si segregation sites in STEM-EDS mapping. The minimum segregation energy of Ca_{Al}¹⁻ is -4.63 eV, which is much lower than those of other Al sites. On the other hand, the minimum segregation energy of Si_{Al}¹⁺ is -0.46 eV, and the site dependence of segregation energy is small. These results suggest that the segregations of Ca_{Al}¹⁻ and Si_{Al}¹⁺ are induced by the structural stability and the local charge compensation with Si_{Al}¹⁺, respectively. Lastly, we reconstructed the Ca/Si co-segregated $\Sigma 13$ GB and evaluated the GB energy, and the most stable structure is matched well with the STEM image. The GB energy of the Ca/Si co-doped GB decreases with the increase in the chemical potentials of Ca and Si, and it becomes lower than that of the pristine GB. This result suggests that, as increasing the doping amount of Ca and Si, they segregate to the GB core and induce the GB structural transformation.

- [1] J. P. Buban et al., Science, 311, 212 (2006).
- [2] T. Futazuka et al., Phys. Rev. Mater. 4 073602 (2020).

9:45 AM CH02.04.05

Atomic-Scale Insights into the Structural Transformations in Cathodes for Multivalent Metal-Ion Batteries Arashdeep S. Thind and Robert F. Klie; University of Illinois Chicago, United States

Multivalent-metal ion batteries are promising and safer alternatives to lithium-ion batteries for next-generation energy storage devices. Most of the multivalent-metal ions, such as calcium (Ca) and magnesium (Mg), and their respective cathode material systems can be sourced from earth-abundant minerals. Moreover, Ca and Mg-ion batteries, based on high-voltage oxide cathodes show high energy density compared to lithium-ion batteries. This makes multivalent-metal ion batteries a cost-effective proposition for a variety of battery technologies. However, multivalent-metal ion batteries often suffer from poor electrochemical stability. A key challenge in achieving higher performance and stability in these material systems is to understand the fundamental structural changes to the cathode at the atomic scale. Such structural changes during electrochemical cycling include cation disorder, planar defects, phase separation, and (de)intercalation mechanisms. In this work, we combine aberration-corrected scanning transmission electron microscopy (STEM), first-principles density functional theory (DFT) calculations, and STEM simulations to develop a fundamental understanding of the structural changes occurring during electrochemical cycling of Ca and Mg-ions into FePO₄ and α -V₂O₅ as cathodes respectively.

During electrochemical cycling of Ca into FePO₄, we observe that the large particles (> 100 nm) show Ca intercalation at the surface with the bulk of the particle showing little to no activity. Moreover, the smaller particles (< 50 nm) exhibit a tendency to phase-separate into CaPO₄. STEM imaging reveals

the direct atomic-scale evidence of Ca intercalation into the FePO_4 olivine structure, where Ca-ions show a preferential arrangement along the [010] orientation. For the Mg-ion batteries, we observe that the Mg intercalation into $\alpha\text{-V}_2\text{O}_5$ is heterogeneous and is accompanied by the formation of a network of low-angle grain boundaries. We hypothesize that there is significant phase separation between various phases of $\text{Mg}_x\text{V}_2\text{O}_5$ and V_2O_5 , such as the fully intercalated $\delta\text{-MgV}_2\text{O}_5$ and fully deintercalated $\alpha\text{-V}_2\text{O}_5$ phases. Our atomic-scale findings for these two model systems can be leveraged by optimizing the materials synthesis to achieve theoretical operating potentials and performance.

Acknowledgments: This work is supported by the Joint Center for Energy Storage Research (JCESR) and Energy Innovation Hub funded by the U.S. Department of Energy (DOE), Office of Science, Basic Energy Sciences.

10:00 AM BREAK

10:30 AM CH02.04.06

Identifying Inhomogeneities in Niobium Superconducting Transmon Qubit Devices Through Advanced Microscopy [Akshay A. Murthy](#)¹, Jaeyel Lee¹, Cameron Kopas², Stephanie Ribet³, Josh Y. Mutus², Thang T. Pham³, Anna Grassellino¹, Roberto dos Reis³, Vinayak P. Dravid³ and Alexander Romanenko¹; ¹Fermi National Accelerator Laboratory, United States; ²Rigetti Computing, United States; ³Northwestern University, United States

Superconducting qubits have emerged as a platform technology for potentially addressing computational problems deemed intractable with classical computing. Despite recent advances enabling multiqubit designs that exhibit coherence lifetimes on the order of hundreds of μs , defects and amorphous oxides continue to curb device performance by dissipating electromagnetic energy. Experimental and theoretical investigations have led researchers to understand quantum decoherence is dictated by deviations from crystalline order on the nanoscale. Thus, the high-resolution nature of electron microscopy makes it an indispensable tool for identification of decoherence sources. Through a combination of scanning transmission electron imaging and diffraction methods, we interrogate the thin metal films integral for superconducting qubit operation and observe structural and chemical features that can potentially serve as decoherence sources. This includes the presence of localized strain at grain boundaries and metal/substrate interfaces. Such localized strain can induce changes in the superconducting critical temperature and superconducting order parameter. Further, by employing the fluctuation electron microscopy technique, we are able to better understand the medium range order present in the amorphous oxides that inevitably form in these systems. Through this analysis we observe a variation in bond distances in the surface oxide. Such variation can lead to low frequency noise, which helps explain previous experimental data highlighting the lossy nature of this oxide. Equipped with these findings, we seek to intelligently fabricate superconducting qubits and extend coherence times.

10:45 AM CH02.04.07

Characterization of Modulated Nanostructure Using Aberration Corrected Scanning Transmission Electron Microscopy (STEM) [Ronit Sawant](#) and Ray Carpenter; Arizona State University, United States

Modulated nanostructures are short-range quasiperiodic composition fluctuations observed in metals, semiconductors, and ceramic alloys and have an important effect on the mechanical, electrical, and magnetic properties of the materials. Their presence is often attributed to spinodal decomposition [1]. The typical wavelength of the modulations ranges from 5 nm to 15 nm in metal alloys [2]. In past, such modulations have been analyzed using x-ray diffraction (XRD), electron diffraction, and diffraction/strain contrast imaging techniques [3]. These investigations gave useful information about the wavelength and strain fields in the modulation but nothing about the composition amplitude of the modulated structure. With the development of field emission sources [4], aberration correctors [5], and ADF imaging for STEM microscopes, measuring the amplitude of the modulation directly and examining the diffused interface is possible. Also, to study the reaction kinetics measurement of the composition amplitude is necessary. In this study, we measure the composition amplitude of the fluctuations directly using STEM HAADF imaging and energy dispersive x-ray (EDS) spectroscopy. Au-Pt alloys with a symmetrical solid-state miscibility gap are used for the investigation of the modulated structure. Three alloys of compositions 60%Pt, 80%Pt, and 40%Pt are analyzed at different temperatures at various aging times for studying the reaction kinetics. Composition variation and the diffused interface across modulations were successfully mapped using atomic resolution EDS spectroscopy. Results show the wavelength, as well as the composition amplitude of the modulations, increases as the alloy is aged for a longer time. As the reaction proceeds towards equilibrium, the amplitude of the fluctuations should increase and reach the equilibrium composition at the end of the tie line at the selected aging temperature. Although the entire specimen region was modulated, variations in both the wavelength and composition amplitude were observed. 1D and 2D modulation were seen along the $\langle 100 \rangle$ directions. These results obtained are in good agreement with the spinodal theories and XRD experimental data [2]. Cellular precipitates were observed along the grain boundary of alloys aged for a longer time. Nucleation and Growth mechanism is responsible for such precipitation reaction and is also a competing reaction along with the spinodal decomposition. Analyzing such cellular precipitates at the grain boundary is very important as it influences fracture behaviors in spinodal alloys. A similar analysis is also being carried out in the Cu-Ti alloy system which has an asymmetrical miscibility gap. The results obtained from this study show that analyzing the compositions of modulated structures using aberration-corrected STEM is possible and therefore a comparison between the spinodal rate theory and experimental kinetics of the modulated structures can be obtained.

References:

- [1] J. W. Cahn (1962), Acta Met.10, 179-183.
- [2] R. W. Carpenter (1967), Acta Met.15, 1567-1572.
- [3] J. Bentley (1989), Ultramicros.30, 157-171.
- [4] A. V. Crewe et al (1975), p. 47 in Physical Aspects of Electron Microscopy and Microbeam Analysis, ed. by Siegel and Beaman, Wiley, New York.
- [5] O. L. Krivanek et al (2008), Ultramicros.108, 179-195.
- [6] The authors acknowledge funding from the Division of Materials Research of the National Science Foundation, and the use of facilities within the John M. Cowley Center for High-Resolution Electron Microscopy at Arizona State University.

11:00 AM CH02.04.08

Determination of the Thermal Expansion Coefficient of the Nanoparticles with *In Situ* Electron Energy Loss Spectroscopy [Bibash Sapkota](#), Serdar Ogut and Robert F. Klie; University of Illinois at Chicago, United States

Our ability to determine the local temperature of a sample inside the electron microscope column is key in measuring the effects of electron-sample interaction and controlling the beam-induced sample changes. Temperature dependence of the plasmon resonance energy of the material can be used to map the local temperature of the material at the nanoscale [1-2] and to determine its thermal expansion coefficient [3]. In this work, we will study the behavior of plasmon energy of In and BaTiO_3 nanoparticles across the phase transition temperature. We will compare the performance of several nanoparticles (Al, Si, In, SrTiO_3 , BaTiO_3) as a nano-thermometer for high-temperature measurement. In addition, we will also utilize a novel approach of non-contact thermometry based on the combination of low-loss electron energy-loss spectroscopy (EELS) with the free electron model to measure the thermal expansion coefficient (TEC) of nanoparticles at the nanoscale. Finally, we will explore the effects (if present) of the particle size, oxygen vacancies, and contamination on this approach of measuring the thermal expansion coefficient as well as the local temperature.

References:

- [1] Mecklenberg et al., Sci. 347, 6222(2015)
- [2] Mecklenberg et al., Phys. Rev. Applied 9, 014005(2018)
- [3] Hu et al., Phys. Rev. Lett. 120, 05590(2018)
- [4] This work was supported by the National Science Foundation (DMR-1831406).

11:15 AM CH02.04.09

Direct Observation of Non-Brownian Motion of Intercalated Atoms in van der Waals Bonded Interfaces [Joachim D. Thomsen](#)^{1,2}, Yaxian Wang¹, Frances M. Ross² and Prineha Narang¹; ¹Harvard University, United States; ²Massachusetts Institute of Technology, United States

Diffusion processes in two-dimensional materials govern several phenomena such as phase transformations, growth by chemical vapor deposition, and doping by substitutional and interstitial atoms. Furthermore, intercalation of foreign atomic species into van der Waals (vdW) bonded materials has been studied for tuning of physical properties (electronic, optoelectronic, magnetic), and for uses in energy and battery applications.

Here, we directly image the diffusion of W atoms using high-angle annular scanning transmission electron microscopy (HAADF-STEM) inside hexagonal boron nitride (hBN)-WSe₂-hBN vdW heterostructures. By using thin (~2 nm thick) hBN crystals which consist of light B and N atoms, we can image the heavier W atoms inside this heterostructure in two different interfaces: directly between the encapsulating hBN layers and in the WSe₂/hBN interface. In combination with density functional theory calculations, we find that the motion of the intercalating W atoms is strongly affected by local defects created by the high-energy electron beam. When measuring the diffusion coefficient for W atoms at the two different interfaces, we find, for similar experimental conditions, a diffusion coefficient that is twice as large at the WSe₂/BN interface compared to the BN/BN.

This work shows that atomic diffusion inside vdW heterostructures can be imaged directly and suggests avenues for creating superlattices inside such heterostructures by engineering defect sites.

SESSION CH02.05: 4D STEM

Session Chairs: Robert Klie and Naoya Shibata

Tuesday Afternoon, November 29, 2022

Hynes, Level 1, Room 101

1:30 PM *CH02.05.01

Using Four-Dimensional-Scanning Transmission Electron Microscopy (4D-STEM) for Large Field-of-View Material Property Measurements and Ptychographic Atomic-Resolution Tomography. [Colin Ophus](#); Lawrence Berkeley National Lab, United States

The past decade of development for scanning transmission electron microscopy (STEM) have been enormously successful, driven primarily by three technological innovations: hardware aberration correction, direct electron detectors, and the transformation of S/TEM into a digital science with the rise of computational imaging. In this talk, I will show how these three developments have enabled four dimensional (4D)-STEM experiments where we record full 2D images of the diffracted STEM probe over a 2D grid of probe positions. I will demonstrate large field-of-view mapping of structure, orientation and strain for materials ranging from structural oxides nanowires to 2D materials. I will also show how these methods can also be combined with complementary techniques such as STEM-electron energy loss spectroscopy or x-ray spectro-ptychography, for multimodal characterization of energy materials. I will briefly describe how modern machine learning methods can be used to extend the range of usable sample thicknesses by untangling the complex nonlinear contrast generated from multiple scattering of the electron beam. Finally, I will show results from ptychographic atomic-resolution tomography, which we use to solve the structure of complex encapsulated nanotube-nanowire materials. All of our methods, algorithms, codes and datasets are freely available to the community in order to promote widespread development of these experimental procedures.

2:00 PM CH02.05.03

Diffraction Image Processing for 4D-STEM to Improve ASTAR Pattern Matching [Nicolas Folastré](#)^{1,2}, [Sunkyu Park](#)^{1,3}, [Edgar Rauch](#)⁴, [Arash Jamali](#)^{5,1}, [Jean-Noël Chotard](#)^{1,2,6}, [Christian Masquelier](#)^{1,2,6}, [Laurence Croguennec](#)^{3,2,6} and [Arnaud Demortière](#)^{1,2}; ¹Laboratoire de Réactivité et de Chimie des Solides (LRCS) – CNRS UMR 7314, France; ²Réseau sur le Stockage Electrochimique de l’Energie (RS2E), France; ³Institut de Chimie de la Matière Condensée de Bordeaux (ICMCB) – CNRS UMR 5026, France; ⁴Laboratoire Science et Ingénierie des Matériaux et Procédés (SIMaP) – Grenoble INP/CNRS/UJF, France; ⁵University of Picardie Jules Verne (UPJV), France; ⁶ALISTORE-ERI – CNRS FR 3104, France

The emergence of new energy materials is related to the development of highly controlled poly-crystal materials exhibiting specific and interesting phase transformation, electronic/ionic conductivity, and optical properties. The scanning TEM is one of the most actively developing analytical methods to characterize these polycrystals from microscopic to atomic scales. The interest in the hyperspectral STEM approach that gathers structural and chemical information in a 4D image stack was mainly based on imaging-spectroscopy techniques such as STEM-EDX and STEM-EELS. Last decade, thanks to a new generation of direct electron detectors, imaging algorithms, precession technique, and highly coherent electron beam, a new approach emerged called 4D-STEM in which diffraction patterns in parallel or convergent beam are acquired in hyperimage stack. In parallel beam condition, automated crystal orientation mapping (ACOM) turns out to be a new powerful tool to characterize polycrystalline materials at the nanoscale by mapping crystallographic properties.

This 4D-STEM method using ASTAR-ACOM system allows to build maps of crystalline phase and orientation, using scanning nano-diffraction with precession with nanometer resolution. The recent use of high-speed cameras, pixelated detectors such as CMOS cameras and hybrid-pixel detectors enabled larger areas to be scanned, and a higher resolution close to 1 nm. However, using a CMOS camera in the column implies strong changes in the acquired images in comparison to the use of a NanoMegs conventional external optical camera, as the quality of the image improves with the increased electron sensitivity and the resolution. As the 4D-STEM ASTAR suite has been optimized for images acquired with the Stingray optical camera (phosphorescent screen), the data preparation should be adapted to fit with images acquired using CMOS camera as Oneview Gatan camera.

The goal of the data preparation methods proposed here is to improve the quality of ASTAR pattern-matching using a dataset of diffraction patterns acquired with a CMOS Oneview camera. The high sensitivity of the CMOS camera and the data filtering developed here modify the diffraction images leading to a compromise between image quality and template matching result quality.

First, modifications inside diffraction patterns are estimated through image quality metrics such as signal-over-noise ratio (SNR), peak signal-over-noise (PSNR), structural similarity index measure (SSIM), mean absolute error (MAE), and root-mean-square error (RMSE). Second, the quality of the pattern-matching process on filtered and reconstructed images is evaluated using index and orientation reliability, defined in the ASTAR software. We demonstrate that the experimental data preparation provides great advantages for the pattern-matching quality result, as it reduces noise overfitting, improves structural similarity index measure, and increases the orientation reliability from average values of 10-15 before to 20-30 after filtering.

The data reduction method applied in this work is a registration and reconstruction code for diffraction images acquired using a CMOS camera, which we use to filter and record the diffraction signal and reconstruct the images upstream of the ASTAR suite pattern-matching software. The essential information of each reflection of a dataset (200*200*512*512) such as intensity, size, and position are recorded in a few minutes with an accuracy of the order 10^{-2} px, with a data reduction factor of the order 10^2 .

In this work, we show that the mapping of crystal structures and orientations provides essential information for the determination of individual particle lithiation mechanisms of cathode materials for Li-ion and Na-ion batteries, as $\text{Na}_x\text{MnV}(\text{PO}_4)_3$ was used in this study. In addition, this image processing method gives more confidence in phase determinations in such polycrystalline materials.

2:15 PM BREAK

2:45 PM CH02.05.04

Defect Contrast with 4D-STEM, Role of Local Order and Symmetry [Stephanie Ribet](#)¹, Colin Ophus², Roberto dos Reis¹ and Vinayak P. Dravid¹; ¹Northwestern University, United States; ²Lawrence Berkeley National Laboratory, United States

Many important material properties are controlled by defects, which break the local order of structures on the nano to atomic scale. Scanning transmission electron microscopy (S/TEM) is an especially apt tool to study structures and their symmetry at relevant length scales. However, there are intrinsic challenges to characterizing these defects with conventional imaging modalities for some materials due to dose, contrast, and probe-size limitations. 4D-STEM experiments, where a diffraction pattern is acquired at each position in real space, can help overcome these obstacles. The combination of the versatility of the available reconstruction techniques and the rich information contained in a diffraction pattern allows for studies of material properties, such as local symmetry, that would not otherwise be possible. Additionally, the modification of the beam through a phase or amplitude plate inserted in the probe forming aperture of a STEM creates another handle to change final image contrast, while reducing dose and highlighting defects. In this presentation, we will show simulations on a variety of structures and illustrate how virtual detectors and beam modification in a 4D-STEM experiment can be used to highlight important changes in local order of materials. We will compare these results to more conventional imaging techniques in light of realistic parameters, such as electron dose and lens aberrations.

3:00 PM CH02.05.05

Development of a Method to Observe Local Atomic Vibrations by STEM Using a Segmented Detector [Koudai Tabata](#)¹, Takehito Seki^{1,2}, Yuichi Ikuhara^{1,3} and Naoya Shibata^{1,3}; ¹The University of Tokyo, Japan; ²JST PRESTO, Japan; ³Japan Fine Ceramics Center, Japan

Aberration-corrected scanning transmission electron microscopy (STEM) is a powerful technique for directly observing atomic structures and chemistry in local regions of materials. Annular dark-field (ADF) method, in which electrons scattered at high angles are detected by an annular detector, is widely used as a useful tool for direct observation of atomic positions. It is known that the electrons scattered at high angles are dominated by thermal diffuse scattering (TDS) [1], which depends on the atomic number and atomic displacement parameter (ADP) of the atoms. It is considered that anisotropic atomic vibrations cause anisotropic TDS, but conventional annular detectors have not been able to measure local atomic vibrations quantitatively, including anisotropy of vibration. On the other hand, segmented detectors [2] can acquire images from multiple detection areas divided in the azimuthal direction, enabling the acquisition of signals that depend on the direction of electron scattering. In this work, we investigate the possibility of direct observation of anisotropic atomic vibrations by atomic-resolution STEM with a segmented detector. First, we performed image simulations based on the quantum excitation of phonons (QEP) multislice approach [3] and extracted the electrons which have scattered by anisotropic atomic vibrations. STEM observation conditions, such as convergence angle, defocus, accelerating voltage, and detector acquisition angle, were optimized to increase the signal due to anisotropic atomic vibrations. We performed experimental STEM observations for a model sample under thus obtained optimal conditions and quantitatively compared the experimental results with the theoretical simulations. Details will be reported in the presentation.

[1] S. J. Pennycook et al. *Ultramicroscopy* 37, 14 (1991).

[2] N. Shibata et al., *Microscopy* 59, 473 (2010).

[3] B. D. Forbes et al., *Phys. Rev. B* 82, 104103 (2010).

3:15 PM CH02.05.06

Compressed 4D-STEM—From Conception to Implementation [Alex W. Robinson](#)¹, Daniel Nicholls¹, Jack Wells¹, Amirafshar Moshtaghpour^{2,1}, William J. Pearson¹, Angus Kirkland^{2,3} and Nigel Browning^{1,4,5}; ¹University of Liverpool, United Kingdom; ²Rosalind Franklin Institute, United Kingdom; ³University of Oxford, United Kingdom; ⁴Pacific Northwest National Laboratory, United States; ⁵Sivananthan Laboratories, United States

Scanning transmission electron microscopy has routinely shown its capability to identify complex structural, mechanical, and electronic properties of crystalline materials. However, there are many more materials where the resolution of the final image is limited by its response to the incident electron beam, and ultimately reliable images and analysis is determined by how beam-sensitive the sample is. Recent developments in compressive sensing for scanning transmission electron microscopy (CS-STEM) has opened new avenues for low dose electron microscopy, as well as increased temporal resolution through subsampling for fixed detector imaging methods such as annular dark field (ADF) and bright field (BF) imaging.

4D-STEM is becoming more common in the field, where at each probe location a convergent beam electron diffraction (CBED) pattern is acquired using a pixelated detector to allow for a higher angular range of information from electron scattering. The CBEDs can then be used to acquire a variety of image types such as (high angle) ADF (HA/ADF), BF, ABF, Centre of Mass, Phase Contrast, Strain Mapping, Holography, and Ptychography. However, due to the nature of the data acquired, the time for acquisition is much slower with respect to fixed detectors, and the data sets are on the order of many gigabytes as opposed to megabytes in standard imaging methods. This means that beam exposure increases and other artefacts such as drift and distortion are heightened through the increased acquisition time.

In order to overcome this, we propose integrating compressive sensing with 4D-STEM to develop a new method which aims to both lower the electron dose and increase speed through real and reciprocal space subsampling. We demonstrate practical implementation of subsampling the pixelated detector and subsampling the spatial probe locations to generate a 4D-STEM dataset that is not only significantly smaller in memory size, but is acquired in

significantly less time than the full acquisition. The data is then reconstructed through an image inpainting algorithm by first recovering the CBED patterns and then in turn using the CBED patterns to recover a variety of subsampled image types. We present the methods and implementation to our STEM, and the potential for ptychographic reconstruction from subsampled data.

3:30 PM CH02.05.07

Local Structure and Polarization in Relaxor and Ferroelectric Tetragonal Tungsten Bronzes Measured by 4D STEM [Stephen Funni](#) and Elizabeth Dickey; Carnegie Mellon University, United States

Classical and relaxor ferroelectrics are critical for many modern technologies, notably as functional materials in transducer and capacitor applications. Prominent, commercially used materials in these categories are lead-based, which is undesirable due to lead's toxicity. In the search for lead-free alternatives, tetragonal tungsten bronze (TTB) oxides have been examined due to their flexible chemistry and wide range of properties, including relaxor and classical ferroelectric behavior.^[1] TTBs commonly exhibit commensurately or incommensurately modulated superlattices, and an empirical link has been established between superlattice type and ferroelectric order.^[2] The modulation includes tilting within the oxygen-octahedral network and related cation displacements. Several studies have attempted to characterize the structure by various methods, though these have been inconclusive to due various inherent technique limitations.^[3,4] An Ama2 unit cell was proposed as a commensurate approximation of the incommensurate modulation.^[5] This model implies the presence, locally, of one of two possible orientations of the modulation. In this work, we seek to provide more detailed information regarding the structure and origin of ferroelectric properties in TTBs using scanning transmission electron microscopy (STEM).

Current state-of-the-art in STEM, including aberration correction and advanced pixelated detectors, allows precise atomic-scale characterization of materials. In this work, we use 4D STEM (a technique in which a complete electron diffraction pattern is collected for each probe position) to analyze the structural modulation and polarization of two TTB compositions: $\text{Ba}_4\text{Nd}_2\text{Nb}_4\text{Ti}_6\text{O}_{30}$, a commensurately modulated classical ferroelectric, and $\text{Ba}_5\text{Sm}_1\text{Sn}_3\text{Nb}_7\text{O}_{30}$, an incommensurately modulated relaxor. We perform two types of experiments at different length scales. The first 4D STEM experiments, nano-beam electron diffraction (NBED), allow us to measure the local modulation orientation and polarization at nanometer-scale resolution over approximately 1 m^2 fields of view from a single dataset. We design custom virtual detectors informed by electron diffraction simulations of the Ama2 cell. To identify the local modulation orientation, we use a virtual detector sensitive to the corresponding superlattice reflections; and for measuring local polarization, we calculate the normalized difference signal between the and disk pairs. The resulting images map these key structural signatures (modulation orientation and polarization) over the scanned region. Next, we study the structure of the materials at atomic resolution using phase contrast imaging from a second set of 4D STEM experiments. We analyze the images using our recently developed vector pair correlation function method^[6] to quantify the ordering of atomic displacements on the anion and cation sublattices, determining the correlation length of the modulation and polar distortions on a sublattice-specific basis. By applying 4D STEM characterization to TTBs we relate structural information from both nanometer and atomic length scales to the materials' functional, macroscopic properties.

[1] V. V. Shvartsman, D. C. Lupascu, *J. Am. Ceram. Soc.* **2012**, *95*, 1.

[2] X. Zhu, M. Fu, M. C. Stennet, P. M. Vilarinho, I. Levin, C. A. Randall, J. Gardner, F. D. Morrison, I. M. Reaney, *Chem. Mater.* **2015**, *27*, 3250.

[3] T. Woike, V. Petricek, M. Dused, N. K. Hansen, P. Fertey, C. Lecomte, A. Arakcheeva, G. Chapuis, M. Inlaur, R. Pankrath, *Acta Crystallogr. Sect. B* **2003**, *59*, 28.

[4] L. A. Bursill, J. L. Peng, *Acta Cryst* **1987**, *43*, 49.

[5] I. Levin, V. Krayzman, G. Cibir, M. G. Tucker, M. Eremenko, K. Chapman, R. L. Paul, *Sci. Rep.* **2017**, *7*, DOI 10.1038/s41598-017-15937-x.

[6] S. D. Funni, Z. J. Yang, M. J. Cabral, C. Ophus, X. M. Chen, E. C. Dickey, *APL Mater.* **2021**, *9*, 091110.

SESSION CH02.06: Poster Session

Session Chairs: Miaofang Chi, Ryo Ishikawa, Robert Klie and Quentin Ramasse

Tuesday Afternoon, November 29, 2022

8:00 PM - 10:00 PM

Hynes, Level 1, Hall A

CH02.06.01

An Accessible Direct Detection Camera for Transmission Electron Microscopy Imaging, Diffraction and *In Situ* Investigation of Materials from 60 – 200 keV [Fernando Castro](#), Benjamin Miller and Cory Czarnik; Gatan, Inc., United States

The ability of direct detection cameras to collect high-quality data with very low dose rates (e.g. $< 20 \text{ e}^-/\text{pixel/s}$) in the transmission electron microscope (TEM) makes them effective tools for investigating any beam-sensitive material or reaction, such as studies on monolayer 2D materials [1]. These cameras are usually optimized for 200 – 300 keV TEM operation to support the most popular materials science and cryo-electron microscopy applications but have lower detection efficiency at lower TEM accelerating voltages. As a result, direct detection cameras have limited performance for emerging applications requiring $\leq 80 \text{ keV}$ to reduce beam damage or improve scattering contrast. Furthermore, properly operating direct detection cameras typically requires more microscopy expertise than operating a scintillator camera, which can be a barrier to collecting the best possible results.

This presentation highlights Gatan's newest direct detection camera – specifically designed to extend the high-quality imaging capabilities of direct detection technology down to 60 keV while streamlining camera operation to improve accessibility for microscopists of all levels of expertise. In particular, the camera uses a new $2\text{k} \times 2\text{k}$ pixel sensor for experiments from 60 – 200 keV and is capable of framerates $> 40 \text{ FPS}$ at full imaging resolution. Results from low-dose *in-situ* heating experiments at $\leq 80 \text{ keV}$ are presented to highlight the camera's high performance for materials research and *in-situ* experiments. New DigitalMicrograph software features for streamlining camera control and data processing are also discussed.

The improved performance of this camera below 200 keV will benefit all TEM experiments requiring both low-dose and low accelerating voltage, such as research on lithium-ion batteries, catalysts, electronics, and more.

[1] Murthy, A. *et al.* Direct Visualization of Electric-Field-Induced Structural Dynamics in Monolayer Transition Metal Dichalcogenides. *ACS Nano* **14**, 1569-1576 (2020)

CH02.06.04

Atomic-Scale Study of Spinel MgV_2O_4 Nanocrystals for Multivalent Ion Battery Cathodes [Francisco J. Lagunas Vargas](#)^{1,2}, Adriana Lee Purano^{1,3},

Grant C. Alexander^{1,2}, Heonjae Jeong^{1,4}, Christian Moscica^{1,2}, Lei Cheng^{1,4}, Jordi Cabana^{1,2} and Robert F. Klie^{1,2}; ¹Joint Center for Energy Storage Research, United States; ²University of Illinois Chicago, United States; ³Tecnologico de Monterrey, Mexico; ⁴Argonne National Laboratory, United States

Mg-ions based batteries have emerged as a promising candidate in the search for post lithium-ion energy storage. Since Mg ions are divalent, batteries based on their transfer inherently offer higher energy densities than those using Li. Additionally, batteries with Mg metal anodes offer a route towards higher gravimetric energy densities needed for applications in electric vehicles, aircraft, and energy grid storage. While Mg ions are comparable in ionic radii to Li ions, their increased reactivity has complicated the search for compatible cathode materials. To date many systems have been explored but few materials for real-world applications have emerged [1]. To overcome this, a fundamental understanding of Mg electrochemistry and solid-state cathode materials are needed. Here we present a study of a spinel vanadium oxides, a cathode material that has been shown to cycle Mg at capacities greater than 170mAh/g [2], using an aberration corrected cold field scanning transmission electron microscopy (STEM) to develop atomic scale structure-property relationships in the material.

In addition to atomic scale imaging, we will utilize electron energy loss spectroscopy (EELS) to map local changes in the density of states (DOS) of the material and conduct a quantitative chemical analysis of the material using energy dispersive spectroscopy (XEDS).

We will show that MgV₂O₄ crystals tend to form well-defined polyhedra with [111], [001] and [110] surface types. The prevalence of each surface type will be examined through a statistical analysis of imaged crystals and the results will be compared to *in-silico* calculations of the associated energies of each surface type. Additionally, we will present atomic-resolution images of the surface reconstructions observed within the first two-three atomic layers on a variety of surface types. Our analysis will include the atomic-scale effects of electrochemical cycling on the crystals. We will show that upon charging a ~5 nm amorphous layer forms on the crystal surface and notably is the region with most pronounced electrochemical activity. The relationship between the crystal surface type and the depth of the surface layer formation will be explored. Finally, by comparing MgV₂O₄ material at different number of cycles (1,20,50) we will present insights into the failure mechanism associated with this material [3].

References

- [1] Ponrouch, Alexandre, et al. "Multivalent rechargeable batteries." *Energy Storage Materials* 20 (2019): 253-262.
- [2] Hu, Linhua, et al. "High capacity for Mg²⁺ deintercalation in spinel vanadium oxide nanocrystals." *ACS Energy Letters* 5.8 (2020): 2721-2727.
- [3] This work is solely supported by the Joint Center for Energy Storage Research (JCESR) and Energy Innovation Hub funded by the U.S. Department of Energy (DOE), Office of Science, Basic Energy Sciences.

CH02.06.06

Advancements in UltraFast Electron Microscopy Darrin Leonhardt¹, Eric Montgomery¹, Chunguang Jing¹, Bart Wyderski¹, Yubin Zhao¹, Spencer Reisbick², Yimei Zhu² and June Lau³; ¹Euclid TechLabs, United States; ²Brookhaven National Laboratory, United States; ³National Institute of Standards and Technology, United States

Abstract: With the growing applications of temporally-resolved electron microscopy for probing basic chemical and electronic phenomena as well as reducing beam-induced damage, a multifaceted approach to ultrafast transmission electron microscopy is provided in this presentation. Traditionally accepted laser techniques with fixed image acquisition times have been complemented by ultrafast rf and microwave-driven techniques that can be synchronized with any sample excitation (laser, rf, thermal) with much faster image acquisition times (from days to minutes), thereby enabling more reliable data and microscope efficiency.

Keywords: ultrafast electron microscopy, stroboscopic, time-resolved imaging, high resolution transmission electron microscopy, beam damage.

Originally a basic research tool for materials science, transmission electron microscopes (TEMs) have seen a renaissance, as they have been applied in nearly every technology-based field. They have become the gold standard of high spatial resolution techniques and the ever-increasing applications from quantum dots to cellular 3D tomography and holography demand a much wider range of imaging capabilities. TEMs are used to connect photonics, nanodevice architecture, and biophysics, each with their individual intrinsic response times on the nanoscale. The continued evolution of applications and maturation of basic TEM instruments have not only created additional sectors in the TEM industry (life sciences, nanotechnology, and semiconductor), but have fostered significant growth in these areas that the new market sectors are comparable in size to the once dominant materials science market [1].

Generally, the picosecond regime is common for interrogating basic material phenomena, then longer time scales are generally necessary as material systems get larger physically. Ultrafast TEM (UTEM) was developed using lasers and photocathodes in the mid-2000s to interrogate time-resolved responses to optical stimuli [2]. While ultrafast lasers were a natural enabler for early research in UTEM, the explosive growth of these new applications based on large molecules (proteins, cells) and new 2D/3D architectures (NEMS/MEMS, nanosheets, spintronics) requires broader temporal capabilities due to their widely varying response times. If we include research focused on the mitigation of radiation damage from the microscope's probe beam, an entirely new set of requirements and process space becomes critical. The material recovery time from beam induced damage between probe pulses, process temperature, sample area, etc., may all become variables to the imaging process. Especially in these cases, complementary enabling technologies (rf, microwave) have been used with simplified and typically improved imaging performance.

This presentation will also present the challenges for growing ultrafast techniques [3,4] and compares these complementary methods to laser UTEM techniques [3,4], for electron microscope users to consider when trying to expand their research capabilities. An update on UEM applications supported by recently developed techniques and extraordinary electron beam characteristics [7] as well as implementation perspectives will also be provided.

References:

- [1] Technavio. (2020). Transmission Electron Microscope Market by Applications, End-user, and Geography – Forecast and Analysis 2020-2024, Infiniti Research Limited.
- [2] A. H. Zewail, *Annu Rev Phys Chem.* **57** (2006), p. 65. <https://doi.org/10.1146/annurev.physchem.57.032905.104748>
- [3] C. Jing, et al., *Ultramicroscopy* **207** (2019), p. 112829. <https://doi.org/10.1016/j.ultramicro.2019>.
- [4] X. Fu, et al., *Sci. Adv.* **6** (2020), eabc3456. <https://doi.org/10.1126/sciadv.abc3456>
- [5] A. Arbouet, et al., in "Advances in Imaging and Electron Physics," ed. P. W. Hawkes (Academic Press, New York) p. 1.
- [6] D. Flannigan and A. Zewail, *Acc Chem Res* **45** (2012), p. 1828. <https://doi.org/10.1021/ar3001684>
- [7] S. Reisbeck, et al., *Ultramicroscopy* **235** (2022), 113497.

8:00 AM *CH02.07.01

Origin of 2DEG Modulation at LaAlO₃/SrTiO₃ Interface Revealed by In-situ TEM Biasing Sang Ho Oh; Korea Institute of Energy Technology, Korea (the Republic of)

Since its discovery the two-dimensional electron gas (2DEG) forming at LaAlO₃/SrTiO₃ (LAO/STO) interface has attracted a lot of research interests of oxide community. Many groups have demonstrated the successful incorporation of 2DEG into field effect transistors or diodes where the field-induced charge modulation is central to the device operation. Although the device technology has been advanced rapidly, the fundamental understanding of the field-induced charge modulation of 2DEG is not fully understood. Here we show comprehensive in-situ analysis of LAO/STO system under electrical stimulus in TEM. Our in-situ inline electron holography successfully visualized the field-induced charge density modulation of 2DEG by the electric field applied normal to the LAO/STO interface. While in-situ electron energy loss spectroscopy (EELS) confirmed no measurable oxygen vacancy migration, atom-resolved STEM-HAADF imaging revealed the polar distortion of B-site atoms in both LAO and STO, which induces the ionic polarization gradient across the interface in the range of -18.6 $\mu\text{C}/\text{cm}^2$ to 18.7 $\mu\text{C}/\text{cm}^2$ depending on applied voltages. The field-induced polar distortion adds additional charges at the interface with amount depending on the difference between LAO and STO. Our in-situ TEM study, as opposed to the previously suggested mechanism based on oxygen vacancy migration, demonstrates that the evolution of polar distortion of LAO under field electric field is key to the charge modulation at LAO/STO interface.

8:30 AM CH02.07.02

Mapping Thermal Signals with STEM EBIC William Hubbard¹, Matthew Mecklenburg² and B. C. Regan^{2,1}; ¹NanoElectronic Imaging, Inc., United States; ²University of California, Los Angeles, United States

Contrast in the transmission electron microscope (TEM) is primarily sensitive to physical and chemical properties that are sometimes of only secondary interest compared to electronic and thermal signals, especially when studying electronic devices. Recent advances in scanning TEM electron beam-induced current (STEM EBIC) imaging have enabled mapping of electronic properties in live devices, including resistance, with high spatial resolution. Here we discuss an additional STEM EBIC capability: mapping temperature in live devices. We acquire STEM EBIC images on Si-based samples patterned with electrodes and small MEMS heaters that produce a micro-scale temperature gradient. As an independent calibration, we also measure temperature on samples by performing plasmon energy expansion thermometry (PEET) on aluminum fiducials. We observe a strong, repeatable temperature dependence for both EBIC modes, with the "standard" EBIC mode having a larger temperature response than secondary electron emission EBIC (SEEBIC). The thermal response was similar for all electrode materials tested, and temperature maps can be generated with just a few minutes of acquisition time followed by relatively simple image calculation.

8:45 AM CH02.07.03

Investigation of Atomic Structure Changes on Resistive Switching Oxide Thin Film (Memristor) Applying In Situ I-V/TEM Deok-Hwang Kwon; Korea Institute of Science and Technology, Korea (the Republic of)

Combining the power of atomic structure imaging in transmission electron microscope (TEM) and current-voltage (I-V) measurement, in-situ I-V/TEM becomes a powerful tool to characterize the nanoscale of materials while applying voltage simultaneously. Particularly in electronic materials, its significant effectiveness was successfully demonstrated over decades. For example, one of the candidates suggested as the next electronic device for neuromorphic computing, the resistive switching phenomenon (also referred to as Memristor) has been highly investigated. With significant interest in a Neuromorphic computing device, massive research has been conducted on its mechanism and applications.

While the resistive switching phenomenon, which is a straightforward thing, occurs when an external potential is applied to a thin film oxide sandwiched between the top and bottom electrodes, its mechanism has remained controversial due to the lacking of direct evidence. A mobile defect such as oxygen vacancy has been frequently inferred to be the reason provoking the phenomenon; however, their physical form and distribution remained elusive. To resolve this issue, I employed in-situ I-V/TEM and directly investigated the switching mechanism in oxide materials. Various oxide thin films were studied as model systems, such as TiO₂, SrTiO₃, and SrFeO₃. Since in-situ I-V/TEM enables the operation of electronic devices in TEM while measuring atomic structure changes simultaneously, the switching area was directly probed and visualized. Chemical analysis employing electron energy-loss spectroscopy was carried out, confirming oxidation state changes of transition metals. High-resolution TEM imaging and chemical information reveal the atomistic mechanism of resistive switching. Also, thermodynamic modeling is established. The deep insight found from these results sheds light on pathways to Memristor and Neuromorphic computing.

9:00 AM CH02.07.04

Cryogenic 4D-STEM of the Charge Density Wave Transition in TaS₂ with In Situ Electric Biasing James L. Hart¹, Saif Siddique¹, Noah Schnitzer¹, Lena F. Kourkoutis^{1,1} and Judy Cha^{1,2,2}; ¹Cornell University, United States; ²Yale University, United States

The layered van der Waals solid TaS₂ exhibits a number of charge density wave (CDW) states. Of particular interest is the commensurate (C) to nearly commensurate (NC) CDW phase transition, which is associated with a strong metal-to-insulator transition ($T_c \sim 150$ K). The transition can be driven by electrical pulses, and is promising for two-terminal electronic devices, e.g., for neuromorphic computing. Nevertheless, our understanding of how the C to NC transition evolves in real-space and in nanoscale (thickness) confinements is limited, both as a function of temperature, and more interestingly, as a function of applied electric field. Here, we approach these questions using cryogenic 4D-STEM (scanning transmission electron microscopy) with *in situ* electrical biasing. We use the HennyZ sample holder, which allows for variable temperature analysis from $\sim 100 - 1000$ K, and has two electrodes for device biasing. With *in situ* STEM temperature sweeps, we observe resistance versus temperature behavior consistent with conventional TaS₂ devices reported in literature, clearly showing the CDW transitions. At base temperature (~ 110 K) in STEM, we use sub-microsecond electrical pulses to drive the C to NC phase transition, and observe electrical switching data consistent with *ex situ* devices. To visualize the transition in real-space, we use scanning nano-beam diffraction, wherein the C to NC phase transition is manifested by a $\sim 2^\circ$ rotation of the CDW wave vector. This work marks a step towards the goal of operating electrical devices within the (S)TEM and directly correlating real-space sample structure with device performance at variable cryogenic temperatures.

9:15 AM CH02.07.05

Atomic Structure of Organic-Metallic MXenes Revealed by Cryo-STEM and EELS Francisco J. Lagunas Vargas¹, Chenkun Zhou², Dmitri V.

Talpin² and Robert F. Klie¹; ¹University of Illinois Chicago, United States; ²The University of Chicago, United States

MXenes ($M_{n+1}X_nT_x$ with $n=1,2$) are a large family of two-dimensional transition metal carbides and nitrides [1]. What distinguishes MXenes from other 2D materials is that they can be functionalized with a variety of T_x surface groups. In 2020, Kamysbayev *et al.* demonstrated that these surface groups can drastically alter the MXenes' properties [2]. For example, they demonstrated a surface group dependent superconducting behavior in Nb_2CT_x . In this contribution we will continue to explore the range of possible surface group terminations by studying a new family of MXenes functionalized with organic surface groups. These metallic-organic hybrid MXenes open the door to the rich and complex space of organic chemistry and combine the structural and electron properties of metallic material. Our analysis will focus on developing an atomic-scale understanding of structure-property relationships in these novel materials.

This study will be conducted using atomic-resolution scanning transmission electron microscopy (STEM), electron energy loss spectroscopy (EELS) and x-ray energy dispersive spectroscopy (XEDS). Using these tools in tandem we will gain insights into the local chemical composition and bonding environment with high spatial resolution.

The focus of our study will be to examine Ti_3C_2 terminated with hydrocarbon chains and aromatic benzene rings. Since organic material is well known to decompose at the electron dosages required for high resolution studies, we will utilize in-situ cooling to liquid nitrogen temperatures to stabilize the organic material. Our analysis will show that cooling sufficiently preserves the organic material so that the unique π and σ bonding for the different amines can be observed in C K-edge spectra. Additionally, we will demonstrate that atomic resolution images of the material can be acquired while preserving the delicate structure of hybrid MXenes. Our in-situ cooling study will also show dynamic processes that occur in hybrid MXenes as the result of interactions with the electron beam. We will show that highly localized defects can be introduced using the electron probe and that the defects lead to a dynamic reorganization of the MXenes layers. [3]

References

[1] Gogotsi, Yury, and Babak Anasori. "The rise of MXenes." (2019): 8491-8494.

[2] Kamysbayev, Vladislav, et al. "Covalent surface modifications and superconductivity of two-dimensional metal carbide MXenes." *Science* 369.6506 (2020): 979-983.

[3] This project is supported by a supported by the National Science Foundation (DMR-1831406) and made use of instruments in the Electron Microscopy Service at the UIC Research Resources Center. The acquisition of UIC JEOL JEM ARM200CF is supported by an MRI-R² grant from the National Science Foundation (Grant No. DMR-0959470) and the upgraded Gatan Continuum spectrometer was supported by a grant from the NSF (DMR-1626065).

9:30 AM CH02.07.06

Conformal Three-Dimensional Interphase of Li Metal Anode Revealed by Low-Dose Cryo-Electron Microscopy Bing Han¹ and Y. Shirley Meng²;

¹University of California San Diego, United States; ²The University of Chicago, United States

Using cryogenic transmission electron microscopy, we revealed three-dimensional (3D) structural details of the electrochemically plated lithium (Li) flakes and their solid electrolyte interphase (SEI). As the SEI skin layer is largely composed of nanocrystalline LiF and Li₂O in amorphous polymeric matrix, when complete Li stripping occurs, the compromised SEI 3D framework buckles and wrinkles. The flexibility and resilience of the SEI skin layer plays a vital role in preserving an intact SEI 3D framework after Li stripping. The intact SEI network enables the nucleation and growth of newly plated Li inside the previously formed SEI network in subsequent cycles, preventing additional large amounts of SEI formation. In addition, cells cycled under the accurately controlled uniaxial pressure can further enhance the repeated utilization of the SEI and improve the Coulombic efficiency (CE) by up to 97%, demonstrating an effective strategy for reducing the formation of additional SEI and inactive "dead" Li.

9:45 AM BREAK

10:15 AM CH02.07.07

Direct Observation of All Atomic Sites in Zeolite by a Novel Low-Dose STEM Technique—Optimum Bright-Field Imaging Kousuke Ooe^{1,2}, Takehito Seki^{2,3}, Kaname Yoshida¹, Yuji Kohno⁴, Yuichi Ikuhara^{1,2} and Naoya Shibata^{1,2}; ¹Japan Fine Ceramics Center, Japan; ²The University of Tokyo, Japan; ³JST PRESTO, Japan; ⁴JEOL Ltd., Japan

Scanning transmission electron microscopy (STEM) enables us to directly observe atomic structures inside materials, which is powerful in unveiling their structure-property relationships. However, one of the most challenging problems in recent years of (S)TEM research is the atomic-resolution imaging of beam-sensitive materials, which have a low resistance to electron irradiation, such as battery materials, porous materials, and organic materials. The conventional STEM techniques such as annular dark-field and annular bright-field (ABF) imaging modes can robustly visualize atomic structures of electron-resistant materials using single annular detectors. For the beam-sensitive materials, however, there is room to improve the dose efficiency to minimize the irradiation damage because these imaging techniques use only a fraction of transmitted electrons for imaging. Recently, a high-speed segmented detector has been developed, which can record almost all the transmitted electrons by multiple detection channels [1]. Herein, we developed optimum bright-field (OBF) STEM using a segmented detector as a more dose-efficient imaging technique [2]. In the OBF method, a STEM image with the highest signal-to-noise ratio for a given detector is reconstructed via Fourier filters designed based on the phase contrast transfer function and the noise-evaluation theory [3]. OBF STEM has approximately two orders of magnitude higher dose efficiency than ABF STEM, and thus, OBF is promising for low-dose observation. Furthermore, by approximating this filtering process, OBF images can be reconstructed in real-time and displayed in sync with the probe scans as well as the conventional STEM imaging. The real-time display function enables operators to tune aberrations and field-of-view even under the low-dose condition. In this research, we applied the OBF STEM technique to the atomic-resolution imaging of zeolites, which are well-known beam-sensitive materials. The low-dose OBF observation successfully visualized all atomic sites, including even oxygen sites, inside the zeolitic framework. Furthermore, we also observed the twin defects in a zeolite and determined its atomic structure directly in combination with the first-principles calculations.

[1] N. Shibata *et al.*, *Journal of Electron Microscopy* **59** (2010) 473-479.

[2] K. Ooe *et al.*, *Ultramicroscopy* **220** (2021) 113133.

[3] T. Seki *et al.*, *Ultramicroscopy* **193** (2018) 118-125.

[4] The authors acknowledge funding from JSPS KAKENHI (Grant Number JP20H05659).

10:30 AM CH02.07.08

Reversible Intercalation of Mg²⁺ in V₂O₅ at Elevated Temperatures Leads to Enhanced Electrochemical Performances Yingjie Yang and Robert F. Klie; University of Illinois at Chicago, United States

Barriers to lithium ion battery development, such as the limited energy density of Li-ion batteries and the scarcity of Li, have led to great interest in exploring multi-valent ionic batteries containing earth abundant intercalation elements, such as magnesium or calcium. Reversible intercalation of Mg²⁺ ions is a crucial part in constructing a stable battery, which, when combined with high capacity, charts a promising pathway towards high performance and

future designs of Mg-ion batteries. High levels of reversible Mg^{2+} intercalation have been reported in α - V_2O_5 by cycling assembled cells at an elevated temperature of 110°C, the benefit of which is retained at room temperature.

Experiments were carried out with assembled cells consisted of pressed V_2O_5 powders as the cathode, ionic liquid $MgTFSI_2$ -PY14TFSI as the electrolyte, and activated carbon cloths or Mg foil as the anode. After cycling at room temperature and 110°C, the samples were characterized structurally with electron microscopy and X-ray absorption spectroscopy. The ex-situ experiments demonstrate that α - V_2O_5 can intercalate at least one mole of Mg^{2+} reversibly at 110°C, as opposed to <0.6 mole at 25°C. The capacity of the α - V_2O_5 is increased 20-fold, from 16 mAh g^{-1} at 25°C to 295 mAh g^{-1} at 110°C, matching the performance of Li-ion batteries. This increase in electrochemical performance is accompanied by structural changes; the morphology of the α - V_2O_5 powders drastically change from platelets to delaminated layers. Particles with delaminated morphologies show the change in Mg content, which echoes with the change in capacity, calculated to be 1 mol Mg^{2+} per mole α - V_2O_5 . These findings pave the road toward reversible Mg-ion batteries with high degrees of Mg^{2+} intercalation and high potential, and current efforts in developing in-situ characterization functionalities will lead to imperative capabilities.

Current research is ongoing to explore in-situ characterization techniques with scanning transmission electron microscope, combined with capabilities of simultaneous heating and electrochemical cycling. If realized, this can open up more possibilities to deepen the understanding of structural and chemical developments during the intercalation process.

10:45 AM CH02.07.09

Dynamic Evolution of All-Solid-State Li-ion Battery Based on LAGP Solid Electrolyte Using *In Situ* Electrochemical TEM Sorina Cretu^{1,2}, Nicolas Folastre^{1,3,4}, David Traodec⁵, Rainer Straubinger⁶, Nynke Krans⁶, Martial Duchamp² and Arnaud Demortiere^{1,3,4}; ¹Laboratoire de Reactivite et Chimie des Solides, France; ²Nanyang Technological University, Singapore; ³RS2E-French Research Network on Electrochemical Energy Storage, France; ⁴ALISTORE- European Research Institute, France; ⁵IEMN, France; ⁶Protochips, United States

The increasing request for electric vehicles (EV) demands high energy density batteries, wide temperature compatibility and improved safety technology. Solid-state Li-ion batteries (SSB)¹ could represent a possible future solution for current battery technology as the liquid electrolyte containing flammable organic materials is replaced by a solid electrolyte (SE) removing the safety concerns. Moreover, SSB technology offers the possibility to use high voltage cathode materials as some SE present wide electrochemical window and also opens the possibility to use lithium metal as anode resulting in batteries with a higher energy density².

SSB performances improved over the last years, but there are still challenges as interfaces, grain boundaries formation, generation of cracks and dendrites during the cycling which needs to be solved in order to make them a sustainable future battery technology²⁻⁴. To get a better insight into the limiting parameters of SSB performances comprehensive information about the dynamic process occurring at the interfaces between the solid electrolyte and the electrodes during the electrochemical reaction at nanoscale are essential, thus *in-situ* experiments are being required. *in situ* Transmission Electron Microscopy (TEM)^{5,6} represents the perfect tool for understanding the failure mechanism in ASSB as it allows us to visualize the interfaces, will enable us to follow the structural changes using electron diffraction and 4D-STEM as well as the chemical changes using EDX and EELS mapping.

During this study, SSB containing $Li_{1.5}Al_{0.5}Ge_{1.5}(PO_4)_3$ (LAGP) oxide solid electrolyte due to their high stability in the air, $LiFePO_4$ (LFP) as positive electrode and $Li_3V_2(PO_4)_3$ (LVP) as negative electrode allowing us to obtain a full inorganic solid-state battery in one single shot using Spark Plasma Sintering (SPS)⁷.

In situ TEM experiment carried out using our microbattery obtained by Focused Ion Beam (FIB) and connected on Protochips chip revealed the simultaneous process of LAGP particle size reduction with the formation of grain boundaries areas between the solid electrolyte grains during the cycling. 4D-STEM analysis performed before and after the *in-situ* TEM cycling experiment revealed the presence of amorphous regions in the SE and electrode mixture after the cycling process suggesting that the grain boundary phase formed after the cycling process is amorphous. The presence of $FePO_4$ (FP) phase structure analyzed by 4D-STEM mapping is consistent with delithiation process occurred over the electrochemical cycling. The phase mapping also revealed a domino-cascade lithiation process with a clear phase separated between LFP and FP grains. Moreover, the presence of Al-rich areas was spotted in the LAGP in the initial state and those areas represented the weak point in the SE as they were the initial point for crack propagation in the battery. STEM-EDX map analysis was performed before and after the cycling process displayed the unexpected presence of carbon in the pristine SE which possibly increased the electronic conductivity and contributed to the crack propagation. EDX map revealed that oxygen signal from the near vicinity of the solid electrolyte/ positive electrode was also diminished after the electrochemical reaction, most likely reacting with the carbon and leading to the formation of $LiCO_3$ producing possible irreversible changes at the interface solid electrolyte/positive electrode.

1. Janek, J. & Zeier, W. G. *Nature Energy* **1**, 1–4 (2016).
2. Hatzell, K. B. *et al. ACS Energy Letters* **5**, 922–934 (2020).
3. Lewis, J. A., Tippens, J., Cortes, F. J. Q. & McDowell, M. T. **1**, 845–857 (2019).
4. Zhao, W., Yi, J., He, P. & Zhou, H. **2**, 574–605 (2019).
5. Fawey, M. H. *et al. Journal of Power Sources* **466**, 228283 (2020).
6. Meng, Y. *et al. Electrochemical Society Interface* 49–53 (2011).
7. Aboulaich, A. *et al. Advanced Energy Materials* **1**, 179–183 (2011).

11:00 AM CH02.07.10

ETEM Study for Monitoring Oxidation Reaction in $LiFePO_4$ Cathode Materials Arnaud Demortiere; Université de Picardie Jules Verne, France

$LiFePO_4$ is turning out to be one of the best candidates for Li-ion battery cathode materials due to its high retention in cycling, a structural stability of the $FePO_4$ phase and containing no-cobalt [1]. Recent developments show the possibility of significantly increasing power densities with morphology and size modifications. However, the $LiFePO_4$ nanoparticles [2] show significant amounts of structural defects according to the synthetic route used. For instance, the presence of Fe atoms in Li crystallographic sites has a significant effect on electrochemical behavior leading to a decreasing in cation diffusion. $LiFePO_4$ also has a high reactivity to O_2 at moderate temperatures (300-500°C depending on the size) leading to the gradual diffusion of Fe from the core to the surface of the material accompanied by the formation of Fe_2O_3 nanoparticles [2]. Therefore, the composition material $Li_xFe_yPO_4$ exhibits very high degree of crystalline defects. These transformations were evidenced by X-ray diffraction and electron diffraction at different temperatures [3]. These olivine compounds outside stoichiometry have an order of defects leading to the formation of a superstructure.

To get a better insight into the mechanisms related to these transformations, *in situ* investigation in a real-time is necessary. Environmental ETEM, in which a pressurized O_2 can be injected, coupled with a heating holder is a perfect characterization platform to monitor oxidation reactivity of $LiFePO_4$ up to 700°C. This project focuses on the study of the structural mechanisms associated with the temperature reactivity of $LiFePO_4$ under an oxidizing atmosphere using environmental TEM (TITAN). The aim is to quantify the kinetics of Fe_xO_y nanoparticle formation, and the appearance of superstructures induced by Fe diffusion from the core to the surface of the material.

After an optimization step of the experimental conditions inside the ETEM, ideal conditions of reaction have been found. For a temperature of 620°C

(DENSolution heating holder), we have started to observe the formation of Fe_xO_x nanoparticle at the surface of LiFePO_4 crystals in a pressure of O_2 (12 mbar). In the figure 1b, the HAADF-STEM image shows clearly Fe_xO_x nanoparticles with a bright contrast and mainly localized at the surface. The figure 1c exhibits the chips used for the heating experiments. ADF images allow to distinguish the LiFePO_4 crystals and the nanoparticle, which can be formed along the surface or with in an elongated way perpendicular to surface. The growth kinetics of these nanoparticles has been quantified from real-time observations. Chemical investigations by EELS spectroscopy using O-K ELNES reveal the strong modification of oxygen valence from LiFePO_4 to Fe_xO_x , as shown in the figure 1d. The high resolution TEM analyses of nanoparticles confirm the presence of $\gamma\text{-Fe}_2\text{O}_3$ structure. The interfaces between LiFePO_4 and Fe_xO_x have been characterized and help us to identify preferential pathway of diffusion during the Fe extrusion process. Finally, 4D-STEM investigation [5] was made to identify each structural phases based on electron diffraction pattern spatially resolved, which is present in the LFP crystals after oxidation reaction.

References: [1] Gibot, P. et al. *Nature Mater.*, 2008, 7, 741-747. [2] Karakulina, O et al. *Nano letters*, 18(10), 6286-6291. [3] Hamelet, S. et al. *J. Mater. Chem.*, 2009, 19, 3979-3991. [4] Hamelet, S. et al. *Chem. Mater.*, 2011, 23, 32-38. [5] Ophus, C. *Microscopy and Microanalysis*, 25(3), 563-582.

11:15 AM CH02.07.11

Nanoscale Multimodal Analysis of Organic Compounds in Beam-Sensitive Nanoparticles by Monochromated STEM-EELS Maeva Chaupard^{1,2}, Ruxandra Gref² and Marta de Frutos¹; ¹Laboratoire de Physique des Solides, France; ²Institut des Sciences Moléculaires d'Orsay, France

Nanomaterials are of great interest for improving existing technologies or engineering new ones. The unique properties of these emergent structures are widely studied in various fields, such as optics, electronics and medicine. As their properties depend on their sizes, local structures and chemical compositions, each nanomaterial requires deep analysis to unravel its specific behaviour. However, most of the used techniques cannot provide information on such nanosystems at the single-particle level.¹ This has led to a strong interest in electron microscopy, which can image the morphology and crystal structure of specimens with atomic resolution. Low-dose cryo-Transmission Electron Microscopy (cryo-TEM) is now commonly employed to study beam-sensitive materials such as organic and hybrid organic-inorganic materials.² In addition to imaging, the latest generation Scanning Transmission Electron Microscopes (STEM) equipped with Electron Energy Loss Spectroscopy (EELS) allow a deep characterisation of specimens down to the atomic scale.³ Thanks to the recent development of monochromated electron sources, spectral resolutions can now reach below 10 meV, allowing access from the far-IR to the X-ray range.⁴

Nevertheless, the analysis of sensitive specimens remains a major challenge for spectromicroscopy. Although recent studies based on vibrational EELS have demonstrated the possibility of damage-free analysis,^{5,6} most of them exhibited no or limited spatial resolution. Here, we report damage-free analysis of organic-inorganic nanoparticles at the nanoscale. It was achieved via EELS experiments using a monochromated STEM equipped with a cryo-holder and a direct electron detector (DED) in low-dose conditions (down to $10 \text{ e}^-/\text{Å}^2$). First, the beam-induced damage was studied in the UV and soft X-ray spectral energy ranges. The DED provides simultaneous acquisition of low-loss and core-loss signals, in order to study the beam-induced chemical reactions. Secondly, the vibrational energy range was explored in the aloe and transmitted modes with a 7 meV spectral resolution. Finally, chemical maps were obtained in the three energy ranges. Here, we demonstrate that STEM-EELS provides damage-free analysis that enables efficient identification of the organic compound distributions across sensitive specimens. Our work opens new possibilities for analysing organic compounds such as polymers and biomolecules.

1. Chaupard, M., de Frutos, M. & Gref, R. Deciphering the Structure and Chemical Composition of Drug Nanocarriers: From Bulk Approaches to Individual Nanoparticle Characterization. *Particle & Particle Systems Characterization* **38**, 2100022 (2021).
2. Danino, D. Cryo-TEM of soft molecular assemblies. *Current Opinion in Colloid & Interface Science* **17**, 316–329 (2012).
3. Egerton, R. F. *Electron Energy-Loss Spectroscopy in the Electron Microscope*. (Springer Science & Business Media, 2011).
4. Li, X. et al. Three-dimensional vectorial imaging of surface phonon polaritons. *Science* **371**, 1364–1367 (2021).
5. Rez, P. et al. Damage-free vibrational spectroscopy of biological materials in the electron microscope. *Nat Commun* **7**, 10945 (2016).
6. Collins, S. M. et al. Functional Group Mapping by Electron Beam Vibrational Spectroscopy from Nanoscale Volumes. *Nano Lett.* **20**, 1272–1279 (2020).

11:30 AM CH02.07.12

Direct Observation of Formation and Decomposition Processes of Sessile Dislocation by In Situ STEM Mechanical Testing Minjian Cao¹, Eita Tochigi¹, Naoya Shibata^{1,2} and Yuichi Ikuhara^{1,2}; ¹The University of Tokyo, Japan; ²Japan Fine Ceramics Center, Japan

The mechanical behaviors of crystalline materials are highly influenced by dislocation glide, known as one of the elementary processes of plastic deformation. In the plastic deformation of FCC metals, sessile dislocation is formed by the reaction between dislocations on different slip planes. Since sessile dislocation is very difficult to glide and has a unique dislocation core structure, it is important to elucidate the atomic behavior associated with the pinning mechanism of sessile dislocation. In-situ transmission electron microscope (TEM) mechanical testing is promising to observe nanoscale dynamics in materials directly. However, conventional in-situ mechanical testing has difficulty for atomic-resolution observations, because of the lack of precise and stable mechanical loading systems. In recent years, micro-electro-mechanical systems (MEMS) technology has been improved and precise loading functions can be assembled within a small chip with a few millimeters square sizes [1].

Here, we combined a MEMS loading device with scanning TEM (STEM) and observed the formation and decomposition processes of sessile dislocation in Au at the atomic level. A thin section cut from an Au substrate was fixed on the actuators of the MEMS device by focused ion beam with controlling its crystal orientation to be observed from [1-10] zone axis. The sample was further thinned, and a sharp notch was introduced to its edge part for enhancing stress concentration. Upon loading the sample stepwise, it was observed that two stacking faults on (111) and (1-1) planes extended from the sample edge and joined at an angle of about 70.5 degrees. This deformation phenomenon corresponds to the surface nucleation and glide of $1/6[11-2]$ and $1/6[112]$ Shockley partial dislocations, and their reaction to form $1/3[110]$ stair-rod type sessile dislocation. With further loading, the $1/3[110]$ stair-rod type sessile dislocation was decomposed into $1/6[11-2]$ and $1/6[112]$ Shockley partial dislocations, and the $1/6[11-2]$ Shockley partial dislocation proceeded into the interior of the sample. The present result shows that the $1/3[110]$ stair-rod type sessile dislocation does not always act as a pinning point under incremental loading conditions. Details will be discussed in the presentation.

[1] T. Sato, et al., *Microel. Eng.*, **164**, 43–47 (2016).

11:45 AM CH02.07.13

Integrating EIS with In Situ TEM in Ceramic Nanofiber Characterization Waynah Lou Dacayan¹, Christodoulos Chatzichristodoulou¹, Zhongtao Ma¹, Wenjing Zhang², Kristian S. Mølhave³ and Søren B. Simonsen¹; ¹DTU Energy, Denmark; ²DTU Sustain, Denmark; ³DTU Nanolab, Denmark

In this work, electrochemical impedance spectroscopy (EIS) was integrated with in situ transmission electron microscopy (TEM) to allow simultaneous electrochemical and structural characterization of functional materials. This is particularly critical in energy conversion technologies where the interdependence of structure and electrochemical properties of the components significantly affect its functionality, consequently governing the overall process efficiency. Presented herein is the application of the EIS-TEM method in the characterization of electrospun nanofiber of $\text{Ce}_{0.9}\text{Gd}_{0.1}\text{O}_{1.95-8}$ (CGO), a

popular material for solid oxide fuel/electrolysis cells (SOCs).

The CGO nanofiber was prepared by combining sol-gel synthesis and electrospinning. With the aid of a micromanipulator inside a scanning electron microscope (SEM), a single nanofiber was separated from the electrospun nanofiber sheet and was transferred to a heating and biasing MEMS chip. With a MEMS chip-based holder, 2-probe EIS measurements were conducted in parallel with TEM characterization inside an environmental TEM (ETEM) at different temperatures from 28°C to 600°C in 2.5 mbar pO_2 gas. EELS spectra were acquired in the same conditions to follow the possible change in the chemical state of the CGO nanofiber.

The CGO nanofiber was found to have a relatively low activation energy (E_a), close to the value associated with small polaron hopping in pure and doped ceria which is particularly observed when exposed to reducing conditions. The EELS analysis, however, shows that the average Ce oxidation state is close to Ce^{4+} at all temperatures, confirming that no beam-induced Ce^{4+}/Ce^{3+} reduction happened in the material. Possibly, the low E_a may be associated with the small grain size of the CGO nanofiber, i.e. ca. 10nm. The EELS results also show that by keeping the beam exposure low, no beam damage occurs on the nanomaterial and that reliable EIS measurements in combination with TEM analysis can be done.

SESSION CH02.08: Magnetic Imaging
Session Chairs: Robert Klie and Andrew Lupini
Wednesday Afternoon, November 30, 2022
Hynes, Level 1, Room 101

1:30 PM *CH02.08.01

Magnetic-Field-Free Atomic-Resolution Scanning Transmission Electron Microscopy [Naoya Shibata](#)^{1,2}; ¹The University of Tokyo, Japan; ²Japan Fine Ceramics Center, Japan

Aberration-corrected scanning transmission electron microscopy (STEM) is a powerful technique to directly observe atomic-scale structures and chemistry of individual defects, such as interfaces, inside materials and devices. However, since high magnetic fields (~2T) are always exerted on samples inside the magnetic objective lens, atomic-resolution observation of magnetic materials has been essentially very difficult. In recent years, we have developed a magnetic objective lens system that realizes a magnetic field free environment at the sample position. Using this objective lens system combined with the state-of-the-art higher order aberration corrector, direct atom-resolved imaging in a magnetic field free environment has been achieved. The details of this magnetic-field-free STEM, currently ongoing developments and material application results will be presented.

2:00 PM CH02.08.03

Atomic-Plane Resolved Magnetic and Chemical Imaging by Chromatic-Aberration Corrected Electron Magnetic Circular Dichroism and Electron Energy Loss Spectroscopy [Xiaoyan Zhong](#)^{1,2,3}; ¹City University of Hong Kong, Hong Kong; ²City University of Hong Kong Shenzhen Futian Research Institute, China; ³City University of Hong Kong Shenzhen Research Institute, China

Electron magnetic circular dichroism (EMCD), experimentally verified by Schattschneider et al. [1] in a transmission electron microscope (TEM) is a method of magnetic spectroscopy as analogous to X-ray magnetic circular dichroism (XMCD). In principle EMCD can offer higher spatial resolution and greater depth sensitivity due to the short de Broglie wavelength and penetration of high-energy electrons compared to XMCD. Under convergent beam illumination with a probe size of 1.8 nm in a scanning TEM, we acquired the EMCD spectra of individual antiphase boundary with a rock salt structure interlayer in inverse spinel $NiFe_2O_4$. [2] However, the larger convergent angle leads to the better spatial resolution and the poorer signal-to-noise ratio (SNR) of EMCD spectra.

We developed the method of atomic-planed resolved (APR) EELS imaging via the ground-breaking combination of spatially resolved electron energy loss spectroscopy (SR EELS) technique [3] and chromatic/spherical aberration (C_c/C_s) correction [4-6] under parallel illumination mode. With the combined approach mentioned above, the delocalization of both elastically and inelastically scattered electrons has been reduced effectively, which allows us to acquire chemical information with atomic plane resolution. In the example of $SrTiO_3$, we obtained electron energy loss (EEL) spectra of Ti $L_{3,2}$ edges from the individual atomic planes by using APR EELS.

Furthermore, we developed the method of atomic-planed resolved (APR) EMCD imaging by combining EMCD and APR EELS with the aid of C_c/C_s correction [7]. In the example of Sr_2FeMoO_6 , we achieved EMCD spectra and quantitative orbital to spin magnetic moment ratio atomic plane by atomic plane. Combining with advanced capability of structural and chemical imaging by using aberration-corrected transmission electron microscopy, all the information including magnetic polarization, atomic configurations and chemical states can be simultaneously accessed from the very same sample region at the atomic scale.

References:

- [1] P. Schattschneider, et al. Nature 441, 486 (2006).
- [2] Z. Li, et al. Advanced Functional Materials 31 (21), 2008306 (2021).
- [3] L. Reimer, et al. Ultramicroscopy 46, 335 (1992).
- [4] K.W. Urban, et al. Physical Review Letters 110, 185507 (2013).
- [5] M. Haider et al. Nature 392, 768 (1998).
- [6] B. Kabius et al. Journal of Electron Microscopy 58, 147-155 (2009).
- [7] Z. C. Wang, et al. Nature Materials 17, 221-225 (2018).

Acknowledgement: Thanks to Z. Li, B. Lin, F.-R. Chen at City University of Hong Kong, G.-H. Huang, H. B. Jiang, Z. C. Wang, R. Yu and J. Zhu at Tsinghua University, L. Jin, A. Tavabi, M. Luysberg, J. Mayer and R. D. Borkowski at Forschungszentrum Jülich, J. Ruzs, V. Kocovski and D. Tyutyunnikov at Uppsala University, Y. Moritomo, H. Yanagihara and E. Kita at University of Tsukuba, H. J. Xiang and J. L. Lu at Fudan University for their contributions. This work was financially supported by National Natural Science Foundation of China (52171014, 52011530124), Science, Technology and Innovation Commission of Shenzhen Municipality (HZQB-KCZYB-2020031, SGDX20210823104200001, JCYJ20210324134402007), the Sino-German Mobility Programme by the Sino-German Center for Research Promotion (M-0265), Science and Technology Department of Sichuan Province (2021YFSY0016), the Research Grants Council of Hong Kong Special Administrative Region, China (E-CityU101/20, G-CityU102/20, CityU 11302121), the European Research Council (856538, “3D MAGiC”), CityU Strategic Interdisciplinary Research Grant (2020SIRG037), the City University of Hong Kong (9610484, 9680291, 9360162, 9610558) and the City University of Hong Kong Shenzhen Research Institute. This work made use of the resources of

the Ernst Ruska-Centre for Microscopy and Spectroscopy with Electrons in Forschungszentrum Jülich, the National Center for Electron Microscopy in Beijing and TRACE TEM center at the City University of Hong Kong.

3:15 PM CH02.08.04

Measuring the Mean Inner Potential of Bernal Graphite Using Off-Axis Electron Holography [Avi Auslender](#)^{1,1}, George Levi¹, Vladimir Ezersky², Oswaldo Diéguez^{1,1} and Amit Kohn¹; ¹Tel Aviv University, Israel; ²Ben-Gurion University of the Negev, Israel

The mean-inner-potential (MIP) of a crystal is the average electrostatic Coulomb potential within a crystal with respect to vacuum. The MIP is a fundamental material property which reflects chemical-bonding and crystallographic surfaces.

We conducted off-axis electron holography experiments on highly-oriented-pyrolytic-graphite (HOPG) in a transmission-electron-microscope to measure the MIP from nanometer-scale volumes of Bernal graphite oriented with respect to the electron beam, along the principal axis or directions in the basal plane. These MIP were related to mean orbital electron radii and diamagnetic susceptibilities in perpendicular planes. Such intrinsic property measurements are challenging because of defect-induced interfaces at basal planes. Indeed, our structural examination of HOPG show stacking faults and planar rotations around the principal-axis, such that measuring intrinsic properties requires probing a volume of $\sim 10^2 \times 10^2 \times 10^2$ nm³.

Experiments on individual Bernal graphite crystals with (0001) basal, or (1-100), (2-1-10) prismatic planes, resulted in MIP of 10.16±0.40 V, 11.37±0.35 V, 12.66±0.41 V, respectively. First-principles calculations from crystalline slabs confirm these anisotropic measurements with 11.72 V, 13.65 V, 14.56 V, respectively. Additionally, these experiments enabled to measure the mean free path for inelastic scattering in graphite of 197keV electrons at a collection angle of 18mrad resulting in 150.6±2.0 nm.

These measured MIP enable to determine projected mean radii of electron orbitals and volume susceptibilities (SI), assuming spherically symmetric charge distribution, at 0.704±0.015Å, (-1.99±0.08)×10⁻⁵; 0.744±0.015Å, (-2.23±0.07)×10⁻⁵; 0.785±0.015Å, (-2.48±0.08)×10⁻⁵.

The measured orbital radii and diamagnetism in the basal plane are comparable to expected values for carbon s-bond hybridization. Increased MIP on prismatic planes is related to s-orbital components, which decrease due to delocalized electrons between basal planes.

2:30 PM BREAK

3:30 PM CH02.08.05

Detection of Graded Magnetic Interface in Iron Oxide Core/Shell Nanoparticles via Electron Magnetic Chiral Dichroism [Daniel del Pozo Bueno](#)^{1,2}, Maria Varela³, Alberto López-Ortega^{4,4}, Alejandro G. Roca⁵, Marta Estrader^{2,2}, Josep Nogués⁵, Francesca Peiró^{1,2} and Sònia Estradé^{1,2}; ¹University of Barcelona, Spain; ²Universitat de Barcelona, Spain; ³Universidad Complutense de Madrid, Spain; ⁴Universidad de Castilla-La Mancha, Spain; ⁵Catalan Institute of Nanoscience and Nanotechnology, Spain

The Electron Magnetic Chiral Dichroism (EMCD) technique has undergone a significant innovation with the improvement in the spatial and energy resolution of advanced electron microscopes in combination with the advancement of data processing methods, providing a wide range of opportunities to carry out magnetic studies at the nanoscale. This technique is analog to the X-ray Magnetic Circular Dichroism (XMCD), offering a better spatial resolution. It was first postulated by C. Hébert et al.¹ in 2003, and experimentally proved it by P. Schattschneider et al.² three years later. It is based on Electron Energy Loss Spectroscopy (EELS), and it identifies the dichroic signals arising from magnetic materials as a difference in intensity in the transition metal white lines (L₃ and L₂) EEL spectra obtained from two symmetric positions of the spectrometer aperture, and the sample oriented in specific conditions.

In this work, we use this technique to investigate the local magnetization of FeO/Fe₃O₄ nanocubes with an antiferromagnetic/ferrimagnetic core and shell respectively, which are of great interest due to their appealing magnetic characteristics and prospective uses. The interface structure in these types of core/shell nanoparticles is crucial for adjusting their characteristics, hence in this study we make use of the EELS spectra obtained by the EMCD technique to characterize the composition while studying the local magnetization.

Since only the shell exhibits a ferrimagnetic behavior, during the experiments, which were conducted at low temperatures with two beams configuration, it was required to explore the dichroic signal from the core and shell regions independently. EEL spectra were acquired for this purpose with a spatial resolution of 0.25 nm and an energy resolution of 0.25 eV. The spectra were then classified using clustering techniques^{3,4}, particularly the k-means algorithm, with each spectrum being identified by its energy loss near edge structure.

As a result, the EMCD measurements along with the EELS analysis (i.e., clustering methods and compositional analysis) have demonstrated that these nanoparticles are composed by four distinct zones, each with a unique magnetic moment, forming an onion-like structure that is concentric. With the magnetic moment being greatest at the surface and decreasing toward the core, and these magnetic zones are spatially correlate with the oxidation and composition gradient⁵. The results demonstrate that the combination of EELS compositional mapping with EMCD can yield incredibly valuable information about the internal magnetic structure and its correlation to the nanostructure of magnetic nanoparticles. Finally, it is important to emphasize the benefits of clustering algorithms in this work for efficiently and accurately analyze the large amount of acquired spectra in the EMCD technique.

Acknowledgements

This work has been supported by the Spanish Ministerio de Economía y Competitividad through the project MAT2016-79455-P, Spanish Research Network RED2018-102609-T, 2017-SGR-292 project from the Generalitat de Catalunya. ICN2 is funded by the CERCA Programme/Generalitat de Catalunya and supported by the Severo Ochoa Centres of Excellence programme, funded by the Spanish Research Agency (AEI, grant no. SEV-2017-0706). Electron microscopy observation was carried out at the Centro Nacional de Microscopia Electrónica- ELECMI sponsored by MICINN MAT2015-66888-C3-3-R and RTI2018-097895-B43.

References

- (1) Hébert; Schattschneider. *Ultramicroscopy* **2003**, *96* (3–4), 463–468.
- (2) Schattschneider; Rubino; Hébert; Ruzs; Kuneš; Novák; Carlino; Fabrizioli; Panaccione; Rossi. *Nature* **2006**, *441* (7092), 486–488.
- (3) Torruella; Estrader; López-Ortega; Baró; Varela; Peiró; Estradé. *Ultramicroscopy* **2018**, *185*, 42–48.
- (4) Blanco-Portals; Peiró; Estradé. *Microscopy and Microanalysis* **2022**, *28* (1), 109–122.
- (5) Del-Pozo-Bueno; Varela; Estrader; López-Ortega; Roca; Nogués; Peiró; Estradé. *Nano Lett* **2021**, *21* (16), 6923–6930.

4:00 PM CH02.09.01

Extremely Noisy 4D-STEM Strain Mapping Using Cycle Consistent Spatial Transforming Autoencoders [Shuyu Qin](#)^{1,2}, Xiyue Zhang³, Chuqiao Shi⁴, Jules Muhizi⁵, Yichen Guo¹, Xinqiao Zhang², Ni Wan⁶, Aditi Krishnapriyan⁷, Michael Mahoney⁷, Yimo Han⁴, Nhan Tran⁸, Colin Ophus⁹, David A. Muller³ and Joshua Agar²; ¹Lehigh University, United States; ²Drexel University, United States; ³Cornell University, United States; ⁴Rice University, United States; ⁵Harvard University, United States; ⁶Washington University in St. Louis, United States; ⁷University of California, Berkeley, United States; ⁸fermilab, United States; ⁹Lawrence Berkeley National Laboratory, United States

Atomic-scale imaging of 2D and quantum materials benefits from precisely extracting crystallographic strain, shear, and rotation to understand their mechanical, optical and electronic properties. One powerful technique is 4D-STEM (4-dimensional scanning transmission electron microscopy), where a convergent electron beam is scanned across a sample while measuring the resulting diffraction pattern with a direct electron detector. Extracting the crystallographic strain, shear, and rotation from this data relies either on correlation strain measurement method (e.g., implemented in py4DSTEM) or determining the center of mass (CoM) of the diffraction peaks. These algorithms have limitations. They require manual preprocessing and hyperparameter tuning, are sensitive to signal-to-noise, and generally are difficult to automate. There is no one-size-fits-all algorithm.

Recently, machine learning techniques have been used to assist in analyzing 4D-STEM data, however, these models do not possess the capacity to learn the strain, rotation, or translation instead they just learn an approximation that almost always tends to be correct as long as the test examples are within the training dataset distribution.

We developed a novel neural network structure – Cycle Consistent Spatial Transforming Autoencoder (CC-ST-AE). This model takes a set of diffraction images and trains a sparse autoencoder to classify an observed diffraction pattern to a dictionary of learned “averaged” diffraction patterns. Secondly, it learns the affine transformation matrix parameters that minimizes the reconstruction error between the dictionary and the input diffraction pattern. Since the affine transformation includes translation, strain, shear, and rotation, we can parsimoniously learn the strain tensor. To ensure the model is physics conforming, we train the model cycle consistently, by ensuring the inverse affine transformation from the dictionary results in the original diffraction pattern.

We validated this model on a number of benchmark tasks including: A Simulated 4D TEM data of WS₂ and WSe₂ lateral heterostructures (noise free) with a ground truth of the strain, rotation and shear parameters. Secondly, we test this model experimental 4D STEM on 2D-heterostructures of tungsten disulfide (WS₂) and tungsten diselenide (WSe₂).

This model shows several significant improvements including: 1. When tested on simulated data, the model can recover the ground truth with minimal error. 2. The model can learn the rotation and strain on noisy diffraction patterns where CoM failed, and outperforms correlation strain measurement method. 3. Our model can accommodate large and continuous rotations difficult to obtain with other methods. 4. Our model is more robust to noisy data. 5. Our model can map the strain, shear and rotation; identify dislocation and ripples; and distinguish background and sample area automatically.

Ultimately, this work demonstrates how embedding physical concepts into unsupervised neural networks can simplify, automate, and accelerate analysis pipelines while simultaneously leveraging stochastic averaging that improves robustness on noisy data. This algorithmic concept can be extended to include other physical phenomena (e.g., polarization, sample tilt), can be used in automated experiments, and can be applied to other applications in materials characterization.

4:15 PM CH02.09.02

Automated Deep Learning Analysis of Large Sets of High-Resolution Transmission Electron Microscopic Data [Nina Gumbiowski](#)¹, [Kateryna Loza](#)¹, [Marc Heggen](#)² and [Matthias Epple](#)¹; ¹University of Duisburg-Essen, Germany; ²Forschungszentrum Jülich GmbH, Germany

High-resolution transmission electron microscopy (HRTEM) is a valuable technique in materials research, especially for nanoscopic materials like metallic nanoparticles. For these materials size, shape and structure determine their biological, chemical and physical properties and subsequently their possible applications. HRTEM can image the size, shape and structure of these nanoparticles both *ex-situ* and *in-situ* (e.g. during annealing experiments). Large quantities of data can be generated by HRTEM with sub-second time resolution. However, the manual analysis of large sets of HRTEM images is tedious and time-consuming and almost not feasible for large sets of *in-situ* data. Here we present a program based on deep-learning techniques such as semantic segmentation and image classification by convolutional neural networks (CNN).

First a semantic segmentation CNN was trained on labelled HRTEM images of metallic nanoparticles to separate the particles from the background. This network was used to allow the extraction of particle shape-related parameters like circularity, equivalence diameter, and Feret diameter. The program needs only a few seconds to analyse a single HRTEM image to yield all the shape-related parameters of interest. The trained CNN can also be used for transfer learning for *in-situ* datasets that contain more background noise. This enables the generation of time-resolved shape-related data of experiments with hundreds or thousands of individual images. Apart from the shape-related information, HRTEM images can also give information about the internal crystallinity of the nanoparticles. To gain crystallographic information, a classification CNN was trained to classify single particles with respect to the crystallographic nature of individual particles (e.g. single-crystalline, polycrystalline).

Such an automated HRTEM image analysis not only speeds up the evaluation of single HRTEM images but it enables to fully use the capabilities of HRTEM on *in-situ* experimental datasets. Furthermore, it reduces fluctuations in the analysis due to a possible operator bias in manual evaluation. This can give more insight into nanoparticle structures and facilitate more in-depth nanoparticle analysis.

4:30 PM CH02.09.03

Convolutional Neural Networks for Anomaly Detection in Scanning Transmission Electron Microscopy [Enea Prifti](#), [Robert F. Klie](#) and [James Buban](#); University of Illinois at Chicago, United States

Identifying point defects and other structural anomalies using scanning transmission electron microscopy (STEM) is important to understand a material's properties caused by the disruption of the regular pattern of a crystal. Thanks to the high spatial resolution of aberration-corrected transmission electron microscopes, atomic-resolution images with a field of view of several hundred nanometers can be taken. Such data, which often contains thousands of atomic columns need to be analyzed. This process has been done manually in the past, but recent developments in machine learning (ML) can be very useful to speed it up. In this contribution, we will utilize a convolutional variational autoencoder (VAE) which, after being trained with a set of bulk samples, generates an example (prediction) of given input images based on the trained features. We will demonstrate that the performance of a VAE in replicating an input image can be used to differentiate between bulk or defects. In the case of a bulk input, the VAE can replicate well the input within a threshold value that can be set by testing the predictions. For a defect input, the VAE will fail to output a prediction within the set threshold, allowing for a clear and automatic distinction of defects.

4:45 PM CH02.09.04

Multi Clustering Detection of 4D-STEM Diffraction Patterns Using NMF Approach [Junhao Cao](#)^{1,2}, [Nicolas Folastre](#)², [Nicolopoulos Stavros](#)³, [Partha Pratim Das](#)³ and [Arnaud Demortiere](#)²; ¹Laboratoire de Réactivité et Chimie des Solides (LRCS), France; ²Centre National de la Recherche Scientifique, France; ³NanoMEGAS, Belgium

Scientific instruments extracting information from materials have recently been improved using devices enable to generate a huge amount of data. The convergence of different techniques, such as direct electron detectors, image processing algorithms, precession technique and high coherent electron beam, leads to the emergence of a new family of hyperspectral analyze called 4D-STEM in which a 4D stack of diffraction patterns are acquired from a scanning region. The result of the 4D mapping extraction provides crucial information about material properties with a high spatial resolution, including signatures of the local structure, orientation, deformation, electromagnetic fields, and other sample-dependent properties.

A single 4D-STEM map can consist of 40k electron diffraction patterns. As a result, scientists need to automatically process datasets using intelligent algorithms and follow a statistical approach. Pattern matching strategy has been used to process 4D-STEM using ACOM software, which is based on the evaluation of a cross-correlation coefficient between experimental pattern and well-known crystallographic structure.

On the other hand, machine learning (ML) has been used in many fields with its strong powerful ability to process datasets such as classification, regression, or clustering. Unsupervised learning is a significant subset of its system, in which the aim is to automatically detect the distribution and the relationship in the huge of unlabeled data in order to discover the similar type of groups in the dataset. Based on the deep application of Machine Learning (ML), the result of material characterization or clustering in the huge dataset has been obtained automatically and clearly by some unsupervised algorithms.

The 4D-STEM acquisition was made using a Tecnai FEI 200kV, equipped with a Gatan Oneview camera operating at 50 frames per second with a scan step size of 2 nm. The large dataset has been acquired with 10,000 diffraction patterns. In our team, we developed in Python an unsupervised method called non-negative matrix factorization (NMF) to discover the grain mapping clustering in the 4D-STEM dataset. Given a 4D-STEM dataset, we firstly transform its 4D form into a 2D array as a consequence of adopting the input request of NMF; secondly, the new dataset corresponds to each clustering generated by the result of matrix decomposition using NMF. Finally, the grain mapping clustering yielded from each new clustering dataset.

Simultaneously, the best number of cluster points chosen depended upon the result of the mean-loss graph after the procedure of Matrix Decomposition with the help of NMF, the different clustering results in different components had been discussed. The influence of different denoising processes was studied on the convergence of NMF components and the accuracy of clustering mapping.

5:00 PM CH02.09.05

Semi-Supervised Machine Learning Workflow for Analysis of Nanostructured Morphologies from Transmission Electron Microscopy Images Shizhao Lu¹, Brian Montz², Todd Emrick² and Arthi Jayaraman^{1,1}; ¹University of Delaware, United States; ²University of Massachusetts Amherst, United States

In the field of materials science, microscopy is the first and often only accessible method for structural characterization. There is a growing interest in the development of machine learning methods that can automate the analysis and interpretation of microscopy images. Typically training of machine learning models require large numbers of images with associated structural labels, however, manual labeling of images requires domain knowledge and is prone to human error and subjectivity. To overcome these limitations, we present a semi-supervised transfer learning approach that uses a small number of labeled microscopy images for training and performs as effectively as methods trained on significantly larger data sets. Specifically, we train an image encoder with unlabeled images using self-supervised learning methods and use that encoder for transfer learning of different downstream image tasks (classification and segmentation) with a minimal number of labeled images for training. We test the transfer learning ability of two self-supervised learning methods: SimCLR and Barlow-Twins on transmission electron microscopy (TEM) domain images. We demonstrate how this machine learning workflow facilitates fast analysis of TEM images of materials containing nanowires, specifically classification of nanowire morphologies (e.g., single nanowires, nanowire bundles, phase separated) as well as segmentation tasks that can serve as groundwork for quantification of nanowire domain sizes and shape analysis. The applicability of the machine learning workflow is further extended to classification of nanoparticle morphologies and identification of different type of viruses from TEM images.

SESSION CH02.10/EQ08.08: Joint Session: Frontiers of Imaging and Spectroscopy in Transmission Electron Microscopy

Session Chairs: Michele Conroy and Quentin Ramasse

Thursday Morning, December 1, 2022

Hynes, Level 1, Room 101

8:00 AM *CH02.10/EQ08.08.01

Uncovering Magnetic Structures with Scanning Transmission Electron Microscopy Juan C. Idrobo; University of Washington, United States

Understanding the variables that controls the size, switching, and pinning of magnetic domain and structures spans the fields of fundamental physics, materials science, as well as storage and logic device technologies. Here, I will discuss our efforts in using scanning transmission electron microscopy (STEM), within differential phase contrast (DPC) imaging and electron energy-loss spectroscopy (EELS), to detect and measure magnetic phases of materials with atomic, and near atomic, spatial resolution. I will discuss the limits of the aforementioned techniques to resolve contributions from spin and orbit to magnetism, and how topological and chiral phases of matter could be investigated in the near future with an electron microscope.

This research was supported by the Center for Nanophase Materials Sciences, which is a DOE Office of Science User Facility. This research used resources of the National Energy Research Scientific Computing Center, which is supported by the Office of Science of the U.S. Department of Energy under Contract No. DE-AC05-00OR22725 with the DOE, and sponsored by the Laboratory Directed Research and Development Program of Oak Ridge National Laboratory, managed by UT-Battelle, LLC, for the U.S. Department of Energy.

8:30 AM CH02.10/EQ08.08.02

Deep Learning Facilitated Analysis of Defects and Alloying in 2D Magnetic Materials Mads A. Weile¹, Julian Klein², Thang Pham², Rami Dana², Xavier Roy³, Daniel Chica³ and Frances M. Ross²; ¹Technical University of Denmark, Denmark; ²Massachusetts Institute of Technology, United States; ³Columbia University, United States

The advent of two-dimensional (2D) magnets [1] enables a myriad of opportunities in nano-spintronics and memory devices. A key requisite for creating nanoscale magneto-electric devices is atomic-level engineering in which materials and stacks are designed with specific properties in mind. An emerging material that is promising for atomic-level control is the magnetic semiconductor CrSBr. [2] Utilizing CrSBr requires understanding the magneto-electric [3] and magneto-optical [4] properties of the defects, involving structural characterization of individual defects by microscopy. Studies on defects are, however, often limited by the fact that few-layer samples are not stable under imaging conditions, resulting in more defects or low signal-to-noise ratio

(SNR) images [2]. Recently, the emergence of machine learning (ML) in the microscopy field has opened opportunities for faster and more accurate analysis than conventional methods in SNR-dominated systems [5]. Merging ML with high-resolution microscopy techniques like scanning transmission electron microscopy (STEM) and scanning tunneling microscopy (STM) provides means to discover new key insights even in materials only a few layers thick.

Here we study defects and dopants in CrSBr and its alloy $\text{CrSBr}_x\text{Cl}_{1-x}$ using a combination of high-resolution microscopy (HAADF-STEM and STM) and advanced ML techniques. We investigate the quantity, type and distribution of defects with the motivation to understand their structural, electronic and magnetic properties. We apply machine learning in the form of convolutional neural networks to analyze alloys and defects and discuss its applicability to multilayer systems. Overall, we conclude that CrSBr and related compounds are interesting material platforms for applying high resolution microscopy techniques in combination with ML to study their defect properties. We expect that understanding how defects affect the structure of CrSBr and related compounds will lead to new insight into the possibilities of engineering tailor-made magneto-electric and magneto-optical devices. Furthermore, we expect that the ML models for investigating such defects can serve as a foundation for finding defects in a variety of similar materials in this challenging setting.

[1] Huang, B. et al. *Nature* **546**, 270–273 (2017)

[2] Klein, J. et al. *arXiv:2170.00037 to appear in Nature Comm.* (2021)

[3] Telford, E. et al. *Nature Mater.* (2022)

[4] Klein, J. et al. *to be submitted* (2022)

[5] Lee, C., et al. *Nano Lett.* **20**, 3369 (2020)

8:45 AM CH02.10/EQ08.08.03

Prediction of Electronic Density of States at Ground State from ELNES/XANES Izumi Takahara, Poyen Chen, Kiyou Shibata and Teruyasu Mizoguchi; The University of Tokyo, Japan

Energy-loss near-edge structure (ELNES) and X-ray absorption near-edge structure (XANES) are powerful tools for characterizing the local atomic and electronic structures of materials. ELNES/XANES is produced by the electronic transition from a core orbital to conduction bands, and thus it basically provides the information reflecting the partial density of states (PDOS) of the conduction band at the excited state of a given material. Although ELNES/XANES gives us valuable information such as chemical bonding and the charge state of a specific atom, the knowledge that can be extracted from the measurements is limited to the information reflecting the conduction band at the excited state. If the information reflecting the entire PDOS at the ground state can also be extracted from ELNES/XANES, materials properties based on PDOS can be evaluated directly from a single spectral measurement and materials developments would be accelerated.

In this presentation, we introduce a novel machine learning (ML) based method for determining the PDOS of valence and conduction band at the ground state from the ELNES/XANES spectra simultaneously. We have carried out density functional theory (DFT) calculations on various structures of Si and prepared a database of Si-K ELNES/XANES and the corresponding PDOS at the ground state. On this database, we have trained a ML model to predict the entire PDOS spectra at the ground state from the ELNES/XANES spectra directly. In the result, our model successfully reproduced the characteristics of the PDOS spectra near the Fermi level. Therefore, we envision the utilization of the ML could be powerful for widening the application of the ELNES/XANES measurements including simultaneous mapping of structure and property in a transmission electron microscope.

9:00 AM *CH02.10/EQ08.08.04

Direct Imaging of Topological Phase Transitions in Polar Skyrmions, Merons and Anti-Merons in Oxide Heterostructures Yu-Tsun Shao¹, Sergei Prokhorenko², Yousra Nahas², Sujit Das³, Zijian Hong⁴, Ruijuan Xu⁵, Swathi Chandrika¹, Fernando Gómez-Ortiz⁶, Pablo García-Fernández⁶, Long-Qing Chen⁷, Harold Y. Hwang⁵, Javier Junquera⁶, Lane W. Martin⁸, Laurent Bellaïche², Ramamoorthy Ramesh⁸ and David A. Muller¹; ¹Cornell University, United States; ²University of Arkansas, Fayetteville, United States; ³Indian Institute of Science, Bangalore, India; ⁴Zhejiang University, China; ⁵Stanford University, United States; ⁶Universidad de Cantabria, Spain; ⁷The Pennsylvania State University, United States; ⁸University of California, Berkeley, United States

Emergent topological textures such as polar vortices and skyrmions in ferroelectric heterostructures have drawn great interest due to the richness of underlying physics and the potential applications in next generation nanodevices. Although concepts like topological protection and phase transitions as a function of temperature, strain, electric field and superlattice periodicity have been already explored in polar topological defects (vortices), the counterparts for polar topological solitons (skyrmions and merons) remain in its infancy. To understand and explore the microscopic details of these transitions requires a characterization method which can track the detailed 3D structure of individual dipole textures. By combining the full four-dimensional phase space information collected by a new generation of direct electron detectors which quantitatively records the momentum distribution of transmitted electrons at every beam position (4D-STEM), dynamical diffraction simulations, and ptychographic phase retrieval algorithm to process the data, we have been able to robustly image the local polarization and chirality in each polar texture.

Upon heating a lifted-off, freestanding $[(\text{PbTiO}_3)_{16}/(\text{SrTiO}_3)_{16}]_8$ superlattice membrane, we study the strain-driven emergence of tetragonal meron lattice from a disordered liquid-like skyrmion state, accompanied by a change in chirality. In the case of freestanding $(\text{SrTiO}_3)_{16}/(\text{PbTiO}_3)_{16}/(\text{SrTiO}_3)_{16}$ trilayer membranes, we explore the creation and annihilation of polar merons and anti-merons in self-assembling labyrinthine patterns when perturbed by the electric-field gradient generated from the focused electron probe. Theoretical insights into this highly degenerate, frustrated system suggest that the transition among various metastable states originates from the intrinsic topological instabilities.

Research supported by AFOSR Hybrid Materials MURI (FA9550-18-1-0480) and ARO ETHOS MURI (W911NF-21-2-0162), facilities support from the NSF (DMR-1429155, DMR-1719875). Researchers at the University of Arkansas also thank the Vannevar Bush Faculty Fellowship Grant No. N00014-20-1-2834 from the Department of Defense.

9:30 AM BREAK

10:00 AM CH02.10/EQ08.08.06

Prediction of Carbon K Edge Spectra of Organic Molecules Using a Graph Neural Network Kiyou Shibata and Teruyasu Mizoguchi; The University of Tokyo, Japan

Recently, in the context of materials informatics, there have been many attempts to replace expensive first-principles calculations with predictions based on low-cost machine learning (ML) models. Although databases of structures and electronic states of various materials are already being developed and play an important role in the study of ML models, it is necessary to expand not only the number of data in the databases but also their contents in order to construct ML models that represent a wide variety of physical properties.

Among various physical properties, we are focusing on the core-loss spectra, which are not only computationally available but also experimentally

measurable by transmission electron microscopy and synchrotron facilities. The core-loss spectra, which are excitation spectra from a core orbital to unoccupied orbitals, directly reflect partial electronic state densities (PDOS) of states excited state and indirectly contain information on ground-state PDOS, and thus on properties related to PDOS. In the context of these backgrounds, we have been performing first-principles calculations on the K-edge core-loss spectra of each independent carbon site in the organic molecules in the QM9 data set [1], which have carbon numbers of 8 or less. We have already reported that the molecular C-K edge spectra can be used to predict the molecular properties [2], and we have recently published these organic molecular C-K edge spectral database [3]. We expect that this database will be used as benchmarks for organic molecule spectral informatics or for the analysis of experimentally obtained spectra.

In this presentation, we present the results of developing a ML model using a graph neural network with the organic molecular structures and an excitation carbon site therein as input and the corresponding site C-K edge spectra as output. After training on the database, our ML model is generally successful in reproducing spectral outlines such as rough features and major peaks.

References

- [1] R. Ramakrishnan, P. Dral, M. Rupp, and O. A. Lilienfeld, *Sci Data* **1**, 140022 (2014).
- [2] K. Kikumasa S. Kiyohara K. Shibata, and T. Mizoguchi, *Adv. Intell. Syst.* **4**, 2100103 (2021).
- [3] K. Shibata, K. Kikumasa, S. Kiyohara, and T. Mizoguchi, *Sci. Data* **9**, 214 (2022).

SESSION CH02.11: Virtual Session: Frontiers of Imaging and Spectroscopy in Transmission Electron Microscopy
Session Chairs: Ali Husain and Quentin Ramasse
Tuesday Morning, December 6, 2022
CH02-virtual

8:00 AM *CH02.11.01

4D-EELS—A Comprehensive Character Technique for the Study of Local Properties Peng Gao; Peking University, China

Phonon plays a fundamental role in mechanical, electrical, optical, and thermal properties of materials. The description of phonons is known as phonon dispersion, i.e., the phonon energy is plotted as a function of the momentum. For practical materials that inevitably contain interface/defect that discontinues the chemical bonds, new phonon modes emerge locally. Although the interface/defect phonon modes are widely discussed in theory, the experimental measurement has been challenging as it requires the combined spatial, momentum and spectral resolutions to probe localized phonon mode at interfaces/defects. Recently, we propose a four-dimensional electron energy loss spectroscopy technique based on the scanning transmission electron microscopy- electron energy loss spectroscopy. By scanning the electron beam in real space of sample while monitoring both the energy loss and the momentum transfer, we are able to reveal position- and momentum- dependent lattice vibrations at nanometer scale with high efficiency. The space, momentum and energy resolutions can be delicately balanced by carefully adjusting experimental parameters, and thus widely tuned to optimize the data acquisitions for specific samples under study.

In this report, we firstly show the principle of 4D-EELS. Then we show some application examples, including the interface phonon dispersion relation for an epitaxial cubic Boron Nitride/Diamond heterointerface [1], and the local phonon dispersion and defect scattering in Boron Nitride Nanotube [2]. We also reveal the interface phonons in AlN on Si and Al [3] and dislocation phonons at Si/Ge interface [4], and discuss how they possibly affect the local interface thermal conductivity. Finally, we prospect 4D-EELS will provide comprehensive information of sample beyond position- and momentum-simultaneously resolved phonon spectra, such as Electron Magnetic Circular Dichroism [5] and so on.

References:

- [1] R. Qi et al., *Measuring Phonon Dispersion at an Interface*, *Nature* **599**, 399 (2021).
- [2] R. Qi et al., *Four-Dimensional Vibrational Spectroscopy for Nanoscale Mapping of Phonon Dispersion in BN Nanotubes*, *Nat. Commun.* **12**, 1179 (2021).
- [3] Y.-H. Li et al., *Atomic-Scale Probing of Heterointerface Phonon Bridges in Nitride Semiconductor*, *Proc. Natl. Acad. Sci.* **119**, e2117027119 (2022).
- [4] Y. Li, B. Han, R. Shi, R. Qi, X. Hao, N. Li, J. Du, J. Chen, and P. Gao, *Atomic-Scale Measurement of Localized Dislocation Phonons at Si/Ge Interface*, arXiv:2206.02329 (2022).
- [5] Y. Li, M. Wu, R. Shi, and P. Gao, *A Slot Aperture Enabled High Efficient and Accurate EMCD from a Single Acquisition of Momentum Resolved EELS*, *Microsc. Microanal.* **26**, 2632 (2020).

8:30 AM *CH02.11.02

Optimal Structural Determination with Focused Probe Electron Ptychography Timothy J. Pennycook, Chuang Gao, Christoph Hofer, Daen Jannis, Armand Béch e and Jo Verbeeck; University of Antwerp, Belgium

Over the past decade advances in camera technology have greatly facilitated 4D scanning transmission electron microscopy (STEM) and electron ptychography. A wealth of information on the probe position dependence of the scattering can be discerned from 4D STEM data, which electron ptychography uses to provide an especially useful means of directly imaging atomic structures. In essence ptychography solves the so called phase problem in electron microscopy, determining the relative phases of the scattered beams. As the phase of the beam electrons is altered by even the weakest of specimen potentials, efficient detection of phase provides a very efficient form of imaging. The dose efficiency of ptychography far exceeds that of Z-contrast annular dark field (ADF), now a mainstay for local atomic structure determination in materials science [1]. However ptychography can also significantly exceed the dose efficiency of phase contrast imaging in plane wave illumination TEM [2], the mainstay technique for the most beam sensitive materials such as proteins. Such TEM based phase contrast provides intensity images rather than actual images of the phase. Furthermore TEM phase contrast images are often complex and difficult to interpret being the result of using the aberration function as a virtual phase plate, with the resulting contrast transfer function generally oscillating to positive and negative values. Ptychography provides a simple single signed transfer function controlled by the convergence angle without the need for aberrations, which would be detrimental to simultaneous ADF imaging.

In addition to pure dose efficiency ptychography also fills another important deficiency of ADF imaging. Light atoms are often hidden in the strong scattering from neighboring heavy elements in the ADF signal. Addressing this gave rise to the popularity of the annular bright field (ABF) modality. Recently centre of mass (CoM) based methods such as integrated CoM have become more popular as they provide superior dose efficiency compared to ABF. However the dose efficiency of ptychography exceeds all of these, and allows heavy and light elements to be seen most clearly. Similarly, the greater dose efficiency should allow more sensitive examination of charge density for looking at effects from bonding, for instance. The ability to correct for the residual aberrations post collection is also a clear advantage for ptychography compared to CoM methods, and is indeed very important for separating true

effects of charge density from those of aberrations.

Phase imaging with electron ptychography is however not entirely free from complications. It can be more difficult to discern different elements than with ADF Z-contrast. Furthermore, as sample thickness increases the projected potentials cause increasingly large changes in the phase of the scattered beams, which eventually wrap around because phase values exist only in the range of 0 to 2π . Thus complex contrast reversals can also occur in ptychography. However these can be simply compensated for by a small defocus. Ensuring that the structures reflect reality is greatly facilitated by simultaneous Z-contrast imaging, easily available with focused probe ptychography. Thus with focused probe ptychography one can have the best of both worlds, Z-contrast and highly efficient phase imaging. With event driven camera technology this can be performed without any loss of speed compared to conventional rapid scan STEM [3].

[1] T. J. Pennycook et al., *Ultramicroscopy* 151, 160-167 (2015)

[2] T. J. Pennycook et al., *Ultramicroscopy* 196, 131-135 (2019)

[3] D. Jannis et al., *Ultramicroscopy* 233, 113423 (2022).

[4] We acknowledge funding from European Research Council grant nos. 802123-HDEM and 823717-ESTEEM3, European Union's Horizon 2020 Research and Innovation Programme grant No. 101017720 and FWO projects G042920N and G042820N.

9:00 AM *CH02.11.03

Solving A Century-Old Problem—Three-Dimensional Atomic Structure of Amorphous Materials [Jianwei \(John\) Miao](#); University of California, Los Angeles, United States

Amorphous materials such as glass, rubber and plastics are ubiquitous in our daily life and have broad applications ranging from telecommunications to electronics. However, due to the lack of long-range order, the 3D atomic structure of amorphous materials had eluded direct experimental determination for more than a century. One experimental method that can in principle address this grand challenge is atomic electron tomography (AET). AET combines high-resolution tomographic tilt series with advanced computational algorithms to resolve the 3D atomic structure of materials without assuming crystallinity, which has been applied to image grain boundaries, anti-phase boundaries, stacking faults, dislocations, point defects, chemical order/disorder, atomic-scale ripples, bond distortion and strain tensors with unprecedented 3D detail. Recently, we advanced AET to determine the 3D atomic positions of monatomic amorphous materials, namely a Ta thin film and two Pd nanoparticles. We observed that pentagonal bipyramids are the most abundant atomic motifs in these amorphous materials. Instead of forming icosahedra, the majority of pentagonal bipyramids arrange into pentagonal bipyramid networks with medium-range order. Molecular dynamics simulations further reveal that pentagonal bipyramid networks are prevalent in monatomic metallic liquids, which rapidly grow in size and form more icosahedra during the quench from the liquid to the glass state. Furthermore, we also used AET to determine the 3D atomic positions of a multi-component metallic glass and quantitatively characterized the short- and medium-range order. We discovered that, although the 3D atomic packing of the short-range order is geometrically disordered, some short-range-order structures connect with each other to form crystal-like superclusters and give rise to medium-range order. We identified four types of crystal-like medium-range order - face-centred cubic, hexagonal close-packed, body-centred cubic and simple cubic - coexisting in the amorphous sample, showing translational but not orientational order. These observations provide direct experimental evidence to support the general framework of the efficient cluster packing model for metallic glasses. We expect that these results pave the way for the determination of the 3D atomic structure of a wide range of amorphous materials, which could transform our fundamental understanding of non-crystalline materials and related phenomena.

1. Y. Yang, J. Zhou, F. Zhu, Y. Yuan, D. Chang, D. S. Kim, M. Pham, A. Rana, X. Tian, Y. Yao, S. Osher, A. K. Schmid, L. Hu, P. Ercius and J. Miao. Determining the three-dimensional atomic structure of an amorphous solid. *Nature* 592, 60–64 (2021).

2. Y. Yuan, D.S. Kim, J. Zhou, D.J. Chang, F. Zhu, Y. Nagaoka, Y. Yang, M. Pham, S. J. Osher, O. Chen, P. Ercius, A. K. Schmid and J. Miao. Three-dimensional atomic packing in amorphous solids with liquid-like structure. *Nature Mater.* 21, 95–102 (2022).

9:30 AM CH02.11.04

Deterministic Creation and Annihilation of Point Defects in 2D Materials Utilizing Electron and Ion Beam Irradiation [Maksim A. Sultanov](#), Wei-Ying Chen, Yulin Lin, Yasuo Ito, Benjamin Diroll, Thomas Gage and Jianguo Wen; Argonne National Laboratory, United States

Deterministic creation of quantum emitters has long been a topic of study for quantum information science (QIS). It is also indispensable to develop techniques enabling deterministic annihilation of vacancy-center quantum emitters. In this work, we utilize irradiation modes of both e-beam and ion beam to introduce point defects in a monolayer of both MoSe₂ and h-BN. An aberration corrected transmission electron microscope (TEM) enables observations with time-resolved atomic-resolution imaging, including dynamic creation and annihilation of defect sites in the monolayer. In situ high-resolution TEM reveals that the annihilation of vacancy clusters using the electron beam can be achieved with an optimal electron beam dose rate. In-situ annealing of irradiated samples has been explored to understand the formation mechanism of desired quantum emitters. Coupled with ex-situ photoluminescence, these approaches allow us a detailed study of the deterministic quantum emitter creation and the correlation with their optical behaviors in 2D materials.

Work performed at the Center for Nanoscale Materials, a U.S. Department of Energy Office of Science User Facility, was supported by the U.S. DOE, Office of Basic Energy Sciences, under Contract No. DE-AC02-06CH11357. The correlation of point defects with optical behaviour is supported by QIS research funding from the U.S. Department of Energy, Office of Science User Facility. Ion irradiation was performed in IVEM-Tandem Facility at Argonne National Laboratory.

9:35 AM DISCUSSION TIME

SYMPOSIUM CH03

Advanced Characterizations of Heterogeneities in Electrochemical Energy Storage Materials
November 28 - December 7, 2022

Symposium Organizers
Peng Bai, Washington University in St. Louis
Donal Finegan, National Renewable Energy Laboratory
Hui Xiong, Boise State University
Yuan Yang, Columbia University

Symposium Support
Silver
Carl Zeiss Microscopy

* Invited Paper
+ Distinguished Invited

SESSION CH03.01: Lithium Metal Batteries
Session Chairs: Peng Bai and Hui Xiong
Monday Morning, November 28, 2022
Hynes, Level 1, Room 103

10:30 AM *CH03.01.01

***In Situ* Electrochemical Liquid Cell Electron Microscopy Study of Electrode-Electrolyte Interfaces** Haimei Zheng; Lawrence Berkeley National Laboratory, United States

The electrode-electrolyte interfaces often play an important role in electrochemical devices, such as batteries or fuel cells. An understanding of the electrode-electrolyte interfacial phenomena can be significant for understanding the device failure mechanisms and improving the device performance. Our development of electrochemical liquid cell transmission electron microscopy (TEM) has enabled direct observation of many dynamic phenomena at electrode-electrolyte interfaces in nanometer resolution and in real time. With the in-situ electrochemical liquid cell TEM setup, we have been made achievements on the studies of lithium dendrite growth, solid electrolyte interphase (SEI), the electrode configuration on alkali metal deposition, etc. We have also studied lithium stripping. As we know that an understanding of lithium stripping is as important as that of lithium plating to achieve significant advances in using lithium metal anodes for high-energy rechargeable batteries. However, there have been limited studies on lithium stripping compared to lithium plating. With in-situ electrochemical liquid cell TEM, we directly observed and compared the stripping behavior of the in-situ grown lithium dendrites and lithium nanograins on the electrodes. We found the sporadic lithium stripping behavior of lithium deposits regardless of their morphology. In addition, SEI chemical mapping with high spatial resolution showed a SEI loss at the end of the lithium metal stripping, illustrating the importance role of SEI in the subsequent cycles.

11:00 AM *CH03.01.02

Cryo and *In Situ* Electron Microscopy Diagnosis Guided Design of Materials for Rechargeable Battery Chongmin Wang; Pacific Northwest National Laboratory, United States

In Situ and operando electron microscopy enable direct observation of process under dynamic operating condition of a device, representatively such as: real time observation of structural and chemical evolution of rechargeable batteries under battery operating condition; finding the active sites of catalyst; monitoring of mass transport during oxidation and reduction; observing nucleation and growth process in a liquid; visualizing defect generation and interaction during deformation; and capturing the response of materials to external stimuluses. In this presentation, I will focus on recent progress on using ex-situ, in-situ, operando and cryo-scanning transmission electron microscopy for probing into the structural and chemical evolution of electrode materials for lithium ion batteries, representatively such as Li and Si anode. I will highlight several recent key observations, which even appear to be well documented, while essentially are poorly understood, therefore limiting the advances of both cathode and anode for better batteries. It would be expected that this presentation can stimulate new ideas as how to attack the bottlenecks for advancing electrode materials design for better batteries. In perspective, challenges and opportunities for developing in-situ electron microscopy for probing both functional and structural materials will also be discussed.

11:30 AM CH03.01.03

Theoretical Understanding of Heterogeneous Nucleation During Lithium Electrodeposition Aashutosh N. Mistry and Venkat Srinivasan; Argonne National Laboratory, United States

Lithium metal anodes are required to transform the present-day Li-ion batteries for storing more energy. A key challenge is to ensure uniform electrodeposition of lithium when the cell is being charged. While most previous studies examine the efficacy of various mechanisms in regularizing an uneven interface^{1,2,3}, the formation of the uneven interface is poorly understood. Whenever lithium deposits on a surface other than pristine lithium, nucleation is observed⁴. Physics-based understanding of this step is essential to identify the factors that govern nucleation and cause nonuniform growth. In this talk, we propose a theoretical description of lithium nucleation and growth during electrodeposition. We show that nucleation during electrodeposition differs from the metallurgical understanding of melt solidification. We correlate such theoretical understanding with experimental observations. We discuss material property targets to tune the nonuniformity associated with the nucleation and early time growth of electrodeposited lithium.

References:

1. Monroe & Newman (2005) *J. Electrochem. Soc.* 152(2) A396, doi: 10.1149/1.1850854
2. Bai, Brushett & Bazant (2016) *Energy Environ. Sci.* 9, 3221, doi: 10.1039/C6EE01674J
3. Barai, Higa & Srinivasan (2018) *J. Electrochem. Soc.* 165(11) A2654, doi: 10.1149/2.0651811jes
4. Pei et al. (2017) *ACS Nano* 17(2) 1132, doi: 10.1021/acs.nanolett.6b04755

11:45 AM CH03.01.04

Characterization and Modeling of High Rate Performance in High Specific Energy Li-Metal Batteries Shashank Sripad¹, Anthony D'Angelo², Xu

Yan³, Brennan Campbell³ and Alexander Bills¹; ¹Carnegie Mellon University, United States; ²24M Technologies, United States; ³Kitty Hawk, United States

One of the key bottlenecks in developing next-generation Li-metal batteries is simultaneously achieving high rate performance along with high specific energy (>400 Wh/kg). Rate performance and specific energy are crucial for enabling applications such as electric aircraft. This study demonstrates the performance of a Li-metal that cell leverages the use of an ultra-thick cathode (>3 times the thickness of conventional cathodes) which presents a path to low-cost manufacturing while coupling it with a Li-metal anode achieves high stack and cell-level specific energies. The discharge rate and discharge current density are characterized in the context of an electric vertical takeoff and landing aircraft. We use a combination of cell-level characterization with novel test protocols along with cell and interface modeling to examine the heterogeneities in current densities. We also develop pathways and approaches to improve the overall discharge rate at the cell level. The tools, methods, and modeling framework presented here will find utility in characterizing Li-metal batteries for high-rate and high-performance applications.

SESSION CH03.02: Multiphysics in Lithium Batteries

Session Chairs: Peng Bai and Aashutosh Mistry

Monday Afternoon, November 28, 2022

Hynes, Level 1, Room 103

1:30 PM *CH03.02.01

Learning Heterogeneous Reaction Kinetics from Images of Li-Ion Battery Nanoparticles Martin Bazant; Massachusetts Institute of Technology, United States

Nanoscale heterogeneity, which often controls the overall rate of electrochemical reactions, is notoriously difficult to measure or model. Here, we show that reaction kinetics and surface heterogeneity can be learned from operando scanning transmission X-ray microscopy (STXM) images of lithium iron phosphate (LFP) nanoparticles undergoing driven phase transformations in Li-ion batteries. Combining a large dataset of STXM images with a thermodynamically consistent electrochemical phase-field model, PDE-constrained optimization, and uncertainty quantification, we extract the LFP free energy and local reaction rate, and verify their consistency with theoretical models. We also simultaneously learn the spatial heterogeneity of the reaction rate, which we find closely matches the carbon-coating thickness profiles obtained through auger electron microscopy. The chemo-mechanical model is validated by ex-situ STXM and X-ray ptychography images. The 6.8% error between the learned model and over 180,000 pixels of image data is close to the experimental noise. Our results unlock the potential of learning nonequilibrium properties from image data that are difficult to measure in traditional electrochemical methods and offers a new non-destructive method of characterizing reactive surface heterogeneity.

2:00 PM CH03.02.02

Microscopic Operando Diagnosis of Li Plating During Full Cell Fast Charging Bingyuan Ma and Peng Bai; Washington University in St. Louis, United States

The fast-charging becomes crucial for electronic devices and electric vehicles (EVs). However, it can result in Lithium (Li) plating on the graphite anode that aggravates the cell degradation and increases the safety risk. In this work, we fabricate Li-ion full cells in transparent glass capillaries as the model system for the practical Li-ion sandwich cells to probe the dynamic evolution in graphite anodes during the fast-charging process and under low temperatures. We observed that Li plating can occur before the cell is fully charged even at a low C-rate and at room temperature. The onset of Li plating is always accompanied by some features in the full cell voltage signal. Our *operando* experiments provide the direct proof that the subtle features in the electrochemical responses are caused by the Li plating, which can be utilized to improve battery management strategy. Mathematical simulations confirm that the local overpotential due to the strong concentration polarization is the root cause of the axial reaction heterogeneity in lithiated graphite and the Li plating. At low temperatures, such polarization becomes stronger and leads to earlier Li plating during the fast charging.

2:15 PM CH03.02.03

Operando Three-Dimensional Mapping of the Two-Phase Reaction Inside Single Cathode Nanoparticles Yifei Sun; Cornell University, United States

The battery stability is related to nanoscale processes such as the structural evolution during the (de)intercalation. The two-phase reaction - one type of structural evolution - is generally considered a slow kinetic process. Yet many high-rate materials such as LiFePO₄ experience phase separation during (dis)charge. Thus, nanoscale characterization techniques are needed to understand the (de)lithiation mechanism and its interplay with local defects in phase-changing materials.

Disordered spinel LiNi_{0.5}Mn_{1.5}O₄ (LNMO) is a promising high-voltage cathode material that experiences an extended period of two-phase reaction when cycling. Operando Bragg coherent diffractive imaging (BCDI) is a powerful technique that maps nanoscale heterogeneity inside the materials. In this study, we measure consecutive diffraction patterns of a single LNMO nanocrystal operando. With the improved phase retrieval algorithm, we map the three-dimensional strain field of the nanocrystal while it undergoes a structural two-phase reaction. The strain mapping confirms two-phase behavior at the single grain level and reveals different mechanisms upon charge and discharge. With its unique ability to track buried single defects, BCDI also elucidates the critical role of local defects in relieving the coherency strain at the interphase during the phase transformation. This nanoscale understanding of reaction kinetics provides new insights into the development of next-generation durable batteries with faster kinetics.

2:30 PM CH03.02.04

Electrochemically Based and Coupled Characterization of Heterogeneity within Battery Electrodes and Interfaces Amy Marschilok^{1,2}; ¹Stony Brook University, United States; ²Brookhaven National Laboratory, United States

Batteries are ubiquitous in our everyday lives and often appear as black boxes. However, the chemistry inherent to their function is diverse and complicated. Examples of mechanistic insight gained from electrochemistry-based and electrochemistry-coupled characterization of battery electrodes and interfaces will be highlighted in this presentation. This will include approaches to distinguish productive and parasitic regions in functional energy storage materials and systems.

2:45 PM BREAK

SESSION CH03.03: Lithium Nucleation and Growth
Session Chairs: Peng Bai and Yan Yao
Monday Afternoon, November 28, 2022
Hynes, Level 1, Room 103

3:15 PM *CH03.03.01

Operando Analysis of Li Plating on Graphite Anodes During Fast Charging of Li-Ion Batteries Neil P. Dasgupta; University of Michigan, United States

The rapidly growing EV market is increasing the demand for fast-charging (<15 min) of high-energy-density Lithium (Li)-ion batteries. However, state-of-art Li-ion batteries with thick graphite electrodes suffer from Li plating when charged at >4C rates. Therefore, to inform mitigation strategies for Li plating under fast-charging conditions, there is a need to improve our fundamental understanding of the Li plating process.

In this work, I will present two recent studies on *operando* detection and characterization of Li plating on graphite anodes. In the first study, plan-view *operando* video microscopy was performed on >3 mAh cm⁻² graphite electrodes during 6C charging [1]. During a 6C charging half-cycle, the cell was used to visualize the spatial heterogeneity of SoC across the electrode surface, and the nucleation and growth of the plated Li. During the subsequent open circuit voltage (OCV) rest and discharge steps, the re-interaction of the plated Li into graphite was also studied. Furthermore, a 3D understanding of the changes across the electrode volume was developed by performing *ex situ* cross-sectional microscopy. Finally, pouch cells were fabricated to confirm the voltage signature associated with dead Li formation in a commercially relevant cell format.

In the second study, we built upon this understanding to demonstrate a new method for *operando* detection of Li plating during fast charging, using incremental capacity (IC) analysis [2]. To identify the electrochemical signature of plating, 3-electrode pouch cells were assembled, allowing for a correlation of the IC curve with the onset of Li nucleation. This was validated using post mortem microscopy, to demonstrate the ability to uniquely identify the onset of Li plating with high resolution. This provides a pathway towards advanced control and mitigation strategies to enable fast charging while eliminating the most deleterious side reactions within the cell.

[1] Y. Chen, K.-H. Chen, A. J. Sanchez, E. Kazyak, V. Goel, Y. Gorlin, J. Christensen, K. Thornton, N. P. Dasgupta, *J. Mater. Chem. A* **9**, 23522 (2021).

[2] Y. Chen, L. Torres-Castro, K.-H. Chen, D. Penley, J. Lamb, N. P. Dasgupta, *J. Power Sources* **539**, 231601 (2022).

3:45 PM CH03.03.02

Suppressing Chemical Corrosions of Lithium Metal Anodes Bingyu Lu¹, Wei-Kang Li¹, Diyi Cheng¹, Bhargav Bhamwala¹, Miguel Ceja¹, Wuriguluma Bao¹, Chengcheng Fang² and Y. Shirley Meng³; ¹University of California, San Diego, United States; ²Michigan State University, United States; ³The University of Chicago, United States

The lithium (Li) metal anode is essential for next generation high energy density rechargeable Li metal batteries. Although extensive studies have been performed to prolong the cycle life of Li metal batteries, the calendar life, which associates with chemical corrosion of Li metal in liquid electrolytes, has not been quantitatively understood. Here, by combing the Titration Gas Chromatography (TGC) method and Cryogenic Focused Ion Beam (Cryo-FIB), we established a quantitative relationship between the chemical corrosion rate and electrochemically deposited Li morphology in various liquid electrolyte systems. We identified that the corrosion rate is dominated by the porosity of the deposited Li. The larger the porosity of deposited Li has, the faster the corrosion rate will be. We further proposed strategies to mitigate the chemical corrosion on Li thus to extend the calendar life of Li metal batteries. By strictly controlling the stacking pressure during Li plating, Li deposits with ultra-low porosity can be achieved, suppressing the corrosion rate to $0.08 \pm 0.16\%$ /day compared with $1.71 \pm 0.19\%$ /day of the high-porosity Li.

4:00 PM CH03.03.03

Understanding the Effect of Surface Energy on Dendrite Growth in Lithium Metal Batteries Madison Morey and Emily Ryan; Boston University, United States

Lithium metal batteries have shown promise in combating the limitations of lithium ion (Li-ion) batteries, including having a theoretical capacity that is an order of magnitude greater than that of the Li-ion battery. However, a main hinderance is the uncontrolled growth of Li dendrites on the anode during cycling. These dendrites lead to a decrease in coulombic efficiencies and can pierce the separator or break off forming “dead lithium” resulting in short circuit and thermal run away. While there has been extensive research into the growth and morphology of Li dendrites, little is known about the nucleation process of Li along the anode surface. The Li growth process is influenced by several factors including surface heterogeneities such as lattice defects and grain boundaries, the overpotential, local lithium ion (Li⁺) concentrations and varying surface energies along the anode.

Due to the nature of the anode surface, it is difficult to observe the complex physics experimentally. Therefore, computational modeling is a powerful tool for understanding dendrite nucleation. It resolves the electrode-electrolyte interface where dendrite growth occurs and can track the complex chemical and physical phenomena contributing to dendrite nucleation and growth. Here a detailed model is presented that uses an extended, concentration dependent Butler-Volmer equation (eBV) with an additional term for nucleation to describe the rate of reaction at the electrode-electrolyte interface. By utilizing the eBV with the nucleation term, the rate at which Li is locally deposited on the anode surface can be carefully tracked along with other important phenomena, i.e. current density, overpotential, and Li⁺ concentrations. In addition, the nucleation term allows tracking of the growth rate of Li nucleates along the surface when influenced by changes in surface energy.

The model is used to study how defects in the anode surface effect dendrite growth. These defects include lattice defects such as substitutional impurities, interstitial impurities, and vacancies in the Li-metal crystal lattice. In addition to surface defects, grain boundaries can also lead to a change in surface energy. Results show that when defects that decrease the surface energy are present, we see a more homogenous growth, while defects that increase the surface energy led to more growth. Thus, understanding the effects of nucleation locations and rates of dendrite growth could lead to the design of engineered surfaces to extend Li metal battery lifetime and performance.

4:15 PM CH03.03.04

In Situ Li Growth Mechanism at Initial Stage by Liquid Phase Transmission Electron Microscopy Yonggoon Jeon, Hayoung Park, Woo Jun Chung

and Jungwon Park; Seoul National University, Korea (the Republic of)

High energy density and cycling stability of Lithium-ion batteries (LIBs) are receiving great attention as LIBs have been essential goods in our life from portable devices to Electric Vehicles (EVs). Lithium metal anode material is one of the most promising options for next generation battery system. Although it has many advantages such as high theoretical capacity, low density and lowest standard electrochemical redox potential, irregular Li deposition on the anode is the biggest obstacle for practical application. Therefore, it is important to understand the dynamics of Li nucleation and growth in the early stages, because it has a decisive influence on uneven surface formation that determines the performance and safety of Lithium Metal Batteries (LMBs). In this aspect, the initial stage of Li plating in Ethylene carbonate/Diethyl carbonate (EC/DEC, 1M LiPF₆) and 1,3-Dioxolane/Dimethoxyethane (DOL/DME, 1M LiTFSI) are investigated by in situ liquid phase transmission electron microscopy. The formation of large Li particles accompanied by low nucleation density and rapid growth is observed in DOL/DME electrolyte, whereas small-sized Li particles are formed with features of high nucleation density and slow growth rate in EC/DEC electrolyte, and the difference in initial nucleation and growth is closely related to SEI structures determining its mechanical and kinetic property. Heterogeneously distributed ionic species in the organic-rich outer layer from EC/DEC induce structural instability and uneven Li⁺ flux, which leads to cracks on the SEI and low kinetics, revealing many nucleation sites and slow growth, respectively. In contrast, flexible components such as amorphous alkoxide and poly(DOL) and uniform multi-layered Li₂O on the surface in the SEI from DOL/DME improve structural stability and ionic conductivity, which facilitates less nucleation sites and fast growth rate. This results are expected to shed light on the understanding of Li dendrite growth in LMBs and rational design of the next-generation battery.

4:30 PM CH03.03.05

Capacity Recovery via Rest Induced Revival of Isolated Lithium in Lithium Metal Batteries Wenbo Zhang, Philaphon Sayavong, Xin Xiao, Solomon Oyakhire, Rafael Vilá, David Boyle, Sang Cheol Kim, Mun Sek Kim, Sarah Holmes, Stacey F. Bent and Yi Cui; Stanford University, United States

Li metal is a promising high energy anode material for future generation rechargeable batteries. However, Li metal anodes face the obstacle of rapid capacity decay, which must be overcome before Li metal battery (LMB) technology can be commercially embraced. The heterogeneity of Li metal morphology¹ and solid electrolyte interphase (SEI)² are two factors which contribute to capacity decay by promoting uneven stripping, leading to the eventual disconnection and isolation of Li metal. Electronically isolated Li cannot partake in electrochemical reactions and therefore contributes to lost capacity. A recent work has demonstrated the recoverability of isolated Li using an electric field to drive spatial progression towards the electrode³, opening a new path to fight capacity decay in LMBs. Hence, a better mechanistic understanding of isolated Li revival through in-operando studies is essential for future work toward improved inactive capacity recovery. However, the phenomenon of isolated Li recovery has not been documented in prior in-operando optical studies most likely due to the large differences in conditions between optical setups and standard cell architecture.

Here we present a novel in-operando optical cell setup which maintains the pressurized environment and performance of standard coin cells, enabling the first-time imaging of Li metal isolation, reconnection, and recovery. Furthermore, this new optical cell platform is used to demonstrate the degradation of residual SEI during rest and how this evolution improves the recoverability of the isolated Li in subsequent cycles. These observations of enhanced lithium recovery after discharged state resting are corroborated by improved cycling performance using a hybrid continuous/rest cycling protocol. Coulombic efficiencies (CE) greater than 100% are achieved in the first rested cycle following continuous cycling. Additionally, titration gas chromatography results also show decreased quantities of isolated Li on current collectors after the rest cycle compared to those which ran continuous cycles, verifying the recovery of isolated Li from prior cycles. By connecting the observations from this novel optical cell with the unique cycling protocol, we reveal not only new insights on the mechanics of isolated Li reactivation, but also inform how residual SEI degradation can enhance inactive capacity recovery.

1. K. N. Wood, E. Kazyak, A. F. Chadwick, K. H. Chen, J. G. Zhang, K. Thornton, N. P. Dasgupta, *ACS Cent. Sci.* **2**, 790–801 (2016).

2. Y. Li, W. Huang, Y. Li, A. Pei, D. T. Boyle, Y. Cui, *Joule*. **2**, 2167–2177 (2018).

3. F. Liu, R. Xu, Y. Wu, D. T. Boyle, A. Yang, J. Xu, Y. Zhu, Y. Ye, Z. Yu, Z. Zhang, X. Xiao, W. Huang, H. Wang, H. Chen, Y. Cui, *Nature*. **600**, 659–663 (2021).

4:45 PM CH03.03.06

Theoretical Analysis of Reaction Inhomogeneity and Lithium Plating Onset at Fast Charge Rates Aleksandar Mijailovic¹, Guanyi Wang², Jian Yang², Wenquan Lu³, Qingliu Wu² and Brian W. Sheldon¹; ¹Brown University, United States; ²Western Michigan University, United States; ³Argonne National Laboratory, United States

Inhomogeneous lithium intercalation of porous electrodes can lead to lithium plating during fast charging. Previous work has demonstrated the effects of inhomogeneous reactions in cathodes and anodes, both on particle and macroscale (i.e., cell) length scales. The effects of mass transport, ionic transport, electrode thermodynamic behavior and reaction kinetic behavior on lithium plating have been studied in the context of reaction inhomogeneity; however, a complete theoretical understanding on how these effects interplay to accelerate lithium metal plating has not been established at high C-rates. Here, analytical and numerical analysis is used to develop a more complete understanding on how these coupled, nonlinear physical and electrochemical effects act together to cause lithium plating. Specifically, it is shown that analytical solutions, which are functions of several nondimensional numbers (the “reaction inhomogeneity parameter” in particular), can predict onset of lithium plating at high C-rates in half-cell anodes. This analytical prediction of lithium plating exhibits surprising accuracy against a calibrated graphite half-cell model, which has highly non-linear behavior (e.g., in the open circuit voltage). These results are compared against *in situ* and *ex situ* experimental observations of lithium plating onset during fast charging. Applications for design and optimization of electrodes with complex architectures are discussed. This work attempts to clarify and unify findings in complicated numerical models to provide guidance in mitigating Li metal plating at high rates.

SESSION CH03.04: Poster Session
Session Chairs: Peng Bai and Hui Xiong
Monday Afternoon, November 28, 2022
8:00 PM - 10:00 PM
Hynes, Level 1, Hall A

CH03.04.01

Quantitative Evaluations of Reaction Heterogeneities in Thick Battery Electrodes Using Operando Focused Beam X-Ray Diffraction Tianyi Li, Fan Wang, Xinwei Zhou, Yuzi Liu and Yang Ren; Argonne National Laboratory, United States

Recently, the use of thick electrodes in lithium-ion batteries has drawn extensive attention as it effectively promotes the cell-level energy density by reducing the fraction of inactive components such as separators and current collectors. However, the spatially non-uniform reaction can easily arise within a thick electrode design due to the sluggish electrolyte transport. Understanding the heterogeneous reaction and preventing its happening are therefore critical as it may result in inferior rate performance, fast capacity degradation, and even safety hazards. Our previous modeling study has demonstrated that the dependence of equilibrium potential on the state-of-charge (SOC) of active materials strongly influences the degree of reaction non-uniformity. Motivated by the modeling predictions, this study aims to experimentally evaluate the reaction heterogeneities in thick electrodes by employing operando focused beam X-ray diffraction (XRD). We will compare two types of nickel rich cathode materials (LiNi_{0.8}Mn_{0.1}Co_{0.1}O₂) with different crystallinities, therefore, quantitatively assess the degree of reaction along the depth direction in electrodes with different charge and discharge rates. A detailed comparison between the experiments and simulations will help us better understand the origin of reaction heterogeneities in electrodes and guide the design of battery materials and structures in the future.

CH03.04.02

Interfacial Studies of Silicon Anode Cycling and Solid Electrolyte Interphase (SEI) Formation on Highly Curved Surfaces [Hyewon Jeong](#), Nathan J. Fritz, Benjamin Zahiri and Paul Braun; University of Illinois at Urbana-Champaign, United States

Silicon is a promising high-capacity anode material for lithium-ion batteries (LIBs) with ten times higher specific capacity (4200 mAh/g) than leading carbon-based anodes (372 mAh/g). However, silicon expands up to 300% by volume during lithiation, which leads to mechanical failure upon cycling. This further results in electrical contact loss and continuous solid electrolyte interphase (SEI) formation from the decomposition of electrolytes on exposed silicon surfaces. To address these challenges, it is paramount to make a uniform and mechanically durable silicon coating on a current collector and stabilize the SEI for extended cycling. Previous efforts include silicon deposition on a 3D-architected nickel scaffold to enable higher silicon loadings and accommodate the volume expansion of silicon during lithiation. Nonetheless, the characteristics of mechanical failure in 3D structure are complex and make it harder to understand silicon expansion and SEI formation simultaneously. Here we reduce the geometry of the 3D nickel scaffold to basic geometries, such as positive, negative, and neutral curvatures to better understand how each highly curved surface plays its role in silicon expansion, SEI formation, and its composition in 3D structured anodes. We adopted chemical vapor deposition (CVD) to achieve conformal and uniform silicon coatings on nickel current collectors and cycled the electrodes at slow rates to form a stable SEI. The intact interface between SEI and silicon anode with the aforementioned curvatures was characterized via a focused ion-beam, followed by scanning transmission electron microscopy (STEM). We used STEM, combined with energy dispersive X-ray spectroscopy (EDS) and electron energy loss spectroscopy (EELS) to investigate the chemical composition and bonding environments of SEI layers at the interface. This approach enabled us to explore how silicon layer changes by tracing oxygen and carbon and the elemental composition of the following SEI layer upon cycling. Our work integrates electrochemistry and high-resolution electron microscopy to reveal for the first time how curvature correlates to chemo-mechanical properties of silicon and SEI formation mechanism. This fundamental understanding should lead to more effective tuning of the properties of next-generation silicon-based batteries.

CH03.04.03

Beyond the Water Electrolysis Potential—A Systematic Study for Different Ionic Carriers on the Electrolyte Performance for Free-Standing Carbon Nanotube Supercapacitors [Juveiriah M. Ashraf](#), Myriam Ghodhbane and Chiara Busa; Technology Innovation Institute, United Arab Emirates

To eliminate electrolyte leakage, the development of safe and flexible supercapacitors necessitates solid-state electrolytes that integrate high mechanical and electrochemical capabilities. *Quasi*-solid-state electrolytes, which constitute a polymer matrix along with an aqueous electrolytic phase, are a viable answer to this problem. Recently, gel electrolytes have gained a lot of attention in flexible and wearable electronic devices due to their remarkable advancements. However, the limitation in the high-performance of such gels hinders the practical usage of such devices. On the electrochemical perspective, the gel electrolyte performances strictly rely on the type of ionic carrier (acidic, alkaline, or salt-based), size of the ion, solvent concentration, type of polymer, as well as the interaction between the polymer and other components. Moreover, the performance of the electrolyte differs with the electrode-electrolyte interface and thus is highly dependent on the electrode material. For this reason, it is vital to carry a parametric study to evaluate the effect of the above stated.

Most studies in literature focus on limited voltage windows, up to 0.8 V or 1 V, below the electrolysis potential of water. However, it is important to study the efficacy of these electrolytes for larger voltage windows for employment in broader applications. The aim of this study is to investigate the effect of several ionic carriers (namely H₃PO₄, KOH and LiCl) for a cell voltage exceeding the water electrolysis potential (1.2 V), that is, up to 1.5 V. The solvent concentration of the architecturally engineered PVA-based electrolytes' performance in free-standing CNT supercapacitor is also evaluated. In addition, the dependency of the electrolyte's mechanical structure for long-term stability is further studied by using the optimized concentration of each (H₃PO₄, KOH and LiCl) by freezing and de-freezing the gel to form membrane-like films because of the creation of increased physical cross-linking with this cycle. The supercapacitors are studied for their capacitance, charge/discharge capabilities as well their long-term stability to determine the optimum electrolyte.

CH03.04.04

Understanding and Controlling Interfacial Reactivity of Silicon Electrodes—Impact of Electrode and Electrolyte Composition [Mallory Vila](#)¹, Wenzao Li¹, Lisa Housel², Shan Yan², Lei Wang², David Bock², Esther S. Takeuchi^{1,2}, Kenneth J. Takeuchi^{1,2} and Amy Marschilok^{1,2}; ¹Stony Brook University, United States; ²Brookhaven National Laboratory, United States

Silicon is an attractive negative electrode material for lithium-ion batteries (LIBs) because of its high theoretical capacity (3579 mAh g⁻¹), low cost, and demonstrated ability to store Li-ions. However, Si experiences limited capacity retention due to significant volume change on (de)lithiation and repeated formation of the solid-electrolyte interphase (SEI) as the silicon evolves with cycling. These factors can contribute to high internal resistance, low Coulombic efficiency, and decreased capacity over cycling.

Appropriate formation of the SEI through electrolyte modification is a promising strategy to address this issue. Previous studies have evaluated the effectiveness of electrolyte additives on the SEI and capacity retention. While it has been long recognized that the electrode/electrolyte interface is critical, it has proven challenging to probe directly often requiring recovery of the active electrodes with subsequent examination risking change from their functional environment. Cell reactions including SEI formation can be elucidated by coupling information from a variety of methods including electrochemistry, x-ray photoelectron spectroscopy (XPS) of recovered electrodes, and isothermal microcalorimetry (IMC). Outcomes from a series of investigations on the reactivity of silicon electrodes of several compositions and electrolyte environments will be highlighted.

CH03.04.05

Characteristic Dual-Domain Structure of Reduced Graphene Oxide and Its Guidance to Higher Specific Capacitance [Jun Beom Kim](#) and Sang Ouk Kim; KAIST, Korea (the Republic of)

Reduced graphene oxide (rGO) has been regarded as an attractive material for diverse energy storage applications such as fuel cells, batteries, and

supercapacitors. Graphene synthesized by the chemical vapor deposition method or graphene oxide (GO) produced by oxidative exfoliation process from graphite has critical drawbacks of poor scalability or poor electrical conductivity to be used as electrochemical electrode materials. In contrast, rGO addresses those limitations of graphene and GO by providing considerable conductivities of both electron and ion due to simultaneously existing components of graphene and GO as well as the advantage of high-yield mass production. For successful applications of rGO to high-performance electrochemical energy storage devices as electrode materials, both high electrical conductivity of rGO and high ion accessibility from the electrolyte to rGO are crucial requirements. The electrical conductivity of rGO,

however, has a trade-off property of ion accessibility. If the electrical conductivity were enhanced by increasing the degree of reduction of rGO [28–32], the ion accessibility from the electrolyte to rGO would decrease due to diminished hydrophilicity with the reduction of the GO component. Thus, optimization between electrical conductivity and ion accessibility is necessary for successful applications of rGO to high performance electrode material. Investigations on the changes of the above two intrinsic properties with the reduction level of rGO had been rarely reported thus far. Furthermore, fundamental and scientific investigations on the nature of rGO surface, e.g., characteristic domain structures of rGO with reduction levels have been never reported.

In this study, the electrical domain structures of rGO were investigated by the conductive atomic force microscopy (C-AFM) technique. This analysis was expected to reveal the amounts and configurations of graphene and GO domains. If the characteristic 2D domain structures were revealed and controlled with reduction level, the optimized domain structure would guide to higher performance of rGO-based electrode materials. The specific capacitance of rGO freestanding sheets was discussed with their characteristic domain structures. In addition, hybrid composite sheets of Fe₂O₃ and MnO₂ ceramic particles mixed with rGO were examined for further enhanced specific capacitance.

CH03.04.06

Synergetic Effect of Surface-Controlled and Diffusion-Controlled Charge Processes of NiP/CoP@NF for High Energy Density Supercapacitor MooYoung Jung; Korea University, Korea (the Republic of)

Since the rapidly increasing concerns about contamination of the environment and demand for energy storage systems, the development of high energy density supercapacitors has been essential. Although the commercial electrode for the supercapacitor has been carbon-based material, other transition metal-based electrode materials, which are pseudocapacitive or battery-like materials, have been researched by lots of academic or commercial groups due to the low energy density of carbon material. In this study, by combining the pseudocapacitive MOF-derived CoP material with the battery-like NiP material, high energy density NiP/CoP electrode material was fabricated. NiP/CoP@NF exhibited superior specific capacitance of 1154.4 F g⁻¹ at 1 A g⁻¹, exhibiting the mixed charging mechanism of both CoP and NiP materials. An asymmetric supercapacitor (ASC) showed a high energy density of 27.7 Wh kg⁻¹ at the power density of 800 W kg⁻¹ with cycle retention of 86.36% at 10000 cycles.

CH03.04.08

Observation of Ir 5d Orbitals in Epitaxial IrO₂ Thin Films Using Resonant Inelastic X-Ray Scattering Seohyoung Chang and Kyeong Jun Lee; Chung-Ang University, Korea (the Republic of)

Transition metal oxides have been considered one of the alternative material systems for energy conversion and storage systems due to their intriguing physical and chemical properties. Specifically, IrO₂ exhibits high activity and better stability under oxygen evolution reaction (OER) than other 4d transition metal oxides, e.g., ruthenates [1]. Ir 5d orbital states in IrO₂ can play an important role in the OER process because of interactions between d orbitals near Fermi level and adsorbates. However, understanding of the process of the model system is yet incomplete due to experimental limitations, specifically spectroscopic techniques.

Here, we measured 5d orbital states in IrO₂ epitaxial thin films grown on TiO₂ substrates using Ir L₃-edge resonant inelastic x-ray scattering (RIXS). Using the RIXS technique, we systematically investigated 5d orbital states near Fermi level and understood the transition between specific orbitals coupled with orientations and strain. For instance, our RIXS measurement demonstrated that the 5d d_{x²-y²} orbital in the plane of edge-sharing of octahedra along [001] dominantly contributed to about 2eV energy loss signal. We propose that the in-situ RIXS techniques combined with an electric field can understand the OER process and explore emergent physical properties.

[1] G. Kwon et al., ACS Catalysis 11 10084 (2021).

CH03.04.09

A Mesoporous Ternary Transition Metal Oxide Nanoparticle Composite for High-Performance Asymmetric Supercapacitor Devices with High Specific Energy Manar M. Hazaa and Nageh K. Allam; The American University in Cairo, Egypt

We report on the optimized fabrication and electrochemical properties of ternary metal oxide (Ti–Mo–Ni–O) nanoparticles as electrochemical supercapacitor electrode materials. The structural, morphological, and elemental composition of the fabricated Ti–Mo–Ni–O via rapid breakdown anodization are elucidated by field emission scanning electron microscopy, Raman, and photoelectron spectroscopy analyses. The Ti–Mo–Ni–O nanoparticles reveal pseudocapacitive behavior with a specific capacitance of 255.4 F g⁻¹. Moreover, the supercapacitor device Ti–Mo–Ni–O NPs//mesoporous doped-carbon (TMN NPs//MPDC) device exhibited a superior specific energy of 68.47 Wh kg⁻¹ with a corresponding power density of 2058 W kg⁻¹. The supercapacitor device shows 100% coulombic efficiency with 96.8% capacitance retention over 11000 prolonged charge/discharge cycles at 10 A g⁻¹.

CH03.04.10

Highly Stable Supercapacitor Devices Based on Three-Dimensional Bioderived Carbon Encapsulated g-C₃N₄ Nanosheets Manar M. Hazaa, Nageh K. Allam, Loujain G. Ghanem and Mahmoud A. Hamza; The American University in Cairo, Egypt

Owing to the increasing demand for sustainable and eco-friendly energy storage devices such as supercapacitors, it is vital to continuously search for highly stable and cost-effective electrode materials with high energy and power densities. Herein, a 3D/2D metal-free mesoporous composite of graphitic carbon nitride (GCN) and bioderived carbon (Bio-C_x) is investigated as an energy storage electrode material. This composite overcomes the low conductivity and low capacitance limitations of GCN while enjoying its high corrosion resistance, high nitrogen content, and unique 2D structure. The GCN/Bio-C_x composite exhibits a fairly wide operating potential window of 1.2 V in 0.5 M H₂SO₄ aqueous electrolyte with a high capacitance of 300 F/g at 1 A/g. This high performance was ascribed to the huge number of available active sites, large surface area, and the unique 3D/2D structure. The assembled device employing the GCN/Bio-C_x composite as the positive electrode and mesoporous nitrogen-doped carbon (MPNDC) as the negative electrode showed an ultrahigh-energy density of 53.72 Wh/kg and a power density of 900 W/kg. The GCN/Bio-C_x//MPNDC device retains ~100% of its initial capacitance after 13 000 charge/discharge cycles with 100% Columbic efficiency.

CH03.04.11

NMC Microparticles with Core-Shell Structure for Cathodes in Li-Ion Batteries Javier Garcia-Alonso¹, Svitlana Nahiriak², David Maestre¹, Bilge Saruhan², Ana Cremades¹ and Bianchi Mendez¹; ¹Universidad Complutense de Madrid, Spain; ²German Aerospace Center (DLR), Germany

The increasing necessity for improvement in energy storage technologies, especially of the mature Lithium-Ion Batteries (LIBs), relies on the advances in the characterization techniques and the materials used in the device. Advanced microscopy and spectroscopy techniques, including *in-situ* measurements, can provide valuable insights to face some of the challenges that this technology faces. In recent years, Ni-Mn-Co (NMC)-based cathodes have gained relevance due to their high specific capacity and thermal stability leading to an improvement of the performance of the LIBs. So far, different approaches have been pursued to improve the synthesis mechanisms, and diverse characterization techniques have been employed in the study of the NMC materials at the microscale.

In this work, NMC core-shell microparticles have been studied by a combination of techniques including scanning and transmission electron microscopy (SEM, TEM), X-ray diffraction (XRD), energy dispersive x-ray spectroscopy (EDS), Raman spectroscopy and X-Ray Photoelectron Spectroscopy (XPS), including *in-situ* techniques as well. Micro-Raman and XRD results indicate the formation of Li-Ni-Mn-Co-O complex oxides presenting the usual layered structure of NMC (R-3m) with the presence of reduced quantities of other structures like spinel phases. This layered structure is directly related to the high capacity and structural stability of NMC cathodes when the battery is cycled. *In-situ* thermo XRD measurements indicate an enhanced formation of NiO as the temperature increases up to 900 °C. The analyzed microparticles exhibited a rounded appearance with an average diameter of 4 μm and variations in their morphology as a function of the temperature used during the synthesis, as observed by SEM and TEM. *In-situ* SEM observations also lead to assess the morphology evolution of the particles with increasing temperature. EDS analysis with variable beam acceleration voltage confirms the presence of a Ni-rich core and a Mn-rich shell with submicrometric dimensions. The presence of Ni allows for a higher capacity but a lower structural stability when cycling, while Mn allows for higher structural stability but lower capacity. Co in small quantities can mitigate the cation disordering inside the crystal structure. SEM and EDS measurements confirm that the morphological and compositional properties of the particles were maintained after the Li introduction. Micro-Raman spectroscopy was also used to understand the variations in the crystalline structure of the particles as a function of the synthesis route and the Li insertion. Finally, *in-situ* XPS measurements at temperatures up to 500 °C and a variable pressure, shows variations in the Mn(3s) and O(1s) core levels, as well as in the electrical conductivity of the samples. These results can lead to achieve a deeper knowledge of the properties of the NMC microparticles in the search of improved performance in LIBs.

CH03.04.12

Development and Implementation of *In Situ* Mossbauer Spectrometry for the Study of Battery Cathode Materials Simon Ji and Hillary Smith; Swarthmore College, United States

Mossbauer Spectroscopy has proven to be a very useful tool for studying the local electron dynamics in iron-containing battery materials. In the hunt for more economical and sustainable battery cathode materials, NaFePO₄ has emerged as a lower-cost and safer alternative to LiFePO₄. We report the development and characterization of an electrochemical cell for *in situ* Mossbauer spectroscopy measurement. The *in situ* setup is used to study changes in the local structure of iron atoms during initial discharge and charge in NaFePO₄ half-cells. We will compare these results to previous *in situ* studies of LiFePO₄. Finally we will compare the initial charge and discharge spectra to those after multiple cycles to provide insights into changes in the cathode material that may result in cell degradation.

CH03.04.13

On the Connection Between Slurry Rheology and Electrochemical Performance of Graphite Anodes in Lithium-Ion Batteries Joseph Sullivan; The University of Rhode Island, United States

Most current lithium-ion battery anodes are prepared from a slurry containing graphite, polyvinylidene fluoride (PVDF), n-methyl-2-pyrrolidone (NMP), and small amounts of conductive carbon black (CB). The rheology of this four-component slurry is an important indicator of its microstructure, that affects the structure of the dried electrode. This in turn has consequences on the electrochemical performance of the anode. We modulate the rheology of the slurry by choosing three different commercially available carbon blacks that are used in lithium-ion batteries and establish a connection between slurry rheology and electrochemical performance. We show that the storage modulus is the key factor that impacts the electrochemical performance.

CH03.04.15

Insights into Battery Systems using *In-situ* and Operando Characterization Methods Nahian Sadique¹, Shan Yan², Lisa House², Lei Wang², David Bock², Esther S. Takeuchi^{1,2}, Amy Marschilok^{1,2} and Kenneth J. Takeuchi^{1,2}; ¹Stony Brook University, United States; ²Brookhaven National Laboratory, United States

Electrochemical energy storage systems, specifically batteries, have become a key component in our society. As demand increases for electric vehicles, and integration of intermittent renewable energy sources, so does the need for high performing, reliable, and cost-effective battery systems to power the applications. Further, as the applications evolve demands for advances in the technology place new requirements on future generations of batteries. Batteries are highly researched and *ex situ* measurements on components outside of the functional environment have been a standard approach for decades. However, these are often ultimately destructive techniques that risk distortion of the original chemical environment and do not capture kinetic phenomena. More recently, *in situ* characterization on a system in a functioning environment but inactive during the measurement and operando measurements during system operation have become more prevalent with the potential to yield unprecedented mechanistic insights. The appeal of these approaches is evidenced by a ~350% increase in publications regarding “batteries and operando” techniques over the past 5 years. Further, coupling the time dimension with spatial resolution, *in situ* and operando characterization over multiple length scales and time domains becomes a powerful approach. The research presented will provide case studies of *in situ* and operando techniques including the use of synchrotron methods applied to several battery systems. The complementary insights gained from the multiple characterization approaches used will be highlighted in terms of insight into functional electrochemistry.

CH03.04.16

Interfacial Behavior of Thio-LISICON Solid-State Electrolyte Under External Pressure Yifan Wu and Shou-Hang Bo; Shanghai Jiao Tong University, China

External pressure can greatly affect the cycling performance of solid-state batteries, although pressure-driven changes in electrochemical processes are still not fully understood. For instance, Li₁₀GeP₂S₁₂ (LGPS) is known to strongly react with lithium metal. However, under external pressure, with the use of additional Li₆PS₅Cl (LPSCl) outer layers forming a sandwich structure, stable cycling over 1800 cycles can be achieved (*Nature*, 2021, 593, 218–222). This finding motivated us to investigate the interfacial behavior of Li/LGPS under external pressure (*i.e.*, 7.5 MPa) to shed light on the improved electrochemical performance. Our results indicate that the growth rate of the interfacial resistance is substantially decreased while the cycle life before open-circuit failure is substantially extended under MPa-scale external pressure. The reactivity between lithium metal and LGPS is extremely severe,

forming island features upon cycling. Using selected area Raman spectroscopy, these "islands" were confirmed to be interfacial decomposition products (primarily Li_2S). Observations were in line with the expected volume expansion of LGPS when reacting with lithium metal. Exertion of the MPa-scale external pressure may take effect in applying mechanical constraints on volume-expanding reactions, thus improve cycling performance with reactive lithium metal. In addition, a lithium depletion layer was founded formed in the interface region by elemental mapping of lithium with time-of-flight secondary ion mass spectrometry (ToF-SIMS), which can contribute to extra interfacial resistance. Chemo-mechanical degradation processes, which are essentially multi-field coupled, were also captured and analyzed with a home-built *in situ* apparatus. *In situ* X-ray diffraction collected at synchrotron light source evidenced the formation of Li_2S as a dominant interface component at the Li/LGPS interface. Moreover, with help of X-ray tomography conducted *in situ*, we tracked the morphology evolution at the interface. Crack initiation, propagation and crosslinking in LGPS and void formation and suppression in lithium metal were followed. With above-mentioned observations, our work marks an important step to understanding the interfacial electrochemical behavior of the Li/LGPS interface under external pressure.

CH03.04.17

Product Selectivity Change by Ag Nanoparticle Modification on Metal Cathode Electrodes for Electrochemical CO_2 Reduction Kazuki Koike^{1,2}, Takeharu Murakami², Satoshi Wada², Atsushi Ogura^{1,3} and Katsushi Fujii²; ¹Meiji University, Japan; ²RIKEN Center of Advanced Photonics, Japan; ³Meiji University MREL, Japan

Electrochemical CO_2 reduction is an effective technique for reducing atmospheric CO_2 concentration, which is one of the causes of global warming. In addition, product control of CO_2 reduction is important for carbon capture and utilization (CCU). The products of CO_2 reduction are known to vary depending on the metal cathode material and the applied voltage. Thus, modification of metal cathode has been studied to control the kinds of products, including the single-crystal surfaces index, alloying with different metals, and the arrangement of multiple metals. In this study, Ag nanoparticle modifications on several kinds of metal surfaces were investigated.

The Ag nanoparticles were sprayed on the electrode surface using a spray machine to modify the electrodes. The evaluations were performed by H-type cells with electrochemical cyclic voltammetry and chronopotentiometry. The reduced products were evaluated by gas chromatography. The surface condition of the electrode before and after the reaction was also evaluated.

It was found that the metal cathode electrode modified with Ag nanoparticles improved the CO_2 reduction ability to CO compared with the bare metal electrode. The surface evaluation results showed that the surface showed dispersed Ag oxide nanoparticles on the metal surface, and it has the possibility of the improvement of CO_2 reduction.

CH03.04.18

Stable Zn Metal Anode Enabled by a Zincophilic Polyanionic Hydrogel Layer Jin-Lin Yang and Hong Jin Fan; Nanyang Technological University, Singapore

The practical application of Zn metal anode for aqueous batteries is greatly restricted by the catastrophic dendrites growth, intricate hydrogen evolution and parasitic surface passivation. Herein, a polyanionic hydrogel film is introduced as a protective layer on Zn anode with the assistance of saline coupling agent (denote as Zn-SHn). The hydrogel framework with zincophilic $-\text{SO}_3^-$ functional group uniformizes the zinc ions flux and transport, and such hydrogel layer chemically bonded on Zn surface obviously suppresses the dendrites formation by guiding the 3D Zn accumulation. Consequently, very stable and reversible Zn stripping and plating at various currents and capacities is achieved. A full cell by pairing the Zn-SHn anode with a $\text{NaV}_3\text{O}_8 \cdot 1.5 \text{H}_2\text{O}$ cathode shows a capacity of around 176 mAh g^{-1} with a capacity retention around 67 % over 4000 cycles at 10 A g^{-1} . The presented polyanionic hydrogel film protection strategy paves a new way for future Zn anode design and safe aqueous batteries construction.

CH03.04.19

Characterizing 2D Materials (Graphite, GO, and GNP) via Physical, Electrical and Electrochemical Techniques Sonjoy Dey and Gurpreet Singh; Kansas State University, United States

The characterization of different materials, specifically carbonaceous materials, requires combinations of different microscopic and spectroscopic techniques. Among the various Spectroscopic techniques widely used for the characterization of 2D materials, electrochemical impedance spectroscopy (EIS) is a robust, simple, non-destructive, and powerful electroanalytical technique that provides a considerable amount of information about kinetics happening inside a battery in a comparatively short period. The spectrum produced due to the EIS measurement gives a couple of important information to the user, such as the reactions occurring in the cathode and anode in separated features. Furthermore, if the time constants are resolvable, EIS provides ample information about the resistance arising from each kinetic step during the electrochemical reaction in the electrodes. Keeping this in mind, this study concerns the characterization of three different carbon allotropes (Graphite, GNP and GO) via different spectroscopic techniques such as Raman Spectroscopy and X-ray photoelectron Spectroscopy. These materials were then used in a sodium-ion half-cell setup as cathode material. Afterwards, three different carbon allotropes were examined and differentiated using EIS due to the discrepancy in the impedance of electrodes with varying depths of charge/discharge cycles. Furthermore, the study involved the investigation of reaction mechanism and kinetics during sodiation/disodiation. Therefore, it was found that electrochemical performance tests and EIS data can embellish the previously obtained results from the spectroscopic techniques and enhance the understanding of fabricating better anodes for sodium-ion batteries.

SESSION CH03.05: Solid-State Electrolytes and Novel Liquid Electrolytes

Session Chairs: Donal Finegan and Matthew McDowell

Tuesday Morning, November 29, 2022

Hynes, Level 1, Room 103

8:30 AM *CH03.05.01

Mechanistic Origin and Role of Heterogeneities in Solid-State Batteries Partha P. Mukherjee, Bairav Sabarish Vishnugopi and Kaustubh G. Naik; Purdue University, United States

Solid-state batteries (SSBs), consisting of a lithium metal anode and an inorganic solid electrolyte, promise to simultaneously improve the energy/power density and safety as compared to the conventional lithium-ion batteries. However, the complex nature of solid-solid interfaces in SSBs pose a wide range of challenges including the morphological instability of the metal anode, microstructure-driven kinetic and transport interactions in the cathode, and interphase formation. To address these limitations, gaining fundamental understanding of the myriad heterogeneities at scales, and their implication on the electrochemical-transport-mechanics interactions at such solid-solid interfaces is critical. In this presentation, we delineate the underlying role of

heterogeneities on the failure onset, degradation, and electrochemical performance of solid-state batteries. The mechanistic interactions due to the spatio-temporal heterogeneity of the underlying electrochemical-thermal-mechanics coupling will be examined.

9:00 AM *CH03.05.02

Elucidating Interfaces in Solid State Batteries Using Advanced Scanning Transmission Electron Microscopy (STEM) [Miaofang Chi](#); Oak Ridge National Laboratory, United States

Designing next-generation energy storage systems, such as solid-state batteries, faces numerous challenges, many of which are related to interfaces. Elucidating interfacial phenomena requires knowledge, not only of atomic-scale structure and chemistry but also of correlated local charge distribution and ion transport that are difficult to probe with existing characterization techniques. Several emerging scanning transmission electron microscopy (STEM) techniques, such as four-dimensional (4D)-STEM, monochromated EELS (electron energy loss spectroscopy), atomic-scale cryogenic and *in situ* environmental microscopy, allow the behavior of electrons, ions, and atoms to be probed, opening opportunities to tackle complex dynamic interfacial questions. In this talk, I will demonstrate how we advance and utilize these techniques to (1) reveal the origin of unexpected dendrite growth within all-solid-state batteries, (2) probe interfacial ion transport behavior, and (3) map space charge region at solid-solid interfaces. Perspectives for the future advancements of these new STEM techniques for research into emerging energy materials and systems will also be provided.

9:30 AM CH03.05.03

Localized Overlimiting Ion Polarization Preceding Metal Penetration in Lithium-Ion Conducting Electrolytes [Peng Bai](#); Washington University in St. Louis, United States

Next-generation high-energy batteries require rechargeable metal anodes, but hazardous dendrites tend to form during recharging, causing short-circuit risk and capacity loss, even with hard and stiff ceramic electrolytes, by mechanisms that still remain elusive. In this presentation, we will first demonstrate a rigorous analysis of the lithium dendrite formation in liquid electrolytes, through the intimate combination of operando experiments and transport models. Our results demonstrated the necessity to differentiate Li whiskers from Li dendrites, induced by different physical processes. Resolving the interfacial instability and metal whiskers led to an ideally smooth, non-porous, ingot-type Na metal plating, which enabled the anode-free Na metal full cells with a record-high retention rate of 99.93% per cycle at 3C charge and discharge. Novel electrochemical tests of garnet-type cubic $\text{Li}_{7-x}\text{La}_3\text{Zr}_{2-x}\text{Ta}_x\text{O}_{12}$ ceramic electrolytes confirmed a similar overlimiting ion polarization and dendrite initiation mechanism mainly through grain boundaries. Our theoretical and experimental discoveries suggest that both liquid and solid electrolytes follow a similar ion polarization process before the onset of localized metal penetration. The success of alkali metal batteries relies on the rational control of both the interfacial kinetics and the bulk ion transport.

9:45 AM BREAK

10:15 AM *CH03.05.04

Multidimensional Characterizations for All-Solid-State Batteries [Yan Yao](#); University of Houston, United States

All-solid-state batteries (ASSBs) are regarded as one of the future energy storage technologies capable of competing with the state-of-the-art Li-ion batteries. Despite significant development, the room temperature long-cycle performance of lithium metal ASSBs still remains a challenge. The failure of a solid-state Li battery may be linked to two primary causes: interfacial resistance increase and Li dendrite growth. The former may be further attributed to electrolyte decomposition and interfacial void formation (*i.e.*, loss of physical contact). Electrolyte decomposition happens in two ways: oxidative decomposition at the cathode active material-electrolyte interface and reductive decomposition at the Li (including dendrites)-electrolyte interface. The complex origins of battery failure necessitate multidimensional characterizations using a combination of tools capable of quantifying the void and dendrites, identifying the chemical and mechanical natures of the Li dendrites and electrolyte decomposition products, and monitoring the processes *in situ*. The tools must also cover a sufficiently large scale, have a spatial resolution of a few nanometers, and be sensitive enough to detect subtle changes in chemical and mechanical properties. These considerations led us to a suite of methods for structural, chemical, and mechanical characterizations that include PFIB-SEM, ToF-SIMS, and nanoindentation-based stiffness mapping. We fabricated solid-state micro-cells with electrochemical performance comparable to their bulk-type cells. Electrochemical tests with temperature control and external pressure monitoring of solid-state cells were demonstrated in an air-free vessel with an integrated *in-situ* cell test platform. We investigate the function of an interlayer between lithium metal anode and solid electrolyte in preventing lithium dendrite formation and allowing reversible lithium plating and stripping over 1000 cycles. With these in-depth understandings, we will be able to predict and optimize the physical and chemical changes that occur in solid-state Li batteries during operation.

This work was supported by the U.S. Department of Energy's Office of Energy Efficiency and Renewable Energy (EERE) under the Vehicle Technologies Program under Contract DE-EE0008864.

10:45 AM *CH03.05.05

Understanding Materials Dynamics in Solid-State Batteries [Matthew T. McDowell](#); Georgia Institute of Technology, United States

Solid-state batteries offer the promise of improved energy density and safety compared to lithium-ion batteries, but electro-chemo-mechanical evolution and degradation of materials and interfaces can play an outsized role in limiting their performance due to the all-solid nature of these systems. Here, I will present my group's recent work using *in situ* and *operando* experiments to understand interfacial evolution and stress changes in solid-state batteries with lithium metal and alloy anodes. *Operando* X-ray tomography is used to reveal interfacial dynamics in solid-state batteries with Li metal anodes. Segmentation and detailed image analysis enable correlation of interfacial contact loss to electrochemical behavior of symmetric cells, and the loss of interfacial contact area at the Li metal interface is found to cause current constriction and cell failure. The unique aspects of interfacial evolution in anode-free solid-state batteries associated with localized lithium depletion, as revealed by X-ray tomography and cryo-FIB, are also discussed. Finally, stack pressure evolution during cycling of full solid-state batteries is measured *in situ* and correlated with fundamental processes within electrode materials and the properties of composite electrode structures. Cells with alloy-based anodes are found to exhibit large (megapascal-level) changes in stack pressure during cycling, with stable capacity and stress changes over long-term cycling. Together, these findings show the importance of controlling chemo-mechanics and interfaces in solid-state batteries.

11:15 AM CH03.05.06

High-Precision Quantifications of Dendrite Initiation Dynamics in Garnet Solid Electrolytes [Rajeev K. Gopal](#) and Peng Bai; Washington University in St. Louis, United States

Solid-state electrolytes have the potential to stabilize lithium metal anodes, which hold the promise to increase the energy density of lithium-ion batteries. However, lithium metal dendrites that occur locally at the solid-solid interface plague the solid-state lithium metal cells during charging, rendering high safety risks in practical applications. While multiple explanations have been proposed, understandings of the dynamics preceding and causing the metal

penetration in solid electrolytes are still not conclusive. Here, by testing hundreds of highly consistent LLZTO samples and utilizing a novel operando technique on conventional cell geometry, we observed consistent and statistically significant phenomena. The characteristic time to dendrite initiation was measured and coincided with the Sand's time scaling traditionally reserved for liquid electrolytes, indicating similar transport limitations in garnet solid electrolytes. Deviations in scaling and additional normalization were also explored. This new fundamental understanding not only explains the electrochemical origin of dendritic initiation but also provides future insight into optimal all-solid-state battery design.

SESSION CH03.06: Thin-Film Solid-State Batteries
Session Chairs: Kent Griffith and Hui Xiong
Tuesday Afternoon, November 29, 2022
Hynes, Level 1, Room 103

1:30 PM *CH03.06.01

Thin Film Solid State Li-Ion Batteries as Model Systems for Understanding Interface Effects A. A. Talin; Sandia National Laboratories, United States

Rechargeable, thin film solid-state Li and Li ion batteries (TFSSLBs) with high specific power and energy density are highly desirable to energize an emerging class of miniature, autonomous microsystems that operate without a hardware for power or communications. TFSSLBs are also attractive for fundamental studies aimed at understanding how battery geometry, dimensions, composition and the resulting interfaces affect performance. For example, thin film fabrication methods enable precise control over electrode and electrolyte thickness, morphology, geometry and interface area. Furthermore, TFSSLBs are vacuum compatible, meaning that techniques that generally require vacuum or controlled ambient such as SEM, TEM, auger electron spectroscopy, secondary ion mass spectroscopy, neutron depth profiling and Kelvin probe force microscopy can be readily applied to characterize TFSSLB, often in operando mode. In my presentation, I will discuss recent experiments aimed at precisely measuring the Li concentration and electric potential profiles across TFSSLBs. When coupled with first principles informed models, the results provide new insights into the factors that determine electrode/electrolyte interface resistance and to materials selection strategies for achieving stable, high performance solid state batteries.

2:00 PM CH03.06.02

Direct Imaging of the Structural and Morphological Evolution of Epitaxial LiCoO₂ Films During Charge and Overcharge Widitha Samarakoon^{1,2}, Jiangtao Hu¹, Miao Song¹, Mark Bowden¹, Nabajit Lahiri¹, Jia Liu¹, Le Wang¹, Timothy Droubay¹, Hua Zhou³, Zhenxing Feng², Jinhui Tao¹ and Yingge Du¹; ¹Pacific Northwest National Laboratory, United States; ²Oregon State University, United States; ³Argonne National Laboratory, United States

Capacity decay of layered cathodes in high voltage applications underscores the need to utilize accurate and precise techniques to understand the underlying mechanisms. Here, we use well-defined epitaxial LiCoO₂ (LCO) films on SrRuO₃/SrTiO₃ (SRO/STO) with controlled orientations and defect structures along with *in situ* electrochemical atomic force microscopy to probe the structural and morphological evolutions during the charge and overcharge processes. We quantitatively show the morphological changes in both reversible delithiation regime and irreversible over-delithiation regime, and correlate the overall electrochemical behaviors to atomic scale defect evolutions in the films. We also observe a significantly lower charging capacity for LCO/SRO/STO(111) compared to that of LCO/SRO/STO(001) films of the same thickness, which is ascribed to the different types of atomic scale defects formed during the film growth process. Our high-resolution scanning transmission electron microscopy (STEM) and electron energy loss spectroscopy (EELS) studies reveal that the antiphase boundaries in LCO/SRO/STO(001) act as viable channels for Li migration but are more susceptible to irreversible phase transitions, which then blocks subsequent Li diffusion. The use of LiCoO₂ thin films also allows us to design epitaxial interfaces and integrate multilayers which can serve as model materials systems for subsequent studies.

2:15 PM CH03.06.03

Unraveling the Stable Cathode Electrolyte Interface in All Solid-State Thin-Film Battery Operating at 5V Diyi Cheng¹, Ryosuke Shimizu¹, Minghao Zhang¹ and Y. Shirley Meng^{2,1}; ¹University of California, San Diego, United States; ²The University of Chicago, United States

Spinel-type LiNi_{0.5}Mn_{1.5}O₄ (LNMO) is one of the most promising 5 V-class cathode materials for Li-ion batteries that can achieve high energy density and low production costs. However, in liquid electrolyte cells, the high voltage causes continuous cell degradation through the oxidative decomposition of carbonate-based liquid electrolytes. In contrast, some solid-state electrolytes have a wide electrochemical stability range and can withstand the required oxidative potential. In this work, a thin-film battery consisting of a LNMO cathode with a solid lithium phosphorus oxynitride (LiPON) electrolyte is tested and their interface before and after cycling is characterized. With Li metal as the anode, this system can deliver stable performance for 600 cycles with an average Coulombic efficiency > 99%. Neutron depth profiling indicates a slight overlithiated layer at the interface prior to cycling, a result that is consistent with the excess charge capacity measured during the first cycle. Cryogenic electron microscopy further reveals intimate contact between LNMO and LiPON without noticeable structure and chemical composition evolution after extended cycling, demonstrating the superior stability of LiPON against a high voltage cathode. Consequently, we propose design guidelines for interface engineering that could accelerate the commercialization of a high voltage cell with solid or liquid electrolytes.

2:30 PM CH03.06.04

Quantitative Elemental Analysis of Silicon Thin-Film Anodes with 100-nm Depth Resolution Xiaoyang Ji, Nathan J. Fritz, Paul Braun and David Cahill; University of Illinois at Urbana-Champaign, United States

The depth distribution of Li as well as other light elements, i.e. C, O, and F, in the electrodes of lithium-ion batteries is significant for understanding mass transport during cycling. In our work, we take advantage of the proton nuclear reactions with Li and F in addition to the elastic scatterings with all elements in electrochemically deposited silicon thin film anodes, and determine the depth distribution of Li, C, O, F, and Si quantitatively at different cycling states of silicon anodes. A high depth resolution of ~20 – 80 nm in nuclear reactions and elastic scatterings is achieved with a glancing exit angle (~80°) of the proton beam, while the resolution of nuclear reactions is higher due to scattered alpha particles with 8-MeV energy. The Li residue is twice of the Si amount in the first ten cycles, indicating rapid accumulation of trapped lithium in the silicon anode. The relative Li atomic concentration compared to Si decreases by ~10% – 50% in the deeper position of the anode. Meanwhile, the amounts of C and O increase by ~100% after the first cycle, but the amounts remain in the later cycling. We also observe larger atomic concentrations of O and F near the surface of the silicon anode, indicative of solid electrolyte interphase (SEI) formation. The quantitative analysis of the heterogeneous element distribution by this non-destructive technique will be useful to further understand the SEI formation and growth and the mechanism of lithium trapping in cycled silicon anodes.

2:45 PM BREAK

SESSION CH03.07: Li-Ion Cathode Structures
Session Chairs: Donal Finegan and Matthew McDowell
Tuesday Afternoon, November 29, 2022
Hynes, Level 1, Room 103

3:15 PM *CH03.07.01

Designing Cathode Microstructures in Lithium Batteries [Feng Lin](#); Virginia Tech, United States

The propagation of redox reactions governs the electrochemical properties of battery materials and their critical performance metrics in battery cells. The recent research progress, especially aided by advanced analytical techniques, has revealed that incomplete and heterogeneous redox reactions prevail in many electrode materials. Advanced high-capacity cathode materials are mostly polycrystalline materials that exhibit complex charge distribution (the valence state distribution of the redox-active cations) due to the presence of numerous constituting grains and grain boundaries. The redox reactions in individual grains typically do not proceed concurrently due to their distinct geometric locations in polycrystalline particles. As a result, these unsynchronized local redox events collectively induce heterogeneous and anisotropic charge distribution, building up intergranular and intragranular stress. Therefore, these polycrystalline materials may exhibit weak mechanical stability, leading to undesired chemomechanical breakdown during battery operation. Grain engineering in polycrystalline materials provides a large playground to modulate the materials properties beyond controlling the chemical composition, and electronic and crystal structures. In particular, the anisotropic ion-conducting pathways in layered oxides make the grain crystallographic orientation a critical factor in determining the modality of the redox reactions in these materials.

This presentation will discuss our recent progress in the design, synthesis, and characterization of cathode microstructures in lithium batteries.

First, we will discuss how the charge distribution is guided by grain crystallographic orientations in polycrystalline battery materials. We elucidate the spatially resolved charge distribution in lithium layered oxides with different grain crystallographic arrangements and establish a model to quantify their charge distributions. While the holistic “surface-to-bulk” charge distribution prevails in polycrystalline particles, the crystallographic orientation-guided redox reaction governs the charge distribution in the local charged nanodomains. Compared to the randomly oriented grains, the radially aligned grains exhibit a lower cell polarization and higher capacity retention upon battery cycling. The radially aligned grains create less tortuous lithium-ion pathways, thus improving the charge homogeneity as statistically quantified from over 20 million nanodomains in polycrystalline particles. This study provides an improved understanding of the charge distribution and chemomechanical properties of polycrystalline battery materials.

Second, we will discuss how the grain arrangement affects the thermal stability of polycrystalline cathode materials in rechargeable batteries. We performed a systematic in situ study on the Ni-rich polycrystalline cathode materials to investigate the fundamental degradation mechanism of charged cathodes at elevated temperatures, which is essential for tailoring material properties and improving performance. Using multiple microscopy, scattering, thermal, and electrochemical probes, we decoupled the major contributors to the thermal instability from intertwined factors. Based on our findings, the cathode grain microstructure has a forgotten yet important role in the thermal stability of polycrystalline rechargeable batteries. Oxygen release, as an important process during the thermal runaway, can be regulated through engineering grain arrangements. The grain arrangement can modulate the macroscopic crystallographic transformation pattern and oxygen diffusion length in layered cathodes to offer more possibilities for cathode material design and synthesis.

3:45 PM CH03.07.02

Reaction Heterogeneity During the Solid-State Synthesis of Ni-Rich Layered Oxide Revealed by *In Situ* Multiscale Investigation [Hayoung Park](#)¹, [Hyeokjun Park](#)^{2,1}, [Sungsu Kang](#)¹, [Yongsoon Jeon](#)¹, [Jihoon Kim](#)¹, [Kisuk Kang](#)¹ and [Jungwon Park](#)¹; ¹Seoul National University, Korea (the Republic of); ²Korea Research Institute of Standards and Science, Korea (the Republic of)

Nickel-rich layered oxides are regarded as promising next-generation cathode materials for high-energy lithium-ion batteries. However, their commercialization has been hampered by their inferior cycle stability, which stems from chemo-mechanical failures ranging from primary to secondary particle. In this work, we investigate the solid-state synthesis of $\text{LiNi}_{0.6}\text{Co}_{0.2}\text{Mn}_{0.2}\text{O}_2$ in real-time to better understand the structural and/or morphological changes during phase evolution. Multi-length-scale observations (aberration-corrected transmission electron microscopy (TEM), in situ heating TEM and in situ X-ray diffraction, etc.) reveal that the kinetic competition between the intrinsic thermal decomposition of the transition metal hydroxide at the core and the topotactic lithiation near the interface determines the overall synthesis, which results in spatially heterogeneous intermediates at the low temperature. The thermal oxidation of the precursor leads to the formation of intergranular voids and intragranular nanopores which are destructive to cyclability. Furthermore, we demonstrate that the pseudo-equilibrium synthetic pathway which promotes topotactic lithiation can mitigate the generation of defective structures and effectively suppress the chemo-mechanical failures.

4:00 PM CH03.07.05

Defect and Interface/Interphase Engineering in Electrode Materials for Metal Ion Batteries [Hui Xiong](#); Boise State University, United States

Rechargeable batteries are promising energy storage technologies to provide high energy and high power for applications such as electric vehicles and electrical grids. Recent studies have shown enhanced electrochemical charge storage in electrodes that contain intentional structural defects (e.g., vacancies and interstitials) or with tailored interfaces/interphases. In this talk, recent works in my group including engineering defects in electrode materials through ion irradiation as well as interface/interphase engineering in metal ion batteries (e.g., Li ion and Na ion batteries) will be discussed. *In situ* and *operando* characterizations that help elucidate the structural and microstructural evolution of the battery materials will be discussed. Perspectives regarding new pathways to design and engineering defects and interfaces in electrode materials with enhanced energy/power for rechargeable batteries will be given.

SESSION CH03.08: Precision Characterization Techniques
Session Chairs: Peng Bai and Hui Xiong
Wednesday Morning, November 30, 2022
Hynes, Level 1, Room 103

8:30 AM *CH03.08.01**Quantifying Functional Variability Between NMC Particles Using Single-Particle Electrochemistry** Yiyang Li; University of Michigan, United States

Heterogeneity is a commonly observed in battery materials at a variety of length scales. While heterogeneity at the electrode or cell level can be studied and understood based on porous electrode transport losses, the intrinsic heterogeneity and variability in electrochemical properties between individual particles is much more challenging to unravel. Most research into particle-level variability utilize microscopy, but this approach is only able to indirectly measure the electrochemistry using a spectroscopic signature. In this work, we present our research utilizing single-particle electrochemistry to directly quantify the electrochemical properties of single particles. By electrochemically cycling many commercial polycrystalline NMC battery particles under nominally identical conditions, we show that the area-specific resistance vary by as much as 5 times within a batch of commercial battery particles. We combine these experimental results with a porous electrode model to show how the electrochemical variability between individual particles ultimately affects the overall macroscopic behavior of the battery electrode.

9:00 AM *CH03.08.02**Evaluating Electrochemical, Chemical and Spatial Heterogeneities During Degradative Oxygen Evolution at Battery Cathodes Using a Novel Scanning Electrochemical Microscopy Toolbox** Abhiroop Mishra, Dipobrato Sarbapalli and Joaquin Rodriguez-Lopez; University of Illinois at Urbana Champaign, United States

Lattice oxygen loss during cathode charging is one of the main limitations for high-voltage lithium ion batteries and a critical player in various surface cathode phenomena including densification cathode electrolyte interphase (CEI) formation, and electrolyte degradation processes. Thus, developing techniques capable of evaluating the degradative O₂ evolution phenomena with high versatility, e.g. with (electro)chemical and spatial resolution and the capability to correlate to other surface phenomena, is pressing towards understanding and designing better cathodes. In this presentation we will discuss a novel in situ oxygen detection strategy using scanning electrochemical microscopy (SECM) in the substrate generation/tip collection mode. By approaching the tip to the substrate within a few microns, we are able to collect the generated O₂ within few milliseconds after its generation at the cathode with unprecedented sensitivity and signal to noise ratio. This allowed us to generate plots that quantified the rate of oxygen evolution vs. electrode potential. Our first results on LiCoO₂, LiNi_{0.33}Mn_{0.33}Co_{0.33}O₂ and LiNi_{0.8}Mn_{0.1}Co_{0.1}O₂ revealed an unprecedented two-stage oxygen evolution behavior from commercial cathodes with an unreported feature at ~3.3 V vs Li⁺/Li during the first charge cycle. At the main oxygen evolution features above ~3.3 V vs Li⁺/Li, SECM mapping highlighted spatial and temporal heterogeneities as the tip was positioned on different evolution sites and at different times. Further exploration using the feedback mode of SECM enables us to correlate the state of the surface to its charge transfer properties. Since such an interface could also be the source of reactive oxygen species (ROS), we have deployed generation-collection techniques and surface-interrogation SECM methods to quantify and evaluate the properties of ROS and radical intermediates formed at the interface, thus highlighting the chemical versatility of our approach. Our SECM toolbox is a unique complement to other methods used to characterize interfacial processes at battery materials, and requires very little sample preparation, being capable of addressing large format electrodes down to individual particles. This tool will help create new prospects for quantitative and spatially resolved investigations of degradation processes in operating lithium ion battery cathodes.

9:30 AM CH03.08.03**Operando Small-Angle Scattering and Cryo-Electron Microscopy to Quantify the Multiphase Nanostructure in Beyond Intercalation-Type Battery Cathodes** Christian Prehal¹, Jean-Marc von Mentlen¹, Heinz Amenitsch², Lionel Porcar³, Stefan Freunberger⁴ and Vanessa Wood¹; ¹ETH Zurich, Switzerland; ²Graz University of Technology, Austria; ³Institut Laue-Langevin, France; ⁴ISTA (Institute of Science and Technology Austria), Austria

Beyond intercalation-type batteries, such as Li-sulfur (Li-S) batteries could be game-changers in many respects: a theoretical specific capacity among the highest of all batteries paired with low cost and sustainability of sulfur. However, insufficient understanding of the mechanism that reversibly converts sulfur into lithium sulfide (Li₂S) via soluble polysulfides hampers the realization of high-performance Li-S cells. Developing (*operando*) experimental techniques with seamless sensitivity from atomic to sub-micrometer length scales is crucial to identifying physicochemical mechanisms and important structure-property relationships.

Here we present *operando* small- and wide-angle X-ray scattering (SAXS / WAXS) and *operando* small-angle neutron scattering (SANS) to track the growth and dissolution of solid deposits from atomic to sub-micron scales during charge and discharge (Prehal et al., preprint: <https://doi.org/10.21203/rs.3.rs-818607/v2>). Stochastic modeling based on the SANS data allows quantification of the chemical phase evolution in real space (Prehal et al. PNAS 118, e2021893118, 2021 & Prehal et al. Nature Communications 11, 4838, 2020). Cryo-scanning transmission electron microscopy with electron energy loss spectroscopy (cryo-STEM/EELS) provides complimentary local structural information. It verifies the model input for analyzing the *operando* scattering data via stochastic modeling. We show that the deposit nanostructure in Li-S batteries consists of the known nanocrystalline Li₂S and a second solid discharge product which we identify as smaller, solid Li₂S₂ particles. Knowing this has important consequences on how to influence the reaction, discharge capacities, and rate performance. Based on the example of Li-S batteries, we demonstrate that structural information on mesoscopic length scales (1 – 1000 nm) is key to understanding complex transformations such as the electrodeposition and stripping of insulating materials in beyond-intercalation-type battery cathodes. *Operando* SAXS/SANS, cryo-STEM/EELS, and stochastic modeling combine the advantages of integral time-resolved structural information, local element-specific microscopy, and quantitative data analysis.

9:45 AM BREAK

SESSION CH03.09: Heterogeneities of Solid Electrolyte Interphase
Session Chairs: Peng Bai and Joaquin Rodriguez-Lopez
Wednesday Morning, November 30, 2022
Hynes, Level 1, Room 103

10:15 AM +CH03.09.01**The Role of SEI Heterogeneity on Charge Transfer Reactions at Li/SEI/Electrolyte Interfaces** Yue Qi; Brown University, United States

Two kinds of charge transfer reactions are critical for the performance and life of lithium battery: the desired *ion transfer* reaction occurring during each charge/discharge cycle, and the undesired *electron transfer* reactions leading to the parasitic chemical decomposition of the electrolyte and solid electrolyte interphase (SEI) formation/growth. The heterogeneous multi-component nature of SEI dominates its ionic and electronic transport properties

and controls these two charge transfer reactions. Density Functional Theory (DFT)-informed multiscale modeling has been providing valuable insights under the scarcity of quantitative experiments. For example, the LiF/Li₂CO₃ interface was demonstrated to increase the ionic conductivity of mixed SEI nanocomposite by forming an ionic space charge region near the interface and promoting more Li-ion interstitials in Li₂CO₃, although LiF itself has low Li-ion conducting carriers and conductivity. On the other hand, the grain boundaries (GBs) in SEI facilitate electron transport pathways, as all GB structures, especially amorphous GBs, have smaller bandgaps than their corresponding single crystals. Some GBs, such as the symmetric Li₂S Tilt Σ 3 GB and the amorphous LiF GB, showed empty electronic states lower than the standard Li⁺/Li⁰ depositing potential. The electron leakage through these grain boundaries will lead to continuous SEI growth and the trapped electrons will facilitate Li metal nucleation inside of SEI. Therefore, a new DFT-informed-phase field model is developed to capture the Li and SEI morphology change simultaneously due to these two charge transfer reactions.

10:45 AM CH03.09.02

First-Principles Modeling of Vinylene Carbonate Reactivity at Li-Metal Electrode—New Insights on SEI Formation Initial Steps Michèle Pavone, Francesca Fasulo and Ana B. Muñoz-García; University of Napoli Federico II, Italy

The metallic lithium (Li) represents the most promising anode material among the next generation of solid-state lithium batteries [1]. An efficient strategy to achieve durable and effective Li-anode batteries is by engineering the solid-electrolyte interphase (SEI) with purposely designed molecules. To this aim, the vinylene carbonate (VC) is one of the most used additives in conventional electrolytes. Some recent experiments proved that the VC promotes the formation of a stable and protective SEI layer between Li metal and electrolyte [2, 3]. Unless the well-known SEI composition, it is difficult to control the VC reactivity, that involves dissociation and polymerization at the electrode surface. Therefore, to dissect these tangled processes, here we present new atomistic insights on VC-Lithium SEI formation via first-principles calculations by Density Functional Embedding Theory (DFET) [4, 5]. Such approach has potentialities for modeling complex reactions at hybrid interfaces in electrocatalysis: it is well suited to combine the best feasible approaches for molecular species (in this case, hybrid HF-DFT for VC molecules and derivatives) and for Li metal electrode (semi-local GGA density functional). Our results highlight different VC dissociation pathways, with formation of reactive radical species and localized cluster of Li₂O and Li₂CO₃. The use of hybrid-DFT-in-DFT embedding is crucial for obtaining energy barriers and qualitative results in agreement with experiments [3]. Overall, the energetics and structural features of these intermediates improve the current understanding of SEI formation process and can be exploited to drive the reactions toward the desired interfacial properties.

[1] J. Janek, W. G. Zeier, *Nat Energy* 1 (2016) 16141.

[2] A. L. Michan et al. *Chem. Mater.* 28 (2016) 8149.

[3] Y. Kamikawa, K. Amezawa, K. Terada, *J. Phys. Chem. C* 124 (2020) 19937

[4] C. Huang, M. Pavone, E. A. Carter, *J. Chem. Phys.* 134 (2011) 154110

[5] C. Huang, A.B. Muñoz-García, M. Pavone, *J. Chem. Phys.* 145 (2016) 244103

11:00 AM CH03.09.03

Unveiling the Role of Electrolyte on Solid-Electrolyte Interphase Formation and Structure of Li Deposit Yaobin Xu¹, Dingchuan Xue², Hao Jia¹, Ruyue Fang², Ji-Guang Zhang¹, Wu Xu¹ and Chongmin Wang¹; ¹Pacific Northwest National Laboratory, United States; ²Pennsylvania State University, United States

The morphology of electrochemically deposited lithium (EDLi) plays critical role on the cycling stability and safety performance of Li metal batteries. However, formidable challenges and shortcomings of Li metal electrode are currently plaguing its practical application, and the two greatest ones are safety and cycle life. Both of which are associated with the dendritic Li deposition morphology.¹⁻⁴ Especially, the key parameters that control the morphologies remain largely obscure. Here we use cryogenic transmission electron microscopy (cryo-TEM) to probe, at atomic level, the features of solid electrolyte interphase (SEI) on Li particle and Li whisker formed in the same coin cell using carbonate electrolyte and ether electrolyte. In the carbonate-based electrolyte, the SEI layer on the Li whisker and Li particle is similarly monolithic amorphous structure, but the composition and spatial distribution of the chemical species within the SEI are distinctively different for Li particle and Li whisker. In the ether-based localized high concentration electrolyte (LHCE), the SEI layer on the Li particle leads to a mosaic structured SEI with few Li₂O nanoparticles embedded, and rich of sulfur (S) in composition, especially at the outer layer SEI (mainly from anion salt decomposition), while the SEI layer of Li whisker displays bilayer structure. The distinctive difference of SEI on Li particle and Li whisker from the same coin cell delineates insight on the direct correlation between features of SEI layer and Li morphology, leading to possible tuning of crucial structural and chemical features of SEI to regulate the morphology of Li deposit.

1. Xu, K., Electrolytes and Interphases in Li-Ion Batteries and Beyond. *Chem Rev* 2014, 114 (23), 11503-11618.

2. Cheng, X. B.; Zhang, R.; Zhao, C. Z.; Zhang, Q., Toward Safe Lithium Metal Anode in Rechargeable Batteries: A Review. *Chem Rev* 2017, 117 (15), 10403-10473.

3. Lin, D. C.; Liu, Y. Y.; Cui, Y., Reviving the lithium metal anode for high-energy batteries. *Nat Nanotechnol* 2017, 12 (3), 194-206.

4. Zou, P.; Sui, Y.; Zhan, H.; Wang, C.; Xin, H. L.; Cheng, H. M.; Kang, F.; Yang, C., Polymorph Evolution Mechanisms and Regulation Strategies of Lithium Metal Anode under Multiphysical Fields. *Chem Rev* 2021.

11:15 AM CH03.09.04

Dissolution of the Solid Electrolyte Interphase and its Effects on Lithium Metal Anode Cyclability Philaphon Sayavong, Wenbo Zhang, Solomon Oyakhire, David Boyle, Yuelang Chen, Sang Cheol Kim, Rafael Vilá, Sarah Holmes, Mun Sek Kim, Stacey F. Bent, Zhenan Bao and Yi Cui; Stanford University, United States

Despite their potential to provide higher energy density rechargeable batteries, Lithium metal anodes (LMA) suffer from low cyclability. The cycle life of LMA is largely tied to the stability and physicochemical properties of the solid electrolyte interphase (SEI), a nanoscale layer that mitigates the thermodynamic instability of Li metal towards the electrolyte. Using cryogenic-TEM, recent studies by Boyle *et al.* and Huang *et al.* suggest that dissolution of SEI components can introduce nanoscopic interphasial heterogeneities in LMAs.^{1,2} Dissolution compromises the efficacy of the passivation layer since additional electrolyte and Li must be consumed to repair the partially dissolved SEI, resulting in a thicker and more heterogeneous layer.^{3,4} Despite its significance, fundamental understanding of SEI dissolution using electrolytes optimized for LMAs remain lacking. More importantly, it is difficult to gauge on how much SEI dissolution can affect cyclability without a quantitative and systematic study of the process.

In this presentation, we will report the utilization of *in-operando* electrochemical quartz crystal microbalance (EQCM) technique to systematically quantify and compare SEI solubility using ether-based electrolytes for LMAs. Correlating SEI solubility results with performance metrics obtained from coulometric experiments allowed us to establish a correlation between solubility, passivity, and cyclability. Building upon this, we illustrate that cycle life can be further extended for one of the best electrolytes by shifting the SEI solubility equilibria. This suggests that the cycle life of a state-of-the-art electrolyte can be extended by decreasing SEI dissolution, illustrating that solubility is another knob that can be tuned to effectively improve cyclability.

Together with EQCM, X-ray photoelectron spectroscopy (XPS) and nuclear magnetic resonance (NMR) spectroscopy results, we reveal that solubility is dependent on not just the SEI's composition, but also the properties of the electrolyte. We show that comparing SEI solubilities solely based on its composition becomes less reliable for high-performance electrolytes. Our analyses indicate that the differences in the amount of anion-derived component in their SEIs become small enough that the physical and chemical property of the electrolytes start to play a more significant role in dissolution. This crucial piece of information could aid in future design of more passivating and stable SEIs by not just tuning the SEI composition, but also tuning the physical and chemical property of the electrolyte to minimize SEI dissolution even more effectively.

References

1. D. T. Boyle, W. Huang, H. Wang, Y. Li, H. Chen, Z. Yu, W. Zhang, Z. Bao, Y. Cui, *Nat. Energy*, **6**, 487–494 (2021).
2. W. Huang, H. Wang, D. T. Boyle, Y. Li, Y. Cui, *ACS Energy Lett.* **5**, 1128–1135 (2020).
3. M. Broussely, Ph. Biensan, F. Bonhomme, Ph. Blanchard, S. Herreyre, K. Nechev, R. J. Staniewicz, *Sel. Pap. Press. 12th Int. Meet. Lithium Batter.* **146**, 90–96 (2005).
4. S. K. Heiskanen, J. Kim, B. L. Lucht, *Joule*, **3**, 2322–2333 (2019).

11:30 AM CH03.09.05

A Comparison of Solid Electrolyte Interphase Evolution on Highly Oriented Pyrolytic and Disordered Graphite Negative Electrodes in Lithium-Ion Batteries Joshua Russell¹, Haoyu Zhu¹, Zongtang Fang², Lan Li^{1,3}, Jeremy May⁴, I. Francis Cheng⁴, Paul H. Davis¹, Eric Dufek² and Hui Xiong^{1,3}; ¹Boise State University, United States; ²Idaho National Laboratory, United States; ³Center for Advanced Energy Studies, United States; ⁴University of Idaho, United States

During the initial cycling of lithium ion batteries (LIBs), the reaction of negative electrode with electrolyte will result in the formation of a thin film on the electrode surface. This film is referred to as solid electrolyte interphase (SEI), the stability of which is essential for practical LIBs. The most commonly used negative electrode material in LIBs is graphite, due to its low working potential for reversible lithium intercalation/deintercalation (≈ 0.1 V vs Li^+/Li), relatively high theoretical capacity of 372 mAh g^{-1} , and good cycling stability. Previous studies have indicated that in graphite, the basal to edge plane ratio, particle size, pore size, degree of crystallinity and surface chemical composition affected the formation of SEI and its stability. The presence of defects in graphite is also a very important factor for SEI formation but has been rarely studied. Here, we investigated the SEI formation on an almost perfect graphite - HOPG (Highly Oriented Pyrolytic Graphite) - and a synthetic defective carbon film - GUITAR (pseudo-Graphite from University Idaho Thermolyzed Asphalt Reaction) - through operando electrochemical atomic force microscopy (EC-AFM). It was found that the defects on GUITAR promoted the electrolyte decomposition and SEI formation at a higher potential. Furthermore, the SEI particles evenly formed and densely packed on the GUITAR surface with a particle size of $172 \text{ nm} \pm 83 \text{ nm}$ and a thickness of about 60 nm. The SEI thickness on this defective electrode surface is three times of that on HOPG (about 20nm). It is also noteworthy that on HOPG, the formed SEI only partially covered the electrode surface, along with the graphite layer delamination from the step edge and bulging on the basal plane. This study showed direct evidence of how structural defects affect SEI nucleation and growth upon cycling.

11:45 AM CH03.09.06

Uncovering Nanoscale Factors of Graphite Solid-Electrolyte Interphase Formation— From Molecular Layers to 3D Nanoarchitecture Yue Chen^{1,2}, Wenkai Wu³, Avishek Dey^{4,2}, Robert Palgrave^{4,2} and Oleg V. Kolosov^{1,2}; ¹Lancaster University, United Kingdom; ²Faraday Institution, United Kingdom; ³Swansea University, United Kingdom; ⁴University College London, United Kingdom

The solid electrolyte interphase (SEI), a passivation layer formed on the battery electrode-electrolyte interface [1], defines fundamental battery properties - its capacity, cycle stability and safety. While understanding the SEI formation holds keys to these, such studies are complicated by the diversity of interlinked surface reactions and complex nanoarchitecture of the anode active material and electrical double layer (EDL) [2]. Such nanoarchitecture predetermines the electrolyte supramolecular interactions, electrical charge and ion transport therefore dominating the initial SEI formation. To date, the real space molecular arrangements of electrolyte solvents/anions inside the EDL and their effects on the SEI formation remain elusive [3].

In this work, we resolve this complex puzzle, using novel solid-liquid characterization tool with a nanoscale spatial resolution for accessing the whole evolution process from initial molecular-scale EDL structures, toward nanoscale 3D SEI structures. We introduce *in-situ* electrochemical 3D nanorheology microscopy (3D-NRM) [4] combined with magnetic excitation molecular-level solvation force spectroscopy and molecular dynamics simulations to explore a matrix of two morphologically dissimilar but chemically identical surfaces of typical carbon electrode material (basal and edge graphene planes) and different solvent-electrolyte systems (strong and weakly solvating electrolytes, as well as ionic liquid electrolyte). These approaches allowed us to get direct insight into the atomistic pictures for the underlying influence of cation's intercalation and solvation structures on the initial SEI formation.

We found that in the traditional ethylene carbonate (EC) based electrolyte, the strong coordination and co-intercalation of EC solvent dominate the electrolyte decomposition, causing the “swelling” of graphite carbon edge planes and thick SEI accumulations, confirming that SEI formation is graphite crystal plane dependent. At the same time, in the weakly solvation and ionic liquid electrolytes, where the first cation solvation sheath is occupied by the fluorine rich anion, the negatively polarized electrode surface builds up a unique and ordered EDL structure resulting in the preferential reductive decomposition of the anion and creating a highly sought after robust SEI layer. We also observe that the solvent/anion coordination structures with lithium/sodium cation within EDL vary from the bulk electrolyte, modifying the LUMO level of the electrolyte and affecting its electrochemical stability. Our understanding of these key interfacial structural factors in SEI formation allows targeting an electrochemically and mechanically robust surface passivation layer and guiding the development of efficient and safe rechargeable batteries.

References

1. Liu, T., et al., In situ quantification of interphasial chemistry in Li-ion battery. *Nat Nanotechnol.* 2019, 14(1): p. 50-56.
2. Rakov, D.A., et al., Engineering high-energy-density sodium battery anodes for improved cycling with superconcentrated ionic-liquid electrolytes. *Nat Mater.* 2020.
3. Li, C.-Y., et al., Unconventional interfacial water structure of highly concentrated aqueous electrolytes at negative electrode polarizations. *Nature Communications*, 2022, 13(1).
4. Chen, Y. et al, Controlling Interfacial Reduction Kinetics and Suppressing Electrochemical Oscillations in $\text{Li}_4\text{Ti}_5\text{O}_{12}$ Thin-Film Anodes, *Advanced Functional Materials* 2021, 31 (43), 2105354.

Wednesday Afternoon, November 30, 2022
Hynes, Level 1, Room 103

1:30 PM *CH03.10.01

Heterogeneous Damage and Network Evolution in Composite Electrodes of Li-Ion Batteries [Kejie Zhao](#); Purdue University, United States

We assess the heterogeneous electrochemistry and mechanics in a composite cathode using synchrotron X-ray tomography, machine learning, and microstructure-resolved computational modeling. We visualize the morphological defects at multi-scales ranging from the macroscopic composite, particle ensembles, to individual single particles. Particle fracture and interfacial debonding are identified in a large set of tomographic data. The mechanical failure of active particles is highly heterogeneous. The difference originates from the polarization of the electrolyte potential, various local conducting environments, and thus the non-uniform distribution of the activation energy for the charge transfer reaction. We model the kinetics of intergranular fracture and interfacial degradation to assess the heterogeneous mechanical damage in composite electrodes. We quantify the influence of the mechanical damage on the metrics of battery performance. The mechanical failure disrupts the conduction path of electrons and results in significant polarization and capacity loss in batteries. More interestingly, the interfacial failure may reconstruct the conductive network and redistribute the electrochemical activities that render a dynamic nature of electrochemistry and mechanics evolving over time in the composite electrodes.

2:00 PM CH03.10.02

Mechanics of Fibre Debonding in Structural Battery Composites [Kai Guo](#), Keith Foo, Bharathi M. Srinivasan and Sridhar Narayanaswamy; Institute of High Performance Computing, Singapore

The concept of providing power in the form of structural energy storage devices, for example structural supercapacitors and structural batteries, are a potentially viable strategy to achieve both high energy density and a load bearing structure. Structural battery composites, a subclass of composite materials, can provide mechanical integrity and energy storage capability simultaneously. A candidate architecture of a structural battery composite are carbon fibres embedded in an electrolyte matrix material. Mechanical failure mechanisms in structural battery composites are not yet well understood, especially when external mechanical loads are applied. We present modelling results for fibre debonding, a key failure mechanism in a structural battery composite made from carbon fibres and polyethylene oxide (PEO) matrix. We derive the energy release rate for fibre debonding under both electrochemical and mechanical loadings using the solution to the Eshelby's inclusion problem. We discuss the coupling effects of Li content in carbon fibres and external mechanical loads on fibre debonding and provide guidelines for reliable operation of the composite structure.

2:15 PM CH03.10.03

In Situ Optical Methods to Quantify Macroscopic Stress Developed on Electrode Materials During Lithiation [Mayukh Nandy](#), Todd Houghton, Haiwei Wu, Hongbin Yu and Candace Chan; Arizona State University, United States

With the advent of mobile electronics, the need for durable high energy density storage devices like lithium-metal batteries has surged many folds in recent times. To transform the electronics industry, this need must be met as more rigid, bulky devices are replaced by their thin, lightweight yet high-performance counterparts. However, the mechanical stress induced due to electrochemical deposition of Li on the surface of the current collector of lithium-metal batteries still remains a major area of concern, directly affecting the durability of the cell. In this paper, two novel non-contact in-situ techniques are used to characterize mechanical stress experienced by electrodes during Li electroplating. Optically transparent electrochemical cells were prepared with a soft Li metal sheet as the reference electrode and Cu coated PET sheet as the working electrode or current collector. Lithium hexafluorophosphate solution in ethylene carbonate and diethyl carbonate (1.0 M LiPF₆ in EC/DEC=50/50 v/v) is used as the electrolyte. The first characterization method involves a camera setup to monitor the bending angle during charge and discharge cycles. The second technique uses the reflection of a helium neon laser beam off the shiny PET surface. The displacement of the reflected beam is observed and further quantified to obtain the change in bending angle. Both methods are sensitive to structural changes during lithiation. Before Li deposition, the cell is first activated using a LSV (linear sweep voltammetry) method at 5mV s⁻¹ and the ending voltage is set to 0 V. During this process, a minor amount of Cu oxide layer on the surface of Cu coated PET is gradually lithiated and the Solid-Electrolyte Interphase (SEI) layer is formed, which is ready for inducing further Li metal deposition. The change in bending angle was recorded with and without the SEI layer formation. Other parameters like charge density, charge time, number of charge-discharge cycles, and idle time between cycles were varied to observe the difference in bending. The angle change is then used to quantify stress. This type of in-situ stress measurement method is particularly useful to test the reliability of electrodes in cells by studying the physical changes of those materials and their surfaces as they interact with lithium.

2:30 PM BREAK

SESSION CH03.11: Alkali-Ion Batteries
Session Chairs: Luxi Li and Hui Xiong
Wednesday Afternoon, November 30, 2022
Hynes, Level 1, Room 103

3:30 PM CH03.11.02

Revealing the Interaction of Li and Na in Layered Oxide Host by Synchrotron X-Rays and Scanning Transmission Electron Microscopy [Grant Hill](#) and Chong Liu; University of Chicago, United States

Insertion materials are key for electrochemical energy storage, but also have important applications in the areas of electrochemical ion separations, desalination, and catalysis. For ion separations, electrochemical extraction with layered cobalt oxides is a promising method for the separation of Li from Na-rich resources. However, the resulting composition and phase of the host material from co-insertion of cations and its relationship to Li separation performance has not been explored. Here, we developed a core-shell structured (NaLi)_{1-x}CoO₂ via non-Faradaic ion-exchange using parent Li_{1-x}CoO₂ with Na ions. Using synchrotron X-rays and scanning transmission electron microscopy, we reveal the phase separation of low vacancy Li-phase (core), high-vacancy Na-phase (shell), and intermediate phase. The spatial distribution and chemical composition of these phases play critical roles to the Li selectivity. Additionally, we investigate the relationship between alkali cation vacancy on the extent of ion-exchange. Using electrochemical intercalation, this material successfully extracted Li from 1:20,000 Li to Na solution to 7.6:1 Li to Na, which is a Li selectivity of 1.5 x 10⁵ over Na. Therefore, this material has

potential application in Li extraction from seawater and other Li containing brines. Beyond application, heterogeneity characterization of ion-exchange and co-insertion processes allows for a deeper understanding of phase transformation and ion transport phenomenon in insertion materials. These insights may guide development of new materials for electrochemical ion separations, energy storage, and other applications.

3:45 PM CH03.11.05

Altering Ca²⁺ Solvation Dynamics at the Electrolyte/Electrode Interface with Cations and Anions Feipeng Yang¹, Kun Qian^{1,2}, Yang Ha¹, Zengqing Zhuo¹, Scott A. McClary³, Ana Sanz-Matias¹, Nathan Hahn³, David Prendergast¹, Kevin R. Zavadil³ and Jinghua Guo¹; ¹Lawrence Berkeley National Laboratory, United States; ²The University of Akron, United States; ³Sandia National Laboratories, United States

Calcium, with its safe, economic, and nontoxic nature, is considered a promising candidate in multivalent battery technologies. It offers the promise of a more than two-fold increase in the volumetric capacity compared to the monovalent lithium-ion batteries. The understanding of the solvation and charge transfer mechanism at the electrolyte/electrode interface and how different types of cations and anions will affect the calcium solvation at this interface is the key to developing novel calcium batteries. To probe the Ca²⁺ coordination at the electrolyte/electrode interface as a function of the type of anions, total electron yield (TEY) mode soft X-ray absorption spectroscopy (XAS) sensitive to the interfacial speciation has been employed under operando electrochemical conditions. Meanwhile, total fluorescence yield (TFY) mode XAS is sensitive to bulk speciation. Calcium bis(trifluoromethanesulfonyl)imide (CaTFSI₂) in tetrahydrofuran (THF) is an attractive electrolyte because of its oxidative stability and high solubility in various solvents. Combining calcium L-edge soft XAS with resonant soft X-ray scattering (RSoXS) through a patterned interface, the solvation and desolvation dynamics of calcium at the electrolyte/electrode interface was deciphered, and the influence of a second cation and anion were investigated. These in-situ/operando synchrotron-based spectroscopic and scattering characterization will answer the fundamental questions regarding the solvation and charge transfer at the electrode/electrolyte interface and benefit the future development of calcium-ion batteries.

SESSION CH03.12: Advanced Characterization of Li-Ion Batteries

Session Chairs: Peng Bai and Feng Lin

Thursday Morning, December 1, 2022

Hynes, Level 1, Room 103

8:30 AM *CH03.12.01

A Macro-to-Nano Zoom Through the Hierarchy of a Lithium-Ion Battery Yijin Liu; SLAC National Accelerator Laboratory, United States

Lithium-ion battery (LIB) is featured by structural and chemical complexities across a broad range of length scales and, ultimately, it is the hierarchy of the battery structure that determines its functionality. It worth highlighting that, the battery degradation is further complicated as the battery is integrated into and operated for powering a compact system. For example, in a set of commercial wireless earbuds, multiple lithium ion batteries in different forms are integrated and each one of them has to frequently interact with their peers, the battery management units (BMU), the printed circuit boards (PCB), microphones, sensors in the device. The study of the battery function, degradation, and failure mechanisms requires a thorough and systematic investigation from the structural, chemical, mechanical, and dynamic perspectives. X-ray-based characterization techniques are playing an important role in this research field.

In this talk, I will review my group's research activities over the past few years by presenting a macro-to-nano zoom through the hierarchy of a standard battery cell using a suite of state-of-the-art X-ray techniques. Damage, deformation, compositional and chemical heterogeneity at different length scales are visualized and are associated to different degradation phenomena and mechanisms. Our results highlight the importance of the battery cathode material's mechanical properties, which evolve upon battery cycling and could significantly impact both the immediate and the long-term cell behaviours. Finally, I will briefly discuss our recent efforts in conducting in-device battery failure analysis, which can provide valuable insights for the next-generation device design. I hope this presentation will ignite enthusiasm and ideas for future collaborations.

9:00 AM CH03.12.02

Synchrotron X-Ray Fluorescence Microscopy for Studying Materials Degradation in Rechargeable Batteries Yuxin Zhang¹, Anyang Hu¹, Luxi Li² and Feng Lin¹; ¹Virginia Tech, United States; ²Argonne National Laboratory, United States

The X-ray fluorescence microscopy (XFM) is a powerful technique that possesses the following advantages: (1) simultaneous detection of multiple elements with high sensitivity, favorably in the sub-ppm range; (2) sufficient spatial resolution; (3) capability of *in situ* measurements under operating conditions and (4) large-area scanning (μm to mm) to ensure statistical representativeness. It is widely applied in the biological and medical areas while receiving less attention in rechargeable batteries. Herein, using the aqueous batteries as a platform, we systematically demonstrate the application of XFM in the battery field. The ex-situ measurements can inform the degradation issues of traditional cathode materials (LiFePO₄, LiMn₂O₄, and LiNi_{0.8}Mn_{0.1}Co_{0.1}O₂) in different electrolytes and quantify the dissolved transition metals (TM) during electrochemical cycling, establishing the correlation between TM dissolution and electrochemical performance. On the other hand, the in-situ experiments can unravel the spatiotemporal evolution of TM in the electrodes and electrolytes upon cycling. Therefore, we are able to use the home-designed in situ cell to directly investigate the electrode-electrolyte interfacial reactions. For example, the evolution of the diffusion layer formed by TM dissolution can be visualized under different electrochemical protocols, and the dissolution/redeposition dynamics of TM can be revealed at the single-particle resolution and electrode-scale statistical analysis. The present work shows the capabilities of XFM in the rechargeable battery field and potentially serves as a guideline for future XFM-related studies.

9:15 AM CH03.12.03

Lithium-Ion Battery Electrode Manufacturing Model Using X-Ray Computed Tomography Characterization Data Jiahui Xu^{1,2}, Alain C. Ngandjong^{1,2}, Chaoyue Liu^{1,2}, Franco M. Zanotto^{1,2}, Oier Arcelus^{1,2}, Arnaud Demortiere^{1,2,3} and Alejandro A. Franco^{1,2,3}; ¹Laboratoire de Réactivité et Chimie des Solides (LRCS), UMR CNRS 7314, France; ²Réseau sur le Stockage Electrochimique de l'Energie (RS2E), FR CNRS 3459, France; ³ALISTORE-European Research Institute, FR CNRS 3104, France

Nowadays, in face of the increasing need for lithium-ion batteries (LIBs), how to achieve higher energy densities while maintaining or reducing costs has been widely studied. To achieve optimization of the performance of batteries, it is essential to understand the influence of parameters at each stage of the LIBs manufacturing process on the architectures of the electrodes, which affects the energy, power, lifetime and safety of the LIB cells. Non-destructive techniques, such as X-ray computed tomography (XCT), are widely used to obtain the microstructure of electrodes, enabling volume-based 3D characterization. However, the characterizing the spatial location of the carbon binder domain (CBD) in the electrode volume is challenging due

to the nano-features and the similarities between X-ray attenuation coefficients of carbon and pores. Extensive works have been done recently to improve the characterization of CBD, such as combining separate scans of high-attenuating $\text{LiNi}_x\text{Mn}_y\text{Co}_{1-x-y}\text{O}_2$ (NMC) and low-attenuating CBD¹, using X-Ray holographic nano-tomography², and using convolutional neural network-based image segmentation methods³.

The ARTISTIC project⁴, funded by the European Research Council, aims at developing a digital twin that enables predicting the electrode architectures and their electrochemical performances from the parameters used at each stage of the LIBs manufacturing process. Such a digital twin is supported by a combination of multiscale modeling⁵⁻⁹ and machine learning (ML)¹⁰. In this work, we present our new computational approach to simulate the manufacturing process of cathodes by taking into account CBD and the realistic shape of $\text{LiNi}_{0.33}\text{Mn}_{0.33}\text{Co}_{0.33}\text{O}_2$ (NMC111) active material particles obtained by X-ray micro-computational tomography (μ -XCT)¹¹. Our methodology encompasses coarse-grained molecular dynamics (CGMD) to simulate the different manufacturing stages, from the slurry, to the drying and the calendaring of the resulting electrodes. The μ -XCT data is segmented through a Random Forest algorithm available in the Image J Trainable Weka segmentation plugin to extract the active material (AM) phase. Then a Watershed-based algorithm is used to separate the individual secondary particles. The input of CGMD model is prepared by substituting the down-sampled voxels of the individual particles by spherical primary AM particles with equivalent volume. The new model captures the variation of the electrode microstructure in the manufacturing process from the particle scale, and the effect of the manufacturing parameters on the electrode heterogeneity. We discuss the changes in porosity, tortuosity factor, electronic conductivity, different phases distribution and pore network during the calendaring process and compare them with the μ -XCT results, which show reasonable agreements. In addition, our approach allows capturing the deformation of the secondary particles during the calendaring process, as well as their possible variation of orientation.

Reference:

1. X. Lu et al., Nat Commun 2020, 11, 2079.
2. T. Nguyen et al., Adv. Energy Mater. 2021, 11, 2003529.
3. Z. Su et al., npj Comput Mater 2022, 8, 30.
4. "ERC Artistic: Home", can be found under <http://www.erc-artistic.eu/>
5. T. Lombardo et al., Batteries & Supercaps 2020, 3, 721.
6. T. Lombardo et al., Energy Storage Materials 2021, 43, 337.
7. A. C. Ngandjong et al., Journal of Power Sources 2021, 485, 229320.
8. A. Shodiev et al., Energy Storage Materials 2021, 38, 80.
9. C. Liu et al., Journal of Power Sources 2021, 512, 230486.
10. M. Duquesnoy et al., ArXiv, 2022. arXiv:2205.01621
11. J. Xu et al., ArXiv, 2022. arXiv:2206.03969

9:30 AM CH03.12.04

Characterization and Modeling of NMC Particle Architectures [Donal Finegan](#); National Renewable Energy Laboratory, United States

The sub-particle architecture of $\text{LiNi}_x\text{Mn}_y\text{Co}_z\text{O}_2$ (NMC) considerably influences the performance of electrodes in Li-ion batteries, yet quantifying sub-particle properties and identify favorable particle architectures remains extremely challenging. In this presentation, progress towards quantifying sub-particle properties that are relevant to the electrochemical and mechanical performance of NMC particles will be covered. Techniques include using accessible and high-throughput 2D electron backscatter diffraction (EBSD) and 3D focused ion beam (FIB) EBSD to quantify the morphology and orientations of sub-particle crystallographic grains. Furthermore, using image-based NMC particle architectures, continuum-level models were developed to spatially and temporally resolve mechanical strain within NMC particles as the morphology of sub-particle grains evolves during lithiation and delithiation. A range of different image-based particle architectures with varying particle size and grain size were explored via continuum level models and the influence of sub-particle architectures on the life and high rate performance of electrodes is clarified.

9:45 AM BREAK

10:15 AM CH03.12.05

Study of Heterogeneous Aging Inside Different Pouch Cell Formats with Equal Chemistry (NMC 622/ Graphite + Silicon) and Operando Monitoring of the Aging Mechanisms [Alexia Bichon](#), Sylvie Geniès, Philippe Azaïs, Didier Buzon, Sébastien Fiette and Olivier Raccurt; Université Grenoble Alpes, France

Lithium-ion batteries (LIBs) present a major challenge for the coming decade as they could be massively implemented in the EVs in order to replace combustion engines. Although they have been extensively studied, some issues remain, particularly with regard to fast charging and the resulting aging mechanisms. When it comes to the choice of electrode materials, compromises must be made between high energy density, safety and fast charging capability. In order to get performant batteries in these three topics, a better understanding of cell behavior at all scales is needed.

The objective of our study is to understand the impact of the cell format on the development of non-uniform aging [1] by establishing links between different scales: materials, electrodes and cell. There are currently several cell formats on the market ranging from a few mAh to several Ah, packaged in flexible or hard cases and with the electrodes stacked or wound. In order to control the different parameters that can influence the aging, we chose to manufacture the electrodes (NMC 622 ($\text{LiNi}_{0.6}\text{Mn}_{0.2}\text{Co}_{0.2}\text{O}_2$) / Graphite + 10% SiOx) and the cells in our lab. By doing this we were able to know the precise chemistry of the electrodes and electrolyte, and to assemble them in the formats we desired. Two different formats were studied: one with a single layer pair of electrodes of 30 mAh and another one, a multi-layer stack of 500 mAh. Having the same chemistry allows for comparison of aging behaviors [2] with minimal influencing parameters, except for cell design. The cells experienced the same protocols at different C-rates and different temperatures and were stopped at different state of health (SoH).

We monitored electrochemical responses of both positive and negative electrodes independently with a reference electrode, allowing the operando follow-up of the aging behaviors. One of the main concerns with LIBs aging is the growth of lithium plating, which is the metallic deposition of lithium ions on the surface of the negative electrode. The growth of lithium dendrites is a major safety issue because they can pass through the separator and create an internal short-circuit in the cell, causing a thermal runaway that can set the battery on fire. Therefore, following the negative electrode potential is crucial to determine the conditions of apparition of lithium plating. We noticed that the depth of discharge of the previous cycle highly influences the next charging profile of the negative electrode. That could bring an explanation about the sudden decrease in capacity observed frequently after the checkup cycles at low current in discharge performed regularly during the cycling test and used to evaluate the effective capacity.

We performed post-mortem analyses in order to correlate electrochemical response of each electrode, capacity fade, and local heterogeneous degradation mechanisms. Using visual inspection, surface analysis techniques such as EDS and XPS, impedance spectroscopy and XRD mapping, we tracked lithiation and degradation heterogeneities at different scale levels: material, electrode and cell.

References

[1] Beck, et al. « Inhomogeneities and Cell-to-Cell Variations in Lithium-Ion Batteries, a Review ». *Energies* 14, no 11 (2021): 3276. [2] Li, X. et al. « Degradation mechanisms of high capacity 18650 cells containing Si-graphite anode and nickel-rich NMC cathode ». *Electrochimica Acta* 297 (2019): 1109-20.

10:30 AM CH03.12.06

Origin of Structural Degradation in Li-Rich Layered Oxide Cathode Tongchao Liu and Luxi Li; Argonne National Laboratory, United States

Li and Mn-rich cathode materials (LMR) that utilize both cation and anion redox can yield substantial increases in battery energy density. However, even though voltage decay issues cause continuous energy loss and impedes its commercialization, prerequisite driving force for this phenomena is a mystery. Here, with *in-situ* nanoscale sensitive coherent X-ray diffraction imaging (BCDI) techniques, we reveal that nanostrain and lattice displacement accumulate continuously during cell operation. Evidence unequivocally shows that this effect is the driving force for both structure degradations and oxygen loss that triggers the well-known rapid voltage decay in LMR. By further leveraging micro to macro length characterizations that span atomic structure, primary particle, multi-particle and electrode level, we demonstrate that the heterogeneous nature of LMR cathodes inevitably causes pernicious phase displacement/strain which cannot be eliminated by conventional doping or coating methods. These results affirm that lattice displacement and nano-strain, which represent commonly occurred but less detectable dynamic structure evolutions, play an undeniable role in structure decomposition and voltage fade. With these fundamental discoveries, we propose mesostructural design as a strategy to mitigate lattice displacement and inhomogeneous electrochemical/structural evolutions, thereby achieving stable voltage and capacity profiles. These findings highlight the significance of lattice strain/displacement in causing voltage decay and will inspire a wave of efforts to unlock the potential of the broad-scale commercialization of LMR cathode material.

10:45 AM CH03.12.09

Developing Operando Liquid-State NMR Spectroscopy of the Electrolyte Inside an Operating Li-Ion Battery to Follow Its State of Charge Khashayar Bagheri^{1,2}, Vincent Sarou-Kanian^{1,2}, Michael Deschamps^{1,2} and Elodie Salager^{1,2}; ¹CNRS, CEMHTI UPR3079, Université d'Orléans, France; ²Réseau sur le Stockage Electrochimique de l'Energie (RS2E), FR CNRS 3459, France

Electrochemical energy storage devices, such as Li-ion or Na-ion batteries, supercapacitors, or hybrid capacitors, are essential for the energy transition. The entire device characterization (*In situ*) is one of the key elements to obtaining a global understanding of the charge and degradation processes. Nuclear Magnetic Resonance (NMR) spectroscopy is one of the techniques of choice thanks to its ability to detect, non-destructively and with atomic selectivity, the liquid, semi-liquid, crystalline, and amorphous contents of the sample.

Operando NMR spectroscopy of Li-ion batteries is challenging due to the strong heterogeneity of the battery, which results in broadening and distortions of the NMR spectrum. Up to now, most Operando NMR studies used ⁷Li NMR spectroscopy to follow lithiation and degradation processes of electrodes displaying highly shifted peaks (lithiation of graphite and silicon, lithium plating). Although the liquid electrolyte located inside the battery provides a narrower and stronger *In situ* NMR signal, it has not been fully exploited until now.

We will present our efforts to use the liquid ¹H NMR signal of the electrolyte solvent (ether carbonates) to “spy” on the electrodes while benefitting from the higher sensitivity of ¹H NMR compared to ⁷Li NMR. Contrary to lithium atoms, hydrogen atoms in the electrolyte solvent are not a direct probe of the state of charge of the electrode. The ¹H NMR spectrum of the electrolyte is however highly sensitive to heterogeneities and interfaces in the battery, especially at the interface with the electrodes.

We demonstrate that the strongly distorted ¹H NMR spectrum of dimethyl carbonate (DMC) in the battery can be used to track the state of charge of the electrodes. A careful analysis of the effect of battery components such as current collectors, separators, and electrodes with various states of charge will be presented. It provides a framework and descriptors for characterizing the distortion of the electrolyte ¹H NMR spectrum arising from the electrodes, with the goal to apply this technique for fast Operando NMR characterization of operating batteries.

11:00 AM CH03.12.10

1D Magnetic Resonance Imaging, High Resolution 2D and Spin Counting Nuclear Magnetic Resonance for Batteries Michael Deschamps^{1,2}, Elodie Salager² and Vincent Sarou-Kanian²; ¹University of Orleans, France; ²CNRS, France

In batteries and supercapacitors, the variation of lithium concentration profiles can be probed with *operando* 1D magnetic resonance imaging (MRI) of spin bearing atoms, while limiting the signal losses stemming from short relaxation times and broad lines in static systems. In such cases, one can observe interesting effects pertaining to the electrode porosity.[1] In model systems with materials displaying low diamagnetic susceptibilities, pulsed-field-gradient diffusion measurements shows the negative effect of carbon black addition on lithium ion self-diffusion.[2]

High-resolution Magic Angle Spinning NMR, on the other hand, can be performed on a wide variety of materials, and provide a wide range information on many atoms such as ⁷Li or ⁶Li, ²³Na and 2D correlation experiments can provide information on defects or phase separation in battery materials.[3]

Moreover, in favorable systems such as lithium titanates, it has been shown that surface fluorination with XeF₂ greatly improves the electrochemical properties. In such systems, high resolution MAS-NMR can help quantify the amount of fluorine in the structure, and the ¹⁹F chemical shift analysis yields information on the fluorine environment. Moreover, spin counting strategies based on HMQC experiments can provide the number of fluorine atoms which are coordinated to lithium ions and help understand what kind of structures are created locally upon fluorination.[4]

[1] M.Tang, V.Sarou-Kanian, P.Melin, J.B.Leriche, M.Ménétrier, J.M.Tarascon, M.Deschamps, E.Salager, 'Following lithiation fronts in paramagnetic electrodes with in situ magnetic resonance spectroscopic imaging', *Nat. Commun.*, **7**, 13284 (2016)

[2] S.J.Tambio, M.Deschamps, V.Sarou-Kanian, A.Etiemble, T.Douillard, E.Maire, B.Lestriez, 'Self-Diffusion of Electrolyte Species in Model Battery Electrodes Using Magic Angle Spinning and Pulsed Field Gradient Nuclear Magnetic Resonance', *J. Power Sources*, **362**, 315-322 (2017)

[3] R.J.Messinger, M.Ménétrier, E.Salager, A.Boulineau, M.Duttine, D.Carlier, J.M.Ateba Mba, L.Croguennec, C.Masquelier, D.Massiot, M.Deschamps, 'Revealing Defects in Crystalline Lithium-Ion Battery Electrodes by Solid-State NMR: Applications to LiVPO₄F', *Chem. Mat.*, **27(15)**, 5212–5221 (2015)

[4] Y.Charles-Blin, D.Flahaut, J.B.Ledeuil, K.Guérin, M.Dubois, M.Deschamps, A.M.Perbost, L.Monconduit, H.Martinez, N.Louvain, 'Atomic Layer Fluorination of the $\text{Li}_4\text{Ti}_5\text{O}_{12}$ Surface: A Multiprobing Survey', *ACS Appl. Energy Mater.*, **2(9)**, 6681-6692 (2019)

SESSION CH03.13: Beyond Traditional Electrodes
Session Chairs: Chong Liu and Hui Xiong
Thursday Afternoon, December 1, 2022
Hynes, Level 1, Room 103

1:45 PM CH03.13.01

Origin of Particle Evolution in SnO_2/ZnO Core/Shell NW-Based Lithium-Ion Battery Anodes Jasmin-Clara Bürger¹, Serin Lee², Sebastian Gutsch¹, Jan Büttner^{1,1,1}, Anna Fischer^{1,1,1}, Frances M. Ross² and Margit Zacharias¹; ¹University of Freiburg, Germany; ²Massachusetts Institute of Technology, United States

Oxide-based active core/shell heterostructures as Lithium-ion battery anode materials, such as the combination of tin oxide (SnO_2) and zinc oxide (ZnO), are known for their improved charge rate and real (measured) specific capacity compared to those of the individual, uncombined materials, due to synergetic effects. In this study, SnO_2/ZnO core/shell nanowires (NWs) with varying ZnO coating thickness are analyzed before and after charge/discharge chronopotentiometry. As well as standard electrochemical analysis, structural and compositional measurements were made using scanning electron microscopy and transmission electron microscopy of as-prepared and post-mortem SnO_2/ZnO core/shell NWs. For small cycle numbers, including the first charge/discharge step and a small number of subsequent cycles, the microscopy techniques revealed a pronounced morphological change in which the straight nanowires converted to a wirelike assembly of connected nanoparticles with increasing ZnO coating thickness of the SnO_2/ZnO core/shell NWs. This behavior was not observed for uncoated SnO_2 NWs, which retained a recognizable NW structure after cycling. Thus, the structural changes known to occur during cycling are not solved by the NW-based morphology, although the material does not fully pulverize. By electron diffraction and scanning transmission electron microscopy-energy dispersive x-ray spectroscopy, the particles formed were investigated crystallographically and compositionally. We discuss these observations in terms of the elemental distribution and lithiation reactions of the materials involved and the possible strategies for optimizing electrical properties and cycling behavior. We also compare the results to the cycling behavior of NWs with different coating materials.

2:00 PM CH03.13.02

Structural and Chemical Evolution in Metastable Niobates During Li-Ion Battery Cycling Kausturi Parui and Megan M. Butala; University of Florida, United States

Electrochemical energy storage systems, such as rechargeable intercalation batteries, are a reliable and efficient medium of portable energy storage, enabling portable electronics and electric vehicles. Intercalation batteries operate on the basic principle that during discharge (delivery of energy), cations (in our case, Li-ions) diffuse along the chemical potential gradient, and during charge these cations diffuse uphill against the chemical potential gradient. Hence, the performance of the battery depends upon the reversible insertion/extraction of a charged species. Niobium oxides, including their Wadsley-Roth phases, have recently drawn interest for intercalation electrodes. Depending upon synthesis conditions, various stable and metastable polymorphs of Nb_2O_5 can result. With an interest in understanding the underlying storage mechanisms, such as those related to their ionic diffusion and capacity, we have used diffraction and total scattering to characterize their initial structures and cycling products. The knowledge of these underlying mechanisms can inform electrode design, including lowering energy barriers along diffusion pathways and mitigating disadvantageous structural changes.

2:15 PM BREAK

SESSION CH03.14: Fuel Cells and Supercapacitors
Session Chair: Peng Bai
Thursday Afternoon, December 1, 2022
Hynes, Level 1, Room 103

3:00 PM CH03.14.01

Suppression of Segregated Species in Solid Oxide Fuel and Electrolysis Cell by Infiltration of Hf—Enhanced Activity and Stability Sanaz Koohfar¹, Tyler Hafen², Jenna Pike², Elango Elangovan² and Bilge Yildiz¹; ¹Massachusetts Institute of Technology, United States; ²Oxeon Energy, United States

Perovskite oxide solid oxide fuel and electrolysis cells (SOFC/SOEC) are one of the most promising energy storage/conversion devices. Solid oxide electrochemical cells have the advantage of fuel flexibility, lower carbon emission, and high efficiency due to high-temperature operation (800 C) which makes SOFC/SOEC more favorable compared to conventional electrolysis devices. However, the operational stability of SOFC/SOEC stands as a major obstacle to the commercialization of these devices. $\text{La}_{1-x}\text{Sr}_x\text{Co}_{1-x}\text{Fe}_x\text{O}_3$ (LSCF) is commonly used in solid oxide electrochemical cells as the oxygen electrode because of the high ionic and electronic conductivity that are essential for oxygen exchange reactions. The high efficiency of LSCF oxygen electrode suffers from degradation over a long period of operation in both fuel and electrolysis modes. Segregation of A-site cation Strontium (Sr) and Lanthanum (La) on the surface of LSCF perovskite electrode has shown to be one of the main factors hindering the long-term stability of these devices. It has been shown that the segregation of Sr and La blocks the active sites which are vital for oxygen exchange. In this work, we show that the stability and activity of porous LSCF perovskite oxide are enhanced by infiltration Hafnium (Hf) through a quantitative electrochemical impedance spectroscopy measurement. An increase in stability of LSCF is directly correlated with the suppression of Sr and La on the surface of LSCF. We use a three-electrode configuration to study the evolution of cathode and anode independently in a symmetric cell of LSCF in ambient air at 800° C. X-ray photoelectron spectroscopy (XPS) and electrochemical impedance spectroscopy (EIS) are used to quantitatively measure oxygen exchange activity and surface chemistry concentration ratios of LSCF as a function of applied polarization. Our results show a significant improvement in oxygen exchange reactions that lead to enhanced activity and stability of LSCF over 300 hours of operation.

3:15 PM CH03.14.02

Probing the Catalytically Active Region in a Nanoporous Gold and Copper Gas Diffusion Electrode to Enhance Highly Selective Carbon Dioxide Reduction Aidan Q. Fenwick¹, Alex Welch¹, Xueqian Li¹, Ian Sullivan¹, Joseph DuChene², Chengxiang Xiang¹ and Harry A. Atwater¹; ¹California

Institute of Technology, United States; ²University of Massachusetts Amherst, United States

We report the use of a nanoporous gold (np-Au) catalyst for CO₂ reduction in a gas diffusion electrode (GDE) and characterize the role of wetting in electrochemical performance. The np-Au catalyst has pores on the order of 20 nm and is crosssectionally isotropic, enabling Faradaic efficiencies for CO of greater than 95% across a wide range of potentials and a maximum partial current density for CO of 168 mA/cm². Secondary ion mass spectroscopy and in-situ copper underpotential deposition were employed to provide insights into catalyst wetting. At a typical CO₂ flow rate of 50 SCCM, approximately half of the catalyst is in contact with the electrolyte during operation and the dry region exists in the bottom half of the nanoporous catalyst. We discuss implications of the nanoporous GDE wetting characteristics for catalyst performance and the design of improved GDE architectures that can maximize the catalytically active area. An analogous nanoporous copper (np-Cu) catalyst was prepared by electron beam vapor deposition of Cu/Al followed by selective chemical etching of the Al. The morphology and catalyst stability under applied potential were studied before and after electrolysis.

3:30 PM CH03.14.03

X-ray Nano-Imaging of Defects in Thin-Film Catalysts via Cluster Analysis Aileen Luo¹, Oleg Y. Gorobtsov¹, Jocienne Nelson¹, Ding-Yuan Kuo¹, Tao Zhou², Ziming Shao¹, Ryan Bouck¹, Mathew J. Cherukara², Martin Holt^{2,2}, Kyle M. Shen^{1,3}, Darrell Schlom^{1,3,4}, Jin Suntivich¹ and Andrej Singer¹; ¹Cornell University, United States; ²Argonne National Laboratory, United States; ³Kavli Institute at Cornell for Nanoscale Science, United States; ⁴Leibniz-Institut für Kristallzüchtung, Germany

Functional properties of transition-metal oxides strongly depend on crystallographic defects; crystallographic lattice deviations can affect ionic diffusion and adsorbate binding energies. Scanning x-ray nanodiffraction enables imaging of local structural distortions across an extended spatial region of thin samples. Yet, localized lattice distortions due, for example, to line defects remain challenging to detect and localize using nanodiffraction, due to their weak diffuse scattering. Here, we apply an unsupervised machine learning clustering algorithm to isolate the low-intensity diffuse scattering in as-grown and alkaline-treated thin epitaxially strained SrIrO₃ films. We pinpoint the defect locations, find additional strain variation in the morphology of electrochemically cycled SrIrO₃, and interpret the defect type by analyzing the diffraction profile through clustering. Our findings demonstrate the use of a machine learning clustering algorithm for identifying and characterizing hard-to-find crystallographic defects in thin films of electrocatalysts and highlight the potential to study electrochemical reactions at defect sites in operando experiments.

3:45 PM CH03.14.04

MOF Promoted Ternary Transition Metal Chalcogenide Embedded Carbon Fabric for Ultra-Long Life Flexible Energy Storage Application Roshan M. Bhattarai, Shirjana Saud and Young S. Mok; Jeju National University, Korea (the Republic of)

Flexible-portable electronic devices have been deemed the future of innovative electronics. Due to the nature of such electronics, conventional power sources may no longer fulfill their physical and/or electrochemical necessities; hence, innovation in flexible power sources is a crucial requirement. Herein, we realized an ultrastable flexible electrode that can be used in various energy storage applications such as supercapacitors and batteries. Firstly, the flexible and conductive carbon fabric was electrochemically deposited with a nickel nanoseed layer (Ni/CC). Then, the ZIF-67 organometallic framework (MOF) nanostructures were grown over the Ni/CC substrate. As grown, nanostructures were then embedded inside the carbon fabric strands through a precise optimization process of varying the calcination temperature and gas concentrations. The Ni-Co-C co-embedded carbon fabric was then sulfurized via a series of carefully optimized hydrothermal conditions. Thus obtained metal sulfide embedded carbon fabric shows an excellent capacity when tested as a supercapacitor electrode in a three-electrode configuration. Moreover, when paired with the biomass-derived activated carbon, the asymmetric supercapacitor device shows almost 100 % of capacity retention even after 40 thousand charge-discharge cycles. Furthermore, several bending and twisting cycles were run to examine the integrity of the active material and no discernible capacity fading is observed. Hence, a unique metal chalcogenide composite electrode/substrate configuration has been proposed as a highly stable electrode material for flexible energy storage applications.

4:00 PM CH03.14.05

Strategic Tuning Of 2D Transition Metal Oxynitride System for Electrochemical Charge Storage Jacob Som¹, Manosi Roy¹, Kaushik Sarkar¹, Brooke Smith¹, Darrah Dare², Xiaochuan Lu³ and Dhananjay Kumar¹; ¹North Carolina Agricultural & Technical State University, United States; ²Cornell University, United States; ³North Carolina Agricultural & Technical State University, United States

Electrocatalytically highly active titanium oxynitride (TiNO) thin films were fabricated using a pulsed laser deposition method for energy storage applications. The elemental composition and nature of bonding were analyzed using x-ray photoelectron spectroscopy (XPS) to reveal the reacting species and active sites responsible for the enhanced electrochemical performance of the TiNO electrodes. A study of the SEM images before and after electrochemical cycling showed a negligible degradation of TiNO sample, suggesting the TiNO electrodes are stable under the cycling conditions. Symmetric supercapacitor devices were fabricated using two TiNO working electrodes separated by ion transporting layer to analyze their real-time performance. The galvanostatic charge-discharge studies on the symmetric cell, fabricated using TiNO films deposited at 300 °C, exhibited the highest specific capacity of 69 mF/cm² at 0.125 mA/cm² with an energy density of 7.5 Wh/cm². The performance of this supercapacitor (300 °C TiNO) device is found to be ~ 22 % better compared to that of 500 °C TiNO supercapacitor with a capacitance retention ability of 95% after 1000 cycles. The thin film fabrication temperature can be employed as a simple and effective tuning strategy to rationally modulate the morphology and the structure of the thin film to achieve a high charge storage performance.

SESSION CH03.15: Virtual Session: Characterizations of Lithium-Ion and Solid-State Batteries

Session Chairs: Peng Bai and Hui Xiong

Wednesday Morning, December 7, 2022

CH03-virtual

8:00 AM CH03.15.01

Spatiotemporal Pattern of Lithiation State in 18650-Type Cell Observed by Compton Scattering Spectroscopy Kosuke Suzuki¹, Naruki Tsuji², Kirsi Jalkanen³, Jari Koskinen³, Kazushi Hoshi¹, Ari-Pekka Honkanen⁴, Hasnain Hafiz⁵, Yoshiharu Sakurai², Mika Kanninen³, Simo Huotari⁴, Arun Bansil⁶, Hiroshi Sakurai¹ and Bernardo Barbiellini^{7,6}; ¹Gunma University, Japan; ²Japan Synchrotron Radiation Research Institute (JASRI), Japan; ³Akkurate Oy, Finland; ⁴University of Helsinki, Finland; ⁵Carnegie Mellon University, United States; ⁶Northwestern University, United States; ⁷LUT University, Finland

Compton scattering technique is a unique technique to visualize the lithiation state on commercialized lithium-ion cells in-situ and in-operando. This technique characterized by high-energy synchrotron X-rays allows a non-destructive observation of a reaction in closed electrochemical cells and enables

analysis quantitatively of the concentration of the lithium. In this study, the Compton scattering technique is applied to a 18650-type cylindrical lithium-ion cell and observed a spatiotemporal pattern of lithiation state, called Turing pattern [1].

The Compton scattering was carried out at the high-energy inelastic scattering beamline BL08W of the SPring-8. X-rays that were monochromatized to 115.56 keV were used. Compton scattered X-rays were measured by Ge solid-state detector. The scattering angle was fixed to 90 degrees. The state of charge of the sample cell was controlled using a potentiostat/galvanostat.

By analyzing obtained Compton scattered X-ray energy spectrum, the change of lithiation state in both the cathode and anode with the charge-discharge cycle is observed and the position of each component of the cell is shifted during the charge is visualized. Moreover, we observed lithiation state oscillation patterns by a depth-resolved analysis of the cathode electrode. This oscillation corresponds to the timescale of the charging curve and the dominating wavelength of the oscillation is related to the size of the grains of the active material. The reason for the appearance of this lithiation oscillation is due to the different mobilities of lithium ions and electrons. Therefore, the existence of the lithiation oscillation implies that the cell can have an optimal cycle speed with a more homogeneous flow of ions.

[1] K. Suzuki et al., Appl. Phys. Lett., 118, 161902, (2021).

8:15 AM *CH03.15.02

Solid-State NMR/MRI Studies of Heterogeneities in Solid-State Batteries Yanyan Hu; Florida State University, United States

Heterogeneities in solid-state batteries affect ion/electron transport and microstructure formation. Solid-state NMR is sensitive to heterogeneities of local structures and dynamics on the atomic, nano-, and meso-scale. Therefore, we have employed advanced NMR spectroscopy and relaxometry to understand how structural heterogeneity affects ion dynamics and transport properties. In addition, heterogeneities on the mesoscale such as at electrode-solid electrolyte interfaces and around grain boundaries promote microstructure formation, which limits critical current densities thus power densities of solid-state batteries. Magnetic resonance imaging combined with tracer-exchange NMR probes how these heterogeneous features evolve under external stimuli and how they affect Li microstructure formation with both spatial and temporal resolution.

8:45 AM CH03.15.05

Study of the Lithium-Plating Phenomenon by *Operando* Nuclear Magnetic Resonance Characterization and Simulation of the Phenomenon for the Optimization of Li-Ion Battery Fast Charge Abdelmounaim Akkouch^{1,2}, Sylvie Geniès², Marion Chandesis², Alexis Martin² and Michel Bardet³; ¹Université de Grenoble Alpes, France; ²CEA-LITEN Grenoble, France; ³CEA-IRIG Grenoble, France

Li-ion batteries (LIBs) are now ubiquitous in our daily lives and are of tremendous importance for our society, with applications ranging from small electronic devices to electric vehicles, but their limited lifetime still presents a great challenge for the generalization of transport electrification; they must be able to accept fast charges, even at low temperatures. However, during charge process at these conditions, formation of metallic lithium on the surface of the negative electrode made of graphite can occur and accelerate the capacity loss of the battery and thus the autonomy of the vehicle. On the other hand, the deposition of lithium metal being rather on the surface of graphite, the interface with the separator has its importance. It has been observed that the pores of the separator can become clogged, blocking the passage of ions and creating local polarizations. In addition, if lithium metal grows in the form of dendrites, the separator can be perforated, which can lead to an internal short circuit in the battery. This degrading mechanism known as Lithium-plating is therefore a key research axis to extend the life of batteries.

Therefore, a more global understanding, in real time, of this phenomenon and its kinetics in function of the local conditions within the negative electrode in a functional lithium-ion cell is needed. In order to develop this understanding, it is crucial to perform *operando* analytical measurements on a working cell that allow monitoring different states-of-charge (SOC) repeatedly, in principle throughout their life cycle, giving access to a multitude of analytical data compared to a single *ex-situ* or *post mortem* analysis. In our study, we perform measurements by ⁷Li *operando* Nuclear Magnetic Resonance (NMR) on practical configuration: LiNi_{0.8}Mn_{0.1}Co_{0.1}O₂ (NMC811)/graphite pouch cells made with industry-grade electrodes and under realistic cycling conditions. This non-invasive and non-destructive technique, is sensitive to both structure and dynamics. The ⁷Li NMR signal of Li ions in graphite electrode was recorded during electrochemical cycling over a wide range of rates enabled us to analyse intercalation processes in the electrode, changes of Li-ion mobility, and Li metal deposition on graphite at high current rate due to an inhomogeneous distribution of ions induced by limitation of diffusion on solid and liquid phases. In our *operando* experiments, with a CC fast charge and a subsequent CV period at 4.2 V, Li deposition starts at around 3.5 V well before the full lithiation of graphite and continues even during the voltage floating. At the end of the CV phase, and due to the drop of the current, the lithium plating starts to interact with its environment by intercalating in the graphite structure or reoxidizing during the following discharge to transform into cyclable lithium.

Another method used to detect the lithium plating is the anode potential measurement through a reference electrode. This method allows us to precisely measure the potential of each electrode rather than following the evolution of the cell voltage. Thermodynamically, anode lithium plating occurs when the anode potential drops below 0 V (vs Li^{+/}Li). Therefore, by performing *operando* NMR measurements with instrumented cells, we monitor the anode potential which allows the lithiation of the graphite electrode and the apparition of lithium plating to be correlated.

The experimental results are used to implement and validate a multi-physics Newman-based model at the scale of the electrode. It allows varying all the influential parameters and model the evolution of discharge capacity loss, sudden capacity loss, and capacity recovery via physics-based mechanisms on the performance model. These different contributions will be more detailed on the presentation.

9:00 AM DISCUSSION TIME

SYMPOSIUM DS01

Symposium Organizers

Alexandra Khvan, National Research Technological University
Alexandra Navrotsky, Arizona State University
Richard Otis, NASA Jet Propulsion Laboratory
Wenhao Sun, University of Michigan

* Invited Paper
+ Distinguished Invited

SESSION DS01.01: Thermodynamics of Metals and Alloys
Session Chairs: Alexandra Navrotsky, Richard Otis and Wenhao Sun
Monday Morning, November 28, 2022
Hynes, Level 2, Room 204

11:00 AM DS01.01.02

Thermodynamic Analysis on a Formation Mechanism of Metastable Carbides During Tempering of Fe-C Martensite Masanori Enoki¹ and Hiroshi Ohtani²; ¹Tohoku University, Japan; ²Toyota Physical and Chemical Research Institute, Japan

The steels obtain quite hard microstructures by martensitic transformation, however, as-quenched martensites cannot be used industrially because of their brittleness. Therefore, a heat treatment called 'tempering' is applied to improve the balance between strength and toughness. During the tempering process, various metastable carbide precipitates are formed with temperature increasing, and their dispersion in the microstructure has a significant influence on the strength of the steel. Therefore, extensive research has been conducted on metastable carbides in this system, however, it is hard to observe the details of metastable carbides by experiment because of the microscopic nature of precipitates in the early stage of aging. Moreover, the reason why precipitates having higher carbon concentration such as η -carbide (Fe_2C) are formed before more stable cementite (Fe_3C) has not been fully considered. For this reason, in this study, thermodynamics analysis based on first principles calculations was applied to reveal the behavior of solid-solution carbon in the matrix during the preliminary stage of the tempering process and the formation mechanism of η -carbide and cementite.

To clarify the thermodynamic behavior of carbon during the preliminary stage of tempering of martensite, structure models were constructed in which carbon occupies three octahedral interstitial sites (denoted as a-site, b-site, and c-site) in BCT-Fe and BCC-Fe. Using these models, the cluster expansion and variation method was applied to evaluate the free energy of formation of solid solutions. Furthermore, the thermal equilibrium distribution of carbon was obtained by Monte Carlo simulation using the effective cluster interactions obtained by cluster expansion method. From the atomic arrangement obtained by this method, the clustering of carbon was observed, and the transition to metastable carbides was investigated from the ordered structure obtained by extracting the clustering region. The nudged elastic band (NEB) method was applied to evaluate the energy barrier in the transition process.

The Monte Carlo simulations for BCT-Fe and BCC-Fe showed well-defined clustering of carbon atoms. Furthermore, the free energies evaluated by the cluster expansion and variation method showed two-phase separations between Fe and Fe_2C compositions, suggesting that these clusters are formed by two-phase separation based on ordering. Two different carbon clusters were identified between BCT-Fe and BCC-Fe. In this study, the energies of transformation from these clusters to η -carbide were further determined from the NEB method. The carbon configuration formed in BCC-Fe resulted in a transition to η -carbide with no energy barrier. On the other hand, in BCT-Fe, the energy barrier of phase transition was found to be comparable to the diffusion energy barrier of carbon atom. The energy barrier values of transition process calculated by the NEB method were compared, and the series of processes for metastable carbide formation was considered as follows. The η -carbide preferentially precipitates at the beginning of tempering, and cementite is newly formed at a higher temperature stage with the rearrangement of carbon atoms. Furthermore, because the barrier energies of Fe lattice deformation obtained from NEB calculations are small, we also argue that the diffusion of carbon atoms plays an important role in the formation of metastable carbides.

11:15 AM DS01.01.03

Uncertainty Reduction and Quantification in Computational Thermodynamics Richard Otis; NASA Jet Propulsion Laboratory, United States

Uncertainty quantification is an important part of materials science and serves a role not only in assessing the accuracy of a given model, but also in the rational reduction of uncertainty via new models and experiments. In this contribution, recent advances and challenges related to uncertainty quantification for Calphad-based thermodynamic and kinetic models are discussed, with particular focus on approaches using Markov chain Monte Carlo sampling methods. General differentiable and probabilistic programming frameworks are identified as an enabling and rapidly-maturing new technology for scalable uncertainty quantification in complex physics-based models, including those for Calphad. Special challenges for uncertainty reduction and Bayesian design-of-experiment for improving Calphad-based models are discussed in light of recent progress in related fields.

11:30 AM DS01.01.04

Uncertainty Driven Computational Thermodynamics Noah H. Paulson and Joshua Gabriel; Argonne National Laboratory, United States

In computational thermodynamics, statistics and uncertainty quantification are critical for evaluating the confidence in predictions and models with substantial potential for impact on materials development and qualification. The role for statistical techniques, especially Bayesian analysis, is not limited to obtaining uncertainty intervals on phase boundaries. These methods can drive the development of selection criteria for the best combinations of datasets and thermodynamic descriptions that support each other for a given material system. We present the results of such uncertainty driven investigations into thermodynamic model development for unary and binary metallic systems. Specifically, we share statistical approaches to Bayesian model selection, parameter inference, uncertainty quantification/propagation, and the automated weighting of both experimental and computed datasets. This will be accompanied by a discussion of the use of statistical techniques in thermodynamics to inform critical design choices and glean scientific insights.

SESSION DS01.02: Metastability
Session Chairs: Alexandra Navrotsky, Richard Otis and Wenhao Sun
Monday Afternoon, November 28, 2022
Hynes, Level 2, Room 204

1:45 PM DS01.02.01

Predicting and Accessing Metastable Phases [Vancho Kocevski](#), James A. Valdez, Benjamin K. Derby, Yongqiang Wang, Ghanshyam Pilania and Blas Uberuaga; Los Alamos National Laboratory, United States

Metastable forms of matter are invaluable to our everyday lives, from advancing technology to understanding biological processes, with their unique properties often offering novel functionality. Despite their importance, synthesizing metastable phases is more art than science, often either serendipitous or trial-and-error. Insight into the amount of stored energy needed to form a metastable phase can aid in their fabrication. Here, we calculate metastable phase diagrams, from which we extract the metastability threshold – the excess energy stored in the metastable phase relative to the ground state. Using lanthanide sesquioxides (Ln_2O_3) as a case study, we demonstrate how metastable phase diagrams provide new insight into their synthesis and irradiation behavior. We find the metastability threshold above which metastable phases cannot be synthesized from thermal decomposition, explaining why non-equilibrium synthesis is required for fabrication of certain metastable phases. We also discuss a reverse relation between the metastability threshold and kinetics at increased temperatures, and their influence on the formation of metastable phases. Lastly, we successfully predict the sequence of metastable phases induced by irradiation in Lu_2O_3 , forming three metastable phases with increasing irradiation fluence and displaying unique irradiation behavior not observed in other materials.

2:00 PM +DS01.02.03

Selectivity in Materials Synthesis with Hyperdimensional Phase Spaces [James R. Neilson](#); Colorado State University, United States

A significant challenge in materials synthesis is to rationally control composition and structure of materials to achieve desired properties. Unfortunately, metastability or glacial reaction kinetics inhibits the search for and synthesis of functional materials. Yet, solid-state metathesis reactions, which have an expanded, hyperdimensional, compositional space from that of the products, often avoid formation of unreactive intermediates. Furthermore, the nominally spectating elements can even impart selectivity between different products. Experimental in situ investigation of reactions (e.g., with synchrotron X-ray powder diffraction) sheds light on how intermediates in the reaction dictate the local chemical potentials that define the reaction pathway. Selectivity results when intermediates provide a direct thermochemical connection between the reactants and a targeted compound, as illustrated for myriad complex manganese oxides. With this discovery, we now envision an approach for predictive, prescriptive materials synthesis and reversible conversion.

2:30 PM DS01.02.04

Direct DFT Calculation of the Bulk and Nanoscale Stability of Icosahedral Quasicrystals [Woohyeon Baek](#) and Wenhao Sun; University of Michigan, United States

The discovery of quasicrystals forced solid-state chemists to revisit traditional assumptions about crystallinity, bonding, stability, and materials formation. Underlying all these questions is a fundamental question: are quasicrystals thermodynamically stable or metastable, but prefer nucleation due to a low surface energy? Density Functional Theory (DFT) is often used to evaluate thermodynamic stability, but quasicrystals are aperiodic and cannot be calculated under periodic boundary conditions. Here, we present a new technique to directly calculate the bulk and surface energies of quasicrystals in DFT. We compute the energies of large quasicrystal nanoparticles, and then fit the bulk and surface energies of the nanoparticles using a Gibbs-Thomson relationship. Using this technique, we evaluate the Tsai-type ScZn and YbCd icosahedral quasicrystals, whose structures have been resolved with atomistic resolution. From the bulk and surface energies, we construct size-dependent phase diagrams, enabling us to determine the bulk and nanoscale (meta)stability of icosahedral quasicrystals.

2:45 PM DISCUSSION TIME

3:00 PM BREAK

3:30 PM DS01.02.06

Synthesis-Structure Relationship Guided by Intermediate and Remnant Metastability [Akira Miura](#)¹, Hiroaki Ito¹, Yuki Nakahira², Yosuke Goto³, Yoshikazu Mizuguchi⁴, Chikako Moriyoshi⁵, Nataly Carolina Rosero-Navarro¹ and Kiyoharu Tadanaga¹; ¹Hokkaido University, Japan; ²QST, Japan; ³National Institute of Advanced Industrial Science and Technology (AIST), Japan; ⁴Tokyo Metropolitan University, Japan; ⁵Hiroshima University, Japan

With increasing demands for producing new functional ceramics materials, the components of materials tend to increase. However, as the number of components increases, the number of metastable and thermodynamically competing phases increases [Science Advances 2016 e1600225]. Kinetic understanding is essential to guide a synthesis-structure relationship of these metastable and thermodynamically competing phases. In-situ measurement is a powerful technique for understanding kinetics and various reactions have been studied [Journal of the American Chemical Society 2016 11031; Advanced Materials 2021 2100312].

Metastable phases can be classified as intermediate and remnant metastability.[Chemistry of Materials 29 (2), 479-489] Intermediate metastable phases are intermediates trapped by kinetic barriers that have never reached the lowest free-energy phase. In contrast, remnant metastable phases are remnants of thermodynamic conditions where they were once the lowest free-energy phase.[Science Advances 2016 e1600225] By understanding these metastable mechanisms, we can rationally design the synthesis recipes.

Here, we investigated the kinetics of solid-state synthesis reactions of $\text{Li}_3\text{YCl}_6/\text{Li}_3\text{HoCl}_6$ solid electrolytes between LiCl and $\text{YCl}_3/\text{HoCl}_3$ powders via in-situ synchrotron X-ray diffraction at different heating rates. The ion radii of Y^{3+} and Ho^{3+} are comparable, so similar reaction mechanisms can be expected. Both reactions formed $\text{Li}_3\text{YCl}_6/\text{Li}_3\text{HoCl}_6$ with disordered Y/Ho before forming $\text{Li}_3\text{YCl}_6/\text{Li}_3\text{HoCl}_6$ with ordered Y/Ho sites. However, the reversibility of these disorder-order transitions differed; that of Li_3YCl_6 was nonreversible while that of Li_3HoCl_6 was reversible. Therefore, Li_3YCl_6 with ordered Y and Li_3HoCl_6 with disordered Ho were found to be stable phases near room temperature.

Accordingly, Li_3YCl_6 with disordered Y and Li_3HoCl_6 with ordered Ho were metastable phases near room temperature. Interestingly, these metastable phases can be classified as intermediate and remnant metastable phases. Li_3YCl_6 with disordered Y was the intermediate metastable phase, which was obtained by heating at a medium temperature not to reach thermodynamic stable Li_3YCl_6 with ordered Y. On the other hand, Li_3HoCl_6 with ordered Ho was the remnant metastable phase, which was once stabilized at high temperature and only available upon quenching. Therefore, even though ion radii of

Y^{3+} and Ho^{3+} are similar, different kinetics between Li_3YCl_6/Li_3HoCl_6 exhibit distinct contrast in the synthesis-structure relationship. We anticipate that f orbital of Ho can change their kinetics.

3:45 PM *DS01.02.07

Materials Thermodynamics at Extreme Conditions—Towards Knowledge-Based Design of Metastable Materials with Advanced Functionalities

Igor A. Abrikosov; Linköping University, Sweden

Recent advances in high-pressure high-temperature (HPHT) experiment allow one to synthesize materials at TPa compression and temperature above 2000 K [1], paving the way towards discoveries of new materials and observations of novel physical phenomena. The exciting capabilities offered by the HPHT synthesis puts on the agenda a challenging task of knowledge-based design of metastable materials with advanced functionalities. At the same time, profound effect of the extreme conditions on the chemistry and physics of materials requires proper theoretical analysis. We review recent advances in theoretical description of materials thermodynamics at extreme conditions, which combines first-principles electronic structure theory with machine learning (ML) tools. We demonstrate that explicit treatment of lattice dynamics is essential for accurate calculations of thermodynamic properties of materials at elevated temperatures, leading to qualitative improvement between theory and experiment for such key targets as mixing enthalpies and phase diagrams. We show that using ML interatomic potentials allows to greatly increase efficiency of simulations at extreme conditions preserving, and even improving their accuracy [2]. Moreover, employing the transfer learning approach, it is possible to predict highly sensitive materials properties, like elastic moduli, without explicit first-principles calculations [3].

Importantly, we demonstrate feasibility of discovering metastable materials with advanced functionalities in HPHT synthesis followed by decompression to ambient conditions. First, we present the case of rhenium nitride pernitride $Re_2(N_2)(N)_2$, discovered at HP (40 to 90 GPa) [4]. Theoretical analysis demonstrated that it should be (meta-)stable, metallic, ultraincompressible and very hard not only at the synthesis pressure, but also at ambient conditions. Experimentally, $Re_2(N_2)(N)_2$ was recovered at ambient conditions, and a route to scale up its synthesis was developed.

Next, we demonstrate that decompression of materials synthesized at HPHT conditions could lead to phase transitions to metastable polymorphs with properties more exciting than those of the original HPHT phases. In particular, it is possible to use HPHT experiments in a search for layered materials, precursors of novel 2D-materials. We illustrate this concept by discoveries of the triclinic phase of beryllium tetranitride $t\text{-}BeN_4$ [5] and pentagonal (p -) phase of NiN_2 [6]. For the former, theoretical analysis predicts that BeN_4 monolayer, the beryllonitrene, represents a qualitatively new class of 2D materials that host anisotropic Dirac fermions. Realization of an ideal Cairo tessellation in $p\text{-}NiN_2$ provides high-pressure route to pentagonal 2D materials.

[1] L. Dubrovinsky, *et al.*, *Nature* **605**, 274 (2022).

[2] A. V. Shapeev, *et al.*, *New J. Phys.* **22**, 113005 (2020).

[3] H. Levämäki, *et al.*, *NPJ Comp. Mater.* **8**, 17 (2022).

[4] M. Bykov, *et al.*, *Nature Commun.* **10**, 2994 (2019).

[5] M. Bykov, *et al.*, *Phys. Rev. Lett.* **126**, 175501 (2021).

[6] M. Bykov, *et al.*, *ACS Nano* **15**, 13539 (2021).

4:15 PM *DS01.02.08

Synthesis and Thermodynamics of $GeNCr_3$ —A New Nitride Superconductor with Orthorhombic Antiperovskite Structure

Andreas Reitz¹, Hanna Pazniak², Chen Shen³, Harish Singh³, Alexandra Navrotsky¹, Hongbin Zhang³, Ulf Wiedwald⁴ and Christina S. Birke^{1,3}; ¹Arizona State University, United States; ²Institut Polytechnique de Grenoble, France; ³Technische Universität Darmstadt, Germany; ⁴Universität Duisburg-Essen, Germany

In contrast to ternary oxides, the number of known ternary nitrides is an order of magnitude lower, which is partially the result of their lower free energy of formation and lower thermodynamic stability. This challenges experimentalists to continuously explore the synthetic parameter space and push towards new nitride phases. Here, we demonstrate the synthesis of a hitherto unknown orthorhombic structure of $GeNCr_3$, which typically crystallizes in a tetragonal structure. As derived from DFT calculations, formation energies of both phases are similar, and we show that orthorhombic $GeNCr_3$ can be stabilized by choosing lower reaction temperatures. According to detailed thermodynamic analysis, the new compound is stable up to 500 °C and exhibits the same phase transitions as the tetragonal phase at higher temperatures. However, its electronic structure is vastly different. According to our theoretical calculations, the new orthorhombic compound exhibits superconducting behavior with a T_C of 7.2 K, which is due to electron-phonon coupling, while the tetragonal $GeNCr_3$ is an antiferromagnet.

4:45 PM DS01.02.09

Thermally-Quenched Metastable Phases in Correlated Electron Systems

Hiroshi Oike^{1,2,3}, Akiko Kikkawa³, Naoya Kanazawa^{1,3}, Manabu Kamitani³, Yasujiro Taguchi³, Masashi Kawasaki^{1,3}, Yoshinori Tokura^{1,3,4} and Fumitaka Kagawa^{1,3,4}; ¹The University of Tokyo, Japan; ²JST, Japan; ³RIKEN Center for Emergent Matter Science, Japan; ⁴Tokyo Institute of Technology, Japan

A large number of electrons that correlate with each other in crystals form ordered phases, such as magnetic orders and superconductivity, analogously to correlated atoms forming crystals. Whereas the most stable phase is uniquely determined once thermodynamic parameters are fixed, it has long been known that metastable crystals can be obtained when their transformation to the most stable phase is kinetically avoided by thermal quenching. It is intriguing whether the principle of quenching can also be applied to correlated electron systems. However, the cooling rates used in measurements of electronic properties are usually limited to a range between 10^{-3} - 10^{-1} Ks⁻¹, and thus the ubiquity of this principle had not been tested. We have been investigating metastability in correlated electron systems with rapid cooling techniques that produce a cooling rate up to 10^8 Ks⁻¹.

Here, we present two cases, metastable magnetism in a chiral magnet MnSi [H. Oike *et al.*, *Nature Phys.* **12**, 62 (2016).] and metastable superconductivity in a transition-metal dichalcogenide IrTe₂ [H. Oike *et al.*, *Science Adv.* **4**, eaau3489 (2018).]. MnSi is a long-studied magnet without inversion symmetry, and, in the last decade, has been attracting a great deal of attention as a material hosting magnetic skyrmions [Y. Tokura and N. Kanazawa, *Chem. Rev.* **121**, 2857 (2020)]. Two kinds of interactions are acting between electron spins in MnSi; ferromagnetic interaction that aligns neighboring spins in the same direction with each other and Dzyaloshinskii-Moriya interaction that twists neighboring spins. The competition between these interactions underlies a variety of spin structures in MnSi, such as spiral phase, where spins are aligned in a plane and modulated in a direction perpendicular to the plane, and skyrmion lattice phase (SkL), where vortex-like spin swirling objects form a lattice. We applied thermal quenching to the phase transition from SkL to spiral phase and found that SkL exists as a metastable state in a temperature range where a spiral phase is free-energetically most stable. Thus, the principle of quenching is demonstrated to work for magnetism.

Then, the principle is deployed to creation of metastable superconductivity. In correlated electron systems, a superconducting phase often has a slightly higher free-energy than other ordered phases of electrons. Therefore, if the formation of such competing orders is kinetically avoided by quenching, a superconducting state is expected to emerge. The target material IrTe₂ undergoes a complex ordering phenomena where the valence of the two-fifths Ir ions

changes from trivalent to tetravalent and accordingly the network structure formed by Te ions deviating from divalent also changes [K.-T. Ko et al., Nature Commun. 6, 7342 (2015)]. We applied thermal quenching to the complex ordering and found that a phase without the ordering exists as a metastable state at low temperatures. As we expected, the metastable phase exhibits superconductivity highlighting that the principle of quenching opens up new frontiers in the exploration of quantum phenomena.

Thus, the ubiquity of the principle is being demonstrated in correlated electron systems. Because such quenching experiments have only been carried out on a limited number of materials, it is expected that new quantum phases will be pioneered when they are applied to a wide variety of materials. More importantly, there may be similarities between correlated atoms and correlated electrons in the mechanism of metastability, as well as similarities in the methods of creating metastable phases. I hope that general concepts would be found through this presentation and subsequent discussions.

SESSION DS01.03: Thermodynamics of Oxides and Functional Materials
Session Chairs: Scott McCormack, Alexandra Navrotsky, Richard Otis, Jiayu Peng and Wenhao Sun
Tuesday Morning, November 29, 2022
Hynes, Level 2, Room 204

8:00 AM +DS01.03.01

Recent Advancements in Thermodynamic Properties of Zircon Structure-Type Materials Xiaofeng Guo¹, Andrew Strzelecki¹, Xiaodong Zhao¹, Paul Estevenon², Hongwu Xu³, Nicolas Clavier⁴ and Rodney Ewing⁵; ¹Washington State University, United States; ²Commissariat à l'énergie atomique et aux énergies alternatives, France; ³Los Alamos National Laboratory, United States; ⁴Université de Montpellier, France; ⁵Stanford University, United States

Zircon structure-types are ternary oxides with an ideal chemical formula of ATO_4 (I_4/amd), where usually A are lanthanides and actinides, with T = As, P, Si, V. This structure accommodates diverse chemistry on both A- and T-sites, giving rise to more than seventeen mineral end-members of five different mineral groups, and forty-five synthetic end-members. Because of their diverse chemical and physical properties, the zircon structure-types are of interest to a wide variety of fields and may be used as ceramic nuclear waste forms and aeronautical environmental barrier coating, to name a couple. To support advancement of their applications, many studies have been dedicated to the understanding of their structural and thermodynamic properties. The emphasis in this review will be on recent advances in the structural and thermodynamic studies of zircon structure-type ceramics, including pure endmembers (*i.e.*, zircon ($ZrSiO_4$), xenotime (YPO_4)), and solid solutions (*i.e.*, $Er_xTh_{1-x}(PO_4)_x(SiO_4)_{1-x}$). Specifically, we provide an overview of the crystal structure, its variations and transformations in response to non-ambient stimuli (temperature, pressure and radiation), and its correlation to thermophysical and thermochemical properties. We hope this up-to-date summary of knowledge of zircon-type materials will help researchers to continue advancing the use of zircon-type materials for applications, such as actinide waste forms and for aeronautical engineering as environmental barrier coatings.

8:30 AM *DS01.03.02

Materials Design for Extreme Environment Applications Using Rare Earth Oxides and Silicates Mackenzie J. Ridley, Cameron K. Miller, Kristyn D. Ardrey, Kathleen Tomko, John A. Tomko, Mahboobe Jassas, Patrick E. Hopkins and Elizabeth J. Opila; University of Virginia, United States

The seventeen rare earths (Sc, Y, and the 15 lanthanides) provide an ideal materials design space for manipulation of phase, composition, and properties. The wide range of cation sizes results in oxygen coordination numbers varying from six to nine, a large number of polymorphs, (see the figures below) and many possible multicomponent rare earth compounds. This variety enables control of properties such as thermal expansion, thermal conductivity, and thermochemical stability in steam and molten siliceous deposits, all important for high temperature coating applications in extreme environments. In this presentation, control of properties through design of rare earth oxides, rare earth monosilicates, rare earth disilicates, and both rare earth apatites and calcium-stabilized rare earth apatite phases are presented with corresponding experimental validation of property control.

9:00 AM DS01.03.03

Stability Design Principles of Manganese-Based Oxides in Acid Jiayu Peng¹, Livia Giordano¹, Timothy Davenport² and Yang Shao-Horn¹;
¹Massachusetts Institute of Technology, United States; ²Raytheon Technologies Research Center, United States

The utilization of low-cost, non-precious catalysts (e.g., metal oxides) in clean energy technologies in acid (e.g., proton exchange membrane fuel cells and electrolyzers) has been severely hampered by the instability of these catalysts at low pHs. While first-row late transition metal oxides based on Fe, Co, and/or Ni have been found with comparable or higher catalytic activity for the alkaline oxygen reduction and oxygen evolution reactions than the precious metal-based counterparts (e.g., Pt and IrO_2), such oxide catalysts are not stable in acid. Mn-based oxides are more acid-stable than those based on late transition metals at moderately acidic pHs, but they still corrode and deactivate in strong acid and after long operation. To address this issue, extensive efforts over the past decades have been focused on mixing active, yet unstable oxides (e.g., Mn oxides) with corrosion-resistant oxides to generate more stable catalysts. However, having a higher fraction of corrosion-resistant elements also results in less catalytically active oxides, indicating an activity-stability trade-off.

To design oxide catalysts (such as Mn-based oxides) with an optimal trade-off or even bypass this limitation, it is essential to establish their stability descriptors in acid. These descriptors can offer a fundamental understanding of oxide dissolution and provide guiding principles to enhance their intrinsic stability. Unfortunately, while the mechanistic insights into the bulk/surface instability of oxides under alkaline or neutral conditions have been established previously, the stability design principles of these oxides in acid are still lacking.

In this work, we employed a library of Mn-based oxides with diverse structures and valence states to establish oxide stability descriptors in acid based on intrinsic electronic structure and energetic parameters. Using time-dependent dissolution experiments and first-principle calculations, greater amounts and faster kinetics of oxide dissolution in acid were correlated with lowered Mn oxidation states, which are accompanied by decreased covalency, weakened Mn-O bonds, and reduced free energy barriers for key reaction steps, including protonation, vacancy formation, and ion solvation. Such design principles were shown broadly with a computational screening across a vast chemical space of ~1,000 Mn-based oxides, where an Mn oxidation state of +4 was found to give rise to the lowest energetic driving force for the dissolution of Mn-based oxides in acid. Moreover, limiting the percentage of ionic metal substituents in oxides and using more acidic substituents were shown to stabilize Mn-based oxides in acid.

Such design principles and mechanistic insights for stabilizing Mn-based oxides in acid are crucial for a wide variety of applications, such as proton exchange membrane fuel cells and electrolyzers. In addition, we envision this method can be extended to a broader chemical space to develop more universal, fundamental relations between the chemistry and electronic structure of transition metal compounds and their stability in acid for clean energy

applications.

9:15 AM DS01.03.04

Effect of Metal, Topology and Dimensionality on the Thermodynamic Stability of ZIFs [Gerson Leonel](#)¹, K Jayanthi¹, Joseph Marrett², Tomislav Frišcić² and Alexandra Navrotsky¹; ¹Arizona State University, United States; ²McGill University, Canada

Zeolitic imidazole frameworks (ZIFs), exhibit remarkable properties including high porosity, and surface area. Their high moisture stability makes them useful for industrial applications. The stabilizing effect of metal nodes (Co(II), Cu(II), and Zn(II)) across different topologies and dimensionalities (2D or 3D) remains unexplored. By employing room-temperature acid solution calorimetry, we quantify the change in enthalpy (ΔH^0_f) for forming the frameworks relative to endmembers (metal oxide plus linker). Enthalpies of formation for Co-ZIF-L, Zn-ZIF-L, SOD-Co(MeIm)₂, SOD-Zn(MeIm)₂, *dia*-Co(MeIm)₂, *dia*-Zn(MeIm)₂, and *dia*-Cu(MeIm)₂ are -44.72 ± 0.76 , -73.74 ± 0.91 , -15.49 ± 0.86 , -20.45 ± 0.94 , -46.18 ± 0.75 , -31.63 ± 1.26 , and -15.03 ± 1.40 kJ.mol⁻¹, respectively. Zn(II) has the greatest stabilizing effect in the 2D dimensionality (ZIF-L) and SOD topology. Co(II) has the greatest stabilizing effect in the *dia* topology. The stabilizing effect of metal nodes is dependent on both topology and dimensionality of the framework.

9:30 AM BREAK

10:00 AM *DS01.03.05

Novel Insight into Defect Behavior of Irradiated Materials—Combined Neutron Total Scattering and High Temperature Calorimetry
Investigation [Maik K. Lang](#); University of Tennessee, United States

We present neutron total scattering combined with high-temperature calorimetry as a new strategy for the characterization of radiation effects in materials. Irradiation experiments were performed at the GSI Helmholtz Center with heavy ions of specific energy of 11.4 MeV/u. The use of such ions (penetration depth: ~100 μm) produces the sufficiently large irradiated sample mass (~150 mg) required for bulk structural and thermodynamic analysis. Neutron scattering was performed at the Nanoscale Ordered Materials Diffractometer at the Spallation Neutron Source (Oak Ridge National Laboratory). High temperature oxide melt solution calorimetry and differential scanning calorimetry was utilized to investigate the thermodynamic properties and energetic evolution using the same set of irradiated samples. We studied various ion-induced structural modifications, such as defect formation (CeO₂), disordering (Er₂Sn₂O₇), and amorphization (Dy₂Ti₂O₇). Our analytical approach demonstrated that irradiation-induced modifications are more complex than previously thought with distinct processes occurring over different length scales and temperature regimes.

10:30 AM *DS01.03.07

Thermal Expansion of Metal Diborides (MB₂ | M = Ti, Zr, Nb, Hf, Ta) up to 3150 C [Scott J. McCormack](#)¹, Fox Thorpe¹, Elizabeth Sobalvarro², Gabriella King², James Cahill², Wyatt Du Frane² and Joshua Kuntz²; ¹University Of California, Davis, United States; ²Lawrence Livermore National Laboratory, United States

Metal diborides (MB₂ | M = Ti, Zr, Nb, Hf, Ta) are considered an ultra-high temperature refractory ceramic due to their relatively low reactivity and high melting point. While these properties are appealing, they also make it difficult to fully characterize their thermochemical and thermophysical properties up to melting. This work will discuss in-situ high temperature X-ray diffraction measurements up to ~3150 C using a conical nozzle levitator system equipped with a 400 W CO₂ laser. The high temperature X-ray diffraction data was used to calculate anisotropic coefficients of thermal expansion. The coefficients were compared amongst the five diborides (MB₂ | M = Ti, Zr, Nb, Hf, Ta). It was found that the anisotropy could be related to the atomic displacement parameters of the metal cations. These thermophysical measurements will be critical in developing ultra-high temperature material systems for applications in hypersonic vehicles, nuclear fission/fusion reactors, and spacecraft.
Prepared by LLNL under Contract DE-AC52-07NA27344

11:00 AM DS01.03.08

Enabling Permanently Nonvolatile Memory Using Materials Thermodynamics [Yiyang Li](#); University of Michigan, United States

The ability to store information using nonvolatile memory is a crucial pillar for computing and modern society. The most common nonvolatile memory, Flash memory, retains state by trapping charge within energy wells; however, such “kinetic” memory will revert back to the thermodynamic equilibrium and therefore lose information, especially under high temperatures and ionizing radiation. A more resilient nonvolatile memory would instead switch between two or more thermodynamically equilibrium states. Using “thermodynamic” memory, there will be no driving force for the material to leave one state for another, and can yield permanent nonvolatility even without kinetic barriers. Composition phase separation, whereby materials with different compositions can have the same chemical potential, provide one avenue towards engineering materials with multiple equilibrium thermodynamic states.

We present our research on how to utilize composition phase separation in nonvolatile, on-chip memory. One promising nonvolatile memory is the resistive random access memory (RRAM), which switches states through the migration of oxygen vacancies in transition metal oxides. It is widely assumed that RRAM is a “kinetic” memory, which retains state because of slow oxygen vacancy diffusion kinetics. However, the experimentally attained retention time is about 10 orders of magnitude longer than the characteristic oxygen diffusion time. Instead, we show that RRAM is a “thermodynamic” memory that retains state using composition-driven phase separation. Moreover, we show how phase separation can also be used to engineer new types of nonvolatile electrochemical memory. These results show the critical importance as well as potential opportunities of modern thermodynamics to memory and other device technologies.

11:15 AM DS01.03.10

Deep Learning-Accelerated Explicit Solvation Thermodynamics in Molten Salts [Yu Shi](#)¹, Stephen Lam² and Thomas Beck³; ¹University of Cincinnati, United States; ²University of Massachusetts Lowell, United States; ³Oak Ridge National Laboratory, United States

Molten salts are an emerging class of ionic liquids that are used in several advanced energy applications including next-generation nuclear reactors, batteries, and thermal energy storage.

In these applications, predicting corrosion and phase change behavior remains a critical challenge. This requires predicting the solvation of structural metals, atmospheric impurities, and a variety of chemical products that are generated during operation. Due to complex structural ordering in these fluids, explicit solvation modeling that includes all atoms surrounding a solute, is required. Furthermore, the need for precise solvation thermodynamics necessitates the use of methods that are chemically accurate ($E \sim 1-4$ kJ/mol). In this work, we simultaneously address these challenges by combining quasicheical theory (QCT), ab initio molecular dynamics (AIMD) simulation based on dispersion-corrected density functional theory (DFT), and deep learning (DL) potentials to accurately predict the solvation free energy of solute ions in molten salt. First, QCT provides an exact partitioning of solvation free energy into three steps that can be directly simulated: 1) formation of a small cavity in solution, 2) insertion of a solute ion into the cavity, and 3) relaxation of cavity and solution around the solute ion. These contributions are determined by thermodynamic integration requiring extended simulation

time and length-scales that are inaccessible to AIMD. As such, ab initio-accurate (<4 meV/atom) neural network potentials were trained to accelerate MD simulation by several orders of magnitude. Lastly, DFT-interaction energies are corrected using Møller-Plesset perturbation theory (MP2) to accurately account for the effects of dispersion and periodic boundary conditions in a finite-size simulation cell. In this work, we show that deep learning potentials can accurately predict molten salt thermodynamics and local coordination structures. We demonstrate the combined methods (DFT-DL-QCT) on molten NaCl, in which we obtain the total excess potentials of Na^+ and Cl^- ions. Moreover, we highlight that dispersion and finite size errors in DFT result in significant errors (13.7 kJ/mol) in calculating solvation free energy, which must be corrected. The calculated excess chemical potential for Na^+/Cl^- was predicted to be -164.8 ± 2.2 kcal/mol, which is in excellent agreement with the benchmark experimental value of -163.5 kcal/mol from thermochemical tables. Here, chemical accuracy in predicting solvation thermodynamics of molten salts is achieved for the first time. These results provide validation of these combined methods for predicting excess chemical potentials, which can be directly used for determining the solubility, corrosion potential, and volatility of dissolved gases and metals in molten salts. This provides motivation for using DFT-DL-QCT to understand solute chemistry in a wide range of molten salt systems in advanced energy applications.

SESSION DS01.04: New Phase Diagram Frameworks
Session Chairs: Alexandra Navrotsky, Richard Otis and Wenhao Sun
Tuesday Afternoon, November 29, 2022
Hynes, Level 2, Room 204

1:30 PM *DS01.04.01

Statistical Mechanics Approaches to Predict Generalized Free Energy Descriptions [Anton Van der Ven](#); University of California, Santa Barbara, United States

The thermodynamic properties of crystalline materials are determined by excitations that occur at the electronic and atomic length scales. Important sources of entropy include chemical disorder, vibrational excitations and magnetic disorder. Atomic and electronic degrees of freedom within a high symmetry parent crystal can lead to symmetry-breaking ordering reactions. The thermodynamic properties of a high symmetry parent crystal and its symmetry-breaking derivative structures can be encapsulated within a generalized free energy description that is a continuous function of composition, strain and suitably defined symmetry-adapted order parameters. This talk will describe methods to calculate generalized free energies with first-principles statistical mechanics approaches. Systematic approaches to identify order parameters for chemical and magnetic ordering reactions and for martensitic structural transformations will also be described. The importance of anharmonicity and magnetic degrees of freedom in determining phase stability in multi-component crystals will be illustrated for technologically important structural and functional materials. Approaches to quantify uncertainty in statistical mechanics simulations will be described.

2:00 PM DS01.04.02

A Robust Framework for the Determination of Magnetic Properties from First-Principles Calculations [Guy C. Moore](#)^{1,2}, [Matthew K. Horton](#)¹ and [Kristin A. Persson](#)¹; ¹Lawrence Berkeley National Laboratory, United States; ²University of California, Berkeley, United States

Moving from the atomistic picture of magnetism to larger length scale models is an important challenge for the design and discovery of technologically relevant magnetic materials. This problem requires increased care for correlated electron systems, such as transition metal oxides, in which multi-body interactions are difficult to model using conventional density functional theory (DFT). In the extension to DFT+U+J, Hubbard U and Hund J values account for on-site coulomb interactions between localized electrons. These Hubbard U and Hund J values are computed using a customized linear response computational workflow suitable for high-throughput DFT applications. We present a framework for obtaining magnetic exchange constants from DFT+U+J using the established single-particle Green's function approach, which can be used to study finite-temperature behavior of lattice models using Monte Carlo methods. The Heisenberg exchange constants are highly sensitive to two important prerequisites: the magnetic ground-state, as well as U and J values. We explore the sensitivity of the magnetic ground state and resulting exchange constants to U and J values. Additionally, we have implemented and benchmarked a "source-free" exchange-correlation magnetic field in VASP. This source-free functional, paired with a custom particle swarm optimization strategy, SpinPSO, has resulted in improved agreement with a variety of magnetic ground-states measured by neutron diffraction. This ground-up computational approach will allow for the discovery of magnetic materials with technological applications ranging from spintronics to cost-effective magnetocaloric materials for magnetic refrigeration.

2:15 PM DS01.04.03

Duality Between Compositional Phase Diagrams and Chemical Potential Diagrams [Jiadong Chen](#) and Wenhao Sun; University of Michigan, United States

Equilibrium phase diagrams are not well-poised to evaluate materials stability under dissolution and growth—for example, corrosion and etching; synthesis and deposition; or solid-solid interfacial reactions. These non-equilibrium situations would be better analyzed by phase diagrams that visualize the tendency for a material to gain or lose chemical species; e.g., with a chemical potential axis. Here, we present a generalized phase diagram framework to mix composition and chemical potential axes, providing a new stability representation that applies to these non-equilibrium situations. Our theoretical framework relies on the geometric duality between convex hulls and half-space intersections; and leads to a computational platform that scales easily to describe high-dimensional phase boundaries and multi-phase coexistence regions. We discuss how to evaluate and interpret the axes, widths, stability windows, and driving forces on the chemical potential diagram, and importantly, how to connect these to real-world laboratory conditions. Altogether, these mixed composition and chemical potential diagrams enable materials scientists to evaluate stability in more diverse chemical environments.

2:30 PM BREAK

3:00 PM *DS01.04.04

Modern Applications of Classical Thermodynamics to Strained Solids—Multiphase Multidomain Temperature-Strain-Stress Diagrams [Bo Wang](#)^{1,2} and [Long-Qing Chen](#)¹; ¹The Pennsylvania State University, United States; ²Lawrence Livermore National Laboratory, United States

It has been well established that strains or stresses can have profound effects on the thermodynamic stability of phase and domain states of solids, and they can be judiciously utilized to tune solid state phase and domain microstructures and thus physical properties. Here, we propose a general thermodynamic framework to efficiently construct multidomain and multiphase diagrams of arbitrarily strained or stressed solids, in analogies to the well-known temperature-composition phase diagrams. We demonstrate the general approach by obtaining the temperature-strain-stress phase and domain diagrams of

diverse solids, including proper ferroelastic ZrH_2 , strongly correlated electron material VO_2 , ferroelectric $PbTiO_3$, and unconventional ferroelectric $Hf_{0.5}Zr_{0.5}O_2$ with coexisting nonpolar and polar phases. Our thermodynamic theory offers a powerful, yet easy to implement, theoretical tool for understanding the thermodynamics of any strained solids and for guiding the strain engineering of their properties.

3:30 PM DS01.04.05

The Geometry of Phase Boundaries on High-Dimensional Phase Diagrams [Wenhao Sun](#)¹, Jiadong Chen¹ and Matt Powell-Palm²; ¹University of Michigan, United States; ²University of California, Berkeley, United States

There are four main varieties of phase diagrams today: 1) Temperature–Pressure; 2) Temperature–Composition; 3) Ellingham (T, μ_{O_2}); and 4) Pourbaix diagrams (pH , Redox potential). However, these 2D phase diagrams do not account for many other forms of thermodynamic work that may be operative during nucleation and growth—such as surface, elastic, electromagnetic and electrochemical work. Here, I will describe a process to lift 2D phase diagrams into higher dimensions, exposing these additional forms of thermodynamic work on the axes. In particular, this involves deriving the geometry of high-dimensional phase boundaries and phase-coexistence regions, which leads to generalized forms of Gibbs' Phase Rule and Clausius-Clapeyron relations. From this geometric foundation, we can construct and deploy phase diagrams with any axes of mixed intensive or extensive variables—providing a powerful new theoretical framework for the design and synthesis of advanced functional materials.

3:45 PM *DS01.04.06

Holistic Integration of Experimental and Computational Datasets Together with Simplified Models for Rapid Establishment of Diffusion Databases [Ji-Cheng Zhao](#) and Wei Zhong; University of Maryland, United States

Discrepancies between experimental and computational datasets are usually hard to reconcile. For the case of diffusion coefficients, large amounts of both experimental and computational data are available to allow careful assessments of the degree of agreements and disagreements. Such rigorous and systematic assessments allow us to take advantage of the best of both datasets and provide complementary data to be used to establish the most reliable diffusion databases. In addition, simple and yet general mathematical models for binary and multicomponent metallic solid solutions are developed to facilitate future database establishment. This talk will use many examples to illustrate the power of such holistic integration and the new models. The talk also calls for systematic calculations and machine-learning predictions of both self-diffusion and impurity (dilute) diffusion coefficients of all elements in fcc, bcc and hcp crystal structures.

4:15 PM DS01.04.07

Connecting Features of Phase Diagram to Diffusive Flow in Alloys [Arindam Raj](#)¹, Naijia Liu¹, Yujun Xie², Sungwoo Sohn¹, Guannan Liu¹ and Jan Schroers¹; ¹Yale University, United States; ²University of California, Berkeley, United States

A general quantitative understanding of microstructure-property-relationships (MPRs) relationships remains elusive, as microstructures are generally very complex, cannot be directly reconstructed by the characteristics of their constituents, and are multiscale in nature (10^{-9} m – 10^{-3} m). We investigate alloys with different phases, viz., solid solutions, intermetallics, and eutectics to demonstrate the diffusive characteristics of these phases under stress gradient. We draw conclusions about the diffusive response of these phases in alloys based on the diffusing flux. Experimentally, this is realized through thermomechanical nanomolding, where we spatially separate the diffusing flux from the alloy feedstock into the pores of the nanomold. The length and composition of these rods can provide us with the diffusion rate and the composition of the diffusive flux. Here, we can probe $\sim 10^{11}$ distinct spots over the microstructure parallelly. We explain these results on the basis of fastest Gibb's free energy degradation rates.

4:30 PM DS01.04.08

A Gaussian Process Based Saddle-Point Search Method for Temperature-Dependent Energy Surfaces [Seyyedfaridoddin Fattahpour](#) and Sara Kadkhodaei; University of Illinois at Chicago, United States

In this work, we present a unique saddle-point search method based on a Gaussian process regression of the temperature-dependent energy surface to simultaneously sample the temperature-dependent energy surface and converge to the saddle point. We showcase the use of this method for solid-state diffusion in bcc phases of titanium and zirconium. These phases are chosen because they exhibit harmonic phonon instabilities, implying that the thermodynamic equilibrium state does not correspond to a local minimum on their Born-Oppenheimer energy surface. Therefore, saddle point search schemes cannot locate the diffusion transition state according to forces drawn from the Born-Oppenheimer energy surface [1]. Instead, forces drawn from an effective temperature-dependent energy surface are necessary to correctly guide the search scheme towards the transition state. In our method, a Gaussian process is used to estimate the temperature-dependent effective energy surface based on stochastically sampled atomic configurations along the transition path. We utilize the dimer and nudged-elastic band algorithms for the saddle point search on the temperature-dependent effective energy surface. Our method provides a useful alternative to methods such as molecular dynamics, which directly simulate diffusive hops.

References

[1] Fattahpour, Seyyedfaridoddin and Davariashstiyani, Ali and Kadkhodaei, Sara. Understanding the role of anharmonic phonons in diffusion of bcc metals. *Phys. Rev. Materials*, 10.1103/PhysRevMaterials.6.023803

4:45 PM DS01.04.09

A Predictive Surface Tension Model for Binary Metallic Solution [Yoongu Kang](#) and In-Ho Jung; Seoul National University, Korea (the Republic of)

Surface tension is very important thermodynamic energy which determine the phase stability in nano-sized materials. For liquid metallic system, many surface tension models have been proposed to reproduce the experimental data but none of the models can predict the surface tension of liquid metallic solution without any model parameters. In this study, we developed a new predictive surface tension model for liquid metallic solution which can predict the surface tension of binary liquid solution only from unary surface energy data. By using well quantified thermodynamic properties like enthalpy and entropy of mixing of binary bulk liquid solution, the surface composition and surface tension of liquid metal can be predicted from the new model. The present model was tested for 50 binary solutions having ideal, positive and negative interaction. In particular, the present model can give successful results for the liquid solutions with strong positive deviation or negative deviation from ideal solution, which have not been well predicted by any previous models.

SESSION DS01.05: Poster Session
Session Chairs: Richard Otis and Wenhao Sun
Tuesday Afternoon, November 29, 2022
8:00 PM - 10:00 PM
Hynes, Level 1, Hall A

DS01.05.01

Ab Initio Study of the Thermodynamic Properties of Amorphous Bismuth Under Pressure Flor B. Quiroga Bañuelos¹, David Hinojosa¹, Isaias Rodríguez¹, Alexander Valladares², Renela M. Valladares² and Ariel A. Valladares¹; ¹Universidad Nacional Autónoma de México, Instituto de Investigaciones en Materiales, Mexico; ²Universidad Nacional Autónoma de México, Facultad de Ciencias, Mexico

The physicochemical properties of amorphous metals and bulk metallic glasses, when subjected to extreme conditions such as low temperatures or high pressures, make them attractive materials for important technological applications [1]. To fully exploit their benefits, it is necessary to understand the electronic and vibrational contributions to their thermodynamic properties, and first-principles calculations have helped to elucidate the physics of this complex materials. Recently, we explored the effects of negative pressures on the superconducting transition temperatures of amorphous Bismuth through the *ab initio* calculation of its electronic structure [2]. Now we will go into studying the thermodynamic properties of this system by calculating the vibrational densities of states (vDoS) using an *ab initio* approach. Specifically, in this work we calculate the vDoS, heat capacity and enthalpy for 3 amorphous samples, two of them subjected each to a positive and to a negative pressure. The amorphous samples were generated by *ab initio* molecular dynamics and our *undermelt-quench method* [3] applied to supercells of 216 atoms with densities: 10.89, 9.81, and 8.91 g cm⁻³ corresponding to a volume of 90%, 100% and 110% of the original volume, respectively. Results will be presented and discussed.

[1] D. C. Hofmann, R. Polit-Casillas, S. N. Roberts, J.-P. Borgonia, R. P. Dillon, E. Hilgeman, et al., *Castable Bulk Metallic Glass Strain Wave Gears: Towards Decreasing the Cost of High-Performance Robotics*. Scientific Reports 6 (2016), 37773.

[2] F. B. Quiroga Bañuelos, D. Hinojosa-Romero, I. Rodríguez, A. Valladares, R. M. Valladares, A. A. Valladares, Poster QT11.06.02 - *Superconductivity in Amorphous Bismuth at Negative Pressures*, 2022 MRS Spring Meeting & Exhibit.

[3] A. A. Valladares, *A new approach to the ab initio generation of amorphous semiconducting structures. Electronic and vibrational studies*, Glass Materials Research Progress, 2008, pp. 61-123. Editor: Jonas C. Wolf and Luka Lange, Nova Science Publishers, Inc. ISBN 978-1-60456-578-2.

DS01.05.02

Heat Capacity of Dense Post-Stishovite Silica Glass from Fast-Scanning Calorimetry Laura Bonatti, B Brugman, Tamilarassan Subramani, Sergey Ushakov, Kurt Leinenweber and Alexandra Navrotsky; Arizona State University, United States

Stishovite is a high-pressure phase of SiO₂ which transforms into a dense glass when heated at ambient pressure to ~500°C. The properties of post-stishovite glass are more similar to densified silica formed by compression above 10 GPa than to standard fused quartz. Despite widespread thermal data on crystalline and glassy SiO₂ phases, the heat capacity of the dense, post-stishovite glass has not been measured. We calibrated a Mettler Toledo Flash DSC 2+ to determine quantitatively the mean heat capacity for post-stishovite glass, as well as crystalline stishovite and TiO₂ in the temperature range of 200 to 350 °C. The calibration was performed using the heat capacity of alumina, titania and zirconia, with an uncertainty of under 17%. Our measured Cp for titania and stishovite agrees within 9% of the reported literature values. The heat capacity for the post-stishovite glass was within 6.6% of the reported literature value for the heat capacity of stishovite between 200 to 350 °C. The developed methodology allows for obtaining quantitative thermochemical data on solid samples in micrograms amounts that are too small for other methods, e.g. new high pressure phases quenched from diamond anvil cell experiments.

DS01.05.03

Iron-Poor Ferrites for Low Temperature CO₂ Conversion via Reverse Water-Gas Shift Thermochemical Looping Eddie Sun, Jimmy Rojas, Gang Wan and Arun Majumdar; Stanford University, United States

CO₂ utilization via the reverse-water-gas-shift (RWGS) reaction for the production of CO and then to long chain hydrocarbons is a potentially scalable method to mitigate rising global CO₂ emissions, if appreciable CO yields can be achieved at low reaction temperatures. Here, we report that Fe_{0.35}Ni_{0.65}O_x achieves, to the best of our knowledge, a record high experimentally measured CO yield of 80 mL-CO/g_{MOx}/cycle at low reaction temperatures (500°C for both oxidation and reduction steps) in a chemical looping (CL) process. This reported yield is an order of magnitude higher than previously reported RWGS-CL metal oxides at 500°C. We identified the composition of the metal oxide Fe_{0.35}Ni_{0.65}O_x using the Calculation of Phase Diagrams (CALPHAD) methodology to screen and filter through many combinations of metal oxides. We then experimentally tested this Fe_{0.35}Ni_{0.65}O_x metal oxide for chemical looping RWGS and utilize x-ray characterization techniques and CALPHAD to find that a spinel-to-metallic phase transition gives Fe_{0.35}Ni_{0.65}O_x its noteworthy CO yield and oxygen capacity. We emphasize the importance of thermodynamics calculations and CALPHAD screening to quickly search through the vast design space of metal oxides to greatly reduce the amount of necessary experimentation.

DS01.05.04

A High-Throughput Framework for Lattice Dynamics Zhuoying Zhu, Junsoo Park and Anubhav Jain; Lawrence Berkeley National Lab, United States

Lattice dynamics of materials are fundamental to their thermal properties, mechanical properties, as well phase transition behaviors. Among thermodynamic quantities that directly follow from harmonic phonons are vibrational free energy, entropy, and heat capacity, which can be easily obtained from well-known methods like density-functional perturbation theory. Obtaining anharmonic IFCs (third-order and higher), which determine thermal expansion, thermal conductivity, and dynamical stability has remained a challenge for longer.

We herein present our generalized automated workflow for lattice dynamical properties. Under the high-throughput framework, we can obtain both harmonic and anharmonic IFCs with HiPhive package and calculate quantities like three-phonon scattering and lattice thermal conductivity using ShengBTE. For phonon dispersions with imaginary modes, one more step of renormalization will be added to obtain temperature-dependent real and stable phonons before computing the thermodynamic quantities.

DS01.05.05

Exploration of Relationship Between Phonons and Cathode Behavior of Battery Materials Using Density Functional Theory Solomon R. Murdock and Hillary Smith; Swarthmore College, United States

LiFePO₄ is a widely used battery cathode material. Both the rising cost of lithium and the environmental impact of lithium mining has sparked interest in

alternative high performance cathode materials. NaFePO₄ has been proposed as an alternative to LiFePO₄ due to its similar chemical formula. Despite this similarity, the ground state structure of NaFePO₄ is maricite while LiFePO₄ has a triphylite structure. Both maricite and synthetic triphylite NaFePO₄ have been observed to display poor cathode performance as compared with LiFePO₄. We performed Density Functional Theory calculations using VASP (Vienna Ab Initio Simulation Package) to determine the phonon dispersions and density of states for LiFePO₄, maricite NaFePO₄, and triphylite NaFePO₄. The relationship between cathode performance and lattice dynamics is explored for all three materials. A better understanding of the relationship between cathode performance and lattice vibrations will aid in the development of cathode technology.

DS01.05.06

A Cluster Expansion of the FeMnNiAlCr High Entropy Alloy [Andrew Pike](#) and Geoffroy Hautier; Dartmouth College, United States

Experimentally, determination of the phase diagram of a five-component high entropy alloy (HEA) is extremely difficult due to the vast number of combinations of compositions and conditions. While computations of phase diagrams from density functional theory (DFT) at 0K are somewhat commonplace, incorporating the temperature effects and disorder present in a real HEA are not handled well directly from DFT. A cluster expansion uses data from DFT to build a model Hamiltonian, which can then incorporate these effects. I will present a cluster expansion for the FeMnNiAlCr HEA system and discuss the search for useful, novel phases in this system from first principles.

DS01.05.08

A Simulation Study on Dynamic Behavior of Equilibrium Polymer-Linked Colloidal Gels [Taejin Kwon](#), Tanner Wilcoxson, Delia Milliron and Thomas Truskett; The University of Texas at Austin, United States

Colloids with limited valence such as patchy particles can form equilibrium gels that are thermodynamically stable. Polymer-linked colloidal gels are promising candidates due to the possibility to tune valence using the macroscopically controllable ratio of linkers to colloids. Still, an understanding of the dynamics of such networks, and how they relate other systems such patchy colloids, is lacking. Using simulations of a coarse-grained model, we show that linked-colloidal networks exhibit dynamic hallmarks of viscoelastic equilibrium gels. Our results demonstrate that network bond persistence time controls structural relaxation. We also find the re-entrant structural and dynamic behavior as a function of linker concentration, centered at the stoichiometric ratio. Increasing or decreasing linker concentration from the stoichiometric ratio results in reduced network connectivity and shorter structural relaxation times. These results provide fundamental insights and suggest new macroscopic strategies for tuning the network connectivity and the dynamical response in colloidal networks.

DS01.05.09

Impact of Materials Property Uncertainty on the Thermodynamic Models of Materials and Reaction Chemistry [Joshua Gabriel](#), Noah H. Paulson and Angel Yanguas-Gil; Argonne National Laboratory, United States

Materials property data is used in the design of engineering components and in the simulation of reactions for process engineering predictions. In this work we present the impact of uncertainty in the fundamental material properties of heat capacity, enthalpy, and Gibbs free energy on two important tools for materials and process design: phase diagrams for alloys and reaction simulators predicting the equilibrium product distributions of reactions. Specifically, we present applications of Bayesian inference and automated weighting of datasets to quantify uncertainty for materials property models in aluminum, the Cu-Mg phase diagram, and the equilibrium product distribution of precursor gas mixtures relevant for silicon carbide synthesis. In thermodynamic models of aluminum [1], we show the importance of selecting computational datasets compatible with experimental datasets in obtaining a thermodynamic property model. In the Cu-Mg phase diagram, we show that the inclusion of unary data for Cu and/or Mg, as part of uncertainty quantification efforts, increases the uncertainty around invariant points in the phase diagrams by 5%. We also present a cost-effective path forward utilizing uncertainty propagation and compare it with the co-optimization of unary and binary data. Finally, we show how the Bayesian automated weighting approach resolves unphysical discontinuities not associated with phase transitions in the context of silicon carbide synthesis in addition to showing the uncertainty in product distributions.

[1] J. J. Gabriel, N. H. Paulson, T. C. Duong, C. A. Becker, F. Tavazza, U. R. Kattner, and M. Stan, *Materialia* 20, (2021) 101216

DS01.05.10

Thermodynamic Assessment of Heat Capacity and Entropy in Fragile Glasses [Colby Stoddard](#) and Hillary Smith; Swarthmore College, United States

The bulk metallic glasses Pt_{80-x}Cu_xP₂₀ where $14 < x < 27$ exhibit high fragility and a sharp glass transition. This results in a large excess entropy of the liquid phase over the crystalline phase. We used a combination of differential scanning calorimetry (DSC) and inelastic neutron scattering (INS) measurements to characterize the thermodynamics in these Pt-Cu-P glasses across a range in compositions. The isobaric heat capacity and vibrational entropy of the amorphous solid, crystalline solid, and supercooled liquid phases are assessed with DSC and INS, respectively. These data are used to calculate the difference in enthalpy, total entropy, vibrational entropy and Gibbs free energy between the solid and liquid phase. A significant increase in heat capacity is observed at the glass transition, but this does not correspond to a large change in the vibrational entropy. Insights into the effect of fragility on these thermodynamic parameters will be discussed.

SESSION DS01.06: Vibrational Entropy and Phonons

Session Chairs: Alexandra Navrotsky, Richard Otis, Jonathan Paras and Wenhao Sun

Wednesday Morning, November 30, 2022

Hynes, Level 2, Room 204

9:00 AM *DS01.06.01

Understanding Static and Dynamic Local Structure—The Nature of Local Dynamic Order in CH₃NH₃PbI₃ and CH₃NH₃PbBr₃ [Michael F. Toney](#); University of Colorado Boulder, United States

Local atomic structure often differs from the global average structure as measured with diffraction and yet the local structure has a profound impact on properties. This structure-function relationship applies in many materials classes, ranging from organics to Li-ion battery cathodes to perovskites. Accurately characterizing this local structure has proven challenging but recent advances in diffuse scattering (“between” Bragg peaks) has enabled local structure determination. In this talk, I will discuss the importance of local structure and how this can be quantified and will demonstrate this for organic-inorganic hybrid halide perovskites. These materials are a recently re-invigorated class of semiconductor that have demonstrated very high efficiencies for

solar cells after just over a decade of research. While the importance of lattice dynamics and dynamical (dis)order have been recognized in these materials, their nature is only poorly known and understood. We used X-ray and neutron diffuse scattering coupled with molecular dynamics to quantify the nature, size, and time scale associated with dynamical local order in $\text{CH}_3\text{NH}_3\text{PbI}_3$ and $\text{CH}_3\text{NH}_3\text{PbBr}_3$ perovskites. We observe that the nominally cubic perovskite consists of dynamical, two-dimensional sheets of lower symmetry tetragonal regions of about 3 nm diameter with several picosecond lifetimes. The implications on halide perovskite properties will be discussed.

9:30 AM DS01.06.02

Enhancing Efficiency and Scope of First-Principles Quasi-Harmonic Approximation Methods Through the Calculation of Third-Order Elastic Constants [Angelo Bongiorno](#); College of Staten Island - CUNY, United States

In this paper we present a computational strategy to calculate from first principles the coefficient of thermal expansion and elastic constants of a material over meaningful intervals of temperature and pressure. This computational strategy relies on a novel implementation of the quasi-harmonic approximation (QHA) to calculate isothermal-isochoric linear and nonlinear elastic constants of a material in a reference state, followed by the use of elementary equations of nonlinear continuum mechanics to extrapolate values of lattice parameters and elastic constants of the material in an arbitrary deformed state. Our implementation of QHA relies on finite deformations, the use of non-primitive supercells to describe a material, a recently proposed technique to calculate generalized mode Grüneisen parameters, and the numerical differentiation of the second Piola-Kirchhoff (thermal) stress tensor to calculate both second-order elastic constants (SOECs) and third-order elastic constants (TOECs) (at finite temperature). We remark that our implementation of QHA involves a manageable computational workflow that, measured in terms of number of deformed configurations, requires only 4, 6, and 10 configurations (including reference state) to calculate the isothermal SOECs of a material with the cubic, hexagonal, and orthorhombic symmetry, respectively. In this paper, we first focus on conceptual and technical details of our methods, then we present the results of selected applications, and we conclude with a discussion of the advantages and limits of our methods. Overall, we envision that the methods presented in

this paper have the potential to be used for the following purposes. One, the calculation from first principles of nonlinear elastic constants (TOECs and potentially fourth-order elastic constants) of materials at finite temperature. TOECs are important coefficients characterizing the non-linear mechanical response of a material subjected to a deformation, and thereby related to properties such as sound attenuation and yield strength. Our QHA method can be used to calculate these nonlinear elastic coefficients at finite temperature for a variety of materials, for which experimental data are still missing or difficult to obtain. Two, the calculation from first principles of isothermal SOECs of materials with the orthorhombic, monoclinic, or triclinic symmetry, i.e. classes of materials that are within the reach of our QHA approach, which is suitable to be applied to study thermoelastic properties of low-symmetry materials. Three, the "rapid" calculation from first principles of the thermal expansion coefficient and SOECs of a material over finite intervals of temperature and pressure (by using our strategy combining QHA calculations and nonlinear continuum mechanics). We remark that our computational strategy is applicable to materials of arbitrary symmetry and complexity, and therefore it could be used to build databases of materials properties at finite temperature, or to investigate the thermoelastic and mechanical properties of, for example, minerals of geological relevance or metal alloys for structural applications.

9:45 AM DS01.06.03

Simulating Phononic and Vibrational Materials Properties on Quantum Computers [Nicolas P. Sawaya](#); Intel Corporation, United States

Quantum computers are poised to massively speed up the simulation of materials and chemistry, if a sufficiently advanced one can be built. Notably, the use of quantum computers to study phononic and vibrational (as opposed to electronic) degrees of freedom has been a relatively unexplored area. Here we discuss a range of quantum algorithms for calculating light-absorption cross-sections, thermal properties, and other quantities resulting from the motion of nuclei. We introduce data encodings with tunable memory-operations trade-offs, as well as more efficient quantum subroutines for calculating light-absorption properties. We end by discussing which classes of materials and quantities of interest are likely to require a quantum computer for accurate simulation.

10:00 AM BREAK

10:30 AM DS01.06.04

Microscopic View of Heat Capacity of Matter [Jaeyun Moon](#)¹, Lucas Lindsay¹ and Takeshi Egami²; ¹Oak Ridge National Laboratory, United States; ²The University of Tennessee, Knoxville, United States

In contrast to thermodynamic properties of solids and gases that are often described by phonon quasi-particles and real particles, respectively, our microscopic understanding of thermodynamics in liquids is lacking due to strong atomic interactions and lack of symmetry. Recent prior works have initiated efforts to understand heat capacity of liquids based on phonon quasi-particles similar to that of solids but often rely on free fitting parameters and questionable assumptions. In this work, we perform instantaneous normal mode and velocity autocorrelation analysis on single element systems under various conditions up to 10^7 K and 1 TPa. Our results suggest that heat capacity of liquids can be expressed by a combination of both quasi-particles and real-particles, leading to a unified framework to describe heat capacity of all three phases of matter: solid, liquid, and gas.

*Supported by the Department of Energy, Office of Science, Basic Energy Sciences, Materials Sciences and Engineering Division.

10:45 AM DS01.06.05

High Thermal Conductivity and Ultrahigh Thermal Boundary Conductance of Homoepitaxial AlN Thin Films [Gustavo Alvarez](#), Ryan Page, Renjiu Hu, Huili G. Xing, Debdeep Jena and Zhiting Tian; Cornell University, United States

Wurtzite aluminum nitride (AlN) has attracted increasing attention for high-power and high-temperature operations due to its high piezoelectricity, ultrawide-bandgap, and large thermal conductivity k . The k of epitaxially grown AlN on foreign substrates has been investigated; however, no thermal studies have been conducted on homoepitaxially grown AlN. In this study, the thickness dependent k and thermal boundary conductance G of homoepitaxial AlN thin films were systematically studied using the optical pump-probe method of frequency-domain thermoreflectance. Our results show that k increases with the thickness and k values are among the highest reported for film thicknesses of 200 nm, 500 nm, and 1 μm , with values of 71.95, 152.04, and 195.71 W/(mK), respectively. Our first-principles calculations show good agreement with our measured data. Remarkably, the G between the epilayer and the substrate reported high values of 328, 477, 1180, and 2590 MW/(m²K) for sample thicknesses of 200 nm, 500 nm, 1 μm , and 3 μm , respectively. The high k and ultrahigh G of homoepitaxially grown AlN are very promising for efficient heat dissipation, which helps in device design and has advanced applications in micro-electromechanical systems, ultraviolet photonics, and high-power electronics.

11:00 AM DS01.06.06

Extension of Transport-Derived Electronic Entropies to the Thermochemistry of High-Temperature Solid Solutions [Jonathan Paras](#) and Antoine

Allanore; Massachusetts Institute of Technology, United States

High-temperature quantification of the entropy of mixing in binary alloys through simulations remains an open challenge in materials thermodynamics. Recent success in using transport-property measurements to rationalize the total entropy of order-disorder and metal-insulator phase transitions in Cu_3Au and VO_2 suggest an empirical link between electronic transport properties and the electronic entropy. Measurements of the Seebeck coefficient and conductivity were conducted in solid-solution and intermetallic forming systems such as Cu-Ni and Fe-Ni at high temperature to assess the extensibility of the transport electronic entropy formalism to binary alloys. Under unipolar transport assumptions, large measured electronic entropy of mixing is reported in Cu-Ni. Similar trends were systematically observed in other high-temperature solid-solutions and their melts.

SESSION DS01.07: Configurational Entropy and Alloy Theory
Session Chairs: Tina Chen, Alexandra Navrotsky, Richard Otis and Wenhao Sun
Wednesday Afternoon, November 30, 2022
Hynes, Level 2, Room 204

1:30 PM *DS01.07.01

Zentropy—A Theory for Prediction of Observables Zi-Kui Liu; The Pennsylvania State University, United States

An emergent property appears when a number of simple entities interact in an environment to form more complex behaviors collectively that any single entity does not exhibit. Emergent properties are hard to predict because the number of interactions between a system's components increases exponentially with the number of components. In principle, the elegant Schrödinger equation in quantum mechanics could address the many-body interactions, resulting in the standard statistical mechanics where the individual entities are pure quantum states with zero entropy and their partition functions related to their internal energies. The applications of the Schrödinger equation to complex systems are made possible by the density functional theory (DFT) that postulates the existence of a unique electron density for the ground state of a system at 0 K. Using the ground and non-ground states as the building entities of complex systems, we propose that the entropy of a complex system is composed of the weighted sum of entropies of its building entities plus the classical statistical entropy among the entities. This new theory, termed as Zentropy theory, stacks up the entropic contributions from electrons to the scale of complex system of interest and result in the partition functions of building entities related to their free energies instead of their internal energies. With the properties of ground and non-ground states obtained from DFT, we show that the emergent properties in some magnetic and ferroelectric systems, previously thought to be explainable exclusively by strongly correlated physics, can be predicted, including singularity at critical points. This further provides a theoretical framework to predict emergent cross phenomena, including thermoelectricity, thermodiffusion, electrocaloric effect, and thermal expansion of material systems (<https://doi.org/10.1080/21663831.2022.2054668>).

2:00 PM DS01.07.02

Modeling Local Structure and Configurational Free Energy of Multi-Component Alloys Below the High-Temperature Limit Andrew Novick¹, Eric S. Toberer¹ and Vladan Stevanovic^{1,2}; ¹Colorado School of Mines, United States; ²National Renewable Energy Laboratory, United States

We present a method for modeling alloys as a statistical ensemble of randomly sampled ordered configurations on a given lattice. Accurately modeling the structure of alloys can require using large supercells to accommodate atomic disorder. However, with increasing supercell size, the set of possible configurations quickly becomes too large to exhaustively simulate; this is especially true for high-entropy compositions. In this work, we show that randomly sampling from the set of all possible configurations allows for the efficient modeling of alloy systems. This is done while still capturing the structural and energetic complexities found in exhaustive sampling. Furthermore, the statistical treatment naturally produces configurational free energy and local atomic structure as a function of the synthesis temperature. The high-temperature limit, implying perfect configurational disorder, is not assumed; neither is the final structure of the alloy. Thus, our method is particularly useful for studying the relationships between the synthesis temperature, short-range order, and local structure. The high-entropy pseudohexary system, $\text{PbTe-PbSe-PbS-GeTe-GeSe-GeS}$, will be studied as a case example. Trends in both the miscibility and structural deviation from the rocksalt structure-type will be discussed, as well as their agreement with experiment.

2:15 PM DS01.07.03

First Principles Calculation of Phase Diagrams of Alloys of Technological Interest Including Configurational and Vibrational Entropic Contributions Wei Shao^{1,2}, Sha Liu^{2,3} and Javier Llorca^{1,2}; ¹Technical University of Madrid, Spain; ²IMDEA Materials Institute, Spain; ³Yanshan University, China

The phase diagram of different alloys of technological interest is predicted from first principles calculations and statistical mechanics including the effect of configurational and vibrational entropy. The formation enthalpy of different configurations was accurately predicted as a function of temperature by means of cluster expansions that were fitted from first principles calculations. The vibrational entropic contribution of each configuration was determined from the bond length vs. bond stiffness relationships for each type of bond and the Gibbs free energy of the different phases was obtained as a function of temperature from Monte Carlo simulations.

The strategy was applied to determine the phase diagram of Al-Cu, Al-Li, Al-Cu-Li alloys and the computed phase diagrams were compared with the current experimental phase diagrams in the literature. Overall, the calculated phase diagrams were in good agreement with the currently accepted experimental phase diagrams and, moreover, they provided new insights and information that is sometimes missing in the experimental phase diagrams due to the limitations imposed by the kinetics of phase changes. This additional information can be very important to optimize the microstructure of these alloys by means of heat treatments.

2:30 PM BREAK

3:30 PM *DS01.07.04

Configurational Entropy in Complex Multi-Component Oxides Gerbrand Ceder; University of California, Berkeley/Lawrence Berkeley National Laboratory, United States

Configurational entropy embodies the composition complexity that materials can exhibit. Ab-initio methods such as the cluster expansion (CE) technique can be used to develop coarse-grained Hamiltonians that parameterize the energy dependence on configurational state but have rarely been used beyond simple binary or ternary metallic alloys. In this presentation, I will demonstrate the application of cluster expansion techniques to complex oxides with a

high number of cation and anion components. The extension of the cluster expansion is non-trivial due to the combinatorial scaling of basis functions, the inability to sample all characteristic cation configurations leading to unavoidable degeneracy in the ab-initio to CE mapping, and the charge neutrality constraint in systems with charged ions. I will show how modern compressive sensing techniques, combined with physical constraints, can be used to build accurate and stable cluster expansions which can be used with Monte Carlo simulations to determine the state of order in complex oxides. These complex expansions have been used to develop DRX cathode materials, which are an exciting earth abundant replacement for current Ni and Co-based cathodes, but often have a high number of cations present, making their thermodynamic assessment difficult.

4:00 PM DS01.07.05

High-Component Ionic Cluster Expansions for Exploring Disordered Spaces [Tina Chen](#)^{1,2}, Julia Yang¹, Peichen Zhong^{1,2}, Luis Barroso-Luque¹ and Gerbrand Ceder^{1,2}; ¹University of California, Berkeley, United States; ²Lawrence Berkeley National Laboratory, United States

Cluster expansions coarse-grain the free energy of multi-component systems based on the possible configurations of species on a disordered crystal lattice. The modeling of configurational energetics in conjunction with Monte-Carlo methods enables finite temperature voltage curve calculations and the computation of phase diagrams. While cluster expansions can in theory be used for systems of any dimensionality, their application has generally been limited to binary or ternary alloys. When applied to high-component ionic systems, a number of practical challenges emerge, including charge-state assignment, atomic relaxations from the fixed lattice, and the fitting of predictive models from a large feature space. We demonstrate techniques to overcome these challenges in the fitting of a cluster expansion to the space of cation-disordered Mn-based spinel, a Li-ion cathode materials space within which the high energy density, high-rate partially disordered spinels lie. We then show how the cluster expansion can evaluate how the level of disorder between the 16d TM sites and vacant 16c octahedral sites affects the electrochemical properties of the disordered spinel. Through this thermodynamic analysis, we illustrate how cluster expansions can be applied to isolate and understand the effects of specific types of disorder.

4:15 PM DS01.07.06

High Entropy Alloys as Glasses and Solid Solutions—Configurational Entropy and Alloy Properties [Mikko Alava](#)^{1,2}, Rene Alvarez-Donado¹, Amin Esfandiarpour¹ and Stefanos Papanikolaou¹; ¹NOMATEN Center of Excellence, Poland; ²Aalto University, Finland

High entropy alloys (HEAs) represent highly promising multicomponent crystals that form concentrated solid solutions (CSS) and may violate traditional thermodynamic rules of mixing, ultimately leading to excellent physical properties. Here, we report on simulations on seven CSS, including Co-Cr-Ni-Fe-Mn elements and we use 1-1 comparisons to corresponding glass phase characteristics, attained through rapid cooling protocols. We determine the behavior of various structural features, including the configurational entropy for a set of CSS in their crystalline and vitreous states numerically using swap Monte Carlo and show that the entropic rule of mixing is not always adequate for predicting alloy formation. We study the stability and formability of crystalline solid solutions, as well as glasses, while following the configurational entropy. An apparent entropic similarity between CSSs and corresponding glasses, leads us to use a Kauzmann-like ansatz, relating the CSS with the emergence of an order/disorder transition, at a composition-dependent temperature. In the context of glasses, a comparison between kinetic and thermodynamic fragilities allows to associate the sluggish diffusion onset to a drop in configurational entropy at the Kauzmann temperature. In analogy to glasses, we classify CSS as strong or fragile in the sense of their ability to migrate across CSS crystal configurations at high temperatures. We argue that the magnitude of the order/disorder transition temperature may predict CSS single-phase stability, as it appears to scale with well known predictors, such as the valence electron concentration (VEC).

4:30 PM DS01.07.07

Short-Range Order in High-Entropy Superalloys—First Principles Theory and Atomistic Modelling [Christopher D. Woodgate](#) and Julie Staunton; University of Warwick, United Kingdom

Short-Range order (SRO) can be either beneficial or detrimental to the properties of novel superalloys. An understanding of phase behaviour and underlying physical mechanisms driving ordering is therefore essential. We present results from an all-electron, first principles, Landau-type theory which enables us to obtain SRO directly, and also to obtain parameters suitable for atomistic modelling to understand incipient order in these materials. Following successful earlier work on the Ni-based superalloys[1], I will present new results on the refractory-based superalloys, which are being studied as candidate materials for components in fusion reactors, due to their exceptional strength, high melting points, and high levels of resistance to radiation. We present a complete description of SRO in the five-component VNbMoTaW and its derivatives. Further, we elucidate the origins of this order and describe the underlying physical mechanisms by which it is driven.

1. C. D. Woodgate, J. B. Staunton, "Compositional Phase Stability in medium-entropy and high-entropy Cantor-Wu alloys from an ab initio all-electron Landau-type theory and atomistic modelling", Phys. Rev. B, **105** 115124 (2022).

4:45 PM DS01.07.08

Short Range Order Corrections to Alloy-Free Energies within the CALPHAD Framework Using the Cluster Variation Method Formalism. [Sayan Samanta](#) and Axel van de Walle; Brown University, United States

The CALPHAD method, traditionally used to model experimental thermodynamic data, also provides an effective way to parametrize alloy free energies computed from first-principles. While the Special Quasirandom Structure (SQS) formalism offers a natural and efficient tool to generate input data for disordered solid solution phases, accounting for short range order (SRO) effects in a computationally efficient way presents a challenge. In this work we utilize the Cluster Variation Method (CVM) method in tandem with the SQS formalism to determine closed-form nonlinear expressions for temperature-dependent SRO corrections to the formation free energies. Our approach, which implements the CVM to any level of accuracy, has been integrated into the sqs2tdb software pipeline. As a proof of concept, we perform a thermodynamic assessment of the Ir-Ru binary alloy with SRO correction and show that under the tetrahedron approximation, the SRO correction to the hcp phase is sufficient to accurately reproduce the known experimental phase diagram.

SESSION DS01.08: Surface Thermodynamics

Session Chairs: Alexandra Navrotsky, Richard Otis, Wenhao Sun and Stephen Yeandel

Thursday Morning, December 1, 2022

Hynes, Level 2, Room 204

9:00 AM DS01.08.01

Direct Ab Initio Calculation of Solid-Liquid Interfacial Energies Anirudh Appachar and [Wenhao Sun](#); University of Michigan—Ann Arbor, United States

States

Solid-liquid interfacial energies are notoriously difficult to measure experimentally. This has led to a dearth of values in the scientific literature, despite their centrality to nucleation and crystal-growth phenomena. Computational approaches can successfully calculate the interfacial energy for isolated systems, but are not easily generalizable across materials spaces: most models rely on material-specific interatomic potentials, calling into question their transferability, or are simply too resource-intensive to scale practically across thousands of materials. Here, we present a slab-based DFT methodology to calculate the oriented solid-liquid interfacial energy of a material and demonstrate its application to four pure-metal systems. We discuss crucial model considerations, including slab dimensions, molecular dynamics simulation parameters, effects of periodic boundary conditions, and quantification of amorphous character. Our methodology will enable systematic investigations of trends in interfacial energy across materials spaces and serve as a source of first-principles data upon which to train future interatomic potentials.

9:15 AM DS01.08.02

Interfacial Free Energies from MD Simulations—Application to $\text{CaSO}_4 \cdot x\text{H}_2\text{O}$ [Stephen Yeandel](#), Colin Freeman and John Harding; The University of Sheffield, United Kingdom

Surfaces are a ubiquitous feature of crystals and play an important role in both nucleation and crystal growth. At the nanoscale surface effects play a large role in the stability of different nanocrystal polymorphs and so can influence the selection of which polymorph is grown. Additionally, surfaces themselves can be sites for heterogeneous nucleation. It is therefore important to fully understand the energetics of crystal surfaces.

The calculation of surface Enthalpies is now routine using Molecular Dynamics simulations. But when the crystal surface is in contact with a liquid it may induce ordering of the liquid, making Entropy an important factor which must also be considered. Thus, what is required is a method for calculating Interfacial Free Energies (IFE), which include both Enthalpic and Entropic contributions.

A general method for calculating IFEs is difficult to construct as it must be able to deal with multiple materials in different physical phases. Previous methods for calculating IFEs often rely on particular properties of the system under study, such as being able to reform bulk material by bring two surfaces together¹, which may in general not be possible.

We present a new, general, method for calculating IFEs which can easily deal with multiple phases as well as complex surfaces. Our method relies on transforming the solid component of the interface into bulk material via an Einstein Crystal; avoiding the need to define an explicit real-space path for the transformation. Furthermore, the efficiency of the calculation is improved as intermediary values may be computed once and re-used for multiple different interfaces.

We have applied our method to the calculation of water interfaces with different members of the $\text{CaSO}_4 \cdot x\text{H}_2\text{O}$ group of materials. This is a particularly challenging system to study due to strong binding between the Ca^{2+} ion and water², the inclusion of water molecules which formally belong to the bulk material but may behave as liquids at the interface, and the presence of surface dipoles for the hemihydrate phase (Bassanite, $\text{CaSO}_4 \cdot 0.5\text{H}_2\text{O}$).

Our results indicate that Entropy accounts for between 55-85% of the IFE in these materials depending on surface cut, in contrast to NaCl where Entropy accounts for approximately only 20%. We also find that in general the IFEs of Bassanite interfaces ($\text{CaSO}_4 \cdot 0.5\text{H}_2\text{O}$) are lower than that of Gypsum ($\text{CaSO}_4 \cdot 2\text{H}_2\text{O}$), indicating a possible reason why Bassanite is often observed first in solution³. Predicted equilibrium morphologies also show good agreement with experimental studies.

[1] Qi, X., Zhou, Y., and Fichtorn, K.A., "Obtaining the solid-liquid interfacial free energy via multi-scheme thermodynamic integration: Ag-ethylene glycol interfaces." *J. Chem. Phys.* **145**,19 (2016) 194108

[2] Byrne, E.H., Raiteri, P. and Gale, J.D., "Computational insight into calcium-sulfate ion pair formation" *J. Phys. Chem. C* **121** (2017) 25956-25966

[3] Van Driessche, A.E.S., Benning, L.G., Rodriguez-Blanco, J.D., Ossorio, M., Bots, P. and García-Ruiz, J.M., "The Role and Implications of Bassanite as a Stable Precursor Phase to Gypsum Precipitation" *Science* **336** (2012) 69-72

9:30 AM BREAK

10:00 AM DS01.08.03

Effect of Solvent on Chemistry at the Electrochemical Interfaces [Oskar Cheong](#)^{1,2}, Michael Eikerling^{1,2} and Piotr Kowalski¹; ¹FZ Juelich, Germany; ²RWTH Aachen University, Germany

Thermodynamics of chemical reactions at the electrochemical interfaces is a driver of performance of electrocatalyst materials. Computational electrochemistry usually neglects effect of solvent on derived thermodynamic, or model these with simple approximations. The reaction free energies depend on the enthalpy and entropy of the reactant species. Usually only enthalpy effects, computed directly by quantum chemistry computational method such as density functional theory (DFT) is taken into consideration. If accounted for, entropy is usually computed as vibrational, translational and rotational parts using gas phase formulas. In the presence of solvent, the cavitation entropy, which results from the rearrangement of the solvents around the solute, can play a fundamental role in determining the reaction free energy. We will present adaptation of existing models for entropy of the solvent phase derived for the bulk solvent (e.g. [1]) to the description of thermodynamics at an interface, using some hints from the *ab initio* simulation studies [2]. The implication for the surface chemistry thermodynamics will be discussed.

[1] A. J. Garza, *J. Chem. Theory Comput.* **15**, 3204–3214 (2019).

[2] C. K. Jung, L. Braunwarth, A. Sinyavskiy, T. Jacob, *J. Phys. Chem. C*. **125**, 24663–24670 (2021).

10:15 AM DS01.08.04

A Novel Application of Metastable Photoacid Molecules in Liquid-State Light-Electricity Energy Transformation [Jaehyeong Bae](#), Haeseong Lim, Jaewan Ahn, Yoon Hwa Kim and Il-Doo Kim; Korea Advanced Institute of Science & Technology, Korea (the Republic of)

Tuning the metastability of a functional chemical can overcome its own functional limitations, including stimuli sources, sensitivity, and reversibility, which determine its ability to design and utilize in practical applications. Compared to its preceding generation of chemical i.e., irreversible photoacid generators, photoacid can release protons upon light irradiation and recombines with them in the dark through a fully reversible reaction. In this presentation, we utilize this reversible and visible-light responsive photoacid to build a novel liquid-state light-electricity energy harvester. Asymmetric light exposure on a photoacid solution contained in a transparent tube generates a pH gradient ($\Delta\text{pH} = 2$) along the exposed and dark regions, which charges the Nernst potential up to 0.7 V across the two electrodes embedded at each end, as if a capacitor. Owing to the reversibility of photoacids, a

photoacid-driven liquid-state photoenergy harvester (PLPH) generates capacitive currents up to 0.72 mA m^{-2} on irradiation. Notably, the transparent nature of the PLPH enables vertical stacking up to 25 units, which multiplies the light-harvesting efficiencies by over 1000%. This unique approach provides a new route to harness solar energy with a form-factor-free design that maximizes spatial and light-use efficiencies.

10:30 AM DS01.08.05

Self-Assembly in Supercritical Fluids—Thermodynamics and Fluid Mechanics [Loren G. Kaake](#); Simon Fraser University, Canada

Photolithography and solution phase self-assembly are the two primary approaches to creating nanostructures. The former is the powerhouse of computing, the latter is the manufacturing method of living organisms; the two share very little common ground. Photolithography is a subtractive process, employed with staggering precision, but typically used with monolithic materials. Solution phase self-assembly is an additive process that can be employed with systems of arbitrary complexity. However, entropy places limits on the precision of the technique, especially over large length scales. In an effort to bridge these non-intersecting methods of manufacturing, we have developed a materials deposition technique that leverages the unique properties of supercritical, near-critical, and/or subcritical fluids. We deposited polymer thin films with high precision on photolithographically patterned substrates allowing us to control the process of self-assembly with photolithography. The technique relies on a solubility behavior contrary to typical polymer solutions which show a monotonic increase in saturation solubility with temperature. Instead, the saturation solubility of a solid solute first increases, and then decreases with increasing temperature as a solution is heated near its critical point. The typical Flory-Huggins approach to polymer solubility fails to model this behavior, as solvent compressibility is a key factor in supercritical media. Alternatively, the Sanchez-Lacombe model can be used to describe solubility behavior in supercritical media, however, it is too complicated to be practical use. We have developed a simple model based on classical thermodynamics which is adequate to describe our observations while still being simple enough to provide qualitative insight into the key factors important in the process. This non-monotonic solubility behavior enables us to precipitate thin films onto heated substrates. The resulting films have a complex micro and nanoscale structure which depends upon pressure, the nature of the substrate, and the presence of solvent additives. We attribute the behavior to the influence of the fluid mechanics as parameterized by the Rayleigh number as well as the influence of surface energy and surface diffusion immediately following deposition. The development of a fuller understanding this process will allow us to more finely control the formation of nanoscale structures with the precision and scalability of photolithography.

1-3

1. Yousefi, N.; Maala, J. J.; Louie, M.; Storback, J.; Kaake, L. G., Physical Supercritical Fluid Deposition: Patterning Solution Processable Materials on Curved and Flexible Surfaces. *ACS Appl Mater. Interfaces* **2020**, *12*, 17949-17956.
2. Yousefi, N.; Saeedi Saghez, B.; Pettipas, R. D.; Kelly, T. L.; Kaake, L. G., Physical supercritical fluid deposition of polymer films: controlling the crystallinity with pressure. *Mater. Chem. Front.* **2021**, *5*, 1428-1437.
3. Yousefi, N.; Saeedi Saghez, B.; Pettipas, R. D.; Kelly, T. L.; Kaake, L. G., The role of solvent additive in polymer crystallinity during physical supercritical fluid deposition. *New J. Chem.* **2021**, *45*, 11786-11796.

10:45 AM DS01.08.06

Ising and Dissipative Particle Dynamics Models of Network Connections Between Engineered Nanoparticles [Xingfei Wei](#) and Rigoberto Hernandez; Johns Hopkins University, United States

Complex engineered nanoparticle (ENP) networks are emergent materials that have a variety of applications, such as drug delivery, flexible electronics, and computing devices. Uncovering the fundamental physics of network connections between ENPs is critical to developing new networked materials. In this work, we use an Ising model to resolve the network connections in regular arrays of ENPs by Monte-Carlo (MC) simulations and mean-field theory (MFT). We compare the theoretical predictions from the Ising model with dissipative particle dynamics (DPD) simulation results. We report the network connections inside four different types of ENP regular arrays, viz. 2D square, 2D hexagonal, 3D cubic and 3D close-packed hexagonal packings. We found that MFT and MC simulations are in good agreement in describing the thermodynamics of the network connections. We also found that the DPD simulations and Ising model MC simulations agree in predicting the resulting network connections at varying temperatures under a range of external E-field strengths.

11:00 AM DS01.08.07

Picowatt Resolution Calorimetry for High-Throughput Screening of Metabolic Rates in Single Cells [Juanjuan Zheng](#) and Joost J. Vlassak; Harvard University, United States

Calorimetry, which measures the heat generated from a sample, is the only technique that provides a direct measure of metabolic rates. However, calorimetry is rarely used in cell and developmental biology due to limitations in sensitivity and throughput. Here, we describe a sensor that has a near order-of-magnitude increase in sensitivity above current state-of-the-art calorimeters and has orders-of-magnitude higher throughput than existing calorimeters. These improvements will push calorimetry into a regime where it can be used for high-throughput screens of single-cell measurements on a broad range of cell types.

These advances are enabled through use of a novel micromachined sensor design that incorporates several key innovations: The first innovation critical to achieving 30-pW sensitivity of our sensor is the use of low-noise thermopiles embedded in a membrane with negligible thermal mass, allowing measurement of minute temperature differences. Second, the use of a differential measurement setup based on multiple references eliminates the effect of thermal gradients due to environmental drift. The key innovations enabling the increased throughput are 1) effective thermal coupling of the capillaries that contain sample and reference(s) to a very sensitive thermometer using capillary forces, and 2) the design of a micromachined sensor with minimal thermal mass, allowing fast (within 30 seconds) thermal equilibration. The combination of high sensitivity and extremely short equilibration times allows for quick signal integration to measure changes in metabolic rate and therefore a high overall sample throughput.

The extraordinary sensitivity combined with the high throughput makes the sensor ideally suited for the direct measurement of metabolic rates and for the study of non-equilibrium processes in a range of materials systems. Calorimetric based screens for small molecules that alter the metabolic rates of cancer cells and bacteria may help identify compounds that are both useful for scientific research and medically beneficial.

1:45 PM *DS01.09.01

Constructing Defect Phase Diagrams from *Ab Initio* Calculations [Tilman Hicke](#)^{1,2}, Ali zendegani¹, Ali Tehrani¹, Omkar Hegde¹, Prince Mathews¹ and Jorg U. Neugebauer¹; ¹Max-Planck-Institut für Eisenforschung, Germany; ²Federal Institut for Materials Research and Testing, Germany

Recent progress in experimental atomic-scale characterization techniques allows one to study the local chemical composition at individual defects such as interfaces, grain boundaries, dislocations and surfaces. These experiments show a surprisingly rich set of structural and chemical phenomena, going well beyond simple Gibbs isotherms. To understand and eventually utilize the large number of possible defect structures, phases and phase transitions, the construction of defect phase diagrams becomes mandatory. In analogy to the well-established concept of thermodynamical bulk phase diagrams they provide direct insight into the thermodynamically most stable defect state as a function of state variables such as temperature, composition, stresses etc. The power and performance of this concept are demonstrated using the example of nonstoichiometric stacking faults in metallic alloys. Our *ab initio* computed defect phase diagrams provide an accurate tool to correctly predict the rich set of experimentally observed defect structures. Based on these insights we will discuss a conceptual framework of how to generalize these findings and to construct defect phase diagrams on a routine basis.

2:15 PM DS01.09.02

A Probabilistic Model for Oxygen Vacancies at the Surface to Explain Oxidation Kinetics of Metals with Protective Oxide Layer [Mehdi Pishahang](#), Nicolas Hadjiconstantinou, Dionysios Sema, Mathew Swisher, Julien Luzzatto, Qingzi Zhu, Youssef Marzouk and Asegun Henry; MIT, United States

This work presents a novel approach towards the oxidation kinetics of metals that form almost perfectly stoichiometric oxide layer upon oxidation. We have developed a model that relates the oxidation kinetics to the probabilistic availability of oxygen vacancies at the surface of the oxide layer. The rate and energy at which oxygen collides to the oxide surface is explained by the Boltzmann-Maxwell distribution. Given that Hf cannot readily possess 3+ valence, the produced undoped HfO₂ has a very small intrinsic concentration of oxygen vacancies. The concentration of oxygen vacancies, as well as the transport rate of the oxygen vacancies at each temperature is calculated from defect formation and barrier gap energetics. Our model demonstrates that it is the probability of gaseous oxygen colliding with oxygen vacancies at the surface of oxide layer which defines the rate of oxidation. Our model studies the Hf oxidation in 3 phases, the first phase is for when fresh Hf is exposed to O₂ for the first time. The very first gaseous oxygens that hit the surface almost all get fully absorbed, until a very thin (1nm) HfO₂ oxide layer is formed. Our calculations estimate phase 1 to take up to 1 microsecond. As soon as the oxide layer is formed the availability of oxygen vacancies at the surface determines the rate of oxidation, as only gaseous oxygens that happen to collide with the oxygen vacancies get absorbed and join the solid. In the third phase, the oxide layer is so thick that the diffusion of oxygen vacancies from bulk to the surface slows down significantly, and therefore becomes the kinetics rate-definer. A set of TGA (thermogravimetric analysis) experiments are performed to analyze and quantify the oxidation kinetics of Hf. These experiments are performed at different isothermal and isobaric conditions with different surface-to-bulk ratios for the solid. The model satisfactorily reproduces the validation experiments.

2:30 PM DS01.09.04

Heterogeneous Melt-Initiation Mechanisms at Interface Junctions and Vertices in Solids Wenkai Pan, Bonan Shen, [Nikita Lisenko](#), Ruobing Song, Jayoung Park and James S. Im; Columbia University, United States

Melting of elemental solids can be identified and appreciated as a particularly simple example of discontinuous phase transitions involving condensed phases. Driven by (1) the need to decipher and understand laser-irradiation-induced melt-mediated microstructure evolution observed in oxide-capped columnar-grained polycrystalline Si films [1], [2], (2) an opportunity to better incorporate the often-overlooked phenomenon of negative-solid/liquid-interface-curvature-stabilized premelting (or “pretransition”) [3], [4] into the field of discontinuous phase transformations in condensed systems, and (3) the interest in identifying and analyzing previously under-recognized and under-analyzed mechanisms and behaviors of phase initiation and propagation in general, we examine in this paper the nature and mechanisms of melt-initiation transpiring heterogeneously at the interfaces, junctions, and vertices that are present within the precursor solids.

Our analysis employs an important thermodynamic element in the classical nucleation theory that pertains to the mechanical-equilibrium-satisfying shapes of the melt; specifically, this requirement dictates that the solid-liquid interfaces predominantly manifested at the interfaces, junctions, and vertices must comply with the contact angle conditions at the involved interfaces while also satisfying the property of constant mean curvature. Simple and idealized Bi-crystal and tri-crystal models are examined to capture the aforementioned microstructural features present in columnar-grained polycrystalline thin films sandwiched by inert oxide layers. Our shape analysis reveals that, at least for the “isomorphic” cases in which the shape of the melt is preserved, there are three distinct cases of melting behavior at these junctions and vertices as a function of the involved liquid wetting angles. Two phase-initiating scenarios involving (1) negative-curvature-induced premelting and stabilized coexistence of solid and liquid phases in thermodynamic equilibrium, and (2) the well- and long-recognized mechanism of site-localized heterogeneous nucleation at junctions and vertices involving unstable equilibrium, are identified [5]. As well, we identify the existence of a wetting-angle parameter space domain within which localized melting at the junctions and/or vertices is specifically prohibited due to the absence of the existence of mechanical equilibrium shape containing these sites. Note that this behavior actually goes against the conventional view that considers vertices and junctions to always be thermodynamically more favorable sites for nucleation due to the presence of additional interfaces than planar interfacial areas.

We will present melt-initiation mechanism diagrams that identify these domains in the contact angle parameter space, and also discuss (1) how our analysis may also be relevant to understanding melt-mediated processing of bulk materials, (2) how localized premelting at junctions and vertices is not sufficient for inducing efficient microstructure evolution of the polycrystalline materials, and accomplishing this at below the bulk melting temperature further requires attaining a local free-growth condition via interface-curvature reducing shape transitions, and (3) trivial extension of our analysis to address the phase-initiation taking place heterogeneously at the edges and corners of embedded single crystals with three distinct wetting interfaces.

[1] V. K. Wong *et al.*, *SID Symposium Digest of Technical Papers*, vol. 48, no. 1, pp. 426–429, 2017

[2] J. S. Im *et al.*, *Journal of Crystal Growth*, vol. 312, no. 19, pp. 2775–2778, 2010

[3] R. Raj, *Acta Metallurgica et Materialia*, vol. 38, no. 8, pp. 1413–1416, 1990

[4] G. P. Johari, W. Pascheto, and S. J. Jones, *J. Chem. Phys.*, vol. 100, no. 6, pp. 4548–4553, Mar. 1994

[5] P. J. Clemm and J. C. Fisher, *Acta Metallurgica*, vol. 3, no. 1, pp. 70–73, 1955

2:45 PM DS01.09.05

Identifying and Analyzing Contact-induced Nucleation of Solids in Supercooled Liquid Thin Films [Bonan Shen](#), Nikita Lisenko, Wenkai Pan, Ruobing Song, Jayoung Park and James S. Im; Columbia University, United States

Motivated, on the one hand, by the need to understand laser-induced melt-mediated crystallization of thin Si films for realizing advanced high-resolution displays, and on the other hand, by the opportunity to investigate discontinuous phase transformations in condensed systems, we are in the process of examining various mechanisms and behaviors that are manifested at the onset of transformations (i.e., new phase initiation and evolution), particularly as

they are encountered in small, confined, and embedded systems.

In this paper, we focus on identifying and thermodynamically describing a new nucleation mechanism, which we refer to as transmorphic nucleation, as can for instance be revealed in considering nucleation of solids transpiring in supercooled and encapsulated liquid thin films. Following the basic framework of classical nucleation theory, we investigate heterogeneous nucleation of solids as the thickness of the film decreases. When the film thickness becomes slightly less than the critical height of the spherical-cap nuclei on one interface, some of the evolving embryos must come in contact with the other interface. When this occurs, we suggest based on thermodynamic and kinetic considerations that these clusters will undergo a sudden and irreversible local-interface-curvature-driven shape transition starting from the point of contact, leading to the formation of clusters with two-interface-defined shapes. Subsequently, some of these clusters will become supercritical and grow (i.e., “nucleated”), while others may still evolve to stay subcritical and dissolve. Note that, in contrast to the well-established thermal mechanism of heterogeneous nucleation in which fluctuation over the energy barrier associated with the critical nucleus corresponds to the point at which supercritical clusters are generated, in transmorphic nucleation, the point at which the embryos come in contact with the interface is explicitly identified as the critical moment for the nucleating clusters to become supercritical (i.e., the free energy change due to the formation of the contacting clusters is argued as being the effective energy barrier of nucleation).

Using a simplified example of a uniform thin film consisting of two interfaces with identical wetting angles, we explicitly and quantitatively identify the conditions under which transmorphic nucleation is encountered, and evaluate the free energy changes associated with the process. We will also discuss (1) how transmorphic nucleation can be manifested in melting of all polycrystalline materials as well as in melting of confined and embedded solids, (2) how our transmorphic nucleation model is distinct from previously suggested transformation pathways, (3) certain analytical and numerical treatments for dealing with complex cluster shapes and interface geometries, (4) the implications on calculating both steady-state and transient rates of transmorphic nucleation, and (5) a more general category of transmorphic transitions that can affect phase initiation and evolution in discontinuous phase transformations.

3:00 PM BREAK

3:30 PM DS01.09.06

Observation of Negative Surface and Interface Energies of Quantum Dots [Jason J. Calvin](#), Amanda Brewer, Michelle Crook, Tierni Kaufman and Paul Alivisatos; University of California, Berkeley, United States

Surface energy is a fundamental property of materials and is particularly important in describing nanomaterials where atoms or molecules at the surface constitute a large fraction of the material. Traditionally, surface energy is considered to be a positive quantity, where atoms or molecules at the surface are less thermodynamically stable than their counterparts in the interior of the material because they have fewer bonds or interactions at the surface. Using calorimetric methods, we show that the surface energy is negative in some colloidal semiconductor nanocrystals, or quantum dots with organic ligand coatings. This implies that the surface atoms are more thermodynamically stable than those on the interior due to the strong bonds between these atoms and surfactant molecules, or ligands, that coat their surface. In addition, we extend this work to core/shell indium phosphide/zinc sulfide nanocrystals and show that the interfacial energy between these materials is highly thermodynamically favorable in spite of their large lattice mismatch. This work challenges many of the assumptions that have guided thinking about colloidal nanomaterial thermodynamics, illustrates the fundamental stability of many technologically relevant colloidal nanomaterials, and paves the way for future experimental and theoretical work on nanocrystal thermodynamics.

3:45 PM DS01.09.07

Significant Entropic Effects Driving Dislocation Nucleation Kinetics at Surfaces [Soumendu Bagchi](#) and Danny Perez; Los Alamos National Laboratory, United States

A wide range of kinetics of material defects are very successfully predicted by harmonic transition state theory (HTST). It is however worth recalling that the accuracy of HTST relies on a set of assumptions whose validity should be assessed on a case-by-case basis. We discuss a key scenario concerning crystal plasticity i.e., the nucleation of dislocations from surface steps, where HTST dramatically fails to reproduce the transition rates observed in direct MD. We show that a simple and efficient procedure to estimate the changes in vibrational entropy along the minimum energy pathway can resolve the discrepancy with HTST and provide quantitatively accurate predictions of the anharmonic kinetics which is otherwise intractable with the existing HTST approaches ubiquitous in describing reactions in materials.

4:00 PM DS01.09.08

Free-Growth-Initiating Shape Transition from Curvature-Stabilized Premelting in Polycrystalline Materials [Nikita Lisenko](#), Wenkai Pan, Bonan Shen, Jayoung Park, Ruobing Song and James S. Im; Columbia University, United States

This work focuses on investigating phase transformation mechanisms in condensed and confined systems, encountered, for instance, in pulsed-laser-induced melting and solidification of columnar-grained polycrystalline Si films [1]. We start by recognizing that, in addition to nucleation and growth [2], interface-curvature-stabilized premelting can also be relevant for initiating the melting transition. This phenomenon involves equilibrium coexistence of liquid regions confined to grain junctions and vertices within the solid matrix. Isolated premelting clusters or interconnected channels can form and be stabilized below the bulk melting point by adopting negative constant mean curvature (CMC) of the solid-liquid interface, as defined by the Gibbs-Thomson equation [3].

We suggest that consideration of the transition from stable coexistence to free growth is important, as it represents an alternative pathway to nucleation and growth for discontinuous phase transformations. For example, during melt-mediated pulsed-laser processing, complete melting of the grain boundary was established [1] as a necessary condition for microstructure evolution, implying that localized premelting alone is insufficient. In this case, the free growth condition can be realized even below the bulk melting point if the temperature is increased enough to allow the premelting regions to expand until isolated regions meet or connected channels completely envelop and eliminate the grain boundary. We argue that a sudden and spontaneous shape transition must occur at this point of change, necessarily leading to an abrupt reduction of the solid-liquid interface curvature below the pre-melt-stabilizing CMC value. Consequently, the liquid region is now at least locally in the state of free growth with finite velocity, even without any further increase in temperature. Due to the abrupt shape change that initiates free growth, we call this phenomenon *transmorphic free growth* (TFG); this is in contrast to other examples of free growth starting with infinitesimal drift velocity after thermal nucleation or continuous shape evolution discussed previously in literature [4,5]. In this work we capture the conditions necessary for TFG analytically and numerically, and assess the transition rate through direct cluster dynamics calculation [6]. Although presented here in the context of laser-induced melting of columnar-grained polycrystalline thin films, this mechanism of shape-change-induced transformation below the equilibrium temperature is also applicable to broader classes of phase transitions in condensed and confined systems.

[1]. V.K. Wong, M. Yu, W. Pan, R. Song, A.K. Suresh, I. Choi and J.S. Im, SID Symp. Dig. Tech. Pap. 48 (1), 426 (2017)

[2]. P.J. Clemm and J.C. Fisher, Acta Metall. 3 (1), 70-73 (1955)

- [3]. H. Hansen-Goos and J. Wettlaufer, Phys. Rev. E 81, 031604 (2010)
 [4]. D. Turnbull and J. Chem. Phys. 18 (2), 198–203 (1950)
 [5]. A. L. Greer, A. M. Bunn, A. Tronche, P. V. Evans and D. J. Bristow, Acta Mater. 48 (11), 2823–2835 (2000)
 [6]. K. F. Kelton, A. L. Greer and C. V. Thompson, J. Chem. Phys. 79, 6261 (1983)

4:15 PM DS01.09.09

Mimicking the Sustainable Anionic Redox Features for Advanced Lithium-Ion Batteries Jaewoon Lee¹, Kyeongjae Cho² and Duho Kim¹; ¹Kyung Hee University, Korea (the Republic of); ²The University of Texas at Dallas, United States

The practical capacity of lithium-ion batteries based on the cationic redox mechanism of transition metals (Ni, Mn, and Co) has almost approached the theoretical capacity. As a breakthrough, anionic redox from oxygen in the oxide frameworks has been highlighted, recently, as it demonstrates additional capacity in high voltage regions. For this reason, the representative oxygen redox activating cathode, Li_2MnO_3 , got attention since it demonstrates over 300 mAh/g at ~4.5 V versus Li^+/Li . However, it usually suffers from various concomitant electrochemical fast degradations such as a very large irreversible capacity and drastic voltage-fading upon cycling. Doping and coating are commonly used to improve the shortcomings of the cathodes. A lot of experiments and computational calculations have reported the influences of the results to elucidate the electrochemical performances and redox mechanisms to suggest new ways of maintaining the first charge capacity/voltage in Li_2MnO_3 . It is not known yet how to practically utilize the pure anion redox capacity of Li_2MnO_3 . In addition, a lot of theories coexist, and some experimental results indicate discrepancies with each other. However, the fast degradation is generally acknowledged from the undesirable transition metal migration which transforms the pristine structure into a spinel-like sequence and oxygen dimerization causing O_2 gas to evolve. However, $5d$ contained lithium-excess cathode (Li_2IrO_3) does not exhibit similar degradation even though the crystal structure is the same as Li_2MnO_3 . However, it is lack of realistic to utilize the Li-excess $5d$ cathode since it is not feasible due to economic reasons. This motivates us to reinvestigate the critical features of Li_2IrO_3 that contribute to reversible anionic redox without hysteric features and mimic the sustainable redox characteristics for harnessing the pure anionic redox in Li_2MnO_3 .

By computational calculations, we figure out the thermodynamic feature of Li_2IrO_3 that there is an unrevealed stacking sequence during (de)intercalation which was not highlighted sufficiently. The calculated voltage behavior concurs with the experimental results when we reflect on the stacking sequence while the normal Li/vacancy mode demonstrates the difference from the experimental result. Since the atomic configuration was not shown in the Li-excess $3d$ metal compound, we did an intensive investigation of the influences of how the stacking sequence can contribute to sustainable oxygen redox in Li_2IrO_3 without structural deformation. From the same point of view, we reinvestigate the Li_2MnO_3 and investigate that the same stacking sequence state is hidden in the (de)lithiation of Li_2MnO_3 so it was not observed from experimental methods. From the exhaustive computational calculations, we verify why the phase does not have a preference in terms of thermodynamics and concentrate that revealing the stacking sequence is significant to rationally utilize the anionic redox in Li_2MnO_3 sustainably. By controlling the anion in Li_2MnO_3 , we elucidate how we can mimic the sustainable redox mechanism in $3d$ metal by suppressing the structural transformation and undesirable oxygen dimerization during (de)intercalation. It has not been reported yet how we can mimic the sustainable oxygen redox characteristics of Li_2IrO_3 in $3d$ metal Li-excess cathode for practical utilization. For these reasons, it has the possibility to extend the battery research area by applying the concept for advanced lithium-ion batteries.

SESSION DS01.10: Virtual Session I

Session Chairs: Alexandra Khvan, Alexandra Navrotsky, Richard Otis and Wenhao Sun

Tuesday Morning, December 6, 2022

DS01-virtual

10:30 AM DS01.10.01

Thermodynamic Analysis of High-Strength Al-Cu-Mg-Si Alloys at High Temperatures Designed by Using Bayesian Learning for Neural Networks Takeshi Kaneshita¹, Shimpei Takemoto¹, Hattori Ayami¹, Yoshishige Okuno¹, Kenji Nagata², Junya Inoue³ and Manabu Enoki³; ¹SHOWA DENKO K.K., Japan; ²National Institute for Materials Science, Japan; ³The University of Tokyo, Japan

We discuss the design of 2000 series high-strength aluminum alloys at high temperatures using Bayesian learning for neural networks and thermodynamic analysis. It is known that the strength of aluminum alloys decreases rapidly above 150°C, so improving the strength at high temperatures is essential for industrial applications. In order to design high-strength alloys, it is necessary to optimize the additive element compositions and the heat treatment conditions such as temperature and time for homogenization, solution processing, and aging. A data science approach using neural networks is suitable for handling such multi-dimensional problems and exploring the optimal process conditions from the vast design space. This study focuses on the thermodynamic calculations of the behavior of the size and dispersion of precipitates affecting the high-temperature strengthening mechanism of designed alloys by the neural network.

10:35 AM *DS01.10.02

Toward a More Accurate But Still Efficient Density Functional Theory for Materials Prediction John P. Perdew; Temple University, United States

Kohn-Sham density functional theory is the workhorse of materials computation. Whether human-designed or machine-learned, approximate density functionals for the exchange-correlation energy become more predictive [1] as they are constrained to satisfy more of the mathematical properties of the exact functional. Meta-generalized gradient approximations (meta-GGAs) that satisfy 17 (SCAN [2]) or 16 ($r^2\text{SCAN}$ [3]), with reduced grid sensitivity) exact constraints can be remarkably accurate for molecules and non-metallic materials, including some that are strongly-correlated [4]. Further improvements for those systems are possible, including self-interaction corrections [5] re-designed to work accurately and efficiently with SCAN-like functionals. Metallic sp and sd solids and liquids, however, have perfect screening of long-range exchange and can be better treated by more local approximations that employ only the local electron density and its low-order derivatives [6].

*Supported by NSF DMR-1939528 and DOE DE-SC0018331 grants.

[1] A.D. Kaplan, M. Levy, and J.P. Perdew, Predictive Power of the Exact Constraints and Appropriate Norms in Density Functional Theory, submitted.

[2] J. Sun, A. Ruzsinszky, and J.P. Perdew, Strongly Constrained and Appropriately Normed Semi-local Density Functional, *Physical Review Letters* **115**, 036402 (2015).

[3] J.W. Furness, A.D. Kaplan, J. Ning, J.P. Perdew, and J. Sun, Accurate and Numerically Efficient $r^2\text{SCAN}$ Meta- Generalized Gradient Approximation, *Journal of Physical Chemistry Letters* **11**, 8208 (2020).

[4] Y. Zhang, C. Lane, J.W. Furness, B. Barbiellini, J.P. Perdew, R.S. Markiewicz, A. Bansil, and J. Sun, Competing Stripe and Magnetic Phases in the Cuprates from First-Principles, *Proceedings of the National Academy of Sciences USA* **117**, 68 (2020).

[5] M.R. Pederson, A. Ruzsinszky, and J.P. Perdew, Self-Interaction Correction with Unitary Invariance in Density Functional Theory, *Journal of Chemical Physics* 140, 121103 (2014) (Communication).

[6] A.D. Kaplan and J.P. Perdew, Laplacian-level meta-generalized gradient approximation for solid and liquid metals, submitted.

11:05 AM *DS01.10.03

Studies on the Electrochemical Thermodynamics and Safety Behavior of Advanced Batteries and Their Materials [Hans-Jürgen Seifert](#); Karlsruhe Institute of Technology, Germany

Layered oxides NMC ($\text{LiNi}_x\text{Mn}_y\text{Co}_z\text{O}_2$) and spinel phases (LiMn_2O_4) are commercially most relevant cathode materials for lithium-ion battery design. However, there is still lack of fundamental knowledge on electrochemical-thermodynamic properties and related safety behavior of these materials and the batteries assembled thereof. The presented work focuses on the investigation of such properties to provide quantitative data for better understanding the performances of lithium-ion batteries in their regular and irregular operational use and during accidents. Experimental electrochemical, thermodynamic and safety studies are combined with computational methods (CALPHAD). We use various calorimetric methods (DSC, Tian-Calvet) for studies of the energetics of battery active materials as well as electrochemical cells. Such data are input for the thermodynamic modeling and calculation. The results are then used to derive fundamental electrochemical and thermal properties. Accelerating Rate Calorimetry (ARC) is used to quantitatively measure the thermal runaway behavior of self-made and commercial coin cells, cylindrical cells and pouch cells, respectively.

11:35 AM DS01.10.04

Computational Prediction of Ligand Curvature-Selectivity Ability on Gold Nanoparticle Surface [Amanda A. Chen](#), Yufei Wang, Krista Balto, Andrea Tao, Joshua Figueroa and Tod Pascal; University of California, San Diego, United States

Organic ligands are foundational in determining the properties and assembly of inorganic nanoparticles. Recent works have focused on ligands that passivate the nanocrystal surface to enable the supramolecular structure to be formed. However, precise nanoparticle surface modification, as a means of controlling the nanoparticle assembly structure, is difficult. Therefore, in this work, we devised a ligand ($\text{CNAr}^{\text{Mes}^2}$) that can achieve site selective binding on gold nanoparticle (AuNP) surfaces, based on curvature. We adopted a variety of computational approaches, namely quantum mechanical electronic structure theory calculations and molecular dynamics (MD) simulations, to obtain microscopic insights into the AuNP/ligand interaction energies, dynamics, solvation properties, and spectroscopy. We were able to compute the ligand adsorption characteristic and further predict the ligand adsorption sites on AuNPs, as quantified by four unique descriptors: the site binding ratio, the edge-binding factor, and the ligand solubility and solvent partition factors. We verified our predictions experimentally using liquid-liquid extraction, transmission electron microscopy, zeta potential measurements and surface-enhanced Raman spectroscopy. Together, our investigations indicate that $\text{CNAr}^{\text{Mes}^2}$ provided good selectivity for AuNPs based on their average sizes, with a separation resolution of $\pm 5 \text{ \AA}$ that is competitive with the state of the art in industry. Our study demonstrates how first-principles based computations can guide experimental design at the nanoscale, to enable novel material physics and commercial processes.

11:40 AM *DS01.10.05

Computational Tools for the Generation and Visualization of High-Dimensional Phase Diagrams [Axel van de Walle](#); Brown University, United States

We present an array of software tools enabling the construction of high-dimensional Calphad databases from first-principles calculations. These tools span the full spectrum of the accuracy vs. computational requirements trade-off, thus fulfilling the needs of both high-throughput efforts and more targeted high-precision modeling. This is accomplished through a generalization of the Special Quasirandom Structure formalism to include short-range order effects and its integration into the Calphad-type compound energy formalism. Another key element is the generalization of the lattice dynamics calculations to allow for a rigorous handling of mechanical instabilities that is consistent with the Calphad formalism. We finally showcase a new visualization tool enabling interactive exploration of 3D cross-section of higher-dimensional phase diagrams and propose a novel way to represent tie-lines in these settings. Applications to high-entropy refractory alloy design are presented.

12:10 PM DISCUSSION TIME

SESSION DS01.11: Virtual Session II

Session Chairs: Woohyeon Baek, Alexandra Khvan, Alexandra Navrotsky, Richard Otis and Wenhao Sun

Tuesday Afternoon, December 6, 2022

DS01-virtual

9:00 PM *DS01.11.01

Phonon Entropy and Thermal Expansion from Inelastic Neutron Scattering and Computation [Brent Fultz](#) and Camille Bernal-Choban; California Institute of Technology, United States

Entropy comes from atomic-scale degrees of freedom. Most of the entropy in materials comes from the vibrations of atoms, which increase in amplitude with increasing temperature. This is "phonon entropy" (or "vibrational entropy"). The important question is usually how the entropy differs, sometimes slightly, between different states of a material (such as a crystal with chemical order or with disorder). Today both ab initio computation and inelastic neutron scattering can provide accurate entropies over a wide range of temperatures. High temperatures are where entropy is most thermodynamically significant, but is also where degrees of freedom become coupled. Normal modes of vibration are no longer independent, and interactions between vibrations and electrons become important. I will describe how such couplings are sorted out and how they alter thermal expansion and other thermophysical properties.

The phonon entropy can be obtained by inelastic neutron scattering in two ways. Most common for thermodynamics are measurements of phonon densities of states (DOS) using polycrystalline samples. Measurements of single crystal dispersions can also be performed. Some principles of the conversion of raw spectra into phonon DOS curves will be described for data from the chopper spectrometer, ARCS, at Oak Ridge National Laboratory. Calculations of phonon dispersions based on density functional theory (DFT) were also performed with both quasiharmonic and anharmonic methods, and compared to the measured phonons at different temperatures.

Three examples of thermodynamic measurements by inelastic neutron scattering will be presented. 1) The first is bcc Cr, which was measured from 6 to 1493 K. Here, the interest was in reconciling the entropy from phonons and electrons with the entropy assessed from calorimetry. This was successful to better than 2% at 1500 K, showing that magnetic contributions to the entropy are negligible at high temperatures. 2) The second is fcc Pd and Pt, which were also accurate to within 2% of calorimetric results. In both cases, this good agreement required accounting for the effects of the electron-phonon interaction on the electronic entropy. 3) The third is diamond-cubic silicon, where the phonon entropy agreed with the calorimetric entropy to about 1%.

For Cr and Si, the change in free energy with temperature and volume was used to calculate the thermal expansion by both quasi-harmonic (QH) and anharmonic (AH) methods. The thermal expansion was calculated successfully by both methods. Curiously, the temperature dependence of the phonons was not calculated successfully by QH theory. The QH model predicted the wrong sign for the thermal shifts of many phonon energies. Some cancellations of errors in thermal shifts of different phonons evidently allow for the success of the QH method for calculating the thermal expansion of Cr and Si. This is not always the case, however. For NaBr, the thermal expansion from the quasi-harmonic method is too small by a factor of four [4], and AH calculations are necessary. It is possible to calculate bulk thermophysical properties with an unreliable microscopic theory, so more incisive measurements of individual phonons are important for our basic understanding of the underlying physics.

1. C. Bernal-Choban, et al., submitted. 2. Y. Shen, et al, PRB 93, 214303 (2016). 3. D.S. Kim, et al. PRB 91, 014307 (2015). 4. Y. Shen, et al., PRL 125, 085504 (2020).

This work is supported by DOE BES award No. DE-FG02-03ER46055.

9:30 PM DS01.11.03

Phase-Field Simulation of Spinodal Decomposition in Fe-Cr-Co Alloys After Ultra-Rapid Cooling in Powder Bed Fusion Additive Manufacturing Yuheng Liu, Daichi Izumikawa, Masayuki Okugawa and Yuichiro Koizumi; Osaka University, Japan

[Introduction] Fe-Cr-Co permanent magnetic alloys are attractive because of the combination of good ductility and tunable magnetic properties. The mechanical and magnetic properties of these alloys are strongly affected by the microstructures of ferromagnetic and paramagnetic phases originating from spinodal decomposition. Lots of experimental investigations and theoretical simulations of the microstructure evolutions in Fe-Cr-Co alloys have been made, and in general, precise multiple-step aging is indispensable to optimize the coercivity and remanence. Recently, the additive manufacturing of the Fe-Cr-Co alloys using powder bed fusion (PBF) has been reported, significantly improving the fabrication efficiency. However, although the segregation of brittle phases can be suppressed commonly in many alloys fabricated by PBF, solidification cellular structures and inter-cellular boundary segregation in stainless steels were observed occasionally^[1]. Moreover, supersaturated vacancies can be introduced by the ultra-rapid cooling conditions of the PBF process. These characteristics of PBF may affect the spinodal decomposition reaction^[2]. Therefore, the objective of this study is to investigate the influences of vacancies on spinodal decomposition by the phase-field simulation and to optimize the aging conditions using the machine learning method. **[Methods]** Phase-Field models considering the concentration of vacancies were used to simulate the spinodal decomposition for the Fe-25Cr-12Co mass% alloy. The diffusivity of vacancies was assumed to decay with time. Besides, the influence of the dimension of the simulation model (the 2D or 3D) was also examined. The simulation results under various aging temperatures, aging times, and cooling speeds were analyzed quantitatively, which was used for machine learning.

[Results] Although the microstructures were qualitatively like the experimental ones, some discrepancies were found. The discrepancy was reduced by using 3D model. The discrepancy in the initial kinetics can be partly attributed to the supersaturated vacancies. However, it was suggested that the inaccuracy of the thermodynamic parameters is also responsible. Therefore, the thermodynamic parameters were modified. The optimization of aging conditions for the PBF process by phase-field simulation will also be discussed.

[References]

[1] T. Voisin et al.: "New insights on cellular structures strengthening mechanisms and thermal stability of an austenitic stainless steel fabricated by laser powder-bed-fusion", *Acta Mater.* **203** (2021) 116476.

[2] H. Iwazako et al.: "Spinodal decomposition in plastically deformed Fe-Cr-Co magnet alloy", *ISIJ International*, **62(6)** (2022), 1268-1274.

9:45 PM DS01.11.04

Phase-Controlled Preparation and Structural Characterization of Five-Cationic High-Entropy Oxides Daehyeon Hong and Yun-Hyuk Choi; Daegu Catholic University, Korea (the Republic of)

In 2015, the first high-entropy oxide (HEO), equimolar (Co_{0.2}Cu_{0.2}Mg_{0.2}Ni_{0.2}Zn)O was successfully synthesized in a bulk ceramic form by Rost et al. using the conventional solid-state reaction method. The authors synthesized the single-phase rocksalt solid solution by sintering the pellet of the five-component mixed powder (MgO-CoO-NiO-CuO-ZnO) at sufficiently high temperatures. The HEO is a new-type inorganic material composed of multiple metal ions with a single-phase structure, and it reveals unexpected properties of high structural stability and superionic conductivity. In this study, the five-cationic HEOs consisting of new compositions are prepared with changes in crystal structure using the solid-state reaction. As a result, rocksalt, spinel, or their mixed phase were obtained in the HEOs depending on sintering temperature. The structure and composition of the synthesized HEOs have been characterized using various methods such as scanning electron microscopy (SEM), transmission electron microscopy (TEM), X-ray diffraction (XRD) method, and X-ray photoelectron spectroscopy (XPS).

9:50 PM DS01.11.05

Ab Initio Thermodynamics for Adsorption of MoO₂Cl₂ on SiO₂ Surface Hyun-Kyu Kim, Na-Young Lee and Yeong-Cheol Kim; KoreaTech, Korea (the Republic of)

As the semiconductor device technology node decreases down below 5 nm, Cu metal resistivity increases due to the increase of diffusion barrier metal portion. Mo or Co metals that require no or less barrier metal have been studied to suppress the resistivity increase with the technology node. MoO₂Cl₂ is a potential precursor for atomic layer deposition of Mo on SiO₂ surface. Density functional theory is applied to calculate its adsorption energy on the surface. Entropy and enthalpy changes with temperature are taken into account to improve the accuracy of its adsorption behavior. Ab-initio thermodynamics is also employed to consider the partial pressure of gas in the reaction chamber.

9:55 PM DS01.11.06

Ab Initio Thermodynamics Study for Phase Separation of Ce_{0.75}Zr_{0.25}O₂ Solid Solution Hyun-Kyu Kim¹, Seol Hee Oh², Jong-Ho Lee² and Yeong-Cheol Kim¹; ¹KoreaTech, Korea (the Republic of); ²Korea Institute of Science and Technology, Korea (the Republic of)

Since CeO₂ shows high oxygen storage/release capacity and this capacity can be further improved by adding ZrO₂, Ce_{0.75}Zr_{0.25}O₂ (CZO) has been studied for catalyst support of vehicles' catalytic converter and fuel electrode of solid oxide fuel cells. Phase separation, however, of CZO under reducing atmosphere at elevated temperatures has been observed experimentally. TEM with EDS shows oxygen-poor and pyro-like phases as intermediates before

being completely separated to almost pure CeO₂ and ZrO₂; CeO₂ and ZrO₂ contain less than 1 % Zr and Ce, respectively. Ab-initio thermodynamics with density functional theory is employed to analyse the phase separation behavior of CZO.

10:00 PM DISCUSSION TIME

SYMPOSIUM DS02

Integrating Machine Learning with Simulations for Accelerated Materials Modeling
November 27 - December 8, 2022

Symposium Organizers

Mathieu Bauchy, University of California, Los Angeles
Ekin Dogus Cubuk, Google
Grace Gu, University of California, Berkeley
N M Anoop Krishnan, Indian Institute of Technology Delhi

Symposium Support

Bronze
Patterns, Cell Press

* Invited Paper
+ Distinguished Invited

SESSION DS02.01: Machine Learning for Materials Simulations I
Session Chairs: Grace Gu and N M Anoop Krishnan
Sunday Morning, November 27, 2022
Hynes, Level 2, Room 210

8:00 AM *DS02.01.01

Improving Materials Modelling with Differentiable Physics [Samuel Schoenholz](#); Google Brain, United States

The last decade has seen explosive progress in machine learning. This rapid growth has been powered by expressive automatic differentiation frameworks that can execute programs efficiently on accelerators (like GPUs and TPUs) and can be orchestrated from high-level languages like Python. Rewriting traditional tools, such as molecular dynamics, in these frameworks can substantially improve workflows in Materials Science, allow us to seamlessly integrate machine learning models into simulations, and open qualitatively new research directions. This talk will describe, and give an update on, JAX MD which is an end-to-end differentiable molecular dynamics simulation library. We will focus on discussing the creative and unique ways in which automatic differentiation has been combined with traditional physics simulation to enable significant improvements in our ability to model and design materials.

8:30 AM *DS02.01.02

Machine Learning for Accelerated Defect Dynamics in Multicomponent Alloys [Ghanshyam Pilia](#), Anjana Talapatra, Anup Pandey, Danny Perez and Blas Uberuaga; Los Alamos National Laboratory, United States

Understanding defect thermodynamics and transport is essential for predicting materials behavior at elevated temperatures. However, despite the exponential increase in computing power, the extreme disparity between atomistic, meso and macro scales prohibits direct brute-force simulations for most materials problems of practical interest. Going forward, realizing the full potential of multiscale modeling of increasingly complex materials through large-scale computing would require effective use of automation and artificial intelligence-based methods. Using defects transport in complex alloys as an example, this talk would provide an overview of the ongoing efforts at the Los Alamos National Laboratory that aim at addressing these challenges through the development of an integrated and automated multiscale simulation capability driven by exascale computing, rigorous uncertainty quantification, and machine learning.

9:00 AM DS02.01.03

Accelerated Convergence of Machine Learning Potentials for the Prediction of Bimetallic Material Properties [Christopher M. Andolina](#) and Wissam A. Saidi; University of Pittsburgh, United States

Machine learning potentials (MLPs) for atomistic simulations have an enormous prospective impact on materials modeling, offering orders of magnitude speedup over density functional theory (DFT) calculations without appreciably sacrificing accuracy in predicting material properties. We show that MLP-based material property predictions converge faster with respect to precision for Brillouin zone integrations than DFT-based property predictions for elemental systems. Further, we explore statistical error metrics to accurately determine *a priori* the precision level required of DFT training datasets for MLPs to ensure accelerated convergence of material property predictions, thus significantly reducing the computational expense of MLP development. We apply this approach to bimetallic systems where the generation of the DFT training data is substantially larger and thereby incurs higher computational

costs. MLPs for the Al-Mg bimetallic system were generated based on this convergence acceleration MLP approach and validated with DFT reference values. The resulting MLPs reproduce elemental and intermetallic Al-Mg systems' general bulk properties such as point defects and non-ground state lattice configurations, mechanical properties, and various surface terminations for miller indices <4 with high fidelity. We use a hybrid Monte Carlo and molecular dynamics (MC/MD) from 200 to 800 K to model Mg surface segregation enthalpies in Al-Mg slabs (Mg = 0 to 20%). The Mg surface segregation enthalpies increase from (111) < (100) < (110), consistent with existing literature. Furthermore, we model the segregation tendencies obtained from the MC/MD simulations by adapting a recently introduced isotherm model for grain boundary segregation, which provides a more accurate model for Mg segregation behavior on surfaces. Our accelerated convergence approach yields accurate and robust material predictions with lower precision DFT training data, providing a more efficient workflow for training MLP atomistic potentials.

9:15 AM DS02.01.04

Machine-Learned Electronegativity Equalization Trained with Chemical Potential and Hardness of Atoms in Molecules [Alexander Davis](#) and Alex Voznyy; University of Toronto, Canada

The electronegativity equalization method relates the energy of systems to two empirically determined parameters of each atom: the chemical potential and hardness. In its original form, these parameters are functions only of atomic number, and can be determined from ionization energies of free atoms or by empirical fitting to computed partial charges. More recently, machine learning has been used to model the dependence of these parameters on an atom's chemical environment. Although the machine learning method makes predictions of these parameters directly, it is trained using a loss function that depends only on the partial charges calculated from them. To our knowledge, accuracy of the predicted chemical potentials and hardness has not been measured directly, since these parameters are presumed unknown for an atom within a molecule.

We performed first-principles calculations of chemical potential and hardness of atoms within molecules using Bader analysis. A series of differently substituted molecules provided a finely sampled curve of energy as a function of charge for each atom, and the parameters were defined as its first and second derivatives. The theoretically calculated chemical potential and hardness serve as a basis for evaluating the performance of a graph neural network model for the dependence of these parameters on chemical environment. They can also be used for training the model, as an alternative to training with partial charges. Electronegativity equalization using these parameters can serve as the basis of a force field, which can be used for relaxing geometries of molecules bound to catalytic surfaces. In the future, similar methods may also be useful in machine-learned versions of semiempirical quantum methods such as Hückel theory, by enabling predictions of the machine learning model to be compared to theory on an atomic rather than molecular level.

9:30 AM DS02.01.05

Learning a Reactive Potential for Silica-Water Through Uncertainty Attribution. [Swagata Roy](#)¹, Johannes P. Duerholt², Federico Zipoli³, Thomas Asche², Leonid Kahle³, Teodoro Laino³ and Rafael Gomez-Bombarelli¹; ¹Massachusetts Institute of Technology, United States; ²Evonik Industries AG, Germany; ³IBM Research-Zurich, Switzerland

Silica has various polymorphs with different properties, leading to its application in various industries including windowpanes, catalysts, aerogels, rubber and plastic. Despite much progress involving atomistic simulations of different forms of silica, small amorphous silica clusters are still a challenge. Quantum mechanical (QM) calculations have been employed to study the stability of silicate clusters but are limited to a few atoms, often extrapolating to trimers only and cannot deal with reactions involving silicate polymerization in water solvent under different environmental conditions of different temperatures, pH of solutions and different concentration ratio of reactants. Classical reactive force fields can scale up to a large number of atoms but lack in accuracy compared to first principle calculations. Recently, the advent of machine-learning models in materials science has enabled replicating QM accuracy with time and length scale compared to empirical potentials.

Neural network-based interatomic potentials (NNIPs) on condensed phase silica and porous crystalline zeolites trained on QM data have proved to be more accurate than classical potentials and have opened doors to large-scale simulations with high-level QM accuracy. We aim to train a reactive NNIP for silicate polymerization reactions in a water solvent. These reactions are significant to understand the formation of precipitated silica as well as the preliminary stage in zeolite crystallization. Our NNIP is based on a rotationally equivariant message passing neural network known as polarizable atom interaction neural network (PAiNN). Our current dataset comprises 210K molecular clusters with forces and energies calculated using a long-range corrected hybrid functional ω B97XD3. Despite training on molecular clusters, we can perform periodic molecular dynamics (MD) simulations and predict the properties of condensed phases.

Hereon, we also propose a new active learning method based on per-atom attribution of model uncertainty to enlarge our dataset with robust and diverse set of molecular configurations. With this method, we can quantitatively identify inter-atomic interactions with high inaccuracy; carve out an atomic environment within a cut-off on which the potential performs poorly, and thus save QM calculation cost. The method involves taking the derivative of the uncertainty of NNIP ensemble with respect to atomic positions and marks highly uncertain inter-atomic interactions. We then select a molecular cluster environment with a high attributed atom at its center for QM calculations and add to training data. Upon running this automated active learning loop for a few generations, we visualize consecutive improvement of attributions on atoms and thus proving the efficiency of this proposed method.

The current NNIP after eight generations of active learning is successful to predict the properties of liquid water as well as reactions involving deprotonation of water and silicate dimerization in a dilute water solvent. The radial density functions (RDFs) of O-O, O-H and H-H in water obtained from molecular dynamics simulations using our NNIP are comparable to experimental and reported results. The self-diffusivity of water at 300K is predicted as $2.26 \pm 0.06 \times 10^{-9} \text{ m}^2/\text{s}$, close to the experimental one ($2.41 \times 10^{-9} \text{ m}^2/\text{s}$) and the density is predicted as 1.08g/cc. The reaction involving deprotonation of water molecule is replicated accurately with enhanced sampling based MD and the pK_w of water is predicted as 17.4, which is close to expected value of 17 (higher than experimental due to quantum nuclear effect). The NNIP further predicts the relative energy of siliceous zeolites with respect to quartz with error of only 1.2 KJ/mol compared to experimental results. This robust NNIP can replicate the reaction path of silicate dimerization and will be further used to replicate deprotonation of orthosilicic acid and then silicate condensation and hydrolysis reactions.

9:45 AM BREAK

10:15 AM DS02.01.06

Large-Scale Screening of Hypothetical Metal-Organic Frameworks for Thermal Conductivity [Meiirbek Islamov](#)¹, Hasan Babaei², Jeffrey R. Long^{2,2,3}, Alan McGaughey⁴, Diego A. Gomez-Gualdron⁵ and Christopher E. Wilmer^{1,1}; ¹University of Pittsburgh, United States; ²University of California, Berkeley, United States; ³Lawrence Berkeley National Laboratory, United States; ⁴Carnegie Mellon University, United States; ⁵Colorado School of Mines, United States

Metal-Organic Frameworks (MOFs) are highly porous, crystalline materials with ultrahigh surface area that are promising for many gas storage, separation, catalysis, and thermoelectric applications. However, their practical utility depends on their ability to rapidly disperse the exothermic heat generated during the gas adsorption process or on their ability to suppress the directed heat flow to maintain the temperature gradient in thermoelectric applications. Despite their significance, the thermal transport properties of MOFs have been mostly overlooked, which resulted in a lack of an in-depth understanding of the universal structure-thermal conductivity relationships for designing MOFs with tailored thermal conductivity. In this work, we performed a high-

throughput screening of hypothetical MOFs for thermal conductivity to establish structure-property relationships. We judiciously selected 10,194 hypothetical MOFs from the *ToBaCCo* database and performed thermal conductivity calculations using classical molecular dynamics simulation and the Green-Kubo method. We included several important structural and compositional characteristics of MOFs such as density, pore size, surface area, void fraction, node-linker mass mismatch, and metal node connectivity in the analysis. We observed that high thermal conductivity favors small pores, high density, small node-linker mass mismatch, and four-connected metal clusters, whereas low thermal conductivity favors large pores and high porosity. Moreover, we discovered six hypothetical MOF structures that exhibited high average thermal conductivity. We also discovered 36 hypothetical MOFs that displayed ultralow thermal conductivity. Interestingly, those six ultrahigh thermal conductivity MOFs share a four-fold coordinated metal nodes, through which the organic linkers are connected in a perpendicular orientation. This suggests that the underlying topology predominantly determines the limits of the thermal conductivity in MOFs.

10:30 AM DS02.01.07

Gradient-Based Optimization of ReaxFF Parameters Using Pytorch for the Study of Silica Precipitation [Yuliia Orlova](#), Swagata Roy and Rafael Gomez-Bombarelli; Massachusetts Institute of Technology, United States

Silica precipitation is a subject of big interest since it occurs in a wide variety of environmental and industrial processes: ceramic and catalytic applications, water heater scaling, biomineralization, coating applications to improve adhesion and wetting properties, and so forth. Even though there are many advances in atomistic simulation research of different forms of silica, the mechanism of silica precipitation has not been fully understood. We propose to study the following process using reactive force-field method (ReaxFF). Despite being a classical force field, ReaxFF can achieve quantum chemical accuracy once the optimal potential coefficients are found. However, the fitting of ReaxFF parameters is a challenge due to the complex functional form of the potential. Several techniques have been proposed to solve this problem, such as genetic algorithms and Monte-Carlo methods. The stochastic nature of these methods requires millions of error evaluations to fit the parameters, which results in excessive optimization times. Recent advances in machine learning made it possible to drastically speed up the process by utilizing the gradient of the potential. In this work, the gradient-based optimization of reactive force-field parameters is performed using Pytorch to apply the method to study silicate polymerization reactions in a water solvent. We have implemented the current ReaxFF potential as a Pytorch model. The model's parameters were fitted to the dataset, which comprises 210K molecular clusters with forces and energies calculated using a long-range corrected hybrid functional ω B97XD3. We have validated the obtained parameters against the kinetic and thermodynamic properties of water and solid silica systems. The optimized potential will be further used to gain insights into the mechanism of silica precipitation.

10:45 AM DS02.01.08

Structure-Property Relation in LiF-NaF-ZrF₄ Molten Salts Using Transferable Deep Learning Potentials [Rajni Chahal](#)¹, Santanu Roy², Shubhojit Banerjee¹, Vyacheslav Bryantsev² and Stephen Lam¹; ¹University of Massachusetts Lowell, United States; ²Oak Ridge National Laboratory, United States

Multicomponent molten salts have been identified as promising candidate coolants in thermal solar energy storage, advanced batteries, and next-generation nuclear reactors due to their desirable heat transfer properties. In many systems, molten salts with multivalent cations have been proposed, which can exhibit intermediate-range ordering that can drive important transport and thermal properties. However, accurately simulating the structure and properties of these systems is challenging due to size limitations in ab-initio molecular dynamics (AIMD), and inaccuracies in classical molecular dynamics (CMD). In this work, we circumvent these limitations using neural network interatomic potentials (NNIP) and show that NNIP-based simulations can predict extended-range structures inaccessible to ab initio molecular dynamics, and thermal properties with higher accuracy than classical potentials. Specifically, the system LiF-NaF-ZrF₄ is studied, which is known as a promising salt candidate for advanced nuclear systems due to its low melting point (operability), and low cost. The transferability of computationally efficient and accurate neural network interatomic potential across a wide phase-space of LiF-NaF-ZrF₄ molten salts is reported. We found that the NNIP trained on only two salt compositions involving 29% and 37% ZrF₄ (eutectics) can accurately simulate a wide range of compositions where ZrF₄ mole fractions (determinant of intermediate-range structure and property) was varied between 11% to 40%. At short range, we found that neural network molecular dynamics (NNMD) agrees well with AIMD, CMD, and Raman spectra observations in predicting the existence of 6, 7, and 8-coordinated fluorozirconate complexes in the melt. In addition, NNMD can accurately predict the changes in the first coordination shell (coordination number, and bond angles) with the variation in multivalent Zr content, which is also supported by Raman spectra data. At intermediate range, NNMD predicts the structural ordering increases with Zr content due to Zr-F clusters/network formation for compositions with greater than 23% ZrF₄. These observations are directly validated by the excellent agreement in theoretical and experimental data. Moreover, we found that in order to capture structure ordering and hence, accurately predict the properties of compositions with higher ZrF₄ content, cell sizes of at least 17 Å need to be simulated, exceeding the size of most AIMD-based simulations that are typically performed. In addition to accurate structure prediction, when evaluating diffusion coefficients, density, and viscosities, NNIP outperforms both AIMD and CMD in predicting the values close to the experimental data. NNIP accurately matches the salt density with the experimental value of 2.79 g/cc at 700°C for a salt composition containing 37 ZrF₄ mole%. For the same composition and temperature, the viscosity value evaluated from NNMD is 4.45 ± 0.16 cP compared to 6.9 cP as reported from experimental measurements. For composition with ~11 mole% ZrF₄ content at ~750°C, the Zr diffusion coefficient calculated by NNMD simulations is 2.03 ± 0.3 cm²/s compared to the experimental value of 2.92 ± 0.3 cm²/s, while CMD predicted value is 0.73 ± 0.1 cm²/s. Overall, this work explored the existence of structural ordering in molten salts that is often overlooked in understanding thermal property trends. New data is generated for a promising salt system, which will inform materials selection in advanced nuclear systems. Further, NNIP's ability to provide a deeper understanding of structure-property relations in multicomponent molten salts containing multivalent cations is systematically demonstrated. NNIP's transferability across a wide range of compositions and thermodynamics conditions opens the possibility of the development of robust and reliable neural network potentials to advance the study of many structurally-complex liquids.

11:00 AM DS02.01.09

Using Density Functional Theory and Machine Learning to Predict the Binding Energies of Metal-Organics to Organic Functional Groups for Hybrid Material Creation [Yifan Liu](#), Emily K. McGuinness, Mark Losego and Rampi Ramprasad; Georgia Institute of Technology, United States

Understanding chemical interactions between organic and metal-organic molecules has wide-ranging interest to the vapor deposition community for creating hybrid organic-inorganic materials via techniques such as molecular layer deposition and vapor phase infiltration (VPI). In the case of VPI, a vapor-phase metal-organic precursor is infused into the bulk of a polymer and becomes incorporated at the nanoscale through either chemical interaction with the polymer or the formation of a non-volatile species via the introduction of a co-reactant. VPI has applicability in a number of industrially relevant fields including the creation of novel organic-inorganic hybrid membranes which have shown enhanced stability in organic solvents, while retaining high permeance and selectivity. Motivated by this application, this work uses density functional theory (DFT) to explore chemical interactions occurring during the VPI of polymer of intrinsic microporosity (PIM-1, a polymeric membrane material) with trimethylaluminum (TMA) and its co-reaction with water. These computations revealed that the coordination between the polymer and metal-organic is a critical mechanism for the formation of the hybrid and its resultant solvent stability. To expand understanding of this critical characteristic and accelerate the design of organic-inorganic hybrid materials, a DFT dataset of computed binding energies was generated from suitable and representative atomic-level models of several common polymer functional groups and over 100 metal-organic precursors. From this dataset, a predictive machine learning model for the binding energy of metal-organic molecules to

polymers has been developed. This predictive model, along with the chemical guidelines obtained from feature analysis, will aid the selection of potential candidates for novel organic-inorganic hybrid membranes as well as hybrid material creation as a whole.

11:15 AM DS02.01.10

Machine Learned Potentials for Reaction Simulations Patrick Reiser¹, Jingbai Li², Steven Lopez² and Pascal Friederich¹; ¹Karlsruhe Institute of Technology, Germany; ²Northeastern University, United States

Machine learned potentials are widely used to describe the potential energy surface of near-equilibrium systems. To accurately explore and predict potential energy surfaces in the region of transition states requires active learning methods. In Li et al. [1], we show how machine-learned potentials can be used to simulate photochemical reactions, which are widely used by academic and industrial researchers to construct complex molecular compounds via mechanisms that often require harsh reaction conditions. Photodynamics simulations provide time-resolved insight into atomistic processes which are required to understand and predict reactivities and chemoselectivities. However, such simulations require thousands of costly quantum mechanical calculations per trajectory, which limits simulations to a picosecond time scale for most organic photochemical reactions. Westermayr et al. introduced a neural network-based method to accelerate the predictions of electronic properties and pushed the simulation limit to 1 ns for a methylammonium cation model system. We have adapted this methodology to develop two software tools, the Python Rapid Artificial Intelligence Ab Initio Molecular Dynamics (PyRAI2MD) tool for active learning-based molecular dynamics simulations, and the NNs4MD library which implements a single interface to a wide range of machine learning methods to be used in molecular dynamics simulations. Using these tools, we studied the cis-trans isomerization of trans-hexafluoro-2-butene and the 4π-electrocyclic ring-closing of a norbornyl hexacyclodiene. We performed a 10 ns simulation for trans-hexafluoro-2-butene in just 2 days and discovered unknown reaction pathways in the ring-closing reaction. The same simulation would take approximately 58 years with traditional multiconfigurational photodynamics simulations. We are currently implementing graph neural networks in NNs4MD, in order to move from molecule-specific models to generalizable potentials.

[1] Li, J., Reiser, P., Boswell, B.R., Eberhard, A., Burns, N.Z., Friederich, P. and Lopez, S.A., 2021. Automatic discovery of photoisomerization mechanisms with nanosecond machine learning photodynamics simulations. *Chemical science*, 12(14), pp.5302-5314.

11:30 AM DS02.01.11

High-Dimensional Neural Network Potential for Liquid Electrolyte Simulations Garvit Agarwal¹, Steven Dajnowicz¹, James M. Stevenson¹, Leif D. Jacobson¹, Farhad Ramezanghorbani¹, Karl Leswing¹, Richard A. Friesner^{1,2}, Mathew D. Halls¹ and Robert Abel¹; ¹Schrodinger Inc., United States; ²Columbia University, United States

The development of rechargeable Li-ion batteries (LIBs) has revolutionized electric vehicles and portable electronic devices. Yet, further advancements are needed to improve the power, safety, reliability, and lifetime of LIBs. Existing classical force fields are not accurate enough to predict bulk properties of LIB materials without time-consuming and customized parametrization. To move towards accurate and reliable modeling of Li-ion battery chemistries, we developed a machine-learned force field for liquid electrolyte simulations. This force field was constructed using the charge recursive neural network (QRNN) architecture, which includes both long-range interactions and global charge redistribution. The force field was trained using only non-periodic (cluster) DFT data, allowing the practical use of more accurate functionals, like the range-separated hybrid ωB97X-D3BJ functional used here, which would be prohibitively expensive for generating large datasets with periodic DFT. In this work we focus on seven commonly used carbonate solvents and LiPF₆ salt in the Li-ion battery technology, but this methodology is generalizable and can be applied to any liquid electrolyte system. Despite only training to cluster DFT data, the predicted bulk thermodynamic properties and transport properties (such as self-diffusivity and viscosity) are in excellent agreement with experimental data. The force field also reproduces the concentration and temperature dependence for viscosity and diffusivity of ions and solvent. Furthermore, we demonstrate the capability of the model to accurately predict the solvation structure of ions in the liquid electrolyte using a comparison of the radial distribution functions with experimental data. This provides a promising path forward for atomistic modeling of challenging battery chemistries.

11:45 AM DS02.01.12

AuTopology—End to End Force Field Parametrization Workflow for Polymer Electrolytes Using Machine Learning Pablo A. Leon and Rafael Gomez-Bombarelli; Massachusetts Institute of Technology, United States

Solid polymer electrolytes (SPEs) are seen as promising alternatives to conventional liquid electrolytes in lithium battery systems due to their low density, mechanical compliance, and low flammability but are challenged by lower ionic conductivity. Molecular dynamics (MD) simulations can be used to guide the design of novel SPEs by allowing quantitative determination of separable anion and cation diffusions as well as local solvation environments and correlated ion motions. Classical potential MD simulations update molecular conformations by the net force on each atom due to covalent and nonbonded interactions. However, these classical potentials are often not well defined for novel systems as they require materials- and local environment-specific parameters such as unique bond stiffnesses which are either meticulously hand-tuned across decades or unchangeable due to proprietary licenses.

In this work, we explore the effects of anharmonic bonded interactions on ionic solvation and conductivity mechanisms in polymer and liquid electrolyte systems. An in-house, machine learning-based workflow, named AuTopology, was used to autonomously learn the interatomic potential parameters for prototypical solid and liquid electrolyte systems at experimentally-relevant concentrations with both harmonic OPLS-based and anharmonic PCFF+-based models from DFT forces as training data. These simulations of tens-of-thousands of atoms were allowed to run for hundreds of nanoseconds to determine the individual anion and cation diffusivities and resulting conductivities. Using this framework and an in-house database of molecular conformations, we have been able to reproduce ωB97XD3-level DFT forces from trained OPLS force fields to within 5.5 kcal/mol-Å. Correlation-based conductivities between the OPLS and PCFF+ models for polyethylene oxide (PEO) and liquid carbonate systems with different lithium salts were found to match legacy parameterizations to the same order of magnitude while matching or improving conductivity predictions relative to experiments.

12:00 PM DS02.01.13

Cement Clinker Microstructure Segmentation Using Machine Learning Mohd Zaki, Sunil K. Gurjar, Siddhant Sharma, Jayadeva Jayadeva and N M Anoop Krishnan; Indian Institute of Technology Delhi, India

Cement is one of the most consumed construction materials. The quality of cement depends upon the clinker which is manufactured using limestone and aluminosilicate sources. The clinker microstructure comprises four phases: alite, belite, tricalcium aluminate, and aluminoferrite. Identifying different components of microstructures is a challenging task which in turn helps the researchers to control the quality of cement. In this work, we first create a dataset by segmenting alite and belite particles in cement clinker microstructure and use supervised machine learning methods to train models for identifying alite and belite regions in the microstructure image. We demonstrate the capability of machine learning models to accurately segment alite and belite regions. Further, we propose the methodology and guidelines to be taken care of while creating the datasets and training machine learning models for clinker microstructure segmentation tasks.

SESSION DS02.02: Machine Learning for Materials Structure and Properties I
Session Chairs: Ekin Dogus Cubuk and N M Anoop Krishnan
Monday Morning, November 28, 2022
Hynes, Level 2, Room 210

8:00 AM *DS02.02.01

Learning from 2D—Machine Learning Models for Effective Properties of Heterogeneous Materials Based on 2D Microstructure Sections Guangyu Hu and Marat Latypov; University of Arizona, United States

Microstructure-property relationships are key to effective design of structural materials for advanced applications. Advances in computational methods enabled modeling microstructure-sensitive properties using 3D models (e.g., finite elements) based on microstructure representative volumes. 3D microstructure data required as input to these models are typically obtained from either 3D characterization experiments or digital reconstruction based on statistics from 2D microstructure images. In this work, we present machine learning (ML) approaches to modeling effective properties of heterogeneous materials directly from 2D microstructure sections. To this end, we consider statistical learning models based on spatial correlations and multi-view convolutional neural networks as two distinct ML strategies. In both scenarios, models are trained on a dataset of synthetically generated 3D microstructures and their properties obtained from micromechanical 3D simulations. Upon training, the models predict properties from 2D microstructure sections. The advantage of the presented models is that they only need 2D sections, whose experimental acquisition is more accessible compared to 3D characterization. Furthermore, the present models do not require digital reconstruction of 3D microstructures.

8:30 AM *DS02.02.02

Machine Learning Based Surrogate Model for Bioinspired Gradient Composites Shu-Wei Chang, Meng-Lin Tsai and Wei-Han Hui; National Taiwan University, Taiwan

Biological materials evolve extraordinary protective systems to survive the competitive environment, thus having outstanding mechanical properties and multifunctionality. For instance, bone and bamboo are both structural bio-composites with superior mechanical properties. In recent decades, understanding the properties of bio-inspired composites has been a popular subdiscipline of material science. The idea of bioinspiration is to learn from biological structural materials and apply novel structural design strategies for the development of composites with superior mechanical properties. In this research, the composite structures are inspired by the topology of bone and the density distribution of bamboo. In order to explore the extreme huge design space of structural materials, we developed a machine learning based surrogate model by using a combination of principal component analysis (PCA) and deep neural networks (DNN) for predicting the entire stress-strain behavior of the bone- and bamboo-inspired composite structures. Our results show that the surrogate model is accurate and efficient for investigating the design space and the proposed approach in this work can be extended to other composite structures to further accelerate material design and optimization.

9:00 AM DS02.02.03

Learning Local Equivariant Interatomic Potentials for Large-Scale Atomistic Dynamics Simon L. Batzner¹, Albert Musaelian¹, Anders Johansson¹, Lixin Sun¹, Cameron J. Owen¹, Mordechai Kornbluth² and Boris Kozinsky^{1,2}; ¹Harvard University, United States; ²Robert Bosch LLC Research and Technology Center, United States

E(3)-Equivariance — the property of a function to transform with the actions of the Euclidean group — has recently emerged as a key design principle in machine learning interatomic potentials. Starting with the high accuracy, sample efficiency, and generalization properties of the NequIP potential [1], a series of other equivariant message passing interatomic potentials has since been proposed. However, all current methods share the message passing paradigm, in which information is iteratively propagated along an atomistic graph. This propagation mechanics, however, severely hinders the time- and length-scales that can be studied with message passing approaches. Here, we introduce Allegro, a strictly local, E(3)-equivariant deep learning interatomic potential that combines the high accuracy of equivariant neural networks with the scalability of local methods. We demonstrate that Allegro not only obtains state-of-the-art accuracy on a variety of benchmarks, but also displays remarkable generalization to out-of-distribution data. We then show how molecular dynamics simulations driven by Allegro predict structure and kinetic of a Lithium phosphate electrolyte with high fidelity. Finally, we demonstrate how the locality of the proposed method enables a simulation of 100 million atoms on reasonable compute resources, enabling a previously impossible combination of accuracy, scale, and computational efficiency.

[1] Batzner et al. (2022). E (3)-equivariant graph neural networks for data-efficient and accurate interatomic potentials. Nature communications, 13(1), 1-11

9:15 AM DS02.02.04

Phase Transformation Prediction by Machine Learning-Crystal Plasticity Finite Element Model (ML-CPFEM) Mehrzad Soltani, Sanjida Ferdousi, Ravi S. Haridas, Rajiv Mishra and Yijie Jiang; University of North Texas, United States

The mechanical properties of alloy are affected significantly by its microstructure. Efforts to touch white area in Ashby's chart for desired material indices to enhance alloy properties have been investigated for the past decades. This target is coming true through improvement in recognizing microstructure of materials and synergy between microstructure and its effect in bulk materials. Plastic deformation originating from defects in materials mingles with microstructural phenomena, including transformation induced plasticity (TRIP), slip, and twinning. It is observed that active microstructural phenomena make materials harder and increase their strength. To understand the mechanism, development of crystal plasticity finite element models (CPFEM) enables us to solve deformation field with the given crystallographic orientation and loading conditions. Over the past few years, emerging research in various fields has been growing in using machine learning (ML) to investigate fundamental constitutive relationships and to accelerate classic numerical modeling. In this study, we leverage a ML model on local crystallography and CPFEM for FCC to HCP phase transformation prediction in a high entropy alloy (HEA). The training data of the ML uses electron backscatter diffraction (EBSD) experimental data before and after deformation and CPFEM simulation results of localized stress and texture evolution during deformation. We use an extreme gradient boosting (XGBoost) ML approach, which repeatedly builds new models and combine them into an ensemble model based on a decision tree. This approach effectively enhances performance for finding optimum model and accelerates searching process. We implement this predictive model in multiple experimental measurements to validate our model. To further understand the driving force for phase transformation, we harness the ML model prediction accuracy to evaluate several different forms of proposed driving force.

9:30 AM DS02.02.05**Formula Graph Self-Attention Network for Representation-Domain Independent Materials Discovery** Achintha A. Ihalage and Yang Hao; Queen Mary University of London, United Kingdom

Material representation is vital in determining the performance of machine learning (ML) models in predicting the properties of materials. There are two main types of materials descriptors, one that encodes crystal structure details and the other that only uses chemical composition with the hope of discovering new materials. Graph neural networks (GNNs) have dominated materials property prediction tasks outperforming their classical ML counterparts given sufficient data. However, current GNNs are limited to only one of the above two avenues due to the lack of a general graph-based material descriptor. In this study, we propose formula graph that unifies composition-only and structure-based materials descriptors for GNNs. We develop a self-attention integrated GNN that assimilates a formula graph and show that the proposed architecture produces material embeddings transferrable between the two domains, opening further research opportunities in crystal structure prediction. The proposed model can outperform some previously reported structure-agnostic models and their structure-based counterparts while exhibiting better sample efficiency and faster convergence. Finally, the model is applied in a challenging exemplar to predict the complex dielectric function of materials and nominate new substances that potentially exhibit epsilon-near-zero (ENZ) phenomena.

9:45 AM BREAK**10:15 AM DS02.02.06****Automated Artificial-intelligence Inverse Design of Polymer Membranes for CO₂ Capture and Separation** Ronaldo Giro, Hsianghan Hsu, Akihiro Kishimoto, Rodrigo F. Neumann, Binquan Luan, Seiji Takeda and Mathias Steiner; IBM Research, Brazil

Climate change is mainly due to CO₂ emissions occurring in energy production and transportation. A set of technologies are being developed to separate and sequester CO₂ emitted by point sources. Polymer membranes show certain advantages with regards to their storage and disposal properties, they allow for passive operation, have high tolerance to SO_x and NO_x content and can be integrated within an existing power plant steam cycle, i.e., post combustion application.

Candidate materials for application in polymer separation membranes must fulfill two key requirements: high CO₂ permeability and high CO₂/N₂ selectivity. However, there is a tradeoff between these two requirements: increasing a material's permeability decreases its selectivity, and vice-versa. Screening the large number of candidate materials for molecular properties requires an automated design and validation process which does not yet exist.

Here, we report our progress in automated discovery of membrane polymers through inverse molecular design. We have computationally generated and validated hundreds of polymer candidates designed for application in post-combustion carbon dioxide filtration. Specifically, we have validated each discovery step, from training dataset creation, via graph-based generative design of optimized monomer units, to molecular dynamics simulation of gas permeation through the polymer membranes. We compare the permeability predictions obtained by AI models and molecular dynamics simulations with experimental results and discuss future extensions of the discovery approach.

10:30 AM DS02.02.07**Lagrangian and Hamiltonian Graph Neural Networks for Molecular Dynamics Simulations** Ravinder Bhattoo, Sayan Ranu and N M Anoop Krishnan; Indian Institute of Technology Delhi, India

Molecular dynamics simulations are used to realistically simulate the material properties. The interatomic potential energy function (PEF) is critical in determining the validity of the results. Such interatomic PEFs are parameterized using density functional theory (DFT). Usually, interatomic PEF is a multi-body function whose functional form is non-trivial to determine. Therefore, estimating the functional form is critical in determining the interatomic PEF and hence the material properties. Herein, we use Lagrangian Graph Neural Network (LGNN) to learn such interatomic PEF in silica glass system. We show that the LGNN model can learn silica interatomic potential for Si-O, O-O and Si-Si interactions. The inductive bias present in the LGNN makes training easier where it can learn from a significantly small dataset as compared to other ML methods. Thanks to the graph architecture, the size of LGNN model is agnostic to the size of system used and hence, learned LGNN model is scalable. We show the zero-shot generalizability of the LGNN model by simulating systems one orders of magnitude larger than the trained one. Further, LGNN architecture is also capable of incorporating the dissipative force due to connected thermostat. Finally, we show the interpretability of LGNN, which directly provides physical insights on the learned model.

10:45 AM DS02.02.08**Examining Graph Neural Networks for Inorganic Crystalline Structures** Sheng Gong¹, Tian Xie^{1,2}, Rafael Gomez-Bombarelli¹ and Jeffrey Grossman¹; ¹Massachusetts Institute of Technology, United States; ²Microsoft Research, United Kingdom

Graph neural networks (GNNs) are widely used to learn the representations of crystal structures from the data. However, there lacks a systematic scheme to analyze and understand the limits of GNNs for capturing crystal structures. In this work, we propose to use human-designed descriptors as a bank of human knowledge to test whether GNNs can capture knowledge about crystal structures behind descriptors. We find that CGCNN and ALIGNN cannot learn primitive cell-level information well. Then, we suggest that, for learning extensive properties, the frequently used average pooling is not a proper choice. Finally, we propose an initial solution, hybridizing descriptors with GNNs, to improve the prediction performance of GNNs for materials properties, especially phonon internal energy and heat capacity with 90% lower errors. All the analysis can be easily extended to other deep representation learning models and human-designed descriptors. This study shows that the fields of deep representation learning and human-designed descriptors can be developed synergically.

11:00 AM DS02.02.09**Predict Microstructure-Property Relationship of Steels and High Entropy Alloy Formation Using Machine Learning** Michael Gao¹, Zongrui Pei¹, Junqi Yin², Elizabeth Holm³, Nan Gao³, Kyle Rozman¹, Ömer Doğan¹, Youhai Wen¹, Jeff Hawk¹ and David Alman¹; ¹National Energy Technology Laboratory, United States; ²Oak Ridge National Laboratory, United States; ³Carnegie Mellon University, United States

Metallurgy and material design have thousands of years' history and have played a critical role in the civilization process of humankind. Composition, processing, microstructure, and materials properties are the four cornerstones in materials research. The traditional trial-and-error method has been unprecedentedly challenged in the modern era when the number of components and phases in novel alloys keeps increasing, with high-entropy alloys as the representative. New opportunities emerge for alloy design in the artificial intelligence era. For the first part of the talk, we will present a successful machine-learning (ML) study using variational autoencoder and a regression model to identify the microstructure images with eye-challenging morphology for a number of martensitic and ferritic steels. The challenge in differentiating performance with respect to microstructure lies in the extreme similarity of

these steel images, where differences seem insignificant to the viewer. The success of the approach is a result of highly optimized neural network structures and fine-tuned parameters therein. The model clearly identified the key role of several elements in the prototypical 9% Cr steel through the formation of the different features of the martensite steels. As such, a new inverse alloy design method is proposed based on neural networks. It demonstrates a systematic approach to design new alloys.

For the second part of the talk, we will present our research progress in predicting solid solution formation to accelerate high entropy alloys research. In the literature various empirical rules are proposed to predict the formation of single-phase solid solution, but many are based on very small datasets and hence are of very limited predictability. In this project, we perform a machine-learning study on a large dataset consisting of 1252 alloys, including binary and high-entropy alloys, and we achieve a success rate of 93% in predicting single-phase solid solution. The present ML results suggest that the molar volume and bulk modulus are the most important features, and accordingly, a new physics-based thermodynamic rule is constructed. The new rule is nonetheless slightly less accurate (73%) than the ML algorithm but employs only the elemental properties and is thus convenient in applications. Finally, the advantages and pitfalls in applying high-throughput screening and ML versus CALPHAD calculations will be discussed.

11:15 AM DS02.02.10

Predictions of Plasmonic Hot Carrier Energies Using Machine Learning [Adela Habib](#), Benjamin Nebgen, Nicholas Lubbers and Sergei Tretiak; Los Alamos National Laboratory, United States

Atomistic simulation of electron dynamics using machine learning provides a pathway to scale computational studies from a few 10s of atoms to device levels with 1000s of atoms, thereby facilitating efficient device design. For example, studies of plasmonic hot carrier-based devices for efficient energy-harvesting has been limited to small scale systems because of the prohibitively expensive quantum-mechanical simulation methods such as nonadiabatic molecular dynamics (NAMD) or real-time time-dependent density functional theory (rt-TDDFT). On the other hand, we have shown that atomistic neural networks (NN) architectures can estimate a time dependent electron density capable of capturing plasmon formation and its subsequent decay into hot carriers, in nanostructures of 500+ atoms, at fractions of the quantum-mechanical simulation time and with minimal quantum-mechanical input data. In this talk, I will present the extension of this work, showing machine-learned hot carriers' distributions evolving over time as functions of their energy. For this purpose, unlike most NN architectures that focus on scalar predictions, we will introduce a network architecture that predicts orbital occupations transforming with tensor algebra. These ML predictions will enable extraction of useful quantities such as electron-phonon scattering lifetimes that are directly comparable with the experimental measurements. Our goal is to explore the transferability of our workflow in pursuit of a scheme for affordable modeling of hot carrier dynamics in systems with thousands of atoms.

SESSION DS02.03: Machine Learning for Materials Structure and Properties II
Session Chairs: Mathieu Bauchy and Ekin Dogus Cubuk
Monday Afternoon, November 28, 2022
Hynes, Level 2, Room 210

1:30 PM *DS02.03.01

Tough Materials by Design—Autonomous Experimentation for Extreme Mechanics [Keith A. Brown](#); Boston University, United States

Energy-absorbing structures are critical to everyday life and span a wide range of design parameters and use cases. For example, some structures – like those in shoes and sporting equipment – must repeatedly absorb energy without permanent damage while others – such as packaging material and the crumple zones of cars – are designed to protect against singular catastrophic events. Despite their ubiquity, developing new energy-absorbing structures is a time consuming and difficult process that requires iterative experimentation. This is in part because energy-absorbing structures are designed to operate under extreme conditions that feature large deformations, high strain rates, and complex self-self interactions that are collectively very difficult if not impossible to accurately capture using simulation alone. Further, the advent of additive manufacturing has meant that the number of potential structures is now effectively innumerable, compounding the slow pace at which structures or components can be optimized for energy absorption.

Our work is based on the hypothesis that autonomous experimentation can accelerate the discovery of novel structures for extreme mechanical properties. At its core, this combines (1) incorporating automation to increase the speed and consistency of experiments and (2) using active learning – a type of machine learning – to iteratively select experiments using all available knowledge. Together, these comprise an autonomous system that iteratively selects and performs physical experiments to efficiently move towards a target goal, namely the discovery of polymeric structures tailored for efficient energy absorption. This system, which we term a Bayesian Experimental Autonomous Researcher (BEAR), can identify high performing structures in ~60 times fewer experiments relative to conventional grid-based searching.[1] Further, we systematically include prior knowledge in the form of finite element analysis and show that even in cases when the property of interest cannot be directly simulated, it is possible to further accelerate optimization using the principles of transfer learning.[2] Extending this concept of transfer learning for mechanical design, we find that experimental data can be used to predict comparatively hard to obtain experimental performance metrics. Specifically, we identify a process for using behavior during quasi-static testing to predict impact performance and use this procedure to identify additively manufactured lattice structures that have optimized impact performance. Using these principles, our present work focuses on combining the BEAR with a novel algorithm for parametrically generating diverse structures known as generalized cylindrical shells in a manner that allows for components to be highly tuned for efficient energy absorption across a wide range of stress thresholds. This database of >10,000 experiments can be used to select parts tailored for specific applications. By expanding the structural and materials palette available to the BEAR, it is possible to vastly shorten the design loop for developing components for extreme mechanics performance.

[1] Gongora, A. E., et al., *Sci. Adv.* **2020**, *6*, eaaz1708.

[2] Gongora, A. E., et al., *iScience* **2021**, *24*, 102262.

2:00 PM DS02.03.02

Predicting Aggregate Morphology of Sequence-Defined Macromolecules with Machine Learning [Debjyoti Bhattacharya](#); The Pennsylvania State University, United States

Self-assembly of dilute sequence-defined macromolecules is a complex phenomenon in which the local arrangement of chemical moieties can lead to the formation of long-range structures. Predicting the aggregation behavior of these macromolecules is challenging due to the lack of effective order parameters, a vast design space, inherent variability, and high computational costs associated with currently available simulation techniques. Here, I present a workflow that can accurately predict the morphology of aggregates self-assembled from sequence-defined macromolecules using supervised machine

learning. I find that regression models with implicit representation learning perform significantly better than those based on engineered features and a Recurrent-Neural-Network-based regressor performs the best out of nine model architectures we tested. Furthermore, I demonstrate the high-throughput screening of monomer sequences using the regression model to identify candidates for self-assembly into selected morphologies. We further investigate training these models by active learning to perform high-throughput screening from an even smaller number of simulation data on the aggregation process for other increasingly complex design scenarios, such as the design of sequences under polydispersity and at varying environmental conditions. Our strategy is shown to successfully identify multiple suitable sequences in every test we performed.

2:15 PM DS02.03.03

Encoding Dynamic Information from Normal Mode Analysis in Graph Representation Learning for Protein Function Prediction Yuan Chiang^{1,2}, Yen-Lin Chen², Wei-Han Hui² and Shu-Wei Chang²; ¹University of California, Berkeley, United States; ²National Taiwan University, Taiwan

The relationship between protein structure and molecular function has fundamental importance for biological science and pharmaceutical application but remains challenging to probe in by experimental approaches. Recent advances in protein function prediction exploit graph-based deep learning approaches to correlate the structural and topological features of proteins with their molecular functions. However, proteins *in vivo* are not static but dynamic molecules that alter conformation for functional purposes. We recently applied normal mode analysis to native protein conformations and augment protein graphs by connecting edges between dynamically correlated residue pairs. In the multilabel function classification task, our method secures a remarkable performance gain based on the dynamics-informed representation. The proposed graph neural network, ProDAR, increases the interpretability and generalizability of residue-level annotations and robustly reflects structural nuance in proteins. We elucidate the importance of dynamic information in graph representation by comparing gradient-weighted class activation maps with and without dynamic information as inputs. Our model learns the dynamic fingerprints of proteins and pinpoints the residues of functional impacts that hold potential interests for protein and drug design.

2:30 PM BREAK

3:00 PM *DS02.03.04

Structure Determination from Theory and Experiment Maria K. Chan; Argonne National Laboratory, United States

Atomistic modeling has been an invaluable tool for determining structure property relationships and materials design. The relevance of the predicted properties, however, relies on the accuracy of the underlying structure. In many cases of scientific and technological interest, such as nanoparticles, grain boundaries and other interfaces, molecular complexes, and materials with short range order, the determination of the underlying structure is nontrivial. We will discuss approaches to combine information computational modeling and forward simulations of experimental data, driven by AI/ML, to determine structures. Examples include FANTASTX (Fully Automated Nanoscale To Atomistic Structures from Theory and eXperiment) and Ingrained [1]. We will discuss how these tools have successfully determined nanoscale structures from x-ray, electron microscopy, and scanning probe microscopy experimental data.

[1]. Schwenker, V. S. Chaitanya Kolluru, J. Guo, X. Hu, Q. Li, M. C. Hersam, V. P. Dravid, R. F. Klie, J. R. Guest, M. K. Y. Chan, "Ingrained: an automated framework for fusing atomic-scale image simulations into experiments," *Small* 18, 2102960 (2022).

3:30 PM DS02.03.05

Feature Blending—An Approach Toward Generalized Machine Learning Models for Property Prediction of MXene Swanti Satsangi, Avani Mishra and Abhishek K. Singh; Indian Institute of Science, India

From studying the atomic structure and chemical behavior to the discovery of new materials and investigating properties of existing materials, machine learning (ML) has been employed in realms that are arduous to probe experimentally. While numerous highly accurate models, specifically for property prediction, have been reported in the literature, there has been a lack of a generalized framework. Herein we propose a novel feature selection approach that enables the development of a unified ML model for property prediction for several classes of materials. It involves an ingenious blending of selected features from various classes of data such that the resultant feature set equips the model with global data descriptors capturing both class-specific as well as global traits. We took accurate band gaps of three distinct classes of 2D materials as our target property to develop the proposed feature blending approach. Using Gaussian process regression (GPR) with the blended features, the ML model developed here resulted in an average root-mean-squared error of 0.12 eV for unseen data belonging to any of the participating classes. The feature blending approach proposed here can be extended to additional classes of materials and also to predict other properties.

Reference: S. Satsangi, A. Mishra, and A. K. Singh, Feature Blending: An Approach Towards Generalized Machine Learning Models for Property Prediction, *ACS Phys. Chem Au*, 2, 16-22 (2022).

3:45 PM DS02.03.06

Machine Learning Coarse Grained Bond Order Models for Characterizing Mesoscale Aggregation in Liquid Mixtures Anirban Chandra^{1,2}, Troy D. Loeffler¹, Micheal Servis², Srikanth Nayak², Pubudu Wimalasiri², Dina Sheyfer², Jyotsana Lal², Gregory B. Stephenson², Maria K. Chan² and Subramanian Sankaranarayanan^{1,2}; ¹University of Illinois at Chicago, United States; ²Argonne National Laboratory, United States

All-atom molecular dynamics simulations provide crucial insights into a variety of physical phenomena. Despite its numerous successes, all-atom models can be extremely computationally intensive for mesoscale systems. Coarse grained models have been able to overcome the computation bottleneck, but the description of interaction between organic molecules, aqueous media, and inorganic ions is often non-trivial. In this work, we present a coarse grained model for accurately capturing the phase behavior of multicomponent liquid-liquid mixtures. We use TrappE-UA model as a stencil and develop a bond-order based description of interactions between the components. Using the developed model we explore phase behavior and critical phenomena in mixtures consisting of organic solvents, surfactants, and water. Furthermore, aided by the reduced computational cost of our CG model we investigate mesoscale structuring in our systems, for e.g., formation of reverse micellar structures. Insights obtained from our simulations are utilized to interpret experiments performed on such systems.

4:00 PM DS02.03.07

Neural-Network Based Atomistic Modeling of Plastic Deformation Mechanisms of Crystalline Molybdenum Stefanos Papanikolaou¹, Franco Pellegrini², Emine Kucukbenli^{3,4}, Javier Dominguez¹, Mikko Alava^{1,5}, Efthimios Kaxiras³ and Amirhossein Naghdi Dorabati¹; ¹NOMATEN CoE, National Centre for Nuclear Research, Poland; ²International School for Advanced Studies (SISSA), Italy; ³Harvard University, Lyman Laboratory 339, United States; ⁴Department of Information Systems, Questrom School of Business, Boston University, United States; ⁵Department of Applied Physics, Aalto University, Finland

Numerical investigations of nano-mechanical testing for metals and alloys require accurate inter-atomic potentials that may predict configurational energies and interatomic forces, consistent with ab initio calculations. In this work, we investigate crystalline molybdenum (Mo), a viable candidate for extreme environments such as fusion reactors [1]. Mechanical properties of Mo, such as nano-indentation hardness, display non-trivial temperature dependence that requires further validation and deeper understanding, beyond classical force fields methods [2]. In this work, we create a Neural-network interatomic potential (NNIP) for nanoindentation and uniaxial tension of pure crystalline Mo to investigate mechanisms of dislocation nucleation and evolution at multiple temperatures, up to 1000K. Elastic constants, dislocation densities, strain maps and slip traces as a function of indentation depth of the system are compared with embedded atom method (EAM) potentials and the advantages and limitations of NNIPs over traditional potentials are reported [3].

[1] J. Byggmatar, A. Hamedani, et al. *Phys. Rev. B*, 100:144105, Oct 2019.

[2] F.J. Dominguez-Gutierrez, S. Papanikolaou, et al. *Materials Science and Engineering: A*, 826:141912, 2021.

[3] Amirhossein Naghdi et al. In preparation (2022).

4:15 PM DS02.03.09

Multi-Scale Neural Network Quantum Molecular Dynamics Simulations for Computational Ferroelectric Topotronics Thomas M. Linker¹, Ken-ichi Nomura¹, Aiichiro Nakano¹, Rajiv Kalia¹, Fuyuki Shimojo², Kohei Shimamura² and Priya Vashishta¹; ¹University of Southern California, United States; ²Kumamoto University, Japan

Recent discoveries of polar topological structures (*e.g.*, skyrmions and merons) in ferroelectric/paraelectric heterostructures have opened a new field of polar topotronics. However, how complex interplay of photoexcitation, electric field and mechanical strain controls these topological structures remains elusive. To address this challenge, we have developed multi-scale neural network quantum molecular dynamics simulation approaches. Our approaches incorporate excited-state neural network quantum molecular dynamics simulations that integrate quantum-mechanical description of electronic excitation and billion-atom machine learning molecular dynamics to investigate far-from equilibrium optical excitation in ferroelectric materials, as well as imbedding of neural-network(NN) force fields for ferroelectric materials within molecular mechanics (MM) based force-fields to provide accurate mechanical properties and stress/strain controls of ferroelectric/paraelectric heterostructures in a novel NN/MM approach. Our multiscale quantum simulations and machine learning methods will boost not only the emerging field of ferroelectric topotronics but also broader opto-mechano-electronic applications

Acknowledgements:

This work was supported as part of the Computational Materials Sciences Program funded by the U.S. Department of Energy, Office of Science, Basic Energy Sciences, under Award Number DE-SC001460. Simulations were performed at the Argonne Leadership Computing Facility under the DOE INCITE and Aurora Early Science programs and at the Center for Advanced Research Computing of the University of Southern California.

4:30 PM DS02.03.10

Exploring the Structure-Energy Landscape of Oxidic Structures on Copper Surfaces with Machine Learning Potentials and Global Optimization Methods Hyun Jun Kim, Giyeok Lee, Seung-Hyun Victor Oh and Aloysius Soon; Yonsei University, Korea (the Republic of)

Copper has established itself as a transcending material in many key technologies [1]. Despite its long history as an essential metal, there are still uncharted areas of research that have not been systematically conducted. The full-scale structure determination of thin film $\text{Cu}_x\text{O}/\text{Cu}(111)$ surfaces is one such example. The $\text{Cu}(111)$ surface is the most stable surface of copper. Therefore, it will be essential to clarify the most relevant surface structure of its oxidized thin film state under targeted synthesis/technical conditions. Although, there have been many articles from both experimental and theoretical investigations that have discovered the most representative surface oxidic structures such as the “8”, “29”, and “44” surface oxides (which covers 8, 29, and 44 times the area of $p(1 \times 1)$ $\text{Cu}(111)$ surface unit cell, respectively) [2,3], it is still unclear whether these “well-known” thin film structures capture the full family of surface oxides on $\text{Cu}(111)$. The objective of this work is to provide a systematic and thorough survey of the potential energy landscape of $\text{O}/\text{Cu}(111)$ by utilizing with global optimization technique (such as the Global Optimization with First-principles Energy Expression, GOFEE) [4] coupled to a Gaussian Approximation Potential (GAP) [5] which utilizes descriptors that distinguish local atomic environments within a structure. Through this work, we hope to guide experiments in characterizing new (meta)stable surface oxides on $\text{Cu}(111)$ and provide accurate atomistic models for further studies in niche applications such as corrosion and energy-related catalysis.

[1] S. J. Kim, S. Kim, J. Lee, Y. Jo, Y.-S. Seo, M. Lee, Y. Lee, C. R. Cho, J.-P. Kim, M. Cheon, J. Hwang, Y. I. Kim, Y.-H. Kim, Y.-M. Kim, A. Soon, M. Choi, W. S. Choi, S.-Y. Jeong, and Y. H. Lee, *Adv. Mater.* **33**, 2007345 (2021).

[2] Y.-J. Lee, T. T. Ly, T. Lee, K. Palotás, S. Y. Jeong, J. Kim, and A. Soon, *Appl. Surf. Sci.* **562**, 150148 (2021).

[3] N. A. Richter, C.-E. Kim, C. Stampfl, and A. Soon, *Phys. Chem. Chem. Phys.* **16**, 26735 (2014).

[4] M. K. Bisbo and B. Hammer, *Phys. Rev. Lett.* **124**, 086102 (2020).

[5] A. P. Bartók and G. Csányi, *J. Quantum Chem.* **115**, 1051 (2015).

SESSION DS02.04: Machine Learning for Materials Structure and Properties III

Session Chairs: Mathieu Bauchy and Grace Gu

Tuesday Morning, November 29, 2022

Hynes, Level 2, Room 210

8:00 AM *DS02.04.01

Topology-Optimized Porous Cellular Material Architectures with Maximized Energy Absorption Josephine V. Carstensen¹, Reza Lotfi², Wen Chen³, Stefan Sznyszewski⁴, Stavros Gaitanos², Jan Schroers⁵ and James K. Guest²; ¹MIT, United States; ²Johns Hopkins University, United States; ³University of Massachusetts Amherst, United States; ⁴Durham University, United Kingdom; ⁵Yale University, United States

With the recent rapid development of manufacturing technologies, there is a growing need for design methods that can leverage the new fabrication possibilities. This includes design methods that can identify novel low-weight porous cellular material architectures. Topology optimization is a free-form generative design method that does not require the designer to have a preconceived notion of the final design layout. It only requires the definition of a design domain (or unit cell of the cellular material architecture) with applied loads and boundary conditions and will seek to efficiently distribute material within this domain. The design problem is traditionally formulated as a formal optimization problem and solved using a rigorous mathematical program, resulting in solutions that typically outperform conventional low-weight designs.

However, most topology optimization used to design the architecture of porous cellular materials focus on extremizing one or more of the elastic properties. Herein, we look to extend the design problem to the nonlinear regime and aim to maximize the energy absorption capacity until failure of the base solid occurs locally. This results in a problem formulation where the nonlinear properties are estimated using a finitely periodic structure. An interesting base material choice for energy absorption is bulk metallic glasses for which we optimize the designs and fabricate them through a thermoplastic processing method. Testing to full densification reveals that the governing mechanisms for these topologically-optimized structures are combinations of buckling and yielding at the strut level. As a consequence, they offer superior total energy absorption over the traditional honeycomb topologies. Investigations of the same topologies made of polyether ether ketone suggest future directions on how to improve the post-peak response of the topology-optimized cellular materials.

A significant challenge in moving beyond the design of extreme elastic properties is the significant increase in nonlinearity of the design space. Considering nonlinear mechanics such as yielding and large deformations makes it difficult for conventional gradient-based optimizers to navigate the design possibilities and identify quality solutions. With the aim of decreasing the current notable requirement for parameter tuning, we initiate an investigation of how machine learning techniques can be leveraged to increase the robustness of the design framework.

8:30 AM DS02.04.02

Development and Validation of Versatile Deep Atomistic Potentials for Metal Oxides [Pandu Wisesa](#), Christopher M. Andolina and Wissam A. Saidi; University of Pittsburgh, United States

Metal oxide systems are of great interest for various technologies such as coatings and thin film applications. Simulating these materials at larger timescales and system sizes remain a challenge for materials modeling. Calculations based on standard density functional theory while accurate are computationally expensive. On the other hand, methods based on atomistic potentials that can be extended to large system sizes and time scales often fail to describe the different oxidation states of metal oxides. Herein we focus on creating machine learning deep neural-network potentials for different metal oxide systems in a systematic and replicable manner using recently introduced method for convergence acceleration of the training set. Each of these potentials are trained on experimentally verified structures without limitations on the selection of their oxidation states. We validate these interatomic potentials by matching various computed material properties with density functional theory. We demonstrate how these interatomic potentials and their associated training data can be used for further studies to reduce the gap between atomistic simulation and experiments, such as polymorphism, interfaces between different phases, crystalline growth, and other transformations that might include changes in composition. Our study, in addition to our previous studies of metals and binary metallic alloys, demonstrates that machine learning potentials are effective in describing systems with mixed levels of ionic/covalent bonding.

8:45 AM DS02.04.03

Machine Learning Based Prediction of Cation Distribution in Complex Spinel Oxides [Guofeng Wang](#) and Ying Fang; University of Pittsburgh, United States

Spinel ferrites with a general chemical formula of AB_2O_4 ($A, B = Fe, Mg, Co, Ni, Cu, \text{ or } Al$) have interesting and technologically relevant magnetic and electrical properties. The crystal structure of spinel AB_2O_4 can be viewed as a superlattice consisting of eight $(2 \times 2 \times 2)$ face-centered cubic unit cells with the lattice sites occupied by oxygen ions. In addition, one eighth of the tetrahedral and one half of the octahedral sites of the lattice are occupied by the A and B cations. In a normal spinel structure, all A ions will lie at the tetrahedral sites whereas all B ions at the octahedral sites. By contrast, half of the B ions will lie at the tetrahedral sites, whereas the octahedral sites are occupied by both A and B ions in an inverse spinel structure. Varying from the normal to inverse structures, the cation distribution in spinel AB_2O_4 could be quantified using degree of inversion which is the fraction of the tetrahedral sites occupied by B ions.

It has been found that both cation chemistry and degree of inversion play an important role in technically relevant properties of spinel oxides. In this study, we have developed and applied a machine learning based computational approach to predict the equilibrium cation distribution in multi-cation spinel oxides at high temperatures. The database was constructed to contain the density functional theory calculated energies of the spinel oxides with various cation distributions. We applied the machine learning techniques (i.e., linear regression and neural network) to find the relation between the system energy and structural features of the spinel oxides and performed the atomistic Monte Carlo simulations to predict the equilibrium cation distribution as a function of temperature for single spinel AB_2O_4 and double spinel $AB_{2-x}C_xO_4$. Our predicted cation distributions for material systems of $CoFe_2O_4$, $NiFe_2O_4$, $MgAl_2O_4$, $CuAl_2O_4$, and $MgAl_{2-x}Fe_xO_4$ are found to agree well with available experimental results.

9:00 AM DISCUSSION TIME

9:15 AM DS02.04.05

Characterization of Recrystallization Microstructure of Steel Alloys by Multi Phase Field Model Assisted by Data Assimilation Technique. [Nam Hoon Goo](#); Postech, Korea (the Republic of)

Recrystallization is a fundamental phenomenon in steel metallurgy. Through recrystallization, we can complete the creation of the desired microstructure. The critical aspects of the microstructure are grain size distribution, grain orientation texture, and precipitated particles.

The John-Mehl-Avrami equation can describe the kinetics; however, we can not yet make a quantitative prediction related to the recrystallization. In this study, we carry out the ICME approach combined with CPFEM and phase field approach. The CPFEM simulation prepares the initial state of recrystallization for cold-rolled steel sheets, and we implemented the phase field calculation with the data assimilation technique. Data assimilation is required to determine the phase field model parameters such as grain boundary energy and mobility. We validate the modelling results with the annealing experiments for various Fe-C alloys. With the framework, we can characterize the recrystallized microstructure. The characterization contains grain size distribution, orientation texture, and the effect of initial conditions, including plastic deformation and precipitates.

9:30 AM DS02.04.06

Dislocations Shape and Dynamics in BCC Medium Entropy Alloys—Classical Modelling with Machine Learning Potentials [Ivan Lobzenko](#)¹, Yoshinori Shihara² and Tomohito Tsuru¹; ¹Japan Atomic Energy Agency, Japan; ²Toyota Technological Institute, Japan

High-entropy alloys (HEA) are excellent structural materials due to their promising mechanical properties. Works on body-centered cubic (BCC) HEAs show increased ductility if group 4 elements are present in the composition [1,2,3]. Theoretical studies of that effect by first-principles modeling are complicated by the essential randomness of HEA atomic structure, which requires large systems. To achieve high accuracy in classical molecular dynamics we have developed interatomic potentials using machine learning of artificial neural networks (we refer to them as ANN potentials). We present in the current work results for two medium-entropy alloys (MEA): MoNbTa and ZrNbTa. Comparison of basic mechanical properties show

decrease of bulk modulus and elastic constants if Mo is substituted with group 4 element Zr.

Edge and screw dislocations are studied. Classical modelling allows construction of big calculation cells, that prevents self-interaction of the dislocation core due to long-range stress field. Moreover, big cells ensures better randomness of alloys, which is vital in simulations of HEA and MEA mechanical properties. Screw dislocation movement is induced by applying shear strain. In case of edge dislocation the shape and energy is studied in the process of migration of the dislocation core between two adjacent easy core configurations. In this way the Peierls barrier is calculated. Results for two MEA are compared to elucidate the role of group 4 element.

Finally, to understand the stress field of dislocations we employ atomic stress calculation scheme in the framework of ANN potentials. Atomic stress calculations is possible based on virial stress definition due to the fact that atomic energy in the ANN scheme ultimately depends on pair distances between atoms.

9:45 AM BREAK

10:15 AM DS02.04.07

Efficient Implementation of Machine Learning-Based Nonlocal Functionals for Molecules and Solids Kyle W. Bystrom and Boris Kozinsky; Harvard University, United States

Machine Learning (ML) has recently gained attention as a means to develop more accurate exchange-correlation (XC) functionals, and in particular could be used to improve XC functionals for solids without using the computationally expensive exact exchange energy. Feature design is one of the main challenges of this approach because the features must include enough nonlocality to capture the complex nonlocal nature of the exact XC functional while also allowing for computationally efficient and scalable implementations. To address this challenge, the CIDER model for designing nonlocal ML functionals is introduced and used to design a nonlocal exchange functional that obeys the uniform scaling rule for exchange. In addition, two efficient methods for evaluating CIDER features are implemented: A quadratic-scaling algorithm for all-electron, molecular density functional theory (DFT) and a quasi-linear-scaling algorithm for plane-wave DFT with the PAW method. Preliminary efficiency and accuracy benchmarks for periodic systems are presented.

10:30 AM DS02.04.09

Molecular Dynamics Simulations of Lattice Thermal Conductivity with Machine-Learning Anharmonic Interaction Jing Wang¹, Jie-Cheng Chen² and Mei-Yin Chou²; ¹Georgia Institute of Technology, United States; ²Academia Sinica, Taiwan

The lattice thermal conductivity of crystals with strong anharmonic interaction is of particular interest, which cannot be adequately evaluated by linearized Boltzmann transport equation. In this work, we adopt compressive sensing, a machine learning technique to obtain high-order force constants from a small amount of training data. By considering strong heredity effects, we show that the dominant anharmonic interactions are short ranged. This largely shrinks the number of force constants needed in the expansion. To calculate the lattice thermal conductivity, molecular dynamics simulations that include anharmonic interactions up to the sixth order are performed. Test results for Si and NaCl will be presented. The anharmonic interaction in NaCl is found to be more significant than that in Si, which is consistent with the fact that NaCl exhibits a smaller thermal conductivity at above 100 K. Simulation results for highly anharmonic thermoelectric materials SnSe and GeSe that exhibit very low thermal conductivity will also be discussed.

10:45 AM DS02.04.10

Predicting the Dynamics of Atoms in Liquids by a Surrogate Machine-Learned Simulator Han Liu and Mathieu Bauchy; University of California, Los Angeles, United States

Molecular dynamics (MD) is a workhorse of computational material science. However, the inner-loop algorithm of MD (i.e., numerically solving the Newton's law of motion) is computationally expensive. Here, we introduce a surrogate machine learning simulator that is able to predict the dynamics of liquid systems with no prior knowledge of the interatomic potential or nature of the Newton's law of motion. The surrogate model consists of a graph neural network (GNN) engine that is trained by observing existing MD-generated trajectories. We demonstrate that the surrogate simulator properly predicts the dynamics of a variety of systems featuring very different interatomic interactions, namely, model binary Lennard-Jones system, silica (which features long-term coulombic interactions), silicon (which comprises three-body interactions), and copper-zirconium alloy (which is governed by many-body interactions). The development of machine-learned surrogate simulators that can effectively replace costly MD simulations could expand the range of space and time scales that are typically accessible to MD simulations.

11:00 AM DS02.04.11

Charge-Density Based Convolutional Neural Networks for Stacking Fault Energy Prediction in Concentrated Alloys Gaurav Arora, Serveh Kamrava, Pejman Tahmasebi, Dilpuneet S. Aidhy and Nathan Linton; University of Wyoming, United States

A descriptor-less machine learning (ML) model based on charge density extracted from density functional theory (DFT) is developed to predict stacking fault energies (SFE) in concentrated alloys. Often, in most ML models, textbook physical descriptors such as atomic radius, valence charge and electronegativity are used as descriptors which have limitations because these properties change in concentrated alloys when multiple elements are mixed to form a solid solution. We illustrate that, within the scope of DFT, the search for descriptors can be circumvented by electronic charge density, which is the backbone of the Kohn-Sham DFT and describes the system completely. The model is based on convolutional neural networks (CNNs) as one of the promising ML techniques for dealing with complex images and data. The performance of our model is evaluated by predicting SFE of concentrated alloys with an RMSE and R2 of 6.18 mJ/m² and 0.87, respectively, validating the accuracy of the proposed approach.

11:15 AM DS02.04.12

Accelerated Development of ReaxFF Forcefields Using Machine Learning Ankit Mishra, Ken-ichi Nomura, Aiichiro Nakano, Rajiv Kalia and Priya Vashishta; University of Southern California, United States

ReaxFF based reactive force field approach has increased the application of reactive molecular dynamics simulation for studying complex material properties and processes. However, complex simulations require careful tuning of model parameters to high quality ground truth data obtained from accurate quantum mechanical methods. Also, a parameter set tuned for a particular system can be extended through optimization to other applications for similar systems since ReaxFF uses fixed functional form representation of all chemical systems. This optimization process is challenging due to large parameter space, especially for multi component chemical systems and therefore, is extremely challenging to achieve. Currently popular local (parabolic interpolation methods, gradient based methods) and global black box optimization methods (Genetic Algorithms, Monte Carlo Methods, Covariance Matrix Adaptation evolution strategy, Particle Swarm Optimization) require hundreds of thousands of error evaluations for complex training tasks and subsequent error evaluation through energy minimization of many several molecules in the training set. Therefore, an efficient optimization scheme is needed for sampling this high dimensional parameter space with many local minima. Here, we demonstrate various machine learning based parameter

optimization scheme, that use a parallel MD agent for environment sampling and utilizing various machine learning methods to efficiently optimize high dimensional parameter sets. These parameter sets can be further fine-tuned by using gradient based gradient approached near local minima to yield high quality parameter sets suitable for a particular problem at hand

Acknowledgments

This work was supported as part of the Computational Materials Sciences Program funded by the U.S. Department of Energy, Office of Science, Basic Energy Sciences, under Award Number DE-SC001460. Simulations were performed at the Argonne Leadership Computing Facility under the DOE INCITE and Aurora Early Science programs and at the Center for Advanced Research Computing of the University of Southern California

SESSION DS02.05: Machine Learning for Materials Structure and Properties IV

Session Chairs: Mathieu Bauchy and N M Anoop Krishnan

Tuesday Afternoon, November 29, 2022

Hynes, Level 2, Room 210

1:30 PM *DS02.05.01

Towards Out of Distribution Generalization in Mechanics Lingxiao Yuan, Harold S. Park and [Emma Lejeune](#); Boston University, United States

There has been an explosion of recent work in applying data driven methods to problems in mechanics, with particular emphasis on designing materials with novel functionality and predicting their properties. While traditional machine learning (ML) methods have enabled such breakthroughs, they rely on the assumption that the training (observed) data and testing (unseen) data are independent and identically distributed (i.i.d). However, when applied to real world mechanics problems with unknown test environments, a well-trained ML model is very sensitive to data distribution shifts and can break down when evaluated on the shifted test dataset. In contrast, out-of-distribution (OOD) problems assume that the data in test environments is allowed to shift, and many methods both within and outside the mechanics community, have been proposed to improve the out-of-distribution (OOD) generalization for ML methods. However, because most of these OOD methods have been developed for classification problems, and further because of the lack of benchmark datasets for OOD regression problems, the efficiency of these methods on regression problems, which are more important than classification for mechanics, is unknown. Therefore, in this work, we perform a fundamental study of OOD generalization methods for regression problems in mechanics. Specifically, we identify three OOD generalization problems: covariate shift, mechanism shift, and sampling bias, and develop two benchmark datasets for each problem based on the well-known MNIST and EMNIST-Letters datasets to investigate the performance of the OOD generalization methods. Our experiments show that for most cases, while the OOD algorithms perform better compared to traditional ML methods on OOD generalization problems in mechanics, there is a compelling need to develop more robust OOD methods that can generalize notions of invariance across multiple OOD scenarios. Overall, we expect that the combination of this study, as well as the benchmark datasets we developed, will enable further development of OOD methods for regression problems.

2:00 PM *DS02.05.02

A Framework for Variational Embedding of Data in Physics-Based Models [Arif Masud](#) and Shoab Goraya; University of Illinois at Urbana-Champaign, United States

This talk presents a physics-constrained data driven method that variationally embeds measured data in the modeling and analysis framework. The physics-based model is augmented with sparse but high-fidelity data through a variationally derived loss function. The structure of the loss function is analyzed in the context of variational correction to the model predictions wherein loss function penalizes the difference in the modeled response from the measured data that represents the local response of the system. The Variationally Embedded Measured Data (VEMD) method results in forward simulations that are not only driven by boundary and initial conditions but are also augmented by real measurements taken at only a small number of observation points. In the context of forward simulations, the proposed approach can be seen as inducing inductive biases that exploit the difference between the computed and measured quantities in the parametric space. With the help of a model problem from elasticity, we show that the proposed method learns from the sparse high-fidelity datasets while preserving conservation properties of the balance laws. Method is applied to a non-smooth model problem and the mathematical attributes of the formulation are investigated in the context of high-fidelity sparse datasets.

2:30 PM DS02.05.03

Transferable Coarse Grained Potentials Enabled by Gaussian Process Regression and Active Learning [Blake Duschatko](#), Jonathan Vandermause, Nicola Molinari and Boris Kozinsky; Harvard University, United States

Despite continuing advances in the development of interatomic potentials, biologically relevant long length- and time-scales remain inaccessible. Recently, machine learning has shown promise in developing sophisticated “bottom-up” coarse grained potentials, wherein the thermodynamic properties of the all-atom system are preserved. Despite the implications of successfully developing these models, a number of roadblocks remain.

In this work, we demonstrate the use of Gaussian process (GP) regression in designing an on-the-fly active learning framework for coarse grained modeling. In particular, we show that the inherent uncertainty of GP’s allow these models to more seamlessly be transferred across chemically adjacent systems, addressing a persistent problem in the field. Moreover, we examine the applicability of this method to a variety of systems and explore ways in which uncertainty can serve as a probe to the fidelity of system property predictions in ways that traditional diagnostics, such as mean force errors, cannot.

2:45 PM BREAK

3:15 PM DS02.05.04

Acceleration of Simulations of Complex Compounds by Dimensionality Reduction of Atomic Cluster Expansion Features [Yu Xie](#), Anders Johansson and Boris Kozinsky; Harvard University, United States

Machine learning interatomic potentials have shown promising accuracy and efficiency with equivariant features. Among those, atomic cluster expansion [1] is proposed recently as a systematic method to expand body orders of the features. However, the dimension of atomic cluster expansion features grows quickly with the number of chemical elements, which limits its performance for complex materials. In this work, we investigate embedding strategies for dealing with multiple chemical elements and basis functions of atomic cluster expansion. Our theoretical and numerical results illustrate that the embedding

method is able to reduce the dimension of the features with almost no loss of accuracy, yielding significant acceleration of machine learning molecular dynamics of complex materials.

[1] Ralf Drautz. Atomic cluster expansion for accurate and transferable interatomic potentials, 2019

3:30 PM DS02.05.05

Learning the Short- and Medium-Range Enthalpic Structural Manifolds of Disordered Materials [Thomas J. Hardin](#)¹, Mark Wilson¹, Michael Chandross¹, Michael L. Falk² and Michael Shields²; ¹Sandia National Laboratories, United States; ²Johns Hopkins University, United States

Enthalpy minimization pulls the local atomic configurations in materials onto a manifold; by parameterizing that enthalpic structural manifold for a particular material, we can obtain a minimal set of structural descriptors that describe the important degrees of freedom in the local atomic configurations in that material. We sampled local atomic configurations from a variety of experimental and simulated glassy materials, compared those configurations using the Gaussian Integral Inner Product distance, and applied hierarchical clustering and diffusion maps to extract low-dimensional discrete and continuous parameterizations of the materials' enthalpic structural manifolds. We used nonlinear regression to interpret these learned parameters in terms of physically meaningful quantities. This presentation will focus on our structure parameterization methodology and physical interpretation of that parameterization, and will also include physical insights gleaned in the process. SNL is managed and operated by NTESS under DOE NNSA contract DE-NA0003525 (SAND2022-8094 A).

3:45 PM DS02.05.06

Specialized Neural Network Interpolant for Accelerated Pair Interaction in Systems of Rigid Bodies [Gusten Isfeldt](#), Jakob Wohlert and Fredrik Lundell; KTH Royal Institute of Technology, Sweden

Motivated by the limitations of conventional coarse-grained molecular dynamics for simulation of large systems of nanoparticles, an approach to enable the use of complex interaction models for nanoparticles derived from molecular dynamics simulation data in large scale simulation through the use of a class of specialized deep neural networks for interpolation in the relative coordinate space of rigid bodies has been developed.

The first layer of the network transforms the relative position and orientation with a flexibly parametrized geometric representation to a form more suitable to conventional fully connected layers, which, followed by a weighted sum can be used to approximate a potential. Through backpropagation of the gradient of the potential, the force and torque on the particles can then be calculated through the geometric representation. Compared to training a more general network on the components of the force and torque vectors, this method has the advantage of being guaranteed to produce an energy conserving interaction, and due to only being trained on a scalar value, requires fewer internal parameters to be trained. Furthermore since the training data is a scalar potential, the network can be trained to replicate models with no obvious gradient. As the parameters of the geometric transformation are trained along with the other weights in the network, the representation becomes optimized for the geometry of the potential.

The network is fitted to a variety of interaction potentials, investigating training and convergence characteristics and noise sensitivity, to demonstrate both the utility and limitations of the method. Additionally, further generalization to use on soft bodies and polydisperse systems is discussed.

4:00 PM DS02.05.07

Neural Network Models of Phase Field Simulations [Haiying Yang](#) and Michael J. Demkowicz; Texas A&M University, United States

We explore the potential for neural networks (NNs) to predict two aspects of microstructure evolution, as represented in simple phase field simulations. First, we train NNs to predict the evolution of microstructures under pre-specified, spatially and temporally varying temperature and bias fields. This problem is amenable to solution by existing NN training methods because each input maps to a unique output. Next, we train NNs to solve the inverse problem, namely: what externally applied temperature and bias fields are required to guide microstructure evolution to a pre-specified target state? In this problem, inputs do not map to unique outputs, necessitating an innovative approach to NN training. Our work suggests that NNs may be useful for finding optimal processing parameters for achieving a desired microstructure.

4:15 PM DS02.05.08

A Representation-Independent Electronic Charge Density Database for Crystalline Materials [Jimmy-Xuan Shen](#)¹, Jason M. Munro², Matthew K. Horton² and Kristin A. Persson^{2,3}; ¹Lawrence Livermore National Laboratory, United States; ²Lawrence Berkeley National Laboratory, United States; ³University of California, Berkeley, United States

In addition to being the core quantity in density functional theory, the charge density can be used in many tertiary analyses in materials sciences from bonding to assigning charge to specific atoms. The charge density is data-rich since it contains information about all the electrons in the system. With the increasing prevalence of machine-learning tools in materials sciences, a data-rich object like the charge density can be utilized in a wide range of applications. The database presented here provides a modern and user-friendly interface for a large and continuously updated collection of charge densities as part of the Materials Project. In addition to the charge density data, we provide the theory and code for changing the representation of the charge density which should enable more advanced machine-learning studies for the broader community.

4:30 PM DS02.05.09

Structure-Property Relationships for Grain Boundaries Using Strain Functional Descriptors and Supervised Machine Learning [Avanish Mishra](#), Sumit Suresh, Khanh Dang, Saryu Fensin, Edward Kober and Nithin Mathew; Los Alamos National Laboratory, United States

Properties of grain boundaries (GBs) are controlled by the types and arrangement of local atomic environments at the boundary. Although it is possible to estimate GB properties by characterizing minimum energy or well-defined GBs, extrapolating these understanding to real GBs is a formidable task. The increased complexity in metastable states of GBs, with variations in atomic arrangement, provides a remarkable opportunity to utilize data-driven methods to establish the structure-property relationships for GBs. A significant challenge in establishing such relationships is the absence of physically meaningful set of descriptors to represent structural arrangement at GBs. Existing descriptor sets can estimate selected properties; however, they fail to provide any physical insights. Strain functional descriptors (SFD), a complete and symmetry-adapted set of descriptors, are ideal for characterizing the local atomic environment at GBs and provides the capability to decompose the atomic arrangement in terms of physically meaningful descriptions such as strains, strain-gradients, and higher order deformations. The presentation will show the application of SFDs for predicting various properties, such as grain boundary energy, atomic energy density, and elastic stiffness tensor on a large (~5000) database of metastable GBs in Cu, using supervised machine learning models. The developed regression models accurately estimate various properties with unprecedented accuracy and exhibit an exceptional performance even for atomic environments in polycrystalline samples.

8:15 AM *DS02.06.01

Global Optimization of Atomic Structures with Machine Learning [Karsten W. Jacobsen](#); Technical University-Denmark, Denmark

Artificial intelligence is paving the way for new approaches to the understanding and design of materials at the atomic and electronic level. Machine learning can provide guidance for high-throughput computational searches and in some situations effectively replace computer intensive electronic structure calculations.

In the talk I shall focus on one particular application of machine learning: the global optimization of atomic structures. The methodology is based on Gaussian processes and uses the calculated model uncertainties to guide the search [1,2]. Furthermore, the machine learning approach allows for an extension of the configuration space to consider atoms, which are not pure elements, but combinations of several elements (for example an atom which is a combination of gold and copper) [3]. This circumvents barriers in the potential energy surface and makes structure determination much more efficient. The approach is illustrated with applications to clusters, surfaces, and bulk systems.

[1] M. K. Bisbo and B. Hammer, "Efficient Global Structure Optimization with a Machine-Learned Surrogate Model," Phys. Rev. Lett., 124, 086102 (2020).

[2] S. Kaappa, E. G. del Río, and K. W. Jacobsen, "Global optimization of atomic structures with gradient-enhanced Gaussian process regression," Phys. Rev. B, 103, 174114 (2021).

[3] S. Kaappa, C. Larsen, and K. W. Jacobsen, "Atomic Structure Optimization with Machine-Learning Enabled Interpolation between Chemical Elements," Phys. Rev. Lett., 127, 166001 (2021).

8:45 AM DS02.06.02

A Deep Learning Model for Formation Energy and Synthesizability of Crystalline Materials [Ali Davariashdiyani](#)¹, Zahra Kadkhodaie² and Sara Kadkhodaie¹; ¹University of Illinois at Chicago, United States; ²New York University, United States

Predicting the stability, synthesizability, and physical properties of hypothetical crystal structures are essential for developing novel materials for different applications. We present a neural network model that predicts the synthesizability and the formation energy of crystals. We created a novel technique to represent crystals by 3D voxel images, which has advantages over the widely used graph representation technique. The advantage of our approach is that the translation and rotation invariance as well as the long-range ordering of crystals naturally arise in the image representation, whereas both are absent in a graph representation. Visual features embedded in these images are learned by convolutional neural networks and are used to predict the synthesizability and formation energy of never-seen-before crystalline materials. We compare the predictions of our model with other available models.

9:00 AM DS02.06.03

Elastic Constants in Ni Based High Entropy Alloys from DFT and Machine Learning [Nathan Linton](#) and Dilpuneet S. Aidhy; University of Wyoming, United States

High entropy alloys (HEAs) present a paradigm shift in materials design. These alloys consist of multiple principal elements randomly distributed on a crystal lattice resulting in enormously large phase space which on the one hand presents large opportunities to unravel novel properties whereas on the other presents an equally large challenge to survey the phase space thereby presenting a data-science challenge. We present a machine learning framework coupled with electronic structure methods whereby properties in complex alloys could be predicted by learning from simpler alloys. The mechanical properties in complex alloys are predicted from the database of the constituent's binary alloys. Specifically, we demonstrate predictions of stiffness constants, Young's modulus, bulk and shear moduli, and Poisson's ratio in ternary, quaternary, and quinary Ni-based alloys with a high-level of accuracy. A major benefit of this approach is that for every new composition discovered, the mechanical properties can be computed using only the existing binary alloy database thereby completely bypassing the computationally expensive calculations.

9:15 AM DS02.06.05

Neuroevolution Guided Discovery of Pathways for Materials Synthesis [Anirban Chandra](#)^{1,2}, Amanda Dufek³, Suvo Banik^{1,2}, Rohit Batra², Isaac Tamblyn^{4,5}, Pierre Darancet², Stephen Whitelam³ and Subramanian Sankaranarayanan^{1,2}; ¹University of Illinois at Chicago, United States; ²Argonne National Laboratory, United States; ³Lawrence Berkeley National Laboratory, United States; ⁴University of Ottawa, Canada; ⁵Vector Institute of Artificial Intelligence, Canada

Discovery and synthesis of materials with tailored properties is an overarching goal of material scientists. Thermodynamic phase diagrams are often a good starting point for designing synthesis protocols, but in typical experimental settings, kinetic effects are often more prominent and therefore determine the feasibility of such protocols. Selective synthesis of polymorphs of a material can also be limited by such kinetic barriers. Here using molecular simulations we investigate how neural networks trained by evolutionary reinforcement learning can generate feasible synthesis pathways for materials. These previously unknown pathways can enable us to optimally synthesize a particular material and simultaneously provide physical insight into the kinetics of phase transitions. Moreover, we also show how our neural networks learn to change thermodynamic variables in order to promote generation of a particular phase, i.e. perform polymorph selection. Transformation pathways in several materials, such as Carbon and Silicon, are discussed here. The presented evolutionary scheme can be applied to investigate a broad range of problems (such as self-assembly, experimental design, and additive manufacturing) wherein transition pathways from one state to another are unknown.

9:30 AM DS02.06.06

Adaptive Learning From Scarce And Multi-Fidelity Materials Data Sanaz Zanjani, Mehdi Shishehbor, Amin Yousefpour and [Ramin Bostanabad](#); University of California, Irvine, United States

Materials modeling and design is typically hampered by two major uncertainty sources: lack of data and model form discrepancies. In this talk, we will present a novel approach based on nonlinear manifold learning that addresses these (and more) uncertainty sources. Our approach is based on latent map Gaussian processes (LMGPs) and aims to leverage multiple data sources to quantify uncertainty sources and, more importantly, provide visually interpretable diagnostic measures that indicate the extent to which different data sources (e.g., experiments, simulations, etc.) agree with one another. We will introduce our approach in both Bayesian and frequentist settings and demonstrate that both perform well in a wide range of applications.

9:45 AM BREAK

10:15 AM DS02.06.07

Conditional Generation of Liquid Solidification by Manipulating the Degrees of Supercooling Using Deep Generative Model Bor-Yann Tseng, Yu-Chen Chien and [Chi Hua Yu](#); National Cheng Kung University, Taiwan

We propose a deep generative model on the learning of physics behind the dendritic solidification development process. Dendritic structure is commonly seen in many different casting processes, which also plays an important role and affects the properties of the final product for freezing casting. However, there is no efficient tool for the researcher to examine the end product with desired properties. In this study, we developed a time-dependent deep generative model to learn to predict the phase change under different cooling conditions. Our model successfully predicts the morphology of different water ices, proving that our model is capable of reproducing the solidification for a complete growth process. Our results also suggest that by controlling the degree of supercooling, we can successfully manipulate the porosity after freeze casting. Our research opens a new avenue for inverse design of casting processes with the desired porosity. This model can be easily extended to different physics systems, such as cell mechanics, metal recrystallization, and two-phase flow.

10:30 AM DS02.06.08

Utilizing AI and TD-DFT Calculated Raman Response to Optimize CVD Synthesis Parameters of K_2CoS_2 [John P. Ferrier](#) and Swastik Kar; Northeastern University, United States

With new materials being theoretically devised using computational techniques, such as Density Functional Theory (DFT), new experimental tactics must be devised to ease the complexities of synthesizing new 2D materials. Given the large parameter control space for experimental synthesis of 2D materials, we propose utilizing an AI model that correlates experimental growth parameters to their resultant sample Raman spectra measurements. Time-Dependent DFT (TD-DFT) is utilized to calculate an approximation for the expected Raman spectra of the desired 2D material using a wavelength-dependent Placzek approximative method [1], allowing the AI model to propose expected growth parameters. In this presentation we will discuss our preliminary results of ultrathin, possibly monolayer growth of K_2CoS_2 , an in-plane antiferromagnetic insulator [2], using these TD-DFT simulations and AI to optimize CVD growth parameters.

References:

- [1] M. Walter, M. Moseler, "Ab Initio Wavelength-Dependent Raman Spectra: Placzek Approximation and Beyond" J. Chem. Theory Comput., 2020, 16, 1, 576-586
- [2] A. B. Sarkar, A. Bansil, A. Agarwal et al., " K_2CoS_2 : A two-dimensional in-plane antiferromagnetic insulator" Phys. Rev. B 102, 035420, 2020

10:45 AM DS02.06.09

Permutation-Invariant Deep Neural Networks for Predicting the Mechanical Properties of Random Cellular Composites [Yuan Chiang](#)^{1,2}, Grace Gu¹ and Shu-Wei Chang²; ¹University of California, Berkeley, United States; ²National Taiwan University, Taiwan

Composite materials hold exciting key to many extraordinary mechanical properties such as reduced weight, high specific strength and toughness, and progressive fracture behavior. Recent advances in additive manufacturing have facilitated the fabrication of complex composite designs. However, searching for the optimal structures and combinations of composite materials has never been a trivial task. Previous machine learning models usually take structured design features (e.g. fixed-size vectors, images, graphs, etc.) as inputs, which usually confines and discretizes the design space. Here we adopt permutation-invariant neural networks to learn the unordered point distributions in a continuous space. We embed the cell centroid distributions of random cellular composites as high-dimensional representation vectors to predict the stress-strain curves obtained from lattice spring model (LSM) simulations. By learning randomly shuffled and reflected cell centroids, our model obeys permutation invariance and reflection symmetry of cellular composite designs. Without discretization in formulation, the model also learns the continuous mapping of spatial coordinates and can embed arbitrary number of cells. Our model could enable high-throughput and flexible composite design and apply to gradient-based optimization.

11:00 AM DS02.06.10

Inverse Design of Architected Metamaterials Using Isogeometric Analysis and Machine Learning [Deepak Kumar Pokkalla](#)¹, Raja Biswas², Seokpum Kim¹ and Vlastimil Kunc¹; ¹Oak Ridge National Laboratory, United States; ²Evonik Digital Labs, Singapore

Architected materials with prescribed mechanical properties are beneficial for diverse engineering applications. With the advent of additive manufacturing, the fabrication of new lattice metamaterials across multiple length scales with unforeseen properties became feasible. However, rapidly identifying complex architectures with prescribed mechanical properties remains a challenge as the present design paradigm relies on traditional finite element analysis and time-consuming topology optimization. Recently, machine learning techniques are explored for the inverse design of metamaterials, albeit only for infinitesimal deformations. We introduce an efficient machine learning approach for rapid inverse design of lattice metamaterials with tailorable nonlinear stress-strain curves and Poisson's ratios. The structure-property map exploring topological design space with distinct lattice structure types, sizes, and shapes generated using isogeometric analysis serves as the training data. With the prescribed nonlinear stress-strain curve and/or Poisson's ratio profile as input, the machine learning framework rapidly identifies the architecture that, when additively manufactured and mechanically tested, replicates the prescribed mechanical response. We rapidly generate soft network metamaterial architectures that mimic human and cat's skin mechanical behavior for biomimetic applications.

11:15 AM DS02.06.11

Representing Polymers as Periodic Graphs with Learned Descriptors for Accurate Polymer Property Predictions [Evan Antoniuk](#), Peggy Li, Bhavya Kailkhura and Anna Hiszpanski; Lawrence Livermore National Laboratory, United States

One of the grand challenges of utilizing machine learning for the discovery of innovative new polymers lies in the difficulty of accurately representing the complex, multi-scale structures of polymeric materials. Although a wide array of hand-designed polymer representations have been explored, there has yet to be an ideal solution for the problems of how to capture the periodicity of polymer structures, as well as how to automatically develop polymer

descriptors without the need for human feature design. In this talk, I will show how we have tackled these problems through the development of our periodic polymer graph representation. Specifically, our pipeline for polymer property predictions is comprised of our polymer graph representation that naturally accounts for the periodicity of polymers, followed by a message-passing neural network (MPNN) that leverages the power of graph deep learning to automatically learn chemically-relevant polymer descriptors. Across a diverse dataset of 10 polymer properties, we find that this polymer graph representation consistently outperforms previous hand-designed representations with a sizable 20% average reduction in prediction error. Our results illustrate how the incorporation of chemical intuition through directly encoding periodicity into our polymer graph representation is responsible for a considerable improvement in the accuracy and reliability of polymer property predictions. We also demonstrate how combining polymer graph representations with message-passing neural network architectures can automatically extract meaningful polymer features that are consistent with human intuition, while achieving better predictive performance than human-derived features. Whereas previous polymer informatics approaches have typically utilized hand-designed descriptors that have been optimized for representing molecules, this work highlights the advancement in predictive capability that is possible if using chemical descriptors that are specifically optimized for capturing the unique chemical structure of polymers.

SESSION DS02.07: Machine Learning for Materials Structure and Properties VI

Session Chairs: Grace Gu and N M Anoop Krishnan

Wednesday Afternoon, November 30, 2022

Hynes, Level 2, Room 210

2:00 PM DS02.07.02

CEGAN—Crystal Edge Graph Attention Network for Multiscale Classification of Materials Environment Suvo Banik¹, Debdas Dhabal², Henry Chan³, Sukriti Manna¹, Mathew J. Cherukara³, Valeria Molinero² and Subramanian Sankaranarayanan³; ¹University of Illinois at Chicago, United States; ²The University of Utah, United States; ³Argonne National Laboratory, United States

Material characterization plays a crucial role in data-intensive and Artificial intelligence (AI)-driven materials design. In machine learning (ML) applications, the characterization task typically involves the use of fingerprints which is followed by a learning algorithm that maps the fingerprint to a user-desired property of interest. Fingerprints or “descriptors” can be of diverse types and scales ranging from atomic to micro-scale as demanded by the application domain. It is highly desirable that a representation of material in feature space should not only be able to differentiate between different structures but also should be simple, unique, complete, and sensitive to the locality of application. Most popular mathematical formulation-based descriptors are often not unique across the systems or suffer from transferability issues across the different application domains. Crystal graphs in this regard are unique and carry a global signature of a crystal network. In this work, we introduce a workflow called CEGAN - Crystal Edge Graph Attention Network - that uses graph attention-based architecture to combine simple edge and angle features of a crystal edge graph to learn unique feature representation and perform multiscale classification of materials belonging to different classes. We first demonstrate a case study where classification is based on their global (Structure-level) representation such as space group and structural dimensionality (e.g., Bulk, Clusters, 2D, etc.). Using representative materials such as carbon and zeolites, we next demonstrate the transferability of our network in successfully performing local atom level classification tasks, such as grain boundary identification and studying nucleation and growth of polymorph in synthesis mixtures. Overall, our approach is agnostic to the material type and allows for multiscale classification of features ranging from atomic-scale crystal structures to heterointerfaces to microscale grain boundaries.

2:15 PM DS02.07.03

CG-RNN—A Recurrent Neural Network for Coarse-Grained Force Field Prediction Eshan C. Singhal¹, Ziji Zhang², Miriam Rafailovich², Peng Zhang² and Yuefan Deng²; ¹The Oakridge School, United States; ²Stony Brook University, United States

Simulating proteins in silico using Molecular Dynamics (MD) provides highly precise physics insights allowing experimentation without the need for laboratory procedure [1]. These simulations, however, require heavy computational workload with atomic level computations which is the major challenge for large proteins at long time scales. Thus, coarse graining (CG) algorithms have been studied which attempt to reduce the problem dimensions of the target allowing for longer simulations and more protein observations with a limited cost of accuracy [1]. Previous methods employed neural networks and graph neural networks with features calculated from the atomic simulation data to predict the energies and forces on each CG atom [2].

We propose a novel architecture by using unidirectional Recurrent Neural Network (RNN) layers to improve accuracy of the algorithm. The intuition of using RNN is natural as it specializes in time series as input data which applies directly to the MD trajectories whereas the existing approach [2] simply utilizes a dense network of linear layers ignoring the time dependency in the inputs. We deploy an RNN layer with 128 input nodes and 100 hidden nodes with 1 layer of Rectified Linear Unit activation. Outputs are passed to a single Dense layer with 100-dimensional inputs and 1-dimensional output. Because of the RNN model's reliance on our data, training batches are made variably sized, allowing for one trajectory per batch instead of a constant size. A $3e-4$ learning rate with 0.3 decay rate and 4.0 lipschitz strength is utilized along with a predetermined Bead Embedding Layer and Gaussian RBF Layer. After learning, the derived CG simulations are compared to the all-atomic (AA) simulations using the non-infinite energy values in the time-lagged Independent Component Analysis (tICA) free energy distributions, with Jensen-Shannon (JS) Divergence and Mean Squared Error (MSE) as evaluation metrics. Preliminary experiments with 1,000-frame Alanine Dipeptide data demonstrate higher model accuracy for the RNN compared to the baseline CGNet model. Followup experiments are conducted with 50 epoch training on Chignolin data with 1.8 million frames to generate 200 simulated CG trajectories with 200 frames each. CG Trajectories are then processed by assigning unit cell angle and lengths corresponding to Chignolin with a distribution range adjusted from the AA domain in the tICA plot. The loss of the baseline model converges at 847.4 while the loss of the CG-RNN model converges at 304.0. For tICA distributions compared with AA simulations, the baseline model produces a JS divergence of 0.20 and MSE of 3.19, and the CG-RNN model has a JS divergence of 0.14 and MSE of 3.17, which indicates that the CG simulations derived from the CG-RNN model produce closer energy distribution with the AA simulations than the baseline model.

Although experimenting on Chignolin demonstrates merit for the CG-RNN approach, validation with larger proteins will be conducted to further verify the benefit of RNN for coarse graining. Additionally, more variations of the RNN types such as GRU or LSTM with variations in hyperparameters will be tested to further improve the accuracy of the CG-RNN approach.

Acknowledgments:

We thank the Garcia Summer Scholars Program for supporting and facilitating this research and the Morin Charitable Trust for funding.

[1] Kmiecik, S., Gront, D., et. al. (2016). Coarse-Grained Protein Models and Their Applications. *Chemical Reviews*, 116(14), 7898–7936.

[2] Husic, B. E., Charron, N. E., et. al. (2020). Coarse graining molecular dynamics with graph neural networks. *The Journal of Chemical Physics*, 153(19),

2:30 PM BREAK**3:30 PM DS02.07.04**

Adaptive Sampling and Variability—Machine Learning for Optimizing Additive Manufacturing Processes [Maher Alghalayini](#)¹, Surya R. Kalidindi², Christiaan J. Paredis¹ and Fadi Abdeljawad¹; ¹Clemson University, United States; ²Georgia Institute of Technology, United States

Additive Manufacturing (AM) has been the subject of active research in recent years due to its potential use in many applications and the flexibility in designs it offers. However, the sensitivity of AM printed materials and their net properties to the processing conditions remains a challenge to the widespread adoption of these emerging techniques. A need, therefore, exists to optimize AM processes to identify the best printing conditions and unlock the true potential of this manufacturing capability. Recent studies show that traditional optimization approaches are inapplicable as AM materials possess significantly high variability in their net properties when the printing is repeated with the same processing parameters. In terms of optimization, sequential designs can be used to explore the high-dimensional AM processing parameter spaces efficiently. In such approaches, the optimization algorithm learns from previously collected data and adaptively proposes new experiments to selectively sample the space where needed the most to optimize the AM process. Sequential designs usually rely on optimizing a given metric in the design space to choose the experiment in the next iteration. However, the AM costs associated with performing one experiment per iteration are typically high, and an efficient novel optimization algorithm that can identify several experiments per a given iteration is needed to lower the costs associated with the optimization.

Herein, we develop an adaptive optimization method that implements machine learning and integrates the variability in the properties of AM materials. Our approach learns from previous experiments and adaptively proposes new locations in the input domain that maximize expected information gain. Gaussian Process Regression and probability calculus are used to explicitly account for variability in the analysis and optimization. In addition to variability, the novelty of our approach lies in the use of utility theory to define the optimization criteria upon which the new experiments are chosen and the flexibility in identifying the number of new design sites and their respective AM samples to be tested during each optimization iteration. The proposed method is tested on simulated data to showcase its performance. More specifically, multimodal response surfaces for both the mean and variability of AM process parameters are used to benchmark our optimization approach. This study is expected to result in an efficient, variability-embracing adaptive optimization method.

3:45 PM DS02.07.05

Uncertainty Quantification of Coarse-Grained Metal Models Using Bayesian Sampling Methods [Abhishek T. Sose](#)¹, [Troy Gustke](#)¹, [Fangxi Wang](#)¹, [Aditya Savara](#)², [Sanket A. Deshmukh](#)¹ and [Soumil Y. Joshi](#)¹; ¹Virginia Tech, United States; ²Oak Ridge National Laboratory, United States

A fundamental understanding of large and complex systems through coarse-grained (CG) molecular dynamics (MD) has become increasingly popular. Due to its lower resolution and faster dynamics, CG MD has become an efficient and economical way to perform MD simulations. However, the accuracy of the parameters used in interatomic potentials significantly affects the simulation performance. In this study, we present the development of new CG embedded atom method (EAM) potentials to describe the interatomic interactions of face-centered cubic (FCC) metals: Gold (Au), Palladium (Pd), Nickel (Ni), Copper (Cu), Aluminum (Al) and Platinum (Pt). Particularly, a CG MD integrated particle-swarm optimization (PSO) method was used to explore the 14 parameter space defined by EAM potential in order to reproduce the physical, mechanical, and thermodynamic properties of their respective metals. These developed models may contain several sources of uncertainty, including errors in numerical and modeling calculations. Hence, to develop a fundamental understanding of the sensitivity of the output to these errors, we describe the uncertainty of input parameters through the learning of output. The following framework was developed to evaluate the uncertainty and accuracy of these developed FF parameters: (i) Using data obtained from simulations of the CG model and various parameter options, a sensitivity analysis using Sobol sampling was performed. (ii) From the sobol data, a Gaussian Process Regression (GPR) model was developed and used as a surrogate model for MD simulations. (iii) By integrating PEUQSE, a Bayesian tool for parameter estimation, and the GP model, further uncertainty quantification (UQ) was accomplished. The stochastic way of identifying high confidence level parameter sets was a more efficient way, rather than a traditional deterministic approach. Specifically, we performed three sampling techniques: Ensemble slice sampling (ESS), Metropolis-Hastings (MH), and the Grid search approach to sample and identify the most probable parameter set. Our results suggest that the convergence and accuracy of the ESS method was faster and computationally cheaper compared to other two methods. With this robust computational framework, hard- and soft-material interatomic potentials can be developed with excellent reliability and accuracy.

This material is based upon work supported by the National Science Foundation under Grant No. DMR-2047743

4:00 PM DS02.07.07

Quantifying Disorder One Atom at a Time Using an Interpretable Graph Neural Network Paradigm [James Chapman](#)^{1,2}, [Yu-Ting Hsu](#)¹, [Xiao Chen](#)¹, [Tae Wook Heo](#)¹ and [Brandon Wood](#)¹; ¹Lawrence Livermore National Laboratory, United States; ²Boston University, United States

At the center of the structure-property paradigm is the fact that macroscopic materials behavior begins at the atomic scale, with local atomic arrangements ultimately coming together to form structural features observed at larger length scales. Characterizing the nature and propagation of these local environments is therefore vital to understanding macroscale structure-property relationships and their evolution. Complicating this endeavor is the fact that the long-range features often depend on structurally disordered atomic environments, which tend to dictate materials functionality. Quantifying the level of atomic disorder within materials is therefore critical to understanding how evolving local structural environments dictate performance and durability. Here, we leverage graph neural networks to define a physically interpretable metric for local disorder. This metric encodes the diversity of the local atomic configurations as a continuous spectrum between the solid and liquid phases, quantified against a distribution of thermal perturbations. We apply this novel methodology to three prototypical examples with varying levels of disorder: (1) solid-liquid interfaces, (2) polycrystalline microstructures, and (3) grain boundaries. Using elemental aluminum as a case study, we show how our paradigm can track the spatio-temporal evolution of interfaces, incorporating a mathematically defined description of the spatial boundary between order and disorder. We further show how to extract physics-preserved gradients from our continuous disorder fields, which may be used to understand and predict materials performance and failure. Overall, our framework provides an intuitive and generalizable pathway to quantify the relationship between complex local atomic structure and coarse-grained materials phenomena.

4:15 PM DS02.07.09

Development of Machine Learned Force Fields for Transition Metals and an Application to Surface Reconstruction [Cameron J. Owen](#)¹, [Steven B. Torrisi](#)^{1,2}, [Yu Xie](#)¹, [Simon L. Batzner](#)¹, [Albert Musaelian](#)¹, [Lixin Sun](#)¹ and [Boris Kozinsky](#)^{1,3}; ¹Harvard University, United States; ²Toyota Research Institute, United States; ³Bosch, United States

The development of accurate and efficient machine-learned force fields is a crucial step in an overall materials discovery workflow that complements experiments with theoretical simulations. In order to facilitate the ongoing development of automated machine learned force fields using tools like

FLARE,[1] Nequip,[2] and Allegro,[3] we have generated a benchmarking dataset of single-element bulk structures with a vacancy defect in order to study the interplay between many body behavior and model performance. This dataset contains ab initio molecular dynamics simulations capturing low-temperature crystalline and melted phases. We investigate the difference in model performance across model architectures, levels of descriptor fidelity, and elements. These results reveal the interplay between elemental properties and model accuracy revealed by differences in performance.

The fidelity of these methods is further assessed by considering the reconstruction of low-index Au surfaces. The workflow results in a MLFF that is able to directly observe these low-index reconstructions, which were previously inaccessible using classical techniques.

[1] Vandermause, J., Xie, Y., et al. Active learning of reactive Bayesian force fields: Application to heterogeneous hydrogen-platinum catalysis dynamics, *Nat. Commun.* Accepted. Also @ arXiv:2106.01949

[2] Batzner, S., Musaelian, A., et al. E(3)-equivariant graph neural networks for data-efficient and accurate interatomic potentials. *Nat. Commun.* 13, 2453 (2022).

[3] Musaelian, A. and Batzner, S., et al. Learning local equivariant representations for large-scale atomistic dynamics. arXiv:2204.05249

SESSION DS02.08: Poster Session
Session Chairs: Grace Gu and N M Anoop Krishnan
Wednesday Afternoon, November 30, 2022
8:00 PM - 10:00 PM
Hynes, Level 1, Hall A

DS02.08.01

Flat Magnetic Bands of Full-Heusler Crystals—Analysis and Prediction with a First Principle Deep Learning Model [Xiuying Zhang](#)¹, Lei Shen¹ and Tong Yang²; ¹National University of Singapore, Singapore; ²The Hong Kong Polytechnic University, China

Materials with flat bands near or at the Fermi level are a promising route towards strongly correlated states, but the properties demonstration has been severely hindered due to the lack of materials for realization of flat bands. Machine learning is a promising way to speed up the unearthing of the flat band materials. Here, we propose a convolutional neural network classification model, which only have the periodic table as the input and thus is called periodic table classifier (PTC), to explore flat bands along the high-symmetry paths around the Fermi level and search for the physics behind it. The full-Heusler crystals are chosen as targets because of its abundance in dataset and its much high symmetry with the space group of 225. The PTC model is trained with the full-Heusler crystals in the AFLOW database and then it can accurately classify the flat bands with the AUC of 0.91 for the test set and 0.88 for the full-Heusler crystals in the materials project (MP) dataset. Visualizing the model also gets some interesting phenomimes. For example, the model regards the number of valence electrons of the crystal as important for the flat band prediction: crystals have a high probability to have flat band around the Fermi level if they have valence electrons of about $12 \times n$ ($n=1,2,3\dots$); crystals have a probability as high as 0.8 to possess flat bands if their number of unfilled d -orbital electrons is around 6, and the larger number of unfilled p -orbital electrons, the smaller flat band probability. The full-Heusler crystals is reach in magnetic crystals and the PTC can also predict both the flat bands and the ferromagnetic full-Heusler compounds with the accuracy of 0.76. Our work not only provide a quick way to enrich the flat band database but also provide the specific direction for searing for the flat bands.

DS02.08.02

Machine Learning Gamma Phonons from Atomic Coordinates [Ryotaro Okabe](#), Zhantao Chen and Mingda Li; Massachusetts Institute of Technology, United States

The phonon¹ of a material describes the dynamics of its constituent atoms in the harmonic approximation, in the framework of the theory of lattice vibrations. The details of the lattice dynamics are of key importance. Especially, phonon at the Gamma point of the reciprocal space gives us important properties such as dielectric constant and the stability of materials.

In this work, we present a machine-learning model that directly predicts phonon band structure only with simple input like atomic coordinates. At the beginning of the machine learning model, the input feature vectors are passed to an embedding layer for dimensionality reduction. In the next part, the Euclidean neural network (E(3)NN)² is then applied to the resulting hidden state and consists of alternating convolution and gated block operations. Here, a convolutional layer operates on the radial distance vectors between atoms in a neighborhood up to a radial cutoff. E(3)NN has made it possible to include 3D rotation, inversion, and translation symmetry in the atomic structures so that high accuracy is reached without data augmentation.

The method we present this time will give us insights about the materials' dynamics. In addition, it is expected that we can expand the tool to predict properties that are difficult to predict, such as the magnetic structures³.

Reference

[1] Petretto et al., *Sci Data* 5, 2018, 180065

[2] Smidt et al., *Phys. Rev. Res.* 2021, 3 (1), L012002.

[3] Rodríguez-Carvajal, et al., *C. R. Physique* 2019, 20, 770–802.

DS02.08.04

Accelerated Computation of Lattice Thermal Conductivity Using Neural Network Interatomic Potentials [JeongMin Choi](#)¹, Kyeongpung Lee¹, Wonseok Jeong² and Seungwu Han¹; ¹Seoul National University, Korea (the Republic of); ²Lawrence Livermore National Laboratory, United States

With the development of the density functional theory (DFT) and ever-increasing computational capacity, an accurate prediction of lattice thermal conductivity based on the Boltzmann transport theory becomes computationally feasible, contributing to a fundamental understanding of thermal conductivity as well as a choice of the optimal materials for specific applications. However, calculation of the anharmonic force constant by DFT is computationally demanding, and the cost steeply increases as the symmetry of the crystal lowers and the number of atoms in the unit cell gets larger. This difficulty has been a bottleneck in theoretical investigation of lattice thermal conductivity of vast materials. Currently, machine learning potentials are garnering attention as a computationally efficient high-fidelity model of DFT, and several studies have demonstrated that the lattice thermal conductivity could be computed accurately via the machine learning potentials. However, test materials were mostly crystals with high symmetries, and the applicability of machine learning potentials to a wide range of materials has yet to be demonstrated. Furthermore, establishing a standard training set that provides

consistent accuracy and computational efficiencies across a wide range of materials would be useful. Our study here addresses these issues by computing lattice thermal conductivities at 300 K using neural network interatomic potentials. Firstly, to select an optimal approach to generate training sets preliminary tests are conducted, and we find that molecular dynamics trajectories at 50–700 K consistently provide results at par with DFT for the test materials. Next, we increase the benchmark cases to 25 materials with diverse symmetries and a wide range of lattice thermal conductivities between 10^{-1} and $10^3 \text{ W m}^{-1} \text{ K}^{-1}$. In contrast to pure DFT approaches, the computational cost in the present approach is uniform over the test materials, yielding a speed gain of 2–10 folds. When a smaller training set is used, the relative efficiency increases by up to ~50 folds without sacrificing accuracy significantly. The current work will broaden the application scope of machine learning potentials by establishing a robust framework for accurately computing lattice thermal conductivity with machine learning potentials.

References

- [1] K. Lee, D. Yoo, W. Jeong, S. Han, *Comput. Phys. Commun.* 242 (2019) 95–103.
- [2] J. M. Choi, K. Lee, S. Kim, M. Moon, W. Jeong, S. Han, *Comput. Mater. Sci.* 211 (2022) 111472.

DS02.08.05

Towards Standardized Polymer Solubility Measurements Using a Parallel Crystallizer [Mona Amrihesari](#), Amari Murry and Blair Brettmann; Georgia Institute of Technology, United States

Recently developed machine learning approaches to understanding material properties provide new opportunities for studying and developing new knowledge about polymers. The vast application of polymers and their sensitivity to many parameters like molecular weight, temperature, morphology, etc. requires developing high throughput experimentation methods that lead to accurate results. It will be vital for developing any prediction model in data science analysis. Although polymer informatics has significantly improved in recent years, using artificial intelligence and machine learning techniques, a significant hurdle in the polymer informatics area is the lack of complete and sufficiently detailed databases. One example where this is a challenge is in developing a dataset for polymer solubility and dissolution, where the classification of “soluble” or “insoluble” is sensitive to molecular weight, concentration, temperature, heating/cooling rate, and other factors that are not always reported or well-controlled. To overcome the challenges with the current dataset on polymer solubility, in this work, we will focus on applying turbidity measurements with precise temperature control technique using a Crystal16 parallel crystallizer. With this method, the experiments are possible to do in reproducible and time-effective ways with minimal human error while also collecting time-resolved dissolution data continuously throughout the experiment. This approach with detailed results in a controllable manner allows us to develop a more information-rich data set for predicting the polymer solubility using machine learning techniques.

DS02.08.06

Hotplate Temperature Studies—On the Need to Characterize the Variability and Reproducibility of Thermal Sources [Kyle Williamson](#), Daniel Herr and Hemali Rathnayake; University of North Carolina at Greensboro, United States

This poster reports the impact of hotplate position on observed temperature and temperature variability. Reaction temperature and variability drive the observed rates and outcomes of many syntheses, such as small-scale reactions on hotplates. Yet, few studies consider whether the hotplate surface consistently and uniformly delivers a targeted reaction temperature. Control charts of five positions on two commercially available hotplates demonstrate significant temperature sensitivity and reproducibility as a function of sample placement position. These results suggest a need for the screening, characterization, and calibration of thermal sources to enhance the reproducibility and credibility of syntheses and mechanistic studies.

DS02.08.07

Development of Coarse Grained Polymer Models by Iterative Boltzmann Inversion and Cross-Entropy Optimization Methods [Wei Han Hui](#) and Shu-Wei Chang; National Taiwan University, Taiwan

Bottom-up computational modeling has been widely used to investigate the material properties of polymer matrix in present years. Molecular dynamics (MD) simulations is the powerful simulation method which could accurately describes the molecular interactions between molecules and thus provide an accurate prediction on the performance of materials. Furthermore, by training coarse grained (CG) models based on full atomistic information, an accurate CG can be developed and used for the study of larger molecular weights to bridge the scales between nanoscale and mesoscale. The CG simulations reduce the degree of freedom of MD and thus increase the time scale and length scale in simulations. To develop a CG force field of a polymer system, the Iterative Boltzmann inversion method (IBIm) is widely used. Recently, many studies have shown that machine learning and deep learning methods (ML/DL) are useful for the development of force fields. In this study, we develop a novel workflow for training CG force field by the integration of IBIm and Cross-entropy optimizer. Our results show that the structural distribution and properties of a full atomistic system are both converged in optimization. The cross-entropy optimizer is able to optimize the loss of polymer conformation and molecular properties and thus provide a suitable CG force field for polymer materials.

DS02.08.08

An Adaptive Optimization System in Multi-Scale and Multi-Objective Wing Structure Using Deep Learning Algorithms [Zilan Zhang](#)¹, Zixiao Wei¹, Francesco Di Caprio² and Grace Gu¹; ¹University of California, Berkeley, United States; ²Italian Aerospace Research Center, Italy

In the aerospace industry, wing design involves multidisciplinary considerations such as material science, aerodynamics, structural architecture, and manufacturing feasibility. The balance between these primary issues and corresponding design parameters is usually hard to achieve. Optimization is hence an essential procedure to assure maximum design efficiency. The conventional optimization method relies heavily on iterative modeling, testing, analysis, and improvement cycle. This process can be time-consuming, costly, and imprecise due to the complexity of the operative conditions. Here we propose an adaptive optimization system built upon a digitized wing structure database and machine learning algorithms, which enable the rapid formulation of multi-scale wing designs for specific performance demands. This system unfolds as two stages of work. The first stage is oriented toward aerodynamic optimization, where Computational Fluid Dynamics (CFD) simulation is exploited to attain performance outputs corresponding to an extensive collection of geometric inputs. A neural network is subsequently utilized for parametric study and finding the optimal wing configuration. The optimization has successfully improved the aerodynamic efficiency of a fixed-wing aircraft by over 4% compared to the average performance of initial geometric inputs when cruising at 0.48 Mach. The second stage work concentrates on the definition of best stacking sequences with composite materials adopted and on the wing box layout. The multi-objective optimization adapts a deep learning schema that lies upon a series of critical structural requirements, such as specific strength, shear flow, cost, margins of safety, etc. To this end, the proposed methodology aims to significantly reduce the computational cost and contribute to better flight performance. With all the merits addressed, the proposed approach will possess great potential for optimizing several aircraft's wing-like sub-components when concerned with different mission environments and load conditions.

DS02.08.09

Machine-Learning Based Prediction of First-Principles XANES Spectra for Amorphous Materials [Haruki Hirai](#), Tomoyuki Tamura, Masayuki

Karasuyama and Ryo Kobayashi; Nagoya Institute of Technology, Japan

In recent years, x-ray absorption spectroscopy (XAS) has become increasingly important for structural characterization of materials. Especially, x-ray absorption near edge structure (XANES) can provide sensitive information on chemical bonds, valence states, and coordination. Conventional interpretation of XANES spectra is based on the so-called “fingerprint” approach in which an experimental spectrum of interest is compared with that of a reference crystalline material. When there are not enough reference spectra, reliable simulations of XANES spectra are necessary. We have already added the computational code of XANES [1] to Quantum Materials Simulator (QMAS) code [2] based on the density functional theory (DFT) within the projector augmented-wave (PAW) method, and applied it to the elucidations of amorphous structures [1] and chemical reactions at interfaces [3]. However, the computational cost of XANES simulation becomes an important issue when we deal with amorphous materials.

In this study, we developed an efficient scheme based on machine learning to predict the theoretical XANES spectra obtained by DFT calculations using only the information of atomic configurations. Our scheme was based on the linear regression model of the structural descriptor. We present a comprehensive prediction of XANES spectra based on atom-centered symmetry functions (ACSF), smooth overlap of atomic positions (SOAP), local many-body tensor representation (LMBTR) and spectral neighbor analysis potential (SNAP). As a test case, we chose amorphous SiO material used as the negative electrode of rechargeable lithium-ion batteries (LIBs), in which the valence states of Si are distributed between 0 and +4. As a result, we could achieve enough prediction accuracy for Si K-edge XANES spectra. Furthermore, we proposed an efficient scheme for the compression of XANES spectral data and the efficient sampling of training data with the active learning approach.

References: [1] T. Tamura et al., Phys. Rev. B 85, 205210 (2012). [2] <http://qmas.jp> [3] T. Tamura et al., Phys. Rev. B 96, 035107 (2017).

DS02.08.11

Design of Showerheads Using Machine Learning for Optimizing Semiconductor Manufacturing Processes Daniel D. Lim¹, Zeqing Jin¹, Meenakshi Mamunuru², Sassan Roham², Xueying Zhao² and Grace Gu¹; ¹University of California, Berkeley, United States; ²LAM Research Corporation, United States

Distribution of uniform gas to the wafer through showerhead is a key technique to fabricate thin film structures for various semiconductor applications. Film thickness uniformity is a critical factor to evaluate the quality of film growth as a non-uniform film may cause a non-functioning die and hence reduce fabrication yields. During the deposition process, film uniformity is largely influenced by flow distribution, where the showerhead is one of the major components that affect the distribution. In this work, we utilize machine learning based optimization algorithms combined with computational fluid dynamics (CFD) simulations to optimize the showerhead design for uniformity of flow by varying the porosity of the faceplate component and inlet pipe structures. Our machine learning model achieves high accuracy on predictions against ground truth with an R-squared value over 99% and a speedup of orders-of-magnitude compared to CFD simulations. The performance difference of various optimization methods such as genetic algorithm, stochastic gradient descent, and Bayesian optimization are presented. Results show that our optimized showerhead design achieves over 10% improvement in film uniformity compared to a conventional showerhead design. Furthermore, sensitivity analysis is conducted to probe fundamentally the most important features that lead to high-performing showerhead designs. It is envisioned that our proposed framework is adaptive to optimize other manufacturing systems and devices that utilize fluid flow mechanisms.

DS02.08.12

CASTING – (A Continuous Action Space Tree Search for INverse desiGn) in Materials Applications Suvo Banik¹, Srilok Srinivasan², Sukriti Manna¹, Troy D. Loeffler², Henry Chan², Pierre Darancet² and Subramanian Sankaranarayanan²; ¹University of Illinois at Chicago, United States; ²Argonne National Laboratory, United States

The most common and popular methods for structure search and optimization are based on evolutionary design. This can often be cumbersome, limited to a few tens of parameters, and fails for large structural configurations or design problems with high degrees of freedom. Reinforcement learning approaches mostly operate in discrete action space such as in the Go game but the applications of that to inverse problems are limited since most inverse problems deal with continuous action space. There are many inverse structural search problems ranging from crystal structure search in material sciences to topology design in Quantum information, where it is highly desirable to optimize structure/configuration to target desired properties or functionalities. We develop CASTING as a scalable framework platform for molecular, crystal structure, defects, topology, device, and component design. We demonstrate the ability of our modified cMCTS algorithm on traditional trial functions. The predicational capability of the CASTING on crystals of 0D, 2D, 3D, polymorphs of carbon and complex system such as perovskite Nickelates. We also compare the cost and prediction performance of our CASTING framework with traditional Evolutionary algorithm-based approaches.

SESSION DS02.09: Machine Learning for Materials Structure and Properties VII

Session Chairs: Mathieu Bauchy and Grace Gu

Thursday Morning, December 1, 2022

Hynes, Level 2, Room 210

8:15 AM *DS02.09.01

Quantum Materials Research at the Nexus of Exascale Simulation, Artificial Intelligence and Quantum Computing Aiichiro Nakano; University of Southern California, United States

Computing landscape is evolving rapidly. Exascale computers have arrived, and quantum supremacy has been demonstrated for several problems, while artificial intelligence (AI) is transforming every aspect of science and engineering. Atomistic simulations at the exa-quantum-AI nexus are revolutionizing quantum materials research. I will describe research on atomically thin two-dimensional and other materials under National Science Foundation (NSF) cybermanufacturing and cybertraining projects using our AI and quantum-computing enabled exascale materials simulator (AIQ-XMaS). Specifically, I will describe excited-state neural-network quantum molecular dynamics (NNQMD) simulations trained by first-principles nonadiabatic quantum molecular dynamics (NAQMD) to prove the exciting concept of picosecond optical, electrical and mechanical control of symmetric breaking in topological ferroelectric skyrmion, skyrmionium and meron for emerging ultralow-power polar topotronics. This research was supported by NSF Future Manufacturing Program, Award 2036359, and NSF Cybertraining Program, Award 2118061. Simulations were performed at Argonne Leadership Computing Facility under DOE INCITE and Aurora Early Science programs and at Center for Advanced Research Computing of the University of Southern California.

8:45 AM DS02.09.02

Billions of Atoms with Machine Learning Interatomic Potentials—Performance Portability of FLARE [Anders Johansson](#), Yu Xie, Cameron J. Owen, Jin Soo Lim, Lixin Sun, Jonathan Vandermause and Boris Kozinsky; Harvard University, United States

Machine learning interatomic potentials (MLIPs) have become a prevalent approach to bridging the gap between slow-but-accurate ab initio calculations and fast-but-inaccurate empirical potentials for molecular dynamics. Among MLIPs, there is a pareto front of models with different tradeoffs between accuracy and speed. The FLARE interatomic potential aims to push the boundary of scalability and performance, while maintaining sufficient accuracy to study complex, reactive systems.

FLARE combines the atomic cluster expansion with a sparse Gaussian process. Bayesian uncertainties enable efficient training with active learning and uncertainty-aware, large-scale molecular dynamics simulations. We implement FLARE in LAMMPS with the Kokkos performance portability library, enabling efficient molecular dynamics simulations on GPUs across a wide range of system sizes. Using 27336 GPUs, we demonstrate state-of-the-art scaling and performance in micrometer-scale heterogeneous catalysis simulations with up to half a trillion atoms [1].

[1] arXiv:2204.12573

9:00 AM DS02.09.03

Effect of Paired Aluminum Sites on the Diffusion of $[\text{Cu}(\text{NH}_3)_2]^+$ in Cu-CHA Predicted by Machine Learning Accelerated Molecular Dynamics [Reisel Millan](#)^{1,2} and [Rafael Gomez-Bombarelli](#)¹; ¹Massachusetts Institute of Technology, United States; ²Polytechnic University of Valencia, Spain

The selective catalytic reduction (SCR) in which ammonia is used as reducing agent (NH_3 -SCR- NO_x) is the current state-of-the-art technology to cope with nitrogen oxides (NO_x) emissions from stationary power plants and diesel vehicles[1,2]. The materials currently employed as catalysts in transport applications are copper-exchanged zeolites, in particular those possessing small-pore structures such as the CHA [3,4]. Operando X-ray absorption and emission (XAS/XES) spectroscopic studies have shown that at low temperature ($T < 473$ K) ammonia liberates the Cu^+ ions from its coordination with the zeolite framework forming mobile $[\text{Cu}(\text{NH}_3)_2]^+$ species. These mobile amino-copper complexes are responsible for the activation of O_2 through the formation of the transient dimeric species $\text{Cu}(\text{NH}_3)_2 - \text{O}_2 - \text{Cu}(\text{NH}_3)_2$ [5-7]. The diffusion of the monomeric $[\text{Cu}(\text{NH}_3)_2]^+$ species to the adjacent cavity through the 8r window is the rate-determining step at low Cu loading. Previous works have shown that the reacting molecules can have a significant impact in the activation free energy and that the diffusion of such species is limited to neighboring cavities[7,8]. The aluminum distribution is another factor that possibly affects the reaction rate but so far remains unexplored[9].

The diffusion of $[\text{Cu}(\text{NH}_3)_2]^+$ complexes through the 8r windows of the CHA is an activated process and therefore the theoretical study of such diffusion requires the use of enhanced sampling techniques. However, the construction of free energy profiles based on DFT is limited to the most relevant cases because of the significant computational cost of umbrella sampling simulations. Machine learning (ML) techniques have already taken special relevance in the area of materials science and heterogeneous catalysis. These techniques provide an opportunity to speed up the costly Born-Oppenheimer molecular dynamics (BOMD) simulations by several orders of magnitude [10]. NN-based interatomic potentials (NNIPs) retain the accuracy of the ab initio training data and can be executed at a computational cost comparable with that of classical force fields.

In this work, we applied NNIPs-based enhanced umbrella sampling (US) simulations to obtain Gibbs free energy profiles for the diffusion of $[\text{Cu}(\text{NH}_3)_2]^+$ complexes through the 8-ring windows of SSZ-13 zeolite for different Al distributions at 423 K representative of the low temperature regime. All interatomic potentials converted to sub-kcal mol^{-1} accuracy for the energies on the corresponding validation set, with a mean absolute error of 0.34 kcal/mol, respectively. The NNIPs are able to reproduce the free energy profiles with an error of 0.4 kcal/mol relative to the DFT counterpart (see Figure 1), at least 400 times faster. The calculated free energy of activation for the diffusion of an isolated $[\text{Cu}(\text{NH}_3)_2]^+$ complex through the 8-ring windows of the chabazite structure is relatively low, 4.3 kcal/mol, showing that this process is fast. An increase in the free energy of activation to 6.7 kcal/mol is observed when a second complex and therefore a second Al are placed in the adjacent cavity (Figure 2). However, when the two Al atoms are placed in the same 8r, through which the diffusion takes place, the free energy of activation decreases by ~ 1.7 kcal/mol (Figure 2), with which the reaction would proceed ~ 10 times faster. Our results show that a fine tuning of the Cu-CHA catalyst can be achieved by controlling the Al distribution, that is, the selective positioning of Al pairs in the same 8-ring window.

9:15 AM DS02.09.05

Going Beyond High Throughput Screening Towards AI in Accelerated Electrolyte Discovery [Vidushi Sharma](#), Maxwell Giammona, Dmitry Zubarev, Tim Erdmann, Andy Tek, Khanh Nguyen and Young-Hye Na; IBM, United States

Discovery of new materials is the key to bringing timely advancements and major breakthrough in the developing technologies. Development of sustainable next generation fast charging batteries for electric vehicles (EV) need a step-forward towards the discovery of non-flammable liquid battery electrolytes. Primary electrolyte systems commonly used for lithium metal batteries are based on ether solvents comprising of 1,2-dimethoxyethane (DME) and a cosolvent 1,3-dioxolane (DOL), both of which are highly flammable. The search and development of sustainable electrolyte formulations for the batteries require collaborative efforts from the disciplines of chemistry, material science and computational simulations. Widely adopted high-throughput screening process for electrolyte discovery involves computational simulations of large set of molecules and screening based on domain intuitive properties. This process manages to accelerate the discovery of new compounds for electrolytes but, the high performance of an electrolyte in a battery goes beyond the sum of the individual compounds. It relies on the complex interactions of those constituent compounds that lead to new, emerging properties of the whole, i.e. the electrolyte *formulation*. There remain significant questions as to how to relate the properties of the individual electrolyte compounds to that of whole; finding the right formulation based on those screened new compounds; and predicting performance of the formulation that contains those compounds as well as their stability over versus the electrodes in a full cell. Artificial Intelligence (AI) methodologies built upon high throughput screening process can expedite the discovery and optimization of both new electrolytes molecules *and* electrolyte formulations which contain them. In this talk, we discuss the synergy of high throughput screening and AI methodologies based on graph theory and inverse design in accelerating the process of electrolyte discovery and formulation optimization. To do this, we apply automated simulation workflows capable of simulating multiple molecular properties such as redox potential and stability, and provide in-silico characterization of the interface chemistries at the electrodes on the fly. Post this, surrogate models built on graph theories establish a structure-composition-performance relationship for the new-found electrolyte formulations and enable the search for electrolyte systems with highest capacity retention and long cycle life.

9:30 AM DS02.09.06

Enzeptional—Enzyme Optimization via a Generative Language Modeling-Based Evolutionary Algorithm [Yves Gaetan Nana Teukam](#)^{1,2}, Matteo Manica¹, Francesca Grisoni² and Teodoro Laino¹; ¹IBM Research Europe - Zurich, Switzerland; ²Technische Universiteit Eindhoven, Netherlands

Enzymes are molecular machines optimized by nature to allow otherwise impossible chemical processes to occur. Besides the increased reaction rates, they present remarkable characteristics to enable more sustainable reactions: mild conditions, less toxic solvents, and reduced waste. Billion years of evolution have made enzymes extremely efficient. However wide adoption in industrial processes requires faster design using in-silico methodologies, a daunting

task far from being solved. The majority of methods operate by introducing mutations in an existing amino acid (AA) sequence using a variety of assumptions and strategies to introduce variants in the original sequence. More recently, machine learning and deep generative networks have gained popularity in the field of protein engineering by leveraging prior knowledge on protein binders, their physicochemical properties, or the 3D structure. Here, we cast the problem of enzyme optimization as an evolutionary algorithm where mutations are modeled via a generalized autoregressive language model trained on fragments of AA sequences from UniProtKB. Relying on a pre-trained language model, we apply transfer learning and train a Random Forest as the scoring model on a dataset of biocatalysed chemical reactions to drive the optimization process. With our approach, using the least amount of assumptions, we can adapt active sites to perform new reactions. Our methodology allows designing enzymes with higher predicted biocatalytic activity, emulating the evolutionary process occurring in nature by sampling optimal sequences modeling the underlying proteomic language.

9:45 AM BREAK

10:15 AM *DS02.09.07

Determining the Phase Diagram of a Machine-Learned Carbon Potential via Nested Sampling [George A. Marchant](#) and Livia Bartok-Partay; University of Warwick, United Kingdom

We detail how the many-body potential energy landscape of a machine-learned (ML) interatomic potential for carbon [1] can be explored by utilising the nested sampling algorithm,[2] allowing for the determination of carbon's phase diagram up to high pressures. The ML potential in question is the GAP-20 model, which was developed in recent years using the gaussian approximation potential methodology to describe the properties of bulk crystalline and amorphous carbon phases with the accuracy of electronic structure methods. With the nested sampling algorithm the 3N-dimensional potential energy surface of the GAP-20 potential can be automatically (and efficiently) sampled at constant pressure, providing a set of configurations with which to test the potential's thermodynamic capabilities. As a point of comparison the phase diagrams of other interatomic potentials - including the ReaxFF, EDIP and Tersoff potentials - are also studied. Despite having been trained on optimised structures at only zero pressure, GAP-20 provides an accurate description of carbon's macroscopic properties up to approximately 200 GPa. Our results also highlight areas for future improvement of the potential.

[1] Rowe P, Deringer VL, Gasparotto P, Csányi G, Michaelides A. An accurate and transferable machine learning potential for carbon. *J Chem Phys.* 2020 Jul 21;153(3):034702.

[2] Pártay LB, Bartók AP, Csányi G. Efficient Sampling of Atomic Configurational Spaces. *J Phys Chem B.* 2010 Aug 19;114(32):10502–12.

10:45 AM DS02.09.08

Htpmd—A Cloud Platform for Automated Analysis of Raw Simulation Data for Polymer Electrolytes Tian Xie¹, Ha-Kyung Kwon², Daniel Schweigert², Sheng Gong¹, Arthur France-Lanord³, Arash Khajeh², Emily J. Crabb¹, Michael Puzon², Chris Fajardo², Will Powelson², Yang Shao-Horn¹ and Jeffrey Grossman¹; ¹Massachusetts Institute of Technology, United States; ²Toyota Research Institute, United States; ³Sorbonne Université, France

Open material databases storing hundreds of thousands of material structures and their corresponding properties have become the cornerstone of modern computational materials science. Yet, the raw outputs of the simulations, such as the trajectories from molecular dynamics simulations and charge densities from density functional theory calculations, are generally not shared due to their huge size. In this work, we provide a cloud-based platform to facilitate sharing of raw data and enable fast post-processing in the cloud to extract new properties defined by the user. As an initial demonstration, our current database includes 6286 molecular dynamics trajectories for amorphous polymer electrolytes and 5.7 terabytes of data. We create a public analysis library at https://github.com/TRI-AMDD/htp_md to extract multiple properties from the raw data, using both expert-designed functions and machine learning models. The analysis is run automatically with computation in the cloud, and results then populate a database that can be accessed publicly. Our platform encourages users to contribute both new trajectory data and analysis functions via public interfaces, and newly analyzed properties will be incorporated into the database. Finally, we create a front-end user interface at <https://www.htpmd.matr.io> for browsing and visualization of our data. We hope the platform provides a new way of raw data sharing for the computational materials science community.

11:00 AM DS02.09.09

Identifying Symmetries with Deep Learning Model [Yichen Guo](#)¹, Shuyu Qin¹, Xinqiao Zhang² and Joshua Agar²; ¹Lehigh University, United States; ²Drexel University, United States

Scientific discoveries rely on extracting understanding from experiment results; however, data collected regularly outpaces human analysis capabilities. In turn, it is common to use computational methods to extract actionable information from scientific data. A fundamental problem with computational methods are that they are bounded by logical rules and thus cannot apply generalized concepts and sentiment. In materials physics, symmetry is one of the most pervasive predictors of structure-property relations. Human identification of symmetry can be time-consuming, inaccurate, and cannot be done at scale. It is essential to create models that can understand this concept. Here, we develop datasets, benchmarks, and DL workflow to classify wallpaper group symmetry.

First, we developed three image datasets based on the 17 wallpaper group symmetries. These datasets are generated by forming symmetry operations on sections of images from the ImageNet dataset, randomly generated noise and artificial atomically resolved images. We apply a Gaussian noise to mimic real data. These datasets with generation metadata provide a predictable benchmark to validate the efficacy of machine learning models. We benchmarked the performance of the deep learning model to identify the symmetries of our three datasets. We trained the ResNet34 model and VGG-19 model with two training strategies: transfer learning and training from random initialization. Results show that current deep learning models can classify images with different symmetry classes with 99.38% accuracy (ResNet34 transfer learning). While, at first pass, it might seem that these models are learning a generalized concept for symmetry, this is a farce. If we cross-validate the performance of a model with a dataset of a different type, the accuracy is only slightly better than a random guess. This highlights challenges in deploying generalized machine learning models for scientific inference, particularly when limited access to training data. As a first step, we demonstrate few-shot learning using neural networks that have symmetry awareness by being pre-trained on symmetry datasets of other forms. The model achieves a 7.55% error rate when trained on 50 images per class dataset, as accurate as models trained on 1000 images per class dataset.

While adding transformations such as Fast Fourier and Radon does not significantly improve the model performance, we achieved marked improvements by adding symmetry-constrained layers. We developed a customized preprocess layer with the ability to detect 2-, 3-, and 4-folds rotation, mirror, and glide transformation. To better test the performance and limitation of this transformation layer, we designed stepwise training experiments to classify the 2-, 3-, and 4-folds rotation and mirror transformed 2D images. The training accuracy improved compared benchmark result only when we preprocess manually defined image region. Compared to the 47.6% accuracy for the P1, P2, and Pm symmetry dataset trained from scratch with the ResNet34 model, the preprocessed dataset gives 85% accuracy. Improvement in cross-entropy accuracy proves that the preprocessing layer can detect the 2-folds and mirror transformation. Still, more effort is required to parsimoniously learn symmetry with neural networks.

All told, we demonstrate the nuanced challenges of designing and benchmarking machine learning models for detecting symmetry. We show that machine learning models can readily give the illusion of solving a benchmark task without actually learning any physically relevant concepts. This work

demonstrates the importance of including physics constraints in machine learning models to improve performance. Developing a model capable of parsimoniously detecting symmetry in the image will tremendously impact crystallographic and microstructural analysis – and could be pipelined into other machine learning models for materials discovery and design.

11:15 AM DS02.09.10

Synthetic Scanning Electron Micrographs Created by Generative Adversarial Networks (GANs) from Artificial Height Maps [Jonas Bals](#)¹ and [Matthias Epple](#)^{1,2}; ¹University of Duisburg-Essen, Germany; ²CeNIDE - Center for Nanointegration Duisburg-Essen, Germany

Scanning electron microscopy (SEM) is a standard method in the morphological analysis of materials, from the nanometer to the centimeter scale. An automated analysis of SEM images helps to save time and also reduces the operator bias when it comes to extract sample parameters like average particle size, particle size distribution, and diversity of particle shapes.

Deep learning and especially deep convolutional neural networks (CNNs) have entered materials science, contributing to image segmentation [1], image classification [2], and object detection [3]. However, a successful training of such machine learning approaches requires a large number of manually annotated training images. Their manual analysis can be extremely time consuming as human evaluators are needed.

The 3D graphics software Blender 3.1.2 [4] was used for artificial image creation, assembling several thousand objects to obtain heightmaps and error-free binary annotation maps. In a second step, we trained a generative adversarial network (GAN) [5] to create a variety of photorealistic SEM images of nanoparticles from these heightmaps.

We have prepared synthetic SEM images as training data by a combination of Blender and GANs. We have first created artificial heightmaps by simulating the dropping of several thousand objects (“nanoparticles”) onto a planar surface with Blender. These objects were typical nanoparticles like spheres, deformed spheres, cubes and truncated cubes, hexagonal plates, rods, or star-shaped particles. The hereby created annotation maps as well as height maps have been used to train two networks. First a GAN to create artificial SEM images, and second a UNet model trained completely on artificial SEM images and binary annotation maps [1]. UNet was then validated against human labelled real data reaching an IoU of 81.7%. This still underperforms human labelled data by 11.76 points. Our method builds on the previously published GAN of [6] and outperforms their annotation map approach by 0.69 points. Notably, we found that a major obstacle to obtain better training data is the addition of the “right amount” of noise to an image created by the GAN. This will require further refinements of the method.

In conclusion, synthetic SEM images prepared by Blender and GANs can be used to create large training data sets for automated analysis of SEM images by machine learning.

[1] Ronneberger, O., Fischer, P., & Brox, T. (2015). In: Navab, N. et al. (Eds.): MICCAI 2015, 234-241

[2] He, K., Zhang, X., Ren, S., & Sun, J. (2016). In: Proceedings of the IEEE CVPR 2016, 770-778

[3] Ren, S., He, K., Girshick, R., Sun, J. (2015). In: Proceedings of the NIPS 2015

[4] Blender Online Community. (2018). <http://www.blender.org>, Last visited: 06.05.2022 11:03

[5] Goodfellow, I., Pouget-Abadie, J., Mirza, M., Xu, B., Warde-Farley, D., Ozair, S., Bengio, Y. (2014)., Proceedings of the NIPS 2014

[6] Rühle, B., Krumrey, J. F., & Hodoroba, V.-D. (2021). Scientific Reports, 11, 4942

SESSION DS02.10: Machine Learning for Materials Structure and Properties VIII

Session Chairs: Mathieu Bauchy and Ekin Dogus Cubuk

Thursday Afternoon, December 1, 2022

Hynes, Level 2, Room 210

1:30 PM *DS02.10.01

Tailoring Molecular Topology to Control the Mechanical Properties of Polymer-Grafted Nanoparticle Assemblies [Sinan Keten](#); Northwestern University, United States

In this talk, I will summarize recent advances in computational design of new polymeric materials that make use of nanoscale topologies, namely brushes and folded loops, that result in exceptional mechanical properties. I will first present systematic coarse-graining and machine-learning approaches that we developed describe molecular and mesoscale mechanics of polymer-grafted nanoparticle systems. Following this, I will present strategies for achieving impact tolerance in soft materials. The first strategy involves the use of star polymers and polymer grafted nanoparticles to improve diametric mechanical properties such as modulus and toughness, while also changing the time-dependence of the mechanical response. The second strategy involves creating nanoparticle interfaces with looped tethers that take inspiration from catch bonds in biological adhesion proteins, which results in molecular seat-belt type interfaces that self-strengthen at high strain rates like shear-thickening fluids. I will conclude with some thoughts on how to translate these theoretical findings to new material concepts that could be explored further with synergistic experiments and simulations.

2:00 PM *DS02.10.02

A Free Energy-Based Framework for Scale Bridging in Crystalline Solids—With Some Use of Machine Learning Methods [Krishna R. Garikipati](#); University of Michigan, United States

The free energy plays a fundamental role in theories of phase transformations and microstructural evolution in crystalline solids. It encodes the thermodynamic coupling between mechanics and chemistry within continuum descriptions of non-equilibrium materials phenomena. In mechano-chemically interacting materials systems, consideration of compositions, order parameters and strains results in a high-dimensional free energy density function. Since its origins lie in the electronic structure, a rigorous representation of the free energy presents a framework for scale bridging in solids. In this study we have been exploring such a framework, while developing practical machine learning methods to contend with high dimensionality and efficient sampling. We have developed integrable deep neural networks (IDNNs) that are trained to free energy derivative data generated by statistical mechanics simulations. The latter are based on cluster Hamiltonians, themselves trained on density functional theory calculations. The IDNNs can be analytically integrated to recover a free energy density function. We combine the IDNNs with active learning workflows for well-distributed sampling of the free energy derivative data in high-dimensional input spaces. This enables scale bridging between first-principles statistical mechanics and continuum phase field models. As prototypical material systems we focus on applications in Ni-Al alloys and in the battery cathode material: Li_xCoO_2 .

2:30 PM DS02.10.04

Graph Recommender System for Ionic Substitution—Discovering New Materials [Elton Ogoshi de Melo](#) and Gustavo Dalpian; UFABC, Brazil

Traditional chemical heuristics have been very important for discovering new inorganic compounds in the past, but as they are usually based on patterns observed on a limited or specific set of materials, they are not generalizable as once thought. Today, as the material scientist can access the data of hundreds of thousands of inorganic materials present in databases, it has become frequent that many Material Science projects have become data-driven, i.e., they use large amounts of materials data and statistical methods, such as Machine Learning, to uncover new patterns and explore the phase space of compounds. In the ML context, recommender systems are widely used in various scientific and nonscientific fields. For instance, in the e-commerce area, these systems recommend users new products by analyzing their past purchased products or by collaborative filtering: a system where a heterogeneous network/graph composed of users and items and their interactions is used as input to recommend new products to users. By using this same principle framework and OQMD's database, we were able to build an analogous graph with the elements in the periodic table together with the set of all described crystal structures' sites as two classes of entities. The relationships between the two classes are given by the occupancy of a site by an element and it is weighted by the compound's thermodynamic stability. The heterogeneous graph is used to build an embedding space with a vector representation for each entity (elements and sites). These vector representations were then used as input to model a recommender system. In addition to finding new materials by uncovering new element-site occupancies, we were also able to analyze the embedding space and find interesting patterns on chemical similarities between elements and the local geometry of sites.

2:45 PM BREAK

3:15 PM DS02.10.05

Machine Learning for Metal Processing Dierk R. Raabe, Jaber Mianroodi and Nima Siboni; Max Planck Institute for Iron Research, Germany

We propose applications based on the use of a deep neural network as fast surrogate models for local stress calculations in inhomogeneous non-linear materials. We show that deep neural networks can predict the local stresses with <4% mean absolute error for the case of heterogeneous elastic media and a mechanical contrast of up to factor of 1.5 among neighboring material domains, while performing 2 orders of times faster than spectral solvers or finite element solvers. Deep neural network models prove suited for reproducing the stress distribution in geometries different from those used for training. In the case of elasto-plastic materials with up to 4 times mechanical contrast in yield stress among adjacent regions, the trained model simulates the micromechanics with an error <7% in one single forward evaluation of the network, without any iteration. The results reveal an efficient approach to solve non-linear mechanical problems, with an acceleration up to a factor of nearly four orders of magnitude for elastic-plastic materials compared to conventional solvers (1). We also show similar applications of the case of heat treatment of metals.

(1) Mianroodi, J.R., H. Siboni, N. & Raabe, D. Teaching solid mechanics to artificial intelligence—a fast solver for heterogeneous materials. *npj Comput Mater* 7, 99 (2021).

3:30 PM DS02.10.06

Improving the Robustness of Deep Learning Interatomic Potentials for Molecular Dynamics Albert Musaelian¹, Simon L. Batzner¹, Nicola Molinari¹ and Boris Kozinsky^{1,2}; ¹Harvard University, United States; ²Robert Bosch LLC Research and Technology Center, United States

Machine learning interatomic potentials promise to make large length- and time-scales accessible to atomistic simulations by approximating the potential energy surface from expensive quantum chemical methods. As in other machine learning problems, the central task is to develop models that learn to generalize in a robust manner beyond the data they were trained on. This challenge is even more pressing for molecular dynamics: incorrect force predictions on even a very small number of atoms in an equally small percentage of time steps can lead the system into unphysical configurations and result in unfaithful dynamics and simulation failure. The recent development of $E(3)$ -equivariant models, exemplified by our NequIP [1] and Allegro [2] architectures, has led to significant demonstrated improvements in accuracy and generalization even with small training sets. In this talk, we will discuss recent efforts to improve the robustness of the accurate simulations NequIP and Allegro can drive at scale.

[1] Batzner, S., Musaelian, A., Sun, L. et al. $E(3)$ -equivariant graph neural networks for data-efficient and accurate interatomic potentials. *Nat Commun* 13, 2453 (2022).

[2] Musaelian, A. and Batzner, S., et. al. Learning Local Equivariant Representations for Large-Scale Atomistic Dynamics. arXiv:2204.05249

3:45 PM DS02.10.07

Voxelized Atomic Structure Framework for Developing Structure-Property Relationships from Density Functional Theory Calculations Matthew C. Barry¹, Michael Chandross², Kristopher E. Wise³, Surya R. Kalidindi¹ and Satish Kumar¹; ¹Georgia Institute of Technology, United States; ²Sandia National Laboratories, United States; ³NASA Langley Research Center, United States

The behavior of material systems is governed by complex physical phenomena taking place over a hierarchy of length scales, making it computationally infeasible to model the full material response with physics-driven simulation methods alone. Machine learning approaches offer new opportunities to efficiently learn the underlying structure-property relationships in material systems using low-computational cost surrogate models trained on expensive physics-based computations. In this talk, we present a comprehensive framework for formulating physics-based, high-fidelity reduced-order material structure-property relationships using density functional theory computations. In this framework, the charge density field is directly utilized as the definition of atomic structure. This provides a complete, purely physics-based definition of the atomic structure that does not require any *ad hoc* feature engineering or idealizations beyond those of the first-principles computations. The spatial features underlying the atomic structure that dictate the physics underlying the material response are then captured by the directionally resolved two-point spatial correlations of the charge density field, projected to a salient low-dimensional feature-space using principal component analysis and correlated to physical properties using Gaussian process regression (GPR). An active learning strategy based on Bayesian experiment design is implemented using the uncertainty quantification provided by GPR to minimize the number of computationally expensive physics simulations required for model training. We utilize this framework to elucidate physical insight into the relationship between chemical composition and bulk modulus in high entropy alloys.

4:00 PM DS02.10.08

DyFraNet—Predicting Fracture Dynamics in Crystalline Solids Using a 2D to 3D Deep Neural Network Yu-Chuan Hsu and Markus J. Buehler; Massachusetts Institute of Technology, United States

We present a novel deep neural network, DyFraNet, to learn from dynamic fracture behaviors in crystalline solids to identify a complete history of fracture propagation. This model can not only forecast future fracture processes but also backcast to elucidate the past fracture history by providing the outcome of a fracture event, from which the model will show what will happen or has happened that led to this failure state. We also show that DyFraNet can capture dynamic fracture mechanics by accurately predicting how cracks develop over time and implying when cracks become unstable. Furthermore, we then use GradCAM to interpret how DyFraNet perceives the relationship between geometric conditions and fracture mechanics and we find DyFraNet pays attention to different areas at different stages during a fracture event. Overall, this approach has great potential to accelerate the exploration of material

design against fracture failures and can be beneficially adapted for different kinds of dynamical engineering problems.

4:15 PM DS02.10.09

A Molecular Dynamics and Machine Learning Approach to Predicting SARS-CoV-2 Spike Protein Denaturation at Varying Temperature and pH Levels Evan Xie¹, Ayush S. Arora², Anya Vaish³, Ziyuan Niu⁴, Peng Zhang⁴, Miriam Rafailovich⁴ and Yuefan Deng⁴; ¹The Pingry School, United States; ²Munster High School, United States; ³Tesla STEM High School, United States; ⁴Stony Brook University, The State University of New York, United States

The SARS-CoV-2 virus has spread globally, causing rapid technological innovation and research on the virus's spike protein (S-protein)^[1]. The viral infection is initiated when the S-protein binds to the human ACE2 receptor^[2]. Understanding the denaturation of the S-protein under various environmental conditions is essential to understanding the virus's infectivity and developing more effective methods of combatting it. Molecular dynamics (MD) simulations can precisely model the S-protein and its structural changes. Previously, these simulations examined only the effect of temperature on S-protein structure^[3]. This project examines both temperature (3°C, 20°C, and 37°C) and pH (pH1, pH2, pH3, pH4, and pH5) and utilizes a novel neural network component to analyze their effects on the protein's root mean squared deviation (RMSD).

The MD simulation is achieved on the open-source Gromacs and the AiMOS supercomputer configured with IBM POWER9 processors and NVIDIA Volta V100 GPUs. The initial structure of the S-protein is 6VXX.pdb, and the force field is the CHARMM27. The TIP3P water box is 21×21×21 nm³ with periodic boundary conditions in all three Carstensen dimensions, and simulations are controlled by the canonical (NVT). The pH values are controlled by the protonation states of the residues in the S-protein following the PROPKA. Charge neutralization and the protonation state accuracy are achieved by adding the Na⁺ or Cl⁻ ions to the solvent.

A weighted K-Nearest Neighbors model, a random forest model, and a neural network were optimized to predict the S-protein RMSD at any temperature and pH. The simulation outputs were processed into training data through averaging, truncating, denoising, and sampling. With this training data, the model predicted the RMSD at each timestep and combined these predictions to predict the entire RMSD vs. time curve. Each model was evaluated with the root mean squared error (RMSE) metric and five-fold cross-validation.

The S-protein conformational changes were measured by the backbone RMSD. (1) The RMSDs of pH3-pH5 were around 0.4 nm at all three temperatures. (2) The pH2 RMSD, as a transition, showed a gap between 37°C and 20°C. The RMSD of 3°C and 20°C increased slightly, while the RMSD of 37°C increased significantly to 0.58 nm. (3) For pH1, the RMSDs of all three temperatures reached around 0.58nm.

The neural network achieved an RMSE of 0.041nm, which was lower than the KNN's RMSE of 0.048nm and the random forest's RMSE of 0.070nm. Another advantage of the neural network was its ability to model a fully continuous function, whereas the KNN and random forest had clusters of input values where they predicted the same RMSD. As the best model, the neural network was used to predict the S-protein's RMSD from 3°C to 37°C and pH 1 to 5, and it illustrated a clear trend that structural change increases as temperature increases and pH decreases.

Further research will involve the adaptation of the MD simulation and machine learning model to other structural metrics for additional insight into S-protein denaturation.

The project is supported by the Stony Brook Garcia Center for Materials Research, the Garcia High School Program, and the Morin Charitable Trust.

[1] Lee, Y., Ng, M., Daniel, K. *et al.* Rapid growth in the COVID-19 era. *MRS Bulletin* **46**, 847–853 (2021). <https://doi.org/10.1557/s43577-021-00185-2>

[2] Kolel-Veetil, M., Sen, A. & Buehler, M.J. Surface adhesion of viruses and bacteria: Defend only and/or *vibrationally* extinguish also?! A perspective. *MRS Advances* **6**, 355–361 (2021). <https://doi.org/10.1557/s43580-021-00079-0>

[3] Liang, D., Song, M., Niu, Z. *et al.* Supervised machine learning approach to molecular dynamics forecast of SARS-CoV-2 spike glycoproteins at varying temperatures. *MRS Advances* **6**, 362–367 (2021). <https://doi.org/10.1557/s43580-021-00021-4>

SESSION DS02.11: Machine Learning for Materials Structures and Properties IX

Session Chairs: Mathieu Bauchy and N M Anoop Krishnan

Friday Morning, December 2, 2022

Hynes, Level 2, Room 210

8:30 AM DS02.11.01

Atomic Structure Generation from Structural Fingerprints Victor Fung^{1,2}; ¹Georgia Institute of Technology, United States; ²Oak Ridge National Laboratory, United States

Data-driven machine learning methods have the potential to dramatically accelerate the rate materials design over conventional human-guided approaches. These methods would help identify or, in the case of generative models, even create novel crystal structures of materials with a set of specified functional properties to then be synthesized or isolated in the laboratory. For crystal structure generation, a key bottleneck lies in developing suitable atomic structure fingerprints or representations for the machine learning model, analogous to the graph-based or SMILES representations used in molecular generation. However, finding data-efficient representations invariant to translations, rotations, and permutations, while remaining invertible to the Cartesian atomic coordinates remains an ongoing challenge. Here, we propose an alternative approach to this problem by taking existing non-invertible representations with the desired invariances and developing a method to reconstruct the atomic coordinates through a global optimization scheme. This can then be coupled to a generative machine learning model which generates new materials within the representation space, rather than in the data-inefficient Cartesian space. In this work, we demonstrate this approach by using conditional variational autoencoders to generate representations from atom-centered symmetry functions, which are then reconstructed to their corresponding atomic positions using the developed optimization method. We are able to successfully generate novel and valid atomic structures of sub-nanometer Pt nanoparticles as a proof of concept. Furthermore, this method can be extended to any suitable structural representation, thereby providing a powerful, generalizable approach towards structure-based generation.

8:45 AM DS02.11.02

Predicting Stable Electron-Exact Clathrate Superstructures via Convolutional Neural Network Frank T. Cerasoli¹, Philip Yox², Kirill Kovnir² and Davide Donadio¹; ¹University of California, Davis, United States; ²Iowa State University of Science and Technology, United States

Clathrate structures consist of nanometer-size polyhedral cages encapsulating guest atoms or molecules that are not directionally bonded to the framework. Compounds in this class of crystal structure have already demonstrated many unique properties, such as ultra-low thermal conductivity and superconductivity. Enforcing electron-balanced compositions, with an average of four electrons per framework site, results in a semiconducting electronic structure and offers utility in electronic devices. To date, only a handful of stable electroneutral tetrel-free clathrates are known, most as ordered superstructures up to eight times larger in volume than the type-I clathrate unit. In this work, new clathrate compounds are predicted computationally and experimentally verified through synthesis. The group III-V A8T27Pn19 clathrate family ($A = \{\text{Na, K, Cs, Rb}\}$, $T = \{\text{Al, Ga, In}\}$, $\text{Pn} = \{\text{P, As, Sb, Bi}\}$) is studied comprehensively with density functional theory (DFT). A crystal graph convolutional neural network (CGCNN) model is trained on the computed clathrates and roughly 500 compounds of similar composition. The model is refined by the results of experimental synthesis and employed to discover other electron-exact superstructures composed from group III-V or II-VI elements.

9:00 AM DS02.11.03

A Physics-Informed Machine Learning Model for Polymer Melt Viscosity [Ayush Jain](#), Arunkumar Rajan and Rampi Ramprasad; Georgia Institute of Technology, United States

Polymer-melt processing is highly dependent on the rheological properties of a given polymer, including melt viscosity. For novel polymers and processes to be industrially viable, the in-situ viscosity must be appropriate for the given application. This viscosity is dependent not only on the polymer identity, but also on the molecular weight (or polydispersity), induced shear rate, and processing temperature. Though phenomenological relationships, motivated by known underlying physics are commonly used to relate these environmental factors to the viscosity, such relationships involve empirical constants obtained by fitting measurements to the phenomenological equations. Predictions of viscosity for new cases are thus generally difficult due to the unavailability of the empirical parameters. Here, we adopt a data-driven approach, with or without physical equation augmentation to predict a set of machine learned models to predict the melt viscosity of polymers as a function of molecular weight, shear rate, and temperature. Our ML models were trained on a data set of 1903 melt-viscosity values pertaining to 93 distinct polymers. Two models, one based on Gaussian-Process Regression (GPR) and the second on Artificial Neural Network (ANN) were first employed, devoid of any physical equation, and trained on the melt-viscosity dataset. Next, we created a HyperNetwork architecture that encodes the known viscosity equations. All three models are critically evaluated to determine the limits of the models with no encoded physics and the extrapolative capabilities of the physics-informed model.

9:15 AM DS02.11.04

Sampling the Thermodynamics of Material Interfaces with Markov Chain Monte Carlo and Machine Learning [Xiaochen Du](#), James K. Damewood, Jaclyn Lunger and Rafael Gomez-Bombarelli; Massachusetts Institute of Technology, United States

Material surfaces often differ significantly from the bulk in both structure and composition. Surface structures depend on temperature, the presence of external chemical potentials (oxygen, hydrogen, water) and applied electrical potential. These surface reconstructions are key because they control the performance of the surface in processes like electrochemistry in batteries, electrocatalysis in fuel cells, adsorption on sensors, etc. While electronic structure simulations can accurately predict the energy of a single surface configuration, they are too expensive to investigate all the possible geometrical and compositional transformations that surfaces can undergo. In order to create accurate models of surfaces that can relate surface composition and structure to external conditions, it is necessary to efficiently sample the thermodynamic distributions of states the surface can access. To this end, we propose integrating Markov Chain Monte Carlo (MCMC) sampling with neural network potentials (NNP) trained on electronic simulations data. We demonstrate the validity of our MCMC model with discrete adsorption sites on the well-known Au(110) missing-row reconstruction. Next, as we show in the GaN(0001) surface reconstruction, adding in continuous relaxation leads to better sampling when the atomic spacing changes near the surface. Finally, we evaluated the effectiveness of our combined MCMC-NNP approach on complex oxide surfaces of the SrTiO₃ perovskite.

9:30 AM DS02.11.05

Fast and Accurate Prediction of Polymer Rheology: Multi-Scale Simulation and Physics-Inspired Machine Learning [Umi Yamamoto](#)¹, Heyi Liang², Kenji Yoshimoto¹, Masahiro Kitabata¹ and Juan J. de Pablo²; ¹Toray Industries, Inc., Japan; ²The University of Chicago, United States

We report two latest advances in enabling fast and accurate prediction of polymer rheology using a bottom-up multi-scale simulation method and a top-down machine-learning approach.

First, a multi-scale simulation method is presented for the prediction of the viscoelastic properties of entangled homopolymer melts. Starting from an atomistic model of a polymer, and introducing two coarser representations (a bead-spring model and a slip-spring model) that successively operate at longer time and length scales, we demonstrate that linear rheology of syndiotactic and atactic polystyrene melts is predicted in good agreement with experiments without requiring experimental parameters as input. Very recently, the same method is applied to another industrial polymer, Nylon 6, leading to reasonable agreement for the molecular-weight dependence of the melt viscosity.

Second, we present a machine-learning framework to construct a predictive model for the dynamic moduli of linear entangled homopolymer. As an initial attempt, using computationally generated data based on Likhthman-McLeish model as a training dataset, it is shown that a straightforward supervised learning with standard algorithms (support vector machine, kernel ridge regression, etc.) provides not-too-bad prediction when an input parameter, the number of entanglements in the present case, is extrapolated. However, the predictive power is non-trivially improved by introducing a polymer physics idea into the learning procedure. Namely, by constructing individual predictive models that specialize in the prediction of distinct relaxation behavior at short, intermediate and long-time scale, and merging them into a single model using a frequency-dependent ensemble method, we are able to predict the storage and loss modulus in quantitative agreement with the training data. This approach is expected to be applicable to more complicated cases where a wider variety of input parameters, e.g. monomer chemical structures, polymer architectures, molecular weight distributions, etc. enter.

Finally, integration of the above two approaches, i.e. generation of polymer rheology data using the multi-scale simulation and construction of accurate predictive models by machine-learning the simulation data, leads to an "ideal" framework where a fast and accurate predictive model for the polymer dynamic moduli can be established via purely in-silico techniques. We will discuss an outlook and latest progress on this front.

9:45 AM BREAK

10:15 AM DS02.11.06

Discovery of Multi-Functional Polyimides through High-Throughput Screening Using Explainable Machine Learning [Lei Tao](#)¹, [Jinlong He](#)¹, [Vikas Varshney](#)², [Wei Chen](#)³ and [Ying Li](#)⁴; ¹University of Connecticut, United States; ²Air Force Research Laboratory, United States; ³Northwestern University, United States; ⁴University of Wisconsin–Madison, United States

Polyimides have been widely used in modern industries because of their excellent mechanical and thermal properties, e.g., high-temperature fuel cells, displays, and aerospace composites. However, it usually takes decades of experimental efforts to develop a successful product. Aiming to expedite the discovery of high-performance polyimides, we utilize computational methods of machine learning (ML) techniques and molecular dynamics (MD)

simulations. We first build a comprehensive library of more than 8 million hypothetical polyimides based on the polycondensation of existing dianhydride and diamine/diisocyanate molecules. Then we establish multiple ML models for thermal and mechanical properties of polyimides based on their experimentally reported values, including glass transition temperature, Young's modulus, and tensile yield strength. The obtained ML models demonstrate excellent predictive performance to identify the key chemical substructures influencing the thermal and mechanical properties of polyimides. The use of explainable machine learning describes the effect of chemical substructures on individual properties, from which human experts can understand the cause of the ML model decision. Applying the well-trained ML models, we obtain property predictions of the 8 million hypothetical polyimides. In such way, we search the whole hypothetical dataset and identify three (3) best-performing novel polyimides that have better combined properties than existing ones through Pareto frontier analysis. For an easy query of the discovered high-performing polyimides, we develop an online platform <http://polyimide.herokuapp.com> that embeds the developed ML model with interactive visualization. Furthermore, we validate the ML predictions through all-atom MD simulations and examine their synthesizability. The MD simulations are in good agreement with the ML predictions, and the three novel polyimides are predicted to be easy to synthesize via Schuffenhauer's synthetic accessibility score. Our study demonstrates an efficient way to expedite the discovery of novel polymers using ML prediction and MD validation. The high-throughput screening of a large computational dataset can serve as a general approach for new material discovery in other polymeric material exploration problems, such as organic photovoltaics, polymer membranes, and dielectrics.

10:30 AM DS02.11.07

Alloy Informatics Using Charge Profiles For Energy and Hydrogen Storage Applications Dario Massa¹, Stefanos Papanikolaou¹ and Efthimios Kaxiras²; ¹NOMATEN Center of Excellence in Multifunctional Materials, (NCBJ), Poland; ²Harvard University, United States

Studies have confirmed the crucial role of solid-state based solutions in hydrogen storage, with respect to liquid or gas states which cannot ensure comparably high amounts of storage per unit volume [1]. The empirical approach is not an option when it comes to the complexity of the quest for hydrogen storage materials, as well as to the strict urgency of a transition to clean and sustainable energy solutions. Here, we pursue machine learning approaches to composition searches for hydrogen storage materials. The compositional space to be explored is extremely vast, and still its vastness is not defined due to the on-going explorations, not only spanning the chemical compositions, but also the dimensionalities of the possible candidate systems [2]. Therefore, there is the need of finding a general predictive approach based on first-principles.

Electron charge profiles shall be illuminating for identifying and classifying local defect properties, thus characterizing alloying, and this is why our machine learning approach is based on the ab-initio analysis of the charge profiles of interstitial hydrogen in pure FCC bulk metallic crystals. Our descriptors are constructed by differential electron charge profiles for a large variety of crystals and also, after analysis of their characterizing local quantities, such as radii and extrema, as well as consider the full profile properties and their integrals. The integration of the profiles and the distinctive features of the effects of hydrogen are discussed, and can be exploited to infer hydrogen mobility in the surrounding matrix, as well as electron clouds motions around hydrogen. After the building of a density dataset, we perform unsupervised machine learning. Basing on preliminary tests we discuss interesting trends between the profile features and the properties of the embedding pure crystals (atomic number, valence electrons, lattice constant, bulk modulus), uncovering compositional relationships (among different crystals) and non-compositional ones (among different hydrogen interstitial equilibrium positions in the same crystals). The results also shed light over the influence that the compressibility of the systems have upon the radii of the hydrogen electron density profiles, which finds interesting connections with the complementary problem of systematically changing an impurity in a same crystal [3].

The results of this study might pave the way to novel material informatics methods for prediction of hydrogen storage behaviours by interpretation of the differential charge density profiles around the defect. Our goals are to understand up to which extent such charge profiles method can be exploited to predict diffusive, as well as the adsorption and desorption properties, overcoming the limited predictive capacity of empirical and thermodynamic based methods.

[1] P. Jena, *J. Phys. Chem. Lett.*, 2011, 2, 206–211.

[2] Xuebin Yu, *et al. Progress in Materials Science*, 2017, 88, 1–48.

[3] L. Messina, *et al. PHYSICAL REVIEW B* 2016, 93, 184302

10:45 AM DS02.11.08

Machine Learning Accelerated Lattice Boltzmann Simulation for Multiscale Platelet Modeling Amit Saha¹, Yicong Zhu², Miriam Rafailovich², Peng Zhang² and Yuefan Deng²; ¹Great Neck South High School, United States; ²Stony Brook University, United States

Background: Cardiovascular disease (CVD) is responsible for upwards of 17.9 million deaths globally per year. CVD-related death commonly occurs on account of platelet-mediated thrombosis. Modeling platelet dynamics is necessary to develop a mechanistic understanding of platelet-mediated thrombosis at multiple scales. Multiscale modeling (MSM) links microscale, mesoscale, and macroscale simulations to speed up computation while maintaining desired accuracy. Previous simulations model platelet aggregation using a MSM model that uses dissipative particle dynamics (DPD) for the shear flow and coarse-grained molecular dynamics (CGMD) for the platelet dynamics. However, the resolution of the fluid particles in the DPD simulation occupies unnecessary computational resources. In contrast, the lattice-Boltzmann method (LBM) may be up to 20-50x faster than DPD while still resolving the relevant fluid phenomena. In this work, we present a machine learning (ML) accelerated LBM for platelet dynamics.

Methods: We evaluate two methods for LBM: the conventional LB algorithm and the ML-LBM model. The conventional LBM solves the discrete Boltzmann equation for velocity distribution functions to predict flow dynamics. An in-silico model of the system was developed for LAMMPS using CGMD for platelets and LBM for fluid dynamics. We initially predicted future dynamics with this framework. The ML-LBM model trains based on existing data to accelerate computation. First, input data is preprocessed by normalization into a series of tensors indicating velocity distributions. The proposed architecture consists of an encoding layer, utilizing a ConvLSTM architecture to effectively resolve system dynamics in both space and time, and a decoding layer, utilizing the ResNet CNN architecture to map these inputs back to the original space. The training process minimizes the Mean Square Error (MSE) loss to iteratively improve predictive accuracy. The model outputs a series of tensors representing the final velocity distribution based on the LB dynamics. Our workflow exports data from LAMMPS, predicts the flow dynamics with the ML model, and then sends these predicted velocity distributions back into LAMMPS. Accuracy was computed by comparison of flow velocity and platelet stresses from our model to CGMD-DPD simulations. Simulations were performed with a total of 4 aggregated platelets and 3 flowing platelets within a box of 16x16x39.1 micrometers, for a total of 1,148,441 particles in the simulation.

Results: The conventional LB algorithm was 9x faster than DPD while maintaining 96.4% and 96.2% accuracy for flow velocity and platelet stress respectively. Evaluation of the ML-LBM yielded a 26x speedup with a 96.1% and 95.8% accuracy for flow velocity and platelet stress respectively. Both algorithms were able to capture major flow dynamics and platelet stresses while evaluating significantly faster than DPD. We attribute the lower accuracy of the machine learning LB model to the inability to effectively learn the dynamics of the platelet-fluid boundary, where lowest accuracy was observed.

Discussion and Future Work: We assessed the relative performance of LB methods in recreating the dynamics of DPD. Both the conventional LB

algorithm and the novel ML-LBM captured the system dynamics of blood flow and platelet stresses. Due to the inherent limitations of LBM, both models used in this study were less accurate near the platelet-fluid interfaces, since LBM cells are much larger than CGMD particles with the added resolution. This added resolution, albeit rather costly, has not caused errors in the platelet dynamics. Future work should implement and assess the efficiency of the ML-LBM method for studying larger and more complex platelet clusters for platelet dynamics modeling.

Acknowledgements: The project is supported by the Garcia High School Program and the Morin Charitable Trust.

11:00 AM DS02.11.09

Coarse Graining to Expedite Molecular Dynamics Simulations of Solvated Fibrinogen [Eric Chen](#)¹, Ziji Zhang², Miriam Rafailovich², Peng Zhang² and Yuefan Deng²; ¹Wayzata High School, United States; ²Stony Brook University, The State University of New York, United States

Accurate molecular dynamics (MD) simulations often require massive computing resources to simulate millions to billions of individual atoms. These all-atomic (AA) simulations are computationally intensive, and often fail to reach long simulation time scales [1]. Coarse graining (CG) alleviates these limitations by reducing an all-atomic model to a skeleton with fewer particles while preserving accuracy by ensuring that the interparticle forces closely resemble those of the all-atomic model [1]. Fibrinogen is especially important in modern biology due to its ability to form fibrin, a protein central to blood clotting and controlling bleeding in vascular injury. A CG model of Fibrinogen with alpha C domains in a vacuum was created by [2] in 2021 using machine learning methods. Our research builds upon the CG model of [2] by solvating it with water to more accurately emulate Fibrinogen's naturally solvated form. Such a solvated model would greatly boost pharmaceutical research in several important areas including thrombosis prevention.

To ensure that our CG model of solvated Fibrinogen accurately emulates an all-atomic model (AA model), we create a control system with the all-atomic 3GHG PDB file. We utilize the structure and force files from [2] for the CG Fibrinogen model. VMD's water box creation tool is employed to solvate both systems. The AA model is solvated with TIP3 water, whereas the CG model is solvated with MARTINI water with the same water box dimensions. We undertake NVT simulations at 310K with Langevin dynamics. To get comparable analyses from the AA model, we group atoms of the resultant AA trajectory into CG beads in the same way the original CG model was formed in [2], referred to as the "mapped all atomic" (MAA) model. For accuracy analysis, we measure the MAA and CG models' root-mean-squared deviation (RMSD), free energy distributions as a function of dihedral angles, and radial distribution functions (RDF).

Our prototyping CG system possesses 85,861 atoms including 15 atoms for Fibrinogen, whereas the AA system consists of 1,186,598 atoms including 42,003 atoms for Fibrinogen in atomistic resolution. On a 2GHz Quad-Core Intel Core i5, the CG model took 41 seconds of wall clock time to complete a 1 picosecond simulated time, while the AA model took 7028 seconds—the CG simulation achieving 172x speedup. After conducting 14.16 nanoseconds of CG simulation with 10 femtoseconds as the time step size and 249 picoseconds AA simulation with 1 femtosecond as the time step size, we conduct our accuracy analyses. The RMSD plot of the MAA model is steeply increasing, matching almost exactly with the CG plot. Because the CG simulation is significantly less computationally expensive, we could continue it beyond the results of the AA simulation until it plateaus at an RMSD value of around 0.37 Å. The dihedral plots of the MAA and CG models all appear very similar, with higher concentrations in similar areas. Likewise, the RDF plots demonstrate highly similar distributions between the two models.

We conclude that our CG model of solvated Fibrinogen utilizes much less CPU time than the AA model while emulating most of the structure properties, meaning that our CG model will feasibly and accurately achieve significantly longer simulation times than the AA model. This will boost future research on Fibrinogen in essential pharmaceuticals and other essential biological fields.

Acknowledgments:

We thank the Stony Brook University Garcia Center for Materials Research, the Garcia Summer Scholars Program, and the Morin Charitable Trust for supporting and facilitating this research.

References:

- [1] Husic, B. E., Charron, N. E., et al. (2020). Coarse graining molecular dynamics with graph neural networks. *The Journal of chemical physics*, 153(19):194101
- [2] Zhang, Z., Zhang, P., et al. (2021). Ai-guided multiscale biomechanical model of fibrinogen: correlating with in vitro results. *International Fibrinogen Research Society Workshop*

11:15 AM DS02.11.10

Use of Machine Learning and Graph Neural Networks for Predicting Hardness Solely Based on the Grain Boundary Microstructure—An Experimental Case Study of Nanoindented Polycrystalline Steel Kamran Karimi and [Stefanos Papanikolaou](#); NOMATEN CoE, Poland

There has been a long-standing notion that alloys' micro/nano hardness is strongly tied to the underlying microstructure. Polycrystals, for instance, consist of multitudes of disoriented grains within a complex polycrystalline network that dictate the mechanical response (i.e. hardness) across nano and micro scales. Nevertheless, the nature of such inherent microstructure-property correlations remains elusive and debated to this date. Conventional physics-based frameworks such as the Hall–Petch relationship empirically describe grain boundary strengthening effects by a single (mean) grain size parameter ignoring inherent grain scale hierarchies and intricate topology of the grain boundary network at micro/nano-structural levels. Here we use a data-driven approach based on the state-of-the-art machine learning (ML) and Graph Neural Net (GNN) model to infer grain-scale hardness from the (initial) grain boundary microstructural information. We trained our GNN model using an Electron backscatter diffraction (EBSD) map containing local lattice orientation information which was supplemented by a nano-mechanical dataset corresponding to a nanoindented polycrystalline steel. The trained ML model was able to make robust predictions of the load-depth curves over a broad range of grain scales. We further investigated that the model performance strongly depends on some certain set of grain-level (topological) attributes such as individual grain size, number of (nearest) neighbors, and grain-grain misorientation angles. On top of mechanical properties (such as hardness), our model can accurately forecast intermittent displacement bursts (i.e. pop-ins) and associated size and statistical distributions solely based on microstructural metrics.

11:30 AM DS02.11.11

Learning the Stress-Strain Fields in Digital Composites Using Fourier Neural Operator Meer Mehran Rashid, Tanu Pittie, Souvik Chakraborty and [M Anoop Krishnan](#); Indian Institute of Technology Delhi, India

The search for high-performance materials has led to advanced composite materials with hierarchical designs. However, designing a superior material with targeted properties and performance is challenging due to the vast design combinations and computational limitations imposed by conventional physics-based solvers. In this study, we use a neural operator-based framework, namely, Fourier Neural Operator (FNO) to learn the mechanical response of 2D digital composites. By just providing the material microstructure to the FNO it predicts the complete stress and strain tensor fields. The model exhibits

zero-shot generalization to unseen arbitrary geometries. Besides, the model demonstrates zero-shot super-resolution capabilities by predicting high-resolution stress and strain fields from low-resolution input configuration images. We show that FNO works for generalized boundary conditions (BCs) by testing the model for different unseen BCs. Furthermore, FNO provides high-accuracy predictions of equivalent stress and von-mises stresses thereby allowing upscaling of the results.

11:45 AM DS02.11.12

Accelerating Calculations of Leonard-Jones Potentials using Physics-Informed Neural Network Yuhe Wei¹, Ziji Zhang², Yicong Zhu², Miriam Rafailovich², Peng Zhang² and Yuefan Deng²; ¹Rutgers Preparatory School, United States; ²Stony Brook University, The State University of New York, United States

Computing Leonard-Jones potentials dominates the computational costs in many simulations involving molecular dynamics (MD), for example, in platelet dynamics that plays an essential role in understanding the mechanisms of blood clotting. The extreme computational workload demand of MD simulations often hinders the study of bioprocess with large spatial and temporal scales. In the recent decades, the rise of machine learning (ML) techniques allows for a significant reduction of computational workload while maintaining the accuracy, by utilizing the ML predictions for MD calculations. Our work aims to simplify the computation of Lennard-Jones (LJ) potentials, which is the intermolecular force fields between interacting platelets, by proposing a generalized equation for theoretically similar ellipsoid models.

Problem Statement: The study considers the two interacting platelets, B_1 and B_2 , to be modeled as ellipsoids, r as the distance between B_1 and B_2 , Φ , Ψ , and θ and as the relative rotation angle of B_1 and B_2 , respectively. Numerical experiments are conducted to generate training samples. We calculated the LJ potential for each 300 thousand random distributed points for each ellipsoid and used Monte Carlo Integration to estimate the double summation over each particle in a fixed form. The length, angle, and distance from center for x , y , z directions are measured to be the independent variables. By using the massive training set with 208,000 samples and 10 independent variables, we train our models to describe the predicted equation that governs the integrated potentials between interacting ellipsoids while significantly reducing the computation time.

The Results: With the numerical training set, we designed a physics-informed neural network (PINN) [1] guided by the proposed equation for LJ potentials with variables of relative distance and orientation (λ_2) between platelets and their respective correction parameters, λ_1 and λ_3 , presented in the equation as $LJP = \lambda_1 \lambda_2 [\lambda_3 (\sigma/r)^7 - (\sigma/r)]$. We used 10 neural network hidden layers each with 20 neurons and employed the Adam optimizer with a learning rate of 0.001. We split the data to training and testing sets into 1:1 ratio to avoid potential overfitting issues. We then trained the data for 15K iterations with the relative orientation (λ_2) as the target output in the neural net framework and use the results to calculate the predicted LJ potential value using the aforementioned equation. Finally, we assess the PINN training with a loss function of root mean square error (RMSE) to penalize the difference between predicted LJ potential and the true LJ potential value. In the range of LJ potential value less than 0, we got a RMSE error of 0.01568. Our learned force-field parameters for orientation (λ_1) and distance (λ_3) are -1.526 and -1.915, respectively.

We learned the parameters for relative orientation and distance for the generalized LJ potential equation to describe the large-scale biophysics systems. The leveraged PINN effectively accelerates the learning process and improve the overall approximation accuracy of the model prediction by embedding the governed physics principles. Our work contributes to thrombosis simulation which could help us better understand the complex risk of blood clotting, providing promising applications to learn the generalized equations of other similar biophysics systems. Future work can investigate other neural network model architectures to improve performance.

Acknowledgment: The project is supported by the Stony Brook Garcia Scholars for Materials Research and funded by Morin Charitable Trust.

References:

[1] Raissi, Maziar, Paris Perdikaris, and George E. Karniadakis. "Physics-informed neural networks: A deep learning framework for solving forward and inverse problems involving nonlinear partial differential equations." *Journal of Computational Physics* 378 (2019): 686-707.

SESSION DS02.12: Machine Learning for Materials Simulations II
Session Chairs: Mathieu Bauchy and N M Anoop Krishnan
Friday Afternoon, December 2, 2022
Hynes, Level 2, Room 210

2:00 PM *DS02.12.01

Multi-Fidelity Scale Bridging Using AI and Machine Learning Subramanian Sankaranarayanan; Argonne National Laboratory, United States

Reinforcement learning (RL) approaches that combine a tree search with deep learning have found remarkable success in searching exorbitantly large, albeit discrete action spaces, as in chess, Shogi and Go. Many real-world materials discovery and design applications, however, involve multi-dimensional search problems and learning domains that have continuous action spaces. Exploring high-dimensional potential energy models of materials is an example. Traditionally, these searches are time consuming (often several years for a single bulk system) and driven by human intuition and/or expertise and more recently by global/local optimization searches that have issues with convergence and/or do not scale well with the search dimensionality. In this talk, we present our recent efforts on the use of RL for parameterization and development of interatomic potential functions. In a departure from discrete action and other gradient-based approaches, we introduce a RL strategy based on decision trees that incorporates modified rewards for improved exploration, efficient sampling during playouts and a "window scaling scheme" for enhanced exploitation, to enable efficient and scalable search for continuous action space problems. We will demonstrate a set of use cases to highlight the efficacy of our RL approach in interatomic potential development for a broad class of materials.

Reinforcement learning (RL) approaches that combine a tree search with deep learning have found remarkable success in searching exorbitantly large, albeit discrete action spaces, as in chess, Shogi and Go. Many real-world materials discovery and design applications, however, involve multi-dimensional search problems and learning domains that have continuous action spaces. Exploring high-dimensional potential energy models of materials is an example. Traditionally, these searches are time consuming (often several years for a single bulk system) and driven by human intuition and/or expertise and more recently by global/local optimization searches that have issues with convergence and/or do not scale well with the search dimensionality. In this talk, we present our recent efforts on the use of RL for parameterization and development of interatomic potential functions. In a departure from discrete action and other gradient-based approaches, we introduce a RL strategy based on decision trees that incorporates modified rewards for improved exploration, efficient sampling during playouts and a "window scaling scheme" for enhanced exploitation, to enable efficient and scalable search for continuous action space

problems. We will demonstrate a set of use cases to highlight the efficacy of our RL approach in interatomic potential development for a broad class of materials.

2:30 PM BREAK

3:00 PM *DS02.12.03

Machine Learning Based Strategies for Materials Discovery and Design [Gwooon Cheon](#); Google Research, United States

With the rapid increase in computational resources and the large-scale datasets of materials, data-driven methods for materials discovery and design are rising to prominence. I will talk about our work on combining high-throughput calculations, data mining and machine learning-based modeling to discover new materials.

3:30 PM DS02.12.04

Accelerated Discovery of Aerospace Materials via Graph Neural Networks and Multiscale Modeling [Mark Polking](#), Lin Li, Kevin Tibbetts, Charles Epstein and Nathan Frey; Lincoln Laboratory, Massachusetts Institute of Technology, United States

The extreme aerothermal conditions encountered in space vehicle re-entry and supersonic flight pose severe challenges for material survivability. Window materials, which must maintain high optical transparency in addition to high mechanical strength, thermal stability, and chemical resistance, pose particular challenges. Here, we demonstrate high-throughput discovery of new high-temperature aerospace window materials using a combination of machine learning-guided materials screening, first-principles materials theory, macroscale modeling with custom thermo-mechanical-optical models, and high-fidelity computational fluid dynamics (CFD) simulations. Our machine learning models, powered by a novel integrated graph neural network (I-GNN) architecture, enable accurate predictions of key thermo-mechanical properties, including thermal conductivity, coefficient of thermal expansion, melting temperature, and other properties. Importantly, by integration of materials physics with GNN models, we demonstrate accurate, temperature-dependent predictions of these properties. Use of these fundamental property predictions as inputs to high-fidelity CFD simulations enables, for the first time, rapid and accurate predictions of macroscale material behavior under realistic aerothermal flow conditions for many thousands of previously unexplored materials. With this approach, several new candidate materials have been identified with combinations of thermal, mechanical, and optical properties that may enable superior performance compared with conventional sapphire windows in the mid-wave and long-wave IR spectral ranges, such as AlReSi and CaZrN₂. Property predictions for these and other top candidate materials have been validated using first-principles calculations with density functional theory and density functional perturbation theory.

3:45 PM DS02.12.05

Exploring Interface Structure Between Perovskite Oxides Using Evolutionary Structure Search and Automated Design of Deep Learning Potentials via Neural Architecture Search [Hong Sun](#)¹, Amit Samanta¹, Vincenzo Lordi¹ and Yayoi Takamura²; ¹Lawrence Livermore National Laboratory, United States; ²University of California, Davis, United States

Perovskite oxides have attracted enormous interest in producing next-generation magnetic and ferroelectric devices. Interfaces between perovskite oxides warrant particular attention as they present distinctive charge transfer reactions and magnetic properties that are often absent in the constituent materials. To harvest the special functionality of perovskite oxide multilayers, developing a mechanistic understanding of their interface phases is imperative to establish materials design principles. In this study, we leveraged evolutionary algorithm and neural architecture search methods to design deep learning potentials and first principles simulations to systematically examine interface structures of La_{1-x}Sr_xCoO_{3-δ}/La_{1-x}Sr_xMnO_{3-δ} (LSCO/LSMO) bilayer system as a function of oxygen deficiency (δ) and strontium concentration (x). Neural network potentials proposed in the literature are typically designed based on intuition and a particular neural network architecture can induce systematic errors into the potential. To overcome this problem, we use a state-of-the-art neural architecture search method to design potentials by optimizing network architectures and hyperparameters over a variety of neural network ensembles. The end products are a set of optimized potentials that then are used to search for interface structures using evolutionary structure search. Since total energies are calculated using an ensemble of potentials, our framework naturally allows us to incorporate uncertainty quantification. To generate our potentials, we use a set of about 800 training structures generated with first principles calculations by using evolutionary structure search. Next, we use these potentials to explore interface structures for different δ and x – this combination of evolutionary structure search and automated design of potentials allowed us to explore over 50,000 interface structures corresponding to 25 distinct δ and x at LSCO/LSMO interfaces. We validate the predictions made using our potentials by (a) performing first principles calculations of energetically favorable structures and comparing them with total energies predicted using our potentials, and (b) comparing predictions with a structure search performed using evolutionary algorithms with first principles calculations (i.e., without potentials). By statistically analyzing the spatial distribution of oxygen vacancies, Sr atoms, and the distortion of Co-/Mn-centered octahedral units, we determine the complex interplay of oxygen vacancy concentration, valence states of transition metal ions, and electronic properties at perovskite oxide interfaces. The fundamental understanding provides useful insights in designing perovskite oxide multilayers with tailored properties for device applications.

This work was performed under the auspices of the U.S. Department of Energy by Lawrence Livermore National Laboratory (LLNL) under Contract DE-AC52-07NA27344. This work was funded by the Laboratory Directed Research and Development (LDRD) Program at LLNL (project tracking code 21-ERD-005). Computing support for this work came from the LLNL institutional computing facility.

4:00 PM DS02.12.06

Early Prediction of Ion Transport Properties in Molecular Dynamics Simulations of Solid Polymer Electrolytes Using Machine Learning [Arash Khajeh](#)¹, Daniel Schweigert¹, Steven B. Torrisi¹, Tian Xie² and Ha-Kyung Kwon¹; ¹Toyota Research Institute, United States; ²Massachusetts Institute of Technology, United States

Solid polymer electrolytes have received much interest for developing a new generation of safe, high-performance Li-ion batteries. To this end, Molecular Dynamics (MD) simulations have been widely used to quickly screen polymer candidates for desirable properties, such as high ionic conductivity and mechanical robustness. Unfortunately, these simulations can be time-consuming, and accurate predictions of these properties can require MD simulation lengths of 20ns or more which correspond to wall clock times on the order of hundreds of hours using conventional computational resources. Therefore, accelerating MD simulations is critical to expedite the screening process, and subsequently, the design of new polymers. In this study, we show that with the correct choice of descriptors, we can make predictions of equilibrated transport properties at 10% of the total simulation time. The new set of descriptors used in the current study combines the configuration of ion clusters with the early time evolution of transport properties. Specifically, we find that descriptors that include information about anion-cation interactions and dynamics of ion transport in the polymer environment outperform features extracted from the molecular structure of the polymers. We show that these descriptors have several advantages over polymer structure-only descriptors, as features can be extracted and predictions made at any time point, increasing the applicability of this method to a wide range of polymer systems, simulation times, and conditions such as different temperatures and concentrations.

4:15 PM DS02.12.07

Combining Density Functional Theory and Machine Learning for Compositional Optimization of Alloyed Perovskite Electrocatalysts [Jessica Karaguesian](#), James K. Damewood, Jaclyn Lunger, Daniel Zheng, Jiayu Peng, Daniel Schwalbe Koda, Yang Shao-Horn and Rafael Gomez-Bombarelli; Massachusetts Institute of Technology, United States

Multicomponent metal oxides, such as perovskite oxides, hold promise for use as sustainable alternatives to Ir-, Ru-, and Pt-based electrocatalysts at scale. Perovskites can accommodate a wide variety of elements in their A- and B-sites, enabling tuning of their structural and electronic properties through compositional alloying. These properties, which are obtainable from density functional theory (DFT) calculations, can be used as low-dimensional descriptors that correlate with experimental stability and activity in, for example, the oxygen evolution reaction (OER). Established descriptors of stability include energy above convex hull and energy above Pourbaix hull, while those for catalytic activity include the difference between oxygen 2p-band center and the Fermi level, the difference between the metal 3d- and oxygen 2p-band centers, as well as oxygen vacancy formation energy. We are therefore presented with a combinatorial problem of determining which A- and B-site compositions optimize such descriptors. The compositional search space for $A_xA'_{1-x}B_yB'_{1-y}O_3$ perovskites with up to two different elements in their A- and B-sites is $O(10^6)$, making it intractable to calculate descriptors exhaustively using DFT. Here, we thus combine high-throughput DFT calculations with crystal graph convolutional neural networks (GCNs) to screen for stability and activity descriptors.

Previous high-throughput screening efforts have largely focused on ABO_3 perovskites, without alloying of the A- and B-sites, or narrow compositional ranges of perovskites with A- and/or B-site alloying. To predict descriptors of highly-alloyed perovskites over a wide cation space, we have used our high-throughput virtual screening platform to generate a dataset of over 10,000 perovskites. Notably, the presented dataset includes over 4,000 $(AA')(BB')O_3$ perovskites with varied A- and B-site alloying ratios and with over 2,000 unique cationic combinations. This significantly increases the amount of available highly-alloyed perovskite DFT data, with previous alloying studies including only a few hundred unique combinations of cations. Moreover, we have generated a dataset of over 2,000 $(AA')(BB')O_3$ perovskites with oxygen vacancies; to our knowledge, the only available high-throughput dataset studying vacancy formation in alloyed perovskites. Using our datasets in combination with data available in the literature, we have trained GCNs to predict the aforementioned descriptors from unrelaxed cubic perovskite structures and used these models to predict descriptors for $O(10^6)$ perovskites containing over 20 different A- and B-site cations, respectively. Leveraging these predictions, we describe trends in the structural and electronic properties of alloyed perovskites across a vast compositional space and work to establish improved structure-property relationships between computed descriptors and experimental catalytic performance. The presented work provides the community with a benchmark dataset for further study of alloyed perovskites and analyses of compositional trends, laying the groundwork for improved design of perovskite electrocatalysts.

4:30 PM DS02.12.08

Deep Learning-Based Prediction of Interfacial Surface Tension of Pendant Droplets Kazi Zihan Hossain, [Sharif Amit Kamran](#), Alireza Tavakkoli and M. Rashed Khan; University of Nevada, Reno, United States

Pendant drops of oxide-coated high-surface tension fluids frequently produce perturbed and distorted shapes that impede surface tension measurements. Eutectic Gallium Indium (eGaIn), a high surface tension fluid coated with a 5nm Gallium Oxide film, falls under this fluid classification, and the recent emergence of eGaIn-based applications often cannot proceed without analyzing interfacial energetics in different environments. The low viscosity, chemical reactivity, and the passive surface oxide have also contributed to the accelerated materials discovery where eGaIn is alloyed with other elements for novel catalysts, bioreactors, and sensor discovery. In this study, for the first time, we are using a regression-based Deep Learning (DL) technique to predict the surface tension of eGaIn that can be extended to analyze any pendant drop. Time and resource-consuming image analysis software with manual intervention is generally used to analyze interfacial surface tension of different fluids. Here, we address the challenges associated with physics-based interfacial energy measurements of eGaIn and introduce a deep convolutional neural network architecture that can be deployed without using Goniometers (interfacial energy measurement instruments). A set of 13081 images were acquired and further analyzed to measure the surface tension. The dataset was split into 10594 training, 1178 validation, and 1309 test samples. We trained various convolutional neural networks on this regression task to accurately predict and compare the pendant drop shape properties. Our best-performing model, ResNet-50v2, achieved a mean absolute error of 0.995 and an R2 value of 99.97%, which signifies a high correlation, and our architecture can predict 99% of the variance in outcome. eGaIn droplets can create a non-axisymmetric shape due to their oxide layer, which cannot be solved with presently available software but can easily be handled with our presented DL technique. In limited-resource settings, our approach can also be deployed with a cell phone, and this deep learning model can be further leveraged to harness the influence of the external environment.

SESSION DS02.13: Virtual Session I: Machine Learning for Materials Processing, Imaging and Properties

Session Chairs: Mathieu Bauchy and Grace Gu

Tuesday Morning, December 6, 2022

DS02-virtual

8:00 AM DS02.13.01

Hybrid Density Functional based Tight Binding-Molecular Mechanics Approach with Machine Learned Potentials for Large-Scale Materials Modeling [Gekko P. Budiutama](#), Sergej Manzhos and Manabu Ihara; Tokyo Institute of Technology, Japan

Density Functional based Tight Binding method (DFTB) has seen a rise in adoption in recent years as it offers both DFT-like accuracy and access to electronic structure as well as scalability for systems where appropriate parameters are available. DFTB is based on the parameterization of interatomic interactions that reduce the cost of calculation when compared to DFT. In DFTB, all interatomic interactions for all atoms of the model have to be pre-parameterized. Conventionally, these parameterizations are performed to multiple DFT calculations and/or reference data. This approach, however, requires a significant number of comparatively high-cost DFT calculations and specific knowledge and skillsets to be performed appropriately, therefore reducing the applicability of DFTB for many heteroatomic materials. In this study, we propose a hybrid approach where interatomic interactions which have little influence on electronic properties are modeled with pairwise interatomic potentials while other interactions are modeled with the conventional Slater-Koster approximation. We demonstrate the usefulness of this method by modeling a large-scale silica-titania interface where the Si-Ti interactions are modeled at the force field level while other interactions are modeled at the DFTB level. The most appropriate functional representation of the potential and its parameters are obtained with a combination of machine learning and gradient-based fitting. The validity of the approximation is verified against DFT on small-scale models. The approach allows the expansion of DFTB application to new materials where Slater-Koster parameters are not yet available.

8:15 AM DS02.13.02

Disconnection Aware Steering of Retrosynthesis Transformer to Facilitate Materials Design Amol Thakkar, Andrea Byekwaso, Alain Vaucher, Philippe Schwaller, Alessandra Toniato and Teodoro Laino; IBM Research-Zurich, Switzerland

Retrosynthetic analysis is the task of breaking down a target molecule into its constituent precursors until a set of commercially available building blocks is reached. At each single step in the sequence, the bonds to be changed and/or functional group interconversions are identified, and the molecule broken into hypothetical precursors. Several deep-learning-based approaches to single-step retrosynthesis treat the prediction of possible disconnections as a translation task, relying on the use of the Transformer architecture [1] and the simplified molecular-input line-entry system (SMILES) [2,3] notation [4-7]. Given a target molecule, these approaches suggest the best set of precursors (i.e. reactants, and possibly other reagents) as the translation's outcome, with the possibility to generate multiple such sets.

However, in their current form, retrosynthetic prediction systems offer the chemist little control over the site at which disconnections are made. As such, this work serves to enable user-defined disconnections for single-step retrosynthetic analysis, enabling steering of transformer models for retrosynthetic prediction. Whereas previous models offer no opportunity to steer the model and remain limited in the disconnections they propose. Thus, paving the ground for a 'human-in-the-loop' component harnessing both expert knowledge and deep learning. To this end, we have investigated methods to enhance user interaction from tagging input molecules, through to dataset augmentation. We additionally introduce and examine the predictions using several metrics beyond topN accuracy, which serves to build an understanding of how the predictions made align with those expected by chemists. Thus, we take a step towards improving decision-making strategies that statistical and machine learning algorithms cannot yet encode due to a lack of relevant training data. Ultimately this serves to enhance a chemist's experience by facilitating user engagement.

[1] Vaswani, A. et al.; Advances in neural information processing systems 2017, 5998–6008. [2] Weininger, D.; J. Chem. Inf. Comput. Sci. 1988, 28, 31–36.

[3] Weininger, D.; Weininger, A.; Weininger, J. L.; J. Chem. Inf. Comput. Sci. 1989, 29, 97–101. [4] Yang, Q. et al.; Chem. Commun. 2019, 55, 12152–12155.

[5] Karpov, P.; Godin, G.; and Tetko, I. V.; International Conference on Artificial Neural Networks 2019, 817–830.

[6] Duan, H.; Wang, L.; Zhang, C.; Guo, L.; and Li, J.; RSC Adv. 2020, 10, 1371–1378.

[7] Schwaller, P. et al.; Chem. Sci. 2020, 11, 3316–3325.

8:30 AM DS02.13.03

Accelerating Material Design with the Generative Toolkit for Scientific Discovery (GT4SD) Matteo Manica¹, Joris Cadow¹, Dimitrios Christofidellis¹, Ashish Dave¹, Jannis Born¹, Dean Clarke¹, Yves Gaetan Nana Teukam¹, Samuel C. Hoffman², Matthew Buchan¹, Vijil Chenthamarakshan², Timothy Donovan¹, Hsianghan Hsu³, Federico Zipoli¹, Oliver Schilter¹, Giorgio Giannone¹, Akihiro Kishimoto³, Lisa Hamada³, Inkit Padhi², Karl Wehden², Lauren McHugh², Alexy Khrabrov², Payel Das², Seiji Takeda³ and John Smith²; ¹IBM Research Europe, Switzerland; ²IBM T.J. Watson Research Center, United States; ³IBM Research Tokyo, Japan

The GT4SD (<https://github.com/GT4SD/gt4sd-core>) is an open-source library to accelerate hypothesis generation in the scientific discovery process that eases the adoption of state-of-the-art generative AI.

GT4SD includes models that can generate new molecule designs based on properties such as target proteins, target omics profiles, scaffolds distances, binding energies, and additional targets relevant for materials and drug discovery.

The library provides an effective environment for the generation of new hypotheses (inference) and for fine-tuning the models to specific domains using custom data sets (models retraining). It is compatible with the majority of popular deep learning frameworks: PyTorch, PyTorch Lightning, HuggingFace Transformers, GuacaMol, Moses, Torchdrug, and serves a wide range of applications ranging from materials science to drug discovery.

GT4SD's common framework makes models easily accessible to a broader community, like AI/ML practitioners developing new generative models who want to deploy with just a few lines of code. GT4SD provides a centralized environment for scientists and students interested in using generative models in their scientific research, allowing them to access and explore a variety of different models — all of which are pretrained. Consistent commands and interfaces for inference or retraining with customizable parameters harmonize the use across the different models.

The development of problem-specific intelligence is made possible thanks to the automatic workflows enabling retraining with users' own data covering molecular structures and properties. The replacement of manual processes and human bias in the discovery process has important effects on downstream applications that rely on the use of AI models, leading to an acceleration of expert knowledge.

In this talk, we will present GT4SD and its main functionalities, ranging from model inference to training and using live applications demos in the context of material science and chemistry.

The session is designed to provide a deep dive for developers and research scientists who want to accelerate their discovery pipelines with generative modeling capabilities.

8:45 AM DS02.13.05

Development of a Machine Learning Interatomic Potential for High-Entropy Alloys Akash A. Deshmukh¹, Manish Sahoo² and Raghavan Ranganathan¹; ¹Indian Institute of Technology Gandhinagar, India; ²Indian Institute of Technology Indore, India

High-Entropy Alloys (HEAs) are alloys of multiple components (usually 5 or more) in nearly equiatomic composition, forming simple solid solutions. Four core effects namely, the high-entropy effect, sluggish diffusion, lattice distortion, and the cocktail effect have enabled HEAs to exhibit excellent mechanical properties such as high hardness, high strength, good corrosion, and wear resistance, unlike traditional alloys. Due to the large compositional space, it is exceptionally difficult to predict promising HEA compositions. Atomistic simulations such as molecular dynamics (MD), Monte Carlo (MC), and first principles (DFT) calculations have provided an alternative to accelerate materials research manifold, thereby reducing the experimental cost, labor, and time involved in the traditional trial-error approach.

Interatomic potentials (IPs) or force fields (FF), are the heart of such simulations and are used for predicting characteristics, describing interatomic interaction, physical, and mechanical properties at varying conditions such as temperature, pressure, and strain rate via molecular simulations. The selection of the appropriate FF is very important for accurate structure-property predictions in HEAs. Although first-principles calculations are the most accurate, small system sizes and small-time scales limit their applicability. Besides, semi-empirical models such as EAM/MEAM are capable of simulating large systems at long time scales with the compromise of accuracy. Being nonparametric in nature, the accuracy of machine learning-based interatomic potentials (MLIP) can be improved by fitting them to different atomic environments and simulation conditions. MLIPs not only combine the advantages of

both first-principles calculations and semi-empirical models but also address the limitations without compromising accuracy. The objective of the work is two-fold: first, we develop an MLIP for the unary molybdenum (Mo) system as a benchmark for testing the efficacy of the potential. This is achieved by training a moment tensor potential (MTP) from the training set that consists of various atomistic configurations during DFT simulations and configurations chosen on the fly during MD simulations, by means of an active learning approach. Specifically, to ensure a reasonable sampling of the phase space, the training set consists of atomic configurations picked up during NVT simulations at 300, 600, and 900 K, with defects such as vacancy and edge dislocation. The accuracy of the MLIP was validated periodically with improved training set by calculating the intrinsic properties such as lattice constant, melting point, and strength. Secondly, this protocol was extended to the CONiCrFeMn HEA. Initially, a defect-free unit cell of the HEA was designed at 300 K using the Special Quasirandom Structure (SQS) approach. Subsequently, defects such as stacking fault, edge dislocation, and vacancy were introduced. Atomic configurations obtained from the defects and at different temperatures (300, 600, and 900 K) form the training set. Again, the accuracy of the MTP was validated against experimental measurements of the lattice constant, melting point, and mechanical properties. We believe that this work will serve as a strong basis for the rapid development of machine learning-based force fields for the exploration of promising HEAs.

9:00 AM *DS02.13.06

Machine Learning Based Design of Composite Structures Seunghwa Ryu; KAIST, Korea (the Republic of)

Despite the technical importance of composite materials and structures, systematic design frameworks for them are limited because conventional optimization techniques face difficulties in handling the high-dimensional design space consisting of an astronomical number of material combinations and configurations as well as a complex nonlinear response beyond the linear response regime. With the advancement of machine learning (ML) techniques, extensive efforts are underway to establish alternative data-driven design frameworks for finding the optimal microstructure, external shape, and processing condition of composite materials and structures. In this talk, I would like to propose systematic composite structure design strategies using machine learning by accounting for the size of design space, dataset size, and the fidelity of the dataset. I will then introduce a few case studies concerning the optimization of nonlinear characteristics such as strength and toughness, design of a composite microstructure with very small dataset which limits the usage of the deep neural network, and the development of composite analysis model with less accurate but large homogenization model dataset with the aid of accurate but small experimental dataset. Additionally, the data-driven optimization of injection molding process parameters will be discussed.

9:30 AM DISCUSSION TIME

SESSION DS02.14: Virtual Session II: Machine Learning for Materials Processing, Imaging and Properties

Session Chair: Jeong-Ho Lee

Tuesday Afternoon, December 6, 2022

DS02-virtual

1:00 PM *DS02.14.01

Graph Neural Networks for Learning System Dynamics Wei Wang; UCLA, United States

Learning multi-agent system dynamics is important yet challenging. The complex interplay among agents is often explained with a one-step discrete model in existing work, which predicts the next observations for all agents given the current observations and their interaction graph. In reality, the interaction graph among agents may evolve over time and not always be observable. Moreover, many real-world systems are continuous in nature and using discretized modeling may significantly impair the precision of nonlinear dynamics. In this talk, I will present our recent work on modeling dynamic interactions using graph neural networks. Our models can jointly learn the latent representations of agent trajectories and the interaction graph in an unsupervised manner over time. Experiments show that they can accurately predict system dynamics especially in the long range and generalize well to low-resource systems that have only few training samples.

1:30 PM DS02.14.02

Combined Machine Learning and Density Functional Theory Approach to Predict Element Distribution of High-Entropy Alloys in Scanning Transmission Electron Microscopy Images Marco Ragone, Abhijit H. Phakatkar, Reza Shahbazian-Yassar, Farzad Mashayek and Vitaliy R. Yurkiv; University of Illinois at Chicago, United States

In comparison to their binary counterparts, high entropy alloys (HEAs) possess many unique properties that make them of high interest for applications in energy storage, bio/plasmonic imaging, catalysis, etc. The information about the element's distribution in columns of HEAs is imperative for a fundamental understanding and to reveal their structure-properties relation. We present a machine learning (ML) framework for the estimation of the element distribution in the atomic columns of HEAs nanoparticles (NPs), using semantic segmentation of high angle annular dark-field (HAADF) scanning transmission electron microscopy (STEM) images. NPs of two distinguished compositions, specifically, PtNiPdCoFe and (MnFeNiCuZn)₃O₄ serve as examples. The ML model is built upon a fully convolutional neural network (FCN), to learn the non-linear correlations between the columns' pixels' intensities in STEM images and the number of atoms of different constituent elements in the atomic columns to resolve the random elements distribution in chemically-complex NPs.¹ The elements motive in NPs with structural characteristics in agreement with the samples observed in the experimental measurements, is obtained using the density functional theory (DFT) calculation. The DFT calculations have been performed using the Vienna Ab Initio Simulation Package (VASP)² and Atomistic Tool Kit (ATK)³, while an FCN has been built using the Tensorflow 2.2⁴.

In order to generate a training dataset of simulated STEM images representing the aforementioned NPs for ML, the multislice algorithm and Gaussian filtering, implemented in the PyQSTEM⁵ Python library, are used. Statistical analysis of the simulated STEM images revealed that the correlation between the columns' pixel intensities and the column heights (CHs) of the constituent elements is highly nonlinear, because of the random distribution, the different electronegativity of the constituent elements, and the crosstalk effect.

After proper training, we illustrate that in the simulated HAADF STEM images, our FCN predicts the majority of the columns correctly with an error of just one atom and with a maximum error of three atoms in 10 nm-sized NPs. Applying the trained network to the experimental HAADF STEM images revealed an overall even distribution of the five constituent elements (i.e., no local clusters of single element rich columns), with inhomogeneous fluctuations with local aggregations at a column level. The mapping of the HEAs element distribution via ML presented in this work allows for a more accurate characterization and engineering of the physical properties of HEAs. Moreover, in addition to the estimation of the number of atoms in the atomic columns of HEAs, our work represents an advancement to the development of computer vision techniques based on statistical learning methods for microscopy analysis, which could be beneficial to a broad area of nanoscience applications.

Authors acknowledge the financial support from the National Science Foundation Award DMR-2055442.

References

1. M. Ragone, M. T. Saray, L. Long, R. Shahbazian-Yassar, F. Mashayek, V. Yurkiv, *Comput. Mater. Sci.* **201** (2022), doi:10.1016/j.commatsci.2021.110905.
2. G. Kresse, J. Furthmüller, *Phys. Rev. B - Condens. Matter Mater. Phys.* **54**, 11169–11186 (1996).
3. Atomistix Toolkit version 2017.2, Synopsys QuantumWise A/S.
4. M. Abadi, A. Agarwal, P. Barham, E. Brevdo, Z. Chen, C. Citro, G.S. Corrado, A. Davis, J. Dean, M. Devin, S. Ghemawat, I. Goodfellow, A. Harp, G. Irving, M. Isard, Y. Jia, R. Jozefowicz, L. Kaiser, M. Kudlur, J. Levenberg, D. Mane, R. Monga, S. Moore, D. Murray, C. Olah, M. Schuster, J. Shlens, B. Steiner, I. Sutskever, K. Talwar, P. Tucker, V. Vanhoucke, V. Vasudevan, F. Viegas, O. Vinyals, P. Warden, M. Wattenberg, M. Wicke, Y. Yu, X. Zheng, TensorFlow: Large-Scale Machine Learning on Heterogeneous Distributed Systems, ArXiv. (2016). <http://arxiv.org/abs/1603.04467>.
5. A. S. U. (2002). C. Koch, Ph.D. Thesis, PyQSTEM.

1:45 PM DS02.14.04

Polycrystal Graph Neural Network Minyi Dai, Mehmet Demirel, Xuanhan Liu, Yingyu Liang and Jiamian Hu; University of Wisconsin-Madison, United States

Graph Neural Network (GNN) has recently emerged as a powerful machine learning model for predicting the properties of molecular and crystal structures, but its application to 3D, topologically complex polycrystalline microstructures still remains scarce. Here, we develop a Polycrystal Graph Neural Network (PGNN) model that permits an accurate prediction of the properties of polycrystalline microstructures by considering the physical features and interactions of both grain and grain boundaries. Trained with 4000 data points, our PGNN model achieves a property prediction error of ~1.5%, which is significantly lower than baseline machine learning models such as ResNet (error ~4%). We also show that such trained PGNN model can be transferred to accelerate and improve the prediction of other physical properties with smaller available data. Our accurate, and transferable PGNN model is well suited for harnessing large-scale datasets of 3D polycrystalline microstructures, which is crucial for realizing accelerated design of polycrystalline materials.

2:00 PM *DS02.14.05

Are Symmetries All We Need? Machine Learning Directions Beyond Equivariance Jonathan W. Godwin; DeepMind, United Kingdom

Machine Learning research for molecular and material simulation has often concentrated on embedding symmetries into the network architecture. A common argument is that embedding such symmetries allows the model to generalise from small amounts of data, and so removes the need to train large models as we do in Natural Language Processing and Computer Vision. In this talk I will argue that this is only partially correct, and that we need to move beyond symmetric architectural improvements.

I'll present evidence that symmetries are not sufficient on their own for learning representations across the periodic table. I'll then show promising evidence that taking inspiration techniques for representation learning and more stable training from other machine learning areas can provide significant performance increases at scale, indicating that we may see an inflection point as we increase the amount of data and compute. Finally, I'll finish by outlining some promising research areas in this direction.

2:30 PM DS02.14.06

Linking Local Atomic Environments to Interfacial Co-Segregation Behavior in NbMoTaW Complex Concentrated Alloy Using Machine Learning Methods Doruk Aksoy and Timothy J. Rupert; University of California, Irvine, United States

Discovery of complex concentrated alloys unveiled a new generation of materials accommodating intricate local atomic environments. Linking these local atomic environments to the co-segregation behavior is instrumental in predicting the interfacial segregation behavior to assess chemical and thermodynamic stability of polycrystals. In this work, the co-segregation landscape of NbMoTaW refractory complex concentrated alloy is studied by employing atomistic simulations coupled with machine learning methods. First, the site availability of every possible combination of interactions (binary, ternary, and quaternary) is obtained at the dilute limit via molecular statics simulations at 0 K. Then, for the same interactions, hybrid Monte Carlo and molecular dynamics simulations are utilized to study chemically complex environments at different compositions. Finally, data-driven methods are employed to create structure property maps, through vectorized local atomic environments and segregation energies. The goal of this work is to gain insights on the effect of interfacial structure on co-segregation behavior rapidly, without the necessity of running costly atomistic simulations. A potential application of this method is to facilitate interfacial design of complex concentrated alloys by using these maps as building blocks.

3:00 PM DISCUSSION TIME

SESSION DS02.15: On-Demand Presentation

Session Chair: Jeong-Ho Lee

Thursday Morning, December 8, 2022

DS02-virtual

7:00 AM DS02.15.01

Accelerated Prediction of Vickers Hardness of Cobalt and Nickel Based Superalloys from Microstructure and Composition Using Advanced Image Processing Techniques and Machine Learning Nikhil Khatavkar, Sucheta Swetlana and Abhishek Kumar Singh; Indian Institute of Science, India

Superalloys are an important class of material that are employed heavily in energy and defence sectors of economy. The high temperature properties of superalloys is the backbone of the aerospace industry due to its applicability in combustion zones of turbine. Vickers hardness is an important property for the selection of this material. In this work, a new approach is developed to establish the structure-property linkages for nickel and cobalt based superalloys. This approach utilizes advanced image processing techniques coupled with machine learning (ML) to estimate the Vickers hardness of the superalloys with unprecedented accuracy. Initially, highly accurate phase separation is achieved for the gamma and gamma-prime phases followed by evaluation of statistical 2-point correlations on the SEM micrographs. These 2-point correlations are an obvious improvement over the conventional microstructure quantification techniques. The correlations are then transformed and ranked according to their variance using principal component analysis (PCA). These transformed correlation along with the composition of the superalloys are then utilized to develop the ML models. The ML models trained using the

Gaussian process regression (GPR) shows unprecedented accuracy with the root mean squared error (RMSE) of 0.14 and R^2 of 0.98. The ML models are unparalleled in the literature and can be of direct applicability to the industry for performance and safety optimization of several important components of aircraft turbines. Further analysis of the model presents numerous trends for increasing the hardness of superalloys. For instance, addition of iron and titanium lead to increase of hardness, while aluminium and tantalum affect the hardness negatively. The ML models developed in this work are trained on the experimental data directly, as opposed to the works on simulated data found commonly. This gives an insurmountable advantage to our ML models in the applicability and transferability. The ML models developed can be generalized for any mechanical property of interest with minimal efforts and can be utilized for accelerated development of new generation of high temperature superalloys.

SYMPOSIUM DS03

Artificial Intelligence Approaches for Energy Materials
November 28 - December 8, 2022

Symposium Organizers

Sijia Dong, Northeastern University
Arun Kumar Mannodi Kanakkithodi, Purdue University
Noah Paulson, Argonne National Laboratory
Logan Ward, University of Chicago

Symposium Support

Silver

Energy Material Advances, a Science Partner Journal

Bronze

Chemical Science | Royal Society of Chemistry
Patterns, Cell Press

* Invited Paper
+ Distinguished Invited

SESSION DS03.01: Materials Discovery
Session Chairs: Arun Kumar Mannodi Kanakkithodi and Noah Paulson
Monday Morning, November 28, 2022
Hynes, Level 2, Room 206

10:30 AM *DS03.01.01

Data-Driven Discovery and Design of Thermoelectric Materials Christopher Wolverton, Northwestern University, United States

Thermoelectrics have potentially significant energy applications, but only if high efficiency materials can be found. However, discovery and design of novel thermoelectrics is particularly challenging, due to the complex set of materials properties that must be simultaneously optimized. Data-driven approaches to discovery and design of materials are a research area that has the potential to significantly accelerate discovery of these energy materials. Here we discuss our efforts at developing and applying data-driven computational techniques that enable an accelerated discovery of novel thermoelectrics. These techniques involve a combination of high-throughput density functional theory (DFT) calculations, inverse design approaches, and machine learning and artificial intelligence based methods. We discuss several recent examples of these methods: (i) inverse design strategies based on a materials database screening to design a solid with a desired band structure, specifically both flat and dispersive components with respect to crystal momentum, (ii) inverse design strategies to identify compounds with ultralow thermal conductivity (iii) an effective strategy of weakening interatomic interactions and therefore suppressing lattice thermal conductivity based on chemical bonding principles, and (iv) the development of crystal graph based neural network techniques to accelerate high-throughput computational screening for materials with ultralow thermal conductivity.

11:00 AM DS03.01.02

A Reinforcement Learning Guided Search for Stable and Functional Inorganic Crystal Structures Jeffrey Law¹, Shubham Pandey², Prashun Gorai^{2,1} and Peter St. John¹; ¹National Renewable Energy Lab, United States; ²Colorado School of Mines, United States

Solid-state batteries (SSBs) are safer, more efficient, and potentially more recyclable than traditional batteries. However, major challenges such as interfacial instabilities remain to be overcome. Well-known solid electrolytes are unstable at the interface with metal anodes (e.g. Li metal) as well as with a high-voltage cathode. While large-scale DFT calculations has enabled functional materials discovery, only a small fraction of the plausible compositions (10^6 - 10^9) can be explored with these relatively expensive computations.

A central problem in using AI to accelerate the search for novel crystalline materials is finding thermodynamically stable structures. Composition-only models lack the accuracy required for assessing stability, especially for polymorphic structures (*I*). Graph neural network (GNN) models can achieve

impressive accuracy, on the order of 1 kcal/mol, in predicting formation enthalpy and energy above the hull; however, the exact input structure is known only after performing expensive DFT relaxation (2, 3). Some progress has been made in predicting stability directly from the unrelaxed structures (4), but the accuracy of these approaches is limited by the degree to which the crystal structure changes during DFT relaxation. In developing models intended to rank the stability of potentially unstable crystal structures, including high-energy hypothetical structures in the training data is critical to achieving reasonable performance (5). In an analogous fashion, training only on fully relaxed energies may bias GNN models to predict lower energies for unrelaxed inputs in high-energy configurations.

Here we develop a reinforcement learning (RL) framework for designing new crystal structures and apply it to the challenge of discovering stable SSB materials. For the surrogate model, we trained a crystal-graph convolutional neural network (CGCNN) on a carefully designed dataset of close to 150,000 final geometries and total energies of three main structure types: ground-state (ICSD), hypothetical battery structures fully relaxed with DFT, and example hypothetical battery structures where only the cell volume is optimized. In this manner, our surrogate model learns to predict a scale-invariant formation energy of the crystal structure in its given coordination, which we subsequently minimize with RL. Validating our top-performing candidates with full DFT relaxations confirms a high percentage of them to be stable while exhibiting large electrochemical stability windows.

1. C. J. Bartel *et al.*, *npj Comput. Mater.* **6**, 1–11 (2020).
2. T. Xie, J. C. Grossman, *Phys. Rev. Lett.* **120**, 145301 (2018).
3. C. W. Park, C. Wolverton, *Phys. Rev. Mater.* **4**, 63801 (2020).
4. K. Pal, C. W. Park, Y. Xia, J. Shen, C. Wolverton, *npj Comput. Mater.* **8**, 1–12 (2022).
5. S. Pandey, J. Qu, V. Stevanović, P. St. John, P. Gorai, *Patterns*. **2** (2021), doi:10.1016/j.patter.2021.100361.

11:15 AM DS03.01.03

Comparing Forward and Inverse Modeling Paradigms—A Case Study on High-Entropy Alloys Arindam Debnath and Wesley Reinhart; The Pennsylvania State University, United States

Refractory High-Entropy Alloys (HEAs) are a promising class of materials for ultra-high-temperature applications including energy generation from gas turbines. In addition to having exceptional mechanical properties at elevated temperatures, these materials can be highly tailored to individual applications by selection of the constituent elements. The relationship between elemental composition and function is challenging to understand and even harder to predict because it is nonlinear, high-dimensional, and results from physical phenomena at many scales. As a result, machine learning is an attractive tool for the empirical design of these materials. While conventional materials design has utilized predictive models to rapidly test hypothesized material compositions in a search for improved ones, more recent generative modeling approaches provide for the possibility of “inverse modeling.”

We have recently developed deep-learning-based generative models including variants on the Generative Adversarial Network (GAN) architecture to perform inverse modeling of refractory HEAs with tailored properties. Generative modeling offers an attractive solution to materials design problems due to its ability to approximate the inverse function directly (i.e., properties to composition) without the need to search the design space. However, we have also faced challenges in training our models on sparse and uncertain experimental data gathered from literature. Here we compare the design of HEAs using these generative models (the “inverse” paradigm) and surrogate regression models (the “forward” paradigm). We discuss the lessons learned from our preliminary work and strategies we are developing to measure the effectiveness of each approach in designing new HEAs for ultra-high-temperature applications.

11:30 AM DS03.01.04

A Unified Active Learning Framework for Designing Energy-Relevant Molecules Shomik Verma¹, Jiali Li², Kevin Greenman¹, Rafael Gomez-Bombarelli¹, Xiaonan Wang^{2,3} and Aron Walsh⁴; ¹Massachusetts Institute of Technology, United States; ²National University of Singapore, Singapore; ³Tsinghua University, China; ⁴Imperial College London, United Kingdom

Solar photovoltaic (PV) technology has received immense, global interest in recent years. Many novel devices have been created beyond conventional silicon solar cells, such as thin film PV, organic PV, and perovskites. Unfortunately, all such single-junction solar cells suffer from an efficiency cap known as the detailed-balance limit, which limits solar cell efficiency to 33.7%. This limit is primarily due to solar cells unable to absorb light below their bandgap, and inefficiently absorbing light above their bandgap.

One strategy to improve PV efficiency is to use certain organic molecules that up- or down-convert photon energies using interplays between their excited states. Two common types of photon conversion processes are triplet-triplet annihilation (TTA) up-conversion and singlet fission (SF) down-conversion. However, designing efficient TTA and SF molecules comes with several challenges. Namely, the design space of organic photon conversion molecules is massive; for example, 166 billion organic molecules exist with less than 17 atoms. Further, experiments or first-principles simulations to evaluate the excited state energies of these molecules are time- and resource-consuming.

Fortunately, large scale virtual screening and inverse design with machine learning are promising solutions, as they allow accelerated evaluation of properties and efficient exploration of chemical space. Supervised machine learning comes with its own challenges, however. As a primarily data-driven method, it is limited by slow acquisition of labeled data for model training. Further, the chemical design space is diverse, so a large amount of labeled data is required for training to ensure sufficient coverage. Finally, tasks may be very different or require non-overlapping data. For these reasons, a model with high accuracy for desired properties is difficult to obtain.

Therefore, it is useful to develop an efficient, unified strategy for generating training sets and suggesting candidate molecules under different conditions. Active learning is one promising strategy for achieving this, as it efficiently explores chemical space. This study presents an active learning framework for designing energy-relevant molecules, where molecules suitable for TTA up-conversion and SF down-conversion are taken as a case study.

First, an ultra-fast chemical simulation method based on machine-learned calibrations to tight binding is developed for accelerating the labeling process. The calibration training set is carefully curated to ensure both breadth of chemical space and depth in space of molecules of interest, namely large aromatic molecules with pi-conjugated bonds.

Next, we use this accelerated labeling to generate a large molecular database and benchmark various active learning strategies with different priorities over this database. Namely, we implement different acquisition functions for both pool-based and generative-based active learning approaches, based on suitability terms developed for target tasks, uncertainty terms derived from surrogate models, and domain knowledge terms for different specific applications.

Finally, a generative machine learning model is developed based on the informative database derived from the unified active learning framework. The

generative model considers both suitability and synthetic accessibility to reduce experimental effort. A pool of molecules suitable for TTA up-conversion and SF down-conversion are proposed, verified with higher-fidelity computational chemistry methods, and finally demonstrated with experiments.

Overall, a unified active learning framework is developed, and molecules suitable for TTA and SF are proposed. The suitability of these materials as photon conversion materials to improve PV efficiency is a promising demonstration of the utility of this approach for designing energy-relevant molecules.

11:45 AM DS03.01.05

Machine-Learning Assisted Discovery of High-Mobility Materials [Husna Anwar](#)¹, Hitarth Choubisa¹, Koen Bertens¹ and Edward H. Sargent^{1,2};
¹University of Toronto, Canada; ²Northwestern University, United States

Machine Learning (ML) models have been shown to accelerate materials discovery by orders of magnitude over traditional computational methods such as density functional theory (DFT)¹. Optical properties, specifically absorption profiles, are very computationally expensive to calculate for alloys, given the large number of configurations available for a single combination of precursors. Additionally, even ML models trained on simulated data often fail to produce physically realizable predictions. Herein we present a multistep ML model that produces new, high-mobility material compositions by predicting their absorption spectra. This model is the first to use a database of experimentally derived compositional data to predict absorption profiles. Absorption profiles contain a rich array of information about material characteristics including bandgap and carrier concentration. The capability of predicting absorption spectra without having to fabricate and characterize thin films is of particular interest for the spectroscopy community². Hence, the first step of our model is trained on various material compositions and predicts their absorption spectra. Given that our chosen database also contains conductivity measurements and synthetic parameters, we further develop our model to calculate the carrier mobility for a given composition using the number of free carriers derived from the absorption profile and conductivity. So, in the second step, the model uses the predicted absorption profile together with conductivity data to train a genetic algorithm (GA) that produces new compositions with high mobilities. We demonstrate the effectiveness of our model by combining it with a segmentation algorithm that identifies materials with bandgaps favorable for optoelectronic applications and verify our results using DFT.

For a given set of precursors, we found that our model produces absorption spectra, at a minimum, 1000 times faster than when we tried to predict the same using DFT. Rather than training on optical data, that may introduce bias in our predictions, we train on three experimental parameters that are key to thin-film fabrication and optimization: compositional stoichiometry, film thickness and annealing temperature. By training on these parameters, we produce a well-generalized model with an R2 value of 0.87. The bandgaps derived from the predicted spectra have a mean absolute error (MAE) of 0.1 eV, a significant improvement over 0.33 eV MAE for current state-of-the-art computational bandgap predictions³.

References:

1. Stein, H. S., Guevarra, D., Newhouse, P. F., Soedarmadji, E. & Gregoire, J. M. Machine learning of optical properties of materials – predicting spectra from images and images from spectra. *Chem. Sci.* **10**, 47–55 (2019).
2. Carbone, M. R., Topsakal, M., Lu, D. & Yoo, S. Machine-Learning X-Ray Absorption Spectra to Quantitative Accuracy. *Phys. Rev. Lett.* **124**, 156401 (2020).
3. Chen, C., Zuo, Y., Ye, W., Li, X. & Ong, S. P. Learning properties of ordered and disordered materials from multi-fidelity data. *Nat. Comput. Sci.* **1**, 46–53 (2021).

SESSION DS03.02: Materials Informatics Methods
Session Chairs: Sijia Dong and Arun Kumar Mannodi Kanakthodi
Monday Afternoon, November 28, 2022
Hynes, Level 2, Room 206

1:30 PM *DS03.02.01

Polymer Informatics—Recent Advances in Algorithms to Solve Forward and Inverse Problems [Rampi Ramprasad](#); Georgia Institute of Technology, United States

Polymers display extraordinary diversity in their chemistry, structure, and applications. However, finding the ideal polymer possessing the right combination of properties for a given application is non-trivial as the chemical space of polymers is practically infinite. This daunting search problem can be mitigated by surrogate models, trained using machine learning algorithms on available property data, that can make instantaneous predictions of polymer properties. I will present a versatile, interpretable, and scalable scheme to build such predictive models. Our “multi-task learning” approach is used for the first time within materials informatics and efficiently, effectively, and simultaneously learns and predicts multiple polymer properties. It is thus a powerful tool to solve “forward materials problems”, i.e., property predictions. I will also discuss new approaches to solve “inverse materials problems”, i.e., identifying materials that satisfy target property criteria. This discussion will include advances made to the genetic algorithm and graph-to-graph translations for polymers. These forward and inverse method developments are expected to have a significant impact on data-driven materials discovery.

2:00 PM DS03.02.04

Fast Optimization of Needle-in-a-Haystack Energy Problems Using Zooming Memory-Based Initialization (ZoMBI) [Alexander E. Siemenn](#)¹, Zekun Ren², James Serdy¹, Basita Das¹, Blake H. Hudspeth¹, Marilyn R. Meyers¹, Emre Tekoglu¹, Myles G. Stapelberg¹, Michael Short¹, Ju Li¹, A. John Hart¹ and Tonio Buonassisi¹; ¹Massachusetts Institute of Technology, United States; ²Singapore-MIT Alliance for Research & Technology, Singapore

Energy materials innovation challenges can require identifying rare combinations of properties at the extremes of distributions. Standard optimization approaches fare well with largely convex and smooth function spaces, but fail in high dimensions, in non-convex spaces with multiple suboptimal local extrema, and with needle-like global optima with local convexity in only a tiny fraction of total function space. Examples of these kinds of problems are searches for specific compositions of matter with constellations of rare user-defined target properties, for example metal alloys with ultrahigh specific strength. With today’s methods’ limitations, experimental searches for novel rare materials require prohibitively large numbers of experiments, even with machine-learning guided exploration.

We believe that addressing this problem requires a multifaceted approach, bringing together simulation, high-throughput experiment, and machine learning methods. To address the ML portion of this challenge, we propose the Zooming Memory-Based Initialization (ZoMBI) algorithm to augment traditional BO methods by zooming in the search bounds of BO based on the extents of the best-performing data points in memory, and then erasing all other memory to accelerate compute. We demonstrate the performance and compute requirements (dimensional scalability) of ZoMBI on a 5-dimensional Ackley

function, a common algorithm benchmarking function, and a 5-dimensional DFT-derived dataset of a rare materials property (negative Poisson's ratio). The ZoMBI algorithm is demonstrated to achieve computing speed-ups of over 400x compared to traditional BO. We also introduce preliminary results from an automated synthesis tool capable of achieving >2000 materials per minute, to explore alloyed materials in the search for rare properties.

2:15 PM DS03.02.05

Variational Method-Based Operator Neural Network for Dynamic Systems in Energy Materials Governed by Gradient Flows [Wei Li](#)^{1,2}, Avtar Singh¹ and Juner Zhu^{1,2}; ¹Massachusetts Institute of Technology, United States; ²Northeastern University, United States

Variational methods have been well established to derive the governing equations of complex, coupled, and nonlinear systems. One example is the gradient flow that entails finding and constructing an appropriate potential energy and inner product to incorporate the kinetics into a variational framework. Gradient flows can be applied to a large variety of physics, including diffusion, phase separation, microstructure evolution, etc., where the governing partial differential equations (PDEs) can be eventually obtained. The conventional numerical methods, such as the finite element method (FEM), have been proven to be effective in solving PDEs. However, it is still challenging for systems with high dimensionality and nonlinearity. Recently, we have witnessed great successes in machine learning (ML) applications in many scientific disciplines. The concept of scientific machine learning was proposed and widely used by many research groups to solve variational problems. One of such approaches is approximating the solutions with ML models and training them by minimizing the energy functional, instead of solving a large set of non-linear equations. An example is the energy-based neural networks. Recently, another approach started to gain increasing attention, which is referred to as operator learning (OL). OL models the mapping from one functional space to another. It has the potential to incorporate solutions with different initial conditions into one algorithm. In this study, we proposed a general variational method-based operator neural network framework for dynamics systems governed by gradient flows. To validate the proposed framework, we investigated several dynamics systems that commonly exist in energy materials, including the linear relaxation kinetics, Allen-Cahn dynamics, and phase-field dynamic fracture. We compared the prediction of the proposed neural network with the FEM solution and found satisfactory agreements. We expect that the trained neural networks can work as surrogate models for energy materials to provide rapid predictions.

2:30 PM BREAK

SESSION DS03.03: Text Mining and Synthesis Prediction
Session Chairs: Noah Paulson and Manuel Tsotsalas
Monday Afternoon, November 28, 2022
Hynes, Level 2, Room 206

3:30 PM *DS03.03.01

Data Driven Methods for Text Mining in Energy Technologies [Elsa Olivetti](#); Massachusetts Institute of Technology, United States

This invited talk will cover the latest in our group's work to extract data to inform development of energy technologies

4:00 PM DS03.03.02

A Holistic Multi-Step Retrosynthesis NLP Model for Plausible Synthetic Pathway Planning in Time Efficient Manner. [Jin Woo Kim](#), Youngchun Kwon, Dongseon Lee and Youn-Suk Choi; Samsung Advanced Institute of Technology, Korea (the Republic of)

The plausible synthetic pathway design is critical for accelerating new material discovery. There can be various precursor candidates for a given target molecule. Also, it usually requires investigation of the vast majority of multi-step pathways to find all available (or purchasable) building blocks, which makes it complex and challenging task. Conventionally, highly skilled experts plan multi-step synthesis strategies utilizing their knowledge and intuition. In recent years, a variety of AI-driven pathway suggestion methods have been developed, leveraging extensive synthetic pathway data with emerging machine learning techniques.

The AI-driven methods have three common components: i) AI model for single-step retrosynthesis, ii) Synthetic tree search algorithm, and iii) Pathway scoring functions. The single-step retrosynthesis model takes the structural representation of a target molecule as an input, then it proposes sets of precursor candidates. It is applied recursively for each synthetic step until all available building blocks are figured out. To prevent combinatorial explosion during the recursive enumeration, tree search algorithms such as Monte Carlo Tree search (MCTS) or hyper-graph exploration method have been employed. Also, pathway scoring functions are devised to select probable nodes (i.e. precursor candidates) to be explored during the tree search. In many cases, scoring functions included some simple heuristic terms such as the number of steps. Also, a recent study proposed pathway evaluation method based on tree-LSTM model for considering tactical synthetic strategies which can be recognized by observing the overall multi-step information, not individual single-step data. The results showed that it provided more plausible pathway suggestions.

The previous methods have shown successful results. However, there are two points to be addressed. First, synthetic step-wise tree search algorithm is still time-consuming part for obtaining the results. Second, even though the current stand-alone evaluation model can view the information of entire synthesis steps, the retrosynthesis AI model can only deal with single-step synthesis data yet. To this end, we propose a novel approach to train AI retrosynthesis model which can suggest multi-step pathways more efficiently. Also, we developed it to learn holistic multi-step pathways, which we expect it to suggest more plausible pathways. There are two key differences from the previous studies. The first one is that we designed a new multi-step pathway representation and the training technique for it. Our representation expresses entire synthesis steps as a string format, so that it contains a whole steps information in a single representation. Then, we adopted the several natural language process techniques to train those data. The other one is that our method does not require synthetic step-wise tree search algorithm, which decreases the computational time.

We validate the performance of our method in terms of its accuracy and elapsed time. First, we trained our model on 28 thousand multi-step synthesis data extracted from Reaxys DB with 8:1:1 (=train:valid:test) split ratio. The top-10 accuracy was 59.1 % and it takes approximately 9 minutes for suggesting multi-step pathways of 2.8 thousand test target molecules with a single core AMD EPYC 7413 CPU and a single A100 GPU. Moreover, we compared our method to the previous approach. For comparison, we devised our baseline model combining single-step retrosynthesis model based on the tied two-way architecture invented in our previous research and the MCTS algorithm. We randomly selected 40 target molecule examples from the test set. The top-10 accuracy of new approach was 37.5 % higher than the conventional one with dramatically decreased elapsed time.

4:15 PM DS03.03.03

The Largest Knowledge Graph in Materials Science—Entities, Relations and Link Predictions Through Graph Representation Learning [Vineeth Venugopal](#)¹, Sumit Pai², Elton Pan¹, Christophe Guéret² and Elsa Olivetti¹; ¹Massachusetts Institute of Technology, United States; ²Accenture Labs, Ireland

Information on materials is available through several platforms - online computational data repositories such as the Materials Project, OQMD, NOMAD etc, scientific literature databases such as Elsevier, Arxiv, Web of Science etc, repositories of experiments such as ICSD, NIST databases, published textbooks, handbooks, industrial datasheets, and more recently in high throughput databases. This data can be structured - eg, the indexed, tabular data in online databases - or unstructured, as in textbooks and scientific literature. Further, while some data is available as numerical or categorical attributes ('melting point', 'space group'), most are delocalised within large chunks of text, or available in images. The presence of multiple streams and modes of data along with the sheer amount of information available at present and being continuously generated taxes human cognition and calls for automated systems that identify, catalog, link, and query information on its own.

Recently, Knowledge Graphs (KGs) have emerged as a tool for integrating data and relational ontologies through versatile graph databases. KGs are the industrial standard for data retrieval and organization as demonstrated by KG use in Google Search, social media sites such as Facebook and LinkedIn, as well as companies with large data inventory such as Ikea and NASA. In the field of materials science as well, several domain specific ontologies and property graphs have been proposed, though the use of knowledge graphs as a relational database tool is not very common at present.

Here we present a knowledge graph in the field of materials science comprising over half a million unique entities and over ten million statements, where each statement is an (entity, relation, entity) triple. The KG covers several topical fields such as inorganic oxides, functional materials, battery materials, metals and alloys, polymers, cements, high entropy alloys, biomaterials, and catalysts. The triples are generated autonomously through data driven natural language processing pipelines and extracted from a corpus of around 6 million published scientific articles. Several informational entities such as materials, properties, application areas, synthesis information, and characterization methods are integrated together with a hierarchical ontological schema, where the base relations are extracted through statistical correlations to which higher level ontologies are appended. Thus the KG is heterogeneous and contains multiple relations between entities. It is shown that a bipartite projection of the base KG leads to comprehensive relational graphs that link materials to their chief attributes and applications and help answer questions such as "what are key attributes of battery materials?" without human intervention.

We use a graph neural network based representational learning method to learn embeddings for entities and their relations which translate the graph data structure to a high dimensional mathematical space in which semantic relations between entities can be formulated as algebraic operations. This can be used not only to query the KG but can also predict new linkages between existing entities, thereby providing a versatile data informed tool for materials development and discovery. Key aspects of the knowledge graph which include entity extraction and link prediction are variously validated and compared with benchmarks where available. Finally, it is shown that the learned embedding representations encrypt physical and chemical information, which lend itself to machine learning in an easy manner.

4:30 PM *DS03.03.04

Natural Language Processing for Data Extraction and Synthesizability Prediction from the Energy Materials Literature Anubhav Jain; Lawrence Berkeley National Laboratory, United States

Historically, both data and knowledge (connections and conclusions based on data) in the materials domain has been recorded mainly as text, figures, or tables in journal articles. Such data is critical to both conventional and machine learning-driven materials discovery. In this talk, I will describe some of our efforts to extract information from the research literature automatically based on natural language processing techniques. For example, data on the dopability of materials is difficult to simulate, but is present either implicitly or explicitly as part of many research studies. Similarly, data on materials synthesis can be difficult or impossible to simulate but can be extracted from the historical research literature. The talk will summarize our most recent progress towards extracting both individual data items as well as "knowledge" (e.g., proposed applications of a chemical composition) in various areas, including extracting materials property data and data pertaining to materials synthesis. Overall, such work may ultimately lead to accelerated energy materials design through access to previously hidden data sets.

5:00 PM DS03.03.05

MOF Synthesis Prediction Enabled by Automatic Data Mining and Machine Learning Yi Luo¹, Saientan Bag², Orysia Zaremba³, Adrian Cierpka⁴, Jacopo Andreato³, Stefan Wuttke³, Pascal Friederich⁴ and Manuel Tsotsalas¹; ¹Institute of Functional Interfaces, Karlsruhe Institute of Technology, Germany; ²Institute of Nanotechnology, Karlsruhe Institute of Technology, Germany; ³Basque Center for Materials, Applications & Nanostructures, Spain; ⁴Institute of Theoretical Informatics, Karlsruhe Institute of Technology, Germany

Metal-organic frameworks (MOFs) are porous materials formed via the connection between metal-centered nodes with organic linkers.¹ With the utilization of different metal nodes and linkers, the topology, pore size, and functional groups of MOFs can be adjusted for high specific surface area, numerous active sites, and mass transfer channels.² This flexibility in the MOF design allows great potential for MOF-based and MOF-derived material in the application in energy storage and conversion.³ Computer-assisted methods have been applied in the acceleration for the design of MOF-based materials.⁴⁻⁶ However, the potential of using machine learning (ML) methods to suggest parameters in MOF synthesis experiments is not well explored. Here, we show an approach of data mining and machine learning (ML) method for rationalization and acceleration of the MOF discovery process by directly predicting the synthesis condition of a new MOF based on its crystal structure.⁷ There are three steps in our approach: 1) Creation of a MOF synthesis database (SynMOF) via automatic extraction of synthesis parameters from scientific literature; 2) Training of multiple ML models on the SynMOF database; 3) Prediction of synthesis conditions for new MOF structures by the ML models. These early-stage ML models, exhibit a good prediction performance, surpassing human expert predictions, which was shown through a synthesis survey from 11 MOF experts worldwide.

References

- (1) Furukawa, H.; Cordova, K. E.; O'Keeffe, M.; Yaghi, O. M. The Chemistry and Applications of Metal-Organic Frameworks. *Science* **2013**, *341* (6149).
- (2) Du, R.; Wu, Y.; Yang, Y.; Zhai, T.; Zhou, T.; Shang, Q.; Zhu, L.; Shang, C.; Guo, Z. Porosity Engineering of MOF-Based Materials for Electrochemical Energy Storage. *Advanced Energy Materials* **2021**, *11* (20), 2100154.
- (3) Adegoke, K. A.; Maxakato, N. W. Porous Metal-Organic Framework (MOF)-Based and MOF-Derived Electrocatalytic Materials for Energy Conversion. *Materials Today Energy* **2021**, *21*, 100816.
- (4) Moosavi, S. M.; Chidambaram, A.; Talirz, L.; Haranczyk, M.; Stylianou, K. C.; Smit, B. Capturing Chemical Intuition in Synthesis of Metal-Organic Frameworks. *Nat Commun* **2019**, *10* (1), 539.
- (5) Luo, Y.; Ahmad, M.; Schug, A.; Tsotsalas, M. Rising Up: Hierarchical Metal-Organic Frameworks in Experiments and Simulations. *Advanced Materials* **2019**, *31* (26), 1901744.
- (6) Ahmad, M.; Luo, Y.; Wöll, C.; Tsotsalas, M.; Schug, A. Design of Metal-Organic Framework Templated Materials Using High-Throughput Computational Screening. *Molecules* **2020**, *25* (21), 4875.
- (7) Luo, Y.; Bag, S.; Zaremba, O.; Cierpka, A.; Andreato, J.; Wuttke, S.; Friederich, P.; Tsotsalas, M. MOF Synthesis Prediction Enabled by Automatic Data Mining and Machine Learning*. *Angewandte Chemie International Edition* **2022**, *61* (19), e202200242.

8:00 AM *DS03.04.01

Reinforcement Learning for Crystal Structure Search [Subramanian Sankaranarayanan](#); Argonne National Laboratory, United States

The most common and popular method for structure search and optimization are based on evolutionary design. This can often be cumbersome, limited to few tens of parameters and fails for large structural configurations or design problems with high degrees of freedom. Reinforcement learning approaches mostly operate in discrete action space such as in Go game but the applications of that to inverse problems is limited since most inverse problems deal with continuous action space. There are a large number of inverse structural search problems ranging from crystal structure search in material sciences to topology design in Quantum information, where it is highly desirable to optimize structure/configuration to target desired properties or functionalities. This talk will provide an overview of our current efforts to perform scalable crystal structure and topology search to discover and design metastable or non-equilibrium phases with desired functionality. We will also discuss our efforts on fingerprinting and use of unsupervised learning to identify crystal structures and critical nuclei from amorphous melts, using zeolites as a representative example.

8:30 AM DS03.04.02

Combining Organic and Inorganic Descriptors for Predictions of Volatility Across Vast Chemical Space [Anand Chandrasekaran](#), Alex K. Chew, Simon D. Elliot, Asela Chandrasinghe, Subodh Tiwari, H. Shaun Kwak and Mathew D. Halls; Schrodinger, United States

Many industries are now leveraging machine learning approaches to predict materials properties that are challenging to measure, necessitating descriptors that are capable of characterizing a wide range of materials. Traditional QSAR/QSPR approaches use machine learning to map 2D molecular structures to a materials' property/label of interest. These 2D structures are usually numerically characterized using bit-based fingerprints that count the number of substructures in a molecule. However, fingerprint-based approaches do not generally perform well for inorganic or metal-containing compounds. Recently, materials informatics descriptors have been developed that span the entire periodic table, capturing both chemical and stoichiometric information of inorganic compounds and alloys. In this work, we utilize a combination of bit-based fingerprints and inorganic descriptors to train machine-learning models that can predict volatility across a huge chemical space of organic and organometallic materials (spanning more than 50 elements). We benchmark a number of different machine learning approaches and show that stacking estimators perform better than a single algorithm/model. These highly accurate models for evaporation temperatures (at different pressures) and vapor pressures (at different temperatures) are invaluable in areas, such as thin film deposition, flavors/fragrances, refrigerants, volatile pollutants and toxicity.

8:45 AM DS03.04.03

Multi-Task Machine Learning Predictors to Combat Data Scarcity—The Examples of Gas Diffusivity and Permeability in Polymers [Brandon K. Phan](#), Kuan-Hsuan Shen and Rampi Ramprasad; Georgia Institute of Technology, United States

Gas transport through polymer membranes is critical in current and emerging applications such as carbon capture, hydrogen recovery and fuel cells. Accurate machine learning (ML) prediction of gas diffusivity in polymers allows us to better control membrane transport properties such as selectivity and permeability and opens up the opportunity to discover novel polymer membrane materials with enhanced performance. However, the accuracy of traditional predictive ML models that are trained on one single property is often constrained by the size of the dataset. To overcome this issue, we created multi-task neural network (NN) models that are trained on both gas diffusivity and permeability to take advantage of larger available permeability data in literature. Such multi-task models exploit the correlations in the data corresponding to the different tasks. In our case, gas diffusivity is related to the ratio of the permeability and solubility. Our multi-task model showed significantly improved R^2 and reduced error for gas diffusivity predictions compared to the single-task model, especially at a small training dataset size. This demonstrated the effectiveness of this multi-task approach on improving the model accuracy when not enough data is available for the property of interest. Moreover, a multi-task gaussian process regression (GPR) model was also trained to test against the NN model. We found that the NN model outperformed the GPR counterpart at almost all training dataset sizes, and also benefited from the better scaling of training time. Overall, we created a multi-task neural network model capable of predicting gas diffusivity in various polymers with a high accuracy. With this model, we will screen existing and new polymers to identify promising polymer membrane materials with improved gas properties.

9:00 AM *DS03.04.04

Enhancing Physics-Based Modeling and Extracting Physics from Data Using Machine Learning [Alejandro Strachan](#); Purdue University, United States

The synergy between principles-based modeling and data science is playing an increasingly important role in materials science and engineering. In addition, there is significant interest in using machine learning (ML) tools to extract physical laws as well as symmetries and associated invariants from data. I will discuss recent progress in machine learning applied to multiscale modeling and in the development of interpretable models that balance accuracy with parsimony.

ML for multiscale modeling. ML interatomic potentials have shown near quantum mechanical accuracy at a fraction of the cost, enabling large-scale atomistic simulations. We developed an iterative approach to address the challenge of generating training data and address the stochastic nature of NN training. I will demonstrate the approach with the development of neural network reactive force fields (NNRF) for the phase change material GeSbTe of interest in electronics. MD simulations with these potentials provide new insight into the process of crystallization from the amorphous state.

Discovery of interpretable physical laws from data. I will introduce parsimonious neural networks (PNNs) that combine neural networks with evolutionary optimization to find models that balance accuracy with parsimony. The power and versatility of the approach will be demonstrated by developing models for classical mechanics and for the melting temperature of materials from fundamental properties. In the first example, the resulting PNNs are easily interpretable as Newton's second law, expressed as a non-trivial time integrator that exhibits time-reversibility and conserves energy, where the parsimony is critical to extracting underlying symmetries from the data. In the second case, the PNNs not only find the celebrated Lindemann melting law, but also new relationships that outperform it in the Pareto sense of parsimony vs. accuracy.

Making workflows and data FAIR. Finally, I will also describe recent developments in nanoHUB, an open cyberinfrastructure for cloud scientific computing, towards making simulation workflows and their data findable, accessible, interoperable, and reusable (FAIR). We introduce Sim2Ls (pronounced sim tools) and the Sim2L Python library that allows developers to create and share end-to-end computational workflows with well-defined and verified inputs and outputs. The Sim2L library makes Sim2Ls, their requirements, and their services discoverable, verifies inputs and outputs, and automatically stores results in a globally accessible simulation cache and results database.

9:30 AM DS03.04.05

A Multi-Task Machine Learning Approach to Predict Molecular Interactions and Diffusivity in Polymers Janhavi Nistane, Lihua Chen, Kuan-Hsuan Shen and Rampi Ramprasad; Georgia Institute of Technology, United States

Understanding the diffusion behavior of organic molecules through polymers is critical for many applications, including fuel production, coatings, and drug delivery systems. Experimental methods to measure diffusivity are usually time and cost-intensive. Further, available experimental data on organic molecular interactions and diffusivity is sparse and covers only limited chemical space. Here, we present a multi-task machine learning (ML) approach to instantaneously predict solvent diffusivity in polymers. The multi-task ML model is trained simultaneously on both available experimental and computational data generated by us using high-throughput classical molecular dynamics simulations. The experimental data is regarded as high-fidelity data; however, this data is only available across a limited chemical space. On the other hand, simulations offer the flexibility to obtain diffusivity values across a vast chemical space. Although there is only semi-quantitative agreement between simulations and experimental values, correlations that do exist between the two classes of data is exploited by the multi-task neural network architecture. This approach tackles the problem of data scarcity while offering a scalable scheme for further data augmentation, enabling the model to co-learn and make predictions more effectively.

9:45 AM DISCUSSION TIME

10:00 AM BREAK

SESSION DS03.05: ML for Perovskites and Interatomic Potentials
Session Chairs: Arun Kumar Mannodi Kanakkithodi and Noah Paulson
Tuesday Morning, November 29, 2022
Hynes, Level 2, Room 206

10:30 AM DS03.05.01

Bayesian Optimization of Perovskite Solar Cells Made by Multiple Short Light Pulses Weijie Xu, Anusha Srivastava, Jessica Grayson and Julia W. Hsu; The University of Texas at Dallas, United States

Photonic curing, a novel processing technique, can promote large-area perovskite crystallization in milliseconds. Photonic curing delivers light pulses from a xenon flash lamp to the sample. The time profile of the pulse can be shaped by utilizing multiple short pulses with custom duty cycles, i.e., micro-pulses. Thus, we can use micro-pulses in photonic curing to design the resulted temperature profiles of perovskite films. Because perovskite films are not exposed to continuous high-intensity light, they can absorb more radiant energy while not being damaged. However, micro-pulse has too many variables—pulse voltage, pulse length, number of micro-pulses, and duty cycles—making it difficult to be optimized by one variable at a time efficiently, which hinders the application of micro-pulses in photonic curing.

In this work, we demonstrate the optimization of micro-pulsed photonic curing with four input variables and aim to achieve the highest PSC power conversion efficiency. Pulse voltage is proportional to the radiant power (W/cm^2) and pulse length is the duration of the pulse (ms). Bayesian optimization (BO) framework is employed to search for the optimal processing conditions in the high-dimensional experimental space. To minimize the optimization time, we perform BO in two steps. Because UV-vis absorbance spectra are quick to measure, we first use UV-vis absorbance to characterize the MAPbI₃ film quality by comparing the absorbance step at MAPbI₃ bandgap (~785 nm) and scattering at longer wavelengths. High-quality MAPbI₃ films should have a large absorbance step at 785 nm and little scattering.[1]Utilizing acquisition function and sequential learning ensures that the ratio between the absorbance step at 785 nm and absorbance above 800 nm is maximized. The first step ensures that we do not spend extra time making solar cells using not promising input variables. Within the narrowed-down input space, our second step exploits the input variables with finer spacings based on device performance. Through iterations, we achieve the global maximum device power conversion efficiency in the input parameter. Visualizing 2D contour plots at every iteration allows the learning results to be understandable by a human. We also examine real-time feature importance using the Shapley Additive Explanation (SHAP) method. Our results demonstrate the feasibility of this two-step BO approach, and we believe that a similar approach can be applied to other processing optimization problems at a lower experimental cost.

This work is supported by NSF CMMI-2109554.

Reference

[1] W. Xu, T.B. Daunis, R.T. Piper, J.W.P. Hsu, Effects of Photonic Curing Processing Conditions on MAPbI₃ Film Properties and Solar Cell Performance, ACS Appl. Energy Mater. 3 (2020) 8636–8645. <https://doi.org/10.1021/acsaem.0c01243>.

10:45 AM DS03.05.02

Machine Learning Prediction of Perovskite Solar Cell Properties Under High Pressure Minkyung Han¹, Chunjing Jia², Yu Lin², Cheng Peng² and Feng Ke^{2,1}; ¹Stanford University, United States; ²SLAC National Accelerator Laboratory, United States

Halide perovskites are promising solar cell materials due to their suitable bandgap range and high tunability. However, materials based on the organic-inorganic (MA)PbI₃ (MA = CH₃NH₃⁺) suffer a chemical instability issue to heat and moisture due to the volatile MA cation, while the all-inorganic Cs-based analogs present a phase instability challenge where the functional perovskite phases are unstable at ambient conditions and spontaneously convert into the thermodynamically stable non-perovskite phase. Therefore, stabilizing the perovskite phases at the room condition is crucial to achieving higher efficiency and commercialization. Tuning the structure by applying pressure and strain is an effective way to modify the stability and electrical properties of perovskite phases. In this work, we investigate the leading structural features that determine the material properties of the perovskites upon compression. We use various machine learning models to train the large-scale dataset obtained from first-principles DFT calculations. This study will provide insights into developing general models to predict the relationship between structural and electrical properties of similar perovskite structures using cost-effective machine learning approaches.

11:00 AM DS03.05.03

Process Understanding of Scalable Perovskite Thin-Film Formation Through Unsupervised Machine Learning of *In Situ* Luminescence Data Felix Laufer¹, Sebastian Ziegler², Fabian Schackmar¹, Edwin A. Moreno Viteri¹, Markus Götz¹, Charlotte Debus¹, Fabian Isensee² and Ulrich W. Paetzold¹;

¹Karlsruhe Institute of Technology, Germany; ²German Cancer Research Center, Germany

High performance perovskite solar cells (PSCs) at laboratory scale show that hybrid metal-halide perovskite semiconductors are a promising absorber material class for the next generation thin-film solar cells. However, transferring the processes to scalable methods that enable large-scale processing remains a key challenge hindering the commercialization of the technology. To enable large-scale and high-throughput production of PSCs, the formation and morphology of perovskite thin-films fabricated by scalable deposition methods needs to be optimized. The perovskite formation process includes the entangled process phases of drying, nucleation and crystal growth, which are crucial for the quality of the perovskite thin-film and must be controlled to obtain thin-films of high optoelectronic quality. Consequently, scaling the technology is complex and demands enhanced understanding of the highly intricate formation process. To improve this understanding and the reproducibility of the scalable thin-film formation process, data-driven machine learning (ML) methods can be employed to accelerate research and process control of large-area perovskite thin-films. For this, a unique, labelled *in situ* photoluminescence (PL) dataset was generated. The dataset contains *in situ* PL data of more than 1,100 PSCs captured during the vacuum-assisted annealing of the blade-coated perovskite thin-films with an in-house-built imaging setup. To generate the ML-based in-line process monitoring dataset, all solar cells were fabricated at the exact same conditions, e.g. layer stack and precursor materials.

In this work, we present unsupervised ML for process understanding of perovskite thin-film formation by employing k-means clustering to our unique *in situ* PL dataset. We show the benefit of acquiring *in situ* PL data during the perovskite formation over *ex situ* PL data by demonstrating the correlation between expert-chosen *in situ* PL features and the power conversion efficiency (PCE) of the corresponding PSCs. Next, we show that k-means clustering creates *in situ* PL clusters that correlate with the performance of the final PSC without prior data encoding assumptions made by a human expert. The correlations display that the *in situ* PL data contains information about the quality of the perovskite thin-film and, consequently, about the performance of the solar cell. Furthermore, we identify detrimental process mechanisms during the formation of the perovskite thin-film using the data science approach. Next to the clusters' performance correlation, differences in the spatial distributions of PL data assigned to the different clusters are identified and reveal substrate areas with adverse thin-film properties. Finally, when applying the trained model to previously unseen data, we find that k-means clustering allows for reasonably good prediction of solar cell performance even though clustering is typically used mainly to explore datasets. In summary, we demonstrate that ML-based in-line processing monitoring of the formation of perovskite thin-films holds great potential and can accelerate the successful commercialization of perovskite thin-film PV.

11:15 AM DS03.05.04

How to Find What is Limiting Your Perovskite Solar Cell Using Bayesian Inference? Basita Das^{1,2}, Thomas Kirchartz^{1,3} and Tonio Buonassisi²; ¹Forschungszentrum Jülich GmbH, Germany; ²Massachusetts Institute of Technology, United States; ³University of Duisburg-Essen, Germany

In a perovskite solar cell, the root cause for underperformance may originate from a large variety of different phenomena such as bulk or interface recombination, transport limitations in the contact layers or bad energy alignment at interfaces. Traditionally, discriminating between these mechanisms has been done by applying a variety of different characterization methods to the samples and then performing some data analysis that often involves fitting the data with analytical equations or numerical models. Such characterizing techniques can be time consuming and often destructive to the device. Furthermore, for the sake of simplicity and to allow fitting the data with a low number of unknowns, the models used for fitting and analyzing the data are often insufficiently complex to really capture all necessary physical phenomena that are relevant to understand the measurement. Ideally one can try to fit more complex device models to the characterization data, but the sheer number of parameters that usually goes into a device simulator, and the correlation between the parameters make the problem intractable. Also, such rudimentary parameter fitting usually gives just one set of parameters that fits the data reasonably well but does not tell us if that combination of parameters is unique or if there are any correlation between the parameters. Information on correlation between parameters is not only important from a device optimization point of view but can also teach us more about the underlying physics controlling the functionality of the device.

In this presentation, we introduce a fast non-destructive method of parameter estimation using Bayesian inference in combination with data current and photoluminescence-voltage measurements taken on perovskite solar cells. From the inferred parameters we identify which region or which layer in our device stack is limiting the performance of our device. Such information is useful to strategize device optimization for better performance. Bayesian inference methods have been previously used in the field of solar cells for well-studied solar cell technologies like Si solar cells as well as for material systems like SnS solar cells where the number of unknown parameters is small [1–3]. In cases where the number of unknowns are few, parameter estimation using only temperature and illumination dependent current voltage (*JVTi*) curves yielded good results.

However, perovskite solar cells have many unknown parameters given it's an emerging PV technology and hence is not as well studied as already established technologies. Perovskite materials are usually intrinsic in nature such that both the electrons and holes matter for carrier transport and recombination and hence increases the number of parameters further. Also, the complex architecture of perovskite solar cell means one requires the knowledge of material parameters of not just the absorber layer but also of the different interfaces and transport layers to fully understand the cause of underperformance. In such scenarios, using only *JVTi* measurements might not be enough to estimate all the desired parameters. In this context we also introduce how combining data from a small number of relatively simple characterization techniques helps in better estimating unknown material parameters.

Also, the Bayesian inference code we developed and the methodology we will introduce is general in nature and can be applied for parameter estimation across fields with just domain expertise of the specific field.

[1] R. E. Brandt, R. C. Kurchin, V. Steinmann, D. Kitchaev, C. Roat, S. Levchenko, G. Ceder, T. Unold, and T. Buonassisi, *Joule* **1**, 843 (2017).

[2] R. Kurchin, G. Romano, and T. Buonassisi, *Comput. Phys. Commun.* **239**, 161 (2019).

[3] R. C. Kurchin, J. R. Poindexter, V. Vähänissi, H. Savin, ¶ Carlos Del Cañizo, and T. Buonassisi, *How Much Physics Is in a Current-Voltage Curve? Inferring Defect Properties from Photovoltaic Device Measurements* (2019).

11:30 AM DS03.05.05

Crystal Structure Prediction of Mixed-Halide Perovskites at Room Temperature Using Machine-Learning Potentials Changho Hong¹, Seungwu Han¹, Yong Youn² and Kanghoon Yim²; ¹Seoul National University, Korea (the Republic of); ²Korea Institute of Energy Research, Korea (the Republic of)

Cesium lead halide perovskites (CsPbI₃) have attracted much attention as a potential candidate for an all-inorganic, high-efficiency solar cell. However, they suffer from short lifetimes because the perovskite phase is unstable at room temperature. To overcome this, recent experiments introduced another halogen element such as Br to stabilize the perovskite structure, which has lower power conversion efficiency than the pure phase. Several computational studies investigated the thermodynamic stability of mixed halides with density functional theory (DFT) calculations and confirmed that the mixing can enhance the stability. However, those computational studies are based on known prototype structures of CsPbI₃, which risks missing unknown phases in mixed-halide perovskites. The heuristic crystal structure prediction (CSP) based on DFT calculations would be necessary in this respect, but it is computationally too expensive to evaluate the energies of numerous candidates.

In this study, we conduct CSP in mixed-halide perovskites (CsPb_{1-x}Br_{3-x}, CsPb_{1-x}Cl_{3-x}) with SPINNER, a recently developed in-house code for CSP using a neural network potential.[1] Using SPINNER, we can explore structures beyond prototypes, with computational costs far less than with the DFT-based approaches. As a result, we identify the most stable phases at 0 K for each stoichiometry. We also estimate the transition temperatures between phases by

calculating finite-temperature free energy. The computed transition temperatures of $\text{CsPbI}_3\text{Br}_{3-x}$ are consistent with experimental observations. In case of Cl, the results indicate that γ -phase with a smaller composition than Br is stable at room temperature. We also find that the predicted γ -phases with mixed-halide are expected to have good optical properties as in CsPbI_3 perovskites. We anticipate that the present findings can contribute to extending the lifespan of solar cells based on all-inorganic lead halide perovskites.

[1] S. Kang et al., *npj Comput. Mater.*, 8, 108 (2022)

SESSION DS03.06: Honoring Marty Green for his Contribution to MRS and the Community
Session Chairs: Arun Kumar Mannodi Kanakkithodi, Austin McDannald, Noah Paulson and Ichiro Takeuchi
Tuesday Afternoon, November 29, 2022
Hynes, Level 2, Room 206

1:30 PM *DS03.06.01

Autonomous Scanning Probe Microscopy—from Imaging to Learning Physics of Local Bias-Induced Transformations in Functional Materials
Sergei V. Kalinin; University of Tennessee, Knoxville, United States

Machine learning and artificial intelligence (ML/AI) are rapidly becoming an indispensable part of physics research, with domain applications ranging from theory and materials prediction to high-throughput data analysis. However, the constantly emerging question is how to match the correlative nature of classical ML with hypothesis-driven causal nature of physical sciences. In parallel, the recent successes in applying ML/AI methods for autonomous systems from robotics through self-driving cars to organic and inorganic synthesis are generating enthusiasm for the potential of these techniques to enable automated and autonomous experiment (AE) in imaging. Here, I will discuss recent progress in automated experiment in scanning probe microscopy, ranging from feature to physics discovery via active learning. The applications of classical deep learning methods in streaming image analysis are strongly affected by the out of distribution drift effects, and the approaches to minimize though are discussed. I will further illustrate transition from post-experiment data analysis to active learning process, including learning structure-property relationships and materials discovery in composition spread libraries. Here, the strategies based on simple Gaussian Processes often tend to produce sub-optimal results due to the lack of prior knowledge and very simplified (via learned kernel function) representation of spatial complexity of the system. Comparatively, deep kernel learning (DKL) and structured Gaussian Processes methods allow to realize both the exploration of complex systems towards the discovery of structure-property relationship, and enable automated experiment targeting physics (rather than simple spatial feature) discovery. The latter is illustrated via experimental discovery of ferroelectric domain dynamics in piezoresponse force microscopy. For probing physical mechanisms of tip-induced modifications, I will demonstrate the combination of the structured Gaussian process and reinforcement learning, the approach we refer to as hypothesis learning. Here, this approach is used to learn the domain growth laws on a fully autonomous microscope. The future potential of Bayesian active learning for autonomous microscopes is discussed.

2:00 PM *DS03.06.02

Reproducible Sorbent Materials Foundry for Carbon Capture at Scale Austin McDannald; National Institute of Standards and Technology, United States

Direct air capture (DAC) is an emerging technology aiming to mitigate climate change by adsorbing CO_2 from ambient air for subsequent use or sequestration. There is a dire need to improve the performance of DAC facilities, as measured by metrics including CO_2 captured per unit energy. This work presents our vision and current progress towards an autonomous sorbent materials foundry for rapidly evaluating materials for DAC. Our initial work focused on machine learning models predicting CO_2 uptake from the sorbent material structure. However, CO_2 uptake alone is not enough to evaluate the fitness of a sorbent for DAC. We subsequently develop more holistic performance metrics for DAC sorbents based on the mixed-gas sorption behavior. For example, knowing the mixed-gas sorption behavior and an choosing a refresh cycle it is possible to calculate intrinsic amount of CO_2 captured per unit energy for the sorbent material. We show how this work fits into a hierarchical framework of autonomous systems accelerating the development of DAC.

2:30 PM *DS03.06.03

Humans and Research Robots: Autonomous Experimentation for Materials Science Benji Maruyama; AFRL/RXA, United States

Autonomous Experimentation is changing the way we do research. We explore the role of human researchers and their partnership with Robot Researchers in the fast-growing area. From job security to job satisfaction to workforce development, there are significant questions and opportunities that arise from the autonomous experimentation movement.

The current materials research process is slow and expensive, taking decades from invention to commercialization. The Air Force Research Laboratory pioneered ARES™, the first autonomous research system for materials development. A rapidly growing number of researchers are now exploiting advances in artificial intelligence (AI), autonomy & robotics, along with modeling and simulation to create research robots capable of doing iterative experimentation orders of magnitude faster than today. Far from displacing human researchers, we expect Autonomous Experimentation to free human researchers to do the “fun,” creative & insightful part of research.

In the future, we expect autonomous experimentation to revolutionize the research process, and propose a “Moore’s Law for the Speed of Research,” where the rate of advancement increases exponentially, and the cost of research drops exponentially. We also consider a renaissance in “Citizen Science” where access to online research robots makes science widely available.

3:00 PM BREAK

3:30 PM *DS01.06.04

Hierarchical Bayesian Data Analysis for Challenging Structural Materials Characterization Problems Brian L. DeCost; National Institute of Standards and Technology, United States

Automated quantitative analysis for structural materials characterization is a challenging task primarily because of the difficulty of physical model specification and optimization. However, potential development of robust online automated quantitative analysis would significantly expand the scope and impact of autonomous platforms for materials development.

Our approach of hierarchical Bayesian analysis of high throughput structural characterization data blurs the lines between machine learning based approaches and conventional nonlinear least squares analysis. This approach allows models to pool information across related samples, and also allows

integration of flexible non-parametric models such as Gaussian Process priors to model functional dependencies between parameters.

We demonstrate how this modeling strategy can provide higher sensitivity for analysis of minority or trace phases in challenging high throughput X-ray diffraction (XRD) data. We will also show how to apply Bayesian modeling workflow to extended X-ray absorption fine structure (EXAFS), a spectroscopic technique that provides insight into local structural and chemistry.

Finally, we will discuss the current limitations of the hierarchical Bayesian modeling approach, and how it may be complemented by other contemporary machine learning based methods.

4:00 PM *DS03.06.05

Autonomous Combinatorial Experimentation [Ichiro Takeuchi](#); University of Maryland, United States

We are incorporating active learning in screening of combinatorial libraries of functional materials. The array format with which samples of different compositions are laid out on combinatorial libraries is particularly conducive to active learning driven autonomous experimentation. For some physical properties, each characterization/measurement requires time/resources long/large enough that true "high"-throughput measurement is not possible. Examples include detection of martensitic transformation and superconducting transitions in thin film libraries. By incorporating active learning into the protocol of combinatorial characterization, we can streamline the measurement and the analysis process substantially. We will discuss some of our latest efforts including real-time autonomous experiment-theory interaction for closed-loop mapping of thin film phase diagrams, and multi-instrument autonomous characterization of library wafers where two different physical properties are simultaneously mapped. Our effort in developing synthesis – measurement closed loops on a combinatorial thin film platform will also be discussed. This work is performed in collaboration with A. Gilad Kusne, H. Liang, A. McDannald, H. Yu, C.-H. Lee, and M. Lippmaa. This work is funded by SRC, ONR, AFOSR, and NIST.

SESSION DS03.07: Poster Session I
Session Chairs: Arun Kumar Mannodi Kanakkithodi and Noah Paulson
Tuesday Afternoon, November 29, 2022
8:00 PM - 10:00 PM
Hynes, Level 1, Hall A

DS03.07.01

DCGANs-Based SOFC Synthetic Image Generation Method [Wonjun Lee](#)¹, Sunjong Bong¹, Tae Ho Shin² and Suyoung Chi³; ¹University of Science and Technology, Korea (the Republic of); ²Korean Institute of Ceramic Engineering and Technology, Korea (the Republic of); ³Electronics and Telecommunications Research Institute, Korea (the Republic of)

Solid Oxide Fuel Cell(SOFC) is attracting attention as a next-generation fuel cell for its eco-friendliness and efficiency. However, surface defects may occur during manufacturing, leading to poor quality and material failure. Deep learning has recently become widespread in research and has been implemented in various applications, including surface defect inspection using computer vision. Though, images that show surface defects are limited, making the dataset class imbalanced, and it becomes problematic. Therefore, we propose a method for generating synthetic data based on Deep Convolutional Generative Adversarial Networks(DCGANs) to solve the limited data problem, train with deep learning, and evaluate it.

DS03.07.02

Inverse Design of BaTiO₃'s Synthetic Condition via Machine Learning [Minjeong Gong](#)¹, Dong-Hwa Seo¹, Young Seog Yoon², Hyun-woo Oh², Suyoung Chi², Seong Hyeok Choi³, HyeonJin Jeong³, Moonhee Choi³ and Sung Beom Cho³; ¹Ulsan National Institute of Science and Technology, Korea (the Republic of); ²Electronics and Telecommunications Research Institute, Moldova (the Republic of); ³Korea Institute of Ceramic Engineering & Technology, Korea (the Republic of)

Due to its high permittivity, barium titanate (BaTiO₃) has attracted attention as a dielectric material for electronic devices. However, the dielectric properties of BaTiO₃ are highly affected by factors such as tetragonality, particle size, impurities, and density. Because these dielectric properties are affected by synthetic conditions, optimizing the synthetic process is required to produce BaTiO₃ with high permittivity and low dielectric loss. Solid-state reaction is attracting attention among synthesis methods because it allows low-cost mass manufactures by using advance technologies for atomization and dispersion of barium carbonate (BaCO₃) and titanium oxide (TiO₂) precursors. However, it is challenging for them to optimize the synthetic processes for targeted permittivity and dielectric loss by a trial-and-error experimental approach due to the large number of combinations of synthetic conditions such as synthetic variables and precursor types affecting their properties. This work suggests a machine learning (ML) approach to find suitable synthesis conditions for achieving target properties of BaTiO₃. We first carried out 370 experiments to synthesize BaTiO₃ using solid-state reactions with various BaCO₃ and TiO₂ precursors of varying purity, particle size, and specific surface area, as well as various synthetic variables for wet mixing, calcination, and sintering, and measured density, permittivity, and dielectric loss. And then, the correlation analysis is performed to figure out the relationship between the synthetic conditions and dielectric properties of BaTiO₃ such as the density, permittivity, and dielectric loss. We discovered that density is highly related with sintering temperature, while permittivity and dielectric loss are correlated with total impurity concentration in BaCO₃. We conduct regression and classification analyses by three models (Random Forest, Gradient Boost and XG Boost) with independent variables as synthetic conditions and dependent variables as dielectric properties. With excellent accuracy, our ML models can predict dielectric properties from synthetic conditions. After then, the ML models predict all possible synthetic conditions. Based on predicted values, synthetic conditions that satisfied target properties are sorted and we call these processes as inverse design. From additionally conducted experiments with ML-guided synthetic conditions, this inverse design based on our ML models allows us to achieve target dielectric properties of BaTiO₃ (density, permittivity, dielectric loss).

DS03.07.03

Development of an Open-Source Adsorption Model for Direct Air Capture [Thomas Sadowski](#)^{1,2}, [Mit Patel](#)^{1,2}, [Jeffery G. Weissman](#)³ and [Christine Broadbridge](#)^{1,2}; ¹Southern Connecticut State University, United States; ²CSCU Center for Nanotechnology, United States; ³Precision Combustion Inc., United States

The continued increase in global energy demand has made it clear the aggressive net-zero targets suggested by the IPCC cannot be attained through conversion to renewables alone. Negative emission technologies such as direct air capture (DAC), are required to remove legacy CO₂ directly from the atmosphere and reduce concentrations back to preindustrial levels. The active element in DAC is a sorbent material that selectively removes CO₂ from the

air stream; however, low atmospheric CO₂ levels severely limit the choice of materials. Physisorbent solids possess the potential to overcome these limitations but can be costly to produce and evaluate, possibly limiting their discovery through traditional trial-and-error physical experimentation and observation. Computational modeling offers a cost-effective alternative approach to rapidly test the efficacy of solid sorbents towards DAC and create optimized models for carbon capture and recovery in an industrial setting. Though such software is commercially available, it can be prohibitively expensive and lacks the ability to model solid-vapor interactions. Hence, there is an acute need to overcome these obstacles to accelerated DAC research efforts. In this study, a computational model was developed to simulate the dynamic adsorption of CO₂ using open-source software supplemented with user-generated code written in Python and implemented as a custom unit operation in the chemical process simulator, DWSIM. To test the accuracy of this model, breakout curves and adsorption isotherms were calculated for activated carbon and compared to experiment, agreeing to within 5%. This framework will provide the basis for a future multivariate sensitivity analysis study to determine the energy duty required for a target sorbent to capture and release a product CO₂ stream with purity from 80 to 98%.

DS03.07.04

High-Throughput Discovery of High-Entropy Alloys Nanocatalysts via Active Learning Approach [Zhichu Ren](#), Ali Abdelhafiz and Zhen Zhang; Massachusetts Institute of Technology, United States

Research solutions aiming to replace existing hydrocarbon fuel technologies with green energy sources have so far been only partially successful. Proton Exchange Membrane Fuel Cells is a very promising candidate for its light weight and high energy density, while its performance and durability are limited by the catalysts used in the cell electrode. Recent studies show that synergistic effects of multiple metals alloyed together yield a material that is even better than noble metal catalysts. Yet, such a very well controlled and precise synthesis of more than tri-metallic nanoparticles is extremely challenging by conventional synthesis techniques at normal/ambient conditions, which are dictated by thermodynamics rules. Ultrafast Joule heating technique is a promising tool to leverage kinetic rules to form meta-stable high entropy alloys by heating and cooling samples within one second. This extreme fast process makes it practical to make the workflow in a high-throughput manner.

The high throughput system consists of a liquid handler, a carbothermal shock setup, and a robotic testing platform. The liquid handling robot allows us to precisely control the composition of each sample, specifically, the ratio between each metal precursor solution. Carbothermal shock is enabled by conducting a large current to a precursor loaded carbon substrate, which can reach above 2000K within hundreds of milliseconds. Once the carbon strips are prepared with the shocking method, a rapid evaluation will be conducted, also in a high-throughput manner. Samples will be cut into pieces and loaded onto testing holders, then a robotic arm will handle sample loading and unloading to the electrocatalytic testing beaker. Testing software is automated using python scripts, as well as data extraction and SQL storage process. The ending step is to run an active learning step, which can analyze the dataset using Bayesian Optimization to generate the suggestion for the next batch of recipes, based on the surrogate model fitted by the Gaussian Process. The newly suggested task will be sent to the liquid handler, forming a closed-feedback optimization loop. Such a high-throughput and autonomous optimization system will greatly enhance the efficiency of finding new high entropy alloy recipes for electrocatalyst application.

DS03.07.05

Trend Analysis and Insight Extractions Using Named Entity Recognition of CO₂RR Literature [Jiwoo Choi](#)^{1,2}, [Kihoon Bang](#)¹, [Suji Jang](#)¹, [Kwang-Ryeol Lee](#)¹, [Sang Soo Han](#)¹ and [Donghun Kim](#)¹; ¹Korea Institute of Science and Technology, Korea (the Republic of); ²Korea University, Korea (the Republic of)

In recent years, big data and artificial intelligence have penetrated materials science research. Currently, most openly available material databases use results derived from computer simulations and not from experiments. Some examples of materials research projects include the Materials Project, Novel Materials Discovery (NOMAD), and Open Quantum Materials Database (OQMD). Unfortunately, it is still difficult to build a large-scale experimental materials database. In this context, the scientific literature is one of the underutilized potential data sources because it contains well-organized experimental data that is easily accessible. An intensive study of natural language processing (NLP) of a huge volume of literature in materials science is required. Data can be automatically extracted from literature using NLP.

Among various research topics in materials science, CO₂ reduction reaction (CO₂RR) catalysis would be an interesting topic to apply NLP. CO₂RR catalysis, a conversion process from carbon dioxides into valuable compounds, would alleviate today's energy crises and environmental problems. Although a large volume of CO₂RR studies have been performed, however the experimental databases have not yet been built. We aim to build a large scale experimental databases using a variety of NLP techniques, and also aim to utilize them to extract research trends or insights, which would benefit the relevant research community.

In this work, we collected papers related to CO₂RR and conducted a study to extract key entities from the papers based on named entity recognition (NER). We provide a universal method to crawl and screen papers of user's interest (in this example, CO₂ electrochemical reduction research) and excluding noise papers using a combination of Doc2Vec and the Latent Dirichlet Allocation (LDA) model: As a result, we collected approximately 4,800 papers. Then, we developed NER models based on long short term memory (LSTM) or bidirectional encoder representations from transformer (BERT). These models were applied to the abstracts of the collected papers so that ten key entities regarding material names (catalyst, electrolyte etc.) and catalytic performances (Faradaic efficiency, current density etc.) are extracted. The average f1-score of MatBERT-based approach is over 85%, greatly exceeding that of LSTM-based approach, indicating the context-inclusive approach is necessary. Additionally, we also investigated over various BERT models, from BERT_base, SciBERT, MatSciBERT, and MatBERT) and their performance comparisons tell that the more domain knowledge is reflected in BERT model, the better the performance we achieve. Lastly, the trend and knowledge extracted from the NER studies in the CO₂RR research field will be discussed.

DS03.07.06

DenseSSD—A Computer Vision Model for Vial-Positioning Detection to Improve Safety in Autonomous Laboratory [Leslie Ching Ow Tiong](#)¹, [Hyuk Jun Yoo](#)^{1,2}, [Na Yeon Kim](#)^{1,2}, [Kwan-Young Lee](#)², [Sang Soo Han](#)¹ and [Donghun Kim](#)¹; ¹Korea Institute of Science and Technology, Korea (the Republic of); ²Korea University, Korea (the Republic of)

Robot-based automation methods for material synthesis have recently garnered much attention because they can substantially accelerate the material development process. Some recent examples were reported, which involves organic or inorganic material synthesis in energy applications (catalysis and photovoltaics) [1-3]. Despite the substantial promise of these methods, surveillance-free environments may lead to dangerous accidents primarily due to hardware control errors. Object detection techniques can play important roles in addressing these safety issues; however, state-of-the-art detectors, including single-shot detector (SSD) models, suffer from insufficient accuracy in environments involving complex and noisy scenes due to uneven visual environments. With the purpose of improving safety in a surveillance-free laboratory, we developed the deep learning (DL)-based object detector, namely, densely connected single-shot detector (DenseSSD) with a densely connected mechanism. For the foremost and frequent problem of detecting vial positions, DenseSSD achieved a mean average precision (mAP) over 95% based on a complex dataset involving both empty and solution-filled vials, greatly exceeding those of conventional detectors; such high precision is critical to minimizing failure-induced accidents. Additionally, DenseSSD was observed to be highly insensitive to the environmental changes, maintaining its high precision under the variations of solution colors or testing view angles. The roughness of DenseSSD would allow the utilized vision module settings to be more flexible. This study verified that DenseSSD is practical for

enhancing safety in an automated material synthesis environment, and it can be extended to diverse applications where high detection accuracy and speed are both needed.

[1] *Nature* **538**, 237-241 (2020)

[2] *Nature* **559**, 377-381 (2018)

[3] *Science* **365**:eaax1566 (2019).

DS03.07.07

Autonomous Laboratory for Bespoke Synthesis of Nanoparticles Using Parallelized Bayesian Optimization Hyuk Jun Yoo^{1,2}, Na Yeon Kim^{1,2}, Leslie Ching Ow Tiong¹, Hee Seung Lee¹, Kwan-Young Lee², Donghun Kim¹ and Sang Soo Han¹; ¹Korea Institute of Science and Technology, Korea (the Republic of); ²Korea University, Korea (the Republic of)

Autonomous laboratories based on robotics and artificial intelligence (AI) has been recently conducted widely for accelerated search of materials. On the other hand, an inverse design that suggest specific synthesis conditions to achieve various target properties is required for bespoke synthesis of materials. However, because the inverse design needs to solve questions in a high-dimensional parameter space, it is greatly complex, so that researchers need to perform enormous numbers of experiments for the inverse design to find the optimal synthesis condition. It is very difficult to predict the next synthesis condition by understanding the correlations between experimental data via human intelligence. Usually, material properties have been individually explored with a single Bayesian optimization (B.O.) model in recent autonomous laboratories; likely leading to successive problems caused by a number of experiments and a lot of physical time although it is more efficient than the high-throughput screening (HTS) process. The conventional B.O. does not share experimental data simultaneously during the entire optimization process. In other words, the inverse design for bespoke synthesis of materials must be performed in parallel for the B.O. models while sharing experimental data in the single variable space. This parallelization allows to accumulate experimental results in the same parameter space without redundant experiment conditions. We tried to optimize the synthesis of silver nanoparticle (Ag NPs) to demonstrate the efficiency of parallelized B.O., in which a home-made automatic apparatus was used for synthesis of Ag NPs. Our automatic synthesis system and B.O. model were used to identify the optimal synthesis condition for various combinations of optical target properties (e.g., λ_{max} , full width half maximum, intensity, etc.) at the same time. Then, we compared the efficiency of HTS, conventional B.O., and parallelized B.O. with increasing the numbers of input synthesis variables and target properties. Our work provides a strong potential to solve the high-dimensional space issue for bespoke design of materials via an autonomous laboratory. In addition, our demonstration of autonomous nanoparticle synthesis will be useful in energy applications such as catalysis, photovoltaics which are made up of nanoparticles.

DS03.07.08

Machine Learning Based Investigation of Optimal Synthesis Parameters for Epitaxially Grown III-Nitride Semiconductors Andrew S. Messecar, Steven Durbin and Robert Makin; Western Michigan University, United States

Materials informatics has demonstrated immense utility in the design and development of synthesis routes for a wide spectrum of materials, ranging from aluminum alloys for additive manufacturing to lead titanate used in aqueous photocathodes for dye-sensitized solar cells. One synthesis route that can benefit greatly from a materials informatics approach is molecular beam epitaxy (MBE). Molecular beam epitaxy offers purity and control in the synthesis of thin-film materials and devices, but its high purity source materials and ultra-high vacuum environment can make finding the optimal growth conditions for a given material costly and time-intensive. A materials informatics approach to MBE can aid in the determination of the optimal synthesis parameters and help reduce the number of runs needed to achieve high quality samples. Recently, machine learning has been used to assist the design of perovskite oxides to be synthesized via molecular beam epitaxy as well as superconducting titanium nitride. Here, we report on initial results that build upon these reported studies by applying statistical learning to plasma-assisted molecular beam epitaxy (PAMBE) growth data to investigate optimal synthesis parameters of PAMBE-grown nitride thin films.

Utilizing the detailed records of over 600 PAMBE nitride thin films grown in a single Perkin-Elmer 430 system, key synthesis parameters such as substrate temperature, substrate lattice mismatch, growth duration, and RF power applied to the plasma source, are associated with the resulting crystallinity (single crystalline, polycrystalline, or amorphous) of the sample as determined by analyzing in-situ acquired reflection high-energy electron diffraction (RHEED) images. Taking the set of synthesis parameters as the predictors and the crystallinity as the categorical response, machine learning algorithms for classification and inference have been implemented to uncover insights regarding the relationship between synthesis parameters and the quality of the PAMBE-synthesized film. Algorithms were implemented using the R open-source programming language, specifically including the “tree”, “rpart” and “randomForest” packages.

The initial results indicate that the temperature of the Knudsen cell with the cation (gallium or indium) source material was the most significant predictor in whether an epitaxial film developed to be single crystalline, which is consistent with conventional wisdom regarding the importance of growing under metal-rich conditions. The complete data set was also divided into separate, focused data sets for gallium nitride and indium nitride, on which a random forest, classification tree and logistical regression were modeled. For gallium nitride films, agreement was found between the results of the classification tree and the random forest, which both found the gallium Knudsen cell temperature to have the greatest impact on the sample's crystallinity, followed by substrate temperature and initial nitrogen pressure. For indium nitride, the logistical regression and random forest model both indicated that the greatest impact on sample crystallinity was the initial nitrogen pressure, followed by substrate temperature and the forward power on the RF plasma source.

These initial results identify key synthesis parameters for obtaining single crystalline nitride thin films, however the differing results among the various statistical algorithms points to an underlying complexity that is not fully captured by these approaches. These results are helping to inform the development of a neural network architecture to be used in predicting crystallinity of PAMBE grown nitride semiconductors based on provided synthesis parameters, while the size of the data set is also being increased by incorporating synthesis and crystallinity data from the literature.

This work was supported in part by the National Science Foundation (grant number DMR-2003581).

DS03.07.09

Towards an Autonomous Combinatorial Co-Sputtering Reactor Davi M. Febba¹, John Mangum¹, Rebecca Smaha¹, Julian Calder¹, Sage Bauers¹, Kendal Johnson¹, Kevin Talley² and Andriy Zakutayev¹; ¹National Renewable Energy Laboratory (NREL), United States; ²Qorvo, Inc., United States

Computational databases can predict novel and promising materials, but those that can be synthesized and subjected to characterization face the challenge of reproducibility. For example, tin-based oxynitride ferroelectric perovskites with band gap in visible, or zinc-based oxynitrides wurtzites with perfect short-range order, have been computationally proposed. However, the oxygen to nitrogen ratio required for these promising properties, such as long-term stability and semiconductor-like charge transport, is difficult to achieve and reproduce.

To answer the question of how to reproducibly synthesize promising computationally predicted materials, a custom-designed co-sputtering reactor “combi-

9" was recently designed and built at NREL. Equipped with four cathodes, this ultra-high vacuum instrument allows the exploration of a wide substrate temperature range, from cryogenic temperatures up to 1000 °C, besides RF and DC substrate biasing. Additional capabilities include real-time deposition data logging of sputtering parameters (such as power, voltage, pressure, gas flow), control of gas distribution to individual targets, time-sequenced shutters, and turbo gate position, all of which enable the user to execute complex programmable synthesis recipes.

However, this automated instrument still requires an expensive and time-consuming trial-and-error approach for synthesis and optimization of novel materials, since the researcher oversees all the sputtering parameters of an experimental campaign to obtain a specific material composition or properties. Therefore, to allow reproducible synthesis of promising materials with minimal human intervention, we are transforming this *automated* instrument into an *autonomous* one, in which a Bayesian algorithm has full control of all sputtering variables, (e.g., plasma powers, gas pressure, substrate temperature, etc.). This algorithm is informed about the process environment by in-situ spectral measurement tools, with the objective to learn how to control the chemical composition of the film, especially its mixed-anion content, during the deposition process.

This presentation will describe this state-of-the-art automated sputtering instrument and discuss our progress towards turning it into an autonomous sputtering reactor, such as estimating film composition from in-situ spectral data, integration among many software platforms, data logging and integration with databases.

DS03.07.10

A Robust Neural Network for Extracting Dynamics from Time-Resolved Electrostatic Force Microscopy Data [Madeleine Breshears](#), Rajiv Giridharagopal, Justin Pothoof and David Ginger; University of Washington, United States

Advances in scanning probe microscopy (SPM) methods such as time-resolved electrostatic force microscopy (trEFM) now permit the mapping of fast local dynamic processes with high resolution in both space and time, but such methods can be time consuming to analyze and calibrate. Here, we design and train a regression neural network (NN) that accelerates and simplifies the extraction of local dynamics from SPM data directly in a cantilever-independent manner, allowing the network to process data taken with different cantilevers. We validate the NN's ability to recover local dynamics with a fidelity equal to or surpassing conventional, more time-consuming calibrations using both simulated and real microscopy data. We apply this method to extract accurate photoinduced carrier dynamics on *n*=1 butylammonium lead iodide, a halide perovskite semiconductor film that is of interest for applications in both solar photovoltaics and quantum light sources. NN extracted dynamics from trEFM measurements confirm previous observations of charging rate heterogeneity across microstructures in the perovskite. Finally, we use SHapley Additive exPlanations (SHAP) to evaluate the robustness of the trained model, confirm its cantilever-independence, and explore which parts of the trEFM signal are important to the network.

DS03.07.11

Deep Learning Models for Predicting the Experimental HOMO and LUMO Orbital Energies Minseok Jeong, Joonyoung Joung, Minhi Han and [Sungnam Park](#); Korea University, Korea (the Republic of)

The highest occupied molecular orbital (HOMO) and lowest unoccupied molecular orbital (LUMO) energies are fundamental properties of molecules. Accurate predictions of the HOMO and LUMO energies of newly-designed molecules are crucial for the efficient development of optoelectronic materials in many research areas such as organic light emitting diodes and organic photovoltaics. Here, we developed a deep learning model to accurately predict the HOMO and LUMO energies of organic molecules based on an experimental database which contains the experimental HOMO and LUMO energies of molecules in solutions, solid states, and the gas phases. Our deep learning model includes the molecule-environment interaction that influences the HOMO and LUMO energies. Our deep learning model based on the experimental database is found to predict the HOMO and LUMO energies within the mean squared error of 0.058 eV. The details and performance of our deep learning model will be presented. In addition, we will demonstrate that our deep learning model can be efficiently used to develop new optoelectronic materials.

DS03.07.12

Development of Machine-Learning Force Fields for Simulating Interfaces in Solid-State Batteries [Kwangnam Kim](#)¹, Aniruddha Dive¹, Andrew Grieder^{2,1,3}, Nicole Adelstein^{3,1}, ShinYoung Kang¹, Liwen Wan¹ and Brandon Wood¹; ¹Lawrence Livermore National Laboratory, United States; ²University of California, Santa Cruz, United States; ³San Francisco State University, United States

There are increasing interests in using machine-learning force fields (MLFFs) in molecular dynamics (MD) simulations to explore local structure and chemistry at complex interfaces that governs the performance of energy storage devices. A number of methodologies has been developed to train MLFFs using ML algorithms (e.g., artificial neural network) and input features that describe local atomic environments. The training data are often collected from highly accurate ab-initio simulation and therefore the trained and validated ML potentials are capable of performing simulations with quantum-level accuracy while achieving thousands of times faster computational speed than ab-initio calculations. In this talk, we will discuss our recent development of MLFFs based on artificial neural network[1,2] to study ion transport kinetics and structural and chemical features at disordered interfaces between garnet-type LLZO solid-electrolyte and cobalt-oxide LCO cathode. The training data was collected from AIMD simulations at a wide range of temperatures and the MLFF is able to predict atomic forces for LLZO, LCO, and the interfaces between them with a DFT level of accuracy. The predicted radial distribution functions, vibrational characteristics of atoms, and ion diffusivities in each system show excellent agreement with those calculated by ab-initio simulations. Also, we will briefly illustrate how the ML force field can be applied to investigate interdiffusion of ions and chemical degradation at the interfaces.

[1] A. Singraber, J. Behler, and C. Dellago, *J. Chem. Theory Comput.* **2019**, *15*, 1827–1840.

[2] A. Singraber, T. Morawietz, J. Behler, and C. Dellago, *J. Chem. Theory Comput.* **2019**, *15*, 3075–3092.

Acknowledgement:

This work was performed under the auspices of the U.S. Department of Energy by Lawrence Livermore National Laboratory under contract number DEAC52-07NA27344. Authors acknowledge funding support from the Vehicle Technologies Office, Office of Energy Efficiency and Renewable Energy, U.S. Department of Energy and computational resource support from the Innovative and Novel Computational Impact on Theory and Experiment (INCITE) program. This research used resources of the Argonne Leadership Computing Facility, which is a DOE Office of Science User Facility supported under Contract DE-AC02-06CH11357.

DS03.07.13

Finite Element Simulation of Resistive Memory Using Fully Coupled Electrothermal and Phase-Field Models [Dongmyung Jung](#) and Kwon Yongwoo; Hongik University, Korea (the Republic of)

Along with phase change memory, resistive memory that utilizes transition metal oxide as switching material can serve as a synapse device in neuromorphic computing systems thanks to its multilevel resistances. In filamentary switching by valence change mechanism, anion vacancies play an important role. When a high electric field is applied inside the insulator, anion vacancies are created and aggregate inside the insulator to form conductive filaments. In existing papers where the finite element analysis of the filament switching was presented, the initial state was the low-resistance state with a

predefined or “assumed” filament shape. Therefore, the forming behavior cannot be predicted for different cell geometry and materials. In this work, we demonstrate our simulation that can predict a full switching cycle of forming, reset, and set operations. The switching material is regarded as a mixture of two phases: high-resistance state (HRS) and low-resistance state (LRS). This mixture is expressed as an order parameter that has 0 and 1 in HRS and LRS phases, respectively. In forming and set operations, new LRS phases are generated, or existing LRS phases are migrated and connected. In reset operation, connected LRS phases are disconnected by dissolution or migration. All these switching behaviors are regarded as the change of the order parameter. At each time step, electrothermal equations are solved to obtain electric field and temperature distributions that determines the driving forces for LRS phase behaviors such as migration, generation, and dissolution. Then, a phase-field equation that is the Cahn-Hilliard equation with migration, sink, and source terms for the LRS phase is solved. Using our simulation, we can reproduce full-cycle current-voltage curves for both unipolar and bipolar switching. We believe that our simulation can serve as an effective tool for the design of cell architecture

DS03.07.14

Supporting Material Synthesis via Research Data Management, Data Mining from Literature and Machine Learning—Metal-Organic Frameworks as Use-Case Manuel Tsotsalas and Christof Wöll; KIT, Germany

In this conference contribution we will present how Metal-Organic Framework (MOF) synthesis data can be managed, sorted, and automatically extracted from literature. In addition, we will show how this synthesis data can be used to support researchers from the field of MOF synthesis via synthesis prediction tools. [1]

The contribution will cover the four aspects (I) electronic lab notebooks (ELN), (II) repositories and archives for material synthesis, (III) automatic data mining using natural language processing (NLP), and (IV) machine learning (ML) to identify patterns from the extracted synthesis data.

In the aspects (I) and (II) we will focus on research data management tools developed / under development by the German National Research Data Infrastructure initiative (NFDI) with a focus on NFDI4Chem and FAIRmat. In this context we will introduce the ELN Chemotion and the Repository and Archive NOMAD and demonstrate how these tools can be implemented in MOF synthesis.

[1] (a) Jalali, M.; Tsotsalas, M.; Wöll, C. MOFSocialNet: Exploiting Metal-Organic Framework Relationships via Social Network Analysis. *Nanomaterials* **2022**, *12*, 704.; (b) MOF Synthesis Prediction Enabled by Automatic Data Mining and Machine Learning. Luo, Y., Bag, S., Zaremba, O., Cierpka, A., Andreo, J., Wuttke, S., Friederich, P. and Tsotsalas, M., *Angew. Chem. Int. Ed.* **2022** e202200242.

[2] The Repository Chemotion: Infrastructure for Sustainable Research in Chemistry P. Tremouilhac, C.-L. Lin, P.-C. Huang, Y.-C. Huang, A. Nguyen, N. Jung, F. Bach, R. Ulrich, B. Neumair, A. Streit, S. Bräse, *Angew. Chem. Int. Ed.* **2020**, *59*, 22771.

[3] (a) The NOMAD laboratory: from data sharing to artificial intelligence C. Draxl and M. Scheffler *J. Phys. Mater.* **2019**, *2*, 036001.; (b) Scheffler, M., Aeschlimann, M., Albrecht, M. et al. FAIR data enabling new horizons for materials research. *Nature* **2022**, *604*, 635–642.

DS03.07.15

Bayesian Optimization of a Scalable Coating Process Using a Self-Driving Laboratory Connor Rupnow, Ben MacLeod, Mehrdad Mokhtari and Curtis Berlinguette; The University of British Columbia, Canada

The commercialization of energy materials can take decades, in part due to the challenge of scaling-up laboratory synthesis techniques for manufacturing. For example, perovskite solar cells were discovered in 2009, but are not yet commercially available. Scaling-up the solution-based fabrication process is widely cited as the major reason for this. To address this challenge, we have designed and built a self-driving laboratory, “Ada”, for autonomously optimizing ultrasonic spray-coating, a scalable coating process. We used this self-driving laboratory to maximize the conductivity of a spray-combustion synthesized Pd coating by optimizing seven experimental variables under the control of a Bayesian optimization algorithm. This optimization yielded coatings with conductivities twice the previous state-of-the-art for spray-combustion synthesis. The best coatings deposited using our vacuum-free process exhibit conductivities comparable to vacuum-sputtered coatings and are directly scalable to larger area substrates with no loss in conductivity. This work shows how self-driving laboratories can contribute to accelerated commercialization of energy materials by rapidly optimizing scalable coating processes.

SESSION DS03.08: Computation Combined with AI

Session Chairs: Sijia Dong and Noah Paulson

Wednesday Morning, November 30, 2022

Hynes, Level 2, Room 206

8:00 AM *DS03.08.01

Data-Driven Prediction of Interphase Reactions for Energy Storage Applications Kristin A. Persson; University of California, Berkeley, United States

Despite decades of work, there is considerable uncertainty regarding the major components of the solid-electrolyte interface (SEI) and its dynamic formation mechanism as a function of electrolyte and anode chemical and structural composition. Here we present a new data-driven first-principles framework using a combination of high-throughput calculations, reaction networks, machine learning and microkinetic modeling. Our automated methodology is based on a systematic generation of relevant species using a general fragmentation/recombination procedure which provides the basis for a vast thermodynamic reaction landscape, calculated with density functional theory. We explore this landscape using stochastic methods and shortest pathfinding algorithms, which yield the most likely reaction pathways which are then refined with transition state calculations and kinetic information. The results of the framework show promise in being able to automatically recover previous insights on single reaction pathways, as well as successfully predicting the early dynamics and competitive nature of the SEI formation. As examples, we present formation mechanisms of major SEI-forming molecules and recover the Peled-like separation of the SEI into inorganic and organic domains resulting from rich reactive competition.

8:30 AM DS03.08.03

Design Flow in Stabilizing Oxygen Redox for Na Layered Oxides—DFT-Assisted Machine Learning Sojung Koo; Kyung Hee University, Korea (the Republic of)

As the demand of electric vehicles grows tremendously for green and sustainable energy environments, the family of Li- and Na-based materials (LIBs and SIBs) have been urged to move toward next generation with remarkable capacities. In particular, Li excess cathode materials exhibit excellent capacity and high potential (>4 V versus Li⁺/Li) resulting from not solely by transition metal (TM) redox, and thus anionic redox is necessary for the extra charges beyond TM redox during Li⁺ (de)intercalation. The high voltage redox which gives excess capacities originates from the oxygen 2p lone pair states in Li⁺-O(2p)-Li⁺ configurations. However, there are serious issues such as the poor cycling stability of anionic redox processes, voltage hysteresis and voltage

fade as a result of the irreversible local structural transformation or lattice oxygen loss. For P2-type $\text{Na}_{0.6}[\text{Li}_{0.2}\text{Mn}_{0.8}]\text{O}_2$ (NLMO), these issues in Li-excess materials have been mitigated as promoted stable electron holes on O^{2-} and showed intriguing reversible oxygen redox with the nonhysteretic voltage for SIBs. This has driven comprehensive explorations of Na-based compounds in spite of its less attention than Li-based materials, in view of the prevention of dimerized oxygen gas-release accompanied by structural distortion. Additionally, Al^{3+} incorporated NLMO (Al-NLMO) exhibits significantly improved reversibility of anion redox as well as maintains nonhysteretic voltage behaviors by stabilization of the oxide framework upon cycling. Extending the voltage range to the high voltage region with extra oxidation of oxygen species leads to an easier oxygen mobility, de-coordination of oxygen from the crystal network, and eventually to vacancies at the neighboring cation sites which drive cation disorder and defects in cathodes. Therefore, the stability or reversibility of oxygen redox is correlated closely with the atomic structure or the local oxygen coordination environment, as elaborated by chemical state of redox-active oxygen showed the isolated Na–O–Li or Li–O–Li O-2p configuration. In terms of this, although cation doping strategies have offered alternative and similarly promising approach toward reversible high energy density materials, the more systematic and comprehensive study could be required to explore crystal structures and atomic configurations compatible with oxygen redox reaction in Li excess system. Theoretical and computational understandings have been powerful in understanding the structural changes in Li-based compounds. Machine-learning potentials have attracted considerable attention because they can provide close to DFT-accurate energies at a fraction of cost, which finds applications to structure prediction of crystals. In this work, first principles calculations and machine learning techniques were adopted to evaluate the oxygen redox behavior of various cation ordering with NaMnO_2 , NLMO and Al-NLMO. First, we propose a probabilistic model assessing the energetically favorable neighboring cation sites for each Li and Al atoms while retaining the crystal structure. Second, the oxygen species formation at the highly charged state of the NLMO and Al-NLMO models, constructed to represent Li-excess and cation-doped, respectively, were evaluated in detail. In addition to the discussion of cation ordering and oxide framework based on atomic- and electronic-level considerations, comprehensive data-driven verification of the structure and thermodynamic energetics with several junction patterns is described. The verification results suggest that the oxygen release from TM intralayer is hindered by Al^{3+} -incorporation with α -Li/Mn ordering, indicating the effectiveness of inactive as a doping element. Via multiple physicochemical and theoretical characterizations, we identify the presence of tailored oxygen species bonds and peculiar morphological structures as the main factors responsible for the improved electrochemical performances of Na layered oxides.

8:45 AM DS03.08.04

Machine Learning-Aided Strategy to Discover Intermetallic Catalysts for the Hydrogen Evolution and the Oxygen Reduction Reactions [Carmen Martínez](#)^{1,2}, José Manuel Guevara¹ and Javier Llorca^{1,3}; ¹IMDEA Materials Institute, Spain; ²Universidad Complutense de Madrid, Spain; ³Universidad Politécnica de Madrid, Spain

The efficiency and rate of hydrogen generating by water splitting are determined by the Hydrogen Evolution Reaction (HER). Similarly, the production of energy from hydrogen in fuel cells by the oxidation of hydrogen into water is limited by the Oxygen Reduction Reaction (ORR). The sluggish kinetics of both reactions are usually improved by using platinum-based catalysts. However, the high cost of Platinum hinders the application of this technology and, at the same time, drives the search for efficient and affordable materials to replace it. Theoretical approaches to predict the catalytic activity of new materials are based on the calculation of the adsorption energies of the intermediate species (-H, O, and OH-) for both the HER and the ORR using Density Functional Theory (DFT) simulations. This strategy has been successfully applied to determine the catalytic activity of late transition metals for both HER and ORR, including the influence of the application of elastic strains in the catalytic performance [1,2].

The extension of this strategy to look for new catalysts based on intermetallic compounds is limited by the dimensions of the chemical space as well as by the computational cost of DFT calculations. Machine learning-based approaches can be used to overcome these limitations, and this is the objective of this talk. Thus, DFT simulations were used to determine the adsorption energies of the intermediate species (-H, O, and OH-) for the HER and ORR in 13 transition metals (Pt, Pd, Ni, Au, Ag, Zn, Cd, Rh, Ir, Ru, Os, Co, and Cu) and around 200 intermetallic compounds with AB and A3B stoichiometries and fcc, bcc, and hcp structures. These intermetallic compounds were among those non-toxic, non-radioactive, stable, and environmentally friendly from the Materials Project database. In addition, the effect of elastic strains was assessed in a subset of the intermetallic compounds, which showed the best catalytic performance. This information was used to train a Decision Tree Regression model using geometrical and electronic descriptors, such as the area of the adsorption hole, the applied strain, and the first ionization energy of the catalyst. This model was used to screen the large chemical space of binary intermetallic compounds at a very low computational cost, thus paving the way for the discovery of affordable catalysts for the HER and ORR.

References

- [1] C. Martínez-Alonso, J. M. Guevara-Vela, J. Llorca, *Phys. Chem. Chem. Phys.* **2022**, 24, 4832-4842.
- [2] C. Martínez-Alonso, J. M. Guevara-Vela, J. Llorca, *Phys. Chem. Chem. Phys.* **2021**, 23, 21295-21306.

9:00 AM DS03.08.05

First-Principles-Informed Machine Learning Study of Defects on the Lithium Metal Surface [Hao Yu](#), Sahar Sharifzadeh, Emily Ryan, Brian Kulis, Tianlun Huang, Kubra Cilingir, Madison Morey and Ziqing Zhao; Boston University, United States

Lithium (Li) metal anode can largely improve the energy density of Li batteries but dendrite formation in the metal prevents its practical implementation. Structural defects on the mesoscale are expected to play the role as precursors to dendrite formation. Here, we combine first-principles density functional theory (DFT) results with machine learning (ML) to study the impact of structural defects on a Li surface. We present a comparison of different ML models for predicting the change in surface energy upon defect formation. We consider the accuracy of available structural descriptors (SOAP, ACSF, MBTR) and show that data sampling impacts our conclusions. We then present a possible approach to bridge the micro- and meso-scales.

9:15 AM DS03.08.06

Machine-Learning Assisted Quantum Materials Discovery And Optimization—Metal-Insulator Transition Compounds [Alexandru Georgescu](#) and James M. Rondinelli; Northwestern University, United States

Metal-insulator transition (MIT) compounds are materials that may exhibit metallic or insulating behavior, depending on the physical conditions, and are of interest due to their correlated properties as well as due to their potential applications in emerging microelectronics, including neuromorphic computing and Mott Field Effect Transistors. Nonetheless, only around 60 materials with a thermally-driven metal-insulator transition are known, and their computational discovery is difficult due to the non-equilibrium nature of the transition, and the complexity of the many-body problem. To address this issue, we have built the first database of all known thermally-driven metal-insulator transition compounds, as well as stoichiometrically related compounds, and a machine-learning based classifier tool to accelerate their discovery - and provided both to the wider public, with no installation required. Using Bayesian optimization techniques, we have also optimized specific materials families to find compounds which are both stable, and may display strong MIT behavior while minimizing the number of calculations. Time permitting, we will present possible new metal-insulator transition oxide compounds identified through a combination of machine learning and DFT calculations, as well as preliminary experimental results on their experimental validation.

References:

- [1] A.B. Georgescu, P. Ren, A.R. Toland, S. Zhang, K.D. Miller, D.W. Apley, E.A. Olivetti, N. Wagner, J.M. Rondinelli, 'Database, Features, and Machine Learning Model to Identify Thermally-Driven Metal-Insulator Transition Compounds', *Chem. Matter*, 2021, 33, 14, 5591-5605

[2] MIT material database: <https://mtd.mccormick.northwestern.edu/mit-classification-dataset/>

[3] ML Classifier: tinyurl.com/mit-classifiers

9:30 AM DS03.08.07

First-Principles and Machine-Learning Assisted High-Throughput Screening for Novel Inorganic Perovskite Solar Cell [Kanghoon Yim](#)¹, Jiho Lee², Wonze Jung^{1,3}, Seungwu Han² and Kihwan Kim¹; ¹Korea Institute of Energy Research, Korea (the Republic of); ²Seoul National University, Korea (the Republic of); ³Chungnam National University, Korea (the Republic of)

In recent years, perovskite-based solar cells have shown a dramatic growth of their efficiency whereas the conventional silicon-based solar cells reached the theoretical limit through decades. However, the hybrid organic-inorganic perovskites (HOIP) which enable the rapid improvement of photovoltaic efficiency suffers from lack of long-term stability. To overcome the instability which originate from their organic components, the development of fully inorganic perovskites with comparable performance could be the solution. In this work, we first investigate the optical and electrical properties of all known ABX_3 inorganic perovskites from the inorganic crystal structure database (ICSD) using density functional theory (DFT) calculations. Though we found several new candidate materials for photovoltaic absorbers, their properties are not expected as promising as reported best materials. To discover new all-inorganic perovskite materials that have good performance and stability simultaneously, we suggest so-called 'double-anion perovskite' as new promising perovskites for solar-cell. While $ABB'X$ -type double perovskite can only replace B-site with element having the same oxidation state, double-anion perovskites can expand possible combinations of A-B metals if chalcogen and halogen elements are mixed in the anion sites. To search the most stable structure of a given combination, we adopt a machine-learning potential based crystal structure prediction method, which is called 'SPINNER'. By combining DFT calculations and machine-learning potential methods, we suggest new all-inorganic double-anion perovskites for photovoltaic absorbers.

9:45 AM BREAK

SESSION DS03.09: Batteries, Life Models, Electrochemistry

Session Chairs: Noah Paulson and Logan Ward

Wednesday Morning, November 30, 2022

Hynes, Level 2, Room 206

10:30 AM *DS03.09.01

Many-Body Materials Graph Networks for Massive-Scale Discovery of Lithium Superionic Conductors [Shyue Ping Ong](#), Chi Chen and Ji Qi; University of California, San Diego, United States

The matterverse is vast and complex. It comprises the infinite combinations of elements of the periodic table in ordered and disordered arrangements. While ab initio techniques can accurately probe the matterverse, the scope of our exploration has been bottlenecked by their high cost and poor scaling. In this talk, I will discuss how graph deep learning models trained on large materials datasets have revolutionized our ability to explore the matterverse at unprecedented scales and accuracy. I will demonstrate how combining the strengths of graph neural networks with many-body interactions provide the means to access the matterverse in all its chemical diversity and structural complexity. Such universal M3GNet interatomic potentials can be applied to perform massive scale screening for novel lithium superionic conductors, as well as for other technological applications.

11:00 AM DS03.09.02

Bio-Inspired Computational Design of Vascularized Electrodes for High-Performance Fast-Charging Batteries Optimized by Deep Learning [Chenxi Sui](#) and Po-Chun Hsu; Duke University, United States

Slow ionic transport and high voltage drop (IR drop) of homogeneous porous electrodes are the critical causes of severe performance degradation of lithium-ion batteries at high charging rates. Nature has already provided plenty of examples like vascular structures to solve this kind of multi-variable transport optimization problem. In this presentation, it is numerically demonstrated that a bio-inspired vascularized porous electrode can simultaneously solve these two problems by introducing low tortuous channels and graded porosity, which can be verified by porous electrode theory. Despite the immense geometrical parameter space of the vascularized electrodes, recent progress in the machine learning algorithm has accelerated the optimization of the complicated topological structures. To optimize the vasculature structural parameters, artificial neural networks are employed to accelerate the computation of possible structures 84 times with high accuracy. Furthermore, an inverse-design searching library is compiled to find the optimal vascular structures under different industrial fabrication and design criteria, based on the structure-property relationships learned by artificial neural networks from the numerical simulation. The prototype delivers a customizable package containing optimal geometric parameters and their uncertainty and sensitivity analysis. Finally, the full-vascularized cell shows a 66% improvement in charging capacity compared to the traditional homogeneous cell under 3.2 C current density in a numerical simulation. This computational research provides an innovative methodology to solve the fast-charging problem in batteries and broaden the applicability of deep learning algorithms informed by numerical simulations to different scientific or engineering areas.

11:15 AM DS03.09.04

Understanding Proton Dynamics near the Superprotonic Phase Transition of Solid-Acid Electrolytes Using Machine Learning Force Fields [Menghang Wang](#), Cameron J. Owen, Yu Xie, Simon L. Batzner, Albert Muelaian, Anders Johansson and Boris Kozinsky; Harvard University, United States

Solid-acid materials CsH_2PO_4 and $CsHSO_4$ exhibit superprotonic behavior above their phase transition temperatures. Due to the high computational cost of ab initio method, previous studies of proton dynamics were limited to a single phase with constant temperature at the scale of hundreds of atoms. While empirical force fields have been applied to study the phase transition specific systems, their accuracy and transferability are limited for the understanding and discovery of new solid-acid materials.

In this work, we build machine learning potentials for CsH_2PO_4 and $CsHSO_4$ data that combining quantum mechanical accuracy, scalability to large systems, as well as long time-scales. First, we collect training data by the Bayesian active learning framework FLARE [1], which utilizes molecular dynamics and uncertainty quantification to sample the configurational space. Then, we train the Allegro neural network potential [2] on the data set. We use the Allegro potential to study proton dynamics and properties near the phase transition by molecular dynamics. Then, we perform large-scale simulations on solid acids to unravel the mechanism of superprotonic behavior around the phase transition. The work flow is transferable to simulate a

wide range of superionic materials, predict their relevant properties, and propose promising candidates for experimental validation.

[1] Xie, Y., Vandermause, J., Ramakers, S., Protik, N., Johansson, A., and Kozinsky, B., Uncertainty-aware molecular dynamics from Bayesian active learning: Phase Transformations and Thermal Transport in SiC. arXiv:2203.03824

[2] Musaelian, A., Batzner, S., Johansson, A., Sun, L., Owen C., M., Kornbluth, M., and Kozinsky, B., 2022. Learning Local Equivariant Representations for Large-Scale Atomistic Dynamics. arXiv:2204.05249

SESSION DS03.10: Manufacturing
Session Chairs: Noah Paulson and Logan Ward
Wednesday Afternoon, November 30, 2022
Hynes, Level 2, Room 206

1:30 PM *DS03.10.01

Multi-Objective Optimization of Lithium Ion Battery Manufacturing by Using Machine Learning Coupled to Physics-Based Process Modeling Alejandro A. Franco; Universite de Picardie Jules Verne, France

In this lecture I present a digital twin for the accelerated optimization of the manufacturing process of Lithium Ion Batteries (LIBs). This digital twin is developed within the context of our ARTISTIC project¹ and it is supported on a hybrid computational approach encompassing a physics-based process modeling workflow and machine learning models, validated with in house experimental data acquired in our battery pilot line.² This digital twin simulates the different steps along the LIB cells manufacturing process, including the electrode slurry, the coating, the drying, the calendaring and the electrolyte infiltration. The physics-based process modeling workflow is supported on the sequential coupling of experimentally-validated Coarse Grained Molecular Dynamics, Discrete Element Method and Lattice Boltzmann simulations which allows predicting the impact of the process parameters on the final electrode microstructures in three dimensions. The predicted electrode microstructures are injected in a continuum performance simulator capturing the influence of the pore networks and spatial location of active material particles and carbon-binder within the electrodes on their electrochemical response. Machine learning models are used to accelerate the physical models' parameterization and to derive surrogate models capturing with high accuracy the predictions of the physics-based modeling workflow. Such surrogate models are incorporated in a Bayesian Optimization-based algorithmic loop which allows to predict which manufacturing parameters to adopt in order to maximize and minimize several electrode properties simultaneously. The predictive and optimization capabilities of our digital twin are illustrated with results for different electrode formulations and manufacturing parameters. Finally, the free online battery manufacturing simulation services offered by the project³ and designed to support the optimization of battery electrodes manufacturing are illustrated through several examples.

1. ERC Consolidator Project ARTISTIC, grant agreement #772873 (<https://www.erc-artistic.eu/>).

2. See our publications here: <https://www.erc-artistic.eu/scientific-production/publications> .

3. T. Lombardo, F. Caro, A. C. Ngandjong, J.B. Hooek, M. Duquesnoy, J. C. Delepine, A. Ponchelet, S. Doison, A. A. Franco. "The ARTISTIC online calculator: exploring the impact of lithium ion battery electrode manufacturing parameters interactively through your browser." *Batteries & Supercaps* 5, no. 3 (2022): e202100324.

2:00 PM DS03.10.02

Maximizing Supercapacitor Capacitance Through Adopting Convolutional Neural Network Guided Bayesian Optimization of 3D Printing JongHyun Kim, Seon Il Kim and WonHyoung Ryu; Yonsei University, Korea (the Republic of)

Supercapacitors are desired in the field of energy harvesting for its high capacitance. Although material properties are the primary factors in determining capacitance, the physical structure is also a dominant factor. 3d printed lattice structures are among preferred structures of supercapacitors as they allow a large surface to volume ratio (SAV). Once the structural rigidity is guaranteed, the printed lines must be narrow to maximize the surface area. Thus, in direct ink writing (DIW) 3d printing, printing parameters are tuned to find an optimal condition under which a uniform and thin line can be printed. However, this process is not only laborious but also costly due to many parameters that can influence printing quality. Recently, there has been a novel trial to implement Bayesian optimization, a technique used in machine learning, to optimize printing parameters [1]. With sample sizes less than 32, the Bayesian optimizer suggested printing conditions of different inks with higher printing resolution. In this work, we introduce a convolution neural network (CNN) guided Bayesian optimization to enhance the performance of supercapacitor through maximizing SAV of 3d-printed lattice electrode. The two optimization goals of high uniformity and narrow width in 3d printed lines are reached through a single scoring method: standard deviation of line widths. Through a camera with 600 x 800 resolution, 800 width measurements are made for each 6.5mm line printed from a 3d printer (Pro4, Nordson) and standard deviation of the measurements are calculated. The Bayesian optimizer attempts to find the global maxima of a surrogate model built from these standard deviation values, fed in negative. Throughout the process, the CNN model guides the Bayesian optimizer to keep its search space within straight line printed regions, preventing costly explorations and reducing total optimization time. The CNN model categorizes the printed lines to discontinuous, straight, coiled, or aggregated and resets the Bayesian optimizer's parameter boundaries when it detects a non-straight line. 7mm x 7mm x 0.72mm lattice structure supercapacitors are made using either graphene oxide (GO) ink or poly(3,4-ethylenedioxythiophene):polystyrene sulfonate (PEDOT:PSS) ink. Three printing parameters: nozzle speed, nozzle height, and pressure, are optimized. Throughout 50 iterations of Bayesian optimization, the CNN model reset the search space 6 times for GO ink and 7 times for PEDOT:PSS ink. Supercapacitors were 3d printed with the optimized parameters and compared to supercapacitors prepared with conventional DIW printing method [3]. For GO and PEDOT:PSS supercapacitor, ligament widths decreased by 78.3% and 82.5% respectively. While ligament spacing was set to 0.3mm, number of unit cells increased by 158.2% and 156.3%, enhancing the pore architecture of the lattice structures. The capacitance, measured by cyclic voltametric method, increased by 121.5% and 108.4%.

Acknowledgement

This work was supported by the National Research Foundation of Korea(NRF) Grant funded by the Korean Government(MSIT) (No. 2020R1A2C3013158)

REFERENCES

- [1] Kalani Ruberu, et al, *Applied Materials Today*, 2020, 22, 100914
- [2] Timothy Erps, et al, *Applied Science and Engineering*, 2021, 7, 22
- [3] Hyunwoo Yuk, et al, *Applied Materials*, 2018, 30, 6

2:15 PM DS03.10.03

AI Guided Manufacturing for Space Applications Todd M. Muller, Hud Wahab, Jacob Heil, Lars Kotthoff, John Ackerman and [Patrick A. Johnson](#); University of Wyoming, United States

Compact printable devices manufactured from lightweight, versatile, and easily stored materials are of interest for in-space manufacturing due to high transportation costs and limited supply chain. Moreover, automated closed-loop experiments could support production during manned and unmanned missions and further limit waste generation. In this article, we demonstrate the use of advanced manufacturing techniques to produce laser-induced graphene temperature and humidity sensors from Kapton. We explore the techniques used to manufacture these sensors, using Bayesian Optimization for single and batch evaluations to interpolate and optimize future experiment parameters from small amounts of data. We also explore the application of these techniques in the development of capacitors for energy storage.

2:30 PM BREAK

SESSION DS03.11: AI for Discovery
Session Chairs: Sijia Dong and Noah Paulson
Wednesday Afternoon, November 30, 2022
Hynes, Level 2, Room 206

3:30 PM DS03.11.01

Data-Driven Discovery of Materials with Tuned Surface Properties for Thermionic Energy Conversion [Peter Schindler](#)^{1,2}, Evan Antoniuk¹, Gowoon Cheon¹, Yanbing Zhu¹ and Evan Reed¹; ¹Stanford University, United States; ²Northeastern University, United States

Data-driven approaches based on high-throughput computational methods have emerged as a new paradigm to facilitate the search through vast chemical spaces for new materials with tuned properties or novel behavior. The rapid increase in available computational data structured in open-source material databases has opened an avenue towards material discovery using data mining and statistically driven machine learning approaches. However, most big material databases like the Materials Project, AFLOW, and NOMAD largely lack to report surface properties like the work function and surface energy, as each bulk material typically has dozens of distinct low-index crystalline surfaces and terminations. The discovery of thermally stable materials with surfaces that exhibit an ultra-low work function (less than 1.5 eV) would allow thermionic conversion of heat (>1500C) directly to electricity with efficiencies exceeding 30% (typical thermionic and thermoelectric converters have efficiencies around 10%). Further, the work function is crucial for band alignment in heterostructures and electron emission devices. Here, we report on a recent advance in our high-throughput workflow using density functional theory (DFT) to calculate both the work functions and the cleavage energies of over 30,000 surfaces that we created from ~2,500 bulk materials, including up to ternary compounds. Moreover, we developed a physics-based approach to featurize surfaces and established a surrogate machine learning model to predict the work function. We find that physical choice of features improves prediction performance such that our random forest model achieves a mean absolute test error 4 times lower than the baseline, comparable to the accuracy of DFT. This surrogate model enables rapid predictions of the work function (~10⁵ faster than DFT) across a vast chemical space. By identifying the Pareto front of material surfaces that have an ultra-low work function as well as low cleavage energy we are able to discover promising, stable material surfaces for application in thermionic energy conversion.

3:45 PM *DS03.11.02

Finding Thermally Robust Superhard Materials with Machine Learning [Jakoah Brgoch](#); University of Houston, United States

Superhard materials with a Vickers hardness >40 GPa are essential in applications ranging from manufacturing to energy production. Finding new superhard materials has traditionally been guided by empirical design rules derived from classically known materials. However, the ability to quantitatively predict hardness remains a significant barrier in materials design. To address this challenge, we constructed an ensemble machine-learning model capable of directly predicting load-dependent hardness. The predictive power of our model was validated on eight unmeasured metal disilicides and a hold-out set of superhard materials. The trained model was then used to screen compounds in Pearson's Crystal Data (PCD) set and combined with our recently developed machine-learning phase diagram tool to suggest previously unreported superhard compounds. Finally, industrial materials often experience tremendous heat during application; thus, we are building a method for predicting hardness at elevated temperatures.

4:15 PM DS03.11.03

Elucidating Precipitation in FeCrAl Alloys Through Explainable AI—A Case Study [Christopher Reynolds](#), Andrew Hoffman, Indranil Roy, Sandipp K. Ravi, Subhrajit Roychowdhury, Bojun Feng and Rajnikant V. Umretiya; GE Global Research, United States

One of the primary challenges of using FeCrAl as a nuclear fuel cladding material is the formation of α' -precipitates that can cause brittleness in the alloy. The precipitation causes hardness change during thermal aging which is sensitive to both alloy composition and experimental conditions (i.e., temperature and time of heat treatment). While this behavior is well known for Al free ferritic stainless alloys, in FeCrAl alloys the effects of Al and Mo additions include both influence on kinetics and thermodynamics. To better understand the influence of composition on this age hardening behavior, artificial intelligence and machine learning have been utilized to interpret a large data set of aging experiments. A Gaussian process regression model was built on the hardness data collected at General Electric Research. Subsequently, for the first time, SHapley Additive exPlanations (SHAP) is leveraged as an explainable artificial intelligence (XAI) tool to understand the effect of feature values in driving the hardness change. This new approach broadens the capabilities of machine learning and artificial intelligence. Several key insights are affirmed and obtained from a material science perspective.

4:30 PM DS03.11.04

Machine-Informed Design of π -Conjugated Molecules with Tuned Optical Properties [Parker Somberger](#)¹, Vinayak Bhat¹, Baskar Ganapathysubramanian² and Chad Risko¹; ¹University of Kentucky, United States; ²Iowa State University of Science and Technology, United States

While organic π -conjugated materials demonstrate great utility in energy generation and storage, lighting, transistors, sensors, and other optical and electronic devices, designing a new molecular material with precise properties for a specific application requires the exploration of a vast chemical space. Molecular generative models show great efficacy for in silico property prediction and design for drug-like molecules. Given this success, these models can have a natural extension to the design of π -conjugated molecules. Here, we will discuss the development of generative normalizing flow models to tune the optical properties of π -conjugated chromophores. The models are trained on the more than 25,000 chromophores and points of optoelectronic data from the Organic Crystals in Electronic and Light-Oriented Technologies (OCELOT) database. The generative models, with a focus on molecules that can be of

interest for singlet fission or thermally activated delayed fluorescence, can quickly generate structures with the aim of tuning the energy gaps between low-lying singlet and triplet excited states. The model optimizes these gaps through sampling a learned chemical space and predicting the gap between a molecule's low-lying singlet and triplet excited states using pretrained message passing neural networks that were trained on the optoelectronic data from OCELOT. Results from the generative models are verified through density functional theory (DFT) and time-dependent DFT (TDDFT) calculations to obtain their optical transitions and frontier molecular orbital energies. Though the models here are focused on robustly tuning optical transitions, the methods can be transferred to optimize additional electronic properties.

SESSION DS03.12: Poster Session II
Session Chairs: Sijia Dong and Logan Ward
Wednesday Afternoon, November 30, 2022
8:00 PM - 10:00 PM
Hynes, Level 1, Hall A

DS03.12.01

Automating Experiments Using Charged Particle Beam Nanofabrication Tools Michael Titze, Edward Bielejec and [Alex Belianinov](#); Sandia National Laboratories, United States

Imaging methods with electrons, ions, and probes have played a central role in modern science and engineering with applications ranging from condensed matter and quantum physics, materials science, chemistry, biology, and medicine. Despite the variability of these approaches in terms of hardware, interaction mechanisms, and extracted information; the fundamental principles of the imaging process remain largely similar. Practically all methodologies map data on grids, to highlight an area of interest pertinent to the given problem. It is no surprise then, that hardware and software developments in the area of machine vision, AI, and decision-making that focus on consumer problems like driving and feature recognition, are now presenting themselves as opportunities for automating aspects of routine scientific processes. This talk exploits the underlying similarities of imaging experiments to combine probe, electron, and ion-based techniques by a common software thread encapsulating image processing and machine-learning algorithms to help focus researchers' efforts on high quality targets and enhance productivity.

Specifically, a combined, transferrable hardware-software toolset aimed at automating routine aspects of the decision-making process in ion exposure, implantation, milling, and deposition will be presented.

DS03.12.02

Semi-Automatic Scheme for Material Search Projects in Early Stage—Developing Practical Solvent-Solubility Prediction Models of Tetraphenylporphyrin Derivatives Securing Chemical-Space Coverage [Raku Shirasawa](#)¹, Ichiro Takemura¹, Shinnosuke Hattori¹ and Yuuya Nagata²; ¹Sony Group Corporation, Japan; ²Hokkaido University, Japan

A semi-automatic molecular exploration scheme to model the solvent-solubility of tetraphenylporphyrin derivatives (TPPs) was designed and implemented. This scheme consisted of the following steps: (1) defining a practical chemical search space, (2) prioritizing molecules in the space using an extended algorithm for submodular function maximization (SFMMOL) without requiring biased variable selection or pre-existing data, (3) synthesis and automatic measurement, and (4) estimating machine-learning (ML) model. The evaluation order of TPPs selected using SFMMOL covered several similar molecules (32% of all targeted molecules, whereas that obtained by random sampling and uncertainty sampling was ~7% and ~4%, respectively) even with a small number of evaluations (10 molecules: 0.13% of all targeted molecules). The top 5 molecules in the order were synthesized, and, in conjunction with commercially available molecules, totally 15 molecules in 16 solvents were evaluated by the automatic measurement of UV-Vis absorption spectra. The derived binary ML classifiers for solute-solvent pair predicted 'good solvents' with an accuracy > 0.8. Consequently, we confirmed the effectivity of the proposed semi-automatic scheme for accelerating the early-stage material search project and expected the scheme applicable to a wider range of material research.

DS03.12.03

Deep-Learning-Based Inkjet Droplet Classification for Jetting Status Evaluation [Eunsik Choi](#)¹, Kunsik An² and Kyung-Tae Kang¹; ¹Korea Institute of Industrial Technology, Korea (the Republic of); ²Konkuk University, Korea (the Republic of)

Inkjet printing is a powerful direct writing process technology of materials, which has been successfully exploited to printed electronics and energy devices including batteries, supercapacitors, fuel cells, and solar cells. Inkjet printing is also an economic and eco-friendly process which deposits microfluidic droplets on a designated area and enables non-contact, additive, maskless patterning in micrometer resolution which reduces materials usage. It can be adopted to print versatile materials into scalable patterns.

Nonetheless, printability or droplet jettability of an ink is not easy to predict owing to the intrinsic complexity of the process depending on ink-nozzle-air interactions. Thus, droplet jetting conditions should be monitored by adept experts to ensure reliability of the process. Moreover, it is unwieldy to predict droplet jetting conditions of multiple nozzles which are the requisite to increase productivity, resulting in incalculable labour costs and application bottleneck.

In this regard, we present a deep learning based method to classify inkjet droplets and evaluate its jetting statuses. MobileNetV2 was used as a pretrained convolutional neural network (CNN) model and its hyperparameters were optimized for the present study. Inkjet droplet frame sets were recorded by an *in situ* CCD camera and each frame was classified by the CNN model. Each classified frame set was accumulated in order of frame time to evaluate the jetting status of the frame set. It was demonstrated for both of single-jet and multi-jet processes.

7,852 frames were used for the single-jet deep learning model and accuracies for training and validation were 0.90 and 0.86, respectively. Jetting statuses were comprehensively evaluated by the accumulated frame classification data. In particular, the jetting status, which is based on frame class-time profile provided complete and perceptive information compared with jetting map, which had been diagnosed from human expert. It was especially valuable for non-expert operators to evaluate the jetting status and to optimize the process based on pulse width (μ s) and pulse amplitude (V).

1,463 frames were gathered from 7 different nozzles for the training and validation of multi-jet model. In addition, 693 frames were generated for the test data of multi-jet model. Multi-jet model proved the accuracies of the training and validation to be 0.97 and 0.98, respectively. Broader distribution of data from differences of the droplet jetting environment was trained by the neural network which resulted in the improved accuracies of the multi-jet model compared with the single-jet model.

Runtime of a frame classification was less than a second, which demonstrated feasibility of the deep learning based real-time process monitoring. The deep learning based inkjet frame classifier could be further developed for autonomous process testing system with numerous nozzles. Moreover, it was applicable to long-term process, while saving plenty of data and frame class-time profiles. On top of that, the droplet classification model was able to be

applied for the other microfluidic jetting processes in that the frames were acquired from shadow images of the ejected inks lighted from strobe LED regardless of ink materials.

The strategy was firstly demonstrated to silver nanoparticle ink jetting process and applicable to the other comprehensive inkjet printing process of materials which can be exploited to fabricate electrodes for energy storage devices. This result shed a light on artificial intelligence based material processing research by using overlooked data during process. Furthermore, it is applicable to large scale process for both academia and industry.

DS03.12.04

Predicting Electronic Properties of Organic π -Conjugated Systems with Graph Neural Networks [Vinayak Bhat](#), Parker Sornberger and Chad Risko; University of Kentucky, United States

Organic π -conjugated molecules have widespread applications namely in field-effect transistors, solar cells, (bio)sensors, and dyes. Accurate estimations of molecular electronic and optical properties using state-of-the-art density functional theory are time-consuming for large systems. Using graph neural network (GNN) and data from the OCELOT database, we trained machine learning (ML) models to predict properties, namely frontier molecular orbital energies, reduction and oxidation energies, relaxation energies, and low-lying singlet and triplet excitation energies. The trained GNNs can provide explanations for the predictions, thereby providing insights into the structure-property relationships. Further, we trained ML models to predict material properties, including the intermolecular electronic couplings between molecular dimers and crystal properties including bandgaps and cohesive energies. These models provide distinct connections between molecular and crystal properties, which we aim to build on as we develop and deploy machine-informed materials design for organic semiconductors.

DS03.12.05

Machine Learning-Assisted Models for Understanding and Optimizing Boiling Heat Transfer on Scalable Random Surfaces [Hyeongyun Cha](#), Yang Zhong and Evelyn N. Wang; Massachusetts Institute of Technology, United States

Boiling is a ubiquitous process in numerous applications, including nuclear power plants, water treatment, and thermal management. However, predicting and enhancing boiling heat transfer performance is notoriously difficult due to the complex nature of the boiling process. Here, we develop supervised machine learning (ML) models based on convolutional neural networks (CNN) to elucidate and predict boiling curves using detailed surface profiles as the only inputs. To train and validate the models, we fabricated a large number of statistically distinct random surfaces using sandblasting, a scalable surface engineering technique to enhance boiling heat transfer. The copper surfaces were sandblasted by aluminum oxide abrasives, and the surface morphologies and roughness were characterized by optical profilometry. Furthermore, the effects of multiple process parameters, including sandblasting medium size, pressure, nozzle distance, sweeping speed, and sweeping pitch, were investigated. The pool boiling experiments were conducted with saturated water in an ambient laboratory condition. The supervised ML models were trained by feeding a variety of surface morphologies with their measured boiling behaviors, which later enabled the models to predict boiling performance solely based on surface morphology. As a result, for a given unobserved random surface, the ML algorithms predicted both the heat transfer coefficient (HTC) and the critical heat flux (CHF) values within a deviation of 10% from experimental results. In addition, we developed the inverse design models based on variational autoencoder (VAE) and generative adversarial network (GAN) to create boiling surfaces for the target boiling performance. The VAE and GAN models were trained and validated with the same training datasets containing different surface morphologies with measured boiling behaviors. The ML models generated surface structures as well as the corresponding manufacturing parameters, which highly matched with the real surface features and the boiling experimental results. This work not only provides optimal boiling surface design guidelines without time-consuming experiments, highly inaccurate empirical correlations (up to 90% error), or extensive computational models (~months), but also enables scalable engineering techniques to be more readily adopted in current energy applications, enhancing performance and enabling a shorter payback period for increased deployment.

DS03.12.06

Real-Time 3D Analysis During Tomographic Experiments Using Tomviz [Jonathan Schwartz](#)¹, Chris Harris², Huihuo Zheng³, Jacob Pietryga^{4,1}, Prashant Kumar¹, Anastasia Visheratina¹, Nicholas A. Kotov¹, Brianna Major², Patrick Avery², Peter Ercius⁵, Utkarsh Ayachit², Berk Geveci², David Muller⁶, Yi Jiang³, Marcus D. Hanwell⁷ and Robert Hovden¹; ¹University of Michigan, United States; ²Kitware, United States; ³Argonne National Laboratory, United States; ⁴Northwestern University, United States; ⁵Lawrence Berkeley National Laboratory, United States; ⁶Cornell University, United States; ⁷Brookhaven National Laboratory, United States

Three-dimensional (3D) characterization across the nanoscale is now possible using scanning / transmission electron microscopes (S/TEM) [1,2]. Unfortunately, tomographic reconstructions can take one to several days to complete depending upon the dataset size or algorithm(s) employed. Even worse, the reconstruction occurs offline, long after all the data has been collected, preventing immediate interpretation during an ongoing experiment. While advancements in detector hardware have boosted throughput with digital data collection, substantial human effort and computational resources are still required to process the deluge of raw data. It has been a longstanding goal to start 3D analysis of specimens in real-time, enabling the immediate assessment of nanoscale structure. Achieving high-throughput electron tomography requires an integrated pipeline that links the microscope hardware to optimized reconstruction algorithms and efficient 3D volumetric visualization.

Here we present interactive 3D visualization that seamlessly runs while experimental projections are collected in an electron microscope using the tomviz platform (www.tomviz.org). Tomviz provides 3D materials structure to scientists in real-time enabling high-throughput specimen interpretation with immediate tomogram visualization [1]. During the experimental acquisition, tomviz monitors for new projections which are continuously appended into the reconstruction process. After a reconstruction updates, tomviz immediately renders the 3D volume. We demonstrate real-time tomography on a helical nanoparticle comprised of a Cysteine amino-acid coordinated with Cadmium (Cys/Cd). The specimen's left-handed chirality is discerned in the first twenty minutes and a high-resolution volume is available within 50% of the experiment (20-30 minutes).

Real-time tomography demands maximally efficient computational speed to ensure the optimization runs faster than the experimental data acquisition rate. Tomograms are reconstructed in parallel with data acquisition and a high-quality 3D reconstruction is available before the experiment completes. The multithreaded pipeline in tomviz enables interactive 3D analysis of the current reconstruction state with minimal impact on performance. A robust graphical user interface allows 3D objects to be rendered as shaded contours or volumetric projections and these objects can be rotated, cropped, or sliced as the reconstruction evolves. Thus, scientists can go beyond superficial inspection to quantify specimen features or internal structure while simultaneously operating the microscope. This immediate feedback can save researchers days of effort as reconstructions are no longer processed offline.

Reference:

- [1] R. Crowther, L. Amos, J. Finch, D. Rosier, A. Klug, *Nature* 226, 421 (1970).
- [2] P. Midgley and M. Weyland. *Ultramicroscopy* 96, 413 (2003).
- [3] Schwartz, *et. al.* Real-Time 3D Analysis During Tomographic Experiments using tomviz. Available at *Research Square* [<https://doi.org/10.21203/rs.3.rs-1061868/v1>]

DS03.12.07

Machine Learning Prediction and Experimental Validation of Novel Materials for Rotating Electrical Machines Shakti P. Padhy¹, Varun Chaudhary¹, Yee-Fun Lim², Kedar Hippalgaonkar¹ and Raju V. Ramanujan¹; ¹Nanyang Technological University, Singapore; ²Agency for Science, Technology and Research, Singapore

Magnetic alloys play a key role in energy conversion, transmission, and utilization. The urgent need for Net Zero energy technologies demand the development of the next generation of high strength magnetic alloys for high frequency rotating electrical machines operating in extreme environments. Multiple properties need to be optimised in such demanding applications. A data-driven approach to develop new Fe-Co-Ni-based alloys for such applications was utilized. A database consisting of the magnetic, electrical, and mechanical properties of Fe-Co-Ni based alloys was curated from the literature. A machine learning (ML) based imputation methodology was utilized to complete the database. A multi-property regression ML model with the lowest mean absolute error (MAE) was chosen to map the composition to the properties. An inverse design strategy was also developed to predict new alloy compositions. Both the multi-property model and inverse design strategy were validated. Fe-Co-Ni ternary alloy compositions were prepared and characterized *via* a high-throughput methodology. New alloy compositions, e.g., Fe₇₃Co₂₄Ni₃ and Fe_{53.6}Co_{36.4}V₄W_{3.5}Cu_{1.3}Al₁Ti_{0.2} with a balanced set of properties for electrical machines applications were identified. This successful strategy can also be deployed for the accelerated development of other classes of materials. This work is supported by the AME Programmatic Fund by the Agency for Science, Technology and Research, Singapore under Grant No. A1898b0043.

DS03.12.08

Data-Driven Approaches to the Electrochemistry of Multi-Component Cathode Materials Peichen Zhong^{1,2} and Gerbrand Ceder^{1,2}; ¹University of California, Berkeley, United States; ²Lawrence Berkeley National Laboratory, United States

The increasing demand in electrical energy storage requires the discovery of high energy density cathode materials for lithium-ion batteries. Disordered rocksalts with Li-excess (DRX) materials are promising candidates as these materials do not require a specific cation chemistry to favor any particular ordering, and can be synthesized with a very wide variety of elements. However, the computational modeling for DRX is difficult as it can be composed from a wide variety of chemistry with site disorder.

In this presentation, we will demonstrate a state-of-art approach to the modeling and prediction of electrochemistry (discharge voltage profile) of DRX materials via a data-driven approach. We applied a deep neural network (DNN) trained directly on a large amount of experimental results. The DNN is trained with an end-to-end learning scheme, that includes the redox information appropriately regularized. The DNN can interpolate and make predictions for compounds that have not yet been tested, which can accelerate the exploration of DRX and other electrode materials.

DS03.12.09

Epitaxial Growth of Silicon Carbide from Molecular Dynamics and Active Learning of Machine Learning Force Field Yu Xie¹, Senja Ramakers^{2,3}, Maximilian Amsler², Thomas Eckl², Ralf Drautz³ and Boris Kozinsky¹; ¹Harvard University, United States; ²Corporate Sector Research and Advance Engineering, Robert Bosch GmbH, Germany; ³Interdisciplinary Centre for Advanced Materials Simulation, Ruhr-Universität Bochum, Germany

The wide-bandgap semiconductor silicon carbide (SiC) has been widely applied to power electronics, nuclear physics, and quantum computing. Epitaxial growth is the primary approach to fabricate high-quality SiC wafers. However, it remains a challenge to understand and control the growth process. Molecular dynamics (MD) provides computational insight on a microscopic scale, but reliability of simulations is often limited by the insufficient accuracy of empirical force fields, whereas *ab initio* MD is too expensive to scale to large length and time scales. Machine learning force fields are shown to be promising with efficiency comparable to empirical force fields and with quantum accuracy. Our Bayesian active learning method [1] has been used for fast training of force fields from first principles. In this work, we incorporate the deposition process with the active learning to train the force field efficiently on the epitaxial growth. We then validate the force field and run large-scale molecular dynamics of the epitaxial growth process. The simulation helps with the understanding of the deposition growth, and can facilitate the control and improvement of the fabrication of high-quality SiC.

[1] Yu Xie et al. Uncertainty-aware molecular dynamics from Bayesian active learning: Phase Transformations and Thermal Transport in SiC. 2022

DS03.12.11

Integrated Neural NLP Pipeline for Autonomous Synthesis Database Extraction from Literature Vineeth Venugopal and Elsa Olivetti; Massachusetts Institute of Technology, United States

The heuristic nature of materials synthesis limits researchers' ability to extend materials genome initiative-type approaches to methods to make novel materials or extend existing materials to new, controlled morphologies and microstructures. A number of recent informatics-based approaches have shown that machine learning models are able to learn synthesis conditions given sufficient data. These data-driven methods should save time and energy in the fabrication of new material compositions and structures. However, machine readable databases of inorganic material fabrication and processing are still limited since the underlying information is present only in unstructured databases such as archives of published scientific literature.

Recent work has shown how Natural Language Processing (NLP) can be used to extract synthesis specific information from texts. Databases for solid state and solution based processing have been made available. The techniques used for these extractions include sequence to sequence tagging algorithms employing recurrent neural networks, large language models, and language dependency parsing using linguistic grammar trees (most often implemented in the popular NLP package, Spacy). While these algorithms are accurate at identifying synthesis specific tokens such as names of the synthesis operations, units, and temperature values, they can be improved when tokens are not proximate in a dependency tree. As a result, the autonomous extraction of synthesis data tends to be error prone and many concurrent data points are required to improve our confidence in a given material -synthesis condition - parameter relation.

We propose a transformer based neural network architecture that directly learns the relations between different entities in a text which is learnt from a custom annotated database of synthesis literature. This approach integrates large language model based named entity recognition systems with neural relational classifiers, thereby creating a unified approach to both entity identification and linkage. Using this approach, the accuracy of extracted synthesis conditions for solid state and solution based processing is greatly increased. This is demonstrated through comparison with extracted public datasets. The results are additionally validated manually. Some reflections on dataset creation and human labeling for NLP tasks is presented as a guideline for the community in extending this approach to non-synthesis datasets.

DS03.12.13

Analysis of Variability in Resistive Memory Originated from Initial Defect Configuration by Fully Coupled Electrothermal and Phase-Field

Models [Chanho Park](#), Dongmyung Jung and Kwon Yongwoo; Hongik University, Korea (the Republic of)

Recently, resistive random-access memory (RRAM) has been profoundly studied to apply to neuromorphic computing. So far, it is hard to use the RRAM as a synapse device because its characteristics are sensitively affected by various factors. In other words, the variability is too severe. Therefore, reducing the variability is one of the major challenges in the RRAM device research. In this work, we investigate the factors affecting the device variability in conductive filament behaviors using a multi-physics simulation that integrates the electrothermal and phase-field models. The initial defect configuration is the source of the variability. With the given defects, the cell architecture, both cell geometry and constituent materials, to reduce the variability in the device characteristics are investigated.

SESSION DS03.13: AI for Characterization
Session Chairs: Sijia Dong and Arun Kumar Mannodi Kanakithodi
Thursday Morning, December 1, 2022
Hynes, Level 2, Room 206

8:00 AM *DS03.13.01

Design and Understanding of Battery and Solar Cell Materials [Maria K. Chan](#); Argonne National Laboratory, United States

Modeling and AI/ML play increasingly important role in the design and understanding of numerous classes of materials. In this talk, we will discuss our work on battery materials including the important question of oxygen redox, and on photovoltaic materials including Cd chalcogenides and perovskite halides.

8:30 AM DS03.13.02

Machine Learning Guided Interrogation of Gas Evolving Electrode Catalyst Activity [Simon Ruffer](#)¹, John Lake¹, Aristana Scourtas^{2,3}, Jim James⁴, Nathan Pruyne⁵, Marcus Schwarting², Ben Blaiszik^{2,3} and Kripa Varanasi¹; ¹Massachusetts Institute of Technology, United States; ²The University of Chicago, United States; ³Argonne National Laboratory, United States; ⁴Georgia Institute of Technology, United States; ⁵Northwestern University, United States

Being able to effectively manage gas evolution at electrochemical electrodes is a major challenge in a wide variety of industrial applications. Perhaps the most important activities where electrochemical bubble generation is critical to control are the chlor-alkali (chlorine gas production) and Hall-Héroult (electrochemical aluminum smelting) processes. Significant effort goes towards mitigating the “anode effect” of the Hall-Héroult process, where carbon dioxide gas inactivates the carbon anode, causing catastrophic increases in overpotential. For the chlor-alkali process, the attachment of bubbles to electrode surfaces accounts for approximately 20% of the overpotential at industrially relevant current densities. Similar inefficiencies and problems are caused during water electrolysis when bubbles adhere to or flood electrodes. As a result, the limiting effects of bubbles restrict the adoption of traditional, low-temperature electrochemical methods for hydrogen generation from renewable electricity. In this way, both understanding and mitigating the negative impacts that bubbles have on electrode performance offer a unique path to enable high performance gas evolving electrochemical technologies, which will play a major industrial role in a renewably electrified future.

These problems motivate this work as we investigate the way that bubble inefficiencies manifest on electrodes by fabricating novel electrodes for studying the effects that adhered bubbles have for electrochemical performance using both hydrogen and oxygen evolution reactions. Despite extensive knowledge of the negative impacts adhered gas bubbles cause at a system level, there is limited fundamental understanding of the extent to which specific mechanisms inactivate active electrode materials. By using surface engineering gas evolving electrode for testing, we can manipulate the micro- and nanoscale electrode morphologies to control bubbles nucleation and bubble/electrode interactions. By developing machine vision algorithms for the detection and tracking of bubbles from electrode surface imaging, we obtain empirical results which oppose the prevailing view held in regard to how bubbles inactivate electrodes. The utility of tracking nucleating and growing bubbles on electrodes’ surfaces can also provide important spatiotemporal information about the activity of the electrocatalyst materials used, not only regarding the inactivation that the bubbles cause. As a result, the machine vision methods developed are also proposed and demonstrated as a useful electrocatalyst screening tool for the evaluation of catalyst materials for gas evolving electrochemical reactions. As a result of these findings and the methods developed, we provide a novel framework for designing gas-evolving electrochemical electrodes and for the discovery of highly active electrocatalyst materials for gas evolving reactions.

8:45 AM DS03.13.03

Multi-Instruments Autonomous Discovery of Phase Change Memory Materials for Nonvolatile Memory Devices [Chih-Yu Lee](#)¹, Haotong Liang¹, Heshan Yu¹, Austin McDannald², A. Gilad Kusne² and Ichiro Takeuchi¹; ¹University of Maryland, United States; ²National Institute of Standards and Technology, United States

Autonomous experimentation enabled by artificial intelligence (AI) facilitates acceleration of materials discovery and design. Investigating materials of complex compositional and structural landscapes requires resource-intensive high-throughput experimentations. Conventionally, we study materials by analyzing data collected from multiple characterization and measurements at different times. However, analyzing these data streams separately cannot exploit shared trends to boost analysis, prediction, and decision making. Herein, a novel approach is proposed to explore structural and functional properties synchronously. The autonomous robot is able to explore phase maps and exploit property optimization simultaneously in the high dimensional space. Multi-instruments run in parallel. The central AI exploits shared trends from the diverse measurement data sources and then employs a multi-objective active learning process to make decisions on the next iteration. The goal is accelerate discovery of optimal materials by learning and utilizing knowledge of composition-structure-property relationships. With this approach, we successfully discover novel materials in the titanium-selenium-tellurium system (TST), which is considered a promising phase change memory (PCM) candidate used in random-access memory. Combining x-ray diffraction and four point probe measurements, structural and functional property maps are established in terms of combinatorial wafer composed of hundreds of various compositions. The algorithm combines active phase mapping of a live x-ray diffraction data stream and multi-objective optimization of functional properties from additional live data streams. We identify a set of materials with identical structural signatures as well as two important features required for nonvolatile memory—large contrast of resistance between amorphous and crystalline states and large resistance in crystalline states. This novel approach again confirms that AI accelerates materials discovery and design.

9:00 AM *DS03.13.04

Generative Materials Informatics—Going Beyond Screening [Taylor D. Sparks](#)¹, Sterling Baird¹, Michael Alverson^{1,2}, Hasan Sayeed¹ and Marianne

Liu¹; ¹University of Utah, United States; ²University of Southern California, United States

Machine learning already enables the discovery of new materials by providing rapid predictions of properties to complement slower calculations and experiments. However, a persistent criticism of machine learning enabled materials discovery is that new materials are very similar, both chemically and structurally, to previously known materials. This begs the question “Can machine learning ever learn new chemistries and families of materials that differ from those present in the training data?” In this talk, I will describe two important tools we are developing to truly move beyond screening to actual discovery. First, I will describe new generative machine learning approaches that can be used to generate structures that do not yet exist, but are likely to. I will compare generative models including variational autoencoders, generative adversarial networks, and diffusion models which have become standard in machine learning for images. I will describe the unique challenges that we face when using tools of this nature to generate periodic crystalline structures. Second, I will describe the Descending from Stochastic Clustering Variance Regression (DiSCoVeR) algorithm to bias the discovery of new suggested materials away from known chemistries in a systematic way towards unintuitive and even unlikely yet promising candidates for new materials.

9:30 AM DS03.13.05

Visual Explanations for the Generation of Dislocation Clusters in Multicrystalline Silicon Using Gradient-Based Techniques [Kyoka Hara](#)¹, Takuto Kojima¹, Kentaro Kutsukake², Hiroaki Kudo¹ and Noritaka Usami¹; ¹Nagoya University, Japan; ²RIKEN, Japan

Multicrystalline materials are often the most common choice for various applications because of their affordable processing. As for solar cells based on multicrystalline absorbers, the conversion efficiency has improved over the years, stimulated by the increasing variety of constituent materials such as silicon, CIS, CdTe, and perovskites. However, device performance tends to be limited by a high concentration of defects that provoke recombination and deteriorate conversion efficiency. Thus, it is essential to reveal how these defects are generated and to control them. In particular, we focus on examining and controlling the formation of dislocation clusters (DCs) in multicrystalline silicon. In order to establish a systematic and comprehensive knowledge on the generation of DCs, we have previously developed a machine-learning based model to estimate the existence of DCs from the microstructures of the sample wafers. This model is constructed with a convolutional neural network. It learns the features of optical images taken of the wafer surface and uses photoluminescence images of corresponding wafers as teacher data. The optical images were taken by a house-made apparatus and inherits crystallographic features such as grain boundaries, grain sizes, and crystal orientations. The photoluminescence images display the locations of DCs. We have previously reported on the techniques regarding this model and the results of the estimations. Promising results have indicated the possibility that some key structures responsible for the generation of dislocation clusters have been successfully extracted from the input images. In this study, we present further analysis of the model's estimations using gradient-based interpretability techniques.

While machine learning has become increasingly powerful and successful, the urgency in interpreting the neural network's decisions has escalated. The reasonings the model makes being a black box, building trust and transparency in machine learning techniques has miles to go. In this case, the neural network has indeed displayed correct estimations on whether dislocations exist or not, but the structures that contribute most to those estimations are masked in the layers. To reveal the model's reasoning in this estimation, we have performed calculations of the gradients flowing into the model's layers using Gradient-weighted Class Activation Mapping (Grad-CAM). The results have been integrated into localization maps showing the most important regions in the input images for the model's decision-making. This provides us with some visual explanations on the microstructures responsible for the generation of DCs.

9:45 AM DS03.13.06

Crystal Structure Reconstruction from X-Ray Diffraction Patterns Based on Supervised Contrastive Learning [Doosun Hong](#)^{1,2}, Tian Xie³, Donghun Kim², Jeffrey Grossman³ and Hyuck Mo Lee¹; ¹Korea Advanced Institute of Science and Technology, Korea (the Republic of); ²Korea Institute of Science and Technology, Korea (the Republic of); ³Massachusetts Institute of Technology, United States

Techniques based on X-ray diffraction (XRD) are the most related to the identification of crystal structures. The latest generation of tools for high-throughput diffraction experiments and simulations has led to collection of a large volume of XRD data. The handling of these large-sized dataset calls for big data and machine learning (ML)-based approaches. Several recent studies were reported, where powder XRD 1D curves were used to classify crystal symmetry such as crystal systems and space groups. However, these studies are limited to identifying crystal symmetry, and not yet extended to the full reconstruction of three dimensional (3D) crystal structure.

In this work, we report a deep learning (DL)-based approach to reconstruct 3D crystal structures from XRD patterns, based on supervised contrastive learning (SupCon). This protocol largely consists of crystallographic prototype classifier and element position assigner. The former process attempts to classify crystallographic prototype, which is one of crystal structure symmetry groups. According to AFLOW, 1,100 prototypes are available today, and each has a unique combination of material composition (stoichiometry), crystal symmetry (Pearson symbol and space group), and Wyckoff position. Using SupCon, we achieved the classification accuracy around 90%, based on the datasets involving 28 prototypes. The latter process is element position assigner, which finds the position of elements as well as lattice parameters for a given prototype. Through our novel protocols leveraging prototype classification, we demonstrate several examples where 3D crystal structures were fully reconstructed from XRD patterns.

We additionally emphasize the importance of SupCon, which is much better in contrasting the subtle differences of similar crystal prototypes than traditional supervised classification methods, which was key to achieving classification accuracy around 90%. This work offers a method to reconstruct 3D crystal structure directly from XRD patterns, which will be useful in understanding the structural information more intuitively.

10:00 AM BREAK

SESSION DS03.14: Intelligent AI and Autonomous Experiments
Session Chairs: Sijia Dong and Logan Ward
Thursday Morning, December 1, 2022
Hynes, Level 2, Room 206

10:30 AM *DS03.14.01

Using Artificial Intelligence to Transform Data into Actionable Knowledge [Jason R. Hattrick-Simpers](#); University of Toronto, Canada

Materials synthesis and measurements are messy, plagued by irreproducibility, outliers, uncertain labels, and are guided by human decisions, assumptions, and biases made while interpreting data. This is only natural but as the materials science field increasingly moves towards AI driven autonomous workflows, automated decision-making is problematic if the AI is trained on ground truth data and models without a means to automatically interrogate their validity. Here I will discuss our recent work across three major thrusts (1) using machine learning to discover unknown unknowns in experimental

analysis, (2) creating physics-based inference models that challenge the assumptions of scientists, and (3) using statistical methods to extract more information from fewer and less complex measurements. The first part of the talk will focus on the how through random seed perturbation and a modification of Cook's distance we were able to identify a major technical issue in the study of molten salt corrosion of high entropy alloys. In the second thrust, we will illustrate that combining evolutionary algorithms with expert heuristics and Bayesian inference we are able to both generate and (in some cases) justify the acceptance of AI generated models over those made by topical experts. Finally, I will discuss how simple statistical models of cross-sectional SEM images can be used to generate 3-D microstructures of membranes.

11:00 AM DS03.14.02

Artificial Intelligence and Human Collaboration in Human-In-The-Loop Materials Science Autonomous Experimentation [Felix Adams](#)¹, A. Gilad Kusne² and Ichiro Takeuchi¹; ¹University of Maryland, United States; ²National Institute of Standards and Technology, United States

Autonomous experimentation uses machine learning and automation to intelligently choose the order of and perform experiments on the fly to achieve goals specified by a user (for example, finding synthesis parameters which optimize a materials property). Autonomous experimentation reduces the time and cost of materials research by achieving research goals with fewer experiments than exhaustive searching and traditional prototyping. While autonomous experimentation can incorporate many sources of information, qualitative human judgement remains an important part of decision making in some individual experiment tasks, which are difficult to automate. We present a method for integrating human input into an autonomous experimental campaign which maps structural phase regions in a high-throughput combinatorial library, demonstrated on the Fe-Ga-Pd system. X-ray diffraction patterns from the Fe-Ga-Pd library are used to predict potential phase maps. During the campaign, the user can indicate phase regions and boundaries based on their materials science knowledge (e.g., known specific material phases or the phase rule). This user input is integrated as a probabilistic prior into a Gaussian Process classifier, the posterior of which is used to choose the next experiment. We will describe the overall procedure and present the campaign results.

11:15 AM DS03.14.03

RoboMapper—On-Chip Robotic Micro-Experimentation Reveals Quantitative Structure-Property Relations in Hybrid Perovskites [Tonghui Wang](#)^{1,1}, Ruipeng Li², Hossein Ardekani^{1,1}, Mahdi Ramezani¹, Ryan Wilmington^{1,1}, Robert Epps¹, Kasra Darabi^{1,1}, Boyu Guo^{1,1}, Milad Abolhasani¹, Kenan Gundogdu^{1,1} and Aram Amassian^{1,1}; ¹North Carolina State University, United States; ²Brookhaven National Laboratory, United States

Solution-processed semiconductors, such as metal halide perovskites (MHPs), have attracted tremendous attention over the past decade, promising to revolutionize the fields of photovoltaics, photonics, and other printed electronic applications. However, given the large compositional and chemical space of modern solution-processed semiconductors, meeting multiple material requirements together with device performance, operational stability, material toxicity and cost, as well as sustainable manufacturing is currently a fundamental challenge that is nearly impossible to overcome using trial-and-error and heuristics approaches. We introduce the RoboMapper, a novel compact robotic laboratory which integrates materials on a chip. We demonstrate end-to-end miniaturized, automated workflow from ink formulation to high-throughput multi-modal characterization for efficient data collection. Compared with traditional manual workflows and existing full-scale serial automation, the RoboMapper is shown to be 5-10 times faster and reduces the material cost, toxic waste, and greenhouse gas emissions by more than an order of magnitude. A state-of-the-art case study on $FA_{1-y}Cs_yPb(I_{1-x}Br_x)_3$ proves the ability of our platform to rapidly establish the quantitative structure-property relationship (QSPR) in a large and complex compositional space and provide accurate and practical guidance for the screening and selection of compositions among a wide range of options with an ideal bandgap as well as improved photostability for different target applications. This platform can be universally applied to solution processable materials such as organic semiconductors, quantum dots, and nanoparticles to pave the way towards the fully autonomous experimentation of ink-based semiconductor materials, ink formulations and (opto)electronic devices co-design with the guidance of artificial intelligence (AI).

11:30 AM DS03.14.04

RoboCoater—Automated, Closed-Loop Bayesian Optimization of Hybrid Perovskite Anti-Solvent Drip [Nathan Woodward](#)¹, Boyu Guo¹, Mihirsinh Chauhan¹, Kasra Darabi¹, Tonghui Wang¹, Milad Abolhasani¹, Kristofer Reyes² and Aram Amassian¹; ¹North Carolina State University, United States; ²University at Buffalo, The State University of New York, United States

Hybrid metal-halide perovskites are a promising material for photovoltaics that have made large strides in power conversion efficiency (PCE) in the past decade due to being an affordable, solution-processible, tunable direct bandgap material. Spin coating is a widely adopted technique for the fabrication of perovskite thin films; however, it is a very strenuous, manual process that can vary person-to-person in each lab. In addition, anti-solvent treatment is a crucial step in the fabrication process. Different anti-solvents and drip parameters are required for varying perovskite systems to achieve the optimal thin film for high PCE devices. Optimization of one-step spin coating of a hybrid perovskite system with an anti-solvent drip is a multiparametric problem that requires many human hours and resources.

Here, we present a fully automated spin coating platform, the RoboCoater, which allows precise control of processing conditions like spin speed, anti-solvent drip timing, drip volume, and on-chuck thermal annealing to achieve accurate and reproducible results that are not feasible by humans. In addition, this platform has integrated in-situ absorbance and photoluminescence measurement capabilities that are synchronized with the spin coating experiment to determine film properties. We have utilized Bayesian Optimization to reduce the time spent to optimize the multiple process parameters of perovskite thin-films in a high-throughput, closed-loop manner to reduce the time and material cost to optimize the perovskite active layer to achieve a higher power conversion efficiency perovskite solar cell. This dramatically reduces the number of person-hours needed to optimize a single anti-solvent for a given perovskite system and allows us to more quickly screen various anti-solvents to find the best performing process parameters. Overall, we have built a compact, modular 3D printed scientific platform that is much more affordable than the large, commercial optical characterization platforms that can run autonomous experimentation for a wide range of solution processable materials. The RoboCoater defines standardized processing conditions for different research labs to achieve repeatable, peer-executed experimentation to help the community advance together.

SESSION DS03.15: Virtual Session I

Session Chairs: Sijia Dong, Arun Kumar Mannodi Kanakkithodi, Noah Paulson and Logan Ward
Tuesday Morning, December 6, 2022
DS03-virtual

8:00 AM *DS03.15.01

Many-Body Perturbation Theory Meets Machine Learning to Discover Singlet Fission Materials [Noa Marom](#); Carnegie Mellon University, United States

Singlet fission (SF), the conversion of one singlet exciton into two triplet excitons, could significantly enhance solar cell efficiency. Molecular crystals that undergo SF are scarce. Computational exploration may accelerate the discovery of SF materials. We have used many-body perturbation theory (MBPT) within the GW approximation and the Bethe-Salpeter equation (GW+BSE) to identify several potentially promising candidate materials [1-4]. However, GW+BSE calculations of the excitonic properties of molecular crystals are impractical for large-scale materials screening. In recent years, machine learning (ML) algorithms have been used increasingly in conjunction with first-principles simulations to accelerate computational design and discovery of materials. We use the sure-independence-screening-and-sparsifying-operator (SISSO) machine-learning algorithm to generate computationally efficient models that can predict the MBPT thermodynamic driving force for SF for a dataset of 101 polycyclic aromatic hydrocarbons (PAH101) [5]. SISSO generates models by iteratively combining physical primary features. The best models are selected by linear regression with cross validation. The SISSO models successfully predict the SF driving force with errors below 0.2 eV. Based on the cost, accuracy, and classification performance of SISSO models, we propose a hierarchical materials screening workflow. Three potential SF candidates are found in the PAH101 set.

- [1] X. Wang, X. Liu, C. J. Cook, B. Schatschneider, and N. Marom "On the Possibility of Singlet Fission in Crystalline Quaterylene", *J. Chem. Phys.* 148 184101 (2018)
- [2] X. Wang, X. Liu, R. Tom, C. J. Cook, B. Schatschneider, and N. Marom "Phenylated Acene Derivatives as Candidates for Intermolecular Singlet Fission", *J. Phys. Chem. C* 123, 5890 (2019)
- [3] X. Liu, R. Tom, X. Wang, C. J. Cook, B. Schatschneider, and N. Marom "Pyrene-Stabilized Acenes as Intermolecular Singlet Fission Candidates: Importance of Exciton Wave-Function Convergence", *J. Phys.: Condens. Matter*, 32 184001 (2020)
- [4] X. Liu, R. Tom, S. Gao, and N. Marom "Assessing Zethrene Derivatives as Singlet Fission Candidates Based on Multiple Descriptors", *J. Phys. Chem. C* 124, 26134 (2020)
- [5] X. Liu, X. Wang, S. Gao, V. Chang, R. Tom, M. Yu, L. Ghiringhelli, N. Marom, *npj Computational Materials* 8, 70 (2022)

8:30 AM *DS03.15.02

Auto-Generating Databases about Batteries and Solar-Cells for Data-driven Materials Discovery Jacqueline M. Cole^{1,2}; ¹University of Cambridge, United Kingdom; ²ISIS Pulsed Neutron and Muon Source, United Kingdom

This talk will introduce the 'chemistry aware' natural processing tool, ChemDataExtractor,[1,2] and illustrate its ability to auto-generate databases on battery and photovoltaic materials and device information. The battery database contains a total of ¼ million data records and includes chemical names of anodes, cathodes and electrolytes as well as five device properties.[3,4] The photovoltaics database contains ½ million data records and includes chemical names and device properties of perovskite-based and dye-sensitized solar cells.[5] The database auto-generation methods are discussed as is the applicability of these large databases to machine-learning pipelines which enable a design-to-device approach to data-driven materials discovery.[6]

References

- [1] Swain and Cole, *J. Chem. Inf. Model.* 2016, 56, 10, 1894–1904 www.chemdataextractor.org
- [2] Mavracic, Court, Isazawa, Elliott, Cole, *J. Chem. Inf. Model.* 2021, 61, 9, 4280–4289 www.chemdataextractor2.org
- [3] Huang, Cole, *Sci. Data* (Springer Nature), 2020, 7, 260 <https://doi.org/10.1038/s41597-020-00602-2>
- [4] Huang, Cole, *J. Chem. Inf. Model.* (2022) DOI: <https://doi.org/10.1021/acs.jcim.2c00035>
- [5] Beard, Cole, *Sci. Data* (Springer Nature), 2022, DOI: 10.1038/s41597-022-01355-w
- [6] Cole, *Acc. Chem. Res.* 2020, 53, 599-610.

9:00 AM DS03.15.03

Screening of Next Generation Ni-Rich Cathode Materials with High Electrochemical Properties via Machine Learning Minseon Kim, Seungpyo Kang and Kyoungmin Min; Soongsil University, Korea (the Republic of)

Ni-rich layered cathode materials are promising candidates to satisfy high energy density and high voltage requirements, but they suffer from degradation during cycling. Ni-rich layered cathodes, such as $\text{LiNi}_x\text{Co}_y\text{Mn}_z\text{O}_2$ (NCM) and $\text{LiNi}_x\text{Co}_y\text{Al}_w\text{O}_2$ (NCA), were extensively investigated to minimize the proportion of Co, which caused price volatility and supply chain problems. Recently, $\text{LiNi}_x\text{Co}_y\text{Mn}_z\text{Al}_w\text{O}_2$ (NCMA), with the minimum Co content and maximum Ni content, was studied owing to its advantages of low manufacturing cost and high theoretical capacity and working potential. However, as the Ni content increases in the cathode, its commercialization is challenging owing to (1) performance degradation and (2) safety issues during electrochemical cycling. Therefore, the development of next-generation Ni-rich cathodes is necessary to resolve these problems.

Density functional theory (DFT) calculations are widely implemented in designing electrode materials owing to their remarkable accuracies and reliabilities. However, DFT calculations require significant computational resources to calculate all possible combinations of candidate materials. This limits the scope of the search for novel materials and the possibilities of fundamental research and development. Thus, to efficiently design next-generation battery materials, narrowing the large design space for cathode materials using artificial intelligence (AI) is necessary. And although various battery-material studies aim to yield cathodes with high voltage and small volume changes, few studies focus on developing prediction models of the average voltage and volume changes of novel materials.

In this study, we developed a machine-learning-based surrogate model to predict the average voltage and volume changes of Ni-rich cathodes with various dopants ($\text{LiNi}_{0.85}\text{D}_x\text{D}'_{(0.15-x)}\text{O}_2$) to determine ideal cathode materials with excellent electrochemical properties. To construct the training database, data regarding 4,401 materials were obtained from the Materials Project. Thirty-three elements were implemented as candidate dopants, suggesting 1,617 potential cathode materials.

We improved the accuracy of predictive models through feature engineering including feature addition and data pre-processing. As a result of adjusting the hyperparameters with Bayesian optimization, the performance improved significantly from the initial to the final model (average voltage: $R^2 = 0.801$ to 0.873 , MAE = 0.404 to 0.323 V; volume change: $R^2 = 0.241$ to 0.561 , MAE = 41.030% to 2.890%).

Using the constructed model, we identified 107 candidate materials. The following are the criteria for selecting cathode materials: (1) The gravimetric energy density should be > 875 mWh/g based on the capacity of Ni-rich compounds (200–250 mAh/g). (2) Based on the potentials (2.7–4.3 V) of recently proposed Ni-rich layered materials, the average voltage should be > 3.5 V. (3) The volume change should be $< 7\%$ based on the Ni-rich compounds (2–9%). 969 materials satisfy criterion (1), 541 satisfy criteria (1) and (2), and 107 satisfy criteria (1)–(3).

The constructed platform may be employed to determine ideal Ni-rich cathode materials with different elemental ratios and compositions, with significantly reduced computational and experimental costs. The model was validated using DFT calculations. We identified 101 Co-free compounds among the candidates and presented a strategy for material selection that could overcome resource limitations. The top ten materials displayed high potentials and capacities and low volume changes without Co, suggesting the potential of developing Co-free cathode materials. The platform used in this study accelerated the screening of unknown materials without extensive calculations. These next-generation cathode candidates may be used in future experimental research regarding cathode material development or predictive models based on constructed databases.

9:15 AM DS03.15.04

Evaluating NMR Chemical Shifts of Ionic Liquids Using Machine Learning Michael O. Ashby¹, Difan Zhang¹, Roger Rousseau² and Vassiliki-Alexandra Glezakou²; ¹Pacific Northwest National Laboratory, United States; ²Oak Ridge National Laboratory, United States

Ionic liquids have a wide range of applications in electrochemistry, engineering, and chemical processes as solvents, catalysts, or reagents. To understand the properties of ionic liquids, Nuclear Magnetic Resonance (NMR) is commonly used because it provides a unique set of chemical shifts that can uniquely characterize an ionic liquid compound. However, due to the versatile categories and complex environments of ionic liquids, it is time-consuming and costly to measure the experimental NMR data for ionic liquids. Although computational methods such as density functional theory calculations provide an alternative way to obtain NMR data, they are limited to small molecular models and are computationally expensive, especially for complex systems. Here, we propose a machine learning approach to evaluate the NMR chemical shifts of ionic liquids. A neural network is trained on an ionic liquid dataset established on experiments and ab initio calculations of ionic liquids. The network can help us to evaluate the NMR data of ionic liquids more quickly and efficiently, as well as predict the NMR data of unknown ionic liquids to accelerate the understanding of their structures and properties. We believe such an approach could be applied beyond the scope of ionic liquids as well as other energy materials, such as optimizing electrolyte solutions to extend the life of flow batteries at a cheaper cost.

9:30 AM DS03.15.05

Crystal-Orientation-Based Analysis on Ingot-Scale Structure of Multicrystalline Silicon Takuto Kojima¹, Kyoka Hara¹, Kentaro Kutsukake², Tetsuya Matsumoto¹, Hiroaki Kudo¹ and Noritaka Usami¹; ¹Nagoya University, Japan; ²RIKEN, Japan

The introduction of defects into multicrystalline silicon during unidirectional solidification growth is expected to be caused by phenomena on various scales, such as microscopic atomic arrangements and macroscopic stress distributions. The crystal orientation of the multicrystalline structure is extensively involved in the occurrence of twinning and the stress distribution around grain boundaries at grain boundaries. In addition, the multicrystalline structure formed by unidirectional solidification grows columnar from nuclei at the bottom of the crucible, and the interior of the columnar structure contains a variety of grain boundaries due to continuous twinning. While the orientation relationship between individual nuclei is random, the orientation relationship due to twinning is crystallographically determined and thus contains information on the grain generation relationship. Therefore, it is expected that the macroscopic crystal orientation distribution can be used to analyze the dynamics of crystal growth. Since obtaining ingot-scale data using conventional diffraction-based methods is difficult, we have developed a method to estimate crystal orientation with a machine learning model using optical images of the surface textured by anisotropic etching as input data. We have achieved the estimation model with an average estimation error of 3.5° (95th percentile < 9°) trained on the crystal orientation distribution obtained by X-ray diffraction [1-3]. In addition, to extract macroscopic features of the multicrystalline structure, we have developed a method to analyze the crystal orientation distribution by attributing the orientation relationship due to twinning to a network graph [4-7]. We will report an ingot-scale analysis of the development of the polycrystalline structure during crystal growth using these methods.

References

- [1] H. Kato et al., IEICE Tech. Report 119 [454], 81 (2020).
- [2] T. Kojima et al., MRM 2021, A4-O3-05.
- [3] K. Hara et al., Abstr. 2021 MRS Fall Meeting, DS01.15.08.
- [4] T. Kojima et al., Abstr. 66th JSAP Spring Meeting, 9a-W611-3, 2019.
- [5] T. Kojima et al., Abstr. 80th JSAP Autumn Meeting, 20a-E314-4, 2019.
- [6] T. Kojima et al., Abstr. 67th JSAP Spring Meeting, 14a-A205-3, 2020.
- [7] T. Kojima et al., Abstr. 2021 MRS Fall Meeting, CH04.09.01.

9:45 AM DS03.15.06

Machine Learning for Anion Exchange Membrane Used by Fuel Cells to Determine the Dominant Factor Controlling Anion Conductivity Yin Kan Phua¹, Tsuyohiko Fujigaya^{1,2,3} and Koichiro Kato^{1,3,4}; ¹Kyushu University, Japan; ²The World Premier International Research Center Initiative, International Institute of Carbon Neutral Energy Research (WPI-I2NER), Kyushu University, Japan; ³Center for Molecular Systems (CMC), Kyushu University, Japan; ⁴Research Institute for Information Technology (RIIT), Kyushu University, Japan

Increasing global demand for clean and sustainable energy has increased attraction towards fuel cell for its zero emissive, sustainable and highly efficient properties. Current mainstream proton exchange membrane fuel cell (PEMFC) faces problems such as sluggish Pt-catalyzed oxygen reduction reaction (ORR) kinetics occurring at the cathode due to low pH operating environment of PEMFC, requiring more Pt to improve ORR reaction rate. In contrast, anion exchange membrane fuel cell (AEMFC) has better ORR reaction kinetics when compared to PEMFC due to the high pH operating environment of AEMFC. This potentially allows the reduction of Pt quantity used in AEMFC compared to PEMFC, thereby bringing down the cost of AEMFC. However, AEMFC carries problems such as low durability and low anion conductivity for the anion exchange membrane (AEM) used as electrolyte membrane in AEMFC, inhibiting it from commercialization. To date, AEM materials research and development (R&D) are carried out through experimental research, requiring huge amount of budget, time, and labor, thereby slowing down the progress of R&D. To solve such issues, high hopes are placed on utilizing machine learning (ML) to accelerate AEM R&D. However, readily available database regarding AEM materials, critical for implementing ML, are not available, and complex structure of AEMs made of functional polymers are difficult to represent in terms understandable by ML models. Hence, a database as well as a method to represent the complex structure of AEM polymers needs to be established to implement ML into the AEM materials research field. In this study, we sought to establish a database that contains both homopolymer and copolymer, represent it using descriptors understandable by ML models, and determine the dominant controlling factor of anion conductivity for AEM materials based on the chemical features information provided by the descriptors. AEM database was made by extracting papers listed in several review papers. Extracted polymer structures were converted to numerical form easily understandable by ML models. For machine learning, objective variable was set as anion conductivity, and explanatory variables were set as anion conductivity measuring temperature and polymer structure in numerical form. The models used in this study are chosen based on their ability to provide high prediction accuracy and difficulty in overfitting, which includes Category Boosting (Catboost), eXtreme Gradient Boosting (XGBoost), Gradient Boosting for regression (GBR) and so on. After training and validating the ML models, R² value was used to evaluate their prediction accuracy. Then, Shapley values for each model when predicting anion conductivity were calculated to determine the dominant controlling factor of AEM polymers. We successfully built a database containing 60 AEM papers worth of data, with 4,014 data points in it. Among the data points, there are 1,200 anion conductivity data points obtained from 180 types of AEM polymer structures. Machine learning models were trained in Python 3.9 using Intel Core i9-11900K. All trained models gave prediction accuracy exceeding 90%, with Catboost model achieving the highest prediction accuracy of 97.7%. To understand the prediction mechanism behind the machine learning models, Shapley values calculated from each ML models showed that anion conductivity measuring temperature carried the highest impact on predicted value. Others include polarizability of the polymer, meaning the polarizability of AEM polymer affects the anion conductivity of AEM heavily. Hence, during the design of AEM polymers, polarizability of the polymer should be increased to achieve higher anion conductivity. This shows that our model successfully determined the dominant control factor for anion conductivity of AEMs, carrying potential to serve as polymer design guidelines in the future.

10:00 AM DISCUSSION TIME

SESSION DS03.16: Virtual Session II
Session Chairs: Noah Paulson and Logan Ward
Tuesday Morning, December 6, 2022
DS03-virtual

10:30 AM *DS03.16.01

Accelerating Battery Research, Development and Deployment Using Machine Learning Kandler Smith; NREL, United States

Batteries are complex multi-physics systems, with weak observability into their underlying physical processes. Physics models have made great strides to answer engineering questions and accelerate scale-up of batteries for 100-kWh-scale electric vehicles and MWh-scale grid energy storage. Yet many challenges still exist. First, with 50+ parameters, electrochemical models of conventional Li-ion batteries are still cumbersome to identify, requiring 3+ months of experiments - a pace too slow to keep up with new product development. Developers often compromise with empirical models that do not directly predict operating limits. Second, complex chemo-mechanical-coupled physics are not fully understood or modeled accurately enough. This slows development of next generation emerging electrode/electrolytes and impedes lifetime prediction/optimization for conventional Li-ion. Semi-empirical reduced-order models predict lifetime, but their supporting aging characterization experiments take 9+ months. Third, battery data comes in many forms, ranging from microscopy/spectroscopy to electrochemical. Streamlined approaches are needed to interpret all of these disparate data sources, distill them, and guide research, design, and deployment decisions.

This talk presents recent progress in application of machine learning to electrochemical and microscopy data, as well as storing that data and supporting models in accessible, searchable formats. Super-resolution generative adversarial networks quantify cracking and damage processes from scanning electron microscopy images of polycrystalline cathodes. Machine learning algorithms interpret electrochemical data to identify physics-based electrochemical models and reduced-order lifetime models. A new battery data hub stores battery R&D data to better coordinate the efforts of researchers and provide uniform access to data and analysis tools.

11:00 AM DS03.16.02

Optimization of Thermoelectric Generators Using Genetic Algorithms Chun-I Wu and Yen-Chen Chu; National Taiwan Ocean University, Taiwan

This research studies optimizing segmented thermoelectric and two-stage thermoelectric generators and using Matlab programming language and Real Number Genetic Algorithm to perform optimization. With different segment lengths and different cross-sectional areas, the material properties of the cold and hot sections can be obtained by calculating the temperature of the material contact surface. The thermal resistivity, electrical resistivity, Seebeck coefficient, and thermoelectric generator output power can also be calculated. After optimization by a genetic algorithm, the output power of the two-stage thermoelectric generator increases by 17.06%, and the output power of the segmented thermoelectric generator increases by 159.32%. Finally, observe the thermoelectric material distribution and temperature changes to make inferences.

11:15 AM DS03.16.03

Autonomous Colloidal Atomic Layer Deposition Amanda A. Volk¹, Robert Epps¹, Kristofer G. Reyes² and Milad Abolhasani¹; ¹North Carolina State University, United States; ²University of Buffalo, United States

Colloidal atomic layer deposition (cALD) is a versatile technique for the solution-phase, room temperature, formation of complex heterostructure nanoparticles.^[1] In cALD, sequences of independent, self-limiting, half reactions are used to grow multi-compositional shells with monolayer precision. Despite the limited number of existing studies, the versatility of this method has allowed for the formation of a diverse set of complex nanostructures, including Au/CdS, Ag/AlO_x, CeO₂/AlO_x, SiO₂/AlO_x, SiO₂/AlPO₄, CdSe/CdS, CdSe/ZnS, PbS/CdS, HgSe/CdSe, HgSe/CdS, HgSe/CdSe, and CsPbX₃/AlO_x.^[2] However, a detailed study of this powerful synthetic route remains challenging due to a variety of factors. Primarily, the multistep and dynamic nature of cALD creates an exponentially growing parameter space. In cALD processes which routinely require over 50 sequential reaction steps, the range of tunable conditions becomes impractically large (> 10¹⁰⁰). Furthermore, optimized cALD reaction conditions at each cycle depend on material properties which cannot easily be measured, such as surface ligand coverage. Experimental designs to elucidate the role of such hidden states, because of an extremely large parameter space, are nearly infeasible as well as highly resource intensive.

In response to the presented challenges, in this work, we designed and developed an autonomous robotic experimentation strategy for accelerated studies of cALD by integrating a modular microfluidic platform with machine learning (ML)-assisted experimental planning.^[3] Using shelling of cadmium sulfide (CdS) onto cadmium selenide (CdSe) quantum dots (QDs) as a case study, we developed a material-efficient microfluidic platform to automatically investigate cALD cycles in sequence, using only a 10 mL biphasic droplet. The developed autonomous robotic experimentation platform is fully automated and modular in design and is capable of on-demand reagent addition, controlled mixing and reaction, online multimodal spectral monitoring, and in-line phase separation. Using the autonomous cALD platform, reagent addition sequences and purification protocols could be varied without hardware reconfiguration. Reaction progress was monitored through a UV-Vis absorption and photoluminescence flow cell positioned at the end of the reactor. The developed autonomous cALD platform could routinely carry out over 1,000 successful reaction step instructions without user intervention.

To demonstrate machine-driven knowledge discovery of the cALD protocol, we directed the ML algorithms to explore different precursor injection and washing sequences up to 20 total injections per starting reactive precursors. After running an exploratory design space search policy over more than 1,000 total injections, we exploited the ML models to identify the optimized injection sequence. Without any prior knowledge of conventional cALD reaction protocols, the integrated system successfully identified an alternative cycled injection sequence substructure that achieved a larger shift in the first absorption peak wavelength and higher photoluminescence intensity than conventional methods (new knowledge generation). The developed intelligent fluidic robot is the first autonomous system to solve a high-dimensional multi-step material synthesis problem in colloidal nanoscience without user guidance and using only in-house generated data. Further implementation of the technologies developed here can lead to more efficient, machine-driven studies of dynamic, highly complex, multi-step, reactive systems.

[1] *J. Am. Chem. Soc.* **2012**, 134, 45, 18585–18590

[2] *ACS Materials Lett.* **2020**, 2, 9, 1182–1202

[3] *Adv. Mater.* **2021**, 33, 2004495

11:30 AM DS03.16.04

Graph Convolutional Neural Network for Projected Density of States Predictions Ihor Neporozhnyi, Oleksandr Voznyy and Zhibo Wang; University

of Toronto, Canada

Machine learning models recently demonstrated prominent results in predicting materials properties and accelerating materials discovery [1]. However, they still fail in predicting complex material properties (particularly bandgaps) or maintaining accuracy in the low-data regime. Graph Convolutional Neural Networks (GCNNs) became the de facto standard for encoding crystal structures of arbitrary size. They showed high accuracy in predicting additive properties of the materials, e.g. total energy, which can be represented as a sum of energies of single atoms. However, we find that they fail to predict atomic interactions that result in delocalized properties, such as molecular orbitals and the resulting electronic bandstructure, even in the simplest 2-level system case.

Here, we developed a material representation that retains the locality of atomic contributions to the final molecular orbitals and band structure. Our GCNN trained on band structure data from the Materials Project database [2] with elements from s, p, d, and f blocks is capable of making accurate predictions of projected densities of states even when training on a dataset with less than 5000 materials.

11:45 AM DS03.16.05

Investigating the Perovskite Solar Cells Layers' Materials Effect on Degradation Curve Shape Using Clustering Algorithms Noor Titan Putri Hartono¹, Hans Köbler¹, Paolo Graniero^{1,2}, Mark Khenkin¹ and Antonio Abate¹; ¹Helmholtz-Zentrum Berlin, Germany; ²Free Universität Berlin, Germany

Despite the high efficiency, addressing the perovskite solar cells (PSCs) degradation issue remains critical for pushing their levelized cost of energy down and making the technology economically feasible to enter the manufacturing stage. Recent studies point out that the most common lifetime metric for solar cells, the T80 lifetime (the time required to reach 80% of initial performance), in PSCs vary due to the difference in degradation curve shape, due to an initial burn-in loss, an initial sharp efficiency increase, and a combination of both. The exact cause of such variations is unknown, which hinders the mitigation efforts for reducing the degradation in PSCs.

In this study, we utilize machine-learning-based clustering algorithms, including dynamic time warping (DTW) and self-organizing map (SOM), to categorize ~1,400 degradation curves of devices degraded under various environmental stressors with different electron- and hole-transport layer, perovskite composition, and contact materials. We also investigate how the various layers affect the shape of the degradation curves, pointing out the layers responsible for specific degradation curve shape. This will be an important step in finding the optimum layer combination, and finally, mitigating the degradation issue in PSCs.

12:00 PM DS03.16.07

Real-Time Parameter Estimation in Electrochemical Systems with Confounding Variables using Neural Network Sarthak Jariwala; PARC, United States

Measuring and estimating parameters of interest in real-time in electrochemical systems remains a challenge. Traditional methods used to characterize the response and estimate parameters of interest are often slow and time-consuming, thus, not applicable for real-time applications. Here, we develop a workflow utilizing physics-based processing and deep learning to estimate parameters and confounding variables with uncertainties in real-time from large amplitude AC Voltammetry (LA-ACV) measurements on electrochemical systems. We demonstrate our approach on a model electrochemical system ($K_3Fe(CN)_6$ in potassium phosphate buffer) to estimate the concentration of redox active species ($K_3Fe(CN)_6$) in the presence of unknown viscosity (confounding variable) with 0.3 mM median absolute error in concentration estimation.

12:15 PM *DS03.16.08

Automated Defect Detection in Electron Microscopy of Radiation Damage in Metals Dane Morgan¹, Ryan Jacobs¹, Mingren Shen¹, Priyam Patki², Matthew Lynch¹ and Kevin Field²; ¹University of Wisconsin--Madison, United States; ²University of Michigan, United States

In this talk, we discuss our recent work on automating detection of defects in electron microscopy images of irradiated metals.¹⁻⁵ Radiation response of materials is a critical design constraint for future nuclear fission and fusion materials. Electron microscopy is widely used to explore defects in crystal structures, but human tracking of defects can be time-consuming, error prone, unreliable, and is not scalable to large numbers of images or real-time analysis. In this work, we discuss application of machine learning approaches to find the location and geometry of different defects in irradiated alloys, such as dislocation loops, black dot interstitial clusters, and cavities. We explore multiple deep learning methods (Faster Regional Convolutional Neural Networks (Faster R-CNN), Mask R-CNN, and You Only look Once (YOLO)) and generally find performance approaching or equivalent that of human accuracy. We explore multiple avenues of assessment, including precision and recall of specific defect identification (F1[endif]-->0.8), accuracy of microstructurally relevant averages (e.g., average defect areal density and size distribution ([endif]-->10% fractional errors), and accuracy of modeled defect dependent macroscopic properties such as hardening (10-20 MPa errors, or about 10% of total hardening), and swelling ([endif]-->0.3% swelling errors). These results suggest that specific images can have significant errors, but averaging over many images yields quite good results. We explore convergence of the results with number of training samples, finding that certain defect types are significantly less well detected, likely due both to their having reduced sampling and greater variability, as well as model limitations for small size features. In addition, our targeted evaluation tests also suggest the best path toward improving future models is not expanding existing databases with more labeled images but instead data additions that target weak points of the model domain, such as images from different microscopes, imaging conditions, irradiation environments, and alloy types. Finally, we discuss the new types of science enabled by the massive data which can be extracted with these approaches, e.g., detailed defect evolution during in-situ irradiations. We will also point to provided cyberinfrastructure to enable use of our models, including Python notebooks tailored for running on Google Colab and cloud accessible models on the Foundry for data, models and science,⁶ which enables inference on new images using only two lines of python code.

References:

- [1] W. Li, K. G. Field, and D. Morgan, "Automated defect analysis in electron microscopic images," *npj Comput. Mater.*, vol. 4, no. 1, pp. 1–9, 2018, doi: 10.1038/s41524-018-0093-8.
- [2] M. Shen *et al.*, "Multi Defect Detection and Analysis of Electron Microscopy Images with Deep Learning," *Accept. Publ. Comput. Mater. Sci.*, 2021.
- [3] M. Shen *et al.*, "A deep learning based automatic defect analysis framework for In-situ TEM ion irradiations," *Comput. Mater. Sci.*, vol. 197, no. November 2020, p. 110560, 2021, doi: 10.1016/j.commatseci.2021.110560.
- [4] K. G. Field *et al.*, "Development and Deployment of Automated Machine Learning Detection in Electron Microscopy Experiments," *Microsc. Microanal.*, vol. 27, no. S1, pp. 2136–2137, 2021, doi: 10.1017/s1431927621007704.
- [5] R. Jacobs *et al.*, "Performance, Successes and Limitations of Deep Learning Semantic Segmentation of Multiple Defects in Transmission Electron Micrographs", arXiv preprint arXiv:2110.08244, 2021.
- [6] R. Chard, *et al.*, "DLHub: Model and data serving for science", *Proc. - 2019 IEEE 33rd Int. Parallel Distrib. Process. Symp. IPDPS 2019* pp. 283–292, 2019. doi:10.1109/IPDPS.2019.00038.; U. of Chicago, U. of Wisconsin-Madison, "Foundry Materials Informatics Environment"(2021). <https://ai-materials-and-chemistry.gitbook.io/foundry/v/docs/>.

12:45 PM DISCUSSION TIME

SESSION DS03.17: On-Demand Presentation
Thursday Morning, December 8, 2022
DS03-virtual

7:00 AM DS03.17.01

A Self-Driving Lab Autonomously Learns to Accurately Dispense Samples via Dynamic Experimental Control [Martin Seifrid](#), Riley Hickman, Emre Alca and Alán Aspuru-Guzik; University of Toronto, Canada

Self-driving labs – automated experiments guided by machine learning (ML) algorithms – have the potential to accelerate discovery of new molecules, materials and processes across a range of disciplines. They can enable researchers to think about their experiments in the context of trends, datasets, and other higher level questions rather than individual experiments by minimizing the necessity for manually performing routine or repetitive tasks.

A central challenge of self-driving labs is building robotic systems capable of carrying out the same wide range of actions and experiments as humans. For example, accurately dispensing both large and very small quantities of material. Currently, this requires careful calibration and testing to determine the correct process parameters for each material, and substantially eats into valuable researcher time. It would therefore be desirable for a robotic systems to be able to teach itself the optimal process parameters autonomously. This would reduce the necessity for human involvement in routine tasks, and boost the efficiency of self-driving labs.

In this talk, I will detail our work toward developing a fully autonomous synthesis platform, enabled by a closed loop of Bayesian optimization and automated experiments, that can optimize its own instrument parameter to accurately dose samples, and learn from its previous experience with optimizing the parameters for other samples in order to further speed up its learning rate. Such systems have the potential to significantly improve the capabilities of self-driving labs, the development of which is often limited by the need to adapt them to each new material.

SYMPOSIUM EN01

Redox Flow Batteries—Materials, Methods and Devices
November 28 - November 30, 2022

Symposium Organizers

Qing Chen, Hong Kong University of Science and Technology
Yi-Chun Lu, Chinese University of Hong Kong
James McKone, University of Pittsburgh
Wei Wang, Pacific Northwest National Laboratory

Symposium Support

Bronze

Gamry Instruments
Journal of Materials Chemistry A
Neware Technology LLC
Pacific Northwest National Laboratory

* Invited Paper
+ Distinguished Invited

SESSION EN01.01: Flow Battery Materials I
Session Chairs: James McKone and Wei Wang
Monday Afternoon, November 28, 2022
Hynes, Level 3, Room 301

1:30 PM *EN01.01.01

Redox Flow Batteries Trends—Chemistries and Materials [Grigorii Soloveichik](#); ARPA-E, United States

Fast growing grid-scale energy storage requires a portfolio of technologies tuned for intermittent renewable energy sources and capable to provide wide range of discharge times up to seasonal storage. Redox flow batteries (RFBs) can occupy an intermediate position with the storage time from several hours

to tens of hours. The amount of stored energy can be adjusted depending on the customer's need by changing the volume of electrolyte storage tanks for rated power, and the system cost could be competitive with other energy storage technologies. The cost reduction remains the major driver in current RFB development, which can be achieved by decreasing costs of the stack via increasing power density and using inexpensive stack components, energy storage media via employing inexpensive active materials and electrolytes, storage tanks via increasing solubility of active materials and BOP (separately or in combination). The former approach targets development of high-power cells based on mainstream vanadium chemistry. The least expensive option is the utilization of earth-abundant inorganic salts (e.g., iron or zinc) and water as solvent. These chemistries are limited by competitive reaction of water splitting. Another option is the use of water-soluble organic compounds, which potential and solubility can be tuned by adding functional groups to the core molecule. However, such tuning requires additional synthetic steps that increase the manufacturing cost and may negate the performance advantage. Non-aqueous RFBs have hypothetically higher (above water splitting threshold) cell potential and higher solubility of tunable active materials. However, this potential was not realized yet, and high cost, low conductivity and flammability of solvents render such RFBs not competitive with aqueous RFBs. Current trends, research needs and tradeoffs for RFBs with stationary (hybrid RFB) and liquid (conventional RFB) electrodes will be discussed. Development of novel ion-selective membranes and chemistries for RFBs was funded by ARPA-E via GRIDS, OPEN, IONICS and DAYS programs. Important lessons from completed projects will be also discussed.

2:00 PM *EN01.01.02

Recent Progress in Organic-Based Aqueous Flow Batteries Michael J. Aziz; Harvard University, United States

The ability to store large amounts of electrical energy is of increasing importance with the growing fraction of electricity generation from intermittent renewable sources such as wind and solar. Wide-scale utilization of flow batteries is limited by the cost of redox-active metals such as vanadium or precious metal electrocatalysts. We have developed high performance flow batteries based on the aqueous redox behavior of small organic and organometallic molecules, e.g. [1-6]. These redox active materials can be inexpensive and exhibit rapid redox kinetics and high solubilities, potentially enabling massive electrical energy storage at greatly reduced cost. We have developed protocols for measuring capacity fade rates, which are particularly important for establishing very low capacity fade rates, and have discovered that the capacity fade rate is determined by the molecular calendar life, which can depend on state of charge, but is independent of the number of charge-discharge cycles imposed [7,8]. We will report the performance of some of the very few chemistries with long enough calendar life for practical application in stationary storage [8], and on progress in reversing capacity fade by recomposing decomposed molecules [9].

- [1] B. Huskinson, M.P. Marshak, C. Suh, S. Er, M.R. Gerhardt, C.J. Galvin, X. Chen, A. Aspuru-Guzik, R.G. Gordon and M.J. Aziz, "A metal-free organic-inorganic aqueous flow battery", *Nature* **505**, 195 (2014), <http://dx.doi.org/10.1038/nature12909>
- [2] K. Lin, Q. Chen, M.R. Gerhardt, L. Tong, S.B. Kim, L. Eisenach, A.W. Valle, D. Hardee, R.G. Gordon, M.J. Aziz and M.P. Marshak, "Alkaline Quinone Flow Battery", *Science* **349**, 1529 (2015), <http://dx.doi.org/10.1126/science.aab3033>
- [3] E.S. Beh, D. De Porcellinis, R.L. Gracia, K.T. Xia, R.G. Gordon and M.J. Aziz, "A Neutral pH Aqueous Organic/Organometallic Redox Flow Battery with Extremely High Capacity Retention", *ACS Energy Letters* **2**, 639 (2017). <http://dx.doi.org/10.1021/acsenerylett.7b00019>
- [4] D.G. Kwabi, K. Lin, Y. Ji, E.F. Kerr, M.-A. Goulet, D. DePorcellinis, D.P. Tabor, D.A. Pollack, A. Aspuru-Guzik, R.G. Gordon, and M.J. Aziz, "Alkaline Quinone Flow Battery with Long Lifetime at pH 12" *Joule* **2**, 1907 (2018). <https://doi.org/10.1016/j.joule.2018.07.005>
- [5] Y. Jing, M. Wu, A.A. Wong, E.M. Fell, S. Jin, D.A. Pollack, E.F. Kerr, R.G. Gordon and M.J. Aziz, "In situ Electrosynthesis of Anthraquinone Electrolytes in Aqueous Flow Batteries", *Green Chemistry*, **22**, 6084 (2020); <https://doi.org/10.1039/D0GC02236E>
- [6] M. Wu, M. Bahari, E.M. Fell, R.G. Gordon and M.J. Aziz, "High-performance anthraquinone with potentially low cost for aqueous redox flow batteries" *J. Mater. Chem. A* **9**, 26709-26716 (2021). <https://doi.org/10.1039/D1TA08900E>
- [7] M.-A. Goulet & M.J. Aziz, "Flow Battery Molecular Reactant Stability Determined by Symmetric Cell Cycling Methods", *J. Electrochem. Soc.* **165**, A1466 (2018). <http://dx.doi.org/10.1149/2.0891807jes>
- [8] D.G. Kwabi, Y.L. Ji and M.J. Aziz, "Electrolyte Lifetime in Aqueous Organic Redox Flow Batteries: A Critical Review" *Chem. Rev.* **120**, 6467 (2020); <https://doi.org/10.1021/acs.chemrev.9b00599>
- [9] Y. Jing, E.W. Zhao, M.-A. Goulet, M. Bahari, E. Fell, S. Jin, A. Davoodi, Erlendur Jónsson, M. Wu, C.P. Grey, R.G. Gordon and M.J. Aziz, "In-situ Electrochemical Recomposition of Decomposed Redox-active Species in Aqueous Organic Flow Batteries" *Nature Chemistry* **14**, in press (2022). <https://doi.org/10.1038/s41557-022-00967-4> ; <http://dx.doi.org/10.33774/chemrxiv-2021-x05x1>

2:30 PM *EN01.01.03

Inroads and Challenges in the Design of Robust, High-Performance Flow Battery Electrolytes Patrick J. Cappillino¹, Shyam K. Pahari¹, Jennifer Bolibok¹, Sara Amin¹, Benjoe Rey B. Visayas¹, Maricris L. Mayes¹, Sundar R. Aravamuthan² and Ertan Agar²; ¹University of Massachusetts Dartmouth, United States; ²University of Massachusetts Lowell, United States

Redox flow batteries (RFBs), in which charge-carrying electrolytes are pumped through electrochemical cells, are a promising energy storage technology. In these systems, the energy capacity scales with the volume of electrolyte stored in tanks, and the power scales with the size of the cell. This decoupling gives RFBs potential advantages for long- and medium-duration grid energy storage applications and a favorable safety profile compared with integrated systems like lithium-ion batteries (LIBs).[1] Furthermore, next-generation RFBs, such as those comprising nonaqueous electrolytes with high voltage active-materials, are an exciting research area, because they may find much wider application. For example, a nonaqueous RFB (NFRB) system that meets or exceeds the energy density of LIBs, while maintaining the flexible architecture of a flow system, could impact distributed energy storage markets.

This presentation will provide a progress update on a bio-inspired NRFB system under development in our laboratories that is based on a molecule known as vanadium bis-hydroxyiminodiacetate (VBH).[2] This molecule, biosynthesis of which evolved in mushrooms, owes its extraordinary stability to natural selection pressure.[2] An NRFB system containing a mixed electrolyte of VBH, as catholyte, and an organic anolyte, both at moderate concentration, will be described. This system operates at a current density approaching state-of-the-art aqueous RFB systems and is stable to exhaustive cycling. Capacity fade from crossover can be restored by rebalancing the electrolyte. I will describe how high stability was achieved and how solubility constraints were overcome, by implementing a combined experimental and theoretical approach.[3-4]

Improving RFB energy density by increasing active-material concentration, while solving one problem, creates another. Inefficiencies due to decreased electrochemical performance and pumping losses in so-called “crowded electrolytes” have been recognized as a fundamental obstacle that must be overcome before NRFB technology can mature.[5] In the last portion of this presentation, I will describe inroads and remaining challenges for two strategies we are pursuing to overcome poor transport in high-concentration NRFB electrolytes. First, a combined theoretical and experimental, structure/function study to understand how nanoscale interactions between ions and solvent molecules impact macroscale transport properties. And second, a “redox targeted” flow battery approach, in which VBH-based electrolyte is combined with a solid storage material to boost the energy density while preserving the high-performance we observe at moderate active-material concentration.[6]

1. Albertus, P.; Manser, J. S.; Litzelman, S., *Joule* 2020, 4 (1), 21-32.
2. Huang, H.; Howland, R.; Agar, E.; Nourani, M.; Golen, J. A.; Cappillino, P. J., *J. Mater. Chem. A* 2017, 5 (23), 11586-11591.
3. Pahari, S. K.; Gokoglan, T. C.; Visayas, B. R. B.; Woehl, J.; Golen, J. A.; Howland, R.; Mayes, M. L.; Agar, E.; Cappillino, P. J., *RSC Adv.* 2021, 11 (10), 5432-5443.
4. Visayas, B. R. B.; Pahari, S. K.; Gokoglan, T. C.; Golen, J. A.; Agar, E.; Cappillino, P. J.; Mayes, M. L., *Chem. Sci.* 2021, 12 (48), 15892-15907.
5. Shkrob, I. A.; Robertson, L. A.; Yu, Z.; Assary, R. S.; Cheng, L.; Zhang, L.; Sarnello, E.; Liu, X.; Li, T.; Preet Kaur, A.; Malsha Suduwella, T.; Odom, S. A.; Wang, Y.; Ewoldt, R. H.; Farag, H. M.; Z, Y., *J. Mol. Liq.* 2021, 334, p. 116533.
6. Egitto, J.; Gokoglan, T. C.; Pahari, S.; Bolibok, J.; Aravamuthan, S. R.; Liu, F.; Jin, X.; Cappillino, P.; Agar, E., *J. Electrochem. En. Conv. Stor.* (in press), <https://doi.org/10.1115/1.4054697>.

3:00 PM BREAK

3:30 PM *EN01.01.04

Solvation Environment Dictates Stability in Benzothiadiazole Flow Battery Solutions Lily A. Robertson^{1,2}, Ilya Shkrob^{1,2}, Shi Li^{1,2}, Haimeng Wang^{1,2}, Garvit Agarwal^{1,2}, Yuyue Zhao^{1,2,3}, Ryan Walsler-Kuntz^{1,4}, Melanie S. Sanford^{1,4}, Rajeev Assary^{1,2}, Lei Cheng^{1,2} and Lu Zhang^{1,2}; ¹Joint Center of Energy Storage Research, United States; ²Argonne National Laboratory, United States; ³Indiana University-Purdue University, United States; ⁴University of Michigan, United States

Redox flow batteries (RFBs) are proposed to fill the supply-demand gap in the renewable energy market. Nonaqueous RFBs are of special interest due to their wider electrochemical windows compared to aqueous systems and compatibility with redox-active organic molecules (redoxmers). However, engineering stability in these systems is highly dependent on redoxmer, electrolyte salt, and solvent. Here, we examine 2,1,3-benzothiadiazole (BzNSN), a negative charge carrier for nonaqueous RFBs. Our previous work revealed significant solvation effects in acetonitrile depending on the cation of the electrolyte, where lithium cations strongly coordinate the BzNSN radical anion and shift its half-wave potential 150-200 mV positive depending on counter-anion. This shift is accompanied by decreased redoxmer stability as shown by spin resonance and symmetric H-cell cycling experiments. We hypothesized that a solvent with strong lithium binding would alleviate the redoxmer-cation chelation effect. For this task, *N,N*-dimethylacetamide (DMA) was explored as preliminary calculations showed that it should interact strongly. Comparing lithium vs. tetraalkylammonium electrolytes showed no shift in half-wave potential in this solvent. Further, there was little change in radical anion stability by spin resonance experiments. Finally, we compared symmetric H-cell cycling of BzNSN in the two solvents in lithium-based electrolyte and found that DMA had successful cycling while the acetonitrile experiment barely cycled. This study reveals the importance of solvation effects in evaluating new materials for nonaqueous RFBs.

The research was financially supported by the Joint Center for Energy Storage Research (JCESR), an Energy Innovation Hub funded by the U.S. Department of Energy, Office of Science, Basic Energy Sciences. The submitted manuscript has been created by UChicago Argonne, LLC, Operator of Argonne National Laboratory (“Argonne”). Argonne, a U.S. Department of Energy Office of Science laboratory, is operated under Contract No. DE-AC02-06CH11357. The U.S. Government retains for itself, and others acting on its behalf, a paid-up nonexclusive, irrevocable worldwide license in said article to reproduce, prepare derivative works, distribute copies to the public, and perform publicly and display publicly, by or on behalf of the Government.

4:00 PM *EN01.01.05

Opportunities and Challenges of Organic Redox Flow Batteries Tianbiao Liu; Utah State University, United States

Aqueous redox flow batteries (AORFBs) represent one promising energy storage technology for integration of renewable energy and balancing the electricity grids because of their technical merits of decoupled energy and power, sustainable and tunable redox active materials, and non-flammable and low cost aqueous supporting electrolytes. This presentation will review recent efforts in developing new flow battery chemistries, including viologen (anolyte), quinone (anolyte), TEMPO (catholyte), ferrocene (catholyte), and ferrocyanide (catholyte). The merits and drawbacks of representative acidic, pH neutral, and alkaline AORFBs will be discussed and compared. A number of research strategies will be discussed to develop high-performance redox active electrolytes to enable energy dense, durable, low-cost flow battery technologies. Particularly, this presentation emphasizes that in-depth mechanistic understandings of redox active electrolytes play crucial roles in developing advanced organic redox flow batteries towards sustainable, long-duration energy storage.

References:

- (1) Luo, J.; Hu, B.; Hu, M.; Liu, T. L. "Status and Prospects of Organic Redox Flow Batteries towards Renewable Energy Storage", *ACS Energy Lett.* 2019, 4, 2220-2240.
- (2) Wu, W.; Luo, J.; Wang, F.; Yuan, B.; Liu, T. L. "A Self-Trapping, Bipolar Viologen Bromide Electrolyte for Aqueous Redox Flow Batteries", *ACS Energy Lett.* 2021, 6, 2891-2897.
- (3) Luo, J.; Hu, B.; DeBruler C. Zhao, Y.; Yuan B.; Hu, M.; Wu, W.; Liu, T. L. "Unprecedented Capacity and Stability of Ammonium Ferrocyanide Catholyte in pH Neutral Aqueous Redox Flow Batteries", *Joule* 2019, 4, 149-163.
- (4) Hu, B.; Luo, J.; Hu, M.; Yuan B.; Liu, T. L.* "A Neutral, Metal Free Aqueous Organic Redox Flow Battery Employing an Ammonium Anthraquinone Anolyte", *Angew. Chem.* 2019, 58, 16629-16636.
- (5) DeBruler C.; Hu, B.; Moss, J.; Liu, X. Luo, J.; Sun, Y.; Liu, T. L. "Designer Two Electron Storage Viologen Anolyte Materials for Aqueous Organic Redox Flow Batteries", *Chem* 2017, 3, 961-978.
- (6) Hu, B.; DeBruler C.; Rhodes, Z.; Liu, T. L. "Long Cycling Aqueous Organic Redox Flow Battery for Sustainable and Safe Energy Storage", *J. Amer. Chem. Soc.* 2017, 139, 1207-1214.
- (7) Liu, T.; Hu, B.; DeBruler, C.; and Luo, J. "Materials for Use in Aqueous Organic Redox Flow Batteries", US patent No., 10,934,258, 2021.
- (8) Liu, T.; Wei, X.; Sprengle, V.; Wang, W. "Aqueous electrolytes for redox flow battery systems", US patent No. 14,690,224, 2016.

4:30 PM *EN01.01.06

Decomposition Mechanisms and Stabilized Organic Catholyte Molecules for Aqueous Redox Flow Batteries Xiaoliang Wei¹, Diqing Yue¹ and Wei

Wang²; ¹Indiana University-Purdue University, United States; ²Pacific Northwest National Laboratory, United States

Redox flow batteries have been widely recognized as promising stationary energy storage solutions for solving the intermittency issue of renewable energies. Owing to the high chemical cost, the state-of-the-art vanadium flow batteries are largely limited in market penetration. Organic redox materials have advantages of structural diversity and tunability, offering an opportunity to harvest exceeding materials properties such as solubility, stability and redox characteristics. In aqueous flow battery systems, organic anolyte molecules are extensively investigated and a variety of promising candidates have been reported such as phenazine, viologen, anthraquinone, etc. However, organic catholyte is an under-addressed area. The major limitation is the often limited chemical stability in aqueous electrolytes, especially for those having high redox potentials. Therefore, a ready urgency lies in understanding the decomposition mechanisms of chosen organic catholyte based on which to develop stable structures.

Here we report the mechanistic analysis of decomposition of TEMPO-based organic catholyte and the resulting development of a highly soluble, highly stable candidate. The unstable TEMPO derivative in the charged cation form is monitored temporally. Based on the evolutions of NMR peaks and pH values in its electrolyte, a decomposition pathway is proposed and a new TEMPO structure is accordingly designed so as to avoid the pathway. The new TEMPO analog exhibits a remarkably high solubility in water and an excellent stability in its charged form. Its solvate structure in water is analyzed and the preferential solvation interactions were suggested. The flow cells using this TEMPO catholyte demonstrate excellent cycling stability under practically relevant conditions. Our result represents a significant advancement in developing soluble, stable organic catholyte molecules to energy-dense, durable aqueous organic flow batteries.

SESSION EN01.02: Flow Battery Methods and Analysis

Session Chairs: Jianbing Jiang and James McKone

Tuesday Morning, November 29, 2022

Hynes, Level 3, Room 301

8:30 AM *EN01.02.01

Electrochemical and Rheological Modeling of Suspension-Based Electrolytes for Redox Flow Batteries Madhu Majji, Bertrand Neyhouse, James Swan and [Fikile Brushett](#); Massachusetts Institute of Technology, United States

Electrochemical energy storage is poised to play a key role in enabling society-wide decarbonization by facilitating the deployment of variable electricity generators and enhancing existing grid infrastructure. Redox flow batteries (RFBs) possess several technology features which are favorable for cost-effective, long-duration energy storage, including independent scaling of power and energy, long service life, and simplified manufacturing [1]. In particular, the battery configuration enables a diversity of electrolyte compositions and cell materials to be considered, either at the beginning of life or during the installation lifetime (e.g., chemistry swaps). While conventional RFBs are based on redox couples dissolved in electrolyte solutions, more recently, suspension-based electrolytes containing solid charge storage materials have emerged as an alternative formulation. Flowable suspensions enable higher capacities (and thus cell energy densities) and unlock new operating modes (e.g., dissolution and precipitation on suspended particles) [2,3]. However, such electrolytes also frustrate traditional approaches to cell design and operation as their complex electrochemical and rheological behavior presents multifaceted tradeoffs [4,5]. By exploring the essential features of these tradeoffs, we aim to better understand fluid dynamic and electrochemical engineering criteria for high-performance flow cells that operate with suspension-based electrolytes.

In this presentation, we develop and apply a one-dimensional model to derive scaling relationships for suspension-based electrolytes in RFBs. Specifically, we investigate connections between rheological (i.e., non-Newtonian behavior, shear stress) and electrochemical (i.e., species and charge transport) phenomena for electrolyte flow through a planar channel. We then identify key dimensionless groups which describe the relative magnitudes of relevant processes within the flowing suspension-based electrolyte. Through scaling analyses, we assess the importance of each parameter under different dynamic and geometric constraints to enable the identification of favorable materials sets and operating conditions. Ultimately, these dimensionless quantities offer a compact representation of the design considerations for suspension-based electrolytes, allowing more informed materials selection, cell engineering, and system formats. Finally, we hypothesize that these results can be generalized to describe flowable and stationary solid suspensions of utility in multiple electrochemical systems.

Acknowledgments

This work was funded by the Skoltech – MIT Next Generation Program. B.J.N gratefully acknowledge the NSF Graduate Research Fellowship Program under Grant Number 1122374. Any opinion, findings, and conclusions or recommendations expressed in this material are those of the authors and do not necessarily reflect the views of the NSF.

References

1. M. L. Perry and A. Z. Weber, *J. Electrochem. Soc.*, **163**, A5064–A5067 (2016).
2. H. Parant et al., *Carbon*, **119**, 10–20 (2017).
3. X. Wang, J. Chai, and J. “Jimmy” Jiang, *Nano Materials Science*, **3**, 17–24 (2021).
4. V. E. Brunini, Y.-M. Chiang, and W. C. Carter, *Electrochimica Acta*, **69**, 301–307 (2012).
5. N. C. Hoyt, R. F. Savinell, and J. S. Wainright, *Chemical Engineering Science*, **144**, 288–297 (2016).

9:00 AM EN01.02.02

Quantifying Chlorine Gas Evolution from Mixed-Acid Vanadium Redox Flow Batteries [Reed Wittman](#), Cassandria E. Poirier, Harry Pratt, Travis M. Anderson and Yuliya Preger; Sandia National Laboratories, United States

Mixed-Acid (MA) Vanadium Redox Flow Batteries (VRFB) improve on standard VRFBs’ energy density via the addition of hydrochloric acid (HCl) to the standard sulfuric acid (H₂SO₄) electrolyte. This improves the stability of the vanadium (V) in the solution, which allows for electrolytes with higher concentrations of V ions and increased operating temperatures. However, the addition of HCl to the system introduces a new safety risk, the evolution of chlorine gas (Cl₂) from the catholyte.

In this study, we cycled an MA VRFB under a range of conditions to understand the fundamental causes of gas evolution. We constructed a single cell MA VRFB using a standard electrolyte composition of 2M H₂SO₄, 5M HCl and 2M V, with a gas analyzer sampling the head space of the catholyte chamber. Cl₂ gas quantity was measured under systematically varied cycling rates and potential holds. The mechanism of gas evolution was determined to be an electrochemical side reaction that occurs when charging the cell beyond 1.5 volts. Depending on the duration the cell was held at high voltage and the

maximum voltage, headspace Cl₂ concentrations between 1 and 4.2% were observed. Overcharging the cell beyond 1.7 volts (the standard VRFB upper limit) generated gas concentrations near 10%. These concentrations represent a significant safety risk that may occur during system operation and need to be mitigated.

Previously it was assumed that the 360 millivolts potential difference between the V⁴⁺/V⁵⁺ (1.00 volts vs SHE) charging reaction in the posolyte and the 2Cl⁻/Cl₂ (1.36 volts vs SHE) gas evolution reaction would prevent Cl₂ gas evolution through electrochemical means. We will discuss how solution chemistry and cell inefficiencies make Cl₂ generation a viable side reaction when charging a cell above 1.5 volts. This new understanding of gas evolution will aid development of safer MA VRFB systems that mitigate Cl₂ formation during operation.

Sandia National Laboratories is a multi-mission laboratory managed and operated by National Technology & Engineering Solutions of Sandia, LLC, a wholly owned subsidiary of Honeywell International Inc., for the U.S. Department of Energy's National Nuclear Security Administration under contract DE-NA0003525.

9:15 AM EN01.02.03

Accelerating High-Throughput Flow Battery Characterization via Temperature-Dependent (Electro) Chemical Kinetics Eric M. Fell and Michael J. Aziz; Harvard University, United States

Aqueous Organic Redox Flow Batteries (AORFBs) have emerged as potentially disruptive technologies for the storage of electrical energy from intermittent renewable sources for use over long discharge durations when the wind isn't blowing, and the sun isn't shining. AORFBs could become preferred solutions for grid-scale storage due to their potentially low-cost active materials, inherent non-flammability, and intrinsic decoupling of energy and power capacities. Our group has previously demonstrated that calendar life, rather than cycle life, limits molecular lifetimes in AORFBs due to various molecular instabilities that lead to side reactions, thus inhibiting performance [1]. To accurately determine molecular fade rates, we utilize potentiostatic holds to avoid artifacts caused by drifts in internal resistance and employ volumetrically unbalanced, compositionally symmetric cell configurations to distinguish molecular fade from membrane crossover. Synthetic efforts have continued to improve molecular design strategies to the point that the most stable molecules degrade at less than 1% per year [2]. With further lifetime increases, the measurement of lower capacity fade rates now necessitates higher precision coulometry methods [3] and the use of thermally accelerated degradation protocols [4,5] to determine which stabilizing approaches are most effective without waiting for multi-month cycling tests to quantify capacity fade.

We have developed a high-throughput setup for cycling AORFBs at elevated temperatures, providing a new dimension in the flow battery characterization space to explore. An in-depth study comparing previously published redox-active organic molecules has been performed using the protocol discussed above. Capacity fade rates as functions of temperature are evaluated in the high-throughput setup using high-precision coulometry, providing the ability to extrapolate fade rates to lower operating temperatures. Collectively, these results highlight the importance of accelerated decomposition protocols to expedite the screening process of candidate molecules for long lifetime AORFBs, which may enable massive grid penetration of intermittent renewable energy.

[1] M.-A. Goulet and M. J. Aziz, "Flow Battery Molecular Reactant Stability Determined by Symmetric Cell Cycling Methods," *Journal of The Electrochemical Society*, **165**, A1466 (2018).

[2] M. Wu, Y. Jing, A. A. Wong, E. M. Fell, S. Jin, Z. Tang, R. G. Gordon, M. J. Aziz, "Extremely Stable Anthraquinone Negolytes Synthesized from Common Precursors," *Chem*, **6**, 1432 (2020).

[3] T. M. Bond, J. C. Burns, D. A. Stevens, H. M. Dahn, and J. R. Dahn, "Improving Precision and Accuracy in Coulombic Efficiency Measurements of Li-Ion Batteries", *Journal of The Electrochemical Society*, **160**, A521 (2013).

[4] D. G. Kwabi, K. Lin, Y. Ji, E. F. Kerr, M.-A. Goulet, D. De Porcellinis, D. P. Tabor, D. A. Pollack, A. Aspuru-Guzik, R. G. Gordon, and M. J. Aziz, "Alkaline Quinone Flow Battery with Long Lifetime at pH 12," *Joule*, **2**, 1894 (2018).

[5] D. A. Stevens, R. Y. Ying, R. Fathi, J. N. Reimers, J. E. Harlow, and J. R. Dahn, "Using High Precision Coulometry Measurements to Compare the Degradation Mechanisms of NMC/LMO and NMC-Only Automotive Scale Pouch Cells", *Journal of The Electrochemical Society*, **161**, A1364 (2014).

[6] Y. Ji, M.-A. Goulet, D. A. Pollack, D. G. Kwabi, S. Jin, D. De Porcellinis, E. F. Kerr, R. G. Gordon, and M. J. Aziz, "A Phosphonate-Functionalized Quinone Redox Flow Battery at Near-Neutral pH with Record Capacity Retention Rate," *Advanced Energy Materials*, **9**, 1900039 (2019).

9:30 AM EN01.02.04

In Situ Reliability Investigation of All-Vanadium Redox Flow Batteries by an Ultra-Stable Reference Electrode Qian Huang¹, Chaojie Song², Alasdair Crawford¹, Zhengming Jiang², Alison Platt², Khalid Fatih², Christina Bock² and David Reed¹; ¹Pacific Northwest National Laboratory, United States; ²National Research Council Canada, Canada

Redox flow batteries (RFBs) have been investigated over the past several decades as a promising energy storage system (ESS) for grid applications due to their unique features that include the separation of energy and power output, high safety, and long cycle life. It is therefore vital but still in severe deficiency to understand the reliability of RFBs, and the mechanisms that cause degradation with time. One of the primary challenges involves the unseparated contributions from individual electrodes due to the lack of a stable reference electrode (RE). In this work, a long-term stable reference electrode is developed for a scaled all-vanadium redox flow battery (VRFB). The newly developed reference electrode demonstrates its high accuracy and long-term stability that enables *in-situ* monitoring of individual electrode potentials throughout hundreds of cycles. By introducing the RE approach to decouple the cathode and anode, the reliability and degradation mechanism of a VRFB is further investigated. This exploratory work will be beneficial for the insight into the reliability/degradation mechanism of a VRFB and future design and development of a stable reference electrode in the practical application of a scaled ESS.

9:45 AM BREAK

10:15 AM EN01.02.05

Understanding the Membrane-Electrolyte System for Designing Aqueous Organic and Metalorganic Flow Batteries Thomas Y. George, Naphtal O. Haya, John P. Deneen, Isabelle C. Thomas, Clifton Wang and Michael J. Aziz; Harvard University, United States

Redox flow batteries with aqueous electrolytes hold promise for large scale energy storage, offering independent scaling of power from the electrochemical

stack and energy stored in tanks of dissolved reactants. The all-vanadium redox flow battery (VRFB) has been the most developed chemistry to date, although more recently organic and metalorganic redox reactants have been proven viable for batteries with long calendar life. Ion exchange membranes for flow batteries must suppress crossover of redox reactants while enabling conductivity of a charge-carrying ion for efficient battery cycling. Studies on VRFBs have shown that the concentration and composition of the solutions contacting the membrane have crucial influence on transport phenomena through the membrane pores. Building on this understanding, the research presented here contributes an evaluation of the effects of iron(II/III) hexacyanide electrolyte concentration and pH on cation exchange membrane performance, which will inform the design of aqueous organic and metalorganic redox flow batteries (AORFB).

In AORFBs, the size and charge numbers of organic molecules and metalorganic complexes afford them more crossover resistance than metal ions like iron or vanadyl, but many of the most stable chemistries use neutral or alkaline electrolytes where sodium or potassium ions carry charge through the membrane. The widely-used cation exchange membrane Nafion has a factor-of-ten reduction in conductivity in potassium form compared to the proton form available in acidic environments. Therefore in AORFBs, ohmic resistance of the membrane is a substantial limiting factor on practical current densities and power densities for battery operation.

The composition and concentration of the electrolyte contacting the membrane influences the water content of the membrane, which determines the pathways available for transport, and hence the conductivity. Here we describe simple methods for conductivity and electrolyte uptake measurements that can be used to screen a variety of membrane materials and electrolytes. We show the influence of both iron hexacyanide concentration and supporting electrolyte (sodium or potassium hydroxide) on water content and conductivity of both Nafion cation exchange membranes and a non-fluorinated, hydrocarbon-based cation exchange membrane from Fumatech (E-620K). These results emphasize that total ion concentration of the electrolyte affects membrane water content, and therefore supporting electrolyte should be minimized when concentrations of redox active species are high enough to provide ionic conductivity. We also show that maximizing the concentration of iron hexacyanide by using mixed cation electrolytes results in increased membrane resistance, signifying that conductivity and volumetric capacity become a tradeoff. Considering membrane and electrolyte properties as an interrelated system supports the design of battery electrolytes for compatibility with a given membrane, and may also accelerate the creation and selection of new membranes tailored for flow batteries.

10:30 AM EN01.02.06

Optimization of Redox Flow Battery Carbon Felt Electrode Mesostructures By Applying Lattice Boltzmann Method and Machine Learning Jia Yu^{1,2}, Marc Duquesnoy^{1,2,3}, Chaoyue Liu^{1,2} and Alejandro A. Franco^{1,2,3}; ¹Laboratoire de Réactivité et Chimie des Solides (LRCS), UMR CNRS 7314, France; ²Réseau sur le Stockage Electrochimique de l'Energie (RS2E), FR CNRS 3459, France; ³ALISTORE-European Research Institute, FR CNRS 3104, France

Carbon felt electrodes constitute state-of-the-art Redox Flow Batteries (RFBs) components because of their high electronic conductivity, high specific surface area, and high porosity. In order to further improve the electrochemical performance of these electrodes, many researchers have investigated different treatment methods, including plasma treatment, thermal, and chemical modifications [1]. However, the geometrical features of the fibrous electrode, which has a significant influence on mass transport (convection) and the anolyte/catholyte utilization rate, are often left from the discussion. This study presents an innovative computational approach that examines the fluid dynamic properties of the anolyte/catholyte flow separately from the electrochemistry behavior in various carbon felt electrode mesostructures. First, electrode mesostructures were generated stochastically based on realistic tuneable manufacturing parameters, including the fiber diameter, electrode density, amount of in-plane and through-plane fibers, and the compression ratio. Afterward, the Lattice Boltzmann Method (LBM) [2–4] was applied to simulate each electrode permeability and the reactive volume ratio, where the latter quantifies the dead volume due to the slow fluid velocity compared with the diffusion coefficient. Finally, based on the results obtained from the LBM, a Bayesian Optimization Algorithm was applied to analyze the datasets and propose promising parameter values corresponding to the optimized anolyte/catholyte utilization rate. This optimization workflow allows analyzing the impact of different manufacturing parameters on fluid dynamic properties and predicting a theoretical optimized carbon felt electrode mesostructure is also identified and tested by computational simulations for charging and discharging conditions.

10:45 AM *EN01.02.07

Microband Electrode Platforms for Identifying Homogeneous and Heterogeneous Factors Limiting Redoxmer Performance for Redox Flow Batteries Michael A. Pence, Oliver Rodriguez Martinez, Inkyu Oh, Nikita Lukhanin, Charles M. Schroeder and [Joaquin Rodriguez-Lopez](#); University of Illinois at Urbana Champaign, United States

Chemical and electrochemical limitations of redox-active species (*redoxmers*) that cause long-term performance losses in redox flow battery devices may not be immediately evident during conventional electroanalytical experimentation. In both aqueous and nonaqueous solutions, effects of uncompensated resistance and non-idealities in the redoxmer response can lead to difficulties in identifying mechanistically complicating factors. Here, we posit that in contrast to $\sim\text{cm}^2$ electrodes typically used for the initial screening of redoxmers, ultramicroelectrodes – electrodes with at least one critical dimension in the micron or sub-micron range – can be used directly or integrated into microfabricated devices to reveal such limitations. Complicating factors can present in the form of heterogeneous, i.e. related to reactivity at the electrodes, or homogeneous, i.e. related to the behavior of the charged molecules in solution. In this talk, we will present our approaches using microfabricated band electrodes (MBEs) and interdigitated array electrodes (IDAs) to tackle these analytical needs for both aqueous and non-aqueous systems. Emphasis will be made on approaches designed to inform on processes at timescales relevant to the flow battery experiment.

In a first example we will discuss an automated generation-collection experiment with IDAs is used to determine the homogeneous rates of decomposition of redoxmers in highly systematic experiments. Taking advantage of several simplifications afforded by this experiment enables the swift estimation of the impact of interfering species, redoxmer concentration, and other electrolyte conditions on the chemical stability of these systems. In a second example, we will show how MBEs are used to obtain heterogeneous kinetics of electron transfer with great versatility, avoiding complications associated with the use of high scan rates in typical cyclic voltammetric experiments at macroelectrodes. We will discuss prospects for integrating these methodologies into systematic experiments similar to those conducted using scanning electrochemical microscopy and associated techniques to promptly identify mechanistic limitations in redoxmer systems.

1:30 PM *EN01.03.01**Minimizing Performance Degradation Due to Crossover in Non-Aqueous Redox Flow Batteries** [Shelley Minter](#); University of Utah, United States

Non-aqueous organic redox flow batteries have been suggested for sustainable grid storage. However, rapid electrolyte crossover between anolyte and catholyte is a problem. Bipolar redox-active molecules are single molecules that undergo both anode and cathode redox reactions and they are an option for addressing this crossover problem. The unique redox chemistry of bipolar redoxmers is commensurate to vanadium species in aqueous redox flow batteries, but enable greater design flexibility and potentially better properties than are otherwise observed. However, there are complex tradeoffs in their properties. Balancing these properties have been incredibly challenging. As such, this talk will discuss the rational design of bipolar redoxmers and the tradeoffs needed to optimize performance. This talk will also discuss ion exchange polymer strategies for minimizing crossover in RFBs.

2:00 PM EN01.03.02**Eutectic Mixing of Quinones—A Strategy for Engineering Highly-Energy Dense Liquid Electrolytes** [Emily Penn](#), Antonio Baclig, Devi Ganapathi and William C. Chueh; Stanford University, United States

To address the low energy density of redox flow batteries, eutectic electrolytes have emerged as an approach to achieving high concentrations of redox-active species. Here we introduce an entropically-driven eutectic mixing approach which, through eutectic mixing of chemically similar redox active species, can be used to engineer highly concentrated liquids composed of nearly all redox active molecules. Demonstrated using quinones, we investigate a ternary benzoquinone eutectic and a binary naphthoquinone eutectic which, if the total charge could be accessed, have a theoretical volumetric capacities of 16.8 and 8.8 M e⁻, respectively. We quantify melting point, ionic conductivity, and viscosity across multiple states of charge. We also explore application to redox flow batteries using a binary naphthoquinone eutectic electrolyte with a protic ionic liquid supporting salt, achieving a volumetric capacity of 37 Ah/L in symmetric static cell cycling. Though reactivity of the redox active quinones and capacity fade during cycling present challenges for the electrolytes in this study, the entropically-driven eutectic approach presents a general framework which could be used to develop highly concentrated, low viscosity electrolytes using redox-active organic small molecules.

2:15 PM EN01.03.03**Multi-Objective Goal-Directed Optimization of De Novo Stable Organic Radicals for Aqueous Redox Flow Batteries** [Peter St. John](#)¹, Shree Sowndarya S. V.², Jeffrey Law¹, David Biagioni¹ and Robert Paton²; ¹National Renewable Energy Laboratory, United States; ²Colorado State University, United States

Advances in the field of goal-directed molecular optimization offer the promise to find feasible candidates for even the most challenging molecular design applications. One example of a fundamental design challenge is the search for novel stable radical scaffolds for an aqueous redox flow battery that simultaneously satisfy redox requirements at the anode and cathode, as relatively few stable organic radicals are known to exist. To meet this challenge, we develop a new open-source molecular optimization framework coupled with a fast, machine learning-derived surrogate objective trained with nearly 100,000 quantum chemistry simulations. The objective function comprises two graph neural networks: one that predicts adiabatic oxidation and reduction potentials and a second that predicts electron density and local 3D environment, previously shown to be correlated with radical persistence and stability. With no hard-coded knowledge of organic chemistry, the reinforcement learning agent finds molecule candidates that satisfy a precise combination of redox, stability, and synthesizability requirements defined at the quantum chemistry level, many of which have reasonable predicted retrosynthetic pathways. The optimized molecules show that alternative stable radical scaffolds may offer a unique profile of stability and redox potentials to enable low-cost symmetric aqueous redox flow batteries.

2:30 PM EN01.03.04**High Performance Nitrogen-Doped Hierarchical Nanostructured Carbon Electrode for Vanadium Redox Flow Batteries** [Gerardo M. Pagano](#)^{1,2}, Simone Fiorini Granieri^{1,2}, Matteo Zago¹, Andrea Casalegno¹ and Fabio Di Fonzo²; ¹Politecnico di Milano, Italy; ²Istituto Italiano di Tecnologia, Italy

In recent years, we have seen an impressive progress in the deployment of renewable energy sources, and in particular of photovoltaics and wind turbines. However, renewable energies have some well-known drawbacks due to their intermittent nature and direct usage of the electricity generated would destabilize the grid. To overcome these problems large scale energy storage systems have drawn great attention in the last few years both from the academic and industrial world. Redox flow batteries (RFB) are emerging as one more promising electrochemical energy storage technologies. Notably, the Vanadium redox flow battery (VRFB) is currently the most widespread technology as it allows for the implementation of strategies that permit to recover the capacity decay induced by ion cross-over. Despite the many advantages, VRFBs have long suffered from low power density, mainly caused by the usage of electrodes which are not optimized for this application. The use of heteroatom dopants, such as nitrogen, phosphor, and boron, is currently the most common method to enhance the performance of carbon electrodes. Nitrogen has been extensively studied as a catalyzer for Vanadium redox reactions, showing exceptional boosts in performance in several works. In a previous work we developed a two-step process based on a plasma enhanced nano-aerosol jet deposition source. Starting from a gas precursor we deposited a nanostructured carbonaceous material on a commercially available substrate, this process allows to increase the current density to 400 mAcm⁻² with an energy efficiency of 80%, that is, 4 times greater than the commercial reference. The two-steps process permits a fine tuning of the properties and structure of the material leading to an exceptionally high surface area and a defect rich structure. The advantage of this process is that nitrogen can be added easily during the deposition phase without the need for any other processing steps. In this work we aim to further increase the performance of our nanostructured electrode by adding nitrogen functionalities to the carbon nanostructure, thus combining the effects of an incredibly high surface area with the excellent catalytic properties of nitrogen. The morphology and chemistry of the synthesized material is analyzed by different techniques such as SEM-EDX, Raman spectroscopy, XPS, BET analysis. The properties of the material are then correlated to the electrochemical properties by testing the material in increasingly complex setups, starting from a three-electrode setup, then in symmetric cell and finally in a full-cell setup. The kinetic activity of the material is studied by cyclic voltammetry and electrochemical impedance spectroscopy. Cyclic voltammetry showed an impressive activity of the electrodes towards the active species, especially towards the V²⁺/V³⁺ couple where a peak-to-peak separation of 65 mV was obtained, which is among the lowest reported in literature. These results were confirmed by EIS, from which the reaction rate constants were calculated following the method proposed by Stimming et al. [1] The addition of nitrogen led to an order of magnitude increase of the reaction rate with respect to the un-doped material. The performance enhancement was then validated by the test in symmetric cell and full cell. Thus, we propose a vertically integrated process, from the synthesis of the material to the final application, which is able to deliver a comprehensive overview on the material properties, its electrochemical performance and the correlation between the two.

[1] Friedl, J., Bauer, C. M., Rinaldi, A., & Stimming, U. (2013). Electron transfer kinetics of the VO₂⁺/VO₂⁺—Reaction on multi-walled carbon nanotubes. Carbon, 63, 228-239.

2:45 PM EN01.03.05

Design High Performance Double Layer Ion Selective Membrane with Porous Boron Nitride and Polyetherimide Tongtai Ji, Xiao Sun, Daxian Cao, Ying Wang, Haoze Ren and Hongli Zhu; Northeastern University, United States

Flow batteries is one of the most attractive large-scale energy storage technologies, while the high cost and ion crossover issues of the commercial ion selective membranes limit scale-up of flow batteries. Herein, we designed a double-layer membrane with a unique bifunctional porous boron nitride (PBN) layer coated on a low cost porous polyetherimide (PEI) layer. PBN, synthesized through a one-step template free method from a precursor with boric acid and excess urea, has high nanoporosity and great stability. Through sonicating in isopropanol, PBN obtained hydroxyl and amino groups during the decomposition of the amorphous part, which increased the hydrophilicity and crystallinity simultaneously. PBN was further mixed with Nafion to constitute the ion selective layer, integrating ion selectivity with proton conductivity. The nanoporous PBN structure decorated by sulfonic acid groups from Nafion formed high-speed proton transfer channels. On the other hand, the nano-sized and tortuous channels from PBN effectively prevented the crossover of other ions and increased the ion selectivity. The ultra-thin (5 μm) PBN ion selective layer was coated on the high ion conductive and low-cost porous PEI layer prepared by nonsolvent induced phase separation method to obtain free-standing membranes with both high mechanical strength and ion conductivity. The PBN-PEI double layer membrane achieved superior coulombic efficiency of 97.02%, voltage efficiency of 93.79%, and energy efficiency of 91.18% at 40 mA cm^{-2} in vanadium redox flow battery compared to the Nafion 115 membrane (coulombic efficiency of 95.01%, voltage efficiency of 92.32%, and energy efficiency of 87.71%). Meanwhile, the PBN-PEI displayed long cycling stability with 700 cycles at 100 mA cm^{-2} . This work presents a novel approach to designing ion selective membrane by imparting ion-exchange groups into the PBN inorganic porous structure to break the tradeoff between ion selectivity and ion conductivity and provides a thread for cost reduction by double-layer design.

3:00 PM BREAK

3:30 PM EN01.03.06

Efficient Prediction of Redox Potentials of First-Row Transition Metal Complexes for Aqueous Targeting Redox Flow Batteries Using Density Functional Theory. Noura Rahbani¹, Emmanuel Baudrin¹ and Piotr de Silva²; ¹Université de Picardie Jules Verne (UPJV), France; ²Technical University of Denmark, Denmark

Targeting redox flow batteries are an emerging alternative to traditional redox flow battery architecture which offer improved energy density *via* an added solid electroactive ‘booster’. For an efficient system, it is imperative that the redox potentials of the soluble redox mediator and the solid match.¹ For this purpose, transition metal complexes are a promising class of redox mediators due to the tunability of their solubility and electrochemical potential, and their safety and sustainability. As such, reliable and time-efficient prediction tools for the redox potentials of transition metal complexes are needed for the discovery of new materials. While density functional theory usually provides a good trade-off between computational cost and accuracy, calculations on organometallic complexes often result in large errors, so they have been used for studying trends of the ligand effect rather than providing accurate predictions.^{2,3} In this communication, we compare redox potential predictions from different solvation methods and levels of theory using an initial experimental data set based on aqueous iron complexes with bidentate ligands complexing through oxygen. Good predictions (MAE= 0.23 V) are obtained using the COSMO-RS solvation model; however, this model is only available through a select list of DFT software. When using the more common implicit solvation models, there is a general deviation from experimental results, irrespective of the level of theory used. We propose that these errors are conveniently corrected by using simple linear regression which yields a good prediction of redox potentials (MAE=0.09 V). The predictive power of this method is also demonstrated by cross-validation using complexes with different metal centers and ligand types.

3:45 PM EN01.03.07

A Spin-Crossover Fe Complex for Low-Cost and Long-Life Aqueous Redox Flow Batteries Donghui Ko, Jantakan Nedsaengtup and Hye Ryung Byon; Korea Advanced Institute of Science and Technology (KAIST), Korea (the Republic of)

The development of low-cost and long-life energy storage systems (ESSs) is essential to alleviate the growing demands for energy and environmental issues. Redox flow batteries (RFBs) are considered promising grid-scale ESSs thanks to the ensured safety, low cost, and decoupled energy and power density. While vanadium has been commercially utilized as the redox-active material in aqueous RFBs, more economical materials such as Fe-based complexes are necessary. Ferrocyanide and ferrocene are representative Fe complexes showing the stable and reversible redox process in aqueous electrochemical cells. However, they suffered from low solubility and chemical instability under acidic and alkaline conditions.^{1,2} Many other Fe complexes even showed unstable nature in the neutral aqueous media due to high sensitivity to water and air.^{3,4} Thus, better molecular designs of Fe complexes are required to extend a Fe-based redox molecular library and understand Fe chemistry in aqueous RFBs. Here we introduced hexadentate Schiff-base ligands to the central Fe ion, which formed the spin-crossover Fe complexes. These spin-crossover Fe complexes showed a correlation between spin state and electrochemical stability. The spin state depended on the strength of the hydrogen bond between the secondary amine group of the ligands and the solvent. The water solvent has a strong hydrogen bonding and increases the electrostatic interaction between the secondary amine group and the Fe metal center. Thus, the percentage of low-spin isomers increases. Besides, the type of functional groups implemented into phenyl rings of the ligands also determined the spin states. We selected the sulfated or hydroxyl groups as representatives of the electron-withdrawing or electron-donating groups, respectively. The electron-withdrawing groups increased the degree of Fe to ligand π -interaction, thereby increasing the ratio of low spin. This trend was inverse for the electron-donating groups. The Evans method reflected the magnetic moment of these Fe complexes according to the functional groups, supporting the relationship between the ligand functional groups and the spin-state of Fe. In cyclic voltammetry, the low-spin Fe complex showed stable 100 cycles with the redox potential at -0.45 V vs. Ag/AgCl. By contrast, the high-spin Fe complex showed the redox potential at -0.53 V vs. Ag/AgCl with poor cyclability. In the aqueous RFB operation, 0.1 M of the low-spin Fe complex showed ~94.4% capacity utilization and achieved 0.004% capacity decay per cycle over 100 cycles, demonstrating a promising candidate as the stable negolyte in aqueous RFBs.

Reference

1. Schrage, B. R.; Zhang, B.; Petrochko, S. C.; Zhao, Z.; Frkonja-Kuczyn, A.; Boika, A.; Ziegler, C. J. *Inorg. Chem.* **2021**, *60*, 10764-10771
2. Luo, J.; Sam, A.; Hu, B.; DeBruiler, C.; Wei, X.; Wang, W.; Liu, T. L. *Nano Energy* **2017**, *42*, 215-221
3. Wen, Y. H.; Zhang, H. M.; Qian, P.; Zhou, H. T.; Zhao, P.; Yi, B. L.; Yang, Y. S. *Electrochimica Acta* **2006**, *51*, 3769-3775
4. Waters, S. E.; Robb, B. H.; Marshak, M. P. *ACS Energy Lett.* **2020**, *5*, 1758-1762

4:00 PM EN01.03.08

Ultrathin MoS₂ Membrane with Low Stacking Fault for Vanadium Redox Flow Battery Ji Soo Roh, Kailing Lin, Robert Dryfe and Mark A. Bissett; The University of Manchester, United Kingdom

Vanadium redox flow battery (VRFB) is one of the most promising sustainable large-scale energy storage systems. In VRFB, a membrane with high proton/vanadium ion selectivity and high proton conductivity is essential for improved cycle life, energy efficiency, and power density of the entire cell. Commercial Nafion membranes are commonly used, but they require a high cost even though they have low ion selectivity and swelling issues. In this

study, we applied MoS₂ as a VRFB membrane material due to its excellent chemical stability. The MoS₂ is vacuum-filtered on porous polymer support to prepare ultrathin membranes, but poor dispersion stability of MoS₂ flakes in solvents has resulted in membrane defects during the filtration process. To decrease the stacking fault, we employed graphene oxide as an additive and used a different solvent system to stabilize the MoS₂ dispersion. As a result, the prepared MoS₂ membranes showed lower vanadium crossover and better chemical stability than the commercial Nafion membrane.

4:15 PM EN01.03.09

An High-Performance Carbon-Nano Onion Electrode for Vanadium Redox Flow Battery Simone Fiorini Granieri^{1,2}, Gerardo M. Pagano^{1,2}, Fabio Di Fonzo¹ and Matteo Zago²; ¹Istituto Italiano Di Tecnologia, Italy; ²Politecnico di Milano, Italy

In order to get rid of fossil fuel energy, continuous production of energy through renewable sources is not sufficient, in fact, a direct connection of renewable energies to the electrical grid would ensure the grid stability. This incompatibility is due to renewable energies intermittency, which requires therefore a coupling with an energy storage system (EES). Among the different EES technologies, the Redox Flow Battery (RFB) is the most promising for the so-called "mid-term storage" (storage up to 12 hours), and in particular the all-vanadium RFB seems to be the most used. Even though RFB has some advantages with respect to lithium ions battery, it still has to overcome some problems, such as the low power density. Power density is determined primarily by the electrodes, these are typically porous carbon media responsible for the production of the electron by a redox reaction with electrolyte. Focusing on electrodes, there are two possible solutions to increase the power density: (i) increasing surface area and (ii) increasing reaction kinetic. Many authors improved the nowadays commercial electrode carbon felt increasing the surface area, e.g. by thermal treatment, or the reaction kinetic, e.g. by bismuth electrodeposition [Zhao, T.S. et al. Energy Storage Material, 2020]. Carbon felt due to its millimeter range thickness suffers from a high overall ohmic resistance, and this feature cannot be neglected when operating the device at high current density. In our work, we propose to increase the surface area of a carbon paper, a 300 μm porous carbon electrode with lower ohmic resistance, by covering the fibers with a turbostratic hierarchical assembly carbon nanostructure, composed of carbon nano onions (CNO). For the deposition of the carbon nano particles, a prototypal deposition method has been adopted, called plasma enhanced, nanoparticle jet deposition, NanoJeD. This deposition method offers a green, high throughput and dry process with potential for easy scale-up. A detailed description of the working principle is shown at the following article [Nava et al., Nanotechnology 29, 2018]. By mean of this deposition technique and a vacuum annealing process, it is possible to maximize the surface area, electrical conductivity and catalytic activity made by the hierarchical assembly of turbostratic CNO. The CNO kinetic properties has been tested by cyclic voltammetry in a three-electrode setup and with electrochemical impedance spectroscopy. From the cyclic voltammetry performed at different scan rate, a net increasing catalytic activity has been observed in both the chemical reaction. At the negative site, which is known to be the limiting one, a separation peak of 80mV at 10mV/sec has been reported, giving a clear indication of quasi-reversibility reaction mechanism. By EIS analysis following the procedure explained in [U. Stimming, ChemPhysChem, 2019] it is possible to extract the kinetic reaction constant, at the negative site a clear increase in kinetic reaction constant with the annealing temperature has been reported, while at the positive site no effect on kinetic reaction constant from the annealing temperature have been observed. The deposited electrode on carbon paper, has been tested with different deposition thicknesses and annealing temperatures in a symmetric cell to evaluate systematically the overpotentials of each configuration towards the V²⁺/V³⁺ and VO(2+)/VO²⁺(+) reactions. A current density sixfold higher with respect to the untreated carbon paper resulted from the test. Combining the high surface area with the high catalytic activity we are able to reach, in a full cell composed of two electrodes per side, a current density of 400 mA/cm² and 600 mA/cm² with an energy efficiency of 81% and 74%, together with an electrolyte utilization of 70% and 59% respectively. Moreover, the stability test showed a low degradation rate, valued in a 1000 cycles test.

4:30 PM *EN01.03.10

Derivatization and Optimization of Iron Bipyridine Complexes for Non-Aqueous Flow Batteries Travis M. Anderson, Claudina X. Kolesnichenko and Cassandra E. Poirier; Sandia National Laboratories, United States

Non-aqueous flow batteries containing earth-abundant elements offer the possibility of higher voltage and a wider temperature range than many of their aqueous counterparts. Here we show the optimization of a symmetric flow battery with baseline Fe(bpy)₃(BF₄)₂ and derivatized Fe(bpy-R)₃(BF₄)₂ (R is electron donating or electron withdrawing groups) to lessen capacity fade and improve energy efficiency over 20 cycles. The cause of the capacity fade in these systems was determined to be ligand shedding in the negolyte upon reduction. Recognizing that the free ligands are often more stable and more tunable, we then evaluated pseudo-symmetric flow batteries containing a family of bipyridinium materials as negolytes with the corresponding iron coordination complex as the posolyte. Methylation of the bipyridine nitrogen sites increased electrochemical stability but left the reduced molecule susceptible to radical-induced bond cleavage and caused poor capacity utilization. Additional functionalization of the bipyridine with carbomethoxy groups resulted in improved battery performance with high Coulombic and voltage efficiency, and improved cycling stability. Current work is underway to look at other iron-organic systems for improved performance.

Sandia National Laboratories is a multi-mission laboratory managed and operated by National Technology and Engineering Solutions of Sandia, LLC, a wholly owned subsidiary of Honeywell International, Inc., for the U.S. Department of Energy's National Nuclear Security Administration under contract DE-NA0003525.

SESSION EN01.04: Poster Session
Session Chairs: James McKone and Wei Wang
Tuesday Afternoon, November 29, 2022
8:00 PM - 10:00 PM
Hynes, Level 1, Hall A

EN01.04.01

Fullerene C₇₆ as a Novel Electrocatalyst for VO²⁺/VO₂⁺ and Chlorine Evolution Inhibitor in All-Vanadium Redox Flow Batteries Nageh K. Allam; American University in Cairo, Egypt

The effect of thermal treatment of carbon cloth and the deposition of fullerene C₇₆ on the performance of the VO²⁺/VO₂⁺ redox reaction was investigated in G1 (H₂SO₄) and G3 (H₂SO₄/HCl, mixed acid) VRFBs. Thermally treated carbon cloth was shown to improve the kinetics of the redox couple due to the increase in its hydrophilicity, graphitic nature, and defects such as oxygen functional groups, which would act as active sites. Incorporation of C₇₆ on treated carbon cloth (TCC) and untreated carbon cloth (UCC) was shown to equally and significantly enhance the reversibility of the electrochemical reaction, as indicated by an average peak separation value of only 109 mV and a charge transfer resistance of 4 Ω, compared to 230 mV for TCC and 403 mV for UCC, in both electrolytes. This could be attributed to C₇₆'s great conductivity, presence of oxygen functional groups, and electron cloud around the nanoparticles, which would appreciably facilitate vanadium adsorption and electron transfer. This also reveals that there is no need to treat carbon cloth before depositing C₇₆; hence saving time and energy. In addition, C₇₆ was demonstrated to hinder chlorine evolution in G3 VRFBs, compared to TCC and

TCC-C₇₆, while also maintaining its stability over a repetitive 100-cycle CV, suggesting its great resistance against corrosion. Overall, the extraordinary reduction in overpotential and facile diffusion of vanadium ions, combined with the hampering of chlorine evolution and its great stability render fullerene C₇₆ as a suitable electrode material towards more efficient VRFBs.

EN01.04.02

Investigation of Iron and Organic-Based Bipolar Redox Molecules for Non-Aqueous Flow Batteries [Cassandra E. Poirier](#), Chad L. Staiger and Travis M. Anderson; Sandia National Labs, United States

Non-aqueous redox flow batteries are being studied as a more attractive option than their aqueous counterparts due to their higher voltage window, less environmental impact, and lower cost of active species. One of the most promising non-aqueous redox chemistries are the ferrocene-phthalimide family of bipolar molecules where the ferrocene moiety is the posolyte and phthalimide is the negolyte. However, only static cell studies of these molecules have been published. We now report full flow cell studies and optimization of these molecules. We also investigate the effects of (1) membrane compatibility, (2) electrolyte volume, (3) functional group, and (4) solvent and supporting electrolyte on battery performance.

Sandia National Laboratories is a multi-mission laboratory managed and operated by National Technology and Engineering Solutions of Sandia, LLC, a wholly owned subsidiary of Honeywell International, Inc., for the U.S. Department of Energy's National Nuclear Security Administration under contract DE-NA0003525.

EN01.04.03

Reversible Metal Ionic Catalysts for High-Voltage Aqueous Hybrid Zinc-Manganese Redox Flow Batteries [Minsoo Kim](#), SooBeom Lee, Jinyeong Choi, Jihan Park and Minjoon Park; Pusan National University, Korea (the Republic of)

Redox flow batteries (RFB) have been considered as a promising candidate for large-scale electrochemical energy storage systems (EES) due to excellent scalability, high efficiency, and long lifetime. Among the various types of redox flow batteries, the aqueous zinc-manganese batteries have attracted tremendous attention due to its intrinsically abundant resources, low-cost and environmentally friendliness. The development of the rechargeable zinc-manganese batteries has focused on the reversible Zn ions insertion and extraction into MnO₂ structures. However, the aqueous zinc-based batteries have fundamental problems such as the dissolution of manganese ions, which usually causes the structure collapse of MnO₂, eventually resulting in a potential degradation with low electrochemical performances. Accordingly, the aqueous-based Mn²⁺/MnO₂ redox couple has been studied to avoid the insertion and deintercalation of zinc ions into crystalline MnO₂, which could prevent the undesirable phase transformation of crystalline MnO₂ structures. Moreover, the acidic and alkaline electrolytes in the aqueous hybrid batteries have been reported to overcome the low operation voltage and effectively use the Mn²⁺/MnO₂ redox couple with a high redox potential ($E = 1.228$ V vs. standard hydrogen electrode (SHE)).

The critical issue for the aqueous-based Mn²⁺/MnO₂ redox couple is low reversibility because of the incomplete dissolution of MnO₂ with the exfoliated dead MnO₂ species. The dead MnO₂ species eventually block the ion transport channel of the membrane and are considered an irreversible species with the main reason for the decreased active areas. Herein, we report the aqueous hybrid zinc manganese redox flow battery (ZMFB) with double-membrane-based three-electrolytes, using an alkaline zinc redox couple ($Zn/[Zn(OH)_4]^{2-}$) and an acidic manganese redox couple (Mn²⁺/MnO₂(s)), showing a high operating voltage of 2.75 V at the state of charge 100%. To improve the manganese redox couple kinetics, we utilized the bismuth nanoparticle embedded carbon felt (BCF) electrode and metal ionic catalysts (MIC) consisting of nickel and magnesium ions. This unique strategy demonstrated the outstanding performance in the aqueous hybrid ZMFB for 150 cycles corresponding to 35 hours at 20 mA cm⁻². It also demonstrated an energy density of 25.2 Wh L⁻¹ with respect to catholyte volume at a concentration of 1 M manganese. Notably, the hybrid ZMFB with BCF-MIC electrode shows an energy efficiency of 89.8% at 15 mA cm⁻². The BCF improved the electrodeposition of MnO₂ by creating atomically reconstructed Bi nanocrystals from dissolved Bi³⁺ ions.

Simultaneously, the use of Ni²⁺ ionic catalysts in catholyte help to maintain the high oxidation state of manganese, resulting in high energy efficiency and long cycle performances with the reversible reaction of metal ionic catalysts. We believe that our approach for the high-voltage aqueous hybrid ZMFB is advantageous for the development of stable and large-scale energy storage systems.

Acknowledgments

This research was supported by Pusan National University BK21 Four Education and Research Division for Energy Convergence Technology. Minsoo Kim is grateful financial support from Hyundai Motor Chung Mong-Koo Foundation. This work was supported by the National Research Foundation of Korea (NRF) grant funded by the Korea government (MSIT) (No.2021R1C1C1008349, NRF-2021R1A4A1022198)

EN01.04.04

Anion Exchange Membrane for Sustainable Vanadium-Manganese Redox Flow Batteries with Reduced Overpotential via Ni-Bi Alloy Oxide Derived Etched Carbon Felt Anode [Jihan Park](#), Minsoo Kim, SooBeom Lee, Jinyeong Choi and Minjoon Park; Pusan National University, Korea (the Republic of)

Recently, intensive studies have been conducted on vanadium/manganese redox flow batteries (V/Mn RFBs) with advantages of abundant element reserves and higher energy density (35 Wh L⁻¹) than VRFBs (20 Wh L⁻¹). Especially, the cell voltage of V/Mn RFBs is 0.5 V higher than VRFB because of the high standard redox potential of the MnO₂/Mn²⁺ couple (1.224 V vs. SHE). Despite these merits, the cycling performance was deteriorated due to disproportionation reaction of the Mn³⁺/Mn²⁺ couple which decay the capacity and power of the V/Mn RFBs. Therefore, previous studies have been focused on improving the reversibility of MnO₂ particles to extend the lifetime of V/Mn RFBs. However, we focused on the loss of cations between anolyte and catholyte through membrane and low redox activity of V²⁺/V³⁺ couple as the main cause of performance degradation.

In this study, two strategies were applied to realize sustainable V/Mn RFBs. First, the cation exchange membrane (CEM) was replaced with an anion exchange membrane (AEM) to prevent the loss of redox-active species and allowed the passage of charge balancing species only. In the V/Mn RFB systems using CEM, the loss of redox-active species was attributed to the attractive force between cations (V²⁺, V³⁺, Mn²⁺, and Mn³⁺) and SO₃⁻ in the cluster network of Nafion 117. On the other hand, the repulsive force between cations and NR₃⁺ in selemion DSV effectively inhibited the net cation transfer through membrane, which was confirmed using ICP-OES and electrochemical performances. Second, the Ni-Bi alloy oxide derived etched carbon felt (NB-ECF) was used as a negative electrode to increase the low redox activity of V²⁺/V³⁺ couple. In particular, the NB-ECF anode significantly improved the reduction activity of V³⁺ ion compared to commercial CF and reduced the overpotential of 191 mV for the V/Mn stack. Additionally, BET, XRD, XPS, and electrochemical analysis demonstrated that NB-ECF provides a large specific surface area, the oxygen functional groups on the carbon surface, and the embedded bi-metal alloy oxide. V/Mn flow battery to which both strategies were applied achieves excellent cycle performance over 70 cycles at 20 mA cm⁻², maintained voltage efficiency above 90%. These novel strategies can be applied to other systems that use cations as redox couple in both tanks and expected to broaden the range of advanced flow batteries through etching of other alloys.

Acknowledgments

This research was supported by Pusan National University BK21 Four Education and Research Division for Energy Convergence Technology. This work was supported by the National Research Foundation of Korea (NRF) grant funded by the Korea government (MSIT) (No.2021R1C1C1008349, NRF-2021R1A4A1022198)

EN01.04.05

Aqueous High-Voltage Zinc-Vanadium Redox Flow Battery with the High-Index Facets Polyhedron $\text{Ce}_{2/3}\text{TiO}_3$ Electrocatalyst Jinyeong Choi, Jihan Park, SooBeom Lee, Minsoo Kim and Minjoon Park; Pusan National University, Korea (the Republic of)

Aqueous redox flow batteries (RFBs) have been considered as the most promising energy storage systems which have several advantages of using inexpensive and nonflammable electrolytes, long lifetime. Most importantly, the independent and tunable power and capacity make it suitable technology for large energy storage systems. Although the reliable cycling performance and stability have been demonstrated, traditional aqueous RFBs still suffer from the limited voltage range and low energy density because of the limited operating voltage by the water splitting voltage of 1.23 V to avoid the hydrogen and oxygen evolutions. In addition, carbon-based electrode materials for RFBs such as carbon paper, graphite felt, and carbon felt were suffered from low electrolyte access to the electrode surface due to the hydrophobic nature which was ascribed to the high graphitization temperature. To overcome the narrow voltage of aqueous RFBs, we demonstrated the hybrid zinc-vanadium RFB with high operating voltage of 2.3 V, which was composed of two-membranes and three-electrolyte reservoirs. According to the Pourbaix diagram, the redox potential of the active materials was mainly affected by pH value. Therefore, we dissolved the zinc redox couple in alkaline solution ($\text{Zn}/[\text{Zn}(\text{OH})_4]^{2-}$, -1.26 V vs standard hydrogen electrode, SHE) to exhibit a higher operating voltage than the zinc redox couple in neutral solution (Zn/Zn^{2+} , -0.76 V vs SHE), allowing the different types of electrolyte combinations. Furthermore, to fully utilize the high voltage of the hybrid zinc-vanadium RFB, we fabricated binary cerium titanium oxide ($\text{Ce}_{2/3}\text{TiO}_3$, hereafter referred to as CTO) with abundant defects and prepared the CTO catalyst ink with mixing Ketjen black (KB) as conductive agent and binder solution, then coated onto the carbon felt electrode for $\text{VO}^{2+}/\text{VO}_2^+$ redox couple. We firstly found that the CTO-KB electrocatalysts could improve the $\text{VO}^{2+}/\text{VO}_2^+$ redox reaction, which could be attributed to synergistic effect of conductive KB. Specifically, the CTO-KB composite electrocatalysts showed a significantly improved peak separation potential (ΔE) of 227 mV, which was 140 mV less than that of the pristine carbon felt electrode. In addition, the reference carbon felt electrode had only 140.95 and 131.08 mA cm^{-2} , whereas CTO-KB represented high oxidation and reduction peak current densities of 167.4 and 159.11 mA cm^{-2} , respectively, and the CTO-KB showed superior performance than other composite electrocatalysts due to the synergistic effect of KB nanoparticles. The abundant defects with edge dislocation, planar defects, and oxygen vacancies were observed in the microstructure of the CTO, which also gave rise to the high catalytic activity. The hybrid zinc-vanadium RFB showed excellent cell efficiency at a current density of 40 mA cm^{-2} and recovered to initial state at the decreased current density. The composite electrocatalysts exhibited higher capacity characteristics than the cell to which pristine CF was applied even after 50 cycles due to low overpotential. As a result, we presented the possibility of driving next-generation energy storage devices with higher efficiencies and showed the possibility of using a high voltage energy storage device using a low potential zinc anode active material.

Acknowledgments

This work was supported by the National Research Foundation of Korea (NRF) grant funded by the Korea government (MSIT) (No.2021R1C1C1008349, NRF-2021R1A4A1022198). This work was supported by Korea Institute of Energy Technology Evaluation and Planning (KETEP) grant funded by the Korea government (MOTIE)(20214000000140, Graduate School of Convergence for Clean Energy Integrated Power Generation). This work was supported by BK21 FOUR Program by Pusan National University Research Grant, 2021.

EN01.04.06

A High-Voltage Aqueous Zinc-Vanadium Redox Flow Battery with Bi-Modal Tin and Copper Clusters by a Continuous-Flow Electrometallic Synthesis SooBeom Lee, Minsoo Kim, Jihan Park, Jinyeong Choi and Minjoon Park; Pusan National University, Korea (the Republic of)

Aqueous zinc-based redox flow batteries are promising large-scale energy storage applications due to its low cost, high safety, environmental friendliness and low redox potential of the zincate couple of $\text{Zn}/[\text{Zn}(\text{OH})_4]^{2-}$ in the alkaline media. However, there have still tremendous obstacles towards practical use, such as zinc dendritic growth during the charging process, resulting in internal short circuit. These can create the dead zinc metal, which accumulate on the porous electrode or membrane and increase the cell resistance. In addition, the formation of the zincates has a problem of a low reversibility in the strong alkaline electrolytes, which can degrade the cycle efficiency and performance. Currently, several methods have been proposed to reduce the zinc dendritic growth in the zinc-based redox flow batteries, such as the surface modification of the carbon felt electrode and membrane developments. However, there were still limitations in terms of the complicated modification process. Also, the water splitting limits the voltage enhancement of the aqueous RFBs, allowing the narrow potential window under 1.23 V. Therefore, it is necessary to develop a low-cost and high energy density aqueous RFB system with the high voltage.

In this work, we report a bi-modal sized tin and copper (Sn, Cu) incorporated carbon felt (SCCF) via a novel multi-step, continuous-flow electrometallic synthesis method to solve the zinc dendrite issue in the zinc-based redox flow batteries. The SCCF electrode lowers the zinc nucleation overvoltage in the zinc symmetric flow battery and zinc-based hybrid redox flow battery, inducing the homogenous zinc plating and suppressing the zinc dendritic growth. A combined electrochemical and computational investigation reveals that the bi-modal tin and copper particles could suppress unwanted alloy formation, such as Cu-Zn alloy, strongly adsorbing zinc without the dendrite formation. The SCCF electrode exhibits 75% improved cycling stability than the pristine carbon felt electrode in the zinc symmetric flow battery. The pH differential hybrid Zn-V redox flow battery with the double membrane, pairing the $\text{VO}^{2+}/\text{VO}_2^+$ catholyte with the $\text{Zn}/[\text{Zn}(\text{OH})_4]^{2-}$ anolyte, affords a high average cell voltage over 2.31 V at 40 mA cm^{-2} . The SCCF electrode in the hybrid Zn-V redox flow battery led to high coulombic efficiency (>99.9%), average energy and voltage efficiency 92.6% and 92.3% over 100 cycles, respectively. We anticipate that this facile preparation method assisted by the continuous-flow electrometallic synthesis and high voltage hybrid Zn-V redox flow battery can pave the way to be large-scale applied in ZFBs, and even expanded into a wide range of energy storage system.

Acknowledgments

This work was supported by the National Research Foundation of Korea (NRF) grant funded by the Korea government (MSIT) (No.2021R1C1C1008349, NRF-2021R1A4A1022198). This work was supported by Korea Institute of Energy Technology Evaluation and Planning (KETEP) grant funded by the Korea government (MOTIE)(20214000000140, Graduate School of Convergence for Clean Energy Integrated Power Generation). This work was supported by BK21 FOUR Program by Pusan National University Research Grant, 2021.

EN01.04.07

Strategies to Mitigate Solvent Degradation to Obtain Deep Reduction Potential Anolytes for Non-Aqueous Redox Flow Batteries Nicolas Daub, Dimitar Georgiev and René Janssen; Technische Universiteit Eindhoven, Netherlands

Redox flow batteries (RFBs) are very promising storage systems in the transition towards renewable energy sources. They can be broadly classified in aqueous and non-aqueous systems. Last-named operate with organic solvents, which allow for a much broader potential window (up to three times higher) compared to water. Combination of organic solvents with organic redox active materials could pave the way for all carbon-based RFBs with superior energy densities compared to aqueous systems.

In this contribution, a new class of organic anolytes will be presented, focusing on their performance as RFB materials in acetonitrile with quaternary ammonium electrolyte salts. To push the limits of energy density, we investigated multi-electron reduction reactions on a single molecule. Current state-of-the-art anolytes for non-aqueous redox flow battery (NARFB) having a deep reduction potential, all contain carbonyl groups.¹⁻⁵ As already proposed by Wei et al.,¹ these anions could possibly attack acetonitrile. Yet, no clear evidence for that was shown. We investigated alkyl terephthalates

which exhibit two consecutive, deep reduction events at about -2.1 and -2.5 V vs Fc/Fc⁺. Upon accessing the second reduction couple, evidence was seen for a deprotonation of acetonitrile. Besides the analysis of the degradation, we suggest a design strategy to mitigate this reaction which results in a suitable anolyte for a NARFB with a deep reduction potential.

¹*ACS Energy Letters* **2016**, 1, 705–711

²*Advanced Energy Materials* **2015**, 5, 1401782.

³*International Journal of Hydrogen Energy* **2017**, 42, 27, 17488.

⁴*ACS Applied Energy Materials* **2019**, 2, 2364.

⁵*Journal of Power Sources* **2020**, 445, 227330.

SESSION EN01.05: Flow Battery Devices
Session Chairs: Patrick Cappillino and James McKone
Wednesday Morning, November 30, 2022
Hynes, Level 3, Room 301

8:45 AM *EN01.05.01

Membrane-Free Redox Flow Batteries Jianbing J. Jiang; University of Cincinnati, United States

While membrane-free batteries have been successfully demonstrated in static batteries, membrane-free batteries in authentic flow modes with high energy capacity and high cyclability are rarely reported. Here, we present a biphasic flow battery with high capacity employing organic compound in organic phase and zinc in aqueous phase. Under ambient flow testing conditions, a capacity retention of 94.5% is obtained over 190 charging/discharging cycles with a Coulombic efficiency of > 99% at a current density of 8.54 mA cm⁻². Self-discharge at full state-of-charge of the membrane-free RFB is negligible (potential drop = 0.78 mV h⁻¹). DFT calculation and *operando* UV-visible and FT-IR spectroscopies are performed to probe minor side reactions during cycling and monitor the water content in the organic electrolyte in real time. The successful demonstration of the prototypical membrane-free battery under flow conditions, together with the developed *operando* spectroscopic techniques, will open a new avenue towards detailed mechanistic studies and practical applications of redox flow batteries for cost-effective energy storage.

9:15 AM EN01.05.04

Efficient Harvesting and Storage of Solar Energy of an All-Vanadium Solar Redox Flow Battery with a MoS₂@TiO₂ Photoelectrode Gengyu Tian; Queen Mary University of London, United Kingdom

Solar redox flow batteries constitute an emerging technology that provides an intelligent alternative for the capture and storage of discontinuous solar energy through the photo-generation of the discharged redox species employed in traditional redox flow batteries. Here, we show that a MoS₂-decorated TiO₂ (MoS₂@TiO₂) photoelectrode can successfully harvest light stored in a solar redox flow battery using vanadium ions redox-active species in both catholyte and anolyte, and without the use of any bias. MoS₂@TiO₂ photoelectrode achieved an average photocurrent density of ~0.4 mA cm⁻² versus 0.08 mA cm⁻² for bare TiO₂ when tested for the oxidation of V⁴⁺ to V⁵⁺, attributed to a more efficient light harvesting and charge separation for the MoS₂@TiO₂ relative to TiO₂. The designed solar redox flow cell exhibited an optimal overall solar-to-chemical output energy conversion efficiency (SOEE) of ~4.78%, which outperforms previously reported solar redox flow batteries. This work demonstrates the potential of MoS₂@TiO₂ photoelectrode to efficiently convert solar energy into chemical energy in a solar redox flow battery, and it also validates the great potential of this technology to increase reliability in renewable energies.

10:00 AM *EN01.05.05

Investigating Indirect Redox-Targeting Reactions for High Energy Density Redox Flow Batteries Sundar R. Aravamuthan¹, Shyam K. Pahari², Shabdiki Chaurasia¹, Jennifer Bolibok², Benjoe Rey B. Visayas², Maricris L. Mayes², Patrick J. Cappillino² and Ertan Agar¹; ¹University of Massachusetts Lowell, United States; ²University of Massachusetts Dartmouth, United States

Redox flow batteries (RFBs) are considered to be one of the key technologies for addressing the intermittency problem in renewable energy sources, due to their unique architecture that allows for unprecedented scalability and flexibility, and cost-effectiveness in long-duration storage [1]. Despite their promise, typical RFBs suffer from low energy density because of the limit imposed by the solubility of the redox active species in the electrolyte [2]. One promising approach to address this limitation is the utilization of solid charge storage materials in the tanks to reversibly reduce or oxidize dissolved species in the electrolyte via indirect redox-targeting reactions without being connected to an external circuit [3–4]. In this way, the capacity is no longer dependent on the concentration of soluble species but rather the quantity of solids in the tanks. This concept [5] demonstrates the promise for exploiting the unique benefits of solid- and liquid-phase redox chemistry, combining the high-energy-density of Li-ion batteries, and the scalability and safety of RFBs.

In this presentation, we demonstrate a high energy density redox-targeting flow battery (RTFB) using a highly stable bio-inspired active material (vanadium(IV/V)bis-hydroxyiminodiacetate (VBH)) and a suitable solid storage material [5]. VBH [2,5] provides an ideal scaffold to investigate the complex electrochemical processes that occur during RTFB operation, which remain virtually unexplored [6]. For the solid storage material, a Prussian Blue Analogue (PBA) is synthesized and coupled with VBH mediators. Our recent efforts on understanding the interplay between two kinetic processes: electrochemical reaction in the flow cell and an indirect redox-targeting reaction in the tank are discussed. Cycling experiments are performed with and without the solid energy booster material to provide evidence that the addition of a compatible solid material greatly improves the energy density. Optimization of the critical parameters such as the amount of solid storage material, the operating current density, and the electrolyte flow rate is presented. Furthermore, an empirical approach to matching RTFB mediators with solid charge storage materials is introduced.

References:

- [1] Z. Li, M. S. Pan, L. Su, P.-C. Tsai, A. F. Badel, J. M. Valle, S. L. Eiler, K. Xiang, F. R. Brushett, Y.-M. Chiang, *Joule*, **1**, 306-327 (2017).
- [2] S. K. Pahari, T. C. Gokoglan, B. R. B. Visayas, J. Woehl, J. A. Golen, R. Howland, M. L. Mayes, E. Agar, P. J. Cappillino, *RSC Adv.*, **11**, 5432-5443 (2021).
- [3] R. Yan, Q. Wang, *Adv. Mater.*, **30**, 1802406 (2018)
- [4] X. Wang, M. Zhou, F. Zhang, H. Zhang, Q. Wang, *Curr. Opin. Electrochem.*, **29**, 100743 (2021).
- [5] J. Egitto, T. C. Gokoglan, S. K. Pahari, J. N. Bolibok, S. R. Aravamuthan, F. Liu, X. Jin, P. J. Cappillino, E. Agar, *ASME. J. Electrochem. En. Conv. Stor.*, (2022) <https://doi.org/10.1115/1.4054697>

[6] M. Moghaddam, S. Sepp, C. Wiberg, A. Bertei, A. Rucci, P. Peljo, *Molecules*, **26**, 2111 (2021).

9:45 AM BREAK

10:30 AM EN01.05.06

Higher Energy Density Mediated Lithium-Sulfur Flow Batteries [Melissa Meyerson](#), Adam Maraschky and Leo J. Small; Sandia National Laboratories, United States

There is a need for safe, reliable, high-capacity storage for long duration energy storage. The low cost and high capacity of sulfur make Li-S batteries ideal for this purpose. However, sulfur has poor electrical conductivity and Li-S batteries are prone to polysulfide shuttling that decreases the battery life. Additionally, lithium metal cannot be cycled at high rates or dendritic growth is produced. We have previously addressed the issues with the S by combining aspects of a static Li-S battery with aspects of a redox targeting system and flow battery. With this system we demonstrated that fundamental Li-S chemistry and novel SEI engineering strategies can be adapted to the hybrid redox flow battery architecture, obviating the need for ion-selective membranes or flowing carbon additives, and offering a potential pathway for inexpensive, scalable, safe MWh scale Li-S energy storage. However, these tests were done at lab scale with low S loadings and limited charge rates, limiting both the energy and power density of the proof-of-concept system. In this study we present recent progress scaling up the system from 2.5 mg_S cm⁻² to over 50 mg_S cm⁻² and increasing the current density from 0.5 mA cm⁻² to 10 mA cm⁻² to decrease the charge/discharge time. The increase in S loading results in an increase in energy density and the increase in applied current increases the power density of the system.

To scale up the flow cell we address limitations of the small-scale architecture including examining the flow field used with the catholyte and the structure of the Li metal anode. We first tested high surface area scaffolds in Swagelok cells to examine the effect of the increased effective surface area and lithiophilic seed materials like ZnO on Li metal deposition independent of the flow cell or S chemistry. Using a high effective surface area anode support enables us to increase the applied current density from 0.5 mA cm⁻² to 10 mA cm⁻² greatly increasing the charge/discharge speed. Furthermore, the addition of a lithiophilic seed layer decreases the nucleation overpotential and encourages uniform Li electrodeposition. A tailored flow field also improves the uniformity of Li deposition on the anode by improving the uniformity of the catholyte flow velocity. These improvements are first evaluated separately and then combined in a mediated Li-S flow battery where cycling rate and capacity retention are compared against a traditional planar Li anode and open flow field.

Sandia National Laboratories is a multi-mission laboratory managed and operated by National Technology and Engineering Solutions of Sandia, LLC., a wholly owned subsidiary of Honeywell International, Inc., for the U.S. Department of Energy's National Nuclear Security Administration under contract DE-NA0003525.

10:45 AM EN01.05.07

A High-Voltage Aqueous Zinc-Based Redox Flow Batteries with Reversible Metal Ionic Catalysts and Bi-Modal Tin and Copper Clusters [Minjoon Park](#), Minsoo Kim, Jinyeong Choi, SooBeom Lee and Jihan Park; Pusan National University, Korea (the Republic of)

With the increasing interest of renewable energy sources, the electrical energy storage (EES) system has received great attention to solve uncertainty of power input and output. Among many EES systems, a redox flow battery is the most promising candidate due to design flexibility for large scale. Recently, low cost and earth abundant transition metal based redox couples have attracted significant attention to replace the expensive vanadium redox couples. Conventional Mn-based aqueous zinc-ion battery is highly safe energy storage system, but low operating voltage (<1.5V) and low energy density limits its broad application in large-scale energy storage system. Recently, a novel aqueous zinc-manganese dioxide redox flow battery is reported. This battery is composed of Mn²⁺ based acidic catholyte and Zn²⁺ based alkaline anolyte, respectively, exhibiting an open circuit voltage of 2.66 V. Also, a neutral electrolyte was located between two different membranes to prevent the cross contamination of acidic and alkaline electrolytes, maintaining the charge balance. However, Mn³⁺ ions suffer from the disproportionation side reaction, lowering battery performance. Thus, the low reversibility of Mn/MnO₂ redox couple should be improved for broad application of Zn-Mn redox flow batteries. In addition, the formation of zinc dendrite should be suppressed when the zinc-based anolyte was used, which could deteriorate the cell performance.

In this work, we report a high voltage aqueous Zn-Mn hybrid redox flow battery with a high operating voltage of 2.75 V at the 100% state of charge. This work is a significant step forward by exploring the pH differential hybrid flow cell with the double-membrane, three-electrolyte configuration. The manganese cathode was deposited on carbon felt electrode with bismuth using carbothermal reduction process. Moreover, metal ionic catalysts are added as solution catalysts. We found that the reversibility of Mn ions was improved, and side reactions were suppressed by adding the metal ionic catalysts, maintaining a higher oxidation state of Mn ions. As a result, our works suggest that the zinc-manganese dioxide redox flow battery can be operated at high voltage with the excellent reversibility. Considering zinc dendrite issues, we introduced the bi-modal sized tin and copper (Sn, Cu) incorporated carbon felt in the negative electrode. The zinc nucleation overpotential was lowered by surface modified carbon felt electrode, also minimizing hydrogen evolution.

Acknowledgements

This work was supported by the National Research Foundation of Korea (NRF) grant funded by the Korea government (MSIT) (No.2021R1C1C1008349, NRF-2021R1A4A1022198). This work was supported by Korea Institute of Energy Technology Evaluation and Planning (KETEP) grant funded by the Korea government (MOTIE)(2021400000140, Graduate School of Convergence for Clean Energy Integrated Power Generation). This work was supported by BK21 FOUR Program by Pusan National University Research Grant, 2021.

SYMPOSIUM EN02

Halide Perovskite Materials, Processing and Devices
November 28 - December 6, 2022

Symposium Organizers

Jin-Wook Lee, Sungkyunkwan University
Carolyn Sutter-Fella, Lawrence Berkeley National Laboratory

Wolfgang Tress, Zurich University of Applied Sciences
Kai Zhu, National Renewable Energy Laboratory

Symposium Support

Bronze

ACS Energy Letters

ChemComm

MilliporeSigma

SKKU Institute of Energy Science & Technology

* Invited Paper
+ Distinguished Invited

SESSION EN02.01: Routes to Higher Performance and Stability

Session Chairs: Jin-Wook Lee and Annamaria Petrozza

Monday Morning, November 28, 2022

Hynes, Level 3, Ballroom B

10:30 AM *EN02.01.01

Research Directions in Perovskite Solar Cell Toward Theoretical Efficiency Nam-Gyu Park^{1,2}; ¹Sungkyunkwan University, Korea (the Republic of); ²SKKU Institute of Energy Science and Technology (SIEST), Korea (the Republic of)

Since the ground-breaking report of the 9.7% efficient and 500 h-stable solid-state perovskite solar cell (PSC) in 2012 based on methylammonium lead iodide, perovskite photovoltaics have been surged swiftly due to high power conversion efficiency (PCE) obtainable via facile fabrication procedure. As a result, a PCE of 25.7% was recorded in 2022. According to Web of Science, number of publications on PSCs increases exponentially since 2012, leading to the accumulated publications of more than 28,000 as of June, 2022. PSC is regarded as a game changer in photovoltaics because of low-cost and high efficiency surpassing the conventional high efficiency thin film technologies. High photovoltaic performance was realized by compositional engineering, device architecture and fabrication methodologies for the past 10 years. Toward theoretical efficiency over 30% along with long-term stability, exquisite control of light absorptivity and photo-excited charges is highly required, along with thermodynamic phase stability. In this talk, light-morphology relation is discussed, where a specific crystal facet is found to have strong interaction with photon, leading to high photocurrent. Compressive strain via wrinkling process is found to control the top surface tensile strain of perovskite film, which is beneficial to charge carrier transport and lifetime. As a result, we could achieve a QSS-measured PCE approaching 25% under one sun illumination.

11:00 AM EN02.01.02

Indoor and Outdoor Performance Tracking of Perovskite Photovoltaic Modules Nutifafa Y. Doumon¹, Michael Owen-Bellini¹, Jack Schall¹, Dana B. Sulas-Kerna¹, Paul Ndione¹, Kent Terwilliger¹, Timothy J. Silverman¹, Michael Deceglie¹, Nikos Kopidakis¹, Ingrid Repins¹, Mickey Wilson¹, Kirsten Perry¹, Robert White¹, Colin Sillerud², Prem Jyoti Singh Rana³, Jinsong Huang³, Zhaoning Song⁴, Michael J. Heben⁴, Yanfa Yan⁴, Devin J. MacKenzie⁵, Reinhold Dauskardt⁶, Angelique M. Montgomery⁷, Bruce King⁷, Joshua S. Stein⁷, Joseph J. Berry¹ and Laura T. Schelhas¹; ¹National Renewable Energy Laboratory, United States; ²CFV Laboratories, United States; ³University of North Carolina at Chapel Hill, United States; ⁴The University of Toledo, United States; ⁵University of Washington, United States; ⁶Stanford University, United States; ⁷Sandia National Laboratories, United States

A little over a decade of intensive research into the enormous potential of metal-halide perovskite (MHP) materials for photovoltaic (PV) applications led to record efficiencies of 25.7% for a single junction cell with 29.8% for tandem/multijunction cells [1]. MHP PV module technology with efficiency around 17.9% [2] is believed to be on the verge of commercialization. However, one of the major bottlenecks of the technology is in its reliability and long-term durability. To date the reported studies of devices in outdoor conditions is small relative to the large volume of work on these materials for photovoltaic applications. Understanding their degradation and failure modes in various environments is critical for advancing the MHP technology even further. And developing accelerated stress tests (AST) underscoring MHP PV failures modes unique to these types of devices sets the ground for qualification testing for perovskite PV modules. In this talk, we highlight the development of accelerated stress test protocols for perovskite PV module reliability testing. We then use a combination of characterization tools for destructive post-mortem analysis. Here we aim to understand the indoor and outdoor performance of modules via in-depth characterization of the MHP films, individual cells, and modules. Modules from different manufacturers, are run through the ongoing prototype indoor AST protocols and are then investigated and compared to those in outdoor field testing to grasp differences if any in their degradation pathways and/or failures modes. We believe these indoor-outdoor cross-examined tests would serve as the foundation for establishing standardized test protocols for MHP modules qualification testing, which are crucial for the technology to break through the PV market.

References:

1. NREL efficiency chart, <https://www.nrel.gov/pv/cell-efficiency.html>; accessed on 05/11/2022
2. NREL efficiency chart, <https://www.nrel.gov/pv/module-efficiency.html>; accessed on 06/08/2022

11:15 AM EN02.01.03

Engineering Ligand Reactivity Enables High-Temperature-Operating-Stable Perovskite Solar Cells So Min Park¹, Mingyang Wei², Jian Xu¹, Kenneth R. Graham³, Michael Graetzel² and Edward H. Sargent¹; ¹University of Toronto, Canada; ²École Polytechnique Fédérale de Lausanne, Switzerland; ³University of Kentucky, United States

Stability remains an area needing improvement on the path to the adoption of perovskite photovoltaics. Perovskite solar cells (PSCs) consisting of interfacial 2D/3D heterostructures via ammonium ligand intercalation have shown promise in the union of performance and stability; however, ligand penetration may contribute to performance degradation in 2D/3D PSCs at elevated temperatures. To date, the 2D/3D approach has not yet produced PSCs that are operating-stable at 85°C – and yet this is a prerequisite for impact on the photovoltaic sector. Here we explore the use of ammonium ligands that are instead non-reactive with the bulk of perovskites, investigating libraries through which we vary ligand molecular structure systematically. Aided by angle-resolved X-ray photoelectron spectroscopy, we find that anilinium exhibits the lowest tendency to penetrate the perovskite film, despite being the

simplest aromatic ammonium ligand – a quality achieved via the introduction of steric hindrance near the ammonium group. We leverage this to synthesize new ammonium ligands, such as fluorinated anilinium, that offer interfacial passivation and simultaneously minimize ligand reactivity. We find experimentally that this reactivity engineering is crucial to overcoming the stability and non-radiative recombination limitations: the new ammonium ligands enable perovskite material stacks that are thermally stable at 85°C, and that simultaneously improve PLQY by a factor of three compared to relevant controls. Using this approach, we report 23.3% certified quasi-steady-state PCE for inverted-structure PSCs; and we document 800-hour T80 (time to 80% of initial PCE) for encapsulated device operated at 85°C and 50% relative humidity, which represents a fourfold enhancement over the operating lifetime of optimized 2D/3D PSC controls. Our strategy of interface engineering provides a facile route to efficient and stable perovskite solar cells.

11:30 AM *EN02.01.04

Addressing the Operational Instability Challenges of Perovskite Solar Cells Yang Yang, Shaun Tan, Yepin Zhao and Qiyu Xing; University of California, Los Angeles, United States

Perovskite solar cells (PSCs) have reached 25.7% power conversion efficiency, but their long-term stability under operational conditions is far behind the standards required for technology commercialization. In this presentation, we summarize our recent progress at UCLA to address the stability of PSCs from the perspective of understanding how the surface/interface energetics, lattice strain, defects, and charge transport affect the degradation of PSCs. Particular attention are on (1) surface passivation and the formation of ideal interface for the NIP structure; and (2) management of ion-migration.

SESSION EN02.02: Characterization and Stabilization of Metastable Phases

Session Chairs: Sascha Feldmann and Ivan Mora-Sero

Monday Afternoon, November 28, 2022

Hynes, Level 3, Ballroom B

1:30 PM *EN02.02.01

Stabilization and Crystallization Control of α -FAPbI₃—Towards Efficient and Stable Perovskite Solar Cells Soeun Shin, Pronoy Nandi, Hyounghmin Park and Hyunjung Shin; Sungkyunkwan University, Korea (the Republic of)

Formamidinium lead triiodide (FAPbI₃) is gaining interest with an optimal band gap of ~ 1.5 eV. Although α -FAPbI₃ is the most thermodynamically stable photoactive phase, it can kinetically stabilize δ -FAPbI₃ in ambient. Many attempts were studied to stabilize the black α -phase, for example, pseudo-halide anion engineering, ionic liquid engineering, and incorporation of additives. Incorporating with methylammonium chloride (MACl) as an additive not only induces the stabilized α -FAPbI₃, but also affects the crystallization kinetics of α -FAPbI₃. Along with the role of methylammonium chloride (MACl) as a ‘stabilizer’ in the formation of α -FAPbI₃, we pointed out the additional role as a ‘controller’ in the crystallization kinetics. Herein, we examined the crystallization process of MACl, as higher concentration of MACl induces slower crystallization kinetics. Which results in larger grain size and [100] preferred orientation in α -FAPbI₃ films as the MACl concentration increased from 10 to 20, 30, and 40%. Microscopic observations, such as electron back-scattered diffraction (EBSD), confocal photoluminescence (PL), time-resolved photoluminescence (TRPL) mapping, and conductive atomic force microscopy (C-AFM), were conducted to examine the optoelectronic properties of [100] preferentially oriented grains. Reduction in the non-radiative recombination, a longer lifetime of charge carriers and less photocurrent deviation between each grain induce higher short-circuit current density (J_{sc}) and fill factor (FF) in α -FAPbI₃ based perovskite solar cells (PSCs) with MACl40%. Resulting the PSCs with MACl40% to attain the highest power conversion efficiency (PCE) of 23.5%. Furthermore, we confirmed these observations by enhancing the grain size and [100] preferred orientation of the MACl10% sample through a two-step heat treatment. As the lower heat treatment induced suppression of nucleation and enhancement of the crystal growth in α -FAPbI₃ films with MACl10%. The two-step processing resulted in an improvement in the PCE from 18.4% to 21.8%. It indicates the impact of adding MACl to control the crystallization kinetics resulting in a preferred orientation and a large grain size. It highlights the importance of crystallization kinetics resulting in desirable microstructures for device engineering.

2:00 PM EN02.02.02

Quantitative Multiscale Diffusion Framework for Halide Perovskites Establishes Stability-Hysteresis-Diffusion Relationship Masoud Ghasemi^{1,1}, Boyu Guo^{1,1}, Chung-Wei Huang², Garrett Baucom^{1,1}, Kasra Darabi^{1,1}, Laine Taussig^{1,1}, Tonghui Wang^{1,1}, Taesoo Kim^{1,1}, Joanna Atkin² and Aram Amassian^{1,1}; ¹North Carolina State University, United States; ²University of North Carolina at Chapel Hill, United States

Anomalous properties such as operational instability and photocurrent hysteresis in metal halide perovskite (MHP)-based devices present a major obstacle to their future commercialization. Halide ion/defect migration has been widely accepted as one of the main mechanisms behind these limiting properties, but a definitive explanation of this relationship has remained elusive. Here, we present a quantitative multi-scale diffusion framework that fully describes halide diffusion in polycrystalline MHPs. By using time-of-flight secondary ion mass spectroscopy (ToF-SIMS) technique we could simultaneously monitor both the fast grain boundary (GB) diffusivity and three to four orders of magnitude slower volume/bulk diffusivity. Our framework reveals an inverse relationship between the diffusion coefficients of GBs (D_{GB}) and volume (D_V) diffusions, such that MHPs (such as MAPbI₃) with a larger D_V also possess a smaller D_{GB} . Importantly, this relationship explains some of the most conflicting observations in the literature, namely that MHPs with improved stability (linked to D_V) typically exhibit reduced hysteresis. This nontrivial relation between volume and GB halide diffusivities is observed across a wide range of MHP systems, including MA- and FA-based iodide and bromide perovskites and is valid when GB passivation approaches are used. The quantitative elucidation of multiscale halide diffusion in polycrystalline MHPs provides an important path toward addressing outstanding issues of stability and hysteresis in MHP device technologies, as will be discussed in this presentation.

2:15 PM EN02.02.03

Addressing Chemical and Thermomechanical Instabilities in Metal Halide Perovskites Across Length Scales Yanan Li, Patrick Lohr, Anton Samoylov, Matthew Dailey and Adam Printz; University of Arizona, United States

The chemical and thermomechanical instabilities of metal halide perovskites represent barriers to long operational lifetimes of perovskite-based devices. There is no single magic bullet to address these instabilities, and so multiple complementary strategies must be undertaken. I will discuss the work by our research group to address these instabilities at multiple length scales, including the effects of the molecular structure and functionality of additives on their interactions with perovskite surfaces, the enhancement of mechanical toughness of perovskite layers by compositing with polymeric nanofibers, and the use of confined volume printing to rapidly produce perovskite films with large grains and reduced surface area of grain boundaries detrimental to stability. Together, these approaches provide one possibly pathway toward significantly increasing the operational lifetimes of perovskite-based devices.

2:30 PM *EN02.02.04

Halide Ion Migration-Induced Instability in Metal Halide Perovskites Preethi S. Mathew, Jeffrey DuBose and Prashant Kamat; University of Notre Dame, United States

Generation of holes through above-bandgap excitation or through electrochemical injection increases ion migration and leads to phase segregation in metal halide perovskites (MHP). The thermodynamic and redox properties of halide perovskites provide a strong driving force for hole trapping and oxidation of iodide species in MHPs. However, mobile halide species within the perovskite lattice take time to migrate and generate halide-rich domains. When in contact with a non-polar solvent, the migration of iodine species is further extended to expulsion of iodine from the perovskite film. Thus, the mobility of halides and their susceptibility to hole-induced oxidation play a crucial role in determining the long-term stability of metal halide perovskites. Strategies to gain kinetic control over ion migration to slow phase segregation are needed to overcome these hurdles and achieve stable mixed halide perovskites. Modification of the perovskite composition through introduction of different cations, halide ions, or introduction of low-dimensional perovskite phases may suppress phase segregation will be discussed. Thus, in achieving stability and improving efficiency of perovskite solar cells and light emitting devices with minimal impacts, suppression of segregation remains the key factor.

3:00 PM BREAK

3:30 PM EN02.02.05

Substrate Functionalization to Improve the Stability of α -FAPbI₃ Andres Felipe Castro Mendez and Juan Pablo Correa Baena; Georgia Institute of Technology, United States

One of the major limitations of the commercialization of perovskite solar is the scalability of the different fabrication processes. In this context, thermal evaporation offers several advantages compared to solution processes, such as higher uniformity, better control of the thickness, deposition of non-soluble materials, and avoiding the removal of solvent orthogonality. Co-evaporation of FAPbI₃ is a promising choice for the fabrication of highly efficient and scalable perovskite solar cells. However, the presence of the non-perovskite hexagonal phase, which is the most stable phase at room temperature, is detrimental to the device's performance. Here, grazing incident wide-angle X-ray scattering (GIWAXS), X-ray diffraction (XRD), and X-ray fluorescence (XRF) techniques are used to understand the role that intermolecular forces (i.e. hydrogen bonds, dipole-dipole, van der Waals) between the perovskite and the substrate plays in determining the crystalline structure and crystallographic orientation of FAPbI₃ deposited by thermal evaporation

3:45 PM EN02.02.06

Water and Oxygen Synergy Induce Undesired Phase Transitions in Formamidinium Lead Iodide Perovskites—Strategies to Stabilize the Perovskite Metastable Phase Juanita Hidalgo¹, Yu An^{2,1} and Juan Pablo Correa Baena¹; ¹Georgia Institute of Technology, United States; ²Tianjin University, China

Formamidinium (FA) lead halide perovskites have shown to be promising materials for solar cells, having achieved a maximum power conversion efficiency greater than 25%. FA-rich compositions have an ideal bandgap close to 1.5 eV and show enhanced thermal stability¹. However, the FA-rich perovskite structure is metastable at room temperature and can easily degrade into non-perovskite hexagonal polytypes. The addition of Cs to the FA-based perovskite has led to a more stable perovskite structure², but not when exposed to humidity. The instability upon humidity exposure is a challenge limiting the efficacy of encapsulating technologies acting as humidity barriers. Beyond the development of encapsulating technologies, it is important to understand the degradation mechanism of FA-rich perovskites when exposed to humidity to design a highly efficient and stable material. The humidity degradation mechanism leading to crystallographic phase transitions in FA-rich perovskites is still poorly understood. Therefore, it is essential to unravel the structural degradation pathways of these materials caused by humidity exposure.

Herein, we studied the phase transformations and degradation kinetics of an FA-rich perovskite, Cs_{0.17}FA_{0.83}PbI₃, upon exposure to humidity, through *in-situ* grazing incidence wide-angle X-ray scattering (GIWAXS). We investigated the effect of the humidity carrier gas (i.e., nitrogen, air) in the degradation pathway of Cs_{0.17}FA_{0.83}PbI₃. Degradation kinetics were investigated and quantified, suggesting that water and oxygen synergy accelerates the non-perovskite FAPbI₃ hexagonal 2H phase formation. Through X-ray photoelectron spectroscopy, we observed that water degradation begins at the surface, where oxygen is present. To study the effect of humidity on the bulk of the film, we observed that iodine content decreases after humidity exposure by X-ray fluorescence maps. For a comprehensive bulk understanding, we synthesized Cs_{0.17}FA_{0.83}PbI₃ powders and studied the structure and vibrational modes before and after humidity degradation. We found that the origins of the phase transitions of the FA-rich perovskite go beyond humidity: oxygen plays an important role in determining the degradation pathway, which starts at the surface of the films. By studying the humidity degradation pathway, we understand how surface passivation, a strategy to enhance charge carrier extraction, can act as a barrier to oxygen and water, preventing the degradation of FA into hexagonal polytypes.

(1) An, Y.; Hidalgo, J.; Perini, C. A. R.; Castro-Méndez, A. F.; Vagott, J. N.; Bairley, K.; Wang, S.; Li, X.; Correa-Baena, J. P. Structural Stability of Formamidinium- And Cesium-Based Halide Perovskites. *ACS Energy Lett.* **2021**, *6* (5), 1942–1969. <https://doi.org/10.1021/acseenergylett.1c00354>.

(2) Lee, J. W.; Kim, D. H.; Kim, H. S.; Seo, S. W.; Cho, S. M.; Park, N. G. Formamidinium and Cesium Hybridization for Photo- and Moisture-Stable Perovskite Solar Cell. *Adv. Energy Mater.* **2015**, *5* (20). <https://doi.org/10.1002/aenm.201501310>.

4:00 PM *EN02.02.07

Defects Activity in Wide and Narrow Bandgap Metal Halide Perovskite Semiconductors Annamaria Petrozza; Istituto Italiano di Tecnologia, Italy

Metal halide perovskites (MHPs) have demonstrated huge potential to build a rich library of materials for a new disruptive optoelectronic technology. The main strength comes from the possibility of easily tune the semiconductor bandgap in order to integrate it in devices with different functionalities – in principle. In reality, this cannot be achieved yet. In fact, while defect tolerance is claimed for MHPs with a bandgap of about 1.6 eV, the model system object of intense investigations, MHPs with lower and higher bandgaps are far from this claim. They show various forms of instabilities which are mainly driven by a strong defect activity.

Here I will discuss our studies on the nature of defects and their photo-chemistry as a function of the semiconductor bandgap and chemical composition in order to identify their role in defining the semiconductor electronic properties and stability.

4:30 PM EN02.02.08

FAPbI₃ Perovskite Solar Cells—Thermal Evaporation vs Solution Processing Terry Chien-Jen Yang^{1,1}, Satyawan D. Nagane^{1,1}, Yu-Hsien Chiang^{1,1}, Affan Iqbal^{1,1}, Tiarnan A. Doherty^{1,1}, Dengyang Guo^{1,1}, Jordi Ferrer Orri^{1,1}, Kyle Frohna^{1,1}, Juliane Borchert^{1,2}, Bart Roose^{1,1}, Miguel Anaya^{1,1} and Samuel

D. Stranks^{1,1}; ¹University of Cambridge, United Kingdom; ²Center for Nanophotonics, AMOLF, Netherlands

Thermal evaporation is an upscalable vacuum deposition technique for fabricating perovskite solar cells (PSCs). The advantages of thermal evaporation include better control of film thickness and reproducibility as well as conformal coating over large substrate areas which could be better suited for multi-junction solar cell fabrication. Furthermore, various thermal sources from inorganic to organic, for example PbI₂, PbBr₂, SnI₂, CsBr, FAI (formamidinium iodide), and MAI (methylammonium iodide) can be used allowing maximum compositional control and flexibility during the solvent-less deposition. To date, evaporation has been far less explored versus more conventional solution processing techniques¹.

The FAPbI₃ perovskite composition has attracted much attention given its optimal bandgap for single-junction PSCs. In this study, we compare the properties of thermally co-evaporated FAPbI₃ (PbI₂ and FAI sources) versus solution processed spin-coated FAPbI₃, by characterizing both pristine FAPbI₃ films and solar cells. We examine chemical properties such as PbI₂ to FAI ratio, structural properties such as the perovskite crystallization conditions, and device architectures comprising different electron/hole transport layers and contacts. In literature, cation (Cs⁺ and MA⁺) or other additives are typically used to improve the properties of the FAPbI₃ perovskite allowing higher efficiency devices and long-term stability as a result of octahedral tilting in their crystal structure².

Interestingly, scanning electron diffraction (SED) results show that thermally co-evaporated FAPbI₃ films exhibit some inherent octahedral tilt in their crystal structure, which results in the slower conversion to the non-perovskite yellow hexagonal δ -phase in air over time. This intrinsic thermodynamic conversion occurs faster in our solution processed pristine FAPbI₃ films as shown through various characterization techniques, which could be due to the different crystallization process or effects of residual solvents. This unwanted conversion of FAPbI₃ is exacerbated in the presence of moisture, heat, and light as shown widely in literature³.

Currently, solution processed FAPbI₃ solar cells have achieved much higher efficiency (record 25.7%⁴) compared to thermally evaporated FAPbI₃ devices (<21%^{5,6}). This is largely due to the fact that vastly more time and effort has been invested in optimizing solution processed PSCs, compared to thermal evaporation. Our work suggests that thermal evaporation could have a marked advantage over solution processing of FAPbI₃ based PSCs and will attract other researchers to further optimize thermally evaporated PSCs. If performance similar to solution processed methods can be achieved, the better scalability will make thermal evaporation a promising route to commercializing PSCs.

References

1. Vaynzof, Y. The Future of Perovskite Photovoltaics — Thermal Evaporation or Solution Processing ? **2003073**, (2020).
2. Doherty, T. A. S. *et al.* Stabilized tilted-octahedra halide perovskites inhibit local formation of performance-limiting phases. *Science (80-.)*. **374**, 1598–1605 (2021).
3. Liu, Z. *et al.* Efficient and Stable FA-Rich Perovskite Photovoltaics: From Material Properties to Device Optimization. *Adv. Energy Mater.* **12**, 1–35 (2022).
4. NREL. NREL Efficiency Chart. *Chart, Best Research-Cell Efficiency* <https://www.nrel.gov/pv/cell-efficiency.html> (2019).
5. Roß, M. *et al.* Co-Evaporated Formamidinium Lead Iodide Based Perovskites with 1000 h Constant Stability for Fully Textured Monolithic Perovskite/Silicon Tandem Solar Cells. *Adv. Energy Mater.* **11**, (2021).
6. Borchert, J. *et al.* Large-Area, Highly Uniform Evaporated Formamidinium Lead Triiodide Thin Films for Solar Cells. *ACS Energy Lett.* **2**, 2799–2804 (2017).

4:45 PM EN02.02.09

Effect of Residual Chloride in FAPbI₃ Film on Phase Stability and Photovoltaic Performance of Perovskite Solar Cell Dong-Ho Kang and Nam-Gyu Park; Sungkyunkwan University, Korea (the Republic of)

The chloride ion in additive is found to have beneficial effect on enhancing photovoltaic performance due to the grain growth of FAPbI₃ perovskite. However, we found that the residual Cl incorporated in crystal lattice can aggravate the crystal phase and device stability. Thus, it is necessary to find an effective way to remove chloride ion from the perovskite film without sacrificing the photovoltaic performance. Here, we report a methodology to improve the stability of perovskite solar cell via elimination of the residual chloride ion. The extended X-ray absorption microstructure (EXAFS) combined with X-ray diffraction (XRD) reveal that the lattice distortion of PbI₆ octahedra is reduced due to the increased (Pb-I) bond distance after removal of chloride ion. The absence of chloride ion, confirmed by X-ray photoelectron spectroscopy (XPS), improves charge carrier lifetime, leading to higher power conversion efficiency (PCE) from 21.57 % for the perovskite film with residual chloride ion to 22.76%, mainly due to the enhancement of open-circuit voltage from 1.129 V to 1.168 V. Long-term stability test for over 1000 h under relative humidity of about 45% shows clearly that the device employing the chloride-removed perovskite film is much less degraded than the control one with perovskite film having residual chloride.

SESSION EN02.03: Poster Session I

Session Chairs: Il Jeon, Jin-Wook Lee, Carolin Sutter-Fella and Wolfgang Tress

Monday Afternoon, November 28, 2022

8:00 PM - 10:00 PM

Hynes, Level 1, Hall A

EN02.03.01

Rational Design of Photoelectrochemical Perovskite-BiVO₄ Tandem Devices for Scalable Solar Fuel Production Virgil Andrei^{1,1}, Judith L. MacManus-Driscoll¹, Robert Hoye², Richard H. Friend¹ and Erwin Reisner¹; ¹University of Cambridge, United Kingdom; ²Imperial College London, United Kingdom

Metal halide perovskites have emerged as promising alternatives to commonly employed light absorbers for solar fuel synthesis, enabling unassisted photoelectrochemical (PEC) water splitting^[1,3] and CO₂ reduction to syngas.^[2,4] While the bare perovskite light absorber is rapidly degraded by moisture, recent developments in the device structure have led to substantial advances in the device stability. Here, we give an overview of the latest progress in perovskite PEC devices, introducing design principles to improve their performance and reliability. For this purpose, we will discuss the role of charge selective layers in increasing the device photocurrent and photovoltage, by fine-tuning the band alignment and enabling efficient charge separation. A further beneficial effect of hydrophobicity is revealed by comparing devices with different hole transport layers (HTLs).^[1,3] On the manufacturing side, we will provide new insights into how appropriate encapsulation techniques can extend the device lifetime to a few days under operation in aqueous media.^[1,2]

To this end, we replace low melting alloys with graphite epoxy paste as a conductive, hydrophobic and low-cost encapsulant.^[3,5] The combined advantages of these approaches are demonstrated in a perovskite-BiVO₄ tandem device archiving selective unassisted CO₂ reduction to syngas.^[4] These design principles are successfully applied to an underexplored BiOI light absorber, increasing the photocathode stability towards hydrogen evolution from minutes to months.^[6] Finally, we take a glance at the next steps required for scalable solar fuels production, showcasing our latest progress in terms of device manufacturing. A suitable choice of materials can decrease the device cost tenfold and expand the device functionality.^[7] Such materials are compatible with large-scale, automated fabrication processes, which present the most potential towards future real-world applications.^[8]

[1] Andrei, V. et al. *Adv. Energy Mater.* 2018, 8, 1801403.

[2] Andrei, V.; Reuillard, B.; Reiser, E. *Nat. Mater.* 2020, 19, 189–194.

[3] Pornrunroj, C.; Andrei, V. et al. *Adv. Funct. Mater.* 2021, 31, 2008182.

[4] Rahaman, M.; Andrei, V. et al. *Energy Environ. Sci.* 2020, 13, 3536–3543.

[5] Andrei, V.; Bethke, K.; Rademann, K. *Phys. Chem. Chem. Phys.* 2016, 18, 10700–10707.

[6] Andrei, V.; Jagt, R. A. et al. *Nat. Mater.* 2022. DOI: 10.1038/s41563-022-01262-w.

[7] Andrei, V.; Ucoski, G. M.; Pornrunroj, C.; Uswachoke, C.; Wang, Q.; Achilleos, D. S.; Kasap, H.; Sokol, K. P.; Jagt, R. A.; Lu, H.; Lawson, T.; Wagner, A.; Pike, S. D.; Wright, D. S.; Hoye, R. L. Z.; MacManus-Driscoll, J. L.; Joyce, H. J.; Friend, R. H.; Reiser, E. *Nature*, accepted.

[8] Sokol, K. P.; Andrei, V. *Nat. Rev. Mater.* 2022, 7, 251–253.

EN02.03.02

Mechanochemistry-Driven Engineering of Cs₄PbX₆/CsPbX₃ (X=Cl, Br, I) Heterostructure for Designing Highly Luminescent Perovskites [Kyeong-Yoon Baek¹](#), [Woocheol Lee¹](#), [Hyungbin Lim¹](#), [Jae Il Kim¹](#), [Richard H. Friend²](#), [Tae-Woo Lee¹](#), [Jeongjae Lee¹](#), [Keehoon Kang¹](#) and [Takhee Lee¹](#); ¹Seoul National University, Korea (the Republic of); ²University of Cambridge, United Kingdom

Embedding metal-halide perovskite emitting particles within an insulating host matrix has proven to be an effective strategy for enhancing and stabilizing the outstanding luminescence properties of perovskites as an emerging class of light emitters [1,2]. Particularly, unexpected bright green emission observed in a nominally pure zero-dimensional cesium-lead-bromide perovskite (Cs₄PbBr₆) has triggered intensive research in better understanding the serendipitous incorporation of emissive guest species CsPbBr₃ within the insulating Cs₄PbBr₆ host [3]. However, a limited controllability over such heterostructural configurations in conventional solution-based synthesis methods has limited the degree of freedom in designing synthesis routes for accessing different structural and compositional configurations of these host-guest species. In this study, we provide means of enhancing the luminescence properties in the nominal Cs₄PbX₆ (X=Cl, Br, I) powder through a guided heterostructural configuration engineering enabled by solid-state mechanochemical synthesis. First, we investigate the reaction kinetics underlying the formation process of Cs₄PbBr₆ [4]. Realized by an in-depth study on time-dependent evaluation of optical and structural properties during the synthesis of Cs₄PbBr₆, we target-design highly luminescent Cs-Pb-Br composite perovskite through promoting the endotaxial formation of Cs₄PbBr₆/CsPbBr₃ heterostructure. Next, we tune the emission wavelength of 520 nm which corresponds to the green emissive Cs-Pb-Br perovskite to the entire visible spectrum range of 410–690 nm. This is achieved through employing the substitution of monovalent halide with other halide components and controlling their stoichiometric ratio in the heterostructural samples (Cs₄PbCl_mBr_{6-m} and Cs₄PbBr_{6-m}I_m) [5]. Our study provides key insights for understanding and designing kinetics-guided synthesis of highly luminescent perovskite emitters and introduces the entire family of 0D/3D heterostructural perovskites for light-emitting applications.

References:

[1] Akkerman, Q. A. et al. *Nat. Mater.* **17**, 394 (2018).

[2] Wang, X. et al. *Nat. Commun.* **10**, 695 (2019).

[3] Wang, L. et al. *ACS Energy Lett.* **5**, 87 (2020).

[4] Baek, K.-Y. et al. *Nat. Commun.* in press (2022).

[5] Lim, H. et al. submitted (2022).

EN02.03.03

Entirely Roll to Roll Coated Perovskite Photovoltaics Enabled by Carbon Ink Formulation [David Beynon](#), Ershad Parvazian, James McGettrick, Rahul Patidar, Rodrigo Garcia Rodriguez, Tom Dunlop and Trystan Watson; Swansea University, United Kingdom

Perovskite photovoltaics have been the subject of intense scientific interest due to their suitability for solution processing, simple device structure and meteoric rise in efficiency. The world record certified efficiency of 25.2% for single junction perovskite solar cells and much of the development leading to this point has been achieved using lab-scale spin-coating methods in controlled environments. This has demonstrated the potential of perovskite solar cells as a competitor of conventional silicon solar cells, however to realise that potential requires an alternative fabrication approach that is capable of high volume manufacture. Spin-coating is an ideal deposition method for the laboratory setting as it allows controlled layer thickness, dynamic drying and rapid solvent evaporation with the potential incorporation of an anti-solvent in a reproducible setup but it suffers high material wastage and scaling challenges that mean it is critical to evolve this process.

Sealing of PSC layers has been achieved in recent studies through roll-to-roll coating techniques with the slot die coating method showing the greatest promise. Slot-die coating is a cost effective coating method that allows significant control in coating and can deposit layers with little material wastage, high control on film thickness and flexibility to coat layers with several stripes. In addition slot-die coating via the roll-to-roll method allows material to be deposited indefinitely (with continuous ink supply) at high line speeds.

Perovskite solar cells are yet to fully transition to roll-to-roll fabrication despite the major impact that this would achieve. The method has been demonstrated on a number of occasions for all-layers (including at this institution) except for the back electrode which has always been deposited via an evaporated metal contact in an off-line process. This means that true fully roll-to-roll perovskites has yet to be achieved.

Printed carbon inks have the potential to provide the solution; however solvent incompatibility, interface incompatibility and incorrect rheology profile mean that simple deposition of a standard carbon ink to finalise the device is not the solution and leads to detrimental printing performance and poor or negligible device performance. Despite recent effort in this field, none of the alternative carbon inks have so far been suitable for application as a R2R top-contact, as they mostly focused on overcoming one of the challenges discussed earlier instead of considering them as one major related issue. Here, we formulate a new carbon ink that has solvent compatible with the perovskite stack and that, crucially, has suitable boiling point for low temperature, high speed processing coupled with very low toxicity (no work place exposure limit). The solid loading of the ink has been optimised for a rheological profile suitable for slot die and we demonstrate the roll to roll slot die coating of the electrode sequentially following the roll to roll coating of the NIP device stack incorporating a low temperature processed PEDOT:PSS p type interlayer. Our work introduces the very first entirely roll to roll devices achieving over 10% efficiency matching equivalent evaporated gold electrodes. This first fully roll-to-roll coated perovskite prototype represents a

game changer in unlocking the potential of industrial scale, high volume, continuous manufacture of perovskite solar cells.

EN02.03.04

Morphology-Controlled Lead-Free Halide Double Perovskite Nanocrystals by Chemical Vapor Deposition [Anupam Biswas](#), Pushpender Yadav, Kyeongdeuk Moon and Seokhyoung Kim; Michigan State University, United States

Materials are vital for the advancement of science and technology in the modern world. Over the last few decades materials like silicon (Si) has dominated the industry owing to their superior stability and reliability. Compared to traditional Si-based technology, lead halide perovskite (LHP) has demonstrated considerable promise for efficient solar energy conversion and light generation. However, the toxicity of lead (Pb) in LHPs is a major barrier that inhibits practical applications. By employing lead-free halide double perovskites, both energy and environmental concerns can be directly addressed. Although lead-free double perovskites have been investigated extensively in the bulk form, their structural behavior and optoelectronic properties have yet to be fully explored in the nanoscale. Here, we present a vapor-phase synthetic control over the size and shape of lead-free double $\text{Cs}_2\text{AgBiBr}_6$ perovskite nanocrystals using a chemical vapor deposition (CVD) system. The synthetic parameters used for the growth control include temperature, deposition position, gas flow rate, and growth time. At optimal conditions, we could obtain a uniform, submicron-sized single-crystals of $\text{Cs}_2\text{AgBiBr}_6$. The structural and compositional properties were characterized by X-ray diffraction (XRD), scanning electron microscopy (SEM), and energy-dispersive X-ray spectroscopy (EDS), which showed good agreement with the known values from the literature. The elemental composition of the CVD-grown $\text{Cs}_2\text{AgBiBr}_6$ was further confirmed along with their corresponding oxidation state by X-ray photoelectron spectroscopy (XPS). We observed an experimentally measured bandgap of 2.1 eV and band-edge photoluminescence at 627 nm with a full-width-half-maximum (FWHM) bandwidth of 150 nm and they are in close agreement with reported values in the literature. We believe our research finding on controlling the morphology and growth of $\text{Cs}_2\text{AgBiBr}_6$ nanocrystals by CVD has the potential to extend to other lead-free halide perovskites and will open a new gateway for the development of future photovoltaics, photodetectors, and related applications.

EN02.03.05

3D Printing of Ruddlesden-Popper Perovskites with High Color Purity and Stability [Sixi Cao](#) and Ji Tae Kim; The University of Hong Kong, Hong Kong

Ruddlesden-Popper (RP) lead halide perovskites have emerged as a new class of tunable two-dimensional semiconductors that demonstrate high performance in optoelectronics due to their enhanced stability and structural tunability^{1,2}. The nanostructured RP perovskites with forms of films or wires are the basic building blocks for manufacturing high-density integration of optoelectronic circuitries and devices^{3,4}. However, their nanostructures are limited due to the complex organic-inorganic layered crystalline features⁵. Some clever methods based on template growth⁶, lithography⁷, inkjet printing⁸ and chemical vapor deposition⁹ have been devised to produce RP perovskite nanostructures but new methods are still in great demand for high-resolution, three-dimensional integration. Furthermore, the engineering challenges associated with how to engineer the perovskite phase in the nanostructure still remains unresolved¹⁰. Here, we report a nanoscale 3D printing method for RP perovskites with programmed shape and crystallinity. The method exploits a femtoliter precursor meniscus formed on a nanopipette to guide RP perovskite crystallization at will under strong evaporation of solvent. Guiding the meniscus in three-dimension leads to the formation of a freeform, freestanding RP perovskite nanowire exhibiting a polycrystalline nature. It is observed that the crystalline feature is successfully controlled in in-situ by adjusting temperature and humidity during the 3D printing process. In this talk, I will present my research progress on the development of 3D printing for RP perovskites and discuss prospects of our work for potential applications in electronics and optoelectronics.

References

- 1 Pan, D. *et al.* Deterministic fabrication of arbitrary vertical heterostructures of two dimensional Ruddlesden-Popper halide perovskites. *Nat Nanotechnol* **16**, 159-165, doi:10.1038/s41565-020-00802-2 (2021).
- 2 Blancon, J. C., Even, J., Stoumpos, C. C., Kanatzidis, M. G. & Mohite, A. D. Semiconductor physics of organic-inorganic 2D halide perovskites. *Nat Nanotechnol* **15**, 969-985, doi:10.1038/s41565-020-00811-1 (2020).
- 3 Quan, L. N., Kang, J., Ning, C.-Z. & Yang, P. Nanowires for Photonics. *Chemical Reviews* **119**, 9153-9169, doi:10.1021/acs.chemrev.9b00240 (2019).
- 4 Chen, J. *et al.* Oriented Halide Perovskite Nanostructures and Thin Films for Optoelectronics. *Chem Rev*, doi:10.1021/acs.chemrev.1c00181 (2021).
- 5 Li, X., Hoffman, J. M. & Kanatzidis, M. G. The 2D Halide Perovskite Rulebook: How the Spacer Influences Everything from the Structure to Optoelectronic Device Efficiency. *Chem Rev* **121**, 2230-2291, doi:10.1021/acs.chemrev.0c01006 (2021).
- 6 Feng, J. *et al.* Single-crystalline layered metal-halide perovskite nanowires for ultrasensitive photodetectors. *Nature Electronics* **1**, 404-410, doi:10.1038/s41928-018-0101-5 (2018).
- 7 Qin, C. *et al.* Stable room-temperature continuous-wave lasing in quasi-2D perovskite films. *Nature* **585**, 53-57, doi:10.1038/s41586-020-2621-1 (2020).
- 8 Jia, S. *et al.* Highly Luminescent and Stable Green Quasi 2D Perovskite Embedded Polymer Sheets by Inkjet Printing. *Advanced Functional Materials* **30**, doi:10.1002/adfm.201910817 (2020).
- 9 Ghoshal, D. *et al.* Catalyst Free and Morphology Controlled Growth of 2D Perovskite Nanowires for Polarized Light Detection. *Advanced Optical Materials* **7**, doi:10.1002/adom.201900039 (2019).
- 10 Liang, C. *et al.* Two-dimensional Ruddlesden-Popper layered perovskite solar cells based on phase-pure thin films. *Nature Energy* **6**, 38+, doi:10.1038/s41560-020-00721-5 (2021).

EN02.03.07

Perovskite and Organic Photoanodes with Low-Temperature Printed Carbon Layer for Solar Water Splitting [Matyas Daboczi](#), Junyi Cui and Salvador Eslava; Imperial College London, United Kingdom

Photoelectrochemical water splitting is a promising way of solar hydrogen generation, however in order to achieve both high efficiency and stability photoelectrodes significant further improvements are needed. Perovskite and organic photoactive materials have attracted great scientific interest by reaching record high single-junction solar cell efficiencies. In this presentation, we will show a cost-effective way of protecting organic (non-fullerene acceptor and polymer donor) as well as all-inorganic perovskite photoactive layers by a printed carbon layer and a functionalised graphite sheet in order to reach both stable (more than 60 hours) and high photocurrents ($> 9 \text{ mA cm}^{-2}$ and $> 15 \text{ mA cm}^{-2}$, respectively). We have developed perovskite photoelectrodes using a low annealing temperature carbon paste with tuned energy level CsPbBr_3 photoactive layer. The effect of 2-dimensional (CsPb_2Br_5) and 0-dimensional (Cs_4PbBr_6) perovskite phases on efficiency and stability will be discussed including ways to control their formation. Photoanodes with stable photocurrents applying the currently best performing organic bulk-heterojunction non-fullerene acceptor photoactive layers will also be presented with particular focus on the role of NiFeOOH co-catalyst. We will share our most recent results towards reaching – instead of the often-reported hours-long – several days long stability at high photocurrent densities close to and above the current state-of-the-art levels.

EN02.03.09

Co-Evaporation and Characterization of Tin Based Perovskite Films For Solar Cell Applications [Joana A. Ferreira Machado](#), Jeremy G. Hiculle, Muhammad U. Farooq, Ajay Singh and Alex Redinger; University of Luxembourg, Luxembourg

Organic-inorganic halide perovskite solar cells have shown a promising increase in power conversion efficiency over the past decade, reaching over 25.5% [1]. Given their low-cost synthesis, perovskites are ideal candidates for the next generation thin film photovoltaics [2]. Nevertheless, the commercialization of this solar cell technology is hindered by the presence of lead in the most efficient halide perovskites, which raises health and environmental concerns [3]. Tin based perovskites are very promising alternatives to the mainstream Pb containing perovskites since they exhibit a lower bandgap, which is closer to the ideal value for single junction devices and they can be used as bottom cells in all perovskite tandem devices [4]. However, they are at present not as efficient and suffer from fast degradation.

In order to make Sn based perovskites a real alternative to the Pb based ones, a thorough understanding of the growth process is indispensable. Here, in order to prevent oxidation, we grow methylammonium tin tri-iodide ($\text{CH}_3\text{NH}_3\text{SnI}_3$) by co-evaporating tin iodide (SnI_2) and methylammonium iodide ($\text{CH}_3\text{NH}_3\text{I}$). We discuss in detail how the growth parameters affect the crystalline structure and the optoelectronic properties of $\text{CH}_3\text{NH}_3\text{SnI}_3$. We show that the $\text{SnI}_2/\text{CH}_3\text{NH}_3\text{I}$ ratio during growth enables to manipulate the texture of the films. Photoluminescence measurements link the changes in crystal structure to the optoelectronic properties of the films.

In addition, we show via X-ray photoelectron spectroscopy (XPS) that the co-evaporated films are free of tin in the +4-oxidation state (Sn^{4+}), contrarily to other methods reported in literature [5-6]. The presence of Sn^{4+} is often linked to the decrease in power conversion efficiency of the tin perovskites due to self-doping [7]. Thus, by avoiding this secondary phase completely, the stability is improved [8]. We show that the absence of oxygen during the whole process is absolutely crucial since films with small amounts of oxygen detected in the XPS spectra, also showed a Sn^{4+} secondary phase. This result provides evidence that the presence of Sn^{4+} in the perovskite films is directly linked to the presence of oxygen.

We use Kelvin Probe Force Microscopy in ultra-high vacuum to assess the local variations in work function. Both the topography and the workfunction maps are smooth and we do not find a prominent grain boundary contrast. A comparison of the workfunction inhomogeneities to other perovskites allows us to conclude that the Sn based perovskites are very homogeneous, which is important for the development of high-performance extraction layers.

[1] H. Min *et al.*, *Nature*, 2021, **598**, 444.

[2] M.A. Green, A. Ho-Baillie, H.J. Snaith, *Nature Photonics*, 2014, **8**, 506.

[3] T. Miyasaka *et al.*, *Advanced Energy Materials*, 2020, **10**, 1902500.

[4] C. Mortan *et al.*, *Physica Status Solidi (A) Applications and Materials Science*, 2019, **216**, 1900209.

[5] N. Balachandran *et al.*, *Journal of Alloys and Compounds*, 2021, **879**, 160325.

[6] Z. Dai *et al.*, *Science China Materials*, 2021, **64**, 2645.

[7] L. Lanzetta *et al.*, *Nature Communications*, 2021, **12**, 2853.

[8] A. Singh *et al.*, under review.

EN02.03.10

Hierarchically Ordered Perovskites with High Photo-Electronic and Environmental Stability via Nanoimprinting Guided Block Copolymer Self-Assembly [Hyowon Han](#), Hyeokjung Lee, Jin Woo Oh, Jihe Jang and Cheolmin Park; Yonsei University, Korea (the Republic of)

The development of a sub-50 nm nanopattern of a thin perovskite film is of significant interest with its excellent photo-electronic properties and environmental stability. By employing nanoimprinting of a moldable perovskite precursor self-assembled with a block copolymer, a thin perovskite nanopattern with excellent photo-electronic stability is developed over a large area. Approximately 40 nm nanodomains consisting of perovskite crystals 10 nm in diameter are templated in the block copolymer, and the registry of the perovskite nanodomains is further guided by the topological pattern with a periodicity of a few hundred nanometers. This method can produce hierarchically controlled nanostructures of the perovskites from molecular crystals to self-assembled domains with tens of nanometer scale and patterned structures of a few hundred nanometers. With an ultrathin top skin layer on a patterned perovskite/block copolymer film developed during the nanoimprinting, the hierarchically ordered perovskite is environmentally stable in ambient conditions over 100 days with its photoluminescence quantum yield of approximately 28 %. Furthermore, the enhanced photoconduction of the perovskite nanocrystals hierarchically structured in the nanopatterns allows for developing the arrays of photodetectors with long-term environmental stability over 90 days.

EN02.03.11

Air and Oxygen Stable Core/Shell Perovskite Nanocrystals for Deep-Blue LED Application [Yongju Hong](#) and Kwangyeol Lee; Korea University, Korea (the Republic of)

The visualization of accurate color information using metal halide perovskites has been explored recently with great fervor, because of their superior optical properties such as high photoluminescence quantum yield (PLQY), and excellent color purity, and facile bandgap tunability. The achievement of white light and accurate color renderings in real-world applications requires the development of efficient and stable perovskite light-emitting diodes to overcome their inherent instability. The cesium lead mixed-halide perovskite nanocrystal system in the form of a well-tailored core/shell structure with a semiconductor shell offers a pathway toward highly stable perovskite-based displays. However, it remains challenging to access the epitaxially well-tailored core/shell architecture because of the limited methodology. Here, we present a systematic strategy for preparing a uniform perovskite core with an epitaxially grown semiconductor shell. We found that post-synthetic treatment is effectively passivating surfaces by defect elimination in the crystalline structure, thereby facilitating the epitaxial growing of the shell and significantly improving the intrinsic stability with high luminescence efficiency. We constructed the perovskite-based light-emitting diodes (LEDs) that exhibit superior external quantum efficiency (EQE) and luminance, representing a performance superior to that of state-of-the-art deep-blue perovskite-LEDs. We anticipate that our core/shell perovskite deep-blue light-emitting devices can greatly facilitate the development of electroluminescent full-color displays using perovskites.

EN02.03.12

Lighting Beyond Blue—Violet Metal Halide Perovskite Light-Emitting Diodes [Manchen Hu](#) and Daniel Congreve; Stanford University, United States

Ultraviolet and violet wavelengths of light are widely used in sterilization (e.g. food, medical equipment), sensing (e.g. gases, fluorescent labels), manufacturing (e.g. 3D printing, lithography), and other applications. However, the commercial violet and ultraviolet light-emitting diodes (LEDs) are based on InGaN/GaN/AlGaN materials grown via metal-organic chemical vapor deposition (MOCVD). This complex fabrication process uses toxic and explosive precursor gases (e.g., $\text{Al}(\text{CH}_3)_3$, $\text{Ga}(\text{CH}_3)_3$) while also requiring high temperatures and high vacuum. In order to increase the viability of UV and violet light-based technologies, it is crucial to explore cheaper and simpler alternatives to this current state-of-the-art. Metal halide perovskite LEDs (PeLEDs) have emerged as promising candidates for next-generation lighting technology, distinguished by high external quantum efficiency (EQE), high emission color purity and tunability, cheap facile solution processability. By rational engineering the perovskite crystallization during spin coating deposition, we have considerably improved the uniformity of 2D perovskite thin films, which leads to a fivefold increment of EQE over the control LED devices. Our PeLEDs emit violet light with a peak at 408 nm and exhibit a champion EQE of 0.41%. We believe this work reveals the strong potential of PeLEDs for violet emission, while simultaneously suggesting a new and simpler pathway towards realizing cost-effective UV LEDs based on metal halide perovskites.

EN02.03.13

On-Demand, 3D Printed Perovskite Nanolasers Shiqi Hu and Ji Tae Kim; The University of Hong Kong, Hong Kong

Inorganic metal halide perovskites are emerging as promising optoelectronic materials due to their strong, tunable, and high-color-purity photo- and electroluminescence, and solution processability¹⁻³. Recently, extensive research has been made to utilize perovskite nanowires as lasers due to their structural benefits such as ultra-compact sizes, highly localized coherent output, and efficient waveguiding^{4,5}. The current fabrication of perovskite nanowires relies on electron beam lithography, photolithography, chemical vapor deposition, solution-phase synthesis, and nanoimprinting. That is to say, these processes are energy- and labor-intensive, which is in stark contrast with the industrial low-cost requirements. Furthermore, technological challenges associated with individual tailoring of nanowire dimensions remain unresolved, making it difficult to manipulate stimulated emission characteristics at the single nanowire level. A new method that can fabricate perovskite nanowires with programmed shape, dimension, and placement is in great demand for addressing the abovementioned issue.

Here, we demonstrate an electrohydrodynamic (EHD) 3D printing of perovskite nanowires for high-performance bespoke lasers. The printed perovskite nanowire presents a two-photon pumped Fabry-Pérot (FP) mode lasing. By adjusting the height of a freestanding nanowire at will, we are able to select the lasing mode and also control the lasing threshold and mode spacing ($\Delta\lambda$). On this basis, we successfully demonstrated the 3D printed nanowires arrays for multi-level anti-counterfeiting security labels by storing information in the cavity-height-dependent features such as the lasing threshold and mode spacing ($\Delta\lambda$), which are unclonable. It is also worth mentioning that the advanced features of our technique such as maskless operation and low-cost production with high stability make it an effective platform to bring the proof-of-concept demonstration into practical commercial application. Likewise, these outcomes not only give us inspiration for the function-oriented design of the nanolaser-based devices but also facilitate the development of high-performance perovskite-based photonic anti-counterfeiting applications. Last but not least, our method could provide an excellent platform to construct scalable, on-demand laser-based photonic devices.

1. Stranks, S. D. *et al.* Electron-hole diffusion lengths exceeding 1 micrometer in an organometal trihalide perovskite absorber. *Science* (80-.). **342**, 341–344 (2013).
2. Braly, I. L. *et al.* Hybrid perovskite films approaching the radiative limit with over 90% photoluminescence quantum efficiency. *Nat. Photonics* **2018** *12*, 355–361 (2018).
3. Lin, K. *et al.* Perovskite light-emitting diodes with external quantum efficiency exceeding 20 percent. *Nat.* **2018** *5627726* **562**, 245–248 (2018).
4. Chen, M. *et al.* 3D Nanoprinting of Perovskites. *Adv. Mater.* **31**, 1–8 (2019).
5. Chen, M. *et al.* Three-Dimensional Perovskite Nanopixels for Ultrahigh-Resolution Color Displays and Multilevel Anticounterfeiting. *Nano Lett.* **21**, 5186–5194 (2021).

EN02.03.14

Dry, Fast and Low-Cost Synthesis Method for Polymer Encapsulated Halide Perovskite Color Converters Bas A. Huisman and Henk J. Bolink; University of Valencia, Spain

Halide perovskites are an interesting candidate for high-end color converters due to their outstanding optical properties¹⁻³. One of the reasons these perovskite color converters are not yet commercialized is due to a lack of fabrication processes which meet the industry standards such as scalability, low cost synthesis and high performance end product. In this talk an easy method to fabricate high luminescent (PLQY>50%) color pure (FWHM~20nm range) halide perovskite color converters is presented. Additionally, the color converters show air stability and temperature stability at 85°C in inert atmosphere for at least a month. The outstanding stability is due to the encapsulation of the perovskite particles with a desired polymer. The fact that the whole process is a dry synthesis technique, there are no difficulties in using additives, different polymers or perovskites. To show the possibilities of this method, MAPbBr₃ with an additive of amantadine hydrochloride is synthesized by dry mechanochemical synthesis together with a desired polymer (here, PMMA, PS and PEO are researched)⁴. The powder is then heated to the glass temperature of the polymer and pressed into a color converter within a couple of seconds. This dry process makes it possible to accurately adjust and change compositions. As a proof of concept a multiple compound color converter, by introducing an extra light emitting polymer (RedF) into the powder, reveals that it is possible to produce a single layer color converter which convert blue light to red and green. The possibility to use one layer to convert both colors, instead of the normally used double layer, reduces the fabrication costs even more and reveals the flexibility of the process. Due to the conditions of this process method and the properties of the color converters, this work shows an interesting route towards synthesis process of polymer embedded halide perovskite color converters for industrialization.

[1]. Deschler, F.; Price, M.; Pathak, S.; Klintberg, L. E.; Jarausch, D.-D.; Hügler, R.; Hü, S.; Leijtens, T.; Stranks, S. D.; Snaith, H. J.; Atati, M.; Phillips, R. T.; Friend, R. H. 1421–1426 *J. Phys. Chem. Lett.* **2014**, *5*, 57. <https://doi.org/10.1021/jz5005285>.

[2]. Protesescu, L.; Yakunin, S.; Bodnarchuk, M. I.; Krieg, F.; Caputo, R.; Hendon, C. H.; Yang, R. X.; Walsh, A.; Kovalenko, M. V. 3692–3696 *Nano Lett* **2015**, *15*, 25. <https://doi.org/10.1021/nl5048779>.

[3]. Song, Z.; Zhao, J.; Liu, Q. Luminescent Perovskites: Recent Advances in Theory and Experiments. *Inorg. Chem. Front.* **2019**, *6*, 2969. <https://doi.org/10.1039/c9qi00777f>.

[4]. Martínez-Sarti, Laura, et al. "Dry mechanochemical synthesis of highly luminescent, blue and green hybrid perovskite solids." *Advanced Optical Materials* **8.4** **2020**: 1901494.

EN02.03.15

Vapor Transport Co-Deposition of Perovskite Photovoltaics Tamar Kadosh, Ella Wassweiler, Harry Tuller and Vladimir Bulovic; Massachusetts Institute of Technology, United States

Halide perovskites have demonstrated remarkably high solar to electrical energy conversion efficiencies and are therefore of great interest for rapid commercialization. Popular solution-based fabrication routes do not lend themselves to rapid scale, up as required. Vapor Transport Deposition (VTD) is beginning to be considered a readily scalable, low-cost technique alternative method for perovskites production. Vapor-based processes promise to overcome many challenges imposed by solution-based techniques. Being solvent-free, they bypass solvent-related challenges, namely uniform coverage of large areas, chemical compatibility, and toxicity. As a low-cost alternative to thermal evaporation, VTD has the potential to deposit organic and inorganic perovskite precursor materials either sequentially or via co-deposition. Furthermore, VTD potentially offers higher tunability of deposition parameters, to enable film growth with improved composition and microstructure control.

We are currently working with a custom-made VTD system, focused on optimization of co-deposition of lead iodide and methylammonium iodide with the aid of carrier gases. We report our progress in investigating the influence of substrate and sublimation temperatures, chamber pressure, and flow rate ratios on the morphology and stoichiometry of the forming perovskite film, and in turn, its photo-active and electronic properties.

EN02.03.16

In Situ Core/Shell Perovskites for Ultra-Bright, Efficient and Stable Light-Emitting Diodes Joo Sung Kim¹, Jung-Min Heo¹, Gyeong-Su Park¹,

Seung-Je Woo¹, Changsoon Cho², Hyung Joong Yun³, Dong-Hyeok Kim¹, Jinwoo Park¹, Seung-Chul Lee¹, Sang-Hwan Park¹, Eojin Yoon¹, Neil Greenham² and Tae-Woo Lee¹; ¹Seoul National University, Korea (the Republic of); ²University of Cambridge, United Kingdom; ³Korea Basic Science Institute, Korea (the Republic of)

Metal halide perovskites are attracting great attention as next-generation light-emitting materials due to their excellent emission properties with narrowband emission. However, perovskite light-emitting diodes (PeLEDs) irrespective of their material types (polycrystalline film or nanocrystals) have not realized high luminance, high efficiency, and long lifetime simultaneously, as they are influenced by the intrinsic limitations related to the trade-off properties between charge transport and confinement in each type of perovskite materials. Here, we report bright, efficient, and stable PeLEDs made of core/shell perovskite nanocrystals obtained using a simple *in-situ* reaction. The ligand passivates the surface defect states, and thereby greatly reduces trap density in films while maintaining good charge-transport properties. Our work sheds great light on the possibility that PeLEDs can be commercialized in the future display industry.

EN02.03.17

All-in-One Process for Film-State Color Patterning of Perovskite Quantum Dot Light Emitting Diodes Junho Kim and Jung-Yong Lee; Korea Advanced Institute of Science and Technology, Korea (the Republic of)

Perovskite quantum dots (PeQDs) are promising material for next-generation display owing to their superior optoelectronic properties. However, the multi-color patterning of PeQDs remains fundamental challenging because the PeQDs are very vulnerable for conventional patterning process containing direct exposure of ultra-violet (UV) ray, electron-beam (E-beam), or polar solvents used as developer. Furthermore, the shorter ligand exchange and halide anion exchange are required to use the PeQDs as active materials and express various emitting-light colors easily in PeQD LED devices. In this study, we propose a novel all-in-one process simultaneously exchanging ligands and halide anions in film-state for enhancing the LED performance, converting emitting-light color, and patterning of cesium lead halide PeQD LEDs for full-color display.^[1] The proposed all-in-one process significantly enhanced the performances of PeQD LEDs by passivating the PeQDs with shorter ligands. The dense passivation with shorter ligands also enhanced the chemical stability of PeQDs. In addition, we fabricated red (R), green (G), and blue (B) LEDs with extremely narrow emission spectra using cesium lead bromide PeQDs and appropriate butylammonium halide solution. Furthermore, the proposed all-in-one process in film-state facilitated rapid color change in localized areas, thereby aiding in realizing fine patterns of narrow widths (300 μm) using simple contact masks. Consequently, the all-in-one process made it possible to from the multi-color patterning without direct exposure of UV ray, E-beam, and developer to PeQD films. Finally, we can fabricate various R/G/B multi-color patterning electroluminescence (EL) LED devices such as R/G/B pixels in a substrate, one pixel containing R/G/B colors between a pair of electrodes, and word-patterned (“KAIST”) LEDs, using the all-in-one process.

[1] J. Kim, K.-W. Seo, S. Lee, K. Kim, C. Kim, and J.-Y. Lee, *Adv. Sci.*, 2022, 9, 2200073.

EN02.03.18

A Novel Strategy for Preparing Chiral Perovskite Nanocrystals with High Chiroptical Activity and Stability Based on Self-Assembly of Achiral Block Copolymer Minju Kim¹, Jiweon Kim¹, Jieun Bang¹, Yu Jin Jang², JaeHong Park¹ and Dong Ha Kim¹; ¹Ewha Womans University, Korea (the Republic of); ²Research Center for Energy and Environmental Sciences, Sungkyunkwan University, Korea (the Republic of)

Chiral hybrid halide perovskites have emerged as promising candidates in next-generation optoelectronic and spintronic applications due to their remarkable chiroptical and electrical properties. However, designing chiral perovskite nanocrystals (NCs) that exhibit high stability as well as outstanding chiroptical performance under ambient condition remains a challenge. In this study, we present a novel and facile strategy to fabricate chiral perovskite NCs based on block copolymer inverse micelles with supramolecular chirality obtained by self-assembly of optically-inactive building blocks, polystyrene-*block*-poly(2-vinyl pyridine) (PS-*b*-P2VP) and DL-alanine (DL-ala). The selective incorporation of perovskite precursors within the confined chiral micellar cores enables effective chirality transfer to the electronic states of perovskite NCs, leading to high chiroptical response at the bandgap with an anisotropy factor of -2.0×10^{-4} , similar to that of chiral octylamine-capped perovskite NCs. In addition, the robust surface passivation of perovskite NCs by PS-*b*-P2VP/DL-ala inverse micelles protects NCs from moisture, heat, and air more efficiently than neat PS-*b*-P2VP inverse micelles, manifesting long-term stability in harsh conditions and long fluorescence lifetime. This approach can not only realize large-scale and low-cost fabrication of chiral perovskite nanostructures but can also be extended to the advanced engineering of chiral perovskite nanostructures by judiciously adjusting block copolymer self-assembly.

EN02.03.19

Low-Dimensional Bismuth and Copper Halide Perovskites for Multilevel Resistive Switching Memory So-Yeon Kim and Nam-Gyu Park; Sungkyunkwan University, Korea (the Republic of)

Here, we report low-dimensional halide perovskite having bismuth or copper metal ion for multilevel resistive switching memory. Layered double perovskite with chemical formula of $\text{BA}_2\text{CsAgBiBr}_7$ was synthesized by phase conversion of 3D $\text{Cs}_2\text{AgBiBr}_6$, which showed endurance of 1,000 cycles and retention time over 2×10^4 s at operational voltage as low as 0.5 V, along with ON/OFF ratio as high as $\sim 10^7$. The ON/OFF ratio of 2D Ag-Bi system was five orders of magnitude larger than those of 3D counterparts. Modification of Schottky conduction at high resistance state (HRS) is found to be responsible for high ON/OFF ratio in 2D structure. 2D $(\text{BzA})_2\text{CuBr}_4$ (BzA = benzylammonium) perovskite was synthesized on Pt substrate, which delivered higher ON/OFF ratio over 10^8 even at lower operational voltage around +0.2 - -0.3 V. Longer endurance of 2,000 cycles was observed with similar Schottky conduction at HRS. A thin film less than 1 micrometer was applied to the low-dimensional $\text{Cs}_3\text{Bi}_2\text{Br}_9$, where synthetic $\text{Cs}_3\text{Bi}_2\text{Br}_9$ powder precursor enabled uniform thin film formation. A bipolar resistive switching behavior was observed. Thin film exhibited reliable cell-to-cell and device-to-device resistive switching behavior. The studied low-dimensional bismuth and copper based halide perovskites showed much better stability under high humidity and at elevated temperature than the 3D and/or lead-based counterparts, which is beneficial for practical applications.

EN02.03.20

Achieving 9.16% Applied Bias Photon-to-Current Efficiency with Monolithic Lead Halide Perovskite Photoelectrochemical Cell Tae Gyun Kim and Jong Hyeok Park; Yonsei University, Korea (the Republic of)

Solar-to-hydrogen conversion from water splitting is of great interest and photoelectrochemical (PEC) cell water splitting is one of the notable technologies for H_2 production. To commercialize PEC water splitting, highly efficient photoanode materials are the governing key factor. Recently, organic-inorganic lead halide perovskite (LHP) materials have emerged as a promising alternative that can overcome the drawbacks of metal-oxide-based photoelectrodes because of their excellent optoelectronic properties such as broad photoresponse range in the solar spectrum, bandgap tunability, and low exciton binding energy. Although LHP-based solar cells can be externally applied to water electrolysis for solar-to-hydrogen conversion, an LHP device with a monolithic configuration for PEC cells is more economically ideal for viable hydrogen production. Herein, we report monolithic PEC cells with a double-cation perovskite solar cell (PSC) connected to a robust 3D oxygen evolution reaction (OER)

catalyst using conductive carbon powders (CCP). CCP has superior conductivity for efficient charge transfer from LHP-based solar cells to OER catalysts. Surprisingly, LHP devices physically interconnected with the OER catalyst by CCP show almost zero current and voltage loss. To achieve an efficient and stable performance in the LHP photoanode, the individual efficiencies and stabilities of the two parts (PSC part and OER catalyst part) should be guaranteed. First, efficiency and stability of the PSC part can be improved by modifying LHP layer. We introduced a smaller cation (methylammonium, MA) to the FAPbI_3 (formamidinium, FA) lattice to stabilize the α -phase by enhancing hydrogen bonding between FA and the PbI_6 octahedron. It was confirmed by UV-vis absorption spectra, X-ray diffraction (XRD), and X-ray photoelectron spectroscopy (XPS). At OER catalyst part, we applied 3D-structured NiFe to an Ni foil substrate to increase the catalytic activity and stability. The 3D porous architecture improves the catalytic activity and stability by facilitating holes supplied from the PSC and increasing the electrochemically active surface area. Finally, integrating optimized PSC part and OER catalyst part, the LHP photoanode exhibits 0.56 V onset potential and a maximum photocurrent density of 24.26 mA/cm^2 at 1.23 V_{RHE} (reversible hydrogen electrode (RHE)), with a 9.16% applied bias photon-to-current efficiency. We further achieve an enhanced stability of 48 h in pH 14 aqueous solution under simulated solar light (1 sun). In summary, we fabricated an LHP-based photoanode using inexpensive CCP as an electrical connector between PSCs and OER catalyst. CCP not only has great conductivity for efficient charge transfer but also is economical for wide deployment. Additionally, we stabilized PSC by using double-cation LHP and optimized the OER catalyst by forming a 3D structure NiFe on the Ni foil. Our LHP photoanode exhibited remarkable performance and durability under continuous illumination in an aqueous electrolyte. We believe that these findings demonstrate the potential of LHP photoanodes with CCP for the future development of low-cost, high-performance, and stable monolithic devices.

EN02.03.21

Scalable Fabrication of High-Performance Perovskite Solar Modules and Their Application to High Power Output Solar Charging Batteries Young Yun Kim, Se-Hee Kim, Nam Joong Jeon and Jungdon Suk; Korea Research Institute of Chemical Technology, Korea (the Republic of)

Rapid climate change and increasing global power demands require active implementation of transition of traditional power sources to renewable energy sources. Perovskite solar cells (PSCs) have been of great interest due to the inherent superior optoelectronic properties of organometallic halide perovskite itself, such as high absorption coefficient, long carrier diffusion length, ambipolar charge transport and solution-processability. Over 25 % of power conversion efficiency (PCE) has been achieved recently for PSCs via composition engineering, optimization of interlayer, and defect management. Aside from the high PCE, the fabrication of PSCs by scalable process in large-area is prerequisite for the PSCs to fully utilize the aforementioned advantages, so to be applied to self-powered personal mobility and electronics, smart textiles, custom-shaped building-integrated photovoltaics, and so on.

Several successful demonstrations of scalable production of PSCs have been reported. However, successful demonstration of fully scalable production of large-area perovskite solar modules (PSMs) is still lacking. The major hurdles to be jumped are uniform wet-film formation via scalable process in large-area, and complete phase conversion of perovskite precursor to photoactive phase. Therefore, reliable scalable production methods should be established including wet-film formation and phase conversion steps.

In addition, the direct integration of energy generation and storage devices have attracted a lot of interest recently in order to correspond to the fluctuation of power input from the Sun and increasing demand for self-powered electronics. However, inherent mismatch of voltage and current range for charging and discharge from PSCs to Li-based batteries is a major obstacle to realize the direct integration between them. Additionally, power output from PSCs under continuous light illumination, and storage capacity from charging-discharging cycles from Li-ion batteries should be retained.

In this work, we successfully demonstrate high-performance PSMs and solar charging batteries by integrating PSMs and Li-ion batteries in a single substrate. All the layers constituting PSMs can be fabricated via solution shearing coating, with optimized rheological and interfacial properties, at a low temperature ($<160^\circ\text{C}$). An electron transporting layer (ETL) is designed to be uniform and compact in large-area, by systematically investigating the effect of leaving group in sol-gel precursor and applying an optimal tin precursor with organic crosslinkers. As a result, high-efficiency over 23% can be achieved, retaining over 80% relative efficiency compared to initial one after over 1000 h. Complete conversion of perovskite precursor to photoactive phase in a large area can be achieved via careful selection of proper antisolvent and bathing in it. PSMs are carefully designed to have a proper area and structure to exactly match the charging voltage-current range of high-capacity Li-ion batteries. Consequently, over 20% efficiency of PSMs and over 14% of overall charging to storage efficiency can be achieved. The photo-charging can be repeatedly conducted over 30 cycles because of stable power output and storage of integrated PSMs and Li-ion batteries.

Ref 1. Young Yun Kim *et al.*, *Nat. Commun.* **11**, 5146 (2020)

EN02.03.22

Green Non-Toxic Cs_3MnBr_5 Phosphor Using Silicon Nitride Nanofilters Using Nanoimprinting Minji Ko, Hyeng Jin Kim, SeungJe Lee, Eunha Hong, Keyong Nam Lee and Young Rag Do; Kookmin University, Korea (the Republic of)

In this study, we tried to reduce impure phases in nonstoichiometric compositions of non-toxic green Cs_3MnBr_5 by using various filtration processes to remove nano and microscale impurities ($> 200\text{nm}$) dissolved in reaction solutions and to induce precipitation of impure phase after crystallization. Green Cs_3MnBr_5 phosphors were synthesized using purified reactant solutions, which filtered with silicon nitride nanofilters through water-based evaporative crystallization. To improve photoluminescence quantum yield (PLQY) of green Cs_3MnBr_5 phosphors, it is necessary to reduce reactant solution impurities such as manganese oxide and undissolved precursors. Therefore, reactant solutions were filtered through silicon nitride nanofilters that included nanopore pattern silicon nitride nanofilters successfully-realized by nanoimprint lithography and etching process on 6 inch Si wafer. The reactant solutions of green Cs_3MnBr_5 phosphors were filtrated using fluid devices with built-in silicon nitride nanofilters with nanopore size adjusted from 50 nm to 200 nm via deposition of Al_2O_3 to increase PLQY. Finally, PLQY of green Cs_3MnBr_5 phosphors synthesized using 50 nm nanopore size silicon nitride nanofilters is 2.3 times higher than that of non-filtrated green Cs_3MnBr_5 phosphors. Therefore, synthesized green Cs_3MnBr_5 phosphors have potential for application to lighting devices and photovoltaic, and other fields. Also, SiN_x nanofilters using nanoimprint lithography have potential for application to chemical purification, biological purification, and other fields.

EN02.03.23

High Luminescence and Efficiency in Perovskite Quantum-Dots -Embedded Thin Film or Fiber Membranes for Light-Emitting Diodes Chi-Ching Kuo, Wei-Cheng Chen and Dai-Hua Jiang; Institute of Organic and Polymeric Materials Department of Molecular Science & Engineering, National Taipei University of Technology, Taiwan

Perovskite quantum dots (PeQDs) have been under commercial and functional development in recent years since they offer outstanding optoelectronic properties and solution processability. However, both insulating ligands around PeQDs and instability impair the performance of photoelectronic devices. Therefore, we introduce multi-step ligands exchange by silver (Ag)- trioctylphosphine (TOP) as short alkyl ligands to reinforce the optical properties and stability for PeQDs and successfully elevated light-emitting diodes characters. The PeQDs with Ag-TOP ligands (Ag@QD) perform higher

photoluminescence quantum yield (PLQY, ~93%), higher exciton binding energy (57.6 meV) with better solvent, temperature, and ambient stability over 1 month presenting better performances on comparison with conventional di-dodecyl dimethyl ammonium bromide (DDAB) or TOP ligands. Nuclear magnetic resonance (NMR), X-ray photoelectron spectroscopy (XPS), and time-resolved photoluminescence (TR-PL) measurement provides clear insight on bilateral affinity in Ag@QD illustrating excellent defect passivation and appropriate steric hindrance. Furthermore, we demonstrate Ag@QD with lower turn-on voltage (~2.8 V), high electroluminescence (~3820 cd/cm²), and high efficiency (EQE ~9.43%). Furthermore, PeQDs with excellent intrinsic properties have been employed universally in optoelectronic applications but undergo hydrolysis even when exposed to atmospheric moisture. In the present study, composite CsPbX₃ (X = Cl, Br, and I) PeQDs were encapsulated with stretchable [poly(styrene-butadiene-styrene); SBS] fibers by electrospinning to prepare water-resistant hybrid membranes as multicolor optical active layers. Brightly luminescent and color-tunable hydrophobic fiber membranes (FMs) with PeQDs were maintained for longer than 1 h in water. A unique remote FMs packaging approach was used in high-brightness perovskite light-emitting diodes.

EN02.03.24

Enhancing Charge Diffusion Length by Pyrene Incorporation in Multi-Cation Halide Perovskites [Yu Jin Lee](#), Taehee Kim, Jung Hwan Lee, Jong Hyeok Park and Dongho Kim; Yonsei University, Korea (the Republic of)

Multi-cation halide perovskites are gathering attention with remarkable optoelectronic properties as materials for light-harvesting and light-emitting applicants. This study suggests strategies to achieve device stability and long carrier diffusion length, which are essential properties in optimizing perovskite device performances. Pyrenes are planar conjugated systems and strong electron donors at the same time, thus can effectively passivate defects at grain boundaries. Due to the large size difference with cations, pyrenes are selectively located in grain boundaries and employed as pi-conjugated bridges to interconnect the adjacent grains. We incorporated pyrene in the precursor with anticipating the effects of suppressing ion migration within the perovskite film and assisting charge carrier transport. Aided by confocal fluorescence lifetime imaging microscopy (FLIM), distribution of photoluminescence (PL) lifetime and charge carrier diffusion dynamics were directly visualized in space and time in pyrene incorporated multi-cation halide perovskites. We suggest that the addition of pyrene precursors reduces spatial energetic disorder at the perovskite surface.

Pyrene is found to enhance emission and increase the PL lifetime at the grain boundaries. A smaller deviation in grain-to-grain emissivity and a more uniform spatial distribution of PL lifetime at the perovskite surface are observed, suggesting reduced grain boundary defects. We also spatiotemporally analyzed the exciton population evolution to study the improvement in diffusion dynamics with pyrene incorporation. Using the trap-state limited diffusion model equation, we tracked the turnover from the normal diffusion and trap-state limited transport regime. Trap depth can be estimated using the Boltzmann relation and can be correlated with diffusion properties. The reduction of trap density by pyrene precursor addition expedites the charge carrier transport and allows longer diffusion length. Pyrene incorporation especially boosted free exciton diffusivity. Thus, diffusivity and charge diffusion length of optically excited states are greatly enhanced to over 1 μm.

[1] Saidaminov, M.I. et al. Multi-cation perovskites prevent carrier reflection from grain surfaces. *Nat. Mater.* **19**, 412–418 (2020).

[2] Álvarez, S.G. et al. Charge Carrier Diffusion Dynamics in Multisized Quaternary Alkylammonium-Capped CsPbBr₃ Perovskite Nanocrystal Solids. *ACS Appl. Mater. Interfaces.* **13**, 37, 44742–44750 (2021).

[3] Seitz, M. et al. Mapping the Trap-State Landscape in 2D Metal-Halide Perovskites Using Transient Photoluminescence Microscopy. *Adv. Optical Mater.* **9**, 2001875 (2021).

EN02.03.26

Lead-Free Double Perovskites—Cs₂Na_{1-x}Ag_xIn_{1-y}Bi_yCl₆ as a Warm White Light Emitter with Unit Efficiency [Daniela Marongiu](#)¹, Fang Liu¹, Angelica Simbula¹, Stefano Lai¹, Luyan Wu¹, Qingqian Wang², Riccardo Pau^{1,3}, Selene Matta¹, Federico Pitzalis¹, Alessio Filippetti¹, Francesco Quochi¹, Michele Saba¹, Andrea Mura¹ and Giovanni Bongiovanni¹; ¹Università di Cagliari, Italy; ²Southern University of Science and Technology, China; ³University of Groningen, Netherlands

Double perovskites have been developed to alternatively replace the divalent cations Pb²⁺ in single perovskite with a combination of a monovalent and trivalent cation, forming structure as A₂BB'X₆. Among them, the compounds Cs₂Na_{1-x}Ag_xIn_{1-y}Bi_yCl₆ can emit warm white light with almost unity quantum efficiency and are thus among the most promising materials for solid-state lighting (1). The emission spectrum is attributed to self-trapped excitons (STEs), the emission efficiency is, however, sensitive to the material composition since it is strictly related to the simultaneous presence of a small percentage of Ag and Bi.

Whether Bi atoms cure extrinsic defects or provide natural recombination centers is still a wide-open question while the addition of Ag has been linked to parity breaking in valence band orbitals, increasing the oscillator strength of the interband optical transitions (2,3).

A comprehensive understanding of the microscopic mechanisms producing the rules for efficient emission is fulfilled by a systematic study of the structural and optical properties as a function of the composition to understand the role of Ag and Bi in the high efficiency emission. Photoluminescence quantum yield (PLQY) measurements are complemented with photoluminescence excitation (PLE) and ultrafast spectroscopy in the form of differential transmission (DT/T) and time-resolved photoluminescence (TRPL). The dynamic of optical excitation is studied to investigate the formation of STEs and their decay times.

Ag atoms are found to promote the formation of STEs that then produce efficient emission. The radiative recombination of STEs is instead favored by the presence of at least 0.1% Bi inhibiting trapping of optical excitations in long-lived, dark STEs thus achieving emission efficiency near unity with a warm white light spectrum in a wide variety of compositions.

Double perovskites realize therefore an almost ideal platform for solid state lighting and these results provide guidance for rational optimization of such compounds in view of the use as phosphors and active materials for LEDs and displays.

References

F. Liu, et al. *EcoMat.* (2020), 2:e12017.

J. Luo, et al. *Nature* (2018), 563, 541–545

M. Ghasemi et al. *Nanophotonics* (2021), 10(8): 2181–2219

EN02.03.27

Ion-Migration-Induced Degradation of Flexible Perovskite Module Under Working Condition [Jiyeon Nam](#), Wonkyu Lee, Hae-Seok Lee, Donghwan Kim and Yoonmook Kang; Korea University, Korea (the Republic of)

In this study, perovskite modules were fabricated on PET flexible substrates. Perovskite light-absorbing layers and ETL (electron transfer layer, SnO₂) are coated using the blade-coating method. The HTL (hole transfer layer, spiro-OMeTAD) layer is spin-coated. The electrodes are deposited by the thermal evaporation method. All patterns are scribed by laser. Modules consist of 10 sub-cells and their area is 5*5cm². Modules used in the experiment are distinguished from the perovskite solar cells fabricated on a rigid substrate like glass in which sub-cells are connected monolithically and patterned. Also, there exist lots of fractures on the modules due to the tensile stress originating from the flexible substrates. In P2, where the Au electrode and perovskite are directly contacted, the decomposition of perovskite and migration of ions occurs. Near the fractures, deep-level defects exist as they do at grain boundaries, where they act as ion transfer channels. Under working conditions with light and electric fields, degradation in the fractures and near the patterns are analyzed. This degradation causes the decomposition of perovskite and the movement of ions, and prevention strategies are needed for the commercialization of modules.

The initial efficiency of the module was 11.03% with 10.3V Voc, Jsc of 1.76mA/cm². Maximum power point (MPP) is tracked in ambient air. The temperature was kept around 33 C and the humidity was maintained below 40%. The modules encapsulated with diffusion barriers were placed under 1 sun illumination. After 25 hours of MPPT, the efficiency decreased to about 50% of the initial efficiency.

We acquired Electro-luminescence (EL) images before and after MPPT and intensities of EL decreased around fractures and P2 patterns. Non-radiative recombination sites can be distinguished from EL images where ion migration occurs followed by the decomposition of perovskite layers.

The series resistance has increased significantly, due to the increase in non-conductive materials such as PbI₂, the byproduct of perovskite layer decomposition. In addition, the shunt resistance decreased slightly, which shows a similar tendency to lock-in thermography (LIT) results. A thermal imaging camera attached to the LIT system senses the Joule heat from the shunt. The number of heating points and their temperature increased. Finally, the element distribution of the module along the depth direction was measured through SIMS analysis. The measurements were performed on the fresh and 25hr-worked modules. Depth profiles are acquired from the neat site, near pattern, and at fractures.

Near the pattern, the intensity of Au was higher than that of the neat area. This shows that Au has diffused from P2 and the top electrode. In the case of fracture, Au was already diffused along with the depth before MPPT, and it spread more after MPPT. Also, the I-2 peak has broadened, which is the result of the decomposition of perovskite.

By comparing the cells with and without applied voltage under light, it is found that the driving force of ion migration is the electric field across the module. In this way, perovskite decomposition and ion diffusion around the pattern and fracture cause changes in Voc and Jsc as well as Rsh and Rs, and affect module stability. In future work, to suppress the ion migration, deposition of the diffusion barrier layer and reforming of HTL and perovskite will be conducted.

EN02.03.28

Defect Passivated All-Inorganic Perovskite Film by Metal-Organic Framework-Assisted Metal-Ion Doping Process for Dual-Mode Image Sensing Display Jin Woo Oh, Hyowon Han, Hyeokjung Lee, Jihye Jang and Cheolmin Park; Yonsei University, Korea (the Republic of)

Crystal engineering based on defect passivation with metal ions doped into halide perovskites is of considerable interest for tailoring the photoelectric properties of perovskites. Herein, a simple and robust approach for doping metal ions into a thin all-inorganic CsPbBr₃ perovskite film by employing metal-organic framework nanoparticles is presented. Zeolitic imidazolate framework-8 nanoparticles, which can adsorb water, are dispersed and embedded in a thin perovskite film. The particles self-decompose at a certain humidity, releasing Zn²⁺ ions into nearby perovskite crystals. The Zn²⁺ ions efficiently passivate the undercoordinated defect sites of the defective perovskite crystals, resulting in environmentally stable, and enhanced photoluminescence of the perovskite with the quantum yield of approximately 14 % more than 24 times greater than that without nanoparticles. Further, a thin Zn-doped CsPbBr₃ film is employed to fabricate arrays of ultraviolet photodetectors, and approximately 90 % of the initial photocurrent is maintained over 15 days in RH 60 %, facilitating the development of a dual-mode image sensor using which programmed images are visualized based on both photocurrent and photoluminescence.

EN02.03.29

Three-Color White Electroluminescence Emission of Perovskite Quantum Dots Mixed with Organic Emitters Hyukmin Kwon, Hayoon Lee, Seokwoo Kang, Sunwoo Park, Seong Jun Kang and Jongwook Park; Kyung Hee University, Korea (the Republic of)

To realize a full-color display in the research field of perovskites or perovskite-structured quantum dots (PeQDs), the development of white-light-emitting devices that operate by emitting light of three primary colors (red, green, and blue) has emerged as an active research topic. In the present study, we report for the first time three color white-light emission with high brightness from white-emitting PeQD organic light-emitting diodes (WPeQD-OLEDs) fabricated using a PeQD material and organic emitters. A WPeQD-OLED bilayer was prepared by depositing a blue-emitting organic layer on top of a CsPb(Br/I)₃ QD layer mixed with N⁹,N¹⁰-Bis(4-(tert-butyl) phenyl)-N⁹,N¹⁰-Di-*o*-Tolylanthracene-9,10-Diamine (*p*-Tb-*o*-Me-TAD), which were spin-coated as red and green emitters, respectively. The WPeQD-OLED device was stable during operation and demonstrated emission of three primary colors. In the WPeQD-OLED device, charge carriers were distributed by an 9-(naphthalen-1-yl)-10-(naphthalen-2-yl)anthracene (α,β -ADN) blue-emitting host material with a deep highest occupied molecular orbital level. The electroluminescence (EL) spectra of the WPeQD-OLEDs showed EL maximum peaks at 460, 527, and 640 nm; the CIE color coordinates of the emitted light were (0.33, 0.40). The EL results confirmed that the maximum luminance was 49,000 cd/m² and the maximum luminance efficiency and power efficiency were 4.48 cd/A⁻¹ and 2.16 lm/W⁻¹, respectively.

EN02.03.30

Atmospheric Humidity Underlies Irreproducibility of Formamidinium Lead Iodide Perovskites Keonwoo Park¹, Maged Abdelsamie², Ji-Sang Park³, Carolin M. Sutter-Fella² and Jin-Wook Lee¹; ¹Sungkyunkwan University, Korea (the Republic of); ²Lawrence Berkeley National Laboratory, United States; ³Kyungpook National University, Korea (the Republic of)

Atmospheric humidity has been considered as a critical factor worsening irreproducibility of the perovskite solar cells (PSCs). The institutional research laboratories, startups, and large enterprises often experience poor reproducibility of the PSC performance, resulting in stagnated development and waste of resources. From a commercial standpoint, such irreproducibility can critically impede quality control and reduce yield and profit margin of the photovoltaic modules. In this study, we reveal critical roles of atmospheric humidity in regulating the formation and crystallization of widely used formamidinium lead triiodide (FAPbI₃) perovskite by in-situ investigations under controlled atmospheric environments. We show that the humidity content during film fabrication underlies significant changes in perovskite stoichiometry, thermodynamic stability, and optoelectronic quality. Thus, well controlled humidity during fabrication of formamidinium perovskite is perhaps indispensable to reproduce phase stable and efficient FAPbI₃-based PSCs.

EN02.03.32

Advance in the Scalable Fabrication of Perovskite Solar Cells Anush Ranka, Inseok Yang, Zhenghong Dai and Nitin P. Padture; Brown University, United States

High performance lab-scale perovskite solar cells (PSCs) with power conversion efficiency (PCE) over 25% have been reported recently. However, most of the reported high-PCE devices have an active area of <0.15 cm², and spin-coating is used to fabricate the perovskite thin films and the electron- and

hole-selective transport layers. While future commercialization of PSCs requires us to move to scalable fabrication methods, an increase in sheet/series resistance, inhomogeneity of the film over large areas, loss in active area due to carrier collectors, *etc.* are inevitable in large scale PSCs. This, along with the technological barriers to entry, makes it difficult to obtain high PCE in PSCs fabricated using scalable processes. To obtain a deeper understanding of the factors that govern these shortcomings, we have investigated the effects of different parameters that need to be controlled to achieve high-quality, large-scale PSCs. We use processes such as chemical bath deposition, and nitrogen 'knife' assisted blade-coating and slot-die coating, and discuss the pros and cons of each process. We begin with controlling factors such as solution composition, nitrogen-knife pressure/speed, *etc.*, that have the biggest effects on the film quality, and then move on to other factors such as molarity, humidity, and substrate roughness, which are more relevant to the device performance. This research aspires to make scalable processes more controllable, reliable, and accessible to the PSCs community.

EN02.03.33

Low-Vacuum Conversion for Sequential Processing of Perovskite Solar Cells [Nathan Rodkey](#), Cristina Roldan-Carmona and Henk J. Bolink; Universitat de València, Spain

Vacuum-based technologies have proven to be a promising route for industrial scale production of perovskite photovoltaics, but performance is still lagging behind its solution-based counterparts. Currently, vapor-based methods such as co-evaporation struggle to grow complex perovskites (6 or more elements), being limited by the number of sources available and the ability to control them. This further limits the ability of many vacuum-based processes to introduce passivating or stabilizing agents. In particular, these are needed for the synthesis of high-efficiency low-bandgap materials (e.g. Sn/Pb) needed for perovskite-perovskite tandems or silicon-perovskite tandems. In this work, we present a conformal, low-vacuum process (1- 100 mbar) for the sequential conversion of evaporated PbI_2 thin-films or co-evaporated $\text{PbI}_2/\text{SnI}_2$ and PbI_2/CsI thin-films. The technique relies on the control of 3 crucial parameters: temperature of the source material, temperature of the substrate, and the working pressure. Using this method, we show fully converted films $>1 \mu\text{m}$ thick, with μm -sized grains for a variety of perovskite compounds: MAPbI_3 , FAPbI_3 , $\text{F}_{1-x}\text{Cs}_x\text{PbI}_3$, $\text{MAPb}_{1-x}\text{Sn}_x\text{I}_3$, and $\text{FAPb}_{1-x}\text{Sn}_x\text{I}_3$. To our knowledge, converting thick films ($>1 \mu\text{m}$) in a 2-step process in this way is previously unreported. Counter-intuitively we find that films with small grains ($<100 \text{nm}$) and PbI_2 or amorphous phases show higher photoluminescence than their large-grained counterparts ($>1 \mu\text{m}$). To circumnavigate this and grow large grains with increased photoluminescence we introduce reactive gasses and/or passivating agents during the conversion process, that appear to quench defects. This method is fully compatible with conformal growth, making it a good candidate for silicon-perovskite tandems. Lastly, these layers are reported in fully vacuum-processed devices, taking advantage of a low-vacuum (1-100 mbar), sequential process with high industrial potential.

EN02.03.34

Stable Near-to-Ideal Performance of a Solution-Grown Single-Crystal Perovskite X-Ray Detector [Kostiantyn Sakhatskyi](#)^{1,2}, Bekir Turedi³, Gebhard Matt^{1,2}, Muhammad N. Lintangpradipto³, Rounak Naphade³, Omar Mohammed³, Sergii Yakunin^{1,2}, Osman M. Bakr³ and Maksym V. Kovalenko^{1,2}; ¹ETH Zurich, Switzerland; ²Empa-Swiss Federal Laboratories for Materials Science and Technology, Switzerland; ³King Abdullah University of Science and Technology, Saudi Arabia

The ideal photodetector is the one able to detect every single incoming photon. In particular, in X-ray medical imaging, the radiation dose for patients can then approach its fundamentally lowest limit set by the Poisson photon statistics. Such near-to-ideal X-ray detection characteristics have been demonstrated with only a few semiconductor materials such as Si and CdTe; however, their industrial deployment in medical diagnostics is still impeded by elaborate and costly fabrication processes. Hybrid metal halide perovskites – newcomer semiconductors – make for a viable alternative owing to their scalable, inexpensive, robust, and versatile solution growth and recent demonstrations of single gamma-photon counting under high applied bias voltages. The major hurdle with perovskites as mixed electronic-ionic conductors, however, arises from the rapid material's degradation under high electric field, thus far used in perovskite X-ray detectors. Here we show that both near-to-ideal and long-term stable performance of perovskite X-ray detectors can be attained in the photovoltaic mode of operation at zero-voltage bias, employing thick and uniform methylammonium lead iodide (MAPbI_3) single crystal (SC) films (up to $300 \mu\text{m}$), solution-grown directly on hole-transporting electrodes. The operational device stability is equivalent to the intrinsic chemical shelf lifetime of MAPbI_3 , being at least one year in the studied case. Detection efficiency of 88% and noise equivalent dose of $90 \text{pGy}_{\text{air}}$ (lower than the dose of a single incident photon) are obtained with 18 keV X-rays, allowing for single-photon counting, as well as low-dose and energy-resolved X-ray imaging. These findings benchmark hybrid perovskites as practically suited materials for developing low-cost commercial detector arrays for X-ray imaging technologies.

EN02.03.35

Designing Perovskite Solar Cells for High-Efficiency Wireless Power Transfer [Francesco Guarnieri](#), Julia Huddy and William J. Scheideler; Dartmouth College, United States

Metal halide perovskites are a promising material system for wireless energy harvesting due to their amenability to flexible form factors offering high power per weight as well as their potential for low cost via high-speed manufacturing. We present an investigation of the performance of high-efficiency planar double cation perovskite solar cells in harvesting monochromatic illumination via Sentaurus TCAD simulations and experimental validation. We provide an examination of metal halide perovskites under a wide range LED illumination profiles in the $\mu\text{W} - \text{mW} / \text{cm}^2$ range, experimentally demonstrating a power conversion efficiency (PCE) above 37%. Our TCAD simulations provide design rules for engineering wide bandgap perovskite cells to maximize wireless power transmission (WPT) for a given monochromatic source. These results also reveal the device physics limiting efficiency for low-intensity constant illumination and very high intensity pulsed illumination profiles. Based on these results, we model perovskite solar cells' potential for high-efficiency medium to long range power transfer at 10 m – 500 m for power levels of 1 mW to 1 W, directly comparing the efficiency against alternative inductive WPT. These results suggest the promising role of perovskite solar cells in powering a more sustainable, battery-free future of the Internet of Things (IoT).

EN02.03.36

Proposal for Novel Direction of Front Transparent Electrodes Towards the Breakthrough of High-Efficiency and Stability Perovskite Solar Cells [Hae-Jun Seok](#), Su-Yeong Choe and Han-Ki Kim; Sungkyunkwan University, Korea (the Republic of)

To attain the Shockley-Queisser limit, unceasing researches have been focused on improving efficiency and stability of perovskite solar cells. However, an aspect overlooked in these studies is the crucial role of transparent conductive electrodes on solar cell performance. So far, despite attempts to develop various front transparent electrodes, research on PSC-only front transparent electrode that surpasses the existing performance is still inadequate. Here we reveal the optimal Sn dopant concentration in In_2O_3 using a co-sputtering process, and develop an advanced perovskite-Sn doped In_2O_3 front electrode that can outperform the commercial front transparent electrodes. As a result, the optimal perovskite-Sn doped In_2O_3 electrode shows ultra-low resistivity, high optical transmittance, smooth surface morphology and markedly enhanced thermal stability. Through these improvements for high-performance perovskite solar cells, we achieve a maximum efficiency of 23.35%. Moreover, the device retained 97.6% initial efficiency after 1000 h maximum power point tracking under continuous 1 sun illumination.

EN02.03.37

Methacrylate-Functionalized Perovskite Nanocrystals Encapsulated by Siloxane Hybrid for Highly Stable Color-Converting Layer in Display Yongmin Shin¹, Hyungwoo Suh², Junho Jang¹, Byoung-Hwa Kwon² and Byeong-Soo Bae¹; ¹Korea Advanced Institution of Science and Technology, Korea (the Republic of); ²Electronics and Telecommunications Research Institute, Korea (the Republic of)

Organic-inorganic hybrid perovskite nanocrystals (PNCs) with ABX₃ crystal structure (A: organic cation, B: metal cation, X: halide anion) have been promised as color-converting material in display, because of their various advantages of low fabrication cost, facile bandgap tunability, very narrow emission bandwidth and high photoluminescence quantum yield, which lead to wide color gamut. However, when they are exposed to heat and light, aggregation or ion migration in PNCs can be generated, causing huge degradation of their optical properties. To overcome these instability issues, various strategies have been suggested such as fabrication of inorganic shell structure and dispersion into polymeric matrix to prevent permeation of oxygen and moisture to surface of PNCs. However, these methods entail complex processes and encounter limited stability due to physical blocking water to PNCs. In addition, to guarantee stability in high temperature with high humidity, the passivation of PNCs by surface ligands with robustness and functionality is also necessary. Therefore, stable PNCs with robust ligand that chemically interacts with the polymer matrix should be developed.

Herein, we report highly stable photoluminescent perovskite nanocrystals (PNCs) to achieve long-term stability in various environments by employing two types of siloxane-based materials (surface ligand and encapsulating matrix). Our approaches are followed: (i) synthesis of PNC passivated by robust methacrylate-functionalized siloxane-based ligand (M-PNC), and (ii) chemical encapsulation of PNCs by siloxane hybrid matrix (M-PNC/siloxane film). Passivation of PNCs by robust ligand induces improved compatibility and rigid chemical cross-linking of between M-PNC and siloxane hybrid matrix, resulting M-PNC/siloxane film maintains PLQY (> 70%) over 100 days in air, water, acid or base solutions, and various polar solvents, 85 °C /85% relative humidity (RH), and continuous blue light irradiation. Fabricated M-PNC/siloxane film presents the homogeneous distribution of M-PNC in siloxane hybrid matrix. To confirm feasibility of our stability enhancement method, we demonstrate M-PNC-based white color-converted organic light-emitting diodes by integrating Cd-based QD as red components, which shows wide color gamut and excellent reliability.

EN02.03.38

Stoichiometry Control of Vapor-Deposited Multication Hybrid Halide Perovskites—From a Single-Source to Solar Cells Tatiana Soto Montero, Suzana Kralj, Wiria Soltanpoor, Junia Shelomi Solomon Sathiaraj, Chris Baeumer and Monica Morales-Masis; University of Twente, Netherlands

Vapor-deposited halide perovskites are highly attractive for the fabrication of monolithic perovskite-silicon tandem solar cells using readily available textured Si bottom cells. However, vapor-deposited halide perovskites have been less explored as top cells as compared to solution-processed or two-step deposited perovskites. Moreover, stoichiometry control remains a challenge for vapor-deposited halide perovskites. Here we explore Pulsed Laser Deposition (PLD) as a single-source room temperature vapor deposition technique of multication halide perovskites. Specifically, we demonstrate that it is possible to fabricate mixed-cation MA⁺:FA⁺ thin films from a single solid target containing tunable MAI:FAI: PbI₂ amounts to achieve the desired film stoichiometry with the photoactive cubic α -phase.

During PLD, a mechanochemically synthesized target containing the desired MA⁺:FA⁺ ratio is ablated pulse by pulse, creating a confined plasma plume that transfers the ablated species towards the substrate. Due to the different atomic masses of the target constituents (H, C, N, Pb, I), excess of MAI/FAI compared to PbI₂ is incorporated to compensate for the losses of volatile compounds upon the laser ablation. Thus, the solid target composition and the MA⁺:FA⁺ cation ratio are critical to growing films with the desired stoichiometry. Using X-ray Photoelectron Spectroscopy (XPS), solid-state Nuclear Magnetic Resonance (NMR), and X-Ray diffraction (XRD), we confirmed the successful transfer of species from target to film with PLD, including the integrity of the molecules and the desired MA⁺:FA⁺ ratio. PLD-deposited films containing 25% to 60% of FA⁺ (MA_{1-x}FA_xPbI₃, x = 0.25-0.60) showed the stabilization of the cubic α -phase. Optical bandgap tuning from 1.61 to 1.55 eV is demonstrated with tuning stoichiometry of the film, as confirmed by photoluminescence, XPS and NMR. MAFA-based compositions are attractive for single junctions applications; however other compositions containing FA-Cs are also promising in terms of wide bandgap for perovskite/silicon tandem solar cells and to improve the stability of MA⁺-free hybrid halide perovskite. Following a similar approach as with the MAFA-based perovskites, the replacement of MA with Cs was furthermore tested, representing a step closer to the desired stoichiometry for wide-bandgap top cells. At the device level, the critical role of the film composition and device contact layers in NIP and PIN configurations will be discussed. Mainly, we found a strong link between PLD parameters to achieve columnar grain growth and tunable composition with the final solar cell performance.

Overall, we demonstrate the potential of PLD as a solvent-free single-source vapor-deposition technique to grow mixed-cation and multi-compound perovskites conformally on several substrates, opening the path for future developments of wide-bandgap perovskite thin-films for monolithic tandem devices with the desired stoichiometry control from a single source.

EN02.03.40

Combinatorial Vacuum-Deposition of Wide Bandgap Perovskites Films and Solar Cells Isidora Susic¹, Lidón Gil-Escrig¹, Adi Kama², Chris Dreessen¹, Francisco Palazon³, Michele Sessolo¹, David Cahen² and Henk J. Bolink¹; ¹Universidad de Valencia, Spain; ²Bar-Ilan University, Israel; ³Universidad Politécnica de Cartagena, Spain

The development of vacuum deposited perovskite materials and devices is partially slowed down by the minor research effort in this direction (at least when compared with the field of solution-processed perovskites), but also from one of its intrinsic characteristics: long timeframe for the optimization of even a single perovskite composition since in one deposition run only a single set of parameters can be used (i.e. set of deposition rates for a certain set of precursors). Combinatorial materials science (CMS) is a method that can be used to accelerate the study of compositionally varying perovskites. When CMS is applied to thin-films, a compositional gradient is deposited on purpose on a single large area substrate, referred to as a library, forming many different compounds or materials in a single deposition run. Here we report the combinatorial vacuum-deposition of wide bandgap perovskites of the type FA_{1-x}Cs_xPb(I_{1-x}Br_x)₃, by using 4 sources and a non-rotating sample holder. From initial deposition rates calculated based on stoichiometry and properties for each precursor, we run a combinatorial deposition and high throughput characterization. By using small pixel substrates, we are able to produce >100 solar cells with different perovskite absorbers in a single deposition run. The materials are thoroughly characterized by spatially resolved and/or high throughput techniques, including optical, morphological and structural techniques. By subsequent fine tuning of the deposition rates, we can alter the gradient and reproduce the best performing formulations in standard depositions with rotation. We extended the method for optimizing wide bandgap CsMAFA triple-cation perovskite solar cells, which are found to be efficient but not thermally stable. With the aim of stabilizing the perovskite phase, we add guanidinium (GA⁺) to the material formulation, and obtained CsMAFAGA quadruple-cation perovskite films with improved thermal stability, as observed by X-ray diffraction and rationalized by microstructural analysis. The corresponding solar cells showed similar performance with a remarkable thermal stability, when compared to the triple-cation perovskite devices.^[1] We believe this approach can encourage the discovery of materials, and serve as a basis to prototype other compositions (low bandgap, lead-free) overcoming the current limitations of vacuum deposition as a research tool for perovskite films.

[1] I. Susic, L. Gil-Escrig, F. Palazon, M. Sessolo, and H. J. Bolink, ACS Energy Lett. 2022, 7, 4, 1355–1363

EN02.03.41

Cold Sintering and Cold Flow of MAPbBr₃ for Large-Area Radiation Detectors Maxwell Tolchin, Sarah Lowum, Ibrahim Dursun, N. C. Giebink and Jon-Paul Maria; The Pennsylvania State University, United States

Methylammonium lead bromide (MAPbBr₃) is classified as a metal hybrid perovskite (MHP), a subset of hybrid organic-inorganic semiconductors with compelling photovoltaic and optoelectronic properties, as well as facile synthesis. Thus, emerging as a candidate to improve current commercial products. While single crystal MAPbBr₃ embodiments have indicated best-known optoelectronic behavior, their integration into commercial utility remains unfeasible due to slow growth kinetics and intensive post-processing procedures. These limitations encourage researchers to investigate new synthetic approaches to shorten production timelines and achieve high-throughput assemblies while maintaining appreciable electronic application viability. One opportunity to reach these industrial advances is through bulk ceramic processing, particularly cold flow (CF) and the cold sintering process (CSP). Keys to these techniques, mild temperatures (< 200 °C) and pressures (< 1 GPa), are favorable industrial fabrication methods. Additionally, CF and CSP provide opportunity for managing microstructure, density, and composition, when adapting single crystal fabrication to size-configurable bulk monolith geometries. Because the coordination of the organic and halogenic components to lead, seen in MAPbBr₃, offers plastic and solubilizing properties amenable to low-temperature CF and CSP.

Herein, MAPbBr₃ crystals prepared via inverse temperature crystallization (ITC) can be densified using CF and CSP into ceramic monoliths with densities near the 100% theoretical limit. The process is scalable from millimeters to several centimeters, drawing interest for bulk polycrystalline radiation detectors which require thick slabs of material. Densification and key morphological responses are shown by altering pressure and temperature, as well as varied liquid and crystalline transport phases in CSP. To connect microstructure to electrical performance, radiation test results show photoelectric response upon hard x-ray exposure and time-of-flight (ToF) *i-v* analysis upon super bandgap laser excitation for carrier mobility. These microstructure-property trends will build our investigation into densification modes that can produce bulk MAPbBr₃ ceramics that are viable, large-area radiation detectors.

EN02.03.42

High Photoluminescence Quantum Yield Near-Infrared Emission from a Lead-Free Ytterbium-Doped Double Perovskite Minh N. Tran, Iver J. Cleveland and Eray S. Aydil; New York University, United States

Redshifting the solar spectrum entering a solar cell by creating near-infrared (NIR) photons from ultraviolet (UV) and blue photons via luminescence down conversion can increase the solar cell's efficiency. Shifting the UV and blue spectrum to NIR reduces thermal losses and the recombination of electron-hole pairs generated from shallow light absorption near interfaces. Ytterbium (Yb) is a well-known luminophore for solar spectral shifting because the Yb³⁺ emission via ²F_{5/2} → ²F_{7/2} electronic transition at 1.24 eV is close to the bandgap of silicon (~ 1.1 eV). Typically, Yb is doped into a host, which absorbs in the UV and visible regions of the electromagnetic spectrum and transfers energy to the Yb³⁺, exciting it from the ²F_{7/2} ground state to the ²F_{5/2} state. The excited Yb³⁺ emits NIR photons at ~1.24 eV upon relaxation. Thus, depositing a layer of a Yb-doped film with high photoluminescence quantum yield (PLQY) on top of a silicon solar cell can improve its solar cell efficiency by modifying the incident solar spectrum. Ideally, all blue (UV) photons are converted to NIR photons, and the maximum possible photoluminescence quantum yield (PLQY) is 100%. However, there is another possibility. If the host bandgap is greater than twice the Yb³⁺ ²F_{5/2} → ²F_{7/2} electronic transition (> 2.5 eV), the energy transfer from the host to Yb³⁺ can be via quantum cutting, a process wherein one UV-blue photon is converted to two NIR photons. PLQY can be >100% in this case with a maximum of 200%. Indeed, Yb-doped CsPbX₃ (X=Cl, Br) have been shown to exhibit quantum cutting with PLQY as high as 190%.¹ However, lead is toxic, and NIR PLQY from CsPbX₃ decreases at high photon fluence.¹ In the search for non-toxic alternatives to CsPbX₃, double and bismuth-based perovskites are emerging as promising hosts because they have high absorption coefficients and tunable bandgaps in the visible range. Specifically, Yb doping of Cs₂Bi₂Br₉, Cs₂AgInCl₆, and Cs₂AgBiBr₆ has been reported.²⁻⁴ Unfortunately, 28%, the highest PLQY from Yb-doped Cs₂AgBiBr₆ thin film, is still much lower than the minimum PLQY estimated to increase solar cell efficiencies (69% for typical Si solar cells).

Herein, we employ physical vapor deposition to synthesize Yb-doped Cs₂AgBiBr₆ films with high PLQY. Cs₂AgBiBr₆ has a stable cubic structure at room temperature and an indirect bandgap of ~2.2 eV. Yb³⁺ ions are hypothesized to replace Bi³⁺ and Ag⁺ ions in the 3D network of corner-sharing [AgBr₆]⁵⁻ and [BiBr₆]³⁻ octahedra. Since the perovskite host sensitizes Yb³⁺, its emission depends strongly on the Yb³⁺ concentration and location in the crystal structure, which are determined by the synthesis conditions. We show that near-infrared PLQY depends strongly on the precursors' evaporation rates and the substrate temperature during the deposition. Ramping the substrate temperature during the deposition promotes the reaction forming Cs₂AgBiBr₆ and helps Yb³⁺ substitute Bi³⁺ and Ag⁺ ions in the crystal structure. Excess BiBr₃ is needed to compensate for the BiBr₃ loss at high substrate temperature and reduce Bi-deficient phase formation. Robust, reproducible, and stable PLQYs as high as 95% are achieved with 8% Yb-doped Cs₂AgBiBr₆ films deposited with excess BiBr₃ and ramping temperature. PLQYs are consistently in the 75-95% range for the excitation energy above the host bandgap (>2.2 eV) and retain 91% of the initial values after two months in the ambient conditions.

References

- 1 D. M. Kroupa, J. Y. Roh, T. J. Milstein, S. E. Creutz and D. R. Gamelin, *ACS Energy Lett.*, 2018, **3**, 2390-2395.
- 2 M. N. Tran, I. J. Cleveland, G. A. Pustorino and E. S. Aydil, *J. Mater. Chem. A*, 2021, **9**, 13026-13035.
- 3 W. Lee, S. Hong and S. Kim, *J. Phys. Chem. C*, 2019, **123**, 2665-2672.
- 4 F. Schmitz, K. Guo, J. Horn, R. Sorrentino, G. Conforto, F. Lamberti, R. Brescia, F. Drago, M. Prato, Z. He, U. Giovanella, F. Cacialli, D. Schlettwein, D. Meggiolaro and T. Gatti, *J. Phys. Chem. Lett.* 2020, **11**, 8893-8900.

EN02.03.43

Synthesis of Violet-Emitting Ruddlesden-Popper Microcrystals of Monolayered Lead Halide Perovskite by Chemical Vapor Deposition Pushpender Yadav, Kyeongdeuk Moon and Seokhyoung Kim; Michigan State University, United States

Organic-inorganic hybrid perovskite (OIHP) has drawn considerable attention owing to the unprecedented rapid advancement of optoelectronic performance both in the bulk and nanoscale. Typically, OIHPs bear an inherent poor stability in ambient conditions, which was resolved by reducing the dimensionality of the materials by incorporating dielectric organic spacer cations. These dimension-reduced Ruddlesden-Popper (RP) layered perovskite shows a range of unique properties including thickness-dependent quantum confinement effects and high luminescent yields. Early research efforts have been primarily devoted towards solution-based methods, to which chemical vapor deposition (CVD) adds a vapor-phase route that is more suited for creating epitaxy and heterointerfaces needed for the fabrication of microelectronics devices. Major challenges such as a high imbalance in vapor pressures of the organic and inorganic precursors need to be addressed to achieve stable growth of single-crystalline nano/microstructures of layered OIHPs. Here, we present a controlled synthesis of RP-phase microcrystals of monolayered OIHP, (C₄H₉NH₃)PbBr₄, using CVD. We have systematically investigated the growth parameters that include temperature, pressure, and gas flow rates to grow morphology-controlled microcrystals, which we summarize in a growth phase diagram. Morphological, structural, and crystallographic properties of our crystals grown at different conditions are characterized by optical microscopy, scanning, and transmission electron microscopy (SEM and TEM), and X-ray diffraction (XRD). The elemental compositions are confirmed by energy-dispersive X-ray spectroscopy (EDS) and X-ray photoelectron spectroscopy (XPS). We observed a sharp excitonic absorption around 400 nm and strong photoluminescence at ~406 nm. The violet emission from the microcrystals indicates the potential to be utilized as a lasing material and for advance

optoelectronic applications. We believe that the fine control of crystallinity, purity, and morphology of $(C_4H_9NH_3)PbBr_3$ microcrystals by CVD opens a new pathway and invigorate more research effort towards the investigation of layered OIHPs for a wide range of optoelectronic applications.

EN02.03.45

Growth of CsPbBr₃ Nanocrystals in a PTFE-Based Microfluidic System Fuqian Yang; University of Kentucky, United States

Understanding the growth of semiconductor nanocrystals in a microfluidic system is of practical importance for continuous fabrication of semiconductor nanocrystals of high quality. We demonstrate the feasibility to synthesize CsPbBr₃ nanocrystals in a PTFE-based microfluidic system via antisolvent method for the synthesis temperature ranging from 303 K to 363 K and study the effects of flow rate and PTFE capillary length on the size of the synthesized CsPbBr₃ nanocrystals. Increasing the flow rate and/or decreasing the PTFE capillary length produce CsPbBr₃ nanocrystals of small sizes. A simple relation is developed between the photoluminescence peak wavelength of the synthesized CsPbBr₃ nanocrystals and the flow rate and supported by the experimental results. The activation energy for the growth of the CsPbBr₃ nanocrystals in the PTFE-based microfluidic system is 2.05 kJ/mol.

This work is supported by the NSF through the grant CMMI-1854554 and CBET- 2018411.

EN02.03.46

High Performance Tin Perovskite Photodetectors Fabricated via Hot Casting Method in Air Kwang Ro Yun, Tae-Ju Lee and Tae-Yeon Seong; Korea University, Korea (the Republic of)

Lead-free tin halide perovskite materials (THP) have emerged as promising candidates for photodetection applications owing to their outstanding optoelectronic properties such as high carrier mobilities ($\approx 10^2$ - 10^3 cm²V⁻¹s⁻¹), narrow bandgaps (1.2-1.4 eV), and low exciton binding energies (≈ 18 meV). However, THP suffers from poor stability in air because Sn²⁺ is easily oxidized to Sn⁴⁺. This “self-doping” effect causes rapid degradation in the performance and reproducibility of THP-based devices. Furthermore, the high-defect density associated with Sn vacancies in the crystal structure creates high mobile holes, resulting in large dark currents and relatively low specific detectivity of THP photodetectors (PDs). Thus, it is essential to be able to adjust “self-doping” effect of THP for the improvement of the performance of THP PDs.

In this study, we prepared lead-free 2D Ruddlesden-Popper perovskite PEA₂SnI₄ films using the nitrogen quenching hot casting (NQHC) method in air. To the best of our knowledge, the formation of THP PDs in air has not been reported because of its vulnerability to oxygen and moisture. By employing dimethyl sulfoxide solvent and SnF₂ additive, air-processed PEA₂SnI₄ films were successfully prepared for PDs. Then, the effects of SnF₂ additive on the optoelectronic properties of the THP films and PDs were investigated. XRD patterns of the PEA₂SnI₄ films show typical diffraction peaks of (001), indicating a layered structure in which an organic spacer is sandwiched between two inorganic sheets. The crystallinity of the films was not affected by the SnF₂ doping concentration. To examine the surface morphology and surface composition of the PEA₂SnI₄, SEM and XPS examinations were conducted. All samples were shown to have a uniform and pin-hole free smooth morphology with large domain sizes. With increasing SnF₂ doping concentration, the peak intensity of Sn⁴⁺ decreased, whereas that of Sn²⁺ increased. This implies that the SnF₂ additive can effectively suppress the formation of Sn vacancies. To investigate the effect of the SnF₂ doping concentration on photodetector performance, PEA₂SnI₄-based photodetectors with different SnF₂ doping concentrations were fabricated. It was shown that the dark current and responsivity of PDs decreased with increasing SnF₂ doping concentration. The addition of SnF₂ was found to be effective in reducing Sn vacancies, background hole concentration and dark current of PDs. However, an excessive SnF₂ concentration (e.g., 30%) did not affect the passivation of Sn vacancies; The optimal doping concentration was observed to be 20%. Consequently, PDs with 20% SnF₂ exhibited a high responsivity of 509 A W⁻¹, excellent specific detectivity of 6.32×10^{13} Jones and fast response time of 0.56 ms. These results show that use of lead-free 2D PEA₂SnI₄ with SnF₂ additives can be an important material system for the fabrication of high-performance optoelectronic devices such as photodetectors and image sensors.

EN02.03.47

Ultra-Fast and On-Demand Fabrication of Multicolor Light-Emitting Diodes and Photodetectors with Perovskite/Polymer Composite Photoactive Layers on Paper and Textile Substrates Junyi Zhao¹, Li-Wei Lo¹, Zhibin Yu² and Chuan Wang¹; ¹Washington University in St. Louis, United States; ²Florida State University, United States

Owing to the unique properties such as tunable bandgap and strong optical absorption, perovskite holds great potential for applications in optoelectronic devices. In this work, we report all-solution-processed perovskite light-emitting diodes (LEDs) and photodetectors (PDs) that are fabricated on a variety of unconventional substrates including paper, textile, plastic film, rubber, metal, and even three-dimensional surfaces using a versatile and low-cost direct handwriting approach. Compared with conventional spin-coating and vacuum-evaporation processes, the handwriting approach enables mask-free patterning and allows even untrained individuals to “draw” a batch of high-performance LEDs/PDs within minutes in a time-efficient and energy-saving manner. One of the greatest challenges associated with implementing optoelectronic devices on paper and textile is the rough surface morphology of the yarn and fiber networks, which could result in nonuniform printed film thickness and leakage current. To address this issue, we have shown that poly(ethylene oxide) (PEO) blended into poly(3,4-ethylenedioxythiophene) polystyrene sulfonate (PEDOT:PSS) could not only help improve the conductivity and stretchability of conducting polymer electrodes, but also help planarize the substrate. For the emissive layer, by substituting the halide elements in the perovskite material (MAPbX₃) and formulating inks with different compositions of two halide elements, we have achieved multicolor LEDs covering the entire visible spectrum on paper substrates. Meanwhile, the brightness and efficiency of LEDs could be further boosted by introducing the butylammonium (BA) group to reduce the perovskite structure dimensionality to form 2D Ruddlesden-Popper perovskite (RPP) structures. Moreover, we have also systematically investigated the perovskite-polymer composite and have shown that the morphology and optoelectronic properties of the perovskite photoactive layer can be tuned by introducing different polymer additives. More specifically, PEO could tune the ink rheology and viscosity to realize more precise and smoother perovskite film deposition; polystyrene (PS) could increase the density and uniformity of crystal arrangement to boost the brightness of LEDs and lower the current leakage; poly(methyl methacrylate) (PMMA) could reduce grain defects and boundaries to benefit the diffusion of carriers for photodetectors. Our hand-drawn LEDs on paper substrates exhibited a brightness as high as 15,225 cd m⁻², a current efficiency of 6.65 cd/A, and a turn-on voltage of 2.4 V; the PDs exhibited an on-off ratio over 10⁴, a responsivity up to 132 mA/W, and a response time of less than 15 ms. Owing to the extraordinary flexibility of each functional layer, the handwritten LEDs on the paper substrate could be bent to a 1 mm extreme curvature radius for over 5000 cycles without decay in performance. In summary, our handwritten perovskite optoelectronic devices are ideally suited for low-cost and large-area application scenarios such as E-Textiles, E-Packaging, and E-Papers with less stringent requirements on resolution.

EN02.03.50

Effects of Residual Intermediate Phase Buried in MAPbI₃ Films on Photocurrent Generation Weijie Xu, Anusha Srivastava, Bishal Bhandari and Julia W. Hsu; The University of Texas at Dallas, United States

Defects and impurities in halide perovskite can have negative effect on device performance and long-term stability. Here, we report an overlooked impurity in MAPbI₃, MA₂Pb₃I₉ (DMSO)₂, which reduces photocurrent generation in perovskite solar cells (PSCs). We observe a substantial loss of the external quantum efficiency (EQE) spectrum at 400 nm in PSCs made by photonic curing despite good device performance. This EQE reduction feature has also

been reported in the literature. We then find that these samples contain $\text{MA}_2\text{Pb}_3\text{I}_8(\text{DMSO})_2$ phase, which is a commonly reported intermediate phase after the addition of DMSO in MAPbI_3 precursors. Previously, $\text{MA}_2\text{Pb}_3\text{I}_8(\text{DMSO})_2$ phase is known to be beneficial by retarding the perovskite growth rate to get high-quality perovskite films. By varying incidence angle in the X-ray diffraction, we show that $\text{MA}_2\text{Pb}_3\text{I}_8(\text{DMSO})_2$ is buried in the substrate/ MAPbI_3 interface. Because the high boiling temperature of DMSO, the result could be explained by the solvent DMSO is hard to escape the precursor films. We further study how $\text{MA}_2\text{Pb}_3\text{I}_8(\text{DMSO})_2$ affects the long-term stability of PSCs. Additionally, the resulting parasitic absorption reduces the photogeneration in the short wavelength region. This is an obstacle while applying PSC as indoor photovoltaics because indoor light-emitting diode spectra are narrower compared to the AM 1.5G. This work is a reminder to the field to rethink the role of $\text{MA}_2\text{Pb}_3\text{I}_8(\text{DMSO})_2$ in MAPbI_3 films and to investigate a mitigation strategy.

This material is based upon work supported by the U.S. Department of Energy's Office of Energy Efficiency and Renewable Energy (EERE) under the Solar Energy Technologies Office Award Number DE-EE0009518.

EN02.03.52

Performance Improvement and Stabilization of Wide-Bandgap Perovskite Solar Cells by Adding Bication Thiocyanate Salt [Mi-Seon Bae](#)¹ and Tae-Youl Yang^{1,2}; ¹Chungnam National University, Korea (the Republic of); ²Korea Research Institute of Chemical Technology, Korea (the Republic of)

In general, Br-rich wide-bandgap perovskite solar cells (PSCs) have higher defect density and deeper trap states than narrow perovskite solar cells. In addition, the halide separation is caused by light and heat, which has been raised as a problem that limits the performance of PSCs. Surface treatment with additional coating with organohalide has been known to be effective to passivate surface defects, however, that requires an additional process with precise thickness control. The addition of ionic liquid additives to the perovskite precursor solution is a simple method and is effective for passivating grain boundaries and surface defects.

In this study, 1-butyl-3-methylimidazolium thiocyanate (BMIM-SCN), a thiocyanate (SCN)-based ionic liquid, is added into a wide-bandgap perovskite material. The ionic liquid passivates uncoordinated lead sites on the grain boundary and the surface of the perovskite material, which ensure the improved quality and long-term stability of PSCs. The secondary additive, $\text{Pb}(\text{SCN})_2$, is additionally included in the perovskite to neutralize the excess charge of BMIM^+ ions and passivates uncoordinated halide defect, thereby improving the performance of the PSCs: High open-circuit voltage (V_{oc}), decreased hysteresis. In addition, enhanced stability to high temperature and light illumination was also observed. The PSCs showed long-term stability of more than 500 hours under AM1.5G-1SUN illumination in ambient air without encapsulation.

EN02.03.53

Inserting Potassium Chloride for Interlayer between Sputtered- SnO_2 and Perovskite to Eliminate the Hysteresis and Enhance the Efficiency of Perovskite Solar Cells [Seok-Hyun Jeong](#), Ji-Seong Hwang, Wonkyu Lee, Sang-Won Lee, Jae-Keun Hwang, Solhee Lee, Hae-Seok Lee, Donghwan Kim and Yoonmook Kang; Korea University, Korea (the Republic of)

In perovskite solar cells (PSCs), Tin Oxide (SnO_2) has been widely used as the electron transport layer (ETL) due to its higher bandgap and higher electron mobility compared to the other metal oxide materials. Generally, SnO_2 is fabricated by a solution-based process (e.g. spin coating, chemical bath deposition) for high-efficiency PSCs. Meanwhile, it has an advantage in commercialization when ETL is deposited using the vacuum deposition method with RF sputtering. However, few studies have been reported on manufacturing PSCs using sputtered- SnO_2 because conventional PSCs with sputtered SnO_2 is subjected to severe hysteresis. It is known that the hysteresis is caused by the defect site that exists at the interface between ETL and perovskite. Additionally, these defect sites induce non-radiative carrier recombination, causing a decrease in open-circuit voltage (V_{oc}) and fill factor (FF) of the device. To solve this problem, a number of studies reported that an increase in V_{oc} and elimination of hysteresis can be achieved by passivating the surface of SnO_2 with various chloride. In this paper, SnO_2 was deposited by RF-sputtering as ETL, and then the surface of as-prepared SnO_2 is passivated with Potassium Chloride (KCl) aqueous solution. Through this surface passivation, it was possible to passivate a defect site that forms traps at the interface with perovskite and change the band alignment for effective electron transport. As a result, the trap density of perovskite is reduced and the efficiency of PSCs is achieved by 21.7% (V_{oc} of 1.11V, FF of 78.2%, and hysteresis index of 2%). This study shows that vacuum-deposited SnO_2 can be adopted by hysteresis-free and high-efficiency PSCs as ETL by inserting KCl between SnO_2 and perovskite.

EN02.03.55

The Influence of Halides on the Interactions of Ammonium Acids with Metal Halide Perovskites [Yanan Li](#)¹, Patrick Lohr¹, Allison Segapeli², Dorian Werner¹, Juliana Baltram¹ and Adam Printz¹; ¹The University of Arizona, United States; ²The University of Texas, United States

Constructing mixed-dimensional 2D/3D metal halide perovskite *via* organic additives incorporation has been demonstrated as a promising approach to simultaneously improve power conversion efficiency (PCE) and stability of perovskite solar cells (PSCs). Amino/Ammonium acids such as 5-aminovaleric acid (5-AVA) or its ammonium/halide salt (5-AVAX) are the most commonly reported additives to prepare 2D/3D perovskites, however, the role of 5-AVA/5-AVAX and how they interact with perovskite are still not fully understood. Here, we systematically investigated the halide effect on the interactions of ammonium acids and perovskite by incorporating pristine 5-AVA and two of its halide salts 5-AVAI and 5-AVACl into MAPbI_3 perovskite and found they showed very different behaviors in directing 2D perovskite formation. Because of the high electronegativity, the Cl in 5-AVACl was strongly bonding with one of the H atoms in the ammonium group then volatilized as HCl, leaving an identical structure to that of 5-AVA. X-ray diffraction (XRD) results showed 5-AVA and 5-AVACl led to a similar Ruddlesden-Popper (RP)-2D structure formation, with a bilayer of 5-AVA^+ between adjacent perovskite sheets. In contrast, 5-AVAI mainly interacted with 3D perovskite surface *via* coordinating interaction of carboxyl group and Pb and did not form 2D perovskite. In addition to structure characterizations, morphology and optical properties of the perovskite films and photovoltaic devices performance were also studied in this work. We hope this work will provide further insight into the role of halides in additives and their effect on molecular interactions in perovskite precursors.

EN02.03.56

A Computational Study of Ammonium Acid Interactions with Metal Halide Perovskites [Patrick Lohr](#), Yanan Li, Krishna Muralidharan and Adam Printz; The University of Arizona, United States

Metal halide perovskite semiconductors exhibit exceptional optoelectronic properties, including high carrier lifetime, high carrier mobility, and extraordinary power conversion efficiencies (PCE) in photovoltaic devices. Despite these favorable characteristics, the thermomechanical and chemical stability of these devices is insufficient to provide robust performance in most real-world scenarios, a significant roadblock to technological relevancy. A key driver of these instabilities are defects that form on the surface of grains during crystallization in polycrystalline perovskite films.

Additive engineering – the addition of organic molecules during perovskite manufacturing – has been demonstrated to inhibit the formation of defect sites in perovskite films and reduce ion migration, enhancing PCE retention. However, the properties that determine an organic additive's ability to passivate defects and coordinate precursor ions during crystallization in perovskite materials are not well-understood on the atomic scale. By using an *ab-initio* modeling approach, we have systematically studied the interactions between the class of multifunctional additives known as 5-aminovaleric acid (5-AVA)

halide derivatives and methylammonium lead iodide perovskite, revealing key molecular insights into the coordination of grain boundaries and the formation of quasi-2D perovskite heterostructures through self-interactions. Combined with experimental evidence, we believe that our results clarify the role of halides and explain the discrepancy of ammonium-chloride salts.

EN02.03.57

Improving the Thermomechanical Stability of High Efficiency Perovskite Solar Cells via Polymeric Nanofiber Reinforcement Anton Samoylov, Nick Swenson, Chi V. Nguyen, Antonio Murrieta, Juliana Baltram, Matthew Dailey and Adam Printz; University of Arizona, United States

Perovskite solar cells (PSC) currently rival traditional silicon and other third-generation solar cells, becoming increasingly investigated for commercial applications due to their compatibility with scalable processing techniques.[1] However, the poor stability of the perovskite photoabsorbing layer—both chemical and thermomechanical—has thus far inhibited the commercial viability of perovskite-based photovoltaics.

We show that the mechanical stability of perovskite thin films can be increased by an order of magnitude by nanocompositing with polymeric nanofibers using a scalable method. We discuss the increase in fracture resistance energy, G_c , in the nanocomposite samples with respect to nanofiber orientation. We demonstrate this platform with commodity polymeric nanofibers including nylon-6,6 and polyvinyl alcohol. The fiber network reduces the mechanical fragility of the PSCs by increasing their fracture energy several-fold, while maintaining comparable morphology, chemical composition, and device efficiencies to pristine perovskite. Improved power conversion efficiency stability of the nanocomposites under accelerated aging conditions is demonstrated. This platform is a promising advance toward the commercial viability of PSCs.

References:

[1] J. Yan, et al. RSC Adv. [10.1039/C4RA07064J] 2014, 4 (82), 43286-43314.

EN02.03.58

Optimization of Vapor Flow Geometry for Highly Uniform Deposition of Perovskite Thin Films Chaeun Yu, Dela Quarme Gbadago, Sungwon Hwang and Naechul Shin; Inha University, Korea (the Republic of)

Organic-Inorganic Hybrid Perovskites (OIHPs) have great potential in photovoltaics (PVs), photodetectors, and light emitting diodes (LEDs) owing to their excellent optoelectronic properties. Currently, a majority of studies on perovskite thin-film fabrication are employing solution-based approaches (*i.e.*, spin-coating), which have limitations in scalable production and suffer from reproducibility. While the vapor deposition method is promising to this end, regulating the as-grown film thickness and roughness over the whole substrate, a prerequisite for highly uniform optoelectronic performance, remains challenging.

In this study, we report the optimization of the flow geometry of vapor precursors to grow high-quality OIHP thin films with uniform thickness over the substrate. By varying the substrate position (e.g., horizontal vs. vertical) relative to the flow direction of vapor precursors in the CVD tube system, we confirmed that the vertical substrate position yielded a more uniform and smooth deposition of the [0001]-oriented lead iodide (PbI_2) primary layers than the horizontal position. Furthermore, the precursor flow simulation based on the computational fluid dynamics (CFD) calculation predicted that the distribution of substrate temperature and molecular transport within the flow boundary layer is more regulated for the vertical position. Interestingly, horizontal flow exhibited a higher degree of uniformity in converting the pre-grown PbI_2 layer into the $\text{CH}_3\text{NH}_3\text{PbI}_3$ perovskite thin film *via* the vapor transport of methylammonium iodide ($\text{CH}_3\text{NH}_3\text{I}$), suggesting that the solid diffusion following intercalation of $\text{CH}_3\text{NH}_3\text{I}$ to PbI_2 layers dominates the conversion process. Our results present a systematic approach to optimizing the vapor-based fabrication of OIHP thin films for uniform optoelectronic properties and scalable production with high reproducibility.

EN02.03.59

Optimization of tin fluoride concentration for enhanced stability in narrow band gap perovskite solar cells Lana M. Kessels, René Janssen and Martijn Wienk; University of Technology Eindhoven, Netherlands

Incorporating tin into mixed-halide lead perovskites has gained considerable attention as it allows for a narrower bandgap (between 1.2 and 1.5 eV), making it suitable for all-perovskite-based tandem solar cells. However, with the incorporation of tin comes the challenge of higher oxidation levels and different crystallization rates. To evade such problems, the processing method is often altered or various additives are added to the precursor solution or applied as a passivation layer. One of the main additives used for tin-containing perovskites is tin fluoride. It has been shown that a certain percentage (ranging between 5 and 10 mol% of the SnI_2 concentration) enhances the performance significantly.^{1,2} Tin fluoride has shown to enhance the number of nucleation sites^{1,3}, allow halide exchange to obtain SnF_4 and SnI_4 , and reduce defects⁵. While most studies focus on enhancing the performance of the device, stability measurements of the device over time are often neglected. In this study, a range of tin fluoride concentrations was tested and analyzed using current tracking at the maximum power point voltage and open-circuit voltage tracking to investigate the stability of the photovoltaic parameters under working conditions. Results show that devices with higher SnF_2 concentrations suffer drastic current density losses when exposed to V_{MPP} or V_{OC} . Instead, a concentration of 4-5 mol% gives a steady current density under these conditions and also yields the overall highest performance. In order to investigate the origin of the discrepancy in stability various methods such as quasi-Fermi level splitting and ultra-sensitive sub-bandgap photocurrent spectroscopy were performed.

1. Chen, Q. *et al.* Unveiling Roles of Tin Fluoride Additives in High-Efficiency Low-Bandgap Mixed Tin-Lead Perovskite Solar Cells. *Adv. Energy Mater.* **11**, 2101045 (2021).
2. Hu, S. *et al.* Optimized carrier extraction at interfaces for 23.6% efficient tin-lead perovskite solar cells. *Energy Environ. Sci.* **15**, 2096–2107 (2022).
3. Xiao, M. *et al.* Tin-Based Perovskite with Improved Coverage and Crystallinity through Tin-Fluoride-Assisted Heterogeneous Nucleation. *Adv. Opt. Mater.* **6**, 1–7 (2018).
4. Pascual, J. *et al.* Fluoride Chemistry in Tin Halide Perovskites. *Angew. Chemie - Int. Ed.* **60**, 21583–21591 (2021).
5. Savill, K. J. *et al.* Impact of Tin Fluoride Additive on the Properties of Mixed Tin-Lead Iodide Perovskite Semiconductors. *Adv. Funct. Mater.* **30**, (2020).

EN02.03.61

Formamidinium Acetate Assisted Antisolvent Free Crystallization of Wide Band-Gap Hybrid Perovskites for Slot-Die Coating Nischal Khakurel¹, Drew Amyx¹, Chandan Q. Howlader¹, Greg Gibson², Yoichi Miyahara¹ and Wilhelmus Geerts¹; ¹Texas State University, United States; ²FAS Holding Group, United States

Mixed halide Hybrid perovskites (HP) poor thermal stability remains a fundamental barrier that can limit their use to a low temperature range. Although formamidinium (FA) based HP are known to be more stable than their Methylammonium (MA) counterparts, they are metastable and transform to the non-photoactive δ -phase over time. The black photoactive α -phase can be stabilized by replacing some of the FA in the lattice with Cesium. Most HP are

deposited using an anti-solvent quenching process - adding an extra layer of complexity to the production process. In this work, we utilize FA based ionic liquid FA Acetate (FAAc) in wide band-gap perovskite $\text{FA}_{0.78}\text{Cs}_{0.22}\text{Pb}(\text{I}_{0.85}\text{Br}_{0.15})_3$ ($\text{Cs}_{22}\text{Br}_{15}$) that assists in nucleation and grain growth of a continuous pinhole free layer without the use of anti-solvent or quenching. We also use the same composition to slot-die coat using nitrogen gas assisted quenching on glass/ITO substrates in ambient conditions.

Inks with various concentrations of FAcAc were made by adding 20, 40, 60, 80, or 100 mg FAcAc/ml in a 1M $\text{Cs}_{22}\text{Br}_{15}$ /N, N-Dimethylformamide solution. θ -2 θ XRD scan were measured prior and after annealing. The pre-anneal XRD scans show intermediate peaks in-between 5 and 10 degrees which do not show up in films spun from ink without FAcAc additive. The post-anneal XRD scans shows peaks of the cubic α -phases. The Scanning electron microscopy images show continuous pin-hole free films for samples spun from inks containing 40 mg/ml or more of FAcAc. It was noticed that the crystallization of HP takes place only after the concentration of FAcAc is equal to or above 40mg/ml. Moreover, the roughness of the films measured with an Atomic Force Microscope decreases from 11 to 8.33nm when the FAcAc concentration is increased from 0 to 40 mg/ml.

The band-gap of these films were determined from UV-Vis spectroscopy and was not affected by the addition of FAcAc to the ink (1.63 eV). The inks were spin-casted into perovskite films to make solar cells (6.25mm²) having the structure: glass/ITO/PTAA/ $\text{Cs}_{22}\text{Br}_{15}$.FAAc/C60/BCP/Al. The champion devices for 40mg/ml, 60mg/ml and 100mg/ml show a power conversion efficiency of 13.63%, 14.82% and 15.12% respectively. Additionally, preliminary slot-die coating experiments in ambient conditions have shown that this ink has a wider printing processing window as it can be coated and results in pin-hole free thin films at chuck temperatures from 30°C-70°C unlike ink without FAcAc additives.

This work was in part funded by NSF through STTR Phase II grant 1927020 and in part by the U.S. Department of Energy's Office of Energy Efficiency and Renewable Energy (EERE) under the Solar Energy Technologies Office Award Number DE-EE0009526. The views expressed herein do not necessarily represent the views of the U.S. Department of Energy or the United States Government.

[1] G. Cotella *et al.*, "One-step deposition by slot-die coating of mixed lead halide perovskite for photovoltaic applications," *Sol. Energy Mater. Sol. Cells*, vol. 159, pp. 362–369, 2017.

[2] M. Fievez *et al.*, "Slot-die coated methylammonium-free perovskite solar cells with 18% efficiency," *Sol. Energy Mater. Sol. Cells*, vol. 230, p. 111189, 2021.

EN02.03.62

A Systematic Vapor-Phase Treatment Process for Efficient Perovskite Solar Cells and Solar Modules [Soyeon Park](#) and Kai Zhu; National Renewable Energy Laboratory, United States

In recent years, the surface passivation using the bulky organic cations in hybrid organic-inorganic perovskite solar cells (HPSCs) have been introduced to boost device efficiency and stability. The precise selection and use of bulky organic cations for surface passivation on 3D perovskite film have enabled fine-tuning of the dimensionality of perovskite and/or suppression of inherently formed defects, leading to enhanced optoelectronic properties and device stability. However, conventional solution process of passivation method using bulky organic cations could face difficulties in controlling and predicting the dimensionality of the resulting capping layer and avoiding the negative affects of the solvent and uneven reaction during the solution process.

In this study, we developed a systematic butylamine-based vapor-phase treatment processing method adapted from an atomic layer deposition (ALD) equipment to perform uniform and reproducible treatment on 3D perovskite films. This new approach has enabled us to fabricate the state-of-art HPSC configuration, with enhanced perovskite optoelectronic properties (charge carrier lifetime and mobility) and much-enhanced device stability. When using this vapor-phase treatment, a power conversion efficiency (PCE) was enhanced for both lab-scale devices and mini-modules with excellent long-term operational stability and environmental stability. Remarkably, the vapor-treated devices exhibited enhanced device stability and efficiency than the solution-treated devices with better reproducibility. We believe that this systematic vapor-phase treatment processing method adapted from an ALD system can provide a general processing strategy of interfacial engineering for future commercial-scale HPSCs development.

EN02.03.63

Novel Method of Recycling Lead Perovskite Solar Cells Using Iodide Solutions [Tanner Y. O'Hara](#); South Dakota School of Mines and Technology, United States

The implementation of green energy solutions has become increasingly common as the global demand for electricity rises along with concerns regarding environmental release. Interest in solar energy has led to the advancement of thin film solar cells, especially lead perovskites as they offer a cheap and simple alternative to existing technologies. Lead perovskite solar cells (PSCs) utilize the compound $\text{CH}_3\text{NH}_3\text{PbI}_3$ as a light harvesting material and have shown promising advancements in power conversion efficiency (PCE) comparable to current products. One hindrance to the large-scale application of PSCs is the use of lead compounds which are highly toxic to humans and the environment. Attempts to replace the lead compounds with those of similar metals such as Sn, Sb, and Bi have resulted in considerably lower PCEs. For this reason lead based perovskites have maintained prominence, and various methods to recycle the panels have been investigated. Unfortunately many of these recycling processes utilize harmful solvents such as DMF, DMSO, and chlorobenzene. The glass backing is often crushed and reduced into scrap, making them unusable for remanufacture.

A novel recycling method utilizing aqueous iodide solutions has proven effective at recovering the lead and preserving the glass substrate for direct remanufacture of new cells. Above a specific concentration of iodide in solution, the solubility of lead begins to increase as several complex ions are formed. Iodide solutions selectively interact with the perovskite photovoltaic (PV) layer and dissolve it from the edge in, allowing for the exfoliation of back contact materials. The back contact material can be physically separated and dissolved lead can be recovered from solution. The glass substrate represents a large portion of the panels material cost, by reusing them for remanufacture the price per panel decreases and minimizes the environmental footprint.

EN02.03.64

Carbazole Based Self Assembly Monolayer as HTL for Highly Efficient Methylammonium Free Mixed Sn/Pb- Based Perovskite Solar Cells [Matteo Pitaro](#)¹, Javier Sebastian Alonso¹, Lorenzo Di Mario¹, Malin B. Johansson², Erik Johansson², Gerrit Boschloo² and Maria Antonietta Loi¹; ¹University of Groningen, Netherlands; ²Uppsala universitet, Sweden

Highly performing mixed tin-lead perovskite materials are among the most promising options as an alternative active layer in perovskite solar cells to reduce Pb content. Moreover, these compounds open the possibility of fabricating full perovskite tandem solar cells, owing to their reduced band gap. The most efficient single junction mixed Sn/Pb perovskite solar cells have been fabricated using methyl ammonium cations (MA^+), and a p-i-n structure where poly(3,4-ethylenedioxythiophene)-poly(styrenesulfonate) (PEDOT: PSS) is implemented as hole transport layer (HTL).¹ However, these record devices show limited stability. Specifically, MA^+ cations easily desorb at high temperature (85 C°) from the perovskite surface, introducing trap states. PEDOT: PSS, due to its hygroscopic and acid nature, reacts with the perovskite active layer, affecting the long term stability.

In this work to improve the thermal stability of these devices, cesium cations (Cs^+) are partially or entirely substituted to MA^+ . The incorporation of Cs^+ cations leads to the contraction of the perovskite crystals, enhancing the organic cations-halides interactions and finally limiting the organic cations

desorption.² To solve the HTL issue, in this work we employ 2-(9H-carbazol-9-yl)ethylphosphonic acid (2-PACz), and [2-(3,6-dibromo-9H-carbazol-9-yl)ethyl]phosphonic acid (Br-2PACz). We fabricate devices in a p-i-n structure, where the intrinsic layer is formed by a $\text{Cs}_{0.25}\text{FA}_{0.75}\text{Sn}_{0.5}\text{Pb}_{0.5}\text{I}_3$ perovskite layer. The perovskite layer deposited on PEDOT:PSS exhibited poor quality and a large number of pin-holes with the champion device efficiency of 16.33%. On the contrary, devices fabricated on 2PACz and Br-2PACz show an enhanced quality of the active layer, leading to an improved efficiency of 18.44% and 19.57% with 2PACz and Br-2PACz, respectively. 19.57% efficiency is a record efficiency for the aforementioned perovskite composition.

¹ <https://doi.org/10.1039/D2EE00288D>

² <https://doi.org/10.1002/aenm.201501310>

EN02.03.65

Lead-Free FASnBr₃/PDMS-Based Flexible Piezoelectric Nanogenerator for Self-Powered Wireless Electronics Md. Masud Rana¹, Asif Abdullah Khan¹, Weiguang Zhu¹, Md Fahim Al Fattah¹, Sathursan Kokilathasan¹, Shazzad Rassel¹, Shuhong Xu², Chunlei Wang² and Dayan Ban¹; ¹University of Waterloo, Canada; ²Southeast University, China

In the modern era of thriving inventions, energy sources play a vital role. Conventional fossil fuel-based energy sources are gradually being replaced by unconventional ones to address imminent challenges, such as inadequacy of resources, environmental pollution, and global warming. Alongside large-scale conventional energy harnessing sources, many unconventional systems including solar, thermoelectric, electrostatic, piezoelectric, and electromagnetic were developed to convert the energy available in the ambient environment into usable electrical energy for self-powered electronic applications.

Following the first reported development of PENGs based on zinc-oxide nanowires in 2006, numerous piezoelectric nanostructures were utilized to construct nanogenerators, such as gallium-nitride nanorods, lead zirconate-lead titanate (PZT) nanofibers, and polyvinylidene fluoride polymer (PVDF) nanofibers. Owing to their high d_{33} value, inorganic perovskite piezoelectric crystals, such as $\text{Pb}(\text{Zr,Ti})\text{O}_3$ (PZT), BaTiO_3 (BTO), and PbTiO_3 (PT), were extensively investigated and explored for their energy-harvesting applications. However, the inherently brittle and rigid nature and requisite high-temperature synthesis of these ceramic materials often limit their applications. Moreover, a major concern and obstacle to commercialization related to traditional lead-based perovskite materials is the environmental toxicity of these materials. After exposure to water, the lead-based materials can easily form a solution containing the life-threatening lead, which may be released to the environment where it can accumulate in the food chain and impose deleterious impacts on ecosystems and human health.

Recently, lead-free flexible piezoelectric nanogenerators (PENGs) have drawn much attention because of the threat posed by lead (Pb)-based piezoelectric materials to the environment. Here, we reported an organic-inorganic hybrid perovskites (OIHP) PENG, which is a combination of lead-free formamidinium tin (Sn) halide perovskite ($\text{CH}(\text{NH}_2)_2\text{SnBr}_3$ (FASnBr₃)) nanoparticles (NPs) and polydimethylsiloxane (PDMS) polymer matrix. The OIHPs combine the advantages from both the organic molecular part and inorganic octahedron of the perovskite structure at a microscopic level, have been the focus of research for quite some time as a potential alternative to ceramics. Besides their distinct optoelectronic properties, OIHPs exhibit great advantages in terms of their compositional variability, structural flexibility, and room-temperature and solvent-based synthesis process.

The fabricated PENGs produced open circuit voltage (V_{oc}) of 94.5V, short-circuit current (I_{sc}) of 19.1 μA , and power density of 18.95 $\mu\text{W}/\text{cm}^2$. The fabricated FASnBr₃@PDMS PENGs was encapsulated between a Cu and PET/ITO electrode. We noticed a 180° change in the phase-hysteresis loop at the time of V-PFM measurements, and also observed a characteristics butterfly feature in the amplitude. Finally, to demonstrate the wireless communication capability an energy-efficient charging circuit was developed which functions in two different steps. In this process, the rectified electrical output from the PENG was stored to a smaller capacitor (1 μF) (step-1 charging). A commercial LTC-3588-1 unit was used to regulate the maximum charging level of this capacitor to 5 V. As soon as the output voltage of this capacitor reaches 5 V, the step-2 charging cycle begins and it transfers a portion of the stored electrical energy to a larger capacitor of 220 μF . In this periodic manner, electronic or wireless circuits can be repeatedly powered up using stored energy from the PENG, thus yielding potential to realize self-powered wireless sensing, structural health monitoring, self-powered implantable biomedical devices, and other critical sensor technologies. This study demonstrates the great potential of lead-free OIHPs materials in next-generation high-performance PENG applications.

SESSION EN02.05: Processing, Toxicity and Extended Applications

Session Chairs: Aram Amassian and Aron Walsh

Tuesday Afternoon, November 29, 2022

Hynes, Level 3, Ballroom B

1:30 PM *EN02.05.01

Toward Commercialization of Perovskite Solar Cells Through Advances in Materials and Process Hyun Suk Jung; Sungkyunkwan University, Korea (the Republic of)

All solid-state solar cells based on organometal trihalide perovskite absorbers have already achieved distinguished power conversion efficiency (PCE) to over 25% and further improvements are expected up to 27%. Now, the research on perovskite solar cells (PSCs) has been moving toward commercialization. To facilitate commercialization of these great solar cells, some technical issues such as long-term stability, large scale fabrication process, and Pb-related hazardous materials need to be solved. Also, flexible perovskite solar cell using plastic substrate can be used in niche applications such as portable electrical chargers, electronic textiles, and large-scale industrial roofing.

This talk is dealing with our recent efforts to facilitate commercialization of perovskite solar cells. For examples, we introduce a recycling technology of perovskite solar cells, which covers the regeneration process of Pb contained perovskite layer as well as recycling process of Au electrodes and transparent conducting oxide glass. Also, simple fabrication technologies for realizing large scale perovskite module are introduced and recent effort for achieving high efficiency module is going to be presented. Precursor technology is of great importance for yielding high efficiency and reproducibility of PSC, which is one of topics in this talk. Finally, recent interesting results regarding ultra flexible perovskite cells will be discussed.

2:00 PM EN02.05.02

Continuous Perovskite Solar Module Manufacturing—Scale-up Challenges and Solutions Rebecca Bolton, Sarah-Jane Potts, Carys Worsley and Trystan Watson; Swansea University, United Kingdom

Transitioning from research to industrial scale manufacture is a challenging task; renewable technology in particular must ensure that the pursuit of highly efficient and highly stable laboratory devices does not impose the requirement for expensive fabrication processes, scarce resources and inadmissible greenhouse gas emissions. Single junction metal halide perovskite cells (PSC), representing the next generation of solar energy harvesting, have recently achieved 25.7% certified efficiency on a lab scale: doubling in less than ten years. Screen-printed triple mesoscopic carbon electrode modules (mCPSC) are

one of the leading perovskite solar cell technologies earmarked for scale-up and commercialisation as a consequence of the inherent lower manufacturing cost and exceptional stability. The reality of scaling from “lab to fab” requires three key stages to be addressed and overcome:

What is the optimum laboratory scale design that can be successfully up-scaled?
What industrial scale optimisation is needed to best replicate the laboratory scale?
How can industrial scale devices be measured and validly compared back to laboratory scale?

This work highlights the difference between a good laboratory cell a good scalable cell and how the end goal of scale-up has directed recent research into laboratory architecture. This includes incidental improvements to full scale modules made from separate studies, such as green perovskite technology research leading to an unexpected improvement in the infiltration process. Industrial scale optimisation to accommodate the batch fabrication of mCPSC modules is also detailed with consideration for further development to continuous production. Notably, the curing and subsequent cooling of triple stack devices constructed on glass substrate is identified as a significant bottleneck for a continuous production line and requires precise optimisation for large area modules. Similarly, the infiltration process is specifically adapted to account for a greater surface tension effect of the perovskite precursor. Finally, recent improvements in technological capability have granted the ability for 520 cm² modules to be measured and accurately correlated to their laboratory scale counter parts; underlining the successful scale-up efforts made in the last year. The culmination of systematically addressing the three key challenges is marked by the construction of a large outdoor array of modules at the Solar Heat Energy Demonstrator (SHED) in Port Talbot, UK. The external data collected from these modules over the last 10 months will be discussed and the route to full scale manufacture presented.

2:15 PM EN02.05.03

Amorphization of Crystalline PbI₂ Stabilizes High Efficiency Perovskite Solar Cells [Shaun Tan](#), Tianyi Huang, Qiyu Xing and Yang Yang; University of California, Los Angeles, United States

Residual PbI₂ in the halide perovskite thin film is known to beneficially increase the performance of perovskite solar cells (PSCs). The residual PbI₂ exists in its crystalline hexagonal phase, distributed along the perovskite grain boundaries. However, it is also known that the presence of this crystalline PbI₂ is a double-edged sword, and sacrifices the long-term operational stability of PSCs. Under illumination, PbI₂ can undergo photolysis to decompose into metallic Pb and I₂ gas – the former constitutes a deep-level trap state, while the latter aggravates the perovskite phase degradation.

In this work, we demonstrate a strategy to suppress the crystallization of residual PbI₂. Synchrotron-based in-situ wide-angle X-ray scattering (in-situ WAXS) measurements were used to monitor the perovskite formation from solution and during thermal annealing, confirming the amorphization of PbI₂ into a secondary, non-crystalline phase. We observed that this amorphization of PbI₂ significantly improved the ambient, humidity, and photo stability of the perovskite thin films. Control experiments on perovskites with residual crystalline PbI₂ showed reduced or comparable stability under the same testing conditions. We verified the universality of our results on a variety of different perovskite compositions. Lastly, our champion devices also reached power conversion efficiencies approaching 25%, with an open-circuit voltage (V_{OC}) loss as low as 0.33 V.

2:30 PM EN02.05.04

Stable Ruddlesden-Popper Phase Inorganic-Cation Pseudohalide 2D Cs₂Pb(SCN)₂Br₂ Perovskite Single Crystal for Photodetector [Chwenhaw Liao](#)^{1,2}, Chu-Chen Chueh² and Anita W. Ho-Baillie¹; ¹The University of Sydney, Australia; ²National Taiwan University, Taiwan

3D metal halide perovskites (ABX₃ where A = Cs⁺, CH₃NH₃⁺, CH(NH₂)₂²⁺; B = Sn²⁺, Pb²⁺; X = Cl⁻, Br⁻, I⁻) have outstanding optoelectronic properties but suffer from poor long term stability or durability. 2D or quasi-2D layered perovskites may be part of the solution by introducing a separation between [PbX₆] octahedron inorganic layers using long carbon chain spacers in the A-site or the X-site. As organic spacers are insulating, appropriate selection is important to ensure the resulting perovskites retain small enough exciton binding energy and sufficient conductivity at least in a vertical direction through each inorganic slab. Here we demonstrate the advantage of X-site substitution over A-site substitution for layered perovskite resulting in much smaller separation between the constituent perovskite layers and hence optoelectronic properties.

This report is the 3rd one on X-site-substituted Ruddlesden-Popper (RP) phase perovskite single crystals since 2015 [1-3] and the first report on inorganic-cation pseudohalide 2D phase perovskite single crystal, Cs₂Pb(SCN)₂Br₂. We have been able to synthesize the crystal at room temperature (lower than those reported previously [1-2]) using the antisolvent vapor-assisted crystallization (AVC) method. Interestingly, the 2D single crystal undergoes first-order phase transformation to 3D cubic CsPbBr₃ above 450K but the transformation is reversible. Mechanisms of reversible transformations will be presented in the conference. A significant advantage of this Cs₂Pb(SCN)₂Br₂ single crystal is its small exciton binding energy of 160 meV, which is one of the lowest values reported for 2D perovskites (n = 1) and is comparable to the quasi-2D A-site substituted RP phase perovskite values. Finally, a Cs₂Pb(SCN)₂Br₂ single crystal photodetector is demonstrated with a respectable responsivity of 8.46 mA W⁻¹ and a detectivity of ≈1.2 × 10¹⁰ Jones at a low bias voltage of 0.5 V.

References

- [1] M. Daub, H. S. Hillebrecht. Synthesis, Single Crystal Structure and Characterization of (CH₃NH₃)₂Pb(SCN)₂I₂. *Angew. Chem.*, **2015**, 127, 11168.
- [2] J. Li, Q. Yu, Y. He, C. C. Stoumpos, G. Niu, G. G. Trimarchi, H. Guo, G. Dong, D. Wang, L. Wang, M. G. Kanatzidis, Cs₂PbI₂Cl₂, All-Inorganic Two-Dimensional Ruddlesden-Popper Mixed Halide Perovskite with Optoelectronic Response. *J. Am. Chem. Soc.*, **2018**, 140, 11085.
- [3] C. H. Liao, C. H. Chen, J. Bing, C. Bailey, Y. T. Lin, T. M. Pandit, L., Granados, J. Zheng, S. Tang, B. H. Lin, H. W. Yen, D. R. McCamey, B. J. Kennedy, C. C. Chueh, A. W. Ho-Baillie. Inorganic Cation Pseudohalide 2D Cs₂Pb(SCN)₂Br₂ Perovskite Single Crystal. *Adv. Mater.*, **2022**, 34(7), 2104782.

2:45 PM EN02.05.05

Utilizing Automated Gas Quenching for Improved Reproducibility in Perovskite Solar Cells [Samantha Kaczaral](#)¹, Samuel Schreiber², Daniel Morales Jr², Keith White², Michael F. Toney^{1,2}, David Moore³ and Michael McGehee^{1,2,3}; ¹University of Colorado, Boulder, United States; ²University of Colorado Boulder, United States; ³National Renewable Energy Laboratory, United States

An automated gas quenching process improves the reproducibility of perovskite solar cells by eliminating processing variables that change over time or from facility to facility. Broad human error can be eliminated by automating the process. Gas quenching, in comparison to antisolvent quenching, prevents the buildup of solvents in the spinning atmosphere. However, a further understanding of how gas quenching parameters can affect perovskite film formation is necessary to develop a robust methodology to create high performing devices. The developed methodology minimizes performance differences between batches of devices and allows for systematic film formation studies.

Gas quenching film formation has previously been studied with respect to the complexing solvent, NMP compared to DMSO. However, our experiments show that film formation changes based on the nitrogen quenching pressure/flowrate. The experiments were done on a 1.73 eV bandgap perovskite with a composition of DMA_{0.1}Cs_{0.3}FA_{0.6}Pb(I_{0.8}Br_{0.2})₂. As the nitrogen quench pressure increases, the homogeneity of the film improves based on XRD analysis.

As the gas quench pressure increases from 30 psi to 80 psi, the ratio of peak area for PVK(100):PbI₂(100) increases from 0.77 to 5.54 respectively. Based on in-situ photoluminescence spectra, PL transients also change as a function of gas quench pressure during the fabrication process. At pressures less than 50 psi, a dual peak is observed in the first 10 seconds of the quench which then homogenizes into a single peak. However, at pressures over 50 psi, only a single peak is observed during the entire duration of film formation.

One explanation of increasing heterogeneity at lower pressures is that certain salts (e.g. PbBr₂, CsI) nucleate first during the spin process when they cannot complex strongly with DMF/NMP. Excess PbI₂ that remains complexed with NMP increases the final film heterogeneity. As pressure increases, the solvents are removed at a faster rate which decreases the PbI₂ remaining in the solvate phase. In-situ GIWAXS data will be shown to describe the structural evolution of the film as a function of quenching pressure.

Film formation using the gas quenching method is less sensitive to the processing environment, compared to the antisolvent method. Gas quenched films show almost identical PL transients during film formation in a solvent free environment and a DMF saturated environment. Dual PL peaks were present at the same location and duration for both environments and the films ended at the same bandgap post quench. For the antisolvent method in a solvent free environment, dual PL peaks were present throughout the entire duration of the spin. However, in a DMF saturated environment, only a single PL peak was present for the duration of fabrication and the post-spin coat bandgap did not match that of the clean environment. Resiliency against solvent buildup during fabrication further improves the reproducibility of our automated gas quench system.

Upon setting up an automated gas quench system at both CU Boulder and NREL, our first observation is that pressure at the nitrogen source outlet is not a sufficient metric for describing our fabrication parameters. The optimum pressure for gas quenching at NREL is 100 psi; however, that caused the perovskite solution to be blasted off the substrate at CU. Based on this observation, it is necessary to report the flowrate of the nitrogen quench instead of the pressure, since tube diameter, curvature, and length can all result in different flowrates for a given input pressure. Using a systematic procedure, multiple researchers at NREL can obtain over 18% devices across multiple batches. The developed methodology can be applied to other facilities to achieve over 18% efficiency across multiple batches. The automated gas quenching process reproducibly resulted in high performing devices and allowed for systematic film formation studies.

3:00 PM BREAK

3:30 PM *EN02.05.06

Taming Defects in Halide Perovskites—Insights from Atomistic and Molecular Simulations [Shuxia Tao](#); Eindhoven University of Technology, Netherlands

Like any other semiconductors, the defects in halide perovskites determine the performance and long-term stability of the resulting optoelectronic devices. Understanding the electronic properties and chemical stability and their interplay are paramount. In this talk, I will present our recent findings on these aspects using atomistic simulations from Density Functional Theory and reactive Molecular Dynamics. By determining the electronic and dynamical properties of several defects, we identify the harmful ones which lead to either recombination losses or chemical degradations. I will also show several strategies to mitigate and passivate these defects. These include engineering compositions of perovskite absorbers/emitters and interfaces in the devices, applying additives and optimizing growth conditions, etc.. The atomistic insights provide a basis for further improving the performance and stability of perovskite devices by optimizing the interplay of these factors.

4:00 PM EN02.05.07

Halide-Dependent Formation Dynamics of 2D Ruddlesden-Popper Phases on 3D Perovskites [Tim Kodalle](#)¹, Carlo Andrea Riccardo Perini², Mriganka Singh¹, Juan Pablo Correa Baena² and Carolin M. Sutter-Fella¹; ¹Lawrence Berkeley National Laboratory, United States; ²Georgia Institute of Technology, United States

While organic-inorganic perovskites achieved competitive power conversion efficiency within a short time¹, they still suffer from insufficient stability². A promising approach to improve their long-term stability is the incorporation of bulky, hydrophobic molecules into the perovskite layer³. The addition of these species onto the 3D perovskite induces the formation of 2D Ruddlesden-Popper (RP) phases, and their formation dynamics along with the effects of these 2D layers on the material's optical/electrical response in solar cells are under intense debate. Recently, we showed that the formation dynamics of these RP phases strongly depend on the choice of the bulky molecules.⁴

In this study, we investigate the role of the halide (Iodine, Bromine, and Chlorine) in Phenethylammonium halides (PEAX) on the formation dynamics of RP phases on triple cation, mixed halide perovskite thin films. Using a multimodal approach combining *in situ* photoluminescence (PL), and *in situ* grazing incidence wide-angle X-ray scattering (GIWAXS) measurements during spin-coating and annealing, we monitor the deposition of the PEAX molecules and investigate the formation mechanics of the subsequently forming RP-phases. We find that the formation dynamics strongly depend on the halide used for the RP phase: In the case of Iodine, we see clear evidence for a slow conversion from the PEAI salt to pure 2D ($n = 1$ in $A'_2A_{n-1}B_nX_{3n+1}$, where A' is PEA, A is Cs,MA,FA, B is Pb, and X is the halide) and quasi-2D ($n > 1$) phases. In the case of PEABr and PEACl, however, we observe a rather fast formation of solely $n = 1$ RP-phases indicating different reaction dynamics and phase stability depending on the halide used. Furthermore, we observe an intermixing of Br and I when PEAI or PEABr is deposited on the I- and Br-containing 3D perovskite but no significant intermixing in the case of the PEACl. The latter might suggest a further increase of the chemical stability of the 2D RP phase with decreasing size of the used halide.

Our results illustrate how multimodal *in situ* characterization can provide mechanistic insights into the 2D layer formation and its interaction with the 3D perovskite. Therefore, it can be utilized to deliberately optimize the annealing sequence targeting an ideal 2D/3D interface satisfying enhanced charge transport and stability. We will further correlate these mechanistic insights with device performance and stability.

References:

- [1] M. A. Green et al., *Prog. In Photov.: Res. & Appl.* 29(7), 2021.
- [2] J. A. Christians et al., *J. Am. Chem. Soc.* 137(4), 2015.
- [3] C. Ma et al., *Nanoscale* 8, 18309, 2016.
- [4] T. Kodalle et al. *Advanced Energy Materials*, Accepted for Publication, 2022. [DOI: 10.1002/aenm.202201490]

4:15 PM EN02.05.08

Does the Solvent Matter?—Influence of the Solvent in Hybrid Halide Perovskites Precursor Solution [Ana Palacios Saura](#)¹, Joachim Breternitz¹, Armin Hoell¹ and Susan Schorr^{1,2}; ¹Helmholtz-Zentrum Berlin für Materialien und Energie, Germany; ²Freie Universität Berlin, Germany

Hybrid halide perovskites (HHPs) are highly promising photovoltaic absorbers not only for using low-cost solution-based processing methods but also for the outstanding increase in power conversion efficiency of solar cells up to 25.5% in 2021[1].

Despite HHPs popularity, the growth mechanism of HHP crystals in solution is still unknown. With this study, we aim to bring more clarity about the precursor arrangement in solution prior to crystallization and how the solvent affects the atomic arrangement in this early state. For this purpose, we applied small angle synchrotron X-ray scattering (SAXS) to investigate precursor solutions of different HHPs (MAPbI₃, MAPbBr₃, MAPbCl₃, MAPb(I,Br)₃ and FAPbI₃) in different common solvents used to synthesize HHPs layers, such as γ -butyrolactone (GBL), dimethylformamide (DMF), dimethyl sulfoxide (DMSO) and mixtures thereof.

SAXS is a non-destructive characterization technique based on the difference between elastic scattering objects in a solution. With SAXS, it is possible to investigate the size and shape of scattering objects ranging between 1 – 100 nm, determining also the distance between adjacent scattering objects and their interaction with each other[2,3]. We performed SAXS experiments at the HZB synchrotron radiation source BESSYII, at the four-crystal monochromator beamline of the Physikalisch-Technische Bundesanstalt[4] using the ASAXS endstation[5]. Samples have been prepared by dissolving binary precursors (e. g. MAI and PbI₂ to synthesize MAPbI₃) in a solvent. The solutions with a concentration of 0.8 M were measured by SAXS 60 minutes after their preparation.

Our measurements show a clear maximum in the scattered intensity at q -values of $\sim 3 \text{ nm}^{-1}$, which holds two essential pieces of information: it demonstrates the agglomeration of scattering objects and the peak position corresponds to the most abundant distance of scattering objects in a range of 2-3 nm. While all solutions show agglomerations, we were able to demonstrate that the size of those agglomerates changes with the composition of HHP precursors, but also with the solvent. Based on this information, we have developed a core-shell model with [PbX₆] octahedra ($X = \text{Cl}, \text{Br}, \text{I}$) in the core surrounded by solvent molecules to describe the scattering objects. The size of the solvent molecules as well as the radii of Pb and halides forming [PbX₆] octahedra were derived from a combination of experimental values from diffraction and computationally obtained electron density distributions. We can explain the solvent dependent variation of the experimentally determined distance between the scattering objects by a core size variation realized by a combination of isolated octahedra or corner-sharing octahedra as core, respectively. Since the solvent molecules can be described as an ellipsoid, their orientation must be taken into account. We can explain the variations of the minimal possible distance between the scattering objects (R_{HS}), evaluated from the structure factor determined by analyzing the SAXS data (using SASfit) by a preferred orientation of the solvent molecules in the solvent shell of the scattering objects. Therefore, the choice of the solvent may not only depend on the precursor solubility but also on their chemical and physical behavior. We will discuss the influences of precursor composition and solvent on the core as well as the solvent shell of the scattering objects, since they have the potential to influence the crystallization process of the HHP and therefore the performance of a device produced from solution processing.

[1] Min et al., Nature, 2021, 598, 444

[2] Schnablegger et al., Anton Paar GmbH, 2013

[3] Flatken et al., J. Mater. Chem. A, 2021, 9, 13477

[4] Krumrey et al., Nucl. Instrum. Methods Phys. Res., Sect. A, 2001, 467, 1175

[5] Hoell et al., DE102006029449, 2007

4:30 PM *EN02.05.09

Formation, Stability and Crystallization in Two-Dimensional Perovskites—From Nanoplates to 2D/3D Interfaces Analyzed by *In Situ* Experiments Ana F. Nogueira; University of Campinas, Brazil

Metal halide perovskite solar cells have reached the recent efficiency breakthrough of 25.6%, higher than silicon polycrystalline photovoltaics. Such fantastic result was only possible due to a precise control and engineering of the morphology, interfaces, defects, and the use of multiple cations in perovskite A-site, as Rb, Cs, MA (methylammonium), FA (formamidinium) and long alkyl cations as phenylethylammonium (PEA). Dimensionality of perovskite materials can be easily controlled by the choice of the cation in the A site, providing structures from zero (0D), one (1D), two (2D) and three-dimensions (3D), amplifying the use of these materials in lighting, lasers and sensors. For tandem perovskite solar cells, a mixture of different anions, as Br and I is also desired to adjust the band gap. Such cocktail of different cations and anions influences not only the structure and dimensionality, but the formation of undesirable phases, halide segregation, defects, etc. They have also a huge impact on device's efficiency and stability.

In this presentation, we will summarize important results using *in situ* experiments to probe the formation of 2D perovskite materials, from nanoplates to micro-sized structures as well 2D/3D interfaces. Dynamics of the formation of these structures and interfaces in solution or solid state, their stability under thermal stress and aggregation, were studied by *in situ* experiments probing the samples with both X-rays and/or visible radiation. For that, we employed time-resolved grazing incidence wide angle X-ray scattering (GIWAXS), small angle X-Ray scattering (SAXS), high-resolution XRD and PL spectroscopy taken at the Brazilian Synchrotron National Laboratory and Lawrence Berkeley National Laboratory.

[1] T. Kodalle, R. Moral, L. Scalón, R. Szostak, M. Abdelsamie, P. E. Marchezi, A. F. Nogueira, C. M. Sutter-Fella, "Revealing the transient formation dynamics and optoelectronic properties of 2D Ruddlesden-Popper phases on 3D perovskites", Advanced Energy Materials, in press, (2022)

[2] R. Szostak, S. Sanchez, P. E. Marchezi, A. Marques, J. C. Silva, M. S. Holanda, H. C. N. Tolentino, A. Hagfeldt, A. F. Nogueira, "Revealing the perovskite film formation using the gas quenching method by in situ GIWAXS: morphology, properties and device performance", Advanced Functional Materials, 31, 2007473 (2021)

[3] A. Sutanto, R. Szostak, N. Drigo, V. Queiroz, P. E. Marchezi, J. C. Germino, H. N. Tolentino, M. Nazeeruddin, A. F. Nogueira, G. Grancini "In Situ Analysis Reveals the Role of 2D Perovskite in Preventing Thermal-Induced Degradation in 2D/3D Perovskite Interfaces", Nano Letters, 20(5) 3992-3998 (2020)

[4] P. E. Marchezi, E. M. Therézio, R. Szostak, H. C. Loureiro, K. Bruening, A. Gold-Parker, M. A. Melo Jr., C. J. Tassone, H. C. N. Tolentino, M. F. Toney, A. F. Nogueira, "Degradation mechanisms in mixed-cation and mixed-halide Cs_xFA_{1-x}Pb(Br_{1-y}I_y)₃ perovskite films under ambient conditions" J. Mater. Chem. A, 9, 9302-9312 (2020)

[5] R. F. Moral, L. G. Bonato, J. C. Germino, W. X. Oliveira, R. Kamat, J. Xu, C. Tassone, D. D. Stranks, M. F. Toney, A. F. Nogueira, "Synthesis of Polycrystalline Ruddlesden-Popper Organic Lead Halides and Their Growth Dynamics", Chemistry of Materials, 31 (22) (2019), 9472-9479

SESSION EN02.07: Surface and Interface Science and Engineering

Session Chairs: Yi Hou and Hyun Suk Jung

Wednesday Afternoon, November 30, 2022

Hynes, Level 3, Ballroom B

1:30 PM *EN02.07.01

Interlayer Engineering in Halide Perovskite Solar Cells Jun Hong Noh; Korea University, Korea (the Republic of)

Halide perovskite solar cells (PSCs) have a typical device structure of polycrystalline thin-film solar cells such as CdTe and CIGS solar cells. PSCs have

surpassed the conventional polycrystalline thin-film solar cells, and now it has become an important issue whether low-temperature solution-processed polycrystalline PSCs can reach the radiative limit like epitaxial GaAs thin-film solar cells. In this talk, our recent approaches to improving the photovoltaic performance of PSCs in terms of the electrical and optical design of PSCs will be discussed. The local electric field design within the perovskite layer between charge transport layers (CTLs) by introducing a wide-bandgap halide layer enabled improved power conversion efficiency. In addition, the boosting radiation of the stacked perovskite layer between CTLs in the complete device by efficient reduction of interfacial non-radiative recombination could also bring performance gain by photon recycling and scattering. The electrical field and optical radiation design by interlayer engineering could be one of the strategies to reach the radiative efficiency limit. Our recent results of oxide CTLs will be discussed to improve the processability and long-term stability of PSCs.

2:00 PM EN02.07.02

Interfacial Toughening in Perovskite Solar Cells Zhenghong Dai and Nitin P. Padture; Brown University, United States

Metal halide perovskites (MHPs) have emerged as the most promising light-absorber materials in the photovoltaic community due to their near-ideal bandgaps and extraordinary optoelectronic properties. However, MHPs are inherently compliant, soft, and brittle. While significant progress has been made in improving the stability of MHPs, perovskite solar cells (PSCs) will also need to be mechanically reliable if they are to operate efficiently for decades. In this context, we study the fracture behavior of PSCs by measuring their cohesion energies (G_c) using double cantilever beam method. By revealing the fractured pathway, we conclude several factors determining the G_c of PSCs including grain size, crystallinity, and interfacial toughness. Also, we report a dual interface reinforcement approach to strategically enhance the interfacial adhesions of two important interfaces in PSCs (electron transporting layer/MHP, and MHP/hole transporting layer), the resulting PSCs demonstrate unprecedented performance, stability, and reliability. This work points to a new route for designing mechanically robust PSCs with long-term durability.

2:15 PM EN02.07.03

Targeted Crystallization of 3D/Polytype Phase Heterostructures in High-Bromide Content Perovskites Joel Smith¹, Margherita Teddei², Pietro Caprioglio¹, Benjamin Gallant¹, Saqlain Chaudhary¹, David Ginger² and Henry Snaith¹; ¹University of Oxford, United Kingdom; ²University of Washington, United States

Mixed-dimensionality metal-halide perovskite films comprising heterostructured interfaces, grain boundaries or surfaces primarily using '2D' phases enable control over optoelectronic properties, interfaces and stability in functional devices. Less explored are low-dimensional polytype phases maintaining ABX_3 stoichiometry, but with mixtures of face- and corner-sharing octahedral arrangements. Here we present our latest data exploring deliberate introduction of targeted polytype phases via both surface treatment and bulk solution additive approaches applied primarily to high-bromide content methylammonium-free perovskite compositions with 1.7 eV and 1.8 eV band gaps. By blade-coating solutions and monitoring using synchrotron-based *in situ* grazing-incidence wide-angle X-ray scattering (GIWAXS) we look at the impact on the crystallization process of different additives. Drawing on the chemical structure and stability of formamidinium, these include ethylenediamine, imidazolium and guanidinium derivatives. From this we find significant differences in the heterogeneity of the perovskite phase and demonstrate enhancements in the ambient stability of these materials. Combining solution characterisation methods including nuclear magnetic resonance (NMR) spectroscopy, we establish a clear understanding of the bridge between solution chemistry, precursor phase formation and resulting material properties across a range of perovskite compositions. Our work provides important insight into the controlled growth of stable perovskite materials by engineering the composition of benign secondary phases.

2:30 PM BREAK

3:30 PM EN02.07.04

Surface Passivation Strategies for Stable Tin Halide Perovskite Solar Cells Studied by Hard X-Ray Photoelectron Spectroscopy Roberto Félix¹, Jorge Pascual¹, Meng Li¹, Mahmoud Hussein¹, Lucas Bodenstein-Dresler¹, Elif Hüsam¹, Claudia Hartmann¹, Regan G. Wilks^{1,1}, Antonio Abate^{1,2} and Marcus Baer^{1,1,3}; ¹Helmholtz-Zentrum Berlin für Materialien und Energie GmbH, Germany; ²University of Naples Federico II, Italy; ³Helmholtz-Zentrum Berlin für Materialien und Energie (GmbH), Germany

Halide perovskite (HaP) solar cells – particularly those using $APbX_3$ [$A = CH_3NH_3^+$ (MA^+), $HC(NH_2)_2^+$ (FA^+), Cs^+ and $X = I, Cl, Br$] as the absorber layer – have recently achieved power conversion efficiencies (η) over 25%, surpassing the record η of well-established photovoltaic technologies based on multicrystalline silicon-wafers or chalcopyrite and cadmium telluride thin-film solar cell absorbers [1]. A major concern related to HaP absorbers is, however, the toxicity of Pb. Ongoing efforts to replace Pb by Sn have so far yielded relatively low-performing solar cells (with record η below 15 % [2]), likely limited by defect formation in the absorber material due to the tendency of Sn to oxidize from Sn^{2+} to Sn^{4+} [3]. To overcome this obstacle, preparation recipes of Sn-based perovskite absorbers routinely include the use of SnX_2 additives (SnF_2 being the mostly widely used) to produce a Sn-rich precursor environment; this is reported to lead to better-quality films, in terms of morphology, decreased presence of secondary phases and Sn^{4+} content [4]. Moreover, it has been demonstrated that the halide anion (e.g., F^-) can influence positively the perovskite crystallization process, in addition to complexing with Sn^{4+} and preventing it from being introduced into the absorber films [5]. Recently, another approach to improving the stability of Sn perovskites has entailed the use of two-dimensional (2D) Ruddlesden-Popper phase-layered perovskites [6,7], where long and/or bulky chain organic cations [e.g., alkylammonium cations, phenyl ethyl ammonium (PEA), etc.] with more hydrophobic properties than A^+ cations (commonly found in HaPs) form a hydrophobic surface (i.e., spacer) expected to prevent oxidizing agents from reaching the absorber. Although the implementation of these strategies is becoming more widespread in Sn-based HaP devices, the underlying passivation/antioxidation mechanisms, as well as the effect of the treatments on the chemical and electronic properties of resulting absorbers, are not fully understood.

Because these strategies focus on the surface nature of the films, characterizations of treated samples by (near) surface sensitive techniques are uniquely suited to provide valuable insight to fill this knowledge gap. For this purpose, we have employed hard X-ray photoelectron spectroscopy (HAXPES) to study the chemical and electronic structure of $FASnI_3$ thin-film sample series treated (i) by using different tin halide additives (i.e., SnI_2 , SnI_4 , $SnBr_2$, SnF_2 and SnF_4) during preparation and (ii) with a combination of bulky and long organic surfactants (i.e., PEACl and perfluorinated carbon chain molecules with varying concentrations) during and after preparation. Employing different excitation energies allows the probing depths of HAXPES measurements to be varied, facilitating a depth-dependent assessment of the effect of the treatments. Evidence of highly heterogeneous Sn and I chemical environments is found for untreated $FASnI_3$ samples (being more pronounced at the surface than towards the bulk of the sample), turning more homogeneous (e.g., exhibiting enhanced Sn^{2+} -character) in samples submitted to performance-enhancing additive treatments. The relation between the HAXPES-determined $[Sn^{2+}]/([Sn^{2+}]+[Sn^{4+}])$ values of the investigated samples and their electronic structure is discussed in this contribution, as well as a comparison of the chemical and electronic properties with the device performance (improvements) of the corresponding solar cells.

[1] NREL Best Research-Cell Efficiency Chart. <https://www.nrel.gov/pv/cell-efficiency.html>.

[2] X. Jiang et al., *J. Am. Chem. Soc.* **2021**, *143*, 10970.

[3] N. K. Noel et al., *Energy Environ. Sci.* **2014**, *7*, 3061.

- [4] C. Hartmann, S. Gupta et al., *ACS Appl. Mater. Interfaces* **2020**, *12*, 12353.
 [5] J. Pascual, M. Flatken et al., *Angew. Chem. Int. Ed.* **2021**, *60*, 21583.
 [6] C. Liang et al., *Energy Environ. Mater.* **2018**, *1*, 221.
 [7] M. Li et al., *ACS Energy Lett.* **2020**, *5*, 1923.

3:45 PM EN02.07.05

Homogeneously Miscible Fullerene Inducing Vertical Gradient in Perovskite Thin-Film Towards Highly Efficient Solar Cells [Il Jeon](#)^{1,2}, Han Y. Woo³, Kyusun Kim¹, Ziang Wu³ and Jiye Han^{1,2}; ¹Sungkyunkwan University, Korea (the Republic of); ²Pusan National University, Korea (the Republic of); ³KU-KIST, Korea (the Republic of)

One of the strategies for obtaining high PCE in PSCs is to use additives for perovskite films. Small amounts of added materials in the perovskite precursor function as a crystal growth template and a crystal growth retarder, which increase the perovskite crystal size and subsequently reduce the interfacial area of grain boundaries. This, in effect, decreases the charge traps that exist at the grain interfaces. Moreover, some additives remain in the perovskite films even after the fabrication, passivating the perovskite defect sites via the Lewis acid-base coordination and sometimes function as charge bridges or charge extractors. A variety of materials have been reported to function as additives and passivation layers, which range from polymers to nanocarbons, such as fullerene derivatives. Among the fullerene derivatives, phenyl-C₆₁-butyric acid methyl ester (PC₆₁BM) has shown promising prospects owing to its high electron affinity and appropriate bandgap. Accordingly, various fullerene derivatives synthesized by modifying PC₆₁BM have been reported. However, there is a significant challenge in using those fullerene derivatives; they are immiscible with polar solvents while most perovskite precursors are dissolved in polar solvents. Conventionally, fullerene additives are either introduced during the antisolvent stage using chlorobenzene (CB) or dispersed directly in the perovskite precursor solution. This restricts the amount of the additives that can be added, and the device architecture to the inverted-type which gives a lower PCE than the normal-type counterparts.

In this work, we attached, triethylene glycol monomethyl ether (TEG) chains to PC₆₁BM to greatly enhance its miscibility with the perovskite precursor. The synthesized TEG-attached PC₆₁BM, [6,6]-phenyl-C₆₁-butyric acid 2-[2-(2-methoxyethoxy)ethoxy]ethyl ester (PC₆₁B-TEG), and a branched substituent with two TEGs-attached PC₆₁BM, [6,6]-phenyl-C₆₁-butyric acid 1-methyl 3-[2-(2,5,8,11-tetraoxadodec-1-yl)-4,7,10,13-tetraoxatetradec-1-yl] ester (PC₆₁B-BiTEG) were highly polar and miscible with the perovskite precursor. Here, we explored three ways to introduce novel fullerene derivatives into PSCs: direct mixing with the precursor prior to film fabrication, overcoating the electron-transporting layer, and overcoating + waiting between drop-casting and spin-coating of the perovskite precursor solution on the overcoated layer of PC₆₁B-TEG to induce gradient dispersion into the perovskite precursor. The initial optimization and tests were conducted using MAPbI₃ (CH₃NH₃PbI₃)-based PSCs. The results showed that the devices in which PC₆₁B-TEG was directly added to the perovskite precursor gave a high open-circuit voltage (V_{OC}), while the overcoating and waiting approaches yielded a high fill factor (FF). We postulate that such a tradeoff arises from the balance between the perovskite grain defect passivation and the electron-transporting (hole-blocking) effect. In either case, an average PCE of ~19.6% was obtained, which is much higher than ~17% of the reference devices without PC₆₁B-TEG. Contrary to our expectation, the newly synthesized PC₆₁B-BiTEG was not as effective as PC₆₁B-TEG, because of its high-lying highest occupied molecular orbital (HOMO) level, which induced charge recombination. Applying the fullerene additive to a more advanced formamidinium/methylammonium mixed cation lead halide (FA_{0.65}MA_{0.35}PbI₃-Cl) system using a combined approach of direct mixing with the precursor and overcoating + waiting techniques manifested even greater effectiveness. A PCE of 23.34% was exhibited when PC₆₁B-TEG was used in FA_{0.65}MA_{0.35}PbI₃-Cl-based PSCs. The same device was taken to a national laboratory for verification and a forward and reverse bias-combined efficiency of 21.24% was officially certified. This, to the best of our knowledge, is one of the highest efficiencies reported among the fullerene additive-used PSCs reported thus far.

4:00 PM *EN02.07.06

Reactive Interfaces—How Metal Oxides Interact with Halide Perovskites and Their Precursors [Selina Olthof](#); University of Cologne, Germany

In optoelectronic devices, the function and performance depends crucially on the proper choice of charge transport layers. In perovskites it turned out that interfaces towards these layers can be rather complex. On the one hand, interface dipoles and band bending occur. But more importantly, the perovskite composition and formation can be significantly influenced by chemical reactions taking place, in particular next to metal oxides.

In this talk, I will summarize our work on a variety of metal oxides such as SnO_x, NiO_x, MoO₃, ZnO, TiO₂ etc. in which we use photoelectron spectroscopy to analyze which components are responsible for the strong interface chemistry. For this, we investigated a variety of different perovskites (i.e. organic vs. inorganic ones, I vs. Br, etc.) as well as the individual perovskite precursors. We find that the reactivity strongly depends on the individual material combination and that different metal oxides show fundamentally different reaction/degradation pathways. Intriguingly, we find that by changing the metal oxide post-treatment we alter the surface defect density and thereby affect the degree of thin film degradation significantly.

Overall, I will show how photoelectron spectroscopy measurements can help to probe and understand the processes going on at these various bottom contact materials which should ultimately help to improve the stability of perovskite related devices.

4:30 PM EN02.07.07

Reconfiguring Perovskite Surface States to Maximise Perovskite Solar Cells [Sam Teale](#), Hao Chen, Bin Chen and Edward H. Sargent; University of Toronto, Canada

Non-radiative recombination rates are orders of magnitude higher at the interfaces of perovskite solar cells (PSCs). Here we illustrate that the cause of interfacial recombination is dependant on both contact type (n-type or p-type) and perovskite composition, each of which must be considered in all-perovskite tandem cells. For example, at p-type contacts, quantum confined (2D) perovskite interfaces have produced single junction cells with > 25% certified power conversion efficiency (PCE), whereas 2D layers hinder charge transport at the n-type contact. Considering composition, we find that the surfaces of wide bandgap (≥40% Br) perovskite films crystallize into PbI₂ and Br-rich perovskite regions which induce recombination. Using surface sensitive spectroscopy, we address the specific problem at each interface of a monolithic all-perovskite tandem: first we tune confinement in 2D layers to improve transport at the n-type contacts, and then remove surface inhomogeneity using diammonium salts in wide bandgap layer. This enables record efficient monolithic perovskite tandems with 2.19 V V_{OC} (89% of the theoretical voltage limit) and > 27% PCE.

4:45 PM EN02.07.08

Understanding Light Induced Dynamic Ion Motion in Metal Halide Perovskite Bilayers Through Surface Photovoltage [Tomi Baikie](#)¹, Philip Calado², Krzysztof Galkowski¹, Zahra Andaji-Garmaroudi¹, Akshay Rao¹, Samuel D. Stranks¹ and Piers Barnes²; ¹University of Cambridge, United Kingdom; ²Imperial College London, United Kingdom

Surface photovoltage measurements (SPV) on highly doped semiconductors, such as those used in commercially available photovoltaics and LEDs, can reveal rich information on photoinduced charge dynamics. However, SPV measurements on mixed ionic-electron conductors, such as perovskites, have been poorly understood. We outline a new understanding of SPV measurements, supported by experimental evidence on perovskite bilayers. Our model, which includes mobile ionic carriers, accurately reproduces these complex SPV measurements, even upon the application of different surface treatments and backing contacts. Importantly, we conclude that the SPV in the perovskite bilayer context is a measurement of the change in potential associated solely

with changes in the net electronic charge within the system. Our understanding of the SPV measurement naturally leads to avenues for the selective control of ion migration in perovskite bilayers, demonstrated here by altering the surface passivation treatment. This opens new avenues for the rational design of strategies to improve the photovoltaic properties of perovskite solar cells and LEDs.

5:00 PM EN02.07.09

In Situ Buried Interface Passivation for Efficient and Stable Perovskite Solar Modules Mingyang Wei¹, Lin Li^{2,1}, Xiong Li² and Michael Graetzel¹; ¹Swiss Federal Institute of Technology Lausanne (EPFL), Switzerland; ²Huazhong University of Science and Technology, China

Scaling-up perovskite solar cells (PSCs) is a prerequisite to the adoption of perovskite photovoltaics. High-performance perovskite solar modules (PSMs) require the passivation of device interfaces; however, this is challenging for the buried interface, i.e., the interface between the bottom charge transport layer (CTL) and perovskites, because the passivating agents on the substrate surface may be redissolved during the perovskite deposition. Here, we report that this limitation can be overcome with in-situ buried interface passivation using nickel oxide (NiO_x) as the bottom CTL – a quality established via directly adding traces of molecular additives into the perovskite precursor solution. Molecular dynamics (MD) simulations indicate that a cyanoacrylic acid-based organic dye, namely BT-T, can achieve monolayer passivation with planar configurations at the perovskite/NiO_x interface. Density functional theory (DFT) calculations reveal that BT-T exhibits a stronger interaction with NiO_x than perovskites. As a result, we find a preference for BT-T molecules to passivate the buried interface during perovskite film formation. The BT-T passivation facilitates interfacial hole transfer and improves the quasi-Fermi level splitting (QFLS) of the perovskite/NiO_x bilayer by ca. 40 meV. Using this strategy, we demonstrate a power-conversion efficiency (PCE) of 22.1% for 1-cm²-sized PSCs and a record-setting PCE of 20.3% (certified stabilized PCE: 18.94%) for NiO_x-based PSMs with an active area of 17.11 cm². The encapsulated PSM retained 90% of its initial PCE (20.1%) following 1000-h maximum power point (MPP) tracking under 1-sun-equivalent light illumination at 50 °C. This work demonstrates the potential of organic dye molecules as scalable and efficient buried interface modifiers for PSMs.

SESSION EN02.08: Poster Session II

Session Chairs: Jin-Wook Lee, Carolin Sutter-Fella and Wolfgang Tress

Wednesday Afternoon, November 30, 2022

8:00 PM - 10:00 PM

Hynes, Level 1, Hall A

EN02.08.01

Utilisation of PEDOT as a Hole Selective Layer for Reproducible Efficient Tin-Based Perovskite Solar Cells with the DMSO-Free Solvent System Ece Aktas¹, Diego Di Girolamo¹, Corinna Ponti¹ and Antonio Abate^{1,2}; ¹University of Federico II, Italy; ²Helmholtz-Zentrum Berlin für Materialien und Energie, Germany

Hybrid metal-organic lead-based perovskite solar cells (PSCs) have shown great performance as a photovoltaic energy source, having comparable high efficiency to commercialised silicon solar cells.¹ Moreover, they are prone to be deposited on variable substrates using cost-effective techniques likewise roll-to-roll processing.² At this point, considering the toxicity of the lead counterparts used will be a critical step in overcoming the commercialization challenge, especially for market niches such as wearable photovoltaics. Tin-based perovskites have gained considerable attention owing to having similar optoelectronic properties to lead-based counterparts such as high charge carrier mobility, small exciton binding energy, and a bandgap close to the ideal value which guarantees a PCE approaching 15%.^{3,4} However, Sn²⁺ quickly oxidizes to Sn⁴⁺ in the presence of oxygen or even with a mildly oxidative solvent system,⁵ limiting their performance in PSCs. Here, we discuss the advantages of adopting water-free poly(3,4-ethylenedioxythiophene) (PEDOT) formulation in hybrid metal-organic tin-based PSCs. We effectively alternated the surface energy of the water-free PEDOT to form a high-quality perovskite film over macroscopic areas. Moreover, we performed a careful perovskite optimization to achieve a power conversion efficiency above 7% for tin-based perovskite solar cells with a DMSO-free solvent system and good operational stability.

1. National Renewable Energy Laboratory. PV Efficiency Chart. <https://www.nrel.gov/pv/cell-efficiency.html> (2022).

2. *Nat. Commun.* **11**, 1–11, (2020).

3. *Energy Environ. Sci.* **14**, 1286–1325, (2021).

4. *J. Am. Chem. Soc.* **143**, 10970–10976, (2021).

5. *Mater. Adv.* **1**, 1066–1070, (2020).

EN02.08.02

Tuning the Surface Potential of Hybrid Perovskite Active Layers Through Interfacial Engineering Using Fluorinated Compounds Riva Alkarsifi^{1,2}, Thierry Buffeteau¹, Lionel Hirsch², Thierry Toupance¹ and Dario M. Bassani¹; ¹University Bordeaux, ISM, CNRS UMR5255, F-33405 Talence, France, France; ²University Bordeaux, IMS, CNRS, UMR 5218, Bordeaux INP, ENSCBP, F-33405 Talence, France, France

Despite the tremendous increase in their overall power conversion efficiency over the past decade, organic-inorganic hybrid perovskite solar cells are still plagued by issues related to their long-term device stability.¹ In particular, the hydrophilicity of the hybrid organic-inorganic perovskite surface due to the ionic nature of the perovskite crystal plays a key role in determining device stability.² In order to improve device stability and performance, the localization of a thin interfacial monolayer can be used to reduce the wettability of the perovskite and also to modify the surface potential of the active perovskite layer.^{1,3} For instance, fluorocarbons possess strong hydrophobicity and exhibit specific binding interactions with the perovskite surface.² Because of this, they may be good candidates for passivating the surface while also optimizing its surface potential.² We investigate self-assembled monolayers on top of the CH₃NH₃PbI₃ surface using various fluorinated molecules with different heteroatoms including tin, phosphorous, and boron. The chemical nature of the fluorinated monolayers, their interaction, orientation, and thickness were investigated by contact angle measurement, X-ray diffraction, X-ray photoelectron spectroscopy, and polarization-modulation infrared reflection absorption spectroscopy. The formation of stable monolayers with specific orientation on top of the perovskite surface was achieved without altering the bulk crystallinity of the active layer as evidenced by XPS. In addition to the increased hydrophobicity of the CH₃NH₃PbI₃ surface, the surface potential of CH₃NH₃PbI₃ was easily tuned over a 160 mV range upon SAMs deposition. This work clearly shows that chemically engineering the composition of the monolayer allows for modifying the perovskite work function, and hence the electrical behavior of the active layer.

¹ Christian M. Wolff *et al.*, *ACS Nano* 2020, 14, 1445–1456

² Weixin Huang *et al.*, *Chem. Mater.*, 2016, 28, 303–311.

EN02.08.03

Hole-Transporting Self-Assembled Monolayer Enables 23.1%-Efficient Single-Crystal Perovskite Solar Cells with Enhanced Stability Khulud M. Almasabi; KAUST, Saudi Arabia

The challenge of growing perovskite single crystals in suitable configurations for efficient photovoltaic devices has severely hindered their exploration as solar cell materials, in spite of their potential to advance perovskite solar cell technology owing to their excellent optoelectronic properties and lower defect densities. While polycrystalline films can be deposited on myriad substrates, perovskite single crystals suitable for high-efficiency devices have only been illustrated on hydrophobic hole transport layers (HTLs, e.g., poly(triaryl amine) (PTAA)), which has restricted the development in both device efficiency and stability. In this work, we report the growth of mixed-cations $\text{FA}_{0.6}\text{MA}_{0.4}\text{PbI}_3$ perovskite single crystals on a hydrophilic self-assembled monolayer (SAM, [2-(3,6-dimethoxy-9H-carbazol-9-yl) ethyl]phosphonic acid), (MeO-2PACz)) HTL surface. Solar cells constructed with SAM MeO-2PACz exhibit improved mechanical adhesion, operational stability, and a record efficiency of 23.1% for single-crystal perovskite solar cells.

EN02.08.04

Solvent Engineering of NiO_x Solutions for Rapid Depositions as Hole Transporting Layers for Flexible Perovskite Solar Cells Peter Armstrong, Sashil Chapagain, Siva Chandra Sekhar Pakanati, Thad L Druffel and Craig Grapperhaus; University of Louisville, United States

State of the art perovskite solar cells (PSCs) have reached record efficiencies on laboratory scale systems. However, transitioning to large scale fabrication of PSCs is still a work in progress. A part of the next steps necessary for upscaling the fabrication of PSCs is the demonstration of uniform charge transport layers, such as metal oxides, at scale. NiO_x is a popular inorganic hole transport material for upscaling as it is easy to produce at scale, is environmentally stable and has been highly successful in small scale systems. Large area deposition of NiO_x nanoparticles has been demonstrated at slow speeds of 5 mm/s by blade coating from aqueous solutions. Increasing deposition speeds to 10 mm/s or 30 mm/s requires the addition of a surfactant to improve surface wetting and film uniformity. The addition of traditional surfactants such as cetrimonium bromide or triton X-100 has been observed to obstruct charge extraction when low temperature annealing is used. Herein, we demonstrate that the addition of short chain alcohols such as isopropanol and tert-butanol effectively improve surface wetting while not interfering with charge extraction when followed by low temperature annealing. Additionally, uniform films were able to be deposited at 2 m/min by blade coating and roll-to-roll slot die coating on ITO coated PET substrates. Changes in zeta potential, surface tension, film uniformity, and power conversion efficiency were quantified as a function of alcohol concentration to identify key traits necessary for high quality film deposition. Films deposited using the optimized solution composition showed improved fill factor, open circuit potential, power conversion efficiency compared to solutions without the alcohols present.

EN02.08.05

Potentiometry of Operating Perovskite-Based Devices with Kelvin Probe Force Microscopy Konstantinos Bidinakis, Shuanglong Wang, Paul Blom, Wojciech Pisula, Tomasz Marszalek and Stefan A. Weber; Max Planck Institute for Polymer Research, Germany

During the past decade, hybrid perovskite materials have attracted considerable attention for application in electronic devices due to the favorable properties their organic and inorganic structural elements grant them. Such devices include solar cells and field-effect transistors (FETs), which exhibit respectable performances with very low production costs. By employing Kelvin probe force microscopy (KPFM), we can scan a probe along the perovskite active area of such devices and quantitatively determine the evolution of potential across them, from one electrode to the other, in order to gain information about their charge transport and charge extraction characteristics. At the same time, we can subject our samples to conditions simulating real-life operation, i.e. application of a gate and source-drain voltage for FETs, or illumination and bias voltages in solar cells.

In this poster, we explain how in-situ nanoscale potentiometry in active devices can help understand the underlying working principles and performance bottlenecks. For example, mapping the potential distribution across the gate channel of FETs revealed that devices with better crystallinity exhibit fewer energetic barriers and a more uniform electric field. These results provide a microscopic explanation for their better performance, as estimated by current-voltage measurements of their transfer characteristics. For solar cells, the perovskite absorbing layer is covered by the layers deposited on top of it and is therefore not readily accessible for a scanning probe measurement. Therefore, a few extra steps are required in order to conduct the experiment: the device is initially cleaved in the direction perpendicular to its constituent layers and subsequently, the exposed cross-section is polished in order to eliminate cross-talk from a rough topography. Here, the potential profiles reveal the charge separating junctions on both sides of the perovskite absorbing layer, as well as the relative barriers for charge extraction at the interfaces with the electron and hole transport layers, which depend on the choice of these materials.

EN02.08.06

Low Temperature Synthesized Y:SnO₂ as an Effective Electron Transport Layer for Inverted Perovskite Solar Cells on Flexible ITO-PET Substrate Sashil Chapagain, Peter Armstrong, Thad L Druffel and Craig Grapperhaus; University of Louisville, United States

Flexible perovskite solar cells (f-PSCs) on plastic substrate have drawn appreciable attention as they have high power-per-weight and potentially wide applications in portable and wearable electronics, aviation, integration in vehicles and buildings, and aerospace. However, the power conversion efficiencies of these f-PSCs are still far below conventional perovskite solar cells on glass substrate. In this study, we investigated the direct deposition of a metal oxide electron transport layer on the top of perovskite for the high-performance f-PSCs. Metal oxide electron transport materials are inexpensive and scalable as compared to their organic counterparts. However, deposition of fully solution-processed metal oxide on perovskite to fabricate f-PSCs is limited by solvent incompatibility of typical metal oxide dispersion media with the underlying perovskite layer and the high processing temperature of metal oxides nanoparticles. Here, we synthesized SnO₂ nanoparticles using the sol-gel method and functionalized them with acetate through ligand exchange allowing their dispersion in anhydrous ethanol. Additionally, we investigated *in situ* yttrium doping of SnO₂ during synthesis. Nonaqueous dispersions of pristine and yttrium doped SnO₂ were directly deposited on the perovskite by blade coating followed by air knife treatment. There was no detectable damage to the underlying perovskite layer as evidenced by x-ray diffraction and scanning electron microscopy. Photoluminescence spectroscopy and device performance statistics confirm superior electron extraction by yttrium doped SnO₂ as compared to pristine one. After yttrium doping, the champion power conversion efficiency was increased above 18% from 15%, which is unprecedented for an inverted device in flexible ITO-PET substrate employing SnO₂ as an ETL. This work highlights the possibilities of the scalable deposition of fully solution-processed metal oxide charge transfer layers directly on the perovskite to achieve highly efficient large-area flexible perovskite solar cells

EN02.08.08

Enabling Perovskite/Perovskite/Silicon Triple Tandem Based on Transparent Conductive Adhesive Lamination Process In Choi, Bonkee Koo and Min Jae Ko; Hanyang University, Korea (the Republic of)

Organic-inorganic hybrid perovskite solar cells (PSCs) are expected to become future renewable energy sources among the emerging photovoltaics.

Perovskite materials are very promising for the tandem solar cells due to the largely tunable band gap energy (E_g). Recently, PSCs based multijunction solar cells are intensively and extensively investigated to achieve higher performance over silicon solar cells. For the fabrication of tandem, conventional vacuum deposition methods have been widely used even though the high-cost and their applications to fabricate multijunction solar cells. However, to realize the simple process to reduce total fabrication cost, simple fabrication process is highly required. Here, we developed a transparent conductive adhesive (TCA) based lamination method for the fabrication of the multijunction solar cell, which is comfortable and cost-effective method. Based on low-temperature and low-pressure lamination conditions, we achieved over 2.2 V open-circuit voltage and 11.16 % power conversion efficiency in perovskite/perovskite/silicon triple-junction solar cells. The TCA lamination method developed through this study is expected to present a new horizon in future research and industrialization of multijunction solar cells.

EN02.08.09

Defect-Stabilized Tin-Based Perovskite Solar Cells Enabled by Multi-Functional Molecular Additives [Jinhyeok Choi](#), Seok Joo Yang and Kilwon Cho; Pohang University of Science and Technology, Korea (the Republic of)

Lead-based perovskite solar cells (Pb-PSCs) with efficiency over 25% and high stability have been reported, however, the toxicity of Pb turns into main hurdle for commercialization of PSCs due to the environmental hazards. Tin-based perovskite solar cells (Sn-PSCs) are most viable candidates for replacing the Pb owing to the high carrier mobility, small exciton binding energy, and narrow optical bandgap. However, facile oxidation of Sn^{2+} and high defect density on surfaces and grain boundaries in Sn-PSCs complicate the task of obtaining highly stable Sn-PSCs. Here, for the first time, a fulleropyrrolidine with a triethylene glycol monoethyl ether side chain (PTEG-1) is introduced as a multi-functional molecular additive to passivate both surfaces and grain boundaries of formamidinium (FA)-based tin triiodide (FASnI_3) perovskites. The ether group and fullerene group in PTEG-1 interact with Sn^{2+} and I^- , respectively, and thereby inhibit formation of Sn^{4+} and I_3^- , which is detrimental to the stability of Sn-PSCs. We observed that this multi-functional molecular additive suppresses non-radiative recombination and increases both power conversion efficiencies (PCEs) and the stability of Sn-PSCs. As a result, Sn-PSCs with PTEG-1 additives exhibited PCEs of 7.40 %, which is accompanied by retaining 65 % of its initial PCE of encapsulated PSCs after 1000 h of exposure to ambient air with light illumination. Our results would provide a guideline for future design of multi-functional molecules with suitable functional groups to fabricate highly stable Sn-PSCs.

EN02.08.10

Perovskite-Based Multijunction Solar Cells for Efficient Continuous Solar-Assisted Water Splitting [Kunal Datta](#)¹, Yifeng Zhao², Bruno Branco¹, Junke Wang¹, Valerio Zardetto³, Nga Phung¹, Dong Zhang^{3,1}, Andrea Bracco¹, Willemijn Remmerswaal¹, Luana Mazzearella², Martijn Wienk¹, Mariadriana Creatore¹, Olindo Isabella² and René Janssen¹; ¹Technische Universiteit Eindhoven, Netherlands; ²Delft University of Technology, Netherlands; ³TNO-Solliance, Netherlands

The intermittency of solar radiation is a key characteristic that impedes the widespread use of photovoltaic systems. As a result, a critical component of any decarbonized energy economy is solar electricity storage for release on demand.^[1] Hydrogen (H_2) evolution through electrochemical (EC) water splitting is an effective method for energy storage due to the high energy density of H_2 fuel. However, present-day H_2 generation relies on byproducts of fossil fuel extraction leading to a high indirect carbon cost.^[2] Photovoltaic (PV)-assisted EC water splitting methods that employ concentrated photovoltaics, on the other hand, use inorganic multijunction devices whose high manufacturing costs can undermine future commercial competitiveness. As a result, a cost-effective PV device delivering high current without light concentration, coupled to a flow EC system, can potentially provide an efficient method for H_2 generation.^[3]

Metal halide perovskite semiconductors have been used to develop high-performance photovoltaic devices. Their tunable optical bandgap, high defect tolerance, and easy processing, are assets that allow their use in efficient multijunction devices.^[4] As a result, high open-circuit voltages can be achieved which results in a high current at the operating potential for water splitting (> 1.23 V). This work describes the development of 1 cm^2 active area all-perovskite and perovskite-silicon tandem solar cells by combining wide-bandgap perovskites with lead-tin based narrow-bandgap perovskite and silicon heterojunction bottom-cells respectively. Upon integrating with continuous flow EC cells, high solar-to-hydrogen (STH) conversion efficiencies can be achieved without using light-concentration techniques.

Mixed-halide wide-bandgap perovskite compositions are developed for each multijunction structure and the defect-rich interface between the perovskite and the electron transport layer is passivated in order to increase radiative yield. Recombination layers in the multijunctions, based on thin atomic layer deposited (ALD) NiO_x (perovskite-silicon) and SnO_x (all-perovskite) layers, are used to maintain charge neutrality while ensuring low interfacial losses. The ALD NiO_x interfacial layer increases surface hydroxyl content, thereby improving the binding of self-assembled hole-transporting monolayer (2PACz) in the top-cell in the perovskite-silicon tandem device.^[5] In the all-perovskite tandem solar cell, the SnO_x layer also acts as a solvent barrier to protect underlying layers from damage from subsequent solution processing steps.^[6] Lastly, advanced optical simulations are used to identify key regions of parasitic absorption and reflection losses, which are mitigated by light-management strategies to yield current-matched tandem devices with a power conversion efficiency of $> 23\%$ (all-perovskite) and $> 25\%$ (perovskite-silicon) in 1 cm^2 active area solar cells. By integrating the device with a flow electrochemical cell using RuO_2 and Pt catalysts for H_2 and O_2 evolution respectively, a continuous water splitting system with a high STH conversion efficiency of $> 18\%$ (with all-perovskite) and $> 21\%$ (with perovskite-silicon) is achieved.

[1] International Energy Agency, *World Energy Outlook 2020*, Paris, 2020.

[2] F. Lehner, D. Hart, in *Electrochem. Power Sources Fundam. Syst. Appl.*, Elsevier, 2022, pp. 1–36.

[3] C. A. Rodríguez, M. A. Modestino, D. Psaltis, C. Moser, *Energy Environ. Sci.* 2014, 7, 3828.

[4] M. T. Hörlantner, T. Leijtens, M. E. Ziffer, G. E. Eperon, M. G. Christoforo, M. D. McGehee, H. J. Snaith, *ACS Energy Lett.* 2017, 2, 2506.

[5] N. Phung, M. Verheijen, A. Todorova, K. Datta, M. Verhage, A. Al-Ashouri, H. Köbler, X. Li, A. Abate, S. Albrecht, M. Creatore, *ACS Appl. Mater. Interfaces* 2022, 14, 2166.

[6] J. Wang, V. Zardetto, K. Datta, D. Zhang, M. M. Wienk, R. A. J. Janssen, *Nat. Commun.* 2020, 11, 5254.

EN02.08.11

In Situ Metrology of Hybrid Halide Perovskite Single Crystals—Investigating Growth Dynamics of Inverse Temperature Crystallisation [Alice Dearle](#), George Lewis, Edward Saunders, Ye Fan, Lucas Mogg, Samuel D. Stranks and Stephan Hofmann; University of Cambridge, United Kingdom

Following the discovery of inverse temperature crystallisation phenomena of single crystal hybrid halide perovskites in specific solvent pairings,^{1,2} the rapid growth of high quality single crystal perovskites by this technique has been widely adopted. This has proven immensely useful in differentiating fundamental material properties from those derived from the granular structure of thin-film counterparts.³ As methods to structurally characterise halide perovskite systems become increasingly intensive, it remains imperative to provide due care to simultaneously advancing our understanding of materials synthesis.

Here, we present an *in-situ* study and analysis of methylammonium lead bromide (MAPbBr_3) single crystal growth. The space-confined inverse

temperature growth of MAPbBr₃ crystals is monitored in real-time using optical microscopy methods examining many relevant experimental conditions including temperature and solute concentration. MAPbBr₃ is selected as an ideal model system, with stable cubic phase within the relevant temperature window of growth and convenient solubility profile. Individual surface facets are monitored and growth rates extracted. We understand this to be the first time that the tracking of individual hybrid perovskite crystal facets has been demonstrated using advanced image analysis techniques. Our method reveals inhomogeneity in the growth rates of crystallographically identical facets and the importance of mass transfer and concentration gradients. Regions of accelerated growth rate lead to excess defect incorporation and diminished crystalline quality within one “single crystal”. We identify the often overlooked complexities of relevant thermodynamic and kinetic crystal growth within the phenomena of inverse temperature crystallisation, the fundamental understanding of which has remained limited since first reported in 2015.

1. Saidaminov, M. I. *et al.* High-quality bulk hybrid perovskite single crystals within minutes by inverse temperature crystallization. *Nat. Commun.* **6**, 7586 (2015).
2. Saidaminov, M. I., Abdelhady, A. L., Maculan, G. & Bakr, O. M. Retrograde solubility of formamidinium and methylammonium lead halide perovskites enabling rapid single crystal growth. *Chem. Commun.* **51**, 17658–17661 (2015).
3. Stavrakas, C. *et al.* Probing buried recombination pathways in perovskite structures using 3D photoluminescence tomography. *Energy Environ. Sci.* **11**, 2846–2852 (2018).

EN02.08.13

High-Efficiency Perovskite Light-Emitting Diodes Enabled by a Combination of Molecular Additives and Self-Assembled Hole Injecting Interlayers Despoina Gkeka, Murali Gedda, Mohamad I. Nugraha, Jafar Khan, Emre Yengel, Iain Hamilton, Frederic Laquai, Donal Bradley and Thomas D. Anthopoulos; KAUST, Saudi Arabia

Low-dimensional hybrid perovskites have recently emerged as promising candidates for light-emitting diode (LED) applications due to their outstanding physical characteristics that include high photoluminescence quantum yield (PLQY), color purity, operating stability and processing versatility. Unfortunately, controlling the microstructure of the solid layers during solution deposition remains very challenging. Introducing molecular additives into the perovskite layer during processing has recently emerged as an effective strategy towards improving both the quality of the formed perovskite layer and the overall performance of the ensuing perovskite LEDs (PeLEDs).

Here we report on the development of highly efficient green PeLEDs based on blends of the quasi-two (q2D) dimensional perovskite PEA₂Cs₄Pb₅Br₁₆ and a known small molecule (SM) organic semiconductor. The presence of the SM enables the formation of single-crystal-like q2D perovskite domains that are uniform, large in size and highly luminescent. We show that combining the q2D-Perovskite:SM blends with self-assembled monolayers (SAMs) as the hole-injecting layers (HILs), results in green emitting PeLEDs that exhibit greatly enhanced performance over pristine perovskite LEDs including, maximum external quantum efficiency (EQE) of 18.6 %, current efficiency of 46.31 cd/A, maximum brightness of $\approx 45,000$ cd m⁻², and a longer operational lifetime. Using a complementary suite of characterization techniques, we show that the improved performance of the blend PeLEDs to originate from multiple synergistic effects including, the enhanced hole-injection due to SAM HILs and the single crystal-like quality of the perovskite phase. Our work highlights perovskite:organic semiconductor blends as promising strategy towards high performance PeLEDs, while the use of SAM HILs creates new opportunities for simpler and more reliable materials for application in next generation light-emitting diodes.

EN02.08.14

Improved Charge Balance in Green Perovskite Light-Emitting Diodes with Atomic-Layer-Deposited Al₂O₃ William B. Gunnarsson, Zhaojian Xu, Nakita K. Noel and Barry P. Rand; Princeton University, United States

Perovskite light-emitting diodes (LEDs) have experienced a rapid increase in efficiency over the last several years and are now regarded as promising low-cost devices for displays and communication systems. However, it is often challenging to employ ZnO, a well-studied electron transport material, in perovskite LEDs due to chemical instability at the ZnO/perovskite interface and charge injection imbalance caused by the relatively high conductivity of ZnO. In this work, we address these problems by depositing an ultrathin Al₂O₃ interlayer at the ZnO/perovskite interface, allowing the fabrication of green-emitting perovskite LEDs with a maximum luminance of 21,815 cd/m². Using atomic layer deposition, we can precisely control the Al₂O₃ thickness and thus fine-tune the electron injection from ZnO, allowing us to enhance the efficiency and operational stability of our LEDs.

EN02.08.16

Large-Area Perovskite Modules with ‘Sol-Gel’ Processed Metal Oxide Charge Transport Layer Soonil Hong¹, Eun Young Park¹, Sooncheol Kwon² and Nam Joong Jeon¹; ¹Korea Research Institute of Chemical Technology, Korea (the Republic of); ²Dongguk University, Korea (the Republic of)

The formation of well-connected metal-oxygen gel networks in ‘sol-gel’ processed transition metal oxide (TMO) interlayer on top of the entire photoactive layer has long been a research goal to ensure large-area PSC modules with high performance and long-term stability; however, it has not yet been achieved because very little is known about the actual nanomorphology from atomic-scale reactions of TMO precursors and its impact on device characteristics. Here, we report for the first time a direct observation of continuous metal-oxygen network in ‘sol-gel’ processed metal oxide film on top of favorable photoactive layer, which can be used as an ideal inner encapsulation layer for achieving large-area organic and perovskite modules with long-term stability. By employing a high-resolution Auger electron spectroscopy, which provide an advantage of short data acquisition times and thus an improved surface sensitivity and accuracy, we successfully obtain the lateral and vertical distribution of chemical components throughout the entire metal oxide thin film surface, indicating that a low surface energy difference at the organic/metal oxide interface allows long-range diffusion of metal ion precursors to promote continuous chemical synthesis associated with oxo-bridge formation. The features of resultant continuous metal-oxygen network can prevent the permeation of surrounding moisture and oxygen into the photoactive layer, resulting in PSC modules with long-term stability, approaching an efficiency of 14.5% and maintaining over 80% of their initial efficiency until 2000 hours with an area of 9.06 cm², respectively.

EN02.08.17

The Role of SnO₂ Processing on Ionic Migration in Multi-Halide Perovskites Holland Hysmith¹, Soyeon Park², Anton V. Ievlev³, Yongtao Liu³, Kai Zhu², Mahshid Ahmadi¹, Joseph J. Berry² and Olga Ovchinnikova³; ¹University of Tennessee Knoxville, United States; ²National Renewable Energy Laboratory, United States; ³Oak Ridge National Laboratory, United States

Moving towards a future of efficient, accessible, and less carbon reliant energy devices has been at the forefront of energy research innovations for the past 30 years. Multi-halide perovskite (MHP) thin films have gained significant attention due to their flexibility of device applications and tunable capabilities for improving power conversion efficiency. Many behavioral aspects to MHP’s are thoroughly investigated: functionality of grain boundaries, recombination effects, ionic migration patterns, and hysteresis. Each avenue serving as gateway to optimize device performance, consideration must be given to chemical synthesis processing techniques.

Chemical Vapor Deposition (CVD) is a widely used technique for thin film coatings due to its ability for producing high volume batches of MHP’s with

larger grain sizes, fewer defects, and fewer grain boundary formations. Additionally, nanoparticle processing has been applied to induce enlargement of grain boundaries, showcasing larger current signals than its MHP counterparts. Therefore, how does common substrate processing techniques (i.e. CVD, nanoparticles, hybrid) influence the behavior of MHP phenomenon such as ion migration and grain boundary formation? Speculated as inducing ionic recombination and driving I-V hysteresis in MHP's, understanding how chemistry can be tuned to reduce such effects would be optimal.

We demonstrate how a hybrid approach of CVD and nanoparticle SnO₂ substrate processing significantly improves the performance of (FAPbI₃)_{0.97}(MAPbBr₃)_{0.03} perovskites in comparison to each technique utilized on its own. Higher performing hybrid devices exhibit fused grain boundary formations, not seen in exclusive CVD or nanoparticle devices. Conductive Atomic Force Microscopy (c-AFM) was used to track fused boundary locations and differentiate them from topographic features. Such fusing behavior has been previously observed to showcase higher counts of current and reduce defects such as halide vacancies.

In summary, to understand the chemistry behavior with respect to each device interface, Time of Flight Secondary Ionization Mass Spectrometry (ToF-SIMS) depth profiling was applied. Migration of K⁺, Na⁺, Ca⁺, FA⁺, MA⁺ was found in hybrid devices, in addition to Ca⁺ and Na⁺ clustering on the perovskite/air layer. Salt clustering could be correlated to the fusing effect demonstrated in the surface morphology imaged in c-AFM. Presence of K⁺ has shown to reduce defects driven by alkali iodides like NaI and Ca⁺ can help with enlarging the bandgap layer in studies where Ca⁺ was used to replace Pb²⁺. Furthermore, reduced separation between positive ion such as MA⁺ and FA⁺ from negative ions can decrease the potential responsible for I-V hysteresis.

EN02.08.19

Oxide/Halide/Oxide Architecture for High Performance Semi-Transparent Perovskite Solar Cells Min Ju Jeong and Jun Hong Noh; Koera university, Korea (the Republic of)

We report a device architecture with n-type oxide/perovskite halide/p-type oxide for the sputtering damage-free semi-transparent perovskite solar cells (PSCs). A p-type nickel oxide (NiO_x) nanoparticle overlayer on a perovskite layer is introduced to act as both a hole transporting layer and buffer layer to avoid sputtering damage during deposition of transparent conducting oxide. The NiO_x based semi-transparent PSCs exhibited superior durability under harsh sputtering conditions such as high temperature and sputtering power, enabling the high quality of transparent electrodes. With optimal sputtering condition for tin-doped indium oxide (ITO) as a top transparent electrode, the semi-transparent device showed an enhanced power conversion efficiency (PCE) of 19.5% (20.5% with a back reflector), which is higher than that of opaque device (19.2%). The semi-transparent devices also showed superior storage stability without encapsulation under 10% relative humidity, retaining over 90% of initial PCE for 1000 hours. By controlling the molar concentration of perovskite solution, we fabricated semi-transparent PSC with a PCE of 12.8%, showing a high average visible transmittance (AVT) of 30.3%. We believe that this architecture with n-type oxide/perovskite halide/p-type oxide presents a cornerstone for the high performance and commercialization of semi-transparent PSCs.

EN02.08.20

High-Performance Semi-Transparent Perovskite Solar Cells Based on 3D-Structured FTO Sucheol Ju, Dongwoo Chae, Soomin Son, Hangyu Lim, Jisung Ha and Heon Lee; Korea University, Korea (the Republic of)

In semi-transparent perovskite solar cells (PSCs), the short-circuit current density (J_{SC}) greatly decreases with an increase in transmittance, and this results in a significant decrease in PCE. Our semi-transparent PSCs were fabricated by controlling the absorption layer thickness and aperture ratio using a 3D-structured FTO manufactured via direct printing and mist-CVD. This strategy has an advantage in that the aperture ratio (transmission/entire area) can be controlled easily by adjusting pattern specification. Also, the 3D-structured FTO enhanced the diffuse transmittance and shortened the carrier travel distance; further, it minimized the decrease in PCE because of an increase in transmittance. Our fully semi-transparent PSCs (F-PSCs) achieved a PCE of 12.0% to 14.6%, and an average visible transmittance (AVT) of 13.4% to 17.0%. These results demonstrate that the parameter of semi-transparent PSCs (transmittance and PCE) can be easily tailored to the application by controlling the specification of the pattern.

EN02.08.22

Cathode Interlayer Engineering with Vacuum Thermal Evaporated N-type Rylene Diimide Derivatives in Highly Efficient Inverted Perovskite Solar Cells Hye Seung Kim and Myoung Hoon Song; Ulsan National Institute of Science and Technology, Korea (the Republic of)

In inverted perovskite solar cells (PeSCs), choosing cathode interlayer plays key role in determining performance of solar cell. Among various processing methods, vacuum thermal evaporation (VTE) is already adopted in electron transporting layer (ETL) such as C₆₀ and cathode interlayer such as bathocuproine (BCP), LiF and Ca in inverted PeSCs. Especially, cathode interlayer have been already utilized to suppress the interfacial resistance and lower the energy barrier between ETL and cathode. N-type rylene diimide derivatives such as perylene diimide (PDI) and naphthalene diimide (NDI) have attracted great attention due to their advantages of easy molecular modification, high electron mobility and good thermal and chemical stability so that have been applied to cathode interlayer by solution processing such as spin-coating method.

In this study, we demonstrate for the first time rylene diimide derivatives such as PDI and NDI family organic small molecules as cathode interlayer candidates using VTE method. Rylene diimide derivatives films show thin thickness about ~5 nm. In comparison with widely used BCP, underlying rylene diimide materials exhibit different silver cathode growth phenomenon. In addition, we compare the effect as a cathode interlayer by considering the energy levels and metal cathode growth phenomenon by the number of amine-functionalized groups of each material. Consequently, the PeSC with N,N'-Bis[3-(dimethylamino)propyl]perylene-3,4,9,10-tetracarboxylic diimide (PDIN) shows an enhanced power conversion efficiency (PCE) of 21.60%, which is higher than that of the PeSC without cathode interlayer and with BCP or NDI-based interlayer. Excluding the solvent consideration in solution processing, PDI-based materials that are easily vacuum thermal evaporated are expected to be in the spotlight in inverted PeSCs for cathode interlayer.

EN02.08.23

Facile Interface Modification via Self-Assembled Monolayer for P-Type Metal Oxide for Efficient and Stable Perovskite Solar Cells Kyeongso Kim, Jae Woong Jung and Jung Jae Do; Kyung Hee University, Korea (the Republic of)

Recently, organic-inorganic hybrid perovskite solar cells (PSCs) received significant attention due to its remarkable progress on record-breaking efficiency of perovskite photovoltaics. P-type metal oxides are an interesting class for robust HTLs of high performance PSCs with high durability, however poor surface morphology and low conductivity are unsatisfactory to achieve ideal optoelectronic properties as HTLs. To overcome these issues, we suggest straightforward strategy of interface modification of metal oxide surface using self-assembled molecule (SAMs) The anchoring the phosphonic acid moiety of SAM form ideal linkage to the metal oxide surface, realizing optimal hole transport pathway at the interface of perovskite absorber and metal oxide HTLs. Moreover, the defect sites at the interface of perovskite/metal oxides successfully passivated by SAMs, providing reduced defect-assisted charge-carrier recombination. As a result, the SAM-passivated NiO_x achieves FA_{0.85}CS_{0.15}PbI₃-based PSCs up to >20% efficiency. There is significant improvement on photovoltaic performances under dim indoor light-emitting diode (LED) conditions (6500 K 1000 lux), 27.19%, 24.84% and 16.05%,

NiO_x/MeO-2PACz, NiO_x and MeO-2PACz each. Details of device and film analyses will be discussed in the presentation.

EN02.08.24

Systematic Design of Conjugated Polymers to Achieve High Efficiency and Thermally Stable Perovskite Solar Cells Sanggyun Kim, Sina Sabury, Austin Jones, John Reynolds and Juan Pablo Correa Baena; Georgia Institute of Technology, United States

Despite significant progress in organic-inorganic hybrid perovskite solar cells (PSCs) with a certified power conversion efficiency of 25.2%, long-term stability remains to be one of the critical challenges for PSC commercialization. While hole transport layers (HTL) play a crucial role in device performance of PSCs, they are shown to be a limiting factor toward achieving long-term stability in devices, stemming from interfacial degradation between perovskites and HTLs, thermal/moisture induced degradation, and ionic migration. Here, we explore new dopant-free conjugated polymer-based HTLs that are resistant to high temperatures. The new conjugated polymers are designed accordingly with various side chains, functional groups, and/or degree of polymerizations to obtain good film-forming properties, high hole mobility, high glass transition temperature (T_g), and suitable HOMO-LUMO energy levels. These new polymers are further incorporated into devices to analyze their effect on perovskite solar cell efficiency and stability at elevated temperature and under illumination over 500 hours.

EN02.08.25

Enhanced Stability of Perovskite Solar Cells with Stoichiometrically Controlled Cobalt Sulfide Functional Nanocrystal Based Hole Transport Layer Wooyeon Kim and Min Jae Ko; Hanyang University, Korea (the Republic of)

Perovskite solar cells (PSCs) have emerged as promising next-generation photovoltaic devices because of their superior optical and electronic properties. In recent years, organic hole transporting material (HTM) based PSCs have been reported with remarkable increase in the photovoltaic performance. As power conversion efficiency (PCE) of PSCs employing organic HTM has dramatically increased, expectations toward commercialization of PSCs are increasing. However, traditional organic HTMs have a couple of issues such as cost and stability. In the view of this limitation, we have developed the new p-type inorganic HTM. Cobalt sulfide compounds are one of the promising materials to replace conventional organic HTMs, which are less expensive and earth-abundant. Nevertheless, synthesis of cobalt sulfide is tricky to control the stoichiometric ratio. Here, we synthesized novel inorganic HTMs as a stoichiometrically adjusted p-type cobalt sulfide nanocrystals (Co_xS_y NCs). Cobalt sulfide nanocrystals synthesized in this study display the excellent hole transport ability owing to its high conductivity and suitable energy levels for hole extraction for PSCs. Co_xS_y NCs HTLs-based PSCs exhibited power conversion efficiency (PCE) nearly comparable to dopants-free spiro-OMeTAD HTM-based PSCs. Especially, the PSCs with mixed Co_xS_y NCs (with undoped Spiro-OMeTAD) HTLs exhibited PCE of 20.48 % which belongs to the high-performance, considering ionic additive-free HTMs. Furthermore, the PSCs employing cobalt sulfide showed an initial efficiency of 92 % even after exposure to 70 % relative humidity for 1000 hours. These new p-type Co_xS_y NCs would support environmentally and economically sustainable development of PSC and diverse optoelectronic area.

EN02.08.26

Effect of Adding Bromine and Changing Temperature on Crystallinity, Phase Segregation and Stability of Methylammonium-Free Lead Halide Perovskites Diana K. LaFollette, Juanita Hidalgo, Carlo Andrea Riccardo Perini and Juan Pablo Correa Baena; Georgia Institute of Technology, United States

One of the ever-present issues with perovskite solar cells (PSCs) is the lack of long-term stability, particularly because popular material methylammonium (MA) lead iodide undergoes a phase transition at 57C and decomposes into PbI₂ even in an inert environment. Past work exploring the formamidinium (FA) and cesium (Cs) compositional space demonstrated that these compositions have increased thermal stability while approaching the impressive efficiency of MA-based PSCs. However, it has still proven to be extremely difficult to stabilize the photoactive phases of these mixed-cation mixed-halide perovskites, due to the favorability of the photoinactive phases at room temperature.

A thorough investigation of 14 compositions with varying Cs-FA and I-Br ratios was carried out using in-situ XRD and in-situ GIWAXS in combination with X-ray fluorescence and X-ray beam induced current. This established that rather than directly matching phase transitions of pure compositions, chemical changes such as varying Cs-FA and I-Br ratios change the relationship between temperature, crystallinity, and phase purity of these mixed-halide compositions. These studies illuminate how and when crystalline phase formation, segregation, and degradation occur. This in turn allows for increased understanding of stability of these compounds from a molecular standpoint, particularly in previously established high performing compounds like Cs_{17%}FA_{83%}PbI₃ and Cs_{17%}FA_{83%}PbI_{83%}Br_{17%}.

EN02.08.27

A Doping Strategy and Mechanism of Magnetron Sputtered Tin Oxide Serving as Electron Transport Layer for Perovskite Solar Cells Shuai Lan, Wenting Zheng and Han-Ki Kim; Sungkyunkwan University, Korea (the Republic of)

Perovskite solar cells (PSCs) using SnO₂ electron transport layers (ETLs), especially the magnetron sputtered SnO₂ ETLs, are faced with the problem of intrinsic point defects. The presence of intrinsic point defects located at the interface between SnO₂ and perovskite results in serious charge recombination, limiting the open-circuit voltage (V_{OC}) and fill factor (FF). In this work, we attempted to passivate the intrinsic point defects in magnetron sputtered SnO₂ via Mg doping so as to minimize the non-radiative charge recombination pathways in the bulk and at the interfaces and boost the device performance of PSCs. Mg is chosen as the dopant for the following two reasons: a) Mg²⁺ ions have a similar ionic radius (71 pm) to that of Sn⁴⁺ ions (69 pm); the introduction of Mg²⁺ into SnO₂ may not lead to a large distortion of lattice constant, which benefits the high carrier mobility. b) The lower valence of divalent Mg dopants than the quadrivalent host Sn atoms will consume the donors and thereby passivate the defects in SnO₂. Taking advantage of Mg doping, the V_{OC} and FF of PSCs were significantly improved, resulting in a champion PCE of 19.55%. This study not only demonstrated a facile method to passivate the defects in low-temperature magnetron sputtered SnO₂ ETL but also reveals the factors influencing the performance of PSCs from the perspective of carrier behaviors in the ETL.

EN02.08.28

Lamination Bonding at Perovskite-Perovskite and Perovskite-Transport Layer Interfaces to Inform Single Junction and Tandem Perovskite Solar Cell Design Clare L. Lanaghan¹, Srinivas K. Yadavalli¹, Jack Palmer², Mengyao Zhang¹, Moses Kodur², Orlando Trejo¹, Sean P. Dunfield², David P. Fenning² and Neil P. Dasgupta^{1,1}; ¹University of Michigan-Ann Arbor, United States; ²University of California San Diego, United States

Perovskite solar cells (PSCs) have achieved similar power conversion efficiency to commercially available options, but still lack operational stability due to unstable interfaces with transport layers and atmospheric induced degradation. Laminated PSCs (L-PSCs) using two half-cell stacks to complete a full device, offer a processing route to relax restrictions on transport layer selection and improve device stability through self-encapsulation. While functional L-PSCs have been previously demonstrated, there is a lack in understanding of how temperature, pressure, time, cell architecture, and lamination interface affect bonding, which will be critical to enable optimization of L-PSCs.

In this study, we explore the optimal bonding of L-PSCs at various interfaces using a range of conditions. Bond quality is quantified by measuring the

interfacial toughness of the system using a double cantilever beam method, as well as calculating the area bonded over the substrate area, and comparing successful bonding conditions with device performance. Design of experiments and predictive statistical analysis are used to identify promising bonding conditions from survey datasets varying the lamination temperature, pressure, and time. A key finding is that the cell architecture has a significant effect on bond quality. Understanding the interplay between lamination conditions and interfacial toughness, area bonded, and device performance is necessary to find regions of optimal bonding. Moreover, deconvolution of how lamination parameters impact mechanical bonding will inform optimization of L-PSCs, strategic development of tandem L-PSCs, and allow design of optimal bonding within the processing constraints of scalable manufacturing.

EN02.08.29

Suppression of Defect Concentrated Planes, Ruddlesden-Popper Faults, via Post Halide Treatment for Blue Perovskite Light Emitting Diodes Ah-young Lee and Myoung Hoon Song; Ulsan National Institute of Science and Technology, Korea (the Republic of)

The one of the critical issues in PeLEDs is low efficiency of blue LEDs. Even though the recent studies have been fabricated the highly efficient red and green perovskite LEDs above 20%, the blue perovskite LEDs still have low efficiency with ~5%. The major factors reducing the efficiency of blue LEDs are non-radiative defects in blue perovskite nanocrystals. Even if the colloidal PNC solutions are well known as the defect tolerant, the PNCs films are no more tolerant to the surface defects. Moreover, the chloride vacancies in mixed halide perovskite induce the deep trap states in PNCs band structure. These non-radiative defect states in blue PNCs films hinder the effective radiative recombination of blue PNCs LEDs during operation. The recent advances show the near unity photoluminescence quantum yield (PLQY) of as-synthesized Cl-based PNCs. Especially, CsPbCl₃ PNCs, expected to large number of deep trap states, also shows near unity PLQY, arranging short-order distance with adding nickel precursors during synthesis. However, efficiency of blue LEDs is still insufficient to follow up the green and red counterparts.

In this study, I hypothesized that the mixed halide synthetic procedures induce several problems inside PNCs. To understand the atomic arrangement of mixed halide blue PNCs, I measured the high-resolution TEM images. In mixed-halide synthetic procedures, stacking faults, called Ruddlesden-Popper faults (RPFs), are introduced inside the PNCs. In contrast, mono-halide PNCs, CsPbBr₃, did not introduce the internal defects. To further deliberate analysis of RPFs, halide intensity mapping near RPFs was conducted with annular dark field images of TEM. The intensity mapping of halide positions revealed the severe intensity drops near RPF. In specific, the halide intensity was dropped in 1st equatorial sites (EQS) and 2nd EQS. The intensity drops can be interpreted as two ways: chloride localization and halide vacancies. To understand the origin of intensity drops, formation energy of chloride substitutions and halide vacancies were calculated. In here, low energy of halide vacancies in 1st and 2nd EQS near RPF were calculated, suggesting the severe defect concentration near RPF. Further, band structures of chloride localization and halide vacancies near RPF were calculated. While chloride localization did not introduce in-gap defect states, halide vacancies introduced the severe in-gap defect states. In summary, unwanted RPF structures were generated during mixed halide blue PNCs synthesis, deteriorating the optical properties of blue PNCs.

Therefore, suppression of blue PNCs was further conducted to obtain highly efficient blue PNCs LEDs. At first, I tried to relieve the internal defects of mixed-halide PNCs (MH-PNCs) with post synthetic dual halide and ligand exchange. In here, MH-PNCs are defined as the blue mixed-halide PNCs synthesized with mixed halide precursors in hot injection and didodecyldimethylammonium chloride (DDAC) was applied to the MH-PNCs for halide and ligand sources, called MHS-PNCs. However, the internal defects were remained even after treating DDAC. That is, the post-synthetic procedures cannot recover the internal defects. I supposed that these kinds of internal defects might degrade the performance of blue MH-PNCs. Therefore, another blue synthetic procedure with post synthetic DDAC treatment toward mono-halide CsPbBr₃ PNCs (CPB-PNCs) was conducted, called post-halide exchange PNCs (PHE-PNCs). In the system, the chloride in DDAC acted as anion exchange precursors, making pure blue PNCs. As expected, PHE-PNCs did not introduce any internal defects. I further compared optical properties of PHE-PNCs with MHS-PNCs in PLQY, showing average 60% of PLQY in PHE-PNCs and average 22% of PLQY in MHS-PNCs. Finally, the device fabrication of MHS-PNCs and PHE-PNCs were conducted, achieving highly efficient blue PNCs LEDs in PHE-PNCs with 2.12% of EQE.

EN02.08.30

Van der Waals Metal Contacts for Estimating Defect Density in Metal Halide Perovskite Thin Films via Space-Charge-Limited Current Measurements Joo-Hong Lee and Jin-Wook Lee; Sungkyunkwan University, Korea (the Republic of)

Reducing a crystal defect density is one of the critical issues for achieving high-performance perovskite optoelectronic devices. For devising effective mitigation strategies, it is imperative to accurately measure the defect density of perovskite thin films. Space-charge-limited current (SCLC) measurement has been commonly used to investigate the defect density of the perovskite thin films. In this study, we show that the physical vapor deposition process of the top metal contact generates unintended defects in underlying metal halide perovskite films to overestimate defect density by more than twofold during conventional SCLC measurement. We suggest an alternative metal contact approach to address this issue using van der Waals metal contact (vdWC) formed by transferring the physically laminated pre-deposited metal onto the perovskite layer. The vdWC approach enables formation of a defect-free metal/perovskite junction for accurate measurement of the defect density. The vdWC can also be a useful platform technology for development of high-performance and reliable electronic devices based on the perovskite thin films.

EN02.08.33

Intact 2D/3D Halide Junction Perovskite Solar Cells via Solid-Phase In-Plane Growth Seungmin Lee¹, Yeoun-Woo Jang^{2,2}, Kyung Mun Yeom¹, Kiwan Jeong², Kwan Choi¹, Mansoo Choi^{2,2} and Jun Hong Noh^{1,1}; ¹Korea University, Korea (the Republic of); ²Seoul National University, Korea (the Republic of)

Ruddlesden-Popper two-dimensional (2D) perovskite in the junction between the three-dimensional (3D) perovskite and hole transporting layer of a device provided not only the effective improvement for performance through the defect passivation on the top of the surface, but also endowed the stability for the device. However, a solution process, general approaches forming 2D (C₄H₉NH₃)₂PbI₄ perovskite on the surface, must accompany a quasi-2D perovskite because it was based on the surface reaction. The intact 2D/3D perovskite bilayer architecture, formed by the "Solid-state Inplane-Growth (SIG)" method, can permit enhancement of performance and stability through the growth of a stable and highly crystalline 2D perovskite on the 3D surface. Also, it was observed that the thickness of intact 2D perovskite depended on an open-circuit voltage and that the built-in potential was formed at the 2D layer in the 2D/3D junction. Thereby, the 2D/3D p-p isotype heterojunction with the thicker 2D layer maximizing the potential furnished the device with a certified 24.35% of quasi-steady-state efficiency with 1.185 V of the open-circuit voltage in 1.55 eV bandgap. The device with intact 2D/3D showed stabilities of 94% of initial efficiency for a damp heat test (85°C/85% relative humidity) after 1,056 h, as well as 98% after 1,620 h under 1-sun illumination.

EN02.08.34

Unveiling the Relationship of the Iodoplumbate Species in the Perovskite Precursor and the Resulting Film SunJe Lee and Jong Hyeok Park; Yonsei University, Korea (the Republic of)

The power conversion efficiency (PCE) of solution-processed (e.g., spin coating, blade coating, and spray coating) organic-inorganic halide perovskite (OIHP) solar cells has been drastically improved. Representatively, since the emergence of OIHP photovoltaics in 2012, the PCE of the photovoltaics exceeds 25% nowadays. Despite this considerable progress, systematic research on precursor solution chemistry and its effects on the film morphology and

photovoltaic parameters has been limited thus far.

In typical halide perovskite precursor solutions, Group 14 transition metal ions (mainly Pb^{2+} and Sn^{2+}) form bonds with other ions or solvent because the d orbitals and s orbitals of transition metals are filled with electrons. Therefore, depending on the position of an anion or a solvent near the empty bond of metal ions, various complexes can be formed in a solution. When lead iodide (PbI_2) is dissolved in the solution, iodide ions (I^-) and solvent (S) coordinate around the lead (Pb^{2+}) center, forming iodoplumbate complexes, i.e., PbIS_5^+ , PbI_2S_4 , PbI_3S_3^- , $\text{PbI}_4\text{S}_2^{2-}$, $\text{PbI}_5\text{S}^{3-}$, and PbI_6^{4-} .

Herein, we report on the tracking of changes in chemical species in a MAPbI_3 precursor solution under solar illumination as an imposed energy and investigate the correlation between the iodoplumbate species development in the solution and the corresponding perovskite film formation. According to the solution Raman spectroscopy and UV-vis spectroscopy, the illuminated OIHP precursors display a higher density of high-valent iodoplumbate along with the detachment of dimethylformamide (DMF) from Pb. As DMF contributes to uncontrolled crystal growth and that higher iodoplumbate species result in crystalline perovskite with fewer defects, we analyzed trap density and electrical properties with conductive AFM (c-AFM). We revealed that trap density of illuminated groups was reduced, and electrical conductivity was significantly enhanced.

Subsequently, we compared the photovoltaic parameters of the control and illuminated groups. The reproducibility significantly increased in the illuminated groups with highly concentrated fill factor and increased short circuit voltage (J_{SC}). Increased photocurrent can also be observed in mixed cation OIHP solar cells, which indicates that analysis of the perovskite precursor chemistry can also contribute to the fabrication of high-quality perovskite thin films in the mixed perovskite system. This discovery shows robust control of perovskite precursor solutions from a simple treatment and suggests that the resulting uniform film may be applicable to various halide perovskite-based devices.

EN02.08.35

Inorganic-Cation Pseudohalide 2D $\text{Cs}_2\text{Pb}(\text{SCN})_2\text{Br}_2$ Perovskite Single Crystal Chwenhaw Liao^{1,2}, Chu-Chen Chueh² and Anita W. Ho-Baillie¹; ¹The University of Sydney Nano Institute, Australia; ²National Taiwan University, Taiwan

While solar cells, light-emitting diodes, photodetectors, and field-effect transistors based on 3D metal halide perovskite with the molecular formula of ABX_3 ($\text{A} = \text{Cs}^+$, CH_3NH_3^+ , $\text{CH}(\text{NH}_2)^{2+}$; $\text{B} = \text{Sn}^{2+}$, Pb^{2+} ; $\text{X} = \text{Cl}^-$, Br^- , I^-) have demonstrated outstanding performance in recent years, 2D or quasi-2D perovskites achieved by space insertions have attracted intensive research effort. This is because of the added stability that accompanies these materials while still inheriting the advantages of 3D counterparts. The versatility of engineer A-site cations or X-site anions in the spacers to achieve lower dimensionality also expands perovskite material choices.

Most of the reported 2D Ruddlesden-Popper (RP) phase lead halide perovskites with the general formula of $\text{A}_{n+1}\text{B}_n\text{X}_{3n+1}$ ($n = 1, 2, \dots$) comprise of layered perovskites separated by A-site-substituted organic spacers. This layered structure is constructed with long carbon chain spacers introducing a large separation between BX_6 octahedron inorganic layers. The organic spacers work as an insulating layer that provides large exciton binding energy and reduces the conductivity in a vertical direction through each inorganic layer. Therefore, the X-site substituted layered perovskite presents a much smaller separation between the constituent perovskite layers than the A-site substituted layered perovskite, moderating the exciton binding energy.

To-date, only three X-site-substituted RP phase perovskites have been reported [1-3]. Herein, we reported the first inorganic-cation pseudohalide 2D phase perovskite single crystal, $\text{Cs}_2\text{Pb}(\text{SCN})_2\text{Br}_2$. It is synthesized by the antisolvent vapor-assisted crystallization (AVC) method at room temperature. The crystal exhibits a standard single-layer ($n = 1$) RP phase structure described in the space group of $Pm\bar{m}n$ (#59) with a slight separation ($d = 1.69 \text{ \AA}$) between the perovskite sheets. Interestingly, the SCN^- anions are found to bend the 2D $\text{Pb}(\text{SCN})_2\text{Br}_2$ framework slightly into a kite-shaped octahedron, limiting the formation of a quasi-2D perovskite structure ($n > 1$). Above 450K, the 2D single crystal undergoes an unusual but reversible first-order phase transformation to 3D CsPbBr_3 ($Pm\bar{3}m$ #221). According to the small separation between perovskite sheets, Pb-Br-Pb coordination can be formed to drive the SCN^- anion away and transform into a more stable 3D CsPbBr_3 structure at high temperatures. Once the temperature cools down to 250K, the existed SCN^- free anions within the grains break the weak Pb-Br-Pb coordination to reconstruct the $\text{Pb}(\text{SCN})_2\text{Br}_2$ octahedral due to the preferable Gibbs energy. Again, due to the small interlayer separation, $\text{Cs}_2\text{Pb}(\text{SCN})_2\text{Br}_2$ exhibits a minuscule exciton binding energy of 160 meV measured by temperature-dependent PL. It is one of the lowest values reported for 2D perovskites ($n = 1$) and comparable to the quasi-2D A-site substituted RP phase perovskite values. Finally, a $\text{Cs}_2\text{Pb}(\text{SCN})_2\text{Br}_2$ single crystal photodetector is demonstrated with a respectable responsivity of 8.46 mA W^{-1} and a detectivity of $\approx 1.2 \times 10^{10}$ Jones at a low bias voltage of 0.5 V.

References

- [1] M. Daub, H. S. Hillebrecht, *Angew. Chem.*, **2015**, 127, 11168.
- [2] J. Li, Q. Yu, Y. He, C. C. Stoumpos, G. Niu, G. G. Trimarchi, H. Guo, G. Dong, D. Wang, L. Wang, M. G. Kanatzidis, *J. Am. Chem. Soc.*, **2018**, 140, 11085.
- [3] C. H. Liao, C. H. Chen, J. Bing, C. Bailey, Y. T. Lin, T. M. Pandit, L., Granados, J. Zheng, S. Tang, B. H. Lin, H. W. Yen, D. R. McCamey, B. J. Kennedy, C. C. Chueh, A. W. Ho-Baillie, *Adv. Mater.*, **2022**, 34(7), 2104782.

EN02.08.40

Application of Black Phosphorus for Interfacial Engineering in Perovskite Solar Cells Damir Aidarkhanov, Zhuldyz Yelzhanova, Gaukhar Nigmatova, Mannix Balanay and Annie Ng; Nazarbayev University, Kazakhstan

Nowadays, the hybrid organic-inorganic perovskite solar cells (PSCs) are considered as the most promising third generation photovoltaic (PV) technology with the highest increasing rate of power conversion efficiency (PCE) among other types of emerging PVs. To date, the PCE values are comparable to the most of the established photovoltaic technologies. Intensive research activities on perovskite materials and their devices have been being performed since last decade, aiming to further boost the device performance including efficiency and stability as well as to accelerate the commercialization progress of the developed technologies via different strategies. The emerging 2D black phosphorus (BP) is a novel class of semiconducting material owing to its unique characteristics, allowing them to become attractive materials for applications in a variety of optoelectronic devices. In this work, the optimized BP materials are incorporated with PSCs at the interface between the electron transport layer and perovskite absorber. Systematic characterizations have been performed on the materials and devices. The obtained results indicate that the incorporation of BP facilitates the crystallization of the perovskite and promotes the carrier transports in PSCs. The device stability with incorporation of BP is also found to be improved significantly.

EN02.08.41

High-Heat and Photo-Stable Perovskite Solar Cells Through Ion Capture Layer Young Wook Noh, Han-Hee Cho and Myoung Hoon Song; Ulsan National Institute of Science and Technology, Korea (the Republic of)

Organic-inorganic hybrid perovskite solar cells (PSCs) have seen a steep rise in power conversion efficiency (PCE) in recent decades and commercialization is just around the corner. Nowadays, they have achieved over 25.5% of PCEs with their excellent properties, such as long diffusion length, high absorption coefficient, and balanced ambipolar carrier transports. In order to commercialize photovoltaic (PV), a product lifetime of at least 20 years is essential, as a conventional crystalline silicon PV module. However, perovskite suffers from low thermal stability and light stability. In this study, we dramatically increased the thermal and light stability of PSCs by introducing a layer capable of inhibiting migration of ions called ion capture layer. Unlike the former materials that block ion migration, a material with tetramethylammonium (TMA^+) and SO_3^- , which are ion groups that could be directly

bonded to iodide and silver ions, was used as the ion capture layer. As a result, PSCs achieved a PCE of 23.3% and maintained >95% of their initial value after >1560 hours at 85 °C heat and retained >80% of their initial PCEs after 700 hours at 1 sun condition.

EN02.08.42

Transparent Electrodes with Enhanced Infrared Transmittance for Semitransparent Perovskite Solar Cells and Four-Terminal Tandem

Applications Hyunmin Jung¹, Geunjin Kim¹, Gyeong Sun Jang¹, Jihoo Lim², Moonyong Kim², Chan Su Moon¹, Xiaojing Hao², Nam Joong Jeon¹, Jae Sung Yun², Helen H. Park¹ and Jangwon Seo¹; ¹Korea Research Institute of Chemical Technology (KRICT), Korea (the Republic of); ²University of New South Wales (UNSW), Australia

Indium oxide doped with titanium and tantulum with high near-infrared transparency is applied to potentially replace the conventional indium-tin-oxide transparent electrode used in semitransparent perovskite devices and top cells of tandem devices. The high near-infrared transmittance of this electrode is possibly explained by the lower carrier concentration suggesting less defect sites that may sacrifice its optical transparency. Incorporating this electrode to semitransparent perovskite solar cells for both the top and bottom electrodes improved the device performance through possible reduction of interfacial defect sites and modification in energy alignment. Furthermore, applying this multi-doped indium oxide to the semitransparent perovskite top cell in four-terminal perovskite-silicon tandem configurations improved the photocurrent response in the bottom silicon cell by more than 7% and 15% without and with an anti-reflection layer, respectively. Finally, effects on the optical and electrical properties and performance of working devices will be addressed, and the mechanisms involved in the enhanced performance will also be discussed.

EN02.08.45

Chloride-Based Additive Engineering for Efficient and Stable Wide-Bandgap Perovskite Solar Cells Xinyi Shen¹, Benjamin Gallant¹, Philippe

Holzhey¹, Joel Smith¹, Melissa McCarthy¹, Karim Elmostekawy¹, Yen-Hung Lin¹, Zhongcheng Yuan¹, Akash Dasgupta¹, Laura Herz^{1,2} and Henry Snaith¹; ¹University of Oxford, United Kingdom; ²TU Munich, Germany

Metal halide perovskite-based tandem solar cells combining absorbers of different bandgaps are promising to achieve light-to-electricity power conversion efficiencies (PCE) beyond the theoretical limits for their single-junction counterparts. However, significant open-circuit voltage deficits present in wide-bandgap perovskite solar cells remain major hurdles for realising efficient and stable perovskite tandem cells. The underlying mechanisms widely believed to be responsible for mediocre wide-bandgap perovskite solar cells include non-radiative interfacial losses,^[1-3] halide segregation,^[4] as well as heterogeneous crystallisation,^[5] resulting in low open-circuit voltage (V_{OC}). Moreover, compared to narrow-bandgap perovskite solar cells (i.e., 1.6 eV and below), wide-bandgap perovskite solar cells exhibit more rapid perovskite degradation under accelerated ageing conditions (e.g., light, moisture, heat and oxygen),^[17] mainly due to the complex composition and processing requirements of this class of perovskite, which can be a great concern for perovskite solar cells stability. Hence, effective strategies to form low-loss and stable wide-bandgap perovskites will be the key to helping the commercial deployment of perovskite tandem solar cells in the near future.

In this study, we report a holistic approach to overcoming challenges in 1.8-eV perovskites by examining a series of chloride additives to engineer intermediate phases during the crystallisation process. Utilizing a carbazole-based self-assembled monolayer as the hole transport layer, synergistic improvement of the perovskite materials, and its interface with the hole transport layer allows us to achieve a maximum power point-tracked PCE (η_{mpp}) of 17% and a steady-state V_{OC} of 1.25 V. In addition, the chloride-modified perovskite material demonstrates improved ambient stability (25 °C, relative humidity = 40% in the air in dark) and suppressed halide segregation compared to no-chloride reference perovskites. In the meantime, we elucidated the role of chloride additives in controlling the intermediate phase formation and detailed subsequent materials properties of chloride-engineered wide-bandgap perovskites. Understanding such underlying mechanisms will help address one of the most challenging aspects in the commercial deployment of perovskite tandem technologies.

[1] J. Wen, Y. Zhao, Z. Liu, H. Gao, R. Lin, S. Wan, C. Ji, K. Xiao, Y. Gao, Y. Tian, J. Xie, C. J. Brabec, H. Tan, *Adv. Mater.* **2022**, e2110356.

[2] W. Chen, Y. Zhu, J. Xiu, G. Chen, H. Liang, S. Liu, H. Xue, E. Birgersson, J. W. Ho, X. Qin, J. Lin, R. Ma, T. Liu, Y. He, A. M.-C. Ng, X. Guo, Z. He, H. Yan, A. B. Djurišić, Y. Hou, *Nature Energy* **2022**, 1.

[3] T. Huang, S. Tan, S. Nuryyeva, I. Yavuz, F. Babbe, Y. Zhao, M. Abdelsamie, M. H. Weber, R. Wang, K. N. Houk, C. M. Sutter-fella, Y. Yang, **2021**, 1.

[4] M. Long, T. Zhang, M. Liu, Z. Chen, C. Wang, W. Xie, **n.d.**, DOI 10.1002/adma.201801562.

[5] S. Mahesh, J. M. Ball, R. D. J. Oliver, D. P. McMeekin, P. K. Nayak, M. B. Johnston, H. J. Snaith, *Energy Environ. Sci.* **2020**, *13*, 258.

EN02.08.46

Photo-Crosslinkable Naphthalene Diimide (NDI) Polymer as Electron Transport Layer for Solution-Processed n-i-p Perovskite Solar Cells

Yangwei Shi^{1,1}, Declan McCarthy², Kevin Ho¹, Fangyuan Jiang¹, Stephen Barlow², Seth R. Marder² and David S. Ginger¹; ¹University of Washington, United States; ²Georgia Institute of Technology, United States

Organic-inorganic halide perovskite has demonstrated great potential in application of photovoltaics with power conversion efficiency (PCE) surging from 3.8% to current record efficiency of 25.7% for a single junction perovskite solar cell. The start-of-art perovskite solar cell usually adopts inorganic metal oxide such as TiO₂, SnO₂ as electron transport layers (ETLs). However, these ETLs generally require high annealing temperature and can cause instability issues due to their photocatalytic nature. Here we report a photo-crosslinkable naphthalene diimide (NDI) polymer with a cinnamate side chain as ETL for solution processed n-i-p perovskite solar cells. Our solar cell device results show that crosslinked NDI polymer exhibit better VOC, FF, PCE, and less hysteresis than its non-crosslinked counterpart. We ascribe this PCE increase to improved perovskite crystallinity and energy level alignment, reduced nonradiative recombination and series resistance of the crosslinked NDI polymer-based perovskite solar cells.

EN02.08.47

Glass-Crystal Transformation Kinetics in a Hybrid Metal Halide Perovskite Akash Singh and David B. Mitzi; Duke University, United States

Metal halide perovskites (MHPs) are the widely celebrated family of crystalline semiconductors that has led to significant advancement in the fields of photovoltaics, emitters, and sensors. Though most of the research is condensed towards studying the crystalline MHPs, the study of MHPs that can access a glassy/amorphous state could help broaden the fundamental understanding of the structure-property relationship as well as their application space.

Our recent discovery of glass formation and reversible crystal-glass switching in an exemplary 2D lead bromide perovskite [1], with distinct optoelectronic properties in either state, has spurred interest into their potential applicability in areas where phase change characteristics could be exploited. To recognize the suitability of glass forming MHPs into such application space, it is imperative to study the kinetics of glass crystallization. Such a study would offer the

potential to understand the underlying nucleation and crystal growth mechanisms, as well as the activation energy requirement to drive such a change, providing important information for prospective phase-change applications.

In this work, we demonstrate the underlying kinetic effects of glass crystallization in a representative MHP family member, [S(-)-1-(1-naphthyl)ethylammonium]₂PbBr₄. By making use of iterative calorimetry and numerical modelling techniques, such as the Ligerio [2] and Kissinger [3] kinetic models, we extract the activation energy of glass crystallization in the studied MHP. The activation energy (~350 kJ/mol) is found to be higher than those determined for most fast-crystallizing chalcogenides but smaller than for most of the stable oxide glasses. Furthermore, the extracted Avrami parameter of ~2 suggests a heterogeneous surface-mediated nucleation mechanism with two-dimensional crystal growth, as also corroborated by in-situ and ex-situ microscopy. Our present work serves as the first study to model the glass crystallization kinetics of MHPs and thus, with the advent of more glass forming MHPs, these results are expected to serve as a starting point for comparing crystallization kinetics parameters as a function of MHP composition and organic cation choice. The results should therefore also help in establishing a framework for selecting suitable candidates for use in new prospective applications for MHPs, such as memory, computing, phase change energy storage, glass-composites, metamaterials, and reconfigurable photonic devices.

[1] Singh, A. et al. *Adv. Mater.* **2021**, *33* (3), 2005868.

[2] Ligerio, R. et al. *J. Mater. Sci.* **1991**, *26* (1), 211-215.

[3] Kissinger, H. E. et al. *J. Res. Natl. Bur. Stand. (U. S.)* **1956**, *57* (4), 217-221.

EN02.08.48

Phase Co-Existence During Hybrid Halide Perovskite Crystallization Mriganka Singh, Maged Abdelsamie, Tim Kodalle and Carolin M. Sutter-Fella; Lawrence Berkeley National Laboratory, United States

Halide perovskites with mixed A- and X-site cations and anions, respectively, are important to overcome challenges such as thermal and structural instability, and moisture sensitivity in single cation MA/FA/CsPbX₃. Triple cation, mixed halide perovskite compositions have been reported to be more thermally stable, exhibit fewer phase impurities, and are less affected by the processing conditions than single cation perovskites. In this work, we present a multimodal in situ study on the formation of Cs_{0.05}FA_{0.81}MA_{0.14}Pb(I_{0.85}Br_{0.15})₃ by combining structural information from grazing-incidence wide-angle synchrotron X-ray scattering (GIWAXS) and optical properties from photoluminescence (PL) spectroscopy. This study covers the predominantly used solvents and solvent systems DMF, DMSO, and mixtures thereof. We are looking at the effect of the solvent used and the application of antisolvent dripping. We find that the non-perovskite delta-FAPbI₃ appears in all crystallization pathways. It is strongly correlated with the antisolvent dripping and temporally close to the perovskite phase formation. It was also found that the delta phase is more stable in DMF than in DMSO systems. These findings provide novel insights into perovskite phase evolution and its correlation with the solvent and antisolvent to allow for better synthetic control.

EN02.08.49

Advanced Characterization of Three-Terminal Perovskite/Silicon Tandem Solar Cells Philipp Tockhorn¹, Philipp Wagner¹, Sebastian Hall¹, Steve Albrecht^{1,2} and Lars Korte¹; ¹Helmholtz-Zentrum Berlin für Materialien und Energie, Germany; ²Technische Universität Berlin, Germany

Perovskite solar cells have been shown to be ideal partners to silicon (Si) in tandem devices due to their flexibility in band-gap engineering by means of compositional variation, and potentially cost-effective fabrication [1,2]. Combining a perovskite top with a silicon heterojunction (SHJ) bottom cell has recently led to a new record power conversion efficiency (PCE) of close to 30% for perovskite/silicon (Si) tandem devices [3]. Most commonly, either a two- (2T) or four-terminal (4T) arrangement of the subcells are studied [1]. In a two-terminal (2T) arrangement, both sub-cells are connected in series in a monolithic device, sharing a common electron and hole contact. In this relatively straightforward device architecture, both sub-cells must, however, provide the same current for optimal operation. Opposed to that, four-terminal (4T) tandems feature electrically decoupled sub-cells with relaxed requirements regarding their respective electrical performance. On the downside, more complex subcell interconnection and potentially intricate module integration are major drawbacks of this concept. As an alternative, here we focus on a third approach that has gained attention only recently for perovskite/Si tandems, namely three-terminal (3T) tandems [4]. In 3T tandems, which are usually realized by using a bottom cell with interdigitated back-contacts (IBC), both subcells feature their own electron contact while sharing a common hole contact (or vice versa) [5]. This arrangement leads to a monolithic architecture that does not require current-matched sub-cells, and therefore combines the main advantages of the more commonly used 2T and 4T tandems. It has been shown that different sub-cell configurations, and especially the type of interconnection scheme, can lead to different electrical behaviors, even if the same materials are used in each case [6,7].

In this contribution, we will report on our recent progress in 3T perovskite/IBC SHJ tandem solar cells with a PCE > 25%. We will focus on different aspects regarding the measurement setup for such devices, the characterization of perovskite and silicon subcells and the visualization of advantages over 2T tandems through measurements and simulations. We will report on the design of a dedicated measurement setup featuring a dual-source source measure unit to accurately characterize the optoelectronic performance of 3T tandems. This is required since the solar cell characteristics of a 3T device cannot be retrieved from a single j-V scan but require simultaneous scanning of two voltages. This measurement setup and a tunable LED-based solar simulator are then used to study the response of 2T and 3T tandems to different illumination conditions. Further, we demonstrate how the individual measurement of the perovskite and Si subcell can be used to understand the behavior of not only 3T but also 2T. In addition to the experimental characterization of 3T, we use energy yield calculations to study the advantageous properties of 3T over 2T tandems. Lastly, we will point out pathways to achieving 3T PCEs in the range of state-of-the-art 2T and 4T tandems.

REFERENCES

[1] T. Leijtens et al., *Nat. Energy* **3** (10), 828-838 (2018).

[2] M. Jošt et al., *Adv. Energy Mater.* **10** (26), 1904102 (2020).

[3] NREL, Best Research-Cell Efficiencies, <https://www.nrel.gov/pv/cell-efficiency.html>, 2022-06-16

[4] P. Tockhorn et al., *ACS Appl. Energy Mater.* **2020**, *3* (2), 1381-1392 (2020).

[5] T. Nagashima et al., Conference Record of the 28th IEEE Photovoltaic Specialists Conference, Anchorage, Alaska, USA, 2000, pp 1193-1196.

[6] E. L. Warren et al., *ACS Energy Lett.* **2020**, *5* (4), 1233-1242 (2020).

[7] P. Wagner et al., Presented at the 11th International Conference on Silicon Photovoltaics, Hamelin, Germany, 2021.

EN02.08.50

Revealing the Role of Graphite and Carbon Black in Carbon Electrodes of Carbon-Based Perovskite Solar Cells Ryuki Tsuji, Kenichirou Tanaka, Kouta Oishi, Takaya Shioki and Seigo Ito; University of Hyogo, Japan

Perovskite solar cells (PSCs) have a photoelectric conversion efficiency of over 20 % and they can be fabricated only by printing and coating processes, so it is expected as next-generation solar cells. However, the back-contact electrode (e.g. Au, Ag) and hole transport materials (e.g. Spiro-OMeTAD) used for PSCs are unstable against water and oxygen, and there is a problem with long-term stability. Therefore, we focused on fully printable carbon-based multi-

porous-layered-electrode PSCs (MPLE-PSCs) which have an electron transport layer (mesoporous TiO₂), an insulation layer (mesoporous ZrO₂), and hole transport/back contact electrode layer (carbon) [1-5]. MPLE-PSCs have long-term stability because the thick carbon layer (~15 μm) can be protected the light absorption layer from ambient water and oxygen. However, MPLE-PSCs have a low efficiency of less than ~18%, so it is necessary to aim for higher efficiency for commercialization. In this work, we focus on carbon electrodes, which have roles of hole transport and back contact. Typically, carbon electrodes are made from a mixture of large-sized graphite particles and nano-sized carbon black. However, the role of each material remains unclear. Therefore, carbon electrodes with different mixing ratios of graphite and carbon black are fabricated and compared. This fundamental comparison reveals the role of carbon materials used in MPLE-PSCs.

A TiO₂ compact layer was deposited by a spray pyrolysis method on patterned FTO glass. Then, porous TiO₂, ZrO₂, and carbon layers were deposited by a screen printing method, and each layer was sintered at 400 to 500 °C. Six mixing ratios of graphite and carbon black for carbon electrodes were prepared: 100-0, 80-20, 65-35, 50-50, 20-80, and 0-100. Finally, (5-AVA)_{0.05}(MA)_{0.95}PbI₃ perovskite precursor solution was drop-casted and permeated through the carbon layer, and the MPLE-PSCs were completed by removing the solvent and crystallizing the perovskite material by heating and drying. Various measurements were performed on the obtained devices.

The results show that the mixing ratio of graphite to carbon black has a significant effect on the performance of MPLE-PSC devices. In the graphite-rich, the open-circuit voltage (V_{oc}) was higher. However, the short-circuit current density (J_{sc}) and fill factor (FF) were low. On the other hand, increasing the ratio of carbon black decreased V_{oc} , but improved J_{sc} and FF. To understand these changes, electrochemical impedance spectroscopy (EIS) and photoluminescence (PL) analysis were performed. The results show that carbon black has the effect of promoting hole extraction and graphite has the effect of efficiently transporting the generated charge. In summary, the MPLE-PSC device achieved maximum performance and a champion efficiency of 13% when graphite and carbon black were in a 50-50 or 20-80 ratio. This study is important for realizing inexpensive and sustainable carbon electrodes not only for PSCs but also for various electronic devices.

References

- [1] A. Mei, *et al.*, *Science* **345**, 295 (2014).
- [2] R. Tsuji, *et al.*, *Electrochemistry* **88**, 418 (2020).
- [3] R. Tsuji, *et al.*, *Photonics* **7**, 133 (2020).
- [4] D. Bogachuk, R. Tsuji, *et al.*, *Carbon* **178**, 10 (2021).
- [5] E. Kobayashi, R. Tsuji, *et al.*, *Cell Rep. Phys. Sci.* **2**, 100648 (2021).

EN02.08.51

Formation of Superlattice in Organometal Halide Perovskite Solar Cells Satoshi Uchida and Hiroshi Segawa; The University of Tokyo, Japan

Recently, perovskite solar cells have become the latest research field among various new generation photovoltaic technologies due to their high performance and potentially low-cost production. The power conversion efficiency has already reached over 25% in 2020 much beyond another solar cells such as CIGS or amorphous Si. The further performance still looks promising toward the Shockley–Queisser limit at around 30%. For that purpose, physical chemistry understanding based on the crystallography must be essential to design the good light harvesting, good charge separation and good charge transfer.

Recently we reported the scientific revelation that the crystal phase of thin film CH₃NH₃PbI₃ consists of the mixture of tetragonal phase and cubic phase. Moreover, bold zebra pattern with d-spacing with 14.2Å (2θ=6.22° for CuKα by XRD) was clearly observed by high resolution TEM with FIB processing that consists with tetragonal and cubic phase superlattice. The typical high magnification In the TEM observation characteristic identity of perovskite can be seen as (1) Phase coexistence (2) Superlattice (3) Nano size domain (10–20nm).

To make more high performance as a solar cell, the crystal phase control with liquid nitrogen quenching just after the hot plate heating was newly examined. The resulting cell performance was impressive, about 2% more than that without Liq. N₂ treatment. Details on TEM observations are also provided for such procedures.

EN02.08.53

Additive Engineering for Enhancing Photovoltaic Performance and Stability of Sn-Pb Alloyed Perovskite Solar Cells Kyu-Woong Yeom and Nam-Gyu Park; Sungkyunkwan University, Korea (the Republic of)

Here, we report on additive engineering in Sn²⁺ and Pb²⁺ bearing precursor solution to improve photovoltaic performance and stability of Sn-Pb alloyed perovskite solar cells. Additives of urea as O-donor and thiourea as S-donor are compared, where oxygen is relatively hard base than sulfur. Photovoltaic performance is higher for the additives than for the control without additive, where thiourea is found to be more effective than urea in enlarging grain size and carrier lifetime. As a result, power conversion efficiency (PCE) of perovskite solar cell employing FA_{0.5}MA_{0.5}Pb_{0.5}Sn_{0.5}I₃ is improved from 14.58% for control (without additive) to 16.00 % for urea and to 18.59% for thiourea. FTIR study on SnI₂ (or PbI₂)-additive adduct shows that the C=S stretching frequency of thiourea is lowered from 729 cm⁻¹ to 721 cm⁻¹ and 708 cm⁻¹ upon interaction with PbI₂ and SnI₂, respectively, which indicates that interaction of S with Sn²⁺ is stronger than that with Pb²⁺. Shift to lower wavenumber is also observed for urea but the degree is marginal for both SnI₂ and PbI₂. Stronger interaction of thiourea with Sn²⁺ than Pb²⁺ is due to increased covalency by interaction of smaller Sn²⁺ ion with soft sulfur bearing thiourea. Thus, the significantly improved performance in the presence of thiourea is ascribed to underlying a kinetic control of crystal growth. X-ray photoelectron spectroscopic study reveals that oxidation of Sn²⁺ is effectively suppressed by thiourea, which is beneficial to not only photovoltaic performance but also phase stability.

EN02.08.54

Enhanced Electron Extraction by Tuning Space-Charge Layer of SnO₂ for Hybrid Perovskite Solar Cells Sarah S. Youn^{1,2}, Jihyun Kim¹, Junhong Na³, William Jo¹ and Gee Yeong Kim²; ¹Ewha Womans University, Korea (the Republic of); ²Korea Institute of Science and Technology, Korea (the Republic of); ³Kyungnam University, Korea (the Republic of)

Perovskite solar cells (PSCs) have shown outstanding performance during the past decade. An important parameter that controls device performance is the charge transport properties at interfaces. Tin oxide (SnO₂) is a widely used electron transport layer (ETL) material in highly efficient perovskite solar cells owing to its superior electrical and optical properties. Therefore, understanding the interfacial effect of ITO/SnO₂ and its role in PSCs is crucial but it is not intensively studied. Here, we employ conductive atomic force microscopy and transfer length method as a function of SnO₂ thickness to identify space-charge effect at the interface. The results show that the critical kink point exists at about 10 nm of SnO₂ thickness, indicating electron depletion and expecting weak charge transfer behavior of the device. A thickness less than 20 nm was favorable for the best PSC performance because charge transport behaviors in the thin SnO₂ layer were modified by electron depletion. This study provides a strategy to tune the electron transport layer and boost the

charge transport behavior in PSCs, making important contributions to optimizing SnO₂-based PSCs.

EN02.08.55

Impact of Halide Composition in Copper Halide-Based Hole Transport Materials on Stability and Performance of Inverted Perovskite Solar Cells Zhaojie Zhang, Hamza Javid, Emily C. Smith and Dhandapani Venkataraman; University of Massachusetts, Amherst, United States

Copper halides are promising hole transport materials for inverted perovskite solar cells (PSCs) due to their advantages of low cost, tunable energy levels, good hole mobility, and excellent stability. However, the understanding of the role of mixed copper halides with fine-tuned energy levels and conducting properties in highly efficient inverted PSCs is still unclear. Here, we demonstrate that using Cu_xBr_{1-x} with an optimized Br/I ratio as HTL leads to a champion power conversion efficiency of 19.2% compared to PTAA (17.7%), CuI (16.6%), and CuBr (17.6%) based PSCs. We systematically investigate the influence of electronic properties of Cu_xBr_{1-x}, including hole mobility, hole density, energy level, and band gap on the performance (V_{oc}, J_{sc}, and FF) and stability of PSCs. We used hyperspectral photoluminescence imaging to quantify charge carrier transport dynamics and recombination loss. PSCs with fine-tuned Cu_xBr_{1-x} have a more homogeneous distribution of quasi-fermi level splitting and more efficient charge extraction, leading to improved fill factor. Cu_xBr_{1-x} also suppresses ion migration and phase segregation in mixed-halide perovskite films. This work provides design guidelines for improving the performance and stability of PSCs by tuning the electronic properties of hole transport layers.

EN02.08.56

Case Study—Applying Benzylamine as a Monoamine Additive Passivation in Wide-Bandgap Perovskites Suer Zhou¹, Yangwei Shi², James Drysdale¹, Joel Smith¹, Margherita Teddei², Jian Wang², Akash Dasgupta¹, Ashley Marshall¹, David Ginger² and Henry Snaith¹; ¹University of Oxford, United Kingdom; ²University of Washington, United States

Silicon/perovskite tandem solar cells are a promising direction for increasing the power output of solar cells past the Shockley-Queisser limit for single junctions. The ideal bandgap of perovskite on top of silicon is around 1.68-1.70eV, which can be achieved by mixed cation, mixed halide perovskites, such as FA_{0.75}CS_{0.25}Pb(I_{0.8}Br_{0.2})₃. However, there are still many challenges for wider bandgap compositions, such as ion migration and phase segregation effects. Under constant laser illumination, these compositions undergo light-induced halide segregation, which will impact the long-term stability during operation.

To stabilize wide-bandgap mixed halide perovskites, we employ benzylamine as a bulk additive. By optimizing the amount of additive in the film, we significantly improved the PLQY and charge carrier lifetime. Compared to applying benzylamine as a surface treatment^{1,2}, the bulk additive approach gave better reproducibility and higher overall device performance. Time-resolved PL and ToF-SIMS reveal that the benzylamine is mostly distributed near the top and bottom surfaces, forming lower dimensional phases. Benzylamine passivates both the grain boundary and surface defects while hindering ion migration. Furthermore, adding benzylamine does not introduce halides that could incorporate into the perovskite and change the bandgap, unlike the more common approach of adding ammonium halides. Perovskite thin films and devices with benzylamine have improved light and moisture stability, beneficial for perovskite/silicon tandem applications.

References

- (1) Zhou, Y.; Wang, F.; Cao, Y.; Wang, J.-P.; Fang, H.-H.; Loi, M. A.; Zhao, N.; Wong, C.-P. Benzylamine-Treated Wide-Bandgap Perovskite with High Thermal-Photostability and Photovoltaic Performance. *Advanced Energy Materials* **2017**, 7 (22), 1701048. <https://doi.org/10.1002/aenm.201701048>.
- (2) Wang, F.; Geng, W.; Zhou, Y.; Fang, H.-H.; Tong, C.-J.; Loi, M. A.; Liu, L.-M.; Zhao, N. Phenylalkylamine Passivation of Organolead Halide Perovskites Enabling High-Efficiency and Air-Stable Photovoltaic Cells. *Advanced Materials* **2016**, 28 (45), 9986–9992. <https://doi.org/10.1002/adma.201603062>.

EN02.08.57

Creation of a Solution Processed Scalable Transparent Top Electrode for Application in Perovskite Solar Cells Jack Horne, Trystan Watson, David Beynon and Chris Griffiths; Swansea University, United Kingdom

Perovskite solar cells frequently rely on a transparent substrate with a non-scalable thermally evaporated TCO for the transmission of photons to the active layers, however, when perovskites are used on an opaque substrate or for semi-transparent applications the top electrodes, which play a critical role in the performance of a solar cell, must instead be transparent to allow photons to reach the active layer, with semi-transparent solar cells too allowing photon to reach the active layers from both sides.

This work presents how single walled carbon nanotubes (SWCNTs) and silver nanowires (AgNWs) can be used in combination to create a low temperature solution processable transparent top electrode for use in opaque substrate-based and semi-transparent perovskite solar cells.

Using a hybrid electrode consisting of low-cost, commercially available inks to create a carbon nanotube in a silver nanowire matrix provides a scalable solution for creating an electrode compatible with roll-to-roll lines. This was achieved through experiments optimising the ratio between the CNT and AgNW solutions using UV-Vis-NIR to measure the transparency and 4-point probe to measure the sheet resistance and repeated over various thicknesses which was further investigated through AFM. The use of opaque substrates, like steel, and the application of a solar cell coated directly onto it provides an additional function outside of their structural uses, giving existing materials the ability to generate electricity utilizing their surface area for energy generation.

This solution processed electrode can be deposited through both spray and slot die coating techniques. The hybrid electrode layer provides improved adhesion over a film of AgNWs alone with the interaction between the CNTs and AgNWs creating a more stable layer reducing the movement of silver ions towards the perovskite. The network of intermeshed nanomaterials creates a high conductivity of charge with the spaces between them creating a small variance in the percentage transmission of wavelength across the visible spectrum.

Using this electrode, we were successfully able to create working perovskite solar cells using both sprayed and slot die deposition with devices performing the same when measure either through a transparent substrate, as in traditional devices, or through the top electrode.

EN02.08.58

Discovering Novel Halide Perovskites Using Multi-Fidelity Machine Learning Panayotis T. Manganaris, Jiaqi Yang and Arun Kumar Mannodi Kanakkithodi; Purdue University, United States

We report a materials design pipeline for halide perovskites. The primary objective being to recommend perovskite alloy compositions corresponding to targeted properties. Here targets are chosen to yield stable compounds with high photovoltaic (PV) performance. Thus, we focus on models of the electronic band gap, decomposition energy (therefore, perovskite stability), and PV efficiency. We use Spectroscopic Limited Maximum Efficiency (SLME) for synthetic data and Power Conversion Efficiency (PCE) for physical data. We use nanoHUB, an NSF-funded, Purdue-based computational repository, to host reproducible notebooks documenting our model development workflow [1]. We also host an interoperable database and inverse design pipeline for public access. Thereby, we enable the scientific community to use and improve these tools. Thus perovskites with alternative optoelectronic properties, possibly targeting quantum computing or metrology, may be discovered. The design pipeline makes recommendations using continuous

surrogate models trained to connect a discretely sampled composition space to the targeted properties. A Genetic Algorithm (GA) selects optimal compositions where fitness involves minimizing euclidean distance between the predicted and targeted properties and by ensuring compositional feasibility.

Our GA optimizer prioritizes exploration so locally optimal candidates can be found without fixating on a small subset of fit regions. GA is also efficient in high dimensional space. In our past published work [2], the discrete alloy space based on a finite supercell experiences combinatorial scaling with supercell size. Going from discrete sampling to continuous surrogate models sees this scaling continue to infinite resolution. We provide machine learning (ML) models for the optimizer to work on: A rigorously optimized Random Forest Regressor (RFR), a Gaussian Process (GP) Regressor, and a Sure Independence Screening and Sparsifying Operator (SISSO) regressor. Naturally, the GA's solutions will only be as good as the ML accuracy.

We subdivide approximately 1000 physical and synthetic records into tables by record accuracy. The largest table of ~500 compounds contains optoelectronic properties simulated using density functional theory (DFT). Here, geometry optimization of pseudo-cubic ABX₃ supercells with arbitrary mixing at each site is followed by static band structure and optical absorption calculations performed at the GGA-PBE level of theory. Also, ~300 compounds were subjected to more expensive hybrid HSE06 computations, both with and without spin-orbit coupling (SOC), for better electronic properties. Finally, ~100 of the same compositions also record experimental measurements for band gap and efficiency.

We combine tables using multi-fidelity modeling techniques so each of our architectures can make predictions with physical accuracy. Currently we use only composition information as descriptors. This simplifies featurization because a composition vector can be procedurally obtained for experimental and synthetic data alike simply by parsing a string encoding the ABX₃ perovskite formula corresponding to each record with relative ease.

No more than this composition vector is needed to make a prediction. However, additional predictors derived from elemental properties easily obtained from the trusted Mendeleev databases are included in model design. Finally, we discuss using state of the art graph based surrogates to extend this optimization loop to non-cubic phases. The nanoHUB pipeline is constantly improving with fresh DFT data, ML models, and design tools.

[1] P. Mangano, et al. MRS ICMS tutorial, 2022. URL <https://nanohub.org/resources/36041?rev=90>.

[2] Mannodi-Kanakkithodi, A., & Chan, M. K. Y. (2022). Data-driven design of novel halide perovskite alloys. *EES.*, 15, 1930–1949. <http://dx.doi.org/10.1039/D1EE02971A>

EN02.08.59

Magnetism in 1D and 2D Hybrid Perovskite Induced Through Water-Assisted Self-Assembly Method Ariany Bonadio, Fernando Sabino, Aryane Tofanello, André L. de Freitas, Vinicius G. de Paula, Gustavo Dalpian and Jose A. Souza; Universidade Federal do ABC, Brazil

Methylammonium lead iodide (MAPbI₃) is an important light-harvesting semiconducting material with excellent optical and electronic properties for the use in optoelectronic devices, including photovoltaic and light-emitting devices. Doping of halide perovskites allows the manipulation of the magnetic, optic, and electronic properties. The successful insertion of magnetic dopants is important to the development of functional devices and is also able to open new potential applications such as in magnetic/semiconducting devices. Therefore, effective strategies to incorporate different ions into the structure have been very appealing. In this work, doped magnetic/semiconducting perovskite microwires have been successfully produced by using a novel strategy involving a self-assembly growth process of [PbI₆]⁴⁻ octahedra chains in the presence of liquid water. In this process, a monohydrate compound with a monoclinic structure is formed. The 1D [PbI₆]⁴⁻ octahedra chains are stabilized by the presence of both water and MA⁺, forming large channels between chains. This monohydrate compound can easily be reversed to MAPbI₃ through heat treatment or in an evacuated atmosphere eliminating the water present in the channels of the structure. Therefore, we were able to produce paramagnetic perovskite microwires by incorporating iron and manganese ions in the organic channels during the recrystallization process. Afterward, the crystal structure collapses into the 3D perovskite structure through thermal annealing, trapping the magnetic ions within the perovskite structure. Structural and morphological studies confirm that the magnetic ions were successfully introduced in the perovskite structure. From first principles calculations, we determined that the magnetic ions are localized in the interstitial sites. Electric transport characterizations were also carried out to study the influence of the two different magnetic ions on the crystal lattice and charge carrier dynamics. 2D ribbon-like magnetic perovskites were also produced by adding large organic molecules along with magnetic ions through this self-assembly growth process. The introduction of large ammonium cation as butylammonium leads to a 2D layered structure alternately stacked insulating organic spacer layer and inorganic BX₆ slabs. The general chemical formula is (L)₂(A)_{n-1}B_nX_{3n+1}, where L is the monovalent organic spacer, A is a monovalent cation, B is a divalent metal cation, X is a halide anion, and *n* represents the number of BX₆ layers. Structural analysis indicated that the 2D perovskite with a mix number of *n* is formed without traces of Fe or Mn binary impurity phases. The hydrophobic organic spacer layer provides a natural protective barrier for the penetration of ions and moisture offering long-term stability in the air atmosphere for the perovskites.

EN02.08.60

Physical Vapor Deposition of Yb-Doped Cesium Lead Halide Perovskites Iver J. Cleveland, Minh N. Tran and Eray S. Aydil; New York University, United States

Recently, ytterbium-doped CsPb(Cl_{1-x}Br_x)₃ (*x*<0.35) perovskite showed efficient quantum cutting, a process wherein photons absorbed at high energies (*e.g.*, > 2.5 eV) generate two photons with energies (~ 1.25 eV) close to the silicon bandgap energy (1.1 eV). The mechanism for this quantum cutting process is not well understood, but the leading theories suggest that Pb vacancy defects in the perovskite efficiently trap excitons and transfer energy to two nearby Yb³⁺ ions, which subsequently emit from the Yb³⁺ ²F_{5/2} → ²F_{7/2} transition.¹ A thin layer of this material on a silicon solar cell can convert blue photons to two near-infrared (NIR) photons, decreasing energy losses due to the relaxation of the high-energy charge carriers to the band edges. In this way, silicon solar cell efficiencies can surpass the Quessier limit. The majority of reports on ytterbium-doped perovskites rely on nanocrystal or solution-based synthesis to make the materials.^{2,3}

We are exploring physical vapor deposition, a solvent-free technique, to synthesize halide-perovskite thin films. Specifically, we deposited CsPb(Cl_{1-x}Br_x)₃ and Yb-doped CsPb(Cl_{1-x}Br_x)₃ films by co-evaporating CsCl, PbCl₂, PbBr₂ and YbCl₃ and controlling the flux of each using quartz crystal microbalances. Films were characterized using x-ray diffraction, scanning electron microscopy, optical absorbance, x-ray photoelectron spectroscopy, photoluminescence, and photoluminescence quantum yield measurements. Specifically, we investigated the effects of deposition temperature, Yb-concentration, stoichiometry, post-deposition annealing, and annealing environment on the structure, morphology, and photoluminescence quantum yield of Yb-doped CsPbCl₃ films formed by PVD and using a combinatorial high throughput approach.

Yb-doped CsPbCl₃ films annealed at 350 °C for 2 hours emitted NIR photoluminescence at ~990 nm (Yb³⁺ ²F_{5/2} → ²F_{7/2} transition, 1.25 eV) with quantum yields (PLQY) exceeding 70%, when excited with photons with energies above the CsPbCl₃ bandgap (*e.g.*, > 3.0 eV). PLQY was maximized at the lowest Yb concentrations and decreased as Yb concentration increased from 2% to 10%. This indicates that not all Yb are optically active. The PLQY is especially sensitive to the annealing environment. For some film compositions, identical films annealed in the air have higher PLQY than films annealed in an N₂-

filled glovebox, and films annealed in an N₂-filled glovebox followed by annealing in the air have even higher PLQY. We hypothesize that grain growth in the glove box followed by oxygen passivation of remaining defects in the air is responsible for the high PLQYs in these films. This PLQY trend with annealing environment, however, is sensitive to the Cs and Yb concentrations as well as the halide composition. For instance, Yb-doped orthorhombic CsPb(Cl_{1-x}Br_x)₃ films with x ~ 0.35 behave differently than Yb-doped cubic CsPbCl₃ films, with annealing in N₂-filled glovebox having the highest PLQY. SEM images show that annealing in air leads to smaller grains. Grain growth is also inhibited when as little as 2% Yb (relative to lead) is incorporated in the film. Surface analysis of Yb-doped CsPbCl₃ films with XPS shows that Yb is detected on the surface of films annealed in a glovebox but missing from the surface of films annealed only in the air.

1. C. S. Erickson, M. J. Crane, T. J. Milstein, D. R. Gamelin, *J. Phys. Chem. C*, 2019, **123**, 12474-12484.
2. D. M. Kroupa, J. Y. Roh, T. J. Milstein, S. E. Creutz, D. R. Gamelin, *ACS Energy Lett.*, 2018, **3**, 2390-2395.
3. T. J. Milstein, D. M. Kroupa, D. R. Gamelin, *Nano Lett.*, 2018, **18**, 3792-3799.

EN02.08.61

Continuous MASn₃ Perovskite Thin Films Deposited by Spin Coating without Antisolvent Treatment Chandan Q. Howlader¹, [Nischal Khakurel](#)¹, Wilhelmus Geerts¹, Greg Gibson² and Maggie Chen¹; ¹Texas State University, United States; ²nTact, United States

Organic-inorganic metal halide perovskite materials have emerging photovoltaic properties, thus high potential for applications in solar cells. Also, they are good competitors to the current market-dominant silicon solar cell as they are cheaper to manufacture. The most efficient perovskite solar cells show a power conversion efficiency of more than 24%. However, they contain lead (Pb), which is harmful to the human body as well as the environment. The most suitable substitute for the lead in the perovskite is tin (Sn) which is less toxic. However, most tin-based perovskite materials require an anti-solvent treatment to start the crystallization for getting a fully covered perovskite thin film. These anti-solvents steps add complexity to the deposition process and are anti-solvents are also often toxic. So, it is also necessary to eliminate the anti-solvent step from the solar cell fabrication process to make it more ecofriendly. In this work, we deposited the methylammonium tin iodide (MASnI₃) without any antisolvent and obtained fully covered perovskite thin films. The crystallization and coverage are highly dependent on the spin speed, spin time and concentration of the perovskite ink. The ink was prepared by dissolving 1 mole of methylammonium iodide (MAI), 1 mole of tin iodide (SnI₂), and 15 mol% of tin fluoride (SnF₂) into a mixed solvent. The mixed solvent contains N, N-dimethylformamide (DMF) and dimethyl sulfoxide (DMSO) of a ratio of 4:1. The perovskite ink was spin-casted at 1000 rpm for 10 s and 6000 rpm for 110s on glass and glass/ITO substrates. The deposited films were cured at 70° C for 10 min on a hot plate inside the glovebox in a nitrogen (N₂) atmosphere. The optical properties of the thin films were determined from UV-Vis, Photoluminescence (PL), ellipsometry and the physical properties from scanning electron microscopy (SEM), atomic force microscope (AFM), and X-ray diffraction (XRD). XRD q-2q scans show that the deposited films have an a-phase MASnI₃ crystal structure with a predominant (001) texture. SEM images show continuous films with large crystallites up to 40 um. The bandgap determined from UV-Vis measurements is approximately 1.25 eV which matches up with the bandgap determined from the PL measurements (1.26 eV) and is similar to what others have found for MASnI₃. The effect of 0, 25 mol%, and 100 mol% MAAc additive in the ink on the properties of the spin cast films was investigated. The MAAc additive increased the PL signal but did not affect the film's morphology observed by SEM images.

This work was in part funded by the Department of Navy's HBCU/MI Program through ONR grant number N00014-19-1-2576 and in part by NSF through STTR Phase II grant 1927020. The authors would like to thank Dr. Holtz of Texas State for training access and help with the PL measurements.

EN02.08.62

High Gain, Stable Infrared Photodetectors Based on Electrospun Triple Cation Perovskite Nanofibers [Min-Woo Kim](#) and Stephanie Lee; New York University, United States

IR photodetectors fabricated using tri-cation (Cs/MA/FA) and dual-anion (Br/I) perovskite as light absorbers exhibit broad light absorption, large charge mobilities, and low-cost fabrication to realize inexpensive but efficient and stable photodetectors. A critical challenge facing their commercialization is their instability under prolonged IR exposure, which can cause parasitic chemical reactions between the perovskite and hole transfer materials (HTMs). Here, we demonstrate stable IR photodetectors based on electrospun tri-cation perovskite fibers infiltrated with hole-transporting π -conjugated small molecule 2,2',7,7'-tetrakis[N,N-di(4-methoxyphenyl)amino]-9,9-spirofluorene (Spiro-OMeTAD). These hybrid perovskite photodetectors show ultra-high gains as well as excellent environmental stability. Operating at a low voltage bias of 5 V, the photodetectors exhibit EQE values up to 3008.9 % under 808 nm irradiation, decreasing only to ~ 2769.8 % after 3 months of storage in air. These values are almost ten times higher than those measured for thin film/HTM photodetectors. Such large EQE values for fiber/HTM photodetectors are attributed to the presence of a high density of charge traps on electrospun fiber surfaces that gives rise to a photomultiplication effect in which photogenerated holes can travel through the active layer multiple times before recombining with trapped electrons. Time-resolved and steady-state photoluminescence measurements and conductive atomic force microscopy mapping revealed that charge transport dynamics are significantly improved in fiber/HTM layers compared to film/HTM layers due to large interfacial areas for exciton dissociation between the two phases in the former case. These results demonstrate the potential of electrospun perovskite hybrid layers to enable the inexpensive fabrication of high-performance IR photodetectors for applications ranging from information technology to imaging.

EN02.08.63

Halide Perovskite Nanocrystal-Enabled Stabilization of Transition Metal Dichalcogenide Nanosheets and Their Photodetective Applications [Hyeokjung Lee](#), Jin Woo Oh, Jihye Jang, Hyowon Han and Cheolmin Park; Yonsei University, Korea (the Republic of)

Transition metal dichalcogenide (TMD) nanosheets exfoliated in the liquid phase are of significant interest owing to their potential for scalable and flexible photoelectronic applications. Although various dispersants such as surfactants, oligomers, and polymers are used to obtain highly exfoliated TMD nanosheets, most of them are electrically insulating and need to be removed; otherwise, the photoelectric properties of the TMD nanosheets degrade. Here, inorganic halide perovskite nanocrystals (NCs) of CsPbX₃ (X = Cl, Br, or I) are presented as non-destructive dispersants capable of dispersing TMD nanosheets in the liquid phase and enhancing the photodetection properties of the nanosheets, thus eliminating the need to remove the dispersant. MoSe₂ nanosheets dispersed in the liquid phase are adsorbed with CsPbCl₃ NCs. The CsPbCl₃ nanocrystals on MoSe₂ efficiently withdraw electrons from the nanosheets, and suppress the dark current of the MoSe₂ nanosheets, leading to flexible near-infrared MoSe₂ photodetectors with a high ON/OFF photocurrent ratio and detectivity. Moreover, lanthanide ion-doped CsPbCl₃ NCs enhance the ON/OFF current ratio to >10⁶. Meanwhile, the dispersion stability of the MoSe₂ nanosheets exfoliated with the perovskite NCs is sufficiently high.

EN02.08.64

Modulation of Film Formation Kinetics to Achieve Perovskite Light-Emitting Diode Emitting Blue Electroluminescence [Yoonseo Nah](#)^{1,2}, Devan Solanki¹, Yitong Dong³, Jason Rohr⁴, Andre Taylor⁴, Shu Hu¹, Edward H. Sargent³ and Dong Ha Kim²; ¹Yale University, United States; ²Ewha Womans University, Korea (the Republic of); ³University of Toronto, Canada; ⁴New York University, United States

Quasi-two-dimensional (Quasi-2D) metal halide perovskite consists of inorganic quantum wells sandwiched with organic spacers. It has attracted enormous interests due to its large exciton binding energy, tunable emission wavelength, and solution processability. In general, solution-processed quasi-2D perovskites contain multiple quantum slabs with a broad phase dispersity. Inhomogeneity induces charge funneling into the smallest bandgap components, which poses a challenge in achieving deep-blue electroluminescence. Here, we report a film modulation strategy that significantly narrows the quantum well distribution. We show that the phase dispersity in perovskite film is significantly narrowed with controlled, simultaneous evaporation of solvent and antisolvent. Our quasi-2D perovskite shows stable deep-blue electroluminescence with a peak emission wavelength of 466 nm and a narrow linewidth of 14 nm. Light emitting diodes records a maximum luminance of 280 cd m⁻² at an external quantum efficiency of 0.1%. This synthetic approach will pave a way to produce new materials that widen the color gamut of next-generation displays.

EN02.08.66

Passivation and Defect Mapping in Lead Halide Perovskites Yenal Yalcinkaya, Pascal N. Rohrbeck and Stefan A. Weber; Max Planck Institute for Polymer Research, Germany

Defect tolerance behaviour of lead halide perovskites makes them significantly important for photovoltaic applications. However, defects at the interfaces such as grain or junction boundaries can result in deep trap states which lead to lower power conversion efficiencies. In this study, we studied effect of some passivation agents on methylammonium-free cesium formamidinium lead iodide (Cs-FAPI) which suffers from phase instability. To this end, we compared the phase stabilities, optical properties, and solar cell efficiencies of pristine and passivated Cs-FAPI films. Finally, we performed time-resolved Kelvin Probe Force Microscopy (tr-KPFM) measurements to map the defects and passivation effect by means of mapping the photovoltage behaviour. This study shows the improvements on Cs-FAPI films and devices by passivation agents on nanoscale.

EN02.08.68

Bulk and Micro-Photoluminescence Studies of Perovskites Stuart Thomson; Edinburgh Instruments Ltd., United Kingdom

Perovskite based solar cells are the subject of intense research interest due to the attractive properties of perovskite; high carrier mobilities, large absorption coefficients, tuneable bandgaps, and long carrier diffusion lengths. One of the challenges in any solar cell design is how to get the charge carriers efficiently out of the device. To aid charge extraction, electron and hole extraction layers are routinely incorporated into the device stack.

One promising material being investigated as a hole extraction layer are vertically aligned carbon nanotubes (VACNTs). The VACNTs can be grown in a grid pattern of 'towers' atop the ITO electrode in order to achieve improved charge extraction while maintaining high optical transmission through the ITO/VACNTs. Photoluminescence response from perovskite materials is proportional to the number of charge carriers in the layer and therefore sensitive to charge extraction into adjacent layers. This makes photoluminescence based techniques invaluable for investigating the performance of new extraction layers. In this work steady-state and time-resolved confocal photoluminescence microscopy and photoluminescence quantum yield studies were used to quantify hole transfer efficiency into the VACNT towers.

EN02.08.70

Lightweight, Floating Perovskite-BiVO₄ Tandem Devices for Scalable Artificial Photosynthesis Virgil Andrei^{1,1}, Geani M. Ucoski¹, Chanon Pornrunroj¹, Demetra S. Achilleos¹, Katarzyna Sokol¹, Judith L. MacManus-Driscoll¹, Robert Hoye², Richard H. Friend¹ and Erwin Reisner¹; ¹University of Cambridge, United Kingdom; ²Imperial College London, United Kingdom

Photoelectrochemical (PEC) artificial leaves hold the potential to lower the costs of sustainable solar fuel production by integrating light harvesting and catalysis within one compact device. However, current deposition techniques limit their scalability, while fragile and heavy bulk materials can affect their transport and deployment. Here, we demonstrate the fabrication of lightweight artificial leaves by employing thin, flexible substrates and carbonaceous protection layers.^[1] Lead halide perovskite photocathodes deposited onto indium tin oxide coated polyethylene terephthalate achieve an activity of 4266 μmol H₂ g⁻¹ h⁻¹ using a platinum catalyst, whereas photocathodes with a molecular Co catalyst for CO₂ reduction attain a high CO:H₂ selectivity of 7.2 under a lower 0.1 sun irradiation. The corresponding lightweight perovskite-BiVO₄ PEC devices display unassisted solar-to-fuel efficiencies of 0.58% (H₂) and 0.053% (CO), respectively. Their potential for scalability is demonstrated by 100 cm² standalone artificial leaves, which sustain a comparable performance and stability of ≈24 h to their 1.7 cm² counterparts. Bubbles formed under operation further enable the 30-100 mg cm⁻² devices to float, while lightweight reactors facilitate gas collection during outdoor testing on a river. The leaf-like PEC device bridges the gap in weight between traditional solar fuel approaches, showcasing activities per gram comparable to photocatalytic suspensions and plant leaves.^[1] The presented lightweight, floating systems are compatible with modern fabrication techniques,^[2] and may enable open water applications, while avoiding competition with land use.

[1] Andrei, V.; Ucoski, G. M.; Pornrunroj, C.; Uswachoke, C.; Wang, Q.; Achilleos, D. S.; Kasap, H.; Sokol, K. P.; Jagt, R. A.; Lu, H.; Lawson, T.; Wagner, A.; Pike, S. D.; Wright, D. S.; Hoye, R. L. Z.; MacManus-Driscoll, J. L.; Joyce, H. J.; Friend, R. H.; Reisner, E., *Nature* 2022, 608, 518–522.
[2] Sokol, K. P.; Andrei, V. *Nat. Rev. Mater.* 2022, 7, 251–253.

EN02.08.71

Hot-Spin Casting Synthesis of Freestanding Cs₂AgBiBr₆ Double Perovskite Facet-Oriented Microcrystals for Efficient Photodetectors Mozakkar Hossain, Md Sariful Sheikh and K. D. M. Rao; Indian Association for the Cultivation of Science, India

Facet-orientated double perovskite (DP) microcrystals (MCs) are of particular interest in optoelectronics due to the special symmetry and homogeneous interfaces, which extend the carrier lifetime and enhance the mobility to realize robust device performance. Here, a simple hot-spin casting method is developed to instantaneously synthesize the highly crystalline lead-free halide DP Cs₂AgBiBr₆ MCs with facet-orientation. The low temperature (130 °C) hot-spin casting synthesis of DP MCs instigates growth only along the highly packed (111) plane attributed to heterogeneous nucleation. The Cs₂AgBiBr₆ DP MCs demonstrate reduced lattice parameters with enhanced light absorbance resulting in decreased bandgap (ΔE_g ≈ 0.23 eV). The facet-oriented DP MCs exhibit the enhancement in photoluminescence and carrier lifetime compared to the nanocrystalline thin-film. Moreover, the DP MCs are successfully transferred on the desired substrate using micro-imprint lithography keeping its original orientation intact. The DP Cs₂AgBiBr₆ MCs-based photodetectors manifest broader spectral response, high detectivity (1.72 × 10¹¹ Jones) and improved external quantum efficiency (EQE, 451%). The freestanding and facet orientated DP MCs synthesis is easily extendable to other types of halide perovskites and has the potential to fabricate high-performance optoelectronic devices.

EN02.08.72

Ultra-high-Resolution Transfer Printing of Light-Emitting Nanocrystals for Next-Generation Advanced Displays Jiwoong Yang¹ and Moon Kee Choi²; ¹Daegu Gyeongbuk Institute of Science & Technology (DGIST), Korea (the Republic of); ²Ulsan National Institute of Science and Technology (UNIST), Korea (the Republic of)

High-resolution patterning techniques that can produce red/green/blue pixels are essential for next-generation advanced displays. Photolithography and inkjet printing have traditionally been applied to create patterns of light-emitting nanocrystals such as CdSe, InP, and perovskite based nanocrystals. However, these methods usually degrade the optical and electrical properties of those nanocrystals because of the severe processing conditions (associated to the use of various chemicals and ultraviolet radiation) and the presence of organic residues (photoresists and additives for photolithography and inkjet printing, respectively).

Here, we present the ultrahigh-resolution transfer printing techniques for next-generation advanced displays. This method does not use wet chemicals and does not remain organics in the created patterns, suggesting its potential to exploit unique properties of light-emitting nanocrystals. The method can produce ultrahigh-resolution colloidal quantum dot patterns.^[1-5] Furthermore, the interfacial engineering between the stamps and nanocrystals broadens its applicability to a variety of materials, including perovskite nanocrystals.^[6] We can successfully fabricate ultrahigh-resolution perovskite patterns, and the external quantum efficiencies of the printed perovskite light-emitting diodes are greater than those of previously reported printed perovskite light-emitting diodes. Our results highlight that the transfer printing is promising for ultrahigh-resolution display applications.

[1] M.K. Choi *et al.* Nature Commun. 6, 7149 (2015).

[2] J. Yang *et al.* Adv. Mater. 28, 1176 (2016).

[3] M.K. Choi *et al.* npj Flex Electron 2, 10 (2018).

[4] J. Yang *et al.* Nano Lett. 21, 26 (2021).

[5] ..., D.-H. Kim*, J. Yang*, M.K. Choi* *et al.* Nanoscale Horiz. 7, 801 (2022).

[6] Unpublished.

EN02.08.73

It's Not All About the Chemical Identity—Strong Impact of Substituent Position in PEAI Based Cations for Realizing Efficient and Stable 2D/3D Perovskite Solar Cells Gorkem Gunbas^{1,2,3}, Ummugulsum Gunes^{1,2,3}, Figen Varlioglu Yaylali^{1,2}, Zeynep Gozukara Karabag^{1,2,3}, Aliekber Karabag^{1,2}, Xiao-Xin Gao³, Olga Syzgantseva⁴, Benu Cel Yildirim^{1,2}, Naoyuki Shibayama⁵, Hiroyuki Kanda³, Alwani Imanah Rafieh³, Liping Zhong³, Andreas Züttel³, Joseph Paul Dyson³, Selcuk Yerci^{1,2,2} and Mohammad Khaja Nazeeruddin³; ¹ODTU-GUNAM, Turkey; ²Middle East Technical University, Turkey; ³École Polytechnique Fédérale de Lausanne, Switzerland; ⁴Lomonosov Moscow State University, Russian Federation; ⁵University of Hyogo, Japan

Perovskite solar cells (PSCs) became a household name in the solar energy community in less than a decade, and rightly so, by combining ease of fabrication and high efficiencies. However, the long-term stability and reproducibility are far from ideal for the commercial implementation of the technology. Stability of PSCs are dependent on several factors and encapsulation can only be a remedy, to a certain extent, for moisture and oxygen related degradations. Interfacial molecular dissociation and ion migration are main concerns for perovskites apart from environmental factors and several approaches have been pursued to address these issues. Surface passivation with 2D perovskites (2DPs) became an impactful strategy to achieve improved stability accompanied with enhanced performance. Phenylethyl ammonium iodide (PEAI) and its derivatives are the mostly commonly utilized cations for 2DPs, although various other cations have been implemented.

We envisioned that strongly electron releasing groups are the clear choice as substituents on PEA, due to their potential to contribute hole extraction and favorable interaction with uncoordinated Pb²⁺ ions. We concentrated on the electron releasing methoxy (-OMe) group substituted at *-ortho*, *-meta*, and *-para* positions of the phenyl ring of PEA to explore not only the effect of the chemical identity but also the effect of substituent position. We developed a three step, straightforward synthetic methodology, which gave us easy access to all target cations. XRD, GIWAXS and SEM analyses confirmed the formation of 2D films on 3D perovskites, independent of the substituent position. PL and TRPL studies revealed that for the *o*-OMe-PEAI treated surfaces, strong passivation, hence, lower defect densities were achieved, compared to reference along with *m*-OMe and *p*-OMe analogues. Device results showed that *o*-OMe-PEAI based cells outperformed the reference, *m*-OMe and *p*-OMe based ones, showing PCEs over 23.3% with excellent V_{oc}(1.2V) and FF(80%). Highest efficiencies for *m*-OMe-PEAI, *p*-OMe-PEAI, and reference cells were 22.2%, 22.6% and 21.4% respectively. Detailed DFT analyses attributed the outlier performance of *o*-OMe-PEAI incorporated cells to the favorable formation energy and desired vertical orientation along with optimal surface coating of the 2DP layer.

One major advantage of 2DP passivation is the increased hydrophobicity of the surface due presence of large organic cations, thus higher stability. Contact angle analyses showed that while all salts showed more hydrophobic character compared to reference, *o*-OMe-PEAI treated surfaces were far superior. Hence, unique orientation of the *o*-OMe-PEAI on 3D perovskite surface improves performance and provides best protection for the 3D perovskite layer against moisture, simultaneously. Long term stability studies are currently underway however, as of 300 hours, *o*-OMe-PEAI based devices preserve 95% of their initial efficiencies whereas reference cells only retain 60%.

Encouraged by these results, we pursued a larger set of cations to gain further insight to the effect of chemical identity and position of substituents on 2DP passivation and device performance. Here, we synthesized 9 salts, with fluorine, chlorine and bromine as the substituents at *-ortho*, *-meta*, and *-para* positions. Interestingly, independent of the halogen, salts substituted at *-meta* position outperformed their *-ortho* and *-para* counterparts (averages = *m*-XPEAI: 23.2%, *o*-XPEAI: 22.5%, *p*-XPEAI: 22.1, ref.: 20.8%). Among different halogens at *-meta* position, *m*-BrPEAI gave only slightly higher PCE. DFT analyses revealed that lower formation energies and higher interfacial dipoles achieved by *meta*-substituted derivatives was responsible for the enhanced performance.

We are currently creating a larger library of ammonium cations with electronically distinct substituents to devise a general set of design principles that could hopefully lead to the optimal material for commercial 2D/3D PSCs.

EN02.08.74

Thiol-Functionalized MoS₂ Induced High Quality α -phase FAPbI₃ Crystal for Efficient Perovskite Solar Cells Yifan Yin¹, Yuchen Zhou¹, Miriam Rafailovich¹ and Chang-Yong Nam²; ¹Stonybrook University, United States; ²Brookhaven National Laboratory, United States

Formamidinium lead iodide (FAPbI₃) has become one of the most promising materials for high performance perovskite solar cells (PSC) due to its ideal band gap and broad light absorption spectrum. However, the readily transformation from black α -phase FAPbI₃ to photoinactive yellow δ -phase makes it difficult to prepare a high-quality phase-pure FAPbI₃ active layer. Meanwhile, the in-plane tensile strain and out-of-plane compressive strain during conventional solution-based film processing technique will cause the lattice mismatches and composition distribution in the polycrystalline multigranular grains, which would further limit the lifetime of PSCs.

Here, we introduced the thiol (3-Mercaptopropionic acid, 3-MPA) functionalized molybdenum disulfide (MoS₂) nanoflakes (NFs) into the FAPbI₃ perovskite layer. The MPA-MoS₂ NFs are incorporated through mixing with FAPbI₃ precursors when preparing the ink. The NFs are believed to serve as the crystallization agent and passivates the defects in the as-prepared films. We tracked the crystallographic evolution during thermal annealing with synchrotron-based in situ grazing-incidence wide angle (GIWAXS). The result shows that the MPA-MoS₂ forms an intermediate structure with FAI at the initial stage then facilitate the orientated growth of FAPbI₃. Moreover, based on the depth-dependent GIWAXS, the FAPbI₃ films with MPA-MoS₂ shows a reduced compressive strain across the film thickness direction. The strong interaction between MPA-MoS₂ and the uncoordinated Pb²⁺ makes the NFs

attached closely to the grain boundaries, which forms efficient heat spreading channels thus modifying the thermal gradient during film preparation. As observed in SEM and XRD, respectively, the MPA-MoS₂ incorporated FAPbI₃ shows increases in average grain size with a 3-fold enhancement in crystalline peak intensity, suggesting the promotion of the perovskite crystal quality after the incorporation of the NFs. In addition, as witnessed in photoluminescence (PL) and lifetime decay measurements, the FAPbI₃ with MPA-MoS₂ NFs functionalized by monolayer of the MPA thiols exhibits quenching in PL intensity and lifetime, indicating more efficient the charge transport likely occurs in the NFs incorporated FAPbI₃. PSCs with MPA-MoS₂ with a champion PCE of 22.3% have been achieved successfully, and the corresponding unencapsulated devices retain over 90% of their initial efficiencies in the ambient environment after 1600 h.

EN02.08.75

Don't Let 'A-Site' Out of Sight—Decisive Role of A-Site Cations in Controlling Band Edge States, Optical Properties and Stability of 0D Hybrid Indium Chlorides Anuraj S. Kshirsagar, Yashpal Singh, Udara Kuruppu, Bruno Donnadieu, Neeraj Rai and Mahesh Gangishetty; Mississippi State University, United States

Organic-inorganic hybrid metal halides have been drawing attention due to their exceptional optoelectronic properties. Like lead halide perovskites, the optoelectronic properties of hybrid metal halides are governed by B-site cations and X-site halides; the frontier orbitals are localized on B and X sites. However, the role of A-site cations remains restricted in governing optoelectronic properties as their electronic levels lie away from the frontier orbitals. Conventionally, A-site cations are only believed to be useful for the stabilization of crystal structure. Rational engineering of A-site cations can offer opportunities to tailor the role of A-site in governing optoelectronic properties beyond structural stabilization. In my presentation, I will discuss the role of three different anilinium-based A-site cations in Sb³⁺-doped zero-dimensional indium chlorides to control optical properties through their contribution to the band edge states. Our experimental and theoretical results demonstrate that with the increase in methyl substitution at the *ortho* position, *p*-orbital contribution near the band edge states increases, leading to the delocalization of the frontier orbitals across organic and inorganic moieties. Sb³⁺-doped 0D indium chlorides exhibit broadband emission with high PLQY (maximum 93%) and excellent stability in a range of polar and non-polar solvents for 21 days, including water.

EN02.08.76

Revealing a New Formamidineum-Based Lead Triiodide Perovskite Material Derived from Chemical Degradation of a Common Additive in High Efficiency Perovskite Solar Cells Benjamin Gallant¹, Elisabeth Duijnste¹, Joel Smith¹, Dominik Kubicki², Harry Sansom¹, Silvia Collavini³, Bernd Sturza¹, Philippe Holzhey¹, Alexandra Ramadan¹, Adam D. Wright¹, Chelsea Xia¹, Murali Gedda⁴, Santanu Saha¹, Marina Filip¹, Thomas D. Anthopoulos⁴, Michael Johnston¹, Robin Nicholas¹ and Henry Snaith¹; ¹University of Oxford, United Kingdom; ²University of Warwick, United Kingdom; ³POLYMAT: Molecular and Supramolecular Materials Laboratories, Spain; ⁴King Abdullah University of Science and Technology, Saudi Arabia

Despite its attractive low band gap, a key challenge for formamidineum lead triiodide (FAPbI₃) is to overcome its inherent ambient phase instability. A range of chemical additives have been employed in FAPbI₃-based solar cells to produce record efficiencies and enhance the stability of the photoactive FAPbI₃ α -phase. Here we grow FAPbI₃ single crystals from a solution containing one such common additive (FAPbI₃-A), which has been widely employed in high-performance solution-processed perovskite solar cells. We demonstrate that FAPbI₃-A crystals are stable against transformation to the photoinactive δ -phase for more than one year under ambient conditions, while FAPbI₃ crystals grown from a neat solution degrade within days. Critically, we reveal via nuclear magnetic resonance (NMR) spectroscopy that this common additive is unstable in solution and does not play an active stabilising role itself, instead degrading fully within minutes to a range of stable products via a complex chemical pathway, which we present. We show that FAPbI₃ crystals grown from a solution containing a certain one of these degradation products (FAPbI₃-D) replicate the enhanced α -phase stability of FAPbI₃-A. By performing a combination of liquid- and solid-state NMR measurements, along with X-ray diffraction (XRD) techniques, we find that previously unreported organic species are present in the FAPbI₃-A and FAPbI₃-D crystals. Remarkably, however, these correspond to neither the common additive, any of its stable degradation products nor any of the intermediates in its degradation pathway. Instead we are able to show that interruption of the degradation pathway by reaction of these intermediates with excess FA⁺ generates alternative organic species in-situ. It is these alternative products that are incorporated into the FAPbI₃ bulk material and lead to α -phase stabilisation. We anticipate that presentation of our new understanding of the complex solution chemistry associated with this common high-performance additive will provide crucial insight for other researchers, immediately enabling more effective and controllable use of it, and direct use of its degradation products, in the fabrication of highly phase-stable α -FAPbI₃ perovskite materials.

SESSION EN02.09: Multi-Junction Cells and Modules
Session Chairs: David Fenning and Michael Stuckelberger
Thursday Morning, December 1, 2022
Hynes, Level 3, Ballroom B

8:30 AM *EN02.09.01

Sn-Pb Perovskite Solar Cells and Modules with Enhanced Efficiency and Stability Jinsong Huang; University of North Carolina-Chapel Hill, United States

Tin-lead (Sn-Pb) narrow bandgap (NBG) perovskites show great potential in both single-junction and all-perovskite tandem solar cells. Sn-Pb perovskite solar cells (PSCs) are still limited by low charge collection efficiency and poor stability. Compared to Pb-perovskites, their degradation is much faster under operation test, despite that they were shown to pass thermal stability tests. Here I will start with our understanding of the issues that limit the light stability of Sn-Pb perovskites. Then I will present our strategies in enhancing the stability using perovskite material modifications and interfacial engineering. I will also present how to upscale the related tandem cells into minimodules with partial processes done in air.

9:00 AM EN02.09.02

Fully Textured Perovskite/Silicon Monolithic Tandems Certified at 29.23% Xin-Yu Chin¹, Deniz Turkyay², Florent Sahlil¹, Peter Fiala², Daniel Jacobs², Kerem Artuk², Quentin Guesnay², Christian Wolff², Quentin Jeangros¹ and Christophe Ballif^{1,2}; ¹Centre Suisse d'Electronique et de Microtechnique, Switzerland; ²Ecole Polytechnique Fédérale de Lausanne, Switzerland

Tandem solar cell technologies have the potential to continue the learning curve of photovoltaics beyond what is achievable with crystalline silicon (c-Si) solar cells as the latter are approaching their practical efficiency limit. Amongst the different options to produce a tandem, stacking a metal halide perovskite cell on a c-Si cell represents the most promising approach to overcome this efficiency limit without significantly increasing production costs. The deposition of a perovskite top cell on a c-Si solar cells however requires certain adaptations, e.g., either flattening or downsizing the front-side

pyramidal texture of the c-Si sub-cell. This texture promises higher photocurrents due to reduced reflection losses and increased trapping of infrared light. However, due to layer conformality/homogeneity challenges, the presence of this texture has also held back advances in performance due to a limited choice of materials and processes to passivate and contact the perovskite absorber.

In this contribution, we will discuss several advances to mitigate voltage and fill factor losses affecting textured tandems. Specifically, the perovskite absorber is deposited here using an “hybrid” evaporation/spin coating process for compatibility with micrometer-sized pyramids. We replace the spiro-derivative hole transport layer with another small-molecule organic compound (TaTM) or a self-assembled monolayer (Me-4PACz). Such HTLs improve open circuit voltage, consistent with the increase in quasi-fermi level splitting extracted via photoluminescence measurement. Moreover, we use a commercially available ligand as an additive in the perovskite synthesis. This additive segregates on the perovskite top surface to alleviate some of the recombination losses occurring at perovskite/ C_{60} electron transport layer interface. The improved interfaces enable the production of single junction cells with a V_{oc} of 1.2 V (for a bandgap of ~1.68 eV) and tandem cell V_{oc} 's of >1.9 V. Combined with the high photocurrent provided by the textured c-Si wafer, these modifications lead to a certified efficiency of 29.23%, an important step towards >30%-efficient tandems featuring an industry-standard c-Si front side.

9:15 AM DISCUSSION TIME

9:30 AM EN02.09.04

Nanostructures Enable Perovskite/Silicon Tandem Solar Cells with Certified Efficiency of 29.80% Philipp Tockhorn¹, Johannes Sutter¹, Alexandros Cruz Bournazou¹, Klaus Jäger¹, Felix Lang², Max Grischek¹, Philipp Wagner¹, Danbi Yoo¹, Martin Stolterfoht², Bernd Stannowski¹, Steve Albrecht¹ and Christiane Becker¹; ¹Helmholtz-Zentrum Berlin für Materialien und Energie, Germany; ²University of Potsdam, Germany

Perovskite/silicon tandem solar cells (PSTSC) recently achieved power conversion efficiencies (PCE) exceeding 29% [1, 2]. So far, the highest efficiencies were obtained for tandem solar cells with fully planar wafer front sides and solution-processed perovskite layers. To further increase the performance of PSTSC, it is important to reduce optical losses by implementation of textures on the perovskite subcell and other advanced concepts [3]. In this work, we present PSTSC with tailor-made sinusoidal nanostructures at the perovskite/silicon interface with 750 nm period nm and 300 nm structure height. The front side of a silicon wafer was nanotextured in a three-step process employing nanoimprint lithography, reactive ion and wet-chemical etching [4]. The back side of the silicon wafers carried random pyramidal textures. Perovskite layers, which are spin-coated on nanotextured silicon bottom cells feature a planar top surface and adapt perfectly to the sinusoidal texture of the wafer. Importantly, these films tend to form less macroscopic pinholes compared to perovskite layers on planar silicon bottom cells, thus increasing the production yield. The nanostructures reduce reflection losses and in turn lead to a small optical gain in the silicon bottom cell.

To further understand the optical effect of the nanotextured interfaces in PSTSC, optical simulations with the finite element solver JCMsuite were conducted. The optical performance was maximized with a global (Bayesian) optimization of several layer thicknesses. Interestingly, for the optimized parameter sets, the simulations find no clear improvement of the nanostructure in comparison to the planar PSTSCs. A detailed sensitivity analysis reveals that the major benefit of the nanostructures is a higher tolerance against variations in thickness of the hydrogenated nano-crystalline silicon oxide (nc-SiO_x:H) layer.

In addition to the optical improvement, we find that the average open-circuit voltage (V_{oc}) of nanotextured PSTSC increases by approximately 15 mV as also confirmed by photo- (PL) and electroluminescence (EL) measurements. These results indicate that —remarkably— the nanotextures improve not only the optical but also the electronic quality of PSTSC. To further improve light management at the rear side of the silicon bottom cell, we integrated a dielectric buffer layer in combination with screen-printed silver grid fingers into the PSTSC [5]. This back contact design allows to mitigate parasitic absorption losses by reducing the thickness of the transparent conductive oxide (TCO) layer and by diminishing plasmonic losses in the silver back contact. With the combination of both investigated light management measures, we achieved a certified PCE of 29.80% (world record, as of 16 June 2022). We are confident that further finetuning of our approach combining nanostructures and dielectric buffer layer will push the PCE of PSTSC well above 30% in the near future.

References

- [1] Al-Ashouri et al., Science (80) 2020;370:1300–9. doi:10.1126/science.abd4016.
- [2] Oxford PV press release <https://www.oxfordpv.com/news/oxford-pv-hits-new-world-record-solar-cell> (accessed June 16, 2022).
- [3] Jäger et al., Nanophotonics 10(8), pp. 1991–2000, 2021.
- [4] Sutter et al., Solar RRL (2020), 4, 2000484.
- [5] Cruz et al., Solar Energy Materials and Solar Cells, Volume 236, 2022

9:45 AM EN02.09.05

Carrier Control in Sn-Pb Narrow-Bandgap Perovskites via 2D Cation Engineering for Efficient and Stable All-Perovskite Tandem Solar Cells Qi Jiang, Jinhui Tong and Kai Zhu; National Renewable Energy Laboratory, United States

Perovskite solar cells (PSCs) represent a competitive photovoltaic (PV) technology with rapid progress of efficiencies reaching a certified 25.5% efficiency for single-junction devices. The bandgap tunability through perovskite composition engineering is attractive for developing ultrahigh-efficiency tandem solar cells, including perovskite/perovskite, perovskite/silicon, or perovskite/thin-film absorber (e.g., CIGS). All-perovskite tandem solar cells are particularly attractive for achieving photovoltaics with power conversion efficiencies above the detailed balance limit of single-junction cells, while retaining the low-cost, light weight and other advantages associated with metal halide perovskite photovoltaics. However, the efficiency and stability of all-perovskite tandem cells are limited by the Sn-Pb-based narrow-bandgap perovskite cells. In this presentation, I will discuss our recent progress on improving Sn-Pb based narrow-bandgap (1.2–1.3 eV) perovskite absorbers by a new 2D additive engineering approach. The structural and optoelectronic properties of the Sn-Pb based perovskite thin films can be significantly tailored by controlling the specific 2D additive composition and structure. Under certain processing conditions, the Sn-Pb perovskite thin films exhibit low dark carrier density, long carrier lifetime, and low surface recombination velocity. These improvements on structural and optoelectronic properties lead to much enhanced performance of Sn-Pb based narrow-bandgap PSCs. When coupling the narrow-bandgap perovskite subcell with a wide-bandgap (>1.7-eV) perovskite subcell, we obtained highly-efficient all-perovskite 2-terminal tandems with excellent long operational stability.

10:00 AM BREAK

10:30 AM *EN02.09.06

Strategies for Preparing Highly Efficient and Stable Perovskite/Si Tandems with Efficiencies over 29% Jin Young Kim; Seoul National University, Korea (the Republic of)

The power conversion efficiency (PCE) of the perovskite solar cells has been improved to 25.7%, which is highest among that of all multi-crystalline solar cells and is gradually approaching to the Shockley-Queisser (SQ) limit. Therefore, perovskite-based tandem solar cells are currently attracting significant

interest as potential candidates for overcoming the SQ limit of single-junction.[1] Among various perovskite-based tandem cells, perovskite/Si tandems are the most attractive combination because their highest certified PCE (29.8%) already surpasses that of the best reported single-junction solar cell (GaAs, 29.1%) [1]. In this presentation, recent progresses in the perovskite-based tandem solar cells researches made in our laboratory will be introduced,[2,3] especially focusing on the key strategies (e.g., photon management and defect passivation) for achieving highly efficient and stable perovskite/Si tandems with efficiencies over 29%. More specifically, the optical/electrical properties of the ITO/C60 window and ITO recombination layers could be optimized with aid of the optical simulation and new 3-terminal characterization platform. The defects located either at the grain boundaries or on the top surface of the wide-bandgap perovskite top cells could be successfully passivated by various additives and their engineering. In addition, a rational strategy for preparing the pure-iodide-based wide-bandgap perovskite top cell that is fundamentally free from the halide segregation (i.e., photostability) issue, and thus, showing excellent stability will be introduced.

References

- [1] NREL Efficiency Chart, rev. 20220126 (<https://www.nrel.gov/pv/cell-efficiency.htm>).
- [2] Kim *et al.*, *Science* 368, 155-160 (2020).
- [3] Park *et al.*, *Adv. Optical Mater.* 9, 2100788 (2021).

11:00 AM EN02.09.07

Universal Lossless Interconnect for Perovskite-Organic and All-Perovskite Tandem Solar Cells. Kai O. Brinkmann¹, Tim Becker¹, Florian Zimmermann¹, Jarla Thiesbrummel^{2,3}, Francisco Pena-Camargo³, Cedric Kreusel¹, Manuel Theisen¹, Tobias Haeger¹, Selina Olthof⁴, Christian Tückmantel¹, Manuel Günster¹, Timo Maschwitz¹, Christine Koch⁴, Dirk Hertel⁴, Pietro Caprioglio², Lorena Perdigón-Toro³, Amran Al-Ashouri⁵, Lena Merten⁶, Alexander Hinderhofer⁶, Leonie Gomell⁷, Siyuan Zhang⁷, Frank Schreiber⁶, Steve Albrecht⁵, Klaus Meerholz⁴, Henry Snaith², Dieter Neher³, Martin Stoltterfoht³ and Thomas Riedl¹; ¹Bergische Universität Wuppertal, Germany; ²University of Oxford, United Kingdom; ³University of Potsdam, Germany; ⁴University of Cologne, Germany; ⁵Helmholtz-Zentrum Berlin, Germany; ⁶University of Tübingen, Germany; ⁷Max Planck Institute for Iron Research, Germany

The concept of multi-junction solar cells is very promising for the future of the solar cell technology, because it provides the potential to overcome fundamental efficiency limits of single-junction devices. The facile bandgap tunability of metal-halide perovskite solar cells renders them particularly attractive for multi-junction architectures. Besides Pb/Sn based perovskite low band gap materials, organic solar cells are becoming increasingly interesting as tandem partner for a perovskite wide bandgap cell. Especially, since the introduction of non-fullerene acceptors has revived the field and enabled organic solar cells with >18% efficiencies and an absorption spectrum extending well into the infrared region.^[1] On the other hand, low gap perovskite materials are almost exclusively based on Sn²⁺ containing structures, where fundamental stability issues are still a serious topic.^[2] However, serious concerns currently exist about photo instability of most non-fullerene organic systems. Now, to alleviate these concerns, we evidenced an outstanding operational stability (~95% PCE remaining after > 5000 h continuous operation) of an organic single junction that is based on the PM6:Y6 active system, if excitons are exclusively generated on the acceptor material Y6 (which is the case in a tandem application).

Aside from the active materials (all-perovskite or perovskite-organic), two terminal tandem cells critically rely on an interconnect that facilitates the recombination of electrons (holes) from the bottom cell with the holes (electrons) from the top cell. In most cases a direct stacking of both cells without dedicated interconnect results in poorly performing devices with s-shaped J-V characteristics. Thus, thin layers (~1 nm) of a metal (Ag or Au) are frequently inserted between top- and bottom-cell.^[3] However, even an Ag-layer as thin as 1 nm already introduces significant optical losses that lower the EQE of the back-cell and the overall J_{sc} of the tandem cell as we could show.

Therefore, we developed an ultra-thin, ALD grown, metal-like indium oxide interconnect. We leverage the unique property of ALD to provide utmost control of layer thickness even on the level of Angstroms, which is impossible with conventional deposition techniques. We show, that 32 ALD cycles are enough to achieve an amorphous and pinhole free indium oxide layer of only 1.5 nm thickness that provides a charge carrier density of 10^{20} cm^{-3} . By this it is able to render the interface between the sub cells ohmic. At the same time the AZO/SnO_x/InO_x layer stack on top of the bottom cell offers a strong protection against the detrimental impact of follow-up processing, which enables swift integration in both perovskite-perovskite and perovskite-organic tandem solar cells. Moreover, due to the very limited thickness, the indium oxide causes only negligible optical losses while simultaneously offering unprecedentedly high shunt resilience.

Finally, by combining the indium oxide interconnect with a multi facet optimization of the wide gap perovskite solar cell, we were able to present high efficiency perovskite-perovskite devices (> 23.5%)^[4] and, even more, we were able to set a new world record for perovskite-organic tandem solar cells (PCE = 24 %).^[5]

This result marks a huge step forward since tandem solar cells are a key topic in order to overcome fundamental efficiency limits of single junction perovskites (realistic PCE potential > 30 %). We could show that ALD grown indium oxide can be utilized for both: high efficiency, tin-perovskite containing all-perovskite as well as world record tin-perovskite free, perovskite-organic tandem solar cells.

- [1] Liu Q, *et al. Science Bulletin* 65, 272-275 (2020).
- [2] Lin R, *et al. Nature Energy* 4, 864–873 (2019).
- [3] Chen X, *et al. Joule* 4, 1594-1606 (2020).
- [4] Thiesbrummel J, Pena-Camargo F, Brinkmann KO, et al (submitted)
- [5] Brinkmann KO, *et al. Nature*, 604, 280 (2022)

11:15 AM *EN02.09.08

Emerging Perovskites-Based Tandem Solar Cells—Towards Efficient, Stable and Commercially Viable Photovoltaics Yi Hou; National University of Singapore, Singapore

The development of perovskite-based tandem solar cells represents a promising strategy to enhance the performance of traditional photovoltaics beyond the single-junction Shockley-Queisser limit. This talk will deliver the rationale behind wide-bandgap perovskite design for the different tandems [1-2], explain how the thin-film-based tandem solar cells reached high efficiencies, and unveil the potential of this technology. The advances reported herein show that it is possible – and powerful – to marry the traditional PVs and perovskite technologies in tandems.

- [1]. Wei Chen, Yudong Zhu, Jingwei Xiu, Guocong Chen, Haoming Liang, Shunchang Liu, Hansong Xue, Erik Birgersson, Jian Wei Ho, Xinshun Qin, Jingyang Lin, Ruijie Ma, Tao Liu, Yanling He, Alan Man-Ching Ng, Xugang Guo, Zhubing He, He Yan, Aleksandra B. Djuricic and Yi Hou. *Nature Energy*, 7, 229 (2022).
- [2]. Fan Fu, Jia Li, Terry Chien-Jen Yang, Haoming Liang, Antonin Faes, Quentin Jeangros, Christophe Ballif, and Yi Hou. *Advanced Materials*, 2106540 (2022).

2:00 PM *EN02.10.01

Stabilization of Photoactive Perovskite Phase for Photovoltaic and LED Applications [Ivan Mora-Sero](#); Universitat Jaume I, Spain

Formamidinium lead iodide (FAPbI₃) is the 3D lead perovskite with the highest theoretical efficiency due to its narrower band gap in comparison with Cs or methylammonium perovskites. Unfortunately, the black phase allowing this narrow bandgap is not the most stable one at room temperature. Here, we show as the fabrication conditions and the interaction with semiconductor quantum dots can boost significantly the stability of FAPbI₃. The interaction of halide perovskite and colloidal semiconductor nanostructures (quantum dots or nanoplatelets) can produce interesting synergistic interactions. We show that the interaction of PbS quantum dots and nanoplatelets can produce the stabilization of FAPbI₃ and FACsPbI₃ perovskite black phase and also the increase of the efficiency, stability and reproducibility of the photovoltaic devices prepared with these halide perovskites. Incorporation of PbS QDs allows the dramatic decrease of the annealing temperature for the formation of black FAPbI₃ phase perovskite thin film, from the 170°C required without QDs to 85°C when QDs are present. In addition, stability of these systems including embedded nanostructures is extended not just for samples prepared in the glove box but fabricated in ambient conditions. These results point to the interest of Perovskite-Quantum Dot Nanocomposites, for further development of advanced optoelectronic devices. Stabilization of tin based perovskite solar cells will be analyzed.

In addition, stabilization of halide perovskite nanoparticles is a necessary step for the development of high performance Halide Perovskite LEDs. Control of post synthetic washing processes allows the preparation of LEDs with enhanced performance and stability.

2:30 PM EN02.10.03

Strain Evolution in Hybrid Perovskite Thin Films Revealed by Simultaneous *In Situ* Multi-Modal Substrate Curvature, Spectroscopic and Structural Characterizations [Boyu Guo](#)^{1,1}, Mihirsinh Chauhan^{1,1}, Nathan Woodward^{1,1}, Gabriel McAndrews^{2,3}, Tonghui Wang^{1,1}, Kasra Darabi^{1,1}, Michael McGehee^{2,2,3} and Aram Amassian^{1,1}; ¹North Carolina State University, United States; ²University of Colorado Boulder, United States; ³National Renewable Energy Laboratory, United States

Hybrid metal halide perovskites are promising to displace other thin film photovoltaic technologies thanks to their high power conversion efficiency (PCE) up to 25.7%, low materials and fabrication costs, and overall ease of manufacturing. Hybrid perovskite thin films deposited on inorganic substrates are believed to exhibit a tensile strain due to mismatch of coefficient of thermal expansion (CTE), which is more than one order of magnitude larger for the hybrid perovskite than typical inorganic substrates like glass and silicon. For photovoltaic devices, the film strain is inevitably present, and several studies have linked device performance and stability to the presence of residual strain. Much effort has therefore been made to engineer the film strain, relying primarily on ex situ characterization methods. Therefore, significant questions remain about the origins of strain, its low magnitude in some instances, and its relationship to solution processing and halide diffusion in hybrid perovskites.

In this work we report, for the first time, integration of multi-beam optical sensor (MOS) experiments together with the entire solution processing and annealing workflows of metal halide perovskite thin films to measure in real time the changes in substrate curvature during solution processing and thin film formation. By combining *in situ* curvature measurements with *in situ* photoluminescence, absorbance, and GIWAXS measurements we reveal, for the first time how the anti-solvent drip triggers the phase transformation of hybrid perovskite near the surface of a supersaturated sol. Phase transformation leads to considerable volume reduction which is felt by the substrate within seconds. This insight reveals that even conversion of a small fraction of the sol into perovskite can cause strain evolution in the substrate, indicating substantial mechanical coupling to the substrate. We go on to demonstrate that thermal annealing causes compressive strain to form due to CTE mismatch, with tensile strain developing during subsequent cooling of the sample. The magnitude of the strain is considerably lower than predicted by the CTE mismatch and points to stress relaxation behavior at elevated temperature, which we will discuss briefly.

2:45 PM EN02.10.05

Role of Ion Migration and Reactivity with Contacts in Halide Perovskite Memristors [Antonio Guerrero](#); Institute of Advanced Materials (INAM), Spain

Halide perovskites are mixed electronic and ionic conductors that find applications in solar cells, light emitting diodes or memory storage devices.¹ The ionic conductivity is connected with the hysteresis observed in the electrical characterization of several electronic devices.² Ions can migrate and will interact with the external contacts *via* physical and chemical interactions leading in some cases to device degradation pathways.³ Ion migration can be used to our advantage to promote formation of conductive and insulating states making them useful as resistive memories (memristors). Here we show that the working mechanism and performance of the memory devices can be tuned and improved by a careful selection of each structural layer. Several configurations are evaluated in which structural layers are modified systematically: the nature of the buffer layer,⁴ nature of the metal contact⁵ and formulation of the perovskite⁶. We show that the properties of the memory device may be modified upon desire from volatile to non-volatile memories. In addition, we also develop an electrical model to account for the observed *j*-*V* response.⁷ Overall, we provide solid understanding on the operational mechanism of halide perovskite memristors that unveils the connection between electronic and ionic conduction.

References

1. Wang, H.; Guerrero, A.; Bou, A.; Al-Mayouf, A. M.; Bisquert, J., Kinetic and material properties of interfaces governing slow response and long timescale phenomena in perovskite solar cells. *Energy Environ. Sci.* **2019**, *12*, 2054-2079.
2. Li, C.; Guerrero, A.; Huettner, S.; Bisquert, J., Unravelling the role of vacancies in lead halide perovskite through electrical switching of photoluminescence. *Nature Communications* **2018**, *9*, 5113.
3. Guerrero, A.; You, J.; Aranda, C.; Kang, Y. S.; Garcia-Belmonte, G.; Zhou, H.; Bisquert, J.; Yang, Y., Interfacial Degradation of Planar Lead Halide Perovskite Solar Cells. *ACS Nano* **2016**, *10*, 218-224.
4. Gonzales, C.; Guerrero, A.; Bisquert, J., Spectral properties of the dynamic state transition in metal halide perovskite-based memristor exhibiting negative capacitance. *Appl. Phys. Lett.* **2021**, *118*, 073501.
5. Pérez-Martínez, J. C.; Mariana, B.; Gonzales, C.; Arredondo, B.; Bisquert, J.; Guerrero, A., *Submitted*.
6. Solanki, A.; Guerrero, A.; Zhang, Q.; Bisquert, J.; Sum, T. C., Interfacial Mechanism for Efficient Resistive Switching in Ruddlesden-Popper Perovskites for Non-volatile Memories. *J. Phys. Chem. Lett.* **2020**, *11*, 463-470.
7. Berruet, M.; Pérez-Martínez, J. C.; Romero, B.; Gonzales, C.; Al-Mayouf, A. M.; Guerrero, A.; Bisquert, J., Physical Model for the Current-Voltage Hysteresis and Impedance of Halide Perovskite Memristors. *ACS Energy Lett.* **2022**, *7*, 1214-1222.

3:00 PM BREAK

3:30 PM *EN02.10.06

Strategies to Tame Complexity and Variability in the Perovskite Composition-Process Space [David P. Fenning](#), Deniz N. Cakan, Zhewen Deng, Connor Dolan, Sean P. Dunfield, Apoorva Gupta, Clark Han, Moses Kodur, Rishi E. Kumar, Eric Oberholtz and Jack Palmer; University of California, San Diego, United States

The compositional and process flexibility of perovskite halides is fundamentally attractive for discovering new materials and advancing figures of merit of existing perovskite technologies. However, the same flexibility also gives rise to challenges in reproducibility across research groups, across operators within single research groups, and across time, slowing cycles of learning. Furthermore, resultant microscopic heterogeneity has been linked to performance and durability losses. Here, steps to automate perovskite solution synthesis are discussed as a means to achieve precise reproduction of processing, allowing for the distinction between process-induced variability and the underlying materials chemistry. Alternative approaches to transport layer and perovskite processing that reduce the use of solvents, relax requirements for solvent compatibility, and show promise for narrow performance variation will also be discussed. Nanoprobe X-ray investigations of resulting perovskite films and devices for single-junction and tandem solar cell applications provide supporting evidence into process dependence on composition, strain and optoelectronic outcomes.

4:00 PM EN02.10.07

Elucidating the Mechanisms of Halide Perovskite Nanocrystal Syntheses Carola Lampe, Kilian Frank, Bert Nickel and [Alexander S. Urban](#); LMU Munich, Germany

Halide perovskite nanoplatelets (NPLs) are a promising material for light-emitting applications, including LEDs and single-photon emitters. Two-dimensional $\text{Cs}_{n-1}\text{Pb}_n\text{Br}_{3n+1}$ NPLs with monolayer-precise control over their thickness can be obtained through a ligand-assisted synthesis. Through quantum confinement, they exhibit narrow and bright photoluminescence (PL) with an emission wavelength tunable between 435 and 515 nm. While the optoelectronic properties of perovskite NPLs are widely understood, little is known about how the synthesis of these promising emitters proceeds, impeding further improvement.

To this end, we developed an in-situ reactor cell to simultaneously acquire small-angle and total X-ray scattering (SAXS and TS) and PL emission at the DESY synchrotron during the synthesis of halide perovskite NPLs with a time-resolution of <50 ms. The NPL synthesis routine is based on combining a PbBr_2 ligand solution and Cs-oleate with a subsequent injection of the antisolvent acetone. The synthesis is carried out in a glass capillary within a copper block with stepper motor-controlled syringe pumps to inject precursor solutions.

An analysis of the SAXS data reveals that the NPLs begin to form immediately upon the combination of the two precursor solutions and not upon injection of the antisolvent. Accordingly, contrary to the common understanding, the $\text{Cs}_{n-1}\text{Pb}_n\text{Br}_{3n+1}$ NPL synthesis is not based on ligand-assisted reprecipitation but on well-defined precursor handling. However, the antisolvent still plays a crucial role, as it induces a superstructure assembly of the NPLs, leading to a greater monodispersity and enabling the sedimentation and purification of the NPLs. Furthermore, we investigated the structural and optical changes during the post-synthetic enhancement step and halide ion exchange within the same experimental setup. The presented combination of in-situ X-ray scattering and PL spectroscopy proves to be a powerful tool for understanding synthetic mechanisms.

4:15 PM EN02.10.08

Universal Mechanism of Luminescence Enhancement in Doped Metal-Halide Perovskite Nanocrystals from Symmetry Analysis [Sascha Feldmann](#); Harvard University, United States

Metal-halide perovskite nanocrystals have demonstrated excellent optoelectronic properties for light-emitting applications. Isovalent doping with various metals (M^{2+}) can be used to tailor and enhance their light emission. Although crucial to maximize performance, an understanding of the universal working mechanism for such doping is still missing. Here, we directly compare the optical properties of nanocrystals containing the most commonly employed dopants, fabricated under identical synthesis conditions. We show for the first time unambiguously and supported by first principles calculations and molecular orbital theory that element-unspecific symmetry-breaking rather than element-specific electronic effects dominate these properties under device-relevant conditions. The impact of most dopants on the perovskite electronic structure is predominantly based on local lattice periodicity breaking and resulting charge carrier localization, leading to enhanced radiative recombination, while dopant-specific hybridization effects play a secondary role. Our results provide specific guidelines for selecting a dopant to maximize the performance of perovskite emitters in the desired optoelectronic devices. <https://arxiv.org/abs/2206.06467> (2022)

4:30 PM *EN02.10.09

How Can Synchrotron Measurements Support the Development of Perovskite Materials and Devices? [Michael E. Stuckelberger](#); Deutsches Elektronen-Synchrotron DESY, Germany

Halide perovskites are arguably the most astonishing materials class of the last decade. The ensemble of uncommon and tunable properties predestines halide perovskites for their exploitation in devices for photovoltaic energy harvesting and sensing – at least theoretically. In practice, the tunability comes at the cost of lacking stability and uniformity, which hampers many large-scale applications.

While great efforts are made to experimentally address the stability and uniformity issues, the nanoscale understanding of halide perovskite materials challenge the characterization community at several levels: How to achieve at the same time nanoscale spatial resolution and large-scale statistics to support findings with evidence? How to disentangle measurement-induced artifacts from material and device properties? How to explore the perovskite chemistry in fully assembled devices in-situ and operando?

Synchrotrons offer X-ray sources with unprecedented intensity that can be exploited in multiple ways – each of them providing deep insight into specific aspects: Imaging in 2D and 3D shows details in buried layers with resolution beyond the diffraction limit of visible light, spectroscopy the nature of chemical bonds, diffraction crystallographic information from structure to lattice distortions.

The entire suite of X-ray modalities can be bundled into multi-modal scanning X-ray microscopy [1]. Advanced X-ray focusing schemes enable raster-scanning halide perovskite samples in multiple dimensions:

- (i) X-ray fluorescence (XRF) unveils the distribution of elements [2]
- (ii) Nano-diffraction (nano-XRD) unveils structural information at sub-grain level
- (iii) X-ray beam induced current (XBIC) unveils the local charge-collection efficiency of devices [3]
- (iv) X-ray excited optical luminescence (XEOL) in temporally- (TR-XEOL) or spectrally-resolved mode (SR-XEOL) unveil the local charge-carrier

lifetime and bandgap

(v) Ptychography unveils the electron density [4]

The simultaneous assessment enables point-by-point correlations [5], ultimately elucidating Materials Paradigm of halide perovskites by shining light on the synthesis-structure-property-performance relationship. Based on measurements at hard X-ray nano- and microprobe endstations at DESY, APS, ESRF, and NSLS II, we will introduce different scanning X-ray microscopy techniques [6] and showcase our latest measurements of halide perovskites.

Finally, we will give an outlook to current developments in the synchrotron world: in the coming years, the most brilliant diffraction-limited storage rings in the US (APS-U) and in Europe (PETRA IV) will bring scanning X-ray microscopy to an entirely new level. Discussing opportunities and challenges in X-ray based metrology, we seek to trigger a discussion about future needs for halide perovskite research and access to hard X-ray nanoprobes to enable efficient and timely use of synchrotron radiation for perovskite materials and devices.

[1] Stuckelberger, M. E., et al., "Engineering solar cells based on correlative X-ray microscopy," *J. Mater. Res.* 32, 1825 – 1854 (2017). doi: 10.1557/jmr.2017.108

[2] Stuckelberger, M. E. et al., "Effects of X-rays on Perovskite Solar Cells," *J. Phys. Chem. C* 124, 17949 – 17956 (2020). doi: 10.1021/acs.jpcc.0c04645

[3] Ossig, C., et al., "X-ray Beam Induced Current Measurements for Multi-Modal X-ray Microscopy of Solar Cells," *J. Vis Exp.* 150 (2019). doi: 10.3791/60001

[4] Schropp, A., et al., "PtyNANI: ptychographic nano-analytical microscope," *J. Appl. Cryst.* 53, 957-971 (2020). doi: 10.1107/S1600576720008420

[5] Stuckelberger, M. E., et al., "Charge Collection in Hybrid Perovskite Solar Cells: Relation to the Nanoscale Elemental Distribution," *IEEE J. Photovolt.* 7 (2017). doi: 10.1109/JPHOTOV.2016.2633801

[6] Kodur, M., et al., "X-Ray Microscopy of Halide Perovskites: Techniques, Applications, and Prospects," *Adv. Energy Mater.* 1903170 (2020). doi: 10.1002/aenm.201903170

SESSION EN02.11: Virtual Session I: Halide Perovskite Materials, Processing and Devices

Session Chair: Jin-Wook Lee

Tuesday Morning, December 6, 2022

EN02-virtual

8:00 AM *EN02.11.01

2D or not 2D? What's Behind Interfacial Engineering in 2D/3D Perovskite Solar Cells Giulia Grancini and Matteo Degani; University of Pavia, Italy

Three-dimensional (3D)/low-dimensional (LD) perovskite solar cells (PSCs) offer an effective strategy to overcome the trade-off between perovskite solar cells device performance and stability. The most successful architecture consists of a bilayered structure where the LDP forms a thin capping layer on top of the 3D bulk, improving the device longevity, while concomitantly simultaneously enhancing increasing the solar cell open circuit voltage and fill factor of the solar cell. Despite being one of the most popular and effective way processing techniques, whether the presence of this surface LDP layer would be - or not-represents the winning crucial path for the future of this technology remains elusive. In particular, atomic layer combined surface and bulk passivation using surface modifiers such as organic dopants, casts the doubts on the effective need for of having an homogeneous LDP cover capping layer. In this talk I will compare recent results obtained in the 3D/LDP configuration with the surfacecation passivation strategy, which can still pushes produce the performances to values comparable to the LDP/3D bilayers. I will providing a comprehensive perspective on the benefits from of the two different strategies, but also presenting how LDP interfaces can play a role in alternative new configurations, such as tandem solar cells [1,2].

Acknowledgements I acknowledge the "HY-NANO" project that has received funding from the European Research Council (ERC) Starting Grant 2018 under the European Union's Horizon 2020 research and innovation programme (Grant agreement No. 802862).

Reference

[1] Degani et al, *Sci Advances* 7, 49, 2021

[2] Degani et al, submitted

8:30 AM EN02.11.03

Highly Performed Near Infra-Red Photodetector and Its Array Based on SnPb Based Perovskites Wallace C. Choy; University of Hong Kong, China

Sn-Pb perovskites have shown their potentials in wide-bandgap photovoltaics and near-infrared photodetection applications which could become alternatives to traditional silicon and inorganic devices. To achieve efficient devices, high-quality and thick Sn-Pb perovskite films featuring well-packed, smooth, pinhole/void-free are highly desirable. Besides, understanding the crystallization kinetics and tuning the crystallization are fundamentally important to reach the Sn-Pb perovskite films, and have been limitedly explored. Herein, we propose an approach of double-side crystallization tuning through low-temperature space-restricted annealing in MA-free Sn-Pb perovskite films. By simultaneously retarding the crystallization in the top of precursor films and promoting the crystal growth of the bottom of precursor films, we achieve high-quality and block-like 1 μm thick Sn-Pb perovskite films with improved crystallinity and reduced trap density [1]. The photovoltaic-mode Sn-Pb perovskite near infra-red photodetectors show a high and flat external quantum efficiency of ~80% at 760-900 nm, a recorded responsivity of 0.53 A/W, and a high specific detectivity of 6×10^{12} Jones at 940 nm. The high-quality Sn-Pb perovskite can also be fabricated on metal/ silicon substrates for promoting direct integration with CMOS electronics and realizing an efficient photodiode imaging array [2].

Meanwhile, with the incorporation of rubidium cation, we can achieve controllable crystallization for growing high-quality films with the improvements of increased crystallinity and strengthened preferred orientation. Our theoretical results show that rubidium incorporation causes lower surface energy of (110) plane, facilitating growth in the dominating plane and suppressing growth of other competing planes. Consequently, the Sn-Pb perovskite photodetectors simultaneously achieve larger photocurrent and lower noise current. Finally, highly efficient UV-VIS-NIR (300-1100 nm) photodetectors with record-high linear dynamic range of 110 dB and 3-dB cut-off frequency reaching 1 MHz are demonstrated. This work contributes to enriching the cation selection in Sn-Pb perovskite systems and offering a promising candidate for low-cost UV-VIS-NIR photodetection [3].

[1] H. Liu, H.L. Zhu, W.C.H. Choy, et al, *Adv. Funct. Mat.* 31, 2010532, 2021.

[2] H.L. Zhu, W.C.H. Choy, et al, *ACS Nano*, 13, 11800, 2019.

[3] H.L. Zhu, W.C.H. Choy, et al, *Adv. Function. Mater.*, 28, 1706068, 2018.

8:45 AM EN02.11.04

Sn-Based Perovskite Solar Cells with Inorganic Hole Transport Layer Liang Wang, Qing Shen and Shuzi Ishi-Hayase; The University of Electro-Communications, Japan

Sn-based perovskite solar cells (PSCs) shows the best power conversion efficiency among all Pb-free-based PSCs due to its ideal narrow bandgap (1.4eV), small exciton binding energy, high carrier mobility and environment friendly. It becomes a potential candidate to replace toxic Pb-based perovskite. Commonly, inverted device structure with PEDOT:PSS as hole transport layer (HTL) are broadly used in Sn-based PSCs. However, the sensitivity of humidity and acidity of PEDOT:PSS limits the improvement of Sn-based PSCs stability and performance because of its nature of Lewis acidity. Therefore, searching inorganic HTL materials is also an important part for industrial application due to their intrinsic stability and low cost. In this study, an inorganic HTL was in-situ prepared by simple method and applied for Sn-based PSCs directly. It shows rapid carrier transportation from perovskite to HTL than that of PEDOT:PSS based. Finally, a 11.97 % power conversion efficiency was obtained, which is comparable to PEDOT:PSS based device (11.68 %).

9:00 AM EN02.11.07

Monolithic All-Perovskite Triple-Junction Solar Cells with Suppressed Non-Radiative and Optical Losses Junke Wang, Lewei Zeng, Aidan Maxwell, Hao Chen and Edward H. Sargent; University of Toronto, Canada

Multijunction solar cells represent an effective approach to surpassing the ~33% power conversion efficiency limit of ideal single-junction devices by piling multiple absorber layers with cascaded bandgaps. Optical simulations suggest that monolithic all-perovskite triple-junction solar cell comprising 2.0 eV, 1.5 eV, and 1.2 eV perovskite absorbers has the potential to reach a high efficiency of 36.6%. Reducing V_{oc} -to-bandgap loss in the wide-bandgap sub-cell and enhancing optical response in the narrow-bandgap sub-cell are key to the performance of such devices.

In this contribution, we report effective strategies to manipulate defects at the buried and top interfaces of wide-bandgap perovskites. A dual surface treatment technique helps reduce the non-radiative recombination losses at the perovskite/charge transport layer heterojunctions, yielding a high open-circuit voltage of over 1.4 V and fill factor of 85% with a 1.98 eV perovskite absorber. Furthermore, an optically benign transparent electrode significantly improves near-infrared absorption in the 1.2 eV narrow-bandgap perovskite sub-cell, resulting in current-matched triple-junction solar cells with a short-circuit current density of over 10 mA cm⁻². After optimization, we demonstrate efficient all-perovskite triple-junction solar cells with power conversion efficiencies of over 26%.

9:15 AM EN02.11.06

Inkjet-printed lead-free red emitting LEDs based on 2D-perovskite PEA₂SnI₄ Giovanni Vescio¹, Jesús Sanchez-Diaz², Gayathri Mathiazhagan¹, Sergi Hernandez¹, Ivan Mora-Sero², Albert Cirera¹ and Blas Garrido¹; ¹Universtat de Barcelona, Spain; ²Universitat Jaume I, Spain

Lead Halide Perovskites (LHPs) have attracted attention over the last decades because of their excellent optoelectronic and semiconducting properties. However, Pb²⁺ presents a great inconvenience in the development procedure of these materials, as it is highly toxic and contaminant. The Sn²⁺ is the most obvious substitute for Pb because of the similar ionic radius and the similar electronic configuration to Pb²⁺, which makes it possible to form a perovskite with a formula ASnX₃ like the lead-based counterparts.

In recent years, 2D halide perovskites have become a striking research spotlight. It is noteworthy that low-dimensional Sn²⁺-based halide perovskites exhibit remarkably enhanced air stability in comparison with their 3D counterparts. Moreover, 2D perovskites presents large exciton binding energy and outstanding thermal stability.

In this work, the stability, because of the large organic cations, and emission properties of single-layer 2D tin perovskite nanoplates with chemical formula PEA₂SnI₄ (PEA= phenylethylammonium) and pure red emission are reported.

An ink solution of PEA₂SnI₄ based on molecular precursors dissolved in DMSO has been prepared for inkjet printing technology. The morphology of inkjet-printed films was characterized via SEM and optical microscopies to observe the uniformity of the films and obtaining the best conditions for producing pin-hole free layers. These results were combined with XPS measurements that allow characterizing the composition of the layers and XRD to determine crystalline structure and micro/nanocrystal size. Finally, optical analysis like absorbance and PL (photoluminescence) spectra allows measuring band gap and confirm that the layers are optically active with the expected narrow red emission at ~630 nm.

The inkjet-printed PEA₂SnI₄-based light-emitting diode (LED) exhibits a maximum external quantum efficiency (EQE) of 1% with an average of 0.7% and a brightness of 30 cd/m², which are comparable to that of the control devices obtained by spin coating. Moreover, lifetime test shows an operating half-life exceeding 3 hours at an initial brightness of 10 cd/m².

This work paves the way for inkjet-printed Cd- and Pb-free perovskite light-emitting devices for a wide variety of low-cost and customizable applications.

9:20 AM EN02.11.08

Efficient 2-Terminal All-Perovskite Tandem Solar Cells by Multisource Evaporation Yu-Hsien Chiang, Miguel Anaya, Kyle Frohna, Hayden Salway, Anna Abfalterer, Bart Roose and Samuel D. Stranks; University of Cambridge, United Kingdom

The rapid screen of perovskite solar cells optimization based on solution-processed methods have achieved historical successfully. The next stage of technology development is to transfer from the lab research to fab production lines. Therefore, another deposition route for scalability and modularity needs to be studied. Our work employs a novel dual-interface treatment to maximize the performance of evaporated perovskite devices, which show great promise when implemented into tandem architectures. We employ a 4-source vacuum deposition method to demonstrate perovskites of the tunable bandgap. Engineering the device architecture via the use of a MeO-2PACz layer as HTM demonstrates a 20.7% PCE in a 1.62 eV bandgap perovskite solar cell, which is among the highest performance in a multisource evaporated system. The use of several sources allows precise control over the halide content in the perovskite composition, which is crucial to enlarge its bandgap and make it relevant for widegap subcells for tandem architectures. Halide segregation is a key factor to consider when designing widegap perovskites and we find that a FA_{0.7}CS_{0.3}Pb(I_{0.66}Br_{0.34})₃ film with a 1.77 eV shows great phase stability under light-soaking, though devices display suboptimal voltages. In order to minimize non-radiative losses, we introduce a surface treatment to passivate the evaporated perovskite that translates into 17.8 % PCE devices with a remarkable Voc of up to 1.26 V, which is among the best in evaporated perovskite solar cells. This method is versatile and reproducible, and we extend it to Pb/Sn-based narrow gap perovskite solar cells reaching a Voc of 0.86 V. Incorporating the narrowgap and widegap perovskite building blocks into a 2-terminal tandem solar cell, we obtain a PCE of 24.1% with a promising Voc of up to 2.06 V, which is unprecedented for a system where either of the subcells is deposited by dry methods. This result represents a major step forward in the realization of third-generation multijunction solar cells of superior performance. Our work opens a myriad of possibilities benefiting from the intrinsically scalable, conformal, and reproducible character of vacuum deposition methods, opening the path to the integration of advanced photonic strategies to push perovskite photovoltaics to their limits.

9:50 AM DISCUSSION TIME

10:30 AM *EN02.12.01

Controlling Spin-Orbit Interactions in Hybrid Metal-Halide Perovskites with Magnetic Doping and Chirality Felix Deschler; University of Heidelberg, Germany

Materials combining the optoelectronic functionalities of semiconductors with control of the spin degree of freedom are highly sought after for the advancement of quantum technology devices and provide exciting avenues for polarized light-emission. In my talk, I will present our efforts on gaining control over spin dynamics and spin-orbit interactions through compositional and structural tuning in solution-processable hybrid perovskite semiconductors. In a first direction, we aim to exploit the exceptional optoelectronic properties of these hybrid perovskites, together with their tolerance in the electronic states to dopants and defects, to make advances towards high-performance dilute magnetic semiconductors. I will discuss how we can employ ultrafast optical spectroscopy for insights into exciton population dynamics and ultrafast optical control of spin dynamics in novel hybrid perovskite materials incorporating transition-metal dopants. In a second direction, we aim to design spin-orbit interactions by tailoring the chiral crystal symmetry of hybrid metal-halide perovskites. I will present our results on chiral lead-free low-dimensional bismuth-based materials, as well as recent advances in maximizing luminescence and polarization in lead-halide systems.

11:00 AM EN02.12.02

Structural and Electronic Characteristics of Double and Mixed Cs₂GeX₆ (X= Br, I, Cl) Perovskite from First Principles David Obada, Simeon Abolade, Syam Kumar and Akinlolu Akande; Atlantic Technological University, Ireland

Lead-free metal halide perovskites are increasingly receiving attention for the commercialization of optoelectronic devices. In this study, first principles simulation using density functional theory has been used to investigate the structural and electronic properties of non-toxic Cs₂GeX₆ (X= Br, I, Cl) with a mixed halide counterpart Cs₂GeBr_xCl_{1-x} (x=0.25, 0.5) using the virtual crystal approximation (VCA). The trend in the gradients observed in the lattice constants of the perovskites followed the increase in ionic radius of the halides. The investigation of the electronic properties showed semiconducting properties for Cs₂GeCl₆ and Cs₂GeBr₆ perovskites, while semiconducting to metallic transitions were observed for the Cs₂GeI₆ and Cs₂GeBr_xCl_{1-x} perovskites. The values obtained for the direct bandgaps of Cs₂GeCl₆ and Cs₂GeBr₆ were 2.28 eV, and 0.93 eV, respectively. The elastic constants calculations showed that the perovskite compounds were mechanically stable. The physics behind the semiconducting to metallic transitions for some of the perovskite compounds studied have been discussed. Our datasets provide useful information for fundamental research on Cs₂GeX₆ perovskites and its practical applications in emerging optoelectronics.

11:15 AM EN02.12.03

Regulating the Spatial Profile of Surface Potential Maximizes Open-Circuit Voltage in Wide-Bandgap Devices Hao Chen, Sam Teale, Bin Chen and Edward H. Sargent; University of Toronto, Canada

Wide-bandgap perovskites (>1.7 eV) are widely used in all-perovskite tandem solar cells, which have the potential to break the Shockley–Queisser limit. However, the open circuit voltage (V_{OC}) deficit in wide-bandgap perovskite solar cells (PSCs) is very large because of the inhomogeneous surface potential and poor energetic alignment between perovskite and ETL, which limits the V_{OC} below 1.3 V. Here, using quasi fermi level measurements, we reveal the key role of increased recombination when the perovskite is in contact with an electron transport layer (ETL). We find common monoammonium surface treatments fail to address this; whereas diammonium molecules modify the perovskite surface states and achieve a more favorable band alignment with a more uniform distribution of the surface potential in space. Processing the perovskite surface with diammonium salts increases the photoluminescence quantum yield of *pin*-stacks 40-fold, and increases the QFLS by 90 meV. Treated 1.78 eV PSCs achieve a certified 1.33 V V_{OC}, and > 19% power conversion efficiency (PCE).

11:30 AM EN02.12.04

A Simple Route to the Synthesis and Deposition of All Inorganic Perovskite CsPbBr₃ Films and Their Photocatalytic Properties Lorenzo Sima^{1,2}, Anna L. Pellegrino^{1,2}, Francesca Lo Presti^{1,2} and Graziella Malandrino^{1,2}; ¹Università di Catania, Italy; ²INSTM, Italy

The compounds belonging to the family of perovskites exhibit a wide range of mechanical, magnetic, and optical properties and for these reasons are currently key materials for many technologies, such as piezoelectrics, photocatalytic systems, and photovoltaic solar cells. Among perovskites, the all-inorganic halide perovskites (AIHPs) with the ABX₃ structure (with A = Cs, Rb; B = Pb, Sn and X = F, Br, I) represent an emerging class of materials that have drawn a growing interest due to the combination of the advantages of containing cheap and abundant elements with the excellent stability of these structures by excluding organic species sensitive to the external environment.

Particularly, our attention is devoted to CsPbBr₃ all-inorganic perovskites, which, among other effects, have emerged for photocatalytic degradation processes of different organic dye compounds. In fact, one of the most challenging applications of AIHP materials regards the wastewater purification process of textile effluents from industrial production. In this field, heterogeneous catalysis under light is widely accepted due to its high efficiency, yield of degradation, and cost effectiveness. For these reasons, CsPbBr₃ in the form of films, being immobilized and not used as a dispersed phase, has the advantage of a simple separation and recovery from the solution. Therefore, a smooth, continuous well-covering thin film on a regular substrate is preferred.

Herein, we report a novel method for the synthesis of CsPbBr₃ films on different substrates such as silicon, glass, quartz, and flexible substrates. The present synthetic strategy is a facile, one-step, and low-temperature approach to the synthesis of Cs-Pb halide perovskite and takes advantage of the Cs and Pb β-diketonate compounds as precursors, allowing, reproducibly and selectively, the synthesis of the CsPbBr₃ phase. The as obtained CsPbBr₃ suspension is deposited onto the substrates by spray deposition at room temperature and atmospheric pressure. This approach reveals to be very simple and extremely versatile and makes it possible to deposit the perovskite on a wide range of different kinds of materials.

Structural, morphological, and compositional analyses of the final products, carried out by X-ray diffraction (XRD), field-emission scanning electron

microscopy (FE-SEM), and Energy Dispersive X-ray analysis (EDX), show the formation of the pure CsPbBr₃ system. Uv-vis spectrophotometric analyses were performed in order to determine the bandgap energy (E_g) of the system. Preliminary results on photodegradation of an organic dye under both visible or UV light irradiation will be presented.

11:45 AM EN02.12.05

Anion Vacancy Defect Passivation of 2D-Layered Tin-based Perovskite Thin-Film Transistor Jaehyeok Cho and Myung-Gil Kim; Sungkyunkwan University, Korea (the Republic of)

Organic-inorganic hybrid perovskites have been intensively investigated for solar cells, optoelectronics and electronic applications with its high light absorption, defect tolerance, and high carrier mobility. Moreover, the hybrid perovskites offer the mechanical flexibility and solution processability. However, it is still challenging to achieve a reliable operation of electronic devices due to ion migration, which may lead to poor field-effect mobility with large current-voltage hysteresis. Such ion migration in perovskite films causes a screening of the applied electric field and thereby adversely impacts the device performance. In this research, we focused on using lead-free tin-based perovskites as the semiconductor in thin-film transistors (TFTs). We introduced anion vacancy suppressing additives in the perovskite precursor to passivate defects at the grain boundaries, thereby improving transistor characteristics. This work provides an effective way to achieve the high-performance in organic-inorganic hybrid perovskite TFT devices.

11:50 AM EN02.12.07

Photoluminescence Quenching Switching from Open- to Short-Circuit as a Figure of Merit for the Efficiency in Perovskite Solar Cells Valerio Campanari¹, Faustino Martelli¹, Antonio Agresti², Sara Pescetelli², Narges Yaghoobi Nia², Francesco Di Giacomo², Daniele Catone¹, Patrick O’Keeffe¹, Stefano Turchini¹, Bowen Yang³, Jiajia Suo³, Anders Hagfeldt³ and Aldo Di Carlo^{2,1}; ¹Consiglio Nazionale delle Ricerche, Italy; ²Università degli Studi di Roma Tor Vergata, Italy; ³Uppsala University, Sweden

The photoluminescence (PL) intensity is often used as an indicator of the performance of perovskite solar cells (PSCs) and indeed steady-state PL is often used for the characterization of these devices and their constituent materials. However, some features of perovskite materials and devices, if not taken adequately into account, could lead to misleading results.^[1] In this work we show that the value of the photoluminescence quenching occurring when the PSCs are switched from open- to short-circuit is an excellent figure of merit (FOM) for the evaluation of the PCS efficiency. Moreover, in order to take into account the large inhomogeneity of the performance in the PCS yield and their temporal instability, we have used a systematic approach to comparison the PCS conversion efficiency and their PL intensity using a large group of PSCs with efficiency varying from 5.63% to 21.5%.

The PSCs were fabricated using different materials both as regards the absorbing materials and the transport layers, different structures, and relatively different fabrication processes. We found that the use of the bare PL intensity in open-circuit (OC) is not a general and reliable indicator of the performances when a large heterogeneous ensemble of devices is used. Instead, considering the values of the PL intensity both at open OC and short circuit (SC)^[2,3], it is possible to correlate the PL intensity to the device power conversion efficiency (PCE) through a FOM based on the quenching of the PL observed in SC conditions ($PL_{Q_{oc-sc}} = (PL_{oc} - PL_{sc}) / PL_{oc}$).^[4] We explain the observed correlation between $PL_{Q_{oc-sc}}$ and the PCE of the device by means of a simplified model based on the carrier density rate equation, in which the extraction time of the photoexcited carriers in the PSC is duly considered. We have also shown that the analysis of $PL_{Q_{oc-sc}}$ using our model can provide a tool to estimate the carrier extraction time in PSCs through a simple cw-PL measurement, provided the carrier lifetime in OC conditions is known. Without suggesting that a PL measurement can substitute a $J-V$ characterization, we point out that our study is an important contribution to the understanding the physical mechanisms underlying carrier recombination and extraction. Moreover, we have found a clear correlation between the increase over time of the PL intensity in SC conditions and the contemporary decrease of the short-circuit current, I_{sc} , a feature that can be easily understood within the framework of our model and FOM.

[1] M. Stolterfoht, C. M. Wolff, J. A. Márquez, S. Zhang, C. J. Hages, D. Rothhardt, S. Albrecht, P. L. Burn, P. Meredith, T. Unold, D. Neher, *Nat. Energy* **2018**, *3*, 847.

[2] T. Du, W. Xu, M. Daboczi, J. Kim, S. Xu, C. T. Lin, H. Kang, K. Lee, M. J. Heeney, J. S. Kim, J. R. Durrant, M. A. McLachlan, *J. Mater. Chem. A* **2019**, *7*, 18971.

[3] M. Stolterfoht, V. M. Le Corre, M. Feuerstein, P. Caprioglio, L. J. A. Koster, D. Neher, *ACS Energy Lett.* **2019**, *4*, 2887.

[4] V. Campanari, F. Martelli, A. Agresti, S. Pescetelli, N. Y. Nia, F. Di Giacomo, D. Catone, P. O’Keeffe, S. Turchini, B. Yang, J. Suo, A. Hagfeldt, A. Di Carlo, *Sol. RRL* **2022**, DOI: 10.1002/solr.202200049.

12:35 PM DISCUSSION TIME

SYMPOSIUM EN03

Beyond Li-Ion Batteries—Low Cost Alternatives Based on Other Chemistries
November 28 - December 6, 2022

Symposium Organizers

Raphaële Clément, University of California, Santa Barbara
Haegyom Kim, Lawrence Berkeley National Laboratory
Shyue Ping Ong, University of California, San Diego
Yan Eric Wang, Samsung Research America

Symposium Support

Silver

Nissan North America, Inc.

SK on Co., Ltd.
Umicore

Bronze
Materials Horizons
MilliporeSigma

* Invited Paper
+ Distinguished Invited

SESSION EN03.01: Na-Ion I
Session Chairs: Haegyum Kim and Yan Eric Wang
Monday Morning, November 28, 2022
Hynes, Level 3, Ballroom C

10:30 AM *EN03.01.01

A Perspective on Sodium-Ion Batteries [Marca M. Doeff](#), Wei Yin and Gozde Barim; Lawrence Berkeley National Laboratory, United States

Sodium-ion batteries (NIBs) have the potential for addressing cost and supply security concerns associated with energy storage for large-scale applications, such as grid storage and electric vehicles. Not only is sodium itself much cheaper and more abundant than lithium, but devices based on sodium also can avoid other strategic, scarce, or costly metals, including cobalt, nickel, and copper. The energy density of state-of-the-art sodium-ion batteries now meets or exceeds that of lithium-ion batteries with lithium iron phosphate cathodes. There are also some potential performance advantages over lithium-ion batteries such as higher power density, better low temperature performance and, possibly, better safety.

A disadvantage, however, is the limited choice of anode materials. Graphite does not intercalate sodium to a useful extent, so hard carbons are the most commonly used negative electrodes in NIBs. The very low potentials at which sodium intercalates into hard carbons means that there is a risk of sodium plating under certain use conditions. We have been investigating titanate anodes as a potential alternative to hard carbon anodes for NIBs. A number of stepped layered ternary or quaternary sodium titanates exist, which intercalate sodium reversibly at moderately low potentials (~0.3-0.6V vs. Na⁺/Na). Some of these exhibit capacities in excess of 200 mAh/g, sometimes greater than that predicted solely by intercalation of sodium into available sites. A kinetic investigation of these interesting materials reveals hybrid redox mechanisms, in which both diffusional (intercalation) and surface (pseudo-capacitive) processes contribute to the electrochemistry. The relative contribution of these processes can be tuned by manipulating the structure; e.g. controlling surface defects, thermal treatments, or heterostructuring. The latter approach involves synthesis of titanate layers interleaved with carbon. This talk will cover these approaches and the electrochemistry of these titanates in detail.

11:00 AM EN03.01.02

A Study on Air Storage Characteristics of O3-type Na[Ni_{1/2}Mn_{1/2}]_{1-x}Fe_xO₂ Cathode Materials for Sodium-Ion Batteries [Jehee Park](#)^{1,2}, [Jihyeon Gim](#)¹, [Seoung-bum son](#)¹, [Dewen Hou](#)³, [Heonjae Jeong](#)¹, [Lei Cheng](#)¹, [Hui Xiong](#)³, [Youngsik Kim](#)², [Christopher Johnson](#)¹ and [Eungje Lee](#)¹; ¹Argonne National Laboratory, United States; ²Ulsan National Institute of Science and Technology, Korea (the Republic of); ³Boise State University, United States

Layered sodium transition metal oxides (Na_xMO₂) have been considered a promising cathode candidate for sodium-ion batteries due to their high theoretical capacity, low cost, easy synthesis, and scalable production ability. However, its poor air storage stability is one of the critical concerns that need to be addressed for practical application. The hygroscopic nature of the Na_xMO₂ cathodes makes them susceptible to hydration, Na extraction, and degradation on the air-exposed cathode surface, leading in turn to further process and performance issues such as gas evolution, slurry gelation, and electrolyte decomposition.[1] These incur extra costs in materials storage, transportation, and cell manufacturing. In this presentation, we will discuss the systematic investigation of the air-storage stability of Na[Ni_{1/2}Mn_{1/2}]_{1-x}Fe_xO₂ cathodes. Compared to Fe-free Na[Ni,Mn]O₂, which has severe moisture sensitivity and poor air-storage properties, the solid solution compounds of Na[Ni,Mn,Fe]O₂ showed significantly improved surface and bulk structural stability under ambient air. The role of Fe and detailed improving mechanism in the air-storage stability of Na[Ni,Mn,Fe]O₂ will be discussed. This presentation will provide useful insight into the cathode design and improvement strategies for practical-scale processing of layered cathode materials for sodium-ion batteries.

Reference

[1] Zhang, Y., Zhang, R., & Huang, Y. (2019). *Frontiers in Chemistry*, 7, 335.

11:15 AM EN03.01.03

Reconfiguring Sodium Intercalation Process of TiS₂ Electrode for a Highly-Stable and Fast-Charging Sodium-Ion Battery by Solvent Co-Intercalation [Jooha Park](#) and Kisuk Kang; Seoul National University, Korea (the Republic of)

Titanium disulfide (TiS₂), which is a well-known first-generation cathode in lithium batteries, has also long attracted a broad interest as a potential electrode candidate for sodium-ion batteries (SIBs) due to favorable sodium intercalation kinetics and semi-metallic nature. However, the reversibility of sodium de/intercalation is far inferior to that of lithium, which has been often attributed to the unfavorable intermediate phase formation upon sodiation, leading to a poor electrochemical cycle life. Herein, we demonstrate that reconfiguring sodium intercalation process *via* partial solvent co-intercalation can induce a significant change in the phase-transition paths for the entire sodium intercalation reactions of Na_xTiS₂ (0 < x < 1), successfully detouring the formation of the unfavorable intermediates. And, it unexpectedly results in a remarkable enhancement of sodium intercalation reversibility, thereby boosting the cycle stability of sodium cell along with high power capability. Our comparative investigations reveal that the sodium intercalation in Diethylene glycol dimethyl ether (DEGDME)-based electrolyte involves a partial pre-intercalation of solvent molecules and subsequently undergoes distinct phase evolutions dissimilar to the bare sodium ion intercalation in conventional electrolytes. The new altered intercalation route allows the Na-TiS₂ cell to deliver a reversible capacity of 93 mAh g⁻¹ over 1,000 cycles with 62 % of capacity retention at as high as 10 C rate. This re-discovery of intercalation behavior of TiS₂ offers a new insight in tailoring the reversibility and kinetics of intercalation process of commonly known electrodes for rechargeable batteries.

11:30 AM EN03.01.04

Impacts of Annealing Temperature on the Properties and Performance of Na₂Fe₂F₇ Cathode Rhiannon M. Kennard¹, Peter Gross¹, Yong-Seok Choi², Darren Ould³, Enrique Sanchez-Perez¹, Christopher Thomas¹, Jethro Pryke¹, Dominic Wright³, David O. Scanlon², Clare Grey³, Serena Cussen¹ and Edmund J. Cussen¹; ¹University of Sheffield, United Kingdom; ²University College London, United Kingdom; ³University of Cambridge, United Kingdom

The development of batteries free of Li, Co, and Ni is critical to meeting demands for grid-scale energy storage. Recent work has shown that weberite-type cathodes with structure Na₂MMF₇ (M = Fe, Ti, etc.) deliver competitive capacities with high energy density and cycling stability, with Na₂Fe₂F₇ performing particularly well. Weberites are also interesting for use as cathodes because their 3D open structure offers many pathways for Na diffusion, while simultaneously avoiding the phase transitions that plague oxide cathodes. In addition, the electronegative F provides open-circuit voltages of > 3V. For fabrication of Na₂Fe₂F₇ to be truly sustainable, the processing temperature must be as low as possible. We therefore investigate how the fundamental properties of Na₂Fe₂F₇ are affected by annealing temperature. From structural analyses, we find that a vacancy-rich weberite is formed at lower temperatures, while a full Na₂Fe₂F₇ weberite forms at more elevated temperatures. Capacity and ion conduction are compared for both phases. We also clarify a debate regarding the polymorph of Na₂Fe₂F₇ via structural refinements and computational analyses. Primary particle size is modified from nanoscale to microscale by increasing the annealing temperature, and the consequences on capacity are explored. In addition, we find that mechanical milling post-synthesis is necessary to achieve good capacity, as large (>50 micron) secondary particles form during annealing. Excessive mechanical milling post-synthesis creates an amorphous phase, which fortunately improves the capacity. This work combines experiment and computation to reveal the fundamental properties of Na₂Fe₂F₇, while simultaneously providing information necessary to the development of this material.

SESSION EN03.02: Na-Ion II
Session Chairs: KyuJung Jun and Yan Yao
Monday Afternoon, November 28, 2022
Hynes, Level 3, Ballroom C

1:30 PM *EN03.02.01

Extending the Low-Temperature Operation of Sodium Metal Batteries [Weiyang Li](#); Dartmouth College, United States

Nonaqueous sodium-based batteries are ideal candidates for the next generation of electrochemical energy storage devices. However, despite the promising performance at ambient temperature, their low-temperature (e.g., < 0°C) operation is detrimentally affected by the increase in the electrolyte resistance and solid electrolyte interphase (SEI) instability. Here, to circumvent these issues, we propose specific electrolyte formulations comprising linear and cyclic ether-based solvents and sodium trifluoromethanesulfonate salt that are thermally stable down to -150°C and enable the formation of a stable SEI at low temperatures. When tested in the Na||Na coin cell configuration, the low-temperature electrolytes enable long-term cycling down to -80°C. Via ex situ physicochemical (e.g., X-ray photoelectron spectroscopy, cryogenic transmission electron microscopy and atomic force microscopy) electrode measurements and density functional theory calculations, we investigate the mechanisms responsible for efficient low-temperature electrochemical performance. We also report the assembly and testing between -20°C and -60°C of full Na||Na₃V₂(PO₄)₃ coin cells.

2:00 PM EN03.02.02

Enabling Low-Cost Molten Sodium Batteries Through Engineered Catholyte-Separator Materials Chemistry [Erik D. Spoeke](#), Adam Maraschky, Melissa Meyerson, Stephen Percival, Stephen Meserole, Lowry Daniel, Martha M. Gross and Leo J. Small; Sandia National Laboratories, United States

Cost-effective, safe, and reliable batteries are expected to be key components of the emerging electrical energy grid. We describe here a new class of low-temperature molten sodium-iodide batteries that employ a molten sodium anode, a solid-state NaSICON ceramic separator, and a low-cost molten salt catholyte. These unique batteries operate near 100°C, a dramatic reduction from the ~300°C operation of traditional molten sodium batteries, and they offer significantly higher voltages (>3.1V) than many other scalable battery chemistries. Enabling this low-temperature operation, however, requires significant understanding and control over materials chemistry and critical interfaces. Here, we will specifically discuss recent discoveries involving chemical interactions at the interface between the NaSICON ceramic and the molten sodium-iodide/aluminum chloride salt catholyte. We will discuss the unexpected dependence of battery cycling performance on molten salt composition and connect the battery performance to specific electrochemical and materials properties of the separator and the salt. In particular, we identify specific impact of catholyte Lewis acidity on key chemical interactions at this critical interface. Understanding these fundamental interactions provides key insights and guidance that are central to designing high performance molten sodium batteries that operate with low-cost catholyte salts.

Sandia National Laboratories is a multimission laboratory managed and operated by National Technology & Engineering Solutions of Sandia, LLC, a wholly owned subsidiary of Honeywell International Inc., for the U.S. Department of Energy's National Nuclear Security Administration under contract DE-NA0003525.

2:30 PM DISCUSSION TIME

2:30 PM EN03.02.06

Operando Electrochemical Dilatometry (ECD)—Monitoring the Dynamic Behavior of Carbon Materials in Sodium-Ion Batteries During Cycling [Ines Escher](#)¹, Guillermo A. Ferrero¹, Mustafa Goktas¹, Yuliya Kravets¹ and Philipp Adelhelm^{1,2}; ¹Humboldt Universität zu Berlin, Germany; ²Helmholtz-Zentrum Berlin, Germany

Due to the continuously increasing demand for energy storage systems research on beyond-lithium technologies has gained much attention. In this field, sodium-ion batteries (SIBs) play an important role due to the greater availability of sodium compared to lithium, no need of critical cobalt as positive electrode material and the possible use of aluminum as current collector, which is cheaper and lighter compared to the commonly used copper.^[1] Carbon electrodes have been effectively applied as negative electrode material in this case. The focus of this abstract is on the investigation of graphite and hard carbon as negative electrode material using operando electrochemical dilatometry (ECD). ECD is a technique that recently gained attention due to the improvement in measurement setups. In contrast to other analytical methods, like X-ray diffraction, that provide information on the structural changes of the active material, ECD gives information on the expansion of the complete electrode, also including inactive components and morphological characteristics. It has been recently used to investigate several electrode materials for sodium- and lithium-ion batteries (LIBs).^[2] Graphite, which is the standard material of choice in LIBs, can not be used with the same, carbonate-based electrolytes, in SIBs, as the formation of binary graphite intercalation compounds is thermodynamically not favorable.^[3] To overcome this issue it was demonstrated that the use of ether-based electrolytes results in the formation of stable ternary graphite intercalation compounds, where the solvent molecules co-intercalate together with the sodium ions into the graphitic lattice.^[4] This reaction results in a large electrode expansion which can be easily followed using ECD. Even though the reaction is highly

reversible a decrease of the electrode expansion is favorable, especially in full cell applications. Herein, the influence of different binder materials as well as the addition of a co-solvent on the electrode expansion has been investigated. The use of CMC (sodium salt of carboxy methylcellulose) as well as the addition of 10 vol% ethylenediamine has shown promising outcomes.^[5]

Hard carbon is so far the standard material in commercial SIBs and benefits from its redox potential close to Na⁺/Na, a storage capacity which is typically between 150-350 mAh g⁻¹ and especially low cost.^[6] Unlike graphite carbonate-based as well as ether-based electrolytes can be used in this case. However, a lot of research has been done to reveal the storage mechanism no clear answer has been found yet. ECD has been applied to get a further understanding of the storage mechanism in hard carbon electrodes. In this case ECD showed that the intercalation process of sodium ions can be divided in three steps, proposing an intercalation – pore filling – plating mechanism. In contrast, a two-step mechanism has been found in the case of lithium ions, assuming an intercalation – pore filling process.^[7]

In conclusion, ECD was found to be a powerful operando tool to investigate the influence of different components (binder, co-solvent) on the co-intercalation of sodium ions in graphite as well as the charge storage mechanism in hard carbon electrodes.

[1] C. Vaalma, D. Buchholz, M. Weil, S. Passerini, *Nat Rev Mater* **2018**, *3*, 1-11.

[2] I. Escher, M. Hahn, G. A. Ferrero, P. Adelhelm, *Energy Technology* **2022**, *10*, 2101120.

[3] O. Lenchuk, P. Adelhelm, D. Mollenhauer, *Phys. Chem. Chem. Phys.* **2019**, *21*, 19378-19390.

[4] B. Jache, P. Adelhelm, *Angew. Chem., Int. Edit.* **2014**, *53*, 10169-10173.

[5] I. Escher, Y. Kravets, G. A. Ferrero, M. Goktas, P. Adelhelm, *Energy Technology* **2020**, *9*, 2000880.

[6] X. Dou, I. Hasa, D. Saurel, C. Vaalma, L. Wu, D. Buchholz, D. Bresser, S. Komaba, S. Passerini, *Mater. Today* **2019**, *23*, 87-104.

[7] I. Escher, G. A. Ferrero, M. Goktas, P. Adelhelm, *Advanced Materials Interfaces* **2021**, *9*, 2100596.

2:45 PM BREAK

2:45 PM EN03.02.07

Influence of Cathode Processing on Cycle Life and Performance of Sodium-Zinc Chloride Batteries Louis Sieuw¹, Tu Lan¹, Enea Svaluto-Ferro¹, Wenjin Ding², Meike Heinz¹ and Corsin Battaglia¹; ¹Empa-Swiss Federal Laboratories for Materials Science and Technology, Switzerland; ²DLR-Institute of Engineering Thermodynamics, German Aerospace Center, Germany

Current commercial sodium-nickel chloride (Na-NiCl₂) batteries possess long design and cycle lives of 20 years and >4500 cycles at 80% depth of discharge, respectively¹. Combined with high cathode loadings and low energy-specific costs, this translates to competitive battery cycle costs of <0.1 \$/kWh/cycle. While this high-temperature (~300 °C) battery technology displays a high potential for large-scale stationary energy storage, the cost of the cell components and their assembly still outranges that of state-of-the-art Li-ion batteries. The replacement of costly nickel, for which demand is increasing, with inexpensive zinc as cathode material, helps to cut down the cell production costs and could provide a sustainable solution for large-scale energy storage applications.

In this study, we assess the electrochemical processes involved in sodium-zinc chloride batteries (Na-ZnCl₂). In particular, we concentrate on understanding the relations between cathode composition, microstructure, capacity, rate limitations, and lifetime of Na-ZnCl₂ cells. Using pellets consisting of zinc powder mixed with rock salt, we investigate the influence of raw materials particle size and compaction pressure on the composite cathode density and electrical conductivity. We further compare the results with those obtained for filamentary nickel and rock salt mixtures to help understand the influence of metal powder morphology on the electronic and ionic conductivities. Moreover, we systematically assess through calculations the influence of secondary electrolyte volume, active metal content, and electrode filling level on cell capacity and pressure evolution at different SOC².

Using the prototype cell design formerly described by our group³, we characterize the successive steps⁴ of the chlorination and de-chlorination reaction of zinc by galvanostatic techniques and electrochemical impedance spectroscopy, as well as cyclic voltammetry. Based on these electrochemical data combined with structural post-mortem characterization, we attempt to resolve the electrochemical processes and degradation mechanisms governing both the efficiency and cycle life of the Na-ZnCl₂ system. By improving the structural understanding of the sodium-zinc chloride cells, we strive to optimize their cycle life, rate performance, and energy efficiency, with the aim of providing a new, cost-efficient generation of batteries for stationary energy storage applications⁵.

1. FZSoNick. Sodium metal chloride battery system, Technical overview. download from fzsonick.com/home (accessed June 13 2022)

2. Heinz, M. V. F., Graeber, G., Landmann, D. & Battaglia, C. Pressure management and cell design in solid-electrolyte batteries, at the example of a sodium-nickel chloride battery. *J. Power Sources* 2021, 228268

3. Graeber, G. et al. Rational Cathode Design for High-Power Sodium-Metal Chloride Batteries. *Adv. Funct. Mater.* 2021, 2106367

4. Lu, X. et al. A novel low-cost sodium-zinc chloride battery. *Energy Environ. Sci.* 2013 6, 1837–1843

5. Sieuw, L. et al. Influence of Cathode Processing on Cycle Life and Performance of Sodium-Zinc Chloride Batteries. To be submitted

3:45 PM DISCUSSION TIME

SESSION EN03.03: Poster Session I: Multivalent and Na-Ion

Session Chairs: Haegyum Kim and Weiyang Li

Monday Afternoon, November 28, 2022

8:00 PM - 10:00 PM

Hynes, Level 1, Hall A

EN03.03.01

Dextrin-DADMAC-MBAA Hydrogel for High Ionic Conductible Flexible Aqueous Sodium Ion Hybrid Battery Jung Woo Hong and HoSeok Park; Sungkyunkwan University, Korea (the Republic of)

For applications in energy storage devices, polymer electrolytes have attracted attention due to their favorable mechanical properties such as flexibility, strain stress, pressure and the ability to reduced reactivity with liquid electrolytes, suppression of dendrite growth. But the disadvantage that the ion conductivity is not as good as that of the liquid electrolyte is hindering the development of the polymer electrolytes. Here in, we demonstrate a high ion-conducting, flexible and double networked (DN) hydrogel films for Sodium Ion Hybrid Battery (SIHB). Hydrogel chain of DADAMC-Dextrin-MBAA is crosslinked by free-radical reaction of Dimethyldiallylammoniumchloride (DADMAC) and N, N'-methylene-bis-acrylamide (MBAA) and Dextrin chain.

In addition, DADMAC and NaClO_4 salt undergo ion exchange reaction that prevents excessive expansion of DADMAC structure (which occurs due to the hydrophilicity of the gel), and also has the advantage of increasing physical properties such as strain stress and pressure. The DDM hydrogel is found to have an ionic conductivity of 31.2 mS cm^{-1} at 25°C , the tensile strength of 8000 KPa, electrochemically stable up to 2.5V.

EN03.03.02

Investigation of Thermodynamic and Structural Properties of Olivine Li- and NaFePO_4 [Elizabeth Brown](#) and Hillary Smith; Swarthmore College, United States

Olivine NaFePO_4 has the potential to be a high performing and cost-effective battery cathode material. However, key differences exist between the behavior of NaFePO_4 and isostructural LiFePO_4 that are not yet fully understood. In this work, the thermodynamic and structural properties of Na_xFePO_4 and Li_xFePO_4 ($0 < x < 1$) are investigated between 300 and 800K. We use neutron powder diffraction to examine the temperature dependent structural change of Na_xFePO_4 for $x=0$, $x=2/3$, and $x=1$ and Li_xFePO_4 for $x=1$ and $x=2/3$. Differential scanning calorimetry provides the isobaric specific heat as a function of temperature. The relationship of structure, specific heat, and entropy will be discussed in the context of improving our understanding of changes induced by ion intercalation and deintercalation.

EN03.03.04

Printed Zinc-Ion Batteries on Hydrogel Reinforced Cellulose Composite for Paper Electronics Peihua Yang¹, Jia Li², Seok Woo Lee³ and Hong Jin Fan⁴; ¹The Institute of Technological Sciences, Wuhan University, China; ²Rolls-Royce@NTU Corporate Lab, Nanyang Technological University, Singapore; ³School of Electrical and Electronic Engineering, Nanyang Technological University, Singapore; ⁴School of Physical and Mathematical Sciences, Nanyang Technological University, Singapore

Paper electronics provides a low-cost and sustainable option for the ever growing demand of Internet of Things (IoT) devices. Batteries are considered as the heart of those energy-consuming paper electronics.[1] Rapid development of flexible electronics not only poses severe challenges to traditional manufacturing methods, but also raises further concerns on their impact on environment. [2] Deriving from abundant biomass, cellulose paper presents an ideal building block for developing flexible and sustainable electronics.[3] Paper electronics could be the raising star of next-generation functional devices, especially in the field of paper-based flexible batteries, sensors, circuits, and diagnostic equipment.[4] Imagine if these devices can be integrated on a piece of paper, it will greatly facilitate the application scenarios and enhance the commercial values. Meanwhile, the compatibility of paper to printing techniques allows facile ink printing of a wide variety of functional materials. [5] Therefore, facile and scalable fabrication of paper-based batteries is crucial to build paper electronics systems.

In our study, we propose polyacrylamide hydrogel reinforced cellulose paper (HCP) for printable zinc batteries and paper electronics. By combining the characteristics of cellulose paper and hydrogel, the composite paper presents favourable mechanical and ionic conductivity properties that are suitable to its function as the separator and electrolyte for zinc batteries. We have realized printing of quasi-solid, biodegradable aqueous Zn-Ni and Zn-Mn batteries and demonstrate its possibility of integrating with other paper electronics. In our strategy, HCP serves as the separator and electrolyte while maintaining its printability as a paper substrate, and electrodes are printed on both sides of the HCP to form flexible batteries. The hydrogel significantly improves the mechanical strength of the cellulose fibers and maintains the ion conductivity of the composite. As a result, the printed batteries are cuttable and flexible without the risk of short of contact failure. The printed zinc batteries deliver remarkable volumetric energy density of $\sim 26 \text{ mWh cm}^{-3}$ (based on total device volume), and feature of cuttability and compatibility with flexible circuits and devices.

Furthermore, The HCP holds great biodegradability as natural cellulose. Polyacrylamide and cellulose are decomposable in the presence of bacteria, fungi, and other microorganisms. When buried in natural soil (roof garden, NTU campus, Singapore), HCP became fractured after two weeks of burial. Hygroscopicity of hydrogel greatly facilitates the growth and reproduction of microorganism. HCP can be completely degraded within four weeks. In addition, the compatibility of the paper batteries with flexible circuits and devices allows the construction of a self-powered paper system that integrates printed battery with solar cells.

In conclusion, we demonstrate the possibility of printed paper batteries and integration with flexible electronics toward the new era of paper electronics. This paper batteries will be an important step to paper electronics when other electronic parts, such as solar cells, can be also printed on the same paper. With the facile synthesis and high performance, the HCP-based printed batteries hold great promise for next-generation sustainable paper electronics.

Abstract original from: [Adv. Sci. 2021, 2103894, DOI: 10.1002/advs.202103894](#)

[1] Printed Batteries: Materials, Technologies and Applications, John Wiley & Sons Ltd, 2018.

[2] Nat. Commun. 2015, 6, 7170.

[3] Adv. Mater. 2018, 30, 1703453.

[4] Adv. Mater. 2021, 33, 2000892.

[5] Adv. Mater. 2018, 30, 1801588.

EN03.03.05

Methylthiourea as Electrolyte Additive Strategy for Zn-Metal Anode Stability and Reversibility of Zn-Ion Batteries [Mahammad Rafi Shaik](#), Jihoon Kim and Sukeun Yoon; Kongju National University, Korea (the Republic of)

Zinc-ion batteries (ZIBs) are considered as a good choice in energy storage technologies due to their high safety and low environmental impact. However, various disadvantages related to Zn dendrite formation, hydrogen generation, and corrosion generated during the charge/discharge process greatly limit the commercialization of ZIBs. Among various electrode components, electrolytes are attracting attention from many researchers because they can solve problems occurring at the anode-cathode interface from a fundamental point of view. Here, we present the use of methylthiourea (MTU) as an electrolyte additive to inhibit the growth of zinc dendrites and obtain smooth Zn deposits. In the presence of MTU, Zn dendrite formation is successfully controlled, the electrochemical performance of the Zn|Zn symmetric cell is significantly improved over 1000 h at a current density of 1 mA cm^{-2} , and stripping of the deposited zinc is uniformly allowed. In addition, the Zn-ion full cell using the $\text{V}_2\text{O}_5/\text{C}$ cathode exhibits consistent capacity retention up to 450 cycles. This study demonstrates that the use of methylthiourea as an electrolyte additive to enhance the electrochemical stability and reversibility of ZIBs can be cost-effective.

EN03.03.06

Fully 3D Printed Aqueous Zinc Ion Batteries for Wearable Electronic Devices [Stefano Tagliaferri](#), Nagaraju Goli, Mauro Och, Maria S. Sokolikova and Cecilia Mattevi; Imperial College London, United Kingdom

Rechargeable Zinc Ion Batteries (ZIBs) based on aqueous electrolytes are among the most promising beyond-lithium energy storage systems, featuring large volumetric capacity, low cost and outstanding safety. The use of Earth-abundant, non-hazardous electrode materials and water-based electrolytes

makes ZIBs ideal power sources to meet the growing energy demand of wearable and portable electronics. Nonetheless, the large-scale commercialization of rechargeable zinc ion batteries is still hindered by significant technological challenges, primarily associated with the low electrochemical reversibility of such systems.

The structural re-design of the electrode architectures is an effective strategy to prolong the cycle life of ZIBs, reducing the local current density at the interface with the electrolyte and promoting a uniform and reversible zinc plating. 3D Printing is a sustainable manufacturing process that can be employed to fabricate electrodes with customized design, *via* the layer-by-layer deposition of suitable inks. The rationally-designed structure of 3D Printed electrodes provides enhanced electrochemical stability and superior specific capacity, simultaneously ensuring uninterrupted charge transport pathways and fast charge transfer inside the device.

Here, we present the fabrication of interdigitated Zinc Ion Batteries entirely *via* the 3D Printing of aqueous ink formulations, specifically tailored for the anode, cathode and gel electrolyte deposition. We electrochemically characterize the battery and we demonstrate it can power commercial wearable devices. We identify that the 3D architecture of the electrodes is crucial in increasing the reversibility of the printed battery, and investigate the degradation processes and electrochemical failure through *post-mortem* characterization.

EN03.03.07

Particle Size and Crystal Structure Engineering of λ -MnO₂ Particles as Cathodes for Zinc-Ion Batteries Zhichu Tang, Wenxiang Chen, Zhiheng Lyu, Oliver Lin, Kaijun Yin, Chen Zhang, Hong Yang, Jian-Min Zuo and Qian Chen; University of Illinois at Urbana-Champaign, United States

We use spinel λ -MnO₂ particles as a model system to study the effect of particle size and crystal structure engineering on Zn-ion diffusion and electrochemical performance in Zn-ion batteries. Through X-ray diffraction and energy-dispersive X-ray spectroscopy analysis, we demonstrate that Zn-ion insertion is enhanced in small nanoparticles (NPs) compared to large micron-sized particles due to larger surface area and solid-solution type phase transition pathway. Meanwhile, poor Zn-ion insertion/extraction reversibility leads to the poor cycling stability of NPs. To improve the cycling performance of λ -MnO₂ NPs, crystal structure engineering is employed to create defects in the spinel lattice. The crystal structure change of λ -MnO₂ is studied by a collocated four-dimensional scanning transmission electron microscopy. Results show that single-crystalline λ -MnO₂ will turn into more disordered polycrystals, which can enhance Zn-ion diffusivity. As a result, the cycling performance of λ -MnO₂ NPs is significantly improved, with a high capacity retention of over 94% after 100 cycles. Our work pinpoints the distinctive impacts of particle size and defects on the ion-diffusion process and cathode performance in Zn-ion batteries, providing guidance for the design of high-performance cathode materials for multi-valent ion batteries.

EN03.03.08

Investigation of the Electrochemistry and Functional Properties of Zn/ Manganese Oxide Rechargeable Aqueous Batteries Daren Wu¹, Lisa Housel², Nahian Sadique¹, Lei Wang², David Bock², Esther S. Takeuchi^{1,2}, Amy Marschilok^{1,2} and Kenneth J. Takeuchi^{1,2}; ¹Stony Brook University, United States; ²Brookhaven National Laboratory, United States

The consistent delivery of clean electrical energy is a global challenge where the current electric grid infrastructure distributes electrical energy from the generation source to the end user.

Widespread integration of inherently intermittent renewable energy sources such as wind and solar into the electric grid electrical energy storage into the electric grid demands incorporation of energy storage. Further, energy storage would enable control over when the electrical energy is used improving grid reliability and resiliency. Thus, stationary energy storage for the electric grid is a critical and timely application for batteries.

Aqueous batteries are desirable candidates for stationary energy storage due to low cost and scalability. In addition, many electrode materials compatible with aqueous electrolytes are earth abundant, and thus may be a cost effective alternative compared traditional lithium-ion battery materials. While batteries with aqueous electrolytes are less flammable than the non-aqueous organic electrolytes employed in lithium-ion battery technologies, they can still undergo problematic degradation processes. Thus, mechanistic understanding of promising aqueous battery chemistries is critical.

Rechargeable aqueous Zn/MnO₂ batteries have received attention for large-scale energy storage applications. Zn metal has a low redox potential (0.76 V vs. SHE) and under mild acidic conditions exhibits an overpotential for hydrogen evolution, enabling a deposition and stripping charge storage mechanism when used as a battery anode. Zn is also non-toxic and has a high theoretical capacity (820 mA/g). Thus, the Zn/MnO₂ system is a potentially high energy density, low cost, and environmentally-friendly chemistry for stationary energy storage.

Advanced characterization approaches were used to investigate the Zn/a-MnO₂ system. The dominant Faradaic mechanisms were probed including determination of the structure and oxidation states of the discharge and charge products. Specifically, operando methods were applied to probe the system and will be discussed in detail.

EN03.03.09

Sodium Vanadium Oxide (NVO) Material Properties—Impact on Electrochemistry and Functional Properties in Zn-Ion Aqueous Batteries Gurpreet Singh¹, Christopher Tang¹, Lisa Housel², Sung Joo Kim², Lei Wang², Yimei Zhu², Esther S. Takeuchi^{1,2}, Kenneth J. Takeuchi^{1,2} and Amy Marschilok^{1,2}; ¹Stony Brook University, United States; ²Brookhaven National Laboratory, United States

Implementation of intermittent renewable energy sources derived from wind and solar power provides interest in the development of safe, sustainable, low cost energy storage including batteries based on aqueous electrolytes. Zn as a negative electrode has a high theoretical capacity (820 mAh/g), low redox potential (-0.76 V vs. SHE), and low toxicity with a voltage window suitable for use with aqueous electrolytes. Vanadium based materials are appealing for aqueous electrochemical energy storage due to the multiple accessible redox states for the vanadium center. Layered vanadates are of interest for Zn-ion batteries as the vanadium redox center allows for high capacity and the layered structure promotes facile ion transfer. In particular, sodium vanadium oxides (NVO) show promise as cathode materials for Zn-ion aqueous batteries. Understanding the parameters that govern the charge storage mechanisms of the Zn/NVO aqueous systems remains of key interest where investigations that tune material properties can provide insight toward ultimately controlling electrochemical outcomes in Zn/NVO systems. Materials properties, their impact on functional electrochemistry such as capacity delivery and capacity retention were determined using methods including synchrotron based x-ray absorption analysis and will be discussed.

EN03.03.10

Ultrasmall ZnMn₂O₄ Cathodes for High-Energy and High-Power Aqueous Zinc-Ion Secondary Batteries [Hiroaki Kobayashi](#)¹, Yuto Katsuyama², Chie Ooka¹ and Itaru Honma¹; ¹Tohoku University, Japan; ²University of California, Los Angeles, United States

Current lithium-ion batteries are widely used for various energy storage devices. However, improvement of LIB performances such as high energy density, cost effective, and safety is urgently required, with increasing demand for lithium-ion batteries (LIBs) as energy storage devices. Rechargeable zinc-ion batteries, using aqueous electrolytes with mild acidity and zinc metal anodes, are promising for stationary power supply due to their environment-friendly, cost-effectiveness, and safety. For high energy density cathode materials, vanadium oxides and manganese oxides were widely developed. However, suitable cathode materials with high capacity and long cycling stability are still progressing. Spinel-type ZnMn₂O₄ is reported as highly cyclable cathode materials, though only one-electron reaction per Mn is available.^[1] Theoretically, two-electron reactions using Mn^{2+/4+} can be utilized in spinel cathode materials.^[2] Here, we apply the ultrasmall ZnMn₂O₄ spinel nanoparticle-graphene composite as cathode material to accelerate the fast Zn intercalation/deintercalation.

The ultrasmall ZnMn₂O₄ spinel was prepared by alcohol reduction process.^[3] The Rietveld analysis of the X-ray diffraction (XRD) pattern suggests the obtained nanoparticles as tetragonal spinel. X-ray absorption spectroscopy (XAS) also shows the valence state of Mn as 3+. According to the Transmission Electron Microscope (TEM) image, primary particles of 5–10 nm were strongly aggregated into micron size secondary particles. The aggregation is effectively suppressed by dispersing graphene into the reaction solution. The ZnMn₂O₄-graphene composite cathode exhibits the reversible capacity of 450 mAh g⁻¹ at 100 mA g⁻¹, a high value because of a reversible two-electron reaction, while ZnMn₂O₄ nanoparticle shows only 300 mAh g⁻¹. Downsizing particles is an effective way to enhance its specific capacity.

[1] L. Chen *et al.*, *J. Power Sources* **425**, 162 (2019).

[2] S. Okamoto *et al.*, *Adv. Sci.* **2**, 1500072 (2015).

[3] H. Kobayashi *et al.*, *RSC Adv.* **9**, 36434 (2019).

EN03.03.11

A Theoretical Investigation of Vanadium-Based Cathodes in Magnesium-Ion Battery [Mai Nguyen](#); University of Texas at Austin, United States

Lithium-ion battery (LIB) technology, first commercialized in 1991 by Sony, has been explored extensively to accomplish many achievements in energy supply throughout past decades due to its high energy density and low self-discharge. Nevertheless, there are still challenges with LIB in cost and scarcity. In addition, the effort of using metal lithium as an anode to increase capacity compared to graphite is limited by the dendrite formation during deposition of Li-ion, which results in problematic and unsafe operation. Magnesium-ion battery (MIB), an alternative to LIB, has received huge interest in the field due to magnesium's higher abundance on Earth's crust, less expensive, a provision of high capacity on the account of two electrons transfer and the negligible dendrite formation on the anode compared to lithium. Despite that, one of the main challenges to MIB technology is the poor cathode cyclability caused by sluggish kinetics of Mg-ion resulting from the high charge density at most cathodes, which can affect the rate capability of the battery. In this work, we are looking at several vanadium oxides, one of the well-known cathode materials: V₂O₅, LiV₃O₈, and V₂(PO₄)₃. These materials have been widely studied in LIB showing great performance during cycling due to its layered and stable structure which indicates a promising material for improving the cathode's cyclability and the battery's rate capability for MIB. Here, we used density function theory (DFT) to predict the theoretical voltages and energy densities of MIB using the magnesium metal anode and the studied vanadium-based cathodes to compare with LIB technology. We found that the MIB's performance resulted in lower voltage but can be compensated by higher capacities in comparison to LIB; as a result, the energy densities of the two batteries can be commensurable. Furthermore, we constructed convex hull phase diagram to predict the process of intercalating Mg-ions into the studied cathodes and then predicted the voltage profile to study the phase boundaries which can affect the kinetics of intercalating ions within these cathodes in MIB. The result found that V₂O₅ and V₂(PO₄)₃ were developing phase boundaries during intercalation of Mg-ions while the flat voltage profile of LiV₃O₈ cathode looks more desirable for the kinetics of intercalating ions. Then, we will further investigate the kinetics characteristics of these vanadium-based cathodes by predicting the ionic conductivity and electrical conductivity which contribute greatly to the rate capability.

EN03.03.12

Mn Binary Nano-Spinel Oxides Toward Mg Rechargeable Battery Cathode with Room-Temperature Operation [Reona Iimura](#), Hiroaki Kobayashi and Itaru Honma; Tohoku university, Japan

With the implementation of the decarbonization policies, the role and demand for storage batteries is significantly growing and changing. Therefore, further improvements for storage battery are required. Mg rechargeable batteries (MRBs), which use Mg metal as anode, are attracting attention as post-Li ion batteries. MRBs have been widely explored because of their high volumetric energy density, low cost and high safety. Regarding MRBs-cathode research, lots of issues such as low potential operation and low cyclability should be resolved. Recently, spinel oxide, MgM₂O₄ (M = Cr, Mn, Fe, Co), has come to draw a lot of attention as a cathode material because of its high potential operation. In particular, MgMn₂O₄ (MMO) is expected to be a high-energy cathode material as it can be used in both Mn^{2+/Mn³⁺} and Mn^{3+/Mn⁴⁺} redox reactions within the potential window of a standard electrolyte (< 3.5 V vs. Mg/Mg²⁺). Nonetheless, oxide-type cathode materials show poor rate capabilities due to the sluggish diffusion rate of Mg-ion in solid derived from the large charge density of Mg²⁺. One effective solution is to make cathode materials nanosized to reduce the diffusion distance in the solid. In our previous work, a cubic nano-spinel MMO was synthesized via alcohol reduction (AR) process and demonstrated the room-temperature operation at full-cell test. However, the observed capacity (100 mAh g⁻¹) is not close to the theoretical capacity (270 mAh g⁻¹), implying that nanosizing cathode materials is not adequate for room-temperature operation. In this study, we focused on changing the structural stability of the redox phase and conductivity using a different transition metal instead of Mg in MMO toward high capacity at room temperature.

Mn binary nano spinel oxides were synthesized by AR process. The appropriate amount of Bu₄NMnO₄ was added into the methanol dissolved with various transition metal salts and this reaction solution was vigorously stirred for an hour. After the reaction, the participants were washed with ethanol, dispersed into tert-butyl alcohol and freeze-dried. The crystalline phase and crystallite size of each spinel oxide were identified by X-ray diffraction and scanning transmission electron microscopy. The obtained sample was mixed with acetylene black and polytetrafluoroethylene at a weight ratio of 60/30/10. Then, these mixtures were pressed onto Al mesh to make a cathode. A coin-shaped full cell consisting of Mg[B(HFIP)₄]₂ / triglyme (HFIP: hexafluoroisopropyl) as electrolyte and a magnesium metal anode was prepared, and charge-discharge tests were conducted at room temperature.

All the synthesized A-Mn spinel (A = Cu, Ni, Co) by AR method showed a single phase of cubic structure from XRD measurements, suggesting that Jahn-Teller effect of Mn³⁺ is suppressed and the metastable cubic structure is obtained. In addition, TEM images revealed that all the synthesized samples have 5 nm-primary particles and electron diffraction patterns attributed to the spinel structure were obtained through Selected Area Electron Diffraction measurements. Regarding charge-discharge tests, Cu-Mn spinel showed much higher discharge capacity than MMO, implying that Mg-ion was easier to be inserted at room temperature. Furthermore, Galvanostatic Intermittent Titration Technique revealed that Cu-Mn spinel has smaller overpotential during discharge than MMO, demonstrating smaller particle resistance.

Therefore, we found that the cathode materials require not only nano-sizing but also smaller particle resistance toward room-temperature operation.

EN03.03.13

Ion-Selective and Chemical-Protective Interphase for Highly Durable Zinc Metal Anode [Sangyeop Lee](#); POSTECH, Korea (the Republic of

The development of sustainable energy sources such as wind, solar, and hydropower has been vigorously studied to overcome global energy crisis and climate change. However, they suffer from uncertainty and instability in power generation since they significantly depend on external environmental factors. As a result, additional energy storage systems are required to manage excess electricity efficiently and transfer energy timely. Rechargeable batteries that enable facile conversion and storage of energy produced, thus, have been extensively investigated as a rational solution for renewable energy sources. Among various candidates, aqueous zinc ion batteries (ZIBs) are studied as the most attractive system owing to the beneficial properties including insensitive manufacturing condition, low material cost, nonflammability, and environmental benignity. However, the practical application of ZIBs is under challenge due to dendritic growth and low electrochemical reversibility of Zn anode. Like other metals, Zn tends to form a dendritic architecture during plating/stripping processes due to inhomogeneous charge distribution. Furthermore, Zn dendrites with large surface area facilitate detrimental side reactions to induce insulating byproducts, corrosion, and hydrogen evolution reaction (HER) in mild acidic electrolytes. The detrimental side reactions incur local environmental change to accelerate dendritic growth and result in low Coulombic efficiency and subsequent capacity fading.

Several strategies reportedly enhance the electrochemical reversibility of Zn anode. In particular, introducing an artificial protective layer is an attractive method because it can be fabricated by a simple coating process and exhibits tunable electrochemical and mechanical properties according to its layer components. Additionally, an artificial protective layer can achieve homogeneous Zn^{2+} transfer through the interphase matrix and prevents direct contact between the aqueous electrolyte and the electrode surface, thereby increasing the lifespan of batteries. However, numerous artificial protective layers are designed with a thick structure to alleviate infinite volume expansion of Zn during the repetitive charge/discharge cycles, while these thick electrochemically inert layers negatively affect to the overall energy density. Also, studies on ion behavior inside the protective interphase still remain in the early stage, while it is required to develop advanced anode materials.

Herein, polystyrene-block-poly(ethylene-ran-butylene)-block-polystyrene-graft-maleic anhydride (SEBS-MA) is introduced as an artificial protective layer for the Zn anode through a simple spin-coating process. The 180 nm-thick SEBS-MA can withstand the volume change of Zn during repetitive charge-discharge processes due to its high stretchability and mechanical robustness. In the SEBS-MA layer, maleic anhydride groups attract Zn^{2+} dissolved in the electrolyte and form a cation transporting channel, leading to a smooth electrode surface without dendritic metal growth. Moreover, this SEBS-MA layer exhibits an ion-selective property, such that only Zn^{2+} can pass through the layer, whereas water molecules and SO_4^{2-} anions are highly restricted. The ion-selective layer could effectively suppresses HER and the formation of detrimental species. Consequently, based on the synergetic effects between the electrode surface stabilization and the uniform ion distribution, the SEBS-MA-coated Zn (Zn@SEBS-MA) symmetric cell demonstrates ultralong cycle life (>3,200 h) at a high current density of 3 mA cm⁻² and an areal capacity of 1 mAh cm⁻². The beneficial effect of SEBS-MA was further investigated using Zn@SEBS-MA|MnO₂ full cells and could realize durable cycle retention 80% after 2,500 cycles. This work provides a facile fabrication process and accessible analysis methods to rationalize the development of high-performance ZIBs.

EN03.03.14

Development of Zinc Ion Battery Anodes by Zinc Electrodeposition on Controllable Three-Dimensional Carbon Framework [Shinnosuke Tachibana](#)¹, Hiroaki Kobayashi¹, Yuto Katsuyama², Akira Kudo¹, Kazuyuki Iwase¹ and Itaru Honma¹; ¹Tohoku University, Japan; ²University of California, Los Angeles, United States

Lithium-ion batteries (LIBs) are widely used as energy storage devices, but their low level of safety, high cost, and unstable supply of lithium metal due to increased demand are challenging. Therefore, environmentally friendly and sustainable energy devices are required. In particular, rechargeable aqueous zinc-based batteries (ZIBs) are expected to be a new electrochemical energy storage device due to their low cost, non-toxicity, and high energy density. However, short circuits due to zinc metal dendrite formation at the anode and poor cycle characteristics due to reduced reversibility have hindered their practical application. Stable and dendrite-free cycling zinc anode with zinc electrodeposition confined in 3D carbon nanotubes network structure has been reported^[1], hence zinc electrodeposition on dense 3D carbon frameworks is an effective approach. 3D printers are gaining attention among the methods for fabricating 3D carbon frameworks^{[2],[3]}. The use of 3D printers for current collector fabrication allows for flexible form factors and scale control on the order of micrometers to centimeters. Therefore, the objective of this study was to develop a high-performance zinc anode material by zinc deposition on 3D carbon modeled by an LCD (Liquid Crystal Display) 3D printer.

3D carbon was designed using computer aided design (CAD). To avoid asymmetric structural parameters, a unit lattice with symmetric framework diameter and vacancies was used in the design. 3D polymer samples were fabricated using an LCD 3D printer (Mars3, ELEGOO) with photo-curing resin (ABS-like resin, SK hompo). The printed samples were rinsed with 2-propanol to remove the uncured resin, dried, and then pyrolyzed in a tube furnace under vacuum at 400 °C for 4 hours and then at 1000 °C for 4 hours. The 3D carbon was subjected to activation treatment (heating under CO₂ atmosphere), and the zinc electrodeposition behavior was evaluated pristine carbon and CO₂ activated carbon. For zinc electrodeposition, 3D carbon was fixed with Au mesh, and the electrolyte was 1M ZnSO₄ aqueous solution, and the current density was 1 mA cm⁻². The zinc electrodeposited 3D carbon samples were investigated by scanning electron microscopy (SEM), energy dispersive X-ray spectroscopy (EDX), X-ray diffraction (XRD), and Raman spectroscopy. To evaluate the electrochemical properties, galvanostatic charge-discharge tests were conducted using a Zn foil and Zn/3D carbon in symmetrical cell.

Pyrolysis reduced it to a quarter of its original size, and even after pyrolysis, it retained its structure at the time of modeling. From the result of SEM observation, there was almost no zinc deposition on the carbon skeleton surface of pristine 3D carbon, but plenty of zinc was deposited on the surface of the carbon skeleton after CO₂ activation treatment. The CO₂ activation treatment was found to increase the specific surface area of the 3D carbon, thereby increasing the number of zinc nucleation sites and achieving uniform zinc deposition. Zinc deposition was also observed inside the CO₂ activated carbon structure, therefore the three-dimensional zinc metal anode was fabricated. Zn/CO₂ activated carbon showed similar low overpotential and long-term cycling stability compared with zinc foil, suggested to be promising as a zinc anode material.

[1] Y Zhou, *et al. J. Mater. Chem. A*, **8**, 11719-11727 (2020).

[2] K Narita, *et al. Adv. Energy Mater.*, **11**, 2002637 (2021).

[3] Xiaolong Li, *et al. Adv. Energy Mater.*, 2000233 (2022).

EN03.03.16

High-Valence Metal-Ion-Preintercalated Vanadium Oxide as High-Capacity Aqueous Zinc-Ion Battery Cathode Material [Sanna Gull](#), Chung-Sheng Ni, Hong-Jyun Huang, Jin-Wei Kang and Han-Yi Chen; National Tsing Hua University, Taiwan

The advantages of aqueous zinc-ion batteries (AZIBs) as high-safety and low-cost energy devices show increasingly large potential in grid-scale storage/supply applications. Nevertheless, finding suitable cathode materials is quite challenging for the further development of aqueous ZIBs. In this work, we design a layered porous structure of the chemically pre-intercalated high-valence metal ions into the interlayers of V₂O₅ (HM-VOH) with a large interlayer spacing of 11.4 Å by using a scalable hydrothermal method in order to improve the electrode performance of AZIBs. As a result, HM-VOH delivers a higher capacity of c.a. 400 mA h g⁻¹ at a current density of 0.1 A g⁻¹ and exhibits an excellent capacity retention of > 80% after 300 cycles at a higher current density of 5 A g⁻¹. In addition, we investigated the Zn²⁺ storage mechanism in this HM-VOH cathode material as well as its associated electrochemical kinetics by using *Operando* synchrotron X-ray diffraction, and *operando* synchrotron X-ray absorption near-edge spectroscopy.

Furthermore, the as-synthesized cathode material can maintain an energy density of $> 280 \text{ Wh kg}^{-1}$ at a high power density of $> 70 \text{ W kg}^{-1}$ which is much higher than the pristine vanadium oxide material. Hence, we found that pre-intercalation of high-valence transition metal ion in the host material allowed rapid diffusion of Zn^{2+} , improved electrical conductivity, and excellent structural reversibility, which can be applied to other advanced battery systems.

EN03.03.17

Electrolyte Engineering for Zn-Ion Batteries—Concentration-Dependent Zn^{2+} Coordination Structure and its Implication on Zn Metal Anode Reversibility Dario Gomez Vazquez¹, Travis P. Pollard², Julian Mars³, Ji Mun Yoo¹, Hans-Georg Steinrück⁴, Sharon E. Bone⁵, Michael F. Toney³, Oleg Borodin² and Maria Lukatskaya¹; ¹ETH Zurich, Switzerland; ²DEVCOM Army Research Laboratory, United States; ³University of Colorado Boulder, United States; ⁴Universität Paderborn, Germany; ⁵SLAC National Accelerator Laboratory, United States

Aqueous secondary zinc ion batteries (ZIBs) are promising systems for grid storage because of their high energy density, low cost, and low safety concern. However, ZIBs have major limitations at their Zn metal anode because it suffers from both, side reaction of water splitting and dendrite formation which affect their coulombic efficiency (CE) and long-term stability, respectively. Recent approaches in electrolyte engineering have shown promising improvements in the cyclic reversibility of Zn metal anodes, including water-in-salt (WIS) electrolytes. While WIS electrolytes effectively increase CE of Zn metal anode through unique solvation structure and suppressed water splitting, its high salt usage, and increased electrolyte viscosity put other limitations on advanced ZIB systems. To implement beneficial effects from WIS into realistic ZIB systems, additional fundamental understanding is required of the correlation between electrolyte concentration, Zn^{2+} coordination environment, electrolyte structure, and resultant Zn plating/stripping efficiency, which has not been properly addressed in the field. Herein, we investigate the electrochemical properties of Zn plating/stripping as a function of electrolyte concentration and structure using a mixed cation $\text{Zn}^{2+}\text{-K}^+$ acetate (OAc) electrolyte: $\text{Zn}_{0.2}\text{K}_{0.8}\text{OAc}_{1.2} \text{ nH}_2\text{O}$ where “n” was varied from 1.5 to 50. Upon increase in concentration, we observed a change in the Zn^{2+} coordination environment and bulk electrolyte properties (e.g. thermal, conductivity and viscosity). We identify optimal electrolyte composition at $n=10$. In this *salt-solvate* electrolyte state we benefit from both WIS-like Zn^{2+} coordination environment and high conductivity and enable high CE $>99\%$ during Zn plating/stripping.

EN03.03.19

Biomimetic Composite Architectural Cathode Material for Ultrahigh Rate Capability and Cycling Life of Na-Ion Battery Kang Ho Shin^{1,2}, Purit Nakhavij³ and HoSeok Park¹; ¹SungKyunKwan University, United States; ²University of California, Los Angeles, United States; ³University of Warwick, United Kingdom

$\text{Na}_3\text{V}_2(\text{PO}_4)_3$ is one of the excellent cathode candidates of sodium ion batteries owing to its high theoretical specific capacity (117 mA h g^{-1}) and operating voltage ($3.4 \text{ V vs. Na/Na}^+$). However, the inferior intrinsic electronic conductivity of NVP limits facile charge transfer, resulting in poor rate capability and long-term cycle stability. In order to overcome these hurdles, studies are being conducted to improve electrical conductivity via forming a composite with a carbon material or doping/substitution of heteroatom. In this work, a composite with reduced graphene oxide (rGO) was fabricated to reduce particle size of NVP, organize a uniform 3D conductive network to minimize capacity loss, and greatly increase electrical conductivity. The composite, called 'BI-NVP', achieved excellent performance of a sodium ion battery and confirmed interfacial stability of NVP-rGO through various post-mortem analysis including HR-TEM and STEM-EELS.

EN03.03.20

Stable Zinc Anodes Enabled by a Zincophilic Polyanionic Hydrogel Layer Jin-Lin Yang and Hong Jin Fan; Nanyang Technological University, Singapore

The practical application of Zn metal anode for aqueous batteries is greatly restricted by the catastrophic dendrites growth, intricate hydrogen evolution and parasitic surface passivation. Herein, a polyanionic hydrogel film is introduced as a protective layer on Zn anode with the assistance of saline coupling agent (denote as Zn-SHn). The hydrogel framework with zincophilic $-\text{SO}_3^-$ functional group uniformizes the zinc ions flux and transport, and such hydrogel layer chemically bonded on Zn surface obviously suppresses the dendrites formation by guiding the 3D Zn accumulation. Consequently, very stable and reversible Zn stripping and plating at various currents and capacities is achieved. A full cell by pairing the Zn-SHn anode with a $\text{NaV}_3\text{O}_8 \cdot 1.5 \text{ H}_2\text{O}$ cathode shows a capacity of around 176 mAh g^{-1} with a capacity retention around 67 % over 4000 cycles at 10 A g^{-1} . The presented polyanionic hydrogel film protection strategy paves a new way for future Zn anode design and safe aqueous batteries construction.

EN03.03.21

Study of Vanadium Oxides at Different Oxygen Flows Prepared by Reactive Magnetron Sputtering and its Evaluation as Cathodes for Lithium Batteries Mackarena Briceño, Juan Fernández, Dario Zambrano, Marcos Flores and Rodrigo Espinoza; Universidad de Chile, Chile

Vanadium pentoxide has intrinsic properties which allow it to obtain electrothermal and thermochemical stability [1]. One of the manufacturing techniques that allow obtaining low thicknesses, homogeneity, and control of the microstructure, is the reactive sputtering magnetron process which also allows to generate different stoichiometries of vanadium oxides and specifically V_2O_5 [1, 2]. The formation of different vanadium oxides mainly depends on the oxygen content of the system [3]. The aim of this work is the study of the effect of oxygen on argon plasma during the process of reactive sputtering and the further influence on the electrochemical performance as electrode. The samples were prepared by DC reactive magnetron sputtering using different oxygen flows and deposited over stainless steel at room temperature. The target was metallic vanadium, while the plasma was argon (15 sccm) combined with oxygen at 1.25, 1.75, 2.25, 2.5, 3.0 and 3.25 sccm. The deposition process was monitored by optical emission spectroscopy (OES), and the samples were characterized by XRD, EDS, Raman confocal spectroscopy, XPS and AFM. In the study of plasma at a constant power of 150W, the OES spectrum exhibited the emission lines of vanadium (458 nm), oxygen (777 nm) and argon (811 nm), showing that the intensity of the V and Ar lines decrease with the increase of oxygen. XRD results demonstrated that the samples were amorphous for all the different oxygen flows. Raman analysis indicated for the sample deposited at 3 sccm, the presence of the V-O-V bonding corresponding to a crystalline structure of the rhombohedral type of V_2O_5 , by the vibrational stretching modes (143 cm^{-1}), and of the V=O bonding by the second flexion vibrational band (995 cm^{-1}). XPS established a correlation between the oxygen flow and the main V oxidation state: V^{+4} at 1.25 O-flow, $\text{V}^{+4}/\text{V}^{+3}$ at 1.75 O-flow and V^{+5} over 2.5 O-flow. A capacity of 280 mAh/g at 1C is observed in the sample with higher oxygen flow in contrast to the samples with lower oxygen flow.

References

- [1] M. Panagopoulou *et al.*, The Journal of Physical Chemistry C, **121**(1), 70–79(2016).
- [2] D. Wruck, S. Ramamurthi *et al.*, Thin Solid Films, **182**(1-2), 79–86(1989).
- [3] L.-J. Meng, R.A. Silva *et al.*, Thin Solid Films, **515**(1), 195–200(2006).

SESSION EN03.04: Multivalent I
Session Chairs: Chunsheng Wang and Yan Zeng
Tuesday Morning, November 29, 2022
Hynes, Level 3, Ballroom C

8:30 AM *EN03.04.01

Grid Storage Batteries from Earth Abundant Elements [Kyeongjae Cho](#)¹, Fantai Kong², Denyce Alvarez², Nestor Solorio², Matthew Bergschneider¹, Youhwan Jo¹, Manifa Noor¹ and Taesoon Hwang¹; ¹The University of Texas at Dallas, United States; ²Hunt Energy Enterprises, United States

Over the last 3 decades, Li ion battery (LIB) production has grown rapidly driven by the mobile device applications and rapid expansion of electric vehicles. Along with these expansions of LIB production, large scale energy storage demands are also rapidly increasing, driven by the increasing renewable energy generation by solar and wind farms. Recent projections of the global energy trends by the US National Academies require replacing the currently growing fossil fuel consumption by renewable energy sources (mainly solar and wind): 30% in 2030 and 50% in 2040. The intermittent and seasonal nature of solar/wind energy generation will require unusually large-scale energy storage capacity for long durations of 4-10 hours or longer. The global energy infrastructure is under rapid transition away from the fossil fuel economy toward renewable energy economy, and there are multiple challenges and opportunities for the current and emerging energy storage technologies. For the large-scale energy storage applications, fundamentally different electrochemistry with intrinsic safety is required based on earth-abundant elements (e.g., Na, K, Zn, Mg, Ca, Al, Fe, Mn) to avoid the competing demands of LIBs for mobile and EV battery applications

Among many emerging beyond LIB chemistries, aqueous zinc ion battery (AZIB) has recently attracted increasing research attentions due to high Zn energy density (5854 Ah l⁻¹ and 820 Ah kg⁻¹), nonflammable nature, good durability, and low cost. Due to the water stability limits, the operating voltage of AZIB is lower than LIB (1.7 V vs. 4 V), but the overall theoretical energy densities are comparable to high ends of LIBs (300 Wh/kg and 500 Wh/L). With further research and development for performance improvements, AZIBs are very promising candidate for grid scale energy storage. The AZIB can be classified based on the electrolyte pH: strongly acidic electrolyte through acid addition, strongly basic electrolyte with alkaline solution, and mild acidic electrolyte with Zn salt solution. Different electrolyte pH leads to different proton electrochemical activity that leads to different electrolyte-electrode interactions, thus fundamental battery operation and degradation mechanism. AZIB with mild acidic electrolyte is an advantageous option due to better safety, lower corrosivity, higher durability, etc. While as both proton and OH⁻ can be active at neutral pH, the fundamental chemistry tends to be more complex. In this work, combined modeling and experimental research progresses are presented to help deepen the understanding on AZIB systems.

9:00 AM *EN03.04.02

Comparisons of Li, Na, K and Mg-Ion Insertion into Layered and Spinel Intercalation Compounds [Anton Van der Ven](#); University of California, Santa Barbara, United States

The electrochemical properties of intercalation compounds commonly used as electrodes in rechargeable batteries are very sensitive to the guest ion that is shuttled between the anode and the cathode. This talk will describe the results of a systematic first-principles statistical mechanics study of guest ion insertion into the layered and spinel forms of A_xMO₂ and A_xMS₂ where A = Li, Na, K, Mg and M = Co, Ti, Ni, Fe and Mn. Differences in the ionic radii and oxidation states of guest ions can lead to important differences in phase stability and diffusion mechanisms. The insertion of large guest ions such as Na and K into layered intercalation compounds, for example, causes a variety of stacking sequence phase transformations in which guest ion coordination by anions switches from octahedral to prismatic coordination. This leads to unique cation-vacancy ordering tendencies and new mechanisms of diffusion. We find that layered Na and K intercalation compounds at intermediate filling are susceptible to Devil's staircase orderings characterized by well-ordered domains that are periodically separated by anti-phase boundaries. The anti-phase boundaries are found to play a crucial role in mediating cation diffusion. The electrochemical properties of spinel are also strongly affected by the guest cation radius and oxidation state. Diffusion over the octahedral sites of spinel is mediated by vacancy clusters, a mechanism that can lead to highly correlated hop sequences. Kinetic Monte Carlo simulations show that correlated diffusion becomes more severe for cations such as Mg with high oxidation states.

9:30 AM EN03.04.03

An Extended Mixed Conduction Governs Cation Transport in Magnesium Cathode Hosts [Aashutosh N. Mistry](#), Ian Johnson, Venkat Srinivasan and Brian Ingram; Argonne National Laboratory, United States

Magnesium batteries have been proposed to complement the existing Lithium-ion technology for the ever-growing battery market¹. While several candidate cathode materials have been identified based on theoretical Mg-ion intercalation capacity, open circuit potential, and cation self-diffusion barriers², the electrochemical response of corresponding electrodes falls short of expectations and is not fully understood³. Of various mechanisms governing the electrochemical response, transport inside active particles is a plausible limitation. In this talk, based on careful electroanalytical measurements, we show that such bulk cation transport is indeed nontrivial, and does not agree with the conventional Li-ion understanding^{4,5}. We propose an extended mixed conduction theory to explain these observations and characterize properties governing the transport behavior. We further discuss the implications of such an unusual behavior to engineering porous electrodes as well as screening new battery intercalation host materials.

References:

1. Ingram (2019) "High Energy Density Insertion Cathode Materials" in *Magnesium Batteries*, pp. 187-207
2. Canepa et al. (2017) *Chem. Rev.* 117(5) 4287, doi: 10.1021/acs.chemrev.6b00614
3. Johnson, Ingram & Cabana (2021) *ACS Energy Lett.* 6(5) 1892, doi: 10.1021/acsenerylett.1c00416
4. Amin, Ravnsbæk & Chiang (2015) *J. Electrochem. Soc.* 162(7) A1163, doi: 10.1149/2.0171507jes
5. Amin & Chiang (2016) *J. Electrochem. Soc.* 163(8) A1512, doi: 10.1149/2.0131608jes

9:45 AM EN03.04.04

Reactivity of Mg Electrolyte Species on MgV₂O₄ Cathode Surface [Heonjae Jeong](#)¹, Dan-Thien Nguyen², D.B. Buchholz³, Guennadi A. Evmenenko³, Jinghua Guo⁴, Feipeng Yang⁴, Paul Redfern¹, Jian Zhi Hu², Justin Connell¹, Venkateshkumar Prabhakaran² and Lei Cheng¹; ¹Argonne National Laboratory, United States; ²Pacific Northwest National Laboratory, United States; ³Northwestern University, United States; ⁴Lawrence Berkeley National Laboratory, United States

Understanding the interaction of electrolyte species and their reduction mechanism at electrode-electrolyte interface is essential for addressing electrolyte instability and surface passivation in multivalent batteries. In this work, reactivities of selected electrolyte species of magnesium bis(trifluoromethanesulfonimide) (Mg(TFSI)₂) in diglyme (G2) electrolyte on the surface of MgV₂O₄ cathode have been studied using a combination of first-principles calculations and experimental approaches such as soft landing of mass-selected electrolyte ions on MgV₂O₄ thin film and x-ray photoelectron spectroscopy analysis of softlanded interfaces. In this talk, we will focus on highlighting the key findings from the calculations of reactivity

and charge transfer of electrolyte species such as $\text{Mg}(\text{TFSI})^+$, $\text{Mg}(\text{TFSI})(\text{G2})^+$, and $\text{Mg}(\text{TFSI})(\text{G2})_2^+$ complexes on MgV_2O_4 (001) cathode surface. Subsequently, their decomposition pathways were investigated by studying the cleavage of C-S bond of TFSI⁻ that yields CF_3 species, and the cleavage of C-O bond of G2 that yields CH_3 or OCH_3 . Our calculations showed that $\text{Mg}(\text{TFSI})^+$ is the strongest adsorbing species on the MgV_2O_4 surface compared to other two. The decomposition reactions studied are generally much more favorable on the MgV_2O_4 surface vs. without the presence of the surface (gas phase) due to the strong stabilization effect of the surface to the decomposed fragments. The decomposition pathway of the TFSI⁻ part to form CF_3 is the most favorable reaction for all three species, followed by the G2 decomposition to form CH_3 . G2 decomposition that forms OCH_3 is endothermic for all three compounds. Our calculations are also corroborated well with the experimental results, wherein XPS analysis reveals the presence of final stable reaction products such MgF_2 , metal oxyfluoride, SO_3^{2-} and C=O due to decomposition of TFSI and G2 part of softlanded electrolyte species. This work reveals the importance of interfacial charge transfer on electrolyte stability at cathode surface. of the influence of reacted products on the formation of interfacial layers are essential for understanding the design principle of stable electrolytes and cathodes in multivalent batteries.

10:00 AM BREAK

10:30 AM *EN03.04.05

Computational Studies of Ca-Ion Materials for Next Generation Multivalent Energy Storage [Peter Zapol](#)^{1,2}, [Haesun Park](#)^{1,3}, [Robert F. Klie](#)^{4,2} and [John T. Vaughan](#)^{1,2}; ¹Argonne National Laboratory, United States; ²Joint Center for Energy Storage Research, United States; ³Chung-Ang University, Korea (the Republic of); ⁴University of Illinois at Chicago, United States

Development of multivalent energy storage with Ca^{2+} working ions shows theoretical promise of high energy density, however it faces numerous challenges. Finding high-voltage Ca cathode materials is a critical step to unleashing the full potential of high-energy-density Ca-ion batteries. First-principles calculations are used to evaluate different battery-related properties of cathode materials including thermodynamic stability, average voltage, energy density, synthesizability, ionic mobility, and electronic structure. To highlight recent advances in calcium-ion chemistry, the calculated properties are related to observed performance. Despite a significant advance in Ca-ion cathode development, the findings highlight the need for further developments.

11:00 AM EN03.04.06

Plating and Stripping Ca-Metal Batteries Using Potassium Hexafluorophosphate in Hybrid Solid Electrolyte Interphases [Paul A. Chando](#), [Jacob Shellhamer](#) and [Ian Hosein](#); Syracuse University, United States

The use of calcium (Ca) metal anodes in batteries is currently challenged by the development of a passivation layer that forms in the Solid Electrolyte Interphase (SEI). The passivation layer is formed from the degradation of the electrolyte onto the surface of the calcium and produces either calcium fluoride (CaF_2) or calcium chloride (CaCl_2). This insulating phase significantly reduces cation movement while continually forming new layers with freshly plated calcium. Reversible plating and stripping of calcium in such systems has been possible but has required either large overpotentials or operating at elevated temperatures. The use of a hybrid SEI is a strategy to mitigate the uncontrolled production of the passivation layer and reduce the overpotentials needed for the plating and stripping of calcium. Here, we report the development of a hybrid Potassium (K) /Ca SEI using symmetrical Ca // Ca cells. The calcium symmetrical cells are cycled for 200 hours at a capacity of 0.15 mAh/cm² with a current density of 0.025 mA/cm². Throughout the lifetime of cycling, the symmetrical cells were able to maintain overpotentials below 2V. Ex-situ X-Ray Diffraction (XRD) of cycling reveals plating and stripping of both calcium and potassium. Scanning Electron Microscope (SEM) cross-sectional views of the calcium electrodes outline clear distinctions between the bulk electrode and the interphase formed from cycling while Energy Dispersive X-Ray (EDX) maps confirm the elements present in the XRD analysis.

11:15 AM EN03.04.08

Improving the Charge Storage of α - MoO_3 Electrodes in Zinc-Ion Batteries via Chemical Incorporation of Dopamine-Derived Carbon [Darrell E. Omo-Lamai](#), [Nazgol Norouzi](#), [Farbod Alimohammadi](#), [Timofey Averianov](#) and [Ekaterina Pomerantseva](#); Drexel University, United States

Orthorhombic molybdenum trioxide (α - MoO_3) is widely studied as an active electrode material for electrochemical energy storage devices, owing to its layered structure, which offers interlayer sites for cation intercalation, and high Mo oxidation state, which generates potential for multiple electron transfer during reversible intercalation of electrochemically cycled cations. However, one significant impediment to the electrochemical properties of α - MoO_3 is its low electrical conductivity, which prevents rapid charge transfer during electrochemical cycling and thus limits charge storage, particularly at high rates of operation. Thus, the attractive strategy to achieve advances in α - MoO_3 electrochemistry is the incorporation of an electrically conductive species to form an intimate heterointerface between the constituting materials.

In this work, a novel MoO_3 -based electrode material containing carbon derived from chemically incorporated dopamine molecules shows an increased capacitance compared to reference α - MoO_3 electrodes in a 5M ZnCl_2 aqueous electrolyte. The material was synthesized *via* a hydrogen peroxide-initiated sol-gel reaction that entailed the oxidization of Mo powder in a dopamine hydrochloride (Dopa HCl) solution. A $(\text{Dopa})_x\text{MoO}_y$ powder precursor was isolated from the metastable gel through freeze-drying, and subsequent hydrothermal treatment (HT) of this precursor at 180°C produced the new MoO_3 material with carbonized Dopa molecules, denoted as HT- MoO_3/C . The reference α - MoO_3 electrodes (α - MoO_3 -ref) were synthesized similarly, but in the absence of Dopa HCl in the initial sol-gel reaction. The appearance of characteristic D and G bands in the Raman spectra and distinct vibrational modes in the FTIR spectra of HT- MoO_3/C confirm the presence of carbon in its structure. SEM images show a uniform nanobelt morphology with fragmentation due to interactions between interlayer Dopa and MoO_3 layers under the conditions of hydrothermal treatment. By means of four-point probe conductivity measurements, the electronic conductivity of rolled films containing 80 wt% HT- MoO_3/C , 15 wt% graphene nanoplatelets (GNPs), and 5 wt% PTFE was determined to be 5.9×10^{-1} S/cm, compared to 2.9×10^{-6} S/cm measured for α - MoO_3 -ref films containing identical ratios of (GNPs) and PTFE, thus confirming improved electron transport in the material synthesized via integration with the dopamine-derived carbon.

HT- MoO_3/C delivered a second-cycle capacitance of 141.4 F/g when cycled at 2 mV/s in a -0.25–0.70 V vs. Ag/AgCl potential window in 5M ZnCl_2 electrolyte, while α - MoO_3 -ref delivered a nearly two-fold smaller second-cycle capacitance of 76.1 F/g under the same conditions. Furthermore, HT- MoO_3/C retained greater capacitance compared to α - MoO_3 -ref at each of the increasing sweep rates when cycled from 1 mV/s to 20 mV/s. The superior performance of HT- MoO_3/C prompted a study of the electrode in an expanded potential window, based on previous reports in which α - MoO_3 showed electrochemical activity at negative potentials vs. Ag/AgCl. The HT- MoO_3/C electrode exhibited a capacitance of 347.6 F/g (178 mAh/g) on the second cycle when cycled from -0.85–1.00V vs. Ag/AgCl at 2 mV/s in 5M ZnCl_2 electrolyte. The increased charge storage of HT- MoO_3/C compared to α - MoO_3 -ref is attributable to facilitated electron transfer in HT- MoO_3/C due to the presence of a tight molybdenum trioxide/carbon heterointerface in its structure as a result of the bottom-up sol-gel approach adopted in its synthesis.

This work demonstrates a new strategy to improve the electrochemical performance of transition metal oxide electrodes for energy storage systems. Integration of oxides with carbon through wet chemistry synthesis approaches that involve carbonization of organic molecules can be used to create pathways for electron transport, leading to improved charge transfer and energy storage properties.

11:30 AM EN03.04.09

Modulation of Surface Chemistry to Overcome the Challenges in Zinc Ion Batteries Jiyun Heo and Hee-Tak Kim; Korea Advanced Institute of Science and Technology, Korea (the Republic of)

Rechargeable aqueous zinc ion batteries (ZIBs) are considered promising candidates for large-scale energy storage systems by virtue of their high safety and low cost. Nevertheless, the application of ZIB has been hesitant because of the low cyclability caused by cathode dissolution, non-uniform Zn deposition, and unwanted hydrogen evolution reaction (HER). In this presentation, we present strategies to overcome the above-mentioned problems in ZIBs via modulating surface chemistry of electrode materials.

Manganese oxide (typically MnO_2) is acknowledged as one of the most promising cathode materials in ZIB due to its high voltage and high specific capacity. However, Mn^{2+} continues to dissolve from MnO_2 , resulting in low capacity retention of MnO_2 . The problematic Mn^{2+} dissolution originates from the charge disproportionation (CD) reaction of Mn^{3+} . Electrically degenerate Mn^{3+} has labile energy states and therefore participates in the relaxation process (CD reaction) producing non-degenerate Mn^{2+} and Mn^{4+} . Several works have notably improved the capacity retention of MnO_2 by coating the surface with physical barriers to prevent Mn^{2+} dissolution. However, these approaches do not address the fundamental cause of the Mn^{2+} formation and only physically suppress the Mn^{2+} dissolution. In order to properly target the underlying cause of Mn^{2+} dissolution, we propose a dicyandiamide-induced cooperative Jahn-Teller distortion (JTD) of Mn^{4+} . Triggering the cooperative JTD of Mn^{4+} alleviates lattice distortion and impedes the CD reaction of Mn^{3+} . Thus, the cycling stability of MnO_2 is improved by more than 170% compared to pristine MnO_2 , and exhibits a 99.9% Coulombic efficiency at 1 C rate condition.

With the increasing demand on high current density and high areal capacity, several issues with negative electrode is also revealed to impinge the cycle life of ZIB. This is particularly true of uneven Zn deposition/dissolution reaction and H_2O decomposition reaction considering that these problems are aggravated under harsh operating conditions, consequently deteriorating the reversibility of Zn electrodes. Although numerous reports have challenged these issues by adopting various strategies, the positive effects have been limited to low current densities, low areal capacities, and low Zn utilizations. Here, we report a polymer of intrinsic microporosity (PIM-1) as an interface modulator and ion regulating layer, which reduces the HER and promotes a uniform Zn deposition/dissolution process. Experimental and computational methods are used to demonstrate that PIM-1 improves the reaction kinetics of Zn metal electrodes by altering the solvation structure of Zn^{2+} ions and increasing the work function of Zn surface. As a result, the PIM-1 coated Zn (PIM-Zn) electrode shows significantly improved cycling stability compared to the bare Zn electrode (1700 h and 340 h at 0.5 mA cm^{-2} , respectively). Moreover, PIM-Zn can operate for more than 200 h at 70% Zn utilization even under 10 mA cm^{-2} and 110 h at 95% Zn utilization of Zn metal electrode. The cycle life of the $\text{Zn}||\text{V}_2\text{O}_5$ full cell is also extended by more than 7 times compared to the cell using bare Zn by adopting the PIM-Zn.

Aqueous ZIB with high safety is an attractive battery system, and there is a persistent consensus that it can partake in the field of future energy storage system. However, it is true that the current technology level of ZIB is far below the level required for commercialization. We believe it is necessary to modulate the surface chemistry of the positive and negative electrode to build better ZIBs.

SESSION EN03.05: Multivalent II

Session Chairs: Howard Qingsong Tu and Anton Van der Ven

Tuesday Afternoon, November 29, 2022

Hynes, Level 3, Ballroom C

1:30 PM *EN03.05.01

Lithium- and Transition Metal-Free Fast-Charging Batteries Yan Yao; University of Houston, United States

Battery technologies available today that offer desirable energy density for transportation are based on lithium chemistry, most of which further require transition metals such as nickel and cobalt in their active materials. The availability of these critical commodity elements in the U.S. could soon be pressured due to the growth of the EV market. To enhance the energy supply chain security of the U.S., we herein propose a battery that will match lithium batteries in terms of energy and power densities without using lithium and transition metals in active materials. Our proposed battery will substitute lithium-based anodes with the energy-dense and abundant magnesium, of which metal the U.S. has a virtually unlimited reserve and has been the world's dominant producer. Transition metal-based cathodes will be replaced by organic materials obtained from oil refineries and biorefineries, of both the U.S. has the largest capacity in the world. The "magnesium-organic" batteries are thus a greener and more reliable domestically available alternative to lithium batteries. Our team's recent breakthrough in the technology has overcome the energy and especially power bottlenecks that have traditionally plagued magnesium batteries, resulting in material-level energy densities of up to 579 Wh/kg and fast charging-discharging capability at 20C. The new ARPA-E project will build on our latest discovery and advance the technology on multiple fronts, including electrode material and electrolyte optimization, cycle life extension, practical cell design, and scale-up of material production and cell fabrication. This work is supported by ARPA-E DE-AR0001548.

2:00 PM EN03.05.02

Cation Symmetry Breaking in Molten-Salt Electrolytes Enables Reversible, Long-Duration Storage in Al Batteries Regina Garcia-Mendez^{1,2}, Jingxu Zheng^{3,1}, David C. Bock^{4,5}, Cherno Jaye⁴, Daniel A. Fischer⁴, Amy Marschilok^{4,5}, Kenneth J. Takeuchi^{4,5}, Esther S. Takeuchi^{4,5} and Lynden A. Archer^{1,2,1}; ¹Cornell University, United States; ²Cornell Energy Systems Institute, United States; ³Massachusetts Institute of Technology, United States; ⁴Brookhaven National Laboratory, United States; ⁵Stony Brook University, The State University of New York, United States

Aluminum is the most earth-abundant metal, is trivalent, and offers a volumetric energy density more than twice that of lithium. It has emerged in recent years as among the most promising candidate materials for cost-effective, long-duration storage of electrical energy in batteries. Scientific discoveries in the past decade have established that rechargeable Al batteries can be created by pairing an Al metal foil with a graphitic carbon sheet in imidazolium-based ionic- AlCl_3 electrolytes. Although such cells are of increasing scientific interest, their utility remains limited by the high cost and environmental sensitivity of the ionic liquid, as well as by the surprisingly poor reversibility of Al electrodes in other electrolyte chemistries. We report that application of *Carnelley's rule* to short-chain alkylammonium chlorides enables design of new families of low-cost alkylammonium chloride- AlCl_3 molten-salt electrolytes that support highly reversible redox reactions at an Al electrode. Through straightforward manipulation of the composition of $[\text{AlCl}_4]^-$ and $[\text{Al}_2\text{Cl}_7]^-$ species in electrochemical cells, we achieve near-unity efficiency for thousands of charge/discharge cycles and conformal Al electrodeposition morphology at a planar substrate. As a first illustration of the practical relevance of our findings, Al||graphite full cell batteries are created and reported to support stable charge/discharge cycling for more than 1000 cycles. Further, the successful development of this new group of electrolytes creates a robust platform to study in detail the working mechanisms of the electrodes using advanced characterization tools. Our findings open up new opportunities for developing simple, cost-effective, room-temperature Al batteries that enable long-duration electrical energy storage.

2:15 PM EN03.05.03

Anodic Hydration $V_2O_5@C$ for Mg-Ion Battery Cathode [Jang Gun](#) and HoSeok Park; Sungkyunkwan University, Korea (the Republic of)

Magnesium-ion batteries are a promising candidate as a next-generation energy storage systems due to high working voltage, high abundance of magnesium metal, and multivalent nature of magnesium-ion. However, finding a suitable cathode material presents a major challenge: low practical capacity and low power density. Due to the strong interaction of the Mg^{2+} ions with the metal oxides commonly used in the cathode. To solve these issues, we demonstrated a novel Mg ion storage mechanism using the in-situ anodic hydration reaction of $V_2O_5@C$. Through In-situ XRD and Solid-state NMR, we observed the development of $V_2O_5@C$ as a high-power energy storage material during anodic hydration of crystal, which displayed a capacity of more than $381.0 \text{ mA h g}^{-1}$ at 0.2 A g^{-1} and $130.4 \text{ mA h g}^{-1}$ at 50.0 A g^{-1} . This work not only provides a new type of cathode material for the magnesium-ion system, but also suggests a new mechanism to prevent the loss of active cations due to irreversible reaction (i.e. formation of solid electrolyte interface (SEI) layer) that occurs in the cathode material during the first charge and discharge.

2:30 PM EN03.05.04

Advanced Investigation of the Electrolyte-Mg Anode Interphase for the Development of Mg-Ion Batteries [Martina Romio](#)¹, Yuri Surace¹, Nicolas Eshraghi¹, Benedikt Herzog², Bruno Eckmann², Damian M. Cupid¹, Johannes Hoffmann² and Marcus Jahn¹; ¹Austrian Institute of Technology, Austria; ²Federal Institute of Metrology METAS, Switzerland

Magnesium-ion batteries (MIBs) represent a promising chemistry to potentially substitute Li-ion technologies in the e-mobility and stationary energy storage applications. This is due to the favourable properties of metallic Mg, such as: abundancy, non-toxic nature, high recycling rate¹, low redox potential (-2.37 vs SHE), safety (smooth Mg^{2+} electrodeposition), as well as divalent character of Mg^{2+} cations which leads to higher theoretical volumetric capacity (3833 mAh/cm^3) than Li (2046 mAh/cm^3) and commercial graphite (760 mAh/cm^3).²

However, the major obstacle in the development of MIBs is the incompatibility of Mg anode with electrolyte formed by mixing simple Mg-based salts (e.g. $Mg(TFSI)_2$, etc.) and polar aprotic solvents (e.g. acetonitrile, etc.). These solutions decompose at the Mg surface forming an electronic and ionic insulating layer, which blocks the electrochemical activity of Mg anode. Conversely, organoborate (Mg -tetrakis(hexafluoroisopropoxy)borate in monoglyme, $MgBOR^3$) or organoaluminate ($1:2 \text{ AlCl}_3:\text{PhMgCl}$ in THF, APC)⁴ ethereal solutions are known to prevent the passivation of the Mg metal anode, allowing the reversible Mg^{2+} electrodeposition.

Despite a great effort has been done in the development of MIB,⁵ very little is known about the formation, evolution and degradation of the solid electrolyte interphase (SEI) formed at the interface between metallic Mg and electrolyte. This work, therefore, aims to investigate the interactions between Mg metal and passivating ($Mg(TFSI)_2$ in monoglyme:diglyme, $Mg(TFSI)_2$ in M:D) and non-passivating ($MgBOR$ and APC) electrolytes combining *ex-situ* and *in-situ* spectroscopic and microscopic techniques with electrochemical testing (cyclic voltammetry, galvanostatic cycling with potential and electrochemical impedance spectroscopy).

As the first step, a successful polishing method was developed to remove the native oxide layer from the surface of Mg discs allowing to expose a bare Mg metal to the electrolyte solutions. The polishing method also enabled to perform scanning microwave microscopy imaging^{6,7} of the Mg metal since a roughness between $1\text{-}2.5 \text{ }\mu\text{m}$ was achieved. This method was applied to MIB technologies for the first time in this work. The Mg discs were then immersed in the electrolyte solutions and an initial deposition of interfacial species (few nm thickness) was observed by SEM when $Mg(TFSI)_2$ in M:D was used, whereas a smooth surface was detected with $MgBOR$ and APC electrolytes. This resulted in different electrochemical behaviours. In fact, symmetric cells ($Mg|Mg$) with $MgBOR$ electrolyte showed a significantly higher cycling stability ($> 250 \text{ h}$) than those with $Mg(TFSI)_2$ in M:D solution. In addition, when the latter electrolyte was used, fluorinated by-products were identified by X-ray photoelectron spectroscopy. To study the SEI formation and growth further, *in-situ* Raman and was employed to establish a correlation between the chemical composition of the electrolyte, the voltage range of the electrochemical tests and cycling time.

References

1. I. R. P. United Nations Environment Programme, (available at <https://wedocs.unep.org/20.500.11822/8702>);
2. J. Niu, Z. Zhang, D. Aurbach, *Adv. Energy Mater.*, **2020**, *10*, 2000697;
3. Z. Zhao-Karger, M. E. Gil Bardaji, O. Fuhr, M. Fichtner, *J. Mater. Chem. A*, **2017**, *5*, 10815–10820;
4. D. Aurbach, Z. Lu, A. Schechter, Y. Gofer, H. Gizbar, R. Turgeman, Y. Cohen, M. Moshkovich, E. Levi, *Nature*, **2000**, *407*, 724;
5. R. Dominko, J. Bitenc, R. Berthelot, M. Gauthier, G. Pagot, V. Di Noto, *J. Power Sources*, **2020**, *478*, 229027;
6. A. Buchter, J. Hoffmann, A. Delvallée, E. Brinciotti, D. Hapiuk, C. Licitra, K. Louarn, A. Arnoult, G. Almuneau, F. Piquemal, M. Zeier, F. Kienberger, *Rev. Sci. Instrum.*, **2018**, *89*, 23704;
7. J. Hoffmann, M. Wollensack, M. Zeier, J. Niegemann, H. Huber, F. Kienberger, in *2012 12th IEEE International Conference on Nanotechnology (IEEE-NANO)*, pp. 1–4.

2:45 PM EN03.05.05

π -Bridge Spacer Embedded Electron Donor-Acceptor Polymer for Flexible Electrochromic Zn-Ion Batteries [Jiyoung Lee](#)¹, Tae Gwang Yun² and Il-Doo Kim¹; ¹Korea Advanced Institute of Science and Technology, Korea (the Republic of); ²Myongji University, Korea (the Republic of)

Zinc ion batteries (ZIBs) have drawn much attention as an alternative to conventional lithium ion batteries due to the high gravimetric/volumetric energy capacities (820 mAh/g , 5855 mAh/cm^3), non-explosiveness, and cost-effectiveness. However, most ZIBs are insufficient to achieve both high energy capacity and multi-functionality (e.g., mechanical flexibility and color visualization), making them undesirable for futuristic smart energy storage systems. In this work, we proposed a π -bridge spacer embedded electron donors-acceptors alternative polymers as cathode materials for multifunctional flexible-ZIBs with high electrochromic and electrochemical performances. This π -bridge spacer endows polymeric skeleton with improved physical accessibility of Zn^{2+} ions and sensitive color variation along the charging–discharging cycles, exhibiting extremely stable cyclability with high specific capacity (95 mAh/g) at very fast rates (8 A/g) and large coloration contrast (40%) under severe mechanical deformation and long-period of time ($\sim 14 \text{ days}$). These results are markedly outstanding than the topological analogue without π -bridge spacer (70 mAh/g at current density of 8 A/g and coloration contrast of 30%) and previously reported other ZIBs. Our strategy to incorporate π -bridge spacer into a polymer network realizes significant electrochromism and electrochemical performance in ZIBs, which paves the way for the future development of smart and stable flexible/wearable electronics.

3:00 PM BREAK

3:30 PM EN03.05.07

Dendrite-Free Zn-Ion Energy Storage Using Hybrid Electrolyte and 3D Printed Electrodes [Nagaraju Goli](#), [Stefano Tagliaferri](#), Apostolos Panagiotopoulos, Mauro Och, Rachael Q. Baxendale and Cecilia Mattevi; Imperial College London, United Kingdom

The rapid growth of miniaturized and customized electronics has initiated constant drive towards efficient energy storage systems, featuring high safety, cost-effective fabrication, and innovative design. Among the various energy storage devices, eco-benign zinc (Zn)-ion capacitors with natural abundance, intrinsic safety, high electrochemical performance, and great compatibility, has nowadays been widely conceded as the most promising power supply for

various portable electronic devices. Nevertheless, the formation of Zn dendrites and unsatisfactory cycling lifetime ascribed by the localized electric field/undesired side reactions on Zn led to an internal short-circuit and diminished electrochemical performance. Various methods have been designed to inhibit the Zn dendrite formation, which include surface modification and electrolyte optimization. Additionally, compared to the planar/thin film cathodes, design of three-dimensional (3D) electrodes with large surface area could be a promising approach to increase energy density of the Zn-ion capacitor. Recently, Direct Ink Writing (DIW) based 3D printing technology is emerging as a novel platform for the scalable development of 3D architected electrodes for high-performance energy storage devices. The 3D printed porous electrodes holds several advantages, including large surface area and can be printable in customized shapes within small footprint areas. Herein, we designed DIW-based 3D printed graphene-carbon nanotubes (Gr-C) electrodes as cathode and hybrid electrolyte for high-energy density and dendrite-free Zn-ion capacitors. The hybrid electrolyte provides two key beneficial features on the anode and cathode, which are: a dynamic electrostatic shield layer and a pH regulating effect which reduces the irreversible side reactions and dendrites. In addition, the high surface area and the good electrical conductivity of the 3D printed 6L Gr-C cathode enable a dual-ion electrochemical mechanism with the hybrid electrolyte, which leads to a maximum capacity of 0.84 mAh cm⁻² and energy density of 0.87 mWh cm⁻² with good cycling stability. The rate performance of the 3D Gr-C//Zn cells are also evaluated using advanced electrochemical methods. This work demonstrates a pathway towards the cost-effective development of efficient electrolytes and highly conductive 3D electrodes for sustainable energy storage devices.

3:45 PM EN03.05.08

Do Solvent Exchange Rate Drives Electrochemical Performance of Multivalent Ions? Ying Chen, Karl T. Mueller and [Vijayakumar Murugesan](#); Pacific Northwest National Laboratory, United States

Solvation structures of metal ions have been considered as one of the key components that influence battery performances. Our work here reports that the solvation dynamics, i.e., how fast the solvents and anions exchange between the free and coordinating states, matters more in multivalent electrolytes due to the stronger interaction between the multivalent cations and the solvents/anions compared to monovalent cations. Based on our previous work on magnesium bis(trifluoromethanesulfonyl)imide (MgTFSI₂) in 1,2-dimethoxyethane (DME), where Mg²⁺ ions form stable fully solvated clusters [Mg(DME)₃]²⁺ at ≥ 0.1 M, we prepare a variety of mixed-solvent electrolytes by maintaining a Mg : DME molar ratio of 1:3 while varying cosolvents ranging from tetrahydrofuran (THF), 2-methyltetrahydrofuran (MeTHF), bis(2,2,2-trifluoroethyl) ether (BTFE), propylene carbonate (PC) to acetonitrile (ACN), trimethylsilyl imidazole (TMSI) and 2-Methoxyethylamine (MEA). Multinuclear (¹H, ¹³C, ¹⁹F, and ¹⁷O) NMR studies of these MgTFSI₂-3DME-cosolvents reveal a wide range of solvation structures with a fraction of DME, cosolvent or TFSI⁻ forms stable first solvation sheath with Mg²⁺. The residence time of coordinating DME or cosolvent can be estimated from ¹H-¹H 2D EXSY NMR, and the coordination power of the cosolvents can be evaluated accordingly and correlated to the physicochemical properties of the cosolvents (coordination asymmetry, donor number, relative permittivity, viscosity, electrostriction, etc.). Furthermore, cyclic voltammograms of these cosolvent electrolytes demonstrate that a shorter-lived solvation shell with faster exchange between coordinating and free solvent/anions can facilitate cation transport, reduce desolvation energy and promote fast charge transfer at the interface, and therefore leads to better reversible magnesium plating and stripping.

4:00 PM EN03.05.09

Conducting Polymer and Zinc-Ion Co-Intercalated Vanadium Oxide Nanofibers for High-Performance Stretchable Zinc-Ion Micro-Battery Jeonguk Hwang, Se Hun Lee, Suheol Kim and [Heejoon Ahn](#); Hanyang University, Korea (the Republic of)

The form of next-generation digital electronic devices has been changed to a wearable design that can be worn or attached to the human body to provide super-connection between people and devices using wireless systems. The wearable electronic device is designed in a stretchable form without shape restriction to secure functionality and wearability. In addition, it is necessary to develop a stretchable battery that can be integrated into a stretchable electronic device to drive a wearable electronic device. Lithium-ion batteries, which are currently the most commonly used batteries, are not suitable as stretchable batteries for wearable electronics due to their flammability and toxicity, which may pose a potential risk to human health. Furthermore, since lithium-ion batteries are manufactured under inert conditions, it is difficult to apply manufacturing processes for stretchable batteries. Recently, aqueous zinc-ion batteries, which have excellent capacity, low price, high safety, and are harmless to the human body, have attracted attention as energy supply devices for wearable electronics. In addition, the aqueous zinc-ion battery has the advantage of being manufactured under ambient conditions where various methods are easily applied, unlike a non-aqueous lithium-ion battery. A wavy-structure strategy has been known as one of the methods for imparting elasticity to objects, and in this strategy, the flexibility of the battery component is inevitably required. However, metal oxides, generally used as the active material for battery electrodes, lack elasticity and flexibility and break easily. As a result, it is difficult to maintain the intrinsic electrochemical performance of the device under repeated deformation. In this study, we developed a stretchable zinc-ion micro-battery with excellent mechanical properties and battery performance. Various strategies such as synthesis of cathode material with improved elasticity and flexibility, pre-zincification, wavy structural design, and assembly technique were applied together to achieve excellent electrochemical performance and mechanical properties of the stretchable zinc-ion micro-battery. Vanadium oxide nanofiber, which is co-intercalated with Zn²⁺ ions and poly 3,4-ethylene dioxythiophene (PEDOT), was synthesized as an active material of the cathode using a facile sonochemical method. The vanadium oxide nanofiber co-intercalated with Zn²⁺ ions and PEDOT showed improved mechanical properties, electrical conductivity, and specific capacity than the vanadium oxide intercalated with only Zn²⁺ ions. In addition, the pre-zincification of the cathode extended the cyclic stability of the stretchable zinc-ion micro-battery. As a result, the stretchable zinc-ion micro-battery exhibited a high areal capacity of 0.15 mAh cm⁻² and maximum energy density of 0.12 mWh cm⁻² at a power density of 0.12 mW cm⁻² and retained 83% of initial capacity over 500 cycles. In addition, the excellent mechanical performance of the stretchable zinc-ion micro-battery was demonstrated while maintaining a capacity of 78.9% during 7000 simultaneous stretching and bending tests. The strategy proposed in this study for fabricating stretchable zinc-ion batteries is expected to contribute to the development of wearable energy storage devices.

4:15 PM EN03.05.10

Correlating Solvation Structure and Interphase Chemistry in Emerging Multivalent Battery Electrolytes [Scott A. McClary](#), Alan Landers, Kathryn A. Small, Paul G. Kotula, Nathan Hahn and Kevin R. Zavadil; Sandia National Laboratories, United States

Multivalent (MV) metals such as Mg and Ca are promising beyond-Li-ion anode materials due to their high gravimetric and volumetric capacities, high abundance in Earth's crust, minimized dendrite formation, and low reduction potentials [1,2]. However, implementing MV metal anodes is challenging because electrolyte constituents spontaneously decompose when in contact with the metal surface, leading to products that are typically ionically insulating. To achieve high-efficiency cycling with a metal anode, a robust solid-electrolyte interphase (SEI) that simultaneously permits sufficient cation transport and blocks electron transport is required. Studying MV SEIs is challenging due to reactivity of metallic anodes with trace contaminants, and little is known about relationships between electrolyte speciation, SEI composition and structure, and electrochemical performance in exemplar electrolytes [3,4]. Our group recently used cryogenic focused ion beam (FIB) and transmission electron microscopy (TEM) to demonstrate that a nanocrystalline CaO layer containing minority calcium borate and carbonate species is an effective SEI for Ca anodes [5]. Supplemental density functional theory (DFT) calculations showed that the unique interfacial solvation structure is key in forming the heterogeneous SEI.

In this contribution, we employ a suite of multimodal characterization techniques to establish correlations between cation solvation structure, SEI chemistry and structure, and electrochemical performance in exemplar Ca and Mg electrolytes. We first quantify Ca²⁺ and Mg²⁺ solvation in ether-based electrolytes

using Raman, nuclear magnetic resonance, and dielectric relaxation spectroscopies in tandem with complementary DFT calculations. We demonstrate control over bulk and interfacial electrolyte speciation via co-salt addition to $\text{Ca}(\text{BH}_4)_2$ and $\text{Mg}(\text{Bhfp})_2$ electrolytes. We then characterize the chemistry and microstructure of electrodeposited Ca and Mg using analytical electron microscopy, X-ray photoelectron spectroscopy, and time-of-flight secondary ion mass spectrometry. We finally conduct chemical and structural mapping of cation-transmissive SEIs using cryo-FIB and TEM, revealing that heterogeneous films are key in enabling MV cation transport. In all cases, we correlate changes in liquid electrolyte speciation and SEI chemistry with improvements in electrochemical performance. Our results provide critical knowledge that will inform design of practical electrolytes and SEIs for rechargeable MV batteries.

This work was supported by the Joint Center for Energy Storage Research, an Energy Innovation Hub funded by the U.S. Department of Energy (DOE) and was performed, in part, at the Center for Integrated Nanotechnologies (CINT), an Office of Science User Facility operated for the U.S. DOE Office of Science. Sandia National Laboratories is a multimission laboratory managed and operated by National Technology & Engineering Solutions of Sandia, LLC, a wholly owned subsidiary of Honeywell International, Inc., for the U.S. DOE's National Nuclear Security Administration under contract DE-NA-0003525. The views expressed in the article do not necessarily represent the views of the U.S. DOE or the United States Government.

References:

- [1] X. Zhang et al. *Advanced Functional Materials* **2020**, 30(45), 2004187.
- [2] Y. Liang et al. *Nature Energy* **2020**, 5(9), 646-656.
- [3] J. Forero-Saboya et al. *Adv. Mat. Interfaces* **2021**, 9(8), 2101578
- [4] N. Leon et al. *Frontiers in Energy Research* **2022**, 9, 802398.
- [5] S. A. McClary et al. *ACS Energy Letters* **2022**, under revision.

SESSION EN03.06: Poster Session II: Li Metal and Silicon Anode
Session Chairs: Shyue Ping Ong and Yan Eric Wang
Tuesday Afternoon, November 29, 2022
8:00 PM - 10:00 PM
Hynes, Level 1, Hall A

EN03.06.01

Spatially Controlled Li Electrodeposition on 3-D Patterned Cu Current Collectors Through Nanometer-Scaled Surface Roughness in Li-Metal Batteries Taegyu Jang, Jin-Hyuk Kang, Sujung Kim, Minyoung Shim and Hye Ryung Byon; KAIST, Korea (the Republic of)

Ever-growing demands for electric vehicles and unmanned aerial vehicle systems require higher energy density of energy storage. The metallic lithium (Li) has been considered a promising negative electrode in lithium-ion batteries, owing to its high specific capacity (3860 mAh/g) and a negative electrochemical reduction potential (-3.04 V vs. SHE). Recently, the Li-free copper (Cu) current collectors have also been developed, called anode-free Li batteries, to improve gravimetric energy density further. However, the dendritic growth of Li during the plating process has caused an electric short-circuit and risk of catching fire for both batteries. Various strategies have been suggested to mitigate this detrimental Li deposition. One of the ideas is to utilize three-dimensional (3-D) current collectors, comprised of alternate receding and protruding parts, to induce selective Li deposition into the receding space. However, many studies showed the preferential Li deposition on the protruding area or edges, which rather promoted vertical Li growth and the electric short-circuit.

Here we show that the nanometer-scale surface roughness of the Cu current collector aided the Li plating at the receding space, which improved cell performance. We designed a 3-D Cu pattern through photolithography, followed by chemical etching using 3.5 mol/kg ammonium persulfate solution. The resulting Cu foil had square patterns of the receding and protruding parts, where the former had $\sim 10 \mu\text{m}$ of offset from the latter surface. They also had a similar Cu oxidation state and surface crystallinity to the pristine Cu foil. However, due to the chemical etching process, the receding area had a rougher surface than the protruding one, measured to be $< 10 \text{ nm}$ of surface roughness. This nanometer-scale roughness in the 3-D Cu foil contributed to two-fold higher capacitance than the flat and pristine Cu foil. In addition, the surface roughness determined the exchange current-density. COMSOL simulation for the 3-D patterned Cu predicted superior local current density at the receding area compared to the protruding part where the enhanced electric field was typically expected. Experimentally, we also observed the selective Li deposition at the receding space thanks to the high surface roughness, better wettability, and high surface energy. COMSOL simulations also indicated that the surface roughness should be dependent on the depth of the receding area if we intended to more intense local current density in this space. Namely, deeper receding areas need more significant roughness. We demonstrated improved Li|Cu cell performances using the resulting 3-D Cu current collectors. This concept guides the design of selective Li deposition in the Li metal and anode-free Li batteries.

EN03.06.02

Dual-Type Gel Polymer Electrolyte for High-Voltage Lithium Metal Battery with Excellent Cycle Life A-Hyeon Ban¹, Su-Jin Pyo¹, Jin-Ah Roh¹, Woo Jin Bae², Hyun-Sik Woo², Jongseok Moon² and Dong-Won Kim¹; ¹Hanyang University, Korea (the Republic of); ²Samsung SDI R&D center, Korea (the Republic of)

Rechargeable lithium metal batteries (LMBs) using lithium metal as an anode are attractive candidates for high energy density power sources in portable electronics and electric vehicles, because the lithium metal offers the highest specific capacity. However, the development of rechargeable lithium metal batteries has been hindered by the high reactivity of lithium metal toward liquid electrolytes and the occurrence of dendrite growth during charge and discharge cycles. Herein, we report a dual-type gel polymer electrolyte composed of anolyte and catholyte, which improves the cycling stability of LMBs. Anolyte is a poly(ethylene oxide) (PEO)-based hybrid electrolyte that can prevent direct contact between lithium metal anode and liquid electrolyte as well as suppress lithium dendrite growth. As a catholyte, the cross-linked gel polymer electrolyte with high ionic conductivity and oxidative stability was used. The Li/LiCoO₂ cell was assembled with dual-type gel polymer electrolyte, and its cycling performance was investigated in the voltage range of 3.0 - 4.48 V at 0.5 C rate. The cell exhibited excellent cycle life with a capacity retention of 87% after 500 cycles, suggesting that dual-type gel polymer electrolyte is promising electrolyte for high-voltage lithium metal batteries.

EN03.06.03

Gel Polymer Electrolyte Based on Localized High-Concentration Electrolyte for Enhancing Cycle Life of Lithium Metal Batteries Ji-Wan Kim¹, Myung-Keun Oh¹, Yeon-A Kim¹, Eun-Ji Kwon², Samuel Seo², Won-Keun Kim², Kyoung-Han Ryu² and Dong-Won Kim¹; ¹Hanyang University, Korea (the Republic of); ²Hyundai Motor Company, Korea (the Republic of)

Lithium metal with high theoretical capacity and low redox potential is one of the promising anode materials for high energy density batteries. However, use of Li metal in conventional liquid electrolyte generates unstable solid electrolyte interphase (SEI) layer on Li metal due to the deleterious reactions between liquid electrolyte and Li metal, which degrades the cycling performance of the battery. To improve the cycling stability, the Li⁺ ion-conductive and stable SEI layer should be formed on Li metal. Recently, high-concentration electrolyte (HCE) or localized high-concentration electrolyte (LHCE) have been studied to form the stable SEI on Li metal, because increasing coordination between Li⁺ and anion is advantageous for forming stable SEI layer. In our study, we synthesized LHCE-based gel polymer electrolyte for forming stable SEI layer and enhancing cycling stability. Dimethoxyethane (DME)-based LHCE containing small amount of cross-linking agent and lithium nitrate (LiNO₃) was used to prepare the cross-linked gel polymer electrolyte. The acrylate groups in cross-linking agent changed the solvation structure of lithium nitrate in LHCE, and increased Li⁺ and nitrate anion coordination, resulting in formation of the inorganic-rich SEI layer composed of Li₃N and Li₂O. The electrochemical characterization of gel polymer electrolyte was performed by linear sweep voltammetry and DC polarization. Spectroscopic analyses such as FTIR, Raman, NMR and XPS were used to investigate solvation structure and SEI layer composition. The Li/NCM cells were assembled with LHCE-based gel polymer electrolyte, and their cycling performance was investigated.

EN03.06.05

Nitrate Additive-Chelate Block Copolymer Micelles Enable Stable Lithium Metal Batteries in Universal Carbonate Electrolytes Sungjin Cho; Postech, Korea (the Republic of)

The inherent instability of lithium (Li) metal anodes against conventional carbonate-based electrolytes (denoted as carbonates) preclude practical Li-metal batteries (LMBs) delivering high-energy and high-power densities. Herein, we propose an innovative strategy based on a thin micelle layer conjunct with Li nitrate (LiNO₃) to enable Li-metal anodes in carbonates without additives. Ionized LiNO₃ is linked with polystyrene-block-poly(2-vinyl pyridine) (S2VP) block copolymer micelles via electrostatic interaction, and planted directly on a Li-metal surface. The rational union between S2VP and LiNO₃ acts effectively to control the deposited Li morphology and to construct a unique solid electrolyte interface layer having a Li-ion conductivity gradient. The use of S2VP/LiNO₃-electrodes enables average high-efficiency (92.6 %) of Li plating/stripping after 100 cycles even at high-temperature. Moreover, S2VP/LiNO₃-Li//LiNi_{0.8}Co_{0.1}Mn_{0.1}O₂ full cells achieve long-stable cycling and high-energy-density (~300 Wh kg⁻¹) under limited-excess Li, high capacity, high current density, and lean carbonates without any additives.

EN03.06.06

“Salt-in-Fiber” Electrolyte Enables High-Voltage Solid-State Supercapacitors Nageh K. Allam¹, Loujain G. Ghanem¹ and Basamat Saif^{2,1}; ¹American University in Cairo, Egypt; ²University of California Santa Barbara, United States

The design of functional solid electrolytes is crucial to developing flexible non-sealing supercapacitors for lightweight, wearable, and portable electronics. Herein, an innovative method was used to fabricate LiCl electrospun electrolyte. A solid-state supercapacitor was assembled using LiCl-containing nanofibers as both an electrolyte and separator, and commercial activated carbon as the positive and negative electrodes, respectively. The morphology and chemical composition of the novel electrolyte was revealed using scanning electron microscopy, energy-dispersive X-ray, Fourier transform infrared, and Brunauer–Emmett–Teller analyses. The electrochemical properties of the solid-state supercapacitor were characterized by cyclic voltammetry, galvanostatic charge-discharge, and electrochemical impedance spectroscopy techniques. Additionally, the performance of the supercapacitor device with the nanofiber electrolyte was compared with that of the aqueous electrolyte-based and hydrogel-based devices. The supercapacitor with the LiCl nanofiber electrolyte exhibited an extended potential window of 2.3 V compared to 1.8 V for the aqueous-based device and 2 V for the hydrogel-based device. Consequently, the specific capacitance and energy density were increased by 9.6 and 44.6%, respectively, when both devices are measured at 1 A/g.

EN03.06.07

Three-Dimensional Si/C Composite Thin Films with Helium-Induced Nanostructures for Use as Anode Materials for Next-Generation LIBs Atsushi Hiramatsu, Kenzo Ibano, Heun T. Lee and Yoshio Ueda; Osaka University, Japan

Lithium-ion batteries are widely used as power sources for portable electronic devices such as PCs and smartphones because of their high voltage and high energy density. Recently, they have also begun to be used in electric vehicles (EVs) and as back-up power sources in times of disaster. In particular, EVs, which have been attracting attention in recent years, require high-output, high-capacity batteries, and there is a need to further increase the capacity of lithium-ion batteries. Silicon (Si) anode (Li₁₅Si₄ chemical composition, capacity density: 4200 mAh/g) is attracting attention as an anode material expected to have higher capacity, replacing graphite (LiC₆ chemical composition, capacity density: 370 mAh/g), which has been used in the past. However, it has been reported that Si anode undergoes large volume changes due to insertion and desorption of Li during charging and discharging, and that the cycle life is shortened due to pulverization [1]. In addition, mechanical crushing of the Si anode during the alloying/de-alloying process during charging/discharging may cause rapid and irreversible capacity reduction and low Coulomb efficiency. One of the methods to solve these problems is the nanosizing of active material particles. Nanoparticles can adapt to large stresses without cracking and shorten the transport distance of electrons and ions. Previous studies have shown that for particle sizes <150 nm, the strain energy stored by electrochemical reactions is insufficient to cause crack propagation in silicon nanoparticles [2]. Another approach to solve the problem of volume change during charging and discharging is the use of composite materials. Since matrix materials do not undergo significant volume changes, they may reduce silicon agglomeration or electrochemical sintering, thereby reducing silicon expansion, maintaining electrode structure, and improving stability. One approach is silicon-carbon composites, the benefits of which include improved electrical conductivity and the buffering effect of the carbon matrix. In addition, carbon additives have the added advantages of excellent ionic conductivity and lithium storage capacity. Based on the above background, in this study, copper was deposited on stainless steel by pulsed laser deposition, and then nano-order Si thin films were fabricated on the copper films by sputtering. The Si nanostructure was then irradiated with helium plasma, and carbon was sputtered onto the surface to create a three-dimensional Si/C thin film. The evaluation of crystal structure properties and the effect on electrochemical performance are reported for these thin films.

[1] K. Rhodes, N. Dudney, E. Lara-Curzio and C. Daniel, “Understanding the degradation of silicon electrodes for lithium-ion batteries using acoustic emission”, *Journal of The Electrochemical Society*, Vol.157, No.12, pp.A1354-A1360

[2] Liu XH, Zhong L, Huang S, Mao SX, Zhu T, Huang JY. 2012. Size-Dependent Fracture of Silicon Nanoparticles During Lithiation. *ACS Nano*.6(2):1522-1531

EN03.06.08

Improving the Initial Coulombic Efficiency and Cycle Stability of Prelithiated SiO Anode Materials by Topological Optimization Ji Young Kim, Dong Jae Chung, Donghan Youn, Won Joon Jeong, Donghyeok Ma, Tae Rim Lee, Seung Tae Kim and Hansu Kim; Hanyang University, Korea (the Republic of)

Silicon monoxide (SiO) is one of the promising anode materials for lithium-ion batteries. However, some chronic problems remain hindering the commercialization of the SiO such as the low initial Coulombic efficiency (ICE) and the poor cyclability. Many efforts were proceeded to solve these problems by prelithiation or coating the surface. In this work, we demonstrated that the ICE and cycle stability of prelithiated SiO can be improved simultaneously by topological optimization of the prelithiated SiO. We identified phase transformation, microstructural evolution and four exothermic reactions during prelithiation of SiO with LiH through X-ray diffraction, NMR, Raman spectroscopy and TG-DSC. We visualized the microstructure of the prelithiated SiO by laser-assisted atom probe tomography and scanning transmission electron microscopy. The prelithiated SiO, heated at 650°C, exhibits a capacity of 1164 mAh g⁻¹ with an ICE of ≈90% and shows remarkable capacity retention of 73.4% after 300 cycles compared to non-optimized homologs. The outstanding electrochemical performances were attributed to the modulated topological arrangement of active Si phase and Li₂SiO₃ inactive buffer phase. Further description of the reaction mechanism will be discussed in the presentation.

EN03.06.10

High Performance Biphasic SiO_x Nanocomposite Anode Material for Lithium Ion Batteries Seungeun Kim¹, Eunjun Park¹, Yeong Eun Kim¹, Juhye Song¹, Da Young Ko¹, Min-Sik Park² and Hansu Kim¹; ¹Hanyang University, Korea (the Republic of); ²Kyung Hee University, Korea (the Republic of)

Silicon oxides(SiO_x) have gained attention as potential candidate of high capacity anode materials for lithium-ion batteries(LIBs) due to their enhanced cycle performance compared to other Si-based materials. However, these materials are insufficient for commercial use owing to poor electrochemical properties and reliability. We propose a biphasic SiO_x composite with a core-shell structure composed of a silicon monoxide(SiO) as core material and Si nanocrystals embedded in SiO_x(Si/SiO_x) as shell material to improve electrochemical performance. Since the Si/SiO_x shell accommodates the volume expansion of the SiO core material during cycling, the long-term cycle performance is improved for up to 350 cycles. More detailed electrochemical properties of biphasic SiO_x composite will be discussed further in the presentation.

EN03.06.14

Analysis of Doped Silicon Anodes in Lithium-Ion Batteries Alexander Suen, Colin Chu, Aaron Hsi, Shyam Annamalai and Neelima Sangeneni; Aspiring Scholars Directed Research Program, United States

Although graphite-based anodes in lithium-ion batteries have been widely accepted as the primary anode material in rechargeable batteries for several decades, we have reached the limit for further exploration, and finding alternative materials is necessary as sustainable battery solutions increase in demand. The abundance and low cost of silicon present silicon anodes as an energy-dense, sustainable alternative to graphite anodes in lithium-ion batteries with a higher reported theoretical capacity of 4200 mAh/g. However, challenges such as significant volume expansion, rapid pulverization, relatively poor conductivity, and unstable SEI layers formed with the use of silicon anodes hinder practical applications. Micro silicon and nano silicon particles under 150 nm in size show promise regarding the challenges while still utilizing the unique energy characteristics of silicon. Due to a larger surface area with smaller particle sizes, this allows for greater charge intercalation with the anode material and the electrolyte without causing significant volume expansion. In order to test micro silicon and nano silicon, we combined them with Nafion and activated Carbon, and sonicated them into inks before depositing them onto our nickel foam electrode. We also created samples with varying amounts of nano silicon with graphite and tested those as well. Then, we analyzed the current against varying voltages using cyclic voltammetry (CV), which was then used to computationally identify the theoretical capacity of the different micro and nano-silicon. Through our computational analysis, we found the theoretical values of our micro silicon and nano silicon anodes. For nano silicon doped with 20% graphite, the areal capacity turned out to be 245 mAh/cm² while the 30% graphite had an areal capacity of 125 mAh/cm². Comparatively, pure nano silicon had an areal capacity of 181 mAh/cm². Nano silicon doped with 10% graphite is still being analyzed and run through CV to determine the areal capacity. We have also analyzed the voltage of our inks over time using an experiment known as galvanostatic charge-discharge (GCD) on our non-doped silicon inks. This will allow us to measure the longevity of our batteries to ensure sustainability and repeatability. In the future, we will continue testing different ratios of micro silicon and nano silicon with new doping materials to find the true optimum combination, wrap up the remaining CV and GCD's to complete the results, and begin testing our materials in coin cell batteries to confirm real-world applications.

EN03.06.15

Borohydrides for Use as Solid-State Electrolytes in Battery Applications Tabbatha A. Dobbins; Rowan Univ, United States

This abstract is based on a review article written to describe the status of borohydrides for use as solid-state electrolytes. In it, crucial breakthroughs are highlighted in solid-state ionic conduction in borohydrides for battery applications. Borohydrides, M^{z+}B_xH_y, form in various molecular structures, for example, nido-M^{z+}BH₄; closo-M^{z+}B₁₀H₁₀; closo-M^{z+}B₁₂H₁₂; and planar-M^{z+}B₆H₆ with M = cations such as Li⁺, K⁺, Na⁺, Ca²⁺, and Mg²⁺, which can participate in ionic conduction. Key parameters which optimize these materials as solid state electrolytes, such as ionic conduction, electrochemical window, high energy density, and resistance to dendrite formation, are discussed. The full phase space of boron-hydrogen chemistry is described. The open structures (for closo-boranes) leads to rapid ionic conduction. The ability to undergo phase transition between low conductivity and high conductivity phases is also described. The remaining challenge of low electrochemical stability of borohydrides is described- with suggestions to mitigate this issue. This poster provides an overview of the current status of borohydrides for solid state electrolyte applications. It additionally recommends approaches which could further expand computational and experimental research efforts.[1]

References:

[1] Dobbins, T.A., Overview of the Structure-Dynamics-Function Relationships in Borohydrides for Use as Solid-State Electrolytes in Battery Applications. *Molecules* 2021, 26,3239. <https://doi.org/10.3390/molecules26113239>

SESSION EN03.07: Na- and K-Ion I
Session Chairs: Raphaële Clément and Yan Eric Wang
Wednesday Morning, November 30, 2022
Hynes, Level 3, Ballroom C

8:45 AM *EN03.07.01

Layered Oxides for High-Power and Durable Na Battery Applications Naoaki Yabuuchi; Yokohama National University, Japan

The urge for the worldwide development of renewable energy production has shed light on the crucial role played by energy storage devices. Among them, Li-ion batteries certainly improved our lives with their high energy density which led them to be widely used in consumer electronics, hybrid and electric

vehicles, and renewable energy storage in grids. However, to guarantee the earth environment sustainability through this worldwide energetic transition, the technological answer should be based on abundant materials. In this context, Na-ion battery arises as the ideal solution, and layered oxides are potentially used for positive/negative electrode materials. Although reversible capacity of Ti-based oxides is small compared with hard carbon, quick charge is possible for Ti-based materials without the sacrifice of safety issues related to Na plating. Moreover, excellent cyclability is achieved as electrode materials.[1-3] In addition, large reversible capacity, which is competitive to layered materials used for Li-ion batteries, is obtained for Mn-based layered oxides.[4] Long-term electrode reversibility is effectively improved by avoiding Jahn-Teller distortion on electrochemical cycling. From these results, we discuss the possibility to design practical and durable sodium ion batteries with high power density.

References

- [1] Y. Tsuchiya *et al.* and N. Yabuuchi, *Chemistry of Materials*, **28**, 7066 (2016).
- [2] R. Umezawa *et al.* and N. Yabuuchi, *Chemical Communications*, **57**, 2756 (2021).
- [3] Benoît D.L. Campéon *et al.* and N. Yabuuchi, *submitted*
- [4] T. Sato *et al.* and N. Yabuuchi, *Energy Material Advances*, **2021**, 9857563 (2021).

9:15 AM EN03.07.02

A Universal Principle of Anionic Redox Chemistry in Li/Na Batteries Donggun Eum and Kisuk Kang; Seoul National University, Korea (the Republic of)

Oxygen redox chemistry provides a novel way to realize the high energy density of electrodes for Li/Na batteries. However, the reaction is accompanied by undesirable structural transformations and electrochemical degradation, which limits its practical use. In this regard, we explore the intimate interaction between local structural changes and oxygen redox chemistry during dynamic battery operation. It is demonstrated that the distinct evolution of oxygen-redox activity and reversibility is governed by the different cation migration mechanisms available within the structure of materials. We found that these cation mechanisms play an important role in determining the stabilization pathway of oxygen oxidation. Although π stabilization of oxygen in the absence of cation migration enhances the reversibility of oxygen chemistry, π -interacting oxygen is gradually replaced by σ -interacting oxygen as the electrochemical cycle progresses, resulting in significant structural changes with O–O dimer formation. These findings provide a unified picture for understanding the interplay between structural evolution and anionic redox chemistry and provide further guidance for designing high-energy Li/Na battery electrodes.

9:30 AM EN03.07.03

Designing Hysteresis Free High-Valent Redox Cathode Materials for Electrochemical Application Iwnetim I. Abate¹ and William C. Chueh²; ¹Massachusetts Institute of Technology, United States; ²Stanford University, United States

Advances in electrochemical devices such as batteries, fuel cells, and water-splitting membranes are making global transition towards clean and renewable energy more possible than ever. Foundational to (electro)chemical and catalytic transformations in these devices are a stable and reversible high-valent redox couples. In particular, the phenomenon of high-valent oxygen redox (anionic redox) in lithium- and sodium-ion positive electrodes has the potential to significantly improve cell energy density by providing additional high voltage capacity beyond that of most transition metal redox couples. However, the additional capacity from (anionic redox) has come at the expense of reduced reversibility in the form of voltage hysteresis and voltage fade. As a result, high valent redox couples have been historically avoided. In this talk, first, I will outline the mechanism and the framework for understanding the source of poor electrochemical reversibility in high valent redox. Second, I will demonstrate a mechanism where structural disorder and voltage hysteresis can be completely avoided. I will finish my talk by discussing a set of actionable design rules to engineer materials for different applications that involve high valent redox couple.

9:45 AM EN03.07.04

A New Differential Electrochemical Mass Spectrometry (DEMS) Setup and Its Application in Sodium Ion Batteries Jonas Geisler¹, Lukas Pfeiffer², Peter Axmann² and Philipp Adelhelm¹; ¹Humboldt Universität zu Berlin, Germany; ²Center for Solar Energy and Hydrogen Research Baden-Württemberg (ZSW), Germany

Many processes in alkali ion batteries lead to the formation of gases. These can be SEI formation, electrolyte decomposition, oxygen release from certain cathodes to name some. These gas formations are relevant for lifetime and safety of the battery cells. Having information about these side reactions is important to fully understand the cell chemistry. This can be the behavior of single parts, like electrode materials or electrolyte solvents, or the more complex interplay in a full cell.

Differential electrochemical mass spectrometry (DEMS) is a powerful method to understand these processes. By measuring the electrochemical behavior and the gases evolving from the cell at the same time, information is gained under which conditions side reactions occur^[1]. This can be state of charge, resting times or temperature changes. While it is such a powerful method, not many DEMS studies have been made on sodium ion batteries (NIBs)^[2]. A better understanding of these side reactions in NIBs is still needed. Therefore, we developed a new DEMS system in our group.

This setup was designed to be comparable to other lab scale cells. So, the results would be comparable over different systems. To do so we took the carrier gas based design of Berkes *et al.* as a starting point for our design^[3]. From there we did some optimizations to make the system suit our requirements.

In the first part of the talk, we want to present the new DEMS system. Here we want to go into detail about the setup and highlight some key features, which can be advantageous compared to other systems. Besides the instrument the way we analyze our measurement data to calculate the gas evolution from full mass spectra is new in the field of DEMS for batteries. This data evaluation algorithm leads to a better signal to gas attribution and more possibilities to verify the results^[4].

In the second part of the talk, we will present results measured with the new system. Here we will show our work on sodium manganese nickel oxide cathodes and hard carbon anodes in half cells and full cells thereof. Comparing the results from half to full cells gives insight into the interplay of the whole cell. The stepwise oxidation of the electrolyte solvent, as well as the cross talk of side products between the electrodes, leads to a complex reaction behavior. To show similarities and differences for different electrolytes, we will present data on carbonate and glyme based electrolytes^[4].

[1] B. Rowden, N. Garcia-Araez, *Energy Reports* **2020**, *6*, 10.

[2] L. Zhang, C. Tzolakidou, S. Mariyappan, J.-M. Tarascon, S. Trabesinger, *Energy Storage Materials* **2021**, *4*, 1616.

[3] B. B. Berkes, A. Jozwiuk, M. Vračar, H. Sommer, T. Brezesinski, J. Janek, *Analytical chemistry* **2015**, *87*, 5878.

[4] J. Geisler, L. Pfeiffer, P. Axmann, P. Adelhelm, "Gas evolution in sodium ion batteries – DEMS setup, data evaluation and a study on sodium nickel manganese oxide cathodes.", *To be submitted*.

10:00 AM BREAK

10:30 AM *EN03.07.05

Probing Interfacial Reactivity in K Batteries with Nuclear Magnetic Resonance Techniques [Lauren Marbella](#); Columbia University, United States

Beyond Li-ion technologies have the potential to diversify the suite of chemistries that can address our energy storage needs in the next few decades. However, we still do not know if the decades of research dedicated to optimizing Li-ion battery performance is transferable to more earth abundant chemistries, such as K-ion batteries. In this talk, I will discuss our research results that show the addition of fluoroethylene carbonate (FEC), a well-known additive used in Li-ion systems, to K-ion batteries led to a drastic decrease in capacity and cell failure in only two cycles. This performance loss in the K system was attributed to the formation of KF and K_2CO_3 species seen in ^{19}F NMR and XPS on the hard carbon anode surface and was correlated with increased resistance in the cell. The high internal resistance is likely due to the fact that binary K compounds exhibit lower dielectric constants than their Li counterparts and higher activation barriers to ion diffusion. Insight from these results underscore the importance of developing experimental tools to screen potential K-ion conductors to design a solid electrolyte interphase (SEI) layer that facilitates K transport.

11:00 AM EN03.07.06

Extremely High-Capacity Design of Hard Carbon for Na- and K-Ion Batteries [Yoko Tanaka](#), Daisuke Igarashi, Kei Kubota, Ryoichi Tatara, Tomooki Hosaka and Shinichi Komaba; Tokyo University of Science, Japan

Non-graphitizable carbon, also known as hard carbon (HC), is a promising candidate for a negative electrode material for Na-ion and K-ion batteries because of its high capacity and good cyclability.¹ The electrochemical properties of HC are significantly affected by the carbon source and synthesis conditions.^{2,3} We have recently synthesized a new type of HC, which delivers a capacity of 478 mAh g⁻¹, by using a freeze-dried precursor of Mg gluconate and glucose mixture.³ In this study, we synthesized HC samples from Mg, Zn, and Ca gluconates (HC-Mg, HC-Zn, and HC-Ca) and electrochemical performance.

The reversible capacities in Na-ion batteries obtained with HC-Mg, HC-Zn, HC-Ca were 383, 418, 258 mAh g⁻¹, respectively. Different reversible capacity obtained could originate from the changes in the size of the micropores in HCs derived from different templates. The irreversible capacities observed at the 1st cycle increased as follows: HC-Zn < HC-Mg < HC-Ca. We also conducted CV to examine the electric double-layer capacitances of the HC-based anodes, and their capacitances were consistent with the trend of variation in irreversible capacities. This suggests that the lower irreversible capacity of HC-Zn was ascribed to lower specific surface area. The charge and discharge behaviors are also examined in K-ion batteries. HC-Zn delivers a larger reversible capacity of 357 mAh g⁻¹, which is much higher than that of graphite (K-GIC).

References

[1] S. Komaba, *et al.*, *Adv. Frnct. Mater.*, **21**, 3859 (2011).

[2] H. Yamamoto, S. Komaba, *et al.*, *J. Mater. Chem. A*, **6**, 16844 (2018).

[3] A. Kamiyama, S. Komaba, *et al.*, *Angew. Chem. Int. Ed.*, **10**, 1574-1580 (2021).

11:15 AM EN03.07.07

Sodium and Potassium Superconcentrated Aqueous Electrolytes for 2 V-Class Aqueous Batteries [Tomooki Hosaka](#), Ayumi Noda, Kento Chiguchi, Rie Takahashi, Kei Kubota and Shinichi Komaba; Tokyo University of Science, Japan

Recently, superconcentrated aqueous electrolytes have attracted significant attention because of their wide potential window compared with conventional aqueous solutions. According to the literature, 21 mol kg⁻¹ LiN(SO₂CF₃)₂ (LiTFSA)/H₂O and 27.8 mol kg⁻¹ Li(TFSA)_{0.7}[N(SO₂C₂F₅)₂ (BETA)]_{0.3}/H₂O electrolytes show potential window of ~2 V and ~3.5 V, respectively.^{1,2} As well as the Li electrolytes, superconcentrated aqueous Na and K electrolytes have been recently studied. In general, aqueous Na and K solutions show higher ionic conductivity than Li counterparts because of their weak Lewis acidity, i.e. weak interaction between the cations and solvents/anions, and consequent small Stokes radii of Na⁺ and K⁺ ions.³ Moreover, these cations with weak Lewis acidity stabilize N(SO₂F)₂⁻ (FSA⁻) anion in highly concentrated aqueous solutions.^{4,5} In order to prepare superconcentrated solutions, both anionic mixing and cationic mixing are effective because larger entropy increase from the solid mixtures to the liquid mixtures at the eutectic mixture makes the liquid phase more stable.

Based on the dual cation and dual anion strategy, we recently reported superconcentrated electrolytes of 33 mol kg⁻¹ Na_{0.45}K_{0.55}FSA/H₂O⁶ and 55 mol kg⁻¹ K(FSA)_{0.6}(OTf)_{0.4}/H₂O electrolytes,⁷ showing the wide potential windows of close to 3 V. In this presentation, we present electrochemical performance and charge-discharge mechanism of aqueous Na- and K-ion batteries using the superconcentrated solutions.

Using the Na_{0.45}K_{0.55}FSA electrolyte, we designed Na/K dual-ion batteries with K₂Mn[Fe(CN)₆] (KMnHCF) positive electrode material and the NASICON-type polyanionic compounds, NaTi₂(PO₄)₃ (NTP) or Na₃V₂(PO₄)₃ (NVP), as negative electrode materials. The NTP||K₂Mn[Fe(CN)₆] cell shows reversible charge-discharge curves with mainly two discharge voltage plateaus located at 1.7 V and 1.3 V and excellent capacity retention. Furthermore, the NVP||K₂Mn[Fe(CN)₆] cell demonstrated a 2 V-class operation.

In the 55 mol kg⁻¹ K(FSA)_{0.6}(OTf)_{0.4} electrolyte, we evaluated K₂Mn_{0.5}Fe_{0.5}[Fe(CN)₆] (KMnFeHCF) positive and PTCDI negative electrodes, which have been utilized for aqueous K-ion batteries using with 22 mol kg⁻¹ KOTf electrolyte.⁸ Both positive and negative electrodes achieved highly reversible charge-discharge for 200 cycles. The cycle performances were much better than either 31 mol kg⁻¹ KFSA or 20 mol kg⁻¹ KOTf electrolytes. Similar to the half cell, the full cell of PTCDI || 55 mol kg⁻¹ K(FSA)_{0.6}(OTf)_{0.4} || K₂Fe_{0.5}Mn_{0.5}[Fe(CN)₆] delivered highly reversible charge-discharge curves for 200 cycles, achieving capacity retention of 96 %.

We will discuss the impact of mixed anions and cations on the electrode reaction, including mobile ionic species and the surface layer of the electrode in the presentation.

References:

1. L. Suo, K. Xu *et al.*, *Science*, 2015, **350**, 938-943.

2. Y. Yamada, A. Yamada *et al.*, *Nat. Energy*, 2016, **1**, 16129.

3. T. Hosaka, S. Komaba *et al.*, *Chem. Rev.*, 2020, **120**, 6358-6466.

4. D. Reber, C. Battaglia *et al.*, *Electrochim. Acta*, 2019, **321**, 134644.

5. S. Ko, Y. Yamada and A. Yamada, *Electrochem. Commun.*, 2020, **116**, 106764.
6. T. Hosaka, S. Komaba *et al.*, *ACS Appl. Mater. Interfaces*, 2022, **14**, 20, 23507.
7. R. Takahashi, T. Hosaka, S. Komaba, *ECSJ Spring Meet.*, 2020, 3119.
8. L. Jiang, Y.-S. Hu *et al.*, *Nat. Energy*, 2019, **4**, 495.

11:30 AM EN03.07.08

High Voltage Potassium Intercalation Cathode Young-Woon Byeon¹, Minjeong Gong², Dong-Hwa Seo² and Haegyom Kim¹; ¹Lawrence Berkeley National Laboratory, United States; ²Ulsan National Institute of Science and Technology, Korea (the Republic of)

Alkali-ion intercalation compounds are the most common cathode materials for rechargeable batteries, including Li-, Na-, and K-ion batteries. For several years, layered oxide cathode materials have been considered promising cathode materials for Na- and K-ion batteries because of their high reversible capacity and high working voltage in Li-ion technology. However, our recent findings demonstrated that the layered oxides may not be good candidates for Na and K intercalation cathodes.^[1] Na and K transition metal oxide compounds have alkali ion deficient composition ($x < 1.0$ in A_xMO_2 , A= Na and K), which leads practical difficulty of realizing Na- and K-ion batteries. This is because all the Na and K ions should come from the cathode in rocking-chair batteries. As the insertion ion size increases, the voltage curve becomes much sloped and the sloped voltage curves cause low specific capacity and low average voltage. Both the problems are attributable to much stronger Na⁻-Na⁺ and K⁻-K⁺ interaction than Li⁺-Li⁺ in the layered oxide structure. In this respect, we propose that polyanion compounds will be better candidates because they have 3 dimensional arrangements of Na and K ions, resulting in longer Na⁺-Na⁺ and K⁺-K⁺ distance and reduced effective interaction between them. We proved this concept using KVPO₄F as a model system of polyanion compounds, which has stoichiometric composition and provides a high average voltage of ~4.3 V (vs. K/K⁺) with a reversible capacity of ~105 mAh/g.^[2]

In this presentation, we will discuss (1) why polyanion frameworks can provide high K intercalation voltages (vs. the layered oxides)^[1-3] and expand our discussion to understand (2) how local structure factors, such as cation and anion substitutions, affect K storage properties and performance with the KVPO₄F model system.^[4]

References

- [1] H. Kim *et al.* *Chem. Mater.* 2018, **30**, 6532.
- [2] H. Kim *et al.* *Adv. Energy Mater.* 2018, **8**, 1801591.
- [3] H. Kim *et al.* *Trends in Chem.* 2019, **1**, 682.
- [4] Y. -W. Byeon *et al.* In preparation.

11:45 AM EN03.07.09

Effects of Ti-Substitution on Electrochemical Properties of KVPO₄F for K-Ion Batteries Xiaoran Yang and Jae Chul Kim; Stevens Institute of Technology, United States

For large-scale energy storage applications, the potassium (K)-ion battery system consisting of electrodes that reversibly intercalate potassium (K) ions have received recent research interest due to the earth-abundance of K resources.¹⁻³ To design K-ion cathodes, materials with open and rigid frameworks are considered desirable due to the large ionic radius of potassium.^{1, 2, 4-8} Particularly, KVPO₄F with a tetrahedral phosphate framework has the potential to achieve effective K storage.^{1, 2, 5} In this presentation, we will demonstrate the impact of partial titanium (Ti) substitution for vanadium (V) on the structure and electrochemical properties of KVPO₄F. We found that kinetics and reversibility of K intercalation and the associated physicochemical properties of Ti-substituted KVPO₄F are strongly coupled with local coordination of K. Ti-substituted KVPO₄F delivers a reversible discharge capacity of ~97 mAh/g at an average working voltage at 4 V over the extended number of cycles. Our results suggest that understanding the K environment can be an effective approach to designing K-ion cathode materials.

Reference:

1. H. Kim, J.C. Kim, M. Bianchini, D.H. Seo, J. Rodriguez-Garcia and G.J.A.E.M. Ceder: Recent progress and perspective in electrode materials for K-ion batteries. *8*, 1702384 (2018).
2. H. Kim, D.H. Seo, M. Bianchini, R.J. Clément, H. Kim, J.C. Kim, Y. Tian, T. Shi, W.S. Yoon and G.J.A.E.M. Ceder: A New Strategy for High-Voltage Cathodes for K-Ion Batteries: Stoichiometric KVPO₄F. *8*, 1801591 (2018).
3. J. Ma, Y. Li, N.S. Grundish, J.B. Goodenough, Y. Chen, L. Guo, Z. Peng, X. Qi, F. Yang and L.J.J.o.P.D.A.P. Qie: The 2021 battery technology roadmap. *54*, 183001 (2021).
4. H. Kim, J.C. Kim, S.H. Bo, T. Shi, D.H. Kwon and G.J.A.E.M. Ceder: K-ion batteries based on a P2-type K_{0.6}CoO₂ cathode. *7*, 1700098 (2017).
5. H. Kim, Y. Tian and G.J.J.o.T.E.S. Ceder: Origin of capacity degradation of high-voltage KVPO₄F cathode. *167*, 110555 (2020).
6. T. Hosaka, T. Shimamura, K. Kubota and S.J.T.C.R. Komaba: Polyanionic Compounds for potassium-ion batteries. *19*, 735 (2019).
7. L. Sharma and A.J.J.o.M.C.A. Manthiram: Polyanionic insertion hosts for aqueous rechargeable batteries. *10*, 6376 (2022).
8. K.-Y. Zhang, Z.-Y. Gu, E.H. Ang, J.-Z. Guo, X.-T. Wang, Y. Wang and X.-L.J.M.T. Wu: Advanced polyanionic electrode materials for potassium-ion batteries: Progresses, challenges and application prospects. (2022).

SESSION EN03.08: Na- and K-Ion II
 Session Chairs: Lauren Marbella and Naoaki Yabuuchi
 Wednesday Afternoon, November 30, 2022
 Hynes, Level 3, Ballroom C

1:30 PM *EN03.08.01

Liquid and Polymer Electrolytes for Potassium-Ion Battery Shinichi Komaba, Tomooki Hosaka, Ryoichi Tatara and Daisuke Igarashi; Tokyo University of Science, Japan

Nonaqueous K-ion batteries have attracted much attention as a potential high-voltage secondary battery owing to the lower standard electrode potential of K⁺/K than that of Li⁺/Li. Our group has demonstrated a 4 V-class KIB of graphite//K₂Mn[Fe(CN)₆] (KMnHCF) with 0.7 mol dm⁻³ KPF₆/EC:DEC electrolyte.² Because of the wide operating potential range, developing nonaqueous electrolytes with higher oxidation stability and the ability to passivate low-potential negative electrodes is one of the major challenges. We will present our recent studies on nonaqueous electrolyte solution, electrolyte additive, and solid polymer electrolyte for KIBs. Based on these results, we provide a design strategy for KIB electrolytes.

KPF6 and KFSa can be used as electrolyte salts because of their sufficient solubility in nonaqueous solvents and their electrochemical stability.³ Highly concentrated KFSa/glyme 4, 5 or KFSa-based ionic liquid (IL)⁶ electrolytes showed high oxidation stability, good passivation ability toward the Al current collector, and stable solid electrolyte interphase (SEI) formation on the negative electrodes. The KPF6-KFSa binary salt electrolyte allows both Al passivation and suitable SEI formation.⁷

Electrolyte additives are critical for the long life of K cells. We found that 1,3,2-dioxathiolane 2,2-dioxide (DTD) successfully passivates the K metal surface.⁸ The DTD addition into nonaqueous electrolytes enables the highly reversible operation of K//KMnHCF cells. Moreover, pretreatment of K metal by a DTD-containing solution enabled the fabrication of 3 V-class all-solid-state K polymer batteries.⁹

References:

- 1 T. Hosaka et al, Chem. Rev., 2020, 120, 6358–6466.
- 2 X. Bie et al., J. Mater. Chem. A, 2017, 5, 4325-4330.
- 3 T. Hosaka et al., Bull. Chem. Soc. Jpn., 2022, 95, 569-581.
- 4 T. Hosaka et al., Chem. Commun., 2018, 54, 8387-8390.
- 5 T. Hosaka et al., J. Mater. Chem. A, 2020, 8, 23766-23771.
- 6 H. Onuma et al., ACS Energy Lett., 2020, 5, 2849-2857.
- 7 T. Hosaka et al., ACS Appl. Mater. Interfaces, 2020, 12, 34873-34881.
- 8 T. Hosaka et al., ACS Energy Lett., 2021, 6, 3643-3649.
- 9 M. Hamada et al., ACS Energy Lett., 2022, 7, 2244-2246.

2:00 PM EN03.08.02

Structural Complexity of K-Ion Prussian Blue Analogue Cathodes [John Cattermull](#), Mauro Pasta and Andrew Goodwin; University of Oxford, United Kingdom

Prussian blue analogues (PBAs) are a framework material that are of great interest for use as cathode materials in Na- and K-ion batteries. Whilst Na-ion PBA batteries have been commercialized for use in stationary storage, the high operating potential of some K-ion PBAs offers the exciting prospect of use in electric vehicles where high specific energy density is critical.

Attempts to maximise the specific capacity of PBA cathodes have been made by eliminating [Fe(CN)₆] vacancies. Whilst making these low-vacancy materials has been made possible by altering the synthesis, optimising the electrochemical performance has proved more challenging. Accessing the full capacity with high retention on cycling is one problem, and achieving the same excellent rate capability of the high vacancy PBAs is also non-trivial.

High-vacancy PBAs have an apparent simple cubic structure, but the low vacancy PBAs with high K-ion content have structural distortions. The subsequent phase transitions on cycling these low-vacancy materials are believed to be responsible for poor capacity retention and rate capability.

PBAs have a parent cubic structure with MN₆ (M = Mn, Fe, Co, Ni, Cu) and FeC₆ octahedra decorating a framework, with K⁺ ions occupying the channels within. At high concentrations of K⁺ in the discharged state of the cathode, the cubic structure is distorted by off-centering of the K⁺ ions in the form of sliding alternate layers. High vacancy PBAs with Jahn-Teller active metals at the nitrogen-coordinated site have a cubic structure, as there is no cooperative alignment of the Jahn-Teller axes. Whereas the same PBAs with a lower vacancy content have a cooperative Jahn-Teller distortion. In fact, it is these two distortions – the slide, and the Jahn-Teller – which are most often responsible for phase transitions on cycling and subsequent structural degradation and/or capacity fade.

To explore the impact of these distortions on the functionality of PBAs we synthesised a material that displayed all of these distortions at once, K₂Cu[Fe(CN)₆]. From a structural perspective, this is the most complex PBA yet characterised: its triclinic crystal structure results from an interplay of cooperative Jahn-Teller order, octahedral tilts, and a collective slide distortion involving K-ion displacements. These different distortions give rise to two crystallographically-distinct K-ion channels with different mobilities. The crystal structure was solved by Rietveld refinement of synchrotron X-ray powder diffraction (XRD) pattern using ISODISTORT in combination with TOPAS. The low symmetry can be explained in theory by the combination of the aforementioned distortion modes, and is justified from good fit to data in the diffraction pattern (Rwp = 1.95%).

Variable-temperature X-ray powder diffraction measurements show that K-ion slides are the lowest-energy distortion mechanism at play, as they are the only distortion to be switched off with increasing temperature. At higher temperatures we propose a decomposition pathway to form a different Prussian blue material from exsolving the copper ions in the framework.

Electrochemically, the material operates as a K-ion cathode with a high operating voltage, and an improved initial capacity relative to higher-vacancy PBA alternatives. On charging, K⁺ ions are selectively removed from a single K-ion channel type and the slide distortions are again switched on and off accordingly. We discuss the functional importance of various aspects of structural complexity in this system, placing our discussion in the context of other related PBAs.

2:15 PM EN03.08.03

Manganese Oxides as Versatile Hosts for Beyond Lithium Ion Electrochemistry [Amy Marschilok](#)^{1,2}, Esther S. Takeuchi^{1,2} and Kenneth J. Takeuchi^{1,2}; ¹Stony Brook University, The State University of New York, United States; ²Brookhaven National Laboratory, United States

Future advances in energy storage systems rely on identification of appropriate target materials and deliberate synthesis of the target materials with control of their physiochemical properties in order to disentangle the contributions of distinct properties to the functional electrochemistry. This goal demands systematic inquiry using model materials that provide the opportunity for significant synthetic versatility and control. Ideally, a material family that enables direct manipulation of characteristics including composition, defects, and crystallite size while remaining within the defined structural framework would be necessary. Accomplishing this through direct synthetic methods is desirable to minimize the complicating effects of secondary processing. This presentation will describe synthetic control of manganese oxide composition and structure with resulting impact on electrochemistry. Attributes specific to beyond lithium ion electrochemistry will be highlighted, including comparisons of function in aqueous and nonaqueous electrolyte systems.

2:30 PM BREAK

3:45 PM EN03.08.04

Oxygen Redox Activity in P2 Layered Oxides as High Energy Cathodes in Na-Ion Batteries—New Design Hints from First-Principles Michele Pavone, Arianna Massaro and Ana B. Muñoz-García; University of Napoli Federico II, Italy

Na-ion batteries (NIBs) are rapidly emerging as promising post-Lithium technology for large-scale applications, thanks to the wide availability and low cost of raw materials [1]. Design and optimization of highly efficient active materials are major issues for their effective deployment [2]. Layered transition metal oxides (Na_xTMO₂) have shown outstanding performances as high-energy cathode materials in NIB cells and exhibited the chance to attain larger specific capacity by enabling anionic reactions at high operating voltage [3, 4]. This represents a new paradigm in the development of positive electrodes, but the O₂/O₂ⁿ⁻/O₂ redox processes need to be finely controlled to prevent the release of molecular oxygen and thus huge capacity loss. We report a first-principles investigation of P2-type Mn-defective layered oxides with different metal doping at the TM site by means of PBE+U-D3(BJ) calculations. Structural and electronic features are dissected for each redox-active element in Na_xTM_{0.25}Mn_{0.68}O₂ (TM = Ni, Fe) materials as function of sodiation degree corresponding to different states of charge. We address the oxygen redox activity by considering the formation of oxygen vacancies and dioxygen metal complexes at low Na loads (i.e., high voltage range). Low-energy superoxide moieties with different coordination geometries are predicted to be formed at $x \text{ Na} = 0.25$ in Mn-deficient sites, while the $x \text{ Na} = 0.125$ content enables the release of molecular O₂ via preferential breaking of Ni-O bonds. Mechanistic insights show that dioxygen formation is driven by the TM-O covalency and unveil that O₂ loss can be effectively suppressed by Fe and Ru doping. Our findings pave the route for the rational design of high-energy Na_xTMO₂ cathodes that feature enhanced reversible capacity and thus boost the development of efficient NIB devices. These outcomes are subject of our recent publications on ACS Energy Letters and Journal of American Ceramic Society [5, 6].

References:

- [1] B. Dunn, et al., *Science*, 334(6058), 928-935 (2011)
- [2] Y. Huang, et al., *ACS Energy Lett.*, 3(7), 1604-1612 (2018)
- [3] Q. Wang, et al., *Nat. Mater.*, 20(3), 353-361 (2021)
- [4] M. Ben Yahia, et al., *Nat. Mater.*, 18(5), 496-502 (2019).
- [5] A. Massaro, et al. *ACS Energy Lett.*, 6, 2470-2480 (2021).
- [6] A. Massaro, et al. *Journal of the American Ceramic Society*, in press (2022),

4:00 PM EN03.08.05

Tape/Freeze-Cast PVDF-HFP/Silica Composite Membranes for Separators in Na-Ion Batteries Chun-Wei Wu¹, Katherine T. Faber¹, Xiaoping Lin² and Hansan Liu²; ¹California Institute of Technology, United States; ²Talos Tech LLC, United States

Separators for Na-ion batteries benefit from directionally aligned pores for shorter transport paths, high porosity, and hydrophilicity for greater electrolyte uptake. This can be achieved by tape/freeze casting of polymeric solutions with ceramic fillers as reinforcements. In this study, the introduction of silica particles from the sol-gel reaction of tetraethoxysilane (TEOS) into poly(vinylidene fluoride-hexafluoropropylene) (PVDF-HFP) membranes is attained by a co-solvent method in conjunction with dimethyl sulfoxide (DMSO). The effects of TEOS on the microstructure, crystal structure, hydrophilicity and mechanical properties of tape/freeze-cast membranes have been investigated. In addition, the effects of silica reinforcement in the composite membrane separators on ionic conductivity, MacMullin numbers and electrochemical performance of NVP/NTP coin cells have been studied. The tape/freeze-cast PVDF-HFP membranes fabricated with DMSO as the solvent exhibit directionally aligned and dendritic pores, while a hierarchical pore morphology with spherical pores on the aligned pore walls is found in membranes fabricated with the addition of TEOS. With the introduction of silica, as confirmed by EDX and FTIR, composite PVDF-HFP/SiO₂ membranes exhibit similar porosities but greater tensile strengths and a noticeable increase in electrolyte uptake and hydrophilicity compared to its unreinforced polymer counterpart. Due to the incorporation of silica, the composite membrane separators show higher conductivities and lower MacMullin numbers. Furthermore, the coin cells with composite membrane separators outperform those with polymer membrane separators and filter papers as separators in capacity retention from charge-discharge and cycling performance tests.

4:15 PM EN03.08.06

Impact of Electrolyte Additives on Interphase Chemistry and Performance in Potassium-Ion Batteries Zachary T. Gossage, Tomooki Hosaka, Tatsuo Matsuyama, Ryoichi Tatara and Shinichi Komaba; Tokyo University of Science, Japan

Potassium-ion batteries are an emerging energy storage technology with promising aspects including high access and good distribution of potassium sources, earth-abundant electrode materials, and voltages comparable to lithium-ion batteries.[1] At the forefront for electrode materials are graphite, as the negative electrode, and Prussian blue analogues, for the positive electrode. While these materials offer good theoretical capacities and redox potentials, their high performance is often achieved in relatively expensive electrolytes based on potassium bis(fluorosulfonyl) amide (KFSA) and potassium bis(trifluoromethanesulfonyl) amide (KTFSa). As an alternative, the costs of the electrolyte could be minimized through low concentration additives in an inexpensive electrolyte, such as potassium hexafluorophosphate (KPF₆) in a carbonate ester solvent.[2] In this work, we explored fluorosulfonyl-type additives that have a similar structure to the electrolyte KFSA, among others, at low concentration (below 10 weight %). We focused on the impact of these additives on graphite and manganese Prussian blue (K₂Mn[Fe(CN)₆]) performance within KPF₆ electrolytes. We found the use of even 1 weight percent of KFSA or dimethyl sulfamoyl fluoride additives could improve the initial charge/discharge coulombic efficiency and subsequent capacity access. We further explored the additive impact on rate performance and charge transfer properties. Lastly, we evaluated the resulting interphase chemistry through surface techniques (e.g. XPS) and other analyses to understand how the additives react at the electrode surfaces. Alike to the additives applied in lithium-ion batteries,[3] we found evidence that small differences in the additive structure can strongly impact the resulting degradation reactions and their subsequent impact on cell performance.

References

- [1] T. Hosaka, et al. *Chem. Rev.* **120**, 6358 (2020).
- [2] T. Hosaka, et al., *ACS Appl. Mater. Interfaces*, **12**, 34873 (2020).
- [3] C. Forestier, et al., *J. Power Sources*, **330**, 186 (2016).

SESSION EN03.09/EN05.10: Joint Keynote Talk
Session Chairs: Alex Bates and Dominika Buchberger
Wednesday Afternoon, November 30, 2022
Hynes, Level 3, Ballroom C

4:30 PM *EN03.09/EN05.10.01

Interfacial Science and Engineering in all Solid-State Batteries—A Comparison Between Li SSB and Na SSB Y. Shirley Meng^{1,2,3}; ¹The University of Chicago, United States; ²Argonne National Laboratory, United States; ³University of California, San Diego, United States

Compared with their liquid-electrolyte analogues, Solid state electrolytes SSEs have drawn increased attention as they promote battery safety, exhibit a wide operational temperature window, and improve energy density by enabling pure metals as anode materials for next-generation rechargeable batteries. Despite suitable mechanical properties to prevent metal dendrite penetration, relatively wide electrochemical stability windows, comparable ionic conductivities, and intrinsic safety, most SSEs are found to be thermodynamically unstable against reactive metals such as Li and Na, where SSE decomposition produces a complex interphase, analogous to the SEI formed in liquid electrolyte systems. An ideal passivation layer should consist of ionically conductive but electronically insulating components to prevent the SSE from being further reduced. Study of the buried interfaces in solid state electrolytes has been challenging. Originating from the structural biology field, cryogenic focused ion beam (cryo-FIB) and cryogenic electron microscopy (cryo-EM) have recently been introduced to battery research, and have proven the ability to preserve and probe reactive metals for quantitative structural and chemical analysis. I will do a comparative study for lithium based and sodium based all solid state battery platforms.

SESSION EN03.10: Poster Session III: Other Chemistry

Session Chair: Naoaki Yabuuchi

Wednesday Afternoon, November 30, 2022

8:00 PM - 10:00 PM

Hynes, Level 1, Hall A

EN03.10.01

Room-Temperature Electrochemical Fluoride (De)Insertion into CsMnFeF₆ Jessica Andrews, Eric McClure, Michael J. Brady and Brent Melot; University of Southern California, United States

Understanding the structural changes induced by cation intercalation has proven crucial to augmenting the performance of Li-ion batteries. However, little work has been done to understand the mechanism of anionic intercalation and its effects on host structures. The possibility of anions serving as charge carriers for electrochemical energy storage provides an alternative frontier to explore a variety of new rechargeable battery materials. Systems that leverage fluoride intercalation have recently been reported, but the solid electrolytes utilized in these cells suffer from low room temperature fluoride conductivity, thereby requiring high operating temperatures and limiting practical use. Recent advancements in liquid electrolytes include salt and solvent combinations that exhibit significant fluoride ion shuttle at room temperature and relatively large electrochemical windows. We will present on the reversible, electrochemical (de)fluorination of CsMnFeF₆ at room temperature using a liquid electrolyte. CsMnFeF₆ can be synthesized via three methods (hydrothermal, ceramic, and mechanochemical), each of which yield products in a defect pyrochlore structure with varying particle sizes and phase purities. After three galvanostatic cycles, approximately one fluoride ion can be reversibly (de)inserted into mechanochemically synthesized CsMnFeF₆ for multiple cycles. Ex-situ X-ray absorption spectroscopy confirms that both Mn²⁺ and Fe³⁺ are redox active. The cell impedance decreases after one cycle, suggesting the formation of fluoride vacancies in early cycles generates mixed-valent Fe and enhances the material's conductivity. Ex-situ synchrotron diffraction shows subtle expansion and contraction of the CsMnFeF₆ cubic lattice on insertion and removal, respectively, during the first two cycles. New reflections intensify in the cycle 3 ex-situ diffraction, corresponding to the formation of a new phase from the topotactic transformation of CsMnFeF₆ in the pyrochlore structure into an orthorhombic polytype that continues cycle reversibly cycle fluoride ions for up to 10 cycles.

EN03.10.02

Polymeric Anchor-Driven Multilinked Graphite Electrode for High-Performance Durable Anion Storage Jieun Kang; Pohang University of Science & Technology (POSTECH), Korea (the Republic of)

A booming market for electric vehicle and stationary energy storage systems has contributed to explosive research efforts to realize impeccable rechargeable batteries. Lithium-ion batteries (LIBs) with high energy density and long lifespan have led the new renaissance of the rechargeable battery market for the past few decades, but their limited theoretical energy density and expensive/finite resources (e.g., lithium (Li), cobalt, nickel) call for the development of next-generation rechargeable batteries with advanced battery chemistry. Among the feasible alternatives, anion intercalation-type batteries such as dual-ion batteries (DIBs) and aluminum-ion batteries (AIBs) have emerged as promising energy storage systems utilizing the inexpensive transition metal-free host materials (e.g., graphite) and anion redox chemistry while delivering compatible energy/power density, cycle life, and safety of rechargeable batteries. Particularly, DIBs have achieved energy density close to commercialized LIBs (~250 Wh kg⁻¹) despite a short research history due to the high-voltage redox reaction of anions (>5.0 V vs. Li/Li⁺). The Li-ions and counter ions (i.e., anions) in the electrolyte are simultaneously stored inside the anode and cathode host during charge-discharge, respectively, and thus shortened diffusion length of each charge-carrier ion significantly improves the rate capability of the DIBs.

High-voltage anion-intercalation into the graphite cathode increases the operating voltage of batteries but entails inevitable structural deterioration (~200% of volume expansion) in repeated anion (de-)intercalation of large-radius anions (e.g., PF₆⁻, FSI⁻, TFSI⁻) into the graphite. Analogous to high-capacity alloying-type anode (e.g., Silicon) in LIBs, such structural issues cause electrically isolated "dead" graphite, electrical contact loss between graphite particles, and the formation of unstable/thick cathode electrolyte interphase (CEI) that blocks the anion diffusion pathway, resulting in the material and/or electrode-level collapse and failure of sustainable anion storage. . Based on studies of large-volume-change materials, several material designs have been proposed to mitigate the degradation of graphite electrodes: (i) Introducing electrochemically anion-inactive inorganic coating layers (e.g., Al₂O₃) that physically encapsulate graphite; (ii) Using porous micro/nanoflake or nanoribbon morphologies to accommodate volumetric expansion during anion (de-)intercalation; (iii) To extend the interlayer spacing of graphite; (iv) Interlayer binding design directly connecting graphene layers with a carboxylic anhydride functionality. Such approaches have achieved significant improvements in battery cycle stability and rate capability. However, adding an electrochemically anion-inactive material lowers the energy density of the battery. Also, the excessively widened specific surface area of the host material causes excessive electrolyte decomposition and CEI generation. Therefore, there is a need for an effective strategy for simply mitigating graphite electrode degradation while overcoming the limitations of existing methods.

Here, we report a high-performance durable graphite electrode using polymeric binders, which are essential for electrodes. A designed high-voltage polymer strongly holds the graphite integrity through the formation of a direct covalent bond with graphite. The graphite electrode with the designed binder shows remarkable rate capability and long-term performance of DIBs and dual-graphite batteries. In addition, it shows superb cell performance even when used for existing LIB graphite anodes. The binder design presented here offers guidelines for further designs of the advanced binder for carbonaceous host material with anion intercalation-type redox chemistry.

EN03.10.03

Changes of Charge Storage Mechanism of Aqueous Battery Depending on pH Youngjae Hong, Changmin Lee and Sung-Yoon Chung; Korea Advanced Institute of Science and Technology, Korea (the Republic of)

Aqueous zinc-ion batteries (AZIB) are the promising candidates for the next-generation energy storage system due to their inherent safe, eco-friendly, and cost-effective characteristics. However, the development for high performance is hindered by the lack of understanding on the charge storage mechanism of AZIB. In fact, there is an ongoing debate on which of the two cations, Zn^{2+} and H^+ , dominantly works as major charge carriers and how much of those contribute to the charge storage of AZIB. Here, we visualized that the charge storage mechanism varies depending on electrolyte pH in AZIB system consist of the orthorhombic α - V_2O_5 cathode. Proton is major charge carrier in acidic (pH=1~2) electrolyte, meanwhile, Zn^{2+} ion is major carrier in near-neutral condition (above pH=4). Furthermore, pH dependency exists not only in zinc ions, but also in other aqueous electrolyte systems such as Na^+ , Mg^{2+} , and Al^{3+} . Finally, we tried to conclude the discussion about Zn^{2+}/H^+ insertion chemistry to some extent by confirming that not only the pH but also the absolute amount of proton can affect the storage mechanism. Through this study, we enable to design an insertion carrier for the aqueous battery system by tuning the salt, concentration, etc.

EN03.10.05

Study of Lithium-Excess Manganese Oxyfluorides with Mn^{2+}/Mn^{3+} Ions for Li Storage Applications Asuka Kanno¹, Naoaki Yabuuchi¹, Issei Ikeuchi², Mitsuhiro Hibino² and Kensuke Nakura²; ¹Yokohama National University, Japan; ²Panasonic Energy Co., Ltd., Japan

To further increase energy density of rechargeable Li batteries, the development of high-capacity positive electrode materials is required. Recently, our group has reported that the use of anionic redox in Li-excess Mn-based oxides as high-capacity positive electrode materials.¹⁾ In this study, this concept is extended to Li-excess Mn-based oxyfluorides, in which higher operating voltage is expected for anionic redox associated with the incorporation of fluoride ions with higher electronegativity.²⁾

Synthesis of oxyfluoride with different compositions has been conducted on the basis of a triangular phase diagram consisting of $LiMnOF$, Li_2MnO_2F , and Li_2MnOF_2 . Single-phase samples are obtained for Li_2MnO_2F with Mn^{3+} ions and $Li_2Mn^{2+}O_{3/2}F_{3/2}$ with Mn^{2+} : $Mn^{3+} = 1:1$, synthesized by mechanical milling. These samples are crystallized into the cation-/anion-disordered rocksalt-type structure with low crystallinity. On the other hand, a single phase sample cannot be obtained for Li_2MnOF_2 with Mn^{2+} ions. Although Li_2MnOF_2 was electrochemically inactive, Li_2MnO_2F and $Li_2Mn^{2+}O_{3/2}F_{3/2}$ deliver a large reversible capacities of $>250 \text{ mA h g}^{-1}$. Note that the capacity retention is partly improved by the enrichment of Mn^{2+} ions with less anionic redox. Based on these results, we will further discuss the possibility of Li-excess manganese-based oxyfluorides with different chemical compositions for Li storage applications.

References

- 1) N. Yabuuchi et al., *Nature Commun.*, 7, 13814 (2016).
- 2) N. Yabuuchi, *Chemical Record*, 19, 690 (2019).

EN03.10.06

Scaled-Up Synthesis of High-Energy Vanadyl Phosphate LIB Cathode Material Jonathan Miller, Krystal J. Lee, Hui Zhou and Stanley Whittingham; M.S. Whittingham Group, United States

Lithium-ion batteries (LIBs) have rapidly become the focus of renewable energy storage over the past decade due to their high cycle life, energy density, and capacity. With the automobile industry preparing for a significant increase in electric vehicle (EV) production, it is more important than ever to develop high-energy cathode materials. These materials should ideally be cobalt and nickel-free. Vanadium is the fourth most abundant transition metal, and moreover can undergo a two redox reaction, from V^{5+} to V^{3+} . Vanadyl phosphate (VOPO 4) has shown increasing promise as a viable cathode material for lithium-ion batteries as it is capable of intercalating up to 2 Li^+ ions reversibly, reaching a capacity that exceeds 300 mAh/g and an energy density higher than commercial NMC cathodes. However, an underlying issue surrounding this material is that it is not commercially available so must be made in-house. ϵ -VOPO 4 with excellent electrochemical performance, reported by our team, was synthesized via a solvothermal method which normally gives a low (~1.5 g) product yield for one batch synthesis. The primary focus of this work is to increase the yield without sacrificing the electrochemical performance. By increasing the concentration of reagents while keeping the amount of solvent constant, VOPO 4 synthesis has been successfully scaled up by a factor of five. Although some particle morphology changes occurred with increased reagent concentration, possibly due to pressure changes inside the reaction vessel, there is no discernible influence on electrochemical performance. By monitoring the physical properties of each synthesis, an optimal procedure will be developed to scale up the production of VOPO 4 to 100 g per batch. This work was supported by the NorthEast Center for Chemical Energy Storage (NECCES).

EN03.10.07

Study of Factors Affecting the Reversibility of Anionic Redox in Mn-Based Li-Excess Layered Oxides Kazuki Yukishita¹, Naoaki Yabuuchi¹ and Tokuhiko Handa²; ¹Yokohama National University, Japan; ²BMW Japan Co., Japan

$Li_{1.2}Co_{0.13}Ni_{0.13}Mn_{0.54}O_2$, a solid solution sample between Li_2MnO_3 and $LiCo_{1/3}Ni_{1/3}Mn_{1/3}O_2$, delivers a large reversible capacity exceeding a theoretical capacity based on cationic redox of transition metal ions by using charge compensation of oxide ions, *i.e.*, anionic redox. However, continuous oxygen loss on charging results in a decrease in average operating voltage, which is known as a critical issue for practical use.¹ In this study, to retain high energy density for $Li_{1.2}Co_{0.13}Ni_{0.13}Mn_{0.54}O_2$, the impact of the substitution of transition metal ions with Al^{3+} ions, which have high ionic bonding characters with oxygen on reversibility of anionic redox and oxygen loss is systematically examined. For comparison, Co-free and Al-substituted Li-excess layered oxides are synthesized and tested as positive electrode materials. Based on these results, we will further discuss the factors affecting the reversibility of anionic redox and the possibility of anionic redox for practical battery applications.

Reference

- 1) Enyuan Hu et al, *Nature Energy*, 3, 690 (2018).

EN03.10.08

Systematic Studies on Li-Excess Mn-Based Oxides with Disordered Rocksalt Structure Nanaka Shimada and Naoaki Yabuuchi; Yokohama National University, Japan

Demand for lithium-ion batteries with higher energy density is rapidly growing all over the world to realize a carbon-free society in the future. Li-excess Mn-based materials based on abundant Mn ions are attracting research interest as cost-effective and high performance electrode materials, and our group has reported that solid solution materials of $LiMnO_2$ and Li_2TiO_3 ($Li_{1.33}Ti_{0.67}O_2$) with disordered rocksalt structure.⁽¹⁾ The solid solution materials deliver a large capacity with reversible cationic/anionic redox. However, the improvement of electrode reversibility is necessary to use anionic redox in practical battery applications. Therefore, in this study, the optimization of chemical compositions and particle sizes in $LiMnO_2$ - Li_2TiO_3 solid solution samples has

been conducted. Through electrochemical and structural characterizations for the optimized materials, we will discuss factors affecting the activation and reversibility of anionic redox for Li-excess Mn-based oxides with the disordered rocksalt structure for lithium-ion battery applications.

Reference:

1) Y. Kobayashi *et al.*, and N. Yabuuchi, *Materials Today*, **37**, 43-55 (2020).

EN03.10.09

Crosslinked Polyacrylate Binder and Electrode Maturation for Si-Based Composite for LIB Shogo Yamazaki¹, Ryoichi Tataru¹, Tomooki Hosaka¹, Hironori Mizuta², Kei Kawano² and Shinichi Komaba¹; ¹Tokyo University Of Science, Japan; ²FUJIFILM Wako Pure Chemical Co. Ltd., Japan

SiO has attracted significant attention as a high-capacity electrode material for Li-ion batteries. The mechanical stability of composite electrodes is critical for ensuring a long-term cycle life because Si exhibits large volume changes during lithiation-delithiation process. The use of partially neutralized crosslinked sodium polyacrylate (CLPA) as a binder for Si electrodes was previously shown to improve the capacity retention^[1]. Moreover, Hernandez et al. reported that a maturation process, wherein the Si electrode slurry was cast onto a Cu foil, following which the pre-dried electrode was stored in a humid atmosphere, improved the cycling performance of the electrode^[2]. Building on these studies, a new CLPA binder was applied; this binder could suppress the electrode volume changes inherent to SiO, which exhibits smaller volume changes than Si. Subsequently, the SiO electrodes were subjected to maturation treatment and its effects on the electrochemical properties and performance were evaluated.

Three kinds of CLPA-based binders were used herein. The carboxyl groups of CLPA were modified by the covalent attachment of functional groups to enhance the mechanical flexibility of the electrode. The modified CLPA samples, with carboxyl functional group contents of 0%, 20%, and 50%, were denoted as CLPA, CLPA-20, and CLPA-50, respectively. Polyvinylidene fluoride (PVDF) or the CLPA-based binders, carbon-coated SiO, and acetylene black were mixed into a slurry, which was subsequently casted onto a Cu foil substrate to prepare negative composite electrodes. The cast electrodes were stored under 92% RH for two days before vacuum drying at 100 °C as part of the maturation process. These electrodes were analyzed using 2032 coin cells with Li metal counter electrodes and a 1 mol dm⁻³ LiPF₆/ethylene carbonate:dimethyl carbonate (1:1, (v/v)) with 2 vol% fluoroethylene carbonate (FEC) electrolyte under charge-discharge cycling in the voltage range of 0.002–1.0 V.

Among the three different binders, the SiO electrode prepared with CLPA-20 showed the highest discharge capacity after 90 cycles. The maturation process increased the discharge capacity and efficiently suppressed the capacity decay. The dispersibility of the electrode constituents was likely improved through changing the chemical structure of the binder polymers and maturation treatment. Thus, the mechanical stability of the electrode was improved and electrolyte decomposition at the active material surface was suppressed.

References:

[1] S. Aoki, S. Komaba *et al.*, *J. Electrochem. Soc.*, **162**, A2245 (2015)

[2] C. R. Hernandez, L. Roué *et al.*, *Adv. Energy Mater.*, **8**, 1701787 (2018)

EN03.10.11

Effect of Carbon Properties on the Lithium-Sulfur Battery Performance H. Merve Bilal, Kagan Yuksel and Damla Eroglu; Bogazici University, Turkey

Lithium-Sulfur (Li-S) batteries have attracted great attention as a beyond Li-ion chemistry because of their high theoretical specific capacity in addition to the natural abundance and low cost of sulfur, the active material in the cathode. Yet, due to the highly complex reaction and shuttle mechanisms in the cell, cell design, specifically the design of cathode materials, is highly determinative of the Li-S battery performance. For instance, the battery performance is vastly sensitive to the type and properties of the carbon in the cathode since Li-S batteries typically use an excess of carbon in the cathode to achieve high electronic conductivity and surface area. In this study, the impact of carbon type and properties on the electrochemical, cell- and system-level performance of the Li-S battery was investigated by combining experimental and modeling techniques. First, the influence of carbon properties on the discharge behavior and cycling performance of Li-S batteries were inspected experimentally for cathodes prepared at different thicknesses (in other words, different S loadings) with three different carbons exhibiting various pore volumes, particle sizes, and specific surface areas: Acetylene Black (AB), Ketjen Black (KB), and Carbon Black (Super C65). Moreover, the influence of S loading on the battery performance was studied for these three different carbons. Following experimental characterization, a system-level performance model projecting the specific energy and energy density of the battery pack as a function of the carbon type and S loading was proposed by modifying the publicly available Battery Performance and Cost (BatPac) model. The performance model considers the experimental dependence of the discharge capacity on the carbon type. It also includes a one-dimensional electrochemical model predicting the area-specific impedance (ASI) and overpotential for each cell component. Subsequently, the variance of the current-voltage relation with the carbon properties was also reflected in the model.

The cycling behavior of Li-S cells with varying sulfur loadings indicates that the carbon used in the cathode has a decisive impact on how the S loading affects battery performance. For instance, Li-S cells with AB present no significant dependence on the S loading, whereas Li-S cells with Super C65 show higher capacity retention at higher S loadings. On the other hand, Li-S cells with KB cannot achieve high performance at higher S loadings, which is quite unexpected due to its considerably higher surface area. The inhomogeneous distribution of S in the cathode may cause this inferior performance. Our results also suggest that carbon properties are more determinative of the cycling performance at higher S loadings. Moreover, the highest pack performance is predicted for Super C65. Interestingly, Li-S cells with both AB and Super C65 cathodes achieve the highest system-level metrics at medium S loadings, where the discharge capacities are maximized. This suggests that the decrease in the cell weight and volume with increasing S loading has a less dominant effect than improving the cell capacity. Our results clearly show that maximizing the energy density and specific energy of the battery pack is critical, and optimizing Li-S cell design based solely on the discharge performance may be misleading.

Acknowledgments

This study was funded by the Bogazici University Research Fund, Grants No: BAP-14443SUP and BAP-20A05D5.

EN03.10.12

Build a High Energy Density Li-S Battery with Long Lifespan Xiaowei Wang¹, Bhargav Bhamwala¹, Saurabh Parab¹, Bingyu Lu¹, Darren H. Tan¹ and Y. Shirley Meng^{2,1}; ¹University of California San Diego, United States; ²The University of Chicago, United States

Commercialization of high energy lithium-sulfur battery is hampered by bottlenecks like low sulfur loading, high cathode porosity, low cycling stability. Herein, we developed a tool box of quantification to identify the limiting factors in Li-S batteries under practical lean Li and electrolyte conditions. As guided by the root reasons identified, we strategically synthesized densely stacked redox-active hexaazatrinaphthylene (HATN) polymer with a surface area of 302 m² g⁻¹ and a very high bulk density of ~1.6 g cm⁻³. Uniquely, HATN polymer has a similar redox potential window to S, which facilitates the binding of Li₂S₈ and its transformation chemistry within the bulky polymer host, leading to fast Li₂S/S kinetics. For another, we designed and synthesized a non-sacrificial NewEle to replace the decomposition-based LiNO₃ to achieve long cycle lifespan of Li-S battery. The compact polymer/S electrode presents a high sulfur loading of ~10 mg_c cm⁻² with a low cathode porosity of 30%. It delivers a high areal capacity of ~10 mAh cm⁻² and good cycling stability

(500+ cycles) at electrolyte-sulfur (E/S) ratio of 5 $\mu\text{l mg}^{-1}$. This work paves the way for achieving practical high energy Li-S battery with long lifespan.

EN03.10.13

Hybrid Supercapacitors—A simple Electrochemical Approach to Determine Optimum Potential Window and Charge Balance [Manar M. Hazaa](#), Nageh K. Allam, Doha M. Sayed and Loujain G. Ghanem; The American University in Cairo, Egypt

In this work, we introduced novel, and simple electrochemical principles to guide the choice of the safe and valid operating potential window profile for carbon-based hybrid supercapacitor. The start vertex potential of the cyclic voltammograms (CVs) is set as the potential of zero charge (PZC). However, the final potential limit is chosen after elucidation of the storage mechanism using the CVs measured at various potential scan rates across the overall examined potential window. In addition, the mass and charge balance of the fabricated hybrid electrodes are rationally designed after evaluation of the potential window of the two separate electrodes. Using those strategies, a record performance merits are achieved of a hybrid device made up of carbon derived from biomass and carbon derived EDTA salt. The assembled device exhibits a specific capacitance 265 F/g at 5 mV/s and 221 F/g at 1 A/g with a high capability rate. Moreover, the device shows exceptional stability over 10,000 cycles with 100% capacitive retention and near 100% columbic efficiency. Most importantly, attaining a battery-like energy level of 99.2 W h/kg is a proof of concept that validates the proposed electrochemical fundamental methods for monitoring the mass ratio balancing of the hybrid cell electrodes.

EN03.10.14

Predicting Electrochemical Stability Window of Polymer Electrolytes with First-Principles Approaches [Pax E. Makhura](#) and Qing Zhao; Northeastern University, United States

Polymer electrolytes in lithium-ion batteries represent an emerging paradigm for energy storage by offering numerous advantages over liquid or solid electrolytes through enhanced resistance to variations in volume of electrodes during charge/discharge process, safety, flexibility, and processability. Overcoming the current limitations of polymer electrolytes necessitates a fundamental understanding of their electrochemical stability window (ESW), which controls polymer electrolyte performance and degradation during charge/discharge cycles. First-principles simulations can provide valuable insights into such properties. However, the widely used density functional theory (DFT) unfortunately engender foundational errors, resulting in incorrect frontier-orbital and band gaps. Here, we carry out a systematic study to accurately and efficiently predict ESW of selected polymer electrolytes. We first identify the most accurate correlated wavefunction (CW) theory methods in predicting ESW of polymers of which experimental data is available. We then develop DFT approximations with enhanced predictive capabilities validated using the CW-predicted properties. These efforts pave the way to reconcile DFT against more computationally demanding approaches and thereby retrieve higher level of accuracy with low computational cost. Our work also assists in the rational design of novel polymer electrolytes with improved electrochemical and physical properties.

EN03.10.15

Unveiling the Charge Storage Behavior in Flower-Like MnMoO₄/Mn-MoS₂ Nanosheet Anode Material by Operando Spectroscopy [Wan-Ju Yu](#), Han-Yi Chen and Ruey-An Doong; National Tsing Hua University, Taiwan

Transition metal disulfides (TMDs) have recently attracted considerable attention on serving as the promising electrode materials for energy storage devices like Li-ion batteries (LIB) due to their rich reaction sites and unique structural features. Molybdenum disulfide (MoS₂) has a high theoretical capacitance (669 mA h g⁻¹) and a low volume expansion rate, which is a promising material for LIB. However, the low cycling stability (<30 cycles) as well as high electric resistance have limited the practical application. Therefore, the combination of TMD with metal oxide such as MnMoO₄ is a possible solution to enhance the cyclability and conductivity of electrode materials for LIB applications. Herein, a binary transition-metal sulfide/oxide, MnMoO₄/Mn-MoS₂ nanosheet (MMSO) grown on nickel foam was developed as the anode material for LIB application. The MMSO electrode was prepared by a two-step hydrothermal method, and the well-distributed sheet structure of MnMoO₄ can freely deposit onto the Mn-MoS₂ surface to form the flower-like heterostructures, which can separately stand onto Ni foam substrate to significantly enhance the electrochemical performance of the active material by increasing the number of active sites as well as by shortening the diffusion path for Li⁺ ions. The electrode exhibits both large mass and areal capacities (1885 mA h g⁻¹ and 3.56 mA h cm⁻²) at a current density 0.5 mA cm⁻² and an outstanding rate capability (2.5 mA h cm⁻²) at a current density 3 mA cm⁻². Moreover, the energy storage mechanism of Mn-MoS₂ nanosheet was unveiled systematically by *operando* synchrotron X-ray absorption near edge structure (XANES) and *in operando* synchrotron X-ray diffraction (XRD) by continuously analyzing the crystal phase and valence state of the material during the charging and discharging process. Based on these observations, the anode material exhibits the conversion-type reaction by reducing Mn-MoS₂ to molybdenum metal (Mo) and Li₂S during lithiation process, and some of Li₂S would be oxidized to elemental sulfur (S₈⁰ or S₄²⁻) at the delithiation process. This reaction leads to the formation of elemental sulfur at about < 1.0 V, and the released sulfur would be further utilized in subsequent reactions to enhance the electrochemical performance greatly. Results in this study have clearly clarified the charging-discharging behaviors of TMD-based materials as the anode of LIB, which can provide a gateway to develop a platform for the utilization of 2-D sulfide materials for energy storage applications.

EN03.10.16

Dual-Single-Atom Enables Bidirectional Catalytic Effect for SRR and SOR in Lithium-Sulfur Battery [Jin-Lin Yang](#) and Hong Jin Fan; Nanyang Technological University, Singapore

Lithium-sulfur battery has been widely considered as one of the most potential candidates for traditional lithium-ion battery owing to its high theoretical capacity (1675 mA h g⁻¹ for sulfur), high energy density (2500 Wh kg⁻¹) and low cost. However, the shuttle effect of lithium polysulfides (Li₂S_x, x=4, 6, 8), the low electrical conductivity of the final products (S₈ and Li₂S), and sluggish redox kinetics greatly impede the practical application of lithium-sulfur battery. Herein, we fabricated a novel hierarchical bidirectional electrocatalyst for sulfur cathode based on single atom engineering. In this structure, hollow carbon polyhedrons with a high specific surface area were modified with Ni-N₄ and Fe-N₄ single atomic sites simultaneously and served as the host for sulfur. From the experimental and DFT calculation results, Ni-N₄ sites could accelerate the liquid-solid conversion (Li₂S₄→Li₂S) while the Fe-N₄ center makes more contribution to the Li₂S oxidation process. Based on such bidirectional catalytic effect, the as-prepared catalyst with dual single atom sites exhibited outstanding rate performance (566 mA h g⁻¹ at 4 C) and remarkable capacity retention in the long-term cycling test (713 mA h g⁻¹ at 1 C after 600 cycles). More importantly, when the sulfur cathode was thickly coated with an areal sulfur loading of around 6 mg cm⁻², a high energy density over 4 mA h cm⁻² (commercial lithium-ion battery) can still be maintained during the cycles. We believe this work could pave a way for the next generation energy storage system investigation.

EN03.10.17

Advanced Electrolyte Development for Next-generation Lithium Batteries [Laisuo Su](#) and Arumugam Manthiram; University of Texas at Austin, United States

Electrolytes connect the two electrodes in a lithium battery by providing Li⁺ transport channels between them. Advanced electrolytes are being explored

with high-Ni cathodes and lithium-metal anodes to meet the high energy density and cycle life goals, but the origin of the performance differences with different electrolytes is not fully understood. In this study, we explored the effect of electrolyte on Li plating morphology and its crystallinity, interphase chemistry on both electrodes, and surface degradation of high-Ni cathodes. We found that advanced electrolytes help form close-packed homogeneous Li morphology on the anode, generate thin and inorganic-rich interphase layers on both electrodes, and reduce surface degradation into spinel and rock-salt phases of high-Ni cathodes, leading to superior cycling performance of lithium batteries. Based on these understandings, we proposed a new concept of electrolyte, namely localized saturated electrolyte (LSE), which can increase the cycle life of lithium batteries based on the Co-free LiNiO₂ cathode by almost an order of magnitude. For example, compared to the conventional electrolyte that retains only 55% of the initial capacity after 200 cycles, the LSE retains a record 81% of the initial capacity after 600 deep cycles at 4.4 V (versus Li/Li⁺). Our work highlights the importance of developing advanced electrolytes for next-generation batteries.

SESSION EN03.11: Solid Electrolyte/Metal Anode I
Session Chairs: Youngmin Ko and Wolfgang Zeier
Thursday Morning, December 1, 2022
Hynes, Level 3, Ballroom C

8:30 AM *EN03.11.01

Apply Machine Learning for Post Li-Ion Batteries—From Research to Engineering Problems [Chen Ling](#); Toyota Research Institute of North America, United States

Batteries dominate the power source of portable electronic devices. Yet in large scale applications the requirement remains to improve the battery performances and reduce the cost. It urges the research of new battery chemistries as well as seeking better strategies for the deployment and recycling. The traditional simulation and experiment methods in battery research usually requires large resources in combination with sophisticated domain knowledge and/or experience to enhance the effectiveness of trial-and-error approaches. In recent years, data-driven approaches have made the way into the research of materials science domain. It is widely recognized that machine learning based technologies offer a fourth paradigm of materials research in parallel to empirical, model-based and computation-based science with the promise of solving challenges intractable through traditional means.

In this talk, we will share our experience on the usage of machine learning in various aspects of battery research and engineering problems. In particular, we show the combination of conventional computational materials science with the emerging data science facilitates the exploration of novel functional materials for all-solid-state batteries. We will also discuss the difference between battery research and battery engineering for the employment of machine learning techniques. Our talk highlights the great potential of machine learning in the development, deployment and management of new battery technologies as a new tool in the arsenal towards the carbon neutrality and electrification.

9:00 AM *EN03.11.02

On the Connections of Thermal and Ionic Transport in Solid Ionic Conductors [Wolfgang Zeier](#); University of Muenster, Germany

The advent of solid-state batteries has spawned a recent increase in interest in lithium and sodium conducting solid electrolytes, especially in the lithium thiophosphates. However, many open questions remain when trying to optimize electrolytes and understand solid state battery chemistries, especially pertaining to the fundamentals of ionic transport.

In this presentation, we will show that single series of substitutions are not sufficient to understand ionic transport bottlenecks and that there is a tremendous influence of lattice dynamics on ionic conductors. By introducing a different approach to understanding ionic motion using phonon occupations, we try to explain so far unexplained behaviors of physical ionic transport and by extending this work we will try to compare ionic and thermal transport properties of solid electrolytes.

9:30 AM EN03.11.03

Computational Understanding of the Role of Local Structures in Superionic Conductivity of Solid-State Electrolytes [Bin Ouyang](#)^{1,2}, [Yingzhi Sun](#)², [Yan Zeng](#)³, [Yan Eric Wang](#)⁴, [Haegyum Kim](#)³ and [Gerbrand Ceder](#)^{2,3}; ¹Florida State University, United States; ²University of California, Berkeley, United States; ³Lawrence Berkeley National Laboratory, United States; ⁴Samsung Research America, United States

The past decades have witnessed a rapid growth of computational aided discovery of novel solid-state superionic conductors. Most advancements have been achieved in discovering novel crystalline frameworks that offer the right bond topology for Li/Na diffusion. However, optimal superionic conductors identified so far in many cases only work with specific stoichiometry and chemical compositions. Such limitation of expanding chemical space in known conductor framework requires a more thorough understanding of the key local structures that evolves when we bring composition modification. In this presentation, we will demonstrate how to control the ionic conductivity by engineering the behaviors of two types of local structures, e.g., cluster ion rotation and local site occupancy conservation. The capability of manipulating cluster ion rotation will be demonstrated with cluster ion substitution of halide-based ionic conductor framework, followed by a high throughput screening and prediction of more halide-based superionic conductors with cluster ion substitution. On the other hand, oxide-based superionic conductors will be used to demonstrate the correlation between local site occupancy conservation and ionic conductivity. It has been found that the need for local site occupancy conservation can lead to very different ion diffusion mechanisms.

9:45 AM EN03.11.04

Minimizing Cathode Volume Change via Design of Microstructure and Mechanical Properties [Howard Qingsong Tu](#), Taylor Kranbuhl and Shafee Farzanian; Rochester Institute of Technology, United States

Integrating the NCM material (high capacity and working voltage) into the composite cathode of solid-state batteries (SSB) is the crucial step for the development of SSBs with high energy density. However, the poor rate capability and the inferior cycling stability of the composite cathode have been observed, which seriously bottleneck its practical implementation. It has been reported these drawbacks are mainly attributed to the contact loss between the cathode particles and solid electrolyte (SE) particles under the random volume expansion-contraction cycles of primary particles inside secondary particles.¹⁻²

The systematic theoretical investigations in this work enable the understanding of the cathode volume change affected by the SE plastic deformation, the

particle size dispersion, and the stress evolution inside the composite. Strategies to minimize the overall volume change and to prevent SE fracture from the modeling will provide important guidance for the experimental optimizations of the composite cathode, and therefore for the final commercialization of the solid-state batteries.

<!--[if supportFields]><b style="mso-bidi-font-weight:normal"> ADDIN EN.REFLIST <![endif-->1. Yan P, Zheng J, Liu J, Wang B, Cheng X, Zhang Y, et al. Tailoring grain boundary structures and chemistry of Ni-rich layered cathodes for enhanced cycle stability of lithium-ion batteries. *Nat Energy*. 2018;3(7):600-5
2. Lin F, Nordlund D, Li Y, Quan MK, Cheng L, Weng T-C, et al. Metal segregation in hierarchically structured cathode materials for high-energy lithium batteries. *Nat Energy*. 2016;1(1):1-8
<!--[if supportFields]><b style="mso-bidi-font-weight:normal"><![endif-->

10:00 AM BREAK

10:30 AM EN03.11.05

Multi-Layer Graphene Mash Membrane Decorated with ZnO Rods for Controlling Dendritic Growth in Lithium Metal Anodes [Dae Yeop Jeong](#) and Won Il Park; Hanyang University, Korea (the Republic of)

Despite an ultimate capacity of ~3,860 mAh g⁻¹ and the lowest negative electrochemical potential (-3.040 V vs. the standard hydrogen electrode) of Li metal anode, it suffers from potential safety hazard and poor cycle lifetime by Li dendrite growth. Here we present a new design strategy for Li metal anode that can circumvent the issues regarding the unwanted Li dendrite growth by inducing position-selective and direction-selective deposition of Li. Deposition of Li is induced by disposing lithiophilic ZnO rods under lithiophobic multi-layer graphene. Owing to the geometric configuration, Li continues to grow in the opposite direction of the counter electrode, that is, toward the current collector. This unusual Li growth depresses the formation of dead Li and prevents a short circuit occurring between the anode and cathode. As a result, the proposed anode showed a significant improvement in cycling performance with no capacity loss over 1400 hours, superior rate characteristics with a Coulombic efficiency higher than 99.9%, and a low overpotential at high current density.

10:45 AM EN03.11.06

Improved Electrochemical Performance of Lithium Metal Batteries with Fluorine Doped SO₂ Based Nonflammable Inorganic Electrolytes [Seong Hoon Choi](#), Jiwhan Lee, Seung Do Mun, Seungeun Kim and Hansu Kim; Hanyang University, Korea (the Republic of)

Lithium metal batteries (LMBs) are one of the most promising candidates for next generation energy storage systems owing to their high energy density. However, the growth of undesired lithium dendrite and low Coulombic efficiency during cycling of LMBs inhibit their commercial applications. The safety issues such as thermal runaway due to lithium dendrite growth must also be addressed for commercialization of LMBs. Herein, we demonstrate LMBs with fluorine doped SO₂ based nonflammable inorganic electrolyte, LiAlCl_{4-x}F_x-3SO₂. The LiAlCl_{4-x}F_x-3SO₂ electrolyte showed enhanced electrochemical performance than that of LiAlCl₄-3SO₂ electrolyte, which could be attributed to more stable solid electrolyte interface induced by the presence of AlCl₃F⁻ anions. Detailed mechanism of LMBs with LiAlCl_{4-x}F_x-3SO₂ inorganic electrolyte will be discussed in the presentation.

11:00 AM EN03.11.08

Fluorinated Ether Co-Solvents for Lithium-Metal Batteries [Lina Kim](#) and Hye Ryung Byon; Korea Advanced Institute of Science and Technology, Korea (the Republic of)

Lithium (Li)-metal batteries (LMBs) have been developed for next-generation energy storages with higher energy density than the current lithium-ion batteries (LIBs). It is attributed to the metallic Li having around a ten-fold higher specific capacity (3,860 mAh g⁻¹) than the graphite. However, interfacial reactions at Li surface are complicated and significantly depend on electrolyte solutions. Carbonate-based electrolyte solutions, which were generally used in the LIBs, were incompatible with the Li and remained poor solid electrolyte interphase (SEI).^[1] Alternatively, Ether-based electrolyte solutions, for example, dimethoxyethane (DME), showed better performance owing to their high reductive potential (< 0.5 V vs. Li/Li⁺) and chemical stability against the metallic Li.^{[2],[3]} Nonetheless, the low oxidative potential (< 4 V vs. Li/Li⁺) of ether-based electrolyte solution was not applicable for the NCM cathode requiring chemical and electrochemical stability over 4.5 V vs. Li/Li⁺. These limitations have restricted the development of LMBs toward high energy density.

We investigated the improved oxidative stability of electrolyte solutions using fluorinated ethers in the LMBs. Recently, fluorinated 1,4-dimethylbutane (FDMB) was designed and tested for the LMBs and anode-free Li batteries.^[4] The inductive effect of fluorine in FDMB significantly raised the oxidative potential up to 6.14 V vs. Li/Li⁺ at the Al electrode, which was correlated with the low HOMO energy level (-7.75 eV).^[4] However, the ionic conductivity of FDMB was lower (5.0 cp at 25 °C) than DME with 1 M LiFSI due to the high intrinsic viscosity and the weak Li⁺ solvation affinity of fluorines. We added 1,2-dimethoxyethane (DME) solvents to FDMB with different ratios and investigated their ionic conductivities, oxidative potentials, and chemical stability with Li. The ionic conductivities and voltage polarizations of symmetric Li cells were improved with increasing DME concentrations. However, the oxidative potentials shift more positively at a higher FDMB amounts. In this presentation, I will show physicochemical properties of FDMB with different DME ratios and their feasibility for symmetric Li cells, Li|LFP, and Li|NCM full cells.

References

- [1] Xu, K. Nonaqueous Liquid Electrolytes for Lithium-Based Rechargeable Batteries. *Chem. Rev.* **2004**, 104, 4303–4418.
- [2] Chibueze, V. A.; Zhao, Y.; Xian K.; Jian, Q.; Yi, C.; Zhenan, B. A New Class of Ionically Conducting Fluorinated Ether Electrolytes with High Electrochemical Stability. *J. Am. Chem. Soc.* **2020**, 142, 7393-7403.
- [3] Jiao, S.; Ren, X.; Cao, R.; Engelhard, M. H.; Liu, Y.; Hu, D.; Mei, D.; Zheng, J.; Zhao, W.; Li, Q.; et al. Stable Cycling of High-Voltage Lithium Metal Batteries in Ether Electrolytes. *Nat. Energy*. **2018**, 3, 739–746.
- [4] Yu, Z.; Wang, H.; Kong, X., et al. Molecular design for electrolyte solvents enabling energy-dense and long-cycling lithium metal batteries. *Nat. Energy* **2020**, 5, 526–533.

11:15 AM EN03.11.09

Elimination of Passivation Layer for Homo-Epitaxial Deposition in Metal Batteries Minsung Baek, [Jinyoung Kim](#), Kwanghoon Jeong and Jangwook Choi; Seoul National University, Korea (the Republic of)

Abstract not Available

SESSION EN03.12: Solid Electrolyte/Metal Anode II
Session Chairs: Pieremanuele Canepa and Chen Ling
Thursday Afternoon, December 1, 2022
Hynes, Level 3, Ballroom C

1:30 PM *EN03.12.01

Disentangling the Complexity of Sodium-Ion Transport in Mixed Polyanion Solid Electrolytes and Electrodes [Pieremanuele Canepa](#); National University of Singapore, Singapore

Rechargeable Li-ion batteries have performed admirably as the linchpin technology enabling today's mobile electronics industry, currently powering hundreds of millions of laptops, cameras, and phones worldwide. However, the energy density required for stationary energy storage devices and electric vehicles are quickly exceeding the limits of commercial Li-ion batteries. Finding alternatives to the Li-ion battery appears a crucial priority in the diversification and modernization of energy storage technologies. Indeed, when life-cycle analysis is examined in the design of batteries, sodium (Na) appears attractive because it can be "harvested" directly from seawater, making Na ~50 times lower in cost than Li. An important class of phosphate electrodes and electrolytes discovered by Hong and Goodenough is the Sodium Super Ionic CONductors (NaSICONs), with chemical formula $\text{Na}_x\text{MM}'(\text{XO}_4)_3$, where M and M' are transition metals and X = Si, P and/or S. NaSICON electrode materials and electrolytes typically display significant Na-ion mobility. In this talk I will show that computational materials science, in particular first principles methodologies, can guide the design of better NaSICON electrode and electrolyte materials, with superior energy densities and improved ion transport. For example, our predictions indicate that suitably doped NaSICON compositions, especially with high silicon content, can achieve high Na^+ mobilities. These findings are relevant for the optimization of mixed polyanion solid electrolytes and electrodes, including sulfide-based polyanion frameworks, which are known for their superior ionic conductivities.

2:00 PM EN03.12.02

Relating Critical Phonon Occupation to Activation Barrier in Fast Lithium-Ion Conductors [Matthias T. Agne](#), Joop Freerichs, Michael Hansen and Wolfgang Zeier; WWU Münster, Germany

The families of $\text{Li}_{10}(\text{Ge}/\text{Sn})\text{P}_2\text{S}_{12}$ and $\text{Li}_6(\text{P}/\text{Sb})\text{S}_5\text{X}$ (X = Cl, Br, I) are, so far, the only Li^+ compounds exceeding 10 mS cm^{-1} at room temperature. The structure and transport of these materials has been widely investigated, and the ionic conductivities have been pushed continually higher, reaching values reasonable for solid state battery operation. From a structural perspective, however, they are markedly different, making them excellent model systems to compare in fundamental investigations. For example, if isotopic substitutions have any impact on ionic transport, known as kinetic isotope effects.

By using a combination of nuclear magnetic resonance spectroscopy and ab initio molecular dynamics to characterize temperature-dependent ion transport, it is demonstrated that the isotopic substitution of ^6Li for ^7Li increases the thermodynamic activation barrier for Li-ion transport in $\text{Li}_{10}\text{SnP}_2\text{S}_{12}$ and $\text{Li}_6\text{PS}_5\text{Cl}$. Although previous studies in Li^+ conductors have indicated that lower vibrational frequencies generally result in lower activation barriers, we find that the lower average vibrational frequency of the $^7\text{Li}^+$ ions results in a larger thermodynamic activation barrier. Unlike the case of proton conductors, the magnitude of the kinetic isotope effect cannot be explained by changes in the zero-point vibrational energy. We propose that the observed changes in activation barrier are related to the differences in critical phonon occupation needed to overcome the local barrier to transport. Our hypothesis is supported by an analytical model, based on the physics of quantum harmonic oscillators, that gives good agreement with experiment. Thus, the kinetic isotope effect provides unique insights into the vibrational perspective and frequency dependence of the activation barrier in these fast Li^+ ionic conductors.

2:15 PM EN03.12.03

Understanding the Role of Charge Carrier Transport in High Performance Silicon-Based Anode Composite for Solid State Lithium-Ion Battery [Moumita Rana](#); University of Münster, Germany

Solid state lithium metal batteries are promising as the next-generation energy storage system due to their high energy density, thermal stability, and volumetric miniaturization.[1] However, the use of Li metal anode is detrimental in terms of catastrophic dendrite formation and Li deposition in the solid electrolyte layer that causes short-circuit, thereby limits the battery cyclability. Besides, the chemical and mechanical instability of the Li-anode-SE interface, and the low earth abundance of lithium establish the need for alternative high-capacity anode development. In this regard, silicon is a potential alternative due to its high theoretical capacity of 4200 mAh/g and formation of lithium-rich alloy (Li_{15}Si) at low electrode potential ($<0.35 \text{ V vs. Li/Li}^+$). However, one of the main bottlenecks to achieve electrochemically stable and high-performance Si based anode is limited electronic and ionic conductivity of silicon. [2, 3] Despite appreciable advances in achieving stable Si based anode, the influence of the transport properties on the rate capability and long-term stability remains unclear.

In this study, we aim to understand the role of effective ionic and electronic conductivity in modulating the electrochemical performance of Si based anodes. First, we have developed Si-based composite anodes with a sulfide solid electrolyte and carbon additive, which significantly improved the ionic and electronic conductivity of the electrode composite, respectively. By systematically varying the ratio of the ion/ electron conducting phases in the silicon anode composite and relating corresponding cell performance with effective transport coefficients we can estimate the limiting conductivity values. The particle size of silicon is also found to significantly influence the effective transport properties, which in turn modulate the rate performance as well as the long-term stability of these anode composites. This study provides a comprehensive understanding on the role of charge carrier transport in achieving high-performance silicon based anode composites for solid-state batteries.

Reference:

[1] Janek, J.; Zeier, W. G. *Nat. Energy* 2016, 1, 16141.

[2] Ohta, N.; Kimura, S.; Sakabe, J.; Mitsuishi, K.; Ohnishi, T.; Takada, K. *ACS Appl. Energy Mater.* 2019, 2, 7005.

[3] Lewis, J.A.; Cavallaro, K. A.; Liu, Y.; McDowell, M. T. *Joule* 2022, doi.org/10.1016/j.joule.2022.05.016.

2:30 PM EN03.12.04

A General Mechanism to Increase Ionic Conductivity by High Entropy Yan Zeng¹, Bin Ouyang^{2,3} and Gerbrand Ceder^{2,1}; ¹Lawrence Berkeley National Laboratory, United States; ²University of California, Berkeley, United States; ³Florida State University, United States

There is increasing interest in high-entropy ceramics due to their successful use to enhance properties in Li-ion cathodes, catalysts, thermal barrier coatings, and thermoelectrics. Attractive because of their good synthesizability and reduced reliance on specific chemistries, it has been unclear whether and how a high-entropy design would be beneficial for developing new and better ion alkali-ion conductors for all-solid-state batteries. In this work, we combine first-principles modeling and experiments to demonstrate the mechanism by which a mixture of multiple principal elements boosts ionic conductivity, regardless of the alkali metal content and crystal framework. We validated our conceptual models and first principles results with experiments that show several orders of magnitude enhancement in the ionic conductivity in oxide materials when the mixing entropy of the metals is increased. This work unveils new opportunities in the vast design space of high-entropy materials and adds a new strategy to the development of novel superionic conductors.

2:45 PM EN03.12.05

Homogenization of Lithium Ion Flux by Utilizing a Solid-state Electrolyte Composite Coupled with a Three-Dimensional Porous Framework for Highly Stable Lithium Metal Batteries Jooyoung Lee, Hyunji Park, Jieun Hwang, Juran Noh and Choongho Yu; Texas A&M University, United States

Lithium metal (Li) has been acknowledged as a holy-grail anode material for the next-generation rechargeable battery due to the high specific capacity (3,860 mAh g⁻¹) and low electrode potential (-3.04 V vs. SHE) over all possible alternatives. However, the non-even dendrite growth on the Li surface and the related rapid capacity fading prevent the commercialization of two dimensional (2D) Li metal itself as an anode. Here we suggest a feasible route of utilizing Li metal as an anode without modifying the other components including cathode and electrolyte by investigating the root cause of the failure when employing the conventional separator and 2D Li metal. In detail, we propose both a highly porous solid-state electrolyte (SE) composite separator which provide more preferential lithium ion (Li⁺) passages through the percolated SE and pore networks and a porous three-dimensional (3D) carbon nanotube (CNT) lithium metal host framework with a large surface area. The proposed SE composite separator showed both a high ionic conductivity (~1.7 mS cm⁻¹) and a high lithium-ion transference number (0.68), which induced the compact and uniform Li plating on the anode side. This could overcome the non-even Li plating issue of the conventional separator. Our in-operando study showed that both the non-uniformly distributed Li⁺ flux through the non-even pores of the conventional induced the localized Li plating and detrimental side effects during large volume changes during the cycling, which give rise to the irreversible capacity fading. By exploiting the SE composite, the homogenized Li⁺ flux was contributed to the compact and uniform Li plating with robust inorganic-rich solid-electrolyte-interphase (SEI) layers. Moreover, by utilizing the large surface area of the 3D CNT framework, both a low Li nucleation overpotential and a low interfacial contact impedance during Li plating compared to the 2D Li metal anode were confirmed. Further comparative tests with the conventional separator/anode corroborated the importance of the synergistic effect between the homogeneous Li⁺ flux and low current density near the anode surface. By coupling the proposed SE composite separator and the 3D CNT anode, full cell tests with conventional cathodes, LiFePO₄ (LFP) and Li[Ni_{0.8}Mn_{0.1}Co_{0.1}]O₂ (NMC811), were conducted. Both LFP and NMC811 full cell represented a long and stable cycling behaviors, ~80% capacity retention at the 750th cycle and 235th cycle for LFP and NMC811, respectively. Finally, the full cell test with a NMC811 cathode with a high active material loading (~4mAh cm⁻²) displayed maximum electrode level-energy densities of 456 Wh kg⁻¹ and 794 Wh L⁻¹, which surpass those of commercial Li-ion batteries based on the conventional separator with a graphite anode pair. This work proposes a readily utilizable solution for raising energy density of the Li battery, which could be a viable option considering only incremental advancement in the conventional cathodes lately.

3:00 PM BREAK

3:30 PM EN03.12.06

Multi-Functional Liquefied Gas Electrolytes for Lithium-Metal Batteries Yijie Yin¹, Yangyuchen Yang¹ and Y. Shirley Meng²; ¹University of California, San Diego, United States; ²The University of Chicago, United States

High-energy density, improved safety, temperature resilience, and sustainability are desirable properties for lithium battery electrolytes, yet these metrics are rarely achieved simultaneously. Inspired by the compositions of clean fire extinguishing agents, we demonstrate inherently safe liquefied gas electrolytes based on 1,1,1,2-tetrafluoroethane and pentafluoroethane that maintain > 3 mS cm⁻¹ ionic conductivity from -78 to +80 °C. As a result of beneficial solvation chemistry and a fluorine-rich environment, Li cycling at > 99% Coulombic efficiency for over 200 cycles at 3 mA cm⁻² and 3 mAh cm⁻² was demonstrated in addition to stable cycling of Li/NMC622 full batteries from -60 to +55 °C. Additionally, we demonstrate a one-step solvent recycling process based on the vapor pressure difference at different temperatures of LGE, which promises sustainable operation at scale. This work provides a route to sustainable, temperature-resilient lithium metal batteries with fire-extinguishing properties that maintain state-of-the-art electrochemical performance.

3:45 PM EN03.12.07

Three-Dimensional Current Collector Construction via Electro-Writing for Reversible Li Plating/Stripping in Anode-Free Li Batteries Yazhou Zhou, Lauren P. Chew and Jae Chul Kim; Stevens Institute of Technology, United States

As one of the promising next-generation energy storage systems, anode-free batteries can have the potential to deliver high energy density with low manufacturing costs compared to conventional lithium batteries[1]. However, the practical use of anode-free batteries faces obstacles due to inevitable problems associated with Li dendrites such as substantial volume change at the anode side and poor Coulombic efficiency from the continuous formation of solid-electrolyte interphases (SEI)[2, 3]. The key to unlocking the true potentials of energy-dense anode-free batteries can be employing functional current collectors that can stabilize SEI and the associate interfaces Li plating and stripping electrochemically and mechanically[4, 5]. Herein, we introduce an electro-writing technique that can fabricate flexible three-dimensional (3D) structures on the Cu current collector. We will demonstrate how the 3D structure can stabilize cycling electrochemically and mechanically in an anode-free battery by engineering the construction materials. Specifically, this presentation will show how the composition, porosity, and thickness of the 3D current collector affect the Li plating/stripping. Our results show that elaboration of the 3D structure leads to stable extended cycle life at 1 mA/cm² against Li metal (>150 times) and at C/5 against LiCoO₂ (>100 times), outperforming conventional anode-free batteries with a planar Cu current collector. We believe that our approach to developing 3D current collectors can promise great opportunities for inexpensive, scalable, and safe anode-free batteries.

Reference:

1. Qian, J., et al., Anode-Free Rechargeable Lithium Metal Batteries. *Advanced Functional Materials*, 2016. 26(39): p. 7094-7102.
2. Liu, J., et al., Pathways for practical high-energy long-cycling lithium metal batteries. *Nature Energy*, 2019. 4(3): p. 180-186.
3. Aurbach, D., et al., Factors Which Limit the Cycle Life of Rechargeable Lithium (Metal) Batteries. *Journal of The Electrochemical Society*, 2000. 147(4): p. 1274.
4. Cheng, Y., et al., Lithium Host:Advanced architecture components for lithium metal anode. *Energy Storage Materials*, 2021. 38: p. 276-298.

5. Louli, A.J., et al., Exploring the Impact of Mechanical Pressure on the Performance of Anode-Free Lithium Metal Cells. Journal of The Electrochemical Society, 2019. 166(8): p. A1291-A1299.

4:00 PM EN03.12.08

Electrolyte Design for Lithium Metal Batteries for Electric Aircraft Youngmin Ko¹, Mike A. Baird^{2,1}, Tofunmi Ogunfunmi², Xinxing Peng¹, Young-Woon Byeon¹, Haegyum Kim¹, Mary Scott² and Brett A. Helms¹; ¹Lawrence Berkeley National Laboratory, United States; ²University of California, Berkeley, United States

Electric aircraft require battery systems with stringent demands for both power and energy density to enable, e.g., vertical take-off and landing (eVTOL), passenger and cargo loading, or long-range flight. Energy density is largely defined by the cell components, as well as the extent to which the full capacity of the cathode is stored on charge and utilized on discharge. For high nickel NMC cathodes (e.g., NMC-811), areal capacities of >5 mAh/g are needed, as are electrolytes that enable charging to >4.2 V vs. Li/Li⁺. Lacking, however, is a deep understanding of electrolyte design rules for minimizing impedance rise (i.e., due to the formation of the cathode-electrolyte interphase, CEI) and cathode fracturing under those criteria. Similarly, for thin Li metal anodes and for anodeless cells, electrolytes that enable high areal ion flux are needed for both power on take-off and landing as well as for fast charge. If realized, then cells for electric aviation with specific capacities of 400–500 Wh/kg would be groundbreaking for the emerging industry. Here, we will discuss design rules for liquid electrolytes that realize the stable operation of Li metal batteries for electric aircraft operating under 3.8 C discharge and a charge cut-off voltage of 4.2 V and 4.35 V. Top performing electrolytes with specific additives enable $\sim 90\%$ and $\sim 70\%$ capacity retention after 500 cycles at a charge cut-off voltage of 4.2 V and 4.35 V, respectively, with Li metal anodes and $>50\%$ capacity retention after 100 cycles in anodeless cells. We find that the additives responsible for these gains in performance function not by improving anode reversibility, but instead on cathode reversibility. By using FIB-SEM and TEM analysis, we show that the additives promote the formation of unique CEI that minimizes impedance growth and significantly reduces the rate of self-discharge. Our strategy may be general to other battery chemistries featuring NMC cathodes, thus accelerating their parallel development to similar gains.

4:15 PM EN03.12.09

The Understanding of Solvation Structures of Localized High Concentration Electrolytes Bin Li; Idaho National Laboratory, United States

Due to its low density (0.534 g/cm³), high theoretical capacity (3,860 mAh/g), and low electrochemical potential (-3.04 V vs. SHE), lithium metal is the ideal anode for electrochemical energy storage to support the transition to cleaner energy technologies. However, there are still key materials issues that inhibit lithium metal from being commercialized for rechargeable battery applications. The chemical and morphological (e.g., grain distribution, surface roughness, etc.) non-uniformity, coupled with the high reactivity of lithium drive heterogeneous solid-electrolyte interphase (SEI) formation, poor ionic flux distribution, active material consumption, and rapid dendrite growth.

The SEI, formed through reaction between electrolyte and electrode, is an inherently passive barrier to continuous consumption of active material that extends the operating voltage window. The ideal SEI should have high ionic conductivity while being electrically insulating to ensure good diffusion kinetics and ion permeability by plating at the SEI/foil interface rather than be consumed at the SEI/electrolyte interface. The SEI must also have good mechanical properties, such as high strength and good flexibility when inevitable non-uniform volume expansion and contraction occurs. One of promising pathways to improve SEI properties and thus harness the highly reactive, yet energetic Li-metal anode is by regulating electrolyte solvation structures beyond that of conventional low-concentration electrolytes (LCEs). Increasing the salt concentration to form high-concentration electrolytes (HCEs) is an effective approach to enable high-performance Li-metal batteries by forming more stable inorganic-rich SEI from anion reduction and reducing parasitic reactions of free solvent molecules. However, increasing salt concentration results in increasing electrolyte viscosity and decreasing ionic conductivity. To mitigate this issue, low viscosity diluent was added to form localized high-concentration electrolytes (LHCE). It was demonstrated that the LHCE formulation largely prevents the formation of Li dendrites due to the formation of inorganic-rich, monolithic SEI and shows excellent cycling performance for Li-metal batteries under practical conditions.

However, the current descriptions on LHCE solvation structure cannot well explain most of experimental phenomena. In our work, the new solvation structure of LHCE was proposed and validated with experiments. The pathways to rationally design LHCE formulation with higher performances based on the new solvation structure were highlighted.

SESSION EN03.13: Other Chemistry I
Session Chairs: Raphaële Clément and Youngmin Ko
Friday Morning, December 2, 2022
Hynes, Level 3, Ballroom C

8:30 AM *EN03.13.01

Batteries with Earth-Abundant Elements Ju Li; Massachusetts Institute of Technology, United States

Low-cost, earth-abundant and easy-to-recycle battery chemistries are key for the impending global energy transition. We provide some examples of proton solid-state battery, Zn-metal battery with aqueous electrolyte, and lithium-sulfur batteries that may compete successfully with lead-acid battery and Li-ion batteries. Full-cell performance evaluation and techno-economic assessment are essential for judging different battery chemistries.

9:00 AM *EN03.13.02

Engineering the Metal Dissolution/Redeposition Dynamics to Control the Structural and Electrochemical Evolution of Battery Electrodes Yuxin Zhang, Anyang Hu and Feng Lin; Virginia Tech, United States

The solid-liquid electrochemical interface offers a two-dimensional environment for geometrically confined interfacial reactions to tailor electrode surface chemistry under operating conditions. Herein, we demonstrate that the dissolution and redeposition kinetics of transition metal cations, a ubiquitous phenomenon at the electrochemical interface, can be manipulated to regulate the chemical composition and crystal structure of the electrode surface as well as the overall electrochemical performance. The presentation will focus on aqueous electrolyte-based battery systems. Foreign cations, either added as electrolyte additives or dissolved from surface coatings, can rapidly participate in the electrode dissolution-redeposition process, and facilitate the establishment of the dissolution-redeposition equilibrium. Furthermore, some ionic polymers, present at the surface of active particles, have strong coordination with dissolved TM cations, reduce the proton transport at the interface and help establish the D/R equilibrium. Our work expands the control over the electrochemical reactions at the solid-liquid interface and provides new insights into interfacial studies in electrochemistry and surface science.

9:30 AM DISCUSSION TIME

9:45 AM EN03.13.04

NMR Studies of Concentrated Aqueous Electrolytes for Low Temperature Batteries Mounesha Garaga¹, Sarah Whittle¹ and Steven G. Greenbaum^{1,2}; ¹Hunter College-CUNY, United States; ²CUNY Graduate Center, United States

Concentrated aqueous electrolytes have received much attention in recent years due to their high ionic conductivity, electrochemical window that significantly exceeds the water electrolysis limit, and surprisingly low freezing point. We present here two projects. In collaboration with Fudan University in China (Fei Wang, Ziyue Li) we have investigated phosphoric acid solutions being considered for proton-based batteries capable of operating at low temperature. ³¹P and ¹H NMR self-diffusion coefficient as well as spin-lattice time relaxation measurements were performed on acid concentrations ranging from 1.25 to 16.6 M. The observed maximum in conductivity at the 5.9 M concentration is attributed to changes in solvation structure and transport mechanism in addition to the usual trade-off between solution viscosity and carrier concentration.

In a second collaborative project with Oregon State University (Alexis Scida, David Ji) we examine concentrated (up to 7 M) aqueous lithium chloride solutions from room temperature down to -40C using a combination of self-diffusion measurements and 1D ¹H, ⁷Li, ¹⁷O, and ³⁵Cl NMR spectra. Along with Raman Spectroscopy and first-principles MD simulations we observe a tendency toward less hydration of the Li⁺ ions and more Li⁺ - Cl⁻ pair formation accompanied by ice-like water clusters upon cooling.

10:00 AM BREAK

10:30 AM EN03.13.06

High-Performance Zinc-Air Batteries with Scalable Metal-Organic Frameworks and Platinum Carbon Black Bifunctional Catalysts Juntao Li, Ivan P. Parkin, Paul Shearing and Srinivas Gadipelli; UCL, United Kingdom

Metal-organic framework (MOF)-related derivatives have generated significant interest in numerous energy conversion and storage applications, such as adsorption, catalysis, and batteries. However, such materials' real-world applicability is hindered because of scalability and reproducibility issues as they are produced by multistep postsynthesis modification of MOFs, often with high-temperature carbonization and/or calcination. In this process, MOFs act as self-sacrificial templates to develop functional materials at the expense of severe mass loss, and the resultant materials exhibit complex process-performance relationships. In this work, we report the direct applicability of a readily synthesized and commercially available MOF, a zeolitic imidazolate framework (ZIF-8), in a rechargeable zinc-air battery. The composite of cobalt-based ZIF-8 and platinum carbon black (ZIF-67@Pt/CB) prepared via facile solution mixing shows a promising bifunctional electrocatalytic activity for oxygen evolution reaction (OER) and oxygen reduction reaction (ORR), the key charge and discharge mechanisms in a battery. ZIF-67@Pt/CB exhibits long OER/ORR activity durability, notably, a significantly enhanced ORR stability compared to Pt/CB, 85 versus 52%. Interestingly, a ZIF-67@Pt/CB-based battery delivers high performance with a power density of >150 mW cm⁻² and long stability for 100 h of charge-discharge cyclic test runs. Such remarkable activities from as-produced ZIF-67 are attributed to the electrochemically driven in situ development of an active cobalt-(oxy)hydroxide nanophase and interfacial interaction with platinum nanoparticles. This work shows commercial feasibility of zinc-air batteries as MOF-cathode materials can be reproducibly synthesized in mass scale and applied as produced.

10:45 AM EN03.13.07

Improved Reversibility of Discharging and Charging Processes in CO₂-Containing Lithium-Oxygen Cells at Low Temperature Jin-Hyuk Kang, Jiwon Park, Moonyoung Na and Hye Ryung Byon; KAIST, Korea (the Republic of)

Lithium-oxygen (Li-O₂) cells suffer from undesired reactions by superoxide radical (O₂^{•-}) intermediate and oxidations at high charging potential. Lithium carbonate (Li₂CO₃) as the main side product was irreversibly deposited over electrodes and only partially decomposed at 4.5 V vs. Li/Li⁺, which caused rapid capacity fading. Interestingly, adding CO₂ gas alters electrochemical and chemical routes in the Li-O₂ cells and allows improving reversibility in galvanostatic discharging-charging processes. The desired reaction is forming a soluble peroxodicarbonate dianion (C₂O₆²⁻). Cycling performances of the Li-O₂/CO₂ cells are associated with the preserved C₂O₆²⁻ without chemical transformation to Li₂CO₃ because the oxidation potential of C₂O₆²⁻ is ~3.75 V vs. Li/Li⁺ at 25 °C, far lower than Li₂CO₃. However, these Li-O₂/CO₂ cells still exhibited low cyclability due to the swift deposition of Li₂CO₃ converted from C₂O₆²⁻ at 25 °C.¹

Here we showed that temperature and aprotic solvents determined the stability and molecular structure of C₂O₆²⁻. The life of the C₂O₆²⁻ species lengthened at low temperatures due to their poor thermal stability. A low temperature below 0 °C was necessitated to preserve the stability of C₂O₆²⁻, while the electrolyte solution should have high ionic conductivity. In addition, the solvents determined the molecular structures of C₂O₆²⁻. The Li⁺ solvating powers of the aprotic solvents explained by the dielectric constants and Gutmann donor numbers caused distinct molecular structures of the C₂O₆²⁻. We observed the anhydride-linkage C₂O₆²⁻ in the tetraglyme. However, the low ionic conductivity of tetraglyme caused large voltage polarization and rapid capacity fading. By contrast, DMAc rendering better Li⁺ solvation produced the peroxy-linkage C₂O₆²⁻ and provided the sufficient ionic conductivity even at -10 °C. Our in-depth study revealed the best cyclability of the Li-O₂/CO₂ (90/10 v/v%) cells with 0.5 M LiNO₃/DMAc at -10 °C. The first charging plateau at 3.75 V (vs. Li/Li⁺) belonging to the C₂O₆²⁻ oxidation process was elongated during the cycles. In addition, the limited amount of Li₂CO₃ was entirely decomposed upon the second charging process, resulting in no capacity fading over 100 cycles. Our positive results encourage us to develop future Li-O₂/CO₂ batteries and Li-air batteries with improved cyclability.

References

1. Marques Mota, F., Kang, J.-H., Jung, Y., Park, J., Na, M., Kim, D.H., and Byon, H.R. (2020). Mechanistic Study Revealing the Role of the Br3-/Br2 Redox Couple in CO₂-Assisted Li-O₂ Batteries. *Adv. Energy Mater.* 10, 1903486. <https://doi.org/10.1002/aenm.201903486>.

11:00 AM EN03.13.08

Modeling the Cathode Area to Predict Lithium-Sulfur Battery Performance as a Function of Materials and Cell Design Busra Abdulkadiroglu, Hilal Bektas and Damla Eroglu; Bogazici University, Turkey

Beyond lithium-ion batteries have attracted significant attraction recently. The lithium-sulfur (Li-S) battery is perhaps the most commonly investigated example as it has a significantly high theoretical energy density. Furthermore, sulfur, which is the active material in the cathode, is an abundant, cheap, and environmentally friendly material. The design of lithium-sulfur batteries affects the performance significantly; both materials properties, such as the conductivity and surface area of the carbon, and cell design factors, such as the carbon-to-sulfur ratio, electrolyte-to-sulfur ratio, and sulfur loading, play an essential role in the discharge performance of the Li-S batteries.

There is an immense effort to model the electrochemical performance of the Li-S batteries in the literature. However, the importance of defining the electrochemically active cathode area has not been considered in the previous reports. This study offers a one-dimensional model for the Li-S battery projecting the initial discharge profile. In the model, the electrochemically active cathode area is defined in a novel way based on the weight fraction of the carbon in the cathode and a reference porosity. The effect of key materials and cell design parameters on the discharge performance is captured

successfully by employing this novel area definition. The results of the model are compared with that of two different models, which use two different electrochemically active area formulas. Furthermore, a mechanistic explanation of the effect of critical design parameters on the battery performance is proposed by investigating the change of the electrochemically active cathode area with carbon properties, carbon-to-sulfur ratio, electrolyte-to-sulfur ratio, and sulfur loading.

The model predictions for the effect of the carbon-to-sulfur ratio on the discharge profile of a Li-S cell present that increasing the carbon-to-sulfur ratio increases the discharge capacity and cell voltage up to a point. However, a further increase in the carbon-to-sulfur ratio does not affect the cell voltage and diminishes the discharge capacity. Considering the experimental findings in the literature, the model successfully predicts the effect of the carbon-to-sulfur ratio on the discharge profile due to the proposed definition of the electrochemically active area. As a result of including a reference porosity in the description of the electrochemically active cathode area in the model, we observe the following trend. The electrochemically active cathode area increases with increasing carbon-to-sulfur ratio up to a point; however, due to the decreasing porosity with increasing carbon-to-sulfur ratio, the increase in the active area stops at high C loadings. This expected trend can only be captured with the proposed cathode area. Similarly, the model successfully projects the impact of electrolyte-to-sulfur ratio and sulfur loading on the discharge behavior of a Li-S cell with the proposed cathode area definition.

The properties of carbon in the cathode have a determinative influence on the discharge performance of the Li-S battery. The offered model can successfully capture the impact of both the carbon surface area and electronic conductivity on the discharge behavior. The carbon surface area controls the electrochemically active area in the model; consequently, the predicted discharge capacities are highly sensitive to this property.

Acknowledgments

Busra Abdulkadiroglu acknowledges support from the Scientific and Technological Research Council of Turkey (TUBITAK) 2209-A National/International Research Projects Fellowship Programme for Undergraduate Students, Application No: 1919B012000712.

11:15 AM EN03.13.09

Room Temperature Electrochemical Cycling of Fluoride in CsMnFeF₆ Brent C. Melot; University of Southern California, United States

This talk will present our group's recent work that reports the first example of a reversible battery based on the electrochemical (de)insertion of F-ions at room temperature. We demonstrate that after three cycles, one full equivalent of F-ions can be reversibly cycled in CsMnFeF₆. Electrochemical impedance spectroscopy and Mössbauer spectroscopy suggests the formation of fluoride vacancies in early cycles generates mixed-valent Fe that enhances the electrical conductivity of the electrode. Furthermore, *ex situ* powder diffraction reveals a subtle expansion and contraction of the cubic lattice during oxidation (insertion) and reduction (removal) respectively, that eventually leads to the evolution of new reflections corresponding to a closely related orthorhombic polytype in later cycles. This topotactic transformation suggests that structural derivatives of the fluorite structure offer a promising class of materials for creating high-performance F-ion insertion electrodes.

SESSION EN03.14: Other Chemistry II
Session Chairs: Feng Lin and Yan Eric Wang
Friday Afternoon, December 2, 2022
Hynes, Level 3, Ballroom C

1:30 PM *EN03.14.01

First Principles Study of Proton Insertion in Aqueous Li- and Na-Ion Battery Cathodes Geoffroy Hautier^{1,2}, Sergi Posada¹ and Gian-Marco Rignanes¹; ¹University Catholique de Louvain, Belgium; ²Dartmouth College, United States

Li- and Na-ion batteries are effective energy storage technologies. Nonetheless, currently used organic-electrolyte batteries present well-known safety problems. Among the alternatives, aqueous batteries could be an interesting choice since they are safe and environmentally benign. However, working with aqueous electrolytes brings new detrimental mechanisms such as proton intercalation. I will report on our recent work aiming at understanding the (de)intercalation chemistry of protons and alkali is one of the keys for designing cathode materials in such aqueous electrochemical cells. We study through first principles computations the competition between alkali and proton intercalation and use these results to rationalize experimental knowledge. I will report mainly on LiCoO₂ and NaCO₂ but discuss also other cathode materials.

2:00 PM EN03.14.03

High-Rate, High-Capacity Electrochemical Energy Storage in Hydrogen-Bonded Fused Aromatics Tianyang Chen, Harish Banda and Mircea Dinca; Massachusetts Institute of Technology, United States

Growing demand for electrifying the transportation sector and decarbonizing the grid requires the development of electrochemical energy storage (EES) systems that cater to a wide variety of energy and power needs. As the dominant EES devices, lithium-ion cells (LICs) and electrochemical capacitors (ECs) typically only offer either high energy or high power. This creates a strong incentive to develop electrode materials that combine the high charge capacity of LICs with the fast charging and long cycling life of ECs, mandating that the material possesses abundant redox-active sites, facile pathways for rapid transport of electrical and ionic charges throughout the electrode bulk. This charge storage mechanism, commonly known as pseudocapacitance, has primarily been identified in redox-active transition metal oxides/nitrides/carbides.

Organic materials offer an alternative, more compositionally diverse materials space for designing pseudocapacitive electrodes from earth-abundant elements. Here, we report bis-tetraaminobenzoquinone (BTABQ) and its polymeric analogue (pBTABQ) as new pseudocapacitive organic materials for EES. They exhibit a high density of redox-active quinone and imine groups and aromatic backbones with extended conjugation. Owing to strong intermolecular hydrogen bonding and donor-acceptor (D-A) π - π interactions, they are insoluble in both organic and aqueous media. They can store up to 310 mAh g⁻¹ and charge in as little as 33 seconds. Charge storage and transport occurs throughout the electrode bulk, even at practical mass loadings, due to extended electronic delocalization and facile ion transport.

2:15 PM EN03.14.04

Cu Based Metal Organic Framework as Electrocatalyst for High Performance Lithium-Sulfur Batteries Aqsa Nazir and Wonbong Choi; University of North Texas, United States

Lithium-Sulfur (Li-S) batteries with high energy and power densities have arisen as one of the most promising secondary batteries but due to Li-polysulfide (LiPSs) shuttle effect, declining discharge capacity and unstable cyclability are main problems. Implementing an effective catalyst which can not only reduce the LiPSs shuttle effect but also increase the conductivity of Li-S battery cathode is prime requirement. Here for the first time, we have

implemented conductive Cu metal-based Metal organic framework (Cu-MOF) as a Li-S battery cathode material. Cu-MOF with tunable pore structure and thread like interwoven morphology has proven itself more efficient electrocatalysts for boosting sulfur conversions, and the innate pores of conductive Cu-MOF helps to trap the LiPSs product towards the cathode side. The well-defined architecture of organic ligands of Cu-MOF also participate to explicate the involved surface-binding mechanisms of S and polysulfide products. Conductive Cu-MOF improve the diffusion rate of Li ions, shackling LiPSs, upsurging conduction of electrons/ions, and regulating the deposition of $\text{Li}_2\text{S}_2/\text{Li}_2\text{S}$ towards cathode side. The Li-S battery having sulfur percolated inside the pores of conductive Cu-MOF shows outstanding long-cycling performance. In this presentation, we will discuss the experimental data and mechanistic understanding of the outstanding battery cell performance. It is believed that introducing sulfur in conducting Cu-MOFs open up new gateways to further utilize other conductive MOFs in the Li-S batteries arena.

2:30 PM EN03.14.05

Real-Time In-Situ Raman Spectroscopy Investigation of Lithium-Sulfur Battery Mechanism Under Lean Electrolyte Condition Pashupati R. Adhikari, Anil D. Pathak and Wonbong Choi; University of North Texas, United States

Lithium-sulfur batteries, which possess high theoretical capacity and energy density (1672 mAh/g and 2500 Wh/kg, respectively) have emerged as the next-generation energy storage systems due to recent developments in electric vehicles (EVs) and portable electronics. However, their development is still hindered due to an incomplete understanding of the complicated reaction mechanism that takes place during charge-discharge. In this work, the underlying mechanism of lithium-sulfur battery during charge-discharge is investigated using LiTFSI-DOL-DME as the electrolyte system. The conversion of elemental sulfur to higher/lower order polysulfides during discharge mainly depends on operating potentials. In-situ Raman spectroscopy is performed at various charge-discharge potentials to investigate such conversion reactions of lithium polysulfides, especially under lean electrolyte condition. In addition, the effect of sulfur loading and E/S ratio in the conversion of elemental sulfur to lithium polysulfides is also investigated. Furthermore, the reaction mechanism, self-discharge reactions, and rates of polysulfide formation and diffusion during the charge-discharge are thoroughly investigated using the in-situ Raman spectroscopy in real-time. The mechanistic understanding of lithium-sulfur battery operation from this study will help the researchers in the future development of electrolyte and electrode materials for lithium-sulfur batteries and beyond.

2:45 PM BREAK

3:15 PM EN03.14.06

Highly Reversible Lithium Phosphorothioate Complexes Catholytes for High Performing Lithium-Sulfur Batteries Peiyu Wang¹, Nick Kateris², Yiwen Zhang¹, Chuanlong Wang¹, Jianmin Luo¹, Hai Wang² and Weiyang Li¹; ¹Dartmouth College, United States; ²Stanford University, United States

Beyond lithium-ion technologies, lithium-sulfur batteries stand out because of their multielectron redox reactions and high theoretical specific energy density (2500 Wh kg⁻¹). However, major challenges in realizing this potential lie in the uncontrollable precipitation of solid $\text{Li}_2\text{S}_2/\text{Li}_2\text{S}$ and irreversible cyclic liquid-solid phase transitions, which cause sluggish reaction kinetics and poor cycle life. This work presents a series of lithium phosphorothioate complexes dissolved in organic solvent as battery catholytes to anchor and store the solid discharge products without precipitation. Such highly reversible and fast all-liquid electrochemical conversion enables superior battery performance with wide-ranging temperature operability (down to -40 °C). Coupled experimental characterizations and density functional theory calculations are utilized to reveal the molecular structures of complexes, the complexation mechanisms, and associated electrochemical reaction mechanisms. This novel complexation chemistry holds great potential for lithium-sulfur batteries as the next-generation energy storage solution to overcome the capacity limitation of intercalation-based chemistries.

3:30 PM EN03.14.07

Data-Driven Prediction of Structure and Dynamic Features of Lithium-Sulfur Electrolytes with an Automated Multi-Scale Computational Infrastructure Rasha Atwi and Nav Nidhi Rajput; Stony Brook University, The State University of New York, United States

Lithium-sulfur (Li-S) batteries continue to be considered promising “beyond lithium-ion” technologies owing to their low cost, natural abundance of elemental sulfur, and high theoretical energy density. However, the dissolution of lithium-polysulfide (LiPS) species formed during cycling in the electrolyte, combined with the insulating properties of sulfur and LiPS are among the most critical factors that impair the achievable specific energy. Many of these challenges are related to the nature and properties of the Li-S electrolyte. The composition and stability of the solid-electrolyte interphase (SEI) layer is also inherently dependent on the electrolyte and its intimate interaction with the Li anode. The selection of solvent in particular plays a crucial role in the transportation of ions and determines the polysulfide solubility and the Li anode stability.

Despite the significant body of work on Li-S electrolyte systems, there is much that is still not understood in terms of the structure-property relationships of Li-S electrolytes and the contribution of the speciation to the overall ionic transport properties. Here, we seek to understand how the replacement of conventional ether solvents with different classes of commonly reported Li-S solvents alters the structure and dynamics of Li-S electrolytes. To do so, we leverage our recently developed high-throughput computational framework (MISPR; <https://github.com/molmd/mispr>) to construct a database of Li-S electrolyte properties from a series of automated density functional theory and molecular dynamics simulations. We find that there is no single descriptor that explains the trends in the polysulfide solubility. We also utilize the output database to highlight on the unique behavior of each solvent class, develop a quantitative model for the primary speciation in solution and its relation to the dynamics, and unravel the underpinnings governing the polysulfide dissolution. This work provides guidelines and crucial information that can accelerate our rational selection of solvents that enable optimal compromise between the solubility of PS species and the transport properties.

3:45 PM EN03.14.08

High-Performance Rechargeable Zinc Sulfur Battery with Deep Eutectic Solvents Shu-Chi Wu, Shin-Yi Tang, Hsiang-Ju Liao, Kuangye Wang, Tzu-Yi Yang, Ling Lee, Ying-Chun Shen and Yu-Lun Chueh; National Tsing-Hua University, Taiwan

Zinc is an attractive anode material due to it possesses the merits of high theoretical capacity, proper redox potential (-0.76 V vs standard hydrogen electrode) and low cost. However, when used in a zinc-sulfur battery, polysulfide rapidly reacts with zinc to form a passivating zinc sulfide (ZnS) film on the zinc metal surface, leading to the capacity decays rapidly. Up to date, it remains challenging to develop high-performance Zn-S batteries. To overcome these issues, non-aqueous electrolyte system composed of deep eutectic solvent (DES), which is combined by choline chloride, ethylene glycol and zinc chloride, is developed in this study. This DES electrolyte provides a wide electrochemical window of 1.8 V, which can stabilize the side reaction during the charge-discharge process. By applying carbon nanotube (CNT)/sulfur composite as cathode material and zinc foil as anode, the battery delivers a specific capacity of 450 mAh g⁻¹ with a flat discharge voltage of 0.8 V and a long-term stability. *Ex-situ* characterization of XRD, XPS, Raman and SEM-EDS mapping reveal that the working mechanism based on the reversible conversion reaction of the Zn-S alloying processes. The utilization of DES on electrolyte for rechargeable battery system opens a new route for high-performance zinc-sulfur batteries.

4:00 PM EN03.14.09

Coarsening Regulated Preventive Magnesium of SiO for High-Performance Lithium Storage Materials [Donghan Youn](#), Nam Gyu Kim, Won Joon Jeong, Dong Jae Chung, Ji Young Kim and Hansu Kim; Hanyang University, Korea (the Republic of)

Silicon monoxide (SiO)-based materials have been intensively investigated as an anode material for high energy density lithium-ion batteries (LIBs) because of their high capacity and superior cycle performance. However, these materials have chronic problems of low initial Coulombic efficiency (ICE), which decreases the energy density of the full cell. Magnesium of SiO is one of the promising candidates for increasing the ICE of SiO-based anode materials. Here, we propose Si/Mg₂SiO₄ nanocomposite materials prepared by endothermic dehydrogenation-driven magnesium of SiO using MgH₂ to improve both ICE and cycle stability. The proposed material shows a much increased ICE up to 89.5% and enhanced long-term cycle performance over 300 cycles compared with pristine SiO and the Si/Mg₂SiO₄ nanocomposite prepared by magnesium of SiO with Mg. The endothermic dehydrogenation of MgH₂ suppressed the abrupt temperature rise during magnesium of SiO, thereby regulating the coarsening of the Si phase in Si/Mg₂SiO₄ nanocomposite, which was revealed by high-resolution transmission electron microscopy with thermogravimetry-differential scanning calorimetry. More detailed material characterizations and electrochemical analysis of the Si/Mg₂SiO₄ nanocomposite material will be discussed in this presentation.

4:15 PM EN03.14.10

Si Microparticles Embedded within Wrinkled-Multilayered-Graphenes for High-Areal-Capacity Lithium-Ion Batteries [Incheol Heo](#), Chanyoung Lee and Won Cheol Yoo; Hanyang University, Korea (the Republic of)

Even nanostructured Si electrodes have demonstrated stable electrochemical performances in lithium-ion batteries (LIBs), complex process and high-cost of nanostructured Si electrodes are far from industry standards. Thus, utilization of commercially available low-cost Si microparticles with high-performance is highly necessary for high-energy-density LIBs. In this presentation, we demonstrate a simple and scalable method to utilize commercially available Si microparticles (*ca.* 7 μm) with wrinkled-multilayered-graphenes (Si-WMGs) for high-areal-capacity LIBs. The WMGs provide not only mechanical flexibility for mitigating large volume change of Si microparticles during deep charge/discharge processes, but also good adhesion property to effectively coalesce Si microparticles, and high electrical conductivity, resulting in binder- and conductor-free thick electrodes. The Si-WMG electrodes showed high initial areal capacities of 12.5 mAh cm⁻² at 0.1 C and 7.1 mAh cm⁻² even at a very high rate of 2 C, with outstanding long-term stability with 5.3 mAh cm⁻² at 2 C for over 240 cycles. Furthermore, a full cell composed of Si-WMG and lithium cobalt oxide presented 3.13 mAh cm⁻² and a stable cycling performance (90.3% retention after 100 cycles) in a practical cell setting, clearly demonstrating the practical applicability of Si-WMG electrodes. Therefore, the WMG as a binder and conductor could be applicable to other electrodes with a large volume change and high mass-loading for high-areal-capacity LIBs.

4:30 PM EN03.14.11

Microgrid-Patterned Silicon Electrode as an Electroactive Lithium Host for Stable and High-Energy Lithium Batteries [Seung-Hyeok Kim](#)^{1,2}, Myeong-Hwa Ryou¹ and Sang-Young Lee¹; ¹Yonsei University, Korea (the Republic of); ²Ulsan National Institute of Science and Technology, Korea (the Republic of)

The ongoing surge in the demand for smart portable electronics, electric vehicles, and large-scale stationary energy storage systems has necessitated the development of high-energy-density lithium (Li) batteries with electrochemical longevity. Li metal has garnered considerable attention as a promising battery anode to achieve this goal owing to its high theoretical gravimetric capacity (3,860 mAh g_{Li}⁻¹) and low redox potential (-3.04 V vs. standard hydrogen electrode). However, the unstable Li plating/stripping cyclability of Li-metal anode has restricted its practical application. To address this issue, Lithium (Li) hosts, which can electrochemically accommodate Li in preformed pores of three-dimensional frameworks, have been investigated as an advanced electrode architecture for high-energy-density Li-metal batteries. However, most of the previous studies on Li hosts utilized electrochemically inert materials for their framework constituents, resulting in the undesired loss of gravimetric/volumetric energy densities of the resulting batteries. Here, we present a microgrid-patterned Si (MPS) electrode as a new electroactive Li host concept (denoted as MPS host). The MPS host is composed of a microgrid-patterned Si electrode active layer on a lithiophilic conductive substrate (*lc*-substrate). The *lc*-substrate is fabricated by electrodepositing a suspension solution (Si nanoparticles/single-walled carbon nanotubes (SWCNTs)) onto a Cu foil. Subsequently, an electrode ink consisting of Si/carbon black/polymeric binders is printed on top of the *lc*-substrate using a microscale direct ink writing (DIW) technique to produce the MPS host. The DIW technique is considered as a facile method for constructing on-demand and complex architectures on arbitrary substrates with high throughput. The underlying design concept of the MPS host is described as follows: (i) owing to its high specific capacity (>3,000 mAh g_{Si}⁻¹), the Si embedded in the microgrids enables the redox capacity of the microgrid frameworks; (ii) a lithiated Si (Li_xSi), which acts as a lithiophilic site, guides the uniform flux of Li-ion toward the MPS host; (iii) the difference in the electronic conductivity of the microgrids and *lc*-substrate regulates the magnitude and direction of the applied electric field, thereby enabling the preferential deposition of Li on the *lc*-substrate; (iv) the ordered pore space formed between the microgrids contributes to the uniform and stable deposition of Li. The resulting MPS host enables a stepwise sequential Si lithiation/delithiation (from the Si in the microgrid frameworks) and Li plating/stripping (inside the pore space between the microgrids) reaction, verifying its unique behavior as an electroactive Li host. In addition, a full cell assembled with the MPS host and LiNi_{0.8}Co_{0.1}Mn_{0.1}O₂ (NCM811) cathode (areal capacity = 3.8 mAh cm⁻²) exhibits high cell energy densities (644 Wh kg_{cell}⁻¹/1,538 Wh L_{cell}⁻¹) and reliable cyclability.

SESSION EN03.15: Virtual Session I: Beyond Li-Ion Batteries I
Session Chairs: Xuelin Guo and Yanyan Hu
Tuesday Morning, December 6, 2022
EN03-virtual

8:00 AM +EN03.15.01

Solid-State NMR Guided Discoveries of Low-Cost, High-Performance Solid Electrolytes [Yanyan Hu](#); Florida State University, United States

Developing low-cost and high-performance solid electrolytes is key to producing inexpensive solid-state batteries. Leveraging cost-effective precursors for synthesizing highly conductive and stable solid electrolytes under mild conditions is a promising approach. We have demonstrated the feasibility of such an approach in several cases, including thiophosphate-, phosphate-, and halide-based solid electrolytes. Solid-state NMR investigations of structure-ion transport correlation have been critical to guiding the synthesis and optimization of these solid electrolytes. In particular, we have employed high-resolution NMR spectroscopy complemented by diffraction techniques to determine long- and short-range structures, NMR relaxometry to probe ion dynamics, NMR diffusometry to measure tracer diffusivity, and electrochemically driven tracer-exchange NMR to map out ion transport pathways. Such a systematic investigation allows for a fundamental understanding of how structural attributes affect different aspects of ion transport properties. In conduction with *in situ* NMR, we can establish synthesis-structure-property relationships, which we use to advise synthesis strategies.

8:30 AM EN03.15.02

Self-Supporting Negative Electrode of Silicon Monoxide Held by Carbon Nanotubes for Stable and High-Capacity Secondary Batteries Tomotaro Mae, Kentaro Kaneko, Mochen Li and Suguru Noda; Waseda University, Japan

Silicon monoxide (SiO) is a promising anode material having high theoretical capacity ($>1710 \text{ mA h/g}_{\text{SiO}}$) with superior stability. However, SiO is used with polymeric binder, conductive filler and heavy current collector of metal [1,2], resulting in low delithiation capacity per electrode mass. Herein, we propose self-supporting SiO-carbon nanotube (CNT) electrode without metal foils nor polymeric binders, being expected to have high delithiation capacity based on electrode mass because CNT is light weight.

Self-supporting electrode was prepared by simple co-dispersion and filtration process [3] using $\sim 1 \mu\text{m}$ -sized SiO particles coated with carbon (SiO/C) and submillimeter-long few-wall CNTs synthesized by our fluidized bed [4] having large specific surface area of $\sim 300 \text{ m}^2/\text{g}$. The SiO/C-CNT ($\sim 1.9 \text{ mg}_{\text{SiO}}/\text{cm}^2$ and $\sim 3.2 \text{ mA h/cm}^2$) was evaluated by half-cell test with a Li foil counter electrode, a polypropylene separator, and an electrolyte (1 M LiTFSI + 0.6 M LiNO_3 , DOL:DME=1:1, v:v). As a condition of electrochemical measurement, the SiO/C-CNT electrode was fully lithiated, fully delithiated, fully lithiated, and then the following cycles were performed with SiO utilization ratios of 42%, 67%, or 100% (1.5, 2, or 3.2 mA h/cm^2). The 1st delithiation capacity per electrode mass achieved $>1200 \text{ mA h/g}_{\text{electrode}}$ at the optimum SiO/C content of 85-90 mass%. The delithiation capacity faded rapidly with the high SiO utilization of 100% and 67% while remained high and stable at 709 $\text{mA h/g}_{\text{SiO}}$ and 584 $\text{mA h/g}_{\text{electrode}}$ for 236 cycles with the moderate SiO utilization of 42%. This is because the moderate SiO utilization keeps the volume change of SiO particles moderate, preventing damage to and regeneration of the solid-electrolyte interphase. And the flexible CNT sponge enabled reversible volume/thickness change of the electrode and retained the electrode structure even after 51st lithiation as evidenced by electron micrographs.

[1] T. Chen, et al., J. Power Sources 363, 126 (2017).

[2] Q. Meng, et al, ACS Appl. Mater. Interfaces 11, 32062 (2019).

[3] K. Hori, et al., J. Phys. Chem. C 123, 3951 (2019).

[4] M. Li, et al., Carbon 167, 256 (2020).

8:35 AM EN03.15.06

Enhancement in Battery Performance of $\text{Na}_2\text{Ti}_3\text{O}_7$ Through Vanadium Doping for Sodium-Ion Batteries Akshita Sharma¹, Katchala Nanaji² and Ashok K. Ganguli¹; ¹Indian Institute of Technology Delhi, India; ²International Advanced Research Centre for Powder Metallurgy and New Materials, India

Sodium-ion batteries are a next-generation and cost-effective alternative to rechargeable lithium-ion batteries. However, there is a substantial reduction in volumetric and gravimetric capacity using sodium ion as a charge carrier. $\text{Na}_2\text{Ti}_3\text{O}_7$ (Sodium titanate oxide-NTO) has a wide direct band gap of 3.07 eV leading to poor performance and high capacity fading after prolonged galvanostatic cycling, limiting the mobility of ions between vacant sites of the structure, which results in low intrinsic electrical conductivity across the material. The above drawback of NTO can be improved by incorporating vanadium into the NTO crystal lattice. This work investigates the varying percentage of doping of vanadium ions in NTO and its overall effect on cell performance with sodium ion as a charge carrier. Various concentration of vanadium ions were substituted in sites of Ti^{4+} sites and the phases were well-characterized by powder XRD, TEM-EDX, HRTEM, ICP, and XPS. Likewise, electrochemical measurements, i.e., EIS, CV, galvanostatic cycling, etc, were carried out in the swagelok cell in two-electrode configuration. The charge-discharge profile has been comparatively analyzed with the varied amount of vanadium in $\text{Na}_2\text{Ti}_{3-x}\text{V}_x\text{O}_7$ at different C-rates to investigate performance and capacity retention. The initial discharge capacity of the V-doped NTO half-cell was improved to 119.46 mAh/g compared to NTO with 98.61 mAh/g at a 0.5 C-rate. Also, there was a significant reduction of 57% in the internal resistance of V-doped NTO half-cell when EIS was recorded between 10 MHz-100 kHz. Cyclic voltammetry study exhibits an increase in the maximum peak current with increasing scan rate, leading to high diffusivity (D_{Na^+}) in the case of $\text{Na}_2\text{Ti}_{3-x}\text{V}_x\text{O}_7$ when compared against $\text{Na}_2\text{Ti}_3\text{O}_7$. The very identical nature of CV profiles of both samples, from 0.1 mV/s to 2 mV/s, is indicative of the pseudocapacitive behaviour of the electrode. The presence of two anodic peaks-0.33V and 0.51V in the cyclic voltammetry of V-doped NTO suggests a biphasic mechanism similar to NTO associated with the transition of $\text{Na}_2\text{Ti}_3\text{O}_7$ to $\text{Na}_{3-y}\text{Ti}_3\text{O}_7$ and then to $\text{Na}_4\text{Ti}_3\text{O}_7$. Thus, our study concludes that doping high valence transition metal ions like vanadium provides enhanced electrochemical performance attributed to the increased conductivity and formation of oxygen vacancies.

8:50 AM EN03.15.07

A Computational Study of the Intrinsic Defect Chemistry of Promising Sodium-Ion Cathode Material $\text{Na}_2\text{FePO}_4\text{F}$ Daniel N. Sykes^{1,2}, Yong-Seok Choi^{1,2} and David O. Scanlon^{1,2,3}; ¹University College London, United Kingdom; ²Faraday Institution, United Kingdom; ³Diamond Light Source, United Kingdom

Long-term viability of Li-ion battery energy storage may be limited by global lithium reserves. Recently, Na-ion batteries (NIBs) have garnered a great deal of attention, particularly because of sodium's natural abundance, its more even distribution across the earth and its lower cost compared to lithium. NIBs are especially attractive for large-scale energy storage systems where cost and life cycle are essential.

To this end, $\text{Na}_2\text{FePO}_4\text{F}$ has been a material of interest as a viable cathode material for sodium-ion storage due to the high discharge voltage and favourable theoretical capacity.¹ Recent work has shown the potential for doping in $\text{Na}_2\text{FePO}_4\text{F}$ cathodes to increase average voltage, reduce band gap and Na-ion diffusion barrier.² Despite its promising performance after doping, the defect chemistry that governs the charge transfer of doped $\text{Na}_2\text{FePO}_4\text{F}$ is yet to be understood, which inhibits the selection of optimum dopants for $\text{Na}_2\text{FePO}_4\text{F}$.

Density Functional Theory (DFT) has been proven to be a powerful tool for investigating the defect chemistry of solid-state materials. In this work, we will present work completed on computationally investigating $\text{Na}_2\text{FePO}_4\text{F}$ using DFT implemented in VASP (Vienna Ab Initio Simulation Package). All calculations have been performed with the hybrid HSE06 (Heyd-Scuseria-Ernzerhof) functional to accurately depict the electronic structures of the defected crystalline structures.³

Based on the above techniques, we investigate the electronic/atomic structures of pristine $\text{Na}_2\text{FePO}_4\text{F}$ and its response to intrinsic defects, which are essential to understanding the doping effect in the future.

Here we elucidated the bulk geometric structure of the material through structural relaxation as well as the most stable magnetic configuration. The electronic structure of the material has also been examined with a Density of States (DOS) and a band structure was obtained. Furthermore, to examine the defect landscape of the material, the different stable phases of $\text{Na}_2\text{FePO}_4\text{F}$ have been investigated. The phase stability region for $\text{Na}_2\text{FePO}_4\text{F}$ has been calculated along with its stable chemical potential regions which is important for understanding of synthesis conditions and defect formations. Lastly, by comparing the formation energies of vacancy defects at different chemical potential conditions, we plotted the transition level diagrams which show the likelihood of different defect formations. The present work provides an insight in improving the key performance indicators (KPIs) of $\text{Na}_2\text{FePO}_4\text{F}$ as a cathode material for NIBs.

1. B. L. Ellis, W. R. M. Makahnouk, Y. Makimura, K. Toghill, L. F. Nazar, *Nature Mater.*, 2007, 6, 749-753
2. D. Jin, H. Qui, F Du, Y. Wei, X Meng, *Solid State Sciences*, 2019, 93, 63-69
3. A. V. Krukau, O. A. Vydrov, A. F. Izmaylov, G. E. Scuseria, *J. Chem. Phys.*, 2006, 6, 224106

9:05 AM EN03.15.08

A Low-Cost Al-Graphite Battery with Urea and Acetamide-Based Electrolytes [Franziska Jach](#)¹, Maximilian Wassner¹, Erica Brendler², Max Bamberg^{1,2}, Gero Frisch² and Ulrike Wunderwald¹; ¹Fraunhofer IISB, Germany; ²Technische Universität Bergakademie Freiberg, Germany

A key challenge facing future battery technologies is finding alternatives for currently used raw materials, which are often expensive and are becoming increasingly scarce. In recent years, Al-graphite batteries have been proposed as a valid alternative to Li-ion systems due to their low-cost and sustainability.^[1]

In contrast to commonly used expensive ionic liquid based electrolytes e.g. [EMIm]Cl/AlCl₃, our reported batteries use urea/AlCl₃ and acetamide/AlCl₃ deep eutectic solvents (DES) as low-cost alternative.^[2]

By carefully selecting amide composition, Al speciation in the DESs can be modified, as confirmed by Raman and NMR spectroscopy. Al₂Cl₇⁻ and AlCl₄⁻ are actively involved in Al dissolution and deposition on the Al electrode, whereas AlCl₄⁻ is intercalated between layers of graphite on the cathode.^[3] Hence, battery performance such as specific capacity, long-term stability and self-discharge is greatly influenced by electrolyte composition as well as structure and morphology of the graphite cathode. We correlate the electrolyte speciation changes with resulting battery performance by systematic electrochemical investigations employing urea and acetamide eutectics of different compositions. The reversible graphite intercalation is examined for minimally processed natural graphite flakes of different particle sizes employing electrochemical methods and Raman spectroscopy.

In addition to this optimization of abundant raw materials, specific capacities can be enhanced by electrochemical treatment of the assembled batteries. Cycling experiments employing urea electrolyte with >8000 cycles, exhibiting a specific capacity of around 50 mAh/g at 2.5 A/g (50C) demonstrate the long-term stability. The development of a corrosion stable pouch cell design allows practical application of these batteries. Thanks to its high rate capability and stable long-term cycle life Al-graphite batteries are a promising candidate for high power applications.

Literature:

- [1] G. A. Elia, N. A. Kyeremateng, K. Marquardt, R. Hahn, *Batteries & Supercaps* **2019**, 2, 83. [2] F. Jach, M. Wassner, M. Bamberg, E. Brendler, G. Frisch, U. Wunderwald, J. Friedrich, *ChemElectroChem* **2021**, 8, 1988. [3] M. Angell, G. Zhou, M.-C. Lin, Y. Rong, H. Dai, *Adv. Funct. Mater.* **2020**, 30, 1901928.

9:40 AM DISCUSSION TIME

SESSION EN03.16: Virtual Session II: Beyond Li-Ion Batteries II
 Session Chairs: Yong-Seok Choi and Shweta Hiwase
 Tuesday Afternoon, December 6, 2022
 EN03-virtual

1:00 PM EN03.16.01

Insights into the Effect of Ti/Zn Dual-Doping on the P3-Type Mn-Ni Based Cathodes for Na-Ion Batteries—Combined First-Principles and Experimental Study [Yong-Seok Choi](#)^{1,2,1}, Stephanie Linnell^{3,2}, A. Robert Armstrong^{3,2} and David O. Scanlon^{1,2,1}; ¹University College London, United Kingdom; ²The Faraday Institution, United Kingdom; ³University of St Andrews, United Kingdom

Having dominated the market for over the past three decades, Li-ion batteries (LIBs) are now faced with a challenge for the use in grid-scale energy storages because of the rarity of Li resources. To meet the growing demands of power sources, Na-ion batteries (NIBs) have emerged as a promising alternative for LIBs owing to the high abundance of sodium. Despite the considerable attention to NIBs, their overall electrochemical performance remains inferior to LIBs because of the less negative redox potential and larger ionic radius of Na^[1,2]. Thus, the development of Na-ion cathodes with high energy densities and long cycle lives are critical for NIBs to be widely applied as an alternative to LIBs.

Among various crystalline phases reported to date, P3-type cathodes can be synthesized at lower temperatures^[3] and have a higher Na content^[4] than P2-type oxides. Moreover, thanks to the prismatic Na sites, P3-type cathodes have larger interlayer space than O3-type counterpart^[3], ending improved rate capability. To maximize the performance of P3-type cathodes, extensive studies have been conducted on doping other elements on the transition metal (TM) sites.^[5] In the journey of research on heteroatom doping, various relationships between dopant property and cathode performance have been suggested: 1) dopant possessing higher electronegativity than TM elements increases thermodynamic redox potentials, according to the inductive effect^[6]. 2) Dopants with lower oxidation states and smaller ionic radii (e.g., Mg²⁺, Al³⁺) widens the interlayer distances while causing TMO₆ octahedra shrinkage, enhancing the rate performance^[7,8]. 3) The redox inactivity of dopants stabilizes the TM layer upon battery cycling, which mitigates the capacity fading^[9]. However, the selection of a single dopant satisfying all above criteria is nearly impossible, as electronegativity is positively correlated with oxidation states and ionic radii. From this perspective, dual or multiple doping is inevitable to design future cathodes with high performance.

In this study, using combined technique of experiments and first-principles calculations, we investigated the effect of two dopants (Ti and Zn) with contrasting properties (electronegativity, oxidation state, and ionic radii) on P3-type Na_{0.7}Mn_{0.75}Ni_{0.25}O₂, aiming for the synergetic effect of dual doping. Galvanostatic cycling test showed that each dopant has different effect on cyclability; Zn and Ti dopants improved the cyclic stability at the early and later stage of cycling, respectively. Furthermore, the redox voltages of Na_{0.7}Mn_{0.75}Ni_{0.25}O₂ decrease after doping, where the degree of decrement is greater for Zn dopant. When both elements are doped, the resulting cathode exhibits greater performance than Zn- or Ti-doped samples in both cyclability and rate performance. Considering the recent interpretations on dopant-property relationships, we interpret the observed behaviours employing first-principles calculations. Finally, based on the conclusions obtained from each dopant effect, we discuss how the combination of dopants with contrasting properties can lead to the improved Na-ion cathodes.

References

- [1] N.Tapia-Ruiz et al., *J. Phys. Energy* 3.3 (2021): 031503
- [2] Y.U. Park, et al., *J. Amer. Chem. Soc.* 135.37 (2013): 13870-13878
- [3] L.Xian, et al., *J. Alloys Compd.* 905 (2022): 163965
- [4] Y. Wang, et al., *Chem. Eng. J.* 360 (2019): 139-147

[5] Y.Li, et al., *Adv. Energy Mater.* 10.27 (2020): 2000927

[6] D.A.Kuznetsov, et al., *Joule* 2.2 (2018): 225-244

[7] N.Tapia-Ruiz et al., *Energy Environ. Sci.* 11.6 (2018): 1470-1479

[8] C. Soares, B. Silvan, **Y.S. Choi**, V. Celorrio, V.R. Seymour, G. Cibin, J.M. Griffin, D.O. Scanlon and N. Tapia-Ruiz, *J. Mater. Chem. A* 10.13 (2022): 7341-7356

[9] S.F. Linnell, E.J. Kim, **Y.S. Choi**, M. Hirsbrunner, S. Imada, A. Pramanik, A.F. Cuesta, D. Miller, E. Fusco, B.E. Bode, J.T.S. Irvine, L.C. Duda, D.O. Scanlon, A.R. Armstrong, *J. Mater. Chem. A* 10.18 (2022): 9941-9953

1:15 PM EN03.16.07

Anode Architecture Design for Enabling Deep Cycling Sodium Metal Anodes **Yue Deng**, Lynden A. Archer, Jingxu Zheng and Prayag Biswal; Cornell University, United States

Rechargeable sodium batteries are of increasing scientific and technological interest as they promise a pathway towards low cost and long-duration electrical energy storage. Versions of these batteries that incorporate metallic sodium as the anode can exhibit high theoretical specific capacity of 1166 mAh/g, low electrochemical potential of -2.71V (vs the standard hydrogen potential), and simplicity. However, sodium metal anodes (SMAs) are plagued with high reactivity and poor electrochemical reversibility that renders that impractical for commercial deployment. In this work we investigate the failure mechanisms of sodium anodes in liquid electrolytes and develop approaches that mitigate the failure modes to enable deep cycling of SMAs. We report that the fundamental cause of premature failure of SMAs is not the loss of morphological control of the plated metal but the inherently poor anchoring/root structure of electrodeposited sodium to the anode current collector. Poorly rooted sodium deposits are prone to break-away (orphaning) from the current collector producing massive levels of dead sodium and poor anode reversibility. Accordingly, we propose two approaches to improve the reversibility of SMAs: 1) utilizing non-planar electrode architectures that provide continuous and morphology agnostic access to the metal at all stages of electrochemical cycling; 2) developing thin metallic interphase coatings with sodium solubilities that undergo reversible alloying reactions with sodium enabling stable root-growth of deposited metal. We show that high reversibility of SMAs can be achieved with simple electrolyte design regardless of the detailed morphology via reinforced root structure originating from non-planar electrode architectures or thin metallic coatings on current collectors.

1:30 PM EN03.16.04

Lithium Insertion into Nearly Empty Type II Silicon Clathrate **Yinan Liu**, Joseph Briggs, Ahmad A. A. Majid, Thomas E. Furtak, Michael Walker, Carolyn A. Koh, P. Craig Taylor and Reuben T. Collins; Colorado School of Mines, United States

We explore thermal diffusion of Li into the guest sites of a nearly empty silicon clathrate framework to synthesize Si-Li clathrate ($\text{Li}_x\text{Si}_{136}$) for electrochemical applications. Silicon clathrates are novel silicon allotropes with a cage-like structure that have been recently investigated as potential anodes. Cubic and amorphous silicon, in fact, are both high density anode materials for the development of lithium-ion batteries. However, the main limitation is the significant volume change after the lithiation process, causing instability or even pulverization of the silicon anodes. In the silicon clathrate materials, initial insertion of Li is expected to occur into the cages, with Li acting as guest atoms and the open-framework structure making them less susceptible to volume expansion during lithiation. Moreover, since Li guests are expected to be donor atoms, lithiated clathrates should exhibit excellent electrical conductivity. These properties make Si-Li clathrates potentially promising for electrochemical applications. Exploring this potential requires the synthesis of Si clathrates with Li atoms in the cages and understanding of Li ionic diffusion in the clathrate lattice. The major barrier to the direct formation of Li-guest clathrates is that unlike Si-Na clathrates which have been formed through the thermal decomposition of a Zintl precursor NaSi phase, the Si-Li phase diagram is more complex and an equivalent LiSi phase, which can decompose into $\text{Li}_x\text{Si}_{136}$ clathrate, has not been demonstrated. In this work, Li insertion into the clathrate structure is made possible by our ability to synthesize extremely low Na type II $\text{Na}_x\text{Si}_{136}$ ($x \sim 0.016$). Low- x $\text{Na}_x\text{Si}_{136}$ is sealed into a quartz ampoule with Li metal under vacuum and annealed at temperatures between 250 to 400 °C. X-ray diffraction (XRD) shows that the clathrate structure exhibits reduced structural stability in the presence of Li converting to polycrystalline or amorphous phases for anneals above 375 °C (or at slightly lower temperatures with high Li content or longer annealing time), while the starting material in the absence of Li shows no change in structure for anneals as high as 400°C for 72 hours. At temperatures < 350°C, the Li diffused clathrate structure is maintained for anneals shorter than 3.5 hr. XRD also shows that the guest content in the material increases after diffusion. Raman shows a frequency reduction due to Li diffusion, especially for higher frequency modes based on a systematic study using Raman line scans. Li guests are expected to be donors and this frequency reduction is consistent with previous reports that donating electrons to the anti-bonding conduction band of Si clathrate causes a reduction in the vibrational frequency. Time of flight secondary ion mass spectrometry confirms the presence of Li, and was used to obtain the ion profiles through the film to extract effective diffusion constants at different temperatures. Electron Paramagnetic Resonance (EPR) was applied to detect low concentration guests and study the interaction of the Li guest with the clathrate cages. EPR results suggest that Li atoms tend to form pairs with other Li or Na atoms in the clathrate structure and diffusion of Li results in a large increase of the free carriers in the clathrate material. Results of this work provide a new method for filling the clathrate cages, potentially allowing several alternative guest atoms to be explored. These findings also provide useful insights into the potential use of Si clathrate as an anode material in Li-ion batteries. This work was supported by National Science Foundation Award 1810463.

1:45 PM EN03.16.05

Intrinsic Defects-Assisted Phase Transition of $\text{Na}_2\text{Ti}_3\text{O}_7$ and its Application for High Performance Na-Ion Anodes **Yong-Seok Choi**^{1,2,1}, Sara I. I. Costa^{3,2}, Nuria Tapia-Ruiz^{3,2} and David O. Scanlon^{1,2}; ¹University College London, United Kingdom; ²The Faraday Institution, United Kingdom; ³Lancaster University, United Kingdom

Na-ion batteries (NIBs), taking advantage of Na being the fourth most earth-abundant element, have emerged as a promising candidate for such applications. Together with cost-effective electrodes, the use of NIBs can bring a radical decrease in cost compared to the widely used Li-ion batteries, while ensuring sustainability.^[1] However, NIBs are still in a developmental research phase and the exploration of proper electrode materials is necessary.^[2] $\text{Na}_2\text{Ti}_3\text{O}_7$, with its large abundance of raw materials, non-toxicity, and high theoretical capacity of 177 mAhg⁻¹,^[3,4] has emerged as one of the most attractive anodes for sustainable NIBs. However, previous tests have shown that $\text{Na}_2\text{Ti}_3\text{O}_7$ suffers from (i) low electrical conductivity and (ii) structural instability, which results in poor electrochemical performance, particularly at high charge/discharge rates. Efforts to improve the cycling stability of sodium titanates have discovered $\text{Na}_2\text{Ti}_6\text{O}_{13}$ which has properties contradictory to $\text{Na}_2\text{Ti}_3\text{O}_7$; $\text{Na}_2\text{Ti}_6\text{O}_{13}$ exhibits high ionic conductivity and structural stability but suffers from low Na storage capacity^[5]. In this regard, proper hybridization of $\text{Na}_2\text{Ti}_3\text{O}_7$ and $\text{Na}_2\text{Ti}_6\text{O}_{13}$ could break the limitations of each structure and offer a composite electrode for high performance NIBs^[6]. One viable approach to synthesize mixed $\text{Na}_2\text{Ti}_3\text{O}_7/\text{Na}_2\text{Ti}_6\text{O}_{13}$ anode is a hydrogenation treatment.^[7] When synthesized with hydrogen gas, some of the $\text{Na}_2\text{Ti}_3\text{O}_7$ spontaneously transforms into $\text{Na}_2\text{Ti}_6\text{O}_{13}$, which provides high-performance $\text{Na}_2\text{Ti}_3\text{O}_7/\text{Na}_2\text{Ti}_6\text{O}_{13}$ hybrid anodes without additional synthesis routes. This procedure typically includes two reactions of O and Na removal, i.e., $2\text{Na}_2\text{Ti}_3\text{O}_7 + \text{H}_2 \rightarrow 2\text{Na}_2\text{Ti}_3\text{O}_{6.5} + \text{H}_2\text{O}$ and $2\text{Na}_2\text{Ti}_3\text{O}_{6.5} + \text{H}_2\text{O} \rightarrow \text{Na}_2\text{Ti}_6\text{O}_{13} + \text{Na}_2\text{O} + \text{H}_2$. Above reactions imply that O and Na vacancy defects formed during the synthesis condition are closely related to the spontaneous phase transition from $\text{Na}_2\text{Ti}_3\text{O}_7$ to $\text{Na}_2\text{Ti}_6\text{O}_{13}$. However, the interplay between defects and phase transition have been neglected to date, and the fundamental driving forces underlying the phase transition remain elusive.

To better understand the role of native defects on the above phase transition behavior, we perform computational analyses on the intrinsic defect chemistry in $\text{Na}_2\text{Ti}_3\text{O}_7$. In particular, using the combined density functional theory (DFT) calculations with hybrid and PBEsol functionals, we replicate the high-temperature synthesis condition and investigate major defects formed during synthesis. The formation energies of the so-formed major defects are used to discuss the charge compensation behaviors and underlying conductivity mechanism, which can help establishing a doping strategy for anodes with improved performance. Furthermore, the effect of intrinsic defects of $\text{Na}_2\text{Ti}_3\text{O}_7$ on its atomic structure were studied to elucidate the origin of the spontaneous phase transition to $\text{Na}_2\text{Ti}_6\text{O}_{13}$, which can potentially guide further optimization of anodes employing phase transitions.

[1] N.Tapia-Ruiz et al., J. Phys. Energy 3.3 (2021): 031503

[2] Chemical reviews 117.21 (2017): 13123-13186.

[3] Advanced Functional Materials 26.21 (2016): 3703-3710.

[4] Nano Energy 18 (2015): 20-27.

[5] Small 12.22 (2016): 2991-2997.

[6] Advanced Science 5.9 (2018): 1800519.

[7] S.I.R. Costa, Y.S. Choi, A.J. Fielding, A.J. Naylor, J.M. Griffin, Z. Sofer, D.O. Scanlon, N. Tapia-Ruiz, Chem. - Eur. J. 27.11 (2021): 3875-3886.

1:50 PM EN03.16.06

Influence of Multiphase Intergrowth on Layered Transition Metal Oxide Positive Electrodes for Sodium-Ion Batteries Eric Gabriel^{1,2}, Kincaid Graff¹, Dewen Hou^{1,2}, Changjian Deng³, Pengbo Wang⁴, Yanyan Hu⁴ and Hui Xiong¹; ¹Boise State University, United States; ²Argonne National Laboratory, United States; ³China Evergrande New Energy Vehicle Group Ltd, China; ⁴Florida State University, United States

Layered transition metal oxides (LTMOs) are a popular class of positive electrode materials for sodium ion batteries (SIBs). Historically, research of LTMO materials as electrodes for SIBs has been focused on single phase materials. On the other hand, multiphase structures with superior properties to single phase materials have gained increased interest in recent years. We demonstrate the preparation of multiphase electrode materials through controlled doping and processing strategies. We observe in the O3-type ternary $\text{Na}_{0.87}\text{Ni}_{0.4}\text{Fe}_{0.2}\text{Mn}_{0.4}\text{O}_2$ (NFM) system that Li doping generates a secondary intergrown Li-rich phase that is mechanically coupled to the primary O3 phase during the first charge/discharge cycle, which suppresses phase transformations seen in the undoped material as observed by operando synchrotron X-ray Diffraction (XRD) measurements. The amount of the Li dopant influences both the structure of the primary O3 phase and the phase fractions of each phase, as shown by synchrotron XRD and neutron diffraction. Li doping also significantly influences the reactivity of the material surface as determined by ²³Na and ⁷Li nuclear magnetic resonance. The phase transformation and surface reaction are shown to be key factors in the cycling stability of the Li doped NFM electrodes.

2:05 PM DISCUSSION TIME

SYMPOSIUM EN04

Advances in the Fundamental Understanding of Halide Perovskites
November 28 - December 7, 2022

Symposium Organizers

Sascha Feldmann, Harvard University
Selina Olthof, University of Cologne
Shuxia Tao, Eindhoven University of Technology
Alexander Urban, LMU Munich

Symposium Support

Gold

LIGHT CONVERSION

Bronze

Software for Chemistry & Materials BV

* Invited Paper

+ Distinguished Invited

SESSION EN04.01: Electronic Structure and Composition Tuning
Session Chairs: Philip Schulz and Shuxia Tao
Monday Morning, November 28, 2022
Hynes, Level 3, Ballroom A

11:00 AM EN04.01.02

The Dominant Static Disorder in Perovskites Originates from Zero-Point Phonon Energy Rather Than Structural Disorder Ardalan Armin;

Swansea University, United Kingdom

Benefiting from recent advancements in the sensitivity of photocurrent spectroscopy¹, in this work, I revisit sub-gap absorption measurements with improved accuracy on state-of-the-art perovskite solar cells based on lead-halides with different numbers of cation components.

Firstly, I demonstrate that the spectral line shape of absorption features associated with mid-gap trap states are strongly influenced by thickness dependent optical cavity effects. Hence, the corresponding spectra, if uncorrected, provide no information about energetic distribution of sub-gap trap states.² I show that the mid-gap trap states lower the photoluminescence quantum yield through SRH recombination and thereby, they cause additional non-radiative voltage loss. These mid-gap traps are present in the bulk of perovskite, but their density is considerably larger at the interface with C60 interlayer.³

Secondly, I show that the determination of the Urbach energy is limited to an uncertainty of 1 meV due to inevitable variations in sub-gap absorption features caused by said cavity effects.⁴ In light of this, we determine the static and dynamic disorder using temperature dependent, ultra-sensitive external quantum efficiency (EQE) measurements. The corresponding static, temperature-independent contributions of the Urbach energy are found to be 3.3 ± 0.9 meV, 4.7 ± 0.3 meV, and 5.1 ± 0.5 meV for single, double, and triple cation perovskite solar cells,⁵ respectively. Defect states with small trap signatures observed in sensitive sub-gap EQE are found not to dominate the perovskite static disorder. Instead, the static disorder in perovskites is only limited by the quantum noise motion of the phonons (zero-point phonon energy), which broadens their potential applicability for realizing quantum devices operating at cryogenic temperatures.

[1] Zeiske, S., Kaiser, C., Meredith, P. & Armin, A. Sensitivity of sub-bandgap external quantum efficiency measurements of solar cells under electrical and light bias. *ACS Photonics* **7**, 256–264 (2019).

[2] Kaiser, C., Zeiske, S., Meredith, P. & Armin, A. Determining ultralow absorption coefficients of organic semiconductors from the sub-bandgap photovoltaic external quantum efficiency. *Adv. Opt. Mater.* **8**, 1901542 (2020).

[3] Warby, J. *et al.* Understanding performance limiting interfacial recombination in pin perovskite solar cells. *Adv. Energy Mater.* **12**, 2103567 (2022).

[4] Kaiser, C. *et al.* A universal Urbach rule for disordered organic semiconductors. *Nat. Commun.* **12**, 3988 (2021).

[5] Zeiske *et al.*, Submitted 2022.

11:15 AM EN04.01.03

Role of Dynamic Symmetry Fluctuations for Band Gaps of Halide Perovskites Stefan A. Seidl¹, Xiangzhou Zhu¹, Guy Reuveni², Christian Gehrman¹, Sebastian Caicedo Davila¹, Omer Yaffe² and David Egger¹; ¹Technical University of Munich, Germany; ²Weizmann Institute of Science, Israel

Thermal effects that include lattice expansion and electron-phonon coupling have been discussed to influence one of the most central physical quantities of halide perovskite (HaP) materials, namely their fundamental band gap. Meanwhile, these systems are known to exhibit outstanding dynamic structural properties and vibrational anharmonicity that is detectable already around room temperature. Here, by combining molecular dynamics and Monte-Carlo calculations, based on density functional theory, with reflectance measurements, we investigate the precise thermal characteristics of the band gap in the prototypical CsPbBr₃ HaP. We find that dynamic fluctuations among crystal symmetries play an important role for the electronic structure of HaPs and impact the band gap in these materials in a profound way. Importantly, we demonstrate that the thermal characteristics of the band gap cannot be rationalized using the average crystal symmetry at a given temperature. Using different levels of vibrational theory, anharmonic vibrational contributions are shown to be connected to the dynamic symmetry fluctuations we describe here. Our work establishes a deep and highly relevant connection between the dynamic structural and optoelectronic properties of HaPs.

11:30 AM *EN04.01.04

Electronic Structure of Bulk and Layered Perovskites. George Volonakis and Claudine Katan; Université de Rennes 1, France

In this talk, we discuss the employment of state-of-the-art electronic structure theory for the materials modelling of novel perovskite and perovskite-like materials in bulk and layers. We first review the current opto-electronic application of Pb-free alternatives, and highlight recent efforts on the front of ‘in silico’ materials design. We discuss the case of halide double perovskites, and explore the link between the type and position of the atomic orbitals in the crystal and their electronic structure. This allows us to propose a classification of the octahedra types based on their electronic structure in existing compounds. Furthermore, we take this approach a step further to analyze different types of perovskite and perovskite-like materials, like the vacancy ordered double perovskites and double salts of Ag and Bi, also known as rudorffites. Finally, we take on the layered derivatives and will discuss insights provided by first-principles calculations to reveal inter-layer interactions in real materials, and establish simplified models to show the charge carrier transport limits one can attain.

SESSION EN04.02: Confinement and Excitonic Effects I

Session Chairs: Alexander Urban and George Volonakis

Monday Afternoon, November 28, 2022

Hynes, Level 3, Ballroom A

1:30 PM *EN04.02.01

Excitons in Chemically and Structurally Heterogeneous Halide Perovskites Linn Leppert; University of Twente, Netherlands

Halide double perovskites are an emerging class of photoactive materials with considerable structural and electronic diversity [1,2, 3] and reliable stability towards heat and moisture under ambient conditions. Contrary to ABX₃ halide perovskites like CH₃NH₃PbI₃, the band edge electronic structure of double perovskites is usually dominated by contributions from two different B site metals. This chemical heterogeneity results in a wealth of different band structure properties many of which can be understood based on simple and intuitive symmetry considerations or calculated with comparably little effort from first principles [4]. The same is true for their quasi-2D counterparts which exhibit pronounced band structure changes in the monolayer limit reminiscent of transition metal dichalcogenides [5, 6]. In contrast, much less is known about the excitonic properties of this class of materials. The calculation of accurate optical spectra is computationally demanding and whether simple physically motivated exciton models like the Wannier-Mott model are reliable for these quaternary, heterogeneous materials, is hard to predict *a priori*.

In this talk I will discuss how first principles numerical modelling techniques such as Green’s function-based many-body perturbation theory can provide an atomistic understanding of excitons in chemically and structurally heterogeneous halide perovskites. I will show that these materials can feature a wide

range of different excitons, from strongly localized, bound, or resonant excitons that fall outside the tenets of the Wannier-Mott model [7] to strongly delocalized, weakly bound Wannier-Mott excitons [8]. Our results can be traced back to the symmetry and orbital character of the band edges of these double perovskites – a consequence of their chemical heterogeneity, and can be tuned via chemical substitution, dimensional reduction, layer thickness and layer stacking. We thus provide a fundamental understanding and reliable design rules for excitons in this family of materials.

- [1] F. Giustino, H. Snaith, ACS Energy Lett. 1, 1233 (2016).
- [2] M. Filip, F. Giustino, Proc. Nat. Acad. Sci. 115, 5397 (2018).
- [3] M. Wolf, B. Connor, A. Slavney, H. Karunadasa, Ang. Chem. Int. Ed. 60, 16264 (2021).
- [4] A. Slavney, B. Connor, L. Leppert, H. Karunadasa, Chem. Sci. 10, 11041 (2019).
- [5] B. Connor, L. Leppert, M. D. Smith, J.B. Neaton, H. I. Karunadasa, J. Am. Chem. Soc. 140, 5235 (2018)
- [6] B. Connor, R.-I. Biega, L. Leppert, H. I. Karunadasa, Chem. Sci. 11, 7708 (2020).
- [7] R. I. Biega, M. Filip, L. Leppert, J. B. Neaton, J. Phys. Chem. Lett. 12, 2057 (2021).
- [8] R. I. Biega, Y. Chen, M. Filip, L. Leppert, in preparation.

2:00 PM EN04.02.02

Excitonic Properties of Vacancy Ordered Double Perovskites—Electron-Hole Coupling and GW Quasi-Particles Bruno Cucco, [Mikael Kepenekian](#) and George Volonakis; Univ Rennes, ENSCR, INSA Rennes, CNRS, ISCR - UMR 6226, France

Over the past decade ABX_3 halide perovskites based on Pb have emerged as a most-promising class of materials. To-date they have been employed for record-breaking solar-cells¹, highly-efficient light-emitters², new photo-catalysts³ and even as X-ray detectors⁴. A_2BX_6 vacancy ordered double perovskites (VODP) are air-stable and environmentally friendly (Pb-free) that have been proposed as alternatives⁵, to halide perovskites. Yet, VODP materials have not achieved the high performance of their Pb-based counterparts. In this work, we thoroughly analyze the properties of the VODP family of materials by employing state-of-art ab initio calculations to unveil the key details of the electronic structure and the effects of electron-hole coupling on the optical properties.

We sample the VODP structures by picking prototypes accordingly to the electronic configuration of the tetravalent metal at the B-site. That is, there are three possible closed-shell metal sites, with valences composed of either *s*-, *p*- or *d*-orbitals. In particular, we select known materials^{5,6,7} Cs_2TeX_6 , Cs_2SnX_6 , and Cs_2ZrX_6 (with X=Br, I) for the groups with a valency comprised of an s, p and d closed-shell, respectively. The structural properties are first investigated, and show how the size of the vacancy, is in fact tuned solely by the size of the halogen. We assess the mechanical stability of each crystalline lattice by means of phonons calculations. The electronic structures are investigated within the GW many-body green's function method, and we obtain band-gaps spanning a range of 1.5-5.0 eV at G_0W_0 . More importantly, we discuss the effects of the substitutional engineering on the dispersion of the electronic bands, and relate our findings to the expected charge carrier mobilities of each type of VODP. The optical and excitonic properties of these compounds are investigated within the independent particle approach, and by solving the Bethe-Salpeter equation (BSE). We report the exciton binding energies and dark-bright exciton exchange splitting for each type of VODP. Finally, we address the exciton symmetries by performing a complete symmetry analysis of the compound's band structure and excitonic wavefunctions, on which a direct link between these and the metal site species is established.

Overall, we explore comparatively the role of electron-hole coupling and GW quasi-particles in VODP materials, and explain its correlation with the choice of the B-metal and X-halide sites. These results shed light on the suitability and the prospect of VODP type might exhibit, due to their opto-electronic and excitonic properties. Finally, we identify the most and least promising materials that could act as photo-active materials or for selective charge transport layers in light-emitting and solar-cell applications.

Acknowledgments

The research leading to these results has received funding from the Chaire de Recherche Rennes Metropole project, and from the European Union's Horizon 2020 program, through a FET Open research and innovation action under the grant agreement No 862656 (DROP-IT).

References

- [1] Amran Al-A. *et al.*, Science **370**, 1300 (2020)
- [2] Yang D. *et al.*, Nat. Commun. **12**, 4295 (2021)
- [3] Pradhan S. *et al.*, Nanoscale Adv. **3**, 1464 (2021)
- [4] Wu. H. *et al.*, Matter **4**, 144 (2021)
- [5] Lee B. *et al.*, J. Am. Chem. Soc. **136**, 15379 (2014)
- [6] Xu Y. *et al.*, ACS Photonics **6**, 196 (2019)
- [7] Cucco B. *et al.*, Appl. Phys. Lett. **119**, 181903 (2021)

2:15 PM *EN04.02.03

Revealing Charge-Carrier Complexes and Interactions in Single Lead-Halide Perovskites Nanocrystal [Brahim Lounis](#); Université de Bordeaux, France

Lead halide perovskites open great prospects for optoelectronics and a wealth of potential applications in quantum optical and spin-based technologies. Precise knowledge of the fundamental optical and spin properties of charge-carrier complexes at the origin of their luminescence is crucial in view of the development of these applications. On nearly bulk Cesium-Lead-Bromide single perovskite nanocrystals, which are the test bench materials for next-generation devices as well as theoretical modeling, we perform low-temperature magneto-optical spectroscopy to reveal their entire band-edge exciton fine structure and charge-complex binding energies. We demonstrate that the ground exciton state is dark and lays several millielectronvolts below the lowest bright exciton sublevels, which settles the debate on the bright-dark exciton level ordering in these materials. More importantly, combining these results with spectroscopic measurements on various perovskite nanocrystal compounds, we show evidence for universal scaling laws relating the exciton fine-structure splitting, the trion and biexciton binding energies to the band-edge exciton energy in lead-halide perovskite nanostructures, regardless of their chemical composition. These scaling laws solely based on quantum confinement effects and dimensionless energies offer a general predictive picture for the interaction energies within charge-carrier complexes photo-generated in these emerging semiconductor nanostructures.

2:45 PM EN04.02.04

Rabi Oscillations of Exciton-Polariton in Phase-Changing Lead Halide Perovskites [Hyeon-Seo Choi](#), Minjee Ko, Jin-Woo Jung, Young-Jun Lee, Taejin Lee, Dongha Kim, Shinbuhm Lee and Chang-Hee Cho; DGIST, Korea (the Republic of)

Organic-inorganic hybrid lead halide perovskites have invoked much interest in cavity quantum electrodynamics due to their excellent excitonic properties

including strong exciton binding energy and high oscillation strength. Interestingly, the perovskites exhibit the crystallographic phase transition, resulting in tunable properties of excitons and polaritons, but the underlying physics remains unexplored. In this work, we have demonstrated tunable Rabi oscillations of exciton-polariton in the lead halide perovskite microcavity, which experiences the phase transition from orthorhombic through tetragonal to cubic phases for varying temperatures. The Rabi splitting can be tuned by the emergence of ferroelectricity to modify the exciton oscillator strength in the noncentrosymmetric tetragonal phase, where the oscillator strength and Rabi splitting are minimized. Our results provide an insight into the emerging functionalities of polariton devices by utilizing the ferroelectric semiconductors, which enable the realization of tunable quantum devices.

3:00 PM BREAK

3:30 PM *EN04.02.05

Exciton-Polaron Quantum Dynamics in Ruddlesden-Popper Metal-Halides [Carlos Silva](#); Georgia Institute of Technology, United States

While polarons --- charges bound to a lattice deformation induced by electron-phonon coupling --- are primary photoexcitations at room temperature in bulk metal-halide hybrid organic-inorganic perovskites (HOIP), excitons --- Coulomb-bound electron-hole pairs --- are the stable quasi-particles in their two-dimensional (2D) analogues. Here we address the fundamental question: are polaronic effects consequential for excitons in 2D-HIOPs? Based on our recent work, we argue that polaronic effects are manifested intrinsically in the exciton spectral structure, which is comprised of multiple non-degenerate resonances with constant inter-peak energy spacing. We highlight measurements of population and dephasing dynamics that point to the apparently deterministic role of polaronic effects in excitonic properties. We contend that an interplay of long-range and short-range exciton-lattice couplings give rise to exciton polarons, a character that fundamentally establishes their effective mass and radius, and consequently, their quantum dynamics. Given this complexity, a fundamentally far-reaching issue is how Coulomb-mediated many-body interactions---elastic scattering such as excitation-induced dephasing, inelastic exciton bimolecular scattering, and multi-exciton binding---depend upon the specific exciton-lattice coupling within the structured excitation lineshape. We measure the intrinsic and density-dependent exciton dephasing rates of the multiple excitons and their dependence on temperature by means of two-dimensional coherent excitation spectroscopy.

4:00 PM EN04.02.06

Tuning the Structure and Dynamics of 2D Hybrid Halide Perovskites [Ferdinand C. Grozema](#); Delft University of Technology, Netherlands

Two-dimensional hybrid perovskites are promising materials for a wide range of opto-electronic applications. Their properties markedly differ from those of their three-dimensional analogues, but they also offer additional routes to engineer their properties by introducing specific functionality in the organic component. One of the key features of 2D hybrid perovskites is their relatively soft structure that allows substantial structural fluctuations, both during synthesis and after deposition. The softness of the material leaves considerable room to manipulate the structure of the inorganic layer through external stimuli such as pressure and adsorption of molecules on the surface, or internal effects such as strain cause by the organic separating layers. The nature of the organic component directly affects the structural and dynamic properties of the inorganic lattice. [1] Such changes in the structure and dynamics translate to changes in the electronic properties of the materials. Therefore, by controlling the structure and interactions in the organic part it is possible to tune important physical parameters of the materials, including the charge carrier mobility, exciton binding energy, carrier lifetime and the decay pathways of charges and excited states.

In this work we computationally explore approaches to engineer the structural and dynamics properties of the 2D perovskite materials by introducing specific organic moieties that have additional functionality. The layer of organic molecules influences the structure and dynamics of the inorganic layer, which also has an immediate effect on the electronic structure. We have performed classical molecular dynamics simulations for a variety of 2D halide perovskites, including Ruddlesden-Popper and Dion-Jacobson structures. We show that the nature of the organic cation determines the average structure and the structural dynamics to a large extent. This indicates that these properties can be tuned significantly by exploiting specific intermolecular interactions in the organic layer. The structure and dynamics of the organic layer directly affect the structure and dynamics of the inorganic layer, for instance the disorder in the octahedral tilt angles. This should lead to marked effect on the steady state electronic properties but also offers a handle to influence the strength and nature of the electron-phonon coupling in these materials.

The soft nature of 2D hybrid perovskites suggest a marked dependence of the electronic properties on external stimuli, for instance the strain in the material. Strain can be introduced by applying external pressure, either uniformly or by bending of the material. Using pressure dependent molecular dynamics simulations we also show that the response to external pressure depends strongly on the nature of the organic layer and also here substantial tuning is possible through structural engineering

[1] M.B. Fridrikson, N. van der Meer, J. de Haas and F.C. Grozema, *J. Phys. Chem. C* **124** (2020) 28201

4:15 PM EN04.02.07

Dimensionality-Controlled Organic Semiconductor-Incorporated Perovskite Quantum Wells [Jee Yung Park](#) and Letian Dou; Purdue University, United States

Two-dimensional organic semiconductor-incorporated perovskites (OSiP) are an emerging family of hybrid materials featuring a built-in quantum well architecture. However, to date, complete tunability in terms of structures and properties has not been established owing to synthetic challenges. Controlling the dimensionality by simultaneously manipulating slab thickness of the inorganic layers while modulating conjugation length of the organic layers is yet to be achieved. Here we demonstrate a general method to synthesize phase pure dimensionality-controlled OSiP single crystals by introducing a novel solvent system. The energy band offsets and exciton dynamics at the organic-inorganic interfaces can therefore be precisely controlled. Furthermore, we reveal that longer and more planar π -conjugated organic cations induce a more rigid inorganic crystal lattice, which leads to suppressed exciton-phonon interactions and superior optoelectronic properties as compared to conventional two-dimensional perovskites. As a demonstration, optically driven lasing behavior with dramatically decreased lasing thresholds was realized.

4:30 PM EN04.02.08

Understanding Sub-Bandgap Luminescence in Ruddlesden-Popper 2D Hybrid Perovskites [Igal Levine](#), Rowan MacQueen, Artem Musiienko, Dorothee Menzel, Hannes Hempel, Lars Korte and Thomas Dittrich; Helmholtz-Zentrum Berlin, Germany

Broad band luminescence, and/or sub-bandgap emission in Ruddlesden-Popper 2D hybrid perovskites (hereinafter termed 2D HaPs) has been widely reported in the literature, and its origin is still under debate, with two possible suggested mechanisms – Self-Trapped Excitons (STEs), vs. defect emission, i.e. radiative recombination via defect states within the bandgap.¹⁻³ The latter is especially important for optoelectronic applications of 2D HaPs, since non-radiative recombination of electronic charge carriers via defect states can strongly limit the performance of devices, especially the open circuit voltage (V_{oc}) of solar cells or the quantum efficiency of light emitting diodes. Distinguishing between the two recombination mechanisms (STE and defect

emission) is challenging, yet of immense importance to identify intrinsic vs. extrinsic limiting factors, and constitutes a necessary step for further device development.

In my talk, I will focus on butylammonium lead iodide (BA₂PbI₄) single crystals, as well as exfoliated layers and thin films, and show how a combination of complementary methods involving both sub-bandgap and supra-bandgap excitation such as photoluminescence, modulated and time-resolved surface photovoltage in the fixed capacitor setup, constant final state yield spectroscopy⁴, and photo-Hall measurements, suggest that *defect states* rather than STE, are the main cause for the sub-band gap emission in BA₂PbI₄. I will discuss the nature of these defect states, their relative position (surface vs. bulk), their energetic position in the bandgap, and their impact on the optoelectronic properties of BA₂PbI₄, compared to its well-studied 3D-analog methylammonium lead iodide (MAPbI₃).

References:

- (1) Kahmann, S.; Tekelenburg, E. K.; Duim, H.; Kamminga, M. E.; Loi, M. A. Extrinsic Nature of the Broad Photoluminescence in Lead Iodide-Based Ruddlesden–Popper Perovskites. *Nat. Commun.* **2020**, *11* (1), 1–8.
- (2) Liang, M.; Lin, W.; Zhao, Q.; Zou, X.; Lan, Z.; Meng, J.; Shi, Q.; Castelli, I. E.; Canton, S. E.; Pullerits, T.; et al. Free Carriers versus Self-Trapped Excitons at Different Facets of Ruddlesden-Popper Two-Dimensional Lead Halide Perovskite Single Crystals. *J. Phys. Chem. Lett.* **2021**, *12* (20), 4965–4971.
- (3) Paritmongkol, W.; Powers, E. R.; Dahod, N. S.; Tisdale, W. A. Two Origins of Broadband Emission in Multilayered 2D Lead Iodide Perovskites. *ACS Publ.* **2020**, *11* (20), 8572.
- (4) Menzel, D.; Tejada, A.; Al-Ashouri, A.; Levine, I.; Guerra, J. A.; Rech, B.; Albrecht, S.; Korte, L. Revisiting the Determination of the Valence Band Maximum and Defect Formation in Halide Perovskites for Solar Cells: Insights from Highly Sensitive Near–UV Photoemission Spectroscopy. *ACS Appl. Mater. Interfaces* **2021**, *13* (36), 43540–43553.

4:45 PM EN04.02.09

Revealing Excitonic Behaviour in Vacancy-Ordered Titanium Perovskites (Cs₂TiX₆) Seán R. Kavanagh¹, Shanti Maria Liga², Gerasimos Konstantatos², David O. Scanlon³ and Aron Walsh⁴; ¹University College London & Imperial College London, United Kingdom; ²ICFO–The Institute of Photonic Sciences, Spain; ³University College London, United Kingdom; ⁴Imperial College London, United Kingdom

High-performance, lightweight solar cells with low-cost and non-toxic substituents are a major target in the field of solar photovoltaics.^{1–4} Perovskite-inspired materials have emerged as promising candidates for this goal, with researchers employing materials design strategies including structural, dimensional and compositional transformations to avoid the use of rare and toxic elemental constituents, while attempting to maintain high optoelectronic performance. These strategies have recently been invoked to propose titanium-based vacancy-ordered halide perovskites (A₂TiX₆) for photovoltaic operation, exhibiting suitable electronic bandgaps, strong optical absorption, benign defect properties, long carrier diffusion lengths and high stability.^{5–9}

Theoretical investigations of the electronic structure of this material, however, consistently overestimate the energy band gap of this material^{5,8,10–15} — the most important property for photovoltaic application. In this work,¹⁶ we reveal strong excitonic effects as the origin of this discrepancy between theory and experiment; a consequence of both low structural dimensionality and orbital localisation.

These findings have important implications for the potential optoelectronic application of these compounds, while also highlighting the crucial importance of frontier-orbital character for chemical substitution materials design strategies.

- (1) Huang, Y.-T.; Kavanagh, S. R.; Scanlon, D. O.; Walsh, A.; Hoye, R. L. Z. *Nanotechnology* **2021**, *32* (13), 132004.
- (2) Wang, Y.[‡] & Kavanagh, S. R.[‡]; Burgués-Ceballos, I.; Walsh, A.; Scanlon, D.; Konstantatos, G. *Nat. Photon.* **2022**, *16* (3), 235–241.
- (3) G. Tang, P. Ghosez, and J. Hong. *J. Phys. Chem. Lett.* **12**, 4227 (2021).
- (4) Huang, Y.-T.[‡] & Kavanagh, S. R.[‡]; Hoye, R. L. Z.; Walsh, A.; Scanlon, D. O. *Nature Communications*. (In review)
- (5) Ju, M.-G.; Chen, M.; Zhou, Y.; Garces, H. F.; Dai, J.; Ma, L.; Padture, N. P.; Zeng, X. C. *ACS Energy Lett.* **2018**, *3* (2), 297–304.
- (6) Liga, S. M.; Konstantatos, G. *J. Mater. Chem. C* **2021**, *9* (34), 11098–11103.
- (7) Chen, M.; Ju, M.-G.; Carl, A. D.; Zong, Y.; Grimm, R. L.; Gu, J.; Zeng, X. C.; Zhou, Y.; Padture, N. P. *Joule* **2018**, *2* (3), 558–570.
- (8) Euvrard, J.; Wang, X.; Li, T.; Yan, Y.; Mitzi, D. B. *J. Mater. Chem. A* **2020**, *8* (7), 4049–4054.
- (9) Maughan, A. E.; Ganose, A. M.; Bordelon, M. M.; Miller, E. M.; Scanlon, D. O.; Neilson, J. R. *D J. Am. Chem. Soc.* **2016**, *138* (27), 8453–8464.
- (10) Cucco, B.; Boudier, G.; Pedesseau, L.; Katan, C.; Even, J.; Kepenekian, M.; Volonakis, G. *Appl. Phys. Lett.* **2021**, *119* (18), 181903.
- (11) Li, W.; Zhu, S.; Zhao, Y.; Qiu, Y. *Journal of Solid State Chemistry* **2020**, *284*, 121213.
- (12) Mahmood, Q.; Hassan, M.; Yousaf, N.; AlObaid, A. A.; Al-Muhimeed, T. I.; Morsi, M.; Albalawi, H.; Alamri, O. A. *Materials Science in Semiconductor Processing* **2022**, *137*, 106180.
- (13) Kong, D.; Cheng, D.; Wang, X.; Zhang, K.; Wang, H.; Liu, K.; Li, H.; Sheng, X.; Yin, L. *J. Mater. Chem. C* **2020**, *8* (5), 1591–1597.
- (14) Liu, D.; Zha, W.; Yuan, R.; Chen, J.; Sa, R. *New J. Chem.* **2020**, *44* (32), 13613–13618.
- (15) Tsuyama, M.; Suzuki, S. *J. Phys. Soc. Jpn.* **2019**, *88* (10), 104802.
- (16) Kavanagh, S. R.; Savory, C. N.; Liga, S. M.; Konstantatos, G.; Walsh, A.; Scanlon, D. O. *ACS Energy Lett.* (In submission)

SESSION EN04.03/EN02.04: Joint Session I: Charge Transport and Defects—Characterization and Modelling

Session Chairs: Wolfgang Tress, Alexander Urban and Kai Zhu

Tuesday Morning, November 29, 2022

Hynes, Level 3, Ballroom A

8:30 AM EN04.03/EN02.04.01

Counting Defects is the Pathway to Understand Degradation in Lead Halide Perovskites Michel De Keersmaecker, Neal R. Armstrong and Erin L. Ratcliff, The University of Arizona, United States

Stability in perovskites is often connected to the presence of electronic defects, but rarely their chemical nature, reactivity and mobility are considered. Only the development of a powerful, quality and durability evaluation tool that allows direct probing of these reactive defect densities under *operando* conditions (i.e. away from equilibrium conditions) is able to correlate their chemical, electronic and physical makeup to irreversible degradation processes in lead halide perovskite films.

In this work, an electrochemical methodology based on a simple half-cell device stack using a "peel and stick" electrolyte top contact that is easily

combined with various existing spectroscopic and surface characterization techniques introduces a new measurement approach to study stability across atomic-to-molecular-to device length scales. Systematic modulation of the potential and the introduction of specific redox probes to support electron and hole injection enables us to draw the most complete electronic band structure of a perovskite and by extension any semiconductor. By reducing charging currents and improving energy resolution, unprecedented detection limits are reached when probing surface defects close to both valence and conduction band with the additional benefit of identifying their (electro)chemical reactivity. Combined with X-ray scattering and photoelectron techniques, we have recently discovered that controlled polarization allows the collection of bias-dependent structural data to gain insight into interfacial and bulk degradation mechanisms during real-time operation.

Overall, this probe has demonstrated to overcome challenges for defect quantification in printable electronic materials and to promote *operando* characterization of perovskites, organic semiconductors, quantum dots, material blends and device stacks, where the removable solid electrolyte functions as the “top contact”. This type of advanced electrochemical characterization platform will prove to be crucial for the quality control of low cost (opto)electronic materials and device stacks as well as the improvement of their stability and durability in order to realize industry-scalable technologies in the field of photovoltaics, charge storage systems, photoelectrochemical cells, etc.

8:45 AM EN04.03/EN02.04.02

Effects of Hole-Transport Layer and Interface Passivation on Photoinduced Halide Segregation in Mixed-Halide Perovskite Solar Cells Vincent J. Lim¹, Alexander J. Knight¹, Robert Oliver¹, Henry Snaith¹, Michael Johnston¹ and Laura Herz^{1,2}; ¹University of Oxford, United Kingdom; ²Technical University of Munich, Germany

Mixed-halide perovskites offer ideal bandgaps for tandem solar cells, but photoinduced halide segregation compromises photovoltaic device performance. We present our recent work [1] wherein we explored the influence of a hole-transport layer, necessary for a full device, by monitoring halide segregation through in situ, concurrent X-ray diffraction and photoluminescence measurements to disentangle compositional and optoelectronic changes. Our work demonstrates that top coating FA_{0.83}CS_{0.17}Pb(Br_{0.4}I_{0.6})₃ perovskite films with a PTAA hole-extraction layer surprisingly leads to suppression of halide segregation because photogenerated charge carriers are rapidly trapped at interfacial defects that do not drive halide segregation. However, the generation of iodide-enriched regions near the perovskite/PTAA interface enhances hole back-transfer from the PTAA layer through improved energy level offsets, increasing radiative recombination losses. It is further found that while passivation with a piperidinium salt slows halide segregation in perovskite films, the addition of a PTAA top-coating accelerates such effects, elucidating the specific nature of trap types that are able to drive the halide segregation process. This report highlights the importance of selective passivation techniques for achieving efficient and stable wide-bandgap perovskite photovoltaic devices.

[1] Lim *et al.* Adv. Funct. Mater. **2022**, 2204825, DOI: 10.1002/adfm.202204825

9:00 AM DISCUSSION TIME

9:15 AM EN04.03/EN02.04.04

Visualizing Macroscopic Inhomogeneities in Perovskite Solar Cells Akash Dasgupta¹, Suhas Mahesh^{2,1} and Henry Snaith¹; ¹University of Oxford, United Kingdom; ²University of Toronto, United Kingdom

Despite the incredible progress made, the highest efficiency perovskite solar cells are still restricted to small areas (<1 cm²). In large part, this stems from a poor understanding of the widespread spatial heterogeneity in devices. Conventional techniques to assess heterogeneities can be time consuming, operate only at microscopic length scales, and demand specialized equipment. We overcome these limitations by using luminescence imaging to reveal large, millimeter-scale heterogeneities in the inferred electronic properties. We determine spatially resolved maps of “charge collection quality”, measured using the ratio of photoluminescence intensity at open and short circuits. We apply these methods to quantify the inhomogeneities introduced by a wide range of transport layers, thereby ranking them by suitability for upscaling. We reveal that top-contacting transport layers are the dominant source of heterogeneity in the multilayer material stack. We suggest that this methodology can be used to accelerate the development of highly efficient, large-area modules, especially through high-throughput experimentation.

9:30 AM *EN04.03/EN02.04.05

Models of Heterogeneity in Metal Halide Perovskites Aron Walsh; Imperial College London, United Kingdom

The deeper you stare at metal halide perovskites, the more imperfections you become aware of. Dilute point defects, such as charged vacancies and interstitials, exist in a diverse landscape of extended defects including dislocations, stacking faults, and grain boundaries. To make matters worse, there are often chemical gradients in the A, B or X crystallographic positions, e.g. in mixed formamidinium/methylammonium, tin/lead, or iodide/bromide systems. I will discuss our growing understanding of these phenomena at the atomic scale drawing from our work from materials modelling [1,2] and linked to multimodal characterisation [3,4]. The use of defect tolerance as a metric to develop and screen (post) perovskite materials will be critically addressed. This research is part of a Leverhulme Trust funded collaboration with the group of Sam Stranks and used the UK National Supercomputer ARCHER2 which is supported by UKRI.

1. Evolutionary exploration of polytypism in lead halide perovskites, Chemical Science 12, 12165 (2021)
2. Giant Huang–Rhys factor for electron capture by the iodine interstitial in perovskite solar cells, Journal of the American Chemical Society 143, 9123 (2021)
3. Performance-limiting nanoscale trap clusters at grain junctions in halide perovskites, Nature 580, 360 (2020)
4. Stabilized tilted-octahedra halide perovskites inhibit local formation of performance-limiting phases, Science 374, 1598 (2021)

10:00 AM BREAK

10:30 AM *EN04.03/EN02.04.06

Charge Carrier Recombination on Different Length Scales in Halide Perovskites Samuel D. Stranks; University of Cambridge, United Kingdom

Halide perovskites are promising materials for next-generation light harvesting and light emission applications. However, an absolute understanding of charge carrier recombination on all relevant length scales is essential to maximise their potential in such applications.

Here, I will outline recent work elucidating charge carrier properties in a range of halide perovskite semiconductors from the macroscale down to the nanoscale. I will report on both 3D systems dominated by free carriers and quasi-2D and 2D systems dominated by exciton recombination, highlighting the interplay between radiative recombination, carrier trapping and carrier diffusion. I will show how these photophysical properties relate to material properties, and how this information can help to further drive material and device performance optimisation.

11:00 AM EN04.03/EN02.04.07

Investigating Lead Halide Perovskites by Synchrotron X-Ray Scanning Tunneling Microscopy Sarah Wiegbold¹, Nozomi Shirato¹, Lea Nienhaus² and Volker Rose¹; ¹Argonne National Laboratory, United States; ²Florida State University, United States

Despite the remarkable success of lead halide perovskites, it was recognized early on that external factors, e.g. light exposure, elevated temperatures, or electric fields can disrupt the perovskite lattice, resulting in non-photoactive phases or even in film decomposition. This phenomenon can be mainly attributed to the ionic bonding character of the lead-halide sub-lattice: both anions and cations can migrate through the perovskite film enabled by bulk and surface defects such as vacancies, interstitials or antisite substitution. Thus, to improve the stability and performance of lead halide perovskites a fundamental understanding of the impact of external factors on the local ionic chemical environment is required, which enables the development of mitigation strategies for applications in photovoltaics and light-emitting diodes.

In this contribution, we present a novel approach to measure the change in the local halide environment in perovskite thin films under applied external electric fields by synchrotron x-ray scanning tunneling microscopy (SX-STM). We investigate the influence of various applied bias polarities on the structural change of the halide ions at the perovskite interface by probing the iodide M_{4,5} absorption edge by x-ray absorption spectroscopy (XAS) in the far field by SX-STM. By performing time-dependent XAS studies, we further track the change in the halide environment under continuous cycling of the applied bias. Additionally, to investigate the impact of the electric field on the spatial variation on the surface, we perform SX-STM experiments in the near field. In this geometry, the STM tip is brought into tunneling range which results in a strong field enhancement, thus local information can be obtained with nanometer resolution. Complemented by theoretical calculations, our results provide an in-depth understanding of crystal structure changes under electric fields investigated by STM.

11:15 AM EN04.03/EN02.04.08

Strain-Induced Domains Introduce Anisotropic Charge Diffusion in Perovskite Absorber Ilka Hermes^{1,2}, Andreas Best², Kaloian Koynov², David S. Ginger³, Liam Collins⁴, Hans-Jürgen Butt² and Stefan A. Weber²; ¹Leibniz Institute for Polymer Research Dresden e.V., Germany; ²Max Planck Institute for Polymer Research, Germany; ³University of Washington, United States; ⁴Oak Ridge National Laboratory, United States

A heterogeneous lattice strain distribution in the polycrystalline absorber layer of perovskite solar cells (PSCs) has been connected to a range of detrimental phenomena including an increase in nonradiative recombination,¹ an acceleration of the material degradation² as well as an overall loss in efficiency.³ On the other hand, during a controlled crystallization via solvent annealing,⁴ the prototype perovskite absorber methylammonium lead iodide releases lattice strain by forming well-ordered subcrystalline periodic domains that alternate in their orientation of the long crystal axis.⁵ Due to their ferroelastic nature, the arrangement of such domains can be influenced by heat treatments above the critical phase transition temperature and external mechanical stress.^{6,7} While the ferroelastic domains appear to exhibit a benign effect on the nonradiative recombination,⁸ we observed in our correlated electromechanical atomic force and spatial and time-resolved photoluminescence microscopy study that the domains introduce an anisotropy in the charge carrier transport: charges diffusing parallel to the domains were faster than charges diffusing perpendicular to the domains.⁹ Moreover, we found that the domains appear to be oriented in a 90° angle with respect to the (110) crystal plane, thus, offering an explanation for the observed improved performance for PSCs, in which the perovskite absorber features a preferential (110) orientation.¹⁰ Here, a faster charge transport parallel to the domains may increase the charge extraction and thereby enhance the efficiency.

1. T. W. Jones, A. Oshero, M. Alsari, M. Sponseller, B. C. Duck, Y.-K. Jung, C. Settens, F. Niroui, R. Brenes and C. V. Stan, *Energy & Environmental Science*, 2019, **12**, 596-606.
2. J. Zhao, Y. Deng, H. Wei, X. Zheng, Z. Yu, Y. Shao, J. E. Shield and J. Huang, *Science advances*, 2017, **3**, ea05616.
3. K. Nishimura, D. Hirota, M. A. Kamarudin, Q. Shen, T. Toyoda, S. Iikubo, T. Minemoto, K. Yoshino and S. Hayase, *ACS Applied Materials & Interfaces*, 2019, **11**, 31105-31110.
4. Z. Xiao, Q. Dong, C. Bi, Y. Shao, Y. Yuan and J. Huang, *Advanced Materials*, 2014, **26**, 6503-6509.
5. I. M. Hermes, S. A. Bretschneider, V. W. Bergmann, D. Li, A. Klase, J. Mars, W. Tremel, F. Laqui, H.-J. Butt, M. Mezger, R. Berger, B. J. Rodriguez and S. A. L. Weber, *The Journal of Physical Chemistry C*, 2016, **120**, 5724-5731.
6. R. M. Kennard, C. J. Dahlman, R. A. DeCrescent, J. A. Schuller, K. Mukherjee, R. Seshadri and M. L. Chabiny, *Chemistry of Materials*, 2020, **33**, 298-309.
7. E. Strelcov, Q. Dong, T. Li, J. Chae, Y. Shao, Y. Deng, A. Gruverman, J. Huang and A. Centrone, *Science advances*, 2017, **3**, e1602165.
8. X. Xiao, W. Li, Y. Fang, Y. Liu, Y. Shao, S. Yang, J. Zhao, X. Dai, R. Zia and J. Huang, *Nature communications*, 2020, **11**, 1-7.
9. I. M. Hermes, A. Best, L. Winkelmann, J. Mars, S. M. Vorpahl, M. Mezger, L. Collins, H.-J. Butt, D. S. Ginger, K. Koynov and S. A. L. Weber, *Energy & Environmental Science*, 2020, **13**, 4168-4177.
10. P. Docampo, F. C. Hanusch, N. Giesbrecht, P. Angloher, A. Ivanova and T. Bein, *Apl Materials*, 2014, **2**, 081508.

11:30 AM *EN04.03/EN02.04.09

Heterointerface and Intragrain Microstructures of Perovskite Semiconductors Yuan Yuan Zhou; Hong Kong Baptist University, China

Heterointerface and intragrain microstructures can be key factors influencing performance of perovskite semiconductors, which have been less studied. In my talk, I will discuss our recent advances on the high-resolution characterization and novel tailoring of these microstructures, advancing our fundamental understanding of microscopic structure-property-performance relationship in perovskites. Specifically, I will demonstrate the design and synthesis of an interpenetrating interface of charge-transport layer/perovskite which mitigates the (opto-)mechanical issue of perovskite solar cells, followed by a discussion on the use of a novel scanning transmission electron microscopy methodology to unravel performance-limiting intragrain interfaces in perovskite solar cells.

SESSION EN04.04: Structure-Property Relations and Stability
 Session Chairs: Linn Leppert and Sarah Wiegbold
 Tuesday Afternoon, November 29, 2022
 Hynes, Level 3, Ballroom A

1:30 PM *EN04.04.01

Inelastic Light Scattering from Disordered Crystals Omer Yaffe; Weizmann Institute, United States

In the past several years, my group investigated the structural dynamics of halide, oxide, and sulfide perovskite crystals by means of Raman scattering. The structural dynamics of the perovskite crystals are fascinating because they exhibit a plethora of anharmonic effects such as soft modes, order-disorder phase transitions, and local fluctuations.

Such effects have significant implications on the electronic properties (e.g. dielectric response, carrier lifetimes, and carrier mobilities) of the crystals, especially at finite temperatures where these properties are invariably truly relevant.

Importantly they may lead to the relaxation of the symmetry-based selection rules for Raman scattering.

On one hand, the resulting Raman spectra are difficult to interpret, on the other, they are rich in information regarding the crystal properties.

In this talk, I will review our journey to unlock the mysteries of perovskite structural dynamics, using Raman spectra.

First, I will demonstrate and discuss a common discrepancy between x-ray diffraction data showing perfect single crystals and Raman data showing disorder.

Next, I will explain how we use generalized models of scattering to settle this discrepancy.

Finally, I will show that the intensity of the scattered light, which is an underused experimental observable, can be utilized to learn much regarding crystal properties such as dielectric response.

2:00 PM EN04.04.02

Structural Dynamics and Sharp Band-to-Band Transitions in Halide Perovskites Sebastian Caicedo Davila, Christian Gehrman, Xiangzhou Zhu and David Egger; Technical University of Munich, Germany

Solar cells based on halide perovskites (HaPs) have achieved remarkable performance, comparable with conventional, high-quality inorganic semiconductors. However, a variety of fundamental aspects in these materials remain enigmatic. For example, an important difference to conventional semiconductors is that HaPs exhibit strong vibrational anharmonicities already at around room temperature, which impact key optoelectronic properties, such as carrier transport, Urbach energy, among others. In this contribution, we investigate the impact that anharmonic lattice dynamics have on the optical absorption of the prototypical HaP, CsPbBr₃. Using molecular dynamics simulations based on density functional theory, we disentangle and better understand the effect of Cs dynamics on the pair-distribution function, as well as its coupling to the Pb-Br framework. Furthermore, we show that large Br displacements occur on planes transversal to the Pb-Br-Pb bonding axis. This *transversality* results in ultrashort dynamic correlations and sharp joint-density of states at finite temperature, as revealed when we contrast the results for HaPs to the case of PbTe, which shares several important properties with CsPbBr₃, but cannot exhibit any *transversality*. Finally, we discuss the interrelations of lattice anharmonicity, structural flexibility and bonding mechanisms in HaPs, and how they can enable their outstanding optoelectronic properties, which could provide guidelines for future materials design.

1. X. Zhu, S. Caicedo-Dávila, C. Gehrman, and D. A. Egger, ACS Appl. Mater. Interfaces 14, 22973 (2022).

2. C. Gehrman, S. Caicedo-Dávila, X. Zhu, and D. A. Egger, Adv. Sci. 9, 2200706 (2022).

2:15 PM EN04.04.03

The Origin of Phase Impurities in FA-Rich Halide Perovskites and Their Impact on Both Performance and Stability Tiarnan A. Doherty¹, Stuart Macpherson¹, Satyawan D. Nagane¹, Dominik Kubicki², Affan Iqbal¹, Elizabeth Tennyson¹, Francesco Simone Ruggeri³, Sofia Kosar⁴, Andrew Winchester⁴, Young-Kwang Jung⁵, Yu-Hsien Chiang¹, Kyle Frohna¹, Miguel Anaya¹, Keshav M. Dani⁴, Aron Walsh⁶, Paul Midgley¹ and Samuel D. Stranks¹; ¹University of Cambridge, United Kingdom; ²University of Warwick, United Kingdom; ³Wageningen University & Research, Netherlands; ⁴Okinawa Institute of Science and Technology, Japan; ⁵Yonsei University, Korea (the Republic of); ⁶Imperial College London, United Kingdom

Halide perovskite materials exhibit promising performance characteristics for low-cost optoelectronic applications. Photovoltaic devices fabricated from perovskite absorbers have reached power conversion efficiencies above 25.5 % in single-junction devices and 29.5% in tandem devices. Formamidinium (FA) lead iodide (FAPbI₃) and FA-rich perovskites are preferred for photovoltaic applications, but their widespread adoption is hindered by the rapid degradation of the desirable corner-sharing cubic (3C) phase to an undesirable wide bandgap, face-sharing, hexagonal (2H) phase under ambient conditions. Alloying FA with small amounts of Cs⁺ and methylammonium (MA) on the A site cation of the ABX₃ perovskite structure has proven a promising strategy for stabilizing photoactive perovskite phases. For example, photovoltaic devices fabricated with compositions such as Cs_{0.05}FA_{0.78}MA_{0.17}Pb(I_{0.83}Br_{0.17})₃ (triple cation) perovskites have achieved high device efficiencies with greatly enhanced reproducibility and ambient stability¹. Recently, there has also been renewed interest in methods to stabilize pure FAPbI₃ through strategies such as the incorporation of MA via treatment with methylammonium thiocyanate vapour², addition of formamidinium formate³ or methylammonium formate⁴.

The mechanism of improved stability obtained from these approaches is generally explained as either originating from a tuning of the Goldschmidt tolerance factor towards the perfect cubic perovskite structure via cation mixing in the case of Triple Cation perovskites^{1,5}, by templating growth of the corner-sharing cubic structure in stabilized-FAPbI₃ perovskites^{2,4}, or by reducing intrinsic defect density³. The key tenet in all these explanations is that the final photoactive perovskite material, regardless of stabilization approach, is a cubic perovskite structure and that this is the structure that should be pursued for optimal stability and performance. Here, we reveal that rather than being cubic, FA-rich perovskites exhibit a slight degree of octahedral tilting that frustrates the transition from the corner sharing photoactive phase to hexagonal photoinactive phases⁶. Local regions of stabilised FA-rich perovskite films that do not exhibit octahedral tilting, transition to nanoscale hexagonal phase impurities that are rich in performance limiting defect clusters⁷. Finally, we show that by modulating the magnitude of octahedral tilting through compositional modification in FA-rich perovskites, the density of these sinister hexagonal phase impurities, and thus overall film photostability, can be tuned. Combined, our talk provides insight into the common origin of performance losses and photostability issues in FA-rich perovskite materials as well as a pathway to mitigate them⁸.

1. Saliba, M. *et al.* Cesium-containing triple cation perovskite solar cells: improved stability, reproducibility and high efficiency. *Energy & Environmental Science* 9,(2016).

2. Lu, H. *et al.* Vapor-assisted deposition of highly efficient, stable black-phase FAPbI₃ perovskite solar cells. *Science* 370, (2020).

3. Jeong, J. *et al.* Pseudo-halide anion engineering for α -FAPbI₃ perovskite solar cells. *Nature* 592, 381–385 (2021).

4. Hui, W. *et al.* Stabilizing black-phase formamidinium perovskite formation at room temperature and high humidity. *Science* 371, 1359–1364 (2021).

5. Kim, J. Y., Lee, J.-W., Jung, H. S., Shin, H. & Park, N.-G. High-Efficiency Perovskite Solar Cells. *Chem. Rev.* 120, 7867–7918 (2020).

6. Doherty Tiarnan A. S. *et al.* Stabilized tilted-octahedra halide perovskites inhibit local formation of performance-limiting phases. *Science* 374, 1598–1605 (2021).

7. Doherty, T. A. S. *et al.* Performance-limiting nanoscale trap clusters at grain junctions in halide perovskites. *Nature* 580, 360–366 (2020).

8. Macpherson, S. *et al.* Local Nanoscale Phase Impurities are Degradation Sites in Halide Perovskites. *Nature* 1–3 (2022).

2:30 PM *EN04.04.04

Looking Inside Halide Perovskites Using On-The-Fly Machine Learning Force Fields Menno Bokdam; University of Twente, Netherlands

Recent developments in the field of high efficiency perovskite solar cells are based on stabilization of the perovskite crystal structure of FAPbI₃ while preserving its excellent optoelectronic properties. Compositional engineering of, for example, MA or Br mixed into FAPbI₃ results in the desired effects, but detailed knowledge of local structural features, such as local (dis)order or cation interactions of formamidinium (FA) and methylammonium (MA), is still limited. This knowledge is, however, crucial for their further development. In this talk, I will present how recent developments in Machine Learning accelerated ab-initio Molecular Dynamics (MD) enable the required length and time scale simulations that can assist in solving some of the open questions. For example, the generated large isothermal-isobaric ensembles can be used to calculate the ¹H-¹H dipolar coupling coefficients that can be compared with those obtained by nuclear magnetic resonance spectroscopy measurements[1]. Furthermore, we can calculate the momentum resolved phonon spectrum by 'measuring' their frequencies and lifetimes directly from velocity auto-correlation functions[2]. We observe that the lifetime of many phonon modes is of the order of the inverse of its frequency. This shows the strong anharmonicity of the potential energy surface of halide perovskites, and the necessity of MD approaches. Overall, there is qualitative and quantitative agreement between experiment and theory on several experimental observables, which leads us to think that the simulated crystals structure trajectories provide a realistic insight into the ionic dynamics of the studied samples.

[1] Helen Grüninger et al. , J. Phys. Chem. C, 125, 3, 1742–1753 (2021)

[2] Jonathan Lahnsteiner and Menno Bokdam, Phys. Rev. B 105, 024302 (2022)

3:00 PM BREAK

3:30 PM *EN04.04.05

Stressing Halide Perovskites—Nanoscale Investigation of the Properties of Perovskite Thin Films Sarah Wiegold¹ and Lea Nienhaus²; ¹Argonne National Laboratory, United States; ²Florida State University, United States

Solution-processed perovskite thin films consist of small grains with a size of 20 - 2000 nm connected by grain boundaries. As a result, there is a vast inhomogeneity in the optical and electronic properties of the different grains/GBs within one film, which can reduce the achievable energy output. In addition, facile ion movement under external stimuli (light or electric fields) adds additional complexity to the system.

To gain insight into the optoelectronic and structural response of the perovskite thin film to these external stressors present under operating conditions, we utilize scanning tunneling microscopy (STM). Single molecule absorption STM (SMA-STM) can probe the local inhomogeneity of the surface properties of the perovskite thin film under illumination by locally mapping the additional photogenerated tunneling current. To understand whether the local changes are caused by optoelectronic changes under illumination or structural changes, we utilize synchrotron X-ray STM (SX-STM). Pump-probe wide-angle X-ray scattering indicates the presence of lattice deformations under optical illumination, highlighting that the photocarriers distort the lattice, and thus, can change the underlying density of states as observed by SMA-STM.

(1) Wiegold, S.; Shirato, N.; Rose, V.; Nienhaus, L. Investigating the Effect of Electric Fields on Lead Halide Perovskites by Scanning Tunneling Microscopy. *J. Appl. Phys.* **2020**, *128*, 125303.

(2) Wiegold, S.; Cope, E.M.; Moller, G.; Shirato, N.; Guzelurk, B.; Rose, V.; Nienhaus, L. Stressing Halide Perovskites with Light and Electric Fields. *ACS Energy Lett.* **2022**, *7*, 2211-2218

4:00 PM EN04.04.06

Multiscale Modelling of Defects in Halide Perovskites—Implications for the Phase Stability and Degradation Reactions Induced by Thermochemical Stress Mike Pols¹, Adri C.T. van Duin², Sofia Calero¹ and Shuxia Tao¹; ¹Eindhoven University of Technology, Netherlands; ²The Pennsylvania State University, United States

The outstanding optoelectronic properties of metal halide perovskites (MHPs) have attracted a lot of attention from the optoelectronic community recently. Despite the significant increase in efficiency, the commercialization of perovskite optoelectronic devices is hampered by long-term stability problems. This is because the common fabrication method, i.e. solution processing, is known to produce polycrystalline films with a wide variety of defects, such as point defects, surfaces and grain boundaries. Although the optoelectronic effects of these defects have been widely studied, a detailed understanding of their impact on the long-term stability, particularly an understanding of the degradation dynamics at the atomic scale, is still lacking.

In this presentation, I will outline our recent advances in studying the dynamical processes and their implications on the stability of halide perovskites using computational multiscale modelling. Our approach combines several levels of theory, including reactive force fields (ReaxFF) [1, 2], density functional tight-binding (DFTB) [3] and machine learned force fields (MLFF) [4]. The multiscale approach allows us to obtain important insights into the dynamical properties at the atomistic scale at various time scales, including phase transitions, phase stability, defect migration and defect-induced degradation reactions in the bulk, at surfaces and near grain boundaries for perovskites with various compositions. The atomistic insights gained in these simulations allow us to propose strategies to passivate and mitigate these defects and thereby stabilize the materials.

References:

[1] **M. Pols**, J.M. Vicent-Luna, I. Filot, A.C.T. van Duin and S. Tao. Atomistic Insights Into the Degradation of Inorganic Halide Perovskite CsPbI₃: A Reactive Force Field Molecular Dynamics Study. *J. Phys. Chem. Lett.* **2021**, *12*, 5519-5525. DOI: <https://doi.org/10.1021/acs.jpclett.1c01192>.

[2] **M. Pols**, T. Hilpert, I. Filot, A.C.T. van Duin, S. Calero and S. Tao. What Happens at Surfaces and Grain Boundaries of Halide Perovskites: Reactive Molecular Dynamics Simulations of CsPbI₃. Submitted. DOI: <https://doi.org/10.48550/arXiv.2205.10545>.

[3] S. Raaijmakers, **M. Pols**, J.M. Vicent-Luna and S. Tao. Refined GFN1-xTB Parameters for Engineering Phase-Stable CsPbX₃ Perovskites. *J. Phys. Chem. C* **2022**, *126*, 22, 9587–9596 DOI: <https://doi.org/10.1021/acs.jpcc.2c02412>.

[4] **M. Pols**, V. Brouwers and S. Tao. On-the-fly Machine Learned Force Fields for Inorganic Halide Perovskites: CsPbX₃ (X = I, Br). In preparation.

4:15 PM EN04.04.07

Mutual Influence of (Anti)Solvents and Precursors on Halide Perovskite Formation Mriganka Singh, Maged Abdelsamie, Tim Kodalle and Carolyn M. Sutter-Fella; Lawrence Berkeley National Laboratory, United States

Halide perovskites with mixed A- and X-site cations and anions, respectively, are important to overcome challenges such as thermal and structural instabilities, as well as moisture sensitivity. Triple cation, mixed halide perovskite compositions have been reported to be more thermally stable, exhibit less phase impurities, and are less affected by the processing conditions than single cation perovskites. In this work, we present a multimodal in situ study on the formation of Cs_{0.05}FA_{0.81}MA_{0.14}Pb(I_{0.85}Br_{0.15})₃ by combining structural information from grazing-incidence wide-angle synchrotron X-ray scattering (GIWAXS) and optical properties from photoluminescence (PL) spectroscopy. This study covers the predominantly used solvents and solvent systems DMF, DMSO and mixtures thereof. We are looking at the solvent-antisolvent interaction and evaluate if the antisolvent induces oversaturation

accompanied by solvate phase formation or if it removes the solvent and thereby suppresses solvate phases. We find that the non-perovskite delta-FAPbI₃ appears in all crystallization pathways. It is strongly correlated with the antisolvent dripping and temporally close to the perovskite phase formation. It was also found that the delta phase is more stable in DMF than in DMSO systems. These findings provide novel insights into solvate and perovskite phase evolution and its mutual correlation with the solvent and antisolvent to allow for better synthetic control.

4:30 PM EN04.04.08

Intrinsic Light Instabilities in Metal Halide Perovskites Jeremy G. Hiculle¹, Muhammad U. Farooq¹, Joana A. Ferreira Machado¹, Ajay Singh¹, Anurag Krishna², Anders Hagfeldt² and Alex Redinger¹; ¹University of Luxembourg, Luxembourg; ²École Polytechnique Fédérale de Lausanne, Switzerland

Solution-processed metal halide perovskite solar cells are currently under the spotlight due to their high-power conversion efficiencies and easy fabrication. However, the commercialization might be hampered by certain drawbacks such as device degradation and hysteresis [1]. Several hypotheses have been formulated concerning the physical origins of the rapid deterioration of the perovskite absorbers, such as vacancies, ion migration, and phase segregation [2-3]. Recent reports in the literature, investigating the perovskite degradation by X-ray photoelectron spectroscopy suggest that X-ray exposure triggers the release of the organic cations as well as the dissociation of PbI₂ into metallic lead Pb(0) and I₂ [4-8]. However, **a fundamental understanding of the role of low energy light (white light) on the intrinsic degradation mechanism taking place in metal halide perovskite is still lacking.**

In this work, we combined scanning probe microscopies (STM, AFM, KPFM), and X-ray photoelectron spectroscopy (XPS) to systematically investigate the effect of light, X-ray, and temperature on the intrinsic stability of the metal-halide (FAPbI₃)_{0.97}(MAPbBr₃)_{0.03} perovskite interface. In contrast to what is usually admitted [6-8], white light has a stronger effect on perovskite degradation as compared to X-rays. Importantly, we show that cooling down the sample helps reduce the formation of Pb(0) and prevents the release of the organic cation during sample analysis. Kelvin Probe microscopy measurements allowed us how to link the losses of the organic cations and iodine to changes in the work function of several hundred meV. The STM measurements reveal drastic changes in the local density of states. We do observe a bandgap shrinkage and strong lateral variations after light exposure. A model, explaining the compositional and electronic changes at the surface will be presented. In addition to providing useful insights into the intrinsic light-induced degradation of perovskite, our findings also offer useful guidelines for more accurate and non-invasive XPS analyses of this highly sensitive material system.

References:

- [1] P Wang *et al.*, *Adv. Funct. Mater.* 29 (47), 1807661 (2019).
- [2] S.G. Motti *et al.*, *Nature Commun.* 12, 6955 (2021).
- [3] W. Zhou *et al.*, *J. Phys. D: Appl. Phys.* 54, 063001 (2021).
- [4] J. Hiculle, *et al.*, *J. Am. Chem. Soc.*, 141, 8, 3515–3523 (2019).
- [5] A. Jamshaid, *et al.*, *Energy Environ. Sci.*, 14, 4541–4554 (2021).
- [6] S. Svanström, *et al.*, *Phys. Chem. Chem. Phys.*, 23, 12479–12489 (2021).
- [7] W.-C. Lin, *et al.*, *npj Materials Degradation* 5:13 (2021).
- [8] M. E. Stuckelberger, *et al.*, *J. Phys. Chem. C*, 124, 17949–17956 (2020).

4:45 PM EN04.04.09

Structural Dependence of Light-Induced Halide Segregation in Mixed-Halide Lower-Dimensional Perovskites Kunal Datta, Alessandro Caiazzo, Zehua Chen, Geert Brocks, Peter Bobbert, Shuxia Tao, Martijn Wienk and René Janssen; Technische Universiteit Eindhoven, Netherlands

The advent of layered Ruddlesden-Popper phases promises the development of efficient lead-halide perovskite optoelectronic devices. Such lower-dimensional phases are more defect tolerant and resistant to environmental stressors, compared to three-dimensional (3D) analogs, leading to high operational stability.^[1] Mixed-halide compositions which are relevant for multijunction photovoltaic applications are, however, poorly characterized and as a result, the occurrence of light-induced instabilities is not well-understood in lower-dimensional phases. In 3D mixed-halide perovskites, such light-induced halide segregation leads to the formation of low-energy iodide-rich phases that act as trap sites, thereby limiting charge-carrier collection and limiting photovoltaic performance.^[2]

This work uses a model phenethylammonium-based series of lower-dimensional perovskites ($n = 1, 2$) and characterizes the occurrence of light-induced halide segregation through time- and temperature-dependent photoluminescence spectroscopy. It is found that the two-dimensional (2D) phase is largely resistant to halide segregation, even at high light intensity. Density functional theory calculations show that this is a consequence of preferential occupancy of halide (iodide and bromide) ions and halide vacancy defects between the axial and equatorial lattice sites which limits ion migration pathways in the 2D phase.^[3]

A co-solvent engineering approach is then used to develop a structurally stratified mixed-halide films with lower-dimensional ($n = 1,2$) phases at the substrate interface and higher-dimensional (approx. 3D) at the air interface, verified by grazing-incidence wide-angle X-ray scattering.^[4] An intermediate quasi-2D phase ($n = 2$) thus formed shows vulnerability to light-induced instability, similar to a 3D phase, with a characteristic red-shift related to the formation of iodide-rich phases. However, the entropic re-mixing of halide ions that occurs in 3D perovskites when stored in dark conditions is absent in quasi-2D phase; this is due to a higher activation barrier for ion migration in the quasi-2D phase which can occur at elevated temperatures to restore the well-mixed phase.

Collectively, these observations show that the structural nature (2D, quasi-2D or 3D) of mixed-halide perovskites plays a strong role in determining iodide-bromide phase stability in mixed-halide compositions. The contrast appears in both the occurrence of halide segregation under illumination and its reversal in the dark, guiding material design decisions for efficient and stable devices based on mixed-halide compositions.

- [1] H. Tsai, W. Nie, J. C. Blancon, C. C. Stoumpos, R. Asadpour, B. Harutyunyan, A. J. Neukirch, R. Verduzco, J. J. Crochet, S. Tretiak, L. Pedesseau, J. Even, M. A. Alam, G. Gupta, J. Lou, P. M. Ajayan, M. J. Bedzyk, M. G. Kanatzidis, A. D. Mohite, *Nature* **2016**, 536, 312.
- [2] K. Datta, B. T. van Gorkom, Z. Chen, M. J. Dyson, T. P. A. van der Pol, S. C. J. Meskers, S. Tao, P. A. Bobbert, M. M. Wienk, R. A. J. Janssen, *ACS Appl. Energy Mater.* **2021**, 4, 6650.
- [3] N. E. Wright, X. Qin, J. Xu, L. L. Kelly, S. P. Harvey, M. F. Toney, V. Blum, A. D. Stiff-Roberts, *Chem. Mater.* **2022**, 34, 3109.
- [4] A. Caiazzo, K. Datta, J. Jiang, M. C. Gélvez-Rueda, J. Li, R. Olletero, J. M. Vicent-Luna, S. Tao, F. C. Grozema, M. M. Wienk, R. A. J. Janssen, *Adv. Energy Mater.* **2021**, 11, 2102144.

EN04.05.01

Manipulating the Fundamental Building Blocks of All-Inorganic Metal-Halide Perovskites Toward Novel Electronic Behavior [Maria C. Folgueras](#), Jianbo Jin, Yuxin Jiang, Mengyu Gao and Peidong Yang; University of California, Berkeley, United States

Metal-halide perovskites are viewed as next-generation semiconductor materials due to their facile solution processability and interesting photophysical and optoelectronic phenomena. The properties of the traditional all-inorganic ABX_3 perovskites ($A = Rb^+$, Cs^+ ; $B = Pb^{2+}$, Sn^{2+} ; $X = Cl^-$, Br^- , I^-) are dominated by the three-dimensional (3D) network of metal-halide $[BX_6]$ octahedra within the crystal structure, as these octahedra serve as both the structural and functional units of the material. Manipulation of these octahedral units thus enables modulation of the perovskite crystal's electronic structure and optoelectronic properties and is traditionally achieved by (1) tuning the crystal's dimensionality, and/or (2) varying the crystal's B-site and X-site elements to form pure-halide and mixed-halide compositions. However, another mode of manipulation is to physically isolate the fundamental octahedral building block within the lattice, as is the case in the zero-dimensional (0D) vacancy-ordered double perovskites of form A_2BX_6 . In particular, all-inorganic Cs_2TeX_6 ($X = Cl^-$, Br^- , I^-) single crystals are an excellent platform for exploring the effect that the isolation of $[TeX_6]^{2-}$ octahedra in the crystal structure has on structural and electronic properties. Serving as the vibrational centers, the isolated octahedra inform the presence of strong exciton-phonon coupling and anharmonic lattice dynamics, as well as the likelihood of a random distribution of 10 octahedral symmetries within the mixed-halide compositional spaces. Serving as the absorbing and emitting centers, the isolated octahedra exhibit compositionally tunable absorption (1.50-3.15 eV) and emission (1.31-2.11 eV) energies. Due to greater molecular orbital overlap between neighboring octahedra with increasing halide anion size, there is a transition from a more molecule-like electronic structure in Cs_2TeCl_6 and Cs_2TeBr_6 – as expected from the effective 0D nature of these single crystals – to a dispersive electronic structure in Cs_2TeI_6 , typical of 3D bulk single crystals. Furthermore, by manipulating the ionic bonding in these crystals, 0D semiconductor perovskite inks of Cs_2TeX_6 are readily produced, in which Cs^+ cations and $[TeX_6]^{2-}$ octahedral complex anions are stabilized in polar aprotic solvents without the presence of ligands. The successful stabilization of the fundamental $[TeX_6]^{2-}$ octahedral molecules in solution creates multifunctional inks with the ability to reversibly transform between the liquid ink and the solid-state perovskite crystalline system in air within minutes, highlighting the crucial role of solvated octahedral complexes toward the rapid formation of phase-pure perovskite structures in ambient conditions. Given that these fundamental octahedral building blocks (with maximum length of 5-6 Å) can be stabilized in solution without ligands (as opposed to colloids, whose stability requires the use of ligands), these inks open the possibility to design new perovskite materials and to probe fundamental energy transfer and electronic properties intrinsic to the octahedral building block.

EN04.05.02

Ultrafast Carrier and Quasiparticle Dynamics in Strongly Confined $CsPbBr_3$ Nanoplatelets [Etienne Socie](#)¹, [Brener RC Vale](#)² and [Jacques-E. Moser](#)¹; ¹EPFL, Switzerland; ²University of Campinas, Brazil

Over the past decade, lead halide perovskites have received considerable attention thanks to their impressive optoelectronic properties. Today, perovskite-based devices are one of the most efficient single-junction solar cells, with a power-conversion efficiency reaching 25.7%. In the same way, nanostructures of the same material emerged with tremendous potential for light-emitting and lasing applications. In addition, their complex and dynamic structure makes them fascinating for fundamental photophysical studies, not only to apply in the context of the device improvements but also for a much broader class of semiconductor materials.

Typically, charge carrier dynamics on the ultrafast and fast (fs to ps) timescales are monitored by time-resolved spectroscopic techniques using ultrashort laser pulses. The aim of this work is to associate transient absorption (TA) and time-resolved photoluminescence (TRPL) spectroscopy for investigating early photophysical mechanisms in low-dimensional perovskite nanocrystals (PNCs). While most available TRPL experimental techniques are limited by a temporal resolution of a few picoseconds, we employ broadband fluorescence upconversion spectroscopy (FLUPS) to obtain 2D spectro-temporal data with a sub-ps time resolution.

After discussing the synthesis and standard characterization of colloidal blue-emitting $CsPbBr_3$ nanoplatelets (NPLs) we investigate the charge carrier dynamics under weak and strong excitation regimes. Under low excitation intensities, the NPL dynamics are dominated by an ensemble of independent excitons and show complex photophysical behaviors. Besides, at high pump fluences, enhanced carrier-carrier interactions induce stable and emissive biexcitons. The properties and recombination mechanisms of the biexcitons follow typical quantum well signatures. Finally, we unveil that the NPLs can easily form a complex with organic acceptors attached at the surface, quenching the material emission. Excitation energy-dependent FLUPS measurements display fast interfacial charge transfer from the perovskite band edge and ultrafast hot carrier transfer from higher energy levels.

EN04.05.03

Difference in Degradation-Induced Trap Formation Between Mixed Lead Tin and Tin Halide Perovskites [Vincent J. Lim](#)¹, [Aleksander M. Ulatowski](#)¹, [Christina Kamaraki](#)^{2,3}, [Matthew T. Klug](#)², [Laura Miranda](#)², [Michael Johnston](#)¹ and [Laura Herz](#)^{1,4}; ¹University of Oxford, United Kingdom; ²Oxford PV, United Kingdom; ³University of Bath, United Kingdom; ⁴Technical University of Munich, Germany

Metal halide perovskites have the potential to surpass the single-junction detailed-balance limit with a tandem device architecture, taking advantage of their bandgap tunability. Mixed lead-tin halide perovskites offer the ideal bandgap as the bottom subcell for such photovoltaic device due to their bandgap bowing effect. However, they suffer from instability in ambient air, more so than their lead counterparts. Likewise, tin halide perovskites, promising for their lead-free nature, also suffer from severe instability. The degradation mechanism in mixed lead-tin halide perovskites has been thought to be similar to that of tin halide perovskites, namely through tin vacancy formation and self p-doping. We highlight our recent work [[Lim *et al.*, Adv. Energy Mater. \(2022\)](#)] wherein we investigated and contrasted the difference in optoelectronic degradation and trap formation between mixed lead-tin and tin halide perovskites in ambient air. Both compositions suffer from optoelectronic degradation, due to trap state formation, over hours of ambient air exposure. However, we report deep trap state formation in lead-tin perovskites during ambient air exposure, which accelerate charge-carrier recombination, without significant impact on charge-carrier mobilities. In contrast, tin-only perovskites undergo shallow tin vacancy trap state formation and hole donation. This report highlights the need for specifically tailored passivation techniques for mixed lead-tin iodide perovskites. We expect such treatments will ultimately improve air stability, facilitating the commercialization of all-perovskite tandem devices.

Lim, V. J.-Y. *et al.*, Air-Degradation Mechanisms in Mixed Lead-Tin Halide Perovskites for Solar Cells, *Adv. Energy Mater.* (2022), 2200847, DOI: 10.1002/aenm.202200847

EN04.05.04

Advanced Kelvin Probe Force Microscopy Methods to Study Mixed Halide Perovskites Pascal N. Rohrbeck¹, Yenel Yalcinkaya^{1,2}, Konstantinos Bidinakis¹, Lukas D. Cavar², Peter Reichel² and Stefan A. Weber^{1,2}; ¹Max Planck Institute for Polymer Research Mainz, Germany; ²Johannes Gutenberg University, Germany

Although perovskite solar cells (PSCs) are a good alternative to silicon solar cells, the basic physics and mechanisms of limiting efficiency are not fully understood.

Atomic force microscopy (AFM) methods are ideal for studying nanoscale electrical devices such as batteries, solar cells, and diodes. Using electrical operation modes enables studying nanoscale surface properties such as contact potential differences^[1], dielectric properties, space charge layers and local photovoltages^[2]. In addition, using a pulsed or AC excitation enables probing dynamics, as well.

In our group, we develop and use the Kelvin probe force microscopy (KPFM) techniques to answer unsolved questions about efficiency losses due to non-radiative recombination processes and stability problems in atmospheric conditions at the nanoscale. These methods, such as time-resolved KPFM (tr-KPFM) and pump-probe KPFM (pp-KPFM), can be used to investigate dynamics in the perovskite like ultra-fast photovoltage behaviour due to migration of excitons or ions.

Also we use frequency-dependent capacity mapping^[3] for investigations in the capacitance, capacitive charging and dielectric properties e.g., at grain boundaries.

This will help to understand the loss mechanism and therefore improve efficiencies of perovskite solar cells in the macroscale.

References:

[1] Gharibzadeh, S.; Fassel, P.; Hossain, I. M.; Rohrbeck, P.; Frericks, M.; Schmidt, M.; Duong, T.; Khan, M. R.; Abzieher, T.; Nejjand, B. A.; Schackmar, F.; Almora, O.; Feeney, T.; Singh, R.; Fuchs, D.; Lemmer, U.; Hofmann, J. P.; Weber, S. A. L.; Paetzold, U. W. Two Birds with One Stone: Dual Grain-Boundary and Interface Passivation Enables >22% Efficient Inverted Methylammonium-Free Perovskite Solar Cells. *Energy Environ. Sci.* 2021, 14 (11), 5875–5893. <https://doi.org/10.1039/d1ee01508g>.

[2] Rohrbeck, P. Untersuchung von lokalen Aufladungsdynamiken an Perowskit-Korngrenzen mit Zeitaufgelösten KPFM Methoden, Max Planck Institut für Polymer Research, 2021.

[3] Reichel, P. Tip-Sample Capacitance in Electrostatic Force Microscopy, University of Mainz, 2021.

EN04.05.05

Limits from Charge Carrier Doping, Mobility and Lifetime on the Potential Performance of Sn and Pb-Based Halide Perovskites Hannes Hempel¹, Klaus Schwarzburg¹, Francisco Pena-Camargo², Martin Stolterfoht², Fatima Akhundova¹, Artem Musiienko¹ and Thomas Unold¹; ¹Helmholtz Zentrum Berlin, Germany; ²University of Potsdam, Germany

Measuring the quantum yield of photoluminescence is a powerful and widely used technique to characterize photovoltaic materials. It can reveal an upper limit for the potential solar cell performance from measurements on neat thin films and can even predict the implied current-voltage (*JV*) characteristics.

However, the contributions from charge carrier doping and lifetimes to the implied voltage are usually not distinguished, and ideal charge carrier transport is assumed for the *JV* prediction. To gain more insights into the performance limiting factors, we use time-resolved photoluminescence, which allows us to determine the charge carrier lifetimes, doping, and mobilities for lead and tin halide perovskites.

Carrier lifetimes are probed under solar AM1.5-equivalent illumination employing sinusoidal modulation as well as under solar AM1.5-equivalent illumination superimposed with a weak pulsed photoexcitation. Such illumination conditions directly yield the relevant lifetime for photovoltaic application and avoid photoluminescence decays that are not connected to charge recombination. The charge carrier lifetimes of a few microseconds measured for lead-based are much larger than the few ns obtained on tin-based perovskites, which translate into larger voltage losses for the tin perovskite solar cells. The doping is accessed from the initial photoluminescence amplitude and increases from $\sim 10^{13} \text{cm}^{-3}$ for lead perovskites to $> 10^{17} \text{cm}^{-3}$ for tin perovskites. This doping of the lead perovskite is much smaller than the photogenerated carrier concentration under solar illumination at open-circuit conditions and also smaller than the charge needed to affect the built-in potential under short circuit conditions. Hence, it has a negligible impact on the solar cell performance and lead-perovskite can be considered intrinsic. In contrast, the doping of the tin-based perovskites is much larger than the photogenerated carrier concentration under solar illumination and partially compensates for the low charge carrier lifetime, and significantly contributes to the implied Voc.

The charge carrier mobility is obtained from the initial decay component of photoluminescence after pulsed photogeneration. For the Pb-based perovskites, the charge carrier diffusion through the thin film takes ~ 100 ns and is described with a mobility of $0.4 \text{ cm}^2/\text{Vs}$, which is in line with complementary Hall measurements. This mobility is significantly lower than the terahertz-derived mobility of $\sim 32 \text{ cm}^2/\text{Vs}$ for the nm-scale intragrain transport and indicates strong transport barriers at grain boundaries which leads to fill-factor losses in the solar cells.

EN04.05.06

Synthesis, Study and Applications of Halide Perovskites at the Ionic Octahedron Level Jianbo Jin¹, Maria C. Folgueras¹, Cheng Zhu¹, Mengyu Gao¹, Lina Quan² and Peidong Yang^{1,3}; ¹University of California, Berkeley, United States; ²Virginia Tech, United States; ³Lawrence Berkeley National Laboratory, United States

Metal halide ionic octahedron, $[\text{MX}_6]^{n-}$ (M = metal cation, X = halide anion), is the fundamental building block and functional unit of metal halide perovskites. The optoelectronic and chemical properties of the extended perovskite solids are dictated by the assembly, connectivity, and interaction of these octahedra. Hence, building up a fundamental understanding at the level of metal halide octahedron will lay the foundation for the synthesis, study, and applications of their solid assembly. The first part of the report will focus on new design principles for constructing new perovskite materials. In particular, when one considers the octahedron as a super ion/atom, the halide perovskites can be described as extended ionic octahedron networks (IONs) stabilized with counterions. Based on the IONs design principle, a new metal halide perovskite ($\text{Cs}_8\text{Au}_{3.5}\text{In}_{1.5}\text{Cl}_{23}$) was successfully synthesized as the first example, where three different metal halide octahedra were packed in the style of ABO_3 -type lattice. In addition to IONs, a new family of (Crown-ether@ A_2) $\text{M}(\text{IV})\text{X}_6$ was achieved with supramolecular molecule crowned alkali metals as the counterions and assembled from a structurally and optoelectronically tunable “dumbbell” structural unit in solution. We will also report how non-ambient conditions affect the packing, connectivity, and configuration of metal halide octahedron, and how it dictate the properties of the solid assembly. Two levels of distortions, including within and among the $[\text{BiBr}_6]^{3-}$ octahedra, have been identified in low-temperature measurements, which reveal the symmetry-related electronic and excitonic behaviors.

EN04.05.08

Cationic Liganding is at the Origin of Quantum Well Orientation and Population Distribution in Reduced Dimensional Perovskites Kasra Darabi, Dovletgeldi Seyitliyev, Boyu Guo, Fazel Bateni, Tonghui Wang, Masoud Ghasemi, Laine Taussig, Milad Abolhasani, Kenan Gundogdu and Aram Amassian; North Carolina State University, United States

Layered hybrid perovskite (LHP) films exhibit highly anisotropic properties including charge and energy transport along quantum wells (QWs), as well as energy and charge transfer between QWs of different sizes. The control of QW orientation and population distribution within LHP films is therefore critically important to various applications ranging from solar cells to LEDs, lasers, and field-effect transistors. It is not surprise, then the hybrid perovskites community has deemed it a scientific and technological imperative to understand the origins of QW orientation and population distribution in LHP films. Despite tremendous recent efforts to understand the mechanism of crystallization in these materials, significant questions remain about the origins of crystalline texture, QW orientation and distribution in LHPs. Here we elucidate the precise solution-to-solid conversion of the sol into the LHP thin film by the aid of using multimodal in-situ characterization techniques such as grazing-incidence wide-angle X-ray scattering (GIWAXS), UV-vis absorption, and photoluminescence (PL). We identify, for the first time, the presence of oriented colloidal templating nanostructures (CTNs) during spin coating at the sol-air interface, that are highly emissive but do not diffract, well before the onset of crystallization of the QWs or 3D phases. According to our in-situ observations along with quantitative analysis, we propose a growth model for CTNs that can explain the underlying reason behind tremendous texture in these thin-films. Furthermore, we test our hypothesis by engineering CTNs during antisolvent drip to manipulate the texture as well as QWs distribution in LHP thin films.

EN04.05.11

Halide Effect on White Light Emission from Low Dimensionality Perovskites Ido Hadar and Bar Bader; The Hebrew University of Jerusalem, Israel

Hybrid halide perovskites are a novel class of semiconductor materials with promising and versatile optoelectronic properties, enabled by their chemically flexible structures and dimensionality. The diversity in the metal ions, halide anions, and organic spacers enables a wide range of materials with highly tunable properties and variable dimensionalities. These materials are studied for various applications such as solar cells, detectors, and light-emitting diodes. The ability to control and adjust the optical properties for a required application is significant. Thus, an improved understanding of the structure and optical mechanisms is crucial.

Specific low-dimensionality hybrid halide perovskites exhibit white-light emission at room temperature, associated with self-trapped excitons (STE), making them ideal candidates for illumination applications. We study the correlation between chemical and structural motifs of low dimensionality (2D, 1D) halide perovskites and their STE emission. Our current research is focused on studying how the composition and specifically exchanging of the halide anions (Br to I or Cl) while maintaining the structural motifs affect the STE properties. We found a reversed correlation between the bandgap energy of these structures and the STE central peak.

EN04.05.12

Spatiotemporal Engineering of Carrier Dynamics by Nanopatterning Halide Perovskite Surfaces Taehee Kim, Do Hyung Chun, Jong Hyeok Park and Dongho Kim; Yonsei University, Korea (the Republic of)

Halide perovskites are popular choice for photoactive layer material in high-performance optoelectronic applications. These devices work by extracting or injecting charge carriers from/into the perovskite layer, through the interface in contact with transporting layers. Thus, in order to exploit the device efficiency to its fullest, it is of critical importance to engineer the charge carrier transport and recombination kinetics at the surface of perovskite layer[1,2]. In-situ nanoscale patterning is an explicit strategy to manipulate the perovskite surface, which benefits both the performance and the ambient stability of perovskite-based devices[3,4]. However, such virtues of nanopatterning crystallization of perovskites remain underrated due to the lack of understanding of the fundamental photophysics beneath.

With the aid of interplay between nanoscale spatial scanning and temporally resolved photon-recording, fluorescence lifetime imaging microscopy (FLIM) provided a powerful means to explore the surface energetics of nanopatterned perovskites. Grain growth process of MAPbI₃ perovskite was assisted by nanopattern template and resulted in a more compact surface morphology with lower grain boundary angle. Nanoscale patterns with various geometry delicately modified the carrier kinetics at grain surfaces. Carrier density dependence of FLIM statistics revealed a large deceleration of bimolecular recombination rate, indicating a broader energetic distribution of carriers accompanied by band structure alteration upon pattern imprinting. Time-resolved imaging of carrier density profile uncovered the enhancement of carrier transport in hole-patterned perovskite, both at top and buried surfaces. Increase in initial diffusivity implies a higher chances of charge extraction, which was attributed to the combined effect of decreased carrier effective mass and reduced defect density at surface by grain boundary healing effect. Solar cell and photodetector devices were fabricated, and performance results suggested an optimal device structure to properly utilize the nanopatterned perovskite surfaces. Robust tuning of surface carrier kinetics proves in-situ nanopatterning a versatile tool for engineering the photoactive layer and should inspire creative design protocols for future optoelectronic devices.

[1] Z. Guo, Y. Wan, M. Yang, J. Snaider, K. Zhu, L. Huang, *Science* 356, 59-62, (2017).

[2] M. I. Saidaminov, K. Williams, M. Wei, A. Johnston, R. Quintero-Bermudez, M. Vafaie, J. M. Pina, A. H. Proppe, Y. Hou, G. Walters, S. O. Kelley, W. A. Tisdale, E. H. Sargent, *Nat. Mater.* 19, 412-418, (2020).

[3] D. H. Chun, Y. J. Choi, Y. In, J. K. Nam, Y. J. Choi, S. Yun, S. Kim, D. Choi, D. Kim, H. Shin, J. H. Cho, J. H. Park, *ACS Nano* 12, 8564-8571 (2018).

[4] D. H. Chun, S. Kim, S. U. Chai, W. Kim, W. Kim, J. H. Lee, R. Rhee, D. Choi, J. K. Kim, H. Shim, J. H. Park, *Nano Lett.* 19, 6498-6505, (2019).

EN04.05.14

Bright Exciton Fine Structure Splitting and Direction Selective Exciton-Phonon Coupling in (PEA)₂Pb_nI_{3n-1} 2D Perovskites Michał Baranowski¹, Katarzyna Posmyk¹, Natalia Zawadzka², Mateusz Dyksik¹, Alessandro Surrente¹, Duncan Maude³, Watcharaphol Paritmongkol⁴, Adam Babinski², Maciej R. Molas², Mirosław Maczka⁵, William Tisdale⁴ and Paulina Plochocka^{3,1}; ¹Wrocław University of Science and Technology, Poland; ²University of Warsaw, Poland; ³Laboratoire National des Champs Magnétiques Intenses, France; ⁴Massachusetts Institute of Technology, United States; ⁵Institute of Low Temperature and Structure Research, Poland

Two-dimensional (2D) metal-halide perovskites have emerged in the recent decade as revolutionary semiconductor materials for light emission and energy harvesting applications. At the same time, 2D perovskites constitute a fascinating playground for fundamental exciton physics studies. Strongly enhanced excitonic effects [1] together with characteristics for ionic crystal coupling of excitonic species to lattice vibration [2], [3] and low symmetry of the crystals challenge our understanding of this elementary excitation. The low symmetry of 2D perovskites lattice affects simultaneously the exciton structure [4] and phonon modes degeneracy [5] leading to nontrivial mutual dependencies between lattice dynamics and electronic excitation resulting in a complex absorption and emission spectrum whose detailed origin is the subject of ongoing controversy.

Here we employ low-temperature polarized magneto-optical spectroscopy to reveal the bright exciton fine structure of (PEA)₂Pb_nI_{3n-1} single crystals. We observe two nondegenerate orthogonally-polarized bright in-plane free exciton states for n=1,2,3 both in reflectance and photoluminescence spectra. We show that the redshifted multiple-peak PL response often ascribed to free exciton transition is a manifold of phonon-dressed states that preserve the polarization of the corresponding FX state[4]. Therefore our results corroborate the most simple picture of exciton FSS derived from symmetry considerations. Moreover, we observe fine structure splitting also for the transition corresponding to exciton phonon replica. Interestingly in this case the energy separation of the two orthogonal states is different than for the zero phonon lines. This strongly indicates the selective coupling of two in-plane exciton states to different non-degenerate high-energy phonon modes, highlighting the importance of the internal lattice symmetry of 2D perovskites for the optical response.

- [1] J.-C. Blancon *et al.*, ‘Scaling law for excitons in 2D perovskite quantum wells’, *Nat. Commun.*, vol. 9, no. 1, p. 2254, Dec. 2018, doi: 10.1038/s41467-018-04659-x.
- [2] D. B. Straus *et al.*, ‘Direct Observation of Electron–Phonon Coupling and Slow Vibrational Relaxation in Organic–Inorganic Hybrid Perovskites’, *J. Am. Chem. Soc.*, vol. 138, no. 42, pp. 13798–13801, Oct. 2016, doi: 10.1021/jacs.6b08175.
- [3] J. M. Urban *et al.*, ‘Revealing Excitonic Phonon Coupling in (PEA)₂(MA)_n–1PbI₃n+1 2D Layered Perovskites’, *J. Phys. Chem. Lett.*, vol. 11, no. 15, pp. 5830–5835, Aug. 2020, doi: 10.1021/acs.jpcllett.0c01714.
- [4] K. Posmyk *et al.*, ‘Quantification of Exciton Fine Structure Splitting in a Two-Dimensional Perovskite Compound’, *J. Phys. Chem. Lett.*, pp. 4463–4469, May 2022, doi: 10.1021/acs.jpcllett.2c00942.
- [5] B. Dhanabalan *et al.*, ‘Directional Anisotropy of the Vibrational Modes in 2D-Layered Perovskites’, *ACS Nano*, vol. 14, no. 4, pp. 4689–4697, Apr. 2020, doi: 10.1021/acsnano.0c00435.

EN04.05.15

Photocatalytic Degradation of Alkyl Halide Molecules and Anion Exchange in Dispersions of CsPbBr₃ Perovskite Nanocrystals Selin Donmez, Sisi Wang and Hedi M. Mattoussi; Florida State University, United States

Since the first successful implementation of bottom-up growth of colloidal cesium lead halide perovskite nanocrystals (PNCs), these materials have generated intense interest and much activity. This has been motivated by the combination of unique photophysical properties with the ionic nature of the semiconducting cores. One interesting property of these materials is the ability to substitute the halide elements in the crystal lattice through anion exchange.

Here, we present a detailed investigation of the photo-assisted anion exchange reaction of CsPbBr₃ NCs dispersed in chlorinated solvents. We probe the kinetics of this process by varying the irradiation source, time, structure of the solvent molecules and the corresponding reduction potentials. We further carry out a thorough characterization of the PNC intermediates during the irradiation period until complete anion exchange, using optical and fluorescence spectroscopy measurements, powder X-ray diffraction (PXRD) and supplement them with x-ray fluorescence spectroscopy (XRF) to track changes in the crystal structure and stoichiometry. Our findings indicate that the PNC acts as a photocatalyst promoting the degradation of solvent molecules, via a dissociative electron transfer process. The transformation requires photons with energy that exceeds the bandgap of the materials. It also generates reactive chloride ions, triggering intensity- and time-dependent anion exchange concomitant with shifting of the optical characteristics of the samples.

EN04.05.17

Valence Band Dispersion of the Structural Ground State CH₃NH₃PbI₃ Studied by Angle-Resolved Photoelectron Spectroscopy Jeehong Park^{1,2}, Soon Sang Huh^{3,4}, Young Woo Choi¹, Soohyung Park⁵, Hyoung Joon Choi¹, Changyoung Kim^{3,4} and Yeonjin Yi^{1,2}; ¹Yonsei University, Korea (the Republic of); ²Van der Waals Research Center, Korea (the Republic of); ³Institute for Basic Science, Korea (the Republic of); ⁴Seoul National University, Korea (the Republic of); ⁵Korea Institute of Science and Technology, Korea (the Republic of)

Lead halide perovskites (LHP) are a novel class of semiconducting materials which have attracted considerable research interest in a wide range of optoelectronic applications due to their long charge carrier lifetimes and carrier diffusion lengths despite the low-cost fabrication methods. Different hypotheses, including the Rashba effects, Fröhlich large polaron formation and ferroelectricity, have been proposed to elucidate the microscopic origin of peculiar charge carrier dynamics of LHPs. Although these effects are generally accompanied by the modifications of their underlying electronic structure, the key experimental evidence has been lacking so far.

Here, we investigate the electronic structure of structural ground state of CH₃NH₃PbI₃, the archetypical hybrid-type LHP material, studied via spin- and angle-resolved photoelectron spectroscopy (ARPES) combined with ab initio density functional theory (DFT) calculations. By establishing careful optimizations of sample preparations and experimental protocols, we present the pristine quality of ARPES with the key spectral features revealed for the first time. With our in-depth analysis of measured electronic dispersions, we comprehensively discuss the Rashba effect and Fröhlich large polaron formation in the uppermost valence band of CH₃NH₃PbI₃.

EN04.05.18

Microstructural Evolution of Perovskite Solar Cells During Thermal Annealing Holger Roehm, Alexander D. Schulz, Tobias Leonhard, Alexander Colsmann and Michael J. Hoffmann; Karlsruhe Institute of Technology, Germany

MAPbI₃ amongst other OMH perovskites is undergoing tetragonal-to-cubic phase transitions within the operational temperature range of solar cells. Many properties of these hybrid perovskite materials, such as piezoelectricity, pyroelectricity, ferroelectricity and ionic conductivity are directly linked to the crystal phase and temperature of the sample. Notably, polar domains that form in MAPbI₃ thin-films during the solar cell fabrication have been observed.^[1,2,3] We have previously shown that poling of these domains can be achieved in an external E-field that is similar to built-in fields in solar cells during operation.^[4]

In this work, we use Piezoresponse Force Microscopy to monitor an evolution of these domains that is triggered by common thermal treatment of perovskite solar cell at 100°C.^[5] Our findings suggest that control over the domain structure in these light absorbing, semiconducting compounds may be essential in order to maximize performance and stability of hybrid perovskite solar cells. In particular, microstructural changes due to stress and strain when the thin-films undergo a tetragonal/cubic phase transition are an often overlooked factor responsible for degradation of perovskite solar cells. We show that local crystal defects can form and vanish both at ferroic domain walls and crystal grains and in turn modulate ionic conductivity and diffusion.

- [1] H. Röhm, *et al.*, *Energy Environ. Sci.* 10, 950-955 (2017) [2] T. Leonhard *et al.*, *Energy Technol.* 7, 1800989 (2019) [3] H. Röhm *et al.*, *Adv. Mater.*, 31, 1806661 (2019) [4] H. Röhm *et al.*, *Adv. Funct. Mater.*, 30, 1908657, (2019) [5] T. Leonhard *et al.*, *J. Mater. Chem. A.*, 9(38), pp. 21845-21858 (2021)

EN04.05.19

Kinetic Origins of High Preferential Crystal Orientation in Quasi-2D Perovskite Solar Cells Lukas Lehner¹, Stepan Demchyshyn¹, Kilian Frank², Alexey Minenkov¹, Dominik Kubicki³, Bekele H. Teklemariam¹, Christoph Putz¹, Niyazi Serdar Saricic¹, Bert Nickel², Markus Scharber¹ and Martin Kaltenbrunner¹; ¹Johannes Kepler University, Austria; ²Ludwig-Maximilian University, Germany; ³University of Warwick, United Kingdom

Pure 2D and mixed 2D/3D perovskites have emerged as a more stable and versatile class of materials for solar cell absorbers compared to their pristine 3D counterparts. However, the large organic cations employed to generate these lower-dimensional structures tend to inhibit charge transport across the device, decreasing performance. Therefore, aligning the organic sheets vertically to the substrate to facilitate unimpeded flow of electrons is critical to realize high power conversion efficiencies. While different methods of achieving such a preferential orientation have been reported, a complete general mechanistic understanding of the process has not yet been put forward. Here, using an organic chloride as an additive and a fluorinated cation as an organic spacer, we

achieve a high degree of preferential crystal orientation of up to 93% and perovskites withstanding 98% relative humidity for more than 10 h without significant degradation. By interrupting the film formation and investigating partially crystallized perovskite films, we can directly observe the initial stages of the crystallization after nucleation. From these observations, together with advanced microscopic and spectroscopic analysis, we are able to formulate a physical and chemical description of the crystallization dynamics that can be expanded to many preferred-orientation-inducing methods. Understanding these general principles behind controlling the nucleation process not only allows the rational design of novel additives for future photovoltaic research, but also more defect tolerant systems as the technology transitions from the lab to roll-to-roll processed mass production.

EN04.05.20

Chemical Engineering of Strain in MAPbI₃ Thin Films [Yenal Yalcinkaya](#)¹, Ilka Hermes², Tobias Seewald³, Katrin Amann-Winkel¹, Lothar Veith¹, Lukas Schmidt-Mende³ and Stefan A. Weber¹; ¹Max Planck Institute for Polymer Research, Germany; ²Leibniz Institute for Polymer Research, Germany; ³Universität Konstanz, Germany

In this study, we introduce a alternative chemical method for adjusting the strain in methylammonium lead iodide (MAPbI₃) perovskite crystals by varying the ratio of Pb(Ac)₂ and PbCl₂ in the precursor solution. To observe the effect of chemical engineering on crystal strain, we used piezoresponse force microscopy (PFM) and X-ray diffraction (XRD) methods. We observed larger ferroelastic twin domains with higher PbCl₂ amount which indicates increased strain. We support our increased strain interpretation with XRD patterns with intensive twinning features. We speculate that this strain behaviour is a result of different evaporation rates of methylammonium acetate and methylammonium chloride which caused a strain gradient as we revealed by time-of-flight secondary ion mass spectroscopy (ToF-SIMS) and grazing incidence x-ray diffraction (GIXRD) measurements. We also observed longer charge carrier lifetimes in MAPbI₃ films with larger twin domains, as time-resolved photoluminescence (TRPL) results revealed. With these results, we demonstrate an easy way to adjust the strain within lead halide perovskite films chemically.

EN04.05.21

Transport and Crystallization Modeling of Perovskite Thin Film Formation [Jesse Starger](#), Aaron Fafarman, Jason Baxter, Nicolas Alvarez and Richard Cairncross; Drexel University, United States

Over the last decade, solution-processing of organometallic halide perovskites has provided a promising path forward for scalable, low-cost photovoltaic devices. A fundamental understanding of crystallization and mass transfer processes in drying thin-films is needed to enable scalable “low energy” processing methods, like slot-die coating, where both solvent mass transfer and crystal growth can drive the microstructure. Absorber layer microstructure, grain size, grain boundaries, and compositional heterogeneity are known to affect device performance, and can be similarly controlled by process parameters such as drying rate and temperature during coating. However, the precise origins of important microstructural features like pinholes, and ultimately the process-structure-performance relationships are difficult to predict.

Here, a 1D transient model for perovskite crystallization at a boundary is developed. The model accounts for lateral solute and solvent gradients parallel to the substrate surface but neglects vertical gradients through the thickness of the wet film. Lateral gradients in a drying film are driven by solute depletion due to crystallization but are counteracted throughout the wet film by evaporation of solvent which depends on the local solvent concentration. Using a first-order rate law for crystallization, crystallization rates over the drying lifetime of the film are shown to vary by an order of magnitude due to rapid depletion of solute in the wet film at the solid-liquid interface when diffusion-limited. The velocity and height of the crystallization boundary is used to predict a solidified crystal film profile which can be adjusted through two convenient dimensionless parameters; a modified Peclet number and a modified Biot number that capture the crystallization (kinetic) and drying (mass transfer) timescales, respectively. The curvature and inflections in the thickness profile are shown to depend on solute concentration at the growing boundary determined by competing crystallization and evaporative driving forces, which also depend on temperature and solvent vapor pressure. By accounting for both crystal growth and thin film drying, this early model sets the foundation for addressing more complex process-structure relationships – such as the development of microstructure in 2D and 3D, predicting local composition and impurity partitioning, engineering solvent mixtures, and enabling novel operating strategies using temperature or solvent gradients.

EN04.05.22

Simulating Self-Trapped Excitonic Emission in Halide ‘Defect Perovskites’ [Christopher Savory](#); University College London, United Kingdom

Inorganic lead halide perovskites have demonstrated comprehensive promise in LEDs, however lower dimensional perovskites and perovskite-like materials, have shown similar self-trapped excitonic behaviour and resultant broadband white light emission.¹ The Pb-free ‘defect perovskite’ Cs₂M^(IV)X₆ (M = Zn, Hf, Sn, X = Cl, Br) compounds,^{2,3} in which half the perovskite ‘B’ site cations are absent, are among those in demonstrating broadband emission – although quantum efficiencies vary between compounds, and the precise mechanism of emission is unclear. Here, we demonstrate how ab initio calculations can shine some light on these issues.

In this study, we simulate an ansatz of the emitting excitonic state using a supercell method with hybrid Density Functional Theory, avoiding the need for the explicit solution of the Bethe-Salpeter equation, while still obtaining accurate estimates of the photoluminescence of the halide defect perovskites – previously used in the simulation of other halide emitters.⁴ Beginning with the successful double perovskite emitter Cs₂AgInCl₆⁵ and its experimental photoluminescence as a benchmark, we move on to the defect perovskite families, and demonstrate the influence of both cation and anion to the excitonic properties – whether the luminescence energy or the barrier to the exciton self-trapping. We also relate these results to the degree of electronic, as well as structural, localization in these systems, and use additional QSGW+BSE calculations available through the code Questaal⁵ to support our results. Through these simulations, we hope to guide the understanding and future synthesis of Pb-free efficient light emitters.

(1) Smith, M. D.; Karunadasa, H. I. *Acc. Chem. Res.* **2018**, *51*, 619.

(2) Abfalterer, A.; Shamsi, J.; Kubicki, D.J.; Savory, C.N.; Xiao, J., *et al. ACS Materials Letters*, **2020**, *2*, 1633-1652

(3) Jing, Y.; Liu, Y.; Zhao, J. and Xia, Z. *J. Phys. Chem. Lett.* **2019**, *10*, 7439-7444

(4) Jung, Y-K., Kim, S.; Kim, Y.C. and Walsh, A. *J. Phys. Chem. Lett.*, **2021**, *12*, 8447-8452

(5) Luo, J.; Wang, X.; Li, S.; Liu, J.; Guo, Y. *et al. Nature*, **2018**, *563*, 541

(6) Pashov, D.; Acharya, S.; Lambrecht, W.R.L.; Jackson, J.; Belashchenko, K.D.; Chantis, A.; Jamet, F.; van Schilfgarde, M. *Comp. Phys. Commun.*, **2020**, *249*, 107065

EN04.05.24

Enhanced Exciton Diffusion in a CsPbBr₃ Binary Nanocrystal Superlattice [Thomas Sheehan](#)¹, Taras V. Sekh^{2,3}, Maksym V. Kovalenko^{2,3} and William Tisdale¹; ¹Massachusetts Institute of Technology, United States; ²ETH Zürich, Switzerland; ³Empa–Swiss Federal Laboratories for Materials Science and Technology, Switzerland

Control of exciton transport is critical for the operation of quantum dot (QD) solids in optoelectronic devices. Exciton diffusion in perovskite QDs typically occurs through Förster resonant energy transfer, which depends on both the optical properties and spatial arrangement of the quantum dots. Recent synthetic advancements have allowed for more control over both these factors in binary nanocrystal superlattices (BNSLs), but the resulting effect on exciton diffusion is not well understood. Here, we use time-resolved photoluminescence microscopy to compare the exciton diffusivity as a function of

temperature in a BNSL containing both 5.3 nm and 17.7 nm CsPbBr₃ QDs, an ordered film of 17.7 nm CsPbBr₃ QDs, and a disordered film of 5.3 nm CsPbBr₃ QDs. We find that although photoluminescence from the BNSL is dominated by emission from the 17.7 nm QDs, the exciton diffusivity is higher in the BNSL than in the ordered 17.7 nm QDs at every temperature. Additionally, at cryogenic temperatures, the exciton diffusivity in the BNSL is about twice as large as the exciton diffusivity in either of the monodisperse samples. Our results demonstrate that the lack of structural disorder in superlattices can lead to more efficient exciton transport.

EN04.05.27

Photo-Induced Charge Carrier Dynamics of Metal Halide Perovskite Yasuhiro Tachibana^{1,2}; ¹RMIT University, Australia; ²Osaka University, Japan

Perovskite solar cells have been recognized as a newly emerging solar cell with the potential of achieving high efficiency with a low cost fabrication process. In particular, facile solution processed cell fabrication facilitated rapid development of optimum cell structure and composition. Over the last few years, the cell efficiency has exceeded 25%.

Highly efficient charge transfer reactions including high charge separation efficiency and swift charge transport are required with minimum charge recombination to achieve the high solar cell performance. Based on previous intensive studies, high efficiency has been achieved by two different film structures: planar heterojunction and mesoporous structures. The latter typically consists of a nanocrystalline TiO₂ film as an electron transport material, lead halide perovskite and *spiro*-OMeTAD as a hole transport material. Several studies were conducted to understand dynamics of electron and hole injections from the perovskite, their charge carrier transport, and interfacial charge recombination.[1-5] Several parameters have been identified to influence these charge carrier dynamics, and therefore the solar cell performance.[1-5] Clarifying these parameters is extremely important to understand the charge transfer mechanisms to further improve solar cell performance.

In this presentation, we will present parameters controlling charge separation and recombination dynamics at the perovskite interfaces employing a series of transient absorption and emission spectroscopies. Nanosecond transient emission spectroscopy (Vis-ns-TES) clarifies charge separation processes, while Vis-NIR submicrosecond-millisecond transient absorption spectroscopies (NIR-smm-TAS) identify charge separation efficiency and charge recombination rates. Correlation of the dynamics results with the solar cell performance will be discussed [1-5].

This work was partly supported by JSPS KAKENHI Grant (19H02813) and (22H02182), and the Collaborative Research Program of Institute for Chemical Research, Kyoto University (grant number 2021-78 and 2022-99), Japan. We would like to acknowledge supports from the Australia-Japan Foundation for the collaborative project between RMIT University and Kyoto University. We also acknowledge supports from ARC DP fund (DP180103815) and ARC LIEF fund (LE200100051), Australia, and Forefront Research Center, Faculty of Science at Osaka University.

References

- [1] Y. Tachibana, et al. *J. Phys. Chem. C*, **119**(35) 20357-20362 (2015).
- [2] Y. Tachibana, et al. *ACS Appl. Mater. Interfaces*, **8**(22) 13957-13965 (2016).
- [3] Y. Tachibana, et al. *J. Photopolym. Sci. Technol.*, **34**(3) 271-278 (2021).
- [4] Y. Tachibana, et al. *Phys. Chem. Chem. Phys.*, **17**(4), 2850 - 2858 (2015).
- [5] Y. Tachibana, et al. *J. Mater. Chem. C*, **5**, 2182 - 2187 (2017).

SESSION EN04.06/EN02.06: Joint Session II: Effects of Composition and Dimensionality
Session Chairs: Jin-Wook Lee, Selina Olthof and Carolin Sutter-Fella
Wednesday Morning, November 30, 2022
Hynes, Level 3, Ballroom A

8:30 AM *EN04.06/EN02.06.01

Symmetry Breaking and Switching in 2D Halide Perovskites David B. Mitzi; Duke University, United States

Detailed crystal structure and symmetry underlie most structure-property correlations in halide perovskites and related semiconductors. For example, symmetry reduction generally may lead to nonlinear optical effects, ferroelectricity, and Rashba/Dresselhaus spin splitting (when accompanied by strong spin orbit coupling). On the other hand, glass-crystal transitions have been used to modulate electrical/optical properties by orders of magnitude and have been used in optical storage disks and phase-change memory. In this talk we will discuss approaches to control ordering and symmetry through organic cation choice and application of external stimuli (e.g., temperature) in 2D metal halide perovskites. Appropriate choice of the organic cation enables reduction of the melting temperature of the hybrids, as well as control over ordering within the melt during cooling, thereby allowing for demonstration of a reversible glass-crystalline transition with distinct kinetics. Further, cation choice can also be used to modulate crystal-to-crystal transition kinetics and can enable stabilizing two different structural types (and crystal symmetries) at the same temperature, depending on thermal cycling. The above approaches to control phase transitions will be discussed and are fundamentally important as well as potentially being of interest for applications connected with degree of crystallinity, symmetry and phase switching.

9:00 AM EN04.06/EN02.06.02

Unveiling Type I Nested Bandgap Heterostructure Arrangement in Two-Dimensional Ruddlesden – Popper Perovskites Xinjue Zhong¹, Xiaojuan Ni², Siraj Sidhik³, Hong Li², Aditya D. Mohite³, Jean-Luc Brédas² and Antoine Kahn¹; ¹Princeton University, United States; ²The University of Arizona, United States; ³Rice University, United States

Two-dimensional (2D) Ruddlesden-Popper perovskites (RPPs) are composed of n layers of inorganic metal-halides sandwiched between bulky organic bilayers, with a general chemical formula $A_2A'_{n-1}M_nY_{3n+1}$ where A and A' are cations, M is a divalent metal, and Y is a halide. RPPs with desirable optoelectronic properties, high structural and chemical tunability and improved environmental stability have been demonstrated as promising alternatives, or additions, to their three-dimensional (3D) counterparts for the fabrication of light-emitting and light-harvesting devices. To achieve successful design for such applications, it is necessary to better understand the electronic properties of these materials, such as their energy level positions and band alignment in 2D/2D and 2D/3D structures. However, these fundamental properties are still under debate because of difficulties in producing phase-pure 2D perovskites with high n values and an absence of reliable characterization of all frontier energy levels. Moreover, a clear determination of exciton binding energies (E_b) in RPPs, which range from a few hundred to tens of meV depending on n , is crucial for understanding charge carrier separation and extraction in solar cells.

Here, we use optical absorption, ultraviolet and inverse photoelectron spectroscopies (UPS / IPES), combined with density functional theory (DFT), to determine the electronic structure of high purity films of $\text{BA}_2\text{MA}_{n-1}\text{Pb}_n\text{I}_{3n+1}$ ($n = 1-5$). We show that the valence band maximum (VBM) and conduction band minimum (CBM) of the films, and their associated ionization energy (IE) and electron affinity (EA), sequentially converge toward those of MAPbI_3 ^[1] as n increases, with corresponding decreasing bandgap. Based on this trend, we demonstrate that the $\text{BA}_2\text{MA}_{n-1}\text{Pb}_n\text{I}_{3n+1}$ series exhibit a type I, nested band gap heterostructure arrangement, consistent with the initial report on the comparison between the $n = 1$ system and bulk MAPbI_3 .^[2] Using DFT calculations for valence and conduction band states, we identify the contribution of organic and inorganic components to the density of states, with the calculated bandgaps consistently following the trend of the experimental results. By combining the electronic and the optical bandgaps, we further determine the exciton binding energy vs. n , the thickness of the inorganic layer. E_b ranges from 320 meV for $n = 1$ down to 100 meV for $n = 5$, which is well fitted by the empirical scaling law developed by Blancon et al.^[3]

These findings on the electronic structures and excitonic effects of $\text{BA}_2\text{MA}_{n-1}\text{Pb}_n\text{I}_{3n+1}$ provide a better understanding of the structure-property relationships in 2D RPPs and give directions for incorporating these materials into optoelectronic devices.

[1] J. Endres, D. A. Egger, M. Kulbak, R. A. Kerner, L. Zhao, S. H. Silver, G. Hodes, B. P. Rand, D. Cahen, L. Kronik, A. Kahn, *J. Phys. Chem. Lett.* **2016**, 7, 2722.

[2] S. Silver, J. Yin, H. Li, J. L. Brédas, A. Kahn, *Adv. Energy Mater.* **2018**, 8, 1.

[3] J. C. Blancon, A. V. Stier, H. Tsai, W. Nie, C. C. Stoumpos, B. Traoré, L. Pedesseau, M. Kepenekian, F. Katsutani, G. T. Noe, J. Kono, S. Tretiak, S. A. Crooker, C. Katan, M. G. Kanatzidis, J. J. Crochet, J. Even, A. D. Mohite, *Nat. Commun.* **2018**, 9, 1.

9:15 AM EN04.06/EN02.06.03

Controlling and Mapping the Dynamic Transformation of Layer-Thickness for Synthesis of Phase-Pure 2D Perovskites Jin Hou¹, WenBin Li¹, Hao Zhang¹, Siraj Sidhik¹, Austin Fehr¹, Jacky Even², Jean-Christophe Blancon¹ and Aditya D. Mohite¹; ¹Rice University, United States; ²INSA Rennes, France

Two-dimensional halide perovskites (2D-HaP) are a sub-class of 3D perovskites (3D-HaP), which imbibe their properties from four exciting classes of novel materials - quantum wells, atomically thin 2D materials, organic semiconductors, and 3D-HaP perovskites. However, there is still a lack of systematic control of the crystallization and purity of 2D-HaP despite the huge amount of efforts on the synthesis of new 2D-HaP families with new organic spacers and tunable quantum thicknesses which will bring additional functionalities and further flexibility. For a 2D-HaP family, each member is identified by the number of perovskite layers (n). A main challenge is: purity is decreasing when targeting higher quantum well thicknesses (generally $n \geq 4$). But high inorganic layer thicknesses are more desirable for their smaller band gaps, closer to 3D-HaP's while maintaining a good stability. The previous attempts to synthesis $n \geq 4$ 2D-HaP all lead to mixed phases in crystals. A lack of control of the purity of the 2D phase can bring several issues, (i) a crystal containing a distribution of n values leads to a heterogeneous film once it is made into light harvesting layer in solar cell. This heterogeneity causes losses in the open circuit voltage, which inevitably lower the efficiency of the device; (ii) Preventing Investigating single- n crystal for fundamental exploration since it relies on the isolation of a crystallite in a heterogeneous bulk crystal, leading to other issues (damages, limitation of size). Indeed reproducibility of phase pure 2D-HaP is a long-existing issue, as the current approach to get a well-defined n member especially for higher n number relies either on a large number of crystallization attempts or isolation from a n -mixing phase. Therefore, a direct, reproducible approach to control the crystallization of a broad range of members from the same family is needed. Despite several attempts in the literature, the classical synthesis (CS) which relies only on the tuning of the precursor stoichiometry has not yield so far a satisfactory control of the purity indicating there are other parameters need to be proposed. Here, we show that both the solution crystallization time and temperature, besides the stoichiometry of precursors, hugely impacts the quantum well layer thickness in the 2D-HaP crystal. By increasing the time of crystallization and/or the temperature of the solution in the classical method of synthesis, the resulting 2D-HaP crystal transforms from lower n -values to higher n -values, shown by X-ray diffraction measurements. To understand the underlying mechanism, we modified the previously reported space confinement method by tuning the annealing time and temperature - termed as thermodynamically controlled space confinement (TCSC) which slows down the crystallization rate of the 2D-HaP crystal in solution allowing us to finely control each of the parameters. In-situ X-ray diffraction and absorption spectroscopy results on the TCSC crystals reveal that increasing the time and/or temperature systematically changes the n -value of the 2D-HaP. In-situ photoluminescence spectroscopy and imaging results demonstrate that the 2D-HaP crystal undergoes layer thickness (n) transformation to higher values through the crystal edge as a function of time. A new machine learning (ML) approach is introduced to accelerate the assisted mapping of the resulting multi-parameter phase diagrams. The ML model is further assessed by in-situ optical spectroscopy results in which intercalation occurs as we increase time of crystallization. Lastly a proof-of-concept synthesis of high n -values ($n=6$) 2D-HaP phase pure single crystals is shown, indicating the ability to fabricate 2D-HaP that are thermodynamically metastable. We also analyzed the transformation behavior in a family of Dion-Jacobson 2D-HaP, indicating that the new growth methodology is universal among 2D-HaP.

9:30 AM *EN04.06/EN02.06.04

Heterointerfaces, Defects and Durability Science in Perovskites Edward H. Sargent^{1,2}; ¹University of Toronto, Canada; ²Northwestern University, United States

Much of the impressive progress in perovskite optoelectronics derives from improved management of interfaces. This includes perovskite:perovskite heterointerfaces, such as between 3D and 2D perovskites, including recent works that allow variously electron-selective vs. hole-selective 2D layers. It also includes management via self-assembled monolayers at the perovskite:contact interface. I will review progress and its links to defect physics and durability science.

10:00 AM BREAK

10:30 AM *EN04.06/EN02.06.05

Stability Challenges in Mixed-Metal and Mixed-Halide Perovskites for Multijunction Solar Cell Applications Laura Herz; University of Oxford, United Kingdom

Organic-inorganic metal halide perovskites have emerged as attractive materials for solar cells with power-conversion efficiencies of single-junction devices now exceeding 25%. Such success has renewed interest in multi-junction cells that may exceed the single-cell Shockley-Queisser efficiency limit. However, a range of remaining challenges and opportunities remain relating to the stability of lead iodide-bromide^[1] and tin-lead iodide^[2] perovskites that currently present the most promising candidates for the required low- and high-energy-bandgap materials, respectively.

In the context of silicon-perovskite tandem cells, we discuss the peculiar mechanisms underlying detrimental halide segregation in mixed iodide-bromide lead perovskites with desirable electronic band gaps near 1.75eV.^[1,3,4] We reveal that, surprisingly, halide segregation results in negligible impact to the THz charge-carrier mobilities.^[4] However, remarkably fast, picosecond charge funneling into the narrow-bandgap I-rich domains leads to enhanced radiative recombination.^[3] Performance losses in photovoltaic devices may therefore potentially be mitigated by deployment of careful light management strategies. We further demonstrate^[4] how a combination of simultaneous in-situ photoluminescence and X-ray diffraction measurements is able to demonstrate clear differences in compositional and optoelectronic changes associated with halide segregation in $\text{MAPb}(\text{Br}_{0.5}\text{I}_{0.5})_3$ and

FA_{0.83}CS_{0.17}Pb(Br_{0.4}I_{0.6})₃ films. While MAPb(Br_{0.5}I_{0.5})₃ exhibits rearrangement of halide ions only in localized volumes of perovskite, FA_{0.83}CS_{0.17}Pb(Br_{0.4}I_{0.6})₃ lacks such low-barrier ionic pathways and is, consequently, more stable against halide segregation. However, under prolonged illumination, it exhibits a considerable ionic rearrangement throughout the bulk material, which may be triggered by an initial demixing of A-site cations, altering the composition of the bulk perovskite and reducing its stability against halide segregation.^[4]

We further discuss the air stability of mixed lead-tin halide perovskites, which provide ideal bandgaps for the bottom subcell of all-perovskite tandem photovoltaic devices. Such degradation pathways are not yet fully understood, especially for the perovskites in the middle of the APb_xSn_{1-x}I₃ solid solution line, which offer the narrowest bandgaps across the range. We contrast the degradation mechanisms of APb_xSn_{1-x}I₃ perovskites, reporting clear differences between mixed lead-tin (x = 0.5) and tin-only (x = 0) perovskites. The dynamic optoelectronic properties, electronic structure, crystal structure, and decomposition products of the perovskite thin films are examined in situ during air exposure. We show that both perovskite compositions suffer from the formation of defects over the timescale of hours, as indicated by a significant reduction in their charge-carrier diffusion lengths. For tin-only perovskite, degradation predominantly causes the formation of energetically shallow tin vacancies and hole doping. However, for mixed lead-tin perovskite, deep trap states are formed that significantly accelerate charge-carrier recombination, yet leave mobilities relatively unaffected. These findings highlight the need for passivation strategies tailored specifically to mixed lead-tin iodide perovskites.

[1] A. J. Knight and L. M. Herz, *Energy Environmental Science* **13**, 2024 (2020).

[2] K.J. Savill, A.M. Ulatowski, and L.M. Herz, *ACS Energy Letters* **6**, 2413–2426 (2021).

[3] S. G. Motti, J. B. Patel, R. D. J. Oliver, H. J. Snaith, M. B. Johnston, L. M. Herz, *Nature Communications* **12**, 6955 (2021).

[4] A. J. Knight, J. Borchert, R. D. J. Oliver, J. B. Patel, P. G. Radaelli, H. J. Snaith, M. B. Johnston, and L. M. Herz, *ACS Energy Letters* **6**, 799 (2021).

[5] V. J.-Y. Lim, A. M. Ulatowski, C. Kamaraki, M. T. Klug, L. Miranda Perez, M. B. Johnston, and L. M. Herz, *Advanced Energy Materials* **12**, 2200847 (2022).

11:00 AM EN04.06/EN02.06.06

Elucidating the Relationship Between A-Site Mixing and Non-Radiative Carrier Capture Lucy Whalley; Northumbria University, United Kingdom

The unusual defect chemistry and physics of lead halide perovskites has attracted significant attention as point defects in these materials are associated with a range of processes including ion diffusion, hysteresis and degradation.^{1,2} While the high voltages and light-to-electricity conversion efficiencies indicate a low rate of non-radiative electron-hole recombination relative to other photovoltaic materials, understanding non-radiative capture processes remains crucial for the development of high-efficiency devices with increased stability.

The most stable materials employ mixed cations on the perovskite A-site, however the reason for this improved performance is not fully understood. While there has been a number of computational defect studies for the single cation compounds, most commonly methylammonium (MA) lead iodide, less is known about the impact of cation mixing on the defect physics of these materials.

We will present results from the quantum chemical simulations of single cation (MA) and mixed cation (Ma/Cs) materials. We will consider both the pristine materials and the materials with an iodine interstitial defect, which has been established as an active site for non-radiative charge trapping.³

First we will demonstrate that cation mixing on the A-site leads to increased octahedral tilting in the minimum energy (relaxed) structures of the pristine materials. This supports previous results which show that octahedral tilts are "locked-in" for the mixed-cation compounds.⁴ We will then analyse the quantum mechanics of carrier trapping at the iodine interstitial. We will show that the lattice relaxation after charge capture is also mediated through octahedral tilting of the inorganic cage, and so can be tuned through A-site composition. Using a computational framework for calculating non-radiative capture rates from first-principles^{3,5} we will quantify the impact that cation mixing has on the rates of electron and hole capture at the iodine interstitial.

Finally, we will demonstrate that due to the rotational motions of the A-site molecular cation after charge capture, the commonly used approximation of linear interpolation for constructing the potential energy surface cannot be applied to this system. Instead, we will discuss the use of Kabsch interpolation and anharmonic potential energy surfaces for systems where rotational motion is significant. Our results highlight the interplay between halide perovskite composition, structural dynamics and defect physics, and we expect these findings to be more widely applicable to systems where dynamic octahedral tilting is evident.

[1] Ni, Z. et al. (2022) *Nat. Energy* **7** 65–73

[2] Yihua Chen et al. (2020) *J. Appl. Phys.* **128** 060903

[3] L. Whalley et al. (2021) *J. Am. Chem. Soc.* **143** 9123–9128

[4] D. Ghosh et al. (2017) *ACS Energy Lett.* **2** 2424–2429

[5] Kim et al. (2020) *J. Open Source Softw.* **5** 2102.

11:15 AM EN04.06/EN02.06.07

Data Driven Composition and Octahedral Engineering of Halide Perovskites Jiaqi Yang, Panayotis T. Manganaris and Arun Kumar Mannodi Kanakkithodi; Purdue University MSE, United States

Halide perovskites are highly desired for optoelectronic applications, because of the excellent tunability of their properties from composition engineering and octahedral distortion and rotation. However, the infinite possibilities of compositions via cation and/or anion-site mixing and octahedral manipulation raise considerable challenges when exploring the stability and properties of halide perovskites, both experimentally and computationally. In this work, we address this issue using high-throughput density functional theory (DFT) computations and discover trends and design rules to aid prediction and screening across large chemical spaces.

We generate a large DFT dataset of ABX₃ halide perovskite alloys with several elemental and molecular choices at A, B and X sites, and arbitrary mixing allowed on each site.¹ This dataset covers ~ 500 compounds across a 14-dimensional ionic space and is currently restricted to alloying with pseudo-cubic 2x2x2 supercells. To further explore property tuning, we create hundreds of random distorted and rotated structures for Cs/MAPbX₃ perovskites (MA = methylammonium, X = I/Br/Cl). Many critical properties are calculated using standard GGA-PBE and hybrid HSE06 functionals, including decomposition and mixing energies, electronic band gap, and Spectroscopic Limited Maximum Efficiency (SLME) based on computed optical absorption spectra.²

A screening process is applied across the dataset of ~ 500 pure and mixed composition perovskites, in terms of the stability, bandgap, deviation from cubicity (to account of any excessive distortion in lattice parameters), degree of octahedral distortion, and finally, some established perovskite stability metrics such as the tolerance and octahedral factors.³⁻⁵ This leads us to 49 stable compositions with attractive properties which are ranked according to SLME and compared with the literature as well as recommended for synthesis and characterization. Using Pearson correlation coefficients and unsupervised learning techniques such as PCA and T-SNE, we unravel qualitative relationships between elemental/molecular combinations, octahedral

distortion, and computed electronic and optical properties. We further develop a unique perovskite descriptor with compositional, physical, and octahedral information, which are used to train regression-based machine learning (ML) models and predict properties of thousands of novel compounds.

In order to make the dataset openly available to researchers, we developed NanoHub⁶⁻⁷ tools that help visualize our entire DFT database, create new structures with arbitrary octahedral distortion and rotation, and make ML predictions for any compositions of interest. The high-throughput DFT framework and tools from this work are promising for accelerating the design of halide perovskites for various applications such as solar cells, photodiodes, electronics, and infrared sensors, and are currently being coupled with active experiments for validation and discovery.

1. Mannodi-Kanakkithodi, *Energy & Environmental Science* 2022, 15, 1930-1949.
2. Yang, J.; A High-Throughput Computational Dataset of Halide Perovskite Alloys. In Preparation.
3. Bartel Christopher, J. *Science Advances*, 5, eaav0693.
4. Sampson, M. D.; *Journal of Materials Chemistry A* 2017, 5, 3578-3588.
5. V. M. Goldschmidt, *Nach Untersuchungen Gemeinsam Mitt. Barth, G. Lunde, W. Zachariasen.*
6. Madhavan, K.; *Nanotechnology Reviews* 2013, 2, 107-117.
7. Klimeck, G.; *Computing in Science & Engineering* 2008, 10, 17-23.

11:30 AM *EN04.06/EN02.06.08

Exploration of the Compositional Space in Methylammonium Free Lead Halide Perovskites for High-Performance Solar Cells Juan Pablo Correa Baena; Georgia Institute of Technology, United States

The certified power conversion efficiency (PCE) of state-of-the-art organic-inorganic metal halide perovskite solar cells (PSCs) has surpassed 25%. The most widely studied methylammonium (MA) lead iodide undergoes a structural phase transition and degradation due to the volatile MA cation, detrimental to the long-term stability of the devices. Formamidinium (FA), used as the majority cation in most PSCs with a PCE of >20%, is thermally more stable and has a more optimal red-shifted bandgap. However, FA with the relatively large ionic radius induces tilted PbI_6 octahedra in FAPbI₃, leading to the photoinactive yellow δ -phase at room temperature. Herein, iodide and FA in FAPbI₃ were gradually replaced by bromide and cesium (Cs) with smaller radius to understand their role on yellow δ -phase suppression and to systematically explore the compositional space via regulating the tolerance factor, revealing the crucial link between the crystal structure and optoelectronic properties of the mixed-cation (FA/Cs) lead mixed-halide (I/Br) perovskite. The FA/Cs-Pb-I/Br films were probed by advanced synchrotron X-ray characterization to understand halide phase segregation, which has been found to be detrimental for solar cell performance.

SESSION EN04.07: Interfaces, Surfaces and Energy Transfer
Session Chairs: Tiarnan Doherty and Carolin Sutter-Fella
Wednesday Afternoon, November 30, 2022
Hynes, Level 3, Ballroom A

1:30 PM *EN04.07.01

Nanoscale Effects in Perovskite Solar Cells Observed by Scanning Force Microscopy Stefan A. Weber^{1,2}, Ilka Hermes^{1,3}, Yenal Yalcinkaya^{1,2}, Pascal N. Rohrbeck¹, Konstantinos Bidinakis¹ and Rüdiger Berger¹; ¹Max Planck Institute for Polymer Research, Germany; ²Johannes Gutenberg University, Germany; ³Leibniz Institute for Polymer Research, Germany

Perovskite solar cells have electrified the solar cell research community with astonishing performance and surprising material properties. However, the widespread commercialization of perovskites in solar cells and other optoelectronic applications still requires a more detailed knowledge about fundamental material properties. My group is specialized in the investigation of these properties on nanometer length scales using scanning force microscopy [1-4].

In 2016, we discovered a distinct nanoscale stripe domain structure in $MAPbI_3$ perovskite crystals that is characteristic for ferro-elastic twin domains [1]. Using a combination of piezoresponse force microscopy (PFM) and photoluminescence microscopy, we found that this domain structure leads to an anisotropic charge transport across the crystal [2]. To utilize this effect in devices, a precise control of the domain configuration would be desirable. To this end, we explored the possibilities of both physical and chemical strain engineering [3]. Next to these intrinsic properties of perovskites, the specific interactions at the various interfaces in devices are of critical importance. To visualize the functionality of different layers, we developed a method to prepare smooth cuts through a solar cell device. We subsequently map the potential distribution across the device using time-resolved Kelvin probe force microscopy (tr-KPFM) [4,5]. We could show that the formation and release of ionic interface charges determine the time scales for current-voltage hysteresis in perovskite solar cells. Our results highlight that precise control over interfaces in perovskite solar cells is the key, not only for controlling and suppressing hysteresis but also for their long-term stability in perovskite solar cells.

[1] Hermes et al. *J. Phys. Chem C*, **120**(10), 5724 (2016).

[2] Hermes et al. *Energy Environ. Sci.* **13**, 4168 (2020).

[3] <https://arxiv.org/abs/2205.00381>.

[4] Weber et al. *Energy Environ. Sci.*, **11**, 2404 (2018).

[5] Hermes et al. *J. Phys. Chem. Lett.*, **9**, 6249 (2018).

2:00 PM EN04.07.02

Nanoscale Charge Carrier Lifetimes Revealed by Intensity Modulated Scanning Kelvin Probe Microscopy Kevin Ho, Rajiv Giridharagopal, Yangwei Shi, Yujing Lin and David Ginger; University of Washington, United States

Halide perovskites are known to be tolerant to defects while exhibiting long carrier lifetimes. At the same time, it is known that lifetimes are spatially-dependent, with grains and grain boundaries exhibiting different levels of nonradiative recombination and therefore different carrier dynamics. In order to approach the radiative efficiency limits in these devices, it is essential to understand the variation of carrier trapping and de-trapping dynamics between grains and grain boundaries and to improve the carrier dynamics at these locations. Here, we use intensity modulated scanning Kelvin probe microscopy (IM-SKPM) to directly image carrier dynamics at the tens of nanosecond timescale, with high spatial resolution on the order of ~80-100 nanometers. We apply IM-SKPM to study the perovskite $FA_{0.83}Cs_{0.17}Pb(Br_{x}I_{1-x})_3$ with varying halide composition. We observe lower carrier lifetimes from IM-SKPM at the

grain boundaries, suggesting that the boundaries are not benign and result in higher carrier trapping. Furthermore, we use IM-SKPM to study how surface passivating agents affect the distribution of carrier lifetimes. The perovskites were passivated with (3-aminopropyl)triethoxysilane (APTMS) which allowed us to investigate the effect of passivation on the local variation of charge carrier dynamics. After passivation, we found that the IM-SKPM lifetimes increased due to a reduction of trap densities. However, a variation in the carrier lifetimes was still observed corresponding to the non-uniformity of the passivator. Importantly, these results show that IM-SKPM can be correlated with the photoluminescence lifetime trends, but at nanoscale spatial resolution far below the optical diffraction limit.

2:15 PM EN04.07.03

Explaining the Negative Capacitance by the Chemical Inductor Effect in Halide Perovskite Cell Devices Juan Bisquert and [Antonio Guerrero](#); University of Jaume I, Spain

A negative capacitance effect is observed in perovskite solar cells and other types of hybrid organic-inorganic solar cells. This effect reduces the resistance and affects the performance of the solar cell as well as the degradation characteristics. We apply the concept of the chemical inductor for a better understanding and control of the negative capacitance. The chemical inductor is a combination of a fast and a slow conduction modes that couple to form an inductor arc in the impedance spectrum. We discuss the interpretation of the slow recombination mechanisms in terms of ion-controlled dynamics and we obtain the information for a better characterization of the hybrid photovoltaic devices.

2:30 PM BREAK

3:30 PM *EN04.07.04

Interface Defects in Halide Perovskite Semiconductor Devices [Philip Schulz](#)^{1,2}; ¹Centre National de la Recherche Scientifique, France; ²Institut photovoltaïque d'Ile de France (IPVF), France

Hybrid organic inorganic metal halide perovskites (MHPs) denote a family of compound semiconductors, which established a novel class of optoelectronics, most prominently known for the perovskite solar cell. While the power conversion efficiency of these photovoltaic devices saw a steep rise in the past decade, tailoring the interfaces between the MHP film and charge transport layer became the major control lever to enhance performance. The use of photoemission spectroscopy to analyze the chemical and electronic properties of these interfaces has been challenging due to many possible chemical reactions at the buried interfaces [1].

Here, we present synchrotron- and lab-based hard X-ray photoelectron spectroscopy (HAXPES) experiments to address the particular chemistry of MHP, beginning with the interface between and SnO₂, grown by atomic layer deposition on top, using photon energies of 2 and 6 keV. We find evidence for the formation of new chemical species (PbO, N and halide-containing compounds) and changes in the energy level alignment at the MHP/SnO₂ interface. The spectra exhibit binding energy shifts that may indicate upward band bending of the MHP energy levels. Assuming flat band conditions at the MHP surface prior interface formation, this upward band bending may form an electron transport barrier detrimental to cell performance.

We also employed the methodology to evaluate lead-free halide perovskite films based on formamidinium tin iodide (FASnI₃), for which tin fluoride (SnF₂) is a commonly used additive enabling a retardation of tin oxidation and a reduction of tin vacancies. We targeted films deposited on the organic hole transport layer PEDOT:PSS. For solar cells with optimized performance, the local SnF₂ distribution in the perovskite bulk and possible chemical reactions at the (buried) interface between PEDOT:PSS and the perovskite film are analyzed by photoelectron spectroscopy using soft (Al Kα) as well as hard (Ga Kα) X-ray photons. Our measurements revealed that SnF₂ significantly improves the layer morphology, but preferably precipitates at the PEDOT:PSS/MHP interface where it forms a SnS interlayer of approximately 1.2 nm thickness induced by a chemical reaction with sulfur-containing groups at the PEDOT:PSS surface. Our work adds a new aspect to the discussion of high-efficiency Sn-based perovskite solar cells which still commonly make use of PEDOT:PSS as HTL material in contrast to Pb-based solar cells, where alternatives to PEDOT:PSS are gaining growing interest [2].

Références

1. S. Béchu, M. Ralaingarisoa, A. Etcheberry, P. Schulz, *Adv. Energy Mater.* **2020**, 201904007
2. J. Zillner, H.-G. Boyen, P. Schulz, J. Hanisch, N. Gauquelin, J. Verbeeck, J. Küffner, D. Desta, L. Eisele, E. Ahlswede, M. Powalla, *Adv. Funct. Mater.* **2022**, 2109649 (DOI: 10.1002/adfm.202109649)

4:00 PM EN04.07.05

Understanding the 2D/3D Heterostructure Interface in Highly Efficient Green PeLEDs [Alexandra Ramadan](#)^{1,2}, Robert Oliver¹, Woo Hyeon Jeong³, Boubacar Traore⁴, Junke Jiang⁴, Bo Ram Lee³, Jacky Even⁴, Claudine Katan⁵ and Henry Snaith¹; ¹University of Oxford, United Kingdom; ²The University of Sheffield, United Kingdom; ³PKNU, Korea (the Republic of); ⁴INSA Rennes, France; ⁵ISCR CNRS, France

Light emitting diodes (LEDs) based on metal halide perovskite semiconductors have attracted considerable research interest due to their potential for low cost, high efficiency LEDs with excellent colour purity and bandwidth. In particular, two dimensional (2D) - three dimensional (3D) hybrid perovskite heterostructures (often described as quasi-2D structures) have been subject to considerable investigation within the perovskite LED community as one route through which to produce highly efficient devices.^{1,2} It has been shown that in these heterostructures the emission wavelength and device performance can be informed by the organic cation used to form the 2D perovskite structure.³ To ensure the optimal continued development of optoelectronic devices based on these structures it is essential that we have a comprehensive understanding of the 2D/3D interface structure and the charge transport across this interface.

To probe this interface we develop a range of quasi-2D perovskite emitting layers, based on a (BABr)_x(CsPbBr₃)_{1-x} (where BA = butylammonium) structure with varying amounts of the 2D perovskite. We implement these emitters in PeLED devices and demonstrate excellent electroluminescence external quantum efficiencies > 16 %. We observe a strong relationship between the 2D content of these heterostructures and the efficiency of the corresponding PeLEDs. We investigate the structure of the 2D-3D heterostructures using X-ray diffraction and observe a mixture of n=1 and n=2 2D-perovskite structures in addition to the 3D perovskite. We comprehensively study the charge carrier dynamics of a range of (BABr)_x(CsPbBr₃)_{1-x} structures using absolute and time-resolved photoluminescence studies. We find that the 2D perovskite only influences the emission profile of our LEDs in specific cases and that the predominant role of the 2D perovskite structure is to confine the size of the 3D perovskite domains and therefore boost the absolute electro- and photoluminescence of the 3D perovskite domains.

To understand the charge transport across the interface between the 2D and 3D perovskite structures we investigate the energetic band alignment using a combination of ultraviolet photoelectron spectroscopy studies (UPS) and density functional theory (DFT) modelling. We demonstrate that charge transfer between the 2D and 3D perovskite structures is determined by the type of 2D structure (whether the structure is n=1 or n=2) and we suggest a route to predicting whether a 2D structure will contribute to the emission of an LED. We show that there is a critical 2D/3D compositional limit for achieving high efficiency devices. Whilst we do not find a mixture of 2D perovskite structures impacts LED efficiency, we show that there is a tight tolerance window for

the $n=1$ perovskite structure and once this window is exceeded it has a large detrimental effect on device performance.

Our work highlights the importance of understanding the 2D/3D heterostructure interface in engineering highly efficient devices and we show our initial results exploring the impact of phase pure 2D/3D perovskite heterostructures on PeLED performance.

1. Liu, Y. *et al.* Boosting the efficiency of quasi-2D perovskites light-emitting diodes by using encapsulation growth method. *Nano Energy* **80**, 105511–105511 (2021).
2. Fakhruddin, A. *et al.* Reduced Efficiency Roll Off and Improved Stability of Mixed 2D/3D Perovskite Light Emitting Diodes by Balancing Charge Injection. *Advanced Functional Materials* **29**, 1904101 (2019).
3. Warby, J. H. *et al.* Revealing Factors Influencing the Operational Stability of Perovskite Light-Emitting Diodes. *ACS Nano* **14**, 8855–8865 (2020).

4:15 PM EN04.07.06

Understanding via Thermal Evaporation How Capping Layers Transform the Lead Halide Perovskite Surface [Carlo Andrea Riccardo Perini](#)¹, Andres Felipe Castro Mendez¹, Tim Kodalle², Carolin M. Sutter-Fella² and Juan Pablo Correa Baena¹; ¹Georgia Institute of Technology, United States; ²Lawrence Berkeley National Laboratory, United States

In this contribution we compare interfaces treated with PEAI, a bulky cation, via solution and via thermal evaporation. We highlight differences in crystallinity, uniformity, and stability of the layers deposited via the two different routes using measurements as SEM, XPS, GIWAXS, and PL mapping. Finally, we test the bulky cation evaporated layers in complete devices stacks, reaching power conversion efficiencies > 20 %. Our observations suggest that bulky-cations deposited via vapor enable superior control of the exposed perovskite surface with respect to solution cast films. Both solution and vapor routes lead to the formation of 2D Ruddlesden-Popper phases at the treated interface, but result in different n , where n is in $A'_{2n-1}B_nX_{3n+1}$, where A' is PEAI, A is Cs, MA, FA, B is Pb, and X is the halide. We also demonstrate the role of interface termination of the underlying 3D perovskite film in the transformation of the 3D perovskite surface to 2D Ruddlesden-Popper structures. The impact of the interface termination is studied by using solution and vapor deposition routes to tailor the non-passivated surface to the stoichiometry desired. Furthermore, the solvent used for deposition via solution of the bulky cations is shown to introduce extra defects at the interface, which can be avoided via vapor depositing the organohalide salts. As a result, solar cells incorporating the vapor deposited layers show an increase in the median power conversion efficiency and better thermal stability than solution deposited films. Our observations indicate that vapor deposition routes are a valid tool to explore the transformation dynamics of the interface and enable a higher degree of control on the formation of the interface, which in turn leads to enhanced efficiency of perovskite solar cells passivated via vapor.

4:30 PM EN04.07.07

Do's and Don'ts of SCLC Analysis for Perovskite Materials [Vincent Le Corre](#); Friedrich-Alexander-Universität Erlangen-Nürnberg, Germany

The space-charge-limited current (SCLC) measurement is one of the most common methods used to study the mobility and defect density in semiconductors. This method has the advantage of separating the measurement of the material properties with respect to electron and hole by the use of single-carrier devices. The apparent simplicity of the method made it very popular in both organic and perovskite photovoltaic research communities. Here, we discuss the often overlooked pitfalls of SCLC analysis for perovskite materials.

First, we introduce a revisited analysis of SCLC measurements on perovskite single-crystals to obtain its trap densities. In fact, simulations clearly show that the presence of mobile ions severely complicates the SCLC analysis. Therefore, we also propose pulsed-SCLC as a new measurement procedure that helps to reduce the impact of mobile ions. We also show that the use of full drift-diffusion fitting of the pulsed-SCLC data allows for more accurate measurements of the mobility but also of both trap and mobile ion densities.

Secondly, we explore the many limitations of SCLC for thin-film perovskite devices. We discuss the importance of reporting the hysteresis, using the appropriate scan speed to do the measurement, and choosing the right charge transport layers. These seemingly experimental 'details' can have a strong influence on both the values of the defect density and the mobility extracted from the SCLC analysis.

SESSION EN04.08: Poster Session II

Session Chairs: Sascha Feldmann, Selina Olthof, Shuxia Tao and Alexander Urban

Wednesday Afternoon, November 30, 2022

8:00 PM - 10:00 PM

Hynes, Level 1, Hall A

EN04.08.03

Fundamental Insights into Halide Ion Migration and Exchange in Perovskite Nanocrystals [Sakiru L. Abiodun](#) and Andrew B. Greytak; University of South Carolina, United States

Halide perovskite nanocrystals have been identified as a prospective candidate for future optoelectronic devices, such as solar cells, LEDs, scintillators, and photo/radiation detectors. Their excellent optoelectronic properties such as large absorption coefficient, high carrier mobility, wide color gamut, long electron-hole diffusion lengths, and tunable bandgap energy are largely responsible for their wide acceptability in various electronic devices. However, despite the recent developments, the problem of instability remains a major obstacle toward their commercialization. For example, ion migration has been reported to cause phase separation in mixed halide perovskite-based optoelectronics which ultimately leads to instability and a decrease in photovoltaic performance. Therefore, many researchers have devoted attention to understanding the process of this ion migration in various mixed halide perovskites $\text{CsPb}(\text{I}_{1-x}\text{Br}_x)_3$ of different compositions. However, to date, the processes underlying this anion migration and exchange remain under debate and largely unclear. Here, we elucidated the processes involved during halide ion exchange and migration in lead perovskite nanocrystals. In addition to this, we also quantify the thermodynamics of this ion exchange, therefore, revealing the origin of phase separation commonly encountered in mixed $\text{CsPb}(\text{I}_{1-x}\text{Br}_x)_3$ halide perovskites-based optoelectronics. Our fundamental understanding of the process of this anion exchange and migration will help provide better-informed guidelines toward engineering perovskite nanocrystals for different applications such as tandem cells and efficient devices for lighting and display technology.

EN04.08.04

(PEA)₂PbI₄ Perovskite Fabry-Perot Microcavity Design [Martin Gomez](#), Victoria Quiros-Cordero, Natalie Stingelin, Carlos Silva and Juan Pablo Correa Baena; Georgia Institute of Technology, United States

Two-dimensional (2D) halide perovskites, multiple quantum-well organic-inorganic heterostructures with confined excitons, exhibit promising light-emitting applications due to their tunable narrow emission bandwidth, high photoluminescence quantum yield and low rates of non-radiative recombination. However, it is still challenging to achieve room temperature lasing from pure 2D perovskites, high crystallinity and reduced grain boundaries are desired to achieve photonic lasing. Grain boundaries are known to increase recombination and impede population inversion. A way to overcome this challenge is by using perovskites as active layers in optical microcavities and exploiting the strong light-matter coupling regime. The extremely light effective mass of exciton polaritons unlocks the possibility of achieving low threshold polariton lasing in which, unlike conventional photonic lasing, there is no need for population inversion. Hence, to further exploit the optical properties of 2D perovskites for lasing applications, more efforts should be invested in the study of 2D perovskite embedded microcavities. Here we have designed, fabricated, and characterized different architectures of (PEA)₂PbI₄ embedded Fabry-Perot cavities and studied the design parameters that lead to strong light-matter coupling.

EN04.08.05

Time-Resolved Kelvin Probe Force Microscopy to Investigate Grains of Mixed Halide Perovskite Solar Cell Material Pascal N. Rohrbeck¹, Yenal Yalcinkaya^{1,2}, Saba Gharibzadeh^{3,3}, Paul Fassel^{3,3}, Konstantinos Bidinakis¹, Ulrich W. Paetzold^{3,3} and Stefan A. Weber^{1,2}; ¹Max Planck Institute for Polymer Research Mainz, Germany; ²Johannes Gutenberg University, Germany; ³Karlsruhe Institute of Technology, Germany

Perovskite solar cells (PSCs) have become a good competitor for silicon-based solar cells. Nevertheless, local defects in the perovskite crystal structures limit the efficiency due to non-radiative charge recombination losses.^[1]

The occurrence of these defects is coupled to the nanoscale structure, e.g., to grain boundaries (GB) and crystal facets. Atomic force microscopy (AFM) methods are ideal for studying nanoscale electrical devices such as batteries, solar cells, and diodes.

Moreover, Kelvin probe force microscopy (KPFM) is a valid method to investigate the local effect of defect passivation on the nanoscale of perovskite materials.^[2] We investigated different perovskite materials by using a Time-resolved kelvin probe force microscopy (tr-KPFM) method. By observing the time- and position-dependent photovoltage, we were able to gain insight into the local defect densities. Further we were also able to uncover the local effect of passivation on individual perovskite grains and grain boundaries by measuring an extended photovoltage decay lifetime.^[1]

The results show that high defect densities in perovskites materials can be avoided with passivation strategies. When improving the efficiencies of perovskite solar cells this method can help to understand the mechanism behind the non-radiative recombination processes and ion migration processes to make them even more competitive to others like Si-based solar cells.

References:

[1] Rohrbeck, P. Untersuchung von lokalen Aufladungsdynamiken an Perowskit-Korngrenzen mit Zeitaufgelösten KPFM Methoden, 2021.

[2] Gharibzadeh, S.; Fassel, P.; Hossain, I. M.; Rohrbeck, P.; Frericks, M.; Schmidt, M.; Duong, T.; Khan, M. R.; Abzieher, T.; Nejjand, B. A.; Schackmar, F.; Almora, O.; Feeney, T.; Singh, R.; Fuchs, D.; Lemmer, U.; Hofmann, J. P.; Weber, S. A. L.; Paetzold, U. W. Two Birds with One Stone: Dual Grain-Boundary and Interface Passivation Enables >22% Efficient Inverted Methylammonium-Free Perovskite Solar Cells. *Energy Environ. Sci.* 2021, 14 (11), 5875–5893. <https://doi.org/10.1039/d1ee01508g>.

EN04.08.06

Plastic Deformation and Fracture in Metal Halide Perovskite Single Crystals and Polycrystalline Bulk Materials Mcaghan Doyle, Madhuja Layek, Zhenghong Dai and Nitin P. Padture; Brown University, United States

Metal halide perovskites (MHPs) have emerged as promising light absorber materials for use in perovskite solar cells (PSCs). Although significant progress has been made in enhancing the efficiency and operational stability of PSCs, their mechanical reliability needs to be improved if they are to operate efficiently for many years. However, the mechanical properties of MHPs have not been fully explored. This is especially important because MHPs possess poor mechanical properties — they are compliant, soft, and brittle. To that end, we have used nanoindentation and micro-indentation to study the plastic deformation and fracture properties of MHP single crystals of various compositions. This includes slip-system analyses, time-dependent creep, environmental effects, and estimation of the fracture toughness. Similar studies are also performed on polycrystalline bulk materials to understand the roles of grain boundaries and anisotropy. Through this we aim to provide a more comprehensive understanding of plastic deformation and fracture of MHPs, which is relevant for understanding and enhancing the mechanical reliability of PSCs.

EN04.08.07

Study of Bi-Doped MAPbI₃ Single Crystal for ETL-Free Perovskite Solar Cell Application Sarah S. Youn¹, Yunae Cho², Gee Yeong Kim³ and William Jo¹; ¹Ewha Womans University, Korea (the Republic of); ²Korea Institute of Energy Research, Korea (the Republic of); ³Korea Institute of Science and Technology, Korea (the Republic of)

Hybrid perovskite single crystals show great potential in photovoltaic applications due to their high stability, absence of grain boundaries, lower intrinsic trap density, and higher carrier mobility compared to polycrystalline thin films. Therefore, the application of thin-film single crystal (THSC) to solar cells is expected to provide improved stability and efficient device performance. To obtain high-quality single crystal solar cells, the space-limited inverse temperature crystallization (ITC) method is widely used in the THSC synthesis process, in which a perovskite single crystal is grown between two hydrophobic hole transport layer (HTL) coated ITO glasses [ref]. After growing the THSC, an electron transport layer (ETL) and electrode are generally deposited on top. In this work, we design an ETL-free device by n-doped perovskite THSC, which reduces one process of continuous layer deposition for solar cell fabrication. Bismuth (Bi) can be used to change the doping concentration in perovskite single crystal. We present the electrical properties of the charge carrier concentration and conductivity changes of Bi-doped MAPbI₃ (MAPI-Bi) and compare it with pristine MAPI by space charge limited current, conductivity (parallel & perpendicular), and scanning probe microscopy measurements. The optical properties are also studied using Raman and PL measurements. Our study will provide an insight to fabricate an ETL-free solar cell device via doping the perovskite layer. By expanding our strategy to p-doped single crystals, a simpler solar cell structure with no charge transport layers can be considered.

[ref] ACS Energy Lett. 2020, 5, 657–662

EN04.08.11

Optically-Induced Long-Lived Chirality Memory in the Color Tunable Chiral Lead-Free Semiconductor (R)/(S)-CHEA₄Bi₂Br_xI_{10-x} (x = 0 - 10) Shangpu Liu¹, Markus W. Heindl¹, Natalie Fehn², Sebastian Caicedo Davila², Lissa Eyre¹, Silva Kronawitter², Gregor Kieslich², David Egger² and Felix Deschler¹; ¹Walter Schottky Institut, Germany; ²Technical University of Munich, Germany

Hybrid organic-Inorganic networks that incorporate chiral molecules have attracted great attention due to their potential in semiconductor lighting

applications and optical communication. Here we introduce the chiral organic molecules (R)/(S)-1-cyclohexylethylamine (CHEA) into bismuth-based lead-free structures with an edge-sharing octahedral motif, to synthesize chiral lead-free (R)/(S)-CHEA₄Bi₂Br_xI_{10-x} crystals and thin films. Using single-crystal X-ray diffraction measurements and density-functional theory calculations, we identify crystal and electronic band structures. We find the difference in the chirality of (R)- and (S)-CHEA₄Bi₂Br₁₀ compound induces opposite spin textures in the x and z directions of band structures. We then investigate the materials' optical properties and find circular dichroism, which we tune by the bromide-iodide ratio over a wide wavelength range from 300 - 500 nm. Further, we employ transient absorption spectra and time-correlated single photon counting to investigate charge carrier dynamics, which show long-lived excitations with unexpected optically-induced chirality memory up to 10s of nanosecond timescales. Our demonstration of chirality memory in a color-tunable and chiral lead-free semiconductor opens a new avenue for the discovery of high-performance, lead-free spintronic materials with optical functionalities.

EN04.08.12

Thermal Annealing-Sensitive Morphology Evolution of Tin-Perovskite Absorbers for Efficient Lead-Free Perovskite Solar Cells [Donghan Kim](#) and Jae Woong Jung; Kyunghee University, Korea (the Republic of)

Tin-based perovskite absorber is the potent candidate for replacing the lead-based perovskite solar cells (PSCs) due to the suitable tolerance factor for perovskite lattice, suitable band-gap, and low toxicity. At present, tin-based perovskite absorbers adopting ABX₃ structure generally suffer from reproducibility and stability issues mainly due to rapid crystal growth and quick oxidation of tin cation. In order to optimize the crystal growth in perovskite absorber layer, we varied the thermal annealing time (duration) of tin-perovskite absorber layer after antisolvent-assisted spin-coating deposition, and the influence of annealing time on the film morphologies and electrical properties were systematically studied. Surprisingly, the film morphology was strongly dependent on the thermal annealing time, and it is found that instantaneous thermal annealing as quick as 1 min is enough to prepare high-quality tin-perovskite absorber layer with compact grains, diminished grain boundaries, and less defect density. And then, no distinct evolution of film morphology was observed after 1 min thermal annealing. For the photovoltaic properties, thermal annealing for 1 min optimally delivered >6% efficiency. Details experiment results and discussion will be presented in the presentation.

EN04.08.15

Quantitative Structure-Property Relationships in Mixed Ion Hybrid Perovskite by Multi-Modal Mapping of Phase Diagrams [Tonghui Wang](#)^{1,1}, Ruipeng Li², Hossein Ardekani^{1,1}, Mahdi Ramezani¹, Ryan Wilmington^{1,1}, Robert Epps¹, Kasra Darabi^{1,1}, Boyu Guo^{1,1}, Milad Abolhasani¹, Kenan Gundogdu^{1,1} and Aram Amassian^{1,1}; ¹North Carolina State University, United States; ²Brookhaven National Laboratory, United States

Hybrid perovskites are part of a highly tunable material class with >1,000 unique compounds and countless mixed-ion alloys currently being investigated for optoelectronic and energy applications. The absence of phase diagrams for mixed ion perovskites limits the establishment structure-property relationships for mixed ion alloys required for optoelectronic applications. We take the view that quantitative structure-property relationships (QSPRs) constructed around phase diagrams provide the most robust framework for materials design and engineering. However, QSPRs are still rare in materials research, let alone in the field of hybrid perovskites. Here, we introduce a new approach to map QSPRs reliably, rapidly and efficiently using research automation combined with on-chip micro-experimentation. We demonstrate the RoboMapper, a compact robotic laboratory which miniaturizes the traditional workflow (formulation, coating/printing) by three to four orders of magnitude to integrate compositional arrays of arbitrary hybrid perovskite composition maps on a single substrate for efficient multi-modal data collection. Compared with traditional manual workflows and existing full-scale serial automation, the RoboMapper is shown to be 5-10 times faster and reduces the material cost, toxic waste, and greenhouse gas emissions by more than an order of magnitude. We successfully demonstrate sophisticated QSPRs for the quaternary system FA_{1-x}Cs_xPb(I_{1-x}Br_x)₃ system that map the structure and phase, optical properties and photostability using multi-modal characterizations, including optical microscopy, micro-diffraction, and micro-photoluminescence. Our QSPR models are demonstrated to be predictive for phase, bandgap and photostability and are tested with targeted bandgaps, such as 1.7eV for perovskite-silicon hybrid tandem solar cells, to discover new compositions exhibiting the ideal bandgap with improved photo-stability in air.

EN04.08.16

The Mechanical Properties of Polycrystalline Metal Halide Perovskite Thin Films and Polycrystalline Bulk Materials [Madhuja Layek](#), Meaghan Doyle, Zhenghong Dai, Hector F. Garces and Nitin P. Padture; Brown University, United States

Over the past years, metal halide perovskites (MHPs) have attracted considerable attention owing to their remarkable application potential in the field of optoelectronics, especially photovoltaics. Despite this keen interest in MHPs, little information can be found on their mechanical properties. However, to manufacture efficient and reliable perovskite solar cells (PSCs) that can operate satisfactorily for decades, it is critical to study the mechanical properties of MHPs which are inherently compliant, soft, and brittle. To that end, here we have employed the curvature-measurement technique to estimate the Young's modulus and coefficient of thermal expansion of polycrystalline MHP thin films of various compositions. Also, we have synthesized MHP powders of different compositions and sintered them into dense polycrystalline bulk pellets and measured their Young's modulus directly using uniaxial compression. This is in an effort to understand the effect of grain size on Young's modulus and other relevant mechanical properties of MHPs. Our aim is to provide an in-depth understanding of the mechanical properties of MHPs, which are key to understanding and enhancing the mechanical reliability of PSCs.

EN04.08.17

Enhanced Crystal Growth of Perovskite Materials [Duane L. Simonson](#); Research Support Instruments, Inc., United States

The design and preparation of durable active materials is a priority for more efficient solar cell and light (LED) source development. The use of perovskite hybrids (such as methylammonium lead halide series) has dominated the attention of researchers over the past few years. Their use is still limited by the longevity issues with temperature, humidity, and other factors. In this work, the use of polymer templates for enhanced perovskite crystal growth is explored. In these systems, the nucleation suppression and growth of very few crystals allows one inch sized bulk crystals to be grown directly (no seeding) from water solutions in very small volumes (100 mL saturated solution). Emphasis on lower toxicity copper, bismuth, and cesium materials will be discussed, along with advanced processing into thin films.

EN04.08.19

A Guide Through the Layered Perovskite Landscape—Mismatch, Inter-Layer Interaction and Perovskitoids [Mikael Kepenekian](#)^{1,2}, Bruno Cucco¹, George Volonakis¹, Claudine Katan^{1,2} and Jacky Even³; ¹Université de Rennes 1, France; ²CNRS, France; ³INSA Rennes, France

If 3-dimensional (3D) halide perovskites have shown spectacular results in optoelectronic devices, they offer limited choice of metals and organic cations. This is not the case of layered (2D) halide perovskites A₂MX₄ (A: organic cation, M: metal ion, X: halide) that impose far less constraints over the chemical design of the organic spacer [2,3]. The number of suitable candidates for A then becomes so large that guidelines would be desirable for the design of future devices. Here, based on computational investigations conducted on experimental and model systems, we propose to contribute to the writing of those rules.

We start by exploring the concept of lattice mismatch [4] that offers a direct insight in the structural stability and optical properties of multi-layered perovskites by considering them as heterostructures formed by single-layer and 3D perovskites [5]. Then, we inspect the interaction between layers that has been shown to have great influence over the optoelectronic properties of the materials [6-8]. We establish the structural parameters governing the amplitude of the interaction as well as its limits. Finally, we present new directions to explore for the design of low-dimensional materials with the recently proposed perovskitoid materials based on a mixing of corner- and edge-sharing octahedra [9].

- [1] B. Saparov, D. B. Mitzi, *Chem. Rev.* **2016**, *116*, 4558.
- [2] L. Pedesseau, M.K. *et al.*, *ACS Nano* **2016**, *10*, 9776.
- [3] C. Katan, N. Mercier, J. Even, *Chem. Rev.* **2019**, *119*, 3140.
- [4] M. Kepenekian *et al.*, *Nano Lett.* **2018**, *18*, 5603.
- [5] E. S. Vasileiadou, M.K. *et al.*, *Chem. Mater.* **2021**, *33*, 5085.
- [6] W. Li *et al.*, *Nat. Nanotechnol.* **2022**, *17*, 45.
- [7] L. Mao, M.K. *et al.*, *J. Am. Chem. Soc.* **2020**, *142*, 8342.
- [8] E. S. Vasileiadou, M.K. *et al.*, *J. Am. Chem. Soc.* **2022**, *144*, 6390.
- [9] X. Li, M.K. *et al.*, *J. Am. Chem. Soc.* **2022**, *144*, 3902.

EN04.08.20

Nano-Volumetric Photoconductivity Mapping for Hybrid Perovskites with Tomographic AFM Luis Ortiz¹, Mingwei Hao², Jingfeng Song¹, Yuanyan Zhou² and Bryan D. Huey¹; ¹University of Connecticut, United States; ²Hong Kong Baptist University, Hong Kong

Thin film solar cells such as the promising hybrid perovskite systems typically possess high densities of grains, grain boundaries, and buried interfaces. Their effects on ultimate device performance and reliability are difficult to ascertain. We employ Tomographic Atomic Force Microscopy (T-AFM), progressively measuring nanoscale photocurrents during tip-induced surface milling, in order to three dimensionally reconstruct the photoconduction network. Specifically, results are presented for perovskite based solar half cells, engineered with continuous layers of SnO_{2-x} or NiO_x between a MAPbI₃ absorber and a conducting back electrode. This isolates electron or hole conduction, respectively, with a clear reversal in the sign of the biased photocurrents and even when directly mapping nanoscale short circuit currents. PCB and Spiro additives concentrated at grain boundaries are further employed, in order to elucidate benefits or disadvantages of interfaces for distinct carrier types. Local, ensemble, and depth dependencies of photocurrents for grains and grain boundaries are thus uniquely considered, thereby informing optimal microstructures for future hybrid perovskite solar cell designs.

EN04.08.24

Directly Probing the Effects of Defect Passivation on Ion Migration in Wide Bandgap Perovskites Justin Pothoof, Rajiv Giridharagopal and David S. Ginger; University of Washington, United States

Wide bandgap halide perovskite (~1.7 eV) materials are the most promising active layers being studied for use in tandem solar cells utilizing silicon (~1.1 eV) as its bottom light harvesting layer. Being solution processible and having an easily tunable bandgap, perovskites can be tailored to fit the already well optimized and established silicon photovoltaic cell to maximize power conversion efficiency. While perovskites are known to be defect tolerant when discussing device performance, those same defects allow for ionic transport through the crystal lattice leading to device instability in the form of phase segregation, hysteresis, and active layer degradation at interphases or electrodes. In wide bandgap perovskites in particular, this ionic motion is exacerbated by the mixed halide composition necessary to achieve a larger energy gap needed in the tandem architecture. Understanding the phenomenon of ion migration and our ability to control it is paramount to the reproducible fabrication of high efficiency and operationally stable photovoltaics. Here, we use a combination of multimodal scanning probe microscopy and photoluminescence characterization to observe the migration of ions in wide bandgap perovskite films. Importantly, we also use this combination of methods to show the benefits of defect passivation schemes in reducing this deleterious ion migration. Defect passivation, often through chemical post-treatment of the perovskite active layer, has been reported to reduce nonradiative recombination. Here we show that passivation also can reduce ion migration and therefore enhance long-term stability. To measure this effect, we utilize electrical and optoelectronic scanning probe microscopy, such as scanning Kelvin probe microscopy and surface photovoltage, to probe ion motion locally and correlate these measurements with photoluminescence lifetimes and intensity. These results enable future investigations of multiple facets of post-processing treatments on optoelectronic properties, such as carrier lifetimes, photoluminescence enhancement, mitigation of ionic migration, and changes in device metrics among other measurements.

EN04.08.26

Direct Observation of Light-Induced Halide Diffusion in 2D Lateral Heterostructures Halide Perovskite Crystals Yanqi Luo¹, Shuchen Zhang², Jia-Shiang Chen¹, Xuedan Ma¹, Junjing Deng¹, Yi Jiang¹, Luxi Li¹, Barry Lai¹, Si Chen¹, Sarah Wigehold¹ and Letian Dou²; ¹Argonne National Laboratory, United States; ²Purdue University, United States

Two-dimensional (2D) halide perovskites with enhanced stability and radiative recombination properties are promising for photovoltaic and light-emitting diode (LED) applications. Recent progress in fabricating lateral heterojunctions of 2D halide perovskites provides a unique platform for creating LEDs with large structural and compositional tunability. However, an improved understanding of the origins of degradation and the interactions with external stimuli within lateral heterostructures needs to be established to overcome stability barriers. In this study, we monitor the evolution of halide diffusion using non-destructive synchrotron-based nanoprobe X-ray fluorescence (Nano-XRF) within various dimensional phenylethylammonium (PEA) based 2D crystals. Upon continuous UV light exposure, the iodine-rich region undergoes rapid sublimation or related photooxidation reactions, while bromine is relatively stable and gradually diffuses/migrates to the previously iodine-rich junction. The degree of bromide diffusion as a function of dimensionality is revealed experimentally in the lateral heterostructures perovskite system for the first time. Understanding the ionic transport mechanism and its driving force is essential for engineering long-lived halide perovskite devices.

EN04.08.30

Assessing *n*-Type Dopability of the Low-Dimensional Metal Halide Cs₃Cu₂I₅ Young-Kwang Jung¹ and Aron Walsh^{1,2}; ¹Yonsei University, Korea (the Republic of); ²Imperial College London, United Kingdom

Low-dimensional metal halides are emerging materials for light-emitting applications due to their unique optical properties (e.g. high photoluminescence quantum yield and giant Stokes shift) [1-4]. Even though their use in other applications including memristors [5] and thermoelectrics [6] has been suggested, fundamental understanding of those compounds is still lacking. For instance, whether we can tune physical properties of low-dimensional metal halides from doping is not known yet. Herein, we identify complex intrinsic defect chemistry of Cs₃Cu₂I₅ — the most well known example of low-dimensional metal halides — and further assess *n*-type dopability of the material using first-principles calculations. We will discuss how different defect properties of Cs₃Cu₂I₅ is from other conventional materials and what dopant will be most effective to make it *n*-type.

- [1] Li, M.; Xia, Z. Recent Progress of Zero-Dimensional Luminescent Metal Halides. *Chem. Soc. Rev.* **2021**, *50*, 2626–2662
- [2] Jun, T.; Sim, K.; Iimura, S.; Sasase, M.; Kamioka, H.; Kim, J.; Hosono, H. Lead-Free Highly Efficient Blue-Emitting Cs₃Cu₂I₅ with 0D Electronic Structure. *Adv. Mater.* **2018**, *30*, 1804547
- [3] Creason, T. D.; McWhorter, T. M.; Bell, Z.; Du, M.-H.; Saparov, B. K₂CuX₃ (X = Cl, Br): All-Inorganic Lead-Free Blue Emitters with Near-Unity Photoluminescence Quantum Yield. *Chem. Mater.* **2020**, *32*, 6197–6205
- [4] Jung, Y.-K.; Kim, S.; Kim, Y. C.; Walsh, A. Low Barrier for Exciton Self-Trapping Enables High Photoluminescence Quantum Yield in Cs₃Cu₂I₅. *J. Phys. Chem. Lett.* **2021**, *12*, 8447–8452
- [5] Yang, J.-M.; Jung, Y.-K.; Lee, J.-H.; Kim, Y. C.; Kim, S.-Y.; Seo, S.; Park, D.-A.; Kim, J.-H.; Jeong, S.-Y.; Han, I.-T.; Park, J.-H.; Walsh, A.; Park, N.-G. Asymmetric carrier transport in flexible interface-type memristor enables artificial synapses with sub-femtojoule energy consumption. *Nanoscale Horiz.* **2021**, *6*, 987–997
- [6] Jung, Y.-K.; Han, I. T.; Kim, Y. C.; Walsh, A. Prediction of high thermoelectric performance in the low-dimensional metal halide Cs₃Cu₂I₅. *npj Comput. Mater.* **2021**, *7*, 51

EN04.08.31

Chiral Nonlinear Optics of Halide Perovskite Under Light-Matter Strong Coupling Daichi Okada and Fumito Araoka; RIKEN Center for Emergent Matter Science, Japan

Light-matter strong coupling is the hybridized state of light and matter, which can be achieved by coherent coupling between an excitonic transition and a resonant optical mode of a cavity, generating two new split exciton-polaritonic energy states, that is the so-called Rabi-splitting. In past years, it has been seen strong coupling can manipulate and enhance various types of materials properties, such as photochemical reactivity, conductivity, rate of energy transfer, nonlinear optical effect, and so on. Because of such interesting quantum nature and potential, many scientists are investigating to deepen the understanding of strong coupling and develop it to various types of materials and physical properties. However, chirality related physical properties has yet been scarcely studied.

In this work, we study nonlinear optical effect in thin films of chiral halide perovskite that are placed either in the strong coupling condition inside a Fabry-Perot (FP) cavity or not (uncoupled condition). Due to the strong excitonic oscillator strength, chiral halide perovskite shows clear Rabi-splitting with a large separation energy of about 0.25 eV. The formation of the strong coupling gives rise to an enhancement of second harmonic generation (SHG) activity by about one order of magnitude at the higher-energy polaritonic band (the so-called, upper polariton). Furthermore, the dissymmetric factor (g-value) of SHG circular dichroism is also modified and improved under the strong coupling, showing inversed and enhanced g-values at upper polaritonic band as well as enhancement of SHG itself. These modifications are linked with changes in the linear circular dichroism and subsequent enhancement of nonlinear electronic/magnetic susceptibility due to the strong coupling. The fact reveals that strong coupling is an effective way to manipulate also the chiral nonlinear optical effect.

SESSION EN04.09: Confinement and Excitonic Effects II
 Session Chairs: Menno Bokdam and Sascha Feldmann
 Thursday Morning, December 1, 2022
 Hynes, Level 3, Ballroom A

8:30 AM *EN04.09.01

2D Perovskite—Exciting Playground for Excitation Studies Paulina Plochocka^{1,2}; ¹CNRS, France; ²Wroclaw University of Science and Technology, Poland

High environmental stability and surprisingly high efficiency of solar cells based on 2D perovskites have renewed interest in these materials. These natural quantum wells consist of planes of metal-halide octahedra, separated by organic spacers. The unique synergy of soft lattice and opto-electronic properties are often invoked to explain superior characteristic of perovskites materials in applications. At the same time such unique synergy creates fascinating playground for exciton physics which challenges our understanding of this elementary excitation. I will demonstrate that even after decade of intense investigation the notation "unique" so often used in case of perovskites deserves serious scrutiny.

First, I will show that in 2D perovskites, the distortion imposed by the organic spacers governs the effective mass of the carriers. As a result, and unlike in any other semiconductor, the effective mass of the carriers in 2D perovskites can be easily tailored. Secondly, I will highlight controversy related to exciton fine structure in different perovskite compounds and demonstrate that the soft lattice can suppress relaxation of excitons to dark state making 2D perovskites great light emitters.

9:00 AM EN04.09.02

Mobile Trions in Two-Dimensional Hybrid Perovskites Sophia Terres¹, Jonas D. Ziegler¹, Yeongsu Cho², Matan Menahem³, Takashi Taniguchi⁴, Kenji Watanabe⁴, Omer Yaffe³, Timothy C. Berkelbach² and Alexey Chernikov¹; ¹Technische Universität Dresden, Germany; ²Columbia University, United States; ³Weizmann Institute of Science, Israel; ⁴National Institute for Materials Science, Japan

Two-dimensional hybrid perovskites are a highly intriguing class of materials. They represent natural quantum well systems composed of alternating inorganic and organic molecular layers. Interesting from the perspectives of both fundamental science and applications, they combine an efficient coupling of electrons to a soft lattice with strong Coulomb interactions between the charge carriers. The latter lead to the formation of tightly bound excitons that are shown to be excellent light emitters and absorbers as well as to determine the transport of optical excitations. Consequently, the physics of excitons in 2D perovskites are currently one of the highly active areas of contemporary research. What remains very difficult to access, however, is the interaction of excitons with free charge carriers – a scenario that is commonly encountered in optoelectronic devices and presents an intriguing case of composite Bose-Fermi quasiparticle mixtures.

Here, we report experimental realization of electrically doped, ultrathin 2D perovskite layers, studied in ambipolar field-effect transistor geometries. We

demonstrate the formation of three-particle charged exciton complexes, known as trions, by detecting photoluminescence spectra as function of gate voltage. In addition, by measuring time- and spatially-resolved profiles of the exciton emission we reveal the impact of exciton-carrier interaction on the exciton mobility. The trion binding energies are found to be in the range of 30 – 50 meV, depending on the sample thickness. Such extremely large values are a direct consequence of strong Coulomb interaction and scale with the exciton binding energies, as shown by theoretical calculations. Moreover, we show that trions can be both localized at cryogenic temperatures but also feature thermally activated, efficient transport already at 50 K. The experimental realization of both tunable and mobile trions brings the topic of exciton-carrier mixtures into the realm of 2D perovskites. It opens up avenues for fundamental research of interacting electronic states in hybrid semiconductors and encourages potential applications involving electrically guided charged exciton currents.

9:15 AM EN04.09.03

Exciton Diffusion in 3D Halide Perovskite Nanocrystal Assemblies Michael F. Lichtenegger¹, Andreas Bornschlegl¹, Jan Drewniok¹, Carola Lampe¹, Nina Henke¹, Andreas Singldinger¹, Maryna Bodnarchuk², Maksym V. Kovalenko² and Alexander S. Urban¹; ¹Ludwig-Maximilians-Universität München, Germany; ²ETH Zurich, Switzerland

Halide perovskite nanocrystals (PNC) have attracted the scientific community for over a decade, but there are still open questions addressing research not only for academic purposes. Among these are PNC stability, maximizing quantum yields, and improving transport performance in thin films. Especially excited-state transport is of tremendous importance for light emission and light-harvesting devices. Surrounded by organic ligands, charge transport is nearly nonexistent in PNC films, rendering energy transfer of excitons the dominant transport mechanism.

We investigate exciton diffusion in films of PNCs cubes and quantum-confined nanoplatelets around room temperature (15-50 °C). Here, diffusion takes advantage of the individual NC size, yielding threefold diffusivity for the largest NCs compared to the smallest ones. Surprisingly, the diffusion process worsens with increasing temperature (up to 50 °C) for all NCs systems. This rate at which this happens differs among the NCs; consequently, the 3 ML NPLs outperform the other NC systems for high temperatures. These two phenomena can be explained by different exciton/free charge carrier ratios present in the NCs. Larger free electron/hole pair ratios decrease the transport efficiency with charge transport irrelevant.

Furthermore, we present unprecedented exciton diffusion results in perovskite nanocrystal films. We investigate an unordered film consisting of 14 nm cubes and highly ordered superlattices comprising either 5 nm or 9 nm large cubes within the range of 9-220 K. Surprisingly, exciton diffusion is higher in the larger PNCs film, irrespective of order for almost all temperatures. Within this temperature range, initially, the diffusivity increases with increasing temperature, reaches a maximum, and drops with increasing temperature for both film types.² We detect three effects whose interplay is responsible for this novel trend. 1) Thermally activated FRET hopping, 2) size-dependent exciton fine level splitting between dark and bright states, and 3) exciton/free charge carrier ratios varying with exciton binding energy (PNC size). This study offers deeper insights into exciton diffusion processes, especially at low temperatures.

9:30 AM DISCUSSION TIME

9:45 AM BREAK

10:15 AM *EN04.09.05

Unconventional Exciton Transport Phenomena in CsPbBr₃ Nanocrystal Solids William Tisdale; Massachusetts Institute of Technology, United States

In some ways, the properties of colloidal CsPbBr₃ nanocrystals resemble those of conventional semiconductor nanocrystals. In other ways, CsPbBr₃ is wholly unique. In this talk, I will present experimental results from our lab using time-resolved emission microscopy to probe the spatiotemporal dynamics of exciton transport in disordered CsPbBr₃ nanocrystal films and nanocrystal superlattices. CsPbBr₃ nanocrystals exhibit a range of novel and unconventional transport behavior, including excitation memory effects, collective phenomena, and record-high values of exciton diffusivity.

10:45 AM EN04.09.07

Ultra-Narrow Room-Temperature Emission from Single CsPbBr₃ Perovskite Quantum Dots Gabriele Rainò^{1,2}, Nuri Yazdani³, Simon C. Böhme^{1,2}, Chenglian Zhu^{1,2}, Marta D. Rossell², Rolf Erni², Vanessa Wood³, Ivan Infante⁴ and Maksym V. Kovalenko^{1,2}; ¹ETH Zurich, Switzerland; ²Empa-Swiss Federal Laboratories for Materials Science and Technology, Switzerland; ³ETH Zürich, Switzerland; ⁴Istituto Italiano di Tecnologia, Italy

Semiconductor quantum dots (QDs) have long been considered artificial atoms, but despite the overarching analogies in the strong energy-level quantization and the single-photon emission capability, their emission spectrum is far broader than typical atomic emission lines. Here,¹ by using ab-initio molecular dynamics for simulating exciton-surface phonon interactions in structurally dynamic CsPbBr₃ QDs, followed by single quantum dot optical spectroscopy, we demonstrate that emission line-broadening in these quantum dots is primarily governed by the coupling of excitons to low-energy surface phonons. Mild adjustments of the surface chemical composition allow for attaining much smaller emission linewidths of 35 - 65 meV (vs. initial values of 70-120 meV), which are on par with the best values known for structurally rigid, colloidal II-VI quantum dots (20 - 60 meV).

Ultra-narrow emission at room temperature is desired for conventional light-emitting devices and paramount for emerging quantum light sources.

Reference

[1] Rainò, G. et al., Nat. Commun. 13, 2587 (2022).
<https://doi.org/10.1038/s41467-022-30016-0>

11:00 AM EN04.09.08

Highly Pure Single-Photon Emission from Single Perovskite QDs Chenglian Zhu^{1,2}, Malwina Marczak^{1,2}, Leon Feld^{1,2}, Simon C. Böhme^{1,2}, Caterina Bernasconi^{1,2}, Anastasiia Moskalenko^{1,2}, Ihor Cherniukh^{1,2}, Dmitry N. Dirin^{1,2}, Maryna Bodnarchuk^{1,2}, Maksym V. Kovalenko^{1,2} and Gabriele Rainò^{1,2}; ¹ETH Zürich, Switzerland; ²Empa-Swiss Federal Laboratories for Materials Science and Technology, Switzerland

Attaining pure single-photon emission is key for many quantum technologies,¹ from optical quantum computing² to quantum key distribution³ and quantum imaging.⁴ The past 20 years have seen the development of several solid-state quantum emitters, but most of them require highly sophisticated techniques (e.g., ultra-high vacuum growth methods and cryostats for low-temperature operation). The system complexity may be significantly reduced by employing quantum emitters capable of working at room temperature. Lead-halide perovskite APbX₃ (A=Cs or organic cation; X=Cl, Br, I) quantum dots (QDs) are one of the desired materials, of particular interest due to their low-cost synthesis, solution processability, tunability of the emission wavelength via size and composition, narrow-band emission, short radiative lifetime (~ns at RT) as well as high photoluminescence quantum yield (QY).^{5,6} Here, we present a systematic study across ~ 170 photostable single CsPbX₃ (X: Br and I) colloidal QDs of different sizes and compositions, unveiling that increasing quantum confinement is an effective strategy for maximizing single-photon purity due to the suppressed biexciton quantum yield. Leveraging the latter, we achieve 98% single-photon purity (g⁽²⁾(0) as low as 2%) from a cavity-free, non-resonantly excited single 6.6 nm CsPbI₃ QDs, showcasing the great potential of CsPbX₃ QDs as room-temperature highly pure single-photon sources for quantum technologies.

References

1. Aharonovich, I., Englund, D. & Toth, M. Solid-state single-photon emitters. *Nature Photonics* **10**, 631-641 (2016).
2. Wang, H. *et al.* Boson sampling with 20 input photons and a 60-mode interferometer in a 10¹⁴-dimensional hilbert space. *Phys. Rev. Lett.* **123**, 250503 (2019).
3. Brassard, G., Lütkenhaus, N., Mor, T. & Sanders, B. C. Limitations on practical quantum cryptography. *Phys. Rev. Lett.* **85**, 1330 (2000).
4. Tenne, R. *et al.* Super-resolution enhancement by quantum image scanning microscopy. *Nature Photonics* **13**, 116-122 (2019).
5. Protesescu, L. *et al.* Nanocrystals of cesium lead halide perovskites (CsPbX₃, X= Cl, Br, and I): novel optoelectronic materials showing bright emission with wide color gamut. *Nano Lett.* **15**, 3692-3696 (2015).
6. Krieg, F. *et al.* Monodisperse long-chain sulfobetaine-capped CsPbBr₃ nanocrystals and their superfluorescent assemblies. *ACS Cent. Sci.* **7**, 135-144 (2020).

11:15 AM *EN04.09.09

Coherent Exciton Transport in Perovskite Quantum Dot Superlattices Libai Huang; Purdue University, United States

The performance of quantum dot (QD) devices in optoelectronic and quantum information applications relies on not only the properties of the individual QDs but also the collective properties arising from interactions between QDs within a solid. The interactions between QDs determine whether long-range coherence and transport can be achieved. Due to their large oscillator strengths, perovskite QD superlattices (SLs) have the potential for exciton superradiance. However, the ultrafast dephasing processes can limit their coherence lengths. We provide a detailed study on the key factors that control exciton delocalization and transport in perovskite QD SLs. Through temperature-dependent and time-resolved photoluminescence microscopy measurements, we demonstrate coherent exciton propagation in highly ordered SLs. We unravel the effect of disorder by comparing SLs with varying degrees of inhomogeneity. Our results point to the exciting opportunities in engineering exciton coherence in perovskite solids.

SESSION EN04.10: Low Dimensional Perovskites—Novel Phenomena and Applications

Session Chairs: Sascha Feldmann and Gabriele Raino

Thursday Afternoon, December 1, 2022

Hynes, Level 3, Ballroom A

1:30 PM *EN04.10.01

Effects of Symmetry Breaking Due to the Bounding Facets of Halide Perovskite Nanocrystals Peter C. Sercel; Center for Hybrid Organic Inorganic Semiconductors for Energy, United States

Halide perovskite nanocrystals are a promising platform for optoelectronic devices such as light sources and displays, and are currently being considered for potential applications in quantum information processing. Such applications hinge on our understanding and control of the exciton fine structure. We begin by reviewing the electron-hole exchange theory for the exciton fine structure in cesium lead halide nanocrystals, which has been shown experimentally to govern the exciton fine structure in these systems [1]. We elaborate on the particular role of the nanocrystal shape in conjunction with long range exchange: To date, models for the fine structure in cuboidal perovskite nanocrystals (e.g., Refs. [1,2]) and in lead halide perovskite nanoplatelets (e.g. Ref. [3]) have assumed the bounding facets in these structures are comprised of the lowest index orthorhombic crystal planes. However, recent studies indicate that, to the contrary, the bounding facets of cuboidal perovskite nanocrystals [4] and cesium lead halide nanoplatelets [5] correspond to the pseudocubic {100} crystal planes. We show that this situation, in general, causes a breaking of the orthorhombic symmetry of the nanocrystals.

In this talk we explore the impact of this facet-related symmetry breaking on the exciton fine structure and optical properties. One consequence is the creation of a bright exciton “fine-structure gap” which can be observed in ensemble-level transient absorption measurements [6]. We predict the existence of chiro-optical effects, which are a manifestation of “extrinsic chirality”, notwithstanding the existence of inversion symmetry in these structures. We will discuss generalizations to other perovskite systems such as two-dimensional hybrid organic/inorganic perovskites.

Acknowledgements

This work was supported by the Center for Hybrid Organic Inorganic Semiconductors for Energy (CHOISE) an Energy Frontier Research Center funded by the Office of Basic Energy Sciences, Office of Science within the US Department of Energy.

References

1. P. Tamarat L. Hou, J.-B. Trebbia, A. Swarnkar, L. Biadala, Y. Louyer, M. I. Bodnarchuk, M. V. Kovalenko, J. Even, and B. Lounis, “The dark exciton ground state promotes photon pair emission in individual perovskite nanocrystals”, *Nat. Commun.*, **11**: 6001 (2020).
2. P.C. Sercel, J. L. Lyons, N. Bernstein, Al. L. Efros, “Quasicubic Model for Metal Halide Perovskite Nanocrystals”, *J. Chem. Phys.*, **151**, 234106 (2019).
3. M. Gramlich, M W. Swift, C. Lampe, J. L. Lyons, M. Doblinger, Al. L. Efros, P. C. Sercel, A. S. Urban, "Dark and Bright Excitons in Halide Perovskite Nanoplatelets", *Adv. Sci. Adv. Sci.*, **2103013** (2021).
4. L. Peng, S. K. Dutta, D. Mondal, B. Hudait, S. Shyamal, R. Xie, P. Mahadevan, and N. Pradhan, “Arm Growth and Facet Modulation in Perovskite Nanocrystals”, *J. Am. Chem. Soc.*, **141**, 16160 (2019).
5. A. Schmitz, F. Montanarella, L.L. Schaberg, M. Abdelbaky, M.V. Kovalenko, and G. Bacher, “Optical Probing of Crystal Lattice Configurations in Single CsPbBr₃ Nanoplatelets”. *Nano Lett.* **21**, 9085 (2021).
6. Y. Han, W. Liang, Y. Li, X. Lin, F. Sun, F. Zhang, P.C. Sercel, K. Wu, Lattice distortion inducing exciton splitting and coherent quantum beating in CsPbI₃ perovskite quantum dots, to be published.

2:00 PM EN04.10.02

Manipulating Chirality of 2D Lead Perovskites via Achiral Isomer Cations Hao Li, Ibrahim Dursun and Qiuming Yu; Cornell University, United States

Hybrid organic-inorganic perovskites have emerged as an important family of materials for optoelectronics with broader applications in solar cells, photodetectors, light-emitting diodes (LEDs), and lasers. As ionic semiconductors, the flexible crystal structures and tunable compositions make it possible to rationally design hybrid perovskites with desired properties. Chiral perovskites demonstrate such possibility and the breakthrough with respect to the development of a new class of chiral semiconductors, which opens up new applications of hybrid perovskites to chiroptoelectronics, ferroelectrics, and

spintronics. One type of chiral perovskites is based on two-dimensional (2D) hybrid organic-inorganic perovskites by incorporating chiral organic ligands between achiral inorganic single layers composed of corner-sharing metal-halide octahedra. As a new class of chiral semiconductors, the chirality of hybrid 2D perovskites is attributed to the symmetry-breaking in the inorganic framework induced by the enantiopure chiral organic cations via asymmetric hydrogen bonding interactions, which transfers the structural chirality across the organic-inorganic interface. In this work, we introduced achiral alkyl isomer cations, n-butylammonium (n-BA⁺) and iso-butylammonium (iso-BA⁺) into the organic layer with chiral organic cations (R/S-MBA⁺). Single phase 2D (R/S-MBA_xnBA_{1-x})₂PbI₄ and (R/S-MBA_yisoBA_{1-y})₂PbI₄ were obtained with x = 0.5 and y = 0.7. The CD signals became strong, and the polarity was flipped by the incorporation of nBA in (R/S-MBA_{0.5}nBA_{0.5})₂PbI₄. We performed density functional theory (DFT) calculations to understand the interaction between organic and inorganic layers and its impact on electronic band structure and band gap. We performed temperature dependent powder XRD and pair distribution function (PDF) measurements using NLSLS-II synchrotron at the Brookhaven National Laboratory to investigate structural variations with temperature to help understanding the observation of the unique behavior exhibited in the temperature dependent circular polarized photoluminescent (CPPL) measurements. We also conducted conventional and circular polarized transient absorption spectroscopy (TAS) to understand the photophysics embedded in these new chiral perovskites. Unlike (R/S-MBA)₂PbI₄ that exhibit red-shifted and broaden CPPL spectra with the increasing of temperature, (R/S-MBA_{0.5}nBA_{0.5})₂PbI₄ and (R/S-MBA_{0.7}isoBA_{0.3})₂PbI₄ show non-shifted CPPL peak and conserved peak width from 10 K -300 K. DFT calculations show stronger hydrogen bonding and more tilted octahedron due to the asymmetric cations on the opposite sides of the inorganic framework. While many phenomena are unknown and needed further investigations, this work provides a new way to manipulate chirality of 2D perovskites, which could lead to broader applications.

2:15 PM EN04.10.03

Characterizing the Circular Polarization-Dependent Refractive Index of Low-Dimensional Chiral Perovskites Shunran Li, Peijun Guo, Conrad Kocoj, Joseph Bennett and Xiaobin Wang; Yale University, United States

Hybrid organic-inorganic perovskites (HOIPs) have recently emerged as promising materials with remarkable light-absorbing and luminescent properties. In two-dimensional hybrid perovskites (2DHPs), chiral ligands can endow the chirality to perovskites and further enable chiral optoelectronic applications such as chiral photoluminescence and chiral photodetection. Currently, the degree of chirality in 2DHPs is represented by their circular dichroism (CD), defined as difference in absorption between left-handed (A_L) and right-handed (A_R) circularly polarized light. However, such characterizations are typically performed on thin film samples in transmission measurements, and the results can be blurred by material thickness and film morphology. Here, we propose and demonstrate the use of chiral complex refractive index (n and k) as a more intrinsic parameter to evaluate the degree of chirality of 2DHPs. From reflectance spectroscopy and the transfer matrix method, we characterize the chirality-dependent n and k for archetypal chiral 2DHPs. Our study provides fundamental insights regarding how chiral ligands impact the intrinsic material optical property and provide guiding principles for the design of chiral perovskites optoelectronic devices.

2:30 PM EN04.10.04

Synthesis, Characterization and Optical Properties of Chiral Metal Halides Ali Azmy¹, Alissa Anderson¹, Alexander Fyffe¹, Nourdine Zibouche², Lukasz Wojtas¹, Minh Tuan Trinh¹ and Ioannis Spanopoulos¹; ¹University of South Florida, United States; ²University of Bath, United Kingdom

Halide perovskites pose as a versatile class of semiconductor materials with exceptional optoelectronic properties and unique structural versatility. They are very competent in applications such as solid-state solar cells and LEDs, but their potential in non-traditional perovskite related research directions such as spintronics is not yet explored. Despite their performance, traditional lead-based perovskites are not suitable for real applications due to toxicity and instability related issues. Double perovskites and lead-free metal halides can eliminate the need for lead, while producing a greener material with equally exquisite optoelectronic features.

Towards this end we synthesized a lead-free metal halide compound based on a chiral linker (L1). Utilization of chiral linkers allows the acquisition of non-centrosymmetric crystalline materials, highly sought after for their nonlinear optical properties (NLO). We present here the synthesis of (L1)₂Sb₂Br₁₀, along with its structural, and optical properties. The material is a wide band gap semiconductor, it crystallizes in the P₂₁ space group, and exhibits asymmetric broad light emission at RT. Second Harmonic Generation (SHG) measurements verify the non-centrosymmetric nature of the structure, while the in-plane azimuthal SHG plot reveals a strong anisotropic signal. This new material poses as an excellent candidate for spintronic applications where important structure-property relationships in terms of spin lifetimes can be extracted.

References

[1] A. Azmi, A. Anderson, A. Fyffe, N. Zibouche, L. Wojtas, M. T. Trinh, I. Spanopoulos, *under submission*. 2022.

2:45 PM BREAK

3:15 PM *EN04.10.05

Controlling Charge, Spin and Light in Lead-Halide Inspired Hybrid Semiconductors Matthew C. Beard; National Renewable Energy Laboratory, United States

In this presentation I will discuss our studies of controlling the charge carrier dynamics, light/matter interactions, and spin populations in metal-halide organic/inorganic hybrid systems. In one effort we are exploring the use of novel organic hybrid systems at and near interfaces to control the carrier dynamics and reduce surface recombination but also to protect grain boundary surfaces from degradation. With respect to controlling spins we have recently studied and developed a novel class of chiral hybrid semiconductors based upon layered metal-halide perovskite 2D Ruddlesden-Popper type structures. These systems exhibit chiral induced spin selectivity whereby only one spin sense can transport across the film and the other spin sense is blocked. From these systems we can achieve a high degree of spin current polarization and injection when used as a contact layer. We have developed novel spin-based LEDs using mixed NCs as the light emitting layer that promotes light emission at a highly spin-polarized interface. The LED spin-polarization is limited by spin-depolarization within the MHP NCs. In a separate effort we have explored the use of chiral copper-halide hybrid systems for circular light polarized detection. Chiral based copper-halide systems combined with highly conductive carbon nanotube networks can be employed to detect circular polarized light with the use of polarizers. Our chiral heterostructure shows high photoresponsivity of 452 A/W, a competitive anisotropy factor of up to 21%, a current response in microamperes, and low working voltage down to 0.01 V. Finally, we have developed novel photocatalyst based upon the unique properties of metal-halide semiconductor nanocrystals and show that such systems can drive multiple electron reactions. These results demonstrate that the emergent properties of organic-inorganic hybrid systems offer unique opportunities in controlling light, charge and spin.

3:45 PM EN04.10.06

Composition Gradient-Enabled Circular Photogalvanic Effect in Epitaxial CsPbBr_xCl_(3-x) Film Ru Jia and [Jian Shi](#); Rensselaer Polytechnic Institute, United States

Inversion symmetry breaking could lead to the creation of Rashba-Dresselhaus magnetic field which plays the key role in spintronic devices. In this project, we propose and develop a composition gradient engineering approach that breaks inversion symmetry in inorganic halide perovskite with strong spin-orbit coupling. We synthesize epitaxial CsPbBr_xCl_(3-x) with Br/Cl composition gradient by a two-step chemical vapor deposition (CVD) approach. Through optoelectronic measurements, we show the presence of circular photogalvanic effect (CPGE) evidencing a Rashba-like spin polarized band structure. By spatially resolved photoluminescence spectra, we find that the observed CPGE is likely a cumulative result of inversion symmetry-broken interfaces featured by abrupt and stepwise composition gradient between the pristine and separated daughter phases. Our work suggests an avenue in engineering the spintronic property of halide perovskite for information processing.

4:00 PM EN04.10.07

Local Symmetry Breaking Drives Spin Accumulation in a Polycrystalline Metal Halide Perovskite [Arjun Ashoka](#), Sascha Feldmann and Akshay Rao; University of Cambridge, United Kingdom

Photoinduced spin-charge interconversion in semiconductors with spin-orbit coupling could provide a route to optically addressable spintronics without the use of external magnetic fields. A central question that remains is whether the resulting spin-associated charge currents are robust to structural disorder, which is inherent to polycrystalline semiconductors, desirable for device applications. Using femtosecond circular polarization-resolved transient absorption microscopy on polycrystalline metal halide perovskite thin films, we observe the formation of micron-scale spin domains on picosecond timescales through spin-associated lateral charge currents. We show that local symmetry breaking, evidenced by micron-scale variations in second-harmonic generation intensity and ferroelectric domains, induces spatially varying Rashba-like spin textures that drive spin-momentum locked currents, leading to local spin accumulation. Local symmetry breaking is only enhanced by increased local structural disorder and our observations suggest that the simultaneous presence of spin-momentum locking will always lead to local spin accumulation. Such structurally disordered Rashba-like materials could provide a new optically addressable platform for ultrafast nanoscale spin-device physics.

4:15 PM EN04.10.08

Tuning the Thermoelectric Properties in Vacuum Deposited Cesium Tin Iodide Thin Films [Paz Sebastia-Luna](#)¹, Unnati Pokharel², Bas A. Huisman¹, Lambert Jan Anton Koster², Francisco Palazon^{1,3} and Henk J. Bolink¹; ¹University of Valencia, Spain; ²University of Groningen, Netherlands; ³Universidad Politécnica de Cartagena, Spain

Thermoelectric generators (TEGs) represent a very promising source of renewable energy, as they directly convert (waste) heat into electricity. Most current thermoelectric materials have important drawbacks, such as toxicity, scarcity, and peak operating temperatures above 300 °C. Herein, we report the thermoelectric properties of different crystalline phases of Sn-based perovskite thin films. A novel 2D phase, Cs₂SnI₄, is obtained through vacuum thermal deposition and easily converted into the black β phase of CsSnI₃ (B-β CsSnI₃) by annealing. B-β CsSnI₃ is a *p*-type semiconductor with a figure-of-merit (ZT) ranging from 0.021 to 0.033 for temperatures below 100 °C, which makes it a promising candidate for applications as the Internet of Things (IoT). The B-β phase is stable under an inert atmosphere but spontaneously oxidizes to Cs₂SnI₆ when exposed to air. In-detail thermoelectric study for both compounds is presented, showing potential for implementation in low temperature operating TEGs.

4:30 PM EN04.10.09

Dielectric Effects in Halide Perovskites Doru C. Lupascu¹, Andrei Karabanov¹, Young Un Jin¹, Niels Benson¹, Kristina Winkler¹, Bernd Marler², Vladimir Shvartsman¹ and [Miriana Vadala](#)¹; ¹University of Duisburg-Essen, Germany; ²Ruhr University Bochum, Germany

The soft nature of the crystal lattices in halide perovskites and related compounds offers a magnificent new realm of properties to these crystals. Among these is the outstandingly large dielectric constant reaching up to very high frequency values. In this contribution we will summarize the state of the art in this field and options to develop new compounds. We will revisit the charge types forming in this class of crystals, the paraelectric and/or ferroelectric contributions. It will be displayed that ferroelectricity is a very rare effect and in most cases is just a misinterpretation of experimental data. Ways to further tune charge carrier mobility will be outlined.

4:45 PM EN04.10.10

Trifluorinated Substitution Strategy to Induce In-Plane Ferroelectricity in Ruddlesden-Popper Layered Hybrid Perovskites [Haining Zheng](#) and Kian Ping Loh; National University of Singapore, Singapore

Two-dimensional (2D) organic-inorganic hybrid perovskites (HOIPs), which possess outstanding optical characteristics, unique structural tunability and customizable elemental composition, have elicited tremendous attention in a wide range of optoelectronic and energy storage applications. One of the most remarkable applications is ferroelectricity-driven non-volatile memory devices. Ferroelectricity, i.e. the characteristic of a material that possesses spontaneous polarization that can be switched by applying external electric fields, has been reported in a number of layered hybrid perovskites, for instance, [2-fluorobenzylammonium]₂PbCl₄ [1], (4,4-difluoropiperidinium)₂PbI₄ [2] as well as the quasi-2D perovskites [n-butylammonium]₂(methylamine)Pb₂Br₇ [3] and (ethylammonium)₄Pb₃Br₁₀ [4]. Nevertheless, on account of the complexity of metal-organic interaction, the precise design and prediction of hybrid perovskite ferroelectrics is still a challenge. In this talk, I will introduce the recently reported design strategy to synthesize perovskite ferroelectrics, including H/F substitution, quasi-spherical theory, homochirality [5] and intercalation-driven strategy [6][7], and also propose a novel trifluorinated substitution strategy that can induce robust in-plane ferroelectricity in Ruddlesden-Popper-phase (RPP) layered hybrid lead chlorine perovskites. The trifluorinated modification of organic ligands can provide additional intermolecular F...F interactions to enhance the strength of the dipole moment and facilitate perovskites to crystallize in ferroelectric space groups. Furthermore, this trifluorinated substitution strategy can also achieve a large spontaneous polarization (*P*_s) of 8.0 μC cm⁻² and a high phase transition temperature (*T*_c) of 415 K, which has been experimentally proved by differential scanning calorimetry (DSC), second harmonic generation (SHG), polarization-electric field (P-E) hysteresis loop and piezoresponse force microscopy (PFM) measurements. This unique trifluorinated substitution strategy offers the possibility to design manipulable memory devices with high operation temperature, shedding the light on multifunctional ferroelectric optoelectronic devices.

[1] Shi, P. *et al. J. Am. Chem. Soc.* **2019**, *141* (45), 18334-18340.

[2] Zhang, H. *et al. J. Am. Chem. Soc.* **2020**, *142* (10), 4925-4931.

[3] Li, L. *et al. J. Am. Chem. Soc.* **2019**, *141* (6), 2623-2629.

[4] Wang, S. *et al. J. Am. Chem. Soc.* **2019**, *141* (19), 7693-7697.

[5] Liu, H. *et al. J. Am. Chem. Soc.* **2020**, *142* (36), 15205-15218.

[6] Wu, Z. *et al. Angew. Chem. Int. Ed.* **2018**, *57* (27), 8140-8243.

[7] Wu, Z. *et al. Nat. Commun.* **2022**, accepted.

10:30 AM EN04.11.03

Carrier Equilibrium in 2D Hybrid Perovskites Thin Crystals Probed with Tandem Ultrafast Optical Spectroscopy Angelica Simbula¹, Luyan Wu¹, Fang Liu¹, Riccardo Pau^{1,2}, Federico Pitzalis¹, Stefano Lai¹, Daniela Marongiu¹, Andrea Mura¹, Francesco Quochi¹, Michele Saba¹ and Giovanni Bongiovanni¹; ¹Università degli Studi di Cagliari, Italy; ²University of Groningen, Netherlands

2D hybrid perovskites (HP) are playing a major role in emerging photovoltaics, thanks also to their long-term stability and high-power conversion efficiency. Despite their outstanding success, the dynamics of photogenerated carriers in these materials, from which their conversion efficiency stems, still needs to be assessed. We can get useful information on photocarrier dynamics thanks to “tandem” ultrafast optical spectroscopy setup, combining transient absorption spectroscopy and time resolved photoluminescence in the same excitation conditions [1]. We report results of tandem spectroscopy applied for the first time to thin crystals of 2D HP (phenethylammonium (PEA)₂PbI₄) in different configurations, both with resonant and non-resonant excitation, and compared with their thin-films counterparts. We believe that our results provide important insights in the photophysics laying under the exceptional optoelectronic properties of these materials.

[1] Simbula, A., et al, *Adv. Optical Mater.* 2021, 9, 2100295. <https://doi.org/10.1002/adom.202100295>

10:45 AM EN04.11.04

Alkyl-Aryl Cation Mixing in Chiral 2D Perovskites Lijiang Yan¹, Manoj K. Jana², Peter C. Sercel³, David B. Mitzi^{2,2} and Wei You¹; ¹University of North Carolina at Chapel Hill, United States; ²Duke University, United States; ³Center for Hybrid Organic Inorganic Semiconductors for Energy, United States

We report 2D hybrid perovskites comprising a blend of chiral arylammonium and achiral alkylammonium spacer cations (1 : 1 mole ratio). These new perovskites feature an unprecedented combination of chirality and alkyl-aryl functionality alongside non-covalent intermolecular interactions (e.g., CH— π interactions), determined by their crystal structures. The mixed-cation perovskites exhibit a circular dichroism that is markedly different from the purely chiral cation analogs, offering new avenues to tune the chiroptical properties of known chiral perovskites, instead of solely relying on otherwise complex chemical syntheses of new useable chiral cations. Further, the ability to dilute the density of chiral cations by mixing with achiral cations may offer a potential way to tailor the spin-based properties in 2D hybrid perovskites, such as Rashba-Dresselhaus spin splitting and chirality-induced spin selectivity and magnetization effects.

11:00 AM EN04.11.06

Survey of acceptor dopants for inorganic halide perovskites John L. Lyons and Michael W. Swift; Naval Research Laboratory, United States

All-inorganic lead halide perovskites, such as cesium lead bromide (CsPbBr₃), are expected to be high-performing light emitters, with potential applications including lighting, displays, and quantum information. All of these applications would benefit from having fully controlled electrical conductivity. However, it has proven difficult to achieve high *p*-type carrier concentrations in these materials. In this work, a wide variety of possible acceptor dopants are evaluated in the halide perovskites, using first-principles calculations based on a hybrid functional with spin-orbit coupling. This approach not only leads to accurate predictions for band structure and band offsets, but also provides a better description of dopant properties. We connect our results with prior work on native defects which are expected to act as compensating species. We show that *p*-type doping is difficult because of two related effects: the moderately high formation energies of acceptor impurities, and compensation by native defects, particularly the lead–cesium antisites (Pb_{Cs}) and bromine interstitials (Br_I). Among the dopants considered, sodium and silver are identified as the most promising acceptors for overcoming these challenges to achieve *p*-type conductivity, and optimum chemical potential conditions for these dopants are identified.

M. W. Swift and J. L. Lyons, *J. Phys. Chem. C* **126**, 12294 (2022).

11:15 AM EN04.11.07

Strain-Induced Structural Distortion, Octahedral Tilting and Bandgap Non-Linearity of 2D Butylammonium Tin Iodide Perovskites—A GGA+SOC Approach Mehreen Javed, Maamar Benkraouda, Noureddine Amrane and Atif Sattar; United Arab Emirates University, United Arab Emirates

Global sustainability challenge requires an immediate shift toward renewable energy resources. Two-dimensional perovskites with long-life stability can be tuned by strain engineering to modulate the structural and electronic properties thus achieving higher solar power conversion efficiency. Herein, we have investigated the influence of biaxial strain ($\pm 3\%$ and $\pm 6\%$) on structural distortion, octahedral tilting, and bandgap tuning of monolayer Butylammonium Tin Iodide (BA₂SnI₄) perovskite through first-principles density functional theory calculations. The prototype structure has a single sheet of corner shared inorganic SnI₄ metal cages sandwiched between Butylammonium (BA) organic spacer cations offering an optically favorable direct bandgap of 1.457 eV, centered at Γ -point. Equivalent biaxial strains (ϵ_{xx} and ϵ_{yy}) are applied along with the directions [100] and [010] of *x*- and *y*-axes respectively, by fractions starting from $\epsilon = -6\%$ to $\epsilon = +6\%$ using a step size of 3%. The lattice parameters *a* and *b* of BA₂SnI₄ are constrained to various values different from their equilibrium lattice parameters, keeping the *c* parameter invariant. Both tensile and compressive strains ($\pm 3\%$ and $\pm 6\%$) applied along the *x*-axis result in smaller bandgaps than strains oriented along the *y*-axis. The cationic and anionic dominance at conduction and valence bands support the defect tolerant tendency, with no trap states in the bandgap. The organic components constitute a larger bandgap than the inorganic part with satisfied quantum and dielectric confinement. Spin-orbit coupling is explored as a more influential phenomenon than the strain effect to tune electronic properties. The strain-induced competing effects of octahedral tilting and structural distortion with bandgap bowing and spin-orbit coupling provide a systematic strategy to tune bandgaps of different optoelectronic device applications.

11:20 AM DISCUSSION TIME

SYMPOSIUM EN05

Solid-State Batteries—Life, Safety and Scalability
November 28 - December 6, 2022

Symposium Organizers

Alex Bates, Sandia National Laboratories
Dominika Buchberger, University of Warsaw
Yue Qi, Brown University
Hongli Zhu, Northeastern University

Symposium Support

Silver

BioLogic USA

Bronze

Chemical Science | Royal Society of Chemistry
Joule, Cell Press
Sandia National Laboratories

* Invited Paper
+ Distinguished Invited

SESSION EN05.01: High Energy Solid-State Batteries Enabled by Anode Design—Li-Dendrite Prevention
Session Chairs: Paul Albertus and Alex Bates
Monday Morning, November 28, 2022
Hynes, Level 3, Room 304

10:30 AM *EN05.01.01

Critical Currents of Lithium Anode Solid-State Batteries with Ceramic Electrolytes Ziyang Ning¹, Dominic Spencer Jolly¹, Dominic Melvin^{1,2}, Guanchen Li¹, Jitti Kasemchainan¹, T. James Marrow¹, Charles Monroe^{1,2} and Peter Bruce^{1,2,3}; ¹University of Oxford, United Kingdom; ²The Faraday Institution, United Kingdom; ³The Henry Royce Institute, United Kingdom

Solid-state batteries using a lithium anode and a ceramic electrolyte promise to improve the energy density and safety of cells. However, there are significant challenges to cycling lithium anode solid-state batteries at practical current densities of several mA cm⁻². Critical currents occur on discharge (stripping) above which cells fail due to voiding at the Li/solid electrolyte interface. Such voiding depends on Li creep rates, which depend on temperature and stack pressure. Dendrites (Li filaments) penetrate the solid electrolyte on charge (plating). Using X-ray computed tomography we have followed in detail how Li dendrites crack Li₆PS₅Cl electrolytes and how the dendrite-cracks propagate across the solid electrolyte. We model the process based on our observations including the process of dry crack propagation. The relationship between cycling conditions, stack pressure and the properties of the solid electrolyte will be discussed. The findings help to inform routes for realising solid-state batteries that avoid short-circuits.

11:00 AM EN05.01.02

Mechanics of Lithium Metal at Nanoscale by EBSD Coupled Nanoindentation Jack Aspinall, David E. Armstrong and Mauro Pasta; University of Oxford, United Kingdom

The fracture of ceramic solid electrolytes, driven by the plating of lithium within cracks, has been identified as one of the fundamental issues to resolve to successfully develop solid-state batteries[1]. Understanding the mechanics of lithium at the nanoscale is therefore essential. In this work, the elastic and plastic properties of lithium are measured by Berkovich nanoindentation within an enclosed argon glovebox system. Lithium is particularly challenging to study due to its high reactivity and softness, preventing the use of traditional surface preparation methods. Using a novel surface preparation methodology, lithium metal samples are characterised by electron backscattered diffraction (EBSD) before and after indentation to allow the dependence of the mechanical properties on crystallographic orientation to be measured, and the stiffness tensor components, moduli and Poisson's ratio to be independently determined using a method first proposed by Vlassak and Nix[2]. The measured stiffness tensor components are C₁₁ = 13.3 GPa, C₁₂ = 11.2 GPa and C₄₄ = 8.8 GPa. These values agree with earlier acoustic works on lithium single crystals within 2%[3]. Hardness measurements show anisotropy according to Schmid's law, with a clear size effect which may explain observed lithium filament propagation. The experiments were repeated across lithium magnesium solid solution alloys from 5 to 20 atomic percent to investigate the change in elastic and plastic properties with solute content.

[1] E. Kazyak, R. Garcia-Mendez, W.S. LePage, A. Sharafi, A.L. Davis, A.J. Sanchez, K.H. Chen, C. Haslam, J. Sakamoto, N.P. Dasgupta, Li Penetration in Ceramic Solid Electrolytes: Operando Microscopy Analysis of Morphology, Propagation, and Reversibility, *Matter*. 2 (2020) 1025–1048. <https://doi.org/10.1016/j.matt.2020.02.008>.

[2] J.J. Vlassak, W.D. Nix, Measuring the Elastic Properties of Materials By Means of Indentation, *J. Mech. Phys. Solids*. 42 (1994) 1223–1245.

[3] T. Slotwinski, J. Trivisonno, Temperature dependence of the elastic constants of single crystal lithium, *J. Phys. Chem. Solids*. 30 (1969) 1276–1278. [https://doi.org/10.1016/0022-3697\(69\)90386-2](https://doi.org/10.1016/0022-3697(69)90386-2).

11:15 AM EN05.01.04

Designing the Ion Exchange Process to Optimize the Tradeoff Between Induced Residual Stress and Ion Transport to Prevent Lithium Filament Growth in Solid Electrolytes [Harsh D. Jagad](#)¹, Stephen Harris², Brian W. Sheldon¹ and Yue Qi¹; ¹Brown University, United States; ²Lawrence Berkeley National Laboratory, United States

Lithium filament propagation in solid state electrolytes (like Lithium Lanthanum Zirconium Oxide LLZO) is stymieing the widespread adoption of Lithium anodes secondary batteries. Sub-surface isovalent Ion Exchange (IX) with a larger cation radius was proposed to prevent the filament propagation by inducing residual compressive stresses (RCS) in the electrolyte. However, several thermodynamic and kinetic tradeoffs need to be optimized. For example, larger ion size induces larger chemical strain and higher RCS but may require higher ion exchange temperature to overcome the large ion substitutional free energy and slow diffusion process. On the other hand, smaller ion size (albeit, still larger than Li⁺) may require higher exchange concentrations to achieve similar vales of RCS, while the high concentration may block Li ion diffusion pathways. Another key challenge is the diffusivity of the exchanged cations in LLZO, which should be sufficient enough to penetrate 1~20 microns in order to suppress crack growth; while being immobile at battery operation conditions. Furthermore, the Li ion diffusivity is also reduced by the ion exchange process, setting an upper limit for the ion exchange concentration and RCS. We compare these tradeoffs for K⁺, Na⁺, Ag⁺ cations to guide the optimization of ion exchange process. Using Density Functional Theory (DFT) informed thermodynamic calculations, a variety of commonly existing precursors (oxides, halides, nitrides, pure metal, etc.) were screened to give the suitable substitutional free energy. The preferred site occupied by the exchanged species in the LLZO is compared for the three cations at various ion-exchange concentrations to understand their impact on diffusion. Molecular Dynamics simulations are then carried out to compare the stress and concentration dependent cation diffusivity. Extrapolating these results to a continuum scale thin film, the macroscopic RCS and the corresponding increase in fracture toughness are evaluated and compared for the various cations. For example, in the case of K⁺, at 3.4% exchange, the RCS induced is close to 1.1 GPa while lowering the Lithium diffusivity by less than a factor of 0.8 at 300K. In summary, the integrated multiscale modelling approach allowed us to optimize the exchange cation size, concentration, ion exchange depth, to balance the increase of RCS and fracture strength while maintaining sufficient Li⁺ diffusivity to alleviate the lithium filament growth problem in solid state electrolytes.

11:30 AM EN05.01.05

Deflection and Arrest of Metal Dendrites—Using Engineered Stresses to Prevent Short-Circuit Failures in Solid Electrolytes [Cole D. Fincher](#)¹, Christos E. Athanasiou^{2,1,3}, Brian W. Sheldon², W. C. Carter¹ and Yet-Ming Chiang¹; ¹Massachusetts Institute of Technology, United States; ²Brown University, United States; ³Georgia Institute of Technology, United States

Metal penetration and electrolyte failure at low current densities threaten the viability of high energy solid-state batteries with metal anodes. Whether metal filaments are driven by mechanical failure or electrochemical degradation of solid electrolytes remains a topic of debate. If internal mechanical forces drive failure, superimposing an external compressive load on the system should balance internal stress buildups and mitigate penetration. Here, we investigate this hypothesis. In-operando microscopy reveals the response of propagating metal filaments to applied loads and electrochemical stimuli. Compressive loads alter the direction of filament propagation, deflecting filament growth and averting cell failure. We develop a simple linear elastic fracture mechanics model which captures many aspects of this behavior. Based upon this analysis, we estimate the impact of applied stack pressure and in-plane stresses on filament propagation within conventional symmetric and full cells. We then chart the in-plane stresses required to prevent dendrite-induced short circuits. Lastly, we outline cell configurations and processing conditions which result in sufficient residual stresses to deflect metal filaments in solid electrolytes via processing. Overall, this work shows experimentally that it is possible to force metal dendrites to follow a tortuous path, thus increasing the time and amount of capacity plated before failure.

SESSION EN05.02: High Energy Solid-State Batteries Enabled by Anode Design
Session Chairs: Dominika Buchberger, David Mitlin, Yue Qi and Hongli Zhu
Monday Afternoon, November 28, 2022
Hynes, Level 3, Room 304

1:45 PM *EN05.02.01

Interfacial Dynamics in Anode-Free Solid-State Batteries [Neil P. Dasgupta](#); University of Michigan, United States

Solid-state batteries (SSB) have seen a dramatic increase in research in recent years because of their ability to address safety challenges associated with flammable liquid electrolytes, and the potential to enable Li metal anodes. Recently there has been an increase in attention paid to anode-free SSB configurations, where all of the lithium inventory in the battery is supplied from the cathode. Accordingly, Li metal is plated out at the interface between a solid electrolyte and a metallic current collector. This enables a N:P ratio of 1, representing a significant increase in the theoretical energy density compared to cells with excess Li metal in the anode. The anode-free configuration unique physical phenomena with regards to chemo-mechanics at the interface, and also represents a valuable platform to quantify the stability and reversibility of Li plating and stripping at solid-solid interfaces.

To probe the dynamic evolution of anode-free solid-state batteries, in this talk, I will present results using a complimentary set of *in situ/operando* methodologies. First, we will explore quantify the impacts of electrochemical cycling conditions and external variables on the voltage signatures and reversibility of anode formation. Comparisons will be made between anode-free cells using state-of-the-art metal oxide and sulfide solid electrolytes. *Operando* video microscopy will be used to study the morphological evolution of the interface, including 3-dimensional analysis using focus variation microscopy. The chemical evolution of SEI formation during the initial anode formation cycle will be explored using *operando* x-ray photoelectron spectroscopy (XPS). The results of these investigations point towards unique processes that occur in anode-free SSBs, including transitions in reaction pathways between SEI formation and Li plating, as well as mechanical evolution of both the Li metal and current collector during nucleation and growth.

2:15 PM EN05.02.02

Uncovering the Effects of Alloy Interfacial Layers in Anode Free Solid-State Batteries Through Cryogenic Focused Ion Beam Characterization [Stephanie E. Sandoval](#), John Lewis and Matthew T. McDowell; Georgia Institute of Technology, United States

In both liquid and solid-state electrolyte (SSE) battery systems, there is growing interest in developing “anode-free” architectures. Anode-free systems feature no active material at the anode current collector and therefore substantially increase the volumetric energy density compared to standard Li-ion batteries. This configuration additionally simplifies manufacturing by removing the need to process lithium metal. During charging of an anode-free cell, Li⁺ ions are removed from the lithiated cathode and electrodeposited as lithium metal on the anode current collector. Upon discharge, lithium is stripped and intercalated back into the cathode. Since there is no excess lithium at the anode, it is essential that deposited lithium is entirely removed to achieve high

Coulombic efficiencies (CE). Thus, it is critically important to understand the nucleation and growth behaviors of lithium in anode-free configurations while exploring methods to spatially control lithium growth. Previous work which probed the effects of alloy interlayers in liquid electrolyte systems using *operando* optical microscopy has found that silver thin films enable higher CE than bare current collectors and cause different deposition and stripping dynamics¹. Silver layers have also shown beneficial effects in enabling long-term cycling of solid-state batteries (SSBs)². Here, we investigate the structural and morphological evolution of alloy interlayers in SSBs using cryogenic focused ion beam (cryo-FIB) methods correlated with electrochemical measurements. Improved CEs are observed using silver and gold thin films compared to bare copper. Performance improvements are investigated using cryo-FIB to probe the Cu| electrodeposited Li| SSE interface. Samples are cooled to -145 °C to stabilize the electrodeposited lithium and minimize interactions between lithium and the gallium ion beam. Once cooled, ~25 mm x ~25 mm x ~25 mm trenches are milled to reveal the solid-solid interface of interest. We observe non-uniform growth on bare copper while uniform lithium growth is observed in silver- and gold- modified interfaces. Interestingly, we observe distinct morphological evolution comparing both alloy interlayers, which also affects cycling behavior. Electrochemical impedance spectroscopy during deposition and stripping is further used to understand and investigate the influence of the alloy interlayers and correlate to morphology evolution. This work provides new understanding of interfacial modification at solid-solid interfaces in SSBs, which will be important for engineering anode-free SSBs.

1. Sandoval, S. E. *et al.* Understanding the Effects of Alloy Films on the Electrochemical Behavior of Lithium Metal Anodes with Operando Optical Microscopy. *J. Electrochem. Soc.* **168**, 100517 (2021).

2. Lee, Y. G. *et al.* High-Energy Long-Cycling All-Solid-State Lithium Metal Batteries Enabled by Silver–Carbon Composite Anodes. *Nat. Energy* **5**, 299–308 (2020).

2:30 PM EN05.02.03

Alloy Anodes for Solid-State Batteries Yonglin Huang, Bowen Shao and Fudong Han; Rensselaer Polytechnic Institute, United States

The serious challenges of utilizing Li metal anodes with solid electrolytes have motivated the research on alternative anodes. Alloy-based anodes have been gaining great interest recently due to their high capacities. Nevertheless, the utilization of alloy anodes cannot prevent Li plating and subsequent cell shorting. In this presentation, we aim to provide our initial understanding of the dendrite formation in alloy-based solid-state batteries by evaluating the dendrite suppression capability of commonly Li alloys including Li-Zn, Li-Si, Li-Sn, and Li-Al. Our results indicate that Li-Al outperforms other alloys in preventing cell shorting. A possible mechanism for the superior performance of Li-Al based on its mechanical properties will also be introduced. While the slightly higher potential of alloy anodes helps to improve the interfacial stability with solid electrolytes, our recent results show that apparent decomposition of thiophosphate-based solid electrolytes occurs when used with Si anodes. The decomposition of solid electrolytes not only leads to a decrease in the first cycle coulombic efficiency which can complicate cell balancing, but also affects the reaction mechanisms in the subsequent cycles. The utilization of cathodic stable electrolytes, for example, hydrides, is therefore important for alloy anodes. Our work highlights that the properties of both the alloy itself and the solid electrolyte should be carefully studied for the future development of alloy anodes for solid-state batteries.

2:45 PM BREAK

3:15 PM EN05.02.05

Initial Coulombic Efficiency of Hard Carbon in All-Solid-State Sodium-Ion Battery Jin An Sam Oh^{1,2}, Grayson Deysher¹, Phillip Ridley¹, Long Hoang Bao Nguyen¹ and Y. Shirley Meng^{1,3}; ¹University of California, San Diego, United States; ²Agency for Science, Technology and Research, Singapore; ³The University of Chicago, United States

All-solid-state sodium ion batteries are highly sought after stationary energy storage systems which can integrate renewal energy into the existing power grid. Among different sodium-ion anodes, hard carbon has a low redox potential, reasonable capacity, and is low cost making it a good candidate in a large-scale format. However, the implementation of hard carbon is hindered by its low initial Coulombic efficiency (ICE) due to formation of solid electrolyte interphase and irreversible sodium trapping. In this study, hard carbon compatibility with a solid-state electrolyte and its initial Coulombic efficiency were studied in detail using X-ray photoemission spectroscopy, electrochemical impedance spectroscopy, and electron microscopy. Additionally, we exploit a method presodiate of the hard carbon to significantly improve the initial Coulombic efficiency. Consequently, the assembled all-solid-state sodium-ions battery with presodiated hard carbon exhibits a higher initial energy density with good reversibility.

3:30 PM *EN05.02.07

Li Metal Solid State Battery Safety Assessed with Calorimetry and Modeling of Large-Format Cells Paul S. Albertus, Nathan Johnson and Bhuvnmita Bhargava; University of Maryland, United States

It is commonly assumed that the introduction of solid-state electrolytes implies the improved safety of high-energy batteries due to the removal of the combustible organic solvents in present Li-ion cells. However, safety is a multifaceted issue that involves thermal runaway onset temperature, self-heating rates, total heat production, maximum temperature, gas or other material release from a cell, thermal runaway prevention mechanisms, and other factors.[1-3] In addition, the use of lithium metal anodes (which melt at 180°C) for high energy density cells may introduce previously unconsidered safety issues due to the presence of molten and reactive lithium metal during a thermal runaway.

This talk will present results on the modeling of thermal runaway in a Li metal solid state battery, under both thermal ramp (e.g., in an oven) and short circuit conditions, with quantitative assessments of the mole fractions of key species in the cell and the temperature.[3] Key assumptions and parameter sensitivities will be shared, to clarify the most important areas for attention and analysis regarding Li metal solid state battery safety. In addition, results from differential scanning calorimetry (DSC) measurements of mg-scale quantities of solid state battery material sets will be presented, which provide quantitative information on onset temperatures and heat flows of key reactions. These experimental results will focus on cells with Li metal, an LLZO-based solid electrode, and metal oxide cathodes.

Finally, perspectives will be given on the early-stage (e.g., for materials and single-layer coin and pouch cells) evaluation of safety for prospective high-energy cells, for which commercial-scale cells (e.g., multi-layer cells of at least several Ah) are not yet available.

References

1. Bates, A.M., et al., Are solid-state batteries safer than lithium-ion batteries? *Joule*, 2022. 6(4): p. 742-755.
2. Inoue, T. and K. Mukai, Are All-Solid-State Lithium-Ion Batteries Really Safe?—Verification by Differential Scanning Calorimetry with an All-Inclusive Microcell. *ACS Applied Materials & Interfaces*, 2017. 9(2): p. 1507-1515.
3. Johnson, N. and P. Albertus, Modeling Thermal Behavior and Safety of Large Format All-Solid-State Lithium Metal Batteries under Thermal Ramp and Short Circuit Conditions. *Journal of The Electrochemical Society*, 2022. 169(6).

SESSION EN05.03: Solid Electrolytes Design for Next Generation Solid-State Batteries I

Session Chairs: Alex Bates and Juner Zhu

Tuesday Morning, November 29, 2022

Hynes, Level 3, Room 304

8:30 AM *EN05.03.01

Residual Compressive Stress as a Proposed General Solution to Dendrite Penetration in Solid Electrolytes [Stephen J. Harris](#)¹, Yue Qi², Brian W. Sheldon², Harsh D. Jagad², Chunmei Ban³, Remi Dingreville⁴, Scott Monismith⁵, Jianmin Qu⁵ and Sydney Morris²; ¹Lawrence Berkeley National Laboratory, United States; ²Brown University, United States; ³University of Colorado Boulder, United States; ⁴Sandia National Laboratories, United States; ⁵Tufts University, United States

Rapid filament growth of lithium is limiting the commercialization of solid state lithium metal anode batteries. Recent work demonstrates that lithium filaments grow into pre-existing or nascent cracks in the solid electrolyte, suggesting that increasing the fracture toughness of the solid electrolytes will inhibit filament penetration. We previously suggested that introducing residual compressive stresses at the surface of the solid electrolyte can provide this additional fracture toughness. In this talk we will discuss ion exchange and ion implantation as methods for introducing residual compresses near the surface of solid electrolytes.

9:00 AM EN05.03.02

Pressure Dependent Studies on Site-Disordered Lithium Superionic Argyrodite Li₆PS₅Br [Vasiliki Faka](#), Matthias T. Agne and Wolfgang Zeier; University of Münster, Germany

The understanding and development of Li⁺ solid ionic conductors is important for solid-state batteries. In the search for novel solid electrolytes for solid-state batteries, lithium argyrodite ionic conductors have been in recent focus owing to their high ionic conductivities and processability. Although atomic site disorder has been systematically studied in these materials, the influence of internal strain resulting from microstructural defects such as dislocations has not. Characterizing the effects of internal strain on ion transport is particularly important given the prevalent use of high energy ball milling in the synthesis and processing of solid-state electrolytes for solid state batteries. In this work, we systematically study the effects of internal strain on the bulk ionic transport of the Li₆PS₅Br argyrodite. We are able to reproducibly induce internal strain by applying uniaxial pressures of 250 – 1500 MPa. Quantification of the bulk internal strain occurs in parallel with a local structural analyses by pair distribution function analysis. The changing ionic conductivity of the different materials is assessed by electrochemical impedance spectroscopy and the lithium-ion mobility is probed by NMR spectroscopy. Together, these results show that the high lithium-ion mobility in Li₆PS₅Br is quantifiably affected by external pressure that results in straining of the material. Not only does this work show that strain engineering may be a new methodology for tuning ion conductors without changing the composition of the material itself, it also shows that the external pressures during solid state battery formation may affect the solid electrolyte permanently.

9:15 AM EN05.03.03

Crystallographic Design of Battery Materials [Ananya Renuka Balakrishna](#); University of Southern California, United States

Solid-state batteries have the potential to enhance energy density and offer greater safety when compared with conventional Li-ion batteries. However, a bottleneck with using a solid-state electrolyte lies in mechanically integrating the solid-state electrolyte with the active materials (electrodes). For example, inserting and extracting Li into electrode lattices expands electrode materials up to 10% in volume. These chemo-mechanical strains in the electrode induce misfit stresses at the electrode/electrolyte interfaces, which weaken the structural integrity and electrical conductivity of the battery material composite. In today's talk, we will show how epitaxial strains in thin-film electrodes can be engineered to deter delamination. We develop a continuum model to explore the interplay between phase-transformation microstructures and substrate strains in thin-film electrodes. We apply this model to the vanadium-oxide system and show how tensile straining of electrodes deters delamination and enhances the reversible cycling of electrode materials. I will also discuss some recent work on crystallographically designing electrode microstructures to mitigate volume changes and fatigue. In this latter project, we draw inspiration from shape-memory alloys to stabilize microstructures that have minimum volume changes and high reversibility. Broadly, our work provides a battery design framework to mechanically engineer electrodes and enhance battery safety and lifespan.

9:30 AM *EN05.03.04

Interfaces and Scaling Relations in Solid-State Batteries [Wolfgang Zeier](#); University of Muenster, Germany

The advent of solid-state batteries has spawned a recent increase in interest in lithium conducting solid electrolytes. However, many open questions remain when trying to optimize electrolytes and understand solid state battery chemistries.

In this presentation, we will explore the current focus of halide-based ionic conductors in solid state batteries and discuss stability limitations in solid state battery cells at the anode as well as the cathode composites.

In a second part, we show the influence of Si type anode materials on the effective transport and behavior of solid-state batteries

Finally, we will discuss that it is not only important to find fast ionic conductors but that for an effective thermal battery management the thermal transport properties of solid ionic conductors need to be explored and understood. Here we will show the diffusive thermal transport nature of solid electrolytes and their different scaling relations that put in question the assumption of Bruggeman transport in solid state batteries.

10:00 AM BREAK

SESSION EN05.04: Fundamental Understanding via Characterization and Modeling I

Session Chairs: Yue Qi and Wolfgang Zeier

Tuesday Morning, November 29, 2022

Hynes, Level 3, Room 304

10:30 AM *EN05.04.01

Structure and Ion Dynamics in Solid Electrolytes Observed by NMR Spectroscopy [Sylvio Indris](#); Karlsruhe Institute of Technology–Institute for Applied Materials, Germany

The correlation between structure and dynamics in different Li and Na solid electrolyte materials was investigated by a combination of different nuclear magnetic resonance (NMR) techniques, including magic-angle spinning NMR, temperature-dependent NMR lineshape analysis, NMR relaxometry, and field-gradient NMR. We are thus able to investigate the dynamics of Li or Na ions on different time scales from some nanoseconds to a few seconds, and thus we can observe the local hopping of these charge carriers as well as the long-range transport over several micrometers. Some examples will be given for Li_3PS_4 , $\text{Li}_6\text{PS}_5\text{Cl}$, $\text{Li}_{0.29}\text{La}_{0.57}\text{TiO}_3$, and NASICON-type structures for Li and Na electrolytes [1-12]. In order to obtain insights into the diffusion pathways inside the crystal structures and the energy landscapes probed by the mobile ions, the NMR results are compared to those obtained by impedance spectroscopy and different diffraction techniques.

- [1] F. Strauss, J. Lin, M. Duffiet, K. Wang, T. Zinkevich, A.-L. Hansen, S. Indris, T. Brezesinski, *ACS Mater. Lett.* **4**, 418-423 (2022).
- [2] R. Schlenker, A.-L. Hansen, A. Senyshyn, T. Zinkevich, M. Knapp, T. Hupfer, H. Ehrenberg, S. Indris, *Chem. Mater.* **32**, 8420-8430 (2020).
- [3] F. Strauss, T. Zinkevich, S. Indris, T. Brezesinski, *Inorg. Chem.* **59**, 12954-12959 (2020).
- [4] R. Schlenker, D. Stepien, P. Koch, T. Hupfer, S. Indris, B. Roling, V. Miß, A. Fuchs, M. Wilhelmi, H. Ehrenberg, *ACS Appl. Mater. Interfaces* **12**, 20012-20025 (2020).
- [5] T. Zinkevich, B. Schwarz, P. Braun, A. Weber, H. Ehrenberg, S. Indris, *Solid State Ionics* **357**, 115486 (2020).
- [6] Z. Liu, T. Zinkevich, S. Indris, X. He, J. Liu, W. Xu, J. Bai, S. Xiong, Y. Mo, H. Chen, *Inorg. Chem.* **59**, 226-234 (2020).
- [7] H. Stöffler, T. Zinkevich, M. Yavuz, A.-L. Hansen, M. Knapp, J. Bednarčík, S. Randau, F. H. Richter, J. Janek, H. Ehrenberg, S. Indris, *J. Phys. Chem. C* **123**, 10280-10290 (2019).
- [8] H. Stöffler, T. Zinkevich, M. Yavuz, A. Senyshyn, J. Kulisch, P. Hartmann, T. Adermann, S. Randau, F. Richter, J. Janek, S. Indris, H. Ehrenberg, *J. Phys. Chem. C* **122**, 15954-15965 (2018).
- [9] C. Dietrich, D. A. Weber, S. J. Sedlmaier, S. Indris, S. Culver, D. Walter, J. Janek, W. G. Zeier, *J. Mater. Chem. A* **5**, 18111-18119 (2017).
- [10] T. Zinkevich, A. Fiedler, M. Guin, F. Tietz, O. Guillon, H. Ehrenberg, S. Indris, *Solid State Ionics* **348**, 115277 (2020).
- [11] M. Kaus, M. Guin, M. Yavuz, M. Knapp, F. Tietz, O. Guillon, H. Ehrenberg, S. Indris, *J. Phys. Chem. C* **121**, 1449-1454 (2017).
- [12] M. Guin, S. Indris, M. Kaus, H. Ehrenberg, F. Tietz, O. Guillon, *Solid State Ionics* **302**, 102-106 (2017).

11:00 AM EN05.04.02

Lithium Deposition Behavior of Anode-Free Solid-State Lithium Secondary Batteries with Carbon-Based Composite Layer Da Young Ko, Donghan Youn, Ji Young Kim and Hansu Kim; Hanyang University, Korea (the Republic of)

Anode-free solid-state lithium secondary batteries are one of the most promising next-generation energy storage systems to improve gravimetric and volumetric energy density. Among various types of solid electrolytes, inorganic sulfide solid electrolytes have drawn attention due to their high ionic conductivity and good scalability. However, low Coulombic efficiency because of its absence of excess lithium source and poor cycle life caused by high chemical reactivity between lithium metal and sulfide solid electrolyte are key issues to be solved. In this work, we compared lithium plating and stripping behaviors of current collectors with and without amorphous carbon-containing composite layer by using various electrochemical and analytical characterization methods. We demonstrate types of material, ratio, or microstructure of the composite layer could affect overall electrochemical performance of the battery. The corresponding morphological difference of deposited lithium will be discussed further in the presentation.

11:15 AM EN05.04.03

Increase in Critical Current Density Due to Mn Rich Secondary Phase Formation in Li Stuffed Garnets Sebastian J. Altus^{1,2}, Innes McClelland^{1,3,2}, Denis Cumming^{4,2} and Edmund J. Cussen^{1,2}; ¹University of Sheffield, United Kingdom; ²The Faraday Institution, United Kingdom; ³ISIS Neutron and Muon Source, United Kingdom; ⁴The University of Sheffield, United Kingdom

Increasing interest in the commercialization of solid-state batteries as an energy source has emphasised the inherent problem of Li dendritic growth.¹ This fundamental mechanism hinders solid state electrolytes from operating at required critical current densities for electric vehicles.^{2,3} In a concerted effort to identify the source of Li dendrite growth researchers have identified high electronic conductivity as the origin for Li dendrite formation in solid electrolytes.⁴

Here we investigated the isovalent doping of Garnet type $\text{Li}_{6.4}\text{La}_3\text{Zr}_{1.4}\text{Ta}_{0.6}\text{O}_{12}$ with the Mn^{4+} cation to enable mixed ionic electronic conduction (MIEC). The ability to introduce small amounts of electronic conductivity would allow for controlled investigations into electrochemical performance and degradation as well as characterize the nucleation and propagation of Li dendrites in a variable electronic conductor. Diffraction analysis following solid state synthesis of $\text{Li}_{6.4}\text{La}_3\text{Ta}_{0.6}\text{Zr}_{1.4-x}\text{Mn}_x\text{O}_{12}$ ($x = 0.035, 0.07, 0.105$) revealed successful stabilisation of the target cubic phase. However, the presence of Ruddlesden popper impurity compound $\text{LiLa}_4\text{MnO}_8$ was also identified. To further investigate the affect of grain boundary located compound on the electrochemical properties, AC impedance and DC polarisation analysis were undertaken. Subsequent measurements revealed only a negligible change in electronic and ionic conductivity with only $x=0.105$ displaying a significant decrease in its ionic conductivity. To elucidate the stability of cycling Li through the solid state electrolyte composite, galvanostatic cycling was performed in a Li/Li symmetrical cell. Here it was found that increasing the dopant level reduced the resistance, thus increasing the critical current density. This was observed up to $x=0.07$ whereupon the secondary compound counteracted the effect and the critical current density decreased. Impedance spectroscopy analysis of Li in contact with the electrolyte revealed the formation of an interphase contribution. This may also be visually seen by a discolouration of the pellet. This work shows that the creation of a composite, where the secondary compound, even at low dopant levels, holding different electrochemical properties to the parent compound may affect important electrochemical attributes of the parent compound.

References

1. Hatzell, K. B. *et al.* Challenges in Lithium Metal Anodes for Solid-State Batteries. *ACS Energy Lett.* **5**, 922–934 (2020).
2. Kasemchainan, J. *et al.* Critical stripping current leads to dendrite formation on plating in lithium anode solid electrolyte cells. *Nat. Mater.* **2019** *1810* **18**, 1105–1111 (2019).
3. Flatscher, F., Philipp, M., Ganschow, S., Wilkening, H. M. R. & Rettenwander, D. The natural critical current density limit for $\text{Li}_7\text{La}_3\text{Zr}_2\text{O}_{12}$ garnets. *J. Mater. Chem. A* **8**, 15782–15788 (2020).
4. Han, F. *et al.* High electronic conductivity as the origin of lithium dendrite formation within solid electrolytes. *Nat. Energy* **4**, 187–196 (2019).

11:30 AM EN05.04.04

Can We Utilise Phonons to Enhance Li-Ion Diffusion? Benjamin A. Williamson and Sverre Magnus Selbach; Norwegian University of Science and Technology, Norway

Solid state electrolytes offer the potential to drastically increase the overall stability of rechargeable lithium batteries as well as provide the means to realise the use of Li-metal anodes maximising the charge capacity of a device. At present, batteries use liquid electrolytes such as $[\text{LiPF}_6]$ which although they possess high ionic conductivities of $1 \times 10^{-2} \text{ S cm}^{-1}$ limit the safe temperature ranges a battery can be operated at as well as forbidding the use of Li-metal anodes due to dendrite formation leading to short circuiting and “thermal runaway”. At present, however, there is a dearth of materials suitable for the role

of a highly conductive, stable, solid electrolyte. Current highly conductive materials such as the agyrodites ($\text{Li}_6\text{PS}_5\text{X}$; $\text{X}=\text{Cl}, \text{Br}$) or LGPS ($\text{Li}_{10}\text{GeP}_2\text{S}_{12}$) typically possess stability issues, whilst more stable materials show low conductivities, e.g. tetragonal LLZO ($\text{Li}_7\text{La}_3\text{Zr}_2\text{O}_{12}$). Understanding the fundamental processes that govern ionic conductivity in such materials has long been a focus of research, however limited information is available on how the intrinsic lattice dynamics of a material influence this, and whether it is a governing factor. In this work we look at understanding the phonon processes between the bulk crystal lattice and a vacancy migration event in the Li-rich antiperovskites (Li_3OX ; $\text{X}=\text{Cl}, \text{Br}, \text{I}$). In studying the phonons in this way, we aim to question how phonon-based descriptors can be applied to materials discovery and whether diffusion processes can be enhanced via external stimuli.

11:45 AM EN05.04.05

The Formation of Residual Li Compounds on Ni-Rich NCM Cathodes and Their Effect on the Electrochemical Performance in LPSCI-Based ASSBs [Burak Aktekin](#), Anja Henss and Jürgen Janek; Justus-Liebig-Universität Giessen, Germany

$\text{LiNi}_x\text{Co}_y\text{Mn}_{(1-x-y)}\text{O}_2$ (NCM) type lithium transition metal oxides with high nickel concentrations have attracted a significant interest as a cathode material in lithium ion batteries due to their high energy density and low cobalt content, however, their reactivity with air during storage/handling and how this affects the electrochemical performance had been overlooked until the recent years. Exposure to H_2O and CO_2 during air storage/handling can lead to formation of LiOH , Li_2CO_3 and also transition metal hydroxides/carbonates.^{1,2} The formation of such Li-compounds can also cause structural changes near the surface of cathode particles.³ Therefore, it is very important to understand how these residual Li compounds are formed and how they affect the electrochemical performance. In all-solid-state batteries (ASSBs), the presence of Li_2CO_3 may improve the electrochemical performance in sulfide-based solid electrolytes,^{4,5} however, there has been no dedicated study aiming to understand relationship between the cell performance and the presence of specific residual Li compounds. In this study, we prepare single crystal $\text{LiNi}_{0.83}\text{Mn}_{0.06}\text{Co}_{0.11}\text{O}_2$ powders with different residual Li amounts and compositions by either carefully controlling the washing, post-annealing, the ambient air exposure (e.g. humidity and CO_2 concentrations) conditions, or applying coatings with an external Li source. Characterization of these powders will be presented with valuable insights gained from a number of analytical techniques such as XPS, TOF-SIMS, TGA-MS, FIB-SEM, acid titration and XRD. In the next step, the relationship between the residual Li type/amount and the electrochemical performance will be evaluated in ASSB cells with $\text{Li}_6\text{PS}_5\text{Cl}$ solid electrolyte and In-Li alloy counter electrode.

- (1) Sicklinger, J.; Metzger, M.; Beyer, H.; Pritzl, D.; Gasteiger, H. A. Ambient Storage Derived Surface Contamination of NCM811 and NCM111: Performance Implications and Mitigation Strategies. *J. Electrochem. Soc.* **2019**, *166*, A2322–A2335.
- (2) Kim, Y.; Park, H.; Warner, J. H.; Manthiram, A. Unraveling the Intricacies of Residual Lithium in High-Ni Cathodes for Lithium-Ion Batteries. *ACS Energy Lett.* **2021**, *941–948*.
- (3) Zhang, L.; Gubler, E. A. M.; Tai, C.-W.; Kondracki; Sommer, H.; Novák, P.; Kazzi, M. El; Trabesinger, S. Elucidating the Humidity-Induced Degradation of Ni-Rich Layered Cathodes for Li-Ion Batteries. *ACS Appl. Mater. Interfaces* **2022**, amsami.1c23128.
- (4) Jung, S. H.; Oh, K.; Nam, Y. J.; Oh, D. Y.; Brüner, P.; Kang, K.; Jung, Y. S. $\text{Li}_3\text{BO}_3\text{-Li}_2\text{CO}_3$: Rationally Designed Buffering Phase for Sulfide All-Solid-State Li-Ion Batteries. *Chem. Mater.* **2018**, *30*, 22, 8190–8200
- (5) Kim, A. Y.; Strauss, F.; Bartsch, T.; Teo, J. H.; Hatsukade, T.; Mazilkin, A.; Janek, J.; Hartmann, P.; Brezesinski, T. Stabilizing Effect of a Hybrid Surface Coating on a Ni-Rich NCM Cathode Material in All-Solid-State Batteries. *Chem. Mater.* **2019**, *31*, 9664–9672.

SESSION EN05.05: Fundamental Understanding via Characterization and Modeling II
Session Chairs: Dominika Buchberger, Megan Diaz, Yue Qi and Hui Wang
Tuesday Afternoon, November 29, 2022
Hynes, Level 3, Room 304

1:30 PM +EN05.05.01

Mechanistic Interrogation of Thermal Stability in Solid-State Batteries [Partha P. Mukherjee](#) and Bairav Sabarish Vishnugopi; Purdue University, United States

Solid-state batteries (SSBs), consisting of an inorganic solid electrolyte and a lithium metal anode are promising next-generation energy storage devices that can deliver high energy and power densities. However, the development of practical SSBs still requires overcoming fundamental challenges related to morphological evolution, transport-kinetics interaction, and electro-chemo-mechanical failure. While a wide range of candidate mechanisms leading to interface instability and failure onset have been studied, their mechanistic implication on the thermal stability at solid-solid interfaces is not understood yet. Due to various factors including the high reactivity of lithium metal, potential for oxygen liberation in the cathode, spatio-temporal evolution of thermal hotspots (e.g., during fast charging) and the propensity for internal short-circuit, the safety of SSBs needs to be critically evaluated. In this presentation, we assess the mechanistic role of thermo-electrochemical interactions, interface stability and interphase growth characteristics that can affect the thermal stability in SSBs.

2:00 PM EN05.05.02

The Role of Anisotropy on the Chemo-Mechanical Failure of Secondary NMC Particles Embedded in a Sulfide-Based Solid Electrolyte Avtar Singh¹, Wei Li¹, Trevor Martin², Donal Finegan² and [Juner Zhu](#)^{3,1}; ¹Massachusetts Institute of Technology, United States; ²National Renewable Energy Laboratory, United States; ³Northeastern University, United States

Lithium-Nickel-Manganese-Cobalt-Oxide (NMC) is being extensively applied as the cathode for solid-state batteries to match the high energy density of metallic anodes. In practice, NMC particles are embedded in the solid electrolyte (SE), forming a composite structure. One of the fundamental challenges for characterization is the co-existence of multiple failure mechanisms. Cracks can initiate and propagate along the grain boundaries between primary particles, through the primary particles, through the SE, or debonding the interface between particles and SE. Therefore, a thermodynamically consistent multi-physics modeling framework was developed to capture all these mechanisms. In order to consider the initiation and propagation of fracture, a regular phase-field fracture variable was employed. A diffused phase-field parameter was introduced to define the transition of chemo-mechanical properties between the grains, grain boundaries, electrolyte, and electrolyte-electrode interfaces. Inspired by the recent experimental evidence that clearly showed that morphological regulation can help mitigate the internal cracks, our model considered two sources of anisotropy, i.e. morphological orientation and crystal orientation. In addition, the concentration-dependent transport and mechanical properties were considered. The present model was implemented in the open-source FEM package MOOSE for solving three state variables: concentration, displacement, and phase-field damage parameter. Various parametric studies were performed to explore the effect of grain morphology and crystal orientation on the chemical-mechanical response of electrode material. The simulation results of this parametric study agreed well with experimental observations that regulated NMC811 particles have significantly fewer cracks than the randomly-oriented NMC532 particles. Ultimately, we applied this model of a polycrystalline particle embedded in a sulfide-based SE to study the

pressure effect on the crack formation and particle fragmentation. Bayesian optimization was used to find the optimal distribution of external pressure on the SE to study three different objectives under the same current density: minimizing the total amount of cracks, minimizing the volume of primary particles that are isolated from Li pathways, or maximizing the coulombic efficiency. Results demonstrated that controlling external pressure can change the electrochemical failure patterns.

2:15 PM EN05.05.03

Towards a Molecular Understanding of the Interfacial Li-Ion Dynamics in Composite Solid-State Electrolytes Under High Polymer Confinement—the Case of Polyethylene Oxide—Li₇La₃Zr₂O₁₂ Composites [Mauricio R. Bonilla](#)¹, [Fabián García Daza](#)², [Henry A. Cortés](#)¹, [Javier Carrasco](#)³ and [Elena Akhmatkaya](#)^{1,4}; ¹Basque Center for Applied Mathematics, Spain; ²The University of Manchester, United Kingdom; ³Centre for Cooperative Research on Alternative Energies (CIC energiGUNE), Basque Research and Technology Alliance (BRTA), Spain; ⁴IKERBASQUE, Basque Foundation for Science, Spain

Composite solid-state electrolytes (CSSEs) comprising a conductive, flexible polymer matrix embedding ceramic filler particles have emerged as a promising option for all-solid-state Li-ion batteries. Understanding the interfacial diffusion of Li⁺ as a function of filler content is crucial to formulating high-performance and cost-efficient CSSE. By considering as a case study a CSSE constituted by ion-conducting Ga³⁺ doped-Li₇La₃Zr₂O₁₂ (LLZO) garnet fillers embedded within a poly (ethylene oxide) and lithium bis(trifluoromethanesulfonyl) imide polymer matrix (PEO(LiTFSI)), we study the interfacial distribution and dynamics of Li⁺ at conditions of high polymer phase confinement in fully amorphous PEO above the melting point, T_m . Such confinement scenario aims to simulate the interstitial space between filler particles in close proximity, which is tantamount to the percolation conditions at which conductivity enhancement has been experimentally observed. By combining classical umbrella sampling calculations, molecular dynamics simulations, and hybrid Monte Carlo methods, we show that the free energy profile associated with the extraction of a Li⁺ ion from the garnet surface is site-dependent and highly asymmetric, suggesting a strong thermodynamic drive towards Li⁺ adsorption onto the garnet phase. Adsorbed Li⁺ is stabilized by exposed oxygens on the garnet surface and oxygens from bound PEO. Only beyond 0.35 nm from the garnet surface, the polymer coordination shell reaches its typical bulk density of 5 oxygens per Li⁺, leading to a slight decrease in the free energy. We also find that this thermodynamic drive towards Li⁺ uptake is counteracted by a kinetic barrier: free polymer chains in the bulk are significantly more mobile than garnet-bound chains. Hence, they can rapidly adapt to coordinate and stabilize incoming Li⁺ ions, dramatically reducing the probability that a Li⁺ ion approaches within 0.35 nm of the garnet surface. Under high polymer confinement (i.e., high filler volume fraction), the overlapping of bound polymer shells from opposite surfaces reduces the availability of free chains, leading to a significant decrease in Li⁺ diffusivity within the interstitial space.

We put forward that understanding Li⁺ diffusion in LLZO:PEO (LiTFSI) CSSEs above T_m , and at conditions of high polymer confinement provides valuable insights to interpret the variation of ionic conductivity with volume fraction *below* T_m (at typical operating conditions). This is because filler particles are surrounded by a layer of amorphous polymer even at room temperature (RT), as filler particles disrupt structural regularity. Based on this premise, we are able to qualitatively describe the experimental variation of RT conductivity with filler content reported in recent experimental work.

2:30 PM EN05.05.04

Unraveling the Grain Boundary Effects in Lithium Lanthanum Titanate (LLTO) Solid Electrolyte [Hyungjun Kim](#)¹, [Patrick Conlin](#)², [Matthew E. Bergschneider](#)², [Hayoung Chung](#)³, [Sung Youb Kim](#)³, [Suk Won Cha](#)¹, [Maenghyo Cho](#)¹ and [Kyeongjae Cho](#)²; ¹Seoul National University, Korea (the Republic of); ²The University of Texas at Dallas, United States; ³Ulsan National Institute of Science and Technology, Korea (the Republic of)

To meet the high energy density and safety requirements of next-generation batteries, all-solid-state batteries (ASSBs) are promising candidates. A lithium metal anode with a high theoretical specific capacity (3860 mAh g⁻¹) and the lowest electrochemical potential (-3.04 V vs. standard hydrogen electrode) is proving to be an essential component in ASSBs. However, solid electrolytes (SEs) in ASSBs still have hurdles to overcome such as lithium metallic phase accumulation, interfacial instability, and unsatisfactory ionic conductivity. Furthermore, solid electrolytes are generally powder-sintered into the polycrystalline phase, and the nature of grain boundaries (GBs) affects the overall performance of solid electrolytes. The polycrystalline solid electrolytes and the effects of GBs are not fully understood yet. In this work, we present a first-principles calculation-based theoretical study that discovers the effect of grain boundaries on ionic and electronic properties in perovskite Li_{3-x}La_{(2/3)-x}TiO₃ (0 < x < 0.167) (LLTO). Since the grain boundaries of SEs have various microstructure configurations, we consider the experimentally observed grain boundary configurations: i) grain boundaries without pore and ii) grain boundaries with pore space. The density functional theory (DFT) studies have uncovered the following properties of LLTO GBs. In pore-free grain boundaries, lithium-ion can enter the grain boundary region without an energy barrier in the aspect of thermodynamics. Moreover, the grain boundary region has an electron insulating feature comparable to bulk LLTO, even differences in A-site composition (0 < x < 0.167) have a negligible effect on electronic conductivity for stoichiometric grain boundaries. Besides, when the A-site distortion occurs at grain boundaries, the grain boundary region exhibits a p-type conductive property but has a high energy barrier for lithium-ion to cross into the grain boundary region. These findings show that the internal lithium metallic phase nucleation does not occur at the interface of firmly connected crystalline grains. On the contrary, in the grain boundaries with pore structure, the pore space has a p-type conductive feature and lithium-ion tends to reside in a neutral charge state. This indicates that the nucleation of the lithium metallic phase begins at the intergranular pore space of solid electrolytes. Based on the thorough investigation of the ionic and electronic properties of various LLTO grain boundaries, consequently, we confirm that the lithium metallic phase nucleates in the solid electrolytes crystalline grains interface rather than at the densely connected solid electrolyte grain boundaries. Our understanding provides an essential insight into the effect of grain boundary on the electrochemical performance of solid electrolytes as well as the crucial properties to be considered in the manufacturing of high electrochemical performance and safety improved solid electrolytes for advanced secondary batteries.

2:45 PM EN05.05.05

Effects of Li Defects on Moisture Stability and Li-Ion Transport Properties on Li₁₀SiP₂S₁₂ Solid Electrolyte—A First-Principles Study [Hou Jen Lai](#) and [Jyh-Chiang Jiang](#); National Taiwan University of Science and Technology, Taiwan

All-solid-state batteries (ASSBs) are expected to replace liquid electrolyte-based lithium-ion batteries (LIBs) as the next-generation rechargeable battery technology to meet the increasing demand for advanced energy storage systems because of their high energy density and safety. Solid electrolytes (SEs) with high Li-ion conductivity are required for ASSBs. Over the years, Li₁₀SiP₂S₁₂ (LSPS) has attracted attention as a promising new Li-ion conductor, as it has the high Li-ion conductivity (2.3 mS/cm). However, the poor chemical stability of sulfide-based electrolytes in the presence of moisture causes the hydrolysis reaction on the LSPS surface, resulting in the formation of toxic H₂S gas. This disadvantage necessitates handling of the LSPS in an inert gas environment, limiting large-scale commercialization. Therefore, improving moisture stability without compromising ionic conductivity of LSPS-based SEs is a critical issue in the development of ASSBs. In this study, we used density functional theory (DFT) calculations to understand the reaction mechanisms of the hydrolysis reaction on the perfect and defective LSPS (101) surface. Furthermore, we investigated the effect of Li vacancy on the Li-ion conductivity of LSPS using ab initio molecular dynamics (AIMD) simulations and statistical thermodynamic methods. The low energy barrier of the hydrolysis reaction on the defective LSPS surface indicated that Li vacancy would decrease the moisture stability of the LSPS surface. On the other hand, the presence of Li vacancy increased Li inter-cage migration, which increased Li ionic conductivity in the LSPS. Our findings show that the Li vacancy has a significant impact on the moisture stability and Li-ion conductivity of LSPS.

3:00 PM BREAK

3:30 PM *EN05.05.06

The Complex Mechanisms that Create High Li-ion Mobility in Oxides and Sulfides Gerbrand Ceder^{1,2}; ¹University of California, Berkeley, United States; ²Lawrence Berkeley National Laboratory, United States

The exciting development of solids with extremely high Li-ion conductivity, higher than that in traditional liquid electrolytes, in the last decade has forced us to rethink the processes that make cations move in solids. Super-ionic Li conductors typically have very high Li concentration so that their conductivity behavior cannot be explained with simple point defect mechanisms. Instead, ideas of concerted motion or highly correlated motion have been proposed. I will discuss our current understanding of the mechanisms that provide high Li-ion conductivity. We find that due to the high screening power of S²⁻ Li mobility in sulfides is mostly determined by local anion coordination and its variation along the migration pathway, making anion topology the main determinant of Li-ion conductivity. As a result, we find that there is little coordinated or concerted motion in sulfides. In contrast, due to the lower screening power of oxides and their lower Li-Li distances, Li-ion conductivity is much more determined by the electrostatic interaction with the other cations, setting the stage for possible concerted motion of multiple ions. I will show how this leads to very specific, but precise rules for selecting structures that may accommodate very fast Li-ion motion.

4:00 PM EN05.05.07

Ion Transport and Interfacial Stability in Fluorine Containing Lithium Argyrodite Electrolytes for Solid-State Lithium-Sulfur Batteries Varun Shreyas, Saransh Gupta, William Arnold, Hui Wang and Badri Narayanan; University of Louisville, United States

Rechargeable solid-state lithium-sulfur batteries (SSLBs) offer tremendous promise as a safe and energy-dense storage technology for use in electric transportation, robotics, and portable electronics. Lithium argyrodites (e.g., Li₇PS₆, and its halogen-doped derivatives) have emerged as a lucrative class of solid-state electrolytes (SSEs) for SSLBs owing to their high Li-ion conductivity (~10⁻³ S/cm), good elastic stiffness (~30 GPa), and low flammability. Despite their promise, SSLBs based on sulfide electrolytes remain far from commercialization due to lack of atomic-scale understanding of ion-conduction, charge transport, structural evolution, and interfacial reactions (e.g., dendrite growth, electrolyte decomposition etc.). Here we employ a combination of density functional theory calculations, and ab initio molecular dynamics simulations to address this challenge for fluorinated argyrodites. Specifically, using accurate materials modeling, we design fluorine-containing argyrodite electrolytes that simultaneously offer enhanced (a) Li-ion conduction facilitated by unique Li-disorder induced by fluorine and other halogen co-dopants, and (b) stability against Li-anode owing to formation of a stable solid-electrolyte interface containing conductive species (Li₃P), alongside LiCl and LiF. We will discuss these results in the context of accelerating design of novel solid-state electrolytes for long-lived, stable, and high-energy density SSLBs.

4:15 PM EN05.05.08

Thermodynamic and Kinetic Stability of Cathode Electrolyte Interface in All Solid-State Li-S Batteries Manas Likhit Holekevi Chandrappa, Swastika Banerjee, Ji Qi, Chi Chen and Shyue Ping Ong; University of California San Diego, United States

Despite the advancements in the Li-S batteries (LSBs), the issues of polysulfide shuttling continues to be a major roadblock it's commercialization. Polysulfide shuttling results in an irreversible loss of active material which results in capacity fading. Replacing liquid electrolyte with solid state electrolytes (SE) holds the promise to mitigate this issue. However, the interfacial stability of these SE/cathode interfaces remains largely unknown. Here, we present a comprehensive evaluation of stability of the SE/cathode interfaces of all the major classes of SEs (oxides, sulfides, nitrides, and halides). Except sulfides SE interfaces all other SE interfaces are predicted to be (electro)chemically unstable. The known Li ion battery (LIB) oxide buffer layers were not found to be suitable to stabilize the oxides and nitride SE interfaces. However, a few sulfide buffer layers such as LiAlS₂, Sc₂S₃, Y₂S₃ can potentially be used as buffer layer for the unstable oxide and halide interfaces. We developed an accurate moment tensor potential (MTP) to study the dynamic stability of SE/cathode interface by taking β-Li₃PS₄ and α-S₈ interfaces as representative example. MD simulations of realistic large-scale interface (>1000s atoms) simulations indicate that this interface is unstable over longer timescales (several ns). Using bond connectivity-based clustering the interface reaction products were analyzed which showed a steady increase in the concentration of several short and long S chains (S_n) at the interface over nanosecond timescales. The presence of several Li polysulfide (Li-S_n) resembling molecules was also detected at the interface. We also confirm that the Li polysulfides are localized at the interface and shows no diffusion into the β-Li₃PS₄.

4:30 PM *EN05.05.09

Effects of Alivalent Doping on Structure and Properties of Na₃SbS₄ Type Superionic Conductors Selim Halacoglu, Yang Li, Varun Shreyas, Badri Narayanan and Hui Wang; University of Louisville, United States

Alivalent doping is a promising strategy to further enhance the ionically conductive properties of solid-state ion conductors. Beside the conductivity, the alivalent dopants also affect the synthesis mechanism, crystalline structure, as well as the electrochemical stability of the doped conductors. In this talk, we will present Na₃SbS₄ as a model material to introduce different types of alivalent anion or cation dopants, and discuss the doping chemistry in sulfide-based solid electrolytes. On the structural studies, we tracked the synthetic process of doped Na₃SbS₄ by in situ neutron diffraction and examined the phase purity and structural stability after different doping treatment. Besides, we also evaluated the ionic conductivity of doped Na₃SbS₄ conductors and established the correlations between dopants and ion transport, as well as the interface stability between the doped Na₃SbS₄ conductors with metallic Na anode. We will also discuss a few strategies for interface stabilization in sulfide-based solid state Na batteries.

SESSION EN05.06: Poster Session: Solid-State Batteries

Session Chairs: Alex Bates and Dominika Buchberger

Tuesday Afternoon, November 29, 2022

8:00 PM - 10:00 PM

Hynes, Level 1, Hall A

EN05.06.02

Phase Evolution and Thermodynamics of Al-Doped Cubic LLZO Studied by High-Temperature X-Ray Diffraction Øystein Gullbrekken¹, Maria Tsoutsouva², Daniel Rettenwander¹, Mari-Ann Einarsrud¹ and Sverre Magnus Selbach¹; ¹Norwegian University of Science and Technology, Norway; ²Onera, France

$\text{Li}_7\text{La}_3\text{Zr}_2\text{O}_{12}$ (LLZO) is a promising solid-state electrolyte for advanced Li-ion batteries due to its high ionic conductivity, non-flammability and high electrochemical stability against Li anodes and high voltage cathodes. However, synthesis of phase pure LLZO is challenging due to easy formation of secondary phases, such as the pyrochlore $\text{La}_2\text{Zr}_2\text{O}_7$, that are detrimental to the performance of a LLZO electrolyte. Although many studies have been performed on the electrochemical performance of LLZO, the understanding of the thermodynamics of the synthesis of LLZO is still lacking.

Here we report on high-temperature X-ray diffraction (HTXRD) following the crystallization of a gel of Al-doped LLZO. Gels with 0, 10 and 20 mol% excess Li were prepared and calcined at 500 °C to remove the volatile components before HTXRD. The powders calcined at 500 °C consisted primarily of $\text{La}_2\text{Zr}_2\text{O}_7$ with trace amounts of Li_2CO_3 and $\text{La}_2\text{O}_2\text{CO}_3$ and were used as starting materials to study the formation of the cubic LLZO phase. During HTXRD the samples were heated from 500 °C to 700 °C in steps of 20 °C, and further to 1000 °C in steps of 50 °C. Upon heating the pyrochlore phase gradually transforms to cubic LLZO. In all samples, cubic LLZO first appears around 600 °C and the pyrochlore phase disappears around 750 °C in the samples with 0 % and 20 % excess Li. We performed two analyses of the sample with 10 % excess Li by HTXRD, one with normal deposition thickness and another with thinner deposition thickness. In the thin sample, cubic LLZO appears at a lower temperature of 560 °C compared to the other experiments. The pyrochlore phase does not fully disappear but instead reappears and crystallizes at the highest temperatures investigated, indicating extensive Li loss from the thin sample. These observations suggest that atmospheric exposure and the relative surface area of powder are important factors for LLZO formation.

To understand the thermodynamics of LLZO formation, we propose the following reaction to take place based on the identified reactants and products: $6.25 \text{Li}_2\text{CO}_3 + 0.25 \text{Al}_2\text{O}_3 + 2 \text{La}_2\text{Zr}_2\text{O}_7 + \text{La}_2\text{O}_2\text{CO}_3 \rightarrow 2 \text{Li}_{6.25-x}\text{Al}_{0.25}\text{La}_3\text{Zr}_2\text{O}_{12-0.5x} + 7.25 \text{CO}_2(\text{g}) + x \text{Li}_2\text{O}(\text{g})$. The enthalpy, entropy and Gibbs energy of the reaction were calculated from literature values and DFT calculations and agree with the experimental observations. Finally, we discuss the significance of the highly disordered Li sublattice for the entropy of cubic LLZO. We believe our findings will contribute to improved understanding of LLZO formation and facilitate the synthesis of high-performance phase pure LLZO electrolytes.

EN05.06.03

Multi-Functional Interface for High-Rate and Long-Durable Garnet-Type Solid Electrolyte in Lithium Metal Batteries Sangwook Han, Kyeongsu Lee and Kisuk Kang; Seoul National University, Korea (the Republic of)

Lithium dendrite growth in solid electrolytes is one of the major obstacles to the commercialization of solid-state batteries based on garnet-type solid electrolytes. Herein, we propose a strategy that can simultaneously resolve both the interface and electronic conductivity issues via a simple one-step procedure that provides multi-layer protection at low temperature. We take advantage of the facile chemical conversion reaction, showing the wet-coated SnF_2 particles on the solid electrolyte effectively produces a multi-functional interface composed of LiF and Li-Sn alloy upon contact with lithium. We demonstrate multi-function enables the remarkably high critical current density up to 2.4 mA cm^{-2} at 25 °C and the stable galvanostatic cycling for over 1000 hours at 0.5 mA cm^{-2} in the lithium symmetric cell. Moreover, the full cell delivers robust cycle life of more than 600 cycles at 1.0 mA cm^{-2} , which is the highest performance at room temperature reported to date.

EN05.06.05

Hybrid Electrolyte Films Incorporating Interfacial-Barrier-Free Garnet-Type Oxide Electrolytes for High-Power-Density Solid-State Batteries Dong Ok Shin, Myeong Ju Lee and Young-Gi Lee; Electronics and Telecommunications Research Institute, Korea (the Republic of)

The key requirement for realizing solid-state batteries where permeable liquid electrolytes (LEs) are replaced with rigid and fragile solid electrolytes, is to form an intimate interface between electrodes and electrolyte layers. To achieve this goal, a hybrid solid electrolyte (HSE) fully using the advantages of both organic and inorganic materials has been considered a promising component. While the inorganic part could contribute to enhancing total conductivity, the organic part could offset the intrinsic drawbacks such as brittleness and fragility of common solid electrolytes. As a proof of concept, a garnet-type $\text{Li}_7\text{La}_3\text{Zr}_2\text{O}_{12}$ (LLZO) ceramic solid electrolyte was employed as a Li-ion conductive filler to construct the HES. However, a formidable challenge facing the LLZO solid electrolyte is its intrinsic surface layer which was inevitably formed in the course of the synthesis process, potentially acting as a resistant interfacial barrier to Li-ion transport. In this work, we demonstrate for the first time that the highly conductive polyvinylidene fluoride (PVDF)-based HSE film incorporating LLZO fillers without the resistive layer through a reliable dry etching process. Such a thin layer mainly consisting of amorphous lithium carbonate has been removed without damaging the core LLZO during the etching process. With optimized the content of LLZO (30 wt% vs. weight of PVDF matrix), the etched LLZO-based HSE film showed the ionic conductivity of $4.05 \times 10^{-4} \text{ S cm}^{-1}$, which was around two times higher than that of the non-etched LLZO-based HSE film. Cycling results with Li symmetric cells of Li/LLZO-PVDF HSE film/Li verified the superior stability of HSE film with etched-LLZO. Particularly, full cell results with SSBs of $\text{LiNi}_{0.6}\text{Mn}_{0.2}\text{Co}_{0.2}\text{O}_2$ /LLZO-PVDF HSE film/Li identified that a high-power-density feature could be obtained in the cell with the HSE film based on etched-LLZO. Moreover, it is revealed that the formation of the chemically modified region at the PVDF/LLZO interface and the resulting promoted Li-ion transport can be furthered in HSEs with etched-LLZO fillers.

EN05.06.06

Stabilization of Cycling Performance of $\text{Li}[\text{Ni}_{0.95}\text{Co}_{0.04}\text{Al}_{0.01}]\text{O}_2$ Cathode Using Thin Film Solid Electrolyte Interlayer Jeon Kim, YeSung Kim, GiMun Han and ChongSeung Yoon; HanYang University, Korea (the Republic of)

The expanding usage of commercial lithium batteries in newer application fields has led to significant attention towards solid electrolytes due to the safety issue with flammable and volatile organic electrolytes. It is expected that practical application of the lithium secondary batteries (LIBs) with the solid electrolytes in order to solve this problem. All-solid-state lithium thin-film batteries (TFBs) are expected to apply to many electrical applications, because of their advantage of safety, long cycle life and form factor based on the solid electrolyte. However, the electrochemical performance of TFBs has been limited by various factors and the interface between the electrolyte and the electrode is one of the key factor of high performing rechargeable all solid state batteries. In this study, we investigated the influence of Solid Electrolyte thin film on cell characteristics and also tried to improve the battery performance compared with liquid electrolytes. Various types of ceramic electrolytes have been employed for improving the performance of LIBs. Among various oxides, NASICONs (NA-Super-Ionic-CONductor) have lower ionic conductivity but are comparatively stable in ambient conditions as well as against commonly used cathode materials. In this work, NASICON-type $\text{LiSnZr}(\text{PO}_4)_3$ (LSZP, hereinafter) ceramics is used for solid state electrolyte material in our experiment. A $\text{Li}[\text{Ni}_{0.95}\text{Co}_{0.04}\text{Al}_{0.01}]\text{O}_2$ (NCA95, hereinafter) system with a high specific capacity was selected as the cathode and LSZP as the solid electrolyte coating. Li was chosen as the anode material. To evaluate the electrochemical properties of the solid electrolyte interlayer, LSZP thin films on the NCA95 Cathode were prepared by RF magnetron reactive sputtering method for Solid electrolyte material in our experiment. The sputtering power and argon pressure of LSZP films have been optimized and are kept constant to reduce interference factors. In this study, We are trying to enhance the cycling performance of discharge capacity by coating thickness of the LSZP. A cells were fabricated in a glove box with Ar atmosphere and investigated by lithiation and electrochemical properties at room temperature. In addition to demonstrating the microstructure and the structural changes during the lithiation of the thin film deposited cathode were followed by ex situ transmission electron microscopy (TEM) to provide structural changes of the microstructure observed between Electrolyte and cathodes. The electrochemical performances of the solid electrolyte interlayer were evaluated using 2032

coin-type half-cells with a lithium (Li) metal anode. The coin cells were cycled between 2.7 and 4.3 V at 30°C. We also investigated the influence of interlayer thickness on cell characteristics and tried to improve the discharge properties. Introducing the thin film solid electrolyte interlayer could improve the battery discharging performance and high stability. The capacity loss rate was decreased with interlayer about 2.3% after 50 charge-discharge cycles. Here, We show that thin film solid electrolyte interlayer process can be considered the practical for commercial applications because of the capacity retention. The batteries with an interlayer revealed better capacity retention and rate characteristics than the pristine one during the charging/discharging, which indicates a promising strategy for the development of ASSBs.

EN05.06.07

Rational Design of Hybrid Electrolytes for All-Solid-State Lithium Batteries Jungdon Suk; Korea Research Institute of Chemical Technology, Korea (the Republic of)

Rechargeable Li-ion batteries have led to a remarkable revolution in consumer electronics, electric vehicles (EV), and energy storage systems (ESS). Especially, EVs are one of the good options for autonomous vehicles and to reduce CO₂ emissions. Rechargeable Li-ion batteries which have been successfully applied to portable electronics are widely used for EVs. However, short driving range due to the limited energy density of Li-ion batteries and safety issues should be overcome to meet a requirement for EVs.

Solid polymer electrolytes (SPEs) and hybrid electrolytes with oxide electrolytes are considered promising electrolytes for next-generation all-solid-state lithium batteries because they have much better safety, flexibility, and mechanical stability in the design of the cells, compared with the liquid electrolytes. Current research on solid polymer electrolytes has focused on poly(ethylene oxide)(PEO)-based polymers, but they are restrictively allowed for practical applications because of their weaknesses such as low ionic conductivity at room temperature and poor electrode/electrolyte interface characteristics. In this presentation, the semi-interpenetrating polymer network PEO-based polymer electrolyte and hybrid electrolytes with oxide electrolytes were used to investigate the performance of Li-polymer batteries by using Ni-rich NMC such as LiNi_{0.8}Mn_{0.1}Co_{0.1}O₂ (NMC811) as cathode materials and carbon-silicon composite or lithium metal as anode materials. All-solid-state batteries are successfully operated at room temperature and 45°C with high rate capability and enhanced cycle performances.

EN05.06.08

High-Temperature Discharge Characteristics of Salt-Coated Solid Electrolyte Hae-Won Cheong, Minu Kim, Tae-Young Ahn, Chaehyeok Han, Kiyoul Kim, Seung-Ho Kang, Yusong Choi and Jang-Hyeon Cho; Agency for Defense Development, Korea (the Republic of)

High-temperature thermal batteries, also called molten-salt batteries, are primary batteries that can be reserved for a long period of up to several decades. The molten salt electrolyte for the thermal battery is a solid insulator that thoroughly prevents self-discharge before activation, but once instantly melted by the pyrotechnic heat source, it becomes an excellent ionic conductor and can supply high-power electricity. Usually, fine MgO powder is added as an inorganic binder to prevent the molten-salt electrolyte from flowing down. Although it is desirable to add a large amount of MgO to hold the liquid electrolyte even under severe acceleration conditions, but if it is excessive, the internal resistance of the cell will increase due to its electrically insulating nature of MgO. Meanwhile, all-solid-state batteries characterized by solid electrolytes have received great attention for their high safety and improved energy density even with high-voltage cathodes. Considering the use for thermal batteries, high-temperature stability and long-term storage properties as well as excellent ionic conductivity of the solid electrolyte are crucially important. The densely sintered body can have high ionic conductivity, however, the poor contact between solids deteriorates the output power capability. In this study, we proposed composite electrolytes that significantly improved the contact area and ionic conductivity by coating the surface of the solid electrolyte with molten salt. It has been shown that the soft salt film coated on the hard surface can also prevent self-discharge and increase the compaction strength. The solid electrolyte used in this study is Li₇La₃Zr₂O₁₂ (LLZO). Discharge performance was tested using disk-shaped LiSi/FeS₂ cells.

EN05.06.09

Highly Stable Solid Hybrid Electrolytes Based on Li-Ion Conductive Li_{6.4}La₃Zr_{1.4}Ta_{0.6}O₁₂ Framework for All-Solid-State Lithium Batteries with High Energy Density and Long Cycle Life Leiwu Tian, Ji-Wan Kim and Dong-Won Kim; Hanyang University, Korea (the Republic of)

All-solid-state lithium batteries (ASSLBs) are one of the best candidates for improving energy density and enhancing battery safety. However, many properties such as ionic conductivity, electrochemical and mechanical stability need to be improved for practical application. In this work, a vertically aligned Li_{6.4}La₃Zr_{1.4}Ta_{0.6}O₁₂ (LLZO) framework composed by three different layers (dense layer, vertical aligned layer and finger liked layer) was prepared by phase inversion method. A framework-based solid hybrid electrolyte (F-SHE) was then obtained by penetrating poly(ϵ -caprolactone) (PCL)-based polymer electrolyte into LLZO framework. The resulting flexible F-SHE exhibited a high ion conductivity of 1.03×10^{-4} S cm⁻¹ at 25 °C, which was attributed to the vertical aligned lithium-ion conductive LLZO framework that provided fast conduction pathway for lithium ions. The lithium symmetric cells assembled with F-SHE showed a long cycling life more than 700 h at 0.3 mA cm⁻², indicating the solid electrolyte promoted a uniform flux for lithium stripping/plating and suppressed the growth of lithium dendrite. The solid-state Li/NCM cell employing F-SHE exhibited good cycling performance in terms of discharge capacity and cycling stability. Our results demonstrate that the F-SHE can be a promising electrolyte for practical application in ASSLBs with enhanced safety and long cycle life.

EN05.06.10

Design of Pyrrolidinium-PEG Ionic Copolyesters for Li-Ion Transport Channels in Polymer Network Gel-Polymer Electrolytes Younggyun Choi and Jong Hyeok Park; Yonsei University, Korea (the Republic of)

Since electric vehicle (EV) accidents from flammable lithium-ion batteries (LIBs) continue to increase, solving the safety issue of LIBs has emerged as an important task. Highly volatile liquid solvents that help solvate and transport Li⁺ are the major cause of the flammability of LIBs. Therefore, replacing liquid electrolytes with solid electrolytes may overcome this safety issue. Even though solid-state electrolytes have advantages over liquid electrolytes, restricted ion transportation in solid-state electrolytes causes poor room temperature ionic conductivity ($\approx 10^{-5}$ to 10^{-2} mS cm⁻¹), which makes solid-state electrolytes difficult to apply to commercial LIBs.

In this work, ionic liquid-based linear polyesters were adapted on solid-state electrolytes. Several ionic polyesters prepared from imidazolium ionic liquid monomers have been previously reported. Imidazolium-polyethylene glycol (Imidazolium-PEG) copolyesters have also been researched, and their electrical and thermal properties are dependent on the length of the PEG segment. However, because pyrrolidinium ionic liquids are more stable and show wider electrochemical windows than imidazolium ionic liquids, pyrrolidinium ionic liquid based polyesters have been prepared and used for solid-state electrolytes. To fabricate a solid-state semi-IPN polymer electrolyte system, a UV-crosslinkable polymer matrix of ethoxylated trimethylolpropane triacrylate (ETPTA) and tailored linear pyrrolidinium-PEG copolyester with carbonate liquid electrolyte were mixed. Well-dispersed pyrrolidinium-PEG copolyester (P_NPEG, N: average molecular weight of PEG) could accelerate Li⁺ transportation between the cathode and anode in the polymer matrix. To optimize battery performance, P_NPEG was synthesized from PEGs with different average molecular weights and pyrrolidinium Bis(trifluoromethanesulfonyl)imide (pyrrolidinium-Tf₂N) ionic monomers. The PEG backbone in P_NPEG promotes Li⁺ transportation through the

interactions between ether groups and Li^+ ions. In addition, ionic liquid monomers in P_NPEG contribute to ion solvation and selective cation transport. In summary, we reported an in situ UV-cured gel polymer electrolyte (GPE) incorporating novel pyrrolidinium-PEG copolyester materials to promote lithium ion transport properties. Well-dispersed $\text{P}_{1000}\text{PEG}$ in the GPE formed ion channels, which were confirmed by SEM images and electrochemical tests. The amorphous polymer structure and low T_g of $\text{P}_{1000}\text{PEG}$ -GPE supported the higher ion conductivity results obtained by XRD and DSC analysis, respectively. In addition, MD simulations showed a lower coordination number between P_NPEG and Li^+ than between pure PEG1000 and Li^+ . As the optimized proportion of $\text{P}_{1000}\text{PEG}$ improved the ion conductivity and stability of the solid-state electrolytes, this study is expected to support advances in solid-state batteries applying $\text{P}_{1000}\text{PEG}$ -based ion channels beyond liquid electrolytes.

EN05.06.11

Study on Mechanical Strength Measurement and Strength Improvement of Sulfide-Based Electrodes [Kiyoul Kim](#), Tae-Young Ahn, Chaehyuk Han, Haewon Jung and Yusong Choi; Agency for Defense Development, Korea (the Republic of)

The thermal battery is a primary battery that is used in special fields such as defense due to its high power and high reliability characteristics. In the thermal battery, a lithium or lithium compound negative electrode and a metal sulfide-based positive electrode system are used. There is always a demand for reducing the weight of the system and a need for the increasing area of electrode. Therefore, it is essential to study the mechanical strength of the electrode and improve its strength. In this research, the strength of the compaction of the positive electrode material was quantitatively measured, and research was conducted to improve the strength for weight reduction and large area. Two methods of measurement were proposed for quantifying the mechanical strength of the electrode of the disk-shaped green compact electrode. The fracture strength of the green compact was measured by the "Monotonic equibiaxial flexural strength test" method proposed by ASTM C1499-09, and the fracture toughness was measured by the double cantilever beam (DCB) test. In order to improve the mechanical strength, the strength according to the powder particle size and the compression pressure was measured. Higher fracture strength and fracture toughness more than double that of green compacts with reference powder grain size and differentiation smaller than $45\mu\text{m}$ were measured. The effect of powder particle size and compression pressure on strength was analyzed through powder characterizations and microstructure observations. In addition, actual electrodes were fabricated and the possibility of battery utilization was verified through discharge tests

EN05.06.13

Investigating Chemo-Mechanical Phenomena in All-Solid-State Lithium Metal Batteries Using *In Situ* Curvature Measurements [Sydney Morris](#)¹, [Jung Hwi Cho](#)¹, [Kunjoong Kim](#)², [Srinath Chakravarthy](#)³, [Xingcheng Xiao](#)⁴, [Jennifer L. Rupp](#)² and [Brian W. Sheldon](#)¹; ¹Brown University, United States; ²Massachusetts Institute of Technology, United States; ³Samsung Semiconductor, Inc., United States; ⁴General Motors Research and Development Center, United States

With increasing interest in the use of solid electrolytes (SE) for lithium-ion and lithium metal batteries, it is important to understand their chemo-mechanical properties and failure mechanisms. A key failure mechanism in the garnet-type solid electrolyte lithium lanthanum zirconium oxide (LLZO) are short circuits caused by Li penetration through the SE once a critical current density (CCD) is reached. Such Li penetration is known to cause fracturing of the SE, highlighting the need to investigate the combined chemo-mechanical phenomena that affect the performance and lifetime of all-solid-state batteries. The unique challenge of evaluating the mechanical driving forces behind this mechanism and how the stresses within the SE evolve during Li plating require careful in situ measurements. This work investigates the evolution of such phenomena within the LLZO using in situ curvature measurements, in both a traditional symmetric Li cell configuration and a novel anode-free configuration. Data was then analyzed in the context of a Finite Element Model (FEM) to quantitatively evaluate stress evolution in the solid electrolyte. Results show that Li metal plating within a surface flaw leads to an accumulation of stress prior to short-circuiting. The combined results of experiments and the FEM suggest that it is critical to minimize surface defects and flaws during the manufacturing of LLZO.

EN05.06.14

A Study of Fabrication and Characterization of Na_xMnO_2 as a Cathode Material for Sodium-Ion Battery [Zia Uddin Mahmud](#) and Kartik Ghosh; Missouri State University, United States

The necessity for electrochemical energy storage technologies is promptly boosted due to the spread of renewable energy sources and the promising market for net-scale battery applications. Sodium-ion batteries (SIB) are a novel battery class due to Na materials' abundance and low cost compared to lithium. Na_xMnO_2 , a sodium-based material is one of the promising candidates for large-scale SIB applications due to the diffusion of Na-ion providing high power density. In the present study, $\text{Na}_{0.44}\text{MnO}_2$ is being prepared by hydrothermal method and investigated Structural, Electrical properties, and describe electrochemical properties of materials. The Materials were characterized using various techniques including X-ray diffraction (XRD), Raman spectroscopy, scanning electron microscopy (SEM), and UV-VIS. The Rietveld refinement performed on the respective XRD pattern led on orthorhombic structure with space group $\text{Pmc}2_1$. We have observed by altering anode materials with graphite, graphene, and a different portion of graphite-graphene mixture affects the efficiency and cycle life. In addition, electronic and structural properties have been modeled employing density functional theory. This synthesis process can be useful for sodium-ion battery applications.

EN05.06.15

Heterogeneous Ion Transport Dynamics in an Organic Ionic Plastic Crystal—With Point Vacancies or at Grain Boundaries [Hyunghick Park](#) and [Bong June Sung](#); Sogang Univ., Korea (the Republic of)

Organic ionic plastic crystals (OIPCs) are a class of solid electrolyte materials. In OIPCs, the interactions between ions are strong enough to form a translationally ordered structure, while the interactions are still weak enough to allow rotational motions of ions. Due to this unique characteristic, dopant ions such as lithium ions can show fast dynamics in the OIPCs. Therefore, OIPCs can be utilized as matrix materials for solid electrolytes. Various ion transport mechanisms through defects have been proposed. However, it is very hard to track ions at the molecular level and understand how these defects facilitate the dynamics in OIPCs via experimental techniques. Hence, the dominant ion transport mechanism in OIPCs is still in debate. In this work, we perform atomistic molecular dynamics simulations to understand the transport mechanisms of matrix and lithium ions in 1,3-dimethylimidazolium hexafluorophosphate ([MMIM][PF₆]) in the presence of defects. We employ two kinds of defects: 1) a point vacancy and 2) a grain boundary. We calculate mean squared displacements (MSDs) and self-part of van Hove correlation functions of ions. We find that both defects facilitate the dynamics of matrix ions and increase the dynamic heterogeneity. However, we observe the anisotropy of structures and dynamics of ions at grain boundaries. Moreover, we calculate non-Gaussian parameters to estimate the timescale (τ_{max}) at which heterogeneous dynamics become maximum. τ_{max} of grain boundary systems are approximately more than 100 ns, while that of point vacancy systems are 10–50 ns. We infer that the difference between these two ion transport mechanisms are the difference in timescales of heterogeneous dynamics.

EN05.06.16

Nanostructure-Designed Interlayer for Anode-Less All-Solid-State Batteries [Seunggoo Jun](#), Yong Bae Song and Yoon Seok Jung; Yonsei University,

Korea (the Republic of)

Owing to their potential of improved energy density and safety compared to conventional lithium-ion batteries, all-solid-state batteries (ASSBs) are considered a promising alternative to accelerate the electrification of power trains. Adopting Li metal anodes for ASSBs has been the Holy Grail as it can maximize the energy density, considering the highest specific capacity (3860 mA h g^{-1}) and the lowest potential (-3.04 V vs. the standard hydrogen electrode (SHE)) for Li metal. However, penetrating growth of Li metal occurs in ASSBs, and various factors, such as grain boundary, defect, and byproduct formation by side reactions of Li-SE, complicates the design of SE/Li interfaces. Recently, Samsung reported the innovative strategy of anode-less ASSBs enabled by the use of carbon-silver layer that prohibits a direct contact between SE and in situ grown Li metal. However, preparation and processability of silver nanoparticles is a potential risk for the practical applications.

In this presentation, we report nanostructure-designed interlayer for anode-less ASSBs. The developed interlayer is intact in ambient atmosphere and facilitates reversible deposition/dissolution of Li metal during charge-discharge.

[1] Lee, Y.G., et al. *Nat. Energy* 2020, 5, 299–308

[2] Lim, H., et al. *Energy Storage Mater.* 2022, 50, 543.

SESSION EN05.07: Solid-State Battery Fabrication—From Materials to Novel Cell Architectures I

Session Chairs: Alex Bates, Dominika Buchberger and Hongli Zhu

Wednesday Morning, November 30, 2022

Hynes, Level 3, Room 304

8:45 AM *EN05.07.01

Development of Next Generation Solid-State Batteries and the Path to Manufacturing [Steven J. Visco](#); PolyPlus Battery Company, United States

A critical difference between conventional rechargeable batteries and solid-state batteries is the substitution of a solid electrolyte for the volatile (and typically flammable) liquid electrolyte. However, this substitution is non-trivial and has significant implications for the structure, performance, manufacture, and cost of solid-state batteries. The scaling and manufacture of polymer electrolytes is relatively straightforward but their low ionic conductivity at room temperature precludes widespread adoption. A number of polycrystalline solid electrolytes have excellent room temperature ionic conductivities, however the difficulty in maintaining solid-solid contacts in composite electrodes is challenging, and the scaling of polycrystalline ceramic sheet is also nontrivial and likely expensive. Oxide glasses have been used successfully in commercial solid-state micro-batteries, but these batteries are made by physical vapor deposition and therefore very expensive to produce. Sulfide glass solid electrolytes have the advantages of being relatively soft and therefore easier to establish solid-solid contacts, and can be scaled using conventional thin glass processing technology. However, sulfide electrolytes are sensitive to moisture which introduces its own complexity in manufacturing. In this presentation we will examine the merits and challenges of each approach and potential paths to commercialization of high energy density solid-state batteries.

9:15 AM EN05.07.03

First-Principles Study on Selenium-doped $\text{Li}_{10}\text{GeP}_2\text{S}_{12}$ Solid Electrolyte—Effects of Doping on Moisture Stability and Li-Ion Transport Properties [Santhanamoorthi Nachimuthu](#) and [Jyh-Chiang Jiang](#); National Taiwan University of Science & Technology, Taiwan

All-solid-state lithium-ion batteries (ASSBs) are currently at the forefront of the search for next-generation energy storage technologies. ASSBs use solid-state electrolytes (SSEs) rather than the liquid electrolyte, allowing for greater safety, higher energy density, and higher output power. Among the different SSEs, the ceramic-sulfide-based solid electrolyte, $\text{Li}_{10}\text{GeP}_2\text{S}_{12}$ (LGPS) has attracted considerable attention because of its comparable ionic conductivity of 12 mS/cm with current organic liquid electrolytes. However, one of the most significant challenges in LGPS is the hydrolysis reactions at the interface, which are intrinsically unstable in ambient humidity, resulting in the release of toxic gas H_2S and, as a result, a significant decrease in ionic conductivity. Hence, improving moisture stability without degrading the ionic conductivity of LGPS-based SSEs is one of the key issues in developing efficient ASSBs. Herein, we report the reactivity of the LGPS surface towards H_2O , subsequent hydrolysis reactions for the H_2S formation, and effective methods to suppress the H_2S evolution on the LGPS surface using density functional theory (DFT) calculations. The pristine LGPS surface is highly unstable towards H_2O at room temperature, where H_2O dissociation occurs spontaneously. However, the H_2O adsorption and its activation are weakened upon the Se substitution on the LGPS surface. By doping the Se atom on LGPS, the H_2S evolution can be suppressed and significantly improve the chemical stability of the LGPS surface. In addition, we predict the Li^+ ion transport properties of both pristine and Se-doped LGPS compounds using ab initio molecular dynamics (AIMD) simulations. The Se-doped LGPS material has a similar bandgap to pristine LGPS; it can have similar decomposition products and low electronic conductivity. The predicted ionic conductivity of Se-doped LGPS is found to be slightly lower than the pristine. These findings suggest that replacing sulfur atoms in LGPS with Se atoms could be an effective strategy for improving moisture stability.

9:30 AM *EN05.07.04

Solid-State Lithium-Metal Battery Technology [Niall Donnelly](#); QuantumScape, United States

The advancement of the battery industry plays a critical role in meeting consumer demand on the performance and efficiency of electric vehicles, however, today's EVs lack the performance, safety and cost required for mass-market adoption of zero-emissions vehicles.

QuantumScape developed the industry's first anode-free cell design, using a nonflammable, noncombustible solid-state separator that will enable extended range, faster charging and safer operating than today's EVs and gas-powered vehicles. Join the session presented by QuantumScape Vice President of Research and Development Niall Donnelly to learn more about QuantumScape and its solid-state lithium-metal battery technology.

10:00 AM BREAK

10:30 AM EN05.07.06

Ultrafast High-Temperature Sintering of Solid-State Electrolytes [Qi Dong](#) and [Liangbing Hu](#); University of Maryland, United States

The synthesis of high-quality solid-state electrolyte membranes is challenging due to the lack of fine control over the grain growth by conventional sintering methods. Herein, we report a unique high-temperature (1500 K) and rapid sintering ($2\text{-}30 \text{ s}$) process called ultrafast high-temperature sintering (UHS) that can tailor the grain growth and densification toward high-quality, high-performance solid-state electrolyte membranes for Li battery applications. In this technique, the high temperature promotes grain growth and removes impurities during sintering. Meanwhile, the short sintering

duration in seconds ensures good tunability from porous to dense microstructures, as well as accurate control on the grain size, distribution, and composition. Using Ta-doped $\text{Li}_7\text{La}_3\text{Zr}_2\text{O}_{12}$ (LLZTO) garnet as a model system, we demonstrate sintering dense solid-state electrolyte membranes with nearly identical grain size and distribution compared to the powders before sintering, along with reduced defects and high relative density. These features contribute to high ionic conductivity ($6.4 \times 10^{-4} \text{ S cm}^{-1}$ at room temperature) and excellent electrochemical stability during Li striping/plating (over 300 h under 0.2 mA cm^{-2}). We further demonstrate sintering solid-state electrolyte with volatile fillers (e.g., LLZTO with Li_3N) toward a dense microstructure, as well as 3D porous solid-state electrolyte scaffolds on various substrates, both showing excellent electrochemical performances. This UHS approach can be further extended to a variety of ceramic conductors for solid-state battery applications.

10:45 AM EN05.07.07

Solid-State Electrodes and Electrolytes with Tunable and Low-Tortuosity Micro-Architected Structures from Nonequilibrium Processing [Anton Resing](#) and Joerg G. Werner; Boston University, United States

The miniaturization of electronics and development of the internet of things (IOT) demands dense and solid-state energy storage on the square millimeter scale, as well as the ability to supply energy over a spectrum of response times. These goals require reimagined processing methods that move beyond planar architectures to create free-standing and active material dense architectures which can serve as the backbone for energy and power dense solid-state batteries (SSBs). Here we introduce a material-agnostic hybrid inorganic phase inversion (HIPI) process as an advanced scalable manufacturing method that results in free-standing solid-state low-tortuosity architectures with anisotropic through-plane material orientation. Critical to their deployment as an active framework in SSBs is the accessible porosity present in the HIPI architectures, resulting from the use of an oligo(ethylene oxide)-based organogel support. The HIPI process can enable both interdigitated electrodes and low-tortuosity solid electrolytes whose relevant feature sizes between 1-20 μm can be tailored by tuning the gelation temperature and nucleation density of the inorganic suspension during the nonequilibrium HIPI process. By tailoring these architectures, the pitch and areal enhancement factor can be adjusted within a multiparameter space to meet both shape constraints and performance demands of specific energy storage applications.

11:00 AM EN05.07.08

Ultimate Design Principles and Fabrication Process for High Energy Density Solid State Pouch Cells Based on Solid Polymer Electrolytes [Jinsoo Kim](#); Korea Institute of Energy Research, Korea (the Republic of)

Solid-state lithium batteries have become promising alternatives to the conventional lithium-ion chemistries for pursuing enhanced safety and higher energy density. Owing to the advancement in the solid electrolytes and the active materials, its energy-storing characteristics are getting evolved in the lab-scale environment, but it is still far from the practical cell engineering perspectives. Here, we are proposing an ultimate design principle for building practically energy-dense solid-state batteries from the microstructure of electrodes to the entire cell architecture. The impact of multiscale parameters on the cell energy density was mathematically evaluated such as 1) gravimetric/volumetric composition, 2) apparent density, 3) areal loading amount in the electrode level, 4) the types of anode materials, 5) the thickness of solid electrolyte membrane, 6) the electrode sheet stacking number, and 7) the cell size. Not only just designing the electrochemical cells, but the fabrication process developments are also quite important to demonstrate the design methodology. To validate our design logic, we also suggest adequate processing methods and made double-layer stacked 200 mAh scale solid-state pouch cells based on the solid polymer electrolyte with PVDF-HFP conjugated to lithium salts and plasticizer as a model system. Thanks to the NCM622-based high active material composition (94 wt%), the areal capacity ($> 4 \text{ mAh cm}^{-1}$) using WIP (warm isostatic press) densification with the freestanding thin lithium metal anode (40 μm), we could verify the energy density as high as 227 Wh kg^{-1} including the whole-cell package, which was certified by the third-party organization. This design principle and the developed process can be applied to the various kind of solid-state batteries, so it might guide the research community to rationally achieve the practical high energy density milestone.

11:15 AM EN05.07.09

On the Use of Photoelasticity for Operando Dendrite-Induced Stress Quantification in Ceramic Electrolytes [Christos E. Athanasiou](#)¹, Cole D. Fincher², Colin Gilgenbach², W. C. Carter², Huajian Gao³, Yet-Ming Chiang² and Brian W. Sheldon⁴; ¹Georgia Institute of Technology, United States; ²Massachusetts Institute of Technology, United States; ³Nanyang Technological University, Singapore; ⁴Brown University, United States

The measurement of stress fields around lithium metal protrusions in solid electrolytes in operating conditions is critical for the design of next-generation, dendrite-resistant solid electrolytes. However, such stress measurements entail inherent experimental difficulties associated with acquiring accurate data at small scales in thin ceramic electrolytes.

By employing the principle of photoelasticity combined with electrochemical cycling in a plan-view cell the aforementioned challenges are bypassed, allowing not only to follow the progression of the dendrite, but also to obtain full field stress information on a propagating dendrite in semi-transparent LLZTO electrolyte. This new experimental methodology will be presented together with a relevant fracture mechanics analysis demonstrating the importance of engineering stress in dendritic propagation at high current densities.

SESSION EN05.08: Solid-State Battery Fabrication—From Materials to Novel Cell Architectures II

Session Chairs: Dominika Buchberger and Yue Qi

Wednesday Afternoon, November 30, 2022

Hynes, Level 3, Room 304

1:30 PM EN05.08.01

Stabilizing the Solid Electrolyte in Inert Atmosphere for Solid-State Battery Fabrication Through Co-Sintering Process [Hari Raj](#)¹, Timothée Fabre², Marlu C. Steil³, Renaud Bouchet² and Valerie Pralong¹; ¹CRISMAT Laboratory, ENSICAEN, Unicaen, CNRS, France; ²Universite Grenoble Alpes, University Savoie Mt Blanc, CNRS, Grenoble INP, LEPMI, France; ³Universite Grenoble Alpes, CNRS, Grenoble INP, SIMAP, France

Climate change due to excessive emission of greenhouse gases has impacted society and ecological life. Therefore, it is an urgent requirement to find alternative renewable (solar and wind) energy sources to replace conventional fossil fuels. Here, low cost, safe and high energy storage devices are required to ensure a continuous energy supply. However, current Li-ion batteries are facing challenges to fulfil the safety and high energy demands of fast-growing market of electric vehicles (EVs) and hybrid electronic vehicles (HEVs). In particular, liquid organic electrolytes used in conventional LIBs have raised the safety issues due to serious fire risk because of its flammability and volatility [1-3].

Therefore, extensive research is being focused to replace liquid electrolyte with suitable solid electrolyte for next-generation (SSBs) [4]. The inorganic

solid electrolytes are well-known for their realistic industrial manufacturing due to higher stability against ambient air and high temperature [5]. The NASICON type $\text{Li}_{1-x}\text{Al}_x\text{Ti}_{2-x}(\text{PO}_4)_3$ (LATP) has shown very promising properties in terms of chemical/thermal stability and low cost. The ionic conductivity of LATP has been reported up to 10^{-4} to 10^{-3} S cm^{-1} at room temperature [6]. If fabrication of SSB is considered by co-sintering process of LATP solid electrolyte and phosphate based cathode materials such as LiFePO_4 , $\text{Li}_3\text{V}_2(\text{PO}_4)_3$, sintering can only be possible in inert atmosphere (Ar/N_2) because these cathode materials are not stable in air at high temperature.

Therefore, by considering more practical approach for SSB fabrication through co-sintering process, present work focuses on sintering behavior of $\text{Li}_{1.4}\text{Al}_{0.4}\text{Ti}_{1.6}(\text{PO}_4)_3$ (LATP) solid electrolyte in argon atmosphere as a function of particle size and sintering conditions. The structural analysis of LATP was done by XRD, morphological study by SEM, particle size analysis by granulometry and densification of pellets was determined by dilatometry techniques. The conductivity measurement of sintered pellets is carried out by AC impedance spectroscopy techniques. At the end of study, we have not only stabilized the LATP in argon atmosphere but also achieved the high conductivity of 8.77×10^{-4} S cm^{-1} at 25 °C for pellets sintered at just 800 °C in argon. The electrochemical study of LATP was also conducted in symmetric cell and with $\text{Li}_3\text{V}_2(\text{PO}_4)_3$ cathode.

1:45 PM EN05.08.02

Investigation Of Nitrogen Doping Of Amorphous Lithium Aluminate As Thin-Film Solid Electrolyte Riccardo Taormina^{1,2} and Fabio Di Fonzo¹; ¹Italian Institute of Technology, Italy; ²Politecnico di Milano, Italy

Solid electrolytes, or fast ion conductors, are characterized by a high ionic conductivity, sometimes comparable to the one of liquid electrolytes. The isotropic and non-periodic structure of amorphous ceramics have shown to contribute to increase the overall ionic conductivity of the material by decreasing the grain-boundary resistive contribution. The formation of high-density phases is responsible for the fast ionic conductivity in polycrystalline electrolytes, but this implies the use of high temperature processing (sintering), limiting the employment of amorphous materials. Current thin-film electrolytes technologies relies mostly on lithium phosphate oxynitride LiPON ($\sigma_{\text{Li}} = 10^{-6}$ S/cm.), which demonstrated that the absence of grain boundaries, allows the formation of lithium small dendrites which can grow inside the material without cracking it, avoiding short life cycle of the battery over high current densities. Gao et al. addressed the limited ionic conductivity of LiPON to the strong bond between the PO₄ group with Li⁺: for this reason, elements with weaker electronegativity than P, such as Al, can generate an ionic bond with O with weaker electrostatic force, regulating the kinetics of Li⁺ transport and speeds up the diffusion process. Lithium Aluminate (LiAlO₂) and Nitrogen-doped Lithium Aluminate (LiAlON) result in a competitive position for the development of an innovative amorphous electrolyte: very few studies have been conducted on the development of lithium aluminate based solid electrolytes at the present time, mainly due to its low processability at the amorphous phase and the low ionic conductivity of the crystalline phase, more common in the traditional sintering processes.

In this preliminary work, it is presented for the first time the possibility to obtain with Pulsed Laser Deposition (PLD), a completely amorphous LiAlO₂ solid electrolyte with a room temperature ionic conductivity of 10-10 S/cm. Thanks to the PLD processing, the grade of polymorphism can be easily controlled as well as film thickness range (10nm up to 10um) and film porosity. By controlling the atmosphere of the process, different content of nitrogen doping has been achieved, promoting the formation of the highly ionic conductive and electronically insulating LiAlON. Electrochemical analysis such as DC polarization and Impedance Spectroscopy, revealed the wide electrochemical voltage stability against lithium metal and the high ionic conductivity of the solid electrolyte. A setup for the direct deposition of the thin film over lithium metal surface is proposed, allowing the realization of symmetric cell test and plating/stripping test. Good protection of Lithium metal substrate has been observed from the LiAlO₂ SSE over 24h in atmosphere, hindering oxidation and degradation of the sample.

1- Nowak, Berkemeier, and Schmitz, "Ultra-Thin LiPON Films – Fundamental Properties and Application in Solid State Thin Film Model Batteries."

2- Gao et al., "Screening Possible Solid Electrolytes by Calculating the Conduction Pathways Using Bond Valence Method."

3- Guan et al., "Superior Ionic Conduction in LiAlO₂ Thin-Film Enabled by Triply Coordinated Nitrogen."

2:00 PM EN05.08.03

Doped NaSICON-Type Solid Electrolytes for Sodium-Ion Batteries from Scalable Spray-Flame Synthesis Mohammed-Ali Sheik¹, Leon Müller¹ and Hartmut Wiggers^{1,2}; ¹University of Duisburg-Essen, Germany; ²Center for Nanointegration Duisburg-Essen (CENIDE), Germany

Solid-state sodium ion batteries are a viable alternative to lithium ion batteries, especially for use in stationary devices, due to the high availability of raw materials and low costs [1] and Sodium Super Ion Conductors (NaSICON) are promising candidates for solid electrolytes in solid-state sodium-ion batteries. They exhibit good mechanical properties, high ionic conductivity and compatibility with sodium metal based anodes enabling high energy density [2]. One of the best studied NaSICON materials is $\text{Na}_3\text{Zr}_2\text{Si}_2\text{PO}_{12}$ (NZSP) with a high ionic conductivity in the order of 10^{-3} S cm^{-1} at room temperature [3, 4]. Conventional synthesis methods of this class of materials such as solid-state reaction and liquid-phase synthesis have several drawbacks due to time-consuming process steps such as milling, high temperature sintering, precipitation, washing and drying steps to obtain the final product [5]. We present spray flame synthesis (SFS) as a new approach for the synthesis of nanosized NaSICON materials. Recent studies have shown that sintering of nanoparticulate NZSP precursors offers several advantages: A high specific surface area, which increases the sintering activity, and short atomic diffusion paths, allowing high homogeneity and phase purity to be achieved at comparatively low sintering temperatures [6]. In SFS, metal salts dissolved in organic solvents are combusted resulting in fine metal oxide particles. They are characterized by transmission electron microscopy (TEM), X-Ray diffraction (XRD) and Raman-Spectroscopy for structural and morphological investigation. Elemental information is obtained via energy-dispersive X-Ray spectroscopy (EDX) and X-Ray photoelectron spectroscopy (XPS). Ionic conductivities of sintered NZSP pellets are measured by impedance spectroscopy.

In our approach, nanoparticles with a median diameter of around 5 nm are obtained. The pristine particles consist of crystalline ZrO₂, homogeneously covered with an amorphous layer consisting of the elements Na, Si, P and O. After a short annealing step for 1h at 1000°C, this mixture can be converted almost quantitatively into the desired rhombohedral NZSP phase. Moreover, aliovalent dopants were successfully added for the synthesis of $\text{Na}_{3+2x}\text{A}_x\text{Zr}_{2-x}\text{Si}_2\text{PO}_{12}$ with A = Mg or Ca. Pressed pellets sintered at 1100°C for 3h to a relative density of ~90% showed - for a material sintered for such a short period of time - a surprisingly high ionic conductivity of up to 10^{-4} S cm^{-1} (Mg-doped).

In conclusion, a novel approach for the preparation of NZSP allowing the phase formation at relatively low temperatures is demonstrated. Spray flame synthesis is an elegant and promising possibility for the scalable production of solid electrolytes, which also holds great potential, especially with regard to further improvement of ionic conductivity through targeted doping.

[1] Y. Wang et al., *Nano Materials Science*, vol. 1, p. 91 (2019)

[2] H. Fu et al., *ACS Mater. Lett.*, vol. 2, p. 127 (2019)

[3] Goodenough et al., *Mater. Res. Bull.*, vol. 11, p. 203 (1976)

[4] S. Narayanan et al., *Solid State Ion.*, vol. 331, p. 22 (2019)

[5] Z. Yang et al., *ChemElectroChem*, vol. 8, p. 1035 (2021)

[6] A. Jalalian-Khakshour et al. *J. Mater. Sci.*, vol. 55, p. 2291 (2019)

2:15 PM EN05.08.04

Cathode Optimization for All-Solid-State Lithium Sulfur Batteries [Yi Lin](#)¹, Rodolfo I. Ledesma², Vesselin I. Yamakov², Ji Su¹, Donald A. Dornbusch³, James Wu³ and Rocco Viggiano³; ¹NASA Langley Research Center, United States; ²National Institute of Aerospace, United States; ³NASA Glenn Research Center, United States

Future electric aircrafts will require energy storage systems with high specific energy (ideally > 500 Wh/kg) but non-flammable, for which all-solid-state lithium-sulfur (Li-S) batteries are a top choice. However, one of the major bottlenecks in attaining the full potential of all-solid-state Li-S batteries is achieving high S utilization while maximizing energy density by using higher S content and higher cathode mass loadings. Since S is electrically non-conductive, the increased loading of S would reduce both ion and electron transport throughout the composite cathode, and thus detrimental to S utilization. Therefore, the composition and the interfaces within the cathode need to be optimized to achieve a balance between increased S content and maximal utilization. In this presentation, we discuss our strategy in preparing cathode composites with various compositions while fine tuning the interfaces of active material S with the solid electrolyte and the carbon additive. By evaluating the cathode performance differences, key parameters and processes in optimizing S utilization for balanced energy density performance may be identified.

2:30 PM BREAK

SESSION EN05.09: Electro-Chemo-Mechanical Coupling in Solid-State Batteries

Session Chairs: Alex Bates and Dominika Buchberger

Wednesday Afternoon, November 30, 2022

Hynes, Level 3, Room 304

3:30 PM EN05.09.01

Mechanistic Analysis of Void Formation in Solid-State Batteries [Bairav Sabarish Vishnugopi](#) and Partha P. Mukherjee; Purdue University, United States

Despite the theoretical promise of solid-state batteries (SSBs) to deliver high energy and power densities, various challenges related to electro-chemo-mechanics, transport and morphological growth at different solid-solid interfaces still need to be addressed. Among the various challenges, the formation and growth of voids in the lithium metal anode during stripping has a critical implication on performance and failure onset. In this presentation, we examine the competing nature of interfacial mechanisms including electro-dissolution, lithium mechanics, vacancy diffusion and ion transport interaction, and the underlying role of heterogeneities on void formation and the evolution of solid-solid point contacts. The mechanistic effect of interfacial roughness, external pressure and temperature on the interface stability, contact area evolution and electrochemical performance will be studied.

3:45 PM EN05.09.02

Evolution of Diffusion-Induced Stress in Lithium Metal Anodes [Kurt Hebert](#); Iowa State University, United States

Stresses in lithium metal anodes determine their stability during inevitable volume changes experienced upon cycling. Lithium deformation in response to stress changes during cycling can initiate surface morphological instabilities which lead to capacity loss, e. g. dendrites, moss, dead lithium etc. Such instabilities are particularly important for solid state batteries where anode-electrolyte interfacial integrity must be maintained. There exist to date limited experimental studies of stress evolution in Li metal anodes, and the mechanistic origins of stress generation are controversial. I will present a model for stress evolution in Li metal anodes during plating and stripping cycles, and detailed comparison of the predictions to an experimental study by J. H. Cho et al. where stress was inferred from measurements of curvature changes during lithium plating and stripping on silicon wafers (Energy Storage Mater. 24 (2020) 281). The model assumes that stress changes originate from grain boundary diffusion of Li atoms into the anode during plating and out of the anode during stripping. Diffusion-induced strain is coupled to viscoplastic deformation of lithium, calculated using an elastic-viscoplastic model due to Narayan and Anand (Extreme Mech. Lett., 24 (2018) 21) The model predictions demonstrate detailed quantitative agreement with experimental transients of wafer-curvature during both plating-open circuit and plating-stripping cycles in a liquid cell. Similar diffusion-induced plastic deformation of lithium anodes may occur in solid-state batteries, where it could contribute significantly to interfacial instabilities.

4:00 PM EN05.09.03

A Thermodynamically Consistent, Phase-Field Electro-Chemo-Mechanical Theory with Account for Damage in Solids—Application to Metal Filament Growth in Solid-State Batteries [Donald Bistri](#) and Claudio V. Di Leo; Georgia Institute of Technology, United States

Solid-state batteries (SSBs) present a promising technology and have attracted significant research attention owing to their superior properties including increased energy density (3860 mAh), wider electrochemical window (0-5V) and safer electrolyte design. From a safety standpoint, SSBs are particularly appealing in that replacement of flammable conventional organic electrolytes with highly conductive, mechanically stiff inorganic solid-state electrolytes (SSEs) can alleviate failure due to short circuit or ignition. However, operation of SSBs is hampered by numerous chemo-mechanical challenges, the most critical one associated with metal filament growth across the SSE.

Filament protrusions can initiate at perturbations of the interface or microstructural heterogeneities and subsequently grow through the SSE, causing the battery to short-circuit. It is critical to understand from both an experimental and modeling perspective the interplay of various mechanisms including morphology of the SSE microstructure, elastic-viscoplastic behavior of Li-metal, critical current density and stack pressure on the morphology of filamentary protrusions across the SSE. While much has been done to understand the interplay of aforementioned mechanisms from an experimental standpoint, theoretical frameworks on modeling of filaments growth in SSBs are still at their infancy and typically simplify dendrites as pressurized cracks under a linear-elastic fracture mechanics (LEFM) approach.

In this work, we propose a thermodynamically consistent phase-field reaction-diffusion-damage theory to investigate the morphology of filament growth across the SSE under varying chemo-mechanical operational conditions. The theory is fully coupled with electrodeposition at the Li metal-SSE interface impacting mechanical deformation, stress generation and subsequent fracture of the SSE. Conversely, electrodeposition kinetics are affected by mechanical stresses through a thermodynamically consistent, physically motivated driving force that distinguishes the role of various chemical, electrical and mechanical contributions. Concurrently, the theory captures the interplay between crack propagation and electrodeposition phenomena by tracking the damage and reaction field using separate phase-field variables such that metal growth is preceded by and confined to damaged regions within the SSE

accessible by Li-metal. This is a critical feature of the theory and confirms experimental observations that the crack front propagates ahead of Li. We specialize the theory and study the role of variations of chemo-mechanical properties (i.e. applied electric potential, SSE fracture energy) on the morphology of metal filament growth and map operational conditions to distinguish between domains of i) stable vs. unstable growth ii) intergranular vs. transgranular growth mode. In doing so, the proposed framework provides a quantitative understanding on mechanisms dictating metal filament growth in SSEs and identifies mitigation strategies to employ in future SSB designs for successful operation.

4:15 PM EN05.09.04

Electro-Chemo-Mechanical Phenomena Governing Dendrite Formation in Solid-State Batteries [Sundeep Vema](#), Dipayan Mukherjee, Joe Stallard, Supreeth Nagendran, Vikram Deshpande, Norman A. Fleck and Clare Grey; University of Cambridge, United Kingdom

Solid electrolyte-based Li-ion batteries can enable energy storage devices with high energy and power densities due to their compatibility with high voltage cathodes (>5 V vs Li/Li⁺) and Li metal anode. Among numerous solid electrolytes, doped Lithium Lanthanum Zirconium Oxide (LLZO) has a high room temperature ionic conductivity ($\sim 10^{-3}$ mS cm⁻¹) and electrochemical stability. LLZO when cycled with Li metal in a symmetrical cell configuration (Li-LLZO-Li), continuous stripping and plating results in the formation of Li metal filaments (dendrites) which nucleate on the cathode, propagate through the solid electrolyte, and short-circuit the cell. The exact phenomena governing the dendrite formation are unclear.

In this work, we have optimized the synthesis and sintering conditions of doped LLZO (both Al and Ga doped) and achieved low interfacial resistance between Li metal and solid electrolyte (<20 Ω cm²). By cycling under constant pressure and temperature, and careful unidirectional plating, we have estimated the true critical current density (CCD) at which a dendrite nucleates and short-circuits the cell. We have also developed an electro-chemo-mechanical model for the nucleation and propagation of dendrites and have corroborated the model with experiments. We show that the process of Lithium ion (Li⁺) transfer from solid electrolyte to Li metal (Li⁰) in a prefilled crack can break open a hard ceramic solid electrolyte and thus create a pathway for Li⁰ to plate inside the crack. We also hypothesize the conditions that dictate whether a dendrite grows in a filled mode, i.e., when a dendrite and crack grow together or in a dry mode, i.e., where the crack grows much faster than the dendrite.

SESSION EN05.11: Solid Electrolytes Design for Next Generation Solid-State Batteries II

Session Chairs: Alex Bates, Megan Diaz, Kelsey Hatzell and Hongli Zhu

Thursday Morning, December 1, 2022

Hynes, Level 3, Room 304

8:30 AM *EN05.11.01

Design of Novel Solid Electrolytes and Fabrication of High-Performance Solid Batteries [Hailong Chen](#); Georgia Institute of Technology, United States

In recent years, a good number of fast ionic conductors have been studied as solid electrolytes for Li-ion or Na-ion batteries. Here we will present our understanding on the advantages and disadvantages of different types for solid electrolytes, including their electrochemical properties, synthesizability, and compatibility in solid cells. Specifically, we will share our recent progresses on rational design of novel sulfide and halide solid electrolytes based on in-depth characterization and understanding of their crystal structure and structure-property relationship. Sulfides commonly offer high room temperature conductivity and good anode compatibility, but their syntheses are tricky and relatively expensive. Halides commonly show lower room temperature conductivity than sulfides, but they are easy to synthesize and stable against air. We will report the crystal structure characterization of sulfide and halide solid electrolytes with using ex situ and in situ high resolution synchrotron X-ray and neutron diffraction and pair distribution function analysis, coupled with variable temperature electrochemical impedance spectroscopy. The design of long-lasting, high-performance solid cell with using the novel electrolytes will also be discussed, including materials selection, cell fabrication and electrochemical testing conditions and protocols.

9:00 AM EN05.11.02

High-Performance and Cost-Effective All-Solid-State Conversion-Type Iron Fluoride Cathode [Bowen Shao](#)¹, Sha Tan², Yonglin Huang¹, Lifu Zhang¹, Jian Shi¹, Xiaoqing Yang², Enyuan Hu² and Fudong Han¹; ¹Rensselaer Polytechnic Institute, United States; ²Brookhaven National Laboratory, United States

The large-scale deployment of lithium-ion batteries requires next-generation cathodes to not contain toxic and expensive elements such as Ni and Co, as well as to provide a higher energy density than existing cathodes. Conversion-type iron fluorides can fulfill these requirements and are being actively pursued by many research groups. Despite being discovered about two decades ago, the commercialization of cost-effective and energy-dense iron fluoride cathodes was obstructed by its low first-cycle redox reversibility, poor cycling stability, and large voltage hysteresis. Here, we demonstrated that these challenges are promising to be overcome by applying halide-based solid electrolytes (SEs). Through detailed ex-situ X-ray diffraction and X-ray absorption spectroscopy investigation, our results showed that halide-based SEs realize the complete intrinsic conversion and reconversion of FeF₂ because of their extinguished electrochemical stability, which cannot be achieved by sulfide SEs. The halide-SE-based all-solid-state FeF₂ cathode demonstrated extraordinary electrochemical performance compared with FeF₂ electrodes in liquid electrolytes, including a high specific capacity (~ 600 mAh/g), a long cycle life (over 100 cycles), a high first-cycle coulombic efficiency ($\sim 100\%$), and high-rate performance. The superior performance can be attributed to the reduced and reversible electrolyte decomposition, avoidance of cation dissolution, and mechanical lockage of electrode particles. Our study also revealed amorphization of FeF₂ cathode with halide SE enhanced the electrode kinetics. Our results demonstrate solidifying the batteries can be used as an effective approach to address the key challenges of iron fluoride cathodes for their practical application.

9:15 AM EN05.11.03

High-Performance All-Solid-State Li-S Batteries Through Advanced Carbon Fiber Decorated with 2D Transition Metal Sulfide [Xiao Sun](#), Daxian Cao and Hongli Zhu; Northeastern University, United States

All-solid-state Lithium-sulfur batteries (ASSLSBs) are considered to concurrently deliver high energy density and safety. Considering the poor electronic conductivity of sulfur, porous carbon has been widely used as the host sulfur and serve as conductive additive to boost the sulfur mass loading and rate performance. However, the conventional porous carbon used in liquid cells exhibits low efficiency in ASSLSBs because it is challenging for the immobile solid electrolytes (SEs) to reach the sulfur confined in the pores distributed in the depth of carbon. The pore structure and distribution highly impact the electrochemical performance of ASSLSBs. Herein, for the first time, we designed a novel carbon fiber with a core-shell structure that processes a layer of micropores located only at the surface via activation by solid potassium hydroxide (KOH). The carbon fibers were fabricated through scalable

electrospinning of polyacrylonitrile followed by carbonization and activation. The obtained polyacrylonitrile-derived porous carbon fibers (named PPCF) possessing an ultrahigh specific surface area of 1519 m²/g provide sufficient sites to host sulfur. Since the porous carbon layer is at the surface, the sulfur within the surface pores has excellent contact with SE; Meanwhile, the dense core provided excellent electron conduction. Therefore, this structurally designed carbon fiber boosted the utilization of sulfur due to enhanced electron and ion accessibilities, accelerated charge transfer, and dramatically promoted the reaction kinetic in the ASSLSBs.

However, the employment of carbon additives can improve the electrical conductivity but accelerate the decomposition of SSEs. Herein, we designed a highly conductive carbon fiber decorated with hybrid 1T/2H MoS₂ nanosheets and applied it in ASSLSBs. The chemical and electrochemical compatibility among MoS₂, sulfur and sulfide SSE can greatly improve the stability of the cathode and therefore maintain pristine interfaces between the different compositions for stable ion and electron transport. The presence of electrical-conductive metallic 1T MoS₂ and its uniform distribution on carbon fiber without aggregation benefit the electron transfer between carbon and sulfur. As a result, our ASSLSB delivered an ultrahigh initial discharge and charge capacity of 1456 mAh g⁻¹ and 1470 mAh g⁻¹ at 0.05 C individually with ultrahigh initial coulombic efficiency and maintained high capacity retention of 78 % after 220 cycles. The extremely high initial coulombic efficiency is attributed to the elimination of shuttle effects through SSE and stable interface. The batteries also obtained a remarkable rate performance of 1069 mAh g⁻¹ at 1 C. This study pioneered the new idea that fabricating the high performance ASSLSBs through developing surface functionalized and stabilized conductive carbon additives in metal sulfides based ASSLSBs.

9:30 AM DISCUSSION TIME

9:45 AM EN05.11.05

All-Solid-State Garnet Type Lithium-Sulfur Battery Enabled by Inorganic Interfacial Engineering and 3D Electrolyte Architectures [Changmin Shi](#), Griffin Godbey and Eric D. Wachsman; University of Maryland, College Park, United States

Current progress in Lithium-Sulfur (Li-S) batteries using garnet electrolytes have involved use of flammable liquid or polymer catholytes to achieve stable cycling due to poor ionic conduction properties of sulfur and the poor interface between sulfur cathodes and LLZO. However, this compromises the safety of “solid-state” batteries. In this work, we propose a novel design which coats our sulfur cathode (Li-S redox material: sulfurized polyacrylonitrile, SPAN) with lithium bis(fluorosulfonyl)imide (LiFSI) to improve SPAN/SPAN and cathode/LLZO interfaces and to provide ionic conductivity in the composite cathode. The LiFSI salt has an ionic conductivity of 1.2×10⁻⁴ S/cm at 60 Celsius degree and 1.9×10⁻⁵ S/cm at 22 Celsius degree, and it is stable in the charge/discharge electrochemical window of SPAN. LiFSI creates Li⁺ ionic conductive pathways which enhance Li⁺ ion transport kinetics through the cathode and its interface with LLZO. With our thin bilayer LLZO architecture^{1,2} we are the first to demonstrate an all-solid-state garnet Li-S batteries that achieved an average discharge capacity of 1400 mAh/g at 0.167 mA/cm² for over 40 cycles and 437 mAh/g at a discharge current density of 0.84 mA/cm² for over 200 cycles both at 60 Celsius degree, using a sulfur mass loading of 1 mg/cm². With a new 3D column architecture, we extended sulfur loading to 7mg/cm² and achieved an exceptionally high discharge capacity of 1569 mAh/g at 0.03C (~0.35 mA/cm²) at 60 Celsius degree using our all-solid-state garnet Li-S battery design, which corresponding to an energy density of 338 Wh/kg and 797 Wh/L.

References:

1. B. Liu, L. Zhang, S. Xu, D. W. McOwen, Y. Gong, C. Yang, G. R. Pastel, H. Xie, K. Fu, J. Dai, C. Chen, E. D. Wachsman, L. Hu, *Energy Storage Mater.* 14, 376–382 (2018).
2. K. Fu, Y. Gong, G. T. Hitz, D. W. McOwen, Y. Li, S. Xu, Y. Wen, L. Zhang, C. Wang, G. Pastel, J. Dai, B. Liu, H. Xie, Y. Yao, E. D. Wachsman, L. Hu, *Energy Environ. Sci.* 10, 1568–1575 (2017).

10:00 AM BREAK

10:30 AM *EN05.11.06

Semi-Solid-State Batteries and Their Path to Commercialization [Joanna Burdynska](#); Factorial Energy, United States

As vehicle electrification advances, the need for high-energy, high-power energy storage solutions increases. The lithium-ion battery (LIB) has emerged as the technology of choice to meet these challenges. Nonetheless, with the ever-increasing battery capacity of cars to increase range, future systems will need to have significantly higher energy densities. At the same time, consumers are pushing for faster charging times [1].

Future lithium-ion batteries may not be able to meet these requirements, especially since their energy density is limited by the given electrode configuration, in particular by the graphite anode. On top of this, safety concerns arise for such high energy systems, as the liquid, organic electrolyte is potentially flammable. To counter such concerns, next generation batteries are intended to employ solid or semi-solid electrolytes (SEs). Those novel electrolytes possess higher thermal stability, thus increase safety, and reduce leakage in the event of fire or crash.

At the same time, those novel electrolytes are intended to allow substitution of the conventional graphite anode with a lithium metal anode. Elemental lithium being light-weight and possessing the most negative electrode potential is the ideal anode material choice and considered the holy grail of batteries. The use of lithium metal would significantly increase the cell energy density and allow electric vehicles to further increase their driving range, while simultaneously allow for faster charging times.

As the prerequisite technologies for the practical solid-state batteries (SSBs) are reported and developed at quicker pace, its commercialization looks very promising. However, there are still problems to be solved.

Highly conductive SEs, high voltage compatible cathodes and high-capacity anodes are good examples of these, however, they still must be verified by applying them to practically large format cells. At the same time, all these components of ASSBs should satisfy requirements of not only the high performance of each material, but also the compatibility between materials, mass production processability, and overall cost.

Along with the cell design-related technology, multi-stacking and cell size upscaling is also crucial. Developed materials and cell technologies must be suitable for mass production not only in terms of materials, but also cells. In general, SSBs using inorganic SEs are more difficult for mass production rather than SSBs using polymer-based and/or semi-solid electrolytes.

Factorial Energy is a leader in the field of semi-solid electrolytes. Prototype cells employing the proprietary Factorial Electrolyte System Technology (FEST™) have demonstrated over 550 cycles when using a state-of-the-art nickel-rich cathode material and a lithium metal anode. Importantly, due to the semi-solid nature of the electrolyte, the cells have shown to perform well at ambient conditions, unlike other solid-state batteries, which require elevated temperatures to operate. After demonstrating the of high performance of semi-solid-state electrolytes Factorial Energy entered into development programs with three major OEMs, Mercedes Benz, Stellantis and Hyundai Motor Corporation. We believe that deep collaboration between battery companies and OEMs will help to accelerate the commercialization of next generation batteries.

The successful commercialization of SSBs strongly relies on the development of the key technologies of its constituents (SEs having high ionic conductivity with high cathodic/anodic stabilities, cathodes having high specific capacity and stable to high oxidation potential, protected thin lithium metals). Also, it should come with the advanced processing including the techniques for upscaling, and cell optimization (i.e. chemical/electrochemical reactivity minimization and interfacial bonding control at the interfaces).

References

- [1] J. Janek, Wolfgang G. Zeier, *Nature Energy*. 1, 16141 (2016)

11:00 AM EN05.11.07

High-Energy and Long-Lasting Lithium Metal Batteries Lithium Employing Garnet Solid Electrolytes and Interlayers Jusik Kim¹, Gabin Yoon¹, Sewon Kim¹, Michael Badding², Zhen Song², Jaemyung Chang² and Dongmin Im¹; ¹Samsung Advanced Institute of Technology, Korea (the Republic of); ²Corning Incorporated, United States

Lithium metal batteries (LMBs) are considered the most promising next-generation battery system because of their high energy density and safety. Significant research effort has been devoted to developing more stable and energy-dense LMBs than the state-of-the-art Li-ion batteries. However, the LMB performance remains unsatisfactory for commercialization, primarily owing to the inability of solid electrolytes to block Li dendrite propagation. Herein, we report that the compatibility between LLZO and lithium metal is crucial for the long-term stability, which can be accomplished by regulating bulk dopants and the corresponding dopant-specific interfacial treatment using protonation/etching. It is demonstrated that LMB using tailored garnet-type $\text{Li}_{7-x}\text{La}_3-z\text{Zr}_{2-4}\text{O}_{12}$ (LLZO) solid electrolytes shows remarkable stability and energy density, meeting the lifespan requirements of commercial applications (cumulative capacity : > 4000 mAh cm⁻² at 3mA cm⁻²).

We further demonstrate highly stable LMB even at room-temperature (25°C) employing garnet-type oxide electrolyte by introducing a carbon-based interlayer with careful interface engineering. It is theoretically and experimentally demonstrated that our design effectively regulated Li deposition away from the solid electrolyte, preventing dendrite penetration. Overall, our garnet-type oxide-based LMB exhibited a high energy density of ~680 Wh/L for over 800 cycles at 25°C without using external pressure, which could meet the cycling requirements and the operating conditions of smartphone batteries, which are represented by: (i) 400 cycles @88% cycle retention without Li metal shorting at the operating current density of 1.6 mA/cm² (0.5 C-rate charging/discharging) and (ii) room-temperature operation under the condition of no external pressure. Moreover, we successfully developed a tape-cast solid electrolyte with a large area (1 inch × 1 inch) and demonstrated excellent cycling performance at 25 °C in a 10-mAh-capacity cell beyond a coin-size cell (~1 mAh).

11:15 AM EN05.11.08

Guiding Principles for Fast Lithium-Ion Diffusion in Oxides KyuJung Jun¹, Yihan Xiao¹, Yan Eric Wang² and Gerbrand Ceder¹; ¹University of California, Berkeley, United States; ²Samsung Research America, United States

Inorganic lithium conductors are one of the most critical components for all-solid-state batteries. While superionic Li-ion conductivity can be found in many materials classes, oxides have the apparent advantage of better electrochemical stability and enhanced safety as compared to sulfide materials. However, achieving high lithium-ion conductivity in oxides has been significantly more challenging due to the lower screening power of the oxygen anions. In contrast to the wide variety of sulfides structures with fast Li-ion motion, oxide frameworks that result in high Li mobility are mostly limited to NASICON-type structures, garnets and perovskites. Moreover, the highest lithium ionic conductivity achieved in oxides is on the order of 1 mS/cm, which is at least one order of magnitude lower than that of the best sulfides.

In this talk, we will present our recent findings [1][2] that let us rationalize how we can achieve high ionic conductivity in oxides and explain why designing oxide lithium superionic conductors requires a conceptually different approach from that in sulfide materials. We find that corner-sharing frameworks of non-Li cations provides high distorted lithium environment as well as sparse cation distribution that allow lithium percolation with minimal electrostatic repulsion, thereby resulting in low activation energies for lithium-ion motion[1]. By embedding the lithium diffusion network into graph representations we demonstrate that an activated local environment is a key feature of compounds with low activation energies[2]. Using these findings, we discover 16 new oxide lithium-superionic conductors and show experimental verification of the high conductivity for one of these materials. Finally, we present an oxide material that is computationally predicted to exhibit ultrafast lithium-ion conductivity over 150 mS/cm at room temperature; the highest ionic conductivity predicted in any inorganic material so far. Our study vastly expands the structural prototypes of oxides with high lithium-ion conductivity and allows the consideration of a more diverse structural and chemical space for solid electrolytes to be used in all-solid-state batteries.

[1] K. Jun, Y. Sun, G. Ceder et al., Lithium superionic conductors with corner-sharing frameworks, *Nat. Mater.*, 2022.

[2] Y.Xiao, K.Jun, G. Ceder et al., Lithium oxide superionic conductors inspired by garnet and NASICON structures, *Adv. Energy Mater.* 2021.

SESSION EN05.12: Solid Electrolytes Design for Next Generation Solid-State Batteries III

Session Chairs: Dominika Buchberger and Reed Wittman

Thursday Afternoon, December 1, 2022

Hynes, Level 3, Room 304

1:30 PM *EN05.12.01

Lithium-Argyrodite Based Solid-State Battery Design and Fabrication Jagjit Nanda; SLAC National Accelerator Laboratory, United States

Lithium-metal based solid-state batteries (SSB) are considered the *holy-grail* of the next generation battery technology for their promise of higher energy density (500 Wh/Kg), safety and providing a flexible platform for integrating a number of solid-electrolytes (SE) and high capacity cathodes to achieve the end goal for users. The talk will highlight on various *state-of-the-art* solid-electrolytes and their key physical and electrochemical attributes for enabling stable electrode-electrolyte interfaces and integration with high capacity cathodes. The design rule for achieving high energy and fast charge SSB will be discussed with specific focus on sulfide based solid-electrolytes. Most of the sulfide-based SE compositions such as Li_3PS_4 and Argyrodite (LiPS_2X ; X= Cl, Br) are thermodynamically unstable against high voltage cathodes such as NMC. Multiple approaches to limit the undesired decomposition of SE at the cathode-SE interfaces and improve capacity retention using interfacial coating and optimizing the cathode composition and architecture. Finally, issue related to anode free configuration using argyrodite based SE will be discussed.

Acknowledgement

This research was conducted at Oak Ridge National Laboratory, managed by UT Battelle, LLC, for the U.S. Department of Energy (DOE) and is supported by Asst. Secretary, Energy Efficiency and Renewable Energy (EERE), Vehicle Technologies Office (VTO) through the Advanced Battery Materials Research (BMR) Program.

2:00 PM EN05.12.02

Interfacial Stability Study of Argyrodite and Nb₂O₅-coated Ni-Rich NMC Under Electrochemical Cycling by Transmission Electron Microscopy Paul Naillou, Adrien Boulineau, Julien Lavie, Eric De Vito and Philippe Azaïs; CEA Grenoble, France

Interfacial phenomena in all-solid-state lithium-ion batteries are extensively studied since they are considered as the main limiting factor for performances and lifetime [1]. Among all electrolytes, $\text{Li}_6\text{PS}_5\text{Cl}$ argyrodite receives great attention due to its high ionic conductivity and its convenience in technological integration [2]. On the other hand, high Ni content in NMC layered oxide cathode materials are known to offer best specific energy density and higher lithium utilization despite higher surface reactivity [3]. Hence, coating materials have been developed in order to inhibit surface degradation and lithium loss through stable SEI formation, such as Niobium-based coatings. However, all solid-state composite electrode based on argyrodite and cathode materials present complex chemical and structural changes that are not yet fully understood. Several approaches have been adopted to enhance comprehension of argyrodite reactivity such as X-ray photoelectron spectroscopy (XPS) [4], electrochemical impedance spectroscopy (EIS) [5], time-of-flight secondary ion mass spectrometry (TOF-SIMS) [6] and ultimately, Transmission Electron Microscopy (TEM) studies have excelled to provide comprehensive and spatially resolved chemical and structural data.

In this context the spontaneous and the electrochemical reactivity of argyrodite $\text{Li}_6\text{PS}_5\text{Cl}$ electrolyte material toward single-crystal Ni-rich NMC cathode material has been investigated. The impact of the Nb_2O_5 coating over the cathode material has also been deeply studied. Most of the characterizations have been led with the help of state of the art TEM-related technics, such as energy-dispersive X-ray spectroscopy (EDX), electron energy loss spectroscopy (EELS) and selected area electron diffraction (SAED). Great care has been taken to work in conditions in which the materials are not altered.

Preliminary study of Nb_2O_5 coating provides details on its crystallinity, thickness, coverage on cathode material, and stability toward lithium diffusion. Cathode material / coating interface has been notably observed on a thin specimen with high resolution imaging coupled with EDX and remarkable details on lithium diffusion through a few nanometers in the coating have been recorded on spectroscopic measurements. With and without this coating, NMC / argyrodite mixture does not show any spontaneous interface generation. However, under electrochemical solicitation, several species have been identified and characterized such as LiCl , P_2S_5 , P_2O_5 , Li_3PS_4 , NiS , and S^0 . The correlation with XPS allowed to point out unrevealed subtleties until now and to discuss degradation mechanisms. The segregation of LiCl toward Li_3PS_4 has been directly observed, validating the theoretical predictions of argyrodite degradation depending on stability window.

Moreover, a novel *operando* TEM characterization technique has been developed to study the interfacial modifications of argyrodite / NMC cells during electrochemical cycling within the TEM. This is the first time such original setup is proposed inside the electron microscopy community: it allows the direct *operando* characterization of the battery while keeping it always prevented from air exposure from the device preparation to the characterization inside the TEM.

The authors gratefully acknowledge the financial support of Umicore for this work and for material providing.

- [1] K. Nie et al., *Front. Chem.* 6 (2018) 616
- [2] N. Kamaya et al., *Nature Mater.* 10 (2011) 682–686
- [3] W. Liu et al., *Angew. Chem. Int. Ed.* 54 (2015) 4440 – 4457
- [4] J. Auvergniot et al., *Solid State Ionics* 300 (2017) 78–85
- [5] D.H.S Tan et al., *ACS Energy Lett.* 4 (2019) 2418–2427
- [6] F. Walther et al., *Chem. Mater.* 31 (2019) 3745–3755

2:15 PM EN05.12.03

A Polycationic Substituted Lithium Argyrodite Superionic Solid Electrolyte Lin Jing¹, Gennady Cherkashinin², Mareen Schäfer¹, Georgian Melinte¹, Sylvio Indris^{1,3}, Aleksandr Kondrakov^{1,4}, Jürgen Janek^{5,1}, Torsten Brezesinski¹ and Florian Strauss¹; ¹Karlsruhe Institute of Technology, Germany; ²Technical University Darmstadt, Germany; ³Helmholtz Institute Ulm (HIU), Germany; ⁴BASF SE, Germany; ⁵Justus-Liebig-University Giessen, Germany

Solid-state batteries are attracting great attention because of potentially higher energy and power densities than conventional Li-ion batteries based on liquid electrolytes. Yet, they are plagued by the development of advanced solid electrolytes, mainly lacking in ionic conductivity and electrochemical stability; thus, the ongoing quest for exploration of new materials and compositions. Despite increasing research interests in high-entropy materials, the effect that configurational entropy has on the charge transport properties remains largely elusive. Recently, we have shown that high-entropy argyrodites can be achieved via polyanionic/cationic substitution, showing a low activation energy ($E_A = 0.22$ eV) and moderate r.t. ionic conductivity (~ 1 mS/cm). However, the possibility of polycationic substitution and the resulting structure-property relationships have not been explored yet. Within this context, we herein report about the influence of polycationic substitution on the Li-ion conductivity in argyrodite superionic conductors. Using electrochemical impedance spectroscopy and ⁷Li pulsed field gradient nuclear magnetic resonance (NMR) spectroscopy, it is found that polycationic substitution leads to a very low activation energy ($E_A = 0.19$ eV) for Li-ion conduction and a high r.t. ionic conductivity of ~ 13 mS/cm. These findings are rationalized via neutron powder diffraction (at 298 K and 10 K) in combination with magic angle spinning NMR spectroscopy. A high S^{2-}/I^- anion site disorder (up to $\sim 10\%$) and redistribution of Li lead to shortened jump distances and therefore facilitated long-range ion diffusion. Finally, it was implemented as SE in bulk-type SSBs. Using XPS analysis we reveal the (electro)chemical degradation upon cycling related to specific elemental constituents. Overall, our results show the possibility of polycationic substitution in lithium argyrodites, thereby opening up large compositional space for the development of novel superionic conductors with improved properties.

2:30 PM EN05.12.04

Amorphous Sodium Chloride Solid Electrolytes with High Ionic Conductivity Phillip Ridley¹, Long Hoang Bao Nguyen¹, Grayson Deysher¹, Jin An Sam Oh¹, Jihyun Jang¹ and Y. Shirley Meng^{2,1}; ¹University of California, San Diego, United States; ²The University of Chicago, United States

Due to the lack of appropriate solid electrolytes possessing a wide electrochemical window that is compatible with both the anode and cathode, separate anolytes and catholytes have been proposed as an approach to realize high performing solid-state batteries. Chloride-based solid electrolytes have emerged as promising catholyte due to their great deformability, excellent electrochemical stability at higher voltages, and good ionic conductivities. While lithium-based chloride solid electrolytes have shown high ionic conductivities ($10^{-4} - 10^{-3}$ S cm^{-1}), the sodium analogues have been scarcely reported and their ionic conductivities significantly lag ($10^{-6} - 10^{-5}$ S cm^{-1}). Consequently, sodium solid-state batteries using chloride catholytes exhibit poor kinetics and lackluster cycling performance at room temperature. Herein, we explore the “Composition–Structure–Conduction property” relationship in the Na–Y–Zr–Cl solid electrolyte system. Experimental observations show that a reduction in crystallinity leads to a significant improvement in the room-temperature ionic conductivity to 10^{-4} S cm^{-1} , which is one of the highest reported in the literature. This high ionic conductivity ultimately translates to improved room-temperature reversible capacity in the battery performance.

2:45 PM EN05.12.05

Revealing Li Dynamics in Mixed Ionic-Electronic Conducting Interlayer of All-Solid-State Batteries Daxian Cao¹, Kenneth Burch², Michael Geiwitz², Kang Xu³, Tongtai Ji¹ and Hongli Zhu¹; ¹Northeastern University, United States; ²Boston College, United States; ³CCDC Army Research

Laboratory, United States

Lithium-metal (Li^0) anode is considered the holy grail of all-solid-state batteries owing to their exceedingly high energy density; in practice, their stability remains unsatisfactory because of the incompatibility between Li^0 and solid-state electrolytes (SEs). One strategy is to introduce an interlayer, which often consists of a mixed ionic-electronic conductor (MIEC), to stabilize the Li^0 . However, how Li ions (Li^+) transport within MIEC remains unknown. Herein, we investigate the Li, including Li^0 and Li^+ , dynamics in a graphite interlayer, a typical MIEC, using *operando* neutron imaging and Raman spectroscopy. Our study reveals the Li evolution during mechano-chemistry and mechano-electrochemistry reactions. During cell assembly, intercalation-extrusion-dominated mechano-chemical reactions transform the graphite into a Li-graphite interlayer consisting of SE, Li^0 , and diluted graphite-intercalation compounds. During battery operation, dictated by the lowest nucleation energy, Li^0 plating preferentially occurred at the Li-graphite|SE interface and then transferred into the Li-graphite interlayer without intercalation. Upon further plating, Li^0 -dendrites formed, inducing short circuits and reverse immigration of Li^0 from the anode to the cathode during charging. Continuum modeling was conducted to explain the Li dynamics. We concluded that with the MIEC interlayer, a lowest nucleation barrier at the Li^0 side is necessary to drive the Li^+ to transport across the MIEC and preferentially deposit onto the Li^0 .

3:00 PM BREAK

SESSION EN05.13: Fundamental Understanding via Characterization and Modeling III

Session Chairs: Alex Bates and Hongli Zhu

Thursday Afternoon, December 1, 2022

Hynes, Level 3, Room 304

3:30 PM +EN05.13.01

High Capacity Lithium Metal Stripping Dynamics in Solid State Batteries Kelsey B. Hatzell; Princeton University, United States

All solid-state batteries (ASSB) can potentially meet the energy density threshold ($900 \text{ Wh} \cdot \text{L}^{-1}$) for next-generation batteries by employing Lithium metal anode and solid electrolyte (SE). However, there is a lack in critical understanding of interfacial chemo-mechanics and ion transport in solid-state batteries which leads to poor cycling performance and dendrite-induced shorting. In this work, we investigate polycrystalline garnet $\text{Li}_7\text{La}_3\text{Zr}_2\text{O}_{12}$ (LLZO), a model solid electrolyte which is pseudo-non-reactive against Li metal. However, Li-LLZO interfaces at high current density initiate substantial void growth, which causes dendrite formation during plating. Stack pressure and temperature are effective means to initiate creep-induced void filling and decreasing charge transfer resistance to enable stable cycling. Applying stack pressure enables Li to deform and creep above yield stress during stripping at high current densities but is not sufficient to prevent cell shorting during plating. We employed a 3-electrode setup to understand the kinetic limitations and morphology changes in Li-LLZO interface during long-term stripping ($5 \text{ mAh} \cdot \text{cm}^{-2}$). The role of cathode-LLZO interfaces was also studied which dictates cyclability and capacity retention in full cells. This work elucidates the role of cathodic and anodic interfacial chemo-mechanics which will contribute to our further understanding electrochemical instability of solid-state batteries.

4:00 PM DISCUSSION TIME

4:15 PM EN05.13.03

Lithium Metal Morphology & Performance Informed by Micro-Computed Tomography Lara Dienemann¹, Ahmed Al-Obeidi², Adrien Stejer³, Iryna Zenyuk³ and Matthew Panzer¹; ¹Tufts University, United States; ²Ionic Materials, United States; ³University of California, Irvine, United States

Alone, *ex-situ* analysis and *postmortem* teardowns often convolute interpretations of lithium metal cell failure modes. In this study, micro-computed tomography renders lithium metal interfaces in various conditions and formats throughout cycling to assist in better understanding the morphology of cycled lithium and its relationship with cycling performance. *Operando* studies link cycling performance with morphology with greater resolution and provide insight into physical phenomena such as deformation of the separator imposed by the lithium metal volume changes. Rolled lithium foils, stack pressure, inorganic-organic hybrid coatings, electrolyte solvent types, and polymer separator morphology is investigated. With this methodology, hairy nanoparticle-based artificial SEIs are found to promote uniform and dense lithium cycling, and their chemo-mechanical interplay which supports this mechanism is studied. Finally, the findings inform best practices in fundamental lithium metal cell design.

4:30 PM EN05.13.04

Interdiffusion Induced Cathode-Electrolyte Interface Instability of Single-Crystalline LLTO Solid Electrolyte Hanseul Choi¹, Hee-Dong Kwak¹, Celesta S. Chang², Min-Ju Choi¹, Jae Young Kim¹, Sangwook Han¹, Sunyoung Lee¹, Mingi Moon¹, Sewon Kim¹, Ho Won Jang¹, Kisuk Kang¹, Jeehwan Kim² and Yun Seog Lee¹; ¹Seoul National University, Korea (the Republic of); ²Massachusetts Institute of Technology, United States

All-solid-state battery using solid electrolyte is promising for next generation energy storage device due to its potential for stability and high energy density. In particular, $\text{Li}_{1-x}\text{La}_{2/3-x}\text{TiO}_3$ (LLTO) ($0.05 < x < 0.167$), a perovskite type solid electrolyte, has shown an ionic conductivity as high as 10^{-3} S/cm at a x of 0.11 as well as air-stability. However, a high interfacial resistance when in contact with an electrode and interfacial instability between the electrode and solid electrolyte caused by electrochemical degradation make it difficult to put LLTO into practical use. Although various efforts including adding an artificial solid electrolyte interface layers such as Al_2O_3 have been employed to mostly mitigate the interface of lithium-metal anodes, the degradation issue at the electrolyte-cathode interface still remains. The interdiffusion of metal-ions between polycrystalline LLTO pellet and LiCoO_2 (LCO) has been reported, however the bulk diffusion without grain boundaries is desirable to evaluate the interdiffusion phenomena and investigate its effects on the Li-ion transport properties of LLTO.

In this study, we investigate the instability of the single crystalline LLTO electrolyte-cathode interface induced by the interdiffusion of metal cations in conventional cathode materials, LCO and $\text{LiNi}_{0.8}\text{Co}_{0.1}\text{Mn}_{0.1}\text{O}_2$ (NCM). We deposit single crystalline LLTO (100) solid electrolyte thin films to exclude the effect of grain boundaries and structural defects of LLTO. Single crystalline LLTO (001) thin-films are deposited by using pulsed laser deposition (PLD) technique epitaxially on SrTiO_3 (001) substrates having a lattice mismatch of 0.8%. The LCO or NCM thin-films are also stacked on LLTO/STO. The structure and the diffusion dynamics between the cathode and the electrolyte are characterized by scanning transmission electron microscopy and X-ray photoelectron spectroscopy with a depth profiling. The interdiffusion of metal cations at the LLTO-LCO interface are measured to be more rapid than that of the LLTO-NCM interface, even with lower deposition temperature. The interfacial resistance of the resulting interfaces from each cathode and the electrolyte are measured through electrochemical impedance spectroscopy. Furthermore, approaches using diffusion barrier layers to mitigate the interdiffusion of ion conductors and cathodes are also discussed.

4:45 PM EN05.13.05

Role of Electronic Passivation in Stabilizing the Lithium LiPON Solid Electrolyte Interphases [Yuheng Li](#)¹, Pieremanuele Canepa¹ and Prashun Gorai²; ¹National University of Singapore, Singapore; ²Colorado School of Mines, United States

The solid-electrolyte interphase (SEI) is crucial to the electrochemical performance of all-solid-state batteries (ASSBs). Theoretical characterization of SEI properties will help understand the origin of interfacial stability (and instability) between solid electrolytes and electrodes. Among solid electrolytes for Lithium(Li)-ion ASSBs, the lithium phosphorus oxynitride $\text{Li}_x\text{PO}_y\text{N}_z$ (LiPON) is one of the most stable against Li metal anode. However, it has been shown that LiPON reacts with Li metal and forms SEIs. The SEI formation stops after a thin layer is formed, but the mechanism that enables this apparent stabilization is unclear. Thermodynamics underpins the defect formation in materials and in turn, creation of electronic charge. Materials for energy storage, including solid electrolytes, are no exception to this fundamental process. Here, we computationally evaluate the electronic passivation of SEIs and its role in stabilizing the Li-LiPON interface. Specifically, we determine the defect and charge carrier concentrations in Li-LiPON SEIs, including Li_2O , Li_3N , Li_3P , and Li_3PO_4 . The defect and charge carrier concentrations were calculated from defect thermodynamics. We then predicted the electronic conductivity of the SEIs under different electrochemical conditions, which correspond to varying potentials to the Li metal anode. Our results reveal that the stoichiometrically abundant and uniformly distributed Li_2O has expectedly negligible electronic conductivity, while the electronically conducting components, such as Li_3N and Li_3P , show preferential distribution in the SEI. We posit that the overall electronically insulating nature of the SEI is responsible for the stability of the Li-LiPON interface. The computational approach adopted here can be extended to reveal the origin of the interfacial stability in other ASSBs.

SESSION EN05.14: Solid Electrolytes Design for Next Generation Solid-State Batteries IV

Session Chairs: Alex Bates, Dominika Buchberger, Yue Qi and Hongli Zhu

Friday Morning, December 2, 2022

Hynes, Level 3, Room 304

8:30 AM *EN05.14.01

Solid Electrolytes for All-Solid-State Batteries Linda Nazar and [Laidong Zhou](#); University of Waterloo, Canada

All-solid state lithium-ion batteries (ASSBs) have emerged as attractive alternatives to conventional liquid electrolyte cells for electrochemical energy storage, owing to their anticipated enhanced safety and higher energy densities. ASSBs are founded on high performance fast-ion conducting solid electrolytes, where the search for improved materials hinges on understanding their intrinsic nature and gaining comprehensive knowledge of the factors that dictate facile Li-ion transport. In turn, incorporating them into high functional ASSBs relies on mastering the interface of the solid electrolyte with the electrode materials.

These topics will be the focus of the presentation based on recent findings in our laboratory. Our correlation of structure with ionic conductivity in a range of newly developed fast ion Li conductors helps understand how cation disorder and a frustrated energy landscape impacts conductivity and activation energy. These considerations lead to exciting new classes of fast-ion conductors, including new argyrodite fast-ion conducting iodides and lithium metal halides. Promising all solid-state Li-ion batteries utilize “bare” NCM-type, Ni-rich lithium metal oxide cathodes coupled with high voltage-stable solid-state electrolytes. Low-resistance “clean” solid-solid interfaces enable room temperature cells with capacities close to their liquid Li-ion counterparts at practical discharge rates over very long-term cycling.

9:00 AM EN05.14.02

Bilayer Dense-Porous LLZO Membranes for High Performance Li-Garnet Solid-State Batteries [HuanYu Zhang](#)^{1,2}, Kostiantyn Kravchuk^{1,2} and Maksym V. Kovalenko^{1,2}; ¹ETH Zürich, Switzerland; ²Empa–Swiss Federal Laboratories for Materials Science and Technology, Switzerland

Currently, the replacement of liquid Li-ion electrolytes with their non-flammable and non-toxic solid counterparts based on $\text{Li}_7\text{La}_3\text{Zr}_2\text{O}_{12}$ (LLZO) with the garnet-type structure is pursued as a compelling approach to improve the energy density, cycling stability, and safety of Li-ion batteries (LIBs).^[1-3] However, Li dendrites form in $\text{Li}_7\text{La}_3\text{Zr}_2\text{O}_{12}$ (LLZO) solid electrolytes due to intrinsic volume changes of Li and the appearance of voids at the Li metal/LLZO interface.^[4] Bilayer dense-porous LLZO membranes make for a compelling solution of this pertinent challenge in the field of Li-garnet solid-state batteries (SSB). Lithium is thus stored in the pores of the LLZO, thereby avoiding (i) dynamic changes of the anode volume and (ii) the formation of voids during Li stripping due to increased surface area of the Li/LLZO interface. The dense layer then additionally reduces the probability of short circuits during cell charging. In this work, we report a method for producing such bilayer membranes utilizing sequential tape-casting of porous and dense layers. The minimum attainable thicknesses are 8–10 μm for dense and 32–35 μm for porous layers, enabling gravimetric and volumetric energy densities of Li-garnet SSBs of 230 Wh kg^{-1} and 830 Wh L^{-1} , respectively. Bilayer LLZO membranes in symmetrical cell configuration exhibit high critical current density up to 6 mA cm^{-2} and cycling stability of over 100 cycles at a current density of 0.1 mA cm^{-2} at an areal capacity limitation of 1 mAh cm^{-2} . The electrochemical performance of LLZO membranes is also assessed in combination with a LiFePO_4 cathode, delivering areal capacities of ca. 0.45 mAh cm^{-2} at a current density of 0.1 C.

Reference

[1] Kim, KJ; Balaish, M; Wadaguchi, M; Kong, L; Rupp, JLM, *Adv. Energy Mater.* **2021**, 11, 2002689.

[2] Xia, S; Wu, X; Zhang, Z; Cui, Y; Liu, W, *Chem* **2019**, 5, 753-785.

[3] Kravchuk, KV; Karabay, DT; Kovalenko, MV, *Sci. Rep.* **2022**, 12, 1177.

[4] Fu, K; Gong, Y; Hitz, GT; McOwen, DW; Li, Y; Xu, S; Wen, Y; Zhang, L; Wang, C; Pastel, G; Dai, J; Liu, B; Xie, H; Yao, Y; Wachsman, ED; Hu, L, *Energy Environ. Sci.* **2017**, 10, 1568-1575.

9:15 AM EN05.14.03

CO_2 -Derived Block Polycarbonate-Ethers for Accommodating the Volume Change in Solid-State Battery Composite Cathodes [Hui Gao](#)^{1,2}, Georgina Gregory^{1,2}, Boyang Liu^{1,2}, Xiangwen Gao^{1,2}, Mauro Pasta¹, Peter Bruce¹ and Charlotte Williams¹; ¹University of Oxford, United Kingdom; ²Faraday Institution, United Kingdom

All-solid-state batteries have gained increasing attention because of their high energy density and safety. Several inorganic solid electrolytes achieved the requirement of lithium-ion conductivity for all-solid-state batteries. However, the rigid and brittle nature of inorganics prevents good interfacial contact

with electrodes. The active materials are subjected to volume change upon charging/discharging. This leads to contact loss between active materials and electrolytes in the composite cathode (including the active material, inorganic solid electrolyte and carbon), resulting in poor cycling stability of the cells. To overcome the contact loss, the polymers can be introduced into cathode composites to improve the interfaces, cohesion and mechanical properties. Herein, we prepare the cathode composite of solid-state batteries by adding purpose-designed triblock polymers, poly(ethylene oxide)-*b*-poly(4-vinyl cyclohexene oxide carbonate)-*b*-poly(ethylene oxide) (PEO-*b*-PC-*b*-PEO). Triblock polymers are synthesized by hydroxyl telechelic PEO as a macroinitiator for CO₂/epoxide ring-opening copolymerization and a well-controlled Mg(II)Co(II) catalyst at 1 bar CO₂. The correlation of ion conductivity and mechanical properties with the block polymer composition is investigated. Three lead polymers are identified. These block polymers show high ionic conductivity (10⁻⁴ S cm⁻¹) at room temperature, lithium-ion transport (t_{Li^+} 0.3-0.62), good electrochemical oxidative stability (> 4 V vs Li⁺/Li) and elastomeric or plastomer properties (G' 0.1 -67 MPa). The solid-state batteries with the block polymer in the LiNi_{0.8}Mn_{0.1}Co_{0.1}O₂ cathode composite demonstrate greater capacity retention than equivalent cells featuring PEO homopolymer or without any polymer.

9:30 AM EN05.14.04

Increasing the Ionic Conductivity of Lithium Carbonphosphonitride Thermosets Through Plasticization and Increased Li Concentration Andrew Purdy, Brian L. Chaloux, Hunter O. Ford, Megan B. Sassin, Christopher A. Klug and Daniel M. Fragiadakis; Naval Research Laboratory, United States

Lithium dicyanamide (LiN(CN)₂) reacts with phosphorus cyanide (P(CN)₃) in a 2:1 or greater mole ratio in any anhydrous non-protic mutual solvent to form a resin. The resin solution is used to coat metal coupons or to impregnate silica fiber paper, which are then cured at temperatures of 200-300 °C, forming adherent, ion conducting films of a completely non-combustible material. When fully cured, those films have a low ionic conductivity, probably due to rigid crosslinking of the thermoset. We found previously that adding compounds to the resin, such as LiCN that contain a higher concentration of Li than LiN(CN)₂, increases the ionic conductivity. Post-cure treatment with diglyme also causes a dramatic conductivity increase, presumably by complexing the mobile Li ions and plasticizing the material. We will report our systematic efforts to increase Li⁺ ion conductivity by introducing small amounts of non-volatile poly(oxoethylene) based plasticizers, and by copolymerizing the resin with other cyano Li monomers to increase the Li concentration. The ionic conductivity and chain motions of these films were characterized by impedance and dielectric relaxation spectroscopy, and test cells with Li foil were constructed and measured. Additionally, the bulk thermoset material was analyzed by solid state NMR. We evaluated how the composition, conductivity, and electrochemical stability of these materials depends on the solvents of preparation and the poly(oxoethylene) and Li cyano additives used. Additionally, combustibility was tested to determine how much plasticizer can be added without compromising the inherent non-flammability of the thermoset materials.

9:45 AM EN05.14.05

Highly Ion-Conductive, Elastic and Adhesive Zwitterionic Polymer Electrolyte for All-Solid-State Lithium Batteries Sangil Kim^{1,2}, Gang Cheng^{1,2}, Kun Wang¹, Yuechen Gao¹, Hyang Seol^{1,2} and Anh Ngo¹; ¹University of Illinois, Chicago, United States; ²ZPore, LLC, United States

Currently, lithium-ion batteries (LIBs) are considered to be one of the most popular energy storage systems for electronic devices supported by high energy density, high operating voltage, and favorable cycling performance. However, commercial LIBs with the organic liquid electrolyte and lithium (Li) salts are associated with critical safety issues such as uncontrollable side reactions, toxic liquid electrolyte leakage, flammability of electrolytes, and poor thermal stability. Therefore, replacing the liquid electrolyte with solid electrolytes is quite necessary. Among several solid ion conductors, solid polymer electrolytes (SPEs) can offer excellent flexibility, interfacial compatibility with electrodes, good processibility, low cost, and light weights that can overcome the limitations of ceramic ion conductors. However, current SPEs often encounter limitations such as poor mechanical strength and dimensional thermal stability, inferior electrochemical stability, and low Li⁺ ion conductivity at room temperature (~10⁻⁵ S cm⁻¹ at room temperature). Here we present a multifunctional solid polymer electrolyte based on zwitterionic polyurethanes (zPU-SPE) for all-solid-state LIBs (SLBs). Our zPU-SPE exhibits a great potential to overcome current technical limitations of conventional SPE materials in SLB applications (e.g., low Li⁺ ion conductivity, inferior electrochemical/mechanical stabilities, unsatisfactory suppression of Li dendrite growth). We designed and synthesized a series of zPU [i.e., poly((diethanolamine ethyl acetate)-co-poly(tetrahydrofuran)-co-(1,6-diisocyanatohexane))]. Our zPU-SPE can host an equal amount of lithium bis(trifluoromethanesulfonyl) imide (LiTFSI) without phase separation (up to 80 wt% of LiTFSI loading). The Li-ion conductivity value of zPU exponentially increases with the addition of LiTFSI and reaches 7.4 × 10⁻⁴ S/cm with Li⁺ transference number of 0.6 at 25 °C, almost 14 times higher than the conductivity of poly(ethylene oxide) (PEO) SPE with ethylene oxide/Li⁺ ratio = 16. In addition, its superior adhesion energy (487.5 J/m² of zPU-SPE vs. 150 J/m² of commercial 3M Scotch Tape) can minimize interfacial resistance between electrode and SPE, and thus cell resistance of 100-μm-thick zPU SPE is as low as 280 W/cm² compared to 1230 W/cm² of the cell with a similar thickness of PEO SPE. Our zPU-SPE also showed an excellent elastic property with a tensile break of 1700% owing to its high density of inter- and intra-molecular hydrogen bonding in polymer matrix. The SLB battery performance of PEO and zPU-SPEs was evaluated using a solid-state Li/SPE/LiFePO₄ cell; the assembled SLB cell was cycled at a constant current rate of 1 C at 25 °C. After a discharge capacity of the cell with zPU-SPE stabilized at 100 mAh g⁻¹ after 15 cycles, there is a negligible capacity decrease (only 3% capacity decrease after 700 cycles), delivering a discharge capacity of 97 mAh g⁻¹ with stable Coulombic efficiency (100%) over entire cycles. However, the discharge capacity of Li/PEO/LiFePO₄ cells drops rapidly to 3 mAh g⁻¹ after 100 cycles. These results demonstrate that the SLB cell assembled with PCB-PTHFU shows high discharge/charge capacity and excellent capacity retention with stable Coulombic efficiency. The good electrochemical performance of the zPU SPE can be attributed to good compatibility with electrodes, low charge transfer resistance at the interface of electrode/electrolyte, and high Li-ion conductivity, strongly suggesting that zPU SPEs are potential candidates for development of high performance of SLBs.

10:00 AM BREAK

10:30 AM EN05.14.06

Tunable Conformal Electrodeposition of Ultra-Thin Polymeric Films for Electrolyte Interphases Wenlu Wang, Anton Resing, Zhaoyi Zheng and Joerg G. Werner; Boston University, United States

Interfaces between materials of various functionalities are omnipresent in solid-state energy-storage devices and partially determine the device performance and degradation due to interfacial incompatibility, instability, resistance, and loss of contact over cycling. Designer three-dimensional (3D) electrolyte-type interphases that bridge battery components and materials with disparate functions, such as the active electrode materials and solid electrolyte, could overcome some of these compatibility detriments and the increase in contact resistance over long-term operation. Additionally, 3D thin-film solid-state batteries as promising candidates for high-performance microscale power sources require 3D ultrathin solid electrolyte interphases, as they take advantage of both short ion diffusion distances for high rate capability with low heat generation, as well as the third dimension for high material loading and energy density. Important characteristics of such electrolyte-type interphases are their capability of electronic insulation and the physical separation of incompatible materials while allowing for ion transport. However, a key challenge of obtaining such functional interphases in batteries is their conformal deposition as thin and uniform coatings on 3D electrode architectures. In this work, we design multifunctional electrochemically active molecules that combine the capability of ionic conduction and molecular permeability with conformal electrodeposition into polymeric thin films that can be uniformly applied to porous electrodes with arbitrary 3D structures. We present an exhaustive exploration of their material-processing-structure-property relationships that reveals the multi-scale control over the ultrathin-film properties. For example, the uniform film thickness is tunable from 10 to 100s of nanometer

through molecular design and electrodeposition conditions, while their molecular permeability and electronic resistance can be tailored from previous to fully blocking. We show that the electrodeposited functional interphases fully coat complex 3D electrode architectures with retention of their functionality in a battery. This work demonstrates that rational molecular design enables the conformal electrodeposition of ultrathin functional coatings with solid polymer electrolyte properties on 3D structured electrodes that will enable designer interphases in various solid-state battery architectures and chemistries.

10:45 AM EN05.14.07

Gradient Ceramics in Polymer Hybrid Electrolyte with Improved Electrochemical Performance for Solid State Li-Ion Batteries Md Yusuf Ali¹, Gerrit Michael Overhoff², Hartmut Wiggers^{1,3} and Gunther Brunklaus²; ¹Institute for Combustion and Gas Dynamics—Reactive Fluids, University of Duisburg-Essen, Germany; ²Helmholtz Institute Münster, Germany; ³CENIDE, Center for Nanointegration, University of Duisburg-Essen, Germany

Solid-state Li-ion batteries have been regarded as one of the most promising candidate for future green energy storage devices due to their safety, low cost, and high energy density properties. Polymer and ceramics electrolytes are attractive candidates to boost the application of lithium metal batteries. Single-ion conducting polymers can reduce polarization and lithium dendrite growth, though these materials are eventually mechanically overly rigid, thus requiring mobilizers such as organic solvents to transport Li ions. Inhomogeneous distribution of the solvent and resulting preferential Li transport pathways might yield favored spots for Li plating, imposing additional mechanical stress and even premature cell short-circuits. On the other hand, ceramic e.g., $\text{Li}_{1.3}\text{Al}_{0.3}\text{Ti}_{1.7}(\text{PO}_4)_3$ (LATP) NASICON based electrolytes are known for better dendrite growth inhibitor, high temperature applicability. Here, we explored a ceramic-in-polymer hybrid electrolyte consisting of a polymer blend of single-ion conducting polymer and PVDF-HFP, including EC:PC as swelling agent, and silane-modified (3-Aminopropyltriethoxysilan (APTES)) LATP particles. The hybrid electrolyte features an oxide-rich layer that notably stabilizes the interphase toward Li metal, enabling single-side lithium deposition for over 700 hours at a current density of 0.1 mA cm^{-2} . Also, the incorporated oxide particles significantly reduce the natural solvent uptake from 140 to 38 wt.% despite maintaining reasonably high ionic conductivities. Its electrochemical performance was evaluated in $\text{LiNi}_{0.6}\text{Co}_{0.2}\text{Mn}_{0.2}\text{O}_2$ (NMC622)||lithium metal cells, exhibiting impressive capacity retention over 300 cycles. Notably, the very thin LiNbO_3 coating of the cathode material further boosts the cycling stability, resulting in capacity retention of 78 % over more than 600 cycles, clearly highlighting the potential of the hybrid electrolyte concept.

11:00 AM EN05.14.08

Polycarbonate Solid Electrolytes for Structural Batteries with Enhanced Mechanical Properties Gerald Singer, Cheng-Tien Hsieh, Yanjun Guo and Yuan Yang; Columbia University, United States

Polymer electrolytes are of increasing importance to replace flammable liquid electrolytes, that can lead to leakage and safety concerns in modern lithium-ion batteries (LIB). Besides the elimination of solvents, polymer electrolytes are light-weight and possess excellent processing, which makes them a great choice for large-scale applications. Most polymers show good mechanical properties but very low intrinsic ion conductivity, which is essential for an electrolyte in batteries. Therefore, a great effort is being made to increase its ion conductivity by adding plasticizers to the polymer matrix to reasonable values ($>0.2 \text{ mS/cm}$), which usually leads to a significant reduction in the mechanical performance. Consequently, only a few examples with reasonable modulus and ion conductivity have been demonstrated so far.

In this study, a polycarbonate-based solid polymer electrolyte (SPE) that shows a combination of good electrochemical and mechanical performance is presented. The SPE can be in-situ polymerized thermally with a glass fiber separator and demonstrates good cycling performance with $\text{LiFePO}_4/\text{Li}$ cells at room temperature. High modulus and strength of the SPE along with good ion conductivity of ca. 0.3 mS/cm enables a strong connection and efficient ion diffusion between the two electrodes. This exceptional combination can be used to improve the mechanical properties of structural batteries on the material-level.

11:15 AM EN05.14.09

In Situ Thermo-Mechanical Characterization and Strain Engineering of LiPON Thin Films Truong Cai¹, Andrew S. Westover², Sergiy Kalnaus², Jung Hwi Cho¹, Christos E. Athanasiou¹, Nancy Dudney² and Brian W. Sheldon¹; ¹Brown University, United States; ²Oak Ridge National Laboratory, United States

High temperature multi-optical-stress sensor (HTMOSS) has been used to characterize the coefficient of thermal expansion (CTE) and yield stress of 1-micron thick LiPON films. Six fully dense, amorphous films were deposited on glass and sapphire substrates. The films were then annealed at temperatures ranging from 80 to 200 C for 3 hours. The CTE of LiPON is found to be approximately $4.1\text{e-}6$, and argued to be independent of the substrate type. Because of this intermediate CTE value, by varying the substrate, we could impose either tension and compression due to thermal mismatch to the film. We observed further that the yield stress of the film is approximately 60 MPa under compression and 100 MPa under tension. Using constant-load hold at and beyond yield point, the films were found to relieve the stress developed during heating with visco-plastic deformation, which led to permanent residual stress during cooling as high as 120 MPa in either tension or compression depending on substrate type. We also found that at annealing temperature higher than 140 C LiPON lost ductility which could be due to composition changes as indicated by XPS measurement. The stress-relief mechanism at constant-load indicates that LiPON may be beneficial as a protective layer against dendrites penetration. Moreover our experimental platform proves that it's an effective method to engineer strain into thin-film solid electrolytes that could be extended to other materials like LLZO or sulfide electrolyte.

11:30 AM EN05.14.10

Fragility and Ion Transport in Silica-Based Ionogels Patricia E. McNeil¹, Thibaud Guillemin², Jean Le Bideau² and Bruce S. Dunn¹; ¹UCLA, United States; ²Université de Nantes, France

The design of electrolytes exhibiting liquid like transport properties with the form and structure of a solid separator is a promising direction for the development of solid-state electrochemical devices, especially solid-state batteries. In recent years, pseudo solid-state electrolytes known as ionogels have emerged as a group of solid phase materials that exhibit the properties of ionic liquids. These materials, which are comprised of two interpenetrating phases, are synthesized using well-known room temperature sol-gel synthesis methods which produce complex open microstructures with various dimensionalities. Ionogels are macroscopically rigid but exhibit liquid-like transport properties due to an ionic liquid (IL) being confined in the nanoscale pores of a sol-gel derived silica matrix. Typically ionogels range from 60-90% IL volume which, in contrast to sol-gel materials that use volatile solvents (e.g., alcohols), are retained in the final material because of the extremely low volatility of ILs. By confining the IL in the mesoscale pores of the sol-gel matrix, ionogels take full advantage of ionic liquid utility, including good chemical stability, high ionic conductivity, thermal stability, and a wide electrochemical window, in combination with a rigid solid backbone.

The present study examines the transport properties for ionic liquids confined within mesoporous materials. The fragility index was determined for several samples with varying microstructures and used to characterize performance as a pseudo-solid electrolyte. Fragility is a measure of the thermal sensitivity of the liquid structure and is described by the fragility index, D . A fragile liquid collapses under weak perturbations and leads to structural re-arrangement. Thus, a fragile liquid exhibits fast dynamical re-arrangement characterized by short relaxation times and non-Fickian diffusion, giving rise to non-Arrhenius behavior. A low D value corresponds to weak molecular interactions, while a high value corresponds to strong molecular interactions. In this

way, fragility is related to molecular mobility with its correlative effect on ionic conductivity and viscosity. In applying these concepts to ionogels, as the complexity of the matrix increases, the fragility index also increases, leading to lower conductivity materials. In our study, the microstructural features influencing conductivity were examined using Archie's law, assuming that the silica matrix conductivity was negligible. This type of analysis is validated for rock matrices and in the current work was extended to pseudo-solid electrolyte materials. Utilizing the concepts presented here, we demonstrate how ionogel samples can approach the conductivity of the unconfined ionic liquid. These conclusions are applicable to a variety of pseudo-solid electrolyte systems and have important implications for the design of solid-state electrochemical devices.

11:45 AM EN05.14.11

Hybrid Quasi-Solid-State Electrolytes—Structure, Dynamics, and Their Effects on Ionic Conductivity [Nyalaliska W. Utomo](#), Minori G. Kitahata, Yue Deng, Xiaotun Liu, Qing Zhao, Tian Tang and Lynden A. Archer; Cornell University, United States

The shift from liquid to solid-state electrolyte has been the focus of many battery electrolyte systems. Solid polymer electrolytes (SPEs) offer advantages such as the suppression of dendrite growth, good electrochemical stability, and low flammability and toxicity. SPEs formed inside an electrochemical cell from monomers and initiators is a strategy employed to overcome electrolyte wetting to active electrode components. The addition of SiO₂ nanoparticles with PEG_{5kDa} tethers hairy nanoparticles (HNPs) modifies the Al(OTf)₃-initiated polymerization of poly(1,3-dioxolane) (poly(DOL)). Time-dependent rheology measurements during polymerization indicate altered macrokinetics and structure. Curiously, the commonly observed soft glassy dynamics in self-suspended hairy nanoparticles (HNPs) are significantly reduced due to the strong interaction between PEG tethers and poly(DOL) chains. This strong interaction leads to co-crystallization –anchoring the nanoparticles to their poly(DOL) host. This anchoring not only enables good dispersion of nanoparticles in the matrix but also opens up more pathways for Li-ion transport as the ether oxygens of both PEG tethers and poly(DOL) chains provide sites for Li-ion hopping. Making use of this regulated Li-ion motion, we are able to increase the room-temperature conductivity of self-suspended HNPs from nS/cm-scale up to 4 mS/cm, four times higher than the golden standard for ether-based SPEs. This favorable ion transport is also reflected in good electrochemical performance in Li||Cu and Li||sPAN (sulfur/poly(acrylonitrile)) cells. Bare, larger microparticles, on the other hand, reduces ionic conductivity in a way predicted by the Maxwell conductivity model up to core volume fractions as high as 40 vol.%. Curiously, at this high core volume fraction, electrolytes have high moduli comparable to solid electrolytes while still possessing liquid-like dynamics.

SESSION EN05.15: Virtual Session: Solid-State Batteries
Session Chairs: Alex Bates and Dominika Buchberger
Tuesday Morning, December 6, 2022
EN05-virtual

8:00 AM *EN05.15.01

Toward Improved Conductivity and Electrochemical Stability of Halide Superionic Conductors for All-Solid-State Batteries Hiram Kwak, Juhyoun Park, Yeji Choi, Mu Chang Lee and [Yoon Seok Jung](#); Yonsei University, Korea (the Republic of)

While lithium-ion batteries using conventional liquid electrolytes have been widely used from portable electronic devices to large-scale applications, such as electric vehicles and energy storage systems, their serious safety concerns have remained unsolved. Moreover, alternative electrode chemistries such as Li metal have not been stabilized by using liquid electrolytes. In this regard, all-solid-state batteries employing inorganic solid electrolytes (SEs) are considered a promising alternative.

Recently, halide SEs, such as Li₃YCl₆, are newly emerging due to their prestigious advantages of excellent electrochemical/chemical oxidation stability and processability. However, a criticism of most halide SEs developed thus far is the use of costly central metal elements, such as Y, Sc, and In, with the only exception of Zr. Several descriptors affecting ionic conductivity of halide SEs have been identified: i) charge carrier concentration which is controlled by aliovalent substitution; ii) structural framework, such as trigonal, orthorhombic, and monoclinic structures; iii) structural disorder, such as disorder of Li⁺ and central metal cation disorder and stacking faults. Meanwhile, the critical drawback of halide SEs, i.e., poor cathodic stability, prohibits their use for negative electrodes, such as Li metal. In this regard, all-solid-state batteries using hybrid SEs using halide and sulfide SEs together would be practically reasonable. However, their compatibility has not been extensively investigated yet.

In this presentation, we report on our recent results of our strategies to develop new halide SEs with improved ionic conductivities and electrochemical/chemical stability. Also, the results of all-solid-state batteries employing developed SEs are discussed.

References

[1] Hiram Kwak, Shuo Wang, Juhyoun Park, Yunsheng Liu, Kyu Tae Kim, Yeji Choi, Yifei Mo, Yoon Seok Jung, *ACS Energy Lett.* **2022**, *7*, 1776.

[2] Hiram Kwak, Daseul Han, Jeyne Lyoo, Juhyoun Park, Sung Hoo Jung, Yoonjae Han, Gihan Kwon, Hansu Kim, Seung-Tae Hong, Kyung-Wan Nam, Yoon Seok Jung, *Adv. Energy Mater.* **2021**, *11*, 2003190.

8:30 AM *EN05.15.02

Mapping and Modeling Physicochemical Fields in Solid-State Lithium Metal Batteries [Shou-Hang Bo](#); Shanghai Jiao Tong University, China

The safety and energy density of solid-state batteries can be, in principle, substantially increased compared with conventional batteries. However, the use of solid-state electrolytes introduces pronounced complexities to the solid-state system because of the strong coupling between different physicochemical fields. This necessitates the development of experimental and theoretical methods to directly trace the evolution of electrochemical, stress, crack and thermal fields upon battery cycling, to fully understand the electrochemical processes. In this talk, I will discuss imaging tools that are developed in our group to track the electrochemical reaction fronts (i.e., electrochemical deposits of lithium metal), stress and crack evolution in 3D during processing and cycling of solid-state lithium metal batteries. We show that the crack formation and stress distribution in solid-state electrolytes are extremely sensitive to the preparation conditions, which, in turn, affect the electrochemical performance of batteries. Further, these imaging data can be combined with theoretical efforts to develop electromechanical and/or electrothermal models for solid-state lithium metal batteries. These works provide a strong basis to understand the strong coupling between different physicochemical fields, a prerequisite to fully unlock the potential of solid-state lithium metal batteries.

9:00 AM EN05.15.04

Investigating the Effects of Doping Layered Lithium Nickel Oxide [Lavan Ganeshkumar](#); University College London, United Kingdom

Lithium-ion batteries have long been established as the leading technology for energy storage devices due to their high energy density and longevity. Common cathode materials for these batteries are layered oxides. LiCoO₂ (LCO) is a popular layered oxide which is commonly used within the electronic

industry. Yet, due to increasing environmental impacts tied with the price of the cobalt, there has been a substantial push for cobalt-free cathode materials, especially for the automotive application. The isostructural compound LiNiO₂ (LNO) has been identified as the ideal replacement for LCO. LNO, with more earth-abundant Ni sources, has the theoretical capacity and voltages comparable to LCO. However, the material cannot fully utilize its theoretical energy density due to its mechanical and thermodynamical instabilities. Recent work has demonstrated that substitution strategies can cater for the instabilities whilst also minimising the reduction in capacity during battery cycling. Still, the underlying chemistry of the improved stabilities of the substituted LNO remain challenging to be elucidated, which has been hidden behind the false ground state structure of R-3m space group. Recently, owing to the Jahn-Teller (JT) distortion, LNO has been found to have the ground state structure with the P21/c space group. Density functional theory (DFT) calculation, with its ability to predict the ground state structures and charge compensation mechanisms, have been an effective tool for investigating solid-state materials with dopants. In this study, we implement DFT in order to fully understand the doped structure with the aim to find a stable nickel-rich cathode with a high theoretical capacity. Using the JT distorted structure, intrinsic point defects have been investigated in these cathode materials. This reveals insight into the experimental observations for LNO and gives an understanding for the charge compensating mechanisms within the pristine system. In addition, by comparing the present results with previous studies, the study will reveal insight into the charge compensating mechanisms as has been established for the pristine system. Lastly, the study explores Mg and W as dopants for LNO due to their notable success established in previous experimental studies. In turn, this will explain the observations of improvements in stability upon addition of the dopants.

9:15 AM EN05.15.05

Sn-Substituted Sulfide Solid Electrolyte Prepared by Liquid-Phase Synthesis for All-Solid-State Batteries Jehoon Woo, Yong Bae Song, Yeji Choi, Jun Pyo Son, Jong Seok Kim and Yoon Seok Jung; Yonsei University, Korea (the Republic of)

Sulfide solid electrolytes (SEs) are widely regarded as one of the most promising candidates for practical all-solid-state batteries (ASSBs) owing to their high ionic conductivities and excellent deformability. However, sulfide SEs are vulnerable to moisture, resulting in the release of toxic H₂S gas and degradation in Li⁺ conductivity when exposed to ambient air. To improve the moisture stability, various compositions have been explored, and their common preparation method has been solid-state synthesis. While liquid-phase synthesis has the potential advantage for mass production, the poor solubility of metal chalcogenides (e.g., SnS₂ and GeS₂) has restricted the available composition to only metal-free ones. Recently, our group developed amine-thiol chemistry enabling liquid-phase syntheses of metal-containing sulfide SEs. In this presentation, we report Sn-substituted sulfide SEs derived via amine-thiol chemistry. The product SEs exhibit improved air-stability compared to conventional metal-free SEs. Mechanical properties of Sn-substituted sulfide SEs are also discussed. Finally, all-solid-state cell performances under practically meaningful conditions such as low pressures are presented.

[1] *Adv. Energy Mater.* **2018**, *8*, 1800035.

[2] *Adv. Mater.* **2022**, 2200083.

9:20 AM EN05.15.06

Anodes Made of Multicoated Nano-Silicon and Graphene Nanoplatelets in Li-Ion Batteries Pin-Yi Zhao, Antonio R. Gonzalez, Bing Li, Yuhuan Liu, Robert Palgrave and Kwang-Leong Choy; University College London, United Kingdom

Silicon anodes are regarded as a near-term practical application by virtue of their high theoretical specific capacity. Despite this, when high-capacity silicon anodes are cycled, they show poor electrical conductivity, considerable volume variation, and severe aggregation. In this study, multicoated anodes are fabricated based on the layered deposition of nano-silicon and graphene nanoplatelets. An innovative, simple, non-vacuum, and cost-effective aerosol-assisted chemical deposition (AACD) technique is designed to deposit a homogeneous composite coating. The multicoated anodes are processed with an organic solvent and deposited on the spacers as current collectors. A fundamental investigation is conducted on critical aspects such as the solvent and nano-silicon concentration. The gaps between the layers accommodate the volume expansion of silicon for superior cycle performance, while the plane of the layers promotes high-rate capability. After 500 discharge/charge cycles, the multicoated composite anode (with 10 wt.% silicon) demonstrates promising capacity retention of 85.8% in Li-ion batteries. The AACD technique combines the benefits of atmospheric pressure chemical vapour deposition and aerosol-assisted chemical vapour deposition, providing an appealing research setting for initial laboratory studies in rechargeable batteries. Furthermore, two ways for presenting cyclic discharge/charge patterns are proposed with generalised algorithms in linear algebra.

Reference: Zhao, Pin-Yi, et al. "Multicoated composites of nano silicon and graphene nanoplatelets as anodes in Li-ion batteries." *Materials Advances*, 2022, 3, 4514 - 4519

9:25 AM EN05.15.08

Li-Garnet Solid-State Batteries—Status, Challenges and Prospects Kostiantyn Kravchuk^{1,2} and Maksym V. Kovalenko^{1,2}; ¹ETH Zurich, Switzerland; ²Empa—Swiss Federal Laboratories for Materials Science and Technology, Switzerland

Solid-state Li-ion batteries based on Li-garnet Li₇La₃Zr₂O₁₂ (LLZO) electrolyte have seen rapid advances in recent years. These solid-state systems are poised to address the urgent need for safe, non-flammable, and temperature-tolerant energy storage batteries that concomitantly possess improved energy densities and the cycle life as compared to conventional liquid-electrolyte-based counterparts. In this presentation, we will review present research pursuits and discuss the limitations in the employment of LLZO solid-state electrolyte (SSE) for solid-state Li-ion batteries. Particular emphasis will be given to the discussion of pros and cons of current methodologies in the fabrication of solid-state cathodes, LLZO SSE, and Li metal anode layers.^[1] Furthermore, we will discuss the contributions of the LLZO thickness, cathode areal capacity, and LLZO content in the solid-state cathode on the energy density of Li-garnet solid-state batteries, summarizing their required values for matching the energy densities of conventional Li-ion systems.^{[2], [3]} Finally, we will highlight challenges that must be addressed in the move towards eventual commercialization of Li-garnet solid-state batteries.

References

[1] K.V. Kravchuk, et al. *Sci. Technol. Adv. Mater.* 2022, 23, 41-48.

[2] K.V. Kravchuk, et al. *Acc. Mater. Res.*, 2022, 3, 411-415.

[3] K.V. Kravchuk, et al. *ACS Energy Lett.*, 2021, 6, 2202-2207.

9:40 AM EN05.15.09

Atomic-Scale Origin of the Low Grain-Boundary Resistance in Perovskite Solid Electrolyte Li_{0.375}Sr_{0.4375}Ta_{0.75}Zr_{0.25}O₃ Ji Qi and Shyue Ping Ong; University of California, San Diego, United States

Oxide solid electrolytes (OSEs) have the potential to achieve improved safety and energy density for lithium-ion batteries, but their high grain-boundary

(GB) resistance is a general bottleneck. In the most well studied perovskite OSE, $\text{Li}_{1-x}\text{La}_{2/3-x}\text{TiO}_3$ (LLTO), the ionic conductivity of GBs is about three orders of magnitude lower than that of the bulk. In contrast, the related $\text{Li}_{0.375}\text{Sr}_{0.4375}\text{Ta}_{0.75}\text{Zr}_{0.25}\text{O}_3$ (LSTZ0.75) perovskite exhibits low GB resistance for reasons yet unknown. Here, we used an active learning moment tensor potential, to reveal the atomic scale structure and composition of LSTZ0.75 GBs. We found that Li depletion, which is a major reason for the low GB ionic conductivity of LLTO, is absent for the GBs of LSTZ0.75. Instead, the low GB resistivity of LSTZ0.75 is attributed to the formation of a nanoscale defective cubic perovskite interfacial structure that contained abundant vacancies, supported by electron energy loss spectroscopies. Our study provides new insights into the atomic scale mechanisms of low GB resistivity and sheds light on using machine learning interatomic potentials to study complex GB structures in solid electrolyte materials.

9:45 AM EN05.15.10

Investigating Dry Room Compatibility of Sulfide Solid-State Electrolytes for Scalable Manufacturing Yu-Ting Chen¹, Maxwell A. T. Marple², Darren H. Tan¹, So-Yeon Ham¹, Baharak Sayahpour¹, Wei-Kang Li¹, Hedi Yang¹, Jeong Beom Lee³, Hoe Jin Hah³, Erik A. Wu¹, Jean-Marie Doux¹, Jihyun Jang¹, Phillip Ridley¹, Ashley Cronk¹, Grayson Deysler¹, Zheng Chen¹ and Y. Shirley Meng⁴; ¹University of California, San Diego, United States; ²Lawrence Livermore National Laboratory, United States; ³LG Energy Solution, Ltd., Korea (the Republic of); ⁴University of Chicago, United States

II-solid-state batteries (ASSBs) are viewed as promising next-generation energy storage devices, due to their enhanced safety by replacing organic liquid electrolytes with non-flammable solid-state electrolytes (SSEs). The high ionic conductivity and low Young's modulus of sulfide SSEs make them suitable candidates for commercial ASSBs. Nevertheless, sulfide SSEs are generally reported to be unstable in ambient air. Moreover, instead of gloveboxes used for laboratory scale studies, large scale production of batteries is usually conducted in dry rooms. Thus, this study aims to elucidate the chemical evolution of a sulfide electrolyte, $\text{Li}_6\text{PS}_5\text{Cl}$ (LPSCl), during air exposure and to evaluate its dry room compatibility. When LPSCl is exposed to ambient air, hydrolysis, hydration, and carbonate formation can occur. Moreover, hydrolysis can lead to irreversible sulfur loss and therefore LPSCl cannot be fully recovered in the subsequent heat treatment. During heat treatment, exposed LPSCl undergoes dehydration, decomposition of carbonate species, and reformation of the LPSCl phase. Finally, LPSCl was found to exhibit good stability in a dry room environment and was subject to only minor conductivity loss due to carbonate formation. The dry room exposed LPSCl sample was tested in a $\text{LiNi}_{0.8}\text{Co}_{0.1}\text{Mn}_{0.1}\text{O}_2$ | LiIn half-cell, exhibiting no significant loss of electrochemical performance compared with the pristine LPSCl, proving it to be compatible with dry room manufacturing processes.

10:00 AM DISCUSSION TIME

SYMPOSIUM EN06

Silicon for Photovoltaics
November 30 - December 7, 2022

Symposium Organizers

James Bullock, The University of Melbourne
Ivan Gordon, IMEC
Emily Warren, National Renewable Energy Laboratory
Xinyu Zhang, Jinko Solar

Symposium Support

Bronze
Jinko Solar Co., Ltd.
National Renewable Energy Laboratory

* Invited Paper
+ Distinguished Invited

SESSION EN06.01: High Performance Si Solar Cells
Session Chairs: James Bullock and Emily Warren
Wednesday Afternoon, November 30, 2022
Hynes, Level 3, Room 301

3:30 PM EN06.01.03

Evaluating the Auger Recombination Temperature Dependence in Crystalline Silicon and the Implication on the Device Efficiency Jorge F. Ochoa-Bueno, Simone Bernardini and Mariana Bertoni; Arizona State University, United States

As the bulk quality and surface passivation of silicon devices improve, the intrinsic recombination processes become increasingly crucial to the performance of solar cells. With higher lifetimes, the operating maximum power point slides to higher injection levels, and the intrinsic Auger lifetime represents the next boundary to the overall device performance. Recently, several authors have proposed revisions to the Auger charge carrier recombination parametrization based on reports of measured lifetimes exceeding previously accepted models. However, these revisions are restricted to room temperature, ignoring solar cell operational temperatures on the field.

We revisit the Auger regime by making the corrections proposed by Black and Niewelt framework and, through the thickness method, analyze the Auger temperature dependence. It is well known that Auger recombination cannot be measured directly; its contribution must therefore be separated from the total measured recombination. By varying the substrate thickness systematically, we experimentally determine the surface recombination, and the bulk lifetime is taken by subtracting the former from the measured effective lifetime. This procedure is conducted at different temperatures. We show that as the temperature increases, the bulk lifetimes significantly exceed those predicted by the recently revised Auger parametrization, which points out the inadequacy of the parameterization to satisfactorily describe the Auger lifetime temperature dependence. These results suggest a strong temperature dependence of the Auger recombination and the need for its characterization at the device operating conditions. The latter is of great importance for calculating the fundamental limiting power conversion efficiency.

In the present work, we experimentally evaluate the Auger lifetime in high-quality float-zone n-type silicon material across a range of temperatures from 300 to 500 K and carrier injection levels representative of the device operating at maximum power point and open-circuit conditions. The radiative recombination is calculated using the widely accepted current values, and by modeling the contributions from the Shockley-Read-Hall recombination, the Auger is separated from other bulk recombination mechanisms. We calculate an ambipolar Auger coefficient $C_{amb}=2.12 \times 10^{-30} \text{ cm}^6\text{s}^{-1}$ in excellent agreement with the most up-to-date parametrization at room temperature. The Auger temperature-dependence experimentally observed can be explained following the quantum mechanical approach proposed by Hangleiter and Häcker. Their approach described the Auger recombination in silicon as enhanced by the presence of scattering and bound states, i.e., excitons, due to the Coulombic interaction among charge carriers. We propose that the enhancement factors g_{eeh} and g_{ehh} exhibit an exponentially decrease with increasing temperature due to the increasing disturbance to the e-h bound states introduced by thermal agitation. Thus, the Auger recombination rate is expected to decrease exponentially with increasing temperature validating the Auger lifetime increment observed. Finally, we evaluate the impact of the experimental Auger temperature dependence on the limit imposed by the intrinsic lifetime on the implied voltage within the analyzed range of injection levels and temperatures and compare it to the results obtained by applying the recently adopted Auger parameterization.

3:45 PM *EN06.01.04

Hot-Wire Chemical Vapor Deposition Techniques for High Efficiency Silicon Heterojunction Solar Cells Kaining Ding; Forschungszentrum Jülich GmbH, Germany

In this contribution we will review the usage of hot-wire chemical vapor deposition (also called catalytic chemical vapor deposition) in crystalline silicon solar cell manufacturing and introduce new approaches how to use this technique to further improve the efficiency of high efficiency silicon heterojunction solar cells. Hot-wire chemical vapor deposition is a plasma-free chemical vapor deposition process, which differs from plasma-enhanced chemical vapor deposition, the current mainstream technology to grow silicon thin-films. This difference allows for a larger extend of decoupling of gas dissociation and film growth, which opens additional possibilities. For example, the deposition rate can be very high without the risk of plasma damage to the surface. Also, material compositions like highly stoichiometric nanocrystalline silicon carbide can be grown. In this contribution we will discuss the growth mechanisms, innovative processes, and industry application of hot-wire chemical vapor deposition.

SESSION EN06.02: Poster Session: Silicon Photovoltaics
Session Chairs: James Bullock, Kaining Ding and Emily Warren
Wednesday Afternoon, November 30, 2022
8:00 PM - 10:00 PM
Hynes, Level 1, Hall A

EN06.02.01

Evaluation of PID Characteristics of Bifacial p-PERC Silicon Photovoltaic Modules by Encapsulant Types Jang Hongjun, Solhee Lee, Sang-Won Lee, Donghwan Kim, Yoonmook Kang and Hae-Seok Lee; Korea University, Korea (the Republic of)

As global warming is getting worse recently because of fossil fuel, renewable energy is getting much attention. Although there are many renewable energies like solar cell, wind power and hydropower, solar cell is becoming main energy source among renewable energy because of economical aspects. Among solar cells, bifacial solar cells composed of glass on both side can receive more light than monofacial solar cells. Therefore, bifacial solar cells are installed about 20GW, which is an increase of about 10 times from 2018. Bifacial p-passivated emitter and rear cell(p-PERC) solar cells are being recording high efficiency so it is mass-produced worldwide. Solar cells are connected to form solar modules, and the modules are connected in series to form strings, and in this process, potential difference occurs between frames and solar cells. When potential difference occurs between the frame of the solar module and the solar cell, potential induced degradation (PID) occurs. If solar cells are (-) biased than frames, then alkaline ions in module glass(soda-lime glass) enter to solar cell, which causes large reduction in power of the solar modules. There are two main mechanisms of PID in p-PERC. First in front side, stacking faults formed and grown by Na^+ ions damage p-n junction of solar cell and result in leakage current and we call this as PID-shunting(PID-s). Second in rear side, Na^+ ions also move to rear side and reduce field effect passivation of AlO_x layer. We call this mechanism as PID-polarization(PID-p). Due to development of wafer process and other passivation skills PID-s is getting decreased, so PID-p in rear side is main cause of power loss. Exact mechanism of PID-p in bifacial p-PERC rear side is not proved yet, so we focused on the PID-p by analyzing change of charges like Na^+ ions. Currently, ethylene vinyl acetate(EVA) is mainly used as an encapsulant for a photovoltaic module because of economical reasons, but in the case of EVA, leakage current flows much due to low volume resistance. And because of high water transmissibility, more moisture moves to solar cells, resulting in more serious PID. Recently, polyolefin elastomer(POE) has been researched as a material that replaces EVA, and POE has high volume resistance, making it more efficient to prevent PID. PID is known to be serious with humid and high temperature conditions. Therefore we fabricated bifacial p-PERC modules with two types of encapsulant(EVA, POE) and applied 85°C/85%RH/1000V condition. After that, we analyzed degree of degradation of two types modules by utilizing Electroluminescence images (EL) and LIV(Light I-V).

EN06.02.02

Field-Induced Radial Junction for Dopant-Free Crystalline Silicon Solar Cells with an Efficiency of over 20% Deokjae Choi and Kwanyong Seo; Ulsan National Institute of Science and Technology, Korea (the Republic of)

Radial junctions on crystalline silicon (c-Si) microwire structures considerably reduce the diffusion length of photo-induced minority carriers required for energy generation by decoupling light absorption and carrier separation in an orthogonal spatial direction. Hence, radial junctions mitigate the need for high-purity materials and thus reduce the fabrication cost of c-Si solar cells. In this study, the formation of dopant-free radial junctions from atomic layer deposition (ALD) of Al_2O_3 on an n-c-Si microwire surface is reported. ALD- Al_2O_3 generates a p^+ inversion layer, which eventually forms the radial junction on the n-c-Si surface. The width of the depletion region induced by the p^+ inversion layer is calculated from PC1D simulation as 900 nm. The

fabricated dopant-free radial junction c-Si solar cells exhibit a power conversion efficiency of 20.1%, which is higher than those of previously reported microwire-based radial junction solar cells. Notably, internal quantum efficiencies of over 90% were obtained in the 300–980 nm wavelength region, thereby verifying the successful formation of radial junctions.

EN06.02.04

A Study of Reflected Light Effect from Module Component with MATLAB Ji-Seong Hwang, Yoonmook Kang, Donghwan Kim and Hae-Seok Lee; Korea University, Korea (the Republic of)

The Paris climate agreement aims to keep the average global temperature rise below 2 °C, and strive to not exceed 1.5 °C. According to a report by the world meteorological organization(WMO), carbon dioxide concentrations reached new highs in 2021, and the global average annual temperature rise was about 1.11 °C (±0.13 °C). Intergovernmental panel on climate change (IPCC) has released its 6th report that forecast 1.5 degree rise between 2021 and 2040. In order to achieve the goal of reducing greenhouse gas emissions, solar energy industry should aim to grow rapidly.

In manufacturing process of photovoltaic module, it is important to reduce cell-to-module power loss(CTM loss). A simulation program Fraunhofer ISE, SmartCalc.Module is the only program to estimate CTM loss. However, this program showed a meaningful error when calculating a mini-module consisting of a single string.

In this research, we studied an effect of reflected light from the area containing non-active component like backsheet and string interconnector. We applied open source MATLAB codes to shingled solar modules that use electrical conductive adhesives to interconnect between cells.

EN06.02.05

Passivation and Carrier Lifetime of Ultra-Thin Film Silicon with Tandem Niobium Oxide and Attached Organosilane Emma J. Pellerin, Julia Martin, Ronald Grimm and Lyubov Titova; Worcester Polytechnic Institute, United States

Tandem junction solar cells with silicon and a dissimilar absorber material pose unique challenges for minimizing interfacial defects between those absorbers. Organic layers would enable flexible, soft, carrier-selective contacts, but silane attachment chemistry to silicon presents its own interfacial defects that must be minimized. A focus on silicon substrates in tandem with deposited niobium oxides, and silane-based organic layers has potential to minimize electronic defects and improve efficiencies. Here, atomic-layer deposition (ALD) deposited ultra-thin niobium oxide layers and wet-chemical processing yielded organosilane monolayers on silicon substrates. Photoelectron spectroscopy quantified surface coverages while microwave-based transient photoconductivity measurements established carrier recombination velocities for these surfaces. Ongoing studies are quantifying the resulting solar energy conversion of the resulting soft-interface tandem junction solar cells.

EN06.02.07

Energy Yield Comparison Between the Mono Facial Module and the Bi Facial Module at the Carport System During 4 Seasons Sungho Hwang¹, Woncheol Jeong¹, Hae-seok Lee¹, Dongchul Suh², Yoonmook Kang¹ and Yongseok Jun¹; ¹Korea University, Korea (the Republic of); ²Hoseo University, Korea (the Republic of)

Both Mono facial and bi facial modules have been major products in the current PV market. Recently, ITRPV predicts the bi facial module's market share will be over than 60% in 2023 because the bi facial module is well known for more power than mono facial module due to light absorption from both sides (not only from front side, but also from rear side). Many researches have shown the yield comparison for both products by simulation or field data from the utility system. In this paper, the yield data analysis for both products has been compared at the carport system in the climate over Korea peninsula during 1 year (4 seasons).

The cell structure is based on the PERC cells with the M4 size wafer. In case of bi facial cell, the rear metal line design is different with the mono facial cell in order to absorb the light from the rear side. Aluminum(Al) paste covers full area of the rear side in case of the mono facial cell and Al covers the part of the rear side with the finger design as like the front design at the bi facial cell. The dielectric structure of the bi facial cell is the same with the mono facial cell which is optimized for maximizing the absorption from the front side. The module BOM (Bill Of Material) of the bi facial module is different with that of the mono facial module, for example, the glass thickness is 3.2 mm for the mono facial module and two glasses with 2.0 mm thickness are used for the bifacial module. EVA thickness is also different. 400um thick EVA for the bi facial module and 500 um EVA for mono facial module are used. In case of the rear glass of the bifacial module, there is no white grid between cells. The average module powers at STC are 422.4 watt on mono facial module and 414.9 watt on bi facial module. Each 15 modules are installed for the each type on the side; thus the climate effect is same. The carport had 5 degrees for north direction and the albedo is Asphalt, but most of time, there are parked cars under the modules, which can bring different albedo.

The annual energy yield is 933.73 kWh/kWp on the mono facial module and 956.98 kWh/kWp on the bi facial module. The bifacial module shows higher energy yield by 23.25 kWh/kWp. All months do not show same phenomenon. For example, May and June data show higher yield value by around 6 kWh/kWp because the large irradiance value on the May and June brings more light absorption from the rear side. From the July, the irradiance value begins to decrease and the temperature shows the highest during 1 year in Korea peninsula climate. At this condition, the delta of July shows decreasing trend. This trend continues up to the Dec(Sprint to Fal). From Jan to March (winter season), the delta of energy yield is almost similar or even minus, which means the yield of the mono facial module shows higher value.. Only 3 months(winter) shows this trend.

Most the dominant parameter for the delta value is the irradiance value at this carport system. The energy yields as the absolute value for both modules show lower value compared with the published values respectively because the Albedo value is low due to the carport structure for the bifacial module and the direction of the carport is to the north for both modules, thus all modules receive relatively lower irradiance. In case of the bifacial module, the delta value of the energy yield between both types is less than the expectation because some parameters such as lower bi-facility value (68.2%) are lower on the bifacial module because both cell types are optimized for absorbing the front light.

EN06.02.08

Effective Near-Infrared Light Management in Silicon Heterojunction Solar Cells for Perovskite/Silicon Tandem Solar Cell Application Yoshio Ohshita¹, Hyunju Lee^{2,3} and Atsushi Ogura^{2,3}; ¹Toyota Technological Institute, Japan; ²Meiji Renewable Energy Laboratory, Japan; ³Meiji University, Japan

Perovskite/silicon tandem solar cells are intensively being investigated as a promising candidate for next generation solar cells combining low costs and high efficiency. Currently, the silicon heterojunction (SHJ) bottom cell technology, which provides high open-circuit voltage values of up to 750 mV, dominates in perovskite/silicon tandem research, and also the latest perovskite/silicon tandem world records are based on SHJ bottom cells [1]. Despite this exciting performance, the tandem solar cell was still limited not only by a relatively low top cell voltage output but also by the bottom-cell photocurrent. For instance, the total photocurrent density of the world record perovskite/silicon tandem solar cell was only 39.6 mA cm⁻² [1]. For comparison, 42.7 mAcm⁻² were reached in the world record SHJ cell [2], which is very close to the theoretical maximum for silicon of about 43.3 mAcm⁻² [3]. An important optical loss mechanism in this tandem cell, in comparison to an optimized single-junction silicon cell, is the increased reflection and reduced absorption in

the near infrared (NIR) part of the spectrum, hence reduced photocurrent in the silicon bottom cell. In particular, on the rear side of SHJ solar cells, an unoptimized transparent conducting oxide (TCO)/metal reflector is the origin of significant losses in the NIR part of the spectrum. These losses come from plasmonic absorption at the TCO/metal interface and from free carrier absorption in the TCO [4,5]. Therefore, the NIR light management becomes increasingly important as short-circuit current in the NIR region has to be increased owing to the increasing interest of using SHJ solar cells as bottom cells in perovskite/silicon tandem solar cells. This contribution demonstrates an improved NIR response of the tungsten-doped indium oxide (IWO)/Ag rear contact in rear-junction SHJ solar cells. The free-carrier concentration and the thickness of the rear IWO layer are optimized in order to minimize the free-carrier and the plasmonic absorption losses without detrimentally affecting the selectivity and the electrical transport properties of SHJ solar cells. In detail, the NIR reflectance of IWO/Ag rear contacts deposited on random pyramid textured silicon wafers can be enhanced by increasing the thickness of IWO layers because of reduced plasmonic absorption at a IWO/Ag interface by increasing the thickness of IWO layers. In addition, 160-nm-thick IWO layers fabricated with an O₂-rich O₂/Ar process gas during remote plasma deposition of the IWO layers, demonstrate the largely reduced free-carrier and plasmonic absorption and the enhanced NIR reflectance of IWO/Ag rear contacts. Furthermore, measured SHJ solar cell parameters such as open-circuit voltage, short-circuit current and fill factor, are shown to be impacted by free-carrier concentration in IWO layers within the investigated ranges. As a result of these optimizations, a significant reduction of the parasitic absorption loss in the NIR part of the spectrum is obtained, leading to a champion SHJ solar cell with a short-circuit current density of up to 40.8 mA/cm² and an efficiency of 22.4%. This work was supported by NEDO.

References

- [1] P. Tockhorn, J. Sutter, A. Cruz, et al., *Research Square*; 2022. DOI: 10.21203/rs.3.rs-1439562/v1.
- [2] K. Yoshikawa, H. Kawasaki, W. Yoshida, et al., *Nature Energy*, 2017, **2**, 17032.
- [3] A. Richter, M. Hermle, S. W. Glunz, *IEEE Journal of Photovoltaics*, 2013, **3**, 1184.
- [4] F.-J. Haug, T. Söderström, O. Cubero et al., *Journal of Applied Physics*, 2008, **104**, 064509.
- [5] Z. C. Holman, M. Filipič, A. Descoedres et al., *Journal of Applied Physics*, 2013, **113**, 013107.

SESSION EN06.03: Photovoltaic Systems and Circular Economy

Session Chairs: Kirstin Alberi and Emily Warren

Thursday Morning, December 1, 2022

Hynes, Level 3, Room 301

8:30 AM *EN06.03.01

Performance and Degradation in Silicon PV Systems Under Outdoor Conditions in Relation to Reliability Aspects of Silicon PV Modules Angèle Reinders^{1,2}; ¹Eindhoven University of Technology, Netherlands; ²University of Twente, Netherlands

The degradation of silicon photovoltaic (PV) modules is one of the key factors to reduce the cost of PV electricity produced by increasing the operational lifetime of PV systems installed in outdoor conditions. To capture degradation in the field, an performance analysis has been executed of monitoring data of over 8400 PV systems. These PV plants are small residential systems with silicon PV modules with a median installed capacity of 6 kWp, primarily installed in Europe, with an average lifetime of 30.5 months. The monitoring data have been stored in the Pearl PV database as time series with 10 min resolution ranging from one to four years from 2010 to 2016 also covering the following metadata: installed capacity, latitude, longitude, azimuth, and tilt angle of the PV modules. ERA5 reanalysis data are used as irradiance data. From the analysis it is found that the annual mean performance ratio across all systems was 76.7 %; and the average yield is 954.9 kWh/kWp per year [1]. On the basis of an analysis of monitoring data, average performance losses between 0.74 %/year and 0.86 %/year were calculated depending on the method used.

To reduce these degradation rates, it is imperative to know the degradation and failure phenomena. Hence, in this presentation an overview is given of the state-of-the-art knowledge on the reliability of silicon PV modules [2]. This overview consists of three parts: firstly, a brief contextual summary about reliability metrics and how reliability is measured. Secondly, a summary of the main stress factors and how they influence module degradation. Finally, a detailed review of degradation and failure modes is presented, which has been partitioned by the individual components within a silicon PV module. This connects the degradation phenomena to the performance of installed PV systems.

From this perspective and through extensive testing and failure analysis, researchers in the field of silicon for photovoltaics could investigate silicon materials in order to reduce stressors and their impact on the long term stability of silicon PV modules installed in the field.

[1] S. Lindig, J. Ascencio-Vásquez, J. Leloux, D. Moser and A. Reinders, "Performance Analysis and Degradation of a Large Fleet of PV Systems," in *IEEE Journal of Photovoltaics*, vol. 11, no. 5, pp. 1312-1318, 2021, doi: 10.1109/JPHOTOV.2021.3093049.

[2] M. Aghaei, A. Fairbrother, A. Gok, S. Ahmad, S. Kazim, K. Lobato, G. Oreski, A. Reinders, J. Schmitz, M. Theelen, P. Yilmaz and J. Kettle, "Review of degradation and failure phenomena in photovoltaic modules," in *Renewable and Sustainable Energy Reviews*, vol. 159, 112160, 2022, doi: 10.1016/j.rser.2022.112160.

Acknowledgements: This presentation is the result of joint collaborations in COST Action PEARL PV involving the following researchers: S. Lindig (EURAC, Italy & University of Ljubljana, Slovenia), J. Ascencio-Vásquez (3E, Belgium & University of Ljubljana, Slovenia), J. Leloux (Lucisun, Belgium), D. Moser (EURAC, Italy), M. Aghaei (Eindhoven University of Technology, the Netherlands & Norwegian University of Science and Technology, Norway), A. Fairbrother (École Polytechnique Fédérale de Lausanne, Switzerland), A. Gok (Gebze Technical University, Turkey), S. Ahmad (UPV/EHU Science Park, Spain & Basque Foundation for Science, Spain), S. Kazim (UPV/EHU Science Park, Spain & Basque Foundation for Science, Spain), K. Lobato (Instituto Dom Luiz, Portugal), G. Oreski (Polymer Competence Center Leoben GmbH, Austria), J. Schmitz (University of Twente, the Netherlands), M. Theelen (TNO Partner in Solliance, the Netherlands), P. Yilmaz (TNO Partner in Solliance, the Netherlands & University of Twente, the Netherlands) and J. Kettle (University of Glasgow, United Kingdom).

9:00 AM EN06.03.03

A Novel Pixelation Approach to Integrate PV for Urban Architecture Conservation Gavin P. Raharjo, Min H. Saw, Shin W. Leow and Mauro Pravettoni; National University of Singapore, Singapore

Conservation of heritage buildings in high density urban context such as Singapore has shifted its paradigm from purely physical preservation to making them functionally relevant for the age through constant redevelopment and repurposing. This opens opportunity for the adoption of modern and innovative technological solutions, such as building-integrated photovoltaics (BIPV), to be a novel approach to value-add these living artefacts; transforming them from energy consumer to clean energy provider. However, integration of standard photovoltaic (PV) module is still deemed inappropriate when it comes to respecting the aesthetics of these conserved buildings, yet it is necessary to populate as much surface as possible to meet the energy demand. Without a

better solution in terms of aesthetics and colour, PV integration on conserved buildings, and even modern structures are limited to the areas out of the public eye. Colourful PV panels for better aesthetic integration are becoming more prevalent. However, it comes with a compromise on PV performance: the ink and frit pigments will absorb and reflect the solar spectrum in particular wavelengths to achieve the desired colour. The light transmittance differs for different colours, and this could cause two issues: i) mismatch losses and ii) potential formation of hot-spots during operation of the PV module. In view of that, in our previous work, we have developed two novel design principles to mitigate mismatch losses and the risk of hot-spot formation in colourful PV modules. The first principle applies a repetitive design across the PV module to achieve uniform cell to cell shading. Secondly, we have studied extensively the relationship between colours, printing parameters and transmittance. By choosing the appropriate colour combinations, as well as printing parameters (e.g. ink thickness) for each colour, different colour areas would have the same amount of transmittance, thus mitigating hot-spots. This lifts the constraints of using repetitive patterns and allows for higher design flexibilities. In this work, the design principle based on colour science is further synthesized into two “pixelation-based” design schemes: (1) Stippling effect: contrasting color tones (eg. dark blue and white) are designed to produce the same level of irradiance transmission under AM 1.5G spectrum. Gradations of light and shade can then be produced by applying the stippling technique to produce an image, while maintaining uniform irradiance on the underlying PV cells.; and (2) Pointillism: a progression of scheme (1), color variation is achieved by extending the equivalent light transmission principle to the design of pixels containing multiple colors. Custom algorithm translating generic raster images to fit this pixel design scheme is also developed. These “pixelation-based” design schemes offer two-fold benefits: (1) allows higher light transmittance to the solar cells and hence improve the electrical efficiency of colourful PV modules; and (2) allows for more flexible image translation for a harmonious BIPV integration on the façade to support urban conservation effort.

9:15 AM *EN06.03.04

Terawatt Scale Sustainability with Silicon PV [Silvana Ovaitt](#); National Renewable Energy Laboratory, United States

We have very ambitious goals and need for decarbonization at the US and World level, which will drive a fast growth in Solar PV manufacturing and deployment. In this talk I'll cover some priorities to de-risk this energy transition, based on module reliability and sustainable materials and energy considerations through the lifetime of solar PV modules. Circular economy is an important concept to start implementing as an industry; some key findings are the importance of striving for long lifetimes, and prioritizing circularity paths tailored for the PV community.

9:45 AM BREAK

SESSION EN06.04: Novel Concepts
Session Chairs: James Bullock and Silvana Ovaitt
Thursday Morning, December 1, 2022
Hynes, Level 3, Room 301

10:30 AM EN06.04.01

Will Pinholes for SiO_x/poly-Si Passivating Contacts Enhance the Passivation Quality? Guangtao Yang, Remon Gram, Paul Procel, Can Han, Zhirong Yao, Yifeng Zhao, Luana Mazzarella, Miroslav Zeman and [Olinto Isabella](#); Delft University of Technology, Netherlands

Poly-Si carrier-selective passivating contacts for c-Si solar cells provide outstanding passivation quality and carrier selectivity as demonstrated in many high-efficiency solar cells architectures [1-12]. Their unique structure consists of two layers. An ultra-thin SiO_x layer chemically passivates the c-Si surface and builds up a potential barrier for the carriers' transport through it [13]. Then, a heavily doped poly-Si layer sits on top of the ultra-thin SiO_x layer. Owing to an optimized doping level, higher within the poly-Si layer and the c-Si surface than in the c-Si bulk, an electrical field is built up at the c-Si interface, enabling field effect passivation and carrier selectivity. The optimization of the doping tail inside the c-Si surface induces an efficient separation of carriers inside the c-Si bulk before they reach the c-Si surface where the defect density, D_{it}, is high. Practically, the doping tail is affected by the thermal diffusion budget (TB) [14] and the properties of the ultra-thin SiO_x layer [15]. However, when annealed at high temperature, the ultra-thin SiO_x layer can be locally broken to form pinholes, which will affect the doping tail and the D_{it} at the c-Si surface [13]. Consequently, the formation of pinholes will influence the passivation quality of the poly-Si passivating contacts. In poly-Si processes one thermal process is conventionally used to activate/diffuse the dopants and to form pinholes in SiO_x, if any. This makes it difficult to study the effect of the SiO_x pinhole formation on the passivation quality. In order to investigate this topic, one needs to decouple these steps.

In this contribution, we effectively decoupled the process of forming pinholes from dopants diffusion by means of a two-step annealing process during the fabrication of our ion-implanted poly-Si passivating contacts. A pre-annealing step before ion-implantation is used to form the pinholes in the SiO_x layer. A second post-annealing step with different TB is used to activate the ion-implanted doping species and enable their diffusion. With a selective etching process based on TMAH [13,16], we monitored the density of the formed pinholes in the pre-annealing step. This enabled us to evaluate the influence of the presence of pinholes and the TB of dopants on the passivation quality of poly-Si passivating contacts.

It is found that, for both n⁺ and p⁺ poly-Si samples, the existence of pinholes can enhance their passivation quality, as long as the pinhole density and the post-annealing TB are not too high (~1x10⁷ cm⁻² and ~2x10¹² cm², respectively). Also, we found that the sensitivity of passivation quality on the pinhole density for n⁺ poly-Si samples is much higher than that for p⁺ poly-Si samples. The enhanced passivation quality is due to the strengthening of the electrical field passivation, owing to the local diffusion of dopants through the pinholes.

- [1] A. Richter, et al., Nat. Energy, 2021.
- [2] R. Peibst, et al., Prog. Photovolt. Res. Appl., 2020.
- [3] G. Nogay, et al., ACS Appl. Mater. Interfaces, 2016.
- [4] B. L. J. Geerligts, et al., Work. Cryst. Silicon Sol. Cells Modul. Mater. Proc., 2016.
- [5] M. Rienäcker, et al., En. Proc., 2016.
- [6] G. Yang, et al., Appl. Phys. Lett., 2016.
- [7] A. Ingenito, et al., Sol. RRL, 2017.
- [8] J. Krügener, et al., Sol. En. Mater. Sol. Cells, 2017.
- [9] Y. Chen, et al., Prog. Photovolt. Res. Appl. 2019.
- [10] W. Wu, et al., 36th EUPVSEC, 2019.
- [11] N. Nandakumar, et al., Prog. Photovolt. Res. Appl., 2019.
- [12] M. Stodolny, et al., 46th IEEE PVSC, 2019.
- [13] R. Peibst, et al., Sol. En. Mater. Sol. Cells, 2016.
- [14] R. Regner, 10th IEEE Int. Conf. Adv. Therm. Process. Semicond., 2002.

[15] F. Feldmann, et al., *Sol. En. Mater. Sol. Cells*, 2019.

[16] H. Steinkemper, et al., *IEEE J. Photovolt.*, 2015.

10:45 AM EN06.04.02

Silicon Microwire Arrays with Nanoscale Spacing for Radial Junction c-Si Solar Cells with an Efficiency of 20.5% Namwoo Kim¹, Deokjae Choi¹, Hyungwoo Kim¹, Han-Don Um² and Kwanyong Seo¹; ¹Ulsan National Institute of Science and Technology, Korea (the Republic of); ²Kangwon National University, Korea (the Republic of)

Structural optimization of microwire arrays is important for the successful demonstration of the practical feasibility of radial junction crystalline silicon (c-Si) solar cells. In this study, we investigated an optimized design of tapered microwire (TMW) arrays to maximize the light absorption of c-Si solar cells, while minimizing the surface recombination, for simultaneously improving the open-circuit voltage and short-circuit current density (J_{sc}). Finite-difference time-domain simulations confirmed that controlling the spacing between the TMWs at the nanometer scale is more effective for increasing the light absorption than increasing the TMW length. The photogenerated current of a c-Si TMW array with a 200 nm spacing was calculated to be 42.90 mA/cm², which is close to the theoretical limit of 43.37 mA/cm² in the 300–1100 nm wavelength range. To experimentally demonstrate the TMW arrays with a nanometer-scale spacing of 200 nm, which cannot be realized by conventional photolithography, we utilized a soft lithography method based on polystyrene beads for patterning a c-Si wafer. The solar cells based on optimized TMW arrays exhibited a J_{sc} of 42.5 mA/cm² and power conversion efficiency of 20.5%, which exceed those of the previously reported microwire-based radial junction solar cells.

11:00 AM EN06.04.03

Enhancement of Light Absorption in Transparent Crystalline Silicon Solar Cells Using Light-Harvesting Film Kangmin Lee, Jeonghwan Park and Kwanyong Seo; UNIST, Korea (the Republic of)

A light-harvesting film is considered as a means to improve the power conversion efficiency (PCE) of solar cells. However, when a light-harvesting film is applied to transparent solar cells, it is difficult to maintain the transparency of transparent solar cells due to the high haze ratio of the film (>95%). In this study, we apply a light-harvesting film onto the selective area, which is the light absorption region of the transparent c-Si solar cells. As a result, the transparent c-Si solar cells with light-harvesting film exhibited a current density (J_{sc}) increase of 2.6 mA/cm² compared with the transparent c-Si solar cells without a light-harvesting film. Therefore, the best device showed a PCE of 15.8% ($J_{sc} = 31.7$ mA/cm², open-circuit voltage (V_{oc}) = 638 mV, and fill factor (FF) = 78.3%) at an average visible transmittance of 20%, while maintaining a low haze ratio (0.95%). Furthermore, the transparent c-Si solar cells with the light-harvesting film have the advantage of minimizing the PCE degradation depending on the angle of light incidence. The transparent c-Si solar cells with light-harvesting film change the J_{sc} are under 4% for incident angles below approximately 50°, whereas that of the reference cells (conventional planar c-Si solar cells) loses over 30% in the same angle range. Hence, the proposed transparent c-Si solar cells present a unique opportunity to develop next-generation transparent solar cells, which would satisfy high efficiency and minimize PCE degradation according to the angle of light incidence.

11:15 AM EN06.04.04

25 cm²-Sized Glass-Like Transparent Crystalline Silicon Solar Cells with an Efficiency of 14.5% Jeonghwan Park, Kangmin Lee and Kwanyong Seo; UNIST, Korea (the Republic of)

Forming light-transmitting structures on c-Si photovoltaics to transmit visible light without wavelength dependency is a promising strategy to realize neutral-color transparent c-Si photovoltaics (c-Si TPVs). However, dry etching, which is used to form a light-transmitting structure on c-Si, inevitably causes nanoscale surface damages such as scallops and plasma-induced damage in c-Si. This aggravates carrier recombination, which decreases the power conversion efficiency (PCE) of c-Si TPVs. Here, we propose an effective chemical treatment method for removing nanoscale surface damage from c-Si microholes. A large-sized neutral-color c-Si TPV after the chemical treatment exhibited a high PCE of 14.5% at a transmittance of 20%. The chemical treatment also enabled systematic control of the hole size (167 nm/sec), and thus, the transmittance was easily tuned from 10% to 70%. Notably, the proposed chemical treatment satisfies the three development factors of 1) high PCE, 2) scaling up, and 3) easy light transmittance tuning of c-Si TPVs.

11:30 AM EN06.04.05

Utilizing Three Terminal IBC-Based Si as a Platform to Study the Durability of Photoelectrodes for Solar Fuel Production Darci Collins^{1,2}, Nathan T. Nesbitt¹, Daniel Tune³, Valentin D. Mihailetchi³ and Emily Warren¹; ¹National Renewable Energy Laboratory, United States; ²Colorado School of Mines, United States; ³International Solar Energy Research Center (ISC) Konstanz, Germany

Three terminal (3T) Si solar cells based on interdigitated back contact (IBC) structures are growing in popularity for the fabrication of tandem solar cells.¹ 3T devices also have potential application in photoelectrochemical fuel-forming applications. The vast majority of photoelectrochemical devices are based on two terminal (2T) semiconductor electrodes. Under illumination, these devices can drive fuel-forming electrochemical reactions coupled to an appropriate catalyst (e.g., the hydrogen evolution reaction or CO₂ reduction). While these devices are still at early stages of research, eventually they will need to operate for long periods of time (years) under diurnal illumination. The operation of photoelectrodes in dark or under diurnal cycling has only received a limited amount of research focus, but may present a problem, as many p-type semiconductor materials and solar cells used as photocathodes oxidize or corrode when not “protected” by the cathodic current present under illumination.² Generally, it is assumed that photocathode devices will sit at open circuit (not passing any current) when not illuminated, but this does not allow the same cathodic protection provided by illumination. Providing cathodic protection to the electrode surface can improve the long-term durability of fuel-forming photocathodes. However, in the dark, 2T p-n junction devices cannot pass appreciable amounts of current in the same direction without going into reverse bias or breakdown.

Using 3T devices as photocathodes can potentially overcome some of these challenges, by providing an alternative pathway to pass current to the electrode surface. We are studying the benefits that a three-terminal (3T) photoabsorber structure can provide for the stability to diurnal cycling and selectivity of solar-driven CO₂R. Using a 3T n/IBC structure (an n-type IBC cell with a conductive n-type front contact fabricated at ISC Konstanz)³ we can operate the device as a standard 2T photocathode when connecting the p⁺ back contact (R) to drive electrochemistry at the front of the cell (F). Additionally, we can also connect the n⁺ back contact (Z) to drive electrochemistry in the dark without needing to drive current backward through the p-n junction. In this talk, we will discuss the electrochemical characterization of 3T Si IBC devices for electrochemical fuel production. We show the performance of these 3T devices in both a standard photovoltaic configuration and as a 3T photocathode for both regenerative and fuel forming reactions. We will show preliminary stability data for these devices and discuss the potential for using a 3T structure for active repair of a photoelectrochemical system.

References:

(1) Warren, E. L. et al., A Taxonomy for Three-Terminal Tandem Solar Cells. *ACS Energy Lett.* **2020**, *5* (4), 1233–1242.

(2) Fu, H. J. et al., Enhanced Stability of Silicon for Photoelectrochemical Water Oxidation through Self-Healing Enabled by an Alkaline Protective Electrolyte. *Energy Environ. Sci.* **2020**, *13* (11), 4132–4141.

(3) Kopecek, R. et al., ZEBRA Technology: Low Cost Bifacial IBC Solar Cells in Mass Production with Efficiency Exceeding 23.5%. In *2020 47th IEEE*

SESSION EN06.05: Tandem Solar Cell and Novel Characterization Approaches
Session Chairs: Kaining Ding and Silvana Ovaite
Thursday Afternoon, December 1, 2022
Hynes, Level 3, Room 301

1:30 PM *EN06.05.01

Interconnection Configurations for Silicon-Based Hybrid Tandem Photovoltaics [Kirstin M. Alberi](#); National Renewable Energy Laboratory, United States

Hybrid tandem solar cells, in which two different photovoltaic absorbers are combined, are increasingly considered as a viable option for extending the efficiency of single junction Si solar cells. Silicon is a natural choice for the bottom sub-cell due to its near-ideal bandgap energy for high tandem power conversion efficiency and its compatibility with both monolithic and mechanically stacked integration approaches. One important yet open design consideration is how the top and bottom sub-cells are connected. Two-terminal, three-terminal and four-terminal interconnection schemes are all options at the cell level. The choice will be dictated in part by the specific top sub-cell absorber material, the ease of fabricating a tunnel junction with the bottom Si sub-cell, and the preferred or established top sub-cell manufacturing methods that are already in place. This talk will cover these interconnection approaches, including voltage matching options at the module level, their benefits and drawbacks, and specific challenges of implementing them with different top sub-cell technologies. Future prospects and near-term research needs will also be discussed.

2:00 PM EN06.05.02

Potential of Si Tandem Solar Cells for PV-Powered Vehicle Applications [Masafumi Yamaguchi](#), Kyotaro Nakamura, Ryo Ozaki, Nobuaki Kojima and Yoshio Ohshita; Toyota Technological Institute, Japan

PV-powered vehicle applications are very attractive for reducing CO₂ emission and creation of new market [1]. Development of high-efficiency (> 30%) and low-cost solar cell modules is very important. Although Toyota Prius and Nissan eNV 200 demonstration cars installed with Sharp's high-efficiency III-V 3-junction solar cell modules with an efficiency of more than 30% have demonstrated longer driving range of 26km/day average compared to 16km/day average for Sono Motors Sion installed with Si back contact solar cell modules with an efficiency of 21.5%, cost reduction of MJ solar cells is necessary for PV-powered vehicle applications. Development of Si tandem solar cells [2] is very promising for cost reduction.

This paper compares analytical results for PV-powered installed with various solar cell modules and actual driving distance of the Toyota Prius demonstration car and Sono Motors Sion. In addition, analytical results for driving distance of PV-powered vehicles installed with various candidate Si tandem solar cells and multi-junction solar cells are shown in this paper.

Solar cell module efficiency impact on driving distance of PV-powered vehicles was calculated. In the calculations, 4kWh/m²/day as solar irradiance, 3m² as module installation area and the charging system efficiency of 73.9% composing of cell temperature correction, maximum power point tracking, DC/DC conversion, and DC charging were assumed. Table 1 shows estimated potential and actual data for driving distance DD of vehicles powered by current solar cell modules. Good agreement between calculated and actual data shows validity of analytical procedure as shown Table 1. Table 2 shows estimated potential of driving distance DD of vehicles powered by candidate Si tandem solar cells including our results and multi-junction solar cells. The III-V 3-junction and Si 3-junction tandem solar cell modules with an efficiency of more than 35% are shown to have potential of driving distance of more than 30 km/day average and more than 50 km/day on a clear day as shown in Table 2.

Table 1. Estimated potential and actual data for driving distance DD of vehicles powered by current solar cell modules

Modules	Efficiency (%)	Estimated DD (km/day)	Actual DD(km/day)
III-V 3-J	32.65	27.0	
III-V 3-J (Prius)	30.9	25.6	25.6
GaAs	25.1	20.8	
Si	24.4	20.2	
Si (Sion)	20	16.6	16
CIGS	19.2	15.9	
Perovskite	17.9	14.8	

Table 2. Estimated potential of driving distance DD of vehicles powered by candidate solar cells

Solar cells	Efficiency (%)	Estimated DD (km/day)
III-V 3-J	39.5	32.8
III-V/Si 3-J	35.9	29.8
III-V/Si 3-J (our study)	34.0	28.2
III-V/Si 2-J	32.8	27.9
III-V/CiGS 3-J	29.3	24.3
Perovskite/Si 2-J	29.8	24.7
Perovskite/perovskite 2-J	28.0	23.2
Perovskite/CIGS 2-J	24.2	20.1

Several losses such as non-radiative recombination, optical and resistance in Si tandem solar cells are discussed in this paper.

References

- [1] M. Yamaguchi et al., *Prog. Photovolt.* **29**, 684 (2021).
- [2] M. Yamaguchi et al., *J. Phys. D: Appl. Phys.* **51**, 133002 (2018).
- [3] M. Yamaguchi et al., *J. Mater. Res.* **32**, 3445 (2017).

2:15 PM EN06.05.03

Novel Technique to Characterize Minority and Majority Carrier Contact Resistivity [Dirk Steyn](#)¹, Matthew Hartenstein¹, William Nemeth², San Theingi², David L. Young², Sumit Agarwal¹ and Pauls Stradins²; ¹Colorado School of Mines, United States; ²National Renewable Energy Laboratory,

United States

In this work we report a novel method of measuring both majority and minority carrier contact resistivities. In the pursuit of highly efficient silicon solar cells, a great deal of research has been done on passivating and selective contacts [1-3]. The contacts of these cell must be well passivating and conductive, and the accurate characterization of contacts is of great importance to silicon PV. The transfer length method (TLM) is widely used to characterize the contact resistivity of PV devices. However, TLM can only be used to measure the majority carrier contact resistivity. To measure the minority carrier contact resistivity with TLM, a contact must be created on the same type of wafer as the minority carrier contact to avoid blocking diode effects. It is not clear that this contact will have the exact same properties as a contact on the original wafer. Our technique can be used to measure the resistance of electrons and holes separately on the same type of wafer used in the final cell, allowing for the accurate characterization of both contacts.

In our method, a thin tunneling oxide is grown on n-Cz silicon. Then heavily doped polysilicon of the same type, either n or p-type, is deposited on both sides of the device to create carrier selective contacts (either electron or hole selecting). The devices have a metal grid on the front, and a full back metal contact (the typical metallization scheme of a bipolar solar cell device). By increasing illumination, the apparent resistance (measured between the front and back metal) of the bulk silicon substrate will approach zero due to increasing wafer conductivity from the high injection of photocarriers, and only the resistance of the contacts will be detected. Under illumination, the effect of the blocking diode is decreased due to increased minority carrier density and a weaker field in the diode. Since the contacts are carrier selective, practically only electrons or holes will conduct through the contact, depending on the contact used, and allows for the measurement of both types of contacts as they would behave in practice. We can then plot the total resistance measured against the inverse of illumination. This gives a very distinct plot that approaches the total contact resistance at the y-intercept. The value of contact resistivity measured in this way has been verified with TLM measurements for n-type contacts on an n-type wafer. We have also characterized the resistivity of p-type contacts on an n-Cz wafer. Unlike the TLM method, we can observe the effects of spreading resistance caused by contact geometry without any additional calculations. This is seen as the total resistance levels out as the inverse of illumination approaches infinity. While this value should ideally correspond to the bulk resistance of the underlying wafer, we observe it to be higher than expected, likely due to spreading resistance between the two contacts.

This technique can give more accurate insight into the causes behind problematic series resistance than TLM and can be used to optimize contact design as well as contact geometry. In addition to the work mentioned above, we will present extensive simulations of this measurement done in Quokka 3, show how this can be used to characterize full devices, and demonstrate how this technique can be used in calculating contact selectivity [1]. We suspect that this method can be used to expand the definition of contact selectivity and will present our investigation of material property effects on selectivity.

References

- [1] Brendel et al., 2016 *IEEE J. Photovoltaics*, vol. 6, no. 6, pp. 1413–1420
- [2] Yan et al., 2022 *Prog. Photovoltaics Res. Appl.*, pp. 1- 17
- [3] Feldmann et al., 2014 *Sol. Energy Mater. Sol. Cells*, vol. 120, pp. 270–274

2:30 PM EN06.05.04

Electrically Detected Magnetic Resonance (EDMR) Spectroscopic Determination of Bulk Defects in n-type Cz Silicon Chirag M. Mule^{1,2}, Vincenzo LaSalvia¹, William Nemeth¹, Fedor Sharov³, Elijah Allridge³, Harvey Guthrey¹, Patrick Lenahan³, Sumit Agarwal² and Pauls Stradins¹; ¹National Renewable Energy Laboratory, United States; ²Colorado School of Mines, United States; ³The Pennsylvania State University, United States

We have produced minicells that exactly replicate the performance of the large area poly-Si/SiO₂ passivated contact cells and measure the Electrically Detected Magnetic Resonance spectroscopic (EDMR) response of the bulk defects in the n-type Cz silicon wafer on them. High efficiency n-type monocrystalline silicon cells with passivated contacts are rapidly gaining global PV market share and are expected to dominate by 2031 [1]. In the current high-performance nCz wafers with lifetimes ~ 20 ms, as little as 10¹⁰ cm⁻³ defects can degrade the cell efficiencies. Electron Paramagnetic Resonance (EPR) can be used for sensitive detection of the bulk defects however the detection limit for EPR is ~10¹¹ cm⁻³. The EDMR can be performed directly on the devices, structures with passivated contacts, fragments of a module, is > 100x more sensitive than the EPR, and senses only the current/performance affecting defects in a cell. The high sensitivity allows EDMR measurements at the room temperatures, avoiding expensive cryogenic equipment. Thus, EDMR has a high potential for the application to advance the Si PV industry.

The high lifetime nCz wafers are prone to various Process-Induced Degradation defects (PIDs) due to thermal processing – oxygen precipitates, vacancies, voids, interstitials etc. We characterize them using EDMR spectroscopy with our unique minicell design and the EDMR at the Penn State University. We use the specific thermal budgets to induce bulk defects: 1) Boron diffusion and deep drive-in (~980°C 10 hr) to induce oxygen precipitates and 2) Tabula Rasa (10 min. 1100°C) in N₂ to induce vacancies in nCz minicell bulk and study them by the EDMR, correlating with the performance loss of the PID-degraded minicells. In the only attempt from the literature by Lang et al [2] the bulk signal intensities are weak, and it is uncertain whether the Pb₀ & Pb₁ signal is coming from the surface or the bulk.

We laser-scribe the nCz Si to 1 mm x 1 cm minicell precursors, which undergo saw damage removal and wet-chemical cleaning. Further, we thermally grow ~1.5 nm tunneling SiO_x and then deposit a-Si: H. We add the doped n⁻ and p⁺ layers through mechanical masks with 10-micron precision and anneal at 850°C to drive the dopants into the a-Si:H layer and crystallize to poly-Si layers. This is followed by Al₂O₃ deposition and Forming Gas Anneal. The minicells are finally metallized with TiAg pads and grids and inserted into the EDMR resonant cavity. The cell process mimics our large area passivated contact cell.

The EDMR were performed both using radiofrequency/low field (prototype of Penn State startup Blue Spin desktop spectrometer) and high field, microwave X-band Bruker system adapted for EDMR. These initial data were taken at room temperature, showed a signal at g-value of 2.006 which corresponds to the Si-dangling bond, likely from the Si wafer surface. This demonstrates the viability of the minicell design, cell processing and the EDMR capabilities.

References –

- [1] International Technology Roadmap for Photovoltaic (ITRPV) SEMI PV Group Europe, 2013, <http://www.itrpv.net/>
- [2] V. Lang, J. D. Murphy, R. J. Falster, and J. J. L. Morton, "Spin-dependent recombination in Czochralski silicon containing oxide precipitates", *Journal of Applied Physics* 111, 013710 (2012) <https://doi.org/10.1063/1.3675449>

2:45 PM BREAK

3:15 PM *EN06.06.01

Architectures for High-Efficiency Crystalline Silicon Solar Cells Miroslav Zeman, Yifeng Zhao, Manvika Singh, Luana Mazzarella, Arthur Weeber and Olindo Isabella; Delft University of Technology, Netherlands

At present, crystalline silicon (c-Si) based solar cells dominate the PV market. There is a continuous effort to improve the conversion efficiency of c-Si solar cells by developing and optimizing different c-Si solar cell architectures.

Front/back-contacted silicon heterojunction (FBC-SHJ) solar cells have exhibited efficiencies well above 26% [1]. To achieve such high efficiencies, the material quality of (*i*)a-Si:H passivating layer is critical, ensuring excellent surface passivation and facilitating charge carrier collections in SHJ solar cells. Fourier-transform infrared spectroscopy (FTIR) was used to study the quality of (*i*)a-Si:H layers deposited in the range from 140°C to 200°C. FTIR results showed that (*i*)a-Si:H films were less dense when deposited at lower temperatures, thus hindering their surface passivation capabilities. However, with additional hydrogen plasma treatments (HPTs), the (*i*)a-Si:H layers deposited at lower temperatures the passivation qualities was significantly improved in contrast to their counterparts deposited at higher temperatures. Further, for monofacial solar cells with screen-printed Ag contacts we observed highest V_{OC} s for cells with (*i*)a-Si:H deposited at the lowest temperature (140°C), however, the related FF s are poorer as compared to their higher temperature counterparts. The optimum trade-off between V_{OC} and FF for the SHJ cells was found with temperatures ranging from 160°C to 180°C. Based on our FTIR study, this trade-off reveals two critical requirements for optimizing the (*i*)a-Si:H layers in high-efficiency SHJ solar cells: (i) excellent surface passivation quality to reduce losses induced by interface recombinations and (ii) less-defective (*i*)a-Si:H bulk to not disrupt the charge carrier collections.

Moreover, reducing indium (In) and silver (Ag) consumption is a crucial challenge for scaling up SHJ solar cell technology towards terawatt level implementation. We performed optical modelling and electrical studies to optimize TCO thicknesses [2]. Instead of standardly used 75-nm-thick tin-doped indium oxide (ITO) on the illumination side, we applied 50-nm-thick tungsten-doped indium oxide (IWO) plus 100-nm-thick SiO_x forming a double-layer antireflection coating (DLARC), which concurrently reduces the thickness of the TCO and improves the optical response of the monofacial SHJ solar cells. To reduce Ag use, we utilized electroplated Cu for forming the front metal grid [3]. The best monofacial SHJ solar cell fabricated in this study achieved V_{OC} of 726.0 mV, J_{SC} of 39.97 mA/cm², FF of 83.3% and efficiency of 24.18%. We demonstrated Cu-plated bifacial SHJ solar cells with DLARCs exhibiting efficiencies > 22% (*n*-side illumination) by applying 25-nm-thick IWO and ITO for *n*- and *p*- contact, respectively [2]. This represents a 78% reduction in TCO use as compared to our lab-standard 75 nm plus 150 nm TCO utilization in monofacial SHJ solar cells.

High-thermal budget carrier selective passivating contacts (CSPCs) based on poly-SiO_x [4],[5],[6], are another excellent candidates for high-efficiency c-Si solar cells. We obtained 690 mV i - V_{oc} on poly-SiO_x / textured c-Si surfaces using the 2-step annealing approach. High passivation quality was achieved for both *p* and *n* type poly-SiO_x CSPCs. With the developed poly-SiO_x CSPCs, we fabricated 4-cm² large, screen-printed single side textured (SST) single junction c-Si solar cell with a certified efficiency of 20.47%. Likewise, a certified efficiency of 18.57% was obtained for a double side textured (DST) cell with poly-SiO_x CSPC.

This work was supported by Dutch NWO Joint Solar Program III.

- [1] LONGi Solar, *news release* (2021)
- [2] C. Han, et al., *Prog. Photovoltaics* (2022)
- [3] C. Han, et al., *Solar RRL*, 2100810 (2022)
- [4] G. Yang, et al., *Appl. Phys. Lett.*, (2018)
- [5] M. Singh, et al., *Sol. Energy Mater. Sol. Cells*, (2020)
- [6] G. Yang, et al., *Prog. Photovolt. Res. Appl.*, (2021)

3:45 PM *EN06.06.02

The Critical Role of TCO Deposition on Solar Cell Performance Monica Morales-Masis; University of Twente, Netherlands

Transparent Conducting Oxides (TCOs) are widely accepted transparent electrodes in a variety of solar cells employing passivating and selective contacts, such as silicon heterojunction (SHJ) solar cells and thin film technologies such as CIGS and perovskite solar cells. Among all possible ways to deposit TCOs, sputter deposition is the most employed technology, both in academia and industry. However, the high kinetic energies of the arriving species during sputtering may damage sensitive functional layers beneath, affecting interface formation, passivation and ultimately device performance. This has motivated the search for alternative sputter system designs or deposition techniques, allowing low damage growth of TCOs on the sensitive layers. Here we explore pulsed laser deposition (PLD) as an alternative low-damage physical vapor deposition technique. PLD is operated at high deposition pressures, promoting thermalization of particles, and therefore reducing the kinetic energy of ablated species. Broadband transparent and high mobility TCOs were developed using wafer-scale (4-inch) PLD with deposition rates on par with lab-scale RF sputtering¹. To investigate the effects of the deposition pressure, we developed ITO with identical sheet resistance (50 Ohm/sq) at deposition pressures three orders of magnitude apart, and applied them as a front TCO in SHJ cells and as rear-contact in semitransparent perovskite cells. The role of the deposition pressure on TCO properties, absorber carrier lifetime and its link to SHJ and perovskite solar cell parameters such as series resistance and fill factor (FF) will be discussed. Strategies to mitigate damage, for each type of cell will be furthermore discussed.

References

- ¹M. Macco et al. *Adv. Electron. Mater.* 3 (5), 1600529, 2017. <https://doi.org/10.1002/aelm.201600529>
- ²Y. Smirnov et al. *Adv. Mater. Technol.* 6 (2), 2000856, 2021. <https://doi.org/10.1002/admt.202000856>

4:15 PM EN06.06.03

Exceptional Surface Passivation and Carrier Transport in Pyramidically Textured N-Type Silicon by Organic Molecules with Sulfonic Acid Head Groups and Perfluoroalkyl Tail Groups Milad Ghasemikashitban, Konstantin Tsoi, Gorkem Gunbas and Selcuk Yerci; Middle East Technical University, Turkey

Improving the passivation quality of the surface in silicon (Si) solar cell is one of the main strategies for enabling higher performance. Excellent passivation schemes have been recently developed, with lifetimes reaching 0.5 sec using, for example, Al₂O₃ and SiN_x dielectric layers with proper (i.e.,

negative and positive for p- and n-type Si, respectively) fixed charges. However, one of the main disadvantages of such dielectrics is the deposition methods requiring vacuum and, possibly, high-temperature annealing steps. Eliminating these steps has the potential to reduce the fabrication costs of silicon solar cells considerably. One family of materials that potentially can provide high passivation of silicon is organic materials. Due to the simplicity of their deposition methods (often fabricated in the room ambience without subsequent thermal annealing), and the capacity to inherently possess high dipole moments and fixed charges, organic materials might deliver the same level of performance as inorganic dielectrics but at a reduced cost. In this regard, we present an investigative study of organic materials with sulfonic acid head groups and perfluoroalkyl tail groups.

We demonstrate minority carrier lifetime values of over 8 ms (an implied open circuit voltage (iV_{oc}) of > 730 mV) with organic materials on textured Czochralski n-type Si wafers, comparable to the passivation level of high-performance inorganic dielectrics. Moreover, we show that only 5% of organic material dissolved in a solution of deionized water (DI) and isopropanol (IPA) is sufficient to passivate the silicon surface. IPA/DI water provides much higher performance compared to alternative solvents (DMSO, ACN, Ethanol, and IPA without water). The critical role of DI water is elucidated. Si surfaces coated with organic materials were investigated using Attenuated Total Reflectance (ATR), Fourier Transform Infrared spectroscopy (FTIR), and X-ray Photoelectron Spectroscopy. Initial results indicate that passivation is mainly provided by the field effect, resulting in a favorable energy band bend bending at the surface of Si. Due to the chemical structure of organic materials and their similarity to those of self-assembling monolayers, we hypothesize that these organic materials form dipoles at the interface generating an electric field and resulting in a favorable band bending. This hypothesis is also supported by contact angle measurements, which reveal high hydrophobicity for surfaces treated with organic materials. These organic materials provide good passivation together with good carrier transport properties. A contact resistance as low as $106 \text{ m}\Omega/\text{cm}^2$ is achieved through n-Si – organic materials – aluminum stacks, which can be further reduced to $15 \text{ m}\Omega/\text{cm}^2$ with a thin layer of LiF_x deposited under Al metal. Lastly, we discuss the stability of organic materials and demonstrate that keeping the samples under nitrogen ambient, at low temperatures (2°C), or adding PCBM ([6,6]-Phenyl C_{61} butyric acid methyl ester) into the solutions improves the stability considerably. A very first proof-of-concept solar cell with organic materials deposited at the rear of the solar cell demonstrated an efficiency of $\sim 17\%$, only 3% lower than the PERC type silicon solar cell produced in the same batch.

Our results prove that organic materials with a head group that anchors to pyramidally textured Si and a tail group that provides a high dipole with a cost-effective, low-temperature fabrication can provide good passivation and charge transport and thus have great potential for providing high-performance solar cells.

SESSION EN06.07: Virtual Session II: Tandem Solar Cells
Session Chairs: Kirstin Alberi and Ivan Gordon
Wednesday Morning, December 7, 2022
EN06-virtual

8:00 AM *EN06.07.01

Pushing Solar Energy Conversion Beyond Today's Efficiency and Cost Limits [Rutger Schlatmann](#)^{1,2}; ¹Helmholtz-Zentrum Berlin, Germany; ²HTW Berlin, Germany

In this talk, we will discuss the detailed material science and engineering aspects of Perovskite/silicon tandem solar cells, that led to a 1 cm^2 sample with 29.8% efficiency. We will focus on adaptations to the standard Silicon Heterojunction bottom cell that enabled high-efficiency tandem values. More in particular, we will discuss optical measures to optimize the bottom cell response in the infrared part of the spectrum. Closely connected to the engineering of the optics, we will discuss the interplay between bottom cell and subsequent top cell optimization. Consequences and potential modifications for industrial implementation will be discussed.

We will also briefly discuss the complicated dynamics, involving both degradation and recovery mechanisms, that are observed in combined indoor and outdoor stability measurements on encapsulated perovskite based tandem cells, which we have monitored for well over a year.

8:30 AM *EN06.07.02

Towards Large Area 4-Terminal Hybrid Perovskite-Silicon Tandems Using Scalable Processing [Arthur W. Weeber](#)^{1,2}; ¹TNO, Netherlands; ²Delft University of Technology, Netherlands

Co-authors from Solliance partners TNO, TU/e, TU Delft and imec will be added to the final paper.

The current PV market is dominated by crystalline silicon solar cells with so-called PERC architecture (Passivated Emitter and Rear Cell). However, the PERC technology is approaching its efficiency limit of about 24% and to maintain the overall 0.5-0.6% absolute annual efficiency improvement, TOPCon (Tunnel Oxide Passivating Contacts) and silicon heterojunctions (SHJ) are seen as the follow-ups. Efficiencies close to and beyond 26% have been achieved in an industrial environment for TOPCon [1] and SHJ [2] respectively. Several large manufacturers are already producing TOPCon and SHJ solar cells and modules. The current world record silicon solar cell is a fully back-contacted SHJ one with an efficiency of 26.7% [3].

For the next step and reaching efficiencies beyond 30% crystalline silicon solar cells can be combined with perovskite solar cells. With a stack of these solar cells in a so-called tandem configuration the solar spectrum can be better utilized. The current world record for a perovskite-silicon tandem is 29.8% and obtained by HZB [4].

Tandem architectures with 2-, 3- or 4-terminals are being researched, and all these configurations have advantages and drawbacks. In this paper we will focus on so-called 4-terminal (4T) perovskite-silicon tandems. The advantage of 4T tandems is that current matching is not required because the component solar cells can operate independently of each other which can result in a higher annual yield. Another advantage of 4T tandems is that bottom cells with different architectures (PERC, TOPCon, SHJ, back-contacted) can be integrated more or less independent of the top-cell layout. A drawback for 4T tandems will be that additional electronics are needed.

We will present our latest results for 4T tandems for small area lab cells, but also for large area cells and modules (area matched). Results of stability and reliability, outdoor monitoring and annual yield modelling will also be shown. So far, we have obtained over 29.5% efficiency for small area tandems with different silicon bottom cell architectures (internal measurements). For large area cells upscaling from spin-coating to slot-die-coating was carried out for the perovskite solar cell. Modules of 100 cm^2 were made using P1, P2 and P3 laser scribing and an efficiency above 16% was obtained for 1.6 eV bandgap perovskite material. Applying this 1.6 eV perovskite solar cell with a SHJ bottom cell and integrating both component cells in an area matched module (100 cm^2) resulted in an efficiency of 25.6% [5].

For lab size perovskite solar cells huge progress has been made with respect to stability and reliability. Several accelerated lifetime test have been passed successfully. Performing outdoor monitoring tests is crucial for tandem PV. At TNO we installed an outdoor facility dedicated to tandems. First results show good outdoor stability over a period of almost a year for the best tandem module configurations [6].

With respect to conventional monofacial PV, the annual yield can be increased by applying bifacial technology. As stated above, in 4T tandems the

component cells can operate independently and with advanced annual yield modelling we have shown a significant higher average generated photocurrent for 4T tandems compared to its 2T counterpart [7]. More details and recent progress will be presented during the conference.

This work has been carried in different Dutch and European project.

- [1] <https://www.jinkosolar.com/en/site/newsdetail/1712>
- [2] <https://www.longi.com/en/news/7469/>
- [3] K. Yoshikawa et al, <http://dx.doi.org/10.1016/j.solmat.20174.06.024>
- [4] https://www.helmholtz-berlin.de/pubbin/news_seite?nid=23248;sprache=en
- [5] V. Zardetto et al, presented at the Tandem Workshop Freiburg 2022
- [6] G. Coletti et al, presented at the Tandem Workshop Freiburg 2022
- [7] Singh et al, <http://dx.doi.org/10.1515/nanoph-2020-0643>

9:00 AM *EN06.07.03

From Three Terminal Tandem Solar Cells to Modules Henning Schulte-Huxel, Robert Witteck, Susanne Blankemeyer and Marc Köntges; Institute for Solar Energy Research in Hamelin (ISFH), Germany

Three terminal tandem (3TT) solar cells require an adapted module integration scheme in order to explore their full efficiency potential. The three terminals allow to extract the power of the top and bottom cell separately. In a string, the wide bandgap top cells are interconnected in parallel to multiple bottom cells, resulting in parallel/series interconnection. This special interconnection has implications for the operation of the subcells, the resulting current path between the subcells, the layout of the cell interconnects and for the system level. Here, we analyze by simulations and experiments the various aspects resulting from the module integration of 3TT depending on the voltage ratio of the top and the bottom cell and their relative orientation, either the sub cells are connected in series and allow a two-terminal (2T) operation (s-type) or they are reverse orientated (r-type). The aim is to present approaches and relevant aspects for modules and systems based on 3T devices, including the integration of bypass diodes as well as the interconnection of modules and their impact on string end losses. The findings also serve as a guide for the design and construction of future 3TT solar cells for optimal module integration. The interconnection is formed by a combination of a typical front-to-back manner and the contacting of back contacted solar cells. For the 1:2 r-type 3TT devices, one interconnect connects the contacts of three adjacent solar cells, resulting in a short length of the interconnect and thus low series resistance losses. All s-type devices and voltage ratios that differ from 1:2 result in longer current paths with the need to pass an intermediate solar cell without contacting it. This requires additional insulating layers on the cells' rear side and causes additional resistive losses as well as material costs. Starting from the cell level perspective, the independent operation of the top and bottom cell is restricted in a string by the requirement of voltage matching of the subcells. However, this type of matching is robust in efficiency with respect to variations in the current of the individual subcells. Apart from the resilience to spectral changes, this also means that 3TT strings can be operated bifacially, unlike 2TT strings that are sensitive for illumination inhomogeneities, allowing a significant increase in energy yield. Furthermore, the series/parallel interconnection provides unique possibilities to protect sensitive perovskite top cells from too high reverse voltages, thus avoiding significant cell degradation. Due to the parallel current path in the interconnection scheme of voltage-matched 3TT cells, they are more robust with respect to partial shading compared to strings of 2T devices. Nevertheless, bypass diodes are required to protect the cells from too high power dissipation in case of shading. For strings with a finite number of cells, string-end losses occur due to the requirement to combine the contacts of the end cells in one terminal. These losses account for at least the power of about one 3TT cell for devices with a 1:2 voltage ratio of the subcells and an r-type configuration. All other 3TT devices have higher string-end losses. One could terminate the strings to integrate the bypass diode, resulting in these string-end losses as will be discussed in detail in the final contribution. However, the 1:2 r-type configuration allows to integrate a bypass diode in parallel to a continuous string, shifting the string-end loss from the substring level of a module to the end of the module string on system level. This means that the string-end loss in a PV system with 20 modules of 72 cells each (1000 V system) accounts to 1/1440 of the power of one r-type 1:2 3TT device, instead of 1/24 as for the module's substring.

9:30 AM *EN06.07.04

Challenges in the Realization of Perovskite/Si Tandem Solar Cells Stephanie Essig; University of Stuttgart, Germany

No doubt commercial Si solar cells will soon be upgraded by combining them with wider bandgap (1.6-1.9 eV) top cells. Such tandem devices allow the reduction of thermalization losses and an efficiency enhancement beyond 30%. While there is a clear trend towards top cells based on low-cost metal halide perovskites, the optimum tandem cell architecture, ideal fabrication process, subcell interconnection, and module integration are still under debate. Furthermore, there is a multitude of interconnection schemes: Most appealing is the monolithic 2-terminal (2T) tandem device architecture with serially connected cells, as known from established (but costly) III-V technology. However, 3-terminal (3T) and 4-terminal (4T) designs also have their pros and cons.

Realization of high-efficiency 2T perovskite/Si tandem cells requires matching the photo currents generated in top and bottom cells. Yet, more technological advancements, like large-scale perovskite cell deposition on textured Si and the development of suitable cell interconnection layers, are needed. The ideal Si bottom cell must be optimized for efficient absorption of the infrared solar radiation. In addition, it features an optically transparent, electrically conductive, and passivating front contact which does withstand subsequent top cell processing. Bottom cell front contacts with similar properties are needed for 3T tandem devices featuring Si cells with interdigitated back contacts (IBC). In contrast to 2T, the 3T configuration does not require current-matching of the subcells. Consequently, and as known from stacked 4-terminal tandems, the energy yield of 3T tandems is more tolerant towards spectral variations and dissimilar degradation behavior of the perovskite top and Si bottom cells.

At the Institute for Photovoltaics (ipv) we investigate various tandem cell architectures and work on the building blocks needed for tandem solar cells. Hence, we develop strategies to implement established c-Si technology into high-efficiency perovskite/Si devices.

10:00 AM DISCUSSION TIME

SESSION EN06.08: Virtual Session I: Interfaces and Contacts
Session Chairs: Kaining Ding and Stephanie Essig
Wednesday Morning, December 7, 2022
EN06-virtual

10:30 AM *EN06.08.01

High-Efficiency Both-Sides-Contacted Silicon Solar Cells—Requirements and Design Options Armin Richter, Ralph Müller, Jan Benick, Bernd Steinhauser, Christian Reichel, Andreas Fell, Martin Bivour, Martin Hermle and Stefan W. Glunz; Fraunhofer Institute for Solar Energy Systems ISE, Germany

The photovoltaic industry is dominated by crystalline silicon solar cells. While interdigitated back contact cells have yielded the highest efficiency, both-sides-contacted cells are the preferred choice in industrial production due to their lower processing complexity. Typically, such industrial cells feature a pn junction at the front surface. In order to identify an ultimate design for both-sides-contacted cells, we have studied here different cell designs at a very high performance level. We demonstrate a very conversion efficiency of 26.0% for a both-sides-contacted silicon solar cell, which exhibits the pn junction at the back surface in form of a full area passivating contact based on poly crystalline silicon. One key feature of this advanced cell structure is the highly transparent front surface based on dielectric passivation layers without any lateral conductivity. A detailed power loss analysis reveals that this cell balances electron and hole transport losses as well as transport and recombination losses in general. On the base of this analysis we performed a systematic simulation study for a variety of different solar cell designs, which led to some fundamental design rules for future >26% efficiency silicon solar cells. We discuss further requirements and design options for these solar cells to improve the device performance even further.

11:00 AM EN06.08.02

Interface Treatments for High-Efficiency MoO_x Based Silicon Heterojunction Solar Cells Liqi Cao¹, Paul Procel^{1,2}, Luana Mazzarella¹, Yifeng Zhao¹, Engin Özkol¹, Jin Yan¹, Can Han¹, Guangtao Yang¹, Zhirong Yao¹, Miroslav Zeman¹ and Olindo Isabella¹; ¹TU Delft, Netherlands; ²San Francisco de Quito University, Ecuador

Silicon based solar cells dominate the market of photovoltaics, which hold the highest potential for green electricity production. A front/back-contacted architecture combined with the silicon-based heterojunction (SHJ) concept realized a world record efficiency of 26.3%¹. However, conventional silicon-based doped layers, which work as carrier selective transport layers, are not optically transparent.

Transition metal oxides are promising candidates for SHJ solar cells due to their advantageous opto-electronic properties. Molybdenum oxide (MoO_x) with high work function (WF) has achieved highly efficient solar cells with 23.5% efficiency². However, depositing high quality MoO_x thin film on top of a-Si:H is challenging due to highly reactive surfaces³. This interaction may result in interfacial oxidation, lower Mo oxidation states and reduced WF^{4,5}. In turn, electrical performances of solar cells featuring MoO_x are poorer³ than standard SHJ devices.

Several attempts have been made to prevent the reaction between MoO_x and (i)a-Si:H. Pre-annealing⁴ of a-Si:H and pre-growth of SiO_x layer⁶ have been proposed as effective ways to prevent the degradation of MoO_x. Nevertheless, those approaches require extra process steps that make MoO_x integration not immediately viable in industrial environment. In our previous work, we proposed a plasma treatment (PT) at MoO_x/(i)a-Si:H interface that demonstrated to mitigate dipole effect and resulted in improved cell performance⁷. After optimizing the interface treatment, even thinner MoO_x layer could be applied.

The solar cells were fabricated using 260±20 μm 4-inch double-side textured n-type <100> FZ wafers. (i)a-Si:H was deposited by plasma-enhanced chemical vapor deposition on both sides, while (n)a-Si:H only at the rear side. We carried out two different plasma treatments on the (i)a-Si:H interface prior MoO_x deposition: one called PT from a mixture of SiH₄, H₂ and CO₂ and another called PTB from a mixture of SiH₄, H₂, CO₂ and B₂H₆. One sample without plasma treatment (noPT) was used as reference to evaluate the efficacy of the proposed method. A thickness series from 1 to 4 nm of MoO_x was thermally evaporated from MoO₃ powder at the pressure of 5×10⁻⁶ mbar. After that, optimized 50-nm and 150-nm thick tungsten-doped indium oxide (IWO) layers were sputtered through a hard mask at front and rear side, respectively, defining six 2×2 cm² solar cells per wafer. As metal contact at the front side, we used room temperature Cu plating⁸ with a metal coverage fraction of 1.575%; at the rear side, 500-nm thick Ag layer was sputtered on the full device area.

We studied the impact of different plasma treatment conditions on MoO_x film quality and cells' performance. MoO_x film quality was assessed based on O vacancies inside the film⁴. The samples with interface treatments contain less O vacancies than the sample without treatment. It is noticeable that the cell precursors endowed with PTB yield higher fill factor (FF) than other types of precursors. Instead, PT and noPT samples benefitted from high short-circuit current density (J_{SC}). Ultimately, PTB and PT samples achieved similar conversion efficiency. For the variation of MoO_x thickness, we observed that even a slightly change in its thickness influences the solar cells' electrical performance drastically. An ultra-thin, ~1.7-nm thick MoO_x layer could provide sufficient field passivation (open circuit voltage, V_{OC} = 721.4 mV) and good opto-electrical properties (FF = 82.18% and J_{SC-illuminated-area} = 40.20 mA/cm²). With our approach we demonstrate world record cell with ISFH-certified conversion efficiency of 23.83%.

¹ LONGi Solar 2021.

² J. Dréon, et al., Nano Energy, 2020.

³ J. Geissbühler et al., Appl. Phys. Lett. 2015.

⁴ M.T. Greiner, et al., Adv. Funct. Mater. 2013.

⁵ M.T. Greiner, et al., Adv. Funct. Mater. 2012.

⁶ J. Tong, et al. ACS Appl. Mater. Interfaces. 2021.

⁷ L. Mazzarella, et al., Prog Photovolt Res Appl. 2020.

⁸ C. Han, et al., Solar RRL 2022.

11:15 AM EN06.08.03

Investigation of Local Parameters of PERC Solar Cells Metallized with Screen Printed Cu-Paste Suchismita Mitra¹, Steve Johnston¹, Steve Harvey¹, Harvey Guthrey¹, Ruvini Dharmadasa², Kevin Elmer², Apolo Nambo², Thad Druffle², Sandra Huneycutt³, Abasifreke Ebong³ and Pauls Stradins¹; ¹NREL, Golden, United States; ²Bert thin films, United States; ³University of North Carolina at Charlotte, United States

We report on copper (Cu) screen print metallization of silicon (Si) solar cells and analyze the performance loss factors due to this new metallization process by mapping of local parameters for large area Passivated Emitter Rear Contact (PERC) solar cells. In order to reach about 40 TW of PV required to transition our planet to renewables, the silver (Ag) should disappear from PV production and get replaced with more abundant and cheaper material. Cu is an excellent alternative to Ag: being cheap and exhibiting similar electrical resistivities. But there are challenges associated with it like easy oxidation, diffusion into the Si cell and recombination activity. Most of the work that has been carried out in case of Cu involves electroplating to get a high aspect ratio metal contact, but it requires additional masking steps like photolithography. Thus, screen printing, a dominant metallization technology, is a potentially inexpensive solution for Cu metallization on c-Si solar cell. The selective emitter PERC cells were developed on M6 sized monocrystalline p-type wafers with a front grid screen-printed with Cu paste and partial Al contacts at the rear side. Although the champion cells have a fill factor (FF) ~77%, we have investigated the solar cells with very low FF (62% to 68%) in order to understand the reason behind the low FF. FF loss analysis indicates that there is ~13.35% loss due to series resistance (R_s), ~4.5% loss due to J₀₂ and a negligible loss of ~0.07% due to shunt resistance (R_{sh}). Our primary motivation for mapping these parameters is to investigate whether the low FF is a result of non-uniformity or overall low value of these parameters. Photoluminescence (PL) imaging was performed at different load conditions including short circuit and open circuit conditions under 1 sun illumination with source excitation of 808 nm and exposure time of 0.5sec. Electroluminescence (EL) imaging was also carried out at different applied voltages in the dark. The PL and EL images at different bias conditions are used to generate the R_s maps. Dark Lock-in Thermography (DLIT) using a thermal camera was measured at a reverse bias and three forward biases (0.508V, 0.547V, 0.631V) which were subsequently used for local IV analysis based on 2-diode model to generate maps for R_{sh}, J₀₁ and J₀₂. Even at short-circuit conditions, the PL images show some bright patches, which indicate that contact formation has

not taken place in those areas. At open circuit conditions, the PL images still show those bright patches at the edges but is very uniform over most the surface. In the EL images, the non-contacted regions are dark, while the remaining areas are quite uniform. Thus, from the PL and EL images at different bias conditions, it is observed that the overall contact formation is uniform barring a few places at the edges indicating that the series resistance is uniform but high over the entire surface. The reason behind the high R_s can be high contact resistance at Cu/Si interface which needs further investigation. The DLIT image in the reverse bias is also mostly uniform and dark over the entire surface supporting our FF loss analysis of low R_{sh} loss. But the DLIT images in the forward biases show non-uniform spots in the interior of the cells which become prominent as higher bias voltages are applied. These spots, which were not visible in EL or PL images indicate non-uniformity of J_{01} and J_{02} . Further studies to investigate the interfaces will be done to understand the source of non-uniformity of J_{01} and J_{02} , diffusion of Cu atoms and the role of the barrier layer between Cu and silicon. We intend to study the diffusion of Cu into Si by SIMS, XRD, TEM, Raman spectroscopy and AFM and present it at the conference. The use of screen printable Cu pastes can reduce the cost of PV production processes to a great extent and hence, is of extreme relevance to the PV community.

11:30 AM EN06.08.04

Electron Transport Layer Design Considerations for Si-based Photocathodes for CO₂ Reduction Joel W. Ager^{1,2}, Rajiv R. Prabhakar², Raphaël Lemerle² and Elif N. Dayi²; ¹University of California, Berkeley, United States; ²Lawrence Berkeley National Laboratory, United States

Use of charge-selective, passivating contacts is responsible much of the recent progress in improving the efficiency of Si-based photovoltaic cells [1]. Designing such contacts for the photoelectrochemical (PEC) environment (i.e. electron transport layers for photocathodes and hole transport layers for photoanodes) has some commonalities with PV but also brings additional challenges and constraints [2]. Focusing on ETLs, materials used for this purpose must be stable in the PEC environment and either be catalytic for the desired reaction (e.g. hydrogen evolution, HER, or CO₂ reduction, CO₂R) or be compatible with a co-catalyst that is. For Si photocathodes used for HER, TiO₂ is widely used: it is stable in the low pH conditions which are typically employed and provides a conductive path to typically used catalysts such as Pt [3].

However, although TiO₂ ETLs appear to be stable at the near-neutral pH conditions used in PEC CO₂R, they also appear to be highly active for the competing HER reaction, which motivates a search for materials which will be more catalytically inert. Consideration of thermodynamic stability rules out many candidates that are used in PV applications (e.g. ITO). We will show that TaO_x synthesized by pulsed laser deposition and RF sputtering has promise as an ETL for PEC CO₂ reduction. Control of the oxygen vacancy concentration enables tuning its conductivity and hence improving its photocurrent densities under CO₂ reduction conditions. Initial work show that while the photovoltage of p-Si/TaO_x junctions is smaller compared to p-Si/TiO₂, TaO_x is catalytically less active for HER. As a result, p-Si/TaO_x/Ta/Au and p-Si/TaO_x/Cu photocathodes produce CO and C1 and 2 products (faradaic efficiencies > 50%), as expected.

As many PV absorber materials are themselves thermodynamically unstable under the strong reducing conditions of PEC CO₂ reduction, investigation of chemically compatible ETLs which also provide surface passivation is warranted. In this context, materials selection strategies, including the use of engineered and multifunctional layers (inspired by those used for PEC HER [4]), will be discussed.

[1] Allen, T. G.; Bullock, J.; Yang, X.; Javey, A.; De Wolf, S. Passivating Contacts for Crystalline Silicon Solar Cells. *Nat. Energy* **2019**, *4*, 914–928.

[2] Hu, S.; Lewis, N. S.; Ager, J. W.; Yang, J.; McKone, J. R.; Strandwitz, N. C. *J. Phys. Chem. C* **2015**, *119*, 24201–24228.

[3] Lin, Y.; Battaglia, C.; Boccard, M.; Hettick, M.; Yu, Z.; Ballif, C.; Ager, J. W.; Javey, A. *Nano Lett.* **2013**, *13*, 5615–5618.

[4] Paracchino, A.; Laporte, V.; Sivula, K.; Grätzel, M.; Thimsen, E. *Nat. Mater.* **2011**, *10*, 456–461.

11:45 AM DISCUSSION TIME

SESSION EN06.09: Virtual Session III: High Efficiency Devices and Material Growth

Session Chairs: James Bullock and Xinyu Zhang

Wednesday Afternoon, December 7, 2022

EN06-virtual

6:30 PM *EN06.09.01

Gettering and Passivation of Impurities and Defects in High Efficiency Silicon Solar Cells Daniel Macdonald, AnYao Liu, Kelvin Sio, Sieu Pheng Phang and Rabin Basnet; Australian National University, Australia

Impurities and defects continue to play an important role in limiting the efficiency of both laboratory and industrial silicon solar cells. In this work, we review recent progress in reducing the impact of some of the most important of these limiting defects through impurity gettering and passivation steps, which occur coincidentally during device fabrication. Since the dominant defects in a material depend very strongly on the crystal growth conditions, we categorise them by the three common silicon crystal growth techniques – Czochralski-grown mono-crystalline silicon, Cast-grown silicon (including both multicrystalline and cast-mono silicon), and Float-Zone silicon.

Czochralski-grown monocrystalline silicon (Cz-Si)

The primary defects in Cz-si, whether p- or n-type, are oxygen-related. In boron-doped p-type silicon, the very well-known Light-Induced Degradation (LID) caused by boron-oxygen defects dominates. Although in principle it is not affected by gettering, hydrogen is widely thought to play a key role in the permanent regeneration of this defect, which is a crucial step in stabilising the high efficiency p-type PERC cells that now dominate the PV industry.

In n-type Cz-Si, which is the preferred substrate for IBC, SHJ and poly-silicon passivating contact solar cells, an important class of defects that sometimes occur during high-temperature processing are the oxygen-related ring defects. These consist of oxygen precipitates, and sometimes their associated dislocations and decorating metallic impurities. Under certain conditions, they can be partially mitigated by impurity gettering and hydrogenation steps. These ring defects can also occur in p-type Cz-Si wafers.

Industrial Cz-Si wafers often also contain traces of dissolved metals such as Fe, which can significantly affect the carrier lifetime, if not removed during processing by gettering. Such gettering can be achieved by phosphorus or boron diffusion, aluminium alloying, doped-poly-silicon layers, and even deposited dielectric films such as silicon nitride and aluminium oxide.

Cast-grown silicon (HP mc-Si and cast-mono Si)

Cast high-performance multicrystalline silicon (HP mc-Si), by design, contains many grain boundaries. Fortunately the recombination activity of these grain boundaries can be significantly reduced after hydrogenation, such as via fired silicon nitride films during cell metallisation. Cast-monocrystalline silicon (cast-mono Si), on the other hand, tends to be dominated by dislocation clusters. These are much more difficult to negate through hydrogenation,

which reduces the achievable efficiency and yield for devices made on such wafers. Both HP mc-Si and cast-mono wafers also contain significant quantities of metallic impurities, some of which are precipitated at structural defects, whilst others remain dissolved. Under the right conditions, they can be gettered to a significant extent during phosphorus or boron diffusions, or by deposited films. This provides a convenient method to identify the metallic species present in these materials.

Float-Zone silicon (FZ-Si)

Although not used in industrial solar cells, Float-Zone silicon (FZ-Si) is often used in research laboratories, partly due to its immunity to oxygen-related LID and ring defects, and very low metallic impurity concentrations. However, due to the addition of nitrogen during crystal growth to control dislocations, they are subject to the formation of nitrogen-vacancy complexes. Once formed, these defects are highly recombination active. However they can be partly mitigated by hydrogenation.

Finally, although hydrogen is helpful in passivating some defects in silicon, it can also cause recombination-active defects when present in excess, such as the widely-researched Light and elevated-Temperature Induced Degradation (LeTID). Since these defects are caused by firing hydrogen-containing dielectric films, they can be found in all three types silicon wafer described above, whether n- or p-type.

7:00 PM *EN06.09.02

High Efficiency Perovskites and Perovskite Tandems via Passivation and Charge Transport Engineering [Kylie Catchpole](#); Australian National University, Australia

Combining perovskites with well-established photovoltaic materials such as silicon is an attractive approach for producing cheap, high efficiency and high voltage solar cells. Perovskite/silicon tandems have the potential for further progress in increasing the efficiency to 30% and beyond provided high efficiency perovskite cells can be demonstrated. We demonstrate a 4-terminal tandem perovskite/silicon configuration in which the efficiency is as high as 27.7% through a passivation approach using 2D perovskites. We also demonstrate efficiency above 22% and fill factor of 86% for a 1cm² single junction perovskite cell using a titanium oxynitride electrode transport layer. We also discuss how high efficiency can contribute to lowering the cost of photovoltaics and to decarbonization, as well as some emerging research challenges as solar transitions to become one of the world's major energy technologies.

7:30 PM *EN06.09.03

Future of Silicon Heterojunction Solar PV Technologies [Akira Terakawa](#)^{1,2}; ¹Panasonic Corporation, Japan; ²Photovoltaic Power Generation Technology Research Association (PVTEC), Japan

A-S/c-Si heterojunction (SHJ) solar cells have been invented in 1990 by Sanyo, which are regarded as a candidate of the main streams of Si solar cells. The history and future prospective of SHJ technologies and applications will be reviewed.

8:00 PM EN06.09.04

Generation Mechanism of Dislocations During Cast Growth of High-Performance Multicrystalline Si Ingots [Yutaka Ohno](#)¹, Hideto Yoshida², Tatsuya Yokoi³, Katsuyuki Mtsunaga³, Koji Inoue¹, Yasuyoshi Nagai¹ and Noritaka Usami³; ¹IMR, Tohoku University, Japan; ²SANKEN, Osaka University, Japan; ³GSE, Nagoya University, Japan

Silicon ingots grown by cast-growth techniques, such as high-performance multicrystalline silicon (hp-Si), have a high productivity at low cost, even though dislocation clusters are frequently generated during the directional solidification. The clusters would degrade the macroscopic electric properties around them, which is much inferior to that in monocrystalline Si solar cells. One important issue to fabricate high quality cast-Si ingots for photovoltaic and electronic applications is, therefore, to control the dislocation generation. The dislocation sources are, however, hardly determined in commercial-scale Si ingots with complicated crystal structure. In the present work, we have found that dislocation clusters are effectively generated at $\Sigma 3$ grain boundaries (GBs) in a commercial hp-Si ingot and discussed the origin of the dislocation generation.

We examined the generation sites on a multiscale by multimodal analysis using optical and electron microscopies, photoluminescence (PL) imaging, finite element stress calculations assisted by crystal growth simulation (CGSIM), and *ab-initio* calculations. A set of alkali-etched wafers cut from a hp-Si ingot was sequentially measured by PL imaging and optical microscopy (OM) [1], and three-dimensional distribution of dislocation clusters and GBs was visualized. The crystal orientation of the grains and GB characters were examined by machine learning using the OM data [2], and a $\Sigma 3$ GB acting as dislocation source was selected. Macroscopic thermal stresses around the GB during the cast-growth was estimated by finite element calculations [3], with the parameters estimated by the relevant crystal growth simulations [4]. The atomistic structure of the GB was examined by transmission electron microscopy (TEM) and scanning TEM (STEM) [5], and local stresses at the GB was discussed by *ab-initio* calculations based on the STEM data. Multiscale analysis of a commercial hp-Si ingot indicates that dislocation clusters can be generated at curved $\Sigma 3$ GBs, around which high thermal stresses are concentrated. The GBs have a stepped structure composed of the symmetric $\Sigma 3$ GB segments lying on {111} and {112}. TEM suggests dislocation generation at the stepped edges, and the Burgers vectors of the dislocations are parallel to the stepped edges. Finite element stress analyses indicate a high shear stress concentrated at the stepped edges. Also, *ab-initio* calculations with STEM data reveal large strains at the GBs, by which the critical stress needed for dislocation generation would be reduced.

This work was supported by JST / CREST, Grant No. JPMJCR17J1 (2018-2023).

[1] Y. Hayama, *et al.*, Sol. Energy Mat. Sol. Cells **189** (2019) 239.

[2] T. Kojima, *et al.*, 17th Symp. on "Photovoltaic Systems for the Next Generation", 2020, PB-25.

[3] K. Yamakoshi, K. Kutsukake, T. Kojima, N. Usami, 2021 MRS Fall Meeting; DS03.13.02.

[4] H. Tanaka, K. Kutsukake, T. Kojima, X. Liu, N. Usami, 82nd JSAP Autumn meeting, 2021, 10a-N203-5.

[5] Y. Ohno, K. Tajima, K. Kutsukake, N. Usami, Appl. Phys. Express **14** (2021) 011002.

8:15 PM EN06.09.05

Al-Catalyzed Si Nanowire Formation on Pre-Etched and Post-Polished Thin Si Substrates for Photovoltaic Application [Wipakorn Jevasuwan](#) and Naoki Fukata; National Institute for Materials Science, Japan

Thin silicon (Si) solar cells have been a candidate to suppress Si material consumption and utilize them as flexible and durable devices. However, the advantage has come with a trading-off in solar cell efficiency. Light absorption loss in thin Si wafers is an important issue to be overcome in order to improve the conversion efficiency. Systems made with one-dimensional (1D) nanostructures of inorganic semiconductors with high crystallinity such as Si nanowires (NWs) are promising to provide significant enhancement by increasing the light trapping and carrier collection area in thin cells owing to the unique NW physical properties [1,2]. From our report [2], vapor-liquid-solid (VLS) growth using aluminum (Al) catalyst of chemical vapor deposition (CVD) on bulk Si(111) wafers was proposed to create single-crystalline SiNWs that resolve the catalyst contamination problem. The developments of vertical-oriented, Al-doped, and smooth surface Al-catalyzed SiNW array formation together with the realization of high-performance SiNW-based

photovoltaic devices have been accomplished. In this study, thin SiNW-based solar cells were further demonstrated. Two different thin and bendable Al-catalyzed SiNW substrates were successfully prepared using simple techniques of pre-chemical etching in HF:CH₃COOH:HNO₃ solution before SiNW formation and post-mechanical polishing with diamond solution after SiNW growth. The formation of Al-catalyzed SiNWs on a pre-etched thin Si substrate was achieved as well as on a post-polished sample by applying optimized conditions from previous studies [2]. Although only one-half of SiNWs was vertically formed along [111] direction on pre-etched samples due to the Si surface roughness, low light reflectance (<10%) of both thin SiNW substrates is comparable. SiNW solar cells fabricated using an axial junction of p⁺-p-n structure [2] on thin pre-etched and post-polished Si wafers could enhance the power conversion efficiency (PCE) up to 6.1% and 6.6%, respectively. Both thin SiNW substrates contribute light trapping qualities while the NW-shaped increases the carrier collecting area compared to thin planar cells. The ease of Al catalyst removal and the capabilities of Al existence as a p-type dopant in SiNWs are also advantageous. The problems of catalyst contamination could be avoided and the process is capable of being scaled up. The photovoltaic characteristics of the best SiNW sample and planar sample with optimizations will be discussed. Further necessitating improvements in SiNW quality and interface engineering is in progress. [1] W. Jevasuwan, et al., JJAP, 56 [8] (2017) 085201. [2] W. Jevasuwan and N. Fukata, Nanoscale. 13 [14] (2021) 6798-6808.

8:20 PM DISCUSSION TIME

SYMPOSIUM EN07

Materials, Modeling and Technoeconomic Impacts for Emergent Applications of Large-Scale Hydrogen
November 29 - December 6, 2022

Symposium Organizers

Mitch Ewan, University of Hawai'i
Thomas Gennett, National Renewable Energy Laboratory/Colorado School of Mines
Alexander Headley, Sandia National Laboratories
Samantha Johnson, Pacific Northwest National Laboratory

* Invited Paper
+ Distinguished Invited

SESSION EN07.01: Solid Oxide Systems
Session Chairs: Mitch Ewan and Alexander Headley
Tuesday Morning, November 29, 2022
Hynes, Level 3, Room 302

8:30 AM EN07.01.01

Fabrication of Highly Conducting Sc and Y Co-Doped ZrO₂ Solid Electrolyte Thin Film on a Porous Electrode Substrate via Facile Method for SOEC Applications Rinlee Butch Cervera and Dale Mhar Alfeche; University of the Philippines Diliman, Philippines

Scandium (Sc) and yttrium (Y) co-doped ZrO₂ (4Sc4YSZ) thin films were fabricated on a porous electrode substrate of NiO-YSZ using a facile drop-coating method. The 4Sc4YSZ powder was synthesized using sol-gel all alkoxide method while the 1:1 wt% composition of NiO and 8YSZ (NiO-YSZ) electrode substrate was synthesized via glycine-nitrate combustion method. The electrode substrate and solid electrolyte powders were characterized first before the half-cell fabrication. For the 4Sc4YSZ sol-gel derived powder, TG/DTA revealed that the powder stabilized at about 1000 degC which is complemented by FTIR results. From the FTIR spectra, the organic functional groups were completely removed after calcination at 1000 degC. The half-cell was then prepared via drop-coating of 4Sc4YSZ on a NiO/YSZ substrate and then characterized for its morphology and conductivity at intermediate temperatures. SEM-EDS revealed a well-distributed and homogeneous elemental composition of the 4Sc4YSZ solid electrolyte thin film on a porous Ni-YSZ electrode substrate. From the conductivity measurements done using electrochemical impedance spectroscopy (EIS), 4Sc4YSZ thin film can be a promising solid electrolyte material due to high total conductivity of about 1.2×10^{-1} S/cm at 700 °C with 0.73 eV activation energy

8:45 AM EN07.01.02

High-Throughput Discovery of Hydrogen Evolution Electrocatalysts in Different Complex Solid Solution Systems Based on Transition Metals Sabrina Baha¹, Simon Schumacher², Alan Savan¹, Corina Andronesuc² and Alfred Ludwig^{1,3}; ¹Materials Engineering, Germany; ²Faculty of Chemistry and CENIDE Center for Nanointegration, Germany; ³Center for Interface-Dominated High Performance Materials, Germany

The efficient production of green hydrogen is one of the most important steps towards the development of a sustainable hydrogen economy. However, in order to advance water electrolysis, new catalyst materials must be found that are ideally based on abundant and cheap elements and further reduce the energy consumption for the hydrogen evolution reaction (HER) [1]. These materials can be based on transition metals. Although individually less active for HER, as compositional complex solid solutions (CCSS) or also named as high entropy alloys (HEAs), their activity can be compared to commercial catalysts [2].

These alloys consist of five or more elements in a compositional range of typically 5-35 at.% and are stabilized by high mixing entropy in a single phase structure. Due to the large number of surface atomic arrangements, there are many different binding energies that can provide an increased density of

optimal or near-optimal binding energies for a given reaction after suitable optimization of the CCSS structure and composition [3]. CCSS have opened up almost infinite possibilities of compositions that need to be discovered in a systematic and material-saving manner [4]. For discovery of new catalysts, we used combinatorial fabrication and high-throughput characterization methods. A thin film with a concentration gradient of each element is deposited on a Si substrate by co-depositing individual elements from five sources, resulting in approximately 340 measurement areas (MAs) of different compositions. These are referred to as material libraries (MLs), which can then be screened using high-throughput methods. The structure and composition of the different MAs are investigated by energy-dispersive X-ray spectroscopy and X-ray diffraction. Using the electrochemical scanning droplet cell technique, we have explored the activity of the different catalyst materials present in the ML for alkaline HER. With only three different MLs in a compositional system, we can investigate more than 1000 different compositions and thus have identified in our work about 350 catalysts of the Cr-Co-Fe-Mo-Ni system with similar or higher electrocatalytic activity than recently reported for alkaline HER in this system [5]. The results show a complex interaction between composition and phases that affect the activity of HER. From these data, we can identify trends as a function of structure, elemental composition, and HER activity. Overall, we can conclude that high Fe and Co contents in the Co-Cr-Fe-Mo-Ni CCSS boost HER activity while an increasing amount of Cr has the opposite effect. In general, CCSS with higher HER activity have higher crystallinity. Still, the composition of the CCSS indicates a stronger influence than the crystallinity on the HER electrocatalytic activity.

- [1] J. Wei, M. Zhou, A. Long, Y. Xue, H. Liao, C. Wei and Z. J. Xu, *Nanomicro Lett.*, 2018, 10, 75.
- [2] G. Zhang, K. Ming, J. Kang, Q. Huang, Z. Zhang, X. Zheng and X. Bi, *Electrochim. Acta*, 2018, 279, 19.
- [3] T. Löffler, A. Ludwig, J. Rossmeiß and W. Schuhmann, *Angew. Chem., Int. Ed. Engl.*, 2021, 60, 26894
- [4] A. Ludwig, *npj Comput. Mater.*, 2019, 5, 70.
- [5] S. Schumacher, S. Baha, A. Savan, C. Andronescu and A. Ludwig, *J. Mater. Chem. A*, 2022, 10, 9981-9987

9:00 AM EN07.01.03

Towards High-Performance, Low-Temperature Solid Oxide Cells with Vertically Aligned Nanocomposite Films [Matthew Wells](#), Adam Lovett and Judith L. MacManus-Driscoll; University of Cambridge, United Kingdom

Low temperature micro solid oxide cells (μ SOCs) represent a key technology in next-generation energy devices for portable applications, offering the highly efficient conversion of electrical to chemical energy (e.g. hydrogen), and vice versa. To date however, the widespread implementation of μ SOCs, and therefore the effective use of hydrogen as a portable energy storage solution, has been prohibited by excessive polarisation resistances at the device electrodes, despite significant progress in materials design.

Vertically aligned nanocomposite (VAN) films have been a leading class of materials in recent performance enhancements in μ SOC design, and in this work we further explore the growth and characterisation of such VAN films. State-of-the-art fluorite and perovskite materials are combined in each of the anode, electrolyte, and cathode layers and the enhancement rendered by the novel VAN structure quantified in each case by electrochemical impedance spectroscopy (EIS). Moreover, films are grown on both single-crystal and more commercially viable polycrystalline/amorphous substrates. This allows for a detailed study of the VAN growth mechanisms for materials of differing crystal structures, while also giving an improved understanding of the importance of crystalline perfection in thin-film μ SOC device performance.

Future progress in low-temperature μ SOC technology will rely heavily on a detailed understanding of the growth mechanisms of state-of-the-art nanostructured materials, such as VAN thin films. By building such an understanding and quantifying the performance enhancements resulting from a wide variety of VAN structures, this study represents an important step towards the realisation of efficient low-temperature μ SOCs for portable applications.

9:15 AM EN07.01.04

Unconventional Highly Active and Stable Oxygen Reduction Catalysts Informed by Computational Design Strategies [Ryan Jacobs](#)^{1,2}, [Jian Liu](#)¹, [Beom Tak Na](#)¹, [Bo Guan](#)^{1,3}, [Tao Yang](#)^{1,3}, [Shiwoo Lee](#)¹, [Greg Hackett](#)¹, [Tom Kalapos](#)^{1,3}, [Harry Abernathy](#)¹ and [Dane Morgan](#)^{1,2}; ¹U.S. Department of Energy National Energy Technology Laboratory, United States; ²University of Wisconsin--Madison, United States; ³NETL Support Contractor, United States

Discovering and engineering new materials with fast oxygen surface exchange kinetics and robust long-term stability is essential for the large scale, economically viable commercialization of solid oxide fuel cell (SOFC) technology. The perovskite catalyst material $\text{BaFe}_{0.125}\text{Co}_{0.125}\text{Zr}_{0.75}\text{O}_3$ (BFCZ75) was predicted to be promising from our recent density functional theory calculations but is unconventional due to its extremely high Zr content and low electronic conductivity.[1] However, we demonstrate that it exhibits oxygen reduction reaction surface exchange rates on par with $\text{Ba}_{0.5}\text{Sr}_{0.5}\text{Co}_{0.8}\text{Fe}_{0.2}\text{O}_3$ (BSCF) and excellent stability at typical operating temperatures.[2] We engineer new composite electrodes integrating BFCZ75 with commercial electrode materials $\text{La}_{1-x}\text{Sr}_x\text{MnO}_3$ (LSM) and $\text{La}_{1-x}\text{Sr}_x\text{Co}_y\text{Fe}_{1-y}\text{O}_3$ (LSCF) and achieve high performance as measured by low area specific resistance (ASR) values, with the LSCF/BFCZ75 ASR values comparable to top performing non-composite electrode materials such as $\text{SrCo}_{0.8}\text{Sc}_{0.2}\text{O}_{3-d}$ [3] $\text{BaNb}_{0.05}\text{Fe}_{0.95}\text{O}_{3-d}$ [4] and $\text{BaCo}_{0.7}\text{Fe}_{0.22}\text{Y}_{0.08}\text{O}_{3-d}$. [5] Considering this result was obtained with simple mixing of commercial LSM/LSCF and as-made BFCZ75 using standard processing methods, the performance of the electrode could be even further improved by optimizing the composition and microstructure. This study successfully demonstrates that modern computational-based materials discovery methods can point to unconventional and novel SOFC electrode design strategies which would have been either inaccessible to experimental techniques (e.g., too many compositions to examine) or ill-advised based on conventional wisdom (e.g., having too low electronic conductivity by virtue of low transition metal content). These novel design strategies can unlock new high-performing SOFC electrode materials with performance rivaling other state-of-the-art novel cathode materials, while also having improved operational stability and utilizing current commercial cathode material production lines, offering a promising path toward the widespread adoption of SOFC energy technology.

References

- [1] Jacobs, R., Mayeshiba, T., Booske, J., Morgan, D. *Material Discovery and Design Principles for Stable, High Activity Perovskite Cathodes for Solid Oxide Fuel Cells*. *Advanced Energy Materials*, 8 (11) (2018)
- [2] Jacobs, R., Liu, J., Na, B.-t., Guan, B., Yang, T., Lee, S., Hackett, G., Kalapos, T., Abernathy, H., Morgan, D., *Unconventional Highly Active and Stable Oxygen Reduction Catalysts Informed by Computational Design Strategies*. *Advanced Energy Materials* 2201203 (2022)
- [3] Chen, D., Chen, C., Zhang, Z., Baiyee, Z. M., Ciucci, F., Shao, Z., *Compositional Engineering of Perovskite Oxides for Highly Efficient Oxygen Reduction Reactions*, *ACS Applied Materials and Interfaces* 7, (16) (2015)
- [4] Dong, F., Chen, Y., Ran, R., Chen, D., Tade, M. O., Liu, S., Shao, Z., *BaNb_{0.05}Fe_{0.95}O_{3-d} as a new oxygen reduction electrocatalyst for intermediate temperature solid oxide fuel cells*, *Journal of Materials Chemistry A* 1 (2013).
- [5] He, W., Wu, X., Yang, G., Shi, H., Dong, F., Ni, M. *BaCo_{0.7}Fe_{0.22}Y_{0.08}O_{3-d} as an Active Oxygen Reduction Electrocatalyst for Low-Temperature Solid Oxide Fuel Cells below 600 C*, *ACE Energy Letters* 2 (2) (2017).

9:30 AM EN07.01.05

Solid-State Synthesis of Layered KIrO_x for the Oxygen Evolution Reaction [Rachael Quintin-Baxendale](#), Maria S. Sokolikova, Ifan E. Stephens and Cecilia Mattevi; Imperial College London, United Kingdom

The current climate crisis means that it is imperative to research new energy solutions, and using green hydrogen formed through electrocatalytic water splitting as a renewable energy storage system is an exciting prospect. Within water electrolyzers, Iridium Oxide is commonly used as a catalyst for the Oxygen Evolution Reaction, the bottleneck reaction of the system on the anode, due to its high stability and activity. However, the low abundance and very high costs of Ir are hindering its commercial application for water electrolysis. Reducing the loading required of the iridium oxide could enable the commercial feasibility of this system, and various methods are gaining increased interest such as nano-structuring, doping and developing new support materials.

Nano-structuring rutile iridium oxide into two-dimensional (2D) nanosheets can offer extremely high surface areas, electron charge-transfer and conductivity abilities, allowing for a drastically reduced mass loading while preserving the catalytic activity. In this work, we synthesise a layered potassium iridate compound which is a precursor of 2D IrO_x . The compound was obtained through a high temperature solid-state reaction, followed by a shorter oxidative deintercalation step to remove potassium ions. Advanced structural characterizations have elucidated the crystal structure. The de-intercalated materials were then tested for oxygen evolution reaction. This approach can pave the way to increase the commercial viability of IrO_x as catalyst for water electrolysis.

9:45 AM BREAK

SESSION EN07.02: Other Technologies
Session Chairs: Thomas Gennett and Alexander Headley
Tuesday Morning, November 29, 2022
Hynes, Level 3, Room 302

10:15 AM EN07.02.01

Insight into the Synergy Between Silver Nanoparticles and Alkaline Anion Exchange Membranes for Power Output [Konnie Duan](#)¹, [Quinton Geller](#)², [Helee Shukla](#)³, [Haoyan Fang](#)⁴, [Md Farabi Rahman](#)⁴, [Aniket M. Raut](#)⁴, [Sean Fang](#)⁵, [Thomas Luong](#)⁶, [Yuhao \(Ben\) Pan](#)⁷ and [Miriam Rafailovich](#)⁴; ¹Harvard-Westlake School, United States; ²Los Alamos High School, United States; ³New Hyde Park Memorial High School, United States; ⁴Stony Brook University, The State University of New York, United States; ⁵Maggie L. Walker Governor's School, United States; ⁶Plano West Senior High School, United States; ⁷Stuyvesant High School, United States

To develop innovative clean energy processes, scientists have been researching alkaline anion exchange membrane fuel cells (AEMFCs), which are currently expensive but can function in salt water and basic environments, unlike other hydrogen fuel cells. Previous studies on proton exchange membrane (PEM) fuel cells showed that monolayer sheets of nanoparticles (NPs) deposited onto Nafion PEMs via the Langmuir Blodgett Trough (LBT) were highly effective in increasing fuel cell power output. Density functional theory (DFT) calculations indicated the existence of a synergy between the surface of the Nafion membrane and the platelet shaped particles, which reduced the activation barrier for the CO oxidation reaction [1,2]. In AEMFCs, a different set of reactions determines the power generated, but a potential synergy between NPs and the membrane surface may still exist and lower the activation barrier. To explore this possibility, we evaluated silver (Ag) NPs, which have been shown to be effective in catalyzing these reactions [3]. We synthesized AgNPs using the Brust method and either deposited a monolayer using the LBT or sprayed AgNPs directly onto parts of the AEMFC. The AEMFCs were treated with dodecanethiol (C_{12})-protected AgNPs under five different conditions: (a) without AgC_{12} NPs, (b) with AgC_{12} NPs deposited using the LBT at 5 mN/m on both sides of the membrane, (c) with AgC_{12} NPs deposited using the LBT at 10 mN/m on both sides of the membrane, (d) with 1 $\mu\text{g}/\text{cm}^2$ of AgC_{12} sprayed on both sides of the membrane, and (e) with 1 $\mu\text{g}/\text{cm}^2$ of AgC_{12} sprayed on both electrodes. Each cell was tested for maximum power density. Approximately the same amount of AgNPs were applied via the LBT with the 10 mN/m surface pressure and each of the airbrush sprays. Each cell was operated with 0.76 mg/cm^2 Pt/C electrodes in ambient conditions at 60°C.

The AEMFC with AgC_{12} NPs sprayed onto the membrane exhibited the highest maximum of 0.556 W/cm^2 (39.7% increase) compared to the other test conditions, which include 0.469 W/cm^2 (17.8% increase) for AgNPs sprayed onto the electrodes, and 0.380 W/cm^2 (4.52% decrease) and 0.451 W/cm^2 (13.3% increase) for the 5 mN/m and 10 mN/m surface pressure depositions, respectively. The control cell had a peak power density of 0.398 W/cm^2 when operated. The membrane spray may have worked better than the electrode spray because of a yet-uncharacterized synergistic effect between the AgNPs and the membrane. The shape of the AgNP may also play a role in the observed effect, as shown by the reduced catalytic activity of deposited AgNPs, which are platelet-shaped after LBT application. The AEMFC with the monolayer deposited at 10 mN/m had a slightly greater maximum power density compared to deposition at 5 mN/m, likely due to the increased quantity of AgNP catalysts. These results clearly demonstrate that a synergy is established when AgNPs are deposited on the membrane for AEMFCs as well. The mechanism of action in AEMFCs, which is most enhanced by sprayed AgNPs on the membrane, appears to be different from that of PEM fuel cells, which showed enhancement when NPs were applied via LBT in previously published work. DFT calculations are in progress in order to elucidate the difference in mechanism.

We acknowledge the Morin Charitable Trust for funding.

[1] Wang, Likun, et al. "Designing nanoplatelet alloy/nafion catalytic interface for optimization of PEMFCs: performance, durability, and CO resistance." *ACS Catalysis* 9.2 (2019): 1446-1456.

[2] Wang, Likun, et al. "Suppression of carbon monoxide poisoning in proton exchange membrane fuel cells via gold nanoparticle/titania ultrathin film heterogeneous catalysts." *ACS Applied Energy Materials* 2.5 (2019): 3479-3487.

[3] Treshchalov, Alexey, et al. "Stabilizer-free silver nanoparticles as efficient catalysts for electrochemical reduction of oxygen." *Journal of colloid and interface science* 491 (2017): 358-366.

10:30 AM EN07.02.02

Multiscale Simulations for Sorption-Diffusion Dynamics Within Polycrystalline Microstructures in the Hydrogen Storage Systems [Younggil Song](#)¹, [Nathan D. Keilbart](#)¹, [Kyoung Eun Kweon](#)¹, [James Chapman](#)^{1,2}, [Yakun Zhu](#)¹, [Jennifer N. Rodriguez](#)¹, [Roger Qiu](#)¹, [Tae Wook Heo](#)¹ and [Brandon Wood](#)¹; ¹Lawrence Livermore National Laboratory, United States; ²Boston University, United States

Within hydrogen storage systems, hydrogen travels various pathways to interact with metals. Metal oxide layers often form near the surface of the storage,

and hence hydrogen diffuses into the layers and find metals to form metal hydrides. In addition, metals and metal oxides are polycrystalline microstructures which have grains with different phases and grain boundaries located between them. The different phases and structural configurations lead to different hydrogen sorption and diffusion dynamics. Therefore, it is important to understand hydrogen sorption-diffusion dynamics within polycrystalline microstructures to enhance efficiency of hydrogen storages.

For the current study, we investigate hydrogen sorption-diffusion dynamics within polycrystalline TiO₂ microstructures using simulations in various length scales and experiments. The TiO₂ layer is typically observed at the surface of the Ti or Ti-based alloys for the hydrogen storage. This layer contains rutile and/or anatase grain structures, and amorphous phases are also existed at the grain boundaries. To identify the thermodynamic properties for the three phases, we use the atomistic simulations and experiments. A thermodynamic analysis of the hydrogen stability using density functional theory can characterize the variation of binding energy from the surface to the deep inside grains. In addition, the binding energy for the amorphous phase are analyzed as a function of the oxygen coordination which shows skew normal distributions. Additionally, we can obtain temperature-dependent hydrogen diffusivities within grains and grain boundaries from experiments and Kinetic Monte Carlo simulations, respectively. Those site-specific binding energies and temperature-dependent diffusivities are imposed into the mesoscale simulations to simulate the hydrogen sorption-diffusion dynamics within different microstructures. Our multi-scale simulations show that hydrogen adsorption is highly linked to the grain sizes within microstructures, which are also observed in experiments. We expect our multi-scale simulations and experiments can elucidate the relation between hydrogen adsorption and microstructures within hydrogen storage systems.

This work was performed under the auspices of the U.S. Department of Energy by Lawrence Livermore National Laboratory under Contract DE-AC52-07NA27344.

10:45 AM EN07.02.03

Design Principles for Transition Metal Nitride Stability and Ammonia Generation in Acid [Jiayu Peng](#), Juan J. Giner-Sanz, Livia Giordano, William Mounfield, Graham Leverick, Yang Yu, Yuriy Román-Leshkov and Yang Shao-Horn; Massachusetts Institute of Technology, United States

Transition metal nitrides have shown great promise for reducing/eliminating the use of expensive precious-metal-based catalysts (e.g., Pt) in proton exchange membrane fuel cells and electrolyzers, but the use of these nitrides in such technologies is still hindered by their dissolution at acidic pHs. Moreover, the decomposition of transition metal nitride catalysts in acid generates ammonia from the protonation of lattice nitrogen, giving rise to many false positives in previous reports of nitride catalysts for electrochemical nitrogen reduction to ammonia. To address these issues, it is essential to establish the stability descriptors of transition metal nitrides in acid. These stability descriptors can not only offer a fundamental understanding of nitride dissolution but also provide new guiding principles to optimize the intrinsic stability of nitrides for diverse acidic applications.

In this work, combining ab initio calculations with synchrotron X-ray spectroscopies, we identified electronic-structure-based design principles governing the extent and kinetics of nitride dissolution and ammonia production in acid. We found that lowering their nitrogen 2p band center with respect to the Fermi level leads to weakened metal-nitrogen bonds, increased labile metallic character, and a reduced barrier for the protonation of lattice nitrogen to produce ammonia, correlating with faster dissolution kinetics of nitrides in acid. Moreover, increasing the solubility of dissolved metal ions was found to be critical in preventing surface oxide passivation to ensure the complete conversion from transition metal nitrides to ammonia. Based on these observations, a mechanistic picture was proposed, where the protonation of lattice nitrogen is critical to trigger nitride dissolution, and this reaction scheme was supported by the pH-dependent dissolution kinetics of nitrides in acid.

These design principles and mechanistic insights for producing ammonia and dissolving metal ions from the decomposition of nitrides in acid are essential for a variety of applications. For example, these stability descriptors can be used to boost the stability of nitride catalysts for proton-exchange membrane fuel cells and electrochemical ammonia synthesis, where the dissolution of nitrides in acid has hindered their functions. Moreover, such descriptors for nitride dissolution and ammonia formation in acid provide emerging opportunities for designing nitride chemistries for distributed, on-demand ammonia generation. Lastly, as nitrides represent an exciting, yet markedly unexplored chemical space, this work provides a blueprint to design multinary nitrides in such a vast chemical space for various acidic applications, including electrocatalysis and beyond.

11:00 AM EN07.02.04

Facile Synthesis of Thiol-Decorated Ag Nanoparticles as Electrocatalyst for CO₂RR [Jinho Hyun](#) and Chanho Pak; Gwangju Institute of Science and Technology, Korea (the Republic of)

Large amount of traditional fossil fuels has been consumed as energy resource with inevitably emitted carbon dioxide (CO₂), one of the greenhouse gases, resulting in the global warming. Electrochemical catalysis is a cost-effective and energy-efficient way to convert CO₂ into valuable products under ambient condition. However, the electrocatalytic reaction involved various pathways suffers from low selectivity and high overpotentials. Therefore, developing the electrocatalysts with the high selectivity and low overpotentials has been the focus of research.

Efficient carbon dioxide reduction reactions (CO₂RR) is required to reduce greenhouse gases and obtain useful carbonaceous chemicals. Electrochemical carbon dioxide reduction (ECR) is one of the most effective methods to reduce carbon dioxide to carbon monoxide and/or other valuable chemicals. Coinage metals, i.e., gold, silver, and copper, are known as catalytic materials for ECR due to their appropriate binding energy for the intermediates (*COOH or *CO). Among them, silver-based catalysts showed high selectivity with relatively low overpotential and low cost. Morphology modification, size engineering and alloying have been conducted to improve ECR performance by promoting the reaction kinetics and selectivity. However, ECR can be improved by not only the enhancement of intrinsic activity but also extrinsic modification of interface.

Molecule-mediated electrocatalysts have been attracted attentions due to their unique electrochemical properties on interface between molecule and surface of electrocatalysts. The molecules around the electrocatalyst could adjust the electronic states of the surface resulting in improved activity and products selectivity. Conventional bulk metal electrodes after the modification of surface of electrodes by molecules showed enhanced ECR performance. We designed and fabricated a Thiol-decorated silver (Ag) nanoparticles on carbon support via simple acid reduction method. The as-prepared electrocatalyst has good dispersion and uniformity in particle size.

1:30 PM *EN07.03.01

Hydrogen Infrastructure and Storage—U.S. DOE Hydrogen and Fuel Cell Technologies Office Perspectives [Zeric Hulvey](#); U.S. Department of Energy, United States

Today there is rapidly increasing interest in utilizing hydrogen to provide clean, reliable power across a number of sectors, including transportation, power generation, energy storage, industrial applications, and chemical production. For many end uses, traditional methods of hydrogen storage and delivery—high pressure gaseous or liquefied hydrogen—will likely not be suitable for large-scale deployment. The U.S. Department of Energy (DOE) therefore remains interested in alternative methods of storage and delivery using materials-based technologies. This presentation will provide an overview of current hydrogen storage and delivery activities funded by DOE's Hydrogen and Fuel Cell Technologies Office (HFTO), with a focus on materials-based R&D. This will include current and future activities by the Hydrogen Materials – Advanced Research Consortium (HyMARC), a national laboratory-led consortium carrying out much of HFTO's materials-based efforts.

2:00 PM *EN07.03.02

Accelerating Development of Hydrogen Storage and Hydrogen Generation Materials through Multi-Faceted Characterization [Sarah Shulda](#)¹, [Philip Parilla](#)¹, [Michael Dzara](#)¹, [Heather Slomski](#)², [Brian Gorman](#)², [David Ginley](#)¹ and [Thomas Gennett](#)^{1,2}; ¹National Renewable Energy Laboratory, United States; ²Colorado School of Mines, United States

Abstract summary for invited talk (full abstract will be submitted at later date):

The importance of a multi-faceted characterization approach for advancing material development to enable H₂ at scale will be discussed. Specific examples highlighting how materials characterization moved the bar forward within hydrogen storage, solar thermochemical hydrogen generation, and high temperature electrolysis will be provided.

2:30 PM BREAK**3:00 PM *EN07.03.03**

Fuel Cell Power—Toyota's Enduring Commitment [Dallas Fox](#); Toyota Motor North America, United States

Toyota's enduring commitment to fuel cells is part of Toyota's broader "Environmental Challenge 2050" strategy. As ever, Toyota believes that the right powertrain for the right application is key to enabling a portfolio which is not only flexible, but also focuses on leveraging the individual strengths each option brings to the table. Whether it be hybrid, plug-in hybrid, battery-electric, or fuel cell, Toyota provides world class options that meet our customers' needs. When it comes to fuel cells, the advantages of high energy density, short refueling time, scalability, and low-to-no energy loss over time come to the fore. In this presentation, you will see how Toyota has explored the wide-ranging industries in which fuel cells can not only provide a marked performance advantage over established powertrains, but also show that better power and clean power don't have to be mutually exclusive. Reliable, powerful, and zero emissions: that's Toyota Fuel Cell.

3:30 PM *EN07.03.04

Design and Cost Analysis of a Liquid Organic Hydrogen Storage System for Enabling Wind and Solar Based Direct Iron Reduction [Hanna Breunig](#)¹, [Fabian Rosner](#)¹, [Peter Valdez](#)², [Dionessius Papadias](#)³, [Kriston Brooks](#)², [Rajesh Ahluwalia](#)³ and [Thomas Autrey](#)²; ¹Lawrence Berkeley National Laboratory, United States; ²Pacific Northwest National Laboratory, United States; ³Argonne National Laboratory, United States

While steel recycling has proven to be energy efficient and low in carbon dioxide intensity, primary steel will still be necessary to meet growing demand for steel, and a recent evaluation of the industry by the IEA suggest new low-emission technologies such as hydrogen (H₂) will be necessary to further lower emissions. Technologies for direct reduced iron (DRI) production using H₂ have been successfully demonstrated with no adverse effects on steel quality. This presents the opportunity for renewably generated H₂, from sustainable regional energy resources, to be coupled with the steel industry. Due to the fluctuations in the availability of renewable power and the continuous nature of the steel-making process, there is a need for H₂ storage carriers to supply cheap, low-carbon emission H₂ and energy continuously during operation. Based upon preliminary analyses of this coupling, it is clear that hydrogen storage is necessary to balance the continuous DRI process and intermittent electricity generation by renewables. Here, we present a concept and technoeconomic analysis of onsite H₂ generation by way of renewable-powered electrolysis. To balance intermittencies, the H₂ is stored using liquid organic hydrogen carriers (LOHCs), specifically methylenecyclohexane (MCH) and dibenzyltoluene (DBT), and H₂ can be regenerated on demand to serve reductant end uses at a steel mill.

We compare these LOHC-based storage systems, using MCH or DBT, with the use of compressed and liquid H₂ for steel mill applications requiring up to 200 TPD H₂ with and without a hypothetical price on carbon. Based on our process design, models and evaluation of the application, we estimate storage cost, storage duration, energy density, specific energy, charge and discharge rate, and efficiency for the storage system. We make recommendations on reasonable near-term values for performance targets based on the necessary requirements of the application and on the performance of business as usual (BaU) and incumbent ironmaking technologies.

4:00 PM PANEL DISCUSSION / RECEPTION

SESSION EN07.04: Poster Session
Session Chairs: Alexander Headley and Samantha Johnson
Tuesday Afternoon, November 29, 2022
8:00 PM - 10:00 PM
Hynes, Level 1, Hall A

EN07.04.03

Doping Effect in SnO₂ Nanoparticles for Catalysts in Polymer Electrolyte Fuel Cells [Takeshi Fukuda](#) and [Seigo Ito](#); University of Hyogo, Japan

Recent energy issues require urgent efforts to realize a decarbonized society around the world. To proceed to the target, development of polymer electrolyte fuel cells (PEFCs) is a topic of great interest, which is related to fuel cell vehicles. Specially, improvement of the cathode catalysts (for oxygen reduction reaction: ORR) is a very important topic for the practical use. Basically, carbon has been utilized for the Pt catalyst due to the electrical conductivity and chemical stability. In this study, metal-doped tin oxide (M-SnO₂) was used as the cathode catalyst support, and the performance was evaluated by

electrochemical measurements irrespective the conductivity of M-SnO₂.

The SnO₂ nanoparticles were synthesized by a solvothermal method. Tin chloride pentahydrate, metal chlorides as doping materials, methanol, and tetramethylammonium hydroxide solution were mixed and stirred to form precursors, which were then placed in a Teflon-lined autoclave for solvothermal synthesis. The reactants were washed with solvent using centrifugation, and the M-SnO₂ powder was obtained. Platinum nanoparticles were deposited on M-SnO₂ by the polyol method using ethylene glycol, to be a platinum-tin oxide-supported catalyst (Pt/M-SnO₂). The resulting catalyst was coated on a rotating-disc glassy carbon electrode for the electrochemical evaluation. Cyclic voltammetry (CV) and linear sweep voltammetry (LSV) were performed, and the results were characterized based on the effective Pt surface area and the activity value of ORR per Pt mass.

Among the M-SnO₂ samples prepared in this study, the highest ECSA value was obtained for Pt/Cu-SnO₂, although the Cu-SnO₂ catalyst support shows no conductivity. In this conference presentation, we will report more detailed results based on the measurements of other samples.

EN07.04.04

Characterization of NaBH₄ Powder Pellets with Heterogeneous Catalysts for Hydrogen-Based Power Systems of Urban Air Mobility Junseok Yoon¹, Byunghui Kim² and Indae Choi³; ¹Korea Institute of Materials Science (KIMS), Korea (the Republic of); ²Changwon National University, Korea (the Republic of); ³Gyeonggi University of Science and Technology, Korea (the Republic of)

Beyond the military purpose, Urban Air Mobility (UAM), commonly known as a drone, has recently become a significant device in the individual consumers and industrial sectors. In this study, to overcome the limitations of conventional battery systems, we investigate the characteristics of nanowire structures with different dimensional catalysts of Co and Ni through the hydrolysis reactions of NaBH₄ powder pellets for the application of UAM. Among the ways to improve the hydrogen conversion rate of the pellets, a small amount of cerium is added to lead the higher hydrophilicity, enhancing the more significant surface contact coverage between catalytic nanowires and the solution in which pellets are dissolved. Compared with other hydrogen supply methods, the advantages of powder pellets with catalysts for hydrogen generation and storage lead to its lightweight and long-distance driving capability, following a wide range of coverage and easy refueling. The reactivity and stability are controlled by adjusting the hydrolysis reaction of NaBH₄ material from the powder pellets, and non-precious metal catalysts are applied while maximizing the hydrogen conversion rate. The effects of influential factors on the improved hydrogen conversion rates are investigated by the optimization of variables (the amount of NaBH₄ powder, the proportion of aqueous solution, the rate of precipitated sodium metaborate, recycling of the water generated from renewable power systems, and maintaining the temperatures during the hydrolysis reaction, etc.). With these results, a novel power generation system with fuel cell equipment using hydrogen gas from NaBH₄ powder pellets is also developed for UAMs and applied for individual mobilities and mobile robots.

* Corresponding author-Indae Choi, indae.choi@gtec.ac.kr

† J. Yoon and B. Kim contributed equally to this work.

EN07.04.05

2D Sulfurized MoS₂ To Reduce Hydrogen Crossover in PEMFCs Shanmukh Kutagulla, Benjamin Stacy, Isabel Caldinho, Nam Le, Brian Korgel and Deji Akinwande; University of Texas at Austin, United States

A fundamental challenge facing proton exchange membrane fuel cells (PEMFCs) is the tradeoff between fuel crossover and conductivity. 2D materials provide a potential avenue to break this relationship through performance increases with thinner membranes. Atomically thin materials are hypothesized to act as sieves to selectively shuttle protons while blocking hydrogen gas based on their crystal structure and resultant pore size.

MoS₂ is a potentially promising material for this application due to a near-ideal pore size, as characterized by XRD, of 2.74 Å based on the (100) d-spacing that sits between the kinetic diameters of water and hydrogen gas. In this study, we examine 2D MoS₂ at various thicknesses (3nm, 6nm, 12 nm) and the resulting effect on H₂ crossover in the cell. All MoS₂ was grown via sulfurization of different thicknesses of molybdenum deposited on c-plane sapphire in a tube furnace and transferred onto a Nafion membrane (15 um). All MoS₂ samples were characterized by Raman spectroscopy. Impedance and LSV crossover data were collected for 3 samples at each thickness.

The results show that trilayer, 3 nm MoS₂ is the most effective hydrogen blocking membrane (54% improvement) while the thicker layers showed progressively lower hydrogen blocking ability. The results also show a surprising inverse relationship between MoS₂ thickness and conductivity, as the thinnest trilayer MoS₂ layer halved conductivity from baseline Nafion, while the thickest 12 nm film illustrated comparable conductivity to the NC700. This unexpected relationship is attributed to the growth dynamics of MoS₂ at different precursor thicknesses, orienting itself from horizontal growth to vertical growth modes, thus changing the effective pore size from the in-plane gap (2.74 Å) to the van der Waals gap (6.15 Å).

Trilayer MoS₂/Nafion MEA's showed superior crossover performance as compared to the baseline NC700, albeit halving conductivity, effectively performing similar to a much thicker membrane. This study thus illustrates the successful growth, transfer, and demonstration of a 2D material to improve the crossover characteristics of a Nafion membrane and provides a roadmap for further use of 2D coatings to enhance membrane performance.

EN07.04.06

Enhanced Photoelectrochemical Performance of WO₃ with Bi-Based Metal-Organic Frameworks and Glycerol Yoonsung Jung¹, Seungkyu Kim² and Sanghan Lee¹; ¹Gwangju Institute of Science and Technology, Korea (the Republic of); ²Korea Institute of Energy Technology, Korea (the Republic of)

Photoelectrochemical (PEC) glycerol oxidation is an economical and nature-friendly energy conversion method that promotes hydrogen production and generates high value-added products using solar energy. Glycerol is a by-product of biodiesel manufacturing processes made from biological sources such as vegetable oils and animal fats. The need for biodiesel is increasing due to environmental problems and rising fossil fuel costs, and production of waste glycerol is also increasing.

On the other hand, glycerol is one of the three hydroxyl groups of alcohols. It is kinetically easily oxidized and thermodynamically requires less energy than water in the oxidation reaction. An oxidized products of glycerol are glyceraldehyde, dihydroxyacetone, glyceric acid, tartaric acid, glycolic acid, formic acid, and oxalic acid. Among them, glycolic acid is more valuable than glycerol and is used as a material for derivatives, degreasers, and skin care products.

Recently, research on PEC glycerol oxidation with various metal oxides has attracted attention. WO₃ is one of the suitable photoanodes for PEC glycerol oxidation owing to appropriate values of band gap (2.5-2.7 eV) and valence band edge position (3.0 V vs. reversible hydrogen electrode (RHE)). Nevertheless, studies on the selectivity and photocurrent improvement of PEC glycerol oxidation by WO₃ photoelectrodes are still insufficient. In order to improve the photocurrent of glycerol oxidation, a utilization of oxygen evolution cocatalysts (OECs) is one of the effective strategies owing to increasing the active area and promoting the charge transfer ability. Especially, Bi-metal organic frameworks (Bi-MOFs) is promising candidate of the OECs because Bi-MOFs is able to provide the high specific surface area, multiple active sites, and good catalytic stability.

We successfully fabricated Bi-MOFs/WO₃ via solvothermal synthesis. With adding glycerol to the electrolyte, the WO₃ photoelectrode shows improved photocurrent performance on the PEC glycerol oxidation reaction (1.14 mA/cm²) than PEC water oxidation reaction (0.17 mA/cm²) at 0.8 V vs. RHE under

1 sun. The main product by glycerol oxidation is a glycolic acid which is converted with selectivity of 80 % among products. Furthermore, the photocurrent is enhanced while maintaining the selectivity (82 %) in Bi-MOFs/WO₃ photoanodes (1.53 mA/cm² at 0.8 V vs. RHE). This study highlights that an eco-friendly and sustainable hydrogen and high value-added product production system based on Bi-MOFs/WO₃ photoanodes which utilize solar energy and waste resulted from biodiesel.

EN07.04.07

Highly Active Cobalt Manganese Oxyhydroxide Added Pt/C Catalyst as ORR for PEFC Maito Tanabe and Seigo Ito; University of Hyogo, Japan

Problem of polymer electrolyte fuel cells (PEFCs) is the high cost and low durability of platinum-supported carbon catalysts (Pt/C). The cost issue is generally due to the high cost of platinum. This problem can be solved by adding other elements to Pt/C to increase the activity of Pt and reduce the amount of Pt used.[1] In this work, we focused on cobalt manganese oxyhydroxide (CMOH), because CMOH has been reported to be highly active as a catalyst for oxygen evolution reaction (OER) in alkaline water electrolysis.[2] In this study, CMOH was utilized to improve the oxygen reduction reaction (ORR) of Pt/C catalysts.

SnO₂ nanoparticles were utilized for the supporting material of CMOH. SnO₂ colloids were dispersed in H₂O. Potassium permanganate and cobalt acetate were added to the solution and stirred to coat CMOH on the SnO₂ surface (as CMOH-SnO₂). The obtained CMOH-SnO₂ was separated from the residue by centrifugation. The CMOH-SnO₂ was redispersed in water and ethanol, and Ketjen black (KB) was added and stirred. After heating, the solution was dried, and the obtained CMOH-SnO₂/KB powder was grinded in an agate mortar. By heating the CMOH-SnO₂/KB powder at 300 °C for 2 hours, cobalt manganese oxide-SnO₂/KB (as CMO-SnO₂/KB) was obtained. Pt-CMOH-SnO₂/KB and Pt-CMO-SnO₂/KB were obtained by depositing platinum on these powders by the polyol method using ethylene glycol. For these electrochemical measurements, a three electrodes system cell was used with a rotating disk electrode coated with catalyst as the working electrode, a platinum wire as the counter electrode, and a reversible hydrogen electrode as the reference electrode with 0.1 M HClO₄ as the electrolyte solution.

Pt-CMOH-SnO₂/KB and Pt-CMO-SnO₂/KB showed lower ECSA values than Pt/KB. By TEM measurements, this is confirmed to be due to the agglomeration of platinum. However, both Pt-CMOH-SnO₂/KB and Pt-CMO-SnO₂/KB showed higher specific activity per Pt surface area. The interaction of CMOH or CMO with Pt may contribute to the enhanced catalytic activity. The improvement in specific activity was higher for Pt-CMO-SnO₂/KB than for Pt-CMOH-SnO₂/KB. This difference may be due to the presence or absence of hydroxyl groups in CMOH. As a result, Pt-CMO-SnO₂/KB successfully increased the oxygen reduction reaction activity (mass activity) per Pt mass compared to Pt/KB.

References

- (1) Y. Bing, *et al.*, *Electrochim. Acta* **77**, 225 (2012).
- (2) R. Jhang, *et al.*, *J. Mater. Chem. A* **6**, 17915 (2018).

EN07.04.08

Hybrid Approach of Phase Separation and Selective Leaching Processes for Multicomponent Alloy Nanostructures and its Application to Hydrogen Storage Alloys Jinwoo Kim¹, So Young Lee^{1,2}, Ji Young Kim² and Eun Soo Park²; ¹Korea Institute of Science and Technology, Korea (the Republic of); ²Seoul National University, Korea (the Republic of)

In contrast to classical bulk alloying processes represented by melting and casting of metal mixtures, the fabrication of multicomponent alloy (MCA) nanostructures such as nanoparticles and nanofoams with more than three elements is often challenging. A few methodologies for directly synthesizing alloy nanostructures up to denary systems have been suggested recently. However, forming alloy nanoparticles inside another metal matrix, instead of inside aqueous media in wet solution-based chemical synthesis, is a fairly well understood strategy in terms of physical metallurgy. Extracting those alloy nanophases chemically from the matrix could provide an alternative way for fabricating novel MCA nanostructures. In this presentation, we introduce a hybrid approach of metallurgical bottom-up and chemical top-down processes for fabricating MCA nanostructures including nanoparticles and nanofoams. The former utilizes the liquid-state phase separation phenomenon that resembles "oil and water", but occurs at nanoscale due to thermodynamic mixing relations among alloying elements and a rapid quenching process. Thermodynamic prediction of immiscible boundary in a temperature-composition space (miscibility gap) plays a key role in designing precursor alloys with MCA nanostructures. Selective leaching, the chemical top-down process for extracting the alloy nanostructures from the precursors, uses the chemical reactivity difference between the embedded nanostructures and the matrix phase against a certain chemical solution. We discuss here how the precise control of alloy composition and cooling rate based on thermodynamic assessments enables to prepare phase-separating precursor alloys for fabricating both nanoparticles and nanofoams with a broad size range. Depending on alloy systems, the atomic structure of alloy nanostructures could be controlled from fully amorphous to nanocrystalline and even into quasicrystalline structure. This unique approach for fabricating nanosized alloys provides an extended methodology to discover novel metallic nanomaterials with promising properties in diverse compositional spaces of MCA systems. We demonstrate how this approach can be applied to fabricate nanostructured alloys for reversible hydrogen storage (e.g. TiFe nanofoams). We also present how controlling the processing parameters influences the ligament size of the nanofoams and eventually manipulates their hydrogen adsorption and desorption behavior by nanoscale size effects.

EN07.04.09

Impact of Ion Exchange Capacity and Counterion Concentration on the Structure-Property Relationship of Pentablock Copolymer Ionomers Andrew White, Thivani Senathiraja and Chris Cornelius; Iowa State University, United States

Proton exchange membranes (PEMs) are becoming more prevalent in many industries as they are integral to many clean energy technologies. The ion transport and physical properties of PEMs can be fine-tuned by altering their morphology to allow a greater degree of efficiency in a wide range of applications. In this study, the impact of ion-exchange capacity (IEC) of pentablock copolymers (PBC(XX)) exchanged with different counterions was used in order to gauge their effects on the morphology and properties of these membranes. The counterions, AlCl₃ and LiCl, were directly introduced into the solvent and were combined with 5wt% PBC blends to produce homogenous solution-cast membranes. The FTIR analysis showed that, in the case of LiCl counterions exchanged with PBC, the interaction energy between the sulfonic acid groups and counterions increases with the concentration of counterions; however, it decreases with an increase in the concentration of sulfonic acid groups. In addition, in the case of PBC exchanged with AlCl₃ counterions, PBC (2.0) membranes showed no impact, while PBC (1.5) exhibited preferential interactions with the counterions. The ion conductivity measured using electron impedance spectroscopy (EIS) showed that, overall, as the concentration and size of counterions increased, the ionic conductivity dropped significantly. However, when the concentration of LiCl is 0.01M, both PBC (1.5) and PBC (2.0) had 38% and 62% higher conductivity values, respectively, when compared to the pure membranes except PBC (1.0). The enhancement in ion conductivity may be due to the rearrangement of the morphology of the PEM to facilitate ion conductivity. The thermal stability studies of PBC (1.5) and PBC (2.0) portrayed higher stability for membranes exchanged with AlCl₃ when compared to LiCl, while PBC (1.0) showed similar stability for both counterions. However, when the IEC of the PBC membranes increased, the thermal stability decreased by 5%. The decrease in the stability may be attributed to the acceleration decomposition due to the presence of sulfonic acid groups. Further studies may include a full morphological study to determine the extent of these changes.

WITHDRAWN NO REG 12/14/22 EN07.04 Enhancing the Oxygen Reduction Reaction on Atomically Dispersed Single-iron FeN₄ Sites Effect of Axial Halogens on Intermediate Adsorption [Sabhapathy Palani](#)¹, Puttikam Raghunath², Amr Sabbah³, Indrajit Shown⁴, Khasim Saheb Bayikadi³, Ming-Chang Lin², Kuei-Hsien Chen^{3,1} and Li-Chyong Chen^{1,1,1}; ¹National Taiwan University, Taiwan; ²National Chiao-Tung University, Taiwan; ³Academia Sinica, Taiwan; ⁴Hindustan Institute of Technology and Sciences, India

EN07.04.12

Selenium-Incorporated Ruthenium Phosphide Nanotubes for Accelerated Hydrogen Evolution Reaction in Alkaline Media [Eunsoo Lee](#) and Kwangyeol Lee; Korea University, Korea (the Republic of)

Hydrogen production *via* electrochemical water splitting is a promising technology that can provide sustainable and eco-friendly energy resources. However, the hydrogen evolution reaction (HER) in alkaline conditions is still challenging owing to the sluggish reaction kinetics from the additional water dissociation step as a formidable hurdle. Due to the superior intrinsic activity of Ru-based electrocatalysts with phosphorous, we synthesized the selenium-incorporated ruthenium phosphides (Se-Ru₂P) nanotubes *via* alternating anion and cation exchange of Cu_{2-x}S hexagonal nanorod templates. Interestingly, selenization of Ru₂P nanotubes could further improve the HER performance after an accelerated durability test (ADT), which might result from the newly formed anion vacant sites during the water electrolysis. Moreover, an in-depth X-ray photoelectron spectroscopic study demonstrated that the Ru-P bonds were more preserved in Se-decorated Ru₂P after ADT than in Ru₂P without Se decoration. Considering these advantages, the Se-Ru₂P nanotubes achieved superior hydrogen evolution catalytic properties with low overpotentials of 39 mV at a current density of 10 mA/cm² in 1.0 M KOH after 15,000 CV cycles. Furthermore, the Tafel slope of Se-Ru₂P nanotubes was only 32.8 mV dec⁻¹, indicating that the introduction of Se can positively alter the reaction kinetics toward the HER in alkaline media.

EN07.04.13

Mosaic CrO/Co₉S₈ Heterostructure with a Maximized Synergy Effect for Hydrogen Evolution in Neutral Media [YeJi Park](#) and Kwangyeol Lee; Korea University, Korea (the Republic of)

Generating hydrogen, an eco-friendly energy carrier, through electrochemical water splitting from the neutral media has attracted considerable attention due to the much less corrosion of the water electrolyzer and the feasibility of the direct usage of seawater sources without pH adjustment. To enhance the catalytic performance in neutral media by modulating the HER mechanism, electrocatalysts with dual-site were required for facilitating fast water adsorption/dissociation and sequential hydrogen desorption, respectively. Therefore, designing the well-defined heterostructures by integrating the H₂O adsorption-active materials with HER-active materials is a promising strategy to heighten the HER performance. Herein, we embedded the numerous oxophilic cluster into the metal sulfide matrix to synthesize the mosaic hetero-nanostructure with the maximized interface, increasing the active sites for hydrogen evolution reaction. The efficient charge redistribution at the interface is significantly enhanced the catalytic performance. This study provides a promising design strategy to synthesize the electrocatalysts with hetero-interface and a realization to understand the fundamental HER mechanism in neutral media.

EN07.04.14

Activating NiO Nanorods via Nitrogen Doping and Vacancy Engineering for Alkaline Hydrogen Evolution Reaction [Jaerim Kim](#)¹, Dong-Seok Kim², Jiye Kim¹, Hyeonwoong Hwang¹ and Jong kyu Kim¹; ¹Pohang University of Science and Technology (POSTECH), Korea (the Republic of); ²Korea Atomic Energy Research Institute, Korea (the Republic of)

Developing efficient and inexpensive electrocatalysts for oxygen evolution reaction (OER) and hydrogen evolution reaction (HER) in alkaline water-electrolysis is of paramount importance in the hydrogen economy to meet future energy demands. Earth-abundant transition metal oxide-based catalysts including NiO have emerged as the active OER catalysts with the advantages of compositional and structural diversity, low cost, easy synthesis, and eco-friendliness. However, they are generally considered inactive towards HER because of limited catalytic active sites, poor electrical conductivity, and inappropriate adsorption abilities. Herein, we show a strategy to activate NiO by using unique ion irradiation technology, which simultaneously creates the nitrogen dopants and oxygen vacancies. An array of three-dimensional (3D) NiO nanorods (NRs) was applied as the scaffold that provides abundant surface active sites and efficient channels for charge transfer and mass transport. Our experimental and theoretical results demonstrate the synergistic effect of nitrogen doping and vacancy engineering via nitrogen-ion irradiation to optimize the hydrogen adsorption and electrical conduction of NiO NRs, which results in the remarkably enhanced alkaline HER performance. Our approach can provide an effective and unique methodology for designing efficient electrocatalysts consisting of earth-abundant elements for electrochemical hydrogen production.

EN07.04.15

Highly Scalable Non-Noble Tri-Metallic Catalyst for Anion Exchange Membrane Electrolyzer Cell (AEMEC) Without Deactivation for Hundreds of Hours Demonstrated in Membrane Electrode Assembly Setup [Ali Abdelhafiz](#)¹, Sameh Elsaidi², Paul Kohl³ and Ju Li¹; ¹Massachusetts Institute of Technology, United States; ²Illinois Institute of Technology, United States; ³Georgia Institute of Technology, United States

Elevated pollution levels due to hydrocarbon fuels combustion and associated global warming effects escalate the necessity to find green alternative energy sources. Other CO₂-free energy sources, such as nuclear energy, is hindered due to elevated costs of dumping the spent nuclear fuel and safety-related mitigation protocols. Thus, Water electrolysis is deemed the most prominent solution towards an economically feasible green hydrogen production. Water electrolysis results in the production of clean hydrogen and oxygen, without any associated carbonaceous emissions. Electricity used in water splitting can be supplied from intermittent and inexpensive sources, such as windmills, where such an electricity can't be stored for prolonged periods due to limited grid-scale battery capacity, for less than half a day. Electrochemical water splitting runs through two separate half reactions: hydrogen evolution reaction (HER) and oxygen evolution reaction (OER). Both reactions are sluggish in nature where an electrocatalyst is essential for the reaction to take place. Catalysts of choice for HER and OER, up to date, are based on noble metals (e.g., Pt, Ir or Ru). In addition to being very expensive, noble metal catalysts suffer from extremely short lifetime and poor efficiency. Therefore, many research efforts have been devoted to discovering efficient, prolonged, and cost-competitive catalysts. Transition metals (TM) have shown great potential in catalyzing HER and OER. OER is considered the bottleneck reaction in water electrolysis. Modulating the metal-oxygen covalency is considered a key to optimize the interaction between the catalyst materials and reaction intermediates. Alloying of different transition metals, heteroatom doping, and/or vacancy creation are prominent strategies to alter the electronic configuration of TM catalyst surfaces to enhance their electrocatalytic activity.

In the presented study, we are demonstrating the utilization of a versatile metal organic framework platform for OER in alkaline aqueous mediums. We carefully studied the effect of tri-metallic Fe, Ni and Co alloying, and their corresponding effect on OER activity and stability. Our synthesized MOF architecture showed a significant enhancement in OER activity due to dynamic chemical state perturbation during OER process, where tri-metallic MOF

turns from metallic to oxide, before converting to the super active oxyhydroxide phase at the OER onset. Catalyst electronic conductivity is a crucial factor to enhance its activity. Our developed synthesis strategy, beside being highly scalable to match industrial demands, successfully fabricated the tri-metallic MOF with a very high surface area and minute crystallite size. Catalytic activity towards OER have been demonstrated in a membrane electrode assembly (MEA) setup in an actual AEMEC device. Results showed a high stability and low overpotential, where catalysts subjected to 1000 mA/cm², recording a potential of 1.85 V. Performance remained stable for over 550 hours of continuous operation without noticeable decay in performance. The presented study is introducing an inexpensive, tremendously stable, and highly active catalyst without any noble metals, which can meet the industrial demands for green hydrogen production.

EN07.04.16

A Valuation Study of Membrane Thickness Selection and Load Cycling on Long-Term Value of PEM Water Electrolysis Systems Efat Mohammadi and Alexander J. Headley; The University of Memphis, United States

As the proportion of energy produced from intermittent renewable energy sources increases, the value of systems capable of storing large quantities of energy will increase as well. Hydrogen, being a very flexible energy storage medium with many end use applications, could play a pivotal role in the future. Polymer electrolyte membrane water electrolyzers (PEMWEs) have been gaining significant attention as a method of producing green hydrogen from intermittent renewable energy sources due to their simplicity, possibility to be designed as a compact system, and suitable dynamic response to the power fluctuations that will be inherent with fluctuating renewable power generation. The highest expenses for electrolysis systems are the membranes, noble metals for the electrocatalysts, as well as the bipolar plates and their coatings. Given the durability concerns for these systems in some conditions and the high upfront cost, they will need to be used in the right applications in addition to being sized and operated appropriately to make them cost-effective. For long term PEMWE performance the weakest component is the membrane, with membrane thinning being one of the most important degradation phenomena in water electrolysis. Though thinner membranes reduce ohmic losses, thereby increasing efficiency they are also more likely to fail more quickly than thicker membranes. Cell durability and safety issues regarding the mechanical strength of thinner membranes in PEMWE, as well as the permeability of gases through the membrane, are critical issues that must be considered. As a result of these two conflicting trends regarding membrane thickness, maximizing the long-term value of an electrolysis system will depend in part on the selection of the proper membrane specifications to maximize their life while minimizing the impact on efficiency.

This is a particularly important consideration for pairing with renewable energy as fluctuating power levels have an impact on PEMWE performance. However, primary studies on PEMWE degradation behavior have shown conflicting results as to how degradation is impacted by power fluctuations. While in some experiments cell voltage performance degradations are reported due to the current ripple, in the others, positive effects of current density switching on PEMWE durability are investigated. This makes valuation studies difficult as it is very unclear how the systems will be impacted by different operational characteristics. It has been suggested by some to leverage the available literature on PEM fuel cell (PEMFC) durability to evaluate electrolyzers as well, but these two technologies contain different materials, boundary and operating conditions which may not make the PEMFC literature useful for PEMWE systems.

Thus, in the present study the effect of membrane thickness selection on long-term value is considered with respect to various degradation trends reported in the literature. The reported performance of PEM electrolyzers are discussed to demonstrate how the value of a PEM electrolysis system could vary depending on the degradation phenomena that occur. Estimates for the effects of membrane thickness and load cycling on PEMWE longevity reported from various sources (including the PEMFC literature) are applied in conjunction with our suggested optimization software to highlight the PEMWE degradation issue. Here we hope to highlight the potential effects for system selection of the gap in PEMWE degradation data and determine the uncertainty that this knowledge gap brings to the realm of system sizing and valuation.

EN07.04.17

Study of the Use of Au-Nanoparticles and Mg Thin-Film Layer as Hole- and Electron-Selective Contacts in TiO₂-Based Photocatalytic Systems Oriol Segura¹, Eloi R. Costals¹, Cristobal Voz¹, Pablo R. Ortega¹, Magno Barcelos², Edoardo Maggi¹, Edgardo Saucedo¹, Jordi Llorca¹, Lluís Soler¹ and Joaquim Puigdollers¹; ¹University of Politecnica-Catalunya, Spain; ²Universidade Federal de São Carlos, Brazil

Photocatalysis is defined as the acceleration of chemical reactions under illumination and in the presence of a catalyst, which absorbs light and participates in the chemical transformation of the products present in the electrolyte. Under illumination, the photocatalytic system photogenerates charge carriers. The different electrochemical energies of these electrons and holes will be used to oxidize or reduce compounds, which translates into interesting applications, such as the generation of hydrogen or the elimination of pollutants. Since the light source comes from the sun, photocatalysis is considered a green technology to convert solar energy into chemical energy.

For the system to be efficient, these charge carriers (electrons and holes) must be physically and energetically separated. The energy separation must be adequate to be able to participate in the chemical reactions of reduction and oxidation, while the physical separation is necessary to avoid their recombination. As occurs in the manufacture of solar cells, the use of selective contacts of electrons and holes is a good strategy to achieve a physical and energetic separation of the photogenerated carriers.

In this work we optimize hydrogen generation from TiO₂ using selective contacts based on Au nanoparticles and thin layers of metallic Mg. Au np acts as a hole transport layer (allowing hole transport and blocking electrons) while Mg acts as an electron transport layer (allowing electron transport and blocking hole transport). Au incorporation is done by sol-gel dip coating method. While the deposition of Mg is carried out by thermal evaporation deposition in high vacuum. The use of shadow masks during the deposition of Mg allows obtaining an interdigitated structure, with TiO₂/Au np fringes and Mg fringes, in what we can call an Interdigitated Front Contact Photocatalytic system.

The global average hydrogen production was 2.8 μmol/(min g) only for the TiO₂ absorber, while in the sample with gold the global average production increases to 66.4 μmol/(min g) due to the catalytic effect of gold nanoparticles. However, for the sample containing Au np plus the Mg layer, the hydrogen generation doubled the generation with respect to the TiO₂/Au sample, with an average total hydrogen production of 133.7 μmol/(min g)

This experimental result can be explained by taking into account the energy diagram of the different layers. The final conclusion is that the TiO₂/Au interface acts as a selective contact of holes, whereas Mg acts as a selective contact of electrons. Additional characterization of the samples was performed by HRTEM, SEM and EDX.

EN07.04.18

Interfacial Band Alignment and Photoelectrochemical Properties of All-Sputtered BiVO₄/FeMO_x (M = Co, Ni, Mn) *p-n* Heterojunctions Renato V. Goncalves¹, Andressa Correa¹, Lucas Rabelo¹, Washington Santa Rosa¹, Niqab Khan² and Sherdil Khan²; ¹University of Sao Paulo, Brazil; ²Federal University of Rio Grande Do Sul, Brazil

BiVO₄ is a well-known *n*-type semiconductor with great potential for photoelectrochemical (PEC) conversion of solar energy into chemical fuels.

Nevertheless, photocurrent densities achieved for bare BiVO₄ photoanodes are still far from their theoretical maximum due to the sluggish water oxidation kinetics and severe electron-hole recombination. In this work, magnetron sputtering deposition was applied for depositing FeMO_x (M = Co, Ni, Mn) cocatalyst layers to induce *p-n* heterojunctions and suppress charge recombination on BiVO₄ photoanodes. The all-sputtered BiVO₄/FeMO_x (M = Co, Ni, Mn) films exhibited higher PEC performance on sulfite oxidation than the bare BiVO₄ photoanode. The *p-n* heterojunction BiVO₄/FeMnO_x exhibited the highest photocurrent density (1.99 mA cm⁻² at 1.23 V vs. RHE) and excellent chemical stability, indicating that the combination of Mn sites on Fe-based oxides provides promising novel cocatalysts materials for PEC applications. Experimental and theoretical techniques were used to investigate the interfacial band alignment and charge transport properties of BiVO₄/FeMO_x (M = Co, Ni, Mn) heterojunctions. The results show that the naive alignment of the individual energy bands of semiconductors, both before and after equilibrium, results in significant potential barriers for the photogenerated charges on the BiVO₄/FeMO_x (M = Co, Ni, Mn) photoanodes, which does not explain its enhanced PEC performance. Therefore, X-ray photoelectron spectroscopy, the Kraut method and the classical band bending model were combined to determine the valence band offsets, potential drops supported in the *n* and *p* layers, and the related depletion widths. Our results show that type II heterojunctions arise in the BiVO₄/FeMO_x (M = Co, Ni, Mn) interface after equilibrium, eliminating the possible potential barriers. Furthermore, the BiVO₄/FeMnO_x film showed a larger space charge region (SCR) characterized by a more intense built-in electric field than other heterojunctions, which explains its higher PEC performance. In summary, this work provides a viable technique for producing photocatalytic heterojunction systems based on metal oxide semiconductors and introduces simple tools for investigating interface effects on photoinduced charge carrier pathways for PEC applications.

EN07.04.20

Anti-Poisoning Carbon Shell-Encapsulated Pt-Based Nanoparticles for Selective Electrochemical Reactions in PAFCs Sourabh Chougule, Sreya Roy Chowdhury, Bathinapatta Sravani, Jiho Min, Yunjin Kim, Keonwoo Ko and Namgee Jung; Chungnam National University, Korea (the Republic of)

In phosphoric acid fuel cells (PAFCs), one of the significant issue is poisoning of Pt-based cathode catalysts by phosphate anions. It is well known that the fuel cell performance decreases by blocking the electrochemically active sites for oxygen reduction reaction (ORR) due to the strong adsorption of phosphate anions on the Pt surface. In this study, we attempt to reduce the poisoning effect by phosphate anions through encapsulating Pt-based nanoparticles by a molecular sieve layer. The structural control of the molecular sieve layer reduces the adsorption of anions and allows gas molecules to selectively penetrate into the Pt surface. In addition, the molecular sieve layer is expected to effectively prevent the dissolution of metal nanoparticles even under harsh conditions during the electrochemical reaction. The electrochemical analysis results suggest that metal nanoparticles coated with a molecular sieve layer having a better antipoisoning capability toward phosphate anion, high selectivity toward ORR with high durability in acid solutions. The durability of the molecular sieve layer-coated metal nanoparticles is demonstrated by accelerated degradation tests (ADTs). Inevitably, designing Pt-based catalysts with an antipoisoning carbon molecular sieve layer provides a highly effective way for use in PAFCs.

EN07.04.22

Understanding the Fundamentals of Hydrogen Degradation in Pipeline Steels Used for Large-Scale Storage and Transport Ting Yang¹, T. A. Venkatesh² and Ming Dao¹; ¹Massachusetts Institute of Technology, United States; ²Stony Brook University, United States

There is considerable interest in repurposing and reusing the multi-billion dollar pipeline infrastructure that is currently used for transporting natural gas for large-scale storage and transport of green hydrogen needed for the hydrogen economy. One of the key technical challenges in transitioning from natural gas networks to hydrogen networks is in understanding the effects of hydrogen on pipeline materials and identifying optimal operating conditions for the reliable and long-term use of the pipeline infrastructure. It is well known that hydrogen degradation (HD), a complex metallurgical phenomenon that combines chemical and physical processes that ultimately reduces material toughness and leads to catastrophic failure, is a key materials challenge to be addressed for enabling the hydrogen economy [1]. In particular, natural gas pipeline steels and pressure vessel steels, most of which are (BCC) ferritic steels, are susceptible to spontaneous failure in the field [2-6]. It is also observed that the hydrogen embrittlement effect is much more pronounced at relatively lower stresses and crack driving forces [7]. In this study, we focus on pure iron, which has a BCC crystal structure, as a model material and investigate the hydrogen embrittlement effect using several experimental approaches, including low cycle fatigue testing with the materials pre-charged with hydrogen and in-situ electrochemical nanoindentation testing of materials with in-situ charging of hydrogen. 304 stainless steel (FCC austenitic steel) is used as reference material. For the materials subjected to low cycle fatigue tensile experiments, fractographic analysis is conducted on the fracture surface to elucidate the effect of hydrogen on the microstructure and mechanical properties. For the materials subjected to in-situ electrochemical nanoindentation, microstructural analysis is conducted to understand the development of insipient plasticity events and dislocation microstructures in localized regions. The embrittlement effects due to hydrogen charging and the differences in dislocation and fracture characteristics are compared between pure iron and 304 stainless steel materials. The insights learned from the hydrogen embrittlement mechanism in pure iron could provide metallurgical design strategies for developing damage-resistant materials for pipeline steels in hydrogen storage and large-scale transport.

References:

1. Li X. et al. *Acta Metallurgica Sinica (English Letters)* 33.6 (2020): 759-773.
2. Pluvinaige G. *International Journal of Pressure Vessels and Piping* 190 (2021): 104293.
3. Birkitt K et al. *International Journal of Hydrogen Energy* 46.23 (2021): 12290-12299.
4. Shang J et al. *Scripta Materialia* 189 (2020): 67-71.
5. Zhou D et al. *International Journal of Hydrogen Energy* 46.10 (2021): 7402-7414.
6. Nguyen TT et al. *Engineering Failure Analysis* 122 (2021): 105242.
7. San Marchi C and Ronevich JA. PVP2022-84757, in *Proceedings of the ASME 2022 Pressure Vessels & Piping Conference (PVP2022)*, July 17-22, 2022, Las Vegas, Nevada, USA.

EN07.04.23

Graphene Oxide-Hydrogen Membrane Fuel Cells Using Ni-Zr Alloy Thin Films Young J. Cho, Shahjahan K. Chowdhury, Sung B. Park and Yong-il Park; Kumoh National Institute of Technology, Korea (the Republic of)

Graphene oxide film (GOM) is an excellent proton conductor at room temperature under humidified conditions, but graphene oxide film fuel cells (GOMFC) exhibit lower maximum power densities compared to Nafion[®] due to fuel crossover, film degradation and loss of surface function. In this study, a double membrane composed of the GOM and a hydrogen permeable Ni-Zr alloy thin film was investigated as an electrolyte membrane for a hydrogen membrane fuel cell (HMFC). In this fuel cell, the graphene oxide-hydrogen film (GOHM) simultaneously serves as an anode catalyst and an electrolyte. A hydrogen-permeable metal thin film of about 40 nm was deposited by DC magnetron sputtering on a 20 μm-thick GOM using a Ni₆₄Zr₃₆ target to complete a double-layer GOHM electrolyte. The fuel cell performance of the fabricated Ni-Zr-based GOHMFC was compared with that of conventional PEMFC.

8:30 AM EN07.05.01

Controlling the Macrostructure of Chromophore Hydrogels for Enhanced Photocatalytic Hydrogen Evolution Jacob E. Kupferberg^{1,2}, Zois Syrgiannis^{1,3}, Luka Dordevic^{1,2}, Eric Bruckner¹, Adam Dannenhoffer¹, Evan Qi¹, Kristen Wek¹, Harry C. Fry⁴, Liam Palmer^{1,2,3} and Samuel I. Stupp^{1,2,3}; ¹Northwestern University, United States; ²Center for Bio-Inspired Energy, United States; ³Simpson Querrey Institute for BioNanotechnology, United States; ⁴Argonne National Laboratory, United States

Solar fuel generation is a promising method of producing stable storage molecules like hydrogen gas using abundant sunlight as an energy source. Self-assembling chromophore amphiphiles based on perylene monoimide (PMI) can form weak hydrogels capable of producing of H₂ in water under visible light illumination. However, the high diffusivity of these gels comes at the cost of poor mechanical stability. We report here on the use the natural biopolymer sodium alginate to both promote self-assembly and immobilization PMI in a robust hydrogel. The PMI-alginate matrix can entrap catalysts in close proximity to PMI photosensitizer to enhance H₂ evolution and enable long-term reusability for up to six days. By changing the diameter and the alginate loading of the PMI-alginate gel, we showed that hydrogen production could be enhanced by reducing the mass transfer distance of reagents through the gel.

The long-aspect ratio of the pi-pi stacked PMI assemblies also enables the formation of a percolation network for electrical conduction within the hydrogel network. In the hydrated state, the chromophore hydrogels displayed photoconductivity under visible light, enabling the application of these 3D hydrogels to electrodes. We then 3D printed this material on an FTO-NiO substrate to create 3D hydrogel photocathodes.

8:45 AM EN07.05.03

Highly Conjugated Covalent Organic Frameworks for the Photocatalytic Generation of Hydrogen Jai-Ram Mistry and Iain A. Wright; Loughborough University, United Kingdom

The development of new conjugated covalent organic frameworks (COFs) designed specifically to maximise hydrogen adsorption and production has been a hot topic in recent years due to the desirable properties COFs possess. High thermal and chemical stability, tuneable pore sizes and charge transport properties as well as the molecular building block approach in their synthesis all make COF's excellent materials for hydrogen storage and production. This coupled with the lack of heavy metals within their structure and within their synthesis make COFs attractive in terms of sustainability.¹

The specific design of compounds with a spiro core have been studied extensively as components of conjugated oligomers and polymers, and their use as organic light emitting diode (OLED) and solar cells.² However, the use of spiro component in COFs has yet to be explored extensively. The C₄ type symmetry in spiro compounds coupled with C₂ symmetry in linkers would provide interesting topologies when considering the dihedral angle in spiro compounds. Varying the linker length also provides a greater insight into the effects this has on pore size and hence and H₂ adsorption.

Furthermore, introducing electron rich donor type molecules within the linkers of the framework furthers the scope of application for these COFs thus allowing them to be used as photocatalysts for photocatalytic evolution of H₂ from water. The high degree of crystallinity favours charge separation and transport, which provides COFs with promising catalytic activity.³ This ties into the growing interest of organics polymeric photocatalyst as well as the growing market for new hydrogen storage and generation materials.

Herein we present a series of highly conjugated spiro core-based COFs designed with two main objectives, to increase hydrogen adsorption rates of COF materials and to further increase the hydrogen evolution rate (HER) seen in current COF photocatalyst materials.

Reference:

- 1 N. W. Ockwig, A. P. Co, M. O. Keeffe, A. J. Matzger and O. M. Yaghi, 2005, 310, 1166–1171.
- 2 R. Pudzich, T. Fuhrmann-Lieker and J. Salbeck, Adv. Polym. Sci., 2006, 199, 83–142.
- 3 C. Dai and B. Liu, Energy Environ. Sci., 2020, 13, 24–52.

9:00 AM EN07.05.04

Glycerol-Assisted Solar-to-Hydrogen Electrolysis in Simple Photoelectrochemical Integrated Systems Zebulun G. Schichtl, Robert H. Coridan, Hamed Mehrabi and Samuel K. Conlin; University of Arkansas, United States

Storing solar energy in the form of hydrogen from water splitting is an attractive replacement for fossil fuels for on-demand energy use. Unassisted solar-driven water splitting is difficult to achieve due to the overall thermodynamics of the reaction and the overpotentials required to drive water oxidation at appreciable rates. The ideal semiconductor material for water splitting would be capable of absorbing a substantial portion of the solar spectrum and generating hydrogen and oxygen at high rates, but this material does not exist yet. The voltage requirements of water splitting are met by designing complex, tandem photoelectrode systems in series but scalability and cost remain major concerns. Glycerol is a co-product of renewable biodiesel synthesis with a well-defined electrooxidation mechanism. The design of solar-to-hydrogen integrated photoelectrochemical (PEC) devices is simplified by replacing water oxidation with crude glycerol electrooxidation. Here, we describe the development of a trimetallic AuPtBi electrocatalyst with increased and sustained electrooxidation activity for crude glycerol. When paired with a hydrogen evolving cathode, the electrolysis system is capable of driving hydrogen evolution at low overall cell potentials (< 0.5 V). We demonstrate the capability for using a single semiconductor light absorber for solar-to-hydrogen production when the anode is performing glycerol oxidation rather than water oxidation. We demonstrate a photoelectrolysis approach using a monocrystalline Si and a GaAs single-junction photovoltaic (PV) in a traditional PV-electrolyzer system, and for an integrated PEC system driven by a copper bismuthate (CuBi₂O₄) photocathode. Finally, we will discuss technical and catalytic metrics that should be considered when comparing these glycerol-assisted integrated systems to other solar-to-fuels technologies.

9:15 AM EN07.05.05

H₂ Production from Photocatalytic Assisted Electrolysis of Water Sang Youn Chae¹, Noyoung Yoon^{2,3}, Adeel Mehmood¹, Oh-Shim Joo² and Eun Duck Park¹; ¹Ajou University, Korea (the Republic of); ²Korea Institute of Science and Technology, Korea (the Republic of); ³Yonsei University, Korea (the Republic of)

Electrolysis of water can be a promising way of producing green hydrogen gaseous because of its zero-carbon emission during the electrolysis process. For green hydrogen production, the electrical power source for electrolysis also should be supplied from a renewable source such as solar light, this is one of

the reasons to increase the production cost of green hydrogen when compared to the production cost of grey hydrogen. Therefore it is important to increase electricity to hydrogen conversion efficiency. In this research, we utilized solar energy via WO_3 photocatalyst for water oxidation reaction and redox couple reduction. For efficient water oxidation and redox couple reduction, the noble-metal co-catalyst decorated WO_3 nanoparticle is designed. And then, the solar energy which is stored in the redox couple is subsequently used in the electrolysis process for hydrogen production reaction. This photolysis-electrolysis tandem system allows largely reduced operating voltage and also led to increased electrical power to hydrogen conversion efficiency.

9:30 AM EN07.05.06

Charge Transport in $\text{SrTiO}_3\text{:Rh}$ and BiVO_4 Nanoparticle Photocatalysts for Z-Scheme Water Splitting [Brian T. Zutter](#)¹, Zejie Chen², Aliya S. Lapp¹, Kenta Watanabe³, Luisa Barrera⁴, Austin Bhandarkar¹, Akihiko Kudo³, Rohini Bala Chandran⁴, Shane Ardo² and A. A. Talin¹; ¹Sandia National Laboratories, United States; ²University of California, Irvine, United States; ³Tokyo University of Science, Japan; ⁴University of Michigan–Ann Arbor, United States

Solar-powered water splitting using nanoparticle photocatalyst suspensions is a promising route to economical, clean hydrogen production. In the Z-scheme approach, hydrogen and oxygen-evolving photocatalysts, such as $\text{SrTiO}_3\text{:Rh}$ and BiVO_4 , are coupled with a redox mediator to improve light absorption compared to single-photocatalyst systems. A key step in the water-splitting process is the separation and transport of photo-excited electrons and holes to the photocatalyst surface. Here we characterize charge transport in individual $\text{SrTiO}_3\text{:Rh}$ and BiVO_4 nanoparticles using a nanoprobe within a scanning electron microscope, and directly map internal electric fields with electron-beam induced current. Charge transport in $\text{SrTiO}_3\text{:Rh}$ particles is limited by bulk defect states within the nanoparticle, in contrast to nearly Ohmic conduction in BiVO_4 nanoparticles. $\text{SrTiO}_3\text{:Rh}$ particles contain insignificant built-in E fields, while BiVO_4 nanoparticles contain built-in E field between different facets of the nanoparticle which can efficiently separate e-h pairs. Inefficient charge transport and lack of built-in electric field explain why the H_2 -evolving $\text{SrTiO}_3\text{:Rh}$ nanoparticles are the limiting component within this Z-scheme system.

9:45 AM BREAK

SESSION EN07.06: Metal Organic Frameworks
Session Chairs: Thomas Gennett and Sarah Shulda
Wednesday Morning, November 30, 2022
Hynes, Level 3, Room 302

10:30 AM *EN07.06.01

Improving Hydrogen Storage in Metal-Organic Frameworks [Michael Hirscher](#)^{1,2}; ¹Max Planck Institute for Intelligent Systems, Germany; ²Advanced Institute for Materials Research, Tohoku University, Japan

Hydrogen storage in nanoporous materials has been attracting a great deal of attention in recent years, as high gravimetric H_2 capacities can be achieved at 77 K using materials with particularly high surface areas. Cryogenic storage by physisorption of hydrogen molecules will safely operate at low pressures, is fully reversible and has fast kinetics.

Experimental data of the gravimetric and volumetric hydrogen uptake have been analysed for many MOFs showing a linear correlation of the gravimetric absolute uptake with the specific surface area (Chahine's rule) [1]. Using the packing density of the powder as well as the single-crystal density, a linear relation is found between the volumetric absolute hydrogen uptake and the volumetric surface area [2]. The specific total volume occupied by a porous material, i.e. the inverse of its packing or single crystal-density, as a function of its specific surface area yields a linear relationship. Based on these results, a phenomenological model is developed for the volumetric absolute uptake as a function of the gravimetric absolute uptake [2]. The key for improving the volumetric storage capacity is closing the gap between the low-density powder towards the theoretical upper limit of the single crystal by either compaction, pelletizing or monoliths. Furthermore, interpenetrated frameworks show generally higher volumetric hydrogen uptakes [3]. Finally, for technical applications the key parameter is the usable or working capacity, which is the amount of hydrogen that can be delivered between the maximum tank pressure and the back pressure required by the end-user [4].

The presentation will give an overview of the current status and discuss future concepts [5,6].

References

- [1] M. Schlichtenmayer, M. Hirscher, *J. Mater. Chem.* 22, 10134 (2012)
- [2] R. Balderas-Xicohtencatl et al., *Energy Technol.* 6, 578 (2018)
- [3] R. Balderas-Xicohtencatl et al., *Energy Technol.* 6, 510 (2018)
- [4] M. Schlichtenmayer, M. Hirscher, *Appl Phys A* 122, 379 (2016)
- [5] D.P. Broom et al., *Int. J. Hydrogen Energy* 44, 7768 (2019)
- [6] L. Zhang et al., *Progress in Energy* in press (2022)

11:00 AM EN07.06.02

Super Proton Conductivity Through Control of Hydrogen-Bonding Networks in Flexible Metal-Organic Frameworks [Nam Ho Kwon](#), Seunghee Han, Jihan Kim and Eun Seon Cho; Korea Advanced Institute of Science and Technology (KAIST), Korea (the Republic of)

Due to the growing concern over climate change and its consequences, it requires the development of renewable energy storage and conversion systems. Fuel cells operating mainly based on hydrogen as a fuel have been considered as an attractive option for sustainable energy conversion. In particular, proton exchange membrane fuel cells (PEMFCs) are recognized as a promising candidate for transportation applications due to their mild operating conditions, high-power density and ultralow emission of pollutants. The design of proton exchange membrane with a high proton conductivity over a wide humidity range remains a challenge to improve the performance of PEMFCs. Moreover, the amorphous nature of the commonly used polymer exchange membrane materials hinders the investigation and control of the proton conduction behavior. Metal-organic frameworks (MOFs) have emerged as a new type of solid-state proton conductor, attributed to their high surface area and porosity as well as high crystallinity and structural tunability. The introduction of functional groups onto the frameworks and guest molecules into the pore spaces of MOFs allows the formation of hydrogen-bonding networks, facilitating proton conduction over a wide humidity range. Furthermore, the crystalline nature of MOFs enables the precise investigation of the hydrogen-bonding networks and the relevant proton conduction mechanism. However, it is still unclear about how the functional groups and non-aqueous proton carriers would simultaneously affect the formation of hydrogen-bonding networks within MOFs. In this regard, flexible MOFs which present a reversible dynamic structural transformation in response to external stimuli can be a suitable host material to unravel the aforementioned issues because of their

potential to control the proton transfer channels.

In this study, we designed a series of imidazole molecule-loaded flexible MOFs (Im@MIL-88B) to modify the hydrogen-bonding networks and the resulting proton conduction characteristics by controlling the breathing behavior. Imidazole molecules were selected as a proton carrier which possibly leads to a full breathing on the flexible framework through the strong host-guest interaction. The breathing behaviors of MIL-88B are tuned by varying the concentration of adsorbed imidazole molecules-Im@MIL-88B-SB (small breathing) and Im@MIL-88B-LB (large breathing)-and introducing functional groups onto MOF ligands-Im@MIL-88B-NH₂ and Im@MIL-88B-SO₃H, also investigating the pristine MIL-88B (no breathing) without the imidazole loading as a control. Im@MIL-88B-LB not only shows a larger breathing effect, but also accommodates a larger amount of encapsulated imidazole into the pore spaces. The proton conductivity of 8.93×10^{-2} S cm⁻¹ at RH 95% and 60 °C for Im@MIL-88B-LB is achieved, which is the highest among N-heterocyclic molecules-loaded proton conducting MOFs reported so far to the best of our knowledge, in spite of mild operating condition. The computation results suggest that the breathing effect induces the pore opening in the frameworks and the mixed configuration of water and imidazole within the transfer channels, contributing to the formation of stable and continuous hydrogen-bonding networks. Interestingly, Im@MIL-88B-LB exhibits the higher proton conductivity than even functionalized Im@MIL-88B, which may be attributed to the high concentration of proton carriers through its large imidazole-dependent structural transformation and self-adaption, while the functional groups in the pores disturb such transformation. Although the functional groups in the channels can facilitate the proton conduction, such effects are offset by the limited breathing behavior, suggesting that dense hydrogen-bonding network of proton carrier is a priority factor in proton conduction. Our investigation provides the promise about the design of hydrogen-bonding networks in proton carrier-loaded systems for facile proton conduction.

11:15 AM *EN07.06.03

Structural Resolution and Mechanistic Insight into Hydrogen Adsorption in Flexible ZIF-7 [Mike McGuirk](#); Colorado School of Mines, United States

Flexible metal-organic frameworks offer a route towards high useable hydrogen storage capacities with minimal swings in pressure and temperature *via* step-shaped adsorption and desorption profiles. Yet, the understanding of hydrogen-induced flexibility in candidate storage materials remains incomplete. Here, we investigate the hydrogen storage properties of a quintessential flexible metal-organic framework, ZIF-7. We use high-pressure isothermal hydrogen adsorption measurements to identify the pressure-temperature conditions of the hydrogen-induced structural transition in ZIF-7. The material displays narrow hysteresis and has a shallow adsorption slope between 100 K and 125 K. To gain mechanistic insight into the cause of the phase transition correlating with stepped adsorption and desorption, we conduct powder neutron diffraction measurements of the D₂ gas-dosed structures at conditions across the phase change. Rietveld refinements of the powder neutron diffraction patterns yield the structures of activated ZIF-7 and of the gas-dosed material in the dense and open phases. The structure of the activated phase of ZIF-7 is corroborated by the structure of the activated phase of the Cd congener, CdIF-13, which we report here for the first time based on single crystal X-ray diffraction measurements. Subsequent Rietveld refinements of the powder patterns for the gas-dosed structure reveal that the primary D₂ adsorption sites in the dense phase form D₂-arene interactions between adjacent ligands in a sandwich-like adsorption motif. These sites are prevalent in both the dense and the open structure for ZIF-7, and we hypothesize that they play an important role in templating the structure of the open phase. We discuss the implications of our findings for future approaches to rationally tune step-shaped adsorption in ZIF-7, its congeners, and flexible porous adsorbents in general. Lastly, important to the application of flexible frameworks, we show that pelletization of ZIF-7 produces minimal variation in performance.

SESSION EN07.07: Fuel Cells

Session Chairs: Alexander Headley and Samantha Johnson
Wednesday Afternoon, November 30, 2022
Hynes, Level 3, Room 302

3:45 PM EN07.07.02

Computational Study of Nanoscale Active Sites in PGM-Free Electrocatalysts for Proton Exchange Membrane Fuel Cells [Guofeng Wang](#) and Boyang Li; University of Pittsburgh, United States

Proton exchange membrane fuel cells (PEMFCs) can convert chemical energy stored in hydrogen fuels to electricity and produce environmentally benign product water. However, the emergent applications of PEMFCs is hindered by the present requirement of expensive Pt group metals (PGM) as their electrocatalysts. To advance PEMFC technology, it is of great interests to develop earth-abundant, non-precious metal based catalysts in replacement of Pt, especially for oxygen reduction reaction (ORR) occurring at the cathode of PEMFCs. In this regard, non-precious transition metal/nitrogen doped carbon (TM-N-C) catalysts have drawn much attention as a promising PGM-free ORR electrocatalyst due to its ORR activity approaching to Pt. However, the chemical structure of the active sites in these TM-N-C catalysts and their catalytic mechanism for ORR and electrochemical stability have not been fully understood. To gain insight into the nature of the nanoscale active sites in the TM-N-C catalysts, we have performed the first-principles density functional theory (DFT) calculations to investigate the progression of ORR on various types of TM-N₄ (TM = Fe, Mn, Co) moiety substitutionally embedded into a graphene layer. On each possible TM-N₄ active site, we calculated the adsorption energies of all the relevant chemical species, namely, O₂, O, OH, OOH, HOOH and H₂O, and the activation energies for O-O dissociation reactions involved in ORR using the DFT method. On FeN₄ and/or CoN₄ embedded in an intact graphene plane, our DFT calculations predicted that the ORR could happen through 4e⁻ associative pathway on the FeN₄ site, whereas follow a 2e⁻ pathway on the CoN₄ site due to high activation energy for O-O bond splitting and extremely weak adsorption of H₂O₂ on the CoN₄ site. Furthermore, we studied and compared the predicted activity and stability on an S1 type FeN₄ site with a porphyrinic architecture and an S2 site FeN₄ sites fully embedded in a graphene layer. Our computational results reveal that the S1 type FeN₄ site will catalyze ORR with the higher onset potential (i.e., higher ORR activity) than the S2 type FeN₄. However, the S1 type FeN₄ site is predicted to exhibit poorer electrochemical stability than the S2 type FeN₄. Our computational predictions are found to agree excellently with recent experimental measurements.

4:00 PM EN07.07.03

Oxygen Evolution Reaction (OER) of Precious-Metal-Free Perovskite Nanocatalysts Made by Spray-Flame Synthesis—Effect of A- and B-Site Substitutions and B-Site Doping [Steven Angel](#)¹, [Adarsh Koul](#)², [Wolfgang Schuhmann](#)², [Christof Schulz](#)^{1,1} and [Hartmut Wiggers](#)^{1,1}; ¹University of Duisburg-Essen, Germany; ²Ruhr-University Bochum, Germany

The sustainable large-scale generation of hydrogen – *via* electrochemical water splitting – demands a large amount – and thus necessarily precious metal-free – active catalyst materials which allow the evolution of H₂ (HER) and O₂ (OER) at high rates while requiring low overpotentials.¹ Especially for the sluggish OER, cost-effective and abundant materials are sought as alternatives to RuO₂ and IrO₂ compounds which are scarce and poorly stable in alkaline electrolytes.² Perovskite-based materials (ABO₃) incorporating lanthanides (A-site) and 3d transition metal ions (B-site) have been identified as such

promising alternatives as their electronic structure and surface defects can be tuned by substituting/doping the A- and B-sites. The synthesis of such compounds is commonly done in time-consuming wet-chemical batch processes followed by a calcination step.^{3,4} Alternatively, the scalable spray-flame synthesis (SFS) allows the formation of functional high-surface-area doped/substituted perovskite nanoparticles in a single step.^{5,6} Using the SFS method, we investigated the A-site ($\text{La}_{1-x}\text{Sr}_x\text{CoO}_3$, $x = 0 - 0.4$) and B-site ($\text{LaCo}_{1-y}\text{Fe}_y\text{O}_3$, $y = 0 - 1$) substitution, and the B-site doping ($\text{LaCo}_{0.94}\text{M}_{0.06}\text{O}_3$ ($M = \text{Cr, Mn, Fe, Ni, Cu}$)) of the LaCoO_3 perovskite. XRD measurements indicated the formation of oxygen-deficient (e.g. LaCoO_{3-d}) trigonal R-3cR structures in the $\text{La}_{1-x}\text{Sr}_x\text{CoO}_3$ series, a transition from the rhombohedrally- to the orthorhombically-distorted perovskite structure at $y > 0.4$ in the $\text{LaCo}_{1-y}\text{Fe}_y\text{O}_3$ series, and the same rhombohedral LaCoO_3 structure in all samples from the $\text{LaCo}_{0.94}\text{M}_{0.06}\text{O}_3$ series. Investigations using XPS measurements revealed a surface enrichment of La^{3+} and Sr^{2+} ions and the presence of Sr-oxides in the $\text{La}_{1-x}\text{Sr}_x\text{CoO}_3$ series, an enrichment of La^{3+} at $y > 0.4$ and the presence of iron in the oxidation state +3 regardless of the concentration (y) in the $\text{LaCo}_{1-y}\text{Fe}_y\text{O}_3$ series, and variable $\text{Co}^{2+}/\text{Co}^{3+}$ ratios (e.g. ~ 0.57 and ~ 0.75 for the Cr- and Ni-doped samples, respectively) depending on the doping element in the $\text{LaCo}_{0.94}\text{M}_{0.06}\text{O}_3$ series. The nanoparticle products were further characterized using TEM/EDX, FTIR, and BET measurements. Selected samples were characterized *via* EXAFS, XANES, and XPS using synchrotron radiation.

For the oxygen-evolution reaction (OER) catalytic performance, the lowest overpotentials – 325, 345, and 397 mV vs. RHE at 10 mA cm^{-2} – were obtained using the $\text{La}_{0.7}\text{Sr}_{0.3}\text{CoO}_3$, $\text{LaCo}_{0.6}\text{Fe}_{0.4}\text{O}_3$, and $\text{LaCo}_{0.94}\text{Ni}_{0.06}\text{O}_3$ samples, respectively. These results point to the relevance of increasing the B–O covalency⁷ and the electrical conductivity⁸ of the perovskite structures and are comparable to the performance of commercial IrO_2 reference⁹ materials (1.59 V vs. RHE at 10 mA cm^{-2}). Relationships between chemical composition, surface properties, and OER activity of the spray-flame synthesized catalysts will be discussed in detail.

References

1. *Electrochemical Science Advances* **2022**, 00 e2100206.
2. *Journal of Materials Chemistry A* **2022**, 10, (5), 2271-2279.
3. *Electrochimica Acta* **2017**, 241, 433-439.
4. *International Journal of Hydrogen Energy* **2018**, 43, (9), 4682-4690.
5. *Proceedings of the Combustion Institute* **2019**, 37, (1), 83-108.
6. *AIChE Journal* **2019**, 66, (1), e16748.
7. *ACS Applied Materials & Interfaces* **2022**, 14, (12), 14129-14136.
8. *Science and Technology of Advanced Materials* **2015**, 16, (2), 026001.
9. *ChemCatChem* **2017**, 9, (15), 2988-2995.

4:15 PM EN07.07.04

Operando STXM and Surface DFT Calculations of Manganese Oxide for Bifunctional Oxygen Electrochemistry Evan Z. Carlson¹, William C. Chueh¹, Michal Bajdich² and J. Tyler Mefford¹; ¹Stanford University, United States; ²SLAC National Accelerator Laboratory, United States

Limited supply of precious metals impedes the scale up of electrolyzer production. To enable 100s of GWs of PEM electrolyzer capacity by 2030, iridium supply must grow by more than 10x.¹ Even transition metal-based alkaline electrolyzers may face constraints as electric vehicles increasingly compete for nickel. Alternatively, catalysts made of cheaper, more abundant manganese could relieve these constraints, if engineered to have comparable activity and stability to the best performing precious metals. The unique bifunctional OER/ORR activity of Mn oxide could also enable electrolyzers that both produce and consume fuel with a single catalyst, achieving even greater material efficiency. Yet rational design of Mn oxide catalysts requires a better understanding of the structural and chemical motifs that lead to high bifunctional performance.

In this talk, we will discuss our investigation of the bifunctional OER & ORR activity of Mn oxide and its unusual pH dependence. Our model system, $\alpha\text{-K}_2\text{MnO}_2$, is among the best reported Mn oxide catalysts for both the OER and the ORR, with ORR activity matching that of Pt. While the OER activity of Mn oxide has been shown to increase at higher pH, we will show that its ORR activity unexpectedly improves as well. We will discuss our attempts to understand this phenomenon with *operando* scanning transmission x-ray microscopy (STXM), which enables spectroscopic investigation of single catalyst particles during reaction with spatial resolution down to 25 nm. Complementary surface DFT calculations provide further evidence for identification of the active crystal facets and insights into the pH-dependency of the OER & ORR mechanisms. We will discuss the implications of this work on the design of bidirectional electrolyzers with low-cost, non-precious metal catalysts.

- 1) IRENA. Green Hydrogen Cost Reduction. **2020**
- 2) Meng, Y. *et al. J. Am. Chem. Soc.* **2014**, 136 (32), 11452–11464.
- 3) Takashima, T. *et al. J. Am. Chem. Soc.* **2012**, 134 (3), 1519–1527.

SESSION EN07.08: Hydrogen Production II
Session Chairs: Alexander Headley and Samantha Johnson
Thursday Morning, December 1, 2022
Hynes, Level 3, Room 302

8:45 AM EN07.08.02

NiFe Nanoalloyed and Nanogranular Thin Films for Oxygen Evolution Reaction Catalysis Luca Ciambriello^{1,2}, Emanuele Cavaliere^{1,2}, Irene Vassalini^{3,4,5}, Ivano Alessandri^{3,4,5}, Matteo Ferroni^{5,4,6}, Rosaria Brescia⁷, Luca Leoncino⁷ and Luca Gavioli^{1,2}; ¹Università Cattolica del Sacro Cuore, Italy; ²Interdisciplinary Laboratories for Advanced Materials Physics (i-LAMP), Italy; ³INSTM, Italy; ⁴University of Brescia, Italy; ⁵INO-CNR, Italy; ⁶CNR-IMM, Italy; ⁷Istituto Italiano di Tecnologia, Italy

The production of hydrogen (H_2), the best alternative to fossil fuels, can be achieved electrochemically through the water splitting, consisting in two half reactions: the oxygen evolution reaction (OER) and the hydrogen evolution reaction, where O_2 and H_2 are obtained from water molecules. The OER is the most thermodynamically demanding part, representing the bottleneck of the entire process. Nanoalloyed materials can overcome the water splitting limitations by serving as efficient OER catalysts with low fabrication costs, towards a large-scale development of H_2 .

On nanostructured materials, the OER catalysis efficiency is mainly determined by the chemical composition and morphology, whose control during the electrode synthesis is of paramount importance.

From the chemical viewpoint metal alloying demonstrates a considerable activity enhancement with respect to pure materials, in particular for transition metals such as NiFe, presented here.

The electrode morphology (including surface roughness and porosity) as determined by micro/nano structures, may improve the efficiency by increasing

the electrochemical surface area. However, a relationship between the catalytic efficiency and the morphological behavior of NiFe electrodes as a function of thickness to unveil the role of porosity, surface area and roughness is missing.

A further fundamental point concerns the mass loading minimization in the electrodes by maintaining the same efficiency with the aim of reducing the synthesis costs. Despite the relevance of this aspect, a thickness dependent investigation of the catalytic efficiency has been limited to noble metals and few non-noble metal compounds.

A third point is the electrode stability in OER operation, influenced by the Ni/Fe oxy/hydroxides phases forming at the interface and by the evolution of the film stoichiometry and morphology during the electrochemical activity. At present, the identification and transformation of the active sites as well as the electrode morphological modifications are still debated.

Here we tackle these issues by synthesizing new nanoalloyed electrocatalysts with nanostructured morphology and high purity chemical composition, employing Supersonic Cluster Beam Deposition (SCBD). The electrodes consist in films with thickness in the 15-88 nm range (corresponding to 5-30 $\mu\text{g}/\text{cm}^2$ loading), composed of NiFe alloy nanoparticles (90%/10% weight fraction). AFM shows that the nanoclusters, having a trimodal size distribution ranging from 0.4 to 3.8 nm, assemble in a porous film with a thickness dependent surface roughness. XPS, reflection and transmission optical spectra reveal a partial NiFe oxidation/hydroxidation, in particular at the film surface, due to the air exposure. The SCBD films show excellent OER catalysis efficiency with a 380 mV overpotential. The electrochemical activity is independent of the film thickness, suggesting an excess of NiFe mass loading in the thicker electrodes and identifying the thinnest film (15 nm) as the most promising low-cost catalyst. Furthermore, a high stability over a set of 1000 accelerated electrochemical cycles is reported. The film OER activity determines considerable structural, morphological and chemical transformations, whose role in the catalysis is under investigation. The film shows an increase of oxide/hydroxide amorphous species, confirmed by a decrease of crystallinity from XRD and a decrease of metallicity from the optical spectra. The effect is accompanied by a film thickness growth measured by AFM, due to the incorporation of chemical species from the electrolyte solution such as $\text{Ni}(\text{OH})_2$, resulting also from electrochemical current/potential curves. This work puts a crucial step toward the thickness optimization of thin films as OER catalysts and the investigation of their stability in electrochemical operation.

9:00 AM EN07.08.03

Optimized 2D Nanostructures for Catalysis of Hydrogen Evolution Reactions Caique Campos and Pedro A. Autreto; Federal University of ABC, Brazil

Hydrogen is one of the most promising energy carriers with energetic transport and storage advantages over fossil fuels. However, commercial H_2 production relies on Hydrocarbon reforming methods, emitting greenhouse gasses (GHG) such as CO_2 [1]. H_2 can be produced without harmful emissions by water splitting in the electrochemical Hydrogen Evolution Reaction (HER). However, this mechanism is limited by the lack of cheap, abundant, and efficient catalysts. The search for new noble-metal-free catalysts has increasingly attracted researchers' interest in the last years, and several prospective materials have been proposed. The Transition Metal Dichalcogenides (TMD) emerged as prospect materials to catalyze HER. These materials exhibit interesting electronic and structural properties. Their catalytic activity can be optimized by increasing active site counting and tailoring electronic properties. Common strategies to optimize TMD catalytic activity comprehend phase engineering and doping [2]. TiSe_2 has emerged as a material with remarkable and extensively investigated properties. The stability of its 1T phase and sensibility of electronic properties to doping can be explored in catalysis. In this work, the catalytic activity of TiSe_2 in HERs is investigated via DFT calculations using the Quantum Espresso package. We employed the Computational Hydrogen Electrode model to conduct a thermodynamic study, evaluating the free energy variation of Hydrogen adsorption, which was reported as a good activity descriptor [3]. We found that the introduction of Pt dopants on the basal plane of the 1T- TiSe_2 enhances the activity of chalcogen sites.

References

- [1] P. J. Megía et al, Energy & Fuels 35 (20), 16403-16415 (2021);
- [2] Voiry D. et al., Adv. Mater., 28: 6197-6206 (2016).
- [3] J. K. Nørskov et al, J. Electrochem. Soc. 152 J23 (2005);

9:15 AM EN07.08.04

Reversible H_2 Storage via High-Temperature Redox Cycling of Fe-Mo Lamellar Foams with High Structural Stability Jacob B. Mack, Samuel Pennell and David Dunand; Northwestern University, United States

Hydrogen storage using Fe-based redox materials represents a potentially inexpensive, environmentally friendly alternative to high pressure gas storage: hydrogen is stored through the reduction of Fe_3O_4 , yielding steam and Fe, and hydrogen is formed via the reversible steam oxidation of Fe. At high temperatures (400-600°C) where the reaction kinetics are favorable, the large volumetric expansion and contraction of the Fe - Fe_3O_4 redox reaction (110%) drives sintering in Fe powder-bed systems, reducing and eventually choking gas access, and thus storage capacity. Unlike a packed bed of Fe powders, lamellar Fe foams, created by freeze-casting, provide free volume for the Fe lamellae to expand during oxidation without sintering to nearby material. However, upon oxidation, Kirkendall porosity develops within the lamellae due to the mismatch in diffusion between Fe and O. As Kirkendall pores coalesce inside lamellae, combined with fracture at lamellae tips from redox stresses, lamellar contact and densification persists. In the past, alloying with redox-inert elements (Ni, Co), has shown promise in stabilizing the Fe lamellae: as Fe is oxidized, a metallic core (Ni- or Co-rich) remains in each lamella, providing an interface that acts as a Kirkendall pore sink, and adhesion to the outer oxide layer to prevent fracture. Upon reduction, the lamellae re-homogenize due to extensive solid solution between Fe and Co/Ni, providing reversibility. Under accelerated cycling degradation studies at 800°C, repeated expansion and contraction of Fe-Ni and Fe-Co however triggers lamellar buckling, which leads to contacting and sintering of neighboring lamellae, and thus choking of the foams.

Here, we develop a strategy to counteract lamellar buckling during redox cycling, by using Mo as an alloying element for Fe foams, with the goal of improving lamellar mechanical strength and preventing their sintering. Freeze-cast Fe-25 at% Mo lamellar foams demonstrate strong sintering inhibition with a stable hierarchical porous structure, having porosity within each lamella, providing further volume for the Fe to expand into upon oxidation. As opposed to the solid solution Fe-Ni and Fe-Co foams studied before, a three-phase mixture of $\alpha\text{Fe-Mo}$, μFeMo , and $\text{Fe}_3\text{Mo}_3\text{C}$ is present, further limiting diffusion, sintering and plastic deformation. Mo, like Fe, is oxidized by steam, leading to a three-phase composition of $\text{Fe}_3\text{O}_4\text{-MoO}_2\text{-Fe}_2\text{Mo}_3\text{O}_8$ at full oxidation. While the expansion from oxidation leads to the densification of the initially porous lamellae, the shrinkage upon reduction restores the internal lamellar porosity, achieving a reversibly porous lamella. Hydrogen reduction yields $\alpha\text{-Fe}(\text{Mo})$ and a nanocrystalline Fe_2Mo phase, which produces a high surface area morphology, further increasing the oxidation rate for subsequent cycles. Buckling from metallic regions present during partial oxidation or reduction proceeds significantly slower, due to the lack of a percolating metallic network. Fracture of ceramic oxides does not cause significant lamellar widening, due to internal porosity, leading to a near constant foam density, without sintering, over the first 10 cycles, as compared to a loss of up to 40% porosity in Fe and 20% in Fe-Ni/Co foams. While lamellar buckling builds up over time in the new Fe-Mo foams, large scale densification is eliminated, since contacting lamellae sinter very slowly. By modifying the lamellar width and length, the extent of buckling can be lowered, further slowing densification. Thus, Mo alloying represents a significant improvement in structural stabilization and reversibility as compared to other Fe-foams.

9:30 AM EN07.08.05

Approaches to Dynamic Electric Model of Polymer Electrolyte Electrochemical Cell (PEEC) for Water Electrolysis Daichi Matsui¹, Katsushi Fujii², Satoshi Wada² and Atsushi Ogura^{1,3}; ¹Meiji University, Japan; ²RIKEN Center of Advanced Photonics, Japan; ³Meiji University MREL, Japan

An energy supply system using hydrogen storage has been proposed with the use of renewable energy [1]. High performance and the toughness of the fluctuated energy are important for clean hydrogen production by using water electrolysis. A polymer electrolyte electrochemical cell (PEEC) is a suitable device for this renewable energy storage. In this report, we focused on this PEEC as devices that convert electricity into hydrogen.

The evaluated PEEC has an electrode area of 12.5 cm² with IrO₂ as the cathode catalyst and Pt as the anode catalyst. The electrolysis voltage is reported to be divided into four main parameters: open circuit potential, activation over potential, ohmic over potential, and concentration over potential [2,3]. The thermal dependences of the PEEC current-voltage characteristics are known to be relatively large. A device model explained with the fundamental electrochemical properties can be explained these static characteristics of PEEC including temperature dependence. However, this model has not been applied for the dynamic characteristics of the PEEC. Thus, the purpose of this report is to investigate the dynamic characteristics of PEEC by comparison with the results of the static device models and the evaluation results of the electrochemical impedance spectroscopy (EIS).

The equivalent circuit for PEEC is usually a single series resistor and double two components connected in parallel, that is, a resistor and a capacitor [4]. The comparison between the EIS results and the static device model was performed to evaluate the dynamic properties of PEEC. The EIS result at the imaginary part zero below the turn-on voltage indicates only the component of series resistance. The comparisons above the turn-on voltage indicate that the series resistance component of EIS is dominated by ohmic over potential and activation over potential in the chemical reaction-based device model. Since the activation over potential is known theoretically, the ohmic over potential can be estimated from the analysis. The two resistance components of EIS with the resistor and capacitor in parallel were found to show the activation over potentials of the anode and cathode, respectively.

A comprehensive device model, which reflects both the static and dynamic characteristics of PEEC, is expected to be proposed from the analysis provided here.

[1] D. Yamashita et al., *Int. J. Hydrogen Energy*, 44 (2019) 27542.

[2] B. Lee et al., *Int. J. Electrochem. Science*, 8 (2013) 235.

[3] V. Liso et al., *Mdpi. J. Energies*, 11 (2018) 3273.

[4] S. Siracusano et al., *Materials*, 11 (2018) 1368.

9:45 AM BREAK

10:15 AM EN07.08.06

Influence of Hierarchical and Conformal Electrodeposition of NiCo₂O₄ Electrocatalyst on Carbon Cloth for Water Oxidation Zahra Albu, Nawal Al Abass and Bandar AlOtaibi; King Abdulaziz City of Science and Technology, Saudi Arabia

To achieve net-zero emissions, consideration of various energy resources is essential for future energy needs. In this regard, green hydrogen production via water electrolysis using renewable energy sources is an attractive route for providing a cleaner energy mix. Water electrolysis has been intensively studied with limited success to produce hydrogen at a very competitive price point. The major bottleneck for widely adopting such a green technology is to find cost-effective electrocatalysts that can efficiently oxidize water and produce hydrogen at practical cost. The best-known oxide electrocatalysts for water evolution reaction (OER) compose of precious metals such as Ru and Ir, which are expensive and impractical for large-scale production. Thus, searching for alternative electrocatalysis based on transition metal oxide is an attractive approach for low-cost electrolysis processes. In this regard, we developed highly efficient hierarchical NiCo₂O₄ porous electrocatalysts on electrochemically treated carbon cloth (CC) using facile and green electrodeposition method. X-ray diffraction spectra and scanning tunneling microscope images confirm the formation of hierarchical NiCo₂O₄ porous structure under study. TEM images of peeled off NiCo₂O₄ particles from CC show that the electrodeposited structure compose of defined nano-sized crystallites of NiCo₂O₄. Additionally, the developed electrode exhibits improved electrocatalytic performance with low overpotential of ~ 290 mV at J = 10 mA/cm² and low Tafel slope of 76 mV/dec. Its superior catalytic activities and durability for OER in alkaline media is mainly attributed to the special hierarchically porous nanostructure that led to enhanced charge transport to more accessible active sites.

10:30 AM EN07.08.07

Role of Fe in Enhancement of OER on Fe-Doped NiOOH Catalyst— Insights from Improved Electronic Structure Calculations Zhengda He, Rebekka Tesch, Michael Eikerling and Piotr Kowalski; Forschungszentrum Juelich, Germany

Low cost, high activity and high stability make Fe-doped NiOOH a good electrocatalyst for oxygen evolution reaction (OER) [1]. Although significant efforts have been dedicated to understand the enhanced electrocatalytic activity of this material [2,3,4,5], the complete information on the atomic scale mechanisms leading to the OER process improvement is still lacking. One of the reasons on the computational side is that the widely used density functional theory with Hubbard U correction for strongly correlated d electrons (DFT+U) is unable to predict correctly the electronic structure of NiOOH, especially its wide band gap [7], leading to contradictory results. In order to solve this problem, we use Wannier function to construct a more realistic projector for calculating the occupation of d-orbitals, severely overestimated by standard DFT+U approach [9]. With this approach, we obtained correct occupations of 3d orbitals for Ni and Fe, and the band gaps for Ni(OH)₂ and NiOOH that are consistent with experimental findings. With this improvements, we investigated the electronic structure spin of Fe in Fe-doped NiOOH. We show that Fe tends to be in low-spin state, which leads to significant decrease in the thermodynamic overpotential for OER. A spin transition from low-spin to high-spin state is predicted at Fe content of 25%, which contributes to the solubility limit of Fe in NiOOH [1]. We will discuss our computational findings against available experimental data, demonstrating important of joint computational and experimental investigation for understanding of catalytic performance of functional materials.

References:

[1] Friebe et al., *J. Am. Chem. Soc.* **137**, 1305-1313 (2015)

[2] Conesa, J. C., *J. Phys. Chem. C* **120**, 18999-19010 (2016)

[3] Martinez, J. M. P., Carter, E. A., *Chem. Mater.* **30**, 5205-5219 (2018)

[4] Tkalych, A. J. et al., *Phys. Chem. Chem. Phys.*, **20**, 19525 (2018)

[5] Rajan, A. G. et al., *J. Am. Chem. Soc.* **142**, 3600-3612 (2020)

[6] Loschen, C. et al., *Phys. Rev. B* **75**, 035115 (2007)

[7] Ratcliff E. L. et al., *Chem. Mater.* **23**, 4988-5000 (2011)

[8] Tkalych A. J. et al., *J. Phys. Chem. C* **119**, 24315-24322 (2015)

[9] Kowalski, P. et al., *Front. Energy Res.* **9**, 653542 (2021)

10:45 AM EN07.08.08

Ni-Based Composite Electrocatalysts for Urea Oxidation Reaction and Molecular Hydrogen Generation Kangwoo Cho; Pohang University of

Science and Technology, Korea (the Republic of)

Urea oxidation reaction (UOR) has been interrogated as an alternative oxidation to decrease the cell voltage in electrochemical water splitting for industrial-scale hydrogen production. The UOR not only enhances the energy conversion efficiency from renewable energy into molecular hydrogen, but also reduces carbon and nitrogen pollution loadings of urea-rich wastewater. Nickel-based catalysts are up-to-date the most widely investigated materials as the UOR electro-catalyst. This presentation introduces our recent findings on Ni-based UOR electro-catalysts that were prepared by i) galvanostatic electro-deposition of mixed metal (oxy)hydroxide (NiFeO_x or NiCoO_x) with variable mixing ratios, ii) potentiostatic dealloying of commercial NiFe alloys under variable pH, and iii) one-pot thermochemical treatment of NiFe alloy foam (NFF), both as substrate and catalyst source to create a self-supporting UOR electro-catalyst. For the anode materials under interrogation, Ni³⁺ in the form of NiOOH served as the active UOR site. The secondary elements (Fe or Co) influenced the Ni^{2+/3+} redox peak potential and current as thoroughly investigated for oxygen evolution reaction (OER) electrocatalysts. This study further revealed that current inflections during potential sweep in the presence of urea could be associated with Ni^{3+/4+} redox peaks. The peak location and intensity continued to change during repetitive scans, due to dynamic dissolution and precipitation of Fe to/from the electrolyte. After the onset of OER, the presence of urea lowered the current responses which should be important consideration for industrial H₂ evolution. On the other hand, oxalic acid treatment of NFF generated prismatic NiFe-oxalate (O-NFF) which marked surprisingly low overpotential and Tafel slope for UOR. The oxalate ligand not only altered the binding site of urea, but also shifted the surface electronic structure of Ni (together with urea), which in-turn affected the rate and potential determining steps. The findings of this study could be further utilized within wastewater electrolysis cell for water-energy nexus.

11:00 AM EN07.08.09

Doped LaMnO₃ for Water Splitting by Density Functional Theory Calculations Ximeng Wang¹, Anuj Goyal², Juan C. Nino¹, Jonathan Scheffe¹, Stephan Lany² and Simon Phillpot¹; ¹University of Florida, United States; ²National Renewable Energy Laboratory, United States

Current solar thermochemical reactors utilize CeO_{2-x} in a two-step redox process. However, the high reaction temperature required for the use of CeO₂ and the large temperature difference between the reduction and oxidation steps drives the search for other materials. Perovskite materials are promising candidates for such water splitting applications. The perovskite ABO₃ formula yields multiple combinations of potential interest, with various A elements (lanthanides) and B elements (transition metals). In this work, focusing on LaMnO₃, we make substitutions of Li, Na, K, Rb, Mg, Ca, Sr, Ba for La-sites and Mg, Zn, Al, Ga, In for Mn-sites. Density functional theory calculations are used to identify candidate materials for water splitting from all these compositions. Thermodynamic stability and oxygen vacancy formation energy (2.5 eV-5.0 eV) are used as criteria to select potential candidates.

This work was supported by the Department of Energy, EERE DE-EE0008840.

Keywords: perovskite, doping, water splitting, density functional theory

11:15 AM EN07.08.10

Tailoring Binding Abilities by Incorporating Oxophilic Transition Metals on 3D Nanostructured Ni Arrays for Accelerated Alkaline Hydrogen Evolution Reaction Jaerim Kim, Hyeonjung Jung, Jeong Woo Han and Jong kyu Kim; Pohang University of Science and Technology (POSTECH), Korea (the Republic of)

Developing efficient and inexpensive electrocatalysts for the hydrogen evolution reaction (HER) in alkaline water electrolysis plays a key role for renewable hydrogen energy technology. The slow reaction kinetics of HER in alkaline solutions, however, has hampered advances in high-performance hydrogen production. Herein, we investigated the trends in HER activity with respect to the binding energies of Ni-based thin film catalysts by incorporating a series of oxophilic transition metal atoms. It was found that the doping of oxophilic atoms enables the modulation of binding abilities of hydrogen and hydroxyl ions on the Ni surfaces, leading to the first establishment of a volcano relation between OH-binding energies and alkaline HER activities. In particular, Cr-incorporated Ni catalyst shows optimized OH-binding as well as H-binding energies for facilitating water dissociation and improving HER activity in alkaline media. Further enhancement of catalytic performance was achieved by introducing an array of three-dimensional (3D) Ni nanohelices (NHs) that provide abundant surface active sites and effective channels for charge transfer and mass transport. The Cr dopants incorporated into the Ni NHs accelerate the dissociative adsorption process of water, resulting in remarkably enhanced catalytic activities in alkaline medium. Our approach can provide a rational design strategy and experimental methodology toward efficient bimetallic electrocatalysts for alkaline HER using earth-abundant elements.

SESSION EN07.09: Hydrogen Production III
Session Chairs: Alexander Headley and Samantha Johnson
Thursday Afternoon, December 1, 2022
Hynes, Level 3, Room 302

1:30 PM EN07.09.01

High-Permeance Hydrogen Selective Membranes Using an Ultrathin Palladium Film Lohyun Kim, Chi Cheng, Aaron Persad, Randall Field and Rohit Karnik; Massachusetts Institute of Technology, United States

Beyond the traditional needs for hydrogen separation in industries, such as H₂/N₂ and H₂/CO₂ in ammonia production, H₂/CH₄ in methane reforming, or H₂/hydrocarbons in petroleum refining, the demand for purified hydrogen has been rising over time and is expected to grow further with transition to a sustainable economy. Emerging applications range from use of hydrogen as an energy carrier, space industry, and nuclear fusion that requires separation and recovery of hydrogen isotopes (deuterium and tritium) from byproduct gases in the reactor.

Membrane technology can be a good candidate for hydrogen separations, owing to several advantages, such as the ease of operation, modularity, and low energy consumption compared to other techniques, such as pressure swing adsorption. Especially, metal composite membranes comprising a metal layer such as palladium (Pd) alloy on porous supports have been spotlighted due to their high H₂ selectivity over other gases and good thermal and mechanical stability. This type of membrane, however, generally requires a several micrometers thick metal layer to cover the porous support without defects. Given that the Pd is very expensive, and permeance decreases with increasing thickness necessitating larger membrane area, the overall cost of hydrogen separation scales approximately as the square of the metal layer thickness.

To address this, we developed an ultrathin Pd composite membrane having a thickness in the range of 100 nm. Gas permeation tests of the Pd film

membrane using a customized gas rig showed a remarkable H₂ and D₂ permeance of ~10⁻⁵ mol/m²×s×Pa, which is ~1,000x higher than the typical permeance of polymeric membrane and ~10x higher than typical Pd membranes which generally require higher temperature to operate. Single-gas H₂ selectivity against He, CH₄, N₂, and CO₂ was about 20, 40, 50, and 60, respectively. The performance of the membrane was evaluated at different temperatures. Unlike the thick Pd composite membranes, which are typically not compatible with temperatures below 600 K due to the phase change of Pd leading to cracks, our membrane showed stable operation at ambient to moderate temperatures and was able to withstand phase change of palladium due to hydrogen while retaining a good selectivity. The change of phase of Pd between alpha and beta was observed as a sharp change in permeance of the membrane with change in partial pressure of H₂ or D₂ as a function of temperature, consistent with the Pd/H₂ and Pd/D₂ phase diagrams.

To quantitatively understand the membrane behavior under different working conditions, we developed a comprehensive gas transport model of the Pd film membrane based on the flow resistance circuit. The configuration of the circuit was determined by considering the potential pathways of the gas species. Several assumptions were made to simplify the numerical calculation. For example, Knudsen diffusion was used to explain the gas transport through the porous support. For the Pd film, the transport was characterized by a solution-diffusion mechanism, and the major kinetic steps, such as surface reactions and bulk diffusion, were included. There are two notable features of the model: 1) the model accounts for the interactions between hydrogen isotopes in Pd film, and 2) the model can be employed regardless of the Pd phase. Good agreement between the theoretical model and the experimental data was observed, which explained the dominant transport mechanism as diffusion of hydrogen through the Pd layer, as well as the selectivity and its dependence on the membrane structure.

Overall, the very high permeance of the reported membranes cuts down the overall use of precious metal and the membrane cost per unit productivity by orders of magnitude. With reasonably good selectivity and ability to operate at ambient to moderate temperatures, the new membranes show potential for various current and emerging hydrogen separation needs.

1:45 PM EN07.09.02

Current Density Improvement Evaluation of Polymer Electrolyte Electrochemical Cells (PEEC) for Hydrogen Generation Using Electrochemical Impedance Spectroscopy Miyuki Nara¹, [Katsushi Fujii](#)¹, Daichi Matsui², Takeharu Murakami¹, Atsushi Ogura^{2,2} and Satoshi Wada¹; ¹RIKEN, RAP, Japan; ²Meiji University, Japan

One of the hydrogen formations from renewable energy is expected to use water electrolysis. Especially, polymer electrolyte electrochemical cell (PEEC) is known as a suitable energy conversion device from renewable electricity to hydrogen because the PEEC is relatively strong for the input energy fluctuation from a reliability point of view.

The energy conversion efficiency improvement of PEEC is an important issue to establish the hydrogen production from renewable energies. The major improvement research for water electrolysis is reducing the operating voltage at the same current density. Therefore, the improvement of the water oxidation catalyst has been discussed because the over voltage of oxygen evolution reaction (OER) is higher than that of hydrogen evolution reaction (HER). However, the device conversion efficiency of PEEC is not defined only by these reaction overpotentials. The series resistance of the PEEC, which is mainly due to the resistance of polymer electrolyte, and ion concentration difference between anode and cathode also affect the device performance. Electrochemical impedance spectroscopy is a powerful tool for the evaluation of these resistances. The spectroscopy can be separated the series resistance, and the resistance due to overpotential at the interface between polymer electrolyte and electrode catalyst interface clearly. Although the reduction of polymer electrolyte resistance has been discussed with the polymer electrolyte thickness, it was found that the reduction with polymer electrolyte treatment also improves the PEEC performance. The overpotential at the interface between polymer electrolyte and electrode catalyst interface was also improved with this treatment. These evaluations clarified that not only the catalytic performance but also the other material properties need to control for the improvement of the PEEC performance.

[1] V. Liso, et al., *Energies* 11 (2018) 3273.

[2] S. Siracusano, et al., *Materials* 11 (2018) 1368.

2:00 PM EN07.09.03

Unveiling the Deceptive Enhancement of Hydrogen Evolution Reaction Overpotential [Nageh K. Allam](#); American University in Cairo, Egypt

Electrochemical hydrogen evolution reaction (HER) is typically studied in a three-electrode system. In this system, several counter electrodes are commonly used to ensure fast kinetics, including Pt, gold, and glassy carbon. However, the extensive application of such electrodes has raised caveats on the contribution of the redox-active species dissolving from such electrodes and redepositing on the surface of the working electrode to the measured overpotential. Consequently, this has been frequently confused with the actual electrochemical signature of the working electrode catalyst, resulting in a deceptive enhancement in the recorded overpotential. This issue becomes more critical when the electrolysis measurements involve an activation step, necessitating the need for alternative counter electrodes that are stable, especially in an acidic medium, which is commonly used as the electrolyte in HER studies. Herein, while we systematically unveil such problems, an alternative counter electrode that overcomes those problems is demonstrated. Specifically, the correlation between the working electrode area to that of the counter electrode, the dissolution rate of the counter electrode, and the potential range used in the activation/cleaning of the surface on accelerating the dissolution rate is explored and discussed in detail. Finally, commercial Ti mesh is demonstrated as an alternative emerging counter electrode, which is proven to be very stable and convenient to study the HER in acidic media.

2:15 PM EN07.09.04

DFT Study of Hydrogen-Evolution Reaction on Mo-Based Alloys [Rodion Belosludov](#), Ruirui Song, Jiuhui Han and Hidemi Kato; Tohoku University, Japan

Electrochemical hydrogen evolution reaction (HER) through water splitting is one of the most effective mechanism among the various hydrogen productions. Although Pt-based catalysts are at present the most active HER catalysts [1], the high cost and scarcity of Pt essentially limit their large-scale practical applications. Therefore, the development of cost-effective and earth-abundant catalysts as alternatives to noble Pt has devoted significant research interest. Among the various materials, intermetallic compounds formed by non-precious transition metals are promising cost-effective and robust catalysts for electrochemical hydrogen production [2]. Using the current theoretical methods it is now possible to study surface chemical reactions in detail and to understand variations in catalytic activity from one catalyst to another as well as compare with available experimental data [3].

Here, we have studied the HER catalytic activity of μ -Co₇Mo₆, μ -Fe₇Mo₆, Mo, Cr₅₀Mo₅₀ heterogeneous catalysts and compared with HER catalytic activity of Pt. The geometry optimization of the selected surface structures, the evaluation of the electronic and thermodynamic properties of the selected compounds and the detailed analysis of their catalytic activities toward hydrogen evolution reaction (HER) through water splitting were performed using the density functional theory calculations implemented in the Vienna Ab initio Simulation Package [4]. The activation barriers have been calculated with the nudged elastic band (NEB) method [5].

The most active catalytic sites toward H₂O, OH and H adsorption have been evaluated for the studied catalysts. The values of the adsorption energies have been calculated and the surface effect on these values have been analyzed based on the geometry of top layers and the electronic structures (Partial density

of states) of catalytic surfaces and the charge transfer between surface atoms and adsorbed species. The obtained results showed that the dissociative adsorption of water is demonstrated to be thermodynamically favorable (exothermic) for $\mu\text{-Co}_7\text{Mo}_6$, $\mu\text{-Fe}_7\text{Mo}_6$, Mo, $\text{Cr}_{50}\text{Mo}_{50}$ catalysts and the lowest activation barrier is found in the case of $\mu\text{-Fe}_7\text{Mo}_6$ one. Based on the calculated DG_{H^*} values, the catalytic activity trend of the order of $\mu\text{-Co}_7\text{Mo}_6 > \text{Mo} > \text{Cr}_{50}\text{Mo}_{50} > \mu\text{-Fe}_7\text{Mo}_6$. In the case of $\mu\text{-Co}_7\text{Mo}_6$, this value is comparable with the DG_{H^*} value calculated for H adsorption on Pt(111) surface. Thus it can be suggested that Mo-based alloys, especially Co_7Mo_6 may be the good candidates for electrolyte fuel cell as substitution of Pt.

REFERENCES

- R. Subbaraman *et al. Science*, 2011, 334, 1256-1260.
H. Shi *et al. Nat. Commun.*, 2020, 11, 1-10.
G. Kresse and J. Furthmüller, *J. Comput. Mater. Sci.*, 1996, 6, 15-50.
G. Henkelman and H. Jonsson *J. Chem. Phys.*, 2000, 113, 9978-9985.

2:30 PM EN07.09.05

Reducing the Noble Metal loading by ALD for Electrocatalysis Sitaramanjaneya M. Thalluri^{1,2}, Raul Zazpe^{1,2}, Hanna Sopha^{1,2} and Jan Macak^{1,2};

¹Center of Materials and Nanotechnologies, University of Pardubice, Czechia; ²Central European Institute of Technology, Brno University of Technology, Czechia

Platinum group metals such as Pt, Ru, Pd, Ir, etc., have superior performance for various catalytic applications.^[1] Due to their scarcity, efforts were being made to reduce or replace these noble metals. Atomic Layer Deposition (ALD) is one among the best technique to facilitate lowering of loading mass on a support of interest.^{[2],[3]} Our efforts in designing processes for different materials on ALD were successful in developing continuous thin films of thickness down to single atom. Due to the governing surface energy variations between noble metals and support surfaces, the growth initiates as nanoparticles (NP) and with a further increase in ALD cycles the agglomeration among NP's dominates over the individual NP size increase, thus developing thin films of relatively higher thickness.

For electrocatalytic applications, it is important to choose the right substrates. Among available substrates, Carbon papers (CP) and Titania nanotube (TNT) layers are best choices considering their physio-chemical properties, availability, vast literature and low costs incurred using these as support substrates in electrocatalysis and photocatalysis. Several surface modifications for CP's and variations on morphological aspects of TNT layers had received a great attention form applied fields due to their improved surface area, conductivity and stability.^{[4],[5],[6]} Uniformly decorating these CP's and TNT layers by nanoparticles or thin films of catalysts proved to be highly efficient with no boundaries on applications.^[7]

ALD is the most suitable technology that can decorate high aspect ratio and high surface area nano architectures.^[8]

The presentation will introduce and describe the synthesis of different noble metal nanoparticles by our ALD tool (Beneq TFS 200) on various aspect ratio TNT layers and CP substrates. It will also include the corresponding physical and electrochemical characterization and encouraging results obtained in electrocatalysis.

References:

1. Huang, Z. F. *et al. Advanced Energy Materials* vol. 7 (2017) 1700544.
2. Yoo, J. E. *et al. Electrochem. commun.* 86, (2018) 6.
3. Anitha, V. C. *et al. J. Catal.* 365, (2018) 86.
4. Sopha, H. *et al. Appl. Mater. Today* 9, (2017) 104.
5. Macak, J. M., Zlamal, M., Krysa, J. & Schmuki, P. *Small* 3, (2007) 300.
6. Liu, C., Sun, C., Gao, Y., Lan, W. & Chen, S. *ACS Omega* 6, (2021) 19153.
7. Dvorak, F. *et al. Appl. Mater. Today* 14, (2019) 1.
8. Zazpe, R. *et al. Langmuir* 32, (2016) 10551.

2:45 PM BREAK

3:15 PM EN07.09.06

Flash Bottom-Up Arc Synthesis of Single Atom Catalysts for Highly Active Alkaline Fuel Cell Electrodes Jae Young Jung¹, Jeong-Gil Kim¹, Min Ji Kim¹, Min Woo Kim¹, Min Seob Kim¹, Pil Kim², Hyung-Kyu Lim³, Sung Jong Yoo¹ and Nam Dong Kim¹; ¹Korea Institute of Science and Technology, Korea (the Republic of); ²Jeonbuk National University, Korea (the Republic of); ³Kangwon National University, Korea (the Republic of)

Single atom electrocatalysts (SACs) mark the beginning of a new era in the field of sustainable energy conversion technologies. The atomically dispersed transition metal-nitrogen-carbon (M-N_x-C) materials emerge as a promising SACs due to their cost effectiveness, extraordinary catalytic activity and selectivity. For a decade, a variety of synthesis strategies have been developed to realize highly active M-N_x-C catalysts. However, the most widely applied synthesis methods need general requirements for either a multistep processes or the use of typically selected metals and carbon supports. It is highly desirable to develop more efficient methods for the fabrication of M-N_x-C catalysts, realizing both simple and simultaneously applicable to various metals and supports.

The construction of hierarchical pore structure is equally important in the field of M-N_x-C catalysts for maximizing electrochemical accessibility to internal/external active area. Unfortunately, the recent studies have focused on maximizing the number of active sites to improve catalytic performance. Simply increasing active site density is not enough solution for more practical energy and environmental applications due to the limited access to the active sites. Therefore, developing the hierarchical pore structure and desirable morphology in M-N_x-C catalysts are crucial for effective mass transport in catalyst layer and utilization of active sites.

In this work, we propose a general strategy for fabricating M-N_x-C catalysts using a flash bottom-up arc discharge method. Our strategy is applicable to a broad type of metals and nanocarbons. This study revealed that nitrogen atoms in buffer gases and ligand atoms in precursor molecules played crucial roles in dispersing and stabilizing metal atoms during nanocarbon synthesis. This work provides a new synthesis protocol and novel design for efficient M-N_x-C catalysts, which may have an impact on the industry of fuel cells. Furthermore, we demonstrate an efficient strategy for developing a hierarchical pore structure in arc nanocarbons with Co-N_x-C sites and improving their oxygen reduction activity. Low temperature thermal annealing in air was highly efficient to generate hierarchical pores by opening internal and interstitial nano-channels in carbon nanohorns. Subsequent ammonia annealing modifies coordination environments and relieves local strain around cobalt atom to form more ideal Co-N₄-C sites. The combined computational and experimental studies proved that the improved kinetic activity of arc-derived Co-N₄-C catalyst is attributed to the ligand-push effect of water molecules on the other side of Co-N₄ sites. In a single-cell experiment, a power density of 742 mW cm⁻² was achieved, which is the remarkably high value among atomic M-N_x-C catalysts using commercialized membrane electrode assemblies (MEAs).

3:30 PM EN07.09.07

3D Geometry-Controlled Superhydrophobic Ni Nanoarrays for Efficient Alkaline Hydrogen Evolution Reaction Jaerim Kim, Sang-Mun Jung,

Hyeonwoong Hwang, Seokho Moon, Yong-Tae Kim and Jong kyu Kim; Pohang University of Science and Technology (POSTECH), Korea (the Republic

of)

Electrochemical water splitting for producing “green hydrogen” is of central importance in the hydrogen economy to meet the global mission of carbon neutrality. Although the hydrogen evolution reaction (HER) under alkaline conditions has many advantages over acidic HER in cost and stability aspects, it typically shows a high overpotential due to sluggish reaction kinetics.

Besides the reactive activity of the catalysts, the H₂ bubble formation due to the limited solubility of products in the electrolyte becomes one of the major causes of the limited catalytic performance. The adhered H₂ bubbles on the catalyst surface can cause reduced active surface sites, blockage of ion pathways, and destruction of catalyst film by inducing a large stretch force. Given these detrimental impacts of the H₂ bubbles on electrochemical performance, more attention should be paid to the management of H₂ bubbles for meeting the demand for large-scale applications.

Exploiting three-dimensional (3D) nanostructures can be a promising approach to minimize the efficiency loss induced by the adhered gas bubble products. Despite the beneficial effects of 3D nanostructured catalysts, the intricate dependencies between H₂ bubble dynamics and the 3D geometry of electrocatalysts remain elusive.

In this study, we systematically investigated the H₂ bubble release behaviors in alkaline HER by introducing arrays of 3D geometry-controlled Ni electrocatalysts. Through the simple and effective oblique angle deposition (OAD) method, the Ni catalysts with planar film and 3D nanorods (NR)-array architectures were fabricated as the geometry-controlled model catalysts. Based on these model catalysts, the relationship among alkaline HER performance, H₂ bubble release behaviors, and the surface wettability in terms of catalyst's geometry was investigated. We observed the tailored wetting states of the Ni catalysts with different porosity, showing the superaerophobic properties on the highly porous Ni NR catalyst. As a result, the highly porous Ni NR catalyst with the superaerophobic nature leads to the accelerated H₂ bubble release through the open pore channels, and thus, remarkably enhanced catalytic activities in alkaline media. Our work can help to deduce the fundamental and practical design rules for efficient alkaline HER catalysts including earth-abundant elements.

3:45 PM EN07.09.09

Modulating the Active Sites of Fe-N-C Catalyst Using Aging Effect for Enhanced Oxygen Reduction Reaction in Alkaline Media [Seon Yeong Lee](#)¹, Han Wool Jang¹, Sung Jong Yoo², Sungho Lee² and Han-Ik Joh¹; ¹Konkuk University, Korea (the Republic of); ²Korea Institute of Science and Technology, Korea (the Republic of)

Fe-N-C catalyst has been regarded as a significant replacement for platinum-group catalyst owing to its outstanding oxygen reduction reaction (ORR) activity in alkaline media. Fe-N_x sites have been recognized as active sites in Fe-N-C catalysts, where a single iron atom is coupled with multiple nitrogen atoms in a carbon matrix. Dual active sites consisting of Fe-N_x sites and iron carbide nanoparticles have recently been proposed as novel active sites for the catalysts, demonstrating improved ORR performance. Both of these types of typical active sites show remarkable activity for ORR, but they are also difficult to synthesize since single atoms should be evenly distributed on the substrate. In this study, we successfully synthesized MOF-derived Fe-N-C catalysts with dense active sites by introducing nano-sized carbon dots (CD) as additional active sites, whose main functional group is pyrrolic N, and controlling the main active sites by simply aging the catalyst for the appropriate duration. Multiple N sites from CD with electronegative force begin electrostatic force with electropositive iron ions throughout the aging process, allowing for a large amount of Fe-N bonding. The ORR activity of the FeNC-24-0.6 and FeNC-48-0.9 catalysts prepared by optimum conditions was superior to that of a commercial Pt/C catalyst. Interestingly, the FeNC-24-0.6 and FeNC-48-0.9 catalysts mainly have dual and single active sites, respectively. However, with accelerated durability cycling, FeNC-24-0.6 exhibited a negative shift in performance, but FeNC-48-0.9 nearly maintained its performance. It was shown that single and dual active sites are both effective for ORR activity, although dual active sites are more susceptible to long-term stability in an alkaline medium. As a result, bringing in extra nitrogen supply and aging at the optimal time is an effective strategy to increase the active site density of Fe-N-C catalysts, and raising the site density of the Fe-N_x structure is more worthwhile than generating secondary active sites to improve ORR performance.

Reference

- [1] Jiang W J, et al., *J. Am. Chem. Soc.*, 138 (2016) 3570–8
- [2] G. -S. Kang, et al., *J. Mater. Chem. A*, 8 (2020) 22379–22388
- [3] Lee, S.Y., et al. *Carbon Lett.* 31, 1349–1355 (2021)

4:00 PM EN07.09.10

Regulating Impurity in Amorphous TiO₂ for Ultra-Stable Photoanode Protection [Yutao Dong](#)¹, Mehrdad Abbasi², Lazarus German¹, Jinwoo Hwang² and Xudong Wang¹; ¹University of Wisconsin-Madison, United States; ²The Ohio State University, United States

On demand of sustainable fuels under irreversible consumption of fossil fuels crisis, hydrogen production from photoelectrochemical (PEC) water splitting can be promising approach to converting solar light into clean hydrogen energy. Silicon (Si) is a feasible semiconductor with small band gap and high industrial maturity, but bare Si suffers deleterious corrosion during photoelectrochemical reaction which largely limited practical application^[1].

Amorphous TiO₂ (a-TiO₂) thin film emerged as an excellent protection layer to avoid Si exposure to corrosive electrolyte directly. However, in comparably thicker a-TiO₂ films, intermediates exhibited conductivity heterogeneity leading to failure in short term^[2]. By lowering the deposition temperature, crystallization behavior could be suppressed to form fully amorphous film but impurities from incomplete ligand exchange reaction were also buried into amorphous film to affect film quality.

In this work, we analyzed the low temperature grown ALD a-TiO₂ film failure process and conducted a water annealing treatment to partially remove chlorine (Cl) impurity to achieve ultra-stable Si photoanode protection performance more than 600 hours. In pristine TiO₂ film, Cl impurity was uniformly distributed into whole TiO₂ and could lead to pinhole formation during electrochemical reaction to allow hydroxide groups to attack Si wafer. As a result, photocurrent density exhibited a continuous decay in PEC stability test. With water annealing treatment on pristine TiO₂ films, cross-sectional scanning transmission electron microscopy (STEM) showed it maintained amorphous phase without any crystallization. X-ray photoelectron spectroscopy (XPS) and long-term electron dispersive spectroscopy (EDS) indicated partial Cl impurity was removed at the top of TiO₂ film to form more stoichiometry TiO₂ film as an excellent protection layer. This work provides a promising approach to obtaining high-quality amorphous TiO₂ film at low temperature deposition and points a pathway to achieve maximum protection of ALD a-TiO₂ coating.

Reference:

- [1] Y. Yu, Z. Zhang, X. Yin, A. Kvit, Q. Liao, Z. Kang, X. Wang, Enhanced photoelectrochemical efficiency and stability using a conformal TiO₂ film on a black silicon photoanode. *Nature Energy*, 2,1-7 (2017).
- [2] Y. Yu[†], C. Sun[†], X. Yin, J. Li, S. Cao, C. Zhang, P. Voyles*, X. Wang*, Metastable Intermediates in Amorphous Titanium Oxide: A Hidden Role Leading to Ultra-Stable Photoanode Protection, *Nano Lett.* 18, 5335–5342 (2018).

4:15 PM EN07.09.11

Mechanism of Charge Accumulation of Poly(heptazine imide) [Seo Goichiro](#)¹, Yuki Saito², Miyu Nakamichi² and Kaname Kanai²; ¹Tokyo University of Science, Japan; ²Tokyo University of science, Japan

In recent years, carbon nitride polymers have attracted enormous interest studied as inexpensive and easy-to-synthesize photocatalysts. Moreover, carbon

nitride polymers has been actively studied because it can generate hydrogen through photocatalytic activity in visible light region around 450 nm unlike TiO₂, which can be activated in ultraviolet light. Through many pioneering work on carbon nitride polymers, several types of new carbon nitrides have been discovered. In particular, poly(heptazine imide) (PHI) is one of the newly carbon nitride polymers, which structure has two-dimensionally polymerized carbon nitride skeleton. Unlike other carbon nitride polymers, PHI has attracted attention not only as a materials that shows high photocatalytic performance in visible light but also shows dark photocatalytic activity. Dark photocatalysis is a function in which the charges generated by light irradiation are stored inside the material and consumed in the dark state, and Lau *et al.* were firstly reported about dark photocatalytic performance of PHI in 2017. Combining the photocatalytic and dark photocatalytic activities of PHI makes it possible to continue generating hydrogen day and night, which cycle is called day-night photocatalysis. If day-night photocatalysis has realized, it is expected to significantly improve the efficiency of hydrogen collection, which has been an important issue for photocatalysts.

Dark photocatalytic activity has also been reported for materials such as TiO₂+WO₃, and it is generally believed that carriers generated by light irradiation accumulate on the surface and exhibit catalytic activity even in the dark state through a state called charge accumulation. In short, it is important to investigate the charge accumulation in detail in order to improve the function of dark photocatalytic activity. For example, studying the charge accumulation phenomenon and improving the amount of stored charge will lead to increase the evolution of hydrogen by dark photocatalytic activity, and also allow the activity to be maintained for longer periods of time in the dark. However, the dark photocatalytic activity of PHI occurs only in solution, making it difficult to analyze changes in electronic and chemical structure, for this reason the mechanism of charge accumulation in PHI has not been discussed from a microscopic perspective.

In this study, we succeeded in solving such a problem by making it possible to take PHI out of the test tube in the form of a gel. The PHI gel (PHIG) can be obtained by mixing PHI and a substance called an ionic liquid, which has an extremely low vapor pressure and a very high viscosity. PHIG has made it possible to carry out many experiments to explore the properties of PHI, including experiments in vacuum such as X-ray photoelectron spectroscopy (XPS) and scanning electron microscopy/energy dispersive X-ray spectroscopy (SEM/EDX). In our study, we found two basic features of PHI, photochromism, which is reversibly changes of molecular structure by light irradiation, and light-driven adsorption of potassium ions, which is a component of PHI. On the other hand, as mentioned above, the charge accumulation phenomenon of PHI can be observed by photoirradiation in PHI. Therefore, we hypothesized that the charge accumulation may be caused by the two characteristics of PHI, and devised a model to explain the phenomenon. More specifically, we considered that the charge accumulation in PHI is caused by three steps: (1) light irradiation generates photocarriers in PHI, (2) photochromism causes narrowing of the energy gap, and (3) the narrowed energy gap acts as a trap and photocarriers are trapped in it. In this presentation, we will discuss the relationship between photochromism, adsorption of potassium ions, and charge accumulation, both of which originate from photoirradiation in PHI and we propose a new model of charge accumulation in PHI based on the results.

SESSION EN07.10: Virtual Session I
Session Chairs: Mitch Ewan and Alexander Headley
Tuesday Afternoon, December 6, 2022
EN07-virtual

1:00 PM *EN07.10.01

Measurement and Modelling of Potential Profiles in Water Electrolysers to Minimize Titanium Use Gareth Hinds; National Physical Laboratory, United Kingdom

Green hydrogen is an essential component of net zero strategies for 'difficult to decarbonize' sectors such as heavy duty transport, domestic heating and industrial processes, but its relatively high price remains a significant challenge. The cost of production using proton exchange membrane water electrolysers (PEMWEs) depends on both CAPEX of the devices and OPEX, which is dominated by the renewable electricity price. The latter is already low and is projected to continue to decrease so reducing CAPEX is the major focus of research efforts.

The assumption of a highly corrosive potential at the anode bipolar plate (BPP) and porous transport layer (PTL) in a PEMWE stack often leads to selection of expensive materials such as platinum-coated titanium. In this talk, a description will be given of a physicochemical model of electrochemical potential distribution in a PTL, validated by *in situ* and *ex situ* electrochemical potential measurement. The model predicts that, under typical PEMWE operating conditions, the corrosive zone associated with the anode polarisation extends only $\approx 200 \mu\text{m}$ into the PTL from the catalyst layer, removing the need for highly corrosion-resistant materials in the bulk of the PTL and at the BPP.

Guided by the model, single cell PEMWE tests were carried out using anode current collectors fabricated from carbon-coated 316L stainless steel. The material was shown to be tolerant to potentials up to 1.2 V vs RHE and when tested *in situ* for 30 days at 2 A cm⁻² showed no evidence of degradation. These results strongly suggest that much of the titanium in PEMWEs may be substituted with cheaper, more abundant materials with no loss of electrolyser performance or lifetime, which would significantly reduce the cost of green hydrogen. The combined modelling and experimental approach developed here shows great promise for design optimisation of PEMWEs and other electrochemical energy conversion devices.

1:30 PM EN07.10.03

Ni-Foam-Graphene-CNTs-SnSeP—An Efficient Electrocatalyst Covering Universal pH Range and Tap Water Splitting for Hydrogen Evolution Reaction Mansi Pahuja, Kehkashan Alam, Kaushik Ghosh and SK Riyajuddin; INST Mohali, India

A day-by-day boost in the hunger of people for renewable energy has to be addressed where green fuel generation via water splitting is a game changer to fossil fuels. The development of rationally designed cost-effective noble-metal free electrocatalyst with high efficiency, and long-term stability has been vigorously pursued. Herein, we report a super-hydrophilic bi-ligand metal phosphide (SnSeP) on the surface of a highly porous Nickel foam-graphene-carbon nanotubes matrix via the facile thermal Chemical Vapour deposition method. The newly developed electrocatalyst renders superior electrocatalytic performance with long-term stability for a minimum of 10 days at a high current density of 250 mA/cm² in each acidic, basic and neutral medium, inferring the commercialization of the catalyst toward industrial-grade application. The excellent electrocatalytic performance is analyzed in terms of low overpotential of 45 mV, 85 mV, and 135 mV at 10 mA/cm² in acidic, basic, and neutral media respectively. Moreover, the as-designed catalyst has shown a noteworthy performance in the smart utilization of tap water in hydrogen fuel production. This work highlights a new insight in adopting a feasible strategy to develop a cost-effective robust electrocatalyst that is capable enough for the facile usage of tap water that could be an attractive paradigm of green fuel synthesis via renewable electrochemical energy conversion.

1:45 PM EN07.10.04

Tuning Interfacial Hydrogen Bonding for Enhanced Hydrogen Evolution and Oxygen Reduction Electrocatalysis Yirui Zhang, Tao Wang, Botao

Designing electrochemical water splitting and its reverse process is crucial for producing hydrogen and achieving high efficiencies for fuel cells. While conventional design of catalysts has focused on tuning the surface electronic structures of electrodes [1] and binding strength of intermediates [2], recent studies show that changing electrolyte compositions, such as spectator cations and pH [3], can also significantly alter catalytic activity and kinetics by orders of magnitude, highlighting new opportunities in tuning non-covalent interactions in the electrolytes to control catalytic activities. We have recently designed an interfacial layer of protic ionic liquids on platinum and gold to tune the oxygen-reduction reaction (ORR) kinetics, where altering the proton activity of organic ionic liquids increases the intrinsic activity by up to five times [4]. The maximum enhancement of kinetics is achieved when the pK_a of the ionic liquid matches that of the reaction intermediate, which is attributed to the strengthened hydrogen bonding between the ionic liquid and reaction products, supported by density functional theory (DFT) calculations and surface-enhanced infrared absorption spectroscopy (SEIRAS).

To further develop design principles for electrolyte engineering and unravel the role of interfacial hydrogen bonding, we have employed a series of water-in-solvent electrolytes for hydrogen evolution and oxidation reactions (HER/HOR). We systematically confine water in organic matrixes, including acetonitrile (ACN) and dimethyl sulfoxide (DMSO), and tune the hydrogen-bonding networks by changing the water concentration (2% - 100% molar ratio) and altering the donor number of organic solvents. Water molecules become more isolated when decreasing the water-to-organic ratio, and water reduction shifts to a more negative potential. The shifts in onset potentials are solvent-dependent, where DMSO-containing electrolytes suppress HER and lower the onset potential compared to ACN-containing electrolytes. The suppression effect of HER with DMSO is attributed to its stabilization effect of isolated water as a result of the high donor number, while the enhancement effect of HER with ACN is due to the promotion of interfacial hydrogen-bonded water. SEIRAS measurements further support the changes in interfacial hydrogen bonding during the reactions, highlighting the role of interfacial hydrogen bonds between organic solvents and water in controlling HER/HOR kinetics.

These findings open up immense opportunities for using non-covalent hydrogen bonding interactions at the electrified interface to control the kinetics of ORR, HER, and beyond. The understanding would also be impactful across other reactions crucial to improving decarbonizing efforts in energy storage, such as CO₂ reduction and aqueous batteries.

References

- [1] Suntivich, J., May, K. J., Gasteiger, H. A., Goodenough, J. B., & Shao-Horn, Y. (2011). *Science*, 334(6061), 1383-1385.
- [2] Seh, Z. W., Kibsgaard, J., Dickens, C. F., Chorkendorff, I. B., Norskov, J. K., & Jaramillo, T. F. (2017). *Science*, 355(6321), eaad4998.
- [3] Huang, B., Rao, R.R., You, S., Hpone Myint, K., Song, Y., Wang, Y., Ding, W., Giordano, L., Zhang, Y., Wang, T., Mui, S., Katayama, Y., Grossman, J. C., Willard, A. P., Xu, K., Jiang, Y., & Shao-Horn, Y. (2021). *JACS Au*, 1(10), 1674-1687.
- [4] Wang, T.*, Zhang, Y.*, Huang, B., Cai, B., Rao, R.R., Giordano, L., Sun, S.G., & Shao-Horn, Y. (2021). *Nature Catalysis*, 4(9), 753-762.

2:00 PM EN07.10.05

Advanced Water Management in Polymer Electrolyte Fuel Cells at Subzero Temperatures: Gas Diffusion Layer with Patterned Wettability

Wenmei Liu^{1,2}, Jongmin Li^{1,1}, Yen-Chun Chen¹, Yang Yao², Sonja Neuhaus³, Alok Goel³, Thomas Justus Schmidt^{1,2} and Pierre Boillat^{1,1}; ¹Paul Scherrer Institute, Switzerland; ²ETH Zürich, Switzerland; ³University of Applied Sciences and Arts Northwestern Switzerland (FHNW), Switzerland

Polymer electrolyte fuel cells (PEFCs) are promising alternatives for automotive and portable applications thanks to zero-emission, low operating temperature, and fast refueling. Water management is a challenge for successful cold-start, as well as stable, long-lasting, and high PEFC performance at subzero temperatures. Sudden freezing of supercooled water leads to rapid voltage degradation, causing cold-start failure^{1,2}. In addition, it causes irreversible damage to cell components, including the membrane, catalyst layer, and gas diffusion layer (GDL), so-called freeze-thaw^{3,4}, which results in a significant reduction of PEFC lifetime.

Our previous work has shown that GDLs with patterned wettability improved water management and cell performance^{5,6} in normal operational conditions. In this presentation, we will show the effects of wettability-patterned GDLs on preventing ice propagation with the following parameters being systematically investigated: GDL substrate, water saturation level, hydrophobic polymeric coating, coating loads, and wettability pattern dimensions. Ex-situ differential scanning calorimetry (DSC) and in-situ advanced calorimetry were used as calorimetric techniques to detect the onset of freezing temperatures of water in GDLs. X-ray tomography was used to visualize the water distribution inside GDLs.

The designed pathways allow the effective separation of water and gas. Individual freezing events were found to happen above -15 °C and below -25 °C in the patterned Toray (250 μm hydrophilic- 1000 μm hydrophobic), which shows the effective prevention of ice propagation in GDLs. Thanks to the improved water management, the ice-free area can diffuse reactant gaseous to allow continuous operation of the cell, which improves the cold-start capability.

1. Wang, S., Sun, Y., Huang, F. & Zhang, J. Freezing Site of Super-Cooled Water and Failure Mechanism of Cold Start of PEFC. *Journal of The Electrochemical Society* **166**, F860-F864 (2019).
2. Jiao, K., Alaefour, I. E., Karimi, G. & Li, X. Cold start characteristics of proton exchange membrane fuel cells. *International Journal of Hydrogen Energy* **36**, 11832-11845 (2011).
3. Alink, R., Gerteisen, D. & Oszcipok, M. Degradation effects in polymer electrolyte membrane fuel cell stacks by sub-zero operation—An in situ and ex situ analysis. *Journal of Power Sources* **182**, 175-187 (2008).
4. Yan, Q., Toghiani, H., Lee, Y.-W., Liang, K. & Causey, H. Effect of sub-freezing temperatures on a PEM fuel cell performance, startup and fuel cell components. *Journal of Power Sources* **160**, 1242-1250 (2006).
5. Former-Cuenca, A. *et al.* Engineered Water Highways in Fuel Cells: Radiation Grafting of Gas Diffusion Layers. *Advanced Materials* **27**, 6317-6322 (2015).
6. Manzi-Orezzoli, V., Siegwart, M., Scheuble, D., Schmidt, T. J. & Boillat, P. Impact of the Microporous Layer on Gas Diffusion Layers with Patterned Wettability II: Operando Performance and Water Distribution Analysis by Neutron Imaging. *J. Electrochem. Soc.* **167**, 064521 (2020).

2:15 PM EN07.10.06

Investigation of Solid-State Metathesis as a Rapid and Convenient Synthetic Method to the Formation of Cobalt-Iron Boride Solid-Solutions and the Effect of Chemical Composition on Electrocatalytic Activity Janaka P. Abeyasinghe and Edward Gillan; University of Iowa, United States

Hydrogen has been gaining popularity as a reliable and environmentally friendly energy source for future energy demands. Water is an abundant source of hydrogen and electrochemical water splitting into hydrogen and oxygen gases is an efficient, effective, and non-greenhouse gas emitting process. The search for cost-effective electrocatalysts for the cathodes and anodes in electrocatalytic hydrogen evolution reaction (HER) and oxygen evolution reaction (OER) that are active at low applied potentials is a subject of great interest. Late transition metal (cobalt, nickel, and iron) compounds have been

extensively studied as electrocatalysts due to their abundance and low cost. Because of their intriguing chemical and physical properties, late transition metal borides are appealing as ideal electrocatalyst with active, long-lasting, and persistent electrocatalytic properties. Borides of cobalt and iron have been investigated and identified as moderate electrocatalysts, both individually and in combination. Some studies have found that a synergistic effect improves electrocatalytic activity of multi-metal combinations as compared to individual metal boride performance. Understanding how synergy works with crystalline cobalt and iron borides and what extent it applies to bulk cobalt iron borides are important research areas. The current study describes cobalt and iron solid-solution formation in crystalline form from rapid and energetic solid-state metathesis reactions using combinations of MCl_2 ($CoCl_2$ and $FeCl_2$) + $Mg + B$. X-ray diffractograms (XRD) show that solid solutions formed in all cobalt and iron compositions, and chemical compositions of solid-solution samples were confirmed using inductively coupled plasma spectroscopy (ICP) and energy dispersive spectroscopy (EDS). Properties of cobalt-iron solid solutions were characterized using scanning electron microscopy, surface area analyzer, and crystallite sizes (XRD peak width), and the results show that structural properties gradually change from one end of the compositional range to the other. These crystalline borides show no evidence of synergy between cobalt and iron in HER electrocatalysis performed in 1.0 M KOH, instead the relative electrocatalytic activity was highest for cobalt boride (10 $mA\ cm^{-2}$ at -223 mV), lowest for iron boride (10 $mA\ cm^{-2}$ at -342 mV), and intermediate for the different solid-solutions compositions. After 24 hours of chronoamperometry, all crystalline cobalt and iron borides showed bulk stability and maintained HER activity. Post-electrochemistry studies confirmed the retention of metal borides after extensive electrochemistry studies.

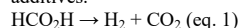
2:45 PM DISCUSSION TIME

SESSION EN07.11: Virtual Session II
Session Chairs: Mitch Ewan and Alexander Headley
Tuesday Afternoon, December 6, 2022
EN07-virtual

9:00 PM *EN07.11.01

High-Pressure Hydrogen Production from Formic Acid Catalyzed by Homogeneous Iridium Complexes Yuichiro Himeda; National Institute of Advanced Industrial Science, Japan

Formic acid as a liquid organic hydrogen carrier has been receiving increasing attention, due to low-toxicity, low-flammability, and biodegradability.[1] We have reported a large number of efficient catalysts for dehydrogenation of formic acid (FADH: eq. 1), which were half-sandwich iridium complexes having *N,N*-bidentate ligands, such as bipyridine and imidazoline. Toward practical hydrogen supply, robust, selective, and efficient catalysts are required. Herein, we describe the development of robust and efficient iridium-based catalysts for high pressure hydrogen production by FADH in water without any additives.



Recently, we have developed robust catalysts for continuous and constant hydrogen supply toward practical use.[2] The catalyst having pyridylpyrazole ligands remained catalytically active for 35 days in FADH at 70 °C to produce hydrogen gas (1.25 m^3) with a TON of 10 million. Furthermore, when the reaction was carried out in closed vessel, the pressure of the evolved gases was raised. In initial studies, the catalyst generated more than 100 MPa, which was composed of H_2 and CO_2 (1:1) without CO by GC analysis.[3] Unfortunately, obvious degradation of the catalyst having 4,4'-dihydroxyl-2,2'-bipyridine ligand was observed under these conditions. The catalyst having 4,4'-diamino-2,2'-bipyridine ligand produced 157 MPa of gases from 21 M of FA solution at 80 °C.[4] It was possible to continuously produce high-pressure and CO-free H_2 by addition of concentrated FA.

[1] *Chem. Rev.* **2015**, *115*, 12936-12973; *Coord. Chem. Rev.* **2018**, *373*, 317-332; *Adv. Energy Mater.* **2019**, *9*, 1801275; *ibid.* **2022**, 2103799; *ibid.* **2022**, 10.1002/aenm.202200817.

[2] *Adv. Synth. Catal.* **2019**, *361*, 289-296.

[3] *ChemCatChem* **2016**, *8*, 886.

[4] *Inorg. Chem.* **2020**, *59*, 4191-4199.

9:30 PM EN07.11.02

Enhancing Gravimetric and Volumetric Ammonia Capacities of Metal-Organic Frameworks via Consecutive Post-Synthetic Modification Dae Won Kim and Chang Seop Hong; Korea University, Korea (the Republic of)

Ammonia is a promising energy vector that can store the high energy density of hydrogen. For this reason, numerous adsorbents have been investigated as ammonia storage materials, but ammonia adsorbents with a high gravimetric/volumetric ammonia capacity can be simultaneously regenerated in an energy-efficient manner remain underdeveloped, which hampers their practical implementation. Herein, we reported Ni_{acryl_TMA} (TMA = thiomallic acid), an acidic group functionalized metal-organic frameworks prepared via double post-synthetic modifications showing top-tier gravimetric ammonia capacity of 23.5 $mmol\ g^{-1}$ and the unprecedented ammonia storage density of 0.39 $g\ cm^{-3}$ at 1 bar and 298 K with facile regeneration. The ammonia storage properties and adsorption mechanism were characterized by ammonia isotherm, NH_3 -temperature-programmed desorption curves, NH_3 breakthrough curves, *in-situ* FT-IR, and DFT-calculation. Detailed synthesis and properties will be presented in the presentation.

9:45 PM EN07.11.03

Relationship Between Anode Deformation and Cell Stress Evolution During Reduction in Solid Oxide Fuel Cells and Electrolysis Cells Junya Tanaka^{1,2}, Kazuhisa Sato¹ and Toshiyuki Hashida¹; ¹Tohoku University, Japan; ²DENSO Corporation, Japan

Solid oxide fuel cells (SOFCs) and solid oxide electrolyte cells (SOECs) are attracting attention as one of next-generation energy devices because of high energy conversion efficiency or non-necessity for expensive catalyst. To commercialize SOFCs/SOECs, it is crucial to ensure their mechanical reliability. Various types of stresses generated in the cells during the lifetime from manufacturing to operation may cause cells failure and system safety degradation. In particular, the anode deformation during reduction is considered to be one of the most important factors causing cell stress changes, but the results reported by previous studies vary, and there are also few reports about the relationship between the anode deformation and cell stress evolution.

In this study, the deformation behavior of anodes with different Ni contents during reduction and the effects of temperature on it were investigated in-situ by a dilatometer and X-ray diffractometry using NiO-YSZ bulk samples which is often used for the anode in SOFCs/SOECs. In addition, the cell stress changes during reduction process are examined by FEM analysis and verified by X-ray diffractometry.

Since YSZ is stable and NiO shrinks under reducing conditions, it was generally assumed that NiO-YSZ shrinks during the reduction process. However, only the sample with the highest Ni content in this measurement was shown to shrink, (specifically, -0.32% strain at 700°C, -0.10% at 800°C and -0.071%

at 900°C), while the other NiO-YSZ samples expanded, (for example, a sample with 27% Ni content showed 0.024% strain at 700°C, 0.013% at 800°C and 0.051% at 900°C). Both the amount of expansion and shrinkage decreased with increasing temperature during reduction. We found that the factor of expansion was the change or release of the residual stress on YSZ side, because the strain change in the NiO-YSZ measured by the dilatometer and that calculated from residual stress change on the YSZ side measured by X-ray diffractometry matched each other in both direction and amount. In addition, it can be explained that the factor of decreasing expansion amount with increasing temperature is also due to the residual stress change on the YSZ side. In the cell configuration, only the anode is deformed unless the cathode is exposed to a reducing environment. Thus, we hypothesized that the factor for cell stress changes during reduction is the anode deformation, and investigated the cell electrolyte stress change by FEM analysis taking into account the anode deformation, creep behavior and temperature dependence of the relevant physical properties. It was also verified by X-ray diffractometry based on the $\cos\alpha$ method. The measured cell was a multilayer structures consisting of an anode, an electrolyte, and an interlayer, which is a structure similar to that of the actual cell. The principal stress on the electrolyte surface was computed from the FEM analysis. Here, the positive side is tensile direction, and the negative side is compressive direction. Specifically, when the anode showed expansion, there were almost no stress changes on the cell electrolyte. However, when the anode showed shrinkage, the residual stress increased by approximately 300MPa on the compressive side during reduction. Then, the residual stresses were relaxed by creep after reduction under both analysis conditions. The experimental results together with the FEM analysis suggest that the anode deformation may control cell stress change during reduction, and the numerical method developed in this study can offer a useful tool for evaluating the cell stress evolution during the reduction process.

10:00 PM EN07.11.04

Functionalization of Graphene Oxide Membranes by (3-Mercaptopropyl) Trimethoxysilane for PEMFCs [Shahjahan K. Chowdury](#), Young J. Cho, Sung B. Park and Yong-il Park; Kumoh National Institute of Technology, Korea (the Republic of)

Graphene oxide membrane (GOM) has promising electrolyte properties in electrochemical devices, including fuel cells and batteries. However, GOM has a much lower proton conductivity in a through-plane direction (σ_{th}) than that of the most commonly known PEMFC electrolyte of Nafion[®] membrane. And the lamellar structure of 2-dimensional graphene oxide (GO) nanosheets show a large anisotropic conductivity, fuel crossover, and negative surface functional groups reduced by hydrogen atmosphere while operating in the PEMFC. In this study, rapid proton-conducting GOMs were synthesized by homogeneous mixing of the diluted (3-mercaptopropyl)trimethoxysilane (MPTS, $HS(CH_2)_3Si(OCH_3)_3$) and GO, i.e., M-GOM, and then oxidizes to supply a proton conduction pathways by obtaining a sulfonic acid ligand (-HSO₃), where MPTS covalently bonded to the surface of GO through the hydrolysis (Si-OCH₃ to Si-OH) and condensation reaction (Si-OH to Si-O-C), and thiol group (-HS) of MPTS was oxidized to accomplish a -HSO₃. Excellent proton conductivity was observed, due to silane-based network formation and a dramatic increase in proton conduction sites. The influence of the fabricated M-GOM on morphology, physicochemical properties, atomic bonding, and crystalline phase are investigated and compared with Nafion[®]. After depositing a hydrogen-permeable metal thin film (Pd) on M-GOM, it is utilized in a hydrogen membrane fuel cell (HMFC), and its operating characteristics are also reported.

10:05 PM EN07.11.05

Nanohybrid Graphene Oxide Membranes for PEMFCs [Shahjahan K. Chowdury](#), Young J. Cho, Sung B. Park and Yong-il Park; Kumoh National Institute of Technology, Korea (the Republic of)

Graphene oxide membrane (GOM) is considered a promising alternative electrolyte due to its hydrophilic nature and fascinating proton conductivity in humidified conditions. However, GOM has a lower proton conductivity than high-performance Nafion^(R) membrane in the through-plane direction (σ_{th}) and GOM loses its surface functional groups by hydrogen gas in anode when operating in PEMFC, resulting in increased electronic conductivity. Therefore, in this research, a highly proton-conducting composite membrane was synthesized using a silanization process between a highly viscous GO solution (5mg/mL) and a diluted (3-mercaptopropyl) trimethoxysilane (MPTS, $HS(CH_2)_3Si(OCH_3)_3$) (0.790 g/mL). The organofunctional group of the thiol group (-SH) was oxidized by hydrogen peroxide (H₂O₂) into a sulfonic acid group (-HSO₃) on the surface of GOM for providing a high-speed proton conduction path along with the functional group of GOM. Moreover, proton conductivity was raised by adding excess MPTS as a binder in the MPTS-modified GO composites (MGCs). The incorporated MPTS into the GO framework was controlled from 1 to 70 wt%, and a suitable ratio of the high-performance electrolyte properties was reported such as excellent proton conductivity, thermally, mechanically and chemically protected from degradation. In addition, the MPTS-derived siloxane structure further enhances the water uptake with dimensional stability and low fuel crossover without damaging the proton transport path in MGCs. The synthesized composite membrane was investigated not only the morphology by FE-SEM, but also the molecular and microstructure analysis using powder X-ray diffraction, X-ray photoelectron spectroscopy, Raman spectroscopy, Fourier-transform infrared spectroscopy, thermogravimetric analysis/differential scanning calorimetry, and UV-Vis spectroscopy. In addition, hydrogen-permeable 40 nm-thick Pd was deposited on the surface of the MGCs to improve the gas tightness and maintain high mechanical stability to prevent degradation of the membrane by hydrogen reduction during the operation of the fuel cell.

10:20 PM EN07.11.06

Pt-Free Cathode for Graphene Oxide-Hydrogen Membrane Fuel Cells [Shahjahan K. Chowdury](#), Young J. Cho, Sung B. Park and Yong-il Park; Kumoh National Institute of Technology, Korea (the Republic of)

Electrocatalysts without precious metals are being actively studied in the field of electrochemical devices, including fuel cells due to their low cost and electrocatalytic activity. Graphene, a new 2-dimensional sp²-hybridized hexagonal (honeycomb lattice) carbon material, provides the noticeable replacing opportunity as an electrocatalyst for oxygen reduction reaction (ORR) because of its excellent chemical, electrical and thermal properties, high catalytic activity, and tolerance against poisoning. In this study, a nitrogen-doped reduced graphene oxide (N-rGO) catalyst for oxygen reduction reaction (ORR) of hydrogen membrane fuel cell was investigated. This process, in this study provides an effective yield and is free of impurities, resulting in the intrinsic catalytic performance. The surface morphology, hydrophobicity and electrical conductivity of the synthesized N-rGO was analyzed by BET and UV-visible spectroscopy. A graphene oxide-hydrogen membrane fuel cells that does not use Pt/C was prepared using the N-rGO electrode and the graphene oxide composite electrolyte membrane modified with 3-mercaptopropyl trimethoxysilane developed in the previous study, and its performance is reported.

10:35 PM EN07.11.08

Power Distribution Control for Improving Lifetime of Proton Exchange Membrane Water Electrolyzers [Keiji Watanabe](#), Daiko Takamatsu, Akio Yoneyama, Futoshi Furuta, Takao Ishikawa and Jun Hayakawa; Hitachi, Ltd., Japan

There is a growing demand for improving lifetime of water electrolyzers in order to reduce the hydrogen production cost. Recently, degradation behaviors of proton exchange membrane (PEM) water electrolyzers operating under fluctuating power such as renewable power sources have been extensively studied. Degradation of electrolyzer appears as increase in the operating voltage (i.e., the overpotential). It was shown that the rate of voltage increase highly depends on the operation parameters such as the current density and the interval of current fluctuation [1,2]. However, it has not been clarified so far what kind of operation control can suppress the degradation of the electrolysis stacks. Here we have developed a novel control technology for improving

lifetime of PEM water electrolyzers.

First, we proposed a control strategy called the Power Distribution Control (PDC) for suppressing the degradation of water electrolyzers. The concept is to decompose a fluctuating power that highly degrades electrolyzers into the power patterns of low-degradation rates. For example, a PEM electrolysis cell operating under the current fluctuation between 2 and 1 A/cm² (mode A) degrades rapidly than that between 2 and 0 A/cm² (mode B) [1]. When two series of stacks (i.e., two strings) operate in mode A, it is possible to distribute the current by the PDC so that one string operates in mode B and the other at a constant current of 2 A/cm² (mode C). It is thus expected that degradation of the stacks can be suppressed by the power distribution. An example of the system architecture to perform the PDC is an array of electrolysis stacks with power converters such as DC/DC converters installed in each string. In order to experimentally validate the effect of PDC, a series of durability tests for a PEM electrolysis cell were performed. A membrane electrode assembly (MEA) composed of a PEM (Nafion 117), an anode catalyst layer (IrO₂), a cathode catalyst layer (Pt/C) and gas diffusion layers was prepared and used for the tests. The rate of cell voltage increase was 111 and 69 μV/h under the operation in mode A (reference) and in the sequence of mode B and C (simulation of PDC), respectively. This result suggests that the degradation rate was reduced by 38% as a result of PDC. As a result of the analysis of current-voltage characteristics, it was found that PDC is particularly effective in suppressing the increase in the activation overvoltage. Furthermore, the degradation mechanism has been investigated by analyzing the degraded sample using synchrotron radiation. Scanning X-ray fluorescence microscopy (SXFM) [3] was performed for obtaining elemental maps of the cross section of the catalyst coated membrane (CCM). An X-ray microbeam 1 μm in diameter was formed, and the distribution of Pt and Ir was obtained. While the distribution of Pt showed little change after the durability test, Ir was observed within the PEM and even near the interface between the PEM and the cathode. Then we performed microbeam X-ray absorption fine structure (XAFS) imaging and estimated the Pt and Ir valence state from the white-line height of Pt and Ir L_{III}-edge X-ray absorption near edge structure (XANES), respectively. It was found that Ir within the PEM is in a higher valence state (Ir^{>4+}) than Ir at the anode (Ir⁴⁺), indicating that highly oxidized IrO_x dissolved and migrated in the PEM. This scenario is consistent with the Pourbaix diagram of Ir [4], where the stable phase changes between IrO₂ (pH = 0) and IrO₄⁻ (pH = 7) during the operation of PEM electrolyzers. Our results demonstrate that PDC is a promising technique for improving lifetime of PEM electrolyzers by suppressing degradation such as Ir dissolution.

[1] C. Rakovsky *et al.*, *J. Power Sources* **342**, 38 (2017).

[2] S. H. Frensch *et al.*, *Int. J. Hydrogen Energy* **44**, 29889 (2019).

[3] A. Yoneyama *et al.*, *J. Instrum.* **15**, P12029 (2020).

[4] M. Pourbaix, "Atlas of Electrochemical Equilibria in Aqueous Solutions" (1974).

10:40 PM EN07.11.09

Selective Oxidation of Aromatic Alcohol and Amine Under Visible-Light Irradiation Using Rh Doped SrTiO₃ Photocatalyst Sayuri Okunaka and Kazuhiro Sayama; National Institute of Advanced Industrial Science and Technology (AIST), Japan

Development of selective organic synthesis using environmentally benign, inexpensive and renewable resources has attracted much attention in both fundamental and industrial chemistry. In particular, selective oxidation of alcohol or amine for the synthesis of fine chemicals and pharmaceuticals has received much attention in chemical research. Recently, selective oxidation using a semiconductor photocatalyst is considered to be one of the most sustainable energy conversion processes with significant advantages of operation under room temperature and utilization of clean, renewable solar light as the driving force. However, TiO₂, which is the famous semiconductor photocatalyst, has the following drawbacks; low photoactivity, poor selectivity and lack of utilization of visible light, and therefore hinder its application. Alternatively, the Rh doped SrTiO₃ (SrTiO₃:Rh) photocatalyst has been known to have a potential that can oxidize organic compounds and produce H₂ from water containing organic media (e.g. methanol) under visible light irradiation. Here, we attempted to use SrTiO₃:Rh as a visible light responsible photocatalyst for selective oxidation of benzyl alcohol or benzylamine, which were chosen as one of the model alcohol or amine derivatives, under visible light irradiation.

10:45 PM EN07.11.10

Tuning the Nanoporous Structure of Cobalt-Iron-Based Nanocomposite via Doping Sulfur and Phosphorus for Charge Storage Application Shiva Bhardwaj^{1,2}, Mahesh Chaudhari^{1,2} and Ram K. Gupta^{1,2}; ¹Pittsburg State University, United States; ²Kansas Polymer Research Center, United States

Running a vehicle needs energy that is derived using fossil fuels mainly (gasoline) leads to the production of greenhouse gases like CO₂, which is the one of the main cause of global warming. So scientists worldwide are looking for clean and sustainable energy for which energy storage devices (ESDs) might be the one solution as they are the past, present, and the future of electric vehicles; without ESDs, these vehicles are not imaginable, providing significant support to the importance of ESDs. Apart from electric vehicles, ESDs have many applications in running electrical and electronic gadgets. The various types of ESDs are batteries, supercapacitor (SC), and fuel cells. Among these fuel cells are the clean and green energy sources, which use hydrogen (H₂) as a fuel. These fuel cells run on the basic principle of water (H₂O) splitting technology. Generally, rare earth metals like Platinum (Pt), Ruthenium (Ru), etc., are used as the electrocatalyst, among which Pt has the lowest possible overpotential ~ 42 mV, but these rare earth metals are expensive. Therefore, researchers worldwide are looking toward the transition metal-based composite. These composites play a vital role in green energy production. This work introduces the use of cobalt-iron (Co-Fe) based composite, which is further followed by the doping sulfur (S) and phosphorus (P) as highly efficient electrocatalyst. The electrocatalyst were synthesized using two facile synthesis routes in which they produce different morphology (nanoflowers and macroparticles). Nanoflowers are produced using the Co and Fe-based precursors via a solvothermal for a week at room temperature. While the macroparticle composite is prepared using a simple co-precipitation method. Their unique structure allows them to have more electroactive sites. Among nanoflowers, the best sample of P-Co-Fe showed an oxygen evolution overpotential of 340 mV at 10 mA/cm² with a Tafel slope of 48 mV/dec along with the hydrogen evolution overpotential of 46 mV to deliver 10 mA/cm². On the other hand, the macroparticle's best sample of P-Co-Fe shows the oxygen evolution overpotential of 330 mV at 10 mA/cm² with a Tafel slope of 63 mV/dec along with the hydrogen evolution overpotential of 61 mV to reach 10 mA/cm². The stability of the prepared electrocatalysts was tested using cyclic linear voltammetry and chronoamperometry. Both the measurements showed high electrocatalytic stability of the prepared samples for over 1,000 cycles of linear voltammetry and 24 hrs of chronoamperometry test. Our research provides a cost-effective and highly efficient electrocatalyst for green energy production.

SYMPOSIUM EN08

Scientific Basis for Nuclear Waste Management
November 28 - December 6, 2022

Symposium Organizers

Claire Corkhill, University of Sheffield
Stephane Gin, CEA Valrho
Josef Matyas, Pacific Northwest National Laboratory
Stefan Neumeier, Forschungszentrum Juelich GmbH

* Invited Paper
+ Distinguished Invited

SESSION EN08.01: Effect of Radiation on Materials
Session Chairs: Tobias Beirau and Mohamed Ruwaid Rafiuddin
Monday Morning, November 28, 2022
Hynes, Level 3, Room 300

11:00 AM EN08.01.02

Radiation damaged zircon and pyrochlore: Mechanical properties and percolation transitions Tobias Beirau¹, Norbert Huber^{2,3}, Edoardo M. Rossi⁴, Marco Sebastiani⁵, Michael Carpenter⁶, Warren Oliver⁶ and Rodney Ewing^{7,8}; ¹Martin Luther University of Halle-Wittenberg, Germany; ²Helmholtz-Zentrum Hereon, Germany; ³Hamburg University of Technology, Germany; ⁴“Roma TRE” University, Italy; ⁵University of Cambridge, United Kingdom; ⁶KLA-Tencor, United States; ⁷Stanford University, United States

Materials with pyrochlore structure ($A_2B_2O_7$), as well as zircon ($ZrSiO_4$) have been proposed as ceramic host phases for the long-term disposal of nuclear waste (especially for actinides, e.g., uranium and plutonium). The decay of incorporated actinides leads to damage in the initially ordered structure. The goal is to better understand the effects of the resulting radiation-damage related structural amorphization and subsequent thermal annealing induced recrystallization on the mechanical properties. The results of modelling [1,2], as well as of experimental work on zircon and pyrochlore, obtained by nanoindentation (CSM and -micro-pillar splitting) and resonant ultrasound spectroscopy [3,4], will be presented to provide a comprehensive picture. Variations in, e.g., elastic modulus (E), hardness (H), and fracture toughness (K_{IC}) have been detected. Percolation theory has found to be appropriate to describe the mainly by alpha-decay induced crystalline-to-amorphous transition. While E and H of pyrochlore and zircon have found to decrease due to radiation-damage, zircon shows an increase in K_{IC} and strong interface effects with increasing amorphous fraction. The recrystallization process in pyrochlore is accompanied by changes in elastic properties and initial heating leads to elastic softening. Zircon and pyrochlore provide useful models for the development of complex ceramics that can be used in high radiation fields.

This research was funded by the Deutsche Forschungsgemeinschaft (DFG, German Research Foundation), No. BE 5456/2-1 (T.B.).

[1] Beirau, T. and Huber, N. (2021) Applied Physics Letters, 119, 131905.

[2] Huber, N. and Beirau, T. (2021) Scripta Materialia, 197, 113789.

[3] Beirau, T., Rossi, E., Sebastiani, M., Oliver, W.C., Pöllmann, H. and Ewing, R.C. (2021) Applied Physics Letters, 119, 231903.

[4] Beirau, T. and Carpenter, M. (2022) Applied Physics Letters, 120, 231901.

11:15 AM EN08.01.03

In Situ Ion Irradiation of Rhabdophane- and Churchite-Type Hydrated Rare-Earth Phosphates Mohamed Ruwaid Rafiuddin; University Of Huddersfield, United Kingdom

Rare-earth phosphates adopting the monazite ($REPO_4$, RE = La to Gd) and xenotime ($REPO_4$, RE = Tb to Lu and Y) structures are proposed as one of the candidate matrices for nuclear waste immobilization applications. Several studies focussing on the effect of radiation and corrosion on the structure of monazite and xenotime materials have been reported in the literature. To the best of our knowledge, the effect of radiation on the structure of metastable polymorphs (rhabdophane – $REPO_4 \cdot H_2O$ (RE = La to Dy) and churchite- $REPO_4 \cdot 2H_2O$ (RE = Gd to Lu and Y)) of the rare-earth phosphate family haven't been reported in the literature. Rhabdophane and churchite phases are proposed as an actinide-solubility controlling phase and is expected to precipitate on the surface of monazite and xenotime materials upon aqueous corrosion of the latter. In the current study, the effect of radiation on rhabdophane ($SmPO_4 \cdot H_2O$, $DyPO_4 \cdot H_2O$) and churchite ($YPO_4 \cdot 2H_2O$, $DyPO_4 \cdot 2H_2O$) materials was studied by irradiating these materials with 650 keV Xe^{2+} ions under in-situ conditions and the structural response were monitored using in-situ TEM (MIAMI facility, University of Huddersfield). Phase-pure rhabdophane and churchite materials were synthesized using wet-chemistry methods at $\sim 25^\circ C - 50^\circ C$. Upon irradiation, these materials transform to the amorphous state at much lower ion-fluences in comparison to their anhydrous counterparts. Amorphous rhabdophane and churchite materials were found to be very sensitive to the electron beam and quickly reverts back to their original crystalline state upon electron beam exposure.

11:30 AM EN08.01.04

Effect of Irradiation on the Aging of Hydrated Gels Obtained from Simplified Borosilicate Glasses Amreen Jan and N M Anoop Krishnan; Indian Institute of Technology Delhi, India

Confinement of radionuclides in borosilicate glass matrix is subject to the durability of vitrified nuclear waste glass in the aqueous medium on the geological time scales under repository conditions. It is now well accepted that under the aqueous condition there is a formation of a hydrated gel layer which is expected to play a significant role. However, the properties of this gel layer are not well understood yet. In this work hydrated gels are obtained from a series of pristine and irradiated borosilicate glasses. These gels are then aged at a temperature, of 2000K. It is observed that, indeed, there is a difference in the properties (connectivity, short and medium-range order) of aged gels formed from pristine and irradiated glass. Aging had a significant effect on the irradiated gels as compared to gels obtained from pristine glasses. Further, the role of medium-range order on the mobility of water is studied and it is observed how different ring distributions (pristine and irradiated) upon aging manifest similarly. mean rings size decrease in pristine gel and its

increase in irradiated gel leads to a decrease in mobility of water across the gel upon aging.

11:45 AM EN08.01.05

Radionuclide Distribution in Irradiated BWR Tie Plate Tomofumi Sakuragi¹, Yuki Nakai², Syuji Yamamoto², Naoto Kume², Tsukasa Sugita², Yu Yamashita² and Hiroyoshi Ueda¹; ¹Radioactive Waste Management Funding and Research Center, Japan; ²Toshiba Energy Systems & Solutions Corporation, Japan

After the fuel reprocessing, the metallic components of spent nuclear fuel assembly including hulls and end pieces are projected to be disposed of in deep underground repositories owing to their high activation and strong contamination. Regarding the current post-closure safety case, the corrosion-related congruent release is assumed as a source term for this nuclear waste where the radionuclides are considered to be homogeneously distributed in the metal matrix. Therefore, the radionuclides distribution is a key factor affecting the leaching behavior especially for end pieces because the change in neutron flux is significant at the fuel edges.

This study investigates the radionuclide content and distribution for a lower tie plate (i.e. bottom end piece of BWR fuel) irradiated with burnup of 35.0 GWd/tHM using the imaging plate (IP) method. The detailed burnup conditions were obtained for the activation calculation by Monte Carlo burnup calculation code (MCNP-BURN2). The contents for ¹⁴C and ⁶⁰Co were obtained by liquid scintillation counting and Ge spectrometry, respectively. The experimental conditions of IP measurement (e.g. exposure time) were set based on those radioactivities. The result of IP method showed that the photostimulated luminescence (PSL) intensity decreased as greater the distance away from near fuel to downward. This trend is in good agreement with the MCNP-BURN2 activation analysis.

This study was carried out as a part of R&D supporting program titled “Advanced technology development for geological disposal of TRU waste (2021 FY)” under the contract with Ministry of Economy, Trade and Industry (METI) (Grant Number: JPJ007597).

This study was carried out as a part of R&D supporting program titled “Advanced technology development for geological disposal of TRU waste (2021 FY)” under the contract with Ministry of Economy, Trade and Industry (METI) (Grant Number: JPJ007597).

SESSION EN08.02: Efficient Capture of Radionuclides
Session Chairs: Kyle Brinkman and Amy Welty
Monday Afternoon, November 28, 2022
Hynes, Level 3, Room 300

1:30 PM *EN08.02.01

Sorbents for Capture of Krypton, and Xenon from Used Nuclear Fuel Off-Gas Streams Amy K. Welty, Meghan S. Fujimoto, Mitchell Greenhalgh and Troy Garn; Idaho National Laboratory, United States

Volatile radionuclides from used nuclear fuel reprocessing (UNF) present significant technical and environmental challenges. Species properties coupled with low concentrations make separation and capture difficult and potentially cost prohibitive. Idaho National Laboratory has spent significant effort developing materials and strategies for the separation and capture of krypton and xenon from UNF off-gas. Tailoring sorbent materials to the harsh conditions of UNF off-gas stream, coupled with rigorous testing designed to challenge material integrity and capability is ongoing. The work is focused on bridging the gap between the fundamental material science and the practical application of those sorbents.

2:00 PM EN08.02.02

Computation-Based Optimization of Functionalized Ni(PyC)2 for Xe and Kr Separation Minbum Kim¹, Alexander Robinson¹, Praveen Thallapally¹, Cory Simon² and Sun Hae Ra Shin¹; ¹PNNL, United States; ²Oregon State University, United States

Known as a next-generation adsorbent, metal-organic frameworks (MOFs) are a promising material for noble gas separation and capture. The Ni(PyC)₂ with a highly Xe/Kr selectivity has optimal pore size and structure for Xe/Kr separation. We synthesized a new Ni(PyC-*m*-NH₂)₂ by appending a functional group to the PyC ligand to increase the Xe/Kr separation selectivity. It showed that the Xe adsorption uptakes increased at low pressure due to the high polarizability of amine group, which indicated that Ni(PyC-*m*-NH₂)₂ (20) has a higher IAST selectivity for Xe/Kr separation than Ni(PyC)₂ (17). The Xe, Kr and Ar adsorption uptakes and selectivities of Ni(PyC-*m*-NH₂)₂ were predicted through simulation, and the simulation results were consistent with the trend of single-component isotherms results. The breakthrough experiment results indicated that the Ni(PyC-*m*-NH₂)₂ showed a higher Xe/Kr separation performance than pristine Ni(PyC)₂ under dynamic flow conditions. These results suggested that Ni(PyC-*m*-NH₂)₂ is a promising adsorbent for Xe/Kr adsorptive gas separation process.

2:15 PM *EN08.02.03

Nanostructured Ceramic Membranes for Hydrogen Isotope Processing Kyle S. Brinkman¹, Jun Gao¹, Yuqing Meng¹, Jianhua Tong¹, James Bechel² and Jake Amoroso²; ¹Clemson University, United States; ²Savannah River National Laboratory, United States

This work explores the use of interfacial hydrated layers in ionic conducting ceramic materials for tritiated water (HTO) adsorption and recovery. Low-temperature water adsorption properties of nanoscale structured ceramics combined with hydrogen isotope exchange in their hydrated layers may provide a low-cost and transformative avenue to address tritium management challenges. Two categories of materials were explored including i) simple oxides (TiO₂), ii) perovskite phases based on zirconates (BaZr_{0.8}Y_{0.2}O_{3-δ} (BZY20), BaCe_{0.7}Zr_{0.1}Y_{0.1}Yb_{0.1}O_{3-δ} (BCZYYb)). Nanostructured membranes were fabricated through multiple sintering methods to investigate the absorption, mobility, and isotope exchange effect. The increased conductivity of nanostructured TiO₂ membrane in the wet atmosphere and its polarization behavior confirm the existence of the proton conductivity in the nanoscale TiO₂ membrane at low temperatures (< 250°C). The difference of proton conductivity in H₂O and D₂O reveals the hopping mechanism of the proton conduction. In addition, the thermo-gravimetric analysis reveals strong water uptake below 250°C resulting in high proton conductivity at low temperatures. Control of interfacial proton conductivity was demonstrated by changing the grain size and porosity of the nanostructured membrane. Furthermore, in-situ Raman and electrical conductivity relaxation techniques were used to quantify isotope exchange rates as a function of temperature. Modeling and process level economic analysis was performed using extrapolation of data from H/D systems, and associated separation factors to understand the potential for tritium absorption and recovery.

References:

J. Gao, Y. Meng, J. H. Duffy, K. S. Brinkman. "Low-Temperature Protonic Ceramic Fuel Cells through Interfacial Engineering of Nanocrystalline BaCe_{0.7}Zr_{0.1}Y_{0.1}Yb_{0.1}O_{3-δ}Electrolytes" *Advanced Energy and Sustainability Research* (2021):2100098
J. Gao, Y. Meng, A. Benton, J. He, L.G. Jacobsohn, J. Tong, K.S. Brinkman. "Insights into the Proton Transport Mechanism in TiO₂ Simple Oxides by In Situ Raman Spectroscopy." *ACS Applied Materials & Interfaces* 12.34 (2020): 38012-38018.

2:45 PM BREAK

3:15 PM EN08.02.04

Adsorption of Uranyl Ions by a Zr-Based Metal-Organic Framework by Density Functional Theory Yuan Liu¹, An Ta¹, Shubham Pandey^{1,2}, Shenyang Hu³, Natalia Shustova⁴ and Simon Phillpot¹; ¹University of Florida, United States; ²Colorado School of Mines, United States; ³Pacific Northwest National Laboratory, United States; ⁴University of South Carolina, United States

Zr-based metal-organic frameworks (Zr-MOFs) have been widely used as ion absorbents for the removal or extraction of toxic and/or radionuclide species from aqueous solutions. However, the mechanisms by which uranyl ions interact with the Zr-MOFs have not been established. Here, the nature of the bonding of a uranyl ion (UO₂²⁺) with a Zr-MOF was determined using density functional theory for nineteen structurally distinct candidate complexes. The results showed that the uranyl ions bond to Zr-MOF with binding energies of the order of 1.5 eV. In the energetically most favorable structure, this strong adsorption is achieved by the formation of bonds between the uranyl ion with one middle oxygen and one edge oxygen in the Zr-MOF metal node. It was also found that the higher the degree of deprotonation of Zr-MOF, the higher the binding energy between Zr-MOF and uranyl ions. This work was supported by the Center for Hierarchical Waste Form Materials (CHWM), an Energy Frontier Research Center (EFRC) funded by the United States Department of Energy Office of Basic Energy Sciences through Award DESC0016574.

3:30 PM EN08.02.05

Cesium Capture via Cationic Faujasite Zeolite An Ta¹, Aoub Daouli², Vanessa Proust³, Agnes Grandjean³, Michael Badawi² and Simon R. Phillpot¹; ¹University of Florida, United States; ²University de Lorraine, France; ³The French Alternative Energies and Atomic Energy Commission (CEA), France

Due to its high aqueous mobility and a half-life of thirty years, Cs¹³⁷ is a primary target for ionic capture during long-term storage of used nuclear fuel. Zeolitic faujasite materials have been demonstrated to be promising candidates for the industrial application of Cs⁺ capture because of their low cost and relatively high stability under radioactive conditions. However, while faujasites have the capability of possessing various cationic species, their relative Cs⁺ ionic exchange performances are yet to be fully established. Here, plane-wave density functional theory calculations are used to thermodynamically survey Cs⁺ exchange with several monovalent cations and assess differences between cationic and acidic faujasite zeolites. The effects of differing alkaline metals and selected transition metals on cationic exchange will be discussed while favorable adsorption sites in HY-2.5 faujasite will also be identified. This work was supported by the Center for Hierarchical Waste Form Materials (CHWM), an Energy Frontier Research Center (EFRC) funded by the United States Department of Energy Office of Basic Energy Sciences through Award DESC0016574.

3:45 PM EN08.02.06

In Situ Powder X-Ray Diffraction Studies of Cs-Exchange in the Zeolite Chabazite Dan Parsons¹, Antony Nearchou² and Joseph Hriljac^{1,2}; ¹Diamond Light Source, United Kingdom; ²University of Birmingham, United Kingdom

The sequestration of relatively long-lived radionuclides such as ¹³⁷Cs (*t*_{1/2} = 30.2 years) from aqueous nuclear waste streams, or from aqueous environments contaminated with nuclear waste, is significant in nuclear waste management. A favoured option for the removal of radioactive cations are zeolites: porous crystalline aluminosilicates adopting framework structures comprising corner-shared [SiO₄] and [AlO₄] tetrahedra, with exchangeable cations occupying the hydrated pores and cages of the framework. Chabazite is a particular zeolite that is efficacious in the selective removal of aqueous Cs⁺ by ion exchange and has been applied in decontamination efforts at Fukushima.^[1] The crystallographic positions occupied by extraframework cations, such as Na, K and Cs, within the chabazite crystal structure are well established when the material contains exclusively one type of cation;^{[2][3]} however, the mechanism by which ion exchange occurs in these materials has not been previously probed despite the inherent advantages to enhancing the understanding of this process.

In this study, powder X-ray diffraction (PXRD) patterns have been collected, on beamline I11 at the Diamond Light Source synchrotron, on chabazite samples as ion exchange occurs, facilitated by a liquid flow cell which elutes a dilute Cs-containing solution through the chabazite sample as data is recorded *in situ*. Cs-ion exchange has been studied for two chabazite samples, one containing sodium (Na-CHA) and the other potassium (K-CHA). Through applying Rietveld refinement to the *in-situ* PXRD datasets, time-resolved structural changes are observed as the constitution of extraframework cations changes within the zeolite, providing a mechanistic understanding of how Cs-ion exchange occurs in these materials.

References

- [1] T. Tsukada, K. Uozumi, T. Hijikata, T. Koyama, K. Ishikawa, S. Ono, S. Suzuki, M. S. Denton, R. Keenan and G. Bonhomme, *J. Nucl. Sci. Technol.*, 2014, **51**, 886 – 893. (n.b. 'chabazite' is referred to by the less common term 'herschelite' in this publication)
- [2] M. Calligaris, A. Mezzetti, G. Nardin and L. Randaccio, *Zeolites*, 1986, **6**, 137 – 141.
- [3] A. Alberti, E. Galli, G. Vezzalini, E. Passaglia and P. F. Zanazzi, *Zeolites*, 1982, **2**, 303 – 309.
- [4] A. J. Celestian and A. Clearfield, *J. Mat. Chem.*, 2007, **17**, 4839 – 4842.

4:00 PM EN08.02.07

In Situ X-Ray Absorption Spectroscopy and Electrochemistry Measurements of Corrosion in Molten Fluoride Salt Boris Khaykovich¹, Guiqiu Zheng¹, David Sprouster², Sean Fayfar¹, Matthew Marshall³, Eli Stavitski⁴ and Denis Leshchev⁴; ¹MIT, United States; ²Stony Brook University, The State University of New York, United States; ³RMD, United States; ⁴Brookhaven National Laboratory, United States

Molten-salt reactors (MSR) are proposed advanced nuclear reactors that utilize molten salts for cooling and solvents for fissile material. Molten salts with dissolved nuclear fuel and fission and corrosion products present challenges due to their corrosive nature, and as such, interactions between the salts and the materials they interface with need to be understood. We are developing new *in-situ* analytical techniques for molten-salt characterization and monitoring, especially near the interfaces between alloys and molten salts. Here, we present our examination of the corrosion of NiCr foils in molten LiF-NaF-KF eutectic (FLiNaK) using a combination of x-ray absorption spectroscopy (XAS) and electrochemistry. We distinguished the oxidation state and coordination numbers of dissolved Ni and Cr, as well as the spatial and temporal distribution of the ions in the solution. We also describe reactions at the electrodes.

4:15 PM EN08.03.01

Structural Characterisation of Advanced Cr & Mn Doped UO₂ Fuels Using X-Ray Absorption Spectroscopy Hannah Smith¹, Luke T. Townsend¹, Ritesh Mohun¹, Theo Cordara¹, Martin Stennett¹, J. Frederick W. Mosselmans², Kristina Kvashnina^{3,4} and Claire L. Corkhill¹; ¹University of Sheffield, United States; ²Diamond Light Source, United Kingdom; ³Helmholtz-Zentrum Dresden-Rossendorf, Germany; ⁴European Synchrotron Radiation Facility, France

Advancements in UO₂ fuel technology are key in the generation of safe and efficient nuclear energy. The doping of UO₂ with transition metals, such as Cr and Mn, provides a method for improving properties, such as increased grain size, improved plasticity, and reduced pellet-cladding interactions. All these enhanced properties result in more accident tolerant and efficient fuels. Despite the implementation of Cr and Mn-doped UO₂ technology within the nuclear industry, there is a lack of fundamental understanding surrounding the local Cr/Mn coordination environment upon incorporation into the UO₂ matrix. Furthermore, the mechanisms by which Cr/Mn are accommodated within the UO₂ lattice are not well established. Here, a variety of spectroscopic techniques, including X-ray absorption spectroscopy (XANES, EXAFS, and HERFD-XANES) and Raman spectroscopy, provide significant insight into mechanisms behind the incorporation of Cr/Mn upon incorporation into the UO₂ structure. In the Mn-doped UO₂ system, Mn²⁺ is substituted onto the U⁴⁺ site, with vacancies and U⁵⁺ forming to maintain charge balance. A similar incorporation mechanism is observed in the Cr-doped UO₂ however, the UO₂ matrix accommodates Cr as a Cr²⁺ on the U⁴⁺ site. Following further heat treatment (to simulate nuclear fuel synthesis), Cr is present as several different species (including, Cr²⁺ and Cr³⁺) in a variety of locations within the UO₂ fuel. The findings of these studies provide significant new insight into the fundamental chemistry behind doped UO₂ fuels and offer new opportunities for advanced nuclear fuels to be further developed and implemented within the nuclear industry.

4:30 PM EN08.03.02

Single Crystal Spectroscopic Studies of Cr doped UO₂—Resolving the Cr Valence and Chemical State of Cr in Chromia Doped Nuclear Fuels Gabriel Murphy¹, Philip Kegler¹, Kristina Kvashnina², Nina Huittinen³ and Sara Gilson³; ¹FZ Juelich, Germany; ²European Synchrotron Radiation Facility, France; ³Helmholtz-Zentrum Dresden-Rossendorf, Germany

As a part of modern nuclear fuels, the use of transition metal elements as dopants, such as Cr, has been shown to increase the in-reactor fuel performance over traditional non-doped variants. The small size of the Cr cation relative to the U⁴⁺ cation results in a low solubility of Cr into UO₂ of approximately 750-1000 ppm depending on the oxygen potential, where higher oxygen potential leads to improved solubility of Cr [1]. Despite this and other advances in the science behind Cr doped UO₂ modern nuclear fuels, significant paucities of information remain such as even the mechanism for incorporation. Pertinently prior to this investigation, there is no definitive conclusion as to the valence state and local environment of Cr within the fuel matrix [2],[3]. Notwithstanding this, we have managed to fabricate Cr single crystals and have studied these using a combination of single crystal X-ray diffraction, electron paramagnetic resonance (EPR) and X-ray absorption spectroscopy (HERFD-XAS/EXAFS). Accordingly, we provide conclusive resolved measurements of the Cr chemical states within the UO₂ matrix, assigning both valence and local structure behaviour. We have further systematically examined the incorporation of Cr doping above and below the solubility limit, providing detailed observation of changes to the lattice parameters and microstructure via synchrotron X-ray powder diffraction measurements and electron microscopy respectively. The results of this investigation will be discussed in detail in linking the local atomic behaviour of Cr in UO₂ to microstructure behaviour in addition to the relevance they have to both modern fuels and spent nuclear fuel disposal.

1. Kegler, P., et al., *Chromium Doped UO₂-Based Ceramics: Synthesis and Characterization of Model Materials for Modern Nuclear Fuels*. Materials, 2021. **14**(20): p. 6160.
2. Cooper, M.W.D., C.R. Stanek, and D.A. Andersson, *The role of dopant charge state on defect chemistry and grain growth of doped UO₂*. Acta Materialia, 2018. **150**: p. 403-413.
3. Sun, M., J. Stackhouse, and P.M. Kowalski, *The + 2 oxidation state of Cr incorporated into the crystal lattice of UO₂*. Communications Materials, 2020. **1**(1): p. 1-8.

4:45 PM EN08.03.03

Rheological Behaviour of Bituminized Waste Products Benoit Dussault, Arnaud Leclerc, Charles Brissot, Antoine Marchal, Jean Baptiste Champenois and Arnaud Poulesquen; CEA Marcoule, France

Bitumen is used since the sixties as confinement matrix of radioactive wastes. The behavior of these bituminized waste products (BWPs) under thermal stress, under ionizing radiation or under leaching conditions has to be assessed. Especially, the determination of the rheological behavior is of primary importance due to its impact on a lot of mechanisms such as the convection, the sedimentation or the migration of gas bubbles generated under irradiation. BWP are elaborated by twin screw extrusion and are mainly composed of 40% in weight of various inorganic salts presenting a spread granulometry, and of 60% in weight of 70/100 pur bitumen. BWPs are thus considered as a non brownian dispersion of salts suspended in a viscoelastic matrix highly thermodependant. Pur bitumen and model BWPs, containing various volume fraction of salts, were synthesized and characterized rheologically as a function of the temperature by using different rheological sequences (creep, flow curve and shear rate step). The results show that the pure bitumen is a newtonian fluid (in the range of 20-200°C) with a strong dependance with the temperature. On the other hand, the BWPs (with the higher load of salts) behave as a yield stress fluid that could be describe by a Herschel Bulkley model. The yield stress depends not only on the volume fraction of salts but also on the temperature as a power law. We will show that this yield stress is related to the adhesion force between the salts and by normalizing the stress by the yield stress, the relative viscosity can be scaled onto a single master curve. Finally, we will illustrate through some examples, that these rheological properties may induce some particular behavior in the flow of the materials under thermal sollicitation but also on the migration and on the bubble size distribution in the case of irradiated BWPs.

5:00 PM EN08.03.04

Investigating the Effect of Fe₂O₃ on the Zirconolite Phase Assemblage Merve Kuman, Laura J. Gardner, Lewis Blackburn, Martin Stennett, Russell Hand and Claire L. Corkhill; University of Sheffield, United Kingdom

The UK has one of the world's largest inventory of civil separated plutonium (PuO₂). There are two potential Pu management strategies being investigated in the UK. One option is re-use within mixed oxide fuel (which is the current UK policy) or alternatively, immobilisation in a ceramic or glass host matrix. The latter could be an option for contaminated PuO₂ stocks (e.g. chlorine contamination) that could be unsuitable for MOX fabrication or a larger portion

of the inventory if deemed necessary [1].

In this study, the efficacy of Fe_2O_3 as a cation charge compensator within zirconolite was investigated, with particular focus on the phase assemblage and microstructure (without the presence of Pu or a surrogate in order to isolate the effect of Fe^{3+} on the zirconolite structure). The Fe-doped zirconolite ceramic structures were fabricated via cold press and sintering method. The conceptual ceramic wasteforms were analyzed via X-ray diffraction (XRD) and Scanning Electron Microscopy/ Energy Dispersive X-ray Spectroscopy (SEM/EDX) methods. Rietveld refinement was performed to determine the effect of Fe^{3+} incorporation on the unit cell parameters of the zirconolite matrix, whilst Mössbauer spectroscopy and X-ray absorption near edge spectroscopy (XANES) data revealed the coordination environment and oxidation state of Fe substitution in which Ti site into the structure. As a result, XRD revealed the phase transformation from zirconolite-2M to -3T, with the increase of Fe concentration and there was an increase in the occurrence of secondary phases, mainly perovskite. The successful incorporation of the charge compensator cation into the zirconolite structure was proved with the change of unit cell parameters, associating with the reduction in volume, and SEM/EDX micrograph. XANES analysis showed that Fe was uniformly present in the Fe^{3+} oxidation state in octahedral coordination.

[1] N.C. Hyatt, Safe management of the UK separated plutonium inventory: a challenge of materials degradation, *npj Materials Degradation* 4(28) (2020).

SESSION EN08.04: Poster Session
Session Chairs: Daniel Gregg and Josef Matyas
Monday Afternoon, November 28, 2022
8:00 PM - 10:00 PM
Hynes, Level 1, Hall A

EN08.04.01

Caustic Scrubber Waste Converted to Aluminosilicates—Structures Determined by Nuclear Magnetic Resonance [John S. McCloy](#), Nick Stone-Weiss and David Bollinger; Washington State University, United States

Several options are proposed for reprocessing of used nuclear fuel from power stations. One possibility is aqueous reprocessing of oxide fuel, which will result in some off-gas of fission products including ^{129}I and ^{14}C , which should be captured and immobilized. Of the four volatile radionuclides that are restricted by the release limits governed by the US regulations (^3H , ^{14}C , ^{85}Kr , and ^{129}I), ^{129}I will require the greatest degree of abatement, whereas ^3H and ^{85}Kr have separate capture and immobilization pathways. Caustic scrubbers (CS) are proposed to be used before sorbent beds to capture radioiodine species. Dissolved anions from the CS are predicted to include I^- , Br^- , Cl^- , OH^- , CO_3^{2-} , NO_3^- , and NO_2^- . One path for immobilization of the high pH CS solutions is to react with kaolinite to form aluminosilicate powders, which can subsequently be consolidated by various means. These aluminosilicates are primarily sodalite phase with amorphous component and minor mixed phases like cancrinite or zeolite Na-P. In the current work, previously reported CS aluminosilicate powders are further characterized by ^{23}Na and ^{27}Al magic angle spinning nuclear magnetic resonance (MAS NMR). These measurements shed light on the structure of crystalline and amorphous species previously identified by X-ray diffraction. The chemical environments probed by NMR are compared to various synthesized and natural standard materials, and ^{23}Na NMR in particular shows that many different chemical environments exist in what appears to be a mixed sodalite assemblage.

EN08.04.02

Simulating Distribution of Carbon in Spent Fuel Cladding of Zirconium Alloys [Teppei Otsuka](#)¹ and Tomofumi Sakuragi²; ¹Kindai University, Japan; ²Radioactive Waste Management Funding and Research Center, Japan

Spent fuel cladding made of zirconium (Zr) alloys would be mechanically compressed as cladding hulls in Japan. In view of waste disposal of the hulls, distribution of radioactive carbon-14 (C-14) produced in a Zr matrix is one of important factors to estimate release behavior of C-14 accompanied with oxidation of the Zr matrix [1]. Although C-14 should be distributed in the Zr cladding matrix by diffusion and precipitation under gradients of concentrations and temperatures during operation of nuclear reactors, it would be potentially relocated by isothermal annealing during a mid-term storage becoming longer before processing of the hulls.

In the present study, diffusion, solution and thermo-transport data for carbon (C) as well as hydrogen (H), nitrogen (N) and oxygen (O) in Zr have been revisited and diffusion data of C in oxygen dissolved Zr (Zr(O)) have been experimentally obtained. Using the transport parameters for C in Zr and Zr(O), distributions of C in the Zr matrix have been simulated under various temperature conditions and periods using numerical calculation of the one-dimensional diffusion equation.

To date, no data of heat of transport, Q^* , for C both in αZr and βZr have been available whereas those for N and O in βZr were reported as $Q^* = +0.925$ and $+1.090$, respectively [2]. Assuming Q^* for C in Zr is positive, initially uniform concentration of C in a wall thickness (0.5 mm) along a radial direction of the Zr cladding tube and diffusion of C for 3 years under the temperature gradient from 573 K to 773 K, C tends to segregate at the cooler side and deplete at the hotter side by thermo-transport but diffuse to the opposite direction with a driving force to minimize a concentration gradient, resulting in formation of a maximum concentration of C in a middle of the wall thickness at around 0.3 mm from the cooler side. Such the concentration non-uniformity disappears during isothermal annealing at 773 K for more than 10 years. In the presentation, effects of dissolved N and O on distribution of C in the Zr matrix will be discussed.

References

- [1] T. Sakuragi, Y. Yamashita, M. Akagi, R. Takahashi, Carbon 14 Distribution in Irradiated BWR Fuel Cladding and Released Carbon 14 after Aqueous Immersion of 6.5 Years, *Procedia Chemistry*, 21 (2016) 341-348.
- [2] Vogel, D. L., Thermotransport of oxygen and nitrogen in beta-zirconium, beta-titanium, niobium and tantalum, Technische Hogeschool Eindhoven (1969).

This study was carried out as a part of R&D supporting program titled “Advanced technology development for geological disposal of TRU waste (2021 FY)” under the contract with Ministry of Economy, Trade and Industry (METI) (Grant Number: JPJ007597).

EN08.04.04

Densification of Nuclear Waste Incinerator Ashes via Hot Isostatic Pressing [Sam Walling](#)¹, H el ene Nonnet² and Claire L. Corkhill¹; ¹University of

Sheffield, United Kingdom; ²CEA, France

The utilisation of Hot Isostatic Pressing (HIP) for the safe, efficient densification of loose simulant radioactive ashes has been investigated. As part of a multinational project looking at pre-disposal thermal treatment of organic material (PREDIS), the University of Sheffield is collaborating with CEA to determine the wastefrom characteristics of specific HIPed ashes.

These ashes arise from processing organic materials surrogates (simulating materials contaminated by α -emitting actinides) within the IRIS process (Installation for Research on Incineration of Solids) in France. It is a multi-step process able to treat high chloride containing wastes via a combined pyrolysis and calcination process. Simulant inactive ashes arising from the IRIS process are comprised of a calcium-zinc aluminosilicate rich material, with a very low level of residual carbon – making these ashes ideal candidates for HIP processing.

HIP trials were undertaken by hydraulically compacting IRIS ashes into stainless steel cans, with no additives or additional components, resulting in a 100 % waste loading. These cans were then processed at 1250 °C with a maximum pressure of 100 MPa. The resultant material was a densified, solidified wastefrom, safely contained within the stainless steel canister. Post-processing characterisation revealed the formation of a polycrystalline material consisting of anorthite, diopside, chlorapatite, leucite, and spinel. Wastefrom-can interactions were observed as a result of the thermal processing, leading to some internal can corrosion and a chromium rich altered wastefrom interface abutting the can wall.

These trials have demonstrated the suitability of HIP towards the processing of such ash materials, resulting in a solidified product with a substantially reduced volume. Though forming a solid product, substantial porosity remains within the final product, creating potential for wastefrom improvements. Further wastefrom optimisation is ongoing to investigate the impact of inclusion of glass forming additives to lower the wastefrom melting temperature and reduce wastefrom-can interactions, along with studies into the long-term aqueous durability of these materials.

EN08.04.05

Powder Processing for Hot-Isostatic Pressing of Nuclear Waste Einar B. Solomon^{1,2}, Ewan Maddrell² and Karl R. Whittle¹; ¹University of Liverpool, United Kingdom; ²National Nuclear Laboratory, United Kingdom

The UK at present holds a substantial stockpile of civilian-owned plutonium dioxide, which recently has been proposed to be predominantly reused as MOX fuel. However, a significant proportion will not be suitable for this use and will need to be immobilized, with the main focus being on ceramic immobilization, using a zirconolite-based system manufactured using hot isostatic pressing. Key to this work has been the reduction of secondary wastes, such as lubricants, which can have an impact on the final wastefrom, whilst at the same time optimize the final product formation. This presentation will examine the options for dry mixing, using lubricants that are both compatible with the process and the final zirconolite wastefrom. Results from analysis of the final products using techniques such as X-ray powder diffraction, electron microscopy, and relative density will be shown, indicating the success of the work in being able to use solid lubricants.

EN08.04.06

Excavation of the Prototype KBS-3 Repository to Begin in 2023 Fredrik Vahlund; SKB, Swedish Nuclear Fuel and Waste Management Co., Sweden

The Prototype Repository is a full-scale experiment in 450 meter-deep crystalline rock at Äspö Hard Rock Laboratory (Äspö HRL). The experiment was initiated in 2001 to simulate the KBS-3 concept developed in Sweden for the disposal of spent nuclear fuel. The experiment consists of four deposition holes, each containing a five meter-tall copper canister surrounded by an eight-tonne bentonite buffer. The canisters are equipped with heaters to simulate heat from the decay of spent nuclear fuel. The deposition holes are located within a 64 meter-long backfilled deposition tunnel.

In the experiment, more than 300 sensors have been installed so that i.e. temperature, pressure, humidity can be measured so that re-saturation and related processes like buffer swelling and homogenisation can be analysed under realistic conditions, including the prevalence of coupled processes and boundary effects, at a scale relevant for analysis of post-closure safety of a repository for spent nuclear fuel.

The experiment also demonstrates the installation and handling of equipment at an industrial scale. Experiences from installing this experiment enabled SKB to argue for the feasibility of constructing and operating a KBS-type repository in their license applications.

The Prototype Repository was planned to run for approximately 20 years, long enough for the buffer to resaturate, given the hydrologic conditions at Äspö HRL. The 20-year experiment timeframe also allows for results from the experiment to be considered in the future, operational license application for the KBS-3 repository.

Excavation of the Prototype Repository will start early 2023 and will continue for two years. During this time a large number samples will be taken to study i.e saturation, homogenisation, swelling and mineral transformation of the clay material, status of the canister, incidence of heat-induced spalling in the deposition hole, and other factors of relevance to post-closure safety.

SESSION EN08.05: Nuclear Waste Immobilization

Session Chairs: Daniel Gregg and Josef Matyas

Tuesday Morning, November 29, 2022

Hynes, Level 3, Room 300

8:15 AM *EN08.05.01

Synroc Technology Options for GEN IV Nuclear Reactor Wastes Daniel Gregg, Rohan Holmes, Lyndon Edwards and Gerry Triani; Australian Nuclear S&T Org, Australia

High feasibility solutions for the safe and responsible management of nuclear wastes generated from the deployment of new nuclear technologies are essential. With regards to public acceptance of new nuclear builds, concerns over the nuclear waste, particularly the intermediate (ILW) and high (HLW) level waste from spent fuel, fall second only to safety. In addition, nuclear regulators now require whole of life strategies which provide an ultimate nuclear waste disposition pathway as part of the approvals process for new nuclear facilities that produce ILW or HLW waste.

The advanced Gen IV reactors currently being commercially developed do not use standard LWR oxide fuel so the currently considered spent fuel storage and disposition options are unsuitable and bespoke waste treatment and disposal solutions are required. Synroc technology is uniquely suited to the treatment of many of these wastes as it employs hot-isostatic processing (HIPing) as a consolidation approach and allows the production of a range of wastefroms (ceramic, glass, and glass-ceramic forms) which can be tailored to the chemical, physical, and radiological properties of the target waste stream

allowing the phases that make up the wastefrom to be tailored to appropriately immobilise the different radioactive species.

This presentation will provide an update of the technical maturity of Synroc Technology for the treatment of nuclear wastes. It will also discuss concepts for candidate wasteforms and processing options for the immobilisation of wastes from advanced reactors, including iodine wastes, graphite-based wastes, advanced fuel wastes, and chloride- and fluoride-molten salt wastes.

8:45 AM EN08.05.02

Investigation of Iron Phosphate Glasses for the Immobilisation of Pyroprocessing Wastes [Daniel Bailey](#)¹, Laura J. Gardner¹, Martin Stennett¹, Mike Harrison², Neil Hyatt¹ and Claire L. Corkhill¹; ¹University of Sheffield, United Kingdom; ²National Nuclear Laboratory, United Kingdom

Potential future fuel cycles may produce used nuclear fuels (UNFs) that are incompatible with aqueous reprocessing routes such as PUREX or UREX. Consequently, alternative routes such as pyroprocessing have seen renewed interest. Pyroprocessing is an electrochemical process and uses a LiCl-KCl eutectic (LKE) to dissolve the UNF which is then refined by means of electrochemistry. U and Pu may be recovered but the salt becomes progressively enriched in fission products, reducing efficiency and necessitating regeneration or replacement of the eutectic. Waste streams with high LKE content are highly challenging due to their low solubility in glass and ceramic wasteforms, high temperature volatility and aqueous solubility. Iron phosphate glasses have been reported to have a relatively high tolerance to the incorporation of chloride. As such, this study presents conceptual iron phosphate glass wasteforms for the immobilisation of these high chloride wastes. These materials have been characterised by powder X-ray diffraction, scanning electron microscopy, X-ray absorption spectroscopy, Raman spectroscopy, Mössbauer spectroscopy and aqueous durability testing. Initial results indicate that these wasteforms possess useful properties and could contribute to a toolbox for the immobilisation of challenging pyroprocessing wastes.

9:00 AM EN08.05.03

Iron Phosphate Glass Waste Forms To Immobilize Salt Waste Stream [Ming Tang](#); Clemson University, United States

Glass waste forms are currently used to stabilize legacy high-level waste (HLW) materials, and glass is the baseline technology for treatment of HLW that would result from reprocessing commercial used nuclear fuel (UNF). Electrochemical reprocessing is one option for The United States Department of Energy (DOE) Office of Nuclear Energy (NE) to reprocess used nuclear fuel in advanced nuclear cycles. During electrochemical reprocessing, used nuclear fuel is dissolved in molten salt (e.g., LiCl-KCl eutectic). Due to the low solubilities (< 1.5 mass% for silicate-based glass) of the chloride/fluoride ions and evolution of Cl₂/F₂ gas from the melt under operation temperature, it is not suitable to employ the borosilicate glasses as the host for the full-salt waste streams. Phosphate glass, especially iron phosphate glass, exhibited promising properties as waste form candidates including good chemical durability; high solubility for many heavy metals (e.g., uranium, cesium, molybdenum), noble metals, and rare earths. However, there are few studies on iron phosphate glass waste forms to immobilize salt waste streams.

In this study, we intend to develop and optimize highly durable and easily processable iron phosphate glass waste form to immobilize the salt streams from advanced nuclear fuel cycle by tailoring the composition of the glasses at intermediate melting temperatures. A simulate salt recipe representing the salt waste stream in our study is 70LiCl-10Li₂O-20SrCl₂ which is based on previous DOE national laboratory reports. For the compositional variation study, different Fe:P ratio vs waste loading in iron phosphate glass waste forms are fabricated; various glass modifiers are added into iron phosphate glass compositions to improve chemical durability and reduce melting temperature. Further, thermal stability, chemical durability, radiation stability tests are performed on these iron phosphate glass and glass waste form samples. Specifically, DTA/TGA measurements are used to understand thermophysical and structure information of these glass waste forms. Monolithic leaching test is performed to study chemical durability of these glass waste forms. Ion beam radiation is used to simulate self-radiation in nuclear waste storage. Various characterization techniques (including XRD, SEM/EDS, TEM, Raman, X-ray CT) are used to characterize structural and chemical information. The study of composition-property-structure correlations of phosphate glasses is aimed to further optimize the waste forms by pushing the limit of salt loading while targeting high chemical durability and easily processing with present technologies. The preliminary result shows promising for iron phosphate glass waste form being an improvement over other candidate waste forms.

9:15 AM EN08.05.04

Scoping Studies of Wasteform Candidates for Li₂SO₄ Bearing Nuclear Waste Immobilisation [Rifat Farzana](#), Pranesh Dayal, Inna Karatchevtseva, Zaynab Aly, Phillip Sutton and Daniel Gregg; ANSTO, Australia

The secondary waste stream generated during Mo-99 production is challenging to immobilise due to the high concentrations of lithium (Li⁺) and sulphate ions (SO₄²⁻), its acidic nature and its activity content. Glass and glass-ceramic wasteforms were explored in the current work as candidates to maximise SO₄²⁻ incorporation, and to provide sufficiently high waste loadings and chemical durability. The base glass systems considered were barium borosilicate glasses with specific compositions selected for targeted phase formation. The highest sulphate incorporation of 2.78 wt.% SO₃ (from waste loading of 11 wt.% as Li₂SO₄) in the glass wasteform was achieved without crystallisation following melting at 1200 °C. An immiscible sulphate layer rich in BaSO₄ and Na₂SO₄ formed on top of the glass at lower temperature (800–1100 °C) and ~65% of the SO₃ was lost during high temperature consolidation. Therefore, tailored glass-ceramic options that can be prepared at lower temperatures with suitably high waste loadings were considered. Single/multi phase ceramics were observed within the glass matrix at 1000 °C with 14–18 wt.% waste loading. Glass and glass-ceramics wasteforms were studied *via* XRD, SEM-EDS, XRF, Raman and thermal analysis. The chemical durability was assessed using the ASTM C1285 Product Consistency Test (PCT) standard protocol and evaluated relative to accepted high-level nuclear waste glasses.

9:30 AM BREAK

10:00 AM EN08.05.05

Effective Immobilization of Iodine with Ag⁰-Aerogel—Different Matrices and Processing Conditions [Josef Matyas](#), Joshua A. Silverstein and Matthew Asmussen; Pacific Northwest National Laboratory, United States

One of the primary challenges for reprocessing of spent nuclear fuel, vitrification of nuclear waste, and development of advanced and innovative reactors and their nuclear fuel cycles is to immobilize iodine into durable and economically viable waste forms. These waste forms must meet criteria of high iodine loading, high chemical durability, and low processing costs. There has been significant progress made over the years with silver-functionalized silica aerogel (Ag⁰-aerogel) as a means for efficient removal and sequestration of iodine from various off-gas streams. The number of lab- and bench-scale consolidation tests with hot isostatic pressing and spark plasma sintering were demonstrated. Also included were other potential pathways such as incorporation of Ag⁰-aerogel into cement or low-temperature melting matrices. The presentation will focus on summarizing different strategies that have been developed to sequester iodine, discuss results from durability tests and conclude with a summary of highlights and a prognosis for future research.

10:15 AM EN08.05.06

Synthesis and Characterisation of Mixed Actinide Oxide Materials for Radioactive Waste Disposition [Claire L. Corkhill](#), Max Cole, Lewis Blackburn, Latham Haigh, Daniel Bailey, Malin C. Dixon Wilkins, Luke T. Townsend, Ritesh Mohun and Hannah Smith; University of Sheffield, United

Kingdom

In this study, we directly evidence the defect chemistry of mixed actinide oxide materials containing Gd^{3+} , within the context of understanding the basic fundamental chemistry of actinide waste immobilisation matrices. Materials were prepared by two different routes (dry mixing and oxalic wet precipitation) and characterised to quantify the incorporation rate and distribution of Gd within the actinide oxide matrix. The thermal treatment of the oxalic powders was refined to improve the uptake of Gd by the final material. Besides measuring the general characteristics of the final sintered materials, such as grain size, density and crystallographic parameters, the defect chemistry was determined using Raman spectroscopy and through analysis of $U M_4$ -edge X-ray absorption near edge spectra, collected in high energy resolved fluorescence detection mode (HERFD-XANES). These data revealed that, despite containing the same amount of Gd, the incorporation method between the two synthesis routes differed. Materials prepared *via* the wet co-precipitation route had defect bands typically associated with the formation of oxygen vacancies, and the HERFD-XANES data evidenced the presence of U^{5+} . Both observations are consistent with the charge-balance mechanism required when Gd^{3+} is incorporated on the actinide oxide lattice sites. Conversely, the materials prepared by the dry mixing route did not evidence the presence of U^{5+} , and the defect bands attributed to oxygen vacancies were significantly reduced.

10:30 AM EN08.05.07

Engineering Dual-Phase Zeolite Composites for Cs-137 and Sr-90 Immobilization [James Reed](#)¹, [Phoebe Allan](#)¹, [Joseph Hriljac](#)^{2,1} and [Thomas Carey](#)³; ¹University of Birmingham, United Kingdom; ²Diamond Light Source, United Kingdom; ³National Nuclear Laboratory, United Kingdom

The control over zeolite selectivity is crucial for numerous industrial applications, including catalysis, gas separation and ion-exchange. In the nuclear industry, natural zeolites are employed for the removal of caesium-137 and strontium-90 from aqueous nuclear decommissioning waste, via an ion-exchange process. However, sourcing a material capable of simultaneous dual-caesium and -strontium removal, such as Mud Hills clinoptilolite, which is currently employed at Sellafield, UK, is challenging. One documented method to improve the strontium affinity of natural mordenites (MOR) and clinoptilolites (HEU) is a structural transformation to a more aluminous Na-P (GIS) structure, achieved by means of a hydrothermal NaOH treatment. However, studies have generally used concentrated NaOH solutions (>2M), ensuring complete transformation into the GIS-type structure, with composite materials seen as undesirable. This work reports the generation of composite zeolites through the partial transformation of polycrystalline mordenite and clinoptilolite aggregates into Na-P, with high levels of chemical control. Subsequently, the ion-exchange performance for cesium and strontium uptake are assessed, granular materials developed and trialed in a rapid, flow system using active nucleotides. The mechanism of transformation and nature of granular composites are also investigated through use of state-of-the-art quasi-simultaneous imaging and diffraction techniques performed at the recently commissioned DIAD beamline, Diamond Light Source.

Four series of composite zeolites were generated through partial transformation of four naturally sourced zeolites, three clinoptilolites and a mordenite. This was achieved through a partial structure transformation into Na-P, where a high level of control is exhibited and a desired blend of zeolite phases can be obtained. Batch ion-exchange experiments highlighted an increase in strontium affinity as the transformation proceeds, at the expense of cesium selectivity. Composites with around an equal blend in phases showed a significant improvement in dual-uptake behavior. Granular composites, suitable for use in ion-exchange beds, were also developed by pre-sieving of the natural zeolite prior to treatment with NaOH. SEM images suggest particle size is retained in this process through crystallization of the new phase on the surface of existing particles. X-ray computed tomography and image-guided micro-diffraction show an 'outer shell' comprised of Na-P, with an intact mordenite interior. This is further confirmed by diffraction tomography data. Similar analysis suggests that fully converted Na-P granules consist of large, spherical sub-particles on the exterior and similar, smaller sub-particles on the interior. These findings suggest the macroscale mechanism to be one of surface dissolution-recrystallisation, resulting in an 'outer shell' encapsulating a partially dissolved interior. The base then penetrates the outer shell, dissolving the interior, which then recrystallizes into Na-P. Containment by the outer shell possibly aids this process by restricting diffusion of aluminosilicate nano-parts into the bulk solution and retaining the original granule morphology.

Rapid ion-exchange data of composites of around a 50:50 mixture of phases shows a remarkable improvement in Sr-90 uptake compared to the parent materials. The enhancement was to such an extent that composite materials exhibited superior Sr-90 affinity when compared to industry standard, Mud Hills clinoptilolite. Critically, this was not at the expense of Cs-137 uptake, which remained high. This work creates scope for a novel route to a host of potential resins from low-cost natural mineral sources, with the added opportunity to tune material compositions for a particular waste stream. Additionally, the potential of the newly commissioned DIAD beamline for advanced materials analysis is showcased.

10:45 AM EN08.05.08

Hot Isostatic Pressing—A Potential Thermal Treatment Process for Pu Immobilisation [Laura J. Gardner](#), [Merve Kuman](#), [Malin C. Dixon Wilkins](#), [Lewis Blackburn](#), [Amber R. Mason](#), [Martin Stennett](#), [Sarah Pepper](#) and [Claire L. Corkhill](#); University of Sheffield, United Kingdom

Hot Isostatic Pressing (HIPing) is a batch thermal treatment process where wastes are heated and compressed within a sealed container under controlled conditions. This results in consolidated high density wastefoms with minimal loss of volatile elements and easy accountability of active inventory [1]. In the UK, HIPing was highlighted as one of the credible options for plutonium immobilisation in the event that disposal is chosen as a management strategy [2]. To help inform the science underpinning larger-scale industrial applications of this technology, the University of Sheffield have a small-scale HIP facility capable of processing radiological simulant wastefoms using an active furnace isolation chamber (AFIC) [3]. The AFIC is designed to function within a conventional HIP set up and provides a novel opportunity in the UK to fabricate and characterise conceptual radioactive wastefoms and gain experience with radiological HIPing. It was under this remit that HIP wastefoms were fabricated as part of a broad research portfolio targeting zirconolite ($CaZrTi_2O_7$) as a single host ceramic wastefom. These trials investigated the bulk phase assemblage and HIP canister-ceramic interactions with a range of potential charge compensation cations (Al^{3+} , Fe^{3+} , Mg^{2+}). Comparison was made with wastefoms produced using typical sintering methods, for which, semi-dynamic static dissolution was performed to understand zirconolite durability. Overall, both HIPing and conventional sintering were determined to yield robust and durable zirconolite ceramic wastefoms across a range of compositions.

[1] M.W.A. Stewart, S.A. Moricca, T. Eddowes, Y. Zhang, E.R. Vance, G.R. Lumpkin, M.L. Carter, M. Dowson, M. James, The use of hot-isostatic pressing to process nuclear waste forms, Proceedings of the 2009 12th International Conference on Environmental Remediation and Radioactive Waste Management ICEM2009, Liverpool, UK, 2009, pp. ICEM2009-16253.

[2] Nuclear Decommissioning Authority, Progress on plutonium consolidation, storage and disposition 2019.

[3] S.A. Moricca, R. Persaud, Active Furnace Isolation Chamber, WO 2018/009782 A1, 2018. <!--![[endif]]---->

11:00 AM EN08.05.09

Solid Solubility in the $CeTi_2O_6$ – $CeTiNbO_6$ System—A Multi-Element Laboratory X-Ray Spectroscopic Study [Malin C. Dixon Wilkins](#)^{1,2}, [Lucy M. Mottram](#)¹, [Martin Stennett](#)¹, [John S. McCloy](#)² and [Claire L. Corkhill](#)¹; ¹The University of Sheffield, United Kingdom; ²Washington State University, United States

Following separation of Pu and/or the minor actinides from spent nuclear fuel, there are currently three possible routes of management: storage above ground (temporarily or indefinitely), reuse within nuclear reactors for further power generation (e.g. as MOX fuels or within inert matrix fuels), or disposal in a tailored wasteform material. Many studies have examined materials for the effective immobilisation of Pu, but the minor actinides have received comparatively little attention. Mineralogical brannerites and aeschynites have both been observed to have become metamict over time, yet samples still retain a significant fraction of their U/Th inventory, suggesting that both phases are significantly durable with respect to aqueous attack, even after partial or full amorphisation. The titanate family of synthetic brannerites includes the prototypical end-members CeTi_2O_6 , UTi_2O_6 , ThTi_2O_6 and PuTi_2O_6 , with only Ce-brannerite being non-radioactive. In this work the Ce-brannerite – Ce-aeschynite system has been examined (following an expected substitution of $\text{Ce}^{4+}_{1-x}\text{Ce}^{3+}_x\text{Ti}_{2-x}\text{Nb}_x\text{O}_6$, with $x = 0, 0.2, \dots, 0.8, 1.0$), with Ce acting as a surrogate for both $\text{Pu}^{3+}/\text{Pu}^{4+}$ and the trivalent minor actinides.

Materials were produced following a solid state route (starting from CeO_2 , TiO_2 , and Nb_2O_5), and reacted at 1350 °C for 48 hrs in an air atmosphere. Materials were analysed using XRD, SEM-EDX, and Raman spectroscopy. Ce L_{3-} edge and Nb K-edge XANES were collected using a laboratory X-ray spectrometer, and utilised to examine the Ce and Nb oxidation states, with further measurements planned at the Ti K-edge to examine the Ti coordination environment in these materials.

The system exhibits significant solid solubility towards the Ce-brannerite endmember, with no aeschynite observed until the target stoichiometry reached $\text{CeTi}_{1.4}\text{Nb}_{0.6}\text{O}_6$ ($x = 0.6$), where it was observed as a minor phase (approx. 7.5 wt.%). Preliminary XANES measurement at the Ce L_{3-} edge and Nb K-edge show that Nb is likely incorporated into the brannerite structure as Nb^{5+} , with an equivalent fraction of Ce^{4+} reduced to Ce^{3+} to retain charge balance. Rietveld refinements show that the Ce-brannerite structure expands significantly to accommodate the larger cations (Ce^{3+} , 1.15 Å; Ce^{4+} , 1.01 Å; Nb^{5+} , 0.78 Å; Ti^{4+} , 0.745 Å), with changes in the unit cell volume of up to approx. 5.5% with increasing Nb substitution. This work further expands the crystal chemistry of the brannerite structure, with significant structural flexibility displayed by the incorporation of up to 0.4 f.u. $\text{Nb}^{5+}/\text{Ce}^{3+}$ (i.e. $\text{Ce}^{3.6+}\text{Ti}_{1.6}\text{Nb}_{0.4}\text{O}_6$).

SESSION EN08.06: Safeguards
Session Chairs: Nicolas Clavier and Josef Matyas
Tuesday Morning, November 29, 2022
Hynes, Level 3, Room 300

11:15 AM *EN08.06.01

Particulate Reference Materials for Nuclear Safeguards—from Hydrothermal Synthesis to Shelf-Life Study Pierre Asplanato^{1,2}, Wassima Zannouh², Anne-Laure Faure¹, Nicolas Dacheux², Fabien Pointurier¹ and Nicolas Clavier²; ¹Commissariat à l'énergie atomique et aux énergies alternatives, France; ²ICSM, France

Particle analyses are a key tool for safeguards verification by the International Atomic Energy Agency (IAEA). They mainly consist in measuring the isotopic composition of individual sub-micrometric particles of nuclear materials. Indeed, despite confinement precautions, nuclear processes may release nanometer to micrometer-sized particles inside the facility. Detection and measurement of the isotopic composition of these particles provide precious information on the activities implemented in the facility, for example by assessing the enrichment rate of a fuel through the $^{235}\text{U}/^{238}\text{U}$ ratio, or the date of the last chemical purification thanks to the $^{230}\text{Th}/^{234}\text{U}$ radio-chronometer. For this purpose, analytical methods based on mass spectrometry techniques, such as Thermo-Ionization Mass Spectrometry (TIMS) and Large Geometry Secondary Ion Mass Spectrometry (LG-SIMS) have been developed and are nowadays applied by a few specialized laboratories in support of the IAEA's nuclear safeguards program. However, because of the low number and extremely small size of the particles of interest, such measurements are always an analytical challenge. Hence, laboratories need reference materials representative of the samples analyzed, i.e. actinide oxide particles with well-known sizes, densities and isotopic compositions, for optimization and qualification of analytical methods and instruments.

Therefore, the synthesis of actinide oxide particles is a field of growing interest. Several production methods based on physical processes were developed, but frequently required specific equipment and cannot be easily implemented in standard nuclear chemistry labs. In this frame, we developed since several years original wet chemistry routes, which aim at precipitating directly morphology-controlled actinide oxides from mixtures of solutions. Such methods are mostly based on the hydrothermal decomposition of An(IV) carboxylate, followed by the hydrolysis of the cations which leads to the formation of amorphous $\text{An}(\text{OH})_4$ samples, finally aging to $\text{AnO}_2 \cdot n\text{H}_2\text{O}$.

The first part of this presentation will cover the multi-parametric studies undertaken to monitor the morphology and the size of UOx and mixed (U,Th)Ox particles. Particularly, the impact of pH, aspartic acid concentration, or mechanical stirring was evaluated, leading to prepare monodisperse microspheres in the 400 nm – 2.5 µm diameter range. In both cases, particles were fired in controlled atmosphere to monitor the final O/M stoichiometry of the samples, then extensively characterized, especially to point out any chemical heterogeneity, or residual porosity.

In a second part, alteration tests of the produced particles will be discussed. These latter were undertaken in various media, with the aim to store these samples as suspensions before use. Preliminary results revealed that only a negligible weight loss occurred after several months in ethanol, while significant modification of the general morphology was observed in presence of water. In addition, first measurements of the isotopic composition of uranium by LG-SIMS led to comparable results between raw and leached samples, the behavior of the particles under the SIMS beam being comparable to typical field sample particles. This set of results then demonstrates the feasibility of producing reference actinide oxide particles through hydrothermal wet chemistry methods, with a large range of chemical compositions and sizes, thus offering various possible applications in the field of nuclear safeguards.

11:45 AM EN08.06.02

Investigation on the Structural Incorporation of Various Dopants into Uranium Oxides in Consideration of Application Requirements as Reference Materials Shannon K. Potts¹, Philip Kegler¹, Giuseppe Modolo¹, Simon Hammerich², Irmgard Niemeyer¹, Dirk Bosbach¹ and Stefan Neumeier¹; ¹Forschungszentrum Jülich GmbH, Institute of Energy and Climate Research – Nuclear Waste Management (IEK-6), Germany; ²Heidelberg University, Institute of Earth Sciences, Germany

In the last few years, an aerosol-based process has been implemented and established in the laboratories of Forschungszentrum Jülich to produce microparticulate uranium oxide reference materials. These microparticulate reference materials with well-defined properties are needed to consolidate the quality controls of the analytical methods used in particle analysis in nuclear safeguards. As a result, these reference materials must fulfill certain requirements. These requirements are specified by the International Atomic Energy Agency (IAEA) to be similar to the U-containing microparticles collected by an IAEA safeguards inspector during in-field verification activities. These so-called environmental samples are analyzed for their isotopic composition by the IAEA's Office of Safeguards Analytical Services and their dedicated Network of Analytical Laboratories (NWAL). In order to further develop analytical methods and quality control of the analytical results from particle analysis to even detect small quantities of fission products, the microparticulate reference materials must be refined. For this purpose, first attempts were made to synthesize Nd-mixed uranium oxide microparticles.

However, due to yield limitations in the μg range, no state-of-the-art analytical methods can be used for the characterization of these materials and the corresponding chemical stability of the mixed microparticles. Therefore, a co-precipitation method was adapted to synthesize bulk-scale comparison materials with various lanthanides and thorium in order to unravel the incorporation mechanism of those dopants into the uranium oxide structure in depth. Through TG-DSC studies on the mixed bulk-scale materials, the temperature range of phase transitions from UO_3 to U_3O_8 were identified and analyzed in dependence on the used dopant. By additional systematic structural investigations of the long- and short-range order phenomena with XRD and Raman, IR, and XAS, respectively the obtained doped UO_3 and U_3O_8 materials could be characterized in more detail. This presentation will show results regarding the incorporation of lanthanides and thorium into the uranium oxide structures and the corresponding phase transformation of the orthorhombic U_3O_8 to the hexagonal U_3O_8 crystal structure. These results will be integrated into the particle production process to design well-defined microparticulate mixed oxide reference materials.

SESSION EN08.07: Containment of Isotopes in Disposal Environments
Session Chairs: Kazuya Idemitsu and Rebecca Lunn
Tuesday Afternoon, November 29, 2022
Hynes, Level 3, Room 300

1:30 PM *EN08.07.01

What Long-Term Diffusion Experiments in Compacted Bentonite Reveal Kazuya Idemitsu, Yaohiro Inagaki and Tatsumi Arima; Kyushu University, Japan

Methods for determining diffusion coefficients include the flow-through method and the profile one. If the diffusion coefficient is small, only the profile method is applicable. In the profile method, the apparent diffusion coefficient can be obtained by setting an appropriate diffusion period. However, if an experiment is conducted with a longer diffusion period, the apparent diffusion coefficient may appear small. This phenomenon is observed in the diffusion of neptunium in compacted bentonite in an atmosphere with high carbonate ion concentrations. One interpretation is that the neptunyl carbonate complex can only pass through a limited size of pores in the compacted bentonite because the complex is so large and negatively charged. In fact, long term diffusion experiment as long as 3 years, the diffusion profile of neptunium in compacted bentonite was exponential, as filtered, and did not change over time. Such exponential profiles have also been observed for relatively large oxo-anions, e.g., molybdate ions. An exponential diffusion profile has also been observed for plutonium in a 20-year iron corrosion environment. With additional information, little plutonium was observed in the iron corrosion products.

2:00 PM EN08.07.02

Functionalized Organoclays for Increased Tc and I Sequestration Elizabeth Gager, Emily Maulden, Nathalie Wall and Juan C. Nino; University of Florida, United States

Nuclear energy production is a promising process for sustainable energy due to its relatively small carbon footprint and low carbon emission. However, the containment of highly mobile isotopes in nuclear waste such as technetium and iodine presents environmental challenges. Therefore, it is imperative to design new buffer materials to immobilize radionuclides to prevent waste from entering water streams. Organoclays, organically modified clays, are promising material systems for sequestration of radionuclides. Focusing on alkyl amine-based modifications, we have recently examined the role of carbon chain length and number of chains on the structure and Tc removal performance for montmorillonite. We will show that Tc removal performance and affinity are increased for longer chains and a greater number of chains. Functionalization with an 8-carbon chain length amine with 2 long chains shows a Tc removal > 90% and K_d of $4700 \pm 300 \text{ mL/g}$ while a single 8-carbon chain length amine shows < 10% removal and K_d of $10 \pm 3 \text{ mL/g}$. Additionally, we will show that the performance of amine functionalized clays can be increased by additional functionalization with a cation such as Fe. For example, montmorillonite modified with a single 16-carbon chain length amine shows a Tc removal of just ~40% while the addition of Fe increases the removal to ~75%. We will demonstrate that these performance increases correlate with structural changes in the functionalized clays captured via Fourier-transform infrared spectroscopy (FTIR) and x-ray diffraction (XRD). Specifically, as the clay's basal plane spacing is increased, the Tc removal performance is also increased and there are associated changes in the orientation and structure within the interlayer of the clay. To better understand the separate effect of the organic and cation modifications on sequestration performance, we will also show the performance in zirconium and amine functionalized clays focusing on the basal plane spacing and CH_2 vibrational bands as a function of concentration.

2:15 PM EN08.07.03

Effects of Hydration on the Stability of Smectite Edge Surface Formation An Ta, Seaton Ullberg and Simon R. Phillpot; University of Florida, United States

Iodine and technetium-99 radionuclides are among those of concern for safe deep geological storage of used nuclear fuel (UNF) due to their high environmental mobility. Smectite clay materials have been considered as an additional protection feature against these isotopes due to their capabilities to capture ions (via adsorption) and to sufficiently swell in the region between vitrified UNF and surrounding rock. Even so, the adsorption behaviors of smectite edge surfaces are yet to be fully understood. Here, plane-wave density functional theory calculations are used to characterize the formation of (010), (100), (110) and (130) of isolated and hydrated edge surfaces of pyrophyllite and montmorillonite. Pyrophyllite is considered as a model for all smectites given its simple form and the consideration of isolated/hydrated surfaces provided the ability to quantifiably survey the impact of hydration on surfaces during termination processes while montmorillonite is a candidate clay material. Specifically, edge distortion will be discussed from a thermodynamic perspective throughout this presentation. This work was supported by funding received from the U.S. DOE Office of Nuclear Energy's Nuclear Energy University Program under Project 20-19198.

2:30 PM EN08.07.04

Sorption Behavior of Cesium and Strontium During the Formation Process of Calcium Silicate Hydrate as a Secondary Mineral Under the Condition Saturated with Groundwater Tsugumi Seki, Reo Tamura, Taiji Chida and Yuichi Niibori; Tohoku University, Japan

Calcium silicate hydrate (C-S-H) is formed also as a secondary mineral in the vicinity of the radioactive waste disposal site by the reaction between calcium (Ca) ions leached from the cement and silicic acid dissolved from the host rock. It is well known that C-S-H significantly absorbs cationic radionuclides as reported by many previous studies. In such researches, C-S-H samples have been once dried after 7 days or more of the curing period from their synthesis. In an actual disposal environment, however, the C-S-H of secondary mineral would be formed under the condition saturated with groundwater. Additionally, C-S-H under a transient condition may also react with nuclides because C-S-H continuously forms and alters by supplying Ca

ions and silicic acid. Therefore, this study examined the sorption behavior of cesium (Cs) and strontium (Sr) during the CSH formation under the condition saturated with groundwater by the sorption experiments without any drying process.

The sorption experiments were conducted with the C-S-H samples adjusted Ca/Si molar ratios to 0.4, 0.8, 1.2, and 1.6. C-S-H was synthesized by mixing calcium oxide, fumed silica, and pure water. The total weight of the solid phase was set to 1.5 g, and the total volume of the liquid phase was 30 mL. The concentrations of Cs or Sr in the samples were set to 1.0 mM with stable isotopes. The sorption conditions were prepared in two types: adding Cs or Sr simultaneously with the C-S-H synthesis (hereinafter referred to as “co-precipitation condition”), and adding Cs or Sr after 30 days of C-S-H curing (hereinafter referred to as “hydration condition”). The reaction periods were selected to 1, 3, 7, and 14 days for co-precipitation conditions and 1, 3, and 7 days for hydration conditions. After the reaction period, the solid and liquid phases were separated by centrifuging and filtering with a 0.20- μm membrane filter. The concentrations of Ca, Si, and Sr were measured by ICP-AES, and that of Cs was measured by AAS. The solid phase was analyzed by Raman spectroscopy and XRD.

In the analysis results of dissolved ions, the concentrations of Ca and Si were negligibly small in the comparison to the amount of Ca and Si used for the C-S-H synthesis, more specifically, the Ca/Si molar ratios of the solid phase were kept almost constant through the experimental period including just after the synthesis. This means that the soluble components quickly reach apparent solid-liquid equilibrium. On the other hand, the Raman spectra of the solid phase showed that the polymerization of the silicate chain in C-S-H progressed with time, and the lower Ca/Si molar ratio increased the degree of polymerization. In addition, the coexistence of amorphous parts and crystalline tobermorite structure was observed in the solid phase just after the C-S-H synthesis by XRD. These suggest that C-S-H continuously alters from its formation even after reaching apparent solid-liquid equilibrium. Besides, as for the sorption of Cs and Sr onto C-S-H, their sorption rates decreased with increasing the Ca/Si molar ratios because the surface charge of C-S-H was negative for the lower Ca/Si molar ratios and positive for the higher ones. Furthermore, these sorption rates were almost constant regardless of the reaction period, the curing period of C-S-H, and the conditions adding Cs or Sr to the C-S-H samples. These suggest that the sorption sites for cations such as silanol groups and interlayers of C-S-H are formed just after the C-S-H synthesis, and hardly change over 30 days or more even if C-S-H gradually alters as mentioned above. The distribution coefficients were estimated to be approximately 1 - 15 mL/g for Cs and 2 - 35 mL/g for Sr under these experimental conditions. As a result, C-S-H which continuously forms as a secondary mineral around the repository is also expected to retard the migration of Cs and Sr because of its sorption property occurring immediately after its formation.

2:45 PM EN08.07.05

Radionuclide Sequestration in Functionalized Montmorillonite Clay from Molecular Dynamics Simulations [Seaton Ullberg](#)¹, Emily Maulden¹, Elizabeth Gager¹, Juan C. Nino¹, Nathalie Wall¹, James Szecsoy², Carolyn Pearce² and Simon Phillpot¹; ¹University of Florida, United States; ²Pacific Northwest National Laboratory, United States

Safe and reliable storage of radioactive waste (vitrified high-level waste (HLW) and spent nuclear fuel (SNF)) is a necessity for effective nuclear power infrastructure. Proper disposal requires buffer materials which can sequester radionuclides such as iodine and technetium for durations of up to 10⁶ years. In this work, the performance of functionalized montmorillonite as a buffer material is evaluated via molecular dynamics (MD) simulations. Functionalizing agents such as alkylammonium, thiol groups, and metallic species react via interlayer exchange to capture the anionic radionuclides which would otherwise be electrostatically repulsed by montmorillonite's net negative charge. The simulations utilize a combination of ClayFF, SPC/e, and OPLSAA potentials to parameterize interactions between the clay sheet, water, and organic functionalizing agents respectively. Differences in performance between a neutral charge pyrophyllite clay, unfunctionalized montmorillonite, and montmorillonite with various functionalizing agents are evaluated to inform an optimal choice for future buffer material applications.

This work was supported by the US Department of Energy Office of Nuclear Energy NEUP Project Number 20-19198.

3:00 PM BREAK

3:30 PM *EN08.07.06

Inhibiting Airborne and Groundwater-Borne Transport of Radionuclides During Decommissioning Operations with Colloidal Silica Grout [Rebecca Lunn](#)¹, Arianna G. Pagano¹, Grainne El Mountassir¹, Claire L. Corkhill² and Joshua Radford²; ¹University of Strathclyde, United Kingdom; ²The University of Sheffield, United Kingdom

Nuclear site decommissioning involves the retrieval and handling of radioactive waste. Waste removal from nuclear reactors and/or storage facilities, such as spent fuel pools and storage silos, represents a potential hazard in terms of radiation exposure for the workforce and the surrounding environment. This may be due to the accidental release of airborne radioactive particulates during waste recovery and transport, or to the loss of radioactive debris upon retrieval due to waste corrosion and degradation. The development of innovative techniques to reduce hazard in decommissioning operations is a critical aspect of site decommissioning.

This study explores the suitability of colloidal silica grouting around radioactive waste, prior to its removal, to reduce radiation exposure during nuclear waste retrieval operations. Colloidal silica is an aqueous suspension of silica (SiO₂) nanoparticles, with average particle size <100 nm. The creation of siloxane bonds (Si - O - Si), typically triggered by the addition of an electrolyte accelerator, leads to the formation of a solid-like network of silica nanoparticles in the form of a hydrogel. Previous work on colloidal silica gel has proved its potential to form low-permeability hydraulic barriers against fluid migration, and to inhibit the diffusion of radionuclides through the gel, making it a promising material for use in retrieval operations.

Here we present research to determine the potential for colloidal silica to be used in a range of decommissioning operations. For example, spent fuel removal requires evidence that colloidal silica hydrogel can maintain its integrity upon exposure to temperatures higher than ambient, typical of the nuclear waste stored within pools and silos. These might be in the range 40-60 °C in standard conditions, but could exceed 100 °C during loss of cooling/loss of coolant accidents. We also consider grouting of particulate wastes prior to their retrieval, during which the grout must prevent particle release, and must not compromise formation of a suitable final wasteform.

Experiments were carried out to simulate colloidal silica grouting operations around objects and particles at temperatures higher than ambient, up to a maximum of 120 °C and to determine their suitability for subsequent vitrification. The effect of the temperature of the grouted object, and of the silica grout properties, on the performance of the gel was explored by a) microstructural analyses using x-ray imaging, to detect the presence and spatial distribution of temperature-induced cracks within the gel, and b) mechanical tensile and shear strength tests at different temperatures and silica concentrations. Experiments were then conducted within a furnace, using contaminated soil samples grouted with colloidal silica, to investigate the additives and processes required to produce a uniform glass and to determine its radionuclide retention. Our results confirm the strong potential of colloidal silica grout to reduce hazard during spent fuel and radioactive waste retrieval operations.

4:00 PM EN08.07.07

The PLEIADES Facility for Long-Term Experimental Investigations of Disposal Environments and Storage—Part of the UK National Nuclear

User Facility Sarah Pepper, Martin Stennett, Clare L. Thorpe, Russell Hand and Claire L. Corkhill; University of Sheffield, United Kingdom

As part of the UK Government's commitment to managing its historical radioactive waste inventory, in addition to any future generated waste, disposal of higher activity waste in a geological disposal facility is considered the safest option. Understanding how radioactive waste and different waste forms respond to storage conditions over extended periods of time is key in developing a robust safety case for disposal in a GDF.

To support this, the PLEIADES (Platform for Long-term Experimental Investigation of Alteration Disposal Environments and Storage) Facility is being established to allow the determination of radio-material corrosion and long-term degradation relevant to radioactive waste storage, disposal and decommissioning associated with legacy, new-build and future fuel cycles.

The facility comprises a suite of laboratories capable of allowing research into radio-material alteration in realistic environments and over extended timescales. Here we will describe the facilities and present some of the research being performed in the facility.

4:15 PM EN08.07.08

Evaluation of the Leaching Behavior of Heavy Metal Including Cement Solidified Waste in Simulated Radioactive Waste Disposal Facility Environment Yulim Lee, Jaeyeong Park and Hyeongjin Byeon; Ulsan National Institute of Science and Technology, Korea (the Republic of)

Radioactive waste containing hazardous substances (mixed waste) frequently occurs around the world for reasons such as radiochemistry, nuclear species analysis, and nuclear decommissioning. These mixed wastes are thoroughly classified and disposed of in the United States, but not dealt with in other countries. Most countries distinct radioactive waste and hazardous waste separately, and there is no clear treatment standard for mixed waste with both properties. Inadequately treated mixed waste could cause crucial issues with both radiation and non-radiation hazard (chemical and biological). For proper disposal of mixed wastes, specific technical standards and regulatory guidelines are required. In order to set these standards, it is possible to consider the application of environmental regulations on hazardous substances. However, there are many differences between non-radioactive waste disposal facilities and radioactive waste depository such as the facility design, post-closure operating standards, and leachate creation. Therefore, rather than simply applying environmental regulations for disposal of mixed waste, appropriate regulations should be established in consideration of the radioactive waste disposal environment.

In this study, the leaching behavior of hazardous substances which is frequently generated from the nuclear industry was tested in the simulated disposal condition. The target harmful substances were selected as lead, cadmium, and antimony focusing on heavy metals, and sample waste was produced by cement solidification method, which is commonly used for the disposal of hazardous and radioactive wastes. The leaching properties of these wastes were tested using TCLP, a leaching test method of hazardous waste, and ANS 16.1, a leaching test method of radioactive waste. Test conditions of leachate pH, leachate composition, and exposure dose were modified and applied to simulate the leachate environment. As a result, it was found that the leachability of the simulated waste increased significantly within the environment of the radioactive waste disposal facility compared to standard leaching test condition. In addition, as a result of the irradiation-leaching test, it was observed that the non-leached heavy metal (Cd) showed leaching though a small amount. Consequently, it was confirmed that Pb and Sb had increased leaching rate in the radioactive waste disposal environment. In the case of lead, it is expected that cement solidification is an inappropriate treatment method due to high leaching amount in cement solidification. Cd was not detected at all in the non-irradiation-leaching experiment, but it was observed that radiation could affect the leaching properties of heavy metals of detection in the irradiation-leaching experiment. Using this approach, it is possible to establish specific regulations for the disposal of mixed waste. It is suggested that wastes containing Pb should be treated with other method than cement solidification. Cd has a highly insoluble property in cement solidification, so cement solidification is considered an appropriate disposal method. In addition, both lead and cadmium show changes in leaching properties as a result of irradiation-leaching experiments, raising the necessity to establish proper leaching criteria in consideration of the expected dose exposure in the disposal facility.

Acknowledgements

This work was supported by the Nuclear safety Research Program through the Korea Foundation Of Nuclear Safety (KoFONS), granted financial resource from the Nuclear Safety and Security Commission (NSSC), Republic of Korea (No. 2003016 & No. 2203028).

4:30 PM EN08.07.09

The Methodologies to Reduce the Thermal Impact of Vitrified Waste from Spent MOX Fuel on Geological Repository Ryo Hamada¹, Tomofumi Sakuragi¹, Hidekazu Asano¹, Toshiro Oniki² and Midori Uchiyama²; ¹Radioactive Waste Management Funding and Research Center, Japan; ²IHI Corporation, Japan

In Japan, the storage of spent MOX fuels discharged from some commercial nuclear power plants has started. In the future, reprocessing, vitrification and final disposal of the spent MOX fuel will be needed in order to reduction of waste volume and radiotoxicity in a potential repository.

Compared to the vitrified waste from spent UO₂ fuels (UO₂-HLW glass), the MOX-HLW glass has high heat generation for a long period, and thus it takes about 300 years to cool down to the same heat generation. So, it is essential to decrease heat generation in order to prevent the bentonite buffer alteration, otherwise the waste volume and repository footprint will be huge.

In this study, 5 options are considered to decrease the bentonite buffer temperature in geological repository for the MOX-HLW glass. One option is minor actinides (MA) separation from high-level liquid waste (HLLW). MA separation is greatly effective to decrease thermal impact because main nuclide of heat generation of MOX-HLW glass is Am-241. MA separation ratio from HLLW requires 80% to lower the bentonite buffer temperature limit of 100 °C. So, the development of MA separation technology is important.

The other options such as long-term storage or low waste loading of MOX-HLW glass, expansion of repository footprint, and mixing with UO₂ and MOX reprocessing liquid waste will be discussed in detail.

This work was carried out as a part of the basic research programs of vitrification technology for waste volume reduction supported (JPJ010599) by the Ministry of Economy, Trade and Industry, Japan.

4:45 PM EN08.07.10

Nuclear Waste from Small Modular Reactors Lindsay Krall^{1,2}, Allison Macfarlane³ and Rodney Ewing⁴; ¹Stanford University (former), United States; ²Swedish Nuclear Fuel and Waste Management Company (current), Sweden; ³The University of British Columbia, Canada; ⁴Stanford University, United States

Small modular reactors (SMRs, *i.e.*, nuclear reactors that produce <300 MW_{elec}, each) have attracted considerable attention because of inherent safety features and reduced cost, but there are remarkably few studies that analyze the impact of SMRs on the back-end of the nuclear fuel cycle, specifically with respect to changes in waste stream management and disposal. Here, we characterize the notional high-, intermediate-, and low-level waste streams for

three, distinct SMR designs in terms of volume, (radio)chemistry, decay heat power, and fissile isotope composition¹. Results reveal that the analyzed water-, molten salt-, and sodium-cooled SMR designs will increase the energy-equivalent volume of nuclear waste in need of management and disposal by two- to thirty-fold relative to an 1100 MW_{elec} pressurized-water reactor. Much of the excess waste volume is attributed to the use of neutron reflectors and/or of chemically reactive fuels and coolants in SMR designs. That said, volume is not the most important parameter for assessing the implications for storage and disposal of a nuclear waste stream; rather the critical issues in the performance of a geologic repository are driven by the decay heat power and the (radio)chemistry of the spent nuclear fuel. SMRs provide no benefit for these two important parameters. For instance, SMRs will not reduce the energy-equivalent generation of geochemically mobile ¹²⁹I, ⁹⁹Tc, and ⁷⁹Se fission products—important dose contributors for various repository designs—relative to a full-scale commercial reactor. Instead, SMR spent fuel will contain relatively high concentrations of fissile nuclides and, therefore, will demand the development of novel approaches to criticality safety during storage and disposal, including increased handling, treatment, and conditioning operations. Since the properties of the waste streams are influenced by neutron leakage, a basic physical process that is enhanced in small reactor cores, SMRs will exacerbate the challenges of nuclear waste management and disposal.

¹Krall, L.M., Macfarlane, A.M., Ewing, R.C. (2022). Nuclear waste from small modular reactors. *Proceedings of the National Academy of Sciences*. 119(23).

SESSION EN08.08: Chemical Durability of Waste Forms
Session Chairs: Claire Corkhill and Jarrod Crum
Wednesday Morning, November 30, 2022
Hynes, Level 3, Room 300

8:15 AM *EN08.08.01

Stage III Glass Corrosion Behavior for Different Glass Compositions at Multiple Temperatures [Jarrod Crum](#), Benjamin Parruzot, Sebastien Kerisit, Richard Daniel, Joelle Reiser, Richard Reyes, Neeway James, Joseph Ryan, Gary Smith and Matthew Asmussen; PNNL, United States

The corrosion of borosilicate waste glass has been studied by groups around the world to understand and estimate the long-term performance of the waste form in the disposal environment. In static conditions, glass first briefly corrodes at the forward rate (Stage I), but the corrosion rate then progressively slows by orders of magnitude to a residual rate (Stage II) due to a combination of solution feedback effects and formation of a stable protective gel layer. However, the corrosion rate can later accelerate above the sustained Stage II corrosion rate, referred to as the resumption (or Stage III) rate. This behavior may be induced by the precipitation of a sink phase, which perturbs the leachate chemistry and stability of the protective gel layer. The sink phases commonly observed during Stage III are zeolite phases, such as analcime, P1, P2, and chabazite. These sink phases act as sources that consume major glass and gel components (alkali, alkaline earth, Al₂O₃, and SiO₂) resulting in accelerated glass corrosion rates. While Stage III behavior has been observed at 70 °C and 90 °C in long-term static testing of crushed glass (e.g., Product Consistency Test), its stochastic nature and long onset times make Stage III corrosion rate measurements extremely challenging. In this work, zeolite seeds (zeolite P1, P2, analcime, and clinoptilolite) were used to induce Stage III behavior at 22 °C, 40 °C, 70 °C, and 90 °C to measure Stage III corrosion rates of low-activity waste glasses and examine resulting alteration products. Results showed that zeolite P2 consistently triggered a Stage III response, the magnitude and persistence of which were correlated to glass composition, solution pH, and temperature. The response to zeolitic seeds varied from transitory acceleration (short events) to sustained linear acceleration to progressively faster acceleration. In many cases, additional zeolite types formed in addition to the original zeolite seeds, which was generally accompanied by a second faster acceleration than the initial response to seeds. Apparent activation energy measurements between 22 °C to 90 °C showed that lower temperature resulted in smaller differences between Stage II and Stage III corrosion rates, along with decreased persistence of Stage III behavior.

8:45 AM EN08.08.02

Predicting the Long-Term Durability of Nuclear Waste Immobilization Glasses Using Machine Learning [Yu Song](#) and [Mathieu Bauchy](#); University of California, Los Angeles, United States

The long-term durability of a glass is a key performance metric for nuclear waste immobilization application. Although some models have been proposed to predict the short-term forward dissolution kinetics of glasses, long-term dissolution is a more complex behavior that is influenced by the glass structure, the feedback from the solution, and the precipitation of secondary phases. This complexity has limited our ability to robustly predict the long-term dissolution rate of nuclear waste immobilization glasses. Here, based on the analysis of a large dataset of vapor hydration tests (VHT), we develop using machine learning a Gaussian Process Regression (GPR) model to predict the long-term durability of glasses. Importantly, GPR models are non-parametric and intrinsically capture the uncertainty of the prediction. We demonstrate that our GPR model features an excellent accuracy. This model allows us to decipher the propensity for each oxide to accelerate or slow down the dissolution kinetics of glasses.

9:00 AM EN08.08.03

The Synthesis and Durability of Cs-Bearing Analogue Glasses Relevant to the Meltdown of the Fukushima Dai-ichi Nuclear Power Plant [Luke T. Townsend](#), Joshua Radford, Sam Walling, Sarah Pepper and Claire L. Corkhill; University of Sheffield, United States

In 2011, the Fukushima Dai-ichi nuclear power plant was hit by a 14 m high tsunami which resulted in one of the worst nuclear disasters in history. As a consequence of the meltdown of reactor units 1-3, radiation was spread widely across Japan (up ~280 km) with radioactivity entering the environment in a variety of forms. A key form of radioactivity was the Cs-bearing microparticle, or CsMP, which consists of glassy silica microparticles embedded with a variety of debris and radionuclides, most prominently ¹³⁷Cs. Due to the small size (~20 μm) of the particles and their distribution throughout the environment in Japan, studying the materials properties of CsMPs is challenging. To this end, analogue glasses have been synthesised with the aim of studying the durability and environmental behaviour of CsMPs, whilst determining the potential for ¹³⁷Cs leaching. Three analogue glasses have been produced based upon compositions of CsMPs scavenged from the environment, with one candidate glass chosen for dissolution testing by the ASTM PCT-B protocol. Over 112 days, the Cs-bearing analogue glass showed dissolution behaviour similar to that reported for soda lime silica glass and was comparable with the limited studies performed on environmentally-sourced single ¹³⁷CsMPs. The results of this study validate the use of analogue glasses in the study of the materials properties of Cs-bearing silica glasses, laying the foundation for further investigation into the durability of CsMPs and informing any environmental remediation or mitigation that may be required.

9:15 AM EN08.08.04

Quantification of the Kinetics and Mechanisms of Dissolution of Full-Scale Simulant UK HLW Glasses Incorporating Post Operational Clean Out (POCO) Waste [Jenny Ayling](#)¹, Adam Fisher¹, Mike Harrison², Clare L. Thorpe¹ and Claire L. Corkhill¹; ¹The University of Sheffield, United Kingdom;

²National Nuclear Laboratory, United Kingdom

As the UK's spent nuclear fuel reprocessing capability draws to a close, a period of Post Operational Clean Out (POCO) of the highly active liquor storage tanks (HASTs) will begin, with the resulting waste vitrified to form a stable disposal product. Since the waste removed from the HASTs is expected to be compositionally different from the HA liquor generated in the last several decades of reprocessing, most notably enriched in molybdenum, an alternative glass composition, containing Ca to promote formation of insoluble CaMoO₄ (powellite) and Zn to improve viscosity, has been developed.

This work focuses on quantifying the dissolution behaviour of full-scale simulant UK HLW CaZn glass, produced at the Waste Vitrification plant, as a function of waste type and waste loading. Glasses containing different waste loadings of Magnox and Thorp calcine blend are compared with glasses containing a blend of simulant calcine derived from high active liquor, HAST and HAST heel waste. Two additional glasses, the International Simple Glass (ISG) and SON68, were also included for comparison.

Dissolution tests were performed for 730 days at 40°C in highly alkaline solution (saturated Ca(OH)₂) on glass monoliths using the ASTM MCC-1 methodology and the release of elements was followed using aqueous analytical techniques. Surface analysis was used to determine the thickness of gel layer formation and to identify secondary phases.

The CaZn glasses displayed similar chemical durability despite differences in composition, microstructure and waste-type, and the dissolution rates consistently lay below SON68, and above the International Simple Glass. The CaZn-Magnox glasses, which were contained a greater proportion of Mg, displayed a higher dissolution rate compared to the CaZn-POCO glasses. These CaZn-POCO glasses showed the lowest rates of Mo dissolution despite having the highest proportion of Mo. This is credited to the durability of the CaMoO₄ crystalline phase even under hyper-alkaline conditions.

9:30 AM EN08.08.06

The Stabilization of Particulate Solid Wastes in Ambient Temperature Waste Forms [Alessandra Lie Fujii Yamagata](#), Matthew Asmussen, Sarah Saslow and Gary Smith; Pacific Northwest National Laboratory, United States

During the processing of nuclear wastes, different particulate solid secondary wastes (SSW) can contain radionuclides and other contaminants. In many cases, these spent particulate materials will require stabilization/blending for disposal. Ambient temperature waste forms, such as cementitious waste forms, are common candidates for the stabilization of SSW due to their low cost, receptiveness to a variety of material types, tailorable properties and ability to meet various waste acceptance criteria. A variety of solid secondary wastes (SSW) have been investigated for stabilization in ambient temperature waste forms, including silver mordenite (AgZ), granular activated carbon (GAC), high efficiency particulate air (HEPA) filters, and organic-based ion exchange resins. This presentation will cover the development and characterization of candidate ambient temperature waste form formulations for the stabilization of these SSW with a focus on overlapping behaviors and unique challenges to specific SSW types.

9:45 AM EN08.08.07

Studies on Properties and Aging Behaviour of Corium Generated Under Severe Accident Conditions [Daniel Serrano Purroy](#), Vincenzo Rondinella and Jakub Kokinda; European Commission, Joint Research Centre Karlsruhe, Germany

During a severe accident, large amounts of volatile fission products, such as caesium and iodine, are released during the core degradation. A significant fraction of the non-volatile ones, including actinides, lanthanides and some of the so-called semi-volatile ones (e.g. barium, strontium), remains trapped in the corium debris. The trapping of low- to non-volatile fission products in corium phases limits the short-term airborne source term during and after the accident. The long term decommissioning and remediation perspectives of the Fukushima Daiichi more than a decade after the accident highlight the importance of adequately assessing the ageing and corrosion behaviour of corium debris and their impact on the "delayed" aqueous source term. In this context, water/corium interaction has to be assessed to be able to estimate the amount and chemical form of fission product that can be released.

In this work, results of ongoing leaching tests on real corium samples from the FPT2 test of the Phébus FP Program are reported. The objective of the FPT2 test was to study the degradation of an irradiated UO₂ fuel bundle and the fission product behaviour under conditions of low steam flow that created reducing conditions. One of the main objectives of the present experiments was to compare to previous tests on TMI-2 corium samples. Indeed considering the "reducing" conditions imposed during the Phébus FPT2 test, a different behaviour of the corium compared to that of TMI-2 could be expected since much more oxidising conditions prevailed during the TMI-2 accident.

Sequential batch leaching experiments at room temperature under ambient atmosphere in static conditions were performed. The composition of the leaching solution was based on the boric acid containing water from the storage tanks (2-2.5g/L). The used vessels were rinsed with 1 M HNO₃ at room temperature. Subsequently, the leachates and the rinse solutions were analysed using ICP-MS to quantify the release kinetics of the fission products and the actinides. Results are discussed in terms of Fraction of Inventory in the Aqueous Phase (FIAP) and dissolution rates, and compared to similar experiments carried out on TMI-2 corium and on LWR UO₂ and MOX spent nuclear fuels. In addition, preliminary surface area characterisation by Raman spectroscopy was carried out.

The present experimental results are part of a programme dedicated to the analysis and the management of LWR after severe accidents. In particular, they will be used to support decommissioning and remediation strategies for the Fukushima Daiichi nuclear power plants.

10:00 AM BREAK

SESSION EN08.09: Challenges of Molten Salt Reactors
Session Chairs: Claude Degueudre and Joanna McFarlane
Wednesday Morning, November 30, 2022
Hynes, Level 3, Room 300

10:30 AM *EN08.09.01

Chemistry of Fission Products in Molten Salt Reactors and Uptake into Waste Forms [Joanna McFarlane](#)¹ and Brian Riley²; ¹Oak Ridge National Laboratory, United States; ²Pacific Northwest National Laboratory, United States

Waste from molten salt reactors is more varied and will need to be handled differently than waste from water-cooled reactors. As the fuel is transported by a carrier salt through the primary heat transfer system, radionuclides generated by fission and transmutation have exposure to several different materials and environments. In addition, the headspace of the fluidic loop, or cover gas system, will also be loaded with radionuclides depending on partitioning between the liquid and vapor phase. The cover gas system is designed to delay radionuclide transport for several months to allow most of the fission products to decay to stable forms. In some designs, the headspace is sealed. In others, the filtered gas is recirculated through the cover gas system.

Hence, certain questions need to be addressed when considering how to manage waste from molten salt reactors. The most important relates to mass accountability for the fission products and actinides and their collection during fuel preparation, reactor operation, maintenance, online processing if used, and post-processing. Each step in the lifecycle of the reactor will generate different waste materials with varying levels of hazard. Waste materials will include the fuel salt itself, structural metals, graphite in some cases, and off-gas filters. In most cases, these materials will need to be processed to form chemically and radiolytically more stable waste forms, to reduce volume, to dissipate decay heat and reduce radiolysis while in storage or in a permanent repository.

Aspects of molten salt waste handling have been reviewed as have chemical hazards associated with pre- and post-processing of reactor materials. There has also been an effort to identify routes to convert chloride and fluoride salts to stable waste forms. This talk will review some of these efforts and identify needs for bridging the gap that exists between designing an operating MSR and developing pathways for safe and secure waste handling.

11:00 AM *EN08.09.02

Analysis of Aerosols and Gases Relevant to Molten Salt Reactor Off-Gas Monitoring Using Laser-Induced Breakdown Spectroscopy [Hunter Andrews](#), Kristian Myhre and Joanna McFarlane; Oak Ridge National Laboratory, United States

Molten Salt Reactors (MSRs) are one category of advanced nuclear reactors receiving increased attention in recent years, as evidenced by significant investments from both government and private industry into MSR technology development. The attractiveness of MSR technology predominately stems from inherent safety features including low pressure operation, passive decay heat cooling, and large negative temperature coefficient of reactivity. A key component of any nuclear reactor is the off-gas system. MSR designs present a unique set of off-gas related challenges due to the fuel being in liquid form. In general, MSR designs will involve an inert cover-gas, such as argon or helium, that is over the liquid fuel. Both stationary and flowing conditions are possible. Volatile species, such as noble gas fission products, and salt aerosols may be partitioned into the cover-gas under both normal and off-normal operating conditions. An off-gas treatment system is therefore required to ensure that radioactive species are not released under any condition. It is expected that although several off-gas treatment systems for MSRs may look similar to those currently in operating reactor designs, there will be differences. A key aspect of developing and deploying these off-gas treatment technologies is instrumentation for monitoring the concentrations of species in the off-gas before and after treatment. Laser-induced breakdown spectroscopy (LIBS) is one of several promising analytical techniques for MSR off-gas monitoring. This contribution will give an overview of MSR off-gas monitoring requirements as well as recent progress on the use of LIBS off-gas monitoring system for MSRs. This will include results from real-time monitoring of various surrogate aerosol streams relevant to MSRs.

SESSION EN08.10: Spent Nuclear Fuel
Session Chairs: Laurent Claparede and Lena Evins
Wednesday Afternoon, November 30, 2022
Hynes, Level 3, Room 300

1:30 PM *EN08.10.01

Spent Fuel Dissolution in Repository Environments [Lena Z. Evins](#); SKB, Sweden

When considering spent nuclear fuel (SNF) for direct disposal, it is necessary to estimate the rate of radionuclide release from this waste form in the repository environment. Since the majority of the radionuclides are contained within the UO₂-matrix of the spent nuclear fuel pellets, the matrix dissolution rate strongly impacts the rate of radionuclide release from the SNF and therefore also the safety assessment. Radionuclides are also located in and on the SNF cladding and other metallic parts of the fuel, and in the gap between the SNF pellets and the cladding. These radionuclides are released more rapidly than those found in the SNF matrix. It is important to quantify these fractions, especially the so-called Instant Release Fraction (IRF), to estimate the effect of this on the safety assessment. Therefore, efforts are made to fully understand the matrix dissolution as well as the fast release of radionuclides observed in SNF leaching experiments [1,2,3]. As soon as it was clear that direct disposal of SNF was likely to be the preferred strategy in some countries, experiments were started to gather radionuclide release data [4]. These first experiments were mainly performed in aerated conditions. Later, there was a focus on reducing conditions, as these are more relevant to the expected repository environment. Many studies published in the last decade have shown that hydrogen in the gas phase can strongly reduce the oxidative dissolution rate [1, 5]. However, some questions still remain regarding the mechanisms and conditions for which the hydrogen is most efficient in this respect. The effects of iron in the system is another important issue [6]. In this contribution, experiments performed under hydrogen and/or corroding iron are reviewed and discussed. Recent advances concerning oxidative and non-oxidative dissolution, gap and grain boundary inventories, as well as fuel microstructure are also presented. As an outlook, some aspects concerning the ongoing and future fuel development, such as fuel with various additives, are also discussed.

References

- [1] Evins, L.Z., Bosbach, D., Duro, L., Farnan, I., Metz, V., Riba, O., 2021. Final Scientific Report. Deliverable D1.26, DisCo project (Grant Agreement 755443), Euratom Research and Training Programme on Nuclear Energy, Horizon 2020 Framework Programme, European Commission.
- [2] Ekeröth, E., Granfors, M., Schild, D. and Spahi, K., 2020. The effect of temperature and fuel surface area on spent nuclear fuel dissolution kinetics under H₂ atmosphere. *Journal of Nuclear Materials*, 531, p.151981.
- [3] Lemmens, K., González-Robles, E., Kienzler, B., Curti, E., Serrano-Purroy, D., Sureda, R., Martínez-Torrents, A., Roth, O., Slonszki, E., Mennecart, T. and Günther-Leopold, I., 2017. Instant release of fission products in leaching experiments with high burn-up nuclear fuels in the framework of the Euratom project FIRST-Nuclides. *Journal of Nuclear Materials*, 484, pp.307-323.
- [4] Forsyth R., 1983. The KBS UO₂ leaching program Summary Report 1983-02-01. SKBF KBS Technical Report 83-86, Swedish Nuclear Fuel Supply

Co/Division KBS.

[5] Puranen, A., Barreiro, A., Evins, L.Z. and Spahiu, K., 2020. Spent fuel corrosion and the impact of iron corrosion—The effects of hydrogen generation and formation of iron corrosion products. *Journal of Nuclear Materials*, 542, p.152423.

[6] Odorowski, M., Jegou, C., De Windt, L., Broudic, V., Jouan, G., Peugeot, S. and Martin, C., 2017. Effect of metallic iron on the oxidative dissolution of UO₂ doped with a radioactive alpha emitter in synthetic Callovian-Oxfordian groundwater. *Geochimica et Cosmochimica Acta*, 219, pp.1-21.

2:00 PM EN08.10.02

Accelerated Dissolution of Doped UO₂-Based Model Systems as Analogues for Modern Spent Nuclear Fuel Under Repository Conditions Philip Kögler, Martina Klinkenberg, Andrey Bukaemskiy, Robert H. Thümmeler, Guido Deissmann, Felix Brandt and Dirk Bosbach; Forschungszentrum Juelich, Germany

Decades of research have demonstrated that spent nuclear fuel is a good waste form supporting its direct disposal in a deep geological repository. Due to the use of doped nuclear fuels (doped with Gd, Al, Cr, etc.) in recent years, a verification of the favourable behaviour of these modern fuels was needed. Here we have studied tailor-made UO₂ model materials that can provide additional insights into the influence of doping on the dissolution behaviour of spent nuclear fuels. Thus, within this work single-effect dissolution studies were carried out using systematically produced and carefully characterised UO₂-based model materials, to provide additional insights into the dissolution behaviour of spent modern LWR-fuels under the post-closure conditions expected in a DGR.

The first step in this study was the development of an optimised synthesis route for the production of UO₂ reference materials, Cr-doped UO₂ as well as Nd- and Gd-doped UO₂ based materials. A special focus was set on a high density of the sintered pellets, control of grain growth and homogeneous distribution of the dopants in the UO₂ matrix.

Here, we present recent results on the dissolution behaviour of these tailor made UO₂ model materials in accelerated static batch experiments using H₂O₂ as simulant for radiolytic oxidants, present in long-term disposal scenarios for SNF in failed container conditions due to the alpha-irradiation of water. In these dissolution experiments, pure UO₂ reference pellets exhibiting different densities and grain sizes, as well as Cr-, Nd-, and Gd-doped UO₂ pellets with varying doping levels, produced using different doping methods and having different grain sizes, were used. In addition, industrially produced Cr- and Cr/Nd-doped UO₂ pellets were used. The dissolution experiments were performed under strictly controlled conditions with respect to exclusion of oxygen, temperature control, and exclusion of light.

This bottom-up approach was followed to understand how the addition of the different dopants into the fuel matrix affects SNF dissolution behaviour. The results of the dissolution experiments indicate that the addition of Cr and the consequential modification of the fuel matrix does not lead to a significant change of the dissolution behaviour of these model materials compared to pure UO₂ reference materials (i.e., dissolution rates agree within an order of magnitude). This is in strong contrast to the dissolution rates of Ln³⁺-doped pellets, which are significantly lower than those of pure and Cr-doped pellets.

2:15 PM EN08.10.03

Hydrogen Inhibition Effect on Spent Nuclear Fuel Matrix Dissolution Under Anoxic/Reducing Atmosphere and Alkaline pH Luis Iglesias Pérez¹, Roberto Gaggiano², Xavier Gaona¹, Michel Herm¹, Tobias Koenig¹, Katrien Meert², Tomas Vandoorne² and Volker Metz¹; ¹Karlsruhe Institute of Technology-Institute for Nuclear Waste Disposal, Germany; ²National Agency for Radioactive Waste and Enriched Fissile Materials (ONDRAF/NIRAS), Belgium

In many countries (United States, Germany, China, etc.), final disposal of spent nuclear fuel (SNF) in deep geological repositories is the preferential option to permanently and safely isolate the radionuclide inventory from the biosphere. In post-closure safety assessments of such facilities, access of water to the emplaced SNF and the consecutive release of radionuclides from the waste is considered. The UO₂ matrix of the SNF retains many radionuclides, which can be released upon its dissolution. Therefore, an improved understanding on the interaction of SNF with pore water solutions under repository conditions is required in safety analyses of deep geological repositories.

In this study, the release of radionuclides from spent UO₂ fuel under relevant geochemical conditions, representative of the Belgian “Supercontainer concept” were investigated. Three leaching experiments with SNF clad pellets were performed in highly alkaline (cementitious) solution and anoxic/reducing atmosphere using autoclaves to analyse the impact of the presence of hydrogen and how influences the hydrogen partial pressure on the release of relevant fission products and actinides.

The SNF specimens, comprising one full and two half pellets in each experiment, were sampled from a fuel rod with an average burn-up of 50.4 MWd/kg_{HM}. The fuel rod was irradiated in the Gösgen pressurised water reactor in Switzerland. Each experiment was divided in two stages, replacing the previous titanium liners and using fresh solution when starting the new stage. The experiments were conducted under different gas atmospheres and total pressures. All other experimental conditions were the same.

- 40 bar of an Ar/H₂ gas mixture with a H₂ partial pressure of 3.2 bar in experiment 40/3.2H.

- 3.75 bar of an Ar/H₂ gas mixture with a H₂ partial pressure of 0.3 bar in experiment 3.75/0.3H.

- 1.0 bar Ar atmosphere (in absence of H₂) during the first stage of experiment 1-40/0; in this experiment the Ar pressure was raised to 8 bars after 497 days until termination of the first stage, 288 days later. Then, the experiment was conducted for another 603 days during the second stage at 40 bar Ar atmosphere.

The findings demonstrate a hydrogen inhibition effect on the dissolution of the fuel matrix (as displayed by an inhibited release of U-238) and on the release of mainly matrix bound radionuclides e.g., Sr-90. Measured uranium and strontium concentrations are lower in the two experiments with hydrogen overpressure compared to respective results of the experiment under solely anoxic conditions. A comparison of the measured U-238 concentrations in the current experiments with calculated solubility limits of respective U(IV) and U(VI) solids indicate that U-238 concentrations approach towards the solubility limit of UO₂(am, hyd) in presence of hydrogen. The observed concentration levels and kinetic data show that the presence of hydrogen inhibits the dissolution kinetics of SNF and favours the formation of a U(IV) solid phase. At the end of the experiments, the Cumulative Fraction of Inventory in Aqueous Phase (CumFIAP) values of Sr-90 are similar to the CumFIAP of U-238. It is concluded that the strontium release behaviour is coupled to the dissolution of the UO₂ matrix.

In the three experiments the CumFIAP values of Cs-137 are several orders of magnitude higher than the respective values of U-238. During the experiments, there was no pronounced effect of the redox conditions on the Cs-137 concentrations or release rates observed.

The fission gases Kr and Xe are continuously released throughout the experiments, too. An effect of the redox conditions on the fission gas release was not detected.

2:30 PM BREAK

3:30 PM EN08.10.04

In Situ Raman Oxidation of Undoped and Zr-Doped UO₂ Sam Karcher and John S. McCloy; Washington State University, United States

Uranium dioxide is used as an analogue for used nuclear fuel (UNF) doped with small amounts of lanthanide and rare-earth elements to simulate fission

products. Structural and thermodynamic data from these materials can be used to help predict the long-term behavior of UNF stored in geological repositories where elevated temperatures, oxidizing environments and eventual groundwater contact may accelerate UNF degradation.

Raman spectroscopy is a particularly useful tool for studying the structures of uranium oxides and defects induced by processes like doping, irradiation, and oxidation.

In this work, the Raman spectra of undoped UO_2 and Zr-doped UO_2 are presented from in-situ heating experiments performed in air at 250°C. After 1 hour, the undoped sample begins to show spectral features indicative of U_4O_9 , whereas immediately after heating the Zr: UO_2 sample shows features of U_4O_9 and U_3O_8 . U_3O_8 features were not observed in the undoped sample even after >10 hours of heating. Accelerated oxidation of Zr: UO_2 compared to undoped UO_2 is consistent with previous work. Optical images of the Zr: UO_2 captured during ramping from 250°C to 400°C show accelerated oxidation along grain boundaries leading to cracking along grain boundaries and eventually intergranular cracking. Raman mapping and principal component analysis together indicate U_3O_8 forms along grain boundaries while grain interiors remain primarily U_4O_9 . Additionally, using 455 nm Raman excitation proved most useful for in-situ experiments; 532 nm gave poor spectra from U_4O_9 and 785 nm gave poor spectra from U_3O_8 .

3:45 PM EN08.10.05

Impact of Lanthanide and PGM Elements on the Chemical Durability and Surface Modifications During Leaching Tests of UO_2 Pellets Mimicking Interim Repository Laurent Claparede, Paul-Henri Imbert, Nicolas Clavier, Stephanie Szenknect and Nicolas Dacheux; ICSM, University Montpellier, CNRS, CEA, France

Managed by ANDRA, the European collaborative research program EURAD aims to federate research efforts and to share scientific and technical knowledge of some 100 European players in the field on the long-term management of radioactive waste. In this context, ICSM/LIME is interested in the chemical durability of spent nuclear fuels under interim storage conditions (i.e. in conditions mimicking their stay in cooling pool).

Due to the complex structure and microstructure of spent nuclear fuels (SNF), the global understanding of their behavior when leaching is very difficult to analyze, although it appears as a very important task. In this study, the role of two families of fission products (FP, i.e. lanthanide and PGM elements) was thus specifically examined. Indeed, in SNF, lanthanide elements are incorporated in the UO_2 structure, inducing redox constraints or formation of oxygen vacancies while PGM elements (Ru, Rh, Pd) are forming metallic inclusions in contact with UO_2 grains.

In order to discriminate the structural, microstructural and chemical impacts of these elements on the chemical durability, a series of simplified model samples has been prepared by direct precipitation of hydroxide-based precursors. A calcination step (800°C, reducing atmosphere) led to fluorine type oxides. After shaping by uniaxial pressing, a sintering step (1600°C, 8 hours, reducing atmosphere) led to dense pellets (up to 90 % and 96 % for PGM and lanthanide doped samples, respectively, considering geometrical measurements and He pycnometry). In addition, the pellets were characterized in terms of microstructure and cationic homogeneity by SEM and X-EDS.

At the macroscopic scale, leaching tests were performed on all the model compounds in conditions mimicking an interim storage, i.e. at pH = 5 and 7, at 50 and 70°C and in the presence (or not) of boron ($5.0 \cdot 10^{-2}$ M). Simultaneously, the monitoring of the solid/liquid interface was performed by ESEM. The normalized dissolution rate of UO_2 during leaching test in $5.0 \cdot 10^{-2}$ M boric acid, at pH = 7 and 50°C reached about $(5.5 \pm 0.1) \times 10^{-4}$ g.m².d⁻¹ (i.e. 0.04% of dissolved material after 300 days of alteration). The presence of PGM elements induced the significant increase of the alteration rate $(2.0 \pm 0.1) \times 10^{-4}$ g.m².d⁻¹ (i.e. 0.2% of dissolved material after 300 days of alteration). Moreover, this dissolution rate reaches 3.3% in the medium at pH = 5. On the other hand, lanthanide elements induced a particular behavior. Indeed, after 80 days of leaching, the uranium concentration was found to be constant in the leachate, suggesting the precipitation of a secondary U-based phase onto the surface of the pellets. This phase is now under characterization.

4:00 PM EN08.10.06

Detailed Investigation of the Microstructure of UO_2 Based Model Systems for Spent Nuclear Fuel Robert H. Thümmel¹, Juri Barthel¹, Martina Klinkenberg¹, Matthew Wolf², Philip Kegler¹, Roger De Souza², Joachim Mayer¹, Dirk Bosbach¹ and Felix Brandt¹; ¹Forschungszentrum Jülich GmbH, Germany; ²RWTH Aachen University, Germany

In safety assessments for the deep geological disposal of high-level nuclear waste, the possibility and results of direct contact between spent nuclear fuel (SNF) and water are considered. In contact with SNF, oxidative species are continuously produced due to the radiation induced hydrolysis of water, which then corrode the SNF, releasing radionuclides [1]. Radiation induced hydrolysis and oxidative dissolution are relevant for early conditions of deep geological waste disposal - depending on the burn up, for the first 6000 to 8000 years. Oxidative corrosion is typical for metals and unusual for oxide ceramics like UO_2 . For many ceramics, grain boundary (GB) dissolution is the dominant dissolution mechanism. However, a detailed mechanistic understanding of the role of microstructure in SNF corrosion is still largely absent. The details of the grain boundary structure have to this day been the subject of just a handful of studies [2]. In a previous work, the microstructure of high burnup SNF was studied, documenting the change in microstructure across the fuel pellet with distinct microstructural regions [3]. To gain a deeper understanding of the effects of individual components on the dissolution kinetics of the complex SNF, a study on UO_2 model systems is used, with a focus on the microstructure and grain boundaries.

In this project, polycrystalline UO_2 samples are synthesised using a co-precipitation method. Besides pure UO_2 , also samples doped with rare earth elements up to a few mass percent are prepared mimicking fission products in SNF [4]. The success of the synthesis is verified by sample density, XRD and SEM. Further extensive microstructure characterization is performed on polished surfaces using EDX, SEM and EBSD. Statistics on grain size, pore size, grain orientation are presented. In the course of the project corrosion experiments will be performed on these samples.

For the purpose of a more detailed analysis of GB structure and their reactivity under oxidizing conditions, the focus is placed on coincidence site lattice (CSL) GBs. CSL boundaries have a comparatively simple structure, which is feasible for modeling. However, this choice requires in experiment to first identify specific GBs and second to extract thin samples suitable for the subsequent transmission electron microscopy (TEM) investigation. The first problem is solved by an efficient EBSD scanning approach, where measurements are only taken near grain boundaries. A pole-figure analysis is performed to determine the crystallographic orientation of the grains and the boundary in order to solve the second problem by extracting a cross-section thin foil using focused ion beam milling. Target of the TEM measurements is to determine the atomic structure including oxygen lattice positions, which play a role in the reactivity of the grain boundaries. The results of these experiments are used as input and crosscheck in molecular dynamic simulations. The simulations are performed to understand the driving forces responsible for the stability of specific GBs and the influence of dopants.

[1] Shoesmith, D. W., Noel, J. J., Hardie, D., & Ikeda, B. M. (2000). Hydrogen absorption and the lifetime performance of titanium nuclear waste containers. *Corros. Rev.*, 18(4-5), 331-360.

[2] Bourasseau, E., Mouret, A., Fantou, P., Iltis, X., Belin, R.C. (2019). Experimental and simulation study of grain boundaries in UO_2 . *J. Nucl. Mater.*, 517, 286–295.

[3] Gerczak, T. J., Parish, C. M., Edmondson, P. D., Baldwin, C. A., & Terrani, K. A. (2018). Restructuring in high burnup UO_2 studied using modern electron microscopy. *Journal of Nuclear Materials*, 509, 245-259.

[4] Kegler, P., Klinkenberg, M., Bukaemski, A., Murphy, G.L., Deissmann, G., Brandt, F. and Bosbach, D., (2021). Chromium Doped UO_2 -Based Ceramics: Synthesis and Characterization of Model Materials for Modern Nuclear Fuels. *Materials*, 14(20), p.6160.

4:15 PM EN08.10.07

Drying of Spent Advanced Gas Reactor Fuel for Storage and Disposal Thomas O. Bainbridge¹, Nicole Hondow¹, Carlos de la Fontaine² and Bruce

Hanson¹; ¹University of Leeds, United Kingdom; ²TUV Sud, United Kingdom

In 2012 the Nuclear Decommissioning Authority took the decision to cease reprocessing spent Advanced Gas-cooled Reactor fuel, with any fuel arisings beyond the contracted amount to be stored pending a decision on whether to classify the fuel as waste for disposal. If the fuel is deemed waste then it will be sent to the high heat generating part of the UK's Geological Disposal Facility (GDF), expected to be in 2075. The current strategy till then is to use extended wet storage while work is being conducted to support dry storage as an alternative and as a pre-treatment for final disposal. The aim of the drying process is to prevent radiolysis of any water left in or on the fuel pin which could lead to both hydrogen and hydrogen peroxide in either the dry store or the GDF. With hydrogen and hydrogen being of particular concern due to hydrogen being explosive and hydrogen peroxide being corrosive. Regarding wet storage the primary concern is that water may seep through the cladding of any failed fuel with stress corrosion cracking the likely cause of this failure. This mechanism causes highly tortuous and branched cracks making characterisation difficult. This work aims to produce a process model to be used to inform the conditions for a future drying procedure. To achieve this two work streams have been set up. The first beign the computational side where the flow through the cracks in the cladding is being modelled and the second, the experimental side, aiming to produce representative crack to aid in validating the process model. Current progress and results will be presented here.

4:30 PM EN08.10.08

Microstructural Characterization of the Critical Regions of Copper Coatings for Canada's Used Nuclear Fuel Containers Liyang Zheng¹, Jason Tam¹, Alex Zhang¹, Jason Giallonardo², Jane Howe¹, Roger Newman¹ and Uwe Erb¹; ¹University of Toronto, Canada; ²Nuclear Waste Management Organization, Canada

For many decades, nuclear energy has been utilized worldwide as an efficient, stable, and sustainable source of electricity with low carbon footprint; however, with increasing amounts of used nuclear fuel, their proper management and disposal has become a challenging issue. In Canada, the Nuclear Waste Management Organization (NWMO) is responsible for the long-term management of Canada's used nuclear fuel. NWMO is developing a deep geological repository (DGR) that consists of multiple engineered barriers to safely isolate the nuclear waste from the environment. In this design, used Canada Deuterium Uranium (CANDU) fuel bundles will be stored in used fuel containers (UFC), which will then be placed underground at a reference depth of approximately 500 m in a suitable rock formation and sealed with bentonite clay.

The UFC is a core component of the multiple-barrier system. In the current design, the inner vessel of the UFC is fabricated from low carbon steel, which comprises a cylindrical shell welded to two hemispherical heads. A minimum 3-mm thick copper layer is applied to the exterior surface of the steel vessel as a corrosion barrier. Two coating techniques are jointly used to coat the entire UFC: the copper coatings on the cylindrical shell and hemispherical heads are applied via electrodeposition (ED), while after loading the fuel bundles into the container, the head is welded to the shell, and the closure-weld zone is copper-coated by the cold spray (CS) process followed by local annealing to impart ductility.

The expected long service life of the UFCs (~one million years) placed high demands on the structural integrity and corrosion resistance of the copper coating. As two deposition techniques are used, it is essential to develop a deeper understanding of how the processing history affects the microstructure, and in turn, the macroscopic properties of the copper coatings. Specifically, the interfaces where ED-Cu and CS-Cu converge might perform differently from the rest of the coatings due to the inherent structural heterogeneity in these regions. In the current study, detailed characterizations including scanning electron microscopy (SEM), electron backscattered diffraction (EBSD) and transmission electron microscopy (TEM) were conducted on the interfacial regions to reveal the microstructural characteristics of different copper coatings (ED, CS, different annealing temperatures), complemented with hardness measurements.

4:45 PM EN08.10.09

Shelf-Life of Uranium Oxide Microparticle Reference Materials and Possible Implications for the Identification of Optimal Storage Conditions Simon Hammerich¹, Shannon K. Potts², Philip Kegler², Stefan Neumeier², Axel K. Schmitt¹ and Mario Tricloff¹; ¹Heidelberg University, Germany; ²Forschungszentrum Jülich GmbH, Germany

Among other tasks, the International Atomic Energy Agency (IAEA) is responsible to verify the peaceful use of nuclear material and technologies concerning the Non-Proliferation Treaty (NPT). Therefore, the IAEA Safeguards were introduced as technical measures to assure the compliance with the NPT by its member states. To secure this, IAEA officials conduct inspections of nuclear facilities all around the world and – among other measures – take swipe samples of surfaces in said facilities. Cotton swipes with collected particles are then sent to the IAEA Safeguards Analytical Service Environmental Sample Laboratory (IAEA SGAS-ESL) and its dedicated Network of Analytical Laboratories (NWAL) to analyze particle elemental and isotopic composition. The quality of these measurements is dependent on the abundance of suitable reference materials. To qualify as potential reference materials, uranium microparticles must be of a size and shape as well as an isotopic and elemental composition similar to the environmental samples. In the Forschungszentrum Jülich (FZJ), uranium microparticles are produced using a Vibrating Orifice Aerosol Generator (VOAG).

A core requirement for distribution of a potential reference material is to guarantee a practical shelf-life. Previous studies of structure and shape of uranium oxide microparticles demonstrated alteration process leading to the formation of uranium hydroxide like schoepite. To further investigate this alteration process, a systematic shelf-life study of VOAG-produced uranium microparticles has been launched in late 2021. In a first part of this study, the influence of different atmospheric conditions was evaluated. Uranium microparticles from the same production batch were deposited on Glass-like Carbon Disks (GCDs) and stored under different atmospheric conditions. The second part of the shelf-life study is related to the long-term stability in different solvent media. The uranium particles used in both approaches were periodically measured using Scanning Electron Microscopy (SEM) and μ -Raman Spectroscopy for structural as well as Large Geometry-Secondary Ion Mass Spectrometry (LG-SIMS) for isotopic investigation. The combination of these aforementioned methods allows to check the long-term stability of uranium microparticles in suspension and under different atmospheric conditions and therefore identify optimal storage conditions for potential reference materials. In this presentation recent results of atmospheric and suspension shelf-life studies will be discussed.

SESSION EN08.11: Virtual Session I: Nuclear Waste Management
Session Chairs: Daniel Gregg and Josef Matyas
Tuesday Morning, December 6, 2022
EN08-virtual

8:00 AM EN08.11.01

Study on Borehole Sealing Corresponding to Hydrogeological Structures by Groundwater Flow Analysis Takuma Sawaguchi, Shizuka Takai, Tsuyoshi Sasagawa, Emiko Uchikoshi, Yusuke Shima and Seiji Takeda; Japan Atomic Energy Agency, Japan

The leakage of radioactive material shall be monitored for the intermediate depth disposal (e.g., 70–100 m from the surface) of relatively high-level, Category 2, radioactive waste in Japan. At the end of the monitoring period, several hundred years later, the monitoring borehole is backfilled and sealed to prevent potential migration pathways for radioactive materials. However, the diameter of borehole is small (e.g., 20 cm) and the depth is several hundred meters, and thus there is a possibility of insufficient backfilling in the borehole. Therefore, a method to confirm whether the borehole is properly sealed should be developed in advance. In this method, it is important to understand the effect of backfill design condition (material selection, layout, permeability, etc.) corresponding to the surrounding hydrogeological structure on the borehole sealing. In this study, groundwater flow analyses were performed for the hydrogeological structures with backfilled boreholes, assuming sedimentary rock area in Japan, to understand what backfill design conditions could prevent significant or early water pathways in the borehole, and to identify the confirmation points of borehole sealing. The analysis area was around and upstream of the borehole; therefore, groundwater flow to the surface was not evaluated. In these analyses, some kinds of backfill design condition proposals, combining bentonite, sand and cementitious materials based on previous studies [e.g., 1-3], were set for each hydrogeologic structure characterized in predominant water-bearing fractures, in aquifers isolated by clay layer and in faults. Whether or not significant water pathways would be formed in the backfilled borehole was considered using flow rate in the borehole and flow path-lines obtained from the analysis. In these analyses, the effect of grouting BDZ (Borehole Disturbed Zone) on borehole sealing were also considered. It was assumed that the grouting BDZ would restore the permeability around borehole increased by boring to that of host rock.

These results indicated the backfill design conditions to prevent water pathways in the borehole and BDZ, such as designing the permeability of bentonite material less than or equal to that of the host rock, and grouting BDZ. In the case considering clay layers and faults, it was also found that if the borehole in the intact rock immediately above these characteristic structures was not backfilled with bentonite material, significant water pathways would be formed.

Acknowledgments: This research was funded by the Secretariat of Nuclear Regulation Authority, Nuclear Regulation Authority, Japan.

References: [1] Sandén, T. et al., Sealing of investigation boreholes –Full scale field test and large-scale laboratory tests, SKB, TR-18-18 (2018). [2]

Jefferies, N. et al., Sealing Deep Site Investigation

Boreholes: Phase 2. Final Report, RWM/03/046 (2018). [3] T. H. Karvonen, Closure of the Investigation Boreholes, POSIVA Working Report 2012-63 (2012).

8:15 AM EN08.11.02

Corrosion of Nuclear Waste Glass in Complex Natural Environments—A Natural Analogue Approach Clare L. Thorpe¹, Garry Manifold¹, Rachel Crawford¹, Christopher Boothman², Katherine Morris², Jonathan Lloyd², Russell Hand¹ and Claire L. Corkhill¹; ¹University of Sheffield, United Kingdom; ²The University of Manchester, United Kingdom

Borosilicate glass is commonly used to immobilise high activity waste liquors and is increasingly considered for low and intermediate activity waste streams¹. Radioactive elements, chemically incorporated in the glass structure, will be released at the same rate as the glass itself dissolves. Understanding the long-term behaviour of glass is therefore important in constructing the safety case for its storage and eventual subsurface disposal. The majority of studies aimed at understanding glass dissolution rates and mechanisms have been conducted at elevated temperatures and under, static, sterile conditions, taking no account of changing geochemistry, adjacent mineralogy or geomicrobiology². Here, a combination of field and laboratory tests are used to explore the behaviour of glasses in complex natural environments.

Alteration observed on glasses from long-term studies, in neutral - high pH, iron rich environments relevant to the subsurface disposal of radioactive waste, is compared to alteration observed in short-term laboratory based tests. In addition to observing the mineralogy of the glass alteration layers, field experiments also aim to identify and characterise the unique microbial communities that colonise the interface between nuclear waste type glasses and their environment. Under laboratory conditions, inactive surrogate nuclear waste glasses, containing the essential nutrients, had a controlling effect on the microbial community that were able to utilize nutrients dissolved from the glass where they were absent in solution. The influence of microbial respiration on the dissolution rate of the glass was found to be complex with some conditions inducing a pacifying effect due to biomineral precipitation whilst other conditions appeared to enhance glass corrosion.

References:

[1] Thorpe CL et al. NPJ Mat Degrad. 2021, 5, 61.

[2] Weaver JL et al. NPJ Mat Degrad. 2021, 5, 11.

8:30 AM *EN08.11.03

The Importance of Secondary Phase Formation in Natural Aqueous Systems M Nieves Rodríguez-Villagra, L.J. Bonales, Abel Milena-Pérez and Hitos Galán; CIEMAT, Spain

Irradiated fuel based on UO₂ is expected to be disposed of in an underground repository according to a “once-through” fuel cycle policy. In addition, those countries that have chosen reprocessing their irradiated fuel will also need this kind of repository, as there is international consensus on this option as the best to properly dispose high-level waste. In any case, after storage times of several thousand years, it is foreseen and accepted that groundwater will penetrate and infiltrate in the emplacement, and will eventually interact with the spent fuel.

As a consequence of water radiolysis, uranium is oxidized from its tetravalent state to the hexavalent uranyl ion, being known to be far more soluble in water than uranium (IV). Then, during the oxidative dissolution and depending of the surface/volume ratio, secondary phases containing uranyl cationic UO₂²⁺ will precipitate at the whole pH range. These secondary phases play an essential role on the radionuclide release in the final disposal environment due to its capacity to seize trace radionuclides, and then, to reduce radionuclides mobility. In fact, some important radionuclides can precipitate into its inner solid structure (e.g. Schoepite UO₃·2H₂O, Becquerelite Ca(UO₂)₆O₄(OH)₆·8H₂O, Soddyite (UO₂)₂SiO₄·2H₂O, Uranophane (H₃O)₂Ca(UO₂)₂(SiO₄)₂·3H₂O, Studtite UO₄·4H₂O).

The objective of this work is to provide an overview of current knowledge on precipitation and dissolution of potential radionuclide-bearing phases under repository relevant conditions. Different approaches carried out are presented, i.e. long-term behavior of natural analogs such as uraninite [1, 2], short-term laboratory coprecipitation experiments [3] and theoretical studies [4,5]. A review of the analysis methods is also presented.

REFERENCES

[1] L. J. Bonales, C. Menor-Salván, and J. Cobos, "Study of the alteration products of a natural uraninite by Raman spectroscopy," *Journal of Nuclear Materials*, vol. 462, pp. 296-303, 2015/07/01/ 2015.

[2] L. J. Bonales, J. M. Elorrieta, C. Menor-Salván, and J. Cobos, "The behavior of unirradiated UO₂ and uraninite under repository conditions characterized by Raman," *MRS Advances*, vol. 1, pp. 4157-4162, 2017.

[3] J. Quiñones, A. González de la Huebra, and A. Martínez Esparza, "Coprecipitation experiments using simulated spent fuel solution in the presence of metallic iron in synthetic bentonitic-granitic water under oxidising conditions," in *Scientific Basis for Nuclear Waste Management XXVIII*. vol. 824, S. Stroes-Gascoyne, J. Hanchar, and L. Browning, Eds., ed San Francisco. USA: Material Research Society, 2004, pp. 425-430.

[4] F. Colmenero, L. J. Bonales, J. Cobos, and V. Timón, "Study of the thermal stability of studtite by in situ Raman spectroscopy and DFT calculations," *Spectrochimica Acta Part A: Molecular and Biomolecular Spectroscopy*, vol. 174, pp. 245-253, 2017/03/05/ 2017.

[5] F. Colmenero, V. Timón, L. J. Bonales, and J. Cobos, "Structural, mechanical and Raman spectroscopic characterization of the layered uranyl silicate mineral, uranophane- α , by density functional theory methods," *Clay Minerals*, vol. 53, pp. 377-392, 2018.

9:00 AM *EN08.11.04

Durability of Iodine Waste Forms [Bill Ebert](#); Argonne National Laboratory, United States

Radioiodine can be captured from off-gas and other waste streams by reaction with metallic silver to generate AgI, which can then be immobilized by microencapsulation in a durable matrix material. Waste forms can be generated by densifying the material used to support the silver or by vitrification in a low-temperature glass. Both the intrinsic durability of AgI and the durability of the encapsulating matrix will contribute to degradation resistance of iodine waste forms in a high-level waste disposal facility and should be taken into account in degradation models. Although AgI is only sparingly soluble under oxidizing conditions, reduction of ionic silver to metallic silver under even moderately reducing conditions will increase the solubility of iodide. The degradation model that is used to represent iodine waste form behavior in simulations used for repository assessments should include a redox-dependence term. Argonne is using a combination of electrochemical and immersion test methods to quantify the dissolution behavior of AgI alone, in galvanic couples, and encapsulated in inert matrix materials. The conceptual basis, testing methods and results, and mechanically-based model being developed for iodide waste forms will be presented.

9:30 AM EN08.11.05

Application of the ASTM C1308 Semi-Dynamic Dissolution Methodology to Ceramic Materials for Radioactive Waste Immobilisation [Amber R. Mason](#), Lewis Blackburn, Laura J. Gardner, Ismail Aldean, Sarah Pepper and Claire L. Corkhill; University of Sheffield, United Kingdom

Semi-dynamic dissolution experiments were performed using the ASTM C1308 methodology, where the dissolution media is renewed periodically, to understand more about the fundamental chemistry of the corrosion behaviour of ceramic wasteforms [1]. Zirconolite ($\text{CaZrTi}_2\text{O}_7$) and pyrochlore ($\text{Gd}_2\text{Ti}_2\text{O}_7$) have frequently been proposed as ceramic wasteform compositions, due to their passive safety, and are known to be chemically flexible and radiation tolerant with excellent overall aqueous durability [2]. However, a recent literature review highlighted a gap in the understanding of the dissolution mechanism of these wasteforms, which the semi-dynamic nature of the C1308 test could elucidate. In this study, the dissolution of a zirconolite and a pyrochlore composition was investigated using the ASTM C1308 test, with an extensive test matrix, where the temperature (40, 60, 90 °C) and dissolution media (0.01M HNO_3 , FIN groundwater and 0.01M LiCl / 0.011M LiOH) were varied. The results have contributed to the understanding of the application of the ASTM C1308 methodology to ceramic materials dissolution, highlighting the merits of this test procedure compared to other commonly used dissolution protocols. This research also supported the development of a standard operating procedure for a series of round robin experiments with partners worldwide to further verify the efficacy and reproducibility of this methodology (allowing direct comparison between different formulations and wasteforms).

9:45 AM EN08.11.06

Exploring a Surrogate of Pellet-Cladding Interaction—Characterization and Oxidation Behavior [M Nieves Rodríguez-Villagra](#), L.J. Bonales, Sergio Fernández-Carretero, Abel Milena-Pérez, Luis Gutierrez and Hitos Galán; CIEMAT, Spain

The thermal gradient at which the nuclear fuel is subjected during operation is one of the reasons of the deformation caused in the pellet, which could affect to its interaction with the cladding. Thus, a potential pellet-cladding contact could take place because of a decrease in the cladding diameter (creep-down due to pressure from the coolant) and an increase in the pellet diameter (thermal expansion, swelling due to the inclusion of solid fission products in the matrix and inter- and intra-granular accumulation of fission gases in pores). Contact between the pellet and the cladding, through a bonding layer called Fuel Cladding Chemical Interaction (FCCI) layer, first occurs at the inter-pellet spaces while a continuing pellet fragmentation (radial and axial cracks) takes place simultaneously. Previous studies conducted on fuel with burnups higher than 55 MWd/kgU^{-1} showed the formation of a restructured region, named as "rim" structure or High Burn-up Structure (HBS) at the periphery of UO_2 pellets [1]. The risk of enhanced Pellet-Cladding Interaction (PCI) grows with burnup. As the burnup increases, some effects turn out to appear in this new region, such as smaller grains (0.1 μm vs initial grains of $\sim 10 \mu\text{m}$ diameter), lattice contraction controlled by recrystallization, higher porosity, hardness decrease and the closure of pellet-cladding gap in fuel rods [2]. The FCCI layer consists in principle of two regions, one closer to the cladding (cubic polycrystalline ZrO_2) and a second nearer to the fuel pellet, characterized by an interphase formed by cubic solid solutions of $(\text{U,Zr})\text{O}_2$ and an amorphous phase, with variable relative concentrations of U and Zr. PCI is considered as a mid-priority process in the investigation of the safety approach for LWR reactor fuel due to the possibility of cladding failure during a power transient. In addition, it could be one of the causes identified as leading to potential fuel failure. Understanding the potential chemical oxidation resistance of UO_2 (matrix fuel) to U_3O_8 as a consequence of ZrO_2/Zr system in case of undetected damaged cladding (zirconium alloy), a potential air intrusion is relevant in terms of assessing fuel cladding integrity.

To gain insight into the PCI response to oxidation, in the present work, a collection of Zr-doped UO_2 (0, 20, 40, 80 and 100 %) pellets were prepared via solid-state synthesis by mimicking the chemical bonding between ZrO_2 and UO_2 . After sintering, the Zr-doped UO_2 monoliths were characterized by (i) surface morphology and average grain size calculation by SEM; (ii) BET Specific Surface Area (SSA) with N_2 ; (iii) evaluation of the purity and the crystalline structure by both XRD and Rietveld Quantitative Phase Analysis (RQPA); (iv) Raman spectroscopy; and (v) geometrical and experimental density obtained by Archimedeian immersion.

The interpretation of these characterizations shows non-uniform distribution of Zr in the UO_2 matrix and ZrO_2 segregation in grain boundaries, presumably because the solubility limit has been reached in the fabrication procedure. Controlled air oxidation of Zr-doped UO_2 samples has been monitored by thermogravimetric analysis (TGA). Based on those results, we observe a profound effect of delayed oxidation with the addition of Zr to UO_2 , and then, an increased resistance of UO_2 to oxidation to U_3O_8 when compared to pure UO_2 pellet.

[1] K. Lassmann, C. T. Walker, J. van de Laar, and F. Lindström, "Modelling the high burnup UO_2 structure in LWR fuel," *Journal of Nuclear Materials*, vol. 226, pp. 1-8, 1995/10/01/ 1995.

[2] U. S. NRC, "Standard Review Plan for Dry Cask Storage Systems Final Report," Washington 2010.

9:50 AM EN08.11.07

Measurements of Thermodynamic Data of Water in Na-Bentonite in the Standard Condition by Relative Humidity Method [Haruo Sato](#); Okayama University, Japan

Buffer material (compacted bentonite) composing engineered barrier in the geological disposal of a high-level radioactive waste develops swelling stress (pressure) by penetration of groundwater from the surrounding rock mass after disclosure. In the past studies, we measured the activity of water and the Gibbs free energy (relative partial molar Gibbs free energy) of water in Na-montmorillonite which is the major component of Na-bentonite by vapor pressure method, and reported a model to analyze the swelling stress of bentonite based on thermodynamic theory. On the other hand, data for the vapor pressure of water in bentonite are limited. In this study, we determined vapor pressure by measuring relative humidity (RH) and temperature for water in Na-bentonite and Na-montmorillonite, and calculated the activity of water and the Gibbs free energy. In addition, we analyzed the swelling stress of bentonite based on the thermodynamic model and discussed by comparing to data reported so far.

Kunigel-V1® and Kunipia-F® (provided from Kunimine Industries Co. Ltd.) were used as a Na-bentonite. The montmorillonite contents of both bentonites are approximately 51 % and 99 %, respectively. Bentonite powder which was dried at 105-110 °C for at least 24 hours in an oven was placed in a polyethylene bottle in an amount of 3.00 g each (repeatability n=3), and slowly adsorbed water vapor in a closed container (vacuum chamber) with 100 % RH for about 9 months. The water content of the bentonite was checked by weighing periodically. Next, RH and temperature sensors and moisturized bentonite powder were placed in the vacuum chamber, and the chamber of which inside pressure was reduced to -95 kPa (6.3 kPa with absolute pressure) or less was submerged in a constant temperature water bath at 25 °C. The RH and temperature in the chamber were measured after 24 hours and the weight of the bentonite was measured. The bentonite sample was returned to the chamber again and the water content of the bentonite was reduced by evacuating for a while, and then the chamber was submerged in a constant temperature water bath again. This operation was carried out every about 24 hours. Thus, RH and temperature were measured as a function of water content (ca. 10-100 %), and the activity of water and the Gibbs free energy as a function of water content were determined.

The activities of water and the Gibbs free energies for both bentonites decreased with decreasing water content in water contents lower than approximately 40 %. This trend is the same as the trend obtained in the past studies. On the other hand, the data (both activities of water and the Gibbs free energies) obtained in this study were slightly higher than conventional data. This indicates that the swelling stress of bentonite slightly decreases than conventional analysis results. This is considered to be due to that conventional data were obtained for purified Na-montmorillonite (no impurities). Although the swelling stresses of bentonite calculated using thermodynamic data obtained in this study were slightly lower than conventional analysis results, those were closer to the measured values than the conventional analysis results.

9:55 AM *EN08.11.08

Molten Salt Fast Reactor with End of Live Waste Disposal or Recycling? Claude A. Degueldre, Joshua Findlay and David Cheneler; Lancaster University, United Kingdom

The Molten Salt Fast Reactor (MSFR) liquid fuel is made of uranium chloride dissolved in sodium or rubidium chloride. ²³⁵U enrichment goes from 0.3% (depleted) for power plant to 20% enriched for research reactor. At End of Live (EoL) the fuel cycle strategies go from the once through then out i.e. full geological disposal (spent fuel, core vessel and structural's of primary) to spent fuel and primary loop material reprocessing and recycling. The late case is emphasized when the chloride of the fuel and from the reflector are made of ³⁷Cl enriched chloride and has to be reprocessed and recycled for economical reason in new fuel and reflector.

The first option would require addition of neutron absorber prior to final geological disposal in a water free environment e.g. in salt dome. The option of Molten Salt drainage in specific tank designed for radwaste disposal would be associated with intelligent barrier to minimise first nuclide release such as ³⁶Cl and ¹²⁶I. Among them Ag or Cu barriers could be envisaged.

The second option deals with the Na/Rb³⁷Cl - ^{depu}U³⁷Cl₄ spent fuel in which case ³⁷Cl has to be, for economic reason, reprocessed for recycling. In memory of Lou Vance, Ansto

10:25 AM DISCUSSION TIME

SYMPOSIUM EN09

Sustainable and Renewable Materials—From Fundamental Science to Applications
November 28 - December 6, 2022

Symposium Organizers

Bichlien Nguyen, Microsoft Research
Eleftheria Roumeli, University of Washington
Julie Schoenung, University of California, Irvine
Ashley White, Lawrence Berkeley National Laboratory

Symposium Support

Bronze

ACS Sustainable Chemistry & Engineering

* Invited Paper
+ Distinguished Invited

SESSION EN09.01: Sustainable Polymers I—Data-Driven Sustainable Polymers
Session Chairs: Bichlien Nguyen and Eleftheria Roumeli
Monday Morning, November 28, 2022
Hynes, Level 3, Room 306

10:30 AM *EN09.01.01

Harnessing the Power of Natural Products Towards the Synthesis of High Performance Materials Samantha L. Kristufek; Texas Tech University, United States

Society is highly dependent upon plastics to add value to everyday life, however, the end-of-life products are highly problematic, especially when they enter into our waterways, crowd our waste streams, and produce nanoplastics that get into the environment. Sustainable polymers have the potential to overcome many of these challenges. Particularly, polymers derived from sugars or polyphenolic compounds that contain degradable moieties in the backbone are of great promise. Through the synthetic manipulations of these natural products, we aim to produce and characterize high performance materials.

11:00 AM EN09.01.02

Manufacture of PHB-Based Biodegradable Composite Film and Evaluation of Mechanical Properties Kwan-Soo Lee, [Jihyeon Kim](#), Nevin Gupta and Jacqueline A. Linn; Los Alamos National Laboratory, United States

Biodegradable plastics can be decomposed into water, carbon dioxide, and biomass by the action of living organisms, typically micro-organisms. Biodegradable plastics are commonly produced with renewable raw materials, micro-organisms, petrochemicals, or combinations of all three. These plastics have been considered as a promising solution to troubleshoot the plastic pollution problem bedeviling the world. Currently, most of biodegradable plastics such as PLA, PBS, PBAT, and PBSA, are degraded in well-managed industrial composting systems providing the specific environments. If products made from these plastics are discarded into conventional waste streams such as landfills, or find their way into the open environment such as rivers and oceans, the potential environmental benefits of the biodegradable plastics are not exploited and can actually exacerbate plastic pollution problems.

Polyhydroxyalkanoates (PHAs) are a class of biodegradable polymers that produced from various micro-organisms. Specific types of PHAs include poly-3-hydroxybutyrate (PHB)s. PHBs have been shown to be biodegradable in less than about one year in various natural and biologically active environments even without the industrial composting systems. Furthermore, PHB's properties are similar to those of conventional petroleum-based polymers (e.g. melting temperature, young's modulus) such as polypropylene (PP), polyethylene (PE), and polyethylene terephthalate (PET). On the other hand, the use of pure PHB has been restricted due mainly to its inherent brittleness, which renders it too frangible for most practical applications. In this study, we have developed a new component of PHB-based polymer composite films using various green additives to overcome the mechanical instability of PHB and optimize the film condition. As a result, the bioplastics films prepared show huge potential, offering 30 times increase of the elongation property with decreasing the melting temperature and the degree of crystallinity. In this presentation, some prototypes of PHB-based packaging (e.g. disposable label, bag) which LANL has developed, will be presented.

11:15 AM EN09.01.03

Intercepting Intermediates in the Depolymerization of Poly(ethylene terephthalate) Shelby Watson-Sanders, Joshua Moncada and [Mark Dadmun](#); University of Tennessee, United States

There is a need to develop new processes for end-of-life plastics to limit waste accumulating and contaminating our environment. One possibility is the chemical recycling of polymer, such as the depolymerization of polyethylene terephthalate (PET). PET is one of the most widely used commercial plastics, which can be depolymerized via glycolysis. In order to broaden the available products from the depolymerization process, we are interested in understanding the evolution of chain structure during chemical recycling. This study therefore monitors the evolution of chain structure in the depolymerization of PET in a heterogeneous reaction as a function of catalyst and reaction temperature. PET, sourced from Coke bottles, is depolymerized by glycolysis catalyzed with the salt of Triazabicyclodecene (TBD) and methanesulfonic acid (MSA) (1:1) or Zinc Acetate (ZnAc) in heterogenous reactions with ethylene glycol (EG). PET was depolymerized with TBD:MSA at 180 C, and with ZnAc at 165 C, 175 C and 185 C. Products of each depolymerization reaction were taken at predetermined intervals to monitor the evolution of chain structure. The chain size as a function of reaction time was determined by NMR (M_n) and intrinsic viscosity (M_v), offering a measure of chain length and dispersity of the chain length (i.e. M_w/M_n) with reaction time.

The depolymerization process entails the interfacial reaction of the EG and insoluble PET, where progress of the reaction forms smaller PET chains that become soluble in EG. This analysis follows the decrease in chain length, and solubility of depolymerized PET in ethylene glycol. Comparison of the two catalysts shows that the decrease in chain length occurs more quickly in the ZnAc catalyzed reaction than the TBD:MSA, where increasing temperature increases the rate of depolymerization. Correlation of reaction rate to change in solubility is underway. Monitoring the dispersity of the PET in the reaction vessel shows that the polymer chain size distribution becomes narrower with depolymerization. These results will therefore provide insight into the mechanism that controls the chain depolymerization and available products from the depolymerization reaction over the course of the reaction.

11:30 AM EN09.01.04

Informatics Pipeline to Identify Polymers Capable of Controllable Depolymerization [Aubrey R. Toland](#), Huan Tran, Lihua Chen, Yinghao Li, McKinley Paul, Kellie Stellmach, Chao Zhang, Will R. Gutekunst and Rampi Ramprasad; Georgia Institute of Technology, United States

Enthalpy of polymerization is a key thermodynamic property to determine if a polymer can be controllably degraded to monomer feedstock at the end-of-use, a capability essential to mitigating the global polymeric waste problem. Due to the favorable thermodynamics of ring opening polymerizations (ROP) in creating depolymerizable polymers, the enthalpy of ROP (ΔH^{ROP}) is the focus of this study. Thanks to a recently developed first-principles computational scheme, a high-quality database for computed ΔH^{ROP} has been developed in order to help overcome the issue of data scarcity present in the current literature. Using this computational database, along with the limited experimental data present in literature, a data-fusion approach has been adopted to create a machine learning (ML) model capable of predicting experimental ΔH^{ROP} near chemical accuracy, ~ 5 kJ/mol. This ML model is then used in conjunction with the first-principles computational method to create a pipeline where the ML method screens the massive chemical space that makes up ROP chemistries, and the most promising candidates are then passed to the first-principles calculations for validation. This iterative process exploits the ML model uncertainty as well as discrepancies between ML predictions and first-principles calculations to create active learning cycles used to optimize the generalizability of the ML model. This informatics pipeline provides an important step towards creating an automated process for the discovery and design of depolymerizable polymers, meant specifically to create plastics that can truly be sustainable.

11:45 AM EN09.01.05

Data-Driven Property Prediction for Accelerated Discovery of Molecular Additives in Robust yet Chemically Deconstructable Thermoset Plastics [Yasmeen S. AlFaraj](#)¹, [Somesh Mohapatra](#)¹, [Peyton Shieh](#)¹, [Keith Husted](#)¹, [Douglas Ivanoff](#)², [Evan Michael Lloyd](#)², [Jeffrey Moore](#)², [Nancy Sottos](#)², [Rafael Gomez-Bombarelli](#)¹ and [Jeremiah Johnson](#)¹; ¹Massachusetts Institute of Technology, United States; ²University of Illinois at Urbana-Champaign, United States

Novel materials discovery approaches are imperative to address time-critical challenges in materials design. Considering that discovery typically precedes and inspires applications, traditional screening methods often rely on arduous and inefficient experimental processes requiring the identification of novel molecules prior to application determination. Recent breakthroughs in data-science approaches have shown great promise for accelerating materials design cycles by leveraging pre-existing data to learn composition-processing-performance models which feed into active learning cycles in experimental lab spaces. However, non-standardized experimental acquisition strategies and sparsity in dataset size variability limits the ability to utilize data-driven

methods for advances in the low-data regime. One such application with limited available data and which poses a time-critical environmental challenge includes the development of thermoset plastics with accessible pathways to deconstructability for improved end-of-life practices and possible reprocessing. More notably, the retention of desirable thermomechanical properties whilst introducing viable pathways to deconstructability remains a challenge. In this work, we propose the use of an ensemble of machine learning models with variable architectures, each trained on distinct parts of a training dataset consisting of data on deconstructable polydicyclopentadiene (pDCPD) thermosets, to overcome the limitations of said low-data regime. We report a closed-loop discovery approach rooted in experimental synthesis, machine learning, and virtual screening to discover potential cleavable comonomer additives (CCAs) which, when introduced in low quantities in accordance with the reverse-gel-point model, enable the degradation of thermosets without compromising desirable thermomechanical properties. Moreover, our approach allows for concurrent prediction of resultant bulk materials properties, introducing tunability into the design process. In this work, we show it is possible to train accurate models on reconstructible pDCPD systems with as few as 101 data points to screen new chemistries and synthetic conditions, whilst predicting and experimentally validating glass transition temperatures within reasonable accuracy. This work lays a ripe foundation for the translation of closed-loop data-driven design cycles for the development of other reprocessable thermoset plastics with tailored thermomechanical properties.

SESSION EN09.02: Sustainable Polymers II—Converging Sustainable Materials Education Efforts/Roundtable

Session Chairs: Samantha Kristufek and Eleftheria Roumeli

Monday Afternoon, November 28, 2022

Hynes, Level 3, Room 306

2:00 PM *EN09.02.01

Sustainable and Degradable Epoxy Resins Containing Multifunctional Lignin-Based Components Megan Robertson, Minjie Shen, Rosalie Berg and Venkatesh Balan; University of Houston, United States

Lignin was investigated as a sustainable source to produce epoxy resins with desirable physical behavior. Epoxy resins are thermoset polymers widely used in composites, coatings and adhesives, with applications spanning automotive and aerospace industries, structural components, and wind turbine blades, among others. Vanillic acid, a product of lignin depolymerization, was investigated as a replacement for conventional diglycidyl ether of bisphenol A (DGEBA) in anhydride-cured epoxy resins. The resulting vanillic acid-based epoxy resins exhibited high glass transition temperatures and similar elongation at tensile behavior as compared to DGEBA-based epoxy resins. The ester groups in the cured network were also leveraged to enhance the end-of-life options for the epoxy resins. The accelerated hydrolytic degradation behavior of the epoxy resins was explored, through monitoring the mass loss after exposure to basic or acidic solutions at moderate temperatures. The vanillic acid-based epoxy resins exhibited rapid degradation, in contrast to the slow degradation rate of the DGEBA-based epoxy resin. The mass loss behavior showed good agreement with predictions with a solid-state kinetic model and chemical analyses confirmed the degradation mechanisms were surface and bulk erosion in basic and acidic solutions, respectively, through ester hydrolysis.

2:30 PM *EN09.02.02

Facile Chemical Modification of Lignin for Synthesis of Lignin-Based Sustainable Polymers Hoyong Chung and Sundol Kim; FAMU-FSU College of Engineering, United States

Lignin is abundant and low-cost biomass polymer that has high concentration of aromaticity. Therefore, the lignin may provide high mechanical and thermal properties which are not easily available from other bioplastics. In addition, because lignin is not a human food, the supply and cost are very stable. However, a natural lignin cannot be used as an original form because of its poor processibility and compatibility with other materials. This presentation will discuss 1) chemical modification of lignin for further material applications and 2) synthesis of well-defined degradable lignin-based polymers. Commonly available kraft lignin, byproduct of paper industry, is not readily processible to produce commodity polymers due to its poor compatibility to other polymers. Thus, a new technology is developed to modify the lignin that possess carboxylic acids in the presence of capping agents. Herein the addition of capping agent is critically important because the capping agent deactivates excessive number of active functional groups on lignin. The remaining a few selected functional groups of lignin works for the next reaction. Without the capping agent, the lignin-based polymer proceeds to unwanted reactions through the excessive functional groups. The unwanted reactions led solubility change and brittleness of the yielding polymers. The modified lignin was then used for a new polyester synthesis. The new lignin-based polyester is a graft copolymer (lignin-graft-poly(ethylene brassylate)) that has strong and stable covalent bonds between lignin and poly(ethylene brassylate) rather than blending of two polymers. The new polymer's main linkage, ester, is scientifically proven biodegradable functional group in natural conditions. The new lignin modification and polymer synthesis method will enable to produce 100% biomass-based and completely biodegradable commodity polymers.

3:00 PM BREAK

3:30 PM *EN09.02.05

Biogenic and Bioinspired Functional Materials for Sustainability Ulrike G. Wegst; Northeastern University, United States

The creation, use and disposal of any engineering product carry with it an environmental burden. On the one hand, materials contribute much to the environmental impact of a product over its lifetime, on the other, materials offer considerable potential to minimize a product's environmental burden. The sustainable and circular economy, which we increasingly desire, requires the development, informed selection and application of new materials that—without compromising product quality—are lighter and less energy intensive, create less toxic by-products, enable a longer product life, are more easily recycled, and whenever possible, use non-critical, renewable or biogenic resources. Presented will be examples for the design and manufacture of biogenic and bioinspired functional materials and how these can be integrated into teaching strategies and tools in support of eco-design and eco-audits, which introduce students to a holistic approach to environmentally-conscious materials selection and its importance at the early stages of the design process. Illustrated will be, how through case studies on the environmentally-conscious redesign of an existing product, students learn to identify and focus on the life phase with the greatest environmental impact, how a trade-off analysis of energy cost of function versus pecuniary cost of function can guide decision making for a given set of design constraints, and whether, in fact, offering a service that would provide the same service unit of the existing product, but at a reduced footprint over the entire life cycle, might be the better solution. Finally, introduced will be the 'Discover Materials!' a "please touch" materials library and exhibition, which links physical materials and product examples, sustainable or not, with software- and web-based selection and information tools and the processes available to students in workshops on campus, in which students can turn materials into technical solutions to engineering problems, or art, or both.

4:00 PM *EN09.02.06

Educating about Critical Raw Materials and Life Cycle Sustainability Assessment Vakhitova Tatiana Vadimovna; Ansys Ltd., United Kingdom

Materials Criticality is not a new topic, but it is taking a stronger place in sustainability discourse now due to various factors, such as an increased complexity and globalisation of supply chains, proliferation of frameworks for Environmental Social and Governance performance (ESGs) disclosure for companies to name just a few. Social risk, related to materials, is getting more and more recognised, similar to environmental impact or a price volatility risk. More research and teaching on the topic of critical raw materials is taking place. An example is a Massive Open Online Course SusCritMOOC, developed by consortium of academics and industry representatives, initiated and funded by the European Institute of Innovation and Technology (EIT RawMaterials). This MOOC has now run on EdEx several times with satellite online and onsite events. In this talk we discuss the topics, surrounding critical materials and how they could be integrated in teaching, provide example of a tool to introduce Social Life Cycle Assessment – Social Impact Audit Tool, developed in-house at Ansys, and, taking a step further, showcase an approach to Life Cycle Sustainability Assessment (LCSA), as a framework for integrating social, economic and environmental impact of a product, based on Mike Ashby's latest LCSA methodology (Ashby, 2022). This is an approach to be used in education and for decision-making.

4:30 PM ROUNDTABLE ON INTEGRATING SUSTAINABLE MATERIALS IN EDUCATION

SESSION EN09.03: Poster Session I: Sustainable Materials

Session Chairs: Bichlien Nguyen and Eleftheria Roumeli

Monday Afternoon, November 28, 2022

8:00 PM - 10:00 PM

Hynes, Level 1, Hall A

EN09.03.01

Bioinspired Amphoteric Sorbent for Water Remediation Kelvin Adrah, Hemali Rathnayake, Sheeba Dawood and Sujoy Saha; University of North Carolina Greensboro, United States

According to UN estimates, 4 billion people will lack access to safe drinking water by the year 2025. This projection can be attributed to rising population and industrialization, resulting in an insurgence of pollutant deposition in water bodies. Heavy metals have been identified as common inorganic contaminants produced in significant amounts by battery manufacturing, metal plating, and mining industries, among other industries. Consumption of these dissolved species in ultra-trace amounts is hazardous to human health. Current water treatment methods such as ion exchange and reverse osmosis are time consuming, generate waste, and costly. Presently, adsorption technology has been adopted in water purification systems to remove heavy metals from water resources due to its effectiveness and low cost, but lacking the high adsorption, environmental sustainability, and versatility. This project aims at overcoming these technical barriers by developing a novel sorbent from biomass by products with high porosity, and high surface area with amphoteric surface properties for selective cleansing of heavy metals in surface water. The sorbent of hierarchical microstructures with a robust metal-organic framework was synthesized by catenating the naturally occurring tannic acid with iron (II) acetate in an aqueous media. The synthesis method follows the green chemistry principles, offering an energy-efficient versatile synthesis method. The chemical composition, shape, physicochemical properties, and colloidal stability of microstructures were investigated using a wide range of characterization techniques. Supporting their amphoteric sorption, Fe (III)-TA microstructures efficiently removed Ag^+ and Cd^{2+} from a highly alkaline synthetic water, with > 96% removal efficiency. Experimental data fitted into Langmuir, Freundlich, and Temkin adsorption isotherms and Pseudo first and second order kinetic models suggests a monolayer adsorption of Ag^+ and Cd^{2+} onto the surface of the microstructures. The effective adsorption of metal ions onto the microstructures is attributed to the highly branched and hydroxyl dense polytopic tannic acid ligand, which provides multiple bonding sites through diverse chemical interactions. These highly porous, amphoteric polyphenol-based metal organic coordination polymers synthesized under environmentally benign conditions are cost-effective and easy to scale-up for pilot or industrial applications. Thus, they offer a great potential for use in tertiary treatment of water remediation.

EN09.03.02

Turning Waste Into Wealth—From Fly Ash to Highly Functionalized Graphitic Anodes by Laser Irradiation for Advanced Sodium-Ion Batteries Eman Alhajji and Husam N. Alshareef; King Abdullah University of Science and Technology, Saudi Arabia

The urgency to develop sodium-ion batteries (NIB) as an eco-friendly alternative to lithium-ion batteries and the issue of massive waste generated by the linear carbon economy are at their peaks. However, the limited sodium-ion intercalation capacity of graphitic anodes hinders the utilization of NIBs, while the costly treatment processes of waste make recycling unfeasible. Laser irradiation of fly ash is an effective approach to enhance Na-ion storage and energy density while simultaneously upcycle waste into a high-value functional material (LFAC). This approach yields three synergistic benefits (1) structurally transforming a soft carbon material into a highly ordered graphitic nanomaterial, (2) increasing carbonylic functional groups on the surface of the electrode, and (3) efficiently producing an additive and binder-free electrode. LFAC anodes exhibit a high first discharge specific capacity of 450 mAh g^{-1} at 0.1 A g^{-1} whereas FAC anodes exhibit 285 mAh g^{-1} . LFAC anodes deliver three times higher capacity than the untreated material, an enhanced reversible capacity of 250 mAh g^{-1} at the current density of 0.1 A g^{-1} after 100 cycles, indicating a slow capacity degradation of 0.2% decay per cycle. In contrast, FAC electrodes demonstrate a low reversible capacity of 80 mAh g^{-1} at a current density of 0.1 A g^{-1} and capacity degradation of 0.3% decay per cycle after 100 cycles. The high intensity of carboxylic functional groups on the surface of LFAC breaks the barriers of Na ion intercalation by increasing the adsorption energy of sodium and enhancing its ion diffusion.

EN09.03.04

Tacky-Free Polyurethanes Pressure-Sensitive Adhesives by Bio-Based Thermoplastic Polyurethane Design from Eco-Friendly Isosorbide Ji-Hong Bae, Won Bin Lim, Jin-Gyu Min, Ju-Hong Lee, Si-Woo Kim and PilHo Huh; Pusan National University, Korea (the Republic of)

A series of Isosorbide-based thermoplastic polyurethanes (ISB-TPUs) were newly developed through the synthetic process by reacting methylene diisocyanate, poly(ethylene glycol) (PEG), and bio-based material isosorbide (ISB) for chain extender based on the different HDI/HDI trimer ratios. The structures of ISB-TPU series were analyzed by Fourier transform infrared spectroscopy and gel permeation chromatography. The changes in the thermal and physical properties due to the hard segment crystallinity were also measured by thermogravimetric analysis, differential scanning calorimetry and universal test machine. The sticking properties of polyurethane pressure-sensitive adhesives (PU-PSAs) depended on both the HDI/HDI trimer ratio and crosslinking-agent composition in the formulation. The differences in the crosslinking-density significantly affected the cohesion, adhesion, and tack in PU-PSA. The formulation of 50 wt% 600PEG and 50 wt% crosslinking-agent and an HDI/HDI trimer ratio of 1.0 led to the optimal balance between the

adhesion and cohesion properties owing to the sufficient tack, high 180-peel strength, and good cohesion. The results showed that biopolyol used in polyurethane can be applied according to the characteristics required in eco-friendly products fields.

EN09.03.05

Reliability and Lifetime of Chemically Sintered Printed Zinc for Highly-Conductive Biodegradable Antennas Carol Baumbauer¹, Anupam Gopalakrishnan², Alyssa Umino¹, Gregory L. Whiting² and Ana C. Arias¹; ¹University of California Berkeley, United States; ²University of Colorado Boulder, United States

Biodegradable or transient electronics are a class of electronics that break down under physiological or environmental conditions into harmless components, offering a solution to the problem of electronic waste generation. Biodegradable electronic devices need conductors to serve as interconnects as well as antennas or inductive loops for wireless power transfer and data communication. In these antennas, conductivity is crucial for functionality, but the majority of biodegradable conductors are significantly less conductive (on the order of 10^3 S/m or less) than their non-degradable counterparts like evaporated copper or printed silver. Additionally, many existing printed biodegradable conductors have functional lifetimes measured in minutes or days, which can be useful in some applications, but is insufficient for applications in which weeks' or months' of data is desired. Higher conductivity, longer-lasting biodegradable conductors are needed.

In recent years, printed zinc treated with acetic acid solution has emerged as a promising biodegradable, highly conductive material, with conductivity greater than 10^5 S/m possible. The low-temperature nature of this process makes it compatible with many biodegradable substrates, which cannot withstand thermal sintering processes. The acid treatment conditions—concentration, exposure time, drying temperature, and drying time—needed to achieve high conductivity are very precise. Small deviations from optimal conditions can cause conductivity to fall by more than four orders of magnitude, rendering devices unusable. These optimal acid treatment conditions also depend on which polymer is used as the ink's binder and on the substrate. Here, we present the optimization of chemically sintered zinc traces, taking binder and substrate material into account. The resulting traces maintain their conductivity for a few weeks.

EN09.03.08

Degradable Silyl Ether-Based Thermoset Under Acidic Condition Boyun Choi and Ho Sun Lim; Sookmyung Women's University, Korea (the Republic of)

Recently, as plastic usage increases, the environmental pollution due to plastic waste is becoming severe. Incomplete degradation of waste plastics produces microplastics, which are difficult to remove by their small sizes. Microplastics, harmful to human health, flow into the marine ecosystem and accumulate in the human body. Many researches are being conducted to develop degradable polymers. However, thermosetting plastics such as epoxy resin used in various industrial fields are still challenging to degrade. In this study, we developed a degradable epoxy thermoset using silyl ether derivative as a curing agent that easily hydrolyzed under acidic or basic conditions. The synthesized silyl ether derivatives were mixed with bisphenol A and formed network structures through thermal curing. To compare the effects of degraded behaviors on the chemical structures of curing agents, we used several types of silyl ether derivatives having different functional groups. The weight loss of the cross-linked epoxy network immersed in HCl solution for a certain time was observed the degradable behavior. As a result, it was confirmed that the crosslinked epoxy network was completely degraded. In addition, curing agents having more sterically hindered functional groups exhibit a slow degraded rate. The results suggest that curing agents containing silyl ether bonds can form the degradable epoxy network, and the rate of degradation can control by chemical structure.

EN09.03.09

Isosorbide-Based Organic-Inorganic Hybrid Materials for Green Chemistry Gwang-Mun Choi, Ki-Seok Jang, Jin-Hyuk Oh, Jiho Joo, Chanmi Lee, Ho-Gyeong Yun, Seok Hwan Moon, In-Seok Kye, Yoon-Hwan Moon, Kwang-Seong Choi and Yong-Sung Eom; Electronics and Telecommunications Research Institute, Korea (the Republic of)

Bio-based plastics using an isosorbide, a 100% biomass obtained from corn starch, have received much attention in last decade due to the demand for low carbon, sustainable growth. In particular, researches on synthesis of isosorbide-based curable resins have been extensively conducted to replace petrochemical-based ones. For example, there are two well-known synthetic methods: an isosorbide-based epoxy resin via etherification reaction of isosorbide with epichlorohydrin¹; an isosorbide-based (meth)acrylic resin via esterification reaction of isosorbide with (meth)acryloyl chloride². However, these methods do not satisfy the green requirements because epichlorohydrin and (meth)acryloyl chloride are severe toxic chemicals for which special precautions is required. Besides, to the best of our knowledge, the isosorbide-based curable resin, which shows superior properties compared with the petrochemical-based one, has not been reported yet. In this study, we demonstrate novel bio-based organic-inorganic hybrid curable resins synthesized by reaction of isosorbide with organofunctional alkoxysilanes. The molecular structure was investigated based on comprehensive understanding by FT-IR, GPC, and NMR analysis, which revealed that isosorbide and alkoxysilane were chemically linked by silyl ether and siloxane bonds. In addition, the thermomechanical properties of cured materials using the isosorbide-based organic-inorganic hybrid curable resins were characterized using DSC, TGA, and rheometer, which showed outstanding properties compared with the petrochemical-based one. For green and sustainable chemistry, we think our material solution can replace petrochemical-based ones and be applicable to advanced semiconductor and display fields.

References

1. J. Hong, D. Radojčić, M. Ionescu, Z. S. Petrović and E. Eastwood, Advanced materials from corn: isosorbide-based epoxy resins. *Polym. Chem.*, 2014,5, 5360-5368
2. Santosh K. Yadav, Kevin M. Schmalbach, Emre Kinaci, Joseph F. Stanzione, Giuseppe R. Palmese, Recent advances in plant-based vinyl ester resins and reactive diluents, *European Polymer Journal*, 2018,98, 199-215

EN09.03.10

A Highly Self-Healable Elastomer Based on Urea Oligomeric Blocks for the Enhanced Mechanical Properties and Long-Term Storage Stability Kiwon Choi¹, Yong Ju Kim¹, Ahyeon Noh¹, Sung Woo Hong² and Min Jae Ko¹; ¹Hanyang University, Korea (the Republic of); ²Korea Institute of Industrial Technology, Korea (the Republic of)

Flexible electronics are enjoying a renaissance with the 4th industrial revolution. However, the change of form factor toward flexibility requires replacing the hard glass with the flexible elastomer as a protective coating layer. The softened surface suffers from repeated cracks and scratches. To address these issues, two kinds of elastomers are developed to strengthen surface hardness and to give self-healing properties. Herein, a highly self-healable elastomer with superior optical and mechanical properties is synthesized based on the urea oligomer in this study. Acrylate-based polyol, linear urea oligomer with isocyanate group at both ends, and cross-linker containing multiple isocyanate groups are blended and the resulting blended precursor is reacted to generate the self-healable elastomer (EUo). The process of oligomer synthesis of urea can successfully ensure processability, thus avoiding potential reactor fouling during commercialization. EUo exhibits a high transmittance (~92%) and low yellow index (~1.5), which makes it applicable to optical-electronic devices as a protective film. The elastomer based on urea oligomer shows remarkable self-healing efficiency (94%), which is extremely enhanced compared to

conventional elastomer without urea oligomer (47%) and the elastomer based on urea diol (62%). This result is due to the strong hydrogen bonding interaction between urethane and urea groups, and we thoroughly analyze this result through a modeling system of FT-IR spectroscopy. Moreover, the strong hydrogen bonding produces a secondary cross-linking network, resulting in enhanced tensile strength (43 MPa) and surface hardness (0.177 GPa). This study suggests a facile strategy that can overcome the conventional trade-off between self-healing property and mechanical robustness that limit the application of self-healing polymers.

EN09.03.12

Green Synthesis of Amino Acid-Based Poly(Ester Urea)s [Katharina Fransen](#) and Bradley Olsen; Massachusetts Institute of Technology, United States

Industrial biotechnology has provided the polymer chemistry community with access to a wide variety of monomers that have traditionally been difficult to synthesize via fossil-fuel based chemistry, leading to new replacements for many of our unsustainable chemistries with both biomass-based and biodegradable polymers. While polyesters based on molecules like furan-dicarboxylic acid (FDCA), ethylene glycol, lactic acid, and 1,3-propanediol have attracted the most attention, these represent a small fraction of all possible polymers and are suitable replacements for only a fraction of synthetic polymers in use today. A complementary set of materials that may be useful for replacing many polyurethanes and polyamides is poly(ester urea)s (PEUs), a known class of biodegradable polymers that can be synthesized from a wide range of amino acids and diols that are easily produced via fermentation in high yield. The monomer chemistry of PEUs consists of both a diol and amino acid, presenting broad opportunities for structural manipulation and tunability to specific applications. However, existing synthetic routes for PEUs are time-consuming, carbon inefficient, and utilize toxic materials necessitating the development of a green chemistry route to produce these promising materials sustainably. We have developed a greener approach to the synthesis of these polymers, making them a truly sustainable biomass-derived and biodegradable chemistry.

EN09.03.14

Closed Loop Recycling of High T_c Biodegradable Polymers by Reactive Distillation [Connor Gallin](#), Won-Woo Lee, Jiangwei Liu and Jeffery Byers; Boston College, United States

A closed loop cycle for polymer production and disposal is needed to handle the estimated half a billion metric tons a year of polymer that will be used by 2050. Current methods for polymer recycling are insufficient to meet this need. Herein, we disclose a simple and inexpensive catalyst system that can readily and selectively depolymerize polyesters and polycarbonates with high ceiling temperatures ($T_c > 200$ °C) back to their constituent monomers. Quantitative recovery of the depolymerized monomer was demonstrated for a variety of aliphatic polyesters and polycarbonates, including the stereoretentive depolymerization of poly(lactic acid) and the depolymerization of polyethylene-like poly(pentadecalactone). The catalyst was readily recyclable for multiple depolymerization batches using the same distillation apparatus, making the method readily adaptable to continuous feed distillations. The catalyst is also capable of carrying out selective depolymerization from a mixture of post-consumer polymers. Finally, monomer recovered from the reactive distillation reactions can be used without further purification to reform the polymer, closing the loop for polymer recycling.

EN09.03.16

Silica Aerogel Preparation and Characterization from Rice Husk by Ambient Pressure Drying [Yang m. Gu](#)^{1,2} and Jin Hyung Lee¹; ¹Korea Institute of Ceramic Engineering & Technology, Korea (the Republic of); ²Hanyang University, Korea (the Republic of)

Rice husk is a promising abundant bioresource for the production of high value added silica materials because it has the highest SiO₂ content among all plant based resources. In this study, silica aerogel are synthesized from rice husk by combining alkali extraction, acid leaching, solvent exchange and ambient pressure drying. Especially, the effect of Trimethylchlorosilane (TMCS)/n-hexane volumetric ratio on the synthesis of silica aerogel was investigated. They were characterized by their properties such as Brunauer-Emmett-Teller theory (BET), X-ray diffraction (XRD), Scanning electron microscope (SEM), Transmission electron microscope (TEM), Thermogravimetric analyzer (TGA), and Fourier transform infrared spectroscopy (FTIR). The synthesis of high value-added silica aerogel from an abundant bioresource can open up new avenues for sustainable and environment-friendly industrial development.

EN09.03.17

Fluoropolymer Based Radiative Cooler Having High Durability for External Environment [Jisung Ha](#), Soomin Son, Dongwoo Chae, Hangyu Lim, Suheol Ju and Heon Lee; Korea University, Korea (the Republic of)

Global warming is accelerating as fossil fuel consumption increases. The global temperature is rising every year due to global warming. According to this environmental issue, exposure of heat stress can reduce people's satisfaction with life in outdoor activities especially in hot summer. Also, it can decrease the efficiency of machine ability. Therefore, a lot of electricity is used for cooling purpose to relieve the heat in the city. In Korea, household electricity consumption is concentrated in August. Also, according to the current trend, the number of days with heat waves is expected to increase further. The increase in electricity consumption leads to an increase in the use of fossil fuels, which is a vicious cycle that causes global warming worse. Passive daytime Radiative cooling (PDRC) can lower the temperature without consuming energy. By reflecting sunlight (0.3-2.5 μ m) and radiating the heat to the space (0K) through the atmosphere's window (8-13 μ m), it can cool the ambient temperature below the radiative cooler. When it is set on rooftop, the building inside temperature goes down. PDRC is new-coming energy saving technology. In this study, we fabricated radiative cooling material in the form of solution and we can obtain white film caused by diffused reflection of nanoparticles. It shows white surface without metal layer so it doesn't cause glare. Fluoropolymer is fluorocarbon-based polymer and it has a high resistance to solvents. Especially, Ethylene Tetra fluoro Ethylene(ETFE) has good chemical resistance among various fluoropolymers. Also, ETFE material has high thermal resistance and its operating temperature is around 520K. In other words, this material can remain at extreme environment. Due to the nature of PDRC installed outside, exposure to weather conditions is inevitable. When acid rain falls in hot summer, normal radiative cooling material which is made of ceramic particle and polymer binder can be degraded by acid and high-temperature, thereafter its cooling performance decrease and durability also downgraded. In this work, ETFE particle is used to make white monolayer with PUA (polyurethane acrylate) for radiative cooling and inside can be cooled easily by coating it thinly on substrate like building outside. ETFE radiative cooler coated on glass substrate shows solar reflectivity of 92.5% and emissivity of 91.7% across atmosphere's window and its calculated cooling power is 95.6W/m². Because ETFE material which is one of fluoropolymer has good high-temperature resistance and high-chemical resistance, we propose PDRC which can operate at high-temperature and chemical environment. ETFE particle cannot solve with organic solvent and also cannot melt at room temperature. Soomin Son et al. fabricated PVDF film using PUA with UV hardening. We dissolved PUA to ethanol and combined white ETFE particle into solution with film forming agent. We fabricated heating chamber which continues to radiate heat by halogen lamp. With 20W lamp, the temperature inside heating chamber can increase up to maximum 400K. By putting ETFE radiative cooling material coated on aluminum on heating chamber, it decreases 24K contrast to ambient temperature when outdoor measurement with heating chamber. By chemical resistance test, we dipped ETFE radiative cooler into sulfuric acid which is same PH range of acid rain during one day with white commercial paint sample (e.g., titanium dioxide-based paint) and zirconia based radiative cooler. Commercial paint sample was yellowed, and also zirconia based radiative cooler was cracked and its film came off. But the film of ETFE radiative cooler was remained and its optical properties was also remained within a small range of error. In this way, ETFE radiative cooling coating hosts promising future in building cooling and it might be also found wide applications in outdoor or devices which of efficiency is sensitive to its

temperature.

EN09.03.18

Easily Recyclable White Polymer Films as Replacement for TiO₂ Pigments Luisa Borgmann, Siegbert Johnsen, Gabriele Wiegand and [Hendrik Hoelscher](#); Karlsruhe Institute of Technology, Germany

Titanium dioxide (TiO₂) has developed in recent decades as a standard white pigment for paints, coatings, films, cosmetics, and foods. But it has repeatedly come under criticism for its potential hazard for the environment and health. Therefore, its use as a food additive has been banned in Europe and further restrictions are expected worldwide. Consequently, replacements are being intensively sought. We, therefore, present a bio-inspired polymer structure that is fabricated via foaming polymers with supercritical CO₂. In that way, tiny nanobubbles are formed inside the polymer, turning the originally transparent material perfectly white. This is a purely structural effect; all other material properties of the respective polymer stay unchanged. Therefore, the respective polymer remains a mono-fraction simplifying recycling dramatically. The process is environmental-friendly and can be utilized with bio-based polymers such as PLA (polylactide) or cellulose acetate and is highly scalable. The foamed films can be used directly and also tolerate further process steps, such as thermoforming.

EN09.03.19

Readily Degradable Thermoset Network Derived from Biomass Resource [Ji Won Joo](#), Ka Hyun Lim and Ho Sun Lim; Sookmyung Women's University, Korea (the Republic of)

Indiscriminate use of non-degradable petroleum-based thermosetting polymers has caused many environmental problems. In particular, plastic waste and microplastics are emerging as major causes of environmental pollution. Therefore, there is growing interest in materials derived from renewable resources such as biomass. These biomass-based polymers offer the benefits of environmentally friendly materials and solve the problem of waste plastic accumulation. In this study, we suggest isosorbide diglycidyl ether (ISEPO) as a sustainable alternative to diglycidyl ether bisphenol A (DGEBA) as an epoxy monomer. The bio-based thermosets with high degradability were cured via a simple cationic polymerization of ISEPO and ester linkages. We discussed the hydrolysis mechanisms according to the contents of ester bonds and examined various factors affecting the degradation of the thermoset. We also identified potential applications for the use of ISEPO as degradable prepregs for the printed circuit boards. It is expected to be a solution to solve the plastic disposal and microplastic problems caused by non-degradable epoxy composites. The presence of degradable connections in the entire thermoset network structure can contribute to solving fundamental environmental problems and even provide a valuable route to recycling.

EN09.03.20

Triboelectric Energy Harvesting System Based on Recyclable Polymers and Electrodes Junseong Ahn^{1,2}, [Jiseok Kim](#)¹, Il-Kwon Oh¹, Jun-Ho Jeong² and Inkyu Park¹; ¹Korea Advanced Institute of Science and Technology, Korea (the Republic of); ²Korea Institute of Machinery and Materials (KIMM), Korea (the Republic of)

As the problem of environmental pollution due to the use of fossil fuels has emerged, interest in eco-friendly and renewable energy has rapidly increased. Especially, triboelectric nanogenerators (TENGs) has a great interest in because they can efficiently harvest wasted mechanical energy at low frequencies. From the first invention of TENG by Prof. Wang's group, TENGs with various advantages such as large effective surface area, operating mode, and efficient energy harvesting system have been actively studied for about 10 years. However, an eco-friendliness and recyclability of TENG itself was rarely considered, and only water-degradable and disposable materials as triboelectric surfaces were selected for eco-friendly and recyclable TENG, which hinders a broad application of TENG in water energy harvesting such as rain, ocean, river, and humid environment. Herein, we propose an all-recyclable TENG (AR-TENG) which consists of thermoplastic polymer, poly(methyl methacrylate) (PMMA) with a nanohole pattern and an electrodeposited ultrathin Pd film for ocean energy harvesting. We chose a PMMA film as a dielectric material because it can be easily dissolved in acetone, nanopatterns can be introduced by thermal nanoimprinting lithography method, and it has a great mechanochemical stability by maintaining its performance after immersion into water and seawater or even 1,000,000 cyclic tests. The proposed AR-TENG has a superior energy harvesting performance with an advantage of large effective contact area by nanopatterns. The practical application of AR-TENG was demonstrated by charging Li-ion batteries using a rectifier, a capacitor, and an ultralow-power step-down regulator with input voltage monitoring and regulation functions. The harvested electrical energy can be stored in Li-ion batteries and it can power the ocean monitoring system which consists of a micro-controller, wireless communication node, various sensors such as salinity sensor, pH sensor, temperature sensor, and oil leakage sensor. We expect that the proposed AR-TENG can provide eco-friendly and effective triboelectric energy harvesting technology considering the mechanochemical stability, recyclability, and eco-friendliness.

EN09.03.21

The Effect of Different Types of Starch on Silicon Anode Binder for High-Performance in Lithium-Ion Batteries [Ohhyun Kwon](#), Seohyeon Jang, Jihyeon Kang, Hojong Eom, Seyoung Choi, Junhyeop Shin, Jongkwon Park and Inho Nam; Chung-Ang University, Korea (the Republic of)

Starch is the most abundant polysaccharide in plants. Starch exists in its native form as semi-crystalline granules that are essentially composed of two main components: linear amylose and highly branched amylopectin. Various type of starch has a different ratio between amylose and amylopectin with different crystallinity. Starch crystallinity is ensured by packing of amylopectin double helices in a unit cell. Several polymorphs characterized by different crystalline structure are differentiated: A, B, and C-type starches which is combination of A-type and B-type starch.

Due to its low cost, abundance, renewability, and continuous structure, starch is considered as one of the polysaccharides with the most potential. Several researchers have vouched to utilize the starch from many sources for the development of solid-state electrolytes, carbon materials, and Li ion battery binders. Despite its benefits, not enough attention is being put towards exploring the applications of starch as a silicon anode binder.

Silicon (Si) is a promising high-capacity anode material for high-energy-density lithium-ion batteries. However, the massive volume change of Si during repeated charge-discharge cycles has been identified as the main origin of insufficient cycle lives of Si anodes. It has been found that binders can contribute substantially to improving their cycle lives. To find a better high performance Si anode binder, we attempted to use a unique starch binder. The presence of several hydroxyl groups in starch can enhance its interaction with the Si particles using the formation of multifaceted hydrogen bonds. Unlike normal polymer binders using silicon anode, starch possesses an intrinsic free volume and periodic crystalline frameworks, which is favorable for a fast Li⁺ transfer.

In this study, the relationships between the structure and properties of the novel starch binder are systematically investigated with the objective of improving electrochemical performance of Li-ion batteries. Corn starch, potato starch and waxy maize only consisting of amylopectin were selected to find out the effect of crystallin differences on Li ion conductivity and the effect of amylose and amylopectin on silicon binders. We reveal that the structure of the crystalline of the starch affects the Li-ion conductivity of the binder. Also, the one-step chemical synthesis was applied in this work to fabricate the binder more efficiently. A-type has a packed structure which restrains the lithium ions' movement. However, B-type has well-defined directional channels that plays a key role in the conduction of lithium ions. During the process of lithiation and delithiation, the structural properties of amylose and amylopectin lead to the formation of SEI layer. Highly branched amylopectin promotes the development of a thick SEI layer at the initial stage, which resulted in a decrease in performance. Due to the potato starch's aforementioned advantages, its electrode displayed a significantly improved cyclic and rate

performance for lithium half battery. The Si anode with the potato starch which has B-type crystallinity could enhance the Li ion conductivity of the binder which in turn, delivers a good electrochemical performance, especially at a high C rate. As expected, the prepared potato starch binder demonstrated a good reversible capacity of 2500mAh/g after 100 cycles at 1C for Li half battery. This systematic study is helpful towards understanding the structural difference starch has on the cycling performance of Si anodes and thus further provides insights for the rational design of novel polymeric binders.

EN09.03.22

Synthesis of Biocompatible Rice Husk-Derived Silica Nanoparticles Jin Hyung Lee^{1,2}, Ji Yeon Park¹, Wonsik Mun³, Jinyoung Chun¹, Yang m. Gu¹, Eun Sung Kan² and Robert J. Mitchell³; ¹Korea Institute of Ceramic Eng. Tech, Korea (the Republic of); ²Texas A&M University, United States; ³Ulsan National Institute of Science and Technology, Korea (the Republic of)

Although silica nanoparticles (SiNPs) can be artificially synthesized, they are also produced naturally within rice plants, but the biocompatibility of these natural SiNPs has thus far remained unknown. Within this study, several different methods (combustion, acid leaching or alkali extraction) to purify SiNPs from rice husks were explored, with an emphasis on their inherent toxicity towards human cell cultures. Whereas acid leaching and alkali extraction both generated highly pure SiNPs (>99.1% SiO₂ vs. 93.1% with combustion), toxicity tests performed with human and mouse cell lines found the alkali-extracted SiNPs to be much less harmful and, consequently, more biocompatible. We explored the toxicity further by incorporating polyethylene glycol (PEG) in the alkali-extracted SiNPs prior to the calcination step to mimic the presence of organic carbon during this step. Not only did the inclusion of PEG render the alkali-extracted SiNPs highly toxic, we found that this depended on the calcination conditions employed.

EN09.03.23

Fully-Recyclable All-Hydrocarbon Multifunctional Yarns for Circular Sustainable Fashion and Aerospace Applications Volodymyr Korolovych, Duo Xu, Rachel Bellisle, Cody A. Paige, Dava Newman and Svetlana V. Boriskina; Massachusetts Institute of Technology, United States

Development of multifunctional, lightweight, durable, and circular materials is critical for high-performance athletic apparel as well as for aerospace and military applications. Most conventional high-performance textiles are blends of multiple polymers, made by combining high-tenacity and elastomer fibers into e.g., polyester-spandex or nylon-spandex yarns. Typically, the elastomer content in such yarns is low, but it renders the textiles non-recyclable, resulting in majority of them ending up in landfills or incinerated. To address this problem, we engineer new high-performance core-sheath elastic yarns that are composed exclusively from all-hydrocarbon polyethylene (PE)-based fibers and exhibit high tensile strength, excellent elastic recovery, resistance to environmental degradation, and full mechanical or chemical recyclability.

The new yarns are fabricated by scalable melt-spinning techniques from PE-based polymer resins derived from either fossil fuels or sugar cane biomass [1]. We demonstrate that these fibers can be engineered through control of their polymer chain structure, crystallinity, and alignment to exhibit mechanical properties spanning the range from single-network elastomers (such as e.g. spandex) to high-performance fibers (such as polyester and nylon). We further engineer multifunctional core-sheath yarns made from a combination of high-performance and elastic PE-based fibers and show that they exhibit reversible elongation between 40% and 100% and breaking force above 9 N [2]. These new yarns are 100% mechanically recyclable at the end of their lifecycle without the loss of performance and enable 75% to 89% reduction in the cradle-to-grave carbon footprint of the textile products composed from either recycled or bio-derived PE resins, respectively.

Other applications that can benefit from a combination of elasticity and high tensile strength of the all-PE yarns as well as their degradation resistance, tunable thermoregulation [3], and radiation shielding capability [3] include medical garments, pilot uniforms, artificial muscles for soft robotics, and skin-tight mechanical counter-pressure (MCP) space suits. In particular, MCP suits offer advantages over conventional gas-pressurized spacesuits, by reducing volume, improving mobility, and enabling natural thermoregulation [4,5]. These suits rely on conventional elastic fibers (elastane and rubber cord) to maintain the necessary pressure and offer little protection from ionizing radiation. The all-hydrocarbon lightweight PE-based flexible yarns offer stretch, moisture wicking, thermal and ionizing radiation control for revolutionizing advanced MCP spacesuits as well as advanced garments for zero-gravity space adventure flights [6]. These materials may help to improve human capability to live and perform in extreme environments, while maintaining material circularity and reducing the environmental footprint needed for their fabrication, maintenance, and disposal.

This work was supported by the DEVCOM Soldier Center through the US Army Research Office (W911NF-13-D-0001), the MIT Deshpande Center, and the United States Navy and NERAMCO LTD (N6833521C0489). We thank the Dow Chemical Company and Braskem for providing polymer resins.

[1] M. Alberghini, et al. *Nature Sustainability* 4,715–724, 2021.

[2] S.V. Boriskina, V. Korolovych, High-performance mono-material hybrid yarns for circular sustainable textiles and soft robotics, MIT 23876 Invention Disclosure, 2021.

[3] S.V. Boriskina, *MRS Energy & Sustainability* 6, E14, 2019.

[4] L. Narici, et al. *Scientific Reports* 7 (1), 1644, 2017.

[5] B. Holschuh, et al, In *AIAA SPACE 2012 Conference & Exposition. AIAA SPACE Forum*, 2012.

[6] L. Tessmer, et al, 3D-knit spacesuit sleeve with multi-functional fibers and tunable compression, submitted to *ACADIA 2022*, University of Pennsylvania, Philadelphia, PA.

EN09.03.24

Biodegradation of PHB-Based Bioplastic Films in Soil Jiyeon Kim, Jacqueline A. Linn and Kwan-Soo Lee; Los Alamos National Laboratory, United States

Plastic materials produced from fossil fuel derivatives cause serious environmental problems due to their non-degradable nature. In general, such synthetic polymers are inexpensive, but their abundance has a significant negative environmental impact. Even most of the bioplastic materials produced currently are non-biodegradable, including Bio-PP, Bio-PET, and Bio-PA. Accordingly, recent research has focused on developing biodegradable polymers such as polymers produced by microorganisms, which have lower carbon footprints and greater ability to be recycled. Recently, Polyhydroxyalkanoates (PHAs) have attracted considerable attention as a biodegradable thermoplastic resin. In particular, polyhydroxybutyrate (PHB), which is the most well-known among PHAs, has been shown to rapidly degrade within 6 months under various natural active environments. The biodegradation of PHB takes place either under anaerobic or aerobic conditions. Implementation of the anaerobic condition will lead PHB to produce H₂O, CO₂, and methane. Under aerobic conditions PHB will produce CO₂ and H₂O. In anaerobic conditions a sludge containing several microorganisms is produced and can degrade PHB in different environments such as soil, salt water, and fresh water. However, soil was found to be the most natural environment for PHB degradation. In this study, we propose a new type of biodegradable bioplastic composite film made of PHB bearing green additives. The green additives implemented to overcome the mechanical instability of PHB and to substantially increase the elongation property of the film. In addition, we have investigated the degradation of two different types of PHB-based biodegradable composite films over a 6 week period in compostable soil. The degradation was evaluated by measuring polymeric material molecular weight loss, crystallinity, mechanical properties, and physical changes within the surface of polymeric films.

EN09.03.25

Wafer-Scale Heterostructured Piezoelectric Bio-Organic Thin Films Jun Li; University of Wisconsin--Madison, United States

Piezoelectric biomaterials are intrinsically suitable for coupling mechanical and electrical energy in biological systems to achieve in vivo real-time sensing, actuation, and electricity generation. However, the inability to synthesize and align the piezoelectric phase at a large scale remains a roadblock toward practical applications. We present a wafer-scale approach to creating piezoelectric biomaterial thin films based on γ -glycine crystals. The thin film has a sandwich structure, where a crystalline glycine layer self-assembles and automatically aligns between two polyvinyl alcohol (PVA) thin films. The heterostructured glycine-PVA films exhibit piezoelectric coefficients of 5.3 picocoulombs per newton or 157.5×10^{-3} volt meters per newton and nearly an order of magnitude enhancement of the mechanical flexibility compared with pure glycine crystals. With its natural compatibility and degradability in physiological environments, glycine-PVA films may enable the development of transient implantable electromechanical devices.

Reference:

[1] "Wafer-scale heterostructured piezoelectric bio-organic thin films." *Science* 373.6552 (2021): 337-342

EN09.03.27

Engineering Proton Exchange Membranes for Hydrogen Fuel Cells from Low Cost Micro Cellulose Filters Yuhao (Ben) Pan¹, Thomas Luong², Sean Fang³, Aniket M. Raut⁴, Haoyan Fang⁴, Md Farabi Rahman⁴, Konnie Duan⁵, Helee Shukla⁶, Quinton Geller⁷, David Sprouster⁴, Rebecca Isseroff⁴ and Miriam Rafailovich⁴; ¹Stuyvesant High School, United States; ²Plano West Senior High School, United States; ³Maggie L. Walker Governor's School, United States; ⁴Stony Brook University, The State University of New York, United States; ⁵Harvard-Westlake High School, United States; ⁶New Hyde Park Memorial High School, United States; ⁷Los Alamos High School, United States

Hydrogen fuel cells are an emerging form of green energy that can produce electricity from hydrogen and oxygen gas with the only by-product being water. However, the fuel cell component materials themselves may not be environmentally sustainable. Currently the material most commonly used for the electrolyte membrane is Nafion, which is a perfluorosulfonic acid polymer created by free radical copolymerization of a perfluorinated vinyl ether sulfonated fluoride co-monomer with tetrafluoroethylene. This has multiple toxic components and hence is not environmentally sustainable. Cellulose has been proposed as an inexpensive renewable alternative material where both microcellulose [1] and nanocellulose [2] have demonstrated the ability to generate power when used as an electrolyte membrane on the fuel cell. However, nanocellulose requires a complex synthesis process where functionalization with strong acids is performed [2]. This research presents a more natural membrane by taking low-cost, bulk-produced commercial cellulose filter papers and treating them with weak acids and a few drops of Resorcinol bis(diphenyl phosphate) (RDP). A power output of approximately 12mW/cm² was obtained from membrane electrode assemblies (MEAs) constructed from filter paper membranes soaked in solutions consisting of a single weak acid with added RDP drops, and operated in air at 60°C with 0.1mg/cm² of Pt at the cathode and anode. This value compared favorably with that of an MEA constructed from nanocellulose produced via the nitro oxidation method and operated under similar conditions which generated 11mW/cm². Treatment of the filter paper membrane to a combination of acids and RDP and incorporation into a similarly constructed MEA yielded a power output of 16mW/cm² when operated under the same conditions. However, operation under O₂ produced a power output of 35mW/cm² which was significantly larger than the 19.1mW/cm² output reported for a nanocellulose membrane operated in O₂. SEM/EDX analysis of the cellulose filter paper membranes shows a phosphate-rich membrane forming between the fibers which possibly explains the lack of hydrogen gas crossover, despite the porosity expected from filter paper construction. Micro-CT analysis of the filter paper membranes further confirms the absence of porosity throughout the entire membrane. Further solid state NMR, as well as XPS is in progress in order to understand the chemical synergy enabled by the combination of acids and RDP.

The authors would like to thank the Morin Charitable Trust and the Office of Naval Research for funding.

[1] Wang, L., et al. (2019). "Operation of proton exchange membrane (PEM) fuel cells using natural cellulose fiber membranes." *Sustainable Energy & Fuels* 3(10): 2725-2732.

[2] Sharma, S. K., et al. (2022). "Nitro-oxidized carboxylated cellulose nanofiber based nanopapers and their PEM fuel cell performance." *Sustainable Energy & Fuels* 6(15): 3669-3680.

EN09.03.28

Opportunities for Cellulose-Based Materials in Sustainable Manufacturing—On Earth and Beyond Shiwei Ng and Javier Gomez Fernandez; SUTD, Singapore

In nature, cellulose is the most abundant structural polysaccharides available from different sources and in different forms. Without extensive modification, it can be used to form composites that mimic natural material synergies and are perfectly integrated within nature's ecology. In circular, closed loop economies where functional objects are manufactured within a geographical region; its diverse utility coupled with material ubiquity and biodegradability drives continuous composite material innovations. More than ever, accentuated supply chain vulnerabilities and resource scarcity accelerates the transition toward circular systems. As materials enabling a sustainable manufacturing strategy within closed loop systems, cellulose-based materials could be a solution for regionalized manufacturing anywhere on Earth; and even ventures beyond Earth where forementioned constraints are further stressed.

Here, to highlight these opportunities where bio-based materials such as cellulose can meet resource constraints challenges for sustainable development on Earth while drawing parallels to similar challenges when establishing sustained human presence beyond Earth, this article presents both preliminary findings of a cellulose-based material solution on Earth as a concrete example and discusses the path for a cellulose-based material solutions to bridge the gap for extra-terrestrial applications.

As a natural source of pure cellulose without requiring intensive chemical post-treatment for contaminant removals like its lignocellulosic counterparts, bacterial cellulose was used to form composites with inorganic elements such as zinc metals, whose use has largely been defined by high energy processes. Due to the high-water holding capacity of bacterial cellulose, the evaporation water drastically reduced volume of composite from wet to dry state, agglomerating zinc particles into a basic functional anode. As a fully water based cellulosic composite, an assembled zinc ion battery sustained a steady coulombic efficiency for nearly 50 cycles. While not ideal without further optimization at this stage, it points the way forward to a more sustainable battery anode. In addition, for applications in other types of battery such as lithium-ion battery, metallic oxides such as zinc-oxide can be precipitated and calcinated within bacterial cellulose pellicle. The presence of zinc-oxide was observed through Scanning Electron Microscopy and verified by X-ray Diffraction to be dispersed within the mesh composite.

From the standpoint of sustainable, alternative cellulose material production without reliance on lignocellulosic resources, regionalized production of pure cellulose could be obtained for land scarce nations without dedicated forestry. Furthermore, as a product of microbial fermentation, industrial waste sugar could be used in its culturing; diversifying feed stock components for production and closing the loop for organic industrial waste. Beyond Earth, any

artificial ecosystem enabling sustained human presence requires organic food resources and produces organic waste. This allows for cellulose and chitin to be extracted from bio converters, heterotrophs and microbial fermentation; laying down the basic materials needed for composites made with in-situ materials.

EN09.03.29

Decarbonization of Chemical Manufacturing Using a Membrane Reactor [Mia Stankovic](#) and Curtis Berlinguette; The University of British Columbia, Canada

Membrane reactors use electricity and water to drive hydrogenation reactions without H₂ gas. In these reactors, a palladium membrane physically separates the site of electrochemical hydrogen formation from the site of chemical hydrogenation. This separation broadens the scope of reaction conditions (e.g., solvents) that can be studied and simplifies reagent handling and purification compared to existing electrochemical hydrogenation methods. We leveraged this feature of the membrane reactor to demonstrate the industrially-relevant hydrogenation of furfural (an important biomass derivative) into furfuryl alcohol (84% selectivity) and tetrahydrofurfuryl alcohol (98% selectivity). To achieve these selectivities, we designed and built a novel membrane reactor design that enabled high-throughput testing of combinations of solvents, catalysts (identities and thicknesses), and applied currents. One key finding was that employing bulky solvents with weak nucleophilicity suppressed side product formation to enable these high selectivities. These solvents are not compatible with conventional electrochemical hydrogenation, but they are compatible with the membrane reactor. This work highlights the utility of the membrane reactor for selective furfural hydrogenation without H₂ gas, and presents the opportunity to decarbonize a >350,000 ton/year hydrogenation industry.

EN09.03.30

Wood Template-Supported Phase Change Materials Composites for Durable and Form-Stable Thermal Energy Storage [Shuang Cui](#)^{1,2}; ¹The University of Texas at Dallas, United States; ²National Renewable Energy Laboratory, United States

To reduce building energy consumption, phase change materials (PCMs) with high transition enthalpies and transition temperatures close to the thermal comfort of humans are desirable for thermal energy storage (TES) in building envelope applications. But traditional high-enthalpy solid-to-liquid PCMs suffer from leakage issues during thermal cycling and thus require encapsulation to be form-stable, which reduces the effective transition enthalpy. Polyethylene glycol (PEG) is a compatible PCM with wood templates (WT). Still, we show that with just PEG infiltrated into the wood, 30 wt% of PEG is stored within wood before detectable phase changes occur, indicating inefficiency of PCM usage. We developed a method to (1) improve the leakage stability of balsa and pine composites (BWT+PCMs and PWT+PCMs) under isothermal conditioning for one month at 50 °C and (2) reduce the inefficiency of the unused PCM within the composites to 10 wt% by incorporating a cross-linkable polymer (<10 wt%). These composites exhibit transition properties as high as 114.2 J/g at 25.4 °C, exhibit no shift in properties after 1000 thermal cycles and retain flexural strengths comparable to the raw balsa and pine wood. Our shape-stabilized WT+PCM composites enrich the functionality of wood materials as both ideal TES material candidates and building construction materials.

EN09.03.31

High-Throughput Coating with Biodegradable Anti-Microbial Pullulan Fibres Extends Shelf-Life and Reduces Weight Loss in an Avocado Model [Huibin Chang](#)¹, [Jie Xu](#)¹, [Luke Macqueen](#)¹, [Zeynep Aytac](#)¹, [Michael Peters](#)¹, [John Zimmerman](#)¹, [Tao Xu](#)¹, [Philip Demokritou](#)^{1,2} and [Kevin K. Parker](#)¹; ¹Harvard University, United States; ²Rutgers, The State University of New Jersey, United States

Food waste and food safety motivate the need for improved food packaging solutions. However, current films/coatings addressing these issues are often limited by inefficient release dynamics that require large quantities of active ingredients. Here we developed antimicrobial pullulan fiber (APF)-based packaging that is biodegradable and capable of wrapping food substrates, increasing their longevity and enhancing their safety. APFs were spun using a high-throughput system, termed focused rotary jet spinning (FRJS), with water as the only solvent, allowing the incorporation of naturally derived antimicrobial agents. Using avocados as a representative example, we demonstrate that APF-coated samples had their shelf life extended by inhibited proliferation of natural microflora and lost less weight than uncoated control samples. This work shows that FRJS is a promising technique to produce scalable, low-cost, and environmentally friendly biodegradable antimicrobial packaging systems.

EN09.03.32

Life Cycle Assessment of Metal Recovery from Perovskite Solar Cells [Emma L. McCalmont](#), [Jon Kellar](#), [Brett Carlson](#), [Tanner Y. O'Hara](#), [Achyuth Ravilla](#), [Gonzalo Rodriguez Garcia](#) and [Ilke Celik](#); South Dakota School of Mines, United States

Perovskite photovoltaic (PVs) cells have created a significant interest over the last few years due to their low-cost and high-power conversion efficiencies. However, the environmental performance of perovskite PV technology can be improved if its material components can be reused. In this study, we focused on the environmental life cycle assessment of recovering metals such as lead, copper, gold, nickel, and silver from the end-of-life perovskite PVs. We assessed the recovered metal efficiencies in the reusing process, determining if recovering and recycling the metals is more sustainable than extracting raw materials. We also focused on the life cycle costing to find ways we can optimize the recovery of these materials and determine the most economically feasible way to separate the cell layer-by-layer. For extracting the back contact material two methods were assessed, physical and chemical. The physical extraction method uses an adhesive to recover the back contact layer while the chemical extraction method uses chlorobenzene, the cost of these processes is no more than \$64.00 per 1 m² of perovskite PV module.

EN09.03.34

Fracture And Fatigue Behavior of Self-Organized Mycelium Nanocomposites— Structure and Mechanical Properties [Precious O. Etinosa](#) and [Wole Soboyejo](#); Worcester Polytechnic Institute, United States

The flexural strength, fracture toughness, fatigue behavior, and resistance-curve behavior of bioprocessed mycelium nanocomposites reinforced with self-organized cellulose fibers were examined in a combined experimental and analytical study. The bioprocessed mycelium nanocomposite blocks were composed of cellulose/hemicellulose hemp-duct with optimized laterite percentage compositions. The compositional dependence of the flexural strength, fracture toughness, and fatigue on different volume fractions of the composite constituents was explored using crack-tip shielding models; small- and large-scale bridging models. The underlying crack-microstructure interactions with the resistance-curve behavior experiments were examined through *in-situ/ex-situ* optical microscopy. The microscopy studies revealed clear evidence of crack bridging by the hemp fibers transverse to the crack propagation. Simulation results from the crack bridging models were shown to be consistent with the experimental data of the resistance-curve behavior. The structural implications of the results are then discussed to provide valuable insights into the design of mycelium biocomposites for potential applications in eco-friendly and sustainable buildings.

EN09.03.35

Active, Selective, and Stable COPROX Catalysts Based on Ceria Aerogel-Supported Cu Nanoparticles Debra R. Rolison, Travis G. Novak, Paul DeSario, Todd H. Brintlinger, Ryan H. DeBlock and Jeffrey W. Long; U.S. Naval Research Laboratory, United States

The size comparability of the networked, covalently bonded nanoparticles (NPs) that define aerogel architectures and the catalytic NPs supported thereon permits a degree of interfacial intimacy uncommon in heterogeneous catalysis. We find that reducing oxide aerogels such as titania and ceria control the catalytically active chemical state of Ni and Cu catalysts at low weight loadings (<5 wt.%) to thermally oxidize CO with high activity and on-stream durability. This morphologically and chemically resilient arrangement of reducing oxide NPs and metal NP yields high activity (mol of product per second per mol of catalyst), low values of T_{50} (temperature of 50% CO conversion), and persistent activity in the presence of gas-phase water. We now show that Cu NPs photodeposited on ceria or gadolinium-substituted ceria aerogels preferentially oxidize CO in H_2 -rich feedstreams, a critical reaction to purify H_2 for use in proton-exchange membrane fuel cells. The catalysts convert >95% of CO with >95% selectivity vs. H_2 and maintain this unprecedented activity for >16 h at 100°C in dry or humidified feedstreams.

EN09.03.36

Developing Fire-Retardant Green Materials For Sustainable Housing Michael Difrieri, Joseph Avalos, Jeanette Cobian-Iñiguez and Lilian P. Davila; University of California, Merced, United States

As human civilization continues to expand, numerous unsustainable resources are exceedingly consumed to satisfy the population's growth needs. To counteract some of the undesirable effects on the environment, researchers are using different approaches to address the challenges related to the fabrication of sustainable housing materials (e.g., reproducibility, reliability, and use of renewable materials) while reducing the carbon footprint arising from the housing industry. Despite current efforts, there are still fundamental limitations in the current fabrication methods of housing materials. To solve those challenges, we have produced a novel waste-derived material (e.g., wood-based insulating material, in combination with ceramic binding agents) to create green materials of varied dimensions for housing applications. This new green material can lead to high-strength load-bearing house components (e.g., walls) and robust weather- and fire-resistant components (e.g., sidings, fences), where burning is not required in the molding process during sample preparation. In this study, we are investigating the fire-retardant properties and structural characteristics of our green material with a biogel coating additive. We have investigated the effect of the biogel coating on our samples using materials characterization techniques (e.g., scanning electron microscopy, SEM) and fire experiments. We have previously evaluated ecological traits (e.g., energy, CO_2 footprint) of the new green material using life-cycle assessment (LCA). Here, we also investigate the effect of biogel coated green samples on the environment via LCA. The hypothesis is that by modifying the biogel coating composition, the impact on the environment could be further decreased. Overall results from this study are in good agreement with recent experiments reported elsewhere independently, and mechanical verification (e.g., fire tests) together with LCA data of the new green material are significant in determining sustainable alternatives compared to other counterparts. This research contributes to improving material discovery by the combination of recyclable sustainable materials, design, low-energy processing methods, fire testing, and LCA evaluation, which allows to define the technical and commercial feasibility of low-cost and sustainable house components.

SESSION EN09.04/SB02.04: Joint Session I: Nanocellulose-Based Materials

Session Chairs: Gustav Nyström and Eleftheria Roumeli

Tuesday Morning, November 29, 2022

Hynes, Level 3, Room 306

8:15 AM INTRODUCTIONARY REMARKS

8:30 AM *EN09.04/SB02.04.01

Mechanisms Underpinning the Mechanical Properties of Lignocellulose-Based Materials Teng Li; University of Maryland, United States

The natural abundance and exceptional intrinsic mechanical properties of cellulose have motivated surging interests in developing lignocellulose-based materials of high performance. Enthusiastic aside, there exist large variations of the mechanical properties of lignocellulose-based materials, far from exhausting the intrinsic potential of cellulose, which essentially result from the lack of mechanistic understanding of the property-governing parameters. This talk discusses the key mechanisms that underpin the mechanical properties of lignocellulose-based materials, with particular focus on those that govern the strength, toughness, as well as flaw sensitivity of lignocellulose-based materials. Such mechanistic understandings shed light on designing lignocellulose-based materials with desirable mechanical properties.

9:00 AM *EN09.04/SB02.04.02

Bioinspired Anisotropic and Multifunctional Nanocellulose Gels Gustav Nyström^{1,2}; ¹Empa, Switzerland; ²ETH Zürich, Switzerland

Nanocellulose represents an important class of sustainable biocolloids that has shown great potential for use in e.g. high strength, optically responsive and thermal insulating materials. To maximize the inherent potential of these colloids in materials requires however a well-controlled organization of the nanocellulose particles across the length scales. In the first part of this talk I will discuss anisotropic structuring of nanocellulose in gels and show examples of how this can be used to control actuation and shape morphing in hydrogels and optimize directional thermal properties including superinsulation in aerogels. In addition to structuring and controlled nanocellulose assembly, the formation of biological, chemical and physical cellulose biohybrid materials has the potential to significantly expand the functionality and application space of these materials. In the second part of this talk I will focus on cellulose biohybrids where at least one other conductive nanomaterial component (e.g. MXenes or carbon nanotubes) has been added to the system and show how this can render multifunctional materials including mechanical sensing hydrogels with dual optical and resistive readout, aerogels with optical birefringence and hydrogels with bioinspired structural colors.

9:30 AM EN09.04/SB02.04.03

Structure-Properties Relations in Reinforced Fibrous Materials—Strength, Toughness and Non-Linear Deformation Catalin R. Picu, Mithun Dey and Shengguang Jin; Rensselaer Polytechnic Institute, United States

Most cellulose products are network materials, that is their mechanical function is provided by a network of fibers. The strength, toughness and mechanical behavior of these materials are of obvious importance during processing and in service. Therefore, it is of interest to establish design methodologies that ensure enhanced properties, based on a fundamental understanding of how the material structure controls mechanical properties in stochastic networks. Establishing such relations is the overarching goal of this work. We focus on reinforced networks, i.e. networks embedded in soft matrix and networks with

particulate or reinforcing fiber additives. We explore by computational means the relation between various structural parameters (network density, fiber orientation, fiber properties and their distribution, flocculation), reinforcement characteristics (reinforcement density and distribution) and the strength, toughness and non-linear deformation of such materials. The talk will outline ways to obtain exceptional properties with minimal amount of reinforcement. These relations can be used in design to develop network materials and, in particular, cellulose-based materials, with exceptional combinations of properties.

9:45 AM BREAK

10:15 AM *EN09.04/SB02.04.04

Hairy Cellulose Nanocrystals—Fundamentals and Emerging Applications Amir Sheikhi; The Pennsylvania State University, United States

For decades, cellulose nanocrystals (CNCs) have been produced by hydrolyzing the disordered (amorphous) regions of cellulose fibrils. These colloidal particles comprise highly ordered arrays of cellulose chains, impeding the physicochemical modifications of inner crystalline layers, which in turn results in limited/compromised dispersion stability, functionalizability and charge, response to external fields, and transport. Nanoengineering cellulose fibrils via controlled oxidation reactions can partially disintegrate the disordered cellulose chains attached to the crystalline body, which yields patchy nanoparticles with a needle-shaped crystalline body (similar to CNCs) attached to two highly functionalized disordered cellulose regions (hairs). This newly emerged class of nanocelluloses are called hairy cellulose nanocrystals (HCNC). The protruding soft brushes from HCNC poles impart significant modifications to the colloidal properties of HCNCs, enhancing their functionality, charge density, stability, and self-assembly. In this presentation, we will discuss our recent progress in understanding the fundamental properties of HCNCs produced from a range of lignocellulosic sources and engineering them for advanced applications, such as rare-earth element recovery, biodegradation, and functional hydrogels. We will show how HCNCs enable several technologies that would otherwise be non-trivial to develop using conventional CNCs. The outcome of our research may leverage universal biomass-based sustainable solutions for several long-lasting industrial challenges in water and healthcare sectors.

10:45 AM EN09.04/SB02.04.05

Advancing Renewable Barrier Packaging with Lignocellulosic and Chitinous Biomaterials Yue Ji¹, Yang Lu¹, Greg Schueneman², Meisha Shofner¹ and Carson Meredith^{1,1}; ¹Georgia Institute of Technology, United States; ²US Forest Products Laboratory, United States

There is strong interest in the introduction of renewable sources of packaging into global society. In particular, flexible barrier packaging and coatings are of interest due to their prevalence in the supply chain, e.g., at least 40% of all packaging is nonrenewable/nonrecycled flexible plastic. Forest-derived cellulose nanocrystals (CNCs) are a promising renewable source, and have been shown to be coatable as films with high oxygen barrier properties. Generally, CNCs are derived by acid hydrolysis processing that leaves pendant sulfate groups, imparting negative charge in aqueous media. Recent work in our group has shown that combining anionic CNCs with renewably sourced cationic nanofibers is a promising approach to developing manufacturable barrier films. Notably, chitin nanofibers (ChNFs) and nanowhiskers (ChNWs), which can be derived from renewable sources including crustacean food waste and fungi, are cationic and form complexes with CNCs that lead to dense barrier films. This talk describes recent innovations in optimizing the synergy between ChNWs and CNCs through careful tuning of the ChNW density and length. We find that optimal deacetylation of the ChNWs leads to formation of layered ChNW/CNC structures with oxygen permeability lower than poly(ethylene terephthalate) (PET), and blended ChNW/CNC structures that have permeability near poly(ethylene-co-vinyl alcohol) (EVOH). We also explore the use of thermal treatment and deposition temperature to further improve the film structures. These bilayers and blends have been applied to a variety of renewable and biodegradable substrates, such as poly(lactic acid) (PLA) and cellulose acetate (CA), as well as recyclable films like poly(ethylene terephthalate) (PET). We will discuss methods to improve the water vapor transport rates of these materials that include thermal and chemical treatments, as well as substrate pairing. Finally, we will discuss data that illustrate the biodegradability of these structures and the potential for recycling and upcycling.

11:00 AM EN09.04/SB02.04.06

Solid-State Adsorption as a Means to Modify Lignocellulosic Surfaces Eero Kontturi¹, Wenyang Xu², Ruige Qi¹ and Panagiotis Spiliopoulos³; ¹Aalto University, Finland; ²Abo Akademi University, Finland; ³Chalmers University of Technology, Sweden

Modifying lignocellulosic surfaces can often be difficult. The modification routes may require special synthetic skills and/or environmentally hazardous chemicals, and their scalability can be questionable. Furthermore, particularly the covalent modification of nanocellulose particles can impair hydrogen bonding in the eventual nanocellulose networks. Here, we demonstrate a conceptually new method for modifying lignocellulosic surfaces by solid-state adsorption of thermoplastic polymers. A thin, so-called Guiselin layer forms on a substrate when a thicker polymer layer is heated above its glass transition temperature or melting point. When the excess polymer is removed by rinsing with a good solvent, the Guiselin layer (usually of 1-10 nm thickness) stays on the surface. This layer has a substantially higher coverage and it is attached more firmly than an adsorbed polymer layer that has been cast by conventional adsorption from a solution. We demonstrate how Guiselin layers of polystyrene and poly(lactic acid) can be applied to simple hydrophobation of a number of different lignocellulosic surfaces: ultrathin cellulose films, cellulose nanopaper, ordinary paper, and wood chips. However, this approach is not limited to mere hydrophobation as virtually any soluble thermoplastic polymer can be applied to Guiselin layer deposition, given that its glass transition temperature or melting point is below the thermal decomposition temperature of cellulose. This includes, for example, certain semi-conducting or responsive polymers that can be combined especially with the recently emerged nanocellulosic substrates by a unique technology.

11:15 AM EN09.04/SB02.04.07

High-Performance Biobased Nanocellulose and Chitin-Based 3D Printing Materials and Smart Coatings Rigoberto C. Advincula^{1,2,3}; ¹Case Western Reserve University, United States; ²The University of Tennessee, Knoxville, United States; ³Oak Ridge National Laboratory, United States

Biobased and renewable feedstocks or derived natural materials for direct utilization (little conversion or synthetic procedures) have been of high interest in materials chemistry. This can be derived from agro-waste or harvested high fiber content grass (*Miscanthus*) or from shrimp-shell waste polysaccharides. Moreover, the use of 3D printing and additive manufacturing has opened up a host of possibilities for bio-inspired materials development. In this regard, the preparation of cellulose nanocrystals (CNC) and cellulose nanofibers (CNF) for polymer nanocomposites is useful as an additive for improving thermo-mechanical properties and improved processability. In this talk, we will focus on the use of polysaccharides and CNC derived from two classes of sources: 1) high fiber and alpha-structure *Miscanthus* grass, Abaca, and coconut fibers. 2) chitosan-derived polysaccharide complexes and CNC. The mode of raw materials can be from processed pulp or directly from coconut coir or agro-waste. These nanofiller materials have been utilized in two types of applications: nanofiller materials for 3D printed parts via stereolithographic apparatus (SLA) and the preparation of smart aerogels and coatings. Chitosan nanomaterials derived from chitin have advantages in terms of functional group interaction with electrostatic charge pairing to form soluble complexes. Likewise in SLA 3D Printing, enable improved biocompatibility and complex materials-design development for biomedical applications. The talk will focus on materials development for 3D printing and coatings and discuss the methods of synthesis, fabrication, and characterization for their specific intended applications.

11:30 AM EN09.04/SB02.04.08

Plant-Derived Nanocellulose as Structural and Mechanical Reinforcement of Freeze-Cast Chitosan Scaffolds for Biomedical Applications Kaiyang Yin^{1,2,3}, Prajan Divakar² and Ulrike G. Wegst^{2,3}, ¹University of Freiburg, Germany; ²Northeastern University, United States; ³Dartmouth College, United States

Despite considerable recent interest in micro- and nanofibrillated cellulose as constituents of lightweight structures and scaffolds for applications that range from thermal insulation to filtration, few systematic studies have been reported to date on structure–property–processing correlations in freeze-cast chitosan–nanocellulose composite scaffolds, in general, and their application in tissue regeneration, in particular. Reported in this study are the effects of the addition of plant-derived nanocellulose fibrils (CNF), crystals (CNCs), or a blend of the two (CNB) to the biopolymer chitosan on the structure and properties of the resulting composites. Chitosan–nanocellulose composite scaffolds were freeze-cast at 10 and 1 °C/min, and their microstructures were quantified in both the dry and fully hydrated states using scanning electron and confocal microscopy, respectively. The modulus, yield strength, and toughness (work to 60% strain) were determined in compression parallel and the modulus also perpendicular to the freezing direction to quantify anisotropy. Observed were the preferential alignments of CNCs and/or fibrils parallel to the freezing direction. Additionally, observed was the self-assembly of the nanocellulose into microstruts and microbridges between adjacent cell walls (lamellae), features that affected the mechanical properties of the scaffolds. When freeze-cast at 1 °C/min, chitosan–CNF scaffolds had the highest modulus, yield strength, toughness, and smallest anisotropy ratio, followed by chitosan and the composites made with the nanocellulose blend, and that with crystalline cellulose. These results illustrate that the nanocellulose additions homogenize the mechanical properties of the scaffold through cell-wall material self-assembly, on the one hand, and add architectural features such as bridges and pillars, on the other. The latter transfer loads and enable the scaffolds to resist deformation also perpendicular to the freezing direction. The observed property profile and the materials' proven biocompatibility highlight the promise of chitosan–nanocellulose composites for a large range of applications, including those for biomedical implants and devices, as is briefly illustrated with examples and outcomes of first in vivo studies.

SESSION EN09.05/SB02.05: Joint Session II: Nanocellulose-Based Materials

Session Chairs: Aji Mathew and Hongli Zhu

Tuesday Afternoon, November 29, 2022

Hynes, Level 3, Room 306

1:30 PM INTRODUCTORY REMARKS

1:45 PM *EN09.05/SB02.05.01

Design of Advanced Filaments from Cellulose Nanofibrils Using a Coaxial Spinning Strategy Lars Wågberg and Michael Reid; KTH, Sweden

The use of flow-focusing for the preparation of filaments from Cellulose I fibrils has allowed for the preparation of ultrastrong, continuous fibres with excellent wet-strength (1). By applying careful hydrodynamic alignment of the fibrils in combination with a colloidal control and locking of the oriented state it is possible to, almost, fully utilize the excellent inherent properties of the CNFs (Cellulose Nano Fibrils). It has also been shown that it is possible to use a simpler, coaxial set-up to prepare oriented filaments where the coaxial alignment also allows for the preparation of interactive filaments using a combination of CNFs and for example Carbon Nano Tubes (CNTs) (2). In this work (2) a core-shell structure was produced where the active components were assembled in a thin layer outside a core of CNFs. In the present work the coaxial spinning strategy has been further expanded by using a coaxial spinning equipment with three channels allowing for the preparation of even more advanced structures. With this set-up it has been possible to prepare filaments containing an external thin layer of high-quality CNFs encapsulating core materials with dimensions from the nano-scale to the macroscale. In this way it has been possible to form filaments containing gases, conductive polymers, nanoparticles and macroscopic fibres modified to meet certain end-use properties. The details behind the preparation of the filaments and the final filaments properties will be discussed.

1. Mittal, N., Ansari, F., Gowda Krishne, V., Brouzet, C., Chen, P., Larsson, P. T., Roth, S. V., Lundell, F., Wågberg, L. and Söderberg, L. D. (2018).

Multiscale Control of Nanocellulose Assembly: Transferring Remarkable Nanoscale Fibril Mechanics to Macroscale Fibers. *ACS Nano*, 12(7), 6378–6388.

2. Marais, A., Wågberg, L., Erlandsson, J., and Söderberg, L. (2020). Coaxial spinning of oriented nanocellulose filaments and core–Shell structures for interactive materials and fiber-reinforced composites. *ACS Applied Nano Materials*, 3(10), 10246–10251.

2:15 PM EN09.05/SB02.05.02

Charge Control on the Surface of Ionic Cellulose Nanocrystal for the Stable Pickering Encapsulation Jonghyun Shin and Jinho Hyun; Seoul national university, Korea (the Republic of)

The charge of surface-active particles is one of the critical factors in Pickering emulsion. It is difficult for charged surfactant particles to form emulsion droplets due to the repulsive force of Coulomb's law against oils with high polarity. In order to form stable emulsion droplets and introduce thermodynamically stable colloidal dispersion between droplets, it is necessary to control the charge of the surface-active materials. Here, we present the CNC surface modification method for controlling charge density from high to low and its effect on the stabilization of Pickering emulsion. The sulfated cellulose nanocrystal (S-CNC) was hydrolyzed with sulfuric acid, and the S-CNC was desulfated with hydrochloric acid at different reaction times to observe the surface charge effect of CNCs on the Pickering encapsulation. In desulfation, we used a low concentration of hydrochloric acid, which does not affect the morphologies of CNCs. Then, the morphologies and surface properties of CNCs were analyzed by TEM, AFM, conductometric assay, zeta potential, FT-IR, and XRD. As a result, the ionic groups on the S-CNCs were successfully substituted for the non-ionic groups without changing CNCs' length and crystal size. After preparing CNCs, to understand the surface effect of CNCs on Pickering encapsulation, we chose n-decane, n-dodecane, n-tetradecane, and n-hexadecane as non-polar oils and chloroform and 1-octanol as polar oils. The stability of Pickering emulsion was evaluated by emulsion phase stability, surface tension, emulsion droplet size, and zeta potential. The dS-CNCs desulfated for 30 h formed small emulsion droplets with high stability for long-term storage. CNCs are potential emulsifiers based on particles. It is critical to control the surface chemistry of CNCs to form a stable Pickering emulsion of oils. These results will find potential utility in pharmaceutical, cosmetic, agriculture, food chemistry, and other related fields.

2:30 PM EN09.05/SB02.05.04

Lignocellulosic Materials in 3D Printing—From Biomedical Applications to Metal Parts Fabrication Rigoberto C. Advincula^{1,2,3}, ¹Case Western Reserve University, United States; ²The University of Tennessee, Knoxville, United States; ³Oak Ridge National Laboratory, United States

Lignocellulosic-based feedstocks are renewable natural materials that are of high interest in materials chemistry for manufacturing. As polysaccharides, their ability to complex with surfactants or metal ions are derived from some of their ligand function and the presence of hydroxyl and carboxylic groups.

Their use of 3D printing has gained ground as both additive and host matrix and gel materials. In this talk, we will focus on the use of lignocellulosic-based polysaccharides isolated from pulp or directly from the raw fiber: 1) polysaccharide complexes and nano cellulose in SLA 3D printing, and 2) Host hydrogels for metal 3D printing. SEM, X-ray, and tensile-compression properties as 3D printed parts were investigated. Their advantages for improved thermo-mechanical properties and biomedical applications will be evident.

2:45 PM DISCUSSION TIME

3:00 PM BREAK

3:30 PM *EN09.05/SB02.05.05

Comparative Study of Lignocellulosic Nanomaterials Production from Different Heterogeneous Waste Feedstocks Renata Bura, Danielle U. Pascoli, Anthony Dichiara, Richard Gustafson and Eleftheria Roumeli; University of Washington, United States

Nanocellulose products may be produced from various heterogeneous waste feedstocks such as agricultural residues, invasive plant species, and other low-cost lignocellulosic biomass, providing economic and sustainability advantages related to the conventional bleached wood pulp feedstock. However, for this to become a reality on a large scale, robust conversion processes that accommodates such heterogeneous feedstocks must be developed. In this study, four different heterogeneous waste feedstocks were utilized (wheat straw, corn stover, reed canary grass, and industrial hemp) to assess the robustness of a novel conversion process previously developed by our group to make lignocellulosic nanomaterials. In our process we utilize inexpensive lignocellulosic feedstock and mild peracetic acid (PAA) pretreatment to produce lignocellulosic nanomaterials (nano and microfibrils) with potential bioplastics applications. PAA was chosen due to its biodegradability, non-toxicity, and high reaction selectivity.

Lignocellulosic nanofibrils (LCNF) and microfibrils (LCMF) were successfully produced from all biomass feedstocks tested, but the original biomass's chemical and physical characteristics influenced the final nanomaterials' properties. The chemical composition and nature of the initial feedstock showed a direct effect on the total mass yields during the process as well as on the surface charge of the final nanomaterials. In addition, the physical characteristics of the feedstock affected the degree of delignification during the reactions, producing materials with different residual lignin contents. This work has demonstrated the successful production of nanomaterials from various low-cost waste feedstocks, advocating for the large-scale production of nanocellulose products in the United States.

4:00 PM DISCUSSION TIME

4:30 PM EN09.05/SB02.05.07

Using Light Scattering to Measure Aggregation of Cellulose Nanomaterials Nayomi Z. Plaza and Carl Houtman; USDA-FS Forest Products Laboratory, United States

As cellulose nanocrystals (CNC) and cellulose nanofibrils (CNF) move to commercial products, simple methods for doing quality control to assess their size, stability and/or dispersion are required. Irreversible aggregation during drying continues to limit the wider commercialization potential of these nanomaterials. If one desires fully dispersed materials, one typically ships slurries, which are 10% solids for CNCs and 1% solids for CNFs. Understanding what governs aggregation and developing simple methods to assess the aggregation state of CNCs and CNFs is essential. We are using a combination of dynamic light scattering (DLS), multiangle static light scattering (MASLS), and small angle light scattering (SALS) to characterize the size (from 5 nm to over 300 nm) and solution behavior of CNC and CNF solutions. SALS is proving to be ideal for identifying aggregates in solution. Moreover, SALS is also being used to measure film products containing cellulose nanomaterials. The scattering of light is proving to be a convenient way to determine the size of the embedded nanomaterials as well as their alignment and dispersion.

4:45 PM EN09.05/SB02.05.08

High Performance Wood Scroll Evaporator for All-Day Evaporation in Saline Water Bokyeong Sohn, Hyunsoo Han, Sangmin Jeon and Minjae Song; Pohang University of Science and Technology, Korea (the Republic of)

A novel all-day evaporator in the form of a scroll is developed by rolling a thin layer of wood. Two different wood layers are used to fabricate a wood scroll with diagonal natural water channels (d-WS) and a wood scroll with parallel natural water channels (p-WS). Vertical water transport through gap channels (i.e., spaces between the overlapping wood layers) is >10 times higher than that through natural water channels. Because only diagonal channels allow water transport across the wood layer, d-WS exhibits good lateral water transport whereas p-WS exhibits poor lateral water transport. The synergistic effect of the gap channels and diagonal channels in d-WS increases evaporation performance. The total evaporation rate of water of d-WS is $9.08 \text{ kg m}^{-2} \text{ h}^{-1}$ in the absence of wind, which increases to $37.95 \text{ kg m}^{-2} \text{ h}^{-1}$ in the presence of 2 m/s wind. These evaporation rates are among the highest values ever reported under similar conditions. Furthermore, the difference between the evaporation rates of p-WS and d-WS increases with height. The higher evaporation rate of d-WS is attributed to the presence of diagonal channels, which enhances lateral water transport to the outermost surface, where dark evaporation occurs. The difference in lateral water transport affects not only the dark evaporation rate but also salt resistance. The evaporation experiments are conducted in a 3.5 wt% NaCl solution under 1 sun illumination. No salt is observed on the top surface of p-WS, but a significant amount of salt is accumulated on the side surface, indicating that the gap channels facilitate sufficient water supply to the top surface, but the microchannels alone fail to supply sufficient water to the side surface. Interestingly, no salt accumulation is observed on both the top and side surfaces of d-WS. The excellent salt resistance of d-WS is attributed to the synergy between its gap channels and diagonal channels, which enables sufficient water supply to the top and side surfaces. The evaporation rate of d-WS does not deteriorate even after 5 days, demonstrating the possibility of long-term operation.

SESSION EN09.06: Bioengineered Polymers, Synthetic Biology Tools in Designing Sustainable Polymers

Session Chairs: Bradley Olsen and Eleftheria Roumeli

Wednesday Morning, November 30, 2022

Hynes, Level 3, Room 306

8:30 AM *EN09.06.01

Sustainable Synthesis of Spider Silk and Other Biopolymers via Photosynthesis Keiji Numata^{1,2}; ¹RIKEN Institute, Japan; ²Kyoto University, Japan

In nature, high-performance biological polymers and composites consist of various organisms and their tissues. Those high-performance biopolymers are

mainly protein/polypeptide, and have therefore been recognized as bioactive and functional material. My research group also reported new findings in spider silk spinning, which is important to design tough structural polymers. However, use of those biopolymers as structural materials is still challenging due to several technical issues. One of the major drawbacks of polypeptide-based materials is their limited synthesis method. To clear the potential issue, my research group is interested in marine purple photosynthetic bacteria as ideal organisms and platforms for production of useful materials to reduce production costs and to contribute sustainable society, because they can utilize sun energy, seawater and carbon dioxide and nitrogen gas in the air for their growth. My research group studies on the photosynthetic bacteria to produce spider silk-like polymers. *Rhodovulum sulfidophilum*, a marine purple non-sulfur photosynthetic bacterium as well as a good polyhydroxyalkanoate (PHA) producer, was genetically engineered for the production of synthetic spider dragline silk protein. The successful construction of photosynthetic microbial host for silk production could reduce the production cost, especially the marine photosynthetic bacteria can fix CO₂ and N₂ with using seawater as a cheap culture medium. To establish the fundamental platforms for photosynthetic bacterial technology, we are currently developing peptide-mediated transformation and protein introduction methods for alga and photosynthetic bacteria. These new methodologies will be able to support the high-throughput characterizations for biopolymer productions.

9:00 AM *EN09.06.02

Modulating the Properties of Functional Biocomposites with Engineered Bacterial Protein Fibers Noemie-Manuelle Dorval Courchesne; McGill University, Canada

Protein-based materials can be genetically customized for a range of applications. In addition to displaying biocompatibility, tunable bioactivity and responsiveness, they represent sustainable alternatives to conventional synthetic polymers. In particular, proteins that self-assemble into higher order structures and can be produced at large scale are of interest for deployment into wearable devices and alternatives for commodity materials like plastics, textiles and electronics. Curli fibers produced as part of the extracellular matrix of *Escherichia coli* bacteria represent a promising protein scaffold, due to their unique physicochemical properties, including their ability to self-repair and their resistance to harsh conditions. Once secreted by bacterial cells, CsgA subunits, the self-assembling repeats of curli fibers, form fibrous structures that can further aggregate, entangle, and gel into macroscopic materials. Among other functionalities, we have genetically encoded in CsgA the ability to fluoresce, to conduct charges, and to respond to stimuli.

Here, I will present an overview of advances that we have made to engineer biocomposite materials containing functional curli fibers. The fibers allow to modulate the mechanical, electrical, self-healing and sensing properties of the composites. First, I will highlight the scalable and simple bioprocesses that we have developed to express, extracellularly secrete, and isolate genetically engineered curli fibers. Then, I will present two main applications of biofunctionalized composites: 1) a curli fiber – conductive polymer composite that exhibits self-healing properties and tunable electrical conductivity dependent on the protein content, and 2) a “living” self-repairing biofilm-based textile in which the curli fibers part of the biofilm’s extracellular matrix act as glue to repair the textile via a water-induced healing mechanism. So far, we have applied curli-functionalized textiles to the fabrication of sweat pH sensors and we foresee several applications of curli-based composites for wearable devices and biocompatible electrodes. These devices enable novel functions that can only be achieved by biological materials, and bring us closer to a bio-based economy.

9:30 AM DISCUSSION TIME

9:45 AM EN09.06.04

Amyloid-Nanocellulose Interactions and Self-Assembly Nico Kummer^{1,2}, Caroline E. Giacomini², Peter Fischer², Silvia Campioni¹ and Gustav Nyström^{1,2}; ¹Empa–Swiss Federal Laboratories for Materials Science and Technology, Switzerland; ²ETH Zürich, Switzerland

Amyloid fibrils from abundant and inexpensive food proteins and nanocellulose in the form of cellulose nanocrystals (CNCs) and nanofibrils (CNFs) are renewable and biodegradable materials with broad ranging applications in water purification, for biomedical engineering and as bioplastics. To increase the mechanical and functional properties of hybrid amyloid-nanocellulose materials, the fundamental understanding of the interactions between the two colloids needs to be improved. Using zeta potential measurements, rheology and atomic force microscopy all experimental evidence point to the importance of electrostatic interactions. We found that entropy-driven polyelectrolyte complexation occurred under pH conditions where the amyloids and nanocellulose particles are oppositely charged, whereas stable co-dispersions are possible above the isoelectric point of the amyloid fibrils, when both amyloids and nanocellulose are negatively charged.

During the polyelectrolyte complexation, the addition of CNCs proportionally increased the elasticity by crosslinking individual fibrils of the hen egg white lysozyme (HEWL) amyloid network. The scaling of the elasticity with amyloid concentration cross-linked with a fixed concentration of CNCs is in agreement with theory (affine thermal model). Finally, strong, transparent hybrid amyloid-nanocellulose hydrogels were fabricated using amyloids from HEWL and beta-lactoglobulin (BLG). The self-assembly was started from stable amyloid-nanocellulose co-dispersions above the isoelectric point of the amyloids and followed by dialysis to decrease the pH and induce amyloid-nanocellulose attraction and cross-linking. In summary, the gained knowledge on colloidal interactions provides an important basis for the design of functional biohybrid materials based on amyloid fibrils and nanocellulose.

10:00 AM BREAK

10:30 AM *EN09.06.05

Green Products for the Red Planet—Sustainable Materials for Human Exploration Lynn J. Rothschild^{1,2}, Ivan Paulino-Lima³, Simon Vecchioni⁴ and Christopher Maurer⁵; ¹NASA, United States; ²Brown University, United States; ³Blue Marble Space Institute Science, United States; ⁴New York University, United States; ⁵Redhouse Studios, United States

Synthetic biology – creating new capabilities with life – promises to create a greener future for planet Earth, from fields as diverse as pharmaceuticals to manufacturing, agriculture and nanotechnology. Progress can be stymied by such considerations as economics, politics, legal and philosophical issues surrounding GMOs. Often solutions to these problems already exist, so it is difficult for a new, superior method to displace the old. As we move humans beyond Earth, to long duration stays in the International Space Station, and then onward to the Moon and Mars, the challenges of supporting human life will need radical new solutions. For example, while life on Earth uses an enzymatic machinery which evolved over 3.5 billion years ago, synthetic biology promises to be able to engineer the systems to adapt to current natural or industrial environments. A focus on solutions off planet require a focus on a circular economy. While there are new constraints, such as worrying about the mass of a solution, constraints offer opportunities for game-changing solutions that will then allow revolutions back on our home planet. Example projects include biomining and fungal-based habitats off planet.

11:00 AM *EN09.06.06

The Power of Biology to Build-Up and Break-Down Polymeric Materials Hal Alper; The University of Texas at Austin, United States

Biology has an exquisite potential to transform the chemical industry. Advances in strain engineering, synthetic biology, and machine learning are leading to a rapid transformation in the reach and potential of bio-based solutions. Within this scope, biotechnology can enable the production of a diverse suite of customized monomers and polymers. On the other side, biotechnology can enable the depolymerization of used polymers. This talk will highlight the

potential for sustainable materials production and reuse through both cell and enzyme processes. Examples include rewired cells for producing polymer precursors, enzymatic plastic waste depolymerization, and conversion of biologically-derived lipids into thermoset plastics. Throughout the talk, there will be a focus on sustainability and the fundamental principles necessary to rewire metabolism and expedite the design-build-test-learn-deploy cycle of engineering for these applications.

11:30 AM *EN09.06.07

Protein-Based Elastomers as Replacements for Polyurethanes Bradley Olsen, Yiping Cao, Wui Yarn Chan, Emil Andersen and Sarah Av-Ron; Massachusetts Institute of Technology, United States

Proteins are biopolymers widely studied for materials applications due to their abundance as waste feedstock and their structural role in producing high performance materials in biological systems. While greater utilization of proteins in materials can provide a sustainable alternative to petroleum-derived polymers, proteins are generally brittle and have high softening temperatures in the absence of plasticizer, making them unsuitable for many applications. Inspired by the chemical and structural similarity between the hard blocks of polyurethanes and the β -strands of proteins, we hypothesized that natural protein materials could be utilized in polyurethane like hard-soft copolymers in order to overcome these limitations and produce sustainable commodity materials.

Simple bioconjugation strategies allow the preparation of polyfunctional proteins that can be co-polymerized with a wide variety of different monomers to produce thermoset plastics. These materials have variable modulus, toughness, and extensibility depending upon the protein content, degree of protein functionalization, and monomer choice. While hydrophilic monomers were first used to enable facile copolymerization with the protein, this leads to strong humidity-sensitivity. To reduce this effect, we developed formulations based on oleophilic monomers using surfactants to compatibilize the protein and monomer before polymerization. This leads to a two-fold reduction in water uptake while preserving the favorable mechanical performance of the materials. Tuning the surface charge of the protein biomass via chemical reaction was further explored in order to control the humidity sensitivity, leading to further stabilization of mechanical properties across a broad range of environmental conditions. Recently, we have also demonstrated that thermal treatment to induce changes in protein conformation can lead to substantial strengthening of the materials, and that this approach generalizes across a wide range of different protein feedstocks and purities. Overall, this work demonstrates the ability to produce biomass-based materials that can mimic the mechanical response of polyurethanes while simultaneously managing moisture uptake, demonstrating promising steps towards a new sustainable material platform.

SESSION EN09.07: Green Structural Materials
Session Chairs: Bichlien Nguyen and Eleftheria Roumeli
Wednesday Afternoon, November 30, 2022
Hynes, Level 3, Room 306

1:30 PM *EN09.07.01

Cement Decarbonization Using Photosynthesis Sarah Williams, Danielle Beatty and Wil V. Srubar III; University of Colorado Boulder, United States

The production of portland cement is responsible for 7% of global carbon dioxide (CO₂) emissions. Multiple strategies, including portland cement clinker substitution with supplementary cementitious materials (SCMs) and carbon capture, utilization, and storage (CCUS), are being explored to decarbonize the cement production process. This presentation will highlight recent research that leverages the carbon capture and storage mechanisms of microalgae to decarbonize cement production. In one study, the pozzolanic reactivity of biosilica extracted from photosynthetic diatoms was investigated as an alternative SCM. In a second study, raw algal biomass was investigated as a carbon-storing set-retarding admixture for portland cement. Finally, biogenic calcium carbonate from microalgae was investigated as a potential carbon-storing mineral replacement for ground limestone in portland limestone cement. In addition to these studies, other opportunities for cement decarbonization that leverage the carbon capture and storage mechanisms of microalgae will be highlighted and discussed.

2:00 PM EN09.07.02

Regenerated Cellulose Structured Materials for Coral Reef Restoration Guillermo A. Reyes¹, Colleen Flanigan² and Orlando J. Rojas¹; ¹Aalto University, Finland; ²Zoe – A Living Sea Sculpture in Cozumel, Mexico

Regenerated cellulose materials using the ionic liquid, 1-ethyl-3-methylimidazolium acetate ([emim][OAc]), were used to produce filaments and 3D-printed meshes *via* wet spinning and Direct-Ink-Writing (DIW); these structures with highly aligned nanofibrils (wide-angle X-ray scattering) simultaneously displayed extensibility (wet strain as high as 39%), and tenacities (up to 2.3 cN/dtex). DIW of the respective gels led to meshes with up to 60% wet stretchability. The IL regenerated structures were demonstrated for reliable performance in marine environments, with prospects of replacing plastic cords and other materials used to restore coral reefs on the coast of Mexico. Additionally, considering the unique ability of alkali dissolved cellulose to absorb CO₂ at room temperature in a non-catalytic, highly reactive media, here a mineralization process is proposed to produce artificial coral-like supports. The resulting Mineralized Cellulose Material (MCM) exhibits tunable flow properties and a wide range of mechanical properties. The synergistic combination of dissolved cellulose and in-situ mineralized CO₂ into calcium carbonate at different Cellulose: Carbonate ratios allows the production of heterogeneous fluid streams with shear-thinning behavior (viscosities from 10² to 10⁷ mPa.s; and storage modulus G' ranging from 10 to 10⁵ Pa). The CO₂ absorption capacity tracks inversely with cellulose concentration. Two types of MCMs are obtained, the first with low cellulose content, namely MCM1 is a dry powder with applications as a flux material for ceramic glazes or cement with porous structures. In contrast, the material with an increased cellulose content, namely MCMh, is a moldable/printable paste that transforms into a tough (stone-like) material after drying. MCMh was tested as an artificial substitute for coral stones in the Gulf of Mexico. LCA results suggest that these technologies bring new opportunities to cellulose and construction industries by removing and utilizing CO₂ emissions for different materials, including the imperative coral reef restoration in the oceans.

2:15 PM EN09.07.03

Use of Waste Bioproducts as a CO₂ Sink in Sustainable Structural Composites Marcos M. Hernandez, Adalee R. Witt, Yuliia Trujillo, Raul C. Gonzalez Esquer, Babetta L. Marrone and Joseph H. Dumont; Los Alamos National Laboratory, United States

The establishment of a bio-based economy that can compensate for the hundreds of megatons of waste generated annually is vital to the successful utilization of waste as a resource. [1] Upon identifying useful waste streams, bio-manufacturing technologies such as sustainable composite materials can

be developed to offset CO₂ emissions. Biomass offers many advantages such as biosequestration, biomineralization, and improved material properties when integrated into such materials. [2, 3, 4] In this study, we incorporate waste from various biological waste streams into cementitious, pressed, and hydrogel materials to develop sustainable composites for applications as structural materials, 3D printing, and fuel pellets. Samples were prepared and characterized using a wide range of chemical, mechanical, and spectroscopic techniques. From this study, we evaluated the effects of waste biomass in sustainable composites for CO₂ mitigation, reduced construction cost, and waste utilization potential.

[1] Gagg, C.R., *Cement and concrete as an engineering material: An historic appraisal and case study analysis*. Engineering Failure Analysis, 2014. 40: p. 114-140.

[2] Oner, A. D. N. A. N., S. Akyuz, and R. Yildiz. "An experimental study on strength development of concrete containing fly ash and optimum usage of fly ash in concrete." *Cement and Concrete Research* 35.6 (2005): 1165-1171.

[3] Dhama, Navdeep K., M. Sudhakara Reddy, and Abhijit Mukherjee. "Biomineralization of calcium carbonates and their engineered applications: a review." *Frontiers in microbiology* 4 (2013): 314.

[4] Cheah, Wai Yan, et al. "Biosequestration of atmospheric CO₂ and flue gas-containing CO₂ by microalgae." *Bioresource technology* 184 (2015): 190-201.

2:30 PM BREAK

3:30 PM EN09.07.05

High pH and Temperature Tolerant Molecular Mimic of Carbonic Anhydrase for Self-Healing Cementitious Material [Rebecca J. Gilchrist](#), Shuai Wang, Nima Rabbar, Suzanne F. Scarlata and Ronald L. Grimm; Worcester Polytechnic Institute, United States

Carbon storage in concrete was recently reinvigorated by the use of carbonic anhydrase to yield an enzymatic self-healing cementitious material. While this material demonstrates high strength and self-healing properties, the reliance on enzymatic catalysis limits the performance based on the two-week lifetime of carbonic anhydrase, and motivates the exploration of non-biological alternatives. We have explored organometallic carbonic anhydrase mimetic materials with a view towards longevity and performance in the highly alkaline environments of cement as well as the high temperatures to which concrete may be subjected. Inspired by bio-relevant carbonic anhydrase mimetics, results with zinc cyclen (cyclen = 1,4,7,10-tetraazacyclododecane) demonstrate high stability at pH above 13 and temperatures above 50 °C with good conversion of gas-phase carbon dioxide to carbonate. We discuss these results in the context of molecular alternatives for self-healing cementitious material and carbon storage in concrete.

3:45 PM EN09.07.06

The Influence of Biomineralized Contaminated Waste Plastics in Reinforced Cement Mortar [Kylee Rux](#), Seth Kane, Michael Espinal, Cecily Ryan, Adrienne Phillips and Chelsea Heveran; Montana State University, United States

The demand for cement infrastructure and plastic products are continuously increasing, and the production of these materials generate greenhouse gas emissions. An additional problem is the low recycling rate of plastics — with only 9% of plastics ever produced being recycled. Instead, these waste plastics are accumulating in landfills and the environment. One contributing factor to low plastic recycling rates is that contamination from food waste and oil necessitates treatment steps that may increase the cost and reduce the quality of recycled plastic. Researchers have made headway against these challenges by using waste plastic as reinforcement in cementitious materials. However, increasing the amount of plastic reinforcement leads to a decrease in composite compressive strength. To combat the loss in compressive strength, it may be possible to use microbially induced calcium carbonate precipitation (MICP) to coat waste plastic in calcium carbonate and improve the strength of plastic-reinforced cementitious materials. The objective of our research was to optimize the amount of clean and contaminated waste plastic that can be added to plastic-reinforced mortar and whether MICP coating of waste plastic enhances the strength. The performance of plastic-reinforced mortar cylinders was investigated using compressive strength tests at a 5%, 10%, and 20% volume replacement for cement. Results indicate that even at a 20% replacement with untreated, clean post-use plastics (HDPE, PVC, LDPE1 (larger chips), and LDPE2 (smaller granules)) produced compressive strengths acceptable for several applications such as foundation walls, garages, and sidewalks. A coating of MICP on clean waste plastic did not significantly improve the compressive strength of the specimens. MICP treatment of oil-coated waste plastics (HDPE, LDPE1, and LDPE2) recovered the strength by 28.28% relative to cylinders containing untreated oil-coated plastics, on average. However, washing the same oil-coated plastics with only water resulted in compressive strengths similar to that of MICP-treated, contaminated plastics. Our results demonstrate that incorporating greater volumes of waste plastics into mortar at optimized replacement ratios could improve the sustainability of cementitious composites by the dual mechanisms of reduced cement production and repurposing plastic waste.

4:00 PM EN09.07.08

Fungal Mycelium as a Scaffold for Biomineralized Building Materials [Ethan T. Viles](#)¹, Erika Espinosa-Ortiz², Arda Akyel², Robin Gerlach², Adrienne Phillips² and Chelsea Heveran¹; ¹Montana State University, United States; ²Montana State University, United States

Concrete manufacturing contributes 5-8% of anthropogenic CO₂ emissions. Biomineralization is a less energy intensive process that could improve the sustainability of building material manufacturing. Microbial biomineralization can occur when ureolytic microbes are cultured in media with urea and calcium (Ca). Ureolysis by microbes increases carbonate alkalinity and pH of the environment—inducing calcium carbonate (CaCO₃) precipitation. Bacterially induced CaCO₃ precipitation (BICP) is used to seal cracks, stabilize soils, and manufacture low weight building materials. Typically, BICP-structures require substantial urea, Ca, and microbial inputs. Biomineralizing a scaffold may increase the efficiency of manufacturing biomineralized materials by templating mineral nucleation for more precise mineralization. Here we draw inspiration from biomineralized tissues, such as bone, which mineralize a compliant scaffold. Fungal mycelium may serve as an environmentally robust scaffold for biomineralization. *Neurospora crassa* is a ureolytic microbe that has the potential for either self-mineralization or exogenous mineralization. The goal of this study was to determine how biomineralization efficiency and biomineral characteristics differ between self-mineralized, abiotically mineralized, and bacterially mineralized fungal scaffolds. *N. crassa* was mineralized using 4 conditions: fungally induced CaCO₃ precipitation (FICP) with malt media (FICP-malt), FICP where urea is the only nitrogen source (FICP-urea), abiotically induced CaCO₃ precipitation (AICP), and BICP where ureolytic bacteria, *Sporosarcina pasteurii*, mineralize the fungal scaffold.

Electron microscopy (EM) and X-ray diffraction (XRD) were used to determine the morphology and elemental composition of scaffolds. For FICP scaffolds, *N. crassa* was cultured for 10 days in media with Ca and urea. For AICP and BICP scaffolds, *N. crassa* was cultured for 5 days in Ca-free medium and then autoclaved. AICP scaffolds were mineralized in a Ca-bicarbonate solution via a pH increase. *S. pasteurii* was first cultured onto BICP scaffolds in Ca free medium, then placed in medium with urea and Ca. Dissolved Ca and urea concentrations, during mineralization, were measured using colorimetric Ca and urea assays. The Ca content of mineralized scaffolds was determined by measuring the mass before and after an acid Ca digest

EM showed different morphologies and mineral attachment locations for all 4 conditions. FICP-malt scaffolds had small Ca minerals coating the top of a mycelium mat. FICP-urea scaffolds did not have a mat of mycelium, but had individual hyphae coated with small Ca minerals. AICP produced Ca minerals

that also coated the outside of the mycelium, but these were much larger than both FICP scaffolds. BICP produced the largest minerals of the 4 conditions, which were incorporated within the mycelium. XRD shows that each condition produced calcite and a minority phase of vaterite. Ca digests showed the FICP-urea scaffolds had the most Ca per weight of scaffold. FICP-malt and AICP both had the least amount of Ca deposited. BICP scaffolds had the second most Ca deposited. FICP-urea samples had lower ureolysis, but a faster decrease of dissolved Ca than FICP-malt samples. BICP showed the most ureolysis and had a faster decrease in dissolved Ca than FICP conditions. AICP scaffolds showed an instantaneous drop of dissolved Ca with the pH increase.

Our results suggests BICP is the most promising technique to mineralize fungal scaffolds as it showed the most ureolysis and the most dissolved Ca loss. The integration of CaCO_3 within the mycelium itself found for BICP scaffolds is promising for conferring strength to biomineralized scaffolds. Future work will include nanoindentation to analyze the material properties of biomineralized fungal scaffolds. Biomineralizing fungal scaffolds with bacteria may lead to new approaches for engineering sustainable building materials.

SESSION EN09.08: Poster Session II: Sustainable Materials

Session Chairs: Bichlien Nguyen and Eleftheria Roumeli

Wednesday Afternoon, November 30, 2022

8:00 PM - 10:00 PM

Hynes, Level 1, Hall A

EN09.08.01

A Chemically Recyclable Thermoplastic Elastomer Synthesized with Redox Switchable Polymerization [Jiangwei Liu](#)¹, Sarah Blosch², Jeffery Byers¹ and John Matson²; ¹Boston College, United States; ²Virginia Tech, United States

Poly(lactic acid) (PLA) as a biodegradable and bio-derived polyester has limited application due to its brittleness. In an effort to increase the flexibility, a redox-switchable catalytic system was developed to make A-B-A' triblock copolymers containing stiff PLA end blocks and a flexible poly(tetrahydrofuran-*co*-epoxide) midblock. The tensile test demonstrated high flexibility of the triblock (strain at break ϵ_b up to 200%) compared with PLLA ($\epsilon_b < 10\%$). The mechanical properties were dependent on the amount of tetrahydrofuran (THF) repeating units in the mid-block: low THF incorporation led to more thermoplastic features while higher THF incorporation resulted in more rubbery materials. In addition to being derived from commodity monomers like lactide and THF, the triblock copolymer can be depolymerized to their constituent monomers. A reactive distillation system with a dual catalyst system was designed that allowed us to recover THF and lactide monomers from the thermoplastic elastomer.

EN09.08.04

Development of Continuous Extraction of Bio-Silica from Rice Husk in Pilot Scale [Ji Yeon Park](#)^{1,2}, Jinyoung Chun¹, Yang m. Gu^{1,2}, Byoungseung Jeon¹ and Jin Hyung Lee¹; ¹Korea Institute of Ceramic Engineering & Technology, Korea (the Republic of); ²Hanyang University, Korea (the Republic of)

The use of renewable biomass, instead of petroleum, could be effective strategy to reach to carbon neutral society. Rice husks can be an alternative to silica raw material because it contains 15~20% of silica. Annually, 194 million tons of rice husk was produced worldwide in 2020. The initial step to use silica in rice husks is extracting silica from rice husk. Generally, alkaline extraction was performed at high temperature and pressure condition to extract silica from rice husks. In this study, the continuous extraction of silica from rice husk has developed at 80°C and atmospheric pressure. First, the optimal conditions of NaOH concentration, reaction temperature and time, and solid/liquid ratio were investigated at a lab-scale. The optimal conditions found in the lab-scale were 80°C reaction temperature, 2.5hr reaction time, 10 wt% solid/liquid ration and 0.5M NaOH. Based on the optimal conditions found in the lab-scale, continuous extraction process was operated in the pilot-scale having 20.2kg/d processing capacity. The stability of the continuous process was proved by operating for 190 hr. The process showed stable during the operation and extraction efficiency was maintained about 82%.

EN09.08.05

Autonomously Self-Healing Effect of Thermoplastic Polyurethane Containing Multiple Self-Healing Moieties [Yoojin Rho](#), Hyojin Kim and Ho Sun Lim; Sookmyung Women's University, Korea (the Republic of)

Inspired by self-healing phenomena in nature such as repairing of plant tissues or the healing of animal skins, there have been many studies about self-healing materials. Normally, materials lose most of their mechanical properties when facing external damage. However, self-healing materials can heal the wound spontaneously or by external stimuli such as light and heat. This self-healing property can extend the life of the material and maintain durability through recovery from damage. Research on self-healable polymers have been shifted from extrinsic to intrinsic self-healing. In extrinsic self-healing, if the healing agents in polymer matrix are not sufficient, repeated healing is limited. In comparison, the surface can be repeatedly cured by intrinsic self-healing methods due to reactions between chains or interactions between supramolecules. In this study, we have developed a thermoplastic polyurethane that is intrinsically healed under the moderate condition due to multiple hydrogen bonding and a disulfide metathesis. The synthesized thermoplastic polyurethane contains ureido-pyrimidinone type supramolecular interactions and aromatic disulfide type dynamic covalent bonds. The results demonstrated that the thermoplastic polyurethane was healed at room temperature in an hour. The mechanical properties of polymers were improved by multiple hydrogen bonding monomers. Also, we extruded these self-healing polymers as fibers via wet spinning technique. Using these fibers, we observed the fibers spooled and packed within silicone droplet. These fibers could be applied to artificial muscles because they stretch or release through the spooling phenomenon like real muscles. Also, it is expected that the mechanical properties of fibers are improved than non self-healable polyurethane fibers due to multiple self-healing moieties on polymers' main chain.

EN09.08.06

Capturing of Inorganic and Organic Pollutants Simultaneously from Complex Wastewater Using Recyclable Magnetically Chitosan Functionalized with EDTA Adsorbent [Monu Verma](#) and [Hyunook Kim](#); University of Seoul, Seoul, Korea (the Republic of)

Herein, we synthesized new and versatile magnetite-doped chitosan-ethylenediaminetetraacetic acid ($\text{Fe}_3\text{O}_4@CS\text{-EDTA}$) composite for simultaneous capturing of multiple heavy metal ions: Hg^{2+} , Cd^{2+} , and Ni^{2+} , and methyl orange (MO) dye from complex wastewater through the adsorption process. We believe that EDTA in the synthesized adsorbent work as a cross-linker as well as a chelating agent for the capturing of heavy metal ions, while the protonated amino groups of CS adsorb MO through electrostatic interaction. In the monocomponent system, the adsorption followed to Langmuir model and gave the maximum adsorption capacities of 232.70 ± 14.30 , 121.40 ± 7.0 , 56.50 ± 2.20 , and $732.10 \pm 72.40 \text{ mg g}^{-1}$ for Hg^{2+} , Cd^{2+} , Ni^{2+} , and MO, respectively. Kinetics data well fitted to the pseudo-second-order (PSO) models, confirmed the chemisorption process. Interestingly, in the case of the

binary component system containing both metals and MO, the adsorption capacity of the adsorbent for the dye was not affected by the metal presence, while the adsorption of metal ions was enhanced with increasing MO concentration. The adsorption mechanism was confirmed by elemental mapping, XPS, and FTIR. Moreover, no significant loss in the adsorption efficiency even after the six continuous adsorption-desorption cycles confirms the great stability and potential of the adsorbent in treating the complex wastewater.

EN09.08.08

Living and Adaptive Microstructures by Combining Laser Printing and Dynamic Covalent Exchange of Alkoxyamines Manuel Tsotsalas; Karlsruhe Institute of Technology, Germany

Two-photon lithography, also known as direct laser writing or 3D laser printing, allows to structure polymer networks in unprecedented definition and can generate interesting optical, mechanical and biomedical properties in the micro and nanoscale. The polymer networks applied usually relies on covalent bonds, lacking dynamic or living characteristics. Inclusion of dynamic and living characteristics to 3D laser printing microstructured polymer networks provides new and exciting possibilities to dynamically modify the molecular structure of the networks, such as crosslinking density or mesh sizes.[1] Such modifications at the molecular level strongly influence important characteristics, such as swelling degree or mechanical properties. For creating polymer network structures containing dynamic and living bonds, it is important to adopt the dynamic covalent chemistry to the radical chemistry applied in the laser printing process.

Here, we include dynamic covalent bonds, based on nitroxide radicals, into the 3D laser printing microstructures. In our approach, dynamic alkoxyamine bonds form during the printing process via trapping of radical species by functionalized nitroxide radicals. The alkoxyamine bonds within the final microstructured polymer networks can afterwards be activated for nitroxide exchange reactions or nitroxide mediated polymerization, providing dynamic, adaptive and “living” properties to the microstructured networks. In addition, the alkoxyamine functionalities provide the networks with self-healing and recyclable properties. [2] [3] [4] [5] [6]

[1] 4D Printing at the Microscale C. Spiegel, M. Hippler, A. Münchinger, M. Bastmeyer, C. Barner-Kowollik, M. Wegener, E. Blasco *Adv. Funct. Mater.* **2020**, 30, 1907615.

[2] Dynamic Covalent Polymer Networks via Combined Nitroxide Exchange Reaction and Nitroxide Mediated Polymerization Y. Jia, Y. Matt, Q. An, I. Wessely, H. Mutlu, P. Theato, S. Bräse, A. Llevot, *Polym. Chem.*, **2020**, 11, 2502.

[3] Recycling and Self-Healing of Dynamic Covalent Polymer Networks with a Precisely Tuneable Crosslinking Degree Q. An, I. Wessely, Y. Matt, Z. Hassan, S. Bräse, M. Tsotsalas *Polym. Chem.* **2019**, 10, 672.

[4] Self-Reporting Refoldable Fluorescent Single-Chain Nanoparticles T. Fischer, S. Spann, Q. An, B. Luy, M. Tsotsalas, J. Blinco, H. Mutlu, C. Barner-Kowollik *Chem. Sci.*, **2018**, 9, 4696.

[5] Radical Exchange Reaction of Multi-Spin Isoindoline Nitroxides Followed by EPR Spectroscopy I. Wessely, V. Mugnaini, A. Bihlmeier, G. Jeschke, S. Bräse, M. Tsotsalas *RSC Advances* **2016**, 6, 55715.

[6] Covalent Adaptable Networks Based on Dynamic Alkoxyamine Bonds. Y. Jia, G. Delaitre, M. Tsotsalas, *Macromol. Mater. Eng.* **2022** Accepted Author Manuscript 2200178. <https://doi.org/10.1002/mame.202200178>

EN09.08.10

Chlorella-Laden Cements for Green Construction Materials—Effects of Algae Incorporation on the Structure and Mechanical Properties of Cement Meng-Yen Lin, Paul Grandgeorge, Andrew M. Jimenez and Eleftheria Roumeli; University of Washington, United States

Concrete industry, which accounts for 5-8% of global CO₂ emissions, raises increasing concerns regarding its environmental impacts. To improve the environmental footprint of cementitious materials, a wide variety of biobased fillers across macro-to-nano scales, including hemp fibers, nanocellulose, and cellulose microfibrils, has been studied. Promising findings on the effects of incorporating such biobased fillers to cementitious materials include improvements on the mechanical properties of the produced composites, as well as enhancement of thermal and acoustic insulation properties. However, limitations involving the use of costly food crops as a source for biobased materials, and the energy-intense processing methods to extract and pretreat such materials prior to introducing them to concrete, have impeded their further applications. Algae-based materials, owing to their high capacity of carbon fixation, rapid growth rate, and capability of growing on non-arable spaces, represent a promising biomass resource for construction materials.

In this work, we investigated the effects of adding a photosynthetic algae, *Chlorella*, in forms of dry powder into Type I/II ordinary Portland cement (OPC) at concentrations ranging from 0.5-15 wt.%. We find that the mixing process, which is crucial to disperse *Chlorella* powder in cement mixture, together with the water absorption capacity and particle sizes of *Chlorella* increase the viscosity and affect the workability of the fresh paste. The compressive strength evolution across 3-91 days is studied and associated with the development of microstructure by scanning electron microscopy. We observed a drastic decrease in strength throughout the entire curing duration with only 5 wt.% addition of *Chlorella*, which suggests a hindrance of the conventional hydration reactions. We further examine the interactions between *Chlorella* and OPC at different concentrations by thermogravimetric analysis (TGA), X-ray diffraction (XRD), Fourier-transform infrared spectroscopy (FTIR), and energy-dispersive X-ray spectroscopy (EDS). Our results show that the presence of *Chlorella* significantly alters the hydration reactions of OPC with the formation of different compounds, which subsequently leads to micro morphological changes and notable difference in macroscopic mechanical properties.

EN09.08.11

Volatile Organic Compound-Free, Eco-Friendly, Colored Lacquer Pallets Derived from Catechol Lipid-Based Bio-Resin Ju Young Shin and Ho Sun Lim; Sookmyung Women's University, Korea (the Republic of)

We report the method for producing volatile organic compound (VOC)-free, eco-friendly, colored lacquer pallets characterized by excellent adhesion strength and strong durability from catechol lipid-based bio-resin extracted from lacquer trees. It is challenging to develop the desired color or predict the color of the lacquer-coated surface as oriental lacquer reflects a shade of dark brown. We focused on the saturation behavior of the color of the coated surface based on the amount of the added pigments. The optical properties of the pigment-containing lacquer were studied using the Kubalika–Munk theory by measuring the degree of absorbance and reflectance. The colors were also observed using the CIE L*a*b color space. Color saturation for the colored lacquer-coated surfaces was achieved at the pigment content of 50 wt.% for red and blue. When the pigment content was 40 wt.%, color saturation was achieved for green and yellow. The results indicated that clear colors that could be observed with the naked eye could be generated without using an excess of pigments. The materials exhibited excellent adhesive properties (5B), and the hardness was 2–3H. In addition, it was observed that with the

progress of the aging time over two years, the color of the lacquer-coated surfaces changed, and a bright and intense surface was formed. The color change could be attributed to the bleaching effect of the oriental lacquer binder. The results reported herein can potentially help in obtaining a green solution for preparing VOC-free colored lacquer pallets and predicting the color development observed for highly decorative and protective coatings.

EN09.08.12

Low-Cost and Efficient Biobased Material for Removal of Noble Metals in Gold Tailing Dam Ruben D. Sinisterra, Vanessa Alves de Paula Soares and Roberto Galery; University Federal-Minas Gerais, Brazil

The technological advance of the industry is an important factor in the increase of environmental pollution by industrial effluents, since high amounts of chemical load, metals, toxic and highly dangerous elements are produced. In Brazil, the mining activity is responsible for providing mineral resources for technological development and source of economic resources, however generates numerous tailings dams. In addition, when the mine is closed, there is a high cost for disposing of wastewater to achieve metals standards established by legislation.

Thus, the treatment of these effluents must be efficient and continuous, and the treatment methods are commonly divided into "active", which requires the addition of alkaline chemicals to neutralize acidity, or "passive". The term "passive treatment" corresponds to biological, geochemical and gravitational processes. Currently, in the short term, most mines use "active treatment" methods such as: neutralization treatment, purification, and recovery of heavy metals, with conventional machines, spent with a large number of chemical products and electric energy.

Among the technologies for the removal of pollutants from industrial and mines effluents, adsorption using biosorbent material has been classified as a low-cost, efficient, and easy-to-implement methodology since they can adsorb metals with high efficiency and being a biodegradable option.

The present technology refers to a method of recovering noble metals, Au (III), Ag (I), Pt (IV) and Pd (II), in wastewater from a gold tailings dam, using seeds from *Bixa Orellana* L and biodegradable nanofibers with Bixin. The recoveries of these noble metals in aqueous solutions containing these metallic ions and in real samples from a gold tailings dam were evaluated.

The noble metals Au (III), Ag (I), Pt (IV) and Pd (II) recovery from aqueous solutions with *Bixa Orellana* L and biodegradable nanofibers with Bixin were carried out at different contact times, pH and amounts. The quantification of metals was carried out using atomic absorption spectroscopy; characterization of seeds and biodegradable nanofibers by TGA, MEV-EDS and Zeta potential. A prove of concept of metal removal using the biosorbent was made with wastewater from a gold tailings dam. The optimal adsorption of Au (III), Ag (I), Pt (IV) and Pd (II) ions were recorded at pH 2, with the addition of a 0.2 mol/L Na₂HPO₄ buffer solution and an acid solution citric acid 0.1 mol/L, the adsorbent concentration between 5 and 200mg/L, at room temperature around 25 °C, under agitation at 50 rpm, after 48h of contact. Solid/liquid separation was performed by centrifugation and metal recovery rates was calculate. The seeds of *Bixa Orellana* L. showed a high degree of selectivity for adsorption of Au (III), where a removal percentage of approximately 84.35% was identified from a gold tailings dam. This technological process, with high efficiency, low cost and commercial value could be serve as alternative to treat industrial effluents, such as the mining industry.

Acknowledgments: The authors would like to thank to the Network for the study, development and application of technologies based on sustainable nanomaterials for the recovery of water from the Doce River basin (N°06/2016), sponsored by the entities: FAPEMIG, CNPQ, CAPES, ANA, FAPES and development in Chemistry Department of UFMG.

EN09.08.13

Modifying Gas Diffusion Electrode with Food Waste-Derived Materials for Enhancing Electrochemical Conversion of CO₂ Ying Chuan Tan¹ and Dan Kai²; ¹Institute of Sustainability for Chemicals, Energy and Environment, Singapore; ²Institute of Materials Research and Engineering, Singapore

The disposal of organic wastes from food sources contributes to undesirable environment impact and the loss of valuable resources. These food wastes usually end up in incineration plants or landfills, which could result in the unintended release of greenhouse gases. Considering that the global population is expected to reach over 9 billion in 2050, the demand of food resources, and thus the production of food waste will increase. Therefore, there is a need to develop strategies to upcycle food wastes toward valuable materials to maximize the utilization of resources while minimizing the environmental impact. In this study, we demonstrated the fabrication of gas diffusion electrodes integrated with food waste-derived materials for the electrochemical conversion of CO₂ to CO. By using commercial Ag nanoparticles as electrocatalysts, the incorporation of the as-prepared food waste-derived materials enhanced the maximum production rate of CO by 48%. At the same time, the faradaic efficiency of CO was improved by 28% at an applied potential of -1.1 V vs RHE. The materials derived from food wastes were shown to improve the conductivity of the gas diffusion electrode, which facilitated the charge transfer between the electrocatalysts to the reactants. This work thus represents an approach to avoid greenhouse gas emissions by valorizing food waste into functional materials, which further enable a more efficient conversion of CO₂ to useful chemicals.

EN09.08.14

Rubber Adhesives and Mixed Mode Recycling to Achieve Over 80% Recycled Content in Rubber Composites Clara Troyano-Valls¹, Sarah Av-Ron¹, Michelle Calabrese², Wui Yarn Chan² and Bradley Olsen¹; ¹MIT, United States; ²University of Minnesota, United States

Diene-based rubbers vulcanized with sulfur are one of the most widely used polymer networks today. Nowhere is their impact more visible than in tires, which form the foundation of our transportation infrastructure. However, the same crosslinking process that imparts desired mechanical properties and chemical resistance makes these thermosets difficult to recycle, frustrating the development of wide-scale and effective methods of rubber waste management. Current rubber mechanical recycling efforts focus on incorporating ground tire rubber (GTR) into other materials as filler. This process yields products with degraded mechanical properties and, as a result, downcycled materials of limited applicability. Chemical recycling via devulcanization, a process in which sulfur crosslinks are cleaved, is similarly unsuccessful: it is energy intensive and cleaves both backbone and crosslink bonds, leading to a partially degraded product [1].

To improve upon existing methods of rubber recycling, our group has developed a GTR coating inspired by tire retreading—an application that requires a strong adhesive to patch two pieces of vulcanized rubber together. We have developed a process and an adhesive formula that increases the performance of GTR and virgin rubber composites by up to 45% as compared to uncoated GTR composites [2]. Here, we present the work further modifying this formula and combining this approach with GTR chemical devulcanization that has enabled us to produce composites containing over 80% post-consumer rubber waste. This optimized composite formulation at this recycle level exhibits superior performance to that of earlier composites containing only 15% post-consumer waste. Structure-property relationships in the material are explored through coating reinforcement, changes in coating to GTR ratios, and matrix material. The goal is to create a coating capable of handling a wide variety of chemically variable post-consumer GTR, incorporating it into high-performing recycled rubber composites.

[1] Asaro, Lucia, Michel Gratton, Saïd Seghar, and Nourredine Aït Hocine. *Conservation and Recycling* 133 (June 2018): 250–62.

[2] Calabrese, Michelle A., Wui Yarn Chan, Sarah H. M. Av-Ron, and Bradley D. Olsen. *ACS Applied Polymer Materials* 3, no. 10 (October 8, 2021): 4849–60.

EN09.08.15

Bio-Trapping of Ureolytic Microorganisms on Sand Surfaces to Enhance Microbially Induced Calcium Carbonate Precipitation [Elif Ugur](#), Recep Avci, Adrienne Phillips and Chelsea Heveran; Montana State University, United States

Microbially induced calcium carbonate precipitation (MICP) has been widely studied for its potential to improve sustainability in the construction industry and geotechnical applications. The presence of urease-producing bacteria is essential for catalyzing the conversion of urea into ammonium and carbonate ions to promote CaCO₃ precipitation. The effectiveness of the MICP process highly depends on the spatial uniformity of the bacterial concentration and CaCO₃ precipitation. In this study, we functionalized sand surfaces with amine groups to trap urease-producing bacteria from the planktonic phase to enhance MICP. The purpose of this study was to investigate the impact of 3-Aminopropylmethylmethoxysilane (AMDES) treatment on microbial viability, attachment, and urea hydrolysis. Bioactive sand surfaces were prepared using 1% AMDES to create positively charged surfaces to promote the adhesion of urease-producing bacteria *Sporosarcina pasteurii* via electrostatic interaction. This approach enables the concentration of urease-producing bacteria on the sand surface, which can then precipitate a full monolayer of CaCO₃ acting as an initial binder to adjacent sand particles. X-Ray Photo Electron Spectroscopy (XPS) was used to confirm the amine groups on the functionalized surface. Zeta Potential measurement was used to understand the changes in surface charges, which proved the negatively charged sand surface becomes positively charged after AMDES treatment. Microbial growth and viability after on AMDES-treated sand were measured using Optical Density (OD₆₀₀), and Confocal laser scanning microscopy (CLSM) of live dead stained cells, respectively, and compared to untreated sand. The results demonstrated that the bio-trapping of microorganisms on AMDES-treated sand surfaces reduced the growth rate of microorganisms and potentially compromised microbial viability. CLSM images of live dead stained cells at 0h showed more bacteria with compromised cell walls attached to AMDES-treated sand. Untreated sand particles did not show any bacterial attachment at 0h. After 24 hours of growth, CLSM images showed no bacterial growth on AMDES-treated sand and untreated sand particles showed densely packed live bacteria. Ureolytic activity was measured using a colorimetric Jung assay. Although the growth of the microorganisms was slowed with the AMDES treatment, ureolytic activity was maintained, and urea was completely hydrolyzed although at a slower rate. The resulting biocemented structures show excellent density and edge definition, which exceed those of conventional MICP. Our results show that bio-trapping of urease-producing bacteria on sand particles may promote uniform and effective biocementation of sand.

EN09.08.16

Porous Scaffolds as Catalysts for New Waste-Reduction Solutions [Miriana Vadala](#), Eva Kroell, Marco Kueppers, Ruth Brunstermann and Doru C. Lupascu; University of Duisburg-Essen, Germany

With the word “scaffolds” a variety of research fields is addressed, ranging from chemistry to medicine, from biology to civil engineering. Scaffolds can be found at different length scales, from supporting structures in construction sites to tissue engineering and bone regeneration. Scaffolds are open porous structures that can be made active by applying a magnetic or electric field or be used as backbone structures for biological and medical purposes. They can be used also as filters, for instance for wastewaters treatment, where hydrogen is produced. Hydrogen production from wastewaters can achieve the dual environmental benefits of waste reduction along with production of high value energy fuel. Moreover, wastewaters can be considered as ideal substrates for biohydrogen production since they are rich in carbon and nitrogen. The addition of nanoparticles (NPs) can improve the biohydrogen production, can promote the bioactivity of hydrogen-producing species and increase the bacterial growth. Micro- or nanosized porous materials possess large surface areas and large pores, which are beneficial for the diffusion, adsorption, and activation of reactants, especially if pores are interconnected. Materials containing porous silicones with excellent mechanical performance, e.g., high compressibility and stretchability, and thermal stability, are in high demand in many practical applications. Recently, porous polydimethylsiloxane (PDMS) materials have been successfully synthesized for selective oil absorption from water. For example, Choi et al. fabricated PDMS sponges with fast oil absorption and excellent recyclability using sugar particles as templates [1]. Zhang et al. prepared PDMS sponges with high oil absorbency by using *p*-xylene as solvent and sugar particles as templates [2]. In this contribution we show our first attempts to fabricate porous scaffolds which can host bacteria colonies and can serve as catalysts for wastewaters treatment. The samples were produced via sugar cube template and consist of PDMS and Fe₂O₃ or TiO₂ nanoparticles. The samples went through several water treatment cycles and maintained their structure without deterioration, creating a suitable environment for bacteria colonies, with consequential hydrogen production.

[1] S. J. Choi, T. H. Kwon, H. Im, D. I. Moon, D. J. Baek, M. L. Seol, J. P. Duarte and Y. K. Choi, ACS Appl. Mater. Interfaces, 2011, 3, 4552–4556

[2] A. J. Zhang, M. J. Chen, C. Du, H. Z. Guo, H. Bai and L. Li, ACS Appl. Mater. Interfaces, 2013, 5, 10201–10206.

EN09.08.17

Pattern-Integrated Paper Li-Ion Microbatteries Through Large-Scale Roll-to-Roll Flexographic Printing [Ying Wang](#), Daxian Cao, Xiao Sun, Haoze Ren, Tongtai Ji and Hongli Zhu; Northeastern University, United States

The large-scale manufacturing of architecture designable lithium-ion (Li-ion) batteries poses a significant challenge but raises an emerging need for enhancing battery performances and enlarging application scenarios. However, traditional methods of manufacturing Li-ion batteries (LiBs) rely on roll-to-roll (R2R) bar coating, which cannot render the customized pattern or structure for fabricated electrodes and limited electrodes' application. To get around this bottleneck, we innovatively introduced the well-developed R2R flexographic printing technology to manufacture pattern-integrated Li-ion electrodes. Compared to alternative electronic printing substrates such as metal, plastic, and glass, the inexpensive and biodegradable cellulosic paper with high printability was selected as a printing substrate to improve printing resolution, reduce cost, and protect the environment. Furthermore, the special pores between the cellulosic fibers in the paper were utilized for transferring ions. Therefore, paper can be used both for a separator in LiBs. In this study, as a novel approach, we integrated large-scale R2R flexographic printing and LiB production to manufacture LiBs with unique patterns, in which flexible and high printable paper was used as both the printing substrate and separator in LiBs. Accordingly, we developed a series of LiFePO₄ (LFP) flexographic printable inks and successfully printed them on thin (25 μm) and lightweight (23.4 g/m²) paper with a large-scale R2R flexographic printer. A high-quality and high-resolution flexographic printed pattern was achieved with 35% solid-content LFP at 80 in/min. Moreover, a thin layer of Al₂O₃ was coated to modify the separator. The flexographically printed paper battery exhibited a high-rate performance (97.2% discharge capacity retention at 2 C of that at 0.1 C) and outstanding capacity stability (~100% discharge capacity retention after 1000 cycles at 3 C). The results highlighted the immense potential of integrating flexographic printing with R2R manufacturing architecture for designable LiBs and using flexible, inexpensive, sustainable, and high printable paper as a printing substrate and separator in printed LiBs for the scalable fabrication of flexible batteries with high-resolution patterns to obtain microbatteries for applications in wearable electronics and bioengineering.

EN09.08.18

Excellent Mechanical and Electrical Properties of Anisotropic Freeze-Cast Native and Carbonized Bacterial Cellulose-Alginate Foams Kaiyan Qiu^{1,2} and [Ulrike G. Wegst](#)^{3,2}; ¹Washington State University, United States; ²Dartmouth College, United States; ³Northeastern University, United States

Native and carbonized freeze-cast bacterial cellulose-alginate (BC-ALG) foams possess an ice-templated honeycomb-like architecture with remarkable properties. Their unique pore morphology consists of two levels of porosity: 20–50 μm diameter pores between, and 0.01–10 μm diameter pores within the

cell-walls. The mechanical properties of the BC-ALG foams, a Young's modulus of up to 646.2 ± 90.4 kPa and a compressive yield strength of up to 37.1 ± 7.9 kPa, are high for their density and scale as predicted by the Gibson–Ashby model for cellular materials. Carbonizing the BC-ALG foams in an inert atmosphere at $1000\text{--}1200$ °C in a second processing step, both pore morphology and mechanical properties of the BC-ALG remain well preserved with specific mechanical properties that are higher than those reported in the literature for similar foams. Also the electrical conductivity of the BC-ALG foams is high at 1.68 ± 0.04 S cm⁻¹ at a density of only 0.055 g cm⁻³, and is found to increase with density as predicted, and as a function of the degree of carbonization determined by both carbonization temperature and atmosphere. The property profile makes freeze-cast BC-ALG foams and their carbonized foams attractive for energy applications and as a sorbent.

EN09.08.19

Fully Fashioned and Curbside Recyclable Mono-Material 3D Textiles Leslie Yan, [Volodymyr Korolovych](#) and Svetlana V. Boriskina; Massachusetts Institute of Technology, United States

3D printing polymer structures onto fabric substrates can be used to develop fully-fashioned, three-dimensional textiles that unlock new functionalities and aesthetics for a wide range of textile-based applications. Moreover, the accessibility of fused-deposition modeling (FDM) 3D printing can streamline the material design and fabrication process, while presenting sustainability advantages with regards to low-waste and localized manufacturing. However, developing these hybrid textiles with traditional filament and fabric types can render high-level material recovery infeasible and present adhesion challenges.

Our work addresses these gaps with a mono-material approach to 3D printing on fabric realized through the lens of polyethylene, producing a textile that is fully curbside recyclable without disassembly. Polyethylene (PE) is among the most popular commodity plastics due to its versatility, affordability, and excellent engineering characteristics. PE offers significant potential as a performance fabric due to its washability and lightweightness, as well as moisture-wicking properties introduced through the standard yarn production process [1-4].

Woven polyethylene fabric was produced from HDPE resin using scalable techniques, then developed into a three-dimensional mono-PE textile through an integrated process utilizing an unmodified FDM 3D printer and commercially-available HDPE printing filament. The digital design workflow for the three-dimensional structures, as well as possible variation in the woven pattern of the textile substrate, enables significant diversity and customizability in the design of the 3D textiles. Moreover, utilization of different densities of PE for either filament or fabric presents an opportunity for optimizing the mechanical performance of the recycle following material recovery. The advantages of the sustainable, three-dimensional PE textile can be leveraged for uses ranging from athletic footwear to space applications.

[1] M. Alberghini, et al, Sustainable polyethylene fabrics with engineered moisture transport for passive cooling. *Nature Sustainability* 4,715–724 (2021).

[2] S.V. Boriskina, An ode to polyethylene. *MRS Energy & Sustainability* 6, E14 (2019).

[3] J.K. Tong, et al, Infrared-transparent visible-opaque fabrics for wearable personal thermal management. *ACS Photonics* 2, 769–778 (2015).

[4] M. Alberghini, et al, Characterisation and modelling of water wicking and evaporation in capillary porous media for passive and energy-efficient applications, *Applied Thermal Engineering*, 188159 (2022).

Acknowledgements: DEVCOM Soldier Center through the US Army Research Office (W911NF-13-D-0001)

EN09.08.20

Electrochemical Properties of Carbon Monolith from Kenaf Fibers Han-Yul Park¹, Minhu Huang², Kyung-Hun Song¹, Jae-Suk Lee² and [Tae-Ho Yoon](#)²; ¹Pai Chai University, Korea (the Republic of); ²Gwangju Institute of Science & Technology, Korea (the Republic of)

Carbon monoliths (CM) were prepared from kenaf fibers via moulding column-shape samples and then pyrolysis at 500, 600, 700 or 800 °C, followed by activation with KOH at 700 °C. Then, the samples were characterized by thermogravimetric analyser (TGA), field-emission scanning electron microscopy (FE-SEM), field-emission transmission electron microscopy (FE-TEM), x-ray photoelectron spectroscopy (XPS), Raman spectroscopy, x-ray diffraction (XRD) and N₂ sorption instrument. The prepared CM was subjected to electrochemical property evaluation via cyclic voltammetry (CV), galvanostatic charge-discharge (GCD) and electrochemical impedance spectroscopy (EIS). The GCD study using a three-electrode system showed that the specific capacitance decreased with higher pyrolysis temperature (PYT), exhibiting the highest specific capacitance of 217 F/g with that from 500 °C pyrolysis. A two-electrode system provided 95.9 % retention upon the 5,000 cycling test as well as the specific capacitance of 212 F/g, being converted to the energy density of 6 Wh/kg at the power density of 215 W/kg.

EN09.08.21

Toxicity of Tin-Based Catalysts on Polymer-Degrading Bacteria [Alex Zappi](#), Katharina Fransen, Sarah Av-Ron, Kristala L. Prather and Bradley Olsen; Massachusetts Institute of Technology, United States

Biodegradable polymers are synthesized using a wide range of transition metal catalysts to control the molecular properties of the final polymer. While catalysts are traditionally chosen only for their efficacy in polymerization, they may also be toxic to microorganisms, impacting the measured biodegradation rate of the final polymer. In particular, catalyst toxicity could cause otherwise biodegradable materials to fail biodegradation testing, undervaluing the actual degradability of the polymer. Tin-based catalysts are widely used to synthesize biodegradable polymers through ring-opening polymerization of lactones due to their availability, cost, and effectiveness; however, their toxicity in environments relative to biodegradation is not well understood. Existing studies suggest toxic effects of tin in aquatic microorganisms with little focus towards the effect on bacteria important for biodegradation. In this study, we first quantify the toxicity of widely used tin-based catalysts in culture media on common soil bacteria with key roles in biodegradation. Using this information to assess the relevant concentration range, we then use clear-zone assays to measure the direct effects of these catalysts on biodegradation of solid state plastics and exemplify the extent of these effects using realistic concentrations of a variety of catalysts doped into commercial polymers. Combined, these results indicate the role that residual catalyst plays in affecting biodegradation results, and the high-throughput methods applied here provide a basis for catalyst screening to identify catalysts that best promote polymer biodegradation.

EN09.08.23

Solar Harvesting Biodegradable Photonic Smart Labels for Mobile Sensing and the Internet of Things (IoT) [Maria Rute Ferreira Andre](#)¹, Gabriela Kovaleski¹, Lilia Dias¹, Lianshe Fu¹, Sonia P. Ventura¹ and Paulo Andre²; ¹University of Aveiro, Portugal; ²Instituto de Telecomunicações, Portugal

Sensors play a key role in the Internet of Things (IoT) providing monitoring inside and outside the communication networks in a multitude of parameters¹. The coupling of optical sensors to smartphones appears as an exciting and affordable strategy to sustainably convert a signal from an optical sensor network into a digital data sequence for the new generation of mobile optical (mOptical) sensing^{1,2}. The opportunity of using luminescent natural renewable materials for smart labels will be addressed, in line with the increasing demand for natural products and underpinned by the recent policies to reduce the environmental impact of industrial processes and products when integrated into a smart and low-waste chain of different products or within a

circular economy approach. Using the concept of colored multiplexed QR codes, bio-based inks will be used to design smart IoT devices to track and sense in real-time² and to address temperature monitoring in buildings³, in which photonic sensors under the configuration of luminescent solar concentrators appear as a solution to integrate energy-generating devices in windows or façades.

Ramalho et al., "Lanthanides for the new generation of optical sensing and Internet of Things", Handbook on the Physics and Chemistry of Rare Earths, doi:10.1016/bs.hpcr.2021.12.001

2. Dias et al., "Smart Optical Sensors for Internet of Things: Integration of Temperature Monitoring and Customized Security Physical Unclonable Functions," IEEE Access, 10, 24433-24443, 2022, doi: 10.1109/ACCESS.2022.3153051

3. Correia et al., "Bio-Based Solar Energy Harvesting for Onsite Mobile Optical Temperature Sensing in Smart Cities", Adv. Sci. 2022, 2104801. doi: 10.1002/adv.202104801

Acknowledgements: CICECO-Aveiro Institute of Materials (UIDB/50011/2020, UIDP/50011/2023, LA/P/0006/2023), Instituto de Telecomunicações (UIDB/50008/2020, UIDP/50008/2020); FCT/MEC, FEDER, PT2020. LMS Dias was supported by 2020.05802.BD. GK acknowledges the financial support through BD/REITORIA/9328/2020.

EN09.08.24

Sugar Derived Nanoporous Carbon Material for CO₂ Direct Air Capture [Amanda Sanchez](#), Guangping Xu, Yongliang Xiong, Yifeng Wang, Sean Dwyer and Hongyou Fan; Sandia National Laboratories, United States

The mitigation of the impact of anthropogenic carbon dioxide is important to the reversal of the trend of the climate change that has been already observed in the world. One of the key approaches for solving this problem is to capture carbon dioxide (CO₂) from the atmosphere in advance of fixation, conversion, or injection into the aquifers for long-term storage. Successful CO₂ capture is further complicated by the fact that nitrogen (N₂) is the dominant gas in the Earth's atmosphere. Thus the separation of carbon dioxide from the mixture of carbon dioxide and nitrogen gases requires economic and environmentally friendly technologies is vital to enable anthropogenic intervention to the reverse of the current trend of climate change.

Current state-of-the-art CO₂ capture technologies involve amine-based chemical sorption in corrosive KOH solution. It is an energy intensive process to regenerate the absorbent. In this work, we synthesized nanoporous carbon material using sugar as precursor to adsorb CO₂ via a physical sorption process to achieve the separation of CO₂ from N₂. We have successfully synthesized both mesoporous and microporous carbon materials utilizing the common table sugar sucrose (C₁₂H₂₂O₁₁) as the carbon precursor material. Addition of polystyrene-block-poly(4-vinylpyridine) (PS-P4VP) or n-Dodecyl beta-D-maltoside (DDM) (C₂₄H₄₆O₁₁) serve as the sugar surfactant and also enhance product porosity. The mesopores synthesized using PS-P4VP are mostly between ~10 nm and ~40 nm. The micropores synthesized using DDM are between 1 – 2 nm. Ongoing work includes characterization of the separation of CO₂ from the mixture of CO₂ + N₂ with the newly synthesized nanoporous carbon materials using mass spectrometry to investigate the relationship between CO₂ separation efficiency and pore size.

The synthesis technology developed will have an important impact in mitigating the negative effect of anthropogenic CO₂ on the climate change. Since the precursor materials for producing the nanoporous materials are cost-effective, abundant, and widely available, and the methods developed in this work for generating the nanoporous materials are environmentally friendly and are sustainable.

SNL is managed and operated by NTESS under DOE NNSA contract DE-NA0003525. SAND2022-8198 A

SESSION EN09.09: Biodegradable Polymers I—Scale-Up and LCA
Session Chairs: Kunal Masania and Eleftheria Roumeli
Thursday Morning, December 1, 2022
Hynes, Level 3, Room 306

8:30 AM *EN09.09.01

Nano-/Bio- Is Not an Either/Or Choice for Composites [Jeffrey P. Youngblood](#); Purdue University, United States

Cellulose Nanomaterials (CN) are attractive materials for possible applications in nanocomposites reinforcement, nanomaterials and biomedicine as they are high strength and stiffness, yet are renewable, biodegradable, non-toxic, cheap, and optically transparent. Here, an overview will be presented on renewable/sustainable nanocomposites based on CN. Specifically, extraction, functionalization and nanocomposite preparation will be covered. We will detail our efforts to characterize CN and CN composite mechanical and thermal properties and understand what factors dictate behavior as well as our efforts at utilizing CN in a variety of application spaces such as for structural composites, infrastructure materials, and food packaging.

9:00 AM EN09.09.02

A Recyclable, Re-Processable Stretchable Conductive Polymer Complex Exhibiting Repeatable Autonomous Self-Healing [Colton Duprey](#)¹, Hadi Rouhi¹, Yang Lu² and Evan K. Wujcik¹; ¹The University of Alabama, United States; ²Georgia Institute of Technology, United States

E-skins and wearable strain sensors are essential for the realization of applications in the broad fields of sensing, soft robotics, and immersive gaming, among many others. These flexible materials can be safely and comfortably adhered to the skin and capable of monitoring human motions with high accuracy, as well as exhibiting excellent durability. However, it is challenging to develop electronic materials that possess the properties of skin: compliant, elastic, stretchable, and self-healable. This work demonstrates a low-energy processing method of producing a polymer complex composed of poly(2-acrylamido-2-methyl-1-propanesulfonic acid), polyaniline, and phytic acid (a transient, plant-based small molecule dopant) for electronic polymer materials. It exhibits ultrahigh stretchability (1935%), repeatable autonomous self-healing ability and linear response to flexion bending, outperforming many current reported wearable strain sensors. Most importantly, the material is recyclable and re-processable, allowing one synthesis to produce a long-lasting lifetime of the sensor material.

9:15 AM EN09.09.03

Strong Backyard-Compostable Bioplastics from Algal and Plant Renewable Resources [Ian Campbell](#), Paul Grandgeorge, Andrew M. Jimenez and Eleftheria Roumeli; University of Washington, United States

Research in sustainable materials continues to produce alternatives to the unsustainable sourcing, manufacturing, and disposal of synthetic plastics. Innovative bioplastics developed during the past decade have properties comparable to commodity plastics. However, seldom are novel bioplastics both biodegradable and only rarely are they truly backyard-compostable. The majority of biodegradable plastics are engineered to degrade only in given controlled, aerobic environments and not in landfills or the biosphere, where they regularly wind up. In this work, we demonstrate the production of plant and algal biocomposites, both from whole-cells and from isolated cellular components. We also introduce varying concentrations of natural plasticizers and adapt processing conditions to tune the bioplastic mechanical and thermal behavior. Processing conditions are controlled via mixing in a twin-screw extruder and during hydraulic pressing of biological matter into bulk materials. By changing the time, temperature, shear rate, and plasticizer content, we develop diverse micro-morphologies and properties. The effects of varying processing conditions and plasticizer concentration on microstructure and mechanical and thermal behavior in the resulting bioplastics are characterized. The micro-morphology of plant and algal bioplastics are evaluated using scanning electron microscopy (SEM). The mechanical properties of the bioplastics are measured (flexural modulus and strength, modulus of resilience) and the thermal stability is assessed by thermogravimetric analysis (TGA). We identify the relationship between the bioplastic composition and processing parameters and the microstructure and mechanical performance. Finally, we measure the mass-loss profiles of the bioplastics during soil burial to assess their compostability.

9:30 AM EN09.09.04

Biopolymer Composites with Tunable Biodegradation Rates [Nicolas A. Lee](#), Hannah Gazdus and Markus J. Buehler; Massachusetts Institute of Technology, United States

The growing environmental impacts of solid waste accumulation have driven an increased demand for biodegradable alternatives to conventional plastics. While several products have begun to gain popularity as biodegradable or compostable plastics, such products still pollute terrestrial and aquatic environments, as they frequently require precise conditions in order to fully decompose. Furthermore, there often exist tradeoffs between a product's shelf stability, mechanical properties, and biodegradability. Here, we characterize biodegradation rates in a series of biopolymer composites, which can be tuned according to their composition. The raw materials in these composites are abundant, organic polymers known to be digestible by common soil organisms. We report relationships between composition and the biodegradation rates of these composites in live-soil environments as well as their degradation rates in aqueous environments. The described biocomposites are solidified from hydrogels containing apple pectin, chitosan (deacetylated chitin), and fibrous delignated cellulose and contain no synthetic binding agents. We demonstrate the suitability of these composites for casting, injection molding, and 3D printing using pneumatic extrusion. This study demonstrates the potential for tunable biopolymer composites to replace bioplastics as a superior alternative to conventional plastic.

9:45 AM EN09.09.05

Degradation of Regenerated Silk Fibroin in Soil, Fresh Water and Marine Environments Augustine Zvinavashe, [Zeina Barghouti](#), Yunteng Cao, Hui Sun, Doyoon Kim, Muchun Liu, Eugene Lim and Benedetto Marelli; Massachusetts Institute of Technology, United States

There is a compelling need to find new materials that meet stringent performance requirements for application in food, water and agriculture industries while addressing biodegradability, circular life cycle, and sustainable sourcing at scale. Regenerated silk fibroin (RSF) is a structural biopolymer with applications in biomedicine, optoelectronics, food, water, and agriculture. Extracted from largely available *Bombyx mori* cocoons through a water-based process, RSF is fabricated into advanced materials that have competitive performance and merits of natural origin and non-toxicity. As a protein, RSF is considered slowly degradable in the human body but as a material it is known to be environmentally stable, and its biodegradation is mostly unknown. In this work, we report for the first time the degradation of silk fibroin films in the soil and water environment as a function of abiotic and biotic factors such as sodium chloride concentration, presence of microorganisms, and bacteriostasis.

Microbial activity was determined to be a key driver for silk film degradation in different environmental conditions. Exogenous bacterial colonization from soil resulted in an accelerated surface degradation, while the encapsulation of a soil-dwelling α -Proteobacteria, *Rhizobium tropici* CIAT 899, in RSF materials at the point of material assembly further accelerated the material degradation, promoting a bulk degradation. It is speculated that the production of proteases by the bacteria, or biofertilizer, contributes to the accelerated biodegradation, and results in the complete degradation of the silk materials considered in soil in 8 weeks.

Studies of biodegradation in freshwater and seawater environments indicated slower biodegradation profiles when compared to the measurements obtained in soil, even when bacteriostats were added. Exposure to seawater resulted in <10% of weight loss in 8 weeks. SF mass loss measurements over time showed that *R. tropici* induced silk fibroin biodegradation in water and the degradation rate was higher at sodium chloride concentrations that allow for the biofertilizers survival (NaCl 50-200mM). A statistically significant decrease ($p < 0.05$) in the mechanical properties (i.e. Young's modulus and hardness) of the SF films exposed to seawater was measured with nanoindentation, when compared to SF films after 8 weeks of exposure to 0, 50, and 100 mM of NaCl solution. These results may suggest that degradation of SF films in seawater and freshwater requires the presence of active heterotrophic bacteria that possess the capability of digesting the silk material.

The effects of silk fibroin polymorphism on degradation in soil was also investigated by modulating beta sheet content with post-processing water annealing and a statistically significant difference of film degradation occurred across time ($p < 0.05$) and across different beta sheets content ($p < 0.05$).

Together, this study shows that RSF biodegradation can be controlled by material design and by regulating the interaction with microorganisms present in the environment. Given the rising need to predict materials' biodegradation in the environment and to embed circular life principles in the design of technical innovations, it will also provide the basis to engineer silk fibroin materials for applications in food, energy, water, and agriculture.

10:00 AM BREAK

10:30 AM *EN09.09.06

Techno-Economic and Life Cycle Analyses of Lignocellulosic Nano-Microfibrils (LCNMF) Production from Wheat Straw Danielle U. Pascoli, Gabriel V. Seufftelli, Anthony Dichiaro, Renata Bura and [Richard Gustafson](#); University of Washington, United States

Lignocellulosic nano- and microfibrils (LCNMF) are sustainable biomass-derived materials with multiple potential applications due to their high surface areas, excellent mechanical properties, and biodegradability. Cellulose nano-microfibrils have not become a commercial product because of high production costs. This work presents techno-economic (TEA) and life cycle analyses (LCA) of lignocellulosic nano-microfibril production from agricultural residues via a newly developed, low cost environmentally friendly process. The standalone process presented is comprehensive, including the areas: 1) Feedstock handling, 2) Pulp and refining, 3) Peracetic acid pretreatment, 4) Mechanical fibrillation, and 5) Wastewater treatment. A facility using 100-tonne wheat straw feedstock per day was modeled with process simulation software with a production capacity of 18,400 tonnes of LCNMF per

year. In the economic analysis we break down the capital and operating costs and establish a LCNMF selling price to achieve a 15% return on investment. In addition, we present the impact of facility size and co-location with an existing biorefinery on the process economics.

Finally, results from LCNMF life cycle analyses, including life cycle global warming potential (100 year) and fossil usage, are presented. This work demonstrates the outstanding economic potential and environmental performance of a standalone process to produce cost-competitive nanocellulose products of small widths (2-17 nm), promoting the commercialization of such products for many applications.

11:00 AM *EN09.09.07

Industrial Decarbonization—Gap and Opportunity for Ammonia, Bioproducts and Cement Carlos Quiroz-Arita; Sandia National Laboratories, California, United States

This research seeks to identify carbon-neutral and carbon-negative processes to decarbonize the U.S. economy within the opportunity space of i) hydrogen and ammonia production, ii) bioresources to bioproducts, and iii) cement and steel. To understand the drivers of sustainability metrics in these decarbonization exemplars, we have developed new models for industrial-scale systems, techno-economics analysis, and life cycle assessment. Our research results show decarbonization opportunities that can significantly decrease Nationwide CO₂ emissions. Sandia's ammonia production process shows promising results that can dramatically reduce energy requirements, resulting in 95% of scenarios at or below -0.017 ton CO₂eq ton NH₃⁻¹. Probabilistic results of algae-derived animal feed and bioplastics show that more than 50% of scenarios can result in negative-net life cycle CO₂eq emissions, which can be improved using more sustainable production of nutrients, i.e., ammonia. Lastly, the resulting probability distribution of emissions from cement varies from 638 to 1,075 kgCO₂eq ton⁻¹ of cement, consistent with the literature, demonstrating that decarbonization strategies that displace direct and indirect emissions in the kiln are priorities to improve the carbon footprint in these systems.

11:30 AM EN09.09.08

Sustainability-by-Design—Achieving State-of-the-Art Performance with Reduced Environmental Impact Anna-Marie Gorman, Amy Clayton and David Johnson; CPI, United Kingdom

Electronic waste generation is predicted to double by 2050 to reach approximately 111 million tonnes per year.¹ Currently only around 20% of this waste is recycled and recycled¹, leaving a significant amount of plastic and heavy metal waste to be released into the environment. The use of printed electronics has grown significantly over the last decade², offering flexible, light, freeform circuits that can be more easily incorporated into products. This however only compounds the problem of increasing waste by adding functionality to everyday objects with a short lifespan. Material selection is a crucial consideration to ensure that e-waste that is not or cannot be recycled will not introduce damaging and long-lasting species into the environment. In this presentation we propose several methodologies that could be used to maximise the potential of printed electronics by reducing health and environmental impacts of associated material sets and processes.

Bio-based binders have long been used in the printed ink industry, with ethyl cellulose and cellulose acetate butyrate being two of the most common. However, these are often paired with harmful and environmentally damaging solvents. By combining the use of Hansen solubility parameters with a safety-by-design approach we have been able to select an array of sustainable solvents with reduced health and environmental impact that can be employed for a range of printing methods. For example, we have demonstrated the use of a renewable and safe solvent benzyl acetate to achieve high conductivity in the range of 10⁻⁵ Ohm-cm, which is comparable to commercial equivalents and doesn't require extraction or special handling conditions.

Other areas that have been explored include selection of bio-derived substrates, assessment of alternative conductive fillers and use of low energy and fast light-based curing and sintering methods.

Finally, we will show how these approaches can lead to developing new materials and processes to enable better recycling, to re-claim high value materials and components that would otherwise be lost to landfill.

(1) *E-waste will double by 2050. Business-as-usual is not an option to cope with it: UN Initiative – SCYCLE*. <https://www.scycle.info/e-waste-will-double-by-2050-business-as-usual-is-not-an-option-to-cope-with-it-un-initiative/> (accessed 2022-06-08).

(2) *MultiBrief: Printed electronics allow technological leap in wearable devices*. <https://exclusive.multibriefs.com/content/printed-electronics-allow-technological-leap-in-wearable-devices/engineering> (accessed 2022-06-08).

SESSION EN09.10: Biodegradable Polymers II—Toxicity and Policy

Session Chairs: Kunal Masania and Eleftheria Roumeli

Thursday Afternoon, December 1, 2022

Hynes, Level 3, Room 306

1:30 PM EN09.10.02

Cannabinoid-Based Bioplastic Conductive Composites for Circular-Lifecycle Medical Electrodes Michael Sotzing¹, John M. Toribio², Amy Pollock², Gregory A. Sotzing² and Alex Chortos¹; ¹Purdue University, United States; ²University of Connecticut, United States

Establishing bioplastics derived from renewable resources as an alternative to petrochemical-derived plastics is an emergent strategy for combating the effects of plastics on the environment. Current bioplastics exhibit uncertain biocompatibility and limited mechanical and processing characteristics. We prepare poly(cannabinoid)s by step growth polymerization of bifunctional carboxylic acids with hemp-derived cannabinoids containing two hydroxyl groups. The resulting thermoplastic poly(cannabinoid)s are the first of their kind to include cannabinoids directly in their polymeric backbone. Homopolymer and copolymer synthesis utilizing a wide variety of available cannabinoids and dicarboxylic acids enables a large range of mechanical properties, in turn promoting development of application-specific materials. Melt and solution processibility of poly(cannabinoid)s broadens fabrication capabilities. The observed natural anti-inflammatory and anti-oxidative behavior of poly(cannabinoid)s provides improved biocompatibility. Furthermore, the capability of poly(cannabinoid)s to degrade through base-catalyzed hydrolysis facilitates repolymerization and reprocessing of polymer composites. The healthcare industry, the second largest producer of waste globally, is a suitable gateway for this nascent materials platform. Medical waste is increasing due to the proliferation of single-use devices such as electrocardiogram (ECG) electrodes that are commonly employed for patient monitoring. We fabricate electrodes composed of tungsten particles, a biodegradable and biocompatible metal, dispersed in a homopolymer of poly(cannabinoid)s. Adhesives are prepared from poly(cannabinoid) copolymers with low glass transition temperature. Fabrication is performed using direct-ink-write printing. Ink rheology

is optimized using solvents such as di(propylene glycol) methyl ether that have minimal impact on the biosphere compared to other organic solvents. Electrodes exhibiting a volume resistivity of 0.2 ohm-meters are demonstrated functionally using ECG acquisition techniques. Poly(cannabinoid)s enable chemical recycling of the electrodes after use. Ester linkages in poly(cannabinoid)s provide a path for facile depolymerization via base-catalyzed hydrolysis. Exposure of electrodes to dilute ammonium hydroxide at 80 degrees Celsius yields cannabinoid monomers, dicarboxylic acids, and tungsten. Concurrently, exposure of tungsten to ammonium hydroxide results in selective etching of surface oxide layers, increasing interparticle electrical conductivity resulting in low volume resistivity of new composites. After hydrolysis, components can be easily separated because the high density of tungsten facilitates centrifugation, whereas the hydrophobicity of the cannabinoids and hydrophilicity of the diacids facilitate chemical separation. To assess the lifecycle of materials post-recycling, we repolymerize poly(cannabinoid)s using reclaimed cannabinoids and carboxylic acids and form composites with recycled tungsten particles to show that functional medical electrodes can be reformed. This chemically-driven circular process ensures the preparation of electrodes that meet the required properties for medical devices, including high reproducibility and high materials purity.

1:45 PM EN09.10.03

Biodegradable Polymers for Reducing Electronic Waste [Kaitlyn E. Crawford](#); University of Central Florida, United States

Plastics enable our modern standard of life from safety and shelter to advanced technologies in electronics and aerospace applications. Thus, we must accelerate fundamental research to innovate advanced polymer materials with new properties. Our modern lifestyle is coming at a severe cost, however, with serious and legitimate economic, energy, and environmental concerns in using plastic. For example, electronic devices, while primarily thought of as agglomeration of metals and semiconductors, are often comprised largely of plastic—up to 90% plastic in some cases. Unfortunately, however, ~50 million tons of electronic waste (e-waste) is generated annually with up to 80% of that waste expected to reach landfills. With the emergence of new electronic technologies, including flexible electronics for human health monitoring, identification of more bio-friendly materials is critical to offset their environmental impact. To this end, the development and integration of degradable materials for wearables can facilitate the decomposition of electronic devices when they are no longer needed. This talk focuses on the development of biodegradable polyesters using step-growth polymerization and incorporation of naturally occurring materials such as polysaccharides. The purpose is to move toward identification of new materials to replace non-degradable plastics in flexible electronics. Included in this talk is a discussion of the synthetic pathways for formation of high glass transition temperature (≥ 80 °C) polyfluorene derivatives and use of polysaccharides with respect to their corresponding structure-property relationships. A demonstration of their use in flexible electronics as either an active component or encapsulating layer, followed by a study of their degradation pathways will also be covered.

2:00 PM EN09.10.04

Biomass-Derived Super Hygroscopic Polymer Films for Sustainable Moisture Harvesting [Youhong Guo](#)^{1,2}, [Weixin Guan](#)² and [Guihua Yu](#)²;

¹Massachusetts Institute of Technology, United States; ²The University of Texas at Austin, United States

Extracting ubiquitous atmospheric water is a sustainable strategy to enable decentralized access to safely managed water. Early efforts on fog capture and dewing enabled the gathering of small water droplets from air, which is only applicable to regions with high relative humidity (RH). The state-of-the-art sorbent-assisted atmospheric water harvesting presents a promising and universal approach for a wide humidity range but remains challenging due to its limited daily water output at low relative humidity ($\leq 30\%$ RH). Here, we will present our newly developed super hygroscopic polymer films (SHPFs) made from renewable biomasses consisting of konjac glucomannan (KGM) and hydroxypropyl cellulose (HPC), exhibiting excellent water uptake of 0.64 g g⁻¹ at 15% RH and 0.96 g g⁻¹ at 30% RH. KGM facilitates the highly porous structures with enlarged air-polymer interfaces for active moisture capture and water vapor transport. Thermoresponsive HPC enables phase transition of SHPFs at a low temperature to assist the release of collected water via hydrophobic interactions. With rapid sorption-desorption kinetics, SHPFs are capable of operating 14-24 cycles per day in arid environments, equivalent to a water yield of 5.8-13.3 L kg⁻¹. Synthesized via a simple casting method using sustainable raw materials, SHPFs highlight the potential for low-cost and scalable atmospheric water harvesting technology to mitigate the global water crisis.

2:15 PM EN09.10.05

Nanocellulose Aerogels as a Solid Template to Induce Protein Aggregation and Amyloid Formation [Ashutosh Sinha](#)^{1,2}, [Nico Kummer](#)^{1,2}, [Tingting Wu](#)¹, [Kevin J. De France](#)¹, [Silvia Campioni](#)¹, [Peter Fischer](#)² and [Gustav Nyström](#)^{1,2}; ¹Swiss Federal Laboratories for Materials Science and Technology, Switzerland; ²ETH Zürich, Switzerland

For decades, amyloid proteins were mostly studied in the context of their roles as contributors to disease. However, the increasing interest in the development of sustainable materials led to researchers exploiting and engineering amyloids for a myriad of functions. These include filtering heavy metals [1], antimicrobial activity [2], and enhancing biocompatibility [3] to name a few.

The formation of amyloids (ordered aggregates) as opposed to disordered aggregates upon protein unfolding is influenced by various factors such as temperature, pH and interfaces. In this research, we focus on the role of interfaces, particularly we are investigating how solid surfaces influence protein aggregation and amyloid formation. Previously, inorganic solid nanoparticles such as silica nanoribbons, carbon nanotubes, quantum dots, and cerium oxide nanoparticles were shown to induce amyloid formation in proteins such as human β 2-microglobulin and Islet Amyloid Polypeptides [4, 5]. However, inorganic and synthetic solid templates are often not sustainable or biocompatible, limiting their utility and acceptability. Therefore, we instead used cellulose, the most abundant biopolymer on earth. Cellulose, obtained from plants, can be converted into cellulose nanofibers with a high surface to volume ratio and cross-linked to form CNF aerogels [6]. In order to induce amyloid formation on their surface, these CNF aerogels were exposed to a solution of hen egg white lysozymes at varying pH. The surface aggregation was studied via various microscopic and spectroscopic methods including FTIR, TIRF, and SEM. Previous reports indicated the adsorption of lysozymes onto the surface of aerogels via electrostatic complexation [7]. Our results indicate not only adsorption of lysozymes, but also the induction of protein aggregation and amyloid formation on the aerogel surface. Additionally, bulk aggregation (or a lack thereof) was investigated using DLS and AFM. By tuning the experimental conditions, amyloid formation was found to either take place exclusively at the aerogel surface or alternatively the presence of aerogels could accelerate bulk aggregation under conditions where little or no lysozyme aggregation was previously reported [2].

Our research provides a new, sustainable method for amyloid aggregation on solid templates. Additionally, the structural integrity of CNF aerogels along with the abundant availability of cellulose provides fascinating new opportunities to create amyloid-cellulose biohybrids.

References:

1. Soon, W.L., et al., *Plant-based amyloids from food waste for removal of heavy metals from contaminated water*. Chemical Engineering Journal, 2022. **445**: p. 136513.
2. Kummer, N., et al., *Self-Assembly Pathways and Antimicrobial Properties of Lysozyme in Different Aggregation States*. Biomacromolecules, 2021.
3. Janssen, M.I., et al., *Coating with genetic engineered hydrophobin promotes growth of fibroblasts on a hydrophobic solid*. Biomaterials, 2002. **23**(24): p. 4847-54.
4. Linse, S., et al., *Nucleation of protein fibrillation by nanoparticles*. Proceedings of the National Academy of Sciences, 2007. **104**(21): p. 8691-8696.
5. Pilkington, E.H., et al., *Star Polymers Reduce Islet Amyloid Polypeptide Toxicity via Accelerated Amyloid Aggregation*. Biomacromolecules, 2017. **18**(12): p. 4249-4260.

6. Wu, T.T., et al., *Dual-porous cellulose nanofibril aerogels via modular drying and cross-linking*. *Nanoscale*, 2020. **12**(13): p. 7383-7394.
7. Severini, L., et al., *Biohybrid Nanocellulose-Lysozyme Amyloid Aerogels via Electrostatic Complexation*. *ACS Omega*, 2022. **7**(1): p. 578-586.

2:30 PM EN09.10.06

Three-Dimensional Printing of Mycelium Hydrogels into Complex Living Materials Kunal Masania; ASM Aerospace Engineering TU Delft, Netherlands

Biological materials constantly adapt to their environment, display low embodied energy, and possess remarkable mechanical properties granted by their hierarchical structures. Adapting these principles to human-made objects promises to disrupt the way we engineer our high-performance critical structures. However, today's engineering materials remain lifeless, and show only limited abilities to adapt and reinforce under load, or to heal and repair in response to damage. Here we harness the livingness of fungal mycelium to reach emerging properties of complex adaptive systems in an engineering context. The potential of the resulting complex material is illustrated by 3D printing living functional skins. We show that fully biobased material is able to autonomously self-heal, self-regenerate and adapt its growth depending on the availability of nutrients in the environment. The adaptive nature of the living mycelium imbues the functional skin thus far inexistent in conventional synthetic materials. To create the animate complex material, we 3D print grid-like structures that provide a mechanically robust architecture combining open airways and a nutrient-rich environment for mycelial growth. The grid is printed using a granulated hydrogel ink that consist of a gelled culture medium inoculated with the fungus. The shaping freedom of the 3D printing process allows us to generate geometries that fulfill specific engineering requirements, such as the encapsulation of robotic parts with a living protective skin. The nutrient concentration in the grid is tuned such that the living mycelium features a balanced growth strategy that combines exploration and exploitation of its surrounding environment. In addition to this decision-making feature, the resulting living material presents several of the hallmarks of complex adaptive systems, such as the emergent behavior of decentralized cells, the efficient processing of information via a scale-free network, the dissipative self-organization processes that promote growth and the organization of building blocks over multiple length scales. This ultimately leads to self-healing, self-regeneration and adaptive properties that are chemically fueled by nutrients in the absence of human intervention.

2:45 PM BREAK

3:15 PM EN09.10.07

Technological Prospecting, Assessment and Scale-Up of Macauba (*Acrocomia aculeata*)-Based Biosorption of Metal Ions from Water Alfonso Martínez Andrade^{1,2}, Julio C. Vargas Sáenz², Angelo M. Denadai³, Ricardo Orlando¹, Leticia Costa¹, Fernanda Costa Pinheiro¹ and Ruben D. Sinisterra¹; ¹Universidade Federal de Minas Gerais, Brazil; ²Universidad Nacional de Colombia, Colombia; ³Universidade Federal de Juiz de Fora, Brazil

Superficial water contamination by anthropomorphic activities and environmental disasters has reached dangerous levels for the water security of humanity, turning this situation in a global concern, which is why the United Nations (UN), in the sixth Objective of Sustainable Development, proposes sanitation and access to clean water for all. Thus, alternative strategies using innovation for metal ions for removal from water is an urgent necessity, where environmental disasters such as those that occurred in Brazil (MG), Mariana (2015) and Brumadinho (2019), have polluted the water to levels that make their consumption unviable. These emerging technologies must ensure synergy with conventional technologies and guarantee economic and environmental viability.

Among the alternatives one could find the bio-based materials, as agricultural waste, for biosorption is a green strategy which helps to the solution of two problems and same time, recovery of polluted water and reuse of biomass materials. The main objective of the present work is the assessment and scale-up of bio-based residual materials for biosorption of metal ions in polluted superficial waters using the residual biomass Macauba (*Acrocomia aculeata*) from the vegetable oil extraction process and its use in the design of adsorption systems with a high fluid dynamic regime.

Chemical treatments of the macauba endocarp with NaOH, H₂SO₄, H₂O₂ and NaClO were evaluated, as well as physical treatment with ultrasound waves, to improve the biosorption capacity. The materials obtained were characterized by TGA, MEV-EDS, X-Ray Fluorescence, metal quantification and Zeta potential. Adsorption tests were carried out, on a laboratory scale, with the metals Al³⁺, Mn²⁺, Pb²⁺ and Fe³⁺ at different conditions of pH, temperature and contact time, and a comparison was made with the use of natural material. Metals quantification was made by atomic absorption. The best results were obtained with the material treated with NaOH, achieving removals above 34% for Fe³⁺, 28% for Mn²⁺, 51% for Pb²⁺ and 46% for Al³⁺, using 100 grams of macauba biomass and 234L/h of flow in a high-rate system.

Considering these results, the potential of this material for scale-up into a continuous separation operation is concluded, for which different strategies, as combination with minerals materials, are being tested to obtain a prototype of a high fluid dynamic regime adsorption system as an innovative strategy. In addition, technology prospection and bibliometric studies were carried out using public and private database, such as Scopus and Questel-Orbit.

Acknowledgments: The authors would like to thank to the Network for the study, development and application of technologies based on sustainable nanomaterials for the recovery of water from the Doce River basin (N°06/2016), sponsored by the entities: FAPEMIG, CNPQ, CAPES, ANA, FAPES and development in Chemistry Department of UFMG.

3:30 PM *EN09.10.09

Overcoming Challenges to Identifying Safer Materials/Products to Per- and Polyfluoroalkyl Substances (PFAS) Mark Rossi; Clean Production Action, United States

In the search to replace per- and polyfluoroalkyl substances (PFAS) in materials and products, how can concerned/relevant parties such as researchers, companies, non-governmental organizations (NGOs), and governments have greater certainty that the alternatives to PFAS are safer and not regrettable substitutes? Regrettable substitutes are alternatives that themselves become problematic; for example, replacing polystyrene foam clamshells with compostable fiber-based (e.g., bagasse) containers made with PFAS.

The entire class of PFAS is now a focus for elimination or restriction in many jurisdictions including state governments and the European Union. This is because over the past few decades PFAS contamination has grown into a serious global health threat due to the ability of these chemicals to persist in the environment for hundreds of years; their presence in almost all human populations; and increasing evidence of their health impacts. PFAS use in all industry sectors is under scrutiny, including food packaging, furniture, apparel/fabrics, firefighting foam, oil and gas, carpets and rugs, and cosmetics.

The journey to safer chemicals in materials and products includes the following stages: a) identify all intentionally added chemicals in the material/product as well as residual chemicals of high concern; b) assess the toxicity of those chemicals; c) avoid known chemicals of high concern; and d) select materials/products with safer chemicals. This journey to safer solutions, for example, to products free of per- and polyfluoroalkyl substances (PFAS) is fraught with many challenges.

Significant challenges to identifying safer alternatives to PFAS and other chemicals of high concern include: 1) confidential business information -- very few materials/products have complete disclosure of all the chemicals intentionally added to the product as well as residual chemicals of high concern to human health or the environment; 2) toxicological capacity -- very few organizations possess the technical capacity to assess the toxicity of the chemicals

in materials/products and to understand how to interpret that data; and 3) availability of materials/products that do not contain chemicals of high concern.

Product certifications provide a unique framework for overcoming these challenges because they create incentives for manufacturers to disclose chemical constituents to a trusted third party with the goal of receiving a product certification that can be used to promote a product for being “PFAS-free” and using preferred chemicals. “PFAS-free” is in quotes because it must be defined, for example as encompassing, no intentionally added PFAS and no residuals above a specified threshold such as 100 parts per million (ppm) per homogeneous material.

To identify PFAS-free and preferred products Clean Production Action developed a certification program called GreenScreen Certified. The methodological requirements for identifying preferred products include: a) chemical ingredient disclosure; b) all chemicals assessed for hazards; c) avoidance of known chemicals or classes (e.g., PFAS) of chemicals of high concern, including carcinogens, mutagens, reproductive or developmental toxicants, endocrine disruptors, persistent/bioaccumulative/toxic chemicals (PBTs), or other similarly toxic chemicals; d) meets analytical testing requirements – for example, for PFAS residuals in the products.

Overall, PFAS-free and preferred products have been identified for significant uses of PFAS, including in firefighting foam, food service ware, furniture and fabrics, textile chemicals, and cleaners and degreasers used in manufacturing.

4:00 PM *EN09.10.10

Sustainable Chemicals and Materials—An Update on Policy Drivers Molly Jacobs; University of Massachusetts Lowell, United States

Our materials economy is extremely reliant on a small number of feedstock chemicals, massive economies of scale and limited innovation – all of which is not sustainable. This dependency on fossil fuel derived chemicals and materials is at the epicenter of the dual crises of climate change and toxic pollution. However, global action on climate change, a growing focus on material circularity and increased attention on a transition towards safer and more sustainable chemistry are generating significant opportunities to rethink and recreate how materials are designed for the future.

Policy is an important driver supporting these changes. Advancing sustainable and renewable polymers and bio-based materials is dependent in part on government policies that help to counter-act the tremendous barrier that unsustainable incumbent materials have on the marketplace. This presentation will provide an update on policy developments, primarily those in the United States (US) and the European Union (EU), that are underpinning progress related to safer and sustainable chemicals, materials and products. Policies to be discussed include the US Sustainable Chemistry R&D Act, policy actions by US States including the California Safer Consumer Products regulation, and a range of policy developments in the EU tied to the Green Deal and the Chemical Strategy for Sustainability.

SESSION EN09.11: Virtual Session
Session Chair: Bichlien Nguyen
Tuesday Morning, December 6, 2022
EN09-virtual

10:45 AM EN09.11.02

Tuning the Mechanical and Dynamic Healing Properties of Bio-Degradable Supramolecular Polylactone Copolymers by Controlling the Arm-Chain Crystallinity Woojin Lee¹, Jae Woo Chung² and Seung-Yeop Kwak^{1,3,4}; ¹Seoul National University, Korea (the Republic of); ²Soongsil University, Korea (the Republic of); ³Research Institute of Advanced Materials, Korea (the Republic of); ⁴Institute of Engineering Research, Korea (the Republic of)

Recently, supramolecular polymeric networks have attracted great scientific interests due to their healing ability of damaged fractures, which can significantly enhance the reliability and sustainability of materials. In particular, the multiple healing capability of supramolecular polymers can be imposed by the dynamic dissociation/re-association of various supramolecular interactions such as hydrogen bonding, ionic bonds, metal-ligand coordination, and π - π interaction etc. In general, most supramolecular polymer networks consist of low T_g amorphous polymeric chains with more dynamic supramolecular bonds for faster healing performances. Although the more dynamic supramolecular polymeric networks, which is composed of flexible chain and rather weaker supramolecular bonds, exhibit an improved healing ability, the mechanically robust supramolecular network structure may not be facilitated. Thus, to resolve these challenges, most research has been focused on developing the alternative supramolecular polymeric network structures with mechanically robustness and excellent healing performances, simultaneously.

In this study, a quadruple hydrogen-bonded supramolecular polylactone copolymer (QSCP) was successfully synthesized using an alkyl-branched ϵ -decalactone (ϵ -DL), which is renewable and bio-degradable ring-shaped lactone derivative, and ϵ -caprolactone (ϵ -CL), via ring-opening copolymerization. The effects of P(ϵ -DL) on structural, mechanical, and dynamic healing properties of QSCP were comprehensively characterized. The degree of polymerization (DP) and segment compositions of QSCP arm-chain are precisely adjusted by controlling the feed monomers-to-core ratio and monomeric fractions. As the composition of ϵ -DL increased for QSCPs, the maximum melting temperature (T_m) and enthalpy (DH_m) values gradually decreased. These indicate that the alkyl-branched P(ϵ -DL) disrupted the formation of hard P(ϵ -CL) crystalline phases. Especially, the prepared QSCP s with ~ 10 mol% of P(ϵ -DL) (i.e., QSCP90) displayed a significantly improved elongation at break (~ 700%) with a highly enhanced tensile strength (~ 6 MPa). In addition, the optically- and mechanically-measured self-healing of QSCP90 were found that the mechanically-damaged QSCP90 was sufficiently recovered after ambient self-healing conditions (50 °C). These results clearly suggested that an optimum composition of arm-chain enabled QSCPs to form the complementary hard/soft multi-phase system, i.e., a hard phase bearing crystalline PCL and a soft phase containing P(ϵ -DL) with quadruple hydrogen bonding moieties, eventually resulting in highly improved tensile properties with a facile healing behavior.

10:50 AM EN09.11.03

Advances in Self-Healing Concrete Lauren Marshall; The American School in London, United Kingdom

With three tonnes utilized per person, concrete is one of the most common building elements in our society. However, cracks in concrete pose dangers to the concrete's strength and structures built with concrete. For decades, the most common method of maintaining safe structures after cracks have developed in concrete has been through replacement with new concrete. This production of concrete leads to approximately eight percent of the world's carbon dioxide emissions.

Identification of methods to significantly reduce the negative impacts associated with cracked concrete as well as newer ideas to minimize the waste associated with cracked concrete will be explored. This presentation will include an examination of the effectiveness and sustainability of various

approaches to self-healing concrete and whether safety concerns associated with repairing concrete through these methods can be adequately addressed.

10:55 AM EN09.11.04

Surface Enhancement of Coir Fibers for Better Bacterial Accumulation [Keshani R. Perera](#) and Madhubhashini Maddumaarachchi; Faculty of Applied Sciences, University of Sri Jayawardenepura, Sri Lanka

Nowadays, contamination of water via pathogenic bacteria, viruses, and parasites is one of the major health problems facing by the society. Therefore, an effective method is essential to rapidly capture the bacteria from water to minimize water contamination by pathogens. The usage of chemical disinfectants in conventional water purification processes has become a challenge due to the formation of carcinogenic by-products and antibiotic-resistant bacterial pathogens. As a solution to that, this study introduces an eco-friendly bacteria capturing strategy using natural coconut fibers as a substrate, which is modified by a novel polymeric coating. This polymer coating consists of an amine functionalized diatomaceous earth/poly(vinyl acetate) composite. Diatomaceous earth (DE) is an inexpensive, environmentally benign, highly porous amorphous silica structure and DE has been treated with a (3-Aminopropyl)triethoxysilane coupling agent to enhance bio-affinity toward bacteria. A poly(vinyl acetate) (PVAc) binder is used to disperse treated DE. PVAc is a nontoxic, eco-friendly thermoplastic adhesive used as a binder to prepare coatings. Alkaline treated coconut fibers were dipped in the treated DE/PVAc composite coating to prepare the modified fibers. The positive charges of the surface amine functionality of the treated DE can promote strong electrostatic interaction with the negatively charged bacterial cell membrane. Further, the pendent propyl group of amine functionality can also play a supplementary role in attracting bacterial pathogens by forming hydrophobic interactions. Fourier transform infrared (FTIR) spectroscopic analysis was conducted to confirm the presence of silane coupling agents on the DE and to characterize the chemical components of (3-Aminopropyl)triethoxysilane treated DE/PVAc coated coconut fiber and raw coconut fiber. The bio-affinity of raw coconut fiber and modified coconut fiber was compared in terms of bacteria capturing ability. Bacterial capturing ability was investigated based on UV spectrophotometer absorbance measurements using *E. coli* bacteria as a model bacteria type. The UV absorbance measurements of the *E. coli* cell suspensions containing modified coconut fibers were gradually decreased over time. Further, the *E. coli* solution containing raw coconut fibers showed an approximately similar absorbance variation to the control sample containing the *E. coli* cells only. The obtained results indicated that the (3-Aminopropyl)triethoxysilane treated DE/PVAc composite coating could be considered as a favorable surface treatment for the coconut fibers for better bacterial accumulation from the aqueous medium.

11:00 AM EN09.11.05

Ureolytically Induced Calcium Carbonate Composites as Bioadhesives [Sobia Anjum](#), Kaylin Clark, Kendall Parks, Chelsea Heveran, Albert Parker and Robin Gerlach; Montana State University, United States

Synthetic adhesives, which currently dominate the adhesives market, are generally petroleum-based and commonly release volatile organic compounds (VOCs) during production or use. Indoor accumulation of VOCs can have detrimental human health effects, and outdoor release of VOCs can have adverse environmental effects (e.g., photochemical smog). Therefore, there is a need for alternative, more sustainable, natural, and natural-synthetic hybrid materials as adhesives. Ureolytically induced calcium carbonate composites (UICCs) are a new design space for sustainable, and low VOC natural adhesives. UICCs are currently used for a broad array of applications, including soil stabilization, concrete remediation, creating subsurface barriers, etc. The aim of this work is to investigate UICC adhesive shear strength and environmental durability.

UICCs are produced by a reaction driven by ureolytic bacteria (e.g., *Sporosarcina pasteurii*) or by crude urease enzyme preparations (e.g., from Jack bean meal). Urea hydrolysis generates carbonate ions, which can form calcium carbonate in the presence of dissolved calcium. The composite adhesive is formed by aggregation of the urease source (bacteria or extracted enzyme), organics, and calcium carbonate precipitates. To test the adhesivity of the UICC adhesives, a modified ASTM D1002.10 method was used. The adhesive was applied to glass and stainless-steel coupons in single lap joint mode, cured, and then tested in tensile extension to measure its shear strength. The shear strength of the adhesives was optimized for glass and stainless-steel surfaces by varying the type of additive (guar gum and soy protein isolate), the concentration of the urease source, and the concentration of calcium ions. UICC shear strength was also evaluated after exposure to various temperatures (-20°C, 25°, 100°C, and 300°C) and relative humidities (50%, 80%, and immersed in deionized water).

The highest shear strength achieved for the UICCs was 2MPa, as compared to the UICC free formulation at 0.2MPa. Image-based surface coverage analysis indicated that the majority of the samples exhibited a mixed failure (both adhesive failure at the composite-surface interface as well as cohesive failure within the composite). Temperature and humidity testing showed that the shear strength of the UICC composite increased by 41% at -20°C, and by 16% at 50% RH. Up to 75% of the initial shear strength was retained at 100°C. This data demonstrates the potential of UICCs for applications as bioadhesives on a range of surfaces and for common environmental conditions.

11:05 AM EN09.11.07

Bio-Inspired Polymer Matrix Based on the Chicken Waste to Novel Polyurethanes [A.A.P.R. Perera](#), K.A.U. Madhushani, Felipe M. de Souza, Tim Dawsey and Ram K. Gupta; Pittsburg State University, United States

Although researchers are focusing on the production of bio-based polyurethane using plant sources, only a few studies have reported the use of animal waste, such as fish oil, in the production of polyurethanes. The amount of chicken waste produced in the United States is staggering, and chicken fat is a valuable by-product of chicken waste and is currently used for a variety of useful purposes. The high unsaturated fatty acids contents in chicken fat make it a prospective alternative source for greener polyurethane formation. This study was conducted to propose a feasible pathway to formulate new low-cost rigid polyurethane foams (RPUFs) with variable mechanical and thermal properties from the chicken fat. The hydroxyl groups were introduced along the fatty acids' chains through simple wet chemical methods. These CF-derived polyols had 96 mg KOH/g hydroxyl group content. The combination of 25–75 wt. % of chicken fat-based polyols with isocyanates formed the semi-rigid, rigid foams with a maximum of 142 kPa compressive strengths that can be further modified for various commercial applications. The characteristics of RPUFs were studied using density, closed-cell content, and scanning electron microscope. As the chicken fat-derived polyol replacement increased to 75 wt.%, the closed-cell content decreased significantly. The thermal behaviors of RPUFs were studied by gradually increasing the percentage of phosphorous-based flame retardant. More importantly, the burning time and thermal stability results revealed that the flame retardant mechanism depends on the matrix of the polyurethane foam. In summary, this work provides an innovative strategy for creating a new alternative source for the polyurethane industry.

11:10 AM EN09.11.08

Green Synthesis of Metal Oxide Nanoparticles Using Mandarin Orange Peels (*Citrus reticulata*) for Phase and Electrochemical Study of Supercapacitor. [Rishabh Srivastava](#), [Shiva Bhardwaj](#) and Ram K. Gupta; Pittsburg State University, United States

Nanoparticle-based materials are the class of significantly emerging materials in all aspects of the field for research in biomedical, pharmaceutical, sensors, and electrical applications which incorporate various branches of science. These nanoparticles can be synthesized using a variety of methods like laser ablation, spark discharge, sputtering, sol-gel, and many more but the products obtained using these methods cause an adverse effect on the environment due to the presence of hazardous, non-biodegradable, and toxic products in nanoparticles. However, green synthesis is one of the solutions to the above-mentioned issues. Therefore, many researchers are pursuing green synthesis methods nowadays where plant parts such as leaves, stems, roots, flowers, and

fruit peels are currently utilized for the fabrication of nanoparticles (NPs) by their extracts. Hence it is considered an inexpensive and eco-friendly method of synthesis where bio-based NPs shows versatile characteristics. These bio-based NPs are widely used in energy storage applications. There are various devices that can store energy like fuel cells, batteries, and supercapacitors (SCs). Among all the energy storage devices (ESDs) SCs show extremely vibrant properties such as fast charge-discharge, high specific capacitance, and cyclic stability. This work includes a facile synthesis route of Cobalt Oxide nanoparticles (CONPs) using Mandarin orange peels. An aqueous extract of orange peel was considered as a precursor which performs a biological reduction mechanism for the synthesis of CONPs from Cobalt nitrate hexahydrate $\text{Co}(\text{NO}_3)_2 \cdot 6\text{H}_2\text{O}$. Additionally, CONPs are also synthesized by using sodium hydroxide (NaOH) as a precursor for the comparative phase study which has been characterized by X-ray diffraction (XRD) and Fourier Transform infrared spectroscopy (FTIR). Furthermore, the obtained NPs are sulfurized and phosphorized to study the effect of morphology and crystalline structure on electrochemical activity. The pseudo-capacitor traits were analyzed by cyclic voltammetry (CV), galvanostatic charge-discharge (GCD), electrochemical impedance spectroscopy (EIS) in 3M KOH, and cyclic stability for over 5000 cycles. The noticeable specific capacitance showed by phosphorized cobalt oxide ($\text{P-Co}_3\text{O}_4$) is 244 F/g at a discharge current density of 1 A/g. Furthermore, the prepared CONPs retain a capacity of more than 82% after 5000 cycles.

11:15 AM EN09.11.09

Molecular Level Studies of Acetic Acid Adsorption and Reactions on Platinum and Nickel Lotanna Ezeonu, Simon Podkolzin, Ziyu Tang, Yue Qi and Fangliang Huo; Stevens Institute of Technology, United States

Pt and Ni-based catalysts are actively studied in the development of improved technologies for the conversion of biomass-derived feedstocks into fuels and chemical feedstocks, specifically for hydrodeoxygenation and steam reforming of bio-oils. Since acetic acid is a component of bio-oils as well as a widely used model compound, it is important to better understand its reactivity on Pt and Ni catalytic surfaces at the molecular level. In this study, acetic acid adsorption and reactions on Pt(111) were studied with infrared reflection absorption spectroscopy (IRAS), temperature-programmed desorption (TPD) and density functional theory (DFT) calculations. The results were compared to Ni(111) and Ni(110) surfaces.

At the dosing temperature of 90 K, acetic acid forms a physisorbed layer on Pt(111). At 140 K, acetic acid predominantly chemisorbs molecularly through its carbonyl oxygen atom. In addition, some dissociative adsorption is observed with the formation of acetate and hydrogen. Annealing to 193 K leads to a mostly complete conversion of molecularly adsorbed acetic acid to acetate species. At 440 K, acetate species decompose, evidenced by desorption of H_2 , CO and CO_2 . In contrast, due to differences in the adsorbed structures, acetate species decompose on Ni(110) at a lower temperature of 425 K. Above 425 K, only residual carbon remains on the Ni surface.

11:20 AM EN09.11.10

Rice Husk Based Biodegradable Cardboards for Packaging Applications Steven Delbove, Deepa Kodali, Siripong Malasri, Louie Lin and Ali Pourhashemi; Christian Brothers University, United States

Rice husk, also known as rice hull, is a byproduct created in the production of rice. With over 500 million tons of rice produced yearly in the world, the supply of rice husk is very high while the usage of it is low. Although United States accounts for only 2% of global rice production, it has become the World's fifth largest exporter with more than 6% of global exports. In 2019 alone, the state of Arkansas has harvested rice in 1,126,000 with an average yield of 7480 pounds per acre. Dried paddy yields around 20% of hull, 15% of stalk and 10% of bran. Taking advantage of this huge sustainable yield, this study focuses on developing the biodegradable cardboard utilizing the discarded rice husk that can be used for packaging applications while lowering the amounts of conventional pulping material. Rice husk contains about 15-25% lignin and 35-40% cellulose and is coarse and abrasive in nature. Hence, the rice husk is softened initially to make it into pulp. This study is aimed to determine the tensile and compressive strength of the paper. Hence, pretreatment of rice husk is performed by using various concentrations of NaOH and the effective pretreatment was observed at 2g of NaOH with 1000 ml of water for 100gms of ricehusk. The mixture thus obtained is blended into pulp and is placed in the trays to dry. When blended and softened, the husk alone was not able to hold any shape when tested in paper making molds. Hence, binding agent was added to the pretreated rice husk to hold the rice husk together and to improve the strength of the specimen. Four specimens were prepared by adding 5g of starch reagent, 5g of tapioca starch, 5g of clear elmers glue and 5g of starch reagent and 5g of elmers glue together. The specimen with tapioca starch was the weakest whereas the specimen with elmers glue and starch reagent was the strongest. The optimization tests with varying amounts of glue and starch reagent were in progress and the tensile and compressive strengths of the cardboards are yet to be determined. However, the studies showed favorable results suggesting that the rice husk together with biodegradable additives can be used to make cardboards for packaging applications.

11:25 AM EN09.11.11

A Flame Retardant Poly(lactic acid) Blend with Modified Cellulose and Ammonium Polyphosphate Minsik Shin¹, Christian Apostol², Allen Bethancourt², Yiwei Fang² and Miriam Rafailovich²; ¹Seoul International School, Korea (the Republic of); ²Stony Brook University, United States

Poly(lactic acid)(PLA), a sustainable and biodegradable polymer, has the potential to be the next generation of eco-friendly materials to replace petroleum based thermoplastic. To further develop PLA applications in a wide range of areas such as tissue engineering, 3D printing, and food packaging, enhancing its flammability and mechanical strength remains challenging as most reinforcing fillers are non recyclable or environmentally destructive. Therefore, it is urgent to design a PLA composite with enhanced flame retardancy and balanced mechanical properties by only using green additives.

Cellulose is a renewable source that received lots of studies when combined with solid phase phosphate flame retardant, namely ammonium polyphosphate (APP), since cellulose generates char under combustion which acts as a physical barrier to stop the flame. APP is reported to effectively increase PLA flame retardancy but deteriorate ductility. While, as other scientific studies show, cellulose incorporated in polymer blend actually strengthens the overall tensile strength and maintains polymer toughness. In a polymer/solid phase flame retardant system, the interfacial energy between the polymer matrix and flame additives is essential to flame resistance performance. Contact angle measurement revealed that the high surface tension of PLA/cellulose and PLA/APP limits the efficiency of flame additives when burnt. Resorcinol bis(diphenyl phosphate) (RDP) can be easily coated with cellulose fibers under mild condition due to strong H-bonding interactions which is elucidated by Fourier Transform Infrared Spectroscopy (FTIR). Based on Young's equation and Owen-Wendt method, RDP lowers the surface tension between each component. Therefore, RDP coated cellulose fibers also act as a compatibilizer in PLA/APP blend, which is correlated with lower Tg analyzed by DMA. So that PLA melt blended with 5%RDP-Cellulose and 5% APP easily passes UL-94 V-0 criteria. The flame retardancy was also confirmed with limiting oxygen index and cone calorimetry. Thermogravimetric analysis (TGA) indicates that PLA/RDP-cellulose/APP has a different thermal decomposition history and higher residue~10% after 800 celsius compared with PLA/untreated cellulose/APP blend. Moreover, the addition of RDP coated cellulose fiber minimizes the negative effect of APP on mechanical properties. Izod Impact and tensile testing showed that the PLA/RDP-cellulose/APP composite has impact strength and tensile strength comparable to those of neat PLA. Work supported by the ERDC (W912HZ-20-2-0054) and the Morin Charitable Trust.

11:30 AM EN09.11.13

Nanocellulose and Carboxymethyl Cellulose Beads as a Protective Matrix for Microbial Inoculants Mariana G. Brondi^{1,2}, Camila Florencio², Luiz Mattoso², Caue Ribeiro² and Cristiane Farinas^{1,2}; ¹Federal University of Sao Carlos, Brazil; ²Embrapa Instrumentation, Brazil

The application of microbial inoculants in agriculture is a sustainable alternative to increase crops productivity and reduce the environmental problems

related to the exacerbated use of agrochemicals. For a successful product, its formulation must provide protection to microorganism from its production to its final application on crops. The use of natural polysaccharides as encapsulation matrices has shown interesting results in the maintenance of cell viability. Matrices of cellulose and its derivatives (nanocellulose, carboxymethyl cellulose, among others) can be interesting to be used in this type of application, since these materials are abundant, renewable and biodegradable. Therefore, this study evaluated the encapsulation of spores of the biocontrol fungus *Trichoderma harzianum* in a green matrix of nanocellulose (CNC) and carboxymethyl cellulose (CMC), through a simple process of ionic cross-linking in a CaCl_2 solution. For beads production, two different polymeric dispersions with the spores (10^9 spores/g polymer) were evaluated: a 5% (w/v) CNC and a mixture of CNC (5%) with CMC (1.5% w/v) in a volume ratio of 3:1. These dispersions were dripped into the salt solution for beads formation. After the coagulation process, the beads were stored wet and under refrigeration. X-Ray microtomography and SEM micrograph showed the uniform distribution of the materials and highlighted the spore's presence within the matrices, respectively. Shelf-life tests showed that the free microorganism presented a much higher viability loss over time than the ones encapsulated. Antagonistic tests showed that the *T. harzianum* spores, encapsulated in both matrices and stored for 1 year, were able to suppress the growth of the phytopathogenic fungus *Fusarium solani*, maintaining its effect as a biocontrol agent. Therefore, our results indicated that both CNC and the composite CNC:CMC are interesting sustainable matrices for improving microbial inoculants protection and shelf-life.

12:05 PM DISCUSSION TIME

SYMPOSIUM EQ01

Progress in Thermoelectrics—From Traditional to Novel Materials
November 28 - December 7, 2022

Symposium Organizers

Sepideh Akhbarifar, The Catholic University of America
Guangzhao Qin, Hunan University
Heng Wang, Illinois Institute of Technology
Sarah J. Watzman, University of Cincinnati

Symposium Support

Gold

National Science Foundation

* Invited Paper

+ Distinguished Invited

SESSION EQ01.01: Computationally-Guided Material Design and Discovery I
Session Chairs: Sepideh Akhbarifar and Heng Wang
Monday Morning, November 28, 2022
Sheraton, 2nd Floor, Back Bay A

10:30 AM *EQ01.01.01

Thermoelectric and Thermionic Transport in MoSe₂ [Mona Zebarjadi](#) and Md. Golam Rosul; University of Virginia, United States

We study the thermoelectric properties of bulk MoSe₂ within relaxation time approximation including electron-phonon and ionized impurity interactions using first-principles calculations. The anisotropy of this 2D layered metal dichalcogenide is studied by calculations of electron mobility in the cross-plane and the in-plane directions. We show that the cross-plane mobility is two orders of magnitude smaller than the in-plane one. The inclusion of van der Waals interactions further lowers the carrier mobility in the cross-plane direction but minimally affects the in-plane one. The results for in-plane electrical mobility and conductivity are in close agreement with experimentally reported values indicating the accuracy of the calculations. In addition to thermoelectric transport, 2D layered heterostructures are appropriate for solid-state thermionic applications. We study electron transport across metal-MoSe₂-metal structures using first-principles calculations combined with Green's function method. We study the effect of the number of layers, the energy barrier, and the asymmetry of the contacts on the performance of MoSe₂-based thermionic converters and show that the key to high-performance thermionic diodes is to make a low-energy barrier, low-resistance metallic contacts and we identify copper as the optimum metallic contact to MoSe₂ based devices.

11:00 AM EQ01.01.02

Symmetry-Guided Design of Thermoelectric Materials [Rinkle Juneja](#)¹, [Tribhuvan Pandey](#)², [Duncan H. Moseley](#)¹, [Raphael P. Hermann](#)¹ and [Lucas Lindsay](#)¹; ¹Oak Ridge National Laboratory, United States; ²University of Antwerp, Belgium

Structural symmetries of crystals put strong constraints on the dynamics of quasiparticles and their associated transport behaviors. Here, I will discuss the role of twist symmetries in a variety of one-dimensional and bulk materials' classes, using first-principles calculations. The symmetry-driven behaviors will be discussed in the context of enforced degeneracies, chirality-induced topological crossings, and quasiparticle interactions governing transport behaviors of thermoelectric materials. The deeper insights into the selection rules for thermal transport and unique scattering observables validated by inelastic

neutron scattering measurements, provide new avenues in designing efficient thermoelectric materials.

The authors acknowledge support from the U. S. Department of Energy, Office of Science, Basic Energy Sciences, Materials Sciences and Engineering Division.

11:15 AM EQ01.01.03

Material Descriptors to Search for Low-Temperature Thermoelectric Materials [Michael Toriyama](#)¹, Adam N. Carranco², G. J. Snyder¹ and Prashun Gorai²; ¹Northwestern University, United States; ²Colorado School of Mines, United States

Thermoelectric (TE) cooling offers an environmentally-friendly and reliable alternative to modern vapor compression cycles that utilize harmful refrigerants. One of the major bottlenecks in adopting TE cooling is the lack of low-temperature TE materials. In this study, we derive computationally-accessible material descriptors from a two-band Boltzmann transport model and predict the TE performance of narrow-gap semiconductors and semimetals. Through analytical modeling, we find that materials exhibiting high asymmetry between the transport distribution functions of electrons and holes yield high TE performance in narrow-gap semiconductors and semimetals. The high asymmetry manifests in the suppression of bipolar conduction. Inspired by the high TE performance of semimetallic Mg₃Bi₂-based materials near room temperature, we apply the material descriptors to search for Zintl phases with narrow and negative band gaps for low-temperature applications. By applying the material descriptors developed in this work, we screened 667 Zintl phases from the Inorganic Crystal Structure Database (ICSD) and identified few phases as promising low-temperature TE candidates. The material descriptors can be generally applied to search for other low-temperature TE materials with narrow and negative band gaps, beyond the Zintl phases considered in this study.

11:30 AM EQ01.01.04

When Power Factor Supersedes zT to Determine Power in a Thermocouple [Duncan Zavanelli](#)¹, Alex Pröschel¹, Joshua Winograd¹, Radion Cherkez² and G. J. Snyder¹; ¹Northwestern University, United States; ²Yuriy Fedkovych Chernivtsi National University, Ukraine

The primary material parameter determining power in a thermoelectric is the figure of merit zT. This figure of merit comes from the requirement for thermal impedance matching between the thermoelectric legs and heat exchangers in an optimally designed thermoelectric module. However, in a thermocouple temperature sensor, the geometry is constrained for temperature sensing. If the geometry is constrained so that the length of the thermoelectric elements is greater than a characteristic length, then the material thermal conductivity becomes less relevant. This makes the power factor the determining material metric for power output in such a device designed for temperature sensing.

11:45 AM EQ01.01.05

Using High-Throughput Calculations and Machine Learning to Understand Electronic Transport in Thermoelectrics [Alex M. Ganose](#)¹, Junsoo Park² and Anubhav Jain³; ¹Imperial College London, United Kingdom; ²NASA Ames Research Center, United States; ³Lawrence Berkeley National Laboratory, United States

The temperature dependence of experimental mobility is commonly used as a predictor of the dominant scattering mechanism in thermoelectric materials. However, if the scattering mechanism is determined incorrectly, this can lead to wildly inaccurate predictions of materials properties, frustrating efforts to optimize devices. In this work, I use a combination of high-throughput workflows and machine learned materials properties to generate a dataset of 24,000 mobility calculations. Based on this dataset, I demonstrate that the temperature-dependence of mobility is not a reliable indicator of the dominant scattering mechanism and instead reveal that many materials long considered to be dominated by deformation-potential scattering are instead controlled by polar optical phonons. This work highlights the potential for data driven approaches to provide insights for materials discovery and optimisation.

SESSION EQ01.02: Magneto-Thermoelectric Transport and Materials

Session Chairs: Sarah J. Watzman and Mona Zebarjadi

Monday Afternoon, November 28, 2022

Sheraton, 2nd Floor, Back Bay A

1:30 PM *EQ01.02.01

Giant Nernst and Thermal Hall Effects in the Weyl Phase of Bi_{1-x}Sb_x Topological Insulators [Joseph P. Heremans](#)¹ and Dung Vu²; ¹The Ohio State University, United States; ²Yale, United States

Single-crystal Bi_{1-x}Sb_x alloys with x>8 at.% are topological insulators (TI's) that become Weyl semimetals in a magnetic field applied along the trigonal axis. When a heat flux is applied parallel to the field, they display the thermal chiral anomaly, also known as the gravitational anomaly [1]. In this talk we present the thermal Hall effect and Nernst effect obtained on samples with x=11 and 15%. The data cross the TI-to-Weyl phase transition with the field along the trigonal direction but the measurement here are carried out with the heat flux perpendicular to the field. The thermal Hall effect is the second largest of any material (only the semimetal Bi has a larger effect, due to the simultaneous presence of electrons and holes). Above 100 K, it is of classical origin. Below 90K, it saturates in field, which cannot be classically explained. The Nernst effect is almost an order of magnitude larger than the Seebeck effect. It is classical above 100 K. However, the Nernst conductivity saturates at a non-zero value below 90K, another non-classical effect and possibly a signature of topological semimetals [2].

[1] Vu et al., Nature Materials **20**, pages1525–1531 (2021)

[2] Kosii et al., Phys. Rev. B **99**, 155123 (2019)

Ackn. NSF MRSEC "Center for Emerging Materials", Grant # DMR 2011876

ONR MURI "Extraordinary electronic switching of thermal transport", Grant # N00014-21-1-2377

2:00 PM EQ01.02.02

Magnetic Fluctuation Enhancement of the Thermoelectric Energy Conversion at a Critical Doping in Magnetic Semimetal Cr_{1+δ}Te₂ [Mohamed M. Atwa](#)¹, Yuita Fujisawa¹, Takatsugu Onishi¹, Markel Pardo-Almanza¹, Mathieu Couillard¹, Keita Harada¹, Tsunehiro Takeuchi^{2,3} and Yoshinori Okada^{1,3}; ¹Okinawa Institute of Science and Technology, Japan; ²Toyota Technological Institute, Japan; ³Japan Science and Technology Agency, Japan

Cr_{1+δ}Te₂ is a self-intercalated transition metal dichalcogenide that hosts tunable electronic filling and magnetism in its semimetallic band structure. Recent angle-resolved photoemission spectroscopy (ARPES) studies have unveiled a systematic shift in this semimetallic band structure relative to the chemical

potential with increased Cr doping. This presentation reports on the temperature and magnetic field dependence of the longitudinal thermopower S_{xx} for different $\text{Cr}_{1+\delta}\text{Te}_2$ compositions. We show that as doping increases, the sign of S_{xx} changes from positive to negative at the critical doping level of $\delta \sim 0.5$. This observed doping-dependent trend in the thermopower is consistent with the evolution of the semimetallic band structure from ARPES. An anomalous enhancement of the thermoelectric response is also observed around $\delta \sim 0.5$, where the formation of a pseudogap and competing magnetic interactions are expected to become prominent. Our findings collectively point to the critical nature of the doping level $\delta_c (\sim 0.5)$ in magnetic semimetal $\text{Cr}_{1+\delta}\text{Te}_2$. Around δ_c , near-Fermi-energy pseudogap formation and magnetic fluctuations play a vital role in enhancing thermoelectric energy conversion.

2:15 PM EQ01.02.03

Doping as a Tuning Mechanism for Magneto-Thermoelectric Effects to Improve zT in Polycrystalline NbP Eleanor Scott¹, Katherine Schlaak¹, Poulomi Chakraborty², Chenguang Fu^{3,4}, Satya Guin^{4,5}, Safa Khodabakhsh¹, Ashley Paz y Puente¹, Claudia Felser⁴, Brian Skinner² and Sarah J. Watzman¹; ¹University of Cincinnati, United States; ²The Ohio State University, United States; ³Zhejiang University, China; ⁴Max Planck Institute for Chemical Physics of Solids, Germany; ⁵Birla Institute of Technology and Science Pilani, India

Weyl semimetals combine topological and semimetallic effects, making them candidates for interesting and effective thermoelectric transport properties. Here, we present experimental results on polycrystalline NbP, which demonstrates a simultaneous existence of a large Nernst effect and a large magneto-Seebeck effect, typically not observed in a single material at the same temperature. We compare transport results from two polycrystalline samples of NbP with previously published work, observing a shift in the temperature at which the maximum Nernst and magneto-Seebeck thermopowers occur, while still maintaining thermopowers of similar magnitude. Theoretical modeling shows how doping strongly alters both the magneto-Seebeck and Nernst thermopowers by shifting the temperature-dependent chemical potential, and the corresponding calculations provide a consistent interpretation of our results. Thus, we offer doping as a tuning mechanism for shifting magneto-thermoelectric effects to temperatures appropriate for device applications, improving zT at desirable operating temperature. Additionally, the simultaneous presence of both a large Nernst and magneto-Seebeck thermopower is uncommon and offers unique device advantages if the thermopowers are used additively. Here, we also propose a unique thermoelectric device which would collectively harness the large Nernst and magneto-Seebeck thermopowers to greatly enhance the output and zT of conventional thermoelectric devices.

2:30 PM EQ01.02.04

Enhanced Thermoelectric Properties Through Carrier Scattering by Localized Nano-Magnetism Junphil Hwang¹, Jae Hyun Yun², Jong-Soo Rhyee², Jungwon Kim³, Sujin Kim¹ and Sung-Jin Kim¹; ¹Ewha Womans University, Korea (the Republic of); ²Kyung Hee University, Korea (the Republic of); ³Institute of Advanced Composite Materials, Korea Institute of Science and Technology(KIST), Korea (the Republic of)

Thermoelectric energy conversion has a lot of attention because of its simple and convenient energy conversion of heat to electricity. In this work, the thermoelectric energy conversion efficiency was enhanced in huge amount by introducing nano-magnetic impurity. The localized spin moment of nano-magnetic impurity interacts with conduction electron spin, resulting scattering of conduction electron. The scattering changes the energy dependence of electron scattering time, inducing decoupling of Seebeck coefficient (S) and electrical conductivity (σ). In general, the S and σ are coupled and limit the enhancement of thermoelectric conversion efficiency. The powerfactor ($S^2\sigma$) was enhanced in whole temperature range, thus the thermoelectric figure of merit, zT was enhanced up to 1.8 at 923 K in Mn doped SnTe nanocomposite. The sophisticated theoretical analysis about electron scattering was conducted using Boltzmann transport equation.

2:45 PM EQ01.02.05

Thermal Hall and Nernst Effects in the Direction of sPin Canting in Antiferromagnet YbMnBi₂ Jiamin Wen¹, Dung Vu¹, Sarah J. Watzman², Claudia Felser³ and Joseph P. Heremans¹; ¹The Ohio State University, United States; ²University of Cincinnati, United States; ³Max Planck Institute for Chemical Physics of Solids, Germany

A large anomalous Nernst effect (ANE) is desirable for thermoelectric applications in transverse geometry, because it leads to simple thermoelectric device construction. YbMnBi₂, a topological antiferromagnet, was demonstrated to have a large ANE conductivity of $\sim 10 \text{ A m}^{-1} \text{ K}^{-1}$, with a magnetic field \mathbf{B} applied along [100], temperature gradient ∇T applied along [001] and Nernst voltage V_N measured along [010], that exceeds observed values in most ferromagnets¹. In this study, we investigated the Nernst effect and thermal Hall effect in a different configuration in which \mathbf{B} is applied along canted ferromagnetic moment direction [110], ∇T along [1-10] and V_N along [001]. In this talk, we present here the experimental data showing that the ANE conductivity is even larger ($30 \sim 70 \text{ A m}^{-1} \text{ K}^{-1}$) than the previously reported value¹. The thermal Hall effect is also anomalously large across the experiment range $40 \text{ K} < T < 300 \text{ K}$ and shows a step in field that suggests the existence of an Anomalous Thermal Hall Effect (ATHE).

*Work supported by the "Center for Emergent Materials", an NSF MRSEC grant # DMR-2011876

1. Pan, Y., Le, C., He, B., Watzman, S.J., Yao, M., Gooth, J., Heremans, J.P., Sun, Y., Felser, C., 2022. Giant anomalous Nernst signal in the antiferromagnet YbMnBi₂. Nature Materials **21**, 203–209 (2021). doi:10.1038/s41563-021-01149-2

3:00 PM BREAK

3:30 PM EQ01.02.06

Magnetically Self-Assembled Stretchable Thermoelectric Devices for Energy Conversion on Skin Byeongmoon Lee¹, Hyeon Cho², Heesuk Kim¹, Yongtaek Hong² and Seungjun Chung¹; ¹Korea Institute of Science and Technology, Korea (the Republic of); ²Seoul National University, Korea (the Republic of)

Compliant forms of thermoelectric devices (TEDs) can provide unprecedented opportunities for skin electronics to be completely untethered, enabling autonomous power systems. For efficient energy harvesting from soft and shape-changing heat sources such as the human body, the TEDs need to conform to complex three-dimensional (3D) surfaces without air gaps that would, otherwise, result in significant heat loss. However, most previous flexible TEDs show limited mechanical conformability due to their bulky inorganic thermoelectric (TE) legs and thick metal electrodes. Recently, soft interconnects such as liquid metals have been utilized to improve the flexibility of TEDs, but the high thermal impedance of elastomer passivation interferes with heat transfer from heat sources to TE materials, significantly reducing their energy harvesting performance.

In this presentation, we will introduce intrinsically stretchable components that can maximize the mechanical conformability and TE performance of compliant TEDs based on the magnetic self-assembly of inorganic particles in elastomeric matrices. Metal particles are magnetically self-assembled into vertical thermal paths in an elastomeric matrix, substantially increasing the through-plane thermal conductivity of elastic platforms. As stretchable interconnects, silver nanowire random networks embedded in the elastomeric platforms efficiently absorb strain energy between inorganic TE legs under deformation. Owing to the soft electrical and thermal conductors, TEDs based on the elastic platforms could form great mechanical and thermal contact with complex 3D heat sources, efficiently harvesting thermal energy from them [1]. In addition, we would like to show unprecedented fully soft TEDs,

where inorganic TE legs are replaced by elastomer composites with magnetically self-assembled TE particles. These results highlight the feasibility of our approach in the realization of high-performance compliant TEDs, paving a new route to fully self-powered electronic skin. The detailed methods and results will be discussed at the conference.

[1] B. Lee et al. *Nature Communications* **11**, 5948 (2020).

3:45 PM EQ01.02.07

First-Principles Calculation of Thermoelectric and Thermomagnetic Transport Effects Using Phoebe Jennifer Coulter, Andrea Cepellotti and Boris Kozinsky; Harvard University, United States

As the need for energy-efficient devices has become more pressing, so has interest in finding ways to enhance the thermoelectric performance of materials. While first-principles methods based on density functional theory can describe these properties, the calculation of transport coefficients can be computationally demanding and memory intensive. To address this challenge, we present ongoing developments to Phoebe [1], a high-performance framework of phonon and electron Boltzmann transport equation solvers with the ability to predict the transport coefficients relevant to thermoelectric performance.

In particular, we will discuss the recent addition of magnetotransport predictions in Phoebe. While transport due to thermomagnetic effects can in some circumstances enhance thermoelectric performance, magnetotransport and thermomagnetic transport effects have rarely been computationally investigated. Using Phoebe, we calculate magneto and thermomagnetic transport coefficients to explore the physics underlying these effects in several materials.

[1] <https://mir-group.github.io/phoebe/>

4:00 PM EQ01.02.08

Validating Experimental Measurement of Electrical Resistivity, Seebeck Coefficient, Hall Coefficient and Nernst Coefficient Using NIST SRM 3451 Matt Beekman, Andrew Jarymowycz, Chad Dutra, Matteo Benedetti, Travis Nichols, Christian Posadas and Kyle Thomson; California Polytechnic State University, United States

Measurement of the four transport coefficients, electrical resistivity, Seebeck coefficient, Hall coefficient, and Nernst coefficient has yielded important experimental insights into features of electronic structure and charge carrier scattering responsible for enhanced thermoelectric performance. While this powerful experimental technique, often referred to as the “method of four coefficients,” remains underutilized in the thermoelectric materials research community, interest in its use has increased in recent years. Like all transport coefficients, thermomagnetic properties like the Nernst coefficient require careful measurement and validation of measurement accuracy, e.g. by using standards or through inter-laboratory comparison. While resistivity measurements can be validated using platinum or other standards, and Seebeck measurements can be validated using the NIST SRM 3451 or 3452, well-defined and widely available standards are not available for Hall or Nernst coefficient. Furthermore, Nernst coefficient measurements are not commonly performed in most research labs, making inter-laboratory comparison nontrivial. Here we describe a method for validating measurement of all four of the above coefficients using a single reference material, namely NIST SRM 3451, mounted for measurement in the same configuration as a research sample, in a single measurement cycle, without the need for inter-laboratory sample exchange. Data for all four coefficients in the temperature range 80 K to 400 K are reported, which will also be of use for researchers wanting to validate new or existing measurement systems in their own laboratory. A comparison of different measurement protocols will also be presented.

4:15 PM EQ01.02.09

New Trick for an Old Dog—From Prediction to Properties of “Hidden” Clathrates Kirill Kovnir; Iowa State University, United States

The zinc-antimony phase space has been heavily investigated due to the structural complexity and abundance of high-performing thermoelectric materials. Consequentially, the desire to use zinc and antimony as framework elements to encage rattling cations to achieve Phonon Glass Electron Crystal properties has remained an enticing goal. Guided by the Zintl electron count prediction we explored the $A\text{-Zn-}Pn$ (A = cation; Pn = As, Sb) phase space via *in-situ* powder X-ray diffraction. *In-situ* studies reveal two “hidden” compounds which can only be synthesized in a narrow temperature range. The *ex-situ* synthesis and crystal growth exposed that compositionally and structurally unique new clathrate-like compounds formed. Single phase synthesis-enabled exploration of the transport properties confirming rattling of guest cations and revealed high Seebeck coefficients and low thermal conductivity. Further optimization of the figure of merit by aliovalent substitutions is computationally analyzed.

4:30 PM EQ01.02.11

Thermal Transport and Outstanding Thermoelectric Properties of 2D-3D Sb₂Te₃ Based Heterostructures with ZT>2.0 Khushboo Agarwal¹, Sergio Gonzalez-Munoz¹, Abhishek Ghosh², Mujeeb Ahmad², Bodh Raj Mehta² and Oleg V. Kolosov¹; ¹Lancaster University, United Kingdom; ²Indian Institute of Technology Delhi, India

While low dimensional and nanostructured materials are long proposed as potential candidates for high performing thermoelectrics (TE), the implementation of these is so far limited [1]. Here we report a large enhancement of the thermoelectric power factor and figure of merit, ZT, in Sb₂Te₃/MoS₂ multilayer structures and Sb₂Te₃/AgSbTe₂ composites with ZT exceeding 2.0 [2]. With thermal conductivity being a defining factor in ZT, we use a novel approach to simultaneously experimentally determine the values of in-plane (k_{xy}) and out-of-plane (k_z) thermal conductivities for multilayer and composite samples with characteristic layer thickness of few nanometres, using scanning thermal cross-sectional microscopy (xSThM). We create a fine near-atomically flat low angle wedge cut on the nanoscale multi-layered TE material via Ar ion beam exit nanopolishing followed by measurement of the local thermal conductance. A simple analytical model is then used to extract the quantitative values of anisotropic thermal conductivities, k_{xy} and k_z as well as to estimate the interfacial thermal resistance between the substrate and sample surface.

For Sb₂Te₃/MoS₂ multilayer structure the thickness and number of layers was optimized to achieve extremely low values of thermal conductivity ($0.7 \pm 0.1 \text{ Wm}^{-1}\text{K}^{-1}$) along with higher values of power factor ($4.97 \pm 0.39 \times 10^{-3} \text{ Wm}^{-1}\text{K}^{-2}$) leading to high values of ZT of 2.08 ± 0.37 at 300 K. For 2D-3D Ag in Sb₂Te₃/AgSbTe₂ composite, the concentration was also optimized to increase values of ZT. Apart of discovering new highly efficient TE materials, the current methodology provides a powerful tool for quantifying the thermophysical properties in thin films and 2D materials with thicknesses on the order from few tens to several hundreds of nanometres, facilitating the search for new efficient thermoelectric and thermal interface and heat-spreading materials.

References

- [1] Vineis, C. J. et al. *Advanced Materials*, 2010, 22 (36), 3970-3980. DOI: 10.1002/adma.201000839 (2010).
- [2] M. Ahmad et al, Engineering interfacial effects in electron and phonon transport of Sb₂Te₃/MoS₂ multilayer for thermoelectric ZT above 2.0, *Advanced Functional Materials*, DOI: 10.1002/adfm.202206384 (2022).
- [3] J. Spieće et al, *Nanoscale*, **24**, 10829 (2021).

SESSION EQ01.03: Poster Session: Progress in Thermoelectrics
Session Chairs: Sepideh Akhbarifar, Heng Wang and Sarah J. Watzman
Monday Afternoon, November 28, 2022
8:00 PM - 10:00 PM
Hynes, Level 1, Hall A

EQ01.03.01

Mobility-Enhanced Thermoelectric Performance in Textured Nanograin Bi₂Se₃, Effect on Scattering and Surface-Like Transport Samaneh Bayesteh¹, Sebastian Sailler¹, Heike Schlörb¹, Ran He¹, Gabi Schierming^{2,1}, Kornelius Nielsch¹ and Nicolas Perez¹; ¹IFW Dresden, Germany; ²Universität Bielefeld, Germany

We report on the effect of artificially generated textures of Bi₂Se₃ in thermoelectric performance and low-temperature magnetoresistance [1]. A set of texturized nanograin Bi₂Se₃ samples was investigated, ranging from predominantly *c*-axis texture to random texture. *c*-axis oriented layered domains rendered the samples highly conducting due to drastically enhanced mobility, up to 1600 cm²V⁻¹s⁻¹ at low temperature, and enhanced both carrier concentration and electrical conductivity. The largest power factor of 800 μWm⁻¹K⁻² and highest 0.14 both at 300K were observed in a sample with a predominantly layered and *c*-axis oriented texture. The carrier scattering mechanism in the samples changed from mostly electron-phonon interaction at in the predominantly layered microstructure, to disorder-related scattering as the texture became random. The weak antilocalization effect was observed predominantly in the random textured samples, pointing towards enhanced surface-like transport channels. The phase coherence length evaluated using the Hikami-Larkin-Nagaoka model resulted in a high value of roughly 600 nm regardless of the texture. In the *c*-axis oriented layered Bi₂Se₃ oxidic insulating inclusions from either Fe₃O₄ or SiO₂ were incorporated. Both insulating phases reduced mobility. However, finely dispersed Fe₃O₄ secondary phase in Bi₂Se₃ resulted in a further increase of 0.2 due to much increased electrical conductivity. The combined effect of layered texture and Fe₃O₄ secondary phase resulted in an overall increase of around 50% compared to a non-textured polycrystal.

[1] Samaneh Bayesteh *et al.*, *Mat. Today Physics* **24** (2022) 100669, DOI: 10.1016/j.mphys.2022.100669.

EQ01.03.02

A General Approach for Exploiting X-Ray Dynamical Diffraction in Material Sciences and Biophysics Rafaela F. Penacchio¹, Mauricio B. Estradiote¹, Milton S. Torikachvili², Cláudio M. Remédios³, Guilherme A. Calligaris⁴, Stefan Kycia³ and Sergio L. Morelhao¹; ¹Institute of Physics, University of São Paulo, Brazil; ²San Diego State University, United States; ³Federal University of Pará, Brazil; ⁴Brazilian Synchrotron Light Laboratory, Brazil; ⁵University of Guelph, Canada

Structural analysis with atomic resolution is, unequivocally, the cornerstone that underpins the development of fundamental areas of human knowledge such as structural biology and materials engineering. On a global scale, billions of dollars are invested annually in equipment and large facilities for structural analysis techniques. Even with all the existing know-how, there are still limits in the resolution of certain structural details capable of unraveling the exact origin of important properties of various organic and inorganic systems. It also applies to standard X-ray scattering and diffraction methods. One way to acquire more detailed structural information beyond that accessible by conventional crystallography is to exploit the X-ray dynamical diffraction (XRDD) phenomenon. It is well-known that XRDD allows direct measurements of diffracted wavefield phases, as extra information on top of the diffracted intensities. Although there are many examples of how to exploit phase measurements [1-4, and references therein], there are a few steps that can be quite difficult for the inexperienced user of the method as it is in its current conception: what are the structural details of a given system accessible by phase measurements only, and how to perform data acquisition and data analysis. In this work, a general approach for exploiting XRDD in virtually any crystal system is presented as implemented into an open-source Python package (PyDDT - Python Dynamical Diffraction Toolkit). It allows experiment planning based on the available Crystallographic Information File (CIF) of the materials. Susceptibility of XRDD to structural details such as valence of chemical species, vacancies and anti-site occupation, internal strain due to foreign atoms, and relative differences in atomic displacement are easily investigated through a differential model structure generation tool inside the PyDDT. Optimum resonant diffraction conditions are also identified in this experiment planning step prior to the actual experiment. After a successful data collection, fast semi-automatic data analysis is carried out by the PyDDT for extracting all structure factor phase information available in the data set. Graphic tools for comparing experimental and theoretical phases conclude the application of the method by stating feasible model structures capable of explaining the XRDD data. Here the application of this approach is demonstrated in a few emblematic cases. Probing electron charges in silicon covalent bonds and in amino acid van der Waals bonds [3], as well as in using resonant diffraction to elucidate vibrational atomic displacements in a thermoelectric crystal [4]. In summary, the PyDDT is demonstrated for probing electronic density and atomic displacements of organic and inorganic crystals using laboratory and synchrotron radiation. This package establishes standard procedures for using this approach of X-ray dynamical diffraction, which now are reproducible by other researchers and transferable to other systems, being a big step toward the spread of the technique.

Financial support of FAPESP (2021/01004-6, 2019/019461-1) and CNPq (310432/2020-0) is acknowledged.

[1] Q. Shen and K. D. Finkelstein. *Solving the crystallographic phase problem with reference-beam diffraction*. *Phys. Rev. Lett.* **65**, 3337 (1990). doi: 10.1063/1.1445828

[2] S. L. Morelhão, S. Kycia. *Enhanced X-Ray Phase Determination by Three-Beam Diffraction*. *Phys. Rev. Lett.* **89**, 015501 (2002). doi: 10.1103/PhysRevLett.89.015501

[3] S. L. Morelhão et al. *X-ray dynamical diffraction in amino acid crystals: a step towards improving structural resolution of biological molecules via physical phase measurements*. *J. Appl. Cryst.* **50**, 689–700 (2017). doi: 10.1107/S1600576717004757

[4] A. Valério et al. *Phonon scattering mechanism in thermoelectric materials revised via resonant x-ray dynamical diffraction*. *MRS Communications* **10**, 265-271 (2020). doi: 10.1557/mrc.2020.37

EQ01.03.03

Challenges and Novel Strategies in High-Performance Thermoelectric Material Engineering Karan Giri, Yan-Lin Wang, Yu-Chieh Shih, Ling-Chun Chao, Chuan-Wen Wang, I-Jung Wang, Yi-Chen Chen, Cheng-Ju Yang, Pei-Hsuan Cho and Chun-Hua Chen; National Yang Ming Chiao Tung University, Taiwan

Thermoelectric (TE) materials have been recognized as promising materials and make a prime contribution to converting waste heat into valuable electrical energy without further loss. In recent decades, researchers have witnessed the development of new and efficient mechanisms/ strategies to optimize the figure of merit (ZT) of these materials to recover low-grade heat more efficiently. The TE materials and devices are of greater importance because of their small size (scalable), lack of moving parts, high reliability, feasibility for miniaturization, lack of noise and pollution, and lack of emission of greenhouse gasses. An application of such characteristics delivers exclusive TE technology for numerous fields or niche applications, such as sensing and wearable electronics, waste low-quality heat recovery, TE refrigeration, aerospace, cogeneration, medical thermostats, zero radiation, and solid-state operation. To fabricate high-performance TE materials, a balanced trade-off between TE parameters is indispensable to optimizing the ZT value and is the key challenge to engineering such thermoelectrics. To achieve the highest ZT value, the maximization of the TE power and the electrical conductivity, and the minimization of the thermal conductivity are essential. To some extent, the hit-and-trial method can be effective in optimizing TE properties. Practically, it is possible to enhance the power factor by aligning and converging the electronic bands, modifying the electronic structure, and creating resonance states. All-scale hierarchical scattering and entropy engineering incorporate all of these outcomes into a single material system. Band flattening and resonant levels are two commonly adopted ways to increase the effective mass which has a significant contribution to optimizing TE performance. The first one can be brought about via the endorsement of dopants accommodating highly localized orbitals which leads to a fall in the overlapped orbitals. The Kane-band model illustrates that band flattening can enhance the bandgap E_g through band dispersion. And in the latter approach, the excess density of states (DOS) can be achieved via electronic coupling and is more efficient at a lower temperature than at a higher temperature because of the variation in relaxation time. Low dimensionality and electronic structural modifications, such as electronic band structure engineering and the creation of extrinsic defects through alloying and nanostructuring to suppress the lattice thermal conductivity (k_l), are efficient strategies to enhance the ZT of TE materials. The confinement of the electrons in low dimensions (D) such as 1D or 2D can improve the performance of TE materials by abruptly altering the electronic DOS. Low-dimensionality strategy is a milestone to initiate the nanostructure (quantum-well, superlattice structures, nanowires) studies in TE materials. When the phonon has a longer mean free path (MFP) than the electron then nanostructuring is an appropriate technique for the optimization of TE properties. The grains or nano-inclusions of a suitable size can be introduced into the specimen to scatter more phonons than the electrons. In the specimen, the interfaces are rationally designed to reduce their effect on charge mobility (μ) and to decouple it with k_l . While adding hierarchical scattering centers into the heavy-band TE materials, the reduction of maintaining high μ is a key to optimizing ZT . For this, the size of these centers should have a dimension larger than the MFP of the charge carrier but smaller than that of the phonon. Some of the high-performance fabrications described in this review paper exhibiting exceptional TE performance include two-dimensional PbTe quadruple layers, both p -type and n -type materials with enhanced values of 2.39 and 2.44 in the mid-temperature range, respectively, and the hole-doped tin selenide polycrystalline samples with a value of ~ 3.1 at 783 K.

EQ01.03.05

P-N Conversion of CrN Films by Oxygen Incorporation and Their Thermoelectric Properties Yi Shuang and Yuji Sutou; Tohoku University, Japan

Thermoelectric properties have been widely studied in bulk materials compared to thin films. However, in some specific applications, such as flexible temperature sensors, small-scale power generation applications and on-chip energy harvesting, thermoelectric thin films are playing a significant role. Traditional thermoelectric thin films showing a high ZT value such as tellurides are limited for the applications at elevated temperatures due to their poor stability, low corrosion resistance and toxicity.^[1,2] Therefore, in the recent years, the transition-metal nitrides and rare-earth nitrides have been developed as a new class of thermoelectric thin films due to their outstanding mechanical properties, relatively low thermal conductivity and a variable range of electrical properties. Among them, chromium nitride (CrN) exhibiting n -type conduction is one of the most promising candidates as they can show a low electrical resistivity together with a large absolute value of Seebeck coefficient. Besides, the high melting point of CrN makes it possible to be used in high-temperature thermoelectric applications. To practically use the n -type CrN into thermoelectric applications, p -type materials are also needed. The best choice of p -type materials is the material with similar crystal structure and thermal properties such as the thermal expansion. In addition, intermixing of atoms or chemical reactions should be avoided between p and n layers. Therefore, it is an ideal way to develop one thermoelectric material with both n - and p -type conducting properties. For example, p -type CrN can be made by alloying with a small amount of Al into n -type CrN.^[3] The alloyed Al element can behave as an electron acceptor that reduces the carrier concentrations of pure CrN and leads to a p -type conducting eventually. Febvrier et al. also proposed a p -type CrN by controlling the stoichiometry without the need for dopants deposited by DC magnetron sputtering at 600 °C. They demonstrated that p -type conduction can be attributed from Cr vacancies, which pushes the Fermi level down in the valence band.^[4] In this study, we proposed a much simpler method to convert the semiconducting type of CrN by introducing oxygen dopants into the CrN film using a radiofrequency (RF) magnetron sputtering at room temperature. By fixing the chamber base pressure to be 10^{-5} Pa and varying the N_2 gas flow rate (f_{N_2}) during reactive sputtering, the oxygen content in the CrN films can be controlled from 6.8 to 12.4 at. %. The n -type CrN can be successfully converted into p -type by tuning the oxygen content. The crystal structure, electrical property and thermoelectric property of the obtained CrN_xO_y thin films were investigated and discussed. The present method to tune the p - n type of CrN_xO_y films is simple and reproducible, which could contribute to a p - n homo-junctions enabling a better application in not only thermoelectric devices, but also wider fields such as photodetectors, selector devices etc. What is more, the room temperature growth of thin film would be beneficial for the flexible and wearable energy-harvesting, and compatible to the MEMS processing.

[1] P. Mannu, M. Palanisamy, G. Bangaru, S. Ramakrishnan, R. Meena, C. L. Dong, A. Kandasami, *Appl. Surf. Sci.* **2020**, *505*, 144115.

[2] R. Lan, S. L. Otoo, P. Yuan, P. Wang, Y. Yuan, X. Jiang, *Appl. Surf. Sci.* **2020**, *507*, 145025.

[3] A. Le Febvrier, N. Van Nong, G. Abadias, P. Eklund, *Appl. Phys. Express* **2018**, *11*, 051003.

[4] A. le Febvrier, D. Gambino, F. Giovannelli, B. Bakhtit, S. Hurand, G. Abadias, B. Alling, P. Eklund, *Phys. Rev. B* **2022**, *105*, 104108.

EQ01.03.06

Effect of Powder ALD Interface Modification on the Thermoelectric Performance of Bismuth Shiyang He, Amin Bahrami and Kornelius Nielsch; Leibniz Institute of Solid State and Materials Science, Germany

In thermoelectric materials, phase boundaries are crucial for carrier/phonon transport. Manipulation of carrier and phonon scatterings by introducing continuous interface modification has been shown to improve thermoelectric performance. In this paper, a strategy of interface modification based on powder atomic layer deposition (PALD) is introduced to accurately control and modify the phase boundary of pure bismuth. Ultrathin layers of Al_2O_3 , TiO_2 and ZnO are deposited on Bi powder by typically 1–20 cycles. All of the oxide layers significantly alter the microstructure and suppressed grain growth. These hierarchical interface modifications aid in the formation of an energy barrier by the oxide layer, resulting in a substantial increase in the Seebeck coefficient that is superior to that of most pure polycrystalline metals. Conversely, taking advantage of the strong electron and phonon scattering, an exceptionally large decrease in thermal conductivity is obtained. A maximum figure of merit, zT , of 0.15 at 393 K and an average zT of 0.14 at 300–453 K were achieved in 5 cycles of Al_2O_3 -coated Bi. The ALD-based approach, as a practical interfacial modification technique, can be easily applied to other thermoelectric materials, which can contribute to the development of high-performance thermoelectric materials of great significance.

EQ01.03.07

Enhancement of Thermoelectric Properties by Magnetic Impurities in Lead-free Thermoelectric Materials Sujin Kim, Junphil Hwang and Sung-Jin Kim; Ewha Womans University, Korea (the Republic of)

Thermoelectric technology has attracted a lot of attention because it enables eco-friendly power generation. The enhancement of thermoelectric

performance is challenging due to its strong inverse interrelationship between electrical conductivity (σ) and Seebeck coefficient (S). In this study, we studied non-toxic IV-VI compound GeTe with magnetic impurities. Our experiments showed an improvement in thermoelectric performance by doping unfilled d-orbital elements. Some of unfilled d-orbital elements were added as magnetic impurities in the GeTe. Previously, we found that magnetic impurities generate exchange interaction and induce additional scattering, resolving their strong inverse correlation between electrical conductivity and Seebeck coefficient. The exchange interactions occur between the spin angular momentum of itinerant electrons and that of magnetic impurities. The exchange interaction between the spin angular momentum of magnetic impurities and itinerant electrons generates the superparamagnetic fluctuation inducing additional scattering reducing thermal conductivity. The magnetic impurities showed synergetic effects of the increasing powerfactor ($S^2\sigma$) and decreasing thermal conductivity (κ) in $zT = S^2\sigma T/\kappa$ resulting enhanced thermoelectric performance of GeTe.

EQ01.03.08

End-On Oriented PEDOT/Graphene Films for Photo-Magneto-Thermoelectric Effect Byeongwan Kim, Cheolhyun Cho and Eunyoung Kim; Yonsei University, Korea (the Republic of)

Orientation control of conductive polymer chain on substrate has been explored for molecular self-assembly engineering, improving the charge transfer, controlling the optical and electronic properties for realizing next-generation flexible electronics. The ordering of conductive polymers in one direction is a key approach to obtain high electrical conductivity and carrier mobility for controlling magnetoresistance and magneto-thermoelectric effect of polymer film. We challenged to align the poly(3,4-ethylenedioxythiophene) (PEDOT) chains perpendicular to the substrate to form end-on orientation. The PEDOT chains were grown on a monomer-functionalized graphene surface that was prepared by using 3D tectons and surface-confined host-guest chemistry. A highly crystalline PEDOT film with end-on orientation showed a reversible magneto-thermoelectric effect and control carrier transport from hot to cold *via* external magnetic fields. The film showed a Seebeck coefficient enhancement and a large magneto-thermoelectric effect. Taking advantage of a high photothermal effect of the film, a photo-magneto-thermoelectric effect was demonstrated to control carrier transport in thin-film *via* external magnetic stimuli with a light source.

EQ01.03.09

Mass Production of Cu_{2-x}Se Nanoparticle for Thermoelectric Bulk Materials with Nanosized Grains via High Concentration Metal Complex Precursor Cheol-hui Ryu¹, Myeongjun Ji¹, Jeong Hyun Kim¹ and Young-In Lee^{1,2}; ¹Seoul National University of Science and Technology, Korea (the Republic of); ²The Institute of Powder Technology, Korea (the Republic of)

Electrical energy consumption is closely related to the growth of economic activity. Energy from fossil fuels causes air pollution, climate change, and global warming due to the release of harmful substances during combustion, so it must be replaced with renewable energy as a result. In accordance with this trend, thermoelectric (TE) technology using waste heat is attracting a lot of attention as an eco-friendly mechanism with high efficiency, wide application temperature range, and high reliability without moving parts. Currently, the medium and high temperature (400-750K) waste heat generated in the industry is being dissipated in a high proportion of more than 60% due to the limit of energy efficiency. Therefore, Cu_{2-x}Se, which has recently been attracting attention among various thermoelectric materials, is a copper-based chalcogenide and has low toxicity and cost-effectiveness. In the high-temperature superior phase above 400K, Cu ions are very disordered and mobile, resulting in very low k_L and high zT values, so the TE efficiency is high in the medium and high-temperature regions. Furthermore, to maximize TE characteristics, a technique for further reducing thermal conductivity by increasing phonon scattering with nano-sized particles through a powder metallurgy process is attracting attention. Although various synthetic methods including hydrothermal, solvothermal, and thermolysis to prepare Cu_{2-x}Se nanoparticles have been developed, they require suitable conditions such as relatively low precursor concentration, high temperature, high vacuum, many numbers of reactants, special experimental arrangements to perform the synthetic procedures. This causes low yield and difficulties in process optimization and commercialization. According to homogeneous nucleation and growth theory, the critical nuclei radius and critical energy to generate specific nuclei depend on a precursor concentration in the reaction medium. In general, the nucleation rate is faster at high precursor concentrations, which means that smaller nanoparticles can be synthesized in large quantities. However, the actual synthesis process using high concentration precursors causes problems in which particles are uneven in size and increase in size. Therefore, a new methodology is needed to solve this problem. In this study, a solution-based mass-production technology of Cu_{2-x}Se nanoparticles was successfully developed using a high-concentration metal complex precursor and ultrasonic energy. This approach can prevent a particle agglomeration by introducing complex molecules and instantaneous uniform energy supply and recovery via ultrasound. Using this facile and cost-effective strategy, Cu_{2-x}Se nanoparticles with an average diameter of 150nm were successfully synthesized at room temperature and atmospheric pressure. In addition, by adjusting the Cu/Se precursor ratio in the starting reaction solution, it was possible to easily control the alpha and beta phase fractions of Cu_{2-x}Se, which greatly contribute to the thermoelectric properties. Then, according to process variables, the physicochemical properties of synthesized nanoparticles were systematically investigated by various analysis methods. After the Cu_{2-x}Se powder of each composition was sintered using Spark Plasma Sintering (SPS), a sample having a nano-sized grain was obtained. Then, the physicochemical properties of the samples prepared according to the Cu/Se composition were systematically analyzed, and the correlation between the composition and the thermoelectric properties was identified through various analysis methods.

EQ01.03.10

Organic Thermoelectrics Thusharika Muthumali and Ryan Chiechi; North Carolina State University, United States

Thermoelectric (TE) materials are a class of materials that can be used to generate electricity from waste heat. For practical TE applications, both p-type and n-type materials must exhibit comparable figures of merit, in order to operate in tandem in a TE generator device. However, n-type materials have so far lagged behind p-type materials. Molecular doping is the key, limiting process to enhancing the performance of n-type materials. It has been demonstrated that n doping efficiency can be increased by lowering the energy of the LUMO level and improving host dopant compatibility. These are, fundamentally, synthetic challenges and we aim to address them as such. In this contribution, we will present our strategies for designing and synthesizing new polymers and dopants to address key properties systematically.

The high doping levels required to maximize performance and the differences in polarity between the host backbone, pendant groups, and ionized dopant molecules can drive deleterious phase separation within the doped film. These challenges can be overcome by tuning the doping concentration and designing pendant groups that interact with and control the dispersion of polar dopants such as 1,3-dimethyl-2-phenylbenzimidazole (DMBI). Improving dopant solubility will lead to uniformity of the films, higher doping efficiency, and increased conductivity.

The energy of the LUMO (conduction band) of the host polymer also plays an important role in increasing doping efficiency in polymeric n-type materials. Manipulating this energy can be achieved by tuning the electronic structure of conjugated polymers. However, electron transfer between the host polymer and the dopant can also be facilitated by introducing electron-rich donor moieties in the dopant, which is why we approach the synthetic challenges to both simultaneously.

EQ01.03.11

Synthesis of Graphene/Cu Nanoparticles by Photoreduction Method for Enhancing Thermoelectric Power Factor Koki Saito, Takashi Shimizu, Shunya Sakane and Hideki Tanaka; Chuo University, Japan

Thermoelectric materials that can directly convert heat to electricity are attracting attention. Their thermoelectric efficiency is usually evaluated by thermoelectric power factor ($S^2\sigma$), where S is Seebeck coefficient and σ is electrical conductivity. Graphene is a promising thermoelectric material due to its high electrical conductivity (σ) derived from its inherent high carrier mobility, good thermal stability and excellent mechanical strength. It has been reported that graphene composited with highly conductive precious metal nanoparticles (Pt, Au, Ag) forms conductive bridges and improves thermoelectric properties by increasing σ [1]. We have focused on copper as alternative metals to precious ones because copper is abundant in the earth and has high electrical conductivity as precious metals. Therefore, the combination of graphene and copper nanoparticles (Cu NPs) is expected to improve the σ . In this study, we synthesized Graphene/Cu nanoparticles (Gr/Cu NPs) by the photoreduction method which does not require environmentally hazardous reductants [2], and evaluated their thermoelectric properties.

Mixed solution of copper acetate and graphene was irradiated with UV light. The resulting precipitates were spin coated and annealed on a glass substrate to form thin films (Gr/Cu NP films). Structure of the thin films was analyzed by X-ray diffraction (XRD), and cross sections and surfaces of the thin films were observed by scanning electron microscopy (SEM). Their electrical conductivity (σ) was measured by van der Pauw method. Their Seebeck coefficient ($S = \Delta V / \Delta T$) was determined by measuring the potential difference (ΔV) and temperature difference (ΔT) by our hand-made system.

SEM images of Gr/Cu NPs showed particles with several dozens of nanometers on the graphene sheet. Cross-sectional SEM images of the thin films showed the thickness of 50–70 nm on the glass substrate. From XRD pattern, the diffraction peak originating from Cu(111) appeared. These results indicate that the nanoparticles observed in the SEM images were Cu NPs. When the dependence on the amount of Cu NPs in the thin film was examined, the electrical conductivity σ showed the highest value at 10 wt%. This value is 1.5 times higher than the graphene thin film, and this indicates the formation of conductive bridges through Cu NPs on the graphene. On the other hand, S showed no significant dependence on the amount of Cu NPs in the thin film. As a result, the power factor ($S^2\sigma$) of the optimized Gr/Cu NP thin films was 1.5 times higher than the graphene thin film.

Acknowledgments

This work was supported by Grant-in-Aid for Early-Career Scientists Grant Number 21K14479 and Grant-in-Aid for Scientific Research (C) Grant Number 19K05187 from JSPS KAKENHI, Japan.

References

- [1] L. L. Shiao et al., Graphene-Metal nanoparticles for Enhancing Thermoelectronic Power Factor. IEEE Transactions on Nanotechnology. 18, 1114 (2019).
- [2] M. Miyagawa, et al., Aqueous synthesis of protectant-free copper nanocubes by a disproportionation reaction of Cu₂O on synthetic saponite. Chem. Commun. 54, 8454 (2018).

EQ01.03.12

Testing the Validity of Wiedemann-Franz Law Using Thermoreflectance-Based Methods in Thin Copper Films Md. Rafiqul Islam¹, John A. Tomko¹, Md Shafkat Bin Hoque¹, Eric Hoglund¹, Sean W. King², Christopher Jezewski², Colin D. Landon², Daniel Hirt¹, Kiumars Aryana¹, Colin Carver², Thomas W. Pfeifer¹ and Patrick E. Hopkins¹; ¹University of Virginia, United States; ²Intel Corporation, United States

To determine the thermal properties of thin metal films, a common approach is to measure their electrical resistivity and then calculate in-plane thermal conductivity employing the Wiedemann-Franz (WF) law and the bulk metal's Lorenz number. However, the implementation of the WF law in calculating thermal conductivity can be refuted because of the Lorenz number deviating from its bulk value owing to thickness-dependent microstructure, inelastic electron-phonon scattering events, and/or point defect density. In this work, we address the dearth of understanding of how thermal and electrical properties of copper (Cu) films scale at nanometer dimensions via independent measurements of the thermal and electrical transport properties. We perform sheet resistance and thermoreflectance-based nanoscale thermal conductance measurements on Cu films ranging from 25 to 500 nm thick, grown by physical vapor deposition (PVD) and electroplating methods. We directly measure the in-plane thermal conductivity of the Cu thin films via time-domain thermoreflectance and steady-state thermoreflectance techniques. We find the in-plane thermal conductivity of thin films deviates at least 15% from the WF law-derived thermal conductivity. This deviation in thermal conductivity of thin films can be attributed to their columnar grain structures and more electron-phonon scattering events compared to the bulk one.

EQ01.03.13

Synthesis of Single Phase α -Cu₂Se Nanowires by Photoreduction Method for Thermo-electrical Application Tatsuki Miura, Kazuki Munakata, Shunichiro Miwa, Shunya Sakane and Hideki Tanaka; Chuo University, Japan

Cu₂Se, a low-toxicity and low-cost p-type semiconductor, has attracted attention for various applications such as thermoelectric materials, photocatalysts, and solar cells due to its optical and electrical properties. Especially, there have been many reports that Cu₂Se exhibited high thermoelectric performance. For further enhancement of thermoelectric performance of Cu₂Se, nanostructuring is effective due to phonon scattering at nanostructure interfaces leading to thermal conductivity reduction. Recently, various Cu₂Se nanostructures have been synthesized. However, Cu₂Se usually shows a complex phase structure depending on temperature and Cu defects because Cu₂Se undergoes a reversible phase transition between the low-temperature phase α -Cu₂Se (monoclinic) and the high-temperature phase β -Cu₂Se (cubic) in the 350–410 K temperature range. Therefore, this makes it difficult to synthesize single-phase Cu₂Se nanostructures. We have focused on the photoreduction method as a synthesis of nanostructures. In the photoreduction method, strong reductant or toxic agent are not used, and the reaction speed is slow. In the synthesis of Cu₂Se nanostructures, the phase structure can be controlled by adjusting the light intensity and irradiation time due to the slow reaction. In this study, we aim to synthesize single-phase α -Cu₂Se nanowires (NWs) by photoreduction method and to evaluate their electronic structures.

Cu₂Se NWs were synthesized by following method briefly. Selenium dioxide and β -cyclodextrin were mixed in distilled water and sonicated. This solution was slowly mixed with L(+)-ascorbic acid solution under continuous stirring. Obtained precipitates were centrifuged and washed. Se NWs were synthesized by redispersion of this precipitates in ethanol [1]. The synthesized Se NWs and copper acetate were mixed in ethanol solution and irradiated with UV light. The product was obtained by centrifugation and Cu₂Se NWs was synthesized. Structural characterization of the prepared samples was performed using scanning electron microscopy (SEM), X-ray diffraction (XRD), energy dispersive X-ray analysis (EDX), and diffuse reflection UV-visible spectroscopy (DR UV-vis).

SEM images showed a nanowire structure with a diameter of about 500 nm and a length of several micrometers. It was found that the nanowire structure was maintained even after photoreduction. The EDX mapping results showed that the nanowires were composed of Cu and Se, and the atomic number ratio of Cu and Se was found to be about 2:1. The diffraction peaks in the XRD pattern of synthesized samples were attributed to α -Cu₂Se. These results indicate that α -Cu₂Se NWs were synthesized from Se NWs by photoreduction method.

DR UV-vis spectra of the synthesized α -Cu₂Se NWs were measured. In the UV-vis absorption spectrum of α -Cu₂Se, the absorption due to the interband excitation from the valence band to the conduction band appears at <800 nm, while the absorption due to the intraband electron excitation in the valence band appears at >800 nm. For the region below 800 nm, the band gap of the sample was obtained by using the equation of Tauc et al [2]. The band gap of synthesized α -Cu₂Se NWs was found to be 1.17 eV. This band gap value was in good agreement with that of bulk α -Cu₂Se (1.20 eV [3]).

Acknowledgments

This work was supported by Grant-in-Aid for Early-Career Scientists Grant Number 21K14479 and Grant-in-Aid for Scientific Research (C) Grant Number 19K05187 from JSPS KAKENHI, Japan.

References

- [1] Qing, L *et al. Chem. Commun.* **1**, 1006 (2006).
[2] Bin Liu *et al. Phys. Chem. Chem. Phys.* **17**, 13280 (2015).
[3] Yizhou You *et al. Phys. Chem. Chem. Phys.* **23**, 9814 (2021).

EQ01.03.16

Enhanced Thermoelectric Properties of CoSb₃-Based Skutterudite by Incorporating Reduced Graphene Oxide Mun Hwi Lee^{1,2}, Woo Hyun Nam¹, Jung Young Cho¹ and Young Soo Lim^{2,2}; ¹Korea Institute of Ceramic Engineering & Technology, Korea (the Republic of); ²Pukyong National University, Korea (the Republic of)

We report a strategy for enhancing thermoelectric properties in CoSb₃-based skutterudite through the incorporation of reduced graphene oxide (RGO). Double-filled *n*-type CoSb₃ (SKD) powder was obtained by encapsulated induction melting and grinding. The SKD-RGO hybrid powder was prepared by coating graphene oxide (GO) onto the SKD powder and followed by a chemical reduction process. The hybrid powder was consolidated into the SKD-RGO bulk composites by spark plasma sintering. Advantageous effects of the RGO incorporation both on the charge and phonon transports were observed in the composites. The electrical conductivity of the composites increased with increasing the RGO content. Although the incorporation of RGO reduced the Seebeck coefficient due to the increase in the carrier concentration, the composites exhibited an improved power factor. Furthermore, lattice thermal conductivity in the composites decreased due to an additional phonon scattering at SKD/RGO interfaces. This study suggests that the incorporation of carbon nanomaterials is a promising way to the simultaneous control of the charge and thermal transports for realizing high thermoelectric performance in skutterudite materials.

EQ01.03.17

Carboxylic Acid Terminal Group Remarkably Enhances Thermopower of Aliphatic Monolayers Jiung Jang and Hyo Jae Yoon; Korea University, Korea (the Republic of)

In molecular thermoelectrics, study of thermopower in molecular junction permits access to physical-organic information about nano-scale thermoelectric energy conversion. Whereas π -extended building blocks have been considered as efficient thermoelectric materials, aliphatic molecules are usually avoided, and the related mechanism of thermoelectric energy conversion remains unclear. In this presentation, we show that replacement of methyl terminal group with carboxylic acid significantly enhances thermopower in self-assembled monolayer (SAM)-based large-area molecular junction. Using the liquid metal junction technique, we formed non-damaging contacts over the delicate surface of SAMs and examined length dependence of Seebeck coefficient. We focused on the following three different series of aliphatic molecules and compared their Seebeck coefficient: mercaptoalkanes (HS(CH₂)_n-CH₃; n=2-10, 12, 14, 16, 18), mercaptoalkanoic acids (HS(CH₂)_{n-1}CO₂H; n=2-8, 11, 12, 16), and methyl mercaptoalkanoates (HS(CH₂)_{n-1}CO₂CH₃; n=2-8, 11, 12). Two interesting features were observed. i) The alkanolic acid molecules led to significant increases in the Seebeck coefficient by up to ~250 %, compared to the alkane molecules of similar lengths. ii) Rather surprisingly, in the short molecular-length regime (n≤5), Seebeck coefficient of alkanolic acid molecules increased as the length of aliphatic backbone increased, whereas the others (mercaptoalkane and mercaptoalkanoate molecules) exhibited linear regression of Seebeck coefficient with increasing the length. Structural analysis over the SAMs and theoretical calculations suggested that the unusual thermoelectric behaviors were attributed to the interplay between the supramolecular disorder in SAM and the electronic interaction between the carboxylic acid terminal group and top electrode, which had significant influence on the energy offset between Fermi level and energy level of accessible occupied molecular orbital.

EQ01.03.19

Moreau Relation and the Nernst Effect in Semiconductors Jean Ghantous, Max Buskirk and Matt Beckman; California Polytechnic State University, United States

An empirical relation first proposed by Moreau and later by Bridgman expresses the Nernst coefficient of a metal as the product of the Thomson coefficient, electrical conductivity, and Hall coefficient. Thus a feature of this relation is that the Nernst coefficient changes sign whenever the slope of the Seebeck coefficient changes sign, behavior that has been observed to hold not only in metals but also in some semiconductors. Here, within the Boltzmann transport theory, we provide an evaluation of the extent to which the Moreau relation applies to semiconductor materials more generally, and specifically in the case of Bi₂Te₃. Implications for interpretation of Nernst measurements for determining charge carrier scattering mechanisms, as well as applications in thermomagnetic energy conversion, will also be discussed.

EQ01.03.20

Progress of Fabricating Heritage Silicon Germanium Unicouples Billy C. Li¹, Sutinee Sujittasakul¹, Vilupanur Ravi^{1,2}, Ike Chi¹ and Jean-Pierre Fleurial¹; ¹Jet Propulsion Laboratory, United States; ²California Polytechnic State University, Pomona, United States

NASA has successfully demonstrated Radioisotope Thermoelectric Generators (RTGs) as an effective power system to support numerous scientific deep space explorations. RTGs have consistently demonstrated their extraordinary reliability and longevity (40 years of continuous operation for Multi-Hundred Watt Radioisotope Thermoelectric Generator (MHW-RTG) on Voyager 1 and 2) while relying on thermoelectric materials and device technologies that were developed in the 1960s and 1970s. Recently, NASA announced plans to reestablish the General Purpose Heat Source-Radioisotope Thermoelectric Generator (GPHS-RTG) with Silicon-Germanium Unicouple(s) for potential future deep-space missions. However, the Silicon-Germanium uncouple production line in industry was discontinued in the late 1990s, resulting in loss of facilities, a combination of legacy equipment obsolescence and scattering of remaining legacy equipment to various government entities, bulk storage of legacy build-to-print procedures, loss of trained and knowledgeable personnel, and a likely loss in qualified vendors. To reduce potential risks due to this obsolescence, NASA's Radioisotope Power Systems program established a SiGe Task Force (NASA RPS DIR-006) in support of the Next-Generation RTG Project (Mod 1). The focus of task force support at NASA's Jet Propulsion Laboratory (JPL) has been on identifying and assessing initial key risks and exploring options relative to reestablishing the GPHS-RTG SiGe uncouple production line. To this end, JPL utilized its existing capabilities and heritage procedures of legacy SiGe uncouple production to conduct "heritage build-to-print" SiGe uncouple fabrication. Performing this "heritage" uncouple assembly and pellets/segments fabrication steps enabled JPL to identify critical processes and evaluate their robustness to variations from available legacy documentation and processes. Here, we report on the results of JPL SiGe uncouple assembly pathfinder practices using Cassini RTG production line ready-to-use parts.

EQ01.03.21

Electrical Alignment of Single-Walled CNTs in Polymer Matrix Toward High Thermoelectric Performances Hyunjin Joh¹, Gopinathan Anoop¹, Seunghyun Jo¹, Hye Jeong Lee^{2,1}, KwangSup Eom¹ and Ji Young Jo¹; ¹Gwangju Institute of Science and Technology, Korea (the Republic of); ²Korea Research Institute of Standards and Science, Korea (the Republic of)

A Thermoelectric generator (TEG), which can convert thermal energy directly to electrical energy, is a promising candidate for renewable energy

converter. Flexible TEGs can easily be attached to heat sources order to reduce heat loss at interfaces rather than rigid inorganic-based TEGs, but their low thermoelectric performance still hinders their being commercialized. The performance of the TEGs can be expressed by thermoelectric figure of merit (ZT), where $ZT = S^2\sigma T/\kappa$, Seebeck coefficient (S), electrical conductivity (σ), and thermal conductivity (κ). These parameters are highly entangled via carrier concentration in pre-existing homogeneous thermoelectric materials, which sets a fundamental limit of ZT in TEGs [1]. A composite consisting of insulating polymer and conducting nanoparticles are suggested to enhance the ZT in flexible thermoelectrics. Such composites provide a high σ via the formation of conducting paths based on nanoparticles and a low κ arising from the energy filtering effect [2]. We chose poly(vinylidene fluoride-trifluoroethylene) (P(VDF-TrFE)) for the polymer matrix and single-walled carbon nanotubes (SWCNTs) as the conducting reinforcement nano-material. In addition, we applied an alternating voltage to align the SWCNTs in the polymer matrix, which provides the high σ as well as the high thermoelectric ZT. Here, we successfully fabricated the freestanding P(VDF-TrFE)-SWCNT composite films with excellent flexibility. At 11.3 CNT wt % sample, thermoelectric Power Factor (PF, where $PF = S^2\sigma$) was measured as $1.25 \mu\text{W}/\text{m}^2\text{K}^2$. After inducing an electric field during the solution process to enhance PF, SWCNTs were aligned in the P(VDF-TrFE) matrix. Therefore, σ was increased ($\sim 500 \text{ S/m}$) much higher than non-aligned samples, while S decreased slightly ($60 \mu\text{V}/\text{K}$) resulting in PF increase up to $1.79 \mu\text{W}/\text{m}^2\text{K}^2$. PF of this composite film remained above 97% even in a highly bent condition (at bending radius under 5 mm), and also remained more than 95% after the 10^5 cycles of the bending test. The freestanding and flexible P(VDF-TrFE)-SWCNT composite films can be attached to any surface and find applications in high-performance flexible thermoelectrics such as wearable devices. To fabricate the thermoelectric composite film, various amounts of powder-type SWCNTs were dispersed in N, N-dimethylformamide (DMF) by magnetic stirring. P(VDF-TrFE) powder was added to the suspension and dissolved. After 24 hours of stirring at room temperature, the suspension was poured into Teflon mold and dried on a hot plate at 60°C under an AC voltage. After 24 hours of drying, P(VDF-TrFE)-CNT sheet is fully dried and peeled off from the mold to be cut into a piece. Raman spectroscopy was used to investigate the alignment of CNTs, and a semiconductor characterization system (Keithley 4200) and Seebeck measurement system was used for the electrical measurement. Differential scanning calorimeter (DSC) and an in-plane thermal diffusivity tester was measured to calculate κ of the film.

EQ01.03.22

SiGe and Mg₂Si Nanostructured Fibers as Thermoelectric Materials for Energy Harvesting Carolina Duque Sierra¹, Jose M. Sojo Gordillo¹, Merce Pacios², Alex Morata¹ and Albert Taracón¹; ¹Catalonian Institute of Energy Research, Spain; ²Universitat Autònoma de Barcelona, Spain

The enormous increase in energy demand for expanding the internet of things (IoT) to create more sustainable cities and communities has led to a much-needed boost in energy sources for low-power microelectronics. Thermoelectric (TE) materials present a versatile and environmentally beneficial option to harvest energy from ambient waste heat to power this transition. Moreover, thanks to nanostructurization, commonly poor TE materials (i.e., silicon) have remarkably enhanced their TE properties; this is the case for nanowires and Si-based fabrics made of nanotubes. Nonetheless, the scalability of Si-based nanostructured materials remains a challenge.

The present work studied Silicon-alloys (SiGe and silicides) nanotube-based fibers due to their integrability in the electronics industry and the abundance and low extraction environmental impact of the herein-used materials. Most importantly, the fabrication of TE nanotubes was up-scaled to large areas. The nanotube-based fabric was fabricated using an electrospun fiber template and chemical vapor deposition (CVD) in a bottom-up approach, allowing the tailoring of the orientation and thickness of nanotubes and the final fabric.

Different strategies to improve Silicon-alloys performance as

TE materials were explored in order to optimize their *Figure of Merit*, $zT = S^2\sigma/\kappa$. The thermal conductivity, κ , was tuned by rapid thermal treatments (RTP) techniques and studied employing Laser Flash Measurements; the Seebeck coefficient, S, was modified by varying the ratio between silicon and the alloying elements and characterized using Seebeck-coefficient equipment. We have also studied the change of the electrical conductivity, σ , by controlling the material's doping and the thickness of the nanostructures. Likewise, a complete morphological and compositional characterization was performed using electron microscopy techniques, EDX, and XRD.

Thus, the suitability of electrospinning and CVD to fabricate large-area TE materials was successfully accessed. Furthermore, the TE properties were investigated, and steps to optimal morphology and compositional conditions of the Si-alloy materials were found.

EQ01.03.23

Effects of PEDOT:PSS Microstructure on the Charge Transport and Thermoelectric Properties Juhyung Park¹, Jae Gyu Jang², Sung Hyun Kim² and Jeonghun Kwak¹; ¹Seoul National University, Korea (the Republic of); ²Wongkwang University, Korea (the Republic of)

Conducting polymer-based thermoelectric (TE) device, which can harvest low temperature waste heat, have great potentials as energy sources for operating various low-power electronic devices. Among various conducting polymers, poly(3,4-ethylenedioxythiophene):poly(styrenesulfonate) (PEDOT:PSS) is one of the most attracting candidates owing to its high electrical conductivity, solution processability, flexibility, and air stability. Various post-treatments have been introduced to increase the thermoelectric properties of the PEDOT:PSS films. These methods have been known to change the crystallinity and relative PSS composition of the PEDOT:PSS films, which determines charge transport. However, how both the crystallinity and composition of the PEDOT:PSS films correlated to their charge transport and thermoelectric properties has not been intensively studied. Here, we present the interdependence of the microstructure (i.e. crystallinity and PSS composition), charge transport and TE properties using PEDOT:PSS films post-treated with various methods. The crystallinity and the composition of the PEDOT:PSS films were carefully characterized with both the grazing incidence wide angle spectroscopy (GIWAXS) and X-ray photoelectron spectroscopy (XPS). The charge transport properties of the films were investigated using theoretical models and the temperature-dependent electrical conductivity.

EQ01.03.25

Preparation and Characterization of Cu-Te Phases Synthesized by Focused Ion Beam Method Nils Braun¹, Vladimir Roddatis², Agnes Mill¹, Sonja Cremer¹, Hagen Bryja¹, Lennart Voß³, Suyang Sun⁴, Lorenz Kienle³, Wei Zhang⁴ and Andriy Lotnyk^{1,5,6}; ¹Leibniz Institute of Surface Engineering (IOM), Germany; ²GFZ German Research Centre for Geosciences, Germany; ³University of Kiel, Germany; ⁴Xi'an Jiaotong University, China; ⁵The Research Institute of Advanced Technologies, China; ⁶Harbin Engineering University, China

Specimen preparation for transmission electron microscopy (TEM) using focused ion beam (FIB) is a commonly used method [1]. An advantage over other methods is site specific specimen preparation that only damages a small area of the sample. However, it also suffers from many disadvantages. Artifacts induced by FIB range from ion implantation and resulting amorphization to thermal effects like phase transitions [2,3]. In this work, we prepared different nanoscale Cu-Te phases from Cu (electrodes) - Sb₂Te₃ (thin films) system [4] using FIB method. Copper chalcogenides have shown promising thermoelectric properties, e.g. high efficiency and tunability, which are key motivations for research on these materials [5].

Sb₂Te₃ thin layers with thicknesses of 17 or 100 nm are epitaxially grown on p-type Si (111) substrates. Samples with a 24 nm thick polycrystalline Sb₂Te₃ thin film are grown on a SiO₂ coated wafer using pulsed laser deposition (PLD) [4]. Cu, Pt/Cu and Cr layers are deposited by magnetron sputtering on top of the Sb₂Te₃ layers. TEM specimens are prepared at varied beam currents using a standard cross-section FIB preparation method [1]. Ion beam parameters are varied and lowered up to 15 kV, 250 pA for the trenching step before lift out. FIB specimens are investigated using advanced methods of aberration-corrected scanning TEM such as atomic-scale HAADF imaging and atomic-scale chemical analysis (EDX and EELS). In situ x-ray diffraction heating of

the Cu-Sb₂Te₃ thin film is performed to confirm structural changes.

Dependent on beam current used during FIB lamella preparation and Sb₂Te₃ layer thickness, hole formation in the Cu layer, thickness change and chemical changes of the Sb₂Te₃ layers are observed. Layer thickness after FIB specimen prepared at normal milling parameters are 28 nm and 23 nm for reduced parameters in a sample with originally 17 nm Sb₂Te₃. Hole formation is also decreased indicating less material transport. The structural changes are confirmed by in situ x-ray diffraction heating in addition. Samples with a 17 nm Sb₂Te₃ layer showed uniform intercalation of Cu while a sample with 100 nm thick Sb₂Te₃ layer exhibited differential intercalation behavior. In specimen prepared from the in situ heated samples Sb₂Te₃ and Cu-Te grains are observed. The introduction of a Pt layer between the Cu electrode and Sb₂Te₃ layers hindered structural changes caused by FIB. The same effect is observed in the heated sample where a Sb layer was formed between the Cu and Sb₂Te₃ layer. Moreover, Cr-Sb₂Te₃ and a Cu-GeTe layer systems showed no modifications of Sb₂Te₃ and GeTe thin films during FIB preparation. In polycrystalline Sb₂Te₃ specimen the intercalation of Cu and formation of new Cu-Te phases was also observed. Here a formation of a tetragonal Cu₂Te phase is found.

This work shows that structural changes in Sb₂Te₃ thin film systems can be induced during FIB specimen preparation of Cu (electrode)-Sb₂Te₃ (thin films) systems. The influence of different factors such as ion beam current, layer stacking sequence, Sb₂Te₃ structure and layer thickness on the formation of Cu-Te phases are evaluated. The changes are thermally induced transitions caused by FIB process, while redeposition of Cu plays a minor role. Similar thermal effects can be observed in heated samples. Other studied systems show no modifications.

Acknowledgements

The authors thank P. Hertel for magnetron sputtering. We acknowledge the financial support by the German Research Foundation (DFG 448667535).

References

- [1] T. Ishitani, et al., *Microscopy* 43 (1994) 322
- [2] J. Mayer, et al., *MRS Bull.* 32 (2007) 400
- [3] R. Schmied, et al., *Phys. Chem. Chem. Phys.* 16 (2014) 6153
- [4] H. Bryja, et al., *2D Materials* 8 (2021) 045027
- [5] T. Wei, et al., *Science China Mater.* 62 (2019) 8

SESSION EQ01.04: Progress in Inorganic Materials—Physics, Design and Characterization I

Session Chairs: Gabi Schierning and Alexandra Zevalkink

Tuesday Morning, November 29, 2022

Sheraton, 2nd Floor, Back Bay A

8:30 AM *EQ01.04.01

Electron Band Engineering for Thermoelectric Semiconductors G. J. Snyder; Northwestern University, United States

Thermoelectric semiconductors typically have complex electronic band structures as it leads to improved performance. This complexity arises from orbital chemistry as well as structure. Band inversion and warping can also lead to complex band structures and unusual electronic properties beyond thermoelectrics such as topological insulating behavior.

The DOS and transport effective masses are commonly used to describe electronic transport in semiconductors using a classical analogy to the kinetic theory of gasses. The Seebeck coefficient can be used conductivity and Hall measurements to characterize the DOS mass [1] and DOS weighted mobility [2] to provide direct experimental characterization of DOS and mobility at room temperature and above. In materials with complex electronic structures the DOS and inertial masses can vary significantly. For example, in many valley electronic structures such as PbTe, with N_v isolated valleys in the Fermi surface, the DOS mass can be high and inertial mass low for high thermoelectric quality factor. High valley degeneracy has been found in many high zT systems such as Bi₂Te₃, Mg₂(Si,Sn), CoSb₃ skutterudites and some Half Heuslers.

In some systems the Fermi surface pockets can be anisotropic and even non-ellipsoidal, such as the tubes of Fermi surface found in SrTiO₃. Tubes or sheets of Fermi surface rather than ellipsoidal pockets leads to a density of states like 1D or 2D low dimensional materials. By engineering the orbital chemistry complex behavior and unusual properties can be devised even in 3D materials.

9:00 AM EQ01.04.03

Discovery and Characterization of an Off-Stoichiometric Stability Region in Combinatorial (Nb,Ta)FeSb Half Heusler Thin Films Dylan J. Kirsch^{1,2}, Joshua Martin¹, Nathan Johnson^{3,4}, Rohit Pant², Ichiro Takeuchi² and Apurva Mehta⁴; ¹National Institute of Standards and Technology, United States; ²University of Maryland, United States; ³Stanford University, United States; ⁴SLAC National Accelerator Laboratory, United States

The NbFeSb ternary system is one of the higher performing p-type Half Heusler (HH) thermoelectrics but has a relatively high thermal conductivity. Several theoretical and experimental reports suggest that forming a solid solution mixture between Nb and Ta could lower lattice thermal conductivity without negatively affecting the electrical transport. Experimental investigations have studied (Nb,Ta)FeSb solid solution mixtures up to (Nb_{0.6}Ta_{0.4})FeSb, which is the Nb/Ta ratio that was found to exhibit the highest thermoelectric figure of merit. However, the effects of an excess or a deficit of Fe or Sb on both the electrical and thermal transport properties have been largely unexplored. There could be additional alloy stoichiometries with more optimized properties. Combinatorial thin film deposition provides an efficient route to synthesize a wide range of stoichiometries on a single substrate, enabling rapid screening of composition/structure/transport property relationships. Here we used combinatorial sputter deposition to investigate thin film mixtures of Sb, Fe, and a Ta_{0.4}Nb_{0.4}Ti_{0.2} alloy target. Room temperature electrical and thermal transport properties were mapped as a function of atomic composition (micro-X-ray Fluorescence) using our custom-built suite of high-throughput measurement instrumentation, which includes a scanning Seebeck coefficient and 4-probe resistivity probe, and a scanning frequency domain thermoreflectance (FDTR) instrument. The structural properties were examined using a high throughput synchrotron X-ray diffraction (XRD) at Stanford Synchrotron Radiation Lightsource. Rietveld refinement of the single phase XRD patterns provide key insights into the role of excess Fe or Sb on the site occupancy and atomic ordering of the HH phase and the resulting electrical and thermal transport properties. A region of off-stoichiometric HH phase stability was identified that exhibits electrical and thermal transport properties which agree with bulk values reported in literature.

9:15 AM EQ01.04.04

Low Thermal Conductivity and Thermoelectric Performance of Zintl Yb₁₀MnSb₉ Leah E. Borgsmiller and G. J. Snyder; Northwestern University, United States

The recently discovered Zintl compound $\text{Yb}_{10}\text{MnSb}_9$ is a thermoelectric material very close in compositional space to high performing materials such as $\text{Yb}_{14}\text{MnSb}_{11}$ and $\text{Yb}_{21}\text{Mn}_4\text{Sb}_{18}$, making it an interesting candidate for high temperature thermoelectric applications. While others have characterized this material's crystal structure, here we measure and report electronic and thermal transport data for bulk polycrystalline $\text{Yb}_{10}\text{MnSb}_9$ up to 825K. We show that this material has ultralow thermal conductivity, likely due to the previously reported complicated crystal structure with partial occupancies. This ultralow lattice thermal conductivity in conjunction with a higher Seebeck coefficient than in other Yb-Mn-Sb compounds, leads to a moderate zT (thermoelectric figure of merit) of about 0.34 at 825K and is likely to peak at a higher value via material optimization. We approximate a bandgap of about 0.4 eV and expect the zT to be able to reach values as high as 0.33 at 725K given adequate doping (which is comparable to $\text{Yb}_{14}\text{MnSb}_{11}$ at that temperature) using a thermoelectric quality factor analysis. Additionally, we suspect that the zT has the potential to reach even higher values by improving the quality factor, B , through grain boundary engineering making it possible to surpass performance of $\text{Yb}_{14}\text{MnSb}_{11}$. Here we provide suggestions for future studies to improve thermoelectric performance. We also suggest that other undiscovered 10-1-9 Zintl compounds with thermoelectric potential likely exist, particularly $\text{Yb}_{10}\text{MgSb}_9$. This work is the first report of thermal conductivity, approximate bandgap, and zT for this $\text{Yb}_{10}\text{MnSb}_9$ compound, and we discuss implications of this material for future thermoelectric study through comparisons to the leading $\text{Yb}_{14}\text{MnSb}_{11}$ material.

9:30 AM EQ01.04.05

High-Entropy Chalcopyrite Materials with Ultralow Thermal Conductivity [Somnath Acharya](#)¹, Junphil Hwang², Kwangrae Kim¹, Woohyun Hwang¹, Aloysius Soon¹ and Woochul Kim¹; ¹Yonsei University, Korea (the Republic of); ²Ewha Womans University, Korea (the Republic of)

Currently, high-entropy alloys are of great interest in material science and engineering research. Unlike conventional alloys, which consist of two or three elements, high-entropy alloys contain multiple principal elements to form a single-phase solid solution with stable crystal structures. Because of its high configuration entropy, high-entropy materials can be more stable at elevated temperatures due to the minimization of Gibbs free energy ($G = H - TS$, where H is enthalpy, S is entropy, and T is temperature). In the context of thermoelectric material, the performance can be greatly improved by optimizing the entropy through lattice thermal conductivity suppression and via improving the crystal structure symmetry resulting in large Seebeck coefficients. Chalcopyrite compounds [(Cu/Ag)(In/Ga)Te₂] have been considered a promising thermoelectric material with high Seebeck coefficients and decent electrical conductivity. Here, we have studied CuGaTe₂-based multicomponent chalcopyrite to investigate their thermal and electrical transport properties. The major drawback of the CuGaTe₂-based compound is high lattice thermal conductivity due to its diamondoid structure. In this study, we observe that Ag and In alloying in $\text{Cu}_{1-x}\text{Ag}_x\text{Ga}_{0.8}\text{In}_{0.2}\text{Te}_2$ leads to the enhancement of power factor and significantly reduces the lattice thermal conductivity. The transport studies and DFT calculation suggest that the power factor enhancement can be justified by the increase of charge carriers while the low lattice thermal conductivity has been explained through a strong phonon coupling between low-frequency optical phonons and heat-carrying acoustic phonons. Additionally, manipulating the configuration entropy via introducing Zn in $\text{Cu}_{1-x}\text{Ag}_x\text{Ga}_{0.8}\text{In}_{0.2}\text{Te}_2$, lowers further lattice thermal conductivity to ~ 0.38 W/m-K at 850 K due to the strengthening of phonon scattering. Therefore, entropy engineering leads to significance improved thermoelectric performance of CuGaTe₂-based material.

9:45 AM BREAK

10:15 AM *EQ01.04.06

Opportunities in Nanoscale and Nanocomposite Thermoelectrics [Ali Shakouri](#); Purdue University, United States

An overview of thermoelectric effects in nanoscale devices and in bulk nanocomposites will be given. Some of the key ideas to increase the material figure-of-merit and the impact on the performance metrics of the energy conversion devices and systems are described. The role of geometry, dimensionality and non-equilibrium effects will be discussed.

10:45 AM EQ01.04.07

Defect Chemistry of Promising N-Type Thermoelectric $\text{Y}_2\text{Ti}_2\text{O}_5\text{S}_2$ [Katarina Brlec](#) and David O. Scanlon; University College London, United Kingdom

One of the many pathways to decreasing the impact of climate change is to increase the efficiency of current fossil fuel based systems. Even the best internal combustion engines suffer from thermal losses where up to 70% of energy is lost as exhaust heat. These losses can be offset to an extent by thermoelectric devices which convert waste heat into useful electrical energy via the Seebeck effect. The efficiency of thermoelectric materials is typically evaluated using the figure of merit (ZT), with some of the best performing materials reaching ZTs of > 2 . [1] However, current state-of-the-art thermoelectric materials contain rare or toxic materials, making them commercially unappealing.

$\text{Y}_2\text{Ti}_2\text{O}_5\text{S}_2$ has been experimentally and computationally studied as a potential battery anode and photocatalyst for water-splitting. [2-4] Our recent work shows the intrinsically n-type $\text{Y}_2\text{Ti}_2\text{O}_5\text{S}_2$ is also a promising high temperature thermoelectric, with ZT exceeding 1 above 850 K at charge carrier concentrations of 10^{19} – 10^{20} cm⁻³. [5] Using hybrid density functional theory we investigate the intrinsic defect chemistry to determine the doping potential. Select n-type extrinsic dopants were considered to establish whether the charge carrier concentrations required for high ZT are indeed achievable.

[1] L. D. Zhao, S. H. Lo, Y. Zhang, H. Sun, G. Tan, C. Uher, C. Wolverton, V. P. Dravid and M. G. Kanatzidis, *Nature*, 2014, **508**, 373–377.

[2] K. McColl and F. Corà, *J. Mater. Chem. A*, 2021, **9**, 7068–7084.

[3] G. Hyett, O. J. Rutt, Z. A. Gál, S. G. Denis, M. A. Hayward and S. J. Clarke, *J. Am. Chem. Soc.*, 2004, **126**, 1980–1991.

[4] Q. Wang, M. Nakabayshi, T. Hisatomi et al., *Nat. Mater.*, 2019, **18**, 827-832.

[5] K. Brlec, K. B. Spooner, J. M. Skelton, D. O. Scanlon, *in submission*. Preprint at 10.26434/chemrxiv-2022-zk09d

11:00 AM EQ01.04.08

New High Performance N-Type Bi₂Te₃-Based Thermoelectric Systems [In Chung](#); Seoul National University, Korea (the Republic of)

Bi_2Te_3 has served as a representative thermoelectric system operating near the room temperature regime. It has been extensively studied to obtain higher thermoelectric figure of merit, ZT. However, there are two major tasks that have to be addressed for broad commercial application of this material system. First, effective doping or alloying for Bi_2Te_3 is so difficult that only few related phases show high thermoelectric performance. As a result, efficient performance-enhancing strategies have been developed in comparison with PbQ (Q = chalcogen) which is a canonical thermoelectric system for intermediate temperature range (500 – 900 K). Second, its n-type performs much inferior to the p-type counterpart, making it challenging to develop their high performance thermoelectric devices. In this presentation, I will present new synthesis methods to stabilize a wide range of new Bi_2Te_3 -based materials. The temperature of a peak ZT can be readily tunable by changing the chemical composition of these series systematically. The best composition exhibits a ZT greater than 1.4, a record-high for n-type thermoelectric materials around atmosphere temperature.

11:15 AM DISCUSSION TIME

11:30 AM EQ01.04.10

Investigating the Effects of Defect Energetics on Phase Boundaries Shapes Adeyoye H. Adekoya and G. J. Snyder; Northwestern University, United States

Thermoelectric (TE) devices which offer a route for energy recovery/production often need to be optimized by doping with other elements to improve the thermoelectric figure of merit (zT), which qualifies the device's efficiency. The solubility of these elements in the bulk system is usually in such dilute concentrations that they can best be described as 0-D defects in an otherwise essentially uniform crystal. Though dilute, the defects can nevertheless be visualized on a phase diagram as providing some width to nominally single-phase regions or so-called line compounds. The width of these phases is known to be set directly by the defect energy of the defects, however, little attention is paid to the shape of these regions despite the fact that the shape of the region directly sets the solubility limits and thus the maximum concentration of defects in addition to providing an understanding of the dominant defects in that system. We discuss the thermodynamic factors that impact the shape of the phase diagrams and show how they can provide a guide to the optimal doping of semiconductors.

SESSION EQ01.05: Progress in Inorganic Materials—Physics, Design and Characterization II

Session Chairs: Ali Shakouri and G. Snyder

Tuesday Afternoon, November 29, 2022

Sheraton, 2nd Floor, Back Bay A

1:30 PM *EQ01.05.01

High-Temperature Elastic Moduli—A Tool for Understanding Chemical Bonding and Thermal Transport in Thermoelectric Materials Alexandra Zevalkink; Michigan State University, United States

Measurements of elastic moduli, in particular as a function of temperature, can play a key role in interpreting trends in lattice thermal conductivity. In addition to providing an accurate measure of sound velocity, the elastic moduli can be used to estimate a thermodynamic Grueneisen parameter using several different approaches. As a case study, this presentation will focus on high-temperature resonant ultrasound spectroscopy measurements of GeSe-AgBiSe₂ alloys. Recently, alloys between IV-VI and I-V-VI₂ semiconductors have been the object of intense investigations, owing to reports of lone-pair induced anharmonicity, ferroelectric instabilities, and spontaneous formation of nanostructures, all of which can contribute to their low thermal conductivity. The GeSe-AgBiSe₂ system is of interest because, within a narrow compositional window, the crystal structure progressively transitions from an orthorhombic structure (*Pnma*), to rhombohedral (*R3m*), to cubic rock salt (*Fm-3m*), with marked consequences on the lattice thermal conductivity. By studying the elastic behavior of the GeSe-AgBiSe₂ system, we can decouple the impact of composition and crystal structure on the sound velocities and phonon scattering rates. Within a given structure type, alloying with Ag and Bi leads to both softening and increased point-defect phonon scattering. However, the transition from rhombohedral to cubic symmetry causes a drastic step-like increase in the elastic moduli, and a corresponding increase in thermal conductivity. Overall, an improved understanding of the elasticity and anharmonicity of complex rock salt alloys may be useful in guiding the design of thermoelectric materials with tailored thermal properties.

2:00 PM EQ01.05.02

Thermoelectric Properties of Thin Film of Metal Chalcogenides Grown on Flexible Substrate by MOCVD and Role of Energy Filtering at Grain Boundaries Giuseppina Pace^{1,2}, Arun Kumar^{1,3}, Pietro Rossi², Mario Caironi², Jean-Luc Battaglia⁴ and Claudia Wiemer¹; ¹Consiglio Nazionale delle Ricerche, Italy; ²Istituto Italiano di Tecnologia, Italy; ³Università degli Studi di Salerno, Italy; ⁴Université de Bordeaux, France

In many industrial processes more than 60% of the energy consumption is wasted into heat. [1] Recovery such heat as well as providing new solution for heat conversion into electricity is a “must be done” effort to contribute to novel green energy solution. This compelling request for sustainable and environmentally friendly energy supplies is driving the study of novel materials to be integrated into thermoelectric generators (TEGs). TEGs have attracted great interest in diverse fields, ranging from electronics to energy storage and conversion. Commercial TEGs are mostly based on bulk thermoelectric materials, providing flat and rigid module devices. However, to enlarge the field of application of such technology, such as micro-cooling ability for solving heat dissipation issues in electronics and light mobile devices for harvesting human body heat, the thermoelectric properties of thin film need to be improved and further investigated. Furthermore, curved and flexible module devices, offer potential for conformable devices enabling the versatile energy harvesting from heat sources of arbitrary geometries. [2]

Here we investigate the thermoelectric properties of Sb₂Te₃ thin films based on phase change metal chalcogenides deposited by Metalorganic Chemical Vapour Deposition (MOCVD) on flexible substrates. [3,4] Differently from other deposition techniques MOCVD enables large area applications, and it is therefore prone to scalable application. The Sb₂Te₃ thin-film growth on the flexible substrate is not commensurate, nevertheless good crystallinity is achieved and an out of plane 001 preferential orientation is achieved also at room temperature. We observed that the electrical and thermal properties of the flexible thin film are preserved even after mechanical stress cycling.

The improvement of the Seebeck coefficient and the increased electrical conductivity following thermal annealing is explained in terms of an energy filtering effect, induced by the formation of larger Sb₂Te₃ crystalline domains contoured by a Te poor boundary phase. Our work highlights the importance of acquiring fundamental knowledge on the proper design of the boundary states and on the optimal interphase engineering, that can reveal to be key aspects to be controlled for the further improvement of thermoelectric performances of novel materials.

References:

- [1] Zeb *et al*, *Renewable and Sustainable Energy Reviews*, **2017**,75, 1142–1155.
- [2] Fan *et al*, *Renewable Sustainable Energy Reviews* **2021**, 137, 110448
- [3] Longo *et al*, *Adv. Mater. Interfaces* **2020**, 7, 2000905.
- [4] Cecchini *et al*, *Small* **2019**, 15, 1901743

2:15 PM EQ01.05.03

Investigating the Role of Vacancies on the Structure, Bonding and Thermoelectric Properties of EuCu_{1-x}Zn_xSb Sevan Chanakian and Alexandra Zevalkink; Michigan State University, United States

The ZrBeSi structure type, consisting of alternating planar hexagonal nets intercalated by a cation layer, can accommodate large vacancy concentrations - up to 50% of the metal species which help form the hexagonal nets. Their tolerance for disorder and varying structural complexity provide routes to

amorphous-like lattice thermal conductivity, making them exciting for thermoelectric applications. Here, we investigate the impact of vacancies on the temperature dependent structural, thermal, and electronic properties of $\text{Eu}_2\text{M}^{1+}_{2x}\text{M}^{2+}_{1-x}\text{Sb}_2$ ($\text{M}^{1+} = \text{Cu}$, $\text{M}^{2+} = \text{Zn}$). The transition from a fully-occupied hexagonal net to one with a quarter of the atoms missing has wide-ranging consequences, particularly for the structural and phononic properties. With increasing vacancy concentration, we observe a non-linear expansion of the hexagonal net and simultaneous contraction in the perpendicular direction. Despite the absence of long-range ordering, pair distribution function analysis from synchrotron X-ray diffraction reveals significant local structural distortions caused by M -vacancies, which leads to strong phonon scattering. It is observed that while the fully-ordered compound, EuCuSb , is a stiff material with moderate thermal conductivity, its half-filled analogue, $\text{EuZn}_{0.5}\text{Sb}$ exhibits soft bonding which corresponds to the decrease in sound velocity. This, combined with increased scattering, leads to a precipitous drop in lattice thermal conductivity in the vacancy-rich $\text{EuZn}_{0.5}\text{Sb}$ samples (0.6 W/mK and 300K). The connection between structure, bonding and electronic properties are not as straightforward. Models incorporating different scattering mechanisms paint varied pictures into the compositional trends in electronic properties, particularly the mobility. These varied explanations of experimental observations warrant further investigation to truly understand how the stability of the planar hexagonal nets influences the electronic properties in the ZrBeSi family of materials.

2:30 PM EQ01.05.04

Metrology, Certification and Release of SRM 3452—High-Temperature Seebeck Coefficient Standard (295 K to 900 K) Joshua Martin¹, Zhan-Qian Lu¹, Winnie Wong-Ng¹, Sergiy Krylyuk¹, Dezhi Wang² and Zhifeng Ren²; ¹National Institute of Standards and Technology, United States; ²University of Houston, United States

To enable instrument validation and interlaboratory data comparison at high temperatures relevant to thermoelectric waste heat recovery, we have completed the development and certification of Standard Reference Material (SRM) 3452: *High-Temperature Seebeck Coefficient Standard (295 K to 900 K)*, now available to the public. SRM 3452 is bar-shaped p-type boron-doped polycrystalline silicon-germanium alloy with a nominal composition of $\text{Si}_{80}\text{Ge}_{20}$. For the SRM 3452 material, we describe the synthesis, anneal-quench procedure, and structural and physical characterization. For the certification measurements, we describe the custom measurement instrumentation, measurement protocols, statistical analysis, the certified Seebeck coefficient values, comprehensive uncertainty budgets, and metrological traceability. Our extensive efforts to identify, reduce, and quantify measurement uncertainties will be emphasized. SRM 3452, together with complimentary SRM 3451: *Low-Temperature Seebeck Coefficient Standard (10 K to 390 K)*, now provide certified reference materials traceable to the International System of Units for Seebeck coefficient measurements within the temperature range 10 K to 900 K with a broad overlap region (295 K to 390 K).

2:45 PM EQ01.05.05

Precision Interface Engineering by ALD in CuNi Alloys Towards High Thermoelectric Performance Shiyang He, Amin Bahrami and Kornelius Nielsch; Leibniz Institute of Solid State and Materials Science, Germany

Phase boundaries play a critical role in the carrier/phonon transport in thermoelectric materials. Herein, a novel technique for surface engineering of thermoelectric materials based on powder atomic layer deposition (pALD) of single/multi-layers of second phase on CuNi powders is presented. Ultrathin layers of various oxides (10–100 cycles of ZnO and Al_2O_3) are uniformly formed on the surface of CuNi alloy particles to validate or refute this idea. The formation of energy barriers and hierarchical interface modifications emerge from the deposition of ZnO/ Al_2O_3 layers, leading in a considerable increase in the Seebeck coefficient. Although there is a slight decrease in electrical conductivity after 50 ALD cycles of ZnO, the increased Seebeck coefficients compensate for the loss and result in a 45% increase in power factor when compared to the pristine sample. In addition, the ZnO/ Al_2O_3 /ZnO multilayer structure was designed to improve electrical resistance at phase boundaries. In coatings with a high cycle number of samples (> 25 cycles ZnO/5 cycles Al_2O_3 / 25 cycles ZnO cycles), the multi-layer structure retained an enhanced power factor while dramatically reducing heat conductivity. At 673 K, a maximum figure of merit (zT) of 0.22 was attained in 44 cycles ZnO/11 cycles Al_2O_3 / 44 cycles ZnO cycles multi-layer samples. When compared to pure CuNi, the zT value increased 144% due to pALD decoupling of thermoelectric parameters, which is comparable to the highest value ever recorded. The pALD technique to surface modification may readily be extended to different thermoelectric materials, assisting in the creation of high-performance thermoelectric materials.

3:00 PM BREAK

3:30 PM *EQ01.05.06

Interface-Dominated Topological Transport in Nanograined Bi_2Te_3 Gabi Schierning¹, Sepideh Izadi¹, Sarah Salloum², Ahana Bhattacharya², Jeong W. Han², Lauritz Schnatmann¹, Stephan Schulz^{2,2} and Martin Mitterdorff²; ¹Bielefeld University, Germany; ²University of Duisburg-Essen, Germany

Bismuth telluride is an excellent thermoelectric material and also belongs to the class of three-dimensional topological insulators. Therefore, surface charge carriers with extremely high mobility exist at the crystal surfaces. This is particularly visible in nanoparticulate samples, provided that the nanoparticles used have sufficient surface purity. Compacted nanoparticulate bulk samples exhibit a high density of interfaces. These samples show a pronounced weak anti-localization in the low-temperature transport behavior as well as a kink in the electrical resistance at about 5 K. Evaluation of the magnetotransport data using the Hikami-Larkin-Nagaoka model yields coherence lengths of up to 200 nm, which is significantly larger than the average grain size in the studied samples. Using terahertz spectroscopy, the average mobility of the surface charge carriers can be estimated to be about 1000 to 10000 $\text{cm}^2\text{V}^{-1}\text{s}^{-1}$ at room temperature. This means that good thermoelectric properties of nanoparticulate Bi_2Te_3 near room temperature are also determined in part by the existence of surface charge carriers.

4:00 PM EQ01.05.08

Phonon Channel Engineering Through Crystal Chemistry and Defects Matthias T. Agne; WWU Münster, Germany

Effective control over thermal transport is often a limiting factor in the development of energy efficient thermal/optical/electronic devices, especially thermoelectric materials that require ultra-low thermal conductivity. In the classic theory of thermal transport by atomic vibrations (phonons) in crystalline materials, heat moves in a manner analogous to a gas, described by a velocity and by scattering events. This is known as the phonon gas model. Thermal transport in amorphous materials is fundamentally different, where heat moves in a manner analogous to an atomic-scale random walk. These phonons can be called diffusons. Only recently have these two perspectives been unified within one theoretical framework, which subsequently shows that phonons in complex crystalline materials can exhibit both gas-like and diffuson-like character. Effective tuning of thermal conductivity thus requires an understanding of both transport “channels.” This talk will discuss materials design strategies in the context of two-channel transport. It will be shown that many ultralow thermal conductivity materials likely have both types of phonon transport, whose relative contributions depend strongly on temperature. Furthermore, factors like chemical composition and material defects may be used to prefer or suppress one channel or the other. This is experimentally demonstrated in several novel thermoelectric materials such as silver argyrodites.

4:15 PM EQ01.05.09

Bipolar Doping of Diamond-Like Semiconductor Hg₂GeTe₄ [Claire Porter](#)¹ and Jiaying Qu²; ¹Colorado School of Mines, United States; ²University of Illinois at Urbana-Champaign, United States

We are in era of unprecedented materials discovery, ushered by the development of rich computational techniques to generate new compositions and structures. However, to create useful state of the art electronic devices, many of these discovered semiconductor compounds require doping to obtain an optimal electronic carrier concentration. In this work, we conduct a thorough investigation of the extrinsic doping of recently discovered candidate thermoelectric material Hg₂GeTe₄, considering the presence of native defects, synthetic growth conditions, and dopant solubility limits.

We start by carrying out a computational analysis of 12 candidate extrinsic dopants, aiming to achieve both high p- and n-type carrier concentrations. Hg₂GeTe₄ is a recently discovered ordered vacancy compound with established regular vacancies in its crystal lattice; our doping strategy focuses on this large interstitial site as an opportunity to introduce donor defects (n-type doping) while suppressing compensating native defects through deliberate synthetic conditions. For p-type doping, we find that Hg-poor growth conditions offer a low energy entry to doping Group 11 dopants on the Hg site, introducing acceptor defects (p-type doping). Experimental results are in good agreement with computation, and we discover that even the most effective n-type dopants (Ga, Zn, In, Sc) are incapable of rendering Hg₂GeTe₄ n-type due to the discrepancy in electronic band effective mass (m_{DOS}^*) between its heavy valence and light conduction band. P-type doping is successful. While Hall data (carrier concentration, Hall mobility) are negative for our most successful n-type dopants, Seebeck coefficients are positive. These anomalous results point to the difficulty in bipolar doping in a material with widely different band masses.

P-type doping of Hg₂GeTe₄ is best realized with Group 11 dopants, of which Ag is the most successful (zT of 0.4 at 200°C). Au is also quite promising, however dopant solubility is impeded by the formation of AuTe₂. Doping Hg₂GeTe₄ with Ag results in the discovery of a Ag quaternary compound (currently undergoing structure/charge flipping analysis to determine the structure of this unknown compound). Cu forms a full solid solution with Hg₂GeTe₄ and has been well studied. We perform a thorough structural analysis of the compound and offer explanations for the different behavior of these 3 Group 11 dopants, including evidence of a C_{2v} distortion in Au-doped HGT analogous to the distortion observed in Au-doped silicon.

N-type doping is more difficulty due to the alloying of the dopant with binary impurity phases in Hg₂GeTe₄, in direct competition with formation of electron-donating defects. Zn, Se, and In are the best n-type dopants according to theory, and experiment confirms these predictions. N-type Hall carrier concentration is realized, but Seebeck coefficients are always positive, suggesting insufficient pushing of the Fermi level into the conduction band. This anomalous result has been well documented in other chemical systems.

Finally, doping strategies are offered for ordered vacancy compounds, where the presence of the vacancy can cause unwanted counter-doping. We also emphasize the importance of paying attention to m_{DOS}^* when attempting bipolar doping.

4:30 PM EQ01.05.10

Selenium Vapor Annealing in Multinary Cubic Selenides Reveals p-Type Dopability via Regulating Hole-Killer Antisite Defects [Hanwhi Jang](#)¹, Michael Toriyama², Stanley Abbey³, Brakowaa Frimpong³, James P. Male², G. J. Snyder², Yeon Sik Jung¹ and Min-Wook Oh³; ¹Korea Advanced Institute of Science and Technology, Korea (the Republic of); ²Northwestern University, United States; ³Hanbat National University, Korea (the Republic of)

Multinary ABX₂-type cubic chalcogenides have attracted significant attention as a promising thermoelectric material because of their intrinsically low lattice thermal conductivity. However, compared to conventional thermoelectric materials, the electronic transport properties of ABX₂ compounds are still poorly understood. For example, it is not clear what types of point defects generate excess carriers in these compounds, resulting in a time- and cost-consuming trial-and-error process for a material discovery. In addition, it is difficult to reproduce the thermoelectric properties of some ABX₂ compounds because the properties of these compounds are highly sensitive to the synthesis environment. Taking AgBiSe₂ as an example, the reported Seebeck coefficient ranges from -450 to 550 μ V/K, implying an uncontrolled carrier concentration and conduction type. Moreover, p-type conductivity of AgBiSe₂ is completely lost above 550 K, implying a generation of unknown hole-killer defects at an elevated temperature. Therefore, a systematic investigation of the electronic properties of these compounds is required. In this presentation, we reveal that Bi-on-Ag antisite defects (Bi_{Ag}) are responsible for low p-type dopability of AgBiSe₂-based cubic thermoelectric materials by first-principles calculations and experimentally demonstrate how to suppress those charged antisite defects via Se vapor annealing to achieve p-type conductivity in AgBiSe₂-based compounds. We rationalize the mechanism of Se vapor annealing to stabilize p-type conductivity by defect formation energy calculations which clearly show an increased Bi_{Ag} formation energy in Se-rich conditions. Moreover, we elucidate the importance of controlling self-doping via the annealing process to capture a signature of band convergence with alloying. This work will pave a way for rationalizing the electronic transport properties of several thermoelectric chalcogenides that suffer from significant phase boundary effects and uncontrolled properties.

SESSION EQ01.06: Device Design, Fabrication and Application I
Session Chairs: Saniya LeBlanc and Jae Sung Son
Wednesday Morning, November 30, 2022
Sheraton, 2nd Floor, Back Bay A

8:15 AM *EQ01.06.01

Distributed Transport Properties (DTP)—Optimally Structured Thermoelectric Material Maximizes Solid State Heat Pump Performance [Doug Crane](#), Bob Madigan and Lon Bell; DTP Thermoelectrics, United States

The novel and optimal structuring of spatially distributed transport properties (DTP) within thermoelectric (TE) elements is introduced and discussed. Using this structuring with currently available materials can produce TE systems with an increase in single-stage maximum temperature differential up to 35% in addition to up to 150% increase in coefficient of performance (COP) and up to 200% increase in heat pumping capacity. A conventional single-stage thermoelectric module operating in cooling mode has a maximum temperature difference of 73K (Th = 300K), whereas a two-stage cascaded device can increase this value up to 107K. One current manufacturer of conventional thermoelectric devices manufactures two-stage cascaded devices with maximum temperature differences that range from 86K to 101K. With DTP, a single-stage device can provide a comparable maximum temperature difference to the conventional two-stage cascaded devices with the potential to reach 100K. The creation of a position-dependent Thompson effect within the elements can partially offset detrimental distortion of the temperature profiles that Joule heating produces. This, combined with locally optimized thermal and electrical transport properties, increases TE element efficiency and thermal power pumping capacity. Closed-form analytic governing equations are presented for TE systems with optimally performing DTP. The unique behavior of DTP TE material systems is described: TE elements

incorporating available TE material with peak ZT at higher temperatures are used at the low temperature side in combination with material with peak ZT at colder temperatures at the high temperature side. Theoretical, numerical, and recent experimental results are reported that quantify performance improvements in maximum temperature difference, COP, and cooling capacity. The development of materials specifically optimized for DTP purposes is discussed along with their projected impact on TE device performance.

8:45 AM EQ01.06.02

Mastering Capillary Forces to Move Silicon Nanowires from Nano to Macro Dario Narducci, Stefano Magagna and Federico Giulio; University of Milano Bicocca, Italy

Silicon nanowires (SiNWs) have been a milestone in the exploitation of nanotechnology as a tool to develop efficient thermoelectric materials. By breaking the unfortunate tie between thermal and electric conductivity, the making of quasi-1D nanostructures let improve Si figure of merit (ZT) at room temperature from a meager 0.01 up to ≈ 1 [1, 2]. Nonetheless, usability of SiNWs in real-world devices has met the hurdles commonly encountered by nanostructures. As noted [3], for most applications thermoelectric devices need bulk materials, exchanging heat over large areas and across macroscopic distances. For SiNWs obtained by extreme lithography [2] this can be hardly obtained at acceptable costs. Instead, bottom-up approaches such as metal-assisted chemical etching (MACE) disclose the possibility of preparing wires with arbitrary lengths over large surfaces, enabling in principle full scalability from the nanoscale to macroscopic systems. However, on the MACE route three issues must be cleared, namely (1) the possibility of obtaining crystalline highly doped SiNWs; (2) the control of capillary forces bundling wires; and (3) the series resistance of the substrate. In this communication we report about the optimization of one-pot MACE to prepare SiNWs with lengths in excess to 0.1 mm [4]. Single-crystalline Si (100) wafers, both p and n-type with doping levels between 10^{15} and 10^{19} cm⁻³, were etched in HF/AgNO₃ solutions at temperatures between 15 and 25 °C. We show that, contrary to previous reports, highly doped SiNWs are crystalline, with an encapsulating amorphized layer of only a few nanometers [4] that may be successfully removed (when needed) by wet etching. Quite independently of the doping, as-prepared SiNWs display bundling because of the capillary forces due to the solvent-wire interaction, ultimately causing SiNWs to bind to each other at their free ends. When supported SiNWs are supposed to act as thermoelectric legs in a device, bundling degrades system performances, as it increases the electrical resistance per area unit. An easy procedure to minimize capillary forces and the subsequent folding of SiNWs will be presented, making a combined use of chemical etching to control SiNW hydrophilicity and of solvent of graded polarity to control solvent-surface interactions. Non-bundled SiNWs also display enhanced (lower) electrical and thermal contact resistances, enabling the fabrication of thermoelectric devices with the conventional II-type geometry [5]. However, capillarity is not always a negative feature. We will report for the first time about the making of unsupported, substrate-free Si ‘nanofelts’, where SiNWs are kept together by random bundling at their opposite ends. Lack of the series thermal and electric substrate resistance along with possibility of obtaining intertwined thick SiNW assemblies discloses exciting novel opportunities to scale thermoelectric nanosystems to the macroscopic scale.

S.M. acknowledges the support received by the Università Italo-Francese through the 2016 Vinci program, grant C3-132.

[1] A. I. Hochbaum, R. Chen, R.D. Delgado, W. Liang, E.C. Garnett, M. Najarian, A. Majumdar, P. Yang, Enhanced Thermoelectric Performance of Rough Silicon Nanowires. *Nature*, 451 (2008) 163.

[2] A.I. Boukai, Y. Bunimovich, J. Tahir-Kheli, J.K. Yu, W.A. Goddard, J.R. Heath, Silicon Nanowires as Efficient Thermoelectric Materials, *Nature*, 451 (2008) 168.

[3] J.P. Heremans, M.S. Dresselhaus, L.E. Bell, D.T. Morelli, When Thermoelectrics Reached the Nanoscale. *Nat. Nanotechnol.*, 8 (2013) 471.

[4] S. Magagna, D. Narducci, C. Alfonso, E. Dimaggio, G. Pennelli, A. Charaï, On the mechanism ruling the morphology of silicon nanowires obtained by one-pot metal-assisted chemical etching, *Nanotechnology*, 31 (2020) 404002.

[5] S. Elyamny, E. Dimaggio, S. Magagna, D. Narducci, G. Pennelli, High Power Thermoelectric Generator Based on Vertical Silicon Nanowires, *Nano Lett.*, 20 (2020) 4748.

9:00 AM EQ01.06.04

Direct Measurement of Peltier Coefficient in Thermoelectric Materials and Devices Mark Lee¹, Hari P. Panthi¹, Ruchika Dhawan^{1,2}, Orlando Lazaro², Andres Blanco² and Hal Edwards²; ¹The University of Texas at Dallas, United States; ²Texas Instruments, United States

Development of thermoelectric (TE) materials and device technology requires the ability to measure fundamental electrical and thermal physical properties such as electrical resistance (R), thermal conductance (K), Seebeck coefficient or thermopower (α) and Peltier coefficient (II) at both device and constituent material levels. The thermopower α governs TE generator operation and is routinely measured by the straightforward procedure of recording open-circuit voltage, V_{oc} , as a function of applied temperature difference ΔT across a sample. Although II is the property that governs TE cooler operation, it is rarely actually measured because of difficulties isolating the Peltier heat flow, III , from often much larger non-Peltier heat sources and flows such as Joule heating, I^2R , and passive Fourier thermal conduction $K\Delta T$, where I is the electrical current through a sample. Instead, the value of II is almost always inferred from the measured α using a theoretical Kelvin relation $II = \alpha T$, where T is the absolute temperature. We recently developed a method for directly and independently determining II on any TE material or device via measurements of the short-circuit current, I_{sc} , and the difference in heat flows between a thermopile held in open-circuit versus short-circuit conditions. This method has several advantages over previous Peltier coefficient measurements; it determines II solely from conventionally measured performance parameters, self-corrects for non-Peltier heat effects, does not require knowing any other material property values, is nondestructive, and does not assume validity of the Kelvin relation. We demonstrate this procedure by measuring II on Bi₂Te₃ near room temperature using a Bi₂Te₃ TE generator. Combined with an independent measurement of α on the same device under the same conditions, we can empirically verify consistency with the Kelvin relation under near-equilibrium conditions to good accuracy. Our method also permits testing the Kelvin relation in TE systems held far from equilibrium.

9:15 AM EQ01.06.05

Barium Titanate Based Materials for Intelligent Thermoelectric Converters with Dynamic Workload Management Mohammad Althehaiban¹, Andrey Berenov¹, Vladimir Getov² and Peter K. Petrov¹; ¹Imperial College London, United Kingdom; ²University of Westminster, United Kingdom

Mobile devices are nowadays an all-pervasive technology. Their number is expected to reach 17.72 billion worldwide by 2024, an increase of 3.7 billion devices compared to 2020 levels¹. A typical cell phone gives off around 0.2 Watts of heat when idle, and closer to a Watt while making a call or running processor-intensive applications. The heat generated by a tablet or laptop is much higher. Almost all this heat is never recovered.

Currently, high and medium-grade heat are the easiest to recover. In contrast, the low-grade heat is usually wasted in the environment, although, it is approximately more than 50% of the entire wasted heat². This is because i) the currently achieved efficiency of the heat to electricity conversion at these temperatures is very low and ii) because, under the condition of constant heat flux generation, it is challenging to maintain a temperature gradient (or heat oscillation) required for the operation of the conventional thermoelectric converters.

In this paper, we will present our latest achievements in developing barium titanate-based materials that could be used to build an intelligent thin film thermoelectric (TFTE) converter attached to a digital system/device with dynamic workload management.

We will review the requirements imposed on the active materials and will compare them with our current results. We will further discuss in detail

materials' structural properties examined using SEM and x-ray diffraction, and their dielectric properties (dielectric permittivity and P-E hysteresis loops) measured in a temperature range between 80-450K at frequencies up to 1MHz. Due to the small heat mass of our TFTE converter, it is possible to achieve a rapid heating-cooling cycle and therefore to recover substantial wasted heat per unit time.

References:

1. <https://www.statista.com/statistics/245501/multiple-mobile-device-ownership-worldwide/>.
2. I. Johnson, et al., (2008) Waste Heat Recovery, <https://tinyurl.com/wkuvftr>;

9:30 AM EQ01.06.06

Effects of Infill Pattern on Thermoelectric Transport in Extrusion-Based Additively Manufactured Elemental Ni and Bi Victoria J. Stotzer, Christian Apel, Eleanor Scott, Sarah J. Watzman and Ashley Paz y Puente; University of Cincinnati, United States

Conventional synthesis and manufacturing of thermoelectric materials is often tedious, time-intensive, wasteful, and expensive with severe limitations in terms of resultant sample geometry and size. While traditional growth techniques have been used for many years in the field, as the interest in thermoelectric devices and environmental efficiency has increased, processing limitations have become abruptly apparent. However, recent popularity for additive manufacturing offers the potential to decrease fabrication time, although success in additive manufacturing has been majorly limited to metals and polymers, while the manufacture of thermoelectric semiconductors has identified many limitations [1]. Current work has not extensively studied how additive manufacturing techniques alter thermoelectric transport. In this work, we approach the problem starting with Ni, whose thermoelectric properties are well established [2], albeit less compelling than those of conventional thermoelectric materials. Specifically, we focus on the particle-laden ink extrusion printing process, which has proven successful with producing bulk Ni samples [3]. Previously, we have shown that extrusion-based additive manufacturing does not alter thermoelectric transport properties of Ni [4]. Through altering printing parameters and sintering techniques, we study the microstructure of printed samples with a specific focus on densification, composition, and pore and crack concentration caused by three distinct infill patterns. We report the effect of these infill patterns on thermoelectric transport through measurements of the temperature-dependence of thermopower, electrical resistivity, and thermal conductivity. We then extend this work to elemental Bi as a more efficient thermoelectric material. Pure Bi has not previously been printed using extrusion-based additive manufacturing; therefore, we present a newly-developed low-temperature method.

[1] A. El-Desouky et al. Mater. Lett. 185, 598-602 (2016).

[2] S. J. Watzman et al. Phys. Rev. B 94, 144407 (2016).

[3] S. L. Taylor et al. Adv. Eng. Mater. 19 (11), 1600365 (2017).

[4] C. D. M. Apel. Thermoelectric Transport in Bulk Ni Fabricated via Particle-Based Ink Extrusion Additive Manufacturing, University of Cincinnati, 2021.

9:45 AM BREAK

10:15 AM *EQ01.06.07

Leveraging Additive Manufacturing to Tailor Thermoelectric Device Configuration, Leg Shape and Transport Properties Saniya LeBlanc; The George Washington University, United States

Additive manufacturing enables unprecedented customization of thermoelectrics at multiple length scales – from nanoscale inclusions to macroscale device shape – potentially all with one manufacturing process. We explore the process-structure-property relationship for laser-based additive manufacturing (specifically laser powder bed fusion) of thermoelectric materials for low and high temperature applications. We determined the process parameters required to form high density parts, and we characterized the nano- and micro-structural features formed in the printed parts. Simulations of the spatial and temporal temperature gradients during processing were used to determine solidification rates and thus predict grain structure, such as the distribution of equiaxed versus columnar grains; the predicted grain structure was compared to the experimentally observed grain structure. Thermoelectric properties (Seebeck coefficient, electrical conductivity, and thermal diffusivity) of printed bulk parts were measured as a function of temperature. The results provide insight about how additive manufacturing can be used to engineer thermoelectric materials and devices at multiple length scales.

10:45 AM EQ01.06.08

Scalable Manufacturing of Textured Thermoelectric Thin Foils of Na_xCoO_2 Nanosheets Rana Ucuncuoglu, Abdelhakim Elmhamdi, Esra B. Karatas Ozkaraca, Elif S. Gur, Ceren Egemen and Mahmut Aksit; Gebze Technical University, Turkey

A novel, industry-compatible nanomaterial processing technique is reported for producing polycrystalline thermoelectric (TE) foils of Na_xCoO_2 nanosheets. In-house produced Na_xCoO_2 nanosheets are chemically modified and coated on polymeric substrates using shear force. By post-heat treatment, Na_xCoO_2 nanosheets in the coated film are re-crystallized into thermoelectric $\text{Na}_{0.7}\text{CoO}_2$ phase while simultaneously burning away the polymer substrate resulting in self-standing textured thin foils of thermoelectric $\text{Na}_{0.7}\text{CoO}_2$ nanosheets. X-ray diffraction (XRD) with point and area detectors is used to confirm the crystalline phase and texturing of the resulting foils. Scanning electron microscopy (SEM) results also indicate the good alignment of Na_xCoO_2 nanosheets in the foil structure. According to SEM images, the thickness of nanosheets in the foil typically varies between 100 and 400 nm. The thickness of the foil can be altered between 9 and 70 μm as measured by cross-sectional SEM. Lateral lengths up to 10 cm can be readily achieved for the produced foils without any obvious indication of potential fundamental limitations to produce even larger foils. Structural changes in Na_xCoO_2 nanosheets are analyzed in detail by Transmission electron microscopy (TEM) after each step of the novel nanomaterial processing method. Finally, thermoelectric properties of the produced foils are measured from 160K to 340K using an in-house built thermoelectric measurement apparatus. Room temperature electrical resistivity of the produced foils can be as low as 3.21 milliohm.cm, whereas their Seebeck coefficients are larger than 65 $\mu\text{V/K}$ in the same conditions.

11:00 AM EQ01.06.10

Scalable Manufacturing of Textured Thermoelectric Thin Films of Bi_2Te_3 Nanosheets Abdelhakim Elmhamdi, Ahmet Furkan Gamli, Elif S. Gur, Esra B. Karatas Ozkaraca, Rana Ucuncuoglu and Mahmut Aksit; Gebze Technical University, Turkey

Many thermoelectric materials have layered crystal structures with anisotropic transport properties. They typically require a high degree of texturing to fully benefit from inherently good thermoelectric properties and possible thermoelectric enhancements from micro-nano structuring. A novel, scalable nanomaterial processing technique is reported for producing textured, polycrystalline thermoelectric foils of Bi_2Te_3 nanosheets. Bi_2Te_3 nanosheets are prepared in-house using a simple solvothermal method. Textured films are then prepared by spraying isopropyl alcohol (IPA) dispersions of the nanosheets on polymeric substrates, followed by shear force application parallel to the substrate plane. The films are then subjected to post-heat treatments to optimize their thermoelectric properties. X-ray diffraction (XRD) patterns of Bi_2Te_3 nanosheets match with JCPDS 15-0863 Bi_2Te_3 reference both before and after

the film preparation and post-heat treatment. The inherently weak [006] peak is almost non-existent in the powder form. In contrast, it is the dominant peak in the post-heat-treated film, indicating the strong orientation of the nanosheets along the substrate plane. The strong texturing in the films is also confirmed with area detector XRD measurements. According to scanning electron microscopy (SEM) images, the Bi₂Te₃ nanosheets have hexagonal shapes with less than 200 nm lateral length. The average nanosheet thickness is ~12 nm as calculated by XRD-Scherrer Broadening crystal size analysis on (006) peak. The thickness of the prepared films can be between 500 to 900 nm. Lateral lengths of more than 5 cm can be achieved for the produced films. Transmission electron microscopy (TEM) is used to observe structural changes in Bi₂Te₃ nanosheets after each step of the novel nanomaterial processing method. The Seebeck coefficient (S) and electrical conductivity (σ) of the produced films are measured from 300K to 350K using an in-house built thermoelectric measurement apparatus. The room temperature S and σ of the produced films are -102 μ V/K and 1.21 10^4 S/m, respectively. According to the mechanical flexibility test, the films can maintain >95% of their initial σ after 1000 bending cycles.

SESSION EQ01.07: Device Design, Fabrication and Application II
Session Chairs: Doug Crane and Joseph Heremans
Wednesday Afternoon, November 30, 2022
Sheraton, 2nd Floor, Back Bay A

1:30 PM EQ01.07.02

Wearable Thermoelectric Generator for Wearable Medical Solutions Jiyong Kim, Eun Kyu Kim, Gimin Park, Bo Min Kang, Hyo Geon Lee, Salman Khan, Seungjai Woo, Sungjin Park, Hyeong Min Yoon, Jae Hyun Kim, Jae Woo Jung, Jun Young Yoon and Woonchul Kim; Yonsei University, Korea (the Republic of)

Patients with medical conditions, including diabetes, require continuous monitoring of the subject's health condition and immediate treatment (e.g., drug injection) to maintain their wellbeing. Nowadays, the development of wearable electronics has made continuous health monitoring possible; for instance, continuous glucose monitors (CGMs) track the glucose level of the wearer and inject insulin *via* insulin pump patches. Nonetheless, conflict arises in terms of their lifetime, such devices should be self-powered so that the external power source need not be replaced. Previously, we have demonstrated that body heat harvesting through a wearable thermoelectric generator (WTEG) allows the operation of a commercial CGM [1] and showed improvement in its power density by attaching a radiatively cooled heat sink [2]. As mentioned before, health monitoring should be followed by immediate treatment of the illness. This study focuses on operating a micropump for drug injection fully powered by a WTEG. The WTEG was carefully designed by integrating the bioheat transfer and thermoelectric phenomena at various environmental conditions. The fabricated WTEG demonstrates power densities up to 13.5 μ W/cm² when the ambient air temperature is 292 K. Also, a handmade low-power micropump consists of a bi-stable electromagnetic actuator wrapped around an energy-storing elastic tube with passive valves. The electromagnetic actuator, capable of injecting 1.5 μ L per 3.76 mJ, can be powered by the stepped-up voltage provided by the WTEG. As the WTEG generates a sufficient amount of power to operate the micropump solely harvested from the human body heat, this study leaps toward a continuous closed-loop diabetes solution.

[1] J. Kim, S. Khan, P. Wu, S. Park, H. Park, C. Yu and W. Kim, *Nano Energy* **79**, 105419 (2021)

[2] S. Khan, J. Kim, K. Roh, G. Park and W. Kim, *Nano Energy* **87**, 106180 (2021)

1:45 PM EQ01.07.03

Geometric Study of Micro Thermoelectric Device with Optimized Contact Resistance Nithin B. Pulumati^{1,2}, Aditya S Dutt^{1,2}, Kangfa Deng¹, Kornelius Nielsch^{1,2} and Heiko Reith¹; ¹Leibniz Institute for Solid State and Materials Research, Germany; ²TU Dresden, Germany

Generation of electricity without leaving a vast carbon footprint represents one of the critical challenges of the 21st century. Around 60% of energy is dissipated in the form of heat while burning fossil fuels. Thermoelectric devices have drawn a wide interest because of its potential to convert waste heat into clean electricity and vice-versa. For applications like in biomedical and Internet of things, μ TEDs need to have a robust packaging so that the devices can be brought in direct thermal contact with the target heat sink and source. The packaging technology developed for macroscopic modules needs improvement as it cannot be applied to μ TEDs due to a large thermal resistance between the capping material and the device which deteriorates its performance. Here, we develop μ TEDs using optimized geometry and contact resistance combined with a novel packaging technique that is fully compatible with on-chip integration.

We developed a process for the fabrication of μ TEDs with vertically free-standing leg pairs without a top plate. The fabricated μ TEDs were embedded in a photoresist for using the device in applications.

The fabrication of the μ TED is based on the combination of photolithographic patterning process with electrochemical deposition of Bi₂(Te_xSe_{1-x})₃ and Te as n-type and p-type thermoelectric materials respectively. Using the optimized geometry and contact resistance, the maximum net cooling temperature and the cycling reliability were enhanced. The geometrically optimized μ TED with low contact resistance showed a maximum cooling of around 10.8K at an applied electrical current of 235mA, a rapid response time of 700 μ s and survived over 100 million cooling cycles in our reliability studies [1]. The fabricated μ TED can be used to scavenge waste heat to provide solid-state electricity for powering electronics and have potential applications in wearable electronics, and wireless sensors. These embedded, optimized, stable and easily scalable μ TEDs open new avenues for widespread applications in biomedical applications, powering internet-of-things devices, and local heat management.

Reference

[1] Dutt, et al., *Adv. Electron. Mater.* (2022): 2101042.

2:00 PM EQ01.07.04

Development Status of Skutterudite-based Thermoelectric Technology for Integration into a Potential Skutterudite-Multi Mission Radioisotope Thermoelectric Generator Thierry Caillat; Jet Propulsion Lab, United States

The flight-proven Multi-Mission Radioisotope Thermoelectric Generator (MMRTG) is currently powering NASA's Mars Curiosity and Perseverance rovers and selected for NASA's Dragonfly mission. The MMRTG design includes sixteen thermoelectric converter modules, each composed of 48 couples of PbTe/TAGS (Lead-Telluride/Tellurium-Antimony-Germanium-Silver) packaged in fibrous insulation and is operated under inert gas in a hermetically sealed environment. The skutterudite (SKD)-MMRTG design in development would be nearly identical except for upgraded 48-couple modules using skutterudite-based couples. While preserving the majority of the flight-qualified MMRTG design, fabrication tooling and flight support equipment, the new skutterudite-based couples would provide a substantial improvement in power output over time.

A team composed of Aerojet Rocketdyne (AR), Teledyne Energy Systems, Inc. (TESI), and NASA's Jet Propulsion Laboratory (JPL) team has been

maturing the SKD technology for integration into a potential SKD-MMRTG. From JPL-transferred skutterudite technology, TESI has developed manufacturing capabilities for skutterudite-based couples as well as 48-couple modules, a building block of the SKD-MMRTG. Life assessment testing of SKD couples is underway at JPL and TESI, with some couples achieving more than three years of continuous time-on-test. Testing of SKD couples and a 48-couple module has shown that their power output is in good agreement with the predicted values. Physics-based life performance prediction models developed at JPL, and a newly developed one at TESI, utilize the couple test data results and analysis to forecast the generator power output. The current best-estimate power predictions for the SKD-MMRTG meets specification requirements and offers up to about 37% more power at End-Of-Design-Life (EODL) than the MMRTG at equivalent operating conditions. The SKD-MMRTG would provide a substantial improvement in power output in the out years, making it ideal for many long-duration, deep-space missions.

3:15 PM *EQ01.07.05

Direct Ink Writing of Three-Dimensional Thermoelectric Materials and Devices Jae Sung Son, Seungjun Choo, Seong Eun Yang, Jungsoo Lee, Keonkuk Kim and Hyunjin Han; Ulsan National Institute of Science and Technology, Korea (the Republic of)

Heat is omnipresent in natural and artificial environments, more than 60% of which is dissipated. Thermoelectric (TE) power generation can provide a unique solution to convert this dissipated, wasted heat into useful energy, that is, electricity. Generally, TE conversion efficiency depends on the material properties and design of the module structure. The geometrical design of thermoelectric legs in modules is important to ensure high power generation but cannot be easily achieved by traditional fabrication processes. At this moment, three-dimensional (3D) printing technology can maximize the flexibility in the design and fabrication of TE modules into more efficient structures. Furthermore, the printing process can significantly reduce the processing cost for the fabrication of TE modules owing to lower energy input and a simplified assembly process. Herein, I present the development of the 3D direct ink writing process applied to a range of different TE materials of Bi₂Te₃, BiSbTe, PbTe, and Cu₂Se-based inorganic alloys. Surface states of TE particles were precisely optimized with the controllable charge states in the presence of anionic inorganic binders, achieving the suitable viscoelasticity of the TE inks to the direct ink writing. The geometrically designed 3D-written TE materials were assembled into power generating systems, in which high efficiencies of energy conversion were achieved by the optimization of heat transfer.

2:30 PM BREAK

3:45 PM EQ01.07.06

Electron Transport in Double-Barrier Semiconductor Heterostructures for Thermionic Cooling Xiangyu Zhu¹, Marc Bescond², Toshiki Onoue¹, Gerald Bastard³, Alwin Philippe³, Carosella Francesca³, Robson Ferreira³, Naomi Nagai¹ and Kazuhiko Hirakawa¹; ¹Institut of Industrial Science - University of Tokyo, Japan; ²IM2NP - Aix Marseille Université, France; ³Laboratoire de Physique de l'ENS, France

Progress in ultrahigh-density ultrahigh-speed electronic-photonic devices has come along with the tremendous generation of heat, resulting from thermalization of hot carriers generated by high electric fields. Cooling technologies are, therefore, indispensable for the continuous development of high-performance devices. Solid-state physics may provide relevant alternative approaches to go beyond the standard cooling techniques based on liquid or air (fans). So far, most of the solid-state solutions rely on the thermoelectric Peltier effect. However, thermoelectric devices operate in the near-equilibrium regime. Furthermore, the cooling efficiency deteriorates due to scattering induced internal Joule heating. Recently, thermionic cooling, which is based on the thermionic emission process, is attracting considerable attention [1]. The thermionic cooling devices operate far from thermal equilibrium. Recently, Chao et al. proposed a thermionic cooling structure with asymmetric double barriers [2]. In this structure, a quantum well (QW) is sandwiched between two potential barriers. The left barrier (the “emitter” barrier) is designed to be thin and tall. Since the emitter barrier is thin, electrons can tunnel from the emitter electrode into the QW by resonant tunneling, which allows only cold electrons to enter the QW. This selective electron injection is the key for enhancing the cooling efficiency. The second barrier (the “collector” barrier) is thick and low. Since the collector barrier is thick, electrons cannot escape the QW by tunneling; instead, they are forced to surpass the collector barrier thermionically (thermionic emission). Indeed, we recently demonstrated that (Al,Ga)As/GaAs asymmetric double-barrier thermionic cooling structures could reduce the electron temperature, T_e , from 300 K down to 250 K by applying a bias voltage to the structure [3,4]. To improve the cooling performance, an understanding of electron transport and optimization of structural parameters are needed.

Here, we investigate electron transport in asymmetric double-barrier (Al, Ga)As/GaAs thermionic cooling heterostructures. Measurements of temperature-dependent current-voltage characteristics confirm that the dominant electron-transport process is a sequential process of resonant tunneling injection into and thermionic emission from the QW cooling layer. The thermal activation energy of the current is found to be strongly dependent on the bias voltage. Furthermore, instead of showing simple thermal activation behavior, the current exhibits rather complicated temperature and voltage dependence, particularly when the thermionic emission barrier is low. To establish a quantitative understanding, we develop an intuitive analytical model for sequential electron transport that explicitly takes into account scattering effects in the thermionic emission process from the two-dimensional QW states to the three-dimensional above-barrier states. The observed temperature dependent sequential current is well explained by the present theory [5].

[1] A. Ziabari, M. Zebajadi, D. Vashaee, and A. Shakouri, Nanoscale solid-state cooling: A review, Rep. Prog. Phys. 79, 095901 (2016).

[2] K. A. Chao, M. Larsson, and A. G. Mal'shukov, Room-temperature semiconductor heterostructure refrigeration, Appl. Phys. Lett. 87, 022103 (2005).

[3] A. Yangui, M. Bescond, T. Yan, N. Nagai, and K. Hirakawa, Evaporative electron cooling in asymmetric double barrier semiconductor heterostructures, Nat. Commun. 10, 4504 (2019).

[4] M. Bescond, D. Logoteta, F. Michelini, N. Cavassi-las, T. Yan, A. Yangui, M. Lannoo, and K. Hirakawa, Thermionic cooling devices based on resonant-tunneling AlGaAs/GaAs heterostructure, J. Phys.: Condens. Matter 30, 064005 (2018).

[5] X. Zhu, M. Bescond, T. Onoue, G. Bastard, F. Carosella, R. Ferreira, N. Nagai, and K. Hirakawa, Electron Transport in Double-Barrier Semiconductor Heterostructures for Thermionic Cooling, Phys. Rev. Applied 16, 064017 (2021)

4:00 PM EQ01.07.07

Direct Ink Writing of Highly Integrated 3D Thermoelectric Generators with Selectively Doped Carbon Nanotubes Seongkwon Hwang¹, Doojoon Jang¹, Byeongmoon Lee¹, Heesuk Kim¹, Jeonghun Kwak² and Seungjun Chung¹; ¹Korea Institute of Science and Technology, Korea (the Republic of); ²Seoul National University, Korea (the Republic of)

With an increase of interest in self-powered electronics, thermoelectric generators (TEGs) have been regarded as the most promising sustainable energy harvesting device to power them due to their reliable energy conversion from heat to electricity regardless of individual circumstances. One of the key requirements of high efficient TEGs is to achieve conformal interfaces on arbitrary-shaped or shape-changing 3D heat sources such as the human body by minimizing heat loss through undesirable air gaps. Specifically, because the temperature difference across thermoelectric (TE) legs would be mostly given in the through-plane in reality, the development of 3D-structured TEGs which could be attached to various types of heat sources is highly desirable. In the last decade, although 3D wavy-structured TEGs or introducing 3D bulk TE legs into deformable platforms have been proposed, still low integration density or limited flexibility would be a bottleneck to achieve maximized energy conversion efficiency.

In this presentation, we will introduce highly integrated 3D TEGs with direct ink writing (DIW) of carbon nanotubes (CNTs) onto an elastomeric substrate and their potential applications. High-performance viscoelasticity *p*- and *n*-type CNT inks were prepared by conducting selective chemical doping, and their rheological properties such as dynamic viscosity, storage modulus and shear yield stress were systematically analyzed according to the concentration of CNTs, which is a key requirement to optimize the DIW process resulting in high-resolution CNT legs. Especially, we directly print CNT inks onto the 3D TEG platforms with 1mm-thick thermal insulators, which can deliver the large temperature difference in the through-plane via optimizing the heat transfer model. Therefore, our TEGs can convert waste heat into electricity by just attaching them to arbitrary-shaped 3D heat sources without any structural assistance.

To deliver improved TE performance, interfacial properties between the TE legs and interconnects and their mechanical properties simultaneously, we have introduced all CNT-based 3D TEGs, which exhibit excellent output power of 32 nW/cm² at $\Delta T = 15$ K. In addition, mechanical reliability and deformability under tensile strain were demonstrated owing to the use of intrinsically soft TEG platforms. To the best of our knowledge, it is the first to employ 3D DIW directly to realize all-CNT-based TEGs to exploit waste heat in the direction of the through-plane. We believe our results pave a promising pathway to realize highly efficient 3D TEGs with a high degree of design freedom for self-powered flexible/or wearable applications. The detailed methods and results will be discussed at the conference.

4:15 PM EQ01.07.08

Thermally Programmable Liquid-Crystalline Thermoelectric Ionogels [Byeongwan Kim](#), Sienoh Park, Cheolhyun Cho, Kyung Tae Park, Wooyoung Lee and Eunyoung Kim; Yonsei University, Korea (the Republic of)

Ionic thermoelectric effect has emerged as a new realm for ionic thermoelectric supercapacitors, energy harvesters, fluorescence ion sensing, and self-healable materials. However, despite significant improvement of ionic thermoelectric performance and several attempts to extend to include other mechanical properties, a temperature-programmable function has not been integrated with ionic thermoelectric materials. Herein, we synthesized thermally programmable ionogels *via* photopolymerization of ionic monomers and hydrophobic nematic monomers in the presence of an ionic liquid. A liquid-crystalline ionogel film showed reversible temperature programmability at designed temperature, at which temperature the nematic-isotropic phase transition occurs by monitoring with polarized optical microscope. The liquid-crystalline ionogel film showed a phase-controlled ionic Seebeck coefficient. To enhance the carrier transport for thermoelectric performance, doped carbon nanotubes were introduced for thermoelectric ionogel device. Taking advantage of high thermoresponsive thermoelectric output, the liquid-crystalline ionogel film was used to demonstrate a self-detectable and wireless fire alarm, which enables detection of elevated temperatures with the naked eye by integrated as a thermal switch for an electrochromic window, a liquid crystal display, or a light-emitting diode. The ionogels could benefit in exploiting autonomous thermoresponsive electronics that can be used to detect and view temperature changes in the environment.

SESSION EQ01.08: Computationally-Guided Material Design and Discovery II

Session Chairs: Anubhav Jain and Heng Wang

Thursday Morning, December 1, 2022

Sheraton, 2nd Floor, Back Bay A

8:15 AM *EQ01.08.01

Efficient Methods for Accurately Calculating Thermoelectric Properties—Electronic and Thermal Transport [Anubhav Jain](#); Lawrence Berkeley National Laboratory, United States

We describe our efforts to aid in new thermoelectric materials discovery through theory-driven approaches. In particular, we focus on two efforts. The first is a new model of carrier transport called AMSET that allows one to model the temperature-dependent Seebeck coefficient and mobility from first-principles at reasonable computational cost. This is achieved by adapting classical scattering equations previously developed for 1D parabolic band semiconductors to complex density functional theory band structures. We will explain the theory behind AMSET as well as comparison against experiment and constant relaxation time approaches typically used in the field. Next, we will describe efforts to efficiently calculate thermal transport using compressed sensing lattice dynamics. Such approaches offer the possibility to calculate temperature-dependent thermal conductivities at a fraction of the computational cost of explicit approaches. For both methods, we will offer comparisons to experiments and offer a perspective on their potential role in uncovering and understanding thermoelectric materials.

8:45 AM EQ01.08.03

Band Inversion-Driven High Valley Degeneracy [Michael Toriyama](#) and G. J. Snyder; Northwestern University, United States

Thermoelectric materials can convert thermal energy to electrical energy and vice versa, enabling low-carbon alternatives for cooling and waste heat recovery. Yet, the low power conversion efficiencies of existing thermoelectric materials remain a challenge. One method to improve the thermoelectric performance of a material is by tuning the valley degeneracy, which we can control by modifying the degree to which the bands are inverted. We generalize this concept of “band inversion-driven high valley degeneracy” and derive simple rules for when inverted-band materials exhibit high thermoelectric performance. Using a combination of *k,p* perturbation theory and Density Functional Theory calculations, we show that electronic bands must be inverted to a critical degree for a material to possess high valley degeneracy. We apply this rule to discover potentially high-performing thermoelectric materials within the *ABX* chemical space of materials. We find that NaCaBi (space group: *P6₃/mmc*) is a promising candidate with a degeneracy of 6 for both the conduction and valence bands, resulting from the high degree of band inversion in the material. Through detailed Boltzmann transport theory-based calculations, we find that NaCaBi can reach zT between 0.4 and 0.8 at 300 K. Our study therefore demonstrates that band inversion is a rational descriptor for identifying high-performing thermoelectric materials.

9:00 AM EQ01.08.04

Substitution of High Oxidation State Cations in *N*-Type Chalcopyrite [Anthony V. Powell](#), Sahil Tippireddy and Paz Vaquero; University of Reading, United Kingdom

Metal sulphides are attractive candidate materials for thermoelectric energy harvesting. In addition to the greater abundance of sulphur compared to its heavier congeners selenium and tellurium, sulphur is also less toxic. There have been significant advances in the performance of *p*-type sulphides, including the binary sulphide, Cu_{2-x}S and materials related to the minerals tetrahedrite, bornite and colusite. However, progress in the *n*-type counterparts has been more modest, with few materials exceeding $ZT = 1$, while the highest performance typically occurs in materials containing toxic elements such as lead.

A major focus of our work on new *n*-type sulphides containing Earth-abundant elements is materials derived from chalcopyrite. Chalcopyrite contains the same Cu₄S building block as in the high-performance binary phase. The presence of additional (Fe) cations suppresses the cation mobility that characterizes phonon liquid electron crystal (PLEC) type behaviour. Although the PLEC character of Cu_{2.4}S contributes to a remarkably low thermal conductivity, it also facilitates copper-ion migration under operating conditions, leading to degradation.

We have sought to utilise substitution with high-oxidation state cations at Cu and Fe sites to manipulate the carrier concentration and hence transport properties of chalcopyrite. Cations such as Sn⁴⁺, Ge⁴⁺ and Cr³⁺ can effect larger changes in carrier concentration per unit of substitution than the more usual dispositive substituents. Figures of merit of ZT > 0.3 at 673 K have been achieved in Sn- and Cr-substituted phases, while values approach ZT = 0.4 on Ge-substitution. These represent a 4- to 5-fold improvement over the stoichiometric end-member phase. However in all cases, substitution leads to increases in carrier concentration that are substantially lower than expected on the basis of formal oxidation states. By application of a range of experimental and computational approaches, we have investigated the origin of this unexpected result. This has led us to identify a variety of new features that introduce additional complexity into the substituted phases.

In Cu_{1-x}Sn_xFeS₂, substitution leads to the formation of small polarons through partial reduction of Fe³⁺ to Fe²⁺. Localized Fe²⁺ states reduce the free-carrier concentration from the expected value, contributing to the maintenance of a relatively high Seebeck coefficient, despite the reduction in electrical resistivity. Substitution also induces a high level of mass and strain-field fluctuation, resulting in lattice softening and enhanced point-defect scattering. This, together with microstructural changes, leads to scattering of phonons with a wide range of mean free paths, and to the observed substantial reductions in thermal conductivity. When iron is partially substituted by germanium however, X-ray photoelectron spectroscopy suggests the lower-than-expected increase in carrier concentration is associated with the presence of germanium in two oxidation states (Ge²⁺/Ge⁴⁺) in the substituted phases. The 4s² lone pair of Ge²⁺ also results in different bonding characteristics to that of the closed-shell Ge⁴⁺ species. This results in a local structural distortion, identified through Pair Distribution Function analysis of synchrotron powder X-ray diffraction data, whereby some germanium cations are displaced from the centre, towards the face of a metal-centered tetrahedron. This local distortion contributes to the observed reduction in thermal conductivity. Collectively, these results reveal an unexpected richness in composition-structure-property relations in *n*-type chalcopyrites that may offer scope for the development of future design strategies for *n*-type sulphide thermoelectrics.

9:15 AM EQ01.08.05

Theoretical Investigation into the Chemical Origins of High Valley Degeneracy in *n*-type Mg₃Sb₂ for Thermoelectric Applications [Madison Brod¹](#), [Shashwat Anand²](#) and [G. J. Snyder¹](#); ¹Northwestern University, United States; ²Lawrence Berkeley National Laboratory, United States

Mg₃Sb₂-based alloys have attracted much attention in recent years as high-performing, low-temperature *n*-type thermoelectrics that are competitive with state-of-the-art Bi₂Te₃. The high valley degeneracy of the conduction band (CB) edge is largely responsible for the excellent thermoelectric performance of Mg₃Sb₂. This high valley degeneracy is due to the fact that the conduction band minimum (CBM) is located at a low-symmetry point in the Γ ALM plane of first Brillouin zone, which has six-fold degeneracy. Moreover, it has been found that alloying Mg₃Sb₂ with Mg₃Bi₂ can further improve thermoelectric performance by increasing the curvature of the conduction band edge, and hence, increasing the electron mobility. In prior works, the highly degenerate CBM in Mg₃Sb₂ has been attributed to interactions between Mg-s orbitals. However, the Mg-s/Mg-s interactions alone cannot explain the changes in transport properties observed upon substitution of Sb with Bi. In this work, we aim to elucidate the chemical origins of the low-symmetry CBM using a combination of density functional theory (DFT), crystal orbital Hamilton population (COHP) calculations, and tight-binding. While, prior studies have not fully considered the importance of Mg/Sb interactions, here, we show that Mg-s/Sb-p interactions play a large role in the formation and shape of the low-symmetry CBM. DFT and COHP calculations show that the strength of Mg-s/Sb-p anti-bonding interactions reach a local minimum near the CBM. Additionally, it is possible to reproduce the low-symmetry CBM using a tight-binding model that considers Mg-s/Sb-p but does not consider Mg-s/Mg-s interactions. Additionally, unlike the Mg-s/Mg-s interactions, Mg-s/Sb-p (and Mg-s/Bi-p) interactions can explain the increase in curvature near the CBM upon Bi alloying on the Sb-site. The findings of this work will allow for improved insights into strategies for tuning electronic transport in Mg₃Sb₂-based alloys and for developing similar materials with high valley degeneracy.

9:30 AM EQ01.08.06

Limits of Thermoelectric Performance with a Bounded Transport Distribution [Jesse Maassen](#); Dalhousie University, Canada

Band engineering is an important strategy that seeks to tailor a material's electronic and scattering properties to improve its thermoelectric performance. This effectively alters the material's transport distribution (TD), which is the central quantity that determines the electronic conductivity, Seebeck coefficient and electronic thermal conductivity. The seminal work of Mahan and Sofo [1] concluded that the thermoelectric figure of merit, ZT, is maximized with a delta function TD – an unbounded distribution. Later studies by Zhou et al. [2] and Jeong et al. [3], exploring different band structures and scattering models, found that ZT is maximized when the width of the TD is finite and that the TD always remains bounded. Assuming a bounded TD, a genetic algorithm search by Fan et al. [4] determined that a boxcar TD is best for ZT.

This talk presents a study that theoretically derives what is the optimal bounded TD and its implications on the limits of thermoelectric performance [5]. To maximize the figure of merit and the power factor the ideal transport distributions are boxcar and Heaviside functions, respectively – the edges of which must be located at specific energies. The optimal power factor is simply limited by the magnitude of the Heaviside TD, and reaches ZT values between 4-5. The optimal figure of merit, which can approach the Carnot limit, is uniquely determined by a key quantity that is proportional to the TD magnitude and temperature, and inversely proportional to the lattice thermal conductivity. These results suggest two general approaches to enhance thermoelectric performance: identify or design materials with TDs that have large magnitude (large distribution of modes, high velocities and/or low scattering) and that possess the ideal boxcar or Heaviside shape (controlled by band structure shape, scattering profile and dimensionality). This study can help guide the search for better thermoelectrics by establishing practical upper limits on performance, and by providing target TDs to guide band and scattering engineering strategies.

[1] Mahan and Sofo, Proc. Natl. Acad. Sci. USA **93**, 7436 (1996).

[2] Zhou, Yang, Chen, and Dresselhaus, Phys. Rev. Lett. **107**, 226601 (2011).

[3] Jeong, Kim, and Lundstrom, J. Appl. Phys. **111**, 113707 (2012).

[4] Fan, Wang, and Zheng, J. Appl. Phys. **109**, 073713 (2011).

[5] Maassen, Phys. Rev. B **104**, 184301 (2021).

Acknowledgements: this research was supported by NSERC and Compute Canada.

9:45 AM BREAK

10:15 AM EQ01.08.07

Inverse Design of Nanoarchitected Three Dimensional Materials for Thermal Transport Applications [Giuseppe Romano](#); Massachusetts Institute of Technology, United States

Owing to phonon-boundary scattering, nanoarchitected materials are a promising platform for tuning thermal transport. Engineering these systems, however, is challenging because the underlying physics must capture momentum-resolved transport, typically addressed by the Boltzmann transport equation (BTE). Borrowing concepts traditionally applied to mechanical compliance optimization, we develop a topology optimization framework for nanoscale heat transport, based upon density-based topology optimization [1]. In practice, the geometry is discretized in pixels (or voxels in three dimensions), to which a fictitious density is assigned. Then, this density is optimized to minimize a given objective function, under constraints. The key aspects of our method are a novel material interpolation method, the Transmission Interpolation Method (TIM), and the solution of the adjoint BTE. In contrast with standard topology optimization methods, where the density is linked to a bulk-related property (e.g. the thermal conductivity), TIM parametrizes an interfacial transmission coefficient. I will show how this approach is able to guarantee a smooth transition between solid and void regions, while ensuring energy conservation along adiabatic walls. After a brief introduction on technical details, I will provide examples on tailoring the effective thermal conductivity tensor in two- and three- dimensional nanoarchitected materials. Conclusion and final remarks will conclude the talk.

[1] Giuseppe Romano and Steven G. Johnson, *Differentiable Phonon Simulations To Optimize Thermal Transport in Nanostructures*.

10:30 AM EQ01.08.09

Finite Element Simulation Approach to Optimize Thermal Behavior in Thermoelectric Interconnected Nanofiber 3D Networks [Germán Alcalá](#)¹, Pablo Cerviño², Marisol Martín-González² and Olga Caballero-Calero²; ¹Complutense University of Madrid, Spain; ²Micro and Nanotechnology Institute (CSIC), Spain

The fabrication of interconnected nanostructures of thermoelectric materials by means of electrochemical growth inside nanoporous templates has been explored recently [1-2]. The production of these networks, especially those produced in high ordered 3D nanoporous alumina templates, have been reported as an excellent method to reduce thermal flux along thermoelectric materials [3]. This approach would allow increasing thermoelectric efficiency by reducing thermal conductivity while having a small effect on electric conductivity.

In the present work we focussed on the fabrication of interconnected nanostructures, using commercial nanoporous filters as templates. In order to optimize the type of structure, and geometrical parameters having an influence on the thermal conductivity of the structure, the thermal behaviour of such nanostructures has been studied using the finite elements method. The use of python script has been a key tool in order to produce the actual geometries, due to the high randomness in parameters such as nanowire section radii, nanowire positions or nanowire orientations. Thermal losses in the nanowire walls have been simplified to a convection model, allowing qualitative comparison between the studied geometries, and facilitating the analysis of the individual geometrical parameters in order to spot the optimal 3D interconnected nanonetwork. This allowed us to determine the optimal parameters leading to the lowest thermal transfer and thermal conductivity, and thus increasing the thermoelectric efficiency.

[1] A. Ruiz-Clavijo, O. Caballero-Calero and M. Martín-González, *Nanomaterials*, 8 (2018) 345 (<http://dx.doi.org/10.3390/nano8050345>)

[2] M. Rauber, I. Alber, S. Müller, R. Neumann, O. Picht, C. Roth, A. Schökel, M.E. Toimil-Molares and W. Ensinger, *Nano Lett.* 11 (2011) 2304–2310 (<https://doi.org/10.1021/nl2005516>)

[3] A. Ruiz-Clavijo., O. Caballero-Calero, C. V. Manzano, X. Maeder, A. Beardo, X. Cartoixa, X. Álvarez and M. Martín-González, *ACS Applied Energy Materials*, 4 (2021). 13556-13566 (<https://doi.org/10.1021/acsaem.1c02129>)

10:45 AM EQ01.08.11

Thermoelectric Performance of CuInTe₂ from First Principles Using Hybrid-DFT and Lattice Dynamics [Sabrine Hachmioune](#)^{1,2,2}, Maheswar Repaka², Zhai Wenhao², Kedar Hippalgaonkar^{2,3} and David O. Scanlon^{1,4}; ¹UCL, United Kingdom; ²Agency for Science, Technology and Research, Singapore; ³Nanyang Technological University, Singapore; ⁴Thomas Young Centre, United Kingdom

Fossil fuels provide 80% of the world's energy¹ and of that energy, an estimated 80% is wasted in the form of heat.² This has motivated world leaders to invest in alternative forms of energy generation.³ One such alternative to be explored is the use of thermoelectric materials (TE).

Thermoelectric materials can convert heat into electricity through the Seebeck effect allowing them to increase the overall efficiency of existing processes, as well as serve as a clean source of electricity. Materials in use today are composed of toxic elements like lead or are plagued by low efficiencies. To measure thermoelectric efficiency, we use the figure of merit, ZT. For comparison, the average ZT of a well-known TE that has been used in many NASA space missions, PbTe is 1.4.⁴

In this work, we explore a chalcopyrite semiconductor, CuInTe₂ (CIT) with an experimental ZT of 1.18 at 850 K⁵ which has been predicted to increase up to 1.72 (10¹⁸ carriers cm⁻³).⁶ The hybrid-DFT functional (HSE06) with spin-orbit coupling (SOC) is used to accurately predict the band structure and the AMSET code⁷ is used to calculate the Seebeck coefficient, electrical conductivity, electronic thermal conductivity, and mobility. We use the supercell approach employed by Phono3py⁸ to calculate third-order phonon-phonon interactions and determine the lattice thermal conductivity. These results allow us to fully calculate the ZT of CIT from first principles where previous theoretical studies have used a semi-empirical approach.⁶

A fundamental understanding of the dopability is key to yielding a proper prediction of the thermoelectric performance, therefore, a study of the full defect chemistry using hybrid-DFT will give insights into realistic doping concentrations by calculating the self-consistent fermi level. We will also assess the effect of different dopants on ZT. This can help guide experimental studies by screening a range of dopants that haven't been studied before in this system such as Sb.⁹

1 Fossil Fuels | EESI, <https://www.eesi.org/topics/fossil-fuels/description>, (accessed 26 April 2022).

2 Q. Bian, *Environ. Syst. Res.*, 2020, 9, 8.

3 P. A. Finn, C. Asker, K. Wan, E. Bilotti, O. Fenwick and C. B. Nielsen, *Front. Electron. Mater.*

4 X. Hao, X. Chen, X. Zhou, L. Zhang, J. Tao, C. Wang, T. Wu and W. Dai, *Front. Energy Res.*

5 R. Liu, L. Xi, H. Liu, X. Shi, W. Zhang and L. Chen, *Chem. Commun.*, 2012, 48, 3818–3820.

6 J. Wei, H. J. Liu, L. Cheng, J. Zhang, J. H. Liang, P. H. Jiang, D. D. Fan and J. Shi, *AIP Adv.*, 2015, 5, 107230.

7 A. M. Ganose, J. Park, A. Faghaninia, R. Woods-Robinson, K. A. Persson and A. Jain, *Nat. Commun.*, 2021, 12, 2222.

8 A. Togo, L. Chaput and I. Tanaka, *Phys. Rev. B*, 2015, 91, 094306.

9 S. Hachmioune et al. (in submission)

11:00 AM EQ01.08.12

Unlocking the Thermoelectric Potential of the Ca₁₄AlSb₁₁ Structure Type—The Case of Yb₁₄ZnSb₁₁ [Geoffroy Hautier](#)^{1,2}, Andrew Justl³, Francesco Ricci², Andrew Pike¹, Giacomo Cerretti⁴, Sabah Bux⁴ and Susan Kauzlarich³; ¹Dartmouth College, United States; ²University Catholique de Louvain, Belgium; ³University of California, Davis, United States; ⁴NASA Jet Propulsion Laboratory, United States

$\text{Yb}_{14}\text{MnSb}_{11}$ and $\text{Yb}_{14}\text{MgSb}_{11}$ are among the best p-type high temperature (>1200 K) thermoelectric materials, yet other compounds of this structure type have not matched their stability and efficiency. Here, we show with first principles computations that the electronic structure features that make these compounds exceptional thermoelectric materials are present across a wide range of chemistries, including materials such as $\text{Yb}_{14}\text{ZnSb}_{11}$ that have shown poor performances. In fact, we show that $\text{Yb}_{14}\text{ZnSb}_{11}$ when phase pure is a high-performance thermoelectric materials. We synthesized phase pure $\text{Yb}_{14}\text{ZnSb}_{11}$ through a new synthetic route utilizing binary precursors which revealed the exceptional high temperature thermoelectric properties, reaching a peak zT of 1.2 at 1175 K. Experimental and theoretical analysis link the previously reported poor performances to the 9-4-9 impurity phase that our new synthesis route eliminated.

SESSION EQ01.09: Thermoelectric Transport in Organic and Composite Materials
Session Chairs: Je-Hyeong Bahk and Heng Wang
Thursday Afternoon, December 1, 2022
Sheraton, 2nd Floor, Back Bay A

1:30 PM *EQ01.09.01

Thermoelectric Transport in Nanotube and Nanowire Network-Based Composites Je-Hyeong Bahk¹, Oluwasegun I. Akinboye¹, Fan Yang², Yu Zhang¹ and Yue Wu²; ¹University of Cincinnati, United States; ²Iowa State University of Science and Technology, United States

High thermoelectric (TE) efficiency of a material can be achieved by promoting high-energy charge carrier transport while simultaneously suppressing thermal transport in the material. This is, however, extremely difficult to achieve in a bulk material because there is a trade-off relationship between the charge and thermal transport. In this talk, we present several strategies of decoupling the charge and thermal transport with nanowire and nanotube networks to enhance the TE efficiency. We focus on carbon nanotube network-based composites, where the three-dimensional nanotube networks provide high-conduction pathways for charge carriers, while the polymer matrix occupying the majority material volume offers suppressed thermal transport. The (sub-)nanoscale junctions between nanotubes can also induce efficient energy-dependent carrier transport via tunneling and energy filtering to enhance the power factor, while suppressing phonon transport across them. We present a comprehensive study on nanotube and nanowire network-based composites including the effects of nanotube doping, modified interfaces with additional nano-inclusions such as bismuth telluride nanoparticles, and the change of network microstructure with excluded volume created by micro-particles.

2:00 PM EQ01.09.02

Thermoelectric and Mechanical Properties of PEDOT:PSS-Coated Ag_2Se Nanowire Composite Fabricated via Digital Light Processing Based 3D Printing Dabin Park and Jooheon Kim; Chung-Ang University, Korea (the Republic of)

In this study, we present a digital light processing (DLP)-based 3D printing method to produce thermoelectric (TE) composites. The UV-curing photoresins are composed of isobornyl acrylate (IBOA), diurethane dimethacrylate (DUDMA), and Phenylbis(2,4,6-trimethylbenzoyl) phosphine oxide (BAPO) is used as the photoinitiator. As TE fillers, poly(3,4-ethylenedioxythiophene)-poly(4-styrenesulfonate)-coated (PEDOT:PSS-coated) silver(I) selenide (Ag_2Se) nanowires (NWs) were used. UV curable photoresins with P- Ag_2Se (2) fillers were then printed with a DLP-based 3D printer. Ag_2Se is widely used as TE materials because of its high electrical conductivity. However, high-electrical conductivity is usually accompanied with high thermal conductivity. Thus, to keep the composite with high electrical conductivity and meanwhile with low thermal conductivity, PEDOT:PSS coating was chosen because PEDOT has a low thermal conductivity. The in-situ synthesis method enables the strong binding of inorganic Se NWs and organic PEDOT:PSS. After synthesizing the P-Se NWs, the P- Ag_2Se composite was formed through the reaction of P-Se and the silver (Ag) precursor solution. As the amount of PEDOT:PSS used in the experiment increased from 1 mL to 3 mL, the composite were named P- Ag_2Se (1), P- Ag_2Se (2), and P- Ag_2Se (3). The successful synthesis of pristine Ag_2Se NWs and P- Ag_2Se was confirmed via field-emission transmission electron microscope (FE-TEM) analysis. The lattice spacing agrees closely with the (200) plane spacing of orthorhombic Ag_2Se with an interplanar spacing of 0.35 nm. It was confirmed that the thickness of the P- Ag_2Se composite coating layer increased as the amount of PEDOT:PSS increased. The temperature-dependent TE properties of prepared P- Ag_2Se composite with different PEDOT:PSS contents were investigated. The electrical conductivity (σ) of the P- Ag_2Se composite increased with an increase in the PEDOT:PSS contents because the PEDOT:PSS can form an electrically conductive network in the PEDOT:PSS-coated Ag_2Se NW, resulting in a high σ . In contrast with the tendency of σ , the absolute value of S of the P- Ag_2Se decreases with increasing PEDOT:PSS contents. The maximum power factor of $\sim 429.18 \mu\text{W}/\text{m K}^2$ was achieved for the P- Ag_2Se composite with ~ 9 wt.% of PEDOT:PSS contents (P(2)- Ag_2Se). Due to its outstanding TE properties, P- Ag_2Se (2) fillers were added to the photoresin as a TE filler with high TE performance. The cured photoresin with 30 wt.% TE fillers are analyzed via FE-SEM. These images illustrate the layered structure of a cured composite and its uniform thickness. Additionally, the FE-SEM images highlight the presence of a large number of wire structures in photoresins.

The mechanical properties of photoresins with various P- Ag_2Se (2) contents are measured. When the filler loading increases, the tensile stress decreases because the P- Ag_2Se (2) filler in the photoresin matrix renders the composite resin brittle. The room-temperature σ of cured composite samples with various TE filler contents (0, 10, 20, and 30 wt.%) are analyzed. The σ of the cured sample increased with ~ 2.87 S/cm to ~ 117.39 S/cm as the amount of TE filler increased from 0 to 30 wt.%. The highest σ value of ~ 117.39 S/cm was obtained in the cured composite with 30 wt.% of P- Ag_2Se (2) fillers, which is much larger than those of photoresins without fillers. The Seebeck coefficient (S) of the composite sample was investigated at room temperature with various P- Ag_2Se (2) contents. The S increases as the contents of P- Ag_2Se (2) increase. The maximum S value of $\sim 81.94 \mu\text{V}/\text{K}$ is found in the cured composite with 30 wt.% of P- Ag_2Se (2). The thermoelectric ZT is calculated with S , σ , and κ . The maximum ZT of ~ 0.02 was achieved from the cured resin with 30 wt.% of P- Ag_2Se composite.

2:15 PM EQ01.09.03

Fully Conjugated Ladder Polymers and Novel Dopants for N-Type Organic Thermoelectrics Donato Ottomano¹, Ryan Chiechi² and Remco W. Havenith¹; ¹University of Groningen (RUG), Netherlands; ²North Carolina State University, United States

Organic thermoelectric materials are systems capable of converting thermal differences into voltage differences. Within a thermoelectric device, the transition between thermal gradient and electric potential results from the diffusion of charge carriers towards the hot side and away from the cold side. This phenomenon is identified as the Seebeck effect, and its coefficient quantifies how rapidly a material responds to a perturbation. The thermoelectric efficiency is directly related to a high electrical conductivity. In contrast, a large thermal conductivity translates in a volatile temperature gradient, which minimizes the voltage difference and limits the diffusion of charge carriers. For these reasons, semiconducting organic polymers are excellent candidates for non-toxic, greener and more versatile thermoelectric applications. To further improve their efficiency, additional charge carriers are injected into these devices via doping. In organic semiconductors, charge carriers move from the frontier orbitals of the dopant towards the undoped species. Therefore, a

greater energy difference between the frontier orbitals of the two species not only guarantees a higher doping efficiency, but enhances the overall thermoelectric performance. In this work, we investigate fully conjugated ladder polymers as n-dopable thermoelectric candidates. Ladder polymers have been shown to perform well as n-type materials in thermoelectric devices, not only on account of their high electrical conductivity, but also their low lying LUMOs rendering them susceptible to reduction by conventional n-dopants. However, they tend to be insoluble and difficult to process. We address these shortcomings by designing and synthesizing novel ladder polymers with solubilizing groups that do not sacrifice performance. Unlike previous reports, we are employing slightly electron donating linkers to avoid overly unreactive monomers which are known to impede the polymerization. In addition, we are incorporating highly electron deficient functionalities within the polymer backbone to further lower the frontier orbitals and improve the doping efficiency. Finally, there is a paucity of n-type dopants and the mechanism of the best-performing dopants remains unclear. We are investigating a class of dopants with readily tunable oxidation potentials that minimally affect their structure, steric bulk and polarity to investigate the role of oxidation potentials without altering other relevant variables. With a deeper understanding of doping mechanisms and with highly electron deficient fully-conjugated ladder polymers, our group points towards record performances in the field of n-type organic thermoelectrics.

2:30 PM EQ01.09.04

Mixed Ionic-Electronic Conducting PEDOT/PAMPS Polymer Composite Films for Transparent and Self-Healable Thermoelectric Harvesters Cheolhyun Cho, Byeongwan Kim and Eunyoung Kim; Yonsei University, Korea (the Republic of)

In these days, a lot of effort is put on energy harvesting technologies. As one of them, thermoelectric (TE) technology which harvests energy through conversion from heat to electricity is a future-oriented technology that contributes to energy reuse and environmental friendliness. However, the existing TE materials have low heat-to-electricity efficiency, so it is difficult to use their harvested energy for operating other devices. As an alternative, ionic polymer could be a promising candidate because it has an excellent energy harvesting property based on the Seebeck effect. In addition to excellent thermoelectric property, ionic thermoelectric materials (iTE) have the advantages of low-cost production, light weight, scalability, and environmental friendliness. However, the lack of electrical properties in the iTE devices is critical because there is little actual energy transfer. In addition, researches on n-type iTE materials have not been progressed much, and they showed lower energy harvesting performance than p-type iTE materials due to the difficulty of the transport of large-sized negative ion carriers.

In this study, we developed mixed ionic-electronic conductor (MIEC) based TE material for better energy harvesting property. Poly(3,4-ethylenedioxythiophene) (PEDOT), an electrical conductive polymer, was co-polymerized in poly(2-acrylamido-2-methyl-1-propanesulfonic acid) (PAMPS), an ionic polymer-based media using ammonium persulfate (APS) as an initiator. Through transmission electron microscopy (TEM) analysis, the core-shell structure of PEDOT-PAMPS and the pi-pi interaction of the PEDOT domain acting as an electrical channel were characterized. We focused on finding an optimized PEDOT concentration that maintains MIEC characteristics while maintaining transparency in a thin film state. APS was additionally doped to the synthesized PEDOT-PAMPS polymer composite, resulting in n-type PEDOT-PAMPS (NPP) composite where bisulfate acts as anionic carrier. A novel n-type ion transport mechanism was designed in consideration of the deprotonation of the sulfonate group of PAMPS and polymer-polymer, polymer-ion interaction. The mechanism was scientifically elucidated through Raman spectroscopy and X-ray photoelectron spectroscopy (XPS) analysis, and bisulfate generation and ion transport were characterized using time-of-flight secondary ion mass spectrometry (ToF-SIMS) and nuclear magnetic resonance (NMR) analysis. In addition, bisulfate-detecting fluorescent material was synthesized to visually show the bisulfate transport in real time when a temperature gradient (ΔT) was given.

The TE properties of NPP films were measured considering humidity, different ΔT , and concentration of components. The optimized NPP film showed a negative ionic Seebeck coefficient of -25.0 mV K^{-1} , ionic power factor of $9.94 \text{ mW m}^{-1} \text{ K}^{-2}$, and an ionic figure of merit of 7.2 at 80% relative humidity and room temperature, which exhibited the highest TE performance in organic materials at room temperature. In addition to excellent TE properties, NPP film with Young's modulus similar to human skin and self-healing property of hydrogel-based composite could be applied to a flexible organic TE module. The TE module with 20 legs generated -2.75 V at a ΔT of 5.5 K, and the flexible band-type TE module attached to the human wrist generated -1.88 V . To emphasize energy harvesting property and transparency, we succeeded in turning on the LED using the capacitor charged by the TE module for the first time using an organic-based TE device, and fabricated a TE module composed of legs dyed with water-soluble ink. In addition, by fabricating a photothermal-thermoelectric combined device, photothermal-to-thermoelectric voltage according to laser power was observed using a light source instead of heat. Various applications using NPP films have demonstrated the practicality and multifunctionality of this novel TE material, and its potential as a promising energy harvester.

2:45 PM EQ01.09.05

Significant Enhancement in the Thermoelectric Properties of Polymers via Ionic or Molecular Energy Filtering [Jianyong Ouyang](#); National University of Singapore, Singapore

Intrinsically conducting polymers such as PEDOT:PSS can exhibit high thermoelectric properties because of their high electrical conductivity. However, their Seebeck coefficient is usually 10^0 - $10^1 \mu\text{V/K}$. Although dedoping can increase the Seebeck coefficient, it is achieved at the sacrifice of the electrical conductivity. A remedy is via energy filtering that can greatly increase the Seebeck coefficient while only slightly affect the electrical conductivity. Here, I will report several novel methods to significantly enhance the thermoelectric properties of polymers by forming composites with ions or organic molecules that can induce energy filtering. The polymer composites can exhibit a very high zT value at room temperature.

3:00 PM BREAK

3:30 PM DISCUSSION TIME

4:00 PM EQ01.09.07

Single Ether-Based Polar Side Chain—A Tool for Controlling the Microstructure and Dopant Location in Polymer Semiconductors for Organic Thermoelectric Devices [Nicolas Leclerc](#)¹, [Pablo Durand](#)¹ and [Martin Brinkmann](#)²; ¹ICPEES-CNRS, France; ²Institute Charles Sadron, France

Combining side chain engineering and controlled alignment of semiconducting polymers is an effective strategy to produce oriented thin films with improved thermoelectric performances. In this contribution, we demonstrate that the substitution of standard linear alkyl side-chains with a chain of identical length including an ether function leads to a new class of slightly polar PBTTT polymers, preserving the ease of synthesis and air stability of alkylated PBTTTs. This side-chain modification improves the structural order of PBTTT backbones and the thermomechanical properties of the polymer. Such polymers can be thus oriented by high temperature rubbing to reach very high dichroic ratios up to 20 thanks to enhanced cohesive forces within side-chain layers. The side chain polarity helps to tune the polymer-dopant interactions. In addition, the single ether-based side-chain approach allows to adjust the ether function position along the side chain, tuning the physico-chemical and TE properties. The conjugation of improved alignment and random orientation of intercalated $F_6\text{TCNNQ}$ dopants helps reach a very high charge conductivity of 10^4 S/cm and a record power factors for organic materials of $2.9 \text{ mWm}^{-1}\text{K}^{-2}$ in the polymer chain direction.

Reference.

P. Durand, H. Zeng, T. Biskup, V. Vijayakumar, V. Untilova, C. Kiefer, B. Heinrich, L. Herrmann, M. Brinkmann, N. Leclerc, *Adv. Energy Mater.*, **2022**, 12, 2103049.

4:15 PM EQ01.09.08

Thermoelectric Power Factor Enhancement of PEDOT:PSS by Formation of Cu₂Se Nanowire Network Structures Shunya Sakane¹, Shunichiro Miwa¹, Tatsuki Miura¹, Kazuki Munakata¹, Takafumi Ishibe², Yoshiaki Nakamura² and Hideki Tanaka¹; ¹Chuo University, Japan; ²Osaka University, Japan

Thermoelectric power factor is represented with $S^2\sigma$, where S and σ are Seebeck coefficient and electrical conductivity, respectively. Recently, organic thermoelectric materials have been attracting attention for their low cost, eco-friendly, and flexibility. For thermoelectric power factor enhancement of organic materials, introduction of inorganic nanostructures is effective. Especially, nanowires (NWs) can bring percolation effect by forming NW network structures, leading to power factor enhancement. As inorganic nanostructures, we focused on Cu₂Se NWs. Cu₂Se is composed of low-cost and abundant elements, and exhibits high thermoelectric power factor at room temperature (RT). In this study, we prepared PEDOT:PSS films containing the Cu₂Se NWs synthesized by photoreduction method [1] for the enhancement of thermoelectric power factor.

Cu₂Se NWs were synthesized as following method. Se NWs were synthesized by mixing SeO₂, β -cyclodextrin, and ascorbic acid, stirring the solution for 4 hours, and redispersing it in ethanol for 4 hours [2]. The Se NWs, ethanol, and copper acetate were added into Milli-Q water, and the solution was irradiated by UV light, forming Cu₂Se NWs (photoreduction method). After that, PEDOT:PSS solution and ethanol dispersion of Cu₂Se NWs were spin coated and annealed at 80 °C alternately on glass with various spin coating number of Cu₂Se NWs. The reference sample of PEDOT:PSS thin film without Cu₂Se NWs was also synthesized. The structures of the NWs and films were confirmed by X-ray diffraction (XRD), scanning electron microscopy (SEM), energy dispersive X-ray spectrometry (EDX). S was measured by hand-made system and σ was measured by van der Pauw method. The S values were also revised by ZEM-3 (ADVANCE RIKO).

From the surface SEM-EDX analysis of PEDOT:PSS/Cu₂Se NWs thin films, Cu, Se and S (from PEDOT:PSS) were observed, indicating that Cu₂Se NWs were covered with PEDOT:PSS. The SEM-EDX image also showed that Cu₂Se NWs were connected to each other, which is NW network structure. Quantitative analysis of EDX demonstrated that the amount of Cu₂Se increased as the spin coating number of Cu₂Se increased. For thermoelectric performance, PEDOT:PSS/Cu₂Se NWs thin films exhibited drastic increase of σ at ~40 wt% as the Cu₂Se amounts increased. This is due to the formation of Cu₂Se NW network structures. This σ value was much higher than that of PEDOT:PSS single thin film. As a result, PEDOT:PSS/Cu₂Se NWs thin films exhibited the enhancement of power factor by formation of Cu₂Se NW network structures.

Acknowledgments

This work was supported by Grant-in-Aid for Early-Career Scientists Grant Number 21K14479 and Grant-in-Aid for Scientific Research (C) Grant Number 19K05187 from JSPS KAKENHI, Japan.

References:

- [1] M. Miyagawa, et al., Aqueous synthesis of protectant-free copper nanocubes by a disproportionation reaction of Cu₂O on synthetic saponite. *Chem. Commun.* 54, 8454 (2018).
- [2] Q. Li, and V. W. W. Yam, High-yield synthesis of selenium nanowires in water at room Temperature. *Chem. Commun.* 1006-1008, (2006).

4:30 PM EQ01.09.09

Phonon Scattering and Vibrational Localization in 2D Embedded Nanoparticle Composites Ongira Chowdhury and Joseph P. Feser; University of Delaware, United States

In this work, a Landauer approach enabled by the Frequency Domain Perfectly Matched Layer Method (FDPML) is used to study phonon transport in a series of large 2D domains with randomly embedded nanoparticles over a wide range of nanoparticle loadings and wavelengths. The effect of nanoparticle packing density on the mean free path and localization length is characterized. We observe that in the Mie scattering regime, the independent scattering approximation is valid up to volume fractions exceeding 10% and often higher depending on the scattering parameter, indicating the mean free path can usually be calculated much less expensively using the number density and the scattering cross-section of a single scatterer. We also study localization lengths and their dependence on particle loading. In the case of heavy particles in a lighter matrix, we have been able to observe localization only at volume fractions >30% using the Landauer approach and only for high frequency modes, exceeding the vibration frequencies of the embedded nanoparticles. Using modal analysis we show that localization in nanoparticle laden materials is primarily due to energetic confinement rather than Anderson localization. Subsequently, we show that by using light particles in a heavy matrix the fraction of confined modes can be substantially increased.

4:45 PM EQ01.09.10

Linking Polaron Signatures to Charge Transport in Doped Thiophene Polymers Anas I. Abutaha¹, Vijila Chellappan², Pawan Kumar² and Kedar Hippalgaonkar^{2,3}; ¹Qatar Environment and Energy Research Institute (QEERI), Hamad Bin Khalifa University (HBKU), Qatar; ²Institute of Materials Research and Engineering, Agency for Science Technology and Research, Singapore; ³Nanyang Technological University (NTU), Singapore

Carrier doping and structural morphology are key knobs to tune thermoelectric transport in conducting polymers. Several characterization methods such as Grazing-Incidence Wide-Angle X-ray Scattering (GIWAXS), Ultraviolet photoelectron spectroscopy (UPS) - inverse photoemission spectroscopy (IPES), and Absorption spectroscopy (Visible- Near Infrared (NIR) spectral region) are required to fully study these knobs. Here, we focus on absorption spectroscopy to understand thermoelectric transport in conducting polymers. Optical signatures of doping are correlated with thermoelectric properties of conducting polymers. Thus, we quantitatively extract the carrier concentration from optical absorption signatures of polarons by linking the absorption ratio of the low energy polaronic peak and neutral excitons in doped thiophene-based films with electrical conductivity and Seebeck coefficient under Boltzmann transport equations (BTE). The rate of change of electrical conductivity with carrier concentration (absorption ratio) differs with variation in doping and/or processing conditions, whereas the Seebeck coefficient decreases monotonically with carrier concentration regardless of doping method as expected. The correlation confirms that charge mobility is a key parameter to improve the thermoelectric performance where the method of doping or process conditions creates wide range of structural disorder controlling charge transport.

SESSION EQ01.10: Virtual Session I: Progress in Thermoelectrics I
Session Chairs: Guangzhao Qin and Sarah J. Watzman
Tuesday Morning, December 6, 2022
EQ01-virtual

8:00 AM *EQ01.10.01

Progress in Transverse Thermoelectric Conversion Using Spin Caloritronics [Ken-ichi Uchida](#)^{1,2}; ¹National Institute for Materials Science, Japan; ²Tohoku University, Japan

Spin caloritronics is the fusion research field based on the combination of spintronics, thermoelectrics, and thermal energy engineering, in which the interplay between spin, charge, and heat currents has been extensively investigated. In this field, many experimental and theoretical studies have focused on the transverse thermoelectric conversion using magnetic materials to clarify its mechanism and utilize unique functionalities [1]. In this talk, we review fundamentals of spin caloritronics and recent progresses in basic and applied studies on the transverse thermoelectric conversion using magnetic materials, *i.e.*, the anomalous Nernst/Ettingshausen effects [2-5] and the Seebeck-driven transverse thermoelectric generation [6-8].

References:

- [1] K. Uchida, W. Zhou, and Y. Sakuraba, *Appl. Phys. Lett.* **118**, 140504 (2021).
- [2] T. Seki, R. Iguchi, K. Takanashi, and K. Uchida, *Appl. Phys. Lett.* **112**, 152403 (2018).
- [3] J. Wang, Y. K. Takahashi, and K. Uchida, *Nature Commun.* **11**, 2 (2020).
- [4] A. Miura *et al.*, *Appl. Phys. Lett.* **115**, 222403 (2019).
- [5] R. Modak *et al.*, arXiv:2203.10737
- [6] W. Zhou *et al.*, *Nature Mater.* **20**, 463 (2021).
- [7] K. Yamamoto *et al.*, *J. Appl. Phys.* **129**, 223908 (2021).
- [8] W. Zhou, T. Hirai, K. Uchida, and Y. Sakuraba, *J. Phys. D: Appl. Phys.* **55**, 335002 (2022).

8:30 AM EQ01.10.02

Globally Optimal Band Structure for Thermoelectrics in Realistic Systems [Junsoo Park](#); NASA Ames Research Center, United States

Observation is made that a linear dispersion in any dimension under acoustic-phonon-deformation-potential scattering theoretically prescribes a constant charge transport distribution, required for the boxcar profile known to maximize the thermoelectric figure of merit. A linear dispersion squeezed by two transport gaps under scattering by phonon deformation then theoretically constitutes a globally optimal qualitative band structure that may arise in realistic materials. Optimum bandwidth and electron velocity are also determined under deformation-potential scattering in three dimensions. The prescriptions lead to constant zT for all temperatures for a given value of lattice thermal conductivity, in agreement with purely analytic results from a boxcar transport distribution. This indicates that for a truly optimal band structure, the electronic part of the performance is temperature-independent, and the temperature-dependence of zT owes solely to that of lattice thermal conductivity.

8:45 AM *EQ01.10.03

Utilizing Band Anisotropy to Enhance the Thermoelectric Power Factor Chenguang Fu, Tiejun Zhu and [Airan Li](#); Zhejiang University, China

The electronic band structure is a “gold mine” for exploring novel strategies that will promote the discovery of good thermoelectrics. Band anisotropy is a key characteristic of electronic structure that broadly exists in a lot of solid materials. Theoretically, valley anisotropy was proposed to benefit the electrical transport of TE materials [1,2]. However, there is still no experimental demonstration to confirm this prediction due to the challenge of the selection of suitable material as a model. Here, taking advantage of the single anisotropic Fermi pocket in p-type Mg₃Sb₂, a feasible strategy of utilizing the valley anisotropy to enhance the thermoelectric properties was demonstrated by synergistic studies of single crystals and textured polycrystalline samples. Compared to the heavy-band direction, improved carrier mobility by a factor of 3 is observed along the light-band direction while the Seebeck coefficient remains similar. Together with lower lattice thermal conductivity, increased room-temperature zT by a factor of 3.6 was found in the light-band direction of the single crystal. Further analysis revealed that the pz orbital, which overlaps more along the light-band direction, leads to the anisotropic valence band. With this knowledge, first-principles calculations of 66 isostructural Zintl phase compounds were conducted and 9 of them were found to display a pz orbital-dominated valence band, which are useful for guiding the development of high-performance p-type Zintl phase TE materials [3].

- [1] *Phy. Rev. Lett.* **110**, 146601 (2013)
- [2] *Phys. Rev. Lett.* **114**, 136601 (2015)
- [3] *Nat. Commun.* **12**, 5408 (2021)

9:15 AM *EQ01.10.04

Thermoelectric Materials Assembled from Nanocrystals [Dmitri V. Talapin](#); University of Chicago, United States

Nano- and mesostructuring of thermoelectric (TE) materials have emerged recently as a new paradigm to enhance the efficiency and manufacturability of TE modules. Switching from materials with large crystal grains to nano- and mesostructured compounds brings to the spotlight fundamentally important problems of morphological stability, grain growth, and inter-grain transport. The chemistry and physics of interfaces in TE devices remain largely underexplored. This is in stark contrast to, e.g., thin-film photovoltaics where grain boundaries have been studied in-depth for many years. We will first discuss the effect of interfaces on charge and heat transport in arrays of semiconductor nanocrystals (NCs) that represent a convenient model of nanostructured TE materials. Next, we will cover new chemical approaches for the rational design of the interfaces in nanostructured TE materials. The NCs themselves can serve as a “solder” for nano- and mesoscopic grains. During mild heat treatment, NCs fill up the voids between particles and act as a “glue” joining grains in hot-pressed pellets or solution-processed films. The chemical design of NC glue allowed for the selective enhancement or reduction of the majority carrier concentration near the grain boundaries, and thus resulted in doped or de-doped interfaces in granular TE materials. Chemically engineered interfaces can be further designed to optimize power factor and thermal conductivity.

9:45 AM DISCUSSION TIME

SESSION EQ01.11: Virtual Session II: Progress in Thermoelectrics II
Session Chairs: Sepideh Akhbarifar and Heng Wang
Wednesday Morning, December 7, 2022
EQ01-virtual

11:00 AM EQ01.11.02

Design and Fabrication of Tetradymites Based Vertically-Oriented Thermoelectric Generators (TEGs) [Mamadou T. Mbaye](#); Norfolk State

University, United States

As the world governments and lawmakers shift to concerted environmentally-friendly policies to achieve net zero in carbon emissions by the year 2050, much interest and discourse are being displayed in scientific fora on how research in renewable energy materials and devices can pave the way to a more sustainable planet. In light of that, thermoelectric materials and devices based on Bi_2Te_3 and its alloys have received renewed attention from industry and academia due to their renewability, large scalability, and commercial viability in producing electricity from waste heat for niche applications in micro refrigeration and small power generation. These materials exhibit the dimensionless figure of merit ZT values around 1, at room temperature and can be utilized to design and fabricate novel, vertical, flexible, wearable, and portable thermoelectric devices. However, for thermoelectric devices to be competitive with fluid-based and other energy-related devices, $ZT \geq 2$ is usually sought. The complexities of achieving high ZT reside in the fact that the dimensionless figure of merit presents a number of conflicting parameters. One cannot change one parameter without the detrimental effect of impacting the others. How then do we navigate the delicate and intricate relationship between the Seebeck coefficient or thermopower S , the electrical conductivity α , and the thermal conductivity K in order to achieve high ZT ? From band engineering to grain boundary scatterings, to multilayer superlattice (SL) structures, thermoelectric researchers worldwide are investigating a plethora of options combined with state-of-the-art techniques to achieve just that. In this work, we designed vertical and flexible thin-film thermoelectric generators (TEGs) based on n-type Bi_2Te_3 , p-type Sb_2Te_3 , and their ternary chalcogenide n-type $\text{Bi}_2\text{Te}_{2.83}\text{Se}_{0.17}$ and p-type $\text{Bi}_{0.4}\text{Sb}_{1.6}\text{Te}_3$ in the form of multilayer superlattice nanostructures using RF magnetron sputtering deposition method. The inclusion of interstitial atoms (Sb and Se) in these nanostructured ternary chalcogenides provides a two-fold benefit as it can greatly reduce the thermal conductivity of the material, due to scattering events of a wide range of phonons carrying heat but also improve the power factor through modification of the electronic structure of the material. In addition, if the layer thickness is in close proximity to the phonon's mean free path (MFP), heat-carrying phonons of different wavelengths (short, medium, or long) can be scattered more effectively at the superlattice interfaces, thereby resulting in the decrease of the lattice thermal conductivity of the material and subsequently the enhancement of the thermoelectric figure of merit. Furthermore, we investigated the optimal growth parameters for each material that will render high thermopower, S , and suitable electrical conductivity, α .

11:15 AM *EQ01.11.03

Defect Design in Thermoelectric Materials—Uniting Computation and Experiment for Tailored Synthesis and Transport Properties [Eric S. Toberer](#); Colorado School of Mines, United States

The application of modern defect physics to thermoelectric materials enables the tailored design of thermoelectric materials with targeted properties.

11:45 AM EQ01.11.04

PRESENTED ON-DEMAND ONLY: Flexible Thermoelectric Generator with Moisture Re-Absorbable Hydrogel Heatsink [Jeong Hun Kim](#), Jong-Pil Im, Seung Eon Moon and Yeriaron Kim; Electronics and Telecommunications Research Institute, Korea (the Republic of)

A thermoelectric generator (TEG) is promising energy harvesting device that can convert heat generated from power plant, furnace and combustion engine to electric energy. Because of the demands for pollutant-free energy source, researches about thermoelectric materials has been widely conducted to utilize it as a renewable energy source. In particular, since many heat sources have a curved shape, interest in flexible TEG (f-TEG) that can be applied here is growing.

In this paper, we made a BiTe-based flexible TEG that can be applied to curved surfaces using a polyimide PCB substrate. By designing the performance of the f-TEG according to the height of the TEG leg (1.5 ~ 3 mm) and the number of pairs (31 ~ 58 pair), and verifying it experimentally, an optimized structure could be derived.

In the case of f-TEG, it is difficult to apply a general fin-type heatsink made of metal, so a hydrogel-based flexible heatsink that can replace it was produced. In the case of utilizing the latent heat of water, high power generation output can be obtained initially, but the performance gradually decreases as water evaporates. To solve this problem, a hygroscopic ion that can reabsorb moisture in the absence of a heat source was introduced. In addition, by controlling the ratio of monomer and crosslinker and solvent, it was confirmed that stable attachment to the f-TEG surface was possible and cracks did not occur even during evaporation. Also, it was confirmed that the f-TEG to which the hydrogel heatsink was applied improved the power generation performance for more than 5 hours, and recovered more than 90% of the initial performance after one night in the atmospheric condition.

The f-TEG was manufactured in the form of an array to produce a system capable of mW-level power generation, and it was confirmed that the voltage was boosted through the power management device to drive the sensor and transmit information using bluetooth.

It is expected that this will be used as a power source for wearable devices and mobile systems that can be driven by themselves using various heat sources including body temperature in the future.

11:50 AM EQ01.11.05

DLC Interlayers Functionalized Bi-Sb-Te-Based Nanoarchitected Films for Achieving High Thermoelectric Performance [Karan Giri](#), Yan-Lin Wang, Yu-Chieh Shih, Chuan-Wen Wang, Ling-Chun Chao, Yi-Chen Chen, I-Jung Wang, Pei-Hsuan Cho, Cheng-Ju Yang and Chun-Hua Chen; National Yang Ming Chiao Tung University, Taiwan

Nanostructuring has become one of the most practically proven and effective strategies in enhancing the thermoelectric figure of merit, which significantly propels thermoelectric materials to the forefront of progress in fundamental research and advanced applications. Accompanied with nanostructuring, heterogenization, which frequently shows excellent synergistic effects with nanostructures, has appeared as an appendable and feasible solution for a further breakthrough. Among numerous hetero-additives, diamond-like carbon (DLC), composed of sp^3 and sp^2 hybrid carbon atoms, is a type of amorphous carbon. Because of its relatively low tuneable thermal conductivity $\sim 10^{-1}-10^{-2} \text{ Wm}^{-1}\text{K}^{-1}$, it may be applied as a potential candidate to suppress the thermal conductivity of the thermoelectric matrix without seriously affecting the overall conductivity.

In this work, we developed a new design concept and methodologies for building quasi-superlattice-like structurally ordered hetero-nanocomposite films for potentially realizing high-thermoelectric performance. According to this design concept, a series of superarchitectures consisting of longitudinally periodic DLC interlayers in latitudinally well-aligned Bi-Sb-Te (BST) based nanostructures were successfully demonstrated for the first time by using dual-beam pulsed laser deposition. The optimized Seebeck coefficient of $\sim 500 \mu\text{VK}^{-1}$ and the corresponding power factor of $\sim 40 \mu\text{Wcm}^{-1}\text{K}^{-2}$ achieved are comparable to or higher than the reported values for BST or BST-based nanocomposites, which evidently originated from the periodically added DLC interlayers, as clarified in the Pisarenko plot. Besides, the periodic presence of the DLC additives was found to instantly refine the grain size of the simultaneously deposited local BST layer and thus effectively reduce the thermal transport as qualitatively evidenced by micro-Raman characterizations. The present work provided a direct insight into the fundamental understanding of the utilization of DLC as functional hetero-additives for structural modulation and thermoelectric enhancement.

12:05 PM DISCUSSION TIME

SYMPOSIUM EQ02

Emerging Materials for Light-Based Quasiparticles, Mie-tronics and Metasurfaces
November 28 - December 7, 2022

Symposium Organizers

Antonio Ambrosio, Fondazione Istituto Italiano di Tecnologia
Viktoriia Babicheva, University of New Mexico
Cheng-Wei Qiu, National University of Singapore
Giulia Tagliabue, École Polytechnique Fédérale de Lausanne

* Invited Paper
+ Distinguished Invited

SESSION EQ02.01: Emergent Phenomena and Light-Based Quasiparticles I
Session Chairs: Viktoriia Babicheva and Stephanie Law
Monday Morning, November 28, 2022
Sheraton, 2nd Floor, Liberty B/C

10:30 AM *EQ02.01.01

“Defects” as Emitters for Quantum Photonics—Imperfections Creating Opportunities [Evelyn Hu](#), Harvard University, United States

We have typically sought out “perfect” materials to produce the best emitters for nano-photonic devices. Recently, however, defect states in wide bandgap semiconductors are defining a new frontier for nano-photonics. This talk will focus on a particular defect state: silicon vacancies in 4H-SiC. Integration of such defects within nanobeam photonic crystal cavities have shown an 80-fold optical enhancement of a Si-vacancy transition with emission at about 860 nanometers. The emitter-cavity coupling produces significant photonic signal amplification, and can serve as a building block, quantum repeater for larger-scale quantum information networks.

The photonic crystal cavities can also serve as “nanoscopes” that allow us to better understand the local environment of the silicon vacancies, the other defects that they encounter, the possible interactions with those defects and pathways to better processing and control of the defects. We will discuss insights provided by the cavities as nanoscopes. The accompanying spin signatures of the silicon vacancies, and the correlations between photon emission and spin modulation provide insights into further applications of these new nanophotonic emitters.

11:00 AM EQ02.01.02

Excitonic Halide Perovskites—A New Room-Temperature Materials Platform for Quantum Simulations. [Wei Bao](#), University of Nebraska–Lincoln, United States

Exciton polaritons, the part-light and part-matter quasiparticles in semiconductor optical cavities, are promising for exploring Bose–Einstein condensation, non-equilibrium many-body physics and analogue simulation at elevated temperatures. However, a room-temperature polaritonic platform on par with the GaAs quantum wells grown by molecular beam epitaxy at low temperatures remains elusive. Here, we address this challenge by adopting a method based on the solution synthesis of excitonic halide perovskites grown under nanoconfinement. Such nanoconfinement growth facilitates the synthesis of smooth and homogeneous single-crystalline large crystals enabling the demonstration of XY Hamiltonian lattices with large sizes. Next, we report the first observation of polariton superfluidity in a Wannier-Mott exciton system at room temperature. Specifically, we demonstrate transitions from a normal fluid to superfluidity and supersonic fluid in both two- and one-dimensional cases in halide perovskite microcavities. In the two-dimensional case, we demonstrated a landmark zero-viscosity superfluid and a supersonic Čerenkov wave pattern at room temperature, on a par with low-temperature GaAs cases for the first time. In the one-dimensional case, we show that the back-reflection can be fully suppressed outside the superfluidity healing length when the polariton superfluid hits a hard potential wall under the critical velocity. With these demonstrations, we further establish perovskites as a promising platform for room temperature polaritonic physics and pave the way for the realization of robust mode-disorder-free polaritonic devices at room temperature.

Nature Materials (2022)
Manuscripts (2022) under review

11:15 AM EQ02.01.03

Topological Hydrodynamic Circulator in Graphene’s Viscous Hall Fluid [Wenbo Sun](#), Todd Van Mechelen, Ashwin K. Boddeti, Sathwik Bharadwaj and Zubin Jacob; Purdue University, United States

Viscous Hall electron fluid in graphene has emerged at the forefront of many-body interacting electron systems due to its low dimensionality and impurity density. It is the first candidate for a non-local topological electromagnetic phase of matter. This 2D topological viscous Hall insulator is characterized by an optical N invariant, fundamentally different from the Chern and quantum spin Hall insulators. Here, we show that this viscous Hall fluid is in a topological electromagnetic phase arising from the repulsive nature of Hall viscosity. This feature is evident by studying the edge magneto-plasmons, which close the low-frequency electromagnetic bandgap for graphene. Based on the unidirectional topological edge plasmons, we design and simulate a topological circulator, which is a chiral quantum radio-frequency (RF) circuit component crucial for information routing and interfacing quantum-classical computing systems. Our work opens practical applications of graphene’s viscous Hall fluid and simultaneously provides an experimental platform for studying topological hydrodynamics of light.

11:30 AM *EQ02.01.04**Creating Bound States in the Continuum Using Superstructure Photonics** [Alexander Cerjan](#); Sandia National Laboratories, United States

In the past decade, symmetry-protected bound states in the continuum (BICs) have proven to be an important design principle for creating and enhancing devices reliant upon states with high-quality (Q) factors, such as sensors, lasers, and those for harmonic generation. However, as I will discuss, it is possible to prove using representation theory that current implementations of symmetry-protected BICs in photonic crystal slabs can only yield BICs at the center of the Brillouin zone and below the Bragg diffraction limit, which fundamentally restricts their use to single- or few-frequency applications. Instead, this limitation must be overcome by altering the system's radiative environment. In this talk I will discuss two separate methods for creating lines of BICs by altering the radiative environment surrounding a photonic slab, i.e., by using a superstructure: First, by using the symmetry of the environment to create a symmetry bandgap in the environment's radiative channels in which slab states with un-represented symmetries are necessarily BICs [1]. Second, by using the environment to reduce the number of radiative channels, enabling the formation of lines of BICs accidentally [2]. The ability to create continuous lines of BIC may have ramifications for enabling multi-frequency and multi-wave vector applications in technologies that leverage these high-Q states.

[1] A. Cerjan *et al.*, *Sci. Adv.*, vol. 7, p. eabk1117, (2021).[2] A. Cerjan *et al.*, *Phys. Rev. Lett.*, vol. 123, p. 023902, (2019).

SESSION EQ02.02: Nanostructures and Optical Response I

Session Chairs: Viktoriia Babicheva and Alexander Cerjan

Monday Afternoon, November 28, 2022

Sheraton, 2nd Floor, Liberty B/C

1:30 PM *EQ02.02.01**Plasmonics in Electronic Topological Materials** [Stephanie Law](#); University of Delaware, United States

Topological insulators (TIs) are materials with an electronic bulk bandgap crossed by surface states that exhibit linear dispersion and spin-momentum locking. Electrons occupying these surface states have low mass and large Fermi velocity due to the linearity of the band structure. The spin-momentum locking of the surface states leads to a reduction in electron scattering, since a change in momentum requires a spin flip. Among other interesting properties, two-dimensional Dirac plasmon polaritons (DPPs) can be excited from these surface electrons. These plasmon polaritons exhibit resonances in the terahertz (THz), a frequency range of interest for chemical identification, imaging, and communication. The TI plasmons inherit the unusual properties of their constituent electrons: the excitations are two-dimensional and massless, similar to those found in graphene. Unlike graphene, TI plasmons should also exhibit spin-momentum locking, leading to a reduction in scattering and an increased plasmon lifetime.

In this talk, I will summarize our past work on exciting DPPs in TI thin films, demonstrating record-high mode indices and long plasmon lifetimes. I will then discuss more recent work on coupling DPPs in adjacent microribbons to tune their frequency, exploring how the DPPs evolve as the TI film thickness is tuned through the topological transition, and synthesizing TI/normal insulator superlattices that house complex DPP modes. I will close by showing evidence for a transition to a THz Dirac hyperbolic metamaterial in multilayer stacks of TIs and normal insulators. These materials have the potential to be powerful components in future THz photonic devices.

2:00 PM EQ02.02.02**Ultra-Low-Loss Anisotropic Image Polaritons in α -MoO₃** [Sergey Menabde](#)¹, [Junghoon Jahng](#)², [Sergejs Boroviks](#)^{3,4}, [Jongtae Ahn](#)⁵, [Jacob Heiden](#)¹, [Do Kyung Hwang](#)⁵, [Eun Sung Lee](#)², [N. Asger Mortensen](#)^{4,4} and [Min Seok Jang](#)¹; ¹Korea Advanced Institute of Science and Technology, Korea (the Republic of); ²Korea Research Institute of Standards and Science, Korea (the Republic of); ³Swiss Federal Institute of Technology Lausanne, Switzerland; ⁴University of Southern Denmark, Denmark; ⁵Korea Institute of Science and Technology, Korea (the Republic of)

Polaritons in van der Waals crystals possess a high degree of field confinement, allowing for the strong light-matter interaction and light manipulation at nanoscale. At the same time, when a polaritonic van der Waals crystal is placed in proximity to a highly conductive metal, the coupling between the collective charge oscillations and their images in the metal results in a manifestation of an even more compressed low-dimensional mode – the image polariton.

We use the near-field optical microscopy and the photo-induced force microscopy to study the hyperbolic image phonon-polaritons (HIP) in orthorhombic molybdenum trioxide (α -MoO₃) – a recently discovered polaritonic van der Waals crystal that supports strongly anisotropic mid-infrared phonon-polaritons. As a low-loss substrate for the image modes, we employ the atomically-flat monocrystalline gold flakes. By leveraging the unique physical properties of the gold crystals, we systematically probe different momentum states on the isofrequency surface and measure the full complex-valued propagation constant of the HIP propagating at different angles to the crystallographic axes of α -MoO₃.

We report an exceptionally long lifetime of phonon-polaritons in α -MoO₃: 4.2 ps and 9.7 ps in the second and the third Reststrahlen bands, respectively, owing to the suppression of all substrate-mediated loss channels in our samples. In contrast, the less confined phonon-polaritons in the α -MoO₃ on SiO₂ substrate have been shown to have a significantly shorter lifetime of ~2 ps in the second Reststrahlen band.

Furthermore, our study reveals the drastically different dispersion properties of the HIP with opposite signs of the group velocity: only the modes with positive group velocity (in the second Reststrahlen band) have both significantly larger momentum and lifetime compared to their counterparts on a dielectric substrate, while the image modes with anomalous dispersion (in the third Reststrahlen band) possess smaller momentum.

Summarizing, our near-field study demonstrates a unique combination of the in-plane anisotropic phonon-polaritons in α -MoO₃, the image mode, and the monocrystalline gold substrate, leading to a manifestation of the hyperbolic image phonon-polaritons with simultaneously greater field compression and larger lifetime compared to the phonon-polaritons in α -MoO₃ on a dielectric substrate. Our results spotlight the HIP in α -MoO₃ as an appealing platform for versatile nanophotonic applications.

2:15 PM *EQ02.02.03**Strong Coupling and Extreme Anisotropy in Infrared Polaritonic Media** [Joshua D. Caldwell](#); Vanderbilt University, United States

The field of nanophotonics is based on the ability to confine light to sub-diffractive dimensions. In the infrared, this requires compression of the wavelength to length scales well below that of the free-space values. While traditional dielectric materials do not exhibit indices of refraction high enough in non-dispersive media to realize such compression, the implementation of polaritons, quasi-particles comprised of oscillating charges and photons, enable such opportunities. Two predominant forms of polaritons, the plasmon and phonon polariton, which are derived from light coupled with free carriers or polar optic phonons, respectively, are broadly applied in the mid- to long-wave infrared. However, the short scattering lifetimes of free-carriers results in

high losses and broad linewidths for the former, while the fast dispersion and narrow band of operation for the latter result in significant limitations for both forms. Here we will discuss the opportunity to implement polaritonic strong coupling between different media in an effort to dictate the polaritonic dispersion relation, and thus, the propagation and resonant properties of these materials. Further, by employing the extreme anisotropy of crystals ranging from two-dimensional materials such as hexagonal boron nitride and transition metal dichalcogenides to low-symmetry monoclinic to triclinic materials, novel optical phenomena such as hyperbolicity and shear polaritons are observed. The talk will highlight ultra-strong coupling between both forms of polaritons in the context of infrared emitters, as a means to control planar propagation using hyperbolic polaritons, an modifying thermal dissipation at ultrafast time scales.

2:45 PM EQ02.02.04

Engineered Near- and Far-Field Optical Response of Dielectric Nanostructures Using Focused Cylindrical Vector Beams [Martin Montagnac](#)¹, Gonzague Agez¹, Sebastien Weber¹, Arnaud Arbouet¹, Aurelien Cuche¹, Guilhem Larrieu², Yoann Brûlé³, Gerard Colas des Francs³, Bruno Masenelli⁴, Vincent Larrey⁵ and Vincent Paillard¹; ¹CNRS-CEMES, France; ²CNRS-LAAS, France; ³ICB, France; ⁴INL, France; ⁵CEA-LETI, France

We present near- and far-field optical properties of silicon nanostructures (Si-NS) under linear polarization (Gaussian beam), and azimuthally or radially focused cylindrical vector beams investigated by finite-difference time-domain method (FDTD) in Meep open-source software. In addition to the preferential excitation of specific electric or magnetic resonance modes as function of the excitation beam polarization, we show in the case of spheroids that shape anisotropy affects the resonance wavelength and the dipole orientation of the magnetic or electric dipole mode. Depending on the spheroid symmetry axis with respect to the electric field orientation, the electric dipole resonance can be split in two peaks, giving quasi-unidirectional scattering, separated by an anapole mode. The optical properties in both the far-field (scattering pattern) and near-field (electric and magnetic field hot spots) can be tuned by changing the excitation polarization at a fixed wavelength and selecting properly the spheroid shape and dimensions. Similar behavior is obtained on nanostructures such as nanocylinders with circular or elliptic section that could be produced by top-down fabrication techniques. As magnetic and electric near field hotspots can be engineered, we present photoluminescence (PL) mappings of Eu³⁺-doped homogenous thin films deposited on Si nanostructures produced by electron beam lithography and reactive ion etching of silicon on silica substrate. On the one hand, we show that the PL enhancement depends on the Si-NS resonance mode at the excitation wavelength. We also evidence that PL maps exhibit a very specific behavior as function of the shape and polarization of the excitation beam. In other words, the PL intensity distribution can be spatially shaped by the near-field, itself shaped by both the excitation beam polarization and the Si-NS properties. On the other hand, we investigate how the PL maps at the emission wavelength for the different kind of emitting dipolar transitions (magnetic dipole at about 590 nm and electric dipole at about 610 nm) are influenced by either the electric or magnetic Local density of States (LDOS). Such work constitutes a first step in the design of Si-NS coupled to quantum emitters that can be optimized for many parameters: both excitation and emission wavelengths, emitting dipole nature and orientation, and emission directivity.

3:00 PM BREAK

SESSION EQ02.03: Nanophotonic and Plasmonic Materials
Session Chairs: Alexander Cerjan and Dmitry Chigrin
Monday Afternoon, November 28, 2022
Sheraton, 2nd Floor, Liberty B/C

3:30 PM EQ02.03.01

Collective Multipole Resonances in Lossy Materials [Amanda Romero](#), [Erik Boldt](#), [James Toomey](#) and [Viktoriia Babicheva](#); University of New Mexico, United States

There is a lot of interest in utilizing metamaterial perfect absorbers and transforming electrodes into hybrid photodetectors, which can enhance their performance. Due to their exceptional properties, lossy materials, such as titanium, nickel, and others, have been a focus of large research efforts. However, because of the high losses, achieving high light confinement and harvesting in the nanostructures of such materials is challenging.

We design resonant nanostructures to achieve efficient light control and dynamic tuning of nanophotonic elements. We have achieved the excitation of strong lattice resonances and larger absorption in the arrays of lossy nanoparticles, which can result in a higher generation of hot electrons. We explore the optical properties of novel nanostructures, intending to use them in laser devices and for enhanced emission.

A universal approach is developed to achieve the design goals of layered nanostructures with low optical losses and high performance. We have shown that further narrowband and broadband photodetector functionality can be improved using a multiple-period array of nanoparticles by manifesting enhancement in the resonances and absorption profiles. These nanostructures can provide high-efficiency hot-electron photoconversion and be applied in hybrid devices and photodetectors.

This work was performed, in part, at the Center for Integrated Nanotechnologies, an Office of Science User Facility operated for the U.S. Department of Energy (DOE) Office of Science by Los Alamos National Laboratory (Contract 89233218CNA000001) and Sandia National Laboratories (Contract DE-NA-0003525). The work is also supported by Contract DE-2375849.

3:45 PM *EQ02.03.02

Metal-Halide Perovskite Hyperbolic Metamaterials [Jacob Scheuer](#); Tel Aviv University, Israel

Hyperbolic metamaterials (HMM) are artificially engineered anisotropic materials. These materials are characterized by their hyperbolic dispersion relation where the in-plane dielectric constants have an opposite sign to the out-of-plane dielectric constants. Recently, HMMs received much attention due to their potential applications in super resolution imaging, absorber, biosensors, extreme polarization anisotropy of photoluminescence just to name a few. Metal-halide perovskites have emerged in recent years as a powerful material system in the field of photonics. Due to their promising electronic and optical properties, tremendous progress has been made in perovskites solar cell performance. In this presentation, I will demonstrate the first realization of HMM using solution processable methyl ammonium lead iodide (MAPbI₃) and plasmonic metal, Au. I will discuss the properties of the HMM within the available parameter space (geometry, wavelength, etc.) in the context of effective medium theory as well as the potential applications

4:15 PM *EQ02.03.03

Extreme Strain Engineering to Control Photon, Electron, Phonon and Polariton Transport in Materials for Energy Applications [Svetlana V. Boriskina](#); Massachusetts Institute of Technology, United States

I will discuss the opportunities and applications enabled by strain-induced deformations in semiconductor and polymer materials. One such application is persistent electric energy generation in flexoelectric devices that can be achieved by harnessing absorption and radiative heat emission in narrow-gap semiconductors with inversion symmetry broken by inhomogeneous strain [1]. Another is static and dynamic control of directional surface plasmon polariton modes propagation in Weyl semimetals or semiconductors under strain [2,3]. I will outline strategies to engineer and characterize the effects of the externally-induced or in-situ strain on the material structure, polarization, and energy transport properties. Finally, I will discuss the opportunities for solid-state cooling and heating applications based on elastocaloric and twistocaloric effects in strain-activated polymer fibers engineered to achieve temperature control, energy storage, and thermal conductivity modulation.

This research has been supported in part by the MIT Lincoln Laboratory under award No. ACC-777 (for the flexoelectric energy harvesting), the Army Research Office under award No. W911NF-19-1-0279 (for the near-field radiative energy transfer), the DOE-BES program under award No. DE-FG02-02ER45977 (for the strain-controlled thermal conductivity) and the MIT-SUSTech Program (for the elastocaloric effects).

[1] B. Lorenzi, Y. Tsurimaki, A. Kobayashi, M. Takashiri, and S. V. Boriskina, "Self-powered broadband photo-detection and persistent energy generation with junction-free strained Bi₂Te₃ thin films," *Opt. Express* 28(19), 27644–27656 (2020).

[2] S. Pajovic, Y. Tsurimaki, X. Qian, and S. V. Boriskina, "Radiative heat and momentum transfer from materials with broken symmetries," *Opt. Mater. Express* 11(9), 3125–3131 (2021).

[3] S.V. Boriskina, M. Blevins, S. Pajovic, There and Back Again: the nonreciprocal adventures of light, *Opt. Photon. News*, Sept. 2022.

4:45 PM EQ02.03.04

Hyper-Doped Silicon Nanoantennas and Metasurfaces for Tunable Infrared Plasmonics Jean-Marie Pouirol¹, Caroline Bonafos¹, Clément Majorel², Peter Wiecha³, Richard Monflier³, Guilhem Larrieu³, Fuccio Cristiano³, Anne-Sophie Royet⁴, Pablo Acosta Alba⁴, Sébastien Kerdiles⁴ and Vincent Paillard¹; ¹CEMES-CNRS, Université de Toulouse, CNRS, France; ²CHREA-CNRS, France; ³LAAS-CNRS, Université de Toulouse, CNRS, France; ⁴CEA-LETI, France

The use of plasmonic or high refractive index dielectric nanoantennas or metasurfaces is a common strategy for increasing optical absorption and scattering and for localizing light at subwavelength dimensions. Because of their low losses and direct compatibility with large-scale production techniques from microelectronics, semiconductor nanostructures and full noble metal nanostructures are attracting increasing interest in the visible spectrum. Those techniques have limitations in the mid-infrared (MIR), namely at wavelengths ranging from 2 to 15 μm , which is the region of relevance for chemical or biological sensing and thermal imaging.

Doped semiconductors^{1,2}, in addition to other properties like shape and size, are a promising choice for plasmonics encompassing a broad infrared spectrum, since their LSPR can be controlled by dopant concentration as well as other parameters like shape and size. Massively doped silicon (Si) nanostructure arrays are logical candidates for mass-producing highly integrated low-cost MIR plasmonic devices.

In this framework, we developed all-silicon-based plasmonic metasurfaces generated by submicrometer tiny doped-Si nanodisks (Si-NDs) by processing hyper-doped overlayers of SOI substrates³. We showed that such nanostructures can support localized surface plasmon resonances that are controlled by the Si free carrier density. By modulating the free carrier concentration between 10^{20} and 10^{21} cm^{-3} , the plasmon can be tuned in a spectral window between 2 and 5 μm ⁴. Active dopant concentrations exceeding 10^{21} cm^{-3} are required to reach the NIR regime. We showed that, despite a large mismatch between the wavelength (25.5 μm) and the Si-ND diameter (100 nm), the LSPR allows for a substantial interaction with IR light, resulting in a loss in transmittance of up to 10% at the resonance⁴. We evaluated the optical characteristics of a single nanodisk as well as the entire metasurface using numerical simulations⁵. They demonstrate excellent agreement with the experimental findings and provide physical insights into the influence of nanostructure form and near-field effects on the metasurface's optical characteristics. Our results open highly promising perspectives for integrated all-silicon-based plasmonic devices for instance for chemical or biological sensing or for thermal imaging.

¹ D. Li, Ning, C. Z. All-semiconductor active plasmonic system in mid-infrared wavelengths. *Opt. Express* 2011, 19, 14594.

² T. Taliercio, P. Biagioni, P. Semiconductor infrared plasmonics, *Nanophotonics* 2019, 8, 949–990.

³ N. Chery, et al. Study of recrystallization and activation processes in thin and highly doped silicon-on-insulator layers by nanosecond laser thermal annealing. *Journal of Applied Physics* 2022, 131, 065301.

⁴ J. M. Pouirol et al. Hyper-Doped Silicon Nanoantennas and Metasurfaces for Tunable Infrared Plasmonics. *ACS Photonics* 2021, 8, 1393-1399.

⁵ C. Majorel, et al. Theory of plasmonic properties of hyper-doped silicon nanostructures. *Opt. Commun.* 2019, 453, 124336.

SESSION EQ02.04: Poster Session
Session Chairs: Viktoriia Babicheva and Alexander Cerjan
Monday Afternoon, November 28, 2022
8:00 PM - 10:00 PM
Hynes, Level 1, Hall A

EQ02.04.01

A Near-Field Tunable Magnetocaloric Thermal Switch Simo Pajovic and Svetlana V. Boriskina; Massachusetts Institute of Technology, United States

The magnetocaloric effect is the phenomenon in which some magnetic materials experience a change in temperature upon an adiabatic change in magnetization. It is well-known that this process can be exploited to achieve magnetic refrigeration and has other potential applications including drug delivery (particularly controlled release) and hyperthermia to treat cancer [1]. In recent years, there has also been an interest in using magnetic fields to manipulate radiative heat transfer, especially in the near-field, where length scales are approximately less than the peak wavelength of the blackbody spectrum and evanescent modes dominate. For example, it is possible to tune the near-field radiative heat transfer between planar doped semiconductors by applying a magnetic field and modulating its magnitude and direction [2]. This is because the applied magnetic field induces off-diagonal elements in the dielectric tensor, which are linked to nonreciprocal modes and magneto-optic effects, as well as uniaxial or biaxial anisotropy, which can give rise to hyperbolic modes. In this work, we have combined the magnetocaloric effect and magnetic control of radiative heat transfer to model a near-field tunable magnetocaloric thermal switch. We have shown that the heat flux between a magnetocaloric material and a magneto-optic material can be controlled via two mechanisms: the temperature change originating from the magnetocaloric effect; and modes such as surface plasmon polaritons and hyperbolic modes that depend on both the magnitude and the direction of the applied magnetic field. Thus, we predict the applied magnetic field enables control over the

directionality of the heat flux—from the magnetocaloric material to the magneto-optic material and vice-versa—and its magnitude, both spectrally and totally. Our work points toward a new class of thermal switches with a potentially wide range of operating temperatures dependent on the Curie temperature of the magnetocaloric material. This work is supported by an ARO MURI (Grant No. W911NF-19-1-0279) via the University of Michigan.

References

- [1] A. M. Tishin, Y. I. Spichkin, *Int. J. Refrig.* 37, 223 (2014).
- [2] E. Moncada-Villa, V. Fernández-Hurtado, F. J. García-Vidal, A. García-Martín, J. C. Cuevas, *Phys. Rev. B* 92, 125418 (2015).

EQ02.04.02

Narrow Bandwidth Polymers and Metal Oxide Interlayers to Improve an Artificial Retina [Leslie Askew](#) and Maxim Shkunov; University of Surrey, United Kingdom

Recent advances in biomedical engineering have led to a growing worldwide effort to develop a retinal prosthesis designed to restore vision to people suffering from retinal dystrophies such as age-related macular degeneration (AMD) and retinitis pigmentosa (RP). Some of this work has involved interfacing degenerative retinas with organic-semiconductor based devices to elicit an electrical response upon illumination in order to initiate a transduction of stimuli through the remaining retinal network, and thus provide a capability to restore vision. Previous work done by our group has demonstrated several conjugated polymers and small molecules with different bandgaps used towards a device prototype for potential vision restoration in full colour by emulating the each photoresponse from the rods and cones of the human eye.[1]

Commercially available prosthetics to date have been designed primarily as solid-state devices requiring transcranial wiring and associated ancillary optical and power components. Recent research into less invasive and more comfortable devices has turned to organic photovoltaic materials that are lightweight, flexible, and relatively low-cost. Moreover, using organics capitalises on their potential biocompatibility and their electrical properties to create arrays of miniature photovoltaic pixels to stimulate neurons in the retinal pathway and may provide a straightforward and reliable basis for durable visual prosthetics.

However, challenges in using carbon-based semiconductors to elicit enough photocurrent to stimulate a cell in the retinal network remain. Firstly, the power conversion efficiency of thin film organic photovoltaics has only recently exceeded 12%, [2-4] a value that is woefully small. Increasing excitation power until a photocurrent is detectable is a common work-around, however, while it might prove functional in a laboratory setting, the unnaturally powerful source may result in catastrophic damage to a prosthetic device in a human body. It would be much more favourable to utilise the electronic properties of additional interfacial materials to improve device performance.

In this study, we report on the characteristics of devices fabricated with a range of organic semiconductor polymers for active layers as part of our development of an artificial retina prototype. Previous work has identified a range of promising small molecules that emulate trichromatic vision (rods and three cones); here we describe improvements made with “off the shelf” polymers with narrow absorption bands that suitably match those of human photoreceptors. Importantly, we employ electron-transporting / hole-blocking metal oxide interlayers at the current collecting electrode to elicit capacitive charge transfer of sufficient magnitude for neuronal stimulation. By reducing the difference in work functions of the electrode and LUMO level of the active materials, a significantly higher photoinduced current can be produced for all of the molecules in this study, and the resulting capacitive nature of charge transfer can help to dramatically reduce peroxide-induced Faradiac reactions in device-neuron interfaces.[5]

1. Shkunov, M., et al., Pixelated full-colour small molecule semiconductor devices towards artificial retinas. *The Journal of Materials Chemistry C*, 2021.
2. Meng, L., et al., Organic and solution-processed tandem solar cells with 17.3% efficiency. *Science*, 2018. 361(6407): p. 1094-1098.
3. Cui, Y., et al., Over 16% efficiency organic photovoltaic cells enabled by a chlorinated acceptor with increased open-circuit voltages. *Nature Communications*, 2019. 10(1).
4. Armin, A., et al., A History and Perspective of Non-Fullerene Electron Acceptors for Organic Solar Cells. *Advanced Energy Materials*, 2021. 11(15): p. 2003570.
5. Ehlich, J., et al. (2022). "Direct measurement of oxygen reduction reactions at neurostimulation electrodes." *Journal of Neural Engineering*.

EQ02.04.04

Spatial Modulation of Radiative Decay Dynamics of Exciton Complexes in WSe₂ Monolayer [Jaeyu Kim](#), Sanghyeok Park, Dongha Kim and Min-Kyo Seo; Korean Advanced Institute of Science and Technology, Korea (the Republic of)

Excitons in transition metal dichalcogenides (TMDs) monolayer possess strong binding energy, valley selectivity, and high quantum efficiency, which are useful for various applications in excitonics, quantum many-body physics, and optoelectronics. TMDs support not only excitons but also a variety of exciton complexes such as biexcitons, charged excitons, and dark excitons that have distinct features and capabilities from excitons: Biexcitons in TMDs have high valley selectivity. Charged excitons can be effectively controlled by the application of electric fields. Dark excitons have a longer intrinsic lifetime and thus can diffuse a longer distance. It has therefore been essential to examine and understand the radiative decay dynamics of exciton complexes in various environmental conditions. The Purcell effect in terms of vacuum field interference has been widely used to control the radiative decay rate of the exciton complexes. However, the radiative decays of the exciton complexes occur at different emission wavelengths and their detailed properties vary from specimen to specimen. The conventional planar mirrors or resonators are not practical to provide the target TMD material with various optical environments depending on the position and emission wavelength at the same time, which is required for investigating the decay dynamics of the exciton complexes systematically.

In this research, we present the spatial modulation of radiative decay dynamics of exciton complexes in the WSe₂ monolayer employing a gradient-thickness mirror (GTM). Our GTM structure consists of the Si/Al (80 nm)/SU8 multilayer. The Al layer acts as a bottom mirror, and the thickness of the SU8 layer gradually changes from 80 to 500 nm over a horizontal distance of 20 micrometers with a slope of ~1°. The flake of hBN (150 nm)/WSe₂ monolayer/hBN (70 nm) was transferred onto the surface of the GTM structure. At a given wavelength, the vacuum field interference and the Purcell effect depend on the thickness of the dielectric SU8 layer. The GTM structure supports a white light interference pattern, in which the constructive/destructive interference conditions for the different emission wavelengths of the exciton (720 nm), biexciton (730 nm), and dark exciton (740 nm) in the WSe₂ monolayer appear at different spatial positions and repeat with different spatial frequencies. As a result, the radiative decay dynamics of each exciton complexes can be modulated in different manners along the direction of the thickness gradient, which enables us to examine the decay dynamics of exciton complexes in the identical WSe₂ monolayer under a variety of conditions.

We measured the photoluminescence (PL) spectrum from the exciton complexes in the WSe₂ monolayer pumped with He-Ne laser via a confocal scanning microscopy. The PL intensity ratio between the exciton complexes, related to their relative radiative decay rates, change depending on the position along the thickness gradient of the GTM structure. We demonstrated that the relative PL intensity ratio of biexcitons to bright excitons spatially changes from ~0.28 to 2.1 with one order of magnitude. We also demonstrated an optical situation where the emission from dark excitons dominates in those of other exciton complexes, which have been difficult to realize due to the weak radiative recombination of the dark exciton. In addition, we were able to systematically investigate the Lamb shift of the bright exciton emission spectrum depending on the vacuum field interference strength.

8:15 AM EQ02.05.01

Thermodynamic Limits of Photon-Multiplier Luminescent Solar Concentrators [Tomi Baikie](#), Arjun Ashoka, Akshay Rao and Neil Greenham; University of Cambridge, United Kingdom

Luminescent solar concentrators (LSCs) are theoretically able to concentrate both direct and diffuse solar radiation with extremely high efficiencies. Photon-multiplier luminescent solar concentrators (PM-LSCs) contain chromophores which exceed 100% photoluminescence quantum efficiency. PM-LSCs have recently been experimentally demonstrated and hold promise to outcompete traditional LSCs. However, we find that the thermodynamic limits of PM-LSCs are different and are sometimes more extreme relative to traditional LSCs. As might be expected, to achieve very high concentration factors a PM-LSC design must also include a free energy change, analogous to the Stoke shift in traditional LSCs. Notably, unlike LSCs, the maximum concentration ratio of a PM-LSC is dependent on brightness of the incident photon field. For some brightnesses, but equivalent energy loss, the PM-LSC has a greater maximum concentration factor than that of the traditional LSC. We find that the thermodynamic requirements to achieve highly concentrating PM-LSCs differ from traditional LSCs. The new model gives insight into the limits of concentration of PM-LSCs and may be used to extract design rules for further PM-LSC design.

8:30 AM *EQ02.05.02

Towards Spectrum Control with Materials Beyond Coin-Age Metals [Marina S. Leite](#); University of California, Davis, United States

Metallic thin films and nanostructures are vital building blocks for next generation nanophotonic devices. Nevertheless, the permittivity of pure metals frequently imposes restrictions on the materials utilized and/or on device performance. Metallic mixtures and alloys embody a promising alternative to engineer the optical response of devices, enabling extra control of the spectrum. I will present our recent advances in photonics achieved using metal alloys, comprising super-absorbers using earth-abundant Al-Cu back reflectors, Pd-Au thin films for catalysis, and photodetectors with enhanced response based on Ag-Au films. An in-depth analysis of experimental and theoretical studies of the metallic mixtures optical properties will be also provided, including their correlation with electronic band structure. In the realm of biodegradable photonics, I will share our results regarding color pixels formed by Mg and MgO. Specifically, the green chemistry reaction between these materials and water enables structural colors to disappear within a few seconds. These devices find applications in environmental science, encryption, and health care. Overall, materials beyond coin-age metals can enable a pathway for further controlling the electromagnetic spectrum.

9:00 AM EQ02.05.03

Uncovering Polar Domains in the Rashba Semiconductor BiTeI Through Piezoresponse Force and Second Harmonic Generation Microscopy [Kevin W. Kwock](#)¹, Thomas P. Darlington¹, Kaiyuan Yao¹, Kai Du², Sang Wook Cheong², Rohit Prasankumar³, Prashant Padmanabhan⁴ and P.J. Schuck¹; ¹Columbia University, United States; ²Rutgers, The State University of New Jersey, United States; ³Intellectual Ventures, United States; ⁴Los Alamos National Laboratory, United States

Nonlinear optics has proven a powerful probe for understanding the intrinsic crystal structure and phase of material. Recently, it has been shown that the 2D class of vdW materials exhibit remarkable nonlinear optical properties. Among the exciting family of 2D materials that are being investigated for their nonlinear optical properties, the Rashba family of semiconductors, including BiTeI, has emerged as an excellent candidate for studying the origins of optical nonlinearities in polar semiconductors. BiTeI and related materials have a large Rashba spin-orbit coupled state, and their large polarity is expected to persist down to the monolayer limit. Here, we used second harmonic generation (SHG) microscopy to show that BiTeI is an extremely nonlinear material using layer-dependent studies and extracting its nonlinear coefficients. This then enabled us to exploit SHG microscopy to image polar domains in BiTeI and correlate it with piezoresponse force microscopy (PFM), providing key insights into the origin of the domains.

9:15 AM EQ02.05.04

Identifying Bacterial Pathogens in Wastewater Samples with Liquid Surface Enhanced Raman Spectroscopy [Liam K. Herndon](#), Farecha Safir, Baba Ogunlade, Halleh Balch, Alexandria Boehm and Jennifer A. Dionne; Stanford University, United States

The ability to accurately identify and monitor bacterial pathogens in environmental samples such as rivers, streams, and wastewater is critical to public health. Our group has recently shown that Raman spectroscopy combined with machine learning (ML) can be a powerful tool for identifying bacterial species, strain, and antibiotic susceptibility [1, 2, 3]. Gold nanorods can enhance the Raman scattering signature, owing to their ability to concentrate the incident light and selectively bind to bacteria via electrostatic interactions. In wastewater, however, anions mask the surface charges of the nanorods, disrupting interactions with bacteria and weakening the Raman enhancement.

Here, we achieve bacterial surface enhanced Raman spectroscopy (SERS) in wastewater by conjugating 12-residue gold-binding peptides (GBPs) to the bacterial surface. These peptides interact with gold through van der Waals interactions, overcoming the need for positive surface charges on the nanorods, and form bonds with gold 10 times more stable than electrostatic interactions [4]. As a proof of concept, we design a plasmid encoding a GBP conjugated to a circularly permuted outer membrane protein X (CPX) scaffold and use this plasmid to express GBPs on the *E. coli* cell surface. We describe the effects of GBP surface expression on adsorption affinity of bacteria to nanorods. Next, we use filtered wastewater samples and spike in GBP-expressing *E. coli* at a concentration of 10^7 cells/ml, a realistic total bacterial concentration for wastewater. With our surface expression of GBPs, SERS can detect *E. coli* at this concentration using only 10 second integration times in a liquid wastewater sample. Finally, to demonstrate broad application to any bacterial species, we conjugate synthetic GBPs to dibenzocyclooctyne (DBCO). These conjugates can be selectively cross-linked to azides via copper-free click chemistry, enabling GBP cross-linking to any bacteria that have been metabolically labeled with azide-conjugated cell wall and outer membrane components. Hence, by combining advances in nanophotonics, ML, and biological engineering, we demonstrate SERS can be used to detect a wide variety of bacterial species and strains in complex environmental samples, allowing rapid and label-free monitoring of a community's bacterial infections through wastewater.

[1] Ho et al., Nat. Comm. 10, 4927 (2019).

[2] Tadesse et al., Nano Lett. 20, 7655-7661 (2020).

[3] Safir et al., ArXiv (2022).

[4] Hnilova et al., Langmuir 24, 12440-12445 (2008).

9:30 AM *EQ02.05.05

Calcite Phonon Polaritons [Jeff Owrutsky](#)¹, Vanessa Breslin¹, Daniel Ratchford¹, Alexander Giles², Chase Ellis¹, Igor Vurgaftman¹ and Joseph Tischler³; ¹Naval Research Laboratory, United States; ²Quantitative Scientific Solutions, LLC, United States; ³The University of Oklahoma, United States

Phonon polaritons are supported within a material-specific spectral region of polar materials called the reststrahlen band, which is bounded by the transverse and longitudinal optical phonons. Surface phonon resonances (SPhPs) are widely recognized in polar semiconductor materials such as SiC and GaN, including our demonstrating active tuning of nanopillar SPhPs and Berreman modes. We have recently shown that phonon resonances are also supported by other materials, including inorganic salts and molecular crystals. Some materials have anisotropic and even hyperbolic optical properties similar to hexagonal boron nitride, in which they behave optically like a dielectric and a metal along different crystal axes. We describe IR reflection results for calcite nanopillar and nanohole arrays which support hyperbolic phonon polaritons (HPs). The HP modes observed in the nanohole arrays appear at higher frequencies than those in the nanopillar arrays. We have developed a qualitative understanding of the nature of the HP modes in the nanohole arrays, in which the modes are most likely confined to the constrictions between holes. In such a model, changing the pitch and/or the diameter of the holes will change the dimensions of the constrictions and result in changing the resonance frequency of the HP modes in a predictable way. Being able to theoretically describe HPs in calcite is a first step towards understanding the nature of these modes in a variety of materials in order to expand the range of phonon polariton materials available for mid-IR nanophotonic applications.

10:00 AM BREAK

SESSION EQ02.06: Synthesis, Processing and Assembly
Session Chairs: Viktoriia Babicheva and Marina Leite
Tuesday Morning, November 29, 2022
Sheraton, 2nd Floor, Liberty B/C

10:30 AM *EQ02.06.01

Emerging Materials for Plasmonics in the Visible Region—From Discovery to Application [Yu-Jung Lu](#); Academia Sinica, Taiwan

Progress in understanding resonant subwavelength optical structures has fueled a worldwide explosion of interest in both fundamental processes and nanophotonic/plasmonic devices for imaging, sensing, solar energy conversion, and information processing. However, plasmonic platforms in the visible region with robust, high performance, thermo-stable, and low-cost remains remain unexplored. In this presentation, I will particularly discuss emerging plasmonic platforms based on transition metal nitrides. I will present an overview of my research works over the past five years on the plasmon-enhanced light-matter interactions in the visible regions and its applications [1-6], including the plasmonic nanolasers [1-2], tunable plasmonic modulators [3], plasmonic phototransistors [4], plasmon-enhanced solar energy harvesting [5], and the refractory plasmonic colors for back-light free displays [6]. My group discovered several unique working mechanisms that utilize plasmonic nanostructures to improve optoelectronic device performance. By engineering the local electromagnetic field confinement, the light-matter interaction strength can be enhanced, which results in efficient energy conversion in the designed nanosystem. The detailed mechanisms and possible applications will be discussed. These results have broad implications for the use of plasmonic crystals/metasurfaces in high-performance optoelectronic devices with efficient energy conversion.

References

- [1] Y-H Hsieh, B-W Hsu, K-N Peng, K-W Lee, C W Chu, S-W Chang, H-W Lin*, T-J Yen*, and [Y-J Lu](#)*, Perovskite Quantum Dot Lasing in a Gap-Plasmon Nanocavity with Ultralow Threshold. *ACS Nano* **14**, 11670 (2020). (Issue cover)
- [2] [Y-J Lu](#)*, T L Shen, K-N Peng, P-J Cheng, S-W Chang, M-Y Lu, C W Chu, T-F Guo, H. Atwater*, Upconversion Plasmonic Lasing from an Organolead Trihalide Perovskite Nanocrystal with Low Threshold. *ACS Photonics* **8**, 335–342 (2021).
- [3] [Y-J Lu](#), R. Sokhoyan, W-H Cheng, G. Kafaie Shirmanesh, A. Davoyan, R. A. Pala, K. Thyagarajan, and H. A. Atwater*, Dynamically Controlled Purcell Enhancement of Visible Spontaneous Emission in a Gated Plasmonic Heterostructure, *Nature Communications* **8**, 1631 (2017).
- [4] H-Y Lan, Y-H Hsieh, Z-Y Chiao, D. Jariwala, M-H Shih, T-J Yen, O. Hess, and [Y-J Lu](#)*, Gate-Tunable Plasmon-Enhanced Photodetection in a Monolayer MoS₂ Phototransistor with Ultrahigh Photoresponsivity. *Nano Lett.* **21**, 3083 (2021).
- [5] M-J Yu, C-L Chang, H-Y Lan, Z-Y Chiao, Y-C Chen, H W H. Lee, Y-C Chang, S-W Chang, T. Tanaka, V. Tung, H-H Chou*, and [Y-J Lu](#)*, Plasmon-Enhanced Solar-Driven Hydrogen Evolution Using Titanium Nitride Metasurface Broadband Absorbers. *ACS Photonics* **8**, 3125–3132 (2021).
- [6] Z-Y Chiao, Y-C Chen, J-W Chen, Y-C Chu, J-W Yang, T-Y Peng, W-R Syong, H W H. Lee, S-W Chu, and [Y-J Lu](#)*, Full-Color Generation Enabled by Refractory Plasmonic Crystals. *Nanophotonics* **11**, 2891-2899 (2022)

11:00 AM EQ02.06.02

Chiral Bio-Inorganic Hedgehogs with Birefringence [Prashant Kumar](#)¹, Emanuele Marino², Alexander Simon¹, Daniel Katz¹, Christopher B. Murray² and Nicholas A. Kotov¹; ¹University of Michigan—Ann Arbor, United States; ²University of Pennsylvania, United States

Spiky hedgehogs can be self-assembled from twisted ribbons formed by gold-copper-cysteine complexes.¹ Furthermore, chirality of these twisted ribbons can be controlled by the cysteine amino acid while their arrangement into supraparticles is guided by the ratio of L- vs D-form during the initial stages of self-assembly. Here we report that the spherically symmetric arrangement of twisted ribbons displays a maltese cross pattern typical of spherulites and liquid crystals under cross-polarizers.² This optical effect is observed at the single particle level³ with tunable diameters of 1-10 um. We investigate the optical effects in chiral hedgehogs using single particle methodology and find that the emergence of Maltese cross pattern is dependent on the sphericity of the supraparticle and the spacing between individual spikes. We understand the interaction of light with hierarchically self-assembled structures through finite-element based electromagnetic simulations and reconstruct the distribution of electromagnetic fields around the hedgehogs in three dimensions. These hedgehogs are omnidispersible in a variety of solvents and offset the limitations of commonly observed organic molecule based spherulitic arrangement for biomolecular sensing under harsh environments.⁴

1. Jiang, W. *et al.* Emergence of complexity in hierarchically organized chiral particles. *Science (1979)* **368**, 642–648 (2020).
2. Shtukenberg, A. G., Punin, Y. O., Gunn, E. & Kahr, B. Spherulites. *Chemical Reviews* **112**, 1805–1838 (2011).
3. Bahng, J. H. *et al.* Mie Resonance Engineering in Meta-Shell Supraparticles for Nanoscale Nonlinear Optics. *ACS Nano* **14**, 17203–17212 (2020).
4. Sivakumar, S., Wark, K. L., Gupta, J. K., Abbott, N. L. & Caruso, F. Liquid crystal emulsions as the basis of biological sensors for the optical detection of bacteria and viruses. *Advanced Functional Materials* **19**, 2260–2265 (2009).

11:15 AM EQ02.06.03

Templated Dewetting of Optical Glasses—A Novel Fabrication Approach of All-Dielectric Metasurfaces Fabien Sorin¹, Pierre-Luc Piveteau¹, Tapajyoti DasGupta² and Louis Martin-Monier³; ¹Ecole Polytechnique Fédérale de Lausanne (EPFL), United States; ²Indian Institute of Science Bangalore, India; ³Massachusetts Institute of Technology, United States

Metasurfaces require the integration of materials with accurate control over position, size and shape for high optical efficiency. This is commonly achieved using well-established lithographic or chemical processes. Nevertheless, such processes suffer from intrinsic limitations over throughput or flexibility, and hence remain difficult to scale up and adapt to large area, flexible or stretchable substrates. Here, we present a novel fabrication approach based on controlled templated fluid instabilities of thin optical glasses, to self-organize a variety of large index contrast all-dielectric metasurfaces. Given the right annealing time-temperature settings, initial film thickness and underlying pattern, the breakup of the film can occur at prescribed locations resulting in nano-objects of tunable position, shapes and sizes. Such control paves the way towards simple fabrication route of advanced 2D and quasi-3D photonic architectures (Das Gupta, Sorin et. al. *Nature Nanotechnology*, 14 (4), 320 (2019); Martin-Monier, Sorin et. al. *Physical Review Applied* 3, 034025 (2021)). Low processing temperatures enable large-scale use of rigid but also unconventional flexible and stretchable substrates. Such structures enable strong electromagnetic field confinement, and are shown to have varieties of applications in sensing, light management and second harmonic generation. In particular, by dewetting successively increasingly thick layers, inter-particle gap down to 10 nm could be achieved. By critically coupling the in-plane diffractive mode with the radiative dipolar mode in such structures, sharp Fano-type resonances are demonstrated in the near visible region. These resonances are exploited to monitor protein monolayer concentrations down to 0.5mg/ml (Das Gupta, Sorin et. al. *Nature Nanotechnology*, 14 (4), 320 (2019)). Tailoring the underlying texture, we will also discuss recent results of chalcogenide based architectures exhibiting high second harmonic conversion efficiency of 10^{-6} in the UV region (Das Gupta, Sorin et. al., *Nanophotonics* 10, 3465 (2021)). Finally, we will further highlight the flexibility of our approach by presenting recent results on highly reflecting all-dielectric nanostructures, as well as tailored architectures for improved index sensing.

11:30 AM *EQ02.06.04

Materials for Active Photonics—Multiphysics Analysis Dmitry N. Chigrin^{1,2}; ¹RWTH Aachen University, Germany; ²DWI Leibniz Institute for Interactive Materials, Germany

The growing demand on reconfigurability in neuromorphic computing, integrated photonics and microwave photonics is attracting increasing attention towards design and optimization of active photonic components. By changing a phase of the phase change material or the state of hydrogel near a functional photonics building block, it is possible to realize (re)configurable, time dependent and (re)programmable components and materials. Phase change materials are materials in which phase transitions can be induced quickly and reversibly, resulting in pronounced changes in their physical properties. Hydrogels are macromolecular cross-linked networks swollen by the solvent in which they are dissolved. The unique property of hydrogels is their ability to dramatically change volume in response to external stimuli. Here we report on our recent developments of a multiphysics description of complex composite active photonic components incorporating phase change materials and hydrogels as their building blocks. Such a multiphysics description requires self-consistent treatment of the electromagnetic, heat transfer, mechanical deformation and phase transition models. Possible applications in the fields of integrated photonics, mid-infrared and microwave metasurfaces are discussed.

SESSION EQ02.07: Performance and Functionality II
Session Chairs: Antonio Ambrosio and Viktoriia Babicheva
Tuesday Afternoon, November 29, 2022
Sheraton, 2nd Floor, Liberty B/C

1:30 PM EQ02.07.01

Luminescent Defects in Ion Irradiated Hexagonal Boron Nitride Giacomo Venturi^{1,2}, Eli Janzen³, James H. Edgar³, Carsten Ronning⁴ and Antonio Ambrosio¹; ¹Fondazione Istituto Italiano di Tecnologia, Italy; ²Politecnico di Milano, Italy; ³Kansas State University, United States; ⁴Friedrich-Schiller-Universität Jena, Germany

Solid-state quantum emitters represent a valuable path for quantum technologies. Engineering and control of single photon emitters (SPEs) in diamond and silicon carbide serve as a benchmark for quantum emission from crystals. However, their intrinsic 3D nature limits some of their applications. 2D materials can circumvent this issue, plus they can also be integrated with standard CMOS technology [1].

In this framework, SPEs in wide bandgap 2D hexagonal boron nitride (hBN) have many advantageous properties including high brightness, photostability, and most importantly, room-temperature operation [2]. Different forms of hBN have been studied ranging from bulk crystals epitaxial films to nanocrystals, and several techniques have been exploited to induce quantum emitting crystal imperfections.

In the present contribution, we characterize the efficacy of ion irradiation to generate emitters in hBN. We compare the throughput of different ions (Ne, Ga, C) in producing the largest number of defects within target hBN flakes. We also tune the ion energy to address a specific penetration depth inside the mechanically exfoliated hBN. Additionally, the ion fluence is also spanned across a wide range.

Irrespectively of the ionic species, a strong and broad peak in the photoluminescence spectra from irradiated hBN always appears at about 820 nm.

Additionally, upon fixing the same implantation depth, gallium irradiated flakes are an order of magnitude brighter.

We conclude that the role of the impinging ions is to trigger the formation of intrinsic defects. We surmise that boron atoms are displaced from lattice sites, creating boron vacancies. These become negatively charged [3] and leads to emission in the NIR.

Such a defect, which can act as a SPE with a spin-dependent optical transition, can be employed for example in quantum communication protocols, where a spin-photon interface is highly desirable.

References

- [1] Aharonovich, Igor, Dirk Englund, and Milos Toth. "Solid-state single-photon emitters." *Nature photonics* 10.10 (2016): 631-641.
- [2] Tran, Toan Trong, et al. "Quantum emission from hexagonal boron nitride monolayers." *Nature nanotechnology* 11.1 (2016): 37-41.
- [3] Gottscholl, Andreas, et al. "Initialization and read-out of intrinsic spin defects in a van der Waals crystal at room temperature." *Nature materials* 19.5 (2020): 540-545.

1:45 PM EQ02.07.02

Massively Parallel Printing of J-Aggregate Dyes for the Formation of Optical Antennas Based on Polariton Resonances Jacob LaNasa, Kyungtae Kim, Andrew C. Jones and Suryakant Mishra; Los Alamos National Laboratory, United States

The utilization of exciton-polariton resonances in dielectric materials represents a novel pathway for the realization of next generation sensors and optical

devices. Recently, the J-aggregation of cyanine dyes has been demonstrated to produce a Frenkel excitonic absorption features strong enough to enable the formation of surface exciton polariton states at room temperatures. The implementation of these optical dyes has an inherent advantage for the development of low cost, optically resonant surfaces, as they can be easily deposited from aqueous solutions to a variety of differing substrates. Here, we demonstrate the massively parallel printing of J-aggregate dyes using polymer pen lithography to fabricate large scale arrays of optical antenna nanostructures. Here, through the control of the contact parameters of the polymer pen array and annealing conditions, we demonstrate the multiplexed fabrication of dye-based optically resonant nanostructures. Reducing structure sizes into the nanoscale to reach sub-wavelength dimensions, we explore the formation of localized exciton polariton resonances in these materials. We further relate the connection between the local morphology of the J-aggregate dye nanostructures to localized optical resonances through a combination of characterization techniques including atomic force microscopy, scattering spectroscopy, and finite element method optical modeling of the near-and far- field optical response.

2:00 PM *EQ02.07.03

Active Metasurface Optics Based on Chalcogenide Phase Change Materials Juejun Hu; Massachusetts Institute of Technology, United States

Phase change materials or PCMs are truly remarkable compounds whose unique switchable properties have fueled an explosion of emerging applications in electronics and photonics. Traditional PCMs suffer from large optical losses even in their dielectric states, which fundamentally limits the performance of optical devices based on the materials. To resolve the issue, we have demonstrated a new PCM Ge-Sb-Se-Te (GSST) with broadband low loss characteristics. In this talk, we will review an array of reconfigurable photonic devices enabled by the low-loss PCM, including electrically tunable metasurfaces, beam steering optics, and parafocal zoom lenses.

2:30 PM BREAK

SESSION EQ02.08: Emergent Materials and Alternative Designs

Session Chairs: Antonio Ambrosio and Viktoriia Babicheva

Tuesday Afternoon, November 29, 2022

Sheraton, 2nd Floor, Liberty B/C

3:00 PM EQ02.08.01

Angstrom-Scale Smoothing of Aluminum Nitride Film Surfaces Using Atomic Layer Etching Haozhe Wang, Azmain Hossain, David Catherall and Austin J. Minnich; California Institute of Technology, United States

Roughness-induced light scattering is an important limitation of the performance of various on-chip optical technologies such as microresonators and quantum photonic integrated circuits. Here, we report a plasma-thermal atomic layer etching (ALE) method which enables etching and smoothing of aluminum nitride (AlN) films with Angstrom-scale precision. The ALE process employs sequential exposures of SF₆ plasma and trimethylaluminum (Al(CH₃)₃, TMA). In each cycle, the surface is fluorinated by fluorine radicals, followed by a ligand-exchange reaction to yield etching. We observed a maximum etch rate of 1.9 Å/cycle at 300 °C as measured using ex-situ ellipsometry. After ALE, the surface roughness of AlN was measured to decrease ~35% from 4.3 Å to 2.7 Å. In addition, the etched surface was found to contain a lower concentration of oxygen compared to the original surface. We anticipate that the ALE process may be applied as a post-treatment to improve the performance of on-chip photonic devices which exploit the simultaneous second-order and cubic-order optical nonlinearities of AlN. ALE processes may be generally applicable to photonic materials to decrease losses arising from surface roughness scattering.

Reference: Wang, Haozhe, et al. "Isotropic plasma-thermal atomic layer etching of aluminum nitride using SF₆ plasma and Al (CH₃)₃" *arXiv preprint arXiv:2209.00150* (2022).

3:15 PM EQ02.08.02

Spontaneous Generation of Magnetically-Active Optical Vortices in Topological Media Dongha Kim, Arthur Baucour, Yun-Seok Choi, Jonghwa Shin and Min-Kyo Seo; Korea Advanced Institute of Science and Technology, Korea (the Republic of)

Vortices, swirling textures with singularities, have been observed in various physical entities. In condensed matter, the emergence of the vortices originates from exotic physical phenomena, such as Bose-Einstein condensation and magnetic flux quantization, that provides quasi-particle nature to the textures. The optical vortex (OV) is an optical analogy to the vortices in other physical entities, exhibiting zero-intensity point with spiral phase distribution in the electromagnetic field. OVs support the orbital angular momentum of light, which provides an extra degree of freedom in fundamental studies and applications, such as optical manipulation, forbidden electronic transition, and classical/quantum information processing. However, the generation of OVs has relied on structural singularities, such as spiral phase plates and metasurfaces, rather than critical phenomena, which prevents the OVs from possessing quasiparticle-like behavior, such as dynamic and interactive characteristics.

In this study, we propose and demonstrate the spontaneous generation of real-space optical vortex and anti-vortex and their active control using an external magnetic field based on a gradient-thickness optical cavity (GTOC) [1]. The GTOC consists of a magneto-optic Ni layer, between two SiO₂ layers, on top of an Al mirror. We found singular solutions in the calculated optical reflection of GTOC depending on the Ni layer thickness (h_{Ni}) in the generalized parameter space of top and bottom SiO₂ layer thicknesses (h_1, h_2), which correspond to the OVs with winding number of $w = \pm 1$. Regarding to the emergence of the OVs, topological phase of given system can be classified as trivial ($h_{Ni} < h_{c1}$ and $h_{Ni} > h_{c2}$) and non-trivial phase ($h_{c1} < h_{Ni} < h_{c2}$), where $h_{c1} = 6.34$ nm and $h_{c2} = 13.15$ nm correspond to the critical points.

We experimentally realized the topological phases of GTOC in an actual media by the bijective projection of the generalized parameter space (h_1, h_2) into real space (x, y). The thickness changes of the top and bottom SiO₂ layers are achieved by non-uniform sputtering in the order of tens of nanometer variation in centimeter-scale distances. We fabricated GTOC samples at trivial ($h_{Ni} = 5, 15$ nm) and non-trivial ($h_{Ni} = 10$ nm) phases and characterized them using confocal reflectance scanning and off-axis holography. For the non-trivial phase, the OVs are observed in the reflection distribution as singular minima and phase singularities. For the trivial phases, weak single minimum and continuous phase distributions are observed.

The most striking point of our topological media is the magnetic field activity. The magneto-optic effect applies an effective change to the optical thickness of the Ni layer, which can perturb the topological phase of GTOC. Under the external magnetic field (B), we observed magneto-optically-driven vortex dynamics, which induce topology- and polarization-dependent movement of the OVs. From $B = -0.5$ to $+0.5$ T, the displacements showed $(\Delta x, \Delta y) = (0.649$ mm, -0.344 mm) and $(-0.385$ mm, 0.010 mm) for the optical vortex ($w = +1$) and antivortex ($w = -1$), respectively, under the right circularly polarized incidence. The displacement directions were reversed when the incidence polarization changed into left circular. Finally, we demonstrated the magnetic-field-induced generation of the optical vortex-antivortex pair at the critical point ($h_{Ni} \sim h_{c2}$) of the topological phase. This is the first observation of field-induced topological phase transition in photonic media. We believe that our findings will pave a way to study topological photonic interactions and

inspire the exploration of quasiparticle-like nature in various topological photonic textures, such as toroidal vortices, polarization/vortex knots, and optical skyrmions.

[1] Kim, D., et al., Spontaneous generation and active manipulation of real-space optical vortex. arXiv:2202.02335 (2022). (Accepted in *Nature*)

3:30 PM EQ02.08.03

Engineering the Spectral and Spatial Dispersion of Thermal Emission Using Phonon Polaritons Guanyu Lu¹, Christopher R. Gubbin², J. R. Nolen¹, Thomas G. Folland³, Katja Diaz-Granados¹, Ivan Kravchenko⁴, Joseph A. Spencer⁵, Marko Tadjer⁵, Don G. Walker¹, Orest J. Glembocki¹, Simone D. Liberato² and Joshua D. Caldwell¹; ¹Vanderbilt University, United States; ²University of Southampton, United Kingdom; ³The University of Iowa, United States; ⁴Oak Ridge National Laboratory, United States; ⁵US Naval Research Laboratory, United States

Every object has a temperature greater than zero Kelvin can emit thermal emission according to the fundamental principles of statistical mechanics. Thermal emission, especially in the long-wave infrared region (LWIR), is of great importance in a variety of fields, including spectroscopy, imaging, communication, and energy management. Recently, the possibility of controlling thermal emission based on nanophotonic structures has been intensively investigated with a view towards a new generation of far-field thermal emitters. Such control is demonstrated in the aspects of engineering narrowband, polarized, and spatial coherent (directional) thermal emission. While narrow-band thermal emitters that provide IR LED-like performance have been demonstrated in photonic crystals, perfect absorber geometries, metallic bullseye structures, and periodic arrays of nanoantennas, spectral tunability and control of the spatial coherence within a given platform is challenging.

We present phonon-polaritonic thermal emitter designs to control the spectral and spatial dispersion of thermal emission. Surface phonon polaritons (SPhPs) are quasiparticles comprising a photon and a coherently oscillating charge on a polar lattice. Localized SPhPs (LSPhPs) can be supported by periodic SiC nanopillars, offering exceptionally high Purcell enhancements that are in excess of plasmonic counterparts, which result from the narrow resonance line widths. We demonstrate that such large-scale narrowband thermal emitters, featuring near-unity absorption, can serve as LWIR sources with effectively no net power consumption, enabling their operation entirely by waste heat from conventional electronics [1]. Furthermore, increasing the complexity of the LSPhPs unit cell can serve to modify the resonant near-field and intra- and inter-unit-cell coupling as well as to dictate spectral tuning in the far-field. We also exploit more complicated unit-cell structures to realize new LSPhPs modes with additional degrees of design freedom [2]. Unlike LSPhPs, which offer no spatial coherence, spatially coherent thermal emission can be induced by a one-dimensional grating with propagating SPhPs. However, only a single spatially coherent mode is supported by purely periodic grating structures. We explore superstructure gratings to enable polaritons with different frequencies/wavevectors in a single grating, manifesting as additional spatial modes in the thermal emission profile [3]. By combining the corresponding virtues of both localized and propagating SPhPs through the introduction of strong coupling, we demonstrate a new hybrid mode with narrowband, spatially coherent thermal emission signature. Additionally, through coupling to a third zone-folded longitudinal optic phonon (ZFLO) mode, the realization of electrically driven emitters is possible [4]. Thus, our results show that phonon polaritons and strong coupling phenomenon enable thermal emitters, which meet the requirements for a host of LWIR applications in a simple, lightweight, and intense emitter.

1. Lu, G., et al., *Narrowband Polaritonic Thermal Emitters Driven by Waste Heat*. ACS Omega, 2020. 5(19): p. 10900-10908.

2. Lu, G., et al., *Collective Phonon-Polaritonic Modes in Silicon Carbide Subarrays*. ACS Nano, 2021.

3. Lu, G., et al., *Multi-frequency coherent emission from superstructure thermal emitters*. Applied Physics Letters, 2021. 118(14).

4. Lu, G., et al., *Engineering the Spectral and Spatial Dispersion of Thermal Emission via Polariton-Phonon Strong Coupling*. Nano Lett, 2021. 21(4): p. 1831-1838.

3:45 PM EQ02.08.04

Applications of Epsilon-Near-Zero (ENZ) Materials to Quantum Systems Jeremy N. Munday; University of California, Davis, United States

The application of epsilon-near-zero (ENZ) materials to photonic devices has resulted in a wealth of fascinating phenomena such as electromagnetic supercoupling, resonance pinning, perfect optical absorption, and ultrafast optical switching. However, the effect of ENZ materials on quantum fluctuations is much less developed. Here, we will present our recent work on use of epsilon-near-zero (ENZ) materials to engineer quantum effects and discuss how they can be applied to various technologies. Specifically, we show how ENZ materials can be used to control the spontaneous emission rate of quantum emitters and present the concept of electromagnetic bandgaps for nanoparticles comprising an ENZ material. Further, we will show how tunable ENZ materials can be used to convert electrical bias into mechanical motion through the modification of the allowed modes within a cavity composed of an ENZ material. Finally, we will discuss the outlook for using the concepts in future device architectures.

4:00 PM *EQ02.08.05

Polaritonic Metasurfaces Andrea Alu; City University of New York, United States

In this talk, I will discuss our recent progress in the area of polaritonics and its role in advancing the field of metamaterials and metasurfaces. Tailored material resonances, based on excitons, phonons, or electronic transitions, can be strongly coupled to light in natural or engineered metasurfaces, unveiling new degrees of freedom for the control of light-matter interactions with light-based quasi-particles. I will discuss how, as the degree of lattice symmetries in the involved materials and in optically engineered structures is reduced, new opportunities emerge in manipulating light and matter at the nanoscale, unveiling giant nonlinearities and topological phenomena in real and reciprocal space.

SESSION EQ02.09: Emergent Phenomena and Light-Based Quasiparticles II

Session Chairs: Viktoriia Babicheva and Augustine Urbas

Wednesday Morning, November 30, 2022

Sheraton, 2nd Floor, Liberty B/C

9:00 AM EQ02.09.01

Photoinduced Excited-State Dynamics in Co-Doped BaFe₂As₂ Superconducting Films Roman Kolodka¹, Alexander Bartenev¹, Ki-Tae Eom², Jong-Hoon Kang², Eric E. Hellstrom³, Chang-Beom Eom², Armando Rua¹ and Sergiy Lysenko¹; ¹University of Puerto Rico at Mayagüez, United States; ²University of Wisconsin-Madison, United States; ³Florida State University, United States

We report on nonlinear optical dynamics and structural reconstruction of Co-doped BaFe₂As₂ single-crystal superconducting films within a broad range of temperatures. Films were grown by pulsed laser deposition on (La,Sr)(Al,Ta)O₃ [LSAT] and LaAlO₃ [LAO] crystalline substrates with epitaxial SrTiO₃ [STO] template buffer layer used for higher epitaxial bonding of BaFe₂As₂. Samples show superconducting transition with T_c~15.5-20 K. Temperature-

dependent optical transmittance measurements in the range from 290 K down to 10 K were conducted using a supercontinuum laser source, revealing a distinct increase of the transmittance within the wavelengths range from $\lambda=400$ nm to $\lambda=1.6$ μm , as the sample temperature drops below T_c . Reflectivity measurements at $\lambda=800$ nm also show an abrupt decrease of the reflectance below T_c . Drude-Lorentz model was applied to fit the optical transmittance spectra in order to demonstrate the contribution of a free-carriers component in the optical signal. The noticeable change of both, carrier scattering rate and plasma frequency near ~ 150 K is associated with the spin density wave (SDW) transition in BaFe_2As_2 . The angle-resolved hemispherical elastic light scattering surface metrology measurements performed with a light scatterometer at cryogenic temperatures indicate that this transition is accompanied by surface reconstruction. High-resolution angle-resolved hemispherical scattering imaging of multi-scale nonequilibrium processes in BaFe_2As_2 reveals that the small change in the elastic energy upon SDW formation results in the splitting of the film into domains due to the same or different structural phases since this process is accompanied by tetragonal-to-orthorhombic phase transition. Several competitive transition processes at ~ 150 K alter the correlation length of the surface and optical properties. In the region of superconducting transition, BaFe_2As_2 films demonstrate abrupt changes in surface morphology (surface autocorrelation length, optical isotropy, and root-mean-square roughness). A strong correlation between the observed temperature dependence of the surface statistics and quasiparticle dynamics near T_c was found. Time-resolved measurements of transient reflectivity performed in a relatively high-fluence regime, of several mJ/cm^2 , reveal a strong dependence of the excited-states-dynamics on sample temperature, morphology, and laser excitation energy. Femtosecond photoexcitation demonstrates complex reflectance traces attributed to two distinct ultrafast processes: (i) instantaneous formation of the nonequilibrium state of quasiparticles with its subsequent thermalization within ~ 3 ps with characteristic time τ_1 , and (ii) slower few-picoseconds phonon-phonon scattering. Temperature-dependence of τ_1 shows its noticeable drop as the temperature rises above T_c . Observed nonlinear optical dynamics correlate with the temperature dependence of the surface morphology near T_c and provide a new understanding of light-induced processes in the superconducting state of BaFe_2As_2 .

9:15 AM EQ02.09.02

Efficient Modulation of Two-Dimensional Excitons via Subwavelength Mie Resonators Jie Fang and Yuebing Zheng; The University of Texas at Austin, United States

Two-dimensional (2D) semiconducting transition metal dichalcogenides (TMDs) have attracted great interests because of their novel excitonic properties, providing new opportunities in nanophotonic devices, excitonic physics, and polaritonic systems. Efficient modulation of the 2D excitons in TMDs is attractive yet challenging. Coupling TMDs with single Mie resonators at the subwavelength scale can be a promising strategy. Here, playing with the electric (ED) and magnetic dipole (MD) modes, we apply single hydrogenated amorphous Silicon nanospheres (a-SiNS:Hs) to facilitate favorable far-field or near-field light manipulations for effective control of TMD excitonic properties. The a-SiNS:Hs Mie resonators are designed via bandgap engineering to support near-zero losses at full visible wavelengths and tunable refractive index based on hydrogen dopants (*Nature Communications* **2020**, *11*, 5055). Different from the high index in typical Mie resonators, a unique moderate refractive index of ~ 2.1 is proposed for broadband and highly interacted ED and MD. The size dependence of Mie resonances is also utilized and sphere diameters from 400 down to 200 nm are chosen for various modulation functions.

(1) Targeting at the directional modulation of far-field excitonic radiation patterns, we control the a-SiNS:H sizes between 300 and 400 nm with partially overlapped ED and MD. The a-SiNS:H Mie resonator is proposed as a highly miniaturized platform for controlling exciton emission through both the excitation and emission processes. Based on the mutual interference of Mie resonances, efficient modulation of directional excitation and exciton emission have been achieved in different TMD materials. A modified Mie theory for dipole-sphere hybrid systems is derived to instruct the optimal design for desirable modulation, leading to the potential of multifunctional integrated photonics. (*Advanced Materials* **2021**, *33*, 2007236)

(2) By coupling single a-SiNS:Hs of 250 to 290 nm in diameters with monolayer WS_2 in water, we successfully tune the WS_2 homogeneous exciton linewidth between 35 and 7 meV at room temperature (RT), providing a practical method to modulate exciton quantum dynamics at the subwavelength scale. Impressively, with an optimal sphere size of 268 nm, we achieve near-intrinsic exciton linewidth at RT, approaching the theoretical limit at 0 Kelvin. The linewidth-narrowing mechanism manifests the dynamic competition between exciton and trion decay channels. Specifically, the a-SiNS:H Mie resonator is designed to selectively boost the trion radiative decay, which breaks the charge balancing in inherently n-doped WS_2 and rebuilds the excitonic relaxation processes with suppressed exciton nonradiative decays. (*Advanced Materials* **2022**, *34*, 2108721)

(3) For a sphere diameter of 240 nm, ED and MD are found to be perfectly overlapped among the whole visible wavelengths. We employ this unique a-SiNS:H Mie resonator for broadband ultra-strong light-matter interactions with 2D excitonic materials. By coupling it with monolayer TMDs, we have achieved multi-Rabi splittings and robust exciton-polariton emission at RT.

In conclusion, by using a moderate-refractive-index a-SiNS:H Mie resonator, we have shown the efficient modulation of 2D TMD excitons in multiple dimensions. The subwavelength nature of the proposed Mie resonator ensures the good coupling efficiency with 2D excitons and practically enables the miniaturization of functional photonic devices.

9:30 AM *EQ02.09.03

Active Epsilon-Near-Zero Optical Materials Aleksei Anopchenko, Sudip Gurung, Christopher M. Gonzalez, David Dang, Leon Zhang, Kent Nguyen, Quynh Dang, Alexander Galkin, Tingwei Liu, Meena Salib and Ho Wai Howard Lee; University of California, Irvine, United States

Epsilon-near-zero materials have been shown to be as one of the most promising optical materials in the recent years as the electromagnetic field inside media with near-zero permittivity has been shown to exhibit unique optical properties. I will review our recent studies on the active linear, nonlinear, and emission properties of conducting oxide and metallic nitride epsilon-near-zero materials. Discovery of novel active materials is fundamental for photonic applications. The epsilon-near-zero (ENZ) materials have been shown to be as one of the most promising optical materials in the recent years as the electromagnetic field inside media with near-zero permittivity has been shown to exhibit unique optical properties, including strong electromagnetic wave confinement, enhanced quantum emission near ENZ media, non-reciprocal magneto-optical effects, unique topological properties, and abnormally large optical nonlinearity. While ENZ optics have been investigated extensively in the last few years, the current commonly used ENZ materials suffer from limited optical enhancement because of the lack of precise control of ENZ frequency, loss, and thickness for efficient ENZ mode excitation. In addition, the active tunability and enhanced nonlinearity and emission properties in ENZ materials have yet been fully experimentally explored. This talk will review our recent studies on the active linear, nonlinear, and emission properties of conducting oxide and metallic nitride epsilon-near-zero materials in planar and optical fiber platforms [1-7]. I will present a method to engineer the field intensity enhancement of the Al-doped zinc oxide (AZO) ENZ thin films synthesized by atomic layer deposition (ALD) technique. I will then discuss the observation of abnormal nonlinear temporal dynamic of hot electrons and enhanced optical nonlinearity in AZO and ITO ENZ thin films under different pump fluences and excitation angles using a degenerate pump-probe spectroscopy technique. I will present the first comprehensive study of photoluminescence from a 2D material placed near ENZ films and its dependence on the losses of materials, as well as the spectral response of such emitters with excitation wavelengths across the ENZ regime. Finally, I will also discuss the first experimental demonstration of optically confined ENZ resonance excitation in an optical fiber waveguide uniformly coated with AZO nanolayer. These studies enrich the fundamental understanding of emission and nonlinear properties on ENZ thin films and the integration of ENZ materials and optical fiber will open the path to revolutionary ultracompact in-fiber optical devices for optical communication, imaging, sensing/laser applications. This work was supported in part by the National Science Foundation (grant number: 2113010), and Air Force Office of Scientific Research (FA9550-21-1-02204) (AFOSR-AOARD, FA2386-21-1-4057)

10:00 AM BREAK

SESSION EQ02.10: Nanostructures and Optical Response II
Session Chairs: Viktoriia Babicheva and Dmitry Chigrin
Wednesday Morning, November 30, 2022
Sheraton, 2nd Floor, Liberty B/C

10:30 AM EQ02.10.02

Control of Nonreciprocal Surface Plasmon Polariton Transport in Weyl Semimetals via Optical Pumping and Strain Engineering Morgan Blevins and Svetlana V. Boriskina; Massachusetts Institute of Technology, United States

Weyl semimetals (WSMs) are a material of emerging interest due to their distinct electronic band structure, which supports pairs of chiral Weyl nodes formed from intersecting, linearly dispersing bands. The Weyl nodes in a pair each act as a source and a sink of Berry curvature respectively, resulting in a net flux of Berry curvature between them and zero Berry flux outside of them in momentum space. The flux of Berry curvature between the Weyl nodes gives rise to the unique, conductive Fermi arc surface states of WSMs.

Either time-reversal symmetry or inversion symmetry breaking is required for the existence of a WSM. Time-reversal symmetry breaking gives rise to the anomalous Hall effect in WSMs. On the other hand, inversion symmetry breaking WSMs have exhibited an exceptionally large bulk photogalvanic effect (PGE) under illumination from linearly polarized infrared (IR) light. This linear bulk PGE results in part from the Berry curvature induced shift current, in which an electron excited by linearly polarized light experiences a spatial shift upon transition from the valence to the conduction band, resulting in a photocurrent without the need for a p-n junction or external field. The detection of mid-IR light with conventional noncentrosymmetric semiconductors is limited by a lack of low energy bandgap materials but is enabled in a WSM by the gapless nature of its bandstructure. The use of the bulk PGE in WSMs has great potential for IR imaging and energy harvesting applications and for surpassing the efficiency limits inherent to p-n junction type detectors [1,2]. In addition to exploiting the bulk PGE, WSM surfaces can be engineered to control the *surface* photogalvanic effects, which opens the door to manipulating both bulk and surface photocurrents in WSMs for enhanced IR detection and devices. Surfaces of WSMs with broken time-reversal symmetry also support non-reciprocal surface plasmon-polariton modes (SPP) propagation, that enable directional energy transfer, Kirchhoff's law violation, and tunable near-field radiative heat transfer [3].

A key step in the development of WSM SPP engineering is to establish means to control them by external stimuli, especially optical stimuli. In this work, we model the impact of the bulk and surface photogalvanic effects as well as material strain on the WSMs surface states. Recent works have shown the Lorentz reciprocity of materials is broken by applying dc currents which produce a Doppler frequency shift of the electron plasma (Fizeau drag) [4]. Here, we exploit the fact that spontaneous photocurrent in WSMs acts as a dc current in the illuminated sample and imparts Fizeau drag on the electron plasma, providing an additional mechanism to control the nonreciprocal behavior of WSM SPPs by optical means. We also compare the impact of the PGE-induced Fizeau drag to the impacts of strain [5] on the SPP modes. A combination of these two mechanisms enables effective means for both static and dynamic control of nonreciprocal SPP propagation.

[1] S. Pajovic, et al, Radiative heat and momentum transfer from materials with broken symmetries: opinion, *Optical Materials Express*, 11(9), 3125-3131, 2021.

[2] S.V. Boriskina, M. Blevins, S. Pajovic, There and Back Again: the nonreciprocal adventures of light, *Opt. Photon. News*, Sept. 2022.

[3] S. Pajovic, et al, Intrinsic nonreciprocal reflection and violation of Kirchhoff's law of radiation in planar type-I magnetic Weyl semimetal surfaces, *Phys. Rev. B* 102(16), 165417, 2020.

[4] K. Y. Bliokh, et al, Electric-current-induced unidirectional propagation of surface plasmon-polaritons, *Opt. Lett.* 43, 963-966, 2018.

[5] Bugaiko, O. & Gorbar, E. & Sukhachov, Pavlo. (2020). Surface plasmon polaritons in strained Weyl semimetals. *Physical Review B*. 102. 10.1103/PhysRevB.102.085426.

This research has been supported by the Army Research Office (W911NF-13-D-0001), Lincoln Laboratory, Massachusetts Institute of Technology (ACC-777), and a Draper Fellowship to M.B.

SESSION EQ02.11: Microstructure, Composition and Nonequilibrium Carrier Dynamics
Session Chairs: Viktoriia Babicheva and Svetlana Boriskina
Wednesday Afternoon, November 30, 2022
Sheraton, 2nd Floor, Liberty B/C

1:30 PM *EQ02.11.01

Nonlinear Optical Response of Two-Dimensional Materials Giulio Cerullo¹, Chiara Trovatello^{1,2} and P.J. Schuck²; ¹Politecnico di Milano, Italy; ²Columbia University, United States

Two-dimensional materials such as graphene and transition metal dichalcogenides (TMDs) show extraordinarily strong second- and third-order nonlinear optical responses which, thanks to their unique electronic properties and despite their atomic thickness, allow a wide range of fundamental studies and technological applications. In this presentation we will discuss some of our recent results on the study of the nonlinear optical properties of two-dimensional materials.

We show that the third-harmonic generation efficiency in graphene can be increased by almost two orders of magnitude by controlling the Fermi energy and the incident photon energy [1]. This enhancement is due to logarithmic resonances in the imaginary part of the nonlinear conductivity arising from resonant multiphoton transitions. Thanks to the linear dispersion of the massless Dirac fermions, gate controllable third-harmonic enhancement can be achieved over an ultrabroad bandwidth, paving the way for electrically tunable broadband frequency converters.

Using semiconducting TMDs, we demonstrate single-pass optical parametric amplification at the ultimate thickness limit, down to a single atomic layer [2]. Second-order nonlinear interaction at the two-dimensional limit bypasses phase-matching requirements and achieves ultrabroad amplification bandwidths. In agreement with first-principle calculations, we observe that the amplification process is independent of the in-plane polarization of signal and pump fields.

We investigate 3R-stacked TMD crystals which combine broken inversion symmetry and aligned layering. By measuring second harmonic generation (SHG) of 3R-MoS₂ with various thickness, from monolayer (0.65 nm) to bulk ($\gg 1 \mu\text{m}$), we present the first measurement of the SHG coherence length ($\gg 530 \text{ nm}$) at 1520nm and achieve record nonlinear optical enhancement from a van der Waals material, $> 10^4$ stronger than a monolayer. We find that 3R-

MoS₂ exhibits similar conversion efficiency as lithium niobate, but with more than 100-fold shorter propagation lengths [3]. Finally, we demonstrate a novel approach for the all-optical control of SHG polarization in MoS₂ and show that this can be used for all-optical modulation of the SHG efficiency with modulation depth close to 100% and speed limited only by the fundamental frequency pulse duration [4].

References

- [1] G. Soavi et al., Broadband, electrically tunable third-harmonic generation in graphene. *Nat. Nanotechnol.* **13**, 583–588 (2018).
- [2] C. Trovatiello et al., Optical parametric amplification by monolayer transition metal dichalcogenides. *Nat. Photon.* **15**, 6–10 (2021).
- [3] X. Xu et al., Towards compact phase-matched and waveguided nonlinear optics in atomically layered semiconductors, *Nat. Photon.*, in press (2022).
- [4] S. Klimmer et al., All-optical polarization and amplitude modulation of second-harmonic generation in atomically thin semiconductors, *Nat. Photon.* **15**, 837 (2021).

2:00 PM EQ02.11.02

Emergent Properties of Noble-Transition Metal Alloys—Near-Infrared Interband Hot-Carrier Generation for Ultrafast Optoelectronic Devices
Orhan Kizilkaya¹, Gregory Manoukian², Sergi Lendinez¹, Luis Manuel¹, Karunya Shirali¹, Tiago R. Leite¹, William Shelton¹, Phillip Sprunger¹, Jason Baxter² and Kevin M. McPeak¹; ¹Louisiana State University, United States; ²Drexel University, United States

Noble-transition metal alloys are a promising class of materials for interband-driven hot hole generation with NIR light.¹ NIR hot-carrier generation in pure, noble metals suffers from insufficient energy to exceed the interband energy threshold (IET) (e.g., > 2 eV), and in pure transition metals, rapid hot-carrier thermalization. Band hybridization in select noble-transition metal alloys can overcome these issues, yielding emergent properties that facilitate tuning the hot-carrier distribution and lifetime.

We deposit disordered Cu_xPd_{1-x} alloy thin films under non-equilibrium conditions and investigate their stoichiometry-dependent optical, structural, electronic, and transient near-infrared absorption properties.² We show experimentally through ultraviolet photoelectron spectroscopy and computationally through the projected density of states calculations that strong hybridization between the Cu 3d and Pd 4d bands exists in the alloy films. Unlike the Au 5d band, the Cu 3d band does not exhibit strong spin-orbit coupling. Therefore, we observe the formation of a common band between the full Cu 3d and Pd 4d bands. This strong d-band hybridization in the alloy films drives emergent behavior across various measurement techniques.

Time-resolved terahertz spectroscopy with near-infrared (e.g., 1550 nm) excitation displays composition tunable electron dynamics. We posit that the negative peak in $\Delta T/T$ below 2 ps from dilute Pd alloys is due to non-thermalized hot-carrier generation and field-driven electron emission. On the other hand, Pd-rich alloys exhibit an increase in $\Delta T/T$ due to thermalization effects upon ultrafast NIR photoexcitation. Cu_xPd_{1-x} alloys in the dilute Pd regime may be a promising material for future ultrafast NIR optoelectronic devices.

1. Sara KF Stofela, Orhan Kizilkaya, Benjamin T Diroll, Tiago R Leite, Mohammad M Taheri, Daniel E Willis, Jason B Baxter, William A Shelton, Phillip T Sprunger, Kevin M McPeak, “A Noble-Transition Alloy Excels at Hot-Carrier Generation in the Near Infrared,” *Advanced Materials* 32 (23), 1906478 (2020)

2. Orhan Kizilkaya, Gregory Manoukian, Sergi Lendinez, Luis D. B. Manuel, Tiago R. Leite, Karunya S. Shirali, William A. Shelton, Phillip T. Sprunger, Jason B. Baxter, Kevin M. McPeak “Emergent Properties from CuPd Alloy Films under Near-Infrared Excitation,” *J Chem Phys* (Under Review)

2:15 PM EQ02.11.03

Nonequilibrium Carrier Dynamics in FeSe_{0.8}Te_{0.2} Roman Kolodka, Alexander Bartenev, Camilo Verbel, Manuel Lozano, Felix Fernandez, Armando Rua and Sergiy Lysenko; University of Puerto Rico, United States

We report on the nonequilibrium dynamics of photoinduced collective excitations in FeSe_{0.8}Te_{0.2} films in a superconducting (SC) state. Epitaxial films were grown on CaF₂ single-crystal substrates by pulsed laser deposition. The SC properties were tuned by varying the strain level by altering the film thickness of the epitaxial film. It was found that increased strain in film can depress SC when the film thickness reaches a threshold minimum, while the increased thickness can result in static domain structure via generation of the dislocation network, but with the introduction of new grain boundaries or microcracks. This fact was observed in angle-resolved light scattering measurements of the surface morphology within a broad temperature range, down to 7 K. It was also found that the surface domains undergo temperature-dependent reorganization when FeSe_{0.8}Te_{0.2} film undergoes a solid-to-solid structural phase transition. Ultrafast time-resolved measurements of reflectivity were performed with 35-fs laser pulse excitation, 1 kHz repetition rate, the central wavelength of 800 nm, and orthogonal polarization for pump and probe pulses. The FeSe_{0.8}Te_{0.2} film was maintained in its SC state at 7.5 K, while excitation fluence was tuned from up to ~10 mJ/cm², sufficiently below the damage threshold. The obtained reflectance traces show three distinct regions attributed to different dynamical processes in the material within the 50 ps time scale: (i) drop of the reflectivity signal within 200 fs, (ii) its subsequent rise within 1 ps, and (iii) much longer process of tens picoseconds. First two processes are associated with collective excitations and photoexcitation of quasiparticles (QP) in FeSe_{0.8}Te_{0.2}. A gradual increase of the excitation energy results in a gradual growth of QP density. Moreover, the QPs decay rate slows down as excitation fluence increases. The transient measurements manifest a gradual time-shift of the specific signal minimum on the reflectivity diagram, since the QPs decay rate slows down as excitation fluence increases. The characteristic time of the process (ii) shows a linear increase with excitation fluence, while the process (i) is more complex. The process (iii) is associated with phonon-phonon scattering demonstrating a decrease of its characteristic time as excitation increasing. This could be a signature of photoinduced structural transformation or a hidden phase in the film. A strong acoustic phonon generation starts at ~100 ps, right after the process (iii) completes. This reveals new features of photoinduced dynamics of superconducting FeSe_{0.8}Te_{0.2} in high excitation regime.

2:30 PM BREAK

SESSION EQ02.12: Extraordinary Physical and Optical Properties
Session Chairs: Viktoriia Babicheva and Svetlana Boriskina
Wednesday Afternoon, November 30, 2022
Sheraton, 2nd Floor, Liberty B/C

3:30 PM EQ02.12.01

Tunable Strong Light-Matter Coupling in Colloidal Transition Metal Dichalcogenide Nanowires Jingang Li^{1,2}, Kan Yao², Yun Huang², Donglei

(Emma) Fan² and Yuebing Zheng²; ¹University of California, Berkeley, United States; ²The University of Texas at Austin, United States

Transition metal dichalcogenides (TMDCs) are an emerging class of materials with extraordinary physical properties, which are investigated for a wide range of electronic, photonic, and optoelectronic applications. While TMDCs have been extensively explored as an excitonic platform with novel optical and electronic functionalities, it is less appreciated that TMDCs also have a high refractive index. The presence of excitons in high-index TMDC nanoresonators enables the formation of unique self-hybridized exciton polaritons, which remarkably enrich the capabilities of nanophotonic systems.

Here, we present strong coupling between excitons and Mie resonances in individual colloidal TMDC nanowires. Molybdenum disulfide (MoS₂) nanowires are chemically synthesized with tailorable dimensions to support tunable Mie-exciton polaritons in visible wavelengths. Compared to previously reported TMDC nanoresonators that are fabricated by lithographical methods (e.g., electron beam lithography), colloidal MoS₂ nanowires provide additional possibilities in the design and fabrication of nanophotonic devices. Specifically, the chemical synthesis approach permits the scalable and high-throughput production of TMDC nanoresonators with tunable optical responses, which can be easily integrated with other techniques for on-demand dispersion, transfer, manipulation, and assembly. Moreover, we show that the MoS₂ excitonic properties and spectral splittings can be optothermally modulated under light illumination, which offers a promising platform for the development of active photonic devices, such as all-optical switches and sensors.

3:45 PM EQ02.12.02

Towards a First-Principles Description of Real Systems in Realistic Cavities with MQED and QEDFT Mark Kamper Svendsen¹, Kristian S. Thygesen¹ and Johannes Flick²; ¹Technical University of Denmark, Denmark; ²Flatiron Institute, United States

Quantum Electrodynamics Density Functional Theory (QEDFT) is a generalization of time-dependent DFT in the presence of quantized modes of the electromagnetic field. QEDFT presents a good compromise between accuracy and computational effort that makes it possible to treat quantum light-matter interactions even for large electronic systems and many modes of the electromagnetic field. At present, however, the light-matter coupling strengths are essentially free parameters and it is unclear how to relate them to a real cavity setup.

In this talk, I will discuss how we can formulate the length-gauge light-matter Hamiltonian in terms of the quantized fields from Macroscopic QED and the extent to which it can be solved using QEDFT. This formulation lets us relate all cavity coupling parameters to the classic Green's function of the electromagnetic field and eliminates all free parameters related to the light-matter coupling strength. Our approach provides a step towards a parameter-free, quantitative description of light-matter interactions in arbitrary electromagnetic environments.

4:00 PM EQ02.12.03

Time-Modulated Conducting Oxide-Based Nanoantennas for Shared-Aperture Multi-Frequency Metasurfaces Raana Sabri and Hossein Mosallaei; Northeastern University, United States

Actively tunable optical nanoantennas are of great importance for dynamic control over the wavefront of light, where real-time and reprogrammable functions are required. Electro-optical tuning mechanisms based on electro-refraction effects induced by the free carriers in doped semiconductors are of growing interest for the realization of active metasurfaces. In particular, indium tin oxide (ITO) is a degenerately doped semiconductor, whose incorporation into the subwavelength unit cells of the geometrically-fixed metasurfaces enables post-fabrication electrical tuning of the optical response at near-infrared frequencies. The epsilon-near-zero transition in the ITO as well as novel design paradigms leveraging high-Q resonant modes allow for extreme light-matter interactions for enhancing the tunability of optical response. Despite the fruitful progress, the operating principle of ITO-integrated quasi-static metasurfaces relies on the modulation of resonant modes between the over- and under-coupled regimes. This limits the performance of such quasi-static metasurfaces to negligibly narrowband regime due to the strong resonant dispersion. Introducing time-modulation into the nanoantennas as an additional degree of freedom, renders a four-dimensional design space and surmounts the limitations of the quasi-static metasurfaces by converting the incident signal at the fundamental frequency to the higher-order sidebands. The phase of higher-order sidebands generated by a time-modulated metasurface can be tuned with uniform amplitude via a non-resonant dispersionless geometric phase shift induced by the modulation phase delay. This dispersionless phase elevates time-modulated metasurfaces beyond their quasi-static counterparts in that it increases the functionality bandwidth, expands the angle-of-view, and minimizes the power coupled into undesired sidelobes by providing access to the full phase span (2π) with uniform amplitude. The current architecture of deep space and local area networks calls for high capacity and high-speed platforms that can simultaneously address multiple users with minimal crosstalk. Time-modulated nanoantennas are promising candidates for multi-frequency functioning as they feature all-angle and all-wavelength optical response due to the access to dispersionless phase span at the sidebands. To demonstrate the adaptive multi-frequency multi-beam steering by the time-modulated metasurface, an array of plasmonic nanostrips integrated with ITO in metal-insulator-metal configuration is considered, wherein two sets of time-varying biasing signals are independently applied to the dual-gated metasurface for modulating the permittivity of ITO in space and time. The aperture of the metasurface is then divided into several interleaved orthogonally modulated sub-array nanoantennas with distinct modulation frequencies to render a shared-aperture metasurface in space and time. The spatially interleaved sub-arrays are programmed to exploit multi-beam scanning via a pixelated control over the modulation phase delays assigned to their constituent elements. The number of sub-arrays and distinct channels can be scaled easily without suffering from crosstalk due to the orthogonality of the channels or the efficient metasurface design. The results point toward high-capacity platforms with low size, weight, and power for next-generation free-space optical (FSO) communication systems.

4:15 PM *EQ02.12.04

Refractory Plasmonics for Energy and Extreme Optics Alexandra Boltasseva; Purdue University, United States

Emerging plasmonic materials such as semimetals (transition metal nitrides and carbides), highly doped semiconductors, 2D and quasi-2D materials such as MXenes are playing an increasingly important role in emerging technologies for sustainable energy and photocatalysis [1]. For example, enhanced hot electrons generation in transition metal nitride nanoparticles compared to conventional materials such as gold enables more efficient light-to-electricity conversion [2,3]. MXenes, a class of 2D nanomaterials formed of transition metal carbides and carbon nitrides, form a promising material platform for tailorable nanophotonics. They offer a number of unusual properties and are being applied to realize novel electromagnetic shields, metal-ion batteries, super capacitors, lasers, and sensors. We utilized the plasmonic response of titanium carbide (Ti₃C₂T_x) MXene thin films in the near infrared spectral window to create a metamaterial for broadband absorption [4] and explore the usage of MXenes for applications in photonics, energy harvesting, and desalination. Expanding the application realm for transition metal nitrides into sustainable, scalable technologies, we also demonstrated ultra-broadband light absorbers with titanium nitride (TiN) nanoparticles obtained through fast, large-scale and environmentally-friendly processes [5]. To advance photonic applications of novel materials further, we apply machine-learning-assisted data analysis techniques coupled with topology optimization and tailorable material platforms to obtain non-intuitive photonic designs for highly efficient optical devices and energy conversion.

Support from the Air Force Office of Scientific Research (grant FA9550-17-1-0243) is acknowledged.

References

- [1] Brongersma, M. L., Halas, N. J. & Nordlander, P. Plasmon-induced hot carrier science and technology. *Nature Nanotechnology* **10**, 25–34 (2015)
- [2] A. Naldoni, U. Guler, Z. Wang, M. Marelli, F. Malara, X. Meng, L. V. Besteiro, A. O. Govorov, A. V. Kildishev, A. Boltasseva, V. M. Shalaev, "Broadband Hot Electron Collection for Solar Water Splitting with Plasmonic Titanium Nitride," *Advanced Optical Materials* **5** (15) 1601031 (August

2017)

[3] A. Naldoni, F. Riboni, U. Guler, A. Boltasseva, V. M. Shalaev, A. V. Kildishev, "Solar-powered plasmon-enhanced heterogeneous catalysis," *Nanophotonics* 5 (1) 112–133 (June 2016)

[4] K. Chaudhuri, M. Alhabeib, Z. Wang, V. M. Shalaev, Y. Gogotsi, A. Boltasseva, "Highly Broadband Absorber Using Plasmonic Titanium Carbide (MXene)," *ACS Photonics* 5 (3) 1115–1122 (2018)

[5] M. Li, U. Guler, Y. Li, A. Rea, E. K. Tanyi, Y. Kim, M. A. Noginov, Y. Song, A. Boltasseva, V. Shalaev, N. A. Kotov, "Plasmonic Biomimetic Nanocomposite with Spontaneous Subwavelength Structuring as Broadband Absorbers," *ACS Energy Letters* 3, 1578–1583 (2018)

SESSION EQ02.13: Virtual Session
Session Chairs: Viktoriia Babicheva and Wei Bao
Wednesday Morning, December 7, 2022
EQ02-virtual

8:00 AM *EQ02.13.01

Germanium and Silicon Nitride Metasurfaces in Photoenergy Conversions Kuo-Ping Chen; National Yang Ming Chiao Tung University, Taiwan

Silicon photonics technology has been widely applied in communication and data centers. In this work, we experimentally demonstrate a special class of true bound state in the continuum (BIC), lattice resonance, and Kerker effect in group IV metasurface, including Si-based semiconductor and germanium (Ge). The photodetection in silicon photonics has become the very important research area. In silicon photonics, germanium (Ge) is an ideal candidate for on-chip photodetection due to the small bandgap of 0.66 eV and the compatibility with the modern CMOS technology. It has widely been used in near infrared (NIR) photodetection. However, the bulky and thick Ge film for photodetector limits the development of system minimization. By the design of metasurface, the absorption in thin Ge metasurface could have much larger absorption than the pure Ge thin-film. In addition, we also present directional emission normal to Si₃N₄ BIC metasurface laser with hybrid surface lattice resonances (SLRs).

8:30 AM EQ02.13.02

Mapping LiNbO₃ Phonon-Polariton Nonlinearities with 2D-THz-THz-Raman (2D-TTR) Spectroscopy Haw-Wei Lin¹, Griffin Mead^{2,1} and Geoffrey A. Blake^{1,1}; ¹California Institute of Technology, United States; ²National Institute of Standards and Technology, United States

Coherent control of vibrational modes is a promising route to achieving ultrafast manipulation of material properties with light. Through excitation of specific phonon modes that are strongly coupled to bulk material properties of interest, researchers have shown examples including enhancement of superconductivity and switching of the magnetic, ferroelectric, and structural phases with ultrafast optical pulses. With the development of intense terahertz (THz) sources, coherent control with THz frequency pulses, which provide phase-sensitive access to phonon modes with no parasitic electronic excitation, has gained significant attention. To achieve this future degree of control over matter, it is essential to characterize the multitude of different linear and nonlinear excitations that occur when pumped with an intense, broadband THz pulse. Lithium niobate (LiNbO₃) is an ideal candidate for developing techniques that can provide detailed information on the potential energy landscape due to its importance in nonlinear THz polaritonic applications. Here, we report two-dimension THz-THz-Raman (2D-TTR) measurements on x-cut LiNbO₃ with selective detection of the third-order nonlinear signal and significantly improved THz bandwidth (up to 9 THz). We demonstrate that 2D-TTR spectroscopy can provide insight into the excitation mechanism, nonlinear phonon-phonon couplings, and sources of anharmonicity in the system. We show that the E(TO₁) and E(TO₃) phonon-polaritons are excited through resonant THz one-photon absorption (1PA) as opposed to THz sum-frequency (SF) excitation. We directly observe THz and Raman nonlinear transitions between the E(TO₁) and E(TO₃) modes. Due to selection rules of the E-symmetry phonon modes, distinct symmetry-allowed Feynman pathways are observed for different THz polarizations. Further, our models show that the set of Feynman pathways observed are induced via mechanical anharmonicity of the phonon-polariton modes as opposed to electronic anharmonicity. Such information is traditionally only available via density functional theory (DFT) calculations. These findings provide a concrete foundation for future coherent control applications. For example, the nonlinear transitions between E(TO₁) and E(TO₃) may be optimized using tailored THz pulse sequences to achieve efficient population transfer between the two modes.

8:45 AM EQ02.13.03

Metasurface Enabled Polarization Sensitive Detection-Aspect Ratio and Design Tolerance for Nanofabrication for the Dielectric Metasurface Element Hosna A. Sultana; University of Alabama, United States

Using the benefit of flat optics metasurface, polarization-sensitive imaging technology has been developing in recent years with a reasonable promise to utilize it as a sensing method. Instead of imaging with light intensity, polarization-sensitive detection can take advantage of the orientation of the electric field to reveal the edge, hidden features, and many details of a target. Metasurface can serve as a stokes intensity splitter based on the incidence polarization state of light, and this utility has become a benchmark of optical sensing. This work explores high contrast dielectric metasurface design with Finite Difference Time Domain (FDTD) simulation to optimize dielectric material choice, layer combination, geometric shape, and assembly to make a total phase, transmission, and polarization control metasurface for 532 nm working wavelength. However, suitable material and design for the total phase control for this wavelength already exist, but the crucial limit of perfect nanofabrication, the design margin, needed to be relaxed. So the main focus of this research is on reducing the height of the nanoantenna and exploring the useful geometric features that can influence the mutual interaction of the metasurface element. For shape optimization, our metasurface element will go beyond the axially rotational symmetric component to affect the orthogonal phase differently. This will continue implementing anisotropic metasurface elements, which may improve the efficiency of detecting scattered light beams as expected from the diverse scattering medium.

9:00 AM EQ02.13.04

Mie Metasurfaces with Multipole Resonances in the Lattice Md Sakibul Islam, Dominic Bosomtwi and Viktoriia Babicheva; University of New Mexico, United States

Recently emerged high-index materials have been a subject of active studies in recent years. Ultra-thin optical elements can be engineered based on transdimensional photonic lattices that include 3D-designed nanoparticles supporting multipole resonances and arranged in 2D arrays to enhance collective effects in the nanostructure. Nanostructures with a high refractive index have been suggested as a promising alternative to conventional metals supporting plasmonic resonances. Here we show that the antennas made out of high-index material support several multipole resonances enabled by the supporting propagating modes with a high effective index and their reflection from the antenna boundaries. Different multipole resonances appear for the large

nanoantenna, as well as a decrease of reflection from the nanoantenna array and highly directional resonant scattering. Transdimensional lattices consisting of resonant nanoantennas in the engineered periodic arrays have great potential to serve as functional elements in flat optical components and photonic devices.

This work was performed, in part, at the Center for Integrated Nanotechnologies, an Office of Science User Facility operated for the U.S. Department of Energy (DOE) Office of Science by Los Alamos National Laboratory (Contract 89233218CNA000001) and Sandia National Laboratories (Contract DE-NA-0003525). The work is also supported by Contract DE-2375849.

9:15 AM EQ02.13.05

Directional Scattering and Quasi-Bound States in the Continuum in All-Dielectric Nano-Antenna Metasurfaces [Dominic Bosomtwi](#) and Viktoriia E. Babicheva; University of New Mexico, United States

Due to their capability to overcome ohmic losses, and the unique ability to manipulate, control and confine electromagnetic waves at the nanoscale dimensions, high index dielectric metastructures have become promising candidates for numerous photonic device applications such as beam steering, imaging, sensing and solar energy harvesting. We numerically study the scattering behavior of an array of silicon nanocylinders, and we show that varying the silicon nanocylinder heights results in the excitation of Fano resonance creating asymmetric scattering spectral profiles. We also demonstrate strong mode coupling behavior called quasi-bound states in the continuum where the modes are localized (trapped) in the nanostructure as a result of suppression of radiative losses leading to a high quality factor due to the disappearance of the width of the Fano lineshape. Our studies also reveal the overlap of the modes between the electric dipole and magnetic dipole moments leading to suppression of light reflectance and transmittance in the metastructure array.

9:30 AM EQ02.13.06

Infrared Plasmon and Phonon-Polaritons in Polar Semiconducting Scandium Nitride (ScN) [Krishna Chand Maurya](#)^{1,1,1}, [Dheemahi Rao](#)^{1,1,1}, [Shashidhara Acharya](#)¹, [Pavithra Rao](#)², [Ashalatha I. Pillai](#)³, [Shankar K. Kumar](#)², [Magnus Garbrecht](#)³ and [Bivas Saha](#)^{1,1,1}; ¹Jawaharlal Nehru Centre for Advanced Scientific Research, India; ²Indian Institute of Science, India; ³The University of Sydney, Australia

Interaction of light with collective free electron oscillations termed plasmon-polariton and with polar lattice vibrations termed phonon-polariton, are essential to confine the light in subwavelength dimensions and for strong optical resonances. Traditionally doped-semiconductors and conducting metal oxides (CMO) are used to achieve plasmon-polaritons in the near-to-mid infrared (IR), while polar dielectrics are utilized for realizing phonon-polaritons in the long-wavelength IR (LWIR) spectral regions. However, demonstrating plasmon- and phonon-polariton in one host material with low loss is challenging due to the mutually conflicting physical property requirements.

In this work, we present high-quality plasmon- and phonon-polaritons in epitaxial polar ScN thin films deposited on (001) MgO substrates using dc-magnetron sputtering in the ultra-high vacuum (1×10^{-9} Torr). As-deposited ScN thin films exhibit an *n*-type carrier concentration of $(2-4) \times 10^{20} \text{ cm}^{-3}$ primarily due to the presence of oxygen impurities. Due to such high carrier concentrations, the Fermi level in ScN resides inside the conduction band, about 0.2-0.3 eV above the band edge. Mg-hole doping is used to reduce the high carrier concentration, and *p*-type ScN is *achieved* along with high hole mobility. Scanning transmission electron microscopy (STEM) is used to characterize the microstructure of the film. Both oxygen and magnesium-doped ScN films deposited in this work on (001) MgO substrates at high-temperatures are epitaxial and nominally single-crystalline with 001 ScN || 001 MgO relationships.

Spectroscopic ellipsometry and Fourier-transform infrared spectroscopy (FTIR) analysis indicate that the highly *n*-type doped ScN thin films exhibit low-loss short-wavelength IR plasmon resonance in the 1500-2500 nm spectral range. Due to the polar semiconducting nature, Mg-doped low carrier concentration ScN also exhibits phonon-polaritons between the 340 cm^{-1} - 677 cm^{-1} spectral range. Excitation of the surface phonon-polariton modes is also demonstrated by polarization-dependent reflectivity measurement in the attenuated-total-reflection (ATR) mode using the Kretschmann configuration. A clear dip in the *p*-/*s*-polarized reflection spectrum at $\sim 1.95 \mu\text{m}$ and at $\sim 16 \mu\text{m}$ correspond to the surface plasmon-polariton (SPP) and surface phonon-polariton (SPhP) resonances respectively.

The plasmonic properties of ScN film are comparable to other IR plasmonic materials such as transparent conductive oxides and doped semiconductors. Also, ScN exhibit a very high figure-of-merit for SPhP propagation compared to its peer materials. Demonstration of plasmon- and phonon-polariton in one host material, ScN through carrier concentration control make it attractive for applications in epsilon-near-zero metamaterials, optical communication, solar-energy harvesting and other nanophotonic applications.

References:

K. C. Maurya, D. Rao, S. Acharya, P. Rao, A. I. K. Pillai, S. K. Selvaraja, M. Garbrecht and B. Saha, "Polar Semiconducting Scandium Nitride as an Infrared Plasmon and Phonon-Polaritonic Material" *Nano letters (In-press, 2022)*.

K. C. Maurya, A. I. K. Pillai, M. Garbrecht and B. Saha, "Simultaneous Light-Harvesting at Visible and Mid-Infrared Frequencies with Epitaxial TiN/Al_{0.72}Sc_{0.28}N/TiN Metal/Polar-dielectric/Metal Metamaterials" *(In-review, 2022)*.

K. C. Maurya, V. M. Shalaev, A. Boltasseva and B. Saha, "Reduced Optical Losses in Refractory Plasmonic Titanium Nitride (TiN) Thin Films Deposited With Molecular Beam Epitaxy" *Opt. Mater. Express. 10, 2679 (2020)*.

9:45 AM *EQ02.13.07

All van der Waals Nanophotonics [Artur Davoyan](#); University of California, Los Angeles, United States

Van der Waals materials have emerged as a promising materials platform for electronics and photonics. In this talk I will overview our recent theoretical and experimental efforts on creating ultra-confined nanophotonics devices. Owing to unique and strong resonances van der Waals materials exhibit very high refractive indices and a strong anisotropy. High reflective index, in turn enables, a conceptually new set of photonic devices that outperform current semiconductor and metallic devices. I will discuss the use of high refractive index transition metal chalcogenides, such as MoS₂, and hexagonal boron nitride for visible and mid-IR nanophotonics. I will show that these van der Waals materials allow extreme optical field confinement in deeply subwavelength structures. Our studies suggest that smaller and more efficient devices may be created with the use of van der Waals materials.

10:15 AM DISCUSSION TIME

SYMPOSIUM EQ03

Plasmonics, Nanophotonics and Metamaterials—From Design to Applications
November 27 - December 8, 2022

Symposium Organizers

Artur Davoyan, University of California, Los Angeles
Ho Wai Howard Lee, University of California, Irvine
Yu-Jung Lu, Academia Sinica
David Norris, ETH Zürich

Symposium Support

Gold

Enli Technology Co., Ltd.

Bronze

ACS Photonics
De Gruyter
Taiwan Semiconductor Manufacturing Company

* Invited Paper
+ Distinguished Invited

SESSION EQ03.01: Active Metasurfaces
Session Chairs: Ho Wai Howard Lee and Yu-Jung Lu
Sunday Morning, November 27, 2022
Hynes, Level 2, Room 202

8:00 AM *EQ03.01.01

Active Metasurfaces in Meta-Imaging Systems [Harry A. Atwater](#); California Institute of Technology, United States

Electro-optically tunable active metasurfaces that enable dynamic modulation of reflection amplitude, phase, and polarization using resonantly excited materials and phenomena are powerful design elements for meta-imaging and computation. We describe the role of such active metasurfaces as cascaded elements in lens-less and single-photon imaging systems. I will describe the features of a lens-less imaging system comprised of active metasurface elements as components, and compare the characteristics to conventional lens-couple image sensors.

8:30 AM EQ03.01.02

Excitonic Beam Steering in Monolayer Molybdenum Diselenide Based Active Metasurfaces [Melissa Li](#), Claudio U. Hail, Souvik Biswas and Harry A. Atwater; California Institute of Technology, United States

We demonstrate dynamic beam steering in an active van der Waals metasurface by combining the large tunability of the complex refractive index near the excitonic resonance in monolayer molybdenum diselenide (MoSe₂) with an array of gold electrodes. While previous demonstrations of reconfigurable metasurfaces depend on the geometric parameters of dielectric or plasmonic Mie resonators, our design relies solely on excitonic resonances which are decoupled from geometric resonances. By varying the voltages between adjacent electrodes, we can control the phase profile of the reflected light from our MoSe₂ metasurface. We generate a momentum space map of the reflected beam by imaging the intensity profile at the Fourier plane with a CCD camera. Our experiments show that at 6 K, the reflected light can be steered to angles between -30° to 30° at the A exciton wavelength of 754 nm. We attribute the dynamic control to the large refractive index modulation of over 200% through tuning the carrier density in MoSe₂ up to $7 \times 10^{12}/\text{cm}^2$. Our results suggest the potential to utilize the tunability of excitonic resonances in two-dimensional transition metal dichalcogenides for wavefront shaping in emerging photonic applications.

8:45 AM EQ03.01.04

Wavefront Manipulation Using Tunable Phase Change Metasurfaces in the Visible Spectrum [Parikshit Moitra](#)¹, Yunzheng Wang^{2,3}, Xinan Liang¹, Li Lu², Alyssa Poh², Tobias W. Mass¹, Robert Simpson², Arseniy Kuznetsov¹ and Ramon Paniagua Dominguez¹; ¹Institute of Materials Research and Engineering, Singapore; ²Singapore University of Technology and Design, Singapore; ³Shandong University, China

Recent advances in wavefront shaping, by complete control of amplitude and phase of the propagating light waves, have been explored with the application of resonant all-dielectric metasurfaces, composed of high-index nano-resonators. However, there is a major limitation, in terms of lack of post-fabrication tunability of their optical responses, as these metasurfaces are commonly fabricated from passive materials. To circumvent this issue, chalcogenide phase

change materials (PCMs) have been incorporated to the design, to bestow a fast and non-volatile tunability of the optical responses. Most of these tunable metasurfaces have been demonstrated in the mid infrared spectrum using Germanium-Antimony-Telluride (GST) PCMs. To lower the absorption loss of GST in the near infrared, selenium (Se) is doped with GST to form Ge-Sb-Se-Te (GSST) to achieve lossless optical properties in the wavelength range longer than 1 μm . However, there have been no demonstrations in the visible frequencies showing complete wavefront control with high efficiency using PCMs due to the lack of lossless and high-index PCMs in the same spectral range. Antimony trisulfide (Sb_2S_3) fits the requirement very well based on its low-loss and high refractive index optical properties in the visible frequencies, along with a sharp index contrast (~ 0.5) between its amorphous and crystalline phases. Here, we demonstrated nanofabrication process development of this novel material using conventional methods to realize high resolution metasurfaces. Having equipped with this fabrication capability, we realized Huygens' metasurfaces with nanoholes etched on to 160 nm thick as-deposited amorphous- Sb_2S_3 film and further demonstrated tunability of transmission resonance by 60 nm and close to 2π optical phase shift upon non-volatile and reversible switching between its amorphous and crystalline phases. With the design based on phase-only manipulation, we further realized reversibly switchable beam steering, tunable holograms and bound-states-in-the-continuum (BIC). We strongly believe that these demonstrations pave the way towards future metasurface devices with dynamic wavefront control viz. high resolution spatial light modulators for AR/ VR applications, tunable flat optics, LiDAR and optical holography.

9:00 AM EQ03.01.05

Wavefront Manipulation Using Chemically and Electrically Driven Geometric Reconfiguration of Polymer Metasurfaces [Siddharth Doshi](#)¹, Anqi Ji¹, Ali Mahdi¹, Scott Keene², Yi-Shiou Duh¹, Skyler Selvin¹, Philippe Lalanne³, Eric A. Appel¹, Mark Brongersma¹ and Nicholas Melosh¹; ¹Stanford University, United States; ²University of Cambridge, United Kingdom; ³LP2N, Université Bordeaux, IOGS, CNRS, France

The optical transfer functions of engineered metasurfaces are defined by the geometric arrangement and material properties of their constituent meta-atoms. Optical metasurfaces have traditionally been fabricated with rigid inorganic materials and accordingly, have geometries that are fixed upon fabrication. Tuning of dynamic metasurfaces based on inorganic materials typically relies on modulation of their refractive index. While significant progress has been made in tuning with semiconductors (by free carrier generation), TMDC monolayers (by exciton generation) and phase change materials, these devices still face challenges including limited index tuning ranges and low power efficiencies.

In contrast, the geometric dimension of polymer materials can be widely reconfigured by a diverse range of stimuli, providing a powerful lever to control optical responses. For example, some thin polymer films can swell by 2-3 times their original thickness in the presence of different solvents or by electrically induced ion uptake. We leverage this property to create dynamically reconfigurable optical metasurfaces that offer control over the intensity and phase of reflected light. Our platform consists of a spacer layer of the widely used and commercially available conducting polymer, PEDOT:PSS, situated between a metallic mirror and plasmonic nano-antennae. The degree of swelling of the PEDOT:PSS spacer is reversibly tuned through fluidic application of solvents with varying degrees of solvation energies. We thereby change the distance between the mirror and plasmonic nano-antennae and hence control the phase of light scattered from individual nano-antennae. We use this platform of "Expansion Plasmonics" to demonstrate high diffraction efficiency beam steering and continuous tuning of colour over a full gamut. Finally, we demonstrate the wider applicability of our platform by tuning our metasurface with other chemical stimuli, including electrochemical control of local ion concentrations. Our work opens the door to the broad integration of a range of polymers, engineered to respond to specific chemical stimuli, into reconfigurable optical elements with applications in bio-sensing, display, and imaging.

9:15 AM BREAK

SESSION EQ03.02: Plasmonic Applications I
Session Chairs: Harry Atwater and Yu-Jung Lu
Sunday Morning, November 27, 2022
Hynes, Level 2, Room 202

10:00 AM *EQ03.02.01

Optical Field and Spin Topologies in Plasmonics and Metamaterials [Anatoly Zayats](#); King's College London, United Kingdom

The ability to engineer and manipulate the properties of optical wavefronts, such as phase, polarisation and amplitude, is very important in numerous applications including imaging, metrology, optical communications as well as biomedical and quantum technologies. Metamaterials and metasurfaces provide a rich playground for both passive and active manipulation of phase and polarisation of light. Engineering spin-orbital angular momentum conversion provides practical opportunities for designing complex vector beams. In this talk, we will discuss optical vector field topologies and their transformations enabled by strongly anisotropic metamaterials and metasurfaces. Field- and spin-skyrmion and meron topologies will be discussed. An anisotropic metamaterial platform for local control of polarisation in complex vector beams, including radial and azimuthal beams, will be presented. The results enable a flexible approach for tailoring complex vector beams and achieving required polarisation patterns on demand for harvesting functionalities and applications of complex light beams with complex polarisation and phase information in numerous photonic and quantum technologies, imaging and metrology.

10:30 AM EQ03.02.02

Nanoscale Imaging of Plasmonic Coupling in Nanorod Dimers/Trimers by UEM [Haihua Liu](#)¹, Prem Singh², Amit Jaiswal², Thomas Gage¹ and Ilke Arslan¹; ¹Argonne National Laboratory, United States; ²Indian Institute of Technology Mandi, India

Replacing electronic signals with light pulses as information carriers is a prime motivation behind research on photonic circuits. Plasmonics based on surface plasmon polaritons, charge collectively oscillating at the interface or surface, is attracting extensive interests because it enables concentration and manipulation of electric fields well beyond diffraction limit via nanoscale structures.[1] Therefore, direct imaging of the plasmonic field and its coupling at the nanoscale between photonics circuit components or plasmonic nanostructures is critical for nanophotonics applications, while scientists in this field mainly rely on theoretical simulation of the plasmonic field by FDTD or other programs. Noble metals such as Au or Ag are among the most popular plasmonic materials because of their strong coupling with light from visible to near-infrared (NIR) wavelengths. The anisotropic optical properties of the Au or Ag nanorods between the long and short axis provide tunable plasmonic energies and alternate ways to manipulate the plasmonic couplings between their dimer or trimer nanostructures depending on their mutual orientations and light polarizations. Photon-Induced Near Field Electron Microscopy (PINEM) developed in ultrafast electron microscopy (UEM) enables scientists to capture the evanescent electromagnetic field on its intrinsic time scale and with nanometer resolution.[2] To gain deeper insights regarding the plasmonic coupling mechanism at the nanometer scale, the dependences of the

plasmonic coupling within the dimer/trimer on laser polarizations and fluences, time, and nanorod mutual orientations were investigated at high spatiotemporal resolution on the newly established scientific UEM platform at Center for Nanoscale Materials, Argonne National Laboratory.

[1] Gramotnev, D.K.; Bozhevolnyi, S.I, Plasmonics beyond the diffraction limit. *Nature Photonics* 2010, 4, 83-91.

[2]. Barwick, B.; Flannigan, D.J.; Zewail, A.H. Photon-induced near field electron microscopy. *Nature* 2009, 462,902-906.

Work performed at the Center for Nanoscale Materials, a U.S. Department of Energy Office of Science User Facility, was supported by the U.S. DOE, Office of Basic Energy Sciences, under Contract No. DE-AC02-06CH11357.

10:45 AM EQ03.02.03

Nanopore Arrays on Free-Standing Plasmonic Nanoassemblies for Electro-Optical Biosensing at Ultra-Low Concentrations [Marzia Iarossi](#)¹, Daniel Darvill^{2,1}, Aliaksandr Hubarevich¹, Jian-An Huang^{3,1}, Yingqi Zhao^{3,1}, Angela F. De Fazio¹, Devin O' Neill¹, Francesco Tantussi¹ and Francesco De Angelis¹; ¹Italian Institute of Technology, Italy; ²Imperial College London, United Kingdom; ³University of Oulu, Finland

In the last two decades, nanopores have been extensively developed to detect and sequence biomolecules, providing powerful biosensing platforms. Typically, nanopore-based sensors are in contact with two compartments filled with an electrolyte solution and under an external bias a certain ionic current can be measured. When molecules are driven by electrophoresis towards the nanopore time-resolved transient fluctuations of the ionic current are observed. From an engineering point of view, solid-state nanopores are the artificial counterpart of biological nanopores and the latter have been even successfully commercialized as sensors at the single-molecule level and sequencing devices by taking advantage of the electrical detection mechanism¹. Nevertheless, solid state nanopores still require further development to properly control the translocation events and collect as much information as possible from the passage of each molecule. For this reason, they have been integrated with plasmonic nanostructures with the aim to couple the electrical readout with an additional sensing modality based on an optical technique, such as, among others, Surface Enhanced Raman Spectroscopy²⁻⁴. Here, we propose an ordered array of nanopores supported on a free-standing plasmonic nanoassembly, which we use to detect DNA fragments both electrically and optically by means of SERS. We show that under resonant illumination the nanoassembly coated with a Au layer is able to highly enhance the electromagnetic field, which is highly confined at the metallic tips of the nanopores supported on the nanoassembly. This implies that the metallic nanopores can be used to detect molecules by SERS in flow-through configuration, taking advantage of the narrow sensing area generated by the plasmonic hotspots inside the nanopores. Since this platform is not based on a single nanopore but on multiple nanopores with high density, we show the detection of DNA at ultra-low concentrations in the femtomolar range. In this regard, nanopore arrays have the potential to overcome the low-throughput of single-nanopore based sensors, which are typically not able to detect molecules at concentrations lower than a few picomolars within a reasonable experimental time⁵. Furthermore, we show that our fabrication approach is based on a well-scalable method, which is based on the assembly of nanospheres, the reshaping of the interstices of the array and finally, the transfer of the nanoassembly on any holey supporting substrate. Hence, being not based on drilling techniques with electron/ion beams of expensive tools, the fabrication approach is advantageous in terms of costs and time. We believe that as a sensing platform based on arrays of nanopores our device could be interfaced with cells for biological applications, in which a significant number of molecules need to be analyzed and discriminated through SERS.

References

1 C. Dekker, *Nat. Nanotechnol.*, 2007, 2, 209–215.

2 Y. Zhao, M. Iarossi, A. Federica, D. Fazio, J.-A. Huang and F. De Angelis, *ACS Photonics*, 2022, 9, 730–742.

3 J. A. Huang, M. Z. Mousavi, Y. Zhao, A. Hubarevich, F. Omeis, G. Giovannini, M. Schütte, D. Garoli and F. De Angelis, *Nat. Commun.*, 2019, 10, 1–10.

4 J. D. Spitzberg, A. Zrehen, X. F. van Kooten and A. Meller, *Adv. Mater.*, 2019, 31, 1900422.

5 L. Xue, H. Yamazaki, R. Ren, M. Wanunu, A. P. Ivanov and J. B. Edel, *Nat. Rev. Mater.* 2020 512, 2020, 5, 931–951.

11:00 AM EQ03.02.04

Integration of Aluminum Plasmonic Nanostructures for Manipulating Organic Ultraviolet Photodetectors [Qiuming Yu](#); Cornell University, United States

Incorporating surface plasmonics into optoelectronic devices can manipulate the performance of devices such as solar cells and photodetectors. This effect has been well-established for metals such as gold (Au), but has not been studied as extensively for metals with UV-range transitions such as aluminum (Al). UV-specific photodetectors have a wide variety of applications including environmental monitoring, scientific research, imaging, and flame and missile detection. Many of the devices currently in use are based on inorganic wide-bandgap materials such as GaN and ZnO, but organic materials offer several advantages over inorganic materials such as flexibility, tunability, and low material cost. In this work, a wide-bandgap (2.4 eV) polymer poly[(9,9-dioctylfluorenyl-2,7-diyl)-alt-co-(bithiophene)] (F8T2) was blended with a fullerene derivative [6,6]-phenyl-C71-butyric acid methyl ester (PC₇₁BM) for device active layers. We integrated Al plasmonic nanostructures into the organic UV photodetectors with the photodiode structures either as a transparent electrode or at the top metal electrode. For the devices with the Al plasmonic nanostructures as the transparent conducting electrodes, we replaced the indium tin oxide (ITO) with Al plasmonic nanohole arrays (Al-NHAs) with the device structure of glass/Al-NHA/PEDOT:PSS/F8T2:PC₇₁BM/LiF/Al, where PEDOT:PSS and LiF were used as hole and electron transport layers, respectively. We applied 3-dimensional finite-difference time-domain (3D-FDTD) electromagnetic simulations to design the Al-NHA to produce strong UV absorption in the active layer and enhanced internal electric field intensity. We successfully fabricated the Al-NHA electrodes using nanosphere lithography and incorporated into photodetectors, which produced two narrow photoresponse peaks with specific detectivity (D*) values of 4.0 x 10⁹ and 4.6 x 10⁹ jones under 340 and 515 nm illumination, respectively, and -2 V bias and one broad photoresponse peak with a peak D* of 8.8 x 10⁹ jones under 450 nm illumination and 2 V bias. For the devices with the Al plasmonic nanostructures at the top metal electrodes, we imprinted nanohemisphere arrays (NHSAs) into the top surface of the active layer (F8T2:PC₇₁BM) in conventional organic UV photodetectors with the structure of glass/ITO/PEDOT:PSS/F8T2:PC₇₁BM/LiF/Al. NHSAs were transferred to the top Al cathode in the following thermal deposition of LiF and Al to generate plasmonic Al nanostructures. 3D-FDTD simulations revealed that the devices with plasmonic NHA top electrodes exhibit stronger UV absorption in the active layer and enhanced electric fields at the interface of the top of the active layer and the Al electrode, especially for devices with thinner active layers. The inclusion of a NHA was found to improve the photoresponse strength, sensitivity and speed through increased UV absorption and enhanced electric fields resulting from angular reflection of light in the active layer and the plasmonic effects of the Al NHA electrode. The novel bias dependent response switching improves the applicability of UV photodetectors through the cost-effective, flexible, and performance-enhancing plasmonic Al-NHA transparent conducting electrodes. Our work also demonstrates that imprinting an NHA into the top of the active layer, thus structuring the top metal electrode, is an effective approach for incorporating performance-enhancing plasmonic nanostructures into organic UV photodetectors.

11:15 AM EQ03.02.05

Enhancing the Broadband Photoresponse of Superconducting Microwire Single Photon Detectors Based on Ag Plasmonic Crystals [Jingwei Yang](#)¹, Tzu-Yu Peng^{2,1}, Jia-Wern Chen¹, Li-Chung Yang^{1,2} and Yu-Jung Lu^{1,2,2}; ¹Research Center for Applied Sciences, Taiwan; ²National Taiwan University,

Taiwan

Superconducting photon detectors (SPDs) have many advantages like low dark noise, low time jitter, and broad detection range. However, there are some trade-offs that should be taken into account during fabricating the device. For example, a superconducting wire with narrower width performs a higher detection efficiency than a wider wire, but its detection area becomes smaller and its critical temperature is suppressed at the same time. On the other hand, a typical nano-meander shows high polarization sensitivity, which is inconvenient in many applications, e.g., quantum communication using MMF coupled systems. To overcome this predicament, we design a superconducting NbN microwire photon detector with gap plasmon enhancement. The gap plasmon resonance in an Al₂O₃ layer between Ag nanostructure and NbN microwire confines a strong electrical field, which destroys the Cooper pairs and further promotes the detection efficiency. For instance, we discovered a localized plasmonic resonance, which resonated at 532 nm wavelength, at the edge of Ag nanocube with 40 nm long and 30 nm thick. Hence, we can enhance the photon response of the detector to the visible range which can attribute to the gap plasmon resonance and the minimum detectable power of light is 4.4 nW. We design 9 different sizes of Ag nanocubes with side lengths of 30 nm to 70 nm (thickness of 30 nm) as a unit cell that resonate at different wavelengths to demonstrate a broadband photon detector with high detection efficiency from visible to NIR. In addition, though the choice of nanocube and microwire makes polarization sensitivity of the device lower, we still can make an SPD with polarization-dependent gap plasmon resonance by the different length-wide ratios of Ag nanoantenna. In the end, we discuss the potential for superconducting microwire photon detector applications, such as large active area, tunable polarization sensitivity, and low time jitter, etc.

11:30 AM EQ03.02.06

Temperature Non-Uniformities in Plasmonic Catalyst Beds: Measuring, Modeling and Implications for Catalysis Man Xu^{1,2}, Lun Cheng¹, Tim den Hartog¹, Roberto Habets¹, Jonathan van den Ham¹, Nicole Meulendijks¹, Francese Sastre Calabuig¹ and Pascal Buskens¹; ¹TNO, Netherlands; ²Delft University of Technology, Netherlands

Distinguishing between photothermal and non-thermal contributions is essential in plasmon catalysis. Use of a tailored optical temperature sensor based on fiber Bragg gratings enabled us to obtain an accurate temperature map of an illuminated plasmonic catalyst bed with high spatiotemporal resolution.^[1] We demonstrate that this fiber optical sensor (FOS) enables accurate temperature measurements at multiple positions inside an illuminated plasmonic catalyst bed realizing monitoring of local temperatures and temperature profiles and gradients. We validate the performance of this FOS sensor using spherical and rod-like alumina-supported Ru nanocatalysts recently developed by our research group for sunlight-powered conversion of CO₂ and H₂ to CH₄.^[2-4] Using the FOS, we measured temperature differences exceeding 50 °C in the top 0.5 mm of the catalyst bed. Furthermore, we discovered differences between the surface temperature and the temperature obtained via conventional thermocouple measurements underneath the catalyst bed exceeding 200 °C. When used and calibrated (emissivity) correctly an IR camera can be used to measure exclusively the surface temperature, and indicate a temperature variation in the x,y-direction. However, an IR camera is unsuited to establish temperature gradients in the z-direction. A low thermal conductivity of 0.04 – 0.08 W m⁻¹ K⁻¹ is found, which causes the large temperature non-uniformity in the NP catalyst bed and should be taken into account when distinguishing between thermal and non-thermal contribution to plasmon catalysis. Using the acquired information of the thermal gradient in the catalyst powders, we developed a simple empirical model to study the photothermal effect. We would also like to point out that the measured temperature gradients will lead to large local deviations in reaction rate, and possible access to additional reaction pathways and mixed reaction mechanisms. Latter may explain differences in selectivity between illuminated reactions and their counterparts in dark. <!--[endif]-->

[1] M. Xu, T. den Hartog, L. Cheng, M. Wolfs, R. Habets, J. Rohlfs, J. van den Ham, N. Meulendijks, F. Sastre, P. Buskens *ChemPhotoChem.* **2022**, *6*, e202100289.

[2] F. Sastre, C. Versluis, N. Meulendijks, J. Rodríguez-Fernández, J. Sweelssen, K. Elen, M. K. Van Bael, T. den Hartog, M. A. Verheijen, P. Buskens *ACS Omega.* **2019**, *4*, 7369-7377.

[3] R. Grote, R. Habets, J. Rohlfs, F. Sastre, N. Meulendijks, M. Xu, M. A. Verheijen, K. Elen, A. Hardy, M. K. Van Bael, T. den Hartog, P. Buskens *ChemCatChem.* **2020**, *12*, 5618-5622.

[4] P. Martínez Molina, N. Meulendijks, M. Xu, M. A. Verheijen, T. den Hartog, P. Buskens, F. Sastre *ChemCatChem.* **2021**, *13*, 4507-4513.

11:45 AM EQ03.02.07

Thin-Film Exsolution of Metal Nanoparticles and Their Galvanic Restructuring for Plasmonically Enhanced Photocatalytic Activity Kevin Gregor Both^{1,1}, Vilde M. Reinertsen^{1,1}, Xiaolan Kang^{1,1}, Dragos Neagu², Øystein Prytz^{1,1}, Truls Norby^{1,1} and Athanasios Chatzidakis^{1,1}; ¹University of Oslo, Norway; ²University of Strathclyde, United Kingdom

The exsolution and precipitation of metal nanoparticles (MNPs) from the bulk of a host material have been studied extensively due to their ability to create well-socketed particles on the host material's surface. This method is particularly useful in catalysis, as these supported catalysts generally have a longer lifetime due to the better adhesion with the substrate. This has been extensively applied to the field of solid oxide fuel cells for electrochemical energy conversion. But, could we apply it to semiconducting materials and improve their photoelectrocatalytic properties?

Most metals considered for exsolution (e.g., Ni, Fe, Co) do not possess notable plasmonic properties, rendering the possibility of increasing the efficiency of wide band gap semiconductors, such as strontium titanate (STO) through the surface plasmon resonance of socketed and plasmonically active nanoparticles. However, silver (Ag) and copper (Cu) can be substituted into STO and forced to exsolve by introducing a reducing environment at elevated temperatures. Moreover, utilizing the principle of galvanic replacement/deposition reaction allows the introduction of other plasmonically active elements, such as gold (Au), despite their inability to be exsolved. We have recently demonstrated this principle by exsolving nickel (Ni) and replacing it with the plasmonically active Au [1].

The direct exsolution or exsolution with subsequent galvanic replacement offer not only the ability to create well-socketed particles, but the latter also ensures that the precious metals are only present on the surface, reducing the amount of precious metals significantly. Moreover, the combination of exsolution and galvanic replacement allows the synthesis of materials with two different MNPs, one located in bulk and one sticking out of the surface. The combination of two plasmonically active elements enables an additional degree of freedom to adjust the absorption spectrum of the final device. In this work, Ag-doped thin films and Cu-doped thin films have been exsolved. Additionally, Ni MNPs created by exsolution have been galvanically replaced by Ag and Au. The samples were characterized by X-Ray Diffraction and electron microscopy (both scanning electron microscopy and scanning transmission electron microscopy), including energy-dispersive X-ray spectroscopy and electron energy loss spectroscopy. These techniques allowed the study of thin films on the nanometer scale. Additionally, the photoelectrochemical performance was determined, and a clear improvement was found between a sample with Au MNPs, and samples without MNPs.

Moreover, the shape, geometry, and the STO-matrix in proximity influence the peak position drastically. Combined with Finite Difference Time Domain

(FDTD) calculations, the results indicate that hot charge carriers are mainly responsible for enhancing photocatalytic properties. Recently, we considered MNPs of two elements close to each other, where one is plasmonically active and the other inactive (i.e., Au and Ni). The plasmonically inactive MNPs showed enhanced absorption while near the plasmonically active MNPs [1]. This configuration is evidence of a reactor-antenna formation, further increasing the possible structures obtained by our proposed methodology.

In brief, thin films with well socketed MNPs were created by exsolution and galvanic replacement. The particles were well dispersed and plasmonically active. The photoelectrochemical response was enhanced in comparison to thin films without MNPs.

[1] Kang, X., Reinertsen, V. M., Both, K. G., Galeckas, A., Aarholt, T., Prytz, Ø., Norby, T., Neagu, D., Chatzidakis, A., Galvanic Restructuring of Exsolved Nanoparticles for Plasmonic and Electrocatalytic Energy Conversion. *Small* 2022, 2201106. <https://doi.org/10.1002/sml.202201106>

SESSION EQ03.03: 2D Photonics I
Session Chairs: David Norris and Anatoly Zayats
Sunday Afternoon, November 27, 2022
Hynes, Level 2, Room 202

1:30 PM *EQ03.03.01

Strong Light-Matter Interactions in Low-Dimensional Excitonic Semiconductors Deep M. Jariwala; University of Pennsylvania, United States

The isolation of stable atomically-thin two-dimensional (2D) crystals has led to a revolution in solid state physics and semiconductor device research over the past decade. A variety of other 2D materials (including semiconductor) with varying properties have been isolated raising the prospects for devices assembled by van der Waals forces.¹ Particularly, these van der Waals bonded semiconductors exhibit strong excitonic resonances and large optical dielectric constants as compared to bulk 3D semiconductors.

I will focus this talk on our recent works in strong light-matter coupling in excitonic 2D semiconductors, namely chalcogenides of Mo and W. Visible spectrum band-gaps with strong excitonic absorption makes transition metal dichalcogenides (TMDCs) of molybdenum and tungsten as attractive candidates for investigating strong light-matter interaction formation of hybrid states.²⁻⁴ We will present our recent work on the fundamental physics of light trapping in multi-layer TMDCs when coupled to plasmonic substrates.⁵

Then, I will show the extension of these results to superlattices of excitonic chalcogenides. These hybrid multilayers offer a unique opportunity to tailor the light-dispersion in the strong-coupling regime.⁶ We will discuss the physics of strong light-matter coupling and applications of these multilayers. If time permits, I will also present our recent work on scalable, localized quantum emitters from strained 2D semiconductors.⁷

Our results highlight the vast opportunities available to tailor light-matter interactions⁸ and building practical devices with 2D semiconductors. I will conclude with a broad vision and prospects for 2D materials in the future of semiconductor electronics and opto-electronics

References:

1. Jariwala, D.; Sangwan, V. K.; Lauhon, L. J.; Marks, T. J.; Hersam, M. C. *ACS Nano* **2014**, *8*, (2), 1102–1120.
2. Jariwala, D.; Davoyan, A. R.; Wong, J.; Atwater, H. A. *ACS Photonics* **2017**, *4*, 2692-2970.
3. Brar, V. W.; Sherrott, M. C.; Jariwala, D. *Chemical Society Reviews* **2018**, *47*, (17), 6824-6844.
4. Anantharaman, S. B.; Jo, K.; Jariwala, D. *ACS Nano* **2021**.
5. Zhang, H.; Abhiraman, B.; Zhang, Q.; Miao, J.; Jo, K.; Roccacaccia, S.; Knight, M. W.; Davoyan, A. R.; Jariwala, D. *Nature Communications* **2020**, *11*, (1), 3552.
6. Kumar, P.; Lynch, J.; Song, B.; Ling, H.; Barrera, F.; Zhang, H.; Anantharaman, S. B.; Digani, J.; Zhu, H.; Choudhury, T. H.; McAleese, C.; Wang, X.; Conran, B. R.; Whear, O.; Motala, M.; Snure, M.; Muratore, C.; Redwing, J. M.; Glavin, N.; Stach, E. A.; Davoyan, A. R.; Jariwala, D. *Nature nanotechnology* **2022**, *17* 182–189.
7. Kim, G.; Kim, H. M.; Kumar, P.; Rahaman, M.; Stevens, C. E.; Jeon, J.; Jo, K.; Kim, K.-H.; Trainor, N.; Zhu, H.; Sohn, B.-H.; Stach, E. A.; Hendrickson, J. R.; Glavin, N.; Suh, J.; Redwing, J. M.; Jariwala, D. *ACS Nano* **2022**, *10.1021/acsnano.2c02974*.
8. Zhang, H.; Ni, Z.; Stevens, C. E.; Bai, A.; Peiris, F.; Hendrickson, J. R.; Wu, L.; Jariwala, D. *Nature Photonics* **2022**, *16*, 311-317.

2:00 PM EQ03.03.02

Room Temperature Mie-Polaritons in a Monolayer WSe₂ Coupled to van der Waals Nanophotonic Structures Yadong Wang¹, Sam Randerson¹, Panaiot Zotev¹, Xuerong Hu¹, Yue Wang², Charalambos Louca¹, Thomas F. Krauss² and Alexander Tartakovskii¹; ¹The University Of Sheffield, United Kingdom; ²University of York, United Kingdom

Dielectric nanostructures exhibit low optical losses and a wealth of distinct Mie resonances in contrast to their plasmonic counterparts (1, 2). Meanwhile, the strong light-matter coupling has attracted long-standing interest due to its fundamental importance in Bose-Einstein condensation, polariton lasing, and potential in quantum optics applications (3). However, strong coupling with relatively broad Mie resonances has been rarely observed. Here, we employ relatively narrow Mie resonances in high-refractive-index WS₂ nanoantennas placed on gold, and demonstrate strong exciton-photon coupling (Mie-polaritons) in monolayer WSe₂ exhibiting room temperature stable excitons with a large oscillator strength.

To achieve the Mie-polaritons, we fabricate nanoantennas by etching thin film WS₂ (30-nm thickness) that is exfoliated on a gold substrate, and then stack a monolayer WSe₂ onto them by using a dry transfer method. We use nanoantennas with radii (*r*) from 83 to 155 nm, which allows gradual tuning of the Mie resonance through the WSe₂ exciton energy. Thanks to the high refractive index of WS₂ and the gold substrate, Mie resonances with a narrow bandwidth of $T_M \approx 105$ meV are achieved in WS₂ nanoantennas, suitable for observation of the strong coupling with WSe₂ excitons. The Mie resonances in the hybrid monolayer WSe₂/nanoantenna structures undergo significant changes compared with bare WS₂ structures. Typical anti-crossing behaviour is observed using dark-field scattering spectroscopy. The energy splitting between the upper (UBP) and low (LPB) polariton branches is fitted as $T_p \approx 86$ meV, which is higher than the value reported in plasmonic systems (~ 50 meV) (4). Considering the linewidth of Mie resonance and neutral exciton ($T_0 \approx 38$ meV), the strong coupling condition is thus satisfied at room temperature. Our results provide a promising platform for the realisation of the strong coupling in nanophotonic structures and controlled light emission in nanophotonics (5-7). Furthermore, one of the keys to our results is the use of hybrid dielectric/metal structures, achievable in a straightforward fashion with layered van der Waals materials.

Reference:

1. A. I. Kuznetsov *et al*, *Science* **354**, aag2472 (2016).

2. L. Sortino *et al.*, *Nature communications* **10**, 5119 (2019).
3. S. Dufferwiel *et al.*, *Nature Photonics* **11**, 497-501 (2017).
4. D. Zheng *et al.*, *Nano letters* **17**, 3809-3814 (2017).
5. L. Sortino *et al.*, *Nature communications* **12**, 6063 (2021).
6. H. Ling, R. Li, A. R. Davoyan, *ACS Photonics* **8**, 721-730 (2021).
7. P. G. Zotev *et al.*, *ACS Nano* doi.org/10.1021/acsnano.2c00802, (2022).

2:15 PM EQ03.03.03

Graphene-Based Mid-Infrared Emitters Geoff Nash, Prarthana Gowda, Dean Patient and Simon Horsley; University of Exeter, United Kingdom

Cost-effective and sustainable mid-infrared light sources are required for applications such as gas sensing and infrared beacons. Semiconductor LEDs are a natural replacement for the conventional incandescent sources still widely used in many applications, but to achieve emission at long wavelengths requires the realization of devices with narrow effective bandgaps, inherently leading to relatively poor internal and external quantum efficiencies. Recently, the technological potential of graphene-based incandescent emitters has been recognized, in part due to the ability of graphene to sustain extremely large current densities. Mid-infrared sources based on such emitters potentially offer an alternative, less complicated, approach to mid-infrared semiconductor LEDs [1], where the low thermal mass of graphene offers the potential for high frequency modulation [2]. Encapsulation of the emitting layer with hexagonal boron nitride allowed devices to run continuously in air for over 1000 hours [3], with the emission spectrum covering the absorption bands of many important gases. The h-BN encapsulation also allows the incorporation of a frequency selective surface metamaterial layer and we have previously shown that a metasurface consisting of ring resonators acts to tailor the broadband thermal emission into a dual band radiation, with measurements of both reflection and emission spectra agreeing well with simulations [4]. Here we describe a simple architecture, consisting of a back-reflector behind a multilayer graphene filament, which we use to produce emitters with wall-plug-efficiencies comparable to state-of-the-art semiconductor cascade LEDs. Such high relative efficiencies demonstrate the feasibility of developing a graphene based mid-infrared light emitting device, which could be more cost effective and sustainable to manufacture than either silicon MEMs or compound semiconductor based alternatives. We show that the spectral characteristics of the emission could also be tailored for specific applications, such as gas sensing, through the incorporation of a metasurface.

- [1] L. M. Lawton, N. H. Mahlmeister, I. J. Luxmoore, and G.R. Nash, "Prospective for graphene based thermal mid-infrared light emitting devices" *AIP Adv.* **4**, 087139 (2014).
- [2] N. H. Mahlmeister, L. M. Lawton, I. J. Luxmoore, and G. R. Nash, "Modulation characteristics of graphene-based thermal emitters", *Appl. Phys. Express* **9**, 012105 (2016).
- [3] H. R. Barnard, E. Zosimova, N. H. Mahlmeister, L. M. Lawton, I. J. Luxmoore, and G. R. Nash, "Boron Nitride Encapsulated Graphene Infrared Emitters", *Appl. Phys. Lett.* **108**, 131110 (2016).
- [4] C. Shi, N. H. Mahlmeister, I. J. Luxmoore, and G. R. Nash, "Metamaterial Graphene Thermal Emitter", *Nano Res.* **11**, 3567 (2018).

2:30 PM EQ03.03.04

Charge Transfer Between Infrared Plasmonic Nanocrystals and Two-Dimensional Semiconductor Michele Guizzardi¹, Michele Ghini², Ilka Kriegel², Giulio Cerullo¹ and Francesco Scotognella¹; ¹Politecnico di Milano, Italy; ²Istituto Italiano di Tecnologia, Italy

Infrared carrier transfer processes are a key technology to harvest energy from light. The standard photovoltaic materials work only in the visible range, but 45% of the emitted light from the sun is in the near-infrared region (NIR).

Indium Tin Oxide (ITO) has a localized surface plasmon resonance (LSPR) in the infrared region tunable between 1.5 μm to 4 μm [1], and it has a bandgap of 3.6 eV. ITO is a transparent material in the visible range. This makes it one of the key materials for the development of infrared plasmonic devices. Charge transfer between infrared plasmonic nanocrystal that absorb in the IR and Two-dimensional semiconductor enables the extraction of charges excited with low-energy photons.

Ultrafast pump-probe spectroscopy has proven to be a powerful technique to study out-of-equilibrium phenomena, being applicable over a broad range of photon energies from THz to x-rays. In pump-probe, a medium is first excited with a short pump pulse and the photoinduced dynamics are probed by a time-delayed broad-band probe pulse.

Here, we used a broadband ultrafast optical spectroscopy to investigate the charge transfer between Indium tin Oxide nanocrystals and a large area Molybdenum disulfide (MoS_2) single layer.

After the excitation of the plasmon, in an ultrafast time scale of around 20fs, we have the plasmon dephasing due to electron-electron scattering, this leads to the generation of the so-called "Drude" electrons around the Fermi level, these carriers are not in equilibrium and they will reach it through e-e scattering. After $\sim 100\text{fs}$ we have generated a hot FD distribution, that will relax by electron-phonon scattering, this process has a different timescale in different materials, however in plasmonic nanocrystal we are in the order of few ps.

When we generate the hot FD, the higher energy electron has enough energy to overcome the Schottky barrier and be transferred into the MoS_2 .

To study this we tuned our Noncollinear optical parametric amplifier to 0.7 eV (1750nm) to be resonant with the infrared plasmon of the ITO and the probe is in the visible region to keep track of the change in the transmitted probe resonant with the MoS_2 excitons, while the ITO have a small negative signal in the visible coming from the ultrafast change in the refractive index.

We were able to see the feature of the A and B exciton of the MoS_2 even if the energy is not enough to excite the exciton of the material, this is a clear sign of plasmon-induced charge transfer from the ITO to the MoS_2 .

We moreover compare the dynamics of directly excited MoS_2 and the one induced by the plasmon to see the difference time constant of the exciton in both cases, when directly and indirectly excited.

- [1] Mryasov, O. N., and A. J. Freeman. "Electronic band structure of indium tin oxide and criteria for transparent conducting behavior." *Physical Review B* **64**.23 (2001): 233111.
- [2] G. V. Hartland, "Optical studies of dynamics in noble metal nanostructures," *Chem. Rev.* **111**, 3858–3887 (2011).

2:45 PM BREAKS

SESSION EQ03.04: Nonlinear Optics
 Session Chairs: Viktoriia Babicheva and Deep Jariwala
 Sunday Afternoon, November 27, 2022
 Hynes, Level 2, Room 202

3:15 PM EQ03.04.01

Vortex Beams for Photonic Metasails and Optomechanical Rotation [Mohammadrasoul Taghavi](#), Mohammadmojtaba Sadafi and Hossein Mosallaei; Northeastern University, United States

It has been proven experimentally that light can generate optical forces while interacting with nano-objects, resulting in various interesting applications such as optical trapping. Inspired by that, lightsailing has been introduced recently as a novel concept, exploiting the radiation pressure of light to reach the relativistic velocities with the hope of exploring the undiscovered universe. Metasurfaces, due to the taking advantage of the generalized Snell's law, can offer the possibility of controlling the wavefront of the reflected/transmitted light to engineer the amplitude and direction of the optical forces to obtain the desired goals. Lightsailing technology seems to be an ideal platform for probing the nearest inhabitable exoplanet within the human lifetime thanks to the exclusive functionalities that the photonic metasurfaces offer. Light tends to carry both the linear and angular momenta while propagating, where the exchange of the former one with the matter can result in linear acceleration, having been the subject of numerous studies so far. The linear momentum exchange between the light and the object exerts an optical force, which can be exploited for accelerating gram-scale space probes. Nevertheless, the transfer of angular momentum to an object will potentially impose a rotational motion, being desirable in a variety of applications. Here, we put our major focus on the study of the rotational behavior of our designed metasail while it exchanges the orbital angular momentum (OAM) with light. The rotational motion of the lightsail will be advantageous in various scenarios, including stability improvement. Moreover, enabling the self-stabilizing mechanism while minimizing the acceleration time in the propulsion stage is one of the key elements to realizing such nanocrafts. Conventional designs of metasails require a parachute configuration with a detached payload for enabling the passive self-stabilizing mechanism. Therefore, spinning the lightsail at high speeds can be introduced as a beneficial tool to provide a new degree of freedom in the stability criteria of the lightsails, which can be exploited to further widen the stability margins. In our study, we design an all-dielectric photonic metasail using multi-objective optimization, which consists of both the reflective and transmissive elements that can provide the required optomechanical performance for reaching the relativistic velocities in an acceptable period of time. Also, we carefully design each unitcell of the metasurface, considering the delicate trade-off between the linear acceleration and rotational motion of the sail. We illustrate the interaction between the vortex beam associated with different OAM states and photonic metasails for achieving desired propulsion performance. Generally, the rotational force would be expected if the incident light is carrying an orbital angular momentum or if the metasail imparts an orbital angular momentum to the incident beam. In the latter case, the propulsion beam upon reflection from a metasail with a broken azimuthal symmetry contains an orbital angular momentum (OAM) which seems to be a viable solution for generating large in-plane rotational torque. Our work addresses in detail the relation between the amount of OAM accompanied by the reflected beam and rotational speed of the sail as well as the linear acceleration. It is shown that a careful design can result in a metasail, having both the desirable linear acceleration and rotational motion, providing the self-stability feature to the sail, simultaneously. We believe that the studies in our work can be used to open a new perspective on the lightsailing field as our results show the impacts of both the linear and rotational motions on the functionality of the metasail.

3:30 PM *EQ03.04.02

Expanding the Materials Palette for Nanophotonics with Super-Mossian and Quantum Materials [Guru V. Naik](#); Rice University, United States

Emerging meta-devices need novel optical materials, both metals and dielectrics, for high performance, flexibility, and large-scale integration. Novel metallic materials or plasmonic materials such as transparent conducting oxides and transition metal nitrides have significantly expanded the scope of nanophotonics in the past. Further improvements are required in dielectrics and tunable dielectrics. Here, I will describe how super-Mossian dielectrics enable high performance and quantum materials enable MHz-fast ultralow-power tunability. Super-Mossian dielectrics are very high index dielectrics that significantly beat the predictions of Moss' rule. The commonly-known form of Moss' rule states that the fourth power of the refractive index of a dielectric inversely scales with its direct bandgap or absorption edge. Thus, the refractive index of dielectrics has an upper limit for a given operating wavelength. However, there are certain materials with special energy band features that can significantly beat Moss' predictions. Here, I will describe how to identify such super-Mossian dielectrics. Also, I will show high-Q dielectric resonances enabled by one such outstanding super-Mossian dielectric, iron pyrite. While a high refractive index is needed for high-quality factor resonators, tunable optical properties are required for reconfigurable and non-linear devices. Low-power tunability is desired in many such devices because of their applications on mobile platforms. Here, I will show how quantum materials offer a paradigm shift in optical tunability. I will describe ultralow-power MHz-fast optical tunability in 1T-TaS₂, a charge-ordered material at room temperature. Finally, I will demonstrate tunable and color-changing metasurfaces built on 1T-TaS₂.

4:00 PM EQ03.04.03

Large Area Periodically Modulated 2D Transition Metal Dichalcogenide Layers Featuring Flat-Optics Light Harvesting [Matteo Gardella](#), Giulio Ferrando, Giorgio Zambito, Maria Caterina Giordano and Francesco Buatier de Mongeot; Università di Genova, Italy

Transition Metal Dichalcogenides (TMDs) are two-dimensional semiconductors featuring high optical absorption coefficient combined with good transport and mechanical properties. Although mechanically exfoliated TMD flakes ensure the best opto-electronic properties, homogeneous large area growth techniques are mandatory for real world applications [1,2]. At the same time, in view of light conversion applications in the extreme thickness regime of 2D-TMDs it is essential to develop effective photon harvesting strategies.

Here we demonstrate that periodic modulation of MoS₂ layers on large area nanostructured samples (either MoS₂ nanostripes arrays or conformal MoS₂ layers grown on top of nanogrooved silica templates) efficiently steers light parallel to the 2D material, exploiting photonic anomalies in the flat-optics regime [3,4].

As a case study, we demonstrate that flat-optics light harvesting in periodically corrugated MoS₂ layers employed as photocatalysts boosts photodissociation of Methylene Blue (MB), a polluting dye molecule commonly used in the textile industry. When illumination occurs at the optimized angles which couple light to the photonic anomalies a two-fold faster photodissociation rate is observed with respect to planar MoS₂ films [6].

In a recent development of our TMD platform, we demonstrated the possibility to stack different 2D-TMDs layers forming large area arrays of van der Waals heterostructures. For this purpose, we developed a custom prototype setup which allows sequential deposition of different TMD layers, MoS₂ and WS₂, by Ion Beam Sputtering. Physical deposition of WS₂ at glancing angles on the nanogrooved silica templates leads to the formation of laterally confined nanostripes which are subsequently coated by a MoS₂ layer, thus achieving maskless deposition of large area arrays of TMD heterostructures. Our preliminary results demonstrate the higher light trapping potential of the TMD heterostructures with respect to single component MoS₂ layers, to be employed as optical sensitizers in water remediation and photocatalytic applications [7].

[1] C. Martella et al., Adv. Mater. 2018, 30, 1705615

[2] C. Martella et al., Adv. Mater. 2017, 1605785

[3] M. Bhatnagar et al., Nanoscale, 2020, 12, s24385-24393

[4] M. Bhatnagar et al., ACS Appl. Mater. Interfaces 2021, 13, 13508–13516

[5] M.C. Giordano et al., under review

[6] G. Ferrando et al., submitted

[7] M. Gardella et al., manuscript in preparation

4:15 PM EQ03.04.04

Optical Customization of Two-Dimensional Exciton Decay Dynamics with Plasmonic Metasurface Sanghyeok Park, Dongha Kim and Min-Kyo Seo; Korea Advanced Institute of Science and Technology(KAIST), Korea (the Republic of)

Excitons in transition metal dichalcogenides (TMDCs) monolayers have been focused on owing to their fascinating physical characteristics such as large binding energy, valley property, and high quantum efficiency. The decay dynamics control of excitons in TMDC monolayer becomes a key issue in various research areas: quantum many-body physics, optoelectronics, valleytronics, and excitonics. The conventional methods applying mechanical strain or electrostatic biasing and implementing defects efficiently control the decay dynamics of excitons. But, those methods accompany the generation of undesired exciton complexes, formation of non-radiative decay channels, and significant changes in the electronic band structure and exciton binding energy. As an alternative method, radiative decay control via optical vacuum field engineering has been suggested. However, the use of typical planar mirrors strictly limits the possibilities of applying further characteristics, such as spectral dispersion, spatial distribution, polarization dependency, and so on, to the dynamics of two-dimensional excitons.

Here, we present the optical customization of the decay dynamics of exciton in MoSe₂ monolayer using plasmonic metasurfaces. The plasmonic metasurface, a square array of Au disks on SiO₂/Au/Si substrate, is covered with hydrogen silsesquioxane (HSQ) to avoid the undesired strain on the MoSe₂ monolayer. The hexagonal boron nitride (hBN) encapsulated MoSe₂ monolayer is transferred on the metasurfaces. The engineered reflection phase shift of the metasurface provides the on-demand vacuum field distribution at the MoSe₂ monolayer depending on the position and frequency. We designed and fabricated three different metasurfaces (A, B, and C) that excite the neutral excitons in the MoSe₂ monolayer at almost the same conditions but make them decay at different rates. With the holography setup, it was experimentally confirmed that the metasurfaces A, B, and C have the same reflection amplitude and reflection phase at the pumping frequency (2.33 eV). On the other hand, the reflection phase changes from destructive interference condition to moderate condition at emission frequency (1.64 eV) depending on the metasurfaces. The metasurface platform controls the radiative decay rate of the neutral exciton in the MoSe₂ monolayer by two orders of magnitude depending on the vacuum field interference. Arranging different metasurfaces in two dimensions enables us to tailor the spatial landscape of exciton radiative decay in a single TMDC flake.

We measured the photoluminescence (PL) spectrum of the neutral exciton in the MoSe₂ monolayer on the metasurfaces, employing a confocal microscope setup. The metasurfaces A, B, and C placed end-to-end resulted in a precise step-wise distribution in the PL intensity. The linewidth and intensity from the Lorentzian fitting of the PL spectra clearly show a positive correlation. The median linewidths at the metasurface A, B, and C are extracted as 2.24, 1.56, and 1.28 meV, respectively. The total decay rate in a two-level system, like excitons, corresponds to the linewidth of the PL spectrum. Employing the coherent optical feedback model, we extract the radiative decay rate from the measured linewidth and reflection phase. We then reveal that the radiative lifetime of the exciton in the TMDC monolayer is successfully controlled by the metasurfaces as desired. We also demonstrated the polarization-dependent radiative decay control of excitons employing an anisotropic metasurface of Au nanorods.

We expect that tailoring the artificial landscape of exciton lifetime by our platform will serve as a building block for the demonstration of advanced exciton transport devices. Also, employing the state-of-the-art metasurfaces will provide more ingredients, such as spectral dispersion, in-plane momentum, and spin/orbital angular momentum, for two-dimensional exciton's decay dynamics.

4:30 PM EQ03.04.05

Atomic Scale van der Waals Nonlinear Optical Metamaterials Bumho Kim¹, Jicheng Jin¹, Zhi Wang¹, Li He¹, Thomas Christensen², Eugene Mele¹ and Bo Zhen¹; ¹University of Pennsylvania, United States; ²Massachusetts Institute of Technology, United States

Material's responses to light are governed by symmetry. For example, the nonvanishing second-order susceptibilities of materials in the 32 point groups have been tabulated and experimentally confirmed. Methods breaking symmetries at interfaces of bulk crystals introduce new electric-dipolar second-order susceptibilities that do not exist in the natural bulk materials, enabling nonlinear metamaterials composed of centrosymmetric dielectrics (Si and Al₂O₃ etc.) and metals (Au, Ag and Al etc.). However, the interfacial nonlinear responses of bulk crystals are inefficient due to the inherently low interface area-to-volume ratio and prevent further miniaturization. The advent of twisted bilayers has provided a new way to create a pristine crystalline interface between two monolayers with an exceptionally low volume fraction. Reconfigured electronic potential in twisted structures enables non-localized nonlinear responses on an atomic scale, promising atomic scale nonlinear optical metamaterials. Most current research focuses on nonlinear responses caused by a superposition of constituent monolayers upon adjusting twist angle or stacking more layers while neglecting interfacial nonlinear responses. Exploring emerging interfacial second-order susceptibilities of van der Waals lattices can bring a new degree of freedom in nonlinear optics, which can be applied to a broad range of nonlinear nanophotonic applications.

In this work, second-harmonic generation (SHG) measurements on $\pm 30^\circ$ twisted bilayer WS₂ unveil the effect of an interfacial second-order sheet susceptibility ($\chi^{(2)}_{s,xyz}$) that does not exist in natural WS₂. In these samples, the interfacial second-harmonic (SH) polarization orientation is solely determined by an interfacial twist orientation. Thus, controlling the twist orientation of trilayer WS₂ enables enhancing and suppressing the interfacial nonlinear response. Furthermore, we devised and demonstrated a twisted quadruple WS₂ with a dominant interfacial nonlinear response ($\chi^{(2)}_{s,xyz} \neq 0$ and $\Sigma\chi^{(2)}_{s,yyy} \approx 0$), which is significantly modified from monolayer WS₂ ($\chi^{(2)}_{s,xyz} = 0$ and $\Sigma\chi^{(2)}_{s,yyy} \neq 0$). The suppression of $\Sigma\chi^{(2)}_{s,yyy}$ in the quad-WS₂ is attributed to a screw axis symmetry. As stacking two quad-WS₂ vertically (octa-WS₂), we observe the interfacial sheet susceptibility increases linearly with the sample thickness, indicating a coherent interference in the thin material. Remarkably, our results demonstrate a new avenue to engineer each component of second-order susceptibilities by twisting and stacking WS₂ layers.

SESSION EQ03.05: Metasurfaces and Metamaterials I

Session Chairs: Artur Davoyan and Stefan Maier

Monday Morning, November 28, 2022

Sheraton, 2nd Floor, Back Bay C

10:30 AM *EQ03.05.01

High-Performance Flat Optics—From Metasurfaces to High-Volume Manufacturing for Consumer Electronics and Communications Federico Capasso; Harvard University, United States

Since the demonstration of the generalized laws of refraction for metasurfaces¹ and the first high performance metalenses², metaoptics has rapidly progressed from the laboratory to manufacturing, propelled by the vision that the foundries that manufacture ICs will manufacture CMOS compatible flat optics using the same semiconductor technology based on deep-UV lithography.^{3,4} This will impact the consumer electronics market in areas such as smart phones and wearable displays for AR/VR. Metasurfaces are now on the market through its partnership with STMicroelectronics, marking the introduction

of this revolutionary optical technology in real-world devices.⁵ I will present recent major advances in cm scale achromatic RGB metalenses for VR by inverse design⁶ and 10 cm metalenses for space optics consisting of 20 billion metatoms.⁷ A compact and highly integrated metasurface-based inverse designed mode multiplexer that takes three single-mode fiber inputs and converts them into the first three linearly polarized spatial modes of a few-mode fiber with high fidelity the C-band (1530–1565 nm) of fiber optics will be presented.⁸ I will conclude with the report of hybrid silicon-organic electrooptic metasurface modulators that use Mie resonances for efficient electro-optic modulation at GHz speeds for free-space communications.⁹

Nanfeng Yu, et al. *Science*, 334, 333 (2011)

Mohammadreza Khorasaninejad, et al. *Science*, 352, 1190 (2016)

Federico Capasso, *Nanophotonics*, 7, 953 (2018)

Alan She et al., *Optics Express*, 26, 1573 (2018)

<https://newsroom.st.com/media-center/press-item.html/t4458.html>; <https://www.metallenz.com>

Zhaoyi Li et al. *Nature Communications*, 13, 2409 (2022)

Joon-Suh Park et al. “All-Glass, Mass-Productible, Large-Diameter Metalens at Visible Wavelength for 100 mm Aperture Optics and Beyond” CLEO 2022

Jaewon Oh et al. *ACS Photonics* 9, 929 (2022)

Ileana-Cristina Benea-Chelms et al. *Nature Communications*, 13, 3170 (2022)

11:00 AM EQ03.05.02

Multi-channel Approach for Secure Metasurface-Based Image Encryption Romil Audhkhasi and Michelle Povinelli; University of Southern California, United States

Recent advances in two disparate but complementary research fields: *metasurfaces* and *hyper-spectral imaging*, suggest exciting new possibilities for the development of secure communication schemes. Metasurfaces can encode information in optical waves by manipulating them in the spatial and spectral domain. On the other hand, hyperspectral imagers can record optical information as a function of both position and wavelength, providing an ideal, complimentary receiver for the transmitted light. Here we introduce a novel, secure communication scheme that takes advantage of the unique opportunities provided by such spatially- and spectrally- multiplexed communication channels. While conventional image encryption approaches perform a 1-to-1 transformation on a plain image to form a cipher image, we propose a 1-to- n transformation scheme. Plain image data is dispersed across n seemingly random cipher images, each transmitted on a separate wavelength channel. The intended recipient converts the cipher images into meaningful information by using a decryption key. We show that the size of our key space grows double-exponentially with the number of channels, providing strong security against both brute force attacks and more advanced attacks based on statistical sampling of the key space. Moreover, our multi-wavelength encryption scheme can be cascaded with traditional 1-to-1 methods, effectively *squaring* the size of the key space. Our results suggest exciting new opportunities for secure transmission in multi-wavelength imaging channels.

11:15 AM EQ03.05.03

Shining Light on the Deep—High Quality Factor Metasurfaces for Real-Time Ocean Observation Halleh Balch¹, Jack Hu¹, Sahil Dagli¹, Varun Dolia¹, Kai Chang¹, Fareeha Safir¹, Greg Doucette², William Ussler², Chris Scholin² and Jennifer A. Dionne¹; ¹Stanford University, United States; ²Monterey Bay Aquarium Research Institute, United States

Phytoplankton are microscopic photosynthetic organisms responsible for half of the global photosynthetic carbon fixation and are an essential part of the earth's carbon cycle. But, under certain conditions, phytoplankton can undergo explosive growth forming dense blooms that can cover hundreds of square kilometers and can release powerful biotoxins (phycotoxins) that contaminate drinking water sources, harming humans and wildlife. Understanding how environmental drivers impact phycotoxin production is key to advancing climate resilience but remains an outstanding challenge due to the difficulty of measuring toxin prevalence and persistence in situ. Predominant methods of studying phycotoxins are based on mass spectroscopy, polymerase chain reaction, and DNA/RNA sequencing. These lab-based methods are costly, require sophisticated infrastructure, and lack remote in situ detection capabilities. Current in situ approaches, such as surface plasmon resonance (SPR), are limited by low sensitivity, poor quantification range, and are challenging to scale.

Here, I will describe the development of a nanophotonic sensor for in situ aquatic toxin detection using surface-functionalized high quality factor (high-Q) silicon metasurfaces. Our metasurfaces are composed of sub-wavelength silicon nanobars with dimensions 500 nm x 600 nm x 160 nm on sapphire substrates. First, we show that by introducing small biperiodic perturbations to the lateral block dimension, free space radiation can be coupled into guided mode resonances to produce high-Q resonances with Q factors exceeding 1,000 in aquatic environments. We demonstrate in simulation and experiment that by varying the biperiodic perturbation from 10 nm to 50 nm, the quality factor can be modulated from a few hundred to nearly 10,000 and that the local electric field can be driven to the silicon surface, increasing the overlap between the probe field and the binding surface by nearly four-fold. We show that long resonance lifetimes together with the increased field penetration at the binding surface results in strong spectral shifts of the resonance mode due to small perturbations to the local dielectric environment. We fabricate our metasurfaces by e-beam lithography and demonstrate that the optical responses of individual resonators can be spatially resolved as individually addressable ‘pixels’ and simultaneously read out as a change in resonance wavelength or as a change to the scattering intensity on a 2D InGaAs CCD array using a home-built infrared optical reflection microscope in a cross-polarized reflection configuration.

We then apply this platform to the detection of two aquatic phycotoxins: domoic acid, a neurotoxin responsible for human and wildlife mortalities, and microcystin, a liver toxin produced by cyanobacteria that poses a threat to drinking and agricultural water supplies. We selectively target domoic acid and microcystin using tailored surface functionalization of self-assembled monolayers (SAM) and a competitive antibody binding assay. We show that domoic acid and microcystin can be directly crosslinked to the metasurface through a step-wise covalent silanization. We observe in both calculations and experiment that consecutive molecular layers generate 0.5 nm - 4 nm shifts to the resonant wavelengths as sequential layers bind to the resonator surface. We then describe selective and quantitative toxin detection using a competitive antibody binding assay, where the metasurface optical signal is inversely proportional to the toxin concentration. Finally, I will discuss the integration of our high-Q metasurfaces with the Environmental Sample Processor (ESP), an autonomous robotic water sampler developed at the Monterey Bay Aquarium Research Institute (MBARI), that offers a pathway for in situ phycotoxin detection, processing, and analysis.

11:30 AM *EQ03.05.04

Lighting Up the Oceans—Real-Time, Multi-Omic Ocean Observation with High-Quality-Factor Metasurfaces Jennifer A. Dionne¹, Halleh Balch¹, Varun Dolia¹, Greg Doucette², William Ussler³ and Chris Scholin³; ¹Stanford University, United States; ²National Oceanic and Atmospheric Administration, United States; ³Monterey Bay Aquarium Research Institute, United States

Phytoplankton are microscopic organisms responsible for half of the global photosynthetic carbon fixation and at least half of the world's oxygen production. The changing climate is driving fundamental shifts in phytoplankton nutrient cycling, with profound impact on marine and freshwater ecosystems. For example, certain phytoplankton taxa can produce powerful biotoxins that harm humans and wildlife, contaminate water sources, and

damage local economies, leading the National Academies to call for the development of *in situ* sensors of phytoplankton nutrient cycling as critical infrastructure needed to advance climate resilience. Predominant methods of studying phytoplankton toxins and their genes are based on tandem mass spectrometry (LC/MS-MS), the polymerase chain reaction (PCR), and DNA/RNA sequencing. These methods are costly, require sophisticated infrastructure, and lack remote, autonomous, real-time detection capabilities that are central to time-series measurements necessary to understand coupled hydrography and climate/ecosystem dynamics.

Here, we present a metasurface-based technology to simultaneously and rapidly measure multiple 'omic' signatures of phytoplankton from aquatic samples. Our high-quality-factor ("high-Q") dielectric metasurfaces produce a large amplification of the electromagnetic field intensity, increasing the response to minute refractive index changes from target binding; simultaneously, the light is beam-steered to particular detector pixels. By combining metasurface design with acoustic bioprinting of samples, we produce microarrays of densely packed sensing pixels, each functionalized with distinct molecular recognition elements. On the same metasurface, we demonstrate specific detection of gene fragments, proteins, and small molecule toxins across hundreds of individual resonators simultaneously. We describe application of this quantitative assay to in-situ molecular analysis of environmental DNA, domoic acid, and microcystin. Finally, we discuss integration of our high-Q metasurfaces with the Environmental Sample Processor, an autonomous robotic water sampler developed at the Monterey Bay Aquarium Research Institute (MBARI), that offers a pathway for in situ phycotoxin detection, processing, and analysis.

SESSION EQ03.06: Radiation Engineering I
Session Chairs: Yu-Jung Lu and Cheng-Wei Qiu
Monday Afternoon, November 28, 2022
Sheraton, 2nd Floor, Back Bay C

1:30 PM *EQ03.06.01

Approaches to Violation of Kirchoff's Law without a Magnetic Field Michelle Povinelli¹, Alok Ghanekar¹, Jiahui Wang² and Shanhui Fan²; ¹University of Southern California, United States; ²Stanford University, United States

Kirchoff's Law of thermal radiation states that for any given angle and wavelength, the absorptivity and emissivity of are equal in steady state. Previous work has achieved violations of Kirchoff's Law only through the use of magneto-optical materials and require the use of an external magnet. Here we introduce an approach to Kirchoff's Law violation using spatiotemporal modulation of the material refractive index. We first introduce a theoretical formalism for calculating absorptivity and emissivity suitable for modulated systems, which fully incorporates the effect of frequency-conversion processes within the material. We show that for nonreciprocal systems with nonzero absorption, Kirchoff's Law may be violated. We introduce a metallodielectric grating design amenable to spatiotemporal modulation through carrier modulation effects and directly calculate the absorptivity and emissivity numerically using finite-element simulations. We show that in addition to nonreciprocal effects in reflection, the absorptivity at fixed angle and wavelength differ. For stronger modulation, we observe directional Rabi splitting, giving rise to even stronger violations of Kirchoff's Law. The results illustrate a potential pathway to achieving non-reciprocal thermal emission without the use of magneto-optical materials.

2:00 PM EQ03.06.02

Tailoring Thermal Emission with Ultrathin Films Jeremy N. Munday; University of California, Davis, United States

The thermal spectrum of hot bodies is well-known and described by Planck's law for blackbody emission. However, for many modern technologies, it is desirably to have significant deviations from this law to achieve directional or wavelength-controlled emission. Many approaches exist, yet difficulties arise due to thermal compatibility of materials at high temperatures, as well as stability of nanostructures when metasurfaces are employed. Here we present an alternative route involving single-layer, ultrathin films. We explored >100 materials that are stable above 2000°C and found combinations that allow for significant tunability of thermal emission throughout the near-infrared frequency range. We have fabricated and tested several material combinations at high temperature and show that the spectrum can be significantly modified using this simple configuration. Using these structures, we optimize the emission spectra of such emitters to match five common thermophotovoltaic cells and show that efficiencies in excess of 45% are achievable at moderate temperatures.

2:15 PM EQ03.06.03

Three-Dimensionally Printable Ultrawhite Radiative Cooler Using Hollow Structured Nanoparticles Seok-Beom Seo, Su-Jin Park, Sunho Jeong and Sun-Kyung Kim; Kyung Hee University, Korea (the Republic of)

Owing to the global consensus on energy-saving, radiative cooling has attracted much interest as a passive thermal management technology. Technically, to cool down objects below ambient temperature, radiative coolers must exhibit low absorption under solar illumination (e.g. $\lambda = 0.3 - 2.5 \text{ mm}$) and high emission in the mid-infrared spectral range (e.g. $\lambda = 8 - 13 \text{ mm}$). It can be achieved by stacking several materials or using a nanoscale photonic structure, which bring an increase in cost and fabrication difficulty.

We use dielectric nanoparticles as an alternative while maintaining the optical properties for sub-ambient radiative cooling. We demonstrated near-perfect reflectance in ultraviolet to near-infrared spectral range using hollow structured silica nanoparticles (HSNPs), owing to the enhanced scattering characteristics of the hollow structure. Note that low absorption and strong reflection in ultraviolet and near-infrared wavelengths are difficult to achieve with conventional silica nanoparticles. HSNPs coated Si shows an average of 0.96 reflectance in the solar spectral range and an average of 0.95 emissivity in the mid-infrared spectral range. We conducted an outdoor cooling experiment on Si wafers. The HSNPs coated Si, covered 8.89% of surface area of full Si wafer, show 4.4°C temperature drop in comparison to bare one.

But one critical issue remains for printability; hollow structured nanoparticles aggregate each other during the solvent evaporation (the final step of printing sequences) and leads to a crack on its surface that diminishes the overall reflectance and durability. We used PVP (Polyvinylpyrrolidone) to prevent aggregation. The PVP molecules are attached to the surface of the HSNPs and impede free motion to fix their coordinates rigidly. The crack-resistant property of the PVP assisted HSNPs paste holds the promise of implementing three-dimensionally printed devices with high precision, such as serpentine-shaped electrodes. In addition, spray coater also can be used to sprinkle HSNPs on a large area due to its great uniformity. We believe that the printable HSNPs developed herein can be extended to a variety of components on arbitrarily designable platforms such as curved or flexible optoelectronic devices.

2:30 PM EQ03.06.04

Electrochemical Dynamic Solar and Mid-Infrared Synergistic Radiative Thermoregulation Chenxi Suj and Po-Chun Hsu; Duke University, United States

The coldness of the deep universe and the hotness of the sun have been considered renewable thermodynamic resources for sustainable thermoregulation. How to utilize both resources showed drastic improvement in the past decade, enabled by the plasmonic and nanophotonic research. Remarkably, the rational photonic and thermal design has pushed forward the power and efficiency of daytime radiative cooling. In this presentation, we will introduce our recent research progress on electrochemical devices that can dynamically switch between solar heating and radiative cooling states, by tuning their optical properties. Such a non-trivial and opposite spectral tuning requires the fabrication of the ultra-wideband transparent conductive electrode, which is transparent in both solar and mid-IR regimes, and the precise control of the plasmonic nanoparticles' morphology during the reversible metal electrodeposition. With the optimization of every device component, this device can maximize its solar reflectivity at the cooling state and minimize its thermal emissivity at the heating state, and thus can serve as the smart building envelope for year-round HVAC energy saving. Ideally, the device can help buildings save 19.2% of HVAC energy across the United States, based on the building energy simulation results. The durable electrodeposition and the broad-band optical spectral tuning ability are confirmed by the DFT simulations and effective medium theory. In addition to the synergistic solar and mid-IR dual-band tuning, our electrochromic device can tune the thermal emissivity with 0.85 contrast based on non-volatile and reversible metal electrodeposition, bringing vast opportunities for applications in space heat management, and thermal camouflage.

2:45 PM EQ03.06.05

Scalable Temperature-Adaptive Radiative Cooler for Thermal Regulation Jiachen Li^{1,2}, Kechao Tang^{3,2,1}, Kaichen Dong^{2,1} and Junqiao Wu^{1,2,2};
¹Lawrence Berkeley National Laboratory, United States; ²University of California, Berkeley, United States; ³Peking University, China

The wavelength range of the mid-infrared atmospheric window matches that of thermal radiation near room temperature, thus the sky is used as a natural heat sink for passive radiative cooling of houses. For decades, experiment works in the field have focused on using static, cooling-optimized material properties to maximize the radiative cooling power of roof coating. However, in cold nights or winter times, especially in climates where heating dominates house energy consumption, the resultant overcooling exacerbates the heating cost and causes more energy consumption over the year. Here we present a different approach to thermal regulation by developing a mechanically flexible and energy-free temperature-adaptive radiative coating (TARC) to minimize the total energy consumption throughout the year, rather than only on hot days. The TARC is a metasurface that optimally absorbs solar energy and automatically adapts its thermal emittance to different ambient temperatures, driven by a photonically amplified metal-insulator transition. We demonstrate its performance in thermal regulation for energy-saving through simulation, lab characterization, and field tests. Simulations based on real climate data show that TARC outperforms existing roof coatings in yearly energy saving in most climates, especially those with substantial seasonal variations. We also develop a scalable process to print TARC in large sizes and at low cost. The scalable fabrication makes TARC a promising product for thermal regulation in other systems such as spacecraft and tents.

Reference:

Tang, Kechao, et al. *Science* 374.6574 (2021): 1504-1509.

3:00 PM BREAK

SESSION EQ03.07: Advanced Nanophotonic Design I
Session Chairs: Artur Davoyan and Yao-Wei Huang
Monday Afternoon, November 28, 2022
Sheraton, 2nd Floor, Back Bay C

3:30 PM EQ03.07.01

Probing ND7/23 Neuronal Cells Before and After Differentiation with SERS Using Sharp-Tipped Au Nanopyramid Arrays Marzia Iarossi¹, Aliaksandr Hubarevich¹, Giuseppina Iachetta¹, Michele Dipalo¹, Jian-An Huang^{2,1}, Daniel D. Price^{3,1} and Francesco De Angelis¹; ¹Istituto Italiano di Tecnologia, Italy; ²University of Oulu, Finland; ³Imperial College London, United Kingdom

The development of local plasmonic nanosensors which can investigate cellular processes, whilst remaining non-invasive, with high sensitivity is still challenging but of great interest in the field of sensing.^[1,2] The use of plasmonic nanostructures for Surface-enhanced Raman spectroscopy (SERS) measurements is one promising route for diagnostics and the measurement of cell activity and cell constituents. SERS allows for highly specific optical data in much shorter acquisition windows for the detection of molecules and markers of interest.

In this work we show the development of a SERS based sensor, which was conceived with the aim of monitoring cell activity and to discriminate cells before and after differentiation.^[3] The SERS sensor is composed of a platform of label-free sharp-tipped Au nanopyramids. To create the array we demonstrate a fabrication technique based on colloidal lithography. We have however altered the technique by using surface charged PS spheres and controlling the pH of the water. This allows us to tune the size of the nanoparticle interstices with sharp definition before metal depositions and achieve tip curvatures of 10nm without the use/cost of mask etching (i.e., reactive ion or plasma etching) or other expensive fabrication routes. Characterisation of the array shows a good matching of both the experimental and simulated optical data, with a plasmonic hotspot confined at the tip of the structure.

The focus of this study was ND7/23 neuronal cells where we performed SERS measurements of the cells both before and after differentiation. We found good success in discriminating the two groups' data by multivariate analysis. From the SERS data we were able to identify fingerprints of both the cell membrane, such as lipids and proteins, and intracellular components, such as RNA/DNA. This shows that the sharp tips of our structure are also able to penetrate the cell membrane and spontaneous poration occurs. A viability test of the cells showed high viability on the sensor and the cells were still found to be in good condition after hours of measurements.

This plasmonic array shows the realisation of a sensing platform which greatly enhances the SERS, with a high signal to noise ratio and reproducibility. This is a structure of interest as we show the development of an efficient SERS sensor based upon a novel facile low-cost fabrication route. The structure is also found to be a good bio-interface with high cell viability and the ability to spontaneously porate the cell. Taking in mind the potential of nanostructured colloidal templates, our fabrication technique is compatible for use with other substrates of interest, including flexible substrates for in-vivo studies. Moreover, the fabrication is very controllable and can be easily tuned to produce NPs with resonances in other wavelength windows of interest.

[1] *Royal Society of Chemistry*, **2018**, 143, 17, 3990; [2] *Nano Lett.* **2013**, 13, 6, 2463; [3] *Sensors Actuators B Chem.* **2022**, 361, 131724.

3:45 PM EQ03.07.02

Direct Imaging of Light-Matter Interaction of Localized Excitonic Emitters Using Tip-Enhanced Scanning Probe Technique Kiyoung Jo¹, Emanuele Marino¹, Jason Lynch¹, Zhiqiao Jiang¹, Natalic Gogotsi¹, Thomas P. Darlington², Mohammad Soroush³, P.J. Schuck², Nicholas Borys³,

Christopher B. Murray¹ and Deep M. Jariwala¹; ¹University of Pennsylvania, United States; ²Columbia University, United States; ³Montana State University, United States

Strong light-matter interaction in nanoscale emitters at optical frequencies using far-field spectroscopic analysis has been a subject of sustained research activity. Yet, direct visualization of the interaction in real space has been restricted by diffraction-limited measurement systems. Here, we perform near-field hyperspectral analysis using scanning probe techniques to image strong light-matter interactions of quasi 2-dimensional emitters on plasmonic Au substrates. We find exciton-polariton formation induced by strong coupling between an excitonic dipole in CdSe/CdS nanoplatelets and a gap mode plasmon in the Au tip under contact mode. Moreover, with the aid of tapping mode measurements, we observe that surface plasmon polaritons launched by excitonic emission from the nanoplatelets propagate in directional and radiative fringe patterns with periods of 317 nm. Extensive optical simulations offer proof that the fringes are the result of a standing wave formed between the tip and the nanoplatelets. Additionally, we find that the fringe shape and its period can be engineered by controlling the exciton dipole orientation of the nanoplatelets, as well as the permittivity ($\epsilon = 3-15$) and thickness (0.7 - 5 nm) of dielectric capping layer on the Au. The fringe patterns are also observed in WSe₂ nano-bubbles and CdSe/CdS nanoplatelets deposited on SiO₂/Si substrate, which implies that phenomenon is universal to localized emitters on various substrates. Our results enable deeper understanding of in-plane, near-field electromagnetic energy transduction from nanoscale emitters with wide implications in nano and quantum photonics.

4:00 PM EQ03.07.03

Ultracompact Imaging Devices by Deep Diffractive Neural Networks [Yilin Zhu](#) and Luca Dal Negro; Boston University, United States

Deep diffractive neural networks (D2NNs) that combine optical diffraction physics and deep learning capabilities have recently been utilized for the inverse design of multi-layered diffractive devices that include pulse shaping elements, broadband filters, and ultracompact dual band lenses with designed spectral and spatial responses. D2NNs are directly trained using error backpropagation within the diffractive layers without the need of training datasets. Moreover, when combined with adaptive loss weight algorithms, these networks achieve a more efficient inverse design of complex phase devices compared with purely data-driven neural network approaches.

In this talk, we present our work on the design, development, and experimental characterization of novel ultracompact diffractive devices based on adaptive-weight D2NN (a-D2NN). Specifically, based on the highly transparent hydrogenated amorphous silicon platform, we will introduce two-layer diffractive devices that operate over multiple visible and infrared spectral bands with designed point-spread functions (PSFs) and optimal focusing efficiency beyond the theoretical limit of single-lens devices. Moreover, we will discuss ultracompact focusing spectrometers (100 μ m-footprint) that achieve <10nm spectral resolution and >50% diffraction efficiency across the visible spectrum. Finally, we will introduce a-D2NN for the inverse design of hyperuniform phase plates (HPPs) and experimentally demonstrate high-fidelity image reconstruction based on fabricated 4-level diffractive devices in silicon. The flexible a-D2NN approach discussed here enables the engineering of multi-layer diffractive optical devices with targeted spectral and spatial responses for advanced multiband imaging and microscopy applications.

4:15 PM EQ03.07.05

A New Option for Efficient Up-Conversion—Crown-Ether-Coordination Compounds [Claud Feldmann](#); Karlsruhe Institute of Technology, Germany

Despite of a rich coordination chemistry, fluorescence is not a salient property of crown-ether coordination compounds until now. Recently, we obtained novel crown-ether coordination compounds such as EuX₂(18-crown-6), Mn₂X₆(18-crown-6)₂ (X: Cl, Br, I), and Mn₂I₄(18-crown-6), which exhibit unprecedented luminescence properties.¹ Thus, they show extremely intense emission, ranging from blue to red light, with outstanding quantum yields of 85-100%. Due to their specific structural features, some crown-ether coordination compounds exhibit intense second-harmonic generation (SHG), where the SHG-generated lines can be used for intrinsic excitation themselves.^{1,2}

Mn₂I₄(18-crown-6), for instance, is able to convert infrared photons (1160-1280 nm) via SHG to green photons (580-640 nm), which are converted to orange photons (605 nm) via photoluminescence.¹ Due to the strong SHG effect and the outstanding quantum yield of the luminescence process, in sum, very efficient up-conversion from infrared light to visible light is possible. With these features, crown-ether coordination compounds can become a new and extremely promising class of compounds for up-conversion and non-linear optics (NLO).

We discuss the promising optical properties – including emission, up-conversion, and NLO effects – of the novel crown-ether coordination compounds and the theoretical and structural background of these unique compounds.

References

1. E. Merzlyakova, S. Wolf, S. Lebedkin, L. Bayarjargal, B. L. Neumeier, D. Bartenbach, C. Holzer, W. Klopper, B. Winkler, M. Kappes, C. Feldmann, *J. Am. Chem. Soc.* **2021**, *143*, 798-804.
2. (a)M. A. Bonnin, C. Feldmann, *Inorg. Chem.* **2021**, *60*, 14645-14654. (b) M. A. Bonnin, L. Bayarjargal, S. Wolf, V. Milman, B. Winkler, C. Feldmann, *Inorg. Chem.* **2021**, *60*, 15653-15658.

SESSION EQ03.08: Poster Session I
Session Chairs: Ho Wai Howard Lee and Yu-Jung Lu
Monday Afternoon, November 28, 2022
8:00 PM - 10:00 PM
Hynes, Level 1, Hall A

EQ03.08.01

Gap-Controlled Core-Satellite Assembly Nanostructures for Efficient Broadband Photocatalytic Hydrogen Evolution [Yonghyeon Kim](#) and Sang Woo Han; Korea Advanced Institute of Science and Technology, Korea (the Republic of)

The development of photocatalysts highly active in the visible-to-near-infrared light region is desired work for efficient solar energy conversion. Here, we introduce a newly designed plasmonic metal-semiconductor hybrid photocatalyst consisting of an Au core-satellite assembly and a crystalline TiO₂ shell. TiO₂ was used as a spacer to control the interparticle gaps between the Au nanocrystals to obtain the core-satellite assemblies. Following the additional growth of TiO₂ and calcination, the Au core-satellite assembly@TiO₂ core-shell nanostructures were successfully synthesized. Depending on the thickness of TiO₂, the gap distance between the core and satellite Au NCs was readily regulated in the same morphological unit. Thanks to this structural controllability, gap distance-dependent plasmonic and photocatalytic properties of Au nanocrystal assembly@TiO₂ structures were clearly elucidated.

Nanostructures possessing the smallest interparticle distances between the core and satellite Au nanocrystals showed superb photocatalytic performance under the visible-to-near-infrared light irradiation attributed to the strong plasmon coupling between the Au nanocrystals and efficient hot electron transfer from the plasmon coupling site to TiO₂.

EQ03.08.02

Spatially Resolved Dynamics of Cobalt Color Centers in ZnO Nanowires by Nanoscale X-Ray Analysis [Christian T. Plass](#)¹, Valentina Bonino², Maurizio Ritzer¹, Lukas R. Jäger¹, Vicente Rey Bakaikoa², Martin Hafermann¹, Jaime Segura Ruiz², Gema Martinez Criado^{2,3} and Carsten Ronning¹; ¹Friedrich-Schiller-Universität Jena, Germany; ²European Synchrotron Radiation Facility, France; ³Instituto de Ciencia de Materiales de Madrid, Spain

Color centers in semiconductors provide properties of great importance for quantum technologies. Their most prominent characteristics are the capability to act as qubits and to offer high quality single photon sources. A promising wide-bandgap semiconductor material for defect-related emission in the visible range is zinc oxide. Creation of color centers in zinc oxide can be achieved by doping it with rare earth elements or transition metals, such as copper, nickel, iron or cobalt. The transition metals provide particularly fast decay times and therefore fast responses. The potential of a coupling platform between single photon emitters and photonic circuits can additionally be gained by embedding such color centers into nanowires, because they provide waveguiding and a cavity for the emitted photons. Investigating the photocarrier dynamics, with respect to the local environment, in such a system is thus of great importance. We apply high spatial resolution synchrotron-based methods to evaluate how the carrier dynamics and the luminescence is influenced by the elemental composition and the local environment of cobalt centers in zinc oxide nanowires. Such systems were previously investigated by different techniques such as photo- or cathodoluminescence measurements. However, these techniques lack crucial complementary information, e.g. spatial or compositional variations of the system, respectively. Simultaneous spatially resolved measurements of the X-ray fluorescence and the X-ray excited optical luminescence provide both information at once. Our findings show an anti-correlation between the band edge emission of the zinc oxide host and the intra-3d cobalt luminescence indicating two competing recombination paths. The luminescence dynamics are temporally resolved with a streak camera providing unique insights into the different decay paths of the intra-shell luminescence of the cobalt atoms incorporated into the lattice of zinc oxide nanowires. Two different exponential decays of the cobalt-related emission are revealed. A fast and newly observed decay is attributed to a recombination cascade within the cobalt atom, resulting from direct excitation.

EQ03.08.06

Photonic Properties of Metal-Dielectric Photonic Crystal OLEDs [David Allemeier](#), Matthew S. White, Khadga Thakuri and Thomas Cleary; University of Vermont, United States

Metal-dielectric photonic crystals (MDPCs) represent a unique class of photonic structures realized through vertically-stacked metallic OLED microcavities. The coupling of multiple microcavities results in hybridization of the cavity modes to form a band of narrow linewidth, tunable emission peaks, expressed directly through the electroluminescence spectrum of the OLEDs. The properties of the photonic band depend sensitively on the resonance states of the underlying unit cells and lie outside the effective medium regime. We discuss the photonic band structure observed in binary (two-cavity) and mono-cell MDPCs and explore the role of the metallic layers in determining the device performance. We examine trends in the state positioning, modal quality factor, and spontaneous emission enhancement as functions of the number of cavities, unit cell geometry, and material properties. The analysis is extended outside the light cone using transfer matrix simulations to discern the waveguided mode structure.

EQ03.08.10

Hydrogenated Zinc Oxide as an Alternative Low-Loss Plasmonic Material with Fano Resonance in Near-IR [Samar Fawzy](#) and Nageh K. Allam; American University in Cairo, Egypt

Low-loss plasmonic materials are of great importance due to their use in many photonic and optoelectronic devices. Doped transparent conducting oxides (TCOs) are potential alternatives to metallic plasmonic materials owing to their reduced losses and the tunability of their complex dielectric function. In this work, first-principles calculations were employed to reveal the role of interstitial hydrogen (H_i) doping in zinc oxide (ZnO) to achieve low losses and excite surface plasmon polaritons (SPPs). Three different concentrations of H_i doping (4.16, 6.25, 8.33%) were investigated. The results show that an H_i concentration as low as 4.16% achieves excellent low-loss plasmonic behavior. The fitted Drude damping parameter at 4.16% H_i doping was found to be lower than that reported for the same aluminum (Al) concentration. Finally, we numerically show that Fano resonance can be excited in near-infrared (IR) using a simple symmetric cylinder with an air hole made of hydrogen-doped ZnO placed on a pure ZnO substrate, revealing its potential use in numerous applications.

EQ03.08.12

Optimizing Up-Conversion Single-Photon Detector for Measurements of Femtosecond Time-Bin Pulse and Photon Echo [Yuta Kochi](#)¹, Yutaro Kinoshita¹, Sunao Kurimura², Kouichi Akahane³ and Junko Ishi-Hayase¹; ¹Keio University, Japan; ²NIMS, Japan; ³NICT, Japan

In a wide range of fields including quantum technology and quantum optics, it is important to measure single-photon-level ultraweak light in the ultrafast range. For measurements with a high signal-to-noise ratio, it is necessary to separate signals from noise in the frequency and/or time domains. However, in conventional electronic single-photon detectors (SPD) such as Si avalanche photodiode (APD) and superconducting nanowire SPD (SNSPD), the dead time and the temporal resolution were limited to 10 ns and 50 ps, respectively. Pulse-pumped frequency up-conversion single-photon detector (UCSPD) is one of the promising candidates to solve these problems. In this method, the signal and pump pulse is incident on a nonlinear crystal, and only the sum-frequency light is extracted by a bandpass filter and detected by a Si APD. By using femtosecond pulses as the pump light, the UCSPD enables dead-time-free measurements with the femtosecond-order temporal resolution. In previous UCSPD research in the ultrafast regime, however, the performance of UCSPD has not been quantitatively evaluated so far [1, 2]. Moreover, ultraweak light measurements from materials using UCSPD have also not been reported so far.

In this study, we developed a UCSPD using commercial PPMgSLT bulk crystals and optimized the experimental conditions such as the crystal length and pump power for measurements of femtosecond single-photon pulses [3]. In addition, we demonstrated the measurements of temporal waveforms of time-bin pulses and photon echo from quantum dots using UCSPD in the femtosecond range.

First, we optimized the performance of the UCSPD. Owing to the group velocity dispersion of the nonlinear crystal, the time delay between the pump and signal pulses is changed as propagating in the PPMgSLT crystal. Therefore, the temporal resolution and up-conversion efficiency strongly depend on the crystal length L. In this study, we estimated the temporal resolution to be 255, 415, 591 fs and the up-conversion efficiencies to be 6.1, 10.1, 10.2 % (the pump power of 300 mW) for L = 1, 2, 3 mm, respectively. By calculating the convolution of the pump and signal waveforms by taking into account the group velocity dispersion, we find that the experimental results of the waveforms and the crystal length dependence of the conversion efficiency can be well explained.

Next, we investigated the dependence of the pump power on the average number of photons at the detection limit. Consequently, the detection limit did not change significantly above 200 mW for any L and reached a minimum value at 300 mW. In this situation, the average number of photons at the detection

limit was 8.6, 3.3, 3.1×10^{-5} /pulse ($L = 1, 2, 3$ mm, respectively). These results indicate that $L = 2$ mm and a pump power of 300 mW are the optimal conditions for UCSPD. These results should be important because they provide guidelines for setting conditions for single-photon-level weak light measurements using UCSPD in the femtosecond range.

Finally, as a demonstration for the measurement of emitted light from materials, we measured photon echo light from broadband quantum memory using quantum dots. The stored light was a femtosecond time-bin signal with a pulse interval of 1 ps, which is the shortest time-bin signal measurement ever reported. This technology is expected to enable quantum communication in the femtosecond range, making possible communications that are 1,000 times faster than previous.

Acknowledgments

This work was supported by MEXT Q-LEAP (No. J PMXS0118067395), and CSRN, Keio University. The quantum dot samples were fabricated with the support of the NICT Advanced ICT Device LABO. The authors would like to thank Prof. R. Shimizu from the University of Electro-Communications for the useful discussion.

References

1. O. Kuzucu, et al., Opt. Lett. 33, 2257 (2008).
2. M. Allgaier, et al., Quantum Sci. Technol. 2, 034012 (2016).
3. Y. Kochi, et al., arXiv, 2205.06957 (2022).

EQ03.08.14

Integration of a Superconducting Nanowire Detector into a Confocal Microscope for TRPL-Mapping: Sensitivity and Time Resolution Volker Buschmann¹, Eugeny Ermilov¹, Christian Oelsner¹, Felix Koberling¹, Jan van Willigen², Guy Brammertz^{3,4,5} and Rainer Erdmann¹; ¹PicoQuant GmbH, Germany; ²Single Quantum, Netherlands; ³Hasselt University, Belgium; ⁴imec, Belgium; ⁵EnergyVille, Belgium

Superconducting Nanowire Single Photon Detectors (SNSPDs) were introduced to the market in 2003 and since then have found a niche in multiple quantum optics applications, due to their outstanding properties such as fast instrument response and high quantum efficiency.¹ The high quantum efficiency is especially important for material science applications in the IR-range beyond 1000 nm, where other available single photon detectors have a low sensitivity, high dark noise, and slow time response.

We have integrated a SNSPD (Single Quantum) into a standard MicroTime 100 confocal photoluminescence lifetime microscope (PicoQuant) in order to compare the performance of different SNSPD designs with a standard IR-PMT for time-resolved photoluminescence (TRPL) measurements and imaging of a CIGS (Cu(InGa)Se₂) device.

While one of the used SNSPDs had a classical single mode fiber coupling to guide the light onto the sensor, the other detector was coupled by an internal multimode fiber instead².

We detected a significant increase in photoluminescence sensitivity of both designs compared to a standard IR-PMT, as well as a several times higher sensitivity of the multimode-fiber coupled nanowire compared to the single-mode fiber one, in spite of comparable photon quantum efficiencies in this wavelength range for the sensor only. The increased sensitivity combined with the lower dark count rate resulted in an increase of the signal-to-noise ratio by more than 2 orders of magnitude compared to the IR-PMT.

The high sensitivity of SNSPDs combined with high temporal resolution (instrument response function of the overall system was below 100 ps) allows to identify and investigate highly quenched micrometer-sized defect sites of the thin-layer CIGS sample even at low illumination levels.

EQ03.08.15

A Near-Perfect Transmissive Metamaterial Heater for Radar Applications Young-Bin Kim, Eun-Joo Lee, Jun-Young Kim and Sun-Kyung Kim; Kyung Hee University, Korea (the Republic of)

Microwaves are used in a variety of industries including mobile communication, satellite broadcasting, aviation altitude meter, and radar sensor, depending on the bandwidth of interest. Specifically, W-band microwaves (a frequency band of 76 to 81 GHz) are used for accurate real-time obstacle detection in radar sensors of smart mobility such as autonomous vehicles and drones. A typical radar module is equipped with a protective cover and an electrical heater, which enables an automobile to navigate even in harsh environments (i.e., icy and frost conditions). However, conventional grid-shaped heaters have a trade-off relationship between microwave attenuation and temperature uniformity because these two features heavily rely on the inherent metallic characteristics of electrodes. To address this issue, we propose a metamaterial-based transparent heater as an effective route to simultaneously achieve both high microwave transmittance and temperature uniformity/electrical conductivity.

We experimentally demonstrated an electrically and thermally interconnected metamaterial-based electrical heater. A properly designed heating electrode induced artificial electromagnetic resonances and it behaves as a low-permittivity dielectric material at W-band frequencies. This enables remarkably high microwave transmission while preserving the electrical conductivity of bulk metal. We also conducted electromagnetic simulations to predict the properties of developed metamaterials and compared their simulated and measured transmission spectra in the $f = 50\text{--}110$ GHz range. The measured spectra were well-matched with the simulated ones; the maximum transmittance was over 90 % near 80 GHz despite the metal filling ratio exceeding 70 %, which was readily tuned by changes in structural variables. Developed metamaterial-based heaters were fabricated based on the standard semiconductor manufacturing process but can be manufactured by other scalable techniques such as three-dimensional printing.

EQ03.08.17

Electro-Optical Chromophores and Polymers for Short-Wavelength NIR Applications Florens R. Kurth^{1,2}, Li Zhao^{1,2}, Tasia Schwenke^{1,2}, Oms Amira¹, Gao Yuqing¹, Emil Agocs^{1,2}, Hans-Hermann Johannes^{1,2}, Henning Menzel^{1,2} and Wolfgang Kowalsky^{1,2}; ¹Technische Universität Braunschweig, Germany; ²Cluster of Excellence PhoenixD, Germany

With the increasing influence of photonics in communication and sensing, especially in integrated circuits, functional optical materials are at the center of this development. The ability to translate an external impulse into an optical signal and vice versa as exhibited by piezo- and elasto-optic, magneto-optic, acousto-optic and electro-optic materials is utilized in modulators, sensing resonators and beam steering devices. In the field of electro-optics (EO), which has long been dominated by periodically poled LiNbO₃, a shift towards specialized applications has driven demand for alternatives with differing properties. Organic electro-optic chromophores exhibit a Pockels effect through the intramolecular movement of electrons along the molecular axis in a donor-acceptor structure upon external stimuli in an electric field. As a part of composite polymer materials, they are compatible with common spin-coating and molding methods and can be integrated into waveguides. This ease of fabrication and the high electro-optical activity r_{33} when compared to LiNbO₃, at specific wavelengths lead to an accessible and low-voltage alternative.

Electro-optic polymer materials are developed to operate at 850 nm (shortwave infrared window) and 980 nm (Nd:YAG) which are two significant wavelengths at the shorter end of the NIR spectrum. The active component of such materials are electro optical (EO) chromophores, which are integrated in a suitable host polymer, mostly amorphous polycarbonate (APC) and poly (methyl methacrylate) (PMMA) and electro-poled to achieve parallel

orientation. A range of molecular parameters such as the dipole moment μ , hyperpolarizability β , the optical absorption and miscibility with the host polymer need to be taken into account. Due to this, the synthesis of EO chromophores is accompanied by DFT calculations which guide the main scaffold and the attachment of side groups. Chromophores with structural variations and their effect on absorption, miscibility and EO activity are shown. Through the utilization of bulky side groups, intermolecular interactions are reduced for more efficient external electro-poling. A copolymer of bulky isobornyl methacrylate and methyl methacrylate has been found to give significantly higher glass transition temperatures and temperature stabilities of the poled state alongside good miscibility. A lower refractive index compared with the more common polycarbonates opens up broader applications in waveguide cladding.

Chromophores with anchor groups have also been synthesized for covalent integration of the chromophores into polymethacrylate and polycarbonate chains. This allows for significantly more stable orientations and prevents agglomeration as the chromophores are held in place by their connection to the main chain.

EQ03.08.18

Enantiomer-Selective Molecular Sensing via Upconverted Chiral Metamaterials [Byunghoon Kim](#)¹, [Kyu-Tae Lee](#)², [Doo-Hyun Ko](#)³ and [Wenshan Cai](#)²; ¹Princeton University, United States; ²Georgia Institute of Technology, United States; ³Sungkyunkwan University, Korea (the Republic of)

Chirality in Nature is a physical property that cannot be superimposable on each other. At the molecular scale, the spatial asymmetry of atomic configuration contributes to a fascinating yet dramatic difference in chemical and physical characteristics. Discriminating enantiomers via optical techniques has been primarily employed since it enables nondestructive characterization; however, enantiomers show these signatures in the ultraviolet region, which limits the versatile application for biochemical species. Here, we proposed a simple but effective method to discriminate chiral molecules via asymmetric behavior of plasmonic metamaterial, leading to the selective optical response in a nonlinear regime. The enantiomers dissimilarly interact with the plasmonic chiral metamaterial, which gives rise to a change in the circular dichroism of chiral metamaterial in the near-infrared region by chirality transfer effect. The distinction of the circular dichroism is clarified by the upconverted photoluminescence in the visible region.

EQ03.08.19

Unidirectionally Aligned Single Bottom Faceted Nanoparticle-Based Plasmonic Nanogap Structures—Design Idea, Fabrication Methods and Applications to Surface-Enhanced Raman Scattering Platform [Jong-Min Lee](#)¹, [Minjun Kim](#)² and [Donghan Lee](#)²; ¹Hallym University, Korea (the Republic of); ²Chungnam National University, Korea (the Republic of)

The significant advantage of utilizing plasmonic nanostructures is strong light-matter interaction on the subwavelength scale. The plausibility of achieving such extreme nano-optical properties can be realized with the help of a nanoparticle-on-mirror (NPOM) system [1]. NPOMs provide highly efficient platforms in the field of nano-plasmonic sensors or energy devices, and they have emerged as strong candidate building blocks. NPOMs were optimized with gaps between nanoparticle and mirror less than 1 nm, which can yield extremely high plasmonic properties. To achieve strong plasmonic properties, the size of the active material to be coupled with the NPOMs platforms is limited to less than 1 nm. As with the simple electromagnetism example problem, the gap size and plasmonic enhancement of NPOMs are inversely proportional to each other. Due to this limitation, the use of large active materials (10 nm or larger, ex: biomolecule, quantum dots) in NPOMs resulted in low plasmonic enhancement.

Herein, we propose an unidirectionally aligned single bottom faceted NPOMs (FNPOM) nanostructure with enhanced plasmonic enhancement, even in the presence of a large gap size exceeding 20 nm. The design started with the simple idea that the relation of the distance between two parallel plane charges and the electric field strength are more gently decrease compared to point charges. Nanoparticle fabrication was performed with vacuum furnace system. Single bottom faceted sphere shape nanoparticles are fabricated under conditions where the surface tension between the substrate and the molten metal is properly balanced. The diameter of the gold nanoparticles formed is about 100 nm, and the plasmonic resonance wavelength is in visible light. FNPOM was successfully fabricated on a 4-inch substrate, and the statistical uniformity based on optical properties is within 10%. The successful demonstration of FNPOM is meaningful in confirming the critical correlation between nanoparticle micromorphology and optical properties.

[1] R. Chikkaraddy, B. de Nijs, F. Benz, S. J. Barrow, O. A. Scherman, E. Rosta, A. Demetriadou, P. Fox, O. Hess and J. J. Baumberg, *Nature*, 2016, 535, 127–130

EQ03.08.20

Towards Integrated Barium Titanate Electro-Optic Modulators Through Epitaxial Film Growth [Larissa Little](#), [David R. Barton](#), [Matthew Yeh](#), [Lorena Britton](#), [Charles Brooks](#), [Marko Loncar](#) and [Julia Mundy](#); Harvard University, United States

Electro-optic modulators are a backbone of the efficient data transfer necessary for modern optical communications. These modulators directly connect a driving electric field with optical properties of a material, and allow for transforming an electrical signal to an optical signal. Modern data centers and high speed internet, as well as sensing systems, heavily rely on these devices. The electro-optic modulators are often bulk crystals with proton-exchanged or titanium-indiffused waveguides, limiting their size, speed, and efficiency. Modern developments in integrated lithium niobate on insulator enables photonic device integration akin to the integrated circuit. In this work, we explore expanding the materials palette for integrated photonic devices with thin film materials such as barium titanate.

The current industry standard for integrated electro-optic modulators are typically Silicon or indium phosphide. Here, carrier injection and dynamics of the modulation mechanism limit performance through optical absorption, operating speed, or half-wave voltage. Bulk lithium niobate devices are also used (electro-optic coefficient $r_{33} \sim 30$ pm/V), but cannot be scaled in the same manner.

We use oxide molecular beam epitaxy to grow high quality, single crystal thin film of non-centrosymmetric materials that have superior electro-optic properties. For example, barium titanate (BaTiO₃) exhibits an extremely high electro-optic coefficient ($r_{42} \sim 900$ pm/V), a reasonably high band gap (> 3 eV), and relatively high refractive index ($n = 2.4$). Additionally, previous work has shown that the ferroelectric properties of BaTiO₃ vary significantly in epitaxially strained thin films. Since ferroelectric and electro-optic properties are both rooted in the crystal structure of these materials, we expect that the electro-optic properties will be equally affected by epitaxial strain.

Here we grow BaTiO₃ on strontium titanate substrates, as well as on a variety of scandate substrates, to understand and characterize the impact of epitaxial strain on the electro-optic tensor of BaTiO₃. Furthermore, in order to facilitate scalability and creation of devices with BaTiO₃, we show our progress in transferring our thin films onto silicon substrates. This is accomplished through growth of a dissolvable interlayer between the growth substrate and the BaTiO₃ that can be used to easily separate the two.

8:00 AM *EQ03.09.01

Beyond Band-Edge Lasing: Plasmonic Lattices with High-Gain Materials Teri W. Odom; Northwestern University, United States

This talk will describe access to new classes of optical modes that can provide feedback for plasmonic nanoscale lasing. We will discuss how quasi-propagating modes supported by plasmonic lattices can be used to facilitate lasing over a continuous range of discrete angles and wavelengths if the modal gain of the material is high enough. Aluminum nanoparticle lattices combined with halide perovskite nanocrystals can exhibit lasing emission from a single device with multiple beams at angles and wavelengths that depend on the gain bandwidth and lattice characteristics.

8:30 AM EQ03.09.02

Towards Tunable Lasing in Thin-Film Lithium Niobate/III-V Cavities David R. Barton¹, Rebecca Cheng¹, Mengjie Yu^{1,2}, Linbo Shao^{1,3}, Hannah Grant⁴, Leif Johansson⁴, Amirhassan Shams-Ansari¹, Dylan Renaud¹ and Marko Loncar¹; ¹Harvard University, United States; ²University of Southern California, United States; ³Virginia Tech, United States; ⁴Freedom Photonics, United States

Thin-film lithium niobate (LN) is a promising platform for high performance chip-scale optical systems, owing to its large electro-optic effect, low-loss waveguides, and wafer scalability. An outstanding challenge for thin-film LN photonics, and many photonic platforms in general, is integration of tunable high-power, low-noise, and narrow-linewidth lasers. Integrated lasers have previously been demonstrated on LN through butt-coupling of high performance DFB lasers and heterogeneous integration of III-V gain material. Further improvements can be made through injection locking with high-Q rings and external cavity laser development.

Here, we demonstrate lasing action from a InP reflective semiconductor optical amplifier (RSOA) using thin-film LN as a wavelength-selective reflector. Our scheme is composed of several integrated components on 600 nm thick x-cut LN. First, we designed low-loss horn couplers to efficiently collect light from the RSOA to the LN chip. Next, we use two cascaded ring resonators with different free spectral ranges and integrated heaters to act as an active thermal filter. We purposefully overcoupled the rings (Q factors ~50,000) to reduce on-chip losses. Finally, we included a narrow-band photonic crystal to act as a partial reflector in the spectral region with the largest optical gain. Our RSOA (Freedom Photonics) emits maximum spontaneous emission at 1590 nm and small-signal gain of 25 dB. The nanofin photonic crystal has a period of 410 nm to match the stop band bandwidth with the maximum gain of the amplifier. We make the mirror partially reflective (R = 70%) by using 150 unit cells.

Our initial demonstration of lasing relies on tunability of the Vernier filter using thermo-optic shifting. We chose ring radii of 120 and 130 microns to set the Vernier FSR similar to the bandwidth of the DBR mirror. After aligning the ring resonances, we estimate the roundtrip reflection to be -17.5 dB, substantially lower than the gain provided by the amplifier. We couple the amplifier to the LN chip, forming a cavity with high reflection only at the optical mode filtered by the Vernier filters within the band gap of the DBR. With proper thermal tuning to manage the mode profiles, we find single-mode lasing over a range of RSOA injection currents from 0.1 A to 0.4 A. We measured both the LI curve and laser linewidth to demonstrate the lasing action of our device. The LI curve shows the clear onset of lasing around 0.1A and saturation above 0.3A. The maximum lasing power we achieved is -9.5 dBm, limited by the distance between the RSOA and input facet of the LN chip. Finally, we measured single mode lasing with sideband suppression ratios greater than 40 dB, and linewidths as low as 250 kHz. Finally, we will discuss progress towards active control and high power, narrow-linewidth lasing using the electro-optic effect in LN. Our results represent progress towards a tunable, robust, and low-cost integrated light source with narrow linewidth and high power, amenable for long haul telecommunication networks, data center optical interconnects, and microwave photonic systems.

8:45 AM EQ03.09.03

M-Point Lasing in Plasmonic Honeycomb Lattices Xitlali G. Juarez¹, Ran Li¹, Jun Guan¹, Thaddeus Reese¹, Richard Schaller^{1,2} and Teri W. Odom^{1,1}; ¹Northwestern University, United States; ²Argonne National Laboratory, United States

Honeycomb lattices can be defined as hexagonal lattices with a two-nanoparticle (NP) unit cell or considered as a superposition of two identical, but inequivalent hexagonal sublattices. Due to their non-Bravais nature, honeycomb NP lattices exhibit unique optical properties. For instance, honeycomb lattices have received attention for their ability to host topological edge states at the Γ and K points of photonic crystals. When the unit cell is redefined to consist of six NPs, edge states can be accessed at the Γ point of the lattice by deforming the unit cell while preserving its C_{6v} symmetry. If a honeycomb lattice is designed with a unit cell consisting of two NPs with inequivalent radii, the mirror and inversion symmetry of the lattice is broken, allowing edge states to emerge at the K points of photonic crystals. To assess the prospects of experimentally realizing topological states in plasmonic honeycomb NP lattices, a deeper understanding of their off-normal, high symmetry points is necessary. This presentation discusses the observation of band-edge states at the M point of Ag NP honeycomb lattices. Honeycomb lattices support the emergence of two surface lattice resonances (SLRs) at the M point: (1) a blue-shifted SLR_{M1} due to coupling of two distinct out-of-plane dipole resonances; and (2) a red-shifted SLR_{M2} resulting from in-plane dipole-dipole coupling. Although honeycomb lattices support two M-point SLR modes, only one mode supported lasing when organic dye solution was used as gain with the Ag NP lattices. This study demonstrates the unique coupling interactions at high symmetry points of non-Bravais plasmonic lattices.¹

1. Juarez, X. G.; Li, R.; Guan, J.; Reese, T.; Schaller, R. D.; Odom, T. W., M-Point Lasing in Hexagonal and Honeycomb Plasmonic Lattices. *ACS Photonics* **2022**, *9* (1), 52-58.

9:00 AM EQ03.09.04

Engineering Strong Coupling in a Nano-Plasmonic Cavity Using Transition Metal Dichalcogenide Nanobubbles Thomas P. Darlington¹, Emanuil Yanev¹, Ravindra Saxena², Vishal Venkatesh², Andrey Krayev³, Deep M. Jariwala² and P.J. Schuck¹; ¹Columbia University, United States; ²University of Pennsylvania, United States; ³Horiba Scientific, United States

In the interaction of light and matter, strong coupling occurs when exchange between a photon and electronic transitions exceeds the relative loss rate leading to hybridization of the optical and electronic states. The behavior is well known in cavity quantum electrodynamics (QED), and is a fundamental ingredient in single photon quantum logic gates [1]. In solid-state systems, many strong coupling phenomena have been explored between different material excitations. Plasmons in particular have attracted great interest owing to their small mode volumes [2], allowing for strong coupling of a plasmon and single quasi-particles excitations such as excitons, potentially recreating in the solid-state, at the nanoscale, and at elevated temperatures many of the phenomena previously studied in traditional trapped atom QED.

Strong coupling between plasmons and excitons has been observed in exciton systems: e.g., J-aggregates [3], and colloidal quantum-dots [4-5]. While these systems offer large coupling strengths, the exciton transition energies are largely fixed, and vary randomly depend on variations in growth conditions. By contrast, transition metal dichalcogenides offer strong exciton and large tunability of exciton energy by applied strain. However, to date strong coupling between plasmons in the excitons in transition metal dichalcogenides has only been achieved in multilayer stacks[6], which have significantly weaker light emission compared to monolayers.

Building off our previous work observing quantum-dot like exciton states in nanobubbles [7], here we show signatures of strong coupling between nanobubble-localized excitons and a gap-mode plasmon mode formed between a scanning near-field optical probe and substrate. By adjusting the gap mode distance, the coupling strength and plasmon energy can be dynamically tuned. Further, by applying pressure with the nano-optical probe the emission energies of localized excitons can be adjusted. When approaching the tip to the nanobubble surface, we observed striking emission peak splitting. Comparing the energy dependence with a coupled oscillator model, we see qualitative agreement of the gap size dependence of the coupled exciton emission. Our results show the promise of engineering room-temperature strong coupling of plasmons with excitons in monolayer semiconductors for use as a model system and for building compact quantum plasmonic-photonic devices.

References:

- [1] A. Reiserer, *et al.*, "A quantum gate between a flying optical photon and a single trapped atom," *Nature*, **508**, 237 (2014)
- [2] J. J. Baumberg, *et al.*, "Extreme nanophotonics from ultrathin metallic gaps," *Nat. Mater.*, **18**, 668 (2019)
- [3] N. T. Fofang, *et al.* "Plexcitonic Nanoparticles: Plasmon-Exciton Coupling in Nanoshell-J-Aggregate Complexes," *Nano Lett.*, **8**, 3481 (2008)
- [4] K-D Park, *et al.*, "Tip-enhanced strong coupling spectroscopy, imaging, and control of a single quantum emitter," *Sci. Adv.*, **5**, 5931 (2019)
- [5] H. Groß, *et al.* "Near-field strong coupling of single quantum dots," *Sci. Adv.*, **4**, 4906 (2018)
- [6] M.-E. Kleeman, *et al.* "Strong-coupling WSe₂ in ultra-compact plasmonic nanocavities at room temperature," *Nat. Comm.*, **8**, 1296 (2017)
- [7] T. Darlington, *et al.* "Imaging strain-localized excitons in nanoscale bubbles of monolayer WSe₂ at room temperature," *Nat. Nano.*, **15**, 854 (2020)

9:15 AM EQ03.09.05

On-Chip Optical Dispersion Management for Femtosecond Pulse Generation David R. Barton¹, Mengjie Yu^{1,2}, Rebecca Cheng¹ and Marko Loncar¹;
¹Harvard University, United States; ²University of Southern California, United States

Dispersive materials properties are a fundamental part of any optical system, and needs to be carefully managed or compensated for in applications spanning spectroscopy, sensing, and communications. Optical pulses in particular are necessarily composed of multiple frequency components, meaning that dispersion management is vital to maintaining high peak power pulses with short time durations. Carefully engineering the dispersive properties of a nanostructured material is one way to manage dispersion in a controllable manner, and can make dispersive elements orders of magnitude smaller than using bulk materials. This offers the ability to sculpt the temporal profile of light with unprecedented control on a chip.

The ability to generate ultrashort, broadband and high-peak-power optical pulses on-chip has been a long-sought-after goal. However, all demonstrations to date rely on a table-top pulse laser source which increases the system complexity, size, and cost, and thus hinders practical applications. In addition, optical pulses can be generated via microresonator frequency comb sources through coupling a continuous-wave laser into a high-quality-factor microresonator. These devices are limited by their low efficiencies (usually <2%), comb-line power and high repetition rates. Therefore, high-power and controllable integrated pulse sources are still missing, a major roadblock for fully integrated nonlinear photonic circuits.

Here we generate femtosecond laser pulses using an integrated electro-optic time lens. Whereas a spatial lens system can focus a collimated laser beam to a spot at its focal plane, a time lens system can compress CW light to a short pulse at a proper dispersive focal length. The key components to build such a spatial/temporal lens system are an aperture, a lens which induces a quadratic phase in space/time, and a diffraction/dispersion medium representing the focal length of the imaging system. In our EO time lens, these roles are played by a single amplitude modulator, one phase modulator, and a dispersive medium (chirped Bragg grating). In the frequency domain, we generate an optical comb spectrum with a flat-top envelope. Without the dispersive medium, the pulse is 16.6 ps long.

To integrate dispersion management on-chip, we designed a chirped Bragg grating based on a nanofin photonic crystal in LN. By linearly chirping the Bragg period from 406.5 nm to 414.5 nm over a length L , we generate the desired group delay dispersion by modifying to total grating length. On a second chip with the chirped grating, we compress the pulse to its bandwidth limit. Fabry-Perot fringes in reflection show spectrally-varying FSR, which we use to compute the group delay. By varying the length of the grating we determine the optimal length for the desired GDD. The generated frequency comb still shows high power and a flat-top spectrum after compression owing to the low loss nature of the grating. Finally, the autocorrelator trace demonstrates a pulse width is 545 fs using a Bragg grating length of 2.25 mm, near the transform limited value. This represents a 25,000 times reduction in the required path length. The loss of our Bragg grating is estimated to be 0.033 dB/mm. Our results represent a tunable, robust and low-cost integrated pulsed light source with CW-to-pulse conversion efficiencies an order of magnitude higher than achieved with previous integrated sources. The novel pulse generator can find applications from ultrafast optical measurement to networks of distributed quantum computers.

9:30 AM BREAK

SESSION EQ03.10: Fundamental of Plasmonics and Metaphotonics I

Session Chairs: Min Seok Jang and David Norris

Tuesday Morning, November 29, 2022

Sheraton, 2nd Floor, Back Bay C

10:00 AM *EQ03.10.01

Nanophotonic Approaches to Controlling Spectral and Directional Thermal Emission Aaswath P. Raman; University of California, Los Angeles, United States

Nanophotonic structures have shown great promise in controlling the spectral and directional nature of thermal emission. Yet thermal emission's intrinsically broadband and omnidirectional nature have posed a fundamental challenge in simultaneously controlling these characteristics. In this talk, we will present our theoretical, computational and experimental approaches to engineering the spectral and directional emissivity in fruitful ways. We will introduce a coupled-mode theory capable of describing highly complex emissivity from multi-resonant systems. We will also describe a tandem ResNet-based inverse design technique that allows for the design of highly complex supercell metasurfaces which exhibit tailored, multispectral emissivity responses. As an example of a system that can benefit from multiple spectral peaks, we will also describe a multi-scale Mie resonant architecture that is simultaneously ultralight and also has enhanced emissivity for novel aerospace applications. Beyond spectral control, we will next discuss our work on enabling anomalous directional control of emissivity over broad spectral bandwidths. In particular we will describe how gradient Epsilon-near-zero (ENZ) photonic structure can enable broadband directional thermal emission. We will also show experimental results on how gradient ENZ thermal emitters can be fabricated from both oxides as well as graded-doped III-V films, enabling new capabilities in the control of thermal emission.

10:30 AM *EQ03.10.02**3D Optical Metamaterials from Colloidal Nanocrystal Assemblies** [Cherie R. Kagan](#); University of Pennsylvania, United States

Colloidal nanocrystals (NCs) have inorganic cores and are commonly synthesized with organic shells. Chemical exchange of the long ligands used in NC synthesis with more compact ligand chemistries reduces the interparticle distance (d) and increases interparticle coupling [1, 2]. Similarly, thermal annealing can decompose ligands, reduce d , and drive NC fusion. We pattern 2D structures using one large-area imprint lithography step. Then, we exploit the different chemical and physical properties of NC assemblies from bulk thin films, to construct NC/bulk bilayer heterostructures that fold into three-dimensional structures upon ligand exchange and/or mild thermal annealing [3-5]. Using this simple fabrication route, we demonstrate 3D chiral metamaterials with configurable bandwidth and reconfigurable optical responses in the infrared.

A. T. Fafarman, S.-H. Hong, H. Caglayan, X. Ye, B. T. Diroll, T. Paik, N. Engheta, C. B. Murray, C. R. Kagan, "Chemically Tailored Dielectric-to-Metal Transition in the Design of Metamaterials from Nanoimprinted Colloidal Nanocrystals," *Nano Lett* 13, 350-357 (2012).

W. Chen, J. Guo, Q. Zhao, P. Gopalan, A. T. Fafarman, Au. Keller, M. Zhang, Y. Wu, C. B. Murray, C. R. Kagan, "Designing Strong Optical Absorbers via Continuous Tuning of Interparticle Interaction in Colloidal Gold Nanocrystal Assemblies," *ACS Nano*, 13, 7493-7501 (2019).

M. Zhang, J. Guo, Y. Yu, Y. Wu, H. Yun, D. Jishkariani, W. Chen, N. J. Greybush, C. Kubel, A. Stein, C. B. Murray, C. R. Kagan, "3D Nanofabrication via Chemo-Mechanical Transformation of Nanocrystal/Bulk Heterostructures," *Adv. Mater.* 30, 1800233 (2018).

J. Guo, J.-Y. Kim, M. Zhang, H. Wang, A. Stein, C. B. Murray, N. A. Kotov, C. R. Kagan, "Chemo- and Thermomechanically Configurable 3D Optical Metamaterials Constructed from Colloidal Nanocrystal Assemblies," *ACS Nano* 13, 1427-1435 (2019).

J. Guo, J.-Y. Kim, S. Yang, J. Xu, Y. C. Choi, A. Stein, C. B. Murray, N. A. Kotov, C. R. Kagan, "Broadband Circular Polarizers via Coupling in 3D plasmonic Meta-Atom Arrays," *ACS Photonics*, 8, 1286-1292 (2021).

11:00 AM EQ03.10.03**Bilayer and Multilayer Moiré Plasmonic Lattices** [Jun Guan](#)^{1,2}, [Jingtian Hu](#)¹, [George C. Schatz](#)¹ and [Teri W. Odom](#)¹; ¹Northwestern University, United States; ²Massachusetts Institute of Technology, United States

Plasmonic nanoparticle lattices can provide a platform for both deep-subwavelength light confinement and strong far-field scattering. However, previous studies mostly focused on how a single layer of a lattice can control the flow of light. This talk describes how bilayer and multilayer plasmonic lattices enable unique optical properties. Superimposing two or more periodic structures resulted in moiré superlattice patterns. We demonstrated that bilayer superlattices combined with dipole emitters can facilitate the engineering of light-emitting characteristics. In addition, we revealed the coupling mechanism in three-layer moiré structures.

11:15 AM EQ03.10.04**Developing Highly Nonlinear Materials and Nanostructures on the Largely Tunable ITO/TiN Platform** [Tornike Shubitidze](#), [Wesley Britton](#) and [Luca Dal Negro](#); Boston University, United States

The engineering of the optical dispersion of thin-film transparent conductive indium tin oxide (ITO) and titanium nitride (TiN) has enabled novel nanostructured materials with largely tunable epsilon-near-zero (ENZ) behavior from the visible to the mid-infrared spectral range as well as optical nonlinearities dramatically enhanced by small refractive index values. Combined with their CMOS compatibility, these materials have been integrated into compact photonic devices and nanostructures that perform efficient nonlinear operations such as sub-picosecond all optical modulation, ultra-fast pulse shaping through frequency translation, and optical time reversal. However, the fundamental mechanisms governing their nonlinear responses remain unclear. In this talk, we use the Z-scan nonlinear optical characterization technique to systematically investigate the complex nonlinear susceptibility $\chi^{(3)}$ and the intensity-dependent refractive index change Δn of ITO samples grown by RF reactive magnetron sputtering followed by post-deposition annealing. Specifically, we study polycrystalline thin films with different microstructural and crystallographic orientations and we demonstrate that post-deposition conditions can modify the crystallographic texture of ITO and further enhance the nonlinear optical properties resulting in a 30X enhancement compared to commercial ITO thin films with similar thickness and optical dispersion. Finally, we discuss opportunities to further control and enhance the optical nonlinearity of ITO using ITO/TiN multilayer stacks with controlled volume fractions, providing large tunability of both ENZ wavelengths and nonlinear responses in the 680nm-1200nm spectral range.

11:30 AM EQ03.10.05**Processing-Dependant Optical and Electrical Properties of Indium Tin Oxide Nanocrystals Thin Films** [Fabio Marangi](#); Politecnico di Milano, Italy

Transparent conducting oxides play a significant role in nowadays electronic devices. Among those, indium tin oxide (ITO) is one of the most relevant materials used for transparent electrodes. Even if the fabrication of ITO-based electronic devices in the form of thin films is mainly carried out by means of sputtering, electrically conductive films may be obtained by the deposition of thin layers of ITO Nanocrystals (NCs) through spin coating and other related wet chemistry techniques. ITO NCs films show interesting properties deriving from the plasmonic behaviour of ITO in the form of small nanoparticles. Localized plasma frequency, which occurs in the infrared, can be tuned by playing around the shape and size of the nanocrystals but also strongly depends on the percentage of doping. Electrical properties of the films are strongly influenced by the properties of the single nanocrystals and morphology of the whole film. Processing conditions during the fabrication of the devices also affect the final conductivity of the films. Electrical conductivity of a number of ITO NCs thin films has been measured as a function of thickness of the films and processing time and temperature, both in controlled atmosphere and in presence of air. Both optical and electrical properties of the films showed to be strongly affected by annealing temperature, regardless of being processed in air or in a controlled environment leading to different outcomes. In particular, films annealed at higher temperature showed greater electrical conductivity but poor optical response in the region of interest. The opposite was observed for lower annealing temperatures. The combination of all those tests allowed the definition of a recipe for the fabrication of ITO Nanocrystals with desired electrical properties and optical response. The plasmonic response of the films can be tuned after deposition, without acting at the single nanocrystal level in terms of doping, size and shape. Even if microscopically influenced by the single nanocrystal, the properties of the system as a film show a macroscopic behaviour deriving from the nanocrystals acting as a whole.

11:45 AM EQ03.10.06**Lateral Permittivity Patterning by Ion Irradiation in CdO Thin Films for Mid-IR Plasmonics** [Angela Cleri](#)¹, [Mingze He](#)², [Joshua Nordlander](#)¹, [Joshua D. Caldwell](#)² and [Jon-Paul Maria](#)¹; ¹The Pennsylvania State University, United States; ²Vanderbilt University, United States

Donor doped cadmium oxide (CdO) thin films demonstrate excellent optoelectronic properties, further enabled by advanced synthesis techniques such as high-power impulse magnetron sputtering (HiPIMS), which yields high quality films with easily controllable transport properties. Tunable carrier concentrations between 10^{19} - 10^{21} cm⁻³ while maintaining mobilities between 300-500 cm²/V-s facilitate low-loss plasmon polaritons spanning the mid-wave infrared (IR). Further, fabricating layered CdO structures with varying thickness and carrier density between each layer has given way to interesting nanophotonic phenomena such as multiple epsilon-near-zero (ENZ) resonances in a single structure, strong coupling between ENZ and surface plasmon polariton modes, and hyperbolic behavior in homoepitaxial structures. By controlling donor dopant levels in individual CdO layers, one controls optical

interfaces in the out-of-plane dimension. Here, we extend this principle to the in-plane dimensions by ion irradiation patterning to locally induce donor defects and achieve lateral permittivity control over relatively large areas. This method creates lateral patterns which exhibit minimal physical interfaces, yet sharp permittivity contrast. In this presentation, we will explore methods for ion irradiation and patterned masks and demonstrate lateral control of optical properties through both near-field and far-field measurements.

SESSION EQ03.11: 2D Photonics II
Session Chairs: Ho Wai Howard Lee and Yu-Jung Lu
Tuesday Afternoon, November 29, 2022
Sheraton, 2nd Floor, Back Bay C

1:30 PM *EQ03.11.01

Properties and Control of Excitons in 2D Semiconductor Heterostructures Tony F. Heinz^{1,2}; ¹Stanford University, United States; ²SLAC National Accelerator Laboratory, United States

In this paper we will describe some of our recent progress in understanding fundamental aspects of excitons in 2D heterostructures in the transition metal dichalcogenide (TMDC) family. For many of these systems, type II band alignment is obtained in stacked layers, causing the lowest-lying optical excited state to be an interlayer exciton. Because of the static dipole moment of these charge-separated states, they are highly tunable by external electric fields, making them interesting sources with readily tunable photon energy by gating available in the visible and infrared spectral ranges. In addition, for crystallographically aligned samples, the moiré potential leads to distinctive exciton localization effects. We will present recent advances in characterizing these states, both through direct optical absorption measurements and through the use of time-resolved, angle-resolve photoemission spectroscopy (tr-ARPES). These methods give us new insight into the radiative lifetime of these states and the degree and nature of exciton localization in moiré structures. In addition to their intrinsic interest, the ability to transfer these materials and to tune them renders them attractive building blocks for integration into photonic devices using meta-materials.

2:00 PM *EQ03.11.02

Image Polaritons in van der Waals Crystals Min Seok Jang and Sergey Menabde; Korea Advanced Institute of Science and Technology, Korea (the Republic of)

Polaritons in two-dimensional materials have been attracting enormous research interest due to their deep-subwavelength field confinement enabling strong light-matter interactions. In this presentation, I introduce a new class of polaritonic modes – image polaritons – that appear when a polaritonic material is in close proximity to a highly conductive metal so that the polaritonic mode couples with its mirror image. The image polaritons constitute an appealing nanophotonic platform, providing an unparalleled degree of optical field compression into nanometric volumes while exhibiting lower normalized propagation loss compared to conventional van der Waals polaritons on nonmetallic substrates. I will cover three different mid-infrared image polaritons in van der Waals Crystals: image plasmons in graphene and image phonon polaritons in h-BN and α -MoO₃.

2:30 PM EQ03.11.03

Measurement of Plasmonic Enhancement of Photoluminescence in Monolayer WSe₂ Stanislav Tsoi, Kathleen McCreary, Marc Christophersen, Hsun-Jen Chuang and Igor Vurgaftman; U.S. Naval Research Laboratory, United States

Recent experimental studies have demonstrated that coupling monolayer transition metal dichalcogenides to plasmonic cavities can significantly enhance their photoluminescence (PL). The present work aims to determine experimentally the magnitude of the plasmonic enhancement in WSe₂. Periodic arrays of gold nanodisks are fabricated using electron beam lithography on Si substrates. The localized plasmon resonance of the nanodisks is characterized using reflectivity measurements. Monolayer flakes of WSe₂ with a lateral size over 30 μm , grown by chemical vapor deposition on separate Si substrates, are transferred on top of the gold nanodisk arrays. Stretching of the flexible monolayer over individual nanodisks creates localized nanoscale regions of WSe₂ under tensile strain, separated by fully relaxed WSe₂ regions between the nanodisks. Accordingly, room-temperature PL recorded from the WSe₂ contains an emission band at 1.65 eV, characteristic of exciton recombination in the fully relaxed monolayer, as well as additional low-energy bands assigned to the strained nano-regions. The strained PL is strongly enhanced when the excitation wavelength approaches the plasmon resonance, consistent with the spatial co-location of the strained nano-regions and the localized plasmonic field. Comparison of the strained PL intensity under the excitation on and off the plasmonic resonance allows us to assess the magnitude of the plasmonic enhancement. The results obtained are in quantitative agreement with numerical simulations.

2:45 PM EQ03.11.04

Van der Waals Nanophotonics Panaiot Zotev¹, Yue Wang², Toby Severs Millard³, Daniel Andres-Penares⁴, Luca Sortino⁵, Nic Mullin¹, Donato Contedua², Mauro Brotons-Gisbert⁴, Sam Randerson¹, Jamie Hobbs¹, Brian Gerardot⁴, Thomas F. Krauss² and Alexander Tartakovskii¹; ¹University of Sheffield, United Kingdom; ²University of York, United Kingdom; ³Imperial College London, United Kingdom; ⁴Heriot-Watt University, United Kingdom; ⁵Ludwig-Maximilians-Universität München, Germany

Nanophotonic structures enable a range of applications including optical waveguiding, Purcell enhancement of emission, low-threshold lasing and higher harmonic generation enhancement. Many research fields and technologies have benefited from nano-scale resonators and waveguides previously fabricated from high refractive index dielectrics such as silicon [1] and III-V materials [2] or noble metals [3]. While these offer a large range of opportunities for both research and technology, van der Waals materials can expand the possibilities of nanophotonics in the visible and near-infrared part of the spectrum due to high refractive indices ($n > 4$) [4], a large range of transparency windows, nonlinear optical properties, and new fabrication possibilities exploiting intrinsic van der Waals forces enabling adhesion to any substrate or between different nanophotonic structures. In order to realize this potential, we extract the dielectric constants of a diverse set of materials including transition metal dichalcogenides (TMDs), III-VI semiconductors, and magnetic layered materials. Employing well established techniques, we fabricate nanoantennas with a range of geometries from these materials and observe Mie resonances as well as strong coupling between the excitonic features of TMDs and anapole modes with Rabi splittings up to 140 meV. After the transfer of a monolayer of WSe₂ onto WS₂ nanoantennas, we observe room temperature Purcell enhancement of emission [5] as well as low temperature formation of single photon emitters with enhanced quantum efficiencies within a system fabricated entirely of layered materials. Due to the weak van der Waals interactions of the nanoresonators and the substrate, we were able to employ an atomic force microscopy cantilever in the repositioning of double-pillar nanoantennas to form ultra-small optical mode hotspots as a result of the small gaps achieved (10 nm) [5]. This post-fabrication technique enables applications such as stable, low-power optical trapping of quantum emitters with Purcell enhancement factors above 150.

3:00 PM BREAK

SESSION EQ03.12: Advanced Nanophotonic Design II
Session Chairs: Yu-Jung Lu and Sergey Menabde
Tuesday Afternoon, November 29, 2022
Sheraton, 2nd Floor, Back Bay C

3:30 PM *EQ03.12.01

Dispersion-Engineered Metasurfaces and RGB-Achromatic Metalens Yao-Wei Huang^{1,2}, Zaoyi Li², Raphaël Pestouric³, Peng Lin⁴, Joon-Suh Park², Cheng-Wei Qiu⁵, Ji-Xin Cheng⁴, Steven G. Johnson³ and Federico Capasso²; ¹National Yang Ming Chiao Tung University, Taiwan; ²Harvard University, United States; ³Massachusetts Institute of Technology, United States; ⁴Boston University, United States; ⁵National University of Singapore, Singapore

In this talk, I will report our recent developments and applications of dispersion-engineered metasurfaces in millimeter-scale diameter RGB-achromatic metalens and potential for future virtual-reality platforms. We demonstrate millimeter-scale diameter, high-NA, submicron-thin, metalenses that achieve diffraction-limited achromatic focusing of the primary colors by exploiting constructive interference of light from multiple zones and dispersion engineering. We also utilize inverse-design framework for aperiodic large-scale complex meta-optics in three dimensions, which alleviates computational cost for both simulation and optimization via a fast-approximate solver and an adjoint method, respectively. To illustrate the potential of this approach, we demonstrate a future virtual-reality platforms by using our meta-eyepieces with a home-built fiber scanning near-eye display or a laser back-illuminated micro liquid crystal display.

Reference:

- [1] Z. Li et al., Science Advances 7(5), eabe4458 (2021).
- [2] Z. Li et al., Nature Communications 13, 2409 (2022).

4:00 PM EQ03.12.02

Triplet Fusion Upconversion Nanocapsules for Volumetric 3D Printing Tracy H. Schloemer^{1,2}, Samuel Sanders², Mahesh Gangishetty², Daniel Anderson², Michael Seitz^{1,2}, Aryn O. Gallegos¹, Christopher Stokes² and Daniel Congreve^{1,2}; ¹Stanford University, United States; ²Rowland Institute at Harvard, United States

Three-dimensional (3D) printing has revolutionized additive manufacturing, but the layer-by-layer process of traditional stereolithography can limit resin selection, shape selection, and material quality. One way to achieve volumetric 3D printing, where a vat of polymerizable resin is patterned by light in three dimensions, is to use triplet fusion upconversion (UC). Triplet fusion UC occurs when a sensitizer molecule absorbs low energy light and generates triplet states, which transfer to the annihilator molecules to ultimately generate an excited singlet state that emits higher energy light to initiate polymerization. To ensure excellent light penetration through the vat of resin and maintain the high sensitizer/annihilator concentrations required, the UC materials are encased in silica to generate robust nanocapsules for suspension in the resin. Fundamental nanocapsule design criteria demonstrates tunable optoelectronic and mechanical properties. By pairing upconverting nanocapsules and photoinitiators tailored to the upconverted light to commercially available printing resins, we generate prints on the centimeter scale with fine details in multiple resins. Importantly, this method uses low energy light to print, as compared to high energy lasers that directly initiate polymerization, which allows for deep light penetration into the vat of resin for volumetric 3D printing.

4:15 PM EQ03.12.03

A General Framework for Scintillation in Nanophotonics Charles Roques-Carmes¹, Nicholas Rivera¹, Ali Ghorashi¹, Steven E. Kooi¹, Yi Yang¹, Zin Lin¹, Justin Beroz¹, Aviram Massuda¹, Jamison Sloan¹, Nicolas Romeo¹, Yang Yu², John Joannopoulos¹, Steven Johnson¹, Ido Kaminer³ and Marin Soljačić¹; ¹Massachusetts Institute of Technology, United States; ²Raith America, United States; ³Technion-Israel Institute of Technology, Israel

Bombardment of materials by high-energy particles (e.g., electrons, nuclei, x-ray and gamma-ray photons) often leads to light emission, known generally as scintillation. Scintillation is ubiquitous and enjoys widespread applications in many areas such as medical imaging, x-ray non-destructive inspection, night vision, electron microscopy, and high-energy particle detectors. A large body of research focuses on finding new materials optimized for brighter, faster, and more controlled scintillation. Recent results have proposed scintillation enhancement relying on photonic effects, either by enhancing the rate of spontaneous emission [1], or through improved light extraction [2].

Here, we develop a general theoretical and experimental framework based on integrating nanophotonic structures into scintillators to enhance their emission, which we coin “nanophotonic scintillators” [3]. To start, we develop a unified and *ab initio* theory of nanophotonic scintillators that accounts for the key aspects of scintillation: the energy loss by high-energy particles, as well as the light emission by non-equilibrium electrons in arbitrary nanostructured optical systems and arbitrary material systems. This theoretical framework allows us, for the first time, to experimentally demonstrate nearly an order-of-magnitude enhancement of scintillation, in both electron-induced scintillation (via direct enhancement of the rate of spontaneous emission by shaping the local density of states), and X-ray-induced scintillation (through improved light extraction from bulk scintillators). Beyond enhancement of the scintillator brightness, which is important from the perspective of many of the above applications, we also show how it is possible to strongly shape the spectral content of the scintillation: showing how the peak wavelength in a broadband scintillator can be changed (e.g., from green to red, for the case of self-trapped holes in silica, using high-Q resonances in photonic crystal slabs). Additionally, we show how our full framework enables us to infer the level diagram of complex defects, based on the dependence of the observed scintillation signal on the energy and flux of impinging high energy particles.

Our theory also allows the discovery of structures that could eventually achieve several orders-of-magnitude scintillation enhancement and shaping of scintillation’s optical properties (e.g. angular, spectral, polarization). The framework and results shown here should enable the development of a new class of brighter, faster, and higher-resolution scintillators with tailored and optimized performances – with many potential applications where scintillators are used.

1. Y. Kurman, A. Shultzman, O. Segal, A. Pick, and I. Kaminer, “Photonic-Crystal Scintillators: Molding the Flow of Light to Enhance X-Ray and γ -Ray Detection,” Phys. Rev. Lett., vol. 125, no. 4, p. 040801, Jul. 2020

2. A. Knapitsch and P. Lecoq, “Review on photonic crystal coatings for scintillators,” Int. J. Mod. Phys. A, vol. 29, no. 30, p. 1430070, Dec. 2015

3. C. Roques-Carmes*, N. Rivera*, et al., "A framework for scintillation in nanophotonics," *Science*, 375.6583 (2022): eabm9293.

4:30 PM EQ03.12.04

Low-Loss, Geometry-Invariant Optical Waveguides with Zero-Index Materials Danjing Wang^{1,2}, Kaichen Dong¹, Jie Yao¹, Jin Hong³ and Junqiao Wu¹; ¹University of California, Berkeley, United States; ²Miller Institute for Basic Research in Science, United States; ³To be updated, United States

Compared to electronic circuits, photonic chips that communicate using light offer a solution to faster computing with the potential for larger bandwidth, faster modulation speed, and lower power consumption. Miniaturization of optical elements is essential in increasing the device density for future photonic circuits, but small-scale optical waveguides based on traditional dielectrics exhibit large radiative loss to the free space when the device size approaches the diffraction limit. In addition, light scattering at the bends and crossings of curved waveguides in Si photonics leads to significant optical loss. In contrast, materials with nearly-zero refractive indices show exotic optical behavior at their interface with conventional dielectrics, which has driven applications ranging from geometry-invariant optical tunneling, nonlinear optics, optical cloaking to thermal emission manipulation.

This presentation will focus on zero-index materials as a cladding layer for low-loss and geometry-invariant optical waveguides, where electromagnetic modes are tightly confined within the dielectric core region. Unlike photonic waveguides based on conventional dielectrics, waveguides with a zero-index cladding layer show the advantage of maintaining a high mode-filling factor for small device sizes close to the diffraction limit. Such tight mode confinement is also tolerant to small permittivity variation in the zero-index materials. Because of a greater numerical aperture for waveguides based on zero-index materials, we found that light propagation is robust to bends in a small radius ($\sim \mu\text{m}$) and geometry variation in the cross section. We also investigated hollow zero-index waveguides that further support low-loss light propagation, where materials absorption is minimized because of the air core. Our work offers critical insights into future designs of low-loss and miniaturized photonic devices.

4:45 PM EQ03.12.05

Photonic Band Gaps in Colloidal Crystals of Chiral Hedgehogs Prashant Kumar, Alain Kadar, Kody Whisnant, Michael Veksler, Sharon Glotzer and Nicholas A. Kotov; University of Michigan–Ann Arbor, United States

Colloidal crystals are desirable for photonic bandgaps, that can be tuned by the change in periodic arrangement of particles. While spherical particles are a trivial shape to crystallize, their monodispersity determines the long-range order that is achievable [1]. Here we report the formation of colloidal crystals from spherically shaped chiral microparticles of gold-cysteine complexes [2]. These microparticles are self-assembled from twisted spikes whose length, width and twist angle can be controlled by physical-chemical parameters such as enantiomeric excess, temperature, and charge screening. Using a mixture of L- and D-cysteine we self-assemble chiral hedgehogs of diameters 1-10 μm , at temperatures of 30-90° C. Machine vision algorithms reveal that 1 μm diameter hedgehogs show higher hexatic order parameter [3] as compared to larger sized hedgehogs. Using two-phase self-assembly we deposit these crystals over 1 cm x 1 cm region through controlled evaporation and study their photonic properties. Inherent chirality of hedgehogs imparts an added dimension to photonic bandgaps by their differential interaction with left- vs right-polarized electromagnetic wave. We evaluate these differences through finite element modeling and generate a band diagram for chiral colloidal crystals.

1. Manoharan, V. N., Elsesser, M. T. & Pine, D. J. Dense packing and symmetry in small clusters of microspheres. *Science* (1979) **301**, 483–487 (2003).
2. Jiang, W. *et al.* Emergence of complexity in hierarchically organized chiral particles. *Science* (1979) **368**, 642–648 (2020).
3. Bernard, E. P. & Krauth, W. Two-step melting in two dimensions: First-order liquid-hexatic transition. *Physical Review Letters* **107**, 155704 (2011).

SESSION EQ03.13: Poster Session II
Session Chairs: Artur Davoyan and Ho Wai Howard Lee
Tuesday Afternoon, November 29, 2022
8:00 PM - 10:00 PM
Hynes, Level 1, Hall A

EQ03.13.01

Dynamic Reflective Structural Color Pixels that Are Color Tunable and On/off Switchable via Electrochemical Metal Deposition Youngji Kim, Cheon Woo Moon and Jerome K. Hyun; Ewha Womans University, Korea (the Republic of)

For reflective color displays (e.g., colored e-reader and e-paper), the ability to tune the color within a single pixel is important for maintaining high brightness. To this end, advances in this direction have been made with dynamic structural colors. However, many designs that actively tune the pixel color across the gamut cannot produce a black color, representing the 'off' mode. In a few cases, the black color is produced only when the color is shifted, indicating that the color shift and intensity are coupled. This is due to the fact that the real and imaginary part of refractive index are coupled through the Kramers-Kronig relation. In this work, we demonstrate how color tuning across a wide gamut and on/off switching with high contrast can be achieved in a single reflective pixel. Our pixel consists of 1D TiO_x grating on a Pt working electrode (and reflector) within an electrochemical cell with electrolyte containing Cu ions and an ITO counter electrode. By electrodepositing Cu inside the dielectric gratings, modal interference between the primary waveguide-array modes changes to produce resonance shifts, appearing as color shifts, when viewed through a cross-polarized configuration. Different colors from resonance wavelength shifts up to ~ 200 nm were observed with a cathodic bias (-1.7V). Black colors were produced during electrodisolution as the Cu becomes disordered and porous by applying an anodic bias (0.7V). This results in plasmonic absorption and depolarization of the reflected light, making the pixel turn "off" with switching contrasts up to ~ 97 %. Based on these results, we demonstrate an actively tunable and on/off switchable image and 3x5 pixel array, showcasing the potential of our approach in dynamic reflective displays.

EQ03.13.03

Effect of The Temperature-Dependent Anisotropic Refractive Index on The Spectral Resonances of $\beta\text{-Ga}_2\text{O}_3\text{:Cr}$ Nanowire-Based Optical Microcavities Daniel Carrasco¹, Manuel Alonso-Orts^{1,2}, Eva Nieto³, Jani Jesenovc⁴, Jose Maria San Juan⁵, Maria Luisa N6⁵, John S. McCloy⁴, Rosalia Serna³, Emilio Nogales¹ and Bianchi Mendez¹; ¹Facultad Ciencias Físicas de la Universidad Complutense de Madrid, Spain; ²University of Bremen, Germany; ³Instituto de óptica, CSIC, Spain; ⁴University of Washington, United States; ⁵Facultad de Ciencias y Tecnología, Universidad del País Vasco, Spain

A field of great interest for photonic applications is semiconductor micro and nanowires, since thanks to the modification of the composition of the material or the creation of artificial optical structures it is possible to control its optical properties.

A key photonic structure is the set of optical micro- and nanocavities based on distributed Bragg reflectors (DBR), obtained by periodic modulations of the refractive index in dielectric media. The creation of this type of structures in semiconductor micro- and nanowires broadens their potential applications as micro and nanoscale light sources.

Among the materials of great interest for this type of applications is gallium oxide in its monoclinic phase (β -Ga₂O₃), a transparent conductive oxide (TCO) that presents a high thermal and chemical stability and high resistance to radiation, key properties for use under extreme conditions. Its bandgap of 4.8 eV results in a transparency range from infrared to deep UV. Among the optically active dopants that efficiently emit light along this transparency range, Cr³⁺ results in an intense photoluminescence (PL) yield in the red-near-infrared (NIR) range due to its intra-ionic transitions. DBR-based optical microcavities made of Ga₂O₃:Cr micro- and nanowires show very interesting applications [1].

An analysis of the thermal dependence of the spectral resonances in such optical cavities was recently reported and applied to develop a new wide-range thermometer [1]. Spatial confinement of light within the cavity results in Fabry-Perot-type NIR-red spectral resonances, whose positions depend on temperature. This effect is mainly due to a change in the refractive index and, to a lesser extent, to a change in the length of the optical cavity. The monoclinic crystal structure results in an anisotropic refractive index, thus being necessary a detailed analysis to fully understand the optical behaviour. However, only a few previous works have been devoted to this topic in β -Ga₂O₃, therefore being still only partially understood [2,3]. In this work, the temperature-dependent refractive indices along the main axes have been obtained experimentally by ellipsometry in bulk monocrystalline β -Ga₂O₃. These results have been implemented in analytical and finite-difference time-domain simulation models of the resonances in the nanowires to further evaluate their spectral behaviour with temperature.

[1] M. Alonso-Orts, D. Carrasco, J. M. San Juan, M. L. N3, A. de Andr3s, E. Nogales, and B. M3ndez, "Wide dynamic range thermometer based on luminescent optical cavities in Ga₂O₃: Cr nanowires," *Small* 18, 2105355 (2022).

[2] I. Bhaumik, R. Bhatt, S. Ganesamoorthy, A. Saxena, A. K. Karnal, P. K. Gupta, A. K. Sinha, and S. K. Deb, "Temperature-dependent index of refraction of monoclinic

Ga₂O₃ single crystal," *Appl. Opt.* 50, 6006-6010 (2011).

[3] C. Sturm, J. Furthm3ller, F. Bechstedt, R. Schmidt-Grund, and M. Grundmann, "Dielectric tensor of monoclinic Ga₂O₃ single crystals in the spectral range 0.5–8.5 eV", *APL Materials* 3, 106106 (2015).

EQ03.13.04

Investigation of Optical Coupling in ZnO Nanowires by μ -PL Measurements [Lukas R. J3ger](#), Francesco Vitale, Christian T. Plass, Edwin Eobaldt and Carsten Ronning; Friedrich-Schiller-Universit3t Jena, Germany

Semiconductor nanowires are a keystone in the miniturization of optoelectronic devices, because they bring the potential to realize compact and low power consumption nanolasers. This is due to their good waveguiding properties, high optical gain and low power consumption.

For many nanoscale applications, the evanescent coupling between two adjacent nanowires may yield interesting consequences, such as frequency selection of the Fabry-Perot modes.

In recent years the optical resonances in nanowire pairs have been investigated for Silicon nanowires, GaN nanowires and CdS nanowires for various arrangements and with disparate measurement techniques.

It is possible to set the nanowire spacing and angle, using nanomanipulation to precisely position ZnO nanowires. In this study, we used this to examine the effect of a varying overlap of the evanescent fields for a chosen nanowire pair. Performing μ -photo luminescence measurements with a pulsed 355nm laser offers three approaches: Emission spectra provide insights into mode selection, a Fourier back focal plane setup may reveal lasing coherence and intensity measurements could show changes in the lasing threshold.

EQ03.13.05

Vertically Stacked Split-Ring Resonators Derived from Block Copolymer Self-Assembly for Polarization-Sensitive Dichroic Responses [Sanghoon Kim](#), Chunghwan Jung, Jungho Mun, Junsuk Rho and Jin Kon Kim; Pohang University of Science and Technology, Korea (the Republic of)

We realized stacked split-ring resonators (SSRRs) arrays from "pagoda-like" nanorods over a large area (~cm²) exhibiting polarization differences in visible and near-infrared (NIR) wavelengths. The lamellar-forming polystyrene-block-poly (methyl methacrylate) copolymer (PS-*b*-PMMA) was confined in cylindrical pores of aluminum oxide (AAO) template grafted by thin neutral brush layers to create this array of "pagoda-like" nanorods. Along the nanorod direction, PS and PMMA lamellae nanodomains with 25 nm were alternately stacked. After the AAO template was removed, "pagoda-like" nanorods were generated by O₂ reactive ion etching. Silver SSRRs formed from the "pagoda-like" nanorods via oblique angle deposition (OAD) exhibit optical polarization differences due to asymmetric architectures. This method of constructing complex nanoscale architectures using block copolymer self-assembly and tilt deposited plasmonic metal could be applied to optical anti-counterfeiting, structural color, and commercial optical components in a large area.

EQ03.13.06

Towards to Fabrication of Plasmonic Conductive Nitrides by Pulsed Laser Ablation for Biomedical Applications [Nikolaos Pliatsikas](#), Spyridon Kassavetis, Aphrodite Koutsogianni, Ilias Fekas, Stavros Panos, Tamara Oduola, Christos Kapnopoulos, Maria Gioti and Panos Patsalas; Aristotle University of Thessaloniki, Greece

Plasmonics is one of the most dynamic and fast-developing scientific and technological fields nowadays. Metal nanoparticles (NPs) with plasmonic response in the Near-Infrared (NIR) spectral range can be applied for biological applications due to the efficient absorption and heating at extremely confined volume in the vicinity of the NPs. "Traditional" plasmonic metal NPs, such as Au and Ag, fail to endure high temperatures and/or the high electric fields of NIR concentrated light, required for biological applications. We could pave the way to emerging plasmonic bio-applications by the fabrication of refractory transition metal nitrides NPs, such as TiN, whose plasmonic performance can extend into the NIR spectral range by varying their stoichiometry or via alloying to form ternary systems. The most promising route to fabricate plasmonic TiN NPs, in terms of reproducibility and ease process upscaling, is by pulsed laser ablation in solvents (LA). As the NIR plasmonics are extremely sensitive to the stoichiometry and/or doping of TiN, LA emerges as the undisputed method of choice, because the ablated NPs retain in the elemental composition of the solid target.

In this work, we present the controlled fabrication of functional refractory and stable plasmonic TiN NPs with absorption in the NIR biological window by LA. The initial targets have been developed by reactive Magnetron Sputtering at room temperature while the final shaping of the colloidal NPs was performed through a laser ablation process by the 532 nm beam of a picosecond laser system and/or by 1064, 532, and 355 nm beam of a nanosecond Nd:YAG pulsed laser system. TiN NPs structure and morphology as well as the quality of the materials have been analyzed by XRD, SEM, EDX, AFM, and XPS. The optical properties of the TiN target materials have been evaluated by NIR-Vis-UV Spectroscopic Ellipsometry, while an optical absorbance characterization was performed on the colloidal TiN NPs. The photothermal properties of these colloidal NPs have also been investigated, and preliminary biocompatibility tests have been carried out using proteins such as albumin and fibrinogen in PBS solvent.

EQ03.13.07

Lithography-Free Fabrications of Chiral Metamaterials with Twisted Micro and Nanowrinkle Patterns Based on Asymmetric Buckling Processes Myonghoo Hwang and Bongjun Yeom; Hanyang University, Korea (the Republic of)

Chiral metamaterials can interact differently with circularly polarized lights, that is determined by their mirror-symmetric structures in three-dimension. Fabrications of the chiral structures in nano and microscales were mostly accomplished by advanced lithography techniques and wet chemical synthesis methods with bio derivatives containing innate molecular chirality. These previous fabrication methods limit wide applications of chiral metamaterials because of high cost in mass production and narrow windows for material selections. Herein, we suggest a facile and general fabrication method based on step-wise buckling processes with biaxial and asymmetric strains for twisted wrinkled patterns in chiral geometry. Soft polydimethylsiloxane substrates were utilized to be biaxially stretched in asymmetric directions. Then, the PDMS surfaces were oxidized by ozone treatment or oxygen plasma to produce hard oxide layers with different moduli from the substrates. By removing in-plane strains in stepwise manner with additional surface treatments, fusilli pasta-shaped twisted wrinkle patterns were produced on top of the substrates. Based on asymmetric angle, degree of strains and the surface treatments, the mirror-symmetric geometries of the twisted wrinkle patterns were controlled, which further utilized for fabrications of various 3D chiral metamaterials. Layer-by-Layer assembly methods for depositions of plasmonic nanoparticles and selective areal depositions over the pattern surfaces were introduced. Optical activity in wide ranges of optical frequencies from visible to THz were realized based on these chiral twisted metapatterns. It is noted that preparations of these materials do not necessitate any lithography or bio-additives, which will be advantageous for facile fabrications of chiral structures for various applications, such as advanced optoelectronic devices, bio sensors and pharmaceutical applications.

EQ03.13.08

Reflection-Enhanced Raman Detection of Single Bacterial Cells Patterned Using Capillary Assembly Joong Bum Lee¹, Minjoon Kim¹, Stefan A. Maier^{2,3,4}, Emiliano Cortés⁴, Yeon Sik Jung¹ and Yoon Sung Nam¹; ¹Korea Advanced Institute of Science and Technology, Korea (the Republic of); ²Monash University, Australia; ³Imperial College London, United Kingdom; ⁴Ludwig-Maximilians-Universität München, Germany

The worldwide prevalence of bacterial infections calls for early diagnostic tools based on rapid, reliable, and accurate identification of pathogenic bacteria. Raman spectroscopy has emerged as an attractive alternative to existing detection techniques to this end, as it offers fast and direct output of molecular fingerprint information. However, an open challenge still remains for Raman detection of bacteria in terms of effectively locating and obtaining reproducible signals from single cells. Herein, we utilize capillary-assisted particle assembly (CAPA) to pattern single bacterial cells into a topographical template which provides a regular alignment of the most Raman active region of the cells as per the geometry of the patterned traps. The supporting template is composed of a highly reflective Ag/SiO₂ film which enhances the inherently weak Raman signals by reflecting the laser for re-excitation of the cells and by reflecting the downward scattered photons towards the detector. The detection platform is simple and provides highly reproducible signature spectra for different bacteria such as *Staphylococcus aureus*, *Salmonella gallinarum*, and *Escherichia coli*. Finally, CAPA is used to directly separate single cells from a suspension of biologically relevant media namely artificial urine, which helps discard additional processes required to isolate the bacteria such as centrifugation. The proposed system can potentially offer new opportunities in clinical settings that require reproducible, simple, and accurate identification of single bacterial cells.

EQ03.13.09

Graphene-Based Antenna Coupled Terahertz Detector Francisco Javier Gonzalez¹, Robert Peale¹, Michael Lodge², Richard Klemm², Masahiro Ishigami², Chris Fredricksen¹ and Ami Rathod²; ¹Truentic-University of Central Florida, United States; ²University of Central Florida, United States

Graphene-based optoelectronic devices has drawn great interest due to its attractive electromagnetic, mechanical, electrical, and thermal properties. Unlike semiconductors graphene has no band gap, therefore can absorb photons from a wide frequency bandwidth efficiently by impedance matching. In graphene photon energy can increase its temperature significantly and due to the very stiff carbon lattice the electron-phonon interaction is weak, making cooling contribution by phonon emission very small. All these characteristics make graphene a good candidate for thermal based photon detectors. Antennas are elements that can be used either to receive or to transmit electromagnetic waves, when used in reception mode electromagnetic waves induce currents in the antenna elements that can be later detected and used for various applications. Antennas have several unique advantages such as polarization sensitivity, directivity, small footprint, tunability and the possibility of integration into electronic and photonic circuits. Antennas have been coupled to thermal detectors, such as bolometers, to increase its frequency response and incorporate some desirable characteristics of the antenna into the antenna-coupled detector, such as a specific bandwidth or polarization dependence. In this work different types of antennas coupled to graphene nanostructures will be evaluated numerically using COMSOL Multiphysics. Results will show the bandwidth, polarization dependence and responsivity of square-spiral, log-periodic and Archymedeian spiral antennas coupled to graphene nanostructures, and the advantages of using each one of those antennas in terahertz detection applications.

EQ03.13.10

Laser-Induced Forward Transfer of Silk Fibroin Periodic Structure—Controlling Mid-Infrared Reflectivity Cleber Mendonca¹, Filipe Couto¹, Kelly Tasso¹, Molirra Santos¹ and Sidney Ribeiro²; ¹University of Sao Paulo, Brazil; ²University of São Paulo State–UNESP, Brazil

Periodic dielectric structures offer an efficient way to control light propagation at micro- and nanoscale. Among many techniques that can produce such types of structures, femtosecond Laser-Induced Forward Transfer (fs-LIFT) is a promising one due to its ability to process different kinds of materials, preserving their integrity. In particular, Silk fibroin (SF), a natural biopolymer, can be processed by fs-LIFT to print well-ordered periodic arrays of microstructures. Due to its high transparency, biocompatibility, and possibilities of functionalization, SF is a suitable material for photonics. In this work, a 2D lattice of hemi-elliptical SF microdroplets was fabricated via fs-LIFT, and finite-element (FEM) simulations were carried out to study their response to electromagnetic radiation in the near to mid-infrared spectral region, considering the influence of the substrate. The simulation results indicated a decrease in reflectivity, which was corroborated by experimental results. In addition, coating the fabricated structures with a higher index dielectric material was shown to enhance the reduction in reflectivity in the mid-infrared spectral region. These results demonstrate a straightforward way to print ordered arrays of SF microstructures in a relatively large area, with potential application as controllable reflectivity coating for the near to mid-infrared spectral region.

EQ03.13.11

Cavity Quantum Electrodynamics on a Single Gold Nanoprobe for Biological Application Kyungwha Chung^{1,2}, Subin Yu^{3,2} and Luke P. Lee^{2,1}; ¹Sungkyunkwan University, Korea (the Republic of); ²Brigham and Women's Hospital, Harvard Medical School, United States; ³Ewha Womans University, Korea (the Republic of)

Cavity quantum electrodynamics (CQED) is an interesting phenomena but difficult to realize. Here, we report the probe that allows strong coupling with biological molecules within a single particle. We accomplish CQED structure in a single gold double nanoring with an intrinsic nanogap of 4-8 nm. We observe topological CQED characteristics in dark-field microscopy measurements.

This CQED probe can be applied to the living cells, showing extraordinary ability to amplify biomolecular signal through strong coupling between the CQED probe and biomolecules. We believe that this 3D CQED nanocavity is a promising nanoprobe for detection of small molecules in the cells and a

platform for breakthrough biomolecular studies.

EQ03.13.13

High-Quality-Factor Dielectric Metasurfaces for Rapid Identification and Classification of Mycobacterium Tuberculosis Using Surface-Enhanced Raman Spectroscopy [Baba Ogunlade¹](#), [Loza Tadesse²](#), [Jack Hu¹](#), [Sahil Dagli¹](#), [Amy Barczak³](#) and [Jennifer A. Dionne¹](#); ¹Stanford University, United States; ²Massachusetts Institute of Technology, United States; ³Ragon Institute, United States

Rapid identification of mycobacterium tuberculosis (MTB) infection and antibiotic susceptibility testing (AST) is essential for effective patient treatment, prevention of community spread, and combating antimicrobial resistance. To date, culture-based techniques remain the gold standard for the identification of TB strains and determination of their antibiotic susceptibility. Unfortunately, such identification and AST can take several days to multiple weeks in well-equipped labs, due to the slow growth rate of MTB. One promising alternative to culture-based cellular fingerprinting is Raman spectroscopy, an optical characterization technique which probes vibrational modes of a sample. It relies upon the inelastic scattering of photons incident on a sample and measures their wavelength shift after interacting with a sample. Raman scattering offers three key advantages over alternative cellular fingerprinting approaches. First, it is label-free and generalizable to all kinds of cells; the intrinsic vibrations of the cells serve as native labels. Second, Raman can be fast, with sub-second acquisition times, and accurately measured with minimal sample preparation. Lastly, because peaks in a Raman spectrum are unique to the vibrational modes of particular biomolecules, Raman cell signatures can be used to assess and monitor the composition, structure, and vitality of that cell and uniquely differentiate it from another cell. Despite these advantages, obtaining and utilizing Raman spectra from cells presents a challenge due to (1) Raman's inherently weak scattering efficiency and low signal-to-noise ratio and (2) its complexity in spectral interpretation.

To address these two issues, we present a combined nanophotonic-machine learning platform that uses resonant nanophotonic surfaces, known as high-quality factor (high-Q) dielectric metasurfaces, to provide critical Raman signal enhancement. Using FDTD simulations, we demonstrate a metasurface of subwavelength silicon nanoblocks that are bi-periodic in length to generate a high Q resonance. These nanoblocks have a width of 120 nm, a bi-periodic length of 430 and 400 nm, and a height of 500 nm. By tuning the nanoblocks' dimensions, we place a high-Q resonance at the Raman excitation wavelength that will be used to enhance the local electric field amplitude as well as a broad magnetic dipole Mie resonance at the MTB's Stokes-shifted Raman region to provide strong, broadband Raman signal enhancement. Collectively, these two resonances provide a maximum Raman signal enhancement of over 105 over a wide spectral range of 1500 cm⁻¹

We fabricate these metasurfaces using electron beam lithography and experimentally verify this enhancement by placing dried MTB bacterial samples on the metasurfaces and measuring their Raman spectra. We use four unique strains of antibiotic-resistant *Bacillus Calmette-Guérin* (BCG), an attenuated form of *Mycobacterium Bovis*, as a model for *Mycobacterium tuberculosis*, as well as a control strain. We classify the antibiotic resistant BCG strains according to their Raman spectra using logistic regression. Specifically, we use a 80/20 train-test split, in which 80% of the data is used to train the model and the remaining 20% is held out and tested on the model in order to evaluate the accuracy of the model. Through this machine learning model, we are able to identify and differentiate the 5 BCG strains with ~98% accuracy. Through this combined nanophotonic-machine learning platform, we have demonstrated a rapid and accurate platform for bacterial identification and classification using Raman spectroscopy.

EQ03.13.14

Light Localization in Multifractal Dielectric Environments [Yilin Zhu](#), [Tornike Shubitidze](#) and [Luca Dal Negro](#); Boston University, United States

Multifractals are heterogeneous structures with multi-scale properties described by a continuous spectrum of fractal dimensions, i.e., the so-called multifractal singularity spectrum. In contrast to traditional fractals, or monofractals, which possess only one global scaling exponent corresponding to the fractal dimension, multifractals have a broad distribution of generalized fractal dimensions and their structural properties exhibit extreme (heavy-tailed) non-Gaussian fluctuations. While the optical properties of fractal structures are well-understood, multiple scattering, light localization and emission phenomena in multifractal dielectric environments remain to be explored. Using rigorous Green's matrix and multi-particle Mie scattering theory, in this talk we systematically investigate light-matter interactions in engineered photonic multifractal media. Specifically, we generate multifractal point patterns from random multiplicative processes with different correlation properties that interpolate in a tunable fashion between random structures, monofractals, and strongly inhomogeneous multifractals. We study photonic structures with different values of dielectric constants and analyze their spectral statistics, optical Thouless conductance, and local density of states. Our findings demonstrate that tailored multifractal dielectrics support scattering resonances with a stronger localization (i.e., smaller localization length) compared to both uniform random and monofractal systems across a broad spectrum extending from visible to infrared wavelengths. Device applications of multifractal media for the demonstration of ultracompact spectrometers and novel broadband lasers will also be presented.

EQ03.13.16

Low Loss Mid-Infrared Plasmonic Waveguides—Extending the Limits of Noble Metals [Mauro David](#), [Elena Arigliani](#), [Alicja Dabrowska](#), [Anna Lardschneider](#), [Masiar Sistani](#), [Daniele Nazzari](#), [Davide Disnan](#), [Ismael C. Doganlar](#), [Hanh T. Hoang](#), [Georg Marschick](#), [Hermann Detz](#), [Ulrich Schmid](#), [Bernhard Lendl](#), [Walter M. Weber](#), [Gottfried Strasser](#) and [Borislav Hinkov](#); TU Wien, Austria

Surface plasmon polaritons (SPPs) combine the high-speed capabilities of photonic circuits with the ability of plasmonic confinement below the diffraction limit. In particular, modes supported at (noble) metal/dielectric interfaces in various configurations have gained great attention owing to their prospects for attractive applications. However, considering such plasmonics as an established technology in the visible (VIS) and near-IR spectral range, plasmonic concepts in the mid-IR spectral range are still in their infancy. This significantly hampers addressing emerging mid-IR applications by chip-scale devices, e.g. in real-time liquid sensing experiments or optical free-space communication. Thus, realizing novel device concepts and introducing new materials aims at mimicking VIS/near-IR properties such as wavelength-scale mode confinement and guiding. Succeeding will enable a novel class of photonic integrated circuits (PICs) with breakthrough performance characteristics like compact chip-scale Mach-Zehnder interferometers, monolithic heterodyne detectors or on-chip logic networks. They all strongly benefit from miniaturization and the use of mid-IR wavelengths.

In this work, we surpass the limitations of traditional noble metal-based plasmonics by exploiting the approach of surface-loading using two different highly transparent mid-IR materials leading to different characteristics. In the first part of this work, we introduce, supported by finite element (FEM) simulations, a new concept of semiconductor-loaded SPPs (SLSPPs), resulting in experimental low-loss, ultra-broadband waveguides covering a full octave between 5.6 μm and 11.2 μm . This is obtained by depositing thin Ge-slabs on a gold layer supported by a Si substrate, allowing to couple and confine mid-IR photons on the wavelength-scale to the chip-surface and efficiently guide them for a few millimetres. Germanium combines multiple advantages including broadband transparency, i.e. low loss, characteristics throughout the mid-IR spectral range, well-known interface characteristics and fabrication protocols from its decades of use in micro- and nano-electronics as well as CMOS compatibility. Its refractive index profile allows the realization of Ge/Au SLSPP waveguides, where >95% of the mode are guided in the surrounding medium, making it highly suitable for monolithic chip-scale liquid spectrometers. Moreover, we exploited previous work on combining high-k dielectrics like HfO_2 , Al_2O_3 and ZrO_2 with Ge for stabilizing its surface-oxides GeO_x . We demonstrate that 10 nm of atomic layer dielectric deposition protects our Ge/Au SLSPP waveguides from being etched in normal water. This opens the pathway towards bio-sensing applications, where water is the most relevant background matrix.

In the second part, we show a novel fabrication technique for spin-coating high-quality polyethylene (PE) films as well as their processing into micrometre-

thick ridges to efficiently confine and guide mid-IR plasmons along the chip surface. In this way, we find a new path to extend the concept of so-called dielectric-loaded SPP (DLSP) structures to the mid-IR and beyond, based on the broad transparency window (2-200 μm) of this material. Therefore, PE can play a similarly important enabling role in the mid-IR as PMMA does at shorter wavelengths.

We show the design (including FEM-simulations), fabrication, and optical characterization of such PE-based DLSP waveguides. This includes the first experimental demonstration of SPPs in PE-based mid-IR plasmonic waveguides. They show capabilities in directing the mode along the chip surface in low-loss straight waveguides and very importantly also adiabatic S-shaped bends (50 μm bending offset along 120 μm waveguide length) with extracted bending losses of <2.5 dB per bend.

Overall, we show for both types of presented waveguides (SLSP & DLSP) total losses of significantly below 20 dB/mm together with their broadband mid-IR plasmonic operation.

EQ03.13.17

Tilt-Rotate Evaporation Colloidal Lithography for Large-Area Nearly-Monodisperse Metasurfaces [MaCayla Caso](#), Michael G. Benton and Kevin M. McPeak; Louisiana State University, United States

Colloidal lithography (CL) has become a key fabrication technique for metasurfaces due to the method's low cost and scalability. Multiple types of structures are fabricated from CL, such as nanohole and nanodot arrays. Controllability of shape, pitch, and size of the features is necessary to tune the optical response of the metasurface. CL allows this control by utilizing assembled colloids as an ordered mask that can be plasma etched to achieve the desired features. Although CL allows for large-scale fabrication the resulting structures are limited in their minimal feature size and uniformity. Reducing the diameter of the polystyrene sphere mask by plasma etching unavoidably increases their coefficient of variation (CV) and deforms their shape, thereby limiting the pitch-to-hole-diameter ratio of the resulting nanohole array (NHA) to less than 3:1 and the minimum hole size to 200 nm with a 10% or better CV. While there has been extensive research on improving the average diameter and defect density in CL derived NHAs, little work has been done in reducing the polydispersity of the hole diameters in the NHAs, especially in the sub-200 nm diameter range.

We show that a modified CL method, tilt-rotate evaporation colloidal lithography (TRE-CL), breaks the trade-off between hole diameter and polydispersity by leveraging glancing angle evaporation, not plasma etching, to adjust the hole size. [1] TRE-CL allows pitch-to-hole-diameter ratios as high as 7:1 and nanohole diameters down to 60 nm while maintaining a nearly constant CV below 10% and hole circularity above 91%. Furthermore, we transfer these hole arrays into ultrathin Si_3N_4 films to fabricate adhesion-layer-free plasmonic Au nanodot arrays down to 70 nm in diameter with 10% CV embedded in Si_3N_4 . TRE-CL allows for large-scale fabrication of uniform metasurfaces quickly and at a low cost while achieving periodic features in the critical 50 – 200 nm regime.

References:

[1] M. J. Caso, M. G. Benton, and K. M. McPeak, *JVST A* 40 (4), 10.1116/6.0001874, (2022). (cover image)

Contact Information:

MaCayla J. Caso: mcaso2@lsu.edu

Michael G. Benton: benton@lsu.edu

Kevin M. McPeak: kmcpeak@lsu.edu

EQ03.13.19

Large Area Flexible Terahertz Textile Metamaterial [Ruben Del Rio Ruiz](#)¹, Aydin Sadeqi² and Sameer R. Sonkusale¹; ¹Tufts University, United States; ²Georgia Institute of Technology, United States

The terahertz and millimeter wave band of the electromagnetic spectrum has been underdeveloped due to the lack of naturally occurring materials that respond at these frequencies. Artificially designed metamaterials offer to fill this terahertz gap by engineering constituent resonant unit cells in large periodic or quasi-periodic arrays. In fact terahertz metamaterials have been developed to demonstrate quite unique properties, such as perfect absorption, amplitude modulation, imager, spatial light modulation, beam steering etc.[1-6] However, current approaches to realizing metamaterials is limited in size to few centimeters and are always rigid due to reliance on expensive cleanroom fabrication process. To truly revolutionize the field of devices that exploit terahertz-matter interaction, we need approaches that allow for large area (meters) metamaterials with arbitrary flexibility and stretchability. Towards that goal, the utilization of common fabrics and advanced textile processing such as stitching or embroidering to design flexible stretchable metamaterial devices on them adds a new dimension enabling terahertz applications. This work presents a millimeter wave and terahertz metamaterial fabrication process on a textile substrate. The fabrication process employs commonly available materials such as pure copper polyester taffeta fabric (PCPTF), thermally activated adhesive mesh, paper adhesive sheets and polyester cotton-based fabric processed using modified textile processing. The material options can be easily expanded to other textile materials in the future. The fabrication process is based on a combination of thermally adhering different materials, laser cutting the metamaterial pattern and peeling the fiducial conductive layer from the final design. A fabrication accuracy down to 0.7mm was easily achieved. It was reproduced eleven times to validate the proposed construction process. The measured average values of the transmission coefficient, and resonance frequency of the designed metamaterial absorbers were 0.09 and 88GHz, respectively. Moreover, the standard deviations of measured transmission coefficient, and resonance frequency equal 0.05 and 0.9GHz, respectively. Interestingly, we realized large area patterns exceeding 10s of centimeters easily, achieved for the first time in literature at these frequencies. These results confirm that novel process flow employing a combination of laser processing, screen printing and textile processing allows realization of large area textile terahertz metamaterials. This will open up new avenues for applications of terahertz metamaterials for the first time.

[1] D. Shrekenhamer, S. Rout, A. Strikwerda, C. Bingham, R. Averitt, S. Sonkusale, and W. Padilla, "High speed terahertz modulation from metamaterials with embedded high electron mobility transistors," *Opt. Express* 19, 9968-9975 (2011).

[2] X. Liu, S. MacNaughton, D. B. Shrekenhamer, H. Tao, S. Selvarasah, A. Totachawattana, R. D. Averitt, M. R. Dokmeci, S. Sonkusale, and W. J. Padilla, "Metamaterials on parylene thin film substrates: Design, fabrication, and characterization at terahertz frequency", *Appl. Phys. Lett.* 96, 011906 (2010).

[3] Saroj Rout and Sameer R. Sonkusale, "A low-voltage high-speed terahertz spatial light modulator using active metamaterial", *APL Photonics* 1, 086102 (2016).

[4] Sameer Sonkusale, Wangren Xu, Saroj Rout, Guoqing Fu, Pramod Singh, "Terahertz metamaterials for modulation and detection," *Proc. SPIE* 9483, Terahertz Physics, Devices, and Systems IX: Advanced Applications in Industry and Defense, 948306 (2015)

[5] Aydin Sadeqi, Hojatollah Rezaei Nejad, and Sameer Sonkusale, "Low-cost metamaterial-on-paper chemical sensor," *Opt. Express* 25, 16092-16100 (2017).

[6] Pramod K. Singh, Konstantin A. Korolev, Mohammed N. Afsar, and Sameer Sonkusale, "Single and dual band 77, 95, 110GHz metamaterial absorbers on flexible polyimide substrate", *Appl. Phys. Lett.* 99, 264101 (2011).

EQ03.13.20

Filterless Infrared Chemical Sensing with Narrowband Thermal Emitters [Thiago S. Arnaud](#)^{1,2}, Guanyu Lu², Mingze He², Ryan Spangler³, Joshua

Nordlander³, Jon-Paul Maria³ and Joshua D. Caldwell^{2,4}; ¹University of Florida, United States; ²Vanderbilt University, United States; ³The Pennsylvania State University, United States; ⁴Sensorium Technological Laboratories, United States

A plasmon polariton is a quasiparticle made from the coupling of a photon with coherently oscillating free charge carriers. A Tamm plasmon mode couples a surface plasmon polariton (SPP) with a distributed Bragg reflector (DBR) that provides a significant reduction in the spectral linewidth of the resonant absorption/emissivity. While this had been demonstrated for thermal emitters and absorbers previously, the periodic nature of the DBR restricted the passbands to a single frequency, while the noble metals employed as the SPP material limited the tunability of the design. Building on prior efforts from our group where we illustrated that an aperiodic DBR with frequency tunable cadmium oxide as our SPP layer can provide a multifrequency, broadly tunable emitter, here, we employ such structures for demonstrating novel gas sensing modalities. We implement a machine-learning algorithm to inversely design the structure of the aperiodic DBR and the carrier concentration of the doped CdO, an n-type semiconductor that we use as the conductive layer to support the Tamm plasmon to optimize the structure for a given spectrum. Due to the tunability of these structures, they can be designed for narrow absorption and thus, thermal emission peaks at an arbitrary spectral position, linewidth and amplitude. This attribute allows for the design of selective infrared sources for chemical sensing, which targets the emission to match the vibrational mode of a desired molecule. Commercially, chemical sensing techniques are typically limited to one target molecule per device due to the dependence of a bandpass filter that is required to eliminate other frequencies where molecular absorption would limit the chemical specificity of the device. Currently, there has not been any successful efforts in discriminating between molecules of nearby vibrational modes without the use of a bandpass filter. By implementing a Tamm-emitter-based sensor, we demonstrate its viability for filterless non-dispersive infrared sensing, while maintaining the ability to also discriminate the response from other molecules. Here the target molecule was CO₂. The vibrational mode of CO₂ however spectrally overlaps with the absorption of CO, making discrimination between the gases challenging in non-spectroscopic methods (e.g. NDIR). A Tamm emitter was designed, fabricated, and tested to achieve CO₂ sensing, with ppm sensitivity, while maintaining its capability to successfully discriminate from the presence of CO gas without the need for an additional bandpass filter. From plotting the ratio of power decrease due to gas absorption as a function of concentration, the Tamm demonstrated higher sensitivity for concentrations of CO₂ than a blackbody with a bandpass filter, while providing the potential for new functionality, such as the ability to incorporate multiple gas sensors within a single platform.

SESSION EQ03.14: Quantum Photonics/Advanced Nanophotonics
Session Chairs: Jennifer Dionne and Yao-Wei Huang
Wednesday Morning, November 30, 2022
Sheraton, 2nd Floor, Back Bay C

8:15 AM *EQ03.14.01

Advancing Photonic Design and Quantum Photonics with Machine Learning [Alexandra Boltasseva](#); Purdue University, United States

Discovering unconventional optical designs via machine-learning promises to advance on-chip circuitry, imaging, sensing, energy, and quantum information technology. In this talk, we discuss photonic design approaches and emerging material platforms for showcasing machine-learning-assisted topology optimization for optical metasurface designs with applications in thermophotovoltaics, reflective optics, and lightsail technology. We demonstrate the effectiveness of autoencoders for compressing the vast design space of metasurfaces into a smaller search space. By employing global optimization via adjoint methods or quantum annealing, one can find the optimal metasurface designs within the smaller space constructed by the autoencoder. The quantum-assisted machine learning framework, named bVAE-QUBO, presented in this work is the first demonstration of a generic machine learning framework that compresses an arbitrary continuous optimization problem into an Ising-model formalism for quantum sampling. When compared to other global optimization techniques, bVAE-QUBO has the potential for quantum speedups and achieving higher quality designs than traditional adjoint optimization methods. The techniques employed in this work extend well beyond the metasurface optimization space and into many inverse design problems for engineering and physics.

8:45 AM DISCUSSION TIME

9:00 AM EQ03.14.03

Highly Uniform and Indistinguishable Scalable Single Photon Source Arrays—Towards Quantum Optical Circuits [Qi Huang](#)¹, [Jiefei Zhang](#)¹, [Swarnabha Chattaraj](#)¹, [Lucas Jordao](#)¹, [Siyuan Lu](#)² and [Anupam Madhukar](#)^{1,1,1}; ¹University of Southern California, United States; ²IBM Thomas J. Watson Research Center, United States

In the field of quantum information processing, realization of integrated quantum optical circuits towards quantum communication, quantum sensing, quantum cryptography, and quantum computation has been a long-sought goal. The biggest obstacle towards achieving such a goal is the lack of an ordered scalable array of on demand single photon sources (SPSs) having sufficient spectral uniformity, near unity brightness, single photon purity and indistinguishability meeting functional requirement for specific applications.

In this talk, I will present our continued study of a unique class of mesa top single quantum dot (MTSQD) in an ordered array [1-3], which is grown using the substrate-encoded size reducing epitaxy (SESRE) approach where surface curvature induced surface stress gradient is exploited as the driving force to have adatoms preferentially migrate from mesa side wall towards pre-patterned nanomesa top. The planarized GaAs/In_{0.5}Ga_{0.5}As MTSQDs grown in a 5x8 array is shown to have high spectral uniformity with standard deviation $\sigma_\lambda \sim 2.8$ nm, within the local wavelength tuning range to bring different MTSQDs into resonance with each other. The highly spectrally uniform MTSQDs show near unity internal quantum efficiency, high single photon purity >99% ($g^{(2)}(0) \sim 0.015$), and high two-photon interference (TPI) visibility of 0.83 ± 0.03 (measured at 11.5K without Purcell enhancement) [4]. The TPI visibility is limited by phonon induced dephasing and can reach ~ 0.92 at 4K. The TPI visibility can be further improved to approach unity with MTSQDs integrated with appropriate photonic structure to provide Purcell enhancement. The reported TPI visibility is one of the best reported amongst various site-controlled QDs [4]. The MTSQDs also show highly uniform behavior in single photon emission purity and TPI visibility. Statistics on these will be discussed. Further work on establishing MTSQDs uniformity across larger arrays, i.e. 10x10 and 50x50 is underway.

Such planarized MTSQDs in an ordered array with near unity quantum efficiency, single photon purity, and indistinguishability, provide a highly promising platform towards realizing quantum optical circuits in a horizontal architecture using well established monolithic or hybrid integration approach that enable on-chip multiphoton interference and entanglement towards various quantum information applications. Work on the integration of MTSQDs to light manipulation units using waveguide and 2D photonic crystal approach is underway.

The work is supported by the Air Force Office of Scientific Research (FA9550-17-1-0353) and the US Army Research Office (W911NF1910025)

[1] J. Zhang et al., *Jour. App. Phys.* 120, 243103 (2016).

[2] J. Zhang, et al., App. Phys. Lett 114, 071102 (2019).

[3] J. Zhang, et al., APL photonics 5, 116106 (2020).

[4] J. Zhang, et al., arXiv:2108.01428 (2021).

9:15 AM DISCUSSION TIME

9:30 AM DISCUSSION TIME

9:45 AM BREAK

SESSION EQ03.15: Lasing and Radiation Engineering II

Session Chairs: Ho Wai Howard Lee and Yu-Jung Lu

Wednesday Morning, November 30, 2022

Sheraton, 2nd Floor, Back Bay C

10:30 AM EQ03.15.01

Exciton-Polaritons in Two-Dimensional Ruddlesden–Popper Perovskites Strongly Coupled with Plasmonic Lattices Jeong-Eun Park^{1,2} and Teri W. Odom²; ¹GIST, Korea (the Republic of); ²Northwestern University, United States

Strong coupling between light and matter can produce hybrid eigenstates known as exciton-polaritons. Although polariton dynamics are important photophysical properties, the relaxation pathways of polaritons in different coupling regimes have seen limited attention. This paper reports the dynamics of hybridized states from 2D Ruddlesden-Popper perovskites coupled to plasmonic nanoparticle lattices. The open cavity architecture of Al lattices enables the coupling strength to be modulated by varying either the lead halide perovskite film thickness or the superstrate refractive index. Both experiments and finite-difference time-domain simulations of the optical dispersion diagrams showed avoided crossings that are a signature of strong coupling. Our analytical model also elucidated the correlation between the exciton/plasmon mixing ratio and polariton coupling strength. Using fs-transient absorption spectroscopy, we found that both the upper and lower polaritons have shorter lifetimes than the excitons and that polaritons can show faster excited state dynamics when they have access to additional energy transfer channels.

10:45 AM EQ03.15.03

Plasmon-Exciton-Polaritons from Nanoparticle Lattices Strongly Coupled to Metal–Organic Framework Ligands Alexander D. Sample, Jun Guan, Jingtian Hu, Thaddeus Reese, Charles Cherqui, Jeong-Eun Park, Francisco Freire Fernandez, Richard Schaller, George C. Schatz and Teri W. Odom; Northwestern University, United States

Strong coupling between light and matter has received significant attention for its interesting fundamental properties and diverse applications. Despite the breadth of work done in this field, the systems capable of achieving strong coupling are still relatively limited. To continue to diversify polariton work, new excitonic materials and cavities must be developed. Surface-mounted metal-organic frameworks (MOF) with a porphyrin-based ligand were synthesized on top of Ag nanoparticle lattices. Angle-resolved transmission measurements of the coupled system reveal a lower energy polariton mode with signature avoided crossing at the exciton energy. With modeling, the upper polariton was predicted and estimated to have a Rabi splitting of 110 meV. By changing the refractive index of the solvent in the MOF, the plasmon energy could be tuned and thus the coupling strength could be controlled from the strong to weak regime. Transient absorption spectroscopy showed that the lower polariton decays rapidly at <500 ps scales, but at later times scales, the decay is slowed by energy transfer from the upper polariton. This work highlights MOFs as an effective molecular exciton and plasmonic lattices as an accessible open cavity for strong light-matter coupling.

11:00 AM EQ03.15.04

Nanostructured Isolation Layer for Enhanced III-Nitride Photonics Performance Ganapathi Subramania¹, Nicholas Karl¹, Keshab Sapkota¹, Zachary Meinelt¹, George Wang¹, Igal Brener¹, Elizabeth Delong² and Daniel Feezell²; ¹Sandia National Laboratories, United States; ²The University of New Mexico, United States

Operation in the visible and ultraviolet frequencies are enabled by III-nitride based nanophotonics that are important for many applications like solid-state lighting, lasers, flat optics and quantum information science. A low refractive index interface cladding region between the high refractive index substrate GaN and the active layer enables the confinement of electromagnetic field in the active layer leading to superior performance. While there are some examples in III-nitrides of low threshold lasing in nanowire array geometry photonic crystals [Sci. Rep. **2013**, 3, 2982] achieving simple optical isolation for membrane PhCs, metasurfaces, and VCSEL structures has been a challenge. In silicon photonics, natural oxide (SiO₂) provides such isolation from the substrate and similarly in III-V semiconductors active GaAs region can be isolated from the substrate by oxidizing an Al_xGa_{1-x}As buffer layer with high Al content. The oxidized Al_xGa_{1-x}As has lower refractive index (~ 1.7) than GaAs (3.5). Since GaN and other III-nitrides do not possess naturally low refractive index oxide other approaches are required to address this challenge. A nanoporous layer with an effective low refractive index formed by electrochemical etching in a highly doped layer of GaN shows to be a promising approach [App. Phys. Lett. **2018**, 112, 041109]. Here we will discuss achieving optical substrate isolation in III-nitride nanowire array-based resonators using electrochemically etched nanoporous layer as well as creating an undercut layer below the active layer. Optical reflectance characterization of the nanowire resonators exhibits the emergence of distinct magnetic and electric dipole resonances depending upon the refractive index of the isolation layer which can be used to characterize the refractive index of the isolation layer.

Sandia National Laboratories is managed and operated by NTESS under DOE NNSA contract DE-NA0003525.

11:15 AM EQ03.15.05

Can Organic Conjugated Polymers, Despite Their Broad Excitonic Linewidth, Serve as Materials for Strong Plasmon-Exciton Coupling? Christopher E. Petoukhoff and Deirdre M. O'Carroll; King Abdullah University of Science & Technology (KAUST), Saudi Arabia

Conjugated polymers are organic molecular semiconductors that are unique materials for next-generation thin-film optoelectronic devices. Because of their low dielectric constant, conjugated polymers support highly localized Frenkel excitons, which have binding energies of over a few hundred meV. These Frenkel excitons are particularly interesting for coupling with light because of their stability at room-temperature, imbuing the polymers with large absorption and emission cross-sections. This makes conjugated polymers particularly suitable for flexible photovoltaic and light-emitting devices, and have

potential for exotic physics such as Bose-Einstein condensation and low-threshold lasing of exciton-polaritons.

When considering plasmon-exciton interactions, the strong coupling regime can be achieved when the rate of energy exchange between the plasmon and exciton exceeds the decay rates of the individual oscillators. When this occurs, the two oscillators hybridize to form new light-matter quasiparticles, called plasmon-exciton polaritons, which have two distinct energies separate from the initial oscillators. This is typically observed when the splitting energy between the two polariton modes exceeds the linewidth of the individual oscillators. Therefore, conventionally, it has been assumed that to achieve strong plasmon-exciton coupling, it is necessary to have narrow plasmon and exciton linewidths.

Plasmonic nanostructures have been employed as an architecture for enhancing light-trapping in conjugated polymer-based solar cells, leading to up to 2-fold enhancement in device efficiencies [1]. When incorporating plasmonic nanostructures into conjugated polymer devices, there have previously been signatures of strong light-matter interactions observed, such as strong splitting in the scattered-light spectra [2,3] and enhanced absorption at the red-edge of the polymer's absorption band. But, is it possible for conjugated polymers, with their broad excitonic linewidths, to serve as materials for strong plasmon-exciton coupling?

Here, we explore two systems to investigate the nature of light-matter interactions between surface plasmons and excitons in conjugated polymers: 1) conjugated polymer-coated Ag plasmonic metasurfaces [2,3] and 2) Ag-conjugated polymer core-shell nanoparticles [4]. We employ dark-field scattered light spectroscopy, finite-difference time-domain simulations, and analytical Mie theory calculations to evaluate the spectroscopic nature of plasmon-exciton coupling. We investigate a range of different conjugated polymers, including P3HT, PCDTBT, and PTB7, as well as model conjugated polymer systems based on vibrationally-dressed Lorentzian oscillators, modified by Frank-Condon factors. We show that conjugated polymer-coated Ag plasmonic metasurfaces exhibited a splitting energy of >1700 meV, far exceeding the linewidths of either the plasmonic metasurface or the conjugated polymer. We predict that for Ag-conjugated polymer core-shell nanoparticles, there exist many conditions to achieve strong coupling by varying different parameters of the Lorentzian oscillators. Finally, we demonstrate the application of these strongly coupled plasmon-exciton polaritons to improve the absorption and carrier generation in hybrid organic-2D mixed-dimensional photovoltaics [5].

- 1) C. E. Petoukhoff *et al.*, *J. Photon. Energy* **5:057002** (2015).
- 2) C. T. Nemes, D. K. Vijapurapu, *et al.*, *J. Nanopart. Res.* **15:1801** (2013).
- 3) C. E. Petoukhoff and D. M. O'Carroll, *Nature Commun.* **6:7899** (2015) 1-13.
- 4) C.E. Petoukhoff *et al.*, *Polymers.* **12:2141** (2020) 1-19.
- 5) C.E. Petoukhoff, *et al. ACS Nano.* **10** (2016) 9899-9908.

11:30 AM EQ03.15.06

Understanding the Confinement Factor—Shaping Light to Optimize Optical Gain [Marianne Aellen](#) and David J. Norris; ETH Zurich, Switzerland

Photonic integrated circuits utilize waveguides to route electromagnetic signals. To amplify these signals, a gain material must be included. In this case, design optimization requires the relationship between amplification and waveguide geometry to be understood. The confinement factor links the gain experienced by the guided mode to the geometry-independent amplification strength of the gain material. Several expressions for the confinement factor have appeared in the literature. Unfortunately, not all of these expressions apply to strongly confined waveguide modes, which are desired in miniaturized optical components. Here, we elucidate the most general description of the confinement factor. Further, we clarify which simplifications have led to other formulations. While related to confinement, these are not generally applicable to the determination of the amplification of a guided mode. Using two numerical examples, we demonstrate the validity and limitation of various expressions of the confinement factor. In high-index-contrast or metallic waveguides, it is typically found that the confinement factor exceeds unity. This counter-intuitive result can be explained by a slowdown of the guided light. Only the general expression of the confinement factor can capture this behavior. Our discussion here provides the necessary understanding to correctly employ the confinement factor for optimization of designs in nanophotonics and plasmonics.

SESSION EQ03.16: Fundamental of Plasmonics and Metaphotonics II

Session Chairs: Marianne Aellen and Ortwin Hess

Wednesday Afternoon, November 30, 2022

Sheraton, 2nd Floor, Back Bay C

1:30 PM *EQ03.16.01

Hybrid Quantum Photonics [Vladimir Shalaev](#)^{1,2}; ¹Purdue University, United States; ²National Quantum Information Science Research Center of the U.S. Department of Energy (DOE), United States

We show that plasmonic enhancement and speedup opens up a means to outpace quantum decoherence^{1,2} and discuss new opportunities for SiN quantum photonic circuitry enabled by recently discovered single-photon sources³ in this technologically important platform

References

- A. Senichev, Z. O. Martin, S. Peana, D. Sychev, X. Xu, A. S. Lagutchev, A. Boltasseva, V. M. Shalaev, Room-temperature single-photon emitters in silicon nitride, *Science Advances*, v. 7, Issue 50 (2021); DOI: 10.1126/sciadv.abj0627
- S. I. Bogdanov, O. A. Makarova, X. Xu, Z. O. Martin, A. S. Lagutchev, M. Olinde, D. Shah, S. N. Chowdhury, A. R. Gabidullin, I. A. Ryzhikov, I. A. Rodionov, A. V. Kildishev, S. I. Bozhevolnyi, A. Boltasseva, V. M. Shalaev, and J. B. Khurgin, Ultrafast quantum photonics enabled by coupling plasmonic nanocavities to strongly radiative antennas (supplement), *Optica* v. 7, pp. 463-469 (2020)
- S.I. Bogdanov, A. Boltasseva, and V.M. Shalaev, Overcoming quantum decoherence with plasmonics, *Science*, v. 364, pp. 532-533 (2019); DOI: 10.1126/science.aax3766

2:00 PM EQ03.16.02

Ultrafast Magnetism Enabled by Nanoplasmonics [Alexandre Dmitriev](#); University of Gothenburg, Sweden

The quest to improve the density, speed and energy efficiency of magnetic memory storage has led to the exploration of new ways of optically manipulating magnetism at the ultrafast time scale, in particular in ferrimagnetic alloys. While all-optical magnetization switching is well-established on the femtosecond timescale, lateral nanoscale confinement and thus the potential significant reduction of the size of the magnetic element remains an outstanding challenge. Thus magnetic memory combining plasmonics and magnetism is poised to dramatically increase the bit density and energy

efficiency of light-assisted ultrafast magnetic storage, thanks to nanoplasmon-driven enhancement and confinement of light [1]. I highlight several recent examples from our work, where we employ plasmon nanoantennas to either funnel electromagnetic energy into ferrimagnetic films assisting the demagnetization at the nanoscale [2], or to build hybrid plasmon-ferrimagnet nanoantennas forming magnetophotonic surface crystals [3,4]. The produced robust magnetophotonic architectures could serve as the building blocks for plasmon-assisted all-optical magnetization switching technology in ferrimagnetic rare earth – transition metal alloys that are the prime candidates to realize in practice femtomagnetic memory storage. In addition, the produced platforms could help realizing the conceptually new high-resolution light incidence direction sensors or systems with multistate ultrafast demagnetization states, potentially opening up for so-far-unforeseen nanomagnetic neuromorphic-like devices operating at femtosecond timescales controlled by light.

[1] N. Maccaferri et al., Nanoscale magnetophotonics, *J. Appl. Phys.*, 127, 080903 (2020).

[2] K. Mishra et al., Ultrafast demagnetization in a ferrimagnet under electromagnetic field funneling, *Nanoscale* 13, 19367 (2021) (journal cover).

[3] R. M. Rowan-Robinson et al., Direction-sensitive magnetophotonic surface crystals, *Adv. Photon. Research* 2100119 (2021) (journal cover).

[4] K. Mishra et al., Ultrafast Demagnetization Control in Magnetophotonic Surface Crystals, *under review* (2022).

2:15 PM EQ03.16.03

Synthesis of Chiral Plasmonic Gold Nanoplates with Broad Chiroptical Activity Eunjeong Jo, Sang Won Im and Ki Tae Nam; Seoul National University, Korea (the Republic of)

Plasmonic chiral nanostructure provides a novel route for extraordinary optical properties such as negative refractive index and light polarization control, and has drawn significant attention in various fields. The symmetry of chiral nanostructures such as helix, gyroid, and the irregular tetrahedron is deeply correlated to chiroptical responses and thus represents an important design parameter. Recently, we demonstrated a new pathway for facile synthesis of the chiral plasmonic nanoparticle by controlling the symmetry of gold nanoparticles utilizing enantioselective interactions on surface kink sites. Particularly, 432 symmetric helicoid nanoparticles were synthesized by breaking the mirror symmetry in single crystalline gold nanoparticles with 4/m 3 2/m symmetry. Here, we aimed to extend further the chiral symmetry of gold nanoparticles and their chiroptical properties. The symmetry of gold nanoparticles can be modulated from that of crystal lattice by inducing single or multiple twin planes in seed nanoparticles. We successfully synthesized chiral gold nanoplates with 3-fold symmetry by using triangular and hexagonal seed nanoplates with 3 2/m symmetry. Chiral gold nanoplates have great significance as they show optical activity in a wide range, from vis to NIR region. This approach provides insight into the changes in optical properties of the gold particles depending on symmetry and can be extended to a material platform for developing next-generation telecommunications and optical devices such as sensors and lidars.

2:30 PM BREAK

SESSION EQ03.17: Plasmonic Applications II
Session Chairs: Seunghoon Han and Jason Valentine
Wednesday Afternoon, November 30, 2022
Sheraton, 2nd Floor, Back Bay C

3:30 PM DISCUSSION TIME

4:00 PM EQ03.17.02

Scalable, Angle-Insensitive Structural Color Printing Using Refractory Metals for High-Temperature Applications Margaret A. Duncan¹, Landin Barney², Mariama Rebello Sousa Dias² and Marina S. Leite¹; ¹University of California, Davis, United States; ²University of Richmond, United States

Structural color systems are growing in popularity due to their myriad of applications ranging from sensing to selective absorption. However, typical structural color devices require nanopatterning, which is difficult to scale up and can have negative environmental effects, or complicated many-layer geometries, which require multiple fabrication steps to achieve their vivid coloration. We utilize the oxidation of several sputtered refractory metal thin films at high temperatures (600°C) to produce four unique three-layer Fabry-Perot-type resonators which each offer vibrant colors with only two fabrication steps: MoO₃/Mo/Si (Purple), RuO₂/Ru/Si (Pink), Ta₂O₅/Ta/Si (Yellow), and WO₃/W/Si (Teal). These optical devices have the added benefit of being thermodynamically stable up to 700°C in an inert environment, making them ideal for high-temperature structural color applications. We heat these samples utilizing *in situ* ellipsometry, allowing very precise control over the thickness of the oxide layers *via* real-time sample characterization during high-temperature oxidation. In addition, we simulate the expected absorption spectra for different thicknesses of the two thin-film layers to determine the full range of colors each material combination can produce, showing that a wide area of the color gamut is accessible for these samples utilizing layer thicknesses of 10 – 100 nm. A detailed and quantitative analysis of the optical response of all refractory metals and their respective oxides will be presented. Our approach of using metals and dielectrics based on refractory metals offers a promising new avenue for structural color fabrication, requiring a single sputtering fabrication step that enable vibrant colors across a large portion of the color gamut.

4:15 PM EQ03.17.03

K-Space Hyperspectral Imaging of Photonic Devices and Metasurfaces by a Birefringent Common-Path Interferometer Armando Genco¹, Cristina Cruciano¹, Matteo Corti¹, Kirsty McGhee², Benedetto Ardini¹, Luca Sortino³, Ludwig Hüttenhofer³, tersilla virgili^{1,4}, David Lidzey², Stefan A. Maier^{3,5,6}, Andrea Bassi¹, Gianluca Valentini¹, Giulio Cerullo¹ and Cristian Manzoni^{1,4}; ¹Politecnico di Milano, Italy; ²The University of Sheffield, United Kingdom; ³Ludwig-Maximilians-Universität München, Germany; ⁴CNR, Istituto di Fotonica e Nanotecnologie, Italy; ⁵Monash University, Australia; ⁶Imperial College London, United Kingdom

Optical microcavities and metasurfaces feature distinctive polarization-dependent energy-momentum dispersions, whose determination is crucial for a broad range of fundamental studies and applications. Planar microcavities confine photons in resonant optical modes, created as a consequence of the out-of-plane constructive interference condition for electromagnetic (EM) waves travelling through the cavity, with a resonant wavelength strictly dependent on the viewing angle. More recently, high refractive index semiconductor nanoresonators have shown optical Mie-resonances in the form of interference of electric and magnetic multipoles, such as the non-radiative anapole excitation, which can also lead to high light confinement within the resonator. Fourier-plane microscopy is a powerful tool for measuring the angular optical response of such devices. The information about the energy-momentum dispersion of such samples can be accessed by exploiting the propagation properties of the EM field through a lens. In fact, when an object is placed in the focus of a lens, the spatial Fourier transform of its field is formed at the lens back focal plane. The momentum space (or k-space) intensity profile can therefore be obtained by imaging a microscope objective back-focal plane on a two-dimensional detector, instead of the object plane. This imaging technique is able to

provide good angular resolution over a wide field of view, but typically losing the spectral information, since it integrates the light intensity over a broad wavelength range. The measurement of the spectrum for each point of the k-space can be then carried out upon insertion of a dispersive spectrometer in the imaging system and using a scanning lens, spanning through the angular field-of-view. However, the intrinsically high losses introduced by the spatial filtering and the dispersive elements impose tedious and alignment-sensitive scans.

In this work, we combine the concept of Fourier-transform hyperspectral imaging, which provides simultaneously a spectrum of the transmitted/reflected/emitted light for each pixel of the image, with k-space microscopy. To this aim, we exploit a common-path birefringent interferometer, placed in the detection path of our microscope, which generates two delayed replicas, whose interference pattern is measured as a function of their delay. The Fourier Transform of the resulting interferogram yields the intensity spectrum as a function of the wavelength for each point of a wide angular field-of-view. Using our technique, we obtain a complete angle- and wavelength-resolved analysis of the samples in just one measurement, with a high throughput. We optimized the technique to get an angular resolution of 0.3° , while ensuring a spectral resolution of less than 0.1 nm in terms of peak shift and 3 THz (4 nm at $\lambda=635\text{nm}$) in terms of peak broadening. In order to demonstrate the capabilities of our technique, we measured the energy-momentum dispersion of complex nanostructured devices. We reconstructed a full 3D map of the dispersion of an organic planar microcavity in the energy-momenta space, clearly evidencing also the polarization dependent behaviour of the resonant cavity modes, owing to the polarizing elements present in the interferometer. Furthermore, we apply our technique for the characterization of a dielectric nanostructured metasurface consisting of an array of GaP nanodisks, revealing an anapole mode with unusual polarization-dependent angular and spectral behaviour. The angular dependence observed for different polarizations is in very good agreement with the results of finite differences time domain simulations. Our approach provides a complete optical characterization of materials and devices with complex angle/wavelength-dependent properties, fundamental for future developments in the fields of topological photonics and optical metamaterials.

4:30 PM *EQ03.17.04

Rapid Bacterial Identification and Antibiotic Susceptibility Testing Using Raman Spectroscopy and Machine Learning Loza Tadesse^{1,2,3}, Chi-Sing Ho³, Baba Ogunlade³, Chris Cundy³, Ahmed Shuaibi^{4,3}, Fareeha Safir³, Pierre Khuri-Yakub³, Stefanie S. Jeffrey³, Stefano Ermon³, Amr Essawi^{5,3} and Jennifer A. Dionne³; ¹UC Berkeley, United States; ²Massachusetts Institute of Technology, United States; ³Stanford University, United States; ⁴Princeton University, United States; ⁵Cairo University, Egypt

Bacterial bloodstream infections account for over 40% of death in hospitals and are one of the most expensive medical conditions in the US. Current diagnostic methods are slow and costly, due to the long bacterial culturing step. Our work utilized Raman spectroscopy for rapid culture-free, sensitive, and specific bacterial identification and antibiotic susceptibility testing. Here, I will present three major milestones that bring Raman closer to clinical application by using machine learning and nanophotonics. First, we achieve high (>99%) species level classification accuracies across 30 major disease-causing bacterial species. Second, we showcase the first of its kind demonstration of a versatile and antibiotic co-incubation free susceptibility testing. Third, we develop a simple liquid well setup for clinical sample handling with uniform Raman spectral enhancement using gold nanorods. Overall, our work opens the door for clinical translation of novel spectroscopy based diagnostic tools for identifying bacterial infections, viral infections such as COVID-19 virus, early cancer detection and drug susceptibility testing by merging machine learning and nanophotonics.

SESSION EQ03.18: Poster Session III
Session Chairs: Po-Chun Hsu and Yu-Jung Lu
Wednesday Afternoon, November 30, 2022
8:00 PM - 10:00 PM
Hynes, Level 1, Hall A

EQ03.18.01

Suppressing Charge Recombination in Photoelectrochemical Cells from Plasmon-Induced Resonance Energy Transfer Young Moon Choi and Jong Hyeok Park; Yonsei University, Korea (the Republic of)

The application of n-type metal-oxide based photoelectrode, such as hematite ($\alpha\text{-Fe}_2\text{O}_3$) and bismuth vanadate (BiVO_4), for the photoelectrochemical (PEC) water splitting has been regarded as a promising approach for clean H_2 production because of their earth abundance and high stability in an aqueous electrolyte. However, their too short hole diffusion length, poor electrical conductance, and inferior oxygen evolution reaction (OER) kinetics deteriorate the PEC response, which limits to reach the theoretical maximum PEC water splitting performance.

In this work, we introduced a 2D nanoamplifier metal film composed of an assembled globular Au nanosphere (AuNS) array with a highly ordered hexagonal pattern (hereafter, Au array) onto the surface of $\alpha\text{-Fe}_2\text{O}_3$ film to enhance the PEC water oxidation through the plasmon-induced resonance energy transfer (PIRET). The Au array is self-assembled on the hexagonally patterned polyurethaneacrylate (PUA) pillar molds and transfer-printed on the surface of the photoanode. The Au array induced the near-field coupling interaction and amplified the electromagnetic field, thus promoting plasmonic energy transfer into the underneath film, resulting in efficient light harvesting in a broadband light spectrum and suppression of charge recombination, which increases the carrier lifetime. The long-lived photogenerated holes at the surface of photoanode were demonstrated from the transient absorption (TA) decay profile. Enhanced charge transfer efficiency was also investigated. Furthermore, the Au array was introduced on the surface of molybdenum-doped BiVO_4 film to demonstrate the high versatility of facile transfer printing Au arrays. Consequently, the transfer-printed Au array resulted in an efficient PIRET effect on both $\alpha\text{-Fe}_2\text{O}_3$ and BiVO_4 films. An over 3.3-fold higher photocurrent density at 1.23 V versus reversible hydrogen electrode (RHE) was achieved for the Au array-incorporated $\alpha\text{-Fe}_2\text{O}_3$ film. As for BiVO_4 , Au array improved the photocurrent density by 1.5-fold more than bare photoanode.

In conclusion, we introduced a 2D arranged Au array in a highly ordered hexagonal pattern onto the surface of $\alpha\text{-Fe}_2\text{O}_3$ and BiVO_4 films via a facile transfer printing process and confirmed the enhanced PEC response through the PIRET effect. The rationally designed Au array film can provide a potential strategy for the versatile application in various light-mediated energy conversion and optoelectronic devices.

EQ03.18.02

Performance Analysis of Materials for Plasmonic Computing Samantha Lubaba Noor¹, Dennis Lin², Pol Van Dorpe², Francky Cathoor² and Azad Naeemi¹; ¹Georgia Institute of Technology, United States; ²imec, Belgium

Plasmonic metal-insulator-metal (MIM) slot waveguide (WG), a promising building block of the plasmonic integrated circuits, has been heavily utilized to explore and demonstrate devices like logic gates, modulators, power splitters, frequency filters, and multiplexers. For the MIM slot WG, the choice of material is critical since it primarily controls the degree of signal attenuation and the extent of confinement of the supported modes. A trade-off always exists between the signal attenuation and mode confinement in plasmonic WGs that define the energy consumption and integration density of the

components, respectively. Therefore, a systematic analysis of the possible material combinations is essential for the MIM WG to optimize the performance of the plasmonic devices. This work presents a comprehensive numerical analysis of the possible material combinations of the plasmonic MIM WG for computation purpose. To demonstrate the material effect on computing related context, the analysis incorporates plasmonic MIM interconnect and MIM majority logic gate as use cases. The potential material combinations are initially selected from material quality factor and CMOS compatibility. For each selected material combinations, the confinement factor, propagation length, and coupling length are calculated for the WG. Also, using the coupling length and power transfer data between two nearby WGs, the WG pitch is optimized considering the trade-off between crosstalk and footprint/integration density of the devices. The manipulated plasmon signal in the MIM WG needs to be converted into current/voltage using a detector for readout purposes. Therefore, the effect of material selection on plasmon detection efficiency is next studied by introducing a Ge-based plasmonic metal-semiconductor-metal (MSM) WG as a plasmon detector. For each material case, the MIM WG width is optimized to match the characteristics impedance of the two WG sections resulting in maximum power transmission. Based on various trade-offs, a system-level holistic performance metric, Emin/bit or minimum required energy to detect a single bit sent from the MIM interconnect/logic gate, is introduced, and compared for all the material combinations. This holistic metric encompasses the effect of signal attenuation, mode confinement, WG coupling efficiency, plasmon detection efficiency, and detection bandwidth. Moreover, signal to noise ratio (SNR) and footprint of the devices are calculated. Lastly, considering the trade-off between Emin/bit, SNR and footprint, the optimized material combination is identified. The study shows that Al and Cu are promising metals for MIM WGs for computing. Regarding dielectrics, SiO₂ offers a low Emin/bit value and large device area, whereas a high-k dielectric material like Si offers a more compact layout at the cost of a higher energy per bit. It is found that Cu-TiO₂-Cu and Al-Al₂O₃-Al are the two optimum material combinations for MIM WG for plasmonic computing circuits.

EQ03.18.03

A Facile Method for Selective Deposition of Metal Nanoparticles into Nanohole Arrays for Recyclable Plasmonic Sensors Pooria Golvari¹, Stephen M. Kuebler^{1,1,1} and Jimmy Touma²; ¹University of Central Florida, United States; ²AFRL/Munitions Eglin AFB, United States

Plasmonic nano-arrays are extensively studied as ultrasensitive vapor sensors [1, 2]. Tunable processes for selective deposition of plasmonic nanoparticles in arrays of host nanoholes are desired for fabrication of next-generation plasmonic devices and sensors. Reported techniques [3, 4] for deposition of gold nanoparticles (AuNPs) into prepatterned nanoholes yield low filling density and are limited to holes created in polymeric substrates which are known to be labile and subject to swelling. We report a method for selective deposition of gold nanoparticles (AuNPs) into nanoholes fabricated in fused silica (FS). Arrays of nanoholes with variable hole size and density are created in the positive resist PMMA by e-beam lithography and transferred into fused silica using cyclic reactive ion etching. The nanoholes are filled with AuNPs using evaporative deposition followed by mechanical rubbing. This simple yet effective approach yields highly selective deposition of AuNPs in nanoholes as small as 150 nm. The effect of the chemical termination of the substrate, the concentration of the AuNPs suspension, and the size and the pitch distance of the nanoholes on the density of AuNPs in the holes was investigated. This approach is being extended to other plasmonic nanoparticles and a variety of substrates. We also demonstrate that the AuNPs can be etched away to reproduce the nanohole array in FS, which can be refilled with fresh nanoparticles. Hence, this method paves the way for recyclable plasmonic sensors that can be regenerated after exposure to analyte.

1. Jiang, J., et al., *Plasmonic nano-arrays for ultrasensitive bio-sensing*. Nanophotonics, 2018. 7(9): p. 1517-1531.
2. Wang, Q. and L. Wang, *Lab-on-fiber: plasmonic nano-arrays for sensing*. Nanoscale, 2020. 12(14): p. 7485-7499.
3. Morakinyo, M.K. and S.B. Rananavare. *Positional control over nanoparticle deposition into nanoholes*. in *11th IEEE International Conference on Nanotechnology*. 2011. IEEE.
4. Morakinyo, M.K. and S.B. Rananavare, *Reducing the effects of shot noise using nanoparticles*. Journal of Materials Chemistry C, 2015. 3(5): p. 955-959.

EQ03.18.07

Gold-Copper Oxide Core-Shell Plasmonic Nanoparticles Rosemary L. Calabro^{1,2}, Stephen F. Bartolucci², John Burpo^{1,1} and Joshua A. Maurer²; ¹United States Military Academy, United States; ²U.S. Army DEVCOM Armaments Center, United States

Noble metal nanoparticles exhibit localized surface plasmon resonance (LSPR) when interacting with light. This property has led to the study of these particles for numerous applications, such as catalysis, energy, biosensing, gas detection, and chemical sensing. One commonly used material in hydrogen sensing is palladium, which can dissociate hydrogen gas and form a hydride, resulting in a shift of the LSPR absorption. Core-shell nanoparticles consisting of a noble metal core and a shell material, such as a transition metal oxide, could provide a material system for hydrogen detection with a more permanent plasmonic shift during exposure to hydrogen compared to palladium. In this work, we show the synthesis of various noble metal core-shell nanoparticles, including gold-copper (I) oxide with spherical, rod, spiked, and bipyramid structures and evaluate their plasmonic behavior and ability to detect hydrogen in colloidal suspensions. In addition, we will discuss the plasmonic properties of these particles and hydrogen sensing ability on various substrates, such as metals.

EQ03.18.08

Seed Mediated Growth of Oxidation Resistant Copper Nanoparticles with Optical Properties Rosemary L. Calabro^{1,2}, John Burpo^{1,1}, Stephen F. Bartolucci² and Joshua A. Maurer²; ¹United States Military Academy, United States; ²U.S. Army DEVCOM Armaments Center, United States

Metal nanoparticles (NPs) exhibit localized surface plasmonic resonance (LSPR) allowing them to span broad applications including energy, catalysis, biomedicine and sensing, and their optical properties can be tuned by changing the size, shape and surrounding environment of the nanoparticles to achieve a LSPR suitable for the desired application. Copper has a low cost, high conductivity, tunable optical properties, and reported LSPR which make copper nanoparticles (CuNPs) an interesting alternative over other noble metal plasmonics. However, the extinction properties of copper nanostructures can be influenced by both interband and intraband transitions, so a deep understanding of the optical properties is required. Copper also suffers drawbacks such as instability and susceptibility to surface oxidation which can further impact the optical properties of the CuNPs. Copper nanoparticles ranging in size from 20-60 nm were synthesized through a seed mediated growth in tetrahydrofuran using polyvinylpyrrolidone (PVP) as a stabilizing agent. Various average molecular weights of PVP were explored and showed influence on both the optical properties and overall shape and size of the resultant NPs where lower molecular weights of PVP resulted in broader spectra and polydisperse particles while higher molecular weights presented narrower spectra with lower polydispersity. The size of the particles could be tuned by changing the PVP amount and by adding acetic acid to the reaction media. Wide angle x-ray scattering measurements show that the particles consist of Cu metal and that no oxide species were present. The particles remained stable in solution for over a month with no shift to the optical properties over time and were resistant to oxidation after addition of water or hydrogen peroxide, or after heating in air. By examining the extinction and true absorbance measurements we determined that all samples had a true absorption peak due to interband transitions at around 590 nm and peaks observed at longer wavelengths were due to scattering effects. The crystallinity and size of these CuNPs was further studied by transmission electron microscopy (TEM) and small angle x-ray scattering (SAXS). Future work will expand on the synthesis strategy to better tune the shape of the copper NPs and we aim to apply this synthesis strategy to prepare other plasmonic metal nanostructures with controlled sizes and optical properties.

EQ03.18.09

Non-Polar GaN Micro-Crystal Array for High-Efficiency Light-Emitting Diodes [Minjoo Kim](#) and Won Il Park; Hanyang University, Korea (the Republic of)

GaN-based micro light-emitting diodes (μ -LEDs) have been considered next-generation displays, given the stable operation for a long time and red, green, and blue light emissions through control of the GaN/InGaN structure and composition. However, GaN nano/micro rod crystals grown in the *c*-axis ([0001]) direction have physical limitations in luminous efficiency due to spontaneous and piezoelectric polarizations. In this work, we employed the epitaxial growth of non-polar GaN nano/micro crystals in the *m*-axis ([1-100]) direction. The key to the vertically exposed *m*-axis GaN relies on the precise rearrangement of the ZnO crystals via shear force. We confirmed that most ZnO crystals over a cm-scale wafer were uniformly re-aligned along the shearing direction. Then, the growth of non-polar GaN crystals and subsequent epi-growth (InGaN/GaN MQW, p-type GaN) were performed in turn. Optical and electroluminescence characterizations showed the enhanced luminous efficiency compared with polar crystals, suggesting that our approach can overcome the performance limitations of *c*-GaN crystals.

EQ03.18.10

Preparation of Metallic Tungsten Oxide Nanoparticles for Visible Upconversion Emission Enhancement [Yuta Osa](#), Mahito Yamamoto and Mitsuru Inada; Kansai University, Japan

It is well known that localized surface plasmon resonance (LSPR) enhances fluorescence from adjacent luminescent materials. This LSPR effect is also effective for infrared (IR) to visible light upconversion emission. Gold and silver nanoparticles are typical nanoparticles with LSPR, but they are not the suitable materials for visible upconversion emission because they absorb visible light. Transition metal oxides are usually transparent in the visible light region but they are insulators. However, they can form metallic phases due to the presence of oxygen defects. In fact, tungsten oxide WO_{3-x} is known to form a metallic phase at $x=0.3$. Therefore, metallic tungsten oxide nanoparticles are one of the candidates for materials to gain upconversion luminescence in the visible range.

In this study, we have prepared metal tungsten oxide nanoparticles with LSPR in the infrared region by sputtering method. Atomic force microscopy revealed that the diameter of these nanoparticles was approximately 50 nm. Hall measurements showed that the nanoparticles were metallic with a carrier density of $5.9 \times 10^{22} \text{ cm}^{-3}$ at room temperature. X-ray diffraction measurements showed that the nanoparticles were crystalline. The nanoparticles had a peak in optical absorption by LSPR at around 960 nm. These results indicate that metallic tungsten oxide nanoparticles have the potential to enhance the upconversion emission from IR to visible light in Er^{3+} doped glass ceramics. Details of upconversion enhancement using LSPR of metal tungsten oxide nanoparticles will be presented and discussed at the meeting.

EQ03.18.12

Efficient and Selective Photocatalytic Conversion of Methanol Using Porous Au-WO₃ and Visible Light [Robert B. Tracy](#) and Christopher C. Landry; University of Vermont, United States

Volatile organic compounds (VOCs) are common pollutants found in indoor and outdoor air. An efficient removal process for high-concentration VOCs can be a challenging task, having a new elimination process would be a crucial development. In the past, we have developed a continuous flow gas-phase reactor to monitor the visible light photocatalytic oxidation of methanol with porous WO_3 and Au loaded WO_3 . Porous WO_3 had a much higher activity than commercial WO_3 and doping with Au improved upon that activity in both samples. In the present studies, we focus on changing the reaction conditions, specifically the concentration of methanol and oxygen to improve upon the visible light photoactivity of porous WO_3 based materials. The change in conditions also have shown to have a major impact on the reaction intermediates and photooxidation pathways on the photocatalytic oxidation of methanol. The continuous flow gas phase reactor was hooked up to a GC-MS which used to monitor the photooxidation process of methanol. EPR and XRD was used to determine the phase of WO_3 . The Lewis acidity of the materials were monitored with the use of TPD. Finally, Nitrogen physisorption was used to monitor the porosity of the materials.

EQ03.18.13

A Surface-Plasmon Enhanced Mid-Infrared Lab-on-a-Chip for Real-Time Reaction Monitoring of Liquids [Borislav Hinkov](#)¹, Florian Pilot¹, Mauro David¹, Andreas Schwaighofer¹, Patricia L. Souza^{1,2}, Benedikt Schwarz¹, Daniela Ristanic¹, Elena Arigliani¹, Laurin Lux¹, Dominik Wacht¹, Felix Frank¹, Hermann Detz^{1,3}, Aaron M. Andrews¹, Bernhard Lendl¹ and Gottfried Strasser¹; ¹TU Wien, Austria; ²Pontificia Universidade Católica do Rio de Janeiro, Brazil; ³Brno University of Technology, Czechia

The mid-infrared (mid-IR) spectral range is highly suitable for selective and sensitive probing of molecules by addressing their fundamental fingerprint absorptions. While high performance gas sensing has already been demonstrated in many different experiments including frequency-comb based techniques and exploiting concepts from direct absorption spectroscopy to photo-acoustics and dispersion spectroscopy, the mid-IR analysis of liquids is still in its infancy. Though recently gaining particular interest, it is still in main parts limited to bulky detection systems like Fourier-Transform Interferometer (FTIR)-based sensors, demanding for liquid films on the order of a few micrometers only. This often results in time-consuming offline analytics, preventing real-time analysis of rapidly changing liquid systems like when undergoing chemical reactions or conformational changes of molecules in the sample.

For enabling the next generation of liquid sensing by going beyond such limitations, we present in this work a novel high-performance monolithic mid-IR sensor. It relies on pioneering quantum cascade (QC) technology by merging a similar wavelength QC laser (QCL) and QC detector (QCD) into one active region and combining it with a novel mid-IR plasmonic concept. Using a surface-sensitive dielectric-loaded surface plasmon polariton (DLSPP) structure, which consists of a SiN-slab on a gold layer, results in a fingertip-sized optical sensor, highly suitable for the monitoring of liquids. In contrast to state-of-the-art systems, its robustness and compactness allow the real-time analysis of dynamical processes in liquids including inline and in-situ measurements by direct exposure to the liquid. In our DLSPP approach, the plasmonic mode propagates along the sample surface, being efficiently guided by more than 95% in the surrounding medium. Our presented FEM-based simulations confirm the preservation of the plasmonic capabilities also in a liquid matrix.

We demonstrate the breakthrough performance of the plasmonic concept implemented into the sensor in an analytical chemistry experiment. We measure the time-dependent conformational changes of the model-protein bovine serum albumin (BSA) with our compact on-chip sensor. Time-resolved measurements are performed by combination of the device with a custom-made 60- μl flow cell for inline measurements at $\lambda = 1620 \text{ cm}^{-1}$. We use a D_2O matrix for reduced background absorption, while maintaining comparable protein unfolding results as in biophysical buffer, i.e. H_2O . BSA unfolds irreversibly from α -helix to antiparallel β -sheets when heated from 20°C to 90°C. In our experiments we obtain the typical protein denaturation curves, following a sigmoidal Boltzmann equation ("s-shaped") with increasing temperature. In good agreement with literature, we observe a decreasing transition temperature with increasing BSA-concentration, confirming the proper operation of our compact sensor. By additionally directly submerging the sensor into a beaker with the protein-analyte and monitoring its absorbance vs concentration curve (calibration line) for increasing BSA concentrations, we can extract the important figures-of-merit of our on-chip device. A comparison with a state-of-the-art attenuated total reflection (ATR-)FTIR reference system reveals the superior performance of our ultra-compact sensor with: 55-times higher absorbance, 120 times lower LOD ($\text{LOD}_{\text{QCLD}} \sim 75 \text{ ppm}$) and coverage

of more than three order of concentrations of 0.0075 % to 9.23 %.

In the second part of this paper, we will show how the plasmonic surface of our sensor can be further enhanced through functionalization. By depositing compatible mesoporous membranes based on ZrO_2 or TiO_2 , molecules can be trapped close to the sample surface. This yields a significant increase in sensitivity by molecule enrichment factors well above 100 (e.g. 162 in a typical setting using a ZrO_2 membrane).

EQ03.18.14

Nickel-Infused Nanoporous Alumina as Tunable Solar Absorber for Desalination [Xuanjie Wang](#) and Shankar Narayan, Rensselaer Polytechnic Institute, United States

Solar energy can alleviate our dependence on traditional energy sources like coal and petroleum. In this regard, the design and performance of solar absorbers are crucial for capturing energy from sunlight. Specifically, for applications relying on solar-thermal energy conversion, it is desirable to construct solar absorbers using scalable techniques that also allow a variation in optical properties. In this study, we demonstrate the ability to tune the spectral absorbance of nickel-infused nanoporous alumina using a scalable and inexpensive fabrication procedure. With simple variations in the geometry of the nanostructures, we enable broadband absorption with a net solar absorbance of 0.96 and thermal emittance of 0.98 and spectrally-selective absorption with a net solar absorbance of 0.83 and thermal emittance of 0.22. We demonstrate a scalable approach involving the use of wicking materials interfaced with the spectrally-selective absorber for the desalination of saline water to get 73% of overall efficiency using a solar flux of one sun. This demonstration of an inexpensive strategy for producing clean water can potentially transform the field of solar-thermal desalination to address the rising demand for water. The simple manufacturing techniques presented in this study to generate nanoengineered surfaces can lead to further advancements in solar absorbers with well-controlled and application-specific optical properties.

EQ03.18.15

Excitonic Properties of sp^3 -Doped (6,5) Single-Walled Carbon Nanotubes as a Single Photon Emitter [Kasidet Jing Trerayapiwat](#)¹, [Diego Barrutia](#)², [Xuedan Ma](#)^{3,4} and [Sahar Sharifzadeh](#)^{1,1}; ¹Boston University, United States; ²Dartmouth College, United States; ³Argonne National Laboratory, United States; ⁴The University of Chicago, United States

Single-walled carbon nanotubes (SWCNTs) doped with sp^3 defects are a promising class of optoelectronic materials with bright tunable photoluminescence and demonstrated single-photon emission (SPE). Experimental and theoretical studies on sp^3 -defective (6,5) SWCNT performed by us suggest that the introduction of the defect leads to presence of a localized unpaired electron around the sp^3 defect site and an in-gap dispersionless state. Here, we study the low-energy excitations associated with this defect state in order to better understand the role of sp^3 defects in SPE. Many-body perturbation theory within the GW/BSE approximation predicts strong excitonic effects with an exciton binding energy of ~ 1 eV for both the pristine and defective (6,5) SWCNT. Additionally, GW/BSE, as well as hybrid time-dependent density functional theory, indicate that the exciton in the enhanced photoluminescence state is a linear combination of the pristine-like transition and that involving the in-gap defect state. Lastly, we present studies of carrier-phonon scattering as a cause of exciton dephasing in sp^3 -defective (6,5) SWCNT by considering electron-phonon and hole-phonon interactions using the independent boson model.

The authors acknowledge financial support from NSF DMR-19005990.

EQ03.18.16

Bright and Highly Uniform, Pure, Indistinguishable, Spatially-Ordered Single Quantum Dot Emitters—Molecular Beam Epitaxial Growth and Structural Characterization [Lucas Jordao](#)¹, [Jiefei Zhang](#)¹, [Qi Huang](#)¹, [Swarnabha Chattaraj](#)¹, [Siyuan Lu](#)² and [Anupam Madhukar](#)¹; ¹University of Southern California, United States; ²IBM T.J. Watson Research Center, United States

A significant step forward in the long-sought goal of on-chip quantum optical circuits is the development of spatially-ordered and spectrally highly uniform and pure single photon emitters provided by a unique class of shape and size controlled single quantum dots, dubbed mesa-top single quantum dots (MTSQDs [1,2]). Quantum dots are the only known solid-state on-demand single photon emitters that have been shown to intrinsically exceed all required quantitative figures-of-merit known for realizing on-chip networks aimed at linear optical quantum computing (LOQC), secure high-capacity quantum communication, and multi-photon entangled states as a basic quantum resource for quantum information processing. The realization of spatially-ordered scalable arrays of MTSQDs while maintaining individual QD characteristics above the threshold [1,4] has thus paved the way for the fabrication and study of quantum optical networks. In this talk we report on (i) the molecular beam epitaxial growth of these remarkable MTSQDs based on the underlying physics of the substrate-encoded size-reducing epitaxy (SESRE) on patterned substrates with judiciously chosen scalable nanomesa arrays, and (ii) their structural and compositional character as determined by scanning transmission electron microscopy (STEM) [4]. The demonstrated uniformity and reproducibility of the SPS characteristics is, for the first time, shown to arise from the unprecedented control on shape, size, and composition of the individual quantum dots across the arrays. Equally significant, such quality is controlled from run-to-run when guided by RHEED-based machine condition transfer function as we demonstrate here.

The SESRE approach enables the formation of single quantum dots of controlled shape and size on mesa-tops for both lattice matched (GaAs/AlGaAs) and lattice mismatched (InGaAs/AlGaAs) material systems. Results of STEM studies provide (i) evolution of the growth front profile through the stages of as-patterned nanomesa size-reduction, deposition of the SQD, and continued growth of the morphology planarizing overlayer; (ii) evidence for the unprecedented control over size and shape uniformity of epitaxial QDs underpinning the spectral uniformity emission (<3 nm) across the arrays [1,4]; (iii) control of SQD lateral positions to an accuracy of <10 nm. The planarization of the MTSQDs [3] makes them naturally suitable for horizontal on-chip integration with light manipulating units (cavity, waveguide, directional coupler) using either standard monolithic integration or hybrid integration with silicon photonics. The MTSQD arrays thus pave the way as a unique platform of quantum emitters for realizing the long-sought on-chip QOCs.

The work is supported by the US Army Research Office (W911NF1910025) and the Air Force Office of Scientific Research (FA9550-17-1-0353).

[1] J. Zhang, arXiv:2108.01428 (2021).

[2] J. Zhang et al., Jour. App. Phys. **120**, 243103 (2016)

[3] J. Zhang, et al., APL photonics **5**, 116106 (2020)

[4] J. Zhang et al. [Under Review]

EQ03.18.17

Study of Far-Field Radiation Pattern in Nano-Photonic Devices and Its Application in Single Small Particle Detection [Abbas Ghaffariefhani](#) and Robert Riehn; North Carolina State University, United States

The optical properties of zero-mode waveguides (ZMW) in metal films has been studied extensively. Here, we investigate the far-field radiation pattern of two zero-mode waveguides surrounded by circular corrugations. We monitor the direction and intensity variation of the transmitted light of the sub-wavelength apertures in the back-focal plane of the microscope objective. Any phase contrast between two holes results in a deflection in the direction or

intensity distribution of light in far-field pattern. We introduce a refractive index contrast between two ZMWs by anchoring a quantum dot within of one of them, which results in a phase difference between holes. Introduction of a phase difference can also be achieved by fabricating two asymmetric ZMWs. We show that in both cases the induced phase variation between two holes lead to a deflection in the far-field diffraction pattern. We find that the complex pattern of the transmitted light can be quantified through a scalar measure of asymmetry along the symmetry axis of the aperture pair. We also demonstrate that asymmetry parameters increase can be controlled by the number of circular rings surrounding ZMWs. Finally, we perform a series of Finite-Difference Time-Domain (FDTD) computational study to propose a new design of double-ZMWs sensors that can be used for small particle detection with higher sensitivity and also applicable to control the direction of the light.

EQ03.18.18

Hybrid Fabrication of High Quality Titanium Nitride Nanostructures for Plasmonic Applications Spyridon Kassavetis, Stavros Panos, Despina Tselekidou, Evi Rabota, Nikolaos Pliatsikas and Panos Patsalas; Aristotle University of Thessaloniki, Greece

Nanomaterials for plasmonic devices have attracted enormous and multidisciplinary interest and efforts over the last decade. However there are few examples of plasmonic devices mainly due to materials issues, since gold and silver, the “traditional” plasmonic materials, show limited tunability of their plasmonic response across the spectra and low melting point, which makes them incompatible with CMOS technology. Transition metals nitrides (TMN) emerge as alternative plasmonic nanomaterials suitable for a wide range of applications from microelectronics to photonics and medicine. The TMN are conductive ceramics with exceptional properties such as substantial electronic conductivity, high melting point (>3000 K), tunable work function, while the TMNs are particularly stable in hostile chemical environments, high temperature, and strong electric fields, such as in lasers. Among them, titanium nitride (TiN) is recently emerging as significant candidate material for plasmonic applications (biosensors, catalysis and photochemistry, solar energy harvesting, photo-detection, and optical storage of information). In this work, we focus on the hybrid fabrication of TiN nanostructures with controlled spacing and tunable dimensions (thickness and lateral dimensions) using a combination of Nanosphere Lithography (NSL) and reactive magnetron sputtering (MS). Several MS techniques such as DC, Closed-Field Unbalanced MS and Highly Power Impulse MS were used with the target to succeed high quality materials. NSL appears as a very promising approach, due to its rapid implementation and compatibility with wafer-scale processes, combines the advantages of both top-down and bottom-up approaches and includes: (a) preparation of the nanospheres colloidal mask, (b) deposition of the desired material in the empty space between the nanospheres and (c) removal/lift-off of the nanosphere colloidal mask to “reveal” the deposited material that keeps the ordered patterning of the mask interstices. Specifically, a suspension of monodisperse polystyrene nanospheres (diameter, $d=552$ nm or $d=175$ nm) was spin coated on a substrate (several substrates were used such as Si (001), glass, and flexible PET to target applications in flexible printed photovoltaics) to form the colloidal mask. A UV ozone process was used to confine the triple-junction vias of the polystyrene mask. Subsequently, the selective growth of TiN was made by the above mentioned MS in Ar/N atmosphere by varying the TiN thickness from 10 to 30 nm, while the MS process parameters were also fine-tuned to increase the directionality of deposited species, TiN crystal quality (low concentration of point defects). In particular, the substrate-to-target distance was maximized to improve geometrical directionality, and a negative bias voltage was used to “guide” the ionic species deep into the vias between the nanospheres. The arrays of ordered TiN nanostructures appear after the lift-off of the mask. The proposed process produces well-defined TiN triangular nanoislands with low concentration of point defects, similar structure with the continuous TiN films of high electrical conductivity and plasmonic performance, and durability at least up to 400° C. Finally it should be noted that TiN is used as a case study as very good representative of other refractory TMNs, such as ZrN, HfN, NbN, and TaN.

Refs: P. Patsalas, N. Kalfagiannis, S. Kassavetis, G. Abadias, D.V. Bellas, Ch. Lekka, E. Lidorikis, Materials Science and Engineering R 123 (2018) 1–55. Panos, S., Tselekidou, D., Kassavetis, S., Fekas, I., Arvanitidis, J., Christofilos, D., Karfaridis, D., Dellis, S., Logothetidis, S. and Patsalas, P., Phys. Status Solidi B, 258 (2021) 2000573

EQ03.18.19

Reversible Photochemical Switching via Plasmonically Enhanced Photoluminescence in a Quasi-Periodic Metallic Nanostructure Byunghoon Kim¹, Kyu-Tae Lee², Wenshan Cai², M. Zahid Hasan¹ and Doo-Hyun Ko³; ¹Princeton University, United States; ²Georgia Institute of Technology, United States; ³Sungkyunkwan University, Korea (the Republic of)

Incorporating metallic nanostructure with fluorophore has offered desirable properties, such as plasmonically enhanced photoluminescence and ultra-sensitive optoelectronic response. The physics behind these improvements is controlling the near-field characteristics as well as finely tuning the wavelength of cavity mode corresponding to the photophysical energy gap of the activator. It leads to achieving a remarkable enhancement of photoluminescence intensity and sensitivity; however, inherent limitations (e.g., the narrowband resonance and restricted wavelength) prevent feasible applications in photochemistry. Here, we’ve achieved broadband photoluminescence enhancement by breaking the symmetry of the periodic metal nanostructure. The proposed quasi-periodic plasmonic platform allows strong electric field localization and intensity enhancement, which leads to the improvement of photoluminescence of photoswitching upconverting nanoparticles while conserving the spectral orthogonality. The accelerated reversible-photoisomerization kinetics is experimentally validated with the amplification of the photoluminescence intensities of the photochromic disulfonyldiarylethene derivatives.

SESSION EQ03.19: Metasurfaces and Metamaterials II
Session Chairs: Ho Wai Howard Lee and Yu-Jung Lu
Thursday Morning, December 1, 2022
Sheraton, 2nd Floor, Back Bay C

8:00 AM *EQ03.19.01

Meta-Optics for Image Processing and Object Classification Hanyu Zheng¹, Quan Liu¹, You Zhou¹, Ivan Kravchenko², Yuankai Huo¹ and Jason G. Valentine¹; ¹Vanderbilt University, United States; ²Oak Ridge National Laboratory, United States

Image processing has become a critical technology in a variety of science and engineering disciplines. While most image processing is performed digitally, optical analog processing has the advantages of being low-power and high-speed though it requires a large volume. Meta-optics provide the advantage of thin form factor optics while also allowing complex transfer functions to be employed. In this talk, I will discuss the use of meta-optics for applications in image processing as well as object classification. Specifically, I will discuss the use of meta-optics as optical front-ends that perform edge filtering as well as identification of higher level spatial features for object classifiers. The meta-optics are designed using end-to-end optimization so that the optical front-end and digital back-end work in harmony. This architecture allows for multiple metasurfaces to be optimized while also allowing us to incorporate noise in the design loop, resulting in robust experimental systems. The meta-optics processors are designed for both coherent and incoherent illumination,

enabling a wide range of use cases that take advantage of both a reduction in processing time and power consumption.

8:30 AM EQ03.19.02

Self-Assembled Plasmonic Metasurfaces Using DNA Origami with Dynamic Optical Response [Mihir Dass](#), Lena Raab, Chris Pauer, Gregor Posnjak and Tim Liedl; Ludwig Maximilians University Munich, Germany

Plasmonic nanoparticles interact strongly with light, concentrating far-field radiation into sub-wavelength volumes, producing effects like near-field coupling. We combine nanosphere lithography and DNA origami placement developed by Gopinath et al.^{1,2} with plasmonic particles and chiral plasmonic metamolecules assembled using gold nanorods and DNA origami to explore the possibility of creating patterned metasurfaces with a dynamic optical response. Since we can fabricate these surfaces on glass, they are compatible with optical techniques like Dark Field and TIRF microscopy. This method enables the creation of optical metasurfaces on the wafer scale and the pursuit of new applications on solid substrates usually incompatible with liquid phase colloidal suspensions.

1. Shetty, R. M.; Brady, S. R.; Rothmund, P. W. K.; Hariadi, R. F.; Gopinath, A. Bench-Top Fabrication of Single-Molecule Nanoarrays by DNA Origami Placement. *ACS Nano* 2021, 15, 7, 11441–11450.

2. Martynenko, I.V.; Ruider, V.; Dass, M.; Liedl, T.; Nickels, P.C. DNA Origami Meets Bottom-Up Nanopatterning, *ACS Nano* 2021, 15, 7, 10769 - 10774.

8:45 AM DISCUSSION TIME

9:00 AM EQ03.19.04

Metasurface-Enhanced Full-Space Structured Light for Depth Sensing [Gyeongtae Kim](#) and Junsuk Rho; Pohang University of Science and Technology, Korea (the Republic of)

Laser-based imaging technology is regarded to be one of the most promising and accurate three-dimensional (3D) depth sensing technologies when combined alongside the rapid advances in computer science. To image 3D objects over a wide field of view (FOV), the laser beams illuminate the objects, and backscattered light is monitored through detectors. Structured light (SL)-based imaging system splits the light into an array of dots or lines over the FOV, enabling imaging of multiple objects simultaneously. So far, diffractive optical elements (DOEs) or spatial light modulators (SLMs) have been used to form the laser spot arrays. However, such architectures suffer from small FOVs, low efficiency, and bulkiness resulting from the large micron-scale pixel size. Here, we propose a metasurface-based SL imaging platform, allowing for subwavelength scale manipulation of incident light. The scattered light from the metasurface covers the full 180° FOV, with a high-density ~10K dot array. The metasurface is composed of a periodic supercell, and the properties of diffraction patterns are analyzed by convolution theorem considering the supercell as a kernel function. As a proof-of-concept, we place face masks one on the laser beam axis and the other 50° apart from axis within distance of 1 m and estimate the depth information from the backscattered light using a stereo matching algorithm. Furthermore, we demonstrate the replication of our metasurface on a glass surface using the nanoimprinting of a nanoparticle-embedded-resin (nano-PER) for high-throughput fabrication.

9:15 AM EQ03.19.05

Terahertz Metamaterial Absorber in Pesticide/Herbicide Detection [Khwanchai Tantiwanichapan](#)¹ and Habibe Durmaz²; ¹National Electronics and Computer Technology Center, Thailand; ²Karamanoglu Mehmetbey University, Turkey

Terahertz (THz) technology has been attracted great interest in many research areas, especially THz plasmonics for sensing applications since intra- and inter-molecular vibrations are within the THz range. The sensitivity of free-space THz detection can be boosted up by use of metamaterials. Here, metamaterial absorber (MA) which are artificial structures in subwavelength scale of the incident light is introduced as a sensing device in THz regime. The operational principle of the MA sensor system is based on trapping the incident electromagnetic field at the interface of metallic antennas and the dielectric layer. These sensors are very sensitive to the change in their surrounding medium; therefore, highly sensitive, label-free, real-time sensing, and non-invasive detection are possible.

This work focuses on the detection of paraquat [(C₆H₇N)₂Cl₂] and glyphosate [N-(phosphonomethyl)glycine] herbicide/pesticide based on the polarization-insensitive THz MA. The MA sensor consisting of a metal-dielectric-metal structure is numerically designed by a commercial electromagnetic solver (CST microwave studio, 2018) software. The spectral response of the MA sensor with different geometrical parameters, such as metallic antenna structure and dielectric thickness is analyzed to optimize the resonance frequency and absorption efficiency. In the sensor fabrication process, general CMOS technology is applied and characterized. Subsequently, the sensing capacity of the THz MA systems is analyzed numerically and measured experimentally for different concentrations of paraquat and glyphosate (5 ppM to 500 ppM). The Fourier Transform Infrared Spectroscopy (FT-IR) is used for measurement from the chip surface with/without paraquat and glyphosate. The experimental results show that the presence of paraquat and glyphosate with concentrations ranging from 5 ppM to 500 ppM in the THz MA sensor surface shifts the spectral position of the absorption peak to the lower frequency. The numerical and experimental results are in good agreement for different concentrations of pesticide molecules. The experimental sensitivity of this THz MA sensor is around 52 GHz/ppM and 89 GHz/ppM for paraquat and glyphosate, respectively. These results indicate that the proposed MA sensor platform has potential use for highly sensitive THz applications in food quality and safety control [1].

Reference

[1] K. Tantiwanichapan and H. Durmaz, "Herbicide/pesticide sensing with metamaterial absorber in THz regime," *Sensors and Actuators A* **331**, 112960 (2021).

9:30 AM BREAK

10:00 AM *EQ03.19.06

Full-Color Non-Dispersive Visible Metalens by Sequentially Stacked Bilayers of HAR SiN Mold and TiO₂ Pillars [Seunghoon Han](#), Hyun Sung Park, Hyeonsoo Park, Hae-Sung Kim, Ki-Deok Bae, Woong Ko, Eun-Hyoun Cho, Jeong Yub Lee and Hyuck Choo; Samsung Electronics, Korea (the Republic of)

We present a new visible metalens, which works as an ideal non-dispersive diffractive lens by providing equal transmission phase profiles over the full-color broadband of light (wavelengths from 400 to 700nm). To implement such engineered dispersion, we sequentially stacked bilayers of meta-structures, i.e., high-index TiO₂ pillars in SiO₂ mold and low-index air holes in SiN mold of high-aspect-ratio (HAR, ~30). When the metalens phase profile is slowly-varying across the device (i.e., low numerical aperture), the dispersion at each location of the metalens through which light propagates can be designed by optimizing the bilayers' structural and material dispersions. As a result, the metalens has polarization independence and high focusing efficiencies (~83%, experiment, improving), which overcomes the limitations of the previous metalens approaches. The high-aspect ratio structuring of ~2μm thick SiN layer is

a key new material opportunity for visible meta-optics. This is an important advancement of the diffractive lens for many emerging applications; Fresnel lenses that have been used for DSLR cameras with refractive lenses are bulky, expensive and suffer various diffractive artifacts, whereas this metalens is thin, mass-producible and suppresses the artifacts significantly. The non-dispersive nature of the metalens allows it to be a basic building block for more complicated dispersion engineered optical systems. Furthermore, the sequentially stacked bilayers will enable new functional metasurfaces at visible frequencies by harnessing its structural and material compositions.

10:30 AM *EQ03.19.07

Advances on Nonlocal Metasurfaces [Andrea Alu](#); City University of New York, United States

In this talk, I will present and discuss our recent advances on metasurfaces based on highly delocalized modes, stemming from long-range resonant interactions and lattice phenomena. Different from conventional metasurface approaches, engineered nonlocality offers tailored spectral control, and at the same time can be tailored in space with large resolution using geometric phase concepts. Their response is ideal for imaging and signal processing applications, and to enhance light-matter interactions. We achieve these features by combining quasi-bound states in the continuum with geometric phase variations in engineered metasurfaces, tailoring at will the supported eigenwaves. The resulting metasurfaces support ultrasharp responses selective to the impinging wave properties, effectively realizing ultrathin transparent films that highly reflect light only when illuminated by selected polarization, frequency and wavefront spatial distribution of choice. The demonstrated wavefront selectivity of nonlocal metasurfaces opens exciting opportunities for augmented reality, secure communications, thermal emission management, optical modulators and enhanced light-matter interactions for nonlinear and quantum optics. In particular, in the talk we demonstrate our recent experimental demonstrations on highly efficient signal processing metasurfaces for polarization imaging, thermal metasurfaces, and other applications of these phenomena.

11:00 AM EQ03.19.08

High Quality Factor Dielectric Metasurfaces for Two-Dimensional Wavefront Manipulation in Transmission [Claudio U. Hail](#), Morgan Foley, Ruzan Sokhoyan and Harry A. Atwater; California Institute of Technology, United States

The strong interaction of light with optical nanostructures plays a critical role in optical sensing, nonlinear optics, and active optical devices. However, for wavefront shaping, the required local, sub-wavelength control over the phase of light limits this interaction, leading to low-quality-factor optical devices. Here, we report on high quality factor dielectric metasurfaces for complete, local wavefront manipulation of near infrared light in transmission mode, and in two dimensions. Our structure consists of high-index dielectric nanoparticles exhibiting strong, lattice-coupled Mie resonances with high quality factors. The local control of these resonances enables setting the phase of transmitted light over a range of $0-2\pi$ with experimentally measured quality factors of up to 295 at a wavelength of $\lambda = 1290$ nm. By appropriately tailoring the dimensions of these dielectric building blocks to attain the desired phase distribution, we experimentally realize wavelength-selective beam deflectors and radial metalenses with a bandwidth of only a few nanometers. Furthermore, we demonstrate the operation under finite illumination apertures (< 50 μm) and oblique incident illumination. This contrasts with other mechanisms for high-quality-factor optical metasurfaces which rely on inherently non-local principles, such as guided mode resonances or symmetry-breaking bound states in the continuum, limiting their application to one-dimensional wavefront shaping or geometric phase tuning, respectively. Our findings demonstrate that local control over the wavefront is successfully attained with high quality factor, opening doors to new applications in active metasurfaces and sensitive, free-space-coupled optical sensing.

11:15 AM EQ03.19.09

Experimental Demonstration of Space-Time Modulated Metasurfaces [Jared Sisler](#), Prachi Thureja, Meir Y. Grajower, Ruzan Sokhoyan and Harry A. Atwater; California Institute of Technology, United States

We experimentally demonstrate operation of a space-time modulated metasurface at 1550 nm in a switchable diffraction experiment. Space-time metasurfaces are a class of tunable metasurfaces that simultaneously impart a spatial and temporal phase gradient to incoming light [1]. Experimentally, this is realized by first modulating all metasurface elements with a high-frequency voltage signal to generate harmonic sidebands of the incident light wavelength. Then, by introducing a time delay to the driving waveform between adjacent metasurface elements, a spatial phase-gradient is created. The phase shift imparted by introducing a time delay to the electrical signal is nonresonant and covers a full 360° range without an associated covariation of amplitude: an issue that has previously limited the performance of tunable metasurfaces. There is currently a surge of interest in the photonics community to produce a space-time optical metasurface because of their potential to enable full 360° phase shift with constant amplitude, multi-channel communication in a single aperture, and nonreciprocal behavior [2,3].

By using a reflective gate-tunable indium-tin-oxide (ITO) based metasurface operating at 1550 nm integrated into an electrical circuit [4], we first demonstrate the generation of multiple harmonics as a function of modulating waveform for frequencies up to 5 MHz. Our device consists of an array of interdigitated plasmonic nanoantennas with two electrical contacts that are initially modulated in-phase such that all harmonics are normally reflected. Next, we offset the electrical waveforms by half a period between the two electrodes such that a spatial binary phase grating is achieved. By doing this, we measured an increase in the intensity of the $\pm 1^{\text{st}}$ diffraction orders, enabling a switchable diffraction functionality. Due to the nonideal properties of our metasurface (i.e., a covarying and nonlinear amplitude and phase response), the efficiency of our device is limited. This can be increased by optimizing the driving waveform to improve the frequency conversion efficiency to a single harmonic using a genetic algorithm and arbitrary waveform generator. Future experiments will use a more complex metasurface design with 32 individually addressable electrodes. This metasurface will operate under the same principle as our current two-electrode device but will be able to demonstrate more complex functionalities such as dynamic steering and focusing. We are further exploring new device architectures and driving schemes that will enable multi-frequency, multi-beam steering as well as the breaking of reciprocity.

[1] Y. Hadad, D. L. Sounas, and A. Alu, "Space-time gradient metasurfaces," *Physical Review B - Condensed Matter and Materials Physics*, vol. 92, no. 10, Sep. 2015, doi: 10.1103/PhysRevB.92.100304.

[2] M. M. Salary and H. Mosallaei, "Time-Modulated Conducting Oxide Metasurfaces for Adaptive Multiple Access Optical Communication," *IEEE Transactions on Antennas and Propagation*, vol. 68, no. 3, pp. 1628–1642, Mar. 2020, doi: 10.1109/TAP.2019.2938613.

[3] S. Taravati and G. v. Eleftheriades, "Microwave Space-Time-Modulated Metasurfaces," *ACS Photonics*, Jan. 2022, doi: 10.1021/acsp Photonics.1c01041.

[4] Y. W. Huang *et al.*, "Gate-Tunable Conducting Oxide Metasurfaces," *Nano Lett.*, vol. 16, no. 9, pp. 5319–5325, 2016.

11:30 AM EQ03.19.10

Tailoring the Spectral Characteristics of Multilayered Chiral Mid-Infrared Metamaterials [Hannah Barnard](#) and Geoff Nash; University of Exeter, United Kingdom

Metamaterials, in particular chiral metamaterials, are of great interest in recent years as they offer potential for application in enhanced sensing techniques [1]–[3]. This is because the structures absorb incident radiation, and confine it to nanoscale regions, which can then be used to probe some analyte. Of particular interest are those materials which absorb mid-infrared (mid-IR) radiation, as the confined fields can then be used to probe the molecular

vibrational frequencies of molecules, which also fall in this spectral region. Here, we present a simulation and experimental study into a particular class of chiral metamaterial, made up of twisted U-shape resonator elements [4]–[6], forming a multi-layered stack. First we scale the dimensions of the structures using simulations, to ensure the resonances fall in the important mid-IR region of the spectrum. Then, the structure is fabricated using standard lithographic techniques to produce gold resonators on an Si/SiO₂ substrate. By measuring the structure in an FTIR spectrometer we demonstrate high levels of circular dichroism (CD), a consequence of the chirality of the structure, in the mid-IR region, for three different configurations [7]. The three configurations discussed include a double layer structure, and two 4-layer structures. Finally, we demonstrate that the spectral position of the metamaterial resonances, and subsequent CD, can be tailored simply by changing the stacking configuration of the layers [7]. We explain this behaviour using a model of the induced magnetic dipoles at each resonance, caused by the coupling of adjacent twisted resonators, when the structure is excited.

This study provides an important insight into the mechanisms of optical activity in an important class of metamaterial, particularly, how to tailor its spectral response. Demonstrating high levels of CD indicates that this structure is strongly optically active in the important mid-IR region, making it a possible candidate for enhanced spectroscopy applications in the future. Further work is underway to investigate the nature of the confined fields produced, how chiral they are, and how accessible they might be to a molecular analyte on the structures surface.

References:

- [1] M. Schäferling, D. Dregely, M. Hentschel, and H. Giessen, “Tailoring enhanced optical chirality: Design principles for chiral plasmonic nanostructures,” *Phys. Rev. X*, vol. 2, no. 3, (2012).
- [2] O. Takayama, “Mid-infrared nanophotonics for biochemical sensing: A review,” *Romanian Reports in Physics*, vol. 72, no. 3., (2020).
- [3] X. Ma, M. Pu, X. Li, Y. Guo, P. Gao, and X. Luo, “Meta-chirality: Fundamentals, construction and applications,” *Nanomaterials*, vol. 7, no. 5. (2017).
- [4] N. Liu, H. Liu, S. Zhu, and H. Giessen, “Stereometamaterials,” *Nat. Photonics*, vol. 3, no. 3, , (2009).
- [5] X. Xiong *et al.*, “Construction of a chiral metamaterial with a U-shaped resonator assembly,” *Phys. Rev. B - Condens. Matter Mater. Phys.*, vol. 81, no. 7, (2010).
- [6] M. Decker, R. Zhao, C. M. Soukoulis, S. Linden, and M. Wegener, “Twisted split-ring-resonator photonic metamaterial with huge optical activity,” *Opt. Lett.*, vol. 35, no. 10, (2010).
- [7] H. R. Barnard and G. R. Nash, “Tailoring the spectral properties of layered chiral mid-infrared metamaterials,” *Appl. Phys. Lett.*, vol. 119, no. 24, (2021).

11:45 AM EQ03.19.11

Mass-Production of Visible Metalenses via Wafer-Scale Printing [Joohoon Kim](#) and Junsuk Rho; Pohang University of Science and Technology, Korea (the Republic of)

Currently, metasurface-based flat optics is going from science to technology transition. A representative example includes a flat and ultra-thin metalens, which has potential to overcome the limitations of conventional optical lenses, such as bulky system, heavy weight, shadowing effect, and chromatic aberration. As an example, typical digital single-lens reflex (DSLR) camera which have a length of over 30 cm and a weight of over 4 kg. On the other side, metalens has near-zero weight and nm-scale thickness. However, their inherent fabrication limitations such as high manufacturing cost, low throughput, and small patterning areas hindered their widespread use. In this abstract, we introduce a new fabrication method for the mass production of visible metalenses. The proposed fabrication method includes an argon fluoride immersion scanner, wafer-scale nanoimprint lithography, and atomic layer deposition. The argon fluoride immersion scanner is used to fabricate a 12-inch master stamp. Once a 12-inch master stamp is imprinted, hundreds of 1-centimeter metalenses can be transferred to the substrate. Since nanoimprint lithography features low cost and high throughput, metalenses can be fabricated with extremely low cost and high throughput. However, a low refractive index of printed resin causes low efficiency. To increase the effective refractive index of printed resin, the printed resin is thinly coated with a high-index film. As a result, the conversion efficiency of the designed meta-atom is drastically increased. In this method, we mass-produced 1-centimeter metalenses on a wafer-scale, even in a laboratory environment. As a proof of concept, a VR device integrated with mass-produced metalenses was demonstrated. Moreover, the proposed method can also be applied to various metasurfaces such as holograms, color filters, and biosensors.

SESSION EQ03.20: Radiation Engineering II
Session Chairs: Seunghoon Han and Yu-Jung Lu
Thursday Afternoon, December 1, 2022
Sheraton, 2nd Floor, Back Bay C

1:45 PM EQ03.20.01

Ultra-Narrowband Mid-Infrared Thermal Emitters Based on Phononic Metasurfaces [Soheil Farazi](#) and Srinivas Tadigadapa; Northeastern University, United States

In this work, we demonstrate a new class of ultra-narrowband coherent emitters in the mid-IR range using bound states in the continuum (BICs) [1]. Most of the existing sources in the mid-IR range are thermal emitters and consequently spontaneous, incoherent, and broadband. Manufacturing a narrowband coherent source is vital in many applications including sensing, lasing, and optical communications. In addition, the ultra-narrowband emitter investigated in this work can pave the way to design and fabricate Vertical Cavity Surface Emitting Lasers (VCSELs) in the 10-12 μm wavelength range.

Although several works have been done to design and fabricate narrowband emitters at visible and near-IR regimes, this goal is still challenging in mid-IR wavelengths. By utilizing polar materials like silicon carbide (SiC) supporting surface phonon polaritons (SPhPs) one can achieve partially coherent emitters with near-unity emissivity [2]. Indeed, the surface waves excited by SPhPs generate thermal radiation with enhanced intensity beyond blackbody radiation; however, the quality factor of the emission peak has thus far been limited due to the intrinsic losses of plasmonic and phononic materials. We have shown by utilizing Friedrich-Wintgen BICs [3], we can establish a high Q -factor coherent source with a near-unity emissivity For both TE and TM polarization. The emission peak of the phononic metasurface has a Q -factor as high as 3,400 which is two orders of magnitude higher than any plasmonic or photonic structure in this wavelength range. Moreover, our simulated results show that the proposed structure has a reasonable fabrication tolerance meaning that any small deviations from the desired construction parameters may not affect the amplitude and Q -factor of the emission peak drastically.

References:

1. Marinica, D., A. Borisov, and S. Shabanov, *Bound states in the continuum in photonics*. Physical review letters, 2008. **100**(18): p. 183902.
2. Greffet, J.-J., et al., *Coherent emission of light by thermal sources*. Nature, 2002. **416**(6876): p. 61.
3. Azzam, S.I., et al., *Formation of bound states in the continuum in hybrid plasmonic-photonic systems*. Physical review letters, 2018. **121**(25): p. 253901.

2:00 PM EQ03.20.02

Dynamically Regulated Radiative Cooling with Continuously Variable Emission Xiaojie Liu¹, Yanpei Tian¹, Fangqi Chen¹, Alok Ghanekar², Mauro Antezza³ and Yi Zheng¹; ¹Northeastern University, United States; ²University of Southern California, United States; ³Institut Universitaire de France, France

Passive radiative cooling drawing the heat energy of objects to the cold outer space through the atmospheric transparent window ($8\ \mu\text{m} \sim 13\ \mu\text{m}$) is significant for reducing the energy consumption of buildings. Daytime and nighttime radiative cooling have been extensively investigated in the past. However, radiative cooling which can continuously regulate its cooling temperature, like a valve, according to human need is rarely reported. In this study, we present a concept of reconfigurable photonic structure for the adaptive radiative cooling by continuously varying the emission spectra in the atmospheric window region. This is realized by the deformation of the one-dimensional Polydimethylsiloxane (PDMS) grating and the nanoparticles embedded PDMS thin film when subjected to mechanical stress/strain. The proposed structure reaches different stagnation temperatures under certain strains. A dynamic tuning in emissivity under different strains results in a continuously variable "ON"/"OFF" mode in a particular atmospheric window that corresponds to the mechanical deformation induced fluctuation of the operating temperatures of the reconfigurable nanophotonic structure.

2:15 PM EQ03.20.04

Directly Violating the Kirchhoff Thermal Law Komron J. Shayegan¹, Souvik Biswas¹, Bo Zhao², Shanhui Fan³ and Harry A. Atwater¹; ¹California Institute of Technology, United States; ²University of Houston, United States; ³Stanford University, United States

The Kirchhoff thermal radiation law provides an inherent constraint on the ability to harness thermal radiation, requiring that the spectral emissivity and absorptivity are equal and exhibit identical angular distributions for a given polarization. This equality is built on the fundamental assumption that all materials obey Lorentz reciprocity. One class of materials that does not satisfy Lorentz reciprocity, and thus can violate the Kirchhoff thermal law, is magneto-optically-active materials. In this work, we experimentally demonstrate a direct inequality between the absorptivity and emissivity in the mid-infrared of a guided-mode-resonant (GMR) structure with a magneto-optical InAs underlayer that breaks time-reversal symmetry, and thus reciprocity, in a moderate external magnetic field. We demonstrate the angular and spectral distribution changes of both the emissivity and the absorptivity in magnetic fields. Furthermore, we use the symmetry of the GMR structure to tune the Kirchhoff violating emission's dispersion and magnetic field dependence. We conclude with an outlook on the dynamic tunability of such structures and their practical implications.

2:30 PM EQ03.20.05

Cooler-free operation (up to 120°C) of microbolometers based on amorphous VO_x thermistor deposited at different growth temperatures Dasom Wang^{1,2}, Ho Won Jang², Dong Hee Park¹ and Won Jun Choi¹; ¹Korea Institute of Science and Technology, Korea (the Republic of); ²Seoul National University, Korea (the Republic of)

The recent growth of the autonomous driving market increased demands for IR image sensors due to the detection capability in the absence of visible light, e.g., night, rainy, or foggy conditions. Since the cost-effectiveness is essential for commercialization of autonomous vehicles, cooler-free operations of IR detectors at high ambient temperature for autonomous vehicles is in high demand. Microbolometers are the most widely used thermal detector in commercial thermal cameras because of its advantages like portability and low cost. However, the upper limit of conventional microbolometers is approximately 70°C since the temperature coefficient of resistance (TCR) is lower than 1 %/K of TCR value that is required for ROICs in microbolometers. Thus, high temperature coefficient of resistance (TCR) value and low resistance is required.

In this work, we report on the amorphous vanadium oxide thin films as thermistor materials for microbolometers. Vanadium oxide thin films were deposited using pulsed DC sputtering processes under different growth temperatures from 160°C to 230°C. We also studied their electrical properties and effects on the performances of fabricated microbolometers. These processes were carried out under 350°C which is suitable for ROIC integration without any doping or annealing process. XRD analysis was carried out to identify the structural properties of thin films and the results show that thin films grown at different temperatures were amorphous phases. The sheet resistances of thin films decrease from 330 to 70 k Ω /sq with increasing growth temperature. XPS analysis confirms that it is due to the increase of oxygen vacancies at higher growth temperature. Amorphous VO_x thin films show non-hysteresis behavior up to 120°C, which in turn shows clear activation energies. The TCR values at room temperature and activation energies of the films increased from 2.44 to 2.8 (%/K) and from 0.145 eV to 0.190 eV by decreasing growth temperature. These thin films also showed higher than 1 %/K of TCR value even at 120°C. Amorphous VO_x based microbolometers have been fabricated using electron-beam lithography and lift-off techniques. Characterizations of fabricated microbolometers were carried out under various ambient temperatures from room temperature to 120°C. Responsivities of fabricated microbolometers based on the amorphous VO_x thermistors change from 1.14×10^3 V/W to 3.04×10^3 V/W at room temperature and from 3.02×10^2 V/W to 9.54×10^2 V/W at 120°C. The fabricated microbolometers showed high frequency operation properties as well. Thermal time constants were from 1.38 to 0.95 ms at room temperature and from 1.77 to 1.22 ms at 120°C which show that the microbolometers are suitable for high-speed camera applications such as autonomous vehicles.

This work reveals the correlations between growth temperatures of vanadium oxide thin films and their electrical properties. Amorphous VO_x based microbolometers showed good performance not only at room temperature but also at high ambient temperature up to 120°C without any cooling device. The results of this work will be highly encouraging for the development of IR detector for autonomous vehicle.

2:45 PM BREAK

SESSION EQ03.21: Metasurfaces and Metamaterials III
Session Chairs: Marianne Aellen and Andrea Alu
Thursday Afternoon, December 1, 2022
Sheraton, 2nd Floor, Back Bay C

3:15 PM *EQ03.21.01

Electrochemically Dynamic Materials for Solar and Radiative Thermoregulation Po-Chun Hsu; University of Chicago, United States

The solar energy has been the cleanest renewable heat sources for humankind. On the other hand, the rest of sky provides the clean cold source via radiative cooling, mitigating the energy consumption for refrigeration and space cooling. While both technologies have been significantly advanced by recent research in photonics and thermal science, there will be a shift of paradigm to combine and dynamically utilize both of them to broaden the

applicability and efficiency for all seasons and climate zones. In this talk, I will summarize recent research progress in this field and introduce our works that use reversible metal electrodeposition to dynamically switch between a plasmonic selective solar absorber and a mid-IR-emitting solar mirror, which can provide year-round HVAC energy saving. Furthermore, the electrochemically variable emittance concept is also applied to ultralow-energy personal thermoregulation, bringing new opportunities in the human-building-energy nexus.

3:45 PM EQ03.21.02

Semiconductor-Based Hyperbolic Metamaterials Dongxia Wei, Patrick Sohr and Stephanie Law; University of Delaware, United States

Traditional metals are good plasmonic materials in the visible spectral range, but do not work well in the infrared (IR). Small gap heavily-doped semiconductors like InAs, InGaAs, and InSb have been shown to be good plasmonic materials in the IR. The carrier density can easily be controlled in these materials, leading to tunable optical properties across wide bandwidths. III-V semiconductors can be grown by molecular beam epitaxy (MBE), an ultra-high vacuum technique in which the materials are grown one atomic layer at a time. This also enables these plasmonic materials to be epitaxially integrated with existing semiconductor-based optoelectronic devices.

MBE is also an excellent technique for the growth of superlattices. A superlattice comprising alternating metal (doped) and dielectric (undoped) layers of subwavelength thickness can act as a hyperbolic metamaterial (HMM). HMMs have an anisotropic dielectric tensor which results in an open, hyperbolic isofrequency surface. The open nature of the isofrequency surface enables HMMs to support the propagation of light with large wavevectors limited only by the subwavelength feature size. In an HMM composed of subwavelength metal and dielectric layers, the modes that support the large wavevector light are called volume plasmon polaritons (VPPs). VPPs are bulk cavity modes that arise from the coupling of surface plasmon polaritons (SPPs) located at the interfaces of the metal and dielectric layers. These features have made HMMs important for studying a variety of light-matter interactions, including negative refraction, subwavelength focusing, subwavelength imaging, modified spontaneous emission, and slow light.

In this presentation, I will describe our results on synthesizing and characterizing semiconductor-based HMMs in the infrared spectral range, explaining how material choice impacts HMM performance, showing far-field thermal emission properties, and demonstrating strong coupling between the HMM VPP modes and epitaxially embedded quantum wells. This work lays the foundation for the creation of new types of IR optoelectronic devices that take advantage of these unusual materials.

4:00 PM EQ03.21.03

A Scalable Metasurface Based Platform for Compact Optical Atomic Clocks Amit Agrawal, Wenqi Zhu, Junyeob Song, Chad Ropp, Vladimir Aksyuk, Andrew Ferdinand, Sindhu Jammi, Grisha Spektor, Scott Papp and Lu Chen; National Institute of Standards and Technology, United States

Over the last decade, flat optical elements composed of an array of deep-subwavelength dielectric or metallic nanostructures of nanoscale thicknesses – referred to as metasurfaces – have revolutionized the field of optics. Because of their ability to impart an arbitrary phase, polarization or amplitude modulation to an optical wavefront as well as perform multiple optical transformations simultaneously on the incoming light, they promise to replace traditional bulk optics in applications requiring compactness, integration and/or multiplexing. Recent demonstrations including imaging, full-Stokes polarimetry, quantum-light generation and LIDAR demonstrate the range of technologies where metasurfaces have already had a significant impact.

In this work, we demonstrate the versatility of wavefront shaping metasurfaces as a compact, efficient and multifunctional interface to: (a) trap single neutral atoms of ^{87}Rb in an optical tweezer trap for application in quantum information science, and (b) trap ensemble of Sr atoms in a magneto-optical-trap (MOT) for realization of a compact optical lattice clock. We further establish a scalable infrastructure for strontium optical-atomic clocks, leveraging advances in visible integrated and metasurface photonics along with a compact, commercially available Sr source and vacuum chamber to reduce the overall SWaP of the physics package. We present experiments with laser cooling and trapping Sr atoms in a metasurface MOT with our compact vacuum chamber and atom source, demonstrating a path toward scalable, compact optical clocks that is completely alignment-free and does not utilize any free-space optics.

In another integration step, combining metasurfaces directly with integrated photonic circuits, replacing bulk optical elements, promises increased complexity and functionality in a batch-fabricated optical microsystem ultimately capable of fully replacing the laboratory optical table. With this goal in mind, we leverage integrated photonic and metasurface optics that interface directly with light from single-mode fibers; and how integration of many such structures on a single chip in a CMOS foundry manufacturable platform enable new capabilities for cold atom atomic clocks and other quantum sensors.

4:15 PM EQ03.21.04

Double Negative Acoustic Metamaterial Reaching Operating at 300 kHz in Water Based on Silicon Microfabricated Unit-Cells Jiaying Wang¹, Florian Allein², Cecile Floer³, Nicholas Boechler¹, James Friend¹ and Oscar Vazquez Mena¹; ¹UC San Diego, United States; ²Le Mans Université, France; ³Université de Lorraine, France

Negative acoustic metamaterials have shown extraordinary novel capabilities such as enhancement of evanescent waves with subwavelength components, negative refractive angle, opposite phase and group velocities, and enhancement of transmission through high-contrast acoustic barriers. This shows enormous promise for medical ultrasound applications. However, a major challenge is increasing their frequency operations. Double negative metamaterials have been demonstrated at 300 Hz(1) and 30 KHz(2), which falls below medical ultrasound range that covers a broad range from 200 kHz to 50 MHz. Herein, we demonstrate a double negative acoustic metamaterial operating at 300 kHz using robust silicon microfabrication technology. The main fabrication novelty is the fabrication of silicon chips as individual unit-cells. Each chip contains sub-100 micron Helmholtz resonators and silicon nitride membranes, which produce negative modulus and negative density behavior, respectively. Then, the silicon chip unit-cells are assembled in water, forming a periodic structure integrating the Helmholtz resonators and silicon nitride membrane that result in a double negative acoustic metamaterial operating at 300 kHz. Our metamaterial consists of an acoustic waveguide 60 μm wide, silicon nitride membranes 200 nm thick, and Helmholtz resonators (500x500x10 μm^3) with a neck with a cross section of (20x10 μm) and a length of 50 μm connecting the Helmholtz resonator to the acoustic waveguide. Our key fabrication strategy is that instead of forming a monoblock structure, we fabricate individual chips, allowing the fabrication of high-resolution micromechanical components, which are then assembled to form the metamaterial. The assembling is done with mechanical screws and using a laser to verify alignment. Silicon and silicon nitride are chemically stable in water and their mechanical properties allows for operation >100 kHz. We present analytical models, finite element method simulations, and laser-doppler vibrometry experimental results that indicate double negative behavior and negative-index propagation in the 0.25-0.35 MHz range. At 300 kHz, Our metamaterial shows a positive group velocity (wave packets carrying information propagate forward) of 200 m/s, but with a negative phase velocity (valleys and peaks moving backwards) of -1750 m/s. The opposite propagation between wave packets and peaks/valleys, together with a close agreement between analytical, simulations and experimental results, provides strong evidence for the negative-index behavior of our metamaterial. We estimate an effective density near -2000 kg/m³ and a modulus of -9 GPa at 300 kHz. The acoustic index with respect to water covers a range from -5 at 0.25 MHz to -1 at 0.35 MHz. Our technology has several advantages: 1) the use of microfabrication tools allows for further reduction in size and increase in frequency operation; 2) the long-term mechanical and chemical stability of silicon

nitride and silicon that open possibilities for using different propagation media besides water; 3) the design flexibility to modify each acoustic component to target specific density/modulus/index value; 4) the fabrication in individual cells also facilitate the integration of membranes and Helmholtz resonators in different 1-D, 2-D and 3-D arrangements. There are also several challenges ahead, such as improving assembling and alignment precision, as well as studying the role of viscosity and damping as sound propagates in structures below 100 um in size.

(1) Lee, S. H.; Park, C. M.; Seo, Y. M.; Wang, Z. G.; Kim, C. K. Composite Acoustic Medium with Simultaneously Negative Density and Modulus. *Phys. Rev. Lett.* **2010**, *104* (5), 054301. <https://doi.org/10.1103/PhysRevLett.104.054301>.

(2) Chen, H.; Li, H.; Zhai, S.; Ding, C.; Li, J.; Luo, C.; Zhao, X. Ultrasound Acoustic Metamaterials with Double-Negative Parameters. *J. Appl. Phys.* **2016**, *119* (20), 204902. <https://doi.org/10.1063/1.4951008>.

4:30 PM EQ03.21.05

Stain-Free Tissue Imaging with Scalable Plasmonic Metasurfaces Do Eun Kim, Juhwan Kim, Soeun Ko, Jin Kyeong Lee, Jang-Hwan Han and Hyeon-Ho Jeong; Gwangju Institute of Science and Technology, Korea (the Republic of)

Label-free tissue diagnostics using plasmonics, a.k.a. histoplasmonics, enables morphological analysis of cells with colorful contrast in the refractive indices between cells and surroundings (Ref. Nature 598, 65, (2021)). However, this method still requires not only cell staining with molecular dyes (hematoxylin and eosin, H&E) for enhanced contrast, but also a regular array of plasmonic nanopatterns via nanolithography, limiting mass-production. We here describe a 'lithography-free' scalable fabrication of plasmonic metasurfaces using a rapid electrostatic coating of nanoparticles and their use for 'stain-free' colorful refractive index imaging of cells. The colloidal solution of negatively-charged plasmonic nanoparticles is casted onto a positively-charged metallic mirror, enabling the rapid (but massive) nanoparticle coating in a random fashion ($> 10\%$ surface coverage for 10 seconds) and thus formulating well-defined solid nanogaps between the nanoparticles and the mirror underneath through the centimeter scale film. Such plasmonic metasurfaces defined with a solid nanogap not only provides the uniform, vivid colors through the entire surface, but are also sensitive to the change in the surrounding refractive index so readily visualize its variation in the extremely localized area (ideally single nanoparticle level) in colors from red to green under an ambient light. More crucially, this metasurface offers the distinct color of the cultured animal cells (3t3-L1, adipose cell, $n= 1.358-1.374$) against the water environment ($n = 1.33$), otherwise impossible to be seen with standard optical microscopy.

In this presentation, the fabrication method of the plasmonic metasurfaces and their theoretical and experimental optical features will be discussed. Furthermore, we will show how to qualitatively model the resonant plasmonic spectra as a function of the refractive index spectroscopically for in-situ colourful imaging of the cultured animal cells.

SESSION EQ03.22: Advanced Nanophotonic Design III
Session Chairs: Viktoriia Babicheva and Yu-Jung Lu
Friday Morning, December 2, 2022
Hynes, Level 2, Room 202

8:30 AM *EQ03.22.01

High-Index Metastructures with Lattice Multipole Resonances Viktorii Babicheva; University of New Mexico, United States

Nanoparticle clusters, such as oligomers, support modes with different symmetries resulting in Fano resonances. Moreover, periodic nanoparticle arrays give rise to lattice resonances at the wavelength close to the Rayleigh anomaly, i.e., effective wavelength in the medium is equal to the array period. Compared to a single nanoscatteer, drastic changes in the metastructure resonances can be induced by arranging nanoparticles into a periodic array. This often facilitates the excitation of additional resonances known as lattice resonances.

In this work, we aim to design efficient directional scatterers and their arrays for metasurfaces and transdimensional metastructures. The combination of different materials in the nanoparticle allows the tune of electric and magnetic resonances of the nanoparticles and achieving broadband overlap. The nanofabrication and characterization include sample preparation, deposition of metals and oxides, as well as optical measurements of reflection and transmission spectra. One or multiple nanoparticles (or scattering elements, or scatterers) are considered in the unit cell of the lattice unit. We introduce mismatched resonances excited in the array and show that the dimensions of scatterers define the type and character of excitations.

This work was performed, in part, at the Center for Integrated Nanotechnologies, an Office of Science User Facility operated for the U.S. Department of Energy (DOE) Office of Science by Los Alamos National Laboratory (Contract 89233218CNA000001) and Sandia National Laboratories (Contract DE-NA-0003525). The work is also supported by Contract DE-2375849.

9:00 AM EQ03.22.02

Pico-Photonics in Silicon Sathwik Bharadwaj, Todd Van Mechelen and Zubin Jacob; Purdue University, United States

The concept of frequency (ω) - momentum (q) dispersion has been extensively studied in artificial dielectric structures such as photonic crystals and metamaterials. However, the $\omega - q$ dispersion of electrodynamic waves hosted in natural materials at the atomistic level is far less explored. Here, we develop a Maxwell Hamiltonian theory of matter combined with the quantum theory of atomistic polarization to obtain the electrodynamic dispersion of natural materials interacting with the photon field. We apply this theory to silicon and discover the existence of anomalous atomistic waves. These waves occur in the spectral region where propagating waves are conventionally forbidden in macroscopic theory. Our findings demonstrate that natural media can host a variety of yet to be discovered waves with sub-nanometer effective wavelengths in the pico-photonics regime. This study bridges the fields of optics and condensed matter physics, spawning a new area of research in material science and engineering.

Reference: arXiv:2203.05734 [physics.optics] (<https://doi.org/10.48550/arXiv.2203.05734>).

9:15 AM EQ03.22.03

Single-Shot Microfabrication of Complex 3D Structures by Volumetric Multiphoton Lithography He Cheng¹, Pooria Golvari¹, Chun Xia¹, Mingman Sun², Meng Zhang², Stephen M. Kuebler^{1,1,1} and Xiaoming Yu¹; ¹University of Central Florida, United States; ²Kansas State University, United States

Multi-photon lithography (MPL) is a technique for fabricating three-dimensional (3D) microstructures with submicron resolution. Arbitrarily complex forms are created by scanning a focal spot in a photoresist using a galvo scanner or a piezoelectric stage to locally induce multi-photon polymerization. The

requirement for point-by-point scanning severely limits the throughput of MPL and hinders its industrial use. Methods for parallel exposure have been explored for improving the fabrication speed in MPL. Various approaches for 2D beam shaping have been used to pattern layers in parallel, but little is known of ways to achieve volumetric exposure, in which whole 3D sub-parts or complete 3D structures are patterned in a single exposure. We recently reported a method for high-throughput fabrication of complex 3D volumes using normal and superposed Bessel beams [1-7]. Complex structures were created in a single static exposure using one or a few laser pulses, including cylinders, needles, and spirals with tunable pitch. Importantly, the pitch distance can be designed to vary along the optical axis, creating “accelerating” or “decelerating” spirals with desired handedness. With complementary horizontal beam scanning, self-supporting matrices of spirals were fabricated in the photoresist SU-8 demonstrating the feasibility of large-scale fabrication. Volumetric exposure increases fabrication throughput by at least two orders of magnitude. This method paves the way for mass production of functional devices using MPL having applications in photonics, microfluidics, bioscaffolds, medicine, and more.

1. Cheng, H.; Xia, C.; Zhang, M.; Kuebler, S. M.; Yu, X., Fabrication of high-aspect-ratio structures using Bessel-beam-activated photopolymerization. *Applied Optics* **2019**, *58* (13), D91-D97.
2. Cheng, H.; Xia, C.; Sun, M.; Zhang, M.; Kuebler, S. M.; Yu, X., Micro-and nanofabrication using Bessel-beam activated photopolymerization. *Journal of Laser Applications* **2020**, *32* (2), 022067.
3. Cheng, H.; Xia, C.; Kuebler, S. M.; Yu, X., Aberration correction for SLM-generated Bessel beams propagating through tilted interfaces. *Optics Communications* **2020**, *475*, 126213.
4. Cheng, H.; Xia, C.; Kuebler, S. M.; Golvari, P.; Sun, M.; Zhang, M.; Yu, X., Generation of Bessel-beam arrays for parallel fabrication in two-photon polymerization. *Journal of Laser Applications* **2021**, *33* (1), 012040.
5. Cheng, H.; Golvari, P.; Xia, C.; Sun, M.; Zhang, M.; Kuebler, S. M.; Yu, X. In *Rapid microfabrication of helical structures for industrial applications*, Advanced Fabrication Technologies for Micro/Nano Optics and Photonics XV, SPIE: 2022; pp 22-29.
6. Cheng, H.; Golvari, P.; Xia, C.; Sun, M.; Zhang, M.; Kuebler, S. M.; Yu, X. In *Volumetric microfabrication of helical structures for industrial applications*, Novel Patterning Technologies 2022, SPIE: 2022; pp 69-75.
7. Cheng, H.; Golvari, P.; Xia, C.; Sun, M.; Zhang, M.; Kuebler, S. M.; Yu, X., High-throughput microfabrication of axially tunable helices. *Photonics Research* **2022**, *10* (2), 303-315.

9:30 AM EQ03.22.04

Optical Microcavities in Luminescent Beta-Ga2O3 Nanowires—Tunability from Near-UV to Near-IR and Wide Range Temperature Sensors

Manuel Alonso-Orts^{1,2}, Daniel Carrasco², Gerwin Chilla¹, Rudolfo Hötzel¹, Jose Maria San Juan³, Maria Luisa N6³, Martin Eickhoff¹, Alicia de Andrés⁴, Emilio Nogales² and Bianchi Mendez²; ¹University of Bremen, Germany; ²University of Complutense-Madrid, Spain; ³Universidad del País Vasco, Spain; ⁴Instituto de Ciencia de Materiales de Madrid (CSIC), Spain

Semiconductor nanostructures-based optical microcavities have attracted much attention for decades. Gallium oxide, an ultra-wide bandgap semiconductor, is currently attracting great interest, especially for its applications in high power electronics [1]. Photonics applications are being parallelly explored, particularly solar-blind UV photodetectors and tunable emitters that take advantage of its 4.8 eV bandgap, allowing wide tunability from the UV to the IR [1]. Indeed, this oxide has shown highly interesting properties as a light emitter in this photonic range.

In this work, we show the use of beta-Ga2O3 nanowire-based photonic structures that result in optical microcavities to be used as resonant, tunable emitters and as thermal sensors. To this aim, microcavities with pairs of distributed Bragg reflectors (DBRs) were created in nanowires by drilling holes with a focused ion beam (FIB) [2] to yield carefully tuned stop bands, i.e. to strongly enhance the reflectivity for specific wavelength ranges. Widely tunable Fabry-Perot (FP) optical resonances are observed in the micro-photoluminescence (PL) spectra obtained from the cavities, which were thoroughly analyzed both experimentally, analytically and through finite-difference time-domain (FDTD) simulations. The results show nice agreement and allow to design and optimize their performance, as demonstrated in two different regions of the spectrum: the blue-NUV [3] and the red-NIR [2].

Finally, a novel design of thermal sensor based on these microcavities is presented [4]. Two different PL features – the R-lines of Cr³⁺ ions and the FP resonances created within the cavity – are monitored, observing a temperature-dependent spectral shift for both of them. Each feature is optimum for a different range, allowing to sense at least from 150 K up to 550 K. Temperature precision is around 1 K and the full width at half maximum of the FP peaks is nearly unchanged in the whole temperature range. These thermometers present a wide dynamic range, high spatial resolution - in the range of microns -, very high thermal and chemical stability and can be used in harsh environments, ideal for high electronic/optical power devices, among other applications.

[1] S. J. Pearton, J. Yang, P. H. Cary IV, F. Ren, J. Kim, M. J. Tadjer, and Michael A. Mastro, *Appl. Phys. Rev.* **5**, 011301 (2018).

[2] M. Alonso-Orts, E. Nogales, J. M. San Juan, M. L. N6, J. Piqueras, B. Méndez, *Phys. Rev. Appl.* **9**, 064004 (2018).

[3] M. Alonso-Orts, G. Chilla, R. Hötzel E. Nogales, J. M. San Juan, M. L. N6, M. Eickhoff, and B. Méndez, *Optics Letters* **46**, 278 (2021).

[4] M. Alonso-Orts, D. Carrasco, J. M. San Juan, M. L. N6, A. de Andrés, E. Nogales, B. Méndez, *Small* **18**, 2105355 (2022).

9:45 AM EQ03.22.05

A System for Measuring Deep Ultraviolet Cathodoluminescence Simo Pajovic¹, Charles Roques-Carnes¹, Steven E. Kooi¹, Nicholas Rivera¹, Ali

Ghorashi¹, Yang Yu², Ido Kaminer³ and Marin Soljačić^{1,1}; ¹Massachusetts Institute of Technology, United States; ²Raith America, Inc., United States;

³Technion-Israel Institute of Technology, Israel

Deep ultraviolet (DUV) radiation plays an essential role in several important technologies, including fluorescence, photolithography, and water purification. However, existing methods of producing DUV radiation have limitations: nonlinear processes (such as those used in Nd:YAG lasers) have limited efficiencies because of phase matching requirements and absorption; the efficiencies of state-of-the-art DUV LEDs (typically based on AlGaN) are limited by defects and electron leakage [1]; and mercury-vapor lamps are plagued with health and safety concerns. Scintillation—light emission from transparent materials due to the passage of high-energy particles—could be a viable alternative, particularly if the high-energy particles are electrons (also known as incoherent cathodoluminescence, or ICL). In this case, it has been predicted that direct bandgap emission could be highly efficient compared to the state of the art [2]. Additionally, the emission spectra of scintillators can be tailored by patterning their surfaces with photonic crystals [3], meaning that ICL-based DUV sources could be tunable in ways conventional ones are not. We have built an experimental setup based on a modified scanning electron microscope capable of measuring both ICL and coherent CL in the DUV (> 130 nm). In our setup, the electron beam impinges on the sample at grazing incidence, causing it to emit light. Emission is collected by a DUV coated reflective objective and sent to a UV monochromator and CCD camera, which finally measures the emission spectrum. Our setup has enabled us to measure DUV emission from wide bandgap materials such as diamond and h-BN and can be used to probe samples with patterned surfaces. We anticipate patterning will lead to spectral shaping and enhancement of DUV ICL based on our simulations of an h-BN nanophotonic scintillator, which showed a wavelength-dependent enhancement of the emitted power by nearly three orders of magnitude [3]. Our work enables the advancement of DUV scintillators and highlights the potential of electron beam pumping to lead to more efficient DUV sources, which would be desirable for all the aforementioned applications. This material is based upon work supported by the US Army Research Laboratory and the US Army Research Office through the Institute for Soldier Nanotechnologies under contract W911NF-18-2-0048.

References

- [1] M. Kneissl, J. Rass, Eds., III-Nitride Ultraviolet Emitters (Springer, Cham, 2016).
 [2] C. A. Klein, J. Appl. Phys. 39, 2029 (1968).
 [3] C. Roques-Carmes, N. Rivera, A. Ghorashi, S. E. Kooi, Y. Yang, Z. Lin, J. Beroz, A. Massuda, J. Sloan, N. Romeo, Y. Yu, J. D. Joannopoulos, I. Kaminer, S. G. Johnson, M. Soljačić, Science 375, eabm9293 (2022).

10:00 AM BREAK

SESSION EQ03.23: Fundamental of Plasmonics and Metaphotonics III
 Session Chairs: Seunghoon Han and Yu-Jung Lu
 Friday Morning, December 2, 2022
 Hynes, Level 2, Room 202

10:30 AM EQ03.23.01

Selective Capture of Hot Electrons/Holes for Plasmon Decay at an Atomically Sharp Metal-Semiconductor Interface Zehao Song and Alois Lugstein; Technical University of Vienna, Austria

Surface plasmon polaritons (SPPs), enabling to operate electro-magnetic waves at nanometer dimension and femtosecond time scale, provide a favourable bridge of combining the compactness of an electronic circuit with the bandwidth of a photonic network. However, this will require the exploration of effective photon to electron and electron to photon converters. Selectively collecting the non-equilibrium hot electrons/holes generated from SPPs decay at Schottky contacts is a promising approach to achieve on-chip hot-carrier photodetectors. Although there are already many studies on hot electron capturing and a few on hot holes, the mechanism is still under debate. This is mainly because the effect is difficult to study separately from common photo-generation and certain metal-smiconductor combinations can only selectively capture either holes or electrons. In this work, we report a gated Schottky diode device with a plasmonic nano-antenna coupled to the monolithic and atomically sharp aluminum-silicon (Al-Si) heterojunction enabling to capture selectively hot holes and/or electrons. Compared to the noble metals gold or silver, Al features an approximately uniform energy distribution, almost the same lifetime and mean free path for hot electrons and holes. The clear geometric separation of the SPPs source and the energy filtering Schottky diode allow precise investigation of the decay of SPPs and the capture of hot charge carriers. Using scanning photocurrent microscopy analysis, we elucidated the electrostatic potential in the ultrascaled Si channel and the tunable Schottky barrier. Using a sophisticatedly split gate configuration, hot electrons or hot holes can be selectively captured with similar external quantum efficiency, demonstrating experimentally the uniform energy distribution of hot electrons/holes energy for SPPs in Al.

10:45 AM EQ03.23.02

Spectral Emissivity Prediction in Multi-Resonator Metamaterials Using Temporal Coupled-Mode Theory Romil Audhkhasi and Michelle Povinelli; University of Southern California, United States

The ability to design thermal emitters with a multi-resonant spectral response is essential for advancement of a wide variety of applications such as thermal management and sensing. To this end, several numerical methods for predicting the spectral response of complex, multi-resonator systems have been investigated. In this work, we propose an alternative semi-analytical approach to spectral prediction based on temporal coupled-mode theory. In our approach, a complex thermal emitter is fully described by a set of coupled-mode parameters, which can be straightforwardly calculated from simulations of single and double resonators. We demonstrate the accuracy of our method by predicting and optimizing spectral response in a coupled, multi-resonator system based on hBN ribbons. Our approach greatly reduces the computational overhead associated with spectral design tasks in coupled, multi-resonator systems. In addition, it provides valuable insights into the relationship between structural parameters and spectral response that is not always possible with purely numerical methods.

11:00 AM EQ03.23.03

Nonreciprocal Photonics Using Surface Waves in the Magnetic Weyl Semimetal $\text{Co}_3\text{Sn}_2\text{S}_2$ Arun Nagpal¹, Christopher Ciccarino², Chandra Shekhar³, Claudia Felser³, Prineha Narang⁴ and Harry A. Atwater¹; ¹California Institute of Technology, United States; ²Stanford University, United States; ³Max Planck Institute for Chemical Physics of Solids, Germany; ⁴University of California, Los Angeles, United States

The demonstrations of a large intrinsic anomalous Hall effect and large nonlinear optical response in Weyl semimetals is attributable to the presence of nontrivial Berry curvature in regions of reciprocal space between recombinant Weyl points. We explore the properties of single crystals of the magnetic Weyl semimetal $\text{Co}_3\text{Sn}_2\text{S}_2$ for non-reciprocal photonics and polaritonic devices. Using Fourier transform infrared spectroscopy and ellipsometry, we characterize the material Mueller matrix at 80K in the MIR range we extract a Kramers Kronig consistent permittivity tensor. With [110]-oriented single crystals, we demonstrate the manifestation of non-equivalent reflection coefficients at $\pm 70^\circ$, induced through the generation of plasmons with a non-reciprocal dispersion. We find for our sample, the non-reciprocity is maximized at 0.17 eV, where the ratio of diagonal and off-diagonal components of the permittivity diverge. We discuss device designs that exploit these relations for use in magnet-less magneto-optical systems.

11:15 AM EQ03.23.04

Arbitrary Space-Time Wave Packet Synthesis Lu Chen^{1,2}, Wenqi Zhu^{1,2}, Pengcheng Huo³, Junyeob Song¹, Henri J. Lezec¹, Ting Xu³ and Amit Agrawal¹; ¹National Institute of Standards and Technology, United States; ²University of Maryland, United States; ³Nanjing University, China

Dielectric metasurfaces, composed of deep-subwavelength nanostructures, can sculpt the phase, amplitude, and polarization of light at the nanoscale. Their multifunctional response at the single-pixel level, combined with compact form-factor and integrability with other CMOS compatible devices make them key components for miniaturized photonic platforms, leading to numerous applications in spatial domain wavefront manipulation of light [1]. Recently, temporal-domain shaping of scalar waveforms of a linearly polarized ultrafast pulse has been demonstrated using dielectric metasurfaces [2, 3]. Here, we show, both theoretically and experimentally, that a single-layer transmission-mode dielectric metasurface can be leveraged to simultaneously and independently tailor the complete spatiotemporal properties of a near-infrared femtosecond pulse. This approach offers the most complete and general control of light field across an ultrabroad bandwidth, enabling synthesis of arbitrary space-time wave packets.

The spatiotemporal profile of a *p*-polarized femtosecond pulse of ≈ 10 fs duration (full-width at tenth-maximum bandwidth of ≈ 80 THz, centered at 800 nm) is tailored by manipulating the constituting discrete frequency lines. A 4-/ Fourier-transform pulse shaper spatially disperses and focuses the frequency lines at the Fourier plane, where a metasurface is positioned to implement a complex masking function sampled by 200 super-pixels. Each super-pixel contains a two-dimensional (2D) array of rectangular silicon nanopillars orientated at 45° with respect to the horizontal direction, providing parallel phase

modulation along the two birefringent axes. In this way, each super-pixel can independently impart a 2D spatial phase function as well as an overall phase-shift to the two orthogonal polarization components of frequency lines that reside within the super-pixel. The shaped frequency lines are then subsequently recombined into a spatiotemporally engineered femtosecond pulse.

This approach, leveraging ultra-high spectral resolution of a Fourier-transform pulse shaper and multifunctional responses at the nanoscale provided by the dielectric metasurface, offers ready design flexibility that can enable the synthesis of a vast variety of complex ultrafast spatiotemporal wave packets. To demonstrate the versatility of this approach, exotic femtosecond pulses, exhibiting a rich set of time-varying instantaneous polarization states and structured wavefronts within a single pulse, are designed and experimentally demonstrated. Comprehensive analysis, including numerical simulations and analytical modeling, are also performed to explain their spatiotemporal evolution.

In conclusion, we have demonstrated tailoring of both the temporal and spatial degrees of freedom of an ultra-broad bandwidth, near-infrared femtosecond pulse using a single-layer transmission-mode dielectric metasurface. Such an approach further promotes the already intriguing applications of metasurfaces, revealing new possibilities in the field of ultrafast science and technology.

[1] N. Yu and F. Capasso, *Nature Materials* **13**, 139 (2014).

[2] S. Divitt, W. Zhu, C. Zhang, H. J. Lezec, and A. Agrawal, *Science* **364**, 890 (2019).

[3] M. Ossiander, Y.-W. Huang, W. T. Chen, Z. Wang, X. Yin, Y. A. Ibrahim, M. Schultze, and F. Capasso, *Nature Communications* **12**, 6518 (2021).

11:30 AM EQ03.23.05

Tailoring the Optical Properties of Zinc Oxide via Bismuth Doping and Co-Doping Strategies—From Birefringence to Metallicity Samar Fawzy, Yehea Ismail and Nageh K. Allam; American University in Cairo, Egypt

We make use of density functional theory to explore the effect of Bi as a high-index dopant on the optical properties of 3 metal-oxide structures: Titanium dioxide (TiO₂), Zirconium dioxide (ZrO₂) and Zinc Oxide (ZnO). It was found that Bi_{Metal} substitutional doping results in reducing the bandgap (E_g) by creating new defect states in the 3 oxides. In case of ZnO, the in-plane refractive index (n_{x,y}) is doubled (>3) over a wide band in mid and far IR, and huge birefringence is obtained compared to other materials in literature. The presence of Oxygen vacancies (O_v) in the structure was found to lower the losses, which was elaborated by the decreased absorption cross section of a sphere of 250 nm radius, using FDTD. At 12% Bi doping, metallicity is obtained with losses lower than Silver, Gold, and Nitrides. Co-doping of Bi with interstitial Hydrogen doping (H_i) or substitutional Aluminium (Al_{Zn}) doping give the same effect, which is increasing both the in-plane and out of plane indices even higher, but on the expense of increasing optical losses.

SESSION EQ03.24: Active Plasmonics
Session Chairs: Claudio Hail and Yu-Jung Lu
Friday Afternoon, December 2, 2022
Hynes, Level 2, Room 202

1:30 PM EQ03.24.01

Tunable Electrical and Optical Properties of Photonic and Plasmonic Multilayer Metastructures Based on Alternative Plasmonic Materials

Cristina Mancarella¹, Liliana Moscardi¹, Lorenzo Stasi¹, Ludovica Tovaglieri¹, Gianluigi Baiardi¹, Giacarlo Terraneo^{1,2}, Vincenzo Caligiuri^{3,4}, Antonio De Luca^{3,4}, Francesco Scotognella^{1,2} and Andrea Li Bassi^{1,2}; ¹Politecnico di Milano, Italy; ²CNST - Italian Institute of Technology, Italy; ³Università della Calabria, Italy; ⁴CNR - Nanotec, Italy

The current research in plasmonic nanotechnologies is focusing on nano-systems with intrinsic multifunctionalities, aimed at reaching large tunability of properties to fulfill at once multiple needs, spanning different applications (optoelectronics, biosensing, solar-energy harvesting). The archetypal plasmonic materials, i.e. noble metals, show limited modulation outside the visible spectrum due to the fixed charge carrier density [1]. This justifies the spreading interest for alternatives (transparent conductive oxides TCOs, transition metal nitrides or oxynitrides) and periodically-arranged multi-phase nanostructures, where the high level of control in carrier concentration is achievable directly at synthesis or with an “active” approach (e.g. external bias). Indeed, several nanoarchitectures have been investigated to modulate optical characteristics of plasmonic metals outside the visible, enhance performances, and eventually activate novel functionalities. Hyperbolic metamaterials especially sustain unique “high-k modes” activated by the periodic alternation of conductors (e.g. noble metals) and dielectrics (e.g oxides) of subwavelength thicknesses [2]. Besides, when increasing the characteristic dimension of layers, Bragg’s reflections start to appear and one-dimensional (1D) photonic crystals can be achieved straightforward [3].

Here, a variety of novel multifunctional nano-structures have been developed, involving alternative materials (TCOs, nitrides and oxynitrides) and original design routes (via pulsed laser deposition PLD) with the aim to explore, from a material science perspective, electrical/optical responses resulting from unusual combinations of materials and properties (transparency, conductivity, tunable VIS-IR plasmonics, active modulation).

For instance, novel TiN-TiO₂ plasmonic multilayers have been realized as hyperbolic metamaterial in the visible, with added advantages determined by the good material affinity and the versatility of TiO₂ as a wide-band gap semiconductor. In addition, the resulting features can benefit from the refractory nature and CMOS compatibility of TiN, along with the possibility to modify the plasmonic response through stoichiometry. Then, original transparent conducting multilayers based on the less-explored Tantalum-doped TiO₂ (Ta:TiO₂) TCO have been obtained directly in a simple one-step synthesis, by alternating conductive (compact) and dielectric (nanoporous) layers of the same TCO achieved by varying the deposition pressure (1-6 Pa O₂). Structural and electrical properties have been optimized to control optical/plasmonic outputs as a function of deposition conditions, doping content and geometrical parameters. Future applications are foreseen as hyperbolic platforms or biosensing devices in the IR, while 1D photonic crystals can be accomplished by customizing compact/porous fraction and dimension of the layers. The proper optimization of material properties leads to an intense photonic band gap, spanning from green to red wavelengths in the visible, which in turn can be actively modulated with an external bias. Finally, the investigation of TiON films as tailorable oxynitrides with expected epsilon-near-zero behaviour, has been started by finely controlling the oxygen content directly during PLD synthesis.

Concluding, these multifunctional meta-devices are application-oriented and possess a cross-disciplinary attitude. Current challenges are related to mastering the material properties and designing devices to prove the real applicability of such meta-structures. Hence, the list of practical applications includes, but is not limited to, VIS or mid-IR biosensors, surface enhanced infrared Raman spectroscopy, optoelectronic elements for color manipulation and thermophotovoltaic emitters.

[1] G.V. Naik et al. *Advanced Materials* **25**, 24, 3264-3294 (2013).

[2] Z. Guo et al. *Journal of Applied Physics* **127**, 071101 (2020).

[3] H. Shen et al. *RCS Advances*, **6**, 4505-4520 (2016).

1:45 PM EQ03.24.02

Helicity-Driven Spin Currents and Magnetization Dynamics in Au-Based Structures Chuangtang Wang and Yongmin Liu; Northeastern University,

United States

Ultrafast helicity-dependent all-optical switching of magnetization by a femtosecond laser pulse has attracted extensive interest, because it holds the promise for future high-rate magnetic storage. Controlling the spin angular momentum transfer from light to magnetic materials is the key to achieve the helicity-dependent switching of a single layer's magnetization. Researchers have found that a capping layer made of heavy metal with large spin-orbital coupling strength, such as Pt, Ta, and W, could enhance the spin momentum transfer, namely optical spin-transfer torque, compared to the direct interaction between the light and magnetic materials. In this work, we will discuss the potential of Au as a better choice for the capping material, because it supports plasmonic resonances which enable both enhanced spin-momentum transfer and nanoscale plasmonic integration. We have studied the magnetization dynamics of Au/Co structures with a time-resolved magnetic-optical Kerr effect spectroscopy. The existence of large spin-transfer torque is observed in the system. The overall efficiency is as high as that in Pt/Co. The mechanism is revealed by the detailed thickness- and wavelength-dependent measurements of magnetization dynamics. Our findings will stimulate future research using Au plasmonic structures to achieve more efficient and denser magnetic storage.

2:00 PM DISCUSSION TIME

2:15 PM EQ03.24.04

Electrically-Switchable Angle-Dependent Plasmonic Coloration [Gyurin Kim](#), Jang-Hwan Han, Hyun Min Kim, Juhwan Kim and Hyeon-Ho Jeong; Gwangju Institute of Science and Technology, Korea (the Republic of)

Optical encryption using plasmonics is a superior concept for security as it offers fade-free rich colorations with viewing-angle and/or polarization dependency.[1] However, such plasmonic coloration typically not only necessitates complex nano-lithographic patterning for multilayered plasmonic systems with their precise nanoscale dimension, but also remains in the production of static image planes.

We here present a 'lithography-free' method to fabricate wafer-scale multi-layered 'active' plasmonic metasurfaces, which show angle-dependent as well as electrically switchable coloration across the whole visible spectra. The physical vacuum growth with substrate cooling allows us to grow a wafer-scale array of dense plasmonic nanoaggregates on a metallic mirror coated with a conductive polymer layer (here polyaniline). Such nanoparticle-on-mirror constructs filled with polyaniline intrinsically possess two dominant gap plasmonic modes, i.e. (i) in-plane coupling between densely-positioned nanoparticles and (ii) out-of-plane coupling between the nanoparticles and the mirror underneath. These two coupling modes can be excited selectively depending on an incident angle of the light and thus reveal a vivid color transition. More crucially, such colors can now be further electrically tunable in response to an external voltage applied ($< 1V$), thanks to the change in the redox states of the polyaniline within the nanojunctions and thus associated refractive indices.[2] With the combinatorial control in the light angle and the electrical input, the single plasmonic metasurface gives rise to rich colorations across the whole visible spectra, potentially useful for 'active' optical information storage and encryption.

In this presentation, the structural design, numerical simulation, fabrication method, optical feature and analysis of the electrically switchable plasmonic metasurfaces will be discussed.

[1] J. Park et. al, Adv. Mat. 2021, **33**, 2007831

[2] J. Peng et. al, Sci. Adv. 2019, **12**, eeaw2205

2:30 PM EQ03.24.05

Microporous Multiresonant Plasmonic Meshes by Hierarchical Micro-Nanoimprinting for Bio-Interfaced SERS Imaging and Nonlinear Nano-Optics [Aditya Garg](#), Elieser Mejia, Wonil Nam, Meitong Nie, Wei Wang, Peter Vikesland and Wei Zhou; Virginia Tech, United States

Due to their low elastic moduli and high permeability to nutrients and oxygen, mesh-like flexible microporous devices confer significant biocompatibility advantages to interface with cell networks and tissues for biomedical sensing or actuation applications. Microporous mesh plasmonic devices have the potential to combine the biocompatibility of microporous polymeric meshes with the capabilities of plasmonic nanostructures to enhance nanoscale light-matter interactions for bio-interfaced optical sensing and actuation. However, scalable integration of dense and uniformly structured plasmonic hotspot arrays with microporous polymeric meshes remains challenging due to the processing incompatibility of conventional nanofabrication methods with flexible microporous substrates. For the first time, we have created microporous multiresonant plasmonic mesh (MMPM) devices via a dissolvable template-based hierarchical micro-/nanoimprinting approach. The MMPMs carry 2-tier nanolaminar plasmonic crystals (NLPCs) consisting of two optically coupled nanodome and nanohole multiresonant sub-systems. The NLPCs can support many hybridized plasmonic modes with spatial overlap and can allow for multiresonant nanoscale light concentration across a wide wavelength range between 400 and 1400 nm. We demonstrate that MMPMs can serve as broadband nonlinear nanoplasmonic devices to generate second-harmonic generation (SHG), third-harmonic generation (THG), and upconversion photoluminescence (UCPL) signals with multiresonant plasmonic enhancement under fs pulse excitation. Moreover, we demonstrate that MMPMs can function as bio-interfaced surface-enhanced Raman spectroscopy (SERS) mesh sensors that enable in-situ spatiotemporal molecular profiling of bacterial biofilm activity. We envision that microporous mesh plasmonic devices can open exciting avenues for bio-interfaced optical sensing and actuation applications, such as inflammation-free epidermal sensors in conformal contact with skin, combined tissue-engineering and biosensing scaffolds for in vitro 3D cell culture models, and minimally invasive implantable probes for long-term disease diagnostics and therapeutics.

3:00 PM BREAK

SESSION EQ03.25: Advanced Nanophotonic Design IV

Session Chairs: Yao-Wei Huang and Yu-Jung Lu

Friday Afternoon, December 2, 2022

Hynes, Level 2, Room 202

3:30 PM EQ03.25.01

Discovery of New Plasmonic Metals Using First-Principles Simulations and Machine Learning Ethan Shapera, Andre Schleife and [Erick I. Hernandez Alvarez](#); University of Illinois at Urbana-Champaign, United States

Discovering new materials with low-loss response to an applied optical field while exhibiting collective oscillations due to intraband transitions is an outstanding challenge for the field of plasmonics. While nanoscale structuring also affects practical applications in this context, here we view this as a materials selection problem: In particular, we aim to address the gap between the large number of a priori candidate materials and high computational cost

to accurately compute optical properties from first principles. We combine the Materials Project database with first-principles simulations and the Drude model. Using density functional theory we compute a training set of geometry-dependent plasmonic quality factors for almost 1,000 materials and train random-forest regressors on this data. Our descriptors ignore crystal structure and are limited to symmetry, quantities obtained using the chemical formula, and the Mendeleev database. Using the trained model we rapidly screen 7,445 candidates and subsequently use density functional theory to compute quality factors for the 233 most promising materials. From this, we identify AlCu_3 , ZnCu , and ZnGa_3 as excellent potential new plasmonic metals and substantiate these results by analyzing their electronic structure and interband optical properties in detail.

3:45 PM EQ03.25.03

Mechanical Deformation Induced Tunable Mid-Infrared Optical Properties [Fangqi Chen](#), Xiaojie Liu, Yanpei Tian and Yi Zheng; Northeastern University, United States

Over the past decade, tremendous efforts have been devoted to the design of metamaterials with ultrahigh absorption. These perfect absorbers can realize the annihilation of incident electromagnetic waves by eliminating reflection and transmission of microwaves, infrared, visible, and ultraviolet. However, the optical properties are usually unchanged due to a rigid structure. In this work, we propose a mechanically stretchable metamaterial composed of polydimethylsiloxane and gold with tunable optical properties in the mid-infrared region. A large variation of absorptances with different gold filling ratios is demonstrated as well as the corresponding electric field distributions. Under moderate uniaxial and biaxial tensions, the proposed two-dimensional grating structure has achieved a dynamic tuning of infrared thermal properties, including a sharp reflectance-absorptance switch. This mechanically stretchable metamaterial can serve different optical and sensing functions due to its facile tunability.

4:00 PM EQ03.25.04

Ultrathin Perfect Absorbing Metamaterial Stacked with Solid and Inverse Antenna Above Metal Ground [Minji Kim](#)¹, Kyungmin Jung¹, Youmee Choi², Seung Sang Hwang² and Jerome K. Hyun¹; ¹Ewha Womans University, Korea (the Republic of); ²Korea Institute of Science and Technology, Korea (the Republic of)

Metamaterials have proven to be effective electromagnetic (EM) wave absorbers with unprecedented control over the properties of the wave. (1-3) To achieve ultracompact, flexible, and lightweight EM absorbers, the ability to perfectly absorb an EM wave with a material much thinner than the wavelength is required. Herein, we demonstrate a metamaterial with extreme subwavelength thickness by introducing a cross-shaped aperture into the bottom metal plane of a conventional three-layer metal patch/dielectric/metal stack. (4) With the stack placed above a metal ground for perfect absorption, a total thickness of only 1/1250 of the working wavelength is achieved. The aperture increases the resonance wavelengths by up to 10-folds by enlarging the inductance of the stack. More specifically, the induced current in the aperture plane must flow around the aperture, creating a magnetic flux that increases with aperture area. Using this approach, we experimentally demonstrate perfect absorption using the appropriate dielectric thickness and loss tangent needed to achieve critical coupling. To the best of our knowledge, our EM absorbers provide the largest wavelength-to-thickness ratios to date. The principles outlined here are general and can be extended to other frequencies.

Reference

1. C. M. Watts, X. Liu, W. J. Padilla, "Metamaterial Electromagnetic Wave Absorbers." *Adv. Mater.* **24**, OP98-OP120 (2012).
2. N. I. Landy, S. Sajuyigbe, J. J. Mock, D. R. Smith, W. J. Padilla, "Perfect Metamaterial Absorber." *Phys. Rev. Lett.* **100**, 207402 (2008).
3. Y. Ra'di, C. R. Simovski, S. A. Tretyakov, "Thin Perfect Absorbers for Electromagnetic Waves: Theory, Design, and Realizations." *Phys. Rev. Appl.* **3**, 037001 (2015).
4. M. Kim, K. Jung, Y. Choi, S. S. Hwang, J. K. Hyun, "Coupled Solid and Inverse Antenna Stacks Above Metal Ground as Metamaterial Perfect Electromagnetic Wave Absorbers with Extreme Subwavelength Thicknesses." *Advanced Optical Materials*, 2101672 (2022).

4:15 PM EQ03.25.05

Compound Meta-Optic for Lossless Complete Field Manipulation [Hanyu Zheng](#)¹, Mingze He¹, You Zhou¹, Ivan Kravchenko², Joshua D. Caldwell¹ and Jason G. Valentine¹; ¹Vanderbilt University, United States; ²Oak Ridge National Laboratory, United States

The ability to independently control the amplitude, phase, and polarization state of light is needed for a wide variety of scientific and industrial applications and generally requires multiple conventional optical elements such as lenses, polarizers, and amplitude masks. The need for multiple elements results in large systems that can be difficult to integrate into compact optical packages. Optical metasurfaces, comprising sub-wavelength scale meta-atoms, provide a versatile platform for manipulating optical waves in a compact form factor, and have been used to create a wide variety of optical elements such as lenses, beam splitters, and waveplates. Metasurfaces, moreover, can go beyond simple replacement of conventional optics by providing novel functionalities including multi-functional imaging, phase-mining, image processing, polarimetry, augmented reality, holography.

Although metasurface-based wavefront control has been demonstrated in the past, independent control of phase and amplitude using a single metasurface comes at the expense of a polarization-dependent response. The involvement of polarizer components introduces loss that can be as high as 90% in some circumstances. Moreover, the symmetric Jones matrix that dictates the transmission of each meta-atom prevents independent control over polarization conversion for orthogonal axes. Spatial multiplexing, on the other hand, can provide independent polarization manipulation over orthogonal states by using interference between the neighboring meta-atoms. However, this method leads to higher diffraction orders due to the use of a larger supercell, limiting the diffraction efficiency in the target order. An alternative approach is the use of multi-layer, compound meta-optics, which harness independent design degrees of freedom in each layer and allow for light redistribution during propagation for realizing near loss-less amplitude and phase functions.

In this work, we expand on the multi-layer meta-optic platform to include polarization by employing end-to-end design optimization. In this platform, birefringent meta-atoms are used for both metasurfaces, enabling independent control over orthogonal polarization states as well as polarization conversion between those states. Redistribution of the wavefront between metasurface layers allows for loss-less, complex-valued wavefront and polarization control, that is not limited by the symmetric Jones matrix. As a proof of concept, we experimentally demonstrate a meta-optic for optical mode manipulation, including a spatial division multiplexer (SDM), an optical mode converter, and a vectorial hologram.

All the demonstrated devices are optimized by an end-to-end inverse design algorithm, which is a stochastic gradient descent (SGD)-based platform, a common approach in machine learning applications. The use of multiple loss functions as well as k -space constraints during optimization avoids overfitting and scattering phase morphology for metasurfaces, allowing for highly improved device performance. In our case, all the devices achieve diffraction efficiency above 80% in experimental measurements. Meanwhile, the meta-optic platform that combines birefringence with the ability to redistribute the wavefront across the aperture, also demonstrates independent and decent control over the amplitude, phase and polarization state. We believe that the increased engineering freedom provided by compound meta-optics will open new avenues for the development of compact optical systems with novel functionalities and applications in quantum entanglement, optical encryption, and optical communications.

4:30 PM EQ03.25.06

Polarization-Selective Non-Volatile Switching in Hybrid Phase-Change Nanowires [June Sang Lee](#)¹, Nikolaos Farnakidis¹, C. David Wright² and

Harish Bhaskaran¹; ¹University of Oxford, United Kingdom; ²University of Exeter, United Kingdom

Polarization, one of the fundamental properties of electromagnetic waves, provides extra physical dimensions for multiplexing optical information and has been essential for applications in optical communication, storage, and encryption. However, such multiplexing properties have been mostly passive thus far, and have not been employed as a tunable factor in optical systems.

Reconfigurable photonics on the other hand, has been rapidly growing. The use of phase change material is established as a functional block for non-volatile photonic and mixed-mode memories with prospective applications in neuromorphic and in-memory computing paradigms. These devices incorporate phase change materials as the reconfigurable elements and have been shown to achieve nanosecond switching performance with large optical modulation over a broad bandwidth. Reconfiguration in phase-change photonic devices is commonly achieved by controlling the intensity or pulse shape of an incident light wave while resonant structures are broadly employed to achieve wavelength-selective operation and enhanced modulation depths. The equivalent functionality in polarization-space is however absent. This significantly limits the addressability of distinct elements in cascaded systems without harnessing full advantages of photonic bandwidths.

Here, we demonstrate for the first time polarization-selective switching in hybrid phase-change nanowires,¹ wherein the optical absorption in the nanowires is modulated by polarization of incoming light. In doing so, the transient temperature profile is controlled to induce reversible switching of the hybridized phase-change element. Our hybrid nanowire consists of a two-layered system of Si/Ge₂Sb₂Te₅ (GST) where dielectric resonance of Si leads the GST to be switched in a polarization-selective manner. Such switching operation is finely modulated by changing the polarization directions, and therefore provides an important degree of freedom for control over the multilevel device states. Using this concept, we demonstrate the polarization-decoupled but electrically-interfaced multi-nanowire system to achieve polarization-selective demultiplexing at highly-confined spatial scales. We further show the use of this system to carry out matrix-vector multiplications with using polarization as a tunable variable. This leads to a huge enhancement of computing density, exceeding that of conventional electronic chips by several orders of magnitude. Our work provides the first such pathway for exploiting polarization to actively modulate device-states with applications ranging from optical encryption/storage to computing.

References

[1] J. S. Lee, N. Farmakidis, C. D. Wright, H. Bhaskaran, "Polarization-selective reconfigurability in hybridized-active-dielectric nanowires", *Sci. Adv.* (2022) doi: 10.1126/sciadv.abn9459

SESSION EQ03.26: Virtual Session I: Fundamental of Plasmonics and Metaphotonics IV
Session Chairs: Po-Chun Hsu and Ren-Min Ma
Tuesday Morning, December 6, 2022
EQ03-virtual

8:00 AM *EQ03.26.01

Structures and Materials for Highly Efficient Non-Linear Optics at the Nanoscale Stefan A. Maier^{1,2}; ¹Monash University, Australia; ²Imperial College London, United Kingdom

Nanophotonic resonators combined with two-dimensional materials are a fertile environment for the development of new approaches for highly efficient non-linear optical devices. Here we will survey our recent work in this regard, focusing on plasmonic or dielectric nanoresonators coupled to a variety of two-dimensional materials. One example is a ring-like resonator structure supporting bound states in the continuum, which due to its compact size is ideal for interfacing with flakes of 2D materials.

We will further present a highly promising class of materials with an extraordinarily high second-order non-linear response, two-dimensional ferroelectric materials.

8:30 AM EQ03.26.03

Characterization of Optical/Electrical Properties and Application of High Crystalline Titanium Nitride Ultrathin Films I-Hung Ho¹, Ching-Wen Chang², Yu-Jung Lu³, Shangir Gwo² and Hyeoung Ahn¹; ¹National Yang Ming Chiao Tung University, Taiwan; ²National Tsing Hua University, Taiwan; ³Academia Sinica, Taiwan

Recently, titanium nitride (TiN) attracts a great attention as a refractory plasmonic material owing to its superior optical properties in the visible and near-infrared spectral regions, high melting temperature, low extinction loss, and excellent mechanical and chemical stabilities. TiN also possesses the epsilon-near-zero (ENZ) point in the shorter end of visible spectrum than gold. One of the many exciting significances of ENZ materials is the strong enhancement of nonlinear optical processes and even higher nonlinear optical effect can be obtained for ultrathin ENZ films or metamaterials, in sharp contrast to conventional high nonlinear response for thick or bulk materials.

In order to realize these excellent performances of TiN, the growth of high quality TiN particularly in the form of ultrathin film is requisite; however, most of previous works on TiN have been reported for the films grown via reactive sputtering, pulsed laser deposition, or atomic layer deposition techniques. Only recently, single-crystalline, stoichiometric TiN films could be realized by the molecular-beam epitaxy (MBE) under the ultrahigh vacuum (UHV) environment. In this work, we will present the growth of TiN ultrathin films with 2–10 nm in thickness and the characterization of optical and electrical properties. Owing to UHV growth, the influence of oxygen-related defects which causes critical degradation of performance is greatly reduced in our MBE-grown TiN epilayers. Formation of continuous and smooth ultrathin TiN films is realized by X-ray diffraction (XRD) and the surface morphology is measured by atomic force microscopy (AFM) and scanning electron microscopy (SEM). The cross-section transmission electron microscope (TEM) image of the 2.4 nm TiN film shows a clear atomic alignment, confirming the growth of high crystalline quality epitaxial film with thickness even down to 2.4 nm.

The optical and dielectric properties of ultrathin TiN epilayers are determined by the reflection/transmittance/absorption measurement and spectroscopic ellipsometry. As the film thickness decreases below 10 nm, the ENZ point of ultrathin TiN epilayers shifts from 480 nm to 550 nm, enabling the realization of tunable plasmonic material. The optical loss also decreases with reduction of film thickness and the optical transmittance increases up to >75% for the 2.4 nm film over the whole visible regime. Electrical properties of the ultrathin TiN films are explored by employing the THz time-domain spectroscopy (THz-TDS) as well as the Hall effect measurement technique. THz-TDS is an optical and non-contact method to characterize the electrical properties of various materials including nanostructured metals, whereas the Hall effect technique is a direct electrical measurement method. THz spectroscopy reveals that the percolation thickness of the MBE-grown TiN epitaxial film is less than 2.4 nm, which is much thinner than the percolation thickness (6–10 nm) of noble metals. More importantly, the conductivities measured by THz-TDS are in excellent agreement with those measured by the Hall effect method. This

is in sharp contrast to previous reports showing a large discrepancy between optically and electrically measured conductivities for ultrathin TiN films fabricated by other techniques in atmospheric environments. The excellent electrical properties of MBE-grown ultrathin TiN films are attributed to their high crystalline quality with the low density of oxygen-related and structural defects. Our results demonstrate the wide potential applications of ultrathin TiN epilayer films as refractory plasmonic material. Additionally, high optical transmittance and electrical conductivity of MBE-grown ultrathin films demonstrate that combined with its high mechanical, thermal, and chemical stabilities, they can serve as a high performance and robust transparent and conductive metal electrode compatible to complementary metal-oxide-semiconductor (CMOS) fabrication technology.

8:45 AM EQ03.26.04

Magnetically Tunable 1D Plasmonic Photonic Crystals [Chaolumen Wu](#), Qingsong Fan and Yadong Yin; University of California Riverside, United States

Structurally colored materials have been attractive for many years due to their vivid colors, long stability, and easy tunability, and within them, plasmonic and photonic nanostructures are two powerful systems to generate structure colors with easy control of the photonic colors. Although promising, the combination of plasmonic resonance and photonic bandgap within a single system is challenging. In this work, 1D plasmonic photonic crystals with angular-dependent structural colors are fabricated by assembling magneto-plasmonic colloidal nanoparticles under an external magnetic field. Different from conventional 1D photonic crystals, the assembled 1D periodic structures show angular-dependent colors from the selective activation of photonic diffraction and plasmonic scattering. Furthermore, the magneto-plasmonic nanoparticle chains can be fixed in an elastic polymer matrix to produce photonic films with angular-dependent as well as mechanically tunable optical properties. Thanks to the easy and precise modulation of magnetic assembly, the orientation of the nanochains within the polymer matrix can be precisely controlled to produce photonic films with desired patterns, showing versatile colors from the backward photonic diffraction and forward plasmonic scattering. This work demonstrates an easy way to combine plasmonic and photonic properties within a single system, showing synergetic optical properties and indicating the potential for the development of programmable optical functions for the applications in color display, optical devices, and information encryption.

9:00 AM EQ03.26.06

Understanding Photovoltage Response of Hexagonal Boron Nitride (hBN)-Graphene-Silver Based 2D van der Waals Heterostructures Towards the Realization of UV-Visible Photodetectors [Debalena Majumder](#); Indian Institute of Science (IISc), India

Various Graphene-plasmonic nanoparticle hybrid devices have paved a way for sensitive photodetection of UV signal leading to multipurpose electrical as well as optoelectronic applications. A single monolayer of graphene (SLG) is sensitized with silver nanoparticles (having size distribution of 50-100nm), such that the electric field close to the nanoparticles generated due to the Localized Surface Plasmon Resonance (LSPR) results in an increased engineered photo response in the UV spectrum. Addition of an intermediate h-BN monolayer to such photodetectors aims to improve the photo response by reducing the substrate effects, interfacial resistance along with the prevention of surface oxidation. The purpose of this study is to investigate the role of 8 different 2d material based composite nanostructures fabricated using layer-by-layer build up technique, which play a determining role in controlling their optical and electronic response.

Raman Spectroscopy analyses the effect of inherent strain and local doping concentration of the graphene monolayer in presence of plasmonic structures. Full width half maxima (FWHMs) of both G and D peak are higher indicating localised strain in case of samples having Gr layer transferred on top of the Ag particles. Whereas the ID/IG ratio when much greater than 1 denotes higher defect concentration in samples due to the formation of sp³ carbon within graphene. Henceforth, significant enhancement is observed in Raman peak intensity with the introduction of HBN to the Gr-Ag composites. The Responsivity study on such samples suggest that the position of the 2D material plays a key role in the anomalous response of these detectors. Further a correlation between optical Responsivity and Resonance plasmonic peak positions with particle distribution and shape analysis was established. Subsequently, each photo response has been deconvoluted into their characteristic rise and fall time zones using an empirical formulation, from which an idea about the effect of intermediate trapping and de-trapping states of these devices can be understood.

10:00 AM DISCUSSION TIME

SESSION EQ03.27: Virtual Session II: Lasing and Radiation Engineering III
Session Chairs: Ho Wai Howard Lee and Yu-Jung Lu
Tuesday Morning, December 6, 2022
EQ03-virtual

10:30 AM *EQ03.27.01

Topological Polarization Singular Laser [Ren-Min Ma](#); Peking University, China

We report a new class of topological polarization singular lasers with high radiation efficiency.

11:00 AM *EQ03.27.02

Control of Nanoscale Heat Generation and Applications for Ultrafast Detectors [Maiken H. Mikkelsen](#); Duke University, United States

Control of light-matter interactions on the deep nanoscale holds the potential to transform a wide variety of optical materials and optoelectronic devices. First, by integrating a plasmonic metasurface with an aluminium nitride pyroelectric thin film, we demonstrate spectrally selective, room-temperature pyroelectric detectors from 660–2,000 nm with an instrument-limited 1.7 ns full width at half maximum and 700 ps rise time (Stewart et al., Nature Materials 19, 158, 2020). Heat generated from light absorption diffuses through the subwavelength absorber into the pyroelectric film producing responsivities up to 0.18 V W⁻¹ due to the temperature-dependent spontaneous polarization of the pyroelectric films. Next, we demonstrate a novel, large-area embedded metasurface architecture that is environmentally robust and capable of spectrally-selective absorption greater than 80 percent spanning from 330-2740 nm (Stewart et al., Nano Letters, in press 2022). These fully encapsulated metasurfaces leverage the capabilities of colloidal plasmonic nanoparticles with various crystallinities, materials, shapes, and sizes to access a larger spectral range and allow for control of nanoscale spatial losses and subsequent heat generation within the constituent elements of the metasurface. Through selection of material, particle size, and shape, these metasurfaces can be designed across the ultraviolet (UV) to short-wave infrared (SWIR) for various hot-electron, photodetection, photocatalysis, and photothermal processes.

11:30 AM *EQ03.27.03

Nanoengineering of Light Absorption—From Hot Carriers to Photothermal Effects [Giulia Tagliabue](#); École Polytechnique Fédérale de Lausanne, Switzerland

In the last decade, optical nanoantennas have revolutionized light manipulation and control at the nanoscale. Light absorption was initially considered a purely detrimental process, reducing the efficiency of optoelectronic devices. Recently, however, it has attracted growing interest, enabling novel light-energy conversion pathways, such as hot carrier harnessing, but also interesting application opportunities based on nanoscale photothermal effects. In this talk, I will first present fundamental aspects of plasmonic hot carrier generation and collection towards photoelectrochemical devices for light energy storage. In particular, I will report the construction, optoelectronic and photoelectrochemical characterization of plasmon-driven devices that operate via hot-hole injection, and I will compare them to their hot electron counterparts [1-4]. I will also show emerging opportunities for plasmonic hot carriers in redox-couple based photoelectrochemical devices and advanced optical design strategies for improving the efficiency [5]. Overall, these results demonstrate the critical role of the metal properties onto hot carrier generation and transport. Thus, I will next report on our recent effort towards the synthesis of record-high aspect ratio gold monocrystalline flakes [6]. In particular, I will discuss how we can leverage them for understanding fundamental electronic processes in metals as well as plasmonic photo-electrochemistry. Finally, I will focus on collective photothermal effects in plasmonic networks and discuss a fast computational method we developed to estimate local temperature maxima and minima. I will conclude with an outlook on applications of hot carriers and photothermal effects in nanoengineered optical antennas.

References

- [1] G Tagliabue, AS Jermyn, R Sundararaman, AJ Welch, JS DuChene, R Pala, AR Davoyan, P Narang, HA Atwater, *Quantifying the role of surface plasmon excitation and hot carrier transport in plasmonic devices*, **Nature Communications** **2018**, 9 (1), 3394.
- [2] G Tagliabue*, JS DuChene*, M Abdellah*, A Habib, DJ Gosztola, Y Hattori, WH Cheng, K Zheng, SE Canton, R Sundararaman, J Sá, HA Atwater, *Ultrafast hot-hole injection modifies hot-electron dynamics in Au/p-GaN heterostructures*, **Nature Materials** **2020**, 19(12), 1312-1318. (* equal contribution)
- [3] JS DuChene*, G Tagliabue*, AJ Welch, WH Cheng, HA Atwater, *Hot Hole Collection and Photoelectrochemical CO2 Reduction with Plasmonic Au/p-GaN Photocathodes*, **Nano letters** **2018**, 18 (4), 2545-2550 (* equal contribution)
- [4] G Tagliabue, JS DuChene, A Habib, R Sundararaman, HA Atwater – *Hot-Hole versus Hot-Electron Transport at Cu/GaN Heterojunction Interfaces - ACS Nano* **2020**, 14, 5, 5788–5797.
- [5] F Kiani, F Sterl, TV Tsoulos, K Weber, H Giessen, G Tagliabue, *Ultra-Broadband and Omnidirectional Perfect Absorber Based on Copper Nanowire/Carbon Nanotube Hierarchical Structure*, **ACS Photonics** **2020** 7 (2), 366-374, 2020
- [6] F Kiani, G Tagliabue, *High Aspect Ratio Au Microflakes via Gap-Assisted Synthesis*, **Chemistry of Materials** **2022**, 34(3), 1278-1288.

12:00 PM EQ03.27.04

Organic Light-Emitting Diode Coupled to Photonic Bound State in the Continuum [Mengfei Wu](#), Son Tung Ha, Ramon Paniagua Dominguez and Arseniy Kuznetsov; Institute of Materials Research and Engineering, Singapore

Lasers based on nanomaterials, such as colloidal nanocrystals, organics, and perovskites, are attractive because of their tunable lasing wavelength, feasibility on a variety of substrates, and facile fabrication. Despite significant progress in optically pumped lasers, nanomaterial-based laser diodes have remained elusive. A typical laser diode consists of a light-emitting diode (LED) integrated with a photonic cavity. Recent efforts have focused on distributed feedback (DFB) cavities, where a grating is patterned into the transparent electrode or emissive layer. Here, we employ a photonic bound state in the continuum (BIC) that arises from an array of out-of-plane dipoles oscillating in phase and has an extremely high quality (Q) factor. Specifically, we fabricate an organic LED (OLED) on a smooth substrate, in which an array of titanium dioxide cylinders is embedded to minimize effects on the electrical performance of the OLED. We demonstrate efficient coupling of the electroluminescence of the OLED to a high-Q BIC mode, paving the way for electrically-driven lasing.

12:15 PM EQ03.27.05

Ultrafast Dynamics Surface Enhanced Fluorescence Through Plasmonic Nanoclusters [Belkis Gökbulut](#); Bogazici University, Turkey

In this work, Perovskite nanowires (NWs) are synthesized and encapsulated by gold nanoparticle clusters in polymer matrix to construct a random medium, which allows surface plasmons of the metal nanoclusters to be confined in subwavelength regions and causes an extreme electromagnetic field concentration to manipulate the fluorescence dynamics of the interacting quantum sources. The strong plasmonic field of the gold nanocluster induces a dramatic enhancement in the Purcell factor ($>10^4$). When the Purcell factor exceeds 10^4 through the intense light confinement based on plasmonic nanoclusters, the ultrafast dynamics surface enhanced fluorescence (UFDSEF) of the light emitters exists to dramatically modify the characteristic properties of the quantum sources. As the internal relaxation rate of the Perovskite quantum sources in a bare polymer is greatly faster than the total decay rate, on the excitation of the plasmonic nanocluster, which surrounds the fluorescent emitters in polymer matrix, the strong electromagnetic field enhances the population rates of the excited states; thus, electrons emit from higher vibrational excited states to the ground states. Then, the total decay rate becomes comparable to the internal relaxation rate, which results in significant changes in the spectral profiles of the quantum emitters. The fluorescence emission signal of the quantum sources surrounded by the plasmonic nanocluster seems to be shifted to the wavelength of 476 nm as the peak wavelength in photoluminescence spectrum of the semiconductor NWs in bare polymer appears at 526 nm. Thus, our photonic design proposed in this work, which consists of semiconductor nanocrystals and plasmonic nanoclusters in polymer matrix, provides a distinctive basis to explore the fluorescence dynamics of the quantum sources through UFDSEF mechanism. The first exploration of the blueshifted photoluminescence signal of the Perovskite NWs is achieved by plasmon-induced intense light-matter interaction. The concept of light concentration in deep subwavelength regions of the random medium provides a significant potential to explore light-matter interaction in photonic-plasmonic environment and to develop highly efficient light-emitting device applications.

12:30 PM DISCUSSION TIME

SESSION EQ03.28: Virtual Session III: Quantum Photonics/Advanced Nanophotonics II
Session Chairs: David Norris and Giulia Tagliabue
Tuesday Afternoon, December 6, 2022
EQ03-virtual

1:00 PM EQ03.28.02

Design and Fabrication of Leaky MoS₂ Split-Nanoring Resonators for Biosensing Application Dipanjan Nandi, Andres A. Forero Pico and Manisha Gupta; University of Alberta, Canada

The emergence of novel atomically thin layered two-dimensional transition metal-dichalcogenides (TMDCs) such as MoS₂ is promising for biosensing [1,2] and optoelectronic applications [3]. In the existing literature, MoS₂ has been explored in field-effect transistor platforms for sensing protein and DNA molecules [4,5]. Recently, stacked heterostructure of MoS₂ and graphene were explored for detecting Rhodamine 6G (R6G) molecules [6] and DNA hybridization [7].

Here we propose a novel nanophotonic device platform using MoS₂ split-nanorings resonators array fabricated on SiO₂/Si substrate. We have explored MoS₂ because of its high refractive index ($n > 4$ [8]) contrast with air and low absorption ($k < 1$ [8]) both at monolayer and bulk. Also, the MoS₂ surface favors bonding with the carboxyl (-COOH) group, which makes it biocompatible. We have conducted finite difference time domain (FDTD) simulations for obtaining the best structural parameters by varying inner and outer diameter (D), periodicity (P), and height (H) of the split-nanorings array to study the resonance properties. We performed FDTD simulations by varying the number of polystyrene particles (100 nm diameter) randomly distributed on the device surface and calculated the resonance wavelength shift with the number of particles increased. Here, we have considered 100 nm-sized polystyrene particles as most of the bioanalytes have a similar refractive index to the polystyrene. One of the best-obtained design parameters is nanoring's outer diameter- 200 nm, inner diameter- 100 nm, the height of MoS₂ nanoring- 150 nm, split gap- 80 nm with unit cell periodicity- 220 nm. The split gap in each nanoring has been introduced to leak out the resonant field available on the MoS₂ surface. Attachment of target bioanalytes on the MoS₂ surface disturbs the resonance field and induces a red-shift at resonance wavelength signifies the presence of bioanalytes and detection sensitivity is obtained by calculating the slope of the resonance shift curve with respect to the bioanalytes concentrations. The large area of uniform MoS₂ thin film will be grown by pulsed laser deposition (PLD) technique on SiO₂/Si substrates and the PLD growth parameters (substrate to target distance, chamber condition, post-growth annealing temperature and duration, number of pulses, etc.) are optimized in our lab. Split-nanoring structures will be patterned by electron beam lithography (EBL) technique on the PLD grown 150 nm MoS₂ thin film and then reactive ion etching (RIE) will be performed to obtain MoS₂ nanoresonators array on SiO₂/Si substrates. Fabricated devices will be characterized by SEM, AFM, and optical reflection measurement will be carried out by our lab-made customized optical setup to get resonance conditions. We will present the design optimization and fabrication process of the MoS₂ nanoresonators array and demonstrate experimental measurements of varying concentrations of polystyrene beads of various dimensions to highlight the biosensing capability of the proposed platform.

References:

1. P. Singh, R. Gupta, M. Sinha, R. Kumar, and V. Bhalla, *Microchim. Acta*, 183, 1501–1506, 2016.
2. S. Li, C. Hu, C. Chen, J. Zhang, Y. Bai, C. S. Tan, G. Ni, F. He, W. Li, and D. Ming, *ACS Appl. Bio Mater.*, 4, 7, 5494–5502, 2021.
3. K. F. Mak, C. Lee, J. Hone, J. Shan and T. F. Heinz, *Phys. Rev. Lett.*, 105, 136805, 2010.
4. D. Sarkar, W. Liu, X. Xie, A. C. Anselmo, S. Mitragotri, K. Banerjee, *ACS Nano*, 8, 3992–4003, 2014.
5. C. Zhu, Z. Zeng, H. Li, F. Li, C. Fan, H. Zhang, *J. Am. Chem. Soc.*, 135, 5998–6001, 2013.
6. M. Alamri, R. Sakidja, R. Goul, S. Ghopry, and J. Z. Wu, *ACS Appl. Nano Mater.*, 2, 3, 1412–1420, 2019.
7. P. T. Loan, W. Zhang, C. T. Lin, K. H. Wei, L. J. Li, C. H. Chen, *Adv. Mater.*, 26, 4838–4844, 2014.
8. C. Hsu, R. Frisenda, R. Schmidt, A. Arora, S. M. de Vasconcellos, R. Bratschitsch, H. S. J. van der Zant, A. C. Gomez, *Advanced Optical Materials*, 7, 1900239, 2019.

1:15 PM EQ03.28.03

Novel Modes of Optomechanical Manipulation by Ultrathin Dielectric Metasurfaces Yujie Luo, Avinash Kumar and Ognjen Ilic; University of Minnesota, United States

Photonic metasurfaces are attracting significant interest due to their remarkable capability to synthesize complex wavefronts, with diverse applications in beam focusing, imaging, and flat optics. In addition to these established applications, an emerging direction in the field is the use of metasurfaces to control optomechanical forces. In this work, we present the underlying principles of using the physics of metasurfaces to control the transfer of mechanical momentum from a beam to the metasurface, leading to contactless pressure that can manipulate and actuate a metasurface. This ability to use metasurfaces to shape the optical forces of light can lead to novel approaches to photonic levitation and propulsion at the macro scale, beyond the limit of current optical manipulation approaches.

We show that highly localized control of the metasurface phase can result in spatial patterns of radiation pressure that gives rise to new steering dynamics, and we present representative designs in all-dielectric and ultrathin configurations. Our analysis further elucidates design-independent limits that govern the intrinsic tradeoff between the optical (e.g., force/torque), mechanical (e.g., mass/moment of inertia) and dynamical response of a metasurface. Finally, we introduce and compare the relevant figures of merit for the interaction between a metasurface and a laser beam and point to optimal metasurface designs for contactless actuation.

1:30 PM EQ03.28.04

An Innovative PCR-Free Nanotechnology for SARS-CoV-2 Sensing Emanuele Luigi Sciuto¹, Antonio Alessio Leonardi², Barbara Fazio^{3,4}, Alessia Irrera^{3,4} and Sabrina Conoci^{1,5,4}; ¹University of Messina, Italy; ²University of Catania, Italy; ³CNR-IPCF, Institute for Chemical-Physical Processes, Italy; ⁴Lab Sens Beyond NANO, Italy; ⁵University of Bologna, Italy

The molecular analysis of Nucleic Acids (NA), DNA and RNA, has become nowadays crucial in many medical fields for early and accurate diagnosis, personalized therapy and preventive screening. It is particularly relevant in the field of the infectious diseases that can catastrophically affect the health of population, as it is the case of the current pandemic of SARS-CoV-2 virus that – up to now – infected up to 434 million of people causing 6 million of deaths worldwide.

In this scenario, the conventional approach for the molecular analysis of SARS-CoV-2 is based on the PCR (Polymerase Chain Reaction) reaction that, although standardized and consolidated, is quite complex and includes multiple laboratory procedures and high cost that limit, *de facto*, its massive use. These limitations make the PCR-based analysis inconsistent with the idea of an efficient patient management, in terms of fast diagnosis and prompt answer to the treatment, and viral outbreaks containment.

The PCR-free approach, that allows a fast, ultrasensitive, low cost and easy to use identification and quantification of the pathogen genome without its amplification, overcomes this issue introducing innovative methodologies suitable for the decentralised and massive infections diagnoses and prevention. In this contribution we present an innovative PCR- and label-free technology for the SARS-CoV-2 genome photoluminescent (PL) detection based on the silicon NanoWires (Si-NWs), one of the most appealing silicon nanomaterials employed in nanodevices for biosensing applications. The strategy involves the surface capture of the whole viral genome via a cooperative hybridization with two complementary capture probes (single stranded DNA) that are

grafted on the Si-NWs surface. The hybridization is, then, optically transduced through the quenching effect of the PL signal that is intrinsically produced by the Si-NWs, due to the quantum confinement at room temperature. The occurrence of a non-radiative phenomena, introduced by the SARS-CoV-2 genome hybridization on the Si-NWs surface, determines the quenching of the PL signal and the PCR- and label-free identification and quantification of the viral RNA, with a Limit of Detection (LoD) of 4 RNA copies, below the LoD of the PCR gold standard method. Moreover, the proposed technology is suitable for Molecular “Point-of-Care” (M-PoC) applications, matching the vision of future home-made infective diagnostic microchips integrated into smart mobile devices (i.e smartphones or smart watches).

1:45 PM EQ03.28.05

Ultrafast Dynamics of Electron Injection from Cu Embedded Nanoparticles in CeO₂ Aerogels [Tara Michael](#), Travis G. Novak, Paul DeSario, Debra Rolison, Jeff Owrutsky, Vanessa Breslin and Adam Dunkelberger; U.S. Naval Research Laboratory, United States

Transition metal oxides such as TiO₂ and CeO₂ are wide bandgap semiconductors with photocatalytic properties used to drive electrical currents and enhance electrochemical reactions. The utility of wide bandgap semiconductors can be extended from the UV and into the visible by embedding metal nanoparticles into the semiconductor. Excitation of localized surface plasmon resonances in the metal nanoparticle generates free electrons that can be injected into the semiconductor and extend the photoactivity range using lower energy photons. In this work, ultrafast transient absorption spectroscopy is used to investigate the hot electron injection from Cu nanoparticles photodeposited onto a CeO₂ aerogel. The Cu nanoparticles are excited with a range of pulsed visible light (300 – 1000 nm) and the appearance of free electrons in the CeO₂ aerogel are detected with mid-infrared light. The transient signals are instrument limited and appear within 300 fs, indicating efficient electron transfer from the Cu nanoparticles into CeO₂. Transient signals are observed over a wide range of probe wavelengths, attributed to free or trapped electrons. Unlike other transition metal oxides, CeO₂ has an additional empty 4f state between its conduction and valence bands that can store electrons and form small polarons. The role of the 4f state in electron-phonon decay is explored by probing the 4f state directly with 266 nm light and 350 nm probe. The dynamics of this system are compared to the findings from a recent publication of TiO₂ films embedded with Au nanoparticles. The results presented here examine the utility of using Cu nanoparticles to enhance the properties of CeO₂ as a photocatalyst.

1:50 PM EQ03.28.06

Whispering Gallery Mode Microdroplet Resonators on 3D-Printed Mounts [Madison S. King](#)¹, Parker Awerkamp², David Hill², Gregory Nordin², Stephanie Hurst¹ and Ryan Camacho²; ¹Northern Arizona University, United States; ²Brigham Young University, United States

Due to their mode stability and high quality (Q) factors; whispering gallery mode (WGM) resonators have a wide range of applications from biological sensing to lasing to quantum optical devices [1]. A variety of geometries and materials, including liquids, can be used to create WGM resonators [2]. There are several existing preparations for microdroplet resonators including suspending a drop on a glass stem [3,4] or suspending a droplet in another liquid [5,6]. These methods range in complexity, preparation time, and accessibility. The fabrication of 3D-prints is easy, quick, and accessible but their inherent surface roughness makes them less than ideal for optical applications. Due to this roughness, 3D-prints result in low-quality WGM resonators and can better serve as mounts for microdroplets. In this work a variety of different liquids, some with high dielectric constants (e.g., propylene carbonate), were characterized as WGM microdroplet resonators. Liquid-crystal WGM resonators with high dielectric constants have been shown to have a tunable geometry with an applied electric field [7]. This tunability of high dielectric materials could be advantageous for these microdroplet WGM resonators.

[1] Vahala, K. J. Optical Microcavities. *Nature* **2003**, *424* (6950), 839–846.

[2] Cai, L.; Pan, J.; Zhao, Y.; Wang, J.; Xiao, S. Whispering Gallery Mode Optical Microresonators: Structures and Sensing Applications. *physica status solidi (a)* **2020**, *217* (6), 1900825.

[3] R. Dahan, L. L. Martin, and T. Carmon, “Droplet optomechanics,” *Optica* **3**(2), 175–178 (2016).

[4] M. Gaira and C. Unnikrishnan, “Integrated table-top facility for the study of whispering gallery modes in dynamic liquid micro-cavities coupled to sub-micron tapered fibers,” arXiv preprint arXiv:1911.01187 (2019).

[5] S. K. Tang, R. Derda, Q. Quan, M. Lončar, and G. M. Whitesides, “Continuously tunable microdroplet-laser in a microfluidic channel,” *Opt. Express* **19**(3), 2204–2215 (2011).

[6] S. Maayani and T. Carmon, “Droplet raman laser coupled to a standard fiber,” *Photonics Res.* **7**(10), 1188–1192 (2019).

[7] Humar, M.; Ravnik, M.; Pajk, S.; Mušević, I. Electrically Tunable Liquid Crystal Optical Microresonators. *Nature Photonics* **2009**, *3* (10), 595–600.

1:55 PM EQ03.28.07

Tuning the Dispersion with Metal and Dielectric Layer Combination for Wavelength Multiplexing Plasmonic Metasurface Design [Hosna A. Sultana](#); University of Alabama, United States

Thin layer plasmonic metasurfaces have offered the exciting features of guided-mode resonance, surface plasmon propagation, and converting propagating wave to surface wave. In nanophotonic devices, especially in waveguide applications, this performance can tune the propagation mode in the dielectric cavity. As the functionality of the plasmonic devices depends on the light dispersion, the wavelength-dependent dispersion engineering for the plasmonic band structure is an essential measure of proper light coupling. The main focus of this study is to select the metal-dielectric layer combination for enhancing the plasmonic mode excitation and channel as the guided mode. The plasmonic metasurface design based on this structure is investigated for their surface plasmon polariton generation. With the metasurface element phase control capability, the long-range or short-range plasmonic coupling maneuver can be utilized in the sensing application. Also, controlling the directionality of the coupled plasmonic wave depending on the incident light wavelength gives the device application in the optical coding.

2:00 PM *EQ03.28.08

Elucidating and Exploiting Hot-Carrier Dynamics in Active and Nonlinear Plasmonic Metamaterials [Wenshan Cai](#); Georgia Institute of Technology, United States

Hybrid plasmonic metamaterials consisting of nanostructured metals and electron-accepting materials serve as an enormously fruitful arena for the investigation and utilization of optically excited energetic carriers. The coherent coupling of electromagnetic radiations to plasmons creates a nonequilibrium distribution of electrons at an elevated temperature, known as hot electrons. The dynamics of such hot carriers has been widely employed for various applications, ranging from the detection of sub-bandgap photons in semiconductors to the production of hydrogen gas via photocatalytic processes.

The generation, transfer, and relaxation of hot carriers also provide a novel route to nonlinear optical effects. For example, the optical Kerr nonlinearity of plasmonic metals provides enticing prospects for developing reconfigurable and ultra-compact all-optical modulators. Although enhanced nonlinear responses of metals are known to enable the optical control of light, the intrinsically slow relaxation dynamics of photoexcited carriers, primarily governed by electron-phonon interactions, impedes sub-picosecond modulation speeds. In this talk, we present femtosecond all-optical modulation in plasmonic systems via the activation of relaxation pathways for hot-electrons at the interface of metals and electron acceptor materials. We show that the relaxation kinetics and the optical nonlinearity can be tuned by leveraging the spectral response of the plasmonic system in the linear regime. Our findings introduce a

generic scheme for achieving sub-picosecond modulation speeds in plasmonic systems, suitable for the ultrafast control of the intensity, polarization, and phase of light upon exchange of energetic hot carriers.

The dynamics of hot carriers in plasmonic system is further exploited for the creation of optically induced second-order nonlinear materials. Second-order optical processes are pivotal to the active modulation and wave mixing of light waves. The inversion symmetry in most materials, however, prevents achieving a bulk χ^2 effect, thereby limiting the portfolio of second-order nonlinear materials. We propose and demonstrate ultrafast conversion of a statically-passive dielectric to a transient second-order nonlinear medium upon the generation and transfer of plasmonically induced hot electrons. Triggered by an optical switching signal, the amorphous dielectric with vanishing intrinsic χ^2 develops dynamically tunable second-order nonlinear responses, which can be leveraged to address the critical need for all-optical control of second-order nonlinearities in nanophotonic systems.

Therefore, the consolidation of the relaxation dynamics of hot electrons with externally induced optical nonlinearity enables a unique opportunity to elucidate the generation, transport, and decay of hot carriers in hybrid plasmonic systems. Conversely, leveraging the ultrafast dynamics of plasmonically induced hot electrons allows us to achieve ultrafast all-optical control of light and realize externally triggered second-order optical nonlinearity in hybrid plasmonic metamaterials.

2:30 PM EQ03.28.09

Passive Transmission Symmetry Breaking Without Non-Reciprocity in All-Dielectric Metagratings Stavroula Foteinopoulou; University of New Mexico, United States

While reflection symmetry can be routinely broken in a passive system by introducing loss the same is not true for transmission symmetry. Passive and linear systems exhibit transmission symmetry because of the reciprocity principle. In other words, it would appear that breaking transmission symmetry in a linear passive system would be synonymous to breaking reciprocity.

In this talk, we will present a specially designed metagrating that possesses several output channels, as a result of higher-order Bragg beams being triggered. We will discuss the transmission response of this system, exhibiting a strong asymmetry, with contrast as high as $\sim 75\%$ [1]. We analyze the underpinning mechanism and explain how a transmission asymmetry in this type of system remains consistent with the reciprocity principle. We further verify such transmission asymmetric behavior with an FDTD numerical experiment.

We believe this transmission asymmetry capability in these simple systems without requiring non-reciprocity can open-up new avenues for photonic components design across the EM spectrum.

[1] S. Foteinopoulou, Breaking Transmission Symmetry Without Breaking Reciprocity in Linear All-Dielectric Polarization-Preserving Metagratings, Phys. Rev. Applied 17, 024064 (2022); <https://doi.org/10.1103/PhysRevApplied.17.024064>

3:00 PM DISCUSSION TIME

SESSION EQ03.29: Virtual Session IV: Advanced Nanophotonic Design V
Session Chairs: Yao-Wei Huang and Yu-Jung Lu
Wednesday Morning, December 7, 2022
EQ03-virtual

8:00 AM *EQ03.29.01

White-Nanorange-Source for Background-Free Nano-Optical Investigation Prabhat Verma; Osaka University, Japan

Plasmonically enhanced spectroscopies, such as the surface-enhanced Raman spectroscopy (SERS) and the tip-enhanced Raman spectroscopy (TERS) have been well utilized for both, sensing tiny amounts of specific molecules, and imaging samples at the nanoscale [1-5]. The most important phenomenon in such measurements is the selective enhancement of Raman signal from the nanometric volume of a sample, which makes it possible to study a sample at extremely high spatial resolution and at a very low concentration. For this purpose, perfect tuning of plasmon resonance wavelength is required, which is achieved by illuminating the plasmonic antenna, such as the apex of a metallic nanotip in TERS or metallic nanoparticles in SERS, with a diffraction-limited focused laser beam. This results in the creation of a nanorange-source in the close vicinity of the antenna through the resonant oscillation of localized surface plasmons. Since the resonance condition is achieved only for a very narrow wavelength range that matches the plasmon resonance for a chosen antenna, the nanorange-source also has a narrow wavelength range. In addition to the creation of a nanorange-source in this process, one also receives an unwanted background scattering that originates from the diffraction-limited illumination of the sample. In some cases, one would like to have a fast wavelength switching or even multiple wavelengths at the nanorange-source without changing the antenna. Also, one would like to avoid unwanted background scattering.

Plasmon nanofocusing [5-7], which is not based on the plasmon resonance, is an alternative method for creating a nanorange-source. It is a phenomenon in which plasmons are excited near the broader end of a tapered metallic structure, which then propagate towards the apex and slow down by adiabatically compressing their energies and eventually stop near the apex where all energy is converted to light creating a strong light field localized at the nanometrically sharp apex of the tapered structure. Here plasmons are excited by coupling propagating photons with plasmons via a grating that works as the plasmon coupler. As the plasmon coupler and the apex of the tapered structure are physically separated by a reasonably large distance, the illuminating light does not fall on the sample, avoiding the unwanted background scattering from direct illumination of the sample. In addition, because one can create a nanorange-source through the propagation of plasmons, rather than the localized resonance, it works over an extremely wide wavelength range. However, the plasmon coupler, that is the grating, can efficiently couple only a narrow wavelength range and imposes a restriction on the wavelength range of the nanorange-source. This can be overcome, if a suitable coupler is created that couples a broad wavelength range or the white light. We found that, if properly designed, a single slit can work as an efficient plasmon coupler for white light, which ultimately results in the creation of a white-nanorange-source. We have recently proposed the generation of a white-nanorange-source through broadband plasmon nanofocusing and successfully exploited it for super-resolution spectral optical imaging, which has exhibited great potential for broadband plasmon nanofocusing not only for optical imaging but also for diverse scientific fields as a novel tiny light source. Here in this talk, we will discuss how to create a white-nanorange-source and how to utilize it in various interesting applications.

[1] P. Verma, *Chem. Rev.* **117**, 6447 (2017).

- [2] P. Verma et al., *Laser Photon. Rev.* **4**, 548 (2010).
 [3] T. Yano et al., *Nature Photon.* **3**, 473 (2009).
 [4] T. Yano et al., *Nature Communications* **4**, 2592 (2013).
 [5] T. Umakoshi et al., *Nanoscale* **8**, 5634 (2016).
 [6] T. Umakoshi et al., *Science Adv.* **6**, eaba4179 (2020).
 [7] K. Taguchi et al., *J. Phys. Chem. C* **125**, 6378 (2021).

8:30 AM *EQ03.29.02

Optical Meta-Devices for Bio-Imaging Mu Ku Chen¹, Yuan Luo² and Din-Ping Tsai¹; ¹City University of Hong Kong, China; ²National Taiwan University, Taiwan

The novel property of optical meta-devices, which consist of meta-antenna made by artificial nanostructures, has attracted a lot of attention lately. Various optical devices based on the specific designs of meta-surfaces are called optical meta-devices. The great advantages of meta-devices are their new properties, lighter weight, small size, high efficiency, better performance, broadband operation, lower energy consumption, and CMOS compatibility for mass production. Given the demand for photonics, many optical meta-devices for the application and control of incident light are being quickly developed for beam deflection and reflection, polarization control and analysis, holography, second-harmonic generation, laser, tunability, imaging, absorption, color display, focusing of light, multiplex color routing, and light-field sensing. Here we demonstrated the optical meta-devices into bio-imaging. In this talk, we report 3 applications, varifocal Moiré meta-lens [1], Meta-lens based light-sheet fluorescent microscopy (MLFSM) [2], and abrupt autofocusing (AAF) meta-lens[3].

Following the Moiré technique, a variable focus dielectric meta-lens is designed and implemented for high-contrast optical sectioning fluorescence microscopy at the visible spectral region. The design principle of Moiré meta-lens and telecentric design is described in detail. We demonstrated telecentric imaging equipped with variable focus meta-lens, which performs high-contrast multi-plane fluorescence imaging for ex vivo mice intestine tissue samples. In addition, Moiré meta-lens-based fluorescence microscopy with the HiLo imaging principle provides fine optical sectioning with invariant image contrast through the entire scanning range. As a clear demonstration of imaging performance for our Moiré meta-lens-based microscope, both standard resolution target and fluorescent microspheres are imaged, with a lateral resolution of $\sim 2 \mu\text{m}$, as well as optical sectioning capability of $\sim 7 \mu\text{m}$. The varifocal Moiré meta-lens with ultra-thin size and compact design may replace its counterpart in any optical system that requires a focus-tunable lens, such as optical coherence tomography and micro-endoscopy for in vivo imaging.

We show the implementation of a metasurface optical element in LFSM for imaging lives biological samples as well. The performance of our LFSM was evaluated by utilizing standard fluorescent microspheres and in vivo imaging of fine structures associated with the developmental process in live *C. elegans*. Results obtained from our systems clearly show internal structures of the *C. elegans* up to cellular resolution for multiple wavelengths. Experimental measurements are compared with the conventional LFSM systems (i.e., without any meta-lenses), and similar image resolution is demonstrated. The results clearly illustrate the capability of the system for biomedical imaging applications. Moreover, the significance of the present techniques lies in the fact that the complexity of the instrument in the illumination is entirely reduced, from tens of centimeters to 800 nm, without affecting any imaging performance, which clearly shows great potential to utilize metasurface optics for miniaturizing microscopic imaging instruments. Applications of meta-lens can be readily extended to illumination, as well as in the detection of LFSM to include all the essential features of meta-surfaces. Metasurface optics can be utilized for many LFSM modalities to achieve novel functionalities, such as meta-lens arrays for light-sheet generation, multi-view/multi-dimensional selective plane illumination microscopy, near-infrared and multi-photon LFSM. Further, by integrating beam shaping techniques in the meta-lens design, exotic light-sheet patterns with an extended field of view and smaller thickness can be achieved. We believe this work is an advancement of the applications of meta-devices in microscopy.

9:00 AM *EQ03.29.03

Geometric Photodetectors for Mid-Infrared Light Cheng-Wei Qiu and Jingxuan Wei; National University of Singapore, Singapore

We will report zero-bias, uncooled, filterless photodetectors in mid-infrared exhibiting colossal discrimination ratio, close-to-perfect CPL-specific response, a zero-bias responsivity of 392 V/W, and a detectivity of ellipticity down to 0.03-degree Hz^{-1/2}. Our approach employs plasmonic nanostructures array with judiciously designed symmetry, assisted by graphene ribbons to electrically read their near-field optical information. It highlights the potential of hybridizing metasurface and semimetals for miniaturized polarimetry.

9:30 AM EQ03.29.04

Plasmonic Sensing Enhancement by Dielectrophoretic Trapping of Bacteria in Total Internal Reflection Ellipsometry Soraya Zangenehzadeh¹, Fenja Schroeder¹, Annalena Eckert¹, Svenja Herdan¹, Max Schittenhelm¹, Emil Agocs^{1,2}, Felix Hirschberg¹, Rebekka Biedendieck³, Hans-Hermann Johannes^{1,2}, Dieter Jahn³ and Wolfgang Kowalsky^{1,2}; ¹Institut für Hochfrequenztechnik, Germany; ²Cluster of Excellence PhoenixD, Germany; ³Institute of Microbiology and Braunschweig Integrated Centre of Systems Biology (BRICS), Germany

Bacterial infection is one of the threats for public health which causes death of millions of people every year. Detection of these microorganisms is important to prevent the prevalence of infectious diseases. There are various bacterial detection methods such as enzyme-linked immunosorbent assay (ELISA) or polymerase chain reaction (PCR) that are time consuming and expensive due to the preparation of antibodies. In recent years, optical biosensors play an important role in analysis and monitoring of binding of biological elements. Spectroscopic ellipsometry analyzes the changes in polarization state of light after reflection or transmission from a surface and determines the optical properties and thickness of the film. These changes in polarization states are studied by the amplitude ratio (Ψ) and the phase difference (Δ) between p- and s-polarized light, respectively. Conventional spectroscopic ellipsometry is limited to monitor bacteria due to the low refractive index contrast between bacterium and its ambient. For this reason, total internal reflection ellipsometry (TIRE) consist of Kretschmann configuration is used to monitor bacterial binding to the functionalized layer. In this configuration surface plasmon polaritons (SPPs) are coupled with an incoming light beam and excited at a specific incidence angle at the metal-dielectric interface. This matching condition causes surface plasmon resonance (SPR) as a sharp dip in reflected light. SPR detects the changes in the refractive index of the sample environment which is in contact to the metal surface. This measurement technique is real-time and non-destructive which makes it reliable for precise detection of bacteria. The aim of this research is to improve the limit of detection (LOD) of surface plasmon resonance by enhancing bacterial mass transport through the effective sensing volume of an evanescent wave in a Kretschmann flow cell. For this purpose, the effect of dielectrophoretic force on the Gram-negative bacterium *Escherichia coli* K12 (*E. coli* K12), a common well investigated apathogenic model strain, is studied in the TIRE structure. Dielectrophoresis (DEP) exerts a force on dielectric particles like bacteria when they experience an asymmetric electric field. In inhomogeneous electric fields, particles will move toward areas of maximum electric field gradient (positive-DEP) and minimum electric field gradient (negative-DEP), respectively.

9:45 AM EQ03.29.05

Self-Assembled Glass Based and Plasmonic Metasurface by Controlled Fluid Instability Tapajyoti DasGupta, Renu R. Sahu, Alwar Samy Ramasamy, Aravindkumar Yelashetty, Ajisha C, Shiju Prasad and Santosh Bhonsle; Indian Institute of Science, India

Modern devices require the tuning of the size, shape and spatial arrangement of nano- objects and their assemblies with nanometer scale precision, over large-area and sometimes soft substrates. Such stringent multi-scale and mechanical requirements are beyond the reach of conventional lithography techniques or simpler self-assembly approaches. In this talk, at first we will demonstrate an unprecedented control over the fluid instabilities of thin glass films as a simple approach for the self-assembly of advanced all-dielectric metasurfaces. We show and model the tailoring of the position, shape, size and inter-particle distance of nano-objects with feature sizes below ten nanometers [1]. This simple and versatile approach can generate optical nanostructures over tens-of-centimeters sized rigid and soft substrates, with better optical performance and a resolution on par with advanced lithography-based processes. By a programmable control of the nanoimprinting method and the initial film thickness we show that we can achieve tunable particle size and lattice using the same master Silicon mold. To underline the potential of our approach, we demonstrate various optical phenomena like a mechanochromic sensor, second harmonic generation with conversion efficiency as high as 10^{-6} , and a Fano resonance with a highest Quality Factor ~ 300 in visible to date [2]. Lastly, we show by tuning just the substrate softness Gallium based liquid metals [3] for the first time could be used as a dynamic metasurface where the optical properties could be tuned in-situ by applying a simple mechanical stress.

References:

- [1] T. Das Gupta et al. Nature nanotechnology, 2019
- [2] T. Das Gupta et al. Nanophotonics, 2021
- [3] L.Martin, T. Das Gupta et al. Adv. Functional Materials, 2021

10:00 AM EQ03.29.06

Self-Assembled Active Deformable Liquid-Metal Based Photonic Nanostructures via Fluid Instabilities Renu R. Sahu, Alwar Samy Ramasamy, Santosh Bhonsle and Tapajyoti DasGupta; Indian Institute of Science (IISc), Bangalore, India

The use of liquid metals, particularly Gallium, and their alloys allow for the fabrication of flexible, bendable, and mechanically reconfigurable devices when deposited on an elastomeric substrate[1]. They have been the choice materials for electronic applications, particularly in the domain of soft and stretchable electronics[2]. Although an excellent optical material due to low comparative loss and UV-based plasma frequency, their applications in the photonic domain have still been limited to the THz region[3]. This is because of its inability to be scaled down to nanoscale owing to their intrinsic large surface tension, thus hindering practical use in visible, dynamic photonic systems with sub 100 nm feature dimensions. However, the possibility of exploiting fluid instabilities for nanofabrication has been well established[4].

In this talk, for the first time we will show a single-step procedure that exploits the fluid instabilities of liquid metal, tending to minimize surface energy by forming spherical droplets of sizes in sub-100nm length scales. By tuning the softness and the temperature of the substrate, the rate of deposition, and the amount of the liquid metal being deposited, we demonstrate a fabrication technique of gallium-based plasmonic thin film with tuneable structural colors for the first time, paving the way toward a novel paradigm in soft photonics and large area reflective displays. By tuning and optimizing a range of experimental parameters, and the choice of substrate material we obtain vibrant coloration encompassing a wide range of chromaticity coordinates as a result of the controlled manipulation of size distribution of Ga nanodroplets. Analysis of scanning electron microscope images for structural characterization of the samples fabricated by our methodology emphasizes the importance of liquid oligomers in the heat-cured Poly-dimethyl siloxane in the formation of non-overlapping Gallium nanodroplets, which is not the case when the oligomers are deliberately removed by toluene treatment. In the latter case, the absence of oligomers results in the formation of nanodroplets without penetration into the substrate, forming a film of nanodrops akin to a thin film over a substrate.

As a proof-of-principle, we show pallets of structural colors, whose advantages can be leveraged in reflective display technologies. The application of the thus-fabricated device also exhibits mechanochromic sensing, which has been characterized to be of high fidelity and reliability, functionalized by exploiting the fluidic properties of Gallium. For at least 1000 cycles of uniaxial stretching and relaxing, the reflectivity spectrum of the sample for a given strain was unchanged, thus proving the reliable reconfiguration of sample response to the application and removal of mechanical strain. The reversible change in the reflectivity spectrum results in the chromaticity coordinates of the sample, hence a visible change in the sample color. Our results have the potential to offer opportunities to dynamically reconfigure thin-film-based functional nanodevices in situ as well as process technology for high throughput fabrication to achieve the same in a single-step method.

References

- [1] Martin Monier, L., Gupta, T. Das Gupta et al. *Adv. Funct. Mater.* **31**, 2021
- [2] Dickey, M. *Advanced Materials* **29**, 2017
- [3] Reineck, P. et al. *Sci. Rep.* **9**, 2019
- [4] Das Gupta, T. et al. *Nat. Nanotechnol.* **14**, 2019

10:20 AM DISCUSSION TIME

SESSION EQ03.30: On-Demand Presentation
Thursday Morning, December 8, 2022
EQ03-virtual

7:00 AM *EQ03.30.02

Two UV Plasmonic Devices by High-Performance Epitaxial Al Metasurfaces—An Ultrasensitive Photodetector and a Surface-Enhanced Resonance Raman Spectroscopic (SERRS) Biosensor Abhishek Dubey¹, Ragini Mishra¹, Yu-Hung Hsieh^{1,2}, Chang Wei Cheng¹, Bao-Hsien Wu¹, Lih-Juann Chen¹, Shanjir Gwo^{1,1,2} and Ta-Jen Yen¹; ¹National Tsing Hua University, Taiwan; ²Academia Sinica, Taiwan

Plasmonics-based devices have been intensively explored in visible and infrared regimes, but scarcely demonstrated in the wide UV regime, mainly because of constrained optical properties of materials. By using epitaxial Al metasurfaces, herein we report two unprecedented plasmonic applications in UV regimes- an ultrasensitive photodetector and a surface-enhanced resonance Raman spectroscopic (SERRS) biosensor. For the first UV plasmonic device, we demonstrated ultrasensitive photodetector with a maximum detectivity ($1.48 \times 10^{15} \text{ cm Hz}^{1/2} \text{ W}^{-1}$) at the on-resonance wavelength of 355 nm. broad bandwidth photodetection through the entire UV regime, and a fast temporal response with a rise time of 51 ms and a fall time of 197 ms,

respectively. For the second UV plasmonic device, we presented an SERRS biosensor. Such a UV SERRS biosensor not only exhibited high signal to noise ratios, but also recorded an SERRS enhancement factor up to 10^6 for extremely thin layer of adenine of 1nm thick. In addition to this egregiously high EF factor, we further exhibit that our SERRS substrate is capable of detecting the single base mutation in the 12-mer ss-DNA.

SYMPOSIUM EQ04

Emerging Chalcogenide Electronic Materials—Theory to Applications
November 28 - December 6, 2022

Symposium Organizers

Rafael Jaramillo, Massachusetts Institute of Technology
Archana Raja, Lawrence Berkeley National Laboratory
Jayakanth Ravichandran, University of Southern California
Akshay Singh, Indian Institute of Science, Bengaluru

Symposium Support

Silver
SEMILAB

Bronze
Lake Shore Cryotronics
Micro Photonics
SPECS Surface Nano Analysis GmbH

* Invited Paper
+ Distinguished Invited

SESSION EQ04.01: Materials Design and Discovery I
Session Chairs: Kaveh Ahadi and Rafael Jaramillo
Monday Morning, November 28, 2022
Sheraton, 2nd Floor, Constitution A

10:30 AM EQ04.01.01

Unexpected Phase-Pure Wurtzite Structure of Nitrogen Doped $\text{ZnSe}_{1-x}\text{Te}_x$ Thin Films Theodore Culman¹, Rachel Woods-Robinson², John Mangum¹, Rebecca Smaha¹, Chris Rom¹, Andriy Zakutayev¹ and Sage Bauers¹; ¹National Renewable Energy Laboratory, United States; ²Lawrence Berkeley National Laboratory, United States

Conventional II-VI and III-V compound semiconductors can be roughly split into two structural categories: zincblende and wurtzite. Both are tetrahedral systems and furthermore, their crystal structures are polytypes with only slight modification to the stacking pattern of honeycomb cation/anion planes. Controlling zincblende-wurtzite polytypism within a single material is a promising way to design semiconductor functionality. In this talk we show that nitrogen doping induces a zincblende-to-wurtzite structural transition in $\text{ZnSe}_{1-x}\text{Te}_x$ when grown as sputter deposited thin films. N-doped $\text{ZnSe}_{1-x}\text{Te}_x$ is prepared from ZnSe and ZnTe source targets with gaseous N_2 as a N source. In some doped films, there is a structural transformation from the usual zincblende to wurtzite. Depending on the temperature and N_2 flow rate during growth, wurtzite can be synthesized across most of the composition range explored, ranging from Te-rich ($x \approx 0.7$) to nearly pure ZnSe ($x \approx 0.1$). Grazing-incidence, wide-angle synchrotron x-ray scattering (GIWAXS) data show that the N-doped $\text{ZnSe}_{0.5}\text{Te}_{0.5}$ alloy forms as phase-pure wurtzite. Temperature-dependent electronic transport measurements collected from N-doped $\text{ZnSe}_{0.5}\text{Te}_{0.5}$ indicate the material is a p-type semiconductor and low-temperature resistivity data are well fit by a transport model dominated by 3D variable range hopping. Scanning electron microscopy reveals voids in the N-doped films that are not present in undoped films. We attribute these microstructural features to N_2 gas trapped during growth, which is confirmed by signals from molecular nitrogen in x-ray absorption spectroscopy data. 0 K formation enthalpy calculations do not completely describe the stability of the wurtzite phase, so we hypothesize that the open microstructure plays a role by increasing the surface energy contribution. This work highlights unexpected polytypism in one of the most studied II-VI semiconductor systems and thus motivates a closer look at other well-studied semiconductor alloys for similar structural diversity.

10:45 AM EQ04.01.02

Computational Prediction of Novel Oxy-Chalcogenides $\text{Ln}_2\text{Ti}_2\text{O}_5\text{Ch}_2$ (Ln=Y, La; Ch=S, Se) Katarina Brlec and David O. Scanlon; University College London, United Kingdom

Ruddlesden Popper (RP) phases $\text{A}_{n+1}\text{B}_n\text{X}_{3n+1}$ ($n = 1, 2, 3$) comprise a versatile and well-studied structural type. The variety of interesting optoelectronic and magnetic properties of RP materials allows for a wide range of applications, from photovoltaics to battery materials. While RP systems are traditionally oxides, several oxynitrides and oxysulphides have been characterised in recent years.

Cation-deficient RP phase $Y_2Ti_2O_5S_2$ has recently shown promise as an n-type thermoelectric with ZT exceeding 1 at high temperatures. [1] However, its thermoelectric performance could be further improved with cation or anion mutation as a lower lattice thermal conductivity is expected with greater variation in ion size due to enhanced phonon scattering.

In this work we use density functional theory (DFT) to predict the properties of previously unknown $La_7Ti_2O_5Ch_2$ ($Ch=S, Se$) and $Y_2Ti_2O_5Se_2$. In total 150 competing phases of the La-Y-Ti-O-S-Se chemical space were studied at hybrid-DFT level to determine the thermodynamic stability window of these novel chalcogenides. Furthermore, we carry out phonon calculations to confirm dynamic stability of these systems and apply hybrid-DFT methods to calculate relevant optoelectronic properties.

[1] K. Brlec, K. B. Spooner, J. M. Skelton, D. O. Scanlon, in submission. Preprint at 10.26434/chemrxiv-2022-zk09d

11:00 AM EQ04.01.03

Innovative $GeSe_{1-x}Te_x$ Chalcogenide Thin Films—From Bonding Mechanism to Phase-Change Material Applications [Martina Tomelleri](#)^{1,2}, Anthony Albanese², Françoise Hippert³, Jean-Yves Raty⁴, Francesco D'acapito⁵, Valentina Giordano⁶, Daniel Benoit¹ and Pierre Noé²; ¹STMicroelectronics, France; ²CEA-LETI, France; ³Univ. Grenoble Alpes, CNRS, France; ⁴Universite de Liege, Institut de Physique B5 Sart Tilman BE, Belgium; ⁵CNR-IOM-OGG c/o ESRF, France; ⁶ILM, UMR 5306 Univ. Lyon 1-CNRS, France

By exploiting their strong optical and resistivity contrast between the amorphous (a-) and the crystalline (c-) phase, chalcogenide phase-change materials (PCMs), such as canonical $Ge_2Sb_2Te_5$ alloy, have made possible to envisage a wide range of application in particular for data storage technology [1]. The difference in bonding mechanism between the a-phase, which is a covalent bonded (CB) structure, and the c-phase, which is governed by the recently introduced concept of “metavalent bonding” (MVB), is responsible for their large property contrast [2]. Many efforts have been devoted to shed light on this unconventional chemical bond, in order to accelerate the discovery of new PCMs with tailored properties for multiple applications. $GeSe_{1-x}Te_x$ alloys, forming a solid solution along the GeSe-GeTe pseudo-binary line, arouse particular interest since they bridge the gap between GeSe, which is a CB material in both its a- and c-phases, and GeTe that is, in its c-state, a prototypical MVB material characterized by outstanding electronic properties such as a high electronic polarizability. Indeed, despite GeTe and GeSe are both IV-VI chalcogenide compounds with an isoelectronic structure, the moderate Peierls distortion in rhombohedral (rh-) c-GeTe (characterized by 3 short and 3 long Ge-Te bonds) enables the formation of MVB, which instead collapses in orthorhombic (orth-) c-GeSe due to the too strong local distortion. In addition to being a model system for fundamental studies, the unprecedented high thermal stability of a-phase of $GeSe_{1-x}Te_x$ films, makes these materials extremely promising for embedded PCM memory applications, for which a data retention at high temperature is crucially needed [3].

$GeSe_{1-x}Te_x$ thin films were deposited by industrial magnetron co-sputtering on silicon and silicon oxide substrate. Their crystallization was monitored by four-point probe resistivity measurement during annealing. The crystallization temperature increases with decreasing Te content, reaching very high a-phase stability. Moreover, the resistivity contrast between a- and c-phase is extremely large for all the studied compositions, except in the case of GeSe. By means of room-temperature X-ray diffraction, Raman spectroscopy and X-ray Absorption Fine Structure on c- $GeSe_{1-x}Te_x$ films, we identified an ortho-structure in GeSe and a rho-MV bonded phase, isostructural to GeTe, in the x range [0.16-1]. This is an unexpected result since, according to the GeSe-GeTe phase diagram, the domain of the rh-phase is restricted to x range [0.48-1], and a covalent-bonded hexagonal phase is stable for x ranging from 0.14 to 0.42 [4]. However, it is precisely the persistence of the rh-structure in our thin films down to $x=0.16$, even if metastable, that allows the formation of MVB giving to the material such unprecedented resistivity contrast upon crystallization. The replacing of a few percent of Se atoms by Te in the covalently bonded Ge-Se network transforms the latter in a MVB material with a unique portfolio of properties. The high thermal stability of GeSe is combined with the wide resistivity contrast provided by MV bonded GeTe in an alloy that remains homogenous after crystallization, thanks to the complete solubility of Te in GeSe. Besides giving the opportunity to explore the transition between CB and MVB, their exceptional combination of properties makes Se-rich $GeSe_{1-x}Te_x$ alloys an extremely promising candidate for integration in phase-change devices requiring high data retention.

[1] P. Noé et al., *Semicond. Sci. Technol.* 33 (2018) 013002. [2] a) J.-Y. Raty et al., *Adv. Mater.* 2019, 31, 1806280 ; b) Kooi, B. J., Wuttig, M., *Adv. Mater.* 2020, 32, 1908302. [3] M. Tomelleri et al., *Phys. Status Solidi RRL*, 2020, 15, 22000451. [4] H. Wiedemeier, P. A. Siemers, *High Temp. Sci.* 1984, 17, 395.

11:15 AM EQ04.01.04

Emerging Amorphous Chalcogenide Thin Films—From Bonding Mechanism to On-Chip Highly Non-Linear Photonic Devices [Anthony Albanese](#)^{1,2}, Jean-Baptiste Dory¹, Jean-Yves Raty^{1,3}, Meryem Ibnoussina², Jean-Baptiste Jager⁴, Anthonin Verdy¹, Francesco D'acapito⁵, Magali Tessaire¹, Mathieu Bernard¹, Aurélien Coillet², Benoît Cluzel² and Pierre Noé¹; ¹CEA-LETI, France; ²ICB, France; ³CESAM, Belgium; ⁴CEA-IRIG, France; ⁵CNR-IOM-OGG c/o ESRF, France

Chalcogenide glasses (ChGs) show a large transparency window in the infrared coupled with outstanding nonlinearities offering tremendous opportunities for achievement of innovative mid-infrared on-chip components. In this work, the amorphous structure and the nonlinear optical properties of As-free amorphous $GeSb_wS_xSe_yTe_z$ chalcogenide thin films are studied. The nonlinear refractive Kerr indices (n_2) of the films were evaluated through modelling of spectroscopic ellipsometry data. The method has been then validated by means of experimental characterization of Kerr indices of a set of selected glassy chalcogenide alloys and SiN_x reference material using advanced nonlinear optical characterizations of waveguides (heterodyne interferometry setup). State-of-the-art and remarkably high n_2 values were obtained for some compositions of the amorphous chalcogenide compounds. Depending on the stoichiometry of the $GeSb_wS_xSe_yTe_z$ ChGs, n_2 can vary of more than one order of magnitude. Besides, Fourier-Transform Infrared (FTIR), Raman and X-ray Absorption (XAS) spectroscopies analysis of the amorphous structure of prototypical chalcogenide alloys in relation with their nonlinear optical properties was used as a basis for *ab initio* molecular dynamics (AIMD) simulations. Thus, the intimal link between local atomic configurations recalling unique “metavalent” bonding (MVB) and optical nonlinearities is unveiled, giving unprecedented clues to control optical nonlinearities of chalcogenide materials.

In this work we evaluated first the n_2 refractive indices of a wide range of $GeSb_wS_xSe_yTe_z$ thin films by means of Sheik-Bahae model, a theoretical model already successfully applied to chalcogenide materials to predict the n_2 . The amorphous as-deposited films exhibit a wide range of n_2 values that show strong dependence on the ChGs composition. The obtained results are well supported by previous study of similar $GeSb_xSe_y$ compounds in the literature. In order to relate optical nonlinearities and structure, four prototypical compositions differing by their n_2 values were selected and finely described by means of advanced optical and structural characterizations. Therefore, the experimental nonlinear coefficients γ of the prototypical Ge-Se-Sb(-N) alloys and SiN_x reference material measured in waveguides using an experimental heterodyne detection setup at 1550 nm are in good agreement with those derived from calculated n_2 Kerr indices using the Sheik-Bahae model. The obtained values are from one to two orders of magnitude higher than that of SiN_x reference sample. A dramatic change of Kerr index depending on the ChGs stoichiometry is observed and related to modifications of the amorphous structure. From the calculation of the bond polarizability, one could relate the origin of the local very high electronic polarizability, related to highly polarizable structural motifs in the amorphous network, to the enhanced optical nonlinearities of the material. These highly polarizable motifs are reminiscent of a unique bonding configuration that recalls the “metavalent” bonding, a unique bonding mechanism at the origin of the huge optical and electrical contrast between amorphous and crystalline state of Phase-Change Materials.

To summarize, the outstanding linear and nonlinear optical properties of selected ChGs at origin of their promising potential of applications for MIR on-

chip components is shown to result from the formation of peculiar structural motifs leading to specific bonding mechanism at the origin of their huge polarizability. In particular, some elements increase dramatically the local electronic polarizability by inducing structural motifs supporting bonds similar to the newly introduced “metavalent” bonding mechanism arising in some local crystal-like motifs. These results pave the way to control and improve further the unique optical properties of ChGs in thin films.

11:30 AM *EQ04.01.05

Ferroelectricity, Superconductivity and Non-Trivial Topology in PbSnTe Heterostructures Athby Al-Tawhid, Antonio Gonzalez, Sam Poage and Kaveh Ahadi; North Carolina State University, United States

Combination of broken inversion symmetry and spin-orbit coupling gives rise to a wide range of exotic superconducting states, such as mixed-parity superconductivity, superconducting Weyl state, and superconducting diode effect. Incipient ferroelectrics e.g., PbTe, are near a polar instability. The emergence of superconductivity has been reported in some of these incipient ferroelectrics upon doping. Many unconventional superconductors, such as the cuprates, pnictides, and heavy fermion systems, occur in close proximity to magnetic fluctuations or magnetic orders, suggesting that these are important ingredients in the superconductivity in these materials. Here, ferroelectricity and superconductivity could be connected or accidental neighbors. Furthermore, the intersection of superconductivity and topologically nontrivial states is a fertile landscape for exciting quantum phenomena, including non-abelian excitations.

IV-VI compounds show a wide range of electronic and polar instabilities. $Pb_{1-x}Sn_xTe$ demonstrates a highly tunable superconductivity and ferroelectricity which are dependent on carrier density and Sn(Pb) concentration. Furthermore, a topological phase transition is expected at $x \sim 0.4$, which inverts the conduction and valence bands for Sn rich compounds. I will report on our recent growth efforts of high quality $Pb_{1-x}Sn_xTe$ heterostructures, using a chalcogenide molecular beam epitaxy (Veeco 930) near the topological phase transition ($x \sim 0.4$). The cross-section high-angle annular dark-field (HAADF) imaging in scanning transmission electron microscopy (STEM) shows abrupt interfaces. X-ray diffraction demonstrates single oriented films. The sheet resistance v.s. temperature demonstrates a metallic-like behavior, $dR/dT > 0$, in doped samples extending to 2 K. The Hall carrier density was measured at various temperatures, resolving the carrier mobility. The carrier mobility is inversely proportional to doping concentration. We report on superconductivity in electron and hole doped $Pb_{1-x}Sn_xTe$ heterostructures and its relation to neighboring ferroelectric and topological phase transitions.

SESSION EQ04.02: Materials Design and Discovery II

Session Chairs: Albert Davydov and Ida Sadeghi

Monday Afternoon, November 28, 2022

Sheraton, 2nd Floor, Constitution A

1:30 PM *EQ04.02.01

Progress in the Synthesis of Device-Grade Chalcogenide Perovskite Thin Films Corrado Comparotto, Kostiantyn Sopiha, Garima Aggarwal and Jonathan Scragg; Uppsala University, Sweden

Functional inorganic materials combining electropositive group-I or group-II elements with transition metals and p-block anions provide some intriguing properties, for example high dielectric polarizability and ferroelectricity in combination with band gaps in the visible light range.^[1] Chalcogenide perovskites such as $BaZrS_3$ are a case in point.^[2] At present, they are being explored as robust, earth-abundant and non-toxic candidates for tandem solar cells where the high polarizability might allow for longer charge carrier lifetimes.

In this contribution, the interesting features of chalcogenide perovskites are summarized. Their structural stability is discussed on the basis of computed formation energies, empirical stability rules and experimental literature. The prevailing picture of a broad family of $(Ca,Sr,Ba)(Ti,Zr)(S,Se)_3$ perovskite compounds is shown to be incorrect: in fact, only $BaHfS_3$ and $BaZrS_3$ are expected to crystallize in the perovskite structure under the appropriate for thin-film solar cell deposition.^[3] All other compounds favor alternative structures (that may nevertheless be worth exploring).

Furthermore, we report our progress in synthesizing chalcogenide perovskites using sputtering routes. The aim is to produce high-quality material suitable for detailed characterization and future device integration, via a fast and flexible route that can be also adapted for a range of related compounds. The main challenges for sputtering chalcogenide perovskites and other compounds containing electropositive group-I or group-II elements are: a) obtaining low oxygen content, to ensure that intrinsic material characteristics can be measured, and b) achieving good crystallization at moderate temperature, for compatibility with device fabrication. Both of these aims can be met using a two-stage growth process consisting of Ba-Zr metal precursor deposition followed by thermal processing in S vapor, although special adaptations are required, as will be described. With suitable procedures, we have grown $BaZrS_3$ films both on Mo-coated and on insulating substrates, with little to no degradation of the substrate, using growth temperatures below 600°C. Finally, the latest results from charge transport measurements, as well as the additional optical and structural characterization of $BaZrS_3$ thin films, will be presented. The impact of process variations, including the influence of S vapor pressure and addition of p-/n-type dopants, will be reported and discussed. References:

[1] R. Jaramillo, J. Ravichandran, *APL Mater.* **2019**, *7*, 100902.

[2] Y.-Y. Sun, M. L. Agiorgousis, P. Zhang, S. Zhang, *Nano Lett.* **2015**, *15*, 581.

[3] K. V. Sopiha, C. Comparotto, J. A. Márquez, J. J. S. Scragg, *Advanced Optical Materials* **2022**, *10*, 2101704.

2:00 PM EQ04.02.02

Understanding Post-Transition Metal Chalcogenide Absorbers—Defects and Beyond-DFT Christopher Savory; University College London, United Kingdom

As we balance the worldwide need for energy with the necessity to move to renewable energy technologies, assembling a diverse array of photovoltaic materials is necessary to overcome such challenges and demands. Silicon is highly abundant and market-dominant, yet energy-intensive to produce and necessitates thick wafers, while established chalcogenide thin-film materials such as CdTe allow strong absorption and the potential for flexible devices but suffer from toxicity and low abundance of constituent elements.^{1,2} Recent work, however, has demonstrated a class of emerging chalcogenide absorbers that offer both more sustainable synthesis and promising optoelectronic properties, and could aid the photovoltaic diversity of the future.

In this talk, I will consider our computational investigations into a selection of these post-transition metal chalcogenide solar absorbers – Sb_2Se_3 , GeSe and $CuSbS_2$ – with a focus on their excitonic properties and defect chemistries. In the first section of the study, we discuss the use of many-body perturbation theory as route to highly accurate band gap prediction. From our initial success in elucidating the nature of the gap in bulk GeSe,³ to looking at the absorption in Sb_2Se_3 and the nature of the excitons in $CuSbS_2$, we show how the QSGW method, with the addition of vertex corrections through the solution of the Bethe-Salpeter equation,⁴ allows understanding and comparison to optical experiments far beyond that possible with standard Density

Functional Theory (DFT).

In the second section, we explore how the unusual structural and chemical environments available to these chalcogenides can both benefit and hamper the defect tolerance of these materials. Our previous work has highlighted how despite possessing a pseudo-1D structure and potentially benign grain boundaries,^{5,6} Sb₂Se₃ suffers from numerous mid-gap defect states that could be hampering open circuit voltage in devices.⁷ In this work, we examine strategies for p-type dopability in the material to improve device performance, in collaboration with the University of Liverpool,⁸ and present simulations of the defect behaviour of GeSe to discuss how elements of this defect chemistry vary between the different post-transition metal chalcogenides. With this understanding, we critique the applicability of defect tolerance in these materials, and assess the promise of emerging chalcogenide absorbers.

- [1] Haegel, N. M.; Margolis, R.; Buonassisi, T.; Feldman, D.; Froitzheim, A. et al. *Science* **356**, 141 (2017)
- [2] Peter, L. M. *Philos. Trans. A. Math. Phys. Eng. Sci.* **369**, 1840 (2011)
- [3] Murgatroyd, P.A.E.; Smiles, M.J.; Savory, C.N.; Shalvey, T.P.; Swallow, J.E.N. et al., *Chem. Mater.* **32**, 3245 (2020)
- [4] Cunningham, B; Gruening, M.; Pashov, D; van Schilfgaarde, M. *arXiv:2106.05759 [cond-mat.mtrl-sci]* (2021)
- [5] Li, Z.; Liang, X.; Li, G.; Liu, H.; Zhang, H.; Guo, J.; Chen, J.; Shen, K.; San, X.; Yu, W.; Schropp, R. E. I.; Mai, Y. *Nat. Commun.* **10**, 125 (2019)
- [6] Zhou, Y.; Wang, L.; Chen, S.; Qin, S.; Liu, X.; Chen, J.; Xue, D.-J.; Luo, M.; Cao, Y.; Cheng, Y.; Sargent, E. H.; Tang, J. *Nat. Photonics* **9**, 409 (2015)
- [7] Savory, C. N.; Scanlon, D. O. *J. Mater. Chem. A* **7**, 10739 (2019)
- [8] Hobson, T.D.C; Shiel, H.; Savory, C.N.; Swallow, J.E.N.; Jones, L.A.H. et al. *in submission* (2022)

2:15 PM EQ04.02.03

Impact of Cation Disorder on Solar Cell Performance in Ternary Chalcogenides (I-III-S₂; NaBiS₂) [Seán R. Kavanagh](#)¹, Yi-Teng Huang², Robert Hoye³, David O. Scanlon⁴ and Aron Walsh³; ¹University College London & Imperial College London, United Kingdom; ²University of Cambridge, United Kingdom; ³Imperial College London, United Kingdom; ⁴University College London, United Kingdom

I-V-VI₂ ternary chalcogenides have recently attracted growing attention as earth-abundant, nontoxic, and air-stable absorbers for photovoltaic applications.¹ In particular, our recent work on the NaBiS₂ & AgBiS₂ members of this family has revealed ultra-strong optical absorption for these compounds – *the highest of all current PV materials*.^{2,3} A key benefit of such intense light absorption is that it allows for ultrathin (<100 nm) solar cell devices, dramatically reducing material consumption, weight and manufacturing demand, directly lowering the cost and facilitating applications in space for example, in addition to benefitting quantum efficiency and photovoltaic (PV) performance.

Our work on AgBiS₂² showed the crucial importance of controlling cation distribution and disorder in these materials, yielding record-breaking efficiencies >9% – the highest of any Bi-based solar absorber.² However, the impact of disorder on the charge-carrier properties in these materials is remains poorly understood. Herein, we investigate the key properties which dictate the relationship between disorder on the cation sublattice and carrier transport in these materials. We find the band-edge orbital character to be a crucial factor in the sensitivity of carrier localisation (and thus solar cell efficiency) to cation disorder, resulting in ultra-fast carrier trapping, despite slow carrier recombination, in NaBiS₂.³

This work reveals the critical role of cation disorder in the photovoltaic performance of these systems, alongside key considerations for future research in this area.

(1) Huang, Y.-T.; Kavanagh, S. R.; Scanlon, D. O.; Walsh, A.; Hoye, R. L. Z. Perovskite-Inspired Materials for Photovoltaics and beyond—from Design to Devices. *Nanotechnology* **2021**, *32* (13), 132004. <https://doi.org/10.1088/1361-6528/abcf6d>.

(2) Wang, Y. † & Kavanagh, S. R. †; Burgués-Ceballos, I.; Walsh, A.; Scanlon, D. O.; Konstantatos, G. Cation Disorder Engineering Yields AgBiS₂ Nanocrystals with Enhanced Optical Absorption for Efficient Ultrathin Solar Cells. *Nature Photonics* **2022**.

(3) Huang, Y.-T. †; Kavanagh S. R. †; R.; Scanlon, D. O.; Walsh, A.; Hoye, R. L. Z. et al. Strong Absorption and Ultrafast Localisation in NaBiS₂ Nanocrystals with Slow Charge-Carrier Recombination. *Nature Communications* (under review)

2:30 PM BREAK

SESSION EQ04.03: Optical and Emergent Properties
Session Chairs: Archana Raja and Jonathan Scragg
Monday Afternoon, November 28, 2022
Sheraton, 2nd Floor, Constitution A

3:00 PM *EQ04.03.01

Opto-Mechanical Structural Transitions in SnSe Driven by Mid-Infrared Light Pulses [Aaron Lindenberg](#); Stanford University, United States

A central goal in materials research is to develop means for controlling and inducing new phases of matter with unique functionalities. With respect to using light to control matter, previous work has mostly focused on above-bandgap or resonant mode excitation, accessing the imaginary part of the dielectric function. Here we present new experimental results using a suite of advanced spectroscopies to show evidence for a novel optomechanical driving force in the chalcogenide material tin selenide (SnSe) using mid-infrared, below-gap femtosecond optical pulses. Femtosecond time-resolved Raman scattering shows an abrupt suppression of Raman modes above a threshold fluence consistent with a distortion towards the high-symmetry rocksalt phase of SnSe. This is further corroborated by transient reflectivity measurements, time-resolved x-ray scattering, and first principles calculations, thereby defining new possibilities for manipulating the structure and functionality of SnSe and related chalcogenide materials.

3:30 PM EQ04.03.02

Visualization of Photoexcited Dynamics in Chalcogenide Materials Grains using State-Of-The-Art Pump-Probe Microscopy and Spectroscopy Techniques [Farnoush Nourigheimesi](#) and [Elham Ghadiri](#); Wake Forest University, United States

In this paper, we integrate a combination of modern and complementary ultrafast transient absorption spectroscopy (TAS) and pump-probe transient absorption microscopy (TAM) techniques to discuss the ultrafast photophysics of efficient photovoltaic materials including Cu₂BaSnS₄Se (CBTSSe) chalcogenides^{1,2} and Cu₂ZnSnS_{4-x}Se_x (CZTSSe). CBTSSe is a recently introduced alternative to Cu(In,Ga)(S,Se)₂ and Cu₂ZnSnS_{4-x}Se_x (CZTSSe). Pump-probe microscopic imaging enables to localize the photoexcitation patterns and early charge carrier kinetics within the grains of only a few hundreds of nanometers and localize the kinetics of photogenerated carriers in each grain with femtosecond time resolution.

We compare the photoexcitation pattern in CBTS and CZTS films and discuss the excited state relaxation within film grains. For CBTS, we spectrally resolve a sharp ground-state bleaching (GSB) peak, formed around the band edge transition. The pump-probe microscopy images are heterogeneously composed of positive and negative regions identifying excited state absorption and ground state bleaching in different grains. For CZTS samples, at identical condition, we observe that the pump-probe microscopy images are homogeneously composed of GSB. The broadband spectrum points to broad GSB absorption extended from visible to near infrared region for CZTS. Our pump-probe microscopy and spectroscopy results, all point to a reduction in shallow defects and band tailing in CBTS relative to CZTS films. The charge carrier relaxation resolved in CBTS single grains, or over an ensemble of grains, however, remains faster compared to CZTS, pointing to the need to perhaps better understand deep traps within this absorber family. Remarkably, we have shown that the unique sensitivity of pump-probe microscopy and sharp electronic transitions allow for detection of small compositional variations,— features that are largely unresolved for ensemble spectroscopy or luminescence measurements.

References:

1. Ghadiri, E.; Shin, D.; Shafiee, A.; Warren, W.S.; Mitzi, D.B.; Grain-Resolved Ultrafast Photophysics in $\text{Cu}_2\text{BaSnS}_{4-x}\text{Se}_x$ Semiconductors Using Pump-Probe Diffuse Reflectance Spectroscopy and Microscopy.
2. Shin, D.; Zhu, T.; Huang, X.; Gunawan, O.; Blum, V.; Mitzi, D. B. Earth-abundant chalcogenide photovoltaic devices with over 5% efficiency based on a $\text{Cu}_2\text{BaSn}(\text{S},\text{Se})_4$ absorber. *Adv. Mater.* **29**, 1606945 (2017).
3. Ghadiri, E.; Zakeeruddin, S.M.; Hagfeldt, A.; Grätzel, M.; Moser, J.-E. Ultrafast charge separation dynamics in opaque, operational dye-sensitized solar cells revealed by femtosecond diffuse reflectance spectroscopy. *Sci. Rep.* **6**, 24465 (2016).
4. Ghadiri, E.; Taghavinia, N.; Zakeeruddin, S. M.; Grätzel, M.; Moser, J.-E. Enhanced electron collection efficiency in dye-sensitized solar cells based on nanostructured TiO_2 hollow fibers. *Nano Lett.* **10**, 1632–1638 (2010).

3:45 PM EQ04.03.03

Pure Spin Photocurrent in Non-Centrosymmetric Crystals—Bulk Spin Photovoltaic Effect Haowei Xu, Hua Wang, Jian Zhou and Ju Li; Massachusetts Institute of Technology, United States

Spin current generators are critical components for spintronics-based information processing. In this work, we theoretically and computationally investigate the bulk spin photovoltaic (BSPV) effect for creating DC spin current under light illumination. The only requirement for BSPV is inversion symmetry breaking, thus it applies to a broad range of materials and can be readily integrated with existing semiconductor technologies. The BSPV effect is a cousin of the bulk photovoltaic (BPV) effect, whereby a DC charge current is generated under light. Thanks to the different selection rules on spin and charge currents, a pure spin current can be realized if the system possesses mirror symmetry or inversion-mirror symmetry. The mechanism of BSPV and the role of the electronic relaxation time are also elucidated. We apply our theory to several distinct material systems, including transition metal dichalcogenides, anti-ferromagnetic MnBi_2Te_4 , and the surface of topological crystalline insulator cubic SnTe .

4:00 PM +EQ04.03.04

The Nature of Metavalent Bonding in Crystals—The Origin of Emergence of Unusual Properties Umesh V. Waghmare, Raagya Arora and C N. Rao; Jawaharlal Nehru Ctr for Adv Sci Research, India

Phase change chalcogenide materials exhibit a remarkable ability to transform reversibly from a covalently bonded amorphous structure to rocksalt crystalline forms considered to exhibit a distinct type of metavalent bonding. An unusual portfolio of anomalous functional properties emerge in the metavalent rocksalt forms, and their origin and electronic mechanisms are yet to be understood. Here, we present first-principles theoretical analysis of the evolution of metavalent bonding along continuous paths in the structural and chemical composition space, starting from distinct covalent, ionic and metallic states. We show that metavalent bonding arises in rocksalt chalcogenides stabilized in weakly broken symmetry states of the parent covalent metal, a simple cubic crystal of Group V metalloid. High electronic degeneracy at the nested Fermi surface of the parent metal drives spontaneous breaking of its translational symmetry with structural and chemical changes, which mediate strong coupling between conduction and valence bands separated by a small energy gap making metavalent crystals highly conductive, polarizable and sensitive to bond-lengths. Stronger changes in structural and chemical fields, however, evolve them discontinuously to covalent and ionic semiconducting states respectively. We predict them to exhibit anomalous second order Raman scattering, adding to the set of their unusual fingerprinting properties. Wannier function analysis reveals multi-centre, mixed bonding and antibonding *pp* and *sp* orbital interactions supporting fractional bond-order and high coordination numbers. Our precise picture of metavalent bonding will guide in design of new metavalent materials with improved thermoelectric, ferroelectric and nontrivial electronic topological properties.

4:30 PM EQ04.03.05

High-Temperature Superconductor FeSe Films Enabled Through Flux Ratio Control Maria Hilse¹, Hemian Yi¹, Cui-Zu Chang¹ and Roman Engel-Herbert^{1,2}; ¹The Pennsylvania State University, United States; ²Paul-Drude-Institut für Festkörperelektronik, Germany

FeSe, a bulk superconductor with a T_C of 9 K has attracted a high level of attention over almost one decade since a skyrocketing boost in T_C was reported for a single unit cell (UC) layer of FeSe grown by molecular beam epitaxy (MBE) on $\text{SrTiO}_3(001)$ to as high as 100 K.[1] FeSe- SrTiO_3 heterostructures have since been fabricated by numerous groups in the field but the record T_C proved extremely difficult to reproduce and thus the mechanism behind it still remains concealed. However, after extensive work in the past, the field appears to agree on certain key “ingredients” in the heterostructure sample preparation that are believed essential for the boost in T_C . Those key players are; 1. an ultra-clean substrate surface of specific double layer of TiO_2 termination typically realized by a chemical and thermal *ex-situ* and additional thermal *in-situ* substrate preparation before growth; 2. ultra-thin – one to few unit cell thickness – limit of FeSe layer thickness; 3. a high number of Se vacancies in the FeSe film ensured through post-growth annealing steps carried out under ultra-high vacuum (UHV) for several hours; 4. followed by a suitable capping layer growth in case films need to be characterized *ex-situ* under ambient pressure due to the rapid oxidation of FeSe in air.

In this talk, we present our findings on FeSe thin film growth by MBE and present a roadmap for high- T_C – as high as 20 K in macroscopic *ex-situ* transport measurements – circumventing above mentioned steps 1, 2, and 3 by simple *in-situ* Se/Fe flux ratio control during FeSe growth. For this study, we have been growing FeSe films of 20-UC-thickness at varying temperature and Se/Fe flux ratios and analyzed the structural and morphological properties of the obtained uncapped FeSe films. Se and Fe fluxes were calibrated before each growth using a heated Quartz crystal microbalance (QCM) and tooling factors for the QCM calibration were extracted from physical thickness measurements by X-ray diffraction (XRD). The substrate surface temperature during growth was monitored with high precision by an infrared (IR) camera system. SrTiO_3 substrates were cleaned in subsequent ultrasonic baths of acetone, isopropyl alcohol, and DI-water and annealed in air to 980 °C for about 1.5 h in a box furnace to realize an atomic terrace surface morphology and additionally annealed in UHV to 600 °C for 2 h to remove adsorbates. Structural and morphological analysis was carried out *in-situ* by reflection high energy electron diffraction (RHEED) and *ex-situ* by XRD and atomic force microscopy (AFM), respectively within 20 min of taking the samples out of the UHV environment to minimize oxidation of the films. The morphology of the films showed a sensitive dependence on the growth temperature and flux ratio spanning from perfectly smooth and continuous films with atomic terraces at 450 °C growth temperature and a low flux ratio of 2.5 to exclusively disconnected island growth of large height but smooth top surfaces at lower temperatures and/or higher flux ratios. Surprisingly, the tetragonal $P4/nmm$ crystal structure of β -FeSe was maintained for all investigated films and the *in-situ* observed diffraction pattern in RHEED also maintained the streaky pattern characteristic for smooth FeSe films even for the samples with the most pronounced island growth resulting in a root mean

square (rms) AFM roughness of more than 18 nm. Smaller flux ratios than 2.5 resulted in mixed β -FeSe/elemental Fe phase samples. FeSe films grown under optimized conditions at 450 °C and a flux ratio of 2.5 (but without any post-growth UHV anneal) and capped with the commonly used FeTe (300 °C) and elemental Te (room temperature) layers yielded superconducting onset temperatures of about 30 K and a T_c of 20 K.

[1] D. Huang, J.E. Hoffman, Monolayer FeSe on SrTiO₃, *Annu. Rev. Condens. Matter Phys.* 8 (2017) 311–336. <https://doi.org/10.1146/annurev-conmatphys-031016-025242>.

SESSION EQ04.04: Defects and Excited States in Low-Dimensional Materials

Session Chairs: Kunal Mukherjee and Mark Polking

Tuesday Morning, November 29, 2022

Sheraton, 2nd Floor, Constitution A

8:30 AM *EQ04.04.01

Tunable Doping for 2D Materials Electronics Albert Davydov¹, Sergiy Krylyuk¹, Huairuo Zhang¹, Bruce Scruggs¹, Zheng Sun², Chandraman Patil³, Volker J. Sorger³ and Joerg Appenzeller²; ¹National Institute of Standards and Technology, United States; ²Purdue University, United States; ³George Washington University, United States

2D materials, including layered metal chalcogenides, enable a broad range of advanced electronic applications. The ability to manipulate electrical properties by doping 2D semiconductors opens a possibility for fabricating ultra-thin p/n junctions and other two-dimensional electronic devices. However, reliable processes for reproducible doping of 2D materials are yet to be developed. This talk will survey various doping approaches of 2D semiconductors from substitutional to electrostatic to charge transfer via surface, followed by the specific example of developing controllable doping of indium selenide layers. The n- and p- type substitutional doping of InSe was conducted via single crystal Bridgman growth using Sn and Zn impurities, respectively. The concentration of Sn atoms in progressively doped n-type InSe samples varied from tens to hundreds of ppm as estimated from the X-ray fluorescence (XRF) and inductively coupled plasma mass-spectrometry (ICP-MS). Electrically active dopant concentration was assessed using van-der-Pauw Hall measurements and compared against the total Sn concentration from XRF and ICP-MS. The talk will conclude with a demonstration of employing electrically tunable indium selenide layers in a p/n homojunction photodetector.

9:00 AM EQ04.04.02

Disorder and Its Effects on Two-Dimensional Transition Metal Dichalcogenides Steven Durbin¹, Krystal R. York¹, Robert Makin¹, Thomas McKnight² and Joan M. Redwing²; ¹Western Michigan University, United States; ²The Pennsylvania State University, United States

Semiconductor transition metal dichalcogenides (TMDs) have an inherent tunability where as the number of layers in the material increases, the band gap decreases and becomes indirect. This property gave rise to several band gap engineering studies for these 2D materials such as heterostructures, strain engineering, and twist angle studies. This work instead focuses on adjusting the band gap energy and other properties by tuning the degree of disorder. Disorder in a lattice refers to a state of a crystalline solid in which not all of the atoms occupy their predicted lattice sites. In other words, a completely ordered lattice would have all of the atoms occupy their equilibrium phase position and a completely disordered lattice would have the atoms randomly distributed over the lattice sites. A disordered state can occur even when the material maintains its predicted stoichiometry since antisite defects can preserve the correct composition. Although disorder in the lattice is typically unwanted, it has been shown to be useful in reliably tuning properties such as the band gap.

The degree of disorder has been quantified using the Bragg-Williams order parameter S to better understand the trends between disorder and significant material properties. This work extracts the order parameter of several of the TMD materials using Raman spectroscopy and SEM, with excellent agreement between these two techniques. For all of the materials in this work, there is a clear linear trend between the band gap values and S^2 , which has previously been experimentally established for other materials like heterovalent ternary materials such as ZnSnN₂ and MgSnN₂, binary materials such as InN and GaN, and elementary materials such as Si.

This work focuses on WSe₂ films grown via metal-organic chemical vapor deposition (MOCVD) on sapphire substrates using a multi-step growth process which involved an initial nucleation step, a ripening step, and a final lateral growth step. This process was chosen as it has shown to achieve large-area, lateral growth of MOCVD grown TMDs in the past. Between each film growth, one process parameter was changed in order to determine how that parameter altered the degree of disorder. The process parameters tested were the substrate temperature, H₂Se flow rate, and length of the individual steps. Additionally, S^2 was also compared to the monolayer coverage and the thickness of the domains, which were extracted using atomic force microscopy to determine if these were the main drivers for the changes seen in the degree of ordering. Exploring the role of process parameters in the context of tuning the degree of disorder can not only allow for a dependable way of controlling of the band gap energy, but also could prove to be a reliable way of controlling other electrical properties such as carrier mobility.

The TMD materials analyzed for this study exhibited an expected continuous linear relationship between the band gap values and S^2 . The amount of coverage and number of layers had the most discernable impact on the S^2 value, showing that as the number of layers or monolayer coverage increased, so too did the degree of ordering. However, process parameters such as the temperature during the nucleation step, H₂Se flow rate, and chamber pressure seemed to have an impact on the degree of ordering as well. Finally, an unexpected result emerged when adjusting the chamber pressure between film growths, which resulted in an ability to control domain alignment and domain directions.

Financial support for research at The Pennsylvania State University was provided by the National Science Foundation through the 2D Crystal Consortium – Materials Innovation Platform (2DCC-MIP) under NSF cooperative agreements DMR-1539916 and DMR-2039351.

Financial support for research at Western Michigan University was funded in part by the National Science Foundation (grant number DMR-2003581).

9:15 AM EQ04.04.03

Explanation of the Opposing Shifts in the Absorption Edge and the Optical Resonance in CuFeS₂ Nanoparticles Yuan Yao; Cornell University, United States

CuFeS₂ nanoparticles are novel intermediate band semiconductors that possess a prominent plasmon-like absorption feature in the visible region (~2.5 eV),

giant optical nonlinearity, and have the potential for post-synthetic tuning of their absorption band. Despite having similar optical properties to other semiconductor plasmonic materials, the quasi-static optical resonance in CuFeS₂ is contributed by collective electronic transitions between filled and unfilled states rather than by a free carrier oscillation.

Size-dependent change of the electronic band structure is one of the key features of nanoparticles in the quantum confinement region, but in CuFeS₂ the optical features follow divergent and conflicting trends that have yet to be explained. Namely, when the particle size decreases the optical resonance feature of CuFeS₂ shows a small redshift while the band gap blueshifts. Since the 2.5 eV absorption feature is contributed by collective electronic transition, we hypothesized that this feature should be subject to quantum confinement effects through modification of the electronic bands. In this paper, we show experimentally that the optical resonance absorption peak redshifts and the optical band gap blueshifts as the particle size decreases. Then, through density functional theory (DFT) and a tight binding modeling, we elucidate the size dependence of the band structure, especially focusing on the change in the intermediate band. Using a Lorentzian oscillator optical model to simulate the absorption spectrum with inputs from the DFT calculated band structure and band shifts from the tight binding model, we find the size-dependent shifts of the optical resonance peak position in CuFeS₂ is due to a tri-band quantum confinement effect that results in both the valence band to intermediate band and intermediate band to conduction band gap expansion that accompanies a decrease in particle size. We also find that the transitions between the intermediate band and conduction band play only a minor role in the optical spectrum. Moreover, the linear optical Lorentzian model predicts the optical resonance peak is tunable across the visible range by partially filling the intermediate band, lowering the conduction band, or expanding the intermediate band.

Overall, in this study, we provide fundamental understandings about the origin of the visible quasi-static resonance in CuFeS₂ nanoparticles and elucidate the correlation between the absorption feature shift and the intermediate-band electronic structure. These results are relevant to other quantum-confined intermediate band systems, which have potential use in optical applications as well as photovoltaic devices.

9:30 AM BREAK

10:00 AM *EQ04.04.04

Dilute Impurities and Bound Excitons in 2D Semiconductors [Goki Eda](#); National University of Singapore, Singapore

Owing to reduced screening, point defects in 2D semiconductors such as monolayer transition metal dichalcogenides (TMDs) can serve as optically addressable quantum dots. However, the density of common defects in TMDs are excessively high, making it challenging to address individual defect states for quantum operations. Accordingly, the physical origin of the localized states also remains elusive, preventing strategic quantum defect engineering. We introduce and optically probe a variety of atomic defects in monolayer TMDs in the dilute limit with the aim of accessing their quantum nature. One example is Nb-doped monolayer WS₂, which is found to exhibit bright sub-gap emission even at ppm concentrations. We show that such emission arises from ionized-acceptor-bound excitons, a three-body charge complex analogous to a negative trion. These bound exciton complexes exhibit sizeable valley selectivity reflecting their partial free exciton character. We further discuss a scanning probe approach to rapidly quantifying impurities in the ultra-dilute limit ($<10^{10}\text{cm}^{-2}$) in ambient conditions.

10:30 AM DISCUSSION TIME

11:00 AM EQ04.04.06

Ab Initio Molecular Dynamics Simulation Study of Oxidation of ZrS₂(001) [Liqiu Yang](#)¹, [Subodh Tiwari](#)², [Aravind Krishnamoorthy](#)¹, [Rajiv Kalia](#)¹, [Aiichiro Nakano](#)¹ and [Priya Vashishta](#)¹; ¹University of Southern California, United States; ²Schrödinger, United States

Abstract

In transition metal dichalcogenides (TMDC) family, ZrS₂ is known for its superior electrical and chemical catalytic properties. Meanwhile, it is easily oxidized, which brings problems in device processing and long-term stability. Although the ZrS₂ oxidation mechanism and oxide growth kinetics has been investigated recently, the atomistic reaction pathway still lacks fully understood. Here, we report *ab initio* molecular dynamics results for studying the oxidation of ZrS₂. Our simulations show the oxidation of ZrS₂(001) surface to be initiated as the adsorption of an oxygen molecule to the ZrS₂(001) surface, followed by oxygen atoms substituting surface sulfur atoms. The recently reported amorphization-assisted-oxidation is found to be linked to the zirconium atoms bonded with inner layer sulfur atoms. We also found the oxygen transport is assisted by bond switching and ring arrangements. The chemical reaction pathways and atomistic mechanisms provided in this work is valuable for device processing and other layered TMDC oxidation.

Acknowledgements

This work was supported as part of the Computational Materials Sciences Program funded by the U.S. Department of Energy, Office of Science, Basic Energy Sciences, under Award Number DE-SC0014607.

11:15 AM EQ04.04.07

Investigation of Oxidation Mechanism in HfS₂ and ZrS₂ TMDs with In Situ Transmission Electron Microscopy [Alexandre Foucher](#), [Kate Reidy](#), [Wouter Mortelmans](#), [Baoming Wang](#), [Seong Soon Jo](#), [Aubrey Penn](#), [Rafael Jaramillo](#) and [Frances M. Ross](#); Massachusetts Institute of Technology, United States

HfS₂ and ZrS₂ transition metal dichalcogenides (TMDs) are of great interest for their potential applications as semiconductors in field effect transistors (FETs), low-power devices and photodetectors. It has been shown that these materials have higher mobility than MoS₂, which makes them promising materials for optical and electric devices. In particular, the oxidation of HfS₂ and ZrS₂ is critical as it can dramatically change their physical properties. In fact, the oxidation of HfS₂ and ZrS₂ can be useful in creating a dielectric layer adjacent to the semiconductor, as needed in FETs. In this work, we performed *in situ* transmission electron microscopy to investigate the oxidation mechanism of HfS₂ and ZrS₂ under O₂ at elevated temperature and compare with MoS₂. Simultaneous *in situ* SEM and STEM-EDS/EELS analysis was performed to show morphological and chemical changes. We demonstrated that S is replaced by O under these conditions and showed increased surface roughness of 2D HfS₂ and ZrS₂. Modifications of the crystal structure, such as the formation of amorphous layers and islands were also observed. Additionally, 4D STEM was performed to show strain and stress in 2D HfS₂ and ZrS₂ upon oxidation. The impact of oxidation was then correlated with modification in optical properties of the oxide, measured by spectroscopic ellipsometry, and modification in electrical and dielectric properties, measured with MOS device. These results provide guidelines to further improve the stability and performance of devices with ZrS₂ and HfS₂ TMDs.

SESSION EQ04.05: Printing 2D Materials
Session Chairs: Yuval Golan and Archana Raja
Tuesday Afternoon, November 29, 2022
Sheraton, 2nd Floor, Constitution A

1:45 PM *EQ04.05.01

Water-Based 2D Material Inks for Printed Electronics Cinzia Casiraghi; University of Manchester, United Kingdom

Solution processing of 2D materials allows simple and low-cost techniques, such as ink-jet printing, to be used for fabrication of heterostructure-based devices of arbitrary complexity. Our group has developed highly concentrated, defect-free, inkjet printable and water-based 2D crystal formulations, by exploiting non-covalent functionalization of 2D materials with pyrene derivatives [1]. Examples of printed heterostructures, containing Chalcogenide inks, such as arrays of photosensors, programmable logic memories, and memristors will be discussed [2-3]. Furthermore, inkjet printing can be easily combined with Chalcogenide materials produced by chemical vapor deposition, allowing simple and quick fabrication of complex circuits on paper, compatible with CMOS technology [4-5].

- [1] Xu et al, *Nanoscale* 13, 460 (2021)
- [2] McManus et al, *Nature Nano*, 12, 343 (2017)
- [3] Peng et al, in preparation
- [4] Conti et al, *Nature comms*, 11 (1), 1-9 (2020)
- [5] Brunetti et al, *npj 2D Materials and Applications* 5, 1-6 (2021)

2:15 PM EQ04.05.02

Generalised Optical Printing of Photocurable Metal Chalcogenides Seongheon Baek and Jae Sung Son; Ulsan National Institute of Science and Technology, Korea (the Republic of)

Optical three-dimensional (3D) printing techniques attract tremendous attention due to the capability of maskless additive manufacturing, enabling cost-effective and straightforward creation of patterned architectures. Despite their potential as alternatives to classical lithography, the printable materials produced by these processes are restricted to photocurable resins, limiting the functioning of printed products and their application regions. Herein, we report a generalised direct optical printing technique to obtain functional metal chalcogenides via digital light processing. We developed universally applicable photocurable chalcogenidometallate inks that could be directly used to create 2D patterns or 3D architectures of various sizes and shapes. Our method may be used to make a wide variety of functional metal chalcogenides for compound semiconductors as well as 2D transition-metal dichalcogenides. Finally, we demonstrate the feasibility of our process that the micro-scale thermoelectric generator with tens of patterned semiconductors was fabricated and evaluated. Our approach shows potential for simple and cost-effective architecturing of functional inorganic materials.

2:30 PM BREAK

SESSION EQ04.06: Materials for Infrared Optoelectronics and Photonics
Session Chairs: Goki Eda and Kevin Ye
Tuesday Afternoon, November 29, 2022
Sheraton, 2nd Floor, Constitution A

3:00 PM *EQ04.06.01

New Functional Metal Chalcogenides Deposited from Solution Yuval Golan; Ben-Gurion University of the Negev, Israel

We review several newly discovered metal-chalcogenide binary phases obtained using solution-based techniques. The new cubic pi-phase of tin sulfide (pi-SnS) reported in 2015 was first obtained using colloidal (surfactant assisted) synthesis, [1] and was later deposited as thin films from aqueous solutions. [2,3] Soon after, the cubic selenide analog, pi-SnSe, was reported. [4] Several "beneficial impurities" were identified, whose presence was found to be essential for stabilization of these metastable phases. [5] More recently, yet another new binary phase of SnSe, the orthorhombic gamma-SnSe, [6] was shown to exhibit intriguing and potentially useful electronic properties. [7] Furthermore, combinatorial liquid flow deposition of metal chalcogenides offers great potential for discovery of new materials and properties. [8] Finally, we will show that caution must be exercised when preparing TEM samples using the dual beam FIB due to sample preparation induced phase transitions. [9]

References

1. A. Rabkin, S. Samuha, R.E. Abutbul, V. Ezersky, L. Meshi, Y. Golan, "New Nanocrystalline Materials: A Previously Unknown Simple Cubic Phase in the SnS Binary System" *Nano Lett.* **15** (2015) 2174-2179.
2. R.E. Abutbul, A. R. Garcia-Angelmo, Z. Burshtein, M.T.S. Nair, P.K. Nair, Y. Golan, "The Puzzle Unraveled: Crystal Structure of Cubic Tin Sulfide in Thin Films", *CrystEngComm* **18** (2016) 5188-5194.
3. R.E. Abutbul and Y. Golan, "Chemical Epitaxy of Cubic SnS on PbS" *CrystEngComm*. **22** (2020) 6170-6181.
4. R.E. Abutbul, E. Segev, S. Samucha, L. Zeiri, V. Ezersky, G. Makov, Y. Golan, "A New Nanocrystalline Prototype Structure: Synthesis and Properties of Cubic π -SnSe", *CrystEngComm* **18** (2016) 1918-1923.
5. R.E. Abutbul and Y. Golan, "Beneficial Impurities in Colloidal Synthesis of Surfactant Coated Inorganic Nanoparticles" (invited review article) *Nanotechnology* **32** (2021) 102001.
6. B. Koren, R.E. Abutbul, V. Ezersky, N. Maman, Y. Golan, "A New Binary Phase in the Tin Monoselenide System: Chemical Epitaxy of Orthorhombic γ -SnSe Thin Films" *RSC Materials Chemistry Frontiers* **5** (2021) 5004-5011.
7. N. Zakay, et al., (2022) in preparation.
8. N. Zakay, O. Friedman, L. Vradman and Y. Golan, "Combinatorial Liquid Flow Deposition of PbS Semiconductor Thin Films", *ACS Industrial & Engineering Chemistry Research* **60** (2021) 15593-15599.
9. B. Koren, O. Friedman, N. Maman, S. Hayun, V. Ezersky and Y. Golan, "Sample preparation induced phase transitions in solution deposited copper selenide thin films" *RSC Advances* **12** (2022) 277-284.

3:30 PM *EQ04.06.02

Infrared PbS Colloidal Quantum Optoelectronics—LEDs and Lasers [Gerasimos Konstantatos](#); ICFO, Spain

Solution Processed CMOS compatible Infrared Optoelectronics is a key enabling technology to revolutionize consumer electronic markets offering unprecedented opportunities for low-cost food quality inspection, environmental monitoring, 3D imaging, automotive safety and night vision applications just to name a few. Recent progress in CMOS compatible CQD photodetectors have addressed the InGaAs image sensor challenge and the next step would be the development of the correspondingly low-cost tunable light sources. In this talk, I will be presenting recent results from my lab at ICFO on highly performant infrared CQD LEDs and downconverting light emitters.

I will present our device architecture approach that allowed us to achieve very high PLQY in conductive solid state QD films that when implemented in a LED stack led to 8% EQE [1]. I will then discuss the optimization of the matrix supply dots that improved charge balance and allowed to reach 8% EQE at high radiance along with a stark improvement in operational stability [2]. I will then elaborate on fine-tuning the energetic potential landscape in the matrix which taken together with optimized optical out-coupling schemes reached a QE of 18% at 1550 nm. The possibility to tune the light spectrum of such QD films by stacking layers of QDs with different bandgaps offers exquisite control over the emission spectrum offering the opportunity to develop solid-state thin film broadband emitters in the SWIR, either optically or electrically excited with implications in SWIR spectroscopy [3].

The second part of my talk will discuss recent progress on infrared CQD lasers comprising doped PbS CQDs integrated in a DFB cavity [4]. Besides this I will present our approach of elongating Auger lifetime by engineering QD solids at the supra-nanocrystalline level offering lasers with improved optical linewidths, reduced thresholds and drastically improved stability [5]. I will also briefly discuss our very recent results of sub-single exciton CQD infrared lasing enabled by optimized doping and adoption of a quantum dot heterostructure.

The last part of my talk, if time allows, will be devoted to a different line of research on how to tune the optical properties of nanocrystals by engineering their atomic configuration. I will show an example of AgBiS₂ NCs whereby cation disorder has been homogenized yielding a material with very high optical absorption coefficient. This material has further been optimized in a solar cell stack leading to a record high PCE of 9% for an extremely thin absorber cell of only 35 nm. [6]

References:

- [1] High-efficiency colloidal quantum dot infrared light emitting diodes via engineering at the supra-nanocrystalline level, *Nature nanotechnology* 14 (1), 72-79, 2019
- [2] Highly Efficient, Bright, and Stable Colloidal Quantum Dot Short Wave Infrared Light Emitting Diodes, *Advanced Functional Materials* 30 (39), 2004445, 2020
- [3] Solid State Thin Film Broadband Short Wave Infrared Light Emitters, *Advanced Materials* 32 (45), 2003830, 2020
- [4] Solution-processed PbS quantum dot infrared laser with room-temperature tunable emission in the optical telecommunications window, *Nature Photonics* 15 (10), 738-742, 2021
- [5] Low Threshold, Highly Stable Colloidal Quantum Dot Short Wave Infrared Laser enabled by Suppression of Trap Assisted Auger Recombination, *Advanced Materials* 34 (3), 2107532, 2022
- [6] Cation disorder engineering yields AgBiS₂ nanocrystals with enhanced optical absorption for efficient ultrathin solar cells. *Nat. Photon.* (2022). <https://doi.org/10.1038/s41566-021-00950-4>

4:00 PM EQ04.06.03

Molecular Beam Epitaxy of SnSe Thin Films for Future Optoelectronic Applications [Wouter Mortelmans](#)¹, [Maria Hilse](#)², [Qian Song](#)¹, [Seong Soon Jo](#)¹, [Kevin Ye](#)¹, [Derrick Shao Heng Liu](#)², [Nitin Samarth](#)² and [Rafael Jaramillo](#)¹; ¹Massachusetts Institute of Technology, United States; ²The Pennsylvania State University, United States

Van der Waals (vdW) layered chalcogenides have strongly direction-dependent properties that make them interesting for certain photonic and optoelectronic applications. Orthorhombic tin selenide (α -SnSe) is a triaxial vdW material with strong optical anisotropy within layer planes, which has motivated studies of optical phase and domain switching. As with every vdW material, controlling the phase and orientation of crystal domains during growth is key to reliably making wafer-scale, high-quality thin films, free from twin boundaries. We demonstrate a fast and easy optical method - that applies to all triaxial vdW materials - to quantify domain orientation in single-phase α -SnSe thin films made by molecular beam epitaxy (MBE). We use our method to confirm a high density of twin boundaries in α -SnSe epitaxial films on MgO substrates, with square symmetry that results in degeneracy between α -SnSe 90° domain orientations. We then demonstrate that growing instead on a-plane sapphire, with rectangular lattice-matched symmetry that breaks the α -SnSe domain degeneracy, results in single-crystalline films with preferred orientation, with twin domains all-but-eliminated. We then perform experiments attempting ferroelastic α -SnSe domain switching and epitaxial stabilization of metastable cubic SnSe using other substrates. Our bottom-up SnSe film syntheses by MBE are enabling for future applications of this vdW material that is particularly difficult to process by top-down methods.

4:15 PM EQ04.06.04

Giant Optical Response in Topological Semiconductors with a Mexican Hat Band Structure [Mark Polking](#)¹, [Haowei Xu](#)² and [Ju Li](#)^{2,2}; ¹Lincoln Laboratory, Massachusetts Institute of Technology, United States; ²Massachusetts Institute of Technology, United States

The infrared (IR) to terahertz (THz) frequencies are the least developed parts of the electromagnetic spectrum for applications. Traditional semiconductor technologies such as laser diodes and photodetectors are successful in the visible light range but face major challenges in the IR/THz range due to weak light-matter interactions. In this work, we theoretically and experimentally demonstrate that topological insulators (TIs), especially those with a Mexican hat band structure (MHBS), can help overcome these challenges. Materials with a MHBS exhibit optical responses 1–2 orders of magnitude larger than those of normal semiconductors at the optical transition edge. Through first-principles calculations, we have discovered a number of MHBS TIs with bandgaps between 0.05 and 0.5 eV and giant absorption coefficients on the order of 10^4 – 10^5 cm⁻¹ at the transition edge. Single-crystal specimens of one of these candidate materials, Pb_{0.7}Sn_{0.3}Se, have been experimentally measured using temperature-dependent spectroscopic ellipsometry over a wavelength range of 1.7–19 μ m. These measurements demonstrate a large enhancement in extinction coefficient characteristic of a MHBS in the vicinity of the absorption edge in agreement with theory predictions. Realization of semiconductors with a MHBS is expected to lead to efficient detectors in the IR/THz range.

4:30 PM *EQ04.06.05

Heteroepitaxial Integration and Defect Structure of IV-VI Semiconductors for Infrared Optoelectronics [Kunal Mukherjee](#), [Leland Nordin](#), [Jarod Meyer](#) and [Pooja Reddy](#); Stanford University, United States

The IV-VI selenide semiconductor family of PbSe-SnSe-GeSe has rich materials physics and device applications[1]. These semiconductors, spanning the rocksalt and layered orthorhombic phases, have long been studied for their unconventional bonding that yields rare properties compared to silicon and III-V materials. We present our results from epitaxial integration of IV-VI semiconductor thin films together with III-V materials using molecular beam epitaxy to understand how we may harness these properties for emerging applications in near- and mid-infrared optoelectronics.

With attractively low temperatures for epitaxy much below 300 °C, we describe the nucleation and growth of IV-VI materials on III-V substrates and study the formation and properties of extended crystal defects that arise due to integration[2]. We find bright band-edge photoluminescence from PbSe epitaxial films on ~8% mismatched GaAs substrates in the mid-infrared (3–4 μm) at room temperature, despite a threading dislocation density exceeding 10⁹/cm². While defects still control the minority carrier lifetime at low injection indicating room for improvement, PbSe samples quickly become Auger-recombination limited at high injection[3]. We present insight into carrier recombination mechanisms in PbSe from temperature, time, and excitation power dependent luminescence studies.

The PbSe/GaAs template also enables us to probe deeper into the growth of thin films of SnSe and the PbSnSe alloys that span orthorhombic-rocksalt phases[4]. We show how the structure of layered orthorhombic and rocksalt films and their defects are set by integration with cubic materials, and present preliminary results exploring this structural phase boundary in epitaxial thin films.

[1] G. Springholz, G. Bauer, Molecular beam epitaxy of IV–VI semiconductor hetero- and nano-structures, *Physica Status Solidi (b)*. 244 (2007) 2752–2767.

[2] B.B. Haidet, E.T. Hughes, K. Mukherjee, Nucleation control and interface structure of rocksalt PbSe on (001) zincblende III-V surfaces, *Phys. Rev. Materials*. 4 (2020) 033402.

[3] J. Meyer, A.J. Muhowski, L. Nordin, E. Hughes, B. Haidet, D. Wasserman, K. Mukherjee, Bright mid-infrared photoluminescence from high dislocation density epitaxial PbSe films on GaAs, *APL Materials*. 9 (2021) 111112.

[4] B.B. Haidet, E. Hughes, K. Mukherjee, Epitaxial Integration and Defect Structure of Layered SnSe Films on PbSe/III–V Substrates, *Crystal Growth & Design*. 22 (2022) 3824–3833.

SESSION EQ04.07: Poster Session: Processing-Structure-Property Relationships in Functional Chalcogenides

Session Chairs: Kunal Mukherjee and Debarghya Sarkar

Tuesday Afternoon, November 29, 2022

8:00 PM - 10:00 PM

Hynes, Level 1, Hall A

EQ04.07.01

Stopping Resistance Drift with High-Field Electrical Stresses and Study of Electronic Transport in Stable Amorphous Ge₂Sb₂Te₅ (GST) Ali Gokirmak, Md Tashfiq Bin Kashem, Raihan Khan, ABM Hasan Talukder, Faruk Dirisaglik and Helena Silva; University of Connecticut, United States

Phase change materials are used for the implementation of the high speed, high density, non-volatile phase change memory (PCM) [1]. However, resistance drift complicates both multi-bit-per-cell implementations and characterization of the amorphous phase of the phase change materials [2,3]. In this work, we stabilized melt-quenched amorphous Ge₂Sb₂Te₅ (a-GST) line-cells (stopped resistance drift) with high electric field stresses at low temperatures (T ~ 85 K) [4-6] and performed a comprehensive study on electric field (0 to ~40 MV/m) and temperature (85 K to 300 K) dependent electronic transport.

The a-GST cells show resistance drift in the whole measurement temperature range with drift coefficients linearly decreasing as a function of 1/KT, extrapolating to zero at 61 K [4-6]. In the low-field regime (< 21 MV/m), current-voltage (I-V) characteristics fit well to a temperature dependent hopping transport model and the voltage stresses do not visibly effect resistance drift. In the high-field regime (> 21 MV/m), we observe a stronger exponential response in current and resistance drift is significantly accelerated. High-field stresses stabilize the cells within a few minutes, reaching resistance values that are normally expected to be reached in months by drifting.

In the low-field regime, we model the electronic transport in the stabilized cells assuming that current is limited by emission of trapped charges from a 'source-trap' to a 'receiving-trap' where the activation energy, hopping distance and relative location of the barrier peak are functions of temperature. The model fits the data extremely well. The fit parameters yield carrier activation energies ranging from 0.22 eV to 0.38 eV, hopping distances increasing from ~ 2 nm to ~ 6 nm for 85 K < T < 300 K, comparable to room temperature values reported in the literature [7]. Our models suggest that the barrier peak appears closer to the receiving-trap at lower temperatures and moves towards the midpoint between the source-trap and the receiving-trap with increasing temperature. The electrical conductivity of a-GST at ~1V ranges from ~2×10⁻¹⁰ S/cm at 85 K to ~5×10⁻⁴ S/cm at 300 K and follows the drifted thin film conductivity of the as-deposited a-GST below the glass transition temperature.

In the high-field regime, we observe a stronger current response to electric field, that becomes clearer at lower temperatures. The differential resistances in the high-field regime converge to a single point at 65.6 +/- 0.4 MV/m for all temperatures and the behavior is distinctly different compared to the low-field regime.

The significant change we observe from the low-field to the high-field regime, at a critical electric field of ~21 MV/m, is possibly due to activation of deeper traps or impact ionization of trapped charges. Band-to-band impact ionization and avalanche breakdown are expected to be less likely at this field strength as the mean free paths of the carriers are expected to be relatively small.

Acknowledgments: This work is supported by US NSF grant # 1711626.

References:

1. S. W. Fong *et al.* *IEEE T. Electron Devices*, 64 (2017): 4374, DOI: 10.1109/TED.2017.2746342
2. D. Ielmini *et al.* *J. Appl. Phys.*, 102 (2007): 054517, DOI: 10.1063/1.2773688
3. M. Le Gallo *et al.* *New J. Phys.*, 17 (2015): 093035, DOI: 10.1088/1367-2630/17/9/093035
4. R. S. Khan, *Doctoral dissertation*, University of Connecticut, 2021.
5. R. S. Khan *et al.* *Appl. Phys. Lett.*, 116 (2020): 253501, DOI: 10.1063/1.5144606
6. R. S. Khan *et al.* *arXiv preprint arXiv:2002.12487* (2020), DOI: 10.48550/arXiv.2002.12487
7. D. Ielmini *et al.* *IEEE Int. El. Devices Meet.*, (2007), DOI: 10.1109/IEDM.2007.4419107

EQ04.07.02

Following the Reaction of Chalcogenide Perovskite BaZrS₃ Prakriti Kayastha, Giulia Longo and Lucy Whalley; Northumbria University, United Kingdom

The perovskite ABX_3 class of materials shows great promise as photovoltaic materials, with low production costs, high efficiencies, and a wide range of tunability through structural and compositional variation. The most successful of these perovskites are lead-based halide perovskites. However, there are several outstanding questions about the toxicity and stability of these materials. Chalcogenide-based perovskites, with a less toxic transition metal on the B-site, have been proposed to address both of these issues. In particular, $BaZrS_3$ has been recently fabricated in the lab but there are relatively few computational studies to support this experimental work. Here we present results from calculations using Density Functional Theory and finite displacement methods. In particular, we will analyze the electronic structure of $BaZrS_3$ and evaluate the dynamical properties and thermodynamics of this system. We will present the calculated IR and Raman spectra of $BaZrS_3$ and its competing phases, and discuss how these predictions can be used to support the synthesis of the material via ball-milling. With this work, we hope to highlight how electronic structure methods can support experimental work and accelerate materials design.

EQ04.07.03

Observation of Defect and Disorder Driven Resistive Switching Properties in Sb_2Se_3 . Jiwoong Yang, Yoonsung Jung and Sanghan Lee; Gwangju Institute of Science and Technology, Korea (the Republic of)

Memristor, two-terminal devices in which their resistance state is able to be switched by an applied voltage, have attracted much research attention owing to their possible application to high density Non-Volatile Memory (NVM). Various candidate materials for developing memristor are being studied to extend Moore's law. Specifically, the chalcogenide-based memristors can produce high memory performance with various strategies for defect engineering, so they have been in the spotlight. Antimony selenide (Sb_2Se_3) is an attractive chalcogenide material due to its unique one-dimensional crystal structure and non-toxicity with earth-abundant components. Despite several attempts to develop memory devices using Sb_2Se_3 , no studies have succeeded in identifying the mechanism, and only a few on/off ratios in resistive switching has been reported. Here in, we have fabricated Sb_2Se_3 memristor with superior resistive switching properties via pulsed laser deposition (PLD). Controlling the working pressure, the Sb_2Se_3 thin films were grown to have a dot structure with void spaces, and the manipulation gives rise to the resistive switching property. We conducted atomic force microscope (AFM) and scanning electron microscope (SEM) measurements to observe the vacant surface morphology.

The on/off current ratio of the memristive Sb_2Se_3 with the vacant structure showed higher performances ($\sim 10^5$), compared to that of Sb_2Se_3 with the highly ordered structure ($\sim 10^1$). It was realized that the on/off resistance ratio varies depending on the applied voltage, and this new memristor switched its resistance state even under microsecond pulsed voltage. Besides, the memory performance was retained continuously after more than 1000 switching cycles. In terms of the conduction mechanism of the memristive Sb_2Se_3 , space charge limited conduction (SCLC) was exhibited at the low resistance state, and the Pool Frenkel emission was dominant during the resistive switching process. In summary, we successfully fabricated a novel memristor device based on Sb_2Se_3 with high performance and low power consumption for the first time.

EQ04.07.04

Crystallographic and Electrical Property Improvement of MBE Grown SnTe Films by Introducing ZnTe Buffer Layers Su Nan, Kaito Tusboi, Shotaro Kobayashi, Kota Sugimoto and Masakazu Kobayashi; Waseda University, Japan

SnTe has attracted lots of attentions because it was predicted to be a topological crystalline insulator (TCI)^[1]. In the previous study, SnTe films are prepared directly on GaAs (100) substrates by molecular beam epitaxy. By controlling the growth temperature T_{sub} and flux ratio of the elemental source Te and Sn J_{Te}/J_{Sn} , SnTe (100) single domain have been achieved. However, Te segregation could be formed when certain growth parameters were used. The crystallographic properties including the film surface morphology and electronic properties are mainly studied in this study, and the improvement by introducing the buffer layer was evaluated.

SnTe layers were grown using elemental sources by conventional MBE with the molecular beam intensity ratio (J_{Te}/J_{Sn}) between 0.7~2.9. The value was tuned by changing the beam intensity of Te. Most of samples were grown at 240°C. According to the result of X-ray diffraction (XRD) measurement, diffraction peaks originated from SnTe were clearly confirmed. A peak originated from hexagonal Te was also observed when samples were grown with excess Te (J_{Te}/J_{Sn} was between 2.9 and 1.5). In the SEM measurements, Smooth surface was confirmed when the XRD of sample exhibited no Te peak while dotted materials were clearly observed on the surface when the hexagonal Te diffraction peak was observed by XRD. The distribution density of that dot was high when the Te diffraction peak signal intensity was strong. Those dotted materials are presumed to be the segregation of pure Te. Those crystallographic properties were improved after introducing the ZnTe layer between SnTe layers and GaAs substrates. The surface smoothness improvement was noticeable. The surface morphology was measured by AFM, and the RMS of the sample grown on the ZnTe layer was 4.9nm, which was much better than other samples grown directly on GaAs substrates.

A standard Hall measurement was performed at room temperature. The sample that didn't include the Te segregation exhibited the resistivity of about ohm. The resistivity was increased as the presence of Te was distinguished. Based on the literatures, the resistivity of SnTe is about $ohm \cdot cm$ ^[2], while the resistivity of Te was around $0.3 ohm \cdot cm$ ^[3] at room temperatures. The higher resistivity is led by the mixing of Te. As a supplement, X-ray fluorescence measurement was also performed, and a similar trend was observed.

The segregation of hexagonal Te took place with the high flux ratio, which degraded the surface morphology and resulted in the poor electronic property of SnTe films. The precise control of the molecular beam intensity and the substrate temperature are the keys to achieve device quality SnTe films.

The introduction of ZnTe buffer layer has clearly improved the surface morphology of SnTe films. This result was useful for achieving TCI properties and device quality SnTe films.

Acknowledge This work was supported in part by the Waseda University Grant for Special Research Projects.

1. L. Fu, Physical Review Letter 106, 106802 (2011).
2. Athwal, I. S., et al. Thin solid films 162 (1988): 1-6.
3. Wang, Dongyang, et al. Journal of Alloys and Compounds 773 (2019): 571-584.

EQ04.07.05

Effect of Cr Doping on the Phase Stability in MnTe Polymorphic-Change Film Mihyeon Kim, Yi Shuang, Daisuke Ando and Yuji Sutou; Tohoku University, Japan

In manganese-tellurium (Mn-Te) binary system, MnTe compound has four polymorphs named α , β , γ , δ -MnTe, which are known to be p-type semiconductors. Interestingly, it has been reported that drastic changes in electrical and optical properties can be obtained between a stable phase of the α -MnTe (NiAs-type hexagonal structure) and a metastable phase of the β -MnTe (wurtzite-type hexagonal structure).^[1-2] In our previous research, we successfully deposited the β -MnTe film by radiofrequency magnetron co-sputtering and the as-deposited β -MnTe thin film shows the polymorphic-change to the α -MnTe at around 455 °C, accompanied by large changes in physical properties.^[3] Because such nonvolatile and reversible change of MnTe goes through melting-free process between two crystalline states, it can achieve a high-speed and low-energy phase change, implying that the MnTe is a promising material for phase-change memory devices. Furthermore, recently we revealed that the polymorphic-change of the MnTe film is closely related

to the stress, [4] which suggests that the electrical properties could be controlled by strain. Such strain-induced physical effects in thin film could be used to develop next-generation semiconductor devices for not only low-powered information storage but also sensor applications. However, to realize the strain-induced polymorphic-change accompanying the change of physical properties, the high polymorphic-change temperature of the MnTe film is still remained as a challenge. The sputtered MnTe film stabilizes in a metastable phase of a wurtzite-type hexagonal structure at room temperature. To control the polymorphic-change temperature from wurtzite-type to NiAs-type structure, we focus on tuning the phase stability of the MnTe film by doping transition metal. Chromium (Cr) is a candidate dopant element that could reduce the polymorphic-transition temperature, because Cr-Te binary system has a stable NiAs-type hexagonal structure at a high temperature region. Various compositions of the Cr-Mn-Te ternary thin films were deposited by radiofrequency magnetron co-sputtering. The structural, electrical and optical changes in the Cr-Mn-Te thin films were carried out at the temperature range of 27 - 500 °C to investigate the effect of Cr doping on the phase stability. The polymorphic-change behavior varied with adding Cr, which suggests that Cr dopant could be effective for controlling the polymorphic-change temperature between NiAs-like and wurtzite-like structures.

- [1] S. Siol, Y. Han, J. Mangum, P. Schulz, A. M. Holder, T. R. Klein, M. F. A. M. van Hest, B. Gorman, A. Zakutayev, *J Mater Chem C* **2018**, *6*, 6297.
[2] R. Woods-Robinson, Y. Han, H. Zhang, T. Ablekim, I. Khan, K. A. Persson, A. Zakutayev, *Chem Rev* **2020**, *120*, 4007.
[3] S. Mori, S. Hatayama, Y. Shuang, D. Ando, Y. Sutou, *Nat Commun* **2020**, *11*, 85.
[4] S. Mori, D. Ando, Y. Sutou, *Mater Design* **2020**, *196*, 109141.

EQ04.07.07

Steep-Switching Operation Condition for Field-Effect Transistor with Series-Connected Phase-Transition Device [Chacho Lim](#)¹, Junmo Park¹, Seunghyun Park¹, Yejo Choi², Chahngwan Shin² and Hyounsub Kim¹; ¹SungKyunKwan Univ., Korea (the Republic of); ²Korea University, Korea (the Republic of)

Steep-switching hybrid phase-transition field-effect transistors (hyper-FETs) have recently been introduced as one approach to breaking through the subthreshold swing limit of 60 mV/dec [1]. However, there are few reports on the effect of the electrical properties of the constituent FETs and phase-transition devices on the switching behavior of hyper-FETs. In this presentation, the boundary conditions for steep-switching operation were studied by comparing the hyper-FETs with various resistance ratios of each constituent device (FET and phase-transition devices). The n-channel metal-oxide-semiconductor FETs (MOSFETs) with various channel lengths (0.5-5 μm) and widths (0.5-5 μm) were prepared, and their drain pads were wired to the phase-transition devices using a probe station. The phase-transition device was fabricated separately by vertically stacking a GeTe₆ film (insulator-metal transition material) and an upper metal-electrode on a heavily doped Si substrate in the form of a 3 mm*3 mm crossbar pattern. The followings are some important observations that will be discussed in detail. The steep slope mode appeared only in a very narrow range of the applied drain voltage, and it consisted of a two-step increase in drain current, i.e., an initial turn-on of the MOSFET followed by abrupt switching of the phase-transition device. Most importantly, because two different types of devices were connected in series, the drain voltage distribution of the two devices was the most critical parameter for a successful steep-switching behavior.

- [1] N. Shukla, Arun V., and S. Datta, *Nature Commun.*, **6**, 7812 (2015).

EQ04.07.08

γ-GeSe—A New Hexagonal Polymorph of Group IV-VI Monochalcogenides [Joong-Eon Jung](#)¹, Sol Lee¹, Han-gyu Kim¹, Yangjin Lee¹, Je Myoung Park², Jeongsu Jang¹, Joonho Kim¹, Sangho Yoon³, Arnab Ghosh¹, Jinsub Park¹, Minseol Kim², Woongki Na², Jonghwan Kim³, Hyoung Joon Choi¹, Hyeonsik Cheong² and Kwanpyo Kim¹; ¹Yonsei university, Korea (the Republic of); ²Sogang University, Korea (the Republic of); ³Pohang University of Science and Technology, Korea (the Republic of)

The family of group IV–VI monochalcogenides has an atomically puckered layered structure, and their atomic bond configuration suggests the possibility for the realization of various polymorphs. Here, we report the synthesis of the first hexagonal polymorph from the family of group IV–VI monochalcogenides, which is conventionally orthorhombic. Recently predicted four-atomic-thick hexagonal GeSe, so-called γ-GeSe, is synthesized and clearly identified by complementary structural characterizations, including elemental analysis, electron diffraction, high-resolution transmission electron microscopy imaging. The electrical and optical measurements indicate that synthesized γ-GeSe exhibits high electrical conductivity, which is comparable to those of other two-dimensional layered semimetallic crystals. The newly identified crystal symmetry of γ-GeSe warrants further studies on various physical properties of γ-GeSe.

EQ04.07.09

Metal Chalcogenide Electrocatalysts for Hydrogen Peroxide Electrosynthesis and the Electro-Fenton Process [Hongyuan Sheng](#)^{1,2}, R. Dominic Ross¹, J. R. Schmidt¹ and Song Jin¹; ¹University of Wisconsin-Madison, United States; ²University of California, Los Angeles, United States

Hydrogen peroxide (H₂O₂) is a powerful oxidant and disinfectant with many applications, but its chemical production poses environmental and safety concerns. Decentralized electrosynthesis of H₂O₂ via the selective two-electron oxygen reduction reaction (2e⁻ ORR) is attractive, which demands high-performance and cost-effective electrocatalysts that are active, selective, and stable in acidic and neutral solutions where H₂O₂ is stable. Metal chalcogenides are an emerging class of 2e⁻ ORR catalysts with diverse and tunable structural motifs for optimizing H₂O₂ electrosynthesis, yet they remain underexplored with poorly understood structure-property relationships. Here, we present our recent computational design and experimental developments of metal chalcogenide-based acidic and neutral 2e⁻ ORR catalysts [1-4], and the resultant new mechanistic understanding and rational catalyst design rules for guiding future catalyst discoveries. The many fundamental and practical factors at the reaction, catalyst, electrode, and device level that impact H₂O₂ electrosynthesis performance are systematically discussed. Metal chalcogenide-based acidic 2e⁻ ORR catalysts can also enable efficient electro-Fenton process for environmental remediation [2,3] and biomass valorization [4].

References:

- [1] *ACS Catal.* **2019**, *9*, 8433-8442.
[2] *Energy Environ. Sci.* **2020**, *13*, 4189-4203.
[3] *ACS Catal.* **2021**, *11*, 12643-12650.
[4] *Nat. Catal.* **2022**, *5*, 716-725.

EQ04.07.10

Morphological Control of 2D Hybrid Organic-Inorganic Semiconductor AgSePh [Watcharaphol Paritmongkol](#)^{1,1}, Woo Seok Lee^{1,1}, Wenbi Shcherbakov-Wu^{1,1}, Seung Kyun Ha¹, Tomoaki Sakurada¹, Soong Ju Oh² and William Tisdale¹; ¹Massachusetts Institute of Technology, United States; ²Korea University, Korea (the Republic of)

Silver phenylselenolate (AgSePh) is a hybrid organic-inorganic two-dimensional (2D) semiconductor exhibiting narrow blue emission, in-plane

anisotropy, and large exciton binding energy. Here, we show that the addition of carefully chosen solvent vapors during the chemical transformation of metallic silver to AgSePh allows for control over the size and orientation of AgSePh crystals. By testing 28 solvent vapors (with different polarities, boiling points, and functional groups), we controlled the resulting crystal size from <200 nm up to a few μm . Furthermore, choice of solvent vapor can substantially improve the orientational homogeneity of 2D crystals with respect to the substrate. In particular, solvents known to form complexes with silver ions, such as dimethyl sulfoxide (DMSO), led to the largest lateral crystal dimensions and parallel crystal orientation. We perform systematic optical and electrical characterizations on DMSO vapor-grown AgSePh films demonstrating improved crystalline quality, lower defect densities, higher photoconductivity, lower dark conductivity, suppression of ionic migration, and reduced midgap photoluminescence at low temperature. Overall, this work provides a strategy for realizing AgSePh films with improved optical properties and reveals the roles of solvent vapors on the chemical transformation of metallic silver.

EQ04.07.11

Photoresponse Effect and P-Type Doping of WS₂ Monolayers Through *In Situ* Niobium Incorporation Neileth J. Stand Figueroa, André do Nascimento Barbosa, Cesar A. Diaz Mendoza and Fernando Lazaro Freire Junior; Pontificia Universidade Católica do Rio de Janeiro, Brazil

Two-dimensional (2D) transition-metal dichalcogenides (TMDs) have been widely studied due to their physical and chemical properties. WS₂ monolayers are atomically thin sheets of isolated sulfur-tungsten-sulfur sandwich arranged in a hexagonal honeycomb-like structure. When imagined from a top-view perspective, this arrangement and bonding make each atomically thin sheet interact very weakly with either the substrate or any adjacent material layer through van der Waals forces. One of the most remarkable properties of some TMDs, such as the WS₂, is the indirect-to-direct bandgap transition when a single atomically thin layer of WS₂ is isolated from the bulk structure. Its bandgap is modified from an indirect bandgap of circa 1.4 eV to a wider direct bandgap of 1.9 eV, with a superior quantum yield compared to MoS₂ monolayers. However, ordinary chemical vapour deposition synthesis yields n-doped WS₂ monolayers, and a roadmap that allows controlling the substitutional doping is of fundamental importance to widen the possibilities of applications in electronics and optoelectronics. In this study, *in situ* Nb doping of WS₂ monolayers was performed through the chemical vapour deposition (CVD) method controlling the Nb and W precursor mass ratios. X-ray photoelectron spectroscopy (XPS) measurements were performed to demonstrate substitutional doping of monolayer WS₂ with Nb. The main effects of Nb incorporation in the lattice were the enhanced luminescence of the doped samples, which was directly related to the Nb₂O₅:WO₃ ratio. Although Raman data using the blue line did not indicate any changes, an overall redshift of the photoemission peak of ~ 30 meV, together with the redshift of 300meV obtained by XPS, suggest that the WS₂ was doped p-type.

EQ04.07.12

Synthesis and Characterization of Germanium Telluride Nanowires Alam Saj¹, Shaikha Alketbi¹, Sumayya M. Ansari¹, Inas Taha¹, Dalaver H. Anjum², Baker Mohammad² and Haila M. Aldosari¹; ¹United Arab Emirates University, United Arab Emirates; ²Khalifa University of Science and Technology, United Arab Emirates

Random access memories (RAMs) made from phase change materials (PCMs) are a promising alternative for the flash memory technology, currently dominating the memory market due to its many appealing traits such as non-volatility, fast read/write performance, excellent scalability, and compatibility with complementary metal-oxide-semiconductor (CMOS) architectures. In fact, the scalability of PCMs is driving this class of materials to be the next successor in the memory industry in the near future. Germanium telluride (GeTe) material is one of the most viable PCMs in this context. In this work, the phase change material GeTe nanowires were fabricated using the vapor-liquid-solid (VLS) growth method. Gold (Au) nanoclusters deposited by a novel approach that has not been used before were used as the metal catalyst to grow GeTe nanowires, which yielded the synthesis of the smallest < 15 nm GeTe nanowires reported to date.

First, size-controlled Au nanoclusters were synthesized using inert gas condensation and dc magnetron sputtering. The impact of magnetron discharge power (P), inert gas flow rate (f), and aggregation length (L) on the diameter and yield of Au nanoclusters was thoroughly investigated. To generate small < 5 nm Au nanoclusters, low P , small L , and large f were needed, and vice versa to produce larger nanoclusters. Optimization of source parameters produced monodispersed nanoclusters of an average size range of 1.7 ± 0.2 nm to 9.1 ± 0.1 nm. Results indicated that Au embryos grew into large nanoclusters via a two-body collision mechanism.

Afterward, the bottom-up synthesis of size-controlled GeTe nanowires growth via Au-catalyzed VLS technique was done by controlling various parameters, namely, growth pressure, inert gas flow rate, growth time, growth temperature, and type of substrate used. GeTe nanowires with an average diameter of ~ 13 nm were produced, the smallest reported to date.

Various characterization techniques were employed to characterize the GeTe nanowires and Au nanoclusters, such as transmission electron microscopy (TEM), scanning electron microscopy (SEM), electron energy loss spectroscopy (EELS), grazing-incidence X-ray diffraction (GIXRD), etc.

SESSION EQ04.08: Materials Innovation Through Solution Synthesis

Session Chairs: Yuval Golan and Ida Sadeghi

Wednesday Morning, November 30, 2022

Sheraton, 2nd Floor, Constitution A

9:00 AM EQ04.08.01

Molecular Design of Low Dimensional Silver Organoselenolate Semiconductors Tomoaki Sakurada^{1,2} and William Tisdale¹; ¹Massachusetts Institute of Technology, United States; ²AGC Inc, Japan

Metal organochalcogenolates (MOCs) have gained a renewed interest as a novel class of hybrid organic-inorganic semiconductors. In contrast to halide perovskites and transition metal chalcogenides, MOCs have strong covalent bonding between organic and inorganic components, offering a unique platform for tuning excitonic properties. Recently, silver phenylselenolate (AgSePh) has attracted attention because of its multiple exciting properties such as narrow blue luminescence, in-plane anisotropy, large exciton binding energy, earth abundant elemental composition, and a scalable synthesis. In this presentation, we will show a new family of AgSePh derivatives with introduced organic functional groups. With modified organic ligands, morphology transformation from 2D sheet to 1D chain structure was induced. We will discuss the effect of organic functionalization on the optical and electronic properties of AgSePh, and show the application of this knowledge toward designing new MOC compounds with improved capabilities

9:15 AM EQ04.08.02

Low-Temperature and Solvent-Free Synthesis and Thin-Film Deposition of Semiconducting Silver Chalcogenide Antiperovskites Paz Sebastia-Luna¹, Nathan Rodkey¹, Joaquin Calbo¹, Adeem S. Mirza², Sigurd Mertens², Koen Vandewal³, Enrique Orti¹, Monica Morales-Masis², Francisco Palazon¹ and Henk J. Bolink¹; ¹University of Valencia, Spain; ²University of Twente, Netherlands; ³Universiteit Hasselt, Belgium

Lead halide perovskites have shown outstanding properties when applied in optoelectronic devices, such as solar cells and light-emitting diodes. Nevertheless, the presence of highly toxic lead together with their low environmental stability might become a bottleneck for their commercialization. Herein we present the synthesis, thin-film deposition, and characterization of silver chalcogenide antiperovskites, as potential alternative optoelectronic materials. Their general formula is Ag_3SX , where X represents a halide. These compounds have potential applications in IR photodiodes and solar cells. We report the fast and solvent-free mechanochemical synthesis of the Br- and I-based species. A proof-of-concept solar cell device is presented via the pulsed-laser deposition of the Ag_3SI powders, achieving a low yet promising power conversion efficiency of 0.07 %.

9:30 AM EQ04.08.03

Solution-Processing of BaMS_3 (M = Ti, Zr, Hf) Materials—A Low-Temperature Route to Chalcogenide Perovskites Jonathan Turnley, Kiruba Catherine Vincent, Apurva A. Pradhan, Shubhanshu Agarwal, Madeleine C. Uible, Suzanne C. Bart and Rakesh Agrawal; Purdue University, United States

While CdTe and $\text{Cu}(\text{In,Ga})(\text{S,Se})_2$ have already proven to be industrially relevant semiconductors, there is broad interest in finding the next generation of metal chalcogenides that are composed of earth-abundant elements, have high intrinsic stability, and have excellent optoelectronic properties. It has been proposed that the sulfide perovskites may satisfy these criteria. BaZrS_3 is the most studied option from this family of materials. Like the halide perovskites, BaZrS_3 has a direct bandgap in the range of 1.7eV to 1.8eV, a high absorption coefficient, and is computationally predicted to be defect tolerant. But unlike the halide perovskites, BaZrS_3 and is known to be highly stable.

To date, the biggest challenges for the chalcogenide perovskites are related to their synthesis. For BaZrS_3 , many synthesis methods rely on solid-state reactions or the sulfurization of BaZrO_3 . In both cases, high temperatures exceeding 800°C are often required. This creates challenges for producing semiconductor devices as most common substrates and contact layers are incompatible with these temperatures. Additionally, these extreme synthesis methods may limit research into related chalcogenide perovskites. For example, there are few reports on the synthesis of BaHfS_3 , all requiring temperatures of at least 1100°C.

Because of the challenges in chalcogenide perovskite synthesis, this work seeks to develop a low-temperature and solution-based deposition approach for BaMS_3 (M = Ti, Zr, Hf) materials. To achieve this, we began with the targeted synthesis of a soluble barium thiolate that can be coated and thermally decomposed into BaS films. The addition of MH_2 nanopowders creates a precursor slurry that can be deposited from the solution-phase. Subsequent sulfurization allows for the conversion to the ternary BaMS_3 material at temperatures below 600°C. Additionally, we investigate alternative delivery methods of the metal hydride precursor in pursuit of device-quality thin films.

In conclusion, this work seeks to take steps towards chalcogenide perovskite semiconductor devices by lowering the synthesis temperature while utilizing a simple solution-based approach.

9:45 AM BREAK

SESSION EQ04.09: Phase Change Functionality in Chalcogenides

Session Chairs: Charles Hages and Hao Zeng

Wednesday Morning, November 30, 2022

Sheraton, 2nd Floor, Constitution A

10:15 AM EQ04.09.01

Novel Applications of ZnTe as an Ovonic Threshold Switching and as a Phase Change Material Oleg Maksimov¹, Katherine Hansen¹, Harish Bhandari¹, Guy Wicker², Habeeb Mousa³, Saidjafarzoda Ilhom³ and Helena Silva³; ¹Radiation Monitoring Devices, United States; ²Ovshinsky Innovation, United States; ³University of Connecticut, United States

The advent of 3D Xpoint non-volatile memory technology has stimulated investigation of novel materials that exhibit efficient and reliable threshold switching behavior. The 3D Xpoint architecture requires each memory element, typically made from phase change material, to be connected in series with a selector element, typically using an ovonic threshold switching (OTS) device [1]. Complex quaternary chalcogenide alloys, such as GeAsSeTe , are usually utilized as selector elements. Ternary chalcogenides, such as $\text{Ge}_2\text{Sb}_2\text{Te}_5$, are used in memory elements. Deposition of these alloys with the exact composition is a non-trivial process. Besides a conformal thin film growth technique both for memory and selector chalcogenides may be beneficial for vertical integration of non-volatile memory.

It was recently demonstrated that polycrystalline thin films of binary chalcogenide ZnTe exhibit switching behavior and have a strong potential for the application in the memory technology in threshold switching devices [2, 3]. Motivated by this report, we conducted study of ZnTe thin films deposited via Atomic Layer Deposition. Upon characterization, we observed that, in addition to the OTS behavior, these exhibit phase change switching with high-speed phase transitions. Such dual behavior of ZnTe opens the opportunity to fabricate both memory elements and selector elements from the same material greatly simplifying the fabrication process.

References:

- [1] Kau, D., Tang, S., Karpov, I. V., Dodge, R., Klehn, B., Kalb, J. A., ... & Spadini, G. (2009, December). A stackable cross point phase change memory. In *2009 IEEE International Electron Devices Meeting (IEDM)* (pp. 1-4). IEEE.
- [2] Kim, T., Kim, Y., Lee, I., Lee, D., & Sohn, H. (2019). Ovonic threshold switching in polycrystalline zinc telluride thin films deposited by RF sputtering. *Nanotechnology*, *30*(13), 13LT01.
- [3] Koo, Y., & Hwang, H. (2018). Zn1-xTe ovonic threshold switching device performance and its correlation to material parameters. *Scientific Reports*, *8*(1), 1-7.

10:30 AM EQ04.09.02

Optimizing Binary to Quaternary Chalcogenides for Ovonic Threshold Switching Selectors in Neuromorphic Applications Jong-Souk Yeo, Chaebn Park, Sang-Heon Park, Deok-Jin Jeon, Young-Min Kim and Su-Bong Lee; Yonsei University, Korea (the Republic of)

Brain-inspired neuromorphic computing has recently emerged as the next-generation information technology that facilitates the innovation from the conventional von-Neumann computing to neuromorphic in-memory computing with remarkable efficiency, operating speed as well as memory density. Realization of neuromorphic computing is possible within the 3D cross-point (X-Point) memory architecture that consists of resistive-switching memory cells to demonstrate synaptic behavior within highly dense structure. However, the adoption of an additional selector cell to each memory cell, thus having

1-selector-1-resistor (1S1R) array, is necessary to ensure reliable operation of the 3D X-Point memory avoiding the issue of sneak current that hinders stable reading and programming of data. For a successful 1S1R integration, the selector is required to meet scalability, short delay time, high on/off ratio, thermal stability, and endurance.

Ovonic threshold switching (OTS) selector based on amorphous chalcogenide film, among many candidates, is considered to have the potential in achieving the aforementioned requirements as demonstrated by S. R. Ovshinsky in 1968. However, optimization of the OTS selector is a difficult task due to the lack of understanding in the switching mechanism behind the OTS phenomenon. In our work, chalcogenide-based OTS selectors ranging from binary to quaternary material systems have been investigated to establish the knowledge on the elemental role to optimize selector performance. Beginning with the binary material system of Si-Te and Ge-Te, the role of Si on thermal stability and of Ge on switching performance are established. Upon proceeding to ternary material systems of Si-Ge-Te as well as N-doped Si-Te and Ge-Te, enhanced features of OTS selectors are achieved that satisfies the selector requirements in electrical performance as well as thermal stability and cyclic endurance simultaneously. The integration of all the elements in the quaternary N-Si-Ge-Te system exhibited the most outstanding characteristics that excel in every device parameter. The investigation of chalcogenides from binary to quaternary material systems enhances our understanding on the elemental roles, thus enabling to optimize the overall performance of OTS selectors for neuromorphic applications.

This research was supported by the Ministry of Trade, Industry & Energy (MOITIE)/Korean Evaluation Institute Industrial Technology (KEIT) (Project No. 10080625) and Korea Semiconductor Research Consortium (KSRC) program for the development of the future semiconductor devices, and by Samsung Electronics Co. Ltd. (Project number IO2102021-08356-01).

10:45 AM *EQ04.09.03

Antimony Trisulfide Programmable Photonics—From Local Structural Transitions to Programmable Photonics Robert Simpson¹, Ting Yu Teo¹, Alyssa Poh¹, Li Lu¹, Yunzheng Wang¹, Jing Ning¹, Parikshit Moitra² and Joel Yang¹; ¹Singapore University of Technology and Design, Singapore; ²A*STAR Institute of Materials Research and Engineering, Singapore

Chalcogenides that exhibit substantial property contrast between different structural phases are of interest for data storage and programmable photonics applications. The most successful data storage materials, such as those that lie along the GeTe-Sb₂Te₃ pseudo-binary compositional tie-line, have a small bandgap and concomitantly, a large optical absorption in the near infrared and visible wavelengths. New phase change materials with a wider bandgap need to be developed for the visible and N-IR photonics applications.

Antimony trisulfide (Sb₂S₃) is an Earth abundant material that is transparent to visible and near infrared light (N-IR). Switching the material between amorphous and crystalline states causes radical property changes that deem it useful for programming the response of visible and N-IR photonics devices. We have demonstrated how Sb₂S₃ can be used to program high resolution micro-displays, dielectric metasurfaces, hyperbolic metamaterials, waveguides, and all-optical neural networks. This presentation will discuss these demonstrations and the underlying structural transitions that are responsible for the property contrast in Sb₂S₃.

11:15 AM *EQ04.09.04

Low-Power Memory Devices Based on Superlattice Chalcogenides Asir Intisar Khan, Xiangjin Wu, Alwin Daus, Sumaiya Wahid and Eric Pop; Stanford University, United States

Phase change memory (PCM) technology could play an important role in future high-density computing systems, including neuromorphic computing. However, PCM based on traditional chalcogenides like Ge₂Sb₂Te₃ (GST) requires relatively large power consumption and suffers from resistance drift [1]. This talk will address our recent efforts to tackle these challenges using various types of superlattice PCM (SL-PCM) materials, made of alternating ultrathin (~nm) layered chalcogenides. From a device perspective, we have demonstrated memory with superlattices based both on GeTe/Sb₂Te₃ [2] and GST/Sb₂Te₃ [3,4], showing up to ~10x lower reset current density and 10x lower resistance drift than control GST PCM with the same mushroom cell structure. We uncovered that the quality of the interfaces within the SL plays an important role in the memory behavior [3,4]; in other words, more good-quality interfaces means better thermal and structural confinement, but interfacial intermixing degrades the drift coefficient. Given that thermal confinement plays such an important role in low-power behavior, we also demonstrated SL-PCM with the lowest switching current density to date (~0.1 MA/cm²) on flexible polyimide substrates, which have ultralow thermal conductivity [5]. Importantly, all our SL-PCM devices show multiple resistance states and scalability with the bottom electrode diameter, offering further promise in ultra-scaled devices.

From a materials perspective, extensive transmission electron microscopy (TEM) revealed van der Waals (vdW)-like interfaces in the superlattices, which facilitate the electro-thermal and structural confinement [2-4]. We found lower cross-plane thermal conductivity and higher electrical anisotropy of the polycrystalline SL stack compared with polycrystalline GST, due to the internal interfaces within the SL [6]. We also explored lateral transport in chalcogenide films and multilayers, measuring good Hall mobilities for GeTe/Sb₂Te₃ superlattices (~18 cm²V⁻¹s⁻¹), 2–3x higher than the other films [7]. These results provide key insights towards new superlattice material design and optimization, and could pave the way to high-density storage and neuromorphic applications using superlattice PCM materials.

[1] S. Raoux, *et al.*, MRS Bull. 39, 703 (2014). [2] A.I. Khan *et al.*, IEEE Electron Dev. Lett. 43, 204 (2022). [3] X. Wu *et al.*, IEEE Electron Dev. Lett. 43, 1669 (2022). [4] A.I. Khan *et al.*, Nano Letters 22, 6285 (2022). [5] A.I. Khan, A. Daus, E. Pop *et al.*, Science 373, 1243 (2021). [6] H. Kwon, A.I. Khan, E. Pop, *et al.*, Nano Letters 21, 5984 (2021). [7] S. Wahid *et al.*, Appl. Phys. Lett. 119, 232106 (2021).

11:45 AM EQ04.09.05

Chalcogenide-Superlattice Interfaces and Intermixing Modulating Phase-Change Memory Performance Asir Intisar Khan¹, Xiangjin Wu¹, Christopher Perez¹, Byoungjun Won², Il-Kwon Oh², Mehdi Asheghi¹, Kenneth E. Goodson¹, H.S. Philip Wong¹ and Eric Pop^{1,1}; ¹Stanford University, United States; ²Ajou University, Korea (the Republic of)

Phase change memory (PCM) based on chalcogenide-superlattices has shown promise with the low-power operation and low resistance drift required for neuromorphic computing applications [1-3]. However, the effects of the *internal* chalcogenide-superlattice interfaces (interface density and degree of intermixing) on superlattice PCM devices are not well understood to date, especially when these interfaces are very dense, just a few Angstroms apart.

Here, we uncover a key correlation between the internal superlattice (SL) interfaces and superlattice PCM (SL-PCM) device performance using nanometer-thin layers of Ge₂Sb₂Te₃ and Sb₂Te₃. We uncover that both switching current density and resistance drift coefficient decrease as the SL period thickness is reduced (i.e., higher interface density) – however, interface intermixing within the SL increases both. The signatures of distinct vs. intermixed interfaces also show up in scanning transmission electron microscopy (STEM), X-ray diffraction (XRD), and thermal conductivity measurements of our SL films.

To understand the role of SL interfaces, we sputtered alternating layers of phase-change chalcogenides Sb₂Te₃ (ST) and Ge₂Sb₂Te₃ (GST) with varying period thicknesses, while keeping the total stack thickness fixed (~65 nm). High-resolution STEM images of a 2/1.8 nm/nm ST/GST SL, reveal atomically sharp interfaces separated by van der Waals (vdW) gaps, representing a good quality SL. In contrast, an ST/GST SL with the sub-nm thin period (0.5/0.45 nm/nm) shows stronger intermixing within layers, more stacking faults, and rougher interfaces. We note that for this SL, the individual ST/GST layers are

smaller than the unit block thicknesses of ST (1 nm) and GST (1.8 nm); therefore, a higher intermixing is expected. XRD spectra for the as-deposited SLs confirm their polycrystallinity, while non-out-of-plane peaks appear in the more intermixed SL spectra.

The measured thermal conductivity of our SLs decreases with the increasing number of interfaces i.e., with decreasing period thicknesses from 16/14.4 nm/nm (4 interfaces) to 2/1.8 nm/nm (32 interfaces). This is attributed to the vdW-like gaps impeding cross-plane thermal transport [4]. However, the thermal conductivity increases for more intermixed SL films due to loss of vdW-like gaps within the SL, also evident from our STEM.

Electrical measurement of our fabricated mushroom-cell ST/GST SL-PCM devices (110 nm bottom electrode diameter) reveals that the reset current (I_{reset}) decreases with an increasing number of SL interfaces, due to improved heat confinement. Low and high resistance states of the devices also increase with more interfaces pointing to higher cross-plane resistivity due to more interfaces. However, a larger I_{reset} in the more intermixed SL-PCM (0.5/0.45 nm/nm) highlights the detrimental effect of intermixing within SL layers. Resistance drift coefficient (ν) also shows a clear trend with the number of interfaces with ν decreasing from GST (no internal interfaces) to SL with 4 interfaces to ST/GST SL with 32 interfaces. On the other hand, deliberate intermixing within SL (0.5/0.45 nm/nm) increases ν . Utilizing such correlation between SL-PCM key performance indicators and SL interface property, we simultaneously achieve low switching current density (3–4 MA/cm²) and low resistance drift coefficient (0.002) in ST/GST SL-PCM, approaching the best corner on the PCM technology.

In summary, we demonstrated that the key material and thermal properties of SLs are controlled by the number of interfaces and their degree of intermixing, which ultimately plays a crucial role in controlling SL-PCM device performance. These results also provide key insights towards new superlattice material design and optimization for SL-PCM technology.

1. A.I. Khan, E. Pop et al., *Science* **373**, 1243 (2021)
2. K. Ding et al., *Science* **366**, 210 (2019)
3. A.I. Khan, E. Pop et al., *IEEE EDL* **43**, 204-207 (2022)
4. H. Kwon, E. Pop et al., *Nano Lett.* **21**, 5984 (2021)

SESSION EQ04.10: Chalcogenide Perovskites
Session Chairs: Rohan Mishra and Robert Simpson
Wednesday Afternoon, November 30, 2022
Sheraton, 2nd Floor, Constitution A

1:30 PM *EQ04.10.01

Growth and Characterizations of Chalcogenide Perovskite Thin Films for Optoelectronics [Hao Zeng](#); SUNY-Buffalo, United States

Recently chalcogenide perovskites have emerged as a new family of semiconductors. With their strong ionicity and defect tolerance, strong light-matter interactions, direct band gap in the visible, high stability, and low toxicity, they have shown promise for opto-electronic applications. However, synthesis of high-quality thin films of such materials remains challenging, partially due to the presence of refractory metal elements such as Zr and Hf. In this talk, I will give a brief overview of the progress made in the past two years in realizing chalcogenide perovskite thin films. I will then discuss our efforts to synthesize BaZrS₃ and other perovskite thin films using pulsed laser deposition and magnetron sputtering, their charge transport and optical properties, and preliminary results on device fabrication and characterizations. Finally, I will layout challenges that need to be addressed to make these materials technologically relevant.

Research supported by NSF CBET-1510121, ECCS-2042085.

2:00 PM EQ04.10.02

Low-Temperature, Solution-Based Synthesis of Luminescent Chalcogenide Perovskite BaZrS₃ Nanoparticles and Their Phase Stability Ruiquan Yang, Alexander Jess, Calvin Fai and [Charles J. Hages](#); University of Florida, United States

Chalcogenide perovskites are an emerging earth-abundant, non-toxic, and robust semiconductor family with the potential to compete with hybrid perovskites as a high-quality photovoltaic absorber. Promising optoelectronic properties have been identified from theory for a number of chalcogenide perovskite compounds. Additionally, increased covalent bonding in the lattice relative to halide perovskites results in enhanced structural stability. However, the cost of structural stability for chalcogenide perovskites can be associated with a high crystallization energy barrier for these materials. As a result, a low-temperature, solution-based synthesis route ideal for realistic semiconductor fabrication has eluded researchers in this area for c. 60 years. In this work, we present the first bottom-up colloidal synthesis of chalcogenide perovskite nanoparticles, demonstrated here for BaZrS₃ which is known to crystallize in the desired distorted perovskite crystal structure. The nanoparticles were synthesized in organic solvent at 330 °C using single-source, reactive metal-dithiocarbamate precursors with a low thermal decomposition temperature, confirmed with XRD, Raman spectroscopy, and HRTEM. The nanoparticles (10–20 nm) are found to be comprised of smaller (3–5 nm) crystalline domains. Promising optoelectronic properties for the nanoparticles are measured, with photoluminescence decay times as high as 4.7 ns.

In addition to the described synthesis, we present a compelling phase stability analysis of sulfide-, selenide-, and telluride-based chalcogenide perovskites based on ionic radii and electronegativity arguments -- related to their increased covalent bonding. A modified tolerance factor for chalcogenide perovskites is proposed, accounting for the expected variations in the bond lengths of constituent atoms in the ABX₃ (X = S, Se, Te) structure. Resulting structural predictions are in good agreement with experimentally reported ABS₃ and ABSe₃ phases. This analysis is a useful tool to identify undesirable phases as well as motivate further experimental research into several unrealized perovskite materials.

2:15 PM EQ04.10.03

Stabilizing BaZr(S,Se)₃ Chalcogenide Perovskite Alloys by Molecular Beam Epitaxy [Ida Sadeghi](#), Dennis Kim, Jack Van Sambeek, James LeBeau and Rafael Jaramillo; Massachusetts Institute of Technology, United States

Symposium EQ04—Emerging Chalcogenide Electronic Materials—Theory to Applications

Chemical intuition, first-principles calculations, and recent experimental results suggest that chalcogenide perovskites are an outstanding class of semiconductors. Chalcogenide perovskites feature the large dielectric response familiar in oxide perovskites, but also have band gap in the VIS-IR and

strong light absorption [1]. Preliminary results suggest that chalcogenide perovskites feature excellent excited-state charge transport properties familiar in halide perovskites, while also being thermally-stable and comprised of abundant and non-toxic elements. Nearly all experimental results on chalcogenide perovskites to-date were obtained on powder samples and microscopic single crystals, and thin film synthesis is in its infancy. The history of complex oxide science teaches us that advances in fundamental understanding and development for applications will hinge on the availability of high-quality, controllable thin film synthesis, and that the best film quality and control is achieved by molecular beam epitaxy (MBE).

We recently reported the first epitaxial synthesis of chalcogenide perovskite thin films by MBE: BaZrS₃ films on (001)-oriented LaAlO₃ substrates [2]. The films are atomically-smooth, and scanning transmission electron microscopy (STEM) data show an atomically-abrupt substrate/film interface. The sulfide perovskite film has a pseudo-cubic lattice constant more than 30% larger than the oxide perovskite substrate. This strain is fully accommodated by a remarkable, self-assembled interface buffer layer that enables epitaxial growth of strain-free films, and that the propensity for buffered epitaxy can be controlled by the H₂S gas flow during growth.

We further demonstrate control of the band gap by alloying BaZrS₃ with Se. We have made the first epitaxial BaZrS_{(3-y)Se_y} films with varying Se composition, up to and including a pure selenide perovskite BaZrSe₃. BaZrSe₃ is theoretically predicted to be stable in a non-perovskite, needle-like phase with very low band gap. We instead stabilized perovskite BaZrSe₃ film on a BaZrS₃ buffer layer grown on LaAlO₃ substrate using MBE. We support these findings with experiments including high-resolution STEM, high-resolution X-ray diffraction (HRXRD), and photocurrent spectroscopy (PCS). The films are smooth with an Rms roughness ranging from 0.65 to 3 nm. The out-of-plane HRXRD measurement confirmed the presence of the perovskite BaZrS₃ buffer layer and the perovskite BaZrS_{(3-y)Se_y} in the films. The in-plane XRD measurements and reciprocal space maps showed that the BaZrS_{(3-y)Se_y} layer grows strained, however, BaZrSe₃ grows relaxed on the BaZrS₃ buffer layer. The PCS measurements on the BaZrS_{(3-y)Se_y} films showed bandgap tunability, with bandgap decreasing from 1.57eV (y=1) to 1.50eV (y=1.3) to 1.49eV (y=2) with increasing Se content.

This work sets the stage for developing chalcogenide perovskites as a family of semiconductor alloys with properties that can be tuned with strain and composition in high-quality epitaxial thin films, as has been long-established for other semiconductor materials.

[1] R. Jaramillo, J. Ravichandran, APL Materials 7(10) (2019) 100902.

[2] I. Sadeghi et al., Adv. Func. Mater., (2021) 2105563.

2:30 PM BREAK

3:30 PM *EQ04.10.04

Skinny Polar Vortices in Quasi-1D Chalcogenides Rohan Mishra¹, Gwan Yeong Jung¹, Guodong Ren¹, Boyang Zhao², Huandong Chen², Di Xiao³ and Jayakanth Ravichandran¹; ¹Washington University in St. Louis, United States; ²University of Southern California, United States; ³University of Washington, United States

Large polar vortices that span several 10's of nanometers in dimensions have been reported in several polar systems such as ferroelectric superlattices and nanowires. In this talk, we will report on the possible formation of atomically thin polar vortex-antivortex pairs in a quasi-1D chalcogenide, BaTiS₃. We will discuss results from first-principles electronic structure calculations and phenomenological modeling that show the various competing structural distortions that can stabilize atomically thin vortices. We will discuss the evolution of such vortices with temperature, strain and electric field. We will end with experimental findings that provide indirect evidence of the presence of skinny vortex-antivortex pairs in BaTiS₃ crystals.

Acknowledgements: This work was supported by ARO through the MURI program with award number W911NF-21-1-0327.

4:00 PM EQ04.10.05

Spectroscopic Evidence for the Formation of Polarons in BaZrS₃ Omer Yaffe; Weizmann Institute, United States

Chalcogenide perovskites combine relatively low band gaps (1.4-2 eV, typical for compound semiconductors) with very high dielectric constants (50-100, typical for insulating perovskite oxides).

We hypothesize that the high polarizability of chalcogenide perovskites stems from large-amplitude thermal fluctuations that also lead to the formation of polarons from photo-excited charge carriers.

In this talk, I will present a test of this hypothesis through a spectroscopic study of single crystals of the prototypical chalcogenide perovskite BaZrS₃. Using temperature-dependent Raman scattering, we establish that the structural dynamics of the crystal are similar to those of insulating oxide perovskites SrTiO₃ and CaTiO₃. Using resonant Raman scattering, we show that photo-excited carriers induce significant symmetry breaking in the crystal lattice - this is experimental evidence for polaron formation. Finally, from temperature-dependent photoluminescence, we show the strong effect of phonons on excited-state recombination pathways.

4:15 PM EQ04.10.06

Perovskite Chalcogenide Thin Films for Photovoltaic Devices Kevin Ye, Jack Van Sambeek, Ida Sadeghi and Rafael Jaramillo; Massachusetts Institute of Technology, United States

Chalcogenides perovskites are candidate materials for solar energy conversion technologies due to their promising optoelectronic properties and chemical stability [1–3]. The prototype chalcogenide perovskite BaZrS₃ is a semiconductor with direct band gap of $E_g = 1.9$ eV, and Shockley-Read-Hall recombination lifetime exceeding 50 ns demonstrated in single crystals; we have also recently demonstrated that E_g can be reduced continuously to 1.4 eV through alloying with Se.

Here we present results of making and testing BaZrS₃ thin-film solar cells in a substrate architecture, as long-established for CIGS technologies. We deposit BaZrS₃ thin films on Mo metal rear contact layers by reactive physical vapor deposition using H₂S. The deposition is similar to our demonstrated synthesis by molecular beam epitaxy (MBE) [4], but BaZrS₃ can also be grown as polycrystalline, non-epitaxial, single-phase thin films. We deposit *n*-type CdS contacts by chemical bath deposition, followed by sputtering ZnO and ITO layers in typical dot-cell geometry. We report results of completed solar cell device tests (I-V and EQE), and quantitative loss analysis based on measured optical and electrical properties of isolated thin-films and device semifactures. We conclude with an outlook for improving device performance and comments on future manufacturability of chalcogenide perovskite solar cells.

1. R. Jaramillo and J. Ravichandran, "In praise and in search of highly-polarizable semiconductors: Technological promise and discovery strategies," APL Mater. 7(10), 100902 (2019).

2. S. Niu, D. Sarkar, K. Williams, Y. Zhou, Y. Li, E. Bianco, H. Huyan, S. B. Cronin, M. E. McConney, R. Haiges, R. Jaramillo, D. J. Singh, W. A. Tisdale, R. Kapadia, and J. Ravichandran, "Optimal Bandgap in a 2D Ruddlesden–Popper Perovskite Chalcogenide for Single-Junction Solar Cells," Chem. Mater. 30(15), 4882–4886 (2018).

3. S. Niu, J. Milam-Guerrero, Y. Zhou, K. Ye, B. Zhao, B. C. Melot, and J. Ravichandran, "Thermal stability study of transition metal perovskite sulfides,"

J. Mater. Res. 33(24), 4135–4143 (2018).

4. I. Sadeghi, K. Ye, M. Xu, Y. Li, J. M. LeBeau, and R. Jaramillo, "Making BaZrS₃ Chalcogenide Perovskite Thin Films by Molecular Beam Epitaxy," Adv. Funct. Mater. 2105563 (2021).

SESSION EQ04.11: Poster Session: Energy Conversion and Sensing

Session Chairs: Archana Raja and Debarghya Sarkar

Wednesday Afternoon, November 30, 2022

8:00 PM - 10:00 PM

Hynes, Level 1, Hall A

EQ04.11.01

Analysis of Potential Induced Degradation Mechanism in CIGS Thin-Film Solar Cells Solhee Lee, Soohyun Bae, Se Jin Park, Yoonmook Kang, Donghwan Kim and Hae-Seok Lee; Korea University, Korea (the Republic of)

Looking at the global photovoltaic (PV) market, the world's PV installation amounted to over 100 GW in 2018, and the increasing trend continued, the installation amount of 150 GW is predicted in 2020 without the influence of COVID-19. In order to increase the economic feasibility of the energy generation source, high energy conversion efficiency, low module degradation rate, and long life must be satisfied. Therefore, in order to ensure long-term reliability of PV module for stable power supply, it is essential to understand and prevent degradation factors. Potential induced degradation (PID) is one of degradation phenomena that has been a problem in the last few years, and it is reported that PV module power is degraded in a short time. The process of PID generation based on the reported literatures is as follows. In the situation where the PV modules are connected in series due to the voltage generation above 600 V corresponding to the system voltage, the frames of modules are also grounded for safety and supporting reasons. And then, a relative potential difference between the grounded electrodes and solar cells inside the modules occurs, and the potential difference increases toward the end of the serial connection. The phenomenon that the leakage current flows in solar cells having a negative potential difference compared to the frame, and eventually the power of the modules decreases, is called PID.

In the case of crystalline silicon solar cells, the mechanism of PID has been identified in both p-type and n-type cases. In CIGS thin film solar cells, since the absorption layer is p-type and Na is injected to some extent to improve the efficiency during solar cell fabrication, it can be expected that Na, like silicon solar cells, can affect the PID mechanism of CIGS solar cells. Indeed, looking at the previous research data on the PID mechanism, the degradation was greater in the case of the sample with high Na concentration and low resistivity. Research to clarify the PID mechanism of CIGS solar cells has been actively conducted until recently. By dark current-voltage (I-V) measurement before and after PID, soda-lime glass (SLG) substrate samples increased diode saturation current and decreased shunt resistance than borosilicate glass (BSG) samples. It can be interpreted by Na effect. In addition, due to secondary ion mass spectrometry (SIMS) and C-V measurement, it was analyzed that the cations accumulate at the junction, thereby decreasing the charge carrier concentration and changing open-circuit voltage (V_{OC}) and efficiency. It is represented through TOF-SIMS 3D tomography in which Na was segregated into a grain boundary after PID. However, the cause of PID in CIGS solar cells has not been clearly defined, and the explanation for the recovery is insufficient. At the cell level, for example in the case of CIGS, accurate understanding of the monolithic series connection structure and PID is an important requirement to resolve degradation fundamentally.

In this study, the PID phenomenon in CIGS module was implemented at cell level to identify the PID mechanism. In particular, the effect of the cover glass on the front of the module structure was excluded, and the research was conducted focusing on the PID phenomenon caused by the glass used as the substrate. First, after devising three voltage application structures for the CIGS cell, voltage was applied to each structure for a certain amount of time, and the voltage application structure was determined while observing changes in the solar cell characteristics. Second, after conducting PID and recovery experiments on the defined structure, PID and recovery tendency were analyzed through light I-V, dark I-V, EQE, and C-V measurements. Changes in the characteristics of the CIGS solar cell by PID were explained as the degradation due to the voltage by comparing with the characteristics in another sample where only temperature was applied.

EQ04.11.02

Investigating the Impact of Intrinsic Defects on Cu₂SiSe₃ for PV Applications Adair Nicolson¹, Seán R. Kavanagh^{1,2}, Graeme Watson³, Robert Palgrave¹ and David O. Scanlon¹; ¹University College London, United Kingdom; ²Imperial College London, United Kingdom; ³Trinity College Dublin, The University of Dublin, Ireland

Metal chalcogenides have seen renewed interest in recent years with the hope that they will deliver stable, non-toxic thin-film solar cells with efficiencies that can match silicon and halide perovskite-based devices.^[1] To this end we have begun an initial investigation into the electronic and optical properties of Cu₂SiSe₃, and it has shown initial promise as a photovoltaic absorber with a calculated band gap of ~1.52 eV and a maximum efficiency of 30% for a 1.5 mm film.

However, a promising band gap and absorption coefficient is not sufficient to determine if a new material will achieve high efficiencies in devices. Non-radiative recombination processes, driven by defect states in the band gap, can drastically reduce carrier lifetimes, and thus performance.^[2] Therefore, in this project we investigate all potential intrinsic defects in Cu₂SiSe₃ to determine how they may affect carrier lifetimes and thus device performance.^[3]

[1] Hadke, S.; Huang, M.; Chen, C.; Tay, Y. F.; Chen, S.; Tang, J.; Wong, L., Chem. Rev., 2021.

[2] Huang, Y.-T.; Kavanagh, S. R.; Scanlon, D. O.; Walsh, A.; Hoye, R. L. Z. Nanotechnology, 2021, 32 (13), 132004.

[3] Nicolson, A. T. J.; Kavanagh, S. R.; Watson, G. W.; Palgrave, R. G.; Scanlon, D. O. Submitted (2022)

EQ04.11.03

Material Design of Monolithic Water-Splitting Device Using Chalcogenide Semiconductors Kana Ueda, Daiki Kanamori and Mutsumi Sugiyama; Tokyo University of Science, Japan

Chalcogenide semiconductors such as Cu(In,Ga)Se₂ (CIGS) and Cu₂SnS₃ (CTS) are used for manufacturing inexpensive thin-film solar cell materials. However, several reports suggested that these materials were inappropriate for photocatalysis owing to their inferior underwater crystal quality and mismatch of band-lineup. Moreover, a water-splitting device requires an external power supply for photoelectrochemical (PEC) performance.

In the future, power generation using hydrogen will be required for not only large-scale systems but also small ones. For example, a small amount of

hydrogen through ultra-small fuel cells is sufficient for driving IoT devices. Therefore, chalcogenide-used water-splitting is a candidate for several applications because chalcogenides have strong durability under venting, heat-cycle, or irradiation. However, the onset potential of photoelectrodes using CIGS or CTS is small due to the small bandgap of the materials. Water splitting with solar and photoelectrochemical cells has been reported to increase the onset potential. Therefore, a monolithic structure for interconnecting solar and PEC cells on the same substrate and fabricating them simultaneously would be appropriate. In this presentation, a new CIGS and CTS thin film based monolithic water-splitting device without external power supply will be proposed. We used chalcogenide materials for both solar cells and water-splitting PEC; hence, fabrication cost and processes of this device was reduced.

The monolithic water-splitting device consisted of a CIGS or CTS solar cell with ZnO:Al / ZnO / CdS / CIGS or CTS / Mo / SLG structure and a photoelectrode with CdS / CIGS or CTS / Mo / SLG structure. The PEC performance in an aqueous solution of 0.1 M NaOH (pH = 9.5) was measured. A Pt wire was used as the counter electrode. Using the CIGS monolithic water-splitting device, the representative onset potential increases to 0.9 V_{RHE}, and the photocurrent density of the device increases to 0.14 mAcm⁻² at 0 V_{RHE}. These results represent a preliminary step toward the potential application of a monolithic water-splitting device using CIGS and CTS.

EQ04.11.04

Band Gap Tunable Inkjet-Printed Buffer Layers for Cu(In,Ga)(S,Se)₂ Solar Cells Alice Debot and Phillip J. Dale; University of Luxembourg, Luxembourg

Buffer layers are essential in thin film solar cells to help form the pn junction and ensure good band alignment between the absorber and the window layers. Inkjet printing has recently gained interest as a deposition method of buffers because of its near 100% material utilization. Compared to a traditional chemical bath deposition (CBD), inkjet printing requires around 50 000 times less solvent and 6500 times less material for synthesising the same buffer layer surface area. Cleaner chemistry and lower waste is an important aspect in industrial production. Various buffer materials can be inkjet-printed and annealed to form layers that when completed into full devices achieve similar efficiencies to the commonly found CBD CdS. We recently deposited Zn(O,S) buffer layers (which is the material used in the current Cu(In,Ga)(S,Se)₂ (CIGS) world record) on CIGS attaining an efficiency higher than the reference CdS [1]. We also showed that In₂S₃ buffer layer can be inkjet printed on CIGS with similar efficiency to a CdS reference device [2] and now we can report here, a printable CdS buffer layer, giving 87% relative efficiency compared to the CBD reference.

CBD deposited buffer layers tend to exhibit band gaps close to their literature bulk values. Here, we show that inkjet printed materials annealed at different temperatures, can exhibit significantly higher values, up to 0.3, 0.7 and 0.9 eV above the bulk band gap for In₂S₃, CdS and Zn(O,S) materials. Previously, it has been shown for silicon that nanoparticles embedded in an amorphous matrix also show higher bandgaps than the bulk value, and this was shown to be a quantum confinement effect [3], irrespective of the crystalline to amorphous matter ratio [4].

To investigate if there is a quantum confinement effect for the inkjet-printed buffer layers the crystal coherence length, a proxy for grain size, was measured with grazing incidence x-ray diffraction (GIXRD) on buffer layers with different band gaps. The exciton Bohr radius of Zn(O,S), CdS and In₂S₃ are calculated to be 1.6, 2.6 and 4.8 nm respectively, based on effective masses values found in literature. Nanoparticles with a radius smaller than the mentioned sizes should then show an increased band gap compared to the bulk value. The Brus equation was used to evaluate the increase of the band gap due to quantum confinement. This approach is simplistic but is considered as a good first qualitative analysis. A variation in the grain radius of In₂S₃ from 3.8 to 3.1 nm increased the band gap by 0.3 eV as predicted using the Brus equation. A similar result was found for Zn(O,S). The grain size of CdS couldn't be extracted for band gaps approaching 3 eV because of a low signal to noise ratio in the diffractograms. This is expected since such a high band gap must result from a 1.5 nm grain radius which would result in a very broadened diffraction peak. Thicker samples could increase the signal to noise ratio, enabling the extraction of the grain size.

A buffer with a wide band gap is preferred to avoid parasitic absorption in the blue region of the solar spectrum thus increasing short circuit current. The ability to tune the band gap via quantum confinement might offer a new way to use relatively narrow band gap buffer layers, such as In₂S₃, and CdS, without them having a parasitic absorption. However, device performance may be impacted by band alignment issues, affecting the open circuit voltage. We will prepare devices where we vary the grain size of the buffer layers and investigate how this affects the solar cell performance.

[1] Chu et al., ACS Appl. Mater. Interfaces. 13 (2021) 13009–13021. <https://doi.org/10.1021/acsami.0c16860>.

[2] Debot et al. Thin Solid Films. 745 (2022). <https://doi.org/10.1016/j.tsf.2022.139096>.

[3] Lusk et al., Phys. Rev. B 89, 075433 (2014) 1–5. <https://doi.org/10.1103/PhysRevB.89.075433>.

[4] Bagolini et al., Phys Rev. ett. 104, 176803 (2010) 1–4. <https://doi.org/10.1103/PhysRevLett.104.176803>.

EQ04.11.05

Effect of Zn-Doped Tin Monosulfide Thin Film Using Atomic Layer Deposition Soo Yeon Kang, Yeonsik Choi, Jangho Bae, Jungtae Kim and Hyeongtag Jeon; Hanyang University, Korea (the Republic of)

Tin monosulfide (SnS), a direct band gap semiconductor compound, has recently received great attention due to its unique properties. In addition, SnS is a promising monochalcogenide two-dimensional materials, each layer consists of a van der Waals (vdW) bonding. Because of low cost, abundant in nature, and non-toxic substance, it is becoming a candidate for future multifunctional devices such as solar cells, optical sensors, batteries, biomedical science and transistors. Among them, it is mainly used in light conversion applications because of its good absorption properties. The most commonly used phase for photovoltaic devices is the orthorhombic α -SnS (herzenbergite), *p* type, which is characterized by a direct optical transition of 1.3–1.6 eV.

The addition of an impurity to the SnS compound has a unique effect on structural, optical, and electronic properties of SnS semiconductor. But there are very few reports on the zinc (Zn)-doped SnS thin films prepared by ALD. Atomic layer deposition (ALD) can be an ideal method for the high conformality with its self-limited reaction. In addition, ALD is a promising method to increase atomic scaling thickness controllability by adjusting the process cycle. With these advantages, we used atomic layer deposition super-cycle Zn-doping. SnS cycle and ZnS cycle are alternately used during a super-cycle process. The number of ZnS cycle varies according to the doping concentration of Zn. The total number of cycles SnS:ZnS is repeated until the desired film thickness is reached.

In this study, we deposited amorphous Zn-doped tin sulfide (SnS_x:Zn) thin films at 100°C using super-cycle ALD and performed post annealing at 400°C for controlling phase transition to SnS. The doping level was changed from [SnS:Zn] = 0% to 10% (every 2%). We developed Zn-doped SnS thin films using Tetrakis-dimethylamino Tin (TDMASn), Diethyl-zinc (DEZ) and H₂S (99.99%) gas as the precursor and reactant. We performed 10 cycles of sulfur passivation before deposition to change the functional group of O-H to S-H on the surface for making more stable chemical energy state of sulfide. The effect of doping on the phase transition and crystal structure of SnS was analyzed through grazing-incidence X-ray diffraction (GI-XRD) and Raman. All the deposited films are polycrystalline SnS and the intensity of the XRD peaks are decreased for the higher Zn concentration. It is because reduction of

crystallinity due to the incorporation of more Zn impurity atoms into the SnS lattice. X-ray photoelectron spectroscopy (XPS) was utilized for chemical binding state. It was confirmed that Zn was well doped through an increase in the ZnS binding peak as the Zn concentration increased. To confirm the band structures and optical properties of a Zn-doped SnS, ultraviolet-visible (UV-vis.) spectroscopy, ultraviolet photoelectron spectroscopy (UPS) and photoluminescence (PL) were investigated. Energy band gap increases by zinc incorporation, exhibited 1.64 eV, 2.10 eV, 2.13 eV, 2.61 eV, 2.85 eV, 2.92 eV for as-dep. 2%, 4%, 6%, 8%, 10% doped samples. Increase of band gap was due to the value of ZnS direct band gap (3.6 eV) is larger than that of SnS. Thus, suitable Zn doping in the SnS thin films can change the optical band structures and other properties for various optical devices. Through this study, we research the effect of Zn-doped tin monosulfide thin films and a variety of optical, chemical, structural characteristics for various multifunctional devices.

EQ04.11.06

Very High Gas Sensing Performance of SnS₂ Material to NO₂ at Room Temperature Miccio O. Melquiades^{1,2}, Ranilson A. da Silva¹ and Marcelo O. Orlandi¹; ¹UNESP, Brazil; ²IFAM, Brazil

Semiconductors based on tin-dichalcogenides have attracted attention in gas sensing application as sensors, as these materials are formed by chemically inert layers bonded by weak van der Waals interactions that promote a high surface-to-volume ratio. It is especially interesting that layers have (001) planes exposed, and this plane present electronic lone pairs, facilitating the adhesion of polar analytes on the material surface. The route of synthesis is a key point to obtain materials with optimal properties. In this context, mechanical grinding stands out for being an easy and low-cost route. Furthermore, this process produces samples with high density of defects, such as vacancies, grain boundaries and stacking faults, and these defects are important for gas detection due to the increased surface reactivity.

In the present work tin-dichalcogenides (SnS₂) was synthesized by high-energy mechanical milling using Sn (Alfa Aesar – 98,8%), Se (Alfa Aesar - 98,8%), and S (Alfa Aesar – 98,8%) precursors. The material phase was confirmed by X-ray diffraction analysis and the particles morphology was observed by scanning electron microscopy. For the gas sensing measurements, first a suspension of the tin-dichalcogenide powder was prepared. Then, devices were produced by drop casting the suspension onto alumina substrates coated with interdigitated platinum electrodes, followed by a heat treatment at 200 °C to remove the solvent and stabilize the material on the substrate.

The gas sensing response of SnS₂ material to NO₂, H₂ and CO analytes was obtained by monitoring the electrical resistance of devices in cycles of 20 min exposure to the analyte followed by 60 min of exposure in dry air. Very high NO₂ (2-100 ppm range) sensor response, from 10² to 10⁶, was observed for temperatures between 25 °C and 300 °C, with devices presenting the highest response at room temperature (25 °C). In addition, devices presented high selectivity to NO₂ at room temperature. The lower detection limit was calculated as 6 ppb, which is much lower (one thousand times) than the Brazilian regulation for NO₂ exposition (6 ppm).

EQ04.11.07

Efficient Polycrystalline N-I-P CdSeTe Thin-Film Solar Cells Enabled by Grain Boundary and Back Contact Interface P-Type Doping Sabin Neupane¹, Xiaomeng Duan², Dengbing Li¹, Yanfa Yan¹, Feng Yan² and Gang Xiong³; ¹The University of Toledo, United States; ²The University of Alabama, United States; ³First Solar Inc., United States

Current state-of-art CdSeTe thin-film solar cells rely on a p-n junction of which the bulk absorber is doped p-type with group-V elements such as As. However the activation of in-situ doped As requires careful engineering of absorber stoichiometry and could potentially induce front interface combination. Furthermore, there is a typical trade-off between high carrier (hole) density and long carrier lifetime. Herein, we report a n-i-p device structure as an alternative to traditional p-type CdTe solar cells. The polycrystalline CdSeTe grain interior is intrinsic, whereas the grain boundaries and back contact interface are p-type doped by ex-situ doping of group V elements such as As, Sb, or Bi. This ex-situ doping method allows to preserve front interface quality, while maintain the high carrier lifetime advantage of the intrinsic absorber. With this approach, we demonstrated n-i-p CdSeTe solar cells with efficiencies on par with our n-p junction-based CdSeTe solar cells doped with Cu or As. Our new approach presents a new strategy for further efficiency improvement of CdSeTe solar cells.

EQ04.11.08

Electromechanical Modulations in Transition Metal Dichalcogenides—Implications for Environmental Sensors Mauricio Bessa¹, Wellington Freitas¹, Natalia Neme¹, Luiz G.P Martins², Ana Barboza³, Matheus Matos³, Mario Mazzoni¹ and Bernardo R. Neves¹; ¹University Federal-Minas Gerais, Brazil; ²Massachusetts Institute of Technology, United States; ³UFOP, Brazil

Transition metal dichalcogenides (TMDs) are key players in the two-dimensional materials nanoarena due to their exquisite optoelectronic properties under a standard environment (room temperature and atmospheric pressure). Nevertheless, they may also portray interesting physical properties under different environments. Here, we show two distinct and significant electromechanical modulations in TMD nanosheets which are tuned by the environmental conditions (applied pressure and adsorbents) [1]. Using scanning probe microscopy techniques, we modify the environmental conditions and observe step-like rises in the electrical response of all studied TMDs (MoS₂, WS₂, MoSe₂, and WSe₂ - monolayers (ML) and few layers (FL)). In a pressure-dependent experiment, we observe an initial electrical response modification at low pressure values (which requires previous exposure to an ambient atmosphere) that is followed by a second modification at higher pressure values (which occurs even without previous exposure to an ambient atmosphere). Experimentally, such electromechanical modulations are characterized by increasing plateaus in the charge injection efficiency, which normally are a signature for gap closure and/or conducting states availability. Our *ab initio* calculations indicate that the first transition is associated with pressure-induced hydrogenation of the chalcogen atom, which results in available conducting states. In the environment of our experiment, water, from the ubiquitous contamination layer atop the samples originated from any previous exposure to ambient atmosphere, is believed to be the current H source. The second modification, observed at high pressures, is associated with both layer-layer approximation (for FL flakes) and bond-angle modification (for both ML and FL flakes). These distinct processes, which are now concomitantly observed in a single experiment [1], evidence the unique environment-related electromechanical behavior of chalcogenide electronic materials.

Despite the physical insights unveiled by our results, it is their possible applicability that makes them stand out. Given the emerging use of chalcogenides at the core of a wide variety of nanoscale sensors, it is natural to foresee a significant impact of the observed electromechanical modulations on the design and operation of environment-related sensor devices, especially when a combination of pressure, temperature, and atmosphere is at play. Therefore, we believe the present work trails a few steps toward more comprehensive applications of the important class of chalcogenide electronic materials.

Reference:

1) Mauricio V. Bessa, Wellington D. Freitas, Natália P. Neme, Luiz G. P. Martins, Ana P. M. Barboza, Matheus J. S. Matos, Mario S. C. Mazzoni, and Bernardo R. A. Neves, Electromechanical Modulations in Transition Metal Dichalcogenide Nanosheets: Implications for Environmental Sensors, *ACS Appl. Nano Mater.* 2021, 4, 11305–11311.

EQ04.11.09

Alloy Broadening Effects in CdZnTeSe Alloy Studied with DFT, HR-XRD, and PL Jonathon Baker and Utpal Roy; Savannah River National

Laboratory, United States

Cadmium Zinc Telluride (CZT) is the leading room-temperature radiation detector material commercially available today. Despite much progress over the past 30 years, today's CZT crystals still suffer from performance-limiting material defects and a commensurate high cost of production. The emerging next-generation material $\text{Cd}_{1-x}\text{Zn}_x\text{Te}_y\text{Se}_{1-y}$ (CZTS) overcomes some of these limitations for radiation detector applications. Here, we present theoretical results and experimental supporting data on how the addition of Se to CZT induces alloy broadening effects, causing an intrinsic degradation in crystal quality regardless of the presence or absence of large crystallographic defects. The impact of this on the use of crystal quality as a performance metric in this alloy space will be discussed.

EQ04.11.10

A Computational Re-Evaluation of Se as a Solar Absorber Alp E. Samli¹, Seán R. Kavanagh^{1,2} and David O. Scanlon¹; ¹University College London (UCL), United Kingdom; ²Imperial College London, United Kingdom

Trigonal selenium (c-Se) was the first material to exhibit the photovoltaic (PV) effect and has recently experience a renaissance in research interest due to its desirable properties (suitable band gap, high earth abundance, low temperature processing and 'simple' chemistry) and potential implementation in silicon tandem cells.¹ Though cell efficiencies have improved much since 1883, c-Se lags behind leading technologies such as silicon and lead-halide perovskites.²

In this work³, we use hybrid density functional theory (DFT) to investigate crystalline selenium's 5 known synthesisable polymorphs (trigonal, rhombohedral, β -monoclinic, γ -monoclinic, δ -monoclinic) and determine the ideal phase for solar cell operation. Trigonal Se has the lowest direct band gap (1.904 eV with spin-orbit coupling) and highest charge carrier mobilities, allowing it to reach the highest efficiencies. Analysis of the optical response shows that c-Se has a theoretical upper limit to its efficiency as a single-junction solar absorber of 23% at a thickness of 2 μm . We calculate the vacuum alignment of the electronic band edges, providing guidance for further optimisation of the absorber contact layers. In addition, we compute the formation energies and charge transition levels of all intrinsic point defects (vacancies and interstitials) at the hybrid DFT level, to characterise the defect chemistry and doping response in this material.

References:

1 M. Zhu, G. Niu and J. Tang, *J. Mater. Chem. C*, 2019, 7, 2199–2206.

2 T. K. Todorov, S. Singh, D. M. Bishop, O. Gunawan, Y. S. Lee, T. S. Gershon, K. W. Brew, P. D. Antunez and R. Haight, *Nat. Commun.*, 2017, 8, 682.

3 A. E. Samli, S. R. Kavanagh and D. O. Scanlon, Submitted, 2022.

EQ04.11.11

Influence of S and Cd Atom on Photoluminescence in Tin Sulfide Films Ayaka Kanai¹, Keina Kusatsu² and Mutsumi Sugiyama²; ¹Nagaoka University of Technology, Japan; ²Tokyo University of Science, Japan

There has been a great deal of interest in research on low-cost and non-toxic semiconductors from both technological and theoretical viewpoints. In particular, tin sulfide (SnS) exhibits appropriate properties as an absorber layer in thin film solar cells, with p-type electrical conductivity, a high absorption coefficient ($\geq 10^4 \text{ cm}^{-1}$), and a bandgap of approximately 1.3 eV. Therefore, it has the potential to be used as an environmentally friendly solar cell material. Recently, a relatively high efficiency exceeding 4% in n-CdS/p-SnS structured solar cells was reported. However, the efficiency of SnS film solar cells remains low for various reasons, including the poorly understood carrier/defect properties of SnS. In highly efficient n-CdS/p-Cu(In,Ga)Se₂ (CIGS) solar cells, the surface of the CIGS layer becomes n-type after chemical bath deposition (CBD) of the CdS layer because of the presence of donors such as Cd on the Cu sites (Cd_{Cu}). This contributes to the relatively high efficiency of CIGS solar cells. However, the fundamental defects in the CdS/SnS interface have not yet been revealed. Therefore, understanding the carrier originating from defects in the CdS/SnS interface is critical for improving device performance. In this study, the effects of Cd and S impurity-related defects in SnS films in the CdS layer were investigated using photoluminescence (PL) measurements.

A 1 μm -thick SnS film was deposited via RF sputtering on Mo-deposited soda-lime glass substrates. The PL spectra of the three CdS/SnS samples subjected to different treatments were investigated to separate the Cd and S impurity-related defects from those in the CdS layer. First, to obtain normal CdS/SnS, a 60 nm-thick CdS buffer layer was deposited on the SnS layer through CBD using an aqueous solution of $\text{CdSO}_4\text{-NH}_3\text{-CH}_4\text{N}_2\text{S}$. Second, to examine the S-related defects in the SnS film, the SnS thin film was sulfurized in a sulfur vapor and N₂ atmosphere before depositing the CdS layer. Finally, to examine the Cd-related defects in the SnS film, Cd partial electrolyte (Cd-PE) treatment was carried out on the SnS film, using the same process as for CBD-CdS but without $\text{CH}_4\text{N}_2\text{S}$ before depositing the CdS layer. PL measurements were carried out for all CdS/SnS using the 532.0 nm line of an Nd:YAG laser as the excitation source. Phase-sensitive detection was carried out from 1200 to 1700 nm using a liquid N₂-cooled Ge photodetector. All experiments were performed using a cryostat at 26 K.

EQ04.11.12

Influence of Ge Inclusion on Surface Morphologies of Cu₂(Sn_{1-x}Ge_x)S₃ Films Grown by Sulfurization of Cu/Sn-S Precursors Ayaka Kanai¹, Mutsumi Sugiyama² and Kunihiko Tanaka¹; ¹Nagaoka University of Technology, Japan; ²Tokyo University of Science, Japan

Recently, next-generation renewable energy devices, such as sensors, solar cells, and water splitting using solar cells, have attracted worldwide attention. Furthermore, there has been a great deal of interest in research on environmentally friendly and low-cost photo-absorber materials from both theoretical and technological viewpoints. For this reason, p-type copper sulfide-based ternary compounds, such as Cu₂SnS₃(CTS), Cu₂GeS₃, and Cu₂SbS₃, which have high absorption coefficients of $\sim 10^4 \text{ cm}^{-1}$, are expected to be used as absorption materials in the future. In particular, the pseudo-ternary alloy Cu₂(Sn_{1-x}Ge_x)S₃ (CTGS) has recently attracted interest because the bandgap energy can be continuously controlled from 0.9 to 1.6 eV by changing the Ge/(Ge+Sn) ratio, x. In addition, compositional grading in the depth direction of the absorber layer in the CTGS film by changing the bandgap can substantially improve the performance, approaching the quality of Cu(In_{1-x}Ga_x)Se₂ (CIGS) solar cells. However, the reported energy efficiency of solar cells using CTGS is still low at approximately 6%. One reason that the surface morphology of CTGS cannot be controlled is the high vapor pressure of germanium sulfide (GeS₂). In addition, the surface roughness of the CTGS thin films increases with increasing x. The increase in the surface roughness of the p-n junction directly affects the electrical properties of the device, resulting in decreased device performance. In this study, to reveal the change in the surface morphology of CTS films by the inclusion of Ge, the effect of sulfurization temperature on the root-mean-square (RMS) roughness of CTGS films was investigated using a laser microscope. To examine the growth mechanism of the CTGS films, cross-sectional secondary ion mass spectrometry (SIMS) measurements were carried out to investigate the distribution of the atomic compositions of the CTGS films.

A Cu/SnS₂ precursor was deposited via RF sputtering on Mo-deposited soda-lime glass substrates. The Ge ratio was controlled by varying the sputtering time of the Ge layer. The CTGS thin films were then sulfurized using sulfur vapor. To investigate the sulfurization mechanism of the Ge-containing Cu/Sn-S precursor, the ramping rate (10°C min⁻¹), high-temperature holding time (5 min), and Ge layer thickness were kept constant. The crystal structures and compounds of the CTS and CTGS films were determined using X-ray diffraction with Cu K α radiation. The RMS roughness of the films was evaluated

using laser microscopy. Depth profiles of the CTGS films were obtained using SIMS. SIMS measurements were carried out using O^{2+} as the primary ion, with acceleration.

EQ04.11.13

Investigations into n-CdTe/p-ZnTe Solar Cells [Luke Thomas](#), Theodore D. Hobson, Laurie J. Phillips and Ken Durose; University of Liverpool, United Kingdom

In this work we use an n-type CdTe absorber layer as opposed to the conventional p-type CdTe layer. The motivation behind this stems from the possibility of high stable n-type doping in the absorber layer which offers high V_{oc} and Ohmic contacting in photovoltaic devices, both of which currently hinder p-type CdTe devices. We explore n-type doping via post-growth and in-situ routes using indium as a dopant with CSS-grown CdTe films and report on the feasibility of doping. We also study the feasibility of ZnTe:Cu as a p-type partner layer in devices.

We have successfully doped CdTe n-type using both post-growth and in-situ methods. Post-growth doping methods trialled include in-diffusion of evaporated indium metal and the annealing of films that had been sprayed with $InCl_3$, in either aqueous or methanolic solutions. Annealing was conducted either in air or under flowing nitrogen. Indium incorporation into the films was confirmed by quantitative SIMS measurements with concentrations up to 10^{19} cm^{-3} . Conductivity type was confirmed as n-type by determination of the Fermi level position from photoemission measurements (XPS).

In-situ n-type doping was achieved by growing CdTe films via CSS from pre-doped melt-synthesized CdTe:In source material. Chemical incorporation of the indium was quantified with ICP-OES and the bulk CdTe:In was verified as n-type with 10^{17} cm^{-3} . Thin film doping densities from SIMS were in the range of 10^{16} - 10^{19} cm^{-3} depending on growth conditions, these films were verified as n-type by photoemission (HAXPES) determination of the Fermi level position.

ZnTe layers were deposited via rf-sputtering and were characterized with surface profilometry, optical spectroscopy, and resistivity and Hall Effect measurements. Copper doping was implemented by evaporating a thin layer of Cu onto the ZnTe surface followed by annealing in an inert atmosphere. With optimized Cu content and annealing temperatures, we fabricated p-type ZnTe layers with sheet resistances below $1000 \Omega/\text{sq}$. Similar processing resulted in carrier concentrations in the range of 10^{16} - 10^{21} cm^{-3} by varying the copper content. Optical spectroscopy measurements showed that Cu-doping did not affect the optical transmission or the band gap of the ZnTe layer.

Devices were then fabricated with the following structure; TEC15/n-CdTe/p-ZnTe/Au. This structure was used in both superstrate and substrate configurations with either thin CdTe absorber layers or thin Au contacts respectively. Devices in the substrate configuration yielded efficiencies up to 1.5% whereas those in the superstrate configuration yielded efficiencies up to 3.5%. Capacitance-voltage measurements confirmed carrier concentrations of around 10^{14} cm^{-3} in the substrate geometry with $3 \mu\text{m}$ CdTe whereas superstrate devices with 800 nm CdTe showed carrier concentrations as high as 10^{16} cm^{-3} .

Work in progress includes investigating CuI as either a hole-transport layer in conjunction with ZnTe or as an individual p-type partner layer to n-CdTe. In addition to this, Au contacts will be replaced with an appropriate transparent contact (such as ITO) for the substrate devices.

EQ04.11.14

Perovskite-Antimony Selenide Tandem Solar Cell [Harigovind Gokul Menon](#), Vijayaraghavan Sankaranarayanan Nair, Al Amin, Xiaomeng Duan, Wenjun Xiang and Feng Yan; University of Alabama, United States

Tandem solar cell represents a promising solar cell technology to overcome the Shockley-Queasier limit in the single-junction solar cell. However, it is a challenge to make an affordable and highly efficient tandem device. Particularly, it is in high demand to use the earth-abundant materials for both the wide bandgap and narrow bandgap sub-cells, respectively. In this work, we reported new tandem solar cells using earth-abundant wide-bandgap perovskite (1.7 eV) and narrow bandgap antimony selenide (Sb_2Se_3 , 1.2 eV). A device-level simulation using SCAPS has been performed to predict the device performance. A prototype tandem cell with device architecture Perovskite/ Sb_2Se_3 has been fabricated to validate the simulation. The experimental results show promising device performance and pave the way to further improve device performance by engineering the device architecture and interfaces.

EQ04.11.15

Wide Bandgap Metal Oxide Buffer Layers on the Eco-Friendly Selenium Thin-Film Solar Cells [Cheng-Ying Chen](#)¹, I-Jui Hsieh², Thi-Thong Ho³, Pochun Chen², Kuei-Hsien Chen³ and Li-Chyong Chen⁴; ¹Department of Optoelectronics and Materials Technology, National Taiwan Ocean University, Taiwan; ²Institute of Materials Science and Engineering, National Taipei University of Technology, Taiwan; ³Institute of Atomic and Molecular Sciences, Academia Sinica, Taiwan; ⁴National Taiwan University, Taiwan

The element selenium (Se) was used in the first solid-state solar cell in 1883 and has a high absorption coefficient and mobility, making it a p-type absorber for wide energy gap (~1.8~2.0 eV) thin film solar cells. In addition, direct bandgap, earth-abundance, simple composition, non-toxicity, low melting point and environmental stability make Se inexpensive and developable for solar cells. However, in the n-type buffer layer perspective, so far, has not been found a suitable buffer layer for modulating conduction band offset (CBO) between n-type buffer layers and p-type Se absorbers.

In this work, we utilized atomic layer deposition (ALD), depositing ZnSnO as buffer layers for p-type Se absorbers. The benefit for using ALD growth ZnSnO can be summarized the as following points: (1) ZnSnO is wide band gap material (~3.2eV); (2) Controllable of Zn and Sn ratio, which can intentionally modulate the CBO become spike type (i.e., $0 < \text{CBO} < 0.5 \text{ eV}$); (3) ALD can effectively growth larger scale of thin-film and precisely control the thickness. Finally, the result presented the $Zn_{1-x}Sn_xO$ ($x=7\%$) under the optimization of ZnO and SnO ratio, the power conversion efficiency can be achieved at about 2.68%.

EQ04.11.16

Realizing High Responsivity Sb_2Se_3 -Based NIR Photodetector by Employing Selenization Process and Controlling Crystallinity [Su K. Kim](#), Hee-Kyoung You, Kwang Ro Yun, Jong-Ho Kim and Tae-Yeon Seong; Korea University, Korea (the Republic of)

Chalcogenide semiconductors (alloys with chalcogen elements) are well known for their stability under heat, moisture, and light exposure. Among these semiconductors, antimony selenide (Sb_2Se_3) is of increasing interest as a suitable light absorber material suitable for solar cells and photodetectors in the visible to near-infrared wavelength range. In particular, photodetectors are of increasing interest because of their applications in optical communications, sensors, and broadband imaging technologies for military systems. Sb_2Se_3 has a narrow band gap, (varying from 1.6 to 1.2 eV by controlling annealing temperature), low toxicity, and high absorption coefficient. However, there is a challenge to be addressed for various applications due to the intrinsically low electrical conductivity of Sb_2Se_3 . Additionally, Se loss occurs during thin film deposition, which negatively affects the characteristics of film and device performance. Thus, to solve the problem, many studies have been conducted to deposit Sb_2Se_3 films with additional Se by annealing with Se powder

and H₂Se gas environment, and Se co-sputtering process. Researches on Sb₂Se₃ films and associated devices have been mainly carried out to improve the performance of solar cells, and studies related to Sb₂Se₃-based photodetectors have not been conducted so far. In this study, we first report on the fabrication of selenized Sb₂Se₃ film-based photodetectors through a facile co-sputtering process. Sb₂Se₃ films were deposited by a sputtering method and were then crystallized by employing an annealing process. To compensate for the loss of Se atoms during deposition, a process of co-sputtering Se and Sb₂Se₃ targets was adopted. The performance of photodetectors fabricated with selenized and unselenized Sb₂Se₃ films was examined. All samples were annealed at temperatures of 150 - 300 °C for 30 min. The XRD results showed that selenized-Sb₂Se₃ films exhibited better crystallinity. The selenized-Sb₂Se₃ films were crystallized at 150 °C, whilst unselenized Sb₂Se₃ films were crystallized at 200 °C. For the unselenized Sb₂Se₃ films, the photocurrent increased with the temperature, whereas the selenized-Sb₂Se₃ films showed maximum current at 250 °C. The 250 °C-annealed selenized-Sb₂Se₃ photodetectors exhibited the responsivity of 1130 mA/W at the light intensity of 200 μW/cm² and the detectivity of 4.62 × 10¹¹ Jones. The rise/fall time of the 250 °C-annealed selenized-Sb₂Se₃ detectors was 4.54 ms/8.50 ms at 200 μW/cm², and sensitivity and external quantum efficiency were 94.2 and 155%, respectively. The fast response time indicates the formation of high crystal-quality films. The bandgap of the selenized-Sb₂Se₃ film was 1.65 and 1.23 eV before and after annealing at 250 °C, respectively. Based on XPS, STEM and AFM results, the improved behaviours of selenized photodetectors will be explained in terms of the formation of donor-like defects, dense crystallinity, and surface characteristics. These results show that the selenization of Sb₂Se₃ films could be a promising process for the fabrication of high-performance NIR photodetectors.

EQ04.11.17

Above Ambient Pressure Synthesis of Antimony Chalcogenide Semiconductors Ivan Cano Prades¹, S Bousseguil¹, Kunal J. Tiwari^{2,1}, Sergio Giraldo¹, Alejandro Navarro Güell¹, Zacharie Jehl Li Kao¹, Marcel Placidi¹, Joaquim Puigdollers¹ and Edgardo Saucedo¹; ¹Universitat Politècnica de Catalunya, Spain; ²Catalonia Institute of Energy Research, Spain

Antimony chalcogenides Sb₂X₃ (X=Se,S,Te) and its alloys have become a topic of active research through the past decade due to their interesting electrical and optical properties stemming from an intriguing quasi-1D crystal structure. Observation of anisotropic charge transport properties coupled with ease of synthesis at relatively lower temperature are important characteristic observed for this class of semiconductor compounds which have been studied both in bulk and thin film form. Amongst the various possible chemical compositions, Sb₂Se₃ has garnered particular attention from the PV community due its ideal 1.3 eV band gap and high absorption coefficient $\alpha > 10^5\text{-}6\text{ cm}^{-1}$ in the visible region, positioning it as a promising absorber layer for thin film photovoltaic applications. State of the art Sb₂Se₃ based thin film solar cell devices have reached a record efficiency = 12% [1] and to the growing community is aiming for much higher values in the short term. Beyond the various strategies being implemented to improve performance, there is also a need to further expand the range of application beyond stand-alone PV by tuning the band gap of the parent Sb₂Se₃ material. The inclusion of halogen elements such as iodine and bromine has been proposed as an interesting strategy to widen the band gap of Sb₂Se₃ making it optically suitable for application in building integrated PV as well as top cell in tandem solar cells [2].

We present here a novel method for the fabrication of antimony chalcogenide thin films and report on recently obtained results on SbSe(I/Br) absorber synthesis. The process relies on the high pressure (> 1 atm) reactive thermal annealing under Se atmosphere and SbI₃ and SbBr₃ precursors at low temperature (≤ 450 degree celsius) for the preparation of SbSeI and SbSeBr semiconductor thin films. A series of optimizations for different experimental conditions such as temperature, pressure, duration etc. were performed leading to the formation of highly *c-axis* oriented chalcogenide semiconductor on Mo coated glass substrates with a unique micro columnar grain morphology. Detailed structural and compositional studies were performed on the as prepared absorber layers in order to study their physical characteristics as well as propose plausible conversion pathway starting from Sb₂Se₃ to SbSeI and SbSeBr. First proof of concept solar cell devices was completed in the substrate configuration of Mo/SbSe(I/Br)/CdS/i-ZnO/ITO and their photovoltaic properties as well as spectral response were investigated. Best performing devices with SbSeI (E_g = 1.6 eV) and SbSeBr (E_g = 2 eV) exhibited V_{oc} = 633 mV and 600 mV respectively, demonstrating the potential of these materials as wide bandgap absorbers. We postulate that the main limitation of the current devices comes from a poor carrier extraction due to the use of a CdS buffer layer with a cliff-like p-n interface and poor coverage due to micro-columnar morphology presenting shunt paths. The replacement of the n-partner layer by a material with a more suited band structure, or the use of electron selective contacts will be discussed as ways to markedly improve performance.

[1] Duan, Zhaoteng, et al. "Sb₂Se₃ Thin Film Solar Cells Exceeding 10% Power Conversion Efficiency Enabled by Injection Vapor Deposition Technology." *Advanced Materials* 34.30 (2022): 2202969.

[2] Nie, Riming, et al. "Efficient and Stable Antimony Selenoiodide Solar Cells." *Advanced Science* 8.8 (2021): 2003172.

SESSION EQ04.12: Virtual Session: Emerging Chalcogenide Electronic Materials

Session Chair: Kevin Ye

Tuesday Morning, December 6, 2022

EQ04-virtual

8:00 AM EQ04.12.01

Fabrication of a Flexible CMOS Image Sensor Integrating Crystalline Selenium Photoconversion Film and Thinned FDSOI Circuit Shigeyuki Imura and Masahide Goto; NHK Science & Technology Research Laboratories, Japan

In a smart society based on the surrounding sensing and monitoring infrastructure, high-performance flexible sensing devices that adapt to various shapes and object movements are necessary. Although flexible sensors using organic and inorganic thin-film transistors have previously been developed to automatically collect and visualize large information around us, a further performance and reliability enhancement of the devices for practical use is required. Here, we demonstrate the flexible silicon (Si)-based complementary metal-oxide semiconductor (CMOS) image sensors with high performance and flexibility by transferring the ultra-thinned CMOS circuits and photoconversion films onto flexible substrates. Combining CMOS circuits on a fully depleted silicon on insulator (FDSOI) substrates [1], which allows very thin device layers, and a crystalline selenium (c-Se) photoconversion film with its outstanding light absorption properties [2] achieves high-performance and excellent flexibility. In this presentation, we discussed substrate thinning and transfer technology, as well as the deposition process of c-Se-based photoconversion film, confirming the mechanical flexibility and operation of thinned CMOS circuits.

The CMOS circuit is formed on the FDSOI wafer with a handle layer, device except for handle layer, and CMOS active layer with thicknesses of 725 μm, 6 μm, and 50 nm, respectively. After dicing into chips and bonding to the temporary fixing substrates, we first ground the handle layer to a thickness of 30 μm mechanically and then removed it using xenon fluoride etching, where the Si is selectively etched and the reaction stopped at the surface of the buried oxide layer. Next, we bonded the device to a 50-μm-thick flexible polyethylene terephthalate (PET) substrate with an adhesive film and removed the temporary fixing substrate after the ultraviolet irradiation. Finally, the photoconversion film, which comprises a 20-nm-thick wide-bandgap n-type gallium

oxide layer, 300-nm-thick p-type c-Se absorption layer, and 30-nm-thick indium tin oxide transparent electrode is directly provided on the CMOS circuit. A c-Se was fabricated by annealing amorphous Se at 200 degrees, whereas tellurium was used as a nucleation layer to prevent Se film from peeling. Consequently, we successfully produced a 6- μm -thick FDSOI device with a 350-nm-thick c-Se-based photoconversion film on a flexible PET substrate.

We compared the characteristics of the drain current-gate voltage of the transferred CMOS circuit with that of the bulk (before transferred) ones, where the gate length is 2 μm . The measurement results reported no significant changes in the characteristics of the devices before and after the transfer, thereby indicating that the thinning and transfer process does not adversely affect the circuit operation. Furthermore, the flexural rigidity (D) of an object is expressed by the following equation [3]:

$$D = Et^3 / 12(1 - \nu^2)$$

where E , t , and ν are the Young's modulus, thickness, and Poisson's ratio, respectively. FDSOI, which is mostly composed of silicon dioxide, has a smaller Young's modulus and Poisson's ratio than Si. Additionally, the thickness of the device, which comprises the photoconversion film and the FDSOI circuit, can be made extremely thin, thereby allowing the device flexibility. Also, the fabricated device can be wrapped around a cylindrical glass rod with a curvature of 6 mm without cracking, confirming its mechanical flexibility.

Conclusively, we developed a fabrication process for a flexible CMOS image sensor that integrates a c-Se-based photoconversion film and a thinned FDSOI circuit. Since this technology enables the flexibility of various Si devices, it can open up new fields of application in image sensors and several high-performance flexible Si devices.

[1] M. Goto et al., IEDM Tech. Dig., 4.2 (2014)

[2] S. Imura et al., Sci. Rep. 10, 21888 (2020)

[3] L. D. Landau et al., Theory of elasticity: volume 7, Elsevier (1986)

8:05 AM EQ04.12.02

PRESENTED ON-DEMAND ONLY: Fabrication and Characteristics of Co_xS_y Thin Films for Gas-Sensing Applications Myeong Gyu Kim and Yun-Hyuk Choi; Daegu Catholic University, Korea (the Republic of)

Transition-metal oxides have been widely studied for detecting toxic and dangerous gases as a semiconductor-type gas sensor. However, those metal oxide-based semiconductor materials usually suffer from high operating temperatures, high noise, and poor selectivity. For this reason, transition-metal sulfides (MoS_2 , WS_2 , etc.) begin to stand out in gas sensors. Despite numerous investigations on the material selection, cobalt sulfides have rarely been studied for the gas sensor application. In this work, gas sensing properties of cobalt sulfide thin films were investigated. Co_xS_y thin films were synthesized by a two-step process using the thermal metal-organic deposition of Co_3O_4 and subsequent sulfidation using a horizontal tube furnace. We have optimized processing temperature and time for the preparation of the Co_xS_y thin films. The gas sensing properties have been investigated with varying gas type and concentration at various operating temperatures. Finally, the gas sensing and structural characteristics of cobalt sulfide thin films were evaluated and demonstrated in terms of processing-structure-property. In addition, the oxidation behaviors on the surface of sensors during the sensor measurements have been examined.

8:20 AM EQ04.12.03

Solar Cells of Antimony Sulfide-Selenide Absorber Thin Films with ZnS-CdS Window Layers Fabiola De Bray Sanchez, M.T. Santhamma Nair and P. Karunakaran Nair; Universidad Nacional Autonoma de Mexico, Mexico

Antimony chalcogenides, Sb_2S_3 and Sb_2Se_3 , and their solid solutions $\text{Sb}_2\text{S}_x\text{Se}_{3-x}$ with band gaps in the 1.88 – 1.1 eV interval are prospective absorber materials for thin film solar cells. In the present work, we used thermal evaporation of commercial Sb_2S_3 and Sb_2Se_3 compounds to obtain the thin films of $\text{Sb}_2\text{S}_x\text{Se}_{3-x}$ with optical band gaps of 1.29 – 1.6 eV, depending on the value of x , and optical absorption coefficients of $> 10^5 \text{ cm}^{-1}$ in the visible region. The films show photoconductivity of $10^{-6} - 10^{-5} \Omega^{-1} \text{ cm}^{-1}$. Heterojunction solar cells of these thin films as absorbers were developed with CdS, ZnO, or ZnS/CdS bilayer as buffer/window on SnO_2 :F-coated glass substrates. With colloidal graphite paste of 0.2 – 1 cm^2 area as the back contacts, the solar cell of glass/FTO/ZnS-CdS/ $\text{Sb}_2\text{S}_x\text{Se}_{3-x}$ /C-Ag structure showed an open circuit voltage of 0.435 V, a short circuit current density of 32.9 mA cm^{-2} , and a conversion efficiency of 7.34 % with Fill Factor, 0.52. We present the details of preparation of the different component films, their properties, and the latest results on the performance of these solar cells.

8:35 AM EQ04.12.04

Tailoring the Optical and Electrical Properties of MoTe_2 via Electrochemical Intercalation of Lithium Ions Alyssa Shiyu Xu, Shunran Li, Mengjing Wang, Joshua Pondick, Peijun Guo and Judy Cha; Yale University, United States

Intercalation of lithium (Li) ions is one of the most effective methods to realize structural transformation and to tune the optical and electrical properties of two-dimensional transition metal dichalcogenides (2D TMDCs). Numerous studies have focused on the phase transition from semiconducting 2H phase to metallic 1T (or 1T') phase in MoS_2 and WS_2 induced by the intercalation of lithium ions. However, few reports explore the effects of lithium intercalation in other TMDCs, such as Mo- or W- ditellurides. In particular, novel electronic and energy devices can be realized using the lithium-intercalated MoTe_2 with its intriguing electrical, topological and catalytic properties.

Here, we report electrochemical lithium intercalation into 1T'- MoTe_2 flakes. The 1T' phase is stable down to 0.9 V of the applied electrochemical voltage using poly(ethylene glycol) methyl ether methacrylate (PEGMA)/ bisphenol A ethoxylate dimethacrylate (BEMA) solid polymer electrolyte and Li anode, and two new phases are observed at 0.7 V (phase I) and 0.4 V (phase II) of the applied electrochemical voltage. At 0.7 V, lightly intercalated phase I is evidenced by the disappearance of the A_g peak at $\sim 77.7 \text{ cm}^{-1}$ and appearance of a new peak at $\sim 86.9 \text{ cm}^{-1}$ in Raman spectroscopy as well as a 10% increase of electrical resistance in two-terminal measurements. For heavily Li-intercalated phase II at 0.4 V, we observe the emergence of additional new peaks at 16.8 cm^{-1} , 109.0 cm^{-1} and 132.8 cm^{-1} in Raman spectroscopy and the dramatic increase of electrical resistance for over 8 folds. *In situ* Hall effect measurements show that the carrier density falls from 10^{15} cm^{-2} of pristine 1T'- MoTe_2 to 10^{14} cm^{-2} (phase I) and 10^{12} cm^{-2} (phase II) despite the supposed electron doping from Li intercalation. Temperature-dependent resistivity measurements further show increasing resistivity with decreasing temperature for phase II, suggesting a gap opening in initially metallic 1T'- MoTe_2 . Our results thus demonstrate electrochemical intercalation of lithium ions as a powerful tool to manipulate phase stability and electron density of 2D TMDCs, and report new phases in MoTe_2 induced by lithium intercalation.

8:50 AM EQ04.12.05

A Gapped Phase in Semimetallic T_d - WTe_2 Induced by Lithium Intercalation Mengjing Wang^{1,2}, Aakash Kumar¹, John Woods¹, Hao Dong¹, Joshua Pondick¹, Alyssa Shiyu Xu¹, Peijun Guo¹, Diana Qiu¹ and Judy Cha^{1,2}; ¹Yale University, United States; ²Cornell University, United States

Lithium intercalation in two-dimensional (2D) materials can introduce useful electronic and structural phase transitions, as enabled by its high electron doping power on the order of 10^{14} e/cm². For example, lithium intercalation can transform semiconducting 2H-MoS₂ into metallic 1T'-MoS₂. Despite the extensive studies of lithium intercalation in MoS₂ and WS₂, the effects of lithium intercalation in 2D transition metal tellurides and thickness effects on intercalation-induced phase transitions have rarely been explored. Herein, we report a reversible structural phase transition in WTe₂ from 2D Weyl semimetal T_d phase to semiconducting T_d' phase by electrochemical lithium intercalation.^[1] We systematically investigated the phase transition dynamics as a function of electrochemical intercalation voltage and layer thickness using combined *in situ* Raman spectroscopy, *in situ* x-ray diffraction, and *in situ* electron transport characterization. Structurally, the new T_d' phase has an in-plane structure resembling the theoretically predicted 2x2 charge density wave (CDW) of monolayer WTe₂ with electron doping.^[2,3] Electronically, the new T_d' phase has an increased longitudinal resistance and a reduction of carrier density both by two orders of magnitude, probed by *in situ* Hall measurements. The more resistive T_d' phase also exhibits an increasing resistance with decreasing temperature, suggesting that this T_d' phase is a semiconductor with a gap opening at the Fermi level. Our *ab initio* calculations further predict that this T_d' phase has an indirect band gap of 0.14 eV and a direct band gap of 0.66 eV, which supports our transport data. Our finding of a new gapped phase, potentially a CDW phase, in a two-dimensional (2D) semimetal demonstrates electrochemical intercalation as a powerful tuning knob for modulating electron density and phase stability in 2D materials. The greatly expanded electronic and structural phase diagram of 2D materials accessible using lithium intercalation will stimulate the research for novel quantum phases, such as topological superconductivity.

[1] M. Wang, A. Kumar, H. Dong, J. M. Woods, J. V. Pondick, S. Xu, D. J. Hynek, P. Guo, D. Y. Qiu, J. J. Cha, *Advanced Materials* **2022**, 2200861.

[2] P. K. Muscher, D. A. Rehn, A. Sood, K. Lim, D. Luo, X. Shen, M. Zajac, F. Lu, A. Mehta, Y. Li, X. Wang, E. J. Reed, W. C. Chueh, A. M. Lindenberg, *Advanced Materials* **2021**, 33, 2101875.

[3] J.-H. Lee, Y.-W. Son, *Physical Chemistry Chemical Physics* **2021**, 23, 17279.

9:05 AM *EQ04.12.06

Structure-Property-Function Relationships of Novel Chalcogenides from Combinatorial Synthesis and High-Throughput Characterization

Thomas Unold; Helmholtz-Zentrum Berlin, Germany

Emerging chalcogenide materials such as BaZrS₃ have raised considerable interest for their attractive optoelectronic properties, earth-abundance and high stability. However, many material properties such as carrier mobilities, carrier densities, defects and band positions are still relatively unclear. Reports of these properties in literature usually refer to few sample studies, with specific synthesis conditions. It would be useful to be construct more general structure-property-function (SPF) relations for which wider regions of the phase-diagram of these multinary materials are explored. We present such SPF relations for combinatorial BaZrS₃ thin films that are synthesized by PLD and sulfurization with large gradients of the Ba/Zr content. We show that SPF relationships obtained by high-throughput XRF, XRD, Raman, UV-Vis, Photoluminescence, Conductivity, THz-Absorption enable important insights in the material properties and their potential application in optoelectronic devices.

9:35 AM *EQ04.12.07

Strategies for Synthesis of Large-Area Epitaxial Transition Metal Dichalcogenides Tanushree Choudhury^{1,2}, Mikhail Chubarov², Haoyue Zhu², Nicholas Trainor², Thomas McKnight², Shruti Subramanian², Danielle R. Hickey², Saiphaneendra Bachu², Tianyi Zhang², Mauricio Terrones^{2,2,2}, Joshua A. Robinson^{2,2} and Joan M. Redwing^{2,2}; ¹Indian Institute of Technology Bombay, India; ²The Pennsylvania State University, United States

Layered 2D transition metal dichalcogenides (TMDs) and their heterostructures have novel and exotic optical and electronic properties. Current research using transferred exfoliated flakes has demonstrated the rich landscape of possible properties and applications that TMDs and their heterostructures exhibit. A major challenge in harnessing the full potential of these materials is the availability of these materials uniformly over a large-scale. Scalable and adaptable synthesis strategies are necessary to obtain pristine epitaxial TMDs and heterostructures. We have developed an epitaxial growth strategy for layered dichalcogenides MX₂ (M=Mo, W and X= S, Se), based on metal organic chemical vapor deposition (MOCVD). This process uses metal hexacarbonyl and hydride chalcogen precursors to deposit monolayers in a cold-wall reactor.

Epitaxial growth of nearly single crystalline TMDs like WS₂ on 2" sapphire wafers is achieved by a multi-step precursor modulation method. In case of conventional 3D substrates, nucleation density is controlled independently by precursor modulation. The lateral growth of these nuclei is promoted while suppressing additional nucleation to form coalesced monolayer films. In-plane X-ray diffraction demonstrates that the films are epitaxially oriented with respect to sapphire. Controlling the growth temperature and chalcogen flux is crucial in establishing an epitaxial relation and achieving oriented growth. Dark-field transmission electron microscopy (DF-TEM) of transferred WS₂ monolayers show ~95% single orientation coverage with minimal bilayer and inversion domains. The key features observed during the growth of MoS₂, WS₂ and WSe₂ will be discussed.

MOCVD synthesis of TMDs is also investigated on 2D substrates like graphene. In this case, we investigate the effect of defects in epitaxial graphene on the growth of transition metal dichalcogenides like WS₂. The defect density in epitaxial graphene, controlled by exposure to a helium plasma for different durations, control the WS₂ nucleation density as well as nucleation sites. The results indicate that the defect generation, and subsequent sulfur incorporation is higher when the buffer layer was present between the SiC substrate the graphene layers. Another key observation was that the plasma treatment modified the WS₂ nucleation sites from step edges to terraces. This impact on the nucleation site was, however, temperature dependent. Additional details about the role of the buffer layer and the impact on the nucleation site and density will be presented.

10:05 AM DISCUSSION TIME

SYMPOSIUM EQ05

Contacts and Interfaces in Optoelectronic Devices
November 28 - December 8, 2022

Symposium Organizers

Stefaan De Wolf, King Abdullah University of Science and Technology
Geoffroy Hautier, University Catholique de Louvain
Monica Morales-Masis, University of Twente
Barry Rand, Princeton University

* Invited Paper
+ Distinguished Invited

SESSION EQ05.01: Perovskites I
Session Chairs: Stefaan De Wolf and Monica Morales-Masis
Monday Morning, November 28, 2022
Sheraton, 2nd Floor, Republic B

10:30 AM *EQ05.01.01

Vapor Phase Deposited Perovskites [Henk J. Bolink](#); University of Valencia, Spain

We will report on the progress on vapor phase deposited perovskites, using novel screening methods and device architectures. The influence of the use of thin organic charge extraction layers, using strong dopants, ionic compounds and other passivators will be described.

11:00 AM *EQ05.01.02

Interactions Between Transport Layer and Active Layer in Organic and Perovskite Solar Cells [Julia W. Hsu](#); The University of Texas at Dallas, United States

Transport layers are essential components of organic and perovskite solar cells (OSCs and PSCs), with functions such as setting up the internal electric field to facilitate charge transport, preventing exciton quenching on the electrodes, and blocking the wrong type of carriers from reaching the electrode. Often transport layers are treated as inert materials in the multi-layered OSCs and PSCs. In this talk, I will highlight a few examples of unforeseen interactions between transport layers and active layers. In OSCs, we find that electron transfer to high work function MoOx hole transport layer (HTL) induces p-doping¹ and highly soluble polyethylenimine (PEI) induced n-doping in the organic active layer,² both resulting in lower short circuit current. In PSCs, we find that NiO can significantly lower the decomposition temperatures of MAPbI₃³ and FAPbI₃⁴ through an interfacial reaction that stabilizes HI and subsequent NiI₂ formation. SnO₂ and ZnO also react with halide perovskites while TiO₂ appears most stable without UV illumination.⁵ The cumulation of these results indicates that the stability of multi-layer devices depends not just on individual layer materials but also their compatibility during processing and operation.

1. Wang, J., Xu, L., Lee, Y.-J., de Villa, M. A., Malko, A. V., and Hsu, J.W.P. (2015). Effects of Contact-Induced Doping on the Behaviors of Organic Photovoltaic Devices. *Nano Letters* *15*, 7627–7632.
2. Wang, J., Xu, L., Zhang, B., Lee, Y.-J., and Hsu, J.W.P. (2017). n-Type Doping Induced by Electron Transport Layer in Organic Photovoltaic Devices. *Advanced Electronic Materials* *3*, 1600458.
3. Thampy, S., Zhang, B., Hong, K.-H., Cho, K., and Hsu, J.W.P. (2020). Altered Stability and Degradation Pathway of CH₃NH₃PbI₃ in Contact with Metal Oxide. *ACS Energy Letters* *5*, 1147–1152.
4. Thampy, S., Zhang, B., Park, J.-G., Hong, K.-H., and Hsu, J.W.P. (2020). Bulk and interfacial decomposition of formamidinium iodide (HC(NH₂)₂I) in contact with metal oxide. *Materials Advances* *1*, 3349–3357.
5. Thampy, S., Xu, W., and Hsu, J.W.P. (2021). Metal Oxide-Induced Instability and Its Mitigation in Halide Perovskite Solar Cells. *The Journal of Physical Chemistry Letters* *12*, 8495–8506.

11:30 AM EQ05.01.03

Probing Metal Oxide Surfaces for Stable and Efficient Perovskite Devices [Sofia Aperi](#)¹, [Selina Olthof](#)², [Geert Brocks](#)^{3,1} and [Shuxia Tao](#)¹; ¹Eindhoven University of Technology, Netherlands; ²University of Cologne, Germany; ³University of Twente, Netherlands

With the rapid advance of metal halide perovskites, refining other materials that comprise a perovskite optoelectronic device becomes all the more urgent. Metal oxides are especially important in such devices, as their favorable charge transport properties and superior stability render them ideal charge transport layers. However, interfacial materials naturally adds another level of complexity to the device, which requires careful characterization and optimization. Here, several studies of metal oxide surfaces will be presented, which using a combination of density functional theory calculations with experimental characterizations aim to understand and improve the oxide interface with perovskites. A variety of topics will be covered, including the reactivity of certain oxide surfaces with perovskite precursors [1], the electronic level alignment at interfaces [2] and the passivation of interfaces with molecular engineering [3]. The atomistic insights obtained from these studies provide important basis for further optimizing the performance of these perovskite devices.

[1] Sofia Aperi, Christine Koch, Geert Brocks, Selina Olthof, and Shuxia Tao, *ACS Appl. Mater. Interfaces* 2022, XXXX, XXX, XXX-XXX

[2] S. Aperi, G. Brocks, S. Tao, *Physical Review Materials*, 4, 085403 (2020)

[3] Jiali Zhang, Renjie Li, Sofia Aperi, Pengyang Wang, Biao Shi, Junke Jiang, Ningyu Ren, Wei Han, Qian Huang, Geert Brocks, Ying Zhao, Shuxia Tao, Xiaodan Zhang, *Solar RRL*, 5, 2100464 (2021)

SESSION EQ05.02: Transparent Electrodes I
Session Chairs: Stefaan De Wolf and Monica Morales-Masis
Monday Afternoon, November 28, 2022
Sheraton, 2nd Floor, Republic B

1:30 PM *EQ05.02.01

Layered Copper Oxychalcogenides for Next Generation P-Type Transparent Conductors Geoffrey Hyett¹, David O. Scanlon², Benjamin A. Williamson³, Zahida Malik¹ and Daniel W. Davies⁴; ¹University of Southampton, United Kingdom; ²University College London, United Kingdom; ³Norwegian University of Science and Technology, Norway; ⁴Imperial College London, United Kingdom

Transparent conducting oxides (TCOs) combine low electrical resistivity with visible light transparency, a combination of properties that have made these materials indispensable to modern technology, being found in the screens of smart phones and portable electronics, in photovoltaic panels and in thermally efficient glazing. However all current commercial TCOs are n-type materials - there are no high mobility p-type transparent conductors (p-TCs) and this is acting as an impediment to many critical technologies. Prior work has identified that layered oxychalcogenides have the potential to fill this p-TCs gap, with the *ZrCuSiAs* structured lanthanum oxychalcogenides, *LaOCuCh* (*Ch* = S, Se and Te), demonstrating band gaps of 2.3 eV to 3.1 eV and reasonably high p-type hole mobility. The key feature of these compounds is the anti-litharge structured copper chalcogenide layer where the *3d* orbitals of the tetrahedral co-ordinated copper(I) hybridise with the chalcogenide orbitals at the top of the valence band to create a highly dispersed band edge. The separation of the copper chalcogenide layer by the lanthanum oxide layer reduces the dimensionality and widens the band gap relative to bulk copper (I) chalcogenides which are not transparent. However although promising, none of the *LaOCuCh* phases combine a sufficiently large band gap with a sufficiently high hole mobility.

In this paper we will report on our work to identify and optimise new p-type transparent conductors through the synthesis of novel layered oxychalcogenide materials which share the same anti-litharge copper layer found in the *LaOCuCh* phases, but with more complex and diverse oxide layers to modulate the structure. We have undertaken a combined computational and synthetic search strategy to investigate structures of the type *A₃B₂O₅Cu₂Ch₂*, *A₄B₂O₆Cu₂Ch₂* and *A₂BO₂Cu₂Ch₂*, where *A* is an alkali or alkaline earth and *B* is a *d*⁰ or *d*¹⁰ closed shell transition or post-transition metal. We abbreviate these to the 325, 426 and 212 structure types. We have taken advantage of the leverage available through computational modelling to consider all the possible combinations of 22 different elements across the *A* and *B* sites in these structures, which after selection for charge order, neutrality and tolerance factor refined down to 150 possible combinations which were then assessed for thermodynamic stability. This greatly accelerated the selection process for synthesis allowing us to identify at least 10 new materials including the following 325 copper sulfides, Ba₃Y₂O₅Cu₂S₂, Ba₃Sc₂O₅Cu₂S₂, Ba₃In₂O₂Cu₂S₂ and Ba₃In₃O₅Cu₂S₂, and copper selenides, Ba₃Sc₂O₅Cu₂Se₂, Ba₃Sc₂O₅Ag₂Se₂ and Ba₃In₂O₅Ag₂Se₂.

These oxychalcogenides and a number of solid solutions between them were synthesized under vacuum using a conventional ceramic synthesis route, at temperatures between 800 °C and 900 °C. Structures were determined by Rietveld refinement of X-ray powder diffraction patterns, and band gaps determined from optical measurements. A comprehensive comparison of experimental and computational results providing the crystallographic and electronic structure of the compounds under investigation has been conducted. We find that the band gaps range from 1.4 eV to 3.3 eV, and that it is possible to band engineer these materials through the selection of different compositions, shifting either the conduction or valence band to control the band gap. We will also report on the transport properties of these compounds, and show that with the diversity of oxide layers available it is possible to control the strain and the geometry in the crucial copper chalcogenide layers, with consequent control of the hole transport properties, and hence their potential as p-type transparent conductors.

2:00 PM EQ05.02.02

Tunneling Junctions on Transparent ITO Electrodes Using Phosphonic Acids for Surface Modification Jane Kardula^{1,2}, Nahid Torabi^{1,2}, Lara Clerici¹ and Ryan Chiechi^{1,3}; ¹Stratingh Institute for Chemistry, Netherlands; ²Zernike Institute for Advanced Materials, Netherlands; ³Department of Chemistry, United States

Since the 1980s, self-assembled monolayers (SAMs) have been used to investigate the electronic properties of molecules in ensemble junctions. They are often formed by contacting a monolayer supported by a planar gold electrode with a conformal metal such as Eutectic Gallium Indium (EGaIn). This material is a non-Newtonian liquid metal alloy, allowing us to form multiple junctions on a single sample in a non-destructive manner. Due to these reasons, replacing the EGaIn electrode for something transparent is not plausible, so instead we target the planar electrode. Suitable candidates for this are transparent conducting oxides (TCOs). We opted for Indium Tin Oxide (ITO) as it is well known, well studied and important in the field of solar cells and diodes.

We formed monolayers of alkyl phosphonates with varying chain lengths and measured the current-voltage characteristics and observed two different regimes of tunneling decay and possibly two regimes of odd-even effect in the monolayers.

2:15 PM EQ05.02.03

Photonic Curing of Hybrid Transparent Electrodes for High-Throughput Solar Cell Manufacturing Robert Piper, Justin Bonner, Weijie Xu and Julia W. Hsu; University of Texas at Dallas, United States

Realizing high-throughput, low-cost perovskite solar cell (PSC) manufacturing is highly sought-after in photovoltaic (PV) research in recent years. To fully achieve roll-to-roll (R2R) manufacturing of PSCs, it is important to consider the flexible transparent electrode (TE). PET/ITO is a commonly used substrate for making flexible PSCs. When optimizing transparent conducting materials, there is a tradeoff between sheet resistance (*R_{sh}*) and optical transparency. Because commercial PET/ITO substrates are made with slow (~ 1 m/min) vacuum deposition processes, they tend to be expensive. Therefore, it would be advantageous to develop a high-throughput, R2R compatible, solution-deposition approach for fabricating the TE on PET substrates. While various solution-deposition processes, such as blade coating or slot-die coating, can achieve the desired web speed of > 10 m/min, there is still a need to improve the post-deposition annealing step. One promising post-deposition processing technique is intense-pulsed-light processing, also known as photonic curing. Photonic curing delivers short (0.01 – 100 ms) pulses of broadband (200 – 1500 nm) light from a xenon flash lamp to the samples. Any materials in the sample stack that absorb light will convert the impinging light pulse into heat within the sample, which drives changes in the sample (calcination, phase change, crystallization, etc.). Photonic curing has three main advantages over thermal annealing: 1. Faster processing speed (milliseconds or seconds). 2. Compatibility with plastic substrates. 3. Smaller physical footprint and less wasted energy. Since the light pulses are on for a short time, the intensity can be high while the total energy delivered to the sample is low, minimizing damage to the plastic substrates.

In this work, a hybrid TE material is fabricated on PET substrates using photonic curing. The hybrid TE material contains a layer of silver nanowires (AgNWs) and a layer of metal-oxide (InO_x, ITO, IZO, etc.). The AgNWs increase the light absorbed by the film during the photonic curing process, which leads to higher processing temperatures, possibly improving the conversion of the metal-oxide layer. The AgNWs also enhance the electrical conductivity of the final TE layer after photonic curing. A AgNW and metal-oxide bilayer is formed by spin coating each solution onto the PET substrate sequentially followed by a single photonic curing process. We use average optical transmittance (*T_{avg}*) from 400 to 700 nm and average *R_{sh}* to evaluate the TE performance. The following photonic curing parameters are varied to optimize *T_{avg}* (maximize) and *R_{sh}* (minimize): Pulse voltage, pulse envelope, number of micro-pulses, duty cycle, number of pulses, and pulse repetition rate. Preliminarily, we also observe a significant impact on the TE properties by the

volume of AgNW deposited during the spin coating deposition step. Using dispense volumes of 80 μL and 20 μL , we achieve samples with $T_{\text{avg}} = 73\%$, $R_{\text{sh}} = 19 \Omega/\text{sq}$, and roughness = 9 nm, and $T_{\text{avg}} = 83\%$, $R_{\text{sh}} = 58 \Omega/\text{sq}$, and roughness = 5.6 nm, respectively, after photonic curing.

This material is based upon work supported by the U.S. Department of Energy's Office of Energy Efficiency and Renewable Energy (EERE) under the Solar Energy Technologies Office Award Number DE-EE0009518.

2:30 PM EQ05.02.04

Computational Prediction and Experimental Realisation of Earth Abundant Transparent Conducting Oxide Ga-Doped ZnSb_2O_6 with Unique Band Alignment Joe Willis^{1,2,3}, Adam J. Jackson⁴, Alex M. Ganose⁵, Anna Regoutz^{1,3}, Tim D. Veal⁶, Robert Palgrave¹ and David O. Scanlon^{1,2}; ¹University College London, United Kingdom; ²Thomas Young Centre, United Kingdom; ³Diamond Light Source, United Kingdom; ⁴Science and Technology Facilities Council, United Kingdom; ⁵Imperial College London, United Kingdom; ⁶University of Liverpool, United Kingdom

Transparent conducting oxides have become ubiquitous in modern opto-electronics, yet the number of materials used for transparent conducting applications is limited to a handful of systems that have been known for the last forty years. Subsequently, one is limited by the work-function of these available post-transition metal oxides when building opto-electronic devices. Therefore, it is desirable to discover new transparent conductors with unique band alignments to bring much needed diversity to the field.

In this work, we use hybrid density functional theory and defect chemistry analysis to demonstrate that tri-rutile zinc antimonate, ZnSb_2O_6 , is an ideal transparent conducting oxide, and identify gallium as the optimal dopant to yield high conductivity and transparency.^[1] To validate our computational predictions, we have synthesised both powder samples and single crystals of Ga-doped ZnSb_2O_6 which conclusively show behaviour consistent with a degenerately doped transparent conductor. The calculated electron affinity is the largest of all known transparent conductors, which could improve contact efficiency in a range of opto-electronic devices and has tremendous implications for organic photovoltaics.^[2]

[1] Willis, J. et al, *chemrxiv*, 2022, <https://doi.org/10.26434/chemrxiv-2022-mz5dc>

[2] Ganose, A. M. and Scanlon, D. O., *J. Mater. Chem. C*, 2016, **4**, 1467

2:45 PM EQ05.02.05

Nanostructured $\alpha\text{-Fe}_2\text{O}_3$ Photoelectrodes with Transparent and Conducting Sb-Doped SnO_2 Films by Atomic Layer Deposition Eunsoo Kim^{1,1}, Hyunwoo Yang^{1,2}, Seongrok Seo^{1,3}, Jong Hyeok Park⁴ and Hyunjung Shin^{1,1}; ¹Sungkyunkwan University, Korea (the Republic of); ²North Carolina State University, United States; ³University of Oxford, United Kingdom; ⁴Yonsei University, Korea (the Republic of)

Wide band gap metal oxides, with incorporation of specific dopants, can take on quite moderate electric conductivity while retaining its intrinsic transparency. This seemingly impossible material property has been one of the essential foundations of modern optoelectronic devices. The fabrication of this layer, so called transparent conducting oxide (TCO), has been mostly done by physical vapor deposition techniques such as sputtering or electron beam evaporation. However, emerging devices with complicated structures requires better step coverages for the geometry with high aspect ratio holes and/or trenches. To meet the requirements, we suggest atomic layer deposition of antimony-doped tin oxide (ATO). By alternatively depositing SnO_x and SbO_x layers as matrix and dopant layers, respectively, we could freely control the dopant concentration in a desired level. The as-deposited films didn't show good conducting properties, but after post-annealing process at 550 $^\circ\text{C}$, the resistivity of the films decreased to $\sim 5 \times 10^{-3} \Omega \text{ cm}$. All the films with different dopant concentrations showed crystalline rutile phase without any suspicious antimony oxide peaks, even up to 20% antimony incorporation, implying that SnO_2 serves well as a matrix for antimony dopant. The composition of the annealed films, with different antimony sub-cycle ratio in ALD super-cycle, were investigated by subsequent XPS analysis. Also, the plasmonic loss features in Sn 3d peaks showed indirect evidence of the existence of extrinsic free carriers. From the Hall effect measurements, we found that the increased antimony content results in the decrease of mobility with the increased carrier concentration. This trade-off ends up with the optimum dopant concentration of 5%. 36 nm thick ATO nanotube array as a demonstration of nanostructured transparent electrode was successfully fabricated and investigated by conductive atomic force microscopy (CAFM), showing ohmic behavior with Ti contact. This nanostructured transparent electrode was adopted for hematite-based photoanode, which consists of ultrathin ($\sim 4 \text{ nm}$) $\alpha\text{-Fe}_2\text{O}_3$ (deposited also by ALD) as an photo-absorbing layer covering 5 μm -long ATO nanotubes' array. The photoanode showed a photocurrent of $\sim 1 \text{ mA/cm}^2$ (@1.23V vs RHE) without any co-catalyst layer. The control samples without ATO conducting layers showed almost no photocurrent, implying that the poor carrier transport ability of intrinsic hematite layer is successfully complemented by the conducting ATO layers.

3:00 PM BREAK

SESSION EQ05.03 Molecular Materials and Devices

Session Chairs: Geoffroy Hautier and Barry Rand

Monday Afternoon, November 28, 2022

Sheraton, 2nd Floor, Republic B

3:30 PM *EQ05.03.01

Novel Charge Transport Materials for Improved Efficiency and Stability of Ultraflexible Organic Solar Cells Kenjiro Fukuda¹, Sixing Xiong², Jiahen Wang^{2,1} and Takao Someya^{2,1}; ¹RIKEN, Japan; ²The University of Tokyo, Japan

Organic photovoltaics, as one of the emerging PVs, has a unique feature of high flexibility by using flexible polymer substrates. By using a substrate and a passivation film with ultimate thinness, ultra-flexible energy harvesting devices can supply powers to wearable sensors on skin or textiles without causing discomfort to wearers [1,2]. The usage of such ultra-thin polymer film typically sacrifices gas barrier properties, and mechanical stresses with small bending radii cause new problems such as delamination at the interface. In this talk, we'll discuss novel charge transport materials to achieve both high efficiency and reliability of ultrathin organic solar cells. The topics will include an organic-inorganic hybrid electron transport layers (ETL) enabling much improved mechanical robustness than a conventional oxide ETL [3], suppression of diffusion of ETL materials after a thermal aging process to enhance the stability of OPVs with non-fullerene active layers [4], and usage of liquid metals as solution-processed top cathodes enabling high-performance fully-solution processed organic photovoltaics [5]. In addition to the performance improvement of organic photovoltaic cells, we'll show a lamination strategy of the ultra-thin organic photovoltaics to a complex curved surface [6].

[1] S. Park et al., *Nature* 561, 516-521 (2018). [2] H. Jinno et al., *Nat. Commun.* 12, 2234 (2021). [3] F. Qin, *Nat. Commun.* 11, 4508 (2020). [4] S. Xiong, *Adv. Sci.* 9, 2105288 (2022). [5] J. Wang, *ACS Appl. Mater. Interfaces*, 14, 14165-14173 (2022). [6] R. Steven, *Adv. Mater.* 34, 2106683 (2022).

4:00 PM EQ05.03.02

Dielectric Surface-Dependent Photogating Phenomenon and Interface Trap Engineering in C8-BTBT Leading to Photo-Induced Synaptic Applications Somi Kim¹, Jihyun Shin¹, Byung Chul Jang² and Hocheon Yoo¹; ¹Gachon University, Korea (the Republic of); ²Kyungpook National University, Korea (the Republic of)

Organic phototransistors (OPTs) are being adopted in considerable research field due to their excellent photo-sensing capabilities, high compatibility with flexible substrates, and simple manufacturing processes. To improve the photoresponsive characteristics, previous OPTs studies have focused on the development of organic semiconductor layers. Exploring a suitable dielectric surface, however, is also an important factor in controlling these photoresponsive properties in OPTs. Nonetheless, research on dielectrics is still lacking. In this talk, we present the dielectric-surface-dependent photogating behavior of 2,7-Dioctyl[1]benzothieno[3,2-b][1]benzothiophene (C8-BTBT) phototransistors. Photogating effect was observed depending on the trap states between C8-BTBT and various dielectric interfaces: cyclic transparent optical polymer (CYTOP), poly(methyl methacrylate) (PMMA), aluminum oxide (Al₂O₃), and silicon dioxide (SiO₂). The photogating effect was not observed in hydrophobic dielectric-based OPTs (CYTOP-based OPTs and PMMA-based OPTs), while the photogating effect was observed in hydrophilic dielectric-based OPTs (Al₂O₃-based OPTs and SiO₂-based OPTs), achieving high sensitivity of $>7.34 \times 10^5 \text{ A A}^{-1}$, detectivity of $>6.32 \times 10^{11}$ Jones, and 20 V shift of turn-on voltage under 400 nm light irradiation. The operation principle of photogating effect was elucidated through a comprehensive study, including an analysis of roughness, morphological investigation, hydroxyl group, and surface energy, according to the dielectric surface. Al₂O₃- and SiO₂-based OPTs have more hydroxyl group than CYTOP- and PMMA-based OPTs, resulting in relatively high surface energies and interfacial trap density of states (N_{it}) values. Through the nearly identical surface roughness (Ra) values for each dielectric by AFM analysis, we demonstrated that the photogating effect is dependent on the interfacial charge trap state by the surface energy, not because of the specific morphological variation between each dielectric surface and semiconductor interface. In addition, we implemented an artificial synapses application using the photogating effect. Optoelectronic artificial synaptic operation using SiO₂-based OPTs accomplishes a recognition rate of more than 95%, whereas, despite the same semiconductor, CYTOP-based OPTs accomplish a recognition rate of 0%. As a result, this research suggests that optimizing the dielectric layer surface characteristics is an important component in modulating photoresponsive properties, and through the implementation of artificial synapses, the possibility of applying optoelectronic devices.

4:15 PM EQ05.03.03

Spectrum Profile Simulation of OLED Materials by Time Dependent Density Functional Theory Nobuhiko Akino; Hosei University, Japan

For the design of emissive materials in organic light emitting diodes, it is highly desired to simulate the spectrum profile, that is, not only the peak wavelength of absorption and/or emission, but also its overall spectrum shape. Especially the emission profile is one of the most important material properties as it determines not only the emission color, but also the device efficiency. For example, the material with sharp spectral profile is essential to achieve a better color gamut and also to avoid any loss by the energy filter for the display applications.

In order to study the spectrum profile of materials, the time dependent density functional theory (TDDFT) has been employed [1]. This is one of the most prominent and widely used methods for calculating excited states of medium-to-large molecules, and it is recognized as a powerful tool for studying electronic transition of molecules. The TDDFT code used in this study is based on the real-space and real-time formalism [2]. One of the advantages of this real-space and real-time formalism is that one can keep the code simple and understand physical meanings as directly as possible. Since this formalism is suitable for large-scale parallel computing, we have been developing its MPI parallelized code which can be applied to large molecules depending on the computer resources.

This approach has so far been applied to some typical organic materials such as poly-(9,9'-dialkyl-fluorene) as a fluorescent material [3], tri(2-phenylpyridinato)iridium(III), Ir(ppy)₃, as a phosphorescent material [4], and 4CzIPN [5] and DABNA-1 [6] as a thermally activated delayed fluorescent (TADF) materials. The results have been suggesting that although some redshift of the peak wavelength is observed, the simulated spectral profiles agree very well with the experimentally observed profiles [7,8].

In the presentation, some TADF molecules will be studied in order to obtain design rules and possibly new molecules with desired spectrum profile.

REFERENCES

- [1] E. Runge and E. K. U. Gross, *Phys. Rev. Lett.* **52**, 997 (1984)
- [2] K. Yabana and G. F. Bertsch, *Phys. Rev.* **B54**, 4484 (1996)
- [3] M. Bernius, M. Inbasekaran, J. O'Brien, and W. Wu, *Adv. Mater.* **12**, 1737 (2000)
- [4] M. A. Baldo, D. F. O'Brien, Y. You, A. Shoustikov, S. Sibley, M. E. Thompson, and S. R. Forrest, *Nature* **395**, 151 (1998)
- [5] C. Adachi, *Jpn. J. Appl. Phys.* **53**, 060101 (2014)
- [6] T. Hatakeyama, K. Shiren, K. Nakajima, S. Nomura, S. Nakatsuka, K. Kinoshita, J. Ni, Y. Ono, and T. Ikuta, *Adv. Mater.* **28**, 2777(2016)
- [7] N. Akino and Y. Zempo, *J. Phys.: Conf. Ser.* **2207** 012039 (2022)
- [8] N. Akino, *MRS Advances* **7**, 310(2022)

4:30 PM EQ05.03.04

Improved Charge Injection of Silver Back Electrodes in Inverted Organic Electronic Devices Using Self-Assembled Monolayers Sneha Sreekumar, Deirdre M. O'Carroll, Marzieh Hydari, Elena Galoppini, Zhongkai Cheng, Hemant Maddali and Krystal House; Rutgers University, United States

OLEDs tend to suffer from low light extraction efficiency when fabricated through conventional methods, in which the devices are built on top of indium-tin oxide on glass. We have developed an inverted method of device fabrication where the device is built on top of the metal electrode, which enables direct patterning of the metal for improved light extraction. However, this method introduces an electronic problem - the creation of a Schottky barrier, where the charge injection at the metal-polymer interface is dependant on the energy difference between the workfunction of the metal and the frontier orbital energy levels of the organic semiconductor. Self-assembled monolayers (SAMs) formed from thiol compounds on metals like Ag and Au electrodes have been used as an important strategy for altering the electronic properties of metal-organic interfaces in organic electronic devices. In this work, we make use of dithiolane compounds that can provide multiple binding sites to the metal, unlike thiol compounds, and, hence, are useful in enhancing the electronic performance of the device. We have fabricated inverted organic semiconducting hole-only devices using Ag back electrodes along with SAMs formed from disulfide lipoic acid-based compounds, in addition to SAMs of a more common long aliphatic chain thiol. Hole-only devices were fabricated on top of the SAM/Ag back electrodes using the organic conjugated polymer F8BT (poly(9,9-dioctylfluorene-alt-benzothiadiazole)) as the semiconducting layer and MoO₃/Au as the top contact layer. Using ultraviolet photoelectron spectroscopy and by conducting current density-voltage tests, it was found that the SAMs formed from (±)-α-lipoic acid(α-LA), iso-lipoic acid(i-LA) and (±)-4-phenylbutyl 5-(1,2-dithiolan-3-yl)(PhBuL) pentanoate improved charge injection by either changing the work function of the Ag or altering the physical interaction between the polymer and the metal surface. We found an increase in the current density of the device of 40-50% in the case of α-LA/Ag and i-LA/Ag compared to bare Ag electrodes. We also employed infrared reflective-absorption spectroscopy to further understand the interaction of the SAMs with the conjugated polymer by comparing SAM/Ag and F8BT/SAM/Ag, and found i-LA and α-LA interacts differently with F8BT because i-LA is oriented more out-of-plane compared to α-LA. On depositing F8BT on α-LA/Ag and i-LA/Ag samples, the orientations of both SAMs are altered, indicating intermolecular interactions are occurring between the SAM

and the polymer. This study has led to an understanding of how the nature of the functional groups of the SAM as well as the number of bonds formed between each SAM molecule and the metal electrode influence the performance of organic semiconductor devices. These results are being further extended to OLED device structures in which we optically engineer the Ag back electrode to include Ag metasurfaces for increased light extraction.

SESSION EQ05.04: Poster Session
Session Chairs: Stefaan De Wolf, Geoffroy Hautier, Monica Morales-Masis and Barry Rand
Monday Afternoon, November 28, 2022
8:00 PM - 10:00 PM
Hynes, Level 1, Hall A

EQ05.04.01

Low-Temperature Fabrication of BaSnO₃ Thin-Films via Solution Combustion [Sushobhita Chawla](#)¹, Garima Aggarwal², Akhilender J. Singh¹ and Balasubramaniam Kavaipatti¹; ¹Indian Institute of Technology Bombay, India; ²Uppsala University, Sweden

We have extended the solution combustion technique used to synthesize La:BaSnO₃ nanoparticles [1, 2] to develop solution-processed thin films at 130 °C. A colloidal ink of a peroxy/superoxy precursor was spin-coated onto a quartz substrate and yielded ~ 100 nm thick, highly crystalline BaSnO₃ films on annealing at 130 °C. This technique allows for facile incorporation of dopants, like La, in the precursor film itself, thereby leading to the synthesis of La:BaSnO₃ at such a low temperature. The structure, morphology, optical and electrical properties of the undoped and La-doped thin films have been determined using X-ray diffraction, scanning electron microscopy, UV-Vis spectroscopy and AC Hall measurements. The obtained films show a transmittance of around 70-80 % in the visible range (400–800 nm). In comparison to the insulating BaSnO₃, the lanthanum doped films obtained at 130 °C are conducting. The procedure developed can be utilised to directly employ BaSnO₃ films in devices having temperature limitations.

[1] Chawla, S., Aggarwal, G., Kumar, A., Singh, A.J. and Kavaipatti, B., "Alcohol Assisted Solution-Combustion Technique for the Synthesis of Phase-Pure BaSnO₃ Nanoparticles at 130 °C", ChemRxiv, 2021.

[2] Chawla, S., Aggarwal, G., Kumar, A., and Kavaipatti, B., "Novel Solution-Combustion Technique for the synthesis of impurity-free BaSnO₃ nanoparticles at 130 °C", *EQ17: Emerging materials for Contacts and Interfaces in Optoelectronics*, MRS Fall 2021, Boston, Massachusetts, USA.

EQ05.04.02

Near-Infrared Phototransistor Using Localized Surface Plasmonic Resonance at ITO Nanoparticle/IGZO Interfaces [Jusung Chung](#), Jong Hyuk Ahn, Jong Bin An and Hyun Jae Kim; Yonsei University, Korea (the Republic of)

Recently, photodetectors sensitive to infrared (IR) light are highly desirable for optoelectronic applications such as telecommunications, imaging sensors, remote sensing, and motion detectors. Enhancing the sensitivity, decreasing the price, and minimizing the power consumption are anticipated to be the primary factors in expanding the market for IR photo-detectors and broadening their applications. Oxide semiconductor materials are the promising candidate for channel material of IR photodetector because of their low dark current, low fabrication cost, and capability. However, most oxide semiconductor materials cannot absorb long wavelength visible light and IR because of their large optical bandgap (above 3.0 eV) so that additional light absorbing layer is essential for detecting IR.

In this paper, we suggested indium-tin-oxide (ITO) nanoparticles for near-IR (NIR) absorption layer for indium-gallium-zinc oxide (IGZO) NIR phototransistor. We deposited ITO nanoparticles using electrohydrodynamic (EHD) printing for selective area deposition minimizing contact with source and drain electrode. Nanoparticle was used for optoelectronic device to enhance photoelectric efficiency using localized surface plasmon resonance (LSPR) which is sensitive to their carrier concentration. Metal nanoparticles exhibit extremely intense narrow absorptions in the lower visible wavelength region due to their relatively high carrier concentrations. ITO has lower carrier concentrations than noble metals, resulting in lower plasma frequencies and resonances in the near-infrared spectrum. ITO has wider absorptions than noble metals due to the greater optical losses. When ITO nanoparticles and IGZO interfaces of phototransistor was illuminated under NIR, LSPR and hot electron injection were occurred. IGZO channel layer effectively captured the photoexcited hot electrons and photo current increased.

We compared electrical characteristics of ITO nanoparticle/IGZO NIR phototransistor according to the deposition method, spin coating and EHD printing. ITO nanoparticle/IGZO NIR phototransistor fabricated by spin coating shows high off current because of contacts between ITO nanoparticle and source and drain electrode. In case of EHD printing, ITO nanoparticle was deposited selectively area without electrode contact resulting in superior switching characteristics with 3.67 cm²/V s of saturation mobility, 1.80 x 10⁷ of on/off current ratio, and 0.82 V/decade of subthreshold swing. Changes in transfer characteristics according to various wavelengths corresponding to infrared (808, 940, 1342, and 1450 nm) with 190 mW/mm² of light intensity were compared to show the light-sensing range of the ITO nanoparticle/IGZO NIR phototransistor. Turn on voltage of ITO nanoparticle/IGZO NIR phototransistor is hardly shifted under the infrared light with wavelength of 940, 1342, and 1450 nm. In case of 808 nm, turn on voltage is negatively shifted from 13 to 11V, which show LSPR occurrence by 808 nm NIR. Next, the change of the transfer characteristics according to the light power density (190, 380, 570, and 760 mW/mm²) with wavelength of 808 nm was measured and each optoelectronic parameters calculated from change of transfer characteristics were compared. In the case of photoresponsivity, there wasn't a linear relationship with the light power density and was randomly distributed in a certain range (2.5 ± 0.5 A/W). However, As the light power density increased, the turn on voltage shifted negatively so that the difference between photo current and dark current at a constant gate voltage increase. Consequently, maximum photosensitivity increased from 22 to 6.38 x 10³ as light power density increase from 190 to 760 mW/mm².

EQ05.04.03

Optimization of Lithium Intercalation of Sputtered Indium Tin Oxide Thin Films [Denisse Cordova Carrizales](#), Rain Wang, Ari Turkiewicz, Johanna Nordlander, Charles Brooks and Julia Mundy; Harvard University, United States

Indium tin oxide (ITO) is the most widely used transparent conductor for optoelectronics, liquid crystal displays, photovoltaic cells, and touch screens. Generally, optical transparency and high electrical conductivity are mutually exclusive, but the carrier density in a conductor can be optimized to a low enough level to allow for optical transmission in the visible region—this optimization is a central factor of transparent conductivity and has even allowed the creation of transparent superconductors. Previously, ITO thin films grown on glass have been electrochemically doped with Na, Li, K, Rb, Cs, Mg, or Ca ions to create optically transparent superconductors. In this work, we use n-butyllithium to intercalate Li ions into ITO thin films sputtered on technologically relevant substrates. Using x-ray diffraction, atomic force microscopy, and resistance-temperature measurements, we refine ITO sputtering growth parameters and n-butyllithium intercalation parameters to optimally adjust optical transparency and electrical conductivity in lithium-doped ITO thin films for transparent superconductivity.

EQ05.04.04

Tuning Photoconductivity Properties of Co₃O₄ Thin Films Ana Luiza Costa Silva¹, Ariano Rodrigues¹, Renato Jasinevicius² and Marcio P. de Godoy¹; ¹Federal University of São Carlos, Brazil; ²University of São Paulo, Brazil

The search for new materials for energy conversion has pointed to several promising candidates. However, many of those demonstrate adverse effects such as toxicity and the production of harmful waste – either caused by the material itself or its synthesis processes. Due to its chemical stability, non-toxicity, availability, and optical absorption in the visible range, Co₃O₄ is a strong candidate for clean-related applications in photo-assisted devices. In this study, we investigate the photoconduction behavior of Co₃O₄ semiconductor films grown by the spray pyrolysis technique. An interesting characteristic of Co₃O₄ is its two optical absorption edges: the first one is in the visible range (~ 2.0 eV) and corresponds to Co²⁺ oxidation state; the second one is in the Vis-NIR region (~ 1.5 eV) and corresponds to the Co³⁺ oxidation state. The photoconductivity measurements were performed at room temperature using different wavelengths to tune the absorption edges. Thus, some excitations benefit the charge transfer between O²⁻ – Co²⁺, while other excitations access only the O²⁻ – Co³⁺. Regardless of the excitation energy, the films show a positive photoresponse (PR), with a reduction in PR (up to 73%) for red excitation. Under excitation near the Co³⁺ absorption edge, the as-grown sample shows the absence of a saturation profile in the PR and a persistent PC. Additionally, annealing effects under different atmospheres play a relevant role in the optical and electrical properties of the films. When annealed in an oxidizing atmosphere, long response and recovery times are noted. In contrast, after annealing in Ar or synthetic air, fast responses are observed. The annealing inhibits the persistence effects for red excitations. Therefore, we can attribute that the deep levels mitigated by annealing are located between the Co³⁺ subband and the valence band.

EQ05.04.05

Low Dielectric Adhesive through Thiol-Ene Click-Reaction for High-Frequency Electronic Devices Ji Won Joo and Ho Sun Lim; Sookmyung Women's University, Korea (the Republic of)

With the continuous growth of 5G communication-based high-speed transmission-reception systems, there is a demand for developing a low dielectric material in high-frequency electronic devices. Since the 5G communication system uses a shorter wavelength than the 4G mobile communication, there is a problem with transmission loss because the rate of absorption by materials during the movement of radio waves is high. For this reason, electronic components such as FCCL for 5G mobile communication must exhibit a low dielectric character to reduce transmission loss. Herein, we proposed a fabrication of a low dielectric adhesive through a thiol-ene click reaction between bismaleimide and multifunctional thiol, applicable to advanced electronic devices for 5G communication. The development of the adhesive with a low dielectric constant at a high-frequency range is indispensable while maintaining high adhesion between a copper foil and a low dielectric polymer sheet. We optimized the composition of the adhesive by controlling the ratios of the compounds with alkene or thiol groups. The dielectric constant (ϵ') measured at 10 GHz ranged from 2.6 to 2.7, which is lower than commercially available adhesives. The peel strength of the low dielectric bond was measured as 1.0 N/mm through a 90° peel test, showing strong adhesion properties between the copper foil and the low dielectric polymer sheet. This low dielectric adhesive could be applied to manufacturing technology of advanced electronic devices for 5G communication in semiconductors, automobiles, mobile phones, and robots.

EQ05.04.06

Hierarchical Metal–Semiconductor–Graphene Ternary Nanostructures with Intimate Coupling for Hydrogen Generation Hayoon Jung and Sang Woo Han; Korea Advanced Institute of Science and Technology, Korea (the Republic of)

There has been significant interest in heteronanostructures with controlled topologies and configurations for designing efficient photocatalysts. Herein, we present a promising solar energy conversion platform constructed by the intimate contact of graphene, semiconductors (TiO₂), and plasmonic metal nanocrystals (octahedral Au nanocrystals) with well-defined configurations. The complete wrapping of TiO₂ shell around Au nanocrystals and the sequential graphene encapsulation over TiO₂ shell were successfully realized by sol-gel, self-assembly methods, and post-calcination. Through core-shell engineering of the ternary nanostructures, as-prepared graphene-encapsulated octahedral Au nanocrystals@TiO₂ core-shell nanostructures became highly responsive to red light illumination. Accordingly, the ternary nanostructures exhibited superior photocatalytic hydrogen production and photocurrent responses to their binary counterparts, single-component nanomaterials, and physical mixture of the constituents under visible light irradiation ($\lambda > 400$ nm) and even under red light irradiation ($\lambda = 700$ nm). A series of mechanistic studies on photocatalysis indicated that the prominent photocatalytic activity of the hybrid nanostructures is attributed to the hot electron transfer from Au nanocrystals and the subsequent injection of the photogenerated electron to graphene, facilitated through the intimate contact among the constituents. This study can provide new insights in designing heteronanostructures for visible and red light responsive photocatalysis.

EQ05.04.07

Room-Temperature Fabrication of Highly-Oriented β -Ga₂O₃ Thin Film on ZnO/AlO_x-Buffered Cyclo-Olefin Polymer Substrate via Excimer Laser Annealing of Amorphous Thin Film Ryoya Kai¹, Tomoaki Oga¹, Satoru Kaneko^{2,1}, Akifumi Matsuda¹ and Mamoru Yoshimoto¹; ¹Tokyo Institute of Technology, Japan; ²Kanagawa Institute of Industrial Science and Technology, Japan

β -form gallium oxides (β -Ga₂O₃) having ultra-wide bandgap ($E_g \sim 5$ eV) attract much attention in the field of optoelectronic applications such as deep-UV sensor and power-electronics [1]. The combination of polymer substrates and oxide thin films such as transparent conductive oxide (TCO) and Ga₂O₃ has been expected to develop the flexible electric devices with features of wearability and lightness. So far, highly oriented crystalline β -Ga₂O₃ thin films have been prepared mostly on the single crystal substrates such as sapphire (α -Al₂O₃) or Si at relatively high temperatures ($\sim 500^\circ\text{C}$). On the other hand, in case of film-growth on polymer substrates, it is necessary to lower deposition temperatures because of low thermal stability of polymers. Excimer laser annealing (ELA) applied in this study have been widely used as a low-temperature crystallization process of polycrystalline silicon for thin-film transistors (TFT's) [2]. Previously, we have developed epitaxial β -Ga₂O₃ thin films on sapphire substrates at room temperature ($\sim 20^\circ\text{C}$) by ELA [3]. In this study, ELA process has been successfully applied to room-temperature fabrication of highly-oriented β -Ga₂O₃ thin films on [c-axis oriented ZnO/amorphous AlO_x] buffered cyclo-olefin polymer (COP) substrates. The structure and properties of the films were characterized via XRD, RHEED and cathode-luminescence spectroscopy.

COP substrates (Zeonor ZF-16, ZEON Co., Japan) with 10×10 mm, thickness of ~ 188 μm and $T_g \sim 163^\circ\text{C}$ were firstly irradiated in air with vacuum-ultraviolet (VUV) light (172nm) to make the surface clean, flat and hydrophilic before the thin film growth. Thin films were deposited on VUV-irradiated COP substrates by pulsed laser deposition (PLD) technique at room temperature using a focused KrF excimer laser beam ($\lambda = 248$ nm, $E \sim 1.2$ J/cm²). Three kinds of multilayered thin film comprising amorphous aluminum oxide (AlO_x), c-axis oriented crystalline ZnO and amorphous GaO_x were sequentially deposited on COP like GaO_x(~ 100 nm)/ZnO(~ 50 nm)/AlO_x(~ 1 μm)/COP [4]. The thin films were subsequently subject to irradiation of non-focused KrF excimer laser beam ($E \sim 0.15$ J/cm²) from the film surface with 300 pulses at room temperature in air. The XRD and RHEED results indicate that solid state crystallization of uniaxial-oriented β -Ga₂O₃ (-201) thin films occurred on the COP substrate, although crystallization of GaO_x thin films after ELA was not observed in case of GaO_x/ZnO//COP and GaO_x/AlO_x//COP thin films. Atomic-scale interface analysis of film/substrate and Ga₂O₃ layer/ZnO layer via high-resolution cross-sectional TEM observation is also to be presented.

- [1] F.-P. Yu et al., *Opt. Mater. Express*, **5**, 1240 (2015).
 [2] T. Sameshima et al., *IEEE Electron Device Lett.*, **7**, 276 (1986).
 [3] D. Shiojiri et al., *Appl. Phys. Express*, **9**, 105502 (2016).
 [4] T. Oga et al., *Jpn. J. Appl. Phys.*, **59**, 128001 (2020).

EQ05.04.08

Electric Conductivity and Structural Modification of Cobalt Oxide Epitaxial Thin Film at Surface by Excimer Vacuum-Ultraviolet Light Irradiation Kenta Kaneko¹, Hiroki Shoji¹, Tomoaki Oga¹, Yuchi Qiao¹, Satoru Kaneko^{2,1}, Mamoru Yoshimoto¹ and Akifumi Matsuda¹; ¹Tokyo Institute of Technology, Japan; ²Kanagawa Institute of Industrial Science and Technology, Japan

Cobalt oxide with rock-salt type (CoO) and spinel type (Co₃O₄) crystal structures are known p-type semiconductors, which have attracted interests because of their thin film device applications in optoelectronics such as hole extracting layer in solar cells, electrochromic layers, and so on [1,2]. The p-type conductivity and crystal phase of cobalt oxide have been modified via controlling chemical states of Co-ions by aliovalent doping such as Li⁺ as well as O₂ partial pressure during the film deposition [3,4]. Meanwhile, UV-ozone treatment has recently been reported as a post-deposition process to control valence of transition-metal oxide semiconductors without doping impurities [5]. Development and understanding structural and conductivity modification technique which does not depend on aliovalent dopants in cobalt oxide thin films would contribute to improve interfacial properties in optoelectronic multilayer devices. Furthermore, our group have been studied on remarkable enhancement of p-type conductivity in nickel oxide thin films by vacuum ultraviolet (VUV) light irradiation. The VUV-light has larger photon energy compared to conventional mercury lamps, which should have impact on controlling the structure and properties due to its high production efficiency of active oxygen species such as ozone O₃ and atomic oxygen O(¹D). In this study, significant variation of conductivity by 4 digits at the surface of cobalt oxide epitaxial thin films was obtained by VUV-light irradiation using a Xe₂* excimer lamp. In addition, the effects of VUV-light irradiation on structure and its correlation with physical properties of cobalt oxide films were also investigated. CoO and Co₃O₄ epitaxial films were phase-selectively deposited on atomically stepped α -Al₂O₃(0001) single crystal substrates by pulsed laser deposition (PLD) technique using a KrF excimer laser (λ =248 nm, d=20ns) and a pure CoO sintered target. The CoO and Co₃O₄ thin films growth took place in O₂ partial pressure of $\sim 1.0 \times 10^{-5}$ Pa and 10⁰ Pa, respectively at low temperatures below 100°C. The cobalt oxide thin films were subsequently introduced to VUV-light treatment procedure using a Xe₂* excimer lamp (λ =172 nm, E~65 mW/cm² at lamp surface) at room temperature in air. The distance between the lamp surface and the films was fixed at 0.5 mm. The resistivity of as-grown CoO epitaxial films measured by four-point probe method was larger than $\sim 1 \times 10^4 \Omega\text{cm}$, although 120 minutes of VUV-light irradiation reduced the value to $\sim 5 \times 10^1 \Omega\text{cm}$ without any dopants. Structural analysis by RHEED observation indicated appearance of a new set of diffraction rods with half spacing due to occurrence of doubly periodic structure near the thin films surface by VUV-light irradiation. Further XRD results confirmed a topotactic phase transition from rock-salt type CoO to spinel type Co₃O₄ while retaining the epitaxial structure. The effect of VUV-light irradiation on the structure and conductivity of cobalt oxide thin films in different oxidation states, the thickness dependence of conductivity and structure, and chemical state analysis of cobalt ions would also be discussed in detail.

- [1] A. E. Shalan et al., *ACS. Apply. Mater. Interfaces*, **8** (2016) 33592-33600.
 [2] W. Estrada et al., *J. Apply. Phys.* **74** (1993) 5835-5841.
 [3] J. van ELP et al., *Phys. Rev. B* **44** (1991) 6090-6103.
 [4] A. Matsuda et al., *Appl. Surf. Sci.* **349** (2015) 78-82.
 [5] G. H. Aydogdu et al., *J. Appl. Phys.* **108** (2010) 113702.

EQ05.04.09

Hetero-Interfaced Anti-Ambipolar Phototransistor Capable of Distinguishing Wavelength Bands of Light Seongjae Kim, Seongin Hong and Hocheon Yoo; Gachon University, Korea (the Republic of)

Phototransistors that convert light signals into electrical signals are being applied to various fields such as optical communication and image sensors [1-2]. The operation mechanisms of phototransistors have usually been described in terms of photoconductive-effect (PC) and photogating-effect (PG). However, detailed studies still lack, such as the change in photocurrent observed as a function of the position of incident light irradiated to the active layer of the phototransistor. In this presentation, we present the result that the photocurrent changes depending on the location of the light irradiated to the active layer of the phototransistor. The highest photocurrent occurs when the irradiated location is the source region. By utilizing the characteristics of the phototransistor based on the location of the incident light, we implemented a hetero-interfaced anti-ambipolar phototransistor (HI-AA phototransistor), where both source and drain electrodes serve as sources for injecting carriers. Therefore, HI-AA phototransistors can expect excellent photoresponse when the incident light is irradiated to the drain electrode as well as the source electrode. As a result, the HI-AA phototransistor composed of channel layers with different bandgaps has a more varied transfer curve than the single-channel phototransistor depending on the wavelength of the incident light and the irradiated position. Therefore, we can distinguish the wavelength band of the incident light through the change in the transfer curve of the proposed HI-AA phototransistor.

References

1. Ferhati, H., and F. Djeflal. "Planar junctionless phototransistor: A potential high-performance and low-cost device for optical-communications." *Optics & Laser Technology* 97 (2017): 29-35.
 2. Lee, Young Tack, et al. "High-performance 2D MoS₂ phototransistor for photo logic gate and image sensor." *ACS Photonics* 5.12 (2018): 4745-4750.

EQ05.04.10

GW-BSE and TDDFT Approaches to the Optical Properties of Organic NIR-II Fluorophores Nguyet N. Pham, Jong S. Park and Seung Geol Lee; Pusan National University, Korea (the Republic of)

Nowadays, organic molecule fluorophores in the second near-infrared window (NIR-II) (1000–1700 nm) have attracted significant attention in life sciences and biomedical applications due to their great resolution and sensitivity. There is a lack of adequate theoretical levels to distribute efficient and accurate estimations of optical and electronic properties of organic NIR-II fluorophores. The standard approach for these calculations previously is time-dependent density functional theory (TDDFT). However, the size and the large excitonic of these compounds are the challenges for computational cost and time. In this work, we used many-body perturbation theory approaches, especially the GW approximation with the Bethe–Salpeter equation (BSE) implemented in Gaussian basis sets based on density functional theory (DFT), to produce the excited state calculations of two NIR molecular fluorophores such as BTC980, and BTC1070, going beyond TDDFT. In this study, we compared TDDFT and GW-BSE calculations through the optical absorption spectra and frontier molecular orbital of these compounds.

Acknowledgments: This work was supported by the Technology Innovation Program (20011133) funded by the Ministry of Trade, Industry & Energy (MOTIE, Korea).

EQ05.04.11

Fabrication of Polymer Dispersed Liquid Crystal Based Switchable Glazing via Vacuum Coupling [Naila Nasir](#), Hyeryeon Hong and Yongho Seo; Sejong University, Korea (the Republic of)

Polymer-dispersed liquid crystals (PDLCs), a significant class of materials have diverse applications in optics and electronics. Highly efficient and systematic buildings can be made utilizing the PDLC based switchable glazing as they exhibit switching behavior from opaque to transparent mode in presence of power supply, thus saving the energy and elucidating the privacy issues. In this work we prepared typical PDLC mixture using commercially prepared polymer NOA 65 and liquid crystals (like C7 and E7). The mixture was transferred on ITO glass using the wire bar coater and the cell was fabricated by coupling the glass in vacuum. No film was used between the glass as in typical roll-to-roll process, thus enhancing the transmittance. Via vacuum coupling, PDLC based switchable glazing can be fabricated on glass substrates instead of plastic polymers which degrade with the passage of time reducing the efficiency. The cells were then cured by irradiating UV light (intensity $\sim 95.4 \text{ mWcm}^{-2}$) leading to polymerization and polymer induced phase separation process. As a result, the liquid crystal forms droplets segregating from polymer matrix. The cells exhibited a switching behavior characterized using oscilloscope and AC voltage driver at different voltages. The transmittance change of $\sim 60\% - 70\%$ was measured with a driving voltage of $60 \sim 70 \text{ V}$. Thus, by using the vacuum coupling process we can fabricate PDLC based switchable glazing on large scale with maximum transmittance and enhanced stability as it is expected a green refurbishing material of the next generation.

EQ05.04.12

Enhancement of Electrochromic Performance of Sputter Grown WO₃ Thin Films [Yong Jun Park](#), Deokyeon Lee and Dong Hun Kim; Department of Materials Science and Engineering, Myongji University, Korea (the Republic of)

Electrochromic devices are expected to improve the quality of human life by being applied to a wide variety of optical devices such as smart windows, automobile head-up displays, sunroofs, and electronic shelf labels. For the electrochromic layers, tungsten oxide (WO₃) thin films have been extensively used due to their advantageous electrochromic performances compared to other electrochromic materials. However, low stability in acid-based electrolytes with low switching speed for coloring/bleaching of WO₃ thin film hinders its entry into the market. Therefore, the guarantee of chemical stability and durability of WO₃ thin films is exigent for practical application to electrochromic devices as well as enhancement of switching speed. In this presentation, we will report two strategies to enhance the electrochromic performance of sputter grown WO₃ thin films. First, we fabricated multilayers of Nb₂O₅/WO₃ thin films with different thicknesses to prevent the structural evolution during electrochemical process improving the cyclic durability. Bilayer thin films provided distinctly enhanced electrochromic performance, higher transmittance modulation, faster coloring and bleaching responses, and higher CE with considerably enhanced long-term cyclic durability than those of a single-layer WO₃ thin films. Second, we incorporated Ag nanoparticles into WO₃ matrix using a composite target. The improved electrical conductivity by incorporating metallic Ag nanoparticles decreased the electrical resistivity compared to that of single WO₃ layer resulting the enhanced electrochromic performances, including charge density, transmittance change, coloration efficiency, and switching speed. This study provides an exciting opportunity for fabrication of devices with enhanced electrochemical properties for application in promising next generation electronic devices.

EQ05.04.13

Interface Engineering for Self-Stratifying Structure of Polymer Blends with Different Surface Energy [Yoojin Rho](#) and Ho Sun Lim; Sookmyung women's university, Korea (the Republic of)

Self-stratifying coatings can realize a complex multi-layered structure through a one-step process. Thus, self-stratification would be an eco-efficient process since it reduces VOC emissions, time of operation, and processing costs. It could become a promising candidate as an eco-friendly coating in various industries such as automobiles and electronic devices. In this work, we have studied a self-stratifying coating system based on an acrylate/epoxy blend. In particular, we systematically characterized the relationship between the interfacial energy difference and the layer separation. Acrylate copolymers with various surface energy were synthesized by conventional free radical polymerization as controlled the content of fluorinated acrylates. The surface energy varied from 42.9 mN/m to 17.9 mN/m according to fluorinated acrylates content. Kinetically, epoxy resin with a high surface energy of 41.4 mN/m and acrylate copolymer with low surface energy was located on the lower and the upper side of the substrate, respectively. The layer separation can be confirmed by the fact that the surface energy of the self-stratified surface was similar to the surface energy of the acrylate copolymer coated surface. In conclusion, homogeneous blends of acrylate and epoxy resins can be successfully stratified when the surface tension difference is greater than 15 mN/m. In addition, self-stratification can solve the dewetting problem of individually coated two-layer substrates with large surface energy differences.

EQ05.04.15

Ohmic Electron Injection by Solution Processed Interlayers [David Trieb](#), Paul Blom and Gert-Jan Wetzelaer; Max Planck Institute for Polymer Research, Germany

Efficient contacts for charge injection and extraction are of paramount importance in organic electronic devices. Here, we show that inserting a thin organic interlayer between the organic semiconductor and the electrode enables the formation of an Ohmic electron contact. This strategy is demonstrated for electron injection into the high mobility n-type organic semiconductor P(NDI2OD-2T), using a 4 nm layer of TPBi as the organic interlayer. The electron injection is evaluated in electron-only devices. Upon inserting the thin organic interlayer, the electron current increases by three orders of magnitude higher compared to an aluminum contact without interlayer. Upon insertion of the interlayer, the electron current becomes space-charge limited, evidencing the formation of an ohmic electron contact. The function of the interlayer is to decouple the electrode from the organic semiconductor electrostatically, whereas direct contact between metal and semiconductor results in a substantial electron-injection barrier, even when using low-work function metals. With the use of a thin organic interlayer, efficient electron injection is achieved with an air-stable aluminum electrode. Furthermore, we also developed a solution-processed method to deposit the thin organic interlayer on top of the semiconductor. With this solution-processing method, electron injection is equally efficient compared to using evaporated interlayers. Finally, to generalize our procedure, we applied it to different organic interlayer materials as well as different organic semiconductors.

EQ05.04.16

Bi-Dopant Redox Ionic Liquids for Transparent Photo-Electrochromic Windows [Jinbo Kim](#), Hwangdong Jang, Byeongwan Kim and Eunyoung Kim; Yonsei University, Korea (the Republic of)

Ionic liquids (ILs) have been widely studied due to their exclusive properties such as stabilities, diversities, modifiability of structure. Recently, ILs containing redox active molecules have been applied in electrochemical energy storage devices such as supercapacitors, batteries, and DSSCs. In this study, we designed the cation structure to explore its effect on the electrochemical property of π -conjugated polymers (CPs) in transparent photo-electrochromic capacitive window (PECW). The potential at electrodes of PECW was precisely controlled, to match the redox reaction and the generated

photo-energy under a light that triggers photocoloration. Capacitance of the PECW was enhanced from bi-dopable system of RILs, which provided p- and n-doping by TFSI and RIL, respectively. The PECW with neutral dye showed high transparency (> 90%) to allow high color contrast (CC > 85%) with a long electrochromic stability. The optimized PECW recorded the high Fig of merit for CC and photocoloration efficiency. The PECW with new RIL provides an integrated model that consists of electrochromic and energy-harvesting layers in one device. Thus the working principle of PECW can be widely applied in energy saving smart windows and multifunctional electrochemical devices.

EQ05.04.17

Effect of Various Hole Transport Layer on the Inverted Quantum Dot Light-Emitting Diodes JunYoung Kim; Gyeongsang National University, Korea (the Republic of)

In this study, we analyzed the hole injection mechanism according to various hole transport layer (HTL) materials and solvents. We compared 3 HTL materials, Poly(9,9-dioctylfluorene-alt-N-(4-sec-butylphenyl)-diphenylamine) (TFB), Poly(9-vinylcarbazole) (PVK), and Poly[bis(4-phenyl) (2,4,6-trimethylphenyl)amine] (PTAA), widely used for HTL. For solvent, Chlorobenzene, P-Xylene, and 1,4-Dioxane were used. We identified which solvent fits each HTL material. In the inverted structure, when each solvent was used on the Quantum Dot(QD), it was confirmed through the solvent washing test that it did not affect the emission layer (EML). As a result of manufacturing the device with the above three materials, it was confirmed that only TFB showed stable luminance. It can be assumed that PVK is caused by too low mobility, and PTAA is caused by high HOMO level compared to Green QD. Since TFB has fast mobility and intermediate HOMO levels between PVK and PTAA, it is considered the most suitable HTL. However, since there is still a large energy barrier between TFB and QD, PVK with a deep HOMO level is thinly placed between TFB and QD to align the energy level. It was confirmed that the device performance was improved. Also, we use PVPy to delay the fast electron injection rate of ZnO as ETL. When the device was manufactured while increasing the thickness to 1.0mg/ml, the leakage current decreased, and the efficiency increased as the thickness increased. Furthermore, the device was manufactured using the various HTLs to evaluate Electroluminescence (EL) characteristics through IVL measurement. In addition, Hole-only Device (HOD) was made to observe the difference in hole conductivity of each HTL material.

EQ05.04.18

Lift-Off Patterning of OLED Active Layer Seunghan Lee¹, Hyobin Ham², Chang Hyeok Lim¹, Hyukmin Kweon³, Do Hwan Kim³, BongSoo Kim² and Moon Sung Kang¹; ¹Sogang University, Korea (the Republic of); ²Ulsan National Institute of Science and Technology (UNIST), Korea (the Republic of); ³Hanyang University, Korea (the Republic of)

Active layer patterning of organic light-emitting diode (OLED) is a key step in achieving full-color display application. Although conventional OLED manufacturing is based on thermal evaporation, solution process-based patterning techniques allows low-cost fabrication of large-area display. In this work, we propose a patterning method for OLED active layer done via a lift-off process. The lift-off process is widely used in conventional semiconductor and display industry, but its applications to OLEDs are limited. This is due to the fundamental issue that process solvents (such as stripper) can dissolve/damage the pre-deposited layer that should be partially lifted-off. In particular, the luminescent small molecules of OLED (such as iridium and platinum complexes) are assembled by weak forces. Herein, we present the use of crosslinkable host and guest organic emitters added with a low-temperature thermal initiator serving as the active layer for OLEDs. The thermally crosslinked active layer shows chemical robustness against subsequent solvent-processes without compromising its luminescence characteristics (indeed we found that the luminescence characteristics are improved upon crosslinking the molecules). More importantly, by initiating the crosslinking reactions below the temperature affecting the chemical/structural properties of photoresist, we can apply the crosslinked active layer to conventional lift-off process to form active layer patterns. Based on this, we successfully fabricate a few microns multicolor patterns with a minimum pattern width of 4um and exceptionally low line-width roughness. We believe that this approach suggests an alternative route to form micrometer-scale patterns of solution processible materials.

EQ05.04.19

Testing Sputter Deposited Zn_{1-x}Mg_xO:Al Conducting Thin Films in LD Structures as p-GaN Ohmic Contacts and Cladding Layers Aleksandra J. Wójcicka¹, Szymon Grzanka^{2,3}, Zsolt Fogarassy⁴, Adel Racz⁴, Erzsébet Dodony⁴, Tatyana Kravchuk⁵, Iryna Levchenko³, Eliana Kaminska³, Piotr Perlin³ and Michal A. Borysiewicz¹; ¹Lukasiewicz Research Network - Institute of Microelectronics and Photonics, Poland; ²TOP-GAN, Poland; ³Institute of High Pressure Physics, Polish Academy of Science, Poland; ⁴Institute for Technical Physics and Material Science, Centre for Energy Research, Hungary; ⁵Technion-Israel Institute of Technology, Israel

Transparent conductive oxides (TCO) are materials that at the same time are transparent and conductive. They can be easily deposited using sputtering deposition and other methods to achieve high quality, low resistivity and high transparency films. One of such materials is indium tin oxide (ITO) that has been applied as standard transparent electrode material in electronic appliances throughout the world. Recently there have been works showing its application potential as top cladding layers in GaN-based laser diode (LD) structures. Due to difficulties in growing thick and highly doped AlGaN top cladding layer by means of epitaxial techniques, sputter deposited ITO was studied as an alternative for the highly doped top layer. Due to the high indium content however, alternatives to ITO are being sought, one of them being aluminium-doped zinc oxide (AZO), or ZnO:Al. This material also has the advantage of bandgap tunability by alloying with Mg, that also influences its refractive index value. Since the appropriate refractive index tuning is crucial for high quality mode confinement in a laser structure, such material is well poised for studies allowing it to replace the AlGaN layer. In this work we study the development of ZnMgO:Al by means of sputter deposition using cosputtering from AZO and Mg sources and a compound ZnO/MgO/Al₂O₃ source with different Mg content. We study the behavior of the films and determine the deposition conditions allowing high quality, monocrystalline film growth on Ga-face p-GaN surfaces, as confirmed by HR-TEM images. We show that the material exhibits ohmic behavior in contact to p-GaN and that its resistivity is low, at $1.5 \times 10^{-3} \Omega \text{cm}$ for the material deposited with no Mg content. When using a source with 15% Mg, the resistivity of the films goes up by a factor of 4 and the Mg content in the films is around 10% with the relation to Zn. Ellipsometric measurements show that the AZO films have a refractive index around 2 for 440 nm that increases to 2.04 for films with 10% Mg. We prepared laser diode test structures and demonstrate here the properties of InGaN laser diodes operating between 420 and 450 nm and study the cladding performance of the films with varying Mg content and deposited by means of both approaches.

This work was supported by the National Centre for Research and Development, Poland, project 'OxyGaN' - M-ERA.NET2/2019/6/2020, by the Hungarian NRDI Fund, grant number 2019-2.1.7-ERA-NET-2020-00002 and by the Israel Ministry of Science, Technology and Space in the frames of the M-era.net Programme.

EQ05.04.22

A Solution Processed Carbon Electrode for High Volume Roll-to-Roll Manufacture of Flexible Perovskite Solar Cells Trystan Watson, David Beynon, Ershad Parvazian, Rahul Patidar, Katherine Hooper and James McGettrick; SPECIFIC, Swansea University, United Kingdom

Recent experiments involving a new carbon electrode demonstrate a true fully roll to roll coated perovskite solar cell via a continuous slot die coating method. All previous reports of roll to roll coated perovskite solar cells have completed the device off-line with an evaporated metal contact. The

application of a wet carbon film continuously and compatibly with an underlying perovskite device stack in a moving web at manufacturing speeds is complex but game-changing. The ability to sequentially deposit all layers of the device stack culminating in a fully working device entirely in-line means that the promise of high volume “liquid in/solar cell out” can be realised.

This multifunctional carbon electrode can be safely deposited on top of a layered solar cell without any deformation or dissolution of the underlying layers. The new contact material overcomes issues of solvent incompatibility, interface incompatibility and narrow rheology and heating process windows.

In this talk we will present the development journey of this new electrode material and the recent successful pilot run of the material. In particular we will show how we formulate a new carbon ink with solvent compatible with the perovskite stack that crucially has suitable boiling point for low temperature, high speed processing coupled with very low toxicity (no work place exposure limit). The solid loading of the ink is optimised for a rheological profile suitable for slot die and we demonstrate the roll to roll slot die coating of the electrode sequentially following the roll to roll coating of the NIP device stack incorporating a low temperature processed p type interlayer. The carbon ink is formulated with solvent system orthogonal with the device stack and with no detrimental action on the perovskite active layer as shown through X-ray diffraction analysis. Electrochemical impedance spectroscopy and steady state photoluminescence analysis reveal that charge transfer at the interface is equivalent to evaporated gold electrodes. Further, the device stack is demonstrated to have no detrimental effect on stability, unencapsulated cells retained 90% of original PCE at atmospheric temperature for 1000 hours and outperform gold electrode cells at elevated temperature.

This work introduces the very first entirely roll to roll devices achieving efficiency matching evaporated gold electrodes. This first fully roll-to-roll coated perovskite prototype promises the possibility of transferring to industrially efficient PV production in the near future.

EQ05.04.23

A Study on Single-Layer Graphene/germanium Interface—Schottky Junction Cesar A. Diaz Mendoza and Fernando Lazaro Freire Junior; Pontificia Universidade Católica do Rio de Janeiro, Brazil

The graphene/semiconductor interface is a building block of advanced electronic devices. Herein, we investigated the interfacial electronic structure of single-layer graphene on germanium substrates from a fundamental perspective. Direct synthesis of single-layer graphene on (100) and (110) faces of Ge was conducted via chemical vapour deposition. The interaction of π electrons of graphene with the Ge substrate was evidence, confirming its electronic coupling with the semiconductor substrate. Moreover, each Ge crystalline orientation obtained relevant features associated with the Schottky contact nature, interface dipoles, band alignment, and energy barrier heights. Such results are essential for new graphene/germanium systems applications, particularly for its integration into the complementary metal-oxide-semiconductor technology.

EQ05.04.24

Self-Powered Near-Infrared Organic Photodiode with Functional Interlayer Yongju Lee, Hyeonjeong Choi, Hyowon Jang, Swarup Biswas and Hyeok Kim; University of Seoul, Korea (the Republic of)

The electromagnetic spectrum consists of ultraviolet (100-400 nm), visible (400-750 nm), and infrared (750-2500 nm) regions, among others. The visible region contains the wavelengths that can be seen by the human eye, and infrared light is outside the red edge of this band when the light emitted from any source or heating element is spectrally dispersed. In the infrared band, the electromagnetic waves with the shortest wavelength are referred to as near-infrared rays (750-1000 nm). An organic photovoltaic capable of generating light in the near-infrared wavelength band was fabricated herein through bandgap matching of the photoactive polymer for sensing in the near-infrared region. In addition, the organic photovoltaic was optimized through a newly synthesized functional intermediate layer; this layer constitutes a hole-transport layer that transfers the holes generated by the photoactive layer to the cathode easily. The material traditionally used for the hole-transport layer is PEDOT:PSS, which has the advantages of excellent heat resistance as well as high electrical conductivity and transparency. However, PEDOT:PSS also has drawbacks, such as cost inefficiency, strong acidity, and high hydrophilicity. We have synthesized a polypyrrole polystyrene sulfonate (PPY:PSS) as a hole-transport material that overcomes these disadvantages and optimized it by adjusting the ratio of PPY to PSS. Next, poly[4,8-bis(5-(2-ethylhexyl)thiophen-2-yl)benzo[1,2-b:4,5-b']dithiophene-2,6-diyl-alt-(4-(2-ethylhexyl)-3-fluorothieno[3,4-b]thiophene)-(2-carboxylate-2-6-diyl)]phenylC70butyric acid methyl ester (PTB7-th:PC₇₀BM) active-layer-based organic photovoltaic was fabricated. Thus, an organic photodiode capable of sensing more effectively in the near-infrared region was developed by inserting the functional interlayer.

EQ05.04.25

Multifunctional Sensing on a Monolithic Optoelectronic Chip Jixiang Jing¹, Hou Yong¹, Kwai Hei Li² and Zhiqin Chu¹; ¹The University of Hong Kong, Hong Kong; ²Southern University of Science and Technology, China

Miniature biosensors which have significant potential in portable applications in various scenarios and designs with features of convenient, reliable, economic, high sensitive, and capable of real-time measurement are highly desirable in nowadays. Herein, we demonstrate a highly refractive index-sensitive sensor based on a micro-scale III-nitride chip that contains a light emitter (LED) and a photodetector (PD). As the LED and PD of the device contains the same InGaN/GaN multi-quantum wells, the PD can directly respond to the emission of the LED. And the flip-chip assembly of the chip enables the exposed sapphire substrate to be in direct contact with external mediums, and the refractive index sensing capability is governed by the change of critical angle and Fresnel reflection at the sapphire/medium interface. Particularly, we demonstrate the monolithic chip exhibits a sensitivity of 7.77 $\mu\text{A}/\text{RIU}$ and a resolution of 6.4×10^{-6} RIU at the LED current of 10 mA. Furthermore, we apply this integrated chip-sensor into detecting different salinity contents, where this sensor shows excellent sensitivity of salinity as 2721.05 nA/(mol/L) (or 465.57 nA/%) and a response time of 0.243 s. In addition, a polymer-based anti-fouling coating on the surface of the sensing chip has been established to significantly improve its long-term stability in mimicked marine water. Additionally, as existing approaches of quantitatively monitoring cellular activities such as fluorescent staining and impedance-based methods are often hindered by their multiple time-consuming preparation steps, sophisticated labeling procedures, and complicated apparatus. Hence, for the first time, we utilize this chip-sensor to quantitatively monitor the progression of different intracellular processes in a label-free manner. As a proof-of-concept demonstration, we explored its applications in 1) cell adhesion dynamics monitoring, 2) drug screening, and 3) cell differentiation studies, highlighting its potential in broad fundamental cell biology studies as well as in clinical applications.

EQ05.04.26

Electrochemiluminescence Devices Exploiting a Floating Electrode Hyeono Yee, Jong Ik Lee, Keonhee Jung, Seunghan Lee, Dong Mok Park and Moon Sung Kang; Sogang University, Korea (the Republic of)

Electrochemiluminescence (ECL) has been recently exploited to form alternative light-emitting devices referred to as electrochemiluminescence devices (ECLDs). The ECL-based light emitting device offers excellent on/off contrast properties due to the self-emissive technology that generates light by itself.

However, ECLDs have two critical issues, low luminance efficiency and short lifetime. Enhancing the luminance can be typically attained by applying a higher voltage, but this, in turn, induces more side reactions and reduces lifetime. Herein, we introduce a novel ECLD structure exploiting a floating electrode, a third electrode in the device without connection to the external power source, placed on top of an ECLD containing two coplanar parallel electrodes. Based on the electric field rearrangement based on the floating electrode, the novel ECLD structure features enlarged emission area (more than 10 times, depending on the geometry of the device), compared to an ECLD in conventional parallel electrode structure. More importantly, the lifetime of the device is extremely increased because excessive current leading to the side reaction and degrades the operational electrodes can be expanded at the formation of additional EDLs near floating electrode.

SESSION EQ05.05: Perovskites II
Session Chairs: Monica Morales-Masis and Barry Rand
Tuesday Morning, November 29, 2022
Sheraton, 2nd Floor, Republic B

8:30 AM *EQ05.05.01

Halide Perovskite Interface Chemistry—Interphases, Redox and Electrochemistry Ross Kerner¹, Moses Kodur², David P. Fenning², Barry P. Rand³, Joseph J. Berry¹ and Kai Zhu¹; ¹National Renewable Energy Laboratory, United States; ²University of California, San Diego, United States; ³Princeton University, United States

Metal halide perovskites have many attractive advantages as semiconductors and optoelectronic materials owing to their rich and unique chemical properties. However, their molecular and ionic constituents readily participate in reduction/oxidation (redox) and Brønsted acid-base reactions in solution as well as the solid-state. Interactions with other materials range from catastrophic to very subtle; the latter are challenging to characterize, yet have significant impacts that ultimately dictate device performance. In this talk, we present several detailed examples of reactivity with oft-assumed compatible materials such as ITO, NiO_x, SnO_x, organic hole transport layers, and noble metals with an emphasis on voltage-induced electrochemical reactions that can destroy performance (corrosion) or result in added functionality (doping). We further describe electrochemical tools to characterize and/or predict chemical compatibility between contact materials and perovskites via methods that are accessible to most research laboratories and industrial entities. The applications of these methods range from accelerating fundamental, mechanistic revelations in the laboratory to providing excellent quality controls built into commercial production lines, and will play a crucial role in enabling technological development and deployment of halide perovskite devices at scale.

9:00 AM *EQ05.05.02

Charge Selective Contacts for Halide Perovskite Semiconductors Philip Schulz^{1,2}; ¹Centre National de la Recherche Scientifique, France; ²Institut Photovoltaïque d'Ile de France (IPVF), France

It has been well documented in previous reports that optoelectronic properties of perovskites can be altered by the substrate (or selective contact) underneath [1], however so far, we do not dispose of any conclusive picture explaining this effect. In the conventional solar cell stack, a thin perovskite layer is usually buried between charge selective layers, making it very challenging to probe its properties. Here, we fabricated a functional lateral heterojunction device, which consists of a substrate with two laterally arranged selective contacts (TiO_x as an electron transport layer and NiO_x as a hole transport layer), onto which a continuous methyl ammonium lead iodide (MAPbI₃) perovskite layer is deposited. Taking advantage of now exposed perovskite surface, we used a series of surface sensitive techniques and advanced optical characterisation techniques, such as ultraviolet and X-ray photoemission spectroscopy (UPS/XPS), X-ray absorption spectroscopy, Kelvin probe force microscopy, and hyperspectral imaging, to measure how substrate selectivity is affecting the optoelectronic properties of the perovskite. We find evidence suggesting that the contact selectivity is inducing a carrier concentration gradient in the perovskite layer across the junction connected to the functionality of the lateral device. Furthermore, we are able to show, that by varying selectivity of the contacts through different oxidation levels we can alter the magnitude of this gradient, which in turn influences built in potential within the sample and hence the device performance [2]. This study provides a baseline for tailoring the selectivity of the contact materials for enhancing performance of perovskite solar cells and opening an avenue for new device architectures including buried cells terminals [3].

Références

1. P. Schulz, L.L. Whittaker-Brooks, B. A. MacLeod, D. C. Olson, Y.-L. Loo, A. Kahn, A. Adv. Mater. Interfaces **2015**, 2, 1400532
2. S. Dunfield, A. Bojar, et al., *Cell Rep. Phys. Sci.* **2021**, 2, 100520
3. D. Regalado, A. Bojar, et al., *Prog. Photovolt.: Res. Appl.* **2021** <https://doi.org/10.1002/pip.3529>

9:30 AM EQ05.05.03

Interfacial Energetics in Organic and Hybrid Solar Cells—Low-Light, Oxides, Light-Soaking and More! Joel Luke¹, Tianhao Lan¹, Charlie Henderson¹, Yi-Chun Chin¹, Luiza Correa², Matyas Daboczi¹, Izabela Bicalho², Heejoo Kim³, Kwanghee Lee³, Diego Bagnis² and Ji-Seon Kim¹; ¹Imperial College London, United Kingdom; ²Oninn, Brazil; ³GIST, Korea (the Republic of)

Interfacial energetics play a key role in defining the operation and performance of organic and perovskite photovoltaics. Of particular importance is the interface between the photoactive layer (PAL) and the hole transport or electron transport layers (HTL and ETLs). This interface affects charge extraction, and influences charge recombination mechanisms in devices. Understanding and optimising these interfaces is therefore of prime importance to improving device efficiencies and achieving market realisation. Here we present several examples of how interfacial energetics affect device performance and determine the slow processes observed in these devices under illumination (i.e. light-soaking effects).

Organic photovoltaics (OPVs), now exceed 18% power conversion efficiency at 1 sun illumination. However, efficiencies still lag behind Si and perovskite solar cells which limits the potential market for OPVs. One promising route to market for OPVs is for targeted low-light and indoor applications where illuminance is orders of magnitude smaller than 1 sun. Under low-light OPVs perform significantly better than silicon solar cells. However, devices considered in the literature so far employ materials or fabrication methods which are not suitable for large scale-up.

We demonstrate the commercial viability of OPVs for low-light applications by utilizing a fully scalable device architecture with upscalable OPV materials. We show superior device performance to silicon and discuss important optimisation parameters. Critically, we identify and characterise a critical light-soaking (LS) effect that is ruinous for low-light performance. Using surface photovoltage (SPV) and energetics measurements we find that this LS effect results from poor electron extraction at the electron transport layer (ETL)/photoactive layer interface due to high density of mid-gap states in the ZnO ETL and poor energetic alignment. We effectively remove this LS effect by employing SnO₂ nanoparticles as ETL, which we then use to demonstrate scale-up potential by fabricating a 21.6 cm² module (1).

We further investigate the properties of the ETL and look at controlling the LS effect by controlling the properties of ZnO. Here we characterise this oxide and compare it to other oxides using wavelength and atmosphere dependent SPV measurements to develop our understanding of these oxide interlayers and their role in device performance.

Additionally, we apply energetics measurements to perovskite solar cells, to understand how the interface between interlayers and perovskite affects device performance (2,3). Perovskite solar cells are also an exciting PV technology due to rapid improvements in power conversion efficiencies, now exceeding 25%. To further improve performance, it is necessary to improve V_{OC} which is sensitive to the choice of interlayer and the recombination processes at the interface.

Here, we look at a range of interlayers, and control their properties e.g. the doping level, or energetics, to modulate the interface with the perovskite. Doing so we are able to pinpoint an interlayer dependent light-soaking effect in large-area blade-coated perovskite cells, and suggest how to avoid this. We also investigate the energetics of an integrated organic/perovskite solar cell, demonstrating the loss mechanisms involved at the different interfaces, and how these affect device performance.

In summary, this presentation will highlight the importance of understanding the energetics and interfaces in a range of optoelectronic devices, and also the key role of SPV measurements to achieve this.

(1) J. Luke, L. Corrêa, J. Rodrigues, J. Martins, M. Daboczi, D. Bagnis, J. S. Kim, *Adv. Energy Mater.* 2021, 2003405.

(2) Y. C. Chin, M. Daboczi, C. Henderson, J. Luke, J. S. Kim, *ACS Energy Lett.*, 2022 7 (2), 560-568

(3) M. Daboczi, I. Hamilton, S. Xu, J. Luke, S. Limbu, J. Lee, M. A. McLachlan, K. Lee, J. R. Durrant, I. D. Baikie, J. S. Kim, *ACS Appl. Mater. Interfaces* 2019, 11, 46808.

9:45 AM EQ05.05.04

Identifying Field Effect Passivation as the Origin of the Voltage Enhancing LiF Interlayer at the Perovskite/C₆₀ Interface Dorothee Menzel¹, Amran Al-Ashouri¹, Alvaro Tejada^{1,2}, Igal Levine¹, Jorge A. Guerra², Bernd Rech^{1,3}, Steve Albrecht^{1,3} and Lars Korte¹; ¹Helmholtz-Zentrum Berlin für Materialien und Energie, Germany; ²Pontificia Universidad Católica del Perú, Peru; ³Technische Universität Berlin, Germany

In metal halide perovskite (MHP) solar cells with p-i-n architecture, the electron selective contact is often realized using the fullerene C₆₀. However, the C₆₀/perovskite interface is known to limit the open circuit voltage (V_{oc}) of the solar cells. This might be caused by non-radiative recombination, an unfavorable conduction band offset at the interface, or a combination thereof [1]. It has been shown that with an ultra-thin interlayer of LiF the V_{oc} can be enhanced by around 50 meV [2], due to reduced non-radiative recombination [3]. Yet, the exact passivation mechanism is still a question of ongoing research.

In this contribution we investigate the effect of such a thin LiF interlayer on the interface of a state-of-the-art multi cation multi halide perovskite composition, Cs_{0.05}(MA_{0.17}FA_{0.83})_{0.95}Pb(I_{0.83}Br_{0.17})₃ (CsMAFA, $E_G = 1.63$ eV), and thermally evaporated C₆₀ by means of photoelectron spectroscopy [4]. MHPs exhibit a characteristically low density of states at the valence band maximum (VBM) [5]. To access the energetic position of the VBM and defect states within the band gap, we employ a rarely used technique: near-UV photoemission spectroscopy in constant final state mode (CFSYS). CFSYS allows to directly trace the density of occupied states with a very high dynamic range of up to seven orders of magnitude. Previously, we were thus able to reveal the VBM and to quantify occupied states in the band gap of CsMAFA [6]. Furthermore, with the low photon energies used here, the information depth is strongly enhanced to 5 – 10 nm and thus, it is possible to study the buried interface of CsMAFA and C₆₀.

We refine our description of the perovskite's valence band [6] to also model the superposition of the perovskite and C₆₀ density of occupied states for thin C₆₀ layers. From a sample with 5 nm C₆₀ thickness, we can then directly determine the offset between the perovskite VBM and the C₆₀ HOMO-edge to 0.55 eV. Furthermore, considering the band gap of the MHP and C₆₀, the LUMO edge is found 0.26 eV below the perovskite CBM. This unfavorable line-up potentially contributes to the V_{oc} limitation by the C₆₀ interface. Interestingly, we find that introducing the LiF interlayer leads to an *enhanced* defect density in the first monolayers of C₆₀, which would lead to an increased trap assisted recombination, thus lower V_{oc} in a cell. Our CFSYS data shows, that this is overcompensated by a reduced hole density in the vicinity of the perovskite/C₆₀ interface, which can be caused by a small dipole and probably a positive fixed charge. Linking to established solar cell technologies, we propose that the LiF evokes a field effect passivation reducing the absolute non-radiative charge carrier recombination and leading to the improved V_{oc} .

[1] Stolterfoht *et al.*, 2019, DOI: 10.1039/C9EE02020A

[2] Al-Ashouri *et al.*, 2020, DOI: 10.1126/science.abd4016

[3] Wolff *et al.*, 2019, DOI: 10.1002/adma.201902762

[4] Menzel *et al.* 2022, accepted for publication in *Advanced Energy Materials*

[5] Zu *et al.*, 2019, DOI: 10.1021/acs.jpcclett.8b03728

[6] Menzel *et al.*, 2021, DOI: 10.1021/acsami.1c10171

10:00 AM BREAK

SESSION EQ05.06: Optoelectronic Devices
Session Chairs: Barry Rand and Philip Schulz
Tuesday Morning, November 29, 2022
Sheraton, 2nd Floor, Republic B

10:30 AM *EQ05.06.01

Theory-Based Insights into Interfacial Effects Influencing the Performance and Stability of Thin-Film Photovoltaics Joel B. Varley; Lawrence Livermore National Laboratory, United States

The transformation and utilization of solar energy with photovoltaics is becoming an increasingly cost-effective renewable energy source to supplant fossil-based alternatives. Rapid and parallel advances in storage solutions like batteries or in chemical bonds via (photo)electrochemical (PEC) processes are further accelerating this transformation. Underpinning all of these technologies are the creation and optimization of complex interfaces required for the desired separation and transfer of charge carriers, chemical reactivity, and stability. First-principles based calculations offer one avenue for providing insight into many of the fundamental details of these heterointerfaces that can so strongly influence device performance. Here we detail many examples of particular relevance to thin-film photovoltaics, such as the choices for particular absorber compositions and heterojunction partners of other layers like buffer layers and transparent contacts, and common deposition and post-processing treatments. Using hybrid density functional theory calculations, we will

discuss how these choices, as well as the role of alloying in different layers, can steer important device variables such as band gap, band offsets, doping and stability. These properties are often interrelated and can complicate device optimization. We will primarily illustrate how understanding these effects have led to gradual improvements in conventional thin-film photovoltaics (e.g. those based on $\text{Cu}(\text{In,Ga})(\text{S,Se})_2$ and CdTe), but will discuss how they are also relevant to alternative absorbers like wider-bandgap chalcopyrites and the hybrid perovskites.

This work performed under the auspices of the U.S. Department of Energy by Lawrence Livermore National Laboratory under Contract DE-AC52-07NA27344 and partially supported by the Department of Energy office of Energy Efficiency & Renewable Energy (EERE) and by the HydroGEN Advanced Water Splitting Materials Consortium, established as part of the Energy Materials Network under the EERE Hydrogen and Fuel Cell Technologies Office.

11:00 AM EQ05.06.02

Size Tunable High-Efficiency Micro-LED Array Grown on Sapphire Nano-Membrane Template [Jungel Ryu](#), Jehong Oh, Sohyeon Park, Yongjo Park and Ho Won Jang; Seoul National University, Korea (the Republic of)

Micro-LED displays are emerging displays with a lot of potential advantages over conventional display technologies. They are new displays with high pixel density, high brightness, superior stability, low energy consumption and most importantly, no limitation in size, capable of covering from micro-displays for AR/VR/MR to large area displays for consumer TV. Recent demonstrations by companies and institutes shows that development of micro-LED technology is in progress. However, further research is needed before they are commercialized. The current micro-LED fabrication process contains singulation of LED film into micro-scale using plasma etching. During the etching process, the active layers are inherently damaged, resulting in degradation in quantum efficiency. Another obstacle is the unacceptable loss of LED film known as kerf loss. The mentioned problems become more crucial as the chip size shrinks, affecting the cost of the micro-LED displays. It is highly desired to establish a scheme to fabricate high-efficiency micro-LEDs without a singulation process.

To fabricate micro-LEDs with self-passivated structures, we proposed a unique growth template called sapphire nano-membrane (SNM). The SNMs are 3D bridge structures consisted of 100 nm thick single crystalline Al_2O_3 . The fabrication process of the SNM array started with photolithography to make photoresist (PR) pattern on a sapphire substrate. Then, an amorphous Al_2O_3 layer with a thickness of 120 nm was deposited by atomic layer deposition. Second photolithography and wet etching by H_3PO_4 solution was conducted to make a discrete SNM array. After removal of PR using acetone, the template was annealed at 1100 °C for 2 hours in air to crystallize the amorphous Al_2O_3 into single crystalline Al_2O_3 through solid phase epitaxy.

An array of discrete micro-LEDs surrounded by a major (0001) plane, and (11-20) and (1-101) planes at sidewalls was grown on SNM template using MOCVD. Self-passivated structure of the fabricated micro-LEDs, with MQWs sandwiched between n-GaN at the core and p-GaN at the outer shell, were confirmed with TEM and STEM. The size of micro-LEDs was controlled by adjusting the width and space of the SNM array. By placing several SNMs closely, larger micro-LEDs were obtained via lateral overgrowth and merge of the GaN. Structural and optical properties of the fabricated micro-LEDs were analyzed to confirm the compliant substrate effect of the SNM. Micro-Raman spectroscopy result showed reduced strain on the GaN and consequent reduction of threading dislocations were confirmed with panchromatic CL analysis. Micro-PL result showed improved internal quantum efficiency and spatially resolved CL analysis showed different spectrums emitted from various facets.

After the growth of LED structures, p-contact metal was formed using e-beam evaporation followed by flip-chip bonding to a target substrate with an electrode array. Utilizing ultra-thin profile of the SNM, micro-LED array was massively transferred to the target substrate via mechanical lift-off process. The micro-LEDs showed improved electrical properties with lower leakage current level compared to dry-etched micro-LEDs. Moreover, our devices showed reduced quantum confined stark effect with negligible wavelength shift depending on the current density change. We assume that it is due to relaxed strain which resulted in reduced band bending. The improved properties were observed regardless of the chip size, implying that the size effect problem in micro-LED display could be controlled using the SNM technique. We believe that results presented in this work would provide a significant step towards the commercialization of micro-LED displays.

This work was supported by the BK21Plus SNU Materials Division for Educating Creative Global Leaders (21A20131912052), National Research Foundation of Korea (NRF) grand funded by the Korea government (MSIT) (2021M3D1A2039641)

11:15 AM EQ05.06.03

Resonant Capacitors with Single Injection Contacts for Bright Light Emission Across the Spectrum [Vivian Wang](#) and Ali Javey; University of California, Berkeley, United States

The range of luminescent materials that can be used in light-emitting devices is typically limited due to material processing and band alignment concerns. We have found that a single device architecture can be used to generate electroluminescence from a wide range of materials simply by depositing the luminescent material on top of a metal-oxide-semiconductor capacitor across which pulsed voltages are applied. By using a carbon nanotube network as the top injection contact, emission spanning the ultraviolet to infrared energy range can be produced using materials such as organic molecules and colloidal quantum dots, even when the lateral charge transport is poor or the film is non-uniform. Charge injection is achieved across different band alignments through transient band bending at the contact, rendering the device generic in the sense that emitter-specific charge injection layers are not needed. Importantly, light emission can be observed at voltages near the optical gap of the emissive material by employing a thin high-k gate oxide layer. Due to the capacitive nature of the device, the device can be driven resonantly to reduce the input voltage even further and achieve high power efficiency. Thus, bright emission can be achieved without complex device structures by using alternating carrier injection from a single contact. Facile fabrication of devices with emission across a broad spectral range may enable new opportunities in optoelectronics.

11:30 AM EQ05.06.04

Visualizing NIR Using Monolithic QD Optoelectric Upconversion Devices in Transmissive Mode [Tae Hyun Kwon](#) and Moon Sung Kang; Sogang University, Korea (the Republic of)

Exploiting of near infrared (NIR) wave is under significant advances in emergence technologies related to night vision, bioimaging, wafer inspections, and security systems. The full use of NIR in such technologies eventually requires converting the "invisible" NIR electromagnetic wave to "visible (Vis)" signal. This can be attained from optoelectric upconversion device, comprising a Vis light-emitting diode (LED) tandemly stacked onto an NIR photodiode (PD). In this work, we fabricate an efficient optoelectric upconversion device based on quantum dots (PbS quantum dots for NIR detection and CdSe quantum dots for Vis output signal). Employing a semi-transparent top electrode, we demonstrate a transmissive-mode device where NIR irradiated through the bottom electrode is upconverted to Vis under bias, which is then emitted through the top electrode. Moreover, not only an upconversion device comprising a single LED stacked onto a single PD (1PD-1LED configuration) is demonstrated, but we also fabricate a tandem device comprising a single PD sandwiched between two LEDs (1PD-2LED configuration). Unlike the upconversion device in 1PD-1LED configuration where only either the electrons or holes generated from photoexcitation are exploited in generating light, the upconversion device in 1PD-2LED configuration allows converting both electrons and holes to Vis. This approach will make significant impact on improving the efficiency of optoelectric upconversion and can provide wider possibility of applications.

11:45 AM EQ05.06.05

Leveraging DFT Atomic-Scale Modeling and Simulation Approaches for Designing Ultrathin 2D-TMD Based Optoelectronic Devices Ugonna C. Ohiri; Northrop Grumman Corporation, United States

Two-dimensional (2D) materials are emerging materials which exhibit very intriguing physical, electronic and optoelectronic properties, such as the ability to grow these thin film materials on a variety of heterogeneous substrates, high refractive indices in the visible-IR wavelength regime, and tunable bandgap engineering with respect to the number of stacked 2D layers.

For example, Group-6 Transition metal dichalcogenides (TMDs) monolayer/bilayer materials (e.g., MoS₂, WS₂, WSe₂, MoSe₂, MoTe₂) demonstrate good semiconducting behavior (e.g., direct bandgap performance in the range of 1-2 eV), strong light-matter interactions, and good detection performance in the visible-near IR regime. Black Phosphorous (bP) and Group-10 Noble TMDs (e.g., PdS₂, PdSe₂, PtS₂, and PtSe₂) have attracted more recent attention as these materials demonstrate higher carrier mobility, wider tunable bandgaps, and can offer great potential for developing next-generation mid-infrared optoelectronic devices.

Here, we report on a deep dive exploration into using density functional theory (DFT) approaches for modeling and simulating various Group-6 and Group-10 2D materials, and the ability to tune the electronic and optical performance when Group-6 and Group-10 TMDs are hetero-structured with each other. These DFT modeling and results will shed light on novel and scalable strategies needed to fabricate Group-6 and Group-10 2D-based heterojunction devices; this presentation will also address critical issues which still need to be addressed for physically realizing these devices into the commercial scale.

SESSION EQ05.07: Transparent Electrodes II
Session Chairs: Geoffroy Hautier and Barry Rand
Tuesday Afternoon, November 29, 2022
Sheraton, 2nd Floor, Republic B

1:30 PM *EQ05.07.01

Hydrogen Behavior at Crystalline/Amorphous Interface of Indium Oxide and Its Role in Carrier Transport, Photoconductivity and Crystallization Julia E. Medvedeva; Missouri University of S&T, United States

Revealing the microscopic behavior of hydrogen in wide-bandgap metal oxides that have been employed as transparent electrodes in many optoelectronic devices, including highly efficient silicon heterojunction solar cells, and that recently became competitive in large-area flexible displays, represents a formidable problem. In oxides, hydrogen may passivate under-coordinated oxygen or metal atoms, forming covalent or ionic H bonds, respectively, and the resulting macroscopic properties depend on the relative formation, distribution, and behavior of the competing H defects. Although the structure and properties of substitutional and interstitial H defects in crystalline oxides, primarily, in In₂O₃, SnO₂ or ZnO, have been studied theoretically, the results cannot be transferred to disordered phases. The ionic nature of metal-oxygen bonding renders a substantial disorder within the short-range structure of the amorphous oxide phases that feature large fractions of under-coordinated oxygen (O) and metal (M) atoms. The wide coordination distributions and strong distortions in the M-O and O-M polyhedra dramatically increase the number of possible locations for hydrogen and the diversity of its immediate neighbor environment. The latter affects the formation, activation and stability of various H defects as well as H mobility through the disordered structure. Therefore, quantum-mechanical and statistically-significant calculations are required to elucidate the complex H behavior in wide-bandgap amorphous oxide semiconductors.

In this work, the role of crystalline-amorphous interfaces in the resulting microscopic behavior of hydrogen in indium oxide is investigated using *ab-initio* molecular dynamics simulations and hybrid density functional calculations. The results of this computationally-intensive work reveal that disorder plays a decisive role in H-induced extended bond reconfiguration which: (i) significantly outweighs the energy gains from passivation of under-coordinated oxygen atoms and nonbonding O-p-orbitals; (ii) stabilizes H defects with ionic bonding (In-H-In) even in the stoichiometric amorphous oxide; (iii) improves the morphology of disordered oxide that widens the conduction bandwidth--in accord with the observed improved mobility; and, most strikingly, (iv) favors the formation of covalent OH bonds that introduce deep trap defects, limiting the number of free carriers.

The results help explain a puzzling experimental observation of atypical semiconductor behavior in H-doped indium oxide, namely, a decreasing number of free carriers as temperature raises. Furthermore, the crystalline/amorphous interfacial model developed in this work in order to establish the structural characteristics of the interface and their effect on the formation, stability, distribution, and properties of H defects, is indispensable to resolve the controversial experimental observations regarding the H role in crystallization, namely, faster crystallization rates upon H doping, yet, decreasing grain sizes with increasing H concentration. Our statistically-significant calculations combined with molecular-dynamics simulations at various temperatures help identify the H defects and defect complexes that are responsible for H pinning, switching and segregation, governing the complex crystallization processes in indium oxide. Last but not least, the results of this work help predict which defects in H-doped indium oxide will be sensitive to photo-illumination and may contribute to the observed negative bias illumination stress instability behavior in thin film transistor devices, one of the major drawbacks hampering commercialization of the wide-bandgap amorphous oxide semiconductors.

2:00 PM EQ05.07.02

Doping and Mobility Limits of Cuprous Iodide Joe Willis^{1,2,3}, Qi Zhou¹ and David O. Scanlon^{1,2}; ¹University College London, United Kingdom; ²Thomas Young Centre, United Kingdom; ³Diamond Light Source, United Kingdom

The quest for p-type transparent conducting materials has challenged researchers for decades. Initial efforts focused on designing p-type transparent conducting *oxides*, such as CuAlO₂,^[1] which generally display good transparency, but fail to reach competitive levels of conductivity. This is because the valence bands of such materials are dominated by highly localised oxygen p states, which trap hole polarons and severely limit the charge carrier mobility.^[2] In recent years, research has moved more towards *non-oxide* materials that have greater delocalisation of the states at the valence band maximum in an effort to improve p-type conductivity.^[3-5]

One such material is cuprous iodide (CuI), which has an optical band gap just shy of 3 eV and displays intrinsic p-type conductivity that can be improved upon intentional doping.^[6] The relatively disperse valence band maximum is formed from the broad overlap of Cu 3d and I 5p orbitals that suggests high hole mobility is possible.

In this work, we investigate Se-doping in CuI using hybrid density functional theory. We compare defect formation energies to both experimentally and computationally determined values from the literature, and examine effects of the dopant on the electronic structure. We compute the charge transport properties of CuI using the AMSET package,^[7] and determine the upper limit of hole mobility. We find that the relatively low dielectric response of CuI

ultimately prevents hole mobility exceeding around $40 \text{ cm}^2 \text{ V}^{-1} \text{ s}^{-1}$ when degenerately doped.

[1] Kawazoe, H. et al, *Nature*, 1997, **389**, 939

[2] Scanlon, D. O. and Watson, G. W., *J. Phys. Chem. Lett.*, 2010, **1**, 3195

[3] Williamson, B. A. D. et al, *Chem. Mater.*, 2017, **29**, 2402

[4] Willis, J. and Scanlon, D. O., *J. Mater. Chem. C*, 2021, **9**, 11995

[5] Willis, J. et al, *Chem. Sci.*, 2022, **13**, 5872

[6] Storm, P. et al, *Phys. Status Solidi RRL*, 2021, **15**, 2100214

[7] Ganose, A. M. et al, *Nat. Comms.*, 2021, **12**, 2222

2:15 PM EQ05.07.03

Transparent Ohmic Contacts to p-GaN by AZO with Subcontact Layers Aleksandra J. Wójcicka¹, Zsolt Fogarassy², Tatyana Kravchuk³, Cecile Saguy³, Eliana Kaminska⁴, Piotr Perlin⁴, Szymon Grzanka⁵ and Michal A. Borysiewicz¹; ¹Lukasiewicz Research Network - Institute of Microelectronics and Photonics, Poland; ²Institute of Technical Physics and Materials Science, Centre for Energy Research, Hungary; ³Technion-Israel Institute of Technology, Israel; ⁴Institute of High Pressure Physics, Polish Academy of Science, Poland; ⁵TOP-GAN, Poland

Thanks to its wide band gap engineered by alloying with Mg and In and its built-in piezoelectric field, gallium nitride (GaN) is the material widely used in optoelectronics, for the fabrication of light emitting diodes (LEDs) and laser diodes (LDs) as well as in high frequency electronics for the preparation of high electron mobility transistors (HEMTs). The steady improvement in the already mature epitaxial technology has enabled interesting device developments, however there are also processing concerns which should be taken into account when optimizing a device. One of such is the design of appropriate contact layers for current biasing of the devices. In the case of LEDs and LDs, it is now being regarded that optically active materials are preferred over metals due to the possibility of their usage for enhancing light confinement or extraction.

In this work we analyze the application of a transparent conducting oxide (TCO) ZnO:Al, or AZO deposited by sputtering as the top contact to p-GaN epitaxial layers and if it is possible to improve its performance by introducing ultrathin subcontact layers at the interface and appropriate surface processing. We see that AZO forms an ohmic contact after annealing at 800°C. What is relevant, the application of subcontact layers of Au and Ni lowers the contact forming temperatures to 600°C and 650°C, respectively and substantially increases the currents under the same bias. These metals were applied since the Ni/Au bilayer is the standard low-resistivity ohmic contact to p-GaN. We analyze the interfacial layer using high resolution TEM, XRD and SIMS to try to understand the mechanism of contact formation. For the Ni we see the formation of NiO spots in cross-section TEM and NiO peaks in the XRD suggesting the presence of NiO is needed for the contact to form. However when we fabricate a sample with NiO directly at the interface instead of Ni, we don't observe ohmic I-V characteristics. This might mean that a more intimate reaction at the interface might take place, which we try to deconvolute using cross-sectional scanning tunnelling microscope. The scheme with Au also yields ohmic behavior however no clear mechanism for this has been yet found. We analyze the influence of the thickness of the Ni and Au layers on the contact formation and also apply an ultrathin Ni/Au bilayer to try to understand the role of each element in contact formation. What is specific, we anneal the contacts in nitrogen instead of the commonly used air, as the oxygen source for the contacts to form is the AZO film itself, as seen from the NiO formation. We also assess the length of the temperature formation step and its influence on the performance.

Finally, we demonstrate light emission from LD structures with the AZO-based contacts and determine their influence on the emission of the light from the diode structure.

This work was supported by the National Centre for Research and Development, Poland, project 'OxyGaN' - M-ERA.NET2/2019/6/2020, by the Hungarian NRDI Fund, grant number 2019-2.1.7-ERA-NET-2020-00002 and by the Israel Ministry of Science and Technology in the frames of the M-era.net Programme.

2:30 PM EQ05.07.04

Transport Properties of AlSbO₄—A Rutile Structured Wide Band Gap Oxide for Optoelectronic Applications and Beyond Bonan Zhu and David O. Scanlon; University College London, United Kingdom

Transparent conducting oxides (TCOs), combining two seeming mutually exclusive properties, are essential components for a range of optoelectronic applications. Existing materials such as indium-doped tin oxides (ITOs) require raw materials that are limited in supply (e.g., In). Hence, cost-effective alternatives are in urgent need¹. Having the same rutile lattice, AlSbO₄ can be seen as a cation mutated version of SnO₂ with Sn (IV) replaced Al (III) and Sb (V). Sb based systems are interesting as Sb (V) is isoelectronic to Sn(IV) and In (III) which are known to yield strongly dispersive conduction bands². In this work, a thorough computational investigation is conducted to assess the potential of AlSbO₄ as a TCO. Despite the early experimental report of a fully cation-disordered structure³, Monte-Carlo simulations based on cluster expansions show a relatively high order-disorder transition temperature of about 1800 K. The 0 K ground state structure is also obtained and found to contain a wide direct band gap of ~4 eV, and an electron effective mass of 0.38 m_e at the conduction band minimum. Band alignment calculations suggest a large electron affinity and ionisation potential, which can be attributed to the strong overlap between Sb 2s and O 2p states, making it a potential contact material. The dopability of this system will also be discussed. Beyond potential TCO applications, a low lattice thermal conductivity is found with the ordered ground state structure, and the possibility of further reduction in conductivity through disordering makes it a potential candidate material for thermal barrier coating.

(1) Ellmer, K. Past Achievements and Future Challenges in the Development of Optically Transparent Electrodes. *Nature Photon* **2012**, *6* (12), 809–817. <https://doi.org/10.1038/nphoton.2012.282>.

(2) Jackson, A. J.; Parrett, B. J.; Willis, J.; Ganose, A. M.; Leung, W. W. W.; Williamson, B. A. D.; Liu, Y.; Kim, T. K.; Hoesch, M.; Ishibe-Veiga, L.; Kalra, R.; Neu, J.; Schmuttenmaer, C. A.; Lee, T.-L.; Regoutz, A.; Veal, T. D.; Palgrave, R. G.; Perry, R.; Scanlon, D. O. Computational Prediction and Experimental Realisation of Earth Abundant Transparent Conducting Oxide Ga-Doped ZnSb₂O₆. **2022**. <https://doi.org/10.26434/chemrxiv-2022-mz5dc>.

(3) Donaldson, J. D.; Kjekshus, A.; Nicholson, D. G.; Rakke, T.; Skoglund, U. Properties of Sb-Compounds with Rutile-like Structures. *Acta Chem. Scand.* **1975**, *29a*, 803–809. <https://doi.org/10.3891/acta.chem.scand.29a-0803>.

2:45 PM EQ05.07.05

Nanostructured Inorganic and Organic Materials for Next Generation Solar-Based Energy Technology Andrea Rubino¹, Andrea Camellini¹, Luca Rebecchi^{1,2}, Michele Ghini¹ and Ilka Krieger¹; ¹Istituto Italiano di Tecnologia, Italy; ²Università degli Studi di Genova, Italy

The next generations of optoelectronic devices for energy production will have to comply with increasingly stringent requirements to promote sustainable development. The main directives concern efficiency, environmental compatibility and easy access on a global scale. In terms of materials, all this translates into the need for abundant, non-toxic, stable compounds with the best optoelectronic properties. An equally intriguing direction concerns the design of composite structures in which it is possible to combine the characteristics of several elements in order to exploit new functionalities. Among the

most promising and widespread materials in various fields of optoelectronics we find the nanocrystals of transparent conductive oxides [1]. The advantages in the use of these nanomaterials derive from the successful convergence of optical transparency/absorption and conductivity and from the easy processability in solution for the formation of thin films. However, recent studies have opened new stimulating perspectives on the use of these metal oxides, especially in the field of light-powered devices. The possibility of increasing their charge density through photodoping makes these materials potential candidates for solar conversion technology, but also for energy storage [2,3]. Another family of compounds at the forefront of emerging energy applications are the quantum dots of graphene (GQD). In this case, their attractive optical and electronic properties come with a very low environmental impact and incredible versatility in terms of functionalization [4]. The synthetic control of these organic structures makes it possible to manipulate and enhance their photo-response and adapt them, for example, to the extraction of positive or negative charges on demand. In such a context, the subsequent charge transfer process is a key aspect in the improvement of the performance and possible multi-charge mechanisms can be a significant upgrade in materials design for advanced light-driven technologies as photovoltaics, photo-catalysis or photo-rechargeable batteries. In this study, we spectroscopically analyzed the behavior of Indium Tin Oxide nanoparticles with respect to the possible photo-induced charge accumulation. Furthermore, we present the potential charge transfer properties of these nanomaterials by means of chemical titration with an oxidizing compound (electron-acceptor) [5]. We extended the same characterization to some GQDs designed to be able to delocalize different charges. The aim of this work target the possible implementation and integration of both materials (creating, for example, composite hetero structures) and multiple charge transfer mechanisms (both electrons and holes) for the development of energy conversion and storage systems.

References

- [1] T. Gatti et al. *Adv. Energy Mater.* 2021, 11, 2101041
- [2] I. Kriegel et al. *Physics Reports* 2017, 674, 1–52
- [3] M. Ghini, et al. *Nanoscale Adv.* 2021, 3, 6628-6634
- [4] L. Qianwen, et al. *Mater. Chem. Front.* 2020, 4.2, 421-436.
- [5] M. Ghini, et al. *Nanoscale*, 2021,13, 8773-8783

3:00 PM BREAK

SESSION EQ05.08: Perovskites III
Session Chairs: Geoffroy Hautier and Monica Morales-Masis
Tuesday Afternoon, November 29, 2022
Sheraton, 2nd Floor, Republic B

3:30 PM *EQ05.08.01

Addressing the Stability and Reliability Challenges in Perovskite Solar Cells via Interfacial Tailoring [Nitin P. Padture](#); Brown University, United States

Most commercial devices, including photovoltaics (PVs), have gone through a familiar research and development trajectory — increasing performance, upscaling, improving stability, and enhancing mechanical reliability — before making it to the marketplace successfully. In this context, perovskite solar cells (PSCs) are likely to be no exception, but little attention has been paid to the latter issue of mechanical reliability. In fact, enhancing the mechanical reliability of PSCs is particularly important and challenging because the low formation energies of MHPs that makes them easy to solution-process renders them inherently poor in mechanical properties: they are compliant (low Young's modulus), soft (low hardness), and brittle (low toughness). To address this perhaps final hurdle in the path towards PSCs commercialization, several rationally designed interfacial tailoring approaches are used. These include grain-coarsening, grain-boundary functionalization, and interfacial engineering. Most importantly, these approaches are designed such that they not only enhance the PSCs mechanical reliability but also increase performance and improve stability. The scientific rationales for these approaches are discussed, together with the presentation of the current results.

4:00 PM EQ05.08.02

Energy Band Alignment in between Perovskites with Different A-Site Molecules and NiO Interlayers for Highly Efficient and Stable Inverted (p-i-n) Perovskite Solar Cells [Hyoungmin Park](#), Soeun Shin and Hyunjung Shin; Sungkyunkwan University, Korea (the Republic of)

To date, most highly efficient perovskite solar cells (PSCs) are based on a normal (n-i-p) structure. However, even normal structure PSCs show higher power conversion efficiency (PCE), the advantage of relatively high stability and applicability to tandem devices draw tremendous attention to the inverted (p-i-n) structure of PSCs. Notoriously, most of inverted PSCs are based on polymer hole transporting layers (HTLs), which restrict the further development of stability due to their hygroscopic and acidic properties. Unlike polymer HTLs, PSCs based on oxide HTLs such as NiO, CuO_x and CuCrO₃ demonstrated more stable than polymer HTLs. Among oxide HTLs, NiO is the most attractive and widely accepted as a potential candidate for HTL in the inverted PSCs. However, surface redox reaction at the surface defects, especially at Ni³⁺ what are detrimental reaction sites with cations and/or halides induced voltage loss, series resistance and band alignment miss-match remained to be solved. In addition, surface properties depending on NiO fabrication methods constrict reproducibility of the inverted PSCs based on the composition of formamidinium (FA) cations which show better device performance due to broad light absorption compared to methylammonium (MA), which are before mainstream of perovskite absorbers. Furthermore, to the best of our knowledge, direct deposition of pure-FAPbI₃ or more than 95% of FAPbI₃ on NiO HTLs was not reported yet. Therefore, a suggestion of appropriate deposition techniques of NiO and analysis of the interfaces between NiO/Perovskite layers still much to be investigated. Among various deposition methods, we choose atomic layer deposition (ALD), because of their pin-hole free, uniform and conformal characteristics. To investigate NiO/Perovskite interface, we fabricated inverted PSCs with three perovskite composition (1) pure MAPbI₃, (2) (CsPbI₃)_{0.05}(FA_{0.83}MA_{0.17})_{0.95}Pb(I_{0.83}Br_{0.17})₃, and (3) FAPbI₃ with trace amount of MAI (hereafter MA, CsFAMA and FA). As the amount of FA cation increased from MA to FA composition, PSCs showed a gradual increase of J_{sc} up to 23 mA/cm² in FA base PSCs. However, open-circuit voltage (V_{oc}) showed the decreasing trends from average V_{oc} around of 1.05 V in MA and 0.99 V and 0.97 V in CsFAMA and FA, respectively. We compared X-ray/Ultraviolet photoemission spectroscopy (XPS, UPS) and Kelvin Probe work-function measurement focusing on energy band matching between NiO/Perovskite interfaces. As a result, we figure out that voltage loss dependence on FA cation ratio is caused by energy level miss-matching between NiO/perovskite interface. In addition to energy band mismatch, in all cases of perovskite compositions, Ni³⁺ defects induced a non-radiative recombination, which could restrict further performance enhancement. We also modified the NiO surfaces with organic substances containing both Lewis bases and pseudo halides. Synergetic effect of Ni³⁺ defects' passivation and suppressed nonradiative recombination significantly enhances the device performances, in particular, FF and V_{oc} . Not only device performance, but also reproducibility of PSCs with MA, CsFAMA and FA composition were increased. Furthermore, the fabricated PSCs were additionally passivated with ALD-grown SnO₂ on top of electron transport layer (ETL). Finally, ALD NiO and ETL dual passivated inverted PSCs showed the enhanced photovoltaic

performances and increased stability. In summary, this study demonstrates facile surface defect passivation and energy level alignment optimization to boost charge extraction of NiO/Perovskite interfaces by Lewis base/Ionic molecules. In addition to NiO surface modification, we adopt ALD SnO₂ layer on top of ETL to enhance electron transport and device stability.

4:15 PM EQ05.08.03

Electronic Structure and Charge Transport at Heterogeneous Functional Interfaces in Solar Energy Conversion Devices Ana B. Muñoz-García and Michele Pavone; University of Naples Federico II, Italy

Solar energy conversion devices are pivotal for the ongoing ecological transition toward a sustainable economic and social development. From re-emerging dye-sensitized solar cells for indoor light-recycling and building integrated photovoltaics [1] to the high-performance perovskite solar cells [2], the conversion of light into electricity involves charge transport across several constituent materials. The heterogeneous functional interfaces among these different materials are key for an efficient and effective conversion process. In this context, the complexity of multi-layered devices hinders a complete and conclusive understanding based on experimental outcomes. For this reason, computational modeling tools based on atomistic and first-principles approaches are at the forefront in the current revolution of materials design and optimization.

Here we will discuss how DFT-based approaches are able to unveil the charge transfer mechanism in several interfaces between optically-active materials and charge-collector layers in different electrochemical environments: (i) at hybrid solid-liquid interface with promising Cu-based molecular redox-couples in dye sensitized photo-anodes [3] and (ii) at heterogeneous interface between lead halide perovskite and molecular/inorganic hole transport materials [4,5] and passivation ligands [6].

Our results provide new insights on the structure-property-functional relationships of different functional materials/interfaces and outline new design principles for further improvements of the corresponding devices.

[1] AB Muñoz-García, I Benesperi, G. Boschloo, JJ Concepcion, JH Delcamp, EA Gibson, GJ Meyer, M Pavone, H Pettersson, A Hagfeldt, M Freitag 2021 *Chemical Society Reviews* 50, 12450-12550

[2] J Young Kim, J-W Lee, H Suk Jung, H Shin, N-G Park 2020 *Chemical Review* 120, 7867-7918

[3] I Benesperi, H Michaels, T Edvinsson, M Pavone, MR Probert, P Waddel, AB Muñoz-García, M Freitag 2022 *Chem* 8, 439-449

[4] A Pecoraro, A De Maria, PD Veneri, M Pavone, AB Muñoz-García 2020 *Physical Chemistry Chemical Physics* 22, 28401-28413

[5] C Coppola, A Pecoraro, AB Muñoz-García, R Infantino, A Dessì, G Reginato R Basosi, A Sinicropi M Pavone 2022 *Physical Chemistry Chemical Physics* <https://doi.org/10.1039/D2CP01270G>

[6] R Grisorio, F Fasulo, AB Muñoz-García, M Pavone, D Conelli, E Fanizza, M Striccoli, I Allegretta, R Terzano, NMargiotta, P Vivo, GP Suranna 2022 *Nano Letters* 22, 4437-4444

4:30 PM EQ05.08.04

Hole Transport Materials Based on PEDOT Derivatives for Perovskite Solar Cells Qiuming Yu; Cornell University, United States

Poly(3,4-ethylenedioxythiophene):poly(styrene sulfonate) (PEDOT:PSS) has been widely used as a hole conducting polymer in many optoelectronic devices, such as light-emitting diodes (LEDs), photodetectors, and solar cells. As a benchmark hole transport material, PEDOT:PSS has the advantages such as solution processability, high transparency, and good flexibility. However, relatively low electrical conductivity and poor electron-blocking capacity of PEDOT:PSS are detrimental to the operational parameters of perovskite solar cells, including open-circuit voltage (Voc), short-circuit current density (Jsc), and fill factor (FF). We proposed a new strategy to modify the electronic, structural, and surface morphological properties of PEDOT:PSS by introducing a hydroxymethyl (-MeOH) or chloromethyl (-MeCl) functional group to ethylenedioxythiophene (EDOT) to form hydroxymethylated-3,4-ethylenedioxythiophene (EDOT-MeOH) or chloromethylated-3,4-ethylenedioxythiophene (EDOT-MeCl) monomers and to further polymerize them to water-soluble poly(hydroxymethylated-3,4-ethylenedioxythiophene):polystyrene sulfonate (PEDOT-MeOH:PSS) or poly(chloromethylated-3,4-ethylenedioxythiophene):polystyrene sulfonate (PEDOT-MeCl:PSS) using the oxidative chemical polymerization method. The introduced functional groups can either modify the work function or the conductivity of PEDOT-MeOH:PSS and PEDOT-MeCl:PSS. We systematically varied the amount of the ferric oxidizing and basic agents and reaction temperature and time in polymerization to control the reaction kinetics, the chain length, and the oxidation state of polymers. We also varied the amount of PSS used in polymerization to control the doping level and work function of synthesized PEDOT-MeOH:PSS and PEDOT-MeCl:PSS. Furthermore, we added ethylene glycol (EG) in the synthesized PEDOT-MeOH:PSS and varied annealing conditions such as in polar solvent environment and EG washing for PEDOT-MeCl:PSS to further tune the microstructures, electrical conductivities and work function of PEDOT-MeOH:PSS and PEDOT-MeCl:PSS thin films. We used Raman scattering spectroscopy to study the backbone structural changes among the benzoid and quinoid conformations and their impacts on the surface morphologies using atomic force microscope (AFM), electrical conductivity using four-probe measurement, and work function using ultraviolet photoelectron spectroscopy (UPS) and cyclic voltammetry (CV). The surface chemical compositions were obtained by x-ray photoelectron spectroscopy (XPS) to confirm the presence of PEDOT-MeCl on the thin film surface. The inverted structured MAPbI₃ perovskite solar cells with PEDOT-MeOH:PSS treated with EG exhibited the enhanced Voc and Jsc because of the enlarged work function and electrical conductivity. Elongated photoluminescence lifetime of MAPbI₃ on PEDOT-MeCl:PSS indicated the strong interaction between Cl⁻ and perovskites. Additionally, the inverted structured MAPbI₃ perovskite solar cells with PEDOT-MeCl:PSS annealed in polar solvent vapor exhibited the enhanced Voc and Jsc because of significantly reduced trap states at the HTL/perovskite interfaces. This work opens the way to develop new hole transport materials for highly efficient inverted perovskite solar cells and other optoelectronic devices with low-cost and solution processability.

4:45 PM EQ05.08.05

Optical Probes of Triplet Exciton Sensitization of Silicon Narumi Wong, Collin F. Perkinson, Alice Q. Wu, William Tisdale, Mouni Bawendi and Marc Baldo; Massachusetts Institute of Technology, United States

To match the growing global energy demand while meeting space and cost limitations, efficiencies of solar cells need to improve. However, the efficiencies of crystalline silicon solar cells, the current industry standard, are approaching the maximum theoretical limit. One method of going beyond this limit is to sensitize the silicon (Si) by using a material that can perform singlet exciton fission (SF), a carrier multiplication process that can create two triplet excitons (electron-hole pairs) from a single photon. Successful transfer of these two triplet excitons to silicon can result in increased photocurrent

and improved efficiencies.

Recent work has shown coupling between Si and the archetype SF material tetracene (Tc) in the presence of passivating interfacial layers of Hafnium oxynitride [1]. Excitation spectra show a boost in the photoluminescence from Si when Tc is photoexcited that may be caused by energy transfer or changes in the silicon passivation [1]. To experimentally distinguish between these phenomena and understand the complex dynamics of excited states and charges at silicon/SF interfaces, we have developed a spectroscopy technique that is robust to the weak and intensity-dependent photoluminescence from silicon. Using combinations of biasing optical pumps and selective modulation of SF rates using a magnetic field, we study structural variations at the interface to probe the mechanism of coupling at Hafnium oxynitride interfaces and other rationally-designed heterostructures. We demonstrate positive contributions from tetracene to silicon photoluminescence that suggest a key role for charge transfer states in realizing solar cell efficiency enhancements from singlet exciton fission.

[1] Einzinger, M., Wu, T., Kompalla, J.F. *et al.* Sensitization of silicon by singlet exciton fission in tetracene. *Nature* **571**, 90–94 (2019).

SESSION EQ05.09: Perovskites IV
Session Chairs: Stefaan De Wolf and Nitin Padture
Wednesday Morning, November 30, 2022
Sheraton, 2nd Floor, Republic B

8:30 AM *EQ05.09.01

Interfaces in Perovskite Optoelectronics – Role of Energy Level Alignment and Interface Chemistry [Selina Olthof](#); University of Cologne, Germany

Optoelectronic devices, such as solar cells, are typically multi-layer stacks in which the absorber layer is sandwiched between metal oxide and/or organic transport layers in order to facilitate charge extraction or block unwanted charge carriers. In perovskite-based devices, the role of this energy level alignment remains to be elusive, and I will present some of our own results based on photoelectron spectroscopy analysis, as well as reports from literature. The effect of energetic alignment on the device performance can more easily be understood in case of inorganic-inorganic interfaces, as for example used as recombination layers in monolithic tandem solar cells. Therefore, I will also present our analysis of a highly efficient $\text{Sn}_x\text{-InO}_x$ interconnect, employed in a record-breaking organic-perovskite tandem solar cell.

However, the energetic alignment and device efficiency are not the only important aspects to consider in a solar cell, device stability is almost equally important. We show that material combinations developed for other thin film technologies (such as organic semiconductors) cannot straight forward be transferred to perovskite devices, as the direct contact to metal oxides can trigger chemical reactions that lead to a partial or to a complete decomposition of the perovskite film. Post treatment of the substrate, or the insertion of thin organic interlayers, can be necessary to stabilize the interface and achieve better stability.

9:00 AM EQ05.09.02

Fully Vacuum Deposited Perovskite Solar Cells in Substrate Configuration [Abhyuday Paliwal](#) and Henk J. Bolink; Institute of Molecular Sciences, University of Valencia, Spain

Vacuum-deposition of perovskite solar cells (PSCs) in substrate configuration on metal thin films and foils is advantageous. Due to the high conductivity of the bottom-metal electrode, the possibility of depositing thick and narrow metal grids on the top transparent electrode for facilitating loss-free charge extraction, and the intrinsic scalability of the vacuum-deposition methods, large-area cells, or subcells for modules can be fabricated with relative ease. However, despite the above, the number of reports focusing on the fabrication of PSCs in substrate configuration remains scarce. In this work, we demonstrate the complete fabrication of inverted PSCs in substrate configuration by vacuum-deposition methods. The resultant devices ($\sim 0.05 \text{ cm}^2$) having a co-evaporated formamidinium methylammonium lead iodide (FAMAPI, E_g of $\sim 1.54 \text{ eV}$) perovskite demonstrate a maximum power conversion efficiency (PCE) of $\sim 19\%$, which is comparable to the maximum PCE of $\sim 19.5\%$ obtained in the superstrate configuration devices and is the highest value reported for a PSC in substrate configuration. The devices in substrate configuration exhibit higher short circuit current density values despite the parasitic absorbance from the front fullerene- C_{60} layer ($> 0.5 \text{ mA/cm}^2$). Furthermore, we discuss the reflection losses in the above two device configurations based on the insights obtained from the transfer matrix-based optical simulations. Next, we observe that the encapsulated devices of both the configurations exhibit similar thermal stability at $85 \text{ }^\circ\text{C}$ (on a hotplate) in an N_2 environment, reaching a t_{80} (time to reach 80% of the original PCE) of ~ 800 hours. Finally, via systematic characterization, we study and identify the degradation mechanisms occurring in the devices and propose recommendations for enhancing their thermal stability. We believe our findings may contribute to the development of large-area, efficient, and thermally stable fully vacuum-deposited PSCs.

9:15 AM EQ05.09.03

Revealing Hole Transporting Properties of Transition Metal Oxides Deposited via Atomic Layer Deposition as Bi-Functional Interlayers to Highly Efficient Perovskite Solar Cells (>23%) [Hyounghmin Park](#), Seonghwa Jeong, Seongrok Seo, Soeun Shin, Eunsoo Kim and Hyunjung Shin; Sungkyunkwan University, Korea (the Republic of)

Power Conversion Efficiency (PCE) of Perovskite Solar Cells (PSCs) is over 25.7%. Despite solar cell's high PCE, low device stability coming from the inherent stability of perovskite absorber remains to be solved and restrict PSCs' commercialization. Currently, the state-of-the-art PSCs used FAPbI_3 (Formamidinium lead tri-iodide) as the main composition. Although pure FAPbI_3 -based PSCs show higher PCE due to a wider absorption spectrum owing to a lower band gap than MAPbI_3 (Methylammonium lead tri-iodide), a spontaneous phase transition from photoactive $\alpha\text{-FAPbI}_3$ to non-photoactive $\delta\text{-FAPbI}_3$ is pointed as a significant challenge. In addition to phase transition issue, low device's stability because of 2,2',7,7'-tetrakis[N,N-di(4-methoxyphenyl)amino]-9,9'-spirobifluorene (Spiro-OMeTAD) which is mainly used as hole transporting layer (HTL) in n-i-p normal structure PSCs is also raised as a challenge. Oxide hole transporting layers (HTL) can be strong candidates. However, the oxide transporting layers generally require high processing temperature and the lack of p-type characteristics inhibits application to PSCs as HTLs. Transition metal oxide (TMO) such as TiO_2 , WO_x , MoO_x and V_2O_{5-x} are also recognized as a solution, but the control of hole transporting properties related to oxidation state of metals in TMO and a proper ohmic junction with organic layer and/or suitable deposition methods without damaging the perovskite absorber layer should be solved in advance. Motivated from here, we adopt atomic layer deposition (ALD) to fabricate TMO as HTLs with low temperature process and intentionally induce oxygen deficient traps to form empty d -bands to induce and further enhance hole transporting properties. With their oxygen deficient trap assisted hole transporting properties as an HTL, we fabricated n-i-p normal structure PSCs of FAPbI_3 and Spiro-OMeTAD with ALD grown TMOs (TiO_2 , MoO_x and V_2O_{5-x}) on top of Spiro-OMeTAD to enhance device stability. During fabrication, we adopt funnel like 2D perovskite passivation layers for defect passivation and

enhance perovskite's stability coming from hydrophobic characteristics.^[1] As a result, highly efficient PSCs of PCE of over 23% with TMOs are fabricated with pin-hole free hole transporting and protection bi-functional ALD layers.^[2,3] The stability of PSCs with ALD TMO layer is over 90% initial PCE after ~ 570 hrs and maintained 94.9% of initial PCE after 130 hrs operating condition without UV cut-off filter. In conclusion, this study demonstrates the application of TMOs as hole transport/protective bi-functional HTLs and ALD as an optimal deposition method without damaging the underlying perovskite absorber. Furthermore, this study shows the possibility that ALD TMO can be also applicable to tandem device fabrication and stable PSCs' commercialization.

9:30 AM EQ05.09.04

Gate/Light Co-Tunable Negative Differential Resistance Behaviors from Small-Molecules Heterostructure Seongjae Kim, Yunchae Jeon and Hocheon Yoo; Gachon University, Korea (the Republic of)

Negative differential resistance (NDR) is a characteristic in which the current decreases as the voltage increases. Recently, these new characteristics have been applied in various fields such as multi-value logic devices and switching circuits [1-3]. In this study, we present an ambipolar transistor that controls NDR characteristics through light and gate voltage bias co-tunability. We fabricated the proposed small-molecules heterostructure device by stacking dinaphtho[2,3-b:2',3'-f]thieno[3,2-b]thiophene (DNTT) on top of N,N'-ditridecyl-perylene-3,4:9,10-tetracarboxylic diimide-C13 (PTCDI-C13). The proposed device shows the electrical characteristics of a typical ambipolar transistor in the dark. When light is irradiated, photocarriers move in the sub-bandgap, resulting in NDR behaviors depending on the gate/light control. While the gate voltage bias was increased from 0 V to 30 V with 10 V increments, the peak voltage was measured at 41 V, 51 V, 60 V, and 69 V, which showed a proportional increase with the gate voltage dependency. In addition, as a result of measuring with different wavelengths of light at a fixed gate voltage ($V_G = 10$ V), NDR characteristics were shown in all wavelength ranges from $\lambda = 400$ to 1,100 nm, and light-tunable characteristics according to the wavelength of light were confirmed. The peak to valley ratio (PVCr) exhibited a maximum of 2.02 A/A at $\lambda = 1,000$ nm light illumination. We also fabricated an array of 9×9 NDR devices to test the reproducibility and uniformity of the induced NDR. All 81 devices constituting the array showed light-induced NDR and gate-shiftable characteristics. Finally, we detected the text image by mapping the PVCr of 81 devices when the text image pattern was irradiated on the 9×9 NDR device array.

References

1. Kim, Kwan-Ho, et al. "A multiple negative differential resistance heterojunction device and its circuit application to ternary static random access memory." *Nanoscale horizons* 5.4 (2020): 654-662.
2. Wang, Miao, et al. "S-Type Negative Differential Resistance in Semiconducting Transition-Metal Dichalcogenides." *Advanced Electronic Materials* 5.9 (2019): 1800853.
3. Cheng, Ruiqing, et al. "Modulation of Negative Differential Resistance in Black Phosphorus Transistors." *Advanced Materials* 33.25 (2021): 2008329.

9:45 AM BREAK

SESSION EQ05.10: Oxides and Wide Bandgap Materials
Session Chairs: Monica Morales-Masis and Joel Varley
Wednesday Morning, November 30, 2022
Sheraton, 2nd Floor, Republic B

10:15 AM EQ05.10.01

Elucidating the Growth Kinetics of *h*MBE-Grown SrTiO₃ via ReaxFF Benazir Fazlioglu Yalcin¹, Adri C.T. van Duin¹ and Roman Engel-Herbert^{1,2}; ¹The Pennsylvania State University, United States; ²Paul-Drude-Institut für Festkörperelektronik, Germany

Titanium(IV) isopropoxide (TTIP), a commonly used metal-organic substance, has tremendous industrial applications since its thermal decomposition produces TiO₂ as a final product. Therefore, it has come into focus as an indispensable component of hybrid molecular beam epitaxy (*h*MBE) systems to grow titanate structures such as SrTiO₃.¹ To have a better understanding of the reaction kinetics of the growth process, reactive force field molecular dynamic simulations (ReaxFF-MD) constitute as a powerful tool which is based on a bond order-based force field that provides a unique opportunity to observe chemical reactions with the continuous bond formation and breaking together with allowing for large simulation sizes.^{2,3} The decomposition pathways and surface interactions can realistically be captured and tracked in the low-pressure conditions present in the deposition experiments. In this study, a SrTiO₃ (001) structure was simulated using ReaxFF molecular dynamics simulations in such a way that one surface of SrTiO₃ is TiO₂ terminated while the other surface is SrO terminated. TTIP molecules and Sr atoms were placed randomly around the SrTiO₃ structure to mimic the *h*MBE growth conditions. Performing the ReaxFF-MD simulations in the presence of TiO₂- and SrO-terminated SrTiO (001) surfaces revealed that the particular surface chemistry of the SrTiO₃ growth front dramatically affected the initialization of the TTIP decomposition process. While the metal-organic precursor TTIP was found to be rather stable with a pronounced tendency to thermally desorb from TiO terminated SrTiO (001) surfaces, its decomposition on SrO terminated surfaces was much pronounced, providing first insights into the intricacies of the hybrid MBE growth process. The major observations that were made based on these simulations are as follows:

- 1) Sr atoms had a clear tendency to go to the surface with TiO₂ termination, 2) TTIP molecules were attracted by the SrO surface and no TTIP can be observed in the vicinity of TiO₂-termination which confirmed the experimental finding that TTIP breaks down at a 40% higher rate on SrO than on bare TiO₂.⁴ 3) As soon as the Sr atoms started making bonds with the TiO₂ surface, TTIP molecules were attracted by Sr atoms and got incorporated into the surface to decompose and to grow the SrTiO₃ structure.

The conclusions that were drawn from the simulations of TTIP decomposition on SrTiO₃ play a critical role in understanding the growth kinetics of *h*MBE in more detail. At this level, one can ask questions such as what are the decomposition reactions of TTIP on SrTiO₃? Do the bonds of the TTIP molecule tend to break between C-O or Ti-O leaving the remaining molecule oxygen-deficient? Does the temperature have any contribution to the types of bond dissociation reactions? How does the steric hindrance of TTIP affect the growth? Can TTIP be replaced by a better-suited Ti-based metal-organic precursor? What is the ideal amount of TTIP molecules that need to be supplied on an 8x8 atom surface? All these questions can be answered via ReaxFF-MD simulations and will be discussed in this talk in detail.

1. Jalan, B., Moetakef, P. & Stemmer, S. Molecular beam epitaxy of SrTiO₃ with a growth window. *Appl. Phys. Lett.* **95**, (2009).
2. Van Duin, A. C. T., Dasgupta, S., Lorant, F. & Goddard, W. A. ReaxFF: A reactive force field for hydrocarbons. *J. Phys. Chem. A* **105**, 9396–9409

(2001).

3. Senftle, T. P. *et al.* The ReaxFF reactive force-field : development, applications and future directions. *Nat. Publ. Gr.* (2016) doi:10.1038/npjcompumats.2015.11.

4. Brahlek, M. *et al.* Frontiers in the Growth of Complex Oxide Thin Films: Past, Present, and Future of Hybrid MBE. *Adv. Funct. Mater.* **28**, 1–41 (2018).

10:30 AM EQ05.10.02

Calcium Titanate Orthorhombic Perovskite-Nickel Oxide Heterogeneous Solar Blind UVC Photodetectors with Unprecedented Long-term Stability Exceeding 500 Days and Their Applications to Real-Time Flame Detection [Subin Lee](#), Taehyun Park, Jaehyun Hur and Hocheon Yoo; Gachon University, Korea (the Republic of)

As the frequency of fires has increased in recent years, the demand for efficient fire monitoring systems has increased. To realize sensitive and wide-range fire monitoring, flame detection based on Ultraviolet-C (UVC) photodetector can be considered a promising approach. Here, we demonstrate a self-powered and real-time flame detector by means of calcium titanate perovskite (CTO) and nickel oxide (NiO) heterostructure. The proposed UVC photodetectors achieve a high solar-blinded rejection ratio (at UVC light/ UVA light) of 80.22 A/A and an on/off switching current ratio of 120 A/A under UVC light and dark states. Furthermore, we emphasize that significantly robust and stable operation of long-term stability is accomplished due to the clean interface between CTO and NiO junction. The proposed UVC photodetectors maintained their UVC sensing operation behavior unchanged even for more than 500 days. Comprehensive investigation including UV-visible spectrophotometer, X-ray photoelectron spectroscopy, capacitance-voltage analysis, atomic force microscope, scanning electron microscope, and electrochemical impedance spectroscopy was performed, which shed light on the operation mechanism in the proposed UVC photodetectors. Furthermore, by controlling the junction properties between the two materials, this study obtained a photovoltaic effect that allows the device to operate at zero voltage bias conditions without external bias. Finally, this study successfully demonstrates real-time flame detection using the proposed CTO and NiO heterostructure. During the test, the UVC photodetectors exhibited a systematic current change in response to the flame intensity variation, enabling quantitative analysis of fire monitoring, and presenting a new possibility for prompt and accurate fire detection.

10:45 AM EQ05.10.03

Optical Control and *In Situ* Detection of Trapped Carrier Dynamics in BiVO₄ Photoanodes [Zhu Meng](#)¹, Shababa Selim¹, Ernest Pastor², Andreas Kafizas¹, James R. Durrant¹ and Artem Bakulin¹; ¹Imperial College London, United Kingdom; ²Institut de Ciències Fotòniques, Spain

In solar water splitting cells, the photon-to-current conversion efficiency is often governed by carrier transport in photoelectrodes. While defects in metal oxides are widely known to play a role in this transport, their multifactorial influence on charge dynamics in photoelectrochemical cells remains largely unexplored. Here we apply a novel 'pump-push-photocurrent' (PPPC) approach to observe the trapping and de-trapping of carriers at intrinsic oxygen vacancies (OVs) of the photoanode bismuth vanadate (BiVO₄). In PPPC, re-activating carriers in OV state with near-IR light produces additional photocurrent, aiding electron extraction after de-trapping. We observe that carrier trapping in BiVO₄ first occurs on ~10 ns time scale, followed by ~20 ms delayed transport-assisted trapping. At the external biases below 0.8 V, OVs states directly affect the device photocurrent via carrier trapping and recombination. The recombination of OV-trapped carriers is suppressed at higher bias (> 1.0 V vs Pt) due to the better spatial segregation of electron and hole space charge layers. These observations show that external bias has multiple effects on device performance via oxygen vacancies, which can be instrumental for development of BiVO₄ photoanodes and photocatalyst materials.

11:00 AM EQ05.10.04

A High-Throughput Approach to Determining Energy-Dependent Impact Ionization Probabilities [Ryan N. Hall](#)¹, Norbert Krause², Francois Ladouceur¹ and Fiacre Rougieux¹; ¹University of New South Wales (UNSW), Australia; ²Silanna Pty Ltd, Australia

Introduction

Impact Ionization plays a critical role in a wide range of devices, including avalanche photodiodes, LED devices, power transistors, and MOSFETS. Carrier generation by Impact ionization is also used in the contacts of emerging wide bandgap optoelectronic devices [1] to efficiently inject carriers, mitigating the doping challenges associated with conventional wide bandgap material systems.

The impact ionization probability is a critical parameter in the search for novel wide-bandgap materials. However, current impact ionization models can be poorly predictive, often assuming a parabolic band dispersion relation or failing to take advantage of recent advances in ab-initio electronic structure calculations. On the other hand, advanced models require the calculation of the transition matrix elements which comes at an immense computational cost, precluding high-throughput studies for material screening and prediction.

For high-throughput material screening, there is a critical need for a fast and accurate model for the impact ionization threshold. In this study, we bridge this critical gap and develop a high-throughput computational method to calculate the impact ionization threshold as a function of the primary carrier momentum and from this, the energy-dependent probability of impact ionization for ultra-wide bandgap semiconductors.

Methodology

The threshold for impact ionization was determined by minimizing the energy of the primary carrier subject to energy and momentum conservation. The band structures were acquired from the Materials Project database, enabling a high-throughput computational study of up to 76,000 materials. These band structures were computed via density functional theory (DFT) using the generalized gradient approximation (GGA). A scissor correction was first applied to the Materials Project band-structure data, utilizing experimental bandgaps where available, and by linear regression of the GGA error elsewhere. The band-structures were then interpolated in k-space, applying the symmetry operations of the associated Brillouin zone (BZ), before implementing interpolation by radial basis functions (RBF), using a basis set of cubic splines. The minimization problem comprises nine continuous variables (the k-point coordinates for each of the non-primary carriers) and three discrete variables; their band indices. Minimization was achieved through brute force over the band combinations and by basin-hopping with sequential least squares programming (SLSQP) for the continuous variables. The impact ionization threshold was computed for primary carriers along high symmetry k-space paths and additionally for some number of random primary momenta (k-points) within the first BZ for k-space interpolation. An energy-dependent impact ionization density of states was computed by integrating the states where the threshold is less than the given carrier energy over the constant carrier energy surface of the band structure. Dividing this by the total DOS gives the energy-dependent impact ionization probability.

Results

In this work, we developed a new model to rapidly calculate the impact ionization threshold of wide bandgap semiconductors based on DFT-calculated band structures. We validate the impact ionization thresholds against measurements in the literature showing that the impact ionization probability is a reliable estimator for the impact ionization scattering rate for high-throughput material screening and prediction. We then use our model to calculate impact ionization probability curves for several conventional ultrawide bandgap material systems including GaN, AlN, β -Ga₂O₃, and MgO, and show a range of

interesting asymmetry in electron/hole impact ionization rates that could be exploited to make more efficient optoelectronic devices.

[1] Impact Ionization Light-emitting Diodes, by N. Krause. (2021, Feb. 18). *US20210050474A*. [Online]. Available: <https://patents.google.com/patent/US20210050474A1/en?qoq=20210050474>

11:15 AM EQ05.10.05

High-Resolution Mapping of Strain Partitioning and Relaxation in InGaN/GaN Nanowire Heterostructures Bumsu Park^{1,2}, Jongil Kim³, Christoph T. Koch⁴, Martin Wolz⁵, Lutz Geelhaar⁵ and Sang Ho Oh^{1,3}; ¹Sungkyunkwan University, Korea (the Republic of); ²CEMES-CNRS, France; ³KENTECH, Korea (the Republic of); ⁴Humboldt-Universität zu Berlin, Germany; ⁵Paul-Drude-Institut für Festkörperelektronik, Germany

Growing an $\text{In}_x\text{Ga}_{1-x}\text{N}/\text{GaN}$ multi-quantum well (MQW) heterostructure in nanowire (NW) form is expected to overcome limitations inherent in conventional light-emitting diodes (LED) based on the planar heterostructure. The epitaxial strain induced in an $\text{In}_x\text{Ga}_{1-x}\text{N}/\text{GaN}$ MQW heterostructure can be relaxed through the sidewalls, which is beneficial to LEDs because a much larger misfit strain with higher indium concentration can be accommodated with reduced piezoelectric polarization fields. The strain relaxation, however, renders a highly complex three-dimensional strain distribution within the small volume of the heterostructure.

Here we show that combined use of scanning transmission electron microscopy (STEM) and dark-field inline holography (DIH) strain mapping can comprehend the strain distribution within an axial $\text{In}_{0.3}\text{Ga}_{0.7}\text{N}/\text{GaN}$ MQW heterostructure embedded in GaN NWs by providing the complementary strain maps which can cover the entire NW, and reveal fine details near the sidewalls. The InGaN QDs feature a faceted hollow dome shape, surrounded by an approximately 10 nm-thick epitaxial GaN shell layer. To quantitatively evaluate the strain partitioning and relaxation, FEM strain mapping was carried out in a systematic way by changing the geometry and shape of the InGaN QDs and also with including the GaN shell.

The overall strain distribution within the NW heterostructure is reproduced well by the geometric phase analysis (GPA) of high-resolution STEM images. Due to the strain partitioning between the InGaN QD and the GaN QB, the compressive in-plane strain in InGaN is reduced but the tensile strain arises in the GaN. The DIH strain mapping allowed the details of local strain distribution to be distinguished with much higher spatial resolution and strain sensitivity. The DIH in-plane strain map shows that the strain across the InGaN QDs is not uniform but tensile and compressive strain alternates in the GaN QB and the GaN shell, respectively, which is consistent with FEM calculations. In addition, while exhibiting almost similar in-plane strains within the QD central plate, interestingly, the out-of-plane strain profiles show a locally different distribution in the growth direction. The piezoelectric polarization calculated using the measured in-plane as well as out-of-plane strain indicates a significant reduction in the piezoelectric field compared to that of an equivalent planar heterostructure. The presence of the opposite sign of strain in the GaN QB and shell across the narrow inclined InGaN facet induces a dramatic reduction of the polarization charges and, therefore, a reduced piezoelectric field. This moderated piezoelectric field at the side facet of the InGaN QD can change the direction of the local piezoelectric field and increase the internal quantum efficiency.

11:30 AM EQ05.10.06

Electronic Structure at $\beta\text{-Ga}_2\text{O}_3(001)/\text{NiO}(001)$ Interface—A Computational Study Cheng-Wei Lee^{1,2}, Andriy Zakutayev^{2,1} and Vladan Stevanovic^{1,2}; ¹Colorado School of Mines, United States; ²National Renewable Energy Laboratory, United States

$\beta\text{-Ga}_2\text{O}_3$ is a promising ultra-wide band-gap oxide ($E_g \sim 4.9$ eV) due to its excellent n-type performance. Furthermore, high-quality and low-cost bulk single crystal can be grown from melt, making it particularly attractive for device fabrication and commercialization. However, no p-type doping has been realized for $\beta\text{-Ga}_2\text{O}_3$, preventing realization of homoepitaxial p-n junction devices. Instead, heterojunctions are needed. $\beta\text{-Ga}_2\text{O}_3(001)/\text{NiO}(001)$ heterojunction was recently shown to have better rectifying performance than $\beta\text{-Ga}_2\text{O}_3/\text{Ni}$ Schottky diodes[1]. Experimental J-V curve indicates existence of interfacial states, but their identity remains unclear. To study the electronic structure of the heterojunction, we utilize the structure-matching algorithm (actual atom-to-atom matching algorithm) developed by Therrin *et al.*[2] and found that the experimentally observed orientations of (001) and (111) are among the top three NiO surfaces that best match the $\text{Ga}_2\text{O}_3(001)$ substrate. Moreover, another critical challenge of modeling such heterojunction lies on the selection of proper XC functionals that can correctly describe the band gaps of $\beta\text{-Ga}_2\text{O}_3$ and antiferromagnetic rock-salt NiO simultaneously. Hybrid functionals like HSE06 are known to reproduce the band gap of $\beta\text{-Ga}_2\text{O}_3$ when an adjusted mixing parameter ($\alpha=0.32$) is used. But HSE06 requires a significantly smaller mixing parameter ($\alpha=0.19$) to reproduce the band gap of NiO (~ 3.5 eV). The nature of homogeneous screening for HSE06 makes it challenging to find a mixing parameter that can describe the electronic structure of the whole heterojunction correctly at the same time[3]. For NiO, the CBM is mostly composed of localized Ni *d* orbital, which can be adjusted via on-site potential[4] while keeping the mixing parameter that reproduces the band gap of Ga_2O_3 well. In this talk, we will show that the HSE06+U method can simultaneously reproduce the respective band gaps of $\beta\text{-Ga}_2\text{O}_3$ and NiO within the interface. As a result, we can identify in-gap interfacial states that affect the band alignment and the position of the Fermi energy. We can also extract the differences in valence and conduction band edges, which differ from values estimated using the electron affinity rule. Our findings reveal the potential interfacial defects and provide the basis for future improvement on its rectifying performance.

[1] arXiv:2204.00112

[2] Therrin *et al.*, *Phys. Rev. Applied* 16, 064064 (2021)

[3] Zheng *et al.*, *Phys. Rev. Materials* 3, 073803 (2019)

[4] Ivády *et al.*, *Phys. Rev. B* 90, 035146 (2014)

11:45 AM EQ05.10.07

Ultra-Thin Metal Capping Layer-Induced Oxygen Deficient Interface for Visible Light Absorption in Indium-Gallium-Zinc Oxide Phototransistors Kyungmoon Kwak, Kyungho Park, Hyukjoon Yoo, Jusung Chung and Hyun Jae Kim; Yonsei University, Korea (the Republic of)

With the advent of next-generation technologies such as the internet of things (IoT) and artificial intelligence (AI), broadband photo sensor technology is considered one of the most significant sensors to recognize vast amounts of the optical signal and allow users to interact with surroundings anywhere via an optical signal. Recently, amorphous oxide semiconductor (AOS) thin-film transistors (TFTs) have gained considerable attention as promising candidates for photosensors due to their excellent characteristics, such as high field-effect mobility, low off-current, high transparency, and large-scale deposition capability. Among AOS materials, indium-gallium-zinc-oxide (IGZO) based TFTs exhibit superior performance and stability. However, there is a critical limitation in detecting visible light by an IGZO phototransistor because of its wide band gap of more than 3 eV. To solve this issue, studies have been reported to broaden the absorption wavelength by adopting an additional absorption layer, such as nanowires, quantum dots, and nanoparticles. However, these studies have the drawbacks of requiring complicated processes and not being suitable for commercialization.

In this research, we propose IGZO phototransistors with an ultra-thin aluminum capping layer (UACL). The UACL is used to generate subgap states in the interface between IGZO and the UACL that allow visible light to be absorbed. To fabricate IGZO phototransistors with the UACL, the IGZO channel was deposited by radio frequency (RF) magnetron sputtering on a SiO_2 (120 nm)/Si substrate. The length and width of the channel were defined as 150 and 1,000 μm , respectively. After the channel layer deposition, indium-tin-oxide (ITO) source and drain electrodes were deposited by RF magnetron sputtering

via shadow mask. Sequentially, the UACL was finely patterned between the source and drain electrodes by RF magnetron sputtering with RF power of 80 W. The deposition time and the shadow mask width of the UACL were adjusted from 0 to 50, 70, 90 seconds, from 50 to 75, 100 μm , respectively. After all deposition processes, IGZO phototransistors with the UACL were simultaneously annealed at 300°C for 1 hour in the air.

The optoelectronic characteristics of IGZO phototransistors with the UACL were enlarged to absorb visible light by modulating the thickness and width of the UACL. It was confirmed that the IGZO phototransistors with the UACL had the highest photoresponse characteristic at the UACL thickness of 10 nm and width of 50 μm . Specifically, we achieved IGZO phototransistors with photoresponsivity of 651.55 A/W, photosensitivity of 1.08×10^8 , and detectivity of 1.19×10^{12} Jones under 5 mW/mm² of green visible light using. The reason for improved optoelectronic characteristics of IGZO phototransistors with the UACL could be assumed that oxygen vacancies and subgap states are generated at the interface between the IGZO layer and the UACL. In general, aluminum (Al), a material with a low standard electrode potential (SEP) and strong oxygen affinity, showed the characteristic of binding to oxygen ions. Therefore, the UACL attracts oxygen ions in the IGZO and generates oxygen vacancies that serve as subgap states. For this reason, IGZO phototransistors with the UACL enable to absorb broadband wavelength over UV visible light. The aforementioned mechanism of the subgap states generated in the interface between the UACL and IGZO is also discussed along with X-ray photoelectron spectroscopy (XPS) and technology computer-aided design (TCAD) simulation analyses. Finally, we revealed that optoelectronic characteristics of IGZO thin film are easy to control substantially depending upon the thickness and dimension of the UACL. This controllability is critical for expanding the range of applications and fine-tuning performance from phototransistor to photo memory, such as neuromorphic devices that use persistent photoconductivity (PPC).

SESSION EQ05.11: Surfaces and Interfaces
Session Chairs: Stefaan De Wolf and Geoffroy Hautier
Wednesday Afternoon, November 30, 2022
Sheraton, 2nd Floor, Republic B

1:30 PM *EQ05.11.02

Site-Selective Atomic Layer Deposition for Surface Defect Amelioration Alex Martinson; Argonne National Laboratory, United States

While ALD is most commonly employed in uniform conformal growth, more selective precursors and processes may allow for more precise synthetic strategies including targeted reaction at subtly unique surface sites including those that lead to electronic defects. The adsorption free energies for molecular and dissociative adsorption of H₂O on TiO₂ and In₂O₃ were calculated to evaluate this strategy as a viable route to step edge and oxygen vacancy selectivity. We predict that selective hydroxylation is possible on several step edges and vacancy sites and further computationally evaluate three metalorganic ALD precursors for their compatibility with the selective hydration strategy. Experimental evidence for delayed nucleation of ALD on rutile (001), (110), and (100) TiO₂ single crystals corroborates predictions of surface dehydration that enables site-selective synthesis.

2:00 PM BREAK

3:00 PM EQ05.11.03

Predicting Thermochemistry and Stability of Metal/Oxide Interfaces Cheng-Wei Lee^{1,2}, Andriy Zakutayev^{2,1} and Vladan Stevanovic^{1,2}; ¹Colorado School of Mines, United States; ²National Renewable Energy Laboratory, United States

Assessing thermochemical stability of metal (and other) contact materials with wide-gap oxides is relevant for device design and fabrication. Experimental databases of standard formation enthalpies can be used for this purpose but are mostly limited to binary oxides. On the other hand, computational databases include not only the binary but also most of the multi-component compounds documented in ICSD and beyond. Building on these and using $\beta\text{-Ga}_2\text{O}_3$ as an example, we perform thermochemical stability analysis based on one of the existing computational databases (NREL MatDB[1]) to predict the stability of metal/ $\beta\text{-Ga}_2\text{O}_3$ interfaces. $\beta\text{-Ga}_2\text{O}_3$ has great n-type performance as power electronics and electron affinity (EA) around 4.0 eV. Based on the Schottky-Mott rule, metals with work functions (WF) around 4.0 eV will be candidates for Ohmic contacts for $\beta\text{-Ga}_2\text{O}_3$. From the stability analysis, we found that Cd, In, Sn, Tl, Pb, and Bi are stable $\beta\text{-Ga}_2\text{O}_3$ and the difference in WF from 4.0 eV is ≤ 0.3 eV. But we also notice that these metal candidates have low melting temperatures (<400 °C) and require very low oxygen partial pressure ($<10^{-10}$ atm) to remain thermochemically stable with $\beta\text{-Ga}_2\text{O}_3$. Our results are also consistent with recent experimental findings[2] that the commonly used Ti contact is not stable with $\beta\text{-Ga}_2\text{O}_3$ at elevated temperature (~ 400 K). To generalize our results to other oxides, we found a correlation between the metal WF and the formation enthalpy of its oxides: Smaller the WF in magnitude (closer to vacuum level), larger the formation enthalpy per oxygen in magnitude. Such correlation suggests that if a metal oxide's EA is smaller or close to the WF of its corresponding metal, other metals with WF close to its EA will likely oxidize in contact with the metal oxide. This suggests that an alternative approach beyond the Schottky-Mott rule is generally needed to select a stable ohmic contact with wide-gap oxides.

[1] <https://materials.nrel.gov/>

[2] Heinselman *et al.*, *Journal of Vacuum Science & Technology A* 39, 040402 (2021)

3:15 PM EQ05.11.04

Tunable Bandgap in Molecular 2D Conductor Composites Raphael Pfattner^{1,2}, Jinghai Li¹, Elena Laukhina², Rossella L. Zaffino¹, Nuria Aliaga-Alcalde¹, Marta Mas-Torrent^{1,2}, Vladimir Laukhin¹, Jaume Veciana^{1,2} and Sergi Riera-Galindo¹; ¹Materials Science Institute of Barcelona (ICMAB-CSIC), Spain; ²Networking Research Center on Bioengineering, Biomaterials and Nanomedicine (CIBER-BBN), Spain

The first BEDT-TTF=bis(ethylenedithio)-tetrathiafulvalene based quasi two-dimensional organic superconductor $\beta\text{-(BEDT-TTF)}_2\text{I}_3$ was reported back in 1984.^[1] Soon it became clear that ion radical salts derived from BEDT-TTF exhibit tunable electronic band structures. Therefore, such molecules are excellent building blocks for engineering a rich and diverse family of organic crystalline metals and semiconductors. Such systems can be further tuned by choosing the nature of the IRs enabling high sensitivity towards strain, pressure, humidity, temperature or even contact-less radiation sensing *i.e.* bolometers.^[2-4] Composites exhibit unique synergistic properties emerging when components with different properties are combined. The tuning of the energy bandgap in the electronic structure of the material allows designing tailor-made systems with desirable mechanical, electrical, optical, and/or thermal properties.^[5] Here, we discuss an emergent insulator-metal transition at room temperature in thin-films comprised of polycarbonate/molecular-metal composites. Temperature-dependent resistance measurements allow monitoring of the electrical bandgap, which is in agreement with the optical bandgap extracted by optical absorption spectroscopy. The semiconductor-like properties of our films, made with bis(ethylenedithio)-tetrathiafulvalene (BEDT-TTF or ET) $\alpha\text{-ET}_2\text{I}_3$ (nano)microcrystals as two-dimensional molecular conductor on one side and insulator polycarbonate as a second ingredient, are attributed to an emergent phenomenon equivalent to the transition from an insulator to a metal. This made it possible to obtain semiconducting films with tunable electrical/optical bandgaps ranging from 0 to 2.9 eV. A remarkable aspect is the similarity close to room temperature of the thermal and

mechanical properties of both composite components, making these materials ideal candidates to fabricate flexible and soft sensors for stress, pressure, and temperature aiming at applications in wearable human health care and bioelectronics.

References:

- E. B. Yagubskii, I. F. Shchegolev, V. N. Laukhin, et.al., JETP Lett., (1984), 39, 12.
E. Laukhina, R. Pfattner, L. R. Ferreras, et. al., Adv. Mater., (2009), 21, 1-5.
R. Pfattner, V. Lebedev, E. Laukhina, et.al., Adv. Electron. Mater., (2015), 1, 1500090.
R. Pfattner, E. Laukhina, L. Ferlauto, et.al, ACS Appl. Electron. Mater., (2019), 1, 1781.
R. Pfattner, E. Laukhina, J. Li, et.al, ACS Appl. Electron. Mater. (2022), 4, 2432.

SESSION EQ05.12: Virtual Session
Session Chairs: Stefaan De Wolf, Geoffroy Hautier and Monica Morales-Masis
Wednesday Morning, December 7, 2022
EQ05-virtual

8:00 AM *EQ05.12.01

Interface Engineering for Enhancing the Performance of Perovskite and Sb₂SSe₃ Solar Cells Lydia H. Wong; Nanyang Technological University, Singapore

In this talk, I will present our group's efforts in enhancing the performance of perovskite solar cell by interface engineering. In the first example, Cu-S and Al-CuS is used as hole transporting layer and found to enhance the stability of perovskite solar cell due to the Pb-S bond at the interface. In the second example, SnO/CdS electron transporting layer is shown to facilitate directional growth of the higher mobility [hk1] planes of Sb₂(S,Se)₃, resulting in power conversion efficiency of >9%.

8:30 AM *EQ05.12.02

High Performance Si and Cu(In,Ga)Se₂ Tandem Solar Cells Based on Wide-Bandgap Perovskites Prepared with Anion-Engineered 2D Additives Daehan Kim¹, Passarut Boonmongkolras¹, Hojin Lee¹, Inyoung Jeong², Kihwan Kim² and Byungha Shin¹; ¹Korea Advanced Institute of Science and Technology, Korea (the Republic of); ²Korea Institute of Energy Research, Korea (the Republic of)

To reach ultrahigh efficiency beyond the Shockley-Queisser limit for single-junction devices, there have been growing interests in applying a perovskite top cell in tandem with a Si or Cu(In,Ga)Se₂ (CIGS) bottom cell. The ideal bandgap for the tandem configuration is ~1.67 to 1.75 eV for the top cell and 1.12 eV for the bottom cell, which, fortuitously, is the bandgap of both Si and CIGS. The bandgap of perovskites can be tuned by (partial) replacement of iodine anions with bromine or chlorine. However, the replacement of I with Br by more than 20%, which is necessary to enlarge the bandgap to ~1.7 eV, leads to stability issues under illumination through phase separation that forms I-rich and Br-rich structures. One approach to stabilize the perovskite is to create a two-dimensional (2D) phase in which sheets of [PbX₆]²⁻ octahedra are separated by an excess number of long-chain molecules that act as a passivation agent. While most of the recent studies have focused on the cation components of the 2D additives, we developed a 2D-3D mixed wide bandgap (1.68 eV) perovskite using a mixture of thiocyanate (SCN) with the more conventional choice, iodine. Through a careful application of atomic resolution transmission electron microscopy, we demonstrated that electrical and charge transport properties as well as the physical location of 2D passivation layers can be controlled with anion engineering of the 2D additives. This approach not only improved device performance but also extended light stability. For a perovskite device, we achieved a PCE of 20.7% that retained > 80% of its initial efficiency after 1000 hours of continuous illumination in working conditions. Taking advantage of the highly efficient and stable wide bandgap perovskite, we have achieved a power conversion efficiency of 26.7% from monolithic two-terminal Si/perovskite tandem solar cells and over 23% from monolithic two-terminal CIGS/perovskite tandem solar cells, the integration details of which will be discussed.

9:00 AM EQ05.12.04

Controllable Aggregation of Conjugated Polymer Monolayer—From Field-Effect Transistors to Integrated Circuits Mengmeng Li; Institute of Microelectronics, Chinese Academy of Sciences, China

In spite of their great potentials in bottom-up organic electronics, it is challenging to fabricate conjugated polymer monolayer field-effect transistors due to intricate crystallization and film formation of conjugated polymers. Here, we demonstrate transistors based on a single molecular layer of a conjugated polymer. The resulting polymer monolayer transistors are highly reproducible and exhibit field-effect mobilities reaching 3 cm² V⁻¹ s⁻¹. The high performance is attributed to the strong interactions of the polymer chains present already in solution leading to pronounced edge-on packing and well-defined microstructure in the monolayer. The high reproducibility enables the integration of discrete unipolar polymer monolayer transistors into inverters and ring oscillators. Real logic functionality has been demonstrated by constructing a 15-bit code generator in which hundreds of self-assembled polymer monolayer transistors are addressed simultaneously. Our results open prospective pathways for bottom-up organic electronics.

9:15 AM EQ05.12.05

Lowering in Resistivity and Ultra-Flattening of AZO Thin Films on Cyclo-Olefin Polymer Substrates via Substrate-Surface Modification for Flexible Optoelectronics Tomoaki Oga¹, Ryoya Kai¹, Hisashi Miyazaki², Satoru Kaneko^{3,1}, Akifumi Matsuda¹ and Mamoru Yoshimoto¹; ¹Tokyo Institute of Technology, Japan; ²National Defense Academy, Japan; ³Kanagawa Institute of Industrial Science and Technology, Japan

ZnO and Al-doped ZnO (AZO) thin films can achieve relatively low resistivity even on amorphous substrates such as oxide glasses. Therefore, in combination with flexible transparent polymer substrates, these conducting thin films are expected to be used in wearable or flexible optoelectronic devices. The thermoplastic cyclo-olefin polymer (COP) used in this study is promising as a flexible substrate for wearable optoelectronics due to its very low moisture absorption, high transparency, and relatively high glass transition temperature (about 150°C), in contrast there are concerns about its thermal properties and surface roughness in comparison with oxide substrates. It might be useful for the growth of highly crystalline oxide thin films on polymeric substrates to modify of the polymer substrate surface to control oxide nucleation and growth direction. It might be useful to modify the polymer substrate surface for growth of highly crystalline oxide thin films on polymer substrates, leading to control of oxide nucleation and growth direction at low temperatures applicable for polymer materials. So far, we reported the atomic-scale patterning on the polymer surfaces having 0.3 nm-high atomic-steps and ultra-flat terraces, by applying thermal nanoimprinting using atomically stepped sapphire (α -Al₂O₃) molds [1]. Significant decrease in the surface roughness and crystallinity improvement was found for the ZnO thin films deposited on the surface-morphology-controlled polymer substrates subject to

nanoimprinting [2]. The insertion of an oxide buffer layer on the polymer substrate will be expected to promote oriented crystal growth of ZnO thin film deposited on it. In this study, we investigate the influence of the oxide buffer layer inserted on the ultra-flat polymer substrate upon the crystal growth and electrical property of ZnO thin films in pulsed laser deposition (PLD) at room-temperature.

Firstly, the surface topography of COP sheets used as the substrates was modified by thermal nanoimprinting (2 MPa, 180°C, 5 min, 10^3 Pa) using a sapphire mold with a 0.3 nm-high atomic step and terrace pattern, followed by PLD using a KrF excimer laser ($\lambda=248$ nm, $d\sim 20$ ns) to form oxide buffer layers such as Al_2O_3 . Subsequently, Al-doped ZnO (AZO; Al: 2 wt%) thin films ($t\sim 200$ nm) were grown at RT by PLD under O_2 gas at 10^{-3} Pa. The AZO thin films grown on the surface-pretreated COP substrates showed very smooth surface without irregularities. The root mean square roughness in $3\ \mu\text{m}$ squares of the AZO thin film on the pretreated COP substrate was reduced from 1.3 nm for the sample on the untreated substrate down to 0.4 nm. The XRD analysis of the diffraction peak attributed to AZO (001) indicated that the crystallinity and growth orientation of AZO thin films on the surface-pretreated substrate were clearly improved compared to the sample grown on an untreated COP substrate. The electrical resistivity of the AZO thin films deposited on the surface-modified COP substrates was decreased to $2.8 \times 10^{-4}\ \Omega\text{cm}$, approximately 30% lower than the films on the untreated substrates. Thus, physical and chemical pretreatments of COP substrate surfaces improved surface smoothness and electrical properties of AZO thin films even on the polymer substrates.

[1] G. Tan et al., *Nanotech.*, **27**, 295603 (2016).

[2] T. Oga et al., *Jpn. J. Appl. Phys.*, **59**, 128001 (2020).

9:50 AM DISCUSSION TIME

SESSION EQ05.13: Virtual Session II

Session Chairs: Stefaan De Wolf, Geoffroy Hautier, Monica Morales-Masis and Barry Rand

Wednesday Morning, December 7, 2022

EQ05-virtual

11:15 AM EQ05.13.03

First Principles Phase Diagram Calculation and Theoretical Investigation of Electronic Structure Properties of $\text{ZnO}_{1-x}\text{Se}_x$ for Photoanode Applications [Arini Kar](#), Balasubramaniam Kavaipatti and Dayadeep S. Monder; Indian Institute of Technology Bombay, India

Terminal solid solutions in the $\text{ZnO}_{1-x}\text{Se}_x$ system ($0 \leq x \leq 0.15$, $0.95 \leq x \leq 1$), exhibit extreme bandgap reduction attributable to band anti-crossing (BAC). In this work, we perform a theoretical investigation of extreme alloying in this system ($0 \leq x \leq 1$). The temperature-composition phase diagram of $\text{ZnO}_{1-x}\text{Se}_x$ is obtained via cluster expansion method and Monte Carlo simulations. For $0 \leq x \leq 0.15$, a solid solution in the wurtzite structure and for $0.8 \leq x \leq 1$, a solid solution in the sphalerite structure is obtained. The alloy system exhibits a miscibility gap in the range $0.15 \leq x \leq 0.8$. Only the solid solutions are seen to obey bandgap reduction predicted by BAC. The band gap of the alloys, calculated using the delta-sol method shows a bowing behaviour as predicted by the BAC model. Difference in the electronegativities of O and Se atoms in the lattice leads to hybridization of O-2p and Se-4p electronic states. Interaction between these electronic states also leads to a split in the valence band edge at O-rich end and a split in the conduction band edge at the Se-rich end. The effective mass, estimated from the density of states, of holes at the O-rich end and that of electrons at the Se-rich end, increases with alloying. These fundamental insights will help in employing suitable alloy compositions for optimal photocurrent density when these materials are used as photoanodes.

11:20 AM EQ05.13.04

Metal Nanostructure Embedded ITO Deposition and Modified Top Transparent Electrode for Emerging Thin-Film Photovoltaics [Ananta Paul](#), Vikas Sharma, Saurabh Gupta, Sudhanshu Mallick and Dinesh Kabra; IIT Bombay, India

The conventional structure of transparent devices is finished with metal oxide as a sputtering damage protection layer and top electrode in general Indium doped tin oxide (ITO). The geometry is designed and investigated considering the inverted solar cell structure (PIN). The work considered is to modify this oxide-electrode junction with the insertion of ultrathin metal in between tin oxide and ITO. In this study, we investigated the effect of process temperature and different metal insertions on the performance of $\text{SnO}_2/\text{metal}(\text{Al}/\text{Au}/\text{Ag})/\text{ITO}$ (SMI) multilayer film. The damage protection layer SnO_2 is prepared by atomic layer deposition. The thermal evaporation system evaporated the metal. The top ITO layer is deposited by RF magnetron sputtering system at different temperatures (25°C, 50°C, and 100°C). Transparent tin oxide $\text{SnO}_2/\text{metal}(\text{Al}/\text{Au}/\text{Ag})/\text{ITO}$ (Hybrid) multilayer electrodes have been prepared on conventional soda-lime glass substrates. The thickness of SnO_2 , M (Al/Au/Ag), and ITO metal films in the multilayered structure was constant at 10, 1, and 200 nm, respectively. The hybrid multilayer electrode films' structural, electrical, and optical properties are investigated. The variation of transmittance and sheet resistance values are dependent on the intermediate metal layers (Al/Ag/Au) and can be tuned accordingly. These hybrid films show a very high average transmittance of $>75\%$ in 300 to 1200 nm and roughness below or average 3 nm. With the observation, we can state that we can tune the electrode properties such as transparency in a particular wavelength and control the electrical conduction by controlling the mobility and carrier number.

11:25 AM EQ05.13.05

UV Light Blocking and Conversion by Porous Europium-Doped Titanium Dioxide ($\text{TiO}_2\text{-Eu}$) Thin Films for Potential Protection of Photovoltaic Devices Kamila Zhumanova and [Timur Atabaev](#); Nazarbayev University, Kazakhstan

In recent years, transparent thin films capable of screening and converting UV photons into visible spectrum gained significant interest in the protection of photovoltaic devices. We investigated the optical properties and UV screening capability of europium-doped titanium oxide ($\text{TiO}_2\text{-Eu}$) thin films deposited by the spin-coating method from a solution precursor for the first time in this study. We showed that $\text{TiO}_2\text{-Eu}$ thin films demonstrate europium concentration-dependent optical properties, and the quantum yield (QY) of the optimized sample was found to be $\sim 10.2\%$. Transmittance and photoluminescence measurements suggested that $\text{TiO}_2\text{-Eu}$ thin film can effectively block UV photons ($\sim 30.5\%$ at 320 nm) at glass substrate and convert them to red emission thanks to ${}^5\text{D}_0 \rightarrow {}^7\text{F}_j$ ($j = 0, 1, 2, 3, \text{ and } 4$) Eu (III) electronic transitions. Photodegradation experiments with Methylene blue (MB) dye revealed that $\text{TiO}_2\text{-Eu}$ thin films offer better UV protection as compared to uncoated samples. We strongly believe that porous $\text{TiO}_2\text{-Eu}$ thin films can be effectively utilized as a UV blocking and light conversion coating.

11:30 AM EQ05.13.06

Spin Coated Indium Tin Oxide for Application as a Transparent Superconductor in Quantum Devices [Madison S. King](#)¹, Emma K. Batson², Karl Berggren² and Stephanie Hurst¹; ¹Northern Arizona University, United States; ²Massachusetts Institute of Technology, United States

The use of solid-state qubits in quantum technologies has created a need for efficient electro-optical transduction to avoid loss that comes with transmitting data at microwave frequencies over optical fibers in a quantum network [1]. Through the integration of superconducting electronics and quantum photonics, efficient transduction and read out of qubits can be achieved. The use of a transparent superconducting material is ideal to avoid efficiency loss in these circuits due to photon absorption. It has been demonstrated that indium tin oxide (ITO), a transparent semiconductor, behaves as a superconductor with a transition temperature (T_c) between 2–4 K when doped to a charge carrier concentration of 10^{21} cm^{-3} [2, 3]. This work is a part of collaborative effort to characterize the structure, composition, and electro-optical properties of superconducting ITO thin films prepared by two different methods. Our prior work has shown that commercially available ITO can be electrochemically reduced, permitting superconductivity. This process has been found to generate a rough nanoparticle layer on the surface of the ITO thin film [4].

Here we present the characterization of ITO thin films with applications as a transparent superconductor prepared by a spin coating method. Atomic force microscopy (AFM), scanning electron microscopy (SEM), and X-ray photoelectron spectroscopy (XPS) measurements provide details on surface and cross-section characteristics of the ITO thin films. The transparency of the thin films has been quantified through ellipsometry along with UV-visible spectroscopy and their T_c values determined.

[1] Lambert, N. J.; Rueda, A.; Sedlmeir, F.; Schwefel, H. G. Coherent Conversion between Microwave and Optical Photons—an Overview of Physical Implementations. *Adv. Quantum Technol.* **2020**, *3* (1), 1900077.

[4] Aliev, A. E.; Xiong, K.; Cho, K.; Salamon, M. B. Reversible Superconductivity in Electrochromic Indium-Tin Oxide Films. *Appl. Phys. Lett.* **2012**, *101* (25), 252603.

[5] Mori, N. Superconductivity in Transparent Sn-Doped In_2O_3 Films. *J. Appl. Phys.* **1993**, *73* (3), 1327–1338.

[6] Batson, E. Reduced indium tin oxide as a transparent superconductor. <https://hdl.handle.net/1721.1/144972> (accessed Sep 13, 2022).

11:35 AM DISCUSSION TIME

SESSION EQ05.14: On-Demand Presentation
Thursday Morning, December 8, 2022
EQ05-virtual

7:00 AM EQ05.14.01

Enhanced Electro-Thermal Properties of Gallium Doped Zinc Oxide (GZO) Thin-Films Transparent Heater Using 3D Printed Mask Technique Jasmine Beckford, Makhes Behera, Sangram K. Pradhan and Messaoud Bahoura; Norfolk State University, United States

There is a growing popularity of incorporation of transparent conducting oxide in domestic applications such as car defrosters, smart windows, and other devices. We fabricated and investigated the different properties of thin film transparent heaters (TFTH) which are made by a 3D printed mask. Gallium doped zinc oxide (GZO) transparent conducting oxide thin film is used as active material and deposited on glass substrate via pulsed laser deposition (PLD) technique. The thin films are ultra-smooth in nature and displayed excellent structural, electrical, optical, and thermal properties. The temperature dependent resistivity is measured using linear four probe methods, and the samples are highly conducting and showed low sheet resistance values. Optical transmission spectra revealed that the samples exhibit high optical transparency value of (>85%). These TFTH also demonstrated excellent joule heating effect. GZO based TFTH performed a consistent joule heating effect for many repeatable measurements with temperature reaching over 50 °C with a low input voltage of 8 V. These findings are encouraging for the use of GZO as a transparent conducting oxide material for applications in low-cost optoelectronics.

7:00 AM EQ05.14.02

Systematic Study of Electro Optic Polymers for Short-Distance Optical Interconnects Li Zhao^{1,2}; ¹Technische Universität Braunschweig, Germany; ²Cluster of Excellence PhoenixD, Germany

Li Zhao ^{1,2,*}, Florens Kurth ^{1,2}, Tasja Schwenke ^{2,3}, Anna Karoline Rüsseler^{2,4}, Emil Agocs ^{1,2}, Hans-Hermann Johannes ^{1,2}, Henning Menzel ^{2,3}, Wolfgang Kowalsky^{1,2}

¹ *Institut für Hochfrequenztechnik, Technische Universität Braunschweig, Braunschweig, 38106, Germany*

² *Cluster of Excellence PhoenixD, Hannover, 30167, Germany*

³ *Institut für Technische Chemie, Technische Universität Braunschweig, Braunschweig, 38106, Germany*

⁴ *Laser Zentrum Hannover e.V., Hollerithallee 8, 30419 Hanover, Germany*

*E-mail address: li.zhao@ihf.tu-bs.de

Electro optic (EO) polymers containing nonlinear chromophore and polymer matrix have attracted great attention due to their large EO activity. Versatile optical devices based on EO polymers like optical switch, optical modulator and so on are already reported. Compared to 1310 and 1550 nm wavelength, the EO activities at the shorter end of near-infrared range (from 800 nm to 1000 nm) for short-distance or frees-space optical interconnects have seldom been studied due to the challenge of absorption band. The work here provides a systematic study on how the molecular engineering affects the properties of these EO polymers, as well as photonic devices. By doping chromophores up to 50 wt%, the electro-optic coefficient as a function of the concentration is examined. To suppress intermolecular interaction at higher loading concentration, site isolating groups are attached to the chromophores. Along with guest host polymers, covalently bonded polymers are also probed. They show much higher long-term temperature stability compared to guest host polymers, which is a critical figure of merit for high-density photonic device array.

The advances in EO polymers make nanophotonic devices wide-band, high frequency and low energy consumption. Optical filter is an indispensable tool for nano-optic platform. Within our cooperation, the EO polymer as active material is integrated between thin-film mirrors which are prepared by ion beam sputtering. The Fabry-Perot interferometer alike device shows a promising frequency filtering and different wavelength range compared to silicon photonics.

The aim of this research is to study nanophotonic EO devices starting from theoretical material design, and up to device characterization. The material data bank built by us offers a good base for optical devices over a wide range of wavelength and under extreme working conditions.

Key words: electro optic polymer, chromophore, optical device.

7:00 AM EQ05.14.03

High-Efficient Photoelectrochemical Water Splitting of the Three-Dimensional ZnO Nanostructure Nanzheng Ji¹, Lingya Yu², Wenhan Cai², Chun-Yu Lee¹, Yongchun Xiao¹, Shujing Sun¹, Kun-Ching Shen³ and Chenlong Chen¹; ¹Chinese Academy of Science Fujian Inet, China; ²Chinese Academy of Science Fujian Inst, China; ³Fuzhou university, China

In recent years, ZnO has attained focus in water splitting applications due to the benefits of low cost, ease of fabrication, and high chemical stability. Here, we proposed a three-dimensional (3D) inclined ZnO nanowire structure via an Au catalyst-assisted vapor-liquid-solid method. This ZnO nanostructure exhibited better photoelectrochemical performance as compared with the ordinary 1D ZnO nanowires because of the increased area for the light-receiving and catalyst reaction. Furthermore, the 3D ZnO structure was doped with nitrogen using a post-annealing process, the photocurrent density of the *N*-doping ZnO was significantly increased from 1.68 mA/cm² to 2.82 mA/cm² at 1.23 V vs. RHE, and the photon-to-current conversion efficiency at 400 nm wavelength reached 7.3%. The strategy of appropriate *N*-doping can effectively increase carrier concentration of samples, and the carrier concentration of the sample annealed for one hour reaches the maximum of 6.54×10^{18} . In this study, the photoelectric properties of ZnO materials were considerably enhanced by constructing a 3D ZnO nanostructure and N doping.

SYMPOSIUM EQ06

Two-Dimensional (2D) van der Waals Materials—Quantum Properties and Electronic and Photonic Devices
November 28 - December 7, 2022

Symposium Organizers

Monica Allen, University of California, San Diego
Ming-Yang Li, TSMC
Doron Naveh, Bar-Ilan Univ
Xu Zhang, Carnegie Mellon University

* Invited Paper
+ Distinguished Invited

SESSION EQ06.01: Quantum and Topological Materials I
Session Chairs: Doron Naveh and Haozhe Wang
Monday Morning, November 28, 2022
Sheraton, 2nd Floor, Back Bay B

10:30 AM *EQ06.01.01

"Slide-Tronics" Moshe Ben Shalom; Tel Aviv University, Israel

A ferroelectric system is presented, only two atoms thick. Its intrinsic electric polarization emerges once stacking diatomic hexagonal layers with parallel lattice orientations. Interestingly, the symmetry of these bilayer crystals translates a minute planner shift between the layers, by one inter-atomic spacing, to a vertical flipping of the structure and its out-of-plane polarization. Owing to the interfacially-confined charge redistribution in these systems, we named the phenomena interfacial ferroelectricity. I will discuss the origin and consequences of this confinement from a real and momentum space perspective and the unique polarization switching mechanism by domain wall sliding observed in our experiments.

"Interfacial ferroelectricity by van-der-Waals sliding"
<https://www.science.org/doi/10.1126/science.abe8177>

11:00 AM *EQ06.01.03

High-Order van der Waals Superlattices and Artificial Quantum Solid Beyond Mechanical Exfoliation and Restacking Xiangfeng Duan; University of California-Los Angeles, United States

The advent of two-dimensional atomic crystals (2DACs) and van der Waals heterostructures (vdWHs) has inspired a new thinking on heterostructure construction beyond the limits of lattice matching requirement. However, the vdWHs explored to date have been largely limited to relatively simple systems with a small number of building blocks. The preparation of high-order vdW superlattices with a larger number of alternating units is exponentially more challenging due to the limited yield and scalability of the commonly used exfoliation-and-restacking strategy. Here I will discuss strategies to create high-order vdW superlattices (vdWLSs). First, by exploiting a capillary-force-driven rolling-up process, we show a series of synthetic VDWHs can be transformed into high-order vdWLSs with alternating atomic layers of widely variable material compositions, electronic band offset dimensions, chirality and topology. Alternatively, we further introduce a molecular intercalation approach to prepare a new family of hybrid superlattices consisting of alternating layers of covalently bonded 2D atomic layers and self-assembled molecular layers, which opens the door to exploit highly versatile molecular design strategies to tailor solid-state materials, enabling artificial materials with designable structural motifs and tunable electronic properties beyond the reach of conventional crystalline solids. We will particularly highlight a recent example of a new class of chiral molecular intercalation superlattices with robust chiral-induced spin selectivity. The formation of high-order vdW superlattices defines a rich artificial materials platform to unlock previously inaccessible physical limits and enable new device concepts beyond the reach of the existing materials.

1:45 PM *EQ06.02.01

Weyl Semimetal Phase in 2D Tellurium Under High Pressure Peide P. Ye; Purdue University, United States

Relativistic Weyl fermion quasiparticles in Weyl semimetal bring the electron's chirality degree of freedom into the electrical transport and give rise to various exotic phenomena. A topological phase transition from topological trivial phase to topological non-trivial phase offers a route to controllable topological electronic devices. Here, we report the Weyl semimetal phase in hydrothermally grown two-dimensional (2D) Tellurium (Te) induced by pressure (up to 2.47 GPa). The highly tunable chemical potential in 2D Te provides a comprehensive understanding of the pressure-dependent electron band structure. The pressure-induced insulator to metal transition, two-carrier transport, and the non-trivial π phase shift in quantum oscillations are observed in the 2D Te Weyl semimetal phase. Our work demonstrates the pressure-induced bandgap closing in inversion asymmetric narrow bandgap semiconductors and opens the door for the electronic transport study on the topological phase transition process.

2:15 PM EQ06.02.02

Excitonic Three-Level System for Quantum Interference in Transition Metal Dichalcogenide Monolayers and Bilayers Jonas M. Bauer, Sebastian Bange, John M. Lupton and Kaiqiang Lin; Universität Regensburg, Germany

Combining atom-like quantum interference phenomena with optoelectronic devices has been a long-standing goal. Few solid-state systems exhibit such quantum interference effects like electromagnetically induced transparency (EIT). We have discovered a new excitonic species, the high-lying exciton (HX), in transition metal dichalcogenide monolayers with almost twice the band-edge A-exciton energy and with a linewidth as narrow as that of band-edge excitons [1]. The coincidence of such high-lying excitonic species at around twice the energy of band-edge excitons explains the efficient exciton-exciton annihilation in TMDC monolayers, and forms a three-level system that enables the excitonic quantum-interference phenomenon revealed in optical second-harmonic generation (SHG) [2]. High-lying excitons in bilayer WSe₂ can be widely tuned by twisting [3] and by the Stark effect, which gives control over the excitonic quantum interference and the corresponding optical nonlinearity. In a monolayer WSe₂ transistor device, an electrical gate controls both the oscillator strength and the detuning of the excitonic transitions and thus the Rabi frequency of the strongly driven three-level system, enabling excitonic quantum interference to be electrically switched on and off in a deterministic fashion.

[1] K. -Q. Lin et al., *Nat. Commun.* **12**, 5500 (2021).

[2] K. -Q. Lin, S. Bange, & J. M. Lupton, *Nat. Phys.* **15**, 242-246 (2019).

[3] K. -Q. Lin et al., *Nat. Commun.* **12**, 1553 (2021).

2:30 PM EQ06.02.03

Nonlinear Interactions of Dipolar Excitons and Polaritons in MoS₂ Bilayers Charalambos Louca¹, Armando Genco², Salvatore Chiavazzo³, Thomas P. Lyons^{1,4}, Sam Randerson¹, Chiara Trovatiello², Peter Claronino¹, Rahul Jayaprakash¹, Kenji Watanabe⁵, Takashi Taniguchi⁵, Stefano Dal Conte², David Lidzey¹, Giulio Cerullo², Oleksandr Kyriienko³ and Alexander Tartakovskii¹; ¹The University of Sheffield, United Kingdom; ²Politecnico di Milano, Italy; ³University of Exeter, United Kingdom; ⁴RIKEN Center for Emergent Matter Science, Japan; ⁵National Institute for Materials Science, Japan

Coherent superposition of light and matter allows for the realisation of half-light half-matter quasiparticles called polaritons. Nonlinear interactions between excitons strongly coupled to light are key for accessing quantum many-body phenomena in polariton systems[1]. Atomically-thin two-dimensional semiconductors provide an attractive platform for strong light-matter coupling owing to many controllable excitonic degrees of freedom[2]. Among these, the recently emerged exciton hybridization opens access to unexplored excitonic species, with a promise of enhanced interactions[3]. In this work [4], we employ hybridized interlayer excitons (hIX) in bilayer MoS₂ to achieve highly nonlinear excitonic and polaritonic effects. Such interlayer excitons possess an out-of-plane electric dipole as well as an unusually large oscillator strength [5]. The latter allows us to realise dipolar polaritons (dipolaritons) in bilayers in optical microcavities with large Rabi splitting. We observe coupling strengths comparable to monolayer intralayer excitons and as much as half of that of intralayer excitons in bilayers.

The dipolar nature of hIX and polariton states in MoS₂ homobilayers results in approximately 8 times stronger nonlinearity compared with their monolayer intralayer exciton [6] counterparts. Namely, we observe saturation and blueshift at much lower exciton densities, which can be explained by the enhanced exciton-exciton coulomb interactions in this system.

We, also, find a further strong enhancement of interaction under simultaneous excitation of inter and intralayer excitons that share the same valence band. Specifically, we observe intralayer excitons blueshift while hIX redshift with the bleaching of hIX occurring at an order of magnitude lower densities than separate illumination. Thus, we report on an overall enhancement of the nonlinearity by nearly two orders of magnitude. Simultaneous excitation provides access to an unprecedented nonlinear regime which we describe theoretically by analysing the excitonic many-body physics and the inter-species cross interactions. We refer to this effect as hole-crowding, and note that, to our knowledge, it was never considered before, requiring specific conditions matched only in TMD bilayers. The presented insight into many-body interactions provides new tools for accessing few-polariton quantum correlations which are highly sought after for fundamental studies and applications in polariton logic networks .

[1] Deng, H., Haug, H. & Yamamoto, Y. Exciton-polariton Bose-Einstein condensation. *Rev. Mod. Phys.* **82**, 1489–1537 (2010).

[2] Dufferwiel, S. *et al.* Valley-addressable polaritons in atomically thin semiconductors. *Nat. Photonics* **11**, 497–501 (2017).

[3] Alexeev, E. M. *et al.* Resonantly hybridized excitons in moiré superlattices in van der Waals heterostructures. *Nature* **567**, 81–86 (2019).

[4] Louca, C. *et al.* Nonlinear interactions of dipolar excitons and polaritons in MoS₂ bilayers. *Preprint* at <https://doi.org/10.48550/arXiv.2204.00485> (2022).

[5] Gerber, I. C. *et al.* Interlayer excitons in bilayer MoS₂ with strong oscillator strength up to room temperature. *Phys. Rev. B* **99**, 1–8 (2019).

[6] Zhang, L. *et al.* Van der Waals heterostructure polaritons with moiré-induced nonlinearity. *Nature* **591**, 61–65 (2021).

2:45 PM EQ06.02.04

The Axial Higgs Mode in RTes Yiping Wang¹, Ioannis Petrides², Grant McNamara¹, Mofazzel Hosen¹, Shiming Lei³, Yueh-Chun Wu⁴, James L. Hart⁵, Jun Yan⁴, Di Xiao⁶, Judy Cha⁵, Prineha Narang², Leslie Schoop³ and Kenneth Burch¹; ¹Boston College, United States; ²Harvard University, United States; ³Princeton University, United States; ⁴University of Massachusetts Amherst, United States; ⁵Yale University, United States; ⁶University of Washington, United States

Charge density wave (CDW) systems can host a variety of emergent modes whose properties are linked to a change or breaking of symmetry; a well studied example is the Higgs (amplitude) mode that breaks translational symmetry. Despite its close resemblance to superconductivity and first prediction in 1955, all CDW to date have revealed s-wave condensation with a scalar Higgs. Uncovering the symmetry properties of collective modes is challenging, usually necessitating very low temperatures and requiring going beyond typical spectroscopic or scattering techniques. Here, we present the study of room temperature Raman spectra of the CDW system RTe_3 (where $\text{R} = \text{La}$ or Gd) and reveal the existence of an axial Higgs mode. We use a polarization-resolved inelastic scattering technique to obtain the Raman tensor associated to the Higgs mode, elucidating the axial vector representation (i.e. a pseudo-angular momentum) and the unconventional nature of the CDW in RTe_3 .

3:00 PM BREAK

3:30 PM *EQ06.02.06

Frank van der Merwe Manufacturing of Bilayer Graphene with ‘Smart’ Processes [Haozhe Wang](#); California Institute of Technology, United States

While the number of exciting physical phenomena observed in bilayer graphene increases, a significant gap persists in transforming these discoveries into practical applications, owing to the small-scale samples obtained via top-down approaches. We realized a layer-by-layer (that is, Frank-van der Merwe) growth mode in large-scale bilayer graphene, with no island impurities, which is unprecedented in any van der Waals-stacked materials. Machine learning is adopted to assist spectroscopy, enabling the ‘smart’ characterization following the chemical vapor deposition. Rather than random sampling on large-area materials, we adapted K-means algorithms to analyze Raman mapping data for precise characterization of stacking order and layer number of graphene. After growth, a transfer is necessary to move bilayer graphene from the growth substrate to a destination substrate with a mandatory sacrificial support layer. This process induces residuals, wrinkles, and cracks, thus deteriorating 2D materials from their intrinsic properties. We utilized the Marangoni effect, also known as the ‘tears of wine’, to enable ‘smart’ transfer by building a surface tension gradient in transfer liquids. We demonstrate our autonomous Marangoni-flow transfer technique can transfer bilayer graphene without a support layer, resulting in residue-free bilayer graphene.

4:00 PM EQ06.02.09

Strong and Localized Luminescence from Interface Bubbles Between Stacked hBN Multilayers [HaeYeon Lee](#)^{1,2}, [Soumya Sarkar](#)³, [Kate Reidy](#)², [Abinash Kumar](#)², [Julian Klein](#)², [Kenji Watanabe](#)⁴, [Takashi Taniguchi](#)⁴, [James LeBeau](#)², [Frances M. Ross](#)² and [Silvija Gradečak](#)³; ¹Columbia University, United States; ²Massachusetts Institute of Technology, United States; ³National University of Singapore, Singapore; ⁴National Institute for Materials Science, Japan

Van der Waals (vdW) layered materials and their heterostructures exhibit extraordinary physical properties while readily allowing out-of-plane deformation, which is of great interest for flexible and conformal electronics. A unique approach to understand the role of mechanical deformation on optoelectronic properties of vdW materials is to take advantage of the bubbles that are formed during the fabrication of vertical vdW heterostructures. Potential applications of bubbles in vdW heterostructures in optoelectronics and photonics have been recently reported due to their unique structure, the resulting strain, and the pressure in the bubble (vdW pressure), however, have been limited to monolayers. Strain engineering of vdW multilayers should present new opportunities in optoelectronics since multilayers of vdW materials exhibit robust optical performance, their bending is different from that seen in a monolayer or in classical plate theory, and multilayers circumvent issues related to exfoliation and manipulation of monolayers. Here, we demonstrate strong and localized luminescence in the ultraviolet region from interface bubbles between stacked multilayers of hexagonal boron nitride (hBN). Compared to bubbles in stacked monolayers, bubbles formed by stacking vdW multilayers show distinct mechanical behavior. We combine experimental measurements and theoretical modeling to elucidate geometry and strain across the bubble, providing insights into bending of vdW multilayers. We then demonstrate a novel approach to modify the bubble geometry by utilizing the polymeric material confined within the bubbles, resulting in strong luminescence and formation of optical standing waves. We observe a strong phonon-coupled luminescence locally from the hBN bubble regions and examine the origin of the optical emission. Our results open a new route to design and modulate microscopic-scale optical cavities in ultraviolet region with controlled dimensions *via* strain engineering in vdW materials, which we suggest will be relevant to both fundamental mechanical studies and stretchable optoelectronic and photonic applications.

4:15 PM EQ06.02.08

Magic-Angle Graphene for Highly Efficient Tunable 2D Photonic Surfaces and Waveguide-Coupled Modulators [Tao Fang](#), [Xiaoxin Wang](#) and [Jifeng Liu](#); Dartmouth College, United States

Tuning the refractive index of optical materials via external stimuli (e.g. electric field, temperature, etc.) has broad applications from optical communications to display technologies. While conventional semiconductor quantum well modulators can achieve a fast and reversible optical tunability, the refractive index change is small ($\Delta n, \Delta k \ll 0.1$). Phase change materials can achieve large $\Delta n > 1$, yet the response is much slower due to the phase transition rate limitation. Tunable 2D photonic surfaces provide a unique opportunity in their atomic thickness and a large refractive index change ($\Delta n, \Delta k > 1$) comparable to phase change materials, while simultaneously offering a response time even faster than conventional semiconductors, enabling unique opportunities in tunable photonic devices. Magic angle graphene (twisted bilayer graphene with the twist angle around 1.1°) is famous for its topological insulator and unconventional superconductivity behavior. However, until now, few studies have been conducted on its applications in photonics to benefit from its unique band structures.

In this research, we extract the optical conductivity and dielectric function of the magic angle graphene by tight-binding model and Kramers-Kronig relations. We then calculated the refractive index of the magic angle graphene at different Fermi levels upon electrical gating. Interestingly, while regular monolayer graphene changes from a semimetal ($n \sim k$) to a dielectric material ($n \gg k$) upon gating at near infrared (NIR) spectral regime, magic angle graphene behaves in the opposite fashion in that its changes from a semimetal to a good metal ($n \ll k$). This behavior gives magic angle graphene a unique application prospective in photonics.

As a demonstration, we use finite element model to design magic-angle graphene based optical devices. We report 2D surface photonic modulators based on coupling between magic angle graphene and regular single-layer graphene to best utilize their opposite behavior upon electrical gating. This modulator can work both in reflective mode and transmission mode, and the former can be applied to efficient modulating retroreflectors for free-space optical communication and light detection and ranging (LiDAR) applications. With optimized parameters and dielectric materials in an optical slot-antenna coupled cavity (SAC), the broadband reflection difference in 1500-2000 nm wavelength range between the on and off states can reach 70%, with a low insertion loss of 0.7 dB and a high extinction ratio of 7 dB almost independent of incident angles. This performance far exceeds our previous design optimization of surface-incident modulator based on regular single layer graphene in a similar optical SAC structure, which only achieved an extinction ratio of 1.62 dB [1]. This device structure also enables a low driving voltage for free-space optical modulation, as opposed to their commercial bulk LiNbO_3 counterparts that require more than 100 V to drive [2].

Our second design is the magic-angle graphene on silicon waveguide electroabsorption modulator. This waveguide could work at the wavelength around 1550 nm with an on-off ratio larger than 14 (> 11 dB extinction ratio) and transmission loss less than 0.013 dB. To increase the absorption difference, we compared slot waveguide vs. channel waveguide structures. According to the previous work on graphene coupled silicon waveguide electroabsorption

modulator, our device can work in a similar infrared region, but our simulation results showed a larger modulation 0.22 dB than their results 0.1 dB. Finally, the device concept for such large refractive change 2D photonic system may also extend to other 2D materials and other electromagnetic wave range. Currently, tunability of flat metalenses and other optical components is of great interest for these 2D surface photonic systems.

References

- [1] S Fu et al. ACS Photonics 6 (1), 50-58
- [2] https://www.thorlabs.com/newgrouppage9.cfm?objectgroup_id=2729

4:30 PM EQ06.02.07

Magnetotransport Properties of MBE-Grown NiTe₂ Zuzanna W. Ogorzalek¹, Bartłomiej Seredynski¹, Slawomir Kret², Wiktoria Zajkowska², Rafal Bozek¹, Mateusz Tokarczyk¹, Michal Baj¹, Michal Grzybowski¹, Wojciech Pacuski¹, Janusz Sadowski^{1,2,3} and Marta Gryglas-Borysiewicz¹; ¹University of Warsaw, Poland; ²Institute of Physics, Polish Academy of Sciences, Poland; ³Linnaeus University, Sweden

The recent discovery of topological semimetals (TSMs) with linear Dirac cone-shaped band dispersion, opened a new path of research in condensed matter physics. In some special TSMs, called type-II TSMs, the Dirac cone is strongly tilted as a result of broken Lorentz symmetry. As a consequence many peculiar physical phenomena, such as angle-dependent chiral anomaly [1], exotic superconductivity [2] and large, positive magnetoresistance [3] appear. Here we focus on the NiTe₂ which has recently been shown to be type-II Dirac TSM with Dirac nodes much closer to the Fermi level (EF) than in other type-II Dirac transition metal di-tellurides (TMDT), which opens possibility to exploit phenomena associated with Dirac carriers in transport [4]. There are a number of methods to obtain high quality crystalline TMDT materials including self-flux method [4-6] and molecular beam epitaxy [7]. The latter method is relatively novel and yet seems promising due to an in-situ monitoring of the growth process with reflection high energy electron diffraction. In this paper, we present a study of the magnetotransport properties of MBE-grown NiTe₂ layers. Hall effect measurements were performed in magnetic fields up to 12 T and in temperature range from 300 K to 1.4 K. Samples were grown on semi-insulating GaAs (111)B, which provides the same crystal symmetry and the lattice parameter close to that of NiTe₂. The growth conditions were adjusted by the substrate temperature and modification of Ni and Te fluxes, which enabled variation of the room temperature resistivity by two orders of magnitude. The resistivity of the samples dropped when temperature was decreased, however the residual resistivity ratio stays relatively low, reaching 10 for the best samples. Possible scattering mechanisms, keeping the value of the low temperature resistivity relatively high, will be discussed. They are of key importance as the Dirac surface states have been observed by ARPES in our NiTe₂ samples, but still, no clear impact of relativistic carriers on electronic transport has been concluded up to now.

This work has been supported by the National Science Centre (Poland), through the project No. 2017/27/B/ST5/02284.

- [1] Lv Y. Y. et al., Phys. Rev. Lett. 118, 096603 (2017)
- [2] Alidoust, M. et al., Phys. Rev. B 95, 155124 (2017)
- [3] Xiong Ali, M. et al. Nature 514 205–208 (2014)
- [4] Chunqiang Xu et al., Chem. Mater. 30, 4823–4830 (2018)
- [5] Qianqian Liu et al., Phys. Rev. B 99, 155119 (2019)
- [6] Wenkai Zheng et al., Phys. Rev. B 102, 125103 (2020)
- [7] Seredynski B. et al, Cryst. Growth Des. 21, 10, 5773–5779 (2021)

SESSION EQ06.03: 2D Electronic and Photonic Devices I
Session Chairs: Monica Allen and Doron Naveh
Tuesday Morning, November 29, 2022
Sheraton, 2nd Floor, Back Bay B

8:30 AM *EQ06.03.01

Zerovalent-Metal Intercalated MoS₂ Hybrids for Optoelectronics Ashwin Ramasubramaniam; University of Massachusetts-Amherst, United States

The intercalation of layered compounds is a promising route for scalable synthesis of 2D heterostructures with novel emergent optoelectronic properties. Here, we investigate, via first principles calculations, the intercalation of zerovalent metals within the van der Waals gap of bulk MoS₂. Specifically, we focus on Cu-MoS₂ and Sn-MoS₂ hybrids that can accommodate Cu and Sn, ranging from clusters to continuous 2D layers within the vdW gap of MoS₂. We study the evolution of the Cu-MoS₂ and Sn-MoS₂ hybrids with increasing metal content and examine the consequences for intercalation energetics and optoelectronic properties as the intercalated metals evolve from disordered clusters to contiguous layers. We identify emergent interfacial plasmons (1-2 eV range) that are unique to these intercalated materials, arising from resonant 2D metallic states within the MoS₂ band gap. Our calculations are shown to be in good agreement with experiments and help explain the enhanced infrared absorption of the Cu-MoS₂ and Sn-MoS₂ hybrids. Overall, our results indicate that intercalation of zerovalent metals in layered materials offers a facile and scalable approach for designing hybrid 2D heterostructures with tunable optoelectronic properties for device applications.

9:00 AM EQ06.03.02

Linear Bulk Photovoltaic Effect in Strain Gradient-Engineered MoS₂ Jie Jiang and Jian Shi; Rensselaer Polytechnic Institute, United States

The theoretical Shockley-Queisser limit of photon-electricity conversion in conventional *p-n* junction could be potentially overcome by the bulk photovoltaic effect that uniquely occurs in non-centrosymmetric materials. Using strain gradient engineering, the flexo-photovoltaic effect, i.e., strain gradient-induced bulk photovoltaic effect, can be activated in centrosymmetric semiconductors significantly expanding material choices for future sensing and energy applications. Here, we propose a strain gradient engineering approach based on the structural inhomogeneity and phase transition of a two-dimensional/three-dimensional (2D/3D) hybrid system. We report an experimental demonstration of the flexo-photovoltaic effect in an archetypal 2D material MoS₂ transferred on a VO₂ microbeam. The experimental bulk photovoltaic coefficient in MoS₂ is orders of magnitude higher than that in most non-centrosymmetric materials. Our findings unveil the fundamental relation between the flexo-photovoltaic effect and a strain gradient in low-dimensional materials, which could potentially inspire the exploration of novel optoelectronic phenomena in strain gradient-engineered materials. The MoS₂/VO₂ hybrid structure sheds light on emerging phenomena and brings new opportunity in 2D/3D interfaces.

9:15 AM EQ06.03.03

Excitonic Properties in 2D Silver Phenylchalcogenolates Woo Seok Lee, Yeongsu Cho, Eric R. Powers, Watcharaphol Paritmongkol, Tomoaki Sakurada, Heather J. Kulik and William Tisdale; Massachusetts Institute of Technology, United States

Silver phenylselenolate (AgSePh) and silver phenyltelluroate (AgTePh) are novel hybrid organic-inorganic two-dimensional (2D) semiconductors. AgSePh and AgTePh are synthesized in the form of three-dimensional crystals consisting of 2D layers bound together by van der Waals forces. Unlike 2D layered perovskites and transition metal dichalcogenides, AgSePh and AgTePh feature strong covalent bonding between organic and inorganic components, forming truly hybrid organic-inorganic semiconductors. However, AgSePh and AgTePh exhibit strikingly different excitonic properties despite having the same crystal structure. Whereas AgSePh exhibit narrow, fast luminescence with minimal Stokes shift, AgTePh exhibits comparatively slow, significantly broadened luminescence with large Stokes shift. In this presentation, we will present the synthesis, structural and optical properties of AgSePh and AgTePh films. Furthermore, we will discuss different physical mechanisms underlying light emission in AgSePh and AgTePh. Using time-resolved and temperature-dependent optical spectroscopy, combined with sub-gap photoexcitation studies, we will show that exciton dynamics in AgTePh are dominated by intrinsic self-trapping behavior, whereas dynamics in AgTePh are dominated by interaction of free-excitons with extrinsic defect states. Finally, we will discuss the origin of exciton self-trapping in AgTePh using density functional theory calculations.

9:30 AM BREAK

10:00 AM *EQ06.03.04

Large Scale Atomically Thin Semiconductor Films for Electronics and Optoelectronics [Jiwoong Park](#); University of Chicago, United States

Two dimensional (2D) electron transport has been one of the most important topics in science and technology for decades. It was originally studied in 3D semiconductors and then continued in 2D van der Waals (vdW) crystals. In this talk, I will start with the large-scale processes for generating 2D crystalline semiconductor transition metal dichalcogenide (TMD) films and superlattices that could be used to fabricate atomically thin integrated circuits cleanly. These large scale TMD films also display novel optical properties depending on the geometry of the film itself and on the geometry of the incident light. I will discuss two examples. First, TMD films grown with nanoscale textures produce optically isotropic films with strongly enhanced absorption. Second, TMD monolayers can be used to form three-atom-thick waveguides with a long (~ 1 cm) propagation length that can be used to generate a novel 2D photonics platform.

10:30 AM EQ06.03.05

Proximity Exchange in 2D Magnets Deduced from a Cr(o-tolyl)₄ Magnetic Sensor [Kathleen R. Mullin](#) and James M. Rondinelli; Northwestern University, United States

Molecular color centers, like Cr(o-tolyl)₄, show promise as a more flexible platform for magnetic sensing with many similarities to more frequently studied quantum magnetic sensors, like diamond NV centers. Using these molecules in thin film geometries would allow for the sensing of magnetic fields over a wide range of distances, angstroms to micrometers, from the analyte. This is particularly important for 2D magnetic materials, such as CrI₃, that have shown large discrepancies in magnetic fields measured by different methods. Past studies have suggested proximity exchange, that occurs between the magnetic substrate and a very close sensor, may be responsible for the discrepancies. To that end, we used density functional theory calculations to understand how the molecular color center, Cr(o-tolyl)₄, adsorbs on a monolayer CrI₃ substrate and how proximity exchange, or wavefunction overlap, impacts the excited states in the Cr(o-tolyl)₄ molecule at different distances from the substrate. Magneto-static modeling is used to predict dipolar interactions between the magnetic sensor and the substrate. By combining these models, we show that at short distances proximity exchange dominates in molecule-substrate interaction, but at further distances the molecule would act as a typical magnetic sensor, with magneto-static effects dominating changes to the energies of the excited state. Our models effectively demonstrate how a molecular color center could be used to measure the magnetic field of a 2D magnet and the role of important distance-dependent interactions that contribute to the field.

This work was supported by the U.S. Department of Energy, Office of Science, Basic Energy Sciences under award DE-SC0019356.

10:45 AM EQ06.03.06

Towards Compact Phase-Matched and Waveguided Nonlinear Optics in Atomically Layered Semiconductors [Chiara Trovatello](#)^{1,2}, Xinyi Xu¹, Fabian Mooshammer¹, Yinming Shao¹, Shuai Zhang¹, Kaiyuan Yao¹, Dmitri N. Basov¹, Giulio Cerullo² and P.J. Schuck¹; ¹Columbia University, United States; ²Polytechnic University of Milan, Italy

Nonlinear frequency conversion provides essential tools for light generation, photon entanglement, and manipulation. Conventional nonlinear optical crystals display moderate second-order nonlinear susceptibilities ($|X^{(2)}| \approx 1-30$ pm/V) and perform well in benchtop setups with discrete optical components. However, such crystals do not easily lend themselves to miniaturization and on-chip integration. Two-dimensional transition metal dichalcogenides (TMDs) possess huge nonlinear susceptibilities ($|X^{(2)}| \approx 100-1000$ pm/V) and, thanks to their deeply sub-wavelength thickness, offer a unique platform for on-chip nonlinear frequency conversion and light amplification. However, due to their atomic thickness, they display a notably lower second harmonic generation (SHG) efficiency ($\eta_{\text{SHG}} = I_{2\omega}/I_{\omega} \approx 10^{-11}$ at $I_{\omega} = 30$ GW/cm²) compared to standard nonlinear crystals ($\eta_{\text{SHG}} = I_{2\omega}/I_{\omega} = 1-50\%$).

The nonlinear conversion efficiency of a TMD could be scaled by increasing the propagation length through the active medium. This is attainable by increasing the number of layers in the TMD sample. However, the nonlinear optical properties of semiconducting TMDs critically depend on their crystallographic symmetry, i.e., 2H (hexagonal) or 3R (rhombohedral). 2H-MoS₂ is naturally centrosymmetric, giving an opposite dipole orientation among consecutive layers. This results in a vanishing nonlinear susceptibility ($|X^{(2)}| = 0$) for crystals with even number of layers and precludes efficient conversion in multilayer 2H-TMDs. In contrast, 3R-MoS₂ naturally combines broken inversion symmetry ($|X^{(2)}| \neq 0$) and aligned layering, representing ideal candidates to boost the nonlinear gain with minimal footprint. The nonlinear optical response of 3R-MoS₂ has been explored in some recent pioneering studies^[1,2], so far focusing on thinner crystals, reporting the quadratic enhancement with the number of layers at the 2D limit, and showing a maximum SHG enhancement of $\approx 10^2$ occurring at specific thickness windows. Pushing towards general application, however, requires higher nonlinear enhancements and thus larger layer number, which in turn leads to more intricate interferences and interactions within the crystal.

Here we measure SHG from multilayer 3R-MoS₂ crystals with variable thickness, using a custom transmittance microscope, and we achieve record nonlinear enhancement from a van der Waals material, $>10^4$ stronger than a monolayer, revealing the intrinsic single-pass upper limits of the material. We provide a comprehensive model, which explains the second-order nonlinearity of 3R-MoS₂ including its phase mismatch and its intrinsic interference effects. We report the first measurement of the coherence length along the ordinary axis, elucidating the role of phase-matching at excitation photon energies close to the telecom band. Furthermore, along the extraordinary axis, we achieve broadly tunable SHG in a waveguide geometry, revealing the coherence length in such a structure for the first time. Upon edge coupling the fundamental wavelength on one side of the flake we detect the SH emission from the opposite edge within our field of view. We observe the characteristic SHG signal modulation with increasing path length, allowing us to quantify the out-of-plane coherence length in 3R waveguide structures. In addition, we also characterize the anisotropic linear optical properties by imaging the propagation of waveguide modes in real space using near-field nano-imaging, identifying the conditions for phase-matched SHG in waveguide geometries^[3].

Our results highlight the potential of 3R-stacked TMDs for integrated photonics, providing critical parameters for designing highly efficient on-chip nonlinear optical devices including periodically poled structures, optical parametric oscillators and amplifiers, and quantum circuits.

[1] Shi, J. et al. *Adv.Mater.* 29, 1701486 (2017).

[2] Zhao, M. et al. *Light: Sci. Appl.* 5, e16131 (2016)

[3] Xu, X., Trovatiello, C. et al. *arXiv:2204.12618* (2022)

11:00 AM *EQ06.03.07

Dual COVID-19 and Influenza Virus Detection via Antibody-Functionalized Graphene Field-Effect Transistors Deji Akinwande; The University of Texas at Austin, United States

The advent of pandemic caused by SARS-CoV-2 (COVID-19) has highlighted the requirement of sensor devices capable of carrying out rapid differential diagnosis of various viruses that may manifest similar physiological symptoms but demand tailored treatment plan. Annually, the world undergoes multiple cycles of seasonal Flu infection which now poses a bigger challenge, exacerbated by the pandemic. In this work, we demonstrate liquid-gated graphene field-effect transistor (GFET) based rapid biosensing device capable of making differential diagnosis between Influenza and COVID-19 viruses. The device consists of four onboard GFETs arranged in a quadruple architecture, where each quarter is functionalized with specific antibody to utilize the antibody-antigen reaction on graphene's surface to indicate the presence of either Influenza or COVID-19. The graphene bio-sensors were successfully tested against a range of concentrations of both the viruses, indicating extremely high sensitivity. Unlike the standard polymerase chain reaction-based testing kits which have a turn-around time of at least three hours, graphene bio-sensors offer a response time of about 10 seconds, hence enabling rapid diagnosis. The antibody functionalized graphene bio-sensor is a suitable platform for the rapid diagnosis of existing and future infectious diseases.

11:30 AM EQ06.03.08

Charge Transfer in Janus 2D Semiconductors and Janus Heterostructures Fabricated by Low-Energy Selenium Implantation Yu-Chuan Lin^{1,2}; ¹The Pennsylvania State University, United States; ²Oak Ridge National Laboratory, United States

Janus transition metal dichalcogenide (TMD) monolayer is relatively new in the family of two-dimensional (2D) materials. In 2D Janus TMDs, such as MSSe (M= W, Mo), one M atomic layer is sandwiched by S and Se atomic layers. This asymmetry perpendicular to the basal plane of 2D Janus TMD results in a built-in dipole moment pointing from Se to S layers. Many theoretical studies have predicted many exciting aspects of 2D Janus TMDs, including electronic band structures, spin properties, piezoelectric, and photocarrier transfer. First, the preparation and properties of 2D WSSe and MoSSe prepared by selenium implantation will be discussed.[1] The plasma plumes of pulsed laser deposition offer controllable hyperthermal kinetic energies to synthesize metastable 2D materials that conventional thin film techniques cannot achieve. Using the plasma plumes, we replace the top S atoms in 2D WS₂ and MoS₂ with Se atoms and convert them to Janus structures. Second, transient absorption measurements reveal that the excitons in 2D Janus TMDs form faster than those in their pristine counterparts by about 30% due to their enhanced electron-phonon interaction by the newly introduced built-in dipole moment.[2] Finally, we study the charge transfer properties of bilayer heterostructures formed by Janus and regular TMDs with photoluminescence and time-resolved pump-probe measurements.[3] The results from three heterostructures with atomic layer sequences of S-W-Se/S-W-S, Se-W-S/S-W-S, and S-W-Se/Se-W-Se reveal that charge transfer from regular to Janus TMDs is ultrafast and independent of the direction of the built-in electrical field (Janus field). On the other hand, the charge transfer from Janus to regular TMDs is directional and controlled by the Janus field: When the current direction is along the field, the charge transfer is ultrafast and efficient, while the field blocks the charge transfer with an opposite charge current direction. The understanding of ultrafast and directional charge transfer between Janus and regular TMDs shows that the Janus structures can be used to make 2D heterostructures with efficient and directional charge transfer properties.

Reference:

[1] Y.-C. Lin, C. Liu, Y. Yu, E. Zarkadoula, M. Yoon, A. A. Puzos, L. Liang, Y. Gu, A. M. Strasser, G. Duscher, M. F. Chisholm, I. Ivanov, C. Rouleau, H. Meyer III, K. Xiao, D. B. Geohegan, "Low-energy implantation into transition metal dichalcogenides for Janus structures" *ACS Nano* (2020), 14, 3896-3906

[2] T. Cheng, Y.-C. Lin[†], Y. Yu, P. Valencia-Acuna, A. A. Puzos, C. Liu, I. N. Ivanov, G. Duscher, D. B. Geohegan, Z. Ni[†], H. Zhao[†] "Excitonic Dynamic in Janus MoSSe and WSSe Monolayers" *Nano Letters* (2021), 21, 931-937 († Corresponding author)

[3] T. Cheng, Y.-C. Lin[†], N. Rafizadeh, D. B. Geohegan, Z. Ni[†], K. Xiao, H. Zhao[†], "Janus Monolayers for Ultrafast and Directional Charge Transfer in Transition Metal Dichalcogenide Heterostructures" *ACS Nano* (2022), 16, 4197-4205 († Corresponding author)

11:45 AM EQ06.03.09

Towards Strain-Tuning Correlations in van der Waals Heterostructures Marshall A. Campbell^{1,2}, Sean Doan¹, Vignesh Chandrasekaran², Michael T. Pettes² and Luis Jauregui¹; ¹University of California, Irvine, United States; ²Los Alamos National Laboratory, United States

Two-dimensional (2D) materials and heterostructures offer a rich environment to study and probe quantum phenomena such as electron correlations, superconductivity, ferromagnetism, and topological effects with great tunability. Controllable in-situ strain in 2D materials offers a novel pathway to control those correlated effects. Transition metal dichalcogenides are one class of 2D materials known for their capability of electronic band tuning and promising photonic applications as they exhibit a direct gap at the monolayer limit. While several studies have been performed on commensurate TMD structures, few strain studies have been performed on twisted structures due to the difficulty in fabricating high-quality samples and the techniques available to apply controllable strain. Here, we present a strain study on twisted homobilayers of WSe₂ on hexagonal Boron nitride (BN). The twisted WSe₂ structure exhibits a moire lattice that alters the electronic band structure and phonon modes. Placing the twisted homobilayers of WSe₂/BN structure on flexible polyethylene terephthalate (PET) substrates enables the application of tunable tensile strain along the axis of substrate bending and orthogonal compressive strain due to the Poisson effect. This provides a controllable method to strain the moire superlattice. We then perform ultralow frequency Raman spectroscopy, photoluminescence spectroscopy, and lifetime measurements to characterize any changes with strain. We observe changes in the low-frequency phonon modes which we attribute to changes in the moire wavelength. Furthermore, we extract the strain applied to the homobilayer WSe₂ by a Gruneisen parameter analysis on phonon mode shift in the E_{2g} and A_{1g} modes. We measure an applied strain of roughly 1% in our samples. We carry on this analysis to observe shifts in the photoluminescence energy and exciton lifetime. We observe a small decrease in the exciton lifetime, but no significant shift in exciton energy at room temperature. Knowing the exact amount of strain applied to a moire lattice is pivotal to characterizing the strain-tunability in these structures. Our methods allow the characterization of the amount of strain applied and the modification of the moire patterns via low-frequency Raman measurements. Our results could pave the way toward strain-tunable electron interactions in strongly correlated systems and the study of strain-driven phase transitions in van der Waals heterostructures.

1:30 PM *EQ06.04.01

MoS₂ Transistors for Back-End-of-the-Line Si Integration [Tomas Palacios](#); MIT, United States

This paper describes our recent work on developing both the material synthesis and the fabrication technology needed to integrate single-layer molybdenum disulfide (MoS₂) devices at the back-end-of-the-line of fully fabricated Silicon CMOS chips. These devices could significantly improve the performance of future Si chips by enabling compact three-dimensional microsystems with shorter interconnects, lower leakage currents, and increased memory.

2:00 PM EQ06.04.02

Transition Metal Dichalcogenides p-n Junctions Fabricated by Plasma-Assisted Edge Doping [Luca Anzi](#), Andrea Tagliabue, Nikil Paithankar and Roman Sordan; Polytechnic University of Milan, Italy

Two-dimensional (2D) transition metal dichalcogenides (TMDCs) have raised great research interest due to their attractive optical and electronic properties. Their semiconducting nature and the low dimensionality make them the perfect candidate for new-generation electronic devices. MoS₂ and WSe₂ are the most promising TMDCs for the fabrication of 2D electronic circuits. However, a reliable technique to modify the carrier type and concentration in these semiconductors is still missing. Three different techniques have been used so far to dope TMDCs: charge transfer, electrostatic, and plasma-assisted doping. Charge transfer doping has been widely used due to a simple fabrication procedure. However, the lack of controllability and the induced carrier scattering make this method unsuitable for small scale devices. Electrostatic doping exploits external gate electrodes and has been used, e.g., to realize a lateral p-n junction with a controllable barrier height and carrier concentration. However, this method cannot be used in realistic applications due to the increased circuit complexity and power consumption. Plasma treatments with fluorinated gases or N₂ have been used to p-dope the MoS₂ surface by substituting S atoms with energetic F or N ions. However, the etching of the surface exposed to the plasma increases the surface roughness, which drastically affects the transport properties of the doped flakes. For this reason, the obtained p-n junctions exhibited relatively low forward current, limiting their use in realistic applications.

Here we demonstrate high-quality p-type MoS₂ and WSe₂ obtained by plasma-assisted edge doping. Ribbons of width of ~ 100 nm were patterned by e-beam lithography on wide-area flakes of MoS₂/WSe₂. The flakes, which initially exhibited an overall n-type behavior, were subsequently etched by SF₆ plasma. The etching incorporated an excess of F atoms at the edges of the ribbon caused by the plasma substitution of S/Se atoms. Due to their acceptor nature, the F atoms increased the concentration of holes in the proximity of the edges. In narrow enough (width < 100 nm) ribbons, the doping from the edges extended through the entire width, leading to an overall p-type conduction. At the interface between the ribbon and the wide part of the flake, a p-n junction was formed due to the opposite carrier type of the two sides.

The edge doping technique preserved the surface integrity of the TMDC flakes. We obtained high-quality MoS₂ p-n junctions with an on/off ratio of ~ 10⁴ and forward current of ~ 50 A/m (normalized to the ribbon width). Such p-n junctions were used to fabricate realistic electronic circuits, e.g., wave rectifiers and amplitude demodulators.

The presented technique for the p-type doping of MoS₂ and WSe₂ could be, in principle, adapted to control the doping type and concentration of any TMDC by choosing a suitable plasma treatment.

2:15 PM EQ06.04.03

Reduced Dopant-Induced-Scattering in Remote Charge Transfer Doped MoS₂ Field-Effect Transistors [Juntae Jang](#)¹, Jae-Keun Kim², Kyungjune Cho³, Keehoon Kang¹ and Takhee Lee¹; ¹Seoul National University, Korea (the Republic of); ²Max Planck Institute of Microstructure Physics, Germany; ³Korea Institute of Science and Technology, Korea (the Republic of)

Two-dimensional (2D) transition metal dichalcogenide (TMDC) semiconductors such as molybdenum disulfide (MoS₂) hold great promise for next-generation electronic devices [1, 2]. From a practical point of view, surface charge transfer doping (SCTD) is known to be an effective method to modulate the electrical properties of 2D semiconductors. However, although SCTD is a facile and non-destructive method, it could also introduce charged impurities that can hinder charge transport [3].

In this study, we overcome the shortcomings of SCTD through demonstrating a remote charge transfer doping by simply inserting a thin hexagonal boron nitride (h-BN) layer (< ~3 nm thickness) between MoS₂ channel and the n-type molecular dopants, benzyl viologen (BV), which was sufficient for achieving a significant charge transfer [4]. First, we characterized the electrical properties of MoS₂ field-effect transistors (FETs) with h-BN interlayer (denoted as “remotely doped” device) and without h-BN (denoted as “directly doped” device) before and after doping with temperature-dependent gated four-point probe measurements which can minimize the effect of phonon scattering and the varying charge injection behaviors due to the BV doping. As a result, we identified a significantly larger enhancement in the mobility of remotely doped device relative to its pristine (un-doped) state than that of directly doped device under similar carrier concentration conditions since the spatial separation of thin h-BN interlayer between BV and the MoS₂ FETs channel suppresses the charged impurity scattering which could be additionally introduced by the SCTD. Next, we conducted the quantitative analysis of the remote doping method in comparison with the conventional direct doping method and our mechanistic study supports the efficient suppression of the dopant-induced charged impurity scattering in the remotely doped MoS₂ channel, corroborated by our theoretical predictions.

Our mechanistic study of the novel doping method promotes the remote charge transfer strategy as a promising way for achieving a wide doping range without compromising the carrier mobility, which is required for high performance emerging electronic and optoelectronic devices based on 2D materials.

2:30 PM BREAK

3:00 PM *EQ06.04.04

Carbon Nanotube Transistors for a Future 3D Logic Technology [Qing Lin](#), Carlo Gilardi, Subhasish Mitra and H.S. Philip Wong; Stanford University, United States

Carbon Nanotube (CNT) Field-Effect Transistors (CNFETs) are promising candidates for future high-performance and energy-efficient digital logic. Gate-All-Around (GAA) CNFETs with doped extensions and multiple layers of high-density CNTs are projected to show up to 7× Energy-Delay Product (EDP) benefits vs. Si FET at the 2 nm technology node [1]. Moreover, CNFETs have already been integrated into silicon industrial manufacturing facilities at relaxed nodes (e.g. through DARPA 3DSoc program, at ADI, and SkyWater Technology Foundry), thus illustrating compatibility with existing fab process

infrastructures [2-3].

Many fundamental building blocks of the CNFET technology have already been demonstrated. In the very near future, it will be possible to integrate all the building blocks achieved thus far to demonstrate a MOSFET-like structure with 35-nm contacted gate pitch, and 20-nm active width that is projected to have performance that far exceeds Si transistors for a 2-nm node logic technology while at the same time can be fabricated in multiple 3D device layers for a future logic technology.

In this talk, I will describe the journey of the worldwide CNT research community that leads up to this important juncture. I will discuss the remaining challenges for CNFET to mature into a manufacturing-ready technology.

References:

- [1] C. Gilardi *et al.*, "Extended Scale Length Theory Targeting Low-Dimensional FETs for Carbon Nanotube FET Digital Logic Design-Technology Co-optimization," *2021 IEEE International Electron Devices Meeting (IEDM)*, 2021, pp. 27.3.1-27.3.4, doi: 10.1109/IEDM19574.2021.9720672.
- [2] T. Srimani *et al.*, "Heterogeneous Integration of BEOL Logic and Memory in a Commercial Foundry: Multi-Tier Complementary Carbon Nanotube Logic and Resistive RAM at a 130 nm node," *2020 IEEE Symposium on VLSI Technology*, 2020, pp. 1-2, doi: 10.1109/VLSITechnology18217.2020.9265083.
- [3] M. D. Bishop *et al.*, "Fabrication of carbon nanotube field-effect transistors in commercial silicon manufacturing facilities." *Nat Electron* **3**, 2020, pp. 492-501, doi: 10.1038/s41928-020-0419-7

3:30 PM *EQ06.04.05

Material and Device Challenges for Low Dimensional Material Transistor Technology Han Wang; Corporate Research, TSMC San Jose, United States

Low dimensional materials including 2D materials and 1D carbon nanotube offer unique properties for potential applications in advanced electronics technology. In this talk, I will give an overview of the activities in low dimensional materials research at TSMC Corporate Research. The prospects and key challenges facing the practical applications of these materials in transistor technology will be discussed. Some of the recent progresses in the 2D and CNT material and device research at TSMC will also be presented.

4:00 PM EQ06.04.06

Effect of Plasma Etching on the Transport Properties and Electrical Stability in Transition-Metal Dichalcogenide Field-Effect Transistors Mohammad Nouri and William S. Wong; University of Waterloo, Canada

The application of two-dimensional (2-D) layered transition metal dichalcogenide (TMDC) for high-performance large-area memory applications requires establishing long-term electrical stability through an understanding of the carrier transport and the effect of the materials processing on the device behavior. A novel approach for creating arrays of thin-film and few-layer molybdenum disulfide (MoS₂)-based field-effect transistors was achieved through a mechanical exfoliation and a dry etching process. The current-voltage (I-V) and electrical stability characteristics showed that the etching process can effectively remove intrinsic bulk defects within the TMDC layers and create few-layer device structures. The as-transferred thin-film transistor (TFT) structures, having thicknesses of ~90 nm, were found to have a trap density of approximately 3×10^{10} cm⁻² per monolayer. This defect density was observed to decrease when the layers were removed using a SF₆/O₂ plasma etching process, resulting in a positive threshold voltage shift in the transistor operation. The process was effective in removing bulk defects in the MoS₂ layers causing a positive threshold voltage shift of +40V with a final threshold voltage of -12V for a 3 nm thick layer. Conversely, the measured transport properties and electrical stability was found to degrade when the thickness of the MoS₂ layer was < 15 nm. This observed degradation was due to the etched backchannel layer moving closer to the active channel region as the TMDC layer was thinned. The transport properties of the transistor were affected by surface states along the backchannel contributing to carrier scattering as the thickness of the semiconductor approached the accumulation layer in the transistor. The same surface states acted as trap centers in the semiconductor degrading the electrical stability of the devices. This effect was becoming more pronounced as the proximity of the TFT backchannel surface approached the active channel region during etching. Finally, the effect of passivation layers on the etched backchannel will be presented for an array of TMDC devices for large-area memory applications.

4:15 PM EQ06.04.07

Giant and Tunable Fano Resonance Induced by Two-Dimensional Metals Kunyan Zhang¹, Rinu A. Maniyara¹, Yuanxi Wang², Maxwell Wetherington¹, Thuc Mai³, Timothy Bowen¹, Chengye Dong¹, Slava Rotkin¹, Angela R. Hight Walker³, Vincent Crespi¹, Joshua A. Robinson¹ and Shengxi Huang^{1,4}; ¹The Pennsylvania State University, United States; ²University of North Texas, United States; ³National Institute of Standards and Technology, United States; ⁴Rice University, United States

Quantum interference between phonons and other quasiparticles brings about fascinating physical phenomena. As an example of phonon coupled to a scattering continuum, Fano resonance is characterized by an asymmetric line shape in the scattering spectrum. Here, we report the giant Fano resonance of folded longitudinal optical phonons in SiC after the intercalation of atomically thin metals, with a resonance strength two orders of magnitude higher than prior reports. A range of physical characteristics, including surface termination, temperature, and excitation wavelength, were used to tune the degree of Fano resonance. The tuning mechanisms were studied by first-principles calculations, which reproduced the intricate phonon behaviors. Our work presents the plethora of tuning knobs for the phonon-related Fano resonance, which paves the way toward constructing quantum interference effects in the nanoscale limit.

4:30 PM EQ06.04.08

High-Performance Ambipolar MoTe₂ Field-Effect Transistors Zhiying Wang¹, HaeYeon Lee¹, Yang Liu¹, Jordan Pack¹, Song Liu¹, Luke Holtzman¹, Kenji Watanabe², Takashi Taniguchi², Cory Dean¹, Qianhui Shi³ and James Hone¹; ¹Columbia University, United States; ²National Institute for Materials Science, Japan; ³University of California, Los Angeles, United States

Two-dimensional (2D) monolayer semiconductors such as transition metal dichalcogenides (TMDs) host a variety of emergent quantum properties and have attracted intense attention in electronics and optoelectronics. For both fundamental studies and novel electronic applications, it is a critical prerequisite to achieve low-resistance contacts on monolayer (ML) TMDs. Semiconductor Molybdenum Ditelluride (MoTe₂) is an attractive material platform in various ways including its ambipolar behavior due to its smaller bandgap of 1.2 eV compared with other TMDs materials and small energy required for the phase transition. However, due to air-instability of ML MoTe₂ and weak Mo-Te bonding, it is challenging to fabricate high performance ML MoTe₂ transistors with low contact resistance. Therefore, there is a lack of fundamental studies of ML MoTe₂ and its applications.

Here, we present several techniques to fabricate electrical contacts on ML MoTe₂: (1) direct deposition of semimetal on ML MoTe₂ (2) insertion of

monolayer spacer as a tunneling barrier between metal contact and ML MoTe₂ and (3) pre-pattern high work function metal contact. High quality MoTe₂ is used for our study, which is synthesized by self-flux method and exhibits defect density as low as $1 \times 10^{11}/\text{cm}^2$. We compare electric performance of ML MoTe₂ field effect transistor fabricated by using different approaches mentioned above. Among those approaches, we have achieved ML 2H-MoTe₂ field effect transistor with low contact resistance which is an order of magnitude lower than the previous report for both electrons and holes at room temperature, by further optimizing the pre-pattern contact structure and device fabrication process. Our results can allow us to have comprehensive insight of the Landau level sequence and correlated states by accessing both electrons and holes region from a single device. It also provides new opportunities in optoelectronics using ML MoTe₂, which is comparable with silicon with similar band gap.

4:45 PM EQ06.04.09

Novel Nanospike Array Electrodes for Enhanced-Performance 50 NM-Channel MoS₂ Thin-Film Transistors Yuchen Zhou, Chankeun Yoon, Xin Xu, Kelly Liang and Ananth Dodabalapur; University of Texas at Austin, United States

There has been a great deal of research interest in scaling down the channel lengths in MoS₂ thin-film transistors (TFTs). However, when the channel length reaches the nanometer scale, transistors start experiencing short channel effects, including low on/off ratio, degraded subthreshold swing, and drain-induced barrier lowering (DIBL), etc. This abstract introduces an alternative to overcome short channel effects for transistors with channel lengths below 100 nm. Conventionally, MoS₂ TFTs have been fabricated with flat edge source and drain electrodes. By changing the shape of the source/drain electrodes into nanospike-like structure, transistors can overcome short channel effects and regain gate control. Furthermore, patterning the source and drain contacts into nanospike array electrodes can improve the on-current of the transistors as well. 50 nm-channel length MoS₂ TFTs with nanospike array electrodes were fabricated along with the conventional flat edge electrodes for direct comparison.

The 17 nm thick source/drain electrodes (Cr/Au) were patterned on 90 nm of SiO₂ coated silicon substrates using electron beam lithography (EBL). Mechanically exfoliated 5 nm few-layer MoS₂ and 20 nm thick hBN were transferred onto the preformed contacts. A 100 nm thick Au top gate was patterned with EBL and thermally evaporated. The nanospike tips are 200 nm wide equilateral triangles with a 1 μm long rectangular base extending orthogonally from conventional flat electrodes. The channel length, defined as the distance between the tips of the source and drain spikes, is approximately 50 nm. The total channel width is 3.4 μm with 5 pairs of nanospikes spaced evenly from each other.

Nanospike electrodes provide a unique bias-dependent charge flow pattern, which is responsible for the improved performance. Enhanced electric field results in increased charge injection from the tips of the nanospike electrodes and improves channel length scaling to sub-50 nm while maintaining excellent current modulation. The spacing between each pair of nanospikes also plays an important role. Larger spacing accentuates the formation of individual charged nanoribbons between source and drain, and the increased channel width from having larger spacing also helps improve the on-current as well. The transfer characteristics of nanospike TFTs demonstrate an on/off ratio of $\sim 10^7$ while this ratio is typically 10^2 or less for devices with flat edge electrodes. Increased drain current (35 μA/μm vs. 25 μA/μm) and reduced contact resistance (40 kΩ μm vs. 52 kΩ μm) are also observed for the nanospike devices.

The 50 nm MoS₂ TFTs was connected in series with a 15 kΩ resistor to assess the characteristics of an inverter. With a supply voltage of 2 V, the circuit is on with an output voltage of 2 V at negative input voltages and an output voltage of near 0 at positive input voltages. The circuit gain was calculated to be approximately 3.75. The intrinsic gain (g_{m,r_0}) of the device reaches 300 in the subthreshold regime, which is much higher than the intrinsic gain that can be achieved by silicon under subthreshold condition. The high intrinsic gain is a result of reduced DIBL and improved sub-threshold swing due to charged nanoribbon formation and enhanced gate control. This opens up the possibility for high performance subthreshold circuits with low power dissipation for applications such as neuromorphic computing and energy efficient logic. In summary, the use of nanospike array source/drain electrodes shows a step towards scalable, multi-functional, and high-performance MoS₂ TFTs.

SESSION EQ06.05: Poster Session
Session Chairs: Ming-Yang Li and Xu Zhang
Tuesday Afternoon, November 29, 2022
8:00 PM - 10:00 PM
Hynes, Level 1, Hall A

EQ06.05.01

Towards Accurate Ionic Relaxation Algorithms for Two-Dimensional Chalcogenide van der Waals Materials Mahmoud el-Attar and Nageh K. Allam; American University in Cairo, Egypt

Recently, two-dimensional (2D) layered materials, known as van der Waals (vdW) materials, have attracted remarkable attention due to their unique electrochemical and physical properties. Transition metal dichalcogenides (TMDs) are 2D materials, which commonly exist in three polymorphs (1T, 2H, and 3R) in a honeycomb structure (hexagonal lattice). From a structure relaxation point of view, the 1T phase has less structural symmetry along the z-direction, rendering it more challenging than the 2H counterpart. Herein, the importance of enabling vdW forces as well as the associated challenges during the simulation of 1T polymorph are tackled. The two most widely used ionic relaxation methods (conjugate gradient and RMM-DIIS) were used for six TMDs (TaS₂, TaSe₂, MoS₂, MoSe₂, WS₂, WSe₂), and the results were compared to those reported in the literature. Moreover, a newly designed advanced conversion algorithm (TPSCA) is developed by incorporating shell scripts, DFT electronic relaxation, and Python coding. The developed algorithm is tested for 1T-TaS₂ to confirm the obtained results and get better insights into the dependence of the energy on the different combinations of those parameters.

EQ06.05.02

Ab Initio Studies of Thermodynamic and Electronic Properties of MoSi₂N₄ Edges Atharva S. Burtel¹, Ashwin Ramasubramaniam¹, Omar Abdelrahman¹ and Andre Muniz²; ¹University of Massachusetts Amherst, United States; ²Universidade Federal do Rio Grande do Sul, Brazil

Recently, a novel 2D nitride, MoSi₂N₄, was successfully fabricated by chemical vapor deposition methods. This 2D nitride displays excellent mechanical and thermal stability and exhibits semiconducting behavior within the bulk. Drawing parallels with other 2D materials that have been studied for optoelectronics and catalysis, we anticipate that the edges of MoSi₂N₄ could host interesting electronic and chemical properties. Here, we present a density functional theory study of the electronic and thermodynamic properties of MoSi₂N₄ edges. We developed a ternary phase diagram, identifying a region of chemical potentials wherein MoSi₂N₄ is stable over competing elemental or binary phases. Based on this phase diagram, we determined the thermodynamic properties of a wide range of armchair and zigzag edges. Using this detailed thermodynamic analysis as a basis, we identify the most favorable edge structures and elucidate the electronic structures of these favorable edges. Our analysis suggests that low-energy edges of MoSi₂N₄ could be of potential

interest in (opto)electronic and/or electrocatalytic applications.

EQ06.05.03

Tunable Optical Pulling Forces Enabled by Bilayer van der Waals Materials [Ziqiang Cai](#); Northeastern University, United States

Light induced forces can be used to manipulate nanoparticles, which have led to various applications in nanotechnology and bioengineering. Among all kinds of light induced forces, the optical pulling force can transport objects towards the source rather than pushing them away, providing a new degree of freedom in particle manipulation. It has been demonstrated that by using hyperbolic metamaterials and photonic crystals, the scattered light possesses increased momentum in the forward direction compared with the incident light, giving rise to optical pulling forces [1, 2]. However, once these photonic structures are fabricated, their properties cannot be tuned, thus the optical force cannot be in-situ changed. On the other hand, people have demonstrated that the momentum topology of the polaritons in graphene/ α -MoO₃ bilayer structure can be changed from the hyperbolic to elliptical via tuning the Fermi level of graphene [3].

In this work, we numerically demonstrate that by utilizing the tunable property of graphene/ α -MoO₃ bilayer structure, under plane-wave illumination, the direction of optical force exerted on the nanoparticle can be switched between pulling and pushing in a broad frequency range (from 851 cm⁻¹ to 952 cm⁻¹) while only tuning the Fermi level of graphene. In the simulation, the carrier mobility and maximum Fermi level of graphene are 3000 cm²/(Vs) and 0.6 eV, respectively, which are achievable in experiment. We point out that such phenomenon can be used in in-situ optical force tuning without changing the light source. We believe that our work can provide more degrees of freedom in applications related to particle manipulations.

1. Jin, R., et al., *Optical Pulling Forces Enabled by Hyperbolic Metamaterials*. Nano Lett, 2021. **21**(24): p. 10431-10437.

2. Li, H., et al., *Momentum-Topology-Induced Optical Pulling Force*. Phys Rev Lett, 2020. **124**(14): p. 143901.

3. Zeng, Y., et al., *Tailoring topological transition of anisotropic polaritons by interface engineering in biaxial crystals*. 2022.

EQ06.05.04

Direct Observation of Stacking Faults and Stacking Domains in the van der Waals Magnet CrI₃ [Myeongjin Jang](#)¹, [Sol Lee](#)¹, [Fernando Cantos-Prieto](#)², [Ivona Košić](#)², [Jong Chan Kim](#)³, [Jun Yeong Yoon](#)¹, [Loukya Boddapati](#)⁴, [Francis Leonard Deepak](#)⁴, [Hu Young Jeong](#)³, [Elton J. Santos](#)⁵, [Efrén Navarro-Moratalla](#)² and [Kwanpyo Kim](#)¹; ¹University of Yonsei, Korea (the Republic of); ²Universitat de Valencia, Spain; ³Ulsan National Institute of Science and Technology, Korea (the Republic of); ⁴International Iberian Nanotechnology Laboratory, Portugal; ⁵University of Edinburgh, United Kingdom

Van der Waals (vdW) stacking is a powerful technique to achieve desired properties in condensed matter systems under the paradigm of layer-by-layer crystal engineering. Here, we show that recently discovered 2D vdW CrI₃ magnets stabilize natural twisted stacking domains in their crystal structure. By using cross-sectional high-angle annular dark-field scanning transmission electron microscopy and electron diffraction, we unveil that multilayer CrI₃ displays an overall monoclinic structure with occasional rhombohedral stacking faults at room temperature. In addition, the appearance of unusual 120° twisted faults along the stacking direction break up the continuity of the structure into twisted domains with a mode thickness of 10 nm. Remarkably, the monoclinic domains show no hint of the structural phase transition to the rhombohedral stacking down to 95 K but the relative populations among different twisting directions display the strong temperature dependence. Our findings indicate that multilayer CrI₃ presents a high degree of domain stacking disorder, shedding light into the longstanding question of its structural phase transition.

EQ06.05.05

Alternating Doping Level in Epitaxial WS₂ Monolayer on Zigzag Au Substrate Using Scanning Tunneling Microscopy [Jeong Won Jin](#)¹, [Bumsub Song](#)², [Soo Ho Choi](#)², [Ki Kang Kim](#)¹ and [Young Hee Lee](#)²; ¹Sung Kyun Kwan University, United States; ²IBS-Cinap, Korea (the Republic of)

Monolayer transition metal dichalcogenides (TMDs) have been extensively investigated owing to their unique physical properties, such as atomically thin nature and tunable electronic properties. Especially, monolayer TMDs require the presence of substrates, which inevitably induces drastic changes to the properties of adlayer materials in various ways including charge doping and strain. Here, employing scanning tunneling microscopy and spectroscopy (STM/S), we characterize the epitaxial WS₂ monolayer grown on the high-index Au surface which was recently introduced as a unique platform for single-crystalline TMD synthesis. Interestingly, alternating doping level of WS₂ ranged from neutral to strong *n*-type with atomically sharp boundaries is observed, and a direct correlation with the zigzag-like morphology of the Au substrate is revealed by STS mapping. From the Fourier analysis, two major superstructures between the WS₂ and substrate are found. This implies that different interlayer coupling may lead to the alternating doping level.

EQ06.05.06

Electrically Tunable Two-Dimensional Homo Junctions for Self-Powered Photodetection [Tengyu Jin](#) and [Wei Chen](#); National University of Singapore, Singapore

Photodetectors play an important role in the future “Internet-of-Things” information society. Two-dimensional (2D) materials-based photodetectors have attracted intense interest from both academic and industrial fields, thanks to their outstanding performances and related interesting electrical, and optoelectronic phenomena. However, controlling the electronic properties of the 2D materials by incorporating impurity dopants is inherently difficult due to the limited physical space in the atomically thin lattices. Here, we report a successful reconfigurable WSe₂ optoelectronic device with a simple localized floating gate structure that allows reversible electrostatic doping of the channel. Fitting the *I*-*V* curve of the lateral p-n homo junction diode formed in this way with the Shockley diode equation reveals an ideality factor of 1.25 and a series resistance of 0.42 MΩ, which are beneficial for highly-efficient photodetection. Under the illumination of a 525-nm laser, the diode manifests high-performance self-powered photodetection. The photocurrent depends linearly on input power, giving an almost constant responsivity (*R*) value of ~0.17 A/W, which is outstanding compared with other 2D materials-based homo junction devices. A maximum EQE of ~51%, FF of ~67%, and PCE of ~5.62% can also be obtained for the p-n homo junction. In addition, the homo junction demonstrates a wide detection spectral range from violet (405 nm) to the near-infrared region (the cutoff near 1,100 nm) and maintains a high *R* for all the wavelengths. This work opens up a promising pathway toward high-performance optoelectronics based on locally electrostatic doped 2D semiconductors.

EQ06.05.07

Electrical Improvement Using PtTe₂/PtSe₂/PtTe₂ Edge Contact Synthesized by Molecular Beam Epitaxy [Hyeon-Sik Kim](#), [Jaehun Jeong](#), [Gihyeon Kwon](#), [Hyunjun Park](#) and [Mann-Ho Cho](#); Yonsei University, Korea (the Republic of)

As the dimensions of channel materials decrease, the importance of the interface between semiconductor and contact metal increases significantly. One-dimensional (1D) edge contact is considered as one of the keys to improve problems resulting from the interface between two-dimensional (2D) transition-metal dichalcogenides (TMDs) and contact metal, overcoming the problems of surface contact, such as surface damage and orbital hybridization. Although several studies have investigated edge contact, there are some problems such as inevitable etching damage and a limited area. Herein, a tellurization method is applied to a specific lateral region to fabricate PtTe₂/PtSe₂/PtTe₂ edge-contact field-effect transistors (FETs) without etching damage. X-ray

photoelectron spectroscopy, Raman spectroscopy, and annular dark-field scanning transmission electron microscopy are used to verify tellurization completion, which is evidenced by the complete transformation of PtSe₂ to PtTe₂ by the substitution of Se atoms with evaporated Te atoms. Furthermore, tellurization is applied to a specific lateral region by utilizing the hexagonal boron nitride to block the detachment of Se atoms and the interdiffusion of evaporated Te atoms. Finally, the 1D edge-contact FETs fabricated by tellurization shows a higher on-off ratio and carrier mobility than the surface-contact FET, owing to the reduction in contact resistance. Therefore, the fabrication method of the PtSe₂-based 1D edge-contact device with free contact resistance can be applied to achieve various 2D TMD-based electrical devices with a high on-off ratio and carrier mobility, which has yet to be demonstrated in large-area TMD-based electrical devices.

EQ06.05.08

Aharonov-Bohm and Quantum Hall Interferometers in Graphene Rings Cynthia I. Osuala, Zitao Tang, Eui-Hyeok Yang and Chunlei Qu; Stevens Institute of Technology, United States

Two-dimensional monolayer graphene exhibits many interesting physical and chemical properties, representing a powerful platform for the development of sensors with various unique advantages [1]. The interference of the electron matter-wave in a mesoscopic graphene ring has important interferometric applications such as the engineering of electron Sagnac gyroscopes [2] and Aharonov-Bohm interferometers [3,4]. Both applications are based on the same mechanism [5] - the electron picks up a different phase while moving along the two arms of the graphene ring with the relative phase being proportional to the applied rotation velocity or the magnetic field.

We will present our theoretical investigations of the Aharonov-Bohm oscillations in a graphene ring structure in the presence of a magnetic field. For a weak magnetic field, the differential conductance oscillates with a fast frequency due to the Aharonov-Bohm effect; as the magnetic field is further increased, the system enters the quantum Hall regime and the conductance diagram in the plane of Fermi energy and magnetic field exhibits the Hofstadter butterfly fractal structure. The dependence of the electric conductance on the radius of the graphene ring, the width of the arms, the position of the leads, the defects on the edge and in the bulk, the spin-orbit interaction, the electric potentials of the side gates, and the thermal fluctuations are systematically studied for a single graphene ring and a few coupled graphene rings. The optimal structure for the control of the quantum transport properties and for the engineering of interferometric devices will be discussed. Our theoretical results and analysis will be useful for graphene transport experiments and the development of graphene interferometers.

References:

- [1] A. Nag, A. Mitra, S. C. Mukhopadhyay, *Sensors and Actuators A*: 270 (2018).
- [2] J. R. E. Toland, C. P. Search, *Physical Letters A*. 374 (2010).
- [3] J. Schelter, P. Recher, B. Trauzettel, *Solid State Comm.* 152, 1411 (2012).
- [4] Y. Ronen, T. Werkmeister, D. H. Najafabadi, A. T. Pierce, L. E. Anderson, Y. J. Shin, S. Y. Lee, Y. H. Lee, B. Johnson, K. Watanabe, T. Taniguchi, A. Yacoby and P. Kim, *Nature Nanotechnology* 16, 563 (2021).
- [5] J. J. Sakurai *Phys. Rev. D* 21, 2993, (1980).

EQ06.05.09

The Ferroelectric Floating Memory (FFM) with the Reconfigurable Operating Voltage Sangyong Park^{1,2} and Jin-Hong Park^{1,1}; ¹Sungkyunkwan University, Korea (the Republic of); ²Samsung Electronics, Korea (the Republic of)

Ferroelectric field-effect-transistor (Fe-FET) is a promising candidate for a synaptic device of the neuromorphic system due to its compatibility with the conventional CMOS structure, fast operation speed, and facilitating conductance control. The electrical characteristics of the synaptic device are mainly determined by the intrinsic properties of the material and fixed after the fabrication process is completed. However, to support the multiple target applications, reconfigurable electric characteristics are required. In this paper, we introduce an alternative ferroelectric memory device, named ferro-floating memory (FFM), that changes the operating voltage region and the dynamic range by using dual operating mechanisms (ferroelectric switching and tunneling mechanisms). The ferro-floating memory (FFM) uses the electrically isolated semiconducting van-der-Waals ferroelectric material, indium selenide (In₂Se₃), as both the ferroelectric memory and charge storage layers. The two operating mechanisms are individually operated because the ferroelectric switching voltage is lower than the tunneling voltage. The electrical potential of the ferro-floating layer is controlled by injecting the charges into the ferro-floating layer with sufficient gate voltage to occur tunneling. The changing of the electrical potential in the ferro-floating layer modulates the channel surface potential and shifts the threshold voltage. As a result, the operating voltage region of the ferroelectric switching operation can be reconfigured by storing the charges in the ferro-floating layer. We experimentally implemented the ferro-floating memory with van-der-Waals materials and confirmed dual-mode operation by the electrical measurement and scanning Kelvin force microscopy (SKFM). The hysteresis of the double sweep I_d - V_g curve is successfully shifted as tunneling voltage is applied. Finally, we apply the dual-mode operation of the ferro-floating memory to the controlling of the threshold voltage variations in an artificial neural network. The effect of controlling variation is verified using our in-house image recognition simulator.

EQ06.05.12

Nanomechanical Characterization of an Antiferromagnetic Topological Insulator Amit Vashist¹, Shuwan Liu¹, Su Kong Chong², Dongwook Kim¹, Rohit Kumar¹, Seng Huat Lee³, Kang L. Wang², Zhiqiang Mao³, Feng Liu¹ and Vikram V. Deshpande¹; ¹The University of Utah, United States; ²University of California, United States; ³The Pennsylvania State University, United States

The antiferromagnetic topological insulator MnBi₂Te₄ (MBT) exhibits an ideal platform to study exotic topological phenomena and magnetic properties. The transport signatures of magnetic phase transitions in the MBT family materials have been well-studied. However, their mechanical properties and magneto-mechanical coupling have not been well-explored. We use nanoelectromechanical systems to study the intrinsic magnetism in MBT thin flakes via their magnetostrictive coupling. We investigate mechanical resonance signatures of magnetic phase transitions from antiferromagnetic (AFM) to canted antiferromagnetic (cAFM) to ferromagnetic (FM) phases versus magnetic field at different temperatures. The spin-flop transitions in MBT are revealed by frequency shifts of mechanical resonance. With temperatures going above T_N, the transitions disappear in the resonance frequency map, consistent with transport measurements. We use a magnetostrictive model to correlate the frequency shifts with the spin-canting states. Our work demonstrates a technique to study magnetic phase transitions, magnetization and magnetoelastic properties of the magnetic topological insulator.

EQ06.05.13

Vanadium Doping/Alloying in Molybdenum Disulfide Monolayers—Characteristic Raman Modes and Tunable Electronic and Magnetic Properties Da Zhou¹, Mingzu Liu¹, Yen Thi Hai Pham², Aaryan Oberoi¹, David Sanchez¹, Ke Wang¹, Andres Fest¹, Alexander J. Sredenschek¹, Na Zhang¹, Humberto Terrones³, Saptarshi Das¹, Manh-Huong Phan² and Mauricio Terrones^{1,1,1}; ¹The Pennsylvania State University, United States; ²University of South Florida, United States; ³Rensselaer Polytechnic Institute, United States

Transition metal doping/alloying is a powerful tool to tailor the optical, electronic, and magnetic properties of semiconducting transition metal dichalcogenides (TMDs). In particular, vanadium doping in tungsten disulfide (V-WS₂) and tungsten diselenide (V-WSe₂) monolayers have demonstrated p-type doping^{1,2} and ferromagnetism at room temperature^{1,3}. Recently, the synthesis of vanadium-doped molybdenum disulfide (V-MoS₂) monolayers had also been reported using powder chemical vapor deposition (CVD) with the study of their optical and electronic properties.^{4,5} Their emergent Raman modes have been explained by the introduction of vanadium atoms into the MoS₂ lattice. However, no systematic study on the origin of these Raman modes as a function of vanadium doping concentration has been reported to date. The magnetic properties of these monolayers were also not investigated. To address these gaps, here we use a liquid precursor CVD method⁶ to grow V-MoS₂ monolayers with doping levels ranging from 0.1 to 8 at%. We then combine Raman spectroscopy using different excitation wavelengths, high-resolution scanning transmission electron microscopy (HR-STEM), and first-principles density functional theory (DFT) calculations to study the interaction of vanadium dopants and sulfur vacancies and how they contribute to the emergent Raman modes. Furthermore, vibrating sample magnetometry (VSM) measurements at room temperature revealed an optimal ferromagnetic signal when the vanadium doping concentration was moderate (2-3 at%). In addition, we fabricated field effect transistors (FETs) on the V-MoS₂ with different vanadium doping concentrations and found the emergence of p-type behavior as the vanadium concentration increased. Our work lays the foundation for future studies on defect engineering for tunable electronic/magnetic properties in magnetic atom doped/alloyed TMD systems.

[1] Zhang, F. *et al.* Monolayer Vanadium-Doped Tungsten Disulfide: A Room-Temperature Dilute Magnetic Semiconductor. *Advanced Science* 7, 2001174 (2020).

[2] Kozhakhmetov, A. *et al.* Controllable p-Type Doping of 2D WSe₂ via Vanadium Substitution. *Advanced Functional Materials* 31, 2105252 (2021).

[3] Pham, Y. T. H. *et al.* Tunable Ferromagnetism and Thermally Induced Spin Flip in Vanadium-Doped Tungsten Diselenide Monolayers at Room Temperature. *Advanced Materials* 32, 2003607 (2020).

[4] Zou, J. *et al.* Doping Concentration Modulation in Vanadium-Doped Monolayer Molybdenum Disulfide for Synaptic Transistors. *ACS Nano* 15, 7340-7347 (2021).

[5] Zhang, J. *et al.* Vanadium-Doped Monolayer MoS₂ with Tunable Optical Properties for Field-Effect Transistors. *ACS Applied Nano Materials* 4, 769-777 (2021).

[6] Zhang, T. *et al.* Universal In Situ Substitutional Doping of Transition Metal Dichalcogenides by Liquid-Phase Precursor-Assisted Synthesis. *ACS Nano* 14, 4326-4335 (2020).

EQ06.05.15

Nanoporous MoS₂ Field-Effect Transistor-Based Biosensor for Ultrasensitive and Selective Biomolecular Detection Junoh Shim¹, Heekyeong Park^{1,2}, Seungho Baek¹, Anamika Sen¹ and Sunkook Kim¹; ¹Sungkyunkwan University, Korea (the Republic of); ²Harvard University, United States

In this work, we incorporate an ultrasensitive and selective biological FET (bio-FET) created by nanoporous molybdenum disulfide (MoS₂). We construct the nanoring of MoS₂ nanopores via block copolymer (BCP) and analyze them by Raman, scanning transmission electron microscopy, and X-ray photoelectron spectroscopy spectra. After fabricating MoS₂ nanopore rings-based bio-FET, we identify edge-selective functionalization by the Au nanoparticle tethering test and the change of electrical property of the bio-FET. And we achieve the ultrahigh sensitivity with the limit of detection of 1 ag/mL for cortisol detection by using MoS₂ nanopore edge rings-based bio-FET. Also we verify the selectivity by performing several control experiments with other biomaterials. This work suggests a probability that nanoporous MoS₂ bio-FET would furnish platforms for biosensors with ultrahigh sensitivity and selectivity.

EQ06.05.17

The High Sensitivity of the Magnetic Exciton in a Non-Magnet Doped van der Waals Antiferromagnet Junghyun Kim^{1,2}, Jonghyeon Kim³, Woongki Na⁴, Pyeongjae Park^{1,2}, Hyeonsik Cheong⁴, Jae Hoon Kim³ and Je-Geun Park^{1,2}; ¹Center for Quantum Materials, Seoul National University, Korea (the Republic of); ²Department of Physics & Astronomy, Seoul National University, Korea (the Republic of); ³Department of Physics, Yonsei University, Korea (the Republic of); ⁴Department of Physics, Sogang University, Korea (the Republic of)

The antiferromagnetic van der Waals (vdW) NiPS₃ is a rare material for studying the exciton physics based on the magnetically ordered system. The extremely narrow linewidth of the exciton peak arising coherently from the Zhang-Rice singlet and triplet states was observed by the photoluminescence (PL) and the optical absorption in the single crystal NiPS₃ [1]. The locality of NiS₆ cluster based on the cluster model calculation was expected to show a stability of the coherent behavior against to the disturbance in the magnetically ordered system. Here, we newly synthesized the antiferromagnetic vdW Ni_{1-x}Cd_xPS₃ which have the non-magnetic dopant Cd replaced in the Ni sites homogeneously throughout the whole crystal. The lattice constant *c* extracted from the XRD pattern expanded linearly, changing by 0.6 % from *x* = 0 to 0.1, following the Vegard's law. From the PL and absorption measurement, we observed that the coherent behavior of magnetic exciton peak shows high sensitivity to the dopant concentration where the Neel temperature relatively maintained showing a linear decrement. Here, we emphasize that we showed the decoherence behavior from the linewidth and peak suppression starts to change drastically even in the magnetically ordered ground state where the non-magnetic dopant broke the spin order locally. Additionally, we simulated the magnetic ground state for doped systems and the magnon linewidth broadening was compared with that from the optical probes. We expect that our work will provide novel magnetic systems with spin ordering for a deeper understanding of the magnetic exciton.

[1] S. Kang *et al.*, *Nature* 583, 285 (2020)

EQ06.05.19

Adhesive Functionalization and Lamination of 2D Materials for Flexible Device Fabrication. Ningxin Li¹, Rui He², Olunloyo Olugbenga³, Tara Jabegu¹, Hedi Ma¹, Diren Maraba¹, Aisha A. Okmi¹, Kai Xiao³, Gangli Wang¹, Pei Dong² and Sidong Lei¹; ¹Georgia State University, United States; ²George Mason University, United States; ³Oak Ridge National Laboratory, United States

In modern microelectronics, flexible device fabrication with two-dimensional (2D) materials which show excellent bendability, and ductility is leading a new trend. The sustainable deformation level of 2D materials before rupture is an important degree that determines the performance of the microelectronic device. Despite the respective progress, strain engineering is lagging due to a major challenge: providing strong adhesion between 2D materials and substrate to avoid slippage. Here, we report a method by employing (3-Mercaptopropyl) trimethoxysilane (MPTMS) for surface functionalization to ensure mechanical strain transferring. By applying different tension strain, we noticed the Raman spectrum shows a red shift of 12.9 cm⁻¹ for monolayer MoS₂ under the maximum strain value at 1.50%. Meanwhile, the magnitude of the Raman spectrum red shift is inversely proportional to the thickness of the 2D

materials. Compared with other physical encapsulation methods, our way provides strong adhesion to the interface through atomic level chemical bonding, reducing the negative impact of slippage effectively which inherits the mechanical flexibility of 2D materials. Moreover, such a strong bonding method allows not only the isolated samples to transfer, but also the complete micro-devices. As such, the difficulty of fabricating devices on flexible substrates can be overcome simultaneously, which develops the flexible micro-device fabrication technology.

EQ06.05.20

Strain Manipulation and the Role of Magnetism for Charge Density Waves in Monolayer VTe₂ Do Hoon Kiem, Min Yong Jeong, Hongkee Yoon and Myung Joon Han; Korea Advanced Institute of Science and Technology, Korea (the Republic of)

Vanadium ditelluride (VTe₂), which is one of the transition metal dichalcogenides (TMDCs), has an intriguing interplay of spin, charge, and lattice degrees of freedom. Motivated by our recent work on crystalline bulk VTe₂ [1], we theoretically investigated the interplay between spin, charge, and lattice in monolayer VTe₂. To understand the controversial experimental reports on several different charge density wave (CDW) ground states, we paid special attention to the 'hidden' role of antiferromagnetism as direct experimental detection may be challenging. Our first-principle calculations show that the 4x1 CDW and the corresponding lattice strain are accompanied by a 'double-stripe' AFM spin order in its ground state. This magnetic phase has the lowest total energy as well as dynamic phonon stability, which supports the group of previous experiments. Interestingly, this ground state is only stabilized by assuming an underlying spin order. Other previously reported phases were found to have significantly high total energy or unstable phonon profiles. By discovering interesting and previously unknown interactions between magnetism and other degrees of freedom, we propose possible strain engineering. The monolayer VTe₂ exhibits a phase transition first to a different CDW structure by applying a tensile strain, and then finally to a ferromagnetically ordered one.

[1] Won, Kiem et al. *Adv. Mater.* 32 (11), 1906578 (2020).

EQ06.05.21

Optical Control of Spin Defects in a van der Waals Magnetic Semiconductor Samuel W. Song¹, Julian Klein¹, Rami Dana¹, Zdenek Sofer², Frances M. Ross¹ and Rafael Jaramillo¹; ¹Massachusetts Institute of Technology, United States; ²University of Chemistry and Technology Prague, Czechia

The van der Waals material CrSBr stands out as a promising 2D magnetic semiconductor due to its high antiferromagnetic ordering temperature $T_{\text{Néel}} \approx 135$ K, near-infrared direct bandgap $E_g \approx 1.55$ eV, and air-stability. In addition to its bulk magnetic order, CrSBr also exhibits a low-temperature magnetic order that is hypothesized to originate from the ferromagnetic polarization of defects [1,2]. A detailed understanding of the mechanisms underlying this defect-induced magnetic order is still needed to fully characterize and better engineer the material's magnetic response.

In this work, we demonstrate optical control of the defect-induced magnetic order in CrSBr single crystals using magneto-optic superconducting quantum interference device (SQUID) magnetometry, which provides high-sensitivity magnetic susceptibility measurements under a controllable external light source. We observe an increase in the zero-field susceptibility of the defect-induced order after exposure to above-bandgap excitation using 405 nm (3.06 eV) illumination. This effect is further amplified upon subsequent excitation using 880 nm (1.41 eV) illumination, which was chosen due to the increased sensitivity of defect absorption at sub-bandgap frequencies [1]. Moreover, we anneal the samples at 400°, 600°, and 800°C to increase defect concentration, which we verify through scanning tunneling microscope (STM) imaging and susceptibility measurements showing increased onset temperatures for the defect-induced magnetic order. For a sample annealed at 800°C, the peak in the enhanced susceptibility (near 70 K) is comparable to or even larger than that of the critical Néel transition at 135 K. From our results, we hypothesize that interactions in the magnetic subsystem of disordered defects arise from the interplay between defect charge states and light-induced carriers, thereby allowing control via illumination. Further exploration of the history-dependence of this interplay relation may lead to the realization of optical control of magnetic interactions between solid-state defect state spin qubits. More broadly, our findings establish CrSBr as an outstanding candidate for further research into tunable optical control of magnetism in 2D semiconductors, with potential applications in spintronics, quantum sensors, and opto-magnetic devices.

[1] Klein, J. *et al.*, Sensing the local magnetic environment through optically active defects in a layered magnetic semiconductor *arXiv:2207.02884 under review* (2022).

[2] Telford, E. J. *et al.*, Coupling between magnetic order and charge transport in a two-dimensional magnetic semiconductor. *Nature Materials* 21, 754–760 (2022).

EQ06.05.22

A Computational Thermodynamic Approach to Modeling the Efficiency of 2D Materials in Space Solar Cells Using a Novel 7-Junction Configuration Calista Wilk and Peide P. Ye; Purdue University, United States

Approximately 3 billion people have never used the internet due to its costs and inaccessibility, particularly in developing countries. To provide these areas with affordable internet, reducing the cost of building and launching satellites has become paramount in the assessment of their design, particularly their solar cells. While three-dimensional semiconductor materials like gallium arsenide (GaAs) have been the main material used in these cells to convert solar energy into electrical energy, two-dimensional (2D) materials like tellurene have demonstrated properties that warrant consideration. This research evaluates the potential of a novel 7-junction space solar cell configuration consisting of manganese phosphorus trisulfide, tungsten disulfide, rhenium disulfide, molybdenum disulfide, molybdenum ditelluride, bismuth oxyselenide, and tellurene to replace current 3-junction configurations using GaAs-based materials. Thermodynamic expressions, including the efficiency of a Carnot heat engine and a geometric optimization approach using the Shockley-Queisser triangle, were analyzed to derive equations for two properties critical to a space solar cell: efficiency and specific power. Computational simulations were run, and the results indicate that a 7-junction space solar cell configuration using 2D materials can enable a maximum efficiency gain of 12%, a mass reduction by over one-fifth, and a specific power output improvement of 54% at lower costs compared to GaAs-based space solar cells. The implications of this study point to the performance and cost feasibility of satellite usage for a broad range of applications, with social and environmental significance.

EQ06.05.23

Bandgap Study of Titanium Oxynitride Photoactive Material System Abiodun Odusanya and Dhananjay Kumar; North Carolina A&T State University, United States

A TiN_xO_y (TiNO) material system has been synthesized in thin-film form using a pulsed laser deposition method. X-ray photoelectron spectroscopic measurements have been carried out to determine the elemental composition of the partially oxidized films to show partial oxidation of TiN to TiNO. In addition, the bandgaps were experimentally measured using UV-Vis. In this paper, we performed a theoretical study through Density Functional Theory (DFT) calculations to theoretically assess the role of oxygen content on the changes in bandgap as well as the variation of the lattice parameter with

increasing oxygen composition. We compared these variations with the experimental data. In our calculations, we systematically evaluate the electronic structures within the context of accompanying perturbation in the defect chemistry associated with the charge balance necessary to accurately determine the corresponding bandgap and lattice parameter of TiNO thin films. Due to the potential application of these TiNO systems which possess excellent photoactive characteristics, this study may open up a new compositional and processing strategy to realize novel optical devices.

This work was supported by the National Science Foundation, NSF-PREM through MRSEC [grant No. DMR-2122067].

SESSION EQ06.06: 2D Electronic and Photonic Devices III

Session Chairs: Doron Naveh and Xu Zhang

Wednesday Morning, November 30, 2022

Sheraton, 2nd Floor, Back Bay B

8:30 AM *EQ06.06.01

2D Amorphous Carbon Dielectric Prepared from Solution Precursor for Nanoelectronics [Qing Cao](#); University of Illinois at Urbana-Champaign, United States

Two-dimensional (2D) semiconductors and semimetals could enable performance and scaling of solid-state electronic devices beyond the limits of those built on their conventional bulk counterparts. However, their suitable accompanying 2D dielectric, ideally in the highly disordered amorphous form to avoid nonuniformity and defects associated with grain boundaries similar to SiO₂ for silicon, has not been identified, which prevents nanoelectronic devices based on low-dimensional nanomaterials from fulfilling their potential. The synthesis of 2D amorphous dielectrics and their integration into electronic devices are challenging due to the metastable nature of amorphous phases. Here we present a scalable and solution-based strategy to prepare large-area and freestanding 2D amorphous carbon monolayers and multilayers as novel dielectrics, from coal-derived carbon quantum dots as precursors. The synthesized 2D amorphous carbon can be transferred to various substrates and is mechanically robust enough to be suspended over cavities without tearing. Structures are fully characterized by Raman, atomic-force microscopy (AFM), X-ray spectroscopy (XPS), and atomic-resolution transmission electron microscopy (TEM). Resulting from their unique amorphous atomic structures, the prepared 2D amorphous carbon demonstrates robust dielectric properties with resistivity higher than 10⁹ Ω/cm and dielectric strength above 20 MV/cm. When utilized as gate dielectrics in graphene transistors, 2D amorphous carbon helps to achieve a low leakage current density below 10⁻⁴ A/cm² with an extremely scaled thickness down to three atomic layers (~1.6 nm) for enhanced electrostatic coupling. Meanwhile, their dangling-bond-free van der Waals interface with graphene leads to mobility twice as high as that of 2D devices employing SiO₂. When implemented as ion-transport media in memristors, the ultrathinness of 2D amorphous carbon bilayer enables forming-free operations of non-volatile memory cells with low voltage (<0.4 V), fast switching time (<20 ns), and low energy consumption (<20 fJ per operation), without sacrificing endurance and retention. The large-number rings in their amorphous Zachariasen regions provide well-defined pathways for the filament formation to minimize device spatiotemporal variability.

9:00 AM EQ06.06.02

Continuous Liquid Metal Printing of High Mobility 2D Oxide Heterostructure Transistors [Andrew B. Hamlin](#), Simon Agnew, Anand P. Tiwari and William J. Scheideler; Dartmouth College, United States

We introduce a new roller-based Continuous Liquid Metal Printing (CLMP) process for low-temperature, in-air deposition of 2D metal oxides, including InO_x and GaO_x. Our R2R compatible printing method uses Van der Waals forces to transfer high-quality, large area (> 30 cm²) 3.5 nm conductive oxide films generated by a self-limiting Cabrera-Mott oxidation mechanism in < 3s. We apply the CLMP method to fabricate InO_x / GaO_x heterostructure thin film transistors (TFTs) at a maximum process temperature of 200 °C. The CLMP 2D GaO_x layers were designed to provide a modulation doping effect at the back-channel of the 2D InO_x, enhancing the free carrier concentration as well as the electronic mobility. The nature of this InO_x / GaO_x heterointerface was further investigated by AFM, Kelvin probe measurements, photoelectronic spectroscopy in air (PESA), and Raman spectroscopy. XRD and TEM characterization reveal that the 2D GaO_x layer is amorphous as deposited, while the 2D InO_x exhibits large, plate-like grains, an electronically advantageous unique property of CLMP InO_x. An average linear mobility improvement from μ₀ = 12.5 cm²/Vs to μ₀ = 17.5 cm²/Vs is observed in comparing pure InO_x channels with InO_x / GaO_x heterostructure TFTs. These heterostructure devices exhibit accumulation mode operation and an average I_{on}/I_{off} of 10⁷. In summary, our work utilizes a breakthrough high-speed Van der Waals printing to fabricate semiconducting 2D oxide heterostructures for applications to displays, photodetectors, and flexible inorganic electronics.

9:15 AM EQ06.06.03

Atomic Layer Deposition Integration of Amorphous Boron Nitride with 2D Semiconductors [Cindy Y. Chen](#)¹, Yu-Chuan Lin¹, Riccardo Torsi¹, Ke Wang¹, Haiying Wang¹, Bangzhi Liu¹, Jessica Kachian² and Joshua A. Robinson¹; ¹The Pennsylvania State University, United States; ²Intel Corporation, United States

2D transition metal dichalcogenides (TMDs) exhibit unique electronic and optical properties and are actively under investigation as transistor channel materials to combat the critical limit in continued transistor scaling. While 2D TMDs are hailed as having no out-of-plane bonding, these systems are rarely defect-free, and the atomic thickness leads to a high susceptibility to environmental factors that reduce layer stability and electronic performance. Encapsulation with insulators is an effective method to not only prevent 2D TMD oxidation and degradation in ambient environment, but also provide a suitable dielectric environment for enhancing 2D device performance. For instance, hexagonal boron nitride (hBN) at the interface between 2D TMD and the oxide substrate can improve the carrier mobility up to an order of magnitude due to dielectric screening from charged impurities and the suppression of surface optical phonon scattering, both of which are commonly present in conventional 3D oxide substrates. Motivated by the robust dielectric properties of BN, we explore atomic layer deposition (ALD) of ultrathin (2-10 nm) BN as a wafer-scale, non-water-based, low-temperature process for 2D TMD encapsulation. Two routes of ALD, plasma-enhanced (PE) and thermal (Th), are explored to understand the impact of ALD precursor and processing parameters on the resulting chemical, structural, and dielectric properties of BN. ThALD, utilizing sequential injections of NH₃ and BCl₃, results in fully amorphous BN (aBN), whereas the increased energy from N₂ plasma generation in PEALD yields nanocrystalline BN with higher surface roughness. Furthermore, using Mo-based TMDs as a test 2D TMD system, we find significant improvement in the thermal and chemical stability of aBN-capped 2D TMD after prolonged periods (> 1 month) of time in ambient air. Finally, we will discuss the impact of aBN encapsulation on the electronic and optical properties of a range of TMDs, with discussion of implications on using aBN as a robust dielectric for 2D-based electronics.

9:30 AM BREAK

10:00 AM EQ06.06.06

Doping 2H-MoTe₂ with a Monolayer Oxide [Anjaly Rajendran](#), Rishi Maiti, Luke Holtzman, Song Liu, Katayun Barmak and James Hone; Columbia University, United States

Direct bandgap van der Waals semiconductors are excellent candidates for optical devices like photodiodes and light emitting diodes due to excellent optical properties and scope for miniaturization. Among these, monolayer Molybdenum Telluride (2H-phase) is a promising material for fabricating optical devices that can work in the Infrared (IR)/ Near-infrared (NIR) regions pertaining to its band gap of 1.1 eV. However, its air sensitive nature makes it extremely hard to find appropriate dopants to form a p-n junction --- heart of any photodetector.

In this work, we demonstrate p-type doping of 2H-MoTe₂ using a monolayer of Tungsten Oxyselenide (TOS) --- an amorphous, stable, and high work-function oxide obtained by self-limiting oxidation of WSe₂. Compared to other p-type doping techniques, this method allows first-passivation-then-doping mechanism that allows to preserve the underlying 2H-MoTe₂. We characterize the doping in MoTe₂ using Raman, PL, and electrical characterization that shows degenerate doping of MoTe₂ using TOS. This is further supported by charge-balance simulations that indicate $> 10^{13}$ cm⁻² doping density. In conclusion, we demonstrate a stable, controllable, degenerate p-type doping technique to dope 2H-MoTe₂ using tungsten oxy selenide (TOS).

10:15 AM *EQ06.06.07

Manipulation and Characterization of Interlayer Exciton Electroluminescence in Atomically Thin Semiconductor Heterostructures [Philip Kim](#); Harvard University, United States

Atomically thin semiconductor heterostructures based on transition metal dichalcogenides (TMDs) offer an electrically tunable platform for developing coherent on-chip optoelectronic devices. Interlayer excitons (IEs) in these systems form out-of-plane dipoles and exhibit long lifetimes owing to the spatial separation of electrons and holes. The bosonic nature of excitons and strong dipolar interactions make them ideal candidates for searching for Bose-Einstein condensation in 2D materials. In this presentation, I will discuss creating high densities of cold, controllable excitons as an essential step toward studying the phase diagram of dipolar exciton gases in MoSe₂/WSe₂ atomically thin heterostructures. Via electrostatic gating, we spatially modulate the vertical electric fields to create a quasi-1D trap for the diffusive IEs, enabling control over the spatial diffusion profile and local IE densities. By electrically modulating density, we reveal a universal linewidth broadening at a critical density in good agreement with the Mott density, independent of the local electrostatic profile. In the second part of the talk, I will demonstrate coherent light emission from the IEs formed by electrically driven carrier injection. We observe a threshold in the electroluminescence of interlayer excitons as we increase the applied forward bias with a balanced injection of electrons and holes. We further characterize the nature of this transition by performing measurements of the second-order correlation function. Strong photon number correlation has been characterized near the threshold IE emission, signaling the quantum correlation of IEs in this regime.

10:45 AM *EQ06.06.08

Interacting Opto-Moiré Quantum Matter [Xi Wang](#); University of Washington Seattle, United States

Transition metal dichalcogenide (TMD) heterobilayers with tunable periodic moiré potentials have emerged as a desirable platform for studying quantum many-body interactions. Strong excitonic responses in TMDs allow optical access to the wealth of correlated physics. In this presentation, I will discuss our recent studies of interactions between moiré excitons and charge carriers trapped in moiré potentials. New excitonic many-body ground states are discovered, which can be tuned by moiré carrier fillings and layer stacking. The integration of optical excitation further enriches the phase diagram of moiré quantum matter. We have observed that the spin-spin interactions between moiré trapped holes can be drastically tuned by optical excitation power, pointing to the excitons mediated long-range exchange interaction between moiré trapped carriers. Our work provides the framework for understanding and engineering electronic and excitonic states in moiré quantum matters.

SESSION EQ06.07: 2D Electronic and Photonic Devices IV

Session Chairs: Qing Cao and Yuxuan Cosmi Lin

Wednesday Afternoon, November 30, 2022

Sheraton, 2nd Floor, Back Bay B

1:30 PM *EQ06.07.01

A Quasiparticle Soup—Phonons, Magnons and Spin-Orbit Excitons in CoTiO₃ [Angela R. Hight Walker](#); National Institute of Standards and Technology, United States

CoTiO₃ has recently been in the spotlight due to its promise of exotic magnetic behavior especially topological magnons. It is a semiconductor with a band gap of ~2.25 eV with the Co²⁺ in edge-sharing octahedra form a stacked honeycomb lattice along the c-axis, with an easy-plane, A-type, antiferromagnetic ordering below 38 K. The spins in each honeycomb plane, which is perpendicular to the c-axis, are ferromagnetically aligned, while the planes are antiferromagnetically aligned with each other. There is significant bond-dependent exchange coupling, which is quite unique for 3d ions. Our magneto-Raman spectroscopic capabilities enable diffraction-limited, spatially resolved optical measurements while simultaneously varying the temperature, laser wavelength and magnetic field to study the photo-physics of layered quantum materials like CoTiO₃. Additionally, coupling to a triple grating spectrometer provides access to low-frequency (down to 6 cm⁻¹, or 0.75 meV) phonon and magnon modes, which are sensitive to magnetic order and interactions. Two magnons are clearly identified and studied as a function of temperature and magnetic field, both parallel and perpendicular to the c-axis. Wild phonon behavior is seen which is corroborated by recent neutron scattering measurements and will be discussed.

2:00 PM EQ06.07.02

Exciton-Charge Auger Limit Photovoltaic Performance of 2D Semiconductor Devices [Timothy L. Atallah](#)^{1,2}, Peng Chen^{3,2}, Zhaoyang Lin², Peiqi Wang², Sung-Joon Lee², Jungqing Xu⁴, Zhihong Huang², Xidong Duan⁵, Yuan Ping⁴, Yu Huang², Justin R. Caram² and Xiangfeng Duan²; ¹Denison University, United States; ²UCLA, United States; ³Southern University of Science and Technology, China; ⁴University of California, Santa Cruz, United States; ⁵Hunan University, China

Two-dimensional semiconductors remain of great interest due to their exotic photophysical and magnetic properties: for example while they are inorganic semiconductors they exhibit strong exciton binding energies due to limited dielectric screening. Furthermore, doping has dramatic impacts on 2D device properties due to planar confinement. However, since they are largely interfacial in nature, devices from 2D materials often are plagued with extrinsic limitations such as chemical disorder or contact effects which limits our ability to observe the intrinsic semiconductor properties within devices. Our work shows we can correlate the exciton lifetime from time resolved photoluminescence to the short circuit photocurrent as function of electrostatic doping

within our Van der Waals contacted tungsten diselenide diode showing that at high doping the charge collection is diffusion limited due to the exciton-charge Auger process. This further supported by our scanning imaging photocurrent microscopy measurements. Hence we are able to correlate the photophysics directly with device performance and show the importance of pristine and non-destructive contacts and the control of charge density to achieve a high quality 2D device.

2:15 PM EQ06.07.03

Probing Charge Transfer of A β -Proteins Examined Using Two-Dimensional Materials as Raman Spectroscopic Platform [Wujoon Cha](#)^{1,2}, Chaejeong Heo^{1,2}, Sang Hyub Lee^{1,2}, Seok Jun Yun³, Byeong Wook Cho^{1,2}, Taewoo Ha^{1,2} and Young Hee Lee^{1,2}; ¹Institute for Basic Science, Korea (the Republic of); ²Sungkyunkwan University, Korea (the Republic of); ³Oak Ridge National Laboratory, United States

We report distinguished charge transfer of amyloid- β (A β) proteins at different aggregation stages with two-dimensional (2D) materials that can potentially be critical for understanding the fibrillization mechanism and developing an early-stage diagnostic method of Alzheimer's disease. We previously identified notable variations in conductance of A β proteins in monomer, oligomer, and fibril forms measured by THz spectroscopy, suggesting significant changes in electronic structures as A β fibrillizes [1]. In this work, we show that A β s exhibit distinct charge-transfer behavior depending on their aggregated states when interacting with monolayer graphene and molybdenum disulfide (MoS₂). In particular, we found that small and soluble A β monomers *p*-doped both graphene and MoS₂ sheets while large and insoluble A β fibrils *n*-doped them. These findings provide critical insights into the electronic properties of A β s that could be essential to identifying the onset of neurotoxic A β fibril formation and developing a rapid, label-free diagnosis based on two-dimensional materials.

In Alzheimer's disease (AD), the accumulation of senile plaques, dominantly composed of fibrillized A β s in the cerebral cortex, has been identified as the primary indication of degeneracy. Therefore, early diagnosis of AD is strongly dependent on the ability to detect the emergence of toxic A β oligomers and fibrils. It has been suggested that charge transfer plays a key role in the formation and the interaction of proteins [2]. Although A β states can be identified based on 'fingerprints' of vibrational modes observed with optical spectroscopies, there is a gap in knowledge about the electronic properties of A β that varies significantly as A β fibrillizes. To address this gap, we used Raman spectroscopy to probe A β proteins interacting with two-dimensional materials that are sensitive to molecular charge transfer.

Graphene, an atomically thin semimetal, and monolayer MoS₂, a semiconductor with a direct bandgap, react sensitively to charge-transfer-induced doping. The shifts in the carrier concentrations and in the Fermi levels can be distinguished from the characteristic Raman bands in graphene (G and 2D) and in MoS₂ (E_{2g} and A_{1g}) [3,4]. Here, we conducted Raman spectroscopy on monolayer graphene and MoS₂ added with A β proteins at different fibrillization stages - monomer, oligomer, and fibril. The graphene and MoS₂ sheets were prepared *via* chemical vapor deposition and transferred on a Si/SiO₂ 300-nm substrate separately. Then, 10 μ M protein solutions were loaded and dried in air for subsequent Raman spectroscopy. A statistically significant (*p*-value < 0.0001) distinction was shown for doping due to monomers and fibrils. Taking the effects of buffer media into account, we observed that, in both graphene and MoS₂, monomer withdrew electrons and *p*-doped while fibril injected electrons and *n*-doped on average. This was evidenced by the upshift(downshift) of G and 2D band, sharpening(broadening) of G band, and decrease(increase) of 2D to G intensity ratio for graphene with monomer(fibril). Similarly, in MoS₂, A_{1g} frequency increased(decreased) and width stiffened(softened) by monomer(fibril). The changes in carrier concentrations were calculated based on the relative positions of the signature Raman bands. In turn, we estimated that the monomers and fibrils shifted the graphene Fermi level by approximately -1.0 eV and +1.9 eV, respectively. The contrary charge-transfer behavior suggests that the electronic states of A β , such as its highest occupied (HOMO) and lowest unoccupied (LUMO) molecular orbital levels, shift significantly as A β fibrillizes. The transition point from *p*-doping to *n*-doping can serve as a marker for the onset of toxic A β aggregates.

[1] Heo *et al.*, ACS Nano, **14**, 6548 (2020).

[2] Cordes *et al.*, Chem. Soc. Rev., **38**, 892 (2009).

[3] Das *et al.*, Nat. Nanotech., **3**, 210 (2008).

[4] Zhong *et al.*, Chem. Soc. Rev., **44**, 2757 (2015).

2:30 PM BREAK

3:30 PM *EQ06.07.04

Application of 2D Materials in Photonic Sensing and Electronics [Thomas Mueller](#); Technische Universität Wien, Austria

The materials that have enabled the information technology revolution over the past decades will soon reach their physical limits. Novel nanomaterials and technologies have therefore become a major focus of current solid-state device research, with two-dimensional (2D) materials being one of the most promising candidates. While much progress has been made on an individual device level, only a few studies have looked into more complex systems. In this talk I will present realizations of electronic and photonic systems, comprising a large number of 2D material-based devices. In particular, I will discuss photosensors that are able to simultaneously sense and process optical images without latency. We achieved both supervised and unsupervised learning and successfully trained the sensors to classify and encode images, that are optically projected onto the chip. Further, I will share our latest results on the heterogeneous integration of 2D materials with arbitrary substrates, including paper, for applications in electronics and integrated photonics. I will present investigations of 2D device variability, its physical origins, and how it affects system performance.

4:00 PM *EQ06.07.05

Coupling of Magnetic and Optical Properties in Transition Metal Phosphorous Trichalcogenide [Efrat Lifshitz](#); Technion-Israel Inst of Tech, Israel

In recent years, van der Waals magnetic materials gained a renaissance of interest due to their potential implementation in modern quantum technologies. The current study focuses on the study of *the transition metal phosphorous tri-chalcogenides semiconductors*, having a general chemical formula MPX₃ (M=1st row transition metals, X=chalcogenides). A single MPX₃ (M=transition metal, X=chalcogenide) layer comprises a honeycomb arrangement (Neel, stripe, or zigzag) of the metal ions, producing an anti-ferromagnetism (AFM). The study tackled a few scientific questions: (1) What mechanism sustains the long-range AFM, and whether the type of magnetic arrangement can be manipulated? Previous work proposed a dominance of spin-exchange coupling among next metal neighbors. To examine this assumption, we examined the magnetic and magneto-optical properties of a benchmark compound, MnPS₃, embedded with different diamagnetic cations (e.g., Zn²⁺). The results designated a sustain of AFM, however, with a reduction of the Neel temperature with the increase of the dopant concentration, followed by a switch of a magnetic arrangement from Neel to Zigzag in layers at Mn: Zn ratio of 1:1, and a complete loss of AFM arrangement with the dominance of Zn ions. The gradual transitions with the increase of Zn content were reflected in shifts and polarization of the magneto-PL spectrum, exposing a magnetic-optical solid correlation. (2) Do other moments (e.g., spin-orbit) dictate spin arrangement? To address this question comparison of magneto-optical properties among a few different compounds (MnPS₃, FePS₃) has been explored. The study designated a unique behavior in FePS₃ compared to the two others, exposing new magnetic phenomena that have not been demonstrated before, supposedly related to strong spin-orbit and an inversion of symmetry breaking (see attached a representative emission spectrum). A full description of the observations

will be discussed at the meeting. The experimental observations were corroborated by considering the electronic properties in the framework of DFT+U studies.

4:30 PM EQ06.07.06

Detection of Circularly Polarized Light with Chiral Molecule Functionalized MoS₂ Ye Wang, Yan Wang, Yiru Zhu and Manish Chhowalla; University of Cambridge, United Kingdom

Emission and detection of circularly polarized photons are essential for quantum computing, spintronics, biosensing, and three-dimensional displays. Thus, materials that can emit and detect circularly polarized light are crucial for enabling new technologies. Here, we demonstrate chemical vapor deposited (CVD) atomically thin semiconductor (MoS₂) coupled with chiral thiol-based amino acids for circularly polarized light (CPL) photodetection. The functionalization was carried out by dipping the CVD MoS₂ sample in a solution of amino acids (concentration = 7.6 mmol in deionised (DI) water). Circular dichroism (CD) spectra show temperature-independent bands between 200 to 500 nm, indicating induction of chirality on functionalized MoS₂. We estimate the degree of functionalization to be 5~7%. The photodetection measurements performed at excitation wavelength of $\lambda = 405$ nm on the functionalized CVD MoS₂ devices show an anisotropy factor (g factor) of $\sim 10^{-1}$ at room temperature for left and right CPL detection. The results suggest that while MoS₂ is non-chiral, functionalization with chiral molecules allows differentiation of different polarizations of light.

4:45 PM EQ06.07.07

Optical Emission in Hafnium Disulphide (HfS₂) Related to Iodine (I₂) Intercalation Natalia Zawadzka¹, Tomasz Wozniak², Marcin Strawski¹, Igor Antoniazzi¹, Zahir Muhammad³, Weisheng Zhao³, Roman Stepniwski¹, Adam Babinski¹ and Maciej R. Molas¹; ¹University of Warsaw, Poland; ²Wroclaw University of Science and Technology, Poland; ³Hefei Innovation Research Institute, Beihang University, China

Hafnium-based transition metal dichalcogenides (TMDs) including hafnium disulphide (HfS₂) have attracted recently more attention of researchers due to their very effective electrical response [1]. This justifies a need to uncover their basic optical and electrical properties.

Along the line of research, we report on optical emission from HfS₂ bulk crystal grown by chemical vapor transport method. The photoluminescence (PL) is investigated in a broad range of temperatures (5-300 K).

The low-temperature emission consists of a series of well-resolved emission lines apparent in the energy range of 1.3-1.5 eV. In order to identify the observed emission lines, classical correlations between the PL intensity at the energies of different emission lines [2] is analysed. A series of spectra measured at different spots of the sample is used in the analysis. The analysis allows to identify two zero-phonon emission lines in the spectrum which intensities are strongly anticorrelated. The zero-phonon lines are accompanied by several phonon replica. The replica involving acoustic (LA, TA) and optical (E_g(TO)) phonons and their combinations are identified.

The observed emission is related to excitons (most likely neutral and charged) in HfS₂ bound to a localizing potential due to neutral iodine molecules (I₂). The I₂ molecules were introduced into the crystal during its growth as iodine is used as a transport agent in the process. The molecules are intercalated in van der Waals gaps between covalently bonded HfS₂ layers. The presence of iodine in the investigated samples was confirmed by secondary ion mass spectroscopy and the sample de-iodization results in the spectrum disappearance which further supports our attribution. Similar low-temperature PL, related to intercalated halogen molecules was previously observed in 2H polytypes of tungsten sulphides/selenides [3].

The space localization of the bound excitons leads to their delocalization in the momentum space. This explains a strong coupling to phonons from a whole Brillouin zone. We note that the energies of phonon replicas in the PL spectra correspond to maxima of the total density of phonon states in bulk HfS₂, rather than to the energies of phonons from particular high-symmetry points of the Brillouin zone.

In conclusion we present for the first time the low-temperature excitonic emission in bulk HfS₂. We analyze the observed PL spectrum using classical correlation method and we identify two "families" of lines attributed to neutral and charged excitons bound by a potential due to iodine molecules in van der Waals gaps. Our attribution is supported by the observation of iodine in the investigated samples by means of secondary ion mass spectroscopy.

[1] S. Lukman, et al. Nature Nanotechnology, 15, 675, (2020)

[2] B. Pietka, et al. Phys. Rev. B87, 035310 (2013)

[3] D. Duchenko, et al. Thin Solid Films, 495, 82, (2006)

SESSION EQ06.08: Quantum Properties and Applications I

Session Chairs: Monica Allen and Qiong Ma

Thursday Morning, December 1, 2022

Sheraton, 2nd Floor, Back Bay B

8:30 AM *EQ06.08.01

New Optical Features and Biosensing Applications of Engineered 2D Materials Shengxi Huang; Rice University, United States

Engineering of 2D materials, such as defect and structural engineering, offers enormous opportunities to realize new material properties. In this talk, I will introduce a nitrogen substitutional defect in 2D transition metal dichalcogenides and new photoluminescence features generated at various wavelengths. I will also discuss how various 2D materials, including the natural and artificially engineered ones, can be used for biosensing to achieve high sensitivity and high multiplexity.

9:00 AM EQ06.08.02

Giant Effective Zeeman Splitting in a Monolayer Semiconductor Realised by Spin Selective Strong Light-Matter Coupling Daniel Gillard¹, Thomas P. Lyons^{2,1}, Charly Leblanc³, Jorge Puebla², Dmitry Solnyshkov^{3,4}, Lars Klompmaker⁵, Ilya Akimov^{5,6}, Charalambos Louca¹, Pranaba Muduli^{7,8}, Armando Genco^{1,9}, Manfred Bayer^{5,6}, Yoshi Otani^{2,7}, Guillaume Malpuech³ and Alexander Tartakovskii¹; ¹The University of Sheffield, United Kingdom; ²RIKEN, Japan; ³Institut Pascal, France; ⁴Institut Universitaire de France, France; ⁵Technische Universität Dortmund, Germany; ⁶Russian Academy of Sciences, Russian Federation; ⁷The University of Tokyo, Japan; ⁸Indian Institute of Technology Madras, India; ⁹Politecnico di Milano, Italy

Strong coupling between light and the fundamental excitations of a two-dimensional electron gas (2DEG) are of foundational importance both to pure physics and to the understanding and development of future photonic nanotechnologies (Smolka et al, 2014; Efimkin et al, 2017; Back et al, 2017; Sidler et al, 2017; Tan et al, 2020; Klein et al, 2021; Roch et al, 2019). Here we study the relationship between spin polarization of a 2DEG in a monolayer semiconductor, MoSe₂, and light-matter interactions modified by a zero-dimensional optical microcavity. We find pronounced spin-susceptibility of the 2DEG to simultaneously enhance and suppress trion-polariton formation in opposite photon helicities. This leads to observation of a giant effective valley Zeeman splitting for trion-polaritons (g-factor > 20), exceeding the purely trionic splitting by over five times. Going further, we observe clear effective optical non-linearity arising from the highly non-linear behavior of the valley-specific strong light-matter coupling regime, and allowing all-optical tuning of the polaritonic Zeeman splitting from 4 to > 10 meV. Our experiments lay the groundwork for engineering topological phases with true unidirectionality in monolayer semiconductors, accompanied by giant effective photonic nonlinearities rooted in many-body exciton-electron correlations.

Our experiments demonstrate the simultaneous manifestation of strong and weak coupling regimes between a photonic mode and a many-body correlated matter excitation consisting of an exciton dressed by electrons in an effective ferromagnetic phase, resulting in a giant Zeeman splitting between trion-polariton modes. We additionally show that laser illumination acts to depolarize the 2DEG via a process of trion valley pseudospin relaxation and subsequent radiative recombination. The resulting Rabi splitting transfer between the two polarization components induces energy renormalization to which we associate large effective interactions. While in this work an EuS film was used to introduce additional free electrons into the flake, similar results should be observed in any MoSe₂ monolayer in which the itinerant carrier density can be raised arbitrarily to give the trion sufficient oscillator strength. Magnetic 2-dimensional materials may also be used to induce 2DEG spin polarization without the need for strong external B-fields (Lyons et al, 2021). Moreover, we note that extremely high laser powers, often pulsed and quasi-resonant, are typically needed to enter regimes of polariton non-linearity, while here the strongest effective interactions occur under low power non-resonant continuous-wave laser excitation. Our work therefore highlights doped MoSe₂ as a flexible system in which to realize and apply ultrastrong low-threshold non linearities, for instance towards TMD-based all-optical logic gates (Amo et al, 2010), or to explore nonlinear topological photonics (Smirnova et al, 2020).

See full article: <https://arxiv.org/abs/2109.05859>

9:15 AM EQ06.08.03

Scanning Tunneling Microscope Characterization of Chalcogen Site Defects in Flux Grown WSe₂ [Madisen Holbrook](#), Luke Holtzman, Song Liu, Katayun Barmak, Abhay N. Pasupathy and James Hone; Columbia University, United States

Within the family of two dimensional (2D) materials, transition metal dichalcogenides (TMDs) have gained much research interest due to their potential for filling the semiconductor role in 2D devices. Defects play a critical role in modifying semiconductor electronic properties, both detrimental by limiting device performance, and beneficial as a tool to engineer the electronic properties. The extreme 2D nature of TMDs leads to a strong sensitivity to defects from confinement and reduced screening.^[1] A number of different atomic defects have already been experimentally observed in TMDs, but connecting each defect species with their impact on the electronic properties is critical. Recent studies have shown that defect concentrations below 10¹¹ cm⁻² are achievable for TMD single crystals synthesized by a self-flux growth method,^[2] but the identity of these defects still remains unclear. Of the possible defects in TMDs, chalcogen vacancies are shown to be the most energetically favorable with the lowest formation energy,^[3] but previous studies have shown that oxygen passivated vacancies are the most abundant defect in CVD grown samples. Here we report the characterization of chalcogen site defects in flux grown WSe₂ using scanning tunneling microscopy and spectroscopy (STM/S). We study the electronic and structural properties of the defects in both bulk and monolayer as-grown WSe₂. We further induce vacancies by thermal annealing in UHV, and oxygen passivate them to show how the defects influence the WSe₂ electronic properties. Our study sheds light on the how one of the most abundant defects in TMDs, chalcogen site defects, can be used to engineer the electronic properties of TMDs.

[1] Q. Liang, et al., *ACS Nano*, **15**, (2021).

[2] D. Edelburg, et al., *Nano. Lett.*, **19**, (2019).

[3] H.-P. Komsa, et al., *PRB*, **88**, (2013).

[4] S. Barja et. al., *Nat. Comm.*, **10**, (2019).

9:30 AM BREAK

10:00 AM EQ06.08.05

Single Photons from Atomically Thin h-BN/WS₂ Heterostructured Bubbles Elena Blundo¹, Salvatore Cianci¹, Federico Tuzi¹, Djero Peteers², Eirini Parmenopoulou¹, Giorgio Pettinari³, Antonio Miriametro¹, Takashi Taniguchi⁴, Kenji Watanabe⁴, Marco Felici¹ and [Antonio Polimeni](#)¹; ¹Sapienza University, Italy; ²Technische Universiteit Eindhoven, Netherlands; ³National Research Council, Italy; ⁴National Institute for Materials Science, Japan

Two-dimensional (2D) crystals represent a vast class of materials with exceptional properties that most often contrast with those of their bulk counterpart. An exemplary case is that of transition metal dichalcogenides (TMDCs), which feature a direct bandgap in the monolayer (ML) form, while they are indirect bandgap semiconductors as soon as their thickness exceeds one layer. Indeed, very high emission efficiency characterizes TMDC MLs in the visible/infrared range. In addition, the robustness of TMDC MLs to mechanical deformations (strain) has been exploited as a tuning "knob" to tailor the optical and electronic properties of 2D crystals [1]. At the same time, strain is also at the basis of the appearance of quantum emitters (QEs) in the photoluminescence (PL) spectra of deformed MLs brought to cryogenic temperatures, a property that has sparked the interest of the nanophotonics and quantum information community.

Starting from the observation that the majority of the QEs seemed to appear in spontaneously strained ML regions, such as at the edges of exfoliated flakes [2] or in naturally occurring wrinkles [3], different methods were employed to generate ordered arrays of "strained" emitters that is an essential step for their integration in photonic devices. So far, top-down approaches were mainly used (see a review in [1]), whereby the deposition of MLs on patterned substrates followed by the exposure to highly energetic charged particles [4] generates spatially controlled emitters.

Here, we present an innovative bottom-up straining method, which avoids etched substrates and allows the control over the position and properties of QEs. Indeed, we show that *low-energy* (10 eV) hydrogen-ion irradiation of *bulk* WS₂ flakes can be exploited to engender localised strains. More specifically, protons penetrate through one layer, leading to the production and accumulation of molecular hydrogen in the first interlayer region. The trapped gas coalesces, causing a local blistering of the material, and thus the formation of ML-thick WS₂ micro/nano-bubbles [5]. The bubbles can be made ordered via lithographic methods [5] and host complex strain fields [6], which drive peculiar interaction phenomena between the ML electronic states [7,8]. However, the bubbles completely deflate for temperatures below the gas-to-liquid transition temperature of H₂ (33 K) [5], thus nullifying strain and hindering the appearance of QEs at cryogenic temperatures. We show that by capping the WS₂ bubbles with few-layer-thick h-BN it is possible to preserve the bubble

shape even at temperatures below 33 K, leading to exciton localization in regions of the bubbles, where the strain gradient is maximum. As a result, the micro-PL spectra of the h-BN-capped bubbles at 5 K feature emission lines as narrow as about 1 meV and spectrally isolated. Finally, autocorrelation measurements performed with a Hanbury Brown & Twiss setup demonstrates the quantum nature of the light coming from the bubbles. This finding provides us with a new route to create ordered arrays of site-controlled QEs with the exciting perspective of coupling them with the nano-mechanical resonator represented by the bubbles' membrane.

- [1] E. Blundo *et al.*, *Appl. Phys. Rev.* **8**, 021318 (2021)
- [2] Y. Koperski *et al.*, *Nat. Nanotechnol.* **10**, 503 (2015)
- [3] A. Branny *et al.*, *Appl. Phys. Lett.* **108**, 142101 (2016)
- [4] K. Parto *et al.*, *Nat. Commun.* **12**, 3585 (2021)
- [5] D. Tedeschi, E. Blundo *et al.*, *Adv. Mater.* **31**, 1903795 (2019)
- [6] E. Blundo *et al.*, *Phys. Rev. Lett.* **124**, 046101 (2021)
- [7] E. Blundo *et al.*, *Phys. Rev. Res.* **2**, 012024 (2020)
- [8] E. Blundo *et al.*, *Phys. Rev. Lett.*, in press

10:15 AM EQ06.08.06

Chemomechanical Modification of Quantum Emission in Monolayer WSe₂ Iqbal B. Utama¹, Hongfei Zeng¹, Tumpa Sadhukhan¹, Anushka Dasgupta¹, S. C. Gavin¹, Riddhi Ananth¹, Dmitry Lebedev¹, Wei Wang², Jia-Shiang Chen², Kenji Watanabe³, Takashi Taniguchi³, Tobin J. Marks¹, Xuedan Ma², Emily A. Weiss¹, George C. Schatz¹, Nathaniel P. Stern¹ and Mark C. Hersam¹; ¹Northwestern University, United States; ²Argonne National Laboratory, United States; ³National Institute for Materials Science, Japan

Two-dimensional (2D) materials such as monolayer WSe₂ have prospective applications in quantum information science because of their capability to host single-photon emitters (SPEs). However, chemical functionalization remains an unexplored parameter space in the design and control of SPEs based on 2D materials, whose atomically thin structure should yield strong tunability with interfacial modifications. Moreover, SPEs in 2D materials are typically generated using a single mechanism such as strain. Here, we report a chemomechanical approach to modify SPEs by using a synergistic combination of localized mechanical strain and non-covalent functionalization with aryl diazonium chemistry. Following a facile diazonium treatment, the dense defect-related emissive states of strained monolayer WSe₂ are simplified into spectrally-isolated SPEs with high photon purity. Our work significantly broadens the possibilities in the parameter space of designing 2D materials-based SPEs by utilizing molecular heterojunction and chemical functionalization approaches.

10:30 AM *EQ06.08.07

Semimetal Device Technology for 2D Semiconductor Electronics Yuxuan Cosmi Lin; Corporate Research, TSMC San Jose, United States

2D semiconductor has emerged as promising candidates for the channel materials in a future ultimately scaled transistor technology. A number of challenges still remain both in terms of material processing and device technologies. The weak interlayer coupling and the unique mesoscopic physics of semimetal/2D semiconductor heterostructures have shown great promises to address some of these fundamental challenges and have demonstrated viable pathways towards scalable and high-performance electronic device technologies based on 2D semiconductors. This talk will summarize our recent research efforts on the material processing and device technologies for semimetal/2D semiconductor electronics. First, I will discuss a wafer-scale semi-automated dry transfer process for monolayer CVD transition-metal dichalcogenides (TMDs) utilizing the weakly coupled interface between semimetal (Bi) and TMDs. Second, our recent progress on semimetal contacts (Bi, Sb) to 2D TMDs for high performance n-type field effect transistor (nFET) technologies will be covered. The thermal stability of these contact technologies will also be evaluated. Finally, I will talk about our computational efforts on the searching of pinning free semimetallic p-type contacts to 2D TMDs.

SESSION EQ06.09: Quantum Properties and Applications II
Session Chairs: Shengxi Huang and Yuxuan Cosmi Lin
Thursday Afternoon, December 1, 2022
Sheraton, 2nd Floor, Back Bay B

1:30 PM *EQ06.09.01

Quantum Properties and Applications of Ultrapure 2D Materials James Hone; Columbia University, United States

This talk will review four areas relevant to the use of 2D materials for achieving novel quantum states and technologies. (1) Synthesis of ultra-pure crystals of transition metal dichalcogenide semiconductors and metals; (2) Studies of quantum transport in semiconducting WSe₂; (3) Novel superconductivity in bilayer MoTe₂; and (4) Applications of 2D heterostructures in superconducting qubits.

2:00 PM *EQ06.09.02

Atomic Layer Etching—Towards the Atomic Limit in Scalable Manufacturing Austin J. Minnich; California Institute of Technology, United States

The figures of merit of photonic and electronic devices based on both 2D and 3D materials are increasingly limited by imperfections introduced in nano fabrication. Further advances in capabilities demands subtractive manufacturing methods with vastly improved precision compared to that of typical methods such as wet etching or plasma-based reactive ion etching. In this talk, I will describe our development of plasma-thermal atomic layer etching which enables engineering of the surfaces of photonic and electronic materials with atomic monolayer precision. Possible extensions to 2D materials will also be discussed.

2:30 PM *EQ06.09.03

Creating and Probing New Phases in Layered Quantum Materials Qiong Ma; Boston College, United States

Over the past decade, van der Waals monolayer crystals and heterostructures have been increasingly recognized as a highly-tunable material platform to create and control novel quantum phases. Remarkably, we can create moiré superlattices with the lattice constant continuously tuned over a wide range, providing artificial potential modulation that is effectively felt by electrons. This has led to a plethora of low-temperature emergent phases in lattices made

out of pure carbon, including magnetism, topology, and superconductivity. In this talk, I will show an unexpected spontaneously ordered electronic phase in graphene moiré superlattices with practical device functionalities, persisting all the way up to room temperature. Also, in order to sensitively detect the symmetry properties of such new electronic orders, I will introduce nonlinear electromagnetic responses in various forms and give an example in which the nonlinear properties are employed not only to detect but also to control an emergent electronic phase with definite chirality in a layered correlated semimetal.

3:00 PM BREAK

3:30 PM EQ06.09.04

Deep-Ultraviolet Photoluminescence Excitation Spectroscopy of Hexagonal Boron-Nitride Crystals Su-Beom Song^{1,2}, Sangho Yoon^{1,2}, So Young Kim^{1,2}, Sera Yang^{1,2}, Seung-Young Seo¹, Soonyoung Cha², Hyeon-Woo Jeong¹, Kenji Watanabe³, Takashi Taniguchi³, Gil-Ho Lee¹, Jun Sung Kim^{1,2}, Moon-Ho Jo^{1,2} and Jonghwan Kim^{1,2}; ¹Pohang University of Science and Technology, Korea (the Republic of); ²Institute for Basic Science, Korea (the Republic of); ³National Institute for Materials Science, Japan

hBN is an indirect and wide bandgap vdW semiconductor forming the indirect gap of ~ 5.96 eV. Despite the indirect bandgap, hBN emits series of strong luminescence lines via strong electron-phonon coupling. Although the physical origin of S-series is verified as phonon-assisted emission from the indirect bandgap of AA' stacked hBN, the physical origin of D-series is largely elusive yet. Cathodoluminescence imaging of D-series has identified that the structural origin is stacking fault in hBN. However, the physical origin of D-series emission is still ambiguous. Here, we employ deep-ultraviolet photoluminescence excitation (PLE) spectroscopy to probe light absorption properties of electronic states for the emission lines of D-series. Our PLE spectra unambiguously demonstrate that all emission lines in D-series originate from inherent stacking faults in hBN crystals.

3:45 PM EQ06.09.05

CVD-Grown Graphene Rings Toward Aharonov-Bohm Oscillations Zitao Tang¹, Siwei Chen¹, Abdus Salam Sarkar¹, Na Liu¹, Stefan Strauf¹, Grzegorz Hader², Chunlei Qu¹ and Eui-Hyeok Yang^{1,1}; ¹Stevens Institute of Technology, United States; ²US army DEVCOM, United States

The Aharonov-Bohm effect (AB Effect) demonstrates that the orbital wave function of a charged particle picks up a different phase when it moves along two different paths in the presence of an external magnetic field. The AB effect has been studied in various semiconductors, including GaAs, InP, InAs, AlGaSb, phosphorene, and Bi₂Se₃ [1–3]. More recently, the AB effect was also demonstrated in mechanically exfoliated graphene nanostructures [4–6]. While these results revealed intriguing electron transport properties in graphene nanostructures, relying on graphene produced using sticky tapes limits its scalability for future practical applications.

Here, we present the fabrication of CVD-grown graphene nanorings and their electron transport measurement under magnetic fields toward achieving AB oscillations. We first fabricated graphene channels to measure the sheet resistance (approx. 1165 Ω) and the mobility (approx. 3400 cm²/V*s), which were found comparable to the values found in the literature [7]. We then fabricated the graphene rings and loaded the device inside an ultra-low vibration cryogen-free cooling closed-cycle cryostat at 4 K for the magnetoresistance measurement under the out-of-plane external magnetic fields up to ± 2 T. The side gate voltage of up to 1 V was also applied to the graphene ring. The results showed low-frequency oscillations from which the AB oscillations were not extracted, and it is likely due to the large universal conductance fluctuations present in the current device.

We are currently working on modifying and improving the device design based on inputs from modeling to isolate the AB oscillations from the noise floor at 4K (note that AB oscillations in exfoliated graphene rings were detected only below 3.5K in the past [4, 6]). In addition, we will encapsulate the device with hBN to improve the environmental stability of electronic properties and room-temperature mobility [8]. We will also consider incorporating Si₃N₄ or Al₂O₃ as the substrate for graphene rings to reduce the back gate leakage/charging effect. The new results will be included in the presentation at the meeting.

References:

- [1] I. Vurgaftman, J. Ć Meyer, and L. Ć Ram-Mohan, *Journal of applied physics*, **89** (11), 5815–5875, (2001).
- [2] M. Grochol, F. Grosse, and R. Zimmermann, *Physical Review B*, **74** (11), 115416, (2006).
- [3] T. Thakur and B. Szafran, *Physical Review B*, **105** (16), 165309, (2022).
- [4] M. Huefner, F. Molitor, A. Jacobsen, A. Pioda, C. Stampfer, K. Ensslin, and T. Ihn, *New Journal of Physics*, **12** (4), 43054, (2010).
- [5] J. Schelter, P. Recher, and B. Trauzettel, *Solid state communications*, **152** (15), 1411–1419, (2012).
- [6] M. Huefner, F. Molitor, A. Jacobsen, A. Pioda, C. Stampfer, K. Ensslin, and T. Ihn, *physica status solidi (b)*, **246** (11–12), 2756–2759, (2009).
- [7] V. E. Dorgan, M.-H. Bae, and E. Pop, *Applied Physics Letters*, **97** (8), 82112, (2010).
- [8] N. Petrone, T. Chari, I. Meric, L. Wang, K. L. Shepard, and J. Hone, *ACS nano*, **9** (9), 8953–8959, (2015).

4:00 PM EQ06.09.06

Imaging Conductance with Atomic Scale Resolution in van der Waals Heterostructures Jawaher Almutlaq¹, Ondrej Dyck², Bevin Huang¹, Hyowon Moon¹, Chitrleema Chakraborty¹, Stephen Jesse² and Dirk Englund¹; ¹Massachusetts Institute of Technology, United States; ²Oak Ridge National Laboratory, United States

Transition metal dichalcogenides (TMDs) are naturally favored for e-beam imaging due to their atomic thickness, semiconducting nature, and heavy atoms that are easy to see under scanning probe techniques. In this project, we use STEM Secondary Electron Beam Induced Current (SEBIC) to image and probe the electrical conductivity and connectivity of the active layers in quantum devices. SEEBIC is an emerging electron microscopy technique for probing the electronic band structure of a material by spatially mapping secondary electrons (SEs) [1,2]. The image signal generated with this technique depends on the device and material parameters including SE generation and emission, work function, and conductivity. The measurement requires special sample preparation and a unique substrate with an electron transparent window for STEM. The method has been initially demonstrated to probe graphene and now it is extended to probe more complex multi-layer Van der Waals (VdW) heterostructures. Our results show that we can distinguish the excitonic and conductive layers and see the WSe₂ monolayer with atomic resolution even though it is buried between layers of h-BN and graphene, while regions of h-BN and graphene could be identified using electron energy loss spectroscopy (EELS). The correlation between local atomic structure and the emergent electronic properties is of paramount importance in the design and fabrication of device architectures. The facilitation of direct measurement and visualization of such properties is expected to provide a critical window into the operational physics of devices spanning sensing, optoelectronics, and quantum information processing.

References

- [1] Dyck, Ondrej, Jacob L. Swett, Andrew R. Lupini, Jan A. Mol, and Stephen Jesse. "Imaging Secondary Electron Emission from a Single Atomic Layer."

Small Methods 5, no. 4 (2021): 2000950

[2] Dyck, Ondrej, Jacob L. Swett, Charalambos Evangelis, Andrew R. Lupini, Jan A. Mol, and Stephen Jesse. "Mapping conductance and switching behavior of graphene devices *In situ*." Small Methods 6, no. 3 (2022): 2101245

4:15 PM EQ06.09.07

Engineering Charge Density Waves Using Interleaved Polytype Heterostructures Suk Hyun Sung¹, Yin Min Goh¹, Nishkarsh Agarwal¹, Noah Schnitzer², Ismail El Baggari³, Kai Sun¹, Lena F. Kourkoutis² and Robert Hovden¹; ¹University of Michigan, United States; ²Cornell University, United States; ³The Rowland Institute at Harvard University, United States

1T-TaS₂ is a prototypical charge-ordered van der Waals (vdW) material that hosts several charge density wave (CDW) phases that spontaneously break crystal symmetries, mediate metal–insulator transitions and compete with superconductivity [1–4]. CDWs in TaS₂ are two-dimensional (2D) and reside within each vdW layer. These low-dimensional quantum states are promising candidates for novel devices [5–8], efficient ultrafast non-volatile switching [9,10], and suggest elusive chiral superconductivity [9,10]. Unfortunately, 2D charge ordering is fragile, and extrinsic and thermal disorder quickly degrades long-range order. Here, we engineer 2D-CDW states by controlling disorder via endotaxial interleaved polytype heterostructures of TaS₂. Furthermore, we explore the temperature vs disorder phase space of octahedrally coordinated TaS₂ using *in-situ* S/TEM to offer a deeper understanding of the system.

Disorder—both extrinsic and thermal—significantly degrades CDWs. Nie, Tarjus, and Kivelson showed that 2D incommensurate (IC)-CDWs in cuprates are long-range ordered only at the zero-disorder limit [11]. Here, we employ endotaxial polytype engineering to substantially decrease disorder to access new regions of the phase diagram where fragile low dimensional quantum states become stable. For example, we show that for octahedrally coordinated TaS₂ the long-range ordered C-CDW (stable < 200 K for 1T) is stable all the way up to ~350 K in interleaved polytype heterostructures [12]. Above ~350 K, the polytype heterostructure recovers long-range order in the IC phase. Furthermore, the hexatic-IC phase exists even above 620 K; in 1T-TaS₂, CDWs completely vanish at ~540 K [13]. Using *in-situ* electron microscopy we can control amount of disorder by directly observing layer-by-layer polytype transformations [12].

In summary, we demonstrate that polytype engineering can stabilize fragile phases such as an ordered IC phase even at high temperatures. In addition, we now provide a schematic phase diagram of octahedrally coordinated TaS₂.

References:

- [1] J Wilson et al., Adv. Phys., **24** (1975) p.117.
- [2] E Navarro-Moratalla et al., Nat. Commun., **7** (2016) 11043.
- [3] R Ang et al., Nat. Commun., **6** (2015) 60981.
- [4] L Li et al., npj Quantum Mater., **2** (2017) 11.
- [5] DN Basov et al., Nat. Mater., **16** (2017) p.1077.
- [6] Y Tokura et al., Nat. Phys., **13** (2017) p.1056.
- [7] MJ Hollander et al., Nano Lett., **15** (2015) p.1861.
- [8] G Liu et al., Nat. Nanotechnol., **11** (2016) 845.
- [9] A Ribak et al., Sci. Adv., **6** (2020) aax9480.
- [10] R Ganesh et al., Phys. Rev. Lett., **113** (2014) 177001.
- [11] L Nie, G Tarjus, and SA Kivelson, Proc. Natl. Acad. Sci., **111** (2014) p.7980.
- [12] SH. Sung et al., Nat. Commun., **13** (2022) p.413.
- [13] SC Bayliss, A Clarke and WY Liang, J. Phys. C: Solid State Phys. **16** (1983) p.L831.

4:30 PM EQ06.09.08

Momentum-Dependent Oscillator Strength Crossover of Excitons and Plasmons in Two-Dimensional PtSe₂ Mark Kamper Svendsen¹, Jinhua Hong², Thomas Pichler³, Kazu Suenaga² and Kristian S. Thygesen¹; ¹Technical University of Denmark, Denmark; ²National Institute of Advanced Industrial Science and Technology (AIST), Japan; ³University of Vienna, Austria

The 1T-phase layered PtX₂ chalcogenide has attracted widespread interest due to its thickness dependent metal–semiconductor transition driven by strong interlayer coupling. While the ground state properties of this paradigmatic material system have been widely explored, its fundamental excitation spectrum remains poorly understood. Here we combine first-principles calculations with momentum (q) resolved electron energy loss spectroscopy (q -EELS) to study the collective excitations in 1T-PtSe₂ from the monolayer limit to the bulk. At finite momentum transfer, all the spectra are dominated by two distinct interband plasmons that disperse to higher energy with increasing q . Interestingly, the absence of long-range screening in the two-dimensional (2D) limit inhibits the formation of long wavelength plasmons. Consequently, in the small- q limit, excitations in monolayer PtSe₂ are exclusively of excitonic nature, and the loss spectrum coincides with the optical spectrum. The qualitatively different momentum dependence of excitons and plasmons enables us to unambiguously disentangle their spectral fingerprints in the excited state spectrum of layered 1T-PtSe₂. This will help to discern the charge carrier plasmon and locally map the optical conductivity and trace the layer-dependent semiconductor to metal transition in 1T-PtSe₂ and other 2D materials.

4:45 PM EQ06.09.09

Intrinsic Supercurrent Non-Reciprocity Coupled to the Crystal Structure of a van der Waals Josephson Barrier Jae-Keun Kim¹, Kun-Rok Jeon², Pranava Sivakumar¹, Jaechun Jeon¹ and Stuart S. Parkin¹; ¹Max Planck Institute of Microstructure Physics, Germany; ²Chung-Ang University, Korea (the Republic of)

The non-reciprocal behavior in dissipative current flows, known as the diode effect, has played a central role in modern electronic devices and circuits. In conventional schemes, non-reciprocity along the current direction arises from spatial inhomogeneity. Recently, it has been shown that when inversion and time-reversal symmetries are both broken, and in combination with a spin-orbit interaction (SOI), even spatially homogeneous systems can provide for diode functionality. By implementing this magneto-chirality with superconductors and matching the superconducting gap with the SOI energy, one can achieve a directional, non-dissipative, supercurrent flow, which is a prerequisite for the realization of future superconducting quantum devices. To date, only a few methods have been developed to intrinsically and/or extrinsically break the inversion symmetry and its mechanisms, especially whether intrinsic or extrinsic, remain elusive.

Here we demonstrate a substantial supercurrent non-reciprocity in a van der Waals (vdW) vertical Josephson junction (JJ) formed with a T_d -WTe₂ barrier and NbSe₂ electrodes that clearly reflects the intrinsic crystal structure of T_d -WTe₂. In combination with time-reversal symmetry breaking by the applied magnetic field, an inherently inversion symmetry breaking of WTe₂ barrier can provide a non-reciprocal supercurrent in NbSe₂/WTe₂/NbSe₂ vdW JJs. The

magneto-chiral characteristics with respect to a mirror plane of WTe_2 strongly support the crystal structure reflected supercurrent non-reciprocity in $NbSe_2/WTe_2/NbSe_2$ vdW JJs. The diode efficiency of the JJs show linear scaling behavior with WTe_2 barrier thickness up to critical thickness, which is predicted theoretically for ballistic JJ. It shows that the supercurrent non-reciprocity of the JJs can be likely related to charge transport mechanism in the barrier. Our results show that 2D materials promise vertical Josephson diodes with high efficiency and tunability. Our approach can be extended to other low-symmetric and twisted vdW systems for accelerating the development of 2D superconducting devices and circuits.

SESSION EQ06.10: Quantum Properties and Applications III
Session Chairs: Siyuan Dai and Yuxuan Cosmi Lin
Friday Morning, December 2, 2022
Hynes, Level 3, Room 306

8:15 AM *EQ06.10.01

Large-Area Single-Crystal 2D Films for Electronic Device Applications [Ki Kang Kim](#)^{1,2}; ¹Institute for Basic Science, Korea (the Republic of); ²Sungkyunkwan University, Korea (the Republic of)

Two-dimensional (2D) materials including graphene, hexagonal boron nitride and transition metal dichalcogenide have been highlighted due to unusual intrinsic physical and chemical properties such as high exciton binding energy and large magnetic resistance, which allows unprecedented electronic applications. To realize the intrinsic material properties and industrial applications, wafer-scaled single-crystal 2D films are highly required. Here, we present the recent progress of single-crystal growth for 2D materials in a wafer scale via the self-collimation on liquid substrate and the epitaxial growth on atomic sawtooth surface. The detailed growth mechanism is discussed accordingly.

8:45 AM EQ06.10.02

Modelling Defective MoS₂ and Au Interfaces in 2D Memristors by Combining DFT with Green's Function Surface Calculations [Gabriele Boschetto](#)¹ and Aida Todri-Sanial^{1,2}; ¹LIRMM, University of Montpellier, CNRS, France; ²Technical University of Eindhoven, Netherlands

Atomically thin single-layer molybdenum disulfide (MoS₂) is a two-dimensional material with highly desirable mechanical, electronic, and optical properties. In addition, its reduced dimensionality and ultra-thin size could enable the fabrication of a new generation of very compact and low-power devices beyond conventional CMOS technology.

In this context, 2D memristors for neuromorphic computing applications [1] based on single-layer MoS₂ present several advantages with respect to conventional devices based on transition metal oxides: good flexibility, high transparency, and the potential to work when applying low voltages (0.1 - 0.2 V), thus allowing the fabrication of very compact and energy-efficient devices.

However, the working mechanism of 2D memristors is still far from being understood: the resistive switching may non-trivially depend on several factors, such as device architecture, metal electrodes, and the quality of the MoS₂ film. Small and extended defects in MoS₂ films, which are introduced during the material growth, are thought to play a crucial role not just in the properties of MoS₂ itself but also in the quality of the metal contact.

Indeed, at present, MoS₂ films are far from being pristine, and there is still much debate around the role of defects in the physics of the device.

Thus, to shed light onto the physics of metal-MoS₂ interfaces, we carry out atomistic computer simulations in the framework of density functional theory (DFT). We employ surface calculations based on the Green's function formalism to construct realistic interfaces and compute surface properties [2]. To model the metal electrode, we choose Au as it is commonly one of the most popular choices, and it has been successfully used to develop 2D memristors [3]. As we aim to bridge the gap between materials' properties and device physics, we investigate the effect of common defects on MoS₂ (i.e., vacancies and substitutions) on the physics and chemistry of Au-MoS₂ interfaces [4].

To the best of our knowledge, this is the first attempt to thoroughly model defective MoS₂ interfaces with DFT coupled with the Green's function formalism.

Ultimately, our study constitutes the first step of a more comprehensive multi-scale modelling approach, in which the aim is to construct a full atomistic-to-device level model that can aid us in elucidating the working mechanism of 2D memristors based on single-layer MoS₂.

[1] EU H2020 NeurONN Project, www.neuronn.eu.

[2] S. Smidstrup et al. "First-Principles Green's Function Method for Surface Calculations: A Pseudopotential Localized Basis Set Approach," Phys. Rev. B, 96, 195309, 2017.

[3] R. Ge et al., "Atomristor: Nonvolatile Resistance Switching in Atomic Sheets of Transition Metal Dichalcogenides," *Nano Lett.*, 18, 434-441, 2017.

[4] G. Boschetto et al. "Ab Initio Computer Simulations on Interfacial Properties of Single-Layer MoS₂ and Au Contacts for Two-Dimensional Nanodevices" ACS Appl. Nano Mater. Just published, 2022.

9:00 AM EQ06.10.03

High-Quality Exfoliation and Integration of Large-Area Transition Metal Dichalcogenide Monolayers with Wafer Bonder [Wenjing Wu](#)^{1,2} and Shengxi Huang^{1,2}; ¹Rice University, United States; ²Penn State University, United States

Transition metal dichalcogenides (TMDCs) monolayers and their heterostructures have attracted tremendous research interests in the past decades, for their remarkable physical properties. However, producing such two-dimensional (2D) monolayers with both desired lateral scale and film quality still needs effort. Here, we report a nifty and generic way to achieve high quality large-area TMDC monolayers and their assembly from bulk crystals, with improved control over cracks and strain based on the Au-assist exfoliation technique. Wafer bonder is used during the process for: 1) applying controllable and uniform force to integrate monolayers onto desired substrates, 2) supporting a high vacuum (HV) environment to eliminate air bubbles between layers, and 3) maintaining the desired temperature. Both optical and electrical characterizations of different TMDC monolayers confirm the high quality over a centimeter scale. This high-throughput method could be beneficial to the fundamental physical studies as well as the electronic and photonic applications of the TMDC materials.

9:15 AM EQ06.10.04

Conformal Growth of Hexagonal Boron Nitride on Silicon-Based Nano-Trenches with High-Aspect Ratio [Jiye Kim](#)¹, Chang-Won Choi¹, Seokho Moon¹, Doh Kyung Yeon¹, Hokyong Jeong^{2,1}, Jaewon Kim^{3,1}, Jaerim Kim¹, Dongwa Lee¹, Si-Young Choi¹ and Jong kyu Kim¹; ¹Pohang University of Science and Technology, Korea (the Republic of); ²Samsung Electronics Memory Division, Korea (the Republic of); ³Samsung Advanced Institute of Technology, Korea (the Republic of)

Hexagonal boron nitride (h-BN) has emerged as a prospective dielectric material for future silicon (Si)-based electronics. Despite notable advances in h-BN synthesis, there are remaining challenges toward real-world applications at the industrial level. h-BN grown on catalytic substrates by using chemical vapor deposition (CVD) should be transferred onto a target substrate, which inevitably induces various deformations of the transferred h-BN such as tears, wrinkles, and incorporation of impurities. Moreover, it is extremely difficult to form a conformal and intact contact between h-BN and a target substrate with 3-dimensional complicated nanostructures, as is the case for CMOS devices, through such a transfer process, which should be addressed for taking advantage of h-BN in the future Si electronics technologies.

Here, we present the direct growth of h-BN film on an array of Si-based nano-trenches with a pitch of 60 nm and the aspect ratio of 7:1 by metal-organic chemical vapor deposition (MOCVD). Few-layer h-BN with a thickness of ~1.67 nm was conformally grown along the nano-trenches consisting of SiO₂ and Si, with an excellent step coverage. The conformal growth mechanism of MOCVD-grown h-BN will be discussed with a combination of state-of-the-art spectroscopic analyses and theoretical calculations. The boron and nitrogen precursors act as the key factor of conformal growth, which can easily diffuse into the nano-trenches and chemisorb on the SiO₂ surface.

9:30 AM EQ06.10.05

EllipsoNet—Deep-Learning-Enabled Optical Ellipsometry for Complex Thin Films Ziyang Wang¹, Yuxuan Lin², Kunyan Zhang¹, Wenjing Wu¹ and Shengxi Huang¹; ¹The Pennsylvania State University, United States; ²University of California, United States

Analysis of optical spectroscopy data often requires intensive model fitting. Reflectometry and ellipsometry are commonly used methods to measure the optical dielectric functions or the complex refractive indices of optical thin films such as 2D materials. However, the available fitting models are extremely computational intense, require calibrations from human-expert and very specific to the optical structures of the samples. The substrate structures need to be simple (a single, thick, and transparent substrate is ideal) and perfectly defined. In addition, ellipsometry also requires expensive setup. In this study, we developed a deep learning method based on an encoder-decoder convolutional neural network that is capable of extracting refractive indices of thin films including 2D materials on arbitrary complex multilayer substrates named EllipsoNet. EllipsoNet is trained with numerically generated data. Without any prior knowledge of stack materials or human intervention, EllipsoNet can predict the complex refractive indices of thin films from experimentally obtained optical reflectance with high accuracies. Kramers-Kronig relations are spontaneously learned by the model without purposely teaching. This approach enables the in-situ optical characterization of functional materials and components in actual complex optoelectronic devices, a task previously not feasible with traditional reflectometry or ellipsometry methods.

9:45 AM BREAK

10:15 AM *EQ06.10.06

Multiscale Simulation of 2D Electronic Devices—From Contact Design to Machine-Learning-Guided Device Optimization Tong Wu¹, Ning Yang¹, Han Wang² and Jing Guo¹; ¹University of Florida, United States; ²University of Southern California, United States

In nanoscale logic and memory devices based on new materials, atomistic scale features of materials and interfaces can play an important role in determining device characteristics and performance. Atomistic simulations of a practical logic or memory device, however, are computationally expensive, which hinders efficient device design. A multiscale approach to device simulation can address the above challenge and achieve physical accuracy and computational efficiency at the same time in device simulations. We have developed a multiscale simulation approach and machine-learning-guided design optimization methods to investigate the metal contacts to 2D materials, 2D-material-based nanoscale transistors, and ferroelectric tunneling junction (FTJ) memory devices, as described below.

To understand and explore low contact resistance to 2D materials, a multiscale simulation approach is developed to simulate the contact transport properties between a semimetal to a monolayer two-dimensional (2D) transition metal dichalcogenide (TMDC) semiconductor [1]. The results elucidate the mechanisms for low contact resistance between semimetal and TMDC semiconductor contacts from a quantum transport perspective. The simulation results compare favorably with recent experiments. Furthermore, the results show that the contact resistance of a Bismuth-MoS₂ contact can be further reduced by engineering the dielectric environment and doping the TMDC material to . The quantum transport simulation indicates the possibility to achieve an ultrashort contact transfer length of ~1nm, which can allow aggressive scaling of the contact size.

At the device level, scaling of transistors near the physical limits imposes significant technological and design challenges. Identifying and understanding optimum designs and trade-offs between multiple design targets, including speed, power or energy, and variability, is necessary. By integrating machine-learning-based optimization methods into device simulation, we developed a multiobjective device design method that can automatically and efficiently identify the most promising device designs that can simultaneously satisfy multiple design objectives [2] for 2D-material-based field-effect transistors (FETs) near the scaling limit. The multiobjective design framework performs gradient-free efficient global optimization based on an active learning method. Optimum designs with the trade-off between transistor speed, power, and variability are identified automatically for 2D FETs by applying the multiobjective design framework. It is shown that the International Roadmap of Devices and Systems (IRDS) target of 2025 and 2028 technology nodes can be met by the identified designs of 2D FETs [2].

The multiscale simulation approach is further applied to simulate 2D-material-based memory devices. Atomically thin van der Waals (vdW) heterojunctions are investigated for ferroelectric tunnel junction (FTJ) device application by combining multiscale simulations from atomistic *ab initio* to quantum transport device simulations with experimental studies [3]. The simulation reveals that low quantum capacitance of graphene, weak electronic hybridization of vdW bonds, and high interface quality free of dangling bonds can lead to extremely large vdW interface barrier height modulation at the graphene-2D ferroelectric (FE) interface [3].

References:

- [1] T. Wu and J. Guo, "Multiscale simulation of semimetal contact to transition metal dichalcogenide semiconductor," submitted, (2022).
- [2] T. Wu and J. Guo, "Multiobjective design of 2-D-material-based field-effect transistors with machine learning methods," *IEEE Trans. Electron Dev.*, (2021), doi: 10.1109/TEDE.2021.3085701
- [3] N. Yang, H. Chen, J. Wu, T. Wu, J. Cao, X. Ling, H. Wang, J. Guo, "Multiscale simulation of ferroelectric tunnel junction memory enabled by van der Waals heterojunction: comparison to experiment and performance projection," Int. Electron Dev. Meeting (IEDM), (2020).

10:45 AM EQ06.10.07

Unraveling the Correlation Between Raman and Photoluminescence in Monolayer MoS₂ Through Machine Learning Models Ang-Yu Lu¹, Luiz G.P Martins¹, Pin-Chun Shen¹, Zhantao Chen¹, Ji-Hoon Park¹, Mantian Xue¹, Jinchi Han¹, Nannan Mao¹, Ming-Hui Chiu^{1,2}, Tomas Palacios¹, Vincent Tung^{2,3} and Jing Kong¹; ¹Massachusetts Institute of Technology, United States; ²King Abdullah University of Science and Technology, Saudi Arabia; ³The University of Tokyo, Japan

Two-dimensional (2D) transition metal dichalcogenides (TMDCs) with intense and tunable photoluminescence (PL) have opened up new opportunities for optoelectronic and photonic applications such as light-emitting diodes, photodetectors, and single-photon emitters. Among the standard characterization tools for 2D materials, Raman spectroscopy stands out as a fast and non-destructive technique capable of probing material crystallinities and perturbations

such as doping and strain. However, a comprehensive understanding of the correlation between photoluminescence and Raman spectra in monolayer MoS₂ remains elusive due to its highly nonlinear nature. Here, we systematically explore the connections between PL signatures and Raman modes, providing comprehensive insights into the physical mechanisms correlating PL and Raman features. Our analysis further disentangles the strain and doping contributions from the Raman spectra through machine learning models. First, we deploy a DenseNet to predict PL maps by spatial Raman maps. Moreover, we apply a gradient boosted trees model (XGBoost) with Shapley additive explanation (SHAP) to bridge the impact of individual Raman features in PL features, allowing us to link the strain and doping of monolayer MoS₂. Last, we adopt a support vector machine (SVM) to project PL features on Raman frequencies. Our work may serve as a methodology for applying machine learning in 2D material characterizations and providing the knowledge for tuning and synthesizing 2D semiconductors for high-yield photoluminescence.

11:00 AM EQ06.10.08

Transition Metal Dichalcogenides—Self-Flux Synthesis, Characterization and Defect Computations [Luke Holtzman](#)¹, Song Liu¹, Preston A. Vargas², Madisen A. Holbrook¹, Richard Hennig², James Hone¹ and Katayun Barnak¹; ¹Columbia University, United States; ²University of Florida, United States

Two-dimensional transition metal dichalcogenides (TMDs) have emerged as a highly attractive class of materials due to their novel optical and electronic phenomena, scalability to sub-nanometer sizes, and potential for electronic and optoelectronic applications. Chemical vapor deposition (CVD) and chemical vapor transport (CVT) have been used to grow monolayers and bulk crystals, respectively, quickly and at high yields. However, these techniques produce highly defective TMDs, negatively impacting the novel properties [1-4]. An alternative synthesis method is self-flux crystal growth, which has been shown to grow bulk TMDs with point defect densities several orders of magnitude lower than those from CVD and CVT [5]. The self-flux-growth uses high-purity elemental precursors limiting impurities and occurs inside of a vacuum sealed quartz ampule. The transition metal dissolves in the excess liquid chalcogen flux at an elevated temperature, then the mixture is slowly cooled to allow for growth of high-quality crystals. In this work, we use the self-flux method to synthesize five different TMDs: MoSe₂, WSe₂, WTe₂, 2H-MoTe₂, and 1T'-MoTe₂. Temperature profiles for growth of the four stable phases are largely similar; however, for the metastable 1T'-MoTe₂ phase, the ampule is removed from the furnace at 900 °C and rapidly quenched instead of slow cooling to room temperature. The material and phase are confirmed using a combination of Raman spectroscopy and x-ray diffraction. The point defect density is determined by counting point defects in several scanning tunneling microscopy (STM) images taken from across a cleaved bulk TMD's surface. To identify the defect chemical identities in self-flux TMDs, density functional theory calculations were used to simulate STM images for various intrinsic defects, and after comparison to experimental images, the simulations suggest the presence of chalcogen vacancies in MoSe₂ and WSe₂, and both metal and chalcogen vacancies in 2H-MoTe₂. Additionally, ab initio modeling is used in conjunction with experimental thermodynamic data to calculate temperature dependent thermal equilibrium defect densities for intrinsic defects of the four stable self-flux TMDs. In WSe₂, the thermal equilibrium defect density of selenium vacancies at the self-flux growth conditions was calculated to be two to three orders of magnitude less than experimental values determined by STM images, suggesting thermal equilibrium has not been reached, and kinetic or residual impurity factors drive increased point defect densities in self-flux TMDs.

[1] D. Rhodes, *et al.*, *Nat. Mater.* 18 (2019), pp. 541-549, <https://doi.org/10.1038/s41563-019-0366-8>

[2] G. H. Han, *et al.*, *Nat. Comm.* 6, 6128 (2015), <https://doi.org/10.1038/ncomms7128>

[3] C. H. Naylor, *et al.*, *Nano. Lett.* 16, 7 (2016), pp. 4297-4304, <https://doi.org/10.1021/acs.nanolett.6b01342>

[4] C. H. Naylor, *et al.*, *2D Mater.* 4 (2017), 021008, <https://doi.org/10.1088/2053-1583/aa5921>

[5] D. Edelberg, *et al.*, *Nano Lett.* 19 (2019), pp. 4371-4379, <https://doi.org/10.1021/acs.nanolett.9b00985>

11:15 AM EQ06.10.09

Printed Memristors on Paper [Jinrui Chen](#), Mingfei Xiao, Nasiruddin Macadam and Tawfique Hasan; University of Cambridge, United Kingdom

Paper is a low-cost, flexible, and biodegradable substrate that could address the ever-growing e-waste problem. It is 10,000 times cheaper than silicon, and 300 times cheaper than the widely used plastic substrate polyimide. However, the progress in electronics on paper-based substrates in the last decade has largely remained focused on transistors and rudimentary sensors. We present the first ever memristor on consumer-grade printing paper. Our MoS₂-based inkjet-printed memristors with Ag and Au electrodes can be fabricated at < 120-celsius degrees. The devices exhibit excellent resistive switching behavior, with a high (10⁶) ON-OFF ratio, and < ±0.5 V operation voltage. Using an intermediate layer of polyethyleneimine, we demonstrate more than 6 stable resistive states and controllable transition from volatile to non-volatile state. We further demonstrate synaptic and neuron functions by integrating the devices into RC circuits. Our versatile memristor platform opens exciting opportunities in artificial synapses for neuromorphic electronics on biodegradable substrates.

11:30 AM EQ06.10.10

Chemical Exfoliation of Tin Monosulfides for Thin Film FETs on Flexible Substrates [Abdus Salam Sarkar](#), Sarah Erickson, Siwei Chen and Eui-Hyeok Yang; Stevens Institute of Technology, United States

Low crystal symmetry and structural in-plane anisotropic orthorhombic group IV_A-VI metal monochalcogenides (MMCs) have recently emerged as novel electronic materials. [1-3] They have a chemical formula, MX (M=Si, Ge, Sn and X=S/Se), with uniquely distorted layered structures. Among them, earth-abundant tin (II) monosulfides (SnS) show rich fundamental physics and anisotropic optical, electrical and mechanical responses originating from their low crystal symmetry [1]. However, the successful isolation of atomically thin SnS single/ultrathin layers is challenging due to strong interlayer interactions attributed to the lone-pair electrons of sulfur (S), which, in turn, makes it difficult to realize low-cost, printed field-effect transistors (FETs). Here, we present a top-down liquid-phase exfoliation (LPE) approach to overcome the challenge by synergistically utilizing the thermal and ultrasound energies that induce hydrodynamic force in the solution, giving rise to the systematic isolation of highly crystalline SnS nanosheets [4, 5]. In the LPE method, tin (II) sulfide granular (>99.99%) trace metals were dissolved in acetone in a glass vial sealed with Teflon tape, followed by cavitation using ultrasonication at 50 W and 40 kHz for 20 hours. After the sonication process, the obtained dark brown solution was centrifuged at 8000 rpm for 15 minutes. The isolated SnS nanosheets were characterized using an atomic force microscope (AFM), transmission electron microscope and Raman/PL spectroscopy. The AFM analysis of isolated SnS dimensionality revealed Gaussian distribution in thicknesses. The average sheet thickness of the nanosheets was ~0.90 nm, affirming the isolation of monolayers or bilayers with high crystallinity. The room temperature Raman spectra of SnS nanosheets exhibited four optically active phonon modes consistent with those of ultrathin layers. The phonon modes peaked at ~100, ~190, ~210 cm⁻¹ correspond to A_g (1), A_g (2), A_g (3) vibrational modes, respectively, while the peak at ~160 cm⁻¹ to B_{3g} orthorhombic mode. The SnS nanosheets formulate a functional ink that can be subsequently deposited by spin/spray coating onto Si/SiO₂ and PET substrates. This chemical exfoliation technique enables large-scale isolation of electronic grade SnS nanolayers for a wide range of applications, including extended area nanoelectronic devices printed from solution to create field-effect transistors (FETs) and phototransistors for flexible electronic applications. Currently, we

are fabricating these FET arrays, which will be included in the presentation at the meeting.

References

- [1] A. S. Sarkar and E. Stratakis, *Adv. Sci.*, 2020, 7, 2001655
- [2] F. Xia, H. Wang, J. C. M. Hwang, A. H. Castro Neto and Li Yang, *Nat. Rev. Phys.*, 2019, 1, 306–317.
- [3] X. Li, H. Liu, C. Ke, W. Tang, M. Liu, F. Huang, Y. Wu, Z. Wu and J. Kang, *Laser Photon. Rev.*, 2021, 15, 2100322
- [4] A. S. Sarkar et al., Under revision in *Adv. Sci.*, 2022
- [5] A. S. Sarkar, S. Erickson and E. H. Yang, *Work in progress*, 2022

11:45 AM EQ06.10.11

Low-Energy Ion Implantation—Range Comparisons Between Theory and Experiment [Michael Titze](#)¹, Jonathan Poplawsky², Alex Belianinov¹ and Edward Bielejec¹; ¹Sandia National Laboratories, United States; ²Oak Ridge National Laboratory, United States

The continued decrease in size of microelectronic devices has created a need for shallower implanted dopant layers. With the recent discovery of two-dimensional (2D) materials, the ultimate limit for shallow layer implant is incorporating material into a single monolayer. Multi-specie focused ion beams (FIB) can operate with a variety of ion species and enable direct-write implantation of specific ions tailored for an exact application. Prior to any ion irradiation experiment, the range of ions in the material needs to be calculated, often predicted by using freely available Stopping and Range of Ions in Matter (SRIM) simulation.

SRIM simulations are in excellent agreement with experiment for high energy light ions, however, for low energy heavy ions, discrepancies between SRIM and observed experimental values have been reported. We use Rutherford backscattering spectrometry (RBS), Secondary ion mass spectrometry (SIMS) and Atom-probe tomography (APT) to measure the depth of heavy ions in silicon following FIB implantation with energies from 1 – 150 keV. The resolution limit of RBS and SIMS is on the order of nanometers, comparable to the implantation depth for few keV ion implants, requiring the use of APT for measuring lowest energy implants because APT is capable of almost angstrom resolution in the 100 direction of single crystalline Si. The difference between SRIM and experimental result is < 10 nm for all investigated ion energies, however due to the low overall range of the ions, the relative error is larger for lower ion energies with 1 keV as the minimum energy investigated showing > 500 % relative discrepancy.

This work was performed, in part, at the Center for Integrated Nanotechnologies, an Office of Science User Facility operated for the U.S. Department of Energy (DOE) Office of Science. Sandia National Laboratories is a multimission laboratory managed and operated by National Technology & Engineering Solutions of Sandia, LLC, a wholly owned subsidiary of Honeywell International, Inc., for the U.S. DOE's National Nuclear Security Administration under contract DE-NA-0003525. The views expressed in the article do not necessarily represent the views of the U.S. DOE or the United States Government. APT research was supported by the Center for Nanophase Materials Sciences (CNMS), which is a US Department of Energy, Office of Science User Facility at Oak Ridge National Laboratory.

SESSION EQ06.11: Quantum Properties and Applications IV
Session Chairs: Ki Kang Kim and Wenjing Wu
Friday Afternoon, December 2, 2022
Hynes, Level 3, Room 306

1:30 PM *EQ06.11.01

Engineer Confined Phononic Light-Matter Waves in van der Waals Materials [Siyuan Dai](#); Auburn University, United States

The manipulation of light at small scales is one of the ultimate goals for modern optics. For this purpose, polaritons—hybrid light-matter waves that propagate in a confined length scale—are typically involved. Recent results of polaritons in van der Waals materials reveal a series of advances, including atomic-scale localization, dynamic tunability, relative low-loss, and topologically protected states. These advances are attributed to the unique physical properties in reduced dimensions and the configurability through van der Waals heterostructuring. In this talk, I will show the engineered merits of photonic lattice waves—phonon polaritons—by van der Waals stacking, structuring, and twisting. Phonon polaritons in van der Waals heterostructures exhibit dynamic tunability, various wavefronts, and new energy-momentum dispersions.

2:30 PM EQ06.11.04

Experimental Quantum Transport in Strained Graphene and SWCNTs – Towards NOEMS [Alexandre R. Champagne](#); Concordia University, Canada

We report new measurements of ballistic charge conductivity in strained suspended graphene, and observe the previously predicted [1] strain-induced scalar and vector potentials. To do so, we built an experimental platform for *in-situ* strain-engineering of quantum transport in 2D materials. This instrumentation permits low temperature (0.3 K) transport in 0 to 9 Tesla magnetic fields. The tunable uniaxial strain (up to 3%) is completely decoupled from the gate-tunable charge density, permitting quantitative understanding of strain effects. We show slippage-free mechanical clamping of high aspect-ratio graphene crystals, where atomically ordered edges are unnecessary for quantitative straintronics. We study in detail transport in a ballistic graphene channel whose length is 90 nm and width is 600 nm. By applying strain in this device, we observe that the strain-induced scalar potential shifts its low energy band structure downward by up to 30 meV. We also show precise control of the gauge vector potential which reversibly suppresses the conductance. We discuss our ongoing experimental progress towards quantum strain engineering in SWCNTs, and present calculations showing their potential for valleytronics and other applications.

We conclude with an overview of a project to integrate *suspended* 2D materials in planar optical cavities towards achieving fully tunable nano-opto-electro-mechanical (NOEMS) systems. We developed a nitrocellulose-based (nail polish) method to manipulate very gently and suspend individual ultrathin 2D materials [2]. Using this method, we assembled optical cavities able to widely tune Raman scattering and absorption in bilayer graphene. [1] A. C. McRae, G. Wei, and A. R. Champagne, *Phys. Rev. Applied* 11, 054019 (2019). [2] I. G. Rebollo, F. C. Rodrigues-Machado, W. Wright, G. J. Melin, A. R. Champagne, *2D Mater.* 8, 35028 (2021).

2:30 PM BREAK

2:45 PM EQ06.11.05

Photon Addition Quantum Module for Enhanced Sensing and Imaging Pankaj K. Jha¹, Hamidreza Akbari¹, Souvik Biswas¹, Claudio Parazzoli², Barbara Capron², Benjamin Koltenbah³ and Harry A. Atwater¹; ¹California Institute of Technology, United States; ²North West Quantum Science, United States; ³The Boeing Company, United States

Single photon sources (SPSs) are one of the building blocks for quantum technologies, including optical quantum computing, quantum communications, and sensing and metrology [1]. Recently, color centers in hexagonal boron nitride (*h*BN) have emerged as a promising candidate for SPS at room temperature [2], which can be localized with nanometric precision [3] as well as exhibit near-lifetime and tunable quantum emission [4]. Here, we show that these *h*BN emitters can be used as a quantum module for photon addition quantum technology for enhanced sensing and imaging applications [5]. In this work, we investigated emission characteristics of an *h*BN quantum emitter pumped off-resonantly with a 532 nm pulsed laser. We quantified the Mandel-Q parameter over several orders of magnitude of observation time scale by tagging every photon and applying temporal gating. We observed the transformation of sub-Poissonian statistics of intensity fluctuations measured over the shorter (tens of nanoseconds) times to super-Poissonian over the longer (tens of microseconds) times. Next, in addition to the pump laser, we triggered the excited quantum emitter quasi-resonantly with a very weak (at the level of single photons) tunable dye laser. De-excitation of the *h*BN quantum emitter can be triggered by the dye laser or occur spontaneously. Using the Hanbury Brown-Twiss setup, we measured two photon counts with and without the *h*BN quantum emitter. We compared the experimental results to those calculated using a light-emitter interaction model. Our experimental results may open the door to using *h*BN quantum emitters for probabilistic coherent amplification of weak optical and thermal signals for applications in sensing and imaging.

References:

- [1] M. D. Eisaman *et al.*, *Rev. Sci. Instrum.* **82**, 071101 (2011).
- [2] T. T. Tran *et al.*, *Nat. Nanotechnol.* **11**, 31 (2016).
- [3] P. K. Jha *et al.*, *Nanotechnology* **33**, 015001 (2022).
- [4] H. Akbari *et al.*, *Lifetime limited and tunable quantum light emission in h-BN via electric field modulation* (in review 2022)
- [5] C. G. Parazzoli *et al.*, "Enhanced Thermal Images of Faint Objects via Photon Addition / Subtraction," in Conference on Lasers and Electro-Optics, OSA Technical Digest (online) (Optica Publishing Group, 2016), paper FTu3C.4.

3:00 PM EQ06.11.06

Disentangling Many-Body Effects in the Coherent Optical Response of a 2D Semiconductor Chiara Trovatiello^{1,2}, Florian Katsch³, Qiuyang Li¹, Xiaoyang Zhu¹, Andreas Knorr³, Giulio Cerullo² and Stefano Dal Conte²; ¹Columbia University, United States; ²Polytechnic University of Milan, Italy; ³Technische Universität Berlin, Germany

Monolayer transition metal dichalcogenides (1L-TMDs) have received increasing attention because of their enhanced light-matter interaction and tightly bound excitons[1]. Measuring and modeling the transient behavior of optically excited carriers and excitons is essential for exploiting TMDs in optoelectronic devices with decreased size[2]. Transient absorption spectroscopy has been extensively used to study exciton scattering processes on an ultrafast timescale. While it has been shown that on a ten- to hundred-ps timescale, the exciton decay dynamics is dominated by thermal effects[3], **the physical origin of exciton dynamics on a ps and sub-ps timescale is still under debate.** In this temporal window, many-body effects lead to a renormalization of the bands, inducing a transient energy shift of the excitonic resonance. Simultaneously, the increase of the electronic temperature after photo-excitation, due to multiple electronic scattering events, broadens the excitonic linewidth. Broadening and shift of the excitonic peak overlap in time with an abrupt absorption reduction due to phase-space filling effect (i.e., Pauli blocking mechanism)[4]. All these processes are difficult to disentangle, and their dynamical interplay determines the complex shape of the transient absorption spectra of TMDs across the bandgap at early time delays (i.e., during and immediately after the pump and probe temporal overlap). In the literature, transient exciton energy shifts have been roughly estimated from pump-probe measurements with contrasting results, e.g., different signs and values depending on the pump energy.

In this work, we measure the transient optical response of 1L-WS₂ on SiO₂ across its optical bandgap. The sample is photoexcited on- and out-of-resonance with respect to the A exciton, and at variable pump fluences below the exciton-Mott transition. In order to capture the origin of the different transient signal shapes, **we fully disentangle absorption reduction, energy shift and broadening of the excitonic peak from the transient optical response, using Kramers-Kronig constrained variational analysis to extract the absorbance spectrum from the measured transient reflectivity ($\Delta R/R$) as a function of pump-probe delay.**

The absorption spectra show a linear variation of all the A exciton peak parameters (i.e. intensity, energy and linewidth) with the pump fluence. We find that **many-body effects are strongly enhanced for resonant excitation**, resulting in a transient blue shift of the A exciton. The shift progressively decreases as the pump is detuned from the resonance and turns into a small red shift when the energy of the pump is close to the B excitonic resonance. The energy shift originates from Coulomb-induced bandgap renormalization while the asymmetric broadening is related to excitation induced dephasing mechanism. **Microscopic calculations based on excitonic Heisenberg equations of motion quantitatively reproduce the non-linear absorbance spectra of the material.**

In conclusion, we provide a more complete picture of the transient optical response of 1L-WS₂ which can finally explain the strong differences observed in the pump-probe spectra following on- and off-resonant excitation. Our combined experimental and theoretical studies give important insights into the complex interplay between many-body correlations and excitonic interactions determining the non-equilibrium response of 1L-TMDs.

- [1] Qiu, D. Y. et al. "Optical spectrum of MoS₂: many-body effects and diversity of exciton states" *Phys. Rev. Lett.* **111**, 216805 (2013).
- [2] Mueller, T. & Malic, E. "Exciton physics and device application of 2D TMD semiconductors" *npj 2D Mater. Appl.* **2**, 29 (2018).
- [3] Moody, G. et al. "Exciton dynamics in monolayer transition metal dichalcogenides." *J. Opt. Soc. Am. B* **33**, C39–C49 (2016).
- [4] Katsch, F., et al. Exciton-scattering-induced dephasing in two-dimensional semiconductors. *Phys. Rev. Lett.* **124**, 257402 (2020).

SESSION EQ06.12: Virtual Session I: Quantum Properties and Applications I
Session Chairs: Monica Allen and Ming-Yang Li
Tuesday Morning, December 6, 2022
EQ06-virtual

8:00 AM *EQ06.12.01

Interlayer Drag Effects in Graphene-Based Electronic Double-Layer Systems Changgan Zeng; University of Science and Technology of China, China

A closely spaced but electronically isolated electronic double-layer system is a fascinating platform to study interlayer quasiparticle interactions and to reveal intriguing interlayer correlated states. Recent progress in the development of graphene and other two-dimensional (2D) electronic systems has sparked renewed interest in the study of interlayer interactions based on vertical 2D heterostructures. Especially, the highly tunable electronic properties of component layers, together with the accessibility of ultra-small interlayer separation, enable the investigation of the drag effect in previously inaccessible regimes.

In this talk, I will present our recent progresses on the interlayer drag experiments in several graphene-based electronic double-layer systems, including: 1) The demonstration of signature carrier-density-dependence of drag resistance between massless and massive fermions in heterostructures consisting of monolayer graphene and bilayer graphene separated by hBN spacer [1]. 2) The discovery of a new type of quantum interference effect in inter-layer Coulomb drag, with the interference pathway comprising different carrier diffusion paths across the two constituent graphene layers [2]. 3) The discovery of a giant and highly-tunable drag effect between graphene and superconducting LaAlO₃/SrTiO₃ heterointerface, wherein a brand-new mechanism of Josephson-Coulomb drag is proposed [3]. These results have important implication for investigating interlayer-coupling-induced fascinating physics via utilizing newly-emerging 2D electronic systems.

References:

- [1] Lijun Zhu et al., *Nano Lett.* 20, 1396 (2020)
- [2] Lijun Zhu et al., Unpublished
- [3] Ran Tao et al., arXiv: 2003.12826v3

8:30 AM *EQ06.12.02

Symmetry Engineering in Nanostructures of Transition Metal Dichalcogenides [Yoshi Iwasa](#)^{1,2}; ¹The University of Tokyo, Japan; ²RIKEN CEMS, Japan

Symmetry often plays crucial roles in the properties and functions of materials. In bulk materials, symmetry is basically determined by the space group of single crystals. In sharp contrast, in nanomaterials, symmetry can be controlled as designed. For instance, graphene and bilayer graphene have totally different symmetry, and needless to say, rolling them into tubular structures makes their symmetry reduced to chiral.

In this presentation, we discuss one of the symmetry sensitive properties, bulk photovoltaic effect, in nanotubes [1], van der Waals (vdW) heterostructures [2], and strained [3] transition metal dichalcogenides (TMD). Bulk photovoltaic effect is the photovoltaic effect of uniform materials without p-n junctions, which have been known as a characteristic property of ferroelectric or polar bulk materials. Monolayer TMD has a trigonal structure, which is a noncentrosymmetric but nonpolar structure. Therefore no bulk photovoltaic effect for random light polarization is expected. However, TMD can be changed to polar structures by making tubular structures, vdW heterostructures with twofold rotational symmetry, or strained 3R structure, and thus bulk photovoltaic effect emerges. The light intensity dependence of photocurrent exhibits a crossover from linear to route mean square dependence, in agreement with the quantum mechanical shift current mechanism. Importantly, the observed photocurrent density is rather large comparing to those in bulk polar materials. The present result may indicate a novel route to create new functionalities based on nanostructures through symmetry engineering.

- [1] Y. J. Zhang et al., *Nature* 570, 349 (2019).
- [2] T. Akamatsu et al., *Science* 372, 68 (2021).
- [3] Y. Dong et al., submitted for publication.

9:00 AM EQ06.12.03

Intercalation Dynamics, Charge Transfer and Defect Correlation in Transition Metal Dichalcogenides/Sapphire Interfaces [Jill Serron](#)¹, Albert Minj¹, Valentina Spampinato¹, Alexis Franquet¹, Yevhenii Rybalchenko^{1,2}, Marie-Emmanuelle Boulon¹, Steven Brems¹, Henry M. Silva¹, Yuanyuan Shi¹, Benjamin Groven¹, Renan Villarreal², Thierry Conard¹, Paul van der Heide¹ and Thomas Hantschel¹; ¹IMEC, Belgium; ²KU Leuven, Belgium

Due to their unique properties, offering prospects in multitudinous applications, two-dimensional (2D) materials have received significant interest in the research community. A pivotal factor to consider is their sensitivity to atmospheric gas species, as experimental observations have shown consistently that defective transition metal dichalcogenides (TMDs) layers interact with oxygen, water, and ambient gasses^{1,2}. Undoubtedly, as commonly used characterization techniques are often performed in an ambient or inert environment, they can contribute to unreliable quality checks. Although, a clear insight on the interaction mechanism with water and ambient has been established for graphene, the key role atmospheric adsorbates play in modifying the material properties of layered TMDs has not yet been fully understood. Therefore, in this work scanning probe microscopy techniques, such as Conductive - Atomic Force Microscopy (C-AFM), Kelvin Probe Force Microscopy (KPFM) and Scanning Tunneling Microscopy (STM) along with Time of Flight - Secondary Ion Mass Spectrometry (ToF-SIMS), are carried out in (ultra-)high vacuum to identify the intercalated adsorbates in the MoS₂/sapphire and WS₂/sapphire systems and to explore the complexity of the adsorption-desorption mechanism. Contact mode experiments reveal a conductivity increase with the removal of intercalated species. Re-exposure to atmospheric ambient proves intercalation to be a rapid process happening in the order of minutes. Our experimental data suggests that the intercalated species are water molecules at the interface, which is supported by ToF-SIMS findings. Moreover, the collected C-AFM data shows a local decrease in conductivity in the water intercalated regions, indicating that a charge transfer occurs to the adsorbates, depleting the *n*-type 2D layer. On the contrary, contact potential differences obtained by KPFM seemingly imply an improvement of *p*-doping over time. However, when considering the 2D screening of substrate interface charges³, this trend can rather be quantitatively interpreted as an enhancement in *n*-doping, which is in consonance with the C-AFM findings. Besides verifying that intercalation takes place at the interface, STM uncovers that the confined water layer (5.6 Å) is comprised of three phases: an ice, a quasi-liquid, and a triple water layer⁴. Lastly, time dependent STM has established a distinct interdependence between water intercalation and the presence of defects. Either defects form selectively and gradually in water intercalated areas or water intercalation is facilitated by pre-existing defects associated to local inhomogeneities in growth. Regardless, this discovery must be factored when evaluating the degradation of device performance with aging. Our work shows that TMD/sapphire samples are prone to water intercalation, which heavily affects the electronic properties, potentially leading to material degradation.

- (1) Tongay, S.; Zhou, J.; Ataca, C.; Liu, J.; Kang, J. S.; Matthews, T. S.; You, L.; Li, J.; Grossman, J. C.; Wu, J. Broad-Range Modulation of Light Emission in Two-Dimensional Semiconductors by Molecular Physisorption Gating. *Nano Lett.* **2013**, *13* (6), 2831–2836.
- (2) Nan, H.; Wang, Z.; Wang, W.; Liang, Z.; Lu, Y.; Chen, Q.; He, D.; Tan, P.; Miao, F.; Wang, X.; Wang, J.; Ni, Z. *Strong Photoluminescence Enhancement of MoS₂ through Defect Engineering and Oxygen Bonding*.
- (3) Castellanos-gomez, A.; Cappelluti, E.; Roldán, R.; Agraït, N. Electric-Field Screening in Atomically Thin Layers of MoS₂: The Role of Interlayer Coupling. **2013**, 899–903.
- (4) Sothewes, K.; Bampoulis, P.; Zandvliet, H. J. W.; Lohse, D.; Poelsema, B. Pressure-Induced Melting of Confined Ice. *ACS Nano* **2017**, *11* (12), 12723–12731.

9:15 AM EQ06.12.04

Twisted van-der-Waal's (vdW) Hetero-Bilayer Stacking Using Polymer to Polymer Transfer [Abdulaziz Almutairi](#)¹, David Schmitt², Jan Philipp

Bange², Wiebke Bennecke², Giuseppe Meneghini³, Daniel Steil², D. Russell Luke⁴, R. Thomas Weitz^{2,5}, Sabine Steil², G. S. Matthijs Jansen², Samuel Brem³, Ermin Malic^{3,6}, Marcel Reutzler², Stefan Mathias^{2,5}, Antonio Lombardo^{7,7} and Stephan Hofmann¹; ¹The University of Cambridge, United Kingdom; ²Georg-August-Universität Göttingen, Germany; ³Philipps-Universität, Germany; ⁴, Georg-August-Universität Göttingen, Germany; ⁵University of Göttingen, Germany; ⁶Chalmers University of Technology, Sweden; ⁷University College London, United Kingdom

Two dimensional layered (2D) materials exhibit outstanding properties that make them excellent candidates for electronic and optoelectronic applications [1]. The lack of surface dangling bonds allows deterministic stacking different 2D materials to form heterostructure without the constraints of lattice matching. These heterostructures are usually referred as van-der-Waals (vdW) heterostructures, and they characteristics resulting from the interaction between their constituent layers. Hence, vdW heterostructures have been extensively used in different type of electronic devices from tunneling field effect transistors (TFETs) to photodetectors (PDs) [2]. In addition, the ability to combine 2D material deterministically permits to stack 2D materials with controlled twist angle between layers resulting in the formation moiré superlattices [3], which in return opens the door for more complex device architecture.

Interface quality between layers has a significant impact on the overall properties of the resulting vdW heterostructure. Therefore, major focus has been dedicated to developing transfer techniques that produce vdW heterostructures with clean interface [4,5]. However, most techniques developed are situational and requires several complicated steps. In fact, most techniques rely on using a polymeric stamp to transfer/stack 2D materials. Hence, techniques that works by stacking on a target substrate faces the issue of dealing with polymer residual on surface of each transferred layer. Whereas approaches that utilize stacking vdW heterostructure on the stamp by picking up layers from different substrates are limited by the size of the flakes exfoliated on holding substrates. This is a major concern for 2D materials such as transition metal dichalcogenides (TMDs) where monolayer flake size is limited if exfoliated on SiO₂.

Here, we investigate polymer to polymer stacking to realize bilayer vdW heterostructures. This approach allows relatively large flakes stacking while maintain relatively clean interface. For this study, WSe₂/MoS₂ hetero-bilayer system was stacked using polydimethylsiloxane (PDMS) to PDMS transfer technique with 9.8±0.8° twist angle. The interface quality was investigated using multidimensional time- and angle-resolved photoelectron spectroscopy (trARPES). Even though PDMS stamps are known for their persistent residuals, the WSe₂/MoS₂ heterostructure demonstrated the formation of interlayer exciton (ILX) which is characteristic of vdW hetero-bilayers and additionally showing a distinct ILX momentum fingerprint which is a direct hallmark of the moiré superlattice [6]. This suggests the forming of clean interface between the two 2D materials. While the technique does not produce blister free heterostructure, polymer to polymer stacking represents a facile stacking technique to produce clean interfaces in hetero-bilayers when advanced approaches are not feasible.

- 1 Lemme, M. C. *et al. Nat Commun* **13**, 1392, doi:10.1038/s41467-022-29001-4 (2022).
- 2 Geim, A. K. *et al. Nature* **499**, 419-425, doi:10.1038/nature12385 (2013).
- 3 Cao, Y. *et al. Nature* **556**, 43-50, doi:10.1038/nature26160 (2018).
- 4 Purdie, D. G. *et al. Nat Commun* **9**, 5387, doi:10.1038/s41467-018-07558-3 (2018).
- 5 Pizzocchero, F. *et al. Nat Commun* **7**, 11894, doi:10.1038/ncomms11894 (2016).
- 6 Schmitt, D. *et al. arXiv*, doi:10.48550/arXiv.2112.05011.

9:30 AM EQ06.12.05

Room Temperature Multiferroicity in Transition Metal Dichalcogenide Bulk Single Crystals Gabriel Cardenas-Chirivi^{1,2}, Karen Vega-Bustos², Jhon Pazos¹, Mario A. Macias Lopez², Oscar Herrera¹, Camilo Espejo³, William López-Pérez³, Jose Augusto Galvis¹ and Paula Giraldo-Gallo²; ¹Universidad Central, Colombia; ²Universidad de los Andes, Colombia; ³Universidad del Norte, Colombia

The search for new and better multiferroicity is arduous. Ferroic orders such as ferroelectricity and ferromagnetism must coexist simultaneously¹. Nonetheless, ferroelectrics tend to be insulators as a need to preserve electric polarization (free charges in metals screen this effect) while ferromagnets are metals in their majority². Coupling among the multiple degrees of freedom allows that the order parameters of one state can be controlled by tuning parameters different from their conjugate variable. Historically, it has been found mainly in 3-dimensional complex oxides and perovskites, such as Cr₂O₃³, YMnO₃⁴, BiFeO₃⁵, among others, or in heterostructures of ferroelectric/ferromagnetic thin-films⁶. Recent advancements in the field of 2D-multiferroics have been done, as for example in the halide compound NiI₂ and Fe-doped In₂Se₃^{7,8}. However, this state has still been elusive for the most widely studied and characterized family of 2D compounds, the transition metal dichalcogenides (TMDs), in spite of theoretical predictions in this respect^{9,10}. In this study, we report the first experimental realization of multiferroic states in TMDs via doping, at room temperature, in bulk single crystals. We observe a coexistence of ferromagnetism and ferroelectricity, revealed in the observation of magnetic hysteresis loops and piezoresponse force microscopy (PFM) measurements, resistive switching effects, Density functional theory (DFT) calculations, and substantial piezoelectricity with similar effective coefficients than its undoped monolayer counterparts¹¹. This work opens the possibility of building devices for new nanoelectronic and spintronic applications.

References

1. Spaldin, N. A., Cheong, S.-W. & Ramesh, R. Multiferroics: Past, present, and future. *Phys. Today* **63**, 38–43 (2010).
2. Hill, N. A. Why Are There so Few Magnetic Ferroelectrics? *J. Phys. Chem. B* **104**, 6694–6709 (2000).
3. Astrov, D. N. The magnetoelectric effect in antiferromagnetics. *Sov. Phys. JETP* **11**, 708–709 (1960).
4. Hanamura, E. & Tanabe, Y. Phase transitions and second-harmonics of ferroelectric and antiferromagnetic RMnO₃. *Phase Transitions* **79**, 957–971 (2006).
5. Kadomtseva, A. M. et al. Phase transitions in multiferroic BiFeO₃ crystals, thin-layers, and ceramics: enduring potential for a single phase, room-temperature magnetoelectric ‘holy grail’. *Phase Transitions* **79**, 1019–1042 (2006).
6. Ueda, K., Tabata, H. & Kawai, T. Coexistence of ferroelectricity and ferromagnetism in BiFeO₃-BaTiO₃ thin films at room temperature. *Appl. Phys. Lett.* **75**, 555–557 (1999).
7. Behera, B., Sutar, B. C. & Pradhan, N. R. Recent progress on 2D ferroelectric and multiferroic materials, challenges, and opportunity. *Emergent Materials* **4**, 847–863 (2021).
8. Song, Q. et al. Evidence for a single-layer van der Waals multiferroic. *Nature* **602**, 601–605 (2022).
9. Tu, Z. & Wu, M. 2D diluted multiferroic semiconductors upon intercalation. *Adv. Electron. Mater.* **5**, 1800960 (2019).
10. Zhong, T., Li, X., Wu, M. & Liu, J.-M. Room-temperature multiferroicity and diversified magnetoelectric couplings in 2D materials. *Natl Sci Rev* **7**, 373–380 (2020).
11. Duerloo, K.-A. N., Ong, M. T. & Reed, E. J. Intrinsic Piezoelectricity in Two-Dimensional Materials. *J. Phys. Chem. Lett.* **3**, 2871–2876 (2012).

9:45 AM EQ06.12.06

Amorphous BN Growth Using CVD and Measurement of RRAM Properties Using the Same Dokyeong Yun; Sungkyunkwan University, Korea (the Republic of)

In this paper, a large array resistive memristor device was manufactured by adjusting the crystal properties of the film by adjusting the growth conditions. It is composed of Au/amorphous/Au as a two-terminal resistive switching device with a Metal/Insulator/Metal (MIM) vertical structure. Changes in the state, thickness and crystal structure of the film were analyzed by adjusting various growth conditions, and it can be seen that it has Boron Nitride characteristics through Raman spectrometers measurement and TEM image. When a voltage is applied to a non-conductive material, RRAM generates a filament through which ions can aggregate and current can flow. Similarly, RRAM with high electrical characteristics was implemented by adjusting growth conditions.

10:00 AM DISCUSSION TIME

SESSION EQ06.13: Virtual Session II: Quantum Properties and Applications II

Session Chairs: Monica Allen and Ming-Yang Li

Tuesday Afternoon, December 6, 2022

EQ06-virtual

1:00 PM *EQ06.13.01

Imaging the Local Band Topology in Magic-Angle Graphene Eli Zeldov; Weizmann Institute of Science, Israel

Topology is a key element governing the electronic and magnetic properties of 2D moiré materials. The topological electronic bands are classified by their Chern number C , which is considered to be a global topological invariant. The Chern number is governed by the Berry curvature that leads to orbital magnetization. Utilizing a scanning superconducting quantum interference device on a tip (SQUID-on-tip), we image the Berry-curvature-induced equilibrium orbital magnetization, thus providing new means to resolve the local band topology on the nanoscale [1]. At integer filling $\nu=1$, we observe a zero-field Chern insulator, which rather than being described by a global topologically invariant C , forms a Chern mosaic of microscopic patches of $C = 1, 0, \text{ or } -1$, the boundaries of which carry chiral edge states. Upon further filling, we find a first-order phase transition due to reconcondensation of electrons from valley K to K' , leading to irreversible flips of the local Chern number and magnetization, and to the formation of valley domain walls giving rise to hysteretic anomalous Hall resistance. The findings shed new light on the structure and dynamics of topological phases in moiré devices.

[1] S. Grover, M. Bocarsly, A. Uri, P. Stepanov, G. Di Battista, I. Roy, J. Xiao, A. Y. Meltzer, Y. Myasoedov, K. Pareek, K. Watanabe, T. Taniguchi, B. Yan, A. Stern, E. Berg, D. K. Efetov, and E. Zeldov, arXiv:2201.06901

1:30 PM EQ06.13.02

Rethinking Deposition at the Scale of an Atom Ondrej Dyck¹, Sinchul Yeom¹, Andrew Lupini¹, Jacob Swett², Dale Hensley¹, Mina Yoon¹ and Stephen Jesse¹; ¹Oak Ridge National Laboratory, United States; ²Arizona State University, United States

The aim of all human action is to rearrange the world into a more preferable state. The field of engineering, with ever increasing degrees of precision, seeks to arrange matter such that desirable functional properties are elicited. With routine fabrication procedures edging into the single digit nanometer scale, one begins to wonder about the bottom. This talk will discuss current efforts at controllably attaching atoms to single and bilayer graphene using an electron beam in a scanning transmission electron microscope. The effects of source and sample temperature on defect and adatom diffusion will be discussed. In addition, the effects of temperature on the rate of healing, desorption, and effective damage rate will be elaborated with a view toward refined top down control. Demonstrations of patterning single atoms and atomic clusters as well as the direct writing of chains of Sn atoms into graphene will be presented.²

(1) Feynman, R. P. There's Plenty of Room at the Bottom. *Engineering and science* **1960**, 23 (5), 22–36.

(2) This work was supported by the U.S. Department of Energy, Office of Science, Basic Energy Sciences, Materials Sciences and Engineering Division (O.D. A.R.L., S.J.), and was performed at the Center for Nanophase Materials Sciences (CNMS), a U.S. Department of Energy, Office of Science User Facility.

1:45 PM *EQ06.13.03

From Metals to Doped Semiconductors—Exploring the Formation and Unique Phenomena in 2D Systems Joshua A. Robinson; The Pennsylvania State University, United States

Two-Dimensional materials are now a main-stay in the sciences, with an ever increasing footprint across the technological world. After the first decade of proof-of-concept studies and demonstration of large area “pristine” 2D semiconductors, our research efforts now aim to advance controllable doping and establish universal methods to identify the doping and carrier concentration in 2D layers. Furthermore, heterogeneous stacking and doping of 2D materials also allows for additional band structure engineering. In this talk, I will discuss recent breakthroughs in two-dimensional atomic layer synthesis and properties, with an emphasis on doping 2D semiconductors, and combining 2D metals with topological insulators to create unique platforms for next generation quantum applications.

2:15 PM DISCUSSION TIME

SESSION EQ06.14: Virtual Session III: Quantum Properties and Applications III

Session Chairs: Ming-Yang Li and Doron Naveh

Wednesday Morning, December 7, 2022

EQ06-virtual

8:00 AM *EQ06.14.01

Single-Crystalline 2D Semiconductor Growth and Device Technology Xinran Wang; Nanjing University, China

2D transition-metal dichalcogenide semiconductors are promising candidates in future electronics due to unmatched device performance at atomic limit and low-temperature heterogeneous integration. In this talk, I will present our recent advances in this area. The main topics include wafer-scale single-crystal epitaxial growth, uniform bi-layer material growth, dielectric integration and Ohmic contact, and heterogeneous integration with mainstream technology. These advances clearly demonstrate the promise of 2D semiconductors in next-generation electronic and optoelectronic applications.

References:

- [1] Weisheng Li et al., Nat. Electron., 2 563 (2019).
- [2] Taotao Li et al., Nat. Nanotech., (2021) DOI: 10.1038/s41565-021-00963-8.
- [3] Wanqing Meng et al., Nat. Nanotech., (2021) DOI: 10.1038/s41565-021-00966-5.
- [4] Zhihao Yu et al. IEDM (2020) DOI: 10.1109/IEDM13553.2020.9371917.
- [5] Lei Liu et al. Nature 605, 69(2022).

8:30 AM EQ06.14.02

De-Wrinkling of the 2D Black Phosphorus Using Electron Beam Irradiation Manpreet Kaur, Himanshu Tyagi and KIRAN S. HAZRA; Institute of Nano Science and Technology, India

The two dimensional van der waals nanomaterials are sensitive to formation of surface corrugations (wrinkles and ripples) during the handling of materials in any scientific experiment. Especially, Black Phosphorous (BP) is affected by formation of such surface corrugations due to their high surface reactivity. The interface disorders such as interface coulomb contaminations, charge traps and local fluctuations in strain, polarised carrier puddles, dielectric screening and suppression of electron transport occur due to such surface corrugations. While numerous efforts have been made to de-wrinkle the flake, the issue is far from resolved. Here, we demonstrate the de-wrinkling process that utilizes electron beam of transmission electron microscope (TEM) for ironing out the wrinkles and ripples of BP flake. Experimental outcomes show the enhancement in crystallinity of the flake under e-beam irradiation due to the evolution of lattice ridden with line defects and declinations into the uniformly spaced parallel lattice planes. The overexposure to e-beam causes buckling of flake and thus the de-wrinkling process is optimized by crucially controlling the electron fluence rates or the exposure time. The hitherto undeveloped electron beam based de-wrinkling of 2D flakes with nanoscale precision is prospective to open up innovative prospects for progress of 2D nanomaterials with reproducible optoelectronic properties.

8:45 AM EQ06.14.03

A Brand New Type of Heterostructure—Dual Additives-Assisted Chemical Vapor Deposition for High-Performance W-Doped MoS₂/MoS₂ Heterostructures Qing Zhang^{1,2}, Dechao Geng³, Wei Chen^{1,2} and Wenping Hu^{1,3}; ¹Joint School of National University of Singapore and Tianjin University, International Campus of Tianjin University, China; ²Department of Chemistry, National University of Singapore, Singapore; ³Department of Chemistry, Tianjin University & Collaborative Innovation Center of Chemical Science and Engineering, China

Chemical techniques for modifying the intrinsic optoelectronic properties of transition metal dichalcogenides (TMDs) have provided tremendous flexibility for multi-functional electronics. The innovative product created by combining two chemical strategies, substitutional doping and heterostructure, is predicted to tune TMD band topologies over a wide range. However, because of the advanced equipment and the unavoidable cross-contamination problem, the regulated synthesis of doped material/pure material heterostructures remains a challenge. To address the issues, a simple dual additives-assisted chemical vapor deposition (DACVD) approach is proposed to synthesis a new type of heterostructure formed by W-doped MoS₂ and pure MoS₂ in a controlled manner. Molten salts lower the melting point of metal oxide precursors, while oxygen plasma pre-treatment on the substrate creates a defect-free surface that allows only pure MoS₂ to be deposited. Following that, doped materials are grown in sub-sequential layers in a controlled manner. The doping ratio can reach as high as 17%. The multilayered pyramid structure reduces contact resistance sufficiently, thus the mobility of multilayer heterostructure is superior to that of conventionally CVD-produced monolayer MoS₂ and multilayer MoS₂. Furthermore, the heterostructure exhibits diode-like characteristics, with a rectification ratio of up to 3.5×10^3 . This work provides ideas and experimental cases for the preparation and application of novel heterostructures.

8:50 AM *EQ06.14.04

Intelligent Infrared Sensing Enabled by Tunable Moiré Quantum Geometry Fengnian Xia; Yale University, United States

In optical sensing, traditionally different types of optical sensors are utilized to measure different physical properties of light. The spectrometer, polarimeter and power meter are used to determine the incident light spectrum, polarization state and power, respectively. It appears that measuring of all the physical properties with a single device is not feasible. Here we introduce a new sensing scheme which challenges this conventional wisdom leveraging the reconfigurable quantum geometric properties in twisted double bilayer graphene (TDBG) and artificial intelligence.

We show that the nonlinear infrared bulk photovoltaic response is largely determined by the quantum geometric properties of Bloch electrons (i.e., Berry connection and curvature). Moreover, due to the tunable quantum geometric properties and the bandstructures in TDBG, the bulk photovoltaic responses in dual-gated TDBG are dependent on the wavelength, the polarization states of the light, and the top and bottom gate biasing voltages of the TDBG device. Utilizing such unique properties of such dual-gated TDBG devices, we were able to generate a photoresponse map as a function of top and bottom gate biases for each incident light with specific power, wavelength and polarization state. Furthermore, we utilized the measured results to train a convolutional neural network (CNN), which was then leveraged to interpret the photoresponse map measured under the unknown excitation light. We showed that such a trained CNN was able to decipher the physical properties of the unknown incident infrared light measured with a single TDBG device.

Our work represents a novel sensing scheme which is ultimately compact but is able to realize the functions of multiple table-top instruments. Moreover, the results also suggest a new pathway for nonlinear infrared photonics research.

*This abstract is prepared based on our recent publication in Nature 604, 266–272 (2022). Contributions from other authors will be discussed in the presentation.

9:20 AM EQ06.14.05

The Overcome Defect at ZnO Thin Film Interface by Self-Assembly of Molecule Buffer Layer Kim Taehyeon; Sungkyunkwan university, Korea (the Republic of)

Tuning defect is very important for top gate devices to control it well. Especially ZnO thin film, which is deposited by ALD (atomic layer deposition) method, have surface defect formation so that it's hard to control top-gate devices.

So, in this study, we introduced self-assembly of molecule(SAM) buffer layer. it's very powerful for adjusting charge transports in ZnO thin film by reducing the trap density at interface. we also report the robust fabrication of ZnO top gate field effect transistors (TG-FET) arrays by using thin SAM buffer layer Al₂O₃ as top gate oxide. Our devices have 12 times higher mobility than origin ZnO thin film and 100,000 higher on/off ratio than device without buffer layer. Using this new platform, we demonstrated a large scale of transistors arrays with high mobility.

9:25 AM EQ06.14.06

Probing Magnetism in Cobalt-Intercalated MoTe₂ Whan Kyun Kim^{1,2}, Ga Young Cho¹ and Woo Jong Yu¹; ¹Sungkyunkwan University, Korea (the Republic of); ²Samsung Electronics, Korea (the Republic of)

Recently, as 2D materials with long-range ferromagnetic order such as Fe₃GeTe₂, Cr₂Ge₂Te₆, CrTe₂, VSe₂, and CrI₃ have been experimentally proven, research on magnetic devices based on them has been actively conducted. On the other hand, various studies have been conducted on magnetic properties generated by defects or implanting magnetic dopants into 2D transition metal dichalcogenide (TMD) with semiconducting or metallic properties. However, from the viewpoint of magnetism, the intercalation method that inserts an additional element between the van der Waals (vdW) planes of TMD has rarely been explored. Intercalation for 2D layered materials can be applied using vapor phase methods, solid phase diffusion, and wet chemical methods. In this study, Co, the 3d transition metal, was inserted between the vdW layers of 2H-MoTe₂ by applying 2 step-intercalation, which was sequentially performed Li-intercalation and Co-intercalation based on the wet chemical method.

n-Butyllithium diluted in hexane has been widely adopted as a reagent for preparing lithium intercalation complexes. Since the reaction is possible at room temperature, only Li ions can be intercalated, excluding by-products. 2H-MoTe₂ with n-type semiconducting behavior undergoes a phase transition to 1T'-MoTe₂ by Li-intercalation for 48 hours. It was confirmed that Li-intercalated MoTe₂ with metallic properties had ohmic contact with the metal electrode. As Li-ions are injected between each MoTe₂ layer, the vdW gap is also increased compared to the pristine. After Li-intercalation, the phase transition to 1T'-MoTe₂ was confirmed by measuring I-V characteristics and the transfer curve. We observed that the source-drain current increased from 20nA to 82nA at 1V due to Li-ion insertion, and current modulation was minimized when applying the back gate voltage.

Next, the intercalation method of Co, a zero-valent transition metal formed by disproportionation redox reaction, was applied to Li-intercalated MoTe₂. Dicobalt octacarbonyl, Co₂(CO)₈, was used as a precursor to providing zero-valent Cobalt (Co(0)) through redox reaction. This redox reaction is carried out in acetone used as a solvent during intercalation for 30 minutes at a reaction temperature of 50°C. Longitudinal magnetoresistance (MR) was measured in a cryogen-free probe station (Lake Shore CRX-VF) with a superconducting magnet by applying an out-of-plane magnetic field at a temperature from 200K to 300K. Our sample showed the MR ratio of 7% at 200K and 4% at 300K around ±2T. We demonstrate that MoTe₂ intercalated with Co has a ferromagnetic order in which resistance changes by an external magnetic field. This study has opened new horizons to the future field of 2D vdW-based magnetic devices.

9:30 AM DISCUSSION TIME

SYMPOSIUM EQ07

Diamond Electronics, Devices and Sensors—From Synthesis to Applications
November 28 - December 6, 2022

Symposium Organizers

Philippe Bergonzo, Seki Diamond Systems
Chia-Liang Cheng, National Dong Hwa University
Anke Krueger, Stuttgart University
Mariko Suzuki, University of Cádiz

Symposium Support

Silver

MUEGGE GmbH
Seki Diamond Systems

Bronze

Applied Diamond, Inc.
EDP Corporation
Fine Abrasives Taiwan CO., LTD.
Fraunhofer USA, Inc.
Qnami AG

* Invited Paper
+ Distinguished Invited

SESSION EQ07.01: Growth I
Session Chairs: Anke Krueger and Oliver Williams
Monday Morning, November 28, 2022
Sheraton, 2nd Floor, Independence East

10:30 AM *EQ07.01.01

Doped Diamond Deposition for Quantum Applications—Opportunities and Challenges Shannon S. Nicley^{1,2} and Jonas N. Becker^{1,2}; ¹Michigan State University, United States; ²Fraunhofer USA Center Midwest (CMW), United States

Diamond is a highly attractive material as a solid-state host for a class of crystal defect spin-based qubits, which exhibit high stability even under ambient conditions. Carbon-12 isotopically purified diamond is also spin free, allowing for exceptionally long coherence times. We will introduce the challenges and opportunities in this field and present the results of our ongoing efforts to improve the charge state stability of defects through the controlled growth of doped diamond and our efforts to identify new defects in diamond with long coherence times and high-quality optical interfaces.

11:00 AM *EQ07.01.02

Cubic Boron Nitride/Diamond Heterostructures Grown by Ion Beam-Assisted Molecular-Beam Epitaxy David F. Storm, Sergey Maximenko, Andrew Lang, Neeraj Nepal, Tatyana Feygelson, Bradford Pate and David Meyer; US Naval Research Laboratory, United States

Cubic boron nitride has several electronic and thermal properties which make it an attractive candidate for high power and high temperature electronic applications: an ultra-wide band gap (6.4 eV, indirect); a high thermal conductivity, second only to diamond; and its capacity to be doped both *n*- and *p*-type. Further, its structural and electronic similarity to diamond hold the potential for novel electronic devices based on c-BN/diamond heterostructures. However, there are numerous challenges associated with growing device-quality layers of c-BN, including the existence of multiple phases of BN; the metastability of the cubic phase at pressures and temperatures typical of vapor-phase growth; and the absence of large-area bulk c-BN crystals, which necessitates heteroepitaxial growth on non-native substrates.

Single crystal epitaxial cubic boron nitride films were grown on (100) oriented IIA diamond substrates by ion beam-assisted molecular-beam epitaxy (MBE) in a custom MBE system equipped with an Ar ion source, a N₂ plasma source, and an electron beam evaporator for supplying elemental boron. Fourier transform infrared spectroscopy indicates these films are fully cubic, and the phase identification is corroborated by x-ray photoelectron spectroscopy. Transmission electron microscopy confirms the presence of an epitaxial c-BN film with isolated misfit dislocations and no indication of h-BN. The interface between the c-BN layer and the diamond substrate is structurally abrupt, and no interlayer between the c-BN film and diamond substrate is seen. It was found that trace amounts of impurities, such as Mg, facilitate the growth of c-BN on diamond by ion-assisted MBE. [1]

[1] D.F. Storm et al., *phys status solidi-RRL* <https://doi.org/10.1002/pssr.202200036> (2022).

11:30 AM EQ07.01.03

Growth Process of 2-Inch-Diameter High-Quality CVD Diamond on Ir/Sapphire Substrate Compared with Ir/MgO Substrate Makoto Kasu¹, Ryo Masaki¹, Koji Koyama² and Seong W. Kim²; ¹Saga University, Japan; ²Adamant Namiki Precision Jewel Co., Ltd., Japan

Diamond is expected to be high power and high efficient devices, superior to SiC and GaN, because diamond possesses higher critical field strength, and thermal conductivity. For the power-device application, the inch-diameter high-quality diamond wafer has been a big challenge. Recently, we have demonstrated the growth of the highest-quality 2-inch-diameter (001) diamond on a (11-20) sapphire substrate.

In this study, we investigate the crystal properties of diamond wafer mainly by XRD in both out-of-plane and in-plane conditions, and observe the surfaces of the Ir buffer layer, bias-enhanced nucleation (BEN)-treated Ir surfaces, and diamond surfaces grown at the initial stage with different diamond growth times on both the (11-20) sapphire and (001) MgO substrates by AFM, XTEM, and EDX. We grew diamonds on Ir/ sapphire and Ir/MgO substrates. We found that Ir buffer layers had compressive stress, diamond layers had tensile stress. Ir buffer layers were concave and diamond layers were convex. However, the magnitude of compressive stress in Ir buffer on sapphire was much less than that on MgO, and the magnitude of tensile stress in diamond grown on Ir/sapphire was much less than that on Ir/MgO. This is a key to the success of a 2-inch diameter high-quality diamond wafer grown on Ir/sapphire.

The (001) Ir buffer surface exhibits atomically flat terraces with atomic steps. However, after the BEN treatment, a ridged surface appears, and diamond island growth begins from the bottom of the ridges during the diamond CVD growth. On Ir/sapphire, quadrangular-pyramid diamond three-dimensional (3D) islands with {111} sidewalls grow first. Subsequently, the sidewall facet changes from {111} to {011} and preferentially coalesced in the <010> direction. In contrast, on Ir/MgO, quadrangular-pyramid diamond 3D islands with {111} sidewalls grow first. Subsequently, the columnar growth proceeds. Consequently, the coalescence of diamond 3D islands on Ir/MgO requires a longer time than that on Ir/sapphire. These different growth processes on Ir/sapphire and Ir/MgO substrates lead to lower threading dislocation density and narrower XRC FWHM for the diamond grown on Ir/sapphire substrates.

11:45 AM EQ07.01.04

Preparation and Analysis of Oxidation on (100) Single-Crystal Diamond Surface Ricardo Vidrio¹, Daniel Vincent¹, Benjamin Bachman², Cesar Saucedo², Maryam Zahedian¹, Zihong Xu¹, Timothy A. Grotjohn³, Shimon Kolkowitz¹, Junyu Lai⁴, Jung-Hun Seo⁴, Robert J. Hamers², Keith G. Ray⁵, Zhenqiang Ma¹ and Jennifer Choy¹; ¹University of Wisconsin–Madison, United States; ²UW-Madison, United States; ³Michigan State University, United States; ⁴University at Buffalo, The State University of New York, United States; ⁵Lawrence Livermore National Laboratory, United States

Applications for oxidized single crystalline diamond surfaces are found in various fields of study, such as controlling the surface conductivity of diamond-based electronics, stabilizing near-surface color centers, and enabling functionalization of the diamond surface for chemical sensing. There are a multitude of oxidation approaches for diamond and diamond-like materials, with similar techniques on identical carbon materials reporting inconsistent oxygen coverages. In this work, several surface treatment methods were performed on (100)-single-crystal diamonds to establish protocols for ensuring that oxidized diamond surfaces can be prepared consistently and analyzed. Our findings indicate that two chemical parameters on the surface, graphitic carbon and molecular contaminants, prove crucial towards interpreting the oxygen coverage on the diamond surface and can account for the inconsistency found in literature.

Diamond surfaces were treated using wet chemical oxidation (which includes exposure to oxidizing acids and hydrogen peroxide, and treatment of a hydrogen-terminated surface with carboxylic acids), photochemical oxidation via UV-illumination, and an atomic layer deposition (ALD) technique using water vapor pulses. Surface analyses were performed primarily with X-ray Photoelectron Spectroscopy (XPS), as well as atomic force microscopy (AFM), and ultraviolet photoelectron spectroscopy (UPS).

XPS peak deconvolution on H-terminated diamond samples shows the presence of C-C, C-H, ether bonds, and Csp² bonding carbon in the bulk. H-terminated diamond surfaces with a subsequent acid treatment show similar results, except for a lower C-H intensity and the addition of a carbonyl peak. All other oxidation methods show only the presence of ether, carbonyls, C-C and Csp² bonded carbon from C1s peak deconvolution. The results show that the O1s surface content tends to be strongly correlated to the presence of surface contaminants and graphitic content. Out of the three wet chemistry oxidation methods, it was found that a tri-acid mixture of sulfuric, nitric, and perchloric acids yielded the least contaminants, with less than 0.1 at %, when compared to the other wet chemical methods. Similarly, the dry oxidation methods, such as the ALD water vapor pulses and the photochemical UV/Ozone treatment, exhibited contaminants at less than 0.7 at % while having O1s at % values of 6 – 7%. However, the O1s peak area showed strong correlation with respect to the intensity of the deconvoluted graphitic peak in the C1s narrow scan. Given the dependence of O1s at % to surface contamination, we

suggest a series of experimental best practices to ensure repeatable and high purity oxygen-terminations on diamond. Furthermore, we advocate that any future reporting of O1s at % content on diamond surfaces have a detailed description concerning the severity of surface contamination and graphitic content. We identify the tri-acid clean, ALD water vapor pulses, and the UV/Ozone illumination as the prime techniques to ensure clean diamond surfaces with O1s at % between 4.8 and 7.1%. Preliminary computational results show that a full monolayer coverage of carbonyl bonds on the Csp3 diamond surface correspond to 6.0 O1s at %. However, these results consider only Csp3 carbon bonds on the diamond and do not account for any Csp2 sites that tend to be prolific on the surface. Future work will look at computational modeling efforts to ascertain how the monolayer coverage changes as a function of different functionalizations on the surface.

SESSION EQ07.02: Sensing I
Session Chairs: Philippe Bergonzo and Chia-Liang Cheng
Monday Afternoon, November 28, 2022
Sheraton, 2nd Floor, Independence East

1:45 PM *EQ07.02.01

Chemical Sensors Based on Diamond—From Lab to Field Applications Emmanuel Scorson^{1,2}; ¹Université Paris-Saclay, France; ²Commissariat à l'énergie atomique et aux énergies alternatives, France

Diamond has been grown in some laboratories by either HPHT process or Plasma-Enhanced Chemical Vapor Deposition (MP-CVD) since a few decades. Single crystal diamond exhibits outstanding properties including a high optical transparency over a broad electromagnetic spectrum, high thermal conductivity approx. five times higher than copper, and acoustic wave velocity close to 19 000 m.s⁻¹. It displays also remarkable mechanical properties with e.g. a Young's modulus exceeding 1000 GPa along with high resistance to fracture, to name a few. Some of these properties remain also remarkable in its polycrystalline form when compare to most other materials. Furthermore, diamond can be doped e.g. with nitrogen or boron during growth, offering electrical properties from semiconducting to quasi-metallic regimes. When heavily doped with boron (~2.10²¹ cm⁻³), the so-called Boron Doped Diamond (BDD) electrodes become attractive electrodes featuring a high potential window > 3V in water and low double-layer capacitance. Moreover, diamond is extremely resilient to corrosion and more generally to chemical attacks. It is also biocompatible, which makes it very attractive for *in-vivo* sensing applications. Finally, the carbon nature of the diamond offers wide opportunities for surface grafting of chemical or biochemical functional groups through highly stable covalent carbon-carbon bonding. One can take advantage of these properties to enhance the analytical performances and stability of chemical/biochemical sensors and this has motivated our research over the last 15 years.

Our work focuses mainly on polycrystalline diamond thin films that can be grown typically on 4 inches silicon substrates, thus offering access to some clean-room processes and potentially large-scale production. As examples, diamond based MEMS devices (microcantilevers, SAW sensors) take advantage both of the mechanical properties of diamond, along with steady carbon interface for convenient bio-functionalization. Our work here focused mainly on the detection of odorant molecules, using biomolecular receptors involved in olfaction in Nature as sensitive layers, including Odorant Binding Proteins (OBPs), Major Urinary Proteins (MUPs) and Olfactory Receptors (OR). Multisensor array instrumentations were developed around this concept, for applications ranging from breathe analysis to security applications. Beside, heavily doped diamond electrodes were developed successfully both as macro- and micro-electrodes for biomedical, pharmaceutical or foodstuff analysis applications. These applications benefit both from the high analytical performances of diamond electrodes in particular due to their low background signals and high reactivity, and high stability and reliability. BDD electrodes offer also significant advantages in electrochemiluminescence (ECL) techniques, which are being investigated for various applications ranging from foodstuff analysis to narcotics detection. A key benefit of BDD electrodes for all of the above applications is certainly that they can be electrochemically reactivated following fouling, sometimes directly in the analytical medium, to maintain high reactivity thus opening the way to reusable sensors and online monitoring.

2:15 PM EQ07.02.02

Proposal of a Common Gate Method Suitable for Multi Sensing Using Diamond Electrolyte Solution Gate FETs Reona Nomoto¹, Hirotaka Sato¹, Yu H. Chang¹ and Hiroshi Kawarada^{1,2}; ¹Faculty of Science and Engineering, Waseda University, Japan; ²The Kagami Memorial Research Institute for Materials Science and Technology, Waseda University, Japan

In this study, we report the pH sensitivity utilizing common-gate Diamond Electrolyte Solution Gate FETs (SGFET)[1].

Since the introduction of SGFETs, the development of multi-ion sensors including pH sensor has been a great interest. Most of the multi-ion monitoring systems utilizing the FETs employ common-source FETs. However, the systems with the common-source FETs have the following drawbacks. In order to operate the common-source multiple sensors, it is required to immerse multiple reference gate electrodes in sample solution and to apply a different gate voltage (V_{GS}) for each FET. Consequently, simultaneous sensing of various ions at various points is not practically performed. Moreover, Ag/AgCl glass electrodes, which are commonly used as the gate electrodes, are difficult to miniaturize, resulting in a larger sensing system with more glass electrodes for detection of a wider variety of ions at many locations. Therefore, multi-sensing with a plurality of FETs at a common gate is desirable. Here, we propose biosensing measurement using a common gate FET that can be sensed by sharing one gate electrode with a plurality of FETs. In general, common-gate FETs are often used as cascade amplifiers and contribute to high output impedance in electronic circuits. The gate of the common-gate FETs is grounded, that is, gate bias is not applied. Instead, source voltage V_{SG} and drain voltage V_{DG} are applied and control drain current I_D . Sensing is also performed by changing only the source voltage V_{SG} and the drain voltage V_{DG} . Therefore, even when a plurality of FETs is used for common gate, only one gate electrode is completed.

In this study, we have investigated whether multi-sensing is actually possible using common-gate SGFETs composed of one gate and plural source drain (SD) probes and the pH sensitivity of SD probes is independently measured.

In this experiment, we utilized two n-channel SGFETs (SGFET 1, SGFET 2) with different threshold voltages. The $I - V$ characteristics of the common-gate SGFETs were measured in the following two ways: 1) measuring each SGFET independently and 2) measuring two both SGFETs operated simultaneously with a common gate electrode.

A Carmody buffer solution was used for each pH solution (pH 2 - 12), and a gate electrode (Ag/AgCl) and SGFET were immersed in the Carmody buffer solution. The $I_D - V_{SG}$ characteristics of the SGFET were measured in the range of $V_{SG} = 0$ to $-2V$ at $V_{DG} = 0V$ from pH 2 - 12. From $I_D - V_{SG}$ characteristics, the $V_{SG} - pH$ characteristics were obtained from the source voltage V_{SG} at a certain drain current value I_D , and the pH sensitivity was calculated from the slope of the $V_{SG} - pH$ characteristics. At common gate, the n-channel SGFET showed high pH sensitivity comparable to the Nernst response (About 59 mV/pH) with -49.4 mV/pH and -48.2 mV/pH. Next, The pH sensitivity of the two SGFETs obtained by multisensing is shown in comparison with the previous results. The pH sensitivity of SGFET1 was -49.4 mV/pH, and the pH sensitivity of SGFET1 in multisensing was -49.7 mV/pH. The pH sensitivity of SGFET2 was -48.2 mV/pH, and the pH sensitivity of SGFET2 in multisensing was -48.0 mV/pH.

It can be seen that the characteristics hardly change when measured with one SGFET and when a voltage is applied to two SGFETs simultaneously and

multi-sensing is performed. The $I_D - V_{SG}$ characteristics of two SGFETs has measured at the same time. From this result, we have shown how simultaneous applying gate voltage to two SGFETs affects the individual characteristics. We confirmed that multi-sensing is possible from the experimental results that , multiple ions can be sensed simultaneously by using FETs having different ion-sensitive films.

[1]K. Igarasi, H.Kawarada et al, Proceedings of the 63rd Annual Meeting of the Japan Society of Applied Physics 19p-H103-16(2016).

2:30 PM BREAK

SESSION EQ07.03: Quantum Applications I
Session Chairs: Philippe Bergonzo and Junko Ishi-Hayase
Monday Afternoon, November 28, 2022
Sheraton, 2nd Floor, Independence East

3:00 PM EQ07.03.01

Diamond for Quantum Technology Applications Paul Quayle¹, Ramon Díaz¹, Thanh Tran¹, Sandra Cita¹, Alex Grotjohn¹, Danyell Morris¹, Luis Hernandez¹, Keith Evans¹ and Timothy Grotjohn²; ¹Great Lakes Crystal Technologies, United States; ²Michigan State University, United States

The performance of nitrogen-vacancy (NV) center diamond is dependent on the crystalline properties of the substrate and N-doped epitaxial layer. The crystallinity of the substrate and epi-layer in terms of lattice curvature, extended defect concentration and chemical purity determines the baseline characteristics of the final devices, which have immense potential to impact a variety of magnetic field and electric field sensing applications. These technologies are enabled by the negatively charged NV⁻ center in diamond which has a spin state that can be optically probed and manipulated. The extreme sensitivity of this spin-state to magnetic fields allows for unprecedented capabilities in magnetic and electric field sensing. In this presentation, we report on the assessment of NV center diamond produced by Great Lakes Crystal Technologies. Samples were synthesized at a variety of conditions to investigate optimum growth conditions. Ensemble NV center dephasing times are correlated with defect characteristics measured using birefringence microscopy and lattice curvature measured by x-ray diffraction mapping. UV-visible and Fourier-transform infrared spectroscopy is used to compare parasitic acceptor-like defects concentrations. Results are reported for samples grown using both natural and isotopically purified carbon sources.

3:15 PM EQ07.03.02

Control and Sensing of Dark-Spin Bath Polarization via a Single Probe Qubit Yuxin Wang¹, Mykyta Onizhuk¹, Jonathan Marcks¹, Benjamin Soloway¹, Paul C. Jerger¹, Nazar Delegan^{2,1}, F. J. Heremans^{2,1}, David Awschalom^{1,2,1}, Giulia Galli^{1,1,2} and Aash Clerk¹; ¹The University of Chicago, United States; ²Argonne National Laboratory, United States

The central spin model, where a single qubit interacts with a collection of neighboring bath spins, provides a paradigmatic model for understanding qubit decoherence in a great variety of quantum platforms ranging from superconducting circuits to solid state defect spins. It is common to treat such spin environment as a classical fluctuating noise source, which can be readily characterized using standard qubit noise spectroscopy techniques. However, a realistic spin bath forms a dynamical object that can be perturbed by evolution of the central spin. Here, we theoretically propose techniques that utilize a single qubit to both polarize and probe its surrounding spin bath. Making use of an effective quench induced by the qubit onto the bath [1], we further show how our method allows a model-free estimation of the effective bath temperature. We discuss how our protocols can be directly implemented using a single NV center spin qubit in diamond, which can interact with either ¹³C nuclear spins or substitutional nitrogen electron spins (P1 centers). We also present numerical calculations based on cluster correlation expansion (CCE) to benchmark our protocols' performance.

[1] Y.-X. Wang, A. A. Clerk, Nat. Commun. **12**, 6528 (2021).

3:30 PM EQ07.03.03

Surface-Activated Direct Bonding of Diamond (100) and Sapphire with High Transparency for Quantum Devices Tetsuya Miyatake¹, Toshiki Iwai¹, Tetsuro Ishiguro¹, Kenichi Kawaguchi¹, Yoshiyasu Doi¹, Shintaro Sato¹, Jeffrel Hermias², Salahuddin Nur² and Ryoichi Ishihara²; ¹Fujitsu Limited, Japan; ²Delft University of Technology, Netherlands

Diamond single crystals with color centers have attracted attention for their application in quantum photonic devices. Owing to the size limitation of diamond substrates, bonding a small diamond substrate to a large mother wafer is crucial for developing large-scale integrated devices. To access the quantum states of color centers using an optical technique, bonding the diamond with a transparent material with low optical loss in the visible region is desired. Sapphire is a promising candidate as a transparent material as it is a single crystal with a large optical bandgap. However, the direct bonding of a diamond substrate with (100) surface orientation is an unexplored challenge for sapphire wafers. In fact, such direct bonding has not been easy for Si wafers [1-5]. Herein, we report the successful direct bonding of diamond (100) substrates and sapphire (1000) wafers using the atom beam-assisted surface-activated bonding method and clarify its mechanism with detailed structural characterizations.

CVD-grown diamond (100) substrates with a size of 4×4 mm² and a thickness of 0.5 mm were used in the experiments. We systematically investigated the relationship between the surface properties and the bonding strength. It was found that atomic-level surface flatness (roughness below 0.1 nm) in a micron-sized area and submicron-level global flatness (roughness below 0.2 μm) in the whole area are important to achieve stable bonding. The diamond and sapphire surfaces were activated using fast atom beam (FAB) irradiation in a vacuum chamber for 600 s, although the diamond/Si bonding studies used the wet-chemical activation process for the diamond surface [1-5]. Subsequently, the substrates were brought into contact under a pressure of 20 MPa at room temperature, resulting in full bonding. No graphite layers were observed on the activated diamond surface through Raman spectroscopy. Thus, a highly transparent bonding interface was realized. Cross-sectional transmission electron microscopy and energy dispersive X-ray spectroscopy revealed that an amorphous AlO_x layer with a thickness of 150–200 nm existed between the diamond and the sapphire single crystal. This intermediate amorphous layer was likely formed during the FAB treatment. The shape of the amorphous layer was deformed to fit the monolayer steps of the diamond surface, indicating its effectiveness as an adhesive layer. This bonding method was effective for the diamond substrates with various impurity concentrations, including very high-purity substrates suitable for quantum devices. Furthermore, it was confirmed that the light emitting from the color center was efficiently extracted from the sapphire side. The shear strength measurement showed that the diamond/sapphire-bonded wafer had a shear strength of 14.41 MPa, approximately nine times higher than that for diamond/Si wafers [1],[2], making it sufficient for device processes. To summarize, we have successfully bonded diamond (100) and sapphire with high transparency, realizing a promising technique for diamond integrated device applications.

[1] T. Matsumae *et al.*, Scr. Mater. **191**, 52 (2021).

- [2] T. Matsumae *et al.*, *Scr. Mater.* 175, 24 (2020).
 [3] T. Matsumae *et al.*, *Jpn. J. Appl. Phys.* 59, SBBA01 (2020).
 [4] S. Fukumoto *et al.*, *Appl. Phys. Lett.* 117, 201601 (2020).
 [5] J. Hermias *et al.*, *Hasselt Diamond Workshop 2022 - SBDD XXVI* (2022).

3:45 PM EQ07.03.04

Synthesis of Spin Defects in Low Dimensionality and Heteropolytypic Platforms for Quantum Applications [Nazar Deleghan](#)^{1,2}, Jonathan Marcks², Xinghan Guo², Katherine Harmon¹, Sean Sullivan¹, Martin Holt¹, Stephan Hruszkewycz¹, Alex High², David Awschalom^{2,1} and F. J. Heremans^{1,2};
¹Argonne National Laboratory, United States; ²The University of Chicago, United States

Wide band-gap semiconductor hosted, optically addressable point-defects are a versatile platform for a number of quantum information science (QIS) applications. These spin qubits are inherently sensitive to their local crystalline, charge, and nuclear spin environments making them ideal for quantum sensing applications. Recent advances in host material growth, nanofabrication, and deterministic defect creation have enabled the ability to engineer the local environment surrounding these spin qubits via the control of host material polytype, isotopic engineering, and host dimensionality. Herein, we present on these advances, highlighting novel low dimensionality (1) and heteropolytypic (2) quantum platforms. These advances will be presented in the context of deterministic integration of these quantum systems with other classical or quantum systems, as a means for local defect control, and as probes of local spin-bath dynamics.

References:

1. X. Guo *et al.*, Tunable and Transferable Diamond Membranes for Integrated Quantum Technologies. *Nano Lett.* **21**, 10392–10399 (2021).
2. K. J. Harmon *et al.*, Designing silicon carbide heterostructures for quantum information science: challenges and opportunities. *Mater. Quantum Technol.* **2**, 023001 (2022).

Supported by US Department of Energy, Office of Science, Basic Energy Sciences, Materials and Sciences Engineering Division

SESSION EQ07.04: Nanodiamond I
 Session Chairs: Arsène Chemin and Chia-Liang Cheng
 Tuesday Morning, November 29, 2022
 Sheraton, 2nd Floor, Independence East

8:30 AM *EQ07.04.01

Virus Capture by Nanodiamond Modified Membranes Henry Bland¹, Isabella Centeleghe², Soumen Mandal¹, Evan Thomas¹, Jean-Yves Maillard² and [Oliver A. Williams](#)¹; ¹Cardiff University School of Physics and Astronomy, United Kingdom; ²Cardiff University, United Kingdom

Nanoscale contaminants such as viruses, industrial dyes and pharmaceutical by-products present serious challenges to health in the water supply, drug manufacture and blood filtration. Of the existing filtration platforms, only ultrafiltration or reverse osmosis can achieve high retention levels of such nanoscale pathogens. These systems are expensive and complex, being mostly limited to centralised water treatment systems. This has led to the development of adsorptive depth filtration (ADF) where contaminants are targeted by van der Waals / electrostatics forces, hydrophobic interactions etc driving contaminant adsorption to the membrane surface. A key advantage of such a technology is that retention is not achieved through size exclusion, allowing much higher flow rates and smaller pressure differentials. It can also enable the removal of nanoscale contaminants by charge whilst allowing larger bodies to pass through the filter. Such approaches are used in blood filtration, virus capture during drug manufacture and virus preconcentration in water monitoring.

In this work¹, quartz filters were modified with hydrogenated diamond nanoparticles, reversing the zeta potential of the membranes from negative to positive across a wide pH range. Untreated quartz filters demonstrate log_{0.2} (35%) retention of viruses (MS2 bacteriophage) whereas the diamond modified ones exhibit at least log_{6.2} (>99.9999%) reduction from feed waters. This is due to the MS2 bacteriophage exhibiting a low isoelectric point, in common with the overwhelming majority of viruses. Thus, it has a negative zeta potential in water and is attracted to the positively charged diamond modified membrane. The modified membrane was also tested with far smaller contaminants such as acid black 2 dye and demonstrated >90% higher retention over the unmodified filter. Finally, the diamond modified filter was compared to commercially available electropositive filter membranes where it demonstrated a consistently higher positive zeta potential over a larger pH range. Thus, diamond modified filters offer higher zeta potentials vs pH and thus higher virus retention over current ADF technologies. These filters are also stable over a wider temperature range and flow than the currently available technology.

¹ H.A. Bland, *ACS Appl. Nano Mater.* **4**, 3252 (2021).

9:00 AM EQ07.04.02

Surface Modification of Nanodiamond for Tailored Interaction in Biological Media Viktor Merz¹, Julia Puck¹, Elisabeth Mayerhoefer² and [Anke Krueger](#)²; ¹Julius-Maximilians-Universität Würzburg, Germany; ²Stuttgart University, Germany

The surface of nanoparticles plays a major role in their interaction with biological systems and media. Especially undesired nonspecific adsorption e.g. of proteins as well as unwanted agglomeration in physiological fluids hamper the application of nanoparticles in biomedicine and related fields. This holds true for nanodiamonds, too.

Here, we present several strategies involving covalent surface functionalization of nanodiamond with peptides, hydrophilic/lipophilic hybrid systems, zwitterions and oligoethers which enable the formation of stable colloidal solutions of nanodiamond even at high ionic concentrations and prevent the formation of a protein corona when such nanodiamonds are exposed to serum proteins.[1]

Complex architectures combining different of these elements have been investigated for their effect on the dispersibility, colloidal stability and inhibition of protein adsorption.

First in vitro experiments confirm the low toxicity and high biocompatibility of these functionalized nanodiamonds.

Such functionalized nanodiamonds can now be used to introduce specific functional moieties, which can then selectively interact with their environment, a prerequisite for sensing, imaging and drug delivery.

[1] Viktor Merz, Julian Lenhart, Yvonne Vonhausen, Maria E. Ortiz Soto, Juergen Seibel, Anke Krueger, *Small* **2019**, 1901551, DOI:

This research has received funding by the Volkswagen foundation under grant agreement number 88 393.

9:15 AM EQ07.04.03

Advances in Preparation and Understanding of Ultrasmall Nanodiamonds Stepan Stehlik^{1,2}, Ales Vlk², Martin Ledinsky², Michel Mermoux³ and Evgeny Ekimov⁴; ¹University of West Bohemia, Czechia; ²Institute of Physics, AS CR, Czechia; ³Univ. Grenoble Alpes, Univ. Savoie Mont Blanc, France; ⁴Institute of High Pressure Physics, Russian Academy of Sciences, Russian Federation

Understanding of diamond properties in ultrasmall region of few nanometers is important, yet challenging task. Since spectroscopic characterization reflects the mass/volume-weighted particle size distribution, only samples containing volumetrically dominant sub-5 nm nanodiamonds (NDs) may be used for reliable characterization. However, conventional detonation nanodiamonds (DNDs) and top-down high-pressure high-temperature (TD_HPHT) NDs do not generally meet this criterion and so additional approaches and synthetic methods are needed.

In this work we show i) isolation of volumetrically-dominant sub-5 nm ND fractions from commercially available DNDs and TD_HPHT NDs by combination of ND size reduction followed by ultracentrifugation [1]; ii) bottom-up HPHT synthesis of sub-5 nm NDs (BU_HPHT NDs) from halogenated adamantanes at 8 GPa with excellent size control in the sub-5 nm region achieved by variation of the synthesis time and temperature [2]. Successful preparation of the sub-5 nm samples of three different ND kinds provides great opportunity not only to compare the typical spectral features of each ND kind but also to investigate size-dependent phenomena such as evolution of the Raman diamond peak parameters (position and full width at half maximum) down to 1.2 nm. Comparison of Raman spectra of DND and TD_HPHT NDs on the sub-5 nm scale reveals clear differences between the two types of NDs. We show that diamond core size, structural quality/defects, and temperature (in)stability caused by laser irradiation during the measurement are key features reflected in the particular NDs' Raman spectrum[1]. Raman spectra of the BU_HPHT NDs exhibit some additional unique features compared to conventional DNDs and TD_HPHT NDs. The most striking is nearly complete absence of sp^2 -C related features in most of the investigated samples. The size-dependent evolution of diamond peak parameters was investigated by multi-wavelength (442, 532, and 633 nm) Raman spectroscopy to identify and/or avoid any heating effect of the excitation laser on the diamond line position. Use of multiple wavelengths also enabled to study dispersion of Raman active bands. We show that down to 2.6 nm the diamond Raman line shift is only minor ($2\text{-}3\text{ cm}^{-1}$) which do not corroborate with the current phonon confinement models often applied to NDs. Only when the size decreases below 2 nm, larger shifts are observed ($8\text{-}9\text{ cm}^{-1}$ for 1.4 nm sample). Finally, we provide analysis of the first-time observed low-frequency ($20\text{-}200\text{ cm}^{-1}$) NDs related Raman scattering signals assigned to "breathing"-like acoustic modes as these signals exhibit clear size dependence. We show that in contrast to diamond Raman line parameters these features are more suitable for size analysis of sub-4 nm NDs as we evidenced a good match with the size values obtained from XRD data (Scherrer's formula)[3].

- [1] S. Stehlik, M. Mermoux, B. Schummer, O. Vanek, K. Kolarova, P. Stenclova, A. Vlk, M. Ledinsky, R. Pfeifer, O. Romanyuk, I. Gordeev, F. Roussel-Dherbey, Z. Nemeckova, J. Henych, P. Bezdicka, A. Kromka, B. Rezek, Size Effects on Surface Chemistry and Raman Spectra of Sub-5 nm Oxidized High-Pressure High-Temperature and Detonation Nanodiamonds, *J. Phys. Chem. C*. 125 (2021) 5647–5669. <https://doi.org/10.1021/acs.jpcc.0c09190>.
 [2] E.A. Ekimov, S.G. Lyapin, Yu.V. Grigoriev, I.P. Zibrov, K.M. Kondrina, Size-controllable synthesis of ultrasmall diamonds from halogenated adamantanes at high static pressure, *Carbon*. 150 (2019) 436–438. <https://doi.org/10.1016/j.carbon.2019.05.047>.
 [3] A. Vlk, M. Ledinsky, A. Shiryayev, E. Ekimov, S. Stehlik, Nanodiamond Size from Low-Frequency Acoustic Raman Modes, *J. Phys. Chem. C*. 126 (2022) 6318–6324. <https://doi.org/10.1021/acs.jpcc.2c00446>.

9:30 AM EQ07.04.04

Controlled Synthesis of Sub-Five-Nanometer Diamond Particles Teng Teng Lyu and Hao Yan; University of North Texas, United States

Diamond nanoparticles in the sub-five-nanometer size regime are crucial for several emerging technologies including subcellular imaging, quantum information processing, and drug delivery. State-of-the-art methods to produce nanodiamonds include mechanical grinding of bulk crystals, decomposition of hydrocarbon molecules, and detonation of explosives. However, no existing technique is capable of precise size control in the sub-five-nanometer regime.

Here we describe a method for controlled synthesis of nanodiamond with 2-5 nm diameter. The key innovation lies in the utilization of metal carbide nanoparticles as carbon sources. The reaction between these metal carbides with metal oxides under high-pressure-high-temperature conditions yields diamond nanoparticles with <5 nm diameter, uniform size, and high crystallinity. The size of the nanodiamond is precisely tuned by the nanostructured carbon precursor. Chemical doping of the precursor allows controlled incorporation of functional defects, enabling these nanodiamonds for key applications as bio-compatible high-resolution fluorescent markers, storage bits for quantum information processing, photon and electron sources as well as vehicles for targeted drug delivery. <!--[endif]-->

9:45 AM BREAK

SESSION EQ07.05: Spin Defects
 Session Chairs: Paul Quayle and Mariko Suzuki
 Tuesday Morning, November 29, 2022
 Sheraton, 2nd Floor, Independence East

10:15 AM *EQ07.05.01

Multiplexed Sensing and Imaging Based on Complex Electronic Spin Manipulation of Nitrogen-Vacancy Centers in Diamond Junko Ishi-Hayase; Keio University, Japan

Nitrogen-vacancy (NV) centers in diamond are promising as highly-sensitive nanoscale quantum sensors for measuring several kinds of physical quantities such as magnetic field, electric field, temperature, pressure, etc^[1]. It is because that spin-triplet electronic ground states of NV centers can be coherently manipulated using microwave (MW) field and optically initialized/readout with long coherence time at room temperature. Optically detected magnetic resonance (ODMR) has been typically used to demonstrate quantum sensing using NV centers. In this study, we propose and demonstrate multiplexed sensor using NV center ensemble in diamond for simultaneously measuring AC magnetic field and temperature.

One of the proposed multiplexed sensors is based on double or triple electron spin resonance transitions induced by simultaneously applying MW and radio-frequency (RF) fields^[2-6]. By utilizing eigenstates under bias magnetic field perpendicular to the NV axis, all transitions between spin-triplet states

can be directly controlled by external MW and RF magnetic fields^[4]. This is much different from the conventional quantum sensing under bias magnetic field parallel to the NV axis. In our method, we generate RF-dressed state or RF-doubly-dressed state by simultaneously irradiating continuous laser, MW and RF fields. The use of these dressed states enables us to implement MHz-range AC magnetic field sensing and temperature sensing using continuous-wave ODMR (CW-ODMR)^[2,3,5,6], the proposed method does not require a pulse sequence unlike conventional methods based on pulsed-ODMR; this greatly simplifies the procedure and apparatus needed for implementation. Moreover, the use of dressed states enables us to improve the sensitivity by suppressing the variances of strain and/or electric field^[6].

Another of the proposed multiplexed sensors is based on simultaneous manipulation of electronic spins of NV centers with different axes by using MW pulses with different frequencies^[7,8]. The simultaneous spin manipulation enables us to improve the sensitivity by synthesizing the signals and suppressing the noise from NV centers with different axes. Here, we demonstrate vector magnetic field sensing and temperature sensing by applying the proposed multi-frequency manipulation technique to spin echo and Ramsey interference measurements in an ensemble of NV centers with random orientations. We find that the sensitivity using the multi-frequency manipulation is better than that using the conventional single-frequency manipulation.

Acknowledgement

This work was done in collaboration with Dr. Matsuzaki, Dr. Watanabe (AIST), Prof. Mizuochi (Kyoto Univ.), Prof. Tokuda (Kanazawa Univ.), Prof. Kobayashi, Dr. Sasaki (Univ. Tokyo), Hayase Laboratory members (Keio Univ.). This work was supported by MEXT Q-LEAP (No. JPMXS0118067395), MEXT KAKENHI (No. 18H01502, 20H05661, 22H01558), and CSRN, Keio University. This work was supported by Leading Initiative for Excellent Young Researchers MEXT Japan and JST presto (Grant No. JPMJPR1919) Japan and Kanazawa University SAKIGAKE Project 2020. YM acknowledges support of Grants-in-Aid for Scientific Research from the Ministry of Education, Culture, Sports, Science, and Technology, Japan (20H05661).

Reference

- [1] L. Rondin, *et al.*, Rep. Prog. Phys. **77**, 056503 (2014).
- [2] S. Saijo, *et al.*, Appl. Phys. Lett. **113**, 082405 (2018).
- [3] T. Yamaguchi, *et al.*, Jpn. J. Appl. Phys. **58**, 100901 (2019).
- [4] T. Yamaguchi, *et al.*, Jpn. J. Appl. Phys. **59**, 110907 (2020).
- [5] K. J. Hallbäck, *et al.*, Proc. SPIE 117004A (2021).
- [6] H. Tabuchi, *et al.*, arXiv:2205.06976 (2022).
- [7] S. Kitazawa, *et al.*, Phys. Rev. A **96**, 042115 (2017).
- [8] K. Yahata, *et al.*, Appl. Phys. Lett. **114**, 022404 (2019).

10:45 AM EQ07.05.02

Bath-State-Dependent Quantum Phase on a Single NV Center Benjamin Soloway¹, Paul C. Jerger¹, Yuxin Wang¹, Mykyta Onizhuk¹, Michael Solomon^{1,2}, F. Joseph Heremans^{1,2}, Giulia Galli^{1,1,2}, Aash Clerk¹ and David Awschalom^{1,2,1}, ¹The University of Chicago, United States; ²Argonne National Laboratory, United States

The central spin model is important for developing qubits as sensors of environmental noise and protecting qubits from decoherence. In both noise spectroscopy and dynamical decoupling protocols, the central qubit is actively controlled. However, the qubit-bath interaction may enable changes in the qubit state to trigger changes in the bath, ultimately modifying the evolution of the qubit [1]. Here, we experimentally observe the self-interaction of the electron spin of the nitrogen vacancy (NV) center in diamond mediated by a bath of polarized ¹³C nuclear spins. We are even able to detect the polarization of the bath using phase-resolved Hahn echo sequences. These techniques may assist in preparing high-fidelity memory states, improving nuclear spin hyperpolarization, and investigating the nature of environmental noise.

- [1] Y.-X. Wang and A. A. Clerk, *Nat. Commun.* **12**, 6528 (2021).

11:00 AM EQ07.05.03

Engineering Color Centers in Isotopically-Controlled Diamond Layers Christian Osterkamp¹, Priyadarshini Balasubramanian¹, Christoph Findler¹, Gerhard Wolff¹, Milos Nesladek² and Fedor Jelezko¹; ¹Ulm University, Germany; ²Hasselt University, Belgium

Nitrogen-vacancy (NV) centers in synthetic tailored diamond are promising and emerging platforms for quantum sensing technologies. The realization of such solid-state based quantum sensors is widely studied and requires reproducible manufacturing of NV centers with controlled spin properties, including the spin bath environment within the diamond crystal. A high nitrogen incorporation rate combined with the controllability of the NV axis alignment, makes <111> oriented diamond an interesting material for the creation of ensembles.

We engineer ¹⁵NVs by nitrogen delta doping during a plasma enhanced chemical vapor deposition (PECVD) process and we are able to produce an isotopically controlled diamond environment by changing the ratio of ¹²C/¹³C atoms in the growth chamber. Moreover, since the presence of ¹³NV hyperfine coupling, as well as the characteristic P1 bath spectrum from ¹⁵N are observed, our growth facilities are capable of tuning a wide range of isotopic compounds within the diamond lattice.

Especially, shallow ensembles can be used for NV based magnetometry optimized for the detection of very small magnetic fields from outside of the diamond itself. Whereby the decoupling of the NV's electronic spins by driving the electronic spin bath and by using dynamical decoupling sequences results in an improved magnetic field sensitivity.

In summary, a non-invasive method is shown to rank NV ensembles regarding their suitability as ultra-sensitive magnetic field sensors. Imaging and electron spin resonance techniques are presented to determine operating figures and precisely define the optimal material for NV-driven diamond engineering. The functionality of the methods is manifested on examples of chemical vapor deposition synthesized diamond layers containing preferentially-aligned, isotopically controlled ¹⁵NV center ensembles. Quantification of the limiting ¹⁵N P1 spin bath, in an otherwise ¹²C enriched environment, and the reduction of its influence by applying dynamical decoupling protocols, complete the suggested set of criteria for the analysis of NV ensemble with potential use as magnetometers.

References:

- Osterkamp et al. (2020), Adv. Quantum Technol., 3: 2000074

11:15 AM EQ07.05.04

High-Density NV Ensemble Produced by Electron Irradiation of Ultra High-Concentration Nitrogen-Doped CVD Diamond Kyosuke Hayasaka¹, Mayu Ueda¹, Kyotaro Kanehisa¹, Kazuki Otani¹, Yuki Ueda¹, Takashi Tani¹, Taisuke Kageura^{1,2}, Shinobu Onoda², Shinpei Enomoto³, Shozo Kono³ and Hiroshi Kawarada^{1,3}; ¹Waseda University, Japan; ²National Institute of Quantum and Radiological Science and Technology, Japan; ³Kagami Memorial Research Institute for Materials Science and Technology, Japan

Negatively charged nitrogen vacancy (NV) centers have potential applications in magnetic sensors and quantum communications [1]. In particular, the sensitivity of magnetic sensors scales with the square root of the quantum coherence time and the total number of NV centers [1]. Therefore, to improve magnetic sensitivity, it is desirable to increase the concentration of NVs while maintaining a long coherence time. Moreover, highly concentrated NV centers have recently emerged as a promising platform for investigating non-equilibrium quantum many-body systems, contributing to the observation of discrete-time crystals [2].

It is desirable to use diamond with a high concentration of nitrogen for the fabrication of high-concentration NV centers. Currently, nitrogen concentrations of at most 2×10^{20} [cm⁻³] have been achieved in CVD diamond [3]. Furthermore, the higher the nitrogen concentration, the more atomic vacancies must be introduced. Electron irradiation with a single-ended accelerator [4] or TEM [5] is often used as a means of forming vacancies.

With TEM, the amount of electron irradiation per unit time can be adjusted by reducing the beam diameter. Therefore, it is possible to irradiate with a high dose of electron beams, which cannot be achieved with an accelerator. TEMs also have the advantage of being more easily accessible than accelerators. Therefore, we irradiated CVD diamonds containing the world's highest concentration of nitrogen ([N]= 8×10^{20} [cm⁻³]) prepared by the MPCVD method with electron beams using a TEM and investigated changes in NV density and spin properties in the irradiated area.

CVD synthesis was performed using a waveguide confined MPCVD system with quartz tube where plasma was confined within the waveguide, with a pressure of 110 [Torr], a microwave power 300 [W], and at a temperature of 850 [°C]. CO₂, N₂, and CH₄ gases were used for homoepitaxial growth. The gas mixture condition was 2%, 8%, and 2%, respectively. The total gas flow rate was fixed at 200 [sccm]. HPHT synthetic (111)-oriented diamond substrate was used.

A 300-keV TEM (JEOL JEM-ARM300F) was used for electron beam irradiation because the minimum electron energy required for defect formation in (111) diamond is 220-keV [6]. After electron irradiation, vacuum annealing was performed at 1000°C for 2 hours. Next, a custom-made laser scanning confocal fluorescence microscope (CFM) was used to estimate the concentration of NV centers from the issue intensity. T_1^* and T_2^* were also measured by Ramsey and Hahn-Echo measurements on the NV ensemble in the electron-irradiated region. As a result, the volume density of the NV ensemble in the electron irradiated region increased with increasing electron dose from 10^{17} to 10^{20} [cm⁻²]; at a dose of 1.0×10^{20} [cm⁻²], the NV volume density reached 2×10^{17} [cm⁻³]. In HPHT diamond ([N]= 3×10^{19} [cm⁻³]), which was used as a comparison, the NV volume density was 4×10^{17} [cm⁻³] after 1.0×10^{20} [cm⁻²] electron doses. Since the NV volume density was on the same order of magnitude as that of HPHT diamond, the concentration of NV centers could be further improved by further irradiation with higher doses in the future. In addition, T_2^* remained 50 ns and T_1^* remained 0.5 μs despite such a high nitrogen concentration in the diamond.

This work was supported by MEXT Quantum Leap Flagship Program (MEXT Q-LEAP) Grant Number JPMXS0118067395.

- [1] V. M. Acosta, D. Budker et al., Phys. Rev. B 80, 115202 (2009).
- [2] S. Choi, S. M. D. Lukin et al., Nature, 543(7644), 221-225 (2017).
- [3] Y. Nakano, N. Tokuda et al., Diamond and Related Materials, 125, 108997 (2022).
- [4] C. Zhang, J. C. Fang et al., J. Phys. D: Appl. Phys. 50 505104 (2017).
- [5] D. Farfurnik, N. Bar-Gill et al., Appl. Phys. Lett. 111, 123101 (2017).
- [6] J. Koike, D. M. Parkin, and T. E. Mitchell, Appl. Phys. Lett. 60, 1450 (1992).

SESSION EQ07.06: Growth II
Session Chairs: Ken Haenen and Shannon Nicley
Tuesday Afternoon, November 29, 2022
Sheraton, 2nd Floor, Independence East

2:00 PM EQ07.06.02

Atmospheric-Pressure Flame Vapor Deposition of Nanocrystalline Diamonds over Large Areas Adrian Manjarrez¹, Kai Zhou¹, Changqiang Chen¹, Yan-Kai Tzeng² and Lili Cai¹; ¹University of Illinois Urbana-Champaign, United States; ²Stanford University, United States

Nanocrystalline diamonds (NCDs) are one of the many carbon allotropes that have attracted great attention for the advancement of many technologies, owing to their superior mechanical, thermal, and optical properties. Yet, their synthesis must be improved for availability at low costs and their widespread application. Here, we report the atmospheric-pressure flame vapor deposition (FVD) synthesis of NCD particles and thin films over an area of more than 28 cm² using methane-hydrogen-air flat flames. Notably, the FVD method unlocks new conditions for diamond growth beyond the previously considered diamond-growth region of the C-H-O phase diagram. Additionally, we demonstrate that the FVD growth of NCDs can be flexibly controlled by tuning the reactant gas composition, substrate material, seeding density, and external electric bias. Overall, with the low cost and simplicity for operation without the need of vacuum, this atmospheric-pressure FVD approach will offer new opportunities to facilitate the scaling-up of diamond synthesis.

2:15 PM EQ07.06.01

Bonding and Integration of CVD Diamond Components in Advanced Industrial Applications Ian Friel¹, Andrew Bennett¹, Julian Ellis¹, Firooz Faili², Teodoro Graziosi¹, Michael Pearson¹ and Daniel Twitchen¹; ¹Element Six (UK) Ltd, United Kingdom; ²Element Six Technologies US Corporation, United States

CVD diamond is a well-established and versatile engineering material which can be manufactured at scale to address a broad range of industrial and consumer sectors, such as defense, semiconductor test and manufacturing, high-end audio, and lab-grown jewelry. Typically, the CVD diamond component is integrated into a larger system to provide an engineering solution which exploits one or more of diamond's remarkable physical properties.

While the successful development of high-quality CVD diamond grades for various optical, electronic, thermal and quantum-sensing applications has been widely reported, the challenges inherent in integrating diamond are less well-understood. Here, many of diamond's properties, such as its chemical inertness, low thermal expansion coefficient, high stiffness and yield stress, as well as low toughness, present barriers to integration, which if not managed successfully can lead to poor adhesion of dielectric and metal coatings, or highly strained components and interface layers vulnerable to failure.

In this paper we discuss bonding and integration challenges and solutions in the context of state-of-the-art optical and thermal applications of CVD diamond, such as high-power Raman lasers, and heat spreaders for high power RF amplifiers.

2:30 PM EQ07.06.03

Strain Engineering of Diamond Microstructures by Trench Filling and Oxidation Keshab R. Sapkota, Andrew Mounce, Tzu-Ming Lu, George Wang

and Ting S. Luk; Sandia National Laboratories, United States

Diamond is considered as the “Mount Everest” of electronic, photonic, and quantum materials due to its outstanding properties, such as an ultrawide bandgap, ultrahigh thermal conductivity, ultrahigh dielectric breakdown strength, high carrier mobility, and hosts of quantum emitters. However, difficulty in doping due to deep dopant levels, indirect bandgap, and difficulty in controlling the color centers’ quantum levels have posed significant challenges to fully utilize diamond in electronic, photonic, and quantum applications. Based on recent theoretical predictions, the bandgap of diamond can be significantly tuned given enough strain. Additionally, it has been demonstrated that strain can manipulate the energy levels in color centers. Therefore, the ability to engineer strain in diamond can be a game changer for diamond based electronics, photonics and quantum applications. However, being the hardest material, diamond is notoriously difficult to strain. Here we present a novel, in-situ, and integrated approach to strain engineer diamond microstructure by growth and oxidation of material (e.g. Si, Al) filled in the micro-fabricated diamond trench. In this study, pairs of diamond fins are fabricated and the trench between fins is filled by poly-Si or Al. The oxidation of trench-filling material exerts stress on the diamond microstructures as a consequence of increased material volume and produces mechanical strain on the microstructures. We will present strain analysis on diamond microstructures as a function of trench dimension, oxidation temperature, and oxidizing materials as measured by electron microscopy and Raman spectroscopy.

*Sandia National Laboratories is managed and operated by NTESS under DOE NNSA contract DE-NA0003525.
(SAND #: SAND2022-8136 A)*

2:45 PM BREAK

SESSION EQ07.07: Nanodiamond II
Session Chairs: Anke Krueger and Stepan Stehlik
Tuesday Afternoon, November 29, 2022
Sheraton, 2nd Floor, Independence East

3:15 PM EQ07.07.02

Fluorescent Nanodiamond-Based Spin-Enhanced Lateral Flow Immunoassay for Detection of SARS-CoV-2 Nucleocapsid Protein and Spike Protein from Different Variants Neha Sharma, Wesley W. Hsiao and Wei-Hung Chiang; National Taiwan University of Science and Technology, Taiwan

Fluorescence Nanodiamonds (FND) have proved to be a promising candidate as biomarkers due to their great optical properties and high biocompatibility. Moreover, FNDs can be easily functionalized with biomolecules such as protein, enzymes. Furthermore, FND do not show photo-blinking, photobleaching and found to have a stable fluorescence and can be used as biomarkers in heterogenous environment due to their no cytotoxicity and biocompatibility. Recent outbreak of Covid-19 lead WHO to announce a pandemic. This disease has infected more than ~500 million people and caused ~6 million deaths. There are several methods to detect corona virus but most of them are required of long-time, expensive and larger laboratory instruments, highly skilled professionals, particular environmental conditions, low specificity and sensitivity. These drawback limits these methods to control that disease at global level. It is necessary to have fast, sensitive and lower cost rapid detection for preventing spread of disease at global level.

Here we report a simple and fast FND based Spin-Enhanced Lateral Flow Immunoassay (SELFIA) for the detection of SARS-CoV-2 virus. Two different antigen from Corona virus, Spike protein and Nucleocapsid protein were detected by SELFIA using FNDs as biomarkers. SELFIA is a homebuilt platform which incident green laser on sample LFIA strips in the presence of electromagnetic field. Antibody functionalized FNDs emit fluorescence when green laser incident on it. The fluorescence signal was detected to photomultiplier tube and amplified signal is received. We successfully detected Spike protein and Nucleocapsid Protein from corona virus from different mutations. This work offers a promising rapid method to detect SARS-CoV-2 with fast, highly sensitive and lower limit of detection (LoD).

3:30 PM EQ07.07.03

X-Ray Absorption Spectroscopy on Nanodiamonds in Water Arsène Chemin¹, Ronny Golnak¹, Jie Xiao¹, Andreas Weisser¹, Benjamin Kiendl², Anke Krueger^{2,3} and Tristan Petit¹; ¹Helmholtz-Zentrum Berlin for Materials and Energy GmbH, Germany; ²Julius-Maximilians-Universität Würzburg, Germany; ³Institut für Organische Chemie, Germany

Easy production of solvated electrons from solar illumination would be a game changer for green chemistry and environmental research. The use of widely available synthetic diamonds to generate solvated electrons upon light irradiation in water has been proposed as a promising strategy to achieve CO₂ or N₂ reduction in liquid phase [1-2]. Free electrons can easily transfer to water because diamonds have a high energetic level of the conduction band and a negative electron affinity when its surface is hydrogenated. At first glance, the large band gap of diamonds (5.5 eV) should only enable excitation from deep UV light, limiting the electrons production using sun. However, CO₂ photo(electro)chemical reduction with visible light has been previously reported [3]. Electron emission mechanisms from visible light radiation remains poorly understood but seems strongly related to the surface state of the diamonds and the interaction with water.

The surface chemistry of the diamonds in water as well as its functionalization, for example with Ru dye, plays a dramatic role on electron excitation and emission. It affects the interfacial properties such as electron affinity or the electron emission and solvation. X-ray absorption spectroscopy (XAS) can be used to characterize the surface states. XAS corresponds to the resonant excitation by X-rays from the core electrons into unoccupied electronic levels allowing a high chemical sensitivity. This provides knowledge on the chemical state of the surface atoms, the density of states and the photoelectron yield. While this characterisation is easily performed into vacuum, measurement in water is much more challenging due to the vacuum requirement for soft X-ray propagation.

In this work, we apply a new technique of XAS in liquid [4] to the characterization of the nanodiamonds film in interaction with water. The nanodiamonds are detonation nanodiamonds functionalized with Ru complex, which showed good photocatalytic properties. A similar method was previously applied to dispersed carbon dots [5]. Measurements were performed at BESSY II synchrotron in Berlin. We used a two electrodes liquid flow-cell with an ultra-thin membrane separating the liquid from the vacuum. The nanodiamonds are deposited on a gold-coated membrane used as working electrode. Here, we show that we can measure the absorption spectrum of nanodiamonds deposited on the membrane and of the water molecules in interaction with the nanodiamonds. The signature from both diamond core and of the functionalized molecules on the nanodiamond surface can be detected. By comparing this measurement to XAS in vacuum, we determine that the interaction with the liquid lead to strong modification of the surface states giving a new insight on possible pathways for the production of the solvated electrons in water.

References

Zhu, D. et al, Photo-illuminated diamond as a solid-state source of solvated electrons in water for nitrogen reduction. *Nat. Mater.* 12, 836–841. (2013).

Zhang, L. et al. Selective Photoelectrochemical Reduction of Aqueous CO₂ to CO by Solvated Electrons. *Angew. Chem.* 53, 9746–9750. (2014)
Knittel, P. et al. Nanostructured boron doped diamond electrodes with increased reactivity for solar-driven CO₂ reduction in room temperature ionic liquids. *ChemCatChem* cctc.202000938. (2020)
Schön, D. et al. Introducing Ionic-Current Detection for X-ray Absorption Spectroscopy in Liquid Cells. *J. Phys. Chem. Lett.* 8, 9, 2087-2092. (2017)
Ren, J. et al. Uncovering the Charge Transfer between Carbon Dots and Water by in Situ Soft X-ray Absorption Spectroscopy. *J. Phys. Chem. Lett.* 10, 14, 3843–3848 (2019)

This project has received funding from the European Commission under the Horizon 2020 grant agreement 665085 (DIACAT) and Volkswagen Foundation under the Freigeist Fellowship No. 89592.

SESSION EQ07.08: Poster Session
Session Chairs: Chia-Liang Cheng and Mariko Suzuki
Tuesday Afternoon, November 29, 2022
8:00 PM - 10:00 PM
Hynes, Level 1, Hall A

EQ07.08.01

Ultra High-Concentration Nitrogen-Doped CVD Diamond with Highest Crystallinity Mayu Ueda¹, Kyosuke Hayasaka¹, Kyotaro Kanehisa¹, Yasuhiro Takahashi¹, Chiyuki Wakabayashi¹, Taisuke Kageura² and Hiroshi Kawarada^{1,3}; ¹Waseda University, Japan; ²National Institute of Advanced Industrial Science and Technology (AIST), Japan; ³Kagami Memorial Research Institute for Materials Science and Technology, Japan

High impurity doping in diamond using microwave plasma chemical vapor deposition (MPCVD) has been actively investigated with many dopants such as boron, nitrogen, and phosphorus. In particular, high concentration doping as high as $2 \times 10^{22} \text{cm}^{-3}$ has been achieved for boron doping [1], whereas the highest concentration for nitrogen is only $2 \times 10^{20} \text{cm}^{-3}$ [2]. The fabrication of highly nitrogen-doped diamond is expected to realize highly sensitive magnetic sensing by NV centers and superconductivity theoretically predicted [3]. In general, increasing the proportion of supplied nitrogen gas degrades the film quality of diamond [4]. On the other hand, it has been reported that supplying carbon and oxygen at a ratio of 1:1 during deposition improves the film quality [5]. Diamonds doped with high concentrations of boron, which has a larger ionic radius than carbon, exhibit crystal expansion in vertical direction [1]. Up to now, there are no reports on crystal distortion in highly nitrogen doped diamonds where nitrogen, has a smaller ionic radius than carbon. In this study, we fabricated diamond and characterized the physical properties of the thin films by Reciprocal Space Mapping (RSM) using a XRD (Bruker D8 DISCOVER) and cross-sectional imaging using a TEM (JEOL JEM-2100F).

CVD synthesis was performed using a waveguide confined MPCVD system with quartz tube where plasma was confined within waveguide, with a pressure of 110Torr, a microwave power 300W and at a temperature of 850°C. CH₄, N₂, and CO₂ gases were used for homoepitaxial growth. The gas mixture conditions are [C,O]=1.2% (common value for C and O), [C,O]=1.5, 2.0%, and [C,O]=4.0% (common value for C and O). The total gas flow rate was fixed at 200 sccm, and samples were prepared by varying the ratio of gases. HPHT synthetic (111)-oriented diamond substrates were used. As a result, the nitrogen concentration of [C,O]=4.0% was $8 \times 10^{20} \text{cm}^{-3}$ from SIMS measurements. It is the world's highest concentration of nitrogen existed in diamond. From the cross-sectional TEM images, it was confirmed that twinning defects were introduced into the epitaxial layer in [C,O]=1.5, 2.0%, and stacking defects were introduced into the epitaxial layer in [C,O]=1.2%. On the other hand, [C,O]=4.0% showed no twins or stacking faults, but dark spots which appeared to be nitrogen aggregation [6] in the epitaxial layer. The origin of these spots must be further investigated. In the Raman spectrum measurement (RENISHAW inVia Basis, 532nm), a peak at 1333cm⁻¹, the Raman peak of diamond, was confirmed for all three samples. [C,O]=4.0% showed the FWHM of 8.6cm⁻¹ at 1333cm⁻¹. The FWHM is comparable to that of HPHT diamond with few defects. High quality nitrogen-doped diamond was produced despite of containing as much as $8 \times 10^{20} \text{cm}^{-3}$ nitrogen. The lattice expansion was calculated from RSM. [C,O]=1.2% exhibited 0.66% expansion in the horizontal direction and 0.20% shrinkage in the perpendicular direction. [C,O]=1.5, 2.0% exhibited 1.47% expansion in the horizontal direction and 0.50% shrinkage in the perpendicular direction. This anisotropic expansion and shrinkage is opposite to those of heavily boron doped samples [1] and is caused by high concentration of nitrogen above $5 \times 10^{20} \text{cm}^{-3}$. However, [C,O]=4.0% exhibited no crystal lattice expansion or shrinkage. The well-crystalline CVD diamond has been fabricated with the highest nitrogen concentration of $8 \times 10^{20} \text{cm}^{-3}$ by using [C,O]=4.0%. It is the most promising condition for high nitrogen incorporation with high quality CVD diamond equivalent to HPHT diamond and can be applied high sensitive NV magnetometry.

[1]T. Kageura, H. Kawarada, *et al.*, *Diam. Mater.* **90**, 181-187(2018).

[2]Y. Nakano, N. Tokuda, *et al.*, *Diam. Mater.* **125**, 108997(2022).

[3]Y. Ma, G. Zou, *et al.*, *Phys. Rev. B* **72**, 014306(2005).

[4]E.Boettger, C. P. Klages *et al.*, *J. Appl. Phys.* **77**, 6332(1995).

[5]P. K. Bachmann, H. Lydtin *et al.*, *Diam. Mater.* **1**, 1-12(1991).

[6]T. Evans, J. Maguire, *et al.*, *J. Phys. C* **14**, L379(1981).

EQ07.08.02

Chemical Mechanical Polishing Rate and Uniformity for Single-Crystalline Diamond Substrates S M Asaduzzaman¹, Aaron M. Hardy², Cristian J. Herrera-Rodriguez¹, Mark Tompkins² and Timothy A. Grotjohn^{1,2}; ¹Michigan State University, United States; ²Fraunhofer USA, Inc., Center Midwest, United States

Diamond has exceptional physical and chemical properties, including maximum hardness, thermal conductivity, and superior chemical erosion resistance. Chemical Vapor Deposition (CVD) diamonds are strong candidates for industrial use but can suffer from the non-uniform thickness and rough surfaces. The development of diamond applications in electronics can be greatly improved by precise polishing that produces minimal damage to diamond substrates. Among the numerous applications, polishing and planarizing operations are needed in the preparation of CVD diamonds for precision machining tools, electronic applications, optical windows, heat spreaders, and bonding of diamonds to other semiconductors. In terms of cost-effective processing and material surface finish, polishing is a crucial and limiting step for diamond applications. Polishing diamonds over the years has been accomplished in several ways. Chemical Mechanical Polishing (CMP) with strong oxidizing slurries to polish CVD diamond films is a promising approach [1-5].

We have studied the CMP process originally developed for the work described in [6] that put a GaAs membrane on a CMP polished diamond substrate/epi-layer. We have looked at quantifying the CMP polishing rate and the uniformity of the polishing across the diamond substrate. This study utilizes High-Pressure High-Temperature (HPHT) diamond samples with a 0-3° degree off-angle from the (001) surface orientation with dimensions of 3.5 x 3.5 mm²

and larger. Since the applications of interest often have epi-layers of diamond grown by the CVD method, we studied the CMP process applied to CVD diamond grown on the HPHT substrates. To study the polishing rates, patterns are etched into the diamond surface so the CMP rate could be measured with the atomic force microscope (AFM) and surface profilometry techniques.

The CMP polishing equipment rotates the polishing wheel and sweeps/rotates the sample while using a self-leveling sample holder to maintain contact between the SCD surface and the grooved ceramic polishing wheel. The self-leveling approach helps achieve a repeatable, uniform, and proportionate material removal. With this approach, roughness can be reduced without too aggressively reducing the thickness or homogeneity of epitaxial layers. The oxidative CMP slurry mixture consists of potassium permanganate (KMnO_4) and boron carbide particles (1-3 μm) with phosphoric acid and DI water also in the slurry.

For determination of CMP removal rates and uniformity, CMP is performed for fixed time intervals with the surface profile of the previously etched structures on the diamond surface measured after each interval. The typical interval time between measurements was 60 minutes. Before and after each hour of CMP operation, microscopic checks, profilometer step scanning, and atomic force microscope (AFM) scans were performed. On the SCD substrate, measurements were performed at multiple locations. The typical CMP removal rates were 100-150 nm/hr. The surface profile scans, and AFM indicate that some material removal also occurs at the bottom of the etch structure as wide trenches and narrow trenches show different depths after CMP processing.

Acknowledgment:

This work was supported by the Michigan Translational Research and Commercialization (MTRAC) program.

References:

1. T. Schuelke, T.A. Grotjohn, *Diam. Relat. Mater.* 32 (2013).
2. H. Luo, K.M. Ajmal, W. Liu, K. Yamamura, H. Deng, *Int. J. Extrem. Manuf.* 3 (2021).
3. Z. Yuan, Z. Jin, Y. Zhang, Q. Wen, *J. Manuf. Sci. Eng. Trans. ASME.* 135 (2013).
4. H. Hocheng, C.C. Chen, *Mater. Sci. Forum.* 505–507 (2006)
5. J. Kühnle, O. Weis, *Surf. Sci.* 340 (1995).
6. S. J. Cho, D. Liu, A. Hardy, J. Kim, J. Gong, C. J. Herrera-Rodriguez, E. Swinnich, X. Konstantinou, G. Y. Oh, D. G. Kim, J. C. Shin, J. Papapolymerou, M. Becker, J. H. Seo, J. D. Albrecht, T. A. Grotjohn, Z. Ma, *AIP Advances.* 10 (2020), doi:10.1063/5.0027864.

EQ07.08.03

Following Polymer Degradation with Nanodiamond Magnetometry Runrun Li, Thea Vedelaar and Romana Schirhagl; University of Groningen, Netherlands

Degradable polymers have been widely used in the biomedical fields, including treatment of cancer, development of vaccines, manufacture of nanoparticles with increased plasma half-life, scaffolds for cell culture, and tissue regeneration or drug delivery. Their main advantages are their non-toxicity as well as great biocompatibility and biodegradability. Many kinds of polymers are used for various biochemical media in medical practice. Hence, it is important to precisely follow the degradation of polymers in real time. Common methods to evaluate polymer degradation encompass atomic force microscopy, gel permeation chromatography, nuclear magnetic resonance, and Raman spectroscopy. However, all of them have limitations, such as the requirement of large sample masses, interference from cellular biomolecules or organelles, and none of them allow for straightforward and time-efficient tracking of polymer degradation in real time with high precision. In this study, we made use of relaxometry or T1 measurements for the first time to track polymer degradation with nanoscale precision, both extracellular and intracellular. The method is a new technique based on fluorescent defects in nanodiamonds, which change their optical properties based on their magnetic surrounding. Since optical signals can be read out more sensitively than magnetic signals, this method enables unprecedented sensitivity down to the nanoscale. Here we investigated an exemplary polymer polylactic acid (PLA), whose degradation product, lactic acid, is eventually converted into H_2O and CO_2 through the citric acid cycle. For extracellular degradation, fluorescent nanodiamonds (FNDs) were incorporated into PLA films that were produced by spin-coating. Then, this thin film was immersed in a degradation medium, which contained Gd^{3+} . Gd^{3+} is a common contrast agent which causes a spin noise. When the film is degraded, Gd^{3+} can come closer to nanodiamonds and thus an increase in spin noise is detected. We found that T1 constants decreased gradually with the erosion of the film exposed to an alkaline condition. In addition, we accessed the mobility of nanodiamonds within the film and indicated the freedom of particles increased under the strong alkaline environment. We also compared T1 data with the conventional methods including quartz crystal microbalance, fourier-transform infrared spectroscopy and atomic force microscopy. The results were in good agreement with each other. For intracellular degradation, PLA conjugated with NH_2 -DOTA-GA was linked to Gd^{3+} by chelate, and then FNDs were loaded to PLA-Gd to form nanoparticles (PLA-Gd-FNDs NPs) by the emulsion method. Afterwards, nanoparticles were taken up by the cells and degradation of PLA in the cells was detected in real time with our home-built T1 magnetometry. In that case we start with low T1 and the Gd^{3+} moves away from the nanodiamonds simultaneously with the PLA when nanoparticles are degraded intracellularly. Therefore, we find an increase in T1. At the same time, we could freely explore the movement of nanodiamonds loaded into PLA nanoparticles as a complement to the T1 results. Unlike traditional methods, T1 measurements provide localized detection with nanoscale resolution, and due to the stability and non-bleaching of nanodiamonds, this technique allows for long-term tracking. T1 and tracking have been used to follow the degradation of PLA in real-time, and we expect that they could be applied to other polymers as well.

EQ07.08.04

Analytical Solution of Electron-Spin Double Resonance Spectra in Diamond Under Strong RF Fields Derived by the Floquet Theory Takumi Mikawa^{1,1}, Yuichiro Matsuzaki^{2,2}, Ryusei Okaniwa^{1,1}, Yuta Nakano^{3,3}, Norio Tokuda^{3,3}, Hideyuki Watanabe² and Junko Ishi-Hayase^{1,1}; ¹Keio University, Japan; ²National Institute of Advanced Industrial Science and Technology (AIST), Japan; ³Kanazawa University, Japan

Detections of radio frequency (RF) magnetic fields with high sensitivity have been demanded in both pure and applied physics. A nitrogen-vacancy (NV) center in diamond has attracted much attention as a RF signal sensor with high sensitivity and high-spatial resolution because of its atomic size and long coherence time at room temperature. While many studies have proposed several methods to sense RF, electron-spin double resonance (ESDR) [1-2] enables to detect RF based on continuous-wave optically detected magnetic resonance (CW-ODMR). Due to its simple setup and sequence, the ESDR is suitable for wide-field sensing. However, previous studies [1-3] can explain the ESDR spectra only for the weak RF and cannot provide any analytical solutions for the characteristic phenomena under the strong RF. In this study, we theoretically and experimentally analyze the ESDR spectra for strong RF by adapting the double-unitary-transformation (DUT) approach [4] in the Floquet theory [5].

In the present of bias magnetic perpendicular to the NV axis, eigenstates of electronic spins of an NV center are represented by the bright state $|B\rangle$, the dark state $|D\rangle$ and $|ms = 0\rangle$. The resonant microwave (MW) magnetic can induce the transition from $|0\rangle$ to $|B\rangle$ or $|D\rangle$, which results in the decrease of photoluminescence (PL) under a green laser excitation (CW-ODMR). The transition between $|B\rangle$ - $|D\rangle$ states can be induced by RF and its resonant frequency depends on the transverse strain and the transverse magnetic field. In the ESDR experiment, the PL intensities were measured by simultaneously irradiating continuous MW and RF with various frequencies. In Refs [1,2], the anti-crossings around $|B\rangle$ - $|D\rangle$ resonant frequency can be observed under

weak RF and well reproduced by the theoretical calculations assuming only rotating wave approximation (RWA). Under the strong RF, however, additional anti-crossings at different RF and MW frequencies appeared that cannot be reproduced using the previous theoretical approach [1,2]. Then, we introduce the Floquet theory treating the time-periodic Hamiltonian of the ESDR. According to the Floquet theory, the state of the NV center under driving RF forms a RF-dressed state by absorbing or emitting any RF-photons. For strong driving fields, we adapt the DUT approach in the Floquet theory to turn the strong driving term into many weak driving terms. Therefore, the analytical solutions of the DUT approach can reproduce the anti-crossings peculiar to strong RF. Moreover, we find that, the anti-crossings peculiar to strong RF are caused by the multi-photon transition where the MW induces the transition between dressed states generated by RF via $|0\rangle$. In contrast, the anti-crossings under the weak RF [1,2] are caused by the one-photon transition between $|B\rangle$ - $|D\rangle$ states.

We use the DUT approach in the Floquet theory to analyze the ESDE and experimentally confirm that the analysis can reproduce the ESDR spectrum with the strong RF. Our result provides the insight into the applicability of Floquet theory for understanding physical properties of NV centers.

Acknowledge

We acknowledge Kent Sasaki and Kensuke Kobayashi for the helpful advice about the experiment setup. This work was supported by MEXT Q-LEAP (No. JPMXS0118067395), MEXT KAKENHI (No. 18H01502, 20H05661, 22H01558), and CSRN, Keio University. This work was supported by Leading Initiative for Excellent Young Researchers MEXT Japan and JST presto (Grant No. JPMJPR1919) Japan and Kanazawa University SAKIGAKE Project 2020. YM acknowledges support of Grants-in-Aid for Scientific Research from the Ministry of Education, Culture, Sports, Science, and Technology, Japan (20H05661).

References

- [1] S. Saijo et al., Appl. Phys. Lett. 113, 082405 (2018).
- [2] T. Yamaguchi et al., Jpn. J. Appl. Phys. 58, 100901 (2019).
- [3] A. K. Dmitriev et al., Phys. Rev. A 100, 11801 (2019).
- [4] Y. Han et al., Phys. Rev. A 101, 022108 (2020).
- [5] J. H. Shirley, Phys. Rev. 138, B979 (1965).

EQ07.08.05

Optical Properties of Silicon Vacancy (SiV) Centers in Nanodiamonds Fabricated by Detonation Process [Yoshiki Saito](#)¹, Yuto Makino^{1,2}, Yosuke Minowa¹ and Masaaki Ashida¹; ¹Osaka University, Japan; ²Daicel Corporation, Japan

Silicon vacancy (SiV) center-containing nanodiamonds (SiV-NDs) have attracted much attention as promising fluorescent probes due to their high biocompatibility and fluorescence properties. SiV centers in bulk diamond exhibit a sharp zero-phonon line (ZPL) with a linewidth of 5 nm in the biomaterial window (650-950nm) [1] at room temperature [2][3]. In addition, the SiV center emission has a large Debye-Waller factor (DWF), concentrating about 70% of the total emission in the ZPL [4]. This sharp photoluminescence is excellent for multicolor bioimaging and for distinguishing of autofluorescence. Recently, Daicel Corporation has demonstrated the synthesis of SiV-NDs by detonation process (SiV-DNDs) [5]. This method has the potential to pave the way for bioimaging applications because it can efficiently produce NDs with a single-digit nm size, which is extremely small compared to NDs produced by other methods. The small size allows non-invasive imaging. However, there is a concern that SiV centers in DNDs may show optical properties different from those of SiV centers in bulk diamond due to their extremely small size. For example, a nitrogen-vacancy (NV) center, another well-studied color center, in DNDs has been reported to show different optical properties from NVs in bulk diamond, such as the extinction of fluorescence caused by defects near the surface and inhomogeneous distribution of the ZPL due to energy level shifts depending on the position of the NV centers [6].

In the present study, we measured photoluminescence and photoluminescence excitation spectra (PLE) and conducted time-resolved photoluminescence measurements to investigate the optical properties of SiV centers in DNDs.

The optical properties were compared with those of typical SiV centers in bulk diamond; in the case of SiV centers in DNDs, the linewidth of ZPL is 14.4 nm at room temperature, which is wider than the line width of SiV centers in bulk diamond. Furthermore, the DWF of the SiV center in DNDs is 0.47, which is reduced to about 70% of that of the SiV center in bulk diamond. The luminescence lifetime of the SiV center in DNDs is 0.56 ns, which is about half of that of the SiV center in bulk diamond. PLE measurements confirmed SiV-DND emission under excitation wavelengths from 390 to 690 nm. PLE spectra is broad and more efficiently excited at longer wavelengths compared to SiV centers in bulk diamond.

We attribute these differences in optical properties to surface effects due to the very small particle size (~10 nm). The enhanced non-radiative transition probability and electron-phonon coupling resulting from the surface effects lead to homogeneous broadening of the ZPL and shorter fluorescence lifetime of the SiV centers in the DNDs. The rise in the low-energy side of the PLE spectrum is also considered to be the tail of the ZPL of the absorption spectrum. Moreover, surface effects cause fluctuations in the energy levels of the SiV centers in each DND. This fluctuation gives rise to the inhomogeneous broadening of the ZPL. However, we demonstrated that the photostability does not change, irrespective of the particle size. In summary, SiV-DNDs show a sharp photostable emission, a wide excitation wavelength range and a high excitation efficiency in the biomaterial window region, suggesting that they are promising fluorescent probes in the field of bioimaging.

- [1] R. Weissleder, et al. Nat. Biotechnol. 19, 316 (2001).
- [2] G. Thiering, A. Gali, Phys. Rev. X, 8, 021063 (2018).
- [3] S. V. Bolshedvorski, et al., ACS Appl. Nano Mater. 2, 4765 (2019).
- [4] S. Häußler, et al., New J. Phys. 19, 063036 (2017).
- [5] Y. Makino, et al., Diam. Relat. Mater. 112, 108248 (2021).
- [6] V.Y. Osipov, et al., Nanoscale Res. Lett. 14, 1 (2019).

EQ07.08.06

Ultrafast Pump-Probe Dynamics of the Unknown 3237 cm^{-1} Diamond Defect Absorption Feature [Terng Junn Keat](#), Daniel J. Coxon, Vasilios G. Stavros, Mark E. Newton and James Lloyd-Hughes; University of Warwick, United Kingdom

The 3237 cm^{-1} absorption feature has often been observed in diamonds alongside the 3107 cm^{-1} feature which originates from the N_3VH defect. Despite the commonplace occurrence of both features, their relationship with each other has long eluded diamond researchers. Furthermore, the vibrational energy dynamics of the 3237 cm^{-1} are entirely unknown. Understanding this is vital in understanding the origins of this feature and its possible interactions with other diamond defects which are of significant interest. For example, the possibility of the 3237 cm^{-1} being a N-H bond vibration suggests that the defect responsible for this feature may act as a nitrogen sink. This is significant when trying to produce and/or characterize the famous NV^- defect, amongst others. Here, we present a thorough investigation on the infrared vibrational dynamics of the unknown 3237 cm^{-1} absorption feature and its relationship with the N_3VH defect. Fourier transformation infrared spectroscopy and ultrafast pump-probe measurements were conducted to establish whether the 3237 cm^{-1} also originated from the N_3VH defect, and if not, how the two defects are related. The vibrational energy states related to the 3237 cm^{-1} feature and their respective relaxation dynamics were also investigated. This, along with theoretical modelling of the unknown defect's energy potential via the Morse

potential model, further provided the dimensionless matrix element and the defect concentration calibration factor needed to quantify this defect from its infrared absorption spectrum.

EQ07.08.07

Sub-Bandgap Electron Emission from Diamond into Vacuum and Water Cesar Saucedo, Nathaniel F. Rieders and Robert J. Hamers; University of Wisconsin–Madison, United States

Diamond has the potential to enable novel photochemistry through the generation of solvated (hydrated) electrons. Hydrogen-terminated diamond surfaces are of particular interest as they exhibit negative electron affinity, allowing for efficient electron emission into vacuum. Due to diamond's large bandgap, photoelectron emission is typically achieved at short wavelengths (<225 nm), although emission using longer wavelengths is possible. Enhancing photoemission at longer wavelengths requires a better understanding of the photophysics involved in the sub-bandgap region. Understanding the energy distribution of emitted electrons and how this distribution depends on the energy of the photoexcitation source is critical for developing models of the sub-bandgap emission process. Our studies provide new insights into the mechanism and the role hydrogen and oxygen terminated surfaces have on the sub-bandgap electron emission into vacuum and water. We have modified a commercial photoelectron spectroscopy system to enable the use of sub-bandgap excitation energies. In addition, we performed photocurrent measurements with the same sub-bandgap excitation energies into water. Using various sub-band gap photon energies, we have measured the energy distribution of photoelectrons emitted from boron-doped (111) H-terminated and O-terminated diamond surfaces as well as emission into water. Initial observations demonstrate that sub-bandgap emission from both H- and O-terminated diamond substrates is possible. The efficiency of sub-bandgap excitation and distribution of emitted electron energies differs between surface terminations.

EQ07.08.08

Electron Emission from Nanodiamond Field Emitters Travis C. Wade¹, David Kerns², Glenn Hess², Keith Warren³ and Jim Davidson²; ¹Evolv Diamonds LLC, United States; ²International FemtoScience Inc., United States; ³Spatial Microsystems, United States

Chemical vapor deposited (CVD) diamond is an attractive material for electron field emitters because of its low or negative electron affinity, excellent mechanical strength, and chemical inertness. Diamond's excellent mechanical strength and chemical stability contribute to excellent durability characteristics. The strong covalent sp³ bonds present in diamond have a stabilizing effect on the electron emission as compared to the weaker ionic bonds present in traditional metal cathodes. Nanocrystalline diamond, (grain size ~ 1 nm - 100 nm), possesses unique properties including deliberate and controlled amounts of sp²-carbon content and n-type electrical conductivity at room temperature.

The authors have demonstrated electron emission from widely spaced nanodiamond pyramidal tip arrays as well as lateral lithographically-patterned field emission arrays. Array tips have not been observed to be physically damaged by extended emission tests on the scales available to scanning electron microscopy (SEM). Methods developed by the authors permit analysis of diamond tip structure and provide a basis for optimization of field emitter composition and performance.

The authors are focused on developing new technologies, sensors and products for operation in extreme environments and applications (e.g., high and low temperature, pressure, radiation, etc.) where no other, or limited, capability currently exists.

EQ07.08.09

Incubation Effect upon FS-Laser Micromachining in CVD Diamond Cleber Mendonca, Lucas Nolasco and Filipe Couto; University of Sao Paulo, Brazil

Diamond is well known for its many remarkable mechanical, thermal, electric and optical properties. Among its unique features, it also presents interesting nonlinear optical effects, thus being a highly desired material for many photonic devices. Therefore, femtosecond laser micromachining can be used as a processing method for such devices due to its high micron/sub-micron resolution, which has been mostly exploited using fs-pulses at 800 nm. Although such a method has been intensively investigated, most experiments were performed by an fs-laser system centered at 800 nm. Thus, in this work, the incubation effect (damage threshold fluence as a function of the number of applied fs-pulses) is studied at 1030, 515, and 343 nm with 216 fs pulses using the zero damage method. By implementing the exponential defect model, the incubation parameter (γ) was determined to be (0.14 ± 0.03) at 1030 nm (0.3 ± 0.1) at 515 nm, and (0.13 ± 0.04) at 343 nm, which indicates that at 515 nm, fewer fs-pulses are necessary to reach the minimum damage fluence value. In addition, a theoretical model of the electron density formed by a single fs-pulse, considering multiphoton excitation and avalanche ionization, was used to interpret the experimental result. Therefore, this work adds to the knowledge of fs-laser micromachining of CVD diamond from near IR to UV, improving such processing technique.

EQ07.08.10

Chemical Mechanical Polishing of Single Crystalline Diamond Epitaxial Layers for Electronics Applications Aaron M. Hardy¹, Cristian J. Herrera-Rodriguez², Matthias Muehle¹, Michael Becker¹, Edward Drown^{1,2}, Nina Baule¹, Mark Tompkins¹, Timothy A. Grotjohn² and John D. Albrecht^{1,2}; ¹Fraunhofer USA Inc., Center Midwest, United States; ²Michigan State University, United States

In order for single crystal diamond (SCD) to be practical as an electronic material for technical applications including solid state electronics, thin (<1 μm), precisely doped epitaxial SCD layers with very low (<1 nm) surface roughness are required. The roughness requirement is especially crucial for fabrication processes utilizing membrane transfer techniques. To meet roughness requirements, a post-growth chemical mechanical polishing (CMP) process may be employed. While the current body of literature gives valuable insight into the material removal mechanism, material removal rates (MRRs), subsurface damage, and resultant roughness¹⁻⁴, there is limited exploration of material removal uniformity or the need for post-growth smoothening of thin, epitaxially grown diamond layers for electronics applications.

To address this, we propose a self-leveling oxidative CMP process targeting repeatable, minimal, and uniform material removal. This process utilizes a ball-joint style self-leveling sample holder to keep the SCD surface in flat contact with a grooved ceramic polishing wheel under the conditions of wheel rotation, sample rotation, and sample sweeping. These innovations seek to meet roughness requirements without unnecessarily affecting the epitaxial layer thickness or uniformity.

In this study, an 8-hour oxidative CMP process was performed on two p⁺ epilayers grown on (100) SCDs cut to 3° off-angle. Five wear trenches were etched into each p⁺ epilayer after growth, and atomic force microscope (AFM) analysis of the trenches was used to evaluate material MRR and material removal uniformity. After CMP, the average roughness decreased from 3.83 nm and 1.57 nm to 0.20 nm and 0.16 nm for the two samples, respectively. The average MRRs for the two samples were found to be 41 nm/hr and 38 nm/hr as measured by mass loss, indicating a good degree of repeatability. Profilometer scans of the diagonals were used to further evaluate macroscale morphology and material removal uniformity.

In addition, we show how this CMP process has been deployed to smoothen p⁺ SCD device layers. The thickness of these layers ranged from 200 – 600 nm before polishing, exhibited typical roughness >2 nm, and displayed hillock formation. By using this process, the p⁺ SCD device layers were smoothened to roughness values typically <0.3 nm, and thinned to target thicknesses between 100 – 300 nm. Subsequently, these samples were used by collaborators for the fabrication of GaAs/diamond n-p diodes and AlGaAs/GaAs/diamond p-n-p heterojunction bipolar transistors (HBTs) by means of a semiconductor grafting membrane transfer process.⁵

Acknowledgement

This work was supported by the Defense Advanced Research Projects Agency (DARPA) and the Office of Naval Research (ONR) under the DREaM program (Grant No. N00014-18-1-2032).

References

1. N. Tatsumi, K. Harano, T. Ito, H. Sumiya, *Diamond and Related Materials*. **63**, 80–85 (2016).
2. H. Yang, Z. Jin, L. Niu, H. Wang, H. Niu, *Diamond and Related Materials*. **125**, 108982 (2022).
3. S. Yuan, X. Guo, S. Zhang, C. Zhang, P. Li, Z. Jin, R. Kang, D. Guo, *Applied Surface Science*. **566**, 150638 (2021).
4. A. Kubota, S. Nagae, M. Touge, *Diamond and Related Materials*. **70**, 39–45 (2016).
5. S. J. Cho, D. Liu, A. Hardy, J. Kim, J. Gong, C. J. Herrera-Rodriguez, E. Swinnich, X. Konstantinou, G. Y. Oh, D. G. Kim, J. C. Shin, J. Papapolymerou, M. Becker, J. H. Seo, J. D. Albrecht, T. A. Grotjohn, Z. Ma, *AIP Advances*. **10** (2020), doi:10.1063/5.0027864.

EQ07.08.11

An Electrochemical Sensor for Chemotherapeutic Agent Methotrexate Based on a Novel Graphitic Nano-Heterostructure Material Reham G. Elfaragy, Mahmoud A. Saleh and Nageh K. Allam; American University in Cairo, Egypt

A novel graphitic material was used to determine, using electrochemical voltammetry, whether methotrexate (MTX) is a chemotherapeutic and immunomodulator medication. The study shows an enhanced response compared to the previous ones. A graphite/CPE exhibits superior electrochemical oxidation and detection capabilities of MTX in biological platforms (plasma, urine) than bare Carbon Paste Electrodes. As part of the characterization of the synthesized graphitic material, several techniques were utilized, including X-ray powder diffraction (XRD), X-ray photoelectron spectroscopy (XPS), UV-visible absorption spectroscopy, scanning electron microscopy, Raman spectroscopy, cyclic voltammetry, square wave voltammetry, and electrochemical impedance spectroscopy. By using density functional theory (DFT), the electronic structure, adsorption energy, band gap, type of interaction, and stable configuration of the graphitic material/CPE used were also investigated. For MTX concentrations in Britton Robinson Buffer (BRB) solution, urine, and plasma, the graphitic/CPE platform demonstrated linear response, with a higher recovery rate and a lower limit of detection (LOD) and limit of quantification (LOQ), compared with existing literature. Several studies using modified graphitic materials/CPE electrodes have shown promising results in terms of reproducibility, stability, and selectivity.

EQ07.08.12

Study on the Growth of High-Quality Diamond Microparticles with Preselected Seeds and Their Practical Applications Tongtong Zhang¹, Madhav Gupta¹, Zhongqiang Wang², Lingzhi Wang¹, Jing Wang³, Qi Wang², Lei Shao³, Kwai Hei Li⁴ and Zhiqin Chu¹; ¹The University of Hong Kong, Hong Kong; ²Peking University, China; ³Computational Science Research Center, China; ⁴Southern University of Science and Technology, China

The diamond materials have demonstrated copious applications in a wide range of areas due to their extraordinary features. Thus, various methods, e.g., chemical vapor deposition (CVD), have been developed to fabricate diamond materials with desired properties. However, the conventional CVD diamonds grown by detonation nanodiamonds (DNDs) seeds are unsuitable for most demanding applications that require diamonds with superior properties. Here, we propose to use our previously developed clean and rounded salt-assisted air-oxidized (SAAO) high-pressure high-temperature (HPHT) nanodiamonds (NDs)¹ as CVD seeds to grow high-quality diamond microparticles on the silicon substrate. The as-grown diamond microparticles are found to contain silicon-vacancy (SiV) centers with superior properties, i.e., significantly increased photoluminescence (PL) emission, narrow linewidth, etc., enabling a wide range of practical applications. For example, ultrasensitive all-optical thermometry measurements with an intrinsic noise floor of ~0.24 °C Hz^{-1/2} are demonstrated by utilizing the SiV centers in the fabricated high-quality diamond microparticles.

At the same time, these chaotic diamond microparticles heterogeneously grown on silicon substrate also have great potential to be used as robust optical anti-counterfeiting labels. The location, size, and shape of each particle are random and unclonable due to the unpredictable CVD fabrication process. Notably, the robust and tunable signals of 1) SiV PL and 2) scattering from diamond microparticles are demonstrated to enable high-capacity optical encryption. Furthermore, this diamond-based anti-counterfeiting label shows extreme stability in various practical application scenarios, e.g., harsh chemical environments, high temperature, mechanical abrasion, and UV light irradiation.

Reference

1. Zhang, T.; Ma, L.; Wang, L.; Xu, F.; Wei, Q.; Wang, W.; Lin, Y.; Chu, Z., Scalable Fabrication of Clean Nanodiamonds via Salt-Assisted Air Oxidation: Implications for Sensing and Imaging. *ACS Appl. Nano Mater.* **2021**, *4* (9), 9223–9230.

EQ07.08.13

Depth Dependence of the Radiative Lifetimes of Shallow Color Centers in Single-Crystalline Diamond Maryam Zahedian, Jietian Liu, Ricardo Vidrio, Shimon Kolkowitz and Jennifer Choy; University of Wisconsin–Madison, United States

Optically active defects in diamond are widely used as bright single-photon sources for quantum sensing, computing, and communication. For sensing applications, the measurement sensitivity and spatial resolution benefit from placing the spin defect in close proximity (within few to tens of nanometers) to the physical quantity being measured. Emission from shallow color centers is affected by the proximity of the emitters to the planar interface which alters their dielectric environment leading to changes in the emission rate and profile. Understanding the characteristics of shallow-color-center emission, including how the radiative lifetime is affected by proximity to the surface, is especially crucial for implementing near-field sensing measurements such as Förster resonance energy transfer and for designing photonic structures to control light-matter interactions with color centers. While it is well-known that the radiative power from an electric dipole decreases as the emitter approaches an interface with a higher-index dielectric, leading to an elongation in the radiative lifetime. For emitters in crystalline solids, modeling of this effect needs to consider the crystal orientation and direction of the surface cut, which can greatly impact the emission characteristics. In this paper, we provide a framework for analyzing the radiative lifetime of shallow (<100 nm) defects, in which optical transitions are derived from electric dipoles in a plane perpendicular to their spin axis. The radiative lifetime of electric dipoles is acquired by integrating their total radiative power where the lifetime of any electric dipole is inversely proportional to its radiative power. We present our calculations and preliminary experimental data for the depth-dependent radiative lifetime for Nitrogen Vacancy (NV) centers in (100)-cut diamond. Our experimental data agree with the calculations, confirming the lifetime elongation of emitters, close to the interface which proposes the feasibility of utilizing lifetime measurements as complementary technique for estimating the color center depth. Our calculations can be adapted for other vacancy defects in diamond and

have been extended to defects along any allowed orientation for diamond with (110) and (111) surface cuts.

EQ07.08.14

Nanostructured Plasmonic Diamond for Marine SERS [Massimiliano Ramsay](#), Alexander C. Pakpour-tabrizi and Richard B. Jackman; Univ College London, United Kingdom

Surface-enhanced Raman scattering, or SERS, is an important optical sensing technique in which inelastic light scattering by molecules is greatly enhanced, enabling trace multi-component chemical detection. SERS typically involves metallic nanoparticles, Au or Ag, supported on a substrate such as Si, onto which the analyte of interest adsorbs. Enhancement arises from local fields generated by plasmon excitation in the NPs. However, SERS substrates degrade rapidly and are not suitable for re-use. Moreover, they are simply too fragile for use in environmentally challenging situations such as ocean analysis.

As a robust substrate for SERS, diamond has ideal optical properties displaying only a single intense peak at 1332cm⁻¹ enabling the signal from many organic species to be detected with little interference. However, the reliance of van-der-Waals forces for NP adhesion to diamond offers little improvement. A solution is to include the NPs within diamond, sufficiently near the surface to retain their plasmonic enhancement of the SERS signal. Metallic NP plasmonics can be significantly affected by dielectric environment, shape and inter-particle interactions. Most methods for Au or Ag NP formation on diamond, lead to a range of NP sizes and separations whose inhomogeneous nature is then reflected in any layer created by overgrowth with diamond by CVD methods; these structures perform poorly as SERS substrates. Here, we have applied Nano-imprint Lithography (NIL) to direct the etching of ordered nano-holes into diamond substrates. Templated de-wetting of Silver films into diamond nano-holes was successfully demonstrated. Diamond was grown over these highly ordered nanoparticles arrays and SERS tests were carried out with sequential oxygen etches enabling the precise diamond over-layer thickness to be controlled. Using this approach exact control over NP size and spacing can be achieved. Excellent SERS performance results; the prospects for these robust diamond SERS substrates in challenging environments will be addressed.

EQ07.08.15

Mechanical Properties of Pentadiamond—A Combined DFT and Reactive Molecular Dynamics Investigation Levi C. Felix¹, Raphael M. Tromer¹, Cristiano F. Woellner², Chandra Sekhar Tiwary³ and [Douglas S. Galvao](#)¹; ¹State University of Campinas, Brazil; ²Federal University of Paraná, Brazil; ³Indian Institute of Technology Kharagpur, Brazil

Recently, a new carbon allotrope called pentadiamond was proposed [1]. It consists of a network of pentagonal rings where both sp² and sp³ hybridization are present. Recent works have shown that pentadiamond presents thermoelectric and optoelectronic [1,2] properties. 3D-printed pentadiamond structures [3] also exhibit the same topology-dependent mechanical behavior of the atomic model. In this work [4], we investigated the mechanical and electronic properties and the thermal stability of pentadiamond using DFT and fully atomistic reactive molecular dynamics (MD) simulations. The mechanical behavior, beyond the elastic regime, was investigated for three deformation modes: compression, tensile, and shear. Under compressive deformation, strong fluctuations in the atomic positions appear, which are responsible for the strain-softening at strains beyond the linear regime. These characterize its plastic flow. As expected, as we increase temperature, Young's modulus values decrease, with changes (up to 300 K) smaller than 10% (from 347.5 to 313.6 GPa). The fracture strain values present a broader variation, from ~44% at 1K to ~5% at 300K.

[1] Y. Fujii, M. Maruyama, N. T. Cuong, and S. Okada, *Phys. Rev. Lett.* 125, 016001 (2020).

[2] R.M. Tromer, L.C. Felix, C.F. Woellner, D.S. Galvao, *Chemical Physics Letters*, 763, 138210 (2020).

[3] L.C. Felix, R.S. Ambekar, C.F. Woellner, B. Kushwaha, V. Pal, D.S. Galvao and C.S. Tiwary, arXiv:2105.10000 (2021)

[4] L.C. Felix, R.M. Tromer, C.F. Woellner, C.S. Tiwary and D.S. Galvao, *Physica B: Condens. Matter Physica B: Condensed Matter* 629, 413576 (2022)

EQ07.08.16

Detailed Atomic Structure Analyses of N-Doped NanoDiamonds [Raul Arenal](#)^{1,2,3}, Fredrik S. Hage⁴, Quentin Ramasse⁴ and Dieter Gruen⁵; ¹Instituto de Nanociencia y Materiales de Aragon (INMA), CSIC-U. Zaragoza, Spain; ²Universidad de Zaragoza, Spain; ³ARAID Foundation, Spain; ⁴SuperSTEM Laboratory, United Kingdom; ⁵Argonne National Laboratory, United States

Ultrananocrystalline diamond (UNCD) film is a crystalline diamond film consisting of 3-5 nm randomly oriented diamond crystallites surrounded by 0.2-0.3 nm wide grain. These films possess exemplary mechanical, electronic and optical properties [1,2]. Under normal process conditions, these UNCD films are highly electrically insulating, but they can become highly conducting when Ar is substituted in the synthesis gas with some N₂ [1, 5]. In this contribution, we have revisited, using aberration corrected microscopes and combining HR(S)TEM and EELS, the structure and local composition of these n-type UNCD films [3-5].

n-type UNCD films are composed of elongated diamond nanocrystals (called nanowires (NWs) [3]). The formation of these NWs is initiated when the N₂ content in the gas phase reaches about 10% in volume. From these studies, we concluded that the insulator-metal transition of these films is strongly correlated with the formation of these diamond NWs. Indeed, these NWs are enveloped by a sp²-based carbon layer that seems to provide the conductive path for electrons [3-6]. Thus, here we will present the atomic structure studies and local EELS analyses developed on these complex films [5]. These results show where the nitrogen is located into these nanostructures and provide insights into their atomic configuration. These aspects provide very important information about the role played by nitrogen in the formation of such nano-objects.

In summary, these studies elucidate crucial questions concerning the local composition (atomic configuration) of these materials. This detailed knowledge is essential for better understanding the outstanding properties of such materials as well as for shedding light on their growth mechanism.

References

[1] O.A. Shenderova & D.M. Gruen, UNCD: synthesis, properties & applic. William Andrew. (2012).

[2] R. Arenal, Review paper, to be submitted.

[3] R. Arenal, P. Bruno, D.J. Miller, M. Bleuel, J. Lal, D.M. Gruen, *Phys. Rev. B* 75, 195431 (2007).

[4] R. Arenal, O. Stephan, P. Bruno, D.M. Gruen, *Appl. Phys. Lett.* 94, 111905 (2009).

[5] R. Arenal, F. Hage, Q.M. Ramasse and D.M. Gruen, to be submitted.

[6] Research supported by the MICINN (project grant PID2019-104739GB-I00/AE1/10.13039/501100011033), Government of Aragon through project DGA E13_20R (FEDER, EU) and European Union H2020 program "ESTEEM3" (823717).

EQ07.08.18

HPHT Growth of High-Quality Diffraction Grade Diamond Substrates for X-Ray Optics Ilya Ponomarev¹, Boris Feigelson², Jeffrey J. Derby³, Scott S. Dossa³, Marc Hainke⁴, Christian Kranert⁴ and Jochen Fredrich⁴; ¹Euclid Beamlabs LLC, United States; ²U.S. Naval Research Laboratory, United States; ³University of Minnesota, United States; ⁴Fraunhofer IISB, Germany

Next-generation of synchrotron and Free-Electron Laser X-ray sources will increase the peak power by several orders of magnitude. In these conditions, X-ray intensity will become too severe for the existing materials. Large, single-crystal diamond is one of the few materials, if not the only one, suitable for high-power X-ray optical applications due to its unique combination of high thermal conductivity, low thermal expansion, and low X-ray absorptivity. We developed the modified High-Pressure High-Temperature (HPHT) temperature gradient growth technology that allows for growing the highest crystalline quality large diamond crystals, with dislocation density of less than 10 cm^{-2} . This near-equilibrium process is carried out under extreme conditions, where diamond single crystals are grown from a molten metal solvent (Fe, Ni, and Co and their alloys) under pressures in excess of 5 GPa and temperatures of 1,600 K and higher. Since there are no available diagnostics to monitor crystal growth in the HPHT cell directly, both indirect experimental growth monitoring and faithful models are needed to connect experimental outcomes to system design and process conditions. We present initial results from a collaboration that includes experimental growth carried out at the Euclid Beamlabs and two modeling efforts by the University of Minnesota and Fraunhofer. X-ray white beam topography of grown crystals is also discussed. This two-fold approach provides rigorous tools to both understand growth in this system and to perform subsequent optimization of growth conditions. In particular, we aim to more fully understand fundamental aspects of diamond nucleation and growth and identify process conditions that will achieve the highest crystalline quality in large diamond crystals.

EQ07.08.19

Steady State, Modulated and Transient Surface Photovoltage Spectroscopy of Diamond Thomas Dittrich¹, Steffen Fengler², Arsène Chemin¹, Peter Knittel³, Igal Levine¹ and Tristan Petit¹; ¹Helmholtz-Zentrum Berlin for Materials and Energie, Germany; ²Helmholtz-Zentrum hereon GmbH, Germany; ³Fraunhofer Institute for Applied Solid State Physics, Germany

Diamond is a promising material for applications in fields of electronics, optoelectronics, spintronics, energy conversion etc. For further development and deeper understanding, there is a need for highly sensitive and contactless characterization of electronic transitions and transport phenomena in single crystal and nanocrystalline diamond and at diamond interfaces. Light induced charge separation in space causes a surface photovoltage (SPV) on photoactive materials which can be studied with highly sensitive techniques such as steady state, modulated and transient SPV spectroscopy [1]. Recently, we developed a charge amplifier in combination with a perforated electrode that allows for complex SPV spectroscopy measurements on ultrawide bandgap semiconductors in dc (Kelvin probe), ac (modulated and transient) regimes at photon energies from near infrared to deep ultraviolet [2] [3] [4]. In this work, measurement principles of steady state, modulated and transient SPV spectroscopy will be explained, highlighting the high sensitivities of these techniques. Examples will be demonstrated for numerous transitions around and below the band gap of diamond which have been distinguished for differently terminated single crystal, polycrystalline and nanocrystalline diamond samples.

Acknowledgement: S. F. and I. L. are grateful to the BMWi (ZIM-KK-5085302DF0 and ZIM-KK-5123601DF0, respectively).

[1] Th. Dittrich, S. Fengler, Surface photovoltage analysis of photoactive materials, World Scientific, 2020.

[2] Th. Dittrich, S. Fengler, N. Nickel, Surface photovoltage spectroscopy over wide time domains for semiconductors with ultrawide bandgap: example of gallium oxide, Phys. Stat. Sol. A 11 (2021) 2100176.

[3] Th. Dittrich, Transient surface photovoltage spectroscopy of diamond, AIP Advances 12 (2022) 065206.

[4] Th. Dittrich, S. Fengler, Transitions in polycrystalline diamond probed by steady state, modulated and transient surface photovoltage spectroscopy, 2022 (submitted).

EQ07.08.20

Using Image Based Artificial Intelligence for *In Situ* Growth Prediction of Single Crystalline Diamond as a Tool to Improve SCD Wafer Dimensions and Growth Yield Matthias Muehle¹, Rohan Reddy¹, Arjun Srinivasan¹ and Elias Garratt²; ¹Fraunhofer USA, United States; ²Michigan State University, United States

Single crystal diamond (SCD) is an attractive wide bandgap semiconductor material for a variety of applications ranging from advanced optics, solid state electronics to thermal management solutions. While lab-scale prototype demonstrations have demonstrated superior performance, utilizing diamond has been prohibitively expensive compared to more mature, commercialized semiconductor materials. This is attributed to the fact the SCD wafer size of suitable quality is smaller than 1 inch, and often as little as small as 3 mm x 3mm. For comparison, the commercially available wafer size for single crystalline Silicon Carbide is beyond 6 inches. A direct result is a lack of process scaling when processing individual diamond applications. The only way to overcome this is by controlling the size and quality of SCD wafers during chemical vapor deposition (CVD) growth to enable realization of wafers 2 inches in size and beyond either. This type of process control can be applied either for epitaxial layer outgrowth, or for tiled wafer growth. We are envisioning to address this challenge by developing an artificial intelligence (AI) based algorithm to predict SCD growth states (size and quality) through use of in-situ RGB images. Once established, this AI growth prediction can be incorporated as control system to increase SCD wafer size and quality, by adjusting process conditions before they achieve critical turnover points.

We are reporting on our efforts on AI algorithm development and validation. First, we installed a full-frame mirrorless interchangeable lens camera equipped with a macro lens to a CVD diamond reactor. Then a cumulative image-based AI pipeline consisting of three inter-connected thrusts was developed to model diamond growth. These are 1) Feature extraction pipeline, for extraction of geometrical features in the recorded imaged, 2) Defect detection pipeline, to extract macroscopic defect features in the recorded images, and 3) Frame prediction pipeline utilizing features, defects and reactor telemetry, to predict future image states 6, 8 and 12 hours into the future.

The objective for the feature extraction pipeline was to isolate and classify accurate pixel masks of geometric features like diamond, pocket holder and background, and their translation into geometrical shapes without the need of human-generated input. Our approach was enhanced to deliver results with high precision within the constraints of being limited to low-volume high-feature-complexity training dataset environments, given that data procurement, requiring physical SCD growth, is extremely time-consuming and expensive. Our best performing DL-based model achieved excellent accuracy metrics of >98% for the pocket holder, diamond top and diamond side features. Similarly, our DL-based defect detection pipeline achieved excellent accuracy metrics (>95%) for detecting center, polycrystalline and edge defects.

Prediction accuracies of ~99.9999% were obtained with minimal information loss between predicted and actual outputs. This constitutes a never-before obtained result of spatiotemporal (AI) prediction of diamond shape from in-situ obtained growth data obtained based on few inputs from data collected within an hour apart. This demonstrates the potential of these algorithms as a machine-intelligence-enabled solution for automated optimization and control of the diamond growth process.

EQ07.08.21

Quantum Diamond Magnetometer Sensitivity Optimized via Supervised Machine Learning Dane W. DeQuilletes, Eden Price and Danielle Braje; Massachusetts Institute of Technology, United States

Defect centers in diamond have the potential to revolutionize the fields of quantum sensing, computing, and communication with the capability to operate at room temperature. For example, defects such as NV (nitrogen-vacancy), SiV, and SnV have already established new performance benchmarks in magnetometers and quantum repeaters. Currently, many of these defects are introduced through destructive methods such as ion implantation where the introduction of unwanted defects leads to poor coherence properties and spectral wandering. Instead, plasma enhanced chemical vapor deposition (PE-CVD) offers an alternative route to achieve higher quality quantum properties from the bottom up, but the large PE-CVD growth parameter space makes it difficult to grow in desirable defects while avoiding formation of others. Here, we develop and apply a supervised machine learning approach with Shapley-based importance ranking and Bayesian optimization to determine the ideal growth parameters that lead to the highest NV⁻ defect yield and best magnetometer sensitivity. Using 15 processing conditions and >100 N-doped diamond samples as a training-test set, we reveal growth temperature and irradiation dose fraction (i.e. V/N_s) as key processing parameters. This work establishes a new methodology to optimize NV defects for magnetometry applications and a starting point for more sophisticated engineering of quantum defects for various quantum technologies.

SESSION EQ07.09: Quantum Applications II
Session Chairs: Philippe Bergonzo and Christian Osterkamp
Wednesday Morning, November 30, 2022
Sheraton, 2nd Floor, Independence East

8:30 AM EQ07.09.01

Precise Current Monitoring over a Wide Dynamic Range for Electric Vehicle Batteries Using Diamond Quantum Sensors Yuji Hatano¹, Jaewon Shin², Junya Tanigawa², Yuta Shigenobu¹, Akimichi Nakazono², Takeharu Sekiguchi¹, Shinobu Onoda³, Takeshi Ohshima³, Takayuki Iwasaki¹ and Mutsuko Hatano^{1,3}; ¹Tokyo Institute of Technology, Japan; ²Yazaki Corporation, Japan; ³National Institutes for Quantum Science and Technology, Japan

Diamond quantum sensors with NV centers potentially have high sensitivity and a wide dynamic range. This feature is advantageous for EV battery monitoring applications. The peak value of EV battery current reaches \pm several hundred amperes. So far, the accuracy of commercially available current sensors with a measurement range of \pm several hundred amperes is about 1 A. On the other hand, the average battery current over the driving hours is about 10 A. Therefore, about a 10% margin is required in the remaining cruising mileage estimation. If the accuracy of the current sensor can be improved to 10 mA while maintaining a maximum range of \pm several hundred amperes, the state of charge (SOC) of the EV battery can be accurately determined and the EV's cruising mileage can be extended by 10%.

In our prototype battery current monitor, a diamond sensor bonded to the end of an optical fiber was attached close to a copper busbar of 20 mm width and 8 mm thickness. The diamond sensor is a $2 \times 2 \times 1$ mm³ type Ib (111) crystal treated by 3×10^{18} cm⁻² EB irradiation and 1000°C annealing for 2 hours. The sensor contains 5-6 ppm NV⁻ centers. A two-tone microwave is applied to the diamond sensor through a copper tape adhered to the sensor. The change in the fluorescence in response to the microwave frequency is the Optically Detected Magnetic Resonance (ODMR) spectrum.

The magnetic field is measured as the resonance frequency difference, that is, the difference between the low and high resonance frequencies in the ODMR. The (111) plane of the diamond sensor is placed perpendicular to the busbar surface as well as parallel to the current direction. The magnetic field at the diamond sensor position caused by the 10 mA busbar current is 170 nT. The sensitivity of 5 nT/ $\sqrt{\text{Hz}}$ enables the 10 mA detection in 1 kHz bandwidth. Three key points to ensure accuracy is as follows:

(1) Differential measurement

Differential measurement using a pair of diamond sensors placed above and below the busbar allows excluding external noise as common mode. Another purpose of the differential measurement is the elimination of the static magnetic field fluctuation caused by the temperature change. Two neodymium magnets are placed several centimeters apart from each other to provide about 20 mT static magnetic field at the diamond sensor so that the low and high resonance frequencies are separated even at the busbar current of \pm several hundred amperes. Two diamond sensors are placed at the midpoint between these magnets, symmetrically positioned vertically across the busbar, so that the static magnetic fields applied to the two sensors are equal. This also eliminates the effect of the static magnetic field change due to the temperature change as common mode.

(2) Stable tracking of resonance frequency

The narrowness of the ODMR linewidth enables to follow the resonance frequency sharply by analog feedback from the photodiode output to the frequency modulation input of the microwave oscillator. On the other hand, the feedback is stable only within the linewidth. Therefore, the carrier frequency of the microwave oscillator should be intermittently adjusted so that the FM modulation amount be kept within the linewidth.

(3) Suppression of transverse magnetic field

To keep precise linearity between the resonance frequency difference and the busbar current, the transverse magnetic field applied to the [111] NV-axis by the busbar current should be minimized. For that purpose, the (111) plane should be carefully aligned perpendicular to the busbar surface as well as parallel to the current direction.

This work was supported by the MEXT Q-LEAP (JPMXS0118067395).

8:45 AM EQ07.09.02

Relaxation Mechanisms of Single Dark Spins in Diamond Jonathan C. Marcks¹, Mykyta Onizhuk^{1,1}, Yuxin Wang¹, Nazar Deegan^{2,2,1}, Masaya Fukami¹, Maya Watts¹, F. J. Heremans^{2,2}, Aash Clerk¹, Giulia Galli^{1,1,2} and David Awschalom^{1,2,2}; ¹The University of Chicago, United States; ²Argonne National Laboratory, United States

Decoherence of nitrogen vacancy (NV) centers limits sensitivity in magnetometry applications ranging from nanoscale NMR to navigation. A main source of decoherence arises from the substitutional nitrogen electron spin (P1 center) bath in the diamond lattice. Much effort has focused on decoupling NV and P1 spin interactions, but a full description of the underlying bath evolution remains incomplete. Here, we study interactions of a single P1 center with surrounding bath spins using a nearby NV center as a polarization source and probe. We present time-resolved measurements of the spin under external

laser and microwave excitation, revealing charge and spin dynamics at a single-P1 level. Alongside experiments we perform cluster correlation expansion (CCE) calculations to determine the structure of our spin bath, demonstrating characterization methods that account for local disorder.

9:00 AM EQ07.09.03

Manipulating Spins in Diamond with Magnetoelastic Films Nathaniel Beaver¹, Bin Luo¹, Seyed M. Abrishami¹, Isabel Martos-Repath¹, Piyush J. Shah², Derek A. Bas², Michael Page², Nian Sun¹ and Paul Stevenson¹; ¹Northeastern University, United States; ²U.S. Air Force, United States

Nitrogen Vacancy (NV) centers in diamond are extraordinarily sensitive magnetometers, capable of resolving picotesla fields. However, the large microwave fields required to control and manipulate the NV center can perturb the sensing target and are an obstacle to real-world deployment, motivating the development of new, efficient, control schemes. Using strain-generated magnetic fields in magnetoelastic (ME) films is a promising approach to addressing these challenges; highly localized magnetic fields can be efficiently generated, reducing power requirements and minimizing sample perturbation. However, the device requirements of NV center sensors are distinct from conventional applications of ME films, requiring new approaches to design and utilization.

In this talk, I will share recent results where coupled surface acoustic wave devices and ME films are used to drive spin transitions in the NV center. Our results highlight the strengths – and limitations – of these devices, revealing the interplay of efficient spin manipulation and increased noise from the magnetoelastic film, and enabling us to outline design principles for constructing hybrid NV center-ME film sensors.

9:15 AM EQ07.09.04

Ab-Initio Theory of Spin-Lattice Relaxation for NV Center in Diamond Gergo Thiering^{1,2}, Matt Cambria³, Shimon Kolkowitz³, Ishita Kemeny³, Ariel Norambuena⁴, Yanfei Li³, Aedan Gardill³, Hossein Dinani⁴, Vincenzo Lordi³, Jerónimo Maze⁶ and Adam Gali^{1,2}; ¹Wigner Research Centre, Hungary; ²Budapest University of Technology and Economics, Hungary; ³University of Wisconsin-Madison, United States; ⁴Universidad Mayor, Chile; ⁵Lawrence Livermore National Laboratory, United States; ⁶Pontificia Universidad Católica de Chile, Chile

Certain defects in diamond are promising candidates as building blocks for quantum information processing. In particular, the nitrogen-vacancy (NV) center in diamond has become one of the leading solid-state qubit contenders to its favorable properties. One of the most remarkable properties is its long spin coherence time: it can reach 1 ms at room temperature and can exceed seconds at cryogenic temperatures. In our present work, we will describe the spin-lattice interaction between S=1 electronic spin of NV center and the lattice phonons by means of density functional theory and experiments for a temperature range between 9 to 474 K in high-purity diamond samples. Spin-lattice relaxation is an intrinsic property of the host material and the defect that can be less obviously engineered like the coherence times by isotope engineering of the host material. As T₁ time is an ultimate limit for the spin coherence, deep insight about the spin-lattice relaxation processes is necessary for control of the NV center and understand this process for akin color centers in solids. Here, we review the first order and second order (Raman) spin-phonon relaxation processes acting between NV center's $|ms = 0\rangle \leftrightarrow |ms = +1\rangle \leftrightarrow |ms = -1\rangle$ spin states. To our best knowledge, only the ultralow temperature regime below 1 K has been discussed for NV center at ab-initio level, to date [1]. In this paper, we discuss the second order Raman transitions that dominate relaxation at high temperatures which is in stark contrast to the case of small molecules [2]. By invoking the ab-initio spin-phonon spectral functions, we propose a novel analytic model in which NV spin-phonon relaxation is characterized by interactions with two distinct groups of quasilocalized phonons which can be described as a double Orbach-process. In summary, we developed an ab-initio framework that can predict the spin-relaxation times and associated limit of coherence times for any spin-1 qubit center in diamond and related materials.

A. G. acknowledges support from the National Research Development and Innovation Office of Hungary within the Quantum Technology National Excellence Program (Project Contract No. 2017-1.2.1-NKP-2017-00001) and the National Excellence Program (Project No. KKP129866) and the Quantum Information National Laboratory sponsored via the Ministry of Innovation and Technology of Hungary, and the European Commission of H2020 ASTERIQS project (Grant No. 820394). We thank the National Information Infrastructure Development Program for the high-performance computing resources in Hungary. G. T. were supported by the János Bolyai Research Scholarship of the Hungarian Academy of Sciences. The acknowledge the high-performance computational resources provided by KIFÚ (Governmental Agency for IT Development) institute of Hungary. Part of this work was performed under the auspices of US DOE by LLNL under Contract DE-AC52-07NA27344.

9:30 AM BREAK

SESSION EQ07.10: Sensing II and Devices I
Session Chairs: Anke Krueger and Emmanuel Scorsone
Wednesday Morning, November 30, 2022
Sheraton, 2nd Floor, Independence East

10:00 AM *EQ07.10.01

Diamond Particles Incorporated Fiber-Optic Probes for Biosensing Purposes Monika Janik^{1,2}, Mateusz Ficek¹, Maciej Glowacki¹, Mateusz Smetana² and Robert Bogdanowicz^{1,2}; ¹Gdansk Univ of Technology, Poland; ²Warsaw University of Technology, Poland

Integration of nanodiamonds with glass fibers is a powerful method of scaling diamond biosensing functionality. In this overview, we report on the volume incorporation approach for the integration of nanodiamond particles with optical fibers and coating with diamond particles to tailor optical sensing properties. The 750 nm and 140 nm diameter diamond particles were applied in those procedures. Manufactured optical fiber probes were analyzed using Raman mapping, SEM, optical and fluorescence spectra. SEM analysis reveals distinctly that the majority of the glass area is covered with single, separated diamond particles. Nanodiamond-doped fiber cross-section revealing a homogenous glass structure with incorporated sectionally nanodiamond particles. Diamond particles are tightly included in the glass structure with a mean adjacent distance of approx. 2.5 μm. Core-incorporated diamond particles allow to guide its fluorescence along the fiber is sensitive to the external environment. Diamonds deposited on the surface of optical-fiber probes tailor their transmittance and provide the interface for biosensing enhancing both optical and electrochemical responses. Following dedicated experimental work, doped diamond particles have the potential of extending the existing models with practical ways of optimizing signal coupling and readout to the guided modes in optical fiber-based biosensing probes.

10:30 AM EQ07.10.02

Multifunctional Diamond Sensor for Deep Ocean Deployment Ralph Jennings-Moors and Richard B. Jackman; Univ College London, United Kingdom

Sequestration of CO₂ in the planets oceans is one approach under consideration as humankind flights to tackle climate change. In this process CO₂ would be pumped to depth greater than 3km where it liquefies and, as it is heavier than water would form permanent lakes on the ocean floor. The potential for CO₂ storage this way is enormous. However, our oceans naturally contain CO₂ at shallow depths and this has the effect of mild acidification of the marine environment - if the acidification is allowed to increase, severe adverse effects on marine life will result. Thus, there is a real need to monitor the pH of oceans over large areas and at many depths should CO₂ sequestration technology become a reality. At present this involves the temporary deployment of large expensive equipment in limited regions of our seas. With the emergence of the internet-of-things (IoT) the concept of a permanently deployed more intelligent far-reaching network of ocean sensors has emerged - should such devices be sufficiently small and robust they could stay in position for years, occasionally rising to the surface to relay data bursts. Diamond is an ideal material for sensor fabrication that must survive in harsh environments and diamond pH sensors have been demonstrated by a number of groups. However, the real value for such devices lies in a multifunctional sensors within a robust housing with encased control electronics for remote operation. Moreover, most sensors demonstrated with diamond technology to date rely upon metal contacts on the sensor face that would readily corrode in the marine environment.

In this paper we show the design and realisation of a diamond sensor with housing suitable for high pressure deployment, where the ocean only sees a diamond face for the sensor. Real-time measurement of pH, dissolved oxygen, water resistivity and temperature are achieved. At the heart of this sensor technology lies conductive patterns of graphitic-like material within the diamond created by a laser direct write-process. The prospects for these devices will be discussed.

10:45 AM EQ07.10.03

Nanocrystalline Diamond Nano-Mechanical Resonators Evan Thomas, Soumen Mandal, William Leigh and Oliver A. Williams; Cardiff University, United Kingdom

Nano-electro-mechanical systems (NEMS) incorporating miniature scale mechanical elements into electronic circuits are of interest in applications ranging from atomic resolution mass spectrometers¹ to single electron spin detectors². For resonating structures, the frequency of operation is proportional to the acoustic velocity of the material from which they are fabricated, making diamond with its unrivalled value of 18000 m/s ideally suited for use in high frequency NEMS with minimal dissipation from scaling induced losses. While offering the benefits of diamond but in thin-film form, the use of nanocrystalline diamond (NCD) for smaller scale NEMS however is often prohibited by its considerable columnar growth induced roughness, complicating fabrication and resulting in significant surface associated dissipation³. In addition, the concentration of strain at the attachment points of typically used geometries is expected to radiate energy away from the device and lead to substantial loss that scales with frequency⁴. Through combining the use of chemical mechanical polished (CMP) stock with advanced geometries it is therefore expected that dissipation can be minimised in thin-film diamond based NEMS⁵.

To this end, metallised doubly clamped and 'free-free' geometry resonators incorporating flexural supports were fabricated from intrinsic NCD films with and without CMP. The devices were then placed in a Quantum Design Physical Property Measurement System at cryogenic temperatures, and actuated magnetotomically through sweeping the frequency of an applied AC signal while in the presence of a static magnetic field^{6,7}. Upon comparing the resulting resonances, a ~5-fold reduction in dissipation was observed upon switching from rough to polished films and the addition of 2nd mode flexural supports, highlighting the benefits of CMP and the use of anchor-loss minimising geometries.

References

1. K. Jensen, *et al. Nat Nano.* **3** (2008), 533-537.
2. D. Rugar, *et al. Nature* **430** (2004), 329-332.
3. X. M. H. Huang, *et al. New J. Phys.* **7** (2005), 247.
4. M. Imboden, *et al. Appl. Phys. Lett.* **90** (2007), 173502.
5. E. L. H. Thomas, *et al. Carbon* **68** (2014), 473-479.
6. K. L. Ekinici, *et al. Appl. Phys. Lett.* **81** (2002), 2253-2255.
7. T. Bautze, *et al. Carbon* **72** (2014), 100-105.

SESSION EQ07.11: Devices II

Session Chairs: Philippe Bergonzo and David Storm
Wednesday Afternoon, November 30, 2022
Sheraton, 2nd Floor, Independence East

1:30 PM EQ07.11.01

3659 V 0.37 A/mm NO₂-Doped P-Channel Diamond MOSFETs Fabricated on Diamond Grown on Misoriented Sapphire Substrates Niloy C. Saha¹, Seong W. Kim², Koji Koyama², Toshiyuki Oishi¹ and Makoto Kasu¹; ¹Saga University, Japan; ²Adamant Namiki Precision Jewel Co., Ltd., Japan

Diamond is an ultra-wide-gap semiconductor for prospective high-power and high-frequency transistors, because it possesses high bandgap energy of 5.47 eV and a breakdown field of >10 MV/cm. A 1-inch-diameter diamond wafers were grown on (11-20) sapphire just substrate without cracking using the micro-needle technique [1]. Very recently, we have demonstrated a 2-inch-diameter (001) diamond wafer without cracking by using a misoriented (11-20) sapphire substrate. The diamond wafer showed the highest crystal quality; the lowest XRC FWHM of 98 arcsec and low dislocation density of $1\sim 2 \times 10^7$ cm⁻² [2]. In this study, we fabricated a NO₂-doped p-channel diamond MOSFETs on a high-quality misoriented diamond substrate, which showed the highest breakdown voltages of 3659 V among diamond FETs.

We used a (001) diamond as a substrate which was grown on a misoriented (11-20) sapphire substrate by 5° toward the [0001] c-direction. The H-terminated diamond substrate was exposed to 2% NO₂ gas diluted in N₂ to perform NO₂ p-type doping. After forming Au ohmic contact, 16-nm-thick Al₂O₃ bi-layer was deposited as a gate insulator layer, and Au gate was formed with a gate length (L_G) of 2 μm with gate-to-drain distance (L_{GD}) varied from 12 μm to 50 μm. Finally, the diamond p-channel was passivated with 16-nm-thick Al₂O₃ bi-layer.

The DC output characteristics of a MOSFET showed a maximum drain current of 372 mA/mm. The gate leakage current was <10⁻⁴ mA/mm and an on/off ratio was determined as 10⁷. The on-resistance was 98.3 Ωmm and transconductance was obtained as 81 mS/mm at V_{GS} of -3 V. The threshold voltage was 4.1 V indicative of normally-ON operation. The maximum field-effect mobility was estimated as 134 cm²/Vs. The maximum off-state breakdown voltage reached 3659 V, which is the highest for diamond FETs.

[1] S.-W. Kim, Y. Kawamata, R. Takaya, K. Koyama, and M. Kasu, *Appl. Phys. Lett.* **117**, 202102 (2020).

[2] S.-W. Kim, R. Takaya, S. Hirano and M. Kasu, *Appl. Phys. Express* **14** 115501 (2021).

1:45 PM EQ07.11.02

Normally-Off Operation in (001) Vertical Diamond MOSFET Using Oxidized Si Termination Diamond Channel Kosuke Ota, Yu Fu, Kento Narita, Chiyuki Wakabayashi, Atsushi Hiraiwa and Hiroshi Kawarada; Waseda University, Japan

The development of p-FETs corresponding to n-FETs is necessary to realize compact, high-power high-speed switching complementary inverters. To date, n-FETs using wide bandgap semiconductor materials such as GaN, SiC, and Ga₂O₃ have been studied extensively, but there are few reports on p-FETs. We have reported vertical diamond MOSFETs using 2-Dimensional Hole Gas(2DHG) which is induced independently of crystal orientation by hydrogen terminated diamond surface(C-H) and high-temperature ALD-Al₂O₃[1-4]. However, all conventional vertical diamond MOSFETs use C-H surface as channel and exhibit normally-on operation (+16 V ~ +30 V) with positively large threshold voltage, and normally-off operation has not been achieved[1-4]. Normally-off operation is essential for industrial power electronic application, and we have already demonstrated normally-off operation in lateral diamond FETs using oxidized Si terminated (C-Si-O) diamond as channel[5-7] which can be applied to vertical devices. In this study, we have fabricated (001) vertical diamond MOSFET with C-Si-O diamond channel and achieved the first normally-off operation(-10.2 V) in vertical diamond FETs. Fabrication process is as follows. A total of 1.5 μm of nitrogen-doped layer was deposited on the (001) p⁺ diamond substrate as current blocking layer by microwave plasma chemical vapor deposition(MPCVD), and trench with depth(W_T) of 3 μm was formed by inductively coupled plasma reactive ion etching(ICP-RIE). After trench formation, a 200 nm regrown undoped layer was deposited by MPCVD to induce 2DHG. Then, SiO₂ was deposited 300 nm as a mask by tetraethyl orthosilicate CVD, and the p⁺⁺ layer(B): 1×10²¹ cm⁻³ was deposited by MPCVD after etching 300 nm of SiO₂ and 40 nm of the Regrown layer in the p⁺⁺ layer growth area by ICP-RIE. At this time, C-Si-O diamond channel was formed by SiO₂ and diamond reaction in reductive and high temperature atmosphere(~1223 K). After SiO₂ mask removal by HF and ICP-RIE, device isolation was performed by oxygen plasma. Then, the source electrode(Ti/Pt/Au) was formed, and 200 nm of Al₂O₃ was deposited as the gate insulator by high-temperature ALD method(450°C) using H₂O as the oxidant. Finally, drain electrode(Ti/Au) was formed on the backside of the substrate and gate electrode(Al) on the surface of the substrate to complete the device.

The lengths of source-source(L_{SS}), source-drain(L_{SD}), effective channel(L_{CH}), gate-drain(L_{GD}), trench width(W_T), and gate width(W_G) were 18 μm, 9.2 μm, 8.8 μm, 0.4 μm, 6 μm, and 25 μm, respectively. The maximum drain current density(I_{D,max}) by the gate width was 8.05 mA/mm. The gate leakage current was less than 10⁻⁹ A at 300 K and on-off ratio was 10⁷. The threshold voltage(V_{th}) was -10.2 V, achieving normally-off operation. For device with different dimensions (L_{SS}: 8 μm, L_{SD}: 9.2 μm, L_{CH}: 8.8 μm, W_T: 4 μm), I_{D,max} was 102 mA/mm, R_{on} was 258 Ω mm, and V_{th} was -1.9 V, confirming normally-off operation. Compared to the threshold voltage of the conventional vertical C-H diamond MOSFET, the threshold voltage was shifted in the negative direction by more than 15 V. This large negative shift of the threshold voltage can be attributed to decrease upward band bending between diamond and Al₂O₃ due to increase the electron affinity of the C-Si-O interface (-0.25 eV)[8] compared to that of the C-H interface (-1.3 eV)[9].

- [1] N. Oi, H. K. et al., Scientific reports, 8(1), 1-10(2018).
- [2] J. Tsunoda, H. K. et al., Carbon 176, 349-357(2021).
- [3] J. Tsunoda, H. K. et al., IEEE TED, 68(7), 3490-3496(2021).
- [4] J. Tsunoda, H. K. et al., IEEE EDL, 43(1), 88-91(2021).
- [5] W. Fei, H. K. et al., APL, 116(21), 212103(2020).
- [6] Y. Fu, H. K. et al., IEEE TED, 69(5), 2236-2242(2022).
- [7] X. Zhu, H. K. et al., Appl. Sur. Sci., 593, 153368(2022).
- [8] A. Schenk, C. I. Pakes et al., J. Phys., Conds. Matt, 29, 025003(2017).
- [9] H. K. et al., Sci. Rep, 7, 42368(2017).

2:00 PM EQ07.11.03

1.6K Operation of Diamond FETs with Superconducting Diamond Sources and Drains Targeting JoFET or SCFET Operation Chiyuki Wakabayashi¹, Yasuhiro Takahashi¹, Taisuke Kageura^{1,2}, Minoru Tachiki³, Shuuichi Ooi², Shunichi Arisawa², Yoshihiko Takano² and Hiroshi Kawarada^{1,4}; ¹Waseda University, Japan; ²National Institute of Advanced Industrial Science and Technology (AIST), Japan; ³National Institute for Materials Science, Japan; ⁴The Kagami Memorial Research Institute for Materials Science and Technology, Japan

Superconducting currents are induced in the semiconductor channels of Josephson field-effect transistors (JoFETs) or Superconductor FETs (SCFETs) by the proximity effect from the superconductor. The carrier depletion or accumulation induced by the applied gate electric field control the critical currents of them. For example, JoFETs or SCFETs are realized by using Al contacts and Ge channels [1]. They can be applied for ultra-high speed and ultra-low power consumption operation of transistors. Furthermore, JoFETs can be used to call the Qubits of quantum computers in cryogenic environments. Boron-doped diamond exhibits superconductivity, with its superconducting transition temperature T_c of 10 K at its boron concentration of 1×10²² cm⁻³ [2] and a few types of Josephson junctions and superconducting quantum interference devices were realized [3][4]. Also, diamond is known as a wide-gap semiconductor. Therefore, it is possible to realize hybrid devices of superconductors and semiconductors with the same material.

We fabricated diamond FETs composed of 2DHG channels induced by hydrogen termination and ALD-Al₂O₃, and Superconducting diamond contacts which were homoepitaxially grown by microwave plasma chemical vapor deposition. The channel length L_{sd} were miniaturized down to 100 nm. The gate width W_g was 100 μm. The insulator Al₂O₃ was deposited by atomic layer deposition method with 10 nm at 573K. The Al gate electrode was deposited by Electron Beam vapor deposition with 100 nm. We evaluated low temperature operations of 2DHG diamond FETs down to 1.6 K with four terminal methods by applying a current instead of a voltage to examine the possibility of realization of JoFETs or SCFETs.

The I-V characteristics of the FET with L_{sd} = 100 nm and W_g = 100 μm were obtained at 1.6 K, 8 K and 12 K. We applied current I_{ds} = 10 μA, 100 μA respectively and applied gate voltage V_{gs} from -3.5 V to 1.0 V in 0.5 V increments. The drain current I_{ds} were modulated by applied gate voltage clearly. It is the first demonstration of diamond FET operated below 2K. The on-resistance R_{on} was 7.9 Ω·mm at 1.6 K at V_{gs} = -3.5 V. This value is about one-fourth of that at 12 K. That's because 1.6 K is well below the superconducting diamond T_c (~10 K) and the resistance of the superconducting diamond source and drain was disappeared. Also, it is possible that the proximity effect from superconducting diamond reduced the resistance of the semiconductor channel. Furthermore, we obtained R-T characteristics from 1.6 K to 12 K by applying bias current of 10 μA at V_{gs} = 0 V, -3.5 V respectively. When the gate voltage was not applied, the resistance drops around 10 K (~T_c) but increase remarkably as the temperature goes down from 10 K. This is because, the barrier of valence band maximum between boron-doped diamond and 2DHG diamond becomes prominent due to the lower temperature (1.6K). However, the increase of the resistance from 10 K down to 1.6 K was reduced by applying gate voltage since the carrier accumulation due to the applied gate voltage cause band bending and holes tunnel through the barrier. In this work, the superconducting current was not observed because the channel mobility at low temperature is decreased by ion scattering.

The 2DHG diamond FET with L_{sd} = 100 nm was operated in cryogenic environments down to 1.6 K. This result suggests that JoFET or SCFET operation would be possible by high mobility 2DHG diamond channel with further miniaturized structure.

- [1] F. Vigneau, S. Franceschi, *et al.* Nano Lett. 19 (2019) 1023-1027
- [2] T. Kageura, HK *et al.*, Diamond and Related Materials 90 (2018) 181-187
- [3] T. Kageura, HK *et al.* Sci. Rep. 9 (2019) 15214
- [4] A. Morishita, HK *et al.*, Carbon 181 (2021) 379-388

2:15 PM EQ07.11.04

2DHG Diamond MOSFETs with Multi-Finger Structure for Gate Width Expansion and Improved RF Characteristics Akira Takahashi; Waseda Univ, Japan

abstract

We have fabricated a high frequency 2DHG diamond MOSFET with air-bridge and multi-finger structure to increase the gate width. DC and RF performance of the double-finger devices and multi-finger devices were compared and investigated. As a result, the multi-finger devices did not degrade the current density due to the increase of gate width (W_{GT}).

1. Introduction

We fabricated 2DHG diamond MOSFET which $W_G=1$ mm using a multi-finger structure. High output power performance is critical for the RF amplifier applications. It is valid for high output to increase actual current by extending the gate width. The device with extended W_G may deteriorate output current because of self-heating, and influence characteristics of devices caused by increase of the gate resistance. In this work, 2DHG MOSFETs with multi-finger structure were fabricated on a diamond substrate, and its DC and RF characteristics were evaluated and compared with those of the double-finger structure.

2. Device information

Devices were fabricated on a (001) diamond substrate. After the boron-doped layer deposited, source and drain electrodes are deposited Ti/Pt/Au (20nm/20nm/90nm). After H-termination and isolation, deposited Al_2O_3 as gate insulator. After that, 100nm of Al was deposited as the gate. The gate length was fixed $L_G=0.5\mu m$ and the source-drain length L_{SD} was fixed $4.0\mu m$. the gate-drain length L_{GD} defined as $2.5\mu m$. The air-bridge over the gate fingers is made of Au ($1\mu m$) after resist application.

3. Result and Discussion

We compared DC characteristics of double-finger structure and multi-finger structure. The result of double-finger device with $W_{GT}=25\mu m \times 2$ at $V_{GS}=-24V$ and $V_{DS}=-40V$, the maximum drain current density I_{Dmax} was 428mA/mm. The result of multi-finger device by air-bridge with $W_{GT}=25\mu m \times 6$ at $V_{GS}=-24V$ and $V_{DS}=-40V$, the maximum drain current density I_{Dmax} was 433mA/mm. Since the drain current densities are almost the same in the double-finger and multi-finger devices the actual current value of multi-finger is almost three times higher than that of double-finger. In multi-finger, the current density is not degraded by gate resistance or heat, because W_{GU} (length of one finger) remains the same even when W_{GT} is increased.

The frequency at MSG and MAG convert, defined f_k , is decreased with increasing gate width. But it is confirmed that the rate of decreasing f_k with the multi-finger device is much smaller than that of double-finger device. Comparing the maximum oscillation frequency (f_{max}) with $W_{GT}=1000\mu m$, double-finger device indicates 4.8GHz and multi-finger device indicates 9.0 GHz. The reason why high f_{max} is obtained with multi-finger is that the gate resistance becomes smaller and the decrease in f_k is smaller, because the W_{GU} is maintained. These results indicate that the multi-finger structure, in which the gate length (W_{GT}) can be increased while keeping the length of one finger (W_{GU}) short, can suppress the decrease in f_{max} and improve the high-frequency performance.

3. Conclusion

In this work, we fabricated 2DHG diamond MOSFETs which $W_{GT} = 1$ mm with multi-finger structure on (001) diamond substrate for RF application and evaluated DC and RF performance. It was also confirmed that the introduction of the multi-finger structure did not cause deterioration in current density as the gate width expanded in association with the increase of gate fingers. In the RF characteristics evaluation, it was found that the multi-finger structure has a smaller rate of decrease in f_k with an increase in gate width, and the maximum oscillation frequency is 9.0 GHz at $W_{GT}=100\mu m \times 10$ whereas 4.8 GHz at $W_{GT}=500\mu m \times 2$. The multi-finger structure makes it possible to fabricate diamond devices in densely integrated structure with much smaller W_S (width of Source electrode between gate fingers). It improves high-frequency characteristics. Because of high thermal conductivity, the device integration is the advantage of diamond compared with GaN.

2:30 PM BREAK

SESSION EQ07.12: Materials Properties
Session Chairs: Robert Bogdanowicz and Anke Krueger
Wednesday Afternoon, November 30, 2022
Sheraton, 2nd Floor, Independence East

3:30 PM EQ07.12.01

Detection of Solvated Electrons from Photoexcited Diamond Nathaniel F. Rieders, Cesar Saucedo and Robert J. Hamers; University of Wisconsin-Madison, United States

Diamond possesses the unique ability to act as a facile and robust electron emitter in both vacuum and non-vacuum environments. While emission into vacuum has been widely studied, much less is known about diamond electron emission into water. Direct detection of electrons photoemitted into water is challenging because of the short lifetime (hundreds of nanoseconds), small cross-section, and near proximity of the electrons to the liquid interface. We have been developing improved methods for detecting solvated electrons at solid-liquid interfaces using transient absorption spectroscopy. Our experiments using a 705 nm detection wavelength (near the maximum of solvated electron absorption) gives rise to intensity changes on the order of $\sim 10^{-3}$ (0.1%), with lifetimes in agreement with expected values. In order to collect the complete solvated electron spectrum and enhance the specificity of detection, we have recently been developing a transient absorption system for complete spectroscopic analysis of solvated electrons produced via diamond photoemission. In this talk we will describe our efforts to detect solvated electrons from diamond into water, and efforts toward complete spectroscopic characterization of the transient absorption spectra. As time permits, we will also discuss the possibility of electron emission from other wide-bandgap materials.

3:45 PM EQ07.12.02

Transient Surface Photovoltage on B-Doped Single Crystal Diamonds—Charge Dynamics and Transfer Arsène Chemin¹, Peter Knittel², Philipp Reinke², Igal Levine¹, Thomas Dittrich¹ and Tristan Petit¹; ¹Helmholtz-Zentrum Berlin for Materials and Energy GmbH, Germany; ²Fraunhofer Institute for Applied Solid State Physics, Germany

Easy production of solvated electrons from solar illumination would be a game changer for green chemistry and environmental research. The use of widely available synthetic diamonds to generate solvated electrons upon light irradiation in water has been proposed as a promising strategy to achieve CO₂ or N₂ reduction in liquid phase [1-2]. Free electrons can be transferred to water because diamonds have a high energetic level of the conduction band and a negative electron affinity when its surface is hydrogenated. At first glance, the large band gap of diamonds (5.5 eV) should only enable excitation from

deep UV light, dramatically limiting the direct application of sunlight for photocatalysis with diamond. However, photogeneration via in-gap states is possible and CO₂ photo(electro)chemical reduction with visible light has been previously reported [3]. In this work, we study separation of photogenerated charge carriers in differently terminated single crystal diamonds using transient surface photovoltage (SPV) spectroscopy under excitation over a wide spectral range below and above the bandgap. Transient SPV spectroscopy with a tunable laser is a contactless and highly sensitive technique probing electronic transitions from near infrared to deep ultraviolet in the time range from several ns to s [4]. It enables us to determine the excitation paths and charge transfer in diamond crystals depending on surface and bulk states. Namely, we determine the influence of the doping states and defects by comparing B-doped diamonds to reference intrinsic crystals and the influence of the surface states by comparing hydrogenated and hydroxylated surfaces. In complement, the surface states of the diamond crystals have been characterized by X-ray absorption spectroscopy performed at the synchrotron BESSY II in Berlin. The excitation of electrons in the diamond crystals with visible light can be related to doping states at low energy and surface state just below the bandgap. The possible emission of these charges from the diamond samples in air and in water have been characterized by photoemission and photocurrent spectroscopies, respectively. While a wide range of excitation leads to charge separation in the diamond crystals, only the excitation related to surface state leads to electron emission.

References

- Zhu, D. et al, Photo-illuminated diamond as a solid-state source of solvated electrons in water for nitrogen reduction. *Nat. Mater.* 12, 836–841. (2013).
Zhang, L. et al. Selective Photoelectrochemical Reduction of Aqueous CO₂ to CO by Solvated Electrons. *Angew. Chem.* 53, 9746–9750. (2014)
Knittel, P. et al. Nanostructured boron doped diamond electrodes with increased reactivity for solar-driven CO₂ reduction in room temperature ionic liquids. *ChemCatChem* cctc.202000938. (2020)
Dittrich, T. Transient surface photovoltage spectroscopy of diamond. *AIP Adv.*, 12, 6, 065206 (2022)

This project has received funding from the Volkswagen Foundation under the Freigeist Fellowship No. 89592.

4:00 PM EQ07.12.03

Electron Emission from Negative Electron Affinity Surfaces of Planar-Type Diamond PIN Diodes Shoya Yamakawa^{1,2}, Hiromitsu Kato², Masahiko Ogura², Yukako Kato², Toshiharu Makino², Ryota Tsukamoto^{1,2}, Daisuke Takeuchi^{2,1} and Ichiro Shoji¹; ¹Chuo University, Japan; ²National Institute of Advanced Industrial Science and Technology (AIST), Japan

Diamond is well-known as an ultimate material because of its superior properties and it is expected to be employed in next-generation power electronic devices. One of the unique properties of diamond is the electron emission from negative electron affinity (NEA) surfaces. A vacuum power switch using a vertical-type PIN diamond diode was reported, which was made use of electron emission from NEA surfaces obtained by hydrogen-termination, and switching at 10kV was demonstrated. [1] The vertical PIN diodes were fabricated on a p-type substrate and the mesa diodes were fabricated by ICP etching, since there is no n-type conductive substrate. Then in this study, we attempted to fabricate planer-type diodes on Ib(111) substrates using selective growth technique, which could avoid damage in the device caused by ICP etching. As a result, the planer-type PIN diodes fabricated successfully showed electron emission by turning on, and the highest electron emission efficiency was close to 1%, which was comparable to the vertical-type one. It means that the planer-type diodes have a potential of high electron emission efficiency as well as the vertical-type ones, even the body was fabricated only by thin-films. Since it is a planer-type, it is possible to apply not only for electron emitters, but also for quantum devices owing to its ease of observation from the top. In this paper, we will introduce such a high potential of the new planar diode-type electron emitters, with the discussion of electron emission mechanism.

<Acknowledgement>

We are grateful for huge collaborations in experiments and discussion from our AIST colleagues and technical staffs. This work was partially supported by MEXT-Program for Creation of Innovative Core Technology for Power Electronics Grant Number JPJ009777, The FUTABA Foundation, and MEXT Quantum Leap Flagship Program (MEXT Q-LEAP) Grant Number JPMXS0118067395. Part of this work was also performed under the Cooperative Research Program of "Network Joint Research Center for Materials and Devices," which was carried out with Dr. Abukawa in Tohoku University.

[1]: D. Takeuchi, S. Koizumi, T. Makino, H. Kato, M. Ogura, H. Ohashi, H. Okushi, S. Yamasaki, "Negative electron affinity of diamond and its application to high voltage vacuum power switches," *Phys. Status Solidi*, 2013.

4:15 PM EQ07.12.04

Compressive Stress in Diamond Nanomembranes Paulius Pobedinskas^{1,2} and Ken Haenen^{1,2}; ¹Hasselt University, Belgium; ²IMEC vzw, Belgium

Nanomembranes (NMs) are very thin (≤ 500 nm) and have very high aspect ratios of thickness to lateral dimension ($\geq 10^4$). This makes them extremely flexible due to the linear decrease of bending strain with thickness. At the extreme thinness, materials fold much easier.¹ When nanocrystalline diamond (NCD) thin films are grown on substrates, which have a higher thermal expansion coefficient than diamond, unavoidably, compressive stress is generated. When a NCD NM is released from such substrate a pattern of wrinkles and wrinkles evolves. The out-of-plane deformation is associated with the onset of an elastic instability, where the total energy is best minimized by the film bending rather than straining in-plane. These deformations strongly affect the electrical properties of B-doped NCD NMs.² Therefore, one cannot disregard the influence of wrinkles when dealing with any type of device that is based on NMs.

In this work, finite element simulations of compressive stress relaxation under gravity in a diamond NM as it is released from a supporting substrate are presented. As NCD consists of hard diamond grains and soft grain boundaries, the Young's modulus and Poisson's ratio are not expected to be the same as in bulk diamond.³ To study the impact of elastic constants on wrinkling, calculations were made with different Young's moduli ($E = 300, 600, 900,$ and 1200 GPa) and Poisson's ratios ($\nu = 0, 0.07, 0.14,$ and 0.21). The initial compressive stress of the NM was varied in the range from 0 Pa up to -6 GPa. When a NCD thin film, which is 150 nm thick and has a compressive stress of up to -10^4 Pa, is released from the substrate as the NCD membrane, it relaxes without forming wrinkles. Symmetrical wrinkles form when the membrane relaxes from -10^5 Pa and higher compression. At absolute stresses larger than -1 GPa the asymmetric wrinkling is dominant. The Young's modulus and Poisson's ratio does not have notable impact on the relaxed membrane shape as stress does. However, the Young's modulus has higher impact on the relaxed membrane area and out-of-plane deformation range than Poisson's ratio. The higher the Young's modulus (or Poisson's ratio), the smaller the area (and out-of-plane deformation range) of the nanomembrane is obtained after the compressive stress relaxation. Finally, the obtained results on wrinkling phenomena are explain through the system's energy minimization.

[1] J.A. Rogers, *et al.*, *Nature* **477**, 45 (2011).

[2] S. Drijkoningen, *et al.*, *Scientific Reports* **6**, 35667 (2016).

[3] C.A. Klein and G.F. Cardinale, *Diamond and Related Materials* **2**, 918 (1993).

8:00 AM *EQ07.13.01

An All-Optical Diamond Voltage Microscope Daniel McCloskey¹, Nikolai Dontschuk¹, Alastair Stacey², Charlie Pattinson¹, Athavan Nadarajah¹, Liam Hall¹, Lloyd Hollenberg¹, Steven Prawer¹ and David A. Simpson¹; ¹University of Melbourne, Australia; ²RMIT University, Australia

The development of fluorescent molecular sensors for imaging voltage changes in biological systems has revolutionized neuroscience, providing a tool to capture neuronal activity over large areas with sub-neuron resolution both *in vitro* and *in vivo* [1–3]. However, the poor photostability of molecular voltage sensors limits recording times to a few minutes [1–3], posing problems for longitudinal studies of network evolution and disease processes. These limitations have led to the uptake of lower-resolution extracellular recording techniques such as multi-electrode arrays (MEAs) for long term neurological research[4,5].

Here, we present an alternate platform for sensitive high resolution voltage imaging using fluorescent, charge-sensitive defects in a transparent diamond substrate [6]. The nitrogen vacancy (NV) defect in diamond possesses three optically distinguishable charge states known to be responsive to voltage changes in solution [7–9]. In this work, we will show that precise electrochemical control of the diamond surface termination, can effectively tune the ensemble charge state population to an optimal composition for voltage sensing consisting exclusively of the fluorescent neutral (NV0) and non-fluorescent positive (NV+) states. Using these charge state sensors, we establish an all-optical diamond voltage imaging microscope (DVIM) capable of real-time imaging of capacitive charge injection by a microelectrode in solution. Finally, we show that this sensing mechanism can be replicated and enhanced in an array of diamond nanopillars, possessing sub-millisecond fluorescence response times and sub-millivolt sensitivity suitable for a host of excitable cell imaging applications.

References:

1. Knöpfel, T. & Song, C. Optical voltage imaging in neurons: moving from technology development to practical tool. *Nature Reviews Neuroscience* 20, (2019).
2. Piatkevich, K. D. et al. Population imaging of neural activity in awake behaving mice. *Nature* 574, (2019).
3. Wang, W., Kim, C. K. & Ting, A. Y. Molecular tools for imaging and recording neuronal activity. *Nature Chemical Biology* 15, (2019).
4. Abbott, J. et al. Extracellular recording of direct synaptic signals with a CMOS-nanoelectrode array. *Lab on a Chip* 20, (2020).
5. Emmenegger, V., Obien, M. E. J., Franke, F. & Hierlemann, A. Technologies to Study Action Potential Propagation With a Focus on HD-MEAs. *Frontiers in Cellular Neuroscience* 13, (2019).
6. McCloskey, D, Dontschuk, N. et al. A diamond voltage imaging microscope. *Nature Photonics* (accepted 13th June 2022).
7. Karaveli, S. et al. Modulation of nitrogen vacancy charge state and fluorescence in nanodiamonds using electrochemical potential. *Proceedings of the National Academy of Sciences* 113, (2016).
8. Grotz, B. et al. Charge state manipulation of qubits in diamond. *Nature Communications* 3, (2012).
9. Krečmarová, M. et al. A Label-Free Diamond Microfluidic DNA Sensor Based on Active Nitrogen-Vacancy Center Charge State Control. *ACS Applied Materials & Interfaces* 13, (2021).

8:30 AM *EQ07.13.02

Formation of Nitrogen Vacancy Center in Diamond for Quantum Sensing Applications Tokuyuki Teraji; National Institute for Materials Science, Japan

Formation and control of electron spin of negatively charged nitrogen vacancy center (NV⁻) in diamond is attracting much attention for next-generation quantum devices. For sensing applications, a relatively large amount of NV⁻ center is required to increase sensitivity. This corresponds to an increase of the total number of sensors. Typically, [NV⁻] of 0.1–3ppm is desired to detect weak magnetic fields. The coherence time of the electron spin T₂ is another important factor for increasing sensitivity, and this value has been reported to be inversely proportional to the density of nitrogen concentration [1]. Considering these facts, we have optimized diamond growth condition for both chemical-vapor deposition (CVD) [2, 3] and high-pressure/high-temperature (HPHT) methods [4]. To prolong T₂, we applied ¹²C isotopic enrichment and improved a crystalline quality of diamond. For obtaining higher [NV⁻], first we improved controllability of nitrogen concentration in the doping range of 0.1–50ppm. Then, NV⁻ center is created in diamond crystals through electron beam irradiation and subsequent vacuum annealing. It is also important to elucidate the creation of point defects other than the NV⁻ center during NV⁻ center formation processes and to understand their effect on T₂, that is, on magnetic sensitivity. We performed electron paramagnetic resonance and photoluminescence measurements from this point of view [5]. In the CVD method, a free-standing diamond (001) single crystals were obtained by cutting the substrate after a growth of nitrogen-doped homoepitaxial diamond thick layer. The dimension of CVD single-crystal plates was typically 3×3×0.5mm³. In the case of HPHT crystals, after the bulk diamond crystals were grown, these crystals were cut parallel to the {111} crystal plane to obtain {111} single crystals. Typical size of the HPHT {111} single-crystal plates was 1.5×1.5×0.4mm³.

The author would like to thank Dr. C. Shinei, Dr. T. Taniguchi, Dr. M. Miyakawa, Dr. K. Watanabe of NIMS and Dr. Y. Masuyama, Dr. H. Abe, Dr. S. Onoda, Dr. T. Ohshima for crystal growth, characterization, and electron beam irradiation processes. This work was partially supported by MEXT Q-LEAP (JPMXS0118068379, JPMXS0118067395), JST CREST (JPMJCR1773), JST Moonshot R&D (JPMJMS2062), MIC R&D for construction of a global quantum cryptography network (JPMI00316), JSPS KAKENHI (No. 20H02187 and 20H05661).

- [1] J. F. Barry *et al.*, *Rev. Mod. Phys.* **92**, 015004 (2020).
- [2] T. Teraji *et al.*, *J. Appl. Phys.* **118**, 115304 (2015).
- [3] T. Teraji *et al.*, *phys. stat. sol. (a)* **212**, 2365 (2015).
- [4] M. Miyakawa *et al.*, *Jpn. J. Appl. Phys.* **61**, 045507 (2022).
- [5] C. Shinei *et al.*, *Appl. Phys. Lett.*, **119**, 254001 (2021).

9:00 AM *EQ07.13.03

Isotopically Engineered Diamond for Quantum Technologies Fedor Jelezko; Ulm University, Germany

We will present a new solid-state architecture for a scalable quantum simulator that consists of strongly interacting nuclear spins formed by doping of diamond lattice with C^{13} isotope. Initialization and read-out of this quantum simulator is enabled by single nitrogen-vacancy centers implanted in diamond. The system can be employed to simulate a wide variety of strongly correlated spin models. We will also discuss the potential of isotopic engineering of diamond nanoparticles for ultrasensitive NMR and MRI.

9:30 AM DISCUSSION TIME

SESSION EQ07.14: Virtual Session II: Growth III
Session Chairs: Philippe Bergonzo and David Simpson
Tuesday Afternoon, December 6, 2022
EQ07-virtual

9:00 PM *EQ07.14.01

Plasma CVD Engineering of Nitrogen-Vacancy Centers in (111) Single Crystal Diamond Hiroimitsu Kato; National Institute of Advanced Industrial Science and Technology, Japan

Negatively charged nitrogen vacancy (NV-) centers will be high importance for a variety of quantum applications. Due to the long coherence time constant of NV- center even at room temperature, applications for quantum sensing, quantum information processing, and quantum register are very promising. Plasma-enhanced chemical vapor deposition (CVD) is one of the major approaches to introduce well-defined NV centers in diamond, as well as electron beam irradiation and ion implantation techniques. N-type Fermi control by phosphorus doping can offer charge-state stabilization of NV center, leading to longer coherent time at room temperature [1-3]. NV centers can be perfectly aligned along [111] axis by CVD growth on (111) surface [4,5]. Electrically excitation of NV defects and related readout with photo current, required to realize chip-scale magnetometers, have also been conducted by using diamond PIN junction diode structure [6-8]. All these achievements are based on our comprehensive progresses of CVD diamond growth, impurity doping, junction management, and device fabrication processes. Details will be discussed focusing on technical aspects peculiar to plasma CVD engineering of diamond NV centers.

Acknowledgements: This work was partially supported by MEXT Q-LEAP (JPMXS0118067395), JST CREST (JPMJCR1773), MIC R&D (JPMI00316), and JST Moonshot R&D (JPMJMS2062).

References: [1] H. Kato, et. al., Appl. Phys. Lett. 109, 142102 (2016). [2] Y. Doi, et. al., Phys. Rev. B 93, 081203(R) (2016). [3] E. D. Herbschleb, et. al., Nat. Commun. 10, 3766 (2019). [4] T. Fukui, et. al., Appl. Phys. Express 7, 055201 (2014). [5] T. Miyazaki, et. al., Appl. Phys. Lett. 105, 261601 (2014). [6] N. Mizuochi, et. al., Nat. Photonics 6, 299 (2012). [7] H. Kato, et. al., Appl. Phys. Lett. 102, 151101 (2013). [8] T. Murooka, et. al., Appl. Phys. Lett. 118, 253502 (2021).

9:30 PM *EQ07.14.02

Diamond Surface Nanostructures: Morphology Control, Formation Mechanism, and Applications Wenjun Zhang; City Univ of Hong Kong, China

The outstanding properties of diamond make it an excellent material for various applications. It is known that the potential applications of materials depend not only on their intrinsic properties, but also on the surface geometries in which they appear. The extreme properties of diamond, however, make it difficult to be structured to a desired geometry. This presentation will review the recent progress in the nano-/micro-structuring techniques of diamond films, in particular a simple and applicable method developed by us to nanostructure diamond (ranging from microcrystalline to nanocrystalline) surfaces using bias-assisted reactive ion etching (RIE) in hydrogen/argon plasmas. Various diamond nanocone/nanopillar/ nanowhisker (nanowire) arrays with high uniformity and tunable density have been achieved by using this method. The effects of initial film structure, surface roughness, and RIE conditions on the size, density, and geometry of nanostructures are revealed. Surface nanostructuring of diamond films is demonstrated to be an effective approach to extend and/or enhance the properties of diamond with respect to its bulk and film counterparts. Example applications of the diamond nanostructures in field electron emission electrode, in situ probing and drug delivery at the cell level, and electrocatalysis are also discussed.

10:00 PM EQ07.14.03

Synthesis and Characterization of Cubic BN / Diamond or Hexagon BN / Diamond Heterostructures Avani Patel¹, Jesse Brown², Saurabh Vishwakarma¹, David J. Smith¹ and Robert J. Nemanich¹; ¹Arizona State University, United States; ²Advent Diamond, United States

Boron nitride exists in various polymorphs, including sp³ bonded cubic (c-BN) or wurtzite (w-BN) and sp² bonded hexagonal or turbostratic structures (h-BN or t-BN). The sp³ bonded c-BN or w-BN may be considered for high power electronics and the sp² bonded h-BN or t-BN may have significant potential as a dielectric layer for surface passivation or as a gate insulator. For the power electronic applications, growth of c-BN or h-BN / diamond heterostructures with highly ordered interface and low interface defect density are essential. In this research, our goal is to form a BN / diamond heterostructure using a three-step approach 1) *in situ* plasma clean, 2) a nucleation step, and 3) an epitaxial growth step. The c-BN or h-BN layers are grown on boron-doped diamond substrates using electron cyclotron resonance plasma-enhanced chemical vapor deposition (ECR PECVD) with gas phase precursors of Ar, N₂, BF₃, H₂ and He. The resulting c-BN or h-BN layers were characterized by *in-situ* X-ray photoelectron spectroscopy (XPS) and cross-sectional Transmission Electron Microscopy (XTEM). In-situ XPS results confirmed the presence of sp² or sp³ BN near the top surface. The TEM measurements were used to observe the nucleation and morphology of the BN / diamond interface. The experimental results demonstrated that the nucleation and growth steps are optimized by controlling the ratio of hydrogen and fluorine at a higher deposition temperature (~ 850 °C). A comparative study of nucleation and growth of BN on (100) and (111) diamond substrates indicates that a reduced hydrogen flow rate in the initial nucleation stage and a higher substrate temperature in the growth stage promotes the growth of c-BN compared to the hexagonal or turbostratic phase of BN.

Research supported through ULTRA, an Energy Frontier Research Center funded by the U.S. Department of Energy, Office of Science, Basic Energy Sciences under award DE-SC0021230.

10:15 PM EQ07.14.04

Frequency-Tunable AC Magnetometry by Using Electronic Spin Triple-Resonance of Nitrogen-Vacancy Center in Diamond Ryusei Okaniwa^{1,1}, Yuichiro Matsuzaki^{2,2}, Tatsuma Yamaguchi¹, Hideyuki Watanabe², Norikazu Mizuochi³, Norio Tokuda^{4,4}, Yuta Nakano⁴, Kensuke Kobayashi^{5,5}, Kento Sasaki⁵ and Junko Ishi-Hayase^{1,1}; ¹Keio University, Japan; ²National Institute of Advanced Industrial Science and Technology (AIST), Japan; ³Kyoto University, Japan; ⁴Kanazawa University, Japan; ⁵The University of Tokyo, Japan

Nitrogen-vacancy (NV) center in diamond is expected to be a practical quantum sensor with high sensitivity and high spatial resolution due to the room-

temperature long spin coherence time and atomic-scale size^[1]. Quantum sensing using NV centers is implemented by measuring spin-dependent photoluminescence (PL) and manipulating spin state by microwave (MW). Pulsed-optimally detected magnetic resonance (pulsed-ODMR) is typically used for AC magnetometry^[2,3]. Although achieving high sensitivity, it can be disadvantage to require sophisticated setup, rapid control and measurements, strong MW pulse irradiations and its calibration. Recently, our group proposed and demonstrated MHz-range AC magnetic field sensing using continuous-wave ODMR (CW-ODMR) which is simpler than pulsed-ODMR^[4,5]. We utilized radio-frequency (RF)-dressed states of NV electronic spins by applying MW and RF magnetic fields (double resonance). However, it is difficult to change the frequency of detectable AC magnetic fields because of an intrinsic strain field in a diamond.

In this study, to avoid such potential drawback, we propose frequency-tunable AC magnetic field sensing by CW-ODMR based on electronic spin triple resonance. In this scheme, the MHz-range magnetic field (target RF) is applied to resonant transition between RF-dressed states generated by another RF field (control RF). Consequently, RF-doubly dressed states is generated and observed by CW-ODMR measurements to estimate the amplitude of target RF field. The target frequency is expected to be varied by controlling the RF-dressed states with changing the control RF field amplitude.

The NV center has spin-1 system described by eigenstates B, D, 0 under applying DC magnetic field perpendicular to the specific NV axis of it. When MW induces the transition from 0 to B(D), the PL intensity decrease (CW-ODMR). By measuring CW-ODMR spectrum with control RF field resonant to B-D transition (7.5 MHz), we observe four dips due to the splitting of B and D levels (RF-dressed states). As increasing the amplitude of control RF field, the splitting energy became larger. Furthermore, we applied the target RF field resonant to the lower transition between the RF-dressed states (5.4 MHz). Consequently, the energy levels of RF-dressed states were split into eight levels. This result demonstrates that RF-doubly dressed states were generated. By sweeping the frequency of target RF field, the anti-crossing structure was observed near the resonant frequency between the RF-dressed states. We found that the splitting energy of the anti-crossing spectra linearly increased as increasing the target RF amplitude. This result demonstrate that the amplitude of the target RF field can be estimated by measuring the splitting energy. Moreover, it is found that the detectable frequency of the target RF field can be tuned by changing the amplitude of the control RF. The obtained signal was larger than our previous work utilizing the RF-dressed states because the coherence time was extended by applying two different driving fields. This result shows that the sensitivity can be improved compared with that for the sensor based on the double resonance.

Acknowledgement

This work was supported by MEXT Q-LEAP (No. JPMXS0118067395), MEXT KAKENHI (No. 18H01502, 20H05661, 22H01558), and CSRN, Keio University. This work was supported by Leading Initiative for Excellent Young Researchers MEXT Japan and JST presto (Grant No. JPMJPR1919) Japan and Kanazawa University SAKIGAKE Project 2020. YM acknowledges support of Grants-in-Aid for Scientific Research from the Ministry of Education, Culture, Sports, Science, and Technology, Japan (20H05661).

Reference

- [1] L. Rondin, *et al.*, Rep. Prog. Phys. **77**, 056503 (2014).
- [2] J. R. Maze, *et al.*, Nature **455**, 644 (2008).
- [3] L. M. Pham, *et al.*, Phys. Rev. B **86**, 045214 (2012).
- [4] S. Saijo, *et al.*, Appl. Phys. Lett. **113**, 082405 (2018).
- [5] T. Yamaguchi, *et al.*, Jpn. J. Appl. Phys. **58**, 100901 (2019).

10:30 PM EQ07.14.05

Fabrication and Characterization of Femtosecond Laser Written Low Loss Depressed Cladding and Half-Ring Waveguides in Diamond Faik D. Ince¹, Yagiz Morova^{1,1}, Umur Yazlar² and Alphan Sennaroglu^{1,1}; ¹Koç University, Turkey; ²Appsilon B.V., Netherlands

We report on the fabrication and characterization of femtosecond (fs) laser written depressed cladding and half-ring waveguides in diamond. The propagation losses of 2.05 dB/cm for the depressed claddings and 1.2 dB/cm for the half rings are the lowest propagation losses reported to date for fs laser written waveguides in diamond. Such low loss values reveal the potential of diamond waveguides in efficient quantum sensing applications.

A polished single crystal CVD diamond was used in the experiments. The sample was positioned on a 3D translational stage and an amplified Ti³⁺:Sapphire laser generating 120 fs pulses at 800 nm and at 1 kHz repetition rate was used during waveguide fabrication. Laser pulses were focused into the sample with a 40X objective. With 100 nJ of incident pulse energy and 0.4 mm/s scan speed, 6 waveguides were fabricated across the full length of the sample. Three of the waveguides had depressed circular cladding, whereas the rest had semi-circular, half-ring configuration. Fabrication depth of depressed cladding waveguides was determined as 100 μm . Core diameter (D) of the depressed claddings was kept constant as 60 μm and the number of written tracks (N) was set as N=36, 48 and 60. Half rings were fabricated directly below the crystal surface to create an interface between air and the waveguide core. Design parameters (D, N) of the three half-ring waveguides were set as (60 μm , 18), (90 μm , 28), and (120 μm , 36).

A He-Ne laser operating at 633 nm was utilized to characterize the waveguides. The laser beam was coupled to the waveguides with a converging lens and the guided beam exiting the waveguide was collimated with an aspheric lens (focal length f=6 mm). In order to reduce the mode mismatch between the focused beam and the waveguide core, converging lenses with focal lengths of f=4, 5 and 7.5 cm were used for half ring waveguides with D=60, 90 and 120 μm , respectively. For the depressed claddings, the optimum focal length for the converging lens was determined as f=7.5 cm.

By comparing the power transmission of the waveguide with the bulk transmission of the crystal, propagation loss was measured as 2.05, 3.04 and 3.99 dB/cm for the depressed cladding waveguides with N=36, 48 and 60, respectively. For the half rings, losses were found as 1.2, 1.8 and 6.1 dB/cm for the waveguides with D=60, 90 and 120 μm , respectively. The trend from the depressed claddings shows that an increase in N increases the propagation loss as well. This trend is expected since the fs laser written tracks introduce graphitic content to the track region, resulting in an increase in the loss of the waveguide due to the optical properties of graphite. We further examined the structure of the written tracks by using Raman microscopy and observed the G-band for graphite at 1575 cm^{-1} , which supports the mentioned trend. For the half rings, results indicate that as the core diameter increases, the propagation loss decreases. This trend is expected also, since increasing the core diameter also increases the size of the unmodified core region in relation to the modified graphitic region.

To summarize, the propagation loss of 2.05 dB/cm is the lowest loss reported to date for fs laser written depressed cladding waveguides in diamond. Results from the depressed cladding waveguide measurements showed that decreasing the number of written tracks reduces the loss. However, since reducing the number of tracks also decreases the refractive index contrast (Δn) and the ability of the waveguides to confine light, an optimum number of written tracks is needed for low-loss guiding. So, use of half-ring waveguides in diamond enables the confinement of light with reduced number of tracks, by taking advantage of the high Δn occurring at the air-waveguide interface. Switching to the half-ring waveguides resulted in propagation losses as low as 1.20 dB/cm, which is the lowest propagation loss reported to date for fs laser written waveguides in diamond.

10:35 PM DISCUSSION TIME

SYMPOSIUM EQ08

Higher-Order Topological Structures in Real Space—From Charge to Spin
November 28 - December 7, 2022

Symposium Organizers

Michele Conroy, Imperial College London
Sinead Griffin, Lawrence Berkeley National Laboratory
Zijian Hong, Zhejiang University
Dennis Meier, Norwegian University of Science and Technology

* Invited Paper
+ Distinguished Invited

SESSION EQ08.01: Probing High-Order Topological Structures I
Session Chairs: Marin Alexe and Michele Conroy
Monday Morning, November 28, 2022
Sheraton, 2nd Floor, Republic A

10:30 AM *EQ08.01.01

Imaging Topological Order at the Picometer-Scale by Electron Ptychography [David A. Muller](#); Cornell University, United States

Electron microscopy is often used to directly image the atomic displacements in ferroelectrics, reaching a precision of a few picometers. As good as this is, it is still not sufficient to robustly measure many ferroic order parameters, including vorticity and higher order moments. Enabled by a new design of electron detector [1,2] that is capable of measuring the complete distribution of momentum transfers at every probe position, we construct a 4-dimensional phase space from which we solve the inverse multiple scattering problem and retrieve the underlying 3-dimensional potential of the sample. The lateral resolution of less than 20 pm is now limited not by the instrument, but by the thermal vibrations of the atoms themselves, and the precision is improved to well below 1 pm [3]. The resulting ptychographic reconstructions have allowed us to image the internal structures of both magnetic and ferroelectric vortices, skyrmions and merons, including their singular points that are critical for accurately describing the topological properties of these field textures.

[1] M. W. Tate, P. Purohit, D. Chamberlain, K. X. Nguyen, R. Hovden, C. S. Chang, P. Deb, E. Turgut, J. T. Heron, D. G. Schlom, D. C. Ralph, G. D. Fuchs, K. S. Shanks, H. T. Philipp, D. A. Muller, and S. M. Gruner. "High Dynamic Range Pixel Array Detector for Scanning Transmission Electron Microscopy" *Microscopy and Microanalysis* **22**, (2016): 237–249.

[2] H. T. Philipp, H. T., M. W. Tate, K. S. Shanks, L. Mele, M. Peemen, P. Dona, R. Hartong, G. Van Veen, Y. T. Shao, Z. Chen, J. Thom-Levy, D. A. Muller, and S. M. Gruner. "Very-High Dynamic Range, 10,000 Frames/Second Pixel Array Detector for Electron Microscopy" *Microscopy and Microanalysis* **28**, (2022): 425–440.

[3] Z. Chen, Y. Jiang, Y.-T. Shao, M. E. Holtz, M. Odstrčil, M. Guizar-Sicairos, I. Hanke, S. Ganschow, D. G. Schlom, and D. A. Muller. "Electron Ptychography Achieves Atomic-Resolution Limits Set by Lattice Vibrations" *Science* **372**, (2021): 826–831

11:00 AM *EQ08.01.02

Coupling of Ferroelectric Domain Walls with Liquid and Magnetic Interfaces [Neus Domingo Marimon](#)¹, Ch. Stefani¹, I. Spasojevic¹, V. Sireus², E. Menendez², J. Sort², Albert Verdaguer² and Gustau Catalan¹; ¹Catalan Institute of Nanoscience and Nanotechnology (ICN2), CSIC and BIST, Spain; ²Universitat Autònoma de Barcelona, Spain

Ferroelectric domain walls strongly interact with its surroundings. In ferroelectrics thin films with exposed surfaces investigated by piezoresponse force microscopy (PFM), the main source of external screening charges is the atmosphere and the water neck, and therefore relative humidity (RH) plays a major role. In this context the speed as well as the creep-factor m describing the domain wall kinetics follow the behavior of water adsorption represented by the adsorption isotherm, indicating that the screening mechanism dominating the switching dynamics is the thickness and the structure of adsorbed water structure and its associated dielectric constant and ionic mobility.[1] On the other hand, the ferroelectrics can couple to other ferroic physical magnitudes in heterostructures such as FE/FM multilayers. In this context, the magnetic structure of magnetoelastic thin films can be manipulated by the tunable piezoelectric strain underneath: here I will show how in this case the dynamics of magnetic domain walls are dominated by the ferroelectric domain walls creating pinning sites that nucleate vortex like structures with predominant out of plane magnetic moments.[2]

Reference(s)

[1] I. Spasojevic, A. Verdaguer, G. Catalan, N. Domingo, Adv. Electron. Mater. 2021, 2100650

[2] Ch. Stefani, V. Sireus, J. Sort, E. Menendez, N. Domingo, *manuscript under preparation*

11:30 AM EQ08.01.03

High-Resolution Electric Field Mapping at Crystal Interfaces by Tilt-Scan Averaged DPC STEM Satoko Toyama¹, Takehito Seki^{1,2}, Bin Feng¹, Yuichi Ikuhara^{1,3} and Naoya Shibata^{1,3}; ¹The University of Tokyo, Japan; ²JST PRESTO, Japan; ³Japan Fine Ceramics Center, Japan

Local electromagnetic field distribution inside materials can be directly observed at high spatial resolution by using differential phase contrast (DPC) imaging in scanning transmission electron microscopy (STEM) [1]. In DPC STEM, momentum transfers of electrons due to electromagnetic fields are

detected by a segmented detector or pixelated detector placed on the bright field region. However, as for crystalline defects such as heterointerfaces, grain boundaries, etc., concomitant diffraction contrast seriously hinders the quantitative electromagnetic fields observation by DPC STEM.

In general, diffraction contrast dramatically varies with a slight change in beam tilt or sample tilt, whereas DPC contrast originates from electric fields and is insensitive to the slight tilt changes. Therefore, by averaging multiple DPC signals acquired with slightly different tilt conditions at the same sample position, the diffraction contrast can be suppressed (averaged) while reinforcing the electric field signals [2]. We have developed tilt-scan averaged DPC (tDPC) STEM system, which can average DPC signals obtained under multiple-beam tilt conditions and suppress diffraction contrast in real-time [3] [4]. tDPC STEM has been successfully applied to observe electric field and electron carriers in GaN-based semiconductor heterointerfaces [5], demonstrating the effectiveness of tDPC STEM.

In this study, we applied tDPC STEM for observing space charge layers in yttria-stabilized zirconia (YSZ) grain boundaries. tDPC STEM observation of YSZ $\Sigma 5[001]/(310)$ grain boundaries revealed that an electric field diverging from the grain boundary was distributed within 15 nm on both sides of the grain boundary. This result indicates the existence of positive charges at the grain boundary core accompanied by surrounding negative charges. On the other hand, little electric field fluctuation was observed at the $\Sigma 5[001]/(210)$ grain boundary. These results suggest that the electric field and the width of the space charge strongly depend on the local structures of the grain boundaries [6]. Details will be discussed in the presentation.

[1] N. Shibata *et al.*, *Acc Chem Res*, 50, 1502, 2017.

[2] T. Mawson *et al.*, *Ultramicroscopy*, 219, 113097, 2020.

[3] Y. Kohno, *et al.*, *Microscopy*, 71, 111 2022.

[4] S. Toyama *et al.*, *Ultramicroscopy*, 238, 113538, 2022.

[5] S. Toyama *et al.*, to be submitted.

11:45 AM EQ08.01.04

Quantitative 3D Imaging of Oxygen Defects in Multiferroic $(\text{LuFeO}_3)_y/(\text{LuFe}_2\text{O}_4)_1$ Superlattices Kasper Hunnestad¹, Hena Das², Constantin Hatzoglou¹, Megan E. Holtz³, Charles Brooks³, Antonius van Helvoort¹, Darrell Schlom³, Julia Mundy⁴ and Dennis Meier¹; ¹Norwegian University of Science and Technology, Norway; ²Tokyo Institute of Technology, Japan; ³Cornell University, United States; ⁴Harvard University, United States

Oxide interfaces are a rich source for novel physical phenomena, ranging from interfacial superconductivity to unusual (multi-)ferroic effects. Over the last decade, significant progress has been made in both the understanding and engineering of oxide interfaces, propelled by the ongoing progress in the development of atomic-scale characterization techniques¹.

Here, we introduce atom probe tomography (APT) as versatile tool for studying oxide interfaces, investigating the 3D atomic-scale structure and chemical composition of $(\text{LuFeO}_3)_y/(\text{LuFe}_2\text{O}_4)_1$ superlattices. This system couples together ferroelectric and ferrimagnetic response, enabling a true multiferroic material with an intriguing display of charge redistribution at polar interfaces². With our APT measurements we are able to reveal a subtle accumulation of charged oxygen vacancies at the LuFe_2O_4 layers which would typically go undetected with conventional microscopy approaches. We quantify the vacancy concentration and discuss their accumulation in relation to calculated defect formation energies, as well as their ability to stabilize an intriguing multiferroic domain structure. In general, this research establishes a new pathway for studying the interaction of interfaces and point defects in oxides, expanding related atomic-scale investigations into 3D with a new level of chemical accuracy.

References

1. Hunnestad, K. A. *et al.* Atomic-scale 3D imaging of individual dopant atoms in a complex oxide. arXiv:2111.00317 (2021).

2. Mundy, J. A. *et al.* Atomically engineered ferroic layers yield a room-temperature magnetoelectric multiferroic. *Nature* **537**, 523–527 (2016).

SESSION EQ08.02: Probing High-Order Topological Structures II

Session Chairs: Ismail El Baggari and Julia Mundy

Monday Afternoon, November 28, 2022

Sheraton, 2nd Floor, Republic A

1:30 PM *EQ08.02.01

Improper Ferroelectrics at the Ultrathin Limit Marta D. Rossell; Empa, Swiss Federal Laboratories for Material Science and Technology, Switzerland

Recently, improper ferroelectrics –materials in which electric polarization arises as a secondary effect of a leading order parameter– are receiving increasing attention. The family of hexagonal manganites (h - RMnO_3 , R = rare earth) is a model system for improper ferroelectricity, where the electric polarization emerges as a byproduct of a primary lattice-trimerizing structural distortion, a combination of tilt and rotation of the MnO_5 bipyramids around the R^{3+} ion. The trimerization is described by a two-component order parameter \mathbf{Q} consisting of the tilt amplitude Q and the angle φ of the MnO_5 bipyramids, but can also be related to the amplitude and phase of the corrugation of the R layer, which is easily visible and quantifiable by HAADF-STEM imaging [1]. However, while bulk h - RMnO_3 bulk crystals have been intensively studied in the last decade, not as much of research at the atomic scale has been conducted on the improper ferroelectric behavior of technologically relevant ultrathin films.

Rather than the depolarizing field being the main challenge to achieving polar thin films, as in proper ferroelectrics, improper ferroelectricity in ultrathin films is determined by the thin-film specific behavior of its driving non-polar order parameter. In YMnO_3 thin films, substrate clamping and critical fluctuations of the order parameter lead to a lowering of the temperature of the phase transition, T_C^{film} . Thus, T_C^{film} decreases smoothly with YMnO_3 thickness and, inexplicably, at room temperature, the spontaneous polarization reaches zero for the two-unit-cell film [2].

Our current work focuses on the investigation of nanoscale confinement effects on the lattice trimerization of ultrathin YMnO_3 films. The structure and properties of the YMnO_3 films, with a special focus on the interfaces, are investigated by using a combination of quantitative (in-situ) HAADF-STEM and STEM-EELS, and density functional calculations. Our results advance the understanding of the evolution of improper ferroelectricity within the confinement of ultrathin films, which is essential for their successful implementation in nanoscale devices, such as ferroelectric tunnel junctions and resistive memories [3].

[1] E. Holtz *et al.* *Nano Lett.* **17**, 5883 (2017).

[2] J. Nordlander *et al.* *Nat. Commun.* **10**, 5591 (2019).

[3] A. Vogel *et al.* *In preparation* (2022).

2:00 PM *EQ08.02.02

Dark-Field and Momentum-Resolved Electron Energy Loss Spectroscopy of Bi_2Se_3 -Based Heterostructures for Spintronics Quentin Ramasse^{1,2}, Vlado Lazarov³ and Demie Kepaptsoglou^{1,3}; ¹SuperSTEM Laboratory, United Kingdom; ²University of Leeds, United Kingdom; ³University of York, United Kingdom

Engineering the structural or chemical architecture of functional materials at the nano or even atomic level enables emergent properties that rely on the interplay between fundamental properties of matter such as charge, spin and local atomic-scale chemistry. A striking illustration of the relevance of this strategy is provided by placing Bi_2Se_3 , a topological insulator (TI) with topologically-protected helical two-dimensional surface states and one-dimensional bulk states associated with crystal defects, in close proximity with graphene. The strong spin-orbit interaction and proximity effects result in subtle and controllable electronic band structure changes at and near the interface, with exciting potential for spintronic applications. Here we probe at high energy resolution the interfaces in a system consisting of Bi_2Se_3 films grown by chemical vapor deposition on epitaxial graphene/SiC(0001), where the number of carbon layers can be carefully controlled to tune possible proximity effects between the film and the substrate. All experiments were carried out on a monochromated Nion UltraSTEM100 MC operated at 60kV, with a probe convergence semi-angle of 31mrad and a beam current of approximately 4pA (after monochromation to $\sim 12\text{meV}$ resolution). Chemical mapping confirms the atomic-level chemistry of the layers, while the specific geometry of the sample offers opportunities for probing directly the spatial localization of electronic states within the graphene layers [1] and at the SiC/graphene and graphene/ Bi_2Se_3 interfaces. Strikingly, the use of a dark-field EELS geometry, using e.g. a set of custom-developed annular apertures, reveals the emergence of locally resolved fine structure in the ultra-low loss region of the spectrum. In addition to a direct interrogation of the chemical bonds between the layers via their vibrational response, these observations are linked to the interplay between the various phonon modes and the Dirac plasmons in the TI layers, whose dispersion is mapped in momentum space with nm spatial sensitivity using a recently developed methodology for nanoscale momentum-resolved spectroscopy [2].

[1] M. Bugnet et al., Phys. Rev. Lett. 128, 116401 (2022)

[2] F.S. Hage et al., Science Advances 4, eaar7495 (2018)

2:30 PM *EQ08.02.03

Real Space Topologies in Ferroelectric Superlattices Ramamoorthy Ramesh; University of California, Berkeley, United States

Complex topological configurations are a fertile playground to explore novel emergent phenomena and exotic phases in condensed-matter physics. I will describe the discovery of polar skyrmions in a lead-titanate layer confined by strontium-titanate layers by atomic-resolution scanning transmission electron microscopy (STEM). Phase-field modeling and second-principles calculations reveal that the polar skyrmions have a skyrmion number of +1 and resonant soft X-ray diffraction experiments show circular dichroism confirming chirality. Such nanometer-scale polar skyrmions exhibit a strong signature of negative permittivity at the surface of the skyrmion, which is furthermore highly tunable with an electric field. They are a new state of matter and electric analogs of magnetic skyrmions, and may be envisaged for potential applications in information technologies.

3:00 PM BREAK

3:30 PM EQ.08.02.00

Predicting Phonon-Induced Spin Decoherence from First Principles—Colossal Spin Renormalization in Condensed Matter Jinsoo Park¹, Jin-Jian Zhou², Yao Luo¹ and Marco Bernardi¹; ¹California Institute of Technology, United States; ²Beijing Institute of Technology, China

Developing a microscopic understanding of spin decoherence is essential to advancing quantum technologies. Electron spin decoherence due to atomic vibrations (phonons) plays a special role as it sets an intrinsic limit to the performance of spin-based quantum devices. Two main sources of phonon-induced spin decoherence - the Elliott-Yafet (EY) and Dyakonov-Perel (DP) mechanisms - have distinct physical origins and theoretical treatments. Here we show a rigorous framework that unifies their modeling and enable accurate predictions of spin relaxation and precession in semiconductors [1]. We compute the phonon-dressed vertex of the spin-spin correlation function, with a treatment analogous to the calculation of the anomalous electron magnetic moment in QED [2]. We find that the vertex correction provides a giant renormalization of the electron spin dynamics in solids, greater by many orders of magnitude than the corresponding correction in vacuum. Our work demonstrates a general approach for quantitative analysis of spin decoherence in materials, advancing the quest for spin-based quantum technologies.

[1] J. Park, Y. Luo, J.-J. Zhou, and M. Bernardi. "Many-body theory of phonon-induced spin relaxation and decoherence." Preprint: arXiv:2208.09575

[2] J. Park, J.-J. Zhou, Y. Luo, and M. Bernardi. "Predicting Phonon-Induced Spin Decoherence from First Principles: Colossal Spin Renormalization in Condensed Matter." Phys. Rev. Lett. (in press) Preprint: arXiv:2203.06401

3:45 PM EQ.08.02.04

Molecular Beam Epitaxy Grown Tantalum Arsenide Weyl Semimetal Zuzanna W. Ogorzalek¹, Janusz Sadowski^{1,2,3}, Jaroslaw Domagala³, Wiktoria Zajkowska³, Slawomir Kret³, Bartlomiej Seredynski¹, Rafal Bozek¹, Wojciech Pacuski¹ and Marta Gryglas-Borysiewicz¹; ¹University of Warsaw, Poland; ²Linnaeus University, Sweden; ³Institute of Physics, Polish Academy of Sciences, Poland

Tantalum arsenide belongs to topological Weyl semimetals (WSM), with unusual electronic and magnetotransport properties. In WSM materials, the combination of distinct features of electronic structure and crystal lattice symmetry - either time reversal or inversion symmetry, leads to occurrence of so called Weyl nodes at the crossing points of two bands without spin degeneracy. The low energy excitations at the Weyl nodes behave as massless Weyl fermions with linear dispersion relations and opposite chiralities. In the band structure of TaAs 12 pairs of Weyl nodes have been identified in the distinct points of the Brillouin zone [1]; but so far TaAs has been obtained only in the form of bulk crystals [1-4]. We have grown TaAs by molecular beam epitaxy (MBE) on commonly used GaAs(001) substrates, in a III-V MBE system equipped with a valved cracker source for arsenic and e-beam source for Ta. TaAs crystallizes in a body-centred-tetragonal structure with the lattice parameters: $a = b = 3.4348 \text{ \AA}$; $c = 11.641$. Using in-situ reflection high energy electron diffraction (RHEED) we observe that in spite of a significant lattice mismatch to zinc-blende GaAs (with lattice parameter $a=5.653 \text{ \AA}$), TaAs grows on GaAs(001) in a fully 2-dimensional layer-by-layer mode, from the very first sub-monolayer deposition stage, with no initial 3-dimensional growth typical for epitaxy on the substrates with a high lattice mismatch. The orientation of TaAs is the same as that of the substrate, i.e. TaAs(001) planes are parallel to GaAs(001), but they are rotated by 45 degrees, hence the [110] in-plane direction of the GaAs substrate is parallel to the [010] one of TaAs. Such configuration decreases the lattice mismatch between TaAs and GaAs, but still it is as big as 19%. The twisting of TaAs(001) layers with respect to GaAs(001) substrate is observed in RHEED, and confirmed by X-ray diffraction and transmission electron microscopy (TEM) measurements. Even though no misfit dislocations are identified in TEM cross-sections visualizing the TaAs/GaAs interface, the TaAs surface morphology revealed by atomic force microscopy exhibits stripe-like structure with about 200 nm long and 20 nm thick planar columnar features parallel to GaAs[-110]. This hampers (so far) applicability of angle resolved photoemission spectroscopy (ARPES) to reveal topological properties typical to Weyl semimetals, such as bulk Dirac cones and surface Fermi arcs, due to much larger dimensions of UV-beam spot used in ARPES, but should not be an obstacle in much more local scanning tunneling spectroscopy measurements. The possibility of obtaining epitaxial layers of TaAs opens a way for integrating this WSM in heterostructures with other materials e.g. ferromagnets or superconductors, which enables investigations of proximity effects, impossible to explore using bulk TaAs crystals accessible so far.

This work has been supported by the National Science Centre (Poland), through the project No. 2017/27/B/ST5/02284, and by the Swedish Research Council through project No. 2017-04404.

- [1] Su-Yang Xu, et. al. *Science*, **349**, (2015), 613.
 [2] B. Q. Lv, et al. *Phys. Rev. X*, **5**, (2015), 031013.
 [3] L. X. Yang, et. al. *Nat. Phys.* **11**, (2015), 728.
 [4] Q. R. Zhang, et. al. *Phys. Rev. B* **100**, (2019), 115138.

4:00 PM *EQ08.02.05

Uncovering Chirality of Skyrmions in Polycrystalline B20 FeGe on Si Kayla Nguyen; University of Illinois at Urbana-Champaign, United States

Understanding chirality, the intrinsic handedness of a system, is important for future technologies using quantum magnetic materials. Of particular interest are magnetic skyrmions which are chiral and topologically protected, meaning that their spin textures can act as barriers from deformation in crystalline grains. However, most electron microscopy studies use Lorentz TEM or holography to investigate chirality of skyrmions in nearly perfect single crystals because Fresnel effects may cause signals from grain structures to be mistaken as magnetism when the two are comparable in size. In this work, we probe nanomagnetism of topological magnetic textures in sputtered thin film of B20 FeGe on Si to study the relationship between magnetic and crystal chirality. Using 4D-STEM, we find that the vorticity and helicity of these magnetic topological phases are coupled to the crystal chirality. Furthermore, our work shows that signals from magnetism can be disentangled from the crystalline effects for sub-micron grains, enabling a way to investigate topological magnetism in the presence of small polycrystalline grains. This methodology is important for spintronics and low-power magnetic memory technologies that rely on scalable techniques for large scale manufacturing of real devices.

- [1] Nguyen, KX et al., *Physical Review Applied*, **17**, 034066 (2022).

4:30 PM EQ08.02.06

Atomic-Resolution Mapping of Metal-Insulator Phase Coexistence in Epitaxially Strained Ca₂RuO₄ Noah Schnitzer¹, Oleg Y. Gorobtsov¹, Ziming Shao¹, Jacob P. Ruf^{1,2}, Berit H. Goodge^{1,3}, Hari P. Nair¹, Darrell Schlom^{1,3,4}, Kyle M. Shen^{1,3}, Andrej Singer¹ and Lena F. Kourkoutsis^{1,3}; ¹Cornell University, United States; ²Max Planck Institute for Chemical Physics of Solids, Germany; ³Kavli Institute at Cornell for Nanoscale Science, United States; ⁴Leibniz-Institut für Kristallzüchtung, Germany

Materials exhibiting metal-insulator transitions (MITs) have a variety of potential technological applications, but in many systems the mechanism of the transition and the coupling of electronic and lattice degrees of freedom are not fully understood. The Ruddlesden-Popper ruthenate Ca₂RuO₄ is a particularly interesting example due to the tunability of its MIT and strong lattice effects. Although both the metallic and insulating phases of Ca₂RuO₄ share the same P4mm symmetry, a structural transition is closely coupled to the electronic transition in which the insulating phase is distinguished by flattened octahedra [1]. The transition is highly sensitive to a variety of external stimuli including electric fields, with a threshold field of only 40 V/cm at room temperature [2], and epitaxial strain, which can tune the transition temperature over a broad range [3]. Notably, the current driven transition can result in extended stripe patterns of metallic and insulating phase coexistence, which are suggested to mediate the significant mismatch strain between the metallic and insulating phases [4, 5].

Here, a 40 nm thick Ca₂RuO₄ film epitaxially grown on LaAlO₃ is characterized through the MIT with scanning transmission electron microscopy (STEM). The compressive epitaxial strain stabilizes a uniform metallic phase at room temperature, but cryogenic STEM measurements reveal that upon cooling below ~230 K nanometer scale stripes emerge with modulated lattice parameters consistent with the insulating phase, forming a coherent extended nanostructure. Measurement of the nanostructure at atomic-resolution over hundreds of nanometers enables visualization of the complex mesoscale phase arrangement, as well as characterization of the atomic structure within the stripes and through the interfaces of the coexisting phases. In addition, nanoscale features such as defects, local strain gradients, and the substrate-film interface can be resolved and correlated with the nanostructure. Finally, taking advantage of recent instrumentation developments [6], the film is measured at atomic-resolution at intermediate temperatures between liquid nitrogen and room temperature, capturing the evolution of the nanostructure through repeated cycles of the MIT.

- [1] Braden, et al. *Physical Review B*, **58**, 847. (1998).
 [2] Nakamura, et al. *Scientific reports*, **3**, 1-6. (2013).
 [3] Dietl, et al. *Applied Physics Letters*, **112**, 031902. (2018).
 [4] Zhang, et al. *Physical Review X*, **9**, 011032. (2019).
 [5] Jenni, et al. *Physical Review Materials*, **4**, 085001. (2020).
 [6] Goodge, et al. *Microscopy and Microanalysis*, **26**, 439-446. (2020).

*Supported by the National Science Foundation (Platform for the Accelerated Realization, Analysis, and Discovery of Interface Materials (PARADIM)) under Cooperative Agreement No. DMR-2039380 and by the U.S. Department of Energy, Office of Science, Office of Basic Energy Sciences, under Contract No. DE-SC0019414.

4:45 PM EQ08.02.07

Quantitative Surface-Magnetic Imaging by SEMPA to Measure the Dzyaloshinskii-Moriya Interaction and Investigate Three-Dimensional Magnetic Topologic Structures Robert Frömter¹, Mona Bhukta¹, Takaaki Dohi¹, Maria A. Syskaki¹, Fabian Kloodt-Twesten², Hans P. Oepen² and Mathias Klau¹; ¹University of Mainz, Germany; ²Hamburg University, Germany

Scanning electron microscopy with polarization analysis (SEMPA) is a versatile tool for high-resolution magnetic surface imaging. The capability of synchronous vector imaging is especially useful for accurately determining the in-plane angle of the local magnetization vector. Domain walls in ultrathin films with DMI and out-of-plane magnetization show a thickness-driven continuous transition from Néel to Bloch orientation, which is due to the 1/d reduction in DMI strength that is competing with the dipolar energy of the wall's magnetic charge. By measuring the DW angle and modeling the dipolar energy the DMI strength can be determined. We present examples for epitaxial, in-situ grown layers of Co/Pt(111) and Co/Ir(111) [1,2], where due to the absence of DMI in the ferromagnet/vacuum interface exactly the DMI of one epitaxially ordered interface can be measured. While UHV conditions are required in SEMPA, there is in fact no strict limitation to imaging in-situ prepared, uncapped magnetic layers. After covering an ex-situ sputtered sample with 1 nm of Pt imaging is still possible, however at reduced magnetic contrast [3]. This enables surface imaging of sputtered multilayer stacks with varied couplings that can host three-dimensional magnetic structures. Of special interest is this for imaging synthetic antiferromagnets [4], where due to the high surface sensitivity of less than one nanometer no contrast reduction from the AF coupled second layer occurs. The combination of high-resolution surface in-plane imaging with micromagnetic simulation and additional, less surface-sensitive microscopy methods allows for successful investigation of such structures. By tilting the sample or using additional techniques like MFM the out-of-plane component of the magnetization gets accessible and thus chiral objects like skyrmions or merons can be identified.

- [1] E.C. Corredor, et al. *Phys. Rev. B* **96**, 060410(R), (2017).

- [2] F. Klodt-Twesten, et al. Phys. Rev. B **100**, 100402(R), (2019).
 [3] S. Kuhrau, et al. Appl. Phys. Lett. **113**, 172403, (2018).
 [4] T. Dohi et al, Nat. Commun. **10**, 5153 (2019).

SESSION EQ08.03: Probing High-Order Topological Structures III
 Session Chairs: Kayla Nguyen and Marta Rossell
 Tuesday Morning, November 29, 2022
 Sheraton, 2nd Floor, Republic A

8:30 AM *EQ08.03.01

Atomic-Scale Visualizations of Topological Defects in Charge Order Superlattices [Ismail El Baggari](#); Harvard University, United States

Charge order is the spontaneous formation of real space superstructures driven by electron-lattice coupling. Similar to other ordered structures such as crystals and magnetic lattices, charge order superlattices may exhibit a variety of defects with emergent properties. Here we use atomic-resolution scanning transmission electron microscopy (STEM) to visualize phase fluctuations and defects in charge order including dislocations, compression and shear deformations. These defects in the superlattice play a key role in nanoscale competition, incommensurate order, and long-range correlations. In particular, STEM shows how topological defects (dislocations) in the charge order lattice of a manganite destroy long-range ordering and host competing charge order instabilities. Non-equilibrium conditions can generate even more complex phase defect structures in charge order superlattices. In the case of 1T-TaS₂ following ultrafast light excitation, we observe the formation of long-lived metastable charge order twins. Remarkably, these twins are delineated by a series of dislocations similar to low-angle grain boundaries. These atomic-resolution STEM visualizations show that charge order is a promising platform for realizing novel topological defects that are often intertwined with competing electronic instabilities.

9:00 AM *EQ08.03.02

Direct Electromagnetic Field Imaging by Atomic-Resolution Differential Phase Contrast STEM [Naoya Shibata](#)^{1,2}; ¹The University of Tokyo, Japan; ²Japan Fine Ceramics Center, Japan

Differential phase contrast imaging in aberration-corrected scanning transmission electron microscopy (DPC STEM) brings the possibility to probe the electromagnetic field distribution in materials and devices down to the atomic scale. Recently, it has been shown that intrinsic magnetic fields of an antiferromagnet can be visualized in real space by this technique. However, when applying this technique to crystal defects such as interfaces and dislocations, concomitant diffraction contrast has been a serious issue. We have developed a novel scanning system to suppress diffraction contrast in DPC images, and quantitative electromagnetic field imaging at defect regions becomes possible. In this talk, several applications of DPC STEM to crystal interfaces will be reported.

9:30 AM *EQ08.03.03

Discoveries of "Hidden" Topologies Occurring Intrinsically Within a Multiferroic Matrix [Lynette Keeney](#)¹, [Kalani Moore](#)², [Eoghan O'Connell](#)², [Sinead M. Griffin](#)³, [Clive Downing](#)⁴, [Louise Colfer](#)¹, [Michael Schmidt](#)¹, [Valeria Nicolosi](#)⁴, [Ursel Bangart](#)² and [Michele Conroy](#)^{5,2}; ¹Tyndall National Institute, Ireland; ²University of Limerick, Ireland; ³Lawrence Berkeley National Laboratory, United States; ⁴Trinity College Dublin, The University of Dublin, Ireland; ⁵Imperial College London, United Kingdom

Single-phase multiferroics intertwine ferroelectric and ferromagnetic properties, providing novel ways to manipulate data and store information, as well as providing opportunities for exploring new chemistry and physics. In practice, due to the fundamental contra-indication between ferroelectricity (empty d^0 electronic structures) and ferromagnetism (occupied d^n electronic structures), single-phase multiferroics are exceedingly scarce. In recent years, we reported the design of such a novel room temperature magnetoelectric multiferroic material that could ideally be suited to future fabrication of revolutionary memory devices. To achieve this design, we took the approach of creating a new layered Aurivillius composition, $\text{Bi}_6\text{Ti}_x\text{Fe}_y\text{Mn}_z\text{O}_{18}$ (B6TFMO; $x = 2.80$ to 3.04 ; $Y = 1.32$ to 1.52 ; $Z = 0.54$ to 0.64), which combines differing types of A -site (Bi^{3+}) and B -site (Ti^{4+} , Fe^{3+} , $\text{Mn}^{3+/4+}$) cations, to drive both ferroelectricity and ferromagnetism within the same structural phase.

While this is a rare breakthrough on its own, in this presentation I will describe how we have lately uncovered remarkable polar topological structures close to regions where the B6TFMO layering is disrupted by naturally occurring structural defects. Here, the internal elastic strain and electrostatic energy gradients are altered to give rise to an inhomogeneous polarisation distribution of polar magnitude and polar rotation angle. Atomic resolution scanning transmission electron microscopy, in conjunction with polar displacement mapping, reveals nominally charged ferroelectric domain walls and non-trivial continuous rotations of ferroelectric polarisation into exotic polar vortex structures. These emergent topological structures hitherto lay "hidden", previously undiscovered within multiferroic B6TFMO, however they occur intrinsically, without the need for an artificial interface and in the absence of external strain engineering.

These distinctive types of 2D topologies are intriguing entities in matter, because they can offer spatially confined emergent functional properties, such as electrical conductivity within an otherwise insulating matrix. The internal characteristic length scales of these polar vortex domain walls (~5 nm) are much more compact than that of their magnetic counterparts (~10 to 100 nm), signifying potential to transcend the limits of classical data storage.

10:00 AM BREAK

10:30 AM EQ08.03.04

Revealing Fast Cu-Ion Motion in CuInP_2S_6 - $\text{In}_{4/3}\text{P}_2\text{S}_6$ Flakes Through the Ferroelectric to Pseudoferroelectric Phase Transition [Marti Checa](#)¹, [Xin Jin](#)^{2,3}, [Sabine Neumayer](#)¹, [Ruben Millan-Solsona](#)^{4,5}, [Michael A. Susner](#)⁶, [Michael McGuire](#)⁷, [Andrew O'Hara](#)², [Gabriel Gomila](#)^{4,5}, [Peter Maksymovych](#)¹, [Sokrates Pantelides](#)² and [Liam Collins](#)¹; ¹Center for Nanophase Materials Sciences, Oak Ridge National Laboratory, United States; ²Vanderbilt University, United States; ³Institute of Physics & University of the Chinese Academy of Sciences, China; ⁴Institut de Bioenginyeria de Catalunya (IBEC), The Barcelona Institute of Science and Technology (BIST), Spain; ⁵Universitat de Barcelona, Spain; ⁶Materials and Manufacturing Directorate, Air Force Research Laboratory, United States; ⁷Materials Science and Technology Division, Oak Ridge National Laboratory, United States

Van der Waals layered materials exhibiting robust room temperature ferroelectricity offer a versatile platform for miniaturization of ferroelectric device technology. Within this class of 2D material systems, CuInP_2S_6 has received a significant degree of interest due to the revelation of ionically mediated polarization switching pathways, multistate ferroelectricity, ionic conduction, and complex interfacial chemistry. Moreover, it is possible to form stable self-assembled heterostructures of ferroelectric CuInP_2S_6 (CIPS) and non-ferroelectric (i.e., lacking Cu) $\text{In}_{4/3}\text{P}_2\text{S}_6$ (IPS), by controlling the targeted

composition and kinetics of synthesis. To date, the properties of CIPS/IPS interfaces naturally forming by in-plane epitaxy have received little attention. In this work, we use an advanced scanning probe microscopy approach to explore in detail the nanoscale variability of the AC ion-transport dependent functional properties (electromechanical, dielectric, and conductive) in CIPS-IPS flakes during the ferroelectric-paraelectric transition. First, we show evidence of a kHz ionically mediated electromechanical response of CIPS in the paraelectric phase (above TC). Second, we reveal the local dielectric constant and ionic conductivity changes across the CIPS-IPS heterostructure, by local in-situ imaging and explaining the dielectric peak of the ferroelectric phase transition with scanning probe microscopy. Finally, we find a temperature enhanced dielectric loss/ionic conductivity at the CIPS/IPS boundary that we propose is a result of enhanced Cu motion at the CIPS/IPS interface as supported by DFT calculations. Our results expose a new insight into polar properties of CIPS and open the possibility for tuning interfacial properties of the CIPS/IPS interface.

10:45 AM *EQ08.03.05

Synthesis of a Quantum Spin Liquid in the Thin-Film Form [Julia Mundy](#)¹, Johanna Nordlander¹, Margaret Anderson¹, Ismail El Baggari² and Charles Brooks¹; ¹Harvard University, United States; ²The Rowland Institute at Harvard University, United States

Magnetically frustrated materials offer a playground for realizing exotic magnetic ground states such as quantum spin ices and spin liquids. Synthesizing such quantum magnets in thin-film form allows further tuning of the magnetic ground state with dimensionality and epitaxial strain as well as the possibility to integrate these states with other functional materials. Here we use reactive oxide molecular beam epitaxy to synthesize thin films of hexagonal TbInO₃. This material is isostructural to the well-studied multiferroic material YMnO₃. Due to a lattice distortion accompanied by an improper ferroelectric polarization at high temperatures, the Tb³⁺ sublattice exhibits a stuffed honeycomb geometry which hosts frustrated magnetism. We study the interplay of ferroelectricity and the frustrated magnetic order in the thin film geometry.

11:15 AM *EQ08.03.06

Magnetolectric Correlations in Inhomogeneous Multiferroics [Manfred Fiebig](#); ETH Zürich, Switzerland

Magnetolectric coupling phenomena in multiferroics were initially treated almost exclusively as bulk effects exhibited by homogeneous materials. In recent years, however, attention has moved to the inhomogeneous distributions of the multiferroic order down to the nanoscale. On the one hand, magnetolectric phase control ultimately happens on the level of the mostly sub-micrometer-sized domains. On the other hand, domain walls, interfaces and thin films are nanoscale and/or topological objects that have been proving to be the source of intriguing magnetolectric coupling effects. In my talk, I will therefore explore the fascinating world of magnetolectric correlations in multiferroics that are inhomogeneous at the nanoscale and demonstrate their enormous potential for new types of correlations. Examples will include [1] a seemingly contradictory coexistence of strong local and forbidden global magnetolectric coupling; [2] conversion of a multiferroic bulk state into a multiferroic domain wall in a non-multiferroic environment; [3] magnetolectric transfer of an order parameter with a joking reference to teleportation.

SESSION EQ08.04: Theory of Higher Order Topological Structures

Session Chairs: Sinead Griffin and Juan Idrobo

Tuesday Afternoon, November 29, 2022

Sheraton, 2nd Floor, Republic A

1:30 PM *EQ08.04.01

A Magnetolectric Multipolar Taxonomy of Topologies [Nicola Spaldin](#); ETH Zurich, Switzerland

We will show how many popular real-space electric or magnetic topologies can be classified in terms of their underlying magnetolectric multipoles. The magnetolectric multipoles form the next-order term, beyond the magnetic dipole, in the multipole expansion of a general magnetization density in a spatially varying magnetic field. They are known to occur in all linear magnetolectric materials, where their simultaneous breaking of time-reversal and space-inversion symmetry is both responsible for the linear magnetolectric effect, and contributes to the surface magnetization. Here we will describe other occurrences of magnetolectric multipoles that are relevant for real-space magnetic and electric topologies in materials. First, we will show that magnetic skyrmions can be classified in terms of magnetolectric multipoles, allowing a straightforward determination of their textures via a magnetolectric response measurement. Then we will show that conventional, non-magnetic ferroelectric materials contain hidden *reciprocal-space* magnetolectric multipoles that should be detectable using magnetic measurements such as Compton scattering. Finally, we will discuss how the magnetolectric multipoles manifest when topologically non-trivial real-space electric structures evolve in time.

2:00 PM *EQ08.04.02

Foundations of Topology in Ferroelectrics [Igor Lukyanchuk](#); University of Picardie, France

During the past decade, it has been realized that various topological structures, arising in ferroelectrics may significantly contribute to their physical properties. Even the simplest topological formation, domain walls (DWs), bring new functional complexity and open a new avenue in the operating of ferroelectric devices at the nanoscale. Here we generalize topological consideration of the nanostructured ferroelectrics to small nanoparticles, nanodots, films, and nanorods and show that the topologically stable *knotted* of the polarization field lines and *topological chirality* results in a wealth of useful functionalities such as optical activity and THz vibrations of DWs.

Importantly, despite the seeming similarity, the origin of topological structures is very different in magnetic and ferroelectric systems. In magnetic systems, it is the local built-in Dzyaloshinskii-Moriya interaction that induces the long-range chiral ordering of topological excitations. At variance, a distinct feature of ferroelectrics is that the topological excitations appear as a result of the spontaneous symmetry breaking due to an interplay of the confinement and depolarization effects where the topological excitations are generated by the long-range interaction of the depolarization charges, $\rho = -\text{div}P$. Upon confinement the polarization field swirls to keep its divergenceless structure, the situation being similar to the incompressible liquid flow in the whirlpools or to the magnetohydrodynamic flow of the plasma interior of the stars. The topological classification scheme of these formations, unified by the constraint of the divergenceless of the vector field is by far more complex than that for the magnetic systems.

We demonstrate that the advanced 3D topological excitations, *vortices*, *skyrmions*, and *Hopfions*, characterized by the nontrivial *linking numbers* and *helicity* arise inside the nanostructured ferroelectrics and mimic the "topology of the Universe". Our consideration is in-line with the ongoing paradigmatic shift in physics, marking the change from deriving properties of the matter out of the local structural symmetries to the global topological paradigm, which describes the fundamental properties of matter on the basis of their invariance under continuous transformations or perturbations.

2:30 PM BREAK

3:00 PM *EQ08.04.03

Chiral Phase Transitions in Topological Phases at Oxide Superlattices Fernando Gómez-Ortiz¹, Pablo García-Fernández¹, Juan M. López², Piusch Behera³, Ramamoorthy Ramesh³ and Javier Junquera¹; ¹University of Cantabria, Spain; ²Instituto de Física de Cantabria, University of Cantabria, Spain; ³University of California, Berkeley, United States

Over the past few years, the existence of materials capable of showing non-trivial topological textures of the polarization pattern has attracted lots of attention triggered by the presumably higher density (due to their smaller sizes) and faster response (phonon frequencies typically range in the THz regime) than their magnetic counterparts making them good candidates for next generation electronic devices. In particular, structures arising in polar oxide nanostructures, due to the delicate interplay between elastic, electrostatic and gradient energies have emerged as a fertile playground to observe novel emergent phenomena and exotic dipole textures. Most studies were performed embedding a prototype ferroelectric (PbTiO₃) in superlattices with a prototype dielectric (SrTiO₃). Theoretical predictions together with an atomically precise synthesis and characterization of materials have led to the observation of flux-closure [1], vortices [2], skyrmions [3] or merons [4] depending on the periodicity, mechanical and electrostatic boundary conditions. This delicate balance and multimimima potential energy surface suggest a very rich phase diagram with novel phase transitions [5-7] together with exotic physical responses such as negative capacitance [8] or chirality [9]. The involved typical sizes and the will of studying the dependence of the polar texture with external stimuli such as temperature or electric fields require the development of new modelling tools. In this respect, second-principles methods [10-11] are emerging as a valuable solution for such a problems.

In this talk, I shall describe the path of phase transitions occurring in the polar vortex chiral structures upon increasing temperature and characterize them with appropriate order parameters [12]. Although the overall polarization is zero throughout the process, the system suffers a first-order first transition from a chiral-crystal to a chiral-liquid of polarization vortices upon increasing temperature. Finally, a second order phase transition is found at higher temperatures where the mirror symmetry is restored and the system becomes a disordered achiral-liquid. Moreover, in the ordered polar vortex phase, under suitable mechanical (epitaxial strain) and electrostatic boundary conditions (built in potential), a deterministic and reversible control of chirality over mesoscale regions have been found under the application of homogeneous electric fields [13]. Second-principles simulations together with second-harmonic generation based circular-dichroism measurements have shown the existence of hysteresis between left- and right-handed chiral states under the application of such electric fields.

We acknowledge the continuous feedback and support of the experimental groups led by Prof. R. Ramesh, L. W. Martin and S. Salahuddin from University of California-Berkeley and by D. A. Muller from University of Cornell. The authors acknowledge financial support from grant PGC2018-096955-B-C41 funded by MCIN/AEI/10.13039/501100011033 and by "ERDF a way of making Europe". FGO acknowledge support from grant FPU18/04661 funded by MCIN/AEI/10.13039/501100011033.

- [1] Y. L. Tang et al. *Science* **348**, 547 (2015)
- [2] A. K. Yadav et al. *Nature* **530**, 198 (2016)
- [3] S. Das et al. *Nature* **568**, 368 (2019)
- [4] Y. J. Wang et al. *Nat. Mater.* **19**, 881 (2020)
- [5] Y. Nahas et al. *Nature* **577**, 47 (2020)
- [6] Y. Nahas et al. *Phys. Rev. Lett.* **119**, 117601 (2017)
- [7] L. Zhou et al. *Adv. Funct. Mater.* 2111392 (2022)
- [8] A. K. Yadav et al. *Nature* **565**, 468-471 (2019)
- [9] P. Shafer et al. *Proc. of the Natl. Acad. Sci. U.S.A.*, **115**, 915-920 (2018)
- [10] J. Wojdel et al. *J. of Phys.: Condens. Matter*, **25**, 305401 (2013)
- [11] P. García-Fernández et al. *Phys. Rev. B*, **93**, 195137 (2016)
- [12] F. Gómez-Ortiz et al. *Phys. Rev. B*, **105**, L220103 (2022)
- [13] P. Behera et al. *Sci. Adv.* **8**, eabj8030 (2022)

3:30 PM EQ08.04.04

Instability of Dynamical Axion Mode Towards Finite-Momentum Jonathan Curtis, Ioannis Petrides and Prineha Narang; Harvard University, United States

The chiral anomaly is a striking signature of quantum effects which leads to violations of the continuity equation for a classically conserved current. In the case of a Weyl semimetal, this leads to a breakdown in the conservation of the chiral-charge current, which is conserved by the classical dynamics. In condensed matter systems this leads to a signature magnetoelectric response associated to anomaly due to the separation of the Weyl points in momentum space. In the presence of strong interactions however, a Weyl semimetal phase become unstable towards spontaneous symmetry breaking. If the chiral symmetry is spontaneously broken this then leads to a Goldstone mode which couples to the chiral anomaly leading to a dynamical magnetoelectric response -- a situation known as a dynamical axion insulator.

Here we consider a simple model of a charge-density wave in a Weyl semimetal and calculate the equations of motion for the Goldstone mode. Surprisingly, we find that the Goldstone mode appears to exhibit a negative phase stiffness, signalling instability of the mean-field towards finite momentum condensation. This is expected to lead to very strong fluctuations in the dynamical anomaly. We suggest a suitable long-wavelength theory which may govern the new axion dynamics in this system and comment on possible signatures.

3:45 PM EQ08.04.05

Coexistence of Kondo Effect and Weyl Semimetallic States in Mn-Doped Mn_xVAI₃ Compounds Kwan-Young Lee and Jong-Soo Rhyee; Kyung Hee University, Korea (the Republic of)

Topological Dirac and Weyl semimetals are a 3-dimensional topological phase of matter, exhibit gapless energy bands with bulk band crossing that lead to the linear band dispersion. Degenerated Dirac bands are separated by breaking of topological symmetries, resulting in the formation of Weyl semimetal. The strong correlation effect in topological Weyl semimetal is a critical issue in condensed matter physics. Recently, one of the strong correlation effect, the Kondo effect, in Weyl semimetal was theoretically proposed but not yet realized experimental point of view. Here we suggest a coexistence of the Weyl semimetal and Kondo effect in disordered Mn-doped Mn_xVAI₃. Dilute magnetic element Mn-doping in type-II Dirac semimetal VAI₃ acts as a magnetic impurities that induces the tuning of its chemical potential so the Dirac points go closer to the Fermi energy and lifts its band degeneracy, leading to the Weyl semimetal topological phase transition. We observed the Kondo effect by several experimental points of view. Especially, the Kondo effect has confirmed by the electrical resistivity minimum at T_K = 40 K, and logarithmic increase of electrical resistivity, magnetic susceptibility, and specific heat divided by temperature with a significant Sommerfeld coefficient at low temperature. Furthermore, in order to confirm the topological phase transition from Dirac to Weyl semimetal, we affirm the experimental suggestion of Weyl semimetallic phase. One of the representative confirmation of the Weyl semimetal is the angle-resolved magnetoresistance, which has revealed the negative longitudinal magnetoresistance below Kondo temperature due to the chiral anomaly in Mn-doped Mn_xVAI₃. At low temperature below Kondo temperature (T ≤ T_K), the exchange interaction by RKKY interaction in Mn_xVAI₃

breaks time-reversal symmetry even in Kondo screening, resulting in the topological phase transition from Dirac to Weyl semimetal. Also the angle-dependent planar Hall effect can manifest the nontrivial Berry phase of matter and the chiral anomaly which elucidates the same physical origin with negative longitudinal magnetoresistance. This research shows the coexistence of the Kondo effect and Weyl semimetallic state in experimental viewpoint as well as the temperature-induced topological phase transition.

4:00 PM EQ08.04.06

How the Interplay of Spin-Orbit Coupling and Correlations Affects the Multipolar Order in $\text{Ba}_2\text{MgReO}_6$ Maximilian E. Merkel and Claude Ederer; ETH Zurich, Switzerland

Double perovskites with an open transition-metal 5d shell are interesting materials because they are influenced by the interaction of correlation and spin-orbit coupling effects, similar to Osmate and Iridate compounds.

Here, we present our study on $\text{Ba}_2\text{MgReO}_6$, an insulating double perovskite with a structural transition at 33 K and a Néel temperature of 18 K. In a previous study with density-functional theory (DFT)+U [1], the authors could correctly describe the two low-symmetry phases but not the cubic, paramagnetic phase above 33 K, which came out metallic.

Using DFT+dynamical mean-field theory (DMFT), we first show that we can obtain the cubic, insulating phase with a moderate Hubbard U, showing the importance of correlations in $\text{Ba}_2\text{MgReO}_6$, which are due to the narrow Re-t_{2g} bands.

We then look at how the interplay of Hubbard U and spin-orbit coupling can trigger a metal-insulator transition to better understand the physics at play here. Finally, we analyze whether charge quadrupoles or hexadecapoles couple more strongly to the phase transition from cubic to tetragonal at 33 K and compare them quantitatively to the DFT+U results.

4:15 PM EQ08.04.08

Crystal Growth of Inter-Metallic Rhodium Compounds Nikola Subotić¹, Mochiku Takahashi², Yoshitaka Matsushita², Osamu Takeuchi¹, Hidemi Shigekawa¹, Takanari Kashiwagi¹ and Kazuo Kadowaki¹; ¹University of Tsukuba, Japan; ²National Institute for Materials Science, Japan

Our previous results on the RhPb_2 intermetallic compound [1] inspired us to search for new Rh compounds that may have topological and superconducting properties. Preliminary investigation of them in the ternary Au-Rh-Pb phase diagram has shown that AuPb_4Rh_5 exists newly [2]. Moreover, resistivity measurements of the grown crystals that had a chemical composition close to AuPb_3Rh_3 (EPMA results) have shown two superconducting transitions at 1.73 K and 2.8 K, which do not correspond to the transition temperatures of superconductors from the binary Au-Pb and Rh-Pb phase diagrams.

Further investigation of the ternary phase diagram yielded unexpected results. The EPMA measurements of grown crystals with an infrared mirror furnace similar to RhPb_2 [1] having the initial molar ratio of Au:Pb:Rh=1:4:1 showed that the crystals are Rh_2Pb_3 , which seems not to exist to our knowledge or in the known binary Rh-Pb phase diagram [3]. This implies that the current understanding of the binary Rh-Pb phase diagram is incomplete.

During the RhPb_2 melting experiments[1], it was noted that Fe does react with the Rh-Pb alloy, indicating that some compounds might form. This inspired us to investigate further other phase diagrams as well. The melting experiments with a muffle furnace have shown that square-plate-like crystals can grow on the surface of the boule from the melt with an initial molar ratio of Au:Fe:Rh:Pb=2:2:1:4. Surprisingly, the EPMA measurements have shown that the grown crystals do not contain Au and Pb and it turns out finally to be FeRh. To our knowledge, this is the first time that single crystals of FeRh are grown from the melted flux of Au and Pb. The inter-metallic FeRh compound has been studied in the past intensively on peculiar ferromagnetic to antiferromagnetic transition, anomalous thermodynamical properties, crystal structural transformation, *etc.* near the stoichiometric 1:1 composition of Fe and Rh. However, the lack of a good single crystal has hindered understanding of these interesting properties of the RhFe intermetallic compound. The single crystal made by our method will enable us to understand more deeply the intriguing RhFe intermetallic compound.

[1] N.Subotić, *etc.* MRS Advances (2022) <https://doi.org/10.1557/s43580-022-00292-5>.

[2] N.Subotić, *etc.* to be published

[3] "Phase Equilibria, Crystallographic and Thermodynamic Data of Binary Alloy, Pb-Rh (Lead-Rhodium)", Landolt-Börnstein -Group IV Physical Chemistry **51** (1998) 321.

SESSION EQ08.05: Poster Session: Higher-Order Topological Structures in Real Space

Session Chairs: Michele Conroy and Dennis Meier

Tuesday Afternoon, November 29, 2022

8:00 PM - 10:00 PM

Hynes, Level 1, Hall A

EQ08.05.01

Characterization of Rare-Earth Titanate Pyrochlore Thin Films Synthesized by Molecular Beam Epitaxy Troy Powell, Margaret Anderson, Ari Turkiewicz, Nicole Taylor, Johanna Nordlander, Charles Brooks and Julia Mundy; Harvard University, United States

Pyrochlores are a class of metal oxide materials with the empirical formula $\text{A}_2\text{B}_2\text{O}_6\text{O}^\bullet$. Both the A^{3+} and B^{4+} sites are filled with select metal, metalloid, or lanthanide cations; the oxygen atoms coordinate roughly as a scalenohedron around the A site and as an octahedron around the B site¹. These specific oxidations and coordinations create the environment for the non-symmetric distribution of electrons in the lattice. This non-symmetric distribution is partially responsible for the 'spin-ice' behaviors of some pyrochlores². These metal cations also exhibit other unique magnetic properties including long-range ordered, spin-glass, and spin-liquid phases³. Here we synthesize thin films of pyrochlores using reactive-oxide molecular beam epitaxy. We study the structural and magnetic properties of rare-earth titanate pyrochlores thin films with a focus on oxidation and oxygen vacancies in these materials. Atomic-force microscopy (AFM) and x-ray diffraction (XRD) are used to verify the quality and identity of our grown films. We used SQUID magnetometry to characterize magnetic properties.

- 1 - Journal of Applied Physics 51, 290 (1980); <https://doi.org/10.1063/1.327368>
 2 - Nature Materials, 13(5), 488–493. <https://doi.org/10.1038/NMAT3924>
 3 - Reviews of Modern Physics, 82(1), 53–107. <https://doi.org/10.1103/RevModPhys.82.53>

EQ08.05.02

Doubled Quantum Spin Hall Effect in α -Antimonene Hsin Lin¹, Baokai Wang², Xiaoting Zhou², Yi-Chun Hung³, Yen-Chuan Lin³ and Arun Bansil²;
¹Academia Sinica, Taiwan; ²Northeastern University, United States; ³National Taiwan University, Taiwan

For a two-dimensional time-reversal symmetric system, the quantum spin Hall phase is assumed to be the same as the Z_2 topological insulator phase in the existing literature because the spin Chern number C_s and the Z_2 invariant yield the same topological classification. Here, by investigating the topological electronic structures of monolayer α -phase group V elements, we uncover the presence of a topological phase in α -Sb, which can be characterized by a spin Chern number $C_s=2$, even though it is Z_2 trivial. Our analysis shows that α -As and Sb share the same band representations at high-symmetry points (HSPs) and would thus both be classified as trivial insulators in terms of topological quantum chemistry (TQC) and symmetry indicators (SIs). However, we demonstrate the existence of a phase transition between α -As and Sb, which is induced by band inversions at two generic k points. In the absence of spin-orbit coupling (SOC), α -As is a trivial insulator, while α -Sb is a Dirac semimetal with four Dirac points (DPs) located away from the high-symmetry lines. Inclusion of the SOC gaps out the Dirac points and induces a nontrivial Berry curvature, endowing α -Sb a doubled quantum spin Hall insulator with a high spin Chern number of $C_s=2$. We further show that monolayer α -Sb exhibits either a gapless band structure or a gapless spin spectrum on its edges as expected from topological considerations.

EQ08.05.03

Electronic Structure Investigation of Magnetic Splitting and Gap Formation in Ferromagnetic Topological Insulator $(\text{Cr}_{0.35}\text{Sb}_{0.65})_2\text{Te}_3$ Chien Wen Chuang^{1,2}, Y. Nakata¹, K. Hori¹, F. M. F. de Groot³, F.-H. Chang², H.-J. Lin², C.-T. Chen², S. Gupta^{1,1,1}, F. Matsukura^{1,1,1}, S. Souma^{1,1}, T. Takahashi^{1,1,1}, T. Sato^{1,1,1} and A. Chainani²; ¹Tohoku University, Japan; ²National Synchrotron Radiation Research Center, Taiwan; ³Utrecht University, Netherlands

We study the temperature (T) dependent electronic structure and magnetic properties of a high Curie temperature ($T_c \sim 185$ K) ferromagnetic topological insulator $(\text{Cr}_{0.35}\text{Sb}_{0.65})_2\text{Te}_3$ using Cr L-edge and Te M-edge x-ray absorption spectroscopy (XAS), x-ray magnetic circular dichroism (XMCD), and angle-resolved photoemission spectroscopy (ARPES). The T -dependent XAS and XMCD results show a systematic and spin-selective splitting of Cr $3d$ and Te $5p$ unoccupied density of states, resulting in a magnetic gap opening. The T -dependent XMCD signal and magnetic gap are consistent with bulk magnetization as well as mean-field theory. The full-multiplet charge-transfer cluster model calculations with a negative charge transfer energy show a good agreement with the experimental Cr L-edge XAS and XMCD spectra. The ARPES measurements show the Dirac-cone topological surface states (SS) below and above T_c , implying that the band inversion between the Sb and Te orbital is maintained even at high Cr doping level, and is consistent with a negative charge transfer energy. These results establish a direct link between Cr $3d$ dopant states and the Te $5p$ SS forming the magnetic gap in $(\text{Cr}_{0.35}\text{Sb}_{0.65})_2\text{Te}_3$.

SESSION EQ08.06: Probing High-Order Topological Structures IV
 Session Chairs: Megan Holtz and Dennis Meier
 Wednesday Morning, November 30, 2022
 Sheraton, 2nd Floor, Republic A

8:45 AM *EQ08.06.01

Investigating Static and Dynamic Properties of Magnetic Hopfions with Advanced X-Ray Spectromicroscopies Peter Fischer^{1,2}; ¹Lawrence Berkeley National Lab, United States; ²University of California, Santa Cruz, United States

Topologically protected magnetic structures, such as skyrmions, are currently an intensely studied topic in the nanomagnetism community due to their scientific beauty and deep fundamental insight into nanoscale spin systems, but also with regard to potential future applications towards low-power, high-density and high-speed information technologies, which are required for the Internet-of-Things (IoT) and beyond [1-3]. Skyrmions are two dimensional chiral solitons where the magnetization smoothly covers a solid angle density of π radians coherently from the center of the spin texture to the opposite magnetization outside of the spin texture [4-5]. Recently, it has been realized, that expanding into the third dimension opens a door to explore highly complex topological magnetic structures that can only exist in 3D [6]. Among those 3D textures are magnetic Hopfions [7], which are three-dimensional knot-solitons with a topological class defined by its linking number. Theory has predicted that magnetic Hopfions can be stabilized, e.g., in chiral magnets. Those systems can host target skyrmions (TSks) which are seen as precursors to Hopfions [8-9]. Our recent research was able to stabilize magnetic Hopfions in tailored magnetic multilayers with a depth varying perpendicular anisotropy, and we confirmed the static properties of those Hopfion textures by a combination of two advanced x-ray spectromicroscopy techniques, specifically surface sensitive X-PEEM and bulk sensitive MTXM which allowed us to delineate Hopfions from TSks and torons [10]. In this presentation, we will discuss our recent experimental studies of the static character of magnetic Hopfions, using advanced X-ray microspectroscopy techniques, as well as results from micromagnetic simulations with high-performance computing (HPC), where we identified a field-driven transition from a Hopfion texture to a toron with distinct dynamics for each of the spin textures [11].

This work was supported by the U.S. Department of Energy, Office of Science, Office of Basic Energy Sciences, Materials Sciences and Engineering Division Contract No. DE-AC02-05-CH1123 in the Non-Equilibrium Magnetic Materials Program (MSMAG).

- [1] A. Fert, N. Reyren and V. Cros, Nature Reviews Materials **2** (7), 17031 (2017).
 [2] S. Woo, K. Litzius, B. Krüger, M.-Y. Im, L. Caretta, K. Richter, M. Mann, A. Krone, R. Reeve, M. Weigand, P. Agrawal, P. Fischer, M. Kläui, G.S.D. Beach, Nature Materials **15**, 501 (2016).
 [3] S. Woo, K.M. Song, H.-S. Han, M.-S. Jung, M.-Y. Im, K.-S. Lee, K.S. Song, P. Fischer, J.-I. Hong, J W Choi, B.-C. Min, H. C. Koo, J. Chang, Nature Comm **8**:15573 (2017)
 [4] H.-B. Braun, Advances in Physics **61** (1), 1-116 (2012).
 [5] A. N. Bogdanov and U. K. Röbber, Physical Review Letters **87** (3), 037203 (2001).
 [6] A. Fernández-Pacheco, R. Streubel, O. Fruchart, R. Hertel, P. Fischer and R. P. Cowburn, Nature Communications **8**, 15756 (2017).
 [7] Y. Liu, R. K. Lake and J. Zang, Phys Rev B **98** (17), 174437 (2018).
 [8] P. Sutcliffe, Journal of Physics A: Mathematical and Theoretical **51** (37), 375401 (2018).
 [9] N. Kent, R. Streubel, C.-H. Lambert, A. Ceballos, S.-G. Je, S. Dhuey, M.-Y. Im, F. Büttner, F. Hellman, S. Salahuddin and P. Fischer, Applied Physics

Letters **115** (11), 112404 (2019).

[10] N. Kent, N. Reynolds, D. Raftrey, I.T.G. Campbell, S. Virasawmy, S. Dhuey, R. V. Chopdekar, A. Hierro-Rodriguez, A. Sorrentino, E. Pereiro, S. Ferrer, F. Hellman, P. Sutcliffe, P. Fischer, Nature Communications 12 1562 (2021)

[11] D. Raftrey and P. Fischer, Phys Rev Lett 127, 257201 (2021)

9:15 AM EQ08.06.02

Controlled Ordering of Room-Temperature Magnetic Skyrmions in a Polar van der Waals Magnet Peter Meisenheimer¹, Hongrui Zhang¹, David Raftrey^{2,3}, Peter Fischer^{2,3}, Robert Birgeneau^{1,2} and Ramamoorthy Ramesh^{1,2}; ¹University of California, Berkeley, United States; ²Lawrence Berkeley National Laboratory, United States; ³University of California, Santa Cruz, United States

Skyrmions are topologically-protected magnetic quasiparticles that are of great interest for their potential use in spintronic memory and logic. This is especially true in systems with native non-centrosymmetry, since the inherent Dzyaloshinskii-Moriya interaction can stabilize a robust topological phase at or near room temperature and zero field. Control and understanding of ensembles of skyrmions is important for realization of devices based on the technology. In particular, the order-disorder transition associated with the 2D lattice of magnetic skyrmions can have significant implications for transport and other dynamic functionality. Here, we investigate the condensation of the skyrmion phase in a polar, Van der Waals magnet. We then demonstrate that we can engineer an ordered skyrmion crystal through structural confinement, demonstrating control over this order-disorder transition on scales relevant for device applications.

9:30 AM BREAK

10:00 AM EQ08.06.05

Ultra-Reactive Domain Liquid Phase in PbTiO₃/SrTiO₃ Superlattices Hugo Aramberri¹, Mónica Graf¹ and Jorge Íñiguez^{1,2}; ¹Luxembourg Institute of Science and Technology, Luxembourg; ²University of Luxembourg, Luxembourg

PbTiO₃/SrTiO₃ superlattices display topological dipole textures in the ferroelectric layer that have recently been found to present excitations in sub-terahertz frequencies. Moreover, a previous work discovered an ultra-reactive phase in these materials in which the thermal activation can cause the domain walls to move spontaneously, resembling the behaviour of a liquid. In this work we employ second-principles models to map the phase diagram of these superlattices, which features three phases that can be deemed as a solid, a liquid and a gas phase. We also use molecular dynamics to study and characterize the dynamic response of these phases. Our findings indicate how the response of these materials can be optimized with respect to the design parameters of the superlattices (layer thicknesses, strain) and temperature. The tuneable sub-terahertz response of these systems makes them interesting candidates for applications in high-speed telecommunications.

10:15 AM EQ08.06.06

Microscopic Origin of Dirac Mass Gap Variation in the Intrinsic Magnetic Topological Insulator MnBi₂Te₄ Mengke Liu^{1,2}, Chao Lei¹, Hyunsue Kim¹, Yanxing Li¹, Lisa Frammolino¹, Jiaqiang Yan³, Allan H. Macdonald¹ and Chih-Kang Shih¹; ¹The University of Texas at Austin, United States; ²Harvard University, United States; ³Oak Ridge National Laboratory, United States

In intrinsic magnetic topological insulators, Dirac surface state gaps are prerequisites for quantum anomalous Hall and axion insulating states. Unambiguous experimental identification of these gaps has proved to be a challenge, however. Here we use molecular beam epitaxy to grow intrinsic MnBi₂Te₄ thin films. Using scanning tunneling microscopy/spectroscopy, we directly visualize the Dirac mass gap and its disappearance below and above the magnetic order temperature. We further reveal the interplay of Dirac mass gaps and local magnetic defects. We find that in high defect regions, the Dirac mass gap collapses. *Ab initio* and coupled Dirac cone model calculations provide insight into the microscopic origin of the correlation between defect density and spatial gap variations. This work provides unambiguous identification of the Dirac mass gap in MnBi₂Te₄, and by revealing the microscopic origin of its gap variation, establishes a material design principle for realizing exotic states in intrinsic magnetic topological insulators.

10:30 AM EQ08.06.08

Spin Texture of 1D Chains of Magnetic Atoms in a Novel Air-Stable 2D Magnet Eugene Park¹, Julian Klein¹, Zhigang Song², John P. Philbin², Aubrey Penn¹, Mads Weile³, Baoming Wang¹, Prineha Narang² and Frances M. Ross¹; ¹Massachusetts Institute of Technology, United States; ²Harvard University, United States; ³Technical University of Denmark, Denmark

Van der Waals 2D magnetic materials have emerged as a novel platform that offers unique optoelectronic, magnetic, and quantum properties.¹ Such low-dimensional spin systems have vast potential in applications such as spintronics and nanoscale magnetic devices. The ability to engineer the structure and defects with respect to magnetic, optical, and electronic properties is critical. For example, an optically active single defect may have potential as a quantum emitter interacting with and embedded in the novel magnetic environment. Air-stable 2D van der Waals magnets are relatively unexplored, making the study of such materials intriguing and helpful for both fundamental research and device design.

Here, we examine the structural properties of the 2D magnet AgCrP₂S₆, a compound that is similar to the family of M₂P₂S₆. Using scanning transmission electron microscopy (STEM), we measure structural parameters, identify the 1D chain structure of magnetic atoms, and visualize the alignment of the magnetic chains between layers with atomic resolution. We also explore the nature of defects and the possibility of controlling defect location using the STEM beam. We expect this crystal structure to offer a high opportunity for anisotropy of its magnetic properties as a 2D van der Waals magnet. By parameterizing a model spin Hamiltonian based on density functional theory calculations, we predict an unusual spin structure that develops from the chain arrangement of the magnetic atoms in this material. We discuss measurements to verify the modelled spin configuration using vibrating sample magnetometry and other techniques. Lastly, we compare the defects, atomic structure transformations, and spin texture with a more studied 2D magnet, CrSBr^{2,3}, to better understand the fundamental properties of defects and structures in these novel air-stable 2D magnetic materials as a basis for future control and application of magnetic and optical properties.

References

1. Gibertini, M., Koperski, M., Morpurgo, A. F. *et al.* Magnetic 2D materials and heterostructures. *Nat. Nanotechnol.* **14**, 408-129 (2019).
2. Klein, J., Pingault, B., Florian, M. *et al.* The bulk van der Waals layered magnet CrSBr is a quasi-1D quantum material. arXiv:2205.13456 (2022).
3. Klein, J., Pham, T., Thomsen, J. D. *et al.* Atomistic spin textures on-demand in the van der Waals layered magnet CrSBr. arXiv:2107.00037 (2021)

1:30 PM *EQ08.07.02

Emergence of Ferromagnetic Topological Surface State in FeSi and Nonlinear Dynamics of Magnetic Domains Naoya Kanazawa; The University of Tokyo, Japan

A chiral compound FeSi is a prototypical example of the strongly-correlated *d*-electron insulators. Its peculiar charge and spin dynamics, which cannot be explained by a simple mean-field picture of nonmagnetic insulators, have provoked many important physical concepts such as *d*-electron Kondo insulator and insulator-to-metal (reversed Mott) transition due to on-site strong Coulomb interaction.

Triggered by recent new insights into topological aspects of correlated insulators, FeSi is attracting renewed attention for its unusual properties. However, it remains highly nontrivial that compounds made of light (and usually common) elements, like FeSi, can bear topological characteristics. As evidenced by the recent numerous researches, the topological insulators necessarily contain heavy (and generally rare) elements with strong spin-orbit coupling (SOC) to protect their topological band structure.

In this study, we successfully demonstrate a novel surface state hosting metallic conduction and ferromagnetic order in FeSi thin film with nonmagnetic bulk state. We identify that the surface state is not categorized into the class of topological insulators but can be described by a central concept in the modern theory of electric polarization, i.e., Zak phase. Owing to the dipolar charge distribution of Zak-phase origin, the surface state produces the strong SOC properties despite the absence of heavy-metal elements. By taking advantage of the emergent SOC, we also realize various types of nonlinear electrical conduction such as unidirectional magnetoresistance and current-induced magnetization switching. These nonlinear responses are rooted in the non-equilibrium spin accumulation and the consequent dynamics of magnetic domains.

Our results shed light on compounds made of common elements and demonstrate rich phenomena related to magnetic-domain dynamics at the new type of topological polar surface.

This work was done in collaboration with T. Hori, Y. Ohtsuka, M. Hirayama, A. Matsui, T. Nomoto, R. Arita, T. Nakajima, T. Hanashima, V. Ukleev, H. Aoki, M. Mogi, K. Fujiwara, A. Tsukazaki, M. Ichikawa, M. Kawasaki and Y. Tokura.

3:00 PM *EQ08.07.03

Skyrmions in Spin-Orbitronics and Orbitronics—Novel Science and Applications in Memory and Non-Conventional Computing Mathias Klauui; University of Mainz, Germany

Novel spintronic devices can play a role in the quest for GreenIT if they are stable and can transport and manipulate spin with low power. Devices have been proposed, where switching by energy-efficient approaches is used to manipulate topological spin structures [1,2].

Firstly, to obtain ultimate stability of states, topological spin structures that emerge due to the Dzyaloshinskii-Moriya interaction (DMI) at structurally asymmetric interfaces, such as chiral domain walls and skyrmions with enhanced topological protection can be used [3-5]. Here we will introduce these spin structures and we have investigated in detail their dynamics and find that it is governed by the topology of the spin structure [3]. By designing the materials, we can even obtain a skyrmion lattice phase as the ground state [4]. Beyond 2D structures, we recently developed systems with chiral interlayer exchange interactions that lend themselves to the formation of chiral 3D structures [6].

Secondly, for ultimately efficient spin manipulation, we use spin-orbit torques, that can transfer more than $1\hbar$ per electron by transferring not only spin but also orbital angular momentum. We combine ultimately stable skyrmions with spin orbit torques into a skyrmion racetrack memory device [4], where the real time imaging of the trajectories allows us to quantify the skyrmion Hall effect [5]. Recently, we determined the possible mechanisms that lead to a dependence of the skyrmion Hall effect on skyrmion velocity [7]. We furthermore use spin-orbit torque induced skyrmion dynamics for non-conventional stochastic computing applications, where we developed skyrmion reshuffler devices [8] based on skyrmion diffusion, which also reveals the origin of skyrmion pinning [8]. Such diffusion can furthermore be used for Token-based Brownian Computing and Reservoir Computing [9].

Beyond dynamics excited by spin-orbit torques the next step is to use orbital currents that generate orbital torques [10]. We have demonstrated that with an additional Cu/CuOx layer, the acting torques can be increased by more than a factor 10 [10]. This effect has been interpreted as resulting from an orbital Hall current that is converted to a spin current. Finally, an interfacial Orbital Rashba Edelstein Effect has been found, highlighting that the orbital analogues of both the spin Hall effect and the spin-based Rashba Edelstein or Inverse Spin Galvanic effect exist [11].

References

- [1] G. Finocchio et al., J. Phys. D: Appl. Phys., vol. 49, no. 42, 423001, 2016.
- [2] K. Everschor-Sitte et al., J. Appl. Phys., vol. 124, no. 24, 240901, 2018.
- [3] F. Büttner et al., Nature Phys., vol. 11, no. 3, pp. 225–228, 2015.
- [4] S. Woo et al., Nature Mater., vol. 15, no. 5, pp. 501–506, 2016.
- [5] K. Litzius et al., Nature Phys., vol. 13, no. 2, pp. 170–175, 2017.
- [6] D. Han et al., Nature Mater., vol. 18, no. 7, pp. 703–708, 2019.
- [7] K. Litzius et al., Nature Electron., vol. 3, no. 1, pp. 30–36, 2020.
- [8] J. Zázvorka et al., Nature Nanotechnol., vol. 14, no. 7, pp. 658–661, 2019;
- [9] R. Gruber et al., arxiv:2201.01618 (Nature Commun. in press (2022)).
- [10] K. Raab et al., arxiv: 2203.14720; M. Brems et al., Appl. Phys. Lett. 119, 132405, 2021.
- [11] S. Ding et al. Phys. Rev. Lett. 125, 177201, 2020; Phys. Rev. Lett. 128, 067201, 2022.
- [11] D. Go et al., EPL 135, 037002 (2021)

2:30 PM BREAK

3:30 PM *EQ08.07.04

Topological Vortex Domains in Quantum Materials Sang Wook Cheong; Rutgers Univ, United States

Engineering of domains and domain boundaries is quintessential for technological exploitation of numerous functional materials. However, it has only recently realized that the configuration of these domains/domain boundaries can have non-trivial topology. We will discuss a new topological classification scheme of domain/domain boundary configurations with Ising-type or two-dimensional order parameters: $Z_m \times Z_n$ domains (m directional variants and n translational antiphases) and Z_l vortices (where l number of domains and that of domain boundaries merge). This classification, with the concept of topological protection and topological charge conservation, has been applied to a wide range of materials such as improper ferroelectric R(Mn,Fe)O₃, antipolar In(Mn,Ga)O₃, hybrid improper ferroelectric (Ca,Sr)₃Ti₂O₇, chiral & helical Cr_{1/3}TaS₂, antiferromagnetic Nd₂SrFe₂O₇ & a-Fe₂O₃,

antiferromagnetic & superconducting $\text{Sr}_2\text{VO}_3\text{FeAs}$, and CDW systems such as 2H-TaSe_2 . We will also discuss the emergent physical properties of domain boundaries, distinct from those of domains. The presented topological consideration provides a basis in understanding the formation, kinetics, manipulation and property optimization of domains/domain boundaries in quantum materials.

4:00 PM EQ08.07.05

Low-Temperature Epitaxial Growth of Anti-Ferromagnetic MnTe at Bi_2Te_3 [Oleg Maksimov](#)¹, Katherine Hansen¹, Harish Bhandari¹, Bryan Rachmilowitz² and Ilija Zeljkovic²; ¹Radiation Monitoring Devices, United States; ²Boston College, United States

There is significant scientific and technological interest in the epitaxial integration of ferromagnetic or antiferromagnetic materials with the topological insulators (TI). This allows the introduction of the ferromagnetic order into a topological insulator system and may lead to the development of novel spin electronic devices. It is anticipated that these heterostructures can be used as novel magnetoresistive random access memory (MRAM) devices with high charge-to-spin conversion efficiency. This implies that TI-based heterostructures can switch between 0 and 1 memory states much more efficiently, while consuming lower energy than the state-of-the-art magnetic tunneling junction-based heterostructures that use transition metals. The TI-based devices will be less susceptible to weak disorder and perturbations since writing process will occur via conventional writing field while electrical read out process will be topologically protected.

A key requirement for an operational heterojunction is a successful coupling of a TI with the magnetic material, which is facilitated by “atomically-clean” and abrupt junction interface. This should involve low-temperature deposition of the magnetic layer on the TI surface. This eliminates usage of the standard magnetic materials growth techniques, such as molecular beam epitaxy (MBE) and pulsed laser deposition, as they require the substrate temperatures greater than 300-350 °C, above what TIs can survive.

Here, we report on the innovative approach to grow a room-temperature antiferromagnetic semiconductor (MnTe) using atomic layer deposition (ALD) and to epitaxially integrate it with the topological insulator (Bi_2Te_3). MnTe films were deposited at $\langle 100 \rangle$ GaAs and $\langle 111 \rangle$ InP. While the MnTe at $\langle 100 \rangle$ GaAs were polycrystalline, epitaxial growth was achieved at closely lattice-matched $\langle 111 \rangle$ InP at temperatures as low as 120 °C. Bi_2Te_3 was grown by MBE at $c\text{-Al}_2\text{O}_3$, *ex-situ* transferred into the ALD system, and used as a template for MnTe growth. High-resolution X-ray diffraction studies demonstrated that epitaxial MnTe growth was achieved at 120 °C. Transmission electron microscopy showed that the MnTe / Bi_2Te_3 interface was atomically sharp. No amorphous and / or disordered regions were present at the interface within the imaged regions. Magnetotransport properties of the ALD-grown MnTe were also studied and will be reported here.

In summary, ALD was successfully used for the low-temperature epitaxial integration of MnTe antiferromagnetic semiconductor with the Bi_2Te_3 topological insulator. This opens the path for the realization of near-room temperature energy-efficient spintronic devices.

4:15 PM EQ08.07.06

Surface Modalities of Stacked 2D Heterostructured Topological Materials [David C. Bell](#) and Austin Akey; Harvard University, United States

Topological materials present new challenges in terms of characterization, in particular how to minimize surface and sample damage while imaging and analyzing surfaces at the direct native level. Therefore, novel approaches are needed in order to correlate materials properties with surface topology. We have adapted LEEM multi-modal techniques such as Low Energy Electron Diffraction (LEED), Photoemission Electron Microscopy (PEEM) and in-situ ARPES with high temperature annealing to study individual surface modalities. We have examined various topological materials in the form of bulk 2D heterostructures, specifically artificially constructed metasurfaces with unique order parameters (spin, lattice, localized charge and collective excitations (such as plasmons)).

It is possible to form, via controlled growth, systems with heterointerfaces in bulk materials. We will present the structure analysis of a novel synthesized material $\text{Ba}_6\text{Nb}_4\text{S}_8$ along with key physical properties. This material naturally realizes vdW coupled heterointerfaces between transition metal dichalcogenide (TMD) monolayers (hexagonal NbS_2 , H-NbS_2) and insulating spacers Ba_3NbS_5 . TEM diffraction taken along the c-axis shows that the hexagonal spacer and TMD layers are commensurate. The electronic band structure can be understood as that resulting from superimposing a periodic potential defined by Ba_3NbS_5 onto monolayer H-NbS_2 . This is similar to the mechanism which yields flat bands and strongly correlated physics in twisted-bilayer graphene and TMD heterostructures. LEEM techniques and Low Voltage electron microscopy has been used to characterize grown materials with high resolution at low beam voltages to directly confirm structural layers, ordering and surface diffraction and relate them to metrics of possible topological material performance.

Acknowledgement

This work was supported by the STC Center for Integrated Quantum Materials, NSF Grant No. DMR-1231319. This work was supported by an MRI grant from the National Science Foundation DMR-1828237 “The acquisition of a Low Energy Electron Microscope for Nanoscience research”

References

- [1] Devarakonda A, Inoue H, Fang S, Ozsoy-Keskinbora C, Suzuki T, Kriener M, Fu L, Kaxiras E, Bell DC, Checkelsky J. G. *Science* Oct 9;370(6513):231-236 (2020).
- [2] Bell D, Erdman N. Low Voltage Electron Microscopy. Bell D, Erdman N, editors. Chichester, UK: John Wiley & Sons, Ltd; (2012)

SESSION EQ08.09: Virtual Session I: Higher-Order Topologies in Real Space II

Session Chairs: Michele Conroy and Zijian Hong

Wednesday Morning, December 7, 2022

EQ08-virtual

8:00 AM *EQ08.09.02

Spectroscopic Studies of the Topological Magnon Band Structure in a Skyrmion Lattice [Markus Garst](#); Karlsruhe Institute of Technology, Germany

When magnons propagate across a non-collinear magnetic texture, they collect a Berry phase that can be interpreted as the flux of a synthetic orbital magnetic field. This Berry flux is related to the topological skyrmion density of the magnetic texture. For a topologically non-trivial skyrmion configuration, the magnon thus experiences a synthetic Lorentz force that bends the quasi-classical trajectories of the magnons. For a skyrmion lattice, the average synthetic field is finite such that the magnons are confined to cyclotron orbits of the corresponding magnon Landau levels. This is reflected in a magnon band structure with finite Chern numbers. Here, we report on a series of spectroscopic studies of this band structure using various techniques that allow to probe different regimes in energy-momentum space: magnetic resonance spectroscopy [1], spin-wave spectroscopy [2], inelastic neutron scattering

[3] and Brillouin light scattering [4,5]. These techniques have been applied to various cubic chiral magnets like MnSi, FeCoSi and Cu₂OSeO₃, that are well described by a universal effective continuum theory parametrized by a few parameters only. The combined data from all techniques are found to be in quantitative agreement with theory.

- [1] R. Takagi, M. Garst, J. Sahliger, C. H. Back, Y. Tokura, S. Seki, Phys. Rev. B **104**, 144410 (2021).
- [2] S. Seki, M. Garst, J. Waizner, R. Takagi, N. D. Khanh, Y. Okamura, K. Kondou, F. Kagawa, Y. Otani, Y. Tokura, Nat. Commun. **11**, 256 (2020).
- [3] T. Weber, D. M. Fobe, J. Waizner, P. Steffens, G. S. Tucker, M. Boehm, L. Beddrieh, C. Franz, H. Gabold, R. Bewley, D. Voneshen, M. Skoulatos, R. Georgii, G. Ehlers, A. Bauer, C. Pfeleiderer, P. Boeni, M. Janoschek, M. Garst, Science **375**, 1025 (2022).
- [4] N. Ogawa, L. Koehler, M. Garst, S. Toyoda, S. Seki, Y. Tokura, PNAS **118**, e2022927118 (2021).
- [5] P. Che, R. Ciola, V. Kravchuk, M. Garst, D. Grundler, unpublished.

8:30 AM *EQ08.09.03

Topological Magnetic Structures and Their Dynamics [Karin Everschor-Sitte](#); University of Duisburg-Essen, Germany

The current-induced dynamics of magnetic structures is quite complex. For example, magnetic skyrmions allow for ‘banana kicks’ in magnetism, i.e., not only a motion of the skyrmions along but also transverse to the current direction. This effect, which has become known as the skyrmion Hall effect [1,2,3], is often disruptive for device applications. In this talk, we will present possibilities of how to eliminate the skyrmion Hall effect [4,5]. As a particular example, we discuss helical phases which provide confined one-dimensional channels for high-speed skyrmion motion. We discuss how skyrmions can be generated in such helical backgrounds and analyze their stability [6].

Moreover, we will address the role played by topology in the physics of the skyrmion Hall effect. For example, it is widely believed that the skyrmion Hall effect, vanishes for overall topologically neutral structures such as (synthetic) antiferromagnetic skyrmions and skyrmioniums due to a compensation of Magnus forces. While this is true for spin-transfer torque-driven skyrmions, we show that this simple picture is generally false for spin-orbit torque-driven objects [7]. We find that the skyrmion Hall angle for spin-orbit torque-driven skyrmions is directly related to their helicity, which imposes an unexpected roadblock for developing faster and lower input racetrack memories based on spin-orbit torques.

- [1] T. Schulz, et al., Nat. Phys. **8**, 301 (2012)
- [2] K. Litzius, et al., Nat. Phys. **13**, 170 (2017)
- [3] W. Jiang, et al., Nat. Phys. **13**, 162 (2017)
- [4] R. Zarzuela, et al., Phys. Rev. B **101**, 054405 (2020)
- [5] K.-W. Kim, et al., Phys. Rev. B **97**, 224427 (2018)
- [6] R. Knapman, et al., J. Phys. D: Appl Phys. **54**, 404003 (2021)
- [7] R. Msiska, et al., Phys. Rev. Appl. **17**, 064015 (2022)

9:00 AM EQ08.09.04

Thermodynamic and Symmetry Aspects of Multiferroic Materials [Jiri Hlinka](#); Czech Academy of Sciences, Czechia

This contribution is aimed to address the trends in multiferroics research in a broader context of thermodynamics and symmetry theory. This would allow me to remind the conference audience about reflections about the multiferroics and their topological defects by the late Prof. Janovec from our Institute. Finally, I would like to address the incomplete analogy between physics of ferromagnets and ferroelectrics in the context of formation of spatially modulated ferroic phases and skyrmion condensate phases.

9:15 AM DISCUSSION TIME

SESSION EQ08.10: Virtual Session II
Session Chairs: Michele Conroy and Zijian Hong
Wednesday Morning, December 7, 2022
EQ08-virtual

10:30 AM *EQ08.10.01

Novel Methods Enabling Characterisation of Topological Structures [Laura Clark](#); University of Leeds, United Kingdom

With reference to structured electron illumination (including electron vortex beams) and four-dimensional STEM algorithm developments (including DPC and ptychography), in this talk I will discuss recent developments of (S)TEM techniques enabling improved characterisation of topological structures.

11:00 AM *EQ08.10.02

Structural Chirality of Polar Skyrmions Probed by Resonant Elastic X-Ray Scattering [Margaret McCarter](#)¹, [Kook Tae Kim](#)², [Vladimir Stoica](#)^{3,4}, [Sujit Das](#)⁵, [Christoph Klewe](#)⁶, [Elizabeth Donoway](#)¹, [David M. Burn](#)⁷, [Padraic Shafer](#)⁶, [Fanny Rodolakis](#)³, [Stephen Lovesey](#)⁷, [Gerrit van der Laan](#)⁷, [Se Young Park](#)², [John Freeland](#)³, [Dong Ryeol Lee](#)² and [Ramamoorthy Ramesh](#)^{1,1,6}; ¹University of California, Berkeley, United States; ²Soongsil University, Korea (the Republic of); ³Argonne National Laboratory, United States; ⁴Pennsylvania State University, United States; ⁵Indian Institute of Science, India; ⁶Lawrence Berkeley National Laboratory, United States; ⁷Harwell Science and Innovation Campus, United Kingdom

The emergence of real-space topological structures, such as ferroelectric and ferromagnetic skyrmions, is an increasingly popular area of research. As the sizes of these structures approach the nanometer-scale, new characterization techniques are required to map out complex polarization profiles in three dimensions. Resonant elastic x-ray scattering (REXS) is often used to study chirality in spin textures such as magnetic skyrmions and domain walls. However, the application of this technique to analogous electric polarization textures is less established. Here, we present a framework for analyzing REXS from an arrangement of charge quadrupole moments [1], which is applied to measurements on polar skyrmions that form in PbTiO₃/SrTiO₃ superlattices. By utilizing circularly polarized x-rays and extended reciprocal space scans, we gain insight into their three-dimensional chiral structure. Furthermore, we determine that both right- and left-handed polar skyrmions coexist, and their relative fraction can be extracted using REXS. This technique can be extended to study ordered electric and/or magnetic phases in similar systems. We discuss how this can be applied to complex structures that emerge in multiferroic BiFeO₃/TbScO₃ superlattices.

[1] K. T. Kim, M. R. McCarter, *et al.*, *Nat. Commun.* **13**, 1769 (2022).

11:30 AM EQ08.10.03

Role of Polarization-Photon Coupling in Ultrafast Terahertz Excitation of Ferroelectrics Shihao Zhuang and Jiamian Hu; University of Wisconsin, Madison, United States

We investigate the role of polarization-photon coupling (specifically, the polarization-oscillation-induced radiation electric field) in the excitation of ferroelectric thin films by an ultrafast terahertz electric field pulse. Analytical formulas are developed to predict how the frequencies and relaxation time of three-dimensional soft mode phonons (intrinsic polarization oscillation) are modulated by the radiation electric field and epitaxial strain. Ultrafast terahertz-pulse-driven excitation of harmonic polarization oscillation in strained single-domain ferroelectric thin film is then simulated using a dynamical phase-field model that considers the coupled strain-polarization-photon dynamics. The frequencies and relaxation time extracted from such numerical simulations agree well with analytical predictions. In relatively thin films, it is predicted that the radiation electric field slightly reduces the frequencies but significantly shortens the relaxation time. These results demonstrate the necessity of considering polarization-photon coupling in understanding and predicting the response of ferroelectric materials to ultrafast pulses of terahertz and higher frequencies.

11:45 AM EQ08.10.04

Ultrafast Carrier Dynamics in Polycrystalline Low Cost Bi₂Se₃ Topological Insulator Valerio Campanari¹, Daniele Catone¹, Patrick O’Keeffe¹, Alessandra Paladini¹, Stefano Turchini¹, Faustino Martelli¹, Matteo Salvato², Nouha Loudaief², Elena Campagna² and Paola Castrucci²; ¹Consiglio Nazionale delle Ricerche, Italy; ²Università degli Studi di Roma Tor Vergata, Italy

Carrier dynamics in Bi₂Se₃ topological insulator thin films of different thickness were investigated by femtosecond transient absorption spectroscopy (FTAS) at 77K and room temperature, by using selected pump energies (from 2.5 eV down to 0.6 eV) and a wide spectrum probe (from 3.6 eV down to 0.9 eV). The fabrication process for growing Bi₂Se₃, that was recently developed^[1], is quick, very inexpensive, easy to control and allows obtaining films of different thickness, endowed with topological properties, during the same procedure. In particular, ultra-thin films deposited on n-doped Si substrates with this method show good rectifying properties suitable for their use as photodetectors in the UV-Vis-IR range. The process consists of two consecutive procedures: first Bi₂Se₃ nanowires/nanobelts are deposited by standard catalyst-free vapor–solid deposition on different substrates positioned inside a quartz tube. Then, the Bi₂Se₃ stuck on the inner surface of the quartz tube is re-evaporated and deposited in the form of ultra-thin films on new substrates at a temperature below 100 °C.

FTAS measurements revealed several resolved bleaching signals that show different temporal dynamics. These spectral components can be attributed to the electron transitions at the various bulk or surface states present in the complex Bi₂Se₃ band structure and to plasmonic resonance of long-range strongly correlated electrons, as recently observed with ellipsometry in the same material.^[2] We point out that the polycrystalline films used for this work show similar absorption spectra and carrier dynamics of epitaxial layers grown by MBE.^[3,4]

Using a pump of low energy, but sufficient to give rise to interband transitions (e.g., 0.6 eV), we have observed absorption bleaching even at energies greater than that of the pump. By a careful study as a function of the pump fluence, we have been able to rule out any multiphotonic contribution to the absorption of the pump. The observation of absorption bleaching at energies larger than that of the pump is attributed to the depletion of the electron population in the bulk valence band (BVB) and/or in the lower Dirac surface states (SS1) that are involved in the interband transition permitted at 0.6 eV. Being the BVB and the SS1 also involved in high-energy transitions, that carrier depletion gives rise to a reduction of the absorption also at the higher energy resonances.

The wide experimental conditions used in our work allow a careful description of the transitions involved in the absorption spectrum and of the photoexcited carrier dynamics, thus providing novel and very useful insights into the properties that allow the fabrication of innovative, low-cost and wide-range photodetectors.

[1] M. Salvato, M. Scagliotti, M. De Crescenzi, P. Castrucci, F. De Matteis, M. Crivellari, S. Pelli Cresi, D. Catone, T. Bauch, F. Lombardi, *Nanoscale* **2020**, *12*, 12405.

[2] T. J. Whitcher, M. G. Silly, M. Yang, P. K. Das, D. Peyrot, X. Chi, M. Eddrief, J. Moon, S. Oh, A. H. Castro-Neto, M. B. H. Breese, A. T. S. Wee, F. Silly, A. Ruydy, *NPG Asia Mater.* **2020**, *12*, DOI: 10.1038/s41427-020-0218-7.

[3] Y. D. Glinka, J. Li, T. He, X. W. Sun, *ACS Photonics* **2021**, *8*, 1191.

[4] T. Jiang, R. Miao, J. Zhao, Z. Xu, T. Zhou, K. Wei, J. You, X. Zheng, Z. Wang, *Chinese Opt. Lett.* **2019**, *17*, 20005.

12:00 PM DISCUSSION TIME

SYMPOSIUM EQ09

Emergent Materials for Low Power Electronics
November 28 - December 8, 2022

Symposium Organizers

Ying-Hao Chu, National Tsing Hua University
Catherine Dubourdieu, Helmholtz-Zentrum Berlin / Freie Universität Berlin
Olga Ovchinnikova, Oak Ridge National Laboratory
Bhagwati Prasad, Indian Institute of Science

Symposium Support

Bronze

CRYOGENIC LIMITED

* Invited Paper
+ Distinguished Invited

SESSION EQ09.01: High K Materials and Large-Area Deposition
Session Chairs: Catherine Dubourdieu and Olga Ovchinnikova
Monday Morning, November 28, 2022
Sheraton, 2nd Floor, Back Bay D

10:30 AM EQ09.01.02

Investigation of the Hetero-Epitaxial Growth Behavior of the Ultrathin Dielectric Films with HfO₂/Al-Doped TiO₂ Bilayer Structure [Dae Seon Kwon](#)¹, [Kun Hee Ye](#)^{1,2}, [In Soo Lee](#)¹, [Junil Lim](#)¹, [Haengha Seo](#)¹, [Tae Kyun Kim](#)¹, [Heewon Paik](#)¹, [Jonghoon Shin](#)¹, [Jung-Hae Choi](#)² and [Cheol Seong Hwang](#)¹; ¹Seoul National University, Korea (the Republic of); ²Korea Institute of Science and Technology, Korea (the Republic of)

The locally hetero-epitaxial growth and interfacial properties of atomic layer deposited (ALD) Al-doped TiO₂ (ATO) and HfO₂/ATO/Ru structure. The locally hetero-epitaxial growth of the ATO films on the Ru substrate could be divided into two stages: the first stage was highly affected by the Ru (and RuO₂) substrate and the second stage was by the ATO itself once the ATO fully covered the Ru substrate. The physicochemical properties of the films at each stage were investigated, supported by computational data, and local lattice-matched growth mechanisms were suggested. At a low thickness (<~4 nm) of the ATO film, the coherent structure of the rutile ATO with *in-situ* formed-rutile RuO₂ was more stable. However, at a higher thickness (>~4 nm), the incoherent structure of the rutile ATO was more stable, leading to the evolution of the new grains with random crystalline orientations. Subsequently, these structural differences in the rutile ATO highly affected the growth of the upper HfO₂ film was suppressed on the ATO film with the appropriate thickness (~2.5 nm). Also, the surface morphology and the interfacial chemical bonding nature of the HfO₂/ATO films depended on the crystalline structure of the rutile ATO films. Finally, the electrical properties of the Pt/HfO₂/ATO/Ru structured capacitors were obtained. Minimum equivalent oxide thickness (EOT) and physical oxide thickness (POT) values were 0.61 nm and 4.28 nm, respectively, while still satisfying the specification of the dynamic random-access memory (DRAM) leakage current density (<10⁻⁷ A/cm² at a capacitor voltage of 0.8 V).

10:45 AM EQ09.01.03

Low Temperature Fabrication of 3D Integrated CMOS Devices by Via-Hole-Less Structure on Flexible Substrate [Seongcheol Jang](#) and [Hyun-Suk Kim](#); Chungnam National University, Korea (the Republic of)

Complementary metal oxide semiconductor (CMOS) inverter is basic building blocks for complex integrated logic circuits, which require both p- and n-type thin film transistors (TFTs). Si-based CMOS shows good performance across n- and p- type transistors, however, Si require high temperature process that is not suitable for next generation flexible devices. Organic, Oxides, and metal chalcogenides are proposed for the high performance p-type TFTs, however, their fabrication process, physical nature, and electrical properties are not suitable for cutting-edge CMOS inverter. There are some reports that compose an inverter with only n-type TFTs, however, they suffer from low output swing, small input capacitance, large power dissipation and poor noise margin. To realize high performance CMOS inverter logic circuit, high performance p-type semiconductor with simple fabrication process is strongly required.

3-dimensional (3D) integration is an emerging technology that can offer minimized system, short interconnection, reducing packaging cost and integrate various devices. As Moore's Law reaches its limits, 3D integration technology becomes increasingly important. There are several 3D integration methods such as wire bonding and 3D through silicon via (TSV). Wire bonding is cheap and mature process, however, the process is only possible around die, low chip connection freedom, require interlayer, and suffer from RC delay. 3D-TSV shows the reduced footprint, improved Si efficiency, reduced RC delay and lower power consumption. However, 3D-TSV strongly limited to Si semiconductor and restricted on the use of other semiconductors. 3D via-hole-less is a novel multilevel integration system that is etchant-free, allows simultaneous metal interconnection, minimizes underlying device degradation and provides high substrate-compatibility.

In this work, we present the 3D integration of n-type ZnON and p-type Te TFTs through 3D via-hole less structure. ZnON is well known n-type materials which shows high field effect mobility. Tellurium (Te) is promise 2D p-type materials which can be fabricated via solution process or evaporation process with very low substrate temperature. Here, Te is deposited by room temperature sputtering system which is cost-effective and allow large area uniformity. To demonstrate the 3D via-hole-less structure, ZnON based n-type TFT and Te based p-type TFT were fabricated on the bottom floor and top floor, respectively. Alumina (Al₂O₃) was deposited by plasma enhanced atomic layer deposition (PEALD) using precursor of TMA and reactant of O₂ for the interlayer dielectric (ILD) and dielectric layer. Overall process temperature is under 200 °C which is suitable for cheap flexible substrate. By using proposed etchant-free 3D via-hole-less structure, 3D stacked inverter was successfully fabricated, showing the high gain of ~20. Finally, flexible 3D via-hole-less CMOS inverter was fabricated on PI substrate.

11:00 AM EQ09.01.04

Solution Combustion-Derived Hf_{0.5}Zr_{0.5}O₂ Ferroelectrics for Negative Capacitance Field Effect Transistors [Pavan Pujar](#), [Hae Won Cho](#) and [Sunkook Kim](#); Sungkyunkwan University, Korea (the Republic of)

Fabricating solution combustion-derived Hf_{0.5}Zr_{0.5}O₂-ferroelectric films for negative capacitors is presented for the first time. The precursor used for the solution combustion reaction to form equimolar hafnia-based ferroelectric, i.e., Hf_{0.5}Zr_{0.5}O₂ are designed to act as both combustible elements and cation sources - Hf and Zr. Jain's method, mainly used for calculating the stoichiometric quantities of precursors in propellant chemistry, has also been modified and applied in the present study. The assumption for this method that molecular oxygen does not take part in the reaction is not only refuted but also stoichiometric combustion in the presence of molecular oxygen is proposed. This reaction is followed by post-rapid thermal processing to crystallize the metastable, non-centrosymmetric orthorhombic phase. The thin-film stacks of ferroelectric and dielectric, Hf_{0.5}Zr_{0.5}O₂/HfO₂, are used to achieve small sub-thermionic swing magnitudes (forward sweep: 25.42 ± 8.05 mV dec⁻¹, reverse sweep: 42.56 ± 4.87 mV dec⁻¹) in 2-dimensional MoS₂ negative capacitance field-effect transistors with a hysteresis of ~40 mV at 1 nA that results in ultra-low-power operation.

11:15 AM EQ09.01.05

Toward Highly Pure Ferroelectric $\text{Hf}_{1-x}\text{Zr}_x\text{O}_2$ Thin Films by Tailoring the Strain in an Unstable Thermodynamic System Yu-Cheng Kao¹, Hao-Kai Peng¹, Kuo-An Wu¹, Yung-Hsien Wu¹ and Pin-Jiun Wu²; ¹National Tsing Hua University, Taiwan; ²National Synchrotron Radiation Research Center, Taiwan

By utilizing the combined analyses of X-ray diffraction (XRD) and X-ray absorption spectroscopy (XAS), a systematic identification on the crystal phases of the polymorphic $\text{Hf}_{1-x}\text{Zr}_x\text{O}_2$ (HZO) thin films with various series of preparation conditions was presented. The results of the rigorous quantitative analysis show that the monoclinic phase (*m*-phase) and the tetragonal phase (*t*-phase) are mutually exclusive and a high fraction of orthorhombic phase (*o*-phase) up to 97% can be achieved under a specific process condition. Based on the observed correlation between the phase fraction and the in-plane strain, the strain-induced activation energy barrier was proposed to clarify the mechanism of kinetic phase transition process. The endurance test of the device, exhibiting that the wake-up degree (remnant polarization variation $\Delta P_r/P_{\text{max}}$) increases exponentially with increasing the content of tetragonal phase in the pristine state, indicating the transition from *t*- to *o*-phases as a possible mechanism of the wake-up effect. Our study presented herein points the way to efficiently optimize the strain towards highly pure orthorhombic HZO thin film through precisely controlling the process parameters, which is beneficial for the future development of ferroelectric devices.

SESSION EQ09.02: Ferroelectrics
Session Chairs: Yunseok Kim and Dennis Meier
Monday Afternoon, November 28, 2022
Sheraton, 2nd Floor, Back Bay D

1:30 PM *EQ09.02.01

The Third Dimension of Ferroelectric Domain Walls Dennis Meier; Norwegian University of Science and Technology, Norway

Ferroelectric domain walls are a paradigmatic example for the rich physics and application opportunities of topological defects. The research on ferroelectric domain walls has revolutionized the way we understand polar structures and triggered the development of conceptually new devices for nanotechnology.^[1] Despite the immense research efforts, we have scratched only the tip of the iceberg. This is because the quasi-2D walls are embedded in 3D materials and, hence, inaccessible to standard nanoscale imaging techniques. From a theoretical point of view, it is clear that the walls within the bulk are not perfectly flat and just like in other 2D systems, such as graphene and transition-metal dichalcogenides, related corrugation phenomena are crucial for their electronic responses.

In my talk, I will discuss the importance of the 3D nanoscale structure for the emergent transport properties at ferroelectric domain walls. By combining tomographic microscopy techniques and finite element modelling, we revealed how electrical currents spread in the complex network of domain walls and topologically protected vortices in ferroelectric ErMnO_3 .^[2] The results demonstrate the impact of curvature effects on the electrical currents in domain wall networks, giving an additional degree of freedom for their control. In addition, I will introduce novel imaging approaches that allow for studying the interaction of domain walls with point defects in 3D with atomic scale resolution.^[3] The results expand previous work on ferroelectric domain walls into the third dimension and reveal new opportunities for domain-wall based multi-level resistance control and unconventional computing.

[1] D. Meier and S. M. Selbach, *Nature Rev. Mater.* 7, 15 (2022)

[2] E. D. Roede, et al., arXiv:2203.05271 (2022)

[3] K. A. Hunnestad, et al., arXiv:2111.00317 (2021)

2:00 PM EQ09.02.02

Atomic-Scale Scanning of Domain Network in Ferroelectric HfO_2 Thin Films Kunwoo Park, Jihoon Kim, Sungsu Kang and Jungwon Park; Seoul National University, Korea (the Republic of)

Since the discovery of ferroelectric HfO_2 films in 2011, great attention has been drawn due to their nano-scale scalability, large polarization and coercive field, and compatibility with silicon-based engineering. The ferroelectricity of HfO_2 -based thin films is commonly attributed to the polar non-centrosymmetric $\text{Pca}2_1$ orthorhombic phase (*o*-phase). The mechanism of *o*-phase stabilization remains unexplained, however, because the ferroelectric HfO_2 films are typically polycrystalline with nanometer-scale domains and those stabilizing effects are probably effective at the nanoscale. There are also additional questions regarding the size, structure, and distribution of ferroelectric domains, the structure of grain boundaries, and their relationship to the overall ferroelectric properties of the HfO_2 films.

Distinguishing different phases of HfO_2 is extremely difficult since the *o*-phase has nearly identical atomic structure to other phases. The position detection of oxygen atoms across a large region, which is required for ferroelectric domain mapping, is also exceptionally challenging due to their low *Z*-number. Therefore, the direct in-plane TEM study of the atomic structure of epitaxial HfO_2 films, with a capability to precisely resolve hafnium and oxygen over a wide area of the film, will be the ideal approach to resolve the above-mentioned questions.

In this work, we intensively studied free-standing ferroelectric Y:HfO_2 films with varying thicknesses from 1.5 to 11 nm. Crystallographic phases, their distribution, and local strain are analyzed according to the thickness using in-plane STEM analysis, which reveals that new high-symmetry and compressively strained polar phase stabilizing the ferroelectric phase is induced at the grain boundaries. Moreover, atomic-scale ferroelectric domain maps obtained through in-plane iDPC-STEM oxygen position mapping reveal a complex arrangement of ferroelectric domains, implying that non-polar regions and point defects in the vertical domain walls cause ferroelectricity weakening.

2:15 PM EQ09.02.03

Multilevel Polarization Switching in Ferroelectric Thin Films Martin F. Sarott¹, Marta D. Rossell², Manfred Fiebig¹ and Morgan Trassin¹; ¹ETH Zürich, Switzerland; ²Empa-Swiss Federal Laboratories for Materials Science and Technology, Switzerland

The switchable bistable polarization in ferroelectrics allows for the binary control of optical, electronic, and catalytic properties that are essential for a wide range of applications. Going beyond the limitation of a binary remanent polarization and using that for evoking strongly non-linear material responses holds great promise for emerging spintronic and neuromorphic concepts. Here, we demonstrate that we can arbitrarily set the magnitude of the remanent ferroelectric polarization at the nanoscale in epitaxial $\text{PbZr}_{0.52}\text{Ti}_{0.48}\text{O}_3$ thin films with a single DC bias. By driving the ferroelectric system towards an instability near the PZT morphotropic phase boundary and controlling the resulting softness via epitaxial strain, we favor the formation of decoupled nanometric 180° domains that exhibit a broad coercive field distribution. Using in-situ optical second harmonic generation and X-ray diffraction, we investigate the emergence of the nanoscopic domain configuration. We then use piezoresponse force microscopy to demonstrate the possibility to locally and reversibly modulate the remanent polarization continuously between depolarized and saturated, while preserving the nanoscopic length scale of the domains. We highlight the direct technological relevance of nanoscale non-binary polarization switching, by showing first, the voltage-controlled tunability

of the nonlinear optical response in our films and second, the quasi-continuous tunability of the tunnel electroresistance in ferroelectric tunnel junctions.

2:30 PM EQ09.02.04

Z-Cut Barium Titanate Electro-Optic Modulators for Silicon Photonics [Agham Posadas](#)^{1,2}, Vincent Stenger³, John DeFouw³ and Alex Demkov^{1,2};
¹The University of Texas at Austin, United States; ²La Luce Cristallina, United States; ³SRICO, Inc., United States

BaTiO₃ (BTO) is a ferroelectric material that exhibits one of the largest Pockels coefficients among electro-optic (EO) materials, with a coefficient as high as 1300 pm/V in the bulk. In addition to the substantially larger Pockels coefficient compared to the alternative LiNbO₃, BTO is much easier to integrate with Si. Epitaxial BTO integrated on Si or Si-on-insulator (SOI) is a promising materials platform for building EO modulators based on the Pockels effect that can be used for fast, low-power optical switches, with applications ranging from sensors to novel forms of computing including neuromorphic and quantum computing.

The complex refractive index for sputter-grown epitaxial BTO films on SOI was characterized over visible and near-infrared wavelengths via variable angle spectroscopic ellipsometry. The resulting index value was 2.280 at 1550 nm. This result was in line with values reported for optical grade BTO films. A slab waveguide loss test was done using a Metricon 2010 prism coupler measurement system with optical loss attachment. Slab loss was measured to be in the range of 1.0 to 1.5 dB/cm for fundamental transverse electric and transverse magnetic modes at 1550 nm wavelength.

The electro-optic modulation was also measured in transmission geometry for a-oriented films, and in slot waveguide geometry for both a- and c-oriented films. The effective Pockels coefficient for the a-oriented films (combination of r_{42} and r_{13} Pockels tensor components) is measured to be 180 pm/V, while that for c-oriented films (r_{33}) is 110 pm/V. These yield V_{π} -L values of 0.42 and 0.3 V-cm, respectively, for the a- and c-oriented films. These results show that off-axis sputtered BTO films can yield electro-optic modulation similar to that of high-quality MBE-grown films and that the material would be suitable for implementation of low power, small footprint Mach-Zehnder interferometer (MZI)-type electro-optic modulators integrated on silicon.

We have fabricated Z-cut waveguide phase-shifters, with the ridge waveguide being etched directly in BTO and designed to support a TM mode signal. One issue with the more common TE mode devices is that fields applied along the X-direction of the crystal to access r_{42} experience an extremely high dielectric constant, typically over 1000. This high dielectric constant directly translates to decreased EO modulation efficiency. In contrast, fields applied along the Z-direction to access the r_{33} Pockels component experience a more typical dielectric constant less than 60. This reduction in dielectric loading can more than offset the reduction in EO coefficient. Another benefit to Z-cut films is that they are more readily poled along the surface normal direction to produce a uniform polarization across the wafer. We show that Z-cut modulators in BTO are suitable for making compact optical switches that can be used in high density optical networks.

2:45 PM EQ09.02.05

Exploring New Functionalities in Antiferroelectric PbHfO₃-Based Material Systems [Megha Acharya](#)¹, Ella Banyas¹, Handong Ling¹, Djamila Lou¹, Maya Ramesh¹, Abel Fernandez¹, Arvind Dasgupta¹, Yizhe Jiang¹, Brendan Hanrahan², Gabriel Velarde¹, Jeffrey Neaton¹, Mark Asta¹, Kristin A. Persson¹ and Lane W. Martin¹; ¹UC Berkeley, United States; ²US Army Research Laboratory, United States

Perovskite-based antiferroelectric (AFE) materials are getting renewed interest due to their unique polar order and to their interesting electric-field-induced AFE-to-ferroelectric (FE) phase transition which make them potential candidates for applications including capacitive energy storage, electromechanical actuation, electrocaloric cooling, low-loss microwave dielectrics, memory, *etc.* – most being crucial for low-power electronics. Such materials have been studied considerably less than their FE cousins and what limited work does exist primarily focuses on a few archetypal systems such as PbZrO₃ and its derived phases. Here, we focus on another candidate AFE system and its interesting properties, namely PbHfO₃.

In this presentation, we will begin by exploring the structural, chemical, and electrical properties of AFE PbHfO₃ as epitaxial thin films. The PbHfO₃ films exhibit characteristic double-hysteresis loops with a saturation polarization $\approx 53 \mu\text{C cm}^{-2}$ at 1.6 MV cm^{-1} . Using chemical modification at both the lead and hafnium sites, we are further able to explore two very different functionalities in the resultant PbHfO₃-based solid solutions, pointing to the versatility of this material system. First, in $\text{Pb}_{1-x}\text{Sr}_x\text{HfO}_3$ we observe a strong increase in the electric-breakdown strength and decrease in hysteretic loss, thus enhancing the capacitive energy storage density (U_f) and efficiency (η) with values as high as $77 \pm 5 \text{ J cm}^{-3}$ (U_f) and $97 \pm 2\%$ (η); well out-performing many known AFE materials.^[1] From there, we explore the $\text{PbHf}_{1-x}\text{Ti}_x\text{O}_3$ system wherein titanium substitution results in the evolution of both the structure and (di)electrical properties. For all compositions studied herein, ferroelectric behavior was observed while the structure undergoes a rhombohedral-to-tetragonal phase transition with increasing titanium content. Further, intermediate $\text{PbHf}_{1-x}\text{Ti}_x\text{O}_3$ compositions (*i.e.*, $x = 0.4-0.55$) exhibited a mixed-phase (rhombohedral + monoclinic + tetragonal) structure akin to the morphotropic phase boundary (MPB) observed in the well-studied $\text{PbZr}_{1-x}\text{Ti}_x\text{O}_3$ system. Owing to the structural evolution, an enhancement in the dielectric response was observed in the intermediate compositions pointing to the presence of an MPB-like behavior therein. Further, we also measured the electromechanical response for all the chemistries revealing the piezoelectric displacement values to be on par with that of $\text{PbZr}_{0.52}\text{Ti}_{0.48}\text{O}_3$ films in the same geometry.^[2]

Ultimately, from the current work, both PbHfO₃-based solid solutions can be viewed as viable alternatives to the prevalent PbZrO₃-based systems, offering comparable, if not better, performance while being relatively less reactive with silicon, thus, lowering the risks of forming detrimental interfacial phases. While each of these studies is one of just a few reports on synthesis and characterization of PbHfO₃-based solid solutions as epitaxial films, they can motivate future research efforts involving more detailed evaluation of mechanisms for polar behavior in AFE and their derived phases, a topic which is less well understood.

References

- [1] M. Acharya, E. Banyas, M. Ramesh, Y. Jiang, A. Fernandez, A. Dasgupta, H. Ling, B. Hanrahan, K. Persson, J. B. Neaton, L. W. Martin, *Adv Mater* 2021, 2105967.
- [2] M. Acharya, H. Ling, D. Lou, M. Ramesh, B. Hanrahan, G. Velarde, M. Asta, K. Persson, L. W. Martin, 2022 (in preparation).

3:00 PM BREAK

3:30 PM *EQ09.02.06

Highly Enhanced Ferroelectricity in HfO₂-Based Ferroelectric Thin Film by Light Ion Bombardment [Yunseok Kim](#); Sungkyunkwan University, Korea (the Republic of)

Continuous advancement in nonvolatile and morphotropic beyond-Moore electronic devices requires integration of ferroelectric and semiconductor materials. The emergence of HfO₂-based ferroelectrics that are compatible with atomic-layer deposition has opened interesting and promising avenues of research. However, the origins of ferroelectricity and pathways to controlling it in HfO₂ are still mysterious. In this presentation, I will present how we are able to enhance ferroelectricity in these materials by local He ion bombardment and discuss the possible competing mechanisms for highly enhanced ferroelectricity. Our piezoresponse force microscopy results indicate that the amplitude of piezoresponse in the ion-bombarded region increased by approximately twofold compared with that in the pristine region and the scanning transmission electron microscopy results show that the large

enhancement of ferroelectricity by He ion bombardment can be caused by a homogeneous distribution of oxygen vacancies and a phase transition to the ferroelectric phase. These findings both reveal the origins of ferroelectricity in this system and open pathways for nanoengineered binary ferroelectrics.

4:00 PM EQ09.02.07

BaTiO₃ Nanostructures on Si Fabricated by Neon Ion Milling Olanyian I. Ibukun^{1,2}, Sebastian Schmitt¹, Dong-Jik Kim¹, Jürgen Albert¹, Rama K. Vasudevan³, Michael Zachman³, Veeresh Deshpande¹ and Catherine Dubourdieu^{1,2}; ¹Helmholtz-Zentrum Berlin für Materialien und Energie, Germany; ²Freie Universität Berlin, Germany; ³Oak Ridge National Laboratory, United States

Ferroelectric nanostructures are of great interest for fundamental studies on scaling effects of ferroelectricity and as building blocks for ferroelectric-based nanoscale devices for low power, high density integrated circuits. In this study, we investigate the ferroelectric properties of BaTiO₃ cylindrical nanostructures on Si. Epitaxial BaTiO₃ thin films were grown by molecular beam epitaxy on SrTiO₃-buffered Si (100) substrates. Nanopillars with different lateral dimensions (from 200 - 500 nm) were then fabricated using focused neon ion milling in a Zeiss Orion Nanofab microscope¹. The unpatterned thin films were first characterized using X-ray diffraction, Raman spectroscopy, and piezoresponse force microscopy (PFM) showing *c*-axis orientation and a ferroelectric behaviour. Ferroelectricity in the neon ion milled nanostructures was investigated using band excitation piezoresponse force microscopy (BE-PFM)² and contact Kelvin probe force microscopy (cKPFM)³. Their crystalline structure, strain state, and polarization were studied at a local scale by scanning/transmission electron microscopy (S/TEM). We find an imprint and a maximal switchable response in the nanostructures that are dependent on their lateral dimension. The information gained from S/TEM will be discussed, emphasizing the effect of the pillar lateral dimensions on the polarization state. Finally, the potential damage caused by the ions during milling will be evaluated.

References

1. Olanyian, I. *et al.* Nanofabrication of barium titanate using noble gas ions, submitted 2022.
2. Jesse, S., *et al.*, The band excitation method in scanning probe microscopy for rapid mapping of energy dissipation on the nanoscale. *Nanotechnology* **18**, 435503 (2007).
3. Balke, N. *et al.* Differentiating Ferroelectric and Nonferroelectric Electromechanical Effects with Scanning Probe Microscopy. *ACS Nano* **9**, 6484–6492 (2015).

4:15 PM EQ09.02.08

Ferroelectricity and Resistive Switching in BaTiO₃ Thin Films with Liquid Electrolyte Top Contact for Bioelectronic Devices Maximilian T. Becker, Poppy Oldroyd, Nives Strkalj, Moritz Mueller, George G. Malliaras and Judith L. MacManus-Driscoll; University of Cambridge, United Kingdom

We investigate ferroelectric- and resistive switching behavior in epitaxial 18-nm-thick BaTiO₃ (BTO) films in a model electrolyte-ferroelectric-semiconductor (EFS) configuration for ferroelectric microelectrode applications [1] in bioelectronics. BTO films are grown by pulsed laser deposition (PLD) on semiconducting Nb-doped (0.5 wt%) SrTiO₃ (Nb:STO) single crystal substrates. The ferroelectric properties of the bare BTO films are demonstrated by piezoresponse force microscopy (PFM) measurements. Cyclic voltammetry (CV) measurements in EFS configuration, with phosphate buffered saline (PBS) acting as liquid electrolyte top contact, reveal characteristic ferroelectric switching peaks in the bipolar current-voltage loop. The ferroelectric nature of the observed switching peaks is confirmed by analyzing the current response of the EFS devices to unipolar voltage signals. Moreover, electrochemical impedance spectroscopy (EIS) measurements indicate bipolar resistive switching behavior of the EFS devices, which is controlled by the remanent polarization state of the BTO layer. Our results represent a constitutive step towards the realization of neuroprosthetic implants and hybrid neurocomputational systems based on ferroelectric microelectrodes.

[1] M. T. Becker, AIP Advances **11**, 065106 (2021) <https://doi.org/10.1063/5.0049202>

4:30 PM EQ09.02.09

Enabling Ultra-Low-Voltage Switching in BaTiO₃ Yizhe Jiang^{1,2}, Eric Parsonnet¹, Alexander Qualls¹, Wenbo Zhao¹, Sandhya Susarla², David Pesquera^{1,3}, Arvind Dasgupta¹, Megha Acharya^{1,2}, Hongrui Zhang¹, Tanay Gosavi⁴, Chia-ching Lin⁴, Dmitri E. Nikonov⁴, Hai Li⁴, Ian A. Young⁴, Ramamoorthy Ramesh^{1,2,1} and Lane W. Martin^{1,2}; ¹University of California, Berkeley, United States; ²Lawrence Berkeley National Laboratory, United States; ³Catalan Institute of Nanoscience and Nanotechnology (ICN2), CSIC and BIST, Spain; ⁴Intel Corporation, United States

While Moore's law, first put forth in 1964, dictates and guides that the density of transistors per chip should double every two years, Dennard scaling, put forth in 1974, which states that the voltage and current should scale with the size of the MOSFET device (*i.e.*, decreasing 30% every year) while maintaining the same power consumption per area, is arguably more important for microelectronics today. Such scaling is, however, getting increasingly difficult each year, especially when devices approach the fundamental physical and quantum limits (*e.g.*, increased leakage current, Boltzmann tyranny, etc.). Since around 2003, we have failed to keep track with Dennard scaling and keeping up with Moore's law has increased in difficulty. Therefore, researchers have started looking for alternative beyond-CMOS approaches to computation, where new physical variables are used for memories and computing logic (or logic-in-memory approaches). Such novel devices rely on order parameters such as spin, polarization, or strain as a pathway to lower power and device metrics, such as operation voltages <100 mV, operation energies <10 aJ/bit, and switching delays <0.1 ns serving as effective marching orders to the community. In this spirit, ferroelectric materials, with their non-volatile polarization states and low read/write energies (*e.g.*, single-crystal BaTiO₃ exhibits switching fields ~1 kV cm⁻¹ and energies ~0.1 J cm⁻³, with a remanent polarization ~26 μC cm⁻²), are exciting candidates for next-generation devices (*e.g.*, ferroelectric-RAMs, ferroelectric-FETs, negative-capacitance FETs, etc.). The performance of ferroelectric thin films, however, has traditionally been significantly worse than their bulk counterparts (*i.e.*, large coercive fields, reduced remanent polarization) thus making them unsuitable for real memories and logic devices.

Here, we will present a pathway to synthesize BaTiO₃ thin films with high-quality and nearly bulk-like properties, including small coercive fields < 10 kV cm⁻¹, small switching energies < 2 J cm⁻³ (*i.e.*, < 2 aJ/bit in a 10×10×10 nm³ device) and relatively large remanent polarization > 10 μC cm⁻². By scaling down the thickness of the films even further, we have also achieved small coercive voltages < 100 mV; an important metric for real applications of these materials. During the process of reducing film thickness, depolarization fields are found to play an increasingly important role, destabilizing the polar order and causing a reduction in remanent polarization. The depolarization fields, however, also suppress the coercive field scaling in BaTiO₃ thin films, stopping it from increasing as the thickness of the film decreases (a trend described by the Janovec-Kay-Dunn scaling law). In our case, we observe essentially thickness-independent coercive field evolution for films < 150 nm in thickness. Switching-dynamic studies, combined with lateral size scaling, predict the possibility for sub-nanosecond switching time in devices as large as 10 μm² (*i.e.*, capacitor diameters ~3.5 μm). Attempts to integrate the BaTiO₃ thin films onto silicon substrates have also been made, showing ferroelectric switching characteristics similar to films grown on scandate substrates, demonstrating the potential of these materials for real applications. We will also discuss recent efforts to further reduce the lateral size of devices to the sub-micron and even hundreds of nanometer length scales and corresponding switching dynamics studies of these devices. In this size regime, different ferroelectric switching mechanisms could co-exist and give rise to different time limits for ferroelectric switching (*e.g.*, RC charging time of the ferroelectric capacitor,

intrinsic domain-growth limit, nucleus size limit, etc.). Moreover, as the lateral size gets smaller, sub-nanosecond switching times are expected. We will explore the ultimate speed limit for switching in these materials.

4:45 PM EQ09.02.10

From Chemical and Structural Considerations to New Stable Nitride Perovskites—A High Throughput Study Bastien F. Grosso¹, Daniel W. Davies¹, Bonan Zhu¹, Aron Walsh² and David O. Scanlon¹; ¹University College London (UCL), United Kingdom; ²Imperial College London, United Kingdom

Nitride perovskites, with ABN_3 formula, have the potential to start a new paradigm in semiconductor devices. In this talk, we present a high throughput study of (AB)- N_3 compositional space and show how candidate materials can be identified using simple chemical and structural considerations. We further thoroughly explore the potential energy surface of our candidate materials using symmetry elements and ab initio random structure searching (AIRSS) in order to identify a possible ground state structure. The outcome of our workflow is twofold. On the one hand, we provide new insights on the ground state structure of already identified candidate compositions and on the other hand we propose new thermodynamically stable, likely synthesizable, nitride perovskites.

SESSION EQ09.03: Integrated Ferroelectrics

Session Chairs: Athanasios Dimoulas and Susan Trolier-McKinstry

Tuesday Morning, November 29, 2022

Sheraton, 2nd Floor, Back Bay D

8:30 AM *EQ09.03.01

Hafnium-Based Ferroelectric Artificial Synapses on Silicon for Low Power In-Memory Computing Athanasios Dimoulas¹, Nikitas Siannas^{1,2}, Christina Zacharaki^{1,2} and Polychronis Tsipas¹; ¹NCSR Demokritos, Greece; ²National and Kapodistrian University of Athens, Greece

The handling of a large number of inhomogeneous data requires artificial intelligence, energy efficiency and security which will all benefit from advancements in neuromorphic computing.

Ferroelectric multistate non-volatile memories based on Si-compatible Zr-doped Hafnia (HZO) [1] show promise for low power analog in-memory computing. They appear in different device "flavors" such as Ferroelectric Random Access Memory (FeRAM), Ferroelectric Field Effect Transistors (FeFET) [2] and Ferroelectric Tunnel Junctions (FTJ). The main focus in this presentation will be on FTJ-based devices which are resistive two terminal devices with non-destructive reading and excellent integration capability at the back-end of line of CMOS.

The work of ferroelectric HZO on Ge (100) substrates prepared by atomic oxygen deposition [3] in an MBE chamber will be presented first, covering performance and reliability characteristics (endurance and retention) [4]. When HZO thickness is scaled below 10nm, as necessary for FTJ devices, ferroelectric loop pinching and reduction of remanent polarization are observed which however recover after field cycling ("wake-up"). This behavior will be explained [5] in terms of depolarization fields in the framework of Landau-Devonshire theory.

Subsequently, it will be shown that MFS devices in the FTJ configuration with 5 nm HZO and SrTiO₃ (STO) semiconductor bottom electrode behave as analog memristors with more than 16 intermediate non-volatile states (corresponding to 4-bit memory cell) which can be accessed by sequential identical or variable width/amplitude pulses. Devices are defined on bulk n-type Nb:STO (NSTO) and 20 nm thick epitaxial SrTiO_{3-δ} on Si (100) substrates deliberately prepared oxygen deficient by annealing in vacuum to induce n-type conductivity to the STO. It is found that the memristor devices on epi-n-STO present a very good yield, robust ferroelectricity and excellent synaptic plasticity (potentiation and depression). The synaptic conductance weights G can be varied between max and min values in a dynamic range $G_{max}/G_{min} > 3$ showing potentiation and depression which emulate a biological synapse. The programming voltage is very low (~ 1-2 V) in full compatibility with voltage scaling trends in advanced CMOS, indicating that our devices are suitable for very low power memory operation. No retention loss was observed at room temperature for $>10^4$ sec.

Finally, future 3D integration schemes directly on Si with side wall FTJs will be discussed which result in very dense cross bar arrays as the main building block of low power analog in memory AI accelerators based on FTJs

Acknowledgements: Funded by the EU H2020 project BeFerroSynaptic-871737

References

- T.S. Boeske et al., *Appl. Phys. Lett.* **99**, 102903 (2011)
- C. Zacharaki et al., *ACS Appl. Electron. Mater* (2022) <https://doi.org/10.1021/acsaem.2c00324>
- C. Zacharaki et al., *Appl. Phys. Lett.*, **114**, 112901 (2019)
- C. Zacharaki et al., *Appl. Phys. Lett.*, **117**, 212905 (2020)
- N. Siannas et al., *Comms. Phys.* (2022), to be published

9:00 AM EQ09.03.03

Ferroelectric Diodes for Reconfigurable Compute-In-Memory Xiwen Liu, John Ting, Fiagbenu Fiagbenu, Jeffrey Zheng, Dixiong Wang, Pariasadat Musavigharavi, Eric A. Stach, Troy Olsson and Deep M. Jariwala; University of Pennsylvania, United States

The deluge of sensors and data generating devices has driven a paradigm shift in modern computing from arithmetic-logic centric to data centric processing. At a hardware level, this presents an urgent need to integrate dense, high-performance and low-power memory units with Si logic-processor units. However, data-heavy problems such as search and pattern matching also require paradigm changing innovations at the circuit and architecture level to enable compute in memory (CIM) operations. CIM architectures that combine data storage yet concurrently offer low-delay and small footprint are highly sought after but have not been realized. Here, we present Aluminum Scandium Nitride (AlScN) ferroelectric diode (FeD) memristor devices that allow for storage, search and neural network-based pattern recognition in a transistor-free architecture. Our devices can be directly integrated on top of Si processors in a scalable, back-end-of-line process. We leverage the field-programmability, non-volatility and non-linearity of FeDs to demonstrated circuit blocks that can support search operations in-situ memory with search delay times < 0.1 ns and a cell footprint $< 0.12 \mu m^2$. In addition, we demonstrate matrix multiplication operations with 4-bit operation of the FeDs. Our results highlight FeDs as promising candidates for fast, efficient, and multifunctional CIM platforms.

9:15 AM EQ09.03.05

Negative Capacitance Electronics—Manipulating Ultrathin Ferroelectricity in HfO₂-ZrO₂ on Silicon Suraj Cheema^{1,1}, Nirmaan Cheema¹, Shang-Lin Hsu¹ and Sayeef Salahuddin^{1,2}; ¹University of California, Berkeley, United States; ²Lawrence Berkeley National Laboratory, United States

The two-dimensional (2D) limit of ferroelectricity has extensive technological implications for the scaling of low power electronics. In particular, the negative capacitance (NC) effect in ferroelectrics has emerged to overcome fundamental computing energy limits [1]. However, advanced semiconductor technology integration requires NC stabilization at the ultrathin regime on silicon, posing significant materials challenges for conventional ferroelectrics.

To address this, we first established ultrathin ferroelectric order down to 1-nm and 5-Å thickness in doped HfO₂ [2,3] and conventionally antiferroelectric ZrO₂ [4], respectively, the same high-κ dielectrics used in today's advanced logic and memory technologies. These binary oxide films grown by atomic layer deposition on silicon boast ultrathin-enhanced polarization signatures [2-4] – in stark contrast to conventional perovskite oxide ferroelectrics – marking a breakthrough towards exploiting ferroic-based phenomena at ultra-scaled dimensions for electronics. Next, we leveraged the competing atomic-scale (anti)ferroelectric orders to design NC in sub-2-nm HfO₂-ZrO₂ superlattices [5] and 1-nm ZrO₂ [6], the gate oxide thicknesses required for today's state-of-the-art transistors and future 3D transistors, respectively. In contrast to previous NC reports, the microscopic origin of NC in these ultrathin films arises from mixed ferroelectric-antiferroelectric order. Furthermore, this work establishes the first demonstrations of capacitance enhancement – smoking-gun evidence of NC – in the technologically-relevant HfO₂-ZrO₂ system. This results in record-low equivalent oxide thicknesses, promising for ultralow-power transistor operation. Accordingly, this seamless materials swap – conventional high-κ dielectric HfO₂-ZrO₂ to (anti)ferroelectric HfO₂-ZrO₂ – demonstrates key performance benefits in NC transistors compared to established semiconductor foundry benchmarks [5,6].

Therefore, leveraging these materials breakthroughs at the 2D limit – ferroelectricity [2-4] and negative capacitance [5-6] – provides a realistic pathway towards energy-efficient electronics via integrated ferroelectrics. And from a thin film perspective, this approach to exploit 3D materials confined to the 2D limit – particularly within this simple binary oxide model system hosting unconventional and emergent ferroelectric size effects [2-4] – offers an atomic-scale approach to unlock previously hidden electronic phenomena [4-6].

[1] S Salahuddin & S Datta. "Use of Negative Capacitance to Provide Voltage Amplification for Low Power Nanoscale Devices. *Nano Lett.* **8**, 405–410 (2008).

[2] S Cheema *et al.* "Enhanced ferroelectricity in ultrathin films grown directly on silicon." *Nature* **580**, 478–482 (2020).

[3] S Cheema *et al.* "One nanometer HfO₂-based ferroelectric tunnel junctions on silicon." *Adv. Electron. Mater.* **8**, 2100499 (2022).

[4] S Cheema *et al.* "Emergent ferroelectricity in subnanometer binary oxide films on silicon." *Science* **376**, 648–652 (2022).

[5] S Cheema *et al.* "Ultrathin ferroic HfO₂-ZrO₂ superlattice gate stack for advanced transistors." *Nature* **604**, 65–71 (2022).

[6] S Cheema *et al.* "Ultralow equivalent oxide thickness via one nanometer ferroelectric negative capacitance." *In preparation.*

9:30 AM BREAK

10:00 AM *EQ09.03.06

New Materials for Three-Dimensional Ferroelectric Microelectronics Susan E. Trolrier-McKinstry; The Pennsylvania State University, United States

Computing accounts for 5 – 15% of worldwide energy consumption. In the U.S., data centers alone consumed approximately 73 billion kWh in 2020. While recent efficiency gains in hardware have partially mitigated the rising energy consumption of computing, major gains are achievable in a paradigm shift to 3D computing systems, especially those that closely couple memory and logic. In the last decade, there have been major changes in the families of ferroelectric materials available for integration with CMOS electronics. This presentation will focus on new ferroelectrics with the wurtzite crystal structure, especially Al_{1-x}B_xN and Zn_{1-x}Mg_xO, as materials that can be deposited at temperatures compatible with the back-end-of-the-line (<400°C). Both sets of materials have large polarizations (75 – 125 μC/cm²), with large, but strongly temperature-dependent coercive fields. The pseudo-activation energy for the coercive fields is on order 20 – 40 meV. As deposited, the films are (predominantly) unipolar. A wake-up process is therefore needed to nucleate new domain orientations; this process differs from the mechanisms for wake-up in perovskite or fluorite-based ferroelectrics.

10:30 AM EQ09.03.08

Ionic Bonds Control Ferroelectric Behavior in Wurtzite Nitrides Keisuke Yazawa^{1,2}, John Mangum¹, Prashun Gorai^{2,1}, Geoff L. Brennecke² and Andriy Zakutayev¹; ¹National Renewable Energy Laboratory, United States; ²Colorado School of Mines, United States

Ferroelectricity enables key integrated technologies from non-volatile memory to precision ultrasound. Wurtzite ferroelectric Al_{1-x}Sc_xN has recently received significant attention because of its enhanced piezoelectric response [1], robust ferroelectricity [2] and Si process compatibility in addition to being the first known ferroelectric wurtzite. Since the discovery of the ferroelectricity of the material system, chemistry, stress, strain, and film thickness have been rigorously investigated to control ferroelectricity in this material system [2-5]. However, the origin and control of ferroelectricity in wurtzite materials is not yet fully understood. Understanding the root cause is important for coercive field engineering and new wurtzite ferroelectric material discovery to achieve low-power electronic applications such as non-volatile memories.

A part of hinderance for understanding the new wurtzite ferroelectric physics comes from the fact that the prior studies of ferroelectricity in Al_{1-x}Sc_xN included explicit and implicit variables such as residual strain state, process parameters, target condition, chamber type, substrate type/treatment, etc. These variables convolute experimental effects, and the resulting data scatter can easily mask important but unrepresented factors such as microstructure and defects. Combinatorial techniques reduce uncontrolled process variables because a single film library can include all samples of interest and also offer significant advantages for rapid screening.

In this talk, we demonstrate that the local bond ionicity, rather than simply the change in tetrahedral distortion, is key to controlling the macroscopic ferroelectric response, according to our combinatorial film synthesis/characterization experiment and computational approach. Across the composition gradient in Sc < 0.35 range and 140 – 260 nm thickness in combinatorial thin films of Al_{1-x}Sc_xN, the pure wurtzite phase exhibits a similar *c/a* ratio regardless of the Sc content, due to elastic interaction with neighboring crystals. The coercive field and spontaneous polarization significantly decrease with increasing Sc content despite this invariant *c/a* ratio, due to the more ionic bonding nature of Sc-N relative to the more covalent Al-N bonds, supported by DFT calculations. Based on these insights, ionicity engineering is introduced as an approach to reduce coercive field of Al_{1-x}Sc_xN² for memory and other applications and to control ferroelectric properties in other wurtzite materials.

[1] M. Akiyama, T. Kamohara, K. Kano, A. Teshigahara, Y. Takeuchi and N. Kawahara, *Adv. Mater.*, 2009, **21**, 593–596.

[2] S. Fichtner, N. Wolff, F. Lofink, L. Kienle and B. Wagner, *J. Appl. Phys.*, 2019, **125**, 114103.

[3] S. Yasuoka, T. Shimizu, A. Tateyama, M. Uehara, H. Yamada, M. Akiyama, Y. Hiranaga, Y. Cho and H. Funakubo, *J. Appl. Phys.*, 2020, **128**, 114103.

[4] K. Yazawa, D. Drury, A. Zakutayev and G. L. Brenneka, *Appl. Phys. Lett.*, 2021, **118**, 162903.

[5] R. Mizutani, S. Yasuoka, T. Shiraiishi, T. Shimizu, M. Uehara, H. Yamada, M. Akiyama, O. Sakata and H. Funakubo, *Appl. Phys. Express*, 2021, **14**, 105501.

10:45 AM EQ09.03.09

Novel Non-Perovskite Ferroelectric Oxides and Nitrides Jon-Paul Maria, John Hayden, Wanlin Zhu, Devin Goodling and Susan Trolier-McKinstry; Pennsylvania State University, United States

Ferroelectricity in wurtzite-based crystals was observed in 2019 and immediately introduced exciting opportunities to explore and discover new structure-property relationships in novel formulation spaces, and to investigate new integration and device implementations given new process compatibilities. The seminal discovery of ferroelectric $\text{Al}_{1-x}\text{Sc}_x\text{N}$ by University of Kiel researchers initiated this excitement and was followed by comparable observations of polarization reversal in the structurally similar $\text{Al}_{1-x}\text{B}_x\text{N}$ and the $\text{Zn}_{1-x}\text{Mg}_x\text{O}$ systems. These observations lead one to speculate that ferroelectricity might be found much more broadly, even “everywhere”, by introducing the appropriate disorder.

In this presentation the structure-process-property relationships in the B-substituted AlN and Mg-substituted ZnO wurtzite systems will be demonstrated. The B-substituted materials exhibit square hysteresis loops with polarization values between $150 \mu\text{C}/\text{cm}^2$ and $120 \mu\text{C}/\text{cm}^2$ when boron concentrations range between 2% and 15% respectively. Coercive field values fall with additional boron, from 5.5 MV/cm to about 5 MV/cm at B saturation. Bandgap values are approximately 5 eV or above in all cases. Material can be prepared between 100 °C and 350 °C with very little difference in electrical properties. W bottom and top electrodes are used in all cases. Capacitors can be prepared down to 50 nm thick before leakage current becomes problematic during low frequency hysteresis measurements.

Comparable results are found in the $\text{Zn}_{1-x}\text{Mg}_x\text{O}$ system. Between 25% and 35% Mg substitution, square hysteresis loops with remanent polarization values above $100 \mu\text{C}/\text{cm}^2$ are readily achieved. Transmission measurements show bandgap values between 4.0 eV and 4.2 eV in this range. In comparison to AlBN, coercive field values for ZMO are as low as 1.7 MV/cm.

In addition to a discussion of properties and preferred synthesis routes, we will discuss the limitations to property engineering and scaling, and provide a complete update on observations/explorations in additional compositional and structural families. Finally, we will present our efforts to integrate these new ferroelectric crystals using “ground rules” that are consistent with the conventional semiconductor back end, addressing issues of temperature, chemical reactions, CMOS-accepted elements, and crystallographic texture.

11:00 AM EQ09.03.10

The Role of Disorder in Ferroelectric Aluminum Scandium Nitride Xiaoman Zhang¹, Andrew C. Meng^{2,3} and Wen J. Meng¹; ¹Louisiana State University, United States; ²University of Pennsylvania, United States; ³University of Missouri–Columbia, United States

Aluminum scandium nitride (AlScN) thin films have shown promise as a potential ferroelectric material for neuromorphic computing hardware applications. We report epitaxial growth of AlScN thin films on Si (111) at 800°C by ultra-high-vacuum reactive sputtering, with Sc compositions ranging from 0-39 at%. Structural characterization using x-ray diffraction and transmission electron microscopy shows the wurtzite to rocksalt structural transition occurring beyond 30 at% Sc. Sc incorporation into aluminum nitride (AlN) introduces two types of disorder. First, phase segregation at intermediate Sc compositions is observed, suggesting a miscibility gap in this alloy. Second, increasing width of nitride film diffraction features in the in-plane direction as the Sc composition increases suggests that disorder is directly related to Sc alloying. From these observations, we can define a disorder parameter and find that ferroelectricity in AlScN is correlated with an optimum level of disorder in the material.

SESSION EQ09.04: Low-Power CMOS
Session Chairs: Catherine Dubourdieu and Sasikanth Manipatruni
Tuesday Afternoon, November 29, 2022
Sheraton, 2nd Floor, Back Bay D

1:30 PM *EQ09.04.01

Quantum Materials Enabling Beyond CMOS Low Energy Compute John Plombon, Punyashloka Debashis, Dmitri E. Nikonov, Mahendra DC, Dominique Adams, Chia-ching Lin, Scott B. Clendinning, Marko Radosavljevic and Ian A. Young; Intel Corporation, United States

Since the proposal of the MESO logic device [1,2] by the Intel Corporation, the search for materials to realize energy efficient computing on the order of 1 aJ/bit has made much progress.

The importance of a highly energy efficient switch is detailed in the Semiconductor Research Corporation Decadal Plan for Semiconductors [3] which highlights that compute energy is a significant and growing percentage of the global energy production and is on an exponential growth path. The development of substantially lower energy switches is a key ingredient in building a sustainable compute ecosystem.

In the proof-of-concept MESO device [4], the magneto-electric (ME) material was BiFeO_3 , the magnet was $\text{Co}_{0.9}\text{Fe}_{0.1}$, and the spin-orbit (SO) coupling material was Pt all deposited on DyScO_3 substrate. The ME material was deposited with pulsed laser deposition (PLD) and the magnet and SO material were deposited with magnetron sputtering (PVD). The ultimate MESO device will most likely be very different from the proof-of-concept device with some or all portions of the stack being deposited by other means meeting manufacturability requirements.

Two areas of disruption will be the substrate and the SO material. One path forward for a substrate compatible with a front-end of line integrated MESO device is epitaxial SrTiO_3 on Si. The path for material integration for back-end of line is wide open and new ideas are to be explored to enable epitaxial materials on amorphous substrates. The area of SO materials is a grand challenge for the research community with the goal of achieving nearly perfectly efficient spin-to-charge conversion in spin-orbit materials, topological insulators or other novel material systems.

The ME stack is within 4x of the goal of +/- 50mV switching voltage [5] but it has challenges of controlling built-in potentials that can easily exceed the switching voltage specification. Understanding, measuring, and controlling built-in potentials of the ME stack is another grand challenge for the research community that needs to be explored. The nano-magnet material will most likely move to a system that is more compatible with the ME complex oxides

and oxide ferromagnets.

Uniting the ME and SO parts of the MESO device will require manufacturable deposition processes that can scale to large substrates. This will require either innovations in the hardware for depositions techniques such as MBE and PLD, typically associated with epitaxial complex oxide film growth, or a transition to appropriately tuned versions of the more traditional high volume film growth techniques of atomic layer deposition (ALD), chemical vapor deposition (CVD) or (off-axis) physical vapor deposition (PVD). The relative merits and readiness of these film growth technologies for the manufacture of the MESO device will need to be explored.

With the need to drive for lower energy consumption for computing evident, this talk will explore the latest status of the MESO logic device as a path forward with a focus on the key role that quantum materials play in its realization.

- [1] Manapatruni, S., Nikonov, D.E. & Young, I.A. Beyond CMOS computing with spin and polarization. *Nature Phys* **14**, 338–343 (2018).
- [2] Manapatruni, S., Nikonov, D.E., Lin, C.C. *et al.* Scalable energy-efficient magnetoelectric spin-orbit logic. *Nature* **565**, 35–42 (2019).
- [3] The Decadal Plan for Semiconductors, Semiconductor Research Corporation (2022).
- [4] D. C. Vaz *et al.*, "Functional Demonstration of a Fully Integrated Magneto-Electric Spin-Orbit Device," *2021 IEEE International Electron Devices Meeting (IEDM)*, 2021.
- [5] B. Prasad *et al.*, *Adv. Mater.* **32**, 2001943, 2020.

2:00 PM EQ09.04.02

Vertically-Integrated, Multivalued Logics from Heterojunction Transistors for Low Power and High-Efficiency Computing Hocheon Yoo; Gachon University, Korea (the Republic of)

Multivalued logic (MVL) circuits can significantly improve data processing efficiency based on additional logic states in new systems, potentially providing the development of high density information computing [1]. Multivalued logic circuits can be implemented by adopting a structure of heterojunction thin-film transistors (H-TR), where p- and n-type thin-film layers with a partial junction of each layer in contact with only one of the source and drain contact electrode. The above-described H-TR structure does not increase the number of transistors required to implement a multi-value logic operation, so that an additional state can be formed during circuit switching while maintaining the existing digital circuit structure. In this talk, I introduce recent efforts in our group to implement MVL by controlling negative differential transconductance (NDT). I also present our representative MLV development examples: (i) full swing ternary logics [2], (ii) asymmetric contact-based ternary logics [3], (iii) flexible ternary logics [3], and (iv) vertically-integrated ternary logics [4]. By presenting a comprehensive strategy for H-TRs-based MVL in various structures, this talk suggests that MVL is one of the emerging applications from new switching behaviors in transistors.

- [1] Yoo, Hocheon, and Chang-Hyun Kim. "Multi-valued logic system: New opportunities from emerging materials and devices." *Journal of Materials Chemistry C* **9**.12 (2021): 4092-4104.
- [2] Yoo, Hocheon, *et al.* "Negative transconductance heterojunction organic transistors and their application to full swing ternary circuits." *Advanced Materials* **31**.29 (2019): 1808265.
- [3] Lee, Chungryeol, *et al.* "Systematic Control of Negative Transconductance in Organic Heterojunction Transistor for High Performance, Low Power Flexible Ternary Logic Circuits." *Small* **17**.46 (2021): 2103365.
- [4] Choi, Junhwan, *et al.* "Vertically stacked, low-voltage organic ternary logic circuits including nonvolatile floating-gate memory transistors." *Nature communications* **13**.1 (2022): 1-10.

2:15 PM EQ09.04.03

High Mobility InAs and InP Grown Directly on Amorphous Dielectrics at BEOL Compatible Temperatures Debarghya Sarkar^{1,2} and Rehan Kapadia²; ¹Harvard University - Massachusetts General Hospital, United States; ²University of Southern California, United States

A fundamental requirement to realize 3D integrated circuits is the ability to integrate single crystal semiconductor devices on the back-end of functional layers within a thermal budget of ~400 °C. Present state-of-the-art methods involve wafer bonding or epitaxial growth and transfer, since directly growing on amorphous materials by traditional epitaxial growth processes like MOCVD and MBE would give polycrystalline films with submicron-scale grains. To that end, a newly introduced and actively developing growth method called Templated Liquid Phase (TLP) has demonstrated the ability to achieve single crystal compound semiconductor mesas of areal dimension ~10µm diameter on diverse amorphous substrates. While initial demonstrations of TLP growth were at temperatures around 500-600 °C, in this presentation we would discuss some of the recent material characteristics and device results achieved and insights obtained, for crystalline InP mesas grown on amorphous dielectrics at temperatures below 400 °C. The optoelectronic quality of InP is optimal when it is grown at 300 °C, a temperature which is low enough to enable back-end-of-line growth on fully fabricated Si complementary metal oxide semiconductor circuits. Excellent on/off ratios are demonstrated by nanosheet transistors fabricated using this low-temperature grown InP, with the fabrication process also entirely carried out at 300 °C or below. InAs grown by this method showed room temperature mobility of ~5800 cm²/V-s, the highest mobility reported for any thin-film semiconductor material system directly grown on a nonepitaxial substrate, and which is close to reported values of epitaxially grown materials.

2:30 PM EQ09.04.04

Tuning Electrical Properties by High Electronegativity Dopant for Ambipolar Zinc Nitride Semiconductor Ji-Min Park¹, Kwun-Bum Chung² and Hyun-Suk Kim¹; ¹Chungnam National University, Korea (the Republic of); ²Dongguk University, Korea (the Republic of)

High-performance complementary metal-oxide-semiconductor (CMOS) integrated devices and circuits are widely used from memory devices to image sensors, logic devices, and switching and driving devices in displays. In the case of silicon-based CMOS, transfer printing technology is essential, which greatly increases the process cost. Therefore, it is necessary to develop NMOS and PMOS fabrication technologies capable of a direct deposition process on a substrate. On the other hand, high-density unipolar p-type and n-type (non-Si based) transistors are each individually fabricated with different semiconductor materials and integrated to form logic circuits. The separation process requirements of circuits further complicate the manufacturing process. In contrast, ambipolar transistors that can implement both p-type and n-type characteristics with a single material, are promising candidates for highly integrated CMOS circuits with effectively simplified designs.

So far, ambipolar semiconductor materials have been mainly reported based on copper nitride or organic/inorganic perovskite. However, copper nitride is not suitable for mass production and commercialization because high-temperature epitaxial growth is required during the deposition process. On the other hand, organic/inorganic perovskite has the advantage of being able to have both n-type and p-type properties as a single material. But, there is a problem that mobility is very low and unstable, so it is easily decomposed in the atmosphere. In order to overcome this limitation, it is necessary to develop a new ambipolar semiconductor material capable of large-scale deposition and excellent electrical properties.

Herein, the nitride-based semiconductor materials fabricated by the sputtering process at room temperature are proposed as the ambipolar semiconductor

material, which is advantageous for a large area and mass production. The fluorine (F) which has the high electronegativity can act as an acceptor when incorporated as an interstitial dopant in the Zn_3N_2 matrix. Therefore, both n- and p-type characteristics can be achieved through a single Zn_3N_2 material by controlling the amount of F during the sputtering deposition process. As a result, F-incorporated zinc nitride TFTs exhibited symmetric ambipolar properties with high field-effect mobility. Also, the CMOS-like inverters composed of two Zn_3N_2 ambipolar TFTs has been successfully implemented with excellent voltage gain characteristics. These characteristics offer the applicability to low-cost, large-area and high-efficiency CMOS circuits.

2:45 PM EQ09.04.05

Controlling Electrical Behavior Using a Magnetic Field in Early-Stage Memrectifiers [Guinevere Strack](#)¹, Jin Ho Kim², Alkim Akyurtlu¹ and Richard M. Osgood²; ¹University of Massachusetts Lowell, United States; ²US Army Combat Capabilities Development Command Soldier Center, United States

Rectification is a nonlinear optical process through which power and energy can be harvested by subtracting photon energies. This process can be harnessed to enable lightweight power generating devices that could eventually replace or supplement finite power sources, such as batteries. Rectennas are antennas, with sub-wavelength dimensions that, at resonance, intensify the electric field when combined with metal-insulator-metal (MIM) barrier structures (diodes) that have nonlinear, asymmetric conductivity. Minimizing the external power required to drive or control device performance will increase the net power output of rectennas. Pulsing a magnetic switch requires very small amounts of input energy, compared to the amount of energy lost in CMOS-style capacitive memory (to leakage currents, currents required to change gate voltages, etc.).

This presentation will focus the fabrication and characterization of an early stage 'memrectifier', comprised of ferromagnetic material. In this effort, we explored the magnetic reconfigurability of simple thin film devices, magnetic 'memrectifiers', which are nonlinear electrical devices that 'remember' a previous state or electrical behavior. Early stage memrectifiers were designed, fabricated, and electrically characterized in the presence of an applied magnetic field. The early-stage memrectifiers were comprised of several nanometric layers (Nb-Nb₂O₅-Co-Au). The ferromagnetic material, Co, was incorporated into the MIM diode to enable changes in electrical characteristics in the presence of a magnetic field. Niobium was deposited as the first metallic layer. The dissimilar metals, Nb and Co, were separated by the niobium oxide dielectric barrier layer, which was deposited in layers of varying thickness. The effect of the dielectric layer thickness, electrical characteristics, and magnetic reconfigurability were measured, and used to direct fabrication and design strategies.

Electrical characterization was carried out and J-V curves were obtained in the presence and absence of a magnetic field. The diode was subjected to three consecutive sweeps to test the repeatability of the electrical properties. On the fourth sweep, a magnet was placed next to the sample during the current-voltage sweep. The magnet was removed and then four more current-voltage sweeps were applied to the diode. The current density increased from 0.049 to 0.81 A cm², a 20-fold change. Control I-V curves obtained on gold films have revealed that the electrical characteristics are slightly changed in the presence of a magnetic field; however, the subsequent current-voltage sweeps revert to the initial electrical characteristics when the magnetic field is removed. Although this preliminary result is promising, additional experiments are needed before concluding that the change in electrical performance is indeed due to the magnetic field's affecting the magnetic materials. In addition, the effect of the applied voltage and current in the presence of the magnetic field on the 'remembered' electrical state will be studied.

3:00 PM BREAK

SESSION EQ09.05: Low-Power Computing and Interconnects
Session Chairs: Olga Ovchinnikova and John Plombon
Tuesday Afternoon, November 29, 2022
Sheraton, 2nd Floor, Back Bay D

3:30 PM EQ09.05.02

Sub-10K Cold-Electron Injection to Silicon at Room Temperature Pushkar K. Gothe¹, [Anthony Martinez](#)¹, Ojas T. Bhayde¹, J. Tyler Gish², M. R. Tiscareno¹, Jiechao Jiang¹, Joseph Ngai¹, Efstathios Meletis¹, Mark C. Hersam² and Seong Jin Koh¹; ¹The University of Texas at Arlington, United States; ²Northwestern University, United States

The root cause of the excessive power consumption (or excessive heat dissipation) of modern large-scale integrated circuits is the intrinsic thermal excitation of electrons that follows the Fermi-Dirac distribution. The hot electrons at the Fermi-Dirac distribution tail overcomes the OFF-state energy barrier of transistors, leading to inadvertent large electron flows and thereby large OFF-state power consumption. Here we represent an approach in which thermally excited electrons are filtered by a quantum well (QW) state and only energy-filtered cold electrons are injected to semiconductor conduction band. We demonstrate that the energy filtering enables transport of extremely cold electrons, whose effective electron temperature can reach as low as 7 Kelvin at room temperature. The electron energy filtering structure was fabricated on a wafer scale using CMOS-compatible processes and materials. The energy filtering stack is composed of source metal (Cr), first tunneling barrier (0.5-1 nm Al₂O₃ or Si₃N₄), QW layer (1-5 nm SnO₂ or 2 nm Cr₂O₃), second tunneling barrier (1.5-2 nm SiO₂), and Si. Electrons are tunneled from the source to a QW state, and then energy-filtered cold electrons are tunneled from the QW state to Si conduction band. Room-temperature current-voltage (I-V) measurements showed extremely abrupt current jumps, which correspond to alignments of the QW levels with the conduction band edge of Si. Differential conductance (dI/dV) plots show narrow peaks, with their FWHMs (full widths at half maximum) only ~2 mV, corresponding to an effective electron temperature of 7 Kelvin at room temperature. This cold-electron injection demonstrated for a Si system has a potential to realize steep subthreshold swing of much less than 60 mV/decade at room temperature, leading to energy-efficient low-power transistors.

This work was supported by the National Science Foundation UTA/NU Partnership for Research and Education in Materials (NSF DMR-2122128). The atomic layer deposition work was supported by the National Science Foundation Materials Research Science and Engineering Center at Northwestern University (NSF DMR-1720139). S.J.K. also gratefully acknowledges support from the National Science Foundation RAPID program (NSF ECCS-2031770).

3:45 PM EQ09.05.03

Growth of Topological Semimetal Cobalt Monosilicide for Scaled Back-End-of-Line Interconnects [Yansong Li](#), Guanyu Zhou and Christopher Hinkle; University of Notre Dame, United States

The resistivity of conventional metal interconnects increases rapidly with decreasing size which causes high energy consumption with severe signal delay.

Electron scattering at surfaces and grain boundaries are found to be the main causes of this size effect. Topological semimetals, which can effectively suppress electron scattering at surfaces, are believed to be promising candidates to replace currently used conventional metals. CoSi, a topological semimetal with multifold fermions, possesses unique topologically protected surface states that are expected to decrease resistivity at scaled dimensions where surface transport dominates.

Here, we demonstrate the growth of CoSi thin films and single-crystal CoSi nanowires. CoSi thin film growth is achieved on c-plane sapphire and GaN substrates by MBE. Multiple characterization techniques including RHEED, HRXRD, and Raman microscopy are utilized for optimizing growth conditions and realizing single-phase CoSi thin film growth. CoSi nanowires are obtained by co-depositing Co and Si on HOPG substrates via MBE. By carefully controlling the Co flux and growth temperature, the CoSi nanowire dimensions and yield can be controlled and the single-crystal and single-phase nature of the CoSi nanowire are confirmed by TEM and EDX. We also demonstrate a new approach to transferring CoSi nanowires from the HOPG substrate to another carrier wafer by only introducing and freezing DI water. And four-probe devices were made on transferred nanowires via electron beam lithography for measuring the CoSi nanowire resistivity. We will discuss both the thin film and nanowire results, including the impact of in-plane texturing as well as the benefits of the nanowire synthesis. We will discuss resistivity vs. dimension and provide an outlook for using CoSi as scaled interconnects. This work was supported by IMPACT, a center in nCORE, a Semiconductor Research Corporation (SRC) program.

4:00 PM EQ09.05.04

Resistivity Scaling in CuTi and CuAl₂ Intermetallics for Narrow Interconnects [Minghua Zhang](#) and Daniel Gall; Rensselaer Polytechnic Institute, United States

The electrical resistivity ρ as a function of thickness $d = 5.8\text{-}149/10.2\text{-}141$ nm of epitaxial CuTi(001) and CuAl₂(001) layers is measured to quantify the resistivity size effect of these compound conductors and evaluate their promise as a replacement material for Cu in highly scaled interconnect lines in microelectronic devices. The layers are deposited by magnetron co-sputtering onto MgO(001) substrates and their epitaxy is confirmed by x-ray diffraction θ - 2θ scans, ω rocking curves and ϕ -scans. The surface morphology is quantified by x-ray reflectivity and atomic force microscopy, and the composition measured by photoelectron spectroscopy and Rutherford backscattering. Data fitting of the measured ρ vs d yields room-temperature electron mean free paths $\lambda = 12.5$ and 15.6 nm for CuTi and CuAl₂, respectively, and bulk resistivities $\rho_o = 19.2 \pm 0.8$ and 7.7 ± 0.4 $\mu\Omega$ cm. Air exposure causes surface oxidation and a resistivity increase for both intermetallic compounds which is attributed to a transition from partially specular to completely diffuse electron surface scattering. CuTi in direct contact with SiO₂ exhibits a 500 times longer failure time than Cu during room-temperature time-dependent dielectric breakdown (TDDB) tests using a 3 MV/cm bias. The overall analysis yields $\rho_o\lambda$ benchmark values of 24×10^{-16} and 12×10^{-16} Ωm^2 , respectively, indicating that the evaluated compound conductors exhibit a conductivity advantage against Cu only if their higher cohesive energies and stability is exploited to achieve liner-free lines.

4:15 PM EQ09.05.05

Amorphous Gallium Nitride by Low-Temperature MOCVD Growth for Back-End-Of-Line Transistors [Tian Sun](#), Guanyu Zhou, Jaemin Shin and Christopher Hinkle; University of Notre Dame, United States

GaN is a promising material for BEOL access transistors due to its high electron mobility, large bandgap (for low leakage), and stability in a hydrogen environment (to minimize V_t variability). However, GaN is normally grown at temperatures (~ 1000 °C) much higher than the 450 °C typically considered BEOL-compatible. Due to the lack of thermal energy, metal-organic chemical vapor deposition (MOCVD) precursor decomposition is less efficient and adatom diffusion is insufficient, preventing the growth of high-quality GaN using typical growth strategies under BEOL constraints.

Amorphous GaN has been proposed as a promising material for electronic applications [1]. Here, we demonstrate the growth of amorphous GaN at BEOL compatible temperatures ≤ 450 °C by MOCVD with electrical properties starting to approach those necessary for access transistors. Through a detailed study of the growth conditions such as the V/III ratio of the precursors and low-temperature BEOL-compatible anneals, we were able to obtain amorphous GaN (as confirmed by XRD) with a 3.2 eV bandgap as measured by UV-Vis. Room temperature mobilities of 10-15 $\text{cm}^2/\text{V}\cdot\text{s}$ are demonstrated and initial transistors exhibit I_{on}/I_{off} ratios greater than 10^7 with subthreshold swings ~ 110 mV/decade. Crystalline GaN, grown using conventional two-step growth methods, shows a steep drop-off in mobility from the 350 $\text{cm}^2/\text{V}\cdot\text{s}$ when grown at 1000 °C down to 0 when grown at 450 °C. Our amorphous GaN grown at 450 °C has electrical properties that are comparable to crystalline GaN grown at ~ 750 °C. We will discuss the role of oxygen incorporation to suppress electron carrier concentrations and will provide detailed characterization of the films from XPS, Raman, TEM, XRD, EDX, and EXAFS.

This work was supported in part by NEWLIMITS, a center in nCORE, a Semiconductor Research Corporation (SRC) program sponsored by NIST through award number 70NANB17H041. This work was also supported in part by the SRC through the Global Research Collaboration (GRC) program.

References

[1] Stumm, P., and D. A. Drabold., *Physical Review Letters* 79 (4),(1997) 677

SESSION EQ09.06: Magnetolectrics and Multiferroics
Session Chairs: Manuel Bibes and Ramamoorthy Ramesh
Wednesday Morning, November 30, 2022
Sheraton, 2nd Floor, Back Bay D

8:15 AM *EQ09.06.01

Voltage and Current Controlled Nanomagnetism for Memory and Logic [Ramamoorthy Ramesh](#); University of California, Berkeley, United States

Complex perovskite oxides exhibit a rich spectrum of functional responses, including magnetism, ferroelectricity, highly correlated electron behavior, superconductivity, etc. The basic materials physics of such materials provide the ideal playground for interdisciplinary scientific exploration with an eye towards real applications. Over the past decade the oxide community has been exploring the science of such materials as crystals and in thin film form by creating epitaxial heterostructures and nanostructures. Among the large number of materials systems, there exists a small set of materials which exhibit multiple order parameters; these are known as multiferroics, particularly, the coexistence of ferroelectricity and some form of ordered magnetism (typically antiferromagnetism). The scientific community has been able to demonstrate electric field control of both antiferromagnetism and ferromagnetism at room temperature. In parallel, there are some very intriguing new developments in SOT based manipulation of magnets. Particularly, the role of epitaxy and electronically perfect interfaces has been shown to significantly impact the spin-to-charge conversion (or vice versa). Under funding from the US Department of Energy and the SRC-DARPA-JUMP funded ASCENT Center, current work is focused on ultralow energy (1 attoJoule/operation) electric

field manipulation of magnetism with both voltage and current, as the backbone for the next generation of ultralow power electronics. We are exploring many pathways to get to this goal. In this talk, I will describe our progress to date on this exciting possibility. The talk will conclude with a summary of where the future research is going.

8:45 AM EQ09.06.02

Magnetization Reversal in BiFe_{0.9}Co_{0.1}O₃ Thin Films 1- Spin Structure and Magnetization Reversal by Electric Field at Room Temperature in Co-Substituted Bismuth Ferrite Thin Film Kei Shigematsu^{1,2}, Keisuke Shimizu¹, Ryo Kawabe¹, Hajime Hojo³, Haruki Shimizu¹, Marin Katsumata¹, Hajime Yamamoto⁴, Ko Mibu⁵ and Masaki Azuma^{1,2}; ¹Tokyo Institute of Technology, Japan; ²Kanagawa Institute of Industrial Science and Technology, Japan; ³Department of Energy and Material Science, Kyushu University, Japan; ⁴Tohoku University, Japan; ⁵Nagoya Institute of Technology, Japan

Electric-field control of magnetism in multiferroic materials is a significant challenging issue on the development of novel low-energy-consuming nonvolatile memory devices. Perovskite bismuth ferrite BiFeO₃ is widely studied multiferroic material because of strong magnetoelectric coupling between the electrical polarization and antiferromagnetic magnetic ordering above room temperature, but BiFeO₃ does not show such spontaneous magnetization due to the presence of cycloidal spin modulation superimposed on G-type antiferromagnetism. Cobalt-substitution is one of the powerful ways to modify the electric and magnetic properties of BiFeO₃. Partial substitution of Co for Fe stabilizes the collinear phase with weak ferromagnetism preserving the *R3c* crystal structure. Neutron powder diffraction and Mössbauer spectroscopy measurements revealed a change in the spin structure from a cycloidal one at low temperature to a collinear one at room temperature. However, because the magnetic structure of BiFeO₃ is quite sensitive to lattice strain, the choice of single crystal substrate for thin film growth is of great importance.

Here we grew a single-phase ferromagnetic ferroelectric BiFe_{0.9}Co_{0.1}O₃ thin film grown on GdScO₃ substrate. The conversion electron Mössbauer spectroscopy on a nearly 100% ⁵⁷Fe-enriched thin film sample revealed the collinear spin structure, whereas the spectrum of the BFO thin film on the same substrate showed a cycloidal spin structure. The value of quadrupole shift was close to that of bulk BFO (-0.20 mm/s) and that of (111)_{pc}-oriented BFO thin films (-0.217 mm/s), strongly suggesting that the spins are aligned perpendicular to the electric field gradient ($V_{zz} > 0$), which was along the polar axis. Further analysis of Mössbauer spectrum revealed that the possible directions of antiferromagnetic spin direction are limited to four, which is quite close to four of six $\langle 121 \rangle$ directions in the easy plane perpendicular to the polarization along the [111] direction. Each ferroelectric domain has four possible magnetization directions, all of which have an out-of-plane ferromagnetic component. The spontaneous magnetization is in four $\langle 110 \rangle$ directions, perpendicular to both antiferromagnetic spin direction and polarization. Magnetization reversal due to 71° ferroelectric switching is expected to occur if the octahedral rotation is accompanied by a change in the antiferromagnetic spin direction.

The correlation between the ferroelectric and ferromagnetic domains was investigated by performing piezoelectric force microscopy (PFM) and MFM on the as-grown BFO thin film. Both PFM and MFM images exhibit a striped domain configuration with four polarization down domains can be seen, indicating the both ferroelectric and ferromagnetic domains are strongly coupled with each other. Magnetization reversal by polarization switching was demonstrated by tip bias of -7 V. In the area where pure out-of-plane 71° domain switching occurred, the magnetic domain structure was also preserved but the contrast of MFM phase was reversed, indicating that the out-of-plane magnetization switched from downward to upward and vice versa in this area. This was the first direct observation of magnetization reversal by the electric field at room temperature. On the other hand, in the area where the striped domain structure is heavily modified, MFM image is also changed largely by the poling, though the contrast is correlated with the ferroelectric domain structure after the poling. These results indicate that an out-of-plane magnetization reversal can be achieved by 71° polarization switching without reconstruction of the ferroelectric domain.

9:00 AM EQ09.06.03

Magnetization Reversal in BiFe_{0.9}Co_{0.1}O₃ Thin Films 2 - Control of Ferroelectric and Ferromagnetic Domains by Trailing Fields Takuma Itoh¹, Marin Katsumata¹, Kei Shigematsu^{1,2} and Masaki Azuma^{1,2}; ¹Tokyo Institute of Technology, Japan; ²Kanagawa Institute of Industrial Science and Technology, Japan

BiFeO₃ (BFO) is the most widely investigated multiferroic material with a large electric polarization along the [111] of pseudocubic cell with a ferroelectric Curie temperature of 1103 K and an antiferromagnetic Néel temperature of 643 K. The presence of a cycloidal spin modulation prohibits the appearance of spontaneous magnetization. Partial Co substitution for Fe changes the spin structure to a collinear one with a spontaneous magnetization owing to the spin canting preserving the large electric polarization [1]. Therefore, BiFe_{0.9}Co_{0.1}O₃ (BFCO) is a multiferroic material with both a large electric polarization and a spontaneous magnetization at room temperature, which are perpendicular to each other. The magnetization reversal accompanying 71° polarization switching in a thin film has been observed at room temperature, which is expected to be utilized in ultra-low power consumption magnetic memory devices [2]. However, it is necessary to understand the behaviors of ferroelectric and magnetic domains during the polarization reversal process and deterministically control the polarization and magnetization direction.

In this study, the polarization of BFCO grown in (001) orientation was controlled in both out-of-plane and in-plane direction by utilizing the effective in-plane electric field, so-called trailing field, resulting from the scanning of the cantilever [3]. The polarization of the as-grown film was limited to four out-of-plane downward directions by self-poling effect. The cantilever was scanned with a bias voltage of -7 V for out-of-plane polarization switching, which resulted in a striped ferroelectric domain with two types of out-of-plane upward polarization affected by the trailing field. Then, the same surface location was scanned with the cantilever, the slow scan direction of which is opposite to the in-plane component of the polarization, with an increased tip bias (-10 V). This process corresponded to increasing an effective in-plane electric field without changing the direction of the out-of-plane electric field. After such in-plane electric field application, the ferroelectric domains were observed by piezoresponse force microscopy (PFM). It was found that all the polarizations were oriented in the direction of the trailing field while maintaining the striped domain. The magnetic domains were also observed by magnetic force microscopy (MFM) and was found to have a striped domain shape similar to that of the ferroelectric domain. From these results, we conclude that in-plane polarization can be controlled by using the trailing field. The magnitude of the electric trailing field generated by -10 V bias voltage was estimated to be about 40 kV/cm⁻¹. Normally, about 200 kV/cm⁻¹ is required for in-plane polarization reversal of BiFeO₃ using planar electrodes, but in this trailing field, in-plane polarization reversal was achieved with only one-fifth of that voltage.

Consequently, we succeeded in changing the polarization direction to any desired direction by controlling three main factors: the sign and magnitude of the voltage between the cantilever and the bottom electrode, and the slow scan direction (the direction of electric trailing field). Magnetic domain imaging by MFM revealed that the ferroelectric and magnetic domains have similar shapes, suggesting a strong correlation between polarization and magnetism, indicating the magnetic domain can also be controlled by the trailing field. The above results suggest that the electric trailing field is a valuable tool to manipulate the ferroelectric and magnetic domains in multiferroic BFO thin films.

[1] H. Hojo et al., Adv. Mater. 29, 1603131 (2017).

[2] K. Shimizu et al., Nano Lett. 19, 1767 (2019).

[3] T. Itoh et al., Appl. Phys. Express 15, 023002 (2022).

9:15 AM EQ09.06.04

Exploring the Correlation Between the Spin-State Configuration and the Magnetic Order in Co-Substituted BiFeO₃ Koomok Lee¹, Kei Shigematsu^{1,2}, Das Hena¹ and Masaki Azuma^{1,2}; ¹Tokyo Institute of Technology, Japan; ²Kanagawa Institute of Industrial Science and Technology, Japan

BiFeO₃ is one of the most actively studied multiferroic materials that exhibits a robust ferroelectric order below ~ 1100 K and an antiferromagnetic (AFM) order below ~ 640 K. Numerous researches have been conducted to explore its potential in effecting electric field control of magnetic order for energy-efficient nonvolatile magnetic memory applications. The magnetic order in BiFeO₃ is complex in nature. Close competition between various magnetic interactions, such as isotropic symmetric exchange (SE), antisymmetric Dzyaloshinskii-Moriya (DM) interaction and single ion anisotropy (SIA), lead to the formation of magnetic orders like the (1) G-type AFM order and (2) long period cycloidal order (~62nm). By partial substitution of Co instead of Fe, its cycloidal order disappears, and a spin canted G-type AFM with saturation magnetization about 0.03μ_B/f.u. perpendicular to the electric polarization has been observed. Moreover, magnetization reversal by electric field was observed in BiFe_{0.9}Co_{0.1}O₃ thin film. Understanding the effect of Co substitution to magnetic order of BiFeO₃ could give us the guideline to enhance the weak spontaneous magnetization of this system which is critical for magnetic memory application.

In the present study, using density functional theory (DFT) calculations and by employing a constructed model spin Hamiltonian and Monte Carlo simulations, we have studied the stability of the canted G-type AFM as a function Co substitution level. Co³⁺ can exhibit various spin states, such as low spin (LS, S=0), intermediate spin (IS, S=1) and high spin (HS, S=2) states. This ambiguity pertaining to the electronic structure of substituted Co³⁺ further contributes to the complexities of the BiFeO₃ system. Our detailed investigations of various properties of BiFeO₃ system as functions of Hubbard U parameter and the concentration of Co³⁺ show that, the spin state of Co³⁺ ion strongly depends on the U value and the high spin state of Co³⁺ is relatively stable. The calculated volume reductions with increase of Co concentrations are in best agreement with the experimental observations corresponding to the mixing of HS and LS of Co. Finite temperature Monte Carlo results considering a wide range of magnetic parameters, lead to the identification of the factors that enhance the stability of the canted G-type AFM phase. We observe that the strong tendency of the HS Co³⁺ to orient in the {111}_{pc} plane, which is perpendicular to the direction of the spontaneous polarization, enhances the stability of the canted G-type AFM phase and on the other hand the formation of the IS state contributes to the increase of the magnitude of net magnetization. Our study indicates the existence of HS and LS Co in the system under investigation and suggests guidelines to enhance the multiferroic properties of BiFeO₃.

9:30 AM EQ09.06.05

Increasing Strain-Mediated Magnetoelectric Coupling in Nanocomposites with Residual Porosity Shreya K. Patel, Christopher Ty Karaba and Sarah Tolbert; University of California, Los Angeles, United States

This work examines the role of nanoscale structure in the control of magnetoelectric coupling in three-dimensional multiferroic composites. Three-dimensional composites allow for a much increased interfacial surface area between the magnetostrictive and piezoelectric components, which in turn can lead to a much enhanced magnetoelectric coupling over traditional planar stack composites. Here, we investigate a composite made up of a solution-processed mesoporous material with the pores filled by atomic layer deposition with the alternate material. Tuning the thickness of the ALD-deposited layer allows for control of final composite porosity. We have found that the strength of magnetoelectric coupling depends heavily on this residual porosity, with higher porosity leading to greater magnetoelectric response. In a composite of mesoporous cobalt ferrite (CFO) filled with only 25% bismuth ferrite (BFO), we have found that an applied voltage on the composite causes a decrease in the saturation magnetization of the composite to about 50% its unpoled value, while the sample filled 100% with BFO shows little change in saturation magnetization. High-resolution X-ray diffraction confirms that the residual porosity is necessary for strain transfer to occur from the piezoelectric to the magnetostrictive component, as the porosity allows for mechanical flexing throughout the film.

9:45 AM BREAK

10:15 AM *EQ09.06.06

A Multiferroic Two-Dimensional Electron Gas Julien Bréhin¹, Yu Chen², Sara Varotto¹, Maria D'Antuono², Daniela Stornaiuolo², Cinthia Piamontezze³, Marco Salluzzo² and Manuel Bibes¹; ¹Unité Mixte de Physique CNRS/Thales, France; ²CNR-SPIN, Italy; ³PSI, Switzerland

Multiferroics are compounds in which at least two ferroic orders coexist – typically (anti)ferromagnetism and ferroelectricity – and whose investigation has been a major area of materials science during the last two decades. While magnetic order can arise in both insulating and metallic compounds, ferroelectricity is in principle only allowed in insulators, although ferroelectric metals were proposed over 60 years ago. Recently, several two-dimensional systems have been reported to behave as ferroelectric metals. Yet, their combination with magnetic order remains elusive. In this work, we show the coexistence of ferroelectricity and magnetism in a SrTiO₃-based two-dimensional electron gas (2DEG). Ti-L_{3,2} edge X-ray linear dichroism data evidences a modulation of the Ti-O polar displacements depending on the ferroelectric polarization direction while transport data reveal a voltage-induced hysteresis of the sheet resistance, reminiscent of the ferroelectric polarization loop. The 2DEG displays anomalous Hall effect and magnetoresistance that can both be modulated and cycled by switching the remanent polarization, demonstrating a magnetoelectric coupling. Our findings provide new opportunities in quantum matter stemming from the interplay between ferroelectricity, ferromagnetism, metallicity and Rashba spin-orbit coupling.

10:45 AM EQ09.06.07

Magnetization Switching and Reading in Magnetoelectric Spin-Orbit Nanodevices at Room Temperature Diogo C. Vaz¹, Chia-ching Lin², John Plombon², Won Young Choi¹, Inge Groen¹, Isabel Arango¹, Andrey Chuvilin¹, Aymeric Vecchiola³, Karim Bouzehouane³, Stephane Fusil³, Vincent Garcia³, Manuel Bibes³, Dmitri E. Nikonov², Hai Li², Punyashloka Debashis², Scott B. Clendenning², Tanay Gosavi², Yen-Lin Huang⁴, Bhagwati Prasad⁴, Ramamoorthy Ramesh⁴, Ian A. Young² and Felix Casanova¹; ¹CIC nanoGUNE, Spain; ²Intel Corporation, United States; ³CNRS/Thales, France; ⁴University of California, Berkeley, United States

In recent years, voltage and frequency scaling of CMOS technology has slowed down, accompanied by increasingly larger power requirements. To assure the continuity of Moore's Law, new beyond-CMOS logic devices need to be found. For this purpose, one of the leading options is the magneto-electric spin-orbit (MESO) logic device, where a combination of quantum materials and spin-based phenomena allows for energy-efficient logic and favourable device scaling [1, 2].

Here, based on the initial MESO proposal, we show voltage-based magnetization switching and reading at room temperature, in Pt/CoFe nanodevices fabricated on a multiferroic BiFeO₃ layer [3, 4]. Switching is performed by application of a voltage pulse to the BiFeO₃, which reverses its ferroelectric and antiferromagnetic state. Through interfacial exchange coupling, the CoFe magnetization is also reversed. Spin-to-charge conversion in the Pt/CoFe nanodevice is then used to probe the magnetization direction of the CoFe element. Additionally, we show PFM and MFM experiments where magnetization switching is imaged after each voltage pulsed applied. We discuss future strategies that need to be followed for the implementation of MESO-based logic circuits [4].

[1] S. Manipatruni et al., Nature 565, 35-42, 2019.

[2] H. Liu et al., IEEE Journal on Exploratory Solid-State Computational Devices and Circuits 5, 1-9, 2019.

[3] C.-C. Lin et al., IEEE International Electron Devices Meeting (IEDM), 37.3.1-37.3.4, 2019.

[4] D. C. Vaz et al., IEEE International Electron Devices Meeting (IEDM), 32.4. 1-32.4. 4, 2021.

11:00 AM EQ09.06.08

Investigation of Ferro- and Antiferromagnetic Memory Structures Using Scanning NV Magnetometry Peter Rickhaus¹, Umberto Celano², Liza Zaper^{3,1}, Alexander Stark¹, Mathieu Munsch¹, Marco Nordmann¹, Hai Zhong¹, Martino Poggio³, Christoph Adelmann², Paul van der Heide², Aurore Finco⁴, Vincent Jacques⁴, Vincent Garcia⁵ and Patrick Maletinsky^{3,1}; ¹Qnami AG, Switzerland; ²imec, Belgium; ³University of Basel, Switzerland; ⁴Universite' de Montpellier, France; ⁵CNRS Thales, France

To improve magnetic memories, significant efforts are made to reduce the size and spacing of magnetic bits. This implies that failures and defects can only be discovered with a non-invasive technique that can resolve small magnetic fields with high spatial resolution. Scanning NV magnetometry (SNVM) is the emerging quantum sensing technique that offers the required sensitivity.

We will demonstrate magnetic images of a few hot candidate materials for future magnetic memory devices. We will look at memory bits in antiferromagnetic chromia, antiferromagnetic cycloids in BiFeO₃ [1], cobalt nanomagnets and ultra-scaled CoFeB nanowires [2]. We will reveal magnetic textures that are undetectable with standard characterization techniques. In this context, we will more broadly discuss the potential of SNVM as a powerful magnetic characterization tool.

[1] Phys. Rev. Applied 17, 044051 (2022)

[2] Nano Lett. 21, 24, 10409–10415 (2021)

11:15 AM EQ09.06.09

Giant Converse Magnetolectric Effect in Co₂-Heusler Alloy/Pb(Mg_{1/3}Nb_{2/3})O₃-PbTiO₃ Multiferroic Heterostructures Takamasa Usami¹, Shumpei Fujii¹, Yu Shiratsuchi^{1,1,1}, Amran M. Yatmeidhy², Shinya Yamada^{1,1,1}, Takeshi Kanashima¹, Ryoichi Nakatani^{1,1,1}, Yoshihiro Gohda^{2,1} and Kohei Hamaya^{1,1,1}; ¹Osaka University, Japan; ²Tokyo Institute of Technology, Japan

The use of ferromagnetic/ferroelectric interfacial multiferroic heterostructures in spintronics devices is expected as a highly efficient method for controlling magnetization vectors by an electric-field (E) [1]. To incorporate the multiferroic heterostructure into the low-power consumption devices, a giant converse magnetolectric (CME) effect is needed, where the CME coupling coefficient over 10^{-5} s/m is required. In this study, we report giant CME coupling coefficients over 10^{-5} s/m in the multiferroic heterostructures with ferromagnetic Co₂-Heusler alloys that are famous as spintronic materials having high spin polarization [2,3].

30-nm-thick Co₂-Heusler-alloy films (Co₂FeSi, Co₂FeAl_{0.5}Si_{0.5}, Co₂Fe_{0.4}Mn_{0.6}Si, and Co₂MnSi) were grown on (011)-oriented Pb(Mg_{1/3}Nb_{2/3})O₃-PbTiO₃ (PMN-PT) substrates with inserting a 0.3-nm-thick Fe layer by molecular beam epitaxy at 300 °C. As a reference, ferromagnetic Fe₃Si (Fe₂FeSi) was also grown on PMN-PT(011). XRD measurements revealed that all the Heusler films are polycrystalline. In addition, we confirmed that the $L2_1$ or $D0_3$ -ordered structures are included in Co₂FeSi, Co₂Fe_{0.4}Mn_{0.6}Si, and Fe₃Si films whereas only the $B2$ -ordered structure is obtained in Co₂FeAl_{0.5}Si_{0.5} and Co₂MnSi films.

The CME effect was characterized by in-plane magneto-optical Kerr-ellipticity measurements and conventional magnetization measurements at room temperature [3]. We found that all multiferroic heterostructures using Co₂-Heusler-alloy films show the 90° rotation of the magnetic easy axis by applying E . In addition, a giant CME coefficient over 10^{-5} s/m was obtained for all the Co₂-Heusler/PMN-PT(011) multiferroic heterostructures. For the Fe₃Si/PMN-PT(011), on the other hand, a small variation in the magnetic easy axis was seen. This study indicates that the presence of Co atoms in Heusler alloys is important to demonstrate the giant CME effect. We note that the use of Co₂-Heusler alloys is also useful to achieve high-performance spintronics devices. This work was partly supported by JST CREST Grant No. JPMJCR18J1 and JSPS KAKENHI Grant No. JP21K14196 and JP19H05616.

[1] J. M. Hu et al., Nat. Commun. 2, 553 (2011).

[2] T. Usami et al., Appl. Phys. Lett. 118, 142402 (2021).

[3] S. Fujii et al., NPG Asia Mater. 14, 43 (2022).

11:30 AM EQ09.06.10

Voltage-Tunable Coupling to a Coplanar Waveguide Resonator Mediated by a Josephson Junction Field Effect Transistor—Part I William M. Strickland, Bassel Heiba Elfeky, Dylan Langone, Ido Levy and Javad Shabani; New York University, United States

Superconducting qubit circuits could benefit immensely from a low power and fast tunability mechanism. This tunability can mediate microwave photon storage for quantum memory, as well as dynamically control qubit-qubit coupling. However, many current implementations of a tunable coupler for superconducting qubits are based on Al-AlO_x-Al Josephson tunnel junctions arranged in a loop controlled via an applied flux through the loop generated by a current on the order of a milliampere. As the system size scales up, the additional heat load will scale as the square of the number of flux lines. Low-power voltage-controlled Josephson junction field effect transistors (JJ-FET) fabricated on superconductor-semiconductor heterostructures have been utilized to make tunable qubits. We present a gate voltage tunable Josephson junction field effect transistor fabricated on an Al-InAs heterostructure embedded in a coplanar waveguide resonator.

We show how the properties of this device make it a viable option for a tunable coupler. We show measurements of the internal quality factor of the materials stack and find that the loss is dominated by the InAlAs buffer layer. By varying the inductance of the junction via a gate voltage tunable critical current, we find that the resonant frequency and external quality factor can be tuned. By completely suppressing the supercurrent flowing through the junction, the coupler can provide full isolation. Electromagnetic field simulations are utilized to understand and solve for the lowest frequency eigenmodes as a function of the Josephson inductance.

*This abstract is the first part of a two-part abstract. The second abstract will be presented by Bassel Heiba Elfeky.

11:45 AM EQ09.06.11

Voltage-Tunable Coupling to a Coplanar Waveguide Resonator Mediated by a Josephson Junction Field Effect Transistor—Part II Bassel Heiba Elfeky, William M. Strickland, Dylan Langone, Ido Levy and Javad Shabani; New York University, United States

Recent advances and innovation in material systems have provided promising solutions for efficient quantum information processing. Understanding how the properties of such materials affect the functionality and coherence of qubit systems is essential. For superconducting qubit platforms, low-power voltage-controlled Josephson junction field effect transistors (JJ-FET) fabricated on superconductor-semiconductor heterostructures have been utilized to make tunable qubits. Here we present a new voltage-controlled coupler system through coplanar waveguide (CPW) resonators.

Here, we show that a gate-tunable JJ-FET fabricated on an Al-InAs heterostructure embedded in a CPW resonator provides the tunability required to make a tunable coupler. By varying the inductance of the junction using a gate voltage which changes the critical current, properties of the resonator such as its

resonance frequency and external quality factor can be tuned. By completely suppressing the supercurrent flowing through the junction, the coupler can provide full isolation. Electromagnetic field simulations are utilized to understand the system's dynamics.

*This abstract is the second part of a two-part abstract. The first abstract will be presented by William M. Strickland.

SESSION EQ09.07: RRAM I

Session Chairs: Regina Dittmann and Bhagwati Prasad

Wednesday Afternoon, November 30, 2022

Sheraton, 2nd Floor, Back Bay D

1:30 PM *EQ09.07.01

Electrochemical Random Access Memory (ECRAM) for Neuromorphic Computing A. A. Talin; Sandia National Laboratories, United States

As we near the limits of conventional digital CMOS technology, new computing paradigms and architectures co-designed with novel materials and new devices are needed to drastically improve energy efficiency and meet the demands of new classes of data-intensive applications. Non-von Neumann computing using neuromorphic systems based on analog, 2-terminal resistive non-volatile memory elements has emerged as a promising approach, but its full potential has not been realized due to the lack of materials and devices with the appropriate attributes. To address this need, 3-terminal device concept based tuning electronic conductance in functional materials through solid-state electrochemical ion-insertion have emerged as a promising approach. These devices are now broadly known as electrochemical random-access memory (ECRAM). Unlike memristors, which require large write currents to drive phase transformations or filament growth, every electron transferred through the external circuit in ECRAM corresponds to the migration of ~ 1 ion used to store analogue information. Like *static* dopants in traditional semiconductors, electrochemically inserted ions increase or decrease the conductivity by locally perturbing a host's electronic structure; however, ECRAM changes the dopant concentration in a *dynamic* and *reversible* manner. The resulting change in conductance can span orders of magnitude, from *gradual* increments needed for analog elements, to *large, abrupt* changes for dynamically reconfigurable adaptive architectures. In my presentation, I will discuss the recent progress in ECRAM devices spanning organic, inorganic, and 2D materials, circuits, architectures and the rich portfolio of challenging, exciting fundamental science questions and how we can harness these to realize a new paradigm for low power neuromorphic computing.

2:00 PM EQ09.07.02

Simulation of Switching Processes Inside Bilayer Valence Change Memory Cells by a Drift-Diffusion Model Nils Sommer¹, Stephan Menzel¹ and Rainer Waser^{1,2}; ¹Peter Grünberg Institute 7, Germany; ²Institute for Materials in Electrical Engineering 2, Germany

Valence change memory (VCM) cells are promising candidates for future nonvolatile storage devices [1]. VCM cells are characterized by their ability to switch between at least two stable resistance states by applying suitable bias voltages. A special structure of VCM cells are bilayer cells consisting of two semiconducting oxide layers, with one oxide serving as a tunnel barrier. Experiments show that a change in resistance of the cell can be caused by the exchange of oxygen between the two oxide layers [2-4]. However, the processes taking place are not yet well understood. We use a drift-diffusion model to simulate the movement of oxygen inside the semiconductor to gain a better understanding of the exchange process between the layers. We investigate the internal electric fields acting as a driving force on the oxygen, as well as the oxygen diffusion process that causes it to return to an equilibrium state. We show that an oxygen exchange deforms the shape of the tunnel barrier and by this changing the resistance of the cell. Further, we show that the change in resistance depends on the permittivity of the oxides.

[1] R. Waser, R. Dittmann, G. Staikov, K. Szot, Adv. Mater. 2009, 21, 2632

[2] A. Gutsche, S. Siegel, J. Zhang, S. Hamsch, R. Dittmann, Frontiers in Neuroscience, 2021, 15, 661261

[3] B. Arndt, F. Borgatti, F. Offi, M. Philipps, P. Parreira, T. Meiners, S. Menzel, K. Skaja, G. Panaccione, D. MacLaren, R. Waser, R. Dittmann, Adv. Funct. Mater., 2017, 1702282

[4] C. Baumer, T. Heisig, B. Arndt, K. Skaja, F. Borgatti, F. Offi, F. Motti, G. Panaccione, R. Waser, S. Menzel, R. Dittmann, Faraday Discuss., 2019, 213, 215

2:15 PM EQ09.07.03

Study of Resistive Switching in Polycrystalline ErMnO₃ Films Rong Wu^{1,2}, Sebastian Schmitt¹, Veeresh Deshpande¹, Florian Maudet¹ and Catherine Dubourdieu^{1,2}; ¹Helmholtz-Zentrum Berlin für Materialien und Energie, Germany; ²Freie Universität Berlin, Germany

Rare-earth hexagonal manganites h-RMnO₃ (R=Y, Er, Ho to Lu) have been widely studied as multiferroic compounds. Recently, resistive switching behavior has been reported in polycrystalline hexagonal YMnO₃ thin films with promising applications for neuromorphic devices [1]. The particular interest in h-RMnO₃ compounds for memristive devices lies in the potential use of their peculiar ferroelectric domain pattern, and especially of their vortex lines where six-fold domains merge.

In this work, we report the evidence of resistive switching behavior in polycrystalline ErMnO₃ thin films. The films (~60 nm thickness) were prepared on Pt/Ti/SiO₂/Si substrates by room temperature RF sputtering and subsequent annealing at high temperature (700-900 °C). They were characterized at the macro and microscale by X-ray diffraction, scanning electron microscopy, and confocal Raman spectroscopy. Metal-ErMnO₃-metal devices were fabricated using Ti/Au top electrodes. The Au/Ti/ErMnO₃/Pt devices exhibit a bipolar resistive switching with a R_{OFF}/R_{ON} ratio larger than 10⁴ and an ultra-low resistance of only 10 Ω in the low resistance state (R_{ON}), which may result in potential applications such as CMOS circuitry with low power consumption [2] and RF power switches [3]. We investigated the impact of electrical programming operations on the performances of the devices to improve their repeatability and endurance. Furthermore, we quantitatively studied the amount of hexagonal and orthorhombic crystalline phases by Raman spectroscopy and conductive atomic force microscopy and addressed the effect of their simultaneous presence on the resistive switching behavior of the films. We will discuss the properties of the different ErMnO₃ phases and the origin of the resistive switching mechanism in the stacks.

References

[1] Bogusz, A., et al. "Resistive switching in polycrystalline YMnO₃ thin films." AIP Advances 4.10 (2014): 107135

[2] Cao, Haichao, and Hao Ren. "A 10-nm-thick silicon oxide based high switching speed conductive bridging random access memory with ultra-low operation voltage and ultra-low LRS resistance." Applied Physics Letters 120.13 (2022): 133502

[3] Pi, Shuang, et al. "Memristors as radiofrequency switches." 2016 IEEE International Symposium on Circuits and Systems (ISCAS). IEEE, 2016

2:30 PM BREAK

SESSION EQ09.08: Low-Power Spintronics
Session Chairs: Bhagwati Prasad and Daniel Worledge
Wednesday Afternoon, November 30, 2022
Sheraton, 2nd Floor, Back Bay D

3:30 PM *EQ09.08.01

Advances in Spin-Transfer-Torque MRAM Daniel C. Worledge; IBM Research, United States

Spin-Transfer-Torque MRAM (STT-MRAM) is an emerging memory technology that possesses a unique combination of non-volatility, high endurance, and ease of integration using standard CMOS processing [1]. Initial applications include 1 Gb standalone memory for use as a write buffer in solid state drives, and embedded non-volatile memory for microcontroller units, as a replacement for embedded Flash. If the switching current can be reduced further, STT-MRAM could potentially be used as a replacement for SRAM in last-level-cache, providing significant system-level performance improvement due to higher density.

Materials innovation lies at the heart of MRAM research, particularly for the materials used in the magnetic tunnel junction, the device used to store, read, and write data. A magnetic tunnel junction consists of metallic magnetic free and reference layers sandwiched around a thin insulating tunnel barrier. This talk will first give an overview of STT-MRAM, including how it works and the application space, and will then review the materials innovations developed at IBM for reducing the switching current.

IBM has had a long history of research and development of STT-MRAM. Spin-transfer-torque switching was invented at IBM in 1996 by John Slonczewski [2], who also invented the magnetic tunnel junction [3] (which was also independently invented by Julliere [4]). High magnetoresistance using MgO tunnel barriers was first published by IBM and AIST in 2004 [5,6]. The development of perpendicularly magnetized STT-MRAM was first published by IBM and Tohoku University in 2010 [7,8]. Since then the IBM MRAM team has focused on reducing the switching current of STT-MRAM in order to enable last-level-cache applications. Key results include demonstrating reliable writing down to write-error-rates of less than $1e-11$ [9], scaling down to 11 nm tunnel junctions switching in only 7.5 uA [10], and demonstrating fast reliable writing using 2 ns write pulses [11]. IBM and TDK jointly published the first demonstration of product-level yields in 2013, using an 8 Mb STT-MRAM product demonstrator [12]. Double magnetic tunnel junctions were developed to further reduce the switching current, by using two reference layers and two tunnel barriers, in order to provide torque to the free layer from both top and bottom interfaces [13]. Theory predicts that a factor of 10 reduction in switching current is possible, for perfect spin-polarization [14]. Most recently, a new device, called the double spin-torque magnetic tunnel junction was demonstrated to reduce the switching current in a similar manner, however without any penalty in the magnetoresistance, by using a low resistance non-magnetic spacer in place of the second tunnel barrier [15]. This exciting breakthrough opens up a path to using STT-MRAM as last-level-cache.

- [1] Andrew D. Kent and Daniel C. Worledge, *Nature Nano.* 10, 187 (2015)
- [2] J.C. Slonczewski, *J. Magn. Magn. Mat.*, Volume 159, Issues 1–2, Pages L1-L7 (1996)
- [3] J. C. Slonczewski, *IBM Technical Disclosure Bulletin* 19, No. 6, 2331-2332 (1976)
- [4] M. Julliere, *Physics Letters A*, Volume 54, Issue 3, Pages 225-226 (1975)
- [5] S.S.P. Parkin et al., *Nature Mater.* 3, 862–867 (2004)
- [6] S. Yuasa, et al., *Nature Mater.* 3, 868–871 (2004)
- [7] D. C. Worledge et al., *IEDM*, p. 12.5.1-12.5.4 (2010)
- [8] Ikeda, S. et al., *Nature Mater.* 9, 721–724 (2010)
- [9] J. J. Nowak et al., *IEEE Magnetics Letters*, vol. 2, Art no. 3000204 (2011)
- [10] J. J. Nowak et al., *IEEE Magnetics Letters*, vol. 7, Art no. 3102604 (2016)
- [11] G. Hu et al., *IEDM*, p. 2.6.1-2.6.4 (2019)
- [12] Y. J. Lee et al., *VLSI-TSA* p1 (2013)
- [13] G. Hu et al., *IEDM*, p. 26.3.1-26.3.4 (2015)
- [14] D. C. Worledge, *IEEE Magnetics Letters*, vol. 8, Art no. 4306505 (2017)
- [15] G. Hu et al., *IEDM*, p. 2.5.1-2.5.4 (2021)

4:00 PM *EQ09.08.02

Topology for Energy Efficient Spintronics Claudia Felser; Max Planck Institute for Chemical Physics of Solids, Germany

Topology, a mathematical concept, recently became a hot and truly transdisciplinary topic in condensed matter physics, solid state chemistry and materials science. All 200 000 inorganic materials were recently classified into trivial and topological materials, such as topological insulators, Dirac, Weyl and nodal-line semimetals, and topological metals [1]. More than 25% of all materials host topological bands around the Fermi energy. Beyond the single particle picture, we have identified first antiferromagnetic topological materials [2]. Experimentally, we have realized ferromagnetic materials, examples are Co_2MnGa and $\text{Co}_3\text{Sn}_2\text{S}_2$. Surprisingly all crossings in the band structure of ferromagnets are Weyl nodes or nodal lines [3]. Mn_3Sn and YbMnBi_2 are examples of non collinear antiferromagnetic Weyl semimetals, which show giant values for the anomalous Hall and Nernst effect [4]. In the context of real space topology, skyrmions and antiskyrmions are a possible new direction for new data storage [5]. Our goal is to identify new quantum-materials for highly efficient spintronics, quantum computing and energy conversion.

1. Bradlyn et al., *Nature* 547 298, (2017), Vergniory, et al., *Nature* 566 480 (2019), Vergniory, et al., *Science* accepted arXiv:2105.09954.
2. Xu et al. *Nature* 586, 702 (2020).
3. Liu, et al. *Nature Physics* 14, 1125 (2018), Belopolski, et al., *Science* 365, 1278 (2019), Guin, et al. *Advanced Materials* 31 (2019) 1806622, Liu, et al., *Science* 365, 1282 (2019), Morali, et al., *Science* 365, 1286 (2019)
4. Pan, et al., *Nature Materials* 21 (2022) 203, Kübler and Felser, *EPL* 120 (2017) 47002 and *EPL*108 (2014) 67001, Nayak, et al. *Science Advances* 2 (2016) e1501870
5. Nayak et al., *Nature* 548 (2017) 561

4:30 PM EQ09.08.03

Large Spin Hall Effects in a Model Epitaxial $\text{BaPb}_{1-x}\text{Bi}_x\text{O}_3 / \text{La}_{0.7}\text{Sr}_{0.3}\text{MnO}_3$ System Isaac Harris¹, Anthony Edgeton², Xiaoxi Huang¹, Reed Yalisoev¹, George Fratian¹, Marcel Mazur³, Lucas M. Caretta¹, Sandhya Susarla^{1,4}, Chang-Beom Eom², Dan Ralph³ and Ramamoorthy Ramesh¹; ¹University of California, Berkeley, United States; ²University of Wisconsin–Madison, United States; ³Cornell University, United States; ⁴Lawrence Berkeley National Laboratory, United States

Spintronics is a promising field centered around next-generation devices that use electronic spin to store and manipulate information. Since there are no ohmic losses inherent in the transfer of spin – for example in magnons or pure spin currents – spintronic devices have the potential to be very energy efficient, and lots of efforts have been taken over the last few decades to apply spintronic principles to make ‘beyond CMOS’ devices. However, one of the major challenges in spintronics is to find material systems with efficient spin-to-charge conversion, and the lack of such model systems has kept practical, energy efficient spintronic applications from being realized. We propose a new pathway for discovering model systems with efficient spin-to-charge conversion in epitaxial oxide heterostructures. We present on one such system, $\text{BaPb}_{1-x}\text{Bi}_x\text{O}_3 / \text{La}_{0.7}\text{Sr}_{0.3}\text{MnO}_3$ (BPBO/LSMO), grown by pulsed laser deposition with excellent crystalline quality characterized by X-ray diffraction and TEM. Using spin-torque ferromagnetic resonance (STFMR) experiments, we measured a spin-orbit torque efficiency of 3 – over an order of magnitude greater than typical spin-orbit coupled metals. We confirm this measurement with samples grown and measured across 3 different labs, along with transverse STFMR and Second Harmonic experiments. We also find an enhancement of the spin-orbit torque efficiency for thinner layers of BPBO, indicating that the epitaxial interface plays an important role in the generation of spin-orbit torques. With a better understanding of the role of the interface in spin-orbit torque generation, and by exploring similar complex oxide systems, we hope to find a model epitaxial oxide heterostructure that can be used for energy efficient spintronic applications.

We acknowledge funding support from SRC-ASCENT for this project.

4:45 PM EQ09.08.04

Current-Induced Switching in Spin-Filter Tunnel Devices Astha Khandelwal¹, Vinod Kumar¹, Yu-Hui Tang², Mark G. Blamire³ and Bhagwati Prasad¹; ¹Indian Institute of Science, India; ²National Central University, Taiwan; ³University of Cambridge, United Kingdom

The Internet of Things (IoT) devices needs to process a vast amount of data at high speed for smooth interfacing with other supplementary devices on the network. However, the current computational architecture is not efficient for this purpose. One of the potential solutions to tackle this issue is to use high-density nonvolatile memory (NVM). Magnetic random-access memory (MRAM) is one of the promising NVM technologies. The magnetic tunnel junction is the building block of the MRAM device. Intensive studies in the FM/B/FM MTJs, where a barrier (B) is separated by two ferromagnetic (FM) electrodes, have demonstrated that the relative orientation of two FM electrodes can be altered by either an external magnetic field or controlled by a spin-polarized current, i.e., the current-induced magnetization reversal via the spin-transfer (STT) or the field-like (FLST) components of the spin torque [1, 2]. The STT-MRAM technology has significant advantages over magnetic-field-switched MRAM, while the main challenge for implementing STT-MRAM is the requirement of high writing current for high-density and high-speed MRAM. Therefore, alternative writing and reading mechanisms for MTJs may provide a viable route towards switching energies per bit smaller compared with CMOS (~1 fJ). To achieve low-energy consumption in next-generation spintronics devices, much attention has shifted to the spin filter effect in ferromagnetic insulator europium chalcogenides [3] and perovskite oxides [4, 5]. So far, the spin-filter devices have been switched by the applied external magnetic field but to make a high-density memory solution, the current/voltage-induced switching would be required. Recently we have observed the current/voltage-dependent switching in SmSrMnO_3 -based devices. The dI/dV vs. V of such spin filter device shows the large change in the dynamic conductance of the device at lower bias and low temperature (below T_c for the ferromagnetic insulator barrier layer). The underlying mechanism of such current dependent switching is not well understood. We have conducted detailed experiments to get a comprehensive understanding of the current-driven switching dynamics in spin-filter tunnel devices. The physical understanding and theoretical model for the experimental observations are being analyzed by both first-principles calculations and a tight-binding model with a self-developed JunPy+LLG package [6, 7]. The current-driven switching in spin-filter tunnel junctions can potentially be used for high-speed and high-endurance non-volatile memory devices for AI and IoT applications.

References:

- [1] S. S. P. Parkin et. al. Nat. Mater. 3, 862 (2004).
- [2] S. Yusa, et. Al., Nat. Mater. 3, 868(2004).
- [3] J. S. Moodera et al., Phys. Today 63, 46 (2010)
- [4] B. Prasad et. al. Nano Lett. 14, 2789 (2014)
- [5] B. Prasad et. al. Adv.Mater. 27, 3079 (2015)
- [6] Y. -H. Tang and B. -H. Huang, J. Phys. Chem. C. 122, 20500 (2018).
- [7] Y. -H. Tang and B. -H. Huang, Phys. Rev. Research 3, 033264 (2021).

SESSION EQ09.09: Poster Session: Emergent Materials for Low Power Electronics

Session Chairs: Ying-Hao Chu and Bhagwati Prasad

Wednesday Afternoon, November 30, 2022

8:00 PM - 10:00 PM

Hynes, Level 1, Hall A

EQ09.09.01

Energy-Efficient Time Series Data Processing Using HfO_2 -Based 2Memristor-1Capacitor Integrated Temporal Kernel Sung Keun Shim, Yoonho Jang, Janguk Han, Jeong Woo Jeon and Cheol Seong Hwang; Seoul National University, Korea (the Republic of)

Recently, Reservoir Computing (RC), a temporal kernel-based computing method that processes input at the reservoir (a fixed recurrent network) and identifies it in the readout layer, has been studied due to its efficient but cost-effective learning in the machine learning field. Several attempts have been made to implement this reservoir functionality through a physical system using diffusive memristors that showed both nonlinearity and fading memory properties [1]. However, the time scale is fixed with the memristor's material properties in the previous studies, making it difficult to adjust the temporal properties of the kernel. In this study, nonvolatile $\text{W/HfO}_2/\text{TiN}$ (WHT) memristor and $\text{TiN}/\text{ZrO}_2/\text{Al}_2\text{O}_3/\text{ZrO}_2/\text{TiN}$ (TZAOT) capacitor-based temporal kernel with an integrated 2memristor-1capacitor (2MIC) structure is proposed to solve the issue with fixed time scale.

HfO₂-based memristor has been widely studied for various applications, including synaptic applications in neuromorphic hardware. Especially, the WHT memristor in this study shows area-dependent electronic bipolar resistive switching behavior, which works as an analog switching device for the integrated temporal kernel. 2M1C kernel is composed of two serially connected memristors (M1, M2) and a capacitor (C1) which is connected in parallel with one of the memristors (M2). WHT memristor works as both a multi-level conductance device and a variable resistance that generates a broad range of RC delays along with C1. By modulating memristors and capacitors in the kernel circuits, time constants of the 2M1C temporal kernel can vary for 10⁶ orders. This study analyzed how each element's characteristics affected the entire kernel properties.

The task of recognizing digit images in the MNIST database was conducted to verify the performance of the temporal kernel. 784 pixel data of MNIST images were binarized, chopped into n-bit pulse sequences, and fed to the kernel as an input signal. The kernel system can separate different pulse streams in terms of the number of pulses and intervals due to its unique delay dynamics through analog memristors. 2M1C kernel maps the processing results with two memristors (M1, M2; dual mapping), which projects the input signals into a higher-dimensional space. The high dimensionality significantly improves the kernel's separability, reducing the whole network's size needed for classification. Mackey-glass time series prediction test was applied to the 2M1C kernel for its data processing ability and showed excellent performance under the broad test conditions compared with previous studies [2,3].

2M1C temporal kernel shows that it can adapt to various tasks, and real-time data processing is possible under broad conditions by modulating M1, M2, and C1 values. The HfO₂-based nonvolatile memristor acts as an analog memory device as well as the dynamics-maker. The kernel machine took 200 ns of time and ~25pJ of energy to process one input pulse, substantially reducing time and energy compared with previous studies [3]. Tunable RC delay and dual mapping techniques further contribute to the kernel's energy-efficient and accurate processing ability.

[1] Du, C. et al. Reservoir computing using dynamic memristors for temporal information processing. *Nat. Commun.* 8.1 (2017): 1-10.

[2] Jang, Y. H. et al. Time-varying data processing with nonvolatile memristor-based temporal kernel. *Nat. Commun.* 12.1 (2021): 1-9.

[3] Moon, J. et al. Temporal data classification and forecasting using a memristor-based reservoir computing system. *Nat. Electron.* 2.10 (2019): 480-487.

EQ09.09.02

High-Performance UV Photodetectors Using Oriented WO₃ Thin Films Grown at Low Temperature in Open Atmosphere [Zhuotong Sun](#)¹, Ming Xiao¹, Weiwei Li², Megan O. Hill¹, Rob Jagt¹, Louis-Vincent Delumeau³, Kevin Musselman³ and Judith L. MacManus-Driscoll¹; ¹University of Cambridge, United Kingdom; ²Nanjing University of Aeronautics and Astronautics, China; ³University of Waterloo, Canada

Tungsten oxide (WO₃), an n-type semiconductor, has many potential applications, e.g. electrochromic devices, photodetectors, photocatalysts, supercapacitors, memristors, electrolyte-gated transistors, etc. In this work, we demonstrate ultraviolet (UV) responsivity in photodetector devices as an exemplar application of WO₃ thin films via a CMOS-compatible atmospheric pressure-spatial chemical vapour deposition (AP-SCVD) method. Films grown on Si at 320°C were conformal over cm², and their orientations were continuously tuned by controlling the deposition rate using unique parameters of AP-SCVD. Even though the films were grown in open atmosphere and did not undergo any further annealing, they showed high responsivity (10⁻³ A/W) in short response time (3.6 s), comparable to the performance of vacuum- or solution- grown films post-processed at temperatures of up to 600°C. More broadly, the films deposited by AP-SCVD have very strong potential for the wide-ranging applications of WO₃.

EQ09.09.03

Understanding the Correlations Between Structure, Electronic Properties and Oxygen Vacancy Migration in Samarium Nickelates [Ranga Teja Pidathala](#), Devang Bhagat, Mirza Galib and Badri Narayanan; University of Louisville, United States

Ever growing advances in artificial intelligence for wide variety of applications ranging from driverless automobiles, unmanned aerial vehicles to healthcare, poses new challenges in developing strong, fast, and powerful data storage and computer processors. Strongly correlated electron materials like samarium nickelates with property of resistive switching can be potential candidate for brain like computing. The metal to insulation (MIT) or insulator to metal (IMT) transition in SmNiO₃ can be triggered by doping electrons in the d-orbital of Ni. In the current study, we have demonstrated that creating oxygen vacancies (OV) in well-defined order (square planar, pyramidal, tetrahedron) triggers the MIT or IMT transition based on its magnetic ordering (A-AFM, E-AFM, FM, G-AFM, S-AFM, T-AFM) in ground state. The structural changes caused due to OV's in SmNiO_{3-δ} changes the electronic properties of oxygen deficient samarium nickelates. We used climbing image nudge elastic band (CI-NEB) implemented in density functional theory (DFT) code to find the activation energies of OV migration with two different pathways, one in ab plane and other along c-axis and activation barriers are 1.15 eV and 0.95 eV respectively. We also studied the effect of different shapes and different concentration of OVs around the OV migration pathway. It is found that in each magnetic ordering, the barrier increases with increase in the shapes (pyramidal, square planar). It is also found that the S-AFM has the least and T-AFM has the highest activation energies, 1.25eV and 1.5 eV respectively. This study will further help us in understanding energy efficient way of triggering the MIT or IMT driven by OV transport in SmNiO_{3-δ} for designing the next generation electronics

EQ09.09.04

Effect of ZrO₂ Seed Layer in Hf_{0.5}Zr_{0.5}O₂ Ferroelectric Device Fabricated by PEALD [Jina Song](#), MinJung Oh and Yoon Chang-Bun; Tech University of KOREA, Korea (the Republic of)

FeRAM (Ferroelectric Random Access Memory) is one of the next-generation memories and has a non-volatile characteristic through the electrical polarization of a ferroelectric. Therefore, research is being conducted as a memory to replace DRAM (Dynamic Random Access Memory), which has a problem of information volatility.

Among the HfO₂-based ferroelectrics, HfO₂ doped with Zr exhibits ferroelectricity in a wide composition range. The best ferroelectricity is measured when the doping concentration is about 50%. Recently, it has been reported that the ferroelectric properties of Hf_xZr_{1-x}O₂ (HZO) films are increased by forming a ZrO₂ seed layer.

In this research, an Hf_{0.5}Zr_{0.5}O₂ ferroelectric layer was formed using PE-ALD (Plasma Enhanced Atomic Layer Deposition). A metal-ferroelectric-metal (MFM) type capacitor was fabricated using TiN with a thickness of 50nm as the Top and Bottom electrodes. First, to analyze the characteristics of the HZO ferroelectric layer according to various lamination methods, the total number of ALD cycles was fixed at 120 cycles, and the HfO₂-ZrO₂ super cycles were set to 4 types: 5cycle-5cycle, 10cycle-10cycle, 20cycle-20cycle, and 60cycle-60cycle. After setting to, each super cycle was repeated 12, 6, 3, and 1 time to form a ferroelectric layer. Second, to investigate the characteristics according to the heat treatment temperature, the specimens in which the ferroelectric layer was deposited using PE-ALD were heat-treated at 450/550/650°C for 30 seconds in a N₂ atmosphere using RTA (Rapid Thermal Annealing). Finally, four types of MFM capacitors were fabricated without or with the Top/Bottom/Top and Bottom seed layers. Electrical characteristics were analyzed using Keithley 4200A-SCS, and the properties of endurance, I-E curve, and Hysteresis curve were compared. In addition, the crystallinity and component ratio of the ferroelectric thin films were analyzed through XRD, XPS, and TEM.

EQ09.09.05

Novel Phase Formation and Magnetism at the Sb₂Te₃/Ni₈₀Fe₂₀ Interface [Alexandria Will-Cole](#)¹, James L. Hart², Adrian Podpirka³, Matthew Matzelle¹,

Nirjhar Bhattacharjee¹, Shreya K. Patel⁴, Sarah Tolbert⁴, Arun Bansil¹, Judy Cha², Don Heiman¹ and Nian Sun¹; ¹Northeastern University, United States; ²Cornell University, United States; ³Johns Hopkins University Applied Physics Laboratory, United States; ⁴University of California, Los Angeles, United States

Bilayer topological insulator/ferromagnet heterostructures are promising for spintronic memory applications due to their low switching energy and therefore power efficiency.¹ Topological insulators have been grown with molecular beam epitaxy (oriented, epitaxial films)^{2,3} and RF magnetron sputtering (amorphous to crystalline oriented films)⁴⁻⁶ and have demonstrated large spin-to-charge conversion efficiencies. However, the reactivity of topological insulators with ferromagnetic films is often overlooked in the spin-orbit-torque literature, even though there are reports that it is energetically favorable for topological insulators to react with metals and form interfacial layers.⁷⁻¹¹ Previously, we have investigated the interface of Bi₂Te₃/Ni₈₀Fe₂₀ and discovered that a novel topological antiferromagnetic phase forms at the bilayer interface due to selective Ni diffusion, which is possibly catalyzed by the topological surface states.¹² In our previous work the Bi₂Te₃ was grown via sputtering on thermal SiO₂/Si, and while it showed *c*-axis orientation, we suspect mosaicity to be present, which may limit the diffusion depth of the Ni into the Bi₂Te₃ film, thus limiting the thickness and uniformity of the interfacial antiferromagnetic phase. In our current work, we have grown Sb₂Te₃ with molecular beam epitaxy to ensure a highly ordered and epitaxial film, with the expectation that the diffusion depth of the Ni into the Sb₂Te₃ may be much deeper, providing a smaller gradient resulting in a more homogeneous antiferromagnetic interlayer. However, we find this interface to be highly complex with multiple phase formations, including a novel antiferromagnetic phase evident by the presence of large, negative exchange bias. We support our findings with temperature dependent magnetometry, high-angle annular dark-field scanning transmission electron microscopy, and theoretical calculations. Despite the complex nature of the Sb₂Te₃/Ni₈₀Fe₂₀ interface, we still observe significant enhancement of the Gilbert damping and reduction of effective in-plane magnetization, which is indicative of spin pumping in this heterostructure – Sb₂Te₃ is a spin sink due to its large spin-orbit-coupling.¹³ This work highlights the role of interfacial chemistry in topological insulator/ferromagnet heterostructures.

1. Y. Cao et al, *iScience*, **23**, 101614, (2020).
2. S. Hsuan Su et al, *ACS Appl. Electron. Mater.*, **3**, 2988-2994, (2021).
3. N.H.D. Kang et al, *Nat. Mater.*, **17**, 808-813, (2018).
4. M. DC et al, *Nat. Mater.*, **17**, 800-807, (2018).
5. W. Jie Wang et al, *Sci. Rep.*, **6**, 25291, (2015).
6. T. Fan et al, *Sci. Rep.*, **12**, 2998, (2022).
7. C.D Spataru et al, *Phys. Rev. B.*, **90**, 085115 (2014).
8. W. Ye et al, *arXiv*, (2015).
9. L.A. Walsh et al., *J. Phys. Chem. C*, **121**, 23551 (2017).
10. S.J. Chang et al., *RSC Adv.*, **8**, 7785–7791, (2018).
11. G. Li and C. Felser, *Appl. Phys. Lett.*, **116**, 070501, (2020).
12. N. Bhattacharjee et al., *Adv. Mater.*, 2108790, (2022).
13. A.A. Baker et al., *Sci. Rep.*, **5**, 7907 (2015).

EQ09.09.06

Crystal Structure and Electric Properties of (100) Ba(Zr_xTi_{1-x})O₃ Thin Films on MgO Substrates by Pulse Laser Deposition Technique Ryo Takahashi¹, Yoshitaka Ehara¹, Yosuke Hamasaki¹, Shintaro Yasui², Shinnosuke Yasuoka², Hiroshi Funakubo², Shinya Sawai¹ and Ken Nishida¹; ¹National Defense Academy, Japan; ²Tokyo Institute of Technology, Japan

Microwave tunable devices are necessary components for next-generation communication applications. Ferrite, semiconductors, and ferroelectrics are typical tunable materials. Especially ferroelectric thin films have been studied for a long time because of their high dielectric constant and low power consumption. Moreover, microwave dielectric materials show advantages in terms of light weight, compactness, low loss, stability in temperature, and low cost in producing of communication devices. To date, (Ba_{1-x}Sr_x)TiO₃ [BST] has become one of the most popular ferroelectric materials studied and used as tunable microwave devices. However, its dielectric loss is still large, and the temperature dependence of the dielectric constant remains insufficient for applications. It is desirable to have not only high dielectric constant and tunability in a certain electric field range but also low dielectric loss. Ba(Zr_xTi_{1-x})O₃ [BZT] solid solutions are also tunable materials with potential use in devices for wireless communications, just above their Curie temperature in a paraelectric state. BZT is a possible alternative to BST in tunable microwave applications Zr⁴⁺ is chemically more stable than Ti⁴⁺ and maintains a low dielectric loss. Furthermore, BZT in the paraelectric phase has higher temperature stability than BST. Therefore, we focused on BZT thin films as a tunable ferroelectric material.

In this work, we fabricated BZT ($x = 0 \sim 1.0$) thin films with 500nm thick by pulse laser deposition [PLD] technique on MgO(100) and (100)_cSrRuO₃/(100)BaZrO₃/(100)MgO substrates. It enables us to obtain preferential (100)-oriented BZT thin films. The structural properties of the films were characterized by x-ray diffraction [XRD] (MRD, PANalytical). Wavelength-dispersive x-ray fluorescence spectrometry [WDX] (PW2404, PANalytical) was carried out to investigate the composition and thickness of BZT thin films. All the XRD patterns showed only (001)/(100) diffraction peaks and no secondary phase. Reciprocal space mappings (RSMs) of BZT thin films showed that BZT thin films grew epitaxially on (100)MgO and (100)_cSrRuO₃/(100)BaZrO₃/(100)MgO substrates. The electrical properties of the BZT thin films were measured by an impedance analyzer (4194A, Agilent). *P-E* hysteresis loops of BZT films become increasingly slim in shape with increasing Zr content because of the decrease in grain size. The dielectric constant dependence of electric field indicated that tunability is high in the region of $x = 0 \sim 0.5$ BZT thin films. The composition dependence of tetragonality, remanent polarization, and dielectric constant suggested that there may be a phase boundary between $x = 0.2$ and 0.3 , and this tendency is similar to BZT ceramics. Therefore, our result suggests that BZT ($x = 0 \sim 0.5$) can be one of the significant candidates for microwave application which requires high tunability and low loss.

EQ09.09.08

Stabilization of Various Polymorph in Multiferroic ScFeO₃ Film Yosuke Hamasaki¹, Shintaro Yasui², Tsukasa Katayama³ and Mitsuru Itoh²; ¹National Defense Academy, Japan; ²Tokyo Institute of Technology, Japan; ³Hokkaido University, Japan

Polar iron oxides, which exhibit both ferroelectricity and (anti)ferromagnetism, are multiferroic materials, which promise potential application for a new type of memory device. Moreover, due to the strong magnetic interaction between Fe³⁺ cations, a higher magnetic order temperature in iron oxides is expected.

It is well known that a perovskite structure is thermodynamically stable in Re³⁺FeO₃ (Re = Rare earth element). While hexagonal ReFeO₃ (h-ReFeO₃) with YMnO₃-type structure which exhibits ferroelectricity and weak-ferromagnetism is metastable. AlFeO₃ and GaFeO₃ have a polar κ-Al₂O₃ structure which is a sesquioxide structure. When we consider crystal structures vs ionic radius of A³⁺ in A³⁺FeO₃, ScFeO₃ is located at the cross point of various kinds of crystal structures.

Thin film fabrication techniques have contributed to the development of novel functional electronic materials and devices. Epitaxial films deposited on single crystal substrates suffering from interfacial strain due to a mismatch in the lattice constants between the film and the substrate allow stabilizing

metastable phases.

In this study, we attempted to stabilize various crystal structures in the film form by selecting the appropriate substrates or using a buffer layer and explored new polar iron oxides.

ScFeO₃ films were deposited on various substrates by pulsed laser deposition (PLD) technique. The crystal structure of films was characterized by X-ray diffraction (XRD) and scanning transmission electron microscope (STEM).

We stabilized five crystal structures: κ -Al₂O₃-, spinel-, corundum-, YMnO₃-, and bixbyite-type structures. XRD and HAADF-STEM were used to identify the phases. Four of the structures were obtained for the first time: κ -Al₂O₃-, spinel-, corundum-, and YMnO₃-type ScFeO₃. Since κ -Al₂O₃- and YMnO₃-type structures are polar, we investigated their ferroelectricity and magnetic properties.

The YMO-type ScFeO₃ film on a perovskite electrode showed a ferroelectric P - E hysteresis loop with $P_r \sim 4.9 \mu\text{C}/\text{cm}^2$. P_s of h -ScFeO₃ was simply calculated using the displacement of the Sc ion evaluated from the HAADF-STEM image. The obtained P_s was $\sim 8.7 \mu\text{C}/\text{cm}^2$, which is consistent with the observed value. HAADF-STEM observations also revealed that at the domain boundary, the Sc displacement pattern of up-center-down was found, indicating a nonpolar region due to its correspondence to the P - $3c$ phase pattern, which was previously reported in an ErFeO₃ epitaxial film. In addition, the domain boundary was not straight compared with a proper ferroelectric perovskite. Magnetic measurements confirmed weak ferromagnetism with $T_N = 195$ K. The T_N value is the highest in hexagonal $ReFeO_3$ and $ReMnO_3$.

The κ -Al₂O₃-type ScFeO₃ film on a Nb doped SrTiO₃ substrate showed a ferroelectric P - E hysteresis loop with $P_r \sim 4 \mu\text{C}/\text{cm}^2$. Although the spontaneous polarization of ε -Fe₂O₃ calculated using Berry's phase is $21 \mu\text{C}/\text{cm}^2$, the observed value is five times smaller than the theoretical value. This discrepancy can be correlated with the three in-plane domains. During polarization switching, because two close-packed oxygen layers shift in opposite directions along the a -axis (i.e., the in-plane direction in the ε -Fe₂O₃ film), this motion is suppressed by collision among the three in-plane domains. Magnetic measurements revealed the weak ferromagnetism with $T_C \sim 295$ K.

EQ09.09.09

Effect of Synthesis Condition on the Piezoelectric and Conductive Properties in BaTiO₃ Ceramics Eunjin Koh¹, Seunghun Kang¹, Choongseop Jeon², Seungyong Lee², Jinbok Shin², Jeongryeol Kim², Jungwon Lee², Donghoon Kim¹ and Yunseok Kim¹; ¹Sungkyunkwan university, Korea (the Republic of); ²Samsung Electro-Mechanics Co., Ltd, Korea (the Republic of)

Ferroelectric materials have been studied in various fields because of their unique properties, such as spontaneous polarization that can be switched by an electric field. In particular, barium titanate (BaTiO₃), which is a lead-free ferroelectric with a high dielectric constant, has been actively studied for applications in electronic devices, including energy storage applications and capacitor applications. Since electric devices have become miniaturized, the need to develop BaTiO₃ with smaller particle sizes and higher capacitance has been increasing. Although chemical modifications such as dopants, accomplished making BaTiO₃ smaller with high capacitance, there was a limitation in that macro-scale analysis techniques, which are not adequate for investigation of the nano-scale properties and mechanisms, have been mainly used. Consequently, to overcome this limitation, it is necessary to use a micro-scale characterization method to analyze the nano-sized particles. In this study, we employ piezoresponse force microscopy (PFM) and conductive atomic force microscopy (CAFM) to study BaTiO₃ ceramics according to the synthesis conditions of sintering temperatures, dopant species (Dy, Mn), and doping methods (oxide, poly). The investigation using PFM and CAFM reveals that the relative piezoresponse and leakage current depend on the sintering temperatures and dopant species. The uniformity of piezoresponse represents the dispersion of dopants which is different from doping methods. Furthermore, topography images revealed that particle size varied with the sintering temperatures, which is related to the dielectric constant. We explored the synthesis conditions that affect the piezoelectric properties and conductive properties of the BaTiO₃ ceramics using atomic force microscopy (AFM). Therefore, our findings can provide an understanding of the effect of the synthesis conditions on BaTiO₃ at a local level.

EQ09.09.11

Invertible Boolean Logic Gates by Probabilistic Computing Based on the Cu_xTe_{1-x}/HfO₂/Pt Threshold Switch Jaehyun Kim, Kyung Seok Woo, Janguk Han and Cheol Seong Hwang; Seoul National University, Korea (the Republic of)

Complex optimization problems can be solved by sophisticated algorithms, burdening modern computers with significant circuit overhead and high computing power. A new concept called probabilistic computing, which uses "p-bits" operating at room temperature, was devised to handle this problem. The p-bit outputs fluctuate between 0 and 1 with time, which is similar to the behavior of binary stochastic neurons in the Boltzmann machine. Therefore, any stochastic element with tunable switching probability, such as magnetic tunnel junctions (MTJs), can be a potential candidate for building the p-bit hardware.^[1,2]

In this study, p-bit hardware was built using the Cu_{0.1}Te_{0.9}/HfO₂/Pt (CTHP) threshold switch. The underlying switching mechanism of the CTHP memristor is based on ionic diffusion and drift of Cu ions, which form volatile conductive filament in the HfO₂ layer. The switching mode can be modulated by the concentration of Cu in the Cu_xTe_{1-x} electrode, which controls the injection of Cu ions into the oxide matrix.^[3] The concentration of Cu was set to 0.1, where the device showed stable threshold switching behavior. The p-bit circuit was built with the CTHP device connected with a series resistor and a comparator to generate fluctuating random binary outputs with time. The random output of the circuit is mainly due to the variation of switching voltage, delay time, and relaxation time of the CTHP filamentary switching. The measured output voltage average shows a sigmoidal relationship with the input voltage, which is the main feature of the p-bits generating probabilistic outputs. Moreover, the circuit offers power, fabrication, and scalability advantages compared with the reported CMOS and MTJ-based p-bit hardware.

Using the CTHP p-bit characteristics, all 16 invertible Boolean logic gates were demonstrated by Python simulation, assuming the hardware architecture of the p-computing network. Aside from the conventional logic operations in the forward direction, an invertible logic gate can infer the inputs of the logic gate from the outputs. The p-bit outputs were generated following the sigmoidal circuit response considering the device variation. The energy functions and input functions determining the probability of the p-bit outputs were calculated in the field-programmable gate array (FPGA) and digital-to-analog converters (DACs). Moreover, the invertible operation of a half adder was confirmed, which shows the potential of the p-computing network to expand into the applications such as complex arithmetic logic units and integer factorization.

[1] Hassan et al., "Quantitative evaluation of hardware binary stochastic neurons." *Physical Review Applied* 15.6 (2021): 064046.

[2] Borders et al., "Integer factorization using stochastic magnetic tunnel junctions." *Nature* 573.7774 (2019): 390-393.

[3] Woo, Kim et al., "A High Speed True Random Number Generator Based on a Cu_xTe_{1-x} Diffusive Memristor." *Advanced Intelligent Systems* 3.7 (2021): 2100062.

EQ09.09.12

Fabrication of Three-Dimensional Vertical Resistive Random Access Memory and Its Interference Phenomenon Induced by Lateral Charge Spreading Soo Kyeom Yong¹, Seung Soo Kim¹, Hae Jin Kim² and Cheol Seong Hwang¹; ¹Seoul National University, Korea (the Republic of); ²The University of Suwon, Korea (the Republic of)

The resistive switching random access memory (ReRAM) has been actively researched for decades as a memory that can store data by changing resistance. Due to its nonvolatile characteristics, ReRAM is being studied as a successor of the NAND Flash memory once it reaches the scaling or stackability limit.

The resistance change mechanism of ReRAM could be either an ionic switching mechanism in which a current path is formed and annihilated by the movement of metal ions or oxygen vacancies, or an electronic switching mechanism in which electrons are trapped or detrapped at the trap sites. Among them, electronic switching has the advantage of improving reliability because the electroforming step is unnecessary. In this work, vertically-integrated ReRAMs (V-ReRAM) with three-word line (WL) stairs were fabricated using the HfO₂ as a resistive switching layer between Pt top and TiN bottom electrodes. After the memory holes with a diameter of ~1 μm were etched into the multi-layers composed of 50 nm-thick SiO₂ (interlayer dielectric) and 25 nm-thick TiN (word line) layers, the 10 nm-thick HfO₂ film was deposited by the atomic layer deposition. Finally, the Pt top electrode was deposited and patterned to complete the V-ReRAM structure. The V-ReRAM had a set voltage of ~6 V, and the ratio of LRS (lower resistance state) current to HRS (higher resistance state) current was >~100. In addition, it showed self-rectifying characteristics allowing < 10 pA current up to -8 V in the negative voltage region, suppressing the sneak current issue. The WLs of V-ReRAM share the resistive switching layer vertically deposited in the hole. Therefore, it could bear the lateral charge spreading problem, which deteriorates the data reliability. This problem was indeed confirmed, where the selected cell's HRS curve shifted toward the LRS curve when the adjacent cells were set to the LRS state. This phenomenon occurred because electrons stored in the adjacent LRS cells were diffused through the resistive switching layer to the selected cell, which causes HRS data retention problems. The interlayer dielectric thickness was increased to solve this problem, but the improvement was only marginal. Therefore, the shallow trap density in the HfO₂ layer, which is the main factor of lateral charge loss, was decreased by plasma treatment. This method confirmed that charge loss in the nearby LRS cells could be minimized. However, the drift of the HRS curve toward the LRS in the selected cell was still observed, indicating unknown reliability issues.

EQ09.09.13

Improvements of Self-Aligned Multi Patterning Spacer Technology by PEALD Sn-Doped SiO₂ Suhyeon Park, Junyoung An, Heejun Yoon and Hyeongtag Jeon; Hanyang University, Korea (the Republic of)

Currently, EUV lithography begins to be adopted in a few patterning processes. But there is technical problem due to the low power of EUV light source and low hardness of EUV PR, self-aligned multi patterning (SAXP) have to be developed. SiO₂ was chosen as a first spacer for self-aligned patterning. However, since SiO₂ has low elastic modulus of 40GPa, spacer should be improved to prevent spacer collapse during further shrinkage of multi patterning. Therefore, SnO₂ is recently emerged as an alternative material. SnO₂ has high modulus and good etch selectivity. But since there are problems of cost and etch issues, we have studied synthesis and characteristics of Sn-doped SiO₂ as a spacer material.

Sn-doped SiO₂ was mainly studied for optical applications using sol-gel or physical vapor deposition(PVD) such as sputtering. However, it is not a suitable for SAXP spacer deposition due to poor step coverage. Atomic layer deposition (ALD) is one of best method to solve above-mentioned problems. Due to self-limited ALD reaction, it has benefits such as excellent step coverage, uniformity, and thickness control. Also, Sn doping is easy to conduct through ALD super-cycles. Particularly, plasma enhanced ALD(PEALD) was utilized, which is driven by a high plasma energy, allowing low process temperatures to prevent thermal stress issue. As above, Sn-doped SiO₂ has been deposited using PEALD.

In this study, we developed low-temperature Sn-doped SiO₂ using BDEAS (Bis-Diethylamino Silane, H₂Si[N(C₂H₅)₂]₂), TDMA-Sn (Tetrakis(dimethylamido)tin(IV), [(CH₃)₂N]₄Sn) and O₂ reactant plasma as the Si, Sn precursor and reactant plasma. We studied about the effect of doping Sn in SiO₂ film by varying the cycle ratio of SnO₂ and SiO₂ and their film properties were evaluated. The ratio of the SnO₂ and SiO₂ deposition cycle was varied from 15(SiO₂) : 1(SnO₂), 9:1, 6:1, 4:1 to 3:1. Auger electron spectroscopy (AES) was utilized to measure the atomic concentration. As the SnO₂ cycle ratio increase, the amount of Sn in the SiO₂ thin film increase. The X-ray photoelectron spectroscopy (XPS) showed that the greater amount of Sn in the SiO₂ thin film, the binding energy of Si2p and Sn3d shift toward lower, and more Si-O-Sn chemical bonding are formed, which increased the number of stiffer ionic bonds. Therefore, the Young's modulus measured by a nanoindenter increased from 39.9GPa at SiO₂ films to 90.9GPa at 3:1 film. However, the hardness results showed a different tendency showing decrease from 34GPa at 15:1 to 2.8GPa at 9:1 then increase to 7.9GPa at 3:1. This is because Sn is not well distributed in the SiO₂ film due to the cyclic system of ALD and the low distribution energy of the low-temperature process, resulting in a bilayer structure of Sn-doped SiO₂/SiO₂/Sn-doped SiO₂/SiO₂ under the conditions of 15:1, 9:1 and 6:1. These results are compensated by X-ray reflectivity (XRR) and Time of Flight secondary ion mass spectrometer (TOF-SIMS) analysis. Moreover, the GPC of SiO₂ and SnO₂ is 1.45Å/cycle, 1.0 Å/cycle. The values of the Sn-doped SiO₂ films are in between value of pure SiO₂ and SnO₂.

EQ09.09.14

A Study on the Al Doping Effect of HfO₂ Thin Films Using PEALD MinJung Oh, Jina Song and Yoon Chang-Bun; Tech University of Korea, Korea (the Republic of)

A memory semiconductor, a component that stores information, is an essential element in all electronic devices. There are many different types of memory semiconductors. Dynamic Random Access Memory (DRAM) and Flash Memory are widely used. Although DRAM has the advantage of processing data at high speed, it is a volatile memory that loses data when no power is supplied. Also, Flash memory has the advantages of being small, light, and robust against physical shocks, but the disadvantage is that the data processing speed is slow. They are reaching the limit of processing the lots of data generated by society.

Research on new memories to replace these devices is continuously being done. FeRAM (Ferroelectric Random Access Memory) is a next-generation memory with only the advantages of DRAM and Flash Memory. It can preserve data even when power is not supplied and process information quickly. This device is one of the representative non-volatile memories using ferroelectrics. It has a memory function by distinguishing '0' and '1' according to the polarization direction, and it can be used as a non-volatile memory by using the characteristic of maintaining polarization even when the voltage is cut off. It is known that the initial ferroelectricity occurs in perovskites such as SrTiO₃, KTaO₃, and CaTiO₃. However, recently, HfO₂ and ZrO₂ thin films have emerged as new types of ferroelectric materials, and many studies have been conducted. Also, HfO₂-based ferroelectric materials are being researched by doping various materials such as Zr, Si, Y, and Al. Among the many dopants, HfO₂ exists in a high dielectric constant structure at high temperatures, so changing the crystal structure with a high dielectric constant at room temperature is crucial. This study studied ferroelectricity by growing a tetragonal HfO₂ thin film by doping with Al. In order to evaluate the non-volatile memory characteristics, a metal-ferroelectric-metal (MFM) structure was fabricated using an Al-doped HfO₂ ferroelectric thin film. The Al:HfO₂ thin film was fabricated using PE-ALD (Plasma Enhanced Atomic Layer Deposition), and the HfO₂ thin film doped with 5-10 mol% Al was deposited by controlling the deposition ratio of HfO₂ and Al₂O₃. TiN was deposited on the upper and lower electrodes to improve the ferroelectricity of HfO₂ by sputtering. Annealing was performed between 500 and 700 degrees to generate crystallinity while removing organic matter. Transmission electron microscope (TEM) analysis was performed to confirm the structure of the thin film. In addition, X-ray photoelectron spectroscopy (XPS) was used to evaluate the Al:HfO₂ doping concentration. The growth of the tetragonal phase according to the heat treatment temperature of Al:HfO₂ was analyzed using XRD. To evaluate the electric properties of the thin film, the leakage current characteristics of Al doped HfO₂ thin films were measured according to the applied voltage. In addition, Polarization (Pr) was measured to confirm the ferroelectric properties.

EQ09.09.15

Physical Unclonable Function Devices Based on Randomness of Grain-Boundary Formation in Calcium Titanate Perovskite Layers Subin Lee and

Hocheon Yoo; Gachon University, Korea (the Republic of)

The stability of physical unclonable function (PUF) devices, regarded as the fingerprint of security applications, is the crucial point. Hence, we present a robust PUF device that maintains its randomness uninfluenced by ambient gases such as O_2 or H_2O . We synthesized calcium titanate (CTO) perovskite layers and controlled their grain boundary morphologies. The grain boundaries were formed differently by the annealing temperature, and as grain boundaries increased, the current value was distributed randomly. We also performed X-ray diffraction, X-ray photoelectron spectroscopy, scanning electron microscope, and UV-Visible spectrophotometer to investigate the CTO morphological change. The fabricated PUF devices which were annealed at 650 °C and 800 °C have different crystal structures, respectively. Through the mentioned comprehensive analysis, we observed that the CTO PUF devices annealed at 800 °C provide increased grain boundaries compared to that of the same CTO annealed at 650 °C. By measuring total 214 PUF devices, we also found that the current values were dispersed randomly at 800 °C annealed device. Based on the CTO morphological control, the algorithm based on generative adversarial networks (GAN) is used and we evaluated the estimation component randomness and inter-hamming distance. As a result, the less grain boundary device was analyzed to have the lop-sided statistics value which cannot operate on the security device. The randomness and inter-hamming distance were 4.16 % and 8 %, respectively. On the other hand, it is investigated that having lots of grain boundaries device has a random value which can form the Gaussian distribution. The randomness and inter-hamming distance were measured to 49.53 % and 46.55 % at 800 °C annealed device. Therefore, we suggest the security device by the simple sol-gel process, having the random current value due to the control of grain boundaries.

EQ09.09.16

Pre-State-Dependent Ternary/Binary Logic Operation Obtained by Ink-jet Printed SWCNT/InO Heterojunction Transistors Somi Kim¹, Seoyeon Jung², Bongjun Kim² and Hocheon Yoo¹; ¹Gachon University, Korea (the Republic of); ²Sookmyung Women's University, Korea (the Republic of)

The conventional von Neumann architecture, in which memory and processor are separated, has limitations in processing speed, energy consumption, and integrated circuits for next-generation electronic products. To solve the bottleneck of the von Neumann architecture, it is desirable to develop a new logic driving operation technique that simultaneously satisfies logic and memory control operation. Here, we present a pre-state-dependent ternary/binary logic inverter using a single-walled carbon nanotube (SWCNT)/ indium oxide (InO) heterojunction anti-ambipolar field-effect transistor (FET), which is reliably formed by an ink-jet printing method. The suggested device has a logic-in-memory characteristic that allows it to operate in ternary or binary mode change depending on the previous state. To be specific, when the previous state is $V_{DD} = 3$ V, the output value at the intermediate input follows the same $V_{DD} = 3$ V, and when the previous state is $G_{ND} = 0$ V, the output value at the intermediate input is half $V_{DD} = 1.5$ V. The maximum DC gain peak of 11.42 V/V in the forward V_G sweep and 19.14 V/V in the reverse V_G sweep, respectively, demonstrated the functions of ternary and binary inverter operation. In the pulsed-measurement, this study also demonstrates the transient operation of the pre-state-dependent ternary/binary logic inverter circuit. Due to the hysteresis in the current-voltage curve of the InO FET used as the n-type FET and the negative transconductance (NTC) region of the anti-ambipolar FET, showing the binary behavior in the reverse bias while the ternary behavior in the forward bias. The device was manufactured by the ink-jet print method, which has multifarious advantages such as low cost, easy manufacturing process, ambient condition manufacturing, and large-area manufacturing.

EQ09.09.17

Organic Charge Modulated Field-Effect Transistor-Based Pressure Sensor Operated by Electrospun Piezoelectric Polymer Taehoon Hwang, Jungyoon Seo and Hwasung Lee; Hanyang University, Korea (the Republic of)

Organic Field Effect Transistor (OFET) was a basic electronic device, and due to its high structure and signal amplification effect, it was receiving high attention for the development of pressure and chemical sensors and its application potential in the field of wearable electronics. However, in the case of an OFET-based sensor, since an active layer that could detect a signal is formed on top of the source/drain or gate electrode and works, the basic component of the device was damaged by external stimuli, and finally the stability of the unit device, There were issues with performance and reliability degradation. Organic Charge Modulated FET (OCMFET) had a characteristic where the voltage applied to the control gate was induced through an insulator and a operating voltage was applied to the floating gate, and depending on the voltage applied to the control gate, it was possible to control the carrier required to operate the element. Also, by configuring the sensing area in the extended floating gate, it could be applied as a sensor and operation of the element without damaging the components of the FET, so it was advantageous in terms of securing the stability of the element. In this study, an OCMFET was fabricated using Dinaphtho[2,3-b:2',3'-f]thieno[3,2-b]-thiophene (DNTT) organic semiconductor and anodized AlOx dielectric, and pressure sensor was fabricated by applying electrospun PVDF-TrFE-elastomeric template with piezoelectric properties to floating gate. The PVDF-TrFE mat fabricated using electrospinning induced the alignment of b-crystals in the polymer by the applied voltage and the strong elongation force applied therewith, so it had high piezoelectric performance without the poling process. In addition, the template was fabricated by impregnating PDMS to impart elastomeric properties to PVDF-TrFE mat. The OCMFET-based pressure sensor developed through this study exhibits stable FET performance, so it can be applied to various wearable sensor fields such as human motion monitoring, biomedical, and artistic intelligence in the future.

EQ09.09.18

Complementary Hybrid Superlattice Semiconductor with Multi-Channel Charge Transport and Mutual Stabilization Jongchan Kim and Myung M. Sung; Hanyang University, Korea (the Republic of)

We present an organic-inorganic hybrid superlattice as an example of near-perfect synergistic integration between organic and inorganic materials to achieve superior properties to those of individual components alone. The complementary hybrid superlattice is a multiple quantum well structure of 4-mercaptophenol organic monolayers and amorphous ZnO nanolayers. We observed multichannel formation in the hybrid superlattice, associated with a high-performance field effect transistor exhibiting excellent charge carrier mobility and steep subthreshold swing with band-like transport. In addition, mutual stabilizations between the organic monolayers and ZnO prevent the operation instability critical in exclusively organic and ZnO semiconductors.

EQ09.09.19

Effect of Biaxial Strain on the Electronic and Magnetic Properties of CuFeS₂ Roman Malyshev¹, Bjørnulf Brekke¹, Ingeborg-Helene Svenum^{2,1}, Sverre Magnus Selbach¹, Christoph Brüne¹, Arne Brataas¹ and Thomas Tybell¹; ¹NTNU, Norway; ²SINTEF Industry, Norway

Antiferromagnetic materials are robust in external magnetic fields. This, along with demonstrated high-frequency switching, enables the development of high-speed electronics. Here, magnetic semiconductors present an opportunity, as they enable doping and epitaxial strain to fine-tune their properties. CuFeS₂ is a thermoelectric, low-bandgap semiconductor and collinear antiferromagnet, with a Néel temperature above 800 K, making it a potential candidate for spin-based devices. Here, we investigate strain-engineering as a tool for controlling physical properties of CuFeS₂, and present a density functional theory (DFT) study on the effect of bi-axial strain on CuFeS₂. Neither tensile, nor compressive, bi-axial strain, +/- 5 %, alters the crystal structure or symmetry. However, the calculations show a small change in magnetic moments with strain, increasing under tensile and decreasing under compressive strain for Fe. For Cu atoms the magnetic moment increases for both tensile and compressive strain. The emergence of a small magnetic moment on the Cu atoms has previously been observed experimentally. The magnetic structure will be compared with changes in the band structure, density of state and the nature of the bands near the Fermi level in order to understand the effect of strain on the transport properties.

EQ09.09.20

The Effect of Molecular Additions to the Spin Transition and Conductivity of Spin-Crossover Molecules Thilini K. Ekanayaka¹, Yuchen Hu², Esha Mishra¹, Jared Paul Phillips³, Saeed Yazdani³, Alpha T. N'Diaye⁴, Jian Zhang⁵, Ruihua Cheng³ and Peter A. Dowben¹; ¹University of Nebraska Lincoln, United States; ²University of Nebraska–Lincoln, United States; ³Indiana University-Purdue University Indianapolis, United States; ⁴Lawrence Berkeley National Laboratory, United States; ⁵Lawrence Berkeley National Laboratory Molecular Foundry, United States

With the increasing interest in organic molecular multiferroic electronic devices, for flexible non-volatile memory, manipulation of conductivity of various spin crossover (SCO) molecular materials has been gaining attention. Spin crossover (SCO) molecular materials are promising bi-stable magnetic materials and have been identified as an attractive candidate for memory devices. SCO molecules are transition metal based complexes which exhibit reversible spin transition between low spin (LS) and high spin (HS) states and can be fabricated into a voltage controlled device. The voltage control spin state switching of these SCO molecular thin film materials has been studied and the spin state switching by voltage leads to nonvolatile conductance change, when combined with an organic ferroelectric layer. But to make a competitive non-volatile memory device out of SCO and an organic ferroelectric, that can compete with silicon technology, there are several key criteria that need to be addressed. Building an SCO memory device with a low on-state resistance has proved to be a major challenge. The spin transition behavior of $[\text{Fe}\{\text{H}_2\text{B}(\text{pz})_2\}_2(\text{bipy})]$ spin crossover molecule has been well studied and has been used as a successful component of a non-volatile memory device, although the on-state resistance is high (approximately 10^3 Ohm.cm). With a molecular ferroelectric gate dielectric layer, molecular SCO $[\text{Fe}\{\text{H}_2\text{B}(\text{pz})_2\}_2(\text{bipy})]$ exhibited an on/off ratio of 4 to 5 and both isothermal switching and nonvolatility was demonstrated in the transistor device geometry. As an approach to increasing the conductivity, so as to increase the on/off ratio of the SCO molecular devices and make smaller devices practical, we have mixed TCNQ (7,7,8,8-tetracyanoquinodimethane) anions with the molecular SCO $[\text{Fe}\{\text{H}_2\text{B}(\text{pz})_2\}_2(\text{bipy})]$. When compared to the pure $[\text{Fe}\{\text{H}_2\text{B}(\text{pz})_2\}_2(\text{bipy})]$ molecular thin film SCO system, the conductivity is enhanced by mixing $[\text{Fe}\{\text{H}_2\text{B}(\text{pz})_2\}_2(\text{bipy})]$ with TCNQ. The spin transition of $[\text{Fe}\{\text{H}_2\text{B}(\text{pz})_2\}_2(\text{bipy})]$ is also perturbed by adding TCNQ. The transistor measurements taken for the $[\text{Fe}\{\text{H}_2\text{B}(\text{pz})_2\}_2(\text{bipy})]$ SCO + TCNQ, with and without a ferroelectric layer, shows large charge trapping in the latter case. The system shows a low charge carrier mobility and higher drift carrier lifetime which is consistent with extensive charge trapping.

EQ09.09.21

BiSb(012) Crystallinity and Strong Spin Orbit-Torque Enhancement Using Insertion Layers HanYin Poh, Calvin Ang and Wen Siang Lew; Nanyang Technological University, Singapore

Topological insulator is a promising candidate for spintronics applications as it has high charge-to-spin conversion due to its time-reversal symmetry and spin-momentum locking in the Dirac surface state. However, the surface state is vulnerable to disruption like exchange coupling to ferromagnet materials. Here, we demonstrate different insertion layer (Ti, Cu, Pt) at the Co/BiSb interface to promote the topological surface state of BiSb(012). The BiSb(012) surface state is in focus based on having 3 Dirac cone at the Γ , which are ideal in obtaining high spin-orbit torque efficiency. The insertion layers induced large spin Hall angle of up to 10.4, that were otherwise negligible without any insertion layer. We further explore the spin-orbit torque efficiency with BiSb thicknesses ranging from 10 to 100 nm. Our results show a rapidly increasing spin-orbit torque efficiency with BiSb thickness that gradually saturates above 30nm. A clear correlation between the spin-orbit torque efficiency and the crystalline size of BiSb(012) was later verified via x-ray diffractometry. Thus, confirming the crystalline orientation of BiSb(012) being the crucial factor to achieve high spin orbit efficiency. Our work paves the way for the adaptation of topological insulators as the new class of spin source material for spintronics applications.

EQ09.09.22

The Effect of Environment on Electronic Structure of Co Spin Crossover Molecules—An XPS, XAS and IPES Study Esha Mishra¹, Ping Wang², Thilini K. Ekanayaka¹, Kayleigh A. McElveen³, Jared Paul Phillips⁴, Mohammad Zaid Zaz¹, Saeed Yazdani⁴, Alpha T. N'Diaye⁵, Duy Le⁶, Rebecca Y. Lai³, Robert Streubel¹, Ruihua Cheng⁴, Talat S. Rahman⁶, Michael Shatruk² and Peter A. Dowben¹; ¹University of Nebraska-Lincoln, United States; ²Florida State University, United States; ³University of Nebraska–Lincoln, United States; ⁴Indiana University-Purdue University Indianapolis, United States; ⁵Lawrence Berkeley National Laboratory, United States; ⁶University of Central Florida, United States

Two valence tautomeric spin crossover cobalt complexes $[\text{Co}(\text{SQ})(\text{Cat})(4\text{-CN-py})_2]$ and $[\text{Co}(\text{SQ})(\text{Cat})(3\text{-tpp})_2]$ have been investigated with a combination of X-ray photoemission spectroscopy (XPS), X-ray absorption spectroscopy (XAS) and inverse photoemission Spectroscopy (IPES) with the aim of ascertaining the unoccupied molecular orbitals that contain both ligand and metal weight. The alignment of the spectroscopic core levels from XAS and IPES validates the existence of unoccupied metal ligand charge transfer state in these cobalt spin crossover systems. These studies demonstrated that the changes to the electronic structure of $[\text{Co}(\text{SQ})(\text{Cat})(4\text{-CN-py})_2]$ and $[\text{Co}(\text{SQ})(\text{Cat})(3\text{-tpp})_2]$, when an interface is created with either of polar organic molecule, poly-D-lysine or semi conducting polymer, polyaniline, is minimal. The metal-ligand unoccupied states have been identified and the states are largely insensitive to the polymer to spin crossover molecular interface, when the spin crossover complex is in the high spin state.

EQ09.09.23

Spin-Polarized Flexoelectricity John D. Cavin and James M. Rondinelli; Northwestern University, United States

Flexoelectricity describes the coupling between electric polarization and a strain gradient. Because it is represented by an even parity rank-4 tensor, it is not prohibited by the presence of inversion symmetry in a crystal in the same way as piezoelectricity. First-principles methods for calculating flexoelectric tensor components have been developed that involve calculating electronic and lattice contributions using various charge-moment and force tensors.¹ In magnetic materials, these charge moments can be spin-polarized – that is, the densities of spin up and down electrons can respond differently to atomic displacement. Based on this principle, we developed a method for calculating spin-polarized flexoelectric tensor components. The existence of spin-polarization in the flexoelectric tensor could be used to create spin-polarized channels of surface charge. We apply our technique to several rock-salt materials with various magnetic orderings to calculate spin-polarized flexoelectric tensor components. We outline a method for experimental confirmation of our work by calculating effective spin-polarized flexoelectric coefficients for particular cases of beam-bending. This work predicts a novel method for developing spin-channels which may be of use in spintronics.

Acknowledgements: This work was sponsored in part by the National Science Foundation through CBET-1729787 and by the Department of Navy, Office of Naval Research, under ONR Award number N00014-16-1-2280. The US Government has a royalty-free license throughout the world on all copyrightable material contained herein.

1. Hong, J. and D. Vanderbilt, *First-principles theory and calculation of flexoelectricity*. Physical Review B, 2013. **88**(17): p. 174107.

EQ09.09.24

Charge Density Waves in Nano Alkali Molybdenum Oxide Bronzes Nick Russo, Yifeng Cao, Jun Cao, Xi Ling, Linda H. Doerrer and Kevin E. Smith; Boston University, United States

New computing paradigms require new materials exploiting novel phenomena. Another likely requirement is that the material be highly scalable and therefore nanosized. Here we present the preparation and characterization of nanoscale $K_0.3MoO_3$ an alkali molybdenum oxide and quasi 1D charge density wave (CDW) material. In bulk $K_0.3MoO_3$, CDWs are accompanied by many nonlinear electronic phenomena, such as hysteresis, nonlinear conductivity, and DC to AC conversion, as well as electrically controllable optical and IR properties. These novel phenomena may have some future potential application in computing.

We first present the synthesis of bulk powder $K_0.3MoO_3$ using redox mechanochemistry and thermal annealing under an inert atmosphere. From this bulk powder we then synthesize nanoscale $K_0.3MoO_3$ by additional mechanochemical ball milling and filtration and then deposit the product on Silicon wafers. We show that the crystal structure of the product is maintained while the average size is reduced with good distribution control using characterization by standards methods including x-ray diffraction and electron microscopy. We then comment on the change in the optical properties and CDW temperature as a function of size.

EQ09.09.25

Propagation Properties of Spin Wave in Non-Magnetic Metal-Covered YIG Waveguide Takumi Koguchi^{1,2}, Kanta Mori¹, Pang Boey Lim², Mitsuteru Inoue¹, Kazushi Ishiyama¹ and Taichi Goto¹; ¹Tohoku University, Japan; ²Toyohashi University of Technology, Japan

Spin-wave devices attract many interests because of their low Joule heating and power consumption. These devices can be categorized into a novel spintronic application and have been studied widely recently. A yttrium iron garnet (YIG) is widely used as a waveguide for these devices because of its low damping constant, meaning a long propagation length. To fabricate the waveguide, many groups etch the YIG to change it into a rectangular parallelepiped. However, the demagnetization field in the etched YIG is non-uniform, and spin-wave propagation properties are degraded. The different internal magnetic field in the YIG waveguide shows different dispersion curve. Hence the preferred wavelength of the spin wave is also different. To improve the propagation properties, we propose to use a metal-covered YIG waveguide in this paper. The wavelength of the spin wave propagating in a YIG waveguide covered by the non-magnetic metal film is two times longer than that in a non-coated YIG waveguide [1]. Thus, the spin wave can be reflected at the boundary between the metal-coated YIG and non-coated YIG area, providing waveguide functions.

We prepared the YIG film epitaxially grown on gadolinium gallium garnet (GGG) substrate. The gold film was deposited onto the YIG film and formed into a waveguide shape using lithography. The <0.5 T magnetic field was applied to this composite perpendicular to the film plane. The forward volume spin wave was excited and detected using a coplanar waveguide connected to a vector network analyzer (VNA). The wavelength of the propagated spin wave was about 9 micrometers, close to previous reports. The spin-wave spectroscopy was obtained, showing the Kittel curve, and splitting peaks because of the wavelength selectivity of the antennas.

Furthermore, the width and length of the waveguide were varied, and spin-wave propagation properties were measured. These results indicated that the non-magnetic metal-covered YIG worked as a waveguide. We do not need to etch the YIG when we use this waveguide, increasing the uniformity of the internal magnetic field and magnetization in the YIG film and intensity of propagated spin wave compared with the previously etched YIG waveguide. Therefore, we demonstrated the usefulness of the non-magnetic metal-covered YIG waveguide.

[1] T. Goto, K. Shimada, Y. Nakamura, H. Uchida, and M. Inoue, "One-dimensional magnonic crystal with Cu stripes for forward volume spin waves," Phys. Rev. Applied 11, 014033 (2019).

EQ09.09.26

Ferroelectric Phase Formation in $Hf_{0.5}Zr_{0.5}O_2$ Using Dual-Step PLD Growth Strategy for MoS_2 Negative Capacitance Field-Effect Transistors Uisik Jeong, Hae Won Cho, Pavan Pujar and Sunkook Kim; Sungkyunkwan University, Korea (the Republic of)

$Hf_{0.5}Zr_{0.5}O_2$ (HZO) is considered a prominent ferroelectric material at the thin film scale, which usually contain cubic(c), monoclinic(m), tetragonal(t) and orthorhombic(o) phases when crystallized. In particular, the asymmetric o-phase has its own ferroelectricity, but it is not easily obtained due to its metastable state. Comparative studies on the HZO grown on Si by pulse laser deposition (PLD) using 1) direct growth (high temperature deposition) and 2) dual step growth (Rapid thermal annealing (RTA) after RT deposition) strategies have been performed. Compared to other processes, PLD is easy to control the oxygen partial pressure, and high energy particles generated by the pulse laser can produce high quality thin film. Although many studies on ferroelectrics have been conducted with the ALD process, there has been no case of applying it to ultra-low power logic applications based on the PLD-HZO. We obtained a polycrystalline HZO by crystallization via direct deposition at a high temperature, whereas a pure o-phase without non ferroelectric m-phase is formed through RTA treatment after RT deposition with maximized ferroelectricity. By capacitance matching with a high-k dielectrics (HfO_2) on HZO grown on a Si, MoS_2 NCFET were driven with subthreshold swing of 20.42 and 26.16 mV/dec in the forward and reverse directions, respectively. By optimizing various parameters of the PLD process to obtain a ferroelectric HZO thin film, and to evaluate the device, it is expected to be a modeling study for the next generation low-power device research.

EQ09.09.27

Exploring the Limits of RKKY Coupling for Synthetic Antiferromagnets Amal El-Ghazaly and Karthik Srinivasan; Cornell University, United States

Synthetic antiferromagnets (SAFs), made from ferromagnet/non-magnetic metal/ferromagnet exchange-coupled heterostructures, represent a crucial component of magnetic tunnel junctions and giant magnetoresistance spin valves. Yet, beyond their usage for pinning the magnetization in these multilayer, ultra-thin-film stacks, the limits of their reach in thicker films and other applications have not been given much attention. The widespread practice is to grow SAFs with a non-magnetic metal spacer layer thickness optimized to achieve the first oscillatory peak for antiferromagnetic interlayer exchange coupling. However, recent work by Waring et al. suggests that when Ru is used as the metal spacer material, the second oscillatory antiferromagnetic exchange coupling peak may, in fact, achieve better antiferromagnetic anisotropy resulting from the fact that the slightly thicker Ru layer provides better uniformity of the grown material film [1]. This increased interlayer exchange coupling manifests itself as a narrower resonance peak with fewer damping losses in the SAF structure, thereby translating to more efficient, low-power operation. Delving deeper into this question of efficiency, the present research work explores the variation in magnetic anisotropy in $Co_{43}Fe_{43}B_{14}/Ru/Co_{43}Fe_{43}B_{14}$ exchange-coupled SAF trilayers. Thicknesses of both the non-magnetic and magnetic layers are experimentally varied to observe the change in RKKY coupling strength.

Varying the thickness of the Ru non-magnetic metal spacer between the two ferromagnetic layers produced the signature oscillatory behavior between ferromagnetic and antiferromagnetic interlayer exchange coupling. In the first set of experiments, Si substrate/ $SiO_2/CoFeB$ (5 nm)/R (t_{Ru})/ $CoFeB$ (5 nm)/Pt (5 nm) trilayer films were grown with a Ru spacer layer thickness varying between $t_{Ru} = 0.25$ to 3.0 nm, in increments of 0.125 nm steps. A single layer of $CoFeB$ with thickness 10 nm (without a Ru spacer in the middle) was also deposited and used to calibrate the total magnetic moment expected from the SAF multilayer films. Upon inspection, the second antiferromagnetic RKKY peak appeared to correspond to the SAF trilayer with a Ru thickness, $t_{Ru} = 1.875$ nm, which was thicker than the 1.1 nm Ru thickness observed by Waring, et al. Nevertheless, by analyzing magnetization hysteresis behavior for each of the grown films, we demonstrate the gradual transitions between interlayer coupling configurations and strengths.

At the optimal antiferromagnetic interlayer coupling, $t_{Ru} = 1.875$ nm, the thickness of the ferromagnetic layers was also varied. For thinner ferromagnetic films, the exchange coupling across the Ru thickness is expected to have a strong effect throughout the entire magnetic thickness. However, as the

ferromagnetic layer thickness increases, the antiferromagnetic interlayer exchange coupling becomes less pronounced. This behavior is seen experimentally as the thickness of the ferromagnetic layer in the stack substrate/SiO₂/CoFeB (t_{FM})/Ru (1.875 nm)/CoFeB (t_{FM})/Pt (5 nm) is varied between t_{FM} = 2.5 nm to 25 nm in steps of 2.5 nm. As expected the antiferromagnetic exchange decreases as the thickness of the ferromagnetic layer it has to act upon increases, corresponding to an overall reduction in the anisotropy. Thus, this research illustrates that optimization of both the non-magnetic metal spacer and the ferromagnetic layer thicknesses can be used to achieve strongly-coupled and highly-efficient synthetic antiferromagnetic films for future low-power integrated systems.

[1] H. J. Waring, N. A. B. Johansson, I. J. Vera-Marun, and T. Thomson, “Zero-field Optic Mode beyond 20 GHz in a Synthetic Antiferromagnet,” *Phys. Rev. Appl.*, vol. 13, no. 3, p. 1, 2020.

EQ09.09.28

Tunable Anomalous Hall Conductivity of Itinerant Ferromagnet CoS₂ Joonyoung Choi¹, Mi Kyung Kim², Wonshik Kyung^{3,4}, Changyoung Kim^{3,4}, Jin-Hong Park⁵, Jun-Won Rhim⁵, Se Young Park⁶ and Younjung Jo¹; ¹Kyungpook National University, Korea (the Republic of); ²Yonsei University, Korea (the Republic of); ³Institute for Basic Science, Korea (the Republic of); ⁴Seoul National University, Korea (the Republic of); ⁵Ajou University, Korea (the Republic of); ⁶Soongsil University, Korea (the Republic of)

The electrical tunability of material is the most important property for the application of new technologies. Modification of anomalous Hall conductivity (AHC) is an example that is required for spin-torque devices or advanced magnetic sensors. In that case, cobalt disulfide (CoS₂) is a suitable material with the potential to increase its AHC a lot. CoS₂ is an itinerant ferromagnet and expected to be a magnetic topological material as it has turned out that there is small gapped Dirac-type dispersion at a little below the Fermi level as a Berry curvature (BC) source, originating AHC. The BC source is along the Γ -M direction in k-space and there are four of it in the first Brillouin zone possessing the same sign, resulting in a large contribution to AHC without canceling out each other. In this work, we measured the AHC of CoS₂, controlling the amplitude of AHC by Fe- (hole) and Ni- (electron) doping, respectively. Purely intrinsic origin and the largest value of AHC have been observed in Co_{0.95}Fe_{0.05}S₂. This result is well consistent with the AHC calculated by LDA+U methods in the energy scale.

EQ09.09.29

Design Principles to Control Non-Bonding States for Highly Tribopositive Property Donghyeon Kang, Jihye Kim, SeongMin Kim and Sang-Woo Kim; Sungkyunkwan University, Korea (the Republic of)

The development of tribopositive materials is highly required to realize durable and high-performance triboelectric generators. Here, we introduce a novel principle to control local dipoles for designing highly tribopositive materials and suggest nitrogen-based dimethylol urea (DMU), diazolidinyl urea and imidazolidinyl urea as promising tribopositive materials. A mechanism by which the nitrogen-based urea materials provide high tribopositive properties was investigated using negative local dipoles formed in the highest occupied molecular orbital composed of non-bonding electrons. Negative local dipole is formed by the electron accumulation around the high electronegative atoms, which attract electrons from bonded atoms and tend to donate their electrons to atoms in other materials, and thus negative local dipole induces the electron donating environment. In addition, we confirm the proposed design protocol by analyzing the charge transfer characteristics of DMU based on the dipole interaction through density functional theory (DFT) calculations, quantitatively.

EQ09.09.30

Hexagonal MnTe - a Conducting Room Temperature Antiferromagnet Kacper P. Kluczyk¹, Katarzyna Gas², Michal Grzybowski¹, Michal A. Borysiewicz³, Tomasz Fas¹, Jan Suffczynski¹, Pawel Skupinski², Krzysztof Graszka², Elzbieta Lusakowska², Andrzej Mycielski², Maciej Sawicki² and Marta Borysiewicz¹; ¹University of Warsaw, Poland; ²Polish Academy of Sciences, Poland; ³Lukasiewicz Research Network - Institute of Microelectronics and Photonics, Poland

The idea of exploiting magnetic state of the antiferromagnets has become especially timely after groundbreaking demonstrations of current-induced control of Néel vector orientation in these materials [1-3]. Not only do these accomplishments motivate to search for new antiferromagnetic platforms, but also to reexamine some old, prototypic materials. One of such classical antiferromagnets is hexagonal MnTe, a semiconductor with a moderate bandgap (E_G ~1.3 eV) and the Néel temperature just above 300 K. This material in a form of thin films has been extensively studied recently pointing to the role of substrate on its electronic properties [4,5].

In this report we present results of studies of bulk hexagonal MnTe, a reference free standing system to its epilayer counterparts. The material is grown from the vapour phase via reaction of tellurium vapors with manganese powder at a temperature adjusted to reduce the formation of other crystallographic phases. A clear magnetic phase transition between the antiferromagnetic and paramagnetic states is observed at about 310 K, in agreement with the previous studies [4,6,7]. Although the samples are polycrystalline the individual grains have their hexagonal c-axis aligned in the same direction. This crystallographic composition is confirmed by observation of uniaxial magnetic anisotropy below the Néel temperature, whose temperature and magnetic field dependence are characteristic for a system with simple antiparallel spin structure within the c-plane but with the Néel vectors equally distributed among three possible orientations differing by 2p/3 [6]. Our findings makes highly unlikely the possibility of the existence of spin-flop processes reported earlier for epitaxial MnTe [4]. The samples are p-type with an activated character of the temperature dependence of the resistivity characterized by the activation energy of 10 meV. A clear anomalous Hall effect is observed with a pronounced hysteresis loop below the Néel temperature. This evokes questions about the origin of this effect in a magnetically compensated material. The possible origin of this effect will be discussed, referring to the novel concept of altermagnetism [8].

References:

- [1] P. Wadley et al. “Electrical switching of an antiferromagnet,” *Science* 351, 587–590 (2016).
- [2] T. Moriyama et al., “Spin torque control of antiferromagnetic moments in NiO,” *Sci. Rep.* 8, 14167 (2018).
- [3] L. Baldtrati et al. “Mechanism of Neel order switching in antiferromagnetic thin films revealed by magnetotransport and direct imaging,” *Phys. Rev. Lett.* 123, 177201 (2019).
- [4] D. Kriegner et al., *Nat. Commun.* 7, 1162 (2016).
- [5] H. Reichlova et al., “Macroscopic time reversal symmetry breaking arising from antiferromagnetic Zeeman effect”, arXiv:2012.15651v1.
- [6] Komatsubara et al., “Magnetic Properties of Manganese Telluride Single Crystals”, *J. Phys. Soc. Jpn.* 18, 356 (1963).
- [7] K. Ozawa et al., *Phys. Lett.* 20, 132 (1966).
- [8] L. Smejkal et al. “Emerging research landscape of altermagnetism”, arXiv:2204.10844.

8:30 AM *EQ09.10.01

Realizing Topological Superconductivity in Ultrathin FeTeSe Films Shuolong Yang; The University of Chicago, United States

Topological superconductors are the material platforms to realize emergent quasiparticles called Majorana zero modes, which are the basic units for nonabelian statistics and topological quantum computation. Earlier material realizations of topological superconductors are semiconductor nanowires coated with low-temperature superconductors, which not only bear substantial manufacturing complications but also remain under debate in terms of the fundamental physics picture. Here we introduce our latest effort using molecular beam epitaxy to fabricate ultrathin $\text{FeTe}_x\text{Se}_{1-x}$ thin films on SrTiO_3 substrates, where the topological surface state is proximity-coupled to its own superconducting bulk. This leads to a robust topological superconducting state which is manifested in the observation of a superconducting Dirac surface state. By systematically varying the Te:Se ratio and the film thickness, we observe the Dirac surface state in ultrathin $\text{FeTe}_x\text{Se}_{1-x}$ films with $x > 0.7$ and thickness > 2 layers. As we thin down the $\text{FeTe}_x\text{Se}_{1-x}$ films, a drastic band structure evolution is identified due to the hybridization of the top and bottom Dirac surface states, which transforms the band structure quickly into a correlated insulating state in the monolayer limit. Our study not only marks the thinnest topological superconducting film ever fabricated so far, but also paves the road towards topological quantum devices based on ultrathin films.

9:00 AM EQ09.10.02

Understanding the Transition from Metal to Hund's Insulator in CaFeO_3 Maximilian E. Merkel and Claude Ederer; ETH Zurich, Switzerland

Strongly correlated materials show great potential for energy-efficient transistors thanks to the sharp metal-insulator transition (MIT) that some of them exhibit. However, this MIT is almost always coupled to a structural distortion, which can lead to fatigue effects and limit the switching frequency. To better understand the different types of distortions, more fundamental knowledge about the complicated physics at work here is needed.

Recently, materials where strong correlations are caused by the Hund's interaction have attracted a lot of attention. In some cases, a dominant Hund's interaction can even lead to the emergence of a charge-disproportionated insulating (CDI) or "Hund's insulating" state, which can cause an MIT. One example is the perovskite transition-metal oxide CaFeO_3 (CFO) with a transition close to room temperature. This transition couples to a structural distortion that creates alternating large and small FeO_6 octahedra, leading to two inequivalent Fe sites with nominal Fe^{5+} and Fe^{3+} charge states.

We study CFO using density functional theory (DFT) and dynamical mean-field theory (DMFT). To characterize the CDI state, we first apply DMFT to a five-orbital Hubbard model applicable to CFO and demonstrate the emergence of the CDI phase [1]. We then investigate the energetics of the transition using fully self-consistent DFT+DMFT calculations, which show that both structural and electronic properties of the CDI state can be well described within DFT+DMFT.

Finally, we discuss the ligand-hole character of the charge disproportionation and analyze the role of the zero or even negative charge-transfer energy in CFO as well as its influence on the emergence of the MIT.

[1] M. E. Merkel and C. Ederer, *Phys. Rev. B* 104, 165135 (2021), doi: 10.1103/PhysRevB.104.165135

9:15 AM EQ09.10.03

Tunable Perpendicular Magnetic Anisotropy in Amorphous $\text{Gd}_x\text{Co}_{1-x}$ Alloys Karthik Srinivasan, Yulan Chen, Ludovico Cestarollo and Amal El-Ghazaly; Cornell University, United States

Amorphous magnetic alloys have been at the forefront in the development of magnetic random-access memory due to their favorable perpendicular magnetic anisotropies (PMA) and deterministic read/write mechanisms with magnetoresistance and spin-orbit torques. While amorphous ferromagnets are well researched, they are limited by low switching speeds (in \sim ns) and constrained in their read/write energy-efficiency by the large angular momentum, which requires a large critical current for switching. Unlike ferromagnets, ferrimagnetically coupled systems offer faster switching dynamics due to their stiffer exchange interactions, minimal stray field due to their lower net saturation magnetization, and tunable anisotropy and net magnetization due to the existence of two counteracting sublattices. Here, we report on amorphous thin films of GdCo that have a ferrimagnetic order (antiparallel spin orientation) with bulk-like PMA and stoichiometries near its magnetic-compensation that coincide with lower total angular momentum compared to ferromagnets and the potential for much higher switching speeds on the order of tens of picoseconds. Sputter-deposited heterostructures of $\text{Ta}(3 \text{ nm})/\text{Pt}(3 \text{ nm})/\text{Gd}_x\text{Co}_{1-x}(\text{t})/\text{Pt}(5 \text{ nm})$ on $\text{Si}/\text{SiO}_2(3 \text{ nm})$ substrates exhibit bulk-like PMA for $\text{Gd}_x\text{Co}_{1-x}$ thicknesses of 5-12 nm and stoichiometries where $x = 18$ -40%. A strong uniaxial anisotropy for out-of-plane magnetization with an anisotropy field (H_k) of 0.24 T was observed when the Gd:Co ratio was 35:65, which is near the composition that results in a magnetic compensation at room temperature. Interestingly, it was found that strong PMA in GdCo is possible only with a non-negligible amount of oxygen in the thin film. Oxygen flow rates were adjusted between 0-0.8 sccm during deposition and a maximum effective anisotropy energy density of $1 \times 10^5 \text{ erg cc}^{-1}$ was obtained for a metal cation to oxygen (R:O) ratio of 50:50, which corresponds to a flow rate of 0.5 sccm. Furthermore, X-ray photoelectron spectroscopy (XPS) revealed that with an increase in oxygen concentration, Co oxidizes preferentially over Gd, resulting in Co-deficient stoichiometries from lower sputter yields at higher oxygen flow rates. Strong PMA is observed in a stoichiometry of $\text{Gd}_{21}\text{Co}_{28}\text{O}_{51}$ with a Gd:Co ratio of 3:4 and an R:O ratio of 1:1, which suggests that the strong ferrimagnetic order likely arises through a superexchange-like coupling between the magnetic cations (R: Gd,Co) via the non-magnetic anion (O) in this amorphous alloy. With the single layer optimized, super-lattice heterostructures could be developed. Even greater PMA is achieved in a heterostructure with 10 repetitions of the $\text{Gd}_{35}\text{Co}_{65}$ alloy. These films exhibit an anisotropy field on the order of 11.6 kOe, which corresponds with switching speeds as low as 30 ps. The combination of ferrimagnetic ordering (lower total angular momentum) in amorphous GdCo (reduced thermal budget) and well-defined pathways for a strong PMA (low-energy magnetization switching due to the very short picosecond-range write pulses required) make these thin films a suitable choice for ultrafast energy-efficient memory devices.

9:30 AM EQ09.10.04

Spin-Resolved Unoccupied States of NiCo_2O_4 Thin Films Arjun Subedi, Corbyn Mellinger, Xiaoshan Xu and Peter A. Dowben; University of Nebraska-Lincoln, United States

Theoretical calculations indicate that NiCo_2O_4 is a half-metal with fully spin polarized carriers [1], although realization of half metallicity is in fact very doubtful [2] especially at finite temperatures. It remains important, nonetheless, to ascertain whether NiCo_2O_4 is a high polarization material and whether the spin polarization has a projection in the plane of the thin film. We observed in-plane net spin polarized unoccupied states of NiCo_2O_4 near Fermi level

using spin-polarized inverse photoemission spectroscopy (SPIPES) which is an extremely surface sensitive technique. Although NiCo₂O₄ is thought to possess a perpendicular magnetic anisotropy, the presence of in-plane spin-resolved unoccupied states could indicate the influence of the surface on magnetic ordering.

[1] P. F. Ndione et al., *Adv. Funct. Mater.* **24**, 610 (2014).

[2] P.A. Dowben and R. Skomski, *J. Appl. Phys.* **95**, 7453 (2004).

9:45 AM BREAK

SESSION EQ09.11: RRAM II
Session Chairs: Aiping Chen and Ying-Hao Chu
Thursday Morning, December 1, 2022
Sheraton, 2nd Floor, Back Bay D

10:15 AM EQ09.11.01

Stimulation Rate-Dependent 1S1R Synapse with Short-Term Plasticity TiO_x-Based Exponential Selector Mun Yin Chee, Putu Andhita Dananjaya, Gerard Joseph Lim and Wen Siang Lew; Nanyang Technological University, Singapore

Short-term plasticity (STP) is an important synaptic characteristic in hardware-based artificial neural networks, as it is suitable for temporal information processing (TIP).^[1-3] However, the STP feature is difficult to be demonstrated in a single non-volatile memory because it requires a certain degree of volatility. Generally, selector devices are implemented with a non-volatile resistive random-access memory (RRAM) in one selector-one RRAM (1S1R) configuration to suppress the sneak current in a crossbar array.^[4,5] In this work, a TiO_x-based selector is introduced not only to suppress the sneak current but also to enable the TIP feature in the 1S1R synaptic device, which consists of a Pt/TiO_x/Pt exponential selector and a Pt/HfO₂/Ti RRAM device. Our measurements reveal that the exponential selector exhibits the STP characteristic, while the RRAM device enables the long-term memory capabilities of the synapse. With the corresponding 1S1R device, an on/off ratio of up to ~ 18 can be achieved under optimised reading conditions. Furthermore, 5000-cycle writing endurance was demonstrated with uniform switching. Moreover, the potentiation and depression synaptic characteristics are realised in the 1S1R device. Thereafter, we experimentally demonstrated the stimulation rate-dependent multilevel switching in the 1S1R device. 4 multilevel states were achieved in the 1S1R synapse using different frequencies of pulses at 100 000 Hz, 50 000 Hz and 100 Hz, demonstrating the TIP capability in the 1S1R device. This work therefore provides a reliable means of producing the TIP capability in a 1S1R device.

References:

- (1) Cho, H.; Kim, S. Enhancing Short-Term Plasticity by Inserting a Thin TiO₂ Layer in WO_x-Based Resistive Switching Memory. *Coatings*. 2020.
- (2) Lee, Y.; Mahata, C.; Kang, M.; Kim, S. Short-Term and Long-Term Synaptic Plasticity in Ag/HfO₂/SiO₂/Si Stack by Controlling Conducting Filament Strength. *Appl. Surf. Sci.* **2021**, *565*, 150563.
- (3) Ohno, T.; Hasegawa, T.; Tsuruoka, T.; Terabe, K.; Gimzewski, J. K.; Aono, M. Short-Term Plasticity and Long-Term Potentiation Mimicked in Single Inorganic Synapses. *Nat. Mater.* **2011**, *10* (8), 591–595.
- (4) Dananjaya, P. A.; Loy, D. J. J.; Chow, S. C. W.; Lew, W. S. Unidirectional Threshold Switching Induced by Cu Migration with High Selectivity and Ultralow OFF Current under Gradual Electroforming Treatment. *ACS Appl. Electron. Mater.* **2019**, *1* (10), 2076–2085.
- (5) Lee, W.; Park, J.; Kim, S.; Woo, J.; Shin, J.; Choi, G.; Park, S.; Lee, D.; Cha, E.; Lee, B. H.; Hwang, H. High Current Density and Nonlinearity Combination of Selection Device Based on TaOx/TiO₂/TaOx Structure for One Selector–One Resistor Arrays. *ACS Nano* **2012**, *6* (9), 8166–8172.

10:30 AM EQ09.11.02

Metal-Hf_{0.5}Zr_{0.5}O₂-Al₂O₃-Metal Ferroelectric Tunnel Junction Stack Optimization for Enhanced ON/OFF Ratio Keerthana S. Nair^{1,2}, Marco Holzer^{1,2}, Catherine Dubourdieu^{1,2} and Veeresh Deshpande¹; ¹Helmholtz Zentrum Berlin, Germany; ²Freie Universität Berlin, Germany

Hafnium dioxide-based ferroelectrics are enabling the integration of ferroelectric devices into CMOS technology due to their stable ferroelectric phase at nanometer thickness. The low-temperature crystallization (around 400°C) further allows Hf_{0.5}Zr_{0.5}O₂ (HZO) based devices to be integrated into the back-end-of-line of CMOS technology. Among the ferroelectric memory devices, ferroelectric tunnel junctions (FTJ) are well-suited for neuromorphic applications due to their ultra-low power consumption and potential to attain multiple resistance states through partial switching of domains from one polarization state to the other. The typical architecture of FTJ devices is metal-ferroelectric-metal, where the ferroelectric layer should be less than 5 nm in thickness and possess a high remnant polarization to achieve a high ON current. As stabilizing high polarization in sub-5 nm thick HZO layer is challenging, an alternate device stack consisting of Metal-Ferroelectric-Dielectric-Metal layers utilizing a thicker ferroelectric layer (~10-12 nm) has recently been demonstrated with a high ON/OFF ratio [1]. In this work, we study CMOS back-end compatible Metal-HZO-Al₂O₃-Metal FTJ with TiN and W metals. Different stacks, by changing the position of the metal electrode and the dielectric, are fabricated to find the optimum configuration for high ON/OFF ratio. It is observed that the ON/OFF ratio is highly dependent on the positioning of the W, TiN electrodes, and the Al₂O₃ dielectric. We will discuss the influence of processing sequence of the layers and the role of resultant interface charge trap density on the FTJ characteristics [2]. The impact of dielectric thickness on ON/OFF ratio will also be discussed. The optimized FTJ device is electrically programmed to demonstrate multiple resistance states through partial switching set and reset operations. The stability of the intermediate states will be discussed based on the endurance and retention characteristics.

[1] V. Deshpande, K. S. Nair, M. Holzer, S. Banerjee, and C. Dubourdieu, *Solid State Electronics*, 186, pp. 108054 (2021).

[2] R. Fontanini, M. Segatto, K. S. Nair, M. Holzer, F. Driussi, I. Häusler, C. T. Koch, C. Dubourdieu, V. Deshpande, and D. Esseni, *IEEE Transactions on Electron Devices*, 1 (2022).

10:45 AM EQ09.11.03

Operando Direct Observation of Filament Formation in Resistive Switching Devices Enabled by a Phase Transformation Molecule Kunqi Hou, Wen Siang Lew and Wei Lin Leong; Nanyang Technological University, Singapore

Conductive filaments (CFs) play a critical role in the mechanism of resistive random-access memory (ReRAM) devices. However, in situ detection and visualization of the precise location of CFs are still key challenges. Herein, we demonstrate for the first time, the use of an organic π -conjugated molecule with phase transformation behavior for the positioning and visualizing of the CFs in the ReRAM devices. The π -conjugated molecule (called TT molecule)

has the capacity to transform its molecular shape between twisted and planar states under varying temperatures, which can be translated into corresponding adaptations in crystallization, aggregation behavior, and optical properties. Hence, based on localized Joule heating generated within filament regions, the π -conjugated molecule exhibited reversible optical transformation and thus reflecting the location of the underlying CF. Customized patterns of CFs were induced and observed by the π -conjugated molecule layer, which confirmed the hypothesis. Additionally, statistical studies on filaments distribution were conducted to study the effect of device sizes and bottom electrode heights, which serves to enhance the understanding of switching behavior and their variability at device level. Therefore, this phase transformation molecule and such approach have great potential in aiding the development of ReRAM technology.

Keywords: phase transformation, π -conjugated molecule, conductive filament, ReRAM, spatial filament mapping

11:00 AM EQ09.11.04

Confined Conducting Filaments in Resistive Random Access Memory by Al₂O₃ Nanodome Shaped Arrays (NDSAs) via Glancing Angle Deposition Technology Toward Neuromorphic Computing [Ying-Chun Shen](#) and Yu-Lun Chueh; National Tsing Hua University, Taiwan

Resistive random access memory (RRAM) is vital to neuromorphic computing applications. However, filamentary RRAM cells are affected by transitions from abrupt switching to analog switching. In this study, we develop Al₂O₃ nanodome shaped arrays (NDSAs) by glancing angle deposition technology (GLAD) to geometrically confine the conducting filaments (CFs), for which conducting atomic force microscopy (C-AFM) was performed to analyze positions and dimensions of filaments. For the Pt/HfO₂/75 % Al₂O₃ NDSAs/TiN device, the dimension of the CFs can be restricted to 10-12 nm, whereas for the Pt/HfO₂/TiN device, the CFs were formed with the dimension of ~50 nm. The device first yielded multiple weak CFs that subsequently transformed into stronger and larger CFs when the coverage of Al₂O₃ NDSAs was reduced to 55 % while Pt/HfO₂/75 % Al₂O₃ NDSAs/TiN device exhibited synaptic features with more linear potentiation and depression, demonstrating the analog switching. The controllable coverages of Al₂O₃ NDSAs render the geometric design more promising as a memristor for future applications in neuromorphic computing.

11:15 AM EQ09.11.05

Waterproof and Flexible Memristive Physically Unpredictable Functions for Highly Secured Neuromorphic Computing System [Jungyeop Oh](#)¹, [Sungkyu Kim](#)², [Junhwan Choi](#)¹, [Sung Gap Im](#)¹, [Byung Chul Jang](#)³ and [Sung-Yool Choi](#)¹; ¹Korea Advanced Institute of Science and Technology (KAIST), Korea (the Republic of); ²Sejong University, Korea (the Republic of); ³Kyungpook National University, Korea (the Republic of)

Recent advances in neuromorphic edge devices and Internet of Things (IoT) technologies have brought the unprecedented expansion of interconnected networks and devices, enabling artificial intelligence (AI) based services to the public. This AI service based on smart IoT devices is an attractive target for cybercriminals because it utilizes remotely connected networks to process large amounts of personal and security-related data. However, it is challenging for the software-based security system, which is subject to physical attack, to combat alone the threat of cybercriminals, therefore a built-in hardware-based security system is essential.

Here, we report that hardware-based security primitives implemented using a physically unclonable function (PUF) that exhibits the high entropy achieved via the random switching nature of a poly(1,3,5-trivinyl-1,3,5-trimethyl cyclotrisiloxane) (pV3D3)-based memristor. The excellent insulating property of pV3D3 induces the thermal dominating reset by localizing the Joule heat generated by the reset high current generated to the conductive filament and enhances the stochasticity of the tunneling distance for randomly ruptured Cu filaments. With high bandgap energy (E_g) (8.25 eV) and low- k (2.2) of the pV3D3, the pV3D3-PUFs exhibit near-ideal entropy, uniqueness, and uniformity as well as reconfigurability. Thanks to the outstanding chemical stability of pV3D3, pV3D3-PUFs show reliable operation under mechanical stress and the water immersion condition for IoT applications in outdoor environments. We demonstrate a 1kbit pV3D3 memristor crossbar array enabling the strong pV3D3-PUF via stochastic in-memory computing, inducing robustness to machine learning attacks of the multi-layer perceptron and the generative adversarial networks. Furthermore, the strong pV3D3-PUF passed the NIST randomness test and showed outstanding PUF performances compared to other emerging PUFs. Finally, we have proposed a protocol for highly secured smart IoT devices with pV3D3-PUF, which is expected to advance the era of hyperconnectivity.

SESSION EQ09.12: RRAM III

Session Chairs: Olga Ovchinnikova and A. Talin

Thursday Afternoon, December 1, 2022

Sheraton, 2nd Floor, Back Bay D

1:30 PM *EQ09.12.01

Rational Design of Redox-Based Memristive Devices for Novel Computing Paradigm [Regina Dittmann](#)^{1,2}; ¹Forschungszentrum Jülich, Germany; ²RWTH Aachen University, Germany

Memristive devices have been a hot topic in nanoelectronics for the last two decades in both academia and industry. Originally proposed as digital (binary) non-volatile random access memories, research in this field was predominantly driven by the search for higher performance solid-state drive technologies (e.g., Flash replacement) or higher density memories (storage class memory). However, based on their large dynamic range in resistance with analog tunability along with complex switching dynamics, memristive devices enable revolutionary novel functions and computing paradigms. In this talk, we will present the current knowledge about the switching and failure mechanisms in different variants of redox-based memristive elements. In particular, we will show direct experimental evidence of the redox-processes gained by *in-operando* spectroscopy and microscopy. Using the quantitative numbers gained from these experiments as input for existing simulations offers a route to less empirical and more predictive models for memristive devices. Based on the microscopic understanding gained from *operando* spectroscopy and modelling, we will show approaches for rational design of material stacks with tailored properties for novel computing paradigm.

2:00 PM EQ09.12.02

Forming-Free Interface-Type Memristors [Aiping Chen](#); Los Alamos National Laboratory, United States

Memristors with excellent scalability have the potential to revolutionize not only the field of information storage but also neuromorphic computing. Conventional metal oxides have been widely used as resistive switching materials in memristors. Defects such as oxygen vacancy and interface play critical roles in filamentary-type resistive switching (RS) devices. In this talk, I will discuss the role of defects such as oxygen vacancy and cation deficiency, moisture, and interface on switching behavior in forming-free memristors.

2:15 PM EQ09.12.03

Effects of Cs Doping on Ion Transport in MAPbI₃ Hybrid Perovskite Memristors Matthew Flynn-Hepford¹, Arya Ahmadi¹, Holland Hysmith¹, Yongtao Liu², Mahshid Ahmadi¹, Anton V. Ievlev², Bobby Sumpter² and Olga Ovchinnikova²; ¹University of Tennessee- Knoxville, United States; ²Oak Ridge National Laboratory, United States

Hybrid perovskite materials have drawn a lot of attention recently for solar energy applications, but the instability of these materials makes long term efficiency a major issue that needs to be addressed. The weak bonding in methylammonium lead iodide (MAPbI₃) that enables ion migration can be leveraged for memristive applications where ion migration needs to be controlled rather than eliminated. We show that in modeled structures, cesium (Cs) doping the MA site (A-site) can enable stronger local bonding with the iodine (I) ions allowing for weak bonding ion conductivity channels that can help control ion migration under applied bias. Cs doped MAPbI₃ films were spin coated on glass/ITO substrates to act as an active layer for memristive devices. Local IV measurements were conducted using an AFM tip and a DC bias was applied to the tip in contact mode in order to induce ion migration. Kelvin probe force microscopy (KPFM) was used to probe the resulting variation in surface potential. The chemical origins of the surface potential variations were investigated using specially resolved time-of-flight scanning ion mass spectroscopy.

2:30 PM BREAK

3:00 PM *EQ09.12.04

Schottky-to-Ohmic Switching in Ferroelectric Memristors Based on Semiconducting Hf_{0.93}Y_{0.07}O₂ Thin Films Moritz Mueller, Maximilian T. Becker, Nives Strkalj and Judith L. MacManus-Driscoll; University of Cambridge, United Kingdom

We demonstrate resistive switching and memristive behavior in devices consisting of ultrathin (4.5 nm) semiconducting, epitaxial ferroelectric Hf_{0.93}Y_{0.07}O₂ (YHO) films on La_{0.7}Sr_{0.3}MnO₃ (LSMO)-buffered, Nb-doped SrTiO₃ (Nb:STO) single crystal substrates with Au top electrodes. Unlike the tunneling-driven current-voltage characteristics of ferroelectric tunnel junctions (FTJs) which utilize ultrathin insulating (fully depleted) ferroelectric films, the semiconducting nature of our YHO films, i.e. the presence of free charge carriers introduced by Y doping, results in radically different current-voltage characteristics. Current-voltage measurements reveal a polarization-modulated transition from Schottky-barrier-controlled charge transport to Ohmic conduction in the YHO devices, which results in a large on/off ratio of up to 540. Moreover, voltage pulse train measurements reveal a broad range of accessible resistance states, which indicates the memristive behavior of the devices. Our results represent an important step towards the development of future non-volatile memory and brain-inspired neuromorphic computing applications based on ultrathin semiconducting ferroelectric films

3:30 PM EQ09.12.05

Controlling Switching Stochasticity in Hybrid Memristors by Vapor-Phase Infiltration Chang-Yong Nam; Brookhaven National Laboratory, United States

Resistive random-access memory (RRAM) is promising for next-generation data storage and non-von Neumann computing hardware. However, tuning device switching characteristics and particularly, controlling their stochastic variation remain as critical challenges. Here, new organic-inorganic hybrid RRAM media are reported whose bipolar switching characteristics and stochasticity can be controlled by vapor-phase infiltration (VPI), an ex situ hybridization technique derived from atomic layer deposition. Hybrid RRAMs based on AlO_x-infiltrated SU-8 feature facile tunability of device switching voltages, off-state current, and on-off ratio by adjusting the amount of infiltrated AlO_x in the hybrid. Furthermore, a significant reduction in the stochastic, cycle-to-cycle variations of switching parameters is enabled by AlO_x infiltration, driven by the infiltration-induced changes in mechanical, dielectric, and chemical properties of organic medium and their influence on the dimension and formation characteristics of conductive filaments. Finally, multi-level analog switching potentially useful for neuromorphic applications are demonstrated, along with direct, one-step device patterning exploiting the negative-tone resist feature of SU-8. With the demonstrated control over switching characteristics and stochastic variation, combined with analog switching and one-step patterning capabilities, the results not only present a novel hybrid medium for RRAM applications but also showcase the utility of VPI for developing new, high-performance hybrid RRAM devices.

SESSION EQ09.13: Low Power Gated Electronic Devices

Session Chairs: Ying-Hao Chu and Shuolong Yang

Thursday Afternoon, December 1, 2022

Sheraton, 2nd Floor, Back Bay D

3:45 PM EQ09.13.01

3D-Stacked Organic Ternary Logic Circuits Utilize Nonvolatile Floating-Gate Memory Changhyeon Lee¹, Junhwan Choi¹, Chungryeol Lee¹, Seung Min Lee¹, Chang-Hyun Kim², Hocheon Yoo² and Sung Gap Im¹; ¹Korea Advanced Institute of Science and Technology, Korea (the Republic of); ²Gachon University, Korea (the Republic of)

Nowadays, a large amount of information is generated in advanced electronic systems such as artificial intelligence (AI) and internet-of-things (IoT). Therefore, the method of increasing information processing density without increasing additional transistor have great attention. Multi-valued logic (MVL) circuits based on heterojunction transistor (HTR) are one solution. However, it is hard to satisfy all the important characteristics of T-inverters including 1) full-swing operation (in the sufficient input voltage (V_{IN}) range), 2) a well-defined intermediate logic state with the proper output voltage ($V_{OUT} \sim$ half of the supply voltage ($V_{DD}/2$), logic "1") and 3) hysteresis-free, low-voltage operation. Herein, Organic ternary logic inverter (T-inverter) with a nonvolatile floating-gate (FG) flash memory is demonstrated. The T-inverter operation was controlled by the channel conductance control of the flash memory systematically. We adopt initiated chemical vapor deposition (iCVD) process, to fabricate vertically stacked 3-dimensional (3D) T-inverter. The vertical stacked structure allows increase the density per area. In the flash memory, ultrathin polymer dielectrics were utilized to obtain low-voltage operation. All process was done by in-situ patterning through shadow mask to achieve via-hole-less metal interconnection. Also, to electrically isolate the 1st layer flash memory and 2nd layer HTR, a 1 μ m-thick interlayer dielectric (ILD) was deposited between the unit devices. For the polymer dielectric layers, poly(2-cyanoethyl acrylate-co-diethylene glycol divinyl ether) [p(CEA-co-DEGDVE)] (named pC1D1) was used as blocking dielectric layer (BDL) in this study. The pC1D1 has high dielectric constant ($k > 6$) and superb insulating performance (breakdown field, $E_{break} > 3$ MV/cm). Poly(1,3,5-trivinyl-1,3,5-trimethyl cyclotrisiloxane) (pV3D3) was also employed as a tunneling dielectric layer (TDL) in the flash memory and also used as gate dielectric layer (GDL) in the HTR. The pV3D3 has low dielectric constant ($k < 2.3$) and provides a non-polar interface for the facilitated charge transport in the organic semiconductors. The programming/erasing voltage (V_{pre}/V_{ers}) was successfully reduced and the operating voltage was less than 5 V, which is low voltage compared to previous organic 3D logic circuits. Fabricated 3D T-inverter showed full-swing operation, ideal intermediate logic value ($\sim V_{DD}/2$), high DC gain exceeding 20 V/V as well as low-voltage operation (< 5 V). Moreover, 3D T-inverter

showed excellent long-term stability (change of output voltage less than 3% after 10⁴s). We believe the 3D T-inverter with flash memory developed in this study is expected to be one of the new platforms that can utilize in high-performance MVL circuits.

4:00 PM EQ09.13.02

Reduction of Operating Current by Device Size Miniaturization in Physical Reservoir Device Utilizing Electrochemical Reactions in Ionic liquid
Takuma Matsuo^{1,2}, Hisashi Shima², Masaharu Yonezawa^{1,2}, Yasuhisa Naitoh², Hiroyuki Akinaga², Toshiyuki Itoh³, Toshiaki Nokami⁴, Masakazu Kobayashi^{1,5} and Kentaro Kinoshita¹; ¹Tokyo University of Science, Japan; ²National Institute of Advanced Industrial Science and Technology (AIST), Japan; ³Toyota Physical and Chemical Research Institute, Japan; ⁴Tottori University, Japan; ⁵NAGASE & CO., LTD., Japan

Physical reservoir computing (PRC), which is a hardware implementation for a unique paradigm of recurrent neural network (RNN) called RC, attracts considerable attention because PRC is of great promise for advanced and low-power information processing (IP) [1]. PRC has a simple layer configuration: an input, reservoir, and output layers. Since the weight update in PRC is carried out only for the weights between the reservoir and output layers, the lower-power IP is strongly expected compared to the conventional RNN. Although various devices have previously been studied as a reservoir layer (i.e., physical reservoir device (PRD)), an appropriate choice of the physical dynamics in PRD is essential in view of the low-power device operation. Electrochemical reactions (ERs) at a liquid/electrode interface, which are known to exhibit the time-varying current response when voltage is applied, becomes a strong candidate because the electrochemical current reduction is expected by decreasing the electrode area [2]. Considering that liquid materials for PRD are required to withstand repeated voltage inputs, ionic liquids (ILs) are quite suitable because they are more resistant to the electrolysis than aqueous solutions. Besides, the ILs can dissolve various metal cations, which influence the electrochemical properties of PRD [3]. Herein, we report the device size dependence of operating current in IL-based PRD and demonstrate IP with the extremely small operating current of about 0.5 μ A. PRDs used in the present study had a square-shaped openings in the insulating SiO₂ layer on a pair of Pt input and output electrode patterns. The side length L of the square was 10, 100, and 300 μ m. By placing the IL droplet on those openings, the Pt/IL interfaces, which were the site of the ERs, were formed. As the IL material, a solvated IL, Cu(Tf₂N)₂:G3=1:1 (Cu-G3), was selected. The IP capability of the IL-based PRD was assessed based on the short-term memory (STM) task accuracy. In the present STM task evaluation, a binary data (0 and 1) stream $u(T)$ was input to the PRD as a triangular shaped voltage pulse (TVP) stream and $u(T-T_{\text{delay}})$, the input signal T_{delay} timestep before, was used as a training data at the timestep T . The sign of the TVP height for 1 and 0 was positive and negative, respectively. For updating the weights between the reservoir and output layers, the linear regression was used. The deposits on the Pt electrode formed during the device operation were investigated by X-ray photoelectron spectroscopy (XPS) after the washout of the IL droplet.

The output current from IL-based PRD showed L -dependent properties. Although the Faradaic current peak was observed in all the devices, the peak width became narrower for the smaller value of L . This result indicates that the ERs in IL-based PRD have a response time lag at the interface. Also, the output current decreased almost in proportional to the value of L^2 , achieving about 0.5 μ A for $L = 10$ μ m. The STM task accuracy slightly decreased with L probably due to the following two factors. One is the cycle-to-cycle variation in the net Pt/Cu-G3 interface area during the operation caused by the deposits on the Pt electrode, which causes the fluctuation in the electrochemical current values especially for smaller L . Another is presumably the cycle-to-cycle variation in the deposit compositional ratio. From the XPS results, it was found that Cu and some Cu compounds were formed on the Pt electrode depending on the applied voltage. The variation in compositional ratio for those materials reasonably causes the different output current even for the same input. Further operating power reduction by the device size miniaturization and IP performance boost in IL-based PRD are expected by realizing more repeatable and reliable ERs.

[1] G. Tanaka et al., *Neural Netw.* 115, 100 (2019).

[2] S. Trasatti et al., *Pure & Appl. Chem.* 63, 711 (1991).

[3] H. Sato et al., *Front. Nanotechnol.* 3, 660563 (2021).

4:15 PM EQ09.13.03

Operating Power Reduction and Information Processing Performance Improvement in Physical Reservoir Device Using Dehydrated Ionic Liquid
Masaharu Yonezawa^{1,2}, Hisashi Shima², Takuma Matsuo^{1,2}, Yasuhisa Naitoh², Hiroyuki Akinaga², Toshiyuki Itoh³, Toshiaki Nokami⁴, Masakazu Kobayashi^{1,5} and Kentaro Kinoshita¹; ¹Tokyo University of Science, Japan; ²National Institute of Advanced Industrial Science and Technology (AIST), Japan; ³Toyota Physical and Chemical Research Institute, Japan; ⁴Tottori University, Japan; ⁵NAGASE & CO., LTD, Japan

Edge computing is attracting considerable attention because the real-time secure and low-power information processing (IP) is expected. Especially for the IoT devices operated under the limited power-supply condition, the IP power reduction becomes crucial in addition to realizing higher performance. Therefore, a machine learning algorithm called reservoir computing (RC), which is a special type of the recurrent neural networks, is intensively investigated as a breakthrough to satisfy those requirements. The network structure of RC is quite simple, consisting of input, reservoir, and output layers. Because only the weights between the reservoir and output layers are updated in RC, the calculation cost reduction is expected. To implement RC by actual devices, physical reservoir devices (PRDs), in which actual physical phenomena plays a role of reservoir, are essential for edge computing and PRDs. We have developed PRD using Faradaic currents (FCs) generated by the electrochemical reactions (ERs) in metal ion-doped ionic liquids (IL), which possess advantages such as a high design flexibility of material properties and an immunity to the electrolysis [1]. Because the FCs generated by ERs are much smaller than the operating currents of solid-state devices, IL-based PRD is suitable for low-power IP [2]. In this study, we focused on the water contained in IL. According to the previous report, about 10 mol% of water can be dissolved even in hydrophobic ILs such as [Bmim][Tf₂N] [3]. Also, it has been reported that the FC observed during the cyclic voltammetry for the dehydrated, low water content IL decreased below one-fourth of that for the high water content IL [4]. Therefore, further lowering of the operating power in the IL-based PRD is reasonably expected by reducing water content in IL.

Herein, we evaluated the influence of water in IL on the operating power and IP performance of IL-based PRDs by comparing the electrical properties measured in the synthesized dry air (SDA) after vacuum dehydration and those measured in moisture-containing air (MCA).

The present PRD had a pair of input and output terminals made of a Pt thin film. To control the location of the ER, those terminals were covered by the insulating SiO₂ layer excepting the 100 μ m x 100 μ m sized square-shaped regions on each terminal. A droplet of 0.4 M Cu ion-doped [Bmim][Tf₂N] was placed between the terminals to form the Pt/IL interface inside the above-mentioned square-shaped regions. Time series data (TSD) consisting of "0" and "1" was input into the device as a triangular-shaped voltage pulse (TVP) stream, and the output current were measured. The signs of the TVP for "0" and "1" were defined to be negative and positive, respectively. TSDs consisting of alternately and randomly aligned "0" and "1" were used to investigate the basic electrical properties and the short-term memory (STM) characteristics of the PRD, respectively. In SDA, as expected, the peak current values during the device operation decreased below about one-fifth of those in MCA. Moreover, the memory capacity, which is a quantitative measure for the STM characteristics, increased by more than 40%. The input-signal-dependence of output current waveforms became more prominent in SDA thanks to decrease in cycle-to-cycle current dispersion due to dehydration and consequently the memory capacity increased.

We successfully demonstrated both the IP power reduction and IP performance improvement of IL-based PRD in SDA. In addition, the difference in the output current waveforms between SDA and MCA suggests that the different ERs occur in the device depending on the water amount in IL. The ERs optimized for the IP task to be executed are crucial for improving the physical RC accuracy.

[1] H. Sato, et al., *Front. Nanotechnol.* 3, 660563 (2021).

[2] Y. Zhong, et al., *Nat. Commun.* 12, 1 (2021).

[3] F. Di Francesco, et al., *Green Chem.* 13, 1712 (2011).

[4] S. Caporali, *et al.*, *Surf. Coat. Technol.* **264**, 23 (2015).

4:30 PM EQ09.13.04

Channelizing the Exemplary ‘Lane Discipline’ of Topological Insulators for Next-Generation Electronics Sagnik Banerjee¹, Koustav Jana², Anirban Basak² and Bhaskaran Muralidharan²; ¹Jadavpur University, India; ²Indian Institute of Technology Bombay, India

Two-dimensional topological insulators (TIs), like monolayer group-IV and V Xenes with large intrinsic spin-orbit coupling, offer electrically tunable phase transitions due to their buckled lattice structure and present exciting prospects for futuristic low-power electronics. These materials possess robust conducting modes with enforced ‘lane discipline’ at their edges, which provide dissipationless channels for carrier transport and are unaffected even in the presence of scattering centers—the primary source of energy dissipation in modern semiconductor devices. These salient features make 2D topological insulators an excellent material choice for several interesting applications in low-power electronics. We discuss a couple of avenues, namely valleytronics and steep-subthreshold transistors, where 2D TIs have an immense potential to make significant contributions.

Firstly, we demonstrate an all-electrical valley filtering device that exploits the topological robustness of 2D TIs. Our device design draws inspiration from the previous proposals based on bilayer graphene in using the valley-polarized interface states appearing at the domain wall between topologically distinct phases. Spatially separating these interface states by the introduction of a large gap quantum spin Hall region in between the states added to their topological robustness and significantly boosted the valley filtering performance of our device. By adopting the scattering matrix formalism on a suitably designed device structure, valley-resolved transport calculations in the presence of non-magnetic short-range disorder have been done to gauge the valley filter performance in practical scenarios. Based on our numerical simulations, we also outline the role of SO coupling strength, device geometry, and other factors while designing an optimized valleytronic filter device with superior efficiency.

Next, we explore the emerging realm of topological transistors where one can achieve a subthreshold slope steeper than the thermionic Boltzmann’s limit, which is indispensable for low-power device operation. Rashba spin-orbit interaction in 2D TIs enables a faster-than-linear response of the band movement to the applied field via the topological quantum field effect that can have encouraging implications in achieving sub-thermionic performance. Combining this with the prevailing advantage of dissipationless ON state conduction via robust, helical edge modes of the TI channel, makes topological quantum field-effect transistors an excellent device choice for ultra-low power electronics. However, realizing a working device design with the above merits requires a deep exploration of the topological quantum field-effect transition physics. Our numerical and analytical calculations highlighted the drawbacks in the subthreshold performance of a primitive design of the topological transistor. This led us to a partial solution to beat the thermionic limit by adopting a modified gating strategy. However, this strategy fails to preserve the dissipationless ON state performance due to bulk modes conduction. We then show that an out-of-plane antiferromagnetic exchange induced in the material via proximity coupling, effectuating transitions between the quantum spin-valley Hall and the spin quantum anomalous Hall phases, allows the ON state to remain topologically robust while surpassing the thermionic limit on the subthreshold performance. Further dephasing studies have been done on all the transistor designs mentioned above to gauge their performance in experimentally-relevant regimes. They reveal the robustness of the topological edge states under momentum relaxation scattering and the effect of varying degrees of momentum relaxation strengths on the subthreshold performances.

Our work thus provides a strong foundation for future investigations on harnessing topological phase transitions in two-dimensional topological insulators for next-generation low-power electronics.

SESSION EQ09.14: Piezoelectrics and Nanogenerators

Session Chairs: Ying-Hao Chu and Bhagwati Prasad

Friday Morning, December 2, 2022

Hynes, Level 3, Room 302

8:45 AM EQ09.14.01

A Novel PVDF-TrFE/KNN Composite Material for Low Power Flexible Electronics Devices Nitika Batra, Rajinder S. Deol, Henam S. Devi, Madhusudan Singh and Bhaskar Mitra; Indian Institute of Technology Delhi, India

Potassium sodium niobate (KNN) has emerged as a lead-free, environment friendly, and highly piezo-active substitute for lead-based piezoelectrics such as PZT [1]. However, it is difficult to deposit thick films of KNN (required for many IoT applications such as energy harvesting) with reasonable compositional control [2]. Additionally, thick piezoceramic films are brittle, and this is a major reliability concern in these devices. On the other hand, organic fluorinated polymer piezoelectric materials such as PVDF, PVDF-TrFE etc., are flexible and compliant but have poor piezoelectric coefficients. Therefore composite materials combining the properties of ceramics, such as a high piezoelectric constant, and polymers, such as flexibility, are attractive. In this work a novel lead-free piezoelectric composite material consisting of sodium potassium niobate (KNN) sol in an organic piezoelectric polymer (PVDF-TrFE) has been developed. We have used KNN sol specifically to reduce the maximum temperature of the process. We investigated KNN sol addition in PVDF-TrFE polymer with material characterization as a function of KNN loading ratio. Piezoresponse force microscopy (PFM) results found the best composition material to have an electromechanical coupling coefficient of $d_{33}=107$ pm/V (whereas PVDF-TrFE's $d_{33} = 19$ pm/V). The addition of KNN contributes toward higher film stiffness (Young’s mod composite = 165.68 MPa and PVDF-TrFE = 161.8 MPa) and also increases surface roughness (23.90 nm for composite and 22.72 nm for PVDF-TrFE) and adhesion force (0.23nN for composite and 0.15nN for PVDF-TrFE) as measured using contact AFM. The current study demonstrated the applicability of this composite by fabricating a flexible energy harvesting device comprising of 2 μ m film deposited by multiple spin coating at 2000 rpm on an Al-coated PET sheet, and a top metal film. After spin coating the layer was heated at 140° C in oven for 2 hours (which is the maximum tempertaure of whole process). The device generates an open circuit voltage of $V_{oc}=2.2V$ while an identical PVDF-TrFE-based device generates $V_{oc}=0.05V$ for the same loading. It is noteworthy that uniform, crack-free films were deposited using a low-temperature, low-thermal-budget method, which is typically a difficult task with piezoceramics, but it was accomplished easily the developed piezo composite.

References:

[1] R. S. Deol, N. Batra, P. Rai, H. S. Devi, B. Mitra, and M. Singh, “A lead-free flexible energy harvesting device,” *Microsystem Technologies*, Jul. 2022.

[2] R. S. Deol, S. Saha, N. Batra, B. Mitra, and M. Singh, “Study of low temperature solution-processed amorphous KNN thin films using PFM,” *MRS Communications*, vol. 11, no. 5, pp. 554–558, Oct. 2021.

9:00 AM EQ09.14.03

Hierarchical Micro-Nano Patterned Modified PDMS Triboelectric Nanogenerator Enhanced by Carbon-Based Nanofillers Mina Shanbedji and Alamgir Karim; University of Houston, United States

Triboelectric nanogenerators (TENGs) have received recent interest in converting unconventional mechanical energy to electricity, particularly as a

sustainable form of energy generation from sources such as wind and friction. Energy conversion in TENGs is based on the triboelectrification and electrostatic induction effects. In this regard, Polydimethylsiloxane (PDMS) elastomer has been widely used as an excellent triboelectric active layer in TENG owing to its high electronegativity as ranked in the triboelectric series of different materials. The TENGs based on PDMS exhibit a relatively high energy conversion efficiency. However, its output electrical characteristics still need more development. Increasing the triboelectric polymer dielectric constant enhances the current density significantly by facilitating the charge transfer from the contact surface toward electrodes. Nanoparticles' presence enhances charge transfer in TENGs due to increasing the polymer matrix's dielectric constant when their concentration meets the percolation threshold. However, the TENGs' performance has not been investigated from the window of dielectric properties of polymer triboelectric active materials. The shape and sometimes the angle of nanoparticles also play a role in the outcome of the polymer's dielectric constant. This research investigates the effect of carbon-based nanoparticles on PDMS nanocomposite/aluminum TENG output, considering the aforementioned factors. The particles are chosen from various molecular shapes and dielectric constants, including carbon black (CB), carbon nanotube (CNT), graphene oxide (GO), and reduced graphene oxide (r-GO). On the other hand, one of the most practical approaches to enhancing the output performance of TENG is modifying the contact area between triboelectric active material layers. Patterning the surface and changing the shape and density of patterns on the surface is assumed to be an effective strategy for this purpose. The uniform and periodic nanoscale morphology of optical discs (CD and DVD) were replicated onto PDMS films. By changing the ratio of carbon black, the resolution of the CB/PDMS composite layer increases at 4 wt% and then decreases, which was explained according to the percolation theory of the conductive particles in the polymer matrix. The voltage and current output follow the same trend as the dielectric constant. The GO nanoparticle also shows the same behavior at the 1.5 wt%, which is the percolation threshold of GO in PDMS. However, the reduced graphene oxide aggregates faster because of not having the oxygen-containing chemical group and earlier percolation threshold. The procedure is followed by a sequential development of hierarchical low amplitude patterns made by etching treatment leading to perpendicular wrinkling from the DVD wrinkle lines. This method creates a hierarchical pattern as a superposition on the optical disc pattern. Our hierarchical topographic designed TENG led to a considerably higher current and voltage output. Due to having an efficient shape with higher roughness compared to the original CD and DVD patterns base and the flat PDMS surface. Here is a mathematical correction offered in the dielectric constant equations based on the PDMS nanocomposite dielectric properties investigation. The PDMS nanocomposite/Al TENG corresponding output for each filler is studied and compared with the dielectric properties of the nanocomposite. The mathematical correction is also reflected in TENG voltage and current equations.

9:15 AM EQ09.14.06

Bulk Ferroelectric Metamaterial with Enhanced Piezoelectric and Biomimetic Mechanical Properties from Additive Manufacturing Jun Li; University of Wisconsin--Madison, United States

Three-dimensional (3D) ferroelectric materials are electromechanical building blocks for achieving human-machine interfacing, energy sustainability, and enhanced therapeutics. However, current natural or synthetic materials cannot offer both a high piezoelectric response and desired mechanical toughness at the same time to meet the practicality. Here, a lamellar ferroelectric metamaterial was created with a ceramic-like piezoelectric property and a bone-like fracture toughness through a low-voltage-assisted 3D printing technology. The one-step printed bulk structure, consisting of periodically intercalated soft ferroelectric and hard electrode layers, exhibited a significantly enhanced longitudinal piezoelectric charge coefficient (d_{33}) of over 150 pC N^{-1} , as well as a superior fracture resistance of $\sim 5.5 \text{ MPa m}^{1/2}$, more than three times higher than conventional piezo-ceramics. The excellent printability together with the combination of both high piezoelectric and mechanical behaviors allowed us to create a bone-like structure with tunable anisotropic piezoelectricity and bone-comparable mechanical properties, showing a potential of manufacturing practical, high-performance, and smart biological systems.

Reference:

[1] Li, Jun, et al. "Bulk ferroelectric metamaterial with enhanced piezoelectric and biomimetic mechanical properties from additive manufacturing." *ACS Nano* 15.9 (2021): 14903-14914.

9:30 AM EQ09.14.07

Modulus-Tunable Triboelectric Nanogenerator for Maximization of In Vivo Ultrasound Transmission with Biocompatible 2-Hydroxyethyl Methacrylate Bosung Kim and Sang-Woo Kim; Sungkyunkwan University, Korea (the Republic of)

Ultrasound-driven triboelectric nanogenerator (TENG) is recently proposed as an energy solution technology for sustainable lifespan of the implantable medical devices (IMDs). While improving the ultrasound transmission to the TENG is urgent to achieve high energy generation, research on materials is hardly being conducted as an initial stage of current research. Here, a biocompatible 2-hydroxyethyl methacrylate (HEMA) is proposed as a both encapsulation and triboelectric layer for a modulus-tunable ultrasound-driven triboelectric nanogenerator (MU-TENG). As an acoustic impedance of HEMA can be modulated to be optimized for the surrounding environment with different contents of crosslinking concentrations, the ultrasound transmission to the MU-TENG can be increased 3.2 times compared to the case of titanium (Ti) packaging. Furthermore, the surface potential of HEMA can be highly increased by adding an ionic monomer, significantly enhancing the triboelectric output performance of the device. Consequently, we verified that the MU-TENG can generate sufficient energy to charge a $100 \text{ }\mu\text{F}$ capacitor under in vivo condition at a rate of $23.9 \text{ }\mu\text{C/s}$, which is 3.7 times faster than the case with a Ti packaging. This strategy of using multi-functional HEMA for high-performance ultrasound-driven TENG could be promising energy solution technology for low-powered IMDs.

SESSION EQ09.15 Virtual Session
Session Chairs: Ying-Hao Chu and Chih-huang Lai
Wednesday Morning, December 7, 2022
EQ09-virtual

8:00 AM EQ09.15.01

Demonstration of Ferroelectric Properties in GaN Alloyed with Sc Masato Uehara¹, Ryoichi Mizutani², Shinnosuke Yasuoka², Takao Shimizu³, Hiroshi Yamada¹, Morito Akiyama¹ and Hiroshi Funakubo²; ¹National Institute of Advanced Industrial Science and Technology, Japan; ²Tokyo Institute of Technology, Japan; ³National Institute for Materials Science, Japan

Traditionally, AlN does not exhibit ferroelectricity owing to its high barrier to polarization inversion. Recently, its ferroelectricity was demonstrated through an alloying with Sc [1, 2]. Its ferroelectricity in wurtzite nitride is a hot topic. The high remanent polarization (P_r) beyond $120 \text{ }\mu\text{C/cm}^2$ of $\text{Sc}_x\text{Al}_{1-x}\text{N}$ is attractive, but the high coercive field (E_c) value is a drawback. We experimentally succeeded in demonstrating the ferroelectricity in GaN by alloying with Sc. Considering that GaN is a mainstream semiconductor used in applications, such as power electronics and high-frequency devices, its ferroelectricity in $\text{Sc}_x\text{Ga}_{1-x}\text{N}$ has received considerable attention.

The ferroelectricity of $\text{Sc}_x\text{Ga}_{1-x}\text{N}$ ($x = 0.35\text{--}0.44$), was demonstrated in metal–ferroelectric–metal stack devices prepared by sputtering. The P_r value obtained from positive-up negative-down measurements was high, exceeding $120 \mu\text{C}/\text{cm}^2$. The E_c of $\text{Sc}_{0.44}\text{Ga}_{0.56}\text{N}$ was approximately $3.6 \text{ MV}/\text{cm}$ at 300 K , which reduced to $3 \text{ MV}/\text{cm}$ at 473 K . Comparison with $\text{Sc}_x\text{Al}_{1-x}\text{N}$ revealed some important things. The P_r value was governed by the wurtzite u -parameter. On the other hand, the E_c values were governed by the Sc concentration rather than the u -parameter, regardless of the host material in $\text{Sc}_x\text{Ga}_{1-x}\text{N}$ and $\text{Sc}_x\text{Al}_{1-x}\text{N}$. This indicates that the origin of the polarization inversion would be around Sc atoms. Moreover, the $P_r - E_c$ diagram shows that the E_c of $\text{Sc}_x\text{Ga}_{1-x}\text{N}$ is lower with an equivalent P_r , compared with that of $\text{Sc}_x\text{Al}_{1-x}\text{N}$. The lower E_c of $\text{Sc}_x\text{Ga}_{1-x}\text{N}$, which had an equivalent P_r value of $\sim 120 \mu\text{C}/\text{cm}^2$, was attractive. This was caused by the dependence of P_r on the u -parameter, dependence of E_c on the Sc concentration, and different u -parameters between $\text{Sc}_x\text{Ga}_{1-x}\text{N}$ and $\text{Sc}_x\text{Al}_{1-x}\text{N}$.

8:05 AM EQ09.15.02

Controlling the Polarity of Scandium Aluminum Nitride (ScAlN) Piezoelectric Thin Films by Using Ge Addition Sri Ayu Anggraini, Masato Uehara, Kenji Hirata, Hiroshi Yamada and Morito Akiyama; National Institute of Advanced Industrial Science and Technology, Japan

A highly c -oriented wurtzite phased scandium aluminum nitride (ScAlN) piezoelectric thin film could exist in nature as aluminum/scandium (Al/Sc) or nitrogen (N) polar thin films. The utilization of multilayers piezoelectric thin films with different polarity can be advantageous for the performance of the device. For example, the performance of a solidly mounted resonator type bulk acoustic wave (SMR-BAW) can be enhanced by using a stack of N-polar and Al-polar piezoelectric thin films [1]. Since ScAlN-based resonators feature a significant improvement from aluminum nitride (AlN)-based resonators, wurtzite phased ScAlN has been extensively studied and has arose as the future material for many promising electronic applications including radio frequency (RF) filters [2-3]. Polarity control of ScAlN-based thin films is expected to bring further improvement in the performance of the current RF filter by enabling it to function at higher frequency range in 5G communication technology. In terms of polarity control, the addition of germanium (Ge) into AlN have been reported to capable of inverting the polarization direction of non-doped AlN from Al-polar to N-polar [1]. However, there are no report on addition of Ge to inverse the polarity of ScAlN. Therefore, in this study, we investigated of the effect of Ge addition on the polarization direction of ScAlN piezoelectric thin films.

The fabrication of the thin films were conducted by using radio frequency (RF) magnetron sputtering system. The concentration of Sc, Ge and Al was controlled by adjusting the power of cathodes during deposition process. In this study, we examine how co-addition of Sc and Ge into AlN on affect the polarity, the crystal structure, lattice parameters and surface state of each element in the thin films. Positive d_{33} value indicates that the thin film has Al/Sc-polarity while negative d_{33} value indicates that the thin film has N-polarity. All $\text{Sc}_x\text{Al}_{1-x}\text{N}$ thin films exhibited positive d_{33} values which indicate that the thin films have Al/Sc-polarity. Depending on the concentration and the ratio of Sc and Ge, co-addition of Sc and Ge into AlN resulted in thin films with negative d_{33} which suggested that the thin films have N-polarity. For example, $\text{Sc}_x\text{Ge}_y\text{Al}_{1-x-y}\text{N}$ thin films with $x = 0.3$ and $y = 0.05\text{--}0.14$ exhibited N-polarity suggesting that co-addition of Sc and Ge into AlN yielded in thin films with inversed polarity. However, addition of Ge was found to unable to inverse the polarity of $\text{Sc}_{0.4}\text{Al}_{0.6}\text{N}$, since the resulting thin films exhibited Al-polarity. Based on these results, it can be inferred that Ge addition can be used not only to control the polarity of AlN but also the polarity of ScAlN, as long as the concentration of Sc is maintained to be less than 40 at.% and Ge concentration is also kept in a certain concentration range. Thus, both concentration and ratio of Sc and Ge are considered to be among the important parameters that control the polarization direction of the resulting thin films.

Acknowledgement

This work was supported by JSPS KAKENHI grant number JP21K04168.

References:

- [1] Mizuno, T. *et al.* In *2017 19th International Conference on Solid-State Sensors, Actuators and Microsystems (TRANSDUCERS)*. 1891.
- [2] M. Akiyama, T. Kamohara, K. Kano, A. Teshigashara, Y. Takeuchi, N. Kawahara. *Adv. Mater.* (2009) 21, 593.
- [3] M. Moreira, T. Torndahl, I. Katardjiev, T. Kubart, J. *Vac. Sci. Technol. A* 33 (2015) 021518.

8:10 AM EQ09.15.03

Study of Tunneling Switching Operation in Various Tunneling Barrier Materials Jeong Hee Shin; Korea Institute of Ceramic Engineering and Technology, Korea (the Republic of)

There has been increasing demand for electronic devices with ultra-high working frequency or speed to process big data quickly, especially in the fields of communications, the military, and aerospace as well as a high performance control process unit (CPU). However, traditional semiconductor switching devices cannot keep up with the demands of increased speed. Typical semiconductor switching devices are generally used a p-n junction and a Schottky barrier which perform a switching operation by combining electron and holes. A short channel length between source and drain is only solution to achieve high speed. It faces limit due to the resolution limit of the fabrication process and the short channel effect. Electron mobility was considered instead of physical dimension. Although high electron mobility transistor (HEMT), based on III-V group materials, is expected to increase the speed, its theoretical frequency limit is less than 1THz, even with several nanometer channel lengths. Thus, we have to solve the problem of switching speed through a new method.

Tunneling phenomenon is key mechanism as fast switching devices due to direct movement of electrons without hole-electron combination. Although tunneling mechanism can provide ultra-high working speeds ($> \text{THz}$), the very low switching ratio results in poor switching efficiency. Improving switching efficiency is highly motivated for high-speed efficient switching elements.

Our strategy is geometric electrode design to increase switching efficiency (On-off ratio). We have already demonstrated the effectiveness of geometric design. We also study various tunneling barriers to maximize it and the phenomenon (Tunneling transition between direct and Fowler-Nordhiem tunneling).

8:15 AM EQ09.15.04

High Performance Metal-Insulator-Metal SrTiO₃ Thin Film Capacitors Integrated on 300 mm Si Wafers for Advanced Technology Nodes Arbab Sen Gupta, Kaan Oguz, I-cheng Tung, Chia-ching Lin, Sou-chi Chang, Anandi Roy, Jason Peck, Brandon Holybee, Rob Jordan, Thomas Hoff, Sudarat Lee, Scott B. Clendenning, Ian A. Young, Uygur E. Avci and Matthew V. Metz; Intel Corporation, United States

Paraelectric Strontium titanate (SrTiO₃) perovskite thin films have recently gained attention in the semiconductor industry. This is due to their high dielectric constant of > 100 at room temperature, low dielectric loss and non-toxicity due to the absence of Lead^{1,2}. Thin films of SrTiO₃ on various electrodes are being studied world-wide to demonstrate practical usage in the domain of Metal-insulator-metal (MIM) capacitors^{3,4}. In this work we demonstrate a high performing two plate MIM capacitor utilizing the SrTiO₃ film integrated on a 300 mm Silicon (Si) wafer. Highly crystalline SrTiO₃ film was grown on crystalline Ruthenium (Ru) electrode using an advanced sputter technique. The complete stack is made of Ru/ SrTiO₃ / Ru thin films, where both the top and bottom Ru electrodes and a (200) oriented SrTiO₃ dielectric film were deposited utilizing back-end of line (BEOL) compatible conditions. Following the completion of the deposition step on the 300 mm Si wafer, the MIM capacitor was integrated in the fabrication facility using a state-of-the-

art integration flow. The resulting devices demonstrated a capacitance density of about 95 fF/um² with an average leakage of 2e⁻⁵ A/cm². This is a capacitance density boost of about 2.5 times compared to our previously reported MIM capacitor⁵. Furthermore, a record low equivalent oxide thickness (EOT) of about 0.4 nm has also been achieved with this MIM capacitor. The development of such a high performing capacitor together with the BEOL compatibility provides a significant advantage in lowering the voltage droop in a power delivery network without any significant area penalty in future technology nodes.

References:

- D. Fuchs *et al.*, *J. Appl. Phys.* 1999, 85, 7362–7369
C. S. Kang *et al.*, *Jpn. J. Appl. Phys.* 1996, 35, 4890
C. B. Kaynak *et al.*, *Microelectronic Engg.* 2011, 88, 1521-1524
M. A. Pawlak *et al.*, *Appl. Phys. Lett.* 2020, 97, 162906
C-Y. Lin *et al.*, *IEEE Intl. Rel. Phys. Symposium*, 2020, pp.1-4

8:30 AM *EQ09.15.05

A Quantum Materials Path to Next-Generation Computing Sasikanth Manipatruni; Kepler, United States

Computing technology is at the core of the information age forming the basis of all of millennium goals of United Nations. However, Computing is at a momentous point today as AI and big data drive massive demand for computational hardware, while historic Moore's law performance scaling is slowing down.

In this talk, I will outline a framework that combines the energy/dimension scaling (Moore's law), computer error rates (Shannon computing) and modern AI architectures (drawing mainly from *Nature Physics* 14, no. 4 (2018): 338), <https://www.nature.com/articles/s41567-018-0101-4>.

A room-temperature quantum materials path to next-generation computing: Next, I describe a quantum and memory materials-centric approach to enable the computing for beyond the CMOS era. I will outline a number of pathways for computing devices that utilize quantum materials. I will generalize the search for the next computing device with a comprehensive list of quantum materials classes.

We will connect various required components of a computing system to the next generation materials. The materials and transductions are classified under switching, interconnects and detection and are tied to the required targets for materials performance. We also identify activity factor (i.e. utilization of logic), memory BW wall (Turing wall) and thermal extraction as the near term limiting factors for computing. Finally, I describe potential ways to build generalized intelligence hardware overcoming interconnect, memory and compute bottlenecks.

9:00 AM DISCUSSION TIME

SESSION EQ09.16: Virtual Session: Magnetism and Spintronics
Session Chairs: Ying-Hao Chu and Chih-huang Lai
Wednesday Afternoon, December 7, 2022
EQ09-virtual

9:00 PM *EQ09.16.01

A Spin-Orbit Torque Device Toward Energy-Efficient Neuronal Population Performance Chih-huang Lai¹, Po-Chuan Chen¹, Rudis Ismael Salinas¹, Chao-Yao Yang² and Sheng-Huai Chen¹; ¹National Tsing Hua University, Taiwan; ²National Yang Ming Chiao Tung University, Taiwan

Precise control over the intermediate states in a spin-orbit torque (SOT) device with multi-levels has been demonstrated a unique strategy toward high dense storage for an analog memory, which bridges the solid-state device and the neuromorphic computing into a newly developed research field in recent years. In this study, we demonstrate a SOT switching mechanism in the devices composed of Pd/Co/Ta trilayer featuring robust stabilization of intermediate magnetic states, which leads to precise controllability and superior stability of multi-levels. Magnetization reversal of Pd/Co/Ta devices by SOT takes place through the gradual nucleation of reversed domains with restricted domain wall (DW) motion due to DW precession over Walker breakdown, which guarantees stable magnetic multi-levels. Furthermore, we demonstrate that individual reversed magnetic domain can be regarded as a single neuron, and the whole device becomes an artificial neuron population (NP). Therefore, the period required for the magnetization reversal can represent the response time of NP. The DW velocity or nucleation rate in SOT devices thus can be corresponding to the interaction between neurons; accelerated DW motion (or nucleation), leading to faster reversal, can mimic the case that excited neurons would influence neighboring ones to quickly respond to stimulus together. We demonstrate that the relationship between stimulus strength and duration, commonly observed in biological NPs, can be achieved in the artificial NP, composed of a Pd/Co/Ta SOT device. Furthermore, we reveal the modification of the response time of artificial NP under the lowest energy consumption by tuning the DW velocity. Our work not only explores the fundamental physics of the SOT dynamics via both experimental imaging and theoretical micromagnetic simulation, but also demonstrates the potential neuromorphic application as a new branch of neuronal population. Our findings will open a revolutionary avenue for establishing biomimetic neurons toward the energy and time efficient neuromorphic technology.

9:30 PM *EQ09.16.02

A Correlated Polar Ferromagnetic Metal by Design Pu Yu; Tsinghua University, China

Polar metals with a combination of conflicting polarization and metallicity have garnered increased interests recently because of their promising functionalities. Adding ferromagnetism into this unique state would offer exciting opportunities to obtain exotic quantum states, analogous to magnetoelectric multiferroites with coupled polarization and magnetization. However, such an intrinsic ferromagnetic polar metal remains elusive, especially in strongly correlated electron systems. Here, we report the experimental realization of coexisting ferromagnetism, polarity, and metallicity in a new 3d transition metal oxide Ca₃Co₃O₈. Here, structural oxygen vacancies order to form a periodic stacking of oxygen tetrahedral monolayers alternating with octahedral bilayers. The magnetic metallic state is confined within the quasi-two-dimensional CoO₆ octahedra layers, while the broken inversion symmetry arises simultaneously from Co displacements, which is further enhanced by the onset of magnetism, indicating an intrinsic strong magnetoelectric coupling. This coupled response and dual absence of spatial-inversion and time-reversal symmetries produce an intrinsic magnetochiral anisotropy with exotic magnetic field-free nonreciprocal electrical resistivity. We also observe an extraordinarily robust topological Hall effect that persists over a broad temperature-field phase space arising from a Rashba-type spin-orbit coupling. Our work not only provides a rich platform to harvest the

fascinating coupling between polar and magnetic states, but also defines a novel design strategy to access a new class of oxide materials with rich properties through ordered oxygen vacancies.

10:00 PM EQ09.16.03

Emergent Magnetodielectric Materials for 5G Antenna Miniaturization—18H Hexaferrites Qifan Li¹, Yajie Chen² and Vincent Harris³; ¹University of Electronic Science and Technology of China, China; ²Rogers Corporation, United States; ³Northeastern University, United States

Antenna miniaturization technology based on traditional materials with high dielectric constant has the disadvantages of low efficiency, narrow bandwidth, and difficulty in impedance matching. Compared to high-permittivity dielectrics, magnetodielectric materials, which exhibit both relative permeability and permittivity greater than unity, can achieve competitive miniaturization performance and bandwidth enhancement due to their less capacitive nature and low electromagnetic energy concentration. The fifth generation (5G) communications call for high-performance magnetodielectric materials with high values of permeability and permittivity, low magnetic and dielectric losses, and high cutoff frequency over the sub-6 GHz frequency bands. Due to limited resonant frequencies and large natural resonance linewidth, conventional microwave ferrites and their composites, which are usually used over the frequency range from several hundred MHz to several GHz, do not meet these requirements.

Here, a unique type of hexagonal ferrites—Mg-Zn 18H hexaferrite ($\text{Ba}_5\text{Mg}_{2-x}\text{Zn}_x\text{Ti}_3\text{Fe}_{12}\text{O}_{31}$), whose crystal structure can be interpreted as the structure of Y-type hexaferrites with intercalation of a three-layered hexagonal barium titanate block into the middle of the T-block, has been synthesized by a solid-state reaction route, and its microwave properties have been comprehensively investigated for the first time. Depending on the Zn content, the polycrystalline Mg-Zn 18H hexaferrite exhibits a saturation magnetization of 1–1.23 kG and a coercivity of 15–68 Oe. The small coercivity indicates the ease of domain wall motion through the lattice upon demagnetization and the great potential for low-loss applications. The permeability and permittivity spectra of the Mg-Zn 18H hexaferrite are extracted from the S-parameters measured with a vector network analyzer over 0.1–10 GHz. Narrow and strong magnetic resonant peaks up to 5 GHz are observed. The magnetic resonance shifts to lower frequencies and slightly broadens with increasing the Zn content. Fitted with the superposition of the domain wall resonance and gyromagnetic spin resonance, the Mg-Zn 18H hexaferrite shows an extremely low damping coefficient of 0.1–0.2, indicating concentrated magnetic loss within the narrow frequency range and implying a narrow ferrimagnetic resonance (FMR) linewidth. The FMR linewidth is confirmed to be 486–660 Oe by a resonant perturbation technique using a TE₁₀ rectangular waveguide resonator at X band. Owing to this remarkably low damping coefficient compared to that of other microwave ferrites, which typically varies from 0.2 to 0.9, Mg-Zn 18H hexaferrite exhibits an excellent magnetic loss tangent as low as 0.06, as well as a small dielectric loss tangent less than 0.006. By modifying the atomic ratio of Zn:Mg in the formula, this low-loss property covers the entire S band from 2 to 4 GHz, representing the best magnetodielectric performance among the reported microwave ferrites for the S band applications. Moreover, the temperature dependence of the damping coefficient is 0.0004 K⁻¹ over the range of 300–410 K, indicating an excellent thermal stability for the temperature variation of most communication applications.

For antenna miniaturization, depending on the Zn content, the miniaturization factor of the Mg-Zn 18H hexaferrite varies from 5.3 to 7.6. As an example, we demonstrate this capability for antenna size reduction by applying the Mg 18H hexaferrite to the substrate material of a 3.6-GHz patch antenna, which shows a miniaturization factor of ~5 and significant bandwidth improvement of ~50–110% over conventional dielectric substrates. These results imply the great potential of the 18H hexaferrites to be Co-free and low-cost alternatives to most microwave hexaferrites and reveal their great technological and commercial value for 5G communications.

10:15 PM EQ09.16.04

Operando XMCD and EXAFS Spectroscopies for Orbital Control by Reversible Strain at Co₂FeSi/PMN-PT Interface Jun Okabayashi¹, Takamasa Usami², Yu Shiratsuchi², Ryoichi Nakatani² and Kohei Hamaya²; ¹The University of Tokyo, Japan; ²Osaka University, Japan

Artificial ferromagnetic/ferroelectric multiferroic heterostructures have been widely investigated from both fundamental and technological aspects. The electric field (*E*) control of magnetism through the interfacial strain modulates the magnetic anisotropy in the magnetic layer. Controlling the magnetic anisotropy by the interfacial strain related to the orbital magnetic moments has a potential for future devices using both spins and orbitals. The relationship between strain and orbital magnetic moments has not been clarified because there were few tools to probe the changes of orbital magnetic moments. We have developed the *E*-induced x-ray magnetic circular dichroism (EXMCD) technique in order to apply *E* to ferroelectric substrate Pb(Mg_{1/3}Nb_{2/3})O₃-PbTiO₃ (PMN-PT), which tunes the interfacial lattice constants of the Heusler alloy Co₂FeSi magnetic layer [1,2]. In this study, we discuss the microscopic origin of inverse magnetostriction effects or orbital-elastic effects concerning the orbital magnetic moments by using the EXMCD with the detection of element-specific local structural changes by extended x-ray absorption fine structure (EXAFS) analysis.

We prepared the samples of 10-nm-thick Co₂FeSi layer grown on single-crystal PMN-PT(011) substrates with thin Fe buffer layer insertion by molecular beam epitaxy at 300 °C. The *E*-induced modulation of the in-plane magnetic properties was characterized by magneto-optical Kerr effect (MOKE) and XMCD, where the XMCD measurement was performed at BL-7A in the Photon Factory (KEK). The partial fluorescence yield mode was adopted to probe the signals more than 10 nm below the sample surfaces. To apply an *E* to the PMN-PT substrate along the [011] direction, a Au(100 nm)/Ti(3 nm) electrode was deposited on the backside of the PMN-PT substrate, where the Co₂FeSi film was utilized as a top electrode [3]. EXAFS during applying *E* for Fe and Co K-edges were also performed at BL-12C in KEK for the same samples.

The MOKE measurements revealed that the magnetic easy axis is along the PMN-PT [100] in-plane direction at *E* = 0 when *E* is changed from +8 kV/cm to 0. By applying *E* of -8 kV/cm, the easy axis changes 90 deg. within the in-plane through the changes of lattice strain of 0.1 % order. The Fe and Co L₂-edge XMCD hysteresis curves also trace the same changes of magnetic anisotropy of 2.5×10⁴ J/m³, which corresponds to the changes of orbital magnetic moments (*m*_{orb}) of the order of 0.01 μ_B. The EXMCD spectra can detect the changes of *m*_{orb} by *E* for both Fe and Co L-edge XMCD, which suggests the relationship between the strain and the orbital moments. Operando EXAFS measurements also detect the change of nearest neighbor distance at Co site. These phenomena can be understood within the orbital moment anisotropy through the spin-orbit interaction which is controlled by applying *E*. We found that EXMCD clarifies the origin of the reversible changes of magnetic anisotropy and links the relationship between macroscopic inverse magnetostriction effects and microscopic orbital moment anisotropy.

This work was partly supported by JST CREST (JPMJCR18J) and JSPS KAKENHI (JP21K14196, JP19H05616).

10:30 PM EQ09.16.05

Thickness Scaling and Low Voltage Operation of Ferroelectric (Al_{1-x}Sc_x)N Films Prepared by Sputtering Method Hiroshi Funakubo¹, Shinnosuke Yasuoka¹, Ryoichi Mizutani¹, Takahisa Shiraishi^{2,1}, Akinori Tateyama¹, Reika Ota¹, Kazuki Okamoto¹, Takao Shimizu^{3,1}, Masato Uehara⁴, Hiroshi Yamada⁴ and Morito Akiyama⁴; ¹Tokyo Institute of Technology, Japan; ²Kumamoto University, Japan; ³NIMS, Japan; ⁴National Institute of Advanced Industrial Science and Technology (AIST), Japan

Observation of ferroelectricity in (Al_{1-x}Sc_x)N films by Fichtner *et al* in 2019 open the nonvolatile ferroelectric memory (FeRAMs) applications with low

power consumption [1]. Large remanent polarization (P_r) beyond $100 \mu\text{C}/\text{cm}^2$ and easy orientation control toward the polar axis of these films enable us to apply not only conventional capacitor type memories, but also resistance-type memories using ferroelectric tunnel junction (FTJ). However, large coercive field (E_c), electric field for polarization switching, must be overcome for low power operation. We ascertained the ferroelectricity for the films down to 9 nm in thickness [2] and for the films deposited without heating [3]. In addition, we get the ferroelectricity for Sc-doped GaN films with lower E_c value than that of $(\text{Al}_{1-x}\text{Sc}_x)\text{N}$ films [4]. In this presentation, we tried to get the large P_r value even for thin films. In addition, we tried to analyze the determination factor of E_c by the analysis of the switching kinetics of $(\text{Al}_{1-x}\text{Sc}_x)\text{N}$ films.

Large P_r beyond $100 \mu\text{C}/\text{cm}^2$ was obtained even for the 12 nm-thick $(\text{Al}_{0.78}\text{Sc}_{0.22})\text{N}$ films prepared under pure N_2 atmosphere [5, 6]. Leakage current density decreased comparing with the films prepared under $\text{Ar}+\text{N}_2$.

E_c value was found to be mainly determined by the crystal anisotropy of the deposited films as well as operation temperature and the frequency.

Temperature dependency of E_c value was almost the same with those of conventional ferroelectric films including $\text{Pb}(\text{Zr}, \text{Ti})\text{O}_3$ and HfO_2 -based ferroelectrics, but its frequency dependency was relatively small. Polarization switching of $(\text{Al}_{1-x}\text{Sc}_x)\text{N}$ films followed Kolmogorov-Avrami-Ishibashi (KAI) model and its switching speed is faster than those of conventional ferroelectric films.

These results show that ferroelectric $(\text{Al}_{1-x}\text{Sc}_x)\text{N}$ nitrides is a promising candidate for memory applications.

[1] Fichtner, *et al.*, J. Appl. Phys., **125**, 114103 (2019).

[2] Yasuoka *et al.*, J. Appl. Phys., **128**, 114103 (2020).

[3] Yasuoka *et al.*, Phys. Status Solidi A, 2170049 (2021).

[4] Uehara *et al.*, Appl. Phys. Lett. **119**, 172901-1-5 (2021).

[5] Mizutani. *et al.*, Appl. Phys. Exp., **14**, 105501 (2021)

[6] Yasuoka *et al.*, J Ceram Soc. Jpn., *accepted*.

10:45 PM DISCUSSION TIME

SESSION EQ09.17: On-Demand Presentation

Thursday Morning, December 8, 2022

EQ09-virtual

7:00 AM EQ09.17.01

Fabrication of Thin-Film Transistor from Amorphous Oxide Semiconductors [Kelsea Yarbrough](#), Makhes Behera, Sangram K. Pradhan and Messaoud Bahoura; Norfolk State University, United States

Thin-film transistors (TFTs) based on amorphous oxide semiconductor (AOS) are moving towards commercial world as a replacement for hydrogenated amorphous silicon (a:Si:H) TFTs in multiple flat-panel applications. AOS TFTs differ from the conventional complementary metal-oxide semiconductor (CMOS) electronic devices. Instead of using a bulk, crystalline semiconductor, AOS TFTs employ thin amorphous materials in which the channel layer is approximately few tens of nanometers. We have fabricated thin film transistor using a shadow mask technology. Shadow mask technology is a technique that allows a desired pattern to be transferrable onto a substrate. Shadow mask technology is similar to photolithography in patterning; however, it is more environmentally friendly, reusable, and cost effective. Shadow mask technology was used to deposit the active layer and the dielectric layer of our devices. The indium-free oxide-based channel material such as aluminum-doped zinc oxide (AZO) is the active material and can be deposited on glass substrate or silicon for TFT applications. High quality AZO thin films are grown using electron beam evaporation on p-type silicon and on glass for characterization purposes. The effect of Al content on zinc oxide crystal lattice are investigated using various characterization techniques. Atomic force microscopy provided thin film roughness, grain size, and surface morphology. X-ray diffraction provided crystal orientation for both dielectric and active layer deposition. Ultra-violet visible spectroscopy is used for transmission percentage and Keithley 4200 semiconductor characterization system provided dielectric performance and transistor characteristics including on/off ratio, mobility, and threshold voltage. We observed a dielectric capacitance as high as 698 pF and a minimum surface roughness of 0.176 nm. The lowest current density observed for dielectric performance is found to be in the magnitude of $10^{-8} \text{ A}/\text{cm}^2$ and transistor saturation current exceeding 1.5 μA . This present work will provide valuable scientific input of AZO TFTs for the improvement of TFT devices.

This work is supported by the NSF-CREST Grant number HRD 1547771 and NSF-CREST Grant number HRD 1036494.

SYMPOSIUM EQ10

Phase-Change Materials for Brain-Like Computing and Memory Applications

November 28 - December 6, 2022

Symposium Organizers

Valeria Bragaglia, IBM Research Europe - Zurich

Juejun Hu, Massachusetts Institute of Technology

Andriy Lotnyk, Leibniz Institute of Surface Engineering

Wei Zhang, Xi'an Jiaotong University

* Invited Paper
+ Distinguished Invited

SESSION EQ10.01: Brain Inspired Computing I
Session Chairs: Hongsik Jeong and Andriy Lotnyk
Monday Morning, November 28, 2022
Sheraton, 2nd Floor, Independence West

10:30 AM INTRODUCTORY REMARKS

11:00 AM *EQ10.01.02

Phase-Change Memory-Based Analog In-Memory Computing for AI Irem Boybat; IBM Research - Zurich, Switzerland

AI systems managed to reach and even exceed human performance in various cognitive tasks, ranging from image recognition to strategic games and to reasoning. AI models continue to grow in size, requiring us to re-think about how to architect computing systems. Analog in-memory computing is one non-Von Neumann approach, where computational tasks are performed in memory by exploiting the physical attributes of memory devices. This talk will focus on phase-change memory-based analog in-memory computing for accelerating deep learning inference and training. The limited analog computational precision will be discussed with particular attention to device non-idealities. Strategies to overcome these at device, circuit, architecture, and algorithmic levels will be reviewed. Analog in-memory computing-based system architectures tailored for various AI application domains, including low-power solutions, will be presented.

11:30 AM EQ10.01.03

Optimization of Interfacial PCM Layers to Enable High Resistance Doped PCM in Mushroom Cell Devices for Analog Computing Kevin W. Brew¹, Injo Ok¹, Ning Li², Timothy Philip³, Benedikt Kersting³, Shun Manita⁴, William Lee⁴, Iqbal Saraf¹, Juntao Li¹, James Demarest¹, Robert Bruce², Cheng-wei Cheng², Christian Lavoie², Takeshi Masuda⁴, Takehito Jimbo⁴, Nicole Saulnier¹, Matthew BrightSky² and Vijay Narayanan²; ¹IBM AI Hardware Center, United States; ²IBM T.J. Watson Research Center, United States; ³IBM Research Europe, Switzerland; ⁴ULVAC, Inc., Japan

The use of mushroom cell PCM as an NVM memristive weight element for analog computing has been a focus of recent progress towards hardware designed for artificial intelligence. A major detriment of standard Ge-Sb-Te based materials (e.g. GST225) typically used in binary memories, is its relatively low resistance and a low crystallization temperature that leads to high power consumption when implemented in an array such as a neural network, and poor resistance-state retention, respectively. By doping PCM with insoluble non-conducting material to form a homogenous mixture (dPCM), the PCM grain sizes are confined, increasing the crystallization temperature, improving retention through increased crystallization temperature. The resistance of the dPCM is also significantly increased, decreasing programming current requirements. There is, however, a limit to the level of doping that can be used for dPCM as high amounts of dopant can create an inability for the device to SET to its crystalline state. In this work, we show how insertion of a thin, undoped or low-doped interfacial PCM layer between the confined bottom electrode heater (BEH) and the bulk dPCM allows for the use of higher doping and more resistive dPCMs to further reduce programming current requirements.

11:45 AM EQ10.01.04

Impact of PCM Noise on the Spiking Restricted Boltzmann Machine via On-Chip Trainable PCM Synapses Uicheol Shin¹, Masatoshi Ishii², Atsuya Okazaki², Megumi Ito², Rasch Malte³, Wanki Kim³, Akiyo Nomura², Suyeon Jang¹, Sung Min Lee¹, Wonseok Choi¹, Kohji Hosokawa², Matthew BrightSky³, Seiji Munetoh² and SangBum Kim¹; ¹Seoul National University, Korea (the Republic of); ²IBM Research-Tokyo, Japan; ³IBM T.J. Watson Research Center, United States

The spiking neural network (SNN) has been highlighted by its brain-like computing based on spike activities which could bring power-efficient performance, further suggested as the next generation of neural networks [1]. However, hardware implementation of SNN is still challenging as to be designed friendly for both hardware and algorithm, to process large amounts of spatiotemporal spike trains efficiently. In this work, we introduce our recent results [2] based on a fully functional chip with a sizable number of 1.4M synaptic phase-change memory (PCM) cells and all the Si CMOS circuits needed for the targeting algorithm, spiking restricted Boltzmann machine (RBM).

To implement the spiking RBM and its training algorithm, event-driven contrastive divergence (eCD) [3], synaptic crossbar unit cells are constructed with 6-transistor/2-PCM-resistor (6T2R) and peripheral stochastic leaky-integrate-and-fire (LIF) neuron circuits on fully silicon-integrated 90nm CMOS technology. A bidirectional, asynchronous, and parallel pulse-signaling scheme over an analog-weighted PCM synapse array is elaborately designed to be fitted with spike-timing-dependent plasticity local learning rule based on eCD. Since the RBM is a two-layer bidirectional neural network with a probabilistic-based algorithm, we elucidate the system basis with on-chip characterization results such as bidirectional LIF operations over various weighted PCM cells and sigmoid-like firing probability via random walk circuitry. A reasonable symmetricity between LIF and BLIF as well as the stochasticity from on-chip stochastic neuron circuits are shown, which are of critical importance to execute the spiking RBM. The densely integrated spiking RBM chip is configured with a field-programmable gate array (FPGA)-based evaluation system to efficiently transfer spike trains through on-chip scan chains to operate RBM algorithm phases. A fully hardware demonstration of pattern inference scored 93% on-chip training accuracy from 100 MNIST digit handwritten image samples. Furthermore, to clarify the generative performances of the spiking RBM chip, we experimentally demonstrated image reconstruction by inputting partial imperfect patterns. Simulation studies are also added to evaluate how well the impact of PCM-based intrinsic $1/f$ noise is suitable for the generative characteristic of spiking RBM. Thanks to well-fabricated units such as neuron circuits and synaptic cells operating asynchronously and parallelly, this work indicates the potential of power-efficient SNN processors by taking inherent advantage of spike sparseness.

*U. Shin and M. Ishii contributed equally to this work.

[1] W. Maass, Neural Networks, 10, 1659, (1997).

[2] U. Shin, M. Ishii et al., Adv. Intell. Syst. 2200034, (2022).

[3] E. Neftci et al., Front. Neurosci, 7, 272, (2014).

1:30 PM *EQ10.02.01

The Metaheuristic Functionality based on Spontaneity of Memristor Devices for Neural Computing Hongsik Jeong; UNIST, Korea (the Republic of)

Memristor devices have been developed as emerging memory devices compensating for the weakness of conventional memory devices such as DRAM and Flash memory. Memristor devices also have been paid attention as synaptic devices for neural computing. The targeting characteristics of memristor devices as emerging memory devices and synaptic devices are very similar such as low power, non-volatility, high speed, etc. However, memristor devices have unique characteristics that conventional memory devices. Recently, some research has been performed to improve the computation ability by using unique characteristics of memristor devices different from those of existing memory devices as synaptic devices.

In this paper, the higher-level metaheuristic function beyond conventional neural computing will be discussed by using the unique characteristics of memristor-based synaptic devices. The metaheuristic algorithm based on the spontaneity of memristor devices makes neural computing more efficient without additional computing energy.

2:00 PM EQ10.02.02

Simulations of Volatile Memristors Based on Vanadium Dioxide—Linking Material Properties to the Dynamics of Neuromorphic Circuits Stefania Carapezzi, Gabriele Boschetto, Corentin Delacour and Aida Todri-Sanial; LIRMM, University of Montpellier, CNRS, France

Volatile memristors have been gathering a lot of attention as devices suitable for technological applications, such as neuromorphic devices and random number generators, to name a few. Their operating mechanism is a sharp and volatile resistivity variation, switching between high and low resistance states. A thorough understanding and modeling of this resistive switching are essential to fully exploiting volatile memristors. In this respect, multi-physics simulations are crucial. This is especially the case when dealing with devices fabricated with innovative materials, where both material growth and device processing are still to be completely controlled. Then, simulations allow to investigate the interplay between different material properties and/or device features that would be otherwise obscured due to the inherent variability of devices.

In this work, we show results of 3D technology computer-aided design (TCAD) electrothermal simulations of volatile memristors based on vanadium dioxide (VO_2). We avail of a dedicated TCAD approach [1], [2], developed to model the resistive switching of VO_2 volatile memristors as induced by the Joule effect. We combine the electrothermal device simulations with SPICE circuit simulations to simulate the dynamics of VO_2 oscillators. VO_2 oscillators have recently attracted a large interest [3] as the main elements for realization of systems of coupled oscillators, or oscillatory neural networks (ONNs), which are circuits whose dynamics resemble that of networks of neurons in the human brain [4]. By our mixed-mode TCAD-SPICE approach, we are able to link realistically VO_2 material properties to the behavior of the oscillator and the dynamics of simple ONN systems, thus being able to simulate realistically the working of ONN circuits as analogue computing engines. Our findings shed light on the coupled thermal and electrical behavior of VO_2 oscillator as well as the behavior of networks of VO_2 oscillators, providing some physical insights into the successful implementation of ONN technology.

Acknowledgments. Authors wish to thank Dr. S. Karg, IBM Research Europe, Zurich, Switzerland, for providing the experimental data used for calibrating the TCAD model and the valuable discussions about the experimental devices. Authors also wish to thank Dr. A. Nejim and Dr. A. Plews, of Silvaco Europe Ltd., Cambridgeshire, United Kingdom, for providing the customized version of PCM model [1] used to simulate the VO_2 material as well as for the useful discussions about the TCAD and mixed-mode simulations.

[1] "Victory Device User Manual", version 1.19.1.C, Silvaco Inc

[2] S. Carapezzi et al., IEEE J. Emerg. Sel. Topics Circuits Syst. 11, 4, 2021. DOI: 10.1109/JETCAS.2021.3128756.

[3] E. Corti et al., Front. Neurosci., vol. 15, 2021. DOI: 10.3389/fnins.2021.628254

[4] A. Todri-Sanial et al., IEEE Trans. Neural Netw. Learn. Syst., 2021. DOI: 10.1109/TNNLS.2021.3107771

2:15 PM EQ10.02.03

Polaron-Induced Metal-to-Insulator Transition in Vanadium Oxides from Density Functional Theory Calculations Jasleen Kaur, Chi Chen, Manas Likhit Holeykevi Chandrappa and Shyue Ping Ong; University of California, San Diego, United States

Neuromorphic computing approaches have gained significant interest by researchers in the last decade to replace the existing von-Neumann architecture for faster, better, and more efficient machinery with ultra-low power consumption. Intending to emulate the human brain, phase-change memory devices have showcased many advantages to be used as an artificial synapse. V_2O_5 , a member of vanadium Magnéli phases, is a Mott insulator known to exhibit temperature-dependent metal-insulator transition (MIT) at 428 K. In this study, we explore a new triggering mechanism to avoid temperature-induced MIT by forming polarons in the low temperature insulating V_3O_5 phase. We observe a decrease in the band gap from 0.63 eV to 0.47 eV in presence of free electron polaron and 0.51 eV for the system containing free hole polaron. The polaron migrations along different directions were compared using NEB calculations for systems containing free as well as bound polarons in the presence of oxygen vacancies. We find the polaron migration to be facile at low temperatures with the barrier ranging around 100 meV along different directions for both electron and hole polaron, achieving an increased conductivity in the insulating phase. Our studies suggest that this material can exhibit polaron-induced MIT at lower temperatures making it a more favorable candidate for nonvolatile memory in comparison to other vanadium oxides.

2:30 PM BREAK

3:00 PM EQ10.02.06

Optimization of Projected Phase Change Memory for Analog In-Memory Computing Inference Ning Li^{1,2}, Charles Mackin³, An Chen³, Kevin Brew¹, Timothy Philip¹, Andrew Simon¹, Iqbal Saraf¹, Geoffrey Burr³, Malte J. Rasch², Abu Sebastian⁴, Vijay Narayanan² and Nicole Saulnier¹; ¹IBM Albany Nanotech, United States; ²IBM T.J. Watson Research Center, United States; ³IBM Almaden Research Center, United States; ⁴IBM Research-Zurich, Switzerland

Phase change memory (PCM) is a promising candidate for non-von Neumann based analog in-memory computing – particularly for inference of previously-trained Deep Neural Networks. PCM with projection liner is designed for resistance drift mitigation. We show that PCM electrical properties-including resistance values, memory window, resistance drift, read noise, can be tuned systematically using the liner in the manufacturable mushroom PCM. We perform a systematic study of these electrical properties and their impact on the accuracy of several deep neural networks (DNN) using the analog AI simulation tool developed at IBM. We show that the DNN accuracy can be improved by the PCM with liner. We analyze the origin of the accuracy improvement and identify the design space for best performance.

We evaluate large neural networks with tens of millions of weights using the PCM with and without liner, and evaluate a variety of DNNs and test datasets at various times after programming, to study the network performance over time for chips using these PCMs. We evaluate PCM devices in various DNN types, including Recurrent Neural Networks (RNNs), Convolutional Neural Networks (CNNs), and Transformer-based networks. We also evaluate the devices using various weight mapping schemes, including a direct weight mapping scheme for one PCM per weight and an optimized weight mapping scheme using multiple PCMs per weight. We show that the accuracy enhancements from PCM with a projection liner are achieved for all these weight mapping schemes as well as for networks with different structure, complexity, type of nonlinear activation functions employed, etc. We also show that the accuracy is improved for both short term and long term after programming. The better long term accuracy of the liner devices is due to the lower drift coefficient and lower drift variability. The better initial accuracy is due to the reduced noise of the liner devices, despite a trade-off of a reduced memory window. We show that the liner device parameters need to be carefully chosen and identify a range of these parameters that enable the most improvement in network accuracy.

3:15 PM EQ10.02.07

Growing Smooth Polycrystalline VO₂ Film on Silicon Platform for Neuromorphic Computing [Olivier Maher](#)^{1,2}, Roy Bernini¹, Nele Harnack¹, Bernd Gotsmann¹ and Siegfried Karg¹; ¹IBM Research-Zurich, Switzerland; ²ETH Zürich, Switzerland

Exploiting the phase transition of VO₂ close to room temperature (68°C) enables many technologies such as optical switches, smart windows, and terahertz antennas. The insulator-metal transition associated with the crystalline phase-change also provides means to fabricate electronic switches and oscillators. Recently, electrically driven VO₂ oscillators have been suggested for new AI-based computing paradigms including pattern recognition, solving optimization tasks, and NP-hard problems [1, 2]. A series of coupled VO₂ devices exploiting self-oscillations induced through an electric current can be harnessed to build an oscillating neural network (ONN) [1, 3, 4]. Being able to process data locally with ONNs offers new power-efficient solutions to bypass the imbalance between the memory access speed and the computational time needed to process such heavy calculations [5, 4]. For the use of VO₂ in industrial computing applications, CMOS-compatible circuits require high material quality concerning uniformity and surface roughness after depositing on a Silicon-compatible substrate such as Silicon oxide [6, 7]. Devices in planar and crossbar configurations have been fabricated to this end. The VO₂ devices sit on a Si/SiO₂ substrate ensuring CMOS compatibility. Fabrication of VO₂ layers on non-crystalline substrates, however, tends to result in polycrystalline films with granular structure and considerable surface roughness [6]. This leads to undesired variability among electrical devices such as our oscillators that needs to be mitigated [7].

In this study, we show how to solve this issue by treating amorphous vanadium oxide films with an annealing step to recover smooth 50 nm-thick film in its crystalline VO₂ form. The amorphous films are deposited by atomic layer deposition (ALD) using TEMAV (Tetrakis[ethylmethylamino] vanadium) and a water-based reaction. We studied different techniques to find a trade-off between crystallization and oxidation rate and phase. One annealing procedure consists of flashing the film with a high energy beam (FLA-50AS, Dresden Thin Film Technology) for 20 ms under oxygen atmosphere (200 mbar) with the sample preheated between 100°C and 310°C. As a reference, the ALD films were annealed by putting the sample in a low oxygen flow chamber (30-40 mTorr) for 10 minutes at a temperature of 520°C. The impact of the different annealing methods on the grain size, the surface roughness, the electric behavior, and the quality of the resulting VO₂ film are studied through Raman Spectroscopy, Atomic Force Microscopy (AFM), and by measuring the resistance of the film at different temperatures. The nature of the underlying oxide layer and its effect on the quality of the VO₂ is also studied to define which configuration leads to the best and most reproducible results.

Our network of VO₂-based oscillators shows the promise of an attractive and scalable computing unit for hardware accelerators [3, 5], thanks to its MHz high-performance switching properties and CMOS compatibility.

This project has received funding from the EU's Horizon 2020 program under projects No 871501 (NeurONN) and No 861153 (MANIC). We thank the operations team of the Binnig and Rohrer Nanotechnology Center (BRNC) at IBM Research Europe - Zurich for their help and support.

3:30 PM EQ10.02.08

VO₂ Insulator-Metal Phase Change Based Neuromorphic Materials and Devices [Haoming Yu](#), Sunbin Deng, Tae Joon Park, Qi Wang, Sandip Mondal and Shriram Ramanathan; Purdue University, United States

Vanadium dioxide (VO₂) undergoes a phase transition from insulating to metallic states through multiple stimulus, including heat, electric field etc. This inspires the use of VO₂ in artificial neurons to emulate the spiking behavior when the metal to insulator transition (MIT) of VO₂ occurs. Defects and non-stoichiometry profoundly affect the electrical properties such as threshold voltage and state retention. Recently, a few research articles have been presented showing the non-volatile synaptic behavior of VO₂ with oxygen vacancies, inspiring additional research in this direction. This proves the bi-functionality of VO₂. In this work, we will discuss properties of stochastic VO₂ neurons based on two connected VO₂ vertical devices. Two-step switching behavior in transient measurements is shown and is demonstrated to be due to the individual switching of the two devices. Furthermore, we show that the interaction of the two devices enables us to control the switching dynamics by locally controlling the temperature. Finally, we will present electrical characteristics of VO₂ films with intentional point defects such as hydrogen and oxygen vacancies to present a phase map of defect concentration, strain versus volatility and its relation to ground state resistance.

3:45 PM *EQ10.02.09

Optimized Weight Programming for Analog Memory-Based Deep Neural Networks [Charles Mackin](#)¹, Malte J. Rasch¹, An Chen¹, Jonathan Timcheck², Robert Bruce¹, Ning Li¹, Pritish Narayanan¹, Stefano Ambrogio¹, Manuel Le Gallo¹, S.R. Nandakumar¹, Andrea Fasoli¹, Jose Luquin¹, Alexander Friz¹, Abu Sebastian¹, Hsinyu Tsai¹ and Geoffrey Burr¹; ¹IBM, United States; ²Stanford University, United States

Analog memory-based deep neural networks provide energy-efficiency and per-area throughput gains relative to state-of-the-art digital counterparts such as graphics processing units. Recent advances focus largely on hardware-aware algorithmic training and improvements to circuits, architectures, and memory devices. Optimal translation of software-trained weights into analog hardware weights—given the plethora of complex memory non-idealities—represents an equally important task. We report a generalized computational framework that automates the crafting of complex weight programming strategies to minimize accuracy degradations during inference, particularly over time. The framework is agnostic to network structure and generalizes well across recurrent, convolutional, and transformer neural networks. As a highly flexible numerical heuristic, the approach accommodates arbitrary device-level complexity, making it potentially relevant for a variety of analog memories. Interestingly, this computational technique can optimize inference accuracy without the need to run inference simulations or evaluate large training, validation, or test datasets. By quantifying the limit of achievable inference accuracy, it also enables analog memory-based deep neural network accelerators to reach their full inference potential.

8:30 AM *EQ10.03.01

Layered Chalcogenide Materials for Phase-Change Memory and Novel Applications Yuta Saito; National Institute of Advanced Industrial Science and Technology, Japan

Te-based chalcogenides are the key for the phase-change memory technology. The conventional phase-change memory relies on a reversible change between amorphous and polycrystalline phases. Recently, for the further improvement of memory performance, heterogeneously structured phase-change materials have been attracted attention. In fact, most conventional phase-change materials such as Sb_2Te_3 and $\text{Ge}_2\text{Sb}_2\text{Te}_5$ crystallize into a layered structure. Therefore, realization of reversible change between amorphous and highly oriented crystalline phases could have a potential to overcome conventional polycrystalline-based materials. In this talk, some examples of layered chalcogenides will be given with respect to fabrication, function, and novel applications.

9:00 AM EQ10.03.02

Finite Element Electro-Thermal Modeling of Interfacial Phase Change Memory Md Tashfiq Bin Kashem, Jake Scoggin, Ali Gokirmak and Helena Silva; University of Connecticut, United States

Phase change memory (PCM) is a high-speed non-volatile memory that utilizes the reversible and rapid transition between conductive crystalline phase and resistive amorphous phase of the phase change material to store information. One major bottleneck for PCM is the large power requirement to heat the active region above crystallization or melting temperature. To counteract this issue, a device engineering technique is to use thin film periodic structure of layers of two phase change materials known as superlattice or interfacial phase change memory (iPCM) [1,2]. The mechanisms behind the improved performance of iPCM are still under investigation, one experimental work indicates similar crystallization and melt-quench based amorphization of these devices as conventional PCM [2]. iPCM structures benefit from accelerated amorphization through increased number of material interfaces and reduced thermal conduction due to thermal boundary resistances (TBR). Moreover, because of difference in melting temperature, electrical conductivity and Seebeck coefficient of different materials constituting the superlattice, such layered structures may have the advantage of melting of only one of the alternating layers assisted by local heating or cooling due to Peltier effect at the interfaces. If the alternating layers are lattice matched, recrystallization (set) time is also expected to be much faster as crystallization can be achieved through templated growth at the interfaces.

In this work, we utilize our finite element phase change model [3-6] in COMSOL Multiphysics platform to perform electro-thermal simulations of reset and set operations on iPCM structures consisting of alternately stacked $\text{Ge}_2\text{Sb}_2\text{Te}_5$ (GST) and GeTe layers [7]. Electric current and heat transfer physics are employed together to account for Joule heating and thermoelectric effects (Thomson heat within a single material and Peltier heat at material interfaces) with temperature dependent Seebeck coefficients, thermal conductivities, electrical resistivities, heat capacities and TBR for each material / material pairs. Latent heat of crystallization and fusion are included in the amorphous-crystalline and solid-liquid transitions respectively [5], causing heat release at the crystal-amorphous boundaries during crystal growth and heat absorption at the grain boundaries during amorphization. High energy sites: grain boundaries and material interfaces are easier to melt, described as heterogeneous melting [6]. Updated current density function [8] and electrical conductivity model of GST [9] are incorporated in the simulation framework.

Our results on iPCM and conventional PCM structures of same dimensions and geometry (20 nm wide, 70 nm long pillar cells) show ~ 50% reduction in reset time and energy and more consistent set for iPCM. We explored the effect of the total number of layers and the thickness of each material in a period on the time and power requirements for memory operations. Increased number of layers improve speed and power efficiency. However, thinner layers may be less stable and more prone to mixing.

Acknowledgment: This work is partially supported by the National Science Foundation under award DMR-1710468.

References:

1. J. Tominaga *et al.*, *phys. status solidi (RRL)*, 13.4 (2019), DOI: 10.1002/pssr.201800539
2. K. L. Okabe *et al.*, *J Appl. Phys.*, 125 (2019), DOI: 10.1063/1.5093907
3. Z. Woods *et al.*, *IEEE T. Electron Devices*, 64 (2017), DOI: 10.1109/TED.2017.2745506
4. Z. Woods *et al.*, *IEEE T. Electron Devices*, 64 (2017), DOI: 10.1109/TED.2017.2745500
5. J. Scoggin *et al.*, *Appl. Phys. Lett.*, 112 (2018), DOI: 10.1063/1.5025331
6. J. Scoggin *et al.*, *Appl. Phys. Lett.*, 114 (2019), DOI: 10.1063/1.5067397
7. M. T. B. Kashem *et al.*, 241st ECS meet., (2022)
8. M. T. B. Kashem *et al.*, *ECS Transactions*, 108 (2022), DOI: 10.1149/10801.0003ecst
9. R. S. Khan *et al.* *arXiv preprint arXiv:2002.12487* (2020), DOI: 10.48550/arXiv.2002.12487

9:15 AM EQ10.03.03

In-Based PCM Heterostructures—Electronic Properties at the Interface and Confinement of Thin Sb Layers Simone Prili¹, Flavia Righi Riva¹, Ernesto Placidi^{2,1}, Adriano Diaz Fattorini³, Caroline Chèze¹, Marco Bertelli³, Massimo Longo³, Raffaella Calarco³ and Fabrizio Arciprete¹; ¹University of Rome Tor Vergata, Italy; ²Sapienza University of Rome, Italy; ³National Research Council-CNR, Italy

In the last years the widespread of internet and the consequent rise of the so called “Internet of Things” led to a significant increase of interconnection of people with each other and especially between objects that surround us. Among the “things” that have benefited the most out of such revolution, modern cars are by far one of the most representative examples: packed with sensors that monitor every aspect of the vehicle as well as the street environment, they constantly collect and analyzed large amounts of data in order to grant the safest and most comfortable driving experience. To achieve this goal, having a performing, embeddable and highly scalable device for the storage and processing of the information is paramount. Among possible different solution for this task, Phase change Random access memories (PCRAM) are by far one of the most promising candidates since they provide non-volatile device characterized by all the above-mentioned properties and can implement in-memory computing for optimization of AI algorithm.

However, current PCRAM benchmark active materials, $\text{Ge}_2\text{Sb}_2\text{Te}_5$ (GST 225) and other alloys lying on the $(\text{GeTe})_m(\text{Sb}_2\text{Te}_3)_n$ pseudo-binary tie line, fail to meet the strict requirements for the implementation in a vehicle. In fact, despite their outstanding performances in devices working in ambient conditions, GST crystallization temperature is too low for the realization of memory devices for automotive applications, for which high stability at temperatures as high as 160°C is mandatory. To address this issue, In-based PCMs, characterized by inherently high crystallization temperature, could be solid candidates

for this goal. Our work focused on two alloys, In-Sb-Te (IST) and In-Ge-Te (IGT), both characterized by high transition temperature [1, 2], which we studied as single films and combined each other in a IST/IGT heterostructure. Amorphous samples were grown at room temperature by thermal evaporation of the constituting elements from ultrapure sources on Si(111)/SiO₂ substrates by means of Knudsen cells in Ultra-High Vacuum conditions (UHV). Performing *in-situ* X-ray and Ultraviolet photoemission spectroscopy (XPS & UPS) we characterized the electronic properties, valence band (VB) and core levels, of the as-grown samples and managed to track composition variations across the IGT/IST interface. Valence band structures of the alloys will be discussed and compared with published density of states computed by *ab initio* molecular dynamics simulation based on DFT. Unexpectedly, the photoemission study of this heterostructure showed that no Sb diffuses through as-grown IGT, leading to the formation of sharp interface completely lacking antimony. This is particularly relevant especially because of the renewed interest towards pure ultrathin Sb [3], a newfound promising PCM itself. In light of this, we have grown Sb/IGT heterostructures employing IGT as confinement material to study the crystallization of pure Sb and, by means of *ex-situ* X-ray diffraction, we characterized Sb/IGT heterostructures featuring Sb layers of different thicknesses to observe the effect of this parameter on the transition temperature.

REFERENCES

1. Saxena N. *et al.*, Sci. Rep. 9, 19251 (2019)
2. Morikawa T. *et al.*, "Doped In-Ge-Te Phase Change Memory Featuring Stable Operation and Good Data Retention," 2007 IEEE International Electron Devices Meeting, 2007, pp. 307-310
3. Salanga M. *et al.*, Nature Mater. 17, 681–685 (2018)

9:30 AM EQ10.03.04

Revelation of the Underlying Switching Mechanism Occurring in van der Waals GeTe/Sb₂Te₃ Superlattices Damien Terebenc¹, Nicolas Bernier¹, Vitomir Sever¹, Niccolo Castellani¹, Jessy Paterson¹, Françoise Hippert² and Pierre Noé¹; ¹CEA, France; ²LMGP, France

Phase-Change Memory (PCM) is widely recognized as the key emerging technology for the next-generation non-volatile memory. In PCM, the information is stored at the nanoscale in two distinct resistive states of a phase-change material: a polycrystalline state corresponding to the Low Resistance State (LRS), and an amorphous state for the High Resistance State (HRS named RESET). The main shortcoming of PCM is the high energy loss occurring within the memory cell, especially during the RESET operation requiring local melting of the phase-change material, followed by quenching of the liquid phase to the amorphous state. Therefore, reducing the heat loss that occurs during the RESET operation has become a tremendous challenge. A breakthrough in memory cell architecture has enabled a reduction in energy waste through improved thermal confinement within the memory cell.^[1] Nevertheless, the architectural approach has reached a technological limit. In this context, materials engineering has become the main asset in order to improve PCMs, by seeking novel materials with undiscovered properties. For instance, GeTe/Sb₂Te₃ van der Waals superlattices (SLs) embedded in PCM have demonstrated outstanding performance. This is evidenced by a decrease in programming currents of the order of 40%, a better cycling endurance, as well as a higher transition speed than conventional Ge₂Sb₂Te₅ alloy located along the GeTe-Sb₂Te₃ pseudo-binary line.^[2] This performance improvement has long been attributed to a novel mechanism of crystal-to-crystal resistive transition as opposed to the amorphous-to-crystal transition of conventional PCM. The change of electronic properties in GeTe/Sb₂Te₃ SLs has first been attributed to the result of coherent switching of Ge atomic planes at the interfaces with Sb₂Te₃ layers, leading to a change in the density of electronic states, hence the name "interfacial Phase Change Memory" (iPCM). However, the underlying switching mechanism occurring in the SL structure is still highly debated in the PCM community.

In this work, we study the memory performances of [(GeTe)₂/(Sb₂Te₃)_X]_n SL with X=2, 4, and 8 nm, as well as the origin of the resistive switching occurring in SL PCM devices. GeTe/Sb₂Te₃ SLs were deposited by magnetron sputtering in a 200 mm cluster tool. They are obtained by a periodic stacking of nanometer-thick crystalline GeTe and Sb₂Te₃ layers oriented along the [001] axis normal to the substrate surface. In the literature, all models describing crystal-to-crystal resistive transition assume the existence of GeTe layers with pure Ge and Te planes within the SL structure. Nevertheless, we revealed by scanning transmission electron microscopy (STEM) that SLs exhibit an atomic structure consisting in stacking of Sb₂Te₃ quintuple layers, and different Ge₂Sb₂Te₅ alloys ranging between 7 to 11 atomic planes.

Subsequently, SLs were integrated in phase-change memory (PCM) devices in a "wall structure", with a polycrystalline GeTe alloy used as reference. [(GeTe)₂/(Sb₂Te₃)_X]_n SL permits to significantly reduce the RESET current (>60%) in PCM compared to devices using conventional polycrystalline phase-change material. STEM imaging coupled with NanoBeam Electron diffraction of a [(GeTe)₂/(Sb₂Te₃)₈]₄ nm SL device previously switched in the HRS, unambiguously revealed the presence of an amorphous area above the heater. This result demonstrates that the resistive switching occurred through a melting-quenching process in SL, as in conventional PCM.^[3] A thorough understanding of programming performance improvement offered by [(GeTe)₂/(Sb₂Te₃)_X]_n SLs related to their atomic structure will be discussed.

References

- [1] A. Redaelli, Ed., Phase Change Memory, Springer International Publishing, Cham, 2018.
- [2] R. E. Simpson, & al, Nature Nanotech 2011, 6, 501.
- [3] D. Terebenc & al, Phys. Status Solidi RRL 2021, 9.

9:45 AM EQ10.03.05

Engineering Superlattice Materials and Interfaces for Improved Resistance Drift and Retention in Phase-Change Memory Xiangjin Wu, Asir Intisar Khan, Pranav Ramesh, Krishna Saraswat, H.S. Philip Wong and Eric Pop; Stanford University, United States

Phase change memory (PCM) is a promising candidate for data storage and neuromorphic computing. However, using traditional phase change materials like Ge₂Sb₂Te₅ (GST), PCM suffers from resistance drift resulting in undesired bit errors and inference accuracy degradation in compute-in-memory [1]. Recently, superlattice (SL) PCM with thin phase change layers has shown promise for low resistance drift [2-4]. However, the origin of low resistance drift and the role of the SL interfaces remain unexplored. At the same time, retention in such SL-PCM also demands attention to ensure its reliable operation.

Here, we uncover a correlation between resistance drift and SL interfaces in a GST based SL-PCM (Sb₂Te₃/GST) and simultaneously shed insight into its origin using temperature-dependent measurements. By controlling the number of SL interfaces, we obtain a low $\nu < 0.01$ and as low as ~ 0.002 measured for 10⁵ seconds in 2 nm/1.8 nm Sb₂Te₃/GST SL-PCM. We also explore the retention in SL-PCM for the first time and demonstrate how the choice of SL layers can enable higher retention.

We fabricated SL-PCM devices with alternating Sb₂Te₃ and GST layers having different period thicknesses (1/number of interfaces). Measured resistance (R) vs. time shows $>10\times$ lower resistance drift in the SL-PCM device ($\nu < 0.01$) vs. GST-only control PCM ($\nu \approx 0.12$), both with ~ 110 nm BE diameter. However, for SL-PCMs the resistance drift increases with fewer SL interfaces (e.g., 4/1.8 nm/nm and 16/14.4 nm/nm SLs). This suggests that nano-confinement and van-der Waals gaps play an important role in reducing the resistance drift. We also find that intermixing and imperfections within SL layers increase the resistance drift.

To understand the origin of low ν in SL-PCM, we extracted conduction activation energy E_a from R vs. temperature (T) measurements, showing lower E_a in SL-PCM with more interfaces. We also find that 2/1.8 nm/nm SL-PCM displays a negligible change in both E_a and high resistance state after 85°C annealing. In contrast, both attributes show an increasing trend upon annealing for SL-PCM with fewer interfaces and for GST (no internal interfaces). This

suggests that less structural relaxation in SL-PCM with more interfaces reduces the resistance drift. The low $v < 0.01$ in our $\text{Sb}_2\text{Te}_3/\text{GST}$ SL-PCM devices is maintained after extensive ($>10^6$) cycling, for various read stress and upon measurement at different read voltages, demonstrating robustness and reliability of the low resistance drift.

Next, we explore the retention of the resistance states in our SL-PCM devices. Our measurement shows that resistance states in $\text{Sb}_2\text{Te}_3/\text{GST}$ SL-PCM devices retain up to a temperature annealing of 85°C for 1 hour. This relatively lower retention in these SL-PCM devices (vs. control GST) originates from the presence of low-retention Sb_2Te_3 layers within the SL. To address this, we replaced Sb_2Te_3 layers within the SL-PCM with TiTe_2 (higher melting T and higher stability) and $\text{Ge}_2\text{Sb}_2\text{Te}_5$ (GST) layers with $\text{Ge}_4\text{Sb}_6\text{Te}_7$ (a phase-change nanocomposite with higher crystallization T), thus conceptualizing $\text{TiTe}_2/\text{GST467}$ superlattice PCM. Our measurements of the $\text{TiTe}_2/\text{GST467}$ SL-PCM devices indeed confirm a significantly higher retention for the resistance states (145°C for 3 hours).

In summary, we uncover the role of interfaces within superlattice (SL) layers in achieving low the resistance drift of SL-PCM and explore the origin of such interface-controlled low resistance drift. By choosing optimized material layers within the SL, we further demonstrate SL-PCM with simultaneously high retention and low resistance drift, promising for multibit storage and neuromorphic computing using SL-PCM technology.

1. A. Sebastian *et al.*, *J. Appl. Phys.*, 124, 111101 (2018)
2. A.I. Khan, E. Pop *et al.*, *Science* 373, 1243 (2021)
3. K. Ding *et al.*, *Science* 366, 210 (2019)
4. A.I. Khan, E. Pop *et al.*, *IEEE EDL* 43, 204-207 (2022)

10:00 AM BREAK

SESSION EQ10.04: In Depth Comprehension of Various PCM Materials I

Session Chairs: Paolo Fantini and Yuta Saito

Tuesday Morning, November 29, 2022

Sheraton, 2nd Floor, Independence West

10:30 AM *EQ10.04.01

Thermodynamics and Kinetics of the Crystallization of Phase Change Materials from Complementary *In Situ* Microscopic Techniques [Melissa K. Santala](#); Oregon State University, United States

Phase change materials (PCMs) are semi-conducting alloys with distinct optical and electrical properties in the amorphous and crystalline phases that make them useful for memory applications. In memory devices, amorphous bits are crystallized in nanoseconds by either laser or Joule heating, but the amorphous phase must also be stable against crystallization for long-term data retention. Crystal growth rates relevant to memory devices span orders of magnitude and fundamental questions regarding PCM crystallization mechanisms remain open, partly due to the difficulty in measuring crystallization kinetics in certain temperature regimes. This talk will cover the application of multiple imaging techniques used to directly quantify crystal growth rates in PCMs over a broad range of temperatures. The measurable growth rates from the different techniques span from $\sim 10^{-9}$ to >10 m/s and the *in-situ* imaging techniques applied include optical microscopy, conventional transmission electron microscopy (TEM), and dynamic TEM, a photo-emission TEM technique with nanosecond-scale time resolution. The use of complementary *in situ* experimental techniques allow the crystal growth rates to be mapped over a large temperature range and can give insights into the crystallization kinetics of PCMs. Nanocalorimetry results using microfabricated devices designed to be using in a TEM holder will be described. These devices enable simultaneous collection of thermodynamic data along with TEM imaging of the crystal growth front. Challenges associated with integrating results from different microscopic techniques and the incorporation nanocalorimetry to probe the thermodynamics of crystallization with simultaneous TEM imaging will be discussed.

11:00 AM EQ10.04.02

Space-Qualified Chalcogenide Materials Through ISS MISSE Exposure —From Property to Application [Hyun Jung Kim](#)¹, Kiumars Aryana¹, Cosmin-Constantin Popescu² and Juejun Hu²; ¹NASA Langley Research Center, United States; ²Massachusetts Institute of Technology, United States

In March 2021, twenty-four samples of various phase change materials (PCMs - $\text{Ge}_2\text{Sb}_2\text{Te}_5$, $\text{Ge}_2\text{Sb}_2\text{Se}_4\text{Te}_1$, and Sb_2Se_3) along with metasurface optical components comprised of these PCMs, were delivered to the International Space Station (ISS) as part of the Materials International Space Station Experiment (MISSE-14) test campaign [1]. Although PCMs have previously been noted for their resilience to various forms of radiation [2], they had not been tested in a realistic space environment until this exposure campaign with joint NASA and MIT collaboration. During the six-month total open exposure time in low earth orbit (LEO), high-resolution cameras scanned and captured photographs of the samples to detect changes as a function of time along with on-orbit measured temperature, UV radiation, total atomic oxygen fluence, and total ionizing radiation doses. The samples were returned to NASA Langley Research Center in March 2022 for post-flight characterization. This duplicated the preflight characterization (i.e., material composition and crystallinity that limits switching speed, index contrast, loss, etc.) conducted before launch.

The space sector has witnessed tremendous growth within the past decade—not only from government agencies but also entrants from the private sector. Future growth in the capabilities of Earth observation, deep space, and planetary surface missions using miniaturized spacecraft platforms can only be sustained by innovations in the design of remote sensors and other sub-systems. Active metasurface optics with enhanced tunability and reconfigurability continues to redefine the boundaries of optical science [3]. The introduction of PCM technology and associated optical devices will help to accelerate the adoption of new architectures for reduced size, weight, power, and cost (SWaP-C) platforms in space.

Here we introduce results obtained from the MISSE-14 mission related to space qualification of PCM-based optic devices and constituent materials. We then discuss our recent work developing active integrated photonic devices and metasurface optics based on PCMs for space applications. This includes tunable and reconfigurable optical metasurface devices to support NASA space communication and LIDAR applications. PCMs are quickly becoming interesting photonics materials but questions related to mission suitability remain, particularly in regard to key properties like figures-of-merit (FOM, $\Delta n/\Delta k$), glass forming temperatures, and phase transition speeds. This talk will describe efforts to afford researchers the ability to have access to cost-effective data on exposure-induced changes to PCM fundamental physical and optical properties to assess their utility for space applications. The MISSE-14 sample exposure campaign allows a complete understanding of the limitations of the PCMs for various space-based electronic and optoelectronic applications.

- [1] Kim, H. J. et al. *Nature Material in procession*, “Versatile spaceborne photonics with chalcogenide phase-change materials” (2022).
 [2] Konstantinou, K. et al. *PNAS*, 115, 5353-5358 (2018).
 [3] Gu, T. et al. *Nature Photon. in processing*, “Active metasurfaces: lighting the path to a sparkling success” <https://arxiv.org/abs/2205.14193> (2022).

11:15 AM EQ10.04.03

Effect of Photoexcitation on Amorphized Ge₂Sb₂Te₅ Line Cells Stabilized by High-field Stress at Cryogenic Temperatures ABM Hasan Talukder, Raihan Khan, Md Tashfiq Bin Kashem, Faruk Dirisaglik, Helena Silva and Ali Gokirmak; University of Connecticut, United States

Phase change memory (PCM), one of the most promising non-volatile memory technologies, utilizes the large resistivity contrast between amorphous and crystalline phases of phase change materials like Ge₂Sb₂Te₅ (GST). PCM devices suffer from resistance drift which causes the amorphous resistance to increase over time, making it hard to implement multi-bit-per-cell operation. We have demonstrated that cell resistances can be stabilized within minutes by accelerating the drift with high-field stresses [2]. In this work, we have investigated the effect of photoexcitation on amorphized GST line cells stabilized by high-field stresses at cryogenic temperatures to understand the phenomena giving rise to resistance drift.

We amorphized GST line-cells at 80 K using 50 ns to 100 ns electrical pulses, stabilized the cells with several high-field voltage sweeps as we record the current, and observed the effect of photoexcitation at different temperatures up to 200 K. The contribution of photoexcited carriers, excited by a white LED, is clearly observed at 80 K in the low-field (< 20 MV/m) range. The photo-response increases with temperature up to ~150 K and remains constant beyond 150 K. The contribution of the photoexcited carriers become harder to observe for T > 250 K due to large number of thermally generated carriers. When the illumination is turned on and off periodically, electrical current flowing through the device shows sudden changes followed by very slow response (up to ~30 minutes at T = 150 K) [3]. The time scale for the slow changes suggests that the changes in the resistance are predominantly due to emptying and filling of charge traps, and not due to thermal perturbations induced on the cells due to exposure to light. The current through the device is insensitive to light but very sensitive to temperature in the high-field regime, and the high-field current does not change with periodic illumination, verifying that the observed response is not due to a thermal perturbation. These experimental results are used to determine the trap levels and the temperature dependence of band-gap of amorphous GST.

Acknowledgment: This work is partially supported by NSF under award ECCS 1711626

References:

- [1] H. -S. P. Wong et al., Proc. of the IEEE, 98 (2010).
 [2] R. S. Khan et al., Dev. Res. Conf. (DRC), 2020.
 [3] R. S. Khan et al., Appl. Phys. Lett., 116 (2020).

11:30 AM *EQ10.04.04

Machine-Learning-Driven Advances in Modelling Phase-Change Memory Materials Volker L. Deringer; University of Oxford, United Kingdom

In this presentation, I will showcase recent advances in machine-learning (ML) based interatomic potentials, and discuss emerging applications to phase-change memory materials.

(Following the email sent 14 June 2022, this is a placeholder / summary entry, which will be amended in due course.)

SESSION EQ10.05: In Depth Comprehension of Various PCM Materials II

Session Chairs: Volker Deringer and Martin Salinga

Tuesday Afternoon, November 29, 2022

Sheraton, 2nd Floor, Independence West

1:30 PM *EQ10.05.01

Comprehensive Review of Contacts to Phase Change Materials Suzanne Mohnhey and Kayla A. Cooley; The Pennsylvania State University, United States

Many devices, including memory and radio frequency switches, rely on the reversible transformation between amorphous and crystalline states of the phase change material. These devices require electrical contacts, and in many cases the contacts limit the overall device or circuit performance. In this presentation, we review the state-of-the-art on electrical contacts to the phase change materials GeTe, Ge₂Sb₂Te₅ (GST), GeCu₂Te₃, and Ge₂Cr₂Te₆. We address topics including contact resistivity, reactivity, thermal stability, and metal solubility. We especially emphasize contacts to GeTe due to our extensive work with this phase change material, and then we build upon our analysis of the metal-Ge-Te systems to include the metal-Sb-Te systems and finally to draw conclusions about contacts to GST.

2:00 PM EQ10.05.02

Simultaneous Thermodynamic and Kinetic Measurements of the Crystallization of an Ag-In-Sb-Te Phase Change Material Using Transmission Electron Microscopy and In Situ Nanocalorimetry Isak McGieson¹, Jim Ciston², Feng Yi³, David LaVan³ and Melissa K. Santala¹; ¹Oregon State University, United States; ²Lawrence Berkeley National Laboratory, United States; ³National Institute of Standards and Technology, United States

An experimental platform using in-situ nanocalorimetry synchronized with high-frame-rate transmission electron microscopy (TEM) imaging has been developed and is being used to investigate the thermodynamics and kinetics of the crystallization of a phase change material (PCM) with a nominal composition of Ag₃In₄Sb₇Te₁₇ above its glass transition temperature. In-situ nanocalorimetry provides more accurate temperature measurements than other in-situ heating platforms as well as the high heating rates necessary to observe PCM crystallization above the glass transition temperature. High-frame-rate direct electron detectors capture the crystal growth in the milliseconds before impingement. The combined activation energy for nucleation and growth, the activation energy just for growth, and the enthalpy of crystallization are calculated from these measurements. Classical models for nucleation and growth are fit against these data using the temperature dependent viscosity as the free parameter. Models that predict the growth rate solely from calorimetry data are checked against the growth rate measurements.

2:15 PM EQ10.05.03

Optical Properties of Sb-Based Phase Change Materials Toward Visible and IR Photonic Applications Kotaro Makino¹, Yuta Saito¹, Shogo Hatayama¹ and Paul Fons^{2,1}, ¹National Institute of Advanced Industrial Science and Technology (AIST), Japan; ²Keio University, Japan

Phase change materials including Ge-Sb-Te (GST) alloys exhibit a significant change in optical properties upon amorphous-crystalline phase change, and hence are promising for programmable optical device applications in the visible and infrared wavelength range. The optical response of a material is governed by the complex index of refraction, namely the refractive index (real part) and the extinction coefficient (imaginary part). Recently, Sb₂S₃, Sb₂Se₃, and Ge₂Sb₂Se₂Te₁ were found to be good alternatives to GST due to their low extinction coefficients for the crystalline phases [1-3], although GST is still useful for some applications based on absorption change.

In this study, we performed first principles calculations to evaluate the optical constants of Sb-based phase change materials Sb₂Te₃, Sb₂S₃, and Sb₂Se₃. Our objective of the current study is to establish a standard computational procedure for further material development. By using Vienna Ab initio Simulation Package (VASP), we obtained complex index of refraction for both crystalline and amorphous phases. We also carried out ellipsometry measurements for sputter-deposited thin films (except for Sb₂Se₃) and found that use of a hybrid functional is crucial for accurate optical property simulations. Based on the simulation and experimental results, we found Sb₂S₃ is considered to be suitable for low-loss applications rely on refractive index change, while Sb₂Te₃ and GST is appropriate for control of absorption as previously reported.

[1] M. Delaney *et al.*, Adv. Func. Mater. 30, 2002447 (2020).

[2] Y. Zhang *et al.*, Nat. Commun. 16, 661, (2021)

[3] L. Lu *et al.*, ACS Nano 15, 19722 (2021).

2:30 PM BREAK

SESSION EQ10.06: Nanoscaling and Single Phase Change Materials

Session Chairs: Juejun Hu and Suzanne Mohney

Tuesday Afternoon, November 29, 2022

Sheraton, 2nd Floor, Independence West

3:00 PM *EQ10.06.01

The Significance of Antimony for Research on Phase Change Materials Martin Salinga; University of Münster - Institute of Materials Physics, Germany

For many years, phase change materials have been improved by mixing additional chemical species into alloys consisting of Ge, Sb and Te leading to rather complex compositions. A few years ago, in stark contrast to this common strategy, it was demonstrated that also pure Antimony can render phase change behaviour when spatially confined. Here, we discuss the role this product of maximal compositional simplification could play for research and applications.

3:30 PM EQ10.06.02

Low Temperature Wet-Chemical Synthesis of Sub-10 nm Sb Nanoparticles Enables the Stabilization of the Amorphous State Through Three-Dimensional Confinement Anne Frommelius^{1,2}, Konstantin Wirth^{1,3}, Thomas Taubner^{1,3} and Ulrich Simon^{1,2}; ¹RWTH Aachen University, Germany; ²Institute of Inorganic Chemistry, Germany; ³First Institute of Physics (IA), Germany

Non-volatility of the structural state together with fast switching times make phase change materials (PCM) extremely useful for data storage applications and showcase great potential for neuro-inspired computing.^[1] The properties of PCM are commonly tuned by precisely changing stoichiometries or doping components, which may lead to phase segregation or degradation under operation.

By addressing these challenges, which arise from the compositional complexity of common PCM, Salinga *et al.* studied the threshold switching properties of mono-elementary Sb thin films, which behaved similarly to commonly known PCM. The retention time of the amorphous state in 3 nm thin films was found to be approximately 50 hours at room temperature.^[2]

In order to explore, whether the amorphous state of elementary Sb can further be stabilized by three-dimensional confinement, we focused our studies on the liquid phase synthesis of sub-10 nm Sb nanoparticles (Sb-NP) in amorphous state. This requires a synthesis route with extraordinary mild reaction conditions, i.e. reaction temperatures well below the crystallization temperature of Sb, which is enabled by a strong reducing agent.

The formation of a BH₃×THF complex allowed us to reduce Sb³⁺ at room temperature to finally yield ligand stabilized amorphous Sb-NP. Powder X-ray diffraction measurements (p-XRD) and transmission electron microscopy revealed sub-10 nm amorphous Sb-NP with long-term stability against crystallization of 7 weeks under ambient conditions. Additionally, the infrared response of amorphous and crystalline Sb-NP was compared using scattering type Scanning Nearfield Optical Microscopy (s-SNOM) and found to have reasonable differences, which allows us to distinguish between the amorphous and the crystalline state. Heating up the amorphous Sb-NP at temperatures above 100 °C led to crystallization which was verified by s-SNOM and p-XRD independently. These results give evidence that the metastable amorphous state of Sb can be further stabilized by our three-dimensional confinement approach.

Future ambitions on laser-induced switching will now focus on a statistical analysis of the phase stability and the implementation of the Sb-NP as PCM into an optically addressable prototype data storage device.

[1] M. Wuttig *et al.* *Designing phase-change materials for universal memory and neuro-inspired computing*, Nat Rev Mater 4, 2019, 150-168.

[2] M. Salinga *et al.* *Monatomic phase change memory*, Nature Mater 17, 2018, 681-685.

3:45 PM EQ10.06.03

Revealing the Crystallization Kinetic in Thin-Film Phase Change Material via 1,000,000 K/s Nanocalorimetry Jie Zhao¹, Jian Hui^{1,2}, Asir Intisar Khan³, Zichao Ye¹, Xiangjin Wu³, Tianxing Lai², Mikhail Efremov⁴, Hong Wang², Eric Pop^{3,3,3} and Leslie Allen¹; ¹University of Illinois at Urbana-Champaign, United States; ²Shanghai Jiao Tong University, China; ³Stanford University, United States; ⁴College of Engineering, United States

Nanosecond switching speeds in phase-change memory (PCM) devices make its material-level kinetic investigation inaccessible for most calorimetric methods. Nanocalorimetry developed in our group provides quantitative insights into this “no man’s land” with a scanning rate up to 1,000,000 K/s (two orders of magnitude higher than other calorimetric studies on PCM) and sample-size (10–40 nm thick) typical of PCM devices. Our preliminary calorimetric study¹ on 20 nm thick Ge₂Sb₂Te₅ (GST), with negligible thermal lag, reveals a single-step Arrhenius process dominated by the growth of

interfacial nuclei with an activation energy of 2.36 eV. Based on numerical simulation, crystallization growth velocity (CGV) is obtained consistent with that measured in PCM cells. This addresses a 10-year-debate originated from the unexpected non-Arrhenius kinetics measured by commercialized chip-based calorimetry, which reports CGV 10^3 – 10^5 higher than that of PCM cells. The viscosity of supercooled liquid GST, modeled from CGV, suggests a fragile-to-strong crossover at ~ 410 °C. Thermal properties of thin-film GST (melting, solidification, and specific heat) are also measured and agree with conventional calorimetry of bulk samples. The methodology developed in the preliminary work will also be applied to the fast kinetic investigation of other novel phase-change materials including, Ag–In–Sb–Te², Ge₄Sb₆Te₇ (high-temperature PCM) and superlattice Sb₂Te₃/GeTe^{3,4}.

[1] Jie, Zhao, et al. "Exploring "No Man's Land"—Arrhenius Crystallization of Thin-Film Phase Change Material at $1\ 000\ 000\ \text{K s}^{-1}$ via Nanocalorimetry." *Advanced Materials Interfaces*, early view (2022).

[2] McGieson, Isak, et al. "Crystallization kinetics and thermodynamics of an Ag–In–Sb–Te phase change material using complementary in situ microscopic techniques." *Journal of Materials Research* 37.7 (2022): 1281-1295.

[3] Khan, Asir Intisar, et al. "Ultralow-switching current density multilevel phase-change memory on a flexible substrate." *Science* 373.6560 (2021): 1243-1247.

[4] Kwon, Heungdong, et al. "Uncovering thermal and electrical properties of Sb₂Te₃/GeTe superlattice films." *Nano Letters* 21.14 (2021): 5984-5990.

4:00 PM EQ10.06.04

Unravelling the Structure and Crystallization Mechanism of Amorphous Nanoparticle Phase-Change Materials Simon Wintersteller and Maksym Yarema; ETH Zürich, Switzerland

Chalcogenide-based phase change materials such as GeTe and Ge-Sb-Te are commonly used for phase-change memory (PCM) applications, where information is stored using a high contrast in the resistivity or refractive index of the amorphous '0' and crystalline '1' state. Data is written to the memory cell using electrical or optical pulses, which crystallize or amorphize the structure through induced Joule heating. As demand for faster memory and higher data density increases, PCM nanoparticles are well suited to act as the building blocks for future ultrasmall memory devices. To realize this and to optimize memory properties, the structure and switching mechanism of nanoscale PCM materials need to be well understood. To this affect we synthesize 5 nm GeTe nanoparticles, coat them in a ZnS shell isolating the effects of coalescence, and compare their structure and crystallization to sputtered 'bulk' GeTe.

The reversible phase transitions in PCM devices are extremely fast, strongly suggesting a close structural resemblance between the amorphous and crystalline phases. In contrast to this, the amorphous structure is generally assumed to consist of a highly random ordering of atoms, which is generally quite distant to the crystalline counterpart. This work uses ultrafast in-situ X-ray absorption spectroscopy (XAS) and theoretical calculations to study and quantify the amorphous structure of bulk and nanoscale GeTe. Through a series of high-temperature XAS measurements, we can slow down the nanosecond crystallization process and consequently provide a detailed crystallization mechanism, which is validated using molecular dynamic (MD) simulations. We argue that crystallization phase transition is diffusionless for Te atoms, while Ge atoms order via cleavage of Ge-Ge homopolar bonds forming Te-Ge-Te intermediate 'bridge' states. In parallel to experimental measurements, we developed a theoretical model of the amorphous structure, consisting of a disordered fcc-type Te sublattice and randomly arranged chains of Ge in tetrahedral coordination. This structure is relaxed using density functional theory (DFT) calculations and strongly matches our experimental data and previous literature on amorphous GeTe.

We apply our new knowledge about amorphous PCM materials to quantify differences between bulk and nanoscale GeTe. Finally, we extend our model to ternary X-Ge-Te systems and study composition effects on their phase-change properties. Our work provides a high-throughput pathway to model and optimize chalcogenide materials for PCM applications and to design scaling rules for sub-10 nm PCM devices.

SESSION EQ10.07: Poster Session
Session Chairs: Valeria Bragaglia and Andriy Lotnyk
Tuesday Afternoon, November 29, 2022
8:00 PM - 10:00 PM
Hynes, Level 1, Hall A

EQ10.07.01

Characterization of In₂Se₃ Crystalline Phase Changes as the Basis for Multilevel Phase Change Memory Nicholas D. Ignacio¹, Saban Hus^{1,2} and Deji Akinwande¹; ¹University of Texas at Austin, United States; ²Oak Ridge National Laboratory, United States

Layered materials such as In₂Se₃ and MoTe₂ have multiple crystal phases with differing electrical properties and can achieve reversible phase changes between them. Compared to transitions between amorphous and crystalline phase in conventional phase change memories (PCM), changes between crystalline phases are expected to have faster and low energy write operations for PCM even compared to interfacial PCM based Sb₂Te₃-GeTe superlattices due to the lower entropy of the crystalline-crystalline phase change. In₂Se₃ PCM have been demonstrated utilizing β and γ as the low and high resistance state respectively, however multilevel switching has not been extensively explored in part due to the stability of the crystalline phases at room temperature (RT).

In this work, we demonstrate the persistence of β phase In₂Se₃ in bulk phase at RT, previously only seen in single-crystal thin films and polycrystalline powders after annealing in an inert environment. Scanning tunneling microscopy (STM) is used to visualize the different phases as well as to measure the band gap with scanning tunneling spectroscopy (STS) after annealing at different temperatures and cooling to RT. After annealing α In₂Se₃ in UHV ($<10^{-10}$ mbar) at 300C for 1 hour, β was found as confirmed by the shift in band gap from 1.27 eV to 0.52 eV. We also report in-situ Raman spectroscopy taken during heating and cooling of monolayer and effective bulk films of In₂Se₃ in both inert atmosphere and in air. We show evidence that upon bulk In₂Se₃ cooling to RT after heating in an inert atmosphere a mixture α and β phases results as compared to annealing in air where β reverts to α upon cooling.

EQ10.07.02

Memristive Behavior of Li Intercalated MoTe₂ for Neuromorphic Computing Rifat Hasan Rupom¹, Eunho Lee², Pashupati R. Adhikari¹, Moonyoung Jung², Dongseok Suh² and Wonbong Choi¹; ¹University of North Texas, United States; ²Sungkyunkwan University, Korea (the Republic of

Recently, memristor has emerged as an electronic neuromorphic device with an ability to control multiple resistance states by memorizing the history of

prior electrical input and mimicking the synapse for neuromorphic computing. Molybdenum ditelluride (MoTe₂) has attracted considerable interest among 2D transition metal dichalcogenides (TMDs) materials, because of its small band gap, tunable 1T'/2H phases, and favorable polycrystalline nature for ion migration. Herein, for the first time, we report lithium (Li) intercalated MoTe₂ neuromorphic device fabricated by a simple sputtering process exhibiting enhanced memristive behavior with varying Li ion concentration at different bias voltages. It is observed that MoTe₂ film effectively enhances the I_{on}/I_{off} and hysteresis current, which is attributed to high ion transport through the grain boundaries in polycrystalline MoTe₂. After ion-intercalation, I_{on}/I_{off} ratio was enhanced from 5 to $>10^3$ at lower sweep voltage with high retention and linearity conductance modulation for pulsative voltage. This work presents insights in making stable and large-scale MoTe₂ memristive device based on sputtered MoTe₂ and ion intercalation method. In this presentation, we will discuss the device performance and its mechanistic investigation.

EQ10.07.03

Tunable, Reversible Glass–Crystal Transitions in Single & Binary Metal–Bis(acetamide) Glasses Mandy Liu¹, Adam H. Slavney¹, Songsheng Tao², Ryan McGillicuddy¹, Cassia Lee¹, Simon J. Billinge² and Jarad A. Mason¹; ¹Harvard University, United States; ²Columbia University, United States

With large electrical or optical contrast across a continuous transition between two phases encoding the logic states of “0” and “1”, phase-change materials provide promises to address growing demand for data storage and processing. While glass–crystal transitions in chalcogenide alloys have long been studied for rewritable data storage and for neuro-inspired computing more recently, challenges remain with their high energy budget and limited structural diversity and tunability. Glassy phases of metal–organic frameworks offer great potential of using coordination chemistry and reticular synthesis to significantly reduce melting temperatures in comparison to chalcogenide glasses, as well as to predictively tune crystallization kinetics. Although recrystallization has rarely been observed in metal–organic glasses, here we report a novel series of two-dimensional networks M(eba)₃[M'Cl₄] (eba = *N,N'*-ethylenebis(acetamide), M/M' = Mn, Fe; M = Mn, Fe, Co, M' = Zn) that undergo low-temperature melting (150–190 °C) and reversible glass–crystal transitions. Their glass transition temperatures (T_g) are well above 298 K, leading to very stable glasses under ambient conditions. This is attributed to the short polyethylene chain in the eba ligand, which restricts the conformational flexibility of the ligand in the melt and therefore reduces the entropy of fusion. The crystallization kinetics and glass stability of these compounds are readily tunable through the judicious selection of different metal cations and by liquid-phase blending to form binary glasses. This high tunability affords exciting opportunities of forming mixed glasses with precisely tuned glass stability and crystallization behavior tailored for a specific application. Notably, a large reflectivity contrast ratio of 3.7–4.8 for a glass–crystal transition is observed in a Co-containing binary glass, which is driven by changes to the coordination environment of Co centers during crystallization and vitrification. Beyond the M(eba)₃[M'Cl₄] system, a binary metal–bis(acetamide) glass with longer polymethylene chain shows two distinct crystallization features, indicating the possibility of accessing multiple near-degenerate states with different optical properties by harnessing the compositional and structural diversity of metal–organic glasses. These results provide new insights into manipulating reversible glass–crystal transitions in metal–organic materials, which has implications for rewritable data storage at lower energy intensities and well-controlled continuous crystallizations for neuromorphic computing.

EQ10.07.04

Spanning Femtoseconds to Seconds in the Photoinduced Response of Antimony Thin Films Sebastian Walfort¹, Daniel T. Yimam², Bart Kooi² and Martin Salinga¹; ¹University of Muenster, Germany; ²University of Groningen, Netherlands

The observable dynamics in electrical devices based on phase change materials span nanoseconds to decades. Any processes on timescales below nanoseconds are obscured by the limited time resolution of electronic circuits. Photonic circuits do not share this limitation [1]. Material dynamics on much shorter timescales are accessible, but must be understood in order to be exploitable in applications. This study investigates the photoinduced dynamics of the phase change material antimony in the time range from femtoseconds to seconds using optical pump-probe spectroscopy.

Certain aspects of the response of crystalline antimony to excitation with short laser pulses have been examined in the past [2]. The short-timescale response is characterized by the displacive excitation of a damped coherent phonon mode [3], the coupling of the hot electron system to the lattice initially leads to a non-thermal population of phonons [4], and in the long-timescale limit the optical contrast between an amorphous and the crystalline state exhibits a film thickness dependence [5]. However, there is no individual study that attempts to elucidate the photoinduced response of antimony in its entirety. Furthermore, the large parameter space of e.g. film thickness, pump fluence, or probe wavelength remains largely unexplored. Exploring, for instance, the role of the film thickness is expected to be especially important in antimony, where confinement below 10 nm already has been shown to influence a range of material properties such as the crystallization kinetics [6], phonon mode frequencies [5] or electronic structure [7]. Varying the thickness of the antimony film, its structural state through in-situ switching, the probing wavelength, pump fluence and base temperature, we measured the complete photoinduced response until its return to equilibrium. Comparison of the different processes across this broad parameter space is enabled by deriving a phenomenological model that can capture the entire response.

REFERENCES

1. T. Yu et al., arXiv:2102.10398 (2021)
2. J. Tominaga et al., Appl. Phys. Lett. 75 (1999) 3114
3. M. Hase et al., J. Phys. Soc. Jpn. 84 (2015) 024708
4. L. Waldecker et al., Phys. Rev. B 95 (2017) 054303
5. Z. Cheng et al., Sci. Adv. 7 (2021) 7097
6. M. Salinga et al., Nat. Mat. 17 (2018) 681
7. P. Zhang et al., Phys. Rev B 85 (2012) 201410

EQ10.07.05

Investigation of Phase-Change Synapse Architectures by Integrating Electro-Thermal and Phase-Field Models Ho Thi Thu Trang and Kwon Yongwoo; Hongik University, Korea (the Republic of)

Phase-change memory is a promising technology for synapse application in neuromorphic computing because it is the most matured among the nonvolatile memory technologies. The PCM utilizes Ge₂Sb₂Te₅ (GST), a chalcogenide material, whose conductive crystalline and resistive amorphous phases correspond to data 0 and 1, respectively. The switching operation typically resembles heat treatment in material processing such as melt-and-quit for amorphization and annealing for crystallization via nucleation and growth. All the switching mechanisms are controlled by Joule-heating through electrical pulses. In this work, we constructed 3D PCM device simulation by integrating electrothermal and phase-field models in COMSOL Multiphysics. Two representative cell architectures are compared from the viewpoint of device performance and synapse application: one is self-heating wall (SHW), and the other is heater-based wall (HBW). Firstly, the device performance comparison including power consumption, on/off ratio, etc is conducted via recrystallization analysis by different falling-times in the range of 10ns and 100ns after reset operation. Secondly, the synapse characteristics are investigated, i.e., the conductance change data, which are obtained by applying a series of short and moderate current pulses for gradual crystallization after a reset pulse. From our simulations, we observe that the set operations by both melt-and-slow cooling and constant pulses (MSCP and CP) consume similar power. In a high-density memory array, the variability in devices is unavoidable. The MSCP with sufficient height can melt GST in all cells, which ensures

successful operation. On the other hand, the CP with a fixed height may fail to crystallize in some cells due the variability. Therefore, the MSCP may be more beneficial than the CP. In case of synapse characteristics, the SHW is superior to the HBW because it consumes less power and shows better linearity and graduality in the synaptic weight.

EQ10.07.06

Cryogenic Operation of Phase Change Memory Down to 4 K [Sohui Yoon](#), Namwook Hur, Hongsik Jeong and Joonki Suh; Ulsan National Institute of Science and Technology, Korea (the Republic of)

Understanding and realizing the memory operations of non-volatile memory cell under extreme conditions such as cryogenic environment is scientifically and technologically crucial. In this work, we demonstrate the cryogenic operation of phase change memory (PCM) at 4 K and extensively investigate its SET/RESET programming characteristics over a wide range of temperatures. On the fundamental side, the temperature dependent behavior of phase transition and its dynamics of $\text{Ge}_2\text{Sb}_2\text{Te}_5$, a textbook example of phase change material, is monitored with the key device metrics including the voltage shift of RESET/SET operation and with varying input pulses (width, fall time, etc), respectively. It will certainly deepen our understanding on the crystallization mechanism toward a longstanding goal of low-power and high-speed PCM. On the applied side, we successfully fabricate PCM devices with a semi-confined cell geometry and demonstrate their reliable operations from room temperature to 4 K, supported by temperature-dependent resistance change. It will, therefore, be a promising option as the interface processing memory component for quantum computing often operated in the mK range.

EQ10.07.07

Three-Dimensional Phase Change Memory Architecture with Cylindrical Sidewall Electrodes [Namwook Hur](#), Beomsung Park, Sohui Yoon, Sangwoo Park, Huimin Lee, Hongsik Jeong and Joonki Suh; Ulsan National Institute of Science and Technology, Korea (the Republic of)

Next-generation computing system beyond the von Neumann architecture requires the development of new hardware components, and memristive devices have been studied to meet such requirements. As a non-volatile memristor unit, phase-change memory (PCM) is highlighted with the proved nano-second level of fast operation speed and reliable device performances with simple fabrication process using conventional complementary metal-oxide semiconductor (CMOS) technology. Thus, it holds a high potential as non-volatile storage and neuromorphic memory devices, but it still requires device-level innovation for ultra-low operation energy and high-density memory cell arrays beyond the widely adopted 2-dimensional planar device configuration, known as mushroom type PCM. In this work, we propose a new three-dimensional (3D) memory architecture with cylindrical sidewall electrode contacts named heater-all-around phase-change memory (HAA-PCM). With the new design principle, it shows effectively low operation energy (~ 1 nJ) compared with the conventional PCM devices in the identical $0.18 \mu\text{m}$ node CMOS fabrication technology. Our 3D HAA-PCM architecture can be applied to the next-generation artificial intelligence (AI) memory which requires ultra-low operation energy and high-density memory cell.

EQ10.07.08

Growth and Microstructure of $\text{GeTe-Sb}_2\text{Te}_3$ Heterostructures Deposited by Pulsed Laser Deposition Sonja Cremer¹, Lennart Voß², Nils Braun¹, Lorenz Kienle² and [Andriy Lotnyk](#)^{1,3,4}; ¹Leibniz Institute of Surface Engineering (IOM), Germany; ²University of Kiel, Germany; ³The Research Institute of Advanced Technologies, China; ⁴Harbin Engineering University, China

Characterized by non-volatility, scalability and fast operating speed Ge-Sb-Te based phase change alloys are well suited compounds for memory devices. Nevertheless, high power consumption and resistance drift turn out to be obstacles for big data application. Heterostructured phase change memory (HS-PCM) is shown to be a promising strategy to overcome these issues. However, underlying structure-property relationships are still highly debated. [1-3] As a first step for systematic performance improvement, we investigated how varying deposition parameters influence the microstructure of $\text{GeTe-Sb}_2\text{Te}_3$ heterostructured thin films.

The samples were grown at room temperature as non-periodic and periodic HS (npHS and pHS, respectively) using pulsed laser deposition (PLD). Advanced transmission electron microscopy combined with X-ray measurement techniques was applied for in-depth analysis of the microstructure.

For the npHS the system deposited using the highest laser fluence consists of alternating GeTe and Sb_2Te_3 layers. A small degree of interdiffusion of Ge into Sb_2Te_3 layers and vice versa is always present getting more pronounced with decreasing layer thickness. In contrast, the thin film grown using the lowest fluence is a single, completely intermixed layer with a composition close to GeSb_2Te_4 . Revealing the deposition rate as a main influence factor for intermixing, the pHS consist of separated layers irrespective of the layer thickness.

GeTe layers within the HS are always amorphous whereas Sb_2Te_3 layers were found to grow nanocrystalline irrespective of laser fluence. As reported for fully crystalline Sb_2Te_3 [4], the nanocrystals are defective consisting of grain boundaries and bi-layer defects. Further characteristics are varying grain sizes and phases. Apart from the main $\{00l\}$ -textured t-phase, c- and vacancy ordered (vo) phase are present. By electron beam exposure this structure transforms into the c-phase, similar as already reported for vo- $\text{Ge}_2\text{Sb}_2\text{Te}_5$ [5].

In conclusion, varying deposition parameters were found to mainly effect the intermixing in $\text{GeTe-Sb}_2\text{Te}_3$ heterostructured thin films. In contrast, irrespective of the deposition parameters and despite the room temperature deposition PLD grown HS are characterized by nanocrystalline Sb_2Te_3 layers. Considering the correlation of nanocrystallinity and improved operation efficiency reported for $\text{Sb}_2\text{Te}_3\text{-GeSb}_2\text{Te}_4$ -HS in literature [6], this work provides insights into the relationship of deposition, structure, and properties of PLD grown $\text{GeTe-Sb}_2\text{Te}_3$ -HS.

Acknowledgements

We acknowledge the financial support by the German Research Foundation (DFG 445693080). We thank Mrs. A. Mill for assistance in the FIB preparation.

References

- [1] A. Lotnyk et al., Appl. Surf. Sci. 536 (2021) 147959
- [2] L. Zhou et al., Adv. Electron. Mater. 6 (2020) 1900781
- [3] X. Li et al., Adv. Funct. Mater. 28 (2018)1803380.
- [4] J.-J. Wang et al., Phys. Status Solidi RRL 13 (2019) 1900320
- [5] A. Lotnyk et al., Acta Mater. 105 (2016) 1
- [6] J. Feng et al., ACS Appl. Mater. Interfaces 12 (2020) 33397

EQ10.07.09

Phase Change Memory from Molecular Telluride Inks [Florian Schenk](#), Darijan Boskovic, Till Zellweger, Alexandros Emboras and Maksym Yarema; ETH Zurich, Switzerland

Phase change memory (PCM) is an emerging data storage technology, where the information is stored by reversible switching of local bits between high-resistance amorphous and low-resistance crystalline phases of a material (logical “0” and “1”, respectively). The data is written by heating to the crystallization temperature (SET process). Vice versa, amorphization erases the data (RESET process).

Traditionally, phase-change material films are deposited via sputtering techniques, lithography, and lift-off. Solution-phase deposition of chalcogenides at ambient temperature and pressure provides a low-cost, scalable, and composition-flexible alternative. Additionally, thin film fabrication from the liquid phase gives access to new geometries of phase change memory devices (i.e., high-aspect ratio and multilayer arrays) and inexpensive high-throughput printing methods. One way to obtain such material inks is to dissolve bulk chalcogenides in an amine-thiol co-solvent. Annealing then forms compact crystalline thin films. This approach has shown its applicability for solar cells, thermoelectrics or resistive memory, but has not been researched for state-of-the-art telluride phase change applications yet.

Here, we synthesize a range of phase change memory material inks by dissolving bulk tellurides in an amine-thiol co-solvent formulation and subsequent purification steps. Deposition via spin-coating yields thin film telluride layers with tunable thickness, low surface roughness, and high crystallinity. We highlight the possibility to obtain stoichiometric binary materials (i.e., Sb_2Te_3 , Se_2Te_3 or Y_2Te_3) as well as composition-tunable ternary materials by admixing rare-earth telluride inks with antimony telluride. This yields homogenous doping in $\text{M}_3\text{Sb}_{2-x}\text{Te}_3$ due to mixing on the molecular scale. We then demonstrate the benefits of ink formulations, e.g. deposition on patterned substrates like grooves and vias. Finally, we fabricate and test tailor-made prototype devices and quantify critical performance metrics such as I-V characteristics, switching behavior and speed, resistance contrast, power consumption, and cyclability of functional phase-change memory devices from molecular inks.

SESSION EQ10.08: PCM for Embedded Applications

Session Chairs: Ali Adibi and Qian Wang

Wednesday Morning, November 30, 2022

Hynes, Level 1, Room 108

8:30 AM *EQ10.08.01

Improving Crystallization Temperature by Ge-Incorporation in $\text{Ge}_x\text{Sb}_y\text{Te}_z$ Phase Change Alloys and Heterostructures for Automotive Applications

Raffaella Calarco¹, Adriano Diaz Fattorini¹, Marco Bertelli¹, Sara De Simone¹, Valentina Mussi¹, Francesco De Nicola¹, Massimo Longo¹, Giuseppe D'Arrigo¹, Inaki Garcia Lopez¹, Antonella Sciuto¹, Stefania M. Privitera¹, Massimo Borghi², Andrea Redaelli², Marie-Claire Cyrille³ and Nguyet-Phuong Tran³; ¹Consiglio Nazionale delle Ricerche, Italy; ²STMicroelectronics, Italy; ³LETI, France

The interest in Phase Change Memory (PCM) devices with improved crystallization temperature is increasing for automotive applications, where devices must be able to operate reliably at high temperatures (> 160 °C) for at least ten years. Alloys like $\text{Ge}_2\text{Sb}_2\text{Te}_5$ (GST225) are already a standard to realize memory devices. However, one of the major disadvantages of GST225 single layers is the low crystallization temperature (T_c), which results in low thermal stability and limited data retention. An interesting option to increase T_c is to grow Ge-rich GST alloys. Here, several $\text{Ge}_x\text{Sb}_y\text{Te}_z$ and $\text{Ge}_x\text{Sb}_2\text{Te}_3$ layers were grown by RF-sputtering and their thermal stability was studied by X-ray diffraction (XRD) and Raman spectroscopy as a function of temperature. The compositional analysis was performed by X-ray fluorescence (XRF). The results showed that both T_c and Ge-segregation amount grow linearly with the Ge-content in the alloys. Among the different possibilities, our approach combines different phase change materials with opposite properties (Sb_2Te_3 , $\text{Ge}_2\text{Sb}_2\text{Te}_5$ and $\text{Ge}_x\text{Sb}_y\text{Te}_z$), also introducing a confinement Ge layer to realize interesting novel test devices. Therefore $\text{Sb}_2\text{Te}_3/\text{Ge}_2\text{Sb}_2\text{Te}_5/\text{Ge}$ heterostructures with a total thickness of 110 nm were deposited by RF sputtering and their thermal stability was analyzed by X-ray diffraction and Raman spectra, evidencing a slower crystallization dynamic (by 50°C) than in $\text{Ge}_2\text{Sb}_2\text{Te}_5$. After optimization, the heterostructures were deposited onto proper single-cell vehicles prepared on Si(001) substrates and metal contacts were nanolithographically (EBL) defined. The subsequent technical analysis (I-V, R-V, R-cycles graphs for the SET/RESET states) showed that the cell has a programming current of 1.2 mA and an endurance of 2×10^5 cycles.

This project has received funding from the European Union's Horizon 2020 research and innovation program under Grant Agreement No. 824957 (“BeforeHand:” Boosting Performance of Phase Change Devices by Hetero and Nanostructure Material Design).

9:00 AM EQ10.08.02

Atomistic Simulations of the Decomposition Pathways of Ge-Rich GeSbTe Alloys for Phase Change Embedded Memories Omar Abou El Kheir and Marco Bernasconi; University of Milano-Bicocca, Italy

The prototypical $\text{Ge}_2\text{Sb}_2\text{Te}_5$ phase change compound displays a crystallization temperature too low for embedded phase change memories of interest for applications in the automotive sector. Ge-rich GeSbTe (GST) alloys are emerging as promising materials for embedded memories thanks to the higher thermal stability of their amorphous phase. Upon crystallization Ge-rich GST alloys undergo a phase separation into Ge and a less Ge-rich GST alloy. This phase separation enhances the crystallization temperature, but it also gives rise to some drawbacks such as a high cell-to-cell variability and a drift of the electrical resistance with time in the set state. The details of the decomposition process are, however, largely unknown. In this work, we report on high-throughput calculations based on Density Functional Theory on the decomposition pathways of Ge-rich GST alloys. We first calculated the formation free energy of GST alloys in the central region of Ge-Sb-Te ternary phase diagram and their distance from the convex hull. These data allowed us to estimate the decomposition propensity of Ge-rich GST alloys which suggested a possible strategy to minimize phase separation by still keeping a high crystallization temperature.

9:15 AM *EQ10.08.03

Ge-Rich Phase Change Heterostructures for Automotive Applications Marie-Claire Cyrille; CEA-Leti, University Grenoble Alpes, France

Phase change memory (PCM) is a mature technology, versatile enough to fulfill the requirements of automotive, Storage Class and neuromorphic applications. Automotive applications have the most stringent specifications as they require high data retention in a large temperature range and soldering

reflow compatibility. Thanks to their ability to sustain high crystallization temperatures, Ge-rich GeSbTe alloys have proven their ability to meet those constraints and have been successfully introduced in advanced CMOS technology nodes such as 28nm FDSOI and 18nm FDSOI. However Ge-rich GeSbTe materials can exhibit phase segregation upon crystallization which induce variability and can prove detrimental to PCM arrays reliability. We have developed Ge-rich GeSbTe heterostructures and multilayers tailored to automotive requirements with the specific goal of delaying phase segregation in order to improve set and reset state resistance variability while maintaining good data retention.

9:45 AM BREAK

10:15 AM *EQ10.08.04

Molecular Beam Epitaxy of Ge-Rich GeSbTe Alloys for Automotive Applications [Stefano Cecchi](#)^{1,2}; ¹University of Milano-Bicocca, Italy; ²Paul-Drude-Institute, Germany

Chalcogenide phase change materials (PCM) have been identified as promising candidates for the development of storage class memories,¹ as well as brain-inspired computing.² GeSbTe (GST) alloys along the GeTe-Sb₂Te₃ pseudo-binary line are employed as the active material in non-volatile solid-state memories.³ Among (GeTe)_m(Sb₂Te₃)_n compounds, Ge₂Sb₂Te₅ (GST225) is so far the best performing material for PCM memory devices. For embedded devices requiring a higher crystallization temperature, e.g. for automotive applications, the use of GST225 is prevented. The tailoring of the crystallization properties of GST by engineering the alloy composition is therefore fundamental. In this framework, GST alloys with Ge-rich composition have shown increased crystallization temperatures proportional to the excess of Ge.⁴ Molecular beam epitaxy (MBE) allows the design of GST alloys with high structural quality, tuning phase, composition and vacancy ordering.⁵ Moreover, it enables the fabrication of superstructures such as multilayers and superlattices with unique control of structural and electrical properties.^{6,7} The presentation will focus on the investigation of GST with Ge-rich composition grown by MBE. Recent results on the crystallization properties of Ge-rich GST films deposited amorphous will be shown.⁸ Strategies to fabricate high-quality epitaxial films with GeTe-rich composition will be discussed next, aimed at controlling the alloy composition between GST225 and GeTe. The characterization of structural, vibrational and ferroelectric properties as function of composition, supported by density functional theory calculations, will be presented.

¹ S.W. Fong, C.M. Neumann, and H.P. Wong, IEEE Transactions on Electron Devices **64**, 4374 (2017).

² A. Sebastian, M. Le Gallo, G.W. Burr, S. Kim, M. BrightSky, and E. Eleftheriou, Journal of Applied Physics **124**, 111101 (2018).

³ S. Raoux, W. Welnic, and D. Ielmini, Chemical Reviews **110**, 240 (2010).

⁴ P. Zuliani, E. Varesi, E. Palumbo, M. Borghi, I. Tortorelli, D. Erbetta, G.D. Libera, N. Pessina, A. Gandolfo, C. Prelini, L. Ravazzi, and R. Annunziata, IEEE Transactions on Electron Devices **60**, 4020 (2013).

⁵ V. Bragaglia, F. Arciprete, A.M. Mio, and R. Calarco, Journal of Applied Physics **123**, 215304 (2018).

⁶ S. Cecchi, E. Zallo, J. Momand, R. Wang, B.J. Kooi, M.A. Verheijen, and R. Calarco, APL Materials **5**, 026107 (2017).

⁷ R. Wang, F.R.L. Lange, S. Cecchi, M. Hanke, M. Wuttig, and R. Calarco, Advanced Functional Materials **28**, 1705901 (2018).

⁸ S. Cecchi, I. Lopez Garcia, A.M. Mio, E. Zallo, O. Abou El Kheir, R. Calarco, M. Bernasconi, G. Nicotra, and S.M.S. Privitera, Nanomaterials **12**, 631 (2022).

10:45 AM EQ10.08.05

Interplay Between Electronic and Structural Properties of Epitaxial and Amorphous Ge-Rich GST Alloys and Heterostructures [Flavia Righi Riva](#)¹, [Caroline Chêze](#)¹, [Giulia Di Bella](#)², [Ernesto Placidi](#)², [Simone Prili](#)¹, [Adriano Diaz Fattorini](#)³, [Stefano Cecchi](#)⁴, [Massimo Longo](#)³, [Raffaella Calarco](#)³, [Omar Abou El Kheir](#)⁵, [Marco Bernasconi](#)⁵ and [Fabrizio Arciprete](#)¹; ¹University of Rome Tor Vergata, Italy; ²Sapienza University of Rome, Italy; ³CNR Institute for Microelectronics and Microsystems-IMM, Italy; ⁴Paul-Drude-Institut für Festkörperelektronik, Germany; ⁵University of Milano-Bicocca, Italy

The impressive amount of data and information generated by modern electronic systems still requires large numbers of fast, cheap, and power-efficient embedded non-volatile memories and processing devices. Modern cars represent an important example of modern electronic system where sensors monitor every aspect of the vehicle as well as the street environment, resulting in a huge amount of collected and analyzed data. In this context, Phase change materials (PCM) based on chalcogenide alloys are a valid technology for the realization of non-volatile memories and are currently attracting much interest also as suitable materials for in-memory computing applications, where a reproducible set of multilevel resistance values is required [1]. Among the PCM most technologically relevant, the ternary (GeTe)_m(Sb₂Te₃)_n alloys (GST) are the most widely used, commonly in the composition Ge₂Sb₂Te₅ (GST 225). Due to its great performances in terms of crystallization speed GST225 is in fact the prototype alloy chosen for most practical uses. However, in view of neuromorphic applications aiming at the emulation of synaptic behavior, improved material properties such as wide programming windows, low resistance drift and, particularly for automotive applications, high crystallization temperature T_x are still mandatory. For this reason, thermally stable PCM have been recently investigated [2], among which Ge-rich Ge-Sb-Te alloys (GGST) were found to be promising candidates for the realization of non-volatile memories working at high temperatures. Furthermore, the combination of different PCM is a valid strategy to tailor the material properties for the realization of embedded devices with optimized performances. Here, we present a photoemission study of amorphous GGST-based bilayer heterostructures grown by Physical Vapor Deposition (PVD), and epitaxial GGST samples grown by Molecular Beam Epitaxy (MBE). Sb₂Te₃/GGST and GST225/GGST heterostructures are obtained by successive partial depositions of amorphous GGST of increasing thickness by co-evaporation in ultra-high vacuum of the constitutive elements from solid source Knudsen cells. The evolution of the electronic properties of the heterostructures are studied *in-situ* during the interface formation by a combination of X-ray and Ultraviolet photoemission spectroscopies (XPS and UPS) and *ex-situ* X-ray diffraction (XRD) and Raman spectroscopy. Information on composition and intermixing of the alloys across the heterostructures and the final stable composition of thick GGST layers are obtained and discussed. Valence bands measured by UPS are compared to the theoretical density of states calculated by DFT. Also, the effects of thermal annealing at increasing temperatures are discussed with particular focus on the role of the interface on the crystallization of the GGST second layer.

Molecular Beam Epitaxial GGST alloys along the pseudo-binary line are also characterized by XPS and UPS and compared to a standard GST225 sample. Results are interpreted based on the current structural models of trigonal GST and their evolution after subsequent annealing steps is discussed.

[1] A. Sebastian et al., *Nat. Nanotech.* **15**, 529 (2020)

[2] C. Chêze et al. *Nanomaterials*, **12**, 1007 (2022)

11:00 AM EQ10.08.06

Innovative GeSe_{1-x}Te_x Alloys—An Opportunity for Embedded Phase-Change Memory Applications [Martina Tomelleri](#)^{1,2}, [Anthony Albanese](#)², [Chiara Sabbione](#)², [Niccolo Castellani](#)², [Valentina Giordano](#)³, [Daniel Benoit](#)¹, [Francoise Hippert](#)⁴ and [Pierre Noé](#)²; ¹STMICROELECTRONICS, France; ²CEA-LETI, France; ³ILM, UMR 5306 Univ. Lyon 1-CNRS, France; ⁴Univ. Grenoble Alpes, CNRS, France

The unique portfolio of properties of chalcogenide phase-change materials (PCMs), such as Ge-Sb-Te and GeTe, has created and continue to provide exceptional opportunities in resistive memory technologies and data storage [1]. Despite their well-established performances, PCM memory still faces a

number of challenges for a large-scale commercialization. In the case of embedded applications such as for automotive market, the thermal stability of the amorphous (a-) phase must be high enough to avoid unwanted crystallization and thus ensure the code integrity and the endurance of the device at high temperature for long time (industrial criteria of 150°C for 10 years) [2]. Until now, no PCM based on a defined and homogenous compound has been able to meet this challenge. The most common approach has been to use chalcogenide Ge-Sb-Te alloys that are highly enriched in Ge with respect to alloys lying on the well-known GeTe-Sb₂Te₃ pseudo-binary line. The crystallization is slowed down by the required out-diffusion of the Ge excess from the PCM crystalline phase. However, while such an approach has contributed to strongly increase the crystallization temperature (T_x) and thus the data retention, the required huge Ge phase segregation upon crystallization is very difficult to master. Therefore, this could hinder the programming of the memory cells leading to a degradation of reliability in device fabrication process [3].

In the present work, we propose the innovative GeSe_{1-x}Te_x alloys, belonging to the GeTe-GeSe pseudo-binary line, as a homogenous material capable to overcome this technological limit [4]. GeSe_{1-x}Te_x thin films with various composition were obtained using magnetron co-sputtering of pure GeSe and GeTe targets in 200/300 mm industrial microelectronic tools. By means of resistance measurements (Four-point probe) as function of temperature, we followed the crystallization of GeSe_{1-x}Te_x thin films and we observed a significant improvement of thermal performances with decreasing x, reaching very high T_x hence leading to unprecedented high thermal stability of the a-phase. In addition, the resistivity contrast between a- and c-phases is extremely large, except for GeSe, reaching about 8 order of magnitude for the lowest Te content. X-ray diffraction has been performed on c-GeSe_{1-x}Te_x films (annealed at 430°C) and a rhombohedral phase isostructural to GeTe has been observed for the entire x range, apart from the c-GeSe that shows an orthorhombic structure. Based on this result, we could exclude the presence of any detrimental phase segregation, confirming the homogeneity of the alloy after crystallization and the complete solubility of selenium in the GeTe phase. Moreover, the presence of the rhombohedral c-structure in GeSe_{1-x}Te_x thin films is beneficial since it promotes the formation of a unique bonding mechanism recently called “metavalent” bonding (MVB), which is responsible for the uncommonly high property contrast between a- and c-phases of PCMs [5]. The combination of high thermal stability and wide resistivity contrast in a homogenous alloy, represent an important breakthrough for embedded resistive memory technology, making Se-rich GeSe_{1-x}Te_x thin films especially attractive for automotive PCM applications requiring high data retention.

[1] P. Noé et al., *Semicond. Sci. Technol.* 33 (2018) 013002. [2] P. Cappelletti et al., *J. Phys. D: Appl. Phys.* 53 (2020) 193002. [3] V. Sousa et al., *Symp. VLSI Tech. Dig.* 2015, T98. [4] M. Tomelleri et al., *Phys. Status Solidi RRL*, 15 (2021) 2000451. [5] a) J.-Y. Raty et al., *Adv. Mater.* 2019, 31, 1806280 ; b) Kooi, B. J., Wuttig, M., *Adv. Mater.* 2020, 32, 1908302.

11:15 AM *EQ10.08.07

PCM Applications—An Historical Review to Look to the Future [Paolo Fantini](#); Micron Technology Inc., Italy

A historical review of the PCM technology from its first proof of concept up to the most recent achievements of the research will be provided. A parallel historical glance to the product development is also proposed as background to lead the discussion on the opportunities that PCM can bring in the actual scenario of memory eco-system. Against the dream of PCM as universal memory, this paper offers guidelines for PCM applications in the widespread scenario separating the Short-time memory (like DRAM, short both for latency and retention) and the Long-time memory (like NAND, long both for latency and retention), thus contributing to the heterogeneous memory eco-system. In particular, Author will reserve a more extensive discussion for PCM in the Storage Class Memory arena and in the neuromorphic and in-memory computing applications.

The SCM arena represents the ideal realm for the PCM technology from the side of performances like speed and endurance, but a 3-D structure integration must be considered to reduce the cost of PCM devices. To this aim, a cross-point stacked solution combining a PCM with an Ovonic threshold switching as selector has been proposed. In a longer-term perspective, more compact cell design, resembling the 3D vertical NAND of today, should be considered. The primary benefit of such a design is the cell being defined in a single lithographic step, thus reducing the cost. A technological challenge to enable the foundation of this kind of Vertical 3D architectures lies in the ability to deposit conformal and composition-controlled chalcogenide films via ALD technique.

PCMs are also strongly considered as electronic analogue of biological synapses able to implement the Spike-Time-Dependent-Plasticity (STDP) mimicking the synapse functionality. PCM can emulate the biological behavior of synapses and it offers multiple advantages such as scalability, reliability, endurance, multiple programming resistance levels giving them a suitable candidate for implementing large-scale synaptic systems.

PCM technology can also play a relevant role in overcoming the performance limits of the von Neumann architecture, based on a strict separation between the computation unit and memory, where data and instructions for the processing unit use the same data bus, leading to the so-called von Neumann bottleneck.

It will be shown as dense Non-Volatile Memory (NVM) crossbar arrays to few nanometer dimensions is a promising path to build computing systems able to overcome the von-Neumann bottleneck, performing the computation on the memory elements, as the human brain efficiently does, thus avoiding the redundant load-and-store operations. There are still many open challenges to make it a reality, like the improvement of the cell endurance with programming cycling, but definitively, PCM can contribute to mimic what biology figures out: doing the compute in memory. The astounding progress through the Moore's scaling law made possible demonstrations of truly remarkable tasks of artificial intelligence (AI), but at the expense of an energy consumption that is orders of magnitude higher than the one of the human brain.

SESSION EQ10.09: Nanophotonics with PCM
Session Chairs: Raffaella Calarco and Melissa Santala
Wednesday Afternoon, November 30, 2022
Hynes, Level 1, Room 108

1:45 PM *EQ10.09.01

New Platforms for Reconfigurable Nanophotonics Enabled by Nonvolatile Phase-Change Materials Sajjad Abdollahramezani and [Ali Adibi](#); Georgia Institute of Technology, United States

Phase-change materials with very large change in their optical properties upon transition between amorphous and crystalline phases are promising candidates to miniaturize the fundamental reconfigurable nanophotonic and metaphotonic building blocks like phase shifters, delay lines, tunable nanoantennas, and reconfigurable spatial light modulators that are essential for a large range of applications including communication, quantum photonics, computing, imaging, and ranging.

This talk is focused on the unique features of nonvolatile phase-change materials for enabling new classes of reconfigurable nanophotonic and metaphotonic devices with subwavelength feature sizes through forming new hybrid material platforms by their integration with dielectric, plasmonic, and more conventional CMOS-compatible integrated nanophotonic materials (e.g., silicon and silicon nitride). The fundamental properties of such devices and their ability for dynamic wavefront engineering as a major functionality for enabling state-of-the-art applications like switching, structural color, and

ranging will be discussed. Practical issues like speed, minimum feature size, power consumption, and agility of such hybrid reconfigurable platforms will be covered, and a list of potential areas of improvement to enable state-of-the-art applications will be presented.

2:15 PM EQ10.09.03

Optical Properties of Innovative GeSe_{1-x}Te_x Phase-Change Material Thin Films for On-Chip Active Components, Non-Linear and Brain-Like Computing Applications [Anthony Albanese](#)^{1,2}, Martina Tomelleri¹, Jean-Baptiste Dory¹, Christophe Licitra¹, Benoît Charbonnier¹, Jean-Baptiste Jager³, Aurélien Coillet², Benoît Cluzel² and Pierre Noël¹; ¹CEA-LETI, France; ²ICB, France; ³CEA-IRIG, France

In this work, the linear and nonlinear optical properties of innovative GeSe_{1-x}Te_x thin films in amorphous as-deposited state as well as after crystallization by annealing are studied. These alloys, obtained by industrial magnetron co-sputtering of GeSe and GeTe targets, belong to the GeSe-GeTe pseudo-binary line lying between the covalent GeSe compound and the “metavalently” bonded GeTe phase-change material (PCM). They are considered as very promising candidates for high temperature non-volatile resistive memory [1], emerging all-optical neuromorphic circuits and IR photonic applications. In fact, they exhibit fast and reversible phase transformations between amorphous and crystalline states with unprecedented large contrast of electronic and optical properties, a very high thermal stability of the amorphous phase compared to other PCMs [1] as well as a high transparency in the NIR-MIR range in both states. By modifying the Te content of the GeSe_{1-x}Te_x thin films, one can tailor their linear and non-linear optical properties for a wide range of innovative optical and photonic applications.

To compare candidate PCMs and evaluate the impact of their optical losses on the performances of optical switch applications, a figure-of-merit was introduced as $FOM = \Delta n / \Delta k$, where $\Delta n = n_{cr} - n_{am}$ and $\Delta k = k_{cr} - k_{am}$, with n and k refractive index and extinction coefficient of the amorphous (am-) and crystalline (cr-) phase, respectively. Ideally, PCMs with large Δn and small Δk are desired. In this work, the best FOM at 1.55 μm wavelength is found for GeSe_{0.4}Te_{0.6}, for which $FOM = 13$, almost 6 times higher than that of GST-225 reference material with a low FOM of 2.3 at 1.55 μm . Moreover, all the studied compositions showed very high FOM values compared to the most promising composition previously proposed in the literature (Ge₂Sb₂Se₄Te₁ alloy with a FOM value of 4.2 [2]). Besides, the high transparency window in the IR, coupled with large optical non-linearities observed in chalcogenide glasses, also offers opportunities for the development of innovative near- and mid-infrared (NIR-MIR) components such as super-continuum (SC) laser sources, optical sensors for gas spectroscopy, IR microlens arrays and all-optical integrated circuits. The non-linear refractive indices n_2 of the am-films were obtained by using the Sheik-Bahae model. The latter is an analytical approach that estimates the n_2 indices using the values of the linear refractive index n and the optical band gap energy E_g^{opt} . Outstanding n_2 values are obtained for all GeSe_{1-x}Te_x am-films in the NIR-MIR range. These values are two to three orders of magnitude higher than that found in SiN_x thin films, considered nowadays as the reference material for on-chip non-linear NIR photonic applications.

To summarize, the study of the optical properties of GeSe_{1-x}Te_x thin films shows that these new exciting PCM compounds offer promising FOM ($\Delta n / \Delta k$) for purpose of optical switch applications requiring high refractive index contrast upon crystallization with limited optical losses, in particular at 1.55 μm . Besides, the amorphous films exhibit a good thermal stability up to crystallization occurring above 300 °C [1], as well as high non-linear refractive index offering promising opportunities for on chip non-linear NIR-MIR devices.

[1] M. Tomelleri, F. Hippert, T. Farjot, C. Licitra, N. Vaxelaire, J.-B. Dory, D. Benoit, V. Giordano, and P. Noël, *Physica Status Solidi (RRL) – Rapid Research Letters* **15**, 2000451 (2021).

[2] Y. Zhang, J.B. Chou, J. Li, H. Li, Q. Du, A. Yadav, S. Zhou, M.Y. Shalaginov, Z. Fang, H. Zhong, C. Roberts, P. Robinson, B. Bohlin, C. Ríos, H. Lin, M. Kang, T. Gu, J. Warner, V. Liberman, K. Richardson, and J. Hu, *Nature Communications* **10**, 1 (2019).

2:30 PM BREAK

3:30 PM *EQ10.09.04

High-Performance Reconfigurable Infrared Metasurfaces with Phase-Change Materials [Kyung-Ah Son](#), Jeong-Sun Moon, Ryan Quarfoth, Hwa-Chang Seo, Chuong Dao, Elias Flores, Hanseung Lee and David Chow; HRL Laboratories, United States

Optical metastructures and metasurfaces are emerging with properties that could support the development of flat optics with aberration correction, ultrathin focusing lenses, resonant absorbers, polarimeters without moving parts, phase shifters, and holograms. Optical metasurfaces consisting of subwavelength optical resonators or antennas can provide control over the phase, amplitude, and polarization of incoming light, beyond what classical refractive and diffractive optical components can offer. Currently, there is growing interest in reconfigurable or tunable metasurfaces, which can add additional functionality enabling multi-functional dynamic optical components. Phase change materials (PCMs) have been recently explored for reconfigurable optical devices such as spatial light modulators [1,2] and metasurfaces [3,4], where the PCM-based reconfigurable resonant absorber concept has been demonstrated with an optical reflectance contrast of 40% - 75% in the Near-Infrared spectral range.

In this talk, we will present large-scale reconfigurable infrared metasurfaces consisting of greater than 30 million pixelated optical antennas integrated with PCM mesa structures over a 1cm x 1cm area, where the metasurfaces demonstrate 99% resonant absorption and state-of-the-art optical reflectance contrast at off-resonant wavelengths.

[1] J. S. Moon et al., *Proc. of SPIE Vol. 10982*, 2019

[2] J. S. Moon et al., *Proc. of SPIE Vol. 11389*, 2020

[3] Y. Zhang et al., *Nat. Nanotechnol.* **16**, 661–666 (2021)

[4] S. Abdollahramezani et al., arXiv:2014.10381 (2021)

4:00 PM *EQ10.09.05

Phase Change Materials for Reconfigurable Nanophotonic Applications [Qian Wang](#); Institute of Materials Research and Engineering, ASTAR, Singapore

Nanophotonics has garnered intensive interests owing to its unique capabilities on unprecedented manipulation of light in the subwavelength regime for high speed and large bandwidth information transmission and computation. However, to rival electronics in terms of integrability and reprogrammability, nanophotonics must evolve into the next generation miniaturized and reconfigurable platforms with tunable properties on demand. Chalcogenide phase-change materials (PCMs), which retain the “memory” of sub-threshold excitations and enable multiple-step gradual phase transition, have been identified as a promising platform for tunable and reconfigurable nanophotonic frameworks for ubiquitous functionalities from imaging and communication to sensing. In our work, we explore the multi-level optical phase transition of chalcogenide phase change material, Germanium-antimony-tellurium (GST), induced by femtosecond laser pulses. The pixelated phase change of GST in sub-micro marks results in a dramatic change in optical properties from amorphous to crystalline states. Various applications are demonstrated including high density data storage, re-writable flat photonics metamaterial, reconfigurable phase change photomask, and multi-step tuning of third harmonic generation. It is believed that the such reconfigurable mechanism of phase change materials will advance photonics in the next-generation light-related applications e.g. all-optical neuromorphic computing, adaptive optics, imaging/display, and engineering, etc.

Acknowledgements: This work is partially supported by the Agency for Science, Technology and Research (A*STAR) under AME IRG Grant Nos. A20E5c0095, and CDF Grant No. C210112044.

SESSION EQ10.10: Virtual Session I
Session Chairs: Wei Zhang and Min Zhu
Tuesday Morning, December 6, 2022
EQ10-virtual

8:00 AM EQ10.10.01

Ab Initio Calculations of the Electronic Properties of the Metastable β' -MnTe Phase for Terahertz Optical Switching Applications Paul Fons¹, Hiroyuki Tsuda¹, Toshiharu Saiki¹, Kotaro Makino², Yuta Saito², Shogo Hatayama², Yuji Sutou³, Yi Shuang³ and Mihyeon Kim³; ¹Keio University, Japan; ²National Institute of Advanced Industrial Science and Technology (AIST), Japan; ³Tohoku University, Japan

α -MnTe, the stable room temperature phase of MnTe, crystallizes in the NiAs hexagonal structure with space group P63/mmm (194). It is a p-type antiferromagnetic semiconductor with a bandgap of about 1.4-1.5 eV. The α -MnTe is known to transform in ambient conditions into the wide (2.7 eV) bandgap p-type β -MnTe semiconducting phase at approximately 1000°C. The β -MnTe phase assumes the Wurtzite structure with space group P6(3)mc (186) while at the same time experiencing a large (20%) decrease in density. The use of MnTe as a phase-change material has been recently reported in the form of an electrical device structure that exhibits bistable behavior and upon Joule heating switches between α -MnTe and a metastable phase β' -MnTe with a negligible change in density with a concomitant 10^3 increase in resistivity.[1] The temperature coefficient of resistivity suggests that the β' phase is semiconducting while TEM measurements indicate that the structure is Wurtzite with the same space group as the β -MnTe. Based upon TEM measurements, it was proposed that the transition from the α and β' phases is displacive in nature, but little is known about the electronic properties of the beta phase.

Recently some of the current authors have explored the use of another phase-change material $\text{Ge}_2\text{Sb}_2\text{Te}_5$ (GST) in optical switching applications in the infrared region. GST, however, suffers from a large extinction coefficient as well as a small contrast in refractive index outside of the infrared region. The use of MnTe as a material for optical interferometric switching offers the possibility of extending optical switching into the terahertz region, however, little is known about the optical and vibrational properties of the different phases of MnTe and in particular the β' -MnTe phase. We have investigated the optical and electrical properties of the α , β , and β' -phases of MnTe using ab-initio calculations with the plane wave code Vasp. We have carried out GGA+U calculations on the different phases using Hubbard U values determined by a self-consistent procedure to determine the equation of state of each phase as well as the dielectric properties of each phase. The calculated bandgap of the β' - was confirmed to be approximately three times that of the α -MnTe phase similar to that experiment trend between the α and β -phases. In addition, the calculated results indicate a small extinction coefficient and a large contrast in refractive index between the α , and β' -phases suggesting that MnTe may be an excellent candidate as a material for terahertz switching applications. Details of the dielectric constants, infrared absorption, equation of state, and other electronic properties will be reported.

[1] S. Mori, S. Hatayama, Y. Shuang, D. Ando, and Y. Sutou. Reversible displacive transformation in mnTe polymorphic semiconductor. Nat. Commun., 11(1):85, 2020.

Acknowledgement: These research results were obtained from research commissioned by National Institute of Information and Communications Technology (NICT), JAPAN.

8:15 AM *EQ10.10.02

Atom Probe Tomography—A Probe for Bond Breaking Experiments Oana Cojocaru-Miredin; RWTH Aachen University, Germany

Laser-assisted field evaporation is studied in a large number of compounds, including amorphous and crystalline phase change materials employing atom probe tomography. This study reveals significant differences in field evaporation between amorphous and crystalline phase change materials. High probabilities for multiple events with more than a single ion detected per laser pulse are only found for crystalline phase change materials. On the contrary, amorphous phase change materials as well as other covalently bonded compounds and metals possess much lower probabilities for multiple events. The origin of this stringent difference between crystalline and amorphous phase change materials has been investigated in this work. In fact, here we demonstrate that the field penetration depth is considerably higher for crystalline phase change materials with metavalent bonding than for amorphous phase change materials with covalent bonding or for metals with metallic bonding. These findings further consolidate the concept of metavalent bonding as being responsible for the outstanding physical properties and unusual bond-breaking behavior in atom probe tomography.

8:45 AM *EQ10.10.03

Ge-Rich GeSbTe Alloys—Material Properties and Devices Stefania M. Privitera; Consiglio Nazionale delle Ricerche, Italy

Enrichment of GeSbTe alloys with germanium has been proposed as a valid approach to increase the crystallization temperature and therefore to address high temperature applications of non-volatile phase change memories, such as embedded or automotive. Despite the achievement of higher crystallization temperature, Ge-rich GeSbTe alloys commonly suffer of segregation of pure Ge, with the formation of less Ge-rich compositions that may adversely affect the device cyclability and endurance. With the aim to find some possible routes to limit the Ge segregation, starting from the compositions along the GeTe-Sb₂Te₃ pseudo-binary line, we investigate several GeSbTe alloys enriched with low or high amount of Ge. The temperature dependence of the electrical properties of the amorphous alloys and the formation of the crystalline phases have been investigated in thin films by in situ electrical measurements and ex-situ structural analysis, determining the formed phases. The segregation and decomposition processes have been also discussed on the basis of density functional theory calculations, identifying the compositions which are expected to be less prone to decompose with Ge segregation. Single cell memory devices with the most promising material have been manufactured and tested. The characterization of the devices confirm the expected material performance. After a forming process, the device operates between two distinct logic states (SET and RESET) with one order of magnitude of resistance contrast, and can be reversibly switched for up to 10^6 cycles. Upon annealing for 1 h, the one order of magnitude resistance contrast is preserved up to 240°C, and the complete crystallization of the RESET state is not observed even for annealing at temperature up to 280°C.

9:15 AM EQ10.10.04

Identifying the Defect States in Chalcogenide Glass for Ovonic Threshold Switching Selector Meng Xu, Rongchuan Gu, Xiangshui Miao and Ming Xu; Huazhong University of Science & Technology, China

The recent development of 3D semiconductor integration technology demands a key component, the ovonic threshold switching (OTS) selector, to suppress the current leakage in the high-density memory chips. Yet, the unsatisfactory performance of existing OTS materials becomes the bottleneck of the industrial advancement. Due to the heavy first-principles computation on disordered systems, a universal theory to explain the origin of mid-gap states (MGS), which are the key feature leading to the OTS behavior, is still lacking. To avoid the formidable computational tasks, we adopt machine learning method to understand and predict MGS in typical OTS materials. We build hundreds of chalcogenide glass models and collect major structural features from both short-range order (SRO) and medium-range order (MRO) of the amorphous cells. After training the artificial neural network using these features, the accuracy has reached ~95% when it recognizes MGS in new glass. By analyzing the synaptic weights of the input structural features, we discover that the bonding and coordination environments from SRO and particularly MRO are closely related to MGS. The trained model could be used in many other OTS chalcogenides after minor modification. The intelligent machine learning allows us to understand the OTS mechanism from vast amount of structural data without heavy computational tasks, providing a new strategy to design functional amorphous materials from first principles.

9:30 AM EQ10.10.05

Combinatorial Exploration of New Phase-Change Memory Materials for Neuromorphic Computing Applications Heshan Yu¹, Asir Intisar Khan², Changming Wu³, Huairuo Zhang⁴, Albert Davydov⁴, Apurva Mehta⁵, Mo Li³, A. Gilad Kusne⁴, Eric Pop² and Ichiro Takeuchi¹; ¹University of Maryland, United States; ²Stanford University, United States; ³University of Washington, United States; ⁴National Institute of Standards and Technology, United States; ⁵Stanford Synchrotron Radiation Lightsource, United States

Neuromorphic computing, one of the non-von Neumann computing architectures, is recently developed to overcome the bottleneck of the data transfer between the processing and memory units in von Neuman computing architecture. As one of the most promising candidates for developing a neuromorphic architecture, phase-change memory materials (PCMs) in both photonic and electronic devices show fast non-volatile multi-level switching between the amorphous and crystalline states, but still have some shortcomings in meeting the demands of the neuromorphic computing, e.g., resistance drift, energy consumption, etc. With the assistance of machine learning, in particular, the closed-loop autonomous systems which can greatly accelerate screening materials for multiple properties, we have systematically performed combinatorial exploration targeting several fundamental properties across a broad composition range of M-Sb-Te ternary systems, where M is a transition metal. The composition spread libraries are fabricated on Si wafers by the co-sputtering method, and their composition ranges are measured by wavelength dispersive spectroscopy. To identify optimized compositions, X-ray diffraction measurements (synchrotron diffraction), Raman spectroscopy, resistance and optical property mapping are carried out. Some compositions are identified to show enhanced properties, e.g., Ge₄Sb₆Te₇ (GST467)^[1], Ti_{10.3}SbTe₂, etc. Compared to the widely-used Ge₂Sb₂Te₅ (GST225), these identified compositions show higher phase-change temperatures and lower melting point temperatures. The electrical devices fabricated using these phase-change memory compositions show clear multi-level switching with low resistance drift and low quenching energy. To determine the microstructure of the identified PCMs, scanning transmission electron microscope (STEM) measurements are carried out. They have revealed that TiTe₂ nanoprecipitates have grown homogeneously inside the Ti-Sb-Te matrix for Ti_{10.3}SbTe₂ and the SbTe nanoprecipitates have grown epitaxially with the GST matrix for GST467. We believe the nanocomposite configurations are playing the role of precursors which facilitate phase transformation processes. The results here suggest that these compositions can be promising for neuromorphic devices. This work is funded by an ONR MURI (Award No. N00014-17-1-2661) and the Center for Innovative Materials for Accelerated Compute Technologies (IMPACT), one of the centers in nCORE, a Semiconductor Research Corporation (SRC) program.

Reference

[1] A. Gilad Kusne et al. *Nat. Commun.* **11**, 5966 (2020)

9:45 AM EQ10.10.06

All-Dielectric Metagratings with Phase-Change Materials for Non-Volatile Reconfigurable Photonics in the MWIR to LWIR Nikolaos L. Tsitsas¹ and Stavroula Foteinopoulou²; ¹Aristoteleio Panepistemio Thessalonikes, Greece; ²University of New Mexico, United States

Non-volatile phase-change materials (PCMs) have opened up a multitude of possibilities in reconfigurable photonics, receiving a growing attention recently partially driven also by the relevance of these platforms to quantum and neuromorphic computing applications. The vast majority of these works focus around telecommunication wavelengths and incorporate GST, a material well known from the electronics industry used for re-writable optical data storage (CD-RW, DVD-RW). GST however can be reconfigured efficiently only at very small thicknesses of about 100 nm which limits transferring its use to MWIR and LWIR applications. Also the rather high optical loss in the crystalline phase of GST limits the range of high performing photonic designs for reconfigurable functionalities.

In this talk, we propose a new PCM-based platform functional in the MWIR to LWIR spectral range that leverages the fully dielectric properties and amorphous phase stability of a new PCM, belonging to a family of Ge-Sb-Se-Te (GSST) alloys [1], together with the strong beam re-direction capabilities of all-dielectric periodic metagratings [2]. We discuss the key underlying mechanisms and design principles of such platform that lead to reconfigurable beam splitting and beam steering. We believe these results are highly relevant in many infrared applications such as infrared components for integrated photonics, long-range lidar, etc.

[1] Y. Zhang et al., Broadband transparent optical phase change materials for high-performance nonvolatile photonics, *Nature Comm.* **10**, 4279 (2019).

[2] N. L. Tsitsas and C. Valagiannopoulos, Anomalous refraction into free space with all-dielectric binary metagratings, *Phys. Rev. Research* **2**, 033526 (2020).

10:00 AM DISCUSSION TIME

SESSION EQ10.11: Virtual Session II
Session Chairs: Juejun Hu and Ming Xu
Tuesday Afternoon, December 6, 2022
EQ10-virtual

6:30 PM EQ10.11.01

Crystallization Simulations of Amorphous Ge-Sb-Te Alloys Wei Zhang; Xi'an Jiaotong University, China

Ge-Sb-Te (GST) alloys are leading phase-change materials for non-volatile memory and neuro-inspired computing.^[1] Upon fast crystallization, these

materials form rocksalt-like phases with large structural and vacancy disorder, leading to an insulating phase at low temperature. Here, a comprehensive description of crystallization, structural disorder, and electronic properties of GeSb_2Te_4 based on realistic, quantum-mechanically based (ab initio) computer simulations with system sizes of more than 1000 atoms is provided.^[2] It is shown how an analysis of the crystallization mechanism based on the smooth overlap of atomic positions (SOAP) kernel reveals the evolution of both geometrical and chemical order. The connection between structural and electronic properties of the disordered, as-crystallized models, which are relevant to the transport properties of GST,^[3] is then studied. Furthermore, it is shown how antisite defects and extended Sb-rich motifs can lead to Anderson localization in the conduction band. Beyond memory applications, these findings are therefore more generally relevant to disordered rocksalt-like chalcogenides that exhibit self-doping, since they can explain the origin of Anderson insulating behavior in both *p*- and *n*-doped chalcogenide materials. References: [1] W. Zhang*, R. Mazzarello, M. Wuttig, E. Ma, *Nat. Rev. Mater.* 4 (2019) 150. [2] Y. Xu, Y. Zhou, X. Wang, W. Zhang*, E. Ma, V.L. Deringer, R. Mazzarello*, *Adv. Mater.* 34 (2022) 2109139. [3] W. Zhang, A. Thiess, P. Zalden, R. Zeller, P.H. Dederichs, J.Y. Raty, M. Wuttig*, S. Blügel, R. Mazzarello*, *Nat. Mater.* 11 (2012) 952.

6:45 PM *EQ10.11.02

Single-Element Switch [Min Zhu](#); Shanghai Institute of Micro-Systems and Information Technology, China

Nonvolatile phase-change memory has been successfully commercialized, but further density scaling below 10 nanometers requires compositionally and structurally homogeneous materials for both the memory cell and the associated vertically stacked two-terminal access switch. The selector switches are mostly amorphous chalcogenide Ovonic threshold switches (OTSs), operating with a nonlinear current response above a threshold voltage in the amorphous state. However, they currently suffer from the chemical complexity introduced by the quaternary or even more diverse chalcogenide compositions used. We present a single-element tellurium (Te) volatile switch with a large (≥ 11 MA/cm²) drive current density, $\sim 10^3$ ON/OFF current ratio, and faster than 20 nanosecond switching speed (Figure 1). The low OFF current arises from the existence of a ~ 0.95 eV Schottky barrier at the Te-electrode interface, whereas a transient, voltage pulse-induced crystal-liquid melting transition of the pure Te leads to a high ON current. Our discovery of a single-element electrical switch may help realize denser memory chips [1, 2].

Key words: Te, single-element, switch, Ovonic threshold switches, phase change memory

REFERENCES

1. J. Shen, S. Jia, N. Shi, Q. Ge, T. Gotoh, S. Lv, Q. Liu, R. Dronskowski, S. R. Elliott, Z. Song, M. Zhu, Elemental Electrical Switch Enabling Phase-Segregation-Free Operation, *Science*, 2021, 374, 1390.
2. R. Calarco and F. Arciprete, Keep it simple and switch to pure tellurium, *Science*, 2021, 374, 1321.

7:15 PM EQ10.11.03

Low-Entropy Phase Transition in Indium Selenide for Integrated Photonic Memory [Tiantian Li](#)^{1,2}, Yong Wang², Wei Li^{2,3}, Anderson Janotti², Stephanie Law² and Tingyi Gu²; ¹Xi'an University of Posts and Telecommunications, China; ²University of Delaware, United States; ³Los Alamos National Laboratory, United States

Optical phase change materials have emerged as key active components in logic and memory units for optical signal processing and storage. Antimony (Sb) based chalcogenides and chalcogenide alloys have been widely adopted in all-optical and optoelectronic memory technologies, including $\text{Ge}_2\text{Sb}_2\text{Te}_5$, $\text{Ge}_2\text{Sb}_2\text{Se}_4\text{Te}_1$, Sb_2Se_3 , and Sb_2S_3 , where the amorphous-to-recrystallization transitions emerge as an energy and speed bottleneck for these O-PCM memories. Distinguished atomic rearrangements in polymorphic layered chalcogenide materials have attracted great attention across multiple disciplines. The lattice constant dependent free energy between crystalline states across at the critical excitation level where the phase transition takes place. The low entropic crystalline-crystalline phase transitions potentially can revolutionize the power efficiency and data throughput in optical memristive devices. The research on crystalline-crystalline structural transitions for electronic memories has been limited to a few publications, and the phase transition pathways remain controversial. In this work, we focus on the transition between two layered crystalline states (α and β) of In_2Se_3 , which have the same underlying rhombohedral crystal system.

Temperature-dependent in-situ high energy x-ray diffraction and derived pair distribution functions reveal that the structural phase transitions between these two layered structures are achieved through 'inter-layer shear glide' and In-Se bond rearrangement. Differential scanning calorimetry measured reversible phase transition temperatures is around 220°C, compared to the melting temperature beyond 600°C in Sb-based O-PCM. The optical transparency at telecommunication wavelength is predicted by first-principal density functional theory calculations. The 0.81eV fundamental bandgap difference between the two states promises sufficient contrast of their refractive index and conductivity, according to Moss's rule and Kramers-Kronig relations. The measured complex refractive index spectra in molecular beam epitaxial grown continuous thin films confirm the optical bandgaps of both states are beyond 1eV. On the device level, nonvolatile all-optical switching is demonstrated in MBE-grown In_2Se_3 -silicon microring resonators with infrared light excited photo-thermal effect. The covered length of the transferred α -state flake on the silicon single-mode waveguide is around 1.5 μm . Transition into β -state was achieved at the exposure energy of 0.25 nJ. The resonance wavelength red-shifted 100 pm. The extinction ratio increased from 4.45dB to 6.27dB. With the linear coupled-mode-theory fitting of those transmission spectra, the extracted intrinsic quality factors were switched between 4,800 (α -state) and 7,500 (β -state), and the coupling quality factor was kept around 5,000. When the exposure energy increased to around 0.56 nJ, the resonance peak shifted back, and the extinction ratio decreased to the original value. The transistor arrays defined on the thin film measure thermally excited resistivity switching from 10^6 to 10^9 Ω cm. The polymorphic O-PCM's optical transparency at telecommunication and low entropic switching may break the power and speed bottleneck for integrated photonic in-memory computing systems.

7:30 PM EQ10.11.04

Mexican-Hat Potential Energy Surface in Two-Dimensional III₂-VI₃ Materials and the Role of Entropy Barrier in Their Ultrafast Reversible Ferroelectric Phase Change [Yu-Ting Huang](#), Nian-Ke Chen and Xian-Bin Li; Jilin University, China

Because of the spontaneous-aligned electric dipole, which can be switched reversibly by an external electric field, ferroelectric materials have been utilized for applications in nonvolatile memories and neuromorphic computing. However, the miniaturization of conventional ABO_3 ferroelectrics is hindered by the depolarization field. Recently, a new kind of two-dimensional (2D) van der Waals layered material, In_2Se_3 , has emerged as a potential solution for low-dimensional ferroelectrics due to its intrinsic ferroelectric polarization at the nanoscale, even down to the limit of a monolayer. At present, the atomic structure and ferroelectricity of the α phase have been firmly identified. However, the study of the paraelectric β phase is still lacking and even its atomic structure is controversial, which limits the speed of the ferroelectric phase transition. Here, using first-principles calculations and molecular dynamics studies, a unique Mexican-hat potential energy surface (PES) is identified for the family of 2D $\text{III}_2\text{-VI}_3$ materials for the first time.^[1] Taking In_2Se_3 as an example, the PES results in an unexpected pseudo-centrosymmetric (paraelectric) β phase where the presumed centrosymmetry is in fact broken at every moment, which resolves the current structural controversy between theory and experiment. We further show that while the α -to- β (ferroelectric-to-paraelectric) phase transition is fast and coherent, assisted by an in-plane shear phonon mode. However, a random distribution of the Se atoms in the trough of the Mexican-hat PES sets up a sizable effective entropy barrier to slow down the β -to- α transition considerably, which will be the origin of the speed limitation of current In_2Se_3 -based ferroelectric devices. If one orders the β phase (due to the formation of in-plane ferroelectric domains), the reverse transition can take place within tens of picoseconds in the presence of a perpendicular electric field. This study unfolds new physics in 2D $\text{III}_2\text{-VI}_3$

materials with important technological implications. Not only it unifies theory with experiment, but also it points to new directions for achieving ultrafast reversible ferroelectric phase change, whereby improving the performance of existing ferroelectric devices, such as memory and neural computing hardware, especially in terms of their integrated storage density and speed.

[1] I. Huang Y-T, Chen N-K, Li Z-Z, Li X-B, et al. Mexican-hat potential energy surface in two-dimensional III₂-VI₃ materials and the importance of entropy barrier in ultrafast reversible ferroelectric phase change. *Appl. Phys. Rev.* 2021;8(3):031413.

7:45 PM *EQ10.11.06

Atomic Imaging of Layered Structure Phase-Change Materials [Jiangjing Wang](#) and Wei Zhang; Xi'an Jiaotong University, China

Fast and reversible phase transitions in chalcogenide phase-change materials (PCMs), in particular, Ge-Sb-Te (GST) compounds, are not only of fundamental interests but also make PCMs based random access memory a leading candidate for nonvolatile memory, and neuromorphic computing devices. Disorder plays an essential role in shaping the transport properties of GST. Recently, increasing efforts have been undertaken to investigate disorder in the layer-structured GST compounds. In this work, we focus on hexagonal GST. We thoroughly characterized the structural and chemical features of the major defects in hexagonal GST at atomic scale through chemi-scanning transmission electron microscopy (STEM) experiments, including the stacking faults, the in-plane and out-plane twin-like structure, and a unique bilayer structure. By combining nanoscale density functional theory (DFT) modelling and simulations, we clarified the underlying reasons of the abundance of these defects and their effects on the electronic and transport properties of hexagonal GST.

8:15 PM DISCUSSION TIME

SYMPOSIUM NM01

Moire Superlattice of 2D Materials
November 29 - December 7, 2022

Symposium Organizers

Johannes Lischner, Imperial College London

Sufei Shi, Rensselaer Polytechnic Inst

Arend van der Zande, University of Illinois at Urbana Champaign

Jairo Velasco, Univ of California-Berkeley

* Invited Paper

+ Distinguished Invited

SESSION NM01.01: Correlated States in Moire Materials

Session Chairs: Sufei Shi and Tiancong Zhu

Tuesday Morning, November 29, 2022

Hynes, Level 2, Room 205

8:30 AM *NM01.01.01

Plethora of Many-Body Ground States in Magic Angle Twisted Bilayer Graphene [Dmitri A. Efetov](#); LMU Munich and Institut de Ciencies Fotoniques, Germany

Twist-angle engineering of 2D materials has led to the recent discoveries of novel many-body ground states in moiré systems such as correlated insulators, unconventional superconductivity, strange metals, orbital magnetism and topologically nontrivial phases. These systems are clean and tuneable, where all phases can coexist in a single device, which opens up enormous possibilities to address key questions about the nature of correlation induced superconductivity and topology, and allows to create entirely novel quantum phases with enhanced interactions. In this talk we will introduce some of the main concepts underlying these systems, concentrating on magic angle twisted bilayer graphene (MATBG) and show how symmetry-broken states emerge at all integer electron fillings [1]. We further will discuss recent experiments including screened interactions [2], Chern insulators [4], magnetic Josephson junctions [4], quantum criticality [5], re-entrant correlated insulators at high magnetic fields [6] and discuss some of the avenues for novel quantum sensing applications [7].

[1] Nature, 574, 653 (2019).

[2] Nature, 583, 375–378 (2020).

[3] Nature Physics, 17, 710 (2021).

[4] arXiv:2110.01067 (2021).

[5] arXiv:2108.07753 (2021).

[6] arXiv:2201.09260 (2021).

[7] arXiv:2111.08735 (2021).

9:00 AM *NM01.01.02

Correlated Electronic States in TMD Moire Superlattices Probed by Microwave Impedance Microscopy [Yongtao Cui](#); University of California Riverside, United States

Moire superlattices formed by angle-aligned multilayer stacks of 2D materials have recently become a rich platform to discover novel electronic states, such as superconductivity, correlated insulators, and magnetism. In this talk, I will talk about our recent work on the study of correlated states in moire superlattices of semiconducting transitional metal dichalcogenides monolayers. We employ scanning microwave impedance microscopy to probe the local conductivity of these moire superlattices. We find that correlated insulating states can appear when the moire superlattice is partially filled with carriers at simple fractional fillings. When additional layers are introduced in the moire structure, we find that the correlated states can be manipulated in various ways. By applying an electric field, the carriers can be driven to populate in two different layers yet still form insulating states, which can be interpreted as an excitonic insulator.

9:30 AM *NM01.01.03

Electronic Control of Magnetism in Magnetic Chern Insulators [Charles Tschirhart](#)¹, [Evgeny Redekop](#)¹, [Lizhong Li](#)², [Tingxin Li](#)³, [Shengwei Jiang](#)³, [Kenji Watanabe](#)⁴, [Takashi Taniguchi](#)⁴, [Martin Huber](#)⁵, [Kin Fai Mak](#)² and [Jie Shan](#)²; ¹UCSB, United States; ²Cornell University, United States; ³Shanghai Jiao Tong University, China; ⁴National Institute for Materials Science, Japan; ⁵University of Colorado Denver, United States

A variety of intrinsic magnetic Chern insulators have been discovered in moiré superlattice systems, including in both graphene and transition metal dichalcogenide heterostructures. Unlike in previously discovered magnetic Chern insulators, fabricated by adding magnetic dopants to thin films of topological insulators, these systems have magnetism supported entirely by electronic interactions intrinsic to the topological bands. This fact helps limit disorder in these systems by removing the need for magnetic dopants, but it also intimately ties the magnetic order to electronic properties of the system, and thus facilitates electronic control of magnetism. I will discuss electronic switching of magnetization in Chern insulators through two different mechanisms: topological contributions to magnetization and intrinsic spin-orbit torques. I will explain how these mechanisms work in practice in twisted monolayer/bilayer graphene and in AB-WSe₂/MoTe₂ using transport measurements and magnetic imaging performed with our nanoSQUID microscope.

10:00 AM BREAK**10:30 AM *NM01.01.04**

Experimental Investigation of Non-Trivial Band Topology and Quantum Geometry in van der Waals Materials [Chun Ning \(Jeanie\) Lau](#); The Ohio State University, United States

The interplay between quantum confinement, non-trivial band topology, symmetries and electronic interactions gives rise to a rich variety of correlated phenomena and topological phases in van der Waals heterostructures. Here I will present our recent works on this topic, focusing on tunable transport of charges and Cooper pairs in quasi-1D topological insulators, emergent magnetism in rhombohedral-stacked few-layer graphene, and strongly renormalized band velocity and experimental evidence for strong-coupled superconductivity that is enabled by quantum geometry in twisted bilayer graphene.

11:00 AM *NM01.01.05

Diverse Nature of Excitonic States in Transition Metal Dichalcogenide Moiré Superlattices [Mit H. Naik](#)^{1,2}; ¹University of California at Berkeley, United States; ²Lawrence Berkeley National Laboratory, United States

Recent experimental measurements have demonstrated signatures of novel exciton states in moiré superlattices of bilayer transition metal dichalcogenides. However, the microscopic nature and origin of these moiré excitons was not well understood, and previous studies relied often on empirically fit models that did not fully account for the electron and hole degrees of freedom of the exciton. We performed state-of-the-art first-principles *GW*-Bethe Salpeter equation calculations and discovered a rich diversity of excitonic states in large-area transition metal dichalcogenide moiré superlattices. These studies, which involve thousands of atoms in the reconstructed moiré unit-cell, are made possible by a novel computational approach we developed, the pristine unit-cell matrix projection (PUMP) method [1]. In rotationally aligned WSe₂/WS₂ moiré superlattice, we find some excitons of a modulated Wannier character and others of a previously unidentified intralayer charge-transfer character [1]. In 57.7° twisted bilayer WS₂, we discover layer-hybridized excitons with in-plane charge transfer character. These characteristics originate from the strong modulation of electron wavefunctions due to atomic reconstructions of the moiré superlattice. Due to the weaker binding and larger spatial extent of the in-plane charge-transfer excitons, they can be strongly modulated by external electrical field, doping charges, and substrate screening. Experimental reflection contrast [1], electron energy loss spectroscopy [2] and scanning tunneling spectroscopy confirm these predictions.

Acknowledgment: This work is supported by the U.S. Department of Energy and the National Science Foundation, and the theoretical studies are done in collaboration with Y. Chan, Z. Li, C. S. Ong, W. Kim, F. H. da Jornada and S. G. Louie.

References:

- [1] M. H. Naik, E. C. Regan, Z. Zhang, ..., F. H. da Jornada, F. Wang and S. G. Louie, "Intralayer charge-transfer moiré excitons in van der Waals superlattices", *Nature* 609, 52–57 (2022)
- [2] S. Susarla, M. H. Naik, ..., F. H. da Jornada, S. G. Louie, P. Ercius and A. Raja, "Hyperspectral imaging of excitons within a moiré unit-cell with a sub-nanometer electron probe", arXiv:2207.13823 (2022)

11:30 AM *NM01.01.06

Moiré Effects Approaching and Within the Bulk Graphitic Limit [Matthew Yankowitz](#); University of Washington, United States

Moiré quantum materials have recently emerged as highly tunable platforms for the study of strongly correlated and topological states of matter. Although first realized in twisted bilayer graphene, a wealth of new physics has recently been discovered in other twisted multilayer graphene structures. Here, I will discuss an array of moiré-driven effects that emerge in the family of twisted $M+N$ graphene multilayers, defined as structures created by stacking and slightly rotating M -layer and N -layer Bernal-stacked graphene sheets. We observe spontaneous isospin symmetry breaking and signatures of non-trivial topology in a wide variety of these structures (e.g., $t1+2$, $t2+2$, $t1+3$, $t2+3$, etc). Although the precise details vary across platforms, we find an apparent universality of the overall correlated phase diagram resulting from the similar flat moiré bands of these different structures. We further discover entirely new types of moiré reconstruction effects upon entering the bulk graphitic limit, in which the total number of graphene layers exceeds ~ 10 (e.g., $t1+10$). The surface moiré potential can strongly modify the transport properties of the entire bulk graphite sheet, indicating the dominant role of the band hybridization at the moiré interface. Our work points toward a general understanding of strongly correlated and topological states, as well as moiré band reconstruction, in multilayer graphitic systems with a single rotated interface.

SESSION NM01.02: Imaging and Tailoring Moire Superlattices
Session Chairs: Jairo Velasco and Matthew Yankowitz
Tuesday Afternoon, November 29, 2022
Hynes, Level 2, Room 205

1:30 PM *NM01.02.01

The Quantum Twisting Microscope [Shahal Ilani](#); Weizmann Institute of Science, Israel

In this talk I will present a fundamentally new type of scanning probe microscope, the Quantum Twisting Microscope (QTM), capable of performing local quantum interference measurements at a twistable interface between two quantum materials. Its working principle is based on a unique tip, made of an atomically-thin two-dimensional material. This tip allows electrons to coherently tunnel into a sample at many locations at once, with quantum interference between these tunneling events, making it a scanning electronic interferometer. With an extra twist degree of freedom, our microscope becomes a momentum-resolving local probe, providing powerful new ways to study the energy dispersions of interacting electrons. I will present various experiments performed with this microscope, demonstrating quantum interference at room temperature, probing the conductance of in-situ twisting interfaces, and imaging local energy dispersions in a variety of quantum materials.

2:00 PM *NM01.02.02

Quantitatively Mapping Relaxation in Moiré Superlattices Using Interferometric 4D-STEM [Daniel K. Bediako](#); University of California, Berkeley, United States

It is now well established that changing the relative orientation and/or lattice constant mismatch between vertically-stacked single atomic layers modulates emergent physicochemical behavior through the formation of moiré superlattices. However, the band structures and emergent physics of moiré materials are highly sensitive to spontaneous structural deformations, namely lattice relaxation (or “atomic reconstruction”) and resulting intrinsic strain fields, in addition to extrinsic/incidental heterostrain. While it is widely accepted that lattice reconstruction universally occurs in moiré superlattices with small twist angles, direct experimental information regarding the mechanics of the relaxation process and the manifestation of intralayer strain remains limited. This knowledge gap presents critical impediments for generating accurate models that would allow the rational design and interpretation of the electronic/optical/photonic behavior in these systems. To address this challenge, we have developed Bragg interferometry, an imaging methodology that translates intensity information from scanning transmission electron microscopy diffraction data into quantitative measurements of intralayer deformations in encapsulated moiré superlattices. This talk will cover insights into measurements of lattice relaxation in twisted bilayer and trilayer graphene, as well as moiré superlattices of transition metal dichalcogenides. The results of this work serve to deepen our understanding of fundamental structure–property relationships in moiré superlattices and provide a framework for leveraging structural distortions and strain as additional tuning knobs for modifying the unique (opto)electronic behavior of these structures.

2:30 PM NM01.02.03

Tailoring Moiré Wavelength in van der Waals Heterostructures via Interfacial Heterostrain from Thin-Film Stress Capping Layers [Mohammad A. Hossain](#)¹, [Yue Zhang](#)¹, [Kelly Hwang](#)¹, [Paolo Ferrari](#)¹, [Edmund Han](#)¹, [Priti Kharel](#)¹, [Tara Pena](#)², [Joe Maduzia](#)¹, [Stephen M. Wu](#)², [Pinshane Y. Huang](#)¹ and [Arend M. van der Zande](#)¹; ¹University of Illinois at Urbana-Champaign, United States; ²University of Rochester, United States

Due to their high deformability, two-dimensional (2D) materials are ideal candidates for using strain engineering to manipulate the electronic structure and material properties. One system ripe for strain engineering is the moiré superlattice created by stacking nearly commensurate 2D layers. Moiré systems show diverse physics, which are extremely sensitive to the structure and size of the moiré superlattice such as “magic angle” superconductivity in bilayer graphene or strongly bound interlayer excitons in reconstructed transition metal dichalcogenide heterostructure superlattices. Most studies use interlayer twist to generate the moiré superlattice. However, generating an interlayer heterostrain has been proposed as a more flexible tool for inducing the moiré superlattice by modulating the relative lattice constant between the layers. Developing new strategies to induce and tailor heterostrains will open up new dimensions of materials design in moiré superlattices.

An enormous opportunity comes by borrowing techniques developed for strain engineering in the semiconductor industry to apply strain to 2D materials by depositing thin film stress capping layers i.e., MgO, MgF₂, etc. [1]. These approaches apply the strain from the top down, suggesting the enticing possibility for controlled heterostrain in 2D heterostructures.

Here, we investigate strain transfer across the van der Waals interface in twisted MoS₂-WSe₂ heterostructures. We deposited MgO through a shadow mask onto a MoS₂-WSe₂ heterostructure, to generate a patterned array of squares with regions covered and not covered by the stressor. We used Raman spectroscopy to measure the E_{1_{2g}} and A_{1g} peak positions between stressed and unstressed regions on the heterostructure and deconvolved the applied strain and doping effects in the MoS₂ layer by extracting the relative shift in both peaks. To quantify the heterostrain between the constituent layers, we deposited the stressor on two opposite stacking configurations: MoS₂(top)-WSe₂(bottom) and WSe₂(top)-MoS₂(bottom). At the center of a square with 30 nm thick MgO, when MoS₂ is the top layer, the applied tensile strain reaches up to 0.8%. In contrast, when MoS₂ is the bottom layer, tensile strain is limited to less than 0.2%, demonstrating that strain transfer to the bottom layer is minimal due to slip at the 2D interface. The magnitude of the applied strain scales with the thickness of the stressor layer, showing the ability to tailor the heterostrain in 2D heterostructures by more than 0.6%/layer.

To understand how quickly the interlayer heterostrain equilibrates away from the localized stressor layer, we performed hyperspectral Raman mapping and generated spatial maps of the local strain and doping. We found that for the top layer, there is a sharp drop in strain at the edge of the stressor, but some strain extends significantly beyond the edge, taking up to 12 μm to reach equilibrium generating an in-plane heterostrain gradient of ~0.06% strain/μm. This indicates that the low friction at van der Waals interfaces allow heterostrains to propagate for long distances.

Heterostrains show strong potential for tailoring the moiré superlattice wavelength: a 1% strain in an aligned bilayer is equivalent to a 0.6 degree twist, while 1% strain can modify the moiré wavelength in 1° twisted bilayer by more 10%. This is the regime where much of the most interesting physics and interfacial mechanics occurs. We will explore the potential for using dark field electron microscopy or scan probe techniques to directly measure modifications to the moiré wavelength induced by heterostrain.

Taken together, heterostrains via stress capping layers show many new opportunities for spatially patterned or anisotropic moiré superlattices.

References:

[1] Peña, T., et al., Strain engineering 2D MoS₂ with thin film stress capping layers. *2D Materials* 2021, 8, 045001.

2:45 PM BREAK

3:15 PM *NM01.02.04

Scanning Tunneling Microscopy of Twisted 2D Semiconductors [Adina Luican-Mayer](#); University of Ottawa, Canada

In this talk we discuss scanning tunneling microscopy studies of ferroelectric domains at symmetry-broken interfaces of marginally twisted WS₂ films. The analysis of the ferroelectric domain network can give detailed information about the deformations in the assembled layers and we demonstrate that one can achieve full control over the conditions for the redistribution of polarization across the domain network.

We discuss two characteristic regimes of domain evolutions: approximately equilateral triangular stacking order domains featuring partial dislocation at the domain boundary, and elongated triangular domain in which the primary domain walls merge, achieving perfect screw dislocation. The domain geometry was found to be well described by a simple string-like model, allowing for parameter-free prediction of domain wall shapes and lengths in the elongated triangle regime.

3:45 PM *NM01.02.05

In Situ Imaging of Atomic Interfaces of 2D Materials [Yichao Zhang](#)¹, Chia-Hao Lee¹, Huijie Ryu², Ji-Hwan Baek², Gillian Nolan¹, Gwan-Hyong Lee² and Pinshane Y. Huang¹; ¹University of Illinois at Urbana-Champaign, United States; ²Seoul National University, Korea (the Republic of)

Scanning transmission electron microscopy (STEM) provides uniquely powerful tools to study the interfacial structure and interactions of 2D materials up to atomic resolution. In my talk, I will discuss how we create and utilize 2D multilayer stacks to create nanoscale laboratories for studying the atomic structure, structural transformations, and properties of 2D interfaces inside the STEM. We utilize graphene encapsulation in combination with a MEMS-based heating holder to conduct in-situ studies of solid-solid phase transformations and interfacial restructuring in 2D transition metal dichalcogenides. Here, graphene encapsulation protects the 2D materials of interest from the vacuum environment of the STEM, enabling in-situ high temperature studies up to 1000°C. We use these structures to directly visualize phenomena such as the layer-by-layer phase transformation of MoTe₂ and the lattice reconstruction of 2D moirés.

4:15 PM *NM01.02.06

Local Spectroscopy of Gate-Tunable Correlated Chern Insulating State in Twisted Monolayer-Bilayer Graphene [Tiancong Zhu](#)^{1,2}; ¹University of California, Berkeley, United States; ²Lawrence Berkeley National Laboratory, United States

Twisting and stacking two-dimensional van der Waals materials provides a versatile platform for investigating emergent quantum phases of matter driven by strong correlation and non-trivial topology. One example is twisted monolayer-bilayer graphene (tMBLG), where correlated Chern insulating states with electrically switchable magnetic order have been recently demonstrated in transport measurements. I will discuss scanning tunneling microscopy (STM) measurements where high spatial resolution provides new insight into the interplay between correlation, topology, and local structural distortion in determining the electronic and magnetic properties of tMBLG. Our STM spectroscopy (STS) provides evidence for the formation of interaction-driven energy gaps at both 1/2- and 3/4- filling of a moiré mini-band in tMBLG. Magnetic-field-dependent STS measurements further indicate a non-zero total Chern number of $C_{\text{tot}} = \pm 2$ for the 3/4-filled correlated insulating state. In certain regions of the sample, we find that the sign of C_{tot} can be reversed via electrostatic gating in a finite magnetic field, consistent with the electrically switchable magnetic order reported in previous transport studies. This electrical reversibility, however, is not universal and depends strongly on the local hetero-strain (relative strain between the monolayer and bilayer graphene) in tMBLG. The electrical switching of magnetic order appears to result from a competition between the orbital magnetization of filled bulk bands and chiral edge states that is highly sensitive to strain-induced distortion of the moiré superlattice. Our finding illustrates the critical role of local environmental factors in shaping correlation and topology in twisted two-dimensional systems.

SESSION NM01.03: Optical Properties of Moire Materials

Session Chairs: Sufei Shi and Stephen Wu

Wednesday Morning, November 30, 2022

Hynes, Level 2, Room 205

8:30 AM *NM01.03.01

Transport of Confined One-Dimensional Excitons at Monolayer Lateral Heterojunctions [Libai Huang](#); Purdue University, United States

Atomically precise lateral heterojunctions based on transition metal dichalcogenides provide a new platform for confining excitons in one-dimensional (1D). Here, we present the transport of 1D interfacial excitons in a type II WSe₂-WS_{1.16}Se_{0.84} lateral heterostructure using ultrafast microscopy with ~200 fs temporal resolution and nanoscale spatial resolution. Our measurements revealed highly mobile 1D interface exciton at room temperature. Strong repulsive exciton-exciton interactions led to enhanced exciton transport along 1D interface than 2D interlayer excitons in conventional transition metal dichalcogenides heterobilayers. These results highlight that atomically thin lateral heterojunctions can be designed as novel “highways” for excitons.

9:30 AM *NM01.03.03

Imaging Correlated Quantum Phases in van der Waals Heterostructures Feng Wang, Michael Crommie, [Hongyuan Li](#) and Ziyu Xiang; Univ of California-Berkeley, United States

Van der Waals heterostructures of atomically thin crystals offer an exciting new platform to design flat electronic bands for novel correlated quantum phases. We systematically study the flat band and associated correlated states in WS₂/WSe₂ moire heterostructures using scanning tunneling microscopy (STM). We reveal that three-dimensional lattice reconstruction plays a key role in determining the flat moire minibands in the WS₂/WSe₂ heterostructure. We further probe correlated electron physics in transition metal dichalcogenide heterostructures, including imaging generalized Wigner crystal states in the WS₂/WSe₂ moire superlattice and the Wigner crystal states in monolayer WS₂.

9:15 AM BREAK

10:00 AM *NM01.03.04

Layer-Modulated Moiré Excitons and Excitonic Insulator Phase in a Heterojunction Moiré Superlattice Zhen Lian¹, Dongxue Chen¹, Xiong Huang², Ying Su³, Mina Rashednia⁴, Lei Ma¹, Li Yan¹, Mark Blei⁵, Li Xiang⁶, Sefaatin Tongay⁵, Dmitry Smirnov⁶, Zenghui Wang⁷, Chuanwei Zhang³, Yong-Tao Cui⁴ and Su-Fei Shi^{1,1}; ¹Rensselaer Polytechnic Institute, United States; ²Columbia University, United States; ³The University of Texas at Dallas, United States; ⁴University of California, United States; ⁵Arizona State University, United States; ⁶National High Magnetic Field Lab, United States; ⁷University of Electronic Science and Technology of China, China

The moiré superlattices of 2D semiconductors exhibit many novel physics phenomena, including moiré excitons and correlated insulating states. While extensive studies have been conducted to investigate the properties of the moiré superlattices between monolayer TMDCs, the effect of the layer degree of freedom on moiré excitons and correlated insulating states remains uninvestigated. In the first part of this work, we demonstrate layer-modulated moiré excitons and correlated insulating states in WSe_2/WS_2 moiré superlattices. We investigate reflectance contrast spectra of WS_2/WSe_2 moiré heterostructures with varying WSe_2 layer number. The layer degree of freedom strongly modifies the resonant energies of the moiré excitons. In addition, the 1L/2L and 1L/3L WS_2/WSe_2 show an extra excitonic peak close to the original WSe_2 A-exciton resonance, a result of the interfacial nature of the moiré coupling. The carrier density to reach each correlated insulating state is the same for 1L/1L, 1L/2L and 1L/3L WS_2/WSe_2 , indicating the moiré flat band is isolated from the trivial valence bands from the additional WSe_2 layers.

Based on the above result, we further show that the valence bands of the 1st and the 2nd WSe_2 layer in 1L/2L WS_2/WSe_2 can be tuned to overlap by applying an electric field. Holes can partially populate the 2nd WSe_2 layer at a total filling of one hole per moiré supercell, which is evidenced by the emergence of exciton-polarons from the 2nd WSe_2 layer. The abrupt changes of peak positions and intensities of moiré excitons suggest that the system is in an insulating state at $n=-1$. From particle-hole transformation, electron-like carriers reside in the moiré flat band of the 1st WSe_2 layer and are bound with holes in the 2nd WSe_2 layer due to strong Coulomb interaction, forming an excitonic insulator phase. Our result demonstrates a new moiré system for the study of correlated many-body physics in two dimensions.

10:30 AM NM01.03.05

Low-Frequency Raman Study in Precisely Controlled Interlayer Twist Angle Using Etchant-Free Thin-Film Transfer Manpreet Boora¹, Yu-Chuan Lin², Chen Chen², Joan M. Redwing² and Jae Yong Suh¹; ¹Michigan Technological University, United States; ²The Pennsylvania State University, United States

Two-dimensional transition metal dichalcogenides (TMDs) have attracted great attention because of their scalability and tunability of optical bandgaps depending on the number of stacked layers. Twisted TMDs have gained even more interest because of the additional degree of freedom arising from the twist angle, which provides a controllable playground for studying phonon-phonon couplings, twist angle-dependent interlayer excitons, and charge transfer dynamics. A monolayer of TMDs has a stoichiometry of MX_2 where M is a transition metal ($M = W$ or Mo) sandwiched between two layers of chalcogen atoms ($X = S, Se$). For twisted bilayer graphene, the magic angle is 1.1° , and the flat band appears only for a narrow range of twist angles ($1.1^\circ \pm 0.1^\circ$). For TMDs, however, there exists a wider range of twist angles, spanning from 4° to 5° . Moreover, long-wavelength Moiré superlattices arise either from a difference in the lattice constant or a twist angle between two stacked layers. These Moiré patterns in twisted TMD bilayers have emerged as a highly tunable platform for studying strongly correlated electron physics.

Our research focuses on the precise control of the interlayer twist angle with a clean and large interfacing area. For making stacked bilayer homo and heterostructures, the individual monolayer used in our research is epitaxially grown coalesced films using the growth method of Metalorganic Chemical Vapor Deposition (MOCVD) on a 2" sapphire substrate. The highlight of our work firstly lies in making controlled twisted bilayer high-quality large-area samples (9 by 9 mm²). The degree of twist angle is controlled using a special transfer stage to stack WS_2 bilayers with a range of twist angles from $0^\circ, 1^\circ, 2^\circ, 3^\circ, 5^\circ, 7^\circ, 9^\circ, 10^\circ, 15^\circ, 20^\circ$ to 30° . The significance of our work includes creativity in stacking these large area bilayers using an etchant-free transfer method. As the monolayer is grown on a sapphire substrate and only the second layer is transferred, it makes the interface between the two layers cleanest which is very important to study the interlayer excitons and phonons. AFM images support the claim of high quality of transferred films as there are no pores or cracks in the films which usually arises in other transfer techniques like wet transfer methods. Our work makes a significant contribution to understanding phonon interactions using Raman spectroscopy for twisted bilayer structures. Low-frequency Raman modes are studied using 488 nm (ultra-frequency laser) excitation to map the dependence of inter-layer breathing and shear modes showing up in the range of -50 cm^{-1} to 50 cm^{-1} wavenumbers. For small twist angles ($2^\circ, 3^\circ$, and 5°) moiré phonons start appearing and then disappears in case of large twist angle. Our works report the first-time mapping of low-frequency Raman modes (-100 cm^{-1} to 100 cm^{-1}) and high-frequency Raman modes using resonant laser 532 nm and non-resonant laser 488 nm excitation source for WS_2 twisted bilayers. We will also discuss the results of temperature-dependent photoluminescence and optical absorption showing the evolution of interlayer coupling in twisted TMDs.

10:45 AM *NM01.03.06

Optical Sensing of Semiconducting Moiré Superlattices Chenhao Jin; UC Santa Barbara, United States

Moiré superlattices formed between two-dimensional (2D) materials provide new opportunities to engineer novel quantum phenomena, as exemplified by the intriguing observations in twisted bilayer graphene (tBLG). Semiconducting transition metal dichalcogenides (TMDCs) represent another distinct class of moiré system, where the low-energy physics is largely captured by a single-band Hubbard model. In this talk, I will discuss our efforts to study semiconducting moiré superlattices with optical spectroscopies. Taking advantage of the strong light-matter interaction in 2D semiconductors, we access various correlated phases with high sensitivity optical probe. The imaging capability further allows us to look into their spatial variations in wide field.

SESSION NM01.04: Synthesis and Mechanical Properties
Session Chairs: Adina Luican-Mayer and Arend van der Zande
Wednesday Afternoon, November 30, 2022
Hynes, Level 2, Room 205

1:30 PM *NM01.04.01

New 2D with Atomically Thin Crystals Jiwoong Park; University of Chicago, United States

2D van der Waals (vdW) crystals provide a powerful materials platform for studying two dimensional (2D) electron transport. In this talk, I will start with the large-scale processes for generating 2D crystalline semiconductor films and superlattices that could be used to fabricate atomically thin integrated circuits. Then we will discuss new directions, where we use these 2D materials to realize non-electronic 2D transport phenomena, for example, observed

from phonons, photons, and mass. These new approaches could empower the development of 2D phononics, 2D photonics, and 2D mechanics.

2:00 PM NM01.04.02

In-Plane Thermal Conductivity of Twisted 2D Materials [Sorren Warkander](#)¹, Zhuowu Wu², AKM Newaz² and Junqiao Wu^{1,3}; ¹University of California, Berkeley, United States; ²San Francisco State University, United States; ³Lawrence Berkeley National Laboratory, United States

The physics of moiré heterostructures and the opportunity to tune the properties of 2D materials via the twist degree of freedom has seen substantial interest in recent years. However, thermal properties, especially in-plane thermal conductivities, have seen minimal study. The large moiré supercell present for 2D materials stacked at small twist angles and the resultant zone folding may lead to reduced in-plane thermal conductivity; shifts in low-energy phonon modes due to twisting may also impact thermal properties. Molecular dynamics simulations for both graphene and molybdenum disulfide predict reduced in-plane thermal transport in twisted structures. For MoS₂ and for graphene at relatively large twist angles, greater suppression is seen for larger moiré supercells; in graphene at small angles a partial recovery of the thermal conductivity has been predicted, implying the existence of a critical twist angle at which thermal conductivity is minimized. Despite these interesting results, experimental work on twisted bilayer systems has been very limited.

We have recently developed a new technique, transducerless time domain reflectance (tTDR), that allows the use of a standard time domain thermoreflectance (TDTR) setup to measure the thermal properties of semiconductors without the requirement of the metal transducer layer typically used in TDTR measurements. This enables the measurement of ultra-thin materials where a transducer layer would thermally short the sample. In this work, we use tTDR measurements to study the in-plane thermal conductivity of suspended 2D materials, seeking to understand the properties of native few-layer samples and twisted bilayer moiré heterostructures.

2:15 PM BREAK

3:15 PM *NM01.04.04

Modulation of Moiré Superlattice and van der Waals Interaction in Stacked 2D Layers [Gwan-Hyong Lee](#); Seoul National University, Korea (the Republic of)

Van der Waals (vdW) heterostructures have attracted widespread attention because of their intrinsic interfacial properties and a large degree of freedom in designing heterointerfaces. It has been demonstrated that moiré superlattice in stacked 2D layers induces unprecedented properties of vdW heterostructures, such as moiré exciton, confined quantum transport, and superlattice reconstructions. In this talk, I will introduce how to modulate moiré superlattice and vdW interaction at the heterointerface of different 2D materials. I will show atomic reconstruction of the twisted transition metal dichalcogenide (TMD) layers into full commensurate phase by using encapsulation annealing with hexagonal boron nitride (hBN). The full commensurate phase of two TMD layers showed strong enhancement of photoluminescence from interlayer exciton, which indicates that the momentum coordinates of two different TMD layers are well aligned after encapsulation annealing. I will also show the abnormal in-plane anisotropic conductivity of MoO₃/graphene heterostructure that has an elongated superlattice due to a large mismatch of lattices and crystal structures. The periodic potential of MoO₃ single crystal deposited on the graphene induces a distortion of the graphene band structure near Fermi level of graphene, leading to electrical anisotropy in the graphene. Our work shows novel strategies to modulate moiré superlattice and vdW interaction in stacked 2D layers.

3:45 PM *NM01.04.05

Strain Engineering 2D Moiré Superlattices [Stephen M. Wu](#); University of Rochester, United States

Strain engineering in electronics has been widely utilized over the last 20 years to enhance carrier mobility in most standard Si-based CMOS fabrication processes. These process-induced strain engineering techniques, engineered from the nanofabrication process itself, are simple, reliable, applied device-to-device, and highly scalable down to the nanometer scale. Here, we talk about how process-induced strain engineering translates to the world of 2D materials, and how this may be applied to twisted bilayer van der Waals heterostructures to deterministically engineer moiré superlattice structure. Using the deposition of high-stress thin films [1-3], we show a high level of control over layer-by-layer strain in magnitude, directionality, uniaxiality/biaxiality, and tension/compression in 2D heterostructures. This is a damage-free process, that is reliable to low temperatures (at least 4 K), highly time stable (at least 14 mos.), and can be used up to the strain soliton creation limit, typically 2% in most transition metal dichalcogenide (TMDC) systems. We show this technique can be used on high-angle twisted bilayers, as well as low-angle twisted bilayers where reconstruction effects dominate. Optical spectroscopy combined with real space moiré visualization will be used to show the effects before and after strain engineering is applied. Discussion about how these strain engineering techniques may be used to tame uncontrolled strains in 2D moiré heterostructures will also be addressed.

[1] T. Peña, et al., *2D Mater.* **8**, 045001 (2021)

[2] A. Azizimanesh, et al., *Appl. Phys. Lett.* **118**, 213104 (2021)

[3] T. Peña, et al., *J. Appl. Phys.* **131**, 024304 (2022)

4:15 PM NM01.04.06

Universal Torsional Periodic Lattice Distortion in Twisted 2D Materials [Suk Hyun Sung](#)¹, Yin Min Goh¹, Hyobin Yoo², Rebecca Engelke³, Hongchao Xie¹, Zidong Li¹, Andrew Ye⁴, Parag B. Deotare¹, Andrew J. Mannix⁵, Jiwoong Park⁴, Liuyan Zhao¹, Philip Kim³ and Robert Hovden¹; ¹University of Michigan, United States; ²Sogang University, Korea (the Republic of); ³Harvard University, United States; ⁴The University of Chicago, United States; ⁵Stanford University, United States

At low twist angles, moiré heterostructures periodically restructure and spontaneously break symmetry to form complex superstructures [1,2,3]. Periodic restructuring of twisted 2D materials is a direct consequence of competition between interlayer van der Waals registry energy and intralayer elastic energy cost. Here, we use a torsional periodic lattice distortion (PLD) model [4] to concisely describe the relaxed superstructure and electron diffraction patterns across a variety of twisted 2D materials. The moiré of twisted bilayer graphene (TBG) periodically unwinds energetically favorable AB/BA stacked regions to increase AB/BA area, and unfavorable AA stacked regions are further twisted to decrease their area. We use a torsional PLD model to describe the in-plane distortion of twisted 2D materials. The torsional PLD (Δ_N) is made-up of three non-orthogonal, transverse distortion waves of equal amplitudes and harmonics thereof.

Torsional PLDs in twisted 2D materials are a universal phenomenon at low twist angles and not limited to TBG [2,3,5,6]. We found evidence of torsional PLD existing in four distinct twisted 2D systems: a) low twist angle TBG, b) 4-layer (4L) of WS₂, c) twisted double bilayer CrI₃ and d) twisted WS₂/MoSe₂ heterostructure. Quantum mechanical multislice simulation [7] of electron diffraction patterns with torsional PLDs applied show good agreement with the experimental diffraction patterns. Notably, for near magic-angle TBG, single-harmonic torsional PLD (Δ_1) matches quantitatively with the experimental SAED patterns [4].

A torsional PLD model reduces the complexity of low-twist angle moiré crystals to a single order parameter across a variety of 2D materials ranging from

graphene, metal dichalcogenides, metal trihalides homostructures to heterostructures of 2D materials.

References:

- [1] H Yoo et al., Nat. Mater. **18** (2019), p. 448. doi: 10.1038/s41563-019-0346-z
- [2] AJ Mannix et al., Nat. Nanotechnol. (2022). doi: 10.1038/s41565-021-01061-5
- [3] H Xie et al., Nat. Phys. **18** (2022), p. 30. doi: 10.1038/s41567-021-01408-8
- [4] SH Sung et al., arXiv:2203.06510 (2022). doi: 10.48550/arXiv.2203.06510
- [5] K Yasuda et al., Science **372** (2021) p. 1458 doi: 10.1126/science.abd3230
- [6] A Weston et al., Nat. Nanotechnol. **15** (2020) p. 592 doi: 10.1038/s41565-020-0682-9
- [7] EJ Kirkland, "Advanced Computing in Electron Microscopy 2nd edition" (2010)

4:30 PM NM01.04.07

Calculation of Mechanical and Thermal Properties of MoS₂ Using Surface Acoustic Waves [Anikeya Aditya](#)¹, Nitish Baradwaj¹, Ankit Mishra¹, Ken-ichi Nomura¹, Aiichiro Nakano¹, Priya Vashishta¹, Rajiv Kalia¹, Kory Burns² and Assel Aitkaliyeva²; ¹University of Southern California, United States; ²University of Florida, United States

Surface acoustic waves (SAWs) propagate along the surface of materials or at the interface between a solid-air, solid-liquid, solid-solid, and solid-vacuum. SAW's energy is confined to the surface (within the depth of one wavelength) and propagates in the two-dimensional (2D) interface region. SAW's velocity depends on the elastic property of the material. Hence SAWs can be used to determine mechanical properties like Young's modulus, and thermal properties like thermal conductivity and diffusivity in 2D materials. In this work, we use the SAWs originating on the MoS₂ monolayer and bilayer to calculate their thermal conductivity and Young's modulus. We also examine the effect of defects like nanopores on SAW propagation and material properties. We investigate how the relative twist in a bilayer and the resulting moire pattern affect the SAW propagation and related properties.

SESSION NM01.05: Virtual Session: Moire Materials
Session Chairs: Johannes Lischner and Arend van der Zande
Wednesday Morning, December 7, 2022
NM01-virtual

8:00 AM *NM01.05.01

Valley-Layertronics in Moiré Superlattices [Wang Yao](#); University of Hong Kong, China

Long wavelength moiré pattern in van der Waals stacked 2D materials has provided a powerful tool towards designer quantum materials that can extend the exotic properties of the building blocks. For band edge carriers located at the Brillouin zone corners (valleys), the interlayer coupling features sensitive dependence on the atomic registry between the constituting layers. In twisted TMDs homobilayers, such coupling in the moiré pattern manifests itself as a location-dependent Zeeman field acting on the active layer pseudospin. Berry curvature arising from such layer pseudospin texture corresponds to a pseudo-magnetic field that realizes fluxed superlattices tunable by twist angle, strain and interlayer bias [1,2], underlying the quantum spin Hall effect in low energy mini-bands. Ultrafast dynamic modulation of the layer pseudospin texture by bias pulse or Terahertz field further introduces pseudo-electric field for spin/valley manipulation [3]. In moiré patterns distorted by non-uniform strains, the interplay of moiré interlayer coupling and strain together leads to non-Abelian Berry phase effects [4]. I will also discuss other manifestations of the moire modulated layer hybridization on carrier topological transport.

The work was supported by Research Grant Council of HKSAR (17306819, AoE/P-701/20, HKU SRF52122-7S05), and the Croucher Foundation.

References

- [1] Hongyi Yu, Mingxing Chen, Wang Yao, Giant magnetic field from moire induced Berry phase in homobilayer semiconductors, Natl. Sci. Rev. 7, 12 (2020).
- [2] Dawei Zhai and Wang Yao, Theory of tunable flux lattices in the homobilayer moire of twisted and uniformly strained transition metal dichalcogenides, Phys. Rev. Materials 4, 094002 (2020).
- [3] Dawei Zhai and Wang Yao, Ultrafast control of moiré pseudo-electromagnetic field in homobilayer semiconductors, Natural Sciences 2(2), e20210101. (2022).
- [4] Dawei Zhai and Wang Yao, Layer Pseudospin Dynamics and Genuine Non-Abelian Berry Phase in Inhomogeneously Strained Moiré Pattern, Phys. Rev. Lett. 125, 266404 (2020).

8:30 AM DISCUSSION TIME

SYMPOSIUM NM02

Nanotubes, Graphene and Related Nanostructures
November 28 - December 7, 2022

Symposium Organizers

Tanja Kallio, Aalto University
Shunsuke Sakurai, National Institute of Advanced Industrial Science and Technology
Yoke Khin Yap, Michigan Technological University
Ming Zheng, National Institute of Standards and Technology

Symposium Support

Bronze
Nanoscale Horizons

* Invited Paper
+ Distinguished Invited

SESSION NM02.01: Synthesis and Characterization I
Session Chairs: Tanja Kallio, Shunsuke Sakurai, Yoke Khin Yap and Ming Zheng
Monday Morning, November 28, 2022
Hynes, Level 2, Room 208

10:30 AM *NM02.01.01

How Much Can We Control the SWNT Atomic Structure During the Floating Catalyst Chemical Vapor Deposition (FC-CVD) Synthesis? Esko Kauppinen; Aalto University, Finland

Floating-catalyst CVD (FC-CVD) is a highly promising technique for the scalable synthesis of single-walled carbon nanotubes (SWNTs). We have been studying FC-CVD systems with several carbon precursor molecules, including CO, C₂H₄, CH₄, ethanol, methanol, isopropanol, and toluene, using mainly iron catalyst nanoparticles, either generated in-situ via ferrocene vapor thermal decomposition or pre-made via the spark discharge aerosol generator. We have determined the SWNT atomic structure i.e. (n,m) distributions directly via the electron diffraction of individual tubes supported by the optical absorption spectroscopy studies. Using ferrocene as the catalyst precursor, CO as the carbon source and CO₂ as the growth promoter, we show that the SWNT (n,m) distribution and the related thin film color can be directly tuned by adjusting the CO₂ concentration. Also, the fraction of metallic tubes can be tuned via adding carbon dioxide. We will present results on the synthesis of mainly semiconducting tubes from ethanol via adding methanol, and also from isopropanol as the carbon source when using nitrogen carrier gas with minor fraction of hydrogen as the carrier gas. The chiral angle distributions from both CO and ethanol are biased towards the armchair side, while those from hydrocarbons are rather flat. The higher the synthesis temperature the broader are the (n,m) distributions when using ferrocene based catalysts. Finally, we will present mechanistic studies addressing the activity of the catalysts on both ferrocene as well as spark generated based systems.

11:00 AM *NM02.01.02

Synthesis of Carbon Nanotube with High Crystallinity and High Aspect Ratio with New Catalyst Precursors Using Deep-Injection Floating Catalyst Chemical Vapor Deposition Seung Min Kim¹, Ji Hong Park^{1,2} and Suryun Oh^{1,3}; ¹Korea Institute of Science and Technology, Korea (the Republic of); ²Korea Advanced Institute of Science and Technology, Korea (the Republic of); ³Gwangju Institute of Science and Technology, Korea (the Republic of)

A floating catalyst chemical vapor deposition (FCCVD) can be a method to continuously synthesize carbon nanotubes (CNTs) with high crystallinity, because CNT synthesis is usually performed at relatively high temperature. Since CNT synthesis by FCCVD occurs in a vapor phase, the gas flow pattern inside the reactor turns out to critically affect the synthesis of CNTs. Based on the understanding of gas flow pattern, a deep-injection FCCVD (DI-FCCVD) technique is developed. In this technique, all reactants are injected directly and rapidly into high-temperature reaction zone through thin alumina tube; this process leads to simultaneous thermal decomposition of well-mixed catalyst precursors and formation of uniformly-sized catalyst particles, and thus synthesis of CNTs with high aspect ratio (AR > 17000) and high crystallinity ($I_G/I_D > 60$) at relatively high production rate (> 6 mg/min). Using DI-FCCVD technique, the effects of new catalyst precursors on CNT synthesis are investigated. Different catalyst precursors have varying thermal decomposition temperatures and catalyst particles with smaller sizes are expected to be formed using a catalyst precursor with high thermal decomposition temperature. Therefore, CNTs with higher aspect ratio from smaller-sized catalysts could be synthesized using catalyst precursors with high decomposition temperature. Four catalyst precursors (ferrocene, acetyl-ferrocene, ferrocene-carboxaldehyde and methyl-ferrocene) are selected according to their electron donating and withdrawing properties of functional groups on ferrocene. The electron donating functional groups activate the ferrocene and help the precursors to decompose at the lower temperature. On the contrary, the electron withdrawing functional groups deactivate the ferrocene and make the precursor decompose at higher temperature. Thermal decomposition behavior of catalyst precursors and subsequent formation of catalyst particles are observed in real time by utilizing *in-situ* transmission electron microscopy (TEM) with increasing the temperature. When we use catalyst precursors with low decomposition temperature (ferrocene and methyl-ferrocene), by changing the sulfur concentration, the catalyst sizes and the properties of synthesized CNTs (productivity, purity, and diameter) are also changing. On the other hand, in the case of catalyst precursors with high decomposition temperature (acetyl-ferrocene and ferrocene-carboxaldehyde), sulfur concentration less critically affects CNT synthesis. CNTs using acetyl-ferrocene are continuously synthesized to have very low impurity (~ 3 wt% of Fe) and very high aspect ratio (AR > 20000) at reasonable production rate. This study can provide new insights towards how to control CNT synthesis using the configuration of the reactor and the characteristics of various catalyst precursors.

11:30 AM *NM02.01.03

Ultra-Long Carbon Nanotube Forest via *In Situ* Supplements of Iron and Aluminum Vapor Sources Hisashi Sugime; Kindai University, Japan

Growth of carbon nanotube (CNT) forests in large scale is one of the main challenges to utilize the attractive properties of CNTs in variety of applications. To date, several groups have reported the growth of centimeter-scale CNT forests, and the maximum length that has been reached is ~2 cm using an iron-gadolinium (Fe-Gd) catalyst on an aluminum oxide (Al₂O₃) support [1]. Nevertheless, with the conventional approaches, there seemed to exist a ceiling preventing growth that went beyond ~2 cm. Therefore, it is necessary to realize a method that achieves longer CNT forests while alleviating the growth termination which is mainly caused by the structural change of the catalyst nanoparticles [2].

In this work, a carbon nanotube forest with a length of 14 cm grew with an average growth rate of $1.5 \mu\text{m s}^{-1}$ and a growth lifetime of 26 h [3]. Several key factors to realize this unprecedented long growth such as catalyst conditions, growth conditions in chemical vapor deposition, and reactor system were clarified. It was found that the combination of the catalyst system of iron/gadolinium/aluminum oxide (Fe/Gd/Al₂O₃) [4] and the in situ supplements of Fe and Al vapor sources at very low concentration was crucially important. A cold-gas system, where only the substrate is heated while keeping the gas at room temperature, was employed to suppress unnecessary reactions and depositions [5]. The long carbon nanotube forest enabled macroscopic measurements of the tensile and electrical properties of the carbon nanotube wires, and it gave several important insights for industrial applications of the carbon nanotubes in the future.

[1] W. Cho et al., *Carbon* **69**, 609 (2014). [2] H. Sugime et al., *ACS Appl. Mater. Interfaces* **6**, 15440 (2014). [3] H. Sugime et al., *Carbon* **172**, 772 (2021). [4] H. Sugime et al., *ACS Nano* **13**, 13208 (2019). [5] H. Sugime et al., *Carbon* **50**, 2953 (2012).

SESSION NM02.02: Synthesis and Characterization II
Session Chairs: Tanja Kallio, Shunsuke Sakurai, Yoke Khin Yap and Ming Zheng
Monday Afternoon, November 28, 2022
Hynes, Level 2, Room 208

1:30 PM NM02.02.01

Pixelated Carbon Nanotube Forest Darian Smalley^{1,1}, Masahiro Ishigami^{1,1} and Robert Peale^{1,2}; ¹University of Central Florida, United States; ²Truventric, United States

Carbon nanotube forests (CNTFs) were grown on a patterned substrate to form square pixelated arrays. Two-level full factorial optimization first determined the best conditions for synthesis by chemical vapor deposition, catalyzed by Fe nanoparticles deposited on oxidized silicon substrates. Varied parameters included growth temperature, growth time, and acetylene-to-hydrogen gas flow rate ratio. Argon was used as a carrier gas. Reactive ion etching of the substrate in oxygen plasma dramatically improved forest growth rates. Uniform square 7x7 pixel arrays were produced by contact photolithography and lift-off of the deposited Fe. Each pixel was subdivided into square islands separated by gaps with different island and gap dimensions, ranging from 4 to 50 microns and 1 to 10 microns, respectively. Uniform CNTF heights were grown with controllable values from 15 to 2500 microns. The results demonstrate the fabrication of thermally and electrically isolated vertically aligned CNTF islands, which have applications to batteries, sensors, infrared absorbers, and IR or electron emitters.

1:45 PM NM02.02.02

Proof of Concepts About Pulling Out Carbon Nanotube Sheets and Yarns—A Molecular Dynamics Study Luís F. Thomazini and Alexandre F. Fonseca; State University of Campinas, Brazil

Although growing carbon nanotube (CNT) forests is well-known today, growing so-called *drawable* CNT forests, i.e., vertically aligned CNT forests that allow for direct pulling out CNT fibers, sheets or yarns, requires certain conditions. There are three main theoretical hypotheses for the mechanism of conversion of vertically oriented bundles of CNTs into longitudinally oriented CNT fibers during pulling out process. The simplest model [1] considers that the vertically aligned CNT bundles interact only by van der Waals forces. By arguing that van der Waals alone is not able to explain why the CNT bundle being pulled out does not simply detach from the rest of the CNT forest, a second model [2] proposes that something else connects the main vertically aligned CNT bundles in drawable forests. It proposes that individual CNTs or small bundles of CNTs connect the main vertically aligned large CNT bundles, also by van der Waals forces. These connections, during the pulling out of one CNT large bundle, move and get accumulated at the opposite extremity of the forest. This accumulation of connections would, then, transfer the pull-out force on the first CNT bundle to the next, thus keeping the process running continuously. The third model [3] also predicts the existence of connections that get around and entwine one or more large CNT bundles. During the pulling out of the first CNT bundle, the connection strengthens the contact with the neighboring vertically aligned CNT bundle and pulls it out. As the three models might hold true for different structures of CNT forests, using tools of classical molecular dynamics (MD) simulations, we decided to investigate the validity of their main features: van der Waals forces, movement of interconnections, transfer of the pulling-out force from the first to the second large CNT bundle and pulling out of the next bundle. Although the size of real CNT forests prohibits their full atomistic simulation, we designed local structural models that are, at the same time, large enough to test and prove the concept of each feature from the pulling out models, and small enough to be atomistically simulated. We show that the concepts behind the pulling out mechanisms of the last two models hold true, so they are really important in the role of converting vertically aligned CNT forests to longitudinal CNT fibers, sheets and yarns. This work was supported by São Paulo Research Foundation (FAPESP), grant #2020/02044-9.

[1] X. Zhang, et al. *Adv. Mater.* **18**, 1505 (2006).
[2] A. A. Kuznetsov, et al. *ACS Nano* **5**, 985 (2011).
[3] C. Zhu, et al. *Carbon* **49**, 4996 (2011).

2:00 PM NM02.02.03

Semiconducting van der Waals Nanocarbon on Boron Nitride Nanotubes Boyi Hao¹, Shiva Bhandari¹, Haiying He², Ravindra Pandey¹, Dongyan Zhang¹ and Yoke Khin Yap¹; ¹Michigan Technological University, United States; ²Valparaiso University, United States

The use of nanocarbon in future electronics is promising and has gained significant attention after the discovery of carbon nanotubes (CNTs) and graphene. The major obstacles are that not all single-walled CNTs are semiconducting as their properties are chiral-dependence, and graphene is metallic and not applicable for digital switching.

In contrast to CNTs and graphene, BNNTs are electrically insulating and optically transparent [1, 2]. The unique properties of BNNTs have enabled the formation of single-electron transistors (SETs) without semiconductors [3]. We have also demonstrated the formation of 2D gold with tunable optical band gaps [4], field-effect transistors (FETs) by Tellurium (Te) atomic chains inside BNNTs [5], and high-brightness fluorophores that could be 1000X brighter than existing dyes [6-8]. Here we will introduce a novel class of carbon electronic materials, nanocarbon functionalized BNNTs with semiconducting characteristics.

Van der Waals nanocarbon is selectively coated on BNNTs without using any catalyst. Raman spectroscopy, scanning transmission electron microscopy (STEM), and electron energy loss spectroscopy (EELS) are used to analyze the structural properties of this nanocarbon. Four-probe scanning tunneling

microscopy further characterized the as-grown nanocarbon on BNNTs for their electronic properties (4-probe STM). Non-linear current-voltage (I-V) characteristics are detected, suggesting that these carbon are not metallic. Furthermore, the transport properties of this nanocarbon are evaluated at various transport lengths ranging from 300 to 800 nm. Interestingly, the turn-on voltages of this nanocarbon drastically decreased with the decrease of the transport lengths. The details of the experimental results and the theoretical modeling will be discussed in the meeting.

References

- [1] J. Wang, *et al.* Nano Letts 5, 2528-2532 (2005).
- [2] (Review) J. Wang, *et al.*, Nanoscale 2, 2028-2034 (2010).
- [3] C. H. Lee, *et al.* Advanced Materials 25, 4544-4548 (2013).
- [4] S. Bhandari, *et al.* ACS Nano 13, 4347-4353 (2019).
- [5] J-K Qin, *et al.* Nature Electronics 3, 141-147 (2020).
- [6] Y. K. Yap, D. Zhang, N. B. Yapici, US Patent Application US20180296705A1.
- [7] (Review) D. Zhang, *et al.* ACS Omega 6, 20722-20728 (2021).
- [8] (Review) D. Zhang, *et al.* J. Maters. Res. (Submitted)

We acknowledge the support from the Department of Energy, the National Science Foundation, and the Center for Nanophase Materials Sciences (CNMS) at Oak Ridge National Laboratory.

2:15 PM NM02.02.04

Dynamic Assembly of Liquid Crystalline CNT and Graphene into Fiber Won Jun Lee; Dankook University, Korea (the Republic of)

One classic strategy for functional fiber is to merge nanomaterials and a thermoplastic/thermoset matrix. Relatively low performance examples based on thermoplastics exist and motivate model systems for studies of the critical constituent parameters and design. To create high performance embodiments, high surface area, longitudinal and interfacial strength should be considered; these fibers will ultimately be combined with the specifically-designed polymeric matrices. State-of-the-art, high performance constituents, based on graphitic carbon nanomaterials such as carbon nanotubes and graphene, have an essentially static structural framework that fails irreversibly without any dynamic response. We propose to re-engineer the constituents to allow a dynamic response to stimulus without irreversible loss of mechanical performance as a fiber. To enable this approach, molecular interactions must respond at the certain levels and timescales without losing their features at the nanoscale. Recent advances in the chemistry of complementary nanomaterials will provide the means to adjust the strength of the interactions. For optimal performance, the constituents will need to be redesigned from the bottom up; however, in many cases, existing materials can be adapted by integrating new, dynamically responsive links, as part of the matrix structure. Whilst we are not intending to follow an explicitly classical approach, it is worth noting that most functional fiber systems integrate liquid crystalline materials with soft, dynamic molecular phases. Our strategy is to introduce strong dynamic (reversible) interactions in a variety of length scales and geometries, in order to explore new strategies for the fabrication of functional fibers. Indeed, precise control over orientational/positional ordering and complex interface of carbon nanotubes and graphene, has paved the hidden way for energy conversion and storage devices.

2:30 PM NM02.02.05

Carbon Nanotube Forest Synthesis by Hydrogen Free Approach Using Fe Catalyst Nanoparticles with Trace Amounts of Noble Metals Shunsuke Sakurai, Maho Yamada, Jinping He, Kenji Hata and Don N. Futaba; National Institute of Advanced Industrial Science and Technology, Japan

Although iron (Fe) represents one of the most industrially used metallic elements because of its abundance and low cost, the ease of Fe oxidation has been a huge energy and environmental burden to produce Fe metal (or steel) for centuries. For the synthesis of carbon nanotubes (CNTs), although Fe metal nanoparticle (NP) catalysts have been widely used, their sensitivity to oxidation requires reduction in a H₂-rich ambient to prepare the metallic Fe catalyst and prevent exposure to oxidative species, before and during the catalytic chemical vapor decomposition (CCVD) of the carbon feedstock and the precipitation of CNTs.

Here, we report a novel hydrogen-free approach to enable the synthesis of tall and vertically aligned CNTs (forest) by fabricating reduced, highly active, and corrosion-resistant Fe-based NP catalysts [1]. We incorporated the trace levels (< 1 at%) of noble metals, such as iridium (Ir) into Fe oxide NPs. The efficient synthesis of tall (>500 μm) CNT forest has been achieved with as little as 0.3 at% Ir by means of a completely hydrogen-free CCVD process, suggesting only a few Ir atoms was required to reduce hundreds of Fe atoms in one Fe oxide NP. Ex-situ X-ray photoelectron spectroscopy (XPS) revealed the reduction of Fe in a hydrogen-free ambient, and also suggested that metallic Ir⁰ catalytically reduced the surrounding Fe oxide.

- [1] S. Sakurai, M. Yamada, J. He, K. Hata, D. N. Futaba, J. Phys. Chem. Lett. 2022, 13, 1879-1885.

2:45 PM BREAK

SESSION NM02.03: Theoretical Study
Session Chairs: Tanja Kallio, Shunsuke Sakurai, Yoke Khin Yap and Ming Zheng
Monday Afternoon, November 28, 2022
Hynes, Level 2, Room 208

3:30 PM *NM02.03.01

Ferromagnetism Due to Spontaneous Symmetry Breaking in a Twisted Bilayer Graphene Nanoflex Ranjit Pati; Michigan Technological University, United States

Twisted bilayer graphene exhibits many intriguing behaviors ranging from superconductivity to anomalous Hall effect to ferromagnetism at a magic angle close to 1°. In this talk, I will demonstrate ferromagnetism in a twisted bilayer graphene nanoflex (TBGNF) arising from spontaneous symmetry breaking. A first-principles density functional theory that does not make any assumption of the electronic structure is used to study the zero-dimensional twisted nanoflex. Our result shows that when the energy gap of a TBGNF approaches zero, electronic instability-induced spontaneous reorganization of electrons leads to the emergence of a stable ferromagnetic gap state with p-orbitals at the boundary of the nanoflex contributing to ferromagnetism [1].

- [1] D. Pant, S. Aryal, S. Mandal, and R. Pati, Nano Lett. 2021, 21, 7548-7554.

4:00 PM NM02.03.02

Numerical Study of a Quantum Graphene Gyroscope [Aron Cummings](#)¹, [Aleandro Antidormi](#)¹, [Grzegorz Hader](#)² and [Eui-Hyeok Yang](#)^{3,3}; ¹Catalan Institute of Nanoscience and Nanotechnology (ICN2), CSIC and BIST, Spain; ²US Army DEVCOM, United States; ³Stevens Institute of Technology, United States

Today, most personal navigation relies on the Global Positioning System (GPS). This system is quite accurate under open sky, but this accuracy can be significantly degraded when satellite signals are blocked by terrain or buildings, or when the receiver is indoors or underground. In daily situations these issues are mostly a minor inconvenience, but in critical situations such as disaster relief or medical emergencies, this can become a matter of life and death.

For this reason, there is a need for personal location and navigation systems that do not rely exclusively on GPS signals. Such a system can be constructed with a combination of accelerometers and gyroscopes – by tracking changes in velocity and in orientation, this would provide accurate location information from a known starting point. This system would also ideally be lightweight, compact, robust, low power, and highly accurate, making it useable in personal handheld devices. The goal of our current research is to develop a gyroscope based on graphene that meets all these requirements.

In this talk, I will present numerical simulations of graphene gyroscopes that can detect rotation through purely electrical means. This is accomplished with the Sagnac effect, a quantum mechanical effect where angular rotation induces quantum interference that results in a modulation of current through a graphene ring, analogous to the Aharonov-Bohm effect.

As revealed by our simulations, we find that a simple ring structure is not sufficient for gyroscope design, and that alternate device configurations are required. I will discuss the potential device configurations that we have discovered, as well as our efforts to optimize the performance of gyroscopes based on such designs.

4:15 PM NM02.03.03

First-Principles Insights for Light-Ion Microscopy of Graphene [Alina Kononov](#)¹, [Alexandra Olmstead](#)¹, [Andrew Baczewski](#)¹ and [Andre Schleife](#)²; ¹Sandia National Laboratories, United States; ²University of Illinois at Urbana-Champaign, United States

The properties of 2D materials are notoriously sensitive to defects and nanostructure, requiring precise characterization methods to verify desirable features. Ion-beam techniques including helium ion microscopy are a promising tool for this purpose. However, optimizing ion beam parameters for 2D materials requires improved understanding of their highly pre-equilibrium response to ion irradiation, which can fundamentally differ from their bulk counterparts. To this end, we simulate single impacts of 0.25 – 200 keV protons and helium ions in free-standing monolayer graphene using real-time time-dependent density functional theory. We find a channel-dependent anomalous effect in the energy transferred by ~6 keV protons that we associate with electron capture from σ and π bands. Furthermore, our first-principles results confirm analytic estimates of a threshold proton energy near 1 keV below which electron emission vanishes. Most importantly, we predict that anisotropic electron emission mechanisms result in up to 3 times stronger signal and 5 times higher contrast for exit-side (forward) emission than the typically detected entrance-side (backward) emission. At the same time, the ion-induced electronic excitations within the graphene delocalize on a sub-fs time scale, rendering their contribution to damage processes negligible. These findings will advance high-resolution, nondestructive imaging techniques for 2D materials.

This material is based upon work supported by the National Science Foundation under Grant No. OAC-1740219. SNL is managed and operated by NTESS under DOE NNSA contract DE-NA0003525.

4:30 PM NM02.03.04

Strain Effect on Optical and Magnetic Properties of Zigzag Two-Dimensional Passivated GaN Nanoribbons: An *Ab Initio* Study [Vijay Kumar Gudelli](#), [Naresh Alaal](#) and [Iman S. Roqan](#); King Abdullah University of Science and Technology, Saudi Arabia

In this work, systematic studies are conducted to investigate the electronic, magnetic, and optical properties of oxygen- and sulfur-passivated zigzag GaN nanoribbons (Z-GaNNRs) using first-principles density-functional theory. Simulation investigations pertaining to Z-GaNNRs of 0.9–5 nm width reveal that edge passivation increases GaNNR stability, whereby O-Z-GaNNRs are more stable than S-Z-GaNNRs and bare Z-GaNNRs. We demonstrate that the stability increases with the GaNNR width. Spin-polarized band structure analyses further show that bare Z-GaNNRs of all widths exhibit metallic properties with an antiferromagnetic (AFM) phase. In contrast, owing to their half-metallic and semiconducting nature, oxygen-passivated NRs (O-Z-GaNNRs) are characterized by ferromagnetic (FM) and AFM phases, respectively. Finally, S-passivated NRs exhibit ferromagnetic metal properties irrespective of their width. We found that the strain significantly affects the entire band structure of Z-GaNNR compared to bulk GaN, allowing the optical and magnetic properties of the material to be modulated. When the effect of strain on the electronic structure of all three GaNNR materials was investigated, at -4% applied strain, metal-to-semiconductor abrupt transitions were observed in bare Z-GaNNR. For O-Z-GaNNR, the applied -4% and -6% strains allow a transition of the magnetic properties from AFM to FM, showing a metal characteristic band structure. In contrast, no change in the electronic and magnetic properties of S-Z-GaNNR with strain is observed. The optical investigations and electron energy loss (EELS) analysis predict that these NRs have weak absorption potential but exhibit plasmonic vibrations in the 10–11 eV range. Although the refractive index of the bare Z-GaNNRs is equal to that of the bulk GaN, the applied strain and chemical passivation modulate its refractive index value. Thus, our results pave the way for novel one-dimensional GaNNR-based optical, magnetic, and photonic applications.

SESSION NM02.04: Poster Session I

Session Chairs: [Tanja Kallio](#), [Shunsuke Sakurai](#), [Yoke Khin Yap](#) and [Ming Zheng](#)

Monday Afternoon, November 28, 2022

8:00 PM - 10:00 PM

Hynes, Level 1, Hall A

NM02.04.01

Magnetic Field Alignment of Fe₃O₄ Functionalized Boron Nitride Nanotubes for Polymer Nanocomposites [Adesewa Maselugbo](#) and [Jeffrey Alston](#); North Carolina Agricultural and Technical State University, United States

Boron nitride nanotubes (BNNTs) are electrically insulating nanomaterials with unique intrinsic properties such as high thermal conductivity, high oxidation resistance, and superior mechanical strength. Polymer matrixes have low thermal conductivity, while BNNTs have excellent axial thermal

conductivity and poor off-axis thermal conductivity. So, there is great interest in using aligned BNNTs as composite filler to increase thermal conductivity for use in aerospace and other advanced thermal interface materials. However, current BNNT nanocomposite thermal transport properties are far from expected and theoretical values. Low thermal performance is largely due to the random orientation of BNNTs within the composite. Controlling the orientation of the BNNTs in the composite is therefore critical for optimizing its performance. The purpose of this work is to manipulate and eventually align BNNTs in nanofluids and polymer composites using magnetic fields.

Magnetic manipulation is accomplished by first modifying BNNTs with iron oxide nanoparticles (Fe_3O_4 , magnetite) to induce paramagnetic susceptibility. Afterwards, functionalized BNNTs are magnetically aligned. This presentation highlights our method of BNNT functionalization with Fe_3O_4 nanoparticles. During the magnetite synthesis process, magnetite nanoparticle growth occurs on the BNNT surface via electrostatic interaction with the iron oxide nanoparticles, ensuring that the intrinsic properties and structure of the BNNT are not affected. Under external magnetic fields the magnetite functionalized BNNT exhibit magnetic responses that allow control over their orientation and position.

NM02.04.02

Tuning Dielectric Properties of Polymer Nanocomposites by Orientation Control of 2-Dimensional Fillers Maninderjeet Singh¹, Priyanka Das², Farzana Likhil¹, Nihar Pradhan² and Alamgir Karim¹; ¹University of Houston, United States; ²Jackson state university, United States

2D materials provide unique opportunities to design and develop next-generation materials and technologies for applications in energy storage, electronics, sensors, separations, and so on. In this work, we discuss the application of 2-D materials for enhancing the capacitive energy density of polymer-2D material-based nanocomposites. We demonstrate using layered 2D materials in the polymer matrices, the dielectric strength, dielectric permittivity, and hence the capacitive energy density can be tuned to develop high energy density capacitors. In particular, we show that using layered 2D Mica materials, the permittivity of the nanocomposites increases by ~100% with filler fraction as low as ~2 wt. % and the dielectric strength increases by ~80%, resulting in a ~400% increase in capacitive energy density. Furthermore, we show the dielectric properties of graphene oxide-based polymer nanocomposites can also be tuned by using nanoplatelet orientation control dictated by confinement effects in thin films. We believe these "orientation controlled" 2D nanofillers in polymer nanocomposites can help design futuristic materials with tunable properties.

*We acknowledge financial support from Kostas Research Institute (KRI) at Northeastern University via US Army DEVCOM Soldier Center Contract W911QY-19-9-0011 and NSF DMR 1901127

NM02.04.03

Acetylene Chain Length Dependence of the Elastic Properties of Graphynes Guilherme B. Kanagae and Alexandre F. Fonseca; State University of Campinas, Brazil

Graphyne (GY) is the name given to a one-atom-thick carbon allotrope composed of acetylene chains of length n , $[-C\equiv C-]_n$, directly connected to themselves, by aromatic rings or sp^2 carbon-carbon ($C=C$) bonds. Seven types of GY structures were originally proposed in the eighties, but the interest on them only increased in the last decade in view of the quest for new 2D materials with non-null band-gap. As the synthesis of graphynes are advancing, it is important to understand and predict the physical behaviors of GYs. Most of the studies about graphynes and their properties are concentrated on $n = 1$ and $n = 2$. Few works reported results on some individual types of GY having $n > 2$. Here, by means of classical molecular dynamics (MD) simulations, a comprehensive study of the dependence of the elastic properties of graphynes on the number, n , of acetylene chains is presented. Young's modulus, shear modulus, Poisson's ratio and linear compressibility of the seven originally proposed types of GYs with $1 \leq n \leq 10$ are calculated. The results are interpreted in terms of structural models and the dependence of these properties on the density of the structures. Some interesting results are: i) the Poisson's ratio of the GY known as α -graphyne with $n = 10$ is about 0.95, the largest value predicted for a 2D symmetric crystal by MD simulations; ii) linear compressibility of all seven types of GY as function of n are calculated for the first time; iii) the GYs known as 14,14,14- and 14,14,18-graphynes present negative linear compressibility along zig-zag direction whose absolute values increase with n ; iv) the 14,14,14-graphyne presents Poisson's ratio larger than unit. Except for the Poisson's ratio, we show that the acetylene length dependence of the elastic properties of all seven types of GYs could be modeled by a simple serial association of n elastic springs. This work was supported by São Paulo Research Foundation (FAPESP), grant #2020/02044-9.

NM02.04.04

Nanostructured High Voltage Insulation Antigoni Konstantinou, Hiep Nguyen, Yifei Wang and Yang Cao; University of Connecticut, United States

A major challenge for power grids and electric drives for electric vehicles is the reliability of insulation systems for their electrical components. Defects related electrical partial discharges are highly undesirable and should be avoided in an insulation system. Such discharges can lead to aging and progressive degradation, resulting in a complete failure of the insulation system and the power apparatus. Polymer composite materials are being developed to tackle this issue by providing higher lifetime of insulation systems with improved performance. Currently, the state-of-the-art material, mica, is used for insulation in today's high voltage power generators, motors and specialty capacitors. Although mica has renowned electrical discharge and high temperature withstanding capabilities, it is limited in use and performance by its brittle and mechanically weak nature. Attempts to strengthen pure mica have been made by incorporating and/or reinforcing with other materials, but the electrical and heat resistance of the final product/material suffer. To address this gap, polymer composites stand out as the ideal candidates to replace mica while offering all the desired properties. Epoxy-based dielectrics are widely used in modern microelectronics as electrical insulation, adhesive, packaging components and in grid-connected energy systems. High thermal conductivity (λ) ($\text{W}/(\text{m}\times\text{K})$), high breakdown strength, low dielectric constant (low- k) and low dielectric loss factor at both ambient and high temperatures are some of the key points that need to be addressed. This work aims to create a nanostructured insulation leading to better insulation performance for future applications such as motors with high-torque density for all-electric propulsion. Therefore, in this study, inorganic fillers were used to enhance an epoxy matrix. One such filler was hexagonal boron nitride (h-BN), a 2-dimensional material with surprisingly high λ of 751 W/mK at room temperature and excellent electrical insulative properties. On the other hand, zinc oxide (ZnO), which is a renowned semiconductive inorganic material, was also added to provide field grading. Samples were prepared with different ratios of inorganic fillers and studied with scanning electron microscopy (SEM), X-ray diffraction (XRD), voltage endurance tests in accordance with IEC 60343 standard, and thermal conductivity measurement (DTC). This work has the potential to address the insulation needs for transportation electrification and renewable energy conversion and integration.

NM02.04.05

Additive Manufacturing of Carbon Nanotube-Filled Thermosetting Resins Via Direct Ink Writing and Radio Frequency Heating and Curing Anubhav Sarmah, Suchi Desai and Micah Green; Texas A&M University, United States

Direct Ink Writing (DIW) is an extrusion-based additive manufacturing method where the print medium is a liquid-phase 'ink' dispensed out of small nozzles and deposited along digitally defined paths. Conventional DIW methods for thermosetting resins rely on the use of viscosity modifying agents, novel crosslinking chemistries, and/or long curing schedules in an oven. Here we demonstrate the use of a co-planar radio frequency applicator to generate an electric field, which can be used to rapidly heat and cure DIW- printed, CNT-filled composite resins. This method avoids the need of an oven or post-curing step. This process consists of a layer-by-layer, print-and-cure cycle which allows for printing of high-resolution, multi-layered structures. Every extruded layer is partially cured using RF before depositing the next layer; this allows the printed part to maintain structural integrity without buckling

under its own weight. The process enables both increased throughput and decreased touch time relative to traditional part manufacturing. Commercial epoxy resin with varied CNT-filler loadings were examined as DIW candidates. Rheological characterization was used to assess both curing kinetics and printing behavior. After printing, the thermo mechanical properties, surface finish, and shape retention of RF-cured samples were evaluated and found to be comparable against samples conventionally cured in an oven. This method of manufacturing establishes RF heating as a suitable alternative to conventional methods, facilitating rapid, free-form processing of thermosetting resins without a mold.

NM02.04.06

Laponite Nanodisks as Platform for Water Purification Arne T. Skjeltop^{1,2} and Larysa Anisimova³; ¹IFE, Norway; ²Giamag Technologies, Norway; ³Institute of Geotechnical Mechanics, Ukraine

Safe and clean drinking water is essential for every human being. However, clean water is sometimes scarce and not readily available due to industrial pollutant activity or runoff from natural geochemical processes. In the present work, it is shown that water quality can be improved by using Laponite as an adsorbent because of a large surface area. Laponite is a synthetic hectorite clay composed of disk-shaped nanoparticles with a diameter of about 20 nm and a thickness of about 1 nm. In a sample of 1 g laponite, there are about 10^{18} particles. The total surface area for adsorption of pollutants will be about 1000 m² with this amount of Laponite.

The underlying idea in the present work was thus to use functionalized laponite decorated with magnetic nanoparticles. This could enable removal of oil and soluble contaminants such as heavy metals, emulsifiers, surfactants, and micro-nano plastic from water flowing in a pipe. To succeed this, one must have magnets with efficient and high yield separation capabilities. For this it is important to have a strong force F acting on the magnetic bodies, given by the following equation:

$$F = V\Delta\chi B \text{grad}B / \mu_0.$$

Here, V is the volume, $\Delta\chi$ is the difference in the susceptibility of the magnetic particles and the surroundings,

$B \text{grad}B$ is the product of the magnetic field B and field gradient $\text{grad}B$, and μ_0 is the vacuum permeability.

Many permanent magnets on the market have large magnetic fields B , but weak field gradients. The GIAMAG magnets have unique and patented designs that produces both very large magnetic fields and high field gradients, resulting in the most forceful magnetic separation available on the market [1,2].

Qualitative and quantitative measurements of water purification will be reported, in particular removing small oil droplets.

Acknowledgments

We wish to acknowledge Henrik Høyer and Keiko Yakabi Diosdado for the initial investigations in the project.

The project has been funded in part by the Research Council of Norway and the Institute for Energy Technology, Norway.

References

[1] www.giamag.com

[2] Arne T. Skjeltop, Paul Dommersnes and Henrik Høyer, "New Forceful Magnetic Bioseparation using GIAMAG Magnet Systems", MRS Advances, 2017, Vol.2 (24), p.1297-1301

NM02.04.08

Carbon Nanotubes and Graphene Flakes Grown Synchronously in the Confined 2D Nanospace of a Layered Silicate Barbara Pacakova¹, Marian Matejdes^{2,3}, Paulo H. Michels Brito¹, Konstanse Seljelid¹, Leander Michels¹, Josef Breu⁴, Steinar Raaen¹ and Jon Otto Fossum¹; ¹Norwegian University of Science and Technology, Norway; ²Slovak University of Technology, Slovakia; ³Slovak Academy of Sciences, Slovakia; ⁴University of Bayreuth, Germany

Carbon nanotubes are typically grown on metal precursors¹⁻³, upon formation of metal-containing nanoparticles^{4,5} that serve as nucleation centers for nanotube formation, such as Fe₃C in the case of Fe as precursor. This process introduces unwanted properties into this pure graphitic system – for example, to introduce intrinsic magnetism into the carbon nanotubes, metal catalyst has to be completely removed, which is not possible in the most cases. However, several studies showing growth of carbon nanotubes on metal free substrates has been reported so far⁴.

As there are no metal nucleation centres in clays, carbon nanotubes grow directly on the edges of the clay SiO₂ nano-sheets. These SiO₂ sheets sandwich octahedral sheets with Mg and Li inside the octahedra, which constitutes the nano-layered structure of the synthetic clay mineral fluorohectorite.

Here we report formation of the metal-free carbon nanotubes in the interlayer of synthetic fluorohectorite clay, by intercalation and subsequent pyrolyzation of different metal-free dyes. Detailed characterization by XRD, XPS, AFM, Raman spectroscopy, as well as magnetic property measurements allow us to describe this system, and postulate possible mechanisms for formation of carbon nanotubes.

References:

1. Sengupta, J. & Jacob, C. The effect of Fe and Ni catalysts on the growth of multiwalled carbon nanotubes using chemical vapor deposition. *J. Nanoparticle Res.* **12**, 457–465 (2010).

2. Rao, R. *et al.* Carbon Nanotubes and Related Nanomaterials: Critical Advances and Challenges for Synthesis toward Mainstream Commercial Applications. *ACS Nano* **12**, 11756–11784 (2018).

3. Rathinavel, S., Priyadarshini, K. & Panda, D. A review on carbon nanotube: An overview of synthesis, properties, functionalization, characterization, and the application. *Mater. Sci. Eng. B Solid-State Mater. Adv. Technol.* **268**, 115095 (2021).

4. Rümmele, M. H. *et al.* Synthesis of carbon nanotubes with and without catalyst particles. *Nanoscale Res. Lett.* **6**, 1–9 (2011).

5. Vejpravova, J., Pacakova, B. & Kalbac, M. Magnetic impurities in single-walled carbon nanotubes and graphene: a review. *Analyst* **141**, 2639–2656 (2016).

NM02.04.10

Synthesis and Characterization of Protein-Derived Graphene Aerogels Bridget Denzer, Mohd Shaharyar Wani and Craig Arnold; Princeton University, United States

Graphene aerogels (GAs) are promising candidates for applications such as energy storage and water purification due to their exceptional porosity, high electrical conductivity, and absorption capabilities. GAs can be synthesized through chemical vapor deposition (CVD), in which the starting materials are freeze-dried then pyrolyzed at high temperatures and atmospheric pressure. The benefit to this method is that many carbon-based precursors can be used as starting materials, making it an extremely promising method for expanding the production of GAs. In this study, we show the successful synthesis of GAs via a template-free CVD method at 900°C using four different proteins precursors: α -lactalbumin, β -lactoglobulin, bovine serum albumin (BSA), and myoglobin. Through SEM, EDS, and Raman Spectroscopy analysis, we show that all four proteins form GAs when pyrolyzed, although their morphologies vary. The pyrolyzed BSA and α -lactalbumin show ordered graphene networks, but β -lactoglobulin and myoglobin have more amorphous structures. Thus,

when changing the protein precursor, the developed GAs show interesting trends in structural morphology, thus suggesting the tunability of GAs based on precursor selection.

NM02.04.11

3D Graphene Based Architectures for Environmental Applications Rabita Mohd Firdaus¹, Claudia De Melo¹, Jean-Francois Pierson¹, Sylvie Migot¹, Mélanie Emo¹, Abdul Rahman Mohamed² and Brigitte Vigolo¹; ¹Institut Jean Lamour, France; ²Universiti Sains Malaysia, Malaysia

Three-dimensional (3D) graphene-based macrostructures, GBMs, also referred to as aerogels, foams or sponges, have drawn immense interest these last ten years due to the combination of interesting properties such as high surface area and porosity, chemical tunability and stability [1]. These GBMs offer high application potential including CO₂ adsorption, water treatment, batteries, sensors, catalysis, etc. However, due to lack of control of the self-assembling process, GBMs often suffer of restacking phenomenon during the assembly phenomenon which significantly lessens the outcome accessible surface. Exploiting the high surface of graphene within these GBMs is particularly important to develop efficient adsorbents for water or air depollution. From literature, it is still not clear which of the physical (pore size, surface area) or the chemical (nature of the surface functional groups or other chemical modification) properties of GBMs impact their adsorption capacity [2]. More recently, combination of graphene with inorganic compounds such as metal-based nanoparticles or thin films to develop hybrid porous nanomaterials is gaining of attention for environmental applications. In this paper, we will provide a comprehensive study about the main issues to overcome development of GBMs and the investigation of their structural properties. Several 2D and 3D all-graphene based materials have been prepared and chemically modified for the purpose to be used for CO₂ capture. Our results show a significant enhancement of CO₂ absorption capacity after activation. The possible involved mechanism will be discussed [3]. Based on more recent results, preparation of alumina-graphene porous hybrids for depollution application will be as well described. Alumina is here deposited by atomic layer deposition providing a well-suitable deposit method for such porous graphene support. Thanks to an in-depth characterization of the prepared 3D graphene-alumina hybrid material by means of high resolution transmission electron microscopy analysis carried out on a thin foil lamella prepared by focused ion beam, we report here a successful preparation of highly porous alumina by a well-controlled method rarely reported.

[1] R.M. Firdaus, N. Berrada, A. Desforges, A.R. Mohamed, B. Vigolo, From 2D Graphene Nanosheets to 3D Graphene-based Macrostructures, Chem.-Asian J. 15 (2020) 2902–2924. <https://doi.org/10.1002/asia.202000747>.

[2] R.M. Firdaus, A. Desforges, A. Rahman Mohamed, B. Vigolo, Progress in adsorption capacity of nanomaterials for carbon dioxide capture: A comparative study, Journal of Cleaner Production. 328 (2021) 129553. <https://doi.org/10.1016/j.jclepro.2021.129553>.

[3] R.M. Firdaus, A. Desforges, M. Emo, A.R. Mohamed, B. Vigolo, Physical and Chemical Activation of Graphene-Derived Porous Nanomaterials for Post-Combustion Carbon Dioxide Capture, Nanomaterials. 11 (2021) 2419. <https://doi.org/10.3390/nano11092419>.

NM02.04.12

Ternary Transition Metal Chalcogenide Nb₂Pd₃Se₈—A New Candidate of One-Dimensional van der Waals materials for Field-Effect Transistor with Its Controlled Doping Characteristic Byung Joo Jeong¹, Kyung Hwan Choi² and Jae-Young Choi¹; ¹Sungkyunkwan University, Korea (the Republic of); ²Sungkyunkwan University Advanced Institute of NanoTechnology, Korea (the Republic of)

Two-dimensional (2D) van der Waals (vdW) materials with a strong in-plane covalent bond and weak interlayer interaction have been intensively studied due to its unique and superior electrical, optical, and thermal properties. However, a complicated and diverse manufacturing process should be required to apply 2D vdW materials into future electronic devices in which various dimensional structures would be mixed. Mixed-dimensional vdW heterostructures have been studied in order to overcome integration limits of 2D materials by converging other *n*D materials, where *n* is 0, 1 and 3. However, one-dimensional (1D) ternary transition metal chalcogenides containing a noble metal such as Pd or Pt have provided great potential in the field of electronic and optoelectronic applications due to their outstanding structural scalability, transport properties and high stability. In this work, we introduce a new ternary transition metal chalcogenide, Nb₂Pd₃Se₈, which was successfully synthesized via chemical vapor transport (CVT) method using iodine as a transport agent. It is demonstrated for the first time that single or few-ribbon Nb₂Pd₃Se₈ nanowires can be effectively isolated by micromechanical exfoliation due to the weakly bonded vdW interaction between the repeating unit structures. Interestingly, density functional theory (DFT) calculation revealed that this thickness-scalable Nb₂Pd₃Se₈ displays a semiconducting characteristic with an indirect band gap of 0.44 eV in bulk and a direct band gap of 0.73 eV in single-ribbon, exhibiting a tunable band gap with indirect-to-direct transition. For further verification, the work functions of Nb₂Pd₃Se₈ nanowires were characterized by scanning Kelvin probe microscopy (SKPM). Given the applicability to electronic devices, FETs were fabricated on the exfoliated Nb₂Pd₃Se₈ nanowires to evaluate electrical transport property, and high performance of n-type semiconducting behavior was achieved with electron mobility as high as 31 cm²V⁻¹s⁻¹, I_{on}/I_{off} ratio of >10⁴ and long-term stability (up to 60 days) in ambient condition. Furthermore, these series of materials have not been studied for controlling its electrical properties as a field-effect transistor. In general, charge transfer on a dangling bond free surface is the most appropriate approach using chemical doping method since direct infiltration of dopant atoms is difficult to adopt for modulating the electrical properties of nanomaterials as their most atoms are exposed to the environment. Therefore, n-type transport characteristics of Nb₂Pd₃Se₈ is modulated through p/n-type chemical doping method using AuCl₃-Nicotinamide adenine dinucleotide (NADH), respectively. As a result of AuCl₃ doping, high performance p-type field-effect transistor (PFET) showing hole mobility up to ~8.6 cm²V⁻¹s⁻¹ was obtained. For the proof of conception, we fabricated homogenous p-n junction diode with ideal rectifying behavior by applying half-doped device structure using encapsulation process. In addition, n-doped Nb₂Pd₃Se₈ shows the high field-effect mobility of 41 cm²V⁻¹s⁻¹ with maintaining I_{on}/I_{off} values of >10⁴ with long-term stability using NADH. Finally, all of the atoms related to each doped properties were discussed in detail through SKPM and X-ray photoelectron spectroscopy (XPS). We believe that this work can highlight a controllable electrical characteristic of 1D vdW semiconductors in nanoelectronic applications.

NM02.04.14

Sensitive Taste Sensors Using Graphene Decorated with Metal or Nafion for High Selectivity to Glucose and pH Chung Won Lee and Ho Won Jang; Seoul National University, Korea (the Republic of)

In recent days, taste sensing have been an important issue in terms of, detecting food quality or sensing various chemical substances from specific materials. This kind of taste sensor mainly uses 2-Dimensional materials such as graphene for sensing rather using lipids or other biological substances. The aim of using 2D materials rather lipids is for longer use; bio-substance based taste sensors have very high selectivity and sensitivity but the life span of the device is short and it is sensitive to external atmosphere. For long term use and daily usage, 2D material based sensors have the advantage to bio-based sensors. Here in, we report graphene based taste sensors graphene decorated with gold for glucose sensing and nafion spin coating on graphene for pH sensing. Graphene is the main source of sensing and the decorated materials help to enhance selectivity by absorbing or penetrating the target material. Gold is well known to have selectivity to glucose and nafion has the ability to selectively penetrate cations. Gold is decorated with e-beam deposition; which thickness is about 2nm. On the other hand, nafion is spin coated onto a graphene transferred substrate.

NM02.04.15

Growth and Morphology Evolution of Plasma-Synthesized Few-Layer Graphene [Claudia-F. Lopez Camara](#), Paolo Fortugno and Hartmut Wiggers; Universität Duisburg-Essen, Germany

Graphene flakes are an attractive material due to their unique properties, making them promising to use for a wide variety of applications. Examples of these applications are using them as additives (to alter electrical, thermal, and mechanical properties of other materials e.g., polymer composites) or to improve the electrochemical performance in supercapacitors and batteries. However, these applications require industrial mass-production quantities of graphene powder, which are still challenging to achieve. To overcome the current batch-to-batch drawbacks from the commonly-used exfoliation processes for mass-production of graphene powder, substrate-free gas-phase plasma synthesis has emerged during the last years as an effective method to continuously synthesize freestanding few-layer graphene (FLG). This technique has the advantage to operate in a continuous mode and the potential to be scalable. During the plasma synthesis, a hydrocarbon precursor is pyrolyzed within a high-temperature plasma region. Downstream of this region, the gaseous carbon species nucleate and form FLG, leading to carbon yields as high as 10 wt%.

This work examines the evolution of growth and morphology of few-layer graphene (FLG) synthesized in a microwave-plasma reactor. Aerosol particles were sampled and characterized from various positions downstream of the plasma zone by spatially-resolved thermophoretic sampling and transmission electron microscopy (TEM), Raman spectroscopy, and BET surface area analysis (BET-SSA).

The initial carbon nucleation has been found to commence close to the plasma zone (at less than 12.4 cm downstream from the plasma nozzle) and at a temperature of ≥ 2500 °C. The initially formed flakes show an increasing level of crumpling with increasing distance downstream from the plasma zone. From the TEM images of samples collected at different heights above the plasma nozzle, we observed a growth and self-folding pattern for FLG, providing a hypothesis for their formation from single- to few-layer graphene when the materials are carried downstream the plasma region. This hypothesis consists of the creation of one-layer ovalene-shaped graphene flakes that self-folds from the sides and crumples while it continues to grow, creating wrinkled FLG flakes as these move further away from the plasma nozzle.

NM02.04.16

Processing Parameters and Their Influence on the Mechanical and Morphological Properties of Non-Woven Polyacrylonitrile/Carbon Nanotube Composite Thin Films [Conor Doyle](#) and Marilyn L. Minus; Northeastern University, United States

This research details observations of the influence of processing parameters on the formation and mechanical performance of non-woven polyacrylonitrile (PAN)/single wall carbon nanotube (SWNT) composite thin films. Solvent-based phase separation promotes the formation of an extended-chain PAN interphase at the SWNT surface as well as a hybrid through-thickness morphology. Previously reported work has documented the mechanical and electrical properties of various weight ratios of SWNT filler and PAN matrix films produced using this method. This current work reports changes in film mechanical and morphological properties resulting from modifications made to several process parameters, namely the overall film diameter and environmental conditions at which residual solvent is removed from films after the initial filtration step. Environmental conditions tested include the drying temperature and clamping pressure used during residual solvent removal. Dynamic mechanical analysis was used to evaluate the development of tensile strength and modulus (i.e., storage and loss moduli). Morphological changes were characterized using optical and electron microscopy. The results to be presented demonstrate the influence of selected processing parameters on the mechanical and morphological quality of non-woven PAN/SWNT composite thin films.

NM02.04.17

AI Toolkit for Accelerated Nanoporous Material Discovery Jonathan Booth¹, [Dan Cunningham](#)², Flaviu Cipcigan², Rodrigo F. Neumann³ and Breannan O Conchuir²; ¹Science and Technology Facilities Council, United Kingdom; ²IBM Research Europe, United Kingdom; ³IBM Research Brazil, Brazil

Crystalline nanoporous materials are widely recognised as promising candidates for carbon capture, due to their large surface area and highly porous structure. Also, there is a vast number of constituent materials which can be synthesised, enabling precise tuning of various chemical and geometric properties. As a result, there is a large design landscape which has triggered extensive research in the community, and the search continues for the best performing candidates. In this work, we present an artificial intelligence toolkit aimed at improving the discovery of materials such as zeolites, metal-organic frameworks, and zeolitic imidazolate frameworks with good adsorption of greenhouse gases, such as CO₂. The toolkit consists of 3 software packages that respectively implement: (1) a linear regression pre-screening of candidate materials using gravimetric surface area as the independent variable. (2) A crystalline graph convolutional neural network that acts as a computationally cheaper surrogate model for in-silico adsorption simulations, and (3) a pair of neural-symbolic techniques for learning the adsorption isotherm as a symbolic function of pressure and temperature, as well as learning logical rules that identify material features and values that constitute good adsorption performance.

For the initial pre-screening, we use a training set of many nanoporous materials, with various geometric features together with a simulated adsorption value, and fit a linear regression model using each feature as the independent variable. This enables simple rules to be created, such as filtering out materials with a gravimetric surface area below a certain threshold. Meanwhile, the crystalline graph convolutional neural network is trained to predict adsorption from an input Crystallographic File (CIF) format, using a similar training set of in-silico adsorption simulations. During inference, the idea is that the linear regression model can act as a (very) cheap pre-screen, before the neural network surrogate model performs additional downstream screening of candidates. This will greatly prune the space of possible candidates that require more computationally expensive simulations, to accurately determine the adsorption.

The neural-symbolic techniques investigate the feasibility of using AIFeynman, a state-of-the-art symbolic regression technique for learning physical equations from a low number of samples that associate pressure and temperature with adsorption. Should a suitable isotherm expression be learned, the obvious benefit is that the adsorption profile can be quickly evaluated for a variety of pressure and temperature values, which will be of interest to industrial applications when performing experiments, since a given implementation may only be able to achieve certain temperature and pressure values. Also, this work explores the use of FastLAS, a state-of-the-art symbolic machine learning technique that learns interpretable, logical rules from training examples. The goal is to supplement the linear regression pre-screen by exploring a search space of possible rules that can be used to filter out materials that lead to poor adsorption. The inherit interpretability enables further analysis of the learned rules by domain experts, to avoid overfitting the pre-screening check to a given training set, which would result in good candidate materials being filtered out.

This work presents an overview of each of the techniques used, alongside experimental results.

NM02.04.18

Suspended, Self-Tearing and Strained Graphene Nanostructures Formed by Nanoindentation [Daniel Sanchez](#)¹, Graham L. Cross² and Robert Carpick¹; ¹University of Pennsylvania, United States; ²Trinity College, Ireland

The nanoindentation of substrate-supported graphene has recently been shown to lead to the formation of spontaneously self-tearing nanoribbons up to several micrometers in length, known as 2D material pleats (2DMPs) [1]. The physical mechanisms driving this phenomenon are not yet fully understood. Moreover, this unprecedented mechanical behavior has potential to be exploited to produce novel stacked structures made of graphene and other 2D materials without the need for traditional transfer methods that suffer from any limitations, such as the polymer contamination of constitutive flakes. In previous work, the yield and uniformity of 2DMPs are modest, and the factors that predict successful 2DMP growth were not established. Here we explored the statistics of 2DMP formation through nanoindentation. We studied graphene of various thicknesses ranging from monolayer to bulk graphite exfoliated on 300 nm SiO₂/Si, facilitated by using protocols that permit large, uniform exfoliated areas. We then created arrays of indents in a periodic grid formation consisting of tens to hundreds of indents on a single flake. We conducted a postmortem analysis of each indent using atomic force microscopy to categorize the indented graphene sites into distinct types of nanostructures. This permits us to quantify, for first time, the percent yield of 2DMPs as a function of multiple parameters including maximum applied load, graphene thickness, and indent spacing. We discovered two previously unseen graphene nanostructures formed through nanoindentation in addition to 2DMPs. Specifically, we observed the formation of unbroken, suspended graphene, as well as graphene that fully conformed to the plastically deformed substrate, establishing a new method for producing suspended graphene and strained graphene. We then explored how proximity between nearest-neighbor indents affects the statistics of which nanostructures form in the indent arrays, demonstrating the role of elastic strain in 2DMP formation. Our analysis provides insight into the stochastic nature of nanostructures formed through nanoindenting, and explores the experimental conditions that affect the yield of desired nanostructures.

[1] J. Annett and G.W. Cross, Nature (2016). DOI: 10.1038/nature18304

NM02.04.19

Plasma-Induced Biocompatible NGQD-Based Hydrogels as Smart and pH Responsive Cancer Therapeutic Agents Darwin Kurniawan¹, Jacob Mathew¹, Michael Ryan Rahardja¹, Hoang-Phuc Pham¹, Neralla V. Rao¹, Kostya (. Ostrikov² and Wei-Hung Chiang¹; ¹National Taiwan University of Science and Technology, Taiwan; ²Queensland University of Technology, Australia

Cancer is none arguably one of the world's most dreadful diseases striking everyone without any exceptions. Current treatments rely on surgical intervention, radiation, and chemotherapeutic drugs which usually not only kill the cancers cells, but also affect healthy cells causing toxicity and severe side effects to the patients or even death. Therefore, it is urgent to develop a drug delivery system (DDS) capable of either passively or actively targeting cancer cells only to avoid all those possible occurring side effects during therapy. Resembling physicochemical and biological properties of extracellular matrix coupled with their biocompatibility and biodegradability, hydrogels with stable 3D hydrated network emerge as suitable candidate for many biomedical applications, including drug delivery, scaffold engineering, wound treatment, antibacterial, and antioxidant.

Here we report rapid and environmental-friendly plasma engineering of microporous carbon-based NGQD hydrogels from a single chitosan biomass using non-thermal microplasmas at ambient conditions without toxic chemicals and high temperature treatment. The highly reactive species derived from the non-equilibrium plasma regime allows simultaneous conversion of NGQDs and initiation of covalent bond formations within the polymeric chitosan network in a short time. Moreover, synergistic effect manifested by the inclusion of NGQDs in the chitosan matrix framework coupled with energetic plasma treatment can accelerate the cross-linking of chitosan to form a robust 3D porous composite without any toxic chemicals and harsh conditions. Endowed by the presence of NGQDs, the fabricated composites have enhanced anticancer drug loading capacity and pH-controlled sustained drug release. Since the fabricated composites also exhibit stable solid-state PL properties, it is envisaged that our method can advance toward a novel combination of therapeutic and monitoring. Our work provides a rational design of carbon-based composite with defined structures and properties suitable not only for biomedical application, but also other emerging applications.

NM02.04.21

The Synthesis and Characterization of Homogeneous High-Quality Graphene Encapsulated Metallic Powders via Plasma Enhanced Rotating CVD Deniz Cakir¹, Omer R. Caylan^{1,2}, Tarik C. Turkoglu¹, Ogulcan Akgun³, Gunce Dugan³, Halil O. Tugrul³, Benat Kockar³ and Goknur Cambaz Buke¹; ¹TOBB University of Economics and Technology, Turkey; ²Bilkent University, Turkey; ³Hacettepe University, Turkey

Graphene added Cu composites are mostly produced by mixing of graphene flakes (synthesized by Hummer's method and derivatives) and Cu powders through methods like ball milling. However, this approach has many issues related to:

- dispersion of graphene in matrix
- formation of interfacial bondings and interfacial products
- presence of structural defects in graphene
- the number of carbon layers in graphene
- presence of defects in the final product (e.g. porosity or interstitials)
- orientation of graphene relative to the loading direction
- weight or volume ratio of graphene

Hence, it is difficult to directly examine the effect of graphene on mechanical properties with this method, and there are conflicting results in the literature. The problems mentioned above are related to the processing, and within the scope of this study, a process design and development has been made by focusing on the homogeneity and reproducibility of the graphene distribution. To produce uniformly dispersed high quality graphene reinforced copper composites: 1 micrometer spherical Cu powders were coated via plasma enhanced CVD (PECVD), then pressed and sintered at 1000 C. The results show that the yield strength and stress values at different strain values of samples produced from graphene powders are considerably higher than the samples without graphene: At room temperature, the yield strength of the graphene samples increased by about 3 times, and the stress values obtained at 30 percent constant strain increased by about 2 times ... achieving a breakthrough in the performance of copper-based materials. The increase in mechanical performance was evaluated with the discussion of Grain size reduction and Strain hardening. This study is supported by TUBITAK grant number 118F491.

NM02.04.24

Graphene-Based Fracture Diodes Levi C. Felix and Douglas S. Galvao; State University of Campinas, Brazil

In nature, it is not rare to find materials with anisotropic fracture strength, such as wood and graphite. Although this anisotropy occurs along very distinct axes of symmetry, they are all centrosymmetric, meaning that such strength values remain unchanged upon inversion along a given axis. It is possible to break this symmetry in fracture behavior by manipulating the microstructure, for instance, with the insertion of triangular-shaped voids. This idea was recently experimentally realized for polymeric plates [1], where linear arrays of triangular holes created a fracture-rectification effect. In this work, we exploited similar ideas for monolayer graphene to determine whether this behavior also occurs at the nanoscale. By inserting triangular voids in graphene membranes, we investigated their fracture patterns under mechanical strain using fully-atomistic reactive molecular dynamics simulations. A preferential direction to fracture propagation was observed, confirming a robust rectification-like behavior [2]. We can design the voids in configurations that can guide the fracture propagation along specific directions but not in their reverse directions, thus characterizing a mechanical (fracture) diode. We also observed

that there is an optimal value spacing between each triangular defect, which enhances the rectification.

[1] N R Brodnik, S Brach, C M Long, G Ravichandran, B Bourdin, K T Faber, and K Bhattacharya, Phys. Rev. Lett. 126, 025502 (2021).

[2] L. C. Felix and D. S. Galvao, Phys. Chem. Chem. Phys. 24(22), 13905-13910 (2022).

NM02.04.25

Effect of Deposition of Graphene Based Nanocomposite Electrodes on Performance of Ultracapacitors Duy Pham, Mohamed Elkholy, Quang Lam and Ashish Aphale; Kennesaw State University, United States

Supercapacitors, also known as ultracapacitors have gained considerable interest due to fast charge/discharge capacity, and superior specific energy and power density. Dual charge storage mechanisms such as electrochemical double layer capacitance (EDLC) and redox based Faradaic processes have been investigated to enhance the performance of supercapacitor devices. Further, the use of hybrid electrodes comprising of polymer or metal oxides along with 2D materials such as graphene, have been studied extensively to demonstrate increase in electrode performance. In this work, potentiostatic polymerization of pyrrole (Py) along with graphene has been conducted to develop freestanding electrode for supercapacitor application. The role of deposition cycles during electrochemical polymerization is investigated and its effect on gravimetric capacitance is studied in aqueous electrolyte. Changes in capacitive behavior of electrode material as a function of deposition cycle will be discussed. Surface/interfacial morphology and chemical characterization results will be discussed to show the effect of deposition cycle during electrode film formation. Results from electrochemical techniques including cyclic voltammetry (CV), galvanostatic charge-discharge (GCD) and electrochemical impedance spectroscopy (EIS) will be presented.

NM02.04.26

Energy Dissipation and Rate-Dependent Deformation Behavior of STF-Integrated PU Foam Nanocomposites Emre Gunduz, Bunyamin Karagoz, Ipek Osken, Kaan Yildiz and Hulya Cebeci; Istanbul Technical University, Turkey

The transportation industry requires high safety at lower weight to protect human life with engineered solutions. Designing energy dissipative polymeric foam composite structures is essential for many applications to withstand impact loadings. Compared to honeycombs, polymeric foams receive great attention as structural components with their outstanding effective stress transfer, viscoelastic properties and increased surface area. Among several polymeric foams, rigid polyurethane foams (PURs) are good candidates presenting high strength and lightweight characteristics. To achieve multifunctionality in PURs, several reinforcing strategies have been applied to integrate micro and nanomaterials through tuning the PUR microstructure. Under impact loadings, shear thickening fluids (STFs) exhibit strong toughening behavior. STFs are Non-Newtonian fluids demonstrating different flow behaviors under applied shear. STFs are colloid suspensions, at low shear rates, particles are oriented, STFs flow easily, thus viscosity decreases. After critical shear rate, hydroclusters occur due to applied shear rate and particle interactions, resist to flow, hence viscosity increases drastically. The minimum viscosity is observed at the critical shear rate. The ratio of minimum to maximum viscosity is specified as the thickening ratio. Viscosity, critical shear rate and thickening ratio are essential performance parameters of STFs.

In this study, we aim to investigate energy dissipation and rate-dependent deformation behavior of STF-integrated PURs (STF/PURs) under cyclic compression tests, dynamic mechanical analysis and impact forces. Fumed silica particles (11 nm) were dispersed in ethylene glycol (EG) under a constant mechanical mixing rate of 500 rpm and sonicated to form the concentrated colloidal suspension for 2.7 to 5.4 h. The process was performed with the similar procedure for all concentrations of STFs and optimized to achieve the best dispersion of silica particles inside EG. Silica nanoparticles at varying weight fractions of 19, 22, 24, 26, and 28 were dispersed in EG to observe the effective shear-thickening phenomenon. Rheological measurements of the STFs were carried out, presenting a thickening ratio between 22.6 to 67.6. The highest thickening ratio was obtained with 26 wt.% silica content.

STF/PURs were prepared with 0.5, 1 and 3 wt.% STFs with 26wt.% silica content. Polyol was the chosen media for dispersion of STFs and was firstly mixed by a mechanical stirrer at 300 rpm for 4.5 h. Then PMDI was evenly stirred with the mixture.

The load-carrying ability of cellular polymer foams relies on their morphological features. Cell edge lengths decrease and density increases with STFs integration. Quasi-static cyclic compression tests were performed in a strain-controlled mode, up to 10%, 40%, and 80% strains with 10 cycles. The applied strain rates were chosen as 0.002, 0.02, and 0.2/s in order to investigate the rate dependency. Compression and specific compression strength were improved by 33% and 10.4% with 1.wt% STF/PURs at 0.2/s, respectively. Loss factors were calculated from cyclic compression test results, 6% enhancement was obtained at 10% strain whereas no significant changes were apparent at higher strains.

Dynamic mechanical properties of STF/PURs were also measured using a dual cantilever fixture. First, strain-sweep tests were performed in order to determine the linear viscoelastic region. Then, frequency sweep tests were performed with 35 μ m amplitude. The linear viscoelastic region was found to be increasing with increasing STFs content. The storage modulus also increased by more than 50% while no significant changes in the loss factor were observed.

In conclusion, STF/PURs demonstrated higher mechanical properties than neat PURs. Energy absorption capabilities of STF/PURs at high strains and strain rates will be investigated by drop weight impact tests in future studies.

NM02.04.28

Effect of Chemical Vapor Deposition Condition on the Aspect Ratio of Vertically-Aligned Carbon Nano Tubes (VACNTs) Fahd M. Rajab; Najran University Faculty of Engineering, Saudi Arabia

Vertically Aligned Carbon Nanotubes (VACNT) are promising core elements in advanced devices of various applications. Their uniform growth can be achieved by chemical vapor deposition (CVD) at specific process conditions using metal seed catalysts. Catalyst lifetime depends on the synthesis processes used to make the catalytic substrates and CVD process conditions. In electron-beam physical vapor deposition, silica oxide substrates are coated with an alumina barrier layer and a catalyst layer. Further diffusion of the catalyst in the barrier layer in the heating step of CVD and insufficient catalytic oxidation can impede catalyst distribution and suppress the growth of VACNT.

CVD is performed at controlled process conditions to grow VACNT utilizing iron seed catalysts of selected layer thicknesses. CVD conditions such as hydrocarbon and water vapor rates are varied to investigate their effect on VACNT structures. The analytical studies include spectroscopic ellipsometry to measure wafer substrate layer thickness, Raman spectroscopy to assess the structures of carbon nanotubes, as well as scanning electron microscopy (SEM) to evaluate VACNT growth density and patterns. Findings show Fe catalyst/Al₂O₃ buffer layer thickness-position effect, and a highly dependent VACNT G/D ratio on reaction conditions and reactant flow ratios.

NM02.04.29

High-Performance Photothermal Conversion of Electrospun Polymer/Carbon Composite Materials Fangqi Chen, Yanpei Tian, Andrew Caratenuto,

Xiaojie Liu and Yi Zheng; Northeastern University, United States

The usage of the abundant solar energy has attracted significant interest in the recent years, and the photothermal absorber with a high energy conversion efficiency due to its broad solar absorption has become a key component in many solar-harvesting applications, such as solar-driven steam generation. In this work, a polycaprolactone nanofiber composite with incorporation of carbon nanotubes or carbon nanoparticles is introduced with an average absorbance of 0.94 and 0.93 in the wavelength of visible and near-infrared light, serving as an excellent broadband solar absorber. The refractive indices of the composite are determined using a Lorentz–Drude oscillator model based on the experimental transmittance spectra. The composite yields an ultrahigh solar absorbance that contributes to an interfacial evaporation rate of $2.00 \text{ kg m}^{-2} \text{ h}^{-1}$ and $1.95 \text{ kg m}^{-2} \text{ h}^{-1}$ for carbon nanotubes and nanoparticle composites, respectively. Compared with other nanofabrication methods, electrospinning has the advantages of simplicity, cost effectiveness, and high efficiency, and it enables scalable fabrication of nanostructured materials. This work sheds light on a low-cost and high-output fabrication method for a nanofiber photothermal absorber composed of a biocompatible and biodegradable polymer and carbon materials.

NM02.04.30

Confinement Effects on the Dielectric Properties of Graphene and Reduced Graphene Oxide Dispersed Polymer Nanocomposite Films Farzana H. Likhil and Alamgir Karim; University of Houston, United States

Much recent research efforts have studied how the incorporation of graphene oxide (GO) and reduced graphene oxide (rGO) impact the frequency dependent dielectric properties in polymer nanocomposite materials. However, few studies explore the effect of film confinement in the micron to sub-micron range of thin film regime. In this film thickness range, that is comparable to the lateral dimensions of the platelet GO and rGO nanomaterials, we can expect film confinement effects on platelet orientation, that also impacts its relative projection area to the applied electric field. Pristine graphene can be achieved by reducing graphene oxide, which has a similar honeycomb structure with both sp^2 and sp^3 carbon imbuing the surface with limited oxygen-based functional groups that can interact with the polymer matrix via a nanometric interfacial zone. In this work we present the nanomaterial loading-frequency dependence of these two fundamental properties, in thin polyvinylidene fluoride (PVDF) film containing GO and rGO of thicknesses ranging from $1 \mu\text{m}$ to $100 \mu\text{m}$. Controlled microwave was used for reducing graphene oxide in a laboratory environment. We will discuss the film finite size effects on the relative response of GO vs. rGO vs. pristine PVDF in terms of their dielectric constant, loss tangent, and AC conductivity data over the frequency range of 1 kHz to 1 GHz using a dielectric spectrometer. We observed that the AC electrical conductivity tends to increase with frequency, but the dielectric permittivity tends to decrease in general, and that the dielectric properties are more frequency sensitive for the $1 \mu\text{m}$ film than the $100 \mu\text{m}$ films. AFM and SEM were used to ascertain the film morphology and quality of these nanocomposite films. This study may provide an insight for development and utilization of GO and rGO based polymer thin films in future electronics

NM02.04.32

Large Polycyclic Aromatic Hydrocarbons as Graphene Quantum Dots—New Ultra Stable and Bright Emitters for Photonics Giuseppe M. Paternò^{1,2}, Qiang Chen³, Francesco Scotognella^{1,2}, Guglielmo Lanzani^{2,1} and Akimitsu Narita⁴; ¹Politecnico di Milano, Department of Physics, Italy; ²Istituto Italiano di Tecnologia, Italy; ³University of Oxford, United Kingdom; ⁴Okinawa Institute of Science and Technology, Japan

Synergistic research efforts in multistep chemical synthesis and state-of-the-art optical spectroscopy have permitted the realization of graphene quantum dots (GQDs) with defined structures, edge configurations and properties, paving the way towards their possible applications in photonics and optoelectronics. One such fruitful feedback loop between synthesis and spectroscopy is represented by the recent development of stable GQDs with zigzag edges, displaying excellent spectral features such as optical gain and strong absorption/emission in the visible/near-infrared regions, which are appealing for applications in photonics.¹

In this talk, I will provide an overview of the latest developments in the advanced spectroscopic investigations of atomically precise GQDs, with particular emphasis on those with zigzag-edged structures. Finally, I will discuss on their application as stable and efficient gain materials in laser devices and as ultrafast optical switcher.

1 G. M. Paternò, Goudappagouda, Q. Chen, G. Lanzani, F. Scotognella and A. Narita, *Adv. Opt. Mater.*, 2021, 2100508.

NM02.04.34

Rapid, Multianalyte Detection of Opioid Metabolites in Wastewater Michael Geiwitz and Narendra Kumar; Boston College, United States

By monitoring opioid metabolites, wastewater-based epidemiology (WBE) could be an excellent tool for real-time information on the consumption of illicit drugs. A key limitation of WBE is the reliance on costly laboratory-based techniques that require substantial infrastructure and trained personnel, resulting in long turnaround times. Here, we present an aptamer-based graphene field effect transistor (AptG-FET) platform for simultaneous detection of three different opioid metabolites. This platform provides a reliable, rapid, and inexpensive method for quantitative analysis of opioid metabolites in wastewater. The platform delivers a limit of detection 2–3 orders of magnitude lower than previous reports, but in line with the concentration range (pg/mL to ng/mL) of these opioid metabolites present in real samples. To enable multianalyte detection, we developed a facile, reproducible, and high-yield fabrication process producing 20 G-FETs with integrated side gate platinum (Pt) electrodes on a single chip. Our devices achieved the selective multianalyte detection of three different metabolites: noroxycodone (NX), 2-ethylidene-1,5-dimethyl-3,3-diphenylpyrrolidine (EDDP), and norfentanyl (NF) in wastewater diluted $20\times$ in buffer.

NM02.04.35

Construction of Nitrogen-Abundant Graphyne Scaffolds via Mechanochemistry-Promoted Cross-Linking of Aromatic Nitriles with Carbide Towards Enhanced Energy Storage Juntian Fan¹, Zhenzhen Yang² and Sheng Dai²; ¹University of Tennessee, United States; ²Oak Ridge National Laboratory, United States

The two-dimensional (2D) graphyne-related scaffolds linked by carbon–carbon triple bonds are an important category of conjugated organic networks demonstrating promising applications in the field of catalysis and energy storage fields. The mechanochemistry-driven methods could afford graphyne-related materials under neat and ambient conditions by leveraging the energy input from mechanochemical treatment to promote the nucleophilic attack reaction of CaC_2 with aromatic halides. However, the scaffolds construction was still limited to the cross-linking of CaC_2 with aromatic halogens and afforded graphyne materials with none or low content of heteroatom doping (e.g., nitrogen), which cannot meet the high charge storage requirements in the electrochemical fields. Development of alternative approaches to afford nitrogen-abundant graphyne materials via the facile mechanochemical procedure is a long-standing challenge.

In this contribution, towards the construction of nitrogen-doped graphyne materials via the mechanochemistry-driven procedure under neat and mild conditions, multiple substituted aromatic halides with enhanced reactivity with CaC_2 were deployed by introducing extra electron-withdrawing cyano groups on the benzene ring, to achieve efficient graphyne scaffolds construction and simultaneous nitrogen-doping. The as-afforded nitrogen-doped graphyne materials delivered enhanced energy storage behaviors in supercapacitor-related applications. Furthermore, the facile mechanochemical treatment

pathway was extended to a non-halogenated monomer with multiple aromatic nitrile groups and electron-deficient properties, which could efficiently react with CaC_2 via the ball milling procedure. Efficient cross-coupling polymerization could be conducted with a low feeding mass ratio (CaC_2 : monomer) of 1:8 in almost quantitative yield. The as-afforded nitrogen-doped graphyne materials were featured by abundant nitrogen-containing species with nitrogen content up to 29.31 wt%, high surface areas up to $865 \text{ m}^2 \text{ g}^{-1}$, and hierarchical architectures composed of micro- and mesopores, which could be tuned by varying the mechanochemical parameters. The unique properties of these materials worked together to deliver promising capacitance (up to 254.5 F g^{-1}) in supercapacitor-related applications, together with good rate performance and attractive cycling stability. The achievements made in this work not only provide monomers with highly conjugated structures coupled with high nitrogen content to construct task-specific graphyne materials, but will also extend the application of related materials in other under-explored fields.

NM02.04.36

The Structure Dependence on the Mechanical Properties of Spiked-Shell Aerographite Particles YueXuan Li, Hiromu Hamasaki and Kaori Hirahara; Osaka University, Japan

Aerographite particles have a micrometer-sized unique shell structure, consisting of radially-aligned hollow carbon nanorods seamlessly connected at their bottoms [1]. Such a morphology brings excellent flexibility under large compression. When the particles were fully-compressed with strain $>70\%$, they can recover their original shapes after unloading. However, the particles tended to accumulate small cracks at strain $>40\%$, which sometimes leads to fracture or fatigue damages on particles in the repetitive compression. We consider that the mechanical properties of aerographite particles can be improved by controlling the properties of their graphitic structures. In this study, we focus on two structural parameters, crystallinity, and thickness of the graphitic layers consisting the aerographite particle, influencing on the mechanical properties. Crystallinities of individual particles were improved by annealing above $1,600^\circ\text{C}$ with keeping their flexible shell morphologies, although the excess heating at $2,000^\circ\text{C}$ caused damage to the shell structure. On the other hand, the layer thickness was controlled by changing the feeding time of the acetylene gas in the fabrication process. The effect of these structural changes on mechanical properties was investigated by performing single-particle-level compressive tests in a scanning electron microscope with the use of nanomanipulation techniques. Experimental results for particles annealed at different temperatures showed that the annealing at $1,600^\circ\text{C}$ had suppressed the fracture of aerographite particles, due to the restraint of crack propagation caused by crystallinity improvement. For particles fabricated with various thicknesses (4-9 nm), all particles with 5 nm layer thickness did not exhibit fracture, even under fully compressed conditions. The decrease of layer thickness induced buckling of the shell along the compressive axial direction when the compressive strain was over 40%. In addition, such a buckling may be related to reducing the accumulation of residual strain during the cyclic compression. Accordingly, improving crystallinity by annealing at $1,600^\circ\text{C}$ and controlling the thickness of the graphitic layers to 5 nm are revealed to be effective options to realize further superior mechanical properties of aerographite particles.

[1] Hirahara, K., Hiraishi, K., Imadate, K., Xu, Z., Hirota, Y., Nishiyama, N., Carbon, Vol.118, (2017), pp.607-614.

NM02.04.37

Electrical Resistance Measurement of a Single Interface Between Carbon Nanotubes Hiromu Hamasaki and Kaori Hirahara; Osaka University, Japan

As carbon nanotubes (CNTs) possess superior thermal and electrical transport properties, they have broad potential applications for flexible devices such as thermoelectric generators. However, the conductivities in CNT assemblies are reduced by several orders of magnitude and strongly depend on the alignment of individual nanotube axes [1]. This is mainly due to the difference of the conductance between intratube and intertube bondings in assemblies. Probably due to the difficulty of the experimental approaches, less is known about transport via a single contact between two neighboring nanotubes than about transport within an isolated nanotube, despite their likely equivalent importance for CNT assembly applications. To deepen understanding of contact transport, a systematic study of the effects of contact length (or area) in simple, parallelly contacted CNTs would be of great importance. Moreover, they could have enormous implications for the transport of other nanomaterial-based assemblies and composites. In this study, we experimentally investigate the electrical resistance of a single parallel contact between two multi-walled CNTs. A nanomanipulation system, equipped in a transmission electron microscope, enables the performance of in situ measurements of electrical resistance for a range of contact lengths [2].

In all cases for MWCNTs with different diameters, the measured resistances as a function of contact lengths showed the same trend; the electrical resistance decreased with increasing contact length. This is qualitatively reasonable as the contact area increases in proportion to the contact length. Here, we cannot directly attribute the measured resistance values to the contact resistance between the CNTs as they were obtained by the two-terminal method. The total resistance can be divided into three elements, namely, the resistance of the individual CNTs, the interfacial resistance between CNTs, and other resistance. Other resistance is generated by components independent of the nature of both CNTs and CNT-CNT contact, therefore it can be assumed to be a constant value. The contact-length-dependent behaviour can be derived from the first two terms, the resistance of the individual CNTs and the interfacial resistance between the CNTs. We found that the measured electrical resistance exhibited two different dependences as a function of the contact length; it was inversely proportional to the contact length when the contact length was small, whereas, it was proportional to the contact length with a negative gradient when the contact length was sufficiently large. We found that the former and latter dependences can be attributed to the resistances of the interface and CNTs, respectively, and derived the electrical conductivity of the single interface and single CNTs from the measurements. The conductivities of a single CNT were comparable to the previous reports. The interface between nanotubes exhibits intermediate conductivity between those of pyrolytic and single-crystal graphite along c-axis. These findings suggest that the interfacial effect becomes effectively small at contact lengths longer than a few hundred nanometers. The present study has fundamental implications for the physics of CNT-based electronics and their applications. This work was supported by JST CREST Grant Number JPMJCR17I5, Japan.

[1] Y. Inoue et al., Carbon, 49, 2437 (2011).

[2] H. Hamasaki et al., Nanoscale, 14, 11529 (2022).

NM02.04.38

Design and 3D Printing of Optimized Electrodes for Supercapacitor Applications Mariana Desirée Reale Batista¹, Swetha Chandrasekaran¹, Bryan Moran¹, Miguel Salazar de Troya¹, Anica Pinongcos², Zhen Wang³, Ryan Hensleigh³, Adam Carleton¹, Manhao Zeng¹, Thomas Roy¹, Dun Lin², Xinzhe Xue², Victor Beck¹, Daniel Tortorelli¹, Michael Stadermann¹, Rayne Zheng³, Yat Li² and Marcus A. Worsley¹; ¹Lawrence Livermore National Laboratory, United States; ²University of California, Santa Cruz, United States; ³University of California, Los Angeles, United States

Supercapacitors have attracted considerable attention within the automotive, aerospace, and telecommunication industries due to their fast charging/discharging ability. The high electrical conductivity and surface area of porous carbons make them attractive candidates for supercapacitor electrodes. Maximizing porous carbon in electrodes (i.e., thick electrodes) is one strategy to further increase energy density of these devices. However, these porous carbons suffer from sluggish charged species transport in thicker electrodes, which limits them to thin electrode designs. In this work, we investigate the use of computer-guided optimization and additive manufacturing to design and print thick porous electrodes with improved performance. Electrodes with optimal performance were designed by topology optimization and printed by projection micro stereolithography (PμSL) using PR48 resin. The PR48 resin was then pyrolyzed (PR48-P) to create the final conductive electrode. The PR48-P electrodes with optimized design exhibited improved capacitance compared to those control electrodes printed as cubic lattice structures. To further improve performance, a new resin was synthesized by

combining graphene oxide (GO) and trimethylolpropane triacrylate (TMPTA). Electrodes printed with 3 wt% GO in TMPTA exhibited improved capacitance retention after pyrolysis compared to PR48-P electrodes. This work demonstrates the benefits of using topology optimization to design electrodes and material development to improve functional properties of 3D printable resins. This work was performed under the auspices of the U.S. Department of Energy by Lawrence Livermore National Laboratory under contract DE-AC52-07NA27344. Lawrence Livermore National Security, LLC.

NM02.04.39

Cellulose Acetate-Assisted Fibrous Carbon Nanotube Networking Film for Scalable Binder-Free Electrodes in Flexible Li-Ion Batteries Ji Hyun Han and Yun Jung Lee; Hanyang University, Korea (the Republic of)

A freestanding cellulose acetate-carbon nanotube (CA-CNT) film electrode is given here to build very flexible and high-energy lithium-ion batteries (LIBs). CA acts as a CNT dispersion agent and a binder-free network former. Simple washing can eliminate practically all of the CA in the CNT electrode while preserving the fibrous CNT network within the electrode. Furthermore, because the CA-CNT film is treated using a standard casting method rather than area-limited vacuum filtering, the CNT film electrode can be produced on a wide scale. The improved electrochemical performance and great flexibility of the complete cell built with CA-CNT-based electrodes are maintained even at high active material loading, which has proven challenging to achieve in the standard format of LIBs. Furthermore, by merely stacking six sheets of the freestanding CNT film electrode, a capacity of 5.4 mA h cm⁻² is produced. Under considerable distortion, the pouch battery performs reliably. We show that a rational CNT electrode design may increase flexibility to greater energy than the conventional arrangement. We anticipate that the suggested freestanding CNT film electrode's low production cost, great flexibility, and outstanding electrochemical performance would hasten the adoption of wearable gears in daily life.

NM02.04.40

First-Principles Computational Study on Li₂C₆₀ Nanoparticle—High-Performance Anode Material for Li-Ion Batteries Dong-Hwa Seo¹, Dae Hyung Lee¹, Linghong Yin², Jiung Cho³, Su Jae Kim², Il Jeon², Injun Jeon², Mihee Park², Minjoon Park², Se-Young Jeong² and Chae-Ryong Cho²; ¹Ulsan National Institute of Science and Technology, Korea (the Republic of); ²Pusan National University, Korea (the Republic of); ³Korea Basic Science Institute, Korea (the Republic of)

In the era of electric vehicles, lithium-ion batteries are demanded to have properties appropriate to electric vehicles, such as high energy density, superior rate performance, and long cycle stability. Unfortunately, current commercialized anode materials are not enough to fulfill all these requirements at once—graphite brings ~370mAh/g of capacity, which is insufficient to satisfy energy density demand, and silicon suffers from poor cycle performance due to severe volume expansion. In this work, the Li⁺ ion storage mechanism and structural evolution, which play a critical role in determining lithium-ion battery performances, are studied with first-principles calculation for face-centered-cubic (FCC) C₆₀ nanoparticle, which is proposed as a high-performance anode material for lithium-ion batteries. Density functional theory (DFT) functionals are benchmarked for various Li_xC₆₀ (x=0, 1, 2, 3, 4, 6, 8, 10, 12, 14) structures generated by genetic algorithm (GA) approach, and Li⁺ ion sites, electrochemical voltages, and phase transition behavior of Li_xC₆₀ are predicted by SCAN+rVV10 DFT functional. These results are well-matched with the in-situ X-ray diffraction analysis and superior electrochemical performance of FCC C₆₀ nanoparticles, the reversible specific capacity of 750 mAh/g at 0.1 A/g and retains coulombic efficiency of 98.7% after 1000 cycles at 5 A/g. Furthermore, it is figured out that competition between electrostatic repulsion and stress occurred by inserted Li⁺ ion governs phase transition behavior. We expect these atomic-level understandings will accelerate the development of superior lithium-ion batteries and electric vehicle dissemination.

Reference

[1] L. Yin,† J. Cho,† S. J. Kim, I. Jeon, I. Jeon, M. Park, M. Park, S. Y. Jeong, D. H. Lee, D.-H. Seo,* C.-R. Cho,* “Abnormal high-lithium storage of pure crystalline C₆₀ nanoparticles”, *Adv. Mater.*, 33, 2104763 (2021), †equally contributed.

SESSION NM02.05: Synthesis and Characterization III

Session Chairs: Tanja Kallio, Shunsuke Sakurai, Yoke Khin Yap and Ming Zheng
Tuesday Morning, November 29, 2022
Hynes, Level 2, Room 208

8:30 AM *NM02.05.01

Unconventional 2D Materials from Liquid Phase Synthesis Kimmo Mustonen¹, Christoph Hofer², Viera Skakalova¹, Alexander Markevich¹, Timothy Pennycook² and Jani Kotakoski¹; ¹University of Vienna, Austria; ²EMAT, Belgium

Current 2D materials largely derive from van der Waals -layered bulk structures. However, only a limited number of such structures exist under ambient conditions, and in total only a few dozen 2D crystals have been successfully synthesized or exfoliated. In contrast to previous contributions, in this talk I will discuss a so far unexplored scheme for liquid phase synthesis of 2D materials that is based on the use of graphene oxide (GO) bilayers acting as a template material and kinetic barrier. The GO layers in the presented scheme are of fundamental importance as they prevent crystal growth along out-of-plane high-symmetry directions, and thus the formation of bulk crystalline solids.

Among countless 2D materials that have been predicted based on first principle computations [1], the β -phase of CuI, which is only stable at a narrow temperature range of 645-675 K [2,3], is a prime example of a material that would be impossible to isolate in its monolayer form via exfoliation. In our recent contribution we have synthesized this particular material inside a GO envelope and via atomically resolved scanning transmission electron microscopy have subsequently characterized its structure in great detail [4]; these results will be discussed in the talk.

The applicability of our synthesis method, however, is not limited to this singular structure. Quite the contrary, we have already applied the same process to several other transition metal halides, including 2D silver iodide and magnetic nickel iodide crystals. Moreover, generalizing this concept should allow access to further exotic layered structures, which will vastly expand the currently available library of 2D materials and their incorporation in devices, hence facilitating their structure and properties to be studied in room temperature.

1. Mounet *et al.* Two-dimensional materials from high-throughput computational exfoliation of experimentally known compounds. *Nature Nanotechnology* 2018, 13, 246–252.

2. Sakuma, Crystal structure of β -CuI. *Journal of the Physical Society of Japan* 1988, 57, 565–569.

3. Keen, D., Hull, S. Determination of the structure of beta-CuI by high-resolution neutron powder diffraction. *Journal of Physics: Condensed Matter* 1994, 6, 1637.

4. Mustonen *et al.* Toward Exotic Layered Materials: 2D Cuprous Iodide. *Advanced Materials* 2022 e2106922.

9:00 AM *NM02.05.02

MXenes Expand the Range of 2D Materials Far Beyond Graphene Yury Gogotsi; Drexel University, United States

Discovery of new materials provides moments of inspiration and shifts in understanding, shaping the dynamic field of materials science. Following the graphene breakthrough, many other 2D materials emerged. Although many of them remain subjects of purely academic interest, others have jumped into the limelight due to their attractive properties, which have led to practical applications. Among the latter are 2D carbides and nitrides of transition metals known as MXenes [1]. The family of MXenes has been expanding rapidly since the discovery of Ti_3C_2 in 2011 [2]. More than 30 different stoichiometric MXenes have been reported, and the structure and properties of numerous other MXenes have been predicted. Moreover, the availability of solid solutions on M and X sites, multi-element high-entropy MXenes, control of surface terminations, and the discovery of out-of-plane ordered double-M *o*-MXenes (e.g., Mo_2TiC_2), as well as in-plane ordered *i*-MAX phases and their *i*-MXenes offer a potential for producing dozens of new distinct structures. This presentation will describe the state of the art in the manufacturing of MXenes, their delamination into single-layer 2D flakes and assembly into films, fibers and 3D structures. Synthesis-structure-properties relations of MXenes will be addressed on the example of Ti_3C_2 . The versatile chemistry of the MXene family renders their properties tunable for a large variety of applications. In particular, the interaction of MXenes with electromagnetic waves can be controlled via their composition and structure. Many MXenes offer high electronic conductivity and outstanding electromagnetic interference shielding. They can also be used in telecommunication, energy, medical and electronic device applications.

References

A. VahidMohammadi, J. Rosen, Y. Gogotsi, The World of Two-Dimensional Carbides and Nitrides (MXenes), *Science*, 372, eabf1581 (2021)
M. Naguib, M. Kurtoglu, V. Presser, J. Lu, J.-J. Niu, M. Heon, L. Hultman, Y. Gogotsi, M. W. Barsoum, Two-Dimensional Nanocrystals Produced by Exfoliation of Ti_3AlC_2 , *Advanced Materials*, 23, 4248-4253 (2011)
X. Li, Z. Huang, C. E. Shuck, G. Liang, Y. Gogotsi, C. Zhi, MXene chemistry, electrochemistry, and energy storage applications, *Nature Reviews Chemistry*, 6 (6), 389–404 (2022)

9:30 AM NM02.05.03

Electrical Control of the Chemical Vapor Deposition of Graphene Jiangtao Wang, Ji-Hoon Park, Ang-Yu Lu and Jing Kong; Massachusetts Institute of Technology, United States

Chemical vapor deposition (CVD) is widely used for the efficient growth of low dimensional materials. The growth mechanism comprises the mass and heat transport, gas phase and surface chemical reaction, and the interaction between the product and the substrate/catalyst. Correspondingly, the controllable parameter space is conventionally focused on the mass flow of each component, the temperature of the reaction chamber and substrate, and the material and structure of the substrate/catalyst. Here, we report that applying voltage on the copper substrate has significant impacts on the growth of graphene. Electrochemical effect and ionic collision effect are observed in different conditions. With the assistance of negative and positive voltage applied on the growth substrate, selective growth and rapid growth of clean monolayer graphene film are achieved, respectively. We anticipate this discovery will open up a new dimension in methodology for the growth of 2D materials.

9:45 AM NM02.05.04

In Situ Observation of Dynamic Changes in Graphene by STEM Hyunjeong Jeong¹, Dong Hoon Shin², Heena Inani³, Kimmo Mustonen³, Clemens Mangler³, Yugyeong Je¹, Jani Kotakoski³ and Sang Wook Lee¹; ¹Ewha Womans University, Korea (the Republic of); ²Delft University of Technology, Netherlands; ³University of Vienna, Vienna, Austria

We investigated *in-situ* observations of the dynamic changes in graphene by external stimuli such as Joule heating and electron beam irradiation. The carbon structure of graphene was directly observed under electron beam irradiation using a scanning transmission electron microscope (STEM). Suspended graphene was prepared on a Silicon nitride membrane substrate with a hole pattern and connected to electrodes. The Joule heating process by applying a high current can accumulate a high temperature in the middle of the suspended graphene region. In the case of the twisted bilayer graphene structure, the periodicity of the Moiré pattern was changed before and after the Joule heating process. This implies that small flakes of graphene may rotate at high temperature. We also report the observation of defect healing in graphene by electron beam irradiation and the Joule heating process.

10:00 AM BREAK

10:30 AM *NM02.05.05

From Carbon Dots and Graphene Quantum Dots to HBCs and Beyond Dirk M. Guldi; University of Erlangen, Germany

Carbon is the key to many technological applications that have become indispensable in our daily life. Altering the periodic binding motifs in networks of sp^3 -, sp^2 -, and sp -hybridized C-atoms is the conceptual starting point for a broad palette of carbon allotropes. The past two decades have served as a test-bed for measuring the physico-chemical properties of low-dimensional carbon with the advent of fullerenes (0D), followed in chronological order by carbon nanotubes (1D), carbon nanohorns, and, most recently, by graphene (2D). These species are now poised for use in wide-ranging applications. Expanding global needs for energy have led to a significant effort to develop alternatives to fossil fuels. While alternative sources for energy are already in use, they comprise a small percentage of the energy demands needed to carry us through the 21st century. No single source will solve the global needs, but the development of photovoltaics has vast potential as a point-of-use power source. Recent work has shown that hybrid photoelectrochemical efforts with a percolation network of photon absorbers coupled to an electron/hole transporter in combination with advanced photon management are the ideal design for realizing breakthroughs in high photon conversion efficiencies suitable for the catalysis of water. I will report on our efforts regarding a unifying strategy to use the unprecedented charge transfer chemistry of carbon dots and HBCs, together in a groundbreaking approach to solving a far-reaching challenge, that is, the efficient use of the abundant light energy around us.

11:00 AM NM02.05.06

The Correlation Effect Between Growth Parameters for Hexagonal Boron Nitride via Machine-Learning Approach Ji-Hoon Park, Ang-Yu Lu and Jing Kong; Massachusetts Institute of Technology, United States

The large-area, high-quality growth of monolayer hexagonal boron nitride (hBN) was realized by the epitaxy through the step-edge guided nucleation on the wafer-scale single-crystalline metal surface. However, a systematic understanding of the growth dynamics based on the growth parameters is required for not only a clear explanation of the growth mechanism but also the synthesis into the desired direction including the reproducibility and functionalization of materials. Here, we synthesized monolayer hBN on single-crystalline Cu (111) at low pressure by chemical vapor deposition method. The nucleation density and flake size of hBN were controlled by the concentration of borazine as a precursor of hBN during the growth process. Furthermore, we systematically investigate the growth mechanism from single parameter to two parameters effect by the Gaussian process method in Machine-learning, allowing us to explore the correlation between growth parameters. This approach will open new insight for the systematic understanding of the growth mechanism of novel materials.

11:15 AM NM02.05.07

Text Mining of CVD Synthesis Recipes for 2D Materials by Natural Language Processing [Ang-Yu Lu](#)¹, Richard Chen¹, Aijia Yao^{1,2}, Ji-Hoon Park¹, Tianyi Zhang¹, Xudong Zheng¹, Nannan Mao¹, Jiangtao Wang¹ and Jing Kong¹; ¹Massachusetts Institute of Technology, United States; ²ShanghaiTech University, United States

Tremendous and precious scientific knowledge is written in text format as journal articles. This enormous unstructured data is challenging for humans to analyze and develop comprehensive perspectives from the past. Recently, natural language processing (NLP) has made significant advances in word embedding, especially with the launch of pre-trained models (e.g., BERT, GPT). Materials science has attempted to apply this breakthrough by converting unstructured data into structured data, but so far this is limited to very general methods and materials, and the provided information is not yet beyond researchers' domain knowledge. In this work, we adopt the state-of-art NLP technique to collect synthesis recipes from journal articles for seven low-dimensional materials, including CNT, graphene, hexagonal boron nitride (hBN), molybdenum disulfide (MoS₂), molybdenum diselenide (MoSe₂), tungsten disulfide (WS₂), and tungsten diselenide (WSe₂). First, we deploy a fine-tuning BERT model without manual annotation by calculating the term frequency of the titles and combining them with our prior knowledge, allowing us to extract CVD-related titles. Furthermore, we apply keyword searching fusion with a fine-tuning BERT model to classify the CVD abstract as Correlation Output, such as monolayer, bilayer, multilayer, and nanostructures. Lastly, we implemented the BERT model for named entities recognition (NER) to extract experimental recipes as Correlation Input. Through statistical analysis, we discover the correlation among the recipes and their results for each material and unravel the synthesis trajectory between different materials. Our work may serve as a methodology for applying natural language processing in optimizing existing 2D materials and accelerating the exploration of new advanced materials.

11:30 AM NM02.05.09

All-Dry Transfer of Large-Area CVD-Graphene Using Vapor Phase Deposited Smart Thermally-Responsive Pressure Sensitive Adhesive Thin Films Kurtulus Yilmaz, Mehmet Gursoy and [Mustafa Karaman](#); Konya Technical University, Turkey

Since its first isolation from graphite using the simple scotch tape method in 2004, extensive effort has been put by the researchers on graphene due to its intriguing properties, such as high electron mobility, superior electrical and thermal conductivity, extraordinary tensile strength and superior mechanical properties. The transparency of a single-layer graphene is excellent, with very low absorption of the incident light. The prerequisite for making use of such extraordinary properties in real-world applications is to synthesize single or few-layer graphene at large scales on different types of application surfaces. Among the different synthesis protocols, chemical vapor deposition (CVD) appeared to be the ideal bottom-up technique to synthesize graphene in large areas and at high qualities. In CVD, graphene is deposited on atomically smooth metallic substrates, which necessitates a post-deposition stage in order to transfer as-deposited graphene to the real application surface. The transfer of graphene from the metallic growth substrate to other substrates must be carried out perfectly without compromising the quality and properties. The conventional methods for the transfer of CVD-graphene adopt poly(methyl methacrylate) (PMMA) as the support layer. This multi-stage "wet" approach has many drawbacks including the structural degradation during the PMMA removing process. Instead of conventional wet approaches, this study demonstrates an all-dry transfer protocol, in which graphene is transferred using "smart" thermally-responsive polymeric thin films possessing switchable adhesive strength depending on the temperature. A pressure sensitive adhesive film based on poly(acrylic acid) and poly(ethylhexyl acrylate) was deposited on a flexible template material using initiated CVD (iCVD) technique. Thus, surface of transfer film coated with smart PSA became a suitable platform for the adhesive transfer of graphene. The structure and morphology of the as-deposited PSA film was tuned precisely by iCVD, which was verified by FTIR and AFM analyses, respectively. There was a sharp decrease in adhesive strength of the as-deposited PSA films with increasing temperature from 25 to 80 °C, which allowed the design of a smart adhesive-based transfer surface acting like a pick&place gripper. In this way, it was possible to remove CVD-graphene from copper surface at large areas (100 mm x 100 mm) uniformly at room temperature and place the same graphene on glass substrates at 80°C. The measurement of optical, electrical and morphological properties of the as-transferred graphene on glass substrates revealed that the PSA-based all-dry technique was superior to the conventional wet technique. PSA-based all-dry technique allowed the re-use of the copper at least three times without compromising the quality of as-deposited graphene, and it was applicable for the transfer of CVD-graphene to different flat application surfaces, including metals and plastic foils.

SESSION NM02.06: Spectroscopy and Optical Study

Session Chairs: Tanja Kallio, Shunsuke Sakurai, Yoke Khin Yap and Ming Zheng

Tuesday Afternoon, November 29, 2022

Hynes, Level 2, Room 208

1:30 PM *NM02.06.01

Quantifying Adsorbed Dispersant Layers on Single-Wall Carbon Nanotubes in Simple and Complex Environments [Jeffrey Fagan](#); National Institute of Standards and Technology, United States

Dispersion of single-wall carbon nanotubes (SWCNT) as individual objects in most liquid environments requires the use of an adsorbing dispersing agent such as a small molecule surfactant, dispersant such as DNA, or polymer chain to modulate the interactions with other nanotubes and the solution. The exact structure and density of these dispersing agents controls the stability of the dispersed nanotubes and affects their electronic and optical properties. Importantly, these molecules also enable a variety of separation methods for SWCNTs to purify them from impurities or to select for classes of SWCNTs such as semiconducting or metallic, or even for single species (n,m) structures. In particular, aqueous two-phase extraction using either cosurfactant competition or selective DNA sequences depend on the adsorbed interfacial dispersant layer to determine the achieved separation.

In this talk I will present the use of analytical ultracentrifugation to determine the adsorbed dispersant density on different nanotube species first for single species and surfactants, and then for complex environments including competing surfactants and polymer molecules. The quantification of the bound

surfactant quantity and identity as a function of solution concentration on the nanotubes enables the direct testing of separation mechanisms and a measurand for optimization of separation conditions.

2:00 PM *NM02.06.02

Electroluminescence from Single-Walled Carbon Nanotubes with Quantum Defects Min-Ken Li^{1,2}, Adnan Riaz^{1,2}, Martina Wederhake³, Karin Fink¹, Avishek Saha⁴, Simone Dehm¹, Xiaowei He⁴, Friedrich Schöppler³, Manfred Kappes¹, Han Htoon⁴, Valentin Popov⁵, Stephen Doorn⁴, Tobias Hertel³, Frank Hennrich¹ and **Ralph Krupke**^{1,2}; ¹Karlsruhe Institute of Technology, Germany; ²Technische Universität Darmstadt, Germany; ³Julius Maximilian University Würzburg, Germany; ⁴Los Alamos National Laboratory, United States; ⁵University of Sofia, Bulgaria

Individual single-walled carbon nanotubes with covalent sidewall defects have emerged as a new class of photon sources whose photoluminescence spectra can be tailored by the carbon nanotube chirality and the attached functional group/molecule. Here we present electroluminescence spectroscopy data from single-tube devices based on (7, 5) carbon nanotubes, functionalized with dichlorobenzene molecules, and wired to graphene electrodes. We observe electrically generated, defect-induced emissions that are controllable by electrostatic gating and strongly red-shifted compared to emissions from pristine nanotubes. The defect-induced emissions are assigned to excitonic and trionic recombination processes by correlating electroluminescence excitation maps with electrical transport and photoluminescence data. At cryogenic conditions additional, gate-dependent emission lines appear which are assigned to phonon-assisted hot-exciton electroluminescence from quasi-levels. Similar results were obtained with functionalized (6, 5) nanotubes. We also compare functionalized (7, 5) electroluminescence data with photoluminescence of pristine and functionalized (7, 5) nanotubes redox-doped using gold(III) chloride solution. This work shows that electroluminescence excitation is selective toward neutral defect-state configurations with the lowest transition energy, which in combination with gate-control over neutral versus charged defect-state emission leads to high spectral purity.

Reference: Min-Ken Li et al., ACS Nano 2022 (doi: 10.1021/acsnano.2c03083)

2:30 PM NM02.06.03

Programmable Helicity in Optically Active One-Dimensional van der Waals Solids Dmitri Cordova¹, Kenneth Chua¹, Tyler Kerr¹, Toshihiro Aoki¹, David Knez¹, Grigorii Skorupskii², Dmitry Fishman¹ and **Maxx Arguilla**¹; ¹University of California, Irvine, United States; ²Princeton University, United States

Long-range helicity in condensed materials has sternly relied on the precise ordering of cooperative intra- and inter-molecular bonding interactions. The exclusivity of these interactions in natural, organic, or molecular systems has limited the conclusive demonstration of aperiodic helical motifs in densely packed solid state lattices. In this talk, we will present a class of 1D van der Waals solids that crystallize as weakly bound helical chains that possess atomic scale order consistent with an aperiodic tetrahelix. We will describe how precise atomic level control of the local coordination environment in these 1D vdW lattices induces helical aperiodicity in periodic helical motifs based on repeating screw axis symmetry motifs. We will also highlight herein that the modularity of vdW lattices allows for the systematic engineering of helical attributes (radius, rise, and twist angle) and band gap energies across the visible to the near-UV spectral window. Owing to the intrinsic non-centrosymmetry of aperiodic helices, we will show that these 1D vdW tetrahelices exhibit visible range second harmonic generation in freestanding crystals from the bulk down to the nanoscale. Lastly, we will demonstrate that the weak vdW interchain interactions in these 1D vdW tetrahelices enables the micromechanical exfoliation into single ~1 nm diameter helical chains. The realization of exfoliable 1D vdW tetrahelices presents a unique materials platform towards understanding the synthetic design rules towards helicity and chirality in low-dimensional solids. Atomically-precise helicity along these length scales will facilitate new opportunities in designing solid state materials towards sub-nanoscale nonlinear chiroptics, long-range spin polarization via chiral induced spin selectivity, and 1D topological helicoid quantum states.

2:45 PM BREAK

3:15 PM *NM02.06.04

Macroscopically Aligned Carbon Nanotubes for Photonics, Electronics and Thermoelectrics Junichiro Kono and **Jacques Doumani**; Rice University, United States

The remarkable flexibility, stable chemical structure, and extraordinary thermal, electrical, and optical properties of carbon nanotubes (CNTs) are promising for a variety of applications in flexible and/or high-temperature electronics, optoelectronics, and thermoelectrics, including wearables, refractory photonics, and waste heat harvesting. However, the long-standing goal in the preparation of CNT ensembles is how to maintain the extraordinary properties of individual CNTs on a macroscopic scale. The polydispersity and randomness remain two main challenges. Here, we will discuss different methods for creating macroscopically aligned CNTs, including spontaneous formation of wafer-scale aligned CNT films via controlled vacuum filtration and production of ultrahigh-conductivity CNT fibers and films through solution spinning and coating. We will then describe the optical, dc and ac electrical, thermal, and thermoelectric properties of these materials. These results are promising for device applications in various fields such as flexible CNT broadband detectors, spectrally selective thermal emitters, and thermoelectric devices.

References:

1. W. Gao *et al.*, "Macroscopically Aligned Carbon Nanotubes for Flexible and High-Temperature Electronics, Optoelectronics, and Thermoelectrics," *Journal of Physics D: Applied Physics* **53**, 063001 (2020).
2. X. He *et al.*, "Wafer-Scale Monodomain Films of Spontaneously Aligned Single-Walled Carbon Nanotubes," *Nature Nanotechnology* **11**, 633 (2016).
3. W. Gao and J. Kono, "Science and Applications of Wafer-Scale Crystalline Carbon Nanotube Films Prepared through Controlled Vacuum Filtration," *Royal Society Open Science* **6**, 181605 (2019).
4. N. Komatsu *et al.*, "Groove-Assisted Global Spontaneous Alignment of Carbon Nanotubes in Vacuum Filtration," *Nano Letters* **20**, 2332 (2020).
5. K. Yanagi *et al.*, "Intersubband Plasmons in the Quantum Limit in Gated and Aligned Carbon Nanotubes," *Nature Communications* **9**, 1121 (2018).
6. W. Gao *et al.*, "Continuous Transition between Weak and Ultrastrong Coupling through Exceptional Points in Carbon Nanotube Microcavity Exciton-Polaritons," *Nature Photonics* **12**, 362 (2018).
7. F. Katsutani *et al.*, "Direct Observation of Cross-Polarized Excitons in Aligned Single-Chirality Single-Wall Carbon Nanotubes," *Physical Review B* **99**, 035426 (2019).
8. W. Gao *et al.*, "Macroscopically Aligned Carbon Nanotubes as a Refractory Platform for Hyperbolic Thermal Emitters," *ACS Photonics* **6**, 1602 (2019).
9. F. R. G. Bagsican *et al.*, "Terahertz Excitonics in Carbon Nanotubes: Exciton Autoionization and Multiplication," *Nano Letters* **20**, 3098 (2020).
10. A. Baydin *et al.*, "Giant Terahertz Polarization Rotation in Ultrathin Films of Aligned Carbon Nanotubes," *Optica* **8**, 760 (2021).
11. Y. Ichinose *et al.*, "Solving the Thermoelectric Trade-Off Problem with Metallic Carbon Nanotubes," *Nano Letters* **19**, 7370 (2019).
12. N. Komatsu *et al.*, "Macroscopic Weavable Fibers of Carbon Nanotubes with Giant Thermoelectric Power Factor," *Nature Communications* **12**, 4931 (2021).

3:45 PM NM02.06.05

Novel Techniques for Characterising Graphene Nanoplatelets Using Raman Spectroscopy and Machine Learning Vicente Orts Mercadillo^{1,2,3}, Ian Kinloch^{1,2,3} and Mark A. Bissett^{1,2,3}; ¹National Graphene Institute, United Kingdom; ²Henry Royce Institute, United Kingdom; ³The University of

Manchester, United Kingdom

A significant challenge for graphene nanoplatelet (GNP) manufacturers is meaningful characterisation in industrial environments. This has been further exacerbated by the recent push to functionalise GNPs for better compatibility within nanocomposite matrices [1]. Raman Spectroscopy is a fast, facile, and accessible technique for graphene characterisation. The heterogeneity of GNP powders requires that hundreds of Raman spectra are acquired and analysed, to achieve a representative sample [2].

In this work commercially available GNPs are plasma oxygenated, aminated and fluorinated. A peak fitting algorithm was developed to reliably fit hundreds of Raman spectra from mappings, and the curve parameters fed into a binary Random Forest classifier to discern between functionalised and unfunctionalised GNPs. This type of classifier can be used to identify which combination of features are most affected by functionalisation, e.g., fluorination primarily alters the I2D/IG ratio and the G peak FWHM.

Furthermore, computer vision was used to demonstrate a proof of concept for rapid factory floor quality control. A convolutional neural network (CNN) was trained to infer the presence of functional groups directly from Raman spectra with high accuracies.

[1] Kinloch, I. A., *Science* 362, 547-553 (2018).

[2] Goldie, S. J., *Acs Appl Nano Mater* 3, 11229–11239 (2020).

4:00 PM NM02.06.07

Graphene-Based Metamaterial for On-Demand Spectral Absorption Tailoring in the Mid-Infrared Romil Audhkhasi, Mashnoon A. Sakib and Michelle Povinelli; University of Southern California, United States

We propose a graphene-based metamaterial to achieve electrically-tunable spectral absorptivity in the infrared. The metamaterial comprises of a periodic array of coupled metal-insulator-metal resonator pairs. Each of these has an electrically tunable resonance wavelength owing to the presence of graphene. The structural parameters of the two resonators in each unit cell are chosen to implement a dark-bright mode coupling scheme in the context of temporal coupled-mode theory. The relative spectral position, and in turn the coupling between consecutive resonators, can be tuned by modulating the Fermi energy of graphene. Using our metamaterial absorber, we demonstrate the ability to modulate the amplitude of spectral features in the infrared. The spectral response of the metamaterial can be tuned from single-peaked to double-peaked absorption or vice versa by tuning the bright resonator towards or away from the dark resonator, respectively. Our results thus suggest the possibility of achieving tunable multi-band absorption using metamaterials composed of multiple coupled resonators. This ability to dynamically modulate spectral absorptivity can potentially benefit several applications such as infrared imaging and thermal management.

4:15 PM NM02.06.08

Surface Charge Induced Exciton Localization in Surfactant-Wrapped Single Walled Carbon Nanotubes Erin E. Christensen, Trevor M. Tumieli, Mitesh Amin and Todd Krauss; University of Rochester, United States

As-synthesized, semiconducting single-walled carbon nanotubes (SWCNTs) are nominally charge neutral. However, ionic surfactants that are commonly used to disperse SWCNTs in solution lead to heterogeneous surface charge buildup along the nanotube. In this presentation, we will discuss how electrostatic force microscopy (EFM) was used to characterize the static-charge interactions between an individual SWCNT and its local environment. EFM is a modification of atomic force microscopy (AFM) which allows for a quantitative determination of localized charges at the nanometer scale. We found nonuniform spatial charge distributions along the nanotube length with widely varying magnitudes ranging between $\pm 15 e$ for dozens of long SWCNTs (> 1.5 microns) solubilized in aqueous suspension using standard ionic surfactants. EFM images after photoexciting the nanotubes show how these distinct, localized regions of charge on the nanotube can act as electrostatic potential barriers for exciton transport. Model calculations indicate that the large inhomogeneous surfactant aggregates along the nanotube warp the potential energy for the exciton which may lead to localized PL in a manner reminiscent of luminescent sp^3 defects, a result that is most apparent in our correlative AFM and single molecule optical measurements. We have been able to correlate single molecule photoluminescence (PL) spectroscopy and AFM images of the same individual SWCNTs and show that charged surfactant covered areas on the nanotube exhibit brighter, redshifted photoluminescence spectra relative to neutral charge regions. Altogether, our experimental results and theoretical work presents a possible explanation for the source of the potential energy minima along the nanotube that localize excitons.

4:30 PM *NM02.06.06

Optical Properties of Bioresource-Derived Colloidal Nitrogen-Doped Graphene Quantum Dots as Biomarkers Elena D. Obraztsova^{1,2}, Pavel V. Fedotov^{1,2}, Darwin Kurniawan³ and Wei-Hung Chiang³; ¹A.M. Prokhorov General Physics Institute, RAS, Russian Federation; ²Moscow Institute of Physics & Technology, Russian Federation; ³National Taiwan University of Science and Technology, Taiwan

The atmospheric pressure microplasma system was utilized to convert a natural low-cost and biocompatible chitosan into nitrogen-doped graphene quantum dots (NGQDs) with adjustable sizes controlled with Photoluminescence (PL) and Raman measurements. The nucleation, growth, and simultaneously N doping of GQDs were achieved. The rapid synthesis does not need the strong acids and bases, toxic solvents and chemicals, as well as high temperature and vacuum conditions [1]. The appearance of NGQDs with diameter of 4-6 nm and graphene-like nuclei has been confirmed by high resolution transmission electronic microscopy (HRTEM) measurements. The QDs with 4 different diameters have been investigated. Then the PL maps (emission vs excitation) have demonstrated a size-dependent position of resonant PL signal. The size-dependent Raman signals were registered under excitation by radiation of He-Cd laser (325 nm). There was a strong PL background in the spectrum under excitation with longer-wavelength radiation. This effect confirms a 0-dimension structure of the material formed.

The synthesized NGQDs can be used for facile and sensitive pH detection with a broad range (pH 1.25 to 13.56) using PL, UV-Visible absorbance and Raman spectroscopies. By adjusting the pH condition during the detection, thereby establishing a rapid screening system for biomarkers, multiple biomolecules including uric acid (UA), folic acid (FA), epinephrine (EP), and dopamine (DA) can be simultaneously detected with high selectivity and sensitivity using a single material only.

This work opens a new approach in biomedical applications of NGQDs as well as in the early detection and diagnosis of diseases and in the development of new drugs.

The work was supported by RSF/MOST Grant no. 20-42-08004 (110-2628-E-011).

[1] D. Kurniawan, W.-H. Chiang, Microplasma-enabled colloidal nitrogen-doped graphene quantum dots for broad-range fluorescent pH sensors, *Carbon* 167 (2020) 675-684.

NM02.07.01

Size Fractionation of Graphene Oxide via Flow Field-Flow Fractionation for Reinforced Graphene Fiber [Hee Jae Choi](#) and Sang Ouk Kim; Korea Advanced Institute of Science and Technology (KAIST), Korea (the Republic of)

Many interesting properties of 2D materials and their assembled structures are strongly dependent on the lateral size and size distribution of 2D materials. Accordingly, effective size separation of polydisperse 2D sheets is critical for desirable applications. Here, we introduced flow field-flow fractionation (FIFFF) for wide-range size fractionation of graphene oxide (GO) up to 100 μm . Two different separation mechanisms are identified for FIFFF, including normal mode and steric/hyperlayer mode, to size fractionate wide size-distributed GOs while employing a crossflow field for either diffusion or size-controlled migration of GO. We confirmed the chemical composition and defect density of GO are directly proportional to its size. Using size fractionated GOs, three different graphene fibers were fabricated. The microstructure of graphene fibers is strongly affected by their building block size. We also investigated the 2D sheet size-dependent mechanical and electrical properties of three different graphene fibers produced from size-fractionated GOs. This FIFFF-based size selection methodology can be used as a generic approach for effective wide-range size separation for 2D materials, including rGO, TMDs, and MXene.

NM02.07.02

Radial-Hierarchy Mesoporous Carbon Sphere with a Hollow Structure for High-Performance Supercapacitors [Hojong Eom](#), Jihyeon Kang, Seohyeon Jang, Seyoung Choi, Ohhyun Kwon, Junhyeop Shin, Jongkwon Park and Inho Nam; Chung-Ang University, Korea (the Republic of)

Supercapacitors are one of the most ideal energy storage systems due to their fast charge-discharge rate, stable cycle performance, and power density. As the electrode materials, the physicochemical properties including surface area, pore size, and structural morphology influence the electrochemical performance of the system. Therefore, significant improvement has been made in the research field of electrode materials for supercapacitors. Various materials could be considered as the proper electrode materials for supercapacitors; however, the carbonaceous materials are the most commonly used as electrodes owing to their large surface area, adjustable pore structure, and high electrical conductivity abundant availability, and excellent electric double-layer properties.

To synthesize suitable carbonaceous materials for electric double-layer capacitors (EDLCs), the morphology of the porous structure is the main parameter. The carbonaceous materials which have proper pore size and structure provide a large surface area for accumulating electrostatic charges and a favorable diffusion pathway for electrolyte ions. Many previous studies have proven that mesoporous carbonaceous material can enhance their electrochemical properties such as adsorption, separation, catalysis, and energy storage capacity, thus broadening their applications. Especially ordered mesoporous carbons (OMCs) such as CMK, FDU, KIT, and MSU have received considerable attention in recent decades. However, the monotonous and relatively long porous channels diminish ion mobility in their form and result in the overall degradation of the energy storage system performance at the high current density. Herein, we report a facile method for the synthesis of a carbon allotrope based on a hollow sphere with a radial mesoporous hierarchy. There has been substantial research on both OMCs and hollow carbon spheres (HCSs), however, the combined structure of the thick mesoporous-shell and hollow-core has rarely been studied until recently. The mesoporous carbon hollow spheres (MCHSs) endow an ordered radial channel and space-saving stacking based on their spherical morphology. Compared to other carbonaceous materials, the MCHSs have the combined advantages of OMCs and shell-like carbon spheres, especially for application in supercapacitors.

To synthesize the MCHSs, hierarchically and radially mesoporous silica was utilized as a template. The dandelion-shaped mesoporous silica spheres have been exploited in various fields since their first report. Here, the mesoporous edge of the dandelion-like silicas (DSSs) was directly replicated, whereas the core of the DSSs was engraved as a hollow structure. This is referred to as the "Dual-templating method." To optimize the structure of the MCHSs, the composition of templates and precursors was changed. The optimal condition (MCHS-0.5) shows well-developed hierarchical and radial mesopores in the carbon shell and hollow core in the center of the carbon sphere. The carbon shell with narrow pore-size distribution and large surface area (1319 m^2/g) provides a short ion-diffusion path and big specific capacitance. Also, the hollow structure endows the space for electrolyte penetration and retention. These structures play a role in improving their electrochemical performance in comparison to the existing carbonaceous materials. The MCHSs show a specific capacitance up to 135.9 F/g at 10 mV/s and present a well-developed EDLC shape at all scan rates (10 to 1000 mV/s) that qualified them as ideal electrode materials for EDLCs. The short pore length and radially interconnected pore structure combined with controlled surface chemistry would be beneficial for improving the energy density and electrical performance of supercapacitors without aggravating their high-power density and long lifecycle.

NM02.07.03

3D Printed Nanocomposites of Hexagonal Boron Nitride Nanosheets Mustafa C. Gorur, Doga Doganay, Mete Batuhan Durukan and [Husnu E. Unalan](#); Middle East Technical University, Turkey

Additive manufacturing is a fast and cost-effective approach to prototype production. Complex shapes can be produced and the product can be optimized for maximum productivity using different print settings. Polylactic acid (PLA) is the most widely used polymer for additive manufacturing due to its easily formable and recycleable nature. In this study, we prepared thermally conductive and electrically insulating 3D printable filaments composed of hexagonal boron nitride nanosheets (BNNSs) and PLA matrix. A filament winder was assembled to produce filaments with a diameter of 1.75 mm. Simultaneously, BNNS additives were exfoliated with shear exfoliation method. Recycling process increased the fabrication yield, where mono or few layer BNNSs were obtained as revealed by detailed characterizations. Exfoliated BNNS showed better thermal diffusion rate in the composite structure compared to the pristine powder. This was due to the prevention of phonon scattering upon decreasing the number of BNNS layers. Detailed characterizations and 3D printed electronic devices that demonstrate the thermal effect of BNNS will be presented.

NM02.07.04

Electrical and Optical Properties of Suspended and Horizontally-Aligned Carbon Nanotubes Under Thermal Light Emission [Hyeonhui Jeong](#)¹, Hyunjeong Jeong¹, Yugeong Je¹, Sungil Jo², Goowhan Jeong² and Sangwook Lee¹; ¹Ewha Womans University, Korea (the Republic of); ²Kangwon National University, Korea (the Republic of)

We have studied the electrical and optical properties of thermal light emission in carbon nanotubes (CNTs). Aligned CNTs were synthesized by chemical vapor deposition on the ST cut single crystal quartz substrate and transferred on the predefined electrode with trench structures. A light emission phenomenon due to the joule heat occurs when a current flows through the suspended CNTs. A voltage was applied to the electrode pad to conduct a current-voltage characteristic and transport study. Based on these results, we found conditions for stable light emission in CNTs, and the optical and

electrical properties changed by light emission were confirmed. Moreover, the details of device fabrication and possible application of our device will be suggested in this presentation.

NM02.07.06

Fabrication of 3D Porous Anode Electrode for Fast Charging Lithium Ion Secondary Battery Using Dry Transfer and Laser Processing Hyungcheoul Shim^{1,2}, Seungmin Hyun^{1,2} and Jung Bin In^{3,3}; ¹Korea Institute of Machinery and Materials (KIMM), Korea (the Republic of); ²Korea University of Science and Technology (UST), Korea (the Republic of); ³Chung-Ang University, Korea (the Republic of)

The development of next-generation secondary batteries hinges on the design of energy storage materials with high-rate properties capable of high-speed charge/discharge. For example, in order to eliminate 'range anxiety,' which is one of the key problems that makes people hesitate to acquire electric vehicles, it is necessary to build a rechargeable battery that can be recharged in minutes.

The high current density applied to the electrode during high-speed charging/discharging, however, generates a lithium ion concentration gradient inside the electrode, which causes a variety of issues. Furthermore, one of the key reasons for the difficulties in creating energy storage materials with high high-rate qualities is the material's inherent properties, such as ion transport restriction.

We used laser processing and a dry transfer procedure to create a negative electrode plate for a lithium ion secondary battery with a surface aligned in a certain orientation. When compared to the existing electrode plate, laser-induced graphene (LIG), a porous three-dimensional nanomaterial generated by laser processing, had a higher specific surface area and a three-dimensional network structure. The fracture surface of the LIG, whose plane orientation was configured in this easy-to-transfer direction, was discovered to have a significant impact on rate capabilities.

A commercially available polyimide (PI) film (thickness: 125 μm , Kapton) was used to make the LIG-based negative plate used in this investigation, which was treated with a CO₂ laser with a wavelength of 10.6 μm . The irradiated laser had a power output of 5.4 W, and the scan speed and pitch were kept at 200 mm/s and 125 μm , respectively. Press-type roll forming was used to transfer the so produced LIG to a copper substrate with a thickness of around 20 μm , with the distance between the rolls controlled between 70 and 200 μm and the specimen feed rate controlled between 10-100 mm/s. For electrochemical evaluation, the negative plate was made up of 2032 typed coin cells, and for material evaluation, scanning electron microscopy (SEM), transmission electron microscopy (TEM), X-ray diffraction (XRD) analysis, X-ray photoelectron spectroscopy (XPS), and Raman spectroscopy were used. Despite applying a high current density of 20 A/g at a loading level of around 3 mg/cm², this electrode obtained a discharge capacity of 114 mAh/g within 3 minutes, corresponding to 95 percent of the material. The great specific surface area of nanomaterials like graphene, as well as the three-dimensional structure in which the surface is oriented in a precise direction due to dry transfer, account for the unusually high rate.

In other words, the lowered internal charge transfer resistance helps to realize high rate characteristics because the holey-structured graphene with high porosity due to laser processing is well stacked in a three-dimensional structure. Furthermore, because the electrode surface is structured in a structure with multiple edge plane exposures, it was feasible to create an anode material with high rate characteristics by shortening the lithium ion transport and diffusion distance.

This method can be easily applied to the current negative electrode material and electrode manufacturing process for lithium ion secondary batteries, and it has the potential to be extended and applied to material manufacturing methods for a variety of applications that improve charge and ion transport.

NM02.07.07

Infrared Thermal Management with Graphene Ihsan Uluturk; US Army Combat Capabilities Development Command Soldier Center, United States

The main purpose of textiles throughout history is to regulate heat flow and provide warmth or decrease excessive heat for the wearer. In recent times, the textile industry has developed new materials that can ensure the wearer stays dry in hot environments and that repel moisture. The main downside of these new textiles, however, is that their electromagnetic response has not been fully optimized, allowing too much radiation to be absorbed and radiated back to the skin, causing the wearer to overheat. Our work is composed of two parts: simulation and experimentation. Simulations will first be conducted to better understand graphene chemistry, as graphene will be screen printed onto textiles for testing.

In this work, heterostructures made of NPG-FeCl₃-Ag mirror are considered, where NPG is nanopatterned graphene. This system is a representative of a Fabry-Perot type of cavity, where incident infrared light interacts strongly with NPG. The thickness of FeCl₃ will be chosen to be a quarter of the infrared wavelength in order for the amplitude of the infrared light to be maximal at the position of the NPG sheet.

Finite-difference time domain (FDTD) simulations show narrow resonance peaks in the absorbance (=emittance) due to localized surface plasmons (LSPs) in NPG. FeCl₃ is intercalated in NPG in order to shift the Fermi energy of graphene to $E_F = -0.6$ eV.

The positions of the resonance peaks can be tuned in the range between 3 mm and 12 mm by means of the number of graphene layers.

When the number of graphene layers is increased, the conductivity is multiplied by the number of layers, which results in a blueshift of the LSP peaks. By increasing the radius of the holes and the period of the hexagonal lattice of holes, the LSP peaks are redshifted.

For highly doped graphene layers with a small layer of FeCl₃ of around 50 nm between graphene and the Ag mirror, the absorbance (emittance) between 3 mm and 12 mm is around 2%, independent of the number of graphene layers. Such heterostructures could be useful for thermal management systems.

Based on the simulation results, we will be fine tuning the graphene chemistry. Resultant graphene paste will be screen printed onto textiles in the form of different geometries. Graphene printed textiles will be characterized using in-house developed Delta T measurement system. In this system, anodized Aluminum with an emissivity of 0.77 is used, which is smaller than the emissivity of human skin (95% to 98%). The anodized aluminum is placed on a hot plate and a thermocouple. The hot plate is heated up to 38 C to simulate the body temperature and standoff is created between textile and hot plate.

Thermocouples will be used to measure the temperature difference between the printed and plain textiles to see if the printing has a significant effect on the thermal management property of textiles.

NM02.07.08

Chiral Sorting of Carbon Nanotubes Using Tripeptides Jack W. Devlin and Isaac Macwan; Fairfield University, United States

There are many potential applications of carbon nanotubes (CNTs) in flexible electronics, biosensors, fuel storage materials and charge storage devices. CNTs can be categorized as either metallic or semiconducting depending on their chirality, which in turn is influenced by the electronic properties based on the delocalization of the fourth electron in the sp² hybridized orbital. Before using CNTs in potential large-scale applications, it is required that they be sorted out and separated based on their chiral vectors into metallic or semiconducting to be used for their respective purposes in electronics and bioengineering. Other methods such as electrophoresis, ultracentrifugation and chromatography have been used in the past to separate CNTs, but have been found to be expensive and lacking efficiency. We propose a study with nine different tripeptides to sort through a mixture of multi-walled (50-90 nm diameter) and single-walled (0.78 average diameter) CNTs. We analyzed the interactions of the tripeptides having glycine as the repeated amino acid at the center of each tripeptide and the positive, negative, polar and non-polar flanking residues. It is found that tripeptides with threonine as one of the flanking residues have a high affinity for metallic CNTs, whereas those with an uncharged polar group or negatively charged group have a high affinity for semiconducting CNTs. Based on our prior simulation data on the different scenarios with different tripeptides and CNTs, we understood the initial interactions between the tripeptides and different chirality CNTs. However, this has never been experimented in a laboratory before. In order to analyze our results, we used a UV/vis spectrophotometer and circular dichroism spectroscopy to show the chirality and hence the nature of the sorted CNTs. In future,

we plan on implementing the sorted metallic multi-walled and single-walled CNTs to fabricate a scaffold that can be electrically stimulated for bioengineering applications of cell culture and communication. The importance of having CNTs as the substrate is to be able to accurately measure the electrical stimuli of cells. CNTs are more suitable due to their sensitivity, greater surface area to volume ratio, and excellent electrical conductivity allowing for a wider range of applications and fabrication from electrodes for neural recording to substrates for stimulating biological cells.

NM02.07.09

Chiroptical Effect in Aligned Carbon Nanotube Films Jacques Doumani^{1,1,2}, Oliver Dewey^{1,1}, Minhan Lou², Yohei Yomogida³, Matteo Pasquali^{1,1,1}, Kazuhiro Yanagi³, Junichiro Kono^{1,1,1} and Weilu Gao²; ¹Rice University, United States; ²The University of Utah, United States; ³Tokyo Metropolitan University, Japan

In this work, we investigate the unique chiroptical response of large-scale aligned films of racemic, chirality-mixture carbon nanotubes (CNTs) prepared using the controlled vacuum filtration technique. The prepared solid-state films display large circular dichroism (CD) signals (45 mdeg/nm) in the ultraviolet (UV) range, peaked at 264 nm and 317 nm. The strength and sign of CD signals depend on sample positions and vary from sample to sample. Detailed scanning electron microscopy studies revealed a rotation of alignment directors between layers in aligned CNT films. This spontaneously formed twisted stack of aligned CNT thin layers during vacuum filtration leads to a structure-induced optical chirality. Finally, we demonstrate that CD signals can be controlled - either enhanced or suppressed - by engineering the vacuum filtration processes, such as tweaking the shape of the filtration-funnel and adding mechanical vibrations.

NM02.07.10

Faradaic Reactive MoS₂-Carbon Frameworks for Ultrahigh-Energy-Density Electrochemical Capacitors Jaehoon Ji and Jong Hyun Choi; Purdue University, United States

The demand for high-performance energy storage devices has grown at an astonishing pace for various applications including portable electronic gadgets and electric automobiles. Among diverse electrochemical energy devices, pseudocapacitors may be one of the promising candidates to fulfill the requirements of high power (e.g., > 3000 W/kg) and energy (e.g., > 50 Wh/kg) densities.¹ The pseudocapacitors can demonstrate not only large capacitive energy storage but also fast rechargeability and long cyclic stability. Despite the excellent characteristics, one major drawback of the pseudocapacitors has overshadowed their practical use. It is their low energy density compared to that of the ion batteries (over 100 Wh/kg).

To overcome the limitation, one may improve the energy storage mechanisms: surface-controlled electrical double-layer capacitance (SDC) and diffusion-controlled faradaic pseudocapacitance (DFC).² The SDC-driven mechanism is highly affected by the specific surface area of the electrodes since it is determined by the extent of accumulated charges at the electrode. On the other hand, the energy storage by the FPC process may originate from the charge transfer between the electrode and the ions via faradaic reaction. Therefore, the energy density of a pseudocapacitor may be boosted by enhancing the surface area and the faradaic reactivity of the electrode.

In this work, we introduce a ternary composite electrode made of carbon nanotubes (CNT), zeolitic imidazolate frameworks (ZIF), and molybdenum disulfide (MoS₂) to improve SDC and DFC simultaneously. The hybrid electrode demonstrates an ultrahigh energy density that can rival those of lithium-ion batteries, while maintaining the excellent properties of capacitors. This was made happen by exploiting the distinct benefits of the heteromaterials and engineering the morphology of the composite. The percolated CNT provide a robust scaffold with high conductivity for a quick charge transfer.³ The carbon networks are coated with porous ZIF structures, allowing a fast ion diffusion and offering a large surface area. In the CNT-ZIF-MoS₂ composite, the MoS₂ layer from topochemical synthesis presents densely-packed petal-like morphologies. The MoS₂ structure was developed to bear many sulfur vacancies which may serve as active sites for faradaic reaction. The hierarchical pseudocapacitor electrode thus increase not only the specific surface area for SPC-based storage but also the considerable faradaic reactivity to boost electric currents and capacitance.

Our ternary pseudocapacitor demonstrates an ultrahigh energy density of over 100 Wh/kg which may be comparable to the performance of typical ion batteries. The composite electrode also demonstrates a quick charging/discharging behavior with a maximum power density of well over 10 kW/kg. Additionally, it shows a highly stable cyclic behavior over 25,000 cycles. The new approach presented in this work may open new possibilities for developing future electrochemical capacitors.

References

1. Choudhary, R. B., *et al.*, *Renewable and Sustainable Energy Reviews* 2021, **145**, 110854
2. Chen, J., *et al.*, *Advanced Energy Materials* 2021, **11**, 2003311
3. Wan, L., *et al.*, *Carbon* 2017, **121**, 330

NM02.07.11

Highly Bendable Graphene Liquid Crystalline Fiber via Molecular Level Lubrication of 0D Nanodiamond Jin Goo Kim and Sang Ouk Kim; Korea Advanced Institute of Science and Technology, Korea (the Republic of)

Graphene fiber, composed of 2-dimensional graphene sheets, is one of the new class of carbon-based fiber with distinctive material properties particularly useful for electro-conductive components for wearable devices. Nowadays, flexible graphene fibers are principally employing soft dielectric additives, such as polymers, which can significantly deteriorate the genuine electrical properties of pristine graphene-based structures. In this research, molecular level lubricating 0-dimensional nanodiamond as an effective physical property modifier is introduced to improve the mechanical flexibility of graphene fibers by relieving the tight interlayer stacking among 2-dimensional graphene sheets. Nanoscale sized nanodiamond effectively increases tensile strain and bending strain of graphene/nanodiamond composite fibers, while maintaining the genuine electrical conductivity of pristine graphene-based fiber. The molecular level lubricating mechanism is elucidated by friction force microscopy in nanoscale via atomic force microscopy as well as by shear stress measurement in macroscopic scale. Resultant highly bendable graphene/nanodiamond composite fiber is successfully weaved into all graphene fiber-based textiles and wearable Joule-heaters, proposing the potential for reliable wearable applications.

NM02.07.12

Development of Neural Network Interatomic Potential for Simulating Evolution of Pt₃Co Nanoparticles Under Electrochemical Conditions Jisu Jung¹, Suyeon Ju¹, Purun-hanul Kim¹, Wonseok Jeong^{2,1}, Jinhee Lee³, Sungwoo Kang^{4,1} and Seungwu Han¹; ¹Seoul National University, Korea (the Republic of); ²Lawrence Livermore National Laboratory, United States; ³Hyundai Motors, Korea (the Republic of); ⁴Samsung Advanced Institute of Technology, Korea (the Republic of)

The proton-exchange membrane fuel cell (PEMFC) converts chemical energy into electrical energy through an oxygen reduction reaction (ORR) in the cathode. However, costly pure Pt nanoparticles cannot meet the target activity for ORR in PEMFC operation for commercialization. While alloying with

non-noble metal reduces the cost and achieves higher activities, it exacerbates the long-term stability due to active dissolution of non-noble metal atoms. Over the last decade, the computational methods within the density functional theory (DFT) have played crucial roles in the rational design of durable alloy catalysts. However, demanding computational costs limited the DFT studies only for small nanoparticles (diameters of 1-2 nm) in comparison with those employed in the actual PEMFC (diameters of 3-4 nm). In this study, we develop neural network interatomic potentials (NNPs) for Pt₃Co nanoparticles with an aim to simulate the dissolution process of actual size nanoparticles. We train the NNPs over various structures in bulk, surface and cluster geometries. In particular, the present training set explicitly includes formation energies and migration barriers of vacancies, which is crucial for realistic simulation of morphological evolution of nanoparticles under electrochemical conditions. The present NNP has root-mean-squared-errors (RMSEs) of 3.8 meV/atom and 0.14 eV/Å, respectively, for the validation dataset. In addition, for out-of-training structures, the NNP produces vacancy formation energies at the surface with the mean-absolute-error (MAE) of 0.09 eV, and migration barriers of vacancies are predicted with MAEs of 0.19 and 0.26 eV at the surface and bulk, respectively, which provides enough accuracy for simulation of dissolution process and ensuing morphological changes. As a demonstration, we execute the kinetic Monte Carlo simulation by NNP and analyze the effect of size, shape, and atomic ordering on the structural evolution. We believe that the newly developed NNPs can contribute to rational design of durable alloy catalysts.

NM02.07.16

Development of Scalable Dispersion Technique of Graphene Nanoplatelets into Polymer Matrix to Improve Electrical and Thermal Conductivities Kazi Imran; SUNY Polytechnic Institute, United States

Fiber reinforced polymer (FRP) composites have exceptional advantage over traditional materials. A primary limitation of these composites for aircraft application is its susceptibility to lightning strike due to poor electrical, thermal properties. First step of this research was to develop processing method for graphene/epoxy nanocomposites. The most attractive property of graphene nanoplatelets is its high electrical conductivity. This conductive graphene may significantly enhance the electrical conductivity of the composites when used it as filler materials in the insulating polymer matrix. The fundamental criteria used for process development was electrical conductivity, process repeatability and scale up to a larger batch of material. The materials chosen in this study are graphene nanoplatelets (xGnP-25), epon 828 epoxy resin. Three types of exfoliation and dispersion techniques were investigated: conventional mechanical mixing, sonication and three-roll mill. The study showed that three-roll mill dispersion is most repeatable, consistent and scalable to larger batches. The optimized process consists of three gap settings (40, 30 and 25 μm) at 200 rpm and three passes for each gap setting. The percolation threshold of xGnP graphene in epon 828 epoxy was found to be 1.0 wt. %. The xGnP/epon 828 nanocomposites showed an increase of eight log cycles in electrical conductivity, 93 % in thermal conductivity and 34 % in fracture toughness over the base epon 828.

NM02.07.17

Developing a Fiber Spinning Process for Ultra-High-Strength PVA/SWNT Composites Kenneth Benson and Marilyn L. Minus; Northeastern University, United States

In this research the interfacial relationship between a high molecular weight polymer polyvinyl alcohol (PVA) polymer and single walled carbon nanotubes (SWCNTs) are studied in order to push the boundaries for spinning a high-strength fiber. Previous research has shown success in such studies relating to the interactions between PVA and SWCNT. However, these fibers were processed in small batches. These PVA/SWCNT systems showed an increased performance in mechanical properties of the spun and drawn fibers when compared to control samples. These increased properties show promising advantages in applications requiring high-strength fiber materials such as ballistics or protection equipment. The scope of this project was to expand upon this initial success and explore a more continuous processing route to process ultra-high-strength (>3 GPa) PVA/SWCNT composite fibers. With the primary goal of achieving the most optimized system for development of this fibers, the process is tailored and controlled to produce fine-tuned high-performance fibers. The results of this work will be discussed.

NM02.07.18

Solution-Processed Tellurium Nanowire Network Structure for Highly Sensitive P-Type Field-Effect Phototransistors Array Kyung Hwan Choi; Sungkyunkwan University, Korea (the Republic of)

Low-temperature-processed semiconductors are an emerging need for next-generation scalable electronics, and these semiconductors need to feature large-area fabrication, solution processability, high electrical performance, and wide spectral optical absorption properties. Although various strategies of low-temperature-processed n-type semiconductors have been achieved, the development of high-performance p-type semiconductors at low temperature is still limited. Here, we report a unique low-temperature-processed method to synthesize tellurium nanowire networks (Te-nanonets) over a scalable area for the fabrication of high-performance large-area p-type field-effect transistors (FETs) with uniform and stable electrical and optical properties. Maximum mobility of 4.7 cm²/Vs, an on/off current ratio of 1×10^4 , and a maximum transconductance of 2.18 μS are achieved. To further demonstrate the applicability of the proposed semiconductor, the electrical performance of a Te-nanonet-based transistor array of 42 devices is also measured, revealing stable and uniform results. Finally, to broaden the applicability of p-type Tenanonet-based FETs, optical measurements are demonstrated over a wide spectral range, revealing an exceptionally uniform optical performance.

NM02.07.21

Bioelectronic Properties of Graphene Oxide Co-Immobilized with Penicillinase in Lipid Langmuir-Blodgett Films Luciano Caseli¹, Fabio A. Scholl¹ and José R. Siqueira Junior²; ¹Federal Univ of Sao Paulo, Brazil; ²Federal University of Triangulo Mineiro, Brazil

Conjugating bioinspired systems with graphene oxide can provide systems with an active layer that combines materials with different functionalities. Bioinspired systems are particularly an interesting alternative for incorporating bioactive species, enabling a molecular environment favorable to some biomolecule properties, such as enzyme activity. In the same sense, graphene oxide (GO), in addition to presenting biocompatibility, has optical and electrical properties that encourage its application in systems of biological interest. In this work, the interaction of the enzyme penicillinase with the phospholipid di-myristoyl phosphatidic acid (DMPA), conjugated with graphene oxide (GO), was studied as Langmuir and Langmuir-Blodgett (LB) films. The incorporation of the enzyme and GO in the phospholipid floating monolayer was evaluated through measurements of surface pressure-area isotherms, surface elasticity, Brewster angle microscopy (BAM), and Polarization-Modulation Infrared Reflection-Absorption Spectroscopy (PM-IRRAS). The Langmuir films were stabilized with the presence of GO, as identified by the results obtained with the employed techniques. They showed that the enzyme was incorporated in the DMPA monolayers, with its secondary structure being preserved, as identified by PM-IRRAS. Also, the interaction of the mixed lipid-enzyme films with GO located in the aqueous subphase of the monolayers in the form of colloidal dispersion could be identified, forming homogeneous films as observed by BAM. The monolayer stabilization supported the transfer of these hybrid films onto solid substrates using the LB technique, characterized by fluorescence spectroscopy and transfer ratio. The enzymatic activities of the solid devices were then measured by using UV-visible spectroscopy. The approach was effective in co-immobilizing penicillinase and GO, which were co-transferred to solid supports as an ultrathin film with the phospholipid. The presence of GO allowed to improve the identification of the signals for penicillinase detection by electronic excitation and luminescent emission. Also, films with GO increased the catalytic efficiency of the devices towards the hydrolysis of the beta-lactam ring. The presence of

GO in the enzyme/lipid LB film not only tuned the catalytic activity of penicillinase, but also conserved its enzyme activity after weeks. The feasibility of the supramolecular device nanostructured as ultrathin films to detect penicillin was assayed in a capacitive electrolyte–insulator–semiconductor (EIS) sensor device. Viability as a penicillin sensor was demonstrated with capacitance/voltage and constant capacitance measurements, exhibiting regular and distinctive output signals for all concentrations used in this work. Therefore, these results may be related to the nanostructured system as an ultrathin film and the synergism between the compounds on the active layer, leading to a surface morphology that allowed a fast analyte diffusion owing to an adequate molecular accommodation, which preserved the penicillinase activity. Therefore, this work demonstrates that the incorporation of graphene oxide in LB films composed of penicillinase and DMPA boosts the biosensing properties of the hybrid ultrathin film as EIS devices for biosensing applications.

WITHDRAWN NO REG 12/14/22 NM02.07 Colloidal Graphene Oxide Irradiation with Nanopulsed Laser for Microfluidics Applications María B. De la Mora Mojica^{1,2}, Miseong Seo¹, Laura Adriana Oropeza-Ramos¹, Oscar Pilloni Choreño^{1,1}, Tupak García-Fernández³, Jean Y. Tovar Sanchez¹ and Mayo Villagrán-Muniz¹; ¹National Autonomous University of Mexico, Mexico; ²CONACyT, Mexico; ³Universidad Autónoma de la Ciudad de México (UACM), Mexico

NM02.07.23

Development of “Electromagnetic Shielding Fabrics” Using Carbon-Nanotube-Composite-Fabrics Mashu Saito and Takahide Oya; Yokohama National University, Japan

We propose a unique electromagnetic shielding based on carbon-nanotube(CNT) composite fabrics that a composite material of the CNT and a fabrics. The electromagnetic wave environment surrounding us diversifies, and various problems are getting obvious currently. As the solution for them, the use of an electromagnetic wave shield (EMS) is attracting much attention. Nowadays, metal is used for the materials of EMS mainly, but the metal has a problem in the cost side or the processing side. For this, we focus on carbon-nanotube (CNT) with the conductivity that is high as substitute materials in this study. Although CNT has difficulty in treating it in a simple substance because CNT usually exists on a nanoscale and powdery state, our approach will solve above problems. Therefore, we may contrive to use it or develop the way for applications such as combining with other materials. In concrete, we compound with CNT and fabrics, fabricate “CNT-composite-fabrics” (CNTCFs) having a superior characteristic of CNT and facilitate the handling of CNT, and propose the “EMS fabrics” based on CNTCFs. To make our CNTCFs, we add 96 mg of multi-walled CNT and 500 mg of dispersant (Sodium Dodecyl Sulfate) in 60 ml of pure water at first. Next, this mixed solution is ultrasonically dispersed for 60 minutes by using an ultrasonic homogenizer to prepare a CNT dispersion. Moreover, we dip a fabric in the dispersion and drying in an oven until water of the dispersion is evaporated, repeat this process several times. As a result, our CNTCFs are obtained. They have unique properties, e.g., flexible and light weight, in addition to showing the shielding effective (SE). In the recent information society, EMS sheets for a high frequency band, the far field (more than a few GHz), are demanded because the information technology develops rapidly and spreads out all over the world.

In this study, we are aiming to develop the feasible level (SE > 30 dB) electromagnetic shielding fabrics. Because it is fabrics, we can apply it to a curtain and a carpet and intercept an electromagnetic wave easily. We perform a performance gain by the introduction of bridge materials and the removal of the dispersant.

As results of measurements, we have found that our CNTCFs has had the SE for the far field (from 0.5GHz to 18 GHz). Moreover, we have also found that the performance of our EMS fabric considerably changes by difference in material and structure of the fabric. In addition, we confirmed that the performance of CNTCFs is improved by increasing the fixation quantity of CNT. We consider that the bridge material is good for CNTCFs because it increases the fixation quantity of CNT by interaction with CNT. Although our CNTCFs does not reach the feasible level yet, obtained results give us hints to improve SE of our EMS fabric.

We believe our CNTCFs will get desired SE and be used as electromagnetic shielding fabrics in near future.

NM02.07.25

Fabrication of Hierarchically Structured Ultralightweight Graphene-Carbon Fiber Aerogel Networks and its Applications Mohd Shaharyar Wani^{1,1}, Sehmus Ozden^{1,1,2} and Craig Arnold^{1,1}; ¹Princeton University, United States; ²Aramco Americas, United States

Seamlessly integrating 2D-graphene (G) and 1D-carbon nanofiber (CF) with hierarchical porosity as a new carbon structure has great potential to offer improved properties for a broad range of applications yet remains largely unexplored. We have developed a scalable and green approach for fabricating hierarchical G-CF aerogels in a covalently bonded network with a density two orders of magnitude lower than previously reported graphene aerogels. We have established insights into the surface structure and chemistry of the developed material and how it depends on the process conditions such as temperature, time, and the precursor protein. Atomistic reactive molecular dynamics simulations are used to explore the assembly mechanism and structural transformations of proteins during the fabrication process. We discuss the application of such materials to desalination and water purification, notably demonstrating that the G-CF-aerogel can significantly improve upon existing materials, removing 99.99% of nano/microplastic contamination from sea water and desalinate by over 98% in seawater using gravity-based filtration, making it promising for water filtration/desalination applications.

NM02.07.27

Mechanical Characterization of Electrospun Boron Nitride Nanotube-Reinforced Polymer Nanocomposite Microfibers Nasim Anjum¹, Ohood Q. Alsmairat², Zihan Liu¹, Cheol Park³, Catharine C. Fay³ and Changhong Ke¹; ¹Binghamton University, The State University of New York, United States; ²University of Texas at Tyler, United States; ³NASA Langley Research Center, United States

Boron nitride nanotubes (BNNTs) possess many extraordinary structural and physical properties and are promising fillers for reinforcing polymers towards lightweight and high-strength nanocomposite materials. The interfacial load transfer in the bulk nanotube-reinforced polymer composite plays a critical role in property enhancement but is difficult to characterize quantitatively. This is in part because the added nanotubes are prone to aggregate and bundle due to inter-nanotube van der Waals interactions. These hard-to-avoid phenomena disrupt the seamless nanotube-polymer interfacial contact as well as nanotube alignment inside the composite, which decreases the bulk property enhancement. Here, we investigate the mechanical properties of electrospun BNNT-reinforced polymethyl methacrylate (PMMA) nanocomposite microfibers. The viscous force in the electrospinning process facilitates the nanotube alignment, which is quantitatively characterized by using polarized Raman spectroscopy techniques. The local load transfer on the BNNT-PMMA interface inside the nanocomposite microfiber is characterized based on *in situ* Raman micromechanical measurements. The effective interfacial shear strengths of 0.1%, 0.5%, and 0.65% BNNT-PMMA microfibers are found to be about 78.4 MPa, 60.9 MPa, and 50.7MPa, respectively, which correspond to substantial improvements in Young’s modulus and tensile strength. The study reveals the constitutive role of the nanotube-polymer interfacial strength in the composite’s mechanical property enhancement. The findings contribute to a better understanding of the process-structure-property relationship and the reinforcing mechanism of nanotube-based nanocomposites.

NM02.07.28

Charge Transport in Covalently Functionalized Single-Walled Carbon Nanotubes for Tunable Electroluminescent Devices [Nicolas F. Zorn](#) and [Jana Zaumseil](#); Heidelberg University, Germany

The controlled covalent functionalization of semiconducting single-walled carbon nanotubes (SWCNTs) with luminescent sp^3 defects gives rise to tunable emission in the near-infrared with increased photoluminescence quantum yields and single-photon emission at room temperature [*ACS Nano* **2019**, *13*, 9259]. To enable their application in electrically driven light sources, a detailed understanding of the impact of sp^3 defects on charge transport within individual nanotubes and nanotube networks is required. Here, we demonstrate that sp^3 -functionalized, polymer-sorted (6,5) SWCNTs still support efficient ambipolar charge transport in nanotube network field-effect transistors (FETs). While both hole and electron mobilities moderately decrease with increasing degree of functionalization, the transistors remain fully operational with high on/off current ratios. Charge-modulated photoluminescence spectroscopy, which exclusively probes the mobile charge carriers in SWCNT networks, confirms that the defects are efficiently sampled by mobile carriers and consequently, sp^3 -functionalized SWCNTs actively participate in the charge transport within the networks [*ACS Nano* **2021**, *15*, 10451]. We further employ optical-pump terahertz-probe (OPTP) spectroscopy, which probes the intrinsic and local charge transport properties (*e.g.*, carrier mobility) in a quantitative and contact-free fashion, to investigate the ultrafast carrier dynamics in sp^3 -functionalized (6,5) SWCNT dispersions and thin films. The maximum photoconductivity and lifetime decrease upon functionalization, corroborating the direct impact of sp^3 defects on intra-nanotube charge transport. For low levels of functionalization (4-10 defects per micrometer), which are relevant for applications, the reduction of intrinsic carrier mobilities is still low. Through combination of (temperature-dependent) OPTP measurements of sp^3 -functionalized SWCNT dispersions and films with electrical measurements of nanotube network FETs, we can separate the contributions of sp^3 defects (intra-nanotube) and nanotube junctions (inter-nanotube) to charge transport in SWCNT networks [*ACS Nano* **2022**, DOI 10.1021/acsnano.2c02199]. When operated in the ambipolar regime, FETs with sp^3 -functionalized SWCNT networks exhibit red-shifted electroluminescence from the defect states that is tunable via the defect concentration. The selective introduction of defects with even further red-shifted emission [*Nat. Commun.* **2021**, *12*, 2119] or the functionalization of other nanotube species such as (7,5) SWCNTs enables us to fabricate electroluminescent devices with tunable emission in the near-infrared and paves the way towards electrically pumped single-photon sources at telecom wavelengths.

NM02.07.29

Synthesis and Structural Investigation of Holey Graphene [Nitul Rajput](#), Meriam Mohammedture, Zineb Matouk, Shroq AlZadjali, Abdulla AlShehhi and Monserrat Gutierrez; Technology Innovation Institute, United Arab Emirates

Research on holey graphene (HG), a structural derivative of graphene has significantly increased in the recent few years. HG possess unique characteristics and properties such as, semiconducting nature, distinctive porous nature with increased surface area, superior chemical reactivity etc. These properties allow researchers and engineers to utilize and explore the material in DNA sequencing, water filtration, to enhance energy storage capabilities, carbon capture etc. However, challenges remain unresolved in controlled synthesis of mass scale HG production with homogeneous pores distribution and precise hole size with controlled defects. In this work, probe sonication and electro-chemical synthesis approaches are implemented to exfoliate few layers of graphene. Subsequently, pores are generated using normal thermal annealing and thermal shock procedures. The synthesized materials are systematically evaluated using various advanced characterization techniques such as, X-ray photoelectron spectroscopy, transmission electron microscopy and Raman spectroscopy. The characterization unfolds novel properties related to intrinsic nature of HG. Eventually, controlled manufacturing of HG with precise hole size and distribution could be obtained with the understanding of the material.

NM02.07.31

Nanoporous Carbon-Based Catalyst for Hydrogen Evolution Reaction [Caique Campos](#) and [Pedro A. Autreto](#); Federal University of ABC, Brazil

Hydrogen is regarded as one of the future fuels due to its sizeable energetic content per unit mass and Eco-friendliness with the potential to fulfill the ever-growing energetic demand. Clean and renewable production of molecular Hydrogen (H_2) in the electrochemical *Hydrogen Evolution Reaction* (HER) is one of the most promising alternatives to Hydrocarbon reforming methods currently employed due to renewability and high purity H_2 yield [1]. However, large-scale implementation of this mechanism requires cheap, efficient, and earth-abundant catalysts as cost-effective alternatives to the benchmark scarce noble-metal materials. Metal-free Carbon-based catalysts have drawn considerable attention, and several graphene-based nanostructures have been extensively investigated [2]. In particular, porous nanostructures with enhanced ions and mass transport properties compared to graphene have interesting HER activity [3]. In this work, we investigate the catalytic activity of graphenylene, a sp^2 carbon allotrope with intrinsic in-plane nanoporous structure, in HERs using DFT as implemented in the *Quantum Espresso package*. We found that metal decoration is a possible strategy to enhance the catalytic activity, optimizing the Hydrogen adsorption free-energy

References:

[1] K. Zeng and D. Zhang, *Progress in Energy and Combustion Science* **36**, 307 (2010);

[2] Jing Zhu and Liangsheng Hu and Pengxiang Zhao and Lawrence Yoon Suk Lee and Kwok-Yin Wong, *Chemical Reviews* **120** (2), 851-918 (2020);

NM02.07.32

Nanomechanical Characterization of Boron Nitride and Carbon Nanotubes-Metal Interfaces [Yingchun Jiang](#)¹, Zihan Liu¹, Chenglin Yi¹, Ning Li², Soumendu Bagchi³, Cheol Park⁴, Huck B. Chew² and Changhong Ke¹; ¹Binghamton University, The State University of New York, United States; ²University of Illinois at Urbana-Champaign, United States; ³Los Alamos National Laboratory, United States; ⁴NASA Langley Research Center, United States

The light, strong and durable characteristics of nanofiber-reinforced metal-matrix nanocomposites (MMNC) hold promise for tackling some of the most demanding applications, such as the body of aerospace vehicles. The reinforcing mechanism in nanofiber-reinforced MMNC critically relies on adequate load transfer on the nanofiber-metal interface. Boron nitride nanotubes (BNNTs) and carbon nanotubes (CNTs) are two of the most promising reinforcing fillers for disruptive MMNC technology due to their ultra-strong, resilient, and low-density properties. However, the understanding of the interfacial load transfer on these nanotube-metal interfaces remains elusive, which has been a major scientific obstacle in the development of the nanotube-reinforced MMNC technology. Here we investigate the mechanical strengths of the interfaces formed by individual BNNTs/CNTs with aluminum or titanium matrices by using *in situ* electron microscopy nanomechanical single-nanotube pull-out techniques. By pulling out individual nanotubes from metal matrices using atomic force microscopic force sensors inside a high-resolution scanning electron microscope, both the pull-out force and the embedded tube length were measured with resolutions of a few nano-Newtons and nanometers, respectively. The load transfer on the nanotube-metal interface is found to follow a shear lag behavior and the interfacial strength is significantly influenced by thermal-induced reaction products. Density functional theory calculations provide insights into the binding interaction and sliding behavior on the nanotube-metal interfaces that are highly dependent on the electronic structure of the underlying chemical bonds. The research findings help to better understand the load transfer on the nanotube-metal interface and the reinforcing mechanism of nanotube-reinforced metal nanocomposites.

NM02.07.34

1D/2D Heterostructure of Gadolinium/2-Methylimidazole Metal-Organic Framework and Graphitic Carbon Nitride Nanosheet for Bifunctional

Electrocatalytic Oxygen Evolution and Reduction Reactions [Saikat K. Kuila](#) and Tarun K. Kundu; Indian Institute of Technology Kharagpur, India

The electrochemical energy generation, conversion, and storage devices are very promising for developing sustainable clean technologies. Fuel cells and metal-air batteries are emerging as powerful energy conversion devices for future energy requirements. Economically feasible electrocatalysts can be engineered to meet these requirements. In this work, a bifunctional electrocatalyst 1D-gadolinium-2-methylimidazole (1D-Gd-2-mim) metal-organic framework (MOF) functionalized 2D-graphitic carbon nitride (2D-g-C₃N₄) heterostructure (1D-Gd-2-mim/2D-g-C₃N₄) is demonstrated for electrocatalytic oxygen evolution reaction (OER) and oxygen reduction reaction (ORR). The electrocatalyst is synthesized through mixing and coprecipitation methods. The synthesized 1D-Gd-2-mim/2D-g-C₃N₄ is characterized using diffraction (X-ray diffraction (XRD)), spectroscopic (Fourier-transform infrared spectroscopy (FTIR) and X-ray photoelectron spectroscopy (XPS)), microscopic (field Emission scanning electron microscopy and corresponding energy dispersive X-ray spectroscopy (FESEM-EDS), high-resolution transmission electron microscopy (HR-TEM), atomic force microscopy (AFM)), thermal (combined thermogravimetry and differential scanning calorimetry (TG-DSC)), surface and pore measurements (Brunauer–Emmet–Teller and Barret–Joyner–Halenda (BET-BJH)) techniques and compared with pristine 2D-g-C₃N₄. XRD and FTIR studies assure the formation of the heterostructure. The synthesized sample shows a remarkably higher specific surface area (322.4 m² g⁻¹) than the pristine 2D-g-C₃N₄ (69.12 m² g⁻¹) and 1D-Gd-2-mim MOF (93.5 m² g⁻¹). The FESEM and HR-TEM micrographs also confirm the (1D/2D) heterostructure formation where the growth of porous nanorod structured 1D-Gd-2-mim MOFs on 2D-g-C₃N₄ nanosheets is evident. High-angle annular dark-field-scanning transmission electron microscopic (HAADF-STEM) analysis of 1D-Gd-2-mim/2D-g-C₃N₄ confirms that all the elements C, N, Gd, and O are uniformly distributed in the nanoporous microstructure. A considerable weight loss (32%) is recorded within a temperature range of (0-900 °C) for 1D-Gd-2-mim/2D-g-C₃N₄, whereas 2D-g-C₃N₄ is fully dissociated after 610 °C, as confirmed by the TG-DSC study. Further, the ORR activity of the synthesized materials is confirmed through the CV plot in the O₂ and N₂ saturated 0.1 M KOH in the potential window of 0.2 to 1.2 V (vs. RHE). Although the ORR onset and ORR peak potential do not improve remarkably over the addition of La-2-mim and Ce-2-mim MOFs into 2D-g-C₃N₄, the limiting current density increases remarkably, confirming the improvement of ORR activity. The 1D-Gd-2-mim/2D-g-C₃N₄ shows a remarkable positive shift of the ORR onset and ORR peak potential along with enhanced limiting current density, which makes it the best ORR performing catalyst among all the synthesized materials. 1D-Gd-2-mim/2D-g-C₃N₄ exhibits higher stability and methanol tolerance capacity than the state-of-the-art catalyst Pt/C. Furthermore, an LSV study using RDE with various rotation speeds reveals that the catalyst follows a four-electron reduction pathway for ORR. Also, the electrocatalyst shows its superiority over the pristine 2D-g-C₃N₄ and state-of-the-art catalyst RuO₂ by depicting the lowest onset potential (1.25 V vs. RHE), overpotential (59 mV), Rct (7 Ω), Tafel's slope (17 mV decay⁻¹), and higher R_f (1.74), as obtained through several OER electrochemical characterizations. The catalyst is also stable from a morphological and OER performance perspective. So, the electrocatalyst executes the bifunctional activity very proficiently, which is highly demanding for fuel cell and metal-air batteries technology. 1D-Gd-2-mim/2D-g-C₃N₄ is a potential candidate as an alternative to the high cost and scarce Pt/C and RuO₂ in energy conversions and storage applications.

NM02.07.35

Advances in the Solvothermal Synthesis of Red-Emitting Carbon Dots Towards Optoelectronic Devices [Antonino Madonia](#)¹, Gianluca Minervini^{2,3,1}, Annamaria Panniello¹, Carlo M. Carbonaro⁴, Teresa Sibillano¹, Cinzia Giannini¹, Angela Terracina⁵, Alice Sciortino⁵, Fabrizio Messina⁵, Maria Lucia Curri^{3,1} and Marinella Striccoli¹; ¹CNR, Italy; ²Polytechnic of Bari, Italy; ³University of Bari "Aldo Moro", Italy; ⁴University of Cagliari, Italy; ⁵Università degli Studi di Palermo, Italy

Designing functional nanomaterials useful for the development of optoelectronic devices is a challenging task. Industry standards demand careful control over both their structural and optical properties, as well as high reliability and resistance to degradation under real-world usage conditions. Furthermore, the development of cost-effective materials obtained from inexpensive, abundant, and environment-friendly sources is deemed a high priority.

In this context Carbon Dots (CDs) have gained much traction. These nanoparticles, mainly composed of Carbon and other readily available elements such as Oxygen, Nitrogen, and Hydrogen, are considered extremely promising for their enticing properties: it is thanks to their intense absorbance, bright photoluminescence, low toxicity and high biocompatibility that such nanomaterials have found their way into the fields of optoelectronics, photocatalysis, and nanosensing among the others.[1] In fact, CDs are renowned for being able to couple molecular-like optical properties to an enhanced photostability,[2] characteristics which work in parallel to their electron-donating capabilities towards the development of hybrid and functional materials.[3]

In recent years the understanding of the relationship between synthetic conditions, structural features, and optical properties of CDs has witnessed impressive progress. Nonetheless, while we are now able to produce carbon-based nanoparticles with high photoconversion efficiencies both in the blue and green regions of the visible light spectrum,[4] the knowledge regarding how to control the synthesis of red-emitting CDs is still lagging behind;[5] as many optical applications necessitate full control over all visible wavelengths, we need to design new synthetic strategies allowing us to overcome this obstacle.

It is with this purpose in mind that we have explored novel approaches aimed at enhancing the red emission of carbon nanoparticles. By developing both synthetic and post-synthetic treatments we were able to isolate CDs displaying high photoluminescence quantum yields in the red region of the light spectrum. Moreover, we have been successful in finely tuning their optical properties by the careful choice of precursors used during the solvothermal synthesis: these results have been achieved by making use of both in-situ surface passivation strategies as well as post-synthetic purification approaches. The synthesized red CDs possess exciting optical properties and result highly resistant to photobleaching under UV irradiation. An in-depth optical and morphological characterization has allowed to rationalize the mechanisms underlying the emission properties of CDs and isolate the centers responsible for the red photoluminescence. These advances can envisage the effective use of carbon dots as viable substitutes for the semiconductor nanoparticles currently used in the domain of optoelectronics, which are often based on toxic and polluting materials. As we are now able to cover the visible light spectrum in its full range, we have been exploring the possibility of using the carbon-based functional nanomaterials for the development of tunable or white light-emitting devices, as first step towards the application in many other photonic or optoelectronic devices.

The Italian MIUR PRIN 2017 CandI2 Project Prot. n. 2017W75RAE is gratefully acknowledged.

[1] Sciortino, A. et al. *C* **4**, 67 (2018).

[2] Terracina, A. et al. *ACS Appl. Mater. Interfaces* (2022).

[3] Madonia, A. et al. *Phys. Chem. Chem. Phys.* **24**, 17654–17664 (2022); Madonia, A. et al. *Materials Research Bulletin* **149**, 111721 (2022); Madonia, A. et al. *J. Phys. Chem. Lett.* **11**, 4379–4384 (2020).

[4] Minervini, G. et al. *Carbon* **198**, 230–243 (2022).

[5] Carbonaro, C. M. et al. *C* **5**, 60 (2019).

NM02.07.36

Fe₃O₄/GO Magnetic Nanocomposite—A Selective Probe for Simultaneous Detection of Carbofuran and Carbendazim Residues by Electrochemistry and LDI-MS [Jutiporn Yukird](#) and Nadnudda Rodthongkum; Metallurgy and Materials Science Research Institute (MMRI), Thailand

Fe₃O₄/GO magnetic nanocomposite is synthesized and applied as a selective probe for simultaneous detection of pesticides (carbofuran and carbendazim) verifying by the high binding energies calculated by density functional theory. Electrochemistry and LDI-MS are selected for screening and quantitative determination of these pesticides. Fe₃O₄/GO modified on electrode enhances electrocatalytic activity of carbofuran and carbendazim and their oxidation

peak currents linearly increase upon the increase of their concentrations in a range of 1- 250 μM with LODs of 0.06 μM and 0.18 μM for CBF and CBZ, respectively. For LDI-MS, after magnetic separation, CBF and CBZ bound with $\text{Fe}_3\text{O}_4/\text{GO}$ are readily ionized leading to high ion abundance with a linear range of 1- 1000 μM . Thus, using $\text{Fe}_3\text{O}_4/\text{GO}$ magnetic nanocomposite along with our detection platform is effective to cover the required detection level of CBF and CBZ residues in the fruits, which are 0.45 μM and 2.5 μM , respectively. Ultimately, $\text{Fe}_3\text{O}_4/\text{GO}$ bound with CBF and CBZ spiked in pear are successfully visualized by imaging-MS verifying the distribution of these pesticides in real pear peel samples.

NM02.07.37

Modification of Surface Tension of a Green Solvent and Surfactants to Enhance Graphene Synthesis Aditi Pangal, Sharada Kittur, Tze Tseng Soh, Jasper Zhang and Neelima Sangeneni; ASDRP, United States

Graphene is the single layer of graphite, made up entirely of carbon. With many favorable properties, such as high conductivity, incredible tensile strength, flexibility, and a lightweight structure, graphene is one of the first choices in the energy storage industry. The problem with graphene arises in its scalability and producibility. Our research finds a process to create high-quality graphene in a cost-effective, scalable, and green manner, for use in supercapacitors. Many papers explore top-down and bottom-up approaches such as redox reactions, flash graphene, epitaxial growth, and chemical vapor deposition (CVD), but they use toxic solvents and costly equipment, both of which are neither good for the environment, nor widely accessible. The most viable solution seemed to be Liquid-Phase Exfoliation, which uses sonication in a solvent to exfoliate the layers of graphite to produce monolayered- or few-layered-graphene. We also tested variability in the time durations of our sonicating machines; the probe sonicator (direct sonication) and the bath sonicator (indirect sonication). By changing the solvent based on its surface tension and surface energy, we tweaked the solvent ratios so that the surface tension of the solvent was similar to the surface tension of graphite, which is 41 mJ/m². This reduces the potential energy between the two materials and makes it easier to overcome the van der Waals forces. In addition, we experimented with different solvents such as dish soap, hand soap, and an ethanol and water mixture, and different surfactants such as curcumin to observe their effects on yield. We found that the hand soap yield had the most contaminants and was also very dense. The best quality graphene came from ethanol and water, and curcumin and water, with a measured CV capacitance of 13.1 F/g. We used different characterization tools such as FTIR, CV, SEM, and GCD to determine how much graphene we had, and what grade of graphene we had, as well as calculating the specific capacitance and long-term capacitance. In the future, we will test more green solvents and surfactants, and we will attempt with the process of magnetic separation to further exfoliate the graphene. We are also planning on using Raman Spectroscopy in the future to characterize graphene. Finding a simpler, greener, and cost-effective method in which graphene can be synthesized will greatly increase its usage in the electrochemical industry as the cost of manufacturing and its scalability is the main obstacle to the widespread use of graphene.

NM02.07.38

Thermodynamic Behavior of Fe Nanoparticles in the Catalyst Layer Controlling Reliable Direct Growth of Electrically Addressable Carbon Nanotube (CNT) Microstructures on Conductive Layers Kwangjun Kim, Minwook Kim and Jong G. Ok; Seoul National University of science and technology, Korea (the Republic of)

Carbon nanotubes (CNTs) are in the spotlight in next-generation energy conversion, toxic gas detection, and biomedical applications due to their excellent electrical and thermal properties. While manipulating individual CNT strands is effective for specific uses, direct growth of microscale (often nanoscale) bundles of CNTs can be practically useful for functional architectures for subsequent uses with higher throughput and wider compatibility. Namely, this approach could not only minimize mechanical and chemical defects occurring during post-growth manipulation, but make the best use of both nanoscale/nanoporous morphology and up-to-mm-scalable/well-aligned structural framework (i.e., CNT forest structure; CFS). However, it is still challenging to control the length, density, and alignment of CNT structures, especially when growing to micropatterned configurations. Addressing these issues in this work, we first have investigated the morphological properties of catalyst metal (Fe) nanoparticles in order to control the nanoporosity and growth length of CNT forests. As the distribution density of Fe nanoparticles increases, the density of the CNT forest increases (reduces the nanoporosity), which enhances the crowding effect between CNT strands and forms a stable CNT forest to facilitate control of growth length. On the contrary, the more decreased the distribution density, the more difficult to control CNT forest formation and growth length. Furthermore, as the diameter of the nanoparticles increases, decrease in both the catalyst lifetime and the distribution density is qualitatively examined. Therefore, we define the distribution density and diameter as morphologic factors, and these factors have been analyzed based on Ostwald-ripening and subsurface diffusion phenomena. As the effects of these phenomena increase, the nanoparticles' diameter-polarization increases while its distribution density reduces. Especially when the catalyst layer is patterned, the effects becomes more pronounced, which is caused by the thermal system change of the surface due to the increase in the thermal exposure area of the support layer and the substrate. Based on this approach, reliable microstructuring the CNT forest can be realized. For more practical and wider uses based on superb electrical/thermal properties of CNTs, growing the CNT microstructure directly on the conductive substrate is highly desired. To this end, we have also conducted morphological analysis of the nanoparticles on conductive titanium nitride (TiN) (instead of typical Al_2O_3). While keeping an eye on Ostwald ripening and subsurface diffusion, we have additionally developed two growth methods for securing the reliable growth length and porosity of CFSs on more rough TiN surfaces: catalyst-rich condition (CRC) and hydrogen-rich condition (HRC). Finally, we have quantitatively optimized the nanoparticle's diameter and distribution density, leading to the reliable direct growth of electrically addressable micropatterned CFSs on the conductive substrates.

Acknowledgment

This work was supported by the National Research Foundation of Korea (NRF) grants (No. 2020R1F1A1073760, No. 2021M3H4A3A02099204, and 2022M3C1A3090850 (Ministry of Science and ICT) and No. 2022R111A2073224 (Ministry of Education)) funded by the Korean Government.

References

1. S. Esconjauregui, S. Bhardwaj, J. Yang, C. Castellarin-Cudia, R. Xie, L. D'Arسي, T. Makaryan, H. Sugime, S. Eslava, C. Cepek, and J. Robertson, Carbon 73, 13-24 (2014).
2. J. Carpena-Núñez, J. A. Boscoboinik, S. Saber, R. Rao, J.-Q. Zhong, M. R. Maschmann, P. R.

NM02.07.39

Tungsten-Containing MXene (W_2Ti) C_2T_x from a Nanolaminated Ternary Carbide for Hydrogen Evolution Reaction Anupma Thakur, Wyatt Highland, Brian Wyatt and Babak Anasori; IUPUI, United States

Two-dimensional transition metal carbides, nitrides and carbonitrides, known as MXenes, have shown great promise as active materials in catalytic applications such as hydrogen evolution reaction. Tungsten (W) containing MXenes are of particular interest as they are predicted to have overpotentials close to Pt based catalysts in the hydrogen evolution reaction (HER) making them candidates for a more sustainable clean energy application. However, the incorporation of W into MXene structure has proven difficult due to the calculated instability of its hypothetical precursor $\text{M}_{n+1}\text{AX}_n$ phases (W_3AC_2 and W_2AC). In this study, we discuss the synthesis of W-containing MXene (W_2Ti) C_2T_x , derived from a nanolaminated ternary carbide (W_2Ti) C_4C_x precursor. The synergistic effect of the W-containing basal plane endows $\text{W}_2\text{TiC}_2\text{T}_x$ MXene with remarkable electrocatalytic HER performance in terms of lowest HER overpotential (~162 mV) and long-term stability of >24 hours under acidic conditions over other $\text{W}_{1.33}\text{CT}_x$ MXenes (~320 mV) and Mo_2CT_x MXenes

(~190 mV). This enhanced HER activity of (W₂Ti)C₂T_x MXene may be linked to W's highly active and ordered basal-plane vacancies. In this direction, more efforts on the continuous exploration of W-containing MXenes with low overpotentials are significant toward the progress of HER catalysts for clean energy applications due to their highly active basal plane.

SESSION NM02.08: Biological and Chemical Study
Session Chairs: Tanja Kallio, Shunsuke Sakurai, Yoke Khin Yap and Ming Zheng
Wednesday Morning, November 30, 2022
Hynes, Level 2, Room 208

8:30 AM NM02.08.01

Molecular engineering of graphene-like two-dimensional conjugated polymers Jie Shen and Yu Han; King Abdullah University of Science and Technology (KAUST), Saudi Arabia

The discovery of graphene—a two-dimensional (2D) crystalline carbon monolayer, has stimulated interest in the rational synthesis of the 2D polymer. Such a promising class of novel organic 2D materials is expected to offer a greater degree of tunability in terms of composition, geometry, and chemical/physical properties compared with graphene, featuring intriguing application perspectives as membranes and in electronics¹. However, the synthesis of crystalline 2D polymer with strong and stable linkages such as C-C bonds has met with limited success up to now. Taking the solution-based synthesis of graphdiyne (a 2D polymer with benzene rings linked by alkyne bonds) as an example, the free rotation of the alkyne–aryl single bonds leads to out-of-plane random growth of the skeleton during the growth and form disordered 3D structure rather than the desired 2D structure. Ultrahigh-vacuum deposition methods have also been reported to fabricate 2D polymers, but the lateral dimensions of the materials thus prepared are usually small (< 1 μm × 1 μm), which requires better control over the reaction thermodynamics and kinetics.

In this presentation, we will report our most recent progress that has been published in *Nature Materials*²: the design and fabrication of ultrathin, larger area, and ordered 2D conjugated-polymer-framework films (~ 5cm²) with thicknesses down to 1 nm through C-C coupling between the designed monomers using surface-confined chemical vapor deposition (CVD). This method is characterized by the use of single-crystalline Cu (111) substrate with atomic flatness and the addition of an organic base into the CVD system, which have proven to be the key factors in promoting the formation of the ordered 2D structure. The fabricated 2D CPF—the organic analogue of graphene, demonstrated a fully π-conjugation and ultramicroporous structure with promising potential for electronic devices and molecular sieving membranes. We have shown that the CPF nanofilms inherently have regular rhombic sub-nanometer (10.3 × 3.7 Å) channels for achieving a superior water and ion separation performance that surpassed those of state-of-the-art membranes. Additionally, the porosity and surface charge of CPF membranes were finely tuned by controlling the CVD conditions, which were further engineered for ion sieving and osmotic energy harvesting. We envisage that the surface-confined CVD synthesis described here can be applied to other classes of monomers, opening a new avenue to construct novel graphene-like architectures at the atomic level with desirable chemical, physical and electronic properties.

References:

1. Nature 542, 423–424 (2017)
2. Nature Materials, DOI: 10.1038/s41563-022-01325-y (2022)

8:45 AM NM02.08.02

Thermodynamics of Charge Regulation During Ion Transport through Silica Nanochannels Cody Ritt^{1,2}, Pedro de Souza¹, Michelle G. Barsukov², Shari Yosinski², Martin Bazant¹, Mark Reed² and Menachem Elimelech²; ¹Massachusetts Institute of Technology, United States; ²Yale University, United States

Ion-surface interactions can alter the properties of nanopores and dictate nanofluidic transport in engineered and biological systems central to the water-energy nexus. The ion adsorption process, known as “charge regulation”, is ion-specific and is dependent on the extent of confinement when the electric double layers (EDLs) between two charged surfaces overlap. A fundamental understanding of the mechanisms behind charge regulation remains lacking. Herein, we study the thermodynamics of charge regulation reactions in 20 nm SiO₂ channels via conductance measurements at various concentrations and temperatures. The effective activation energies (E_a) for ion conductance at low concentrations (strong EDL overlap) are ~2-fold higher than at high concentrations (no EDL overlap) for the electrolytes studied here: LiCl, NaCl, KCl, and CsCl. We find that E_a values measured at high concentrations result from the temperature dependence of viscosity and its influence on ion mobility, whereas E_a values measured at low concentrations result from the combined effects of ion mobility and the enthalpy of cation adsorption to the charged surface. Notably, the E_a for surface reactions increases from 7.03 kJ mol⁻¹ for NaCl to 16.72 ± 0.48 kJ mol⁻¹ for KCl, corresponding to a difference in surface charge of -8.2 to -0.8 mC m⁻², respectively. We construct a charge regulation model to rationalize the cation-specific charge regulation behavior based on an adsorption equilibrium. Our findings show that temperature- and concentration-dependent conductance measurements can help indirectly probe the ion-surface interactions that govern transport and colloidal interactions at the nanoscale—representing a critical step forward in our understanding of charge regulation and adsorption phenomena under nanoconfinement.

9:00 AM *NM02.08.03

A Wavelength-Induced Frequency Filtering Method for Fluorescent Nanosensors *In Vivo* Michael S. Strano and Volodymyr Koman; Massachusetts Institute of Technology, United States

Fluorescent nanosensors hold the potential to revolutionize life sciences and medicine. However, their adaptation and translation into the in vivo environment is fundamentally hampered by unfavourable tissue scattering and intrinsic autofluorescence. Here we develop wavelength-induced frequency filtering (WIFF) whereby the fluorescence excitation wavelength is modulated across the absorption peak of a nanosensor, allowing the emission signal to be separated from the autofluorescence background, increasing the desired signal relative to noise, and internally referencing it to protect against artefacts. Using highly scattering phantom tissues, an SKH1-E mouse model and other complex tissue types, we show that WIFF improves the nanosensor signal-to-noise ratio across the visible and near-infrared spectra up to 52-fold. This improvement enables the ability to track fluorescent carbon nanotube sensor responses to riboflavin, ascorbic acid, hydrogen peroxide and a chemotherapeutic drug metabolite for depths up to 5.5 ± 0.1 cm when excited at 730 nm and emitting between 1,100 and 1,300 nm, even allowing the monitoring of riboflavin diffusion in thick tissue. As an application, nanosensors aided by WIFF detect the chemotherapeutic activity of temozolomide transcranially at 2.4 ± 0.1 cm through the porcine brain without the use of fibre optic or cranial window insertion. The ability of nanosensors to monitor previously inaccessible in vivo environments will be important for life-sciences research, therapeutics and medical diagnostics.

9:30 AM NM02.08.04

Nanotube-Based High Brightness Fluorophores with Controllable Brightness Yoke Khin Yap¹, Nazmiye Yapici², Rodney Oakley², Xiuling Liu², Steve Tokarz² and Dongyan Zhang¹; ¹Michigan Technological University, United States; ²StabiLux Biosciences, United States

Nanotubes have been used for various mechanical, electrical, and biomedical applications. Here we describe a new nanotube technology for producing high brightness fluorophores (HBFs) that can be 1000 times brighter than any known dyes [1]. The brightness of HBFs is widely tunable, with a molar extinction coefficient (ϵ) ranging from 10^7 to 10^9 , more than three orders of magnitude higher than existing dye. The physics and chemistry in designing these HBFs will be presented in the meeting. Results indicated that the brightness of HBFs based on boron nitride nanotubes (BNNTs) is 450% higher than those based on carbon nanotubes (CNTs).

Biomedical detection relies on various non-invasive techniques such as fluorescent microscopy and flow cytometry. Organic dyes and fluorescent proteins are widely used for these applications where fluorophores are specifically bound to the target biomolecules. The brightness of dyes is important for sensitive and accurate detection. Organic dyes are low cost but not as bright as protein dyes such as PE (extinction coefficient, $\epsilon = 2.5 \times 10^6 \text{ M}^{-1} \text{ cm}^{-1}$; quantum yield, QY = 0.8) and APC ($\epsilon = 7.0 \times 10^5 \text{ M}^{-1} \text{ cm}^{-1}$, QY = 0.68). According to the physics of fluorescent brightness, one can produce bright dyes by enhancing QY and ϵ [2]. There have been tremendous effort reporting the design of new molecules with high quantum yield (QY ranging from 0 to 1). In contrast, we focused on designing HBFs by controlling ϵ , which can be tuned across several orders of magnitude. Our HBFs are constructed by organizing arrays of organic dye with polymeric linkers. Nanotubes are used as the nano-carriers of these dye-linker structures. We found that the brightness of HBFs based on BNNTs can be 450% higher than that based on CNTs. Such enhancement is due to the electrically insulating and optically transparent (band gap of 6eV) nature of BNNTs [2-5]. As a result, we can maintain the QY of dye molecules organized on BNNTs without fluorescent quenching. Furthermore, the conjugation efficiency of the dye-linkers on BNNTs is much higher than that on CNTs. All these contribute to the higher brightness of HBFs based on BNNTs.

[1] Y. K. Yap, D. Zhang, N. B. Yapici, US Patent Application US20180296705A1.

[2] (Review) D. Zhang *et al.* ACS Omega **6**, 20722 (2021)

[3] (Review) J. Wang, C. H. Lee, Y. K. Yap, *Nanoscale* **2**, 2028 (2010)

[4] C. H. Lee, *et al.*, *Advanced Materials* **25**, 2544 (2013).

[5] J. K. Qin, *et al.*, *Nature Electronics*, **3**(3), 141 (2020).

High-brightness fluorophores (HBFs) are developed by StabiLux Biosciences and commercialized as NovoLux[®] dye. This project is supported by the National Science Foundation (IIP 1521057, IIP 1738466), M-TRAC for Life Sciences Innovation Hub co-managed by the University of Michigan and the Michigan Economic Development Corporation (MEDC), Small Company Innovation Program (SCIP), and the Michigan Emerging Technologies Fund (ETF).

9:45 AM BREAK

10:15 AM NM02.08.05

Demanding More from Graphene-Based Sensors—Design and Development of a Multi-Functional GFET with Dielectrophoresis Enhanced Sensing Capabilities Nezhueyotl Izquierdo, Ruixue Li and Steven Koester; University of Minnesota, United States

The demand for low-cost, rapid readout, point-of-care medical diagnostics was exposed by the SARS-CoV-2 pandemic. Graphene-based field-effect transistor (GFET) sensors have emerged as an effective platform for medical diagnostics of clinical biomarkers, such as DNA, RNA, proteins, and antibodies. Commercialization of sensors requires target specificity, sensor sensitivity, and a short sensor response time for target analyte detection.

Our group's previous work on graphene-based DEP devices has demonstrated an ultra-strong (> 10-times) DEP force compared to metal electrodes, as the DEP force magnitude is dependent on the electrode thickness [1]. An applied dielectrophoresis (DEP) force imparts a pseudo-selective trapping mechanism. Target analytes, such as DNA, are mobilized from suspension and localized at the graphene channel DEP trap sites. Graphene provides advantageous material properties for both a GFET sensor and DEP device applications. Graphene, a semi-metal with high carrier mobility and surface-to-area ratio, is well suited as a FET sensor channel material. Functionalized GFET sensors have demonstrated high specificity, sensitivity, and stability in biological buffers [2]. However, detecting low concentrations of biomolecules (e.g., DNA) with GFETs typically requires a long incubation time (>30 minutes) and is therefore not suitable for rapid readout detection.

Here we present our recent work to improve the standard three-terminal GFET sensor by incorporating dielectrophoresis as a strategy to reduce the required response time and improve the sensor sensitivity. The novel 4-terminal graphene-based sensor device structure can operate in three distinctive modes: DEP, GFET, and dielectrophoresis-assisted GFET (DEP-GFET). The DEP-GFET device is realized and capable of sensing shifts in the graphene channel's electrical properties (e.g., V_{Dirac} , I_{DS}). An applied DEP force attracts particles suspended in the solution and traps target particles at the graphene channel edge region. The GFET component of the DEP-GFET device thereby measures the electrical response to the trapped particles. Fluorescence microscopy analysis of the DEP-GFET device demonstrates the effectiveness of DEP-trapped fluorescent particles (i.e., fluorescent polystyrene beads and DNA-YOYO-1) at the graphene channel edge. After 10 seconds of applied DEP, the fluorescence intensity at the graphene channel trapping edges is increased by 25-times. Trapped particles are sensed by measuring V_{Dirac} shifts after two minutes of applied DEP. Thus, the target analyte is locally concentrated at the graphene channel edges, reducing the required sensing response time by up to 30-times. Compared to GFETs that rely on diffusion, the DEP-GFET device overcomes diffusion limitations by increasing target analyte concentrations locally at the graphene sensor channel region by 25-times and reducing the response time by approximately 30-times. These findings support a strategy for significantly reducing response time, a crucial metric for sensor performance, via the development of a 4-terminal GFET with dielectrophoresis enhanced sensing capabilities.

1. Barik, A. *et al.* Nat Commun **8**, 1867 (2017).

2. Beraud, A. *et al.* Analyst, **146**, 403-428 (2021)

10:30 AM NM02.08.06

Penta Nitrogen Coordinating Single Atomic Cobalt with Oxidized Carbon Black to Boost 2-Electron Oxygen Reduction Reaction for H₂O₂ Mass Production Jae Won Choi and Jong Min Kim; Korea Institute of Science and Technology, Korea (the Republic of)

The process of two-electrons ($2e^-$) oxygen reduction reaction (ORR) offers a sustainable and decentralized alternative to the traditional multi-step anthraquinone process and hazardous direct synthetics for hydrogen peroxide (H_2O_2) production. However, considering the future commercialization, high-performance H_2O_2 electrocatalysts with economical cost should be designed rationally. Single-atom catalyst (SAC) has been attracting attention as a

promising candidate for 2e⁻ ORR catalyst due to its maximum atom-utilization efficiency, and unique and tunable electronic structure. Among the transition metal candidates such as Fe, Ni, and Co which lead to 2e⁻ ORR, it has been proven experimentally and theoretically that Co has the most favorable binding free energy with intermediate for H₂O₂ generation. Co-N₄, a metalloenzyme that exists in nature, is a representative Co SAC. However, Co-N₄ is kinetically favorable for the 4e⁻ ORR pathway, resulting in H₂O as a final product. Thus, a strategy to improve the selectivity and activity for H₂O₂ generation by tailoring the coordination environment around the Co SAC is required. Here, the Co-N₅-O-C single-atom catalyst (SAC) combined with highly coordinated Co-N₅ moieties and electro-withdrawing epoxides group nearby is developed by anchoring cobalt phthalocyanine (CoPc) on oxidized carbon support through the coordination of metal complex. The synergy effect between sufficient neighbor epoxy O and Co-N₅ centers can help boost both selectivity and activity for H₂O₂ production significantly. Specifically, the epoxy-rich Co-N₅-O-C structure shows excellent selectivity (85.6% at 0.75 V vs. RHE) in alkaline electrolytes, exceeding more than 15% higher selectivity than that of epoxy-deficient Co-N₅-C. Meanwhile, an ultrahigh mass activity was achieved, exceeding all other reported catalysts for 2e⁻ ORR by far. Supported by theoretical calculations, it is found that Co-N₅ moiety shows a lower overpotential of 2e⁻ ORR than Co-N₄ and the presence of epoxy groups near the Co-N₅ centers further decrease the overpotential, resulting in the enhanced activity of H₂O₂ electrosynthesis. Besides, a comparable high H₂O₂ production rate was also obtained by applying the Co SAC in a three-phase flow cell device, with around 80% faradaic efficiency remaining under 24 hours of testing.

10:45 AM NM02.08.07

Electrochemical Exfoliation and Chemical Functionalization of 2D Materials Mark A. Bissett, Yuling Zhuo and Ian Kinloch; University of Manchester, United Kingdom

Two-dimensional (2D) materials such as graphene and molybdenum disulfide (MoS₂) have been investigated widely for applications in energy storage, including supercapacitors, due to their high specific surface area, potential redox activity, and mechanical flexibility. Although graphene is an ideal material for supercapacitor electrodes due to its high specific surface area, most of the surface area is not accessible to ions due to the restacking of graphene, thus leading to low specific capacitance. Recently, many reports have been published on graphene composites and functionalized graphene to improve this ion-accessibility. In this work, we demonstrate several examples of simultaneous electrochemical exfoliation and functionalization of 2D materials in which the restacking can be reduced (for example, the inter layer spacing between graphene layers is increased by grafted diazonium salts) and the electrochemical properties of these electrodes (such as energy density) can be improved.

Additionally, electrodes comprising either solely graphene or MoS₂ have previously failed to reach their potential due to restacking of the layered structure and poor electrical conductivity. In our work we demonstrate composite electrodes formed by electrochemically functionalizing the graphene so that the negatively charged surface can self-assemble with positively charged chemically exfoliated MoS₂ (1T-MoS₂) to give an alternating layered structure. These alternately restacked 2D materials were then used to produce supercapacitor electrodes, and their energy storage properties were characterized.

Finally, we report a facile and scalable procedure of fabricating chemically functionalized thin (~4 nm) MoS₂ layers. We demonstrate that 2H-MoS₂ can be simultaneously electrochemically exfoliated and functionalized along with graphene. The aryl diazonium salts used for functionalization have not only been successfully grafted onto the 2H-MoS₂, as verified by X-ray photoelectron spectroscopy (XPS) and Raman spectroscopy, but also aids the exfoliation process. These electrochemical exfoliation and functionalization techniques could be extended to other types of 2D materials, introducing different functional species to adjust to specific application requirements.

Zhuo, Y.; Prestat, E.; Kinloch, I. A.; Bissett, M. A., *ACS Applied Energy Materials* **2022**, 5 (1), 61-70.

Zhuo, Y.; Kinloch, I. A.; Bissett, M. A., *J. Electrochem. Soc.* **2020**, 167 (11), 110531.

He, D.; Marsden, A. J.; Li, Z.; Zhao, R.; Xue, W.; Bissett, M. A., *Electrochimica Acta* **2019**, 299, 645-653.

He, D.; Marsden, A. J.; Li, Z.; Zhao, R.; Xue, W.; Bissett, M. A., *J. Electrochem. Soc.* **2018**, 165 (14), A3481-A3486.

11:00 AM NM02.08.08

Functional Single-Walled Carbon Nanotubes for Real-Time Wireless Chemical Sensors Seung-Ho Choi, Joon-Seok Lee, Won-Jun Choi and Seon-Jin Choi; Hanyang University, Korea (the Republic of)

Carbon nanotubes (CNTs) are attractive nanomaterials considering their high electrical conductivity and aspect ratio, leading to the development of innovative electronic devices. In particular, CNTs are widely employed as sensing layers for application in chemical sensors due to their efficient electrical transduction properties. Nevertheless, the stable surface chemical property of pristine CNTs with sp² bond hybridization hinders sensitive and selective detection of a target analyte. In this regard, various surface modification techniques are proposed by altering surface chemistry and imposing chemical reactivity toward analytes. There are two types of surface functionalization techniques of CNTs; covalent and non-covalent functionalization techniques. The covalent functionalization technique results in the disruption of the electrical property of CNTs by breaking sp² carbon bonds, which limits the degree of surface modification. On the other hand, the non-covalent functionalization of CNTs can induce a high degree of surface modification while maintaining high electrical conductivity, thereby leading to sensitive detection of analytes.

In this presentation, I will introduce the recent progress of non-covalently functionalized single-walled carbon nanotubes (SWCNTs) for applications in chemiresistive sensors.[1-4] Functional polymers were synthesized by decorating selector groups, which can have a chemical interaction with target analytes such as gas molecules and ionic species in solution. In particular, a functional polymer of poly(4-vinylpyridine) (P4VP) was employed and further modified by introducing dual-hydrogen bond donors (e.g., thiourea, squaramide, and croconamide) as selectors. The chemiresistive sensing layer of SWCNTs was non-covalently functionalized by wrapping with functional polymers. As a result, real-time electrical transduction was achieved upon the injection of a chemical analyte with high sensitivity and selectivity. For example, a large resistance transition of functional P4VP-SWCNT composite was obtained with the sensitivity [(R-R₀)/R₀ (%)] of 120% at 16.7 mM toward acetate anion. The chemiresistive sensor was integrated with a wireless sensing module for application in real-time wireless detection. The proposed SWCNT-based sensing platform with functional polymers can be applied in various fields such as environmental monitoring and healthcare.

[1] S.J. Choi, B. Yoon, J.D. Ray, A. Netchaev, L.C. Moores, T.M. Swager, Chemiresistors for the Real-Time Wireless Detection of Anions, *Adv. Funct. Mater.*, 30(2020), 1907087.

[2] S.J. Choi, B. Yoon, S.B. Lin, T.M. Swager, Functional Single-Walled Carbon Nanotubes for Anion Sensing, *ACS Appl. Mater. Interfaces*, 12, 25(2020), 28375-28382.

[3] B. Yoon, S.J. Choi, Selective acetate recognition and sensing using SWCNTs functionalized with croconamides, *Sens. Actuators B*, 346(2021), 130461.

[4] B. Yoon, S.J. Choi, T.M. Swager, G.F. Walsh, Flexible Chemiresistive Cyclohexanone Sensors Based on Single-Walled Carbon Nanotube-Polymer Composites, *ACS Sens.*, 6, 8(2021) 3056-3062.

1:30 PM NM02.09.01

Electrochemical Performances of Nickel Nitride/Buckypaper Hybrid Materials Salah Eddine Ben Razzouq¹, Mélanie Emo¹, Sylvie Migot¹, Zafar Ibutopo², Jean-Francois Pierson¹ and Brigitte Vigolo¹; ¹Univ of Lorraine, France; ²University of Sindh, Pakistan

The production of hydrogen using clean processes is one of the main challenge of the next decade. Water electrolysis is a promising method to produce green hydrogen. However, platinum-based materials are the state of the art electrocatalyst for the hydrogen evolution reaction (HER). Among the platinum free materials suitable for such application, transition metal nitrides are efficient and cost effective materials for hydrogen production. Buckypapers (BPs) are thin self-supported sheets of interlaced carbon nanotubes (CNTs) that show interesting high flexibility and chemical stability in electrolytes. The objective of the present work is to determine electrochemical performances of nickel nitride (Ni_xN) thin films deposited on buckypaper substrate. To the best of our knowledge, such hybrid carbon-nitride has never been reported before. In this work, a special attention is devoted to evidence the beneficial combination and synergistic effects between the rough BP and the nickel nitride thin film for their efficiency in HER, including crystallographic and microstructure aspects.

BPs with a thickness of approx. 80 μm have been prepared by the widely known dispersion-filtration method after dispersing CNTs by sonication in water with the help of an anionic surfactant (sodium dodecyl sulfate). In a second step, the outcome BP disks of 40 mm diameter have been coated by nickel nitride thin films using a reactive magnetron sputtering process. By varying the deposition duration, the thickness of the nickel nitride layer was fixed to 150, 200 and 300 nm. Ni_xN thin films have been also deposited on flat substrates (silicon wafer and polished nickel foil). The films deposited on these various substrates have been characterized by scanning electron microscopy, X-ray diffraction (XRD) and Raman spectroscopy. Thin foil lamella prepared by focused ion beam have been characterized by transmission electron microscopy and electron energy loss spectroscopy.

Our results show that the stoichiometry of the nitride films strongly depends on the nitrogen flow rate introduced into the sputtering chamber. At low nitrogen flow rate, pure Ni_3N films have been evidenced by XRD and Raman, while Ni_2N films have been formed at high nitrogen flow rate. Whatever the nature of the substrate (BP, Si or Ni) the sputtered films exhibit a columnar microstructure. Using flat substrates, the columns clearly grow along the direction perpendicular to the surface. Due to the BP roughness, the growth of nickel nitride on BP show an inclination which leads to a less dense and porous microstructures. Contrary to the commonly used liquid phase approach used to prepare the electrocatalysts of poorly controlled morphology and composition, such Ni_xN / BP hybrid materials of well controlled microstructure, rarely reported in the field, are highly desired for electrochemical reactions.

1:45 PM NM02.09.02

Enhancing $LiNi_{0.6}Mn_{0.2}Co_{0.2}O_2$ Based Lithium Battery Electrode Performance by Incorporating SWNTs Seyedabolfazl Mousavihashemi, Katja Lahtinen and Tanja M. Kallio; Aalto University, Finland

Enhancing lithium batteries cycle life and efficiency are essential from both economic and sustainability perspective. On the other hand, battery energy and power densities have to be improved to meet increased energy storage capacity expectations for portable and mobile applications. Today $LiNi_{0.6}Co_{0.2}Mn_{0.2}O_2$ is the most popular lithium battery positive electrode active material because of its relatively high energy density. However, it suffers from relative low conductivity limiting the achieved power density and efficiency at high power operation. Moreover, durability of nickel rich active material calls for enhancement. Preparing a 3D composite electrode from the active material and single-walled carbon nanotubes (SWNTs) is an attractive approach to solve these issues as SWNTs can offer the electrode such desired properties as high electrical conductivity and excellent mechanical and (electro)chemical durability.

In this study, we have investigated implications of incorporating SWNTs in a lithium battery positive electrode. The focused is on optimizing performance of $LiNi_{0.6}Co_{0.2}Mn_{0.2}O_2$ based battery electrodes by adjusting the SWNT amount, but also SWNT surface treatment is considered. The relevance of adding SWNTs in the composite electrode structure is verified in various electrochemical half cell experiments. The origin of the favorable properties and effects brought by SWNTs have been investigated using various structural analysis methods and in-situ electrochemical characterizations.

By optimizing the composite electrode structure, a 3D SWNT network around the active battery material particles is shown to improve the wiring between the particles, and the particles to the current collector. This results in enhanced electron transfer leading to an increment in the positive electrode power density and energy efficiency. That is reflected as enhanced electrochemical lithium (de)insertion reactions, in particularly at high charge/discharge currents. The best performance is reached when the SWNTs are subjected to a mildly oxidizing pre-treatment to increase the electrode wetting though this has an adverse effect on the electron transfer properties.

Our investigations reveal that another benefit brought by SWNTs for the 3D composite electrode is mitigation of mechanochemical aging. This results from hindering electrode volume changes during lithium (de)insertion in the active battery material as SWNTs entangled around the $LiNi_{0.6}Co_{0.2}Mn_{0.2}O_2$ particles decreases irreversible height changes occurring during both the formation cycle and continuous cycling. Our results suggests that this is also reflected as suppression of harmful side reactions indicated by an increase in the coulombic efficiency.

Summarizing, incorporating an optimized amount of modified SWNTs in a $LiNi_{0.6}Co_{0.2}Mn_{0.2}O_2$ based lithium battery positive electrode simultaneously enhances electrode power and energy density and cycling stability. Hence, all the above-mentioned important properties can be improved by incorporating highly conductive and durable carbon nanomaterials in a battery positive electrode structure.

2:00 PM NM02.09.03

Electronic Sensitivity of Individual SWCNT as a Model to Distinguish the Internal Confined Water from Adsorbed Water Said Pashayev^{1,2}, Romain Lhermerout^{1,3}, Christophe Roblin¹, Rudy Desgarceaux^{1,4}, Rémi Jelinek¹, Saïd Tahir¹, Vincent Jourdain¹, Rasim Jabbarov², François Henn¹ and Adrien Noury¹; ¹Laboratoire Charles Coulomb (L2C) - UMR5221 du CNRS, Montpellier, France, France; ²Institute of Physics, Azerbaijan National Academy of Sciences, Baku, Azerbaijan, Azerbaijan; ³Laboratoire Interdisciplinaire de Physique, Univ. Grenoble Alpes & CNRS, Grenoble, France, France; ⁴Institut d'Electronique et des systèmes (IES), Univ. Montpellier & CNRS, Montpellier, France, France

Carbon nanotubes (CNTs) possess extraordinary mechanical, thermal, and electrical properties due to their atomically perfect structure and sp²-hybridization. Recently, Single-wall CNTs (SWCNTs) have become an interesting host for the nanoscale confinement of fluids, with a wealth of surprising phenomena appearing: spontaneous filling, frictionless mass transport, unusual phase diagram, etc[1]. Most of these phenomena are still under debate and call for experimental confirmation. But the field is struggling with finding experimental approaches sensitive enough to carry out measurements at the level of individual nanotubes. SWCNT field effect transistors (SWCNT-FETs) showed that the electronic properties of SWCNTs are sensitive to their diameter,

defects, doping, adsorbates, and environment[2], [3].

In this contribution, we demonstrate that individual carbon nanotube field effect transistors (CNTFET) are excellent tools for this aim, for the first time allowing to precisely identify water confined inside the nanotube. By studying the electrical performances of several unopened and opened CNTFETs submitted to various atmosphere and temperature treatments, i.e. dry air, humidity, secondary vacuum, and current annealing, we show that it is possible to distinguish water being outside and inside the nanotube, just outside, or the nanotube free from water. We thus observed that for opened SWCNT both secondary vacuum and current annealing move threshold gate voltage towards more negative values, while for closed SWCNT secondary vacuum had no effect compared to current annealing. To sum up, the current annealing treatment is essential to distinguish water adsorbed outside from water confined inside. We show that this behavior is universal, as all devices' metallicities behave similarly, provided that the surface of the nanotube is pre-cleaned by current annealing. We will also discuss the mechanisms behind the coupling of electronic transport and the presence of water.

Our results open up the possibility to use CNTFET for instance reliable, selective, and sensitive chemical and biological sensors, and also, to resolve the long-standing questions in the nanofluidic community about the behavior of water under nanoscale confinement.

References:

- [1] T. A. Pascal, W. A. Goddard, and Y. Jung, "Entropy and the driving force for the filling of carbon nanotubes with water," *Proc. Natl. Acad. Sci.*, vol. 108, no. 29, pp. 11794–11798, 2011, doi: 10.1073/pnas.1108073108.
- [2] D. Cao *et al.*, "Electronic sensitivity of carbon nanotubes to internal water wetting," *ACS Nano*, vol. 5, no. 4, pp. 3113–3119, 2011, DOI: 10.1021/nn200251z.
- [3] I. Heller, A. M. Janssens, J. Männik, E. D. Minot, S. G. Lemay, and C. Dekker, "Identifying the mechanism of biosensing with carbon nanotube transistors," *Nano Lett.*, vol. 8, no. 2, pp. 591–595, 2008, DOI: 10.1021/nl072996i.

2:15 PM NM02.09.04

Carbon Nanotube-Based Flexible Memory Devices for Neuromorphic Computing Yutaka Ohno, Takeshi Watanabe, Koki Tatsumi, Atsushi Kawaguchi and Adha Sukma Aji; Nagoya University, Japan

The increasing information needed to be processed in the artificial intelligence (AI) era requires a breakthrough in a novel computing paradigm. Brain-inspired computing using hardware-based synaptic devices, such as memristors, is gaining attention due to its ability to mimic the biological synapse connections. Reservoir computing is a novel neural network computing method that has advantages in processing a high amount of data at a short computing time and low training cost while maintaining low power consumption. Here, we report physical reservoirs based on carbon nanotube (CNT) memory devices, such as memristors and thin-film transistors (TFTs) with hysteresis. First, CNT/HfO₂/CNT memristors were fabricated by sandwiching a thin HfO₂ insulator between two CNT network films. Ultra-dense memristors can be obtained by connecting multiple electrodes to the bottom and top CNT films. Each combination of two electrodes can act as a memristor because the current path will be different for each due to the network structure of the CNT films. We demonstrated Pavlov's dog training regime to the system. We also explored the potential of CNT TFTs with hysteresis as a memory device for reservoir computing. NARMA (nonlinear autoregressive moving average) tasks have been demonstrated by using CNT TFTs with multiple nodes.

2:30 PM BREAK

3:30 PM *NM02.09.05

All-Carbon Nanomaterial Inks for Print-in-Place, Recyclable and Water-Based Electronics Aaron D. Franklin; Duke University, United States

For decades we've been hearing about the promise of printing electronics directly onto any surface. However, despite significant progress in the development of inks and printing processes, reports on fully, direct-write printed electronics continue to rely on excessive thermal treatments and/or fabrication processes that are external from the printer. In this talk, recent progress towards print-in-place electronics will be discussed; print-in-place involves loading a substrate into a printer, printing all needed layers, then removing the substrate with electronic devices immediately ready to test. A key component of these print-in-place transistors is the use of inks from various nanomaterials, including: 2D graphene and hexagonal boron nitride, and 1D carbon nanotubes. Using an aerosol jet printer, these mixed-dimensional inks are printed into functional 1D-2D thin-film transistors (TFTs) without ever removing the substrate from the printer and using a maximum process temperature of 80 C with most processing occurring at room temperature. Using a similar print-in-place process, completely recyclable printed transistors will be discussed, fabricated entirely using nanoscale carbon-based inks. These recyclable devices exploit a printed crystalline nanocellulose (CNC) ionic dielectric. Finally, the same set of carbon-based inks will be demonstrated for use in all-aqueous (completely water-based) printed CNT-TFTs, eliminating dependence on processing with harsh solvents. These demonstrations give evidence for an electronic future involving devices with fabrication and/or function that goes beyond what is possible with traditional semiconductor technologies.

4:00 PM NM02.09.06

Screen-Printed Resistive Gas Sensors Based on Functionalized Carbon Nanotubes and Electronic Design for Selective Detection of Carbon Monoxide and Hydrogen Christopher Landorf, Marriana Nelson, Rebekah Baggett and Zun (Cathy) Chen; Brewer Science, Inc., United States

Often the most challenging aspect of research in nanostructured materials is getting the materials into a form where they can be manipulated without changing the desired properties of the nanomaterial. Brewer Science has developed a unique method for solving this problem by using solubilizing pi-bonders reacted with the carbon nanotubes in a superacid environment. The resulting carbon nanotubes can be dispersed in water, alcohols, and other polar solvents without the need for surfactant, producing a novel environment for the functionalization of the solubilized carbon nanotubes.

Films made of these materials are remarkably conductive, achieving less than 400 Ω /square at 85% transmittance. These carbon nanotubes can be spray coated, placed in alcohols for ink-jet printing, or dispersed in glycols for screen printing. The resulting films can support short current pulses, which, by modulating their frequency, can be used to control the temperature of the film.

In addition to making good inks, these dispersions can be used as a reaction medium to functionalize them with active materials, such as metal oxides, peptides, or polymers, to make them respond electronically to a targeted analyte or environment. In this talk, I will describe how we made tin(IV) oxide-functionalized carbon nanotubes and how we used our pulsed temperature control scheme to sense multiple analytes with only one screen-printed pixel by distinguishing the different optimal reaction temperatures of carbon monoxide and hydrogen.

4:15 PM NM02.09.07

Solution Processable Carbon Nanotubes on Shrinkable Polymer for Enhanced Porosity and Conductivity for Sensing Application Lana Joharji and Nazek El-Atab; King Abdullah University of Science and Technology, Saudi Arabia

Carbon nanotubes (CNTs) have a huge potential in electronic devices applications such as sensors and transistors due their high electric conductivity and stability. More specifically, a wide range of carbon-based nanomaterials, including carbon nanotubes (CNTs), have been used as humidity sensing medium due to their high conductivity, electrical sensitivity, and chemical stability. In terms of fabrication, various methods for coating/depositing CNTs on various substrates have been previously demonstrated, however, they are either complicated with a lot of material waste, or they require stamping to achieve dense

and uniformly dispersed CNTs. In this work, we report a new process flow for achieving a porous, yet more conductive mesh of solution processable CNTs with minimized waste based on drop casting on a shrinkable polymer. Thus, even when a single droplet of the solution is used, the shrinking effect allows improving the resulting film conductivity. Metrology showed that by increasing the heating time at a specific temperature (e.g., 110°C), the CNTs channel area decreases (e.g., 1.3% after 1 min), however, the volume overall increases. This was confirmed using the profilometer where the thickness of the film was increased by 42% at 110°C after 1 min. Moreover, the overall increase in the volume was verified using the porosity test which showed an increasing in the CNTs surface area ~10 times when heated at 130°C for 3 min. Due to the shrinking effect, the CNTs experience a compressive stress which was confirmed by Raman spectroscopy, which showed a shifting of the G peak from 1571 to 1575 after 1 min of heating at 110°C. Moreover, Hall measurements using the physical property measurement system (PPMS) showed that the conductivity of the CNTs film increased by 92.4% after shrinking while the mobility decreased by 44.9%. In fact, the charge density in the CNTs increases under the experienced compressive strain which makes its effect dominant on the overall increase in the film conductivity, despite the degradation in the charge mobility. As an application, the CNTs mesh was used in humidity sensing application. A micro probe system was used to test the device at different humidity levels. The system was connected to the humidity control system, N₂ supply, DI water, and Keithley 4200A-SCS system. The resistive based sensors were tested with and without the shrinking effect. The humidity level was changed from 10% to 90% with a step of 10% and the devices showed a higher change in resistance after shrinking and thus a higher sensitivity compared to the initial intact devices. For instance, with a 30% relative humidity (RH), the resistance increased by 16.3% after 3 min of heating to achieve the shrinking effect compared to 8.7% for the initial device, while at 70% RH, these numbers change to 25.4% and 20.7%, respectively.

4:30 PM NM02.09.08

Measuring TCR of High Purity Semi-Conducting CNT Networks for Super Sensitive Bolometric Infrared Detectors Tomo Tanaka^{1,2}, Miyamoto Toshie^{1,2}, Megumi Kanaori², Norika Fukuda¹ and Ryota Yuge^{1,2}; ¹NEC Corporation, Japan; ²National Institute of Advanced Industrial Science and Technology (AIST), Japan

Uncooled infrared sensors of bolometer type have a wide range of applications such as security, military, food inspection, health care, and automotive camera. Currently, the highly sensitive and low-cost device development is key issue for further expansion of demand. The bolometer is an infrared detector for radiant heat by means of an infrared absorber having a temperature sensitive electrical resistance material. Infrared radiation strikes the absorber material heating it and thus changing resistor material resistance. Therefore, bolometer's performance is strongly limited by temperature coefficient of resistance (TCR) of the resistor. The conventional resistor is generally based on vanadium oxide (VO_x) with TCR of about -2%/K [1] and an outstanding resistor is essential to achieve highly sensitive infrared detectors. Recently, single-walled carbon nanotubes (SWCNTs) have been expected as promising materials with high TCR, low resistivity, and high chemical stability. The TCR of -2.1%/K has already been obtained by semiconducting SWCNT films extracted by density gradient method [2]. Further, conventional bolometer which is named microbolometer has a suspended structure for heat separation between the absorbing layer and the substrate, and these are suspended structure with micro electro mechanical system (MEMS) process.

Therefore, we have tried to develop low-cost and high sensitivity bolometer with SWCNTs as resistor material [2]. In this study, we fabricated high TCR bolometer with printed process that was not MEMS process by using the high purity semiconducting SWCNT network films above 98% and the parylene C film which is the low thermal conductivity material as a thermal separation layer and evaluated its device structure and electrical property.

The pristine SWCNTs are fundamentally a mixture of both semi-conducting and metallic SWCNTs. To extract the semi-conducting SWCNTs, "Electric-field inducing Layer Formation (ELF)" method was used, which is our original method [3]. ELF method is the remarkable promising technique to extract semi-conducting SWCNTs with high purity and excellent electrical transportation property by carrier-free electrophoresis using non-ionic surfactant. To show capability of SWCNT bolometers, we measured TCR of the semi-conducting CNT networks which are extracted from various type of commercial SWCNTs.

The sample fabricating process is described below. First, Ti/Au electrodes as a source drain were deposited on a Si substrate, and SiO₂ was sputter-deposited on the surface. Each electrode was exposed by SiO₂ etching. Then a (3-Aminopropyl) triethoxysilane monolayer was formed on the SiO₂ which remaining between the two electrodes, and semi-conducting SWCNTs which is extracted by ELF method were dispersed. The Si chip was mounted on a ceramic carrier, and the temperature dependence of the electrical characteristics of the CNT network between the source and drain electrodes was measured in a liquid nitrogen cryostat at around room temperature. TCR was calculated using each temperature's resistance. The maximum TCR was close to -6%/K, which was larger than the commercial bolometer's resistor material. This shows the superiority of high purity semiconducting SWCNTs extracted by the ELF method. Furthermore, the relationship between the morphology of CNT networks and its electrical characteristics was also obtained.

Acknowledgments: This study was supported by Innovative Science and Technology Initiative for Security Grant No. JPJ004596, ATLA, Japan.

[1] C. Chen, et. al., *Sen. Act. A. Phys.* 90, 2001, 212.

[2] K. Narita, et. al., *Sen. Act. A.* 195, 2013, 142.

[3] K. Ihara, et. al., *J. Phys. Chem. C*, 115, 2011, 22827.

SESSION NM02.10: Poster Session III

Session Chairs: Tanja Kallio, Shunsuke Sakurai, Yoke Khin Yap and Ming Zheng

Wednesday Afternoon, November 30, 2022

8:00 PM - 10:00 PM

Hynes, Level 1, Hall A

NM02.10.01

Highly Antistatic Polypropylene/Polyaniline Coated Graphene Nanocomposites Pralhad Lamichhane, Dilli Dhakal, Siddhesh Chaudhari, Clinton Switzer and Ranji Vaidyanathan; Oklahoma State University, United States

Polypropylene (PP) is a commodity polymer widely used for many practical applications including structural materials for electronic devices and automobiles, packaging, and fuel cells. Reinforcing PP with graphene nanoplatelets (GNP) increases the multifunctionality of PP. Higher GNP content in PP enhanced the electrical properties of the material. However, a uniform mixture of GNP in the material is difficult to achieve because of the poor dispersion compatibility between PP and GNP. The GNP tends to agglomerate due to inherent van der Waals forces. In this study, GNP was encapsulated with polyaniline (PANI) to improve the dispersion as well as compatibility with PP. The PANI-GNP nanocomposites were synthesized by in-situ polymerization, and concentrations of nanofiller in PANI-GNP/PP composites were varied at 5, 10, 15, and 20 wt%. The dispersion and compatibility were

validated by various characterization techniques such as FTIR, Raman spectroscopy, XRD, and SEM. In addition, mechanical and electrical properties were studied using DMA, DSC, TGA, flexural test, un-notched impact strength, and resistivity. The electrical conductivity and mechanical tests confirmed that 10 wt% PANI-GNP filled PP can make the best antistatic material with improved mechanical strength.

NM02.10.03

Electrochemical Sensitive Determination of Chemotherapeutic and Immunomodulator Agent Methotrexate Enabled by Novel Graphitic Nano-Heterostructure Material Reham G. Elfarargy, Mahmoud A. Saleh and Nageh K. Allam; American University in Cairo, Egypt

In this study, we report the electrochemical voltametric determination of methotrexate (MTX) chemotherapeutic and immunomodulatory agent with a novel graphitic nano-heterostructure (GNHS) material. In comparison with the previous studies, it shows a higher and enhanced peak transduction. In our research, our GNHS/CPE exhibits superior electrochemical oxidation and detection of MTX in buffer and biological fluids (plasma, urine) than bare Carbon Paste Electrodes (CPE). The synthesized GNHS material has been characterized using X-ray powder diffraction (XRD), X-ray photoelectron spectroscopy (XPS), UV-visible absorption spectroscopy, scanning electron microscopy, Raman spectroscopy, cyclic voltammetry, square wave voltammetry, and electrochemical impedance spectroscopy. In addition, the electronic structure, adsorption energy, band gap, type of interaction, and stable configuration of the used GNHS/CPE have been studied by using density functional theory (DFT). Under optimized conditions, the GNHS/CPE platform showed a linear response for the MTX concentrations in Britton Robinson Buffer (BRB) solution, urine, and plasma with high recoveries and lower limit of detection (LOD) and Limit of Quantification (LOQ) in comparison to the current literature. In addition, reproducibility, stability, and selectivity studies show promising results for the modified GNHS/CPE electrode.

NM02.10.04

Molecular Interactions at the Interface of C - Reactive Protein (CRP) and Poly Vinyl Alcohol (PVA) in the Presence of Carbon Nanotubes Ryan Baker and Isaac Macwan; Fairfield University, United States

Many diseases typically trigger an immune response producing biomarkers, which are largely proteins present in blood, other body fluids or tissues indicating the presence of that disease. A common detection method for certain diseases is therefore, the detection of abnormal amount of a certain protein in the body. One example of this is a cardiac inflammatory C-reactive protein (CRP), which is commonly seen to result from a heart disease. Nanotechnology and biosensors can be used to detect the levels of CRP in blood plasma before they get to more extreme levels, leading to an early detection of the disease as pointed out by previous studies. The goal of this project is to simulate the interactions between the inflammatory protein, CRP, a polymer, Polyvinyl Alcohol (PVA), and Carbon Nanotubes (CNTs) using molecular dynamics through simulation software called Visual Molecular Dynamics (VMD) and nanoscale molecular dynamics (NAMM). Atomic-level models (coordinates) of the CRP protein and PVA are acquired through the protein data bank database while the pristine 20nm long CNTs with chirality (15,15) and (12,20) are modeled through the Nanotube builder modeling program within VMD. Molecular simulations of the individual PVA, CRP and CNT controls as well as an entire system with PVA and CRP interacting between the two CNTs are carried out based on the CHARMM (Chemistry at HARvard Molecular Mechanics) parameters. Furthermore, TIP3 water model along with neutralizing salt concentration is used to create a waterbox for real-time interactions as currently such data is lacking in the literature. Stability analysis is performed using RMSD (root mean square deviation), distance between center of mass, salt bridges, hydrogen bonds, secondary structure analysis and conformational energies of the system using VMD plugins and TCL scripts. Exhaustive analysis involving electrostatic energy evaluation of individual molecules, Van der Waals energies between the molecules, optimal adsorption cut-offs using the criteria of interaction energies and number of participating adsorbed atoms as well as interfacial water molecules and their hydrogen bonds is also performed on the simulated molecular trajectories at the nano-bio interface. It is expected that the information obtained from these simulations will be used to develop electrospun PVA/CNT nanofibrous scaffold based electrochemical biosensor to detect biomarkers similar to CRP.

NM02.10.07

Reliable Carbon Nanotube Paste Emitters Producing High Current Density for X-Ray Tubes by Improving Cohesion and Adhesion Through Chemically Reactive Fillers SeonAe Byun¹, Sayed Zafar Abbas¹, Jeung Choon Goak¹, Sora Sim², Choul Ho Lee² and Naesung Lee¹; ¹Sejong University, Korea (the Republic of); ²Vatech, Korea (the Republic of)

Carbon nanotubes (CNTs) with one-dimensionally rolled-up graphene structures have been spotlighted as an electron emission material for cold cathodes, thanks to their extremely high aspect ratios of lengths to diameters, excellent electrical conductivity, superior mechanical strength and outstanding chemical stability. A paste screen printing method, which has been mostly used to fabricate commercial CNT field emitters, is engaged in this study. The paste, usually composed of CNTs, inorganic nanoparticle fillers, organic binders and solvent, should be made to possess an appropriate viscosity for easy printing. Performance of CNT paste emitters is mainly determined by two factors: dispersion of CNTs and fillers; adhesion to a substrate and cohesion of paste. When adhesion and cohesion are weak, the paste may be peeled off from the substrate or partly from the paste by strong electrostatic forces exerted on CNT emitters during field emission, which may unfortunately cause catastrophic arcing and permanent damage. If adhesion and cohesion are too strong, it can be difficult to carry out surface activation to expose CNTs above the surface by delaminating the topmost surface layer of the paste. Thus, the paste adhesion and cohesion should be controlled in an appropriate range. The pastes were fabricated using Al, Ni and AlN nanoparticle fillers. This study made effort to impart appropriate adhesion and cohesion of CNT pastes by controlling formation of intermetallic compounds of aluminides at the paste-substrate interface and inside the paste. The paste was screen-printed on Kovar (54Fe-29Ni-17Co) substrates, fired at 400°C in air to remove organic matters and annealed in vacuum at 830°C to form intermetallic compounds. High-temperature vacuum annealing produced nickel aluminides on the substrates and also inside the paste. Al seems to react with Ni of the Kovar substrate and Ni filler inside the paste, improving the paste-substrate adhesion and the paste cohesion, respectively. X-ray diffraction, transmission electron microscopy, energy dispersive x-ray spectroscopy, and x-ray photoelectron spectroscopy were engaged to characterize the aluminide formation. Vacuum-sealed x-ray tubes were fabricated using the CNT paste emitters with high adhesion and cohesion which generated high current density. The x-ray tubes were normally operated at high current density for an extended period of time.

NM02.10.09

High Quality Growth and Transfer of Bilayer Graphene on Sapphire Sivasakthya Mohan, Yuqian Gu, Dmitry Kireev, Deji Akinwande and Kenneth Liechti; The University of Texas at Austin, United States

Dry transfer of graphene from its growth substrate through mechanical delamination is a quick, effective, and clean transfer method that overcomes the disadvantages of traditional wet transfer approaches such as long processing times, polymeric residues, and harsh chemical exposure of the transferred films [1]. However, it is difficult to use graphene grown on a copper foil, which is a widely used growth substrate, in the dry transfer process due to its lack of mechanical rigidity and relatively high adhesion energy. Thin copper films deposited on silicon wafers have been used to overcome this challenge. However, a very high initial thickness of copper film needs to be deposited to avoid dewetting problems that occur at the high graphene growth temperatures. To this end, we have studied the metal-free synthesis of graphene on sapphire substrates, which has been shown in literature to have a sufficiently low adhesion energy with graphene [2].

In this work, we have performed atmospheric pressure chemical vapor deposition growth of bilayer graphene directly on sapphire at conventional metal CVD temperatures. The as-grown graphene was characterized using Raman spectroscopy, scanning electron microscopy (SEM), atomic force microscopy (AFM) and X-ray photoelectron spectroscopy. Prior to growth, the sapphire substrates were annealed in air at high temperatures to achieve a suitable surface reconstruction of the sapphire surface needed to grow high quality graphene. The annealing improved the quality of the as-grown graphene as confirmed by the reduction in the D/G Raman peak ratio of the graphene. With annealing we have achieved a D/G ratio as low as 0.15 for the graphene grown at 1050C, which is among the lowest reported values in literature, thus proving the graphene to be of high quality. Graphene based transistors were fabricated from the as-grown films and electrical characterization was done to extract field-effect mobility.

Furthermore, fracture experiments have been conducted over a range of mode-mixes on laminated beam specimens consisting of a sapphire/graphene/epoxy/sapphire stack, using a dual actuator loading device. At each mode-mix, we extracted the toughness and normal and shear components of the traction-separation relation of the interface between graphene and sapphire. The high quality of the transferred films was confirmed by Raman mapping, SEM and AFM and electrical characterization. The variation of the interactions with mode-mix adds the potential of switchable adhesion for 2-step dry transfer processes, where higher adhesion is required to remove the graphene from the growth substrate but lower adhesion is required to deposit it on the target substrate.

References

1. Na, S. R., et al. "Clean graphene interfaces by selective dry transfer for large area silicon integration." *Nanoscale* 8.14 (2016): 7523-7533.
2. Dou, Zhipeng, et al. "Atomic mechanism of strong interactions at the graphene/sapphire interface." *Nature communications* 10.1 (2019): 1-5.

NM02.10.10

3D Bioprinting of Soft Polymeric Nanocomposites Subha Parvathi Madamuthu, Nikshiptha Mulagada, Roshan Kumar Bhatta and Prabir Patra; University of Bridgeport, United States

3D bioprinting uses a combination of natural and synthetic materials for a useful tissue scaffold. 3D Printing of biomaterials is a customized method to provide a chance to diffuse different cell types at desired locations. Using the in-situ bioprinting tissue scaffold could be made. Alternatively in ex-situ bioprinting, there is a need for cross-linking of cell formulation. Here we report the 3D printing of a photocurable nanomaterial scaffold using Flavin mononucleotide, a synthetic equivalence of DNA with graphene nanoparticles.

Flavin is an important coenzyme for a few oxidative enzymes. It is the principal form in which RIBOFLAVIN is found in cells and tissues. Flavin Mononucleotide (FMN) is a biomolecule produced from vitamin B2 and is an important luciferin (i.e., bioluminescent cofactor).

Graphene-based materials are non-toxic and demonstrate excellent electrochemical and optical properties, as well as the capability to adsorb a variety of aromatic biomolecules through a π - π stacking interaction and/or electrostatic interaction, which make them ideal materials for constructing biosensors and loading drugs. Graphene's biocompatibility, large surface area, excellent mechanical properties, and ease of functionalization make it a unique material for bone tissue and stem cell research. GO substrates allow cell adhesion and proliferation and have been shown to be capable of increasing the differentiation of stem cells into the osteogenic lineage.

It is also anticipated that graphene scaffolds could play a role in tissue engineering and regenerative medicine. A graphene scaffold with stem cells has been studied and explored by researchers thus the cells not only did survive, but also divided, proliferated, and morphed into neuron-like cells.

In this research, 3D bioprinting of the mixture of graphene nanoparticles, flavin mononucleotide, and gelatin was performed. We used the R3BEL Mini printer which runs on extrusion-based printing technology, and pronterface as a printer control software tool. Using the same tools, a mixture of Alginate, Bowmans Albumin, and Hydroxyapatite as a nanocomposite has also been synthesized to print bone-like structure.

The customized photocuring nanomaterial was prepared at room temperature. A 5ml syringe with a 22-gauge blunt-tip needle was filled with 4ml photocurable nanomaterial. We printed FMN containing graphene and gelatin biomaterial on a petri dish (100 mm diameter). To print the bone-like structure we used a G-code printer file.

This research is still in progress; after overcoming the existing obstacles, we plan to use FTIR, UV-Vis, XRD, and SEM to analyze the surface properties of our custom-made photocurable nanomaterial scaffold.

This work presented stable structures of 3D printed hydroxyapatite and photocurable polymers as soft nano composite biomaterials.

NM02.10.12

Multifunctional Inorganic Nanomaterial Aerogel Assembled into fSWNT Hydrogel Platform for Ultrasensitive NO₂ Sensing Hee-Jin Cho¹, Il-Doo Kim¹ and Sung Mi Jung²; ¹Kaist, Korea (the Republic of); ²Korea Institute of Toxicology, Korea (the Republic of)

Facile fabrication of multifunctional porous inorganic aerogels remains an outstanding challenge despite the considerable demand for extensive applications. Here, we present the production of a multifunctional porous inorganic nanomaterial aerogel by controllable surface chemistry of a functionalized SWNT (fSWNT) hydrogel platform for the first time. The versatile functional inorganic nanoparticles can be incorporated uniformly on the porous 3D fSWNT hydrogel platform through a facile dip coating method at ambient conditions. The morphology of the multifunctional inorganic aerogel is manipulated by designing the fSWNT hydrogel platform for different requirements of applications. In particular, Pt-SnO₂@fSWNT aerogels exhibit high porosity and uniformly distributed ultrafine Pt and SnO₂ on the fSWNT platform with controllable particle size (1.5–3.5 nm), which result in significantly high surface area (393 m² g⁻¹). The ultrafine Pt-SnO₂@fSWNT aerogels exhibit highly sensitive (14.77% at 5 ppm) and selective NO₂ sensing performance even at room temperature due to the increased active surface area and controllable porous structure of the ultrafine aerogel, which can provide fast transport and penetration of a target gas into the sensing layers. The newly designed multifunctional inorganic aerogel with ultrahigh surface area and high open porosity is a prospective materials platform of high performance gas sensors, which could be also broadly expanded to widespread applications including catalysis and energy storages.

NM02.10.13

Advanced Polymer Hybrid Materials with Anisotropically Aligned Carbon Nanotubes Sunwoo Kim and Woo-Jae Kim; Ewha Womans University, Korea (the Republic of)

Carbon nanotubes (CNTs) have been reported their high tensile strength, electrical conductivity, and thermal conductivity. Even though CNTs are utilized as conductive materials in various fields, the studies are focused on CNT-dispersed conductive sheets. However, the anisotropic property of CNTs enables vertically aligned CNTs to have much higher mechanical strength and electrical conductivity. Despite the versatility of polymers, their applications are limited due to the weak strength and the poor electrical conductivity. Thus, some studies have improved their properties by adding conductive materials like CNTs. Particularly, the anisotropic properties of CNTs can fortify polymers to lightweight hybrid polymers with high strength and electrical conductivity. For this purpose, a method of coating polymers on vertically synthesized CNT forests was suggested, but the process is complicated, and it is very difficult to produce the hybrid polymer of large area. We suggest a much more simple and effective process for anisotropically aligned carbon nanotubes (A-CNT)-polymer hybrid materials. In the pre-polymer solution, mildly oxidized CNTs were arranged in the vertical direction by electrophoresis. Electric fields for the arrangement were formed by alternating currents through indium tin oxide (ITO) electrodes. The polymer was

subsequently cured by ultraviolet radiation and the aligned CNTs were fixed in the polymer. The A-CNT-polymer showed higher strength in compression tests compared to the CNT-polymer before the arrangement. In addition, the parallel direction to A-CNT promoted the much lower resistance for the electric current. Low-weight composition of CNTs can efficiently fortify the mechanical and electrical properties of the polymer. The excessive addition of CNTs seems to reduce the mechanical strength of the photocurable polymer. This low-weight and multi-functional hybrid materials can be developed to bodies of vehicles, ballistic materials, or membranes for fuel cells.

NM02.10.14

Covalently Functionalized Graphene for Chemical Separation Membranes [Taishu Yoshinaga](#), Shao-Xiong Lennon Luo, Quynh P. Ngo and Timothy Swager; Massachusetts Institute of Technology, United States

Chemical modifications of graphene oxide (GO) afford functionalized graphene with versatile characteristics. A Johnson-Claisen rearrangement is one of [3, 3] sigmatropic rearrangements to synthesize covalently functionalized graphene. Specifically, allylic alcohols on the GO surface are applied to the Claisen rearrangement to form ethyl ester groups anchored to the GO sheet through a robust carbon-carbon bond. These functional groups and robust carbon bonds survive in thermal and reductive conditions, indicating this functionalized graphene's significant potential in applications in harsh conditions.

GO-based membranes are promising candidates as a pressure-driven non-thermal method to mitigate global energy use and to cope with environmental concerns in water purification and chemical separations because of their favorable characteristics: high water permeability, two-dimensional structures, and mechanical strength. There is a particular need for energy-intensive weak black liquor (WBL) concentration in the kraft pulping process. WBL is a high alkaline corrosive fluid with polymers, other organic molecules, inorganic salts, and total solids of ~18% and is processed at high temperatures of up to 95 °C. Although WBL is concentrated to ~75% solids via the evaporation processes to create biofuels, even partial concentration with non-thermal technology to ~30% solids significantly reduce energy requirements and are beneficial for economics and environments.

We herein focused on further chemical modifications of the robust graphene material prepared by the Claisen rearrangement of GO to apply its membrane for WBL concentration that is processed in the harsh conditions. To increase the hydrophilicity and water permeability of the graphene, we saponified the ester groups under base conditions to generate carboxylic acid groups. A narrowed interlayer spacing of the graphene sheet also lowers water permeation; therefore, we then amidated the hydrophilic graphene under mild conditions using linear diamines. These diamines can contribute to not only the expansion of the interlayer spacing but also the cross-linking between the graphene sheets. Water-dispersible graphenes with various interlayer spacings were successfully synthesized, and we prepared membranes from each graphene material. Large molecules (~1 kDa) were selectively excluded, and WBL was concentrated at a stable rate and water permeation thanks to the expanded interlayer spacing and hydrophilicity. These versatile water-dispersible graphenes represent promising membrane materials in WBL concentration and other chemical separations.

NM02.10.15

Development of Graphene/Silicon Composite Based Lithium Ion Battery Anode [Tarik C. Turkoglu](#), Eren Atli, Omer R. Caylan and Goknur Cambaz Buke; TOBB University of Economics and Technology, Turkey

The need for energy storage devices is growing constantly, requiring the development of more efficient, high-capacity batteries. Due to their superior properties compared to conventional batteries, lithium-ion battery cells have become the most popular energy storage units, and they are now widely used in our daily lives. The most common application area for Li-ion batteries is electric vehicles. The Li-ion battery cells used in electric cars are expected to have a short charging time, a long cycle life, a low weight per volume, and a large storage capacity. The anode structure of Li-ion batteries should be enhanced to obtain these desirable features. The most commonly utilized active material in the battery anode structure is graphite. Although graphite's electrical conductivity and extended service life are superior to those of its alternatives, its low charge capacity and small surface area require further development. Silicon is another common component in Li-ion batteries. Silicon can store ten times more Li ions than graphite; nevertheless, anodes made of Si rather than graphite degrade more quickly and have a shorter service life due to structural fragmentation produced by high-volume fluctuations during charge/discharge cycles. Because of its enormous surface area, mechanical and electrical capabilities, and chemical resistance, graphene, a two-dimensional honeycomb structure of carbon atoms, has a lot of potential to solve these challenges. As a result, the purpose of this research is to use a Gr/Si composite structure to improve the energy storage capacity, mechanical characteristics, and chemical resistance of a battery anode. Top-down processes such as high vacuum furnaces, wet chemistry, and the flash method are used to make Gr for Gr/Si composites. The morphology of synthesized materials is examined using OM, TEM, and SEM. Raman spectroscopy is used to examine their structure. BET analysis is used to determine the surface area of the composite anode material. Electrochemical characterization methods will be used to determine the charge capacity of Gr/Si composites, which will be reported.

NM02.10.16

Ultrashort Pulsed Laser Induces Graphene on Woods and Leaves for Green Electronics [Truong-Son D. Le](#), Han Ku Nam, Dongwook Yang, Younggeun Lee, Young-Ryeul Kim, Seung-Woo Kim and Young-Jin Kim; Korea Advanced Institute of Science and Technology, Korea (the Republic of)

In recent years, we have witnessed a tremendous demand for electronic devices that leads to a massive amount of electronic waste and rapid exhaustion of non-renewable resources. Accordingly, green electronics has received much attention to minimize the negative impact of electronic waste and pave the way toward the sustainable development of our society. Functional nanomaterials are essential components in green electronics in which graphene is highly attractive owing to outstanding electrical, mechanical, and thermal properties. Graphene has been used in various advanced applications ranging from academia to industry. Until now, graphene can be synthesized via liquid-phase exfoliation, mechanical exfoliation, chemical vapor deposition, and reduction of graphene oxide. Nevertheless, there is a lack of an efficient, low-cost, and eco-friendly synthesis method to realize the full potential of graphene.

Herein, we have developed a facile fabrication of pre-designed graphene electrodes on arbitrary woods and leaves in ambient conditions utilizing ultraviolet femtosecond laser pulses. Compared with conventional lasers, the femtosecond laser shows distinct advantages due to ultrashort pulse durations, extremely high peak intensities, and nonlinear interactions with carbon materials. The mechanism of LIG formation was extensively studied in which the heat accumulation of repetitive laser pulses increases the base temperature at the laser-irradiated area to carbonize the precursors, and the intense ultrashort laser pulses induce sufficiently high temperature to transform amorphous carbon into LIG. The formation of LIG was confirmed and characterized using electrical measurement, scanning electron microscopy (SEM), transmission electron microscopy (TEM), Raman spectroscopy, and X-ray diffraction (XRD). The resultant LIG electrodes on woods and leaves exhibited sheet resistances of 10 and 23.3 Ω /sq, respectively. Especially, the sheet resistance of LIG electrodes could be easily controlled via the laser writing parameters. SEM images revealed three-dimensional porous structures formed during the laser-induced carbonization and graphitization processes. These porous structures possess a high active surface area which enhances ion diffusion and is beneficial for sensing and energy storage applications. High-resolution TEM images showed graphene flakes with a typical lattice spacing of 0.355 nm. In order to demonstrate the potential of LIG on woods and leaves, we fabricated green graphene thermistors, micro-supercapacitors, and pseudo-capacitors. The as-produced devices exhibit comparable or better performance than other state-of-the-art graphene-based devices. Thus, the use of low-cost, abundant,

renewable, and biodegradable green materials not only allows the mass production and commercialization of green electronics but also develops a sustainable future.

NM02.10.17

Twisted Graphene Growth on Graphene/SiC Template Using Sequential Thermal Processes in Vacuo Without Air Exposure Yao Yao¹, Taiki Inoue¹, Yoshihiro Kobayashi¹, Makoto Takamura² and Yoshitaka Taniyasu²; ¹Osaka University, Japan; ²NTT Basic Research Laboratories, Japan

Twisted few-layer graphene (FLG) has recently attracted great attention due to the emergence of exotic electrical properties [1]. In a previous study, we reported that the FLG was synthesized by overlayer growth of graphene on a monolayer graphene template (MLGT) using a chemical vapor deposition (CVD) method. We found that moiré pattern appears in the lattice structure of the grown graphene two-dimensional (2D) island and the grown 2D graphene islands have random twisted angles. The coalescence process of graphene islands with various twist angles was indicated by temperature and pressure dependence of graphene island size [2]. In this study, based on understanding the growth mechanism of twisted FLG, we further developed the growth conditions of SiC to optimize the MLGT. By reducing the nucleation sites on the MLGT, large-area lateral growth of twisted graphene can be realized.

The MLGT used in previous studies was possibly contaminated with adsorbates due to air exposure during the step-by-step processes of MLGT formation and overlayer graphene growth in different vacuum chambers. In order to obtain a cleaner MLGT surface with fewer nucleation sites, the epitaxial growth process on SiC and the CVD process on MLGT/SiC were continuously performed in an argon atmosphere in an infrared heating furnace. Raman spectroscopy, atomic force microscopy (AFM), and scanning tunneling microscopy (STM) were used to evaluate the surface features and morphology of the samples.

We obtained high-quality MLGT on 6H-SiC (0001) surfaces at 1700 °C in an argon environment at ~1 bar. We verified the uniform single crystal surface of MLGT by STM and Raman spectroscopy under the epitaxial growth process. Graphene islands with twisted structures were sequentially synthesized in vacuo without air exposure with optimized CVD conditions. Using AFM to measure several representative locations on the surface, we observed twisted FLGs on the MLGT grown under the CVD process. By comparing with previous results [2], the twisted FLG under sequential thermal processes shows a significant reduction in nucleation sites and step-edge nucleation.

The coalescence growth process shows that twisted graphene islands nucleate very closely in the initial nucleation stage. Then, graphene islands gradually approach each other in lateral directions as they grow [2]. This mechanism is exactly the opposite of the thermodynamics-based energetics principle that the chemical potential of carbon atoms and their diffusion length on the graphene surface should be reduced. This suggests that the roughness of the surface directly affects the nucleation efficiency in our growth model. Therefore, in the study of sequential thermal processes in vacuo without air exposure, the clean MLGT surface with reduced initial nucleation sites can effectively provide enough space for lateral growth. It is expected to make further progress in the large-area lateral growth of twisted graphene.

[1] R. Negishi et al., Phys. Status Solidi B **257**, 1900437 (2020).

[2] Y. Yao et al., Nanotechnol. **33**, 155603 (2022).

NM02.10.18

Scanning Nonlinear Dielectric Microscopic Investigation of Mechanically Exfoliated WSe₂/SiO₂ and Suspended WSe₂ Koki Takano, Kohei Yamasue, Toshiaki Kato, Toshiaki Kato and Yasuo Cho; Tohoku University, Japan

Transition metal dichalcogenides (TMDs) have semiconductor properties that make them applicable to various devices even at a thickness of a few atomic layers or less. However, the electrical characteristics of ultra-thin TMD devices are often affected by the quality of the interface between the TMD layers and the substrate. TMD based field-effect transistors may exhibit hysteresis phenomena in their transfer characteristics due to high trap density at the interface. In this context, a suspended structure making TMD layers off the substrate may be effective for avoiding the influence from the interface. To demonstrate the effectiveness of the suspended structure, here we investigate the field-effect carrier doping on a suspended WSe₂ by scanning nonlinear dielectric microscopy (SNDM). SNDM is a near-field microwave based scanning probe microscopy method permitting the dominant carrier concentration imaging (dC/dV imaging) through the detection of the variation in the tip-sample capacitance [1]. The dC/dV image can reflect the polarity of the dominant carriers (p- or n-type) and their concentrations in a nanoscale. We measured three-layer WSe₂ suspended on 40 nm-height Au wires on a SiO₂/Si substrate. For comparison, we also observed 3-10 layer WSe₂ on the same substrate, which was prepared by a Scotch method. Ideally, WSe₂ shows an ambipolar characteristics on dc-bias voltages. To avoid the carrier injection from the tip to the sample during the measurement, we used a special tip insulating the tip apex from the sample. The insulating tip was prepared by forming a 10 nm-thick SiO₂ layer on a commercial conductive microcantilever. We obtained dC/dV images for different dc-bias voltages to investigate field-effect carrier doping. The WSe₂/SiO₂ sample showed a highly hysteretic carrier doping effect. In contrast, the suspended WSe₂ showed an ideal ambipolar behavior without significant hysteresis. We also investigate the spatial density distributions of interface trap by local deep level transient spectroscopy (local DLTS) based on SNDM. Local DLTS showed that interface trap density was high at the WSe₂/SiO₂ interface, while it was below the detectable level in the suspended WSe₂. These results demonstrate that the suspended structure is effective for exploiting the intrinsic characteristics of atomic-layer WSe₂ without the influence from the interface. This work is supported in part by a Grant-in-Aid for Scientific Research (20H02613, 16H06360) from JSPS, Japan.

References:

[1] Y. Cho, Scanning Nonlinear Dielectric Microscopy: Investigation of Ferroelectric, Dielectric, and Semiconductor Materials and Devices. Elsevier, ISBN 978-0-08-102803-2, 2020.

NM02.10.19

Measurements of the Intrinsic Bending Stiffness of Ultrathin 2D Materials Yingchun Jiang¹, Dingli Wang¹, Wenyang Qu¹, Sri Sridhar², Soumendu Bagchi³, Huck B. Chew² and Changhong Ke¹; ¹Binghamton University, The State University of New York, United States; ²University of Illinois at Urbana-Champaign, United States; ³Los Alamos National Laboratory, United States

Bending stiffness is one of the intrinsic fundamental mechanical properties of two-dimensional (2D) van der Waals materials (such as graphene, hexagonal boron nitride (h-BN), and molybdenum disulfide (MoS₂)) and is relevant to many of their applications. While their in-plane elastic properties have been investigated extensively, their bending rigidity remains not well-understood which is mainly due to the elastic anisotropy of these 2D crystals. Individual sheets in 2D crystals are stacked together by weak van der Waals interactions, and interlayer shear deformations result from the out-of-plane deformation. Repeatable experimental measurements of the bending stiffness of 2D materials remain a difficult task because of their small sizes. Remarkable scattering among the reported values in the literature poses challenges to consensus understanding and application of the 2D materials. Here we investigate the intrinsic bending stiffness of monolayer or few-layer graphene, h-BN, and MoS₂ by probing their self-folding deformation on flat substrates using atomic force microscopy (AFM) and by molecular dynamics simulations and density functional theory (DFT) calculations. The self-folding deformation of 2D materials is formed as a result of an energy balance between bending deformations and adhesion interactions. The bending stiffness is obtained from the measured folding deformation using a nonlinear continuum mechanics model. The results show that the bending stiffness of few-layer 2D materials follows a power function with thickness, and h-BN flakes of two to six layers are found to possess much higher bending rigidities than their carbon analogy,

graphene, which are in good agreement with atomistic simulations. Despite that MoS₂ reportedly possesses a lower tensile modulus than graphene and h-BN, its bending stiffness is found to be much higher than that of same-layer graphene and h-BN. The study reveals quantitatively how the interlayer shear interaction contributes to the out-of-plane deformability of multilayered 2D materials.

NM02.10.20

From Structures to Applications—Designing Diverse Architectures of 3D Porous Graphene Oxide and Reduced Graphene Oxide Through Pickering Emulsion Templating Yiwen Chen, Gabriele Capilli, Thomas Szkopek, Simon D. Tran and Marta Cerruti; McGill University, Canada

Graphene oxide (GO) is an oxidized graphene derivative containing hydrophilic oxygen functional groups and hydrophobic sp² graphene domains. GO sheets are stable in water; thus, they are ideal building blocks to assemble the 2D GO from aqueous suspensions into 3D architectures with large surface area and availability for functionalization. GO is an interesting starting material as one can further reduce GO and obtain reduced graphene oxide (rGO) to restore the properties of graphene, such as mechanical strength and electrical conductivity. The broad applications of graphene-based porous materials demand fabrication methods that are simple and yet can create complex architectures and compositions. However, it remains a challenge to assemble GO into porous materials mainly based on GO or rGO with controllable pore size, different interconnectivity, and tunable compositions. GO Pickering emulsion templating is a potential solution to fabricating well-defined graphene-based architectures. GO sheets can stabilize Pickering emulsions because of their amphiphilicity. By controlling the formation of emulsions, one can directly prepare porous GO templated by emulsion droplets. In this study, we used GO Pickering emulsion strategy to obtain porous GO and rGO materials with complex architectures, interconnected or closed pores, and tunable compositions tailored to different applications. We first introduced a dual-templating approach involving emulsion and ice as templates, to create GO, rGO, and composite scaffolds which have interconnected hierarchical structures with variable pore size and composition designed for bone tissue engineering. We developed stable GO emulsions in which GO flakes serve as both stabilizers and matrix builders. Upon freezing and drying these emulsions, large pores are templated by the oil droplets, and small pores by ice crystals formed in the water phase, whose sizes can be controlled by freezing temperatures. The complex architectures are tailored for bone tissue engineering, and we showed GO scaffolds are excellent substrates for mesenchymal stem cell penetration and growth. We subsequently introduced rGO/cobalt oxide porous electrodes for selective seawater electro-oxidation through GO emulsion templating. By adjusting the GO assembly on emulsion droplets, we generated closed pores templated by GO emulsions enclosing Co₃O₄ particles in the oil droplets. After reduction, the pore walls composed of rGO are permeable to water and gases while limiting the diffusion of dissolved ions like chloride to the cobalt oxide particles deposited on the internal walls of rGO pores. The closed rGO pores and the enclosure of cobalt oxide particles improved the electrode's selectivity for water oxidation application. In summary, our study based on GO Pickering emulsions allows us to control the architecture and composition of GO, rGO and composite porous materials. With appropriate design of the GO Pickering emulsions and the architecture of porous materials, one can enhance the performance of GO and rGO based porous materials for a variety of applications.

NM02.10.21

Electrical and Mechanical Properties of Homogeneous CNT/Cu Composite Wire Made from Copper Nanoparticles Supported CNT Yarn Yoku Inoue, Kosuke Tanaka, Takayuki Nakano and Yoshinobu Shimamura; Shizuoka University, Japan

Compositing highly conductive copper with lightweight, strong carbon nanotubes (CNTs) is expected to produce innovative materials that possess all of these characteristics. In this work, we fabricated a homogeneous composite of aligned CNTs and copper by nanoparticle-functionalized CNT dry spinning. Copper complexes were reacted with CNTs in the gas phase to support copper nanoparticles a few nm in diameter on CNT forests. Then the dry-spun CNT webs were fabricated into yarns, introducing Cu nanoparticles inside the yarn structure. The copper nanoparticles decorating the CNTs enabled high-yield copper electroplating inside the CNT yarn. By DC electroplating copper on the CNT yarn, homogeneous CNT/Cu composite wires were fabricated. The electrical conductivity of the composite wire at room temperature was found to be of a magnitude that followed the proportion of copper, and the current flowed through the copper portion. However, since the temperature coefficient of resistance was smaller than that of copper, the composite wire showed superior specific conductivity in the high-temperature region above 350 K compared to the conductivity of commercial copper. Since the resistance was less likely to increase on the high-temperature side, the current capacity was higher than that of copper. On the other hand, the tensile strength was significantly higher than that of copper in the tensile properties. The results followed the mixing rule of CNT bundles and copper, indicating a good homogeneous mixture of CNTs and copper.

NM02.10.22

Direct Laser Conversion of Transparent Polymers into Laser-Induced-Graphene for Realizing Ultra-Thin Optics Younggeun Lee, Dongwook Yang, Han Ku Nam, Truong-Son D. Le, Young-Ryeul Kim, Seung-Woo Kim and Young-Jin Kim; Korea Advanced Institute of Science and Technology, Korea (the Republic of)

Optical systems include refractive, reflective, and diffractive optical elements. Modern industries have mostly adopted refractive lenses out of these. Fundamentally, the optical lens has evolved from glasses for correcting the human eye's imaging capability, to miniaturized cameras inside the mobile phones for taking pictures or face-recognition-based unlocking, also to LIDAR sensors for image processing in autonomous vehicles. Although such refractive lens systems are widespread, they cannot be reduced in terms of the weight and size due to the required geometrical thickness of the refractive material and the volume for performance. Here, we suggest a direct-laser-patterning of diffractive optical elements by converting transparent polymers into laser-induced-graphene (LIG) to realize ultra-thin and light-weight optical system. Colorless polyimide (CPI) was used as the transparent polymer, which is one of the well-known materials for its strong chemical and abrasion resistance. A femtosecond pulse laser was utilized to pattern a diffractive lens to enable non-thermal laser patterning with higher patterning resolution and minimal material damage. CPI is transparent in the visible wavelength region, so it is difficult to process the CPI using a visible laser system (e.g., green laser at 532 nm). Therefore, we imposed an ultra-violet laser (at 343 nm center wavelength) in this fabrication process through the third harmonic generation of a 1030-nm ytterbium-doped fiber femtosecond laser. The transparent CPI film has relatively a high absorption coefficient in ultraviolet region, so it is possible to convert CPI to LIG efficiently even at low laser intensities. An ultra-thin Fresnel zone plate was patterned successfully with a 5- μ m linewidth. The resulting diffractive optics have focal lengths ranging from a few millimeters to hundreds of millimeters.

Two key applications of the realized ultra-thin diffractive optics will be introduced in the presentation; the first one is the micro-endoscopic optical coherence tomography and the other one is the micro-satellites optical communication. Firstly, a more compact micro-optical coherence tomography (OCT) was realized by replacing the existing graded-index (GRIN) lens to an ultra-thin diffractive LIG lens with the astigmatism correction capability. Secondly, we applied ultra-thin LIG optics to satellite applications where weight and volume reduction is crucial. Solar sensors for satellite position control were realized with LIG lens with a 10- μ m thickness and 10-g weight while providing a higher attitude control resolution.

NM02.10.24

Graphene-Based Nano-Electro-Mechanical Resonator for Radio Application Yugyeong Je¹, Dong Hoon Shin², Hyunjeong Jeong¹ and Sang Wook Lee¹; ¹Ewha Womans University, Korea (the Republic of); ²Delft University of Technology, Netherlands

In this work, the electro-mechanical properties and RF (Radio Frequency) applications of graphene nano-electro-mechanical resonators have been studied.

The graphene resonators were fabricated in suspended structures on the PMMA (poly(methyl methacrylate)) trench. The resonance frequency of the graphene resonators was measured by an optical measurement method using a laser interferometer. The resonance frequency of the graphene resonators was measured in the megahertz range, which could be tuned by electrostatic actuation. For radio applications, the audio signal was mixed with the input AC frequency by Frequency Modulation (FM). The resonance frequency shift by FM changed the amplitude of mechanical resonance of the graphene resonators. The graphene nano-electro-mechanical radio reproduced the input audio signal audible to the human ear by amplitude demodulation.

NM02.10.25

Stretchable Strain Sensors Fabricated Using a Highly Crystalline Reduced Graphene Oxide/Carbon Nanotube Composite Yuna Himura¹, Chikako Ishiguro¹, Zizhao Xu¹, Taiki Inoue¹, Yuta Nishina² and Yoshihiro Kobayashi¹; ¹Osaka University, Japan; ²Okayama University, Japan

Graphene and carbon nanotubes (CNTs) have excellent electrical and mechanical properties as well as biocompatibility, making them attractive materials for electronic components of wearable devices. Freeze-dried graphene forms a highly porous three-dimensional structure which retains high conductivity and elasticity due to a 3D network, making it an effective material for strain sensors [1]. Superior properties of graphene for the sensors have been reported to improve by composite formation with the CNTs [2]. In previous studies, however, graphene has been produced in a large scale from graphene oxide (GO) by chemical process or thermal treatment at relatively low temperatures below 1000 °C. Consequently, crystalline quality of reduced graphene oxide (rGO) remains low due to insufficient reduction, and it should be improved for enhancing the sensor performance. By using our unique thermal process under ethanol at 1500°C to produce the high-quality rGO [3], this study developed a stretchable strain sensor using highly crystalline and porous 3D graphene [4]. Sensor performance was improved by introducing CNTs in our devices, after optimizing the sensor structure. Water dispersions of GO [5] and CNTs synthesized by the super-growth method were mixed and freeze-dried at two different freezing rates to form 3D sponge structures. Then, the sample was thermally treated at 1500 °C in an ethanol atmosphere to reduce and repair the GO. Scanning electron microscopy (SEM) was used to observe the sample structure, and Raman spectroscopy was used to evaluate the crystallinity of graphene and CNTs. To fabricate the strain sensor, the sponge sample was connected to copper wires and sandwiched between polydimethylsiloxane (PDMS) films, followed by curing at 80 °C. The sensor performance was evaluated based on the gauge factor (GF) value, which is calculated as the ratio of resistance change to strain change. SEM observation revealed that the porosities of the sponge and the size of aggregated rGO flakes were changed by the freezing rate. The composite sponge of rGO and CNTs formed by rapid freezing resulted in increased sensor durability. The initial resistance of the sensor is on the order of several ohms because of the low defect density of rGO and CNTs. The addition of CNTs improved the linearity of the sensor response, but the GF value decreased. By optimizing the sensor thickness and the connection direction of the copper wires, the sensor durability and sensitivity were significantly improved. The optimized sensor showed a GF value of 15 for over 10 trials at 150 % strain. The stretchable strain sensor demonstrated the constant resistance change in response to finger bending and stretching. High-porosity and high-quality composites of rGO and CNTs are promising as stretchable conductive materials for strain sensors with potential applications in wearable devices.

[1] S. Li et al., ACS Appl. Electronic Mater. **2**(2020)2282.

[2] X. Xie et al., Compos. Part A Appl. Sci. Manuf. **135**(2020)105932.

[3] T. Ishida et al., Appl. Phys. Express **9**(2016)025103

[4] Z. Xu et al., Carbon **185**(2021)368.

[5] N. Morimoto et al., Sci. Rep. **6**(2016)21715.

NM02.10.26

Hydrogen Storage Material of Fe-Doped Magnesium Supported by Graphene Yuto Hosono and Mitsuo Notomi; Meiji University, Japan

Magnesium (Mg) is an abundant resource of all elements and one of the most prospective hydrogen storage materials because of its large hydrogen storage capacity (7.6 wt.%). Magnesium hydride (MgH₂) has a high dehydrogenation temperature (approximate 450 °C), which restricts broad applications and should be reduced for a wide range of applications. There is one of the solutions that we compound Fe and/or graphene into Mg. Fe, which has electrons in the *d* orbital and plays the role of a catalyst for hydro- and dehydrogenation, can promote the dissociation of one hydrogen molecule adsorbed on the surface to two hydrogen atoms and the desorption of absorbed hydrogen from the interface with MgH₂ (called overflow effect and hydrogen-pump effect respectively). Graphene, which generally has a higher specific surface area and electron mobility, is expected not only to be a scaffold but also to facilitate hydrogen absorption and desorption reactions as electron source. Since graphene oxide and defects of graphene have significantly lower electron mobility, one may have to prepare the perfect structure of graphene with fewer defects. Although there are some studies to discuss the effect of the addition of graphene by computer simulation, there are few studies to evaluate the effect of the damage degree of graphene structure on its hydrogen desorption properties with some experiments and to obtain any quantitative results.

Firstly, we prepare less-defected graphene by liquid-phase exfoliation (LPE) method in the procedure as follows. We mix up graphite with salt by ball milling and dissolve as-milled graphite in an organic solvent. The graphite in the solvent separates each layer, i.e., graphene, by sonication and centrifugation in the solution for 5 and 30 minutes respectively, and then we dry the only supernatant of the solution for a little powder. Secondly, we compound Mg, Fe, and graphene by high-energy ball milling under an Ar atmosphere for 5-25 hours and then complete the samples as nano-sized powder. In this preparation of the compounds, we consider some conditions to achieve the most effective dispersion of Fe and graphene around Mg, which are the appropriate state of graphene before adding into Mg and the order of adding each material.

The degree of perfect structure in graphene may be estimated quantitatively from the intensity ratio (I_D/I_G) of the disorder and defect peak (D peak), which is derived from *sp*³ defect, vacancy-like defects and/or edge defects, to the carbon-*sp*² peak (G peak), which is derived from planar configuration bonding, with Raman spectroscopy. We use the graphene with under $I_D/I_G = 0.4$ (graphene oxide: around 1.0, reduced graphene oxide: 0.8 ~ 1.5) in this experiment. The particle size and surface morphology in the samples may be observed with scanning electron microscopy (SEM). The layer spacing and crystallinity of graphene, as well as crystalline phases such as hydrides before and after hydrogenation, may be determined by X-ray diffraction (XRD). The hydrogen storage capacity may be obtained by pressure-composition-temperature (PCT) measurement (based on JIS H 7201) using the Sievert apparatus designed by ourselves under lower hydrogen pressure (< 1.0 MPa). The dehydrogenation temperature may be measured with differential scanning calorimetry (DSC). From the results, we may find making conditions of the most appropriate compound with the processing.

NM02.10.27

Micro-Mechanical Characterization on Amorphous Carbon and Its Nanoporous Structures Zhongyuan Li¹, Ayush Bhardwaj², James J. Watkins² and Seok-Woo Lee¹; ¹University of Connecticut, United States; ²University of Massachusetts Amherst, United States

Carbon-related nanostructured materials have a strong potential as a mechanical reinforcement material due to their strong ionic/covalent C-C bond, which restricts the motion of dislocation, the carrier of plasticity. However, their brittleness and relatively high density limits their structural application. In this study, therefore, we have developed amorphous carbon with almost no short-range ordering and its nanoporous structures, where the ligand thickness is only around 10nm, by rapid thermal annealing of Brush block copolymer and Phenol formaldehyde. To evaluate the mechanical response, we perform the nanoindentation tests and in-situ compression tests on a micropillar, which was fabricated by utilizing focused-ion-beam milling. Both fully dense and nanoporous structures exhibit a large compressive fracture strain up to ~40% with a significantly high work hardening rate. Raman spectroscopy before and

after compression test revealed that this unusual plasticity results from dynamic change in distribution of sp² and sp³ bonds. During plastic deformation, the number of sp² bonds decreases but the number of sp³ bonds increases. Carbon atoms, which have sp² bonds, seem to be reconfigured to form sp³ bond, which is thermodynamically preferable under compression. In addition, we found that both compressive fracture strength and compressive maximum strength are nearly independent of porosity unlike the hardness that scales with the porosity. We think that the porosity-independent strength could be related to the size-affected strength of nanoscale ligand. Larger pores reduce the density, but the size reduction of ligand enhances its strength. These two contributions compensate each other, leading to the negligible change in strength of the entire nanoporous structure. Interestingly, all structures, both fully dense and nanoporous structures, in our study demonstrate the modulus of resilience much higher than most engineering materials due to their low Young's modulus, implying that amorphous carbon materials have an exceptional capability to absorb and release the mechanical energy per a given volume. However, yield strength of our fully dense amorphous carbon was found to be slightly lower than that of amorphous carbon published in other works. Complete diffuse diffraction pattern indicates that our amorphous carbon possesses the almost complete random arrangement of carbon. This liquid-like structure could be beneficial to lower mass density but does not seem to be desirable to obtain high strength. It would be necessary to control the distribution of a short-range ordering to obtain the improved yield strength without sacrificing the mass density and the ductility much by optimizing the synthesis condition or performing the post thermal-mechanical treatment. All these efforts will pave a new pathway to create light, strong, and tough carbon nanostructures for their future structural applications.

NM02.10.28

Deposition of Multilayer Graphene Using Pulsed Laser Deposition Yuxuan Wang, Neil Alford and Peter K. Petrov; Imperial College London, United Kingdom

Since being discovered in 2004, graphene keeps on gaining more and more attention from various research areas. While the wide application of single-layer graphene is still challenging due to the intrinsic defect of traditional mechanical exfoliation and CVD method, the multilayer (2-10 layers of graphene) graphene (MLG) thin films are becoming more and more popular in applications that require a replacement of traditional metals. Multilayer graphene attains a better trade-off between expense and physical property. It is not to mention the unconventional superconductivity in the magic-angle bilayer graphene that was discovered recently¹. Thus, it is important to develop a quick and simple method to grow multilayer graphene on the desired substrate.

In this study, MLG thin films are grown without catalyst on Si/SiO₂, strontium titanate (STO) and boron nitrate substrates by pulsed laser deposition (PLD). The substrate is heated to 800°C at the rate of 50°C/min in the vacuum level of 3 × 10⁻⁵ Torr. Then 500 pulses of a 248nm excimer laser with a frequency of 10Hz are shot to a graphite target. Once the deposition is finished, the substrate is cooled at various rates to 300°C before a further natural cooling to room temperature. To explore the effect of the annealing process on the quality of graphene, the samples were subject to a 5min annealing at 800°C before the cooling process. Finally, to examine the influence of deposition mode on graphene, the 500 laser pulses were divided into 5 groups of 100 pulses, separated with a 10s time interval in between.

The Effect of cooling rate and laser energy on the property of MLG is studied using the samples grown on Si/SiO₂ substrates, while the influence of the annealing process and deposition mode on the MLG is studied on the samples grown on STO substrates. For characterisation, a Raman spectrometer, atomic force microscope and 4x probe electrical measurement are used.

The measured thickness of the MLG grown on Si/SiO₂ substrate was about 2nm indicating that the number of graphene layers is approximately 6. The mean roughness of all the graphene samples measured using AFM was in the range of 100-300pm.

We found that the MLG on all the three substrates show a high D peak and broadened 2D in the Raman spectrum. This can be explained as wrinkled MLG with defects and disorder². According to the Raman result, cooling rate, annealing process and different deposition modes have a marginal effect on the MLG quality.

The electrical measurements have further confirmed this observation. The resistance of graphene on Si/SiO₂ is at the same level when 30-90°C/min cooling rates were used. High resistance of the graphene was measured when cooled at a rate of 10°C/min. However, the measurement uncertainty associated with this experiment was much higher. The post-deposition treatment (annealing process and the altered deposition mode) had a negative effect on the resistance of the graphene grown on the STO substrate.

The graphene resistance improvement occurs only when the laser energy was increased from 435mJ to 735mJ. Then the corresponding resistance of the graphene on the Si/SiO₂ substrate was reduced by three folds. This result was attributed to the improved compactness of MLG.

Thus, we propose the PLD technique as a quick and simple method to produce MLG thin films with electrical conductivity similar to the one of the commercial CVD graphene.

Reference

1. Cao, Yuan, et al. "Unconventional superconductivity in magic-angle graphene superlattices." *Nature* 556.7699 (2018): 43-50.
2. Kaniyoor, Adarsh, and Sundara Ramaprabhu. "A Raman spectroscopic investigation of graphite oxide derived graphene." *AIP Advances* 2.3 (2012): 032183.

NM02.10.29

Nanoarchitected Schwarzites and Tubulanes with Ultrahigh Energy Absorption and Resilience Peter Serles¹, Alianna Maguire², Jun Lou², Pulickel Ajayan² and Tobin Filleter¹; ¹University of Toronto, Canada; ²Rice University, United States

Nanoarchitected materials represent the frontier of low-density metamaterials that can achieve specific strengths and specific stiffnesses beyond the theoretical limit for solid materials. These nanoarchitected materials combine three synergistic effects – nanoscale size effects of individual elements, high performance constituent materials, and optimized shape factors – which are enabled through nanoscale additive manufacturing by two photon polymerization (2PP).¹ Of particular interest, post-2PP pyrolysis enables the printed 3D design to be converted to a mechanically high-performance carbon which has demonstrated rubber-like behaviour due to its nanoscale size and flaw tolerance.^{2,3}

Leveraging the high mechanical performance of nanoarchitected carbon produced by 2PP and pyrolysis, we form Schwarzite and Tubulane structures which are designed from p-type Schwarz minimal surfaces and aligned cross-linked carbon nanotube architectures, respectively. These structures are optimized to minimize stress concentrations and therefore demonstrate specific strengths beyond the theoretical limit when subject to compression testing with failure strengths of several GPa at =50-70%. It is demonstrated that the strength and stiffness increase by nearly an order of magnitude as the wall-thickness of the architecture is reduced from several micron to several hundred nanometers, indicating the role of nanoarchitecture and size effects.

Due to the flaw intolerance of the constituent pyrolyzed carbon, the nanoarchitectures exhibit ultra-high failure strain often exceeding $\epsilon=40\%$ when the wall-thickness is on the order of several hundred nanometers. This equates to an enormous absorption of mechanical energy and the structures demonstrate nearly complete recoverability when subject to cyclic loading up to $\sigma_r=95\%$. The modulus of resilience (U_R) represents the elastic energy absorption, and it is demonstrated that the nanoarchitected Schwarzite and Tubulane structures exhibit U_R more than an order of magnitude greater than Kevlar and other defence materials.

We thus employ the nanoarchitectures towards absorption of dynamic energy including micro-ballistic impact testing at sub- and super-sonic velocities and atomic force microscope vibration damping from kHz to MHz frequency ranges. Both of these unique dynamic loading conditions demonstrate clear applications where the high dynamic performance of these nanoarchitected materials is vastly superior to conventional materials such as Kevlar and rubber. Nanoscale additive manufacturing of these optimized Schwarzschild and Tubulane geometries thus demonstrates that the successes achieved in nanoarchitected materials can be further extended towards dynamic loading conditions with wide-reaching implications from vibration control and damping in device design, to resilient materials for aerospace, or lightweight ballistic impact materials for defence.

1. Zhang, X., Wang, Y., Ding, B. & Li, X. Design, Fabrication, and Mechanics of 3D Micro-/Nanolattices. *Small* vol. 16 (2020).
2. Zhang, X. *et al.* Theoretical strength and rubber-like behaviour in micro-sized pyrolytic carbon. *Nature Nanotechnology* **14**, 762–769 (2019).
3. Serles, P. *et al.* Mechanically Robust Pyrolyzed Carbon Produced by Two-Photon Polymerization. *Carbon* (2022).

NM02.10.30

Copper Single-Atom Catalyst on N-Doped Carbon Nanoparticle for Methane Partial Oxidation Hyesung Lee and Sang-Yup Lee; Yonsei University, Korea (the Republic of)

Methane is an abundant natural resource whose reserve is estimated as 187 trillion m³. Global methane gas production increases rapidly every year, however, methods of long-distance transportation of the liquefied methane and conversion into valuable chemical products are lagged behind because of the high binding energy of a C-H bond (about 100 kcal/mol). Conversion of methane to methanol is one strategy to overcome transportation and economic issues. Currently, methane is generally converted to methanol via a two-step process; first, methane is converted to syngas at a high-temperature and high-pressure condition and then transformed further into methanol. To make this energy-consuming process simple, various catalysts have been explored that convert methane into methanol in a single step. In nature, the enzyme of methane monooxygenase (MMO) found in methanotrophs converts methane directly into methanol during the metabolic process. Recent progress in structural biology revealed that the active site of MMO, specifically particulate MMO (pMMO), has a single-atom copper active center coordinated with three histidine imidazoles and a carboxylate. Inspired by this enzyme structure, a single-atom copper catalyst is developed on the N-doped carbon support and is examined for its catalytic activity. The catalyst is prepared by pyrolysis of the copper-doped zeolitic imidazolate framework-8 (Cu-doped ZIF-8). For the synthesis of the catalyst, single-atom copper sites are constructed at the nodes of ZIF-8 first by doping and then pyrolyzed to convert the imidazole linkers into N-doped carbon. The N-doped carbon stabilizes single-atom copper by coordinating with the nitrogen species and provides a large specific surface area and high physical/chemical stability in acid/base solutions. Due to the stability of the N-doped carbon, oxidative degradation of the catalyst support is reduced remarkably. The coordination structure and oxidation state of the copper active center are extensively scrutinized to have a CuN₄ structure, which is similar to that of pMMO. Catalytic conversion of methane to methanol is promoted with the increase of copper content; however, excessive copper doping generates metallic copper clusters that repress the methane partial oxidation. Besides the copper content, other reaction parameters such as reaction temperature, the concentration of oxidants, and carbonization conditions are influential for the catalytic activity. Too high temperature and oxidant concentrations result in the overoxidation of methane to produce CO₂ and formic acids. This study offers a way to synthesize a catalyst for methane partial oxidation producing liquefied products and contributes to accounting for the reaction pathway of pMMO.

SESSION NM02.11: Electrical Related Study II

Session Chairs: Tanja Kallio, Shunsuke Sakurai, Yoke Khin Yap and Ming Zheng
Thursday Morning, December 1, 2022
Hynes, Level 2, Room 208

8:30 AM *NM02.11.01

Tunable Nonreciprocal Electrical Transport in 2D Tellurium with Different Chirality Peide P. Ye; Purdue University, United States

Tellurium (Te) is an elemental semiconductor with a simple chiral crystal structure. Te is fundamentally a 1D van der Waals material. Te in a two-dimensional (2D) form synthesized by solution-based method shows excellent electrical, optical, and thermal properties. In this work, the chirality of hydrothermally grown 2D Te is identified and analyzed by hot sulfuric acid etching and multi-angle high-resolution transmission electron microscopy. The gate-tunable nonreciprocal electrical transport is observed in 2D Te with different chirality, providing a possibility for the realization of controllable polarized spins for spintronic applications. The opposite band evolution of different-handedness 2D Te under magnetic field reveals the fundamental relationship between the spin-orbit coupling and the symmetry of the crystal structure. Our work shows that 2D Te is an ideal material system for studying the chirality-related electrical transport properties and crystal growth mechanism.

9:00 AM NM02.11.02

Molecular Doping of Bottom-Gate/Top-Contact Nanotube Network Field-Effect Transistors for Flexible Electronics Jan M. Gotthardt and Jana Zaumseil; Universität Heidelberg, Germany

Due to their electrical and mechanical properties, networks of semiconducting single-walled carbon nanotubes (SWCNTs) are of interest as active layers in low-power, low-voltage, high-frequency flexible electronics. However, their intrinsically ambipolar charge transport leads to high power dissipation in integrated circuits.

Here, we report the fabrication of bottom-gate/top-contact field-effect transistors (FETs) with SWCNT networks as semiconducting layer and an ultrathin hybrid dielectric consisting of 5 nm aluminium oxide and a self-assembled monolayer (SAM) of an alkyl phosphonic acid. These FETs show ambipolar behaviour and can be operated at low voltages (less than 2 V). Charge carrier mobilities and contact resistance can be optimized by the choice of SAM^[1] and SWCNTs. The influence of contact and gate electrode overlap on the parasitic capacitance and the contact resistance is investigated. With the use of molecular organic dopants, *e.g.* ttmgb^[2,3] or F4TCNQ, purely n- or p-type channel FETs can be realized. These thin film FETs can be fabricated on rigid glass substrates and also on thin polyimide (PI) films with no change in the device performance upon removing the PI film from the support substrate. With their bendability and purely n- or p-type performance these transistors are suitable for the application in integrated complementary circuits for flexible electronics.

References

- [1] Schiefl et al., *Adv. Mater. Interfaces* **2016**, *3*, 1600215.
- [2] Schneider et al., *ACS Nano* **2018**, *12*, 5895.
- [3] Gotthardt et al., *ACS Appl. Electron. Mater.* **2021**, *3*, 804.

9:15 AM NM02.11.03

Freestanding Electrode for Wearable Supercapacitor Enabled by Sole Carbon Nanotube Liquid Crystalline Fiber Hayoung Yu^{1,2}, Dong-Myeong Lee¹, Nam Dong Kim¹, Seung Min Kim¹ and Hyeon Su Jeong¹; ¹Korea Institute of Science and Technology, Korea (the Republic of); ²Gwangju Institute of Science and Technology, Korea (the Republic of)

With the development of wearable devices and the miniaturization of various home appliances, fiber-type solid-state supercapacitors (FSSCs) are attracting a lot of attention as a wearable storage device. As an electrode material in FSSCs, CNT fibers (CNTF) based on liquid crystal (LC) spinning have been considered as a promising candidate due to the remarkable properties of electrical conductivity ($\sim 10 \text{ MS m}^{-1}$), excellent mechanical strength ($\sim 4 \text{ GPa}$), light weight and good flexibility. However, ironically, the highly densified structure of LC CNTF with clean sp^2 carbon surface acts as disadvantages to directly apply as an electrode for FSSCs. Efforts have been made to increase the electrochemical activity of CNTF mainly by enlarging the specific surface area of CNTF and/or complexing the fibers with pseudocapacitive materials (e.g. metal oxide and conducting polymers). Unfortunately, these post treatments not only require additional complicated process, but also deteriorate intrinsic properties of CNTF. Thus, it is desirable to enhance the electrochemical activity of CNTF without additional material or post-process.

In this study, we fabricate LC CNTF from surface functionalized CNTs, followed by investigating its electrochemical activity without any additional materials for direct use as a freestanding electrode for wearable supercapacitors. Oxygen-containing functional groups ($-\text{COOH}$ and $-\text{OH}$) are introduced onto the surface of CNTs by well-known acid treatment and lyotropic LC phase thereof is developed for use as a dope for wet-spinning. The structure, properties of CNTFs and its electrochemical activity are systemically investigated as a function of the degree of fictionalization. Interestingly, functionalized CNTF shows better mechanical property of 0.67 N tex^{-1} and electrical property of 3 MS m^{-1} than those of pristine CNTF (0.25 N tex^{-1} , 1 MS m^{-1}). Moreover, the functionalized CNTF exhibits a specific capacitance of 140 F g^{-1} at 0.5 A g^{-1} while the pristine CNTF shows 21 F g^{-1} at 0.5 A g^{-1} , demonstrating that it is possible to enhance electrochemical activity without additional material or post-process. A solid state FSSCs prepared with symmetric structure shows reasonable energy density of 9.2 Wh kg^{-1} at a power density of 700 W kg^{-1} . The study on the electrochemical activity of CNTF as a function of functionalization provide a new insight for the development of fiber-shaped energy storage device.

9:30 AM NM02.11.04

Large Thermoelectric Power Factor in Flexible and Robust Few-Walled Carbon Nanotube Yarn by Ultra-High Temperature Annealing Yasuhiko Hayashi¹, Jun Kametaka¹, Shinya Nakahori¹, Takeshi Nishikawa¹, Aung Ko Ko Kyaw² and Hiroo Suzuki¹; ¹Okayama University, Japan; ²Southern University of Science and Technology, China

Carbon nanotube (CNT) yarn is one of the potential thermoelectric (TE) materials owing to its narrow band-gap energy, high charge carrier mobility, and excellent mechanical property, which is conducive for flexible and wearable devices. One of the critical challenges is the tuning of electrical and thermal transport since they interrelate against the high performance of TE properties. Although the thermal and electrical properties of CNT yarns are likely to enhance their properties by the extremely high-temperature annealing using Joule heating process, the phenomena underlying the improvement of properties have not clarified yet.

Here, we propose a way to improve the power factor of CNT yarns fabricated from few-walled carbon nanotubes (FWCNTs) by two-step method; Joule-annealing in the vacuum followed by doping with p-type dopants, 2,3,5,6-tetrafluoro-7,7,8,8-tetracyanoquinodimethane (F4TCNQ). FWCNT yarns ($15 - 20 \mu\text{m}$) were fabricated from the CNT array using a dry spinning method with a rotation speed of 500 rpm and a drawing speed of 300 mm/min. Joule-annealing was accomplished by passing a current of $\sim 73 \text{ mA}$ and voltage of $\sim 56 \text{ V}$ under vacuum condition at around $1-2 \times 10^{-4} \text{ Pa}$ for 1 min. Doping was performed with various concentrations of F4TCNQ such 1, 2.5, 5 and 10 mg/ml, respectively. Then CNT yarns were dipped into the F4TCNQ solution for 6 hrs. Seebeck Coefficient Measurement System was used to measure the thermoelectric properties such as Seebeck coefficient, electrical conductivity and power factor, which has a special sample-attachment to measure the thin film or wire specimen.

Results show that doping after Joule-annealing can lead to a higher thermoelectric power factor of CNT yarn. Specifically, FWCNT yarn doped with 2.5 mg/ml F4TCNQ exhibited a power factor of $2250 \mu\text{W m}^{-1} \text{ K}^{-2}$, which is one of the highest values among the p-typed doped CNT yarn. Moreover, pretreatment by Joule-annealing is confirmed to be an effective way to improve Seebeck coefficient due to the transformation of (semi) metallic to semiconductor behavior. The significant improvement of Seebeck coefficient and electrical conductivity after Joule-annealing followed by p-type doping can be qualitatively explained by applying the power-law model on relaxation time approximation to the single band. Fermi energy of the pristine CNT yarn is -0.0037 eV , which is very near to the top of the valence band. After Joule-annealing, Fermi level rises to 0.071 eV and it behaves like an intrinsic semiconductor, dominating phonon scattering. Therefore, Seebeck coefficient improves significantly after Joule-annealing. After doping, the location of Fermi level moves down to -0.053 eV .

Based on our results, the combination of Joule-annealing and doping can pave a way to enhance the thermoelectric properties of FWCNT yarn.

9:45 AM BREAK

10:15 AM *NM02.11.05

Spin Splitting of Dopant Edge State in Magnetic Zigzag Graphene Nanoribbons Felix R. Fischer^{1,2,3}; ¹Univ of California-Berkeley, United States; ²E O Lawrence Berkeley National Laboratory, United States; ³Kavli Energy NanoScience Institute, United States

Since their original inception the class of ZGNRs, graphene nanoribbons lined by hydrogen terminated zigzag edges, have been associated with unusual magnetic edge states. Computational models predict that the zig-zag edges in ZGNRs host spin-polarized edge-states that are coupled ferromagnetically along one edge and antiferromagnetically coupled across the width of the ribbon. Despite recent advances in the bottom-up synthesis of GNRs the unique magnetic edge-structure of ZGNRs has long been obscured from direct observation by an unusually strong hybridization of the zigzag edges with the surface states of the underlying support. To access the elusive edge magnetism in ZGNRs we developed a novel and broadly applicable technology that effectively decouples the highly reactive spin-polarized edge states of ZGNRs from the underlying metallic growth substrate. Introduction of a superlattice of substitutional nitrogen-atom dopants along the edges of a ribbon not only facilitates the electronic decoupling but introduces a highly sensitive local magnetic sensor. Differential conductance scanning tunneling spectroscopy shows a "Zeeman-like" spin splitting of the two electrons in the nitrogen lone-pair by the spin-polarized frontier bands of ZGNRs revealing a large exchange field corresponding to $B_{\text{eff}} \sim 1000 \text{ T}$ lining the edges of the ribbon.

10:45 AM NM02.11.06

In-Liquid Dual-Harmonic KPFM for the Study of Electronic Properties of Single Layer Graphene Marta D. Fernández¹, Elena del Corro¹, Liam Collins², Martí Checa², Xavier Illa³, Antonio P. Pérez¹ and Jose A. Garrido^{1,4}; ¹Catalan Institute of Nanoscience and Nanotechnology, Spain; ²Oak Ridge National Laboratory, United States; ³Centro de Investigación Biomédica en Red en Bioingeniería, Biomateriales y Nanomedicina (CIBER-BBN), Spain; ⁴ICREA, Spain

Graphene, a biocompatible 2D material with unique properties – electrical, optical, mechanical and chemical- is widely investigated as a key part of electronic devices aimed to perform in the biomedical field. More specifically, electrodes and transistors are fabricated using graphene as the active

material for sensing and brain activity recording, among other applications^{1,2}.

Dual-Harmonic Kelvin probe force microscopy (DH-KPFM) is used in this work to measure the work function of chemically-grown single layer graphene, deposited on different substrates, in contact with an aqueous electrolyte to evaluate its dependence on the electronic nature of the substrate, the pH and the ion strength of the electrolyte. In-liquid DH-KPFM is also used in this project to obtain information about the surface potential distribution along a device (graphene transistor) in a liquid environment, and the measurement of the contact resistance values in that media. Contact resistance in graphene transistors affects its performance and is caused, among other parameters, by the work function differences between graphene and the contacting metals³. Knowing the values of the contact resistance of a standard fabricated device will enable the optimization of the fabrication procedure. To the best of our knowledge, this parameter has never been measured using in-liquid DH-KPFM. Hence, the novelty of this work and its contribution to the field is remarkable. Other techniques such as Raman spectroscopy, electrochemical impedance spectroscopy, X-ray and ultraviolet photoelectron spectroscopy complement the experimental work, providing information about graphene's doping level and its dependence on the ionic environment and the substrate; furthermore, we will also discuss the effect of chemical residues present on the graphene surface.

References

Masvidal-Codina, E., Illa, X., Dasilva, M., et al (2019) High-resolution mapping of infraslow cortical brain activity enabled by graphene microtransistors, *Nature Mater.*

Garcia-Cortadella, R., Schwesig, G., Jeschke, C., et al (2021) Graphene active sensor arrays for long-term and wireless mapping of wide frequency band epicortical brain activity, *Nat Commun.*

F. Giubileo, A. Di Bartolomeo (2017) The role of contact resistance in graphene field-effect devices, *Prog. Surf. Sci.*

11:00 AM NM02.11.07

Advanced Fuel Cell Catalyst Based on Graphene Marie Heitzmann^{1,2}, Gerard Gebel^{1,2} and Laure Guetaz^{1,2}, ¹Commissariat à l'énergie atomique et aux énergies alternatives, France; ²Université Grenoble Alpes, France

Carbon blacks supported Pt, currently widely used as electrocatalysts in Polymer Electrolyte Membrane Fuel Cells (PEMFC) are thermochemically unstable in PEMFC operating conditions. This is especially true at the cathode side where, on top of relatively elevated temperature (80°C) and acidic conditions, both the potential and the relative humidity may be high. The resulting carbon oxidation is partially responsible for the PEMFC performance decrease observed over time. Hence, long term durability still needs to be improved in order to consider PEMFC as credible alternatives to conventional power sources for automotive, stationary or portable applications.

Much effort have been directed to identify and synthesize alternative carbon materials as catalyst supports for PEMFCs. One strategy to decrease carbon support corrosion is to use carbon with high extent of graphitization, which is supposed to decrease defect sites on the carbon structure, where carbon oxidation starts [1], [2]. However high graphitic content of carbon can be a brake for particle nucleation and dispersion. Among the different forms of carbon, graphene, a monolayer of graphite, has attracted increasing attention because of its unique two-dimensional (2D) single sheet of sp² carbon in a hexagonal arrangement. Graphene possesses unique properties, such as high charge-carrier mobility (up to 10⁵ cm² V⁻¹ s⁻¹), super conductivity, ambipolar electric field effect, high mechanical strength (130 GPa), quantum Hall effects at room temperature, and high surface area (2,600 m² g⁻¹). These properties make graphene ideal for a wide potential applications such as in nanoelectronics, electrode support for catalysts in electrochemical energy systems, chemical and biological sensors, composite materials and biotechnology.

Although graphene exhibits an attractive range of properties as catalyst supports for fuel cells, it suffers from a serious issue. Integration of such catalyst in catalyst layer (CL) is complex due to the high cohesive van der Waals attractions between graphene sheets, named also pi-stacking of graphene layers, leading to serious blocking of the active surface area. To overcome this phenomena, one solution consists to add spacers or additives in graphene sheets such as carbon black, carbon nanotube or urea to be intercalated into Pt/graphene [3].

In this work, platinum catalysts were synthesized on Graphene support, nanocharacterised, processed in ink and incorporated in fuel cell. Several techniques of MEA fabrication were used: CCB (catalyst coated backing), CCM (catalyst coated membrane) or CCM by decal (transfer on inert substrate). We investigated these new active layers at the cathode side in term of electrocatalytic performance and compared the electrochemical properties of these hybrid materials with a commercial Pt/C catalyst using carbon blacks as carbon support. Moreover, the use of additive was also studied to enhance performance by aerate active layer and avoid pi-stacking of graphene layer.

The goal of this work is to demonstrate that MEA fabrication has an huge impact on performance but also on durability, and the use of graphene based carbon supports can be promising in effectively reducing the carbon corrosion and then increase lifetime of the cell if CL are assembled correctly. Accelerated stress test has been done in 25 cm² fuel cell setup with two types of test : AST for carbon support from DOE and fuel cell Dynamic Load Cycle, FC-DLC cycles.

The GrapheneCore3 European program funds this work.

11:15 AM NM02.11.08

II-Orbital Mediated Charge Transfer Channels in Functionalized Graphene Andrea Casotto^{1,2}, Giovanni Drera¹, Daniele Perilli³, Sonia Freddi^{1,4}, Stefania Pagliara¹, Michele Zanotti¹, Luca Schio⁵, Alberto Verdini⁵, Luca Floreano⁵, Cristiana Di Valentin³ and Luigi Sangaletti¹; ¹Università Cattolica del Sacro Cuore, Italy; ²University of Notre Dame, United States; ³Università degli Studi di Milano-Bicocca, Italy; ⁴KU Leuven, Belgium; ⁵CNR-IOM, Lab. TASC, Italy

Functionalization makes graphene (Gr)-based materials extremely appealing for several applications, such as photonics, optoelectronics, and sensing, [1,2] provided that clear information on the charge transfer mechanisms at the interface can be obtained. Indeed, in the case of layered materials or two-dimensional semiconductors, the operation of electronic devices cannot be separated from the control of the generation and flow of charge carriers at the surface or through the junction that is present at the interface between two layers.

Organic molecules are often chosen to functionalize Gr since they can form covalent bonds with the carbon atoms of the lattice after chemical [3] or electrochemical [4] treatments, but also can be deposited on the surface through physisorption, as done in this work with the formation of a single-molecule thick layer of Nickel Phthalocyanine (NiPc) on a monolayer Gr substrate. Moreover, the selection of aromatic scaffolds allows the formation of π -stacked layers, whose electronic properties are possibly altered by the π -orbitals interactions, even when there is no formation of chemical bonds.

Indeed, in this presentation, I will deal with the characterization of the interlayer electron transfer channels in a NiPc-Gr heterointerface, probed by the employment of both experimental techniques (Resonant Photoelectron and X-Ray Absorption Spectroscopies) and DFT calculations. The discussion will bring evidence that the relaxation pathway, which occurs in the femtosecond timescale, involves only π -symmetry orbitals, that are opportunely oriented in a π -stacked flat layer. This allows the transfer of electrons from the molecules, selectively excited thanks to the synchrotron radiation's photon energy tunability, to the p-doped Gr layer, unveiling the potential of this particular nanoarchitecture for the application in electronic devices.

References

- [1] K. S. Novoselov, A. K. Geim, S. V. Morozov, D. Jiang, M. I. Katsnelson, I. V. Grigorieva, S. V. Dubonos, and A. A. Firsov, *Two-Dimensional Gas of Massless Dirac Fermions in Graphene*, *Nature* **438**, 197 (2005).
- [2] F. Schedin, A. K. Geim, S. V. Morozov, E. W. Hill, P. Blake, M. I. Katsnelson, and K. S. Novoselov, *Detection of Individual Gas Molecules Adsorbed on Graphene*, *Nat. Mater.* **6**, 652 (2007).
- [3] S. Freddi, M. C. R. Gonzalez, P. Carro, L. Sangaletti, and S. De Feyter, *Chemical Defect-Driven Response on Graphene-Based Chemiresistors for Sub-ppm Ammonia Detection*, *Angew. Chemie Int. Ed.* **61**, e2022001 (2022).
- [4] G. Ambrosio, A. Brown, L. Daukiya, G. Drera, G. Di Santo, L. Petaccia, S. De Feyter, L. Sangaletti, and S. Pagliara, *Impact of Covalent Functionalization by Diazonium Chemistry on the Electronic Properties of Graphene on SiC*, *Nanoscale* **12**, 9032 (2020).

SESSION NM02.12: Virtual Session I
Session Chairs: Shunsuke Sakurai, Yoke Khin Yap and Ming Zheng
Tuesday Morning, December 6, 2022
NM02-virtual

10:30 AM NM02.12.01

Tunable WS₂ Nanotubes from Ga-Ion Seeding Sabrya E. van Heijst and Sonia Conesa-Boj; Delft University of Technology, Netherlands

Two-dimensional layered materials have attracted a lot of attention following the discovery of graphene and the demonstration of its remarkable properties. This renewed interest resulted in the discovery of numerous new 2D layered materials, including 2D materials of the transition metal dichalcogenide (TMD) family. A key feature of these materials is that the reduction of the number of layers is accompanied by the modification of the local electrical and optical properties. Furthermore, it has also been shown that this tunability is not restricted to two-dimensional nanosheets, but is also present within the one-dimensional configuration. In this context, TMD-based one-dimensional nanotubes benefit from unique properties that strongly depend on their chirality, diameter, and number of walls. The ability to control these parameters, and thus tune the properties of the nanotubes, is an essential requirement to deploy TMD nanotubes for realistic application, yet achieving such tunability at the nanofabrication level remains a challenge. Here we report on an approach by means of which WS₂ nanotubes of uniform diameter were fabricated and the investigation of their local electronic properties. We find that by implanting gallium ions in a tungsten film and subsequent annealing, highly uniform tungsten oxide nanowires could be fabricated. The sulfurization of these nanowires results in multiwall, close-ended WS₂ nanotubes with similar diameters. These WS₂ nanotubes are then characterised by using advanced transmission electron microscopy techniques, including high resolution electron energy loss spectroscopy. Our results demonstrate how the proposed gallium-assisted synthesis method provides an efficient way of controlling the morphology of WS₂ nanotubes, and thus tuning the electronic properties of these one-dimensional TMD structures, paving the way for the use of WS₂ nanotubes in nanotechnology applications.

10:35 AM NM02.12.02

Experimental Methods for Nanofluidics—Focus on Sealing Technology for Delicate Nanomaterials Said Pashayev^{1,2}, Romain Lhermerout^{1,3}, Christophe Roblin¹, Eric Alibert¹, Jérôme Barbat¹, Rudy Desgarceaux^{1,4}, Rémi Jelinek¹, Edouard Chauveau¹, Clement Delacou¹, Saïd Tahir¹, Vincent Jourdain¹, Rasim Jabbarov², François Henn¹ and Adrien Noury¹; ¹Laboratoire Charles Coulomb (L2C) - UMR5221 du CNRS, France; ²Institute of Physics, Azerbaijan National Academy of Sciences, Azerbaijan; ³Laboratoire Interdisciplinaire de Physique, Univ. Grenoble Alpes & CNRS, France; ⁴Institut d'Electronique et des systèmes (IES), Univ. Montpellier & CNRS, France

Water is essential to live organisms and human societies as the primordial solvent of life. The primordial role of water can be related to its unique physical properties particularly due to the structure of its hydrogen bond network or its dipolar moment. In extreme confinement situations, such as inside nanoscale channels, important modifications of these features are expected. Thus, many theoretical works predicted that confined water in extremely small diameter pores exhibits both unusual phase behavior[1] and structure, compared to bulk water. Thanks to their stiffness, hydrophobic smooth surface, and high aspect ratio, Single Wall Carbon Nanotubes (SWCNT) can be considered as a model nanochannel to get insight into the confinement of water molecules. For instance, it was calculated that the phase of confined water in SWCNT whose diameter is smaller than 1.4nm, behaves as ice-like water with structures from single-file water chains to pentagonal or hexagonal structures depending on the SWCNT diameter [2]. On the other hand, it has been shown from experimental [3] and theoretical [4] calculations that water diffusion in SWCNT is significantly enhanced. Expanding our fundamental understanding of water properties when it is confined in SWCNTs can yield substantial progress in desalination, drug delivery, energy harvesting, etc. applications. Although there are many numerical simulations reported on this system, only a few experimental works have been achieved and it remains a challenging task to get experimental proof of water behavior in such a confined environment.

One of the main challenges to experimentally measuring the properties of nanoconfined water is to be able to fabricate fully sealed microchips. Sealing is a central process for micro and nanofluidic chip fabrication, yet only a few materials can be used, as they must be chemically inert, vacuum compatible, resistant to temperature change, and must have no electrical effect.

In this presentation, I will present a new sealing technology based on SU8 epoxy resist. We show that our bonding method is reliable and versatile for microfluidic, as it can be patterned by photolithography down to micrometric dimensions. It is thus found that a 30 μm high and 20 μm thick wall made of SU8 can sustain relatively pressures up to ~5 bars. We also measured ions permeation through the SU8 walls and found that it is similar or even better to PDMS. The electrical test shows no significant perturbation of electrical devices down to the sensitivity of our measurement set-up, i.e. pA, which makes the SU8 wall resistivity several orders of magnitude higher than that of carbon nanotubes. In addition, our sealing technology turned out to be chemically stable even at high temperatures. Importantly, it does not require plasma activation (contrary to PDMS), therefore it is perfectly suited for the fabrication of delicate nanochannels such as carbon nanotubes.

I will discuss ongoing work to distinguish the effect of water confined inside of the individual single-wall NT based on analyzing the change of the conductance shape. Our preliminary data show that water confined inside the NT mainly influences the gate hysteresis (charge transfer or doping) of NT, rather than its conductance or the carriers mobilities.

1. Takaiwa D, Hatano I, Koga K, Tanaka H. Phase diagram of water in carbon nanotubes. *Proc Natl Acad Sci.* 2008;105(1):39-43.

doi:10.1073/pnas.0707917105

2. Pascal TA, Goddard WA, Jung Y. Entropy and the driving force for the filling of carbon nanotubes with water. *Proc Natl Acad Sci.*

2011;108(29):11794-11798. doi:10.1073/pnas.1108073108

3. Holt JK, Park HG, Wang Y, et al. Sub-2-Nanometer Carbon Nanotubes. 2006;312(May):1034-1038.

4. Thomas JA, McGaughey AJH. Water flow in carbon nanotubes: Transition to subcontinuum transport. *Phys Rev Lett.* 2009;102(18):1-4.

10:40 AM NM02.12.03

Nanofibrous Carbon Hybrids for Low-Cost Tailored Device Production Mark Atwater; Liberty University, United States

Carbon nanostructures have great potential, which has been largely unrealized in a significant commercial sense. The primary challenges are often related to efficient production at scale and control of device architecture. Carbon nanofibers (CNFs) are a potential alternative to carbon nanotubes, albeit with some loss of performance in terms of electrical or mechanical properties. The countervailing assets, however, are their simplicity in production and diversity in morphology. They have been studied in various aspects of synthesis and functionality for decades, but in recent years a new process for creating bulk devices in situ has been developed. This technique, the constrained formation of fibrous nanostructures (CoFFiN) process, allows free-standing, nonwoven carbon structures to be created repeatedly and reliably at low cost. A recent adaptation has also demonstrated the ability to create hybrid structures incorporating other carbon materials into the fibrous network, which results in a shorter processing time and higher surface area. These CNF hybrids can be made with precise geometries, are strong and robust, and can be tailored to possess a diverse range of properties, making them suitable for electronic devices, composite reinforcement, filtration and purification, etc. The current state of the art, comparison to other nanofibrous structures, and ongoing developments will be discussed.

10:45 AM NM02.12.04

Effects of Mechanochemical Activation on the Structural, Magnetic and Optical Properties of Yttrium Iron Garnet-Graphene Nanoparticles Monica Sorescu¹, Sarah Glasser¹, Felicia Tolea², Andrew Craig¹, Mihaela Sofronie² and Jennifer Aitken¹; ¹Duquesne University, United States; ²National Institute of Materials Physics, Romania

Yttrium iron garnet nanoparticles have potential applications in sensing and microwave devices. In this study, nanoparticles systems were exposed to mechanochemical activation by high-energy ball milling for 0, 2, 4, 8 and 12 h. The samples were subsequently characterized by Mossbauer spectroscopy, X-ray powder diffraction (XRPD), magnetic measurements and optical diffuse reflectance spectroscopy. The 0-h specimens were analyzed by considering 2 sextets in the Mossbauer spectra, corresponding to the tetrahedral and octahedral sites of the yttrium iron garnet structure. The spectra of the milled samples were fitted with a third sextet with the hyperfine magnetic field characteristic to hematite and a quadrupole-split doublet representing superparamagnetic particles of the yttrium iron perovskite (yttrium orthoferrite) phase. The mechanism of the ball milling activation was found to be consistent with the decomposition of the garnet into yttrium iron perovskite and iron oxide phases. A different set of yttrium iron garnet samples was milled with graphene nanoparticles (3 nm in diameter) and analyzed using the same techniques. Examination of the quadrupole doublet's abundance as function of ball milling time indicated that graphene slowed down the precipitation of the perovskite. The increased linewidth of the doublet showed that the carbon from graphene preferentially entered the lattice of the yttrium orthoferrite. The coercive field of the sample milled with graphene is greater than that of the garnet and is even greater when longer milling times are employed and the particle size is smaller. The saturation magnetization decreases with decreasing particle size for prolonged milling due to the occurrence of the antiferromagnetic yttrium iron perovskite phase. The enhanced absorption in the infrared region could be associated with the incorporation of carbon from graphene in the lattice of the yttrium orthoferrite.

10:50 AM NM02.12.05

3D Printing of 3D Graphene—Material Characterization, Properties, Applications and Post Processing to Enhance the Properties Vamsi Krishna Reddy Kondapalli¹, Derek DeArmond¹, Kyle Brittingham¹, Xingyu He¹, Mahnoosh Khosravifar¹, Safa Khodabakhsh¹, Boyce Collins², Sergey Yarmolenko², Ashley Paz y Puente¹ and Vesselin Shanov^{1,1}; ¹University of Cincinnati, United States; ²North Carolina A&T State University, United States

Over the years multiple efforts resulted in the development of various versions of 3D Graphene via chemical and non-chemical routes. 3D printing of graphene-based polymer inks and aerogels has been considered efficient and promising among the other processes given the advantages of this approach. However, the resultant 3D graphene structures highly rely on a binder or ice support to stay intact. The presence of a binder or another non-graphene phase hinders the translation of the excellent graphene properties into the 3D structure. Here we report 3D-shaped 3D graphene (3D²G) synthesized by combining 3D printing with atmospheric pressure chemical vapor deposition (CVD) process. 3D²G structures produced in various shapes and sizes were characterized using scanning electron microscopy, image analysis, X-Ray Diffraction, micro-CT, 2D Raman spectroscopy, thermogravimetric analysis (TGA), and electrical and electrochemical measurements. By changing the printing design, properties like electrical conductivity, electrochemical behavior, mechanical strength, and structural porosity can be tailored without any requirement for doping or chemical post-processing. The obtained material consists of close to 100% 3D graphene and reveals high thermal stability of up to 500°C in air. As synthesized, 3D²G can be exposed to mechanical compression which converts it to a shiny thin sheet thus causing a significant increase in its density, electrical conductivity, tensile strength, and Young's modulus. This work brings together two advanced manufacturing approaches, CVD and 3D printing, thus enabling the synthesis of high-quality, binder-free 3D²G structures with a tailored design and properties that appeared to be suitable for multiple applications.

11:00 AM DISCUSSION TIME

SESSION NM02.13: Virtual Session II
Session Chairs: Shunsuke Sakurai, Yoke Khin Yap and Ming Zheng
Tuesday Afternoon, December 6, 2022
NM02-virtual

9:00 PM *NM02.13.01

Visualizing Current Pathways for the Evaluation and Improvement of the CNT-Polymeric Composite Properties Naoyuki Matsumoto; National Institute of Advanced Industrial Science and Technology, Japan

At AIST, our mission is to bring or “bridge” invention with industry and to contribute to society through the development of new technologies. With this in mind, over the past few years, our team has placed significant effort in developing carbon nanotube (CNT)-polymeric composites, mainly rubber and resin, using our proprietary “Super Growth” CNTs [1] and other commercially available single and multi-walled CNTs. Thus far, we have reported the successful development and commercialization of CNT rubber composites (O-rings) possessing long lifetime, high heat resistance, and high-pressure resistance [2] as well as CNT resin composites exhibiting excellent heat resistance and impact resistance using PEEK, a super engineering plastic [3]. The development of these fabrication technologies enables application of these materials in manufacturing and mainstream uses. In this way, we are able to fulfil our mission to contribute the development of materials and technologies for the betterment of society.

To best design the material to possess the required mechanical, electrical, or thermal properties, understanding of the pertinent governing mechanisms is necessary. Furthermore, the nature of the CNT dispersion in the composite matrix is well known to have significant effect on the formation of a 3-D network structure, i.e., percolation, but evaluation of the dispersion state within a composite for a nano-sized filler is challenging. In this presentation, I will show CNT rubber/resin composites that we have developed and put to practical use, as well as evaluation techniques we have used to visualize and understand the dispersion of CNTs in these composites. Specifically, I will introduce an analysis method using actual rubber/resin composites, focusing on lock-in heat analysis [4-6] and nano-indentation [7]. Through this approach, the homogeneity of the dispersion within the rubber can be characterized through the visualization of the distribution in current pathways. I will show how the application of these characterization techniques aids in the property improvement of our fabricated composites.

- [1] K. Hata, D. N. Futaba, et al. *Science* 306, 1362 (2004).
- [2] S. Ata, et al. *Nano Letters* 12, 2710 (2012).
- [3] S. Ata, et al. *Polymer* 176, 60 (2019).
- [4] T. Morimoto et al., *Scientific Reports* (2019).
- [5] B. Thi et al., *Carbon* (2019).
- [6] H. Nakajima et al., *Science Advances* (2019).
- [7] N. Matsumoto et al. in preparation.

9:30 PM *NM02.13.03

The Material Systems and Performance Limits of CNT Radiofrequency Devices Li Ding and Lian-Mao Peng; Peking Univ, China

Carbon nanotube (CNT) is considered a promising material for building radiofrequency (RF) field-effect transistors (FET) up to terahertz frequencies. This is because CNT has extremely high carrier mobility and saturation velocity, as well as ultra-small intrinsic gate capacitance. Earlier studies on the electronic properties of CNT FETs used individual semiconducting CNTs. But FETs built on individual CNTs can provide at best tens uA which is too low for real applications and the output impedance of the device cannot match the conventional 50 Ω RF measurement standards. Chemical vapor deposition (CVD) based CNT arrays with high-quality were also extensively examined for building RF devices. While promising results were achieved, for example on frequency doublers and mixers, the performance of devices based on CVD arrays of CNTs is severely limited by the low array density and material purity.

Currently, most research efforts are focused on using solution-derived CNTs for preparing thin films. Before 2020, only randomly oriented network of CNTs were widely available for research, and in few cases parallel arrays of CNTs were reported but with limited purity of 99.99% and density of lower than 100 CNT/um. Steady progress on RF performance had been made using these network and low-purity and density arrays, and in particular researchers in Carbonics Inc. pushed the current-gain and power-gain cut-off frequencies of CNT RF FETs to $f_r=75$ GHz and $f_{max}=102$ GHz using CNT arrays; and researcher from Peking University achieved $f_r=103$ GHz and $f_{max}=107$ GHz using network of CNTs. An important breakthrough was made in 2020 by researchers from Peking University, they first developed a multiple-dispersion and sorting process that resulted in extremely high semiconducting purity of better than 99.9999%; and then a dimension-limited self-alignment procedure for preparing well aligned CNT arrays with a tunable array density of 100 to 200 CNTs/um. Top-gate FETs fabricated on the so prepared CNT arrays show a current-gain and power-gain cut-off frequencies of 540 GHz and 306 GHz respectively.

In addition to the channel material, the choice of substrate is also of crucial important for achieving the ultimate performance limit of CNT based RF FETs. The substrate may affect the RF performance of a FET via dielectric permittivity for high speed and dielectric strength, and thermal conductivity for high power. Among all insulating materials, diamond is of particular interest for carbon-based electronics because it is composed of the same carbon element as CNT and has suitable low dielectric permittivity (5.5), strong dielectric strength (1000 kV/cm) and high thermal conductivity (2000 W/mK). Diamond substrate is thus the most suitable substrate for CNT RF devices. Our preliminary results show that we can indeed fabricate well-aligned CNT array-based RF devices on diamond and achieve respectively 245 and 200 GHz of current-gain and power-gain cut-off frequencies. These values are still lower than that achieved using silicon as the substrate, which might be due to the process divergence derived from different substrates. And the device fabrication processes needs to be further optimized on diamond substrate. It is expected that significant improvements on both speed and power could be achieved in RF devices based on aligned CNT arrays on diamond substrate, further pushing the limit into the ballistic terahertz regime in the near future.

10:00 PM NM02.13.04

ML Prediction of Nano-Porous Aerogels Material Properties Omid Aghababaei Tafreshi, Zia Saadatnia, Shahriar Ghaffari-Mosanenzadeh, Chul Park and Hani E. Naguib; University of Toronto, Canada

Due to the high prediction performance and low computational cost, machine learning (ML) based tools have been widely implemented in the field of material science for materials innovation, material design, deriving insights, and material properties prediction. In this context, the application of ML in the field of porous materials, particularly nanostructured aerogels, only rose to prominence recently. Despite many attempts to tailor and optimize the performance of nanostructured aerogels, the current methodologies mostly rely on experimental approaches, and thus further development of novel aerogels with optimum performance is greatly restricted. Considering the prolonged synthesis process, costly materials and equipment, and the necessity of analyzing microstructure and properties of aerogels, developing a ML platform can facilitate data-driven materials innovation and accelerate prediction of the material properties of nanostructure aerogels. Therefore, in this study, we report the application of artificial neural network (ANN) as an effective ML tool for properties prediction of nanostructured organic aerogels. Through optimizing the ANN network parameters, ANN architecture is constructed. Data mining is performed, and selected descriptors are chosen as the input for the model. Various properties, namely compressive modulus, density, and porosity of nanostructured aerogels, are predicted, and ANN performance is analyzed via evaluation metrics.

10:05 PM NM02.13.05

Boron Nitride Nanosheets Can Induce Water Channels Across Lipid Bilayers Leading to Lysosomal Permeabilization Xuliang Qian; Nanyang Technological University, Singapore

While the interaction between 2D materials and cells is of key importance to the development of nanomedicines and safe applications of nanotechnology, still little is known about the biological interactions of many emerging 2D materials. Here, an investigation of how hexagonal boron nitride (hBN) interacts with the cell membrane is carried out by combining molecular dynamics (MD), liquid-phase exfoliation, and in vitro imaging methods. MD simulations reveal that a sharp hBN wedge can penetrate a lipid bilayer and form a cross-membrane water channel along its exposed polar edges, while a round hBN sheet does not exhibit this behavior. It is hypothesized that such water channels can facilitate cross-membrane transport, with important consequences including lysosomal membrane permeabilization, an emerging mechanism of cellular toxicity that involves the release of cathepsin B and generation of radical oxygen species leading to cell apoptosis. To test this hypothesis, two types of hBN nanosheets, one with a rhomboidal, cornered morphology and one with a round morphology, are prepared, and human lung epithelial cells are exposed to both materials. The cornered hBN with lateral polar edges

results in a dose-dependent cytotoxic effect, whereas round hBN does not cause significant toxicity, thus confirming our premise.

10:10 PM NM02.13.06

Reservoir Computing Using Vertically Aligned Graphene/Diamond Heterojunctions Yuga Ito¹, Akiho Nakazuru¹ and Kenji Ueda^{2,1}; ¹Nagoya University, Japan; ²Waseda University, Japan

Recently, reservoir computing (RC) using various physical phenomena such as laser light, rippling water surface, memristors, etc., which have complicated dynamics, has been paid much attention. Higher speed learning and prediction with lower calculation cost is expected to be realized by implementing the physical phenomena to the reservoir system. However, the research on physical RC had only just started, and physical reservoir systems suitable for high speed and high efficiency computing has been seeking.

In this study, we show that it is possible to perform physical RC by using vertically aligned graphene (VG)/diamond heterojunctions, which are found to show multiple photo-memory [1] and brain-mimic optoelectronic memory functions [2], recently, and recognize simple digits (0~9) by using the junctions for the first time.

Heterostructures of VG and boron-doped semiconducting diamond were grown *in situ* by using microwave plasma CVD. VG/diamond junctions were fabricated using the heterostructures by a standard photolithographic process and reactive ion etching (RIE). Current-voltage characteristics of the VG/diamond junctions were measured at room temperature (R. T.) in air with or without photo-irradiation by using visible LEDs.

Conducting behaviors of various VG/diamond junctions formed in different growth conditions were examined during and after irradiating 10 optical pulses with positive bias voltage. Conductivity values of the junctions were increased step-by-step in response to each optical pulse and decayed with different relaxation time (τ). From results of Raman spectroscopy and TEM measurements, the relaxation time of the junctions were decreased as the interlayer distances of interfacial graphene layers were increased. It is suggested that the distances were controlled by the volume of sp^3 type defects in the layers, and photo-memory functions of VG/diamond junctions were changed depending on the sp^3/sp^2 ratio of the VG layers, which could be controlled by changing the growth temperature and the oxygen ratio during CVD growth. VG/diamond junctions with shorter-term memory functions ($\tau = 1.9$ s) could be fabricated based on these results.

RC using the VG/diamond junctions was performed. First, simple digits (0~9) were shown by binary 5*4 images as shown below. As a note, you can see number "2" by tracing the positions of 1 in the images.

----- (5*4 images (= 20 pixels) of the number "2" shown by 1 or 0 (binary image)) -----

```
0 1 1 0
1 0 0 1
0 0 1 0
0 1 0 0
1 1 1 1
```

These images were decomposed into each raw containing 4 sequential pixels, like 0110, 1001, ..., and optical pulses correspond to each raw were irradiated to the junctions. For example, in the case for first line of number "2", the junctions were irradiated by sequential pulses of light-off (0), on (1), on (1), and off (0) because the first line of the images of "2" was shown by "0110". Each conductivity value of the junctions was memorized after irradiation by each sequential pulse, and five conductivity values were obtained. The conductivity of the junctions was changed in a complex way because of short-term memory functions of them. The five conductivity values are different for each digit, and it is possible to recognize each digit (0~9) after transferring them to the simple, two-layered neural network. In this study, 50 images of simple digits were used to evaluate recognition accuracy. As a result, we have obtained excellent recognition ratio of above 90%. These results indicate that the VG/diamond photomemristors work as physical reservoirs and can be used as novel brain-mimic devices with both photo-memory and computing functions.

Ref.: [1] K. Ueda et al., Appl. Phys. Lett. 117 (2020) 092103, [2] Y. Mizuno, Y. Ito, and K. Ueda, Carbon. 182 (2021) 669. [3] Du et al., Nature. Comm. 8 (2017) 2204.

10:15 PM NM02.13.07

Modification of Hexagonal Boron Nitride to Control Vanadyl Species for Selective Catalytic Reduction of Nitrogen Oxides with Ammonia Myeung-Jin Lee^{1,2}, Bora Jeong^{1,3}, Hanguy Im^{1,3}, Su-Jin Kim^{1,2}, Bora Ye¹, Seungho Cho² and Hong-Dae Kim¹; ¹Korea Institute of Industrial Technology, Korea (the Republic of); ²Ulsan National Institute of Science and Technology, Korea (the Republic of); ³Pusan National University, Korea (the Republic of)

Hexagonal-BN is generally known as stable material from RT to 1000 °C at air atmosphere, and has high chemical stability. It is, therefore, used in fields to need thermal and chemical stability, and porous structure obviously gives a variety of properties in ceramic. In this work, modification to porous structure can be confirmed and intentionally obtained from h-BN by catalytic etching of TMOs below 1000 °C. Catalytic etching occurs during calcination which can be confirmed via intersection of between theoretical Ellingham diagram and experimental TGA. At that temperature, TMOs move in a specific preferred direction, and porous h-BN thereby has stuck particles. Existence of highly dispersed TMOs in final product makes it possible to be used as selective catalytic reduction (SCR) catalysts, one of green technologies, through only single step process. A commonly abatement technology of NOx is selective catalytic reduction with NH₃ (NH₃-SCR) as reductant, and vanadium-based catalyst is commercialized with titanium dioxides (TiO₂) and tungsten as promoter, V₂O₅-WO₃/TiO₂. However up to present, because operating temperature of V-based catalyst is the range from 300 to 380 °C, the necessary of modified V-based catalyst capable of operation in the lower temperature due to further tighten environmental regulation in various fields in the future. Generally, vanadium exists in four common oxidation states (+5, +4, +3, and +2), among which V⁴⁺ is the better SCR performance than general oxidation state, V⁵⁺. Therefore, the vanadyl oxidation states are main factor in modifying V-based catalyst for widening to lower temperature drive. The ratio of V⁴⁺ is further higher proportion by interacting between vanadium and tungsten oxides on a hexagonal boron nitride (h-BN) during calcination. The doped vanadium oxides can be confirmed in tungsten oxides structure via theoretical Hume-Rothery rule and experimental results. We can also confirm the enhanced performance of deliberately etched catalyst in both of powder and green-body states, honeycomb and coated type.

SESSION NM02.14: Virtual Session III
Session Chairs: Shunsuke Sakurai, Yoke Khin Yap and Ming Zheng
Wednesday Morning, December 7, 2022
NM02-virtual

8:00 AM *NM02.14.01

Single Crystal Metal Foils and Single Crystal Graphene and Single Crystal F-Diamane [Rodney S. Ruoff^{1,2}](#); ¹Ulsan National Institute of Science and Technology, Korea (the Republic of); ²Institute for Basic Science, Korea (the Republic of)

We have converted polycrystalline foils (copper, nickel, cobalt, platinum, palladium) to single crystal foils (Science 2018) and used single crystal Cu(111) foils to synthesize single crystal graphene having folds (several articles in ACS Nano and Advanced Materials), while single crystal Cu-Ni(111) "alloy" foils have yielded fold-free and wrinkle free single crystal graphene (Nature 2021), and at higher nickel concentrations, relatively large area single crystal AB-stacked bilayer graphene (Nature Nanotechnology 2020) that was converted to fluorinated diamane (C2F) by exposure to XeF₂ (Nature Nanotechnology, also 2020). Our Ni(111) foils were used to make large area single crystal hexagonal boron nitride films in collaboration with Hyeon Suk Shin and team members (Nature 2022). I look forward to presenting these topics and to the interesting questions from colleagues. Our work supported by IBS-R019-D1.

8:30 AM NM02.14.02

Nano-Nanocomposite Membrane Based on Cellulose-Nanofiber and Carbon Nanotubes for Low-Pressure Reverse Osmosis Systems [Juan L. Fajardo Diaz¹](#), [Aaron Morelos-Gomez^{1,1}](#), [Rodolfo Cruz-Silva^{1,1}](#), [Kazuki Ishii²](#), [Tomoharu Yasuike²](#), [Takahiro Kawakatsu²](#), [Ayaka Yamanaka³](#), [Syogo Tejima³](#), [Kazuo Izo¹](#), [Shigeru Saito¹](#), [Jun Maeda¹](#), [Kenji Takeuchi^{1,1}](#) and [Morinobu Endo^{1,1}](#); ¹Shinshu University, Japan; ²Kurita water industries LTD, Japan; ³Research Organization for Information Science & Technology, Japan

A nano-nanocomposite polymeric membrane based on multiwalled carbon nanotubes (CNT), cellulose nanofibers (CNF), and polyamide was used to produce high purity water in a low-pressure reverse osmosis system. The PA-CNT/CNF membranes were physicochemically characterized in order to track the influence of adding different loads of cellulose nanofiber, the influence of isopropanol (IPA) used as a diluting agent, and a sodium nitrate (NaNO₂) post-treatment applied after membrane synthesis. The mixture of CNF/CNT had a significant influence on membrane roughness, hydrophobicity, and the type of functional groups at the surface compared with a plain PA membrane. The incorporation of CNF improves the water permeation while the CNT structure supports the salt rejection at low pressure (0.75 MPa) RO filtration. A significant amount of experiments showed how the concentration of isopropanol also positively influenced the water permeation and salt rejection at low concentrations but negatively impacted both rejection and permeation at higher concentrations. In the case of the post-treatment with NaNO₂, this improves both water permeation and salt rejection. In the end, a CNF concentration between 3 wt. % to 6 %, IPA concentration between 4% to 6%, and treated with NaNO₂ revealed salt rejections above 99 % and water flux above the 1 m³/m²day. The best performance showed a salt rejection of 99.47% and water permeation of 1.65 m³/m²day, very competitive compared with commercial systems like ES20, ES40 (From Nitto-Denko), and BW60 (Dupont). Rejection analysis of selective ions like Ca, Si, and B salts was performed. The PA-CNT/CNF membrane expands the operation time compared with NSF-certified commercial systems for high-purity water production tested with a Si, Ca, and Na mixed solution. The PA-CNT/CNF membrane maintains a Ca rejection of 97.5% with an increased permeability by 1.8 times and a boron rejection of 50.4%. A 2 inches module was built using the PA-CNT/CNF membrane and was tested in a more realistic environment. Its performance compared with a commercial module (TW30), the PA-CNT/CNF module showed an increase of 14.3% over the water flux production before its saturation. This PA-CNT/CNF polymeric nanocomposite has shown a very competitive performance for the rejections of Si, Na, Ca ions and the production of HPW in a low-pressure RO system.

8:45 AM NM02.14.03

Multimodal Artificial Intelligence System for Virtual Screening of Complex Nanocomposite Materials [Shun Muroga¹](#), [Yasuaki Miki¹](#), [Takashi Honda²](#), [Hiroshi Morita¹](#), [Toshiya Okazaki¹](#) and [Kenji Hata¹](#); ¹National Institute of Advanced Industrial Science and Technology, Japan; ²Research Association of High-Throughput Design and Development for Advanced Functional Materials (ADMAT), Japan

Eternal challenge for materials scientists is exploring high-performance materials from the vast expanse of chemical space for targeted properties. Recent progress of data-centric science (i.e. materials informatics or process informatics) accelerate the discovery of new materials, especially in the fields of chemical compounds, solid-state inorganic materials, and materials with periodic ordered structures. Since conventional methods are machine learning of descriptors from atoms or chemical bonds in the structures, the material structures must be precisely defined. However, complex composite materials are dominant in our daily life, such as polymer composites, metal alloys, slurry, fabrics, and so on. Their whole structures cannot be defined by atoms and chemical bonds due to their complexity of multiple phases, hierarchy of structures, and non-periodic features. Therefore, advanced methodology of materials and process informatics for such complex composite materials would enlighten materials scientists to overcome the limitations of materials discovery.

In this study, we propose a method for virtual screening of complex composite materials, namely multimodal artificial intelligence system. Multimodal AI means inference from different inputs like human's perception simultaneously using multiple senses (e.g., visual, auditory, haptic), which has not been investigated in the fields of materials. Our concept of multimodal AI of materials is that integrating the multiple different data of characterizing physical structures and chemical structures leads to sufficient inference of properties of complex composite materials.

Here, polymer nanocomposite thermosets are fabricated as model materials. The polymer nanocomposites consist of complex components: five different matrices of acrylate curing monomers, two curing additives, and three reinforcing fillers including single-walled carbon nanotube, chopped carbon fiber, spherical alumina. Both physical structures (arrangements of fillers) and chemical structures (matrices and additives and their interactions) were evaluated to achieve the prediction of mechanical and electrical properties of polymer nanocomposites. The physical structures of polymer nanocomposites were measured by optical microscope, while the chemical structures of those were characterized by attenuated total reflection mid-infrared spectroscopy and Raman spectroscopy.

Proposed multimodal AI system can be divided into two steps. First step is generation of multiple characterization data. Characterization data (image, IR spectrum, Raman spectrum) of corresponding conditions (e.g., compositions of matrices, additives, fillers) can be virtually generated by generative adversarial neural networks. Second step is prediction of properties of materials from characterization data. Eight different (mechanical, electrical) properties of materials can be estimated by a deep learning model of integrating the inputs of image, IR spectrum, and Raman spectrum. By introducing these two steps using deep learning models, we have achieved the virtual screening dealing with such complexity of structures. Our system can generate characterization data and predict properties of 100,000 conditions of materials, which is equivalent to 20,000 times faster than real experiments. We strongly believe that the proposed concept of multimodal AI for complex composite materials overcomes previous limits and has a potential of applying to various materials and processes.

This work was supported by a project (JPNP16010) commissioned by the New Energy and Industrial Technology Development Organization (NEDO). Computational resource of AI Bridging Cloud Infrastructure (ABCI) provided by National Institute of Advanced Industrial Science and Technology (AIST) was used.

9:00 AM NM02.14.04

Production and Characterization of Arc-Discharged Carbon Nanotubes Using High Purity Natural Vein Graphite as Electrodes [Himasha Appuhami](#), [Tharaka Dissanayake](#) and [Asurasinghe Kumarasinghe](#); University of Sri Jayawardanapura, Sri Lanka

Carbon nanotubes (CNTs) have garnered worldwide attention in the past few years due to their exceptional electrical, thermal, elastic, and functionalization

properties. CNTs are a tubular form of carbon made up of a lattice of carbon hexagons folded into nanometer-scale multi-walled(MWCNTs) or single-walled (SWCNTs) tubes. Manufacturing high-quality carbon nanotubes have been expensive and challenging for industrial applications. Although production methods such as chemical vapor deposition (CVD) are currently used for large-scale production of CNTs, their quality and purity do not meet the demands of specific applications. Therefore, the arc-discharge method has been suggested as a practical approach to alleviating this problem in producing CNTs. In the arc-discharge process, carbon electrodes generate the arc between the two electrodes inside the inert gas-filled chamber where CNT is built on the cathode while consuming the anode. The cost associated with purchasing high-purity carbon electrodes hinders the production of high-quality CNT using the arc discharge method. Alternatively, high purity natural graphite electrodes, readily available in some parts of the world, can be used as electrodes obviating the need to use commercially purchased carbon electrodes. Hence an arc-discharge system was built using high-purity vein graphite as electrodes (Carbon purity of > 99.5 % wt, obtained from the Bogala mines in Sri Lanka). The two electrodes were mounted inside a closed vessel (14.34 L), where the position of the anode was fixed, and the cathode was moved back and forth using a linear actuator consisting of a stepper motor. The arc-discharging was performed inside the closed vessel filled with Argon (Ar) under the pressure of 100 mmHg and with a direct current (DC) supply of 100 A and 70 V, maintaining a 1-2 mm gap between the electrodes. Thus, by varying the arc-discharging time, CNT samples were prepared and collected carefully by scraping the cathode tip. Without further purification, the as-produced samples were characterized using Raman spectroscopy and Scanning electron microscopy (SEM). G band, D band, and noticeable radial breathing mode (RBM) were observed in the Raman spectrograph of the sample produced at 40 s (Sample A) constant arc-discharging. A slight D' split was also observed in the G band peak, indicating that the CNTs should be MWCNTs; Moreover, the D/G ratio was 0.83 (83%), which revealed a high depletion ratio, but the samples were unpurified and contained copious of amorphous carbon. In contrast, only G and D band peaks were recognizable in the sample produced with 60 s (Sample B) constant arc discharging, where no distinguishable RBM peak was observed, which is a sign of the non-existence of CNTs. The above results were confirmed by the further characterization of samples using SEM, where the dispersed CNTs were observed in the SEM image of sample A, while no CNTs were observed in sample B. In conclusion, the newly-home-built arc-discharge system was capable of producing CNTs; however, further research is required to determine the correlation between production variables and characteristics of CNTs.

9:05 AM NM02.14.06

Investigation of the Formation of Free-Standing Graphene Nanoflakes from Ethanol in a Pilot-Scale Plasma Reactor Frederik Kunze¹, Ivan Radev², Edward Nürenberg², Fabian Puslat², Tim Huelser¹ and Sophie Marie Schnurre¹; ¹Institut für Energie- und Umwelttechnik e.V.(IUTA), Germany; ²The Hydrogen and Fuel Cell Center ZBT GmbH, Germany

The interest in 2D materials has increased enormously since the discovery of graphene in 2004. The extraordinary electrical, mechanical and optical properties offer a great potential to improve a wide range of applications. However, this requires a deeper fundamental understanding of the formation of graphene and a resulting synthesis pathway that provides the necessary process conditions for efficient graphene formation. A potential synthesis route for the continuous production of few-layer graphene is the plasma-assisted gas-phase synthesis. In this work, we utilize a pilot-scale microwave plasma reactor with a frequency of 915 MHz and a maximum power of 50 kW [1] to convert ethanol into few-layer graphene to work out the influence of the carbon concentrations on the characteristics of the formed few-layer graphene. For that purpose, ethanol is evaporated and subsequently passed through an argon-hydrogen plasma. To increase the carbon concentration, the feeding rate of EtOH is stepwise adjusted from 200 g/h to 800 g/h. The produced graphene powders are collected on filter membranes and then analyzed ex-situ by different methods. Imaging measurement methods such as scanning and transmission electron microscopy are used to determine the general shape and morphology of the different graphene samples. At low carbon concentration in the plasma, typical graphene sheets are formed almost exclusively. If the carbon concentration increases due to an increased EtOH feeding rate, there is a shift towards the formation of soot-like particles between the graphene sheets. Raman spectroscopy shows peak intensity ratios of 0.85 to 0.86 for I_D/I_G ratio and 0.94 to 0.99 for $I_{D'}/I_G$ ratio for all samples, indicating relatively high sp^2 hybridization, low defect density as well as low number of layers. However, the results reveal that Raman spectroscopy is not able to clearly distinguish and display the fraction of soot-like particles seen on SEM and TEM images by different peak intensity ratios. A better indicator is the electrical conductivity of the material, which is in the end also a crucial factor for potential applications. Therefore, the electrical conductivity and the apparent density of the graphene powders as a function of compression force were investigated in a specially designed powder conductivity test cell by a quasi-four electrode test principle. The measurement of the electrical conductivity shows a similar trend as already suspected from the evaluation of the SEM and TEM images. A decreased carbon concentration leads to a reduced formation of soot particle-like structures and thus also to a higher electrical conductivity of the material. The highest specific conductivity of $\sigma = 3,19$ S/cm and $\rho = 0.23$ g/cm³ at 100 N cm⁻² is obtained for graphene produced with the EtOH feeding rate of 200 g/h, which is 8.6 times higher than the commercial graphene CP-0080-HP-0010 (IoLiTec Ionic Liquids Technologies GmbH, thickness 1-10ML; size 0.5-3 μ m; 250 €/g, $\sigma = 0.37$ S/cm and $\rho = 0.12$ g/cm³ at 100 N cm⁻²). This work demonstrates that low-defect graphene can be produced continuously in a pilot-scale plasma reactor at production rates up to 2.5 g/h. However, it is also shown that the production of graphene from ethanol with conversion rates in the range of 0.6 to 1.2 % based on the carbon mass flow rate is currently still very inefficient and cannot be easily increased by using a pilot-scale reactor. Nevertheless, this synthesis route remains one of the most promising for the production of high-quality few-layer graphene.

Work is performed under the scope of IGF-Project 21784 N funded by the Federal Ministry for Economic Affairs and Climate Action on the basis of a decision by the German Bundestag (IGF-Project 21784 N) and by the German Research Foundation (DFG) (SCHN 1387/1-2, 651051).

[1] F. Kunze et al. / Powder Technology 342 (2019) 880–886

9:10 AM NM02.14.07

Oxidative Chemical Vapor Deposition (oCVD) Synthesis of Molecularly Imprinted Polypyrrole Nanotube for the Detection of CA-125 Protein Faruk Can¹, Tugce Akkas¹, Hazal Sakar², Lokman Uzun³ and Gozde O. Ince^{1,2}; ¹Sabancı University Nanotechnology Research and Application Center, Turkey; ²Sabancı University, Turkey; ³Hacettepe University, Turkey

Field-effect transistor (FET) based biosensors have been widely used in various applications such as medical diagnosis, health and environmental monitoring. The performance of the FET biosensors are determined by anchoring specific probes on the conducting channel for target biomolecules. In the past two decades, molecularly imprinted polymers (MIPs) have attracted much attention as a robust and cost-effective alternative to natural bioreceptors such as enzymes and antibodies. MIPs are artificial template-made receptors which have the ability to recognise specific target molecules. Here, we present a novel FET biosensor incorporated with a molecularly imprinted polypyrrole nanotube (MIPN) for the selective detection of CA-125 ovarian cancer biomarkers. Polypyrrole (PPy) nanotube used in the FET biosensor has been obtained via oxidative chemical vapor deposition (oCVD) which is a highly efficient solvent-free, vacuum-based technique for the synthesis of conductive polymers. Thanks to the flexibility of this method, MIPN has been conveniently synthesized by coating conformally the sacrificial porous structured templates in the presence of target protein. Particularly, imprinting the target molecule on the nanotube surface has provided extremely high surface area which leads to enhancement in selectivity of the sensor. Furthermore, the oCVD synthesis has enabled higher electrical conductivity for the resulting PPy nanotube by tuning deposition parameters such as oxidant/monomer ratio, substrate temperature and reaction pressure. Synthesized MIPN has been integrated onto the interdigitated array Au electrode to make a conductive bridge between source and drain terminals and biosensor platform has been assembled from chip device, microfluidic channel and custom made chip holder for

real-time measurement. The present study has provided useful insight into preparing a novel molecularly imprinted polymer nanotube with various target protein molecules by using oCVD technique.

Acknowledgments

This work was supported by the Scientific and Technological Research Council of Turkey (TUBITAK), Grant No: 119Z342.

Keywords: oxidative chemical vapor deposition, molecularly imprinted polymer, polypyrrole nanotube, FET biosensor

9:15 AM NM02.14.08

MWCNT/Rubber Composites for Pressure Sensing Application Dilusha J. De Silva, Hansini Abeysinghe, Thusitha N. Etampawala and Indhika Wanniarachi; Faculty of Applied Sciences, University of Sri Jayewardenepura, Sri Lanka

The development of various types of sensors to make our living much more comfortable has become a forefront research topic in the modern world. Pressure sensor is one such development. Even though there are different pressure sensors, developing an easy handle, and low-power sensor specifically to measure in-situ pressure change of passenger and industrial tires in motion remains a challenge. Developing a sensing material with flexibility and stretchability to withstand the harsh conditions of tires while being compatible with the tire material is one of the main challenges faced during the production of such pressure sensors. The use of piezoresistive sensing materials is quite a significant approach for this matter. Therefore, in this work, rubber-based piezoresistive materials, which could embed to the tire, were developed. Since rubber materials are electrically insulative, highly conductive Multi-Walled Carbon Nanotubes (MWCNTs) were incorporated to the rubber matrix to obtain the piezoresistive effect. π orbitals of MWCNTs being more delocalized to the outer area of their cylindrical structure and having σ bonds slightly out of the plane, σ - π rehybridization occurs making them mechanically stronger, electrically and thermally more conductive. Therefore, it was assumed that the use of MWCNTs to develop piezoresistive rubber compounds, which could withstand the high loads and harsh conditions as a more promising solution. Since rubber is flexible and stretchable, once a certain amount of pressure is applied on the material, it tends to compress. The rubber vulcanizate obtained after milling MWCNTs with rubber would have evenly spread MWCNTs across the rubber matrix. Therefore, when the rubber matrix gets compressed under certain pressure, the electron tunneling distances between the MWCNTs would reduce. Since MWCNTs are nanoscale 1D cylindrical tubes with delocalized π -electron cloud, under the applied pressure they would form more conductive networks across the rubber composite resulting in low resistance compared to its original form. It was identified that the types of rubber and composition of MWCNTs of the composite would affect the piezoresistive behavior of the composite. Therefore, in this study, 20 phr MWCNT incorporated natural rubber (NR), ethylene propylene diene monomer rubber, nitrile rubber, butadiene rubber, and styrene-butadiene rubber composites were tested for their piezoresistive behavior to identify the most suitable rubber matrix. MWCNT/NR composite showed the highest resistance change of more than 1000 folds of its original resistance when a load of 200 kN was applied and removed in a certain time interval. Therefore, it became evident that NR shows better flexibility and relaxation compared to other synthetic rubber lattices. Then, MWCNT/NR composites with varying MWCNT compositions of 10, 20, 30, and 40 phr were developed to observe their piezoresistive behavioral change under a range of loads. All these composites showed a similar pattern in exponential decrease of their resistance with increasing pressure. However, when applying high-pressure values in the range of 2000 – 12000 kNm⁻² their logarithmic resistance (log R) showed a linear reduction with increasing of pressure. At low-pressure values, log R reduced exponentially and move to a plateau around 500 kNm⁻². However, a linear relationship is expected even at low-pressure values, if the MWCNT composition is comparable with the percolation threshold value. Since the resistance values depend on the thickness of rubber composites, all these data were collected under a constant thickness. Currently, the development of a digital prototype of a piezoresistive pressure sensor to measure the real-time, in-situ pressure changes based on the obtained data is in progress. Here the analog signal is converted to a voltage signal via a potential divider under a low power supply and obtaining the real-time pressure reading to a display via Bluetooth.

9:20 AM *NM02.14.09

High-Brightness Fluorophores for Cell Phenotyping Nazmiye Yapici^{1,2}, Rodney Oakley¹, Xiuling Liu^{1,2}, Dongyan Zhang² and Yoke Khin Yap²; ¹Stabilis Biosciences, United States; ²Michigan Technological University, United States

Flow cytometry (FCM) is a laser spectroscopy technique that detects, counts, and sorts thousands of cells per second. For example, FCM enables cell phenotyping by characterizing the population of clusters of differentiation (CD) on cells. Laser-induced fluorescence from fluorophores conjugated with antibodies can identify various CD on cell surfaces. The multiparametric and high throughput capabilities have made FCM a standard technique for research and clinical laboratories to characterize stem cells, cancer cells, nucleic acids, etc.

We have developed a platform technology to produce high-brightness fluorophores (HBFs, NovoLux dye) for use in FCM. Our unique technology allows us to tune the fluorescent brightness of HBFs to desired levels (10X to 1000X brighter than commercial dyes). We can use any organic dye molecules to formulate HBFs to emit at desired fluorescent wavelengths. To date, we have developed Four types of HBFs: NovoLux 405, NovoLux 488, NovoLux 560 and NovoLux 640. The molar extinction coefficient (ϵ) of NovoLux dyes can be as high as 10^7 to 10^{10} M⁻¹ cm⁻¹ [1-3]. It is several orders of magnitude higher than any existing dye (ϵ for FITC is 7.8×10^4 M⁻¹ cm⁻¹, for Rhodamine B is 7.5×10^4 M⁻¹ cm⁻¹, for Cy5.5 is 2×10^5).

This unique property allows our HBFs to increase the staining index of some rare biomarkers (CD127, CD 19, etc.) in FCM measurements. The spectral properties, fluorescent brightness tunability, and application of NovoLux dyes in FCM will be presented in the meeting.

9:50 AM DISCUSSION TIME

SESSION NM02.15: Virtual Session IV
Session Chairs: Shunsuke Sakurai, Yoke Khin Yap and Ming Zheng
Wednesday Afternoon, December 7, 2022
NM02-virtual

9:00 PM *NM02.15.01

Semiconductor Nanochannels in Metallic Carbon Nanotubes by Thermomechanical Chirality Alteration Dai-Ming Tang¹, Sergey V. Erohin², Dmitry G. Kvashnin³, Victor A. Demin³, Ovidiu Cretu¹, Song Jiang⁴, Lili Zhang⁴, Peng-Xiang Hou⁴, Guohai Chen⁵, Don N. Futaba⁵, Yongjia Zheng⁶, Rong Xiang⁶, Xin Zhou¹, Feng-Chun Hsia¹, Naoyuki Kawamoto¹, Masanori Mitome¹, Yoshihiro Nemoto¹, Fumihiko Uesugi¹, Masaki Takeguchi¹, Shigeo Maruyama⁶, Hui-Ming Cheng^{4,7,8}, Yoshio Bando⁹, Chang Liu⁴, Pavel B. Sorokin² and Dmitri Golberg^{10,1}; ¹National Institute for Materials Science, Japan; ²National University of Science and Technology MISIS, Russian Federation; ³Emanuel Institute of Biochemical Physics, Russian Federation; ⁴Institute of

Metal Research, Chinese Academy of Sciences, China; ⁵National Institute of Advanced Industrial Science and Technology (AIST), Japan; ⁶The University of Tokyo, Japan; ⁷Shenzhen Geim Graphene Center, Tsinghua-Berkeley Shenzhen Institute, China; ⁸Shenzhen Institute of Advanced Technology, Chinese Academy of Sciences, China; ⁹University of Wollongong, Australia; ¹⁰Queensland University of Technology (QUT), Australia

Carbon nanotubes have a helical structure where the chirality determines them to be metallic or semiconducting. Using in situ transmission electron microscopy,^[1] we applied heating and mechanical strain to alter the local chirality and thus to control the electronic properties of individual carbon nanotubes. A transition trend towards larger chiral angle region was observed and explained in terms of orientation-dependent dislocation formation energy. Controlled metal-to-semiconductor transition was realized to create nanotube transistors with a semiconducting nanotube channel covalently bonded between metallic nanotube source and drain. In addition, quantum transport at room temperature was demonstrated for the fabricated nanotube transistors with the channel length down to 2.8 nanometers.^[2]

References

[1] D.-M. Tang *et al.* *Ultramicroscopy*, **194**, 108, (2018).

[2] D.-M. Tang *et al.* *Science*, **374**, 1616 (2021).

9:30 PM NM02.15.02

Towards CO₂ Electroreduction into Carbon Nanotubes in Molten Salt Electrolytes Andrew B. Wong; National University of Singapore, Singapore

This talk will detail our efforts to study and control the electroreduction of CO₂ into nanostructured carbons such as carbon nanotubes and present our insights about factors that are relevant to morphology control. In the high-temperature molten salt electrolytes, the role of experimental conditions will be discussed in the context of controlling the morphology of the products. Moreover, the role of this high-temperature approach to CO₂ reduction within the broader efforts toward scalable electrochemical CO₂ conversion also will be discussed.

9:45 PM NM02.15.03

Evaluation of Hole Doping Performance of Single-Walled Carbon Nanotubes with Boron Compounds Naoki Tanaka^{1,2}, Aoi Hamasuna¹ and Tsuyohiko Fujigaya^{1,2,3}; ¹Kyushu university, Japan; ²WPI-I2CNER, Japan; ³Center for Molecular Systems, Japan

Neutral organoboron compounds often show electron acceptance due to the vacant 2p orbital on boron and act as p-type dopants for organic semiconductors with electron-donating properties.¹ Therefore, most of the organic semiconductors have heteroatoms such as nitrogen, oxygen, and thiophene with lone pair electrons that can coordinate to vacant orbitals on the boron. On the other hand, for carbon materials such as single-walled carbon nanotubes (SWCNTs) consist of only carbon atoms without lone pair electrons, the effect of doping with organoboron compounds has not rarely been studied. In this study, we investigated p-type doping of SWCNTs by monoboranes and diboranes as organoboron compounds and the thermoelectric properties of the p-type doped SWCNT sheets.

P-type doped SWCNT sheets were prepared by immersed SWCNT sheets (4 mm × 14 mm × 30 μm) into THF solution of boron compounds and shaking at 30 °C for 24 hours. Electrical conductivity measurements of the SWCNT sheets revealed a significant increase in conductivity compared with pristine SWCNT sheets when using tris(pentafluorophenyl)borane (BCF) and bis(catecolato)diboron (B₂cat₂). In addition, the Seebeck coefficient of the SWCNT sheets were lower than that of pristine SWCNT. From these results, these dopants can serve as efficient hole-dopants for SWCNTs. Interestingly, the electrical conductivity of these doped SWCNT sheets increased with exposure to air. We considered that the proton generated by the reaction of boron dopants on the surface of SWCNTs with water in air caused hole doping in the SWCNTs.²

References-

[1] G. C. Bazan and T.-Q. Nguyen *et al.*, *Nature Materials* **2019**, *18*, 1327. [2] J. Jang *et al.*, *Adv. Energy Mater.* **2020**, *10*, 2003521.

9:50 PM NM02.15.04

Development of Air-Stable n-Type Doped Single-Walled Carbon Nanotube Sheet by Lewis Acids and Bases Naoki Tanaka^{1,2}, Aoi Hamasuna¹ and Tsuyohiko Fujigaya^{1,2,3}; ¹Kyushu university, Japan; ²WPI-I2CNER, Japan; ³Center for Molecular Systems, Japan

The chemical doping of single-walled carbon nanotubes (SWCNTs) using electron donor and acceptor molecules is a crucial step for controlling the frontier orbital energy gap of SWCNTs. This means that SWCNTs are promising materials for electronics applications such as thermoelectric conversion and thin-film transistors, due to their flexibility, stability, and light weight.^{1,2,3} For efficient thermoelectric generation, both p-type and n-type thermoelectric materials are required. However, SWCNTs act as p-type semiconductors owing to the hole doping by water and oxygen in air. Therefore, many efforts to develop n-type SWCNTs have been performed mainly by chemical doping using electron donors.^{4,5,6} Recently, our group reported that the boryl radical produced by cleavage of the boron-boron bond of bis(pinacolato)diboron (B₂pin₂) by coordinated pyridines to boron can serve as an electron dopant in SWCNTs.⁷ However, the n-doped SWCNTs did not show long-term air stability. In this study, we used tetrahydroxydiboron (B₂(OH)₄) in place of B₂pin₂ as the boron source and various pyridines to study the effect of the chemical structure of the boron to the n-doped air-stability.

Electron doping of SWCNTs was performed by mixing SWCNT sheets (4 mm × 14 mm × 30 μm), B₂(OH)₄ (1.0 eq.), and pyridine derivatives (0.5 eq.) in THF solvent and shaking at 40 °C for 24 hours. Upon using 4-cyanopyridine (4-CNPy), 4-phenylpyridine (4-PhPy), and 4-carboxypyridine (4-COOHPy), the doped SWCNT sheets showed negative Seebeck coefficient values and higher electrical conductivity than pristine SWCNTs, indicating the electron-doping from the corresponding boryl radicals to SWCNT. Interestingly, the n-doped SWCNT sheets prepared with B₂(OH)₄/4-Phpy revealed n-type properties for more than 50 days in air. X-ray photoelectron spectroscopy of the n-doped SWCNTs with B₂(OH)₄/4-Phpy showed that the dopant coverage on SWCNTs was much higher than that of other dopants. In addition, the distance between the dopant cation and the SWCNT was shorter than when B₂pin₂/4Phpy was used as a dopant. Therefore, we consider that n-type stability is not only related to the amount of coverage, but also to the interaction between SWCNT and dopant.

References-

[1] E. Jougelet, C. Mathis and P. Petit, *Chem. Phys. Lett.* **2000**, *318*, 561. [2] J. Kong and H. Dai, *J. Phys. Chem. B* **2001**, *105*, 2890. [3] L. Brownlie and J. Shapter, *Carbon* **2018**, *126*, 257. [4] M. Shim, A. Javey, N. W. S. Kam and H. Dai, *J. Am. Chem. Soc.* **2001**, *123*, 11512. [5] J.-Y. Choi and Y. H. Lee *et al.*, *J. Am. Chem. Soc.* **2009**, *131*, 327. [6] Y. Nonoguchi and T. Kawai *et al.*, *Sci. Rep.*, **2013**, *3*. [7] N. Tanaka and T. Fujigaya *et al.*, *Chem. Commun.* **2021**, *57*, 6019-6022.

9:55 PM NM02.15.05

Mechanics of Biosurfactant Aided Liquid Phase Exfoliation of 2D Materials Xuliang Qian¹, Matteo Andrea Lucherelli², Céline Corcelle², Alberto Bianco² and Huajian Gao^{1,3}; ¹Nanyang Technological University, Singapore; ²CNRS, Immunology, Immunopathology and Therapeutic Chemistry, UPR 3572, University of Strasbourg, ISIS, 67000, France; ³Institute of High Performance Computing, A*STAR, Singapore

Biosurfactant-aided liquid-phase exfoliation (LPE) is emerging as a biocompatible, green, economical, safe, and efficient approach to prepare two-

dimensional (2D) materials for biomedical applications. However, relatively little is known about the molecular mechanisms of this process. Herein, we present the first study of how flavin mononucleotide (FMN) interacts with hexagonal boron nitride (hBN) nanosheets in the context of LPE. We demonstrate that FMN molecules can self-assemble on hBN via π - π interactions, as well as intermolecular hydrogen bonds (H-bonds) between the isoalloxazine moieties. Binding free energy analysis has shown FMN to be an efficient surfactant for LPE of hBN in water. According to the theoretical simulations, stable water suspension of hBN were experimentally obtained by LPE using FMN. With this work, we aim to exemplify how molecular dynamics (MD) simulation can predict and guide empirical LPE experiments, direct the surfactant screening and improve scalable production of 2D materials for biomedical applications.

10:00 PM NM02.15.06

A Near Infrared Fluorescent Nanosensor for Spatial and Dynamic Measurements of Auxin, Indole-3-Acetic Acid, in Living Plants [Thinh D. Khong](#)^{1,2}, Kien V. Vu^{3,1}, Benny Jian Rong Sng^{3,1}, Ian Kin Yuen Choi^{3,4}, Thomas K. Porter⁵, Xun Gong⁵, Nguyen H. Nguyen³, Chunyi Mervin Ang¹, Minkyung Park⁵, Tedrick Thomas Salim Lew^{5,6}, Suh In Loh¹, Riza Ahsim¹, Hui Jun Chin^{1,3}, Gajendra P. Singh¹, Mary B. Chan-Park^{1,2}, Nam-Hai Chua^{1,3}, Michael S. Strano^{1,5} and In-Cheol Jang^{1,3,4}; ¹Singapore-MIT Alliance for Research and Technology, Singapore; ²Nanyang Technological University, Singapore; ³Temasek Life Sciences Laboratory, Singapore; ⁴National University of Singapore, Singapore; ⁵Massachusetts Institute of Technology, United States; ⁶Agency for Science, Technology and Research, Singapore

As climate change stresses global agricultural production, there is urgency to understand auxin signaling, particularly Indole-3-Acetic Acid (IAA), in living plants – a hormone critical for plant growth and yield, as well as the response to environmental stimuli such as phototropism or gravitropism. This goal is confounded by the lack of reversible sensors that report IAA directly, instead indirect visualization of IAA has relied on downstream genetic or metabolic reporters. Herein, we demonstrate a novel near infrared (nIR) fluorescent nanosensor for the spatial and temporal measurement of IAA *in planta* using Corona Phase Molecular Recognition (CoPhMoRe). The IAA nanosensor shows high specificity in detecting IAA *in vitro* and was validated *in planta* by measuring IAA levels in β -estradiol induced *XVE::iaaM Arabidopsis* plants. The sensor works across different plant species and allows the visualization of dynamic changes to IAA distribution and movement in leaf tissues, validating a reaction and diffusion model for IAA. We also demonstrate the application to the detection of transient IAA concentrations and its spatial diffusion in *Nicotiana benthamiana* leaf at the early stage of shade avoidance syndrome, observing preferential transport along the leaf margins. The results obtained from nanosensor measurements suggest different kinds of auxin transport between the vascular and non-vascular tissue in *N. benthamiana* leaf, and highlight the overall utility of this type of sensor to understand plant signaling pathways.

10:05 PM NM02.15.07

A Near Real-Time Physics-Informed Machine Learning-Based Solution of the Reaction-Diffusion Equation for Lithium Intercalation in Nanostructured Silicon Anodes Using Lower-End Computational Hardware Tarun Bijanapally, Tanish S. Tak, [Tejveer S. Anand](#) and Madhusudan Singh; Indian Institute of Technology Delhi, India

Analytical modeling of intercalation of lithium in silicon anodes is expected to be valuable in understanding the role of various kinds of resulting stress in failure of batteries based on these high capacity anodes. Recent work[1] has indicated that it is challenging to obtain the exact solution of lithium concentration as a function of space (r) and time(t), using conventional methods that involve reducing the order of the governing partial differential equation (PDE), even in the natural geometry of the problem: spherical polar coordinates. While exact analytical solutions were obtained with some effort due to the inherent symmetry of the problem, this is expected to be impossible for more realistic models of operation that may involve the use of asymmetric Li injection and extraction contacts in battery devices, interaction of electrolyte with anodes, etc. In this work, we report on the application of a physics-informed neural network model using a loss function expressed as the sum of the residuals of the PDE operator (f), initial value function, and boundary conditions, with backward propagation of node weights (implemented using Python Torch and TensorFlow libraries running on Google Colab to mimic the use of low-end hardware). The model uses spacetime (r,t) coordinates as inputs, and the lithium concentration in a host material ($C(r,t)$) as the output vector of the neural network. In the initial training, we have used the previously obtained exact solutions for a hollow silicon sphere (inner and outer radii: 200 and 500 nm, respectively) exposed to $[Li]=1 \text{ mol/m}^3$. The model includes: number of datasets for r (N_r) and t (N_t), training data sets for boundary conditions ($N_b=1000$), and PDE collocation points ($N_f=10000$) for calculation of residuals(f). A moderate sized dataset of size [2000,2000] when used for (N_r,N_t) results in an average training loss ($E_{A,tr}$) of 1.021×10^{-5} and an average test loss ($E_{A,te}$) of 0.0163 (2 hidden layers, 5 iteration loops, 32 nodes / layer). When the number of points for each dataset is doubled ([4000,4000]), $E_{A,tr}$ is reduced to 6.45×10^{-6} and $E_{A,te}$ to 0.0106. As the number of hidden layers is increased from 2 to 3 in an effort to reduce the testing loss further, memory limitations forced us to limit the maximum dataset size to [3000,3000]. This process actually doubled the testing loss from 0.014 to 0.028, which might suggest an over-determined backpropagation problem in the neural network. Reduction of number of hidden layers to 1 slightly increases the testing loss. The optimal dataset parameters for the problem are thus for dataset size [4000,4000], $N_b = 1000$, $N_f = 10,000$, with two hidden layers of 32 nodes each. An increase in the sampling of the residual function f to 100,000 points does not lead to significant changes in testing loss with significant increase in training time, suggesting that the parameters obtained are near optimal. This initial work has thus been useful in establishing optimal starting points for potential near real-time (~120 seconds) distributed cloud computing of intercalation of lithium in silicon. Conventional machine-learning based predictive systems with high precision are often implemented on high performance computing environments, which is inconsistent with real-time monitoring and predictive maintenance needs of automotive batteries without relying on ubiquitous high-end networked computing. We are currently training the model for various boundary conditions to the surface of the hollow silicon sphere with variable diffusion coefficient and its coupled application with diffusion-induced stress (DIS), reaction-induced stress (RIS), etc. The method developed in this work opens an approach to analyzing electrode stress evolution during charging and discharging cycles in near real-time, with applications in on-board prediction of preventative maintenance/replacement schedules of batteries.

References:

[1] Anand et al, MRS Spring Meeting, 2021 (ST05.00.05).

10:10 PM NM02.15.08

Real-time and Simultaneous Detection of Salicylic Acid and ROS Production in Living Plants Upon Biotic and Abiotic Stresses Using Single-Walled Carbon Nanotube Based Sensors [Chunyi Mervin Ang](#)¹, Jolly Madathiparambil Saju², Sarangapani Sreelatha², Thinh D. Khong¹, Thomas K. Porter³, Suh In Loh¹, Song Wang¹, Gajendra P. Singh¹, Nam-Hai Chua^{2,1}, Michael S. Strano^{3,1} and Rajani Sarojam^{2,1}; ¹Singapore MIT Alliance for Research and Technology, Singapore; ²Temasek Life Sciences Laboratory, Singapore; ³Massachusetts Institute of Technology, United States

Salicylic acid (SA) is an important plant hormone, which controls various aspects of development and mediates plant response to mainly biotic stress. In this work, we developed a SA plant nanobionic sensor, which enables non-destructive and real-time monitoring of SA in living plants. The SA nanosensor is discovered by *in vitro* screening of single-walled carbon nanotubes (SWNTs) wrapped with different cationic co-polymers, against a list of common plant hormones analytes. This sensing strategy is known as corona phase molecular recognition (CoPhMoRe) which relies on amphiphilic co-polymers acting as synthetic antibodies that bind to specific target analytes, as well as disperse SWNTs in aqueous medium. Upon binding to SA, the SA nanosensor achieved a selective 35% near-infrared (nIR) fluorescence quenching response whereas nIR fluorescence remains relatively invariant upon addition of other key plant hormones. *In planta* validation of the sensor was achieved in *Arabidopsis thaliana* (*A. thaliana*) mutants with altered SA levels, and in non-

model *Brassica rapa subsp. chinensis* (Pak Choy) vegetable infected with black rot causing bacteria. To unravel the interplay between SA and redox signals during biotic and abiotic stress responses, the SA nanosensor is further multiplexed with a H₂O₂ nanosensor in the same leaf to monitor the unique ROS and SA signaling waveforms simultaneously, in response to bacterial infection and wounding. This resolves a longstanding goal of the plant biology field to uncover the sequential links between different plant signaling pathways with the nanosensors providing spatiotemporal information as the plant mounts an integrated stress response.

10:20 PM DISCUSSION TIME

SYMPOSIUM NM03

Colloidal Quantum Dots for Emerging Technologies
November 28 - December 6, 2022

Symposium Organizers

Federico Rosei, Université du Québec

Marinella Striccoli, CNR - IPCF

Alberto Vomiero, Luleå University of Technology

Haiguang Zhao, Qingdao University

* Invited Paper
+ Distinguished Invited

SESSION NM03.01: QD Synthesis I
Session Chair: Dmitri Talapin
Monday Morning, November 28, 2022
Hynes, Level 2, Room 209

10:30 AM *NM03.01.01

The Dream of the Perfect Nanocrystal David J. Norris; ETH Zurich, Switzerland

Quantum dots are nanometer-sized crystallites of semiconductor that have a roughly spherical shape. Due to extensive research, quantum dots are now commercially used as a robust fluorescent material in displays and lighting. However, even with our best procedures, state-of-the-art samples still contain particles with a distribution in size and shape. Because this causes variations in their optical properties, their performance for applications is reduced. This leads to a fundamental question: can we achieve a sample of semiconductor nanocrystals in which all the particles are exactly the same? In this talk we will discuss this possibility by examining two classes of nanomaterials. First, we will consider thin rectangular particles known as semiconductor nanoplatelets. Amazingly, nanoplatelet samples can be synthesized in which all crystallites have the same atomic-scale thickness (e.g., 4 monolayers). This uniformity in one dimension suggests that routes to monodisperse samples might exist. After describing the underlying growth mechanism for nanoplatelets, we will then move to a much older nanomaterial—magic-sized clusters (MSCs). Such species are believed to be molecular-scale arrangements (i.e., clusters) of semiconductor atoms with a specific (“magic”) structure with enhanced stability compared to particles slightly smaller or larger. Their existence implies that MSC samples can in principle be the same size and shape. Unfortunately, despite three decades of research, the formation mechanism of MSCs remains unclear, especially considering recent experiments that track the evolution of MSCs to sizes well beyond the “cluster” regime. Again, we will discuss the underlying growth mechanism and its implications for nanocrystal synthesis. Finally, we will present an outlook if perfect nanomaterials can be obtained.

11:00 AM *NM03.01.02

Designing Polymer Ligands to Enable Stabilization, Inter-Phase Transfer, Encapsulation and Structural Transformations of Colloidal Nanocrystals Nikolai Gaponik; TU Dresden, Germany

In this talk, I will discuss how the embedding of colloidal nanocrystals into polymer matrices can be governed by the proper choice of ligands. The ligands can be designed to contain specific polymer or oligomer chains providing direct and unlimited compatibility with desired polymers. The specially designed ligands may not only improve colloidal stability, but also influence the crystallinity of the inorganic colloidal nanoparticles and their composition. Combination of various polymers as co-ligands or the application of custom-designed co-polymers are also powerful tools for controlling the nanoparticle processability. The designed nanoparticle/polymer hybrids can be processed in the form of inks for printing and spraying, in the form of solutions suitable for shaping and casting and as functional bulk solids. Their potential for the applications in the solid-state-lighting, display technologies and photovoltaics will be demonstrated.

11:30 AM NM03.01.03

Self-Driving Fluidic Laboratory for Autonomous Development of Metal Halide Perovskite Nanocrystals Fazel Bateni¹, Kristofer G. Reyes² and Milad Abolhasani¹; ¹North Carolina State University, United States; ²University at Buffalo, The State University of New York, United States

Fully-inorganic lead halide perovskite (LHP) nanocrystals (NCs) have recently been demonstrated to outperform conventional II-VI semiconductor NCs in printed photonic devices. The solution-processability and ionic nature of LHP NCs have resulted in intriguing optical and optoelectronic properties, including near-unity photoluminescence quantum yield (PLQY) and narrow emission linewidth. Despite their potential, the widespread adoption of LHP NCs by clean energy technologies have been limited due to the high content of lead (Pb^{2+}) ions in the NCs. One potential solution to reduce the high Pb content of LHP NCs is to incorporate metal cation dopants that have similar optoelectronic properties (e.g., manganese, Mn^{2+}) to not only reduce the toxicity level but also introduce new properties into the host LHP NCs. However, the high-dimensional design space of metal cation-doped LHP NCs impedes comprehensive mapping of the colloidal reaction space and search for the best-performing material with desired phase stability and optical properties one-at-a-time trial-and-error experimentation approach.

The recent emergence of artificial intelligence (AI)-assisted experiment-selection strategies provide an accelerated route to explore the synthesis universe of novel advanced functional (nano)materials. However, the conventional batch reactors utilized for synthesis, development, and characterization of LHP NCs are time-, material- and labor-intensive and their process efficiency is limited due to their irreproducible heat/mass transport rates, high precursor consumption/waste generation rates, and lack of proper NC in-situ characterization probes for the real-time and rapid process control and optimization. Microfluidic platforms with their reproducible and intensified heat and mass transfer rates, small reactor footprint, facile in-situ characterization, and reduced reagent consumption/waste generation provide a miniaturized and reliable alternative to batch reactors for integration with AI-assisted experiment selection strategies. The result of such integration is a closed-loop 'self-driving fluidic lab (SDFL)'.

In this work, we present a modular SDFL for the accelerated development and fundamental mechanistic studies of pristine and metal cation-doped LHP NCs. The SDFL utilizes, for the first time, a two-stage strategy for the sequential halide exchange and cation doping of LHP NCs to autonomously explore the synthesis and doping design space of LHP NCs. The SDFL utilizes active learning to build an accurate "digital twin" of the multi-stage LHP NC synthesis chemistry (prediction accuracy >85%) within a limited experimental budget (60 experiments). We then employ the digital twin to study the fundamental formation and doping mechanisms of LHP NCs and identify the key process parameters controlling the optical/optoelectronic properties of the in-flow synthesized NCs. The SDFL uses the active learning-guided surrogate model to autonomously manufacture metal cation-doped LHP NCs with the targeted optical properties in less than 90 min per target material. The modularity of the developed SDFL makes it uniquely suited for accelerated formulation-synthesis-property relationship mapping required for discovery and development of next-generation of printable clean energy materials.

11:45 AM NM03.01.04

Accelerated Synthesis of Colloidal Quantum Dots in Multi-Stage Microfluidic Reactors [Fernando Delgado-Licona](#), Robert Epps and Milad Abolhasani; North Carolina State University, United States

Since their discovery more than three decades ago, quantum dots (QDs), have been used as a high-performing solution-processed optical/optoelectronic material in a multitude of applications across energy, chemical, and biomedical industries. The success of QDs in devices has been driven by their intriguing optical and optoelectronic properties that can be precisely tuned via controlling their morphology, size, and chemical composition. However, recent environmental and health restrictions have prioritized the synthesis of potentially benign QD alternatives (e.g., indium phosphide, InP) to QDs containing carcinogenic elements. Specifically, core-shell InP/ZnSe/ZnS heteronanostructure is considered a promising non-toxic material candidate that could reach desirable optical properties (high quantum yield and narrow emission linewidth) similar to the cadmium-based QDs. Despite the potential of InP-based QDs for next-generation photonic devices, their high-dimensional design space because of the multi-stage synthesis nature makes it extremely challenging for manual batch reactors to comprehensively explore. An attractive platform for the accelerated synthesis space exploration and intensified manufacturing of emerging colloidal QDs are continuous flow strategies, due to their facile integration with in-situ characterization techniques, intensified heat and mass transfer rates, high material efficiency, and superior reproducibility when compared to traditional batch synthesis techniques. However, matching the QD quality obtained in multi-stage batch reactors and microfluidic reactors remains a challenge. Due to the significant difference in the microreaction environments of batch and flow reactors, solely "translating" the synthetic process parameters and protocol such as temperature profiles as well as rate and sequence of precursor addition and residence times in continuous multi-stage flow reactors is not sufficient to achieve high performing QDs.

In this work, we present a modular library of 2D and 3D flow reactors to achieve maximum flexibility and reconfigurability for the controlled and intensified synthesis of InP QDs. We demonstrate the significance of both time- and temperature-to-distance transformations achieved through the reconfiguration of our flow reactor modules to optimize the multi-stage QD synthetic route. Thus, achieving high-quality InP QDs in continuous flow reactors. We report a systematic study of the multi-stage flow synthesis of InP QDs, utilizing *in-situ* absorption spectroscopy *via* both hot-injection and heat-up synthesis methods followed by the analysis and optimization of reaction cycling for sequential core growth. Furthermore, the resulting continuous flow synthesis protocol is up to an order of magnitude shorter than previously reported batch protocols. Further adoption of the developed modular flow chemistry strategies in this work could provide access to the unexplored design and synthesis space regions of the other colloidal QDs beyond InP QDs.

SESSION NM03.02: QD Synthesis II
Session Chair: Justin Caram
Monday Afternoon, November 28, 2022
Hynes, Level 2, Room 209

1:30 PM *NM03.02.01

Nanocrystal-Derived Inorganic Aerogels and Their Applications [Alexander Eychmueller](#); TU Dresden, Germany

The focus of my talk will be laid on gels and aerogels manufactured from a variety of different (semiconductor and metal) colloidal nanoparticles. These "New inorganic aerogels"¹ carry an enormous potential for applications which is largely related to their extremely low density and high porosity providing access to the capacious inner surface of the interconnected nanoobjects they consist of.

This will be exemplified with electrocatalytic applications of metal aerogels. An example is the recently developed facile strategy for the controllable synthesis of nanoparticle-based bimetallic Pt-Ni aerogels with high surface area and large porosity, which act as highly active and stable catalysts for the oxygen reduction reaction in polymer electrolyte fuel cell cathodes.² For gaining highest performance of these catalysts the surface chemistry³ as well as the formation mechanisms have to be studied and tuned.^{4,5}

Further applications⁶ I will touch upon include a continuous droplet reactor for the production of millimeter sized spherical aerogels,⁷ hybrid plasmonic-aerogel materials as optical superheaters with engineered resonances,⁸ size-tunable Gold aerogels as durable and misfocus-tolerant 3D substrates for multiplex SERS detection,⁹ and the catalytic activity and selectivity in methanol steam reforming by of intermetallic compounds.¹⁰

References

- [1] C. Ziegler, A. Wolf, W. Liu, A.-K. Herrmann, N. Gaponik, A. Eychmüller, *Angew. Chem. Int. Ed.* 56, 9745 (2017).
- [2] S. Henning, H. Ishikawa, L. Kühn, J. Herranz, E. Müller, A. Eychmüller, T.S. Schmidt, *Angew. Chem. Int. Ed.* 56, 10707 (2017)
- [3] X. Fan, S. Zerebecki, R. Du, R. Hübner, G. Marzum, G. Jiang, Y. Hu, S. Barcikowski, S. Reichenberger, A. Eychmüller, *Angew. Chem. Int. Ed.* 59, 5706 (2020).
- [4] R. Du, J. Wang, R. Hübner, X. Fan, I. Senkowska, Y. Hu, S. Kaskel, A. Eychmüller, *Nat. Comm.* 11, 1590 (2020).
- [5] a) H. Ishikawa, S. Henning, J. Herranz, A. Eychmüller, M. Uchida, T.J. Schmidt, *J. Electrochem. Soc.* 165, F2 (2018), b) S. Jungblut, J.-O. Joswig, A. Eychmüller, *J. Phys. Chem. C* 123, 950 (2019), c) S. Jungblut, J.-O. Joswig, A. Eychmüller, *Phys. Chem. Chem. Phys.* 21, 5723 (2019), d) R. Du, Y. Hu, R. Hübner, J.-O. Joswig, X. Fan, K. Schneider, A. Eychmüller, *Science Advances* 5, 4590 (2019), e) P. Chauhan, K. Hiekel, J.S. Diercks, J. Herranz, V.A. Saveleva, P. Kavlyuk, A. Eychmüller, T.S. Schmidt, *ACS Mater. Au* 2, 278 (2022).
- [6] X. Jiang, R. Du, R. Hübner, Y. Hu, A. Eychmüller, *Matter* 4,54 (2021).
- [7] L. Thoni, B. Klemmed, M. Georgi, A. Benad, S. Klosz, A. Eychmüller, *RSC Adv.* 10, 2277 (2020).
- [8] B. Klemmed, L.V. Besteiro, A. Benad, M. Georgi, Z. Wang, A.O. Govorov, A. Eychmüller, *Angew. Chem. Int. Ed.* 59, 1696 (2020).
- [9] L. Zhou, Y. Peng, N. Zhang, R. Du, R. Hübner, X. Wen, D. Li, Y. Hu, A. Eychmüller, *Adv. Opt. Mater.* 9, 2100352 (2021).
- [10] a) C. Ziegler, S. Klosz, L. Borchardt, M. Oschatz, S. Kaskel, M. Friedrich, R. Kriegel, T. Keilhauer, M. Armbrüster, *Adv. Funct. Mat.* 26, 1014 (2016), b) N. Köwitsch, L. Thoni, B. Klemmed, A. Benad, P. Paciok, M. Heggen, I. Köwitsch, M. Mehring, A. Eychmüller, M. Armbrüster, *ACS Catalysis* 11, 304 (2021), c) N. Köwitsch, L. Thoni, B. Klemmed, A. Benad, P. Paciok, M. Heggen, A. Eychmüller, M. Armbrüster, *J. Phys. Chem. C* 125, 9809 (2021).

2:00 PM NM03.02.02

Single Photons from Silver Dopant Cations in CdSe Nanoplatelets William F. Girten, Mitesh Amin and Todd Krauss; University of Rochester, United States

Quasi-two-dimensional cadmium selenide (CdSe) nanoplatelets (NPLs) have garnered significant research attention in recent years due to their extremely narrow band-edge exciton photoluminescence (PL) linewidths, well-defined absorbance features, and short PL lifetimes. Adding small amounts of aliovalent dopant ions to the NPLs, such as silver, gives rise to a broad and red-shifted dopant-related emission. However, the origin and photophysical properties of the dopant-related emission are not well understood for NPLs. We will discuss NPL photophysical measurements of Ag-doped 4.5 monolayer CdSe NPLs as a function of their lateral size and relative dopant concentrations. We have found that that NPLs with the same concentration of incorporated silver ions but varying lateral areas show large differences in the PL efficiency (relative to the excitonic PL) from the dopant. Furthermore, PL from individual NPLs show dual emission from both the band edge exciton and the dopant state, indicating a homogeneous doping process across the ensemble. Dopant PL intensity and spectral fluctuations across individual NPLs indicate a dynamic hole trapping process which may reflect a heterogeneous distribution of Ag atoms substitutionally placed across the lattice, which is supported by high-resolution electron microscopy images. Under ambient conditions, the dopant emission state also exhibited pronounced photon antibunching with a $g_2(0) = 0.24$, potentially providing a bright, efficient single photon source, which would have potentially important implications for the transmission of quantum information using light. Overall, our findings illustrate the importance of NPL morphology as it relates to the unique single particle photophysics of doped CdSe NPLs.

2:15 PM NM03.02.03

Liquid-Based Ternary Colloidal Nanoparticles for Tunable Phase Change Optics Dhananjeya Kumar Vsa, Helena Weigand, Matthias Can, Simon Wintersteller, Florian Schenk, Artemios Kavounis, Olesya Yarema, Rachel Grange and Maksym Yarema; ETH Zurich, Switzerland

Phase change memory (PCM) materials have gained major interest and revival since their utility in optical data storage discs. This is due to the tunable contrast in material properties such as complex refractive index and electrical conductivity between amorphous and crystalline states. The most heavily studied PCM materials fall in the pseudo-binary tie line of GeTe and Sb₂Te₃. Aside from Sb, doping GeTe with elements such as Pb, Bi, Cu, and Sn has been shown to improve power efficiency, induce faster crystallization, and enhance phase-contrast during switching. Currently, vacuum technology is heavily used for the fabrication of PCM. Despite having the advantages of producing high-quality thin film and good stoichiometry control, vacuum technology has limited combinatorial throughput and flexibility for new materials discovery. Colloidal inorganic nanoparticle chemistry has shown great promise for versatility in synthesizing new materials and cost-effective translation to device applications through liquid-based fabrication routes. Here, we report a facile hot injection synthesis approach to prepare a library of ternary nanoparticles, M₂Ge_{1-x}Te (where M is Sn, Cu, Pb, Bi), which are promising for PCM applications. We then investigate two material systems, namely SnGeTe (SGT) and CuGeTe (CGT), in more details. We utilize the chemical tunability of the synthesis to achieve varied compositions and phases in the SGT and CGT nanoparticles. Using high-temperature *in-situ* XRD experiments we find that increasing the Sn-doping lowers the crystallization temperature while Cu shows the opposite with respect to stoichiometric GeTe nanoparticles. We explain these observations from the viewpoint of local atomic arrangements of SGT and CGT nanoparticles, using X-ray absorption spectroscopy. Furthermore, we present thin-film fabrication through an inorganic ligand-exchange route and spin coating, which we characterize for optical properties in the amorphous and crystalline state using ellipsometry. From this we identify a reflectivity contrast and that SGT and CGT show the most pronounced difference in the refractive index of 0.9 at 1070 nm and 0.51 at 1490 nm respectively. Finally, we demonstrate an optical utility by fabricating a simple reflective stack with SGT nanoparticle thin film sandwiched between ITO layers of tunable thickness on Al mirror. We discuss the change in reflection spectra and optical contrast of the stack in the context of reflective display applications. Our work paves the way to simple fabrication of other photonic PCM applications, including near-IR metalenses, tunable filters, and beam steerer.

2:30 PM BREAK

3:00 PM NM03.02.04

Zinc-Free Synthesis of High-Quality Indium Phosphide Quantum Dots Covering a Large Size Range Ranjana Yadav¹, Winnie Ling², Céline Rivaux¹, Christine S. Pierre¹ and Peter Reiss¹; ¹CEA Grenoble, IRIG/SyMMES (UMR5819 CEA-CNRS-UGA), France; ²Institut de Biologie Structurale (IBS), France

Indium phosphide QDs hold great promises for use in displays and LEDs and are widely considered a safer alternative to toxic Cd-based QDs.[1] Even though significant progress has been made in their synthesis, using non-pyrophoric phosphorus precursors it is still highly challenging to achieve narrow emission linewidths and to reach the near-infrared spectral range. The addition of zinc carboxylates to the synthesis of InP QDs has become commonplace with the goal to reduce the size distribution and increase the PLQY [2]. However, lattice doping by zinc can lead to shallow hole traps inducing spectral broadening, large Stokes shift, and long PL lifetimes.[3]

We present a novel Zn-free synthetic pathway for high-quality InP QDs. As-synthesized InP QDs are tetrahedral-shaped with tunable sizes from 3 nm to 9 nm without secondary additions of precursors. The first excitonic is tunable from 450 nm to 700 nm by changing the reaction conditions. These core QDs

have been subsequently overcoated with a thin ZnS shell at a temperature as low as 140°C to avoid alloying and doping of the core lattice. The emission of the InP/ZnS QDs was tunable up to 728 nm with a NIR PL linewidth of only 48 nm (FWHM). The obtained InP/ZnS QDs also exhibit a much lower Stokes shift and significantly shorter PL lifetime compared to the reported data. Finally, the reaction mechanism underlying the novel synthetic scheme was elucidated by NMR spectroscopy.

[1] Reiss, P.; Carrière, M.; Lincheneau, C.; Vaure, L.; Tamang, S., Synthesis of Semiconductor Nanocrystals, Focusing on Nontoxic and Earth-Abundant Materials. *Chem. Rev.* **2016**, *116* (18), 10731-10819.

[2] Kim, Y.; Lee, S., Investigating the role of zinc precursor during the synthesis of the core of III-V QDs. *Chem. Commun.* **2022**, *58* (6), 875-878.

[3] Janke, E. M.; Williams, N. E.; She, C.; Zherebetsky, D.; Hudson, M. H.; Wang, L.; Gosztola, D. J.; Schaller, R. D.; Lee, B.; Sun, C.; Engel, G. S.; Talapin, D. V., Origin of Broad Emission Spectra in InP Quantum Dots: Contributions from Structural and Electronic Disorder. *J. Am. Chem. Soc.* **2018**, *140* (46), 15791-15803.

3:15 PM NM03.02.05

Synthesis and Characterization of Cu-Doped PbS Nanocrystals Patrick Yee, Sarah Britzman, Paul Cunningham, R Stroud, Katherine Burgess and Janice Boercker; U.S. Naval Research Laboratory, United States

Excitonic PbS nanoparticles have shown excellent infrared photosensitivity, but their limited diffusion lengths of photoexcited charge carriers result in poor device efficiencies. They also have slow radiative recombination rates that limit the performance of light-emitting diodes. To counter some of these limitations, we have developed a synthetic method for incorporating copper into PbS nanocrystals starting with Cu_{2-x}S core nanocrystals. Time-resolved photoluminescence spectroscopy shows a shorter photoluminescence lifetime relative to PbS nanocrystals but a comparable photoluminescence quantum yield, indicating faster radiative decay rates. HAADF-STEM EDS maps show two populations of nanocrystals: plasmonic Cu-rich nanocrystals and excitonic Pb-rich nanocrystals. This ratio of these populations can be tuned by changing the starting Cu_{2-x}S core size or changing the reaction concentration. When smaller Cu_{2-x}S cores and higher reaction concentrations are used, we can create a single population of Cu-doped PbS nanocrystals. With larger Cu_{2-x}S cores and lower reaction concentrations, we can create a single population of plasmonic Cu_{2-x}S/PbS core/shell nanocrystals.¹ ICP-OES measurement show that the atomic Cu:Pb ratio in these new Cu-doped PbS nanocrystals is as low as 0.005:1. In addition to controlling the population ratio of plasmonic Cu-rich nanocrystals and excitonic Pb-rich nanocrystals, we also see a blueshift of the exciton energies with decreasing size. These new Cu-doped PbS nanocrystals lie on a sizing curve (1st exciton transition energy vs nanocrystal diameter) distinct from that of pure PbS nanocrystals, while also showing shorter photoluminescence lifetimes and faster radiative decay rates making them a promising as a new material for infrared single-photon emitters.

1. Yee, P. Y.; Britzman, S.; Mahadik, N. A.; Tischler, J.G.; Stroud, R.M.; Efros, A. L.; Sercel, P.C.; and Boercker, J. E. Cu_{2-x}S/PbS Core/Shell Nanocrystals with Improved Chemical Stability. *Chem. Mater.* **2021**, *33*, 17, 6685-6691.

3:30 PM NM03.02.06

Cadmium-Free and Efficient Type-II InP/ZnO/ZnS Quantum Dots and Their Application for LEDs Gunçem O. Eren¹, Sadra Sadeghi¹, Houman Bahmani Jalali¹, Maximilian Ritter², Mertcan Han¹, Isinsu Baylam¹, Rustamzhon Melikov¹, Asim Onal¹, Fatma Oz¹, Mehmet Sahin³, Clewa W. Ow-Yang⁴, Alphan Sennaroglu¹, Rainer T. Lechner² and Sedat Nizamoglu^{1,1,1}; ¹Koç University, Turkey; ²Montanuniversitaet Leoben, Austria; ³Abdullah Gul University, Turkey; ⁴Sabancı University, Turkey

Because of the spatial separation of electron-hole wavefunctions, type-II quantum dots (QDs) are considered to have a poor photoluminescence quantum yield (PLQY). In recent studies, cadmium-based type-II QDs with high PLQY have been reported¹. However, due to its toxic environment, it is required to develop non-toxic and efficient type-II QDs. Herein, we demonstrate highly efficient heavy toxic metal-free type-II InP/ZnO/ZnS core/shell/shell nanostructures².

InP core structure is synthesized by the hot injection technique. Consecutive ZnO and ZnS shells are grown by thermal decomposition and successive ionic layer adsorption (SILAR), respectively. Optimization studies of ZnO and ZnS shell thickness result in a highly efficient nanostructure that has a PLQY of 91%. The effect of ZnO and ZnS shell growth on the non-linear absorption and ultrafast decay properties is investigated via femtosecond pump-probe spectroscopy.

Small-angle X-ray scattering (SAXS) and transmission electron microscopy (TEM) measurements were used to determine the size and shape of the core/shell/shell QDs. The SAXS analysis shows that multiple ZnS shell growth induces the transition of nanocrystals from spherical to ellipsoidal shape which is in accordance with TEM results. Finally, we integrate the core/shell/shell QDs into light-emitting diode (LED) die in liquid state to reduce the host-material effect. The resulting liquid-LED device exhibited 9.4% of external quantum efficiency (EQE) and 6.8% of power conversion efficiency (PCE), respectively, making it the most efficient type-II-based LED to date. This research found that cadmium-free type-II QDs can achieve significant levels of efficiency, which could lead to new devices and nanomaterials for bioimaging, display, and lighting.

Keywords: cadmium-free, type-II band alignment, liquid LED

Reference:

(1) Ca, N.; Hien, N.; Luyen, N.; Lien, V.; Thanh, L.; Do, P.; Bau, N.; Pham, T. Photoluminescence properties of CdTe/CdTeSe/CdSe core/alloyed/shell type-II quantum dots. *Journal of Alloys and Compounds* **2019**, *787*, 823-830.

(2) Eren, G. O.; Sadeghi, S.; Bahmani Jalali, H.; Ritter, M.; Han, M.; Baylam, I.; Melikov, R.; Onal, A.; Oz, F.; Sahin, M. Cadmium-free and efficient type-II InP/ZnO/ZnS quantum dots and their application for LEDs. *ACS Applied Materials & Interfaces* **2021**, *13*, 32022-32030.

Acknowledgment: S.N. acknowledges support from the European Research Council (ERC) under the European Union's Horizon 2020 Research and Innovation Programme (grant agreement no. 639846). S.N. also acknowledges the support of the Turkish Academy of Sciences (TUBA-GEBIP; The Young Scientist Award Program); the Science Academy of Turkey (BAGEP; The Young Scientist Award Program); and Bilim Kahramanlari Derneği (The Young Scientist Award Program).

8:30 AM *NM03.03.01

Molecular and Nanostructured Semiconductors—Unique Opportunities for Light Harvesting and Light Emission [Richard R. Lunt](#); Michigan State University, United States

The presence of excitons in organic, molecular, and nanocluster materials offer new opportunities for low-cost photovoltaics (PV) and light-emitting systems and provide prospects for unique energy applications. In the first part of the talk, I will introduce our pioneering work on developing transparent photovoltaics (TPV) and transparent luminescent solar concentrators (TSLC) that are creating new paradigms for solar harvesting. These devices are specifically enabled by the manipulation of excitonic semiconductor materials with selective and tuneable harvesting in the near-infrared and ultraviolet components of the solar spectrum. I will discuss key photophysical properties, outline the thermodynamic and practical limits to these new classes of materials and devices, and discuss their optimization and commercialization for a range of applications from buildings to agricultural spaces. I will also outline key protocols necessary to accurately characterize TPVs and TLSCs. In the second part of the talk, I will describe our work on developing phosphorescent nanocluster based light emitting diodes and describe the role of cation/halogen/ligand substitutions on the electroluminescent properties. These inorganic phosphorescent emitters are based on metal halide nanoclusters and nanocluster salts, which have high stability, high abundance, and high quantum yield, and therefore have strong potential as a low cost alternative to organic phosphorescent emitters in a range of applications

9:00 AM NM03.03.02

Near-Unity Biexciton Emission Quantum Yield in CdS/CdSe/CdS Quantum Shells Andrew Marder¹, James Cassidy², Dulanjan Harankahage², Mikhail Zamkov² and [Anton Malko](#)¹; ¹The University of Texas at Dallas, United States; ²Bowling Green State University, United States

Non-radiative Auger recombination is the primary multiexciton loss mechanism in colloidal nanocrystals and an impediment for prospective optoelectronic applications. Recent developments of new core/shell nanocrystal quantum dots (NQDs) with suppressed Auger recombination rates has opened the possibility for studying multicarrier states using single particle time-resolved photoluminescence (PL) spectroscopy. We recently developed a new class of semiconductor NQDs, CdS/CdSe/CdS “nanoshells” where excitons are localized in a large spherical CdSe shell, rather than in a small volume of the core of a conventional “core/shell” NQD. Here, we demonstrate that a quantum shell geometry strongly inhibits Auger processes, resulting in extraordinary improvements to biexciton (BX) quantum yield (QY) and multiexciton (trions and BX) lifetimes. From time-correlated PL of multistate blinking trajectories, the lifetimes and QY of neutral and charged excitons (trions) in individual dots are experimentally measured and a non-statistical scaling model is employed to calculate multiexciton QYs, radiative lifetimes and Auger decay rates. These results are corroborated by second-order correlation (“antibunching”) statistics of BX QY to confirm the validity of the scaling model. By varying the quantum well volume in CdS_{bulk}/CdSe/CdS quantum shells (CdS core diameter ranging from 4.5 to 8 nm), we demonstrate that larger-core nanoparticles exhibit the strongest suppression of Auger decay, corresponding to BX QY of nearly 100%. A combination of ultralong (>15 ns) BX emission lifetimes and strong exciton-exciton repulsion in large-core samples allowed demonstrating low-threshold amplified spontaneous emission (ASE) and large modal gain values for BX transitions. The observed combination of long BX lifetimes and large quantum yields makes the quantum shell geometry a promising candidate for light-emitting and lasing applications.

9:15 AM NM03.03.03

Interpretation of Heteroepitaxy Process on Colloidal III–V/II–VI Nanocrystals [Yeongho Choi](#), Donghyo Hahm, Wan Ki Bae and Jaehoon Lim; Sungkyunkwan University, Korea (the Republic of)

Construction of heterostructures on colloidal nanocrystals (NCs) is one of essential strategies to apply them for various optoelectronic applications such as biomarkers, displays, lightings or solar cells. Many literatures on the heteroepitaxy of NCs have focused on proper processing conditions like ligand types, precursors, or reaction temperatures to accomplish desired morphology and interface. The functionality and its performance of heterostructured NCs are primarily determined by the quality of interface, whether it contains undesired defects or not. In solution phase heteroepitaxy, unfortunately, detailed picture is veiled how elements are participating in epitaxial layer formation and how interfacial defects can be eliminated during the growth. Use of long hydrocarbon ligands may hinder adsorption, surface diffusion, and epilayer formation of metal ions delivered from precursors. We merely perform trial-and-error approaches to find optimal synthetic conditions to realize defect-less heterointerfaces.

In this study, we will propose III-V/II-VI heteroepitaxy on colloidal NCs associated with transfer of surface ligands to alkylphosphine intermediates. Using InP and ZnSe as a III-V seed and a II-VI epitaxy material, we probed association and dissociation of surface ligands as well as organometallic precursors using varied temperature ³¹P, ⁷⁷Se and ¹H nuclear magnetic resonance. We confirmed that trioctylphosphine selenide, representative anion precursor, transfers Se to NCs' surface by accepting carboxylate ligands to form oleyloxytrioctylphosphonium. And incoming zinc oleate leaves Zn to NCs' surface by donating oleate ligands to oleyloxytrioctylphosphonium to form dioctyltrioctylphosphorane. Absence of ZnSe vibrational mode in InP NCs covered with Zn and Se adatoms implies that they form loose Zn-Se monomer networks, not crystalline epitaxial layer. We confirmed the presence of energetic barrier to convert the Zn-Se monomer network to the ZnSe epitaxial layer. This transformation barrier is primarily associated with the oxidized sites preventing association of Zn-P and In-Se bonds and the steric hindrance on the adsorption of zinc oleates.

Understanding on surface chemistry of heteroepitaxy allowed us to devise novel heteroepitaxy process quoting uniform and defect-less III-V/II-VI heterointerface. We chose type-I InP/ZnS core/shell NCs as our test bed because of intrinsic difficulty in uniform ZnS epilayer growth originating from large lattice mismatch of 7.8%. We accomplished near unity photoluminescence quantum yield despite very thin, 1~2 ZnS epitaxial layers. Nearly defect-free heterointerface can be inferred from monoexponential photoluminescence decay. We believe that our finding will contribute to realize heterostructure NCs with superb optoelectronic properties.

9:30 AM *NM03.03.04

Carbon Quantum Dots—A Sustainable Nanoplatfom in Sensing and Energy Applications [Rafik Naccache](#); Concordia University, Canada

significant interest for the development of novel applications in the physical and life sciences. This is especially true for luminescent nanoparticles, which have been investigated for the development of sensors, imaging/diagnostic probes, display and solar cell applications. Recently, a relatively new class of luminescent nanomaterials, namely carbon dots, has come to light. Carbon dots, sometimes known as carbogenic dots, are carbon, oxygen, nitrogen and hydrogen containing materials with the first two elements typically accounting for ~90% of their elemental composition. Moreover, they are water dispersible and can be prepared from an abundant number of inexpensive sources including small molecules such as citric acid, amino acids, sugars and even waste. While they are small in size (typically 1-10 nm), they can offer a high quantum yield of fluorescence, a process that is controlled through passivation of the surface with an organic reagent. Of particular interest are their optical properties, which can be tailored via careful selection of the starting precursors and the desired synthesis route resulting in the ability to generate fluorescence from the blue to the near infrared regions of the spectrum. In addition to their versatile optical properties, these carbon dots are generally known to have low cytotoxicity and good biocompatibility. Combined with their small size and versatile optical properties, developing carbon dots as a nanoplatfom can be achieved as these nanodots lend themselves for integration in a myriad of applications most notably in sensing and catalysis, among others. Our work focuses on achieving a fundamental understanding of the synthesis of these carbon dots in order to control their size and achieve homogenous surface chemistry and optical properties. We take advantage of the large surface area to volume ratio and study their binding to heavy metals in water in an effort to develop novel environmental sensing tools. Finally, we

exploit their surface chemistry and study their catalytic behaviour in the transformation of refined and waste oils to clean biofuel.

10:00 AM BREAK

10:30 AM *NM03.03.05

Colloidal Chemistry in Molten Inorganic Salts Justin Ondry, Aritrajit Gupta, Wooje Cho and Dmitri V. Talapin; University of Chicago, United States

Many functional nanomaterials used for catalysis, healthcare, solid-state lighting, and displays are synthesized by colloidal techniques. The scope of chemical transformations accessible to colloidal chemists is determined by the stability and compatibility of solvents and surfactants used as a reaction medium. For example, very few traditional solvents can handle temperatures above 400C, while many inorganic phases require even higher temperatures to form. We are developing comprehensive understanding of a novel class of colloidal systems, colloids in molten inorganic salts. Nanoparticles of different transition metals, semiconductors, oxides, and magnetic materials can form true colloids in molten inorganic salts. The colloidal stability of nanoparticles in molten salts could not be explained by traditional electrostatic and steric stabilization mechanisms. Our experimental and computational studies point to the importance of the long-range ion correlations in the molten salt near the nanocrystal interface.

In addition to the fundamental exploration of new colloidal systems, molten salts expand the boundaries for solution synthesis of many nanomaterials that have been out of reach for colloidal chemists. We have used molten salts to synthesize colloidal GaAs, $\text{In}_x\text{Ga}_{1-x}\text{As}$, $\text{In}_x\text{Ga}_{1-x}\text{P}$ and GaN quantum dots, which resisted numerous synthetic attempts for over two decades. By further developing colloidal chemistry in molten salts, we hope to enable synthetic routes toward various functional nanomaterials previously considered unsynthesizable by colloidal methods.

11:00 AM NM03.03.06

Lifetime Blinking in InP/ZnSe_xS_{1-x}/ZnS Quantum Dots Yu Jin Lee¹, Dae-Yeon Jo², Taehee Kim¹, Jung-Ho Jo², Jumi Park¹, Heesun Yang² and Dongho Kim¹; ¹Yonsei University, Korea (the Republic of); ²Hongik University, Korea (the Republic of)

We report the observation of ‘lifetime blinking’ in interface alloyed environment-friendly InP/ZnSe_xS_{1-x}/ZnS quantum dots (QDs) with optimal composition. Auger recombination is known to be one of the major drawback factors for self-emitting quantum dot light-emitting diode (QLED) devices. When unwanted Auger recombination is sufficiently suppressed, the charged states of QDs emit comparably to the neutral states of QDs. Rather than common blinking properties of QDs where the charging and discharging results in fluctuation in photoluminescence (PL) intensity, only lifetime variations were observed under substantial suppression of Auger recombination. The lifetime fluctuation despite nonblinking emission is referred to as ‘lifetime blinking’ and is only observed in high-quality QDs with high trion quantum yields and low non-radiative Auger rates. To the best of our knowledge, this study is the first to observe lifetime blinking in non-Cd-based QDs.

We scrutinize the effect of various ZnSeS midshell compositions on QD performance and uncover the relationship between shell structure/composition and QD performance. Negative trion Auger recombination dynamics are studied through ensemble photoelectron doping experiments and single-dot analysis. Interface alloying successfully reduces lattice difference and smoothen confinement potential, and therefore, substantially suppresses unwanted Auger recombination. Non-radiative Auger rates drastically decrease from 0.41 ns⁻¹ to 0.022 ns⁻¹ with the introduction of a smooth shell interface. As the Auger process is suppressed, ‘lifetime blinking’ is observed since the trion quantum yield of gradient shell QD is enhanced to 81% by a factor of 4.5 compared to that of the discrete QD. Properties regarding PL peak width, including spectral diffusion and single-dot PL peak width, are also improved with the introduction of gradient shells due to reduced lattice mismatch between shells and increased charge trapping energy barrier. Yet, these performance improvements are found to be composition-dependent, requiring ZnSe rich midshell to prevent lattice strain in the interface of the core and the shell from arising. We anticipate the presented result to act as a stepping-stone towards developing environmentally friendly QLEDs with high performance.

[1] Lee, Y. et al. Effectual Interface and Defect Engineering for Auger Recombination Suppression in Bright InP/ZnSeS/ZnS Quantum Dots. *ACS Appl. Mater. Interfaces* **14**, 10, 12479–12487 (2022)

[2] Lee, S. et al. The effects of discrete and gradient mid-shell structures on the photoluminescence of single InP quantum dots. *Nanoscale*. **11**, 23251–23258 (2019)

[3] Park, Y. et al. Effect of Interfacial Alloying versus “Volume Scaling” on Auger Recombination in Compositionally Graded Semiconductor Quantum Dots. *Nano Lett.* **17**, 9, 5607–5613 (2017)

[4] Kim, T. et al. Negative Trion Auger Recombination in Highly Luminescent InP/ZnSe/ZnS Quantum Dots. *Nano Lett.* **21**, 5, 2111–2116 (2021)

[5] Cragg, G & Efros, A. Suppression of Auger Processes in Confined Structures. *Nano Lett.* **10**, 1, 313–317 (2010)

11:15 AM NM03.03.07

Shape-Tuned Multiphoton Emission in Single-Crystalline InP Nanotetrapods Taehee Kim¹, Youngsik Kim², Seongmin Park³, Kyoungwon Park⁴, Zhen Wang³, Sang Ho Oh³, Sohee Jeong³ and Dongho Kim¹; ¹Yonsei University, Korea (the Republic of); ²Samsung Display, Korea (the Republic of); ³Sungkyunkwan University, Korea (the Republic of); ⁴Korea Electronics Technology Institute, Korea (the Republic of)

Semiconductors are essential building blocks of modern lifestyles. As their properties are dictated by the fate of photogenerated exciton, manipulating exciton behavior has been a primary goal of nanomaterials[1]. Analogous to molecular chemistry, in which the functionality of a molecule is dictated by the intramolecular exciton-exciton interactions, it is inevitable to expand this understanding into the framework of semiconductor nanomaterials. Strong spatial confinement in nanocrystals (NCs) and quantum dots gives rise to their unusual excitonic characteristics. When highly confined at all three dimensions (i.e. spherical NCs), tightly bound multiexciton states rapidly decay via Auger recombination. As confinement becomes released as in rod- or wire-shaped NCs, recombination mechanism of multiexciton states is altered due to the change in a way multiple excitons interact. This inspired a straightforward strategy of NC shape tuning to tailor interactions between adjacent excitons[2].

Nanotetrapods exhibit unique branched geometry that enabled a precise control over their excited-state orientation and provided a novel dimensional configuration for exciton-exciton interactions. Time-resolved single particle spectroscopy revealed a transition from single to multiphoton emitter occurring at the critical tetrapod arm length ($L_{\text{arm}} = a_B$) of the material. This transition was mediated by the geometry-driven arm-localization of individual exciton. Excited-state anisotropy dynamics was unveiled by polarization-controlled ultrafast spectroscopy, by which the evolution of exciton confinement dimension from 3D(dot)-like to 2D(rod)-like confinement was observed as the arm length increased. Collective behavior of interacting multiple excitons in long-armed ($L_{\text{arm}} > a_B$) nanotetrapods enabled the unprecedented geometric manipulation of memory effect in single NC luminescence. Tunability of exciton-exciton interactions prove nanotetrapods a useful system to explore the interplay of multiple quantum states, extending the applicability of the new class of single-crystalline nanomaterials[3].

[1] X. Peng, L. Manna, W. Yang, J. Wickham, E. Scher, A. Kadavanich, A. P. Alivisatos, *Nature* **404**, 59, (2000).

[2] Y. Kim, H. Choi, Y. Lee, W. K. Koh, E. Cho, T. Kim, H. Kim, Y. H. Kim, H. Y. Jeong, S. Jeong, *Nat. Commun.* **12**, 4454, (2021).

[3] T. Kim, Y. Kim, S. Park, K. Park, Z. Wang, S. H. Oh, S. Jeong, D. Kim, *Adv. Mater.* **34**, 2110665, (2022).

11:30 AM NM03.03.08

Facile Synthesis of Giant CdHgSe/Cd(Hg)SeS Core/Shell Quantum Dots with Large-Stokes-Shift High-Quantum-Yield Near-Infrared Photoluminescence via Chlorine-Mediated Ripening Gyu-dong Lee¹, Wonseok Lee², Andrew M. Smith² and Sung Jun Lim¹; ¹Daegu Gyeongbuk Institute of Science and Technology, Korea (the Republic of); ²University of Illinois at Urbana-Champaign, United States

Emitters having high photoluminescence quantum yield (QY), controllable absorption and emission wavelengths and minimal fluorescence intermittency are required for various applications, including biomedical imaging and optoelectronic devices. One of the promising emitters that satisfies these requirements is a giant quantum dot (GQD) having a core/thick shell structure. In a GQD, absorption and emission wavelengths can be tuned independently by controlling the composition and dimension (diameter or thickness) of the core and the shell, respectively. Moreover, the thick shell effectively decouples the electronic states of the core from the surface states and suppresses Auger recombination to improve QY and photostability. These advantages allowed GQDs to be served as light sources for solid state lighting and fluorescent probes for tracking individual biomolecules in biological environment. However, conventional methods for the synthesis of core/thick shell QDs, such as successive ionic layer adsorption and reaction (SILAR) or continuous precursor injection, were time-consuming processes.

In this work, we fabricated a new GQD having a CdHgSe/Cd(Hg)SeS core/thick shell structure exhibiting a large-Stokes-shift high-QY NIR emission. Unlike conventional GQDs synthesized from aforementioned time-consuming processes, our GQDs were prepared via a facile route utilizing chlorine-mediated ripening. The new ripening synthesis can grow CdHgSe/Cd(Hg)SeS core/thick shell (>20 monolayers, MLs) QDs in a short time (<1 h) through a single heat-up reaction. Briefly, CdHgSe/CdS core/thin shell QDs (~1.6 MLs) (average diameter ~4.5 nm) with NIR emission (λ_{em} ~900 nm; QY > 40%) were prepared by the SILAR process, then heated to ~240 °C in the presence of a small amount of chloroform to initiate ripening. The core/thin shell QDs were stable at elevated temperatures before chloroform addition. Also, mass spectrometry analysis of the intermediate species showed the production of metal chlorides and chalcogen species during ripening, confirming that chlorine plays a crucial role in ripening. The ripening process increased the average QD diameter to ~15 nm, suggesting that only ~3 % of the initial CdHgSe/CdS core/thin shell QDs were grown into GQDs by consuming the rest as the shell precursors. Interestingly, little change in the photoluminescence spectra was observed during ripening, whereas NIR emission QY were increased > 70%. In addition, the effective absorption onset showed a significant blueshift to ~600 nm during ripening due to the rise of an intense absorption band of the thick Cd(Hg)SeS shell, increasing the Stokes shift to ~300 nm (~0.7 eV). The new synthetic process based on chlorine-mediated ripening will enable facile synthesis of various types of core/shell QDs and our GQDs will be used as efficient light sources in various applications including bioimaging and optoelectronic devices.

11:45 AM NM03.03.09

Understanding the Blinking Mechanism in Strongly Confined Lead Bromide Perovskite Quantum Dots Chenjia Mi, Matthew Atteberry and Yitong Dong; University of Oklahoma, United States

Strongly confined lead bromide perovskite quantum dots (PQDs), benefit from their high photoluminescence (PL) quantum yield, defect tolerance and fast radiative emission rate, possess the potential of making high purity single photon emission sources that are “bright and blue” (high emission rate with high energy of emitted photon), which can be used directly in photonics for quantum information technologies, or as a quantum excitation light source to trigger quantum photon emission from traditional emitters.

The phenomenon that the quantum dots (QDs) have PL intermittency greatly exceeds their radiative lifetime, commonly known as “blinking”, hinders their potential applications. Decades of effort has been put on studying the blinking mechanism of traditional QDs and currently three types of mechanisms are widely acknowledged: 1. Auger recombination from trions formed by exciting a charged QD (with the opposite charge carrier being deep-trapped or ejected), namely “Auger-blinking”; 2. photoactivation of interband states causing the band-edge charge carriers to non-radiatively recombine, namely “BCNR-blinking”; 3. photo- or electrical activation of intraband states causing the interception of hot-carriers, namely “HC-blinking”. However, few studies have focused on strongly confined colloidal PQDs, of which the materials are just recently made available by advances in syntheses. Compared to traditional II-VI or III-V QDs, PQDs are more ionic with friable surface, and are believed free from deep hole traps that commonly exist in II-VI QDs to cause Auger-blinking.

In this work, the blinking mechanism of a model type of single CsPbBr₃ PQDs were studied in comparison to commercial CdSe/ZnS core-shell QDs. The latter is considered standard samples to make lateral comparison with previous studies. Mono-dispersed colloidal PQDs with >80% PL quantum yield (75% for single PQDs, estimated with PL lifetime) are prepared. The single PQD emission was measured, and the blinking statistics associated with fluorescence lifetime-intensity distribution (FLID) analyses were performed to study the PL “on”/“off” states distribution and corresponding lifetimes. The PL quantum yield of single CdSe/ZnS QDs varies from 90% to 50%, and there coexist Auger-blinking and BCNR-blinking. FLID analyses show that the BCNR-blinking is dominating at low excitation power, while Auger-blinking become more significant at increased power, where the “off” state also increases. We have not observed HC-blinking in CdSe QDs. The results are consistent with previous reports.

In CsPbBr₃ PQDs, higher excitation power also leads to higher “off” time. However, the blinking mechanism is different in almost all other aspects. At low power, the FLID analyses suggest Auger blinking is the major contributor. Surprisingly, despite the trion Auger recombination is expected to be fast due to the small size, the “off” probability of PQDs is rather insignificant compared to CdSe QDs with similar “on” brightness that show Auger-blinking. The result indicates that the Auger-like behavior in PQDs stems from a “weak trion”, which consists of a charge in PQD is partially stabilized by the distortion of the lattice (a polaron) with an exciton. The latter weakly couples with the polaron and yields a slow Auger pathway compared to radiative recombination. With increased power the PQDs show BCNR-blinking which is attributed to the friability of the un-shelled PQDs surface.

In conclusion, our strongly confined PQDs exhibit suppressed blinking, despite Auger process is expected to be fast as a result of their small size. The blinking suppression is achieved possibly by formation of polaron that weakens the Auger effect. These results illustrate the direction for rational design and optimization of lead halide PQDs towards this application.

SESSION NM03.04: Nanoparticle Properties
Session Chairs: Alexander Eychmueller and Alexander Govorov
Tuesday Afternoon, November 29, 2022
Hynes, Level 2, Room 209

1:30 PM *NM03.04.01

Ultrafast Spectroscopy to Reveal the Origin of Double Emission, Optical Gain and the Role of Dopants in Engineered Semiconductor Nanocrystals Margherita Zavelani-Rossi^{1,2}, Andrea Camellini¹, Haiguang Zhao³, Sergio Brovelli⁴, Ranjani Viswanatha⁵, Isabella Concina⁶ and Alberto Vomiero^{6,7}; ¹Politecnico di Milano, Italy; ²CNR, Italy; ³Qingdao University, China; ⁴Università degli Studi di Milano-Bicocca, Italy; ⁵Jawaharlal Nehru Centre for Advanced Scientific Research, India; ⁶Luleå University of Technology, Sweden; ⁷Università Ca Foscari, Italy

Semiconductor nanocrystals (NCs) are appealing materials for a variety of photonics applications. Key advantage is the possibility to tailor their optical response by controlling the electronic structure (“wave function engineering”) through the synthesis. Beyond single wavelength band-edge photoluminescence (PL), other regimes have been demonstrated such as intragap emission, simultaneous emission on two different wavelengths, amplified spontaneous emission and laser emission. Relevant results have been obtained with heterostructured and doped NCs. The luminescent properties are primarily governed by exciton decay, which can follow different routes. Exciton relaxation occurs on few-picosecond timescale, so ultrafast techniques are required to follow the process.

In this talk, we present studies carried out by broadband ultrafast pump-probe spectroscopy technique, with 100-fs time resolution. We analysed different CdSe/CdS and PbS/CdS NCs (core/shell, dot-in-rod, dot-in-bulk, with sharp or graded interface) [1-4] and CdSeS and CdZnSe doped NCs [5,6], showing single and dual colour PL, optical gain, laser emission and intragap emission. We studied the exciton dynamics to get insights on the photophysics. Studies on CdSe/CdS and PbS/CdS heterostructures allowed us to access the decoupling of core and shell excitons and to reveal the exciton barrier known as “dynamic hole-blockade effect”. We clarified the photo-physics of double emission, suppression of Auger recombination and optical gain, describing the role of the volume and of the interface [1-3].

Experiments on CdZnSe NCs doped with Mn and on CdSeS NCs with sulfur vacancies, enabled us to disclose the emergence of a transient Mn³⁺ state, in the relaxation process, responsible for intragap emission [5] in the first case, and a donor state below the conduction band [6] in the latter case.

Moreover, we studied ZnO NCs decorated with Ag nanoparticle and we described the carrier redistribution in the plasmonic hot-electron/semiconductor junction [7]. We retrieved information for efficient light harvesting/detection schemes, combining high photon absorption with high carrier transfer/generation.

In conclusion, we discussed the ultrafast exciton dynamics in different NCs and we showed that the information retrieved are important for the control of NC functionalities and so for the design of devices such as lasers [8], photovoltaic and photoelectrochemical (PEC) cells [9], ratiometric sensors [10].

[1] G. Sirigu, A. Camellini, H. Zhao, L. Jin, F. Rosei, A. Vomiero, M. Zavelani-Rossi, *Phys. Rev. B* 96, 155303 (2017)

[2] V. Pinchetti, F. Meinardi, A. Camellini, G. Sirigu, S. Christodoulou, W. K. Bae, F. De Donato, L. Manna, M. Zavelani-Rossi, I. Moreels, V. I. Klimov, S. Brovelli, *ACS Nano* 10, 6877 (2016)

[3] H. Zhao, G. Sirigu, A. Parisini, A. Camellini, G. Nicotra, F. Rosei, V. Morandi, M. Zavelani-Rossi, A. Vomiero, *Nanoscale* 8, 4217 (2016)

[4] R. Krahn, M. Zavelani-Rossi, M. G. Lupo, L. Manna, G. Lanzani, *Appl. Phys. Lett.* 98, 063105 (2011)

[5] K. Gahlot, K.R. Pradeep, A. Camellini, G. Sirigu, G. Cerullo, M. Zavelani-Rossi, A. Singh, U. V. Waghmare, R. Viswanatha, *ACS Energy Lett.* 4, 729 (2019)

[6] F. Carulli, V. Pinchetti, M. L. Zaffalon, A. Camellini, S. Rotta Loria, F. Moro, M. Fanciulli, M. Zavelani-Rossi, F. Meinardi, S. A. Crooker, S. Brovelli, *Nano Lett.* 21, 6211 (2021)

[7] M. Gilzad Kohan, S. You, A. Camellini, I. Concina, M. Zavelani-Rossi, A. Vomiero, *J. Mater. Chem. C* 9, 15452 (2021)

[8] M. Zavelani-Rossi, R. Krahn, G. Della Valle, S. Longhi, I. R. Franchini, S. Girardo, F. Scotognella, D. Pisignano, L. Manna, G. Lanzani, F. Tassone, *Laser & Photonics Reviews* 6, 678 (2012)

[9] L. Jin, G. Sirigu, X. Tong, A. Camellini, A. Parisini, G. Nicotra, C. Spinella, H. Zhao, S. Sun, V. Morandi, M. Zavelani-Rossi, F. Rosei, A. Vomiero, *Nano Energy* 30, 531 (2016)

[10] J. Liu, H. Zhang, G. S. Selopal, S. Sun, H. Zhao, F. Rosei, *ACS Photonics*, 2479 (2019)

2:00 PM *NM03.04.02

The Study of Magnetically Doped Metal-Chalcogenide and Halide-Perovskite Nanocrystals, by Optically Detected Magnetic Resonance Spectroscopy [Efrat Lifshitz](#); Technion-Israel Inst of Tech, Israel

The incorporation of magnetic impurities in semiconductor colloidal nanocrystals has garnered broad scientific and technological interest during the past decade due to their tunable magneto-optical properties and consequent potential utility in various spin-related technologies. This work brings a comprehensive study of a few different magnetic dopants (Mn²⁺, Ni²⁺, Cu²⁺) in metal-chalcogenide and halide perovskite nanocrystals, utilizing optically detected magnetic resonance (ODMR) spectroscopy. This methodology directly sees individual spins, uncovering spin-exchange interaction between resident carrier and a dopant spin at a local site, and thus, reflecting knowledge on long-standing debates about the involvement of the dopants in the photophysics of the semiconductors. More specifically, Mn²⁺ dopant in CdSe/CdS seeded rods enhanced the electron-dopant spins by selective positioning of the dopant at the CdS-shell regime. Ni²⁺ dopants in CsPbBr₃ perovskite materials showed a spin-exchange interaction with a hole-resident spin, whose existence could be detected due to the reduction of motion fluctuations by the dopants at the substituted position. The ODMR Cu²⁺ doped CdSe/(CdS, ZnS) were recently investigated compared to that of CuInS₂ QDs. This study showed a joint involvement of a Cu-activated center in the two families of compounds however via a different mechanism; A band-to-Cu recombination with a weak electron-hole spin-exchange interaction was found in the Cu-doped QDs, but, a self-trapped exciton emission with a strong electron-hole exchange constant in Cu-based QDs. Furthermore, nuclei spin effects were pronounced in the magnetic resonance transitions. The described studies exposed spin interaction on atomistic local sites, uncovering information blurred by simple optical methodologies.

2:30 PM NM03.04.03

Photo-Induced Charge Carrier Dynamics at Semiconductor Quantum Dots/TiO₂ Interface [Yasuhiro Tachibana](#)^{1,2}; ¹RMIT University, Australia; ²Osaka University, Japan

Semiconductor quantum dot (QD) is one of the most attractive nanomaterials to be applied for solar energy conversion devices. With their relatively large extinction coefficients and a wide light absorption range over visible wavelengths, QDs can be effective light absorbers. However, despite their attractive optical properties, when they are employed in solar cells, their function, particularly exciton states, charge separation and recombination dynamics has not been well understood. Their relations to the solar cell function are still not clear.

We have reported charge separation and recombination dynamics at the QD and TiO₂ interface,^[1] and relationship of the nanostructures with the solar cell performance.^[2,3] We have also reported novel synthesis of several types of QDs with a narrow size distribution to control the potential energy levels of the conduction and valence bands ^[4,5]. In this presentation, we will discuss underlying key parameters such as interfacial nanostructure controlling charge carrier dynamics at QD / TiO₂ interface.

This work was partly supported by JSPS KAKENHI Grant (19H02813) and (22H02182), and the Collaborative Research Program of Institute for Chemical Research, Kyoto University (grant number 2021-78 and 2022-99), Japan. We would like to acknowledge supports from the Australia-Japan Foundation for the collaborative project between RMIT University and Kyoto University. We also acknowledge supports from ARC DP fund (DP180103815) and ARC LIEF fund (LE200100051), Australia, and Forefront Research Center, Faculty of Science at Osaka University.

References

[1] Y. Tachibana, et al. *J. Phys. Chem. C*, **119**(35) 20357-20362 (2015).

- [2] Y. Tachibana, et al. *ACS Appl. Mater. Interfaces*, **8**(22) 13957-13965 (2016).
[3] Y. Tachibana, et al. *J. Photopolym. Sci. Technol.*, **34**(3) 271-278 (2021).
[4] Y. Tachibana, et al. *Phys. Chem. Chem. Phys.*, **17**(4), 2850 - 2858 (2015).
[5] Y. Tachibana, et al. *J. Mater. Chem. C*, **5**, 2182 - 2187 (2017).

2:45 PM NM03.04.04

High-Efficiency Two-Step Spin-Exchange Auger Photoemission from Manganese-Doped Quantum Dots Valerio Pinchetti¹, Clement Livache¹, Ho Jin^{1,2}, Whi Dong Kim¹, Igor Fedin¹ and Victor I. Klimov¹; ¹Los Alamos National Laboratory, United States; ²The University of New Mexico, United States

Photoemission is a process wherein a material emits free electrons upon its illumination with electromagnetic radiation. Typically, it requires energetic ultraviolet or even X-ray photons. Here we show that using CdSe colloidal quantum dots (CQDs) heavily doped with manganese (Mn), we can realize this process with visible light. The observed effect is enabled by extremely fast (<300 femtoseconds) spin-exchange Auger energy transfer from excited Mn ions to an intrinsic CQD exciton. Since the rate of this process outpaces that of intra-band cooling, the high-energy 'hot' electron produced by the first Auger-excitation step can be efficiently promoted further into the external 'vacuum' state via one more Mn-to-CQD energy-transfer step. This CQD ionization pathway exploits exceptionally large up-hill energy gain rates associated with the spin-exchange Auger process (>10 eV ps⁻¹) and leads to photoemission efficiencies of more than 3%, orders of magnitude greater than in the case of undoped CQDs. We demonstrate that using this phenomenon, we can achieve high-yield production of solvated electrons (>3% internal quantum efficiency), which makes it of considerable utility in visible-light-driven reduction photochemistry. Other potential applications include low-cost, visible-light-driven photocathodes and advanced photoconversion.

3:00 PM BREAK

3:30 PM *NM03.04.05

Semiconductor Nanocrystals as Photooxidative Catalysts in Organic Media Xiao-Min Lin¹ and Elena Shevchenko^{1,2}; ¹Argonne National Laboratory, United States; ²The University of Chicago, United States

Semiconductor nanocrystals (NCs) are extensively studied for photocatalytic applications. CdSe/CdS nanorods (NRs) with a CdSe core and CdS shell enable maximization of solar absorption and conversion of a broad range of visible spectra to chemical energy. The spatial separation of the electrons and holes reduces the recombination rate and increases the probability of photogenerated carries to be extracted. Photocatalytic reaction utilizing both photogenerated electrons and holes could lead to synthesis of a broad range of high value products in organic solvents. Majority of photocatalytic studies on cadmium chalcogenide heterostructures are mainly conducted in aqueous media (e.g., hydrogen generation), with holes scavenged by sacrificial electron donors to prevent oxidation of semiconductor NCs. Using aerobic oxidative coupling of thiophenol in organic media as a model reaction, we show that photogenerated holes in CdSe/CdS core-shell nanorods can be efficiently extracted and CdSe/CdS nanorods can serve as an efficient visible-light photocatalyst at a very low concentration (~1.5 × 10⁻⁴ mol%). We show that primary amines play an important role in the transformation of thiols into disulfides by forming a soluble thiolate in nonpolar solvent. Using time-resolved optical spectroscopy and electron paramagnetic resonance spectroscopy, we show that thiolate can efficiently extract the photogenerated holes from CdSe/CdS nanorods and transform into disulfide in organic solvent. Our data indicate that there are two reaction pathways responsible for S-S coupling of thiolate upon illumination of CdSe/CdS nanorods. We show that instead of scavenging of photogenerated holes by sacrificial species for prevention of photo corrosion of CdSe/CdS nanorods, the photogenerated holes can be efficiently used for oxidative organic synthesis.¹ We will discuss the perspectives of photooxidative catalysis in organic solvents using semiconductor NCs.

1. Sha, Y.; Lin, X.-M.; Niklas, J.; Poluektov, O. G.; Diroll, B. T.; Lin, Y.; Wen, J.; Hood, Z. D.; Lei, A.; Shevchenko, E. V., Insights into the extraction of photogenerated holes from CdSe/CdS nanorods for oxidative organic catalysis. *Journal of Materials Chemistry A* **2021**, *9* (21), 12690-12699.

4:00 PM NM03.04.06

Temperature and Magnetic Field Dependence of Photoluminescence Lifetimes Reveal the Electron-Hole Recombination Mechanism in Colloidal CuInS₂ Quantum Dots Malgorzata Szymura¹, Magdalena Duda¹, Miriam Karpinska¹, Tomasz Kazimierzczuk², Roman Minikayev¹, Magdalena Parlinska-Wojtan³ and Lukasz Klopotoski¹; ¹Institute of Physics, Polish Academy of Sciences, Poland; ²Faculty of Physics, University of Warsaw, Poland; ³Institute of Nuclear Physics Polish Academy of Sciences, Poland

We present experimental evidence that the photoluminescence (PL) in copper indium sulphide (CuInS₂) quantum dots (QDs) occurs through a recombination of a delocalized electron and a localized hole (i.e., a free-to-bound mechanism). More specifically, we study the PL dynamics in a temperature range between 2 and 300 K and in magnetic fields up to 10 T and demonstrate that the results cannot be explained by assuming a recombination of band-edge excitons. On the other hand, the results are consistent with the free-to-bound mechanism in which the hole is localized at the d-shell of copper ions.

CuInS₂ QDs (and I-III-VI compound QDs in general) attract significant attention as more environmentally friendly alternatives to cadmium and lead chalcogenide QDs. Despite years of research, the optical properties of these nanostructures are not fully understood. Although most experimental results point to the free-to-bound process as the underlying mechanism of electron-hole recombination, some theoretical and experimental reports claim that the PL can be due to an excitonic process.

In this work, we find that the PL decays are strongly non-exponential underlining a strong inhomogeneity of the recombination rates. The extracted average PL lifetimes shorten with increasing the temperature. Crucially, when increasing the temperature from 2 K, we find that the short lifetime components are less sensitive to temperature change. We argue that this effect is incompatible with the excitonic mechanism while expected for the free-to-bound mechanism, where the position of the Cu ions within a QD governs the recombination rates. Furthermore, we investigate the PL decays recorded in two circular polarizations as a function of the magnetic field. This allows us to evaluate the spin relaxation rates. The rates are two orders of magnitude smaller than for CdSe QDs, which exhibit excitonic PL. On the other hand, the rates are on the same order as those evaluated for Cu-doped CdSe, in which the free-to-bound mechanism is responsible for the PL. We argue that the low spin relaxation rates originate from a limited interaction of the electron-hole pairs with the QD surface. Finally, we show that the PL polarization exhibits a particular temporal dependence: the equilibrium polarization decays with the time delay from the excitation laser. This effect can be interpreted as originating from a negative correlation between the fine structure splitting of the luminescent excited state and the PL lifetime. Crucially, this correlation is expected for the free-to-bound mechanism, while an opposite, positive correlation, is well established for excitonic photoluminescence. Thus, our results strongly support the free-to-bound recombination process as responsible for the PL of CuInS₂ QDs.

4:15 PM NM03.04.07

Photoluminescence Signatures of Energy Transfer in CuInS₂ Colloidal Quantum Dot Films Pushkar S. Joshi, Magdalena Duda and Lukasz

Klopotowski; Institute of Physics Polish Academy of Sciences, Poland

In this work, we demonstrate spectroscopic signatures of energy transfer (ET) in a solid film prepared from CuInS₂ colloidal quantum dots (QDs). Energy transfer in colloidal QDs has been a highly studied area in pursuit of applications such as solar cells. The size-dependent optical properties of QDs make them ideal candidates for such exploration. The environmentally safer QD materials such as CuInS₂ (CIS) have not been explored as much as Pb and Cd chalcogenide QDs in this regard. The significant Stokes shift of CIS and the scope for changing its stoichiometry provide additional parameters, which may influence ET efficiency. Here, we study steady-state photoluminescence (PL) and time-resolved photoluminescence (trPL) on QD films and solutions. Comparison of the results between the film and solution samples unveils three signatures of ET in QD films: (i) red-shift of the film PL spectrum, (ii) increase/decrease of the relative PL decay rate at the blue/red end of the film PL spectrum, and (iii) presence of a PL rise dynamics at the red end of the film PL spectrum. In agreement with studies on other QD systems, all these effects point to an ET from small to large QDs within the ensemble. The CIS QDs studied here are synthesized at 230°C for 1 minute with Cu-to-In precursor ratio of 1:4. The PL spectrum of QDs in solution form peaks at 652 nm and exhibits a broad full width at half maximum (FWHM) of about 100 nm. This is the sign of the presence of highly inhomogeneous QD size distribution in the ensemble. The PL peak of the same ensemble when drop cast to form a solid film is red-shifted by over 50 nm (140 meV) to 705 nm. Since the FWHM of the film PL hardly changes from the solution PL, we interpret the red-shift as a signature of non-radiative ET from donor QDs of smaller sizes to the larger acceptor QDs when deposited as a film. The spectrally integrated PL lifetime in solution phase is of the order of 300 ns while for the films is shorter, i.e., of the order of 200 ns. The faster PL decays point to the existence of additional recombination channels in the case of films. Furthermore, the spectrally resolved trPL studies unveil the shortening of PL lifetimes from the red end of the spectrum to the blue end. In solution phase, the lifetimes at the red and blue ends relative to that of the peak are 1.3 and 0.6, respectively. This shows that the QD ensemble exhibits an intrinsic spectral dependence of the lifetimes. On the other hand, in the film, the lifetimes at the red and blue ends relative to that of the peak are 1.6 and 0.32, respectively. Thus, in the film form, an additional contribution to the spectral dependence of lifetimes is manifested. An analogous effect was previously ascribed to non-radiative ET within inhomogeneous ensembles of QDs. Accordingly, we interpret this additional contribution as a result of ET between donors and acceptors in the film. This conclusion is further supported by the observation of PL rise dynamics at the red end of the film spectrum, which is absent in the case of the solution trPL. The existence of rise time at the red end together with very short decay at the blue end can be explained by the non-radiative transfer of energy from the small QDs into the larger QDs. Similar effects are observed with varying degrees in 4 other CIS QD ensembles made of different QD sizes and Cu-to-In precursor ratios. Results for all samples support the conclusion that ET occurs in CIS QD films. For more detailed insight into this effect, the future research will include temperature dependent studies and fine selection of QD-sizes to assert an improved control over ET.

4:30 PM NM03.04.08

Stimulated Emission from Bulk-Like CdS Quantum Dots Through Strong Band Gap Renormalization Ivo Tanghe¹, Margarita Samoli¹, Isabella Wagner², Servet A. Cayan¹, Ali H. Khan³, Kai Chen², Justin Hodgkiss², Iwan Moreels¹, Dries Van Thourhout¹, Zeger Hens¹ and Pieter Geiregat¹;
¹University Ghent, Belgium; ²Victoria University of Wellington, New Zealand; ³S.N. Bose National Centre for Basic Sciences, India

Nanostructured semiconductors are heavily investigated for their applications in light emission such as light emitting diodes and, more challenging, lasers. Using quantum confined Cd-based QDs, several groups have shown light amplification and ensuing lasing action in the red part of the spectrum. Although further work is necessary to reduce gain threshold densities for efficient lasing action, there has been some push toward moving away from the current red gain band region, toward green emission.

In this work, we take a look at weakly confined “giant” CdS Quantum Dots, which display disruptive optical gain properties in the green optical region. While showing similar gain thresholds compared to state-of-the-art materials, the gain window (440-600nm), magnitude (up to 50000/cm) and gain lifetime (up to 3ns) vastly outpace other materials in the same optical region.

These remarkable results are explained by using a bulk semiconductor gain model, which is possible due to the large size of the CdS Quantum Dots (8-12 nm). We can very accurately reconstruct the gain window with this model, by including large bandgap renormalization (up to 70 meV). This inclusion helps us to understand the gain mechanism in these particles.

SESSION NM03.05: Nanoparticle Assembly
Session Chairs: Elena Shevchenko and Marinella Striccoli
Wednesday Morning, November 30, 2022
Hynes, Level 2, Room 209

8:30 AM *NM03.05.01

Mesoscale Quantum Confined Nanoplatelets Stephanie Tenney and Justin R. Caram; University of California, Los Angeles, United States

We have synthesized mesoscale semiconductor (II-VI) nanoplatelets (NPLs) for the first time using colloidal seeded growth. These nanoplatelets are quantum-confined and atomically precise but grown to a length scale compatible with conventional optical imaging and microscopic manipulation offering an opportunity to bridge the application space between nanocrystals and 2D materials. Using CdTe as a model system we develop a seeded growth procedure, show the parameters which control extension, and apply them to a variety of thicknesses and compositions. In-situ spectroscopy demonstrates that addition onto the nanoplatelet seeds is not continuous, and likely occurs through ripening. Finally, we use correlative optical and electron microscopy to demonstrate that at large sizes, PL mapping of the entire structure can be resolved including spatial inhomogeneities. Overall, these results show that nanoplatelets can be compared to 2D semiconductors while maintaining the advantages of scalable colloidal synthesis, thickness tunability and solution processability.

9:00 AM NM03.05.02

Single Photon Emitting Arrays by Capillary Assembly of Colloidal Semiconductor CdSe/CdS Nanocrystals Matteo Borelli¹, Cynthia Vidal², Sergio Fiorito¹, Alina Myslovska³, Dimitrie Cielecki², Iwan Moreels³, Riccardo Sapienza² and Francesco Di Stasio¹; ¹Istituto Italiano di Tecnologia, Italy; ²Imperial College London, United Kingdom; ³Ghent University, Belgium

Interest in the physics and materials science of nanocrystals (NCs) has exponentially increased over the last couple of decades. Colloidal semiconductor NCs present remarkable properties in sight of optoelectronic device fabrication, as they are synthesized by wet chemistry methods that offer a seemingly endless amount of freedom on the parameters that determine their optoelectronic properties such as crystal size, shape, crystallinity, chemical composition and architecture (e.g. core/shell NCs). All these various optoelectronic devices are based on thin films; however, complex small-footprint devices

exploiting single NCs require controlled placement of isolated NCs on particular sites of a planar surface and this step is not easily achievable as for quantum-dots fabricated by pure top-down methods. For example, a specific emerging application of isolated colloidal semiconductor NCs is to employ them as single photon sources, in the emerging fields of quantum communication, computing and encryption.¹ A whole range of techniques have been explored to place colloidal NCs from solution to a controlled site on a solid substrate.² In particular, a method called capillary assembly, exploits the force exerted on NCs at the interface between the moving meniscus of the solution solvent and a solid substrate to allow the entrapment of NCs in pre-patterned features on the surface, typically realized by means of lithographic methods such as electron beam lithography.³ However, most results in literature employ metallic NCs in the fabrication of plasmonic metasurfaces and polymeric colloidal units; while the placement of semiconductor NCs has been less explored. The controlled placement of colloidal semiconductor NCs remain crucial in sight of the fabrication of small footprint optoelectronic nanodevices built around them.

In this work, we show the fabrication of periodic arrays of giant shell CdSe/CdS NCs by a capillary assembly method based on a simple and fast drop casting technique. Before proceeding with the array fabrication, the CdSe/CdS NCs have been overcoated with a SiO₂ shell. The large area arrays here presented (2500 holes over 100×100 μm²) contain hundreds of single NCs filled holes, each. The nanoholes filling efficiency follows a Poisson distribution, with 60% of the nanoholes containing one or more NCs. We have characterized the arrays with steady state and time-resolved photoluminescence, and photon correlation measurements. We associated the morphological data collected by scanning electron microscopy with optical data to unveil how the effective density of single photon emitters depends on an interplay between NCs photoluminescence quantum yield and Poisson statistics of the nanohole filling process. That is, why we observe single photon emission by nanoholes filled with multiple NCs. We believe the proposed technique is the first step toward the realization of affordable and reproducible arrays of single photon sources based on colloidal semiconductor NCs. Most importantly, the technique enables future implementation of addressable networks of nanodevices, such as single-NC light-emitting diodes, and it should be applicable to a wide range of semiconductor NCs with variable composition and shape.

References

- (1) Thomas, S.; Senellart, P. The Race for the Ideal Single-Photon Source Is On. *Nat. Nanotechnol.* **2021**, *16* (4), 367–368. <https://doi.org/10.1038/s41565-021-00851-1>.
- (2) Zhang, H.; Kinnear, C.; Mulvaney, P. Fabrication of Single Nanocrystal Arrays. *Adv. Mater.* **2020**, *32* (18), 1904551. <https://doi.org/10.1002/adma.201904551>.
- (3) Ni, S.; Isa, L.; Wolf, H. Capillary Assembly as a Tool for the Heterogeneous Integration of Micro- and Nanoscale Objects. *Soft Matter* **2018**, *14* (16), 2978–2995. <https://doi.org/10.1039/C7SM02496G>.

9:15 AM NM03.05.03

Coupling Interactions of Molecular Assembled Colloidal Quantum Dot in Solution and Solid-State Carlo N. Dibenedetto^{1,2}, Elisabetta Fanizza^{1,2}, Rosaria Brescia³, Liberato De Caro³, Cinzia Giannini², Angela Agostiano^{1,2}, Maria Lucia Curri^{1,2} and Marinella Striccoli²; ¹University of Bari "Aldo Moro", Italy; ²CNR, Italy; ³Istituto Italiano di Tecnologia, Italy

The design of colloidal quantum dots (QDs) assemblies, as well as the investigation of their interactions, mutual and with the surrounding chemical-physical environment, is of great interest for increasing the performance of QD based optoelectronic devices. The coupling, which occurs when only a few QDs are organized in molecular assembly at suitable interparticle distance, can promote electron/energy transfer processes and coherent interactions, relevant for novel technological applications. Here, small molecular assemblies of QDs have been properly prepared by playing with the nanocrystal surface chemistry in solution, and then deposited samples have been fabricated, maintaining the assemblies individuality, to further investigate the electronic coupling between the nano objects in solid state.

Specifically, molecular assemblies composed by colloidal CdSe QDs of same (homo) and different (hetero) sizes,^[1,2] connected by short alkyl chain dithiols, have been prepared in solution. The interparticle distance has been finely tuned by varying the chain length of the bifunctional linker down to sub-nanometer range. Depending on their size, separation distance and mutual energy levels position, an extensive spectroscopic examination has allowed to attribute the coupling mechanisms between the QDs. The findings demonstrate the higher heteroassemblies' potential in terms of transfer rate for charge transfer/wavefunction delocalization, taking advantage of the contact zone's cascade-like energy levels. FRET systems, on the other hand, would greatly benefit from the design of homoassemblies, which can couple more efficiently via an energy transfer mechanism due to quasi iso-energetic electronic states.

The next step has been the fabrication of solid-state architectures, realized depositing the molecular assembly of QDs prepared in solution by means of dithiols or diamines as linkers, on a quartz substrate properly functionalized with an amino terminated self-assembled-monolayer (SAM). The presence of SAM guarantees the effective anchorage of the nano-objects to the substrate and ensures a good uniformity of the deposition. Layer-by-Layer approach has been used as deposition technique and every layer of QD molecular assembly has been alternated with a long molecular spacer, in order to maintain as much as possible the "molecular" nature of the assemblies. For comparison, samples in which the QD capping ligands have been completely exchanged with short bifunctional linker have been fabricated in order to connect collectively all the QDs in the layer, as usually used in conventional optoelectronic devices. The use of amines or thiols deeply influences the morphology of the assemblies, giving rise to fascinating flowered or roundly shaped hierarchical structures, respectively. The spectroscopic investigation reveals interesting electronic properties of these structured materials, that can add another brick to the knowledge of these systems.

[1] Dibenedetto C.N., Fanizza E., Brescia R., Kolodny Y., Remennik S., Panniello A., Depalo N., Yochelis S., Comparelli R., Agostiano A., Curri M.L., Paltiel Y., and Striccoli M.; Coupling Effects in QD Dimers at Sub-Nanometer Interparticle Distance. *Nano Research* (2020), 13(4), 1071-1080. DOI: 10.1007/s12274-020-2747-3

[2] Dibenedetto C.N., Fanizza E., De Caro L., Brescia R., Panniello A., Tommasi R., Ingrosso C., Giannini C., Agostiano A., Curri M.L., and Striccoli M.; "Coupling in Quantum Dot Molecular Hetero-Assemblies" *Mat. Res. Bul.*, (2021). DOI: 10.1016/j.materresbull.2021.111578

This work has been financially supported by the H2020 FET project COPAC (Contract agreement n.766563).

9:30 AM NM03.05.04

Superfluorescence in Lead Halide Perovskite Nanocrystal Assemblies and Giant Nanocrystals Etsuki Kobiyama¹, Gabriele Raino^{2,3}, Ihor Cherniukh^{2,3}, Yuliia Berezovska^{2,3}, Maryna Bodnarchuk^{2,3}, Rainer F. Mahrt¹, Maksym V. Kovalenko^{2,3} and Thilo Stoefler¹; ¹IBM Research GmbH Zurich Research Laboratory, Switzerland; ²ETH Zürich, Switzerland; ³Empa–Swiss Federal Laboratories for Materials Science and Technology, Switzerland

Cooperative effects among electric dipoles lead to drastic changes in photon emission processes. In particular, spontaneous synchronization of dipole oscillation leads to an emission of an intense burst of photons, so-called superfluorescence (SF). Because SF is based on coherent interactions among excited dipoles, the SF response reflects the presence of quantum many-body states. As lead halide perovskite nanocrystals (NC) exhibit giant oscillator

strength and long dephasing times, they have been shown to be excellent solid-state SF platforms^[1]. So far, several types of perovskite NC systems, e.g., mono-component or binary component NC assemblies, exhibit SF^[1,2]. However, how the different structures of the material systems affect the SF process is not fully elucidated yet.

Here, we investigate the photoluminescence (PL) dynamics in several NC assemblies with different lattice geometry. By analyzing the characteristic signatures of SF, e.g., excitation-dependent decay acceleration, super-linear power law of emission intensity, and ringing of emission pulses, we found that the volume fraction of perovskite NCs within the assemblies is a pivotal factor in supporting SF^[3]. Besides, we studied SF dynamics in the different types of material systems, namely bulk-like giant NCs. We observed the characteristic SF signatures with lower excitation power than NC assemblies. Furthermore, we observed that the dominant emission process gradually evolves from SF to amplified spontaneous emission by increasing the temperature.

Our results show that SF responses depend on material systems' geometry or structure (bulk or NC assemblies). The results suggest the possibility of controlling SF responses and quantum many-body states by engineering the geometry or structure of the material systems.

[1] G. Rainò *et al.*, Nature 563, 671-675 (2018)

[2] I. Cherniukh *et al.*, Nature 593, 535-542 (2021)

[3] I. Cherniukh *et al.*, ACS Nano 15, 16488-16500 (2021)

9:45 AM NM03.05.05

Short-Ranged Attractive Forces Enable the Self-Assembly of Binary Nanocrystal Superlattices Emanuele Marino¹, R. Allen LaCour², Timothy C. Moore², Sjoerd van Dongen¹, Austin W. Keller¹, Shengsong Yang¹, Daniel J. Rosen¹, Guillaume Gouget¹, Esther H. Tsai³, Cherie R. Kagan¹, Thomas E. Kodger⁴, Sharon Glotzer² and Christopher B. Murray¹; ¹University of Pennsylvania, United States; ²University of Michigan–Ann Arbor, United States; ³Brookhaven National Laboratory, United States; ⁴Wageningen University & Research, Netherlands

The self-assembly of nanocrystals into binary superlattices enables the targeted integration of orthogonal physical properties, like photoluminescence and magnetism, into a single superstructure, unlocking a vast design space for multifunctional materials. Yet, the formation of binary nanocrystal superlattices remains poorly understood, restricting the use of simulation to predict structure and properties of the final superlattices. Here, we use *in situ* scattering experiments to unravel the time-dependent self-assembly of nanocrystals into 3D binary superlattices, and molecular dynamics simulations to obtain interparticle interactions consistent with experimental observations. We show definitively that short-ranged, attractive interparticle forces are necessary to obtain the binary crystalline phases observed in experiment. The short-ranged attraction stabilizes these crystalline phases relative to fluid phases, dramatically enhancing their formation kinetics over the purely repulsive interactions of the hard-sphere model. In these conditions, the formation of binary nanocrystal superlattices proceeds through homogeneous nucleation in the absence of intermediate ordered structures. These results establish a robust correspondence between experiment and theory, paving the way towards *a priori* prediction of binary nanocrystal superlattices.

10:00 AM BREAK

10:30 AM NM03.05.06

Chiral Conjugated Polymer/Perovskite Quantum Dot Nanowired-Hybrids Juhong Min, Junho Hwang, Seon-Mi Jin and Eunji Lee; Gwangju Institute of Science and Technology, Korea (the Republic of)

Recently, chiral semiconductor quantum dots with chiral ligand have attracted attention because of potential applications such as chiral memory effect and tunable circularly polarized luminescence (CPL) property. Especially, chiral perovskite quantum dots recently receive attention as next-generation circularly polarized photodetectors and spintronic memory devices with high external quantum efficiency and tunable band gap. However, the chirality of perovskite can be degraded during ligand exchange of the organic ligands surrounding the perovskite quantum dot for the hybrid system. I assume that a more easily controlled and stable chiral perovskite system can be induced by arranging the achiral perovskite quantum dot along the self-assembled chiral polymer template in the solution state. Crystalline-driven self-assembly of a conjugated polymer in a solution state is promising high performance optoelectronic devices with excellent charge carrier transport through the solution. Herein, we report the synthesis of chiral enantiomer containing conjugated building block and self-assembly in water as a green solvent for an ecofriendly large scale solution process. Additionally, through co-assembly between chiral conjugated nanowires and achiral perovskite quantum dot, we successfully generated chiral conjugated polymers/perovskite nanoparticles (NPs) hybrid nanowire with preferred handedness. A controlling array of perovskite quantum dots on the chiral self-assembly template was defined by 3D TEM tomography. This work is expected to suggest a new hybrid system to enhance the chirality parameter, circularly polarized luminescence property and synergistic functional application with perovskite quantum dots on the chiral conjugated template.

10:45 AM NM03.05.07

Approaching Bulk Mobility in PbSe Colloidal Quantum Dots 3D Superlattices Jacopo Pinna, Razieh Mehrabi, Dnyaneshwar Gavhane, Majid Ahmadi, Suhas Mutalik, Loredana Protesescu, Bart Kooi, Giuseppe Portale and Maria Antonietta Loi; University of Groningen, Netherlands

Progress in optoelectronics has been hindered by the discrete nature of band gap for inorganic semiconductors and the difficulty of tuning both band gaps and transport properties for a given material. Semiconducting colloidal quantum dots (CQDs) have been in the spotlight thanks to their wide tunability and solution-based synthesis. It is in particular the ability to change the bandgap with their dimensions that makes them excellent candidates for the fabrication of optoelectronic metamaterials, while several other physical properties can be controlled by composition and surface chemistry.

In particular, lead chalcogenides CQDs (PbS, PbSe) have the potential to revolutionize the field of light emission and detection in the short-wavelength infrared range thanks to their tunable bandgap between 800-3000 nm. In this spectral range there is poor or no availability of cheap bulk semiconductors that can be used in applications like telecommunications and sensing in automated transport. Therefore, growing interest in this family of CQDs has risen especially in the last decade. But technological application has been limited by the poor transport properties of thin films fabricated with such materials. This is due to the fact that implementations in devices is performed with techniques that yields disordered films and charge transport is limited by the thermally activated hopping mechanism.

More recently, the self-assembly of CQDs in ordered arrays, the so called superlattices, has been proposed as a solution to the problem. Superlattices are expected to lead to coherent transport through minibands therefore approaching the electronic properties of the bulk counterparts. While the shape and truncation of these quantum dots are highly favorable for self-assembly, as shown by several work on 2D systems, the poor control on the ordering from the nanoscale to the mesoscale, on the electronic coupling and on surface trap passivation has led to the observation of rather disappointing charge transport properties. In the current state-of-the-art reports, electron field-effect mobilities of 24 cm²/Vs have been reported for 2D superlattices (1) and of 2.13 cm²/Vs for the 3D ones (2).

Here we report the self-assembly of highly ordered 3D superlattices with tunable structure and thickness (single layer precision). The superior quality of the fabricated samples is demonstrated with a combination of advanced structural characterization techniques like atomic resolution electron microscopy and grazing incidence X-Ray scattering. We observe coherence lengths in the order of 100 nm in the in plane direction while the superlattice is fully coherent

along its entire thickness. This outstanding ordering, combined with the excellent large scale morphology, results in record electron mobilities up to 257 cm²/Vs as measured in a field effect transistor using ionic gel as gate dielectric. This value is not only approaching the bulk mobility but it is a record among any self-assembled superlattice with fully quantum-confined nanocrystals as building blocks.

(1) D. M. Balazs, B. M. Matysiak, J. Momand, A. G. Shulga, M. Ibáñez, M. v. Kovalenko, B. J. Kooi, M. A. Loi, Electron Mobility of 24 cm² V⁻¹ s⁻¹ in PbSe Colloidal-Quantum-Dot Superlattices. *Advanced Materials*. 30 (2018).

(2) A. Abelson, C. Qian, T. Salk, Z. Luan, K. Fu, J. G. Zheng, J. L. Wardini, M. Law, Collective topo-epitaxy in the self-assembly of a 3D quantum dot superlattice. *Nature Materials*. 19, 49–55 (2020).

11:00 AM NM03.05.08

Multicomponent Nanocrystal Superlattices Comprising Lead Halide Perovskite Nanocubes [Ihor Cherniukh](#)^{1,2}, Gabriele Rainò^{2,1}, Taras V. Sekh^{2,1}, Thilo Stoefler³, Max Burian⁴, Alex Travesset⁵, Modestos Athanasiou⁶, Andreas Manoli⁶, Rohit A. John^{2,1}, Denys Naumenko⁷, Heinz Amenitsch⁷, Grigorios Itkos⁶, Rolf Erni⁸, Rainer F. Mahrt³, Maryna Bodnarchuk^{1,2} and Maksym V. Kovalenko^{2,1}; ¹Empa - Swiss Federal Laboratories for Materials Science and Technology, Switzerland; ²ETH Zurich, Switzerland; ³IBM Research Europe — Zurich, Switzerland; ⁴Paul Scherrer Institute, Switzerland; ⁵Iowa State University, United States; ⁶University of Cyprus, Cyprus; ⁷Graz University of Technology, Austria; ⁸Empa – Swiss Federal Laboratories for Materials Science and Technology, Switzerland

Cesium lead halide perovskite nanocrystals (NCs), owing to their outstanding optoelectronic properties (high oscillator strength of bright triplet excitons, slow dephasing, minimal inhomogeneous broadening of emission lines), are promising materials for creating coherent macroscopic states that can be utilized in quantum applications. Perovskite NCs self-assembled into ordered superlattices (SLs) with simple cubic packing of cubic NCs have been shown to emit ultrafast (*ca.* 20 ps) superfluorescent light. Further advancement in the field, required for programmable tuning of the collective emission and for building a theoretical framework, relies on the higher-level, exquisite structural engineering of the perovskite NC structures, wherein the use of additional building blocks may allow control over the mutual arrangement and orientation of perovskite nanocubes. We present a wide structural diversity in multicomponent, long-range ordered SLs obtained by shape-directed co-assembly of cubic CsPbBr₃ NCs with the spherical, truncated cuboid, and disk-shaped NCs. When combined with spherical Fe₃O₄ or NaGdF₄ NCs, SLs of five structure types form, namely, NaCl-, AlB₂-, and novel, uncommon to all-sphere assemblies AB₂- as well as quasi-ternary ABO₃- and ABO₆-types with cubes occupying B- and O-sites. Targeted incorporation of truncated cuboid PbS NCs on B-sites results in the formation of ternary ABO₃-type SLs. We then demonstrate the effect of superlattice structure on the collective optical properties. Combining perovskite nanocubes with other shape-anisotropic building blocks extends the library of accessible SL structures. With truncated cuboid PbS NCs as a larger component, in addition to binary NaCl-, AlB₂- and ABO₃-type SLs, CuAu-type SL was obtained. Co-assembly of CsPbBr₃ nanocubes with larger disk-shaped LaF₃ NCs results in the formation of six columnar structures with AB, AB₂, AB₄, and AB₆ stoichiometry. In the systems with comparable dimensions of nanocubes (8.6 nm) and nanodisks (6.5–12.5 nm), other, non-columnar structures are observed, such as ReO₃-type SL, featuring intimate intermixing and face-to-face alignment of disks and cubes. With large and thick NaGdF₄ nanodisks the orthorhombic SL resembling CaC₂ structure with clusters of CsPbBr₃ NCs was obtained. In the above-mentioned structures, 8.6 nm perovskite nanocubes exhibit a high degree of orientational ordering. We also explore the substrate-free assembly methods that allow obtaining binary supraparticles and free-floating SL films comprising perovskite nanocrystals.

[1] Cherniukh, I.; Rainò, G.; Stöferle, T.; Burian, M.; Travesset, A.; Naumenko, D.; Amenitsch, H.; Erni, R.; Mahrt, R. F.; Bodnarchuk, M. I.; Kovalenko, M. V. Perovskite-Type Superlattices from Lead Halide Perovskite Nanocubes. *Nature* 2021, 593, 535–542.

[2] Cherniukh, I.; Rainò, G.; Sekh, T. V.; Zhu, C.; Shynkarenko, Y.; John, R. A.; Kobiyama, E.; Mahrt, R. F.; Stöferle, T.; Erni, R.; Kovalenko, M. V.; Bodnarchuk, M. I. Shape-Directed Co-Assembly of Lead Halide Perovskite Nanocubes with Dielectric Nanodisks into Binary Nanocrystal Superlattices. *ACS Nano* 2021, 15, 16488–16500.

[3] Cherniukh, I.; Sekh, T. V.; Rainò, G.; Ashton, O. J.; Burian, M.; Travesset, A.; Athanasiou, M.; Manoli, A.; John, R. A.; Svyrydenko, M.; Morad, V.; Shynkarenko, Y.; Montanarella, F.; Naumenko, D.; Amenitsch, H.; Itkos, G.; Mahrt, R. F.; Stöferle, T.; Erni, R.; Kovalenko, M. V.; Bodnarchuk, M. I. Structural Diversity in Multicomponent Nanocrystal Superlattices Comprising Lead Halide Perovskite Nanocubes. *ACS Nano* 2022, 16, 5, 7210–7232

SESSION NM03.06: Theory and Modeling
Session Chairs: Iwan Moreels and Valerio Pinchetti
Wednesday Afternoon, November 30, 2022
Hynes, Level 2, Room 209

1:30 PM *NM03.06.01

Sub-Nanosecond Radiative Decay Time of Excitons in Large Size Nanocrystals and Nanoplatelets [Alexander L. Efros](#); Naval Research Laboratory, United States

Sub-nanosecond radiative decay time was first observed for weakly bound excitons in bulk semiconductors and was understood in terms of the phenomenon known as giant oscillator strength (GOS).¹ GOS is a quantum phenomenon connected with coherent excitation of excitons over entire volume of exciton localization and is counterintuitive because the radiative decay time is inversely proportional to this volume. Consequently, it was predicted theoretically² that exciton weakly confined in a spherical nanocrystal (NC), which radius *a* is much larger than the exciton radius *a_{ex}* is characterized by GOS which strength, $f_{\text{NC}} = f_0(a/a_{\text{ex}})^3 \gg f_0$, where *f₀* is the exciton oscillator strength. Indeed ~ 100 ps radiative decay times was observed in CuCl³ and large size CsPbX₃ (X=Cl,Br,I) perovskite NCs.⁴ The sub-nanosecond radiative decay time connected with GOS was also observed in quantum wells and nanoplatelets.⁵ In all cases the superfast radiative decay time observed generally at liquid helium temperatures increases with temperature. In my talk I will discuss the origin of the GOS of excitons and their sub-picosecond decay time, the effect of the temperature and line broadening in in nanoplatelets.

¹ E. I Rashba and G. E. Gurgenishvili, Edge absorption theory in semiconductors. *Sov. Phys. Solid State*, **4**, 759-760 (1962).

² A. L. Efros and A. L. Efros, Interband absorption of light in a semiconductor sphere, *Sov. Phys. Semicond*, **16**, 772-775 (1982).

³ T. Itoh and T. Kiriwara, Excitons in CuCl Microcrystals Embedded in NaCl, *J. Lumin.* **31–32**, 120–122 (1984).

⁴ M. A. Becker, *et al.* “Bright triplet excitons in caesium lead halide perovskites,” *Nature*, **553**, 189-193 (2018).

⁵ S. Ithurria, M. D. Tessler, B. Mahler, R. P. S. Lobo, B. Dubertret, A. L. Efros, Colloidal Nanoplatelets with Two- Dimensional Electronic Structure. *Nat. Mater.* **10**, 936–941 (2011).

2:00 PM NM03.06.02

Density Functional Theory Investigation of Trap States in Indium Phosphide Quantum Dots [Ezra A. Alexander](#), Matthias Kick and Troy Van

Voorhis; MIT, United States

Cadmium selenide, one of the premier quantum dot (QD) materials for light emission, solar cells, and biomedical imaging, is highly toxic to both humans and the environment. Alternative, nontoxic III-V QDs are held back by a high density of surface-localized mid-gap states, which trap photoexcited charge carriers and reduce device efficiency. Despite the prevalence of density functional theory (DFT) in past investigations of surface trapping in the II-VI family of QDs, very few studies have applied DFT to the substantially different III-V family of QDs. In this work, we show that trap states can form in indium phosphide QDs as the result of both 2- and 3-coordinate surface indium and phosphorous atoms. However, not all 3-coordinate surface atoms lead to localized midgap states; in particular, structures with many 3-coordinate surface atoms often form delocalized surface states near the band edge. Moreover, we observe the formation of both trap-inducing phosphorous dimers and trap-inert indium dimers on the surface of our model dots. Ultimately, our results suggest that a single-atom picture is insufficient to explain the surface trapping in indium phosphide QDs, hinting at new passivation strategies for improving nontoxic III-V QD devices.

2:15 PM NM03.06.03

Exciton Fine Structure in Lead Salt Nanocrystal Quantum Dots [Serguei Goupalov](#)^{1,2}, Ivan Avdeev², Mikhail Nestoklon² and Eougenious Ivchenko²; ¹Jackson State University, United States; ²Ioffe Institute, Russian Federation

Lead salt (PbX, X = S, Se, Te) quantum dots (QDs) are widely used in optoelectronics and *in vivo* fluorescence imaging due to tunability of their fundamental optical transition with the QD size within the near-infrared and mid-infrared ranges. These materials have both conduction and valence band extrema located at the four L points of the Brillouin zone forming four inequivalent anisotropic valleys. This leads to a high degeneracy of the energy spectrum in bulk materials which is partially lifted in QDs, resulting in the exciton fine structure. Understanding and controlling the exciton fine structure in PbX QDs is of key importance for full utilization of their unique optical properties.

We report a tight-binding calculation of the exciton ground-state fine structure in PbS QDs of different sizes and shapes, complemented by a thorough symmetry analysis [1]. We show that the exciton fine structure in PbX QDs is governed by the competition of two main mechanisms [1,2]. One is the electron-hole exchange interaction which can be best understood within the isotropic $\mathbf{k}\mathbf{p}$ model and is not sensitive to QD shape or valley anisotropy. This interaction has both intra-valley and inter-valley parts and promotes formation of a single ultra-bright state. Emergence of the ultra-bright state is a manifestation of valley coherence which is akin to super-radiance in the reciprocal space. The other competing mechanism is mixing of the valley states due to the scattering at the QD surface. The lower cubic symmetry of the crystal lattice dictates that exciton states from different valleys form combinations representing basis functions of irreducible representations of the symmetry group. While the inter-valley electron-hole exchange interaction tries to arrange the exciton states from different valleys in a fully symmetric combination, valley mixing favors combinations prescribed by the lattice symmetry. Thus, valley mixing distorts the ultra-bright state and leads to redistribution of its oscillator strength among 8 radiative triplets allowed by the symmetry. The radiative triplet having lowest energy is responsible for low-temperature photoluminescence and has radiative lifetime in the microsecond range in agreement with experimental findings. The exciton fine structure splittings between various bright states in core/shell PbS/CdS colloidal nanocrystals have been directly measured by means of single-QD spectroscopy at cryogenic temperatures and are in agreement with the results of our calculations [3].

[1] I. D. Avdeev, M. O. Nestoklon, and S. V. Goupalov, *Nano Lett.* **20**, 8897 (2020).

[2] S.V. Goupalov, E.L. Ivchenko, and M.O. Nestoklon, arXiv:2203.10295.

[3] Z. Hu, Y. Kim, S. Krishnamurthy, I.D. Avdeev, M.O. Nestoklon, A. Singh, A.V. Malko, S.V. Goupalov, J.A. Hollingsworth, and H. Htoon, *Nano Lett.* **19**, 8519 (2019).

2:30 PM BREAK

3:30 PM *NM03.06.04

Plasmonic Nanocrystals and Hybrids with Complex Shapes for Hot Electron Generation and Photochemistry [Alexander Govorov](#) and Oscar Avalos-Ovando; Ohio University, United States

The generation of energetic (hot) electrons and the photoheating are intrinsic properties of any optically excited plasmonic nanocrystal [1,2]. In addition, high-energy hot electrons and phototemperature contribute to the kinetic processes observed in colloidal nanocrystals, metal-semiconductor hybrids, plasmonic Schottky photodetectors, and metastructures [1,2]. In this talk, we will focus on the theory of hot electron injection and present related applications for plasmonic photochemistry and plasmonic photocatalysis [3,4,5,6].

[1] L. Chang, L. V. Besteiro, J. Sun, E. Y. Santiago, S. K. Gray, Z. Wang, A. O. Govorov, *ACS Energy Lett.*, **4**, 10, 2552-2568 (2019).

[2] L. V. Besteiro, P. Yu, Z. Wang, A. W. Holleitner, G. V. Hartland, A. O. Govorov, *Nano Today*, **27**, 120-145 (2019).

[3] T. Liu, L.V. Besteiro, T. Liedl, M.A. Correa-Duarte, Z. Wang, A. Govorov, *Nano Letters*, **19**, 1395–1407 (2019).

[4] L. Khosravi Khorashad, L. V. Besteiro, M. A. Correa-Duarte, S. Burger, Z. M. Wang, A.O. Govorov, *J. Am. Chem. Soc.*, **142**, 9, 4193–4205 (2020).

[5] O. Ávalos-Ovando, L.V. Besteiro, A. Movsesyan, G. Markovich, T. Liedl, K. Martens, Zh. Wang, M.A. Correa-Duarte, and A.O. Govorov, *Nano Letters* (2021); DOI: 10.1021/acs.nanolett.1c02479.

[6] A. Movsesyan, E. Y. Santiago, S. Burger, M. A. Correa-Duarte, L. V. Besteiro, Zh. Wang, and A.O. Govorov, *Advanced Optical Materials* (2022); <https://doi.org/10.1002/adom.202102663>.

4:00 PM NM03.06.05

Computational Investigation of Generation of Entangled Photon Pair from Biexcitonic-to-Exciton Cascade Decay in Semiconductor Nanoparticles [Arindam Chakraborty](#); Syracuse University, United States

This computational work aims to investigate the generation of entangled photon pairs in quantum dots. Entangled photon pairs (EPP) are important in quantum optics and are essential for quantum information, quantum teleportation, quantum key distribution, and controlled logic operations. Semiconductor nanoparticles such as quantum dot (QD) are especially well suited for EPP generation and have been proven to have high-entanglement fidelity, extraction efficiency, and photon indistinguishability.

Accurate description of biexcitonic and exciton states are crucial for accurate prediction of generation of EPPs. In this work, we have used the frequency-dependent geminal-screened electron-hole interaction kernel method (FD-GSIK) for treating the excitonic and biexcitonic states. The FD-GSIK is a first-principles, explicitly-correlated, real-space method that avoids using unoccupied orbitals to construct the electron-hole interaction kernel by performing a complete infinite-order diagrammatic summation of particle-hole excitations and deriving a renormalized R_{12} real-space electron-hole correlator operator. The FD-GSIK method also bypasses the computationally expensive AO-to-MO integral transformation step by computing all integrals directly in the real-space numerically using Monte Carlo integration. The frequency-dependent component of the FD-GSIK method implements the necessary quasiparticle

screening needed for describing biexcitonic states.

In this work, the combination of dressed-atom approach and FD-GISK method was applied to investigate exciton binding energies and biexciton binding energies for large quantum dots ($\text{Pb}_{140}\text{S}_{140}$, $\text{Pb}_{140}\text{Se}_{140}$, $\text{Cd}_{144}\text{Se}_{144}$). Chemical insights from biexciton binding energies, exciton binding energies, fine-structure splitting, oscillator strengths, degree of entanglement, and time-dependent electron-hole recombination probability for these quantum dots will be presented. The results from these calculations demonstrate the efficacy of the FD-GISK method for capturing electron-hole correlation and treating 2-electron 2-hole excitation in large clusters and nanoparticles. Future and ongoing work in this direction including enhancing photon-entanglement characteristics by optimizing surface ligands and adding core/shell heterojunctions will be discussed.

4:15 PM NM03.06.06

First Principles Simulations of $\text{Hg}_x\text{Cd}_{1-x}\text{S}$ and $\text{Hg}_x\text{Cd}_{1-x}\text{Se}$ Optical Properties Erick I. Hernandez Alvarez, Andrew M. Smith and Andre Schleife; University of Illinois at Urbana-Champaign, United States

Mercury cadmium chalcogenide quantum dots (QDs) are promising fluorescent materials for bio-imaging and device applications due to facile tuning of their emission wavelength from the visible to short wave infrared (SWIR; 900 – 2000 nm). High-quality nanocrystals are achieved via cation exchange-mediated synthesis as de novo syntheses of alloy nanocrystals are hard to control. While the relative degree of exchange of cadmium to mercury is used to control the emission wavelength, precise control of the final emission wavelength remains elusive. A first-principles prediction of the relationship between the mercury-to-cadmium ratio in the alloyed QDs and their optical properties can inform the design and synthesis of these materials.

This talk will describe calculated optical spectra of both bulk mercury cadmium chalcogenide materials and nanocrystals composed of HgS, HgSe, CdS, and CdSe. We used density functional theory to calculate the band gap energies and the optical properties via complex dielectric functions and absorption spectra of zinc blende $\text{Hg}_x\text{Cd}_{1-x}\text{S}$ and $\text{Hg}_x\text{Cd}_{1-x}\text{Se}$ alloys as a function of alloy composition. We then applied the generalized quasi-chemical approximation to describe the relationship between band gap energies and optical features with respect to the material composition under different synthesis conditions, including thermodynamic equilibrium. We found that the optical absorption features at the band edge are highly sensitive to even a small mercury fraction ($x < 0.2$) in the material. We considered the effects of spin-orbit coupling and found that while it did alter the band gap energies by up to 0.5 eV, the complex dielectric function features were similar and only shift in energy. Our bulk alloy calculations are consistent with trends observed experimentally and our nanocrystal calculations can be used to adjust the energy range to account for the effect of quantum confinement. Together these results can be used to identify target compositions of mercury cadmium alloy QDs needed to achieve desired optical properties.

4:30 PM NM03.06.07

Rapid Evaluation of Time Dynamics and Excitation Spectra of Quantum Dots Matthias Kick, Ezra A. Alexander and Troy Van Voorhis; Massachusetts Institute of Technology, United States

QDs have attracted a lot of interest in recent years due to their potential use in solar cells, light-emitting diodes (LEDs), displays, photo-detectors and biological sensing and imaging. Due to their size (1-10 nm) their electronic structure resembles that of both a molecule and a solid. At the band edges QDs show a set of discrete states like those in a molecule, while the orbitals lying deeper in the bands form a continuum resembling the electronic structure of a solid. The size of the quantum dots makes their optical properties difficult to describe from a theoretical perspective. For example, a CdSe/ZnS core shell QD, with a diameter of around 2 nm, consists of more than 500 atoms, possible ligand atoms not included. This QD is on the upper end of what is possible to describe computationally, but is still rather small compared to the experimentally observed average size of 3.5 nm. Moreover, hybrid density functional theory (DFT) is required to obtain reasonable accuracy for semiconductors, which further increases the computational cost. Furthermore, in order to reveal the full optical properties of QDs one needs to apply time-dependent DFT (TDDFT). However, the high computational cost of TDDFT, on top of everything mentioned previously, usually allows the computation of only a few, low-lying excited states for rather small QDs. In this computational study, we present a way to obtain accurate excitation spectra for quantum dot sizes which are not feasible by current standard TDDFT approaches. By combining of short real-time propagation TDDFT (RT-TDDFT) and approximated linear-response TDDFT (LR-TDDFT), we are able to rapidly obtain excitation spectra for the entire optical range. We demonstrate the capabilities of our approach by studying the optical properties of CdSe/ZnS core shell QDs.

4:45 PM NM03.06.08

Theoretical Optical Performances of Semiconductor Nanocrystals for Image Sensors and Photovoltaics Applications Bilal Chehaibou¹, Christophe Delerue¹, Gabriel Mugny², Peter Reiss³ and Arthur Arnaud²; ¹Institut d'Electronique, de Microélectronique et de Nanotechnologie, France; ²STMicroelectronics, France; ³CEA, France

Colloidal quantum dot (CQD) thin films are emerging materials that are expected to be used more and more in the microelectronics industry. One of their greatest strengths lies in the capability to tune their optical properties across a wide spectral range by changing their size, shape, and composition. Due to these excellent optical properties, research on QDs has experienced extremely rapid development during the last few decades, accompanied by the emergence of various semiconductor materials (II-VI, III-V, IV-VI, and group IV) and various technologies relying on QD thin films (LEDs, displays, photovoltaics, image sensors), driven also by their low-cost synthesis and easy integration into conventional microelectronic fabrication flows.

QD thin films are made of chemically-synthesized semiconductor nanocrystals, embedded in an insulating matrix made of organic and/or inorganic ligands. The role of these ligands is to passivate dangling bonds on the surface of the QDs, stabilize both mechanically and chemically the QDs, and allow charge carrier transfer between QDs without affecting their optical absorptions. As a consequence, it is important to model the dielectric behavior of the QD thin films and see how the properties of the ligands matrix and the choice of the nanocrystals' shape, composition, and size impact the final performances of the CQD thin films.

In this presentation, we will present a methodology to predict the optical properties of CQD thin films based on nanocrystal quantum simulations coupled with effective medium theory. By using Tight-Binding (TB) simulations, we computed the electronic structure of several nanocrystals of different sizes and made of various bulk semiconductors to find empirical laws describing the evolution of the QDs' optical bandgap as a function of their diameter. For all these materials, we then determined the influence of the QD size on the oscillator strength [1], enabling us to establish empirical laws to forecast the absorption coefficient and optical dielectric permittivity of single QDs. We then used the Bruggeman formula [2] to extrapolate the complex optical indices of thin films made of QDs embedded in a ligand matrix [3]. This allowed us to assess the influence of the ligand and volume fraction on the optical performances. Adjusting the model parameters (QD size, ligand length, and volume fraction), we provided an abacus giving the maximum theoretical optical performances of CQD thin films for various semiconductor materials.

Finally, using the optical indices calculated previously, we performed stack diode simulations using the transfer matrix method (TMM), to see how intrinsic CQD film absorption impacts the design and the quantum efficiency of photodiodes embedding QDs.

The presented work thus provides a detailed understanding of the various physical and chemical parameters at the origin of the optical properties of QDs as

well as elements allowing to compare the performances of QDs with other photosensitive materials used in photonics, image sensors, and photovoltaics. It provides a useful resource and a guide for chemists and physicists synthesizing and characterizing new types of QD.

[1] Moreels, I.; Lambert, K.; Smeets, D.; De Muynck, D.; Nollet, T.; Martins, J. C.; Vanhaecke, F.; Vantomme, A.; Delerue, C.; Allan, G.; et al. Size-Dependent Optical Properties of Colloidal PbS Quantum Dots. *ACS Nano* **2009**, *3*, 3023–3030

[2] Choy, T. C. *Effective Medium Theory*; Oxford University Press, 2015

[3] Chehaibou, B., Izquierdo, E., Abadie, C., Cavallo, M., Khalili, A., Dang, T. H., ... & Delerue, C. Complex Optical Index of PbS Nanocrystal Thin Film and their Use for Short Wave Infrared Sensor Design. *Nanoscale* **2022**, *7*

SESSION NM03.07: Poster Session

Session Chairs: Justin Caram, Alexander Govorov, Iwan Moreels, Marinella Striccoli, Oomman Varghese and Alberto Vomiero

Wednesday Afternoon, November 30, 2022

8:00 PM - 10:00 PM

Hynes, Level 1, Hall A

NM03.07.01

Effect of Redox-Active Ligand Shell on Photocatalysis by Cadmium Sulfide Quantum Dots Florence Dou and Brandi Cossairt; University of Washington, United States

The chemical manufacturing industry accounts for 10% of global energy consumption and 7% of total greenhouse emissions. Endergonic reactions are performed under high temperatures and pressures, but photocatalysis offers a carbon neutral route under ambient conditions. Colloidal quantum dots (QDs) are efficient photocatalysts of organic reactions due to their high extinction coefficients, wide absorption profiles, and highly tunable band edge potentials. Despite the ligand shell taking up such a large portion of the surface, there have only been a few studies probing fundamental effects of the ligand shell on catalysis. These studies typically explore the effect of ligand sterics and surface accessibility, but not ligand electronic properties. Herein, we design a redox-active ligand shell that actively participates in shuttling charge from QD to reactants. We functionalise the surface of our QDs with a series of carboxylic acid derivatives of ferrocene (Fc). We demonstrate that these ligands are efficient quenchers of the excitonic hole. We next test the effect of this hole-accepting ligand shell on a carbon-carbon coupling reaction wherein the rate-limiting step is hole transfer from QD to substrate. We find that the rate of reaction depends on both the driving force for hole transfer and the binding strength of Fc ligands in a dynamic ligand shell. Our findings indicate that direct hole transfer is still more efficient than a hole shuttle, however our strategy seems to protect the surface of the catalyst from oxidation and subsequent aggregation.

NM03.07.02

Antibiotic-Resistant Bacteria Biosensor via Quantum Dot and DNA Hybridization on Magnetic Silica Nanoparticles Guncem O. Eren¹, Alexander Kleimann², Saad Ullah Khan¹, Siti Nurul Aisyiyah Jenie³, Holger Schönherr^{2,2} and Sedat Nizamoglu^{1,1}; ¹Koç University, Turkey; ²University of Siegen, Germany; ³Research Centre for Chemistry, National Research, and Innovation Agency (BRIN), Indonesia

Among the pathogenic bacteria, *Staphylococcus aureus* (SA), which is one of the most common human pathogens, is particularly prone to resistances to most antibiotics. Due to its severe infection disease burden, SA is a worldwide concern in health care facilities¹. In order to screen patients in hospital admission, to analyse the pathways of resistance spread and to administer the appropriate treatment, it is required to develop on-site tests, which are rapid, ultrasensitive, selective, economic and sustainable². In this regard, nanoparticle-enabled techniques provide unique ways to combine the aforementioned properties with the requisite high performance³.

In our study, we aim to design a sandwich DNA hybridization biosensor to detect bacterial infections via genomic DNA by fluorescence. Non-toxic and highly efficient InP/ZnS core/shell QDs and functional porous silica nanoparticles (NPs) are used for signaling and separation process, respectively. InP core QDs are synthesized via amine-derived synthetic approach. The red-shift in the absorption spectra occurs with the ZnS shell, which demonstrates the increase of the size of QDs. After the ZnS shell growth, InP/ZnS core/shell QDs exhibit comparatively narrow PL emission with a 58 nm of full width at half-maximum (FWHM) and 77.5% of photoluminescence quantum yield (PLQY). Time-resolved PL (TRPL) decay measurements show that the average lifetime of the InP/ZnS QDs is 38.33 ns. In order to make the QDs water-soluble, ligand exchange process is performed using MPA.

Porous silica NPs, which possess (a) superparamagnetic or (b) fluorescent properties by incorporating iron oxide or dye molecules such as Rhodamine B, are produced. The MPA-capped InP/ZnS QDs are used as alternative label. The surface of the silica particles is functionalized by a passivating polymer brushes grafting from polymerization. Moreover, to 'catch' complementary DNA molecules, polymer brushes are functionalized via EDC-NHS chemistry technique. Transmission electron microscopy (TEM), X-ray Photoelectron Spectroscopy (XPS) results confirm the functionalization of silica NPs.

Keywords: *Staphylococcus aureus*, DNA Hybridization, nanotechnology

References:

(1) Tacconelli, E. Global Priority List of Antibiotic-Resistant Bacteria to Guide Research, Discovery, and Development. **2017**.

(2) Ebrahimi, M. M. S.; Laabei, M.; Jenkins, A. T. A.; Schönherr, H. Autonomously sensing hydrogels for the rapid and selective detection of pathogenic bacteria. *Macromolecular Rapid Communications* **2015**, *36*, 2123-2128.

(3) Krismastuti, F. S. H.; Bayat, H.; Voelcker, N. H.; Schoonherr, H. Real time monitoring of layer-by-layer polyelectrolyte deposition and bacterial enzyme detection in nanoporous anodized aluminum oxide. *Analytical chemistry* **2015**, *87*, 3856-3863.

Acknowledgement: S.N. acknowledges support by the Technological Research Council of Turkey (TUBITAK) with Project No. 119N544, H.S. acknowledges funding by the Federal Ministry of Education and Research (BMBF) (FKZ: 01DP20005). S.N.A.J would like to acknowledge funding from the JFS SEA-EU/LPDP NAPARBA Project Grant No. SEAEUROPEJFS19ST-117.

NM03.07.03

Synthesis of Eco-Friendly and Stable I-III-VI QD Impregnated Al₂O₃ Microbeads Eunha Hong, Minji Ko, Yun Jae Eo, Seo Yeon Shin, Soyeon Yoon and Young Rag Do; Kookmin university, Korea (the Republic of)

Recently, ternary I-III-VI quantum dots (QDs) such as Zn-Cu-InS and Zn-Ga-In-S have received much attention as replacements for the toxic Cd- and Pb-

based QDs used in optoelectronic devices. Broadband green and red emitting I-III-VI QD-impregnated Al_2O_3 ($\text{QD@Al}_2\text{O}_3$) microbeads, for application to down-converted white light-emitting diodes (DC-WLEDs), were synthesized in a stable and easy-to-use QD material using an integrated synthetic process of electro-spray and rapid hydrolysis to be applied to down-converted white light-emitting diodes (DC-WLEDs). An aluminum tri-sec-butoxide solution was chosen as a rapid hydrolysis precursor, which; this material contains QDs to and can realize a spherical form of $\text{QD@Al}_2\text{O}_3$ powders during the electro-spraying process. To improve the stability of I-III-VI QDs, we treated them with zirconium isopropoxide ($\text{Zr}(\text{PrO})_4$) during the synthesis process. The photoluminescence quantum yields (PLQYs) of the resultant green $\text{Zr}(\text{PrO})_4$ -Zn-Ga-In-S and red $\text{Zr}(\text{PrO})_4$ -Zn-Cu-In-S QD solutions were 94.5% and 95%, respectively. Their PLQY values and operational stability were improved by via reduction of reducing the ligand loss via passivation and by the encapsulation role of the $\text{Zr}(\text{PrO})_4$ complex over the QD surface in the $\text{Zr}(\text{PrO})_4$ -treated $\text{QD@Al}_2\text{O}_3$ powders. A WLED single package implemented with GR $\text{Zr}(\text{PrO})_4$ -treated $\text{QD@Al}_2\text{O}_3$ microbeads showed comparable luminous efficacy ($\text{LE} = 77.0 \text{ lm/W}$) with a high color rendering index (> 92). The LE of a WLED with $\text{Zr}(\text{PrO})_4$ - $\text{QD@Al}_2\text{O}_3$ microbeads was improved by 41% compared to that of a WLED with pristine $\text{QD@Al}_2\text{O}_3$ microbeads. We also realized relative LE stability tests of green and red $\text{QD@Al}_2\text{O}_3$ microbead films at 60 mA for over an application time for of 72 hours. The electro-spraying hydrolysis process of QDs and a reactive metal alkoxide solution provides a simple and novel synthetic platform process to produce easy-to-use spherical QD-embedded solid materials for PL-DC applications into of future QD-based lightings and displays.

NM03.07.04

Highly Efficient (>9%) Lead-Free AgBiS_2 Colloidal Nanocrystal/Organic Hybrid Solar Cells [Changjo Kim](#) and Jung-Yong Lee; Korea Advanced Institute of Science and Technology, Korea (the Republic of)

Colloidal nanocrystals (NCs) have received considerable attention in optoelectronics because of their high reproducibility in synthesis, solution processability, near-infrared (NIR) absorption, and facile bandgap tunability. In particular, solar cells using lead chalcogenide-based NCs, such as lead sulfide (PbS) and lead selenide (PbSe), have exhibited high power conversion efficiencies (PCEs) of over 13% and 10%, respectively. Despite their high PCEs, there has been growing interest in chalcogenide-based NCs combined with lead-free cations (since lead is not environmentally friendly), such as silver, copper, bismuth, indium, zinc, and antimony. Although various combinations of binary and ternary compound NCs have been developed as photoactive materials, their performances are still inferior to those of lead-based NCs. Silver bismuth disulfide (AgBiS_2) NCs have attracted attention as suitable alternatives owing to their narrow bulk bandgap, high extinction coefficient, and light absorption in NIR region. Recently, PCE of 9.17% was achieved in NC/organic hybrid structure, but there was not enough discussion on the NC/organic interfacial electronic structure. Therefore, issues such as the low open-circuit voltage (V_{OC}) compared to the bandgap of the AgBiS_2 NCs and the unoptimized energy level structure at the NC/organic hole transporting layer (HTL) interface should be resolved for higher performance of devices. In this study, a design strategy to obtain efficient energy level structure in AgBiS_2 NC/organic hybrid solar cells is proposed.^[1] By selecting PBDB-T-2F as an HTL with a lower highest occupied molecular orbital level than that of PTB7, the V_{OC} of the device is increased. Furthermore, iodide- and thiolate-passivated AgBiS_2 NC surfaces are generated using tetramethylammonium iodide (TMAI) and 2-mercaptoethanol (2-ME), which leads to the energy level optimization of NCs for efficient charge extraction. This improves the PCE from 3.3% to 7.1%. In addition, the polymer is replaced with a PBDB-T-2F:BTP-4Cl blend to achieve a higher short-circuit current density through complementary absorption. Accordingly, an AgBiS_2 NC-based solar cell with a PCE of 9.1% is fabricated.

I. C. Kim, I. Kozakci, J. Kim, S. Y. Lee, J.-Y. Lee, *Adv. Energy Mater.* 2022, 2200262.

NM03.07.05

Downconverting Mn/Yb Codoped CsPbCl_3 Nanocrystals for Silicon-Based Tandem Solar Cell Application [Hyunju Lee](#)^{1,2}, Yoshio Ohshita³ and Atsushi Ogura^{1,2}; ¹Meiji Renewable Energy Laboratory, Japan; ²Meiji University, Japan; ³Toyota Technological Institute, Japan

Silicon-based tandem solar cells are intensively being investigated as a promising candidate for next generation solar cells combining low costs and high power conversion efficiency potential than currently dominating, but inherently limited, single-junction solar cells. For instance the world record efficiency of perovskite/silicon tandem solar cells is 29.8% [1] which is well above ideal efficiency of single-junction silicon solar cells. Despite this exciting performance, the tandem solar cell was still limited not only by a relatively low perovskite top cell voltage output but also by the silicon bottom-cell photocurrent. For instance, the total photocurrent density of the world record perovskite/silicon tandem solar cell was only 39.9 mA cm^{-2} [1]. For comparison, 42.7 mA cm^{-2} was reached in the world record SHJ cell [2], which is very close to the theoretical maximum for silicon of about 43.3 mA cm^{-2} [3]. An important optical loss mechanism in this tandem cell, in comparison to an optimized single-junction silicon cell, is the increased reflection and reduced absorption in the near infrared (NIR) part of the spectrum, hence reduced photocurrent in the silicon bottom cell. In addition, the highest reported current density for perovskite/silicon tandem solar cells has not yet reached 21 mA cm^{-2} [4]. Therefore, the enhancement of the light absorption in both perovskite top cell and silicon bottom cell becomes increasingly important to achieve cell efficiency $> 30\%$. Meanwhile, doped lead-halide perovskite (LHP) nanocrystals have emerged as unique materials combining strong, tunable broadband absorption in the ultraviolet region of the spectrum with visible and NIR photoluminescence quantum yields (PLQYs) approaching 99% [5] and 200% [6] at ambient temperature, respectively. These remarkable properties make doped LHP nanocrystals an extremely promising candidate for spectral shaping in high-efficiency solar cells. Previous theoretical assessments of such downconversion material has predicted single-junction efficiencies up to 40% [7]. In this contribution we report the synthesis of $\text{Mn}^{2+}/\text{Yb}^{3+}$ codoped CsPbCl_3 nanocrystals through a hot-injection technique. The resulting nanocrystals show a unique triple-wavelength emission covering ultraviolet/blue, visible, and near-infrared regions. In addition, owing to the high PL QYs, the codoped nanocrystals are demonstrated to be used as efficient emitters in downconverting layers, with the enhanced external quantum efficiency of silicon solar cells compared to that of using solely Mn^{2+} doped CsPbCl_3 nanocrystals. This study presents a new model system for enriching doping chemistry studies and future applications of LHP nanocrystals. This work was supported by NEDO.

References

- [1] P. Tockhorn, J. Sutter, A. Cruz, et al., *Research Square*; 2022. DOI: 10.21203/rs.3.rs-1439562/v1.
- [2] K. Yoshikawa, H. Kawasaki, W. Yoshida, et al., *Nature Energy*, 2017, **2**, 17032.
- [3] A. Richter, M. Hermle, S. W. Glunz, *IEEE Journal of Photovoltaics*, 2013, **3**, 1184.
- [4] F. Fu, J. Li, T. C.-J. Yang, et al., *Advanced Materials*, 2022, 2106540.
- [5] S. Ji, X. Yuan, S. Cao, et al., *The Journal of Physical Chemistry Letters*, 2020, **11**, 2142.
- [6] T. A. Cohen, T. J. Milstein, D. M. Kroupa, et al., *Journal of Materials Chemistry A*, 2019, **7**, 9279.
- [7] T. Trupke, M. A. Green, P. Würfel, *Journal of Applied Physics*, 2002, **92**, 1668.

NM03.07.07

Enhanced Stability of Quantum Dots via Core-Shell Type Organic-Inorganic Hybrid Encapsulation [Jeong Min Moon](#), Young Soo Seo and Jung Woo Park; interface lab, Korea (the Republic of)

Quantum dots (QDs), semiconductor nanoparticles with outstanding optical properties, is currently used in QD display. However, in the form of submicron

sized capsule, it still easily lose optical properties by oxidative degradation caused by external factors such as heat, oxygen, and moisture. Many encapsulation methods have been suggested but its reliability is still unsatisfactory for applications including QD-(O)LED or molecular diagnosis. In this study we developed a core-shell type encapsulation method where QDs are encapsulated with organic-inorganic hybrid with tens to hundreds nanometer in size via one-step process. Individual QD is surrounded by the hybrid and then aggregates to form a core and additional hybrid builds a shell. It is noted that during the process quantum yield has not been reduced. Barrier performance of the hybrid structure was performed in two ways. The hybrid capsule was kept at 60°C water solution for a month. And also it was mixed with polymer via a melt-mixing process at 180°C to fabricate a film which was exposed under blue light (450 nm) or at 60°C/95% relative humidity for a month. Quantum yield, emission wavelength and FWHM of the samples were unchanged indicating that the hybrid shell effectively prevented oxygen and water vapor penetration to the core. The hybrid structure and optical properties was mainly confirmed by TEM and PL analysis.

NM03.07.08

Spectroscopic Insight into High Luminescence Efficiency of Isotropic InP/ZnSe/ZnS Quantum Dots [Jumi Park](#)¹, Yu-Ho Won², Yongseok Han², Hyun-Mi Kim³, Eunjoo Jang² and Dongho Kim¹; ¹Yonsei University, Korea (the Republic of); ²Samsung Advanced Institute of Technology, Korea (the Republic of); ³Korea Electronics Technology Institute, Korea (the Republic of)

In this study, we propose a strategy to increase the luminescence efficiency in eco-friendly InP quantum dots (QDs). When synthesizing InP/ZnSe/ZnS QDs, we manipulated the shell growth rates by controlling the ZnSe shell growth temperature.¹ In a pristine synthesis of InP/ZnSe/ZnS QDs, ZnSe shell growing was conducted at 320 °C and these QDs exhibit irregular shell shape. Meanwhile, isotropic InP/ZnSe/ZnS QDs with regular shell can be prepared at a high reaction temperature (340 °C), which facilitates ZnSe shell growth on random facets of the InP core. HR-STEM images showed that the InP/ZnSe/ZnS QDs with irregular shell have considerable stacking faults and twin defects. On the contrary, isotropic QDs presented a well-ordered crystalline structure and good structural quality without stacking faults. In other words, fast ZnSe crystal growth eliminates the stacking faults leading to anisotropic crystal growth.

These isotropic QDs achieved a photoluminescence quantum yield (PL QY) improvement of nearly 20%. To investigate the correlation between the QD morphology and the emission properties, we analyzed the PL blinking and ultrafast charge carrier dynamics. Time- and space-resolved PL measurements showed that the charge trapping significantly decreases in isotropic QDs. The excitation wavelength-dependent transient absorption kinetics revealed that hot hole trapping is considerably suppressed for QDs with regular shape. These results highlight that QD shape-dependent PL QYs are ascribed to the degree of the hole trapping. The tactic, growing the ZnSe shell fast at the elevated reaction temperature, significantly reduced the hole trapping and improved the PL QY of InP/ZnSe/ZnS QDs. Our findings shed light on the relationship between QD shapes and hot carrier dynamics and present a way to design highly luminescent QDs for further promising display applications.

¹ *Small* **2022**, 2105492

NM03.07.09

Swelling-Induced Surface Instability of Crosslinked Nanocrystals [Seyoung Park](#) and Moon Sung Kang; sogang university, Korea (the Republic of)

Colloidal assemblies of semiconductor nanocrystals (NCs) are promising active materials for electronics/optoelectronic devices. These materials are typically processed into thin films based on solution processes. Chance of swelling of these assemblies during the processing can dramatically affect the morphology of the film. Here, we report experimental study on mechanical instability of crosslinked nanocrystal assemblies swollen by various solvents. When a crosslinked NC film is attached to a rigid substrate, swelling induced compressive strain causes delaminated buckling of the film from the substrate. To investigate the feature of delamination, we control the delamination through experimental parameters such as the solvent-colloids interaction parameter, the degree of crosslinking, and the surface energy. The mathematical model of delamination offers a physical approach to elucidate the properties of delamination including wavelength and amplitude. Also, the experimental parameters are substituted to mismatch strain, modulus of film, and adhesion energy, respectively. Finally, we apply various physical models of film delamination describe our observation.

NM03.07.11

Predicting Coherent Nanocrystal Orientation in PbS Superlattices by Minimizing Ligand Packing Frustration [Eliza Price](#) and William Tisdale; Massachusetts Institute of Technology, United States

For many optoelectronic device applications, colloidal nanocrystals (NCs) must be assembled into ordered superlattices (SLs). Since the SL structure influences the photophysics of NC thin films, it is desirable to obtain robust engineering control over SL topology. A number of factors influence the self-assembly of colloidal NCs, such as the well-studied impact of nanocrystal size and shape. In more recent years, the importance of both bound and unbound organic ligands on self-assembly outcomes has been highlighted; the ligand length, ligand coverage, bound and unbound ligand fractions, and ligand interactions can all influence the resulting NC SL structure. In this work, we consider how the classic influence of nanocrystal shape can impact ligand packing frustration and influence the coherent orientation of non-spherical NCs in superlattice structures. Through the application of the freely jointed chain model to predict conformational entropy, we find that minimizing the packing frustration of the ligand layer may explain experimental observations of NC alignment in NC SLs. We validate our model by comparing to prior X-ray scattering data showing the kinetics of PbS superlattice formation. These data show that as solvent is evaporated, the SL exhibits a Bain-like distortion, contracting from an fcc to bcc structure, and the coherent NC tilt relative to the substrate changes from 9.7° to 0° [1]. In future work, other contributions to the free energy of NC SL formation may be considered in an effort to create a coarse-grained, thermodynamic model capable of predicting superlattice structure.

1. M. C. Weidman, D. M. Smilgies, and W. A. Tisdale, "Kinetics of the self-assembly of nanocrystal superlattices measured by real-time in situ X-ray scattering," *Nature Materials*, vol. 15, no. 7, pp. 775–781, 2016, doi: 10.1038/nmat4600.

NM03.07.12

Lead Chalcogenide Quantum Dot Assembly and Attachment on Fluid Interfaces [Wenxin Qi](#), Isaiah Y. Chen and Paulette Clancy; Johns Hopkins University, United States

The formation of tiles composed of quantum dots are thought to constitute a new class of self-assembled nanostructured material. Understanding the dynamic physicochemical processes that govern the assembly of quantum dot monomers at a functionalized fluid interface is crucial for material processing strategies. However, the mechanism of this assembly and attachment is still unclear. What is clear is that a functionalized liquid interface potentially provides more control in the diffusion, coupling, and orientation of the nanocrystals (NCs), which increases the complexity of the assembly process. To investigate this self-assembly process, we look to insight from the fundamental molecular-level interactions; we use Molecular Dynamics (MD) simulations to watch NCs assembly on a surfactant monolayer. The specific model system studied here was composed by lead chalcogenide nanocrystals, covered with lead oleate molecules and assembling on a monolayer composed of 1,2-dipalmitoyl-sn-glycero-3-phosphocholine (DPPC) molecules. In this approach, a reactive force field is used to model the interactions between species in the system. For the PbS NCs, we use the existing Simple Molecular

Reactive Force Field (SMRFF) as an effective force field. The ligands and DPPC molecules are represented by the OPLS force field. All the simulations aimed to reveal the role of the nature of the surface monolayer. Before testing the impact of monolayer parameters, we used density functional theory to confirm that the energy barrier for ligand dissociation was high and are unlikely to detach readily. We adjusted the density of the DPPC molecules in the monolayer from 0.5 to 2.5 molecules/nm² to determine the effect of ML density on assembly and attachment behavior of NCs on a DPPC monolayer. We studied the degree of NC in-plane and out-of-plane orientation during the process and the alignment and tendency to form interconnecting bridges. We found that the NCs prefer to diffuse and assemble rather than interacting with the monolayer. Our studies of the interaction energy and the potential of mean force (PMF) provide quantitative metrics for the interaction between the NCs and the monolayer. We show that there is a similar trend in the interaction energy between NCs and monolayer, which can help us to predict an optimal monolayer structure for NC assembly. We also studied the effect of hydrocarbon chain length in the monolayer molecule, varying the molecule from DPPC to DLPC and DMPC. This property indicates that NC assembly is facilitated by shorter lipid molecules.

NM03.07.13

Indium Phosphide Magic Sized Clusters: Templates for Synthesizing Chiral Nanomaterials [Youngjae Ryu](#) and Sungjee Kim; Pohang University of Science and Technology, POSTECH, Korea (the Republic of)

Chiral materials are of great interest promising various applications that include asymmetric catalysis, chiral sensing, polarization control, and gene engineering. Compared to metallic nanoparticles and II-VI group semiconductor nanoparticles, chiral properties of III-V group semiconductor nanomaterials are less explored. Herein, we aim to understand the chiroptical activities of III-V semiconductor magic sized clusters (MSCs), also known as quantum dot (QD) intermediates. We introduce chiral InP MSCs with unprecedented large circular dichroism signals compared to previously reported chiral semiconductor nanocrystals. To investigate the chiroptical origins of our chiral MSCs, characterizations using XPS, FT-IR, Raman, XRD, TGA, and EXAFS are conducted to explore ligand geometry and structural properties. It is discovered that chiral ligands are bound to MSC surface by double anchoring modes, with both thiolate and carboxylate group. Based on the structural characterizations, the inorganic core was observed to exhibit low-symmetry polytwistane structures. Similar sized chiral InP QDs are prepared as the control counterpart, where their optical chirality was marginal. The low crystal symmetry and large transition dipole moments are attributed to the high chiroptical activity of MSCs. Interestingly, chiral MSCs can induce chiroptically active QDs when used as templates (or seeds) to synthesize the QDs. Halide atoms (Cl, Br, I) can be introduced as dopants into MSCs, which also alters the chiroptical properties. Our findings emphasize the unique characteristics of MSCs as prospective chiral materials and gives intuition on designing chiroptical nanomaterials.

NM03.07.14

Integration of Synaptic Phototransistors and Quantum Dot Light-Emitting Diodes for Visualization and Recognition of UV Patterns [Hyojin Seung](#) and Dae-Hyeong Kim; Seoul National University, Korea (the Republic of)

Neuromorphic photodetectors feature photon-triggered synaptic plasticity, which enables efficient image recognition. However, even with a synaptic device, the visualization and recognition of invisible ultraviolet (UV) patterns are still challenging owing to intense background noise. Here, we develop an integrated device of synaptic phototransistors (SPTs) and quantum dot light-emitting diodes (QLEDs) for noiseless visualization and efficient recognition of UV patterns through on-device preprocessing inspired by all-or-none potentiation of synapse. The SPTs convert noisy UV inputs into a weighted photocurrent, which is applied to the QLEDs as a voltage input through an external current-voltage converting circuit. The QLEDs exhibit threshold switching characteristics, *i.e.*, they either derive the exponentially increasing current output and visible illumination by the suprathreshold input voltage or nearly zero current output and no visible illumination by the subthreshold input voltage. The preprocessed image data obtained by the SPT-QLED has an exponentially amplified signal-to-noise ratio, which is helpful for high-accuracy image recognition based on deep neural networks.

NM03.07.16

Upconversion Photoluminescence Properties of High Quantum Yield Nitrogen Doped Graphene Quantum Dots Synthesized by Pulsed Laser Ablation [Muhammad Shehzad Sultan](#)¹, Vladimir I. Makarov¹, Wojciech Jadwisnienczak², Brad R. Weiner¹ and Gerardo Morell¹; ¹University of Puerto Rico at Río Piedras, United States; ²Ohio University, United States

The graphene quantum dots (GQDs), a zero-dimensional graphene quantum structure, have triggered an intense research worldwide. GQDs possess unique optical, chemical and physical properties as compared to conventional quantum dots (QDs), such as low toxicity, biocompatibility, optical stability, chemical inertness, high photostability and good water-solubility and therefore hold great application potential in biomedical, optoelectronics and energy storage devices. The doping of GQDs with heteroatoms is one of the most effective ways to tune their photoluminescence emission and to increase quantum yield. In this study, we developed a novel approach to synthesize high-quality Nitrogen-doped graphene quantum dots (N-GQDs) with high quantum yield, via irradiation of s-triazene in a solution with benzene by using pulsed laser. The TEM, HRTEM, XPS, XRD, Raman spectroscopy and FTIR were carried out to observe the morphology, size distribution, crystalline structure and to prove successful doping of GQDs with nitrogen atoms. To observe optical properties of as synthesized N-GQDs, the UV-vis and Photoluminescence measurements were carried out. The as-synthesized NGQDs exhibit high quality crystalline structure of graphene with an average size of about 3.7 nm. A high quantum yield was exhibited by the obtained N-GQDs as compare to the pristine GQDs. The obtained N-GQDs with oxygen-rich functional groups exhibit a strong emission and excellent upconversion PL properties. These outcomes result in an ample opportunity for the biomedical and optoelectronic applications.

NM03.07.17

In(Zn)P Core-Multishell Colloidal Quantum Dots Engineering for Narrow FWHM and Enhanced Bright Green-Luminescence via Halide and Alcohol Surface Treatment [Derrick Allan Taylor](#)¹, Justice Agbeshie Teku¹, Sinyoung Cho¹, Weon-Sik Chae², Seock-Jin Jeong¹ and Jong-Soo Lee¹; ¹Daegu Gyeongbuk Institute of Science and Technology, Korea (the Republic of); ²Korea Basic Science Institute, Korea (the Republic of)

Semiconductor colloidal quantum dots (CQDs) have made remarkable progress since their discovery as multifunctional materials due to their attractive size-tunable electronic and optical properties, low-cost production, high efficiency, and high stability. Cd, Hg, and Pb containing CQDs have reached commercial-scale optical properties, yet they are restricted in commercial applications due to their toxicity. For the light-emitting display applications, indium phosphide (InP) QDs have emerged as the best intrinsically low toxic alternative for Cd and Pb-based QDs but still lag in the optical properties of emission linewidth and size dispersity with its counterpart CdSe. In this work, we report the importance of precisely controlling the reaction kinetics of InP QDs by a two-step growth process to achieve uniform size distribution (<4% polydispersity index). Engineering the shell coating to reduce interfacial defects yielded high photoluminescence quantum yield (PLQY) and surface treatment with halides and alcohols enhanced the PLQY through improved surface defect passivation. After the sample purification, the as-synthesized core-multishell QDs exhibited a bright green emission with a very high quantum yield and the narrowest emission linewidth of 71% and 33 nm, respectively. This work aims to expand the understanding of InP QDs synthesis and open up a new surface treatment approach using alcohol.

NM03.07.18

Colloidal Synthesis of Blue Emitting Cadmium Free ZnSe-ZnSeTe Core-Multishell Quantum Dots. Justice Agbeshie Teku, Derrick Allan Taylor, Bowon Moon, Somi Lee and Jong-Soo Lee; Daegu Gyeongbuk Institute of Science and Technology (DGIST), Korea (the Republic of)

Size-tunability, narrow optical properties, high efficiency, low cost of production, and good stability of colloidal semiconductor quantum dots (QDs) are one of the most promising candidates for future light-emitting materials for display. Due to toxicity and environmental concerns of well-developed Cd and Pb-based QDs, researchers and the display industries have tried to develop an alternative to the Cd and Pb-based QDs with similar optical properties. The Indium Phosphide (III – V) QDs, has proven to be a perfect alternative to Cd and Pb-based QDs due to their optical properties similarity. However, the development of Blue InP QDs compare to the Red and the Green remains a major challenge to date. In this work, we developed a non-InP and Cd-Pb free Blue emitting ZnSe-ZnSeTe core-multishell QDs by carefully controlling and optimizing the growth of the core and the shell. The designed synthesis procedure has multiple intermediate shelling, with gradient ZnSeS shelling and outer ZnS shelling. To enhance surface passivation and luminescence the surface of the QDs was treated with halides. The as-synthesized QDs show a pure blue emission (450 – 455nm), symmetrical PL spectra (absence of defect associated with Te materials), the narrowest FWHM for Te-based QDs, and improved PLQY. Our work has a great outcome to be implemented into the RGB patterning system, efficient QLED fabrication, and full-color panel displays.

NM03.07.20

Flexible and Transparent Electrode of Hybrid Ti_3C_2Tx MXene–Silver Nanowires for High-Performance Quantum Dot Light-Emitting Diodes Wei Jiang and Cheolmin Park; Yonsei University, Korea (the Republic of)

The development of electrodes with high conductivity, optical transparency, and reliable mechanical flexibility and stability is important for numerous solution-processed photoelectronic applications. Although transparent Ti_3C_2Tx MXene electrodes with high conductivity are promising, their suitability for displays remains limited because of the high sheet resistance, which is caused by undesirable flake junctions and surface roughness. Herein, a flexible and transparent electrode has been fabricated which is suitable for a full-solution-processed quantum dot light-emitting diode (QLED). An MXene-silver nanowires (AgNWs) hybrid electrode (MXAg) consists of a highly conductive AgNWs network mixed with solution-processed MXene flakes. Efficient welding of wire-to-wire junctions with MXene flakes yields an electrode with a low sheet resistance and a high transparency of approximately $13.9 \Omega \text{ sq}^{-1}$ and 83.8%, respectively. By employing a thin polymer buffer layer of poly (methyl methacrylate) (PMMA), followed by mild thermal treatment, a hybrid PMMA-based MXene-AgNWs (MXAg@PMMA) electrode which the work function of an MXAg hybrid FTE physically embedded in PMMA (MXAg@PMMA) can be tuned by controlling the amount of MXene in a hybrid film facilitates the development of a high performance solution-processed QLED that exhibits maximum external quantum and current efficiencies of approximately 9.88% and 25.8 cd/A, respectively, with excellent bending stability. This work function-tunable flexible transparent electrode based on solution-processed nanoconductors provides a way to develop emerging high-performance, wearable, cost-effective, and soft electroluminescent devices.

NM03.07.21

The Study of QDs-TiO₂ Nanocomposites for Solar Fuels Production Francesca S. Freyria¹, Nicola Blangetti¹, Sandra Doria^{2,3}, Simelys Hernandez¹, Mariangela Di Donato^{2,3}, Maela Manzoli⁴, Sergio Brovelli⁵ and Barbara Bonelli¹; ¹Politecnico di Torino, Italy; ²LENS - European Laboratory for Non-Linear Spectroscopy, Italy; ³Institute of chemistry of organometallic compounds (ICCOM), Italian National Research Council (CNR), Italy; ⁴University of Torino, Italy; ⁵Università degli Studi di Milano-Bicocca, Italy

During these last decades, we are facing every day an increase of both energy shortage and environmental pollution due to the still voracious use of fossil fuels to produce energy. In this scenario, solar energy conversion is an encouraging approach to address these crucial issues, especially because the current global energy consumption in a year could be easily covered by the bihourly solar energy that strikes the Earth.¹ Taking inspiration from leaves, an environmental-friendly way to produce renewable fuels is to exploit the incident solar photon energy to drive energetically uphill reactions such as the water splitting and CO₂ conversion. Currently, one of the most applied photocatalyst is TiO₂ due to its great efficiency, affordable cost and contained toxicity. The three main crystalline phases of TiO₂ are anatase (indirect band gap), rutile and brookite (direct band gap), whose presence and possible heterojunction formation can affect the photogenerated electrons and holes and, consequently, the final photocatalytic efficiency.^{2,3} The crystalline structure of the TiO₂ photocatalyst has been tuned by adopting template-free synthesis followed by a mild thermal treatment. One of the main drawbacks of the TiO₂ is its inability to absorb visible and NIR photons. Colloidal quantum dots (QDs) are receiving great attention to be applied either as sensitizer or as photocatalyst thanks to their excellent optoelectronic properties.¹ NIR emitting toxic-metal-free CuInS₂ (CIS QDs) were chosen as sensitizer for different types of TiO₂ substrates.⁴ We have been testing the photocatalytic behavior for CO₂ reduction under simulated sunlight at 1 Sun (i.e., 100 mW/cm² of intensity) with pure and mixed TiO₂ phases coupled with different loading amounts of CIS QDs. The structure and the properties of QDs-TiO₂ nanocomposites have been investigated with different techniques, such as X-ray powder Diffraction (XRPD) with Rietveld refinement for quantitative phase analysis, Diffuse Reflectance (DR) UV-Vis spectroscopy, N₂ adsorption/desorption at -196 °C, electrophoretic mobility (ζ -potential), FT-IR measurements, X-rays photoelectron spectroscopy (XPS) and electron microscopy (TEM/SEM). Charge transfer and recombination processes are under study by using different spectroscopy techniques. Preliminary chromatographic analyses show a different amount of C₁ and C₂₊ products based on the polymorphs types present in the nanocomposite.

- (1) Freyria, F. S. . In *Nanostructured Catalysts for Environmental Applications*; Piumetti, M., Bensaid, S., Eds.; Springer International Publishing, 2021; pp 214–248.
- (2) Vequizo, J. J. M.; Matsunaga, H.; Ishiku, T.; Kamimura, S.; Ohno, T.; Yamakata, A. *ACS Catal.* 2017, 7 (4), 2644–2651.
- (3) Manzoli, M.; Freyria, F. S.; Blangetti, N.; Bonelli, B. *RSC Adv.* 2022, 12 (6), 3322–3334.
- (4) Shen, F.; Que, W.; Liao, Y.; Yin, X. *Ind. Eng. Chem. Res.* 2011, 50 (15), 9131–9137.

SESSION NM03.08: QD Based Devices I
Session Chairs: Alexander Efros and Richard Lunt
Thursday Morning, December 1, 2022
Hynes, Level 2, Room 209

8:30 AM *NM03.08.01

Colloidal Quantum Dot Laser Diodes Victor I. Klimov and Clement Livache; Los Alamos National Laboratory, United States

Colloidal quantum dots (CQDs) combine superior light-emission characteristics of quantum-confined semiconductors with chemical flexibility of molecular systems. These properties could, in principle, enable solution processable laser diodes with an ultrawide range of accessible colours. However,

the realization of such devices has been hampered by fast optical gain decay due to nonradiative Auger recombination and poor stability of CQD solids at high current densities required for the lasing regime. Recently, we have resolved these problems and achieved a lasing regime with electrically pumped CQDs. The active layer of our devices is made of novel “compact continuously graded CQDs” (ccg-CQDs) that feature strongly suppressed Auger recombination and a large material gain coefficient. The ccg-CQDs are incorporated into an LED-like device stack assembled of low-loss materials and engineered so as to maximize optical field confinement within the CQD layer. The developed design allows us to boost the modal gain coefficient for the active medium and to reduce optical losses in the adjacent charge transport/injection layers. Further, we incorporate an integrated photonic structure which allows for highly efficient light trapping in the CQD waveguiding layer. To lessen the deleterious influence of thermal effects, we reduce the injection area with a small “current-focusing” aperture inserted into a hole injection path and use a pulsed bias to drive our devices. Using this approach, we achieve the lasing effect due to electrically excited stimulated emission from the CQDs. These prototype CQD laser diodes demonstrate a low-threshold laser action at both the band-edge, 1S (637 nm) and the excited-state, 1P (586 nm) transitions at room temperature.

9:00 AM NM03.08.02

Improved Infrared Photoresponse Through Coupling of Lead Sulfide Colloidal Quantum Dots and Amorphous Selenium Håvard Mølnås¹, HariPriya Kannan¹, Atreyo Mukherjee², Shlok Joseph Paul¹, A.H. Goldan² and Ayaskanta Sahu¹; ¹New York University, United States; ²Stony Brook University, The State University of New York, United States

Infrared photodetectors are playing an increasingly important role in our modern society, and the use of colloidal quantum dot active layers have reduced the complexity at which these detectors can be fabricated and tuned. However, a compromise between maximizing charge transfer and absorbance is often necessary to optimize detector performance. Amorphous selenium (a-Se) is known for its uniform properties and ease of deposition scalable to a large area, as well as its ability to provide avalanche gain via hole impact ionization at high applied electric fields. In this work, we combine an a-Se hole transport layer with a lead sulfide (PbS) colloidal quantum dot active layer in order to decouple charge transport and absorption, and we show that this is beneficial for the infrared photoresponse. Although more work remains to improve device performance and stability, preliminary specific detectivity of 2.5×10^{11} Jones at 980 nm and 3dB frequency of 2.5 MHz demonstrate that this technology has the potential to compete with and surpass the current state of the art.

9:15 AM NM03.08.03

A Path to Heavy Metal-Free Infrared Photodetection Using Silver Selenide Colloidal Quantum Dots Shlok Joseph Paul, Håvard Mølnås, Michael R. Scimeca, Navkawal Mattu, Ingrid J. Paredes, Minh N. Tran, Eray S. Aydil and Ayaskanta Sahu; New York University, United States

The deployment of infrared cameras has so far been limited to military and defense applications because of the high costs involved in high temperature epitaxy and hybridization (1). The advent of low cost colloidal quantum dot (QD) infrared detectors will help persuade device adoption in the commercial detector markets. However so far toxic heavy metal compounds like Lead and Mercury chalcogenides have dominated the QD Photodetector space (1,2). In this work we establish a route to environmentally benign Near Infrared (NIR: 0.7 - 1.4 μm) and Short Wave Infrared (SWIR: 1.4 - 3 μm) active Ag_2Se CQDs. Herein we study the dynamics of an alternate Ag_2Se synthesis with exquisite size control. We report the effects of various parameters (Synthesis Time, Injection Temperature, Growth Temperature and Precursor Ratios) and highlight the size tunable excitonic peak and room temperature photoluminescence observed in the NIR and SWIR regions. Furthermore, we demonstrate IR active devices using ligand exchanges with short chain molecules such as 3-Mercaptopropionic acid (MPA), Thiocyanate (SCN) and 1,2-Ethanedithiol (EDT). Our results demonstrate that an EDT/HCl/IPA mixture results in a room temperature responsivity $\sim 50\text{mA/W}$ at 1150 nm. To the best of our knowledge, this device provided the highest responsivity at 1150 nm among Ag_2Se photoconductors to date. Prior work (3) has shown tunable absorption into the MIR (3-5 μm) as well and future work will involve fabricating photodiodes using these MIR particles.

References:

- 1) Pejovic, V. (n.d.). Infrared colloidal quantum dot image sensors. IEEE Xplore.
- 2) Gréboval, C., Chu, A., Goubet, N., Livache, C., Ithurria, S., & Lhuillier, E. (2021). Mercury chalcogenide quantum dots: Material Perspective for Device Integration. *Chemical Reviews*, 121(7), 3627–3700. <https://doi.org/10.1021/acs.chemrev.0c01120>
- 3) Scimeca, M. R., Mattu, N., Paredes, I. J., Tran, M. N., Paul, S. J., Aydil, E. S., & Sahu, A. (2021). Origin of Intradband optical transitions in Ag_2Se colloidal quantum dots. *The Journal of Physical Chemistry C*, 125(31), 17556–17564. <https://doi.org/10.1021/acs.jpcc.1c05371>

9:30 AM NM03.08.04

Unraveling the Transition Dipole Orientation in Lead Halide Perovskite Nanoplatelets and Its Role in QD-LED Light Outcoupling Efficiency Tommaso Marcato, Sudhir Kumar and Chih-Jen Shih; ETH Zürich, Switzerland

In recent years, quantum dot light-emitting diodes (QD-LEDs) have arisen as ideal candidates to compete with organic light-emitting diodes (OLEDs) in display applications. The outstanding photophysical characteristics of colloidal semiconductor nanocrystals (NC), especially CdSe, InP and lead-halide perovskites (LHP), have led to a rapid surge in their use as active layers in high-efficiency devices, with multiple reports of external quantum efficiencies (EQE) surpassing 20%. To date, the major steps in enhancing device efficiency have come from the development of passivation strategies to reduce NC defects and boost internal quantum efficiency (IQE). As IQE approaches unity, the major bottleneck to device efficiency remains light outcoupling. A well-known intrinsic strategy for improving light extraction in OLEDs is transition dipole moment (TDM) engineering. Accordingly, EQEs approaching 40% have been demonstrated by designing efficient phosphorescent or thermally activated fluorescence (TADF) emitters with preferential orientation of their TDMs parallel to the device substrate.

At the same time, recent studies on few-monolayer-thick colloidal CdSe nanoplatelets (NPLs) have shown highly anisotropic TDM orientation, suggesting that similar strategies might be extended to QD-LEDs. Inspired by these results, we wanted to tackle the following fundamental question: can we develop a model to understand and predict the TDM orientation in semiconductor NC films?

In general, in contrast with organic semiconductor molecules, inorganic materials tend to have highly symmetric crystal lattices, leading to isotropic electronic structure and strong degeneracy at the band-edge. However, nanostructuring offers the possibility of introducing favorable symmetry breaking and anisotropy by controlling the NC shape. In this talk, I will first present a multiscale model of the preferential horizontal TDM orientation in LHP NPLs that highlights three fundamental contributions: (i) anisotropic conduction band Bloch states and large fine exciton splitting, (ii) anisotropic dielectric screening, (iii) ordered assembly in thin film. This model identifies the NPL thickness and the film order parameter as the two fundamental degrees of freedom allowing for continuous tuning of the TDM orientation.

We showed that these criteria can already be satisfied in devices by inducing the formation of 2D ordered assemblies of LHP anisotropic NCs on a hole transport layer with low surface energy. This resulted in a ratio of horizontal dipoles up to 0.75, which allowed our optimized green QD-LEDs to achieve peak EQE up to 24.96%.

9:45 AM NM03.08.05

Perovskite Quantum Dots on Polymer Matrix for Stretchable LED Geon-Hui Lee¹, Xiwen Gong² and Sei Kwang Hahn¹; ¹Pohang University of Science and Technology, Korea (the Republic of); ²University of Michigan–Ann Arbor, United States

Most intrinsically stretchable LEDs are developed using a polymer emitting layer, but the organic LED cannot produce vivid colors because of its low color purity with large full width half maximum (FWHM). In the case of organic LED, the FWHM is about 70-90 nm and it achieved 96% of the National Television Standards Committee (NTSC) standard in the Commission Internationale de l'éclairage (CIE) chromaticity chart. However, perovskite quantum dot (QD) LED can produce vivid colors due to its high color purity (low FWHM). The perovskite QD LED has 15~25 nm of FWHM and it achieved 140% of the NTSC standard CIE chromaticity chart. Accordingly, the perovskite QD LEDs can reproduce a vivid image closer to natural color than organic LEDs. Here, we developed an intrinsically stretchable perovskite QD LED by introducing perovskite QD in the semiconducting polymer matrix. The energy band of the polymer matrix must be larger than the energy band of perovskite QD for the energy transfer to perovskite QD. In addition, the polymer matrix has to interact with the perovskite QD physically, so the perovskite QD should be evenly dispersed in the polymer matrix. The stretchable LED was fabricated using the polymer matrix, which had a larger band gap and physical interaction with perovskite QD on the TPU substrate. The fabricated LED could be stretched up to 75% and emitted light under strain with high color purity (~18 nm of FWHM). This intrinsically stretchable LED would be successfully harnessed for stretchable free-form wearable devices, enabling accurate bio-signal analysis and phototherapy for various biomedical applications.

10:00 AM BREAK

10:30 AM *NM03.08.06

Colloidal CdSe/CdS Quantum Dots as Bright and Tunable Single-Photon Emitters [Iwan Moreels](#)¹, Francesco Di Stasio² and Riccardo Sapienza³; ¹Ghent University, Belgium; ²Istituto Italiano di Tecnologia, Italy; ³Imperial College London, Togo

Single-photon emitters are a key component of quantum technology, and often based on epitaxial quantum dots, NV-centers in diamond, or strongly attenuated lasers. However, colloidal quantum dots are becoming a viable, solution-processed alternative. For instance, in contrast with epitaxial quantum dots, they can operate at room temperature, and their emission can be tuned to any desired wavelength by simply controlling the composition and size of the quantum dots. In addition, their inherent nanoscale dimensions allows for miniaturization, and on-chip implementation.

In this talk, I will discuss how to synthesize highly fluorescent CdSe/CdS colloidal quantum dots that show (nearly) no intermittence.¹ Next, as these quantum dots have intrinsic fluorescence lifetimes that extend beyond 100 nanosecond, I will show how one can increase the emission rate by charging them with up to 20 electrons, which increases the radiative recombination rate, while at the same time the nonradiative Auger rate remains suppressed due to the proper choice of quantum dots core and shell dimensions.² Finally, I will demonstrate that the single-photon emission can be improved by spectrally filtering out the biexciton emission, which, due to the unique features of our quantum dots, can be performed at room temperature due to the exceptionally large blue shift of the biexciton emission.³ In particular, this blue shift is achieved by exploiting strain and piezoelectric fields in our CdSe/CdS pure-phase wurtzite quantum dots, which is known to increase the electron-hole separation and exciton-exciton repulsive interactions, especially for quantum dots with a large CdSe core.^{4,5}

[1] S. Christodoulou et al., *J. Mater. Chem. C* **2014**, 2, 3439

[2] S. Morozov et al., *Sci. Adv.* **2020**, 6, eabb1821

[3] S. Morozov et al., *ArXiv211109090 Cond-Mat Physicsphysics* **2021**

[4] S. Christodoulou et al., *Nat. Commun.* **2015**, 6, 7905

[5] A. Polovitsyn et al., *ACS Photon.* **2018**, 5, 4561-4568

11:00 AM NM03.08.07

Novel Detection System for the Characterization of Single Photon Sources Based on a SPAD Array Detector [Davide Piccinotti](#), Eli Slenders, Matteo Barelli, Giuseppe Vicidomini and Francesco Di Stasio; Fondazione Istituto Italiano di Tecnologia, Italy

Future quantum technologies promise to deliver unprecedented computing power, guarantee secure communications, and yield ultra-high precision measurements. In quantum optics, the capability to analyze quantum signatures of the emitted light from single photon sources is essential and current experimental configurations offer limited capabilities for the metrology of quantum-light sources. So far, the primary method to probe non-classical properties of light is measuring the second order correlation function ($g^{(2)}(\tau)$) with a Hanbury-Brown and Twiss (HBT) intensity interferometer. Most of these experiments use single-photon counting detectors based on avalanche photodiodes or superconducting nanowires. These are so-called "click detectors", since the arrival of a single photon causes the detector output state to move from 0 to 1 followed by a dead-time, where photon detection is not possible. Therefore, click detectors cannot discriminate the number of photons present in a light field at a given time offering limited capabilities for the metrology of quantum-light sources. Hence, the development of detectors capable to resolve the number of photons hitting them (so-called photon-number-resolving (PNR) detectors) is crucial for many applications in quantum-information science. Single photon avalanche diode (SPAD) array detectors provide PNR functionality by having the incoming photons hitting an array of parallel SPADs. Here, we take advantage of the exceptional properties of SPAD array detectors for the implementation of a new detection method for the measurement and analysis of single photons emitted by colloidal quantum dots (QDs). The data collected with this system provide a complete characterization of the analyzed single photon emitter giving information on the lifetime, antibunching effect and enable also quantum-imaging microscopy. In order to evaluate the performance of this new detection system, we performed spectroscopic measurements of photons correlation using commercial single photon detectors in Hanbury-Brown and Twiss (HBT) configuration on a sample composed by an array of 50x50 holes filled with single QDs. This type of sample enable us to compare directly the measurements performed with both experimental configurations on the exact same colloidal QDs. The work proposed here could lead to a new technological platform for the characterization of single photon sources that overcomes the limitation of conventional standard click detectors in HBT configuration.

11:15 AM NM03.08.08

Mid-infrared Electroluminescence of HgTe Colloidal Quantum Dots [Xingyu Shen](#), John Peterson and Philippe Guyot-Sionnest; The University of Chicago, United States

HgTe colloidal quantum dots show great potential in many infrared regions because of the zero band gap of bulk HgTe. They have been explored for infrared detection as photoconductors, photovoltaics, and phototransistors, and for electroluminescence in the short-wave region (< 2.5 μm). Here, we report mid-infrared electroluminescence using HgTe CQD photovoltaic devices previously designed for mid-IR detection.

Mid-infrared electroluminescence is challenging because of the low photoluminescence efficiency. To reach a certain radiance, a much higher operation current is required, compared to visible devices. This could relax the requirement of band alignment between layers, but gives extra challenges on material stability and device efficiency. Strong thermal signal from Joule heating also becomes a consideration.

Using a p-n HgTe homojunction sandwiched between ITO and a gold electrode, we demonstrate band-edge electroluminescence at 4 μm (and at 2.5 μm with smaller HgTe quantum dots) when operated at forward bias modulated at 100 kHz. Fast modulation helps reduce the contribution from thermal

emission. By comparing the photoluminescence and electroluminescence of the same device, we found that the electroluminescence efficiency at low current was limited by the photoluminescence efficiency of the quantum dots while the diode structure provided efficient electron-hole recombination. The power efficiency is limited by the resistance of transparent electrode, and we show that the efficiency can be improved through the incorporation of a metal conductive grid.

11:30 AM NM03.08.09

Siloxane-Encapsulated Perovskite Quantum Dot Nanocomposites for Highly Stable Color-Converting White Organic Light-Emitting Diodes Junho Jang^{1,1}, Young-Hoon Kim², Yongmin Shin^{1,1}, Byoung-Hwa Kwon³ and Byeong-Soo Bae^{1,1}; ¹Korea Advanced Institute of Science and Technology, Korea (the Republic of); ²Hanyang University, Korea (the Republic of); ³Electronics and Telecommunications Research Institute, Korea (the Republic of)

Perovskite quantum dots (PQDs) have emerged as a high-performance color converting materials in displays because of low material cost, facile color tunability depending on size or composition, high photoluminescence quantum yield (PLQY), and very narrow emission spectra, which allow them to achieve wide color gamut. Although they show high optical performance, PQDs in humid or high temperature environments are vulnerable to decomposition of perovskite crystals, to ion migration, and to development of metastable states. Stability of PQDs have been increased by various methods such as formation of an inorganic shell, Janus structures, and QD/polymer nanocomposites. However, such strategies still showed limited stability of PQDs under ambient air or in water, and entail complex processes to prevent aggregation of QDs in polymer matrixes. Moreover, PQDs that are stable under harsh conditions (acid or base solutions, polar solvents, high temperature with high humidity) have not been reported. Especially methylammonium (CH_3NH_3^+ , MA) based PQDs decay faster in the presence of moisture than do others such as formamidinium or cesium or mixed cation based PQDs even it can be fabricated by simple process. Therefore, highly stable and uniformly dispersed OIHP NP composites without complex processes such as ligand-exchange and formation of an inorganic shell are desirable.

Herein, we report a simple but effective materials-design approach to achieve extraordinarily-long stability of crosslinked MA lead bromide (MAPbBr_3) QDs in various environments (air, water, chemicals, high temperature (85 °C) with high relative humidity (85%RH) (85 °C/85%RH)) by employing sol-gel derived methacrylate-functionalized siloxane hybrid matrix. The methacrylate in the siloxane matrix induces a chemical crosslinking with unsaturated hydrocarbon in acid and base ligands in PQDs at a molecular scale, to form a crosslinked perovskite QDs (CPN) that prevents decomposition of MA from the perovskites and achieves homogeneous distribution of QD in the siloxane matrix. Moreover, the low concentration of moisture that diffuses through the siloxane matrix during aging can chemically heal surface defects in the QDs, and thereby reduce nonradiative recombination in CPN. As a result, CPNs showed high PLQY of $\approx 70\%$ which remained for >600 d in air, water and acid or base solutions, and various polar solvents, and for >100 d under 85 °C/85%RH. We demonstrate wide color gamut and stable color-converting white LEDs and OLEDs by integration with red-emissive Cd-based QDs. Moreover, water- and chemical-persistent CPNs were successfully applied to cell proliferation which has been impossible with water-sensitive materials with toxic elements (e.g., Cd and Pb).

SESSION NM03.09: QD Based Devices II

Session Chair: Nikolai Gaponik

Thursday Afternoon, December 1, 2022

Hynes, Level 2, Room 209

1:30 PM NM03.09.02

Exciton-Polaritons Arising from CdSe Nanoplatelets Strongly Coupled to Dielectric Optical Cavities Ovishek Morshed and Todd Krauss; University of Rochester, United States

Exciton-polaritons, arising from the strong coupling of excitons with the confined cavity photon modes, are an emerging platform for exploring light-matter interactions at the nanoscale. However, the use of organic molecules for generating polaritons poses a fundamental limitation to the magnitude of light-matter interactions due to their short lifetime and relatively small transition dipoles. Our focus lies on studying the coupling between CdSe nanoplatelets (NPLs) and metal-dielectric Fabry-Perot (FP) optical cavities. The large oscillator strength of NPLs along with exceptionally narrow photoluminescence linewidth makes them a promising candidate for achieving strong light-matter coupling. We have found that NPLs strongly couple to FP cavities with a Rabi splitting of 83 meV, characterized from angle-resolved reflectance and photoluminescence measurements. Numerical simulations using mixed quantum-classical dynamics accurately model our experimental data, providing a fundamental explanation for the observed spectra. Specifically, the light emission properties of the polariton are highly dependent on the coupling of dark (i.e., uncoupled) exciton states with the upper and lower polariton states, as well as their relative photonic character. Also to be presented will be measurements of the polariton photoluminescence lifetime in the strong coupling limit. Our work provides a new platform for investigating cavity-mediated physical and chemical processes which could potentially unlock new types of chemical reactions.

1:45 PM NM03.09.03

Electrically Excited Multi-Color Amplified Spontaneous Emission from Colloidal Quantum Dots Namyoungh Ahn, Clement Livache and Victor I. Klimov; Los Alamos National Laboratory, United States

Solution-processable materials, including organic semiconductors, perovskites, and colloidal quantum dots (QD), have been under intense investigation as optical-gain media for future laser technologies. However, the realization of electrically driven laser action with these materials still remains an unrealized objective. Colloidal continuously-graded QDs (cg-QDs) have recently emerged as a promising system for achieving lasing with electrical excitation.

Thanks to strong suppression of Auger recombination, they showed optical gain under electrical pumping and allowed for demonstrating dual-function devices that operated as an optically pumped laser and a high-brightness light-emitting diode (LED).¹⁻³ Notably, cg-QDs exhibit good stability at current densities of over 1 kA cm^{-2} , which allowed for realizing unusual two-band electroluminescent (EL) wherein the higher-energy 1P feature was more intense than the band-edge 1S emission.² This is indicative of very high per-dot excitonic occupancies that were sufficient to generate strong, broad-band optical gain spanning the 1S and 1P transitions. However, light amplification due to stimulated emission from the QDs was not observed because of strong optical losses in charge-conducting layers of the EL device.³ Here, we tackle this problem but integrating QDs with a specially engineered photonic waveguide. Using this approach, we maximize the mode confinement factor for the gain-active QD layer and reduce the field intensity in the optically lossy charge conducting layers. As a result, the developed devices generate large net optical gain under pulsed bias and demonstrate ASE-type laser action at three optical transitions (abbreviation 'ASE' stands for 'amplified spontaneous emission').⁴ The realization of the ASE regime is indicated by multiple observables including a super-linear growth of the EL intensity above the ASE threshold, a pronounced line narrowing, the emergence of preferred polarization, high directionality of edge-emitted light, and an exceptionally high output intensity which reaches $\sim 2 \text{ kW cm}^{-2}$.

1. H. Jung, N. Ahn, V. I. Klimov, *Nature Photonics*, **15**, 643-655 (2021)

2. H. Jung, Y.-S. Park, N. Ahn, J. Lim, I. Fedin, C. Livache, V. I. Klimov, *Nature Communications*, **13**, 3734 (2022)
3. N. Ahn, Y.-S. Park, C. Livache, J. Du, K. Gungor, J. Kim, V. I. Klimov, arXiv preprint arXiv:2204.01929 (2022)
4. N. Ahn, C. Livache, V. Pinchetti, H. Jung, H. Jin, Y.-S. Park, V. I. Klimov, under review, (2022)

2:00 PM NM03.09.04

Ultrathin High-Resolution Optoelectronic Devices for Skin-Attachable Electronic Applications Moon Kee Choi¹ and Jiwoong Yang²; ¹Ulsan National Institute of Science and Technology, Korea (the Republic of); ²Daegu Gyeongbuk Institute of Science and Technology (DGIST), Korea (the Republic of)

Soft electronic devices, in particular healthcare-related ones, have been intensively studied over the past decade due to their unique advantages in wearable applications over the conventional rigid electronics, including conformal contacts on human skin and high deformability that minimizes unwanted inflammatory responses. To achieve the soft nature in high performance electronics and to apply this technology to wearable biomedical electronics/optoelectronics, several strategies have been employed, such as the designed assembly of high-quality nanomaterials, combination of unconventional manufacturing processes with existing micro-processing technologies, new design of individual devices with deformable structures, and disease-specific system-level integration of diverse soft electronics. Here, we describe ultrathin high-resolution optoelectronic devices for skin-attachable electronic applications. New dry transfer printing techniques using intaglio trench and elastomeric stamp are demonstrated for the high resolution RGB sub-pixels up to ~2500 pixels per inch. Ultrathin high-resolution red-green-blue quantum dot LEDs and perovskite LEDs can be utilized next-generation skin-attachable electronic tattoo, transparent smart display, and display of healthcare monitoring wearable devices.

2:15 PM BREAK

2:45 PM NM03.09.05

Printed Quantum Dots—Graphene IR Photodetector on a Curved Surface Gökhan Kara¹, Sami Bolat¹, Khushdeep Sharma¹, Patrik Rohner¹, Matthias J. Grotevent^{1,2}, Dmitry N. Dirin³, Dominik Bachmann¹, Roman Furrer¹, Luciano F. Boesel¹, Yaroslav E. Romanyuk¹, Dimos Poulidakos³, Maksym V. Kovalenko^{3,1}, Michel Calame^{1,4} and Ivan Shorubalko¹; ¹Empa – Swiss Federal Laboratories for Materials Science and Technology, Switzerland; ²Massachusetts Institute of Technology, United States; ³ETH – Swiss Federal Institute of Technology Zurich, Switzerland; ⁴University of Basel, Switzerland

Shortwave infrared (SWIR) imaging is well known for night vision and seeing through foggy weather conditions. Thus a perfect match for autonomous driving, it is also used for environmental pollution monitoring or smart farming. Furthermore, the integration into smart textile patches is of great interest for human health monitoring of vital signs or wound healing in particular. The lack of monolithic integration with CMOS read-out circuits (ROIC) and the high-temperature processes used to fabricate state-of-the-art InGaAs detectors, though, limits its potential for broad commercial use. Low dimensional materials offer an easy technological edge to launch the next generation of SWIR photodetectors. Phototransistors based on graphene as the channel layer and PbS QDs for light-to-charge conversion, benefit from conformal adaptation and solution processing enabling novel device architectures for high-quality imaging at low light levels.

Most commonly though, detectors are fabricated on flat substrates and the deposition of QDs is performed by spin coating, dip coating, or drop-casting. This limits the substrate choice, wastes a lot of material, and does not allow selective deposition on desired regions only. Here, we present two different emerging drop-on-demand approaches for optoelectronic applications. On the one hand, by electrohydrodynamic nanoprinting of PbS QDs, we reach sub-micrometer resolution with an exceptional film thickness control in the nanometer range suited for small pixel dimensions. With inkjet printing, on the other hand, we can cover large areas (print head speed up to 500 mm/s) with a resolution below 50 µm. In particular, we demonstrate an inkjet-printed phototransistor on a flat rigid substrate (Si/SiO₂), reaching a 1.8 µm spectral cut-off wavelength. Our temperature versus gate voltage map reveals responsivities in the order of 10³ A/W at the first excitonic peak of 1.6 µm wavelength. To demonstrate the versatility of this technological approach, we wrap graphene around a polymer optical fiber with a diameter of 1 mm and print PbS QDs on these active areas solely. We then use this smart cladding layer to detect light (telecom wavelength of 1.3 µm and 1.55 µm) propagating through the fiber without interrupting its path.

3:00 PM NM03.09.06

Quantum Dot-Based Near-Infrared-Sensitive Optoelectronic Biointerface for Neurostimulation Onuralp Karatum, Humeyra Nur Kaleli, Guncem O. Eren, Afsun Sahin and Sedat Nizamoglu; Koc University, Turkey

Optoelectronic neural interfaces offer non-genetic and wireless bioelectronic neuromodulation via light. For minimally invasive communication with neurons inside the deep neural structures, transition of optoelectronic neural interfaces to near-infrared (NIR) spectrum is critical. Colloidal quantum dots (QDs) have size-tunable absorption that can cover visible and infrared wavelength spectrum. QDs also have high absorption coefficient that enables fabrication of thin and flexible optoelectronic devices. In this study, we demonstrated a wireless, and flexible QD-based optoelectronic neural interface that can evoke light-induced action potentials in primary hippocampal neurons via 780 nm light in tissue transparency window.¹ We designed a multilayer photovoltaic device architecture with an ultrathin QD layer of 25 nm to generate a safe capacitive ionic current and integrated supercapacitor ruthenium oxide (RuO₂) into the return electrode for improving the photogenerated charge density. Fully solution-processed neural interfaces preserve their functionality after different stability tests and show low in vitro cytotoxicity. Overall, our results disclose the potential of QDs for tether-free bioelectronic photomodulation of neurons in tissue transparency window.

References

- (1) Karatum, O.; Kaleli, H. N.; Eren, G. O.; Sahin, A.; Nizamoglu, S. Electrical Stimulation of Neurons with Quantum Dots via Near-Infrared Light. *ACS Nano* **16**, 5, 8233-8243 (2022)

3:15 PM NM03.09.07

A Living System for Robust Photocatalytic Hydrogen Evolution from CdSe Quantum Dots Emily Edwards¹, Jana Jelušić¹, Kevin McClelland¹, Wesley Chiang¹, Ryan Kosko¹, Sanela Lampa-Pastirk², Kara Bren¹ and Todd Krauss¹; ¹University of Rochester, United States; ²Nazareth College, United States

Developing systems that interface nanomaterials and microorganisms is an attractive approach to solar fuels production that can take advantage of the extraordinary properties of both components. For example, nanomaterials have been utilized to provide electrons to microorganisms in photo(electro)chemical processes to fuel metabolic pathways for desired products. While semiconductor nanocrystals are known to be highly active and robust photocatalysts for hydrogen evolution, their use is for all practical purposes severely hampered by the need for an inexpensive and sustainable source of electrons from oxidative side of the reaction. Direct water oxidation is thermodynamically challenging and inefficient, and consequently, easily oxidized electron donors are typically supplemented in high concentrations to drive photocatalysis, which is a major limitation. Here, an alternative approach to constructing living bio-nano artificial photosynthetic systems will be discussed.

Rather than catalysis regulated by electron transfer *from* the nanomaterial *to* the microorganism, we show that exceptional photocatalytic activity of semiconductor nanocrystals (NCs) is sustained by extracellular electron transfer (EET) *from* electrogenic bacteria *to* the NCs. In our fully light-driven system, *Shewanella oneidensis* MR-1 (MR-1), a non-photosynthetic facultative anaerobe, respire CdSe NCs, via EET. Under illumination from visible light (530 nm LEDs), we observe sustained H₂ evolution from the NCs for over a week without the requirement of an external voltage. EET from MR-1 is a natural anaerobic respiratory process, and thus, replenishing the growth medium allows catalysis to continue over a second week. To test the hypothesis that the H₂ production in the complete system results from bacterial respiration of CdSe NCs, the MR-1 gene knockout variant *hyaA* (*ΔhyaA*) was used. This variant of MR-1 has impaired hydrogenase activity, and thus is not expected to produce H₂ on its own. Indeed, *ΔhyaA* cultures produced no detectable H₂ over the course of one week. However, the system consisting of *ΔhyaA* and CdSe NCs, produced H₂ at a similar rate and efficiency to the wild type MR-1, confirming that respiration of CdSe NCs was essential and sufficient to complete the oxidative portion of the catalytic cycle. There exists many possible barriers to MR-1 EET directly to colloidal NCs: surface area needed for bacterial adhesion, the oxidative damage from photocatalytic processes, biocompatibility of the NCs, and efficiency of electron transfer. The strategy we will outline demonstrates that these challenges are surmountable in a remarkably simple system and suggests a new solution to the oxidative roadblock in NC photocatalysis. Success here opens the door to pairing this strategy with a host of different NC photocatalytic reactions to yield sustainable systems for NC-mediated photocatalysis.

3:30 PM NM03.09.08

Carrier Transport in Colloidal Nanocrystal Arrays [Mengxia Liu](#); Yale University, United States

Colloidal nanocrystals are an emerging type of solution-processed semiconductors that offer a powerful platform for the scalable manufacturing of optoelectronic devices. Understanding carrier dynamics and transport in nanocrystal is crucial for unlocking their full potential for optoelectronic applications. This presentation will introduce a novel optical methodology to investigate the nanoscale photophysics in thin film semiconductors and present the direct visualization of non-equilibrium carrier propagation in PbS nanocrystal arrays. I will discuss the impact of nanocrystal polydispersity on carrier dynamics, the influence of imbalanced carrier transport on solar cell performance, how these can be controlled and optimized through novel materials processing and structure engineering. These findings offer promising strategies to harness transport phenomena for more efficient optoelectronic devices.

SESSION NM03.10: QD Based Devices III
Session Chair: Marinella Striccoli
Friday Morning, December 2, 2022
Hynes, Level 2, Room 209

8:30 AM *NM03.10.01

0D-1D Nano-Heterostructures for Solar Energy Conversion [Oomman K. Varghese](#); University of Houston, United States

The advent of zero dimensional (0D) nanomaterials such as quantum dots (QD) of semiconductors has brought renewed expectations in direct solar energy conversion technologies such as solar photovoltaics and photoelectrochemical (PEC) fuel generation. The few-atom construction of the QDs furnishes them with very large surface area relative to volume leading to unique characteristics. The phenomena such as quantum confinement effects and associated blue shift in the absorption edge are not only scientifically intriguing but also capable of bringing paradigm shifts in the solar power as well as fuel generation technologies. The efficiency of the single junction devices from these technologies can reach levels significantly beyond the Shockley-Queisser limit utilizing phenomena such as multiple exciton generation and hot carrier extraction. While this milestone has not yet been achieved, there has been substantial improvements in the efficiency of the QD based solar cells. These solar cells have utilized materials from chalcopyrites to inorganic iodide perovskites as light absorbers and the efficiency has reached 18%. Carbon dots and band gap engineered QDs of wide band gap materials such as boron nitride appeared promising for solar PEC water splitting and carbon dioxide reduction. It has also been demonstrated that the potentials of the quantum dots can be extended further if they are supported by high surface area ordered nanostructures. This presentation will review the advances in supported QD based solar cells and solar fuel generation processes.

9:00 AM NM03.10.03

Near-Infrared Photodetectors Based on Silver Chalcogenide Colloidal Quantum Dots [Neil Graddage](#), Jianying Ouyang and Jianping Lu; National Research Council Canada, Canada

Detection of near-infrared (NIR) radiation is essential for a wide variety of applications in industries as varied as healthcare to agriculture. In the healthcare application space in particular, NIR radiation shows good penetration of tissue with low scattering making it ideal for a variety of diagnostic sensors. The primary spectral ranges for this sensing are commonly referred to as NIR-I between 650 nm to 950 nm, and NIR-II from 1000 nm to 1400 nm. The first window can be partially detected by Si based detectors, which are commonplace and low cost, though limited in form factor. The second window typically requires detectors using materials such as InGaAs, which perform well but are expensive to fabricate and also limited to rigid form factors. Therefore the identification of materials capable of photodetection in these regimes while compatible with solution-based fabrication techniques such as printing is of significant interest, as it could result in low-cost devices which can be integrated into new form factors such as wearable electronics.

Colloidal quantum dots (CQDs) are a class of materials which offer tunable optoelectronic properties and solution processibility. A number of CQD materials have shown promise for NIR detection, however primary materials have all been Pb based, with associated toxicology concerns. This has inspired a search for less toxic alternatives. One such family of materials identified are silver chalcogenides, in particular Ag₂Se and Ag₂Te. To date there has been much interest in these materials, but little reported synthesis optimisation and demonstration in photodiodes, which is essential for low power applications. In this work we investigate the potential for these materials for use in NIR sensitive photodiodes, optimising synthesis and developing novel structures to enable such devices.

We developed Ag₂Se based photodiodes with sensitivity in the NIR-II window. Ag₂Se CQDs were synthesised using a hot injection method. We achieved CQDs with a mean diameter of 3.7 nm and a narrow size distribution by employing a secondary phosphine. These CQDs were then used in a photodiode structure which included a porous TiO₂ scaffold inspired by dye-sensitised solar cells. This structure maximises the absorption of the Ag₂Se CQDs, while minimising the risk of device shorting due to the high conductivity of the Ag₂Se CQDs. The ligand exchange process used for CQD layer fabrication is compatible with low-temperature substrates, and devices demonstrated an EQE of over 1% at a wavelength of 1150 nm and sensitivity up to 1400 nm. We also developed Ag₂Te based photodiodes. Ag₂Te CQDs synthesis was comprehensively optimised by investigation of multiple factors including feed ratio, ligand selection and synthesis method. After optimisation we achieved relatively large Ag₂Te QDs with distinct excitonic absorption peaks (~1050–1450

nm) and a PL emission peak from 1.3–1.7 μm . These Ag_2Te CQDs were used to fabricate photodiode devices which demonstrated sensitivity beyond 1400 nm, with an EQE of 0.14% and a responsivity of ~ 1.5 mA/W at 1400 nm.

The combination of good material processability, exciting material properties and promising device performance has demonstrated that silver chalcogenide CQDs offer a reduced-toxicity route for low-cost additive fabrication of NIR-II photodiodes. Further work is still needed to improve device performance and unlock the full potential of these materials.

References:

- Graddage, N. & Ouyang, J. et al., Near-Infrared-II Photodetectors Based on Silver Selenide Quantum Dots on Mesoporous TiO_2 Scaffolds, *ACS Appl. Nano Mater.* 2020, 3, 12, 12209–12217 (2020) doi: <https://doi.org/10.1021/acsnm.0c02686>
- Ouyang, J. et al, Ag_2Te Colloidal Quantum Dots for Near-Infrared-II Photodetectors, *ACS Appl. Nano Mater.* 2021, 4, 12, 13587–13601 (2021) doi: <https://doi.org/10.1021/acsnm.1c03030>

9:15 AM NM03.10.05

Hybrid Inorganic/Organic Nano-Systems for the Development of Light-Driven Storage Devices Andrea Camellini, Michele Ghini, Andrea Rubino and Ilka Kriegel; Istituto Italiano di Tecnologia, Italy

The efficient harvesting of solar radiation and subsequent steady-state storage of photo-charges are now becoming one of the main challenges for the development of sustainable energy sources. The growing demand to reduce the usage of rare^[1] and toxic materials, as well as the need to overcome current limitations in solar energy storage (such as the intermittent nature of the source and inevitable conversion losses) calls for completely innovative approaches. A promising new approach relies on combining light absorption, charge separation, and storage into one single set of solution-processable, environmentally friendly, and Earth-abundant materials as well as the possibility to exploit light-driven multi-electron and hole transfer reactions to improve the charge-storage capability. In this direction, hybrid inorganic/organic nano-systems employing metal oxides nanocrystals (MO NCs) and graphene quantum dots (GQDs) are emerging as potential candidates to fulfill these purposes. In this work, by means of spectro-chemical tools, we investigate the ability of MO NCs (Sn doped In_2O_3 NCs) to quasi-permanently accumulate electrons upon UV light illumination^[2] as well as their efficient extraction^[3]. Moreover, by using a widely employed electron-acceptor molecule, namely F4TCNQ, we show the potential of specifically functionalized GQDs to store one hole in their ground state. These evidences point toward the possibility to exploit hybrid inorganic/organic nano-systems as novel multi-charge accumulation components for the development of solution-based light-driven storage devices.

References:

- ^[1] Gatti et al. “Opportunities from Doping of Non-Critical Metal Oxides in Last Generation Light-Conversion Devices,” *Advanced Energy Materials*, 2021, 11, 2101041
- ^[2] Ghini et al. “Photodoping of metal oxide nanocrystals for multi-charge accumulation and light-driven energy storage,” *Nanoscale*, 2021, 13, 8773–8783.
- ^[3] Ghini et al. “Multi-charge transfer from photodoped ITO nanocrystals,” *Nanoscale Advances*, 2021, 3, 6628–6634

9:30 AM BREAK

10:00 AM NM03.10.06

$\text{CuInS}_2/\text{ZnS}$ Colloidal Quantum Dots as a Luminescent Nanothermometers Magdalena Duda¹, Kamil Sobczak², Roman Minikayev¹, Elzbieta Dynowska¹, Bozena Sikora¹ and Lukasz Klopotoski¹; ¹Polish Academy of Sciences Institute of Physics, Poland; ²University of Warsaw, Poland

In this work, we present the performance of $\text{CuInS}_2/\text{ZnS}$ (CIS/ZnS) quantum dots (QDs) employed as fluorescent nanothermometers. We find that both the intensity and wavelength of the photoluminescence (PL) peak is sensitive to temperature and optimize the growth time of ZnS for maximum thermometer sensitivity.

CIS/ZnS QDs are particularly suitable for bio-applications because of environmentally friendly synthesis and absence of photobleaching. Moreover, the size-dependent photoluminescence (PL) and absorption, low power excitation, and long PL lifetimes make them ideal fluorescence markers. In this work, we demonstrate a dual functionality of CIS/ZnS QDs: as biolabels and nanothermometers.

We synthesised CuInS_2 QDs, according to the method described in Ref. [1]. As a result, we obtained CIS QDs with a pyramidal shape, chalcopyrite structure, and an average size of about 2.3 nm. As recently reported, CIS QDs exhibit significant cytotoxicity. In order to produce non-toxic QDs, a ZnS layer was grown around the CIS QD cores as reported in Ref. [2]. We investigated 5 samples with ZnS growth time varied from 0 to 180 minutes. Increasing the growth time resulted in a blue-shift of the PL peak from 673 to 606 nm. Concomitantly, the PL quantum yield increased from 0.9% to 13%. Due to dodecanethiol capping ligands, as-synthesized QDs were hydrophobic. The use of QDs as nanothermometers requires aqueous environment. Therefore, QDs were encapsulated by micelles, as reported in Ref. [3]. To test the optical and thermal stability of the hydrophilic QDs, the PL was measured in 2 hours and 3 cycles of temperature changes from 20°C to 54°C. After this time, the PL intensity decreased only by up to 15%. The nanothermometers were then calibrated by measurements in steps of 2°C. Increasing the temperature to 54°C, resulted in a PL intensity decrease by up to 70%. We interpret this decrease as a result of thermal activation of non-radiative processes. Moreover, the PL peak red-shifted by up to 10 nm. We interpret the red-shift as a result of closing of the band gap. The two effects afford a precise calibration of the nanothermometer. We found the highest sensitivity — reaching 1.3 %/°C — is at least comparable to other QD systems. Confocal imaging demonstrated successful entering of CIS/ZnS QDs into HeLa cells. Finally, preliminary Presto Blue cell viability assay revealed negligible CIS/ZnS QD cytotoxicity in HeLa cells.

[1] Li L., et al., *Am. Chem. Soc.* 2011, 133, 5, 1176–1179

[2] Speranskaya E. S., et al., *Langmuir* 2014, 30, 25, 7567–7575

[3] Zhang H., et al., *J. Mater. Chem. B*, 2019, 7, 2835–2844

Acknowledgments

This work was supported by National Science Centre Poland grant no. 2019/35/B/ST3/04235 and has been done in the NanoFun laboratories co-financed by the European Regional Development Fund within the Innovation Economy Operational Program, the Project No. POIG.02.02.00-00-025/09/. The research was also partially supported by the project no. UMO-2016/22/E/NZ1/00656.

10:15 AM NM03.10.07

Quantum Dot Mimetics of SARS-CoV-2 for Understanding Origins of Neurologic Disease Associated with Long Covid Wesley Chiang, Harris Gelbard and Todd Krauss; University of Rochester, United States

Colloidal semiconductor quantum dots (QDs) are exceptional fluorescent probes for bioimaging applications; their enhanced photophysical properties, such

as photostability and brightness, compared to conventional fluorophores are essential for achieving high-resolution precision. Additionally, the synthetic tunability of QD emission makes them viable candidates for multiplexed imaging and various biosensing applications. However, conventional applications of fluorescent probes, including QDs, investigate biomolecular interactions by conjugation of a biomolecule to the probe. While such material design is functionally justifiable for single proteins, such designs are incompatible with probing the function of more complex structures such as protein aggregates or virus particles in a manner that is representative of their native environment.

Thus, to study the physicochemical interactions relevant to SARS-CoV-2 mediated disease in the central nervous system (CNS), we have constructed a QD biomimetic for SARS-CoV-2 (COVID-QDs) with a focus on achieving high structural fidelity to native virus particles. The COVID-QDs act as a proxy for SARS-CoV-2 virus particles by accurately mimicking the general shape, size, and surface density of spike proteins. Specifically, the COVID-QDs were constructed by linking SARS-CoV-2 spike (S) proteins to polymeric phospholipid chains that formed a micellar envelope around the QDs; this forms a decorated capsid-like structure in native virus particles. By ensuring structural fidelity, we are able to fluorescently probe the physicochemical interactions between COVID-QDs and various cell types in a context that better reflects the native function of SARS-CoV-2.

We found that the COVID-QDs mediate dysfunction in a model system for the neurovascular unit, comprising endothelial cells, neurons, and glia. Interestingly, by correlating fluorescent micrographs, acquired by structured illumination, with functional biological assays, we have determined that the COVID-QDs primarily bind to the endothelial cells, leading to increased inflammation and leakage. This functional modulation of the endothelial cells by the COVID-QDs subsequently results in inflammation of the neuroglia underneath the endothelial monolayer. Our data shows that the dysfunction of the neural cell types is not mediated by direct interaction with COVID-QDs that have migrated through the endothelial monolayer. These results add to a body of evidence indicating that the neurological effects associated with COVID-19 are primarily driven by inflammation through virus particle-mediated dysregulation of the endothelium. Furthermore, we have identified a potential small molecule that could reverse the effects of the COVID-QDs, leading to inhibition of inflammation in both the monolayer and the CNS.

SESSION NM03.11: Virtual Session: QD
Session Chairs: Marinella Striccoli and Alberto Vomiero
Tuesday Morning, December 6, 2022
NM03-virtual

8:30 AM *NM03.11.01

Evolution of Colloidal Compound Semiconductor Quantum Dots and Magic-Size Clusters [Kui Yu](#); Sichuan University, China

The synthesis of photoluminescent (PL) colloidal semiconductor quantum dots (QDs) has been performed as an empirical art, while colloidal semiconductor magic-sized clusters (MSCs) are reported as a side product. Their growth relation has been addressed only in a limited fashion, with different opinions expressed in the literature. It is critical to develop fundamental understanding, especially regarding the pre-nucleation stage also called the induction period (IP). Here, I will talk about chemical reactions including the effect of the impurity in tri-*n*-octylphosphine (TOP) in Part 1 and the nucleation pathway with the proposed two-pathway model (Yu) in Part 2. For the latter, we suggest that there are two individual pathways in the pre-nucleation stage of QDs. The self-assembly of metal (M) and chalcogenide (E) precursors followed by the formation of binary II-VI ME MSCs inside each assemble depicts Pathway 1. The LaMer model of the classical nucleation theory (CNT) describes Pathway 2. The two pathways are inter-connected via a special intermediate, called the precursor compound (PC) of MSCs. I will introduce our latest advances on the PC-enabled pathway (with monomer substitution or addition) for transformations among various MSCs, as well as on the PC-enabled synthesis of various nano-species. Hopefully, this presentation brings a deeper understanding into the pre-nucleation stage of QDs. We believe that the synthesis of colloidal nanocrystals is slowly and quietly transforming from an empirical art to science.

References

1. Yu, K. et al Effect of tertiary and secondary phosphines on low-temperature formation of quantum dots. *Angew. Chem. Int. Ed.* **2013**, *52*, 4823–4828.
2. Yu, K. et al A Two-pathway model for the evolution of colloidal compound semiconductor quantum dots and magic-size clusters. *Adv. Mater.* **2022**, *34*, e2107940.

9:00 AM *NM03.11.02

Heterostructures Involving Halide Perovskite Nanocrystals and Chalcohalide Nanocrystals [Liberato Manna](#); Istituto Italiano di Tecnologia, Italy

Halide perovskite semiconductors can merge the highly efficient operational principles of conventional inorganic semiconductors with the low temperature solution processability of emerging organic and hybrid materials, offering a promising route towards cheaply generating electricity as well as light. Following a surge of interest in this class of materials, research on the corresponding halide perovskite nanocrystals (NCs) as well has gathered momentum in the last years. Another class of materials that has been recently investigated by us is that of metal chalcohalides. These materials offer a broad solid-state chemistry and they been investigated for applications in solar energy conversion, thermoelectrics, hard radiation detection, and superconductivity. Among them, lead chalcohalides have been rarely studied in the past. We have recently reported the synthesis of a series of lead chalcohalides, by means of colloidal approaches, delivering phases and compositions that had not been previously identified in the bulk. These materials present indirect band gaps, they emit in the NIR region of the spectrum at cryogenic temperatures and have unique crystal structures. We will also show our recent results on the synthesis and advanced characterization of heterostructured nanocrystals in which one domain is a lead chalcohalide and the other domain is a cesium lead halide perovskite. The two domains are separated by a flat, atomically defined, epitaxial interface. In these materials, the photogenerated carriers are separated at their interface, and as such they might be promising in applications ranging from catalysis to photovoltaics. We will also discuss how halide perovskite nanocrystals can be used to template the synthesis of chalcohalide nanocrystals in phases and compositions that are different from the case in which the latter are homogeneously nucleated. This templating effect is due to the formation of an epitaxial interface between the two materials. In a second step, the perovskite domain can be selectively etched, delivering the free standing chalcohalide nanocrystals. This use of perovskite nanocrystals as disposable templates is new and can be used as a tool to discover new materials.

9:30 AM *NM03.11.03

Colloidal Nanoparticles Decorated Graphene—Functional Materials Towards Energy Conversion and Sensing Applications [M.L. Curri](#)^{1,2};

¹Consiglio Nazionale delle Ricerche, Italy; ²University of Bari, Italy

Graphene (G) is an extraordinary material for advanced devices, due to its superior electrical conductivity, (electro)catalytic activity and surface chemical

reactivity. The last enables the implementation of non-covalent routes for its decoration with inorganic nanostructures, thus resulting in hybrid nanocomposites exhibiting original and ingenious combination of the properties of both G and inorganic components. Nanoparticles (NPs) prepared via colloidal chemistry approaches possess original size- and shape-dependent properties and are particularly suited for decorating G [1,2], thanks to the possibility to engineer their surface chemistry. Different types of colloidal nanomaterials, as NIR emitting PbS quantum dots, oxides as TiO₂ and plasmonic Au NPs, have been used to decorate G, [1-3] and the nanocomposite materials have been thoroughly investigated, from a morphological, spectroscopic, electrical and (photo)electrochemical points of view. Distinct decoration approaches have been designed, both for immobilizing pre-synthesized inorganic NPs onto the G based structures, and for performing *in situ* synthesis. In both strategies, suitable anchoring molecules are key element to enable a close interaction between G and NPs and thus direct the chemical and electronic properties of the resulting hybrids. In all the investigated systems, a controlled and uniform NP coverage has been obtained. The photoactivity and photoelectrochemical behavior of the hybrid nanocomposites demonstrate that this class of materials holds a great promise for photo-conversion, sensing and life science applications [4-6]. Selected examples of nanocomposites will be described and their possible integration in devices presented.

Acknowledgements: The research has been supported by the Bilateral Italy-USA "Projects of major importance" founded by Italian Ministry for Foreign Affairs and International Cooperation (MAECI) (Prot. nr. MAE00568722022-04-0), and the Italian PON Ricerca e Innovazione (2014-2020) ECOTEC (ARS 01_00951) and BEST-4U (ARS01_00519) projects.

References

- [1] C. Ingrosso, M. Corricelli, A. Disha, E. Fanizza, G. V. Bianco, N. Depalo, A. Panniello, A. Agostiano, M. Striccoli, M. L. Curri (2019) Carbon, 152, 777-787.
- [2] C. Ingrosso, G. V. Bianco, M. Corricelli, R. Comparelli, D. Altamura, A. Agostiano, M. Striccoli, M. Losurdo, M. L. Curri, G. Bruno (2015) ACS Applied Materials & Interfaces 7 (7), 4151-4159; C Ingrosso, V Valenzano, M Corricelli, A Testolin, V Pifferi, GV Bianco, R Comparelli, N Depalo, E Fanizza, M Striccoli, A Agostiano, I Palchetti, L Falciola, ML Curri (2021) Carbon, 182, 57-69.
- [3] C. Ingrosso, M. Corricelli, F. Bettazzi, E. Konstantinidou, G. V. Bianco, N. Depalo, M. Striccoli, A. Agostiano, M. L. Curri, I. Palchetti (2019) J. Mater. Chem. B., 7, 768-777.
- [4] F. Bettazzi, S. Laschi, D. Voccia, C. Gellini, G. Pietraprazia, L. Falciola, V. Pifferi, A. Testolin, C. Ingrosso, T. Placido, R. Comparelli, M. L. Curri, I. Palchetti (2018) Electrochimica Acta, 276, 389-398.
- [5] C. Ingrosso, G. V. Bianco, V. Pifferi, P. Guffanti, F. Petronella, R. Comparelli, A. Agostiano, M. Striccoli, I. I Palchetti, L Falciola, ML Curri, G Bruno (2017) J. Mater. Chem. A, 5, 9307.

10:00 AM NM03.11.04

High-Performance Green and Blue Quantum-Dot Light-Emitting Diodes by Suppressing the Electron Leakage Yunzhou Deng¹, Feng Peng², Yao Lu¹, Xitong Zhu¹, Wangxiao Jin¹, Jing Qiu¹, Jiawei Dong¹, Yanlei Hao¹, Dawei Di¹, Yuan Gao³, Tulai Sun⁴, Ming Zhang², Feng Liu², Linjun Wang¹, Lei Ying², Fei Huang² and Yizheng Jin¹; ¹Zhejiang University, China; ²South China University of Technology, China; ³Nanjing Technology Corporation Ltd., China; ⁴Zhejiang University of Technology, China; ⁵Shanghai Jiao Tong University, China

Solution-processed light-emitting diodes (LEDs) using colloidal quantum dots (QDs) as the emissive layers (EMLs) have emerged as a promising class of color-pure, low-cost and large-area electroluminescent (EL) devices. Progress in synthetic chemistry and surface chemistry have enabled CdSe-based QDs with near-unity photoluminescent (PL) quantum yields and outstanding photostability across the visible spectral range. However, the EL performances of QDs incorporated into QD-LEDs, especially for the blue-color devices, are still inferior to their PL properties. This apparent "EL-PL gap" implies the inefficient generation of excitons in the operating QD-LEDs with short wavelengths. Hence, in order to fully exploit the potential of QDs in EL applications, in-depth understanding on the charge dynamics in electrical excitation of QDs as well as the associated efficiency-loss mechanism is demanded.

Here, we report our recent findings [1] of the disorder-enhanced electron leakage from the wide-bandgap QDs to amorphous hole-transport layers (HTLs), which was identified as the limiting efficiency-loss channel in the blue QD-LEDs. According to the parasitic emission from HTLs in EL spectra of the QD-LEDs, we revealed that the electron leakage from QDs to HTLs is more severe in green and blue QD-LEDs than that in red QD-LEDs. Our theoretical work shows that the unique electron-transfer dynamics from QD (rigid) to organic (flexible) materials, which are distinctive from those at organic/organic and inorganic/inorganic interfaces, are greatly enhanced due to the different strength of energetic disorder in the two materials. To resolve this problem, we develop hole-transport polymers, i.e., poly[(9,9-dioctylfluorenyl-2,7-diyl)-alt-(9-(2-ethylhexyl)-carbazole-3,6-diyl)] (PF8Cz), with shallower lowest unoccupied molecular orbital (LUMO) energy level and reduced energetic disorder.

By using the PF8Cz HTLs, we realized high-performance green and blue LEDs with high peak external quantum efficiencies (28.7% and 21.9%, respectively) and wide high-efficiency luminance windows. The QD-LEDs also show superior operational stability with the T95 lifetimes (initial luminance: 100 cd m⁻²) of ~580,000 h for green and ~4,400 h for blue QD-LEDs, respectively. The advance in device performance demonstrates that our design of HTL/QD interfaces can effectively block the electron leakage and enable ~100% conversion of the injected charge carriers into emissive excitons. We expect that our strategy could offer a general approach to eliminating electron leakage in solution-processed LEDs incorporating organic-HTL/inorganic-EML interfaces.

Reference

- [1] Deng, Y., Peng, F., Lu, Y. et al. Solution-processed green and blue quantum-dot light-emitting diodes with eliminated charge leakage. *Nat. Photon.* (2022).

10:15 AM NM03.11.05

Mid-Infrared Photodiodes Using HgTe Colloidal Quantum Dots John Peterson and Philippe Guyot-Sionnest; The University of Chicago, United States

HgTe colloidal quantum dot photodetectors offer an inexpensive alternative to the conventional, epitaxially grown, mid-infrared detectors. Recent work describing the thermodynamic limits of these materials suggest that their long Auger lifetime may allow for better performance over such conventional detectors in that region. Previous work has produced HgTe quantum dot photodiodes which are background limited at cryogenic temperatures. However, they exhibited a ~20-fold decrease in the quantum efficiency from 150K to 300K.

Modeling the IV curves has helped to better understand the mechanism of this limited performance. The temperature dependence, the origin of the shunt resistance (recombination mechanisms) and the series resistance (electrodes and the dots themselves) are rather well understood with a simple model. This model suggests that, in the regime where the shunt resistance is on the order of the series resistance, the quantum efficiency is expected to drop substantially. Modifications to the p and n-doping as well as microfabrication methods have been applied to increase the shunt resistance of the devices relative to the series resistance. Methods of producing low resistance, transparent electrodes for the infrared have also been explored. The diffusion length of the materials used requires that these devices remain thin, and so microfabrication is also employed to enhance to optical absorption of the diodes. Together, these efforts to improve single element detectors allow for higher temperature thermal imaging with this technology, closer to the

thermodynamic limit of the material.

10:30 AM NM03.11.06

Fabrication and Characterization of Four-State Inverter utilizing Quantum Dot Gate Field-Effect Transistors (QDGFETs) Bilal Khan¹, Raja Gudlavalleti¹, Roman Mays¹, Evan Heller² and Faquir Jain¹; ¹University of Connecticut, United States; ²Synopsis Corporation, United States

Abstract: This paper presents experimental results of nMOS quantum dot gate field-effect transistor (QDG-FET) based four-state inverter fabricated and tested with Si/SiO₂ and Ge/GeO₂ quantum dots (QD). The site-specific self-assembly of SiOx-cladded Si and GeOx-cladded Ge QD layers in the gate region implements both the driver and load FETs in enhancement nMOS inverters. A four-state inverter will allow reduction of FET count in logic block in microprocessors.

Keywords: QDGFET, Multi-State, Multi-Bit, Inverters

I Introduction: Quantum dot gate (QDG) FETs exhibiting three-state I-V characteristics have been reported using two layers of thin barrier SiOx-cladded Si quantum dots in the gate region [1]. This has been followed by reports of four-state QDG-FETs and enhancement mode inverters using self-assembled Si-Ge quantum dots [2]. This paper presents new results presented in our recent paper [3]. Moore's law states that the number of transistors doubles every two years [4], and reducing transistor size sub 5nm presents challenges.

II QDG-FET comprising of 2 layers of SiOx-Si and 2-layers of GeOx-Ge QDs: A quantum dot (QD) is a semiconductor structure that is confined in all three dimensions. A QD has two main layers, a small semiconductor core such as Si or Ge surrounded by a cladding layer of either SiOx or GeOx respectively. The cladding layer acts as a barrier layer which helps to trap charge inside the quantum dots. When a number of quantum dots are placed next to each other they form a quantum dot superlattice (QDSL). The formation of a QDSL results in mini energy bands which allows the FET device to exhibit multiple states [1]. Three-state inverters using SiOx-Si and GeOx-Ge QDG-FETs have been reported [1, 2]. We are reporting the QDG-FET based inverter employing both SiOx-Si QDs and GeOx-Ge QDs in the gate region that resulted in four-states for the inverter. In this device, we have two layers of cladded Si QD layers over tunnel gate oxide and two additional layers of Ge QDs are self-assembled on Si QDs. Every two layers of QDs provides a new threshold voltage which can be used to program the inverter at different states. The QDs are assembled using a colloidal solution over the gate region via a self-assembly method in which QDs are deposited on the p-Si channel region over the tunnel gate oxide. The Si sample was placed in the colloidal solution for 3 minutes after which an annealing process was performed, this was done for every two layers of QDs.

III Conclusion: Formation of a Si QDSL and Ge QDSL in the gate region results in a four-state inverter. QD-NVRAMs have been experimentally demonstrated with a fast erase/write time [5]. The integration of QDG-FETs with QD-NVRAMs has been envisioned [6]. Finally, Moore's law is prolonged by using extra states exhibited in QDG-FETs.

1. F. C. Jain et. al. "Device and circuit modeling using novel 3-state quantum dot gate FETs," *2007 ISDRS*, 2007, pp. 1-2, doi: 10.1109/ISDRS.2007.4422254.

2. M. Lingalugari et al. "Novel multi-state quantum dot gate FETs using SiO₂ and lattice-matched ZnS-ZnMgS-ZnS as gate insulators," *Journal of Electronic Materials*, 42, pp. 3156-3163, 2013.

3. B. Khan et. al. "Fabrication and Characterization of nMOS Inverters Utilizing Quantum Dot Gate Field Effect Transistor (QDGFET) for SRAM Device" *IJHSES*, 31, no. 01n04, Mar. 2022

4. C. A. Mack, "Fifty Years of Moore's Law," *IEEE TSM*, 24, pp. 202-207, May 2011.

5. M. Lingalugari et. al. "Quantum Dot Floating Gate Nonvolatile Random Access Memory Using Quantum Dot Channel for Faster Erasing", *Electronic Lett.*, 54, 36, 2018.

6.F. Jain et. al. Integrating QD-NVRAMs and QDC-SWS FET based logic for multi-bit computing, *IJHSES*, 31, pp.2240020-1, 2022.

10:35 AM DISCUSSION TIME

SYMPOSIUM NM04

2D MXenes—Synthesis, Properties and Applications
November 28 - December 6, 2022

Symposium Organizers

Babak Anasori, Indiana University-Purdue University
Yohan Dall'Agnese, University College London
Agnieszka Jastrzebska, Warsaw University of Technology
Pooi See Lee, Nanyang Technical University

Symposium Support

Platinum

Murata Manufacturing co., Ltd.

Bronze

King Abdullah University of Science and Technology (KAUST)
MDPI
MilliporeSigma

* Invited Paper
+ Distinguished Invited

SESSION NM04.01: MXenes Synthesis and Structure I
Session Chairs: Babak Anasori and Agnieszka Jastrzebska
Monday Morning, November 28, 2022
Hynes, Level 2, Room 201

10:30 AM *NM04.01.01

Synthesis, Properties and Applications of MXenes Beyond $Ti_3C_2T_x$ Yury Gogotsi and Christopher E. Shuck; Drexel University, United States

MXenes are potentially the largest class of 2D materials discovered so far. With a general formula of $M_{n+1}X_nT_x$, M is an early transition metal (Ti, V, Nb, Ta, etc.), X is C and/or N, T_x represents the surface groups (-O, -OH, -F, -Cl), and $n = 1-4$, over 30 stoichiometric phases have already been discovered, with many more predicted computationally. MXenes have been widely studied owing to their exceptional properties, including hydrophilicity, scalability, mechanical strength, thermal stability, redox capability, and ease of processing. While the majority of research has focused on $Ti_3C_2T_x$, each MXene composition has its own unique optical, electrical, and mechanical properties. The incorporation of two metals into MXenes further imparts novel properties, and stabilized structures that cannot be formed otherwise. For ordered double transition metal MXenes, this allows for the incorporation of elements such as Cr, giving these MXenes unique magnetic properties. One other important class of MXenes are solid-solution MXenes, where multiple elements are randomly distributed within the M layers. These MXenes exhibit tunable properties that are directly related to their chemistry, whether optical, electronic or electrochemical. Moreover, solid-solution MXenes allow for the synthesis of MXenes with unique structures, such as $M_2X_4T_x$. By studying these, and other MXenes, it allows us to understand why MXenes have the properties they do, allowing us to rationally produce MXenes with desired properties.

11:00 AM *NM04.01.02

Two-Dimensional Transition Metal Carbo-Chalcogenide “TMCC” Bridging the Gap Between MXene and TMDC Ahmad Majed¹, Manish Kothakonda¹, Fei Wang¹, Eric N. Tseng², Kaitlyn Prenger¹, Xiaodong Zhang¹, Per O. Persson², Jiang Wei¹, Jianwei Sun¹ and Michael Naguib¹; ¹Tulane University, United States; ²Linköping University, Sweden

A new two-dimensional (2D) materials family of transition metal carbo-chalcogenides (TMCCs) can be considered as a merge between two well-known families of 2D materials: MXenes and transition metal dichalcogenides (TMDCs), at the atomic scale. In this presentation, we will report on the synthesis, characterization, and properties of 2D Nb_2S_2C and Ta_2S_2C which are the first two members of TMCCs. Both are delaminated from their parent multilayered counterpart via electrochemical lithiation followed by liquid exfoliation in water. Electronic and magnetic properties of Nb_2S_2C multilayers were studied, a superconductivity transition is observed at 7.55 K. The effect of delamination on the electrochemical performance of Nb_2S_2C as electrode materials for Li-ion batteries was examined, and the delaminated Nb_2S_2C was found to surpass both multilayered Nb_2S_2C and delaminated NbS_2 in terms of capacity and stability. In addition, *Ab initio* calculations predicted elastic constant of TMCCs to be 50% higher than that of TMDCs.

11:30 AM NM04.01.03

Anhydrous Etching of MAX Phases for Faster and More Efficient Synthesis of MXenes Taegon Oh¹, Seungjun Lee^{1,2} and Chong Min Koo³; ¹Korea Institute of Science and Technology, Korea (the Republic of); ²Korea University, Korea (the Republic of); ³Sungkyunkwan University, Korea (the Republic of)

Anhydrous synthesis of MXene facilitates the control over the surface functionalization and the final physicochemical properties. Here, we propose a novel anhydrous etching solution, consisting of high-boiling-point dimethylsulfoxide as organic medium, NH_4HF_2 as etchant, CH_3SO_3H as acid, and NH_4PF_6 as intercalant. This anhydrous solution does not only enable one to increase the reaction temperature up to 100 °C for accelerating the etching and delamination of Ti_3AlC_2 MAX crystals, but also suppresses the destructive side reaction of the produced $Ti_3C_2T_x$ MXene flakes. Consequently, the etching reaction is completed in 4 h at 100 °C and produces high-quality monolayer $Ti_3C_2T_x$ MXene with an electrical conductivity of 8,200 S cm^{-1} and a yield of over 70%. The synthesized $Ti_3C_2T_x$ exhibits more F-terminations than conventional aqueous $Ti_3C_2T_x$. The atypical surface structure of $Ti_3C_2T_x$ MXene leads to an exceptionally high ultimate tensile strength (167 ± 8 MPa), which is about 5 times larger than the ones synthesized in aqueous HF solution (31.7 ± 7.8 MPa).

SESSION NM04.02: MXenes Synthesis and Structure II
Session Chairs: Babak Anasori, Agnieszka Jastrzebska and Brian Wyatt
Monday Afternoon, November 28, 2022
Hynes, Level 2, Room 201

1:30 PM +NM04.02.01

Quat Derived Nanomaterials and Their Properties Michel W. Barsoum; Drexel Univ, United States

One- (1D) and two-dimensional (2D) materials offer advantages that their 3D counterparts do not. To produce such materials in *bulk* there are two conventional approaches: bottom-up and top-down. MXenes are an excellent example of the latter. The main drawback of this approach is high cost in first making the layered solid and then the many steps needed to etch and delaminate them. The bottom-up approach is in principle much more scalable. There are several bottom-up approaches, the one of interest here is the sol-gel approach common in the processing of ceramic powders, especially oxides of Ti and Si. The main disadvantages of this approach are the need to rely on the solubility of the precursor salt or compound in water and the need for a calcination and/or hydrothermal step that is usually needed to crystallize the products made at lower temperatures. In trying to etch the MAX phases without HF, we stumbled on a very powerful method to make 1D and 2D materials. The general idea is to dissolve inexpensive, non-water soluble, precursors in quaternary ammonium cation salts, or quats, at temperatures < 100 °C under ambient pressures for a few days. The aim of this talk is to describe the resulting materials and some of their properties in two systems: Ti and Mn. In the former, we converted 10 binary and ternary titanium carbides, nitrides, borides, phosphides, and silicides into anatase-based, 1D sub-nano filaments ≈ 6x10 Å in cross-section that self-assemble into 2D flakes

by immersing them in a tetramethylammonium hydroxide, TMAH, solution at temperatures in the 50 to 85 °C range. The 2D flakes are quite well-ordered in the stacking direction. In some cases, the conversion is 100 % precluding the need for centrifuges, filters, etc. We currently routinely make 100 g batches in a lab setting. In some cases, we also make mesoscopic powders. Electrodes made from some of filtered films performed well in lithium-ion and lithium-sulphur systems. These materials also biocompatible and reduce the viability of cancer cells thus showing potential in biomedical applications. In the Mn-case, five water-insoluble Mn-bearing precursors, viz. Mn_3O_4 , Mn_2O_3 , MnB, Mn_5SiB_3 , and Mn_2AlB_2 , were converted to birnessite 2D MnO_2 flakes, that are remarkably crystalline. Here again, the precursor powders are immersed in 25 wt. % TMAH aqueous solutions at 50 °C to 80 °C, for 4 to 2 days, respectively. The 2D sheets demonstrate reversible O_2 electrocatalysis with activities comparable to those of a commercial Pt/C catalyst. Synthesizing 1D and 2D materials in bulk, at near ambient conditions, starting with non-layered precursors (e.g., TiC, Mn_3O_4) could usher a new age where 1D and 2D materials can be mass produced inexpensively using earth abundant elements and a green process.

2:00 PM NM04.02.02

Synthesis and Characterization of 2D MoN Crystals and the Effects of Process Parameters Omer R. Caylan, Elif Okay, Derya Karadeniz and Goknur Cambaz Buke; Tobb University of Economics and Technology, Turkey

Molybdenum Nitride (MoN), hardest superconducting material is estimated to have a critical superconducting temperature of 16 K. Although that these properties attract the attention of many researchers, there are limited studies investigating the effects of process parameters of chemical vapor deposition synthesis of MoN crystals. The melt catalyst method in which a catalyst (Cu or In) is placed on top of a metal foil (Mo) and after reaching the melting temperature of the catalyst, synthesis gasses (CH_4 , NH_3) are supplied to produce 2D MXene materials such as Mo_2C and MoN. This method is advantageous to produce large area 2D crystals with reduced defects and once the process is optimized, the reproducibility and reliability of the method is makes it perfect for advanced electronic applications. We studied the effects of process parameters (effect of catalyst, catalyst thickness, catalyst type, reaction temperature, growth duration, gas amounts) on the growth of 2D MoN crystals and discussed the results. SEM, EDS and OM studies are used to investigate the morphology of these crystals and to further understand the structure of the produced crystals Raman spectroscopy, XPS, TEM and XRD studies are used. We also showed that it is possible to synthesize Molybdenum CarboNitride structures by treating previously synthesized Mo_2C crystals with ammonia gas. This is the first study that investigates the transition of priorly synthesized Mo_2C crystals to MoCN and MoN. Depending on the ammonia exposure duration, Mo_2C crystals can be replaced by MoN crystals completely. For future work, it is aimed to find the corelation between superconducting transition temperature with the different nitriding durations. This study is based on work supported by the Air Force Office of Scientific Research under Award Number FA9550-19-1-7048.

2:15 PM NM04.02.03

Large Flakes of $Ti_3C_2T_x$ MXene Mikhail Shekhiryev¹, Jeffrey Busa¹, Christopher E. Shuck¹, Angel Torres², Saman Bagheri², Alexander Sinitskii² and Yury Gogotsi¹; ¹Drexel University, United States; ²University of Nebraska–Lincoln, United States

The size of individual flakes is critical for 2D materials and their devices. For materials produced *via* a top-down approach, such as graphene oxide produced from graphite, every step of the synthesis process, including the particle size of the precursor and the exfoliation protocol, affects the size of the resultant material. The size, in turn, affects the properties of assembled films and fibers, and the synthesis of ultra-large flakes has been a target for multiple dedicated studies.

Titanium carbide MXene ($Ti_3C_2T_x$) is one example of 2D material produced *via* a top-down approach by selectively etching Al from the parent Ti_3AlC_2 phase, followed by delamination of the multilayer material into individual flakes. $Ti_3C_2T_x$ has found promise in multiple applications, including energy storage, flexible electronics, and membranes, where the size of the flakes is an important parameter, and the increased average size can be beneficial. In this work, we will discuss the factors affecting the lateral size of MXene and ways to synthesize ultra-large individual flakes. Starting with the synthesis of the MAX precursor, etching, and delamination, each step of the process affects the resulting flake size. In particular, the delamination process is critical and must be controlled to achieve large individual flakes of MXene. We will demonstrate a new soft delamination protocol, which preserves the size of the flakes and provides an approach to fabricating individual flakes of up to 40 μm in lateral size.

2:30 PM *NM04.02.04

Two-Dimensional Materials from Selective Etching—MXenes and Beyond Johanna Rosen; Linkoping University, Sweden

Formidable efforts are invested world-wide on two-dimensional (2D) materials research. Most 2D materials are based on van der Waals crystals, that can be mechanically exfoliated (*cf.* graphene). The primary exception, two-dimensional metal carbides and nitrides (MXene), is produced by chemical exfoliation, i.e. selective etching of recurring layers in 3D layered precursor solids. The first MXene, Ti_3C_2 , was first reported in 2011, and since then the family has increased drastically, to also include members with in-plane and out-of-plane ordering of metal atoms, and high entropy metal configurations. Synthesis of new MAX phases designed as precursors for specific MXenes have been crucial for this development, being inspired from exploratory theoretical predictions in uncharted structural and compositional space. The present talk will briefly summarize our work in this area, and show some light on how MXene development can serve as inspiration for selective etching of other layered solids. One such example is a new type of chemically ordered, quaternary metal borides, that can be chemically exfoliated into 2D sheets, and selectively prepared in multilayer form, as delaminated single-layer sheets in colloidal suspension, or as additive-free filtered films, for property evaluation. Furthermore, future two-dimensional materials from selective etching will be discussed, looking beyond MXenes and 2D materials derived from metal borides. Based on the vast library of layered solids, new families of 2D materials are expected through an interplay of computationally driven atomistic design and development of new chemical exfoliation pathways.

3:00 PM BREAK

3:30 PM NM04.02.05

Direct Synthesis and Chemical Vapor Deposition of Vertically Aligned MXene Di Wang¹, Chenkun Zhou¹, Alexander Filatov¹, Wooje Cho¹, Francisco Lagunas², Mingzhan Wang¹, Chong Liu¹, Robert F. Klie² and Dmitri V. Talapin¹; ¹University of Chicago, United States; ²University of Illinois at Chicago, United States

MXenes are attracting ever growing attention for applications in energy storage, electromagnetic interference (EMI) shielding, superconductivity, and catalysis. Traditional preparation of MXenes involves high-temperature synthesis the MAX phase followed by its chemical etching and exfoliation. This synthetic route has high energy consumption, and uses large amounts of hazardous HF or Lewis acidic molten salts. The development of fast, facile, and atom-economic synthetic methods would greatly facilitate widespread practical applications of the rapidly developing family of functional MXenes. An ideal approach would involve direct interconversion of inexpensive precursors into MXenes bypassing intermediate MAX phases. Here we report direct synthesis of Ti_2CCl_2 MXene via novel chemical reactions. The reactions are easily scalable, inexpensive, energy efficient, and more environmentally friendly compared to the traditional route. The directly synthesized MXene also showed excellent energy storage capacity for Li-ion intercalation. Besides convenience and scalability, the direct synthesis route offers new synthetic modalities not compatible with traditional MAX phase etching methods. Thus, we demonstrated chemical vapor deposition (CVD) synthesis of Ti_2CCl_2 , Ti_2NCl_2 , Zr_2CCl_2 , and Zr_2CBR_2 MXenes, producing

carpets of MXene sheets oriented perpendicular to substrate. Such orientation makes MXene surface easily accessible for ion intercalation and exposes catalytically active edge sites.

Overall, direct synthesis and CVD of MXenes opens up new options in making previously unrealized MXenes and fabricating MXene devices. The development of vapor phase synthesis further expands the capabilities for integration of 2D MXenes into electronic and optoelectronic devices, including cross-platform integration with silicon microelectronics.

3:45 PM *NM04.02.06

Highly Conductive MXene with Improved Environmental Stability for Electronics [Shun Sakaida](#), Akari Seko, Masashi Koyanagi and Takeshi Torita; Murata Manufacturing Co., Ltd., Japan

With growing interest in two-dimensional (2-D) materials group and their outstanding properties, considerable attention has been paid to a family of 2-D transition metal carbides (MXene). Herein we summarize our recent works on electrically conductive MXene, especially for $Ti_3C_2T_x$, in thin-film state at humid conditions. Our scale-up production system provides high quality crystalline MXene flakes to exhibit remarkable electrical conductivity as high as 18000 S/cm at 5 μm thickness. Several techniques were successfully used to monitor the stability of MXene dispersion and the fabricated films. X-ray crystallographic studies indicated that the interlayer spacing change by water uptake has a significant effect on the conductivity, and therefore further investigation to prevent degradation are highly required for applications under humid condition at high temperature.

4:15 PM *NM04.02.07

Formation and Characterization of 2D Mo_2C Crystals via Biased CVD Omer R. Caylan¹, Furkan Turker^{1,2}, Omer Tarik Ogurtani³ and [Goknur Cambaz Buke](#)^{1,2}; ¹TOBB ETU, Turkey; ²The Pennsylvania State University, United States; ³Middle East Technical University, Turkey

2D ultrathin transition-metal carbides (TMCs), nitrides (TMNs), and carbonitrides are a family of important functional nanomaterials for various applications due to their properties that are directly dependent on the structure of the crystals, which can be controlled by processing. MXenes formed by wet etching which may consist of defects and surface functional groups (due to the use of acids) are especially useful for applications like composites, energy storage; however, for advanced electronics it is necessary to develop a versatile technique to produce high quality MXenes with controlled thickness, area, and high reproducibility.

Biased CVD is a promising technique to produce large area MXenes. In Biased CVD, a stack of metal substrate (e.g. Mo and Cu) is exposed to a volatile precursor (e.g., CH_4) which decomposes on the substrate surface (e.g., Cu) and reacts with the Metal (e.g., Mo) that is biased towards the surface to produce the desired deposit (e.g., Mo_2C). It is called biased because the catalyst layer (Cu) is used like a diode: Cu lets Mo atoms to diffuse through Cu to the surface but does not let carbon atoms to diffuse through Cu (due to the difference in solubilities). Hence the diffusion is simply called biased.

Studies in literature showed that the morphology and the thickness of Mo_2C crystals are strongly affected by catalyst type, thickness, composition, and the simultaneous graphene growth during CVD. To produce controlled morphology (thin, large area, high quality MXene crystals), the understanding of the growth mechanism via biasing reaction is crucial. However, it is still not clear and reproducible control of thickness and morphology is still a problem. Although it is revealed that simultaneous graphene growth affects the morphology and the thickness of Mo_2C crystals; there are conflicts in literature and the effect of its presence on the Mo_2C formation is not well understood. Moreover, fundamental physico-chemical and kinetic parameters related to the bulk and surface diffusion (associated with graphene, M and X) are missing in the literature and there is lack of data on the nucleation and growth kinetics of MXenes for physico/chemical modelling.

In this presentation, we present an investigation on the controlled growth of thin Mo_2C crystals on both Cu and In substrates via CVD using CH_4 . SEM, EDS, Raman spectroscopy, XPS, and XRD studies show that hexagonal Mo_2C crystals, which are orthorhombic, grow along the [100] direction together with graphene and an amorphous carbon thin film on Cu and In, respectively. The growth mechanism is examined and discussed in detail, and a model is proposed. AFM studies agree well with the proposed model.

This material is based on the work supported by the Air Force Office of Scientific Research (Award number: FA9550-19-1-7048).

4:45 PM POSTER SPOTLIGHT PRESENTATIONS

SESSION NM04.03: Poster Session I: MXenes Synthesis, Structures and Mechanical Properties

Session Chairs: Babak Anasori, Yohan Dall'Agnese, Agnieszka Jastrzebska and Pooi See Lee

Monday Afternoon, November 28, 2022

8:00 PM - 10:00 PM

Hynes, Level 1, Hall A

NM04.03.01

New Methods of Functionalizing Organic Molecules onto 2D Ti_3C_2 MXene Surfaces [Alicia Tripp](#) and Robert J. Hamers; University of Wisconsin–Madison, United States

2D transition metal carbides, nitrides, and carbonitrides (MXenes) have unique and tunable physical, chemical, and mechanical properties that drive their application in chemical sensing, energy storage, and water purification. Among these properties, the excellent dispersion of Ti_3C_2 MXene in water remains one the most important for applications that require solution processibility. However, MXene susceptibility to oxidation in aqueous environments remains a challenge for suspension storage and environmental applications. While there are many computational works that predict property changes for MXenes with altered surface chemistry, successful and controlled experimental manipulation of MXene surfaces remains challenging. This work investigates new methods of controlled MXene surface functionalization that take advantage of the material's intrinsic -OH and -O surface terminations. These methods are based on past group work involving the formation of organic molecular monolayers on metal oxides with hydroxylated surfaces. The organic molecules were bound to the metal oxide surface through alkoxy bonds, and the monolayers were found to be stable in aqueous environments. Current work utilizes X-ray photoelectron spectroscopy and Fourier-transform infrared spectroscopy to elucidate the intrinsic and altered surface chemistry of lab synthesized 2D Ti_3C_2 MXene. This work is important for the development of a simple and controlled functionalization method for MXenes with the potential to bind a wide variety of molecules to the surface.

NM04.03.02

Ultrathin, Single Crystal Tungsten Carbide Phases via Liquid-Metal-Assisted Chemical Vapor Deposition—Controlled Synthesis and Superconducting Transitions

Alexander J. Sredenschek, David Sanchez, Jiayang Wang, Da Zhou, Susan B. Sinnott, Mauricio Terrones, Morteza Kayyalha and Le Yi; The Pennsylvania State University, United States

The transition metal carbide (TMC) family, historically studied as refractory metals for chemical and mechanical applications, is receiving increasing attention in the ultrathin limit. The study of TMCs has been extended to this limit first with the isolation of MXenes, atomically-thin layers of TMCs bound by interlayer van der Waals (vdW) forces;¹ and second with the development of a liquid-metal-assisted chemical vapor deposition (LMCVD) approach to produce nonlayered, ultrathin TMC (UThTMC) crystals with tunable lateral size (1-10 μm) and controllable thickness (less than 100 nm).² MXenes are typically produced as high yield, textured powders, while UThTMCs are high quality, single crystal platelets, ideal for electronic transport studies. Tungsten carbides have received little attention in the ultrathin limit, never isolated in the MXene family due to the lack of proper tungsten precursors. LMCVD, then, is an alternative method to produce ultrathin tungsten carbides as demonstrated in two studies.^{3,4} These LMCVD studies typically produce one carbide phase, and to promote the study of novel UThTMCs phases, we probe the growth parameters to determine whether different tungsten carbide phases can be isolated. In this work, we use LMCVD to synthesize WC and W_2C phases via copper/tungsten (Cu-W) and gallium/tungsten (Ga-W) substrates, respectively. Moreover, we perform detailed structural and transport property characterization to understand the carbide phase-dependent transport properties in these ultrathin crystals.

In our LMCVD approach, we use two substrates, Cu-W and Ga-W, and tune remaining growth parameters to form tungsten carbide nanoplatelets. Scanning electron microscopy reveals differences in the carbide morphology, with triangular and hexagonal crystalline platelets formed on Cu-W and Ga-W, respectively. Moreover, we find that these crystals are ultrathin *via* atomic force microscopy measurements. To determine the crystal structure of these platelets, we carry out selected area electron diffraction, X-ray diffraction, and planar and cross-sectional transmission electron microscopy, and we find that the tungsten carbide is isolated in two phases with high crystallinity: WC (P-6m2) on Cu-W, and W_2C (Pbcn, P6₃/mmc, or P-3m1) on Ga-W, corroborated with first principles density functional theory calculations of the tungsten carbide equation of state. We also measure the superconducting transition temperatures and critical fields of both tungsten carbide phases.

Our work highlights some of the challenges inherent to the phase and polymorph identification of UThTMCs. While we can distinguish between WC and W_2C phases, further studies are required to determine the W_2C polymorph in the Ga-W system, and we conclude that we have one or more of the Pbcn, P6₃/mmc, and P-3m1 polymorphs. Our results suggest that proper choice of substrate in LMCVD can lead to novel, single crystal UThTMCs, and these carbide phases require careful structural characterization to identify accurately.

References

1. Anasori, B., Lukatskaya, M. R., & Gogotsi, Y. *Nat. Rev. Mater.* **2**, (2017).
2. Xu, C. *et al. Nat. Mater.* **14**, 1135–1141 (2015).
3. Zeng, M. *et al. Nano Energy* **33**, 356–362 (2017).
4. Wang, C. *et al. Adv. Electron. Mater.* **5**, 1–7 (2019).

NM04.03.03

The Synthesis and Characterization of Mo_2CT_x Mxene by Hydrothermal Etching with Different Fluoride Salts for EMI Shielding Applications

Elif Okay¹, Omer R. Caylan^{1,2}, Eren Atli¹, Begum B. Incecik^{1,3} and Goknur Cambaz Buke¹; ¹TOBB University of Economics and Technology, Turkey; ²Bilkent University, Turkey; ³Roketsan Missiles Industries Inc., Turkey

MXenes are the novel two-dimensional metal carbides or nitrides derived from their MAX phases. Recently discovered MXenes, attracted the attention of many researchers and widely studied for the applications of energy storage, catalysis, gas sensing, wastewater treatment etc. More than twenty MXenes have been successfully synthesized and Mo_2CT_x holds a great potential due to its theoretically predicted electrochemical, thermoelectric properties and chemical stability. Nonetheless, the long synthesis duration which can amount up to several days due to the strong bonding between the Mo-Ga atoms is challenging. In order to overcome this problem, scientist have used hydrothermal etching and lowered the duration drastically. Additionally, due to the hazardous nature of hydrofluoric acid, there have been studies on using HCl as etchant in hydrothermal conditions to increase the chemical potential between gallium and chloride ions which have proven successful. In this study, the hydrothermal etching of $\text{Mo}_2\text{Ga}_2\text{C}$ to produce Mo_2CT_x using different fluoride salts with hydrochloric acid and only using hydrochloric acid is investigated and effects of different salts (LiF, BaF_2 , MgF_2 and MnF_4) and no salt is discussed. The fluoride salts are mixed with hydrochloric acid to obtain in-situ hydrofluoric acid, and two different reaction temperatures for the hydrothermal etching process is studied (140 °C and 160 °C) for 24 hours (5-7 days for HCl). The synthesized MXenes are characterized by; SEM and EDS for investigating morphology and chemical composition, and XRD for structural analysis. After studying the process parameters, such as temperature and etchant type on the synthesis of Mo_2CT_x powders, Mo_2CT_x powders are hand-mixed with epoxy resin with differing weight percentages to produce epoxy/ Mo_2CT_x composites. Then these samples' electromagnetic interference shielding effectiveness performance is measured. The EMI Shielding properties of Mo_2C Mxene composite is reported for the first time in this study. EMI Shielding properties of the epoxy/Mxene composites are reported in accordance with "ASTM D4935 Standard Test Method for Measuring the Electromagnetic Shielding Effectiveness of Planar Materials" using a vector network analyzer in the frequency range of 1.5–10 GHz. This study is supported by Air Force Office of Scientific Research grant number FA9550-19-1-7048.

NM04.03.05

Kinetics and Mechanism of MXene Synthesis

Mark Anayee, Christopher E. Shuck, Mikhail Shekhirev and Yury Gogotsi; Drexel University, United States

The family of 2D carbides and nitrides called MXenes has grown to encompass numerous structures and compositions. These materials have been explored in a variety of applications such as energy storage, wireless communication, optoelectronics, and medicine because of their high electrical conductivity, redox-active surfaces, plasmonic behavior and other attractive properties. MXenes are typically derived via topochemical etching of atomically thick layers from precursor layered MAX phases using aqueous corrosive etchants. Knowledge of the reaction mechanism and process kinetics are of fundamental importance for synthesis and property control of MXenes. Prediction of the optimal synthesis approaches will facilitate new MXene composition discovery and prediction of optimal processing time as a function of various parameters will also facilitate scaling up wet chemical synthesis of MXenes for industrial use. Despite their importance, such studies have been challenging because of the atomic thickness of the A-element layers being etched and the aggressive etchants that hinder in-situ studies. Herein, we explore various ex-situ techniques to probe the effect of critical etching parameters on the structure, chemistry, and properties of the resulting MXenes; as well as develop an in-situ analytical technique to quantitatively measure the etching kinetics through byproduct hydrogen gas collection and tracking; and finally develop an in-situ optical microscopy and profilometry technique to directly visualize the structural evolution during the etching reaction. Through these methods, we are able to derive empirical models for prediction of etching kinetics, and gain a fundamental understanding of how the etching reaction starts, proceeds, and finishes.

NM04.03.06

Strategies for Optimizing Etching and Delamination Toward High-Quality $Ti_3C_2T_x$ MXenes [Annabelle Harding](#), Anupma Thakur, Karis Davidson, Nithin Chandran Balachandran Sajitha, Brian Wyatt and Babak Anasori; IUPUI, United States

MXenes, two-dimensional (2D) transition metal carbides, nitrides, or carbonitrides, are a rapidly growing family of nanomaterials that have potential uses ranging from energy storage, catalysis, and electromagnetic interference shielding to medical applications. To recognize these applications, it is known that etching and subsequent delamination play a vital role in the quality and scalability of MXenes. Here, we present the experimental strategies to synthesize the most studied MXene, $Ti_3C_2T_x$, using different precursor powder, etching conditions, and delamination methods. For etching, we compare different etchants, including hydrofluoric acid (HF)/hydrochloric acid (HCl) mix and HCl/lithium fluoride (LiF) mix, and conditions such as time and temperature. For delamination, we investigate the effect of time, temperature, and environment (air or argon) on the quality of the $Ti_3C_2T_x$ MXene. We analyze the resultant $Ti_3C_2T_x$ MXene using x-ray diffraction, scanning electron microscopy, and electrical conductivity to illustrate the relation between different synthesis methods on the quality of single-to-few layer MXene flakes of $Ti_3C_2T_x$. With this detailed synthesis study on etching and delamination methods, we suggest updated optimal parameters for the synthesis of high quality $Ti_3C_2T_x$ MXenes.

NM04.03.07

3D Assembly of 2D Molybdenum Carbide(Mo2C) Using Chemical Vapor Deposition [Syam S. Ravuri](#), Sandeep Gorantla, Krzysztof Lis and Alicja Bachmatiuk; Sici Badawczej Lukasiewicz PORT-Polish Center for Technology Development, Poland

Among the burgeoning of novel MXene materials, Molybdenum carbide stands out as they are successfully synthesized by conventional selective chemical etching and chemical vapour deposition growth methods. Molybdenum carbide (Mo2C) is garnering growing research attention due to their interesting chemical and electronic properties. Their properties make them a promising material for future electrochemical energy storage applications. In this work, we show the 3D self-assembly architectures of 2D Molybdenum carbide grown successfully using a chemical Vapor deposition for the first time, to the best of our knowledge. Our controllable CVD approach allows to engineer several aspects of the as grown Mo2C flakes, in particular their orientation of growth with respect to the surface of growth substrate. The as synthesized Mo2C was further investigated by X-ray diffractometry, Raman spectroscopy, scanning electron microscopy and aberration-corrected scanning transmission electron microscopy to gain understanding of the influence of growth conditions on their chemical and structural characteristics.

NM04.03.08

MXenes-Mining—A Decade with MXenes [Yiannis Georgantas](#), Francis Moissinac, Mark A. Bissett and Sarah J. Haigh; University of Manchester, United Kingdom

MXenes is a family of transition metal carbides, nitrides or carbonitride materials that includes more than 20 different chemical compounds, that can be each synthesized with different methods and post-processed in multiple ways, enabling them to be used in a variety of applications. Consequentially, several thousand articles have been published that either mention MXenes or target them. Herein, we have gathered 15,116 articles since 2011, including the first publication about MXene, up to 31 December 2021 from 12 main scientific journal publishers (1. Cambridge University Press, 2. Elsevier (ScienceDirect), 3. Institute Of Physics Publishing (IOP), 4. John Wiley & Sons: Wiley Online (Wiley), 5. Nature Publishing Group (Nature), 6. Oxford Academic Press, 7. SAGE, 8. Springer, 9. Taylor & Francis, 10. American Association for the Advancement of Science (AAAS), 11. Royal Society of Chemistry (RSC) and 12. American Chemistry Society (ACS)). We visualize the results in a range of graphs and figures and try to find trends, correlations between them, but also to identify the gaps that this domain may have for future investigations. We probe the growth of MXenes through the year, statistical occurrence of keywords, MXenes' properties, cluster of applications, specific applications, synthesis methods, which MXenes have been investigated the most over the last decades, 3D architectures, theoretical against experimental articles and combinations of these areas. On one hand, it is obvious that the MXenes research community grows every year dramatically, but on the other hand the investigations are very limited towards specific aspects of this 2D family. Initially, the scientific body has related MXenes with the Ti_3C_2 and there is very little attention for the rest of the materials. Hence, the properties and the applications that are targeted are also limited and on the way that Ti_3C_2 can achieve high performance. There is the need to investigate MXenes further than the titanium carbides, to gain a more comprehensive knowledge for these 2DMs from their synthesis to in what applications can be used. In addition, the problems that occur from the HF-based synthesis also must addressed either with post-process of the MXenes or by using a different path to synthesize these extortionary 2DMs, such as alkali treatment, electrochemical-etching and molten salts; especially the last one, due to the homogeneous surface chemistry of MXenes which is the most crucial advantage and disadvantage of these materials at the moment.

NM04.03.09

Mussel-Inspired Interface Engineering of $Ti_3C_2T_x$ MXene for Practical Applications [Gang San Lee](#) and Sang Ouk Kim; Korea Advanced Institute of Science and Technology, Korea (the Republic of)

Two-dimensional (2D) MXene has shown enormous potential in scientific fields, including energy storage and electromagnetic interference (EMI) shielding. Unfortunately, MXene-based material structures generally suffer from mechanical fragility and vulnerability to oxidation. Herein, mussel-inspired dopamine successfully addresses those weaknesses by improving interface interaction and ordering in MXene assembled films. Dopamine undergoes *in situ* polymerization and binding at MXene flake surfaces by spontaneous interfacial charge transfer, yielding an ultrathin adhesive layer. Resultant nanocomposites with highly aligned tight layer structures achieve approximately seven times enhanced tensile strength with a simultaneous increase of elongation. The ambient stability of MXene films is also greatly improved by the effective screening of oxygen and moisture. Interestingly, angstrom thick polydopamine further promotes the innate high electrical conductivity and excellent EMI shielding properties of MXene films. This synergistic concurrent enhancement of physical properties proposes MXene/polydopamine hybrids as a general platform for MXene-based reliable applications. Furthermore, tight interfacial integration between MXene and polydopamine can be extended to MXene-based three-dimensional nanocomposite capacitive pressure sensor applications.

SESSION NM04.04: MXenes Synthesis, Structures and Surfaces

Session Chairs: Yohan Dall'Agnese and Pooi See Lee

Tuesday Morning, November 29, 2022

Hynes, Level 2, Room 201

8:00 AM NM04.04.01

Observation of Chemical Short-Range Order, Lattice Distortion and Defect Structure in High-Entropy Transition Metal Carbides Xiangyu Zhu¹, Zijiao Wu², Qingxiao Wang³, Yuan Wu², Xiongjun Liu², Hui Wang², Suihe Jiang², Zhaoping Lu² and Moon Kim¹; ¹The University of Texas at Dallas, United States; ²University of Science and Technology Beijing, China; ³King Abdullah University of Science & Technology, Saudi Arabia

In recent years, multiple principal elements of two-dimensional transition metal carbides (MXenes) and its precursor high entropy (HE) MAX phase have been synthesized successfully. Mixing multiple transition metals opened a new ideology to explore the attainable chemistries and led to the discovery of new properties of the MAX & MXene family. It has been reported that HE MXenes show improved conductivity, charge storage capacity, and catalytic ability, as well as superior mechanical properties, as compared with single transition metal MAX. The unprecedented physicochemical properties were found to be closely related to short-range orderings, local lattice distortion, sluggish diffusion, and other features resulted from high configuration entropy.

This work aims to provide fundamental information on structural & chemical configurations at the atomic scale via the S/TEM characterization of HE MXene & MAX materials. The primary equipment used for characterization is JEOL ARM 200F and FEI Titan Themis 300, equipped with a spherical aberration corrector to achieve sub-angstrom imaging resolution and sub-nano spatial resolution. The STEM shows a hexagonal crystal structure of the MAX phase (space group P63/mmc, 194), and stress analysis indicates a strong correlation between lattice distortion and configurational entropy. The detailed chemical arrangement of multiple transition metals was revealed by atomic resolution EDS mapping while the HE MXene lattice and defect configuration was analyzed by Z-contrast (HAADF) images. The apparent atoms exhibit a stochastic arranged variation in brightness, revealing the randomly multiple principal atomic occupation. Our preliminary results offer a chance to garner in-depth understanding of the complex mechanism among multicomponent HE MAX & MXene materials.

8:15 AM NM04.04.02

Using Multiple M-Elements to Understand the Chemistry and Structure of MXenes Christopher E. Shuck, Marley Downes, Jonathan Shochat and Yury Gogotsi; Drexel University, United States

MXenes are potentially the largest class of 2D materials discovered so far. With a general formula of $M_{n+1}X_nT_x$, M is an early transition metal (Ti, V, Nb, Ta, etc.), X is C and/or N, T_x represents the surface groups (-O, -OH, -F, -Cl), and $n = 1-4$, over 30 stoichiometric phases have already been discovered, with many more predicted computationally. This class of materials has been widely studied owing to their exceptional properties, including hydrophilicity, scalability, mechanical strength, thermal stability, redox capability, and ease of processing. Because MXenes inherit their structure from MAX phase precursors, understanding MAX phase synthesis leads to control over flake size, defect density, and chemical composition of the resultant MXene. One understudied, yet important class of MXenes are solid-solution MXenes, where multiple elements are randomly distributed within the M layers. Herein, a set of multi-M chemistries (Mo, V, Ti, Nb) are used to study the effect of structure and chemistry on MXenes. While solid-solution MXenes have unique and tunable chemical, optical, and electronic properties, they also enable the formation of novel MXenes that cannot exist otherwise. By choosing specific chemistries, we can then begin to understand fundamental aspects of MXene chemistry and structure.

8:30 AM *NM04.04.03

In Situ Transmission Electron Microscopy of MXenes Per O. Persson; Linköping University, Sweden

Technical developments that have improved the optical performance in transmission electron microscopes have also enabled significant developments of in situ and in operando experiments under the electron beam. In the field of MXenes, in situ investigations have hitherto remained scarce, although there is much to learn about the interactions between MXene and ambient gas or liquid.

In the present talk, I will review state of the art technical possibilities and their boundary conditions. I will also review our efforts to understand the interactions between MXene, gas and vapor, and how results from these interactions help build an understanding for the stability of MXene and MXene terminations.

9:00 AM NM04.04.04

The Surface Science of MXenes Chenkun Zhou, Di Wang, Vladislav Kamysbayev and Dmitri V. Talapin; University of Chicago, United States

Two-dimensional (2D) transition-metal carbides and nitrides (MXenes) show impressive performance in applications, such as supercapacitors, batteries, electromagnetic interference shielding, or electrocatalysis. These materials combine the electronic and mechanical properties of 2D inorganic crystals with chemically modifiable surfaces, and surface-engineered MXenes represent an ideal platform for fundamental and applied studies of interfaces in 2D functional materials.

The comprehensive understanding of MXene surfaces will be required for prescriptive engineering of their physical and chemical properties. We discuss general strategies to install and remove surface groups by performing substitution and elimination reactions. Successful synthesis of MXenes with oxo-, imido-, thio-, seleno-, or telluro- terminations, as well as bare MXenes (no surface termination), and hybrid organic-inorganic MXenes are demonstrated. The description of MXene surface structure requires an intricate mix of concepts from the fields of coordination chemistry, self-assembled monolayers and surface science. MXene surface groups control biaxial lattice strain, phonon frequencies, electrochemical performance, the strength of electron-phonon coupling, making MXene surfaces not spectators but active contributors to conductivity, superconductivity and catalytic activity.

9:15 AM NM04.04.05

Hybrid Organic-Inorganic Two-Dimensional Metal Carbide MXenes with Amido- and Imido-Terminated Surfaces Chenkun Zhou¹, Di Wang¹, Francisco Lagunas², Benjamin Atterberry³, Alexander Filatov¹, Aaron Rossini³ and Dmitri V. Talapin¹; ¹The University of Chicago, United States; ²University of Illinois Chicago, United States; ³Iowa State University, United States

Two-dimensional (2D) transition-metal carbides and nitrides (MXenes) show impressive performance in applications, such as supercapacitors, batteries, electromagnetic interference shielding, or electrocatalysis. These materials combine the electronic and mechanical properties of 2D inorganic crystals with chemically modifiable surfaces, and surface-engineered MXenes represent an ideal platform for fundamental and applied studies of interfaces in 2D functional materials. A natural step in structural engineering of MXene compounds is the development and understanding of MXenes with various organic functional groups covalently bound to inorganic 2D sheets. Such hybrid structures have the potential to unite the tailorability of organic molecules with the unique electronic properties of inorganic 2D solids.

Here, we introduce a new family of hybrid MXenes (*h*-MXenes) with amido- and imido-bonding between organic and inorganic parts. The description of *h*-MXene structure requires an intricate mix of concepts from the fields of coordination chemistry, self-assembled monolayers and surface science. The optical properties of *h*-MXenes reveal coherent coupling between the organic and inorganic components. *h*-MXenes also show superior stability against hydrolysis in aqueous solutions.

9:30 AM *NM04.04.06

Synthesis of New Types of MAX Phases as Precursors for Novel MXenes Rose Snyder¹ and Christina S. Birkel^{1,2}; ¹Arizona State University, United

States; ²Technische Universität Darmstadt, Germany

Transition metal-based carbides that belong to the family of MAX phases are an intriguing class of materials and have attracted a lot of attention as precursors for the relatively young class of 2D materials, the family of MXenes. Our group utilizes a diverse set of synthesis techniques to prepare new MAX phases as well as known ones with unique morphologies. Cr₂GaC in the shape of carbonaceous microwires, hollow and full microspheres as well as hitherto unknown carbonitride phases, such as Cr₂GaC_{1-x}N_x and V₂GaC_{1-x}N_x, are a few examples of our recent works. We strive to exfoliate these compounds into the respective 2D structures to study their electrochemical properties. All products are structurally characterized by diffraction and electron microscopy techniques.

10:00 AM BREAK

10:30 AM NM04.04.07

Ti₄C_(3-y)N_yT_x: New 2D Carbonitride MXenes Derived from New 413 Carbonitride MAX Phases [Anika Tabassum](#)¹, Christopher E. Shuck², Kaitlyn Prenger¹, Ahmad Majed¹, Yury Gogotsi² and Michael Naguib¹; ¹Tulane University, United States; ²Drexel University, United States

Being a single member of carbonitride family, Ti₃CNT_x exhibited unique properties and behavior compared to its carbide counterpart in applications including energy storage, electromagnetic shielding, optics, sensing, etc. It had been the only carbonitride MXene for more than 10 years until we reported on Ti₂C_{0.5}N_{0.5}T_x in 2021 which exhibited the highest specific capacity among all reported multilayer MXene electrodes. Previously, we have also shown that Ti₃CNT_x is an excellent electrocatalyst for hydrogen evolution reaction with an onset potential of 56 mV which is significantly lower than that of Ti₃C₂T_x. All of the reports of carbonitride MXenes support the hypothesis that replacing carbon partially with nitrogen in X sites can increase the number of electrons as well as active sites in MXenes. Hence, we focused on enriching the carbonitride MXene family with new members to gain a further understanding of the synthesis and property of carbonitrides. It is noteworthy to mention that synthesis of carbonitride MXene is challenging due to the lower stability of nitride MXenes compared to carbides and also the lower number of Carbonitride MAX Phases to start with. Herein, for the first time, we report on the synthesis of new four titanium carbonitride MXenes Ti₄C_(3-y)N_yT_x (y = 2.2, 2.4, 2.6, and 2.8) derived from four new 413 MAX phases. By tuning the synthesis conditions using potassium fluoride and hydrochloric acid and changing various etching parameters we realized Ti₄C_(3-y)N_yT_x MXenes from Ti₄AlC_(3-y)N_yT_x (y = 2.2, 2.4, 2.6, and 2.8). MXene thin films were also achieved by delaminating the multilayers. The synthesis of Ti₄C_(3-y)N_yT_x (y = 2.2, 2.4, 2.6, and 2.8) MXenes is unique because this is the first study of carbonitride MXenes' where carbon to nitrogen ratio has been modified systematically in X sites. Finally, we will present our new findings on their performances in electrochemical energy storage.

10:45 AM *NM04.04.08

Molten Salt Assisted Synthesis and Oxidation Kinetics of Water-Dispersible Ti₃C₂T_x and Nb₂CT_x MXene Nanosheets [Micah Green](#), Kailash Arole, Jodie Lutkenhaus and Miladin Radovic; Texas A&M University, United States

Despite numerous prior reports of molten salt etching of MAX phases, there have been few successful reports of water-dispersible MXene nanosheets, and none for Nb-based MXenes. We recently demonstrated that molten salt etching can be used to create water-dispersible Ti₃C₂T_x nanosheets. Here we demonstrate the synthesis and aqueous dispersion of Nb₂CT_x nanosheets via molten salt etching by utilizing a KOH wash to add hydroxyl group to obtain water-dispersible Nb₂CT_x nanosheets. However, little is known about the oxidation of molten salt etched MXenes compared to acid-etched MXenes. Our results indicate slower oxidation kinetics for MXenes etched by molten salts, which may be due to the decreased amount of oxygen-containing terminal groups.

11:15 AM *NM04.04.10

Understanding Chemistry of 2D Transition Metal Carbides and Carbonitrides (MXenes) to Prolong Stability [Vadym Mochalin](#); Missouri University of Science and Technology, United States

A large family of two-dimensional transition metal carbides and nitrides (MXenes) raises interest for many applications due to their high electrical conductivity, mechanical properties [1], potentially tunable electronic structure [2], nonlinear optical properties [3], and the ability to be manufactured in the thin film state [4]. However, their chemistry that is key to development of these applications, still remains poorly understood [5,6]. In this presentation we will discuss recent progress in understanding fundamental MXene chemistry and harnessing it for suppressing unwanted reactions and prolonging stability of these materials.

For example, suppressing oxidation and hydrolysis at high pH was demonstrated as an effective way to prolong shelf-life and stability of MXene aqueous colloids [7].

Other selected examples illustrating connections between understanding MXene chemistry and development of their applications will also be considered.

References

1. Y. Li, S. Huang, C. Wei, C. Wu, V. N. Mochalin, *Nature Communications*, 10, 3014 (2019)
2. M. Naguib, V. N. Mochalin, M. W. Barsoum, Y. Gogotsi, *Advanced Materials*, 26(7), 992-1005 (2014)
3. J. Yi, L. Du, J. Li, L. Yang, L. Hu, S. Huang, Y. Dong, L. Miao, S. Wen, V. N. Mochalin, et al., *2D Materials*, 6, 045038 (2019)
4. Y. Dong, S. Chertopalov, K. Maleski, B. Anasori, L. Hu, S. Bhattacharya, A. M. Rao, Y. Gogotsi, V. N. Mochalin, R. Podila, *Advanced Materials*, 30(10), 1705714 (2018)
5. S. Huang, V. N. Mochalin, *Inorganic Chemistry*, 58(3), 1958 (2019)
6. S. Huang, V. N. Mochalin, *ACS Nano* 14(8), 10251-10257 (2020)
7. S. Huang, V. N. Mochalin, Combination of High pH and Antioxidant Improves Chemical Stability of Two-Dimensional Transition Metal Carbides and Carbonitrides (MXenes) in Aqueous Colloidal Solutions, *Inorganic Chemistry*, (2022 in press)

SESSION NM04.05: MXenes Synthesis, Mechanical Properties and Tribology

Session Chairs: Babak Anasori and Majid Beidaghi

Tuesday Afternoon, November 29, 2022

Hynes, Level 2, Room 201

1:45 PM NM04.05.02

MXenes as Possible Solid Lubricants—Effects of Termination, Vacancies and Intercalated Water on the Resistance to Sliding and Oxidation of

Titanium-Based MXenes [Edoardo Marquis](#), Michele Cutini, Francesca Benini and Maria Clelia Righi; University of Bologna, Italy

Understanding the interlayer interaction in two-dimensional (2D) transition metal carbides and nitrides (MXenes) is important to improve their exfoliation/delamination process and application in (nano)-tribology. The layer-substrate interaction is also essential in (nano)-tribology as effective solid lubricants should be resistant against peeling-off during rubbing. In our study, Ti-based MXenes with both homogeneous and mixed terminations are modeled using density functional theory (DFT). An *ad-hoc* modified dispersion correction scheme is used, capable of reproducing the results obtained from a higher level of theory. The nature of the interlayer interactions, comprising van der Waals, dipole-dipole, and hydrogen bonding, is discussed along with the effects of MXene sheet's thickness and C/N ratio. Our results demonstrate that terminations play a major role in regulating MXenes' interlayer and substrate adhesion to iron and iron oxide and, therefore, lubrication, which is also affected by an external load. Using graphene and MoS₂ as established references, we verify that MXenes' tribological performance as solid lubricants can be significantly improved by avoiding -OH and -F terminations, which can be done by controlling terminations via post-synthesis processing. Our study on the interaction of Ti-based MXenes with water molecules confirms their extremely high hydrophilicity. The presence of -OH groups and vacancies on the surface inevitably strengthens their interaction with water. The dissociative chemisorption of water is found to be a favorable process when it occurs on both MXene' edges and surface' vacancies cluster, leading to material degradation. Our results try to explain the mechanisms of the spontaneous oxidative degradation of MXenes under aqueous environment. These results are part of the "Advancing Solid Interface and Lubricants by First Principles Material Design (SLIDE)" project that has received funding from the European Research Council (ERC) under the European Union's Horizon 2020 research and innovation program (Grant agreement No. 865633).

2:00 PM *NM04.05.03

Role of Heterogeneities on the Mechanical Strength and Deformation of 2D MXene Flakes—Insights from Atomistic Models and Simulations [Gabriel Plummer](#)¹ and Garritt J. Tucker²; ¹NASA Ames Research Center, United States; ²Colorado School of Mines, United States

The mechanical properties of MXenes are of crucial importance in a number of applications currently being studied, including electrochemical energy storage, flexible electronics, and structural composites. However, the difficulty of performing mechanical characterization experiments on 2D materials has limited the study of these important properties. Ab initio computational techniques have helped to fill in some knowledge gaps, but the length scale limitations of these methods preclude the study of more realistic MXenes containing heterogeneities such as point defects and surface terminations. Atomistic simulations, operating at larger length-scales, provide a solution, enabled by the recent development of a highly scalable bond-order interatomic potential for the titanium carbide MXenes. Large-scale simulations utilizing this potential can be used to study both in-plane and out-of-plane elastic properties as well as fracture behavior, crucially eliminating any system size effects. Results indicate a typical tradeoff between in-plane strength and out-of-plane flexibility depending on MXene structure and composition. The inclusion of surface vacancies has a deleterious effect on MXene mechanical properties, which may be unavoidable due to the harsh nature of MXene synthesis. However, via appropriate surface termination engineering, these effects can be mitigated and, in some cases, even overcome entirely. These newly gained insights at the atomic-scale should help inform synthesis and post-processing techniques seeking to produce mechanically superior MXenes.

2:30 PM BREAK

3:00 PM NM04.05.04

Ti₃C₂T_x MXene—Silicon Carbide for High Temperature Applications [Nithin Chandran B S](#)^{1,2}, Kartik Nemani^{1,3}, Yooran Im³, Ravi Kumar² and Babak Anasori^{1,3}; ¹Purdue School of Engineering and Technology, Indiana University-Purdue University Indianapolis, United States; ²Indian Institute of Technology Madras, India; ³Indiana University-Purdue University Indianapolis, United States

2D transition metal carbides (MXenes) are promising as additives in ceramic systems due to their high temperature phase stability of their resulting carbides and in-plane stiffness. High temperature annealing studies on Ti₃C₂T_x MXene have shown phase transformation to lamellar, non-stoichiometric cubic TiC_x. Silicon carbide (SiC) is known for the high hardness, high wear resistance and stability for a wide range of temperatures. However, the low fracture toughness limits monolithic SiC applications. A ceramic structure with layers of TiC can potentially improve the fracture toughness of SiC. In the present work, we investigated the tailorable preparation of green bodies of nanometer thin Ti₃C₂T_x MXenes with SiC powders via electrostatic self-assembly, in a surfactant-free, scalable aqueous media. Because of negative surface charges (zeta potential of -35 to -50 mV) of MXene flakes, they can be mixed with SiC in pH ~ 5 and lead to a uniform self-assembly of Ti₃C₂T_x and SiC, thereby eliminating the need for additional surfactants. Prepared green bodies are sintered by pressure-assisted pulsed current sintering. Addition of 2D MXene fillers into SiC system improves the densification and lowers the sintering time and temperature. The effect of temperature, dwell time and pressure on the densification of the green bodies are studied, which can provide insights on the role of MXenes in improving SiC mechanical properties and their stability.

3:15 PM NM04.05.05

US Army DEVCOM Soldier Center Technology Needs—Applied Research Opportunities for MXenes [Joshua R. Uzarski](#); US Army DEVCOM Soldier Center, United States

The US Army DEVCOM Soldier Center is the Army's Warfighter-centric research facility. To continuously improve protection and effectiveness of our Soldiers, new technologies, particularly in advanced materials are needed. The MXene research community has continued to demonstrate the vast potential and feasibility of MXenes in accelerating the performance of many relevant technologies. Of particular interest to the Department of Defense community, and specifically at Soldier Center, are water filtration and remediation, portable power and energy generation and storage, sensors, environmental protection, and signature management. This presentation will focus on providing an overview of these critical needs areas, highlighting prior and on-going MXene research with direct relevance to the Soldier Center mission.

3:30 PM MXENES PLATINUM SPONSOR SPECIAL TALK BY YASUNORI HIOKI

3:35 PM POSTER SPOTLIGHT PRESENTATIONS

SESSION NM04.06: Poster Session II: MXenes Electrochemistry, Electronic and Optical Properties, Sensing and Bio Applications

Session Chairs: Babak Anasori, Yohan Dall'Agnese, Agnieszka Jastrzebska and Pooi See Lee

Tuesday Afternoon, November 29, 2022

8:00 PM - 10:00 PM

Hynes, Level 1, Hall A

NM04.06.01

Ordered Double Transition Metal MAX Phases and Their Etching into MXenes—Synthesis and Electrochemical Studies [Yaqoob Khan](#) and Husnu E. Unalan; Middle East Technical University, Turkey

Ordered Double Transition Metal MXenes (DTMs) and their MAX phases are a more recent addition to the rapidly growing MXene family of 2D materials. The few reports published on the electrochemical charge storage properties of DTMs suggests that they perform much better than their mono metal counterparts. This is true for both ordered and solid solution DTMs. Despite the theoretical predictions on the stability of a number of double transition metal MAX phases, only a few have been synthesized and etched into their corresponding MXenes. In attempt to scale up the synthesis and processing of DTMs, we present the synthesis and structural studies of ordered $\text{Mo}_2\text{TiAlC}_2$, $\text{Cr}_2\text{TiAlC}_2$, $\text{Cr}_2\text{Ti}_2\text{AlC}_3$ and solid solution $\text{Ti}_2\text{NbAlC}_2$ MAX phases and their etching into corresponding MXenes. In-situ high temperature XRD data collected on the admix of activated metal powders was used to optimize and model the MAX phase synthesis in high temperature tube furnace. Electrochemical studies such as CV, EIS and CCD of the DTMs compared with $\text{Ti}_3\text{C}_2\text{Tx}$ will be presented and discussed.

Note: This abstract was submitted initially to the MRS-spring meeting but couldn't be presented due to late issuance of US visa to the author.

David Pinto et al., "Synthesis and Electrochemical Properties of 2D Molybdenum Vanadium Carbides – Solid Solution MXenes," *J. Mater. Chem. A* 8, no. 18 (2020): 8957–68, <https://doi.org/10.1039/D0TA01798A>.

Likui Wang et al., "Adjustable Electrochemical Properties of Solid-Solution MXenes," *Nano Energy* 88 (2021): 106308, <https://doi.org/https://doi.org/10.1016/j.nanoen.2021.106308>.

Babak Anasori et al., "Two-Dimensional, Ordered, Double Transition Metals Carbides (MXenes)," *ACS Nano* 9, no. 10 (October 27, 2015): 9507–16, <https://doi.org/10.1021/acsnano.5b03591>.

NM04.06.02

MXene Scrolls—A Vanadium Carbide (V_2C) Papyrus-Like Structure for Energy Applications [Yiannis Georgantas](#), Francis Moissinac, Mark A. Bissett and Sarah J. Haigh; University of Manchester, United Kingdom

V_2C MXene theoretically has one of the highest energy capacitance properties compared to other MXenes and as a result there is big interest toward this area. Herein, we report one of the purest V_2C results without any impurities (V_2AlC , AlF_3 , etc.) through "in-situ" HF synthesis at $<60^\circ\text{C}$ (No need for autoclave) with high delamination rate and low oxidation level due to the self-assembling nanoscrolls of single and/or few flakes of V_2C during the post-synthesis procedure of the intercalation/delamination step with an organic solvent (e.g. quaternary ammonium salt: TMAOH, TPAOH, TBAOH). The morphology and structure of the V_2CT_x MXene was characterized by X-ray diffraction, scanning/transmission electron microscopy, Raman spectroscopy, X-ray photoelectron spectroscopy and BET Surface Area Analysis. Furthermore, the papyrus-like V_2C structure capacitance properties are investigated by cyclic voltammetry, galvanostatic charge–discharge and electrical impedance spectroscopy.

NM04.06.03

Evaluation of Oxidation Processes in $\text{Ti}_3\text{C}_2\text{T}_x$ MXene Using *In Situ* Electrochemical Raman Spectroscopy [Kateryna Shevchuk](#), John Wang and Yury Gogotsi; A.J. Drexel Nanomaterials Institute, United States

MXenes, a large family of two-dimensional materials, have attracted a lot of interest due to their large chemistry space and the diverse chemical, electrical, mechanical, and optical properties. In particular, MXenes' metallic conductivities and redox-active surfaces make them attractive for electrochemical energy storage. Recently, we demonstrated that partial oxidation of $\text{Ti}_3\text{C}_2\text{T}_x$ MXene led to enhanced pseudocapacitance in water-in-salt electrolyte by cycling the material at 1.2 V vs. Ag wire. However, there is a fine line between partial oxidation of $\text{Ti}_3\text{C}_2\text{T}_x$ MXene and complete oxidation that leads to the formation of titania and carbon. The extent of oxidation is difficult to measure with conventional X-ray and electron-based techniques. Raman spectroscopy has proven to be a powerful technique for detecting the degradation of $\text{Ti}_3\text{C}_2\text{T}_x$ MXenes. This work focuses on using *in situ* electrochemical Raman spectroscopy to analyze the oxidation processes in $\text{Ti}_3\text{C}_2\text{T}_x$ MXenes at a high anodic potential. The findings allow us to expand the knowledge of MXene electrochemistry and its degradation processes to achieve higher energy density in MXene-based energy storage devices.

NM04.06.04

Tuning the Nitrogen Reduction Reaction Activity of the Ti_2N Nitride MXene Through Modifying pH and Electrolyte Choice Denis Johnson and [Abdoulaye Djire](#); Texas A&M University, United States

Electrochemical nitrogen reduction reaction (NRR) is used to convert atmospheric nitrogen (N_2) to ammonia (NH_3) at ambient conditions. In general, acidic electrolytes are used for NRR to provide protons (H^+) for the electrocatalytic reduction process. However, this leads to a low NH_3 selectivity due to the formation of the H_2 by-product via the hydrogen evolution reaction (HER). Recently, we showed that a Ti_2N MXene is active and selective for NRR in acidic electrolyte. We demonstrated that this new catalyst works through a Mars-van Krevelen (MvK) mechanism instead of the conventional associative/dissociative mechanisms. However, the effect of pH and electrolyte on the catalytic activity and selectivity was not well understood. Here, we investigate these effects by performing experiments in varying electrolytic conditions and pH values and develop relations between pH, electrolyte choice, and performance. The Ti_2N nitride MXene was synthesized via an oxygen-assisted molten salt fluoride etching technique and characterized through XRD, SEM, and FTIR spectroscopy. Our findings showed that changing pH does not affect the onset potentials for NRR, but does affect yield and selectivity. Alongside this, it was also found that pH changes the charge storage and HER performance of the material. It was found that as pH increases, selectivity towards NH_3 production increases due to the lower concentration of H^+ able to participate in the HER. Favorable NRR selectivity values were obtained in non-aqueous protic electrolytes, such as 2-picoline/trifluoro-acetic acid because of the suppression of HER. These findings are being expanded to other MXene materials to advance our knowledge of the reactivity of MXenes in NRR, and to design optimal electrolytic conditions for the production of NH_3 through NRR.

NM04.06.06

***In Situ* Conversion of V_2CT_x MXene in CS_2 Ambient to Boost Sodium-Ion Battery Anodes Performance** Gang Huang, [Zahra Bayhan](#) and Husam N. Alshareef; King Abdullah University of Science and Technology, Saudi Arabia

Transition metal carbides and nitrides (MXenes) materials have distinctive properties that make them suitable for storing various mobile metal ions. For instance, MXenes have layered structures with large interlayer spacing, high electrical conductivity, and chemical diversity. However, MXenes lose

electrical conductivity and redox activity due to restacking of the layers. Additionally, the uncontrolled attachment of surface functional groups like O, OH, and F influence their pristine electrochemical characteristics.

It is possible to take advantage of the properties of MXene by deriving hybrid materials from MXene. We developed a facile but efficient method to convert $V_2C_2T_x$ MXene into $V_2S_3@C@V_2S_3$ heterostructures within 1 minute. Our results indicated that hybrid materials synergistically improve the performance of NIBs by combining the advantages of individual 2D materials.

The synergistic effect is shown in this unique design by alleviating conductivity, structural degradation, and sluggish kinetics of V_2S_3 . Whereas the carbon interlayer in the anode behaves like flexible conductive support and an anchoring network. Moreover, the ultrathin V_2S_3 nanosheets and the V_2S_3 -C heterointerfaces enhance the Na^+ adsorption and migration abilities. As a result, this $V_2S_3@C@V_2S_3$ anode achieves a highly reversible capacity (628 mAh/g at 0.1 A/g) and excellent rate performance (477 mAh/g at 10A/g), and impressive cycling stability (2000 cycles at 20 A/g, record-high value). Considering the rich compositional diversity of MXene, the in-situ conversion strategy developed here can be extended to construct a wide range of high-performance electrode materials for advanced batteries.

NM04.06.07

Molecular Dipole Assisted Tuning of Work Function in $Ti_3C_2T_x/n$ -Si and $Ti_3C_2T_x/p$ - Sb_2Se_3 Heterojunctions Kunal J. Tiwari^{1,2}, Elói R. Costals², Francesc Xavier², Axel Medaille^{1,2}, Sergio Giraldo², Marcel Placidi², Cristóbal Voz², Joaquim Puigdollers², Edgardo Saucedo² and Zacharie Jehl Li Kao²; ¹Catalonia Institute of Energy Research, Spain; ²Universitat Politècnica de Catalunya, Av. Eduard Maristany, 16, 08019 Barcelona, Spain., Spain

MXene-class materials have emerged as promising candidates in areas currently dominated by graphene, transition metal dichalcogenide (TMD) and related 2D materials, and hold several assets for applications to energy related fields including storage and conversion. Since the first report of $Ti_3C_2T_x$ synthesis in 2011 [1], this ever growing family of materials has garnered significant attention from the research community owing to their remarkably tunable physicochemical properties and ease for large area synthesis using low-cost methods. $Ti_3C_2T_x$ MXene has been utilized as a functional layer/additive in various opto-electronic devices such as solar cells, photodetectors etc. [2]. $Ti_3C_2T_x$ has particularly shown remarkably promising results when used as charge selective contacts in conventional c-Si and Perovskite solar cells [3]. The high conductivity, fully tunable work function, and thickness dependent transparency coupled with a high chemical stability make $Ti_3C_2T_x$ an ideal material to partner with Si and possibly other emerging chalcogenide thin film absorbers as a replacement of the standard p-n junction.

In the present work, we aim at investigating the interplay of a model MXene/c-Si interface with different organic molecular dipole interlayers in terms of carrier transport, carrier selectivity, and chemical compatibility. Initially, a screening of different organic dipoles is performed to identify the most suitable candidates out of PEDOT, PEI, PAMAM, APTES. Multilayer MXene is synthesized from the bulk Ti_3AlC_2 MAX phase through Minimum Intensive Layer Delamination (MILD) technique and 2D sheets are subsequently deposited by drop casting and spray coating on the n-Si/dipole stack. Optimization routes are investigated to tune the band alignment at the MXene/n-Si interface by using the self-assembled mono layers of different organic dipoles. An in-depth characterization of the as prepared MXene sheets by means of XPS, Raman Spectroscopy, AFM and other methods is presented to assess the chemical and structural properties of the heterojunctions, along with the complete electrical characterization of the MXene/n-Si Schottky diodes where the fundamental properties of the interface formed between the 2D charge selective contact and the 3D semiconductor are investigated. Additionally, optoelectronic properties of first proof of concept devices, both solar cells as well as photodetectors, are reported and the complete set of results is presented in regard to the state of the art. Finally, the use of MXene in combination with emerging Sb_2Se_3 photovoltaic absorbers is investigated using the c-Si as reference framework.

References:

- [1] Naguib, Michael, et al. "Two Dimensional Nanocrystals: Two Dimensional Nanocrystals Produced by Exfoliation of Ti_3AlC_2 (Adv. Mater. 37/2011)." *Advanced Materials* 23.37 (2011): 4207-4207.
- [2] Wang, Yizhou, et al. "MXenes for energy harvesting." *Advanced Materials* (2022): 2108560.
- [3] Aydin, Erkan, et al. "Scaled Deposition of $Ti_3C_2T_x$ MXene on Complex Surfaces: Application Assessment as Rear Electrodes for Silicon Heterojunction Solar Cells." *ACS nano* 16.2 (2022): 2419-2428.

NM04.06.08

Industrial-Scale MXene-Contacted Silicon Heterojunction Solar Cells with >20% Power Conversion Efficiency Jehad K. El-Demellawi, Erkan Aydin, Stefaan De Wolf and Husam N. Alshareef; King Abdullah University of Science and Technology, Saudi Arabia

Two-dimensional (2D) transition metal carbides (MXenes) are of great interest as electrode materials for a variety of applications, including photovoltaics (PV), thanks to their tunable optoelectronic properties, high metallic conductivity, and attractive solution-processability. However, thus far, MXene electrodes have only been exploited for small-scale solar cells with modest power conversion efficiencies (PCEs). Hence, herein, to unveil the potential of MXene electrodes at the industrial level, we implemented a scalable spray coating technique to deposit highly conductive (ca. 8000 S/cm) $Ti_3C_2T_x$ MXene films via an automated spray system. We successfully employed these $Ti_3C_2T_x$ films as rear electrodes for silicon heterojunction (SHJ) solar cells. The conformal alignment of the MXene flakes on the random pyramidal textured silicon wafers has provided an intimate contact with the underneath ITO, leading to >20% PCE over both small (4.2 cm²) and large (243 cm², i.e., using industry-sized 6-inch pseudo-square wafers) cell areas. Notably, the $Ti_3C_2T_x$ -rear contacted devices have almost retained 99% of their initial PCE after 600+ days of ambient air storage. Their performance is comparable with state-of-the-art solar cells contacted with sputtered silver electrodes, offering a potential cost reduction for SHJ solar cells. Besides, such high-throughput fabrication of large-scale MXene-based devices brings this technology closer to industrial maturity.

NM04.06.09

A Moisture-Stable MXene-Based OLED for Free-Form Displays with Long-Term Stability So Yeong Jeong¹, Yonghee Lee², Yongmin Jeon³ and Kyung C. Choi¹; ¹Korea Advanced Institute of Science and Technology (KAIST), Korea (the Republic of); ²National Nano Fab Center (NNFC), Korea (the Republic of); ³Gachon University, Korea (the Republic of)

In current research on free-form displays to provide hyper-interconnection between users via e-textiles or e-skins, 2D Titanium Carbide MXene is emerging as an attractive material, specifically as an alternative electrode in flexible devices to brittle ITO and other transparent conducting polymers. MXenes provide high transparency, metallic conductivity, tunable work function, and solution-processability.^[1-4] The use of MXene electrodes in OLED devices is expected to drive an exceptional technical advance in the display research field. OLED devices have demonstrated excellent compatibility with free-form displays, by virtue of their high flexibility, low power consumption and heat, light weight and nanometer-scale thickness. The synergetic effect of the MXene material and OLED devices offers a new paradigm in free-form displays. However, the low moisture-stability of the MXene OLED remains a major challenge. The MXene electrode and organic constituent layers are easily oxidized under water or high humidity conditions. Therefore, a reasonable passivation system which can protect them from the moisture molecules is required. If it can be realized, the advanced development of matrix-form transparent MXene OLEDs which are capable of displaying complex information will follow.

In this work, we developed a highly moisture-stable MXene OLED by exploiting an encapsulation system that combines a water-resistant TiO_2 based nanolaminate layer/ SiO_2 -siloxane polymer/attachable PET. Despite the near-room temperature process (40°C), the TiO_2 based nanolaminate layer showed outstanding impermeability (WVTR on the order of 10^{-5} g m⁻²day⁻¹) even with nanoscale thickness (30 nm) due to its low residual stress.^[5] The SiO_2 -

siloxane polymer contained compressive stress that could be used to offset the tensile residual stress of the TiO₂-based nanolaminate layer, reducing the total residual stress of the barrier to zero.^[5,6] And then, to achieve not only physical scratch resistance but also water endurance, ultra-thin PET (30m) was attached to the top of the device. Using the encapsulation system, a highly stable MXene OLED was fabricated which exhibited a long life-time in ambient conditions (> 2,000 hours). In addition, the MXene OLED displayed a stable J-V-L (current density-voltage-luminance) curve after repetitive high curvature (1,000 times / 1.5 mm) folding deformation, and maintained 70% of its initial luminance after water immersion for 6 hours. In conclusion, the proposed development is expected to be applicable to deformable see-through displays in smart windows, automotive displays and augmented reality systems and provide a technical model that can advance MXene applications.

- [1] M. Alhabeab, K. Maleski, B. Anasori, P. Lelyukh, L. Clark, S. Sin, Y. Gogotsi, *Chem. Mater.* **2017**, *29*, 7633.
[2] S. Ahn, T. H. Han, K. Maleski, J. Song, Y. H. Kim, M. H. Park, H. Zhou, S. Yoo, Y. Gogotsi, T. W. Lee, *Adv. Mater.* **2020**, *32*, 1.
[3] S. Lee, E. H. Kim, S. Yu, H. Kim, C. Park, T. H. Park, H. Han, S. W. Lee, S. Baek, W. Jin, C. M. Koo, C. Park, *Adv. Funct. Mater.* **2020**, *30*, 1.
[4] S. Lee, E. H. Kim, S. Yu, H. Kim, C. Park, S. W. Lee, H. Han, W. Jin, K. Lee, C. E. Lee, J. Jang, C. M. Koo, C. Park, *ACS Nano* **2021**, *15*, 8940.
[5] S. Y. Jeong, H. R. Shim, Y. Na, K. S. Kang, Y. Jeon, S. Choi, E. G. Jeong, Y. C. Park, H. E. Cho, J. Lee, J. H. Kwon, S. G. Im, K. C. Choi, *npj Flex. Electron.* **2021**, *5*, 1.
[6] A. Behrendt, J. Meyer, P. Van De Weijer, T. Gahlmann, R. Heiderhoff, T. Riedl, *ACS Appl. Mater. Interfaces* **2016**, *8*, 4056.

NM04.06.10

Probing Changes in the Electronic Structure of Ti₃C₂ MXene Sheets with Electron Energy-Loss Spectroscopy [Asra Hassan](#)^{1,2}, Josh Kennedy¹, Hilmar Koerner¹, Jinwoo Hwang² and David McComb²; ¹Air Force Research Laboratory, United States; ²Ohio State University, United States

Layered metal carbides and nitrides (MXenes) are a rapidly expanding family of 2D material that have attracted substantial research interest due to their unique properties of hydrophilicity, good metallic conductivity, and structural diversity. Surface terminations are a natural consequence of the MXene synthesis, traditionally consisting of O, OH, and F. The location of these surface-terminating functional groups and/or their chemical nature play a crucial role on the overall MXene properties and affects their performance in different applications. Therefore, to better understand how MXenes properties are governed by their surface terminations, and to develop design strategies that are independent of surface composition, a detailed atomic resolution understanding of electronic structure of MXene is needed. In this contribution, we present fundamental studies aimed at understanding the role of surface functional groups on modifying the electronic structure and related optical properties of single and multilayer Ti₃C₂T₂ (T refers to surface termination group) MXene sheets using aberration-corrected STEM-EEL. This work furthers our understanding of MXene chemistry-property relationships and opens the door to termination-engineered MXenes.

NM04.06.11

Probing Photoexcited Free Carrier Dynamics of Two-Dimensional MXene, Nb₂C, Using Ultrafast Terahertz Spectroscopy [Andrew M. Fitzgerald](#)¹, Laura Londono², Javery Mann¹, Kiana Montazeri³, Michel W. Barsoum³ and Lyubov Titova¹; ¹Worcester Polytechnic Institute, United States; ²Rhode Island College, United States; ³Drexel University, United States

Discovered in 2013, 2D niobium carbide (Nb₂C) MXene has been shown to have many extraordinary properties, such as high photothermal conversion efficiency, strong electron-phonon interactions, strong optical absorption in the near-infrared, and even saturable optical absorption. These unique properties of Nb₂C render this MXene potentially useful for a variety of applications, including photonic and optoelectronic devices and even photothermal cancer therapy. Here, we employ both terahertz time-domain spectroscopy (TDS) and time-resolved terahertz spectroscopy (TRTS) to investigate intrinsic and photoinduced conductivity and dynamics of optically injected carriers with 1.55 eV and 3.1 eV excitations in order to understand the photoinduced processes taking place in Nb₂C. We find that the photoinduced conductivity in this MXene shows an initial rapid decay over a picosecond time scale, followed by a much longer-lived component that lasts for nanoseconds. We also observe that the long-range conductivity is strongly limited by the nanoflake boundaries. We explore the impact of post-synthesis treatments on the carrier lifetime and mobility with the goal of optimizing its optical response for applications in photocatalytic and optoelectronic devices. A. M. Fitzgerald acknowledges support by NSF NRT CEDAR Fellowship, Award Number 2021871.

NM04.06.12

Dynamics of Photoexcitation in Ti₃C₂T_z, Mo₂Ti₂C₃T_z, and Nb₂CT_z 2D MXenes [Erika Colin-Ulloa](#)¹, Kiana Montazeri², Michel W. Barsoum² and Lyubov Titova¹; ¹Worcester Polytechnic Institute, United States; ²Drexel University, United States

MXenes are two-dimensional (2D) transition metal carbides, nitrides and carbonitrides with a general formula M_{n+1}X_nT_z, where M is a metal, X = C or N, and n = 1–3; T_z denotes surface terminations such as –OH, –O, and/or –F. Unlike most other 2D materials, MXenes are intrinsically metallic. They have a high density of states at the Fermi due to a large contribution from transition metal d-orbitals. Many of them also exhibit strong surface plasmon modes in the visible to infrared range. High conductivity, pronounced plasmonic properties and optical nonlinearities, high damage thresholds for exposure to high-intensity laser light suggest MXenes as a promising platform for optoelectronic devices and underscore the need to understand dynamics of photoexcitations in these materials.

We investigate the photoexcited carrier dynamics in three different MXenes, in Ti₃C₂T_z, Mo₂Ti₂C₃T_z, and Nb₂CT_z, using ultrafast transient optical absorption, which provides access to excited state dynamics and changes in the optical absorption the visible range. We find that absorption at the proposed plasmon peak is suppressed by the photoexcitation, with an absorption bleach recovery time increasing with increasing intrinsic free carrier density: recovery time is the fastest in Nb₂CT_z, and it is slower in Mo₂Ti₂C₃T_z and in Ti₃C₂T_z.

Uncovering the exact mechanisms behind the observed rich palette of MXene optoelectronic properties and their relationship to MXene chemistry, structure, and morphology, will lay foundations for MXene-based and visible photonic devices.

NM04.06.15

EMI Shielding Mechanisms of Pristine MXene Films [Roman Rakhmanov](#), Gennady Friedman and Yury Gogotsi; Drexel University, United States

The rapid development of Internet of Things (IOT) and new generations of telecommunication networks bring forward a demand for thin, lightweight shielding materials and microwave circuit components. MXenes, two-dimensional (2D) transition metal carbides, nitrides, and carbonitrides, are a large family of 2D materials that are promising for use in EMI shielding, antennas, transmission lines, etc., owing to their high electrical conductivity. However, the underlying mechanisms are currently unknown. This work focuses on experimental and theoretical methods for extracting electromagnetic properties of MXene films in the microwave region. This, coupled with the variety of chemistries and structures available to MXenes gives rise to unprecedented tunability of their properties, creates the possibility to adjust MXenes for specific applications and provides a roadmap to their stable performance.

NM04.06.16

Development of TeNWs/MXene (Ti₃C₂T_x) Nanohybrid-Based Flexible Piezoresistive Pressure Sensor for Wireless Safety Communication Using

Morse Code Vivek Adepu, Manav Tathacharya, Raghuram CS and Parikshit Sahatiya; BITS-Pilani, Hyderabad Campus, India

Due to the growing need for personal safety applications for emergency communication purposes, two-dimensional (2D) and one-dimensional (1D) nanomaterials-based physical sensors have been actively examined for communication applications owing to their captivating properties such as tunable semiconducting properties, high electrical conductivity/mobility, etc.[1] The combination of Tellurium (Te) nanowires (NWs) and MXene (2D/1D nanohybrid) has not been explored as the active material in fabricating flexible, piezoresistive sensors which provide exciting electromechanical properties.[2], [3] In this perspective, 2D $\text{Ti}_3\text{C}_2\text{T}_x$ film was deposited on cellulose paper substrate followed by 1D Te NWs using the vacuum filtration method to fabricate the piezoresistive pressure sensor. The fabricated sensor was later encapsulated in polydimethylsiloxane (PDMS) and utilized as a wireless communication system button. The fabricated sensor displayed an admirable sensitivity of 6.032 kPa^{-1} (applied pressure $\sim 1.477 - 3.185 \text{ kPa}$) and outstanding stability of ~ 2500 cycles. The underlying transduction mechanism of the TeNWs/ $\text{Ti}_3\text{C}_2\text{T}_x$ nanohybrid pressure sensor for enhancement in sensor current at the metal-semiconductor junction was explained by the increment of tunneling current upon applying external pressure owing to the decrement in an interlayer resistance of the 2D $\text{Ti}_3\text{C}_2\text{T}_x$ and tunneling distance between 1D Te NWs. Furthermore, an android application was developed to wirelessly receive data *via* Bluetooth from the fabricated piezoresistive sensors connected to a microcontroller. In addition, the application displayed the pattern based on the pressure load acting on the sensors as a Morse dash or dot. Also, it can be used similarly to a telegraph to send complex messages such as "HELP." The effective demonstration of a TeNWs/MXene nanohybrid-based flexible, low-cost and biodegradable physical sensor opens new avenues in wireless monitoring and communication applications.

References:

- [1] S.-T. Han *et al.*, "An Overview of the Development of Flexible Sensors," *Adv. Mater.*, vol. 29, no. 33, p. 1700375, 2017.
- [2] X. Li, C. Wang, Y. Cao, and G. Wang, "Functional MXene Materials: Progress of Their Applications," *Chem. – An Asian J.*, vol. 13, no. 19, pp. 2742–2757, 2018.
- [3] F. Liang and H. Qian, "Synthesis of tellurium nanowires and their transport property," *Mater. Chem. Phys.*, vol. 113, no. 2, pp. 523–526, 2009.

NM04.06.17

Evaluating Cellular Stress and Phototoxicity of Photothermal Stimulation on Neurons Yingqiao Wang¹, Jane E. Hartung², Adam Goad³, Michael S. Gold², Yury Gogotsi³ and Tzahi Cohen-Karni¹; ¹Carnegie Mellon University, United States; ²University of Pittsburgh, United States; ³Drexel University, United States

Photothermal modulation is a remote and non-genetic technique to control neural activities with high spatiotemporal resolution and cell-type specificity. During the modulation, the interface between photothermally active nanomaterial and neuron is illuminated with light pulses, leading to transient local temperature rise which will elicit an action potential. Recently, we demonstrated that two-dimensional nanoflake, $\text{Ti}_3\text{C}_2\text{T}_x$ (MXene), is an outstanding candidate for photothermal modulation of neural activity with low needed incident energy per pulse. However, the safety of $\text{Ti}_3\text{C}_2\text{T}_x$ flakes for neural modulation is unknown. Namely, cytotoxicity of $\text{Ti}_3\text{C}_2\text{T}_x$ flakes, phototoxicity, and hyperthermia damage. Here, we investigated the biosafety of $\text{Ti}_3\text{C}_2\text{T}_x$ flakes across multiple assays, including viability, cellular stress (mitochondria membrane potential), and oxidative stress to determine the safety threshold of photothermal modulation. We demonstrated that culturing neurons on a ca. 100 nm $\text{Ti}_3\text{C}_2\text{T}_x$ film and illuminating it with laser pulses (635 nm) with incident energy from 2 - 14 μJ per pulse and different pulse frequencies (1 pulse, 1 Hz, and 10 Hz pulses) neither reduced the cell viability nor generated cellular stress. The upper limit of this safety range is higher than the needed incident energy for neural excitation ($< 10 \mu\text{J}$). However, applying laser pulses with high incident energy (e.g., 22 μJ per pulse) will result in irreversible damage. We further investigated the generation of reactive oxygen species (ROS) and revealed that culturing neurons on $\text{Ti}_3\text{C}_2\text{T}_x$ film will not induce ROS generation. The safety evaluation with multiple assays will guide the design of the operation parameters and protocols of photothermal modulation both *in vitro* and *in vivo*.

NM04.06.18

Solution-Processed 2D MXene/Silver Nanowire Transparent Conducting Electrode for Light-Emitting Diodes Bongjun Choi¹, Byoung Wan Lee¹, Sang Hyuk Im² and Youngseok Kim¹; ¹Korea Electronics Technology Institute, Korea (the Republic of); ²Korea University, Korea (the Republic of)

2D titanium carbide (Ti_3C_2) MXene is a suitable candidate as a transparent conducting electrode (TCE) for optoelectronic devices due to its high conductivity, high work function ($\sim 5.1 \text{ eV}$), and decent optical transparency. Although MXene TCE with high conductivity is a promising electrode for optoelectronic devices, their eligibility as a TCE for displays is still challenging due to their high sheet resistance compared to conventional TCE such as indium tin oxide (ITO). To fabricate the highly conductive MXene TCE, well exfoliated two-dimensional MXene with a large flake size of MXene is essential. Herein, we synthesized 2D MXene through the minimally intensive layer delamination (MILD) method with an additional delamination process with Couette-Taylor reactor which can realize the well delaminated 2D MXene. Ascribed to the ultra exfoliated 2D MXene formation, the MXene TCE film which is achieved by simple solution processing showed high optical transparency and low sheet resistance of 75.8% at 550nm and 132.5ohm/sq. Furthermore, we introduced the 2D MXene/Silver Nanowire (AgNW) hybrid TCE to enhance the conductivity further. The optimized hybrid TCE showed 72.6% optical transparency at 550nm and 18.03ohm/sq sheet resistance respectively which are 6.04 times improved values in terms of the figure of merit (FoM). In order to adapt MXene/AgNW hybrid TCE as a transparent bottom electrode for organic light-emitting diodes (OLEDs), we patterned hybrid TCE by using the photolithography process and lift-off technique. The hybrid TCE-based OLEDs exhibited clear red electroluminescence (EL) peak at 620nm. They showed a maximum external quantum efficiency (EQE), current efficiency (CE), and luminance of 5.25%, 5.25cd/A, and 7563cd/m² respectively. Furthermore, the hybrid TCE was readily formed on a flexible poly(ethylene terephthalate) (PET) substrate by using a solution process. The hybrid TCE gave rise to the enhancement of flexibility of OLEDs. These works demonstrate the potential of 2D MXene/AgNW TCE in flexible optoelectronic devices.

NM04.06.19

L-cys/AuNPs/ Ti_3C_2 -MXene Modified Thread Electrode for Non-Invasive Sweat Cortisol Sensor Thidarut Laochai¹, Jutiporn Yukird², Nadtinan Promphet², Jiaqian Qin², Orawan Chailapakul^{1,3} and Nadnudda Rodthongkum^{2,4}; ¹Chulalongkorn University, Thailand; ²Metallurgy and Materials Science Research Institute, Thailand; ³Electrochemistry and Optical Spectroscopy Center of Excellence (EOSCE), Thailand; ⁴Center of Excellence in Responsive Wearable Materials, Thailand

Non-invasive electrochemical immunosensor is developed by fabricating L-cysteine/gold nanoparticle/titanium carbide (L-cys/AuNPs/ Ti_3C_2 -MXene) onto the thread electrode surface for the detection of sweat cortisol to indicate adrenal gland disorders. Herein, Ti_3C_2 -MXene and AuNPs offer high surface area, high electrochemical conductivity and facilitate antibody immobilization leading to enhanced immunosensor sensitivity. The morphologies of MXene are characterized using transmission electron microscope (TEM) and the surface morphologies of the L-cys/AuNPs/ Ti_3C_2 -MXene modified thread are investigated by scanning electron microscope (SEM) coupled with energy dispersive X-ray spectroscopy (EDX). For the functionalization of antibodies, a direct conjugation between antibody and antigen is performed. Anti-cortisol antibodies are covalently immobilized onto L-cys/AuNPs/ Ti_3C_2 -MXene modified on thread-based electrode using 1-ethyl-3-(3-dimethylaminopropyl) carbodiimide and N-hydroxysulfosuccinimide coupling agents to enhance the sensor specificity. The electrochemical measurements are performed on a potentiostat using cyclic voltammetry (CV) and electrochemical impedance spectroscopy (EIS) for the electrode characterization and amperometry for determination of cortisol from the current change by using a solution of 5 mM

[Fe(CN)₆]^{3-/4-} in 0.5 M KCl. The detection principle is based on the decrease of oxidation current towards the antigen-antibody binding interaction owing to blocking of electron transfer process by cortisol. This system offers two linear ranges from 5 to 40 ng/mL ($R^2 = 0.9880$) and from 40 to 180 ng/mL ($R^2 = 0.9560$) with a limit of detection (LOD) of 0.54 ng/mL with negligible effect from interferences. Furthermore, this immunosensor provides high specificity towards cortisol detection with high reproducibility, and long-term storage stability. Ultimately, this immunosensor is successfully applied for the detection of cortisol in artificial sweat with satisfactory results.

NM04.06.20

Patterned Titanium Carbide (Ti₃C₂T_x) MXene Electrode for Electrochemical Detection of Phosphates [Shiseido Robinson](#), Thiba Nagaraja, Rajavel Krishnamoorthy and Suprem R. Das; Kansas State University, United States

The discovery of two-dimensional transition metal carbides and carbonitrides (*MXene*) has laid the foundation of layered materials for number of potential future applications. The material embodies countless desired properties such as hydrophilic surfaces, high electrical conductivity, large surface to volume ratio and efficient absorption of electromagnetic waves. The unique properties of these 2D layered *MXene* materials have been explored largely in energy storage devices and electromagnetic shielding applications for decades. More recently, the material has attracted enormous interest in the field of chemical and biomolecule sensing owing to its varied chemical structure and ease of functionalization for sensitive and selective detection of different analytes. Phosphorus in the form of phosphates is an essential nutrient for many biological, environmental and agricultural processes that often needs strict monitoring to avoid detrimental effects. However, the complex oxidation states of phosphate in various pH conditions and its interferences with many ions in natural waters and the human body have made it difficult to develop a reliable and accurate method of sensing. Hence, the development of low cost, highly sensitive sensor materials are imperative for the rapid detection of phosphates. In this study, we explored the large-scale exfoliation of the widely studied Ti₃C₂T_x *MXene* materials by adopting minimally intensive layer delamination (MILD) etching route. Controlled chemical exfoliation conditions lead to selective removal of Al layer from Ti₃AlC₂ to form few layer *MXene* that are confirmed from structural and morphological conditions such as XRD, SEM, and AFM. The exfoliated Ti₃C₂T_x was used as an active electrochemical sensing platform for detection of phosphate by exploiting the redox behavior of phosphate complexed with molybdenum. The sensing of phosphates in the presence of interfering ions indicated low detection limit and high sensitivity along with a large linear detection range with reliable performance. Such an application of 2D *MXene* could make it a potential candidate for future environmental monitoring and sensing.

SESSION NM04.07: MXenes Electrochemistry
Session Chairs: Swapnil Ambade and Yohan Dall'Agnese
Wednesday Morning, November 30, 2022
Hynes, Level 2, Room 201

8:30 AM *NM04.07.01

Effects of Synthesis Conditions on the Properties of MXenes Emre Kayali¹, Brian Wyatt², Babak Anasori² and [Majid Beidaghi](#)¹; ¹Auburn University, United States; ²Indiana University–Purdue University Indianapolis, United States

Recent research on the synthesis of *MXene* shows a strong dependence of *MXene* properties on the synthesis conditions. *MXenes* are synthesized by selective etching of A-layer atoms from the structures of MAX phases. So far, several etching processes have been introduced, and recent reports show that the morphology of the synthesized *MXenes*, their size, their surface chemistry, and the amount and the type of various defects in their structures depend on their synthesis conditions. Therefore, synthesis conditions inevitably control the physical and chemical properties of *MXenes*, and understanding these processing-structure-property relationships may lead to innovative new ways to tune the properties of *MXenes* for a variety of applications. This talk will first provide a short review of the effects of synthesis methods and conditions on the structure and morphology of *MXenes*. Then, some of our recent work on tuning various properties of *MXenes* by changing synthesis conditions will be discussed. In particular, the effects of etching parameters on the electrical, electrochemical, and mechanical properties of the various *MXenes* will be presented.

9:00 AM NM04.07.02

High-Performance V₂C MXene/Bilayered V₂O₅ Asymmetric Aqueous Supercapacitors [Mohit Saraf](#), Teng Zhang, Timofey Averianov, Armin VahidMohammadi, Ekaterina Pomerantseva and Yuriy Gogotsi; Drexel University, United States

Two-dimensional transition metal carbides and nitrides (*MXenes*) have shown great potential in electrochemical energy storage applications. Their high electrical conductivity coupled with surface redox reactions make them suitable candidates for high-rate pseudocapacitive energy storage. However, *MXene* supercapacitors often exhibit a limited voltage at higher anodic potentials due to possible oxidation. One of the possible strategies to expand their voltage is by pairing them with suitable candidates such as oxides to design asymmetric supercapacitors. Among them, lithium intercalated bilayered V₂O₅ (Li-V₂O₅) is one of the promising candidates thanks to its high capacity and improved structural stability. In this study, we have explored free-standing films of lithium intercalated V₂C *MXene* (Li-V₂C) as negative electrode with Li-V₂O₅-CNT as positive electrode in aqueous LiCl electrolyte. This results in an electrochemically stable 2 V supercapacitor with high energy density and good cycling stability. The work highlights that *MXenes*, beyond Ti₃C₂, have great possibilities in electrochemical energy storage applications.

9:15 AM NM04.07.03

Understanding the Effects of Transition Metal Intercalation on Electronic and Electrochemical Properties of Ti₃C₂T_x MXene [Shianlin Wee](#)¹, Evgeniya Vorobyeva¹, Netanel Shpigel², Dario Gomez Vazquez¹, Fabio La Mattina³, Akhil Tayal⁴, Erik Mayr^{1,3}, Inge K. Herrmann^{1,3} and Maria Lukatskaya¹; ¹ETH Zurich, Switzerland; ²The Hebrew University of Jerusalem, Israel; ³Empa - Swiss Federal Laboratories for Materials Science and Technology, Switzerland; ⁴Deutsches Elektronen-Synchrotron DESY, Germany

MXenes are two-dimensional (2D) transition metal carbides, nitrides and/or carbonitrides.^[1] It is well-established that *MXenes* can be intercalated by a variety of cations, both chemically and electrochemically.^[2] Predominant attention so far has been devoted to the studies of the intercalation of alkaline and alkaline earth cations such as Li⁺, K⁺, Na⁺, Mg²⁺ or alkylammonium cations into Ti₃C₂T_x *MXenes*.^{[3][4]} Transition metal ions and clusters are known for their attractive electrochemical response.^{[5][6]} However, the effects of intercalation of transition metal ions on electronic and electrochemical properties of *MXenes* have not been explored in detail.

Herein, we studied the effects of intercalated Cu ions on Ti₃C₂T_x and vice versa, with the purpose of providing a comprehensive understanding on how the chemical, physical and electrochemical properties of both pre-intercalated transition metal ion and *MXene* itself were altered. Specifically, in-situ Raman and electrochemical quartz crystal microbalance (EQCM) were used to track the changes of chemical speciation in between the confined environment of

Cu-Ti₃C₂T_x layers during charging/ discharging in aqueous electrolytes. In addition, in-situ X-ray absorption spectroscopy (XAS) was applied to track the oxidation changes of both intercalated Cu ions and Ti atoms of the MXene under different applied potentials, providing insights into the charge transfer between Cu ions and Ti₃C₂T_x. We discovered that the interactions between Ti₃C₂T_x and Cu ions resulted in altered electronic and electrochemical properties compared to the Cu²⁺ ions in solution and pristine Ti₃C₂T_x. Using Cu²⁺ and Ti₃C₂T_x MXene as an example, this work offers mechanistic understanding of the interactions between multi-valent transition metal and MXene layers, providing foundation for the rational design and utilization of transition metal ion intercalants to tune properties of MXenes for their applications in different electrochemical systems and beyond.

[1] B. Anasori, M. R. Lukatskaya, Y. Gogotsi, *Nature Reviews Materials* **2017**, 2, 16098.

[2] M. R. Lukatskaya, O. Mashtalir, E. Ren Chang, Y. Dall'Agnese, P. Rozier, L. Taberna Pierre, M. Naguib, P. Simon, M.W. Barsoum, Y. Gogotsi, *Science* **2013**, 341, 1502-1505.

[3] J. Li, H. Wang, X. Xiao, *Energy & Environmental Materials* **2020**, 3, 306-322

[4] M. Ghidui, S. Kota, J. Halim, A. W. Sherwood, N. Nedfors, J. Rosen, V. N. Mochalin, M. W. Barsoum, *Chemistry of Materials* **2017**, 29, 1099-1106.

[5] D. Göhl, H. Rueß, M. Pander, A. R. Zeradjani, K. J. J. Mayrhofer, J. M. Schneider, A. Erbe, M. Ledendecker, *Journal of The Electrochemical Society* **2020**, 167, 021501.

[6] M. Esmailirad, A. Baskin, A. Kondori, A. Sanz-Matias, J. Qian, B. Song, M. Tamadoni Saray, K. Kucuk, A. R. Belmonte, P. N. M. Delgado, J. Park, R. Azari, C. U. Segre, R. Shahbazian-Yassar, D. Prendergast, M. Asadi, *Nature Communications* **2021**, 12, 5067.

9:30 AM NM04.07.04

Electrochemical Properties of MXene Electrodes in Aqueous Zinc Electrolytes Kyle Matthews¹, Armin VahidMohammadi¹, Danzhen Zhang¹, Liyuan Liu², Patrice Simon² and Yury Gogotsi¹; ¹Drexel University, United States; ²Université Paul Sabatier Toulouse III, France

MXenes are a family of two-dimensional (2D) transition metal carbides, nitrides and carbonitrides, with a general structure of M_{n+1}X_nT_x, where M is the transition metal, X is carbon or nitrogen, T represents the surface terminations (F, O, OH), and n can vary from 1-4. MXenes have shown promise in multiple electrochemical systems including aqueous supercapacitors and non-aqueous batteries containing monovalent cations. However, there have been limited works studying the electrochemical properties of these materials in aqueous electrolytes with multivalent cations such as Zn²⁺ and Mg²⁺. MXenes have high (electro)chemical stability in halide zinc electrolyte systems unlike many oxide materials. Herein, the charge storage mechanism of Ti₃C₂T_x was studied in multiple Zn containing aqueous electrolytes. In-situ XRD and in-situ UV-Vis were employed to monitor the intercalating species and redox response in the electrodes. Ti₃C₂T_x electrodes could deliver battery-like performance at low rates with supercapacitor performance at high rates. This work demonstrates the potential of using MXenes in zinc ion capacitors and zinc hybrid energy storage devices.

9:45 AM BREAK

10:15 AM NM04.07.06

Wearable Energy Storage with MXene Textile Supercapacitors for Real World Use Alex Inman¹, Tetiana Hryhorchuk¹, Lingyi Bi¹, John Wang¹, Ben Greenspan², Taylor Tabb², Eric Gallo², Armin VahidMohammadi¹, Genevieve Dion¹, Andreea Danielescu² and Yury Gogotsi¹; ¹Drexel University, United States; ²Accenture Labs, United States

Successful implementation of wearable electronics requires practical wearable energy storage systems that can meet certain power and energy metrics. However, flexible, stretchable, and truly textile-grade energy storing platforms have so far remained missing from most e-textile systems due to the insufficient performance metrics of current available materials and technologies. Two-dimensional (2D) transition metal carbides and nitrides (MXenes) offer unique combinations of properties including metallic conductivity, high specific capacitance, hydrophilicity, and solution processability, as well as mechanical flexibility and robustness that render these materials promising for flexible wearable energy storage technologies. Here we demonstrate textile-based electrochemical capacitor devices with high areal loading of Ti₃C₂T_x that can be integrated in series via a stacked design approach and meet the real-world power requirements for wearable electronics. A demo textile supercapacitor with 5 cells in series and a footprint area of 25 cm² and a MXene loading of 24.2 mg cm⁻² could operate in a 6 V voltage window delivering an energy density of 0.401 mWh cm⁻² at a power density of 0.248 mW cm⁻², and an areal capacitance of 146 mF cm⁻² at a 0.16 mA cm⁻² discharge current. The MXene textile supercapacitor powers a temperature monitoring system requiring high current densities with wireless data transmission to a receiver for 96 minutes. This initial report of a MXene textile supercapacitor powering a practical peripheral electronics system demonstrates the potential of this family of 2D materials to support a wide range of devices such as motion trackers and biomedical monitors in a flexible textile form factor.

10:30 AM NM04.07.07

MXene-Derived Chemically Pre-Potassiated Bilayered Vanadium Oxides as Cathodes in Non-Aqueous K-Ion Batteries Timofey Averianov and Ekaterina Pomerantseva; Drexel University, United States

As demand for Li-ion batteries (LIBs) continues to rise, concerns about the scarcity of raw materials like lithium present a challenge for large-scale distribution of energy storage devices. Potassium ion (K-ion) batteries (PIBs) present an attractive alternative to devices based on lithium ions due to the abundance of potassium in the earth's crust and potassium's lower cost to lithium. However, many traditional electrode materials cannot reliably accommodate potassium ions due to the ion's large ionic radius. As a result, materials with interlayer regions tailored for K⁺ ion accommodation and diffusion are necessary to fully realize potassium-ion batteries.

Potassium-preintercalated bilayered vanadium oxide (KVO) has been previously identified as a suitable cathode material for K-ion batteries due to its wide d-spacing of 9.65 Å and high theoretical capacity through multiple reversible vanadium reduction steps. Aqueous synthesis of KVO from an α-V₂O₅ precursor produces particles with one-dimensional (1D) nanorod/nanobelt morphologies with promising performance as electrodes in PIBs, but substantial capacity fading during cycling. Alternatively, use of vanadium-based 2D MXene as a precursor has been shown to produce chemically preintercalated bilayered vanadium oxides (BVOs) with centrally nucleated 2D nanosheet morphologies, akin to a flower. Cycling of these nanoflower BVOs resulted in improved cycle-life stability and rate performance in Li-ion batteries as compared to the performance of α-V₂O₅-derived BVOs. In this work we explored if similar improvements may be possible for K-ion batteries. We report, for the first time, the electrochemical behavior of MXene-derived δ-K_xV₂O₅•nH₂O (KVO) electrodes in non-aqueous K-ion cells. Through this study, the KVO synthesis, processing, and cycling conditions that produced the most promising performance have been identified. Initial cycling of the KVO between 2.0 – 3.7 V showed stable cycling with comparable capacities (~70 mAh/g) of other KVOs, but it was found that water content in the hydrated KVO limited cycle stability when the potential limits were extended. Interlayer water dynamics and reactivity can cause parasitic reactions, such as electrolyte decomposition, poorly reversible formation of foreign compounds and vanadium oxide structure transformation, leading to the capacity decay. Vacuum drying the KVO powder at 200°C and vacuum drying the prepared electrode film at 120°C significantly stabilized cycling performance, even when cycling down to 1.5 V, due to the partial removal of the interlayer water molecules. Cycling of the vacuum-dried materials/electrodes up to 4.3 V appeared to introduce new electrochemical behavior with minimal improvements to stability. In the interest of highlighting cathodic performance, 2.0 – 3.7 V was kept as the operating potential window. We show that by adequately drying before and after electrode fabrication, the MXene-derived δ-K_xV₂O₅•nH₂O electrodes demonstrated enhanced electrochemical stability while maintaining improved specific

capacities in K-ion batteries.

10:45 AM NM04.07.08

Photonic Curing of PDMS Intercalated Ti_3C_2 MXenes for Li-Ion Batteries Electrode [Najma Khatoon](#), Binod Subedi, Ahmad Majed, Shipping Wang, Julie Albert, Michael Naguib and Douglas B. Chrisey; Tulane University, United States

Silicon-based nanomaterials are promising candidates for rechargeable anode material in Lithium-ion batteries (LIBs), due to their higher theoretical specific capacity, and low lithium insertion potential. The challenge to utilize these tremendous properties of Si for LIBs is to decrease volume changes and capacity loss during the lithiation/delithiation process along with dealing with their poor electrical conductivity and low lithium-ion diffusivity. Dispersing Si in a carbon like matrix is one of the approaches to tackle these challenges. Titanium carbide ($Ti_3C_2-T_x$), where T_x are surface terminations, is a class of two-dimensional materials called MXenes. Ti_3C_2 have high conductivity and excellent Li-ion diffusion properties. Herein, PDMS (Polydimethylsiloxane) is intercalated in Ti_3C_2 (with d-spacing ~ 1 nm) for introducing the silicon within layers of MXene. The intercalated MXene (with d-spacing ~ 12 nm) is further processed by a unique process of photonic curing to convert intercalated PDMS to silica (SiO_2), leaving behind Si nanomaterial within the MXene layers. The as-converted silica ash on outer surface of MXene will protect it from oxidation due to its oxygen diffusion resistant ability. Photonic curing of 5K and 25K PDMS intercalated MXene is carried out at 350 V, 450 V and 550 V bank voltage for 7 pulses. Our results show that using PulseForge photonic curing of PDMS intercalated MXene changes the d-spacing from 12 nm to ~ 5 nm using a 450 V bank voltage, 7 pulses, and $28 Jcm^{-2}$ overall fluence. The change in d-spacing and loud photoacoustic signal during the process implies that photonic curing removed organic part of PDMS and left mostly SiO_2 . Cyclic voltammetry of cured PDMS intercalated MXene shows that reversible electrochemical reactions are stable with continued cycling. We aim to cure the intercalated MXene under vacuum and reactive gas environment, with varying pressure for controlling nucleation and growth of intercalated material. The present work shows that the photonic curing process is a promising instantaneous and roll-to-roll amenable synthetic route for low-cost large scale-controlled synthesis of Si-MXenes composite with the ability to tune the Si nanostructure within the MXenes layers.

SESSION NM04.08: MXenes for Clean Environment

Session Chairs: Babak Anasori and Anupma Thakur

Wednesday Afternoon, November 30, 2022

Hynes, Level 2, Room 201

1:30 PM NM04.08.01

Tailoring of the Exterior Transition Metal on the Electrocatalytic Performance of Double Transition Metal MXenes [Anupma Thakur](#), Nithin Chandran Balachandran Sajitha, Brian Wyatt, Wyatt Highland and Babak Anasori; Indiana University-Purdue University, United States

Two-dimensional transition metal carbides, known as MXenes, have shown great promise as active materials in catalytic applications such as the hydrogen evolution reaction. Double transition metal (DTM) MXenes, in which two different transition metals occupy the metal sites, can enhance the tunability of MXenes electrocatalytic properties. The transition metal occupying the outer atomic layers controls the HER performance based on their basal plane activity. We investigated out-of-plane ordered DTM MXenes, with inner layers of transition metal (M' : Ti) sandwiched by outer layers of different transition metals (M : Mo, W, Cr) in a layered $M_2M'C_2T_x$ structures. We demonstrate the role of exposed basal plane transition metals on the HER catalytic activity of these out-of-plane ordered DTM MXenes and compare their behaviour to a mono-transition metal MXene, $Ti_3C_2T_x$. $W_2TiC_2T_x$ MXene shows the lowest HER overpotential under acidic conditions over $Mo_2TiC_2T_x$, $Cr_2TiC_2T_x$ and $Ti_3C_2T_x$ MXenes. The improved electrocatalytic performance of $W_2TiC_2T_x$ can be due to the presence of tungsten atoms in the outer M' layers. Additionally, we assessed $W_2TiC_2T_x$ MXene for its long-term stability of more than 24 hours. Our findings, further demonstrate MXenes are precious-metal-free 2D flakes with highly HER active basal planes as well as promising and tunable electrocatalysts for clean energy applications.

1:45 PM NM04.08.02

Copper-Modified 2D Transition Metal Carbide (MXene) Electrocatalysts for CO_2 Reduction [Shiba P. Adhikari](#), Alice Gao, Sixbert Mohuza and Zachary Hood; Argonne National Laboratory, United States

Abstract for NM04 - 2D MXenes—Synthesis, Properties and Applications

Copper-Modified 2D Transition Metal Carbide (MXene) Electrocatalysts for CO_2 Reduction

Shiba P. Adhikari¹, Alice Gao^{1,2}, Sixbert Mohuza¹, and Zachary D. Hood¹

¹*Applied Materials Division, Argonne National Laboratory, Lemont, IL 60439, USA*

²*University of Illinois Urbana-Champaign, Champaign, IL 61801, USA*

Carbon capture and sequestration, as well as industrial decarbonization, are among the primary methods to tackle rising carbon dioxide (CO_2) concentrations in the atmosphere. The CO_2 reduction reaction (CO_2RR) has long been recognized as a promising strategy to capture and convert industrial CO_2 which may help to reduce atmospheric pollution strongly associated with climate change.^[1] Although multiple strategies have shown CO_2 reduction to C1 and C2 liquid fuels, two major hurdles still exist for the most recent examples of catalysts for this reaction, namely 1) the preparation of the catalysts is generally complicated, and 2) the selectivity of the catalysts towards specific C1 and C2 products requires better control.^[2] Here, we present recent results highlighting new Cu-based MXene electrocatalysts that overcome the preparation and CO_2RR selectivity issues. The preparation of these electrocatalysts leverages reductive adsorption of Cu ions directly onto hydroxy-terminated $Ti_3C_2T_x$ ($T_x = -O, -OH, etc.$)^[3] that yields unique metal-ceramic heterostructures with tunable nanoscale hierarchy.^[4] This hierarchy is important towards the structure-property relationships for C1 and C2 production during the CO_2RR . The Cu-based MXene electrocatalysts involved in this study reveal the importance of electrocatalyst selection for enhanced selectivity on electrocatalytic C2 production. These insights suggest new approaches for controlling the MXenes' behavior for optimal characteristics for the CO_2RR .

Acknowledgements:

This material is based upon work supported by Laboratory Directed Research and Development (LDRD) funding from Argonne National Laboratory, provided by the Director, Office of Science, of the U.S. Department of Energy under Contract No. DE-AC02-06CH11357.

References:

Bushuyev, O.S., De Luna, P., Dinh, C.T., Tao, L., Saur, G., van de Lagemaat, J., Kelley, S.O. and Sargent, E.H., What should we make with CO_2 and how can we make it? *Joule*, 2018, 2(5), 825-832.

Handoko, A. D.; Chen, H.; Lum, Y.; Zhang, Q.; Anasori, B.; Seh, Z. W., Two-dimensional titanium and molybdenum carbide MXenes as electrocatalysts for CO_2 reduction. *Science* 2020, 23 (6), 101181.

Naguib, M.; Mochalin, V. N.; Barsoum, M. W.; Gogotsi, Y., 25th anniversary article: MXenes: a new family of two-dimensional materials. *Advanced*

2:00 PM *NM04.08.03

MXene Surface Functionalization for Energy Storage and Catalysis Zdenek Sofer; University of Chemistry and Technology Prague, Czechia

The surface chemistry of MXene can be modified and tuned in order to tune its properties by covalent functionalizations and chemical modifications. The surface chemistry of MXene including introduction of various heteroatoms like chalcogens (S, Se, Te) as well as covalent functionalization of MXene surface will be discussed. Changes of MXene termination significantly improve performance of MXene for supercapacitor applications as well as water splitting. Introduction of zwitterion molecules was used to significantly enhanced capacitance of MXene in both aqueous and non-aqueous electrolytes including ionic liquids. For these modification were used triethoxysilane linkers which is universal tools for introduction of different functionalities on various MXene surface (like $Ti_3C_2T_x$, V_2CT_x , Nb_2CT_x) including various zwitterion molecules and complex supramolecular structures like alpha- and beta-cyclodextrin. Functionalized MXene were used to improve compatibility with polymer matrix for 3D printing of MXene using FMD method providing highly conductive materials for energy storage applications and electromagnetic shielding.

2:30 PM BREAK

3:30 PM NM04.08.04

Optical Properties and Photocatalytic Activity of the Oxidation Stabilized $Ti_3C_2T_x$ MXene Agnieszka M. Jastrzebska, Dominika Bury, Michal Jakubczak and Muhammad A. Purbayanto; Warsaw University of Technology, Poland

Two-dimensional (2D) MXenes are well known for their excellent photocatalytic properties. However, their oxidation stability is far from satisfactory, which makes controlling the photocatalytic processes challenging. Herein, we investigate the influence of oxidative stabilization of delaminated MXene on its optical and photocatalytic properties. The model 2D $Ti_3C_2T_x$ MXene was synthesized via two well-established approaches such as HF/TMAOH (TMAOH-MXene) and minimum intensive layer delamination with HCl/LiF (MILD-MXene) coupled with L-ascorbic acid (Vit.C) stabilization. Our approach revealed that the TMAOH-MXene showed a wider optical band gap than MILD-MXene. The MILD-MXene was therefore most efficient, showing almost 100 % effectiveness in the photocatalytic decomposition of model dyes. The industrial viability was achieved on a commercial textile dye, having a 100-times higher concentration than model dyes. The MILD-MXene needed only several seconds of UV-light and simulated white light irradiation to fully decompose the commercial dye. Further in-detail analysis at various visible light ranges showed that irradiation with 625 nm (red light) gave the highest efficiency of dye decomposition with MILD-MXene catalyst. The photocatalytic mechanism was associated with the interplay between surface dye adsorption and reactive oxygen species (ROS) generated by the MXene under light irradiation. However, excellent dye adsorption was a major driving force in the process. Importantly, both MXenes could be further successfully reused while retaining about 70 % of their activity. Collectively, the obtained results revealed that oxidative stabilization with Vit.C preserved MXene's original surface functionalization. It was further possible to understand MXene's genuine properties such as optical activity and performance in the photocatalytic process, thus supporting its practical use in industrial water remediation technologies.

3:45 PM NM04.08.05

Scalable and Sustainable Production of $Ti_3C_2T_z$ MXene and Fluorine Recovery from Wastewater Through Cryolite Precipitation Michael Carey and Michel W. Barsoum; Drexel University, United States

Traditional synthesis of $Ti_3C_2T_z$ MXene obtained by the selective etching of aluminum from Ti_3AlC_2 MAX phase with hydrofluoric acid, requires a large amount of water to obtain a colloidal suspension of few to single flake $Ti_3C_2T_z$. Typically, the amount of water needed is about 640-800 mL per gram of MXene, as this volume is thought to both wash away residual salts formed in the etching process, and to bring the solution pH to neutral at which point a stable colloidal MXene suspension forms. While MXenes have been shown to be quite promising in terms of their performance across a wide variety of applications, their widescale production has lagged. One of the limiting steps at this time is the large cost of their production and the need for fluorine in the etching medium. Additionally, the treatment of HF containing wastewater is both a major industrial and environmental concern. For MXene production to occur at industrial scales, the large amount of acidic wastewater that is currently a byproduct of its methods of production must be addressed. Furthermore, the presence of F⁻ in this wastewater is problematic as this treatment is quite costly and produces a large amount of industrial waste sludge that becomes difficult to dispose of due to environmental regulations. Herein we show that by modifications made to the synthesis process, we can obtain $Ti_3C_2T_z$ colloidal suspensions with 75% less water utilized in the washing procedure. Additionally, the fluorine in the remaining wastewater can also be recovered through the precipitation of cryolite, Na_3AlF_6 , a value-added compound used extensively in the aluminum production cycle. This cryolite can then be used as a quantitative tool to determine the efficiency of aluminum extraction from Ti_3AlC_2 MAX phase, allowing for optimization of parameters such as etching time, temperature, reagent concentrations, and/or pH of etchant.

SESSION NM04.09: MXenes Electronic, Photonic and Electromagnetic Interference Shielding Applications

Session Chairs: Mikhail Shekhirev and Christopher Shuck

Thursday Morning, December 1, 2022

Hynes, Level 2, Room 201

8:30 AM NM04.09.01

Significant Enhancement in the Seebeck Coefficient and Power Factor of a Thermoelectric Polymer Through the Incorporation of MXene Jianyong Ouyang; National University of Singapore, Singapore

Thermoelectric (TE) materials are important for sustainable development because they can directly convert heat into electricity. Compared with inorganic TE materials, conductive polymers have demonstrated unique advantages. But their TE properties, particularly the Seebeck coefficient, must be greatly enhanced for practical application. Here, I will present the significant enhancement in the Seebeck coefficient and thus the overall thermoelectric properties of poly(3,4-ethylenedioxythiophene):poly(styrenesulfonate) (PEDOT:PSS) that is the most popular thermoelectric polymer through the incorporation of MXene. MXene can enhance the Seebeck coefficient from 23 up to 57.3 $\mu V K^{-1}$ and the power factor from 44.1 to 155 $\mu W m^{-1} K^{-2}$. This is the first time to achieve the enhancement in the Seebeck coefficient of a p-type TE polymer by an n-type filler.

8:45 AM NM04.09.02

Molecular Doping of $Ti_3C_2T_x$ MXene Yields Surface-Termination-Independent Tunable Work Function [Jehad K. El-Demellawi](#), Ahmed E. Mansour, Omar Mohammed and Husam N. Alshareef; King Abdullah University of Science and Technology, Saudi Arabia

MXenes are highly regarded for their localized surface plasmons (SPs), broadband optical absorption, and tunable work functions. These unique features strongly depend on the dipole moments between the transition metal (*e.g.*, Ti) and the functional surface species (T_x) of MXenes. Hence, tailoring the surface terminations of MXenes is expected to alter their work functions, plasmon energies, and optical properties simultaneously, making it hard to modify one property (*e.g.*, work function) without affecting the other properties. In this work, we introduce an alternate method for surface-termination-independent controlling of the work function of $Ti_3C_2T_x$ MXene *via* a well-controlled molecular doping process. Utilizing Tris(4-bromophenyl)ammoniumyl hexachloroantimonate, *viz.* magic blue (MB), as a dopant, we finely tune the work function of $Ti_3C_2T_x$, achieving an increase of ~ 500 meV. The incremental changes in the work function of our spray-coated $Ti_3C_2T_x$ films (20-nm-thick) are proven to be entirely independent of T_x , as denoted by the invariant absorption and relaxation dynamics of the transversal (out-of-plane) plasmonic band throughout the doping process. Using ultraviolet and X-ray photoemission spectroscopy (UPS and XPS) along with electron paramagnetic resonance (EPR) spectroscopy, we attribute the work function modulation to an electron transfer from the energy states below the Fermi level in $Ti_3C_2T_x$ to the dopant cations, accompanied by the physisorption of the dopant anions (antimony hexachloride) on the MXene surface, leading to the formation of polarons as additional charge carriers. The demonstrated ability to engineer the work function of MXenes without altering their surface-termination-dependent properties (*e.g.*, SPs) allows for higher operational degrees of freedom, which is alluring for MXene-based device applications.

9:00 AM NM04.09.04

Environmentally-Stable High Work Function Titanium Carbide MXene for Large-Area Organic Light-Emitting Diodes [Huanyu Zhou](#)¹, Shin Jung Han¹, Hyeon-Dong Lee¹, Danzhen Zhang², Mark Anayee², Seung Hyeon Jo¹, Gogotsi Yury² and Tae-Woo Lee¹; ¹Seoul National University, Korea (the Republic of); ²Drexel University, United States

This paper presents a transparent conducting electrode (TCE), which is an environmentally-stable two-dimensional titanium carbide ($Ti_3C_2T_x$, MXene) that has a high work function WF. High-temperature annealing reduced the d-spacing of $Ti_3C_2T_x$ from 1.33 to 1.06 nm; the result was a highly-compacted thin film that can resist inward diffusion of moisture intercalants. The MXene had high WF = 5.84 eV, which is the highest yet; it was achieved by p-type molecular doping using perfluorosulfonic acid. With benefits from the highly compacted structure of $Ti_3C_2T_x$ and superior chemical stability of overcoated PFSA, the p-doped $Ti_3C_2T_x$ exhibited only a 4.8% increase in sheet resistance with WF maintained > 5.60 eV even after 22-day exposure to ambient air. Lastly, the $Ti_3C_2T_x$ TCE was successfully applied as the anode for both large-area and ten-by-ten passive matrix flexible organic light-emitting diodes on 6 cm \times 6 cm substrates. The significant increases in environmental stability and WF provides a new method to develop practical applications of MXene as TCEs for optoelectronics and photovoltaics.

9:15 AM NM04.09.05

Scalable Wet-Spinning of MXene Assembly and Their Applications [Rohan B. Ambade](#) and Tae Hee Han; Hanyang University, Korea (the Republic of)

MXenes, a fascinating large family of two-dimensional (2D) layered transition metal carbides and nitrides, have aroused substantial interest in various applications owing to their unprecedented ultrahigh metallic conductivity, mechanical properties, and hydrophilicity. This work demonstrates scalable, straightforward, continuously controlled, additive-free wet-spinning assembly of 2D titanium carbide ($Ti_3C_2T_x$) MXene fibers. MXene flakes are perfectly aligned under a mechanical drawing force using concentrated MXene colloids in a coagulation bath to produce $Ti_3C_2T_x$ MXene fibers *via* a wet-spinning process. The wet-spun $Ti_3C_2T_x$ MXene fibers demonstrated excellent electrical conductivity and mechanical properties. As a result, $Ti_3C_2T_x$ MXene fiber-based miniaturized devices are promising for portable applications. Furthermore, the $Ti_3C_2T_x$ MXene hybrid fibers with the synergistic effect of gas-adsorption and electronic properties significantly improved NH_3 sensing response ($\Delta R/R_0 = 6.77\%$) at room temperature for wearable gas sensors. Additionally, fabricated wet-spun $Ti_3C_2T_x$ MXene fibers are integrated into electrical wires to switch on a light-emitting diode light and transmit electrical signals to earphones to demonstrate their application in electrical devices. Furthermore, the wet-spun electroconductive $Ti_3C_2T_x$ MXene fibers exhibited an enhanced electrochemical performance when assembled as supercapacitor applications. Thus, we envisage that these exciting features of 2D $Ti_3C_2T_x$ MXene hybrid fiber materials will provide a novel pathway for designing next-generation portable miniaturized devices.

10:00 AM *NM04.09.06

MXene Surface Chemistry for Electronic and Energy Applications [Chong Min Koo](#); Sungkyunkwan University, Korea (the Republic of)

Surface chemistry controls not only the physicochemical, electrochemical, and optoelectronic properties, but also environment stability and processability of nanomaterials. MXenes have been attracted in many electronic, electrochemical, and optoelectronic applications, due to their high electronic conductivity (~ 15000 S/cm), hydrophilicity, and solution processability. MXenes, transition metal carbides/carbonitrides/nitrides, are a very large family of 2D materials with the general formula $Mn+1XnTx$, where M, X, Tx, and n represent transition metal(s), carbon or nitrogen, surface terminal groups such as -OH, -O and -F, and integers ranging from 1 to 4, respectively. The surface terminations determines the surface properties of MXenes. In this presentation, the presenter will briefly demonstrate two ways to control the surface chemistry of MXenes, including anhydrous synthesis and post-surface functionalization methods. The developed surface chemistry not only control the surface functionality and physicochemical properties of MXenes, but also enables preparation of stable MXene dispersions with good oxidation stability. The surface chemistry also provides an opportunity to prepare printable flexible MXene electrodes for various applications including EMI shielding, flexible joule heater, LED display and energy storage.

10:00 AM BREAK

10:30 AM NM04.09.07

2D Transition Metal Carbides and Carbonitrides (MXenes) for Electromagnetic Interference (EMI) Shielding [Aamir Iqbal](#) and Chongmin Koo; Sungkyunkwan University, Korea (the Republic of)

2D Transition Metal Carbides and Carbonitrides (MXenes) for Electromagnetic Interference (EMI) Shielding

Aamir Iqbal¹, and Chong Min Koo^{1}*

¹School of Advanced Materials Science and Engineering, Sungkyunkwan University, 2066 Seobu-ro, Jangan-gu, Suwon, Gyeonggi-do 16419, Republic of Korea

*Corresponding author: chongminkoo@skku.edu (C. M. Koo)

Two-dimensional (2D) MXenes are a newly discovered family of transition metal carbides, nitrides, and carbonitrides. Their outstanding electrical conductivities of $>10^4 \text{ S cm}^{-1}$ in 2D morphology, low density, mechanical flexibility, easy processability, and structural controllability extends their application scope to compete with existing conventional 2D materials. $\text{Ti}_3\text{C}_2\text{T}_x$, the representative candidate of the MXene family, exhibits an EMI shielding effectiveness of 92 dB at 45 micrometer thickness, whereas a 55-nanometer thick film can provide 99% shielding against EMI, which is outstanding for highly compacted electronics. A transition metal carbonitride, Ti_3CNT_x MXene, with a moderate electrical conductivity provides a shielding effectiveness of 116 dB at 40 micrometer thickness, higher than the more-conductive $\text{Ti}_3\text{C}_2\text{T}_x$ or metal foils of the same thickness. This exceptional shielding performance of Ti_3CNT_x was achieved by thermal annealing and is attributed to an anomalously high absorption of electromagnetic waves in the layered metamaterial-like porous structure. With high absorption of EM waves at minimal thickness, MXenes are ideal for real applications in smart 5G electronics.

Keywords: Transition metal carbides, carbonitrides, MXenes, electromagnetic shielding, porous structure.

10:45 AM NM04.09.08

The Environmental Impacts of $\text{Ti}_3\text{C}_2\text{T}_x$ MXene Synthesis for Electromagnetic Interface Shielding of Communication Satellites [Mostafa Dadashi Firouzjaei](#)¹, [Daqian Jiang](#)¹, [Mark Elliott](#)¹ and [Babak Anasori](#)²; ¹The University of Alabama, United States; ²Indiana University-Purdue University Indianapolis, United States

Scaling up and environmental impacts associated with nanomaterials synthesis is a major challenge in the industries nowadays. As one of the cutting-edge nanostructures, MXenes, have significantly impacted materials science and nanotechnology since their discovery in 2011. Theoretical calculations have predicted more than 100 possible compositions of MXenes, and lab-scale fabrication of more than 40 MXene structures has been reported to date. The unique characteristics of MXenes have made them an ideal fit for a wide variety of applications, including energy storage, environmental, electronics, communications, gas, and liquid separations and adsorption, biomedical, and optoelectronics. By 2021, MXenes have already shown promise in several research areas, including energy storage devices, electromagnetic interference shielding, nanocomposites, and hybrid materials. In parallel, new applications are emerging where MXenes outperform other nanomaterials, such as in tribology. Despite all the new development in the MXenes field, there is no study of the environmental impacts of MXene synthesis. Here, we investigate the environmental impacts associated with the fabrication of $\text{Ti}_3\text{C}_2\text{T}_x$ MXene as a coating layer for electromagnetic interface (EMI) shielding of communications satellites. We use aluminum and copper as an external normalization alternate to show the gaps and recommend solutions for improving the scalability of the $\text{Ti}_3\text{C}_2\text{T}_x$ MXene. Two $\text{Ti}_3\text{C}_2\text{T}_x$ synthesis systems, a small laboratory scale (19.2 g per batch) and a large laboratory scale (800 kg per batch) were compared. We also investigated the use of TiO_2 instead of Ti for the synthesis of the MXene precursor as well as the effects of laboratory location on the environmental impacts of MXene. In summary, this work would help through the more efficient and environmentally friendly synthesis of MXenes, which is vital for considering the scale-up of MXenes.

11:00 AM NM04.09.09

$\text{Ti}_3\text{C}_2\text{T}_x$ MXene Film with High Electrical Conductivity and Moisture Resistance [Akari Seko](#), [Shun Sakaida](#) and [Takeshi Torita](#); Murata Manufacturing Co., Ltd., Japan

With high metallic conductivity, a new family of two-dimensional transition metal carbides (MXene) is a promising candidate for electronics. However, one of challenges in MXene application is poor stability to moisture, degradation of electrical properties by swelling (lattice expansion by water intake) and oxidation [1, 2]. For applications in the field of electronics, MXene with improved environmental stability (e.g. no significant degradation under 60°C/RH85%) is highly required. A number of works has been reported to improve MXene stability in humid conditions, including surface modification [3], but most of them have resulted in ruining their superior properties derived from diversity in surface terminating groups. In this work, we propose a facile strategy to fabricate MXene films exhibiting excellent conductivity and stability under 60°C/RH85% without tailoring of MXene surface functional groups.

References

- [1] Voigt, C. A.; Ghidui, M.; Natu, V.; Barsoum, M. W. Anion Adsorption, $\text{Ti}_3\text{C}_2\text{T}_x$ MXene Multilayers, and Their Effect on Claylike Swelling. *J. Phys. Chem. C* **2018**, 122 (40), 23172–23179.
- [2] Iqbal, A.; Hong, J.; Ko, T. Y.; Koo, C. M. Improving oxidation stability of 2D MXenes: synthesis, storage media, and conditions. *Nano Converg.* **2021**, 8 (1), 1–22.
- [3] Chen, W. Y.; Lai, S. N.; Yen C. C.; Jiang X.; Peroulis D.; Stanciu A. Lia. Surface Functionalization of $\text{Ti}_3\text{C}_2\text{T}_x$ MXene with Highly Reliable Superhydrophobic Protection for Volatile Organic Compounds Sensing. *ACS Nano* **2020**, 14 (9), 11490–11501.

SESSION NM04.10: MXenes Sensing and Biomedical Applications

Session Chairs: [Mostafa Dadashi Firouzjaei](#) and [Anupma Thakur](#)

Thursday Afternoon, December 1, 2022

Hynes, Level 2, Room 201

1:30 PM *NM04.10.01

Automatic MXene Strain Sensor Design via Active Learning and Data Argumentation for Soft Machines [Po-Yen Chen](#); University of Maryland, United States

Emerging soft machines require high-performance strain sensors to achieve closed-loop feedback control. Predicting the performance of a soft robotic sensor from its composition and morphology is nearly impossible with traditional computational approaches. Machine learning (ML) is a versatile tool to uncover complex correlations between fabrication recipes and sensor performance, yet the limited acquisition rate of high-quality data hinders the development of high-accuracy prediction models at the device level. In this talk, I will demonstrate our recent work of using an ML model to predict device-level performance and recommend new material compositions for soft machine applications. I will present a three-stage ML framework to construct a prediction model capable of automating the design of strain sensors across a wide strain range from $<0.5\%$ to 350%. First, a support-vector machine classifier is trained by using 351 compositions of various nanomaterials, including $\text{Ti}_3\text{C}_2\text{T}_x$ MXene nanosheets, single-walled carbon nanotubes, and polyvinyl alcohol. Second, through 12 active learning loops, 125 strain sensors are stagewise fabricated to enrich the multi-dimensional dataset. Third, data augmentation is implemented to synthesize $>10,000$ virtual data points followed by genetic algorithm-based selection to optimize the prediction accuracy of ML model. An ultimate prediction model is finally constructed and able to (1) predict sensor characteristics based on fabrication recipes and (2)

recommend feasible fabrication recipes for adequate strain sensors. As final demonstrations, model-suggested strain sensors are integrated into soft gripper and batoid-like swimmer to endow them with real-time sensing capabilities.

2:00 PM NM04.10.02

Scalable Production of MXene Dip-Coated Yarns and Cords Lingyi Bi^{1,1}, William Perry¹, Robert Lord¹, Stepan Vorotilo¹, Alex Inman¹, Tetiana Hryhorchuk¹, John Wang¹, Vitaliy Balitskiy², Veronika Zahorodna², Oleksiy Gogotsi², Genevieve Dion¹ and Gogotsi Yuri¹; ¹Drexel University, United States; ²Materials Research Center, Ukraine

Fibers, yarns, and textiles have long established themselves in many sectors of society from our daily wear to medicine and structural composites. The rise of the Internet of Things (IoT) has prompted incorporation of conductive materials into textiles that enable real-time monitoring of external stimuli (e.g., stretch, pressure, temperature, and humidity) and body responses. Sensors, antennas, energy storage sources need to be incorporated into textiles. New functions, such as IR stealth, EMI shielding or passive and active temperature control, can be enabled by conductive or optically active coatings. Among the many conductive materials and fabrication methods demonstrated, few met the performance and cost requirements of real-world applications. MXenes are an emerging class of 2D nanomaterials that possess excellent electrical conductivity, attractive optical/plasmonic properties, solution processability and hydrophilic surfaces, making them ideal for imparting conductivity to textiles in a simple dip coating fashion. In this work, a high throughput continuous coating method was demonstrated with a customized automatic yarn dip coater. Thanks to the shear force present in the dip coater and the preferred interactions between Kevlar and MXene, viscous MXene solutions and fast coating speeds could be used. Kilometers of highly conductive MXene coated Kevlar cords were produced with consistent quality. Tensile test with *in-situ* electrical resistance tracking showed the multifunctionality of $Ti_3C_2T_x$ coated Kevlar for composites, both as structural reinforcement and damage sensing.

2:15 PM NM04.10.03

UV-Crosslinked Ti_3C_2 MXene Composite Hydrogel for Selective Detection of Neurotransmitters Mina Kim, Nakwon Choi, Seon Joon Kim and Hyejeong Seong; Korea Institute of Science and Technology, Korea (the Republic of)

Detecting neurotransmitters in the system is critical to diagnosing nervous system diseases. Many studies have been reported to produce high-performance sensors for sensing dopamine. Among the various materials, 2-dimensional Ti_3C_2 MXene, which is highly conductive and electrochemically active, has been investigated to detect neurotransmitters including dopamine, uric acid, and serotonin. However, MXene oxidizes quickly in aqueous conditions, hindering MXene from being widely applicable for biosensing applications.

Herein, we report a composite of MXene and poly (ethylene glycol) diacrylate (PEGDA), enabling selective detection of neurotransmitters. PEGDA is a porous, UV-cross-linkable material with a low degradation rate, protecting MXenes from oxidation in aqueous conditions. The composite thickness was easily controllable by changing UV irradiation time and the guide mold. Also, the composite structure was porous enough to assist small molecules diffused inside, facilitating electrochemical detection of neurotransmitters.

Electrochemical detection of dopamine was confirmed via cyclic voltammetry (CV) and differential pulse voltammetry (DPV), confirming that the composite could detect dopamine in aqueous conditions up to 50 nM. The limit of detection (LOD) is estimated to be lower than 50 nM, suggesting our MXene composite hydrogel would be further applicable for detecting neurotransmitters sensitively but selectively.

2:30 PM BREAK

3:00 PM NM04.10.04

Immune Profiling and Single-Cell Label-Free Detection of Two-Dimensional MXenes by Mass Cytometry and High-Dimensional Imaging Laura Fusco^{1,2,3}, Arianna Gazzi^{1,4}, Christopher E. Shuck², Marco Orecchioni⁵, S enar Mickael D'Almeida⁶, Darawan Rinchai³, Eiman Ahmed³, Leeat Ahmed⁷, Davide Bedognetti³, Yuri Gogotsi² and Lucia Delogu¹; ¹University of Padua, Italy; ²Drexel University, United States; ³Sidra Medicine, Qatar; ⁴University of Trieste, Italy; ⁵La Jolla Institute for Allergy and Immunology, United States; ⁶Ecole Polytechnique F ed erale de Lausanne (EPFL), Switzerland; ⁷Weizmann Institute of Science, Israel

There is a critical unmet need to detect and image two-dimensional (2D) materials within single cells and tissues while surveying a high degree of information from single cells. Here, we propose a versatile multiplexed label-free single-cell detection strategy based on single-cell mass cytometry by time-of-flight (CyTOF) and ion-beam imaging by time-of-flight (MIBI-TOF). [1] This strategy, "Label-free single-cell tracking of 2D materials by mass cytometry and MIBI-TOF Design" (LINKED), enables nanomaterial detection and simultaneous measurement of multiple cell and tissue features. As a proof of concept, we selected a set of 2D materials, transition metal carbides, nitrides, and carbonitrides (MXenes), to ensure mass detection within the cytometry range while avoiding overlap with more than 70 currently available tags, each able to survey multiple biological parameters. In addition, MXenes have received substantial attention for their promise as biomedical nanotools. [2-5]

First, we demonstrated their detection and quantification in 15 primary human immune cell subpopulations. Together with the detection, mass cytometry is used to capture several biological aspects of MXenes, such as their biocompatibility and cytokine production after their uptake. *In vivo* biodistribution experiments using a mixture of MXenes in mice confirmed the versatility of the detection strategy and revealed MXene accumulation in the liver, blood, spleen, lungs, and relative immune cell subtypes. Finally, we applied MIBI-TOF to detect MXenes in different organs revealing their spatial distribution. The label-free detection of 2D materials by mass cytometry at the single-cell level, on multiple cell subpopulations, and in multiple organs simultaneously, is expected to enable exciting new opportunities in biomedicine.

References:

1. Fusco L. *et al.* Immune Profiling and Multiplexed Label-Free Detection of 2D MXenes by Mass Cytometry and High-Dimensional Imaging. *Advanced Materials*, 2022, 2205154.
2. Gogotsi, Y. & Anasori, B. The Rise of MXenes. *ACS Nano*, 2019, 13, 8491.
3. Fusco L. *et al.* Graphene and other 2D materials: a multidisciplinary analysis to uncover the hidden potential as cancer theranostics. *Theranostics*, 2020, 10, 5435.
4. Unal M.A. *et al.* 2D MXenes with antiviral and immunomodulatory properties: a pilot study against SARS-CoV-2. *Nano Today* 2021, 38, 101136.
5. Gazzi A. *et al.* Photodynamic Therapy Based on Graphene and MXene in Cancer Theranostics. *Front. Bioeng. Biotechnol.*, 2019, 7, 295.

3:15 PM NM04.10.05

The Behavior of MXenes in Biological Media Swapnil Ambade, Robert Brown, Aditi Gupta, Michal Zalzman and Zeev Rosenzweig; University of Maryland, United States

The rapidly growing family of ultrathin layered two-dimensional (2D) transition metal carbides, nitrides, and carbonitrides, referred to as MXenes are steadily advancing as novel inorganic nanosystems for various electronic and optoelectronic applications. The metallic conductivity, hydrophilic nature,

and other unique physicochemical properties qualifies 2D MXenes to meet the requirements of biomedicine such as in stem cell research. Stem cell therapies show great promise for the cure of neurological disorders, as stem cells can serve as cell replacement, while also secreting factors to enhance endogenous tissue regeneration. We investigate the impact of outstanding electrical and surface functional properties of MXenes in the application areas of stem cells. Our synthesis strategies allow us to synthesize highly conductive and stable colloidal aqueous dispersions of MXenes that are coated or drawn as films. These freestanding films of MXenes exhibit electrical conductivities ranging from 10 S.cm^{-1} ($\text{V}_4\text{C}_3\text{T}_x$ MXene) to $20,000 \text{ S.cm}^{-1}$ ($\text{Ti}_3\text{C}_2\text{T}_x$ MXene). By the virtue of such high electrical conductivities, MXene nanosheets are explored as interfaces for regulating stem cells. The stem cells grown using a technology that allows for the culture of stem cells in combination with 3D printing technology can be translated to novel therapies for bone regeneration and reconstruction. Stem cells cultured on MXene films enable higher synchronous electrical activities and higher proliferative ability. Our preliminary results suggest that owing to the 2D network, MXenes can be engineered as guided bone regeneration membranes that serve as a scaffold to induce stem cell attachment. This study is an important step toward understanding the potential of MXenes in stem cell research and biomedicine, in general.

3:30 PM NM04.10.06

Stability of $\text{Ti}_3\text{C}_2\text{T}_x$ MXene Electrode Arrays Under Different Sterilization Conditions [Spencer R. Averbeck](#), Brendan B. Murphy, Doris Xu and Flavia Vitale; University of Pennsylvania, United States

Recently, $\text{Ti}_3\text{C}_2\text{T}_x$ MXene has attracted increasing interest for use in sensing and stimulation applications for monitoring electrophysiological activity in the body. The electrochemical properties of MXene-based electrode arrays have consistently demonstrated superior recording quality with increased signal to noise ratios (SNR) compared to clinically standard arrays. Further, the high capacitance of the MXene nanostructure paired with the large charge injection capacity (CIC) make these devices very desirable for high-quality, micron-scale recording and electrical stimulation. For MXene wearable and implantable devices to become clinically and commercially viable, however, they must be able to withstand routine sterilization procedures. Standard sterilization modalities used widely across the world include steam autoclave sterilization at 120°C , Ethylene Oxide (EtO) gas, and hydrogen peroxide (H_2O_2) plasma. Here, we present a comprehensive analysis of the structural, functional, and electrical effects of these common sterilization protocols on thin-film spray-coated $\text{Ti}_3\text{C}_2\text{T}_x$ neural microelectrode arrays as well as $\text{Ti}_3\text{C}_2\text{T}_x$ infused 'MXtrodes'. To confirm that bacteria could be effectively eradicated from the $\text{Ti}_3\text{C}_2\text{T}_x$ MXene devices, *E. Coli* inoculated samples were first tested in each sterilization machine, and the resulting colony-forming units (CFU) were counted. Across all sterilization modalities, the bacterial colony units were below the threshold of detection which confirmed the devices could be effectively sterilized. Post-sterilization analysis reveals that for both autoclave and EtO sterilized devices, the crystalline structure, contact adhesion, and electrical properties remain unchanged. Furthermore, there were no changes in the XRD and Raman spectra for autoclave or EtO sterilized thin-films or MXtrodes. Finally, electrochemical impedance and conductivity were statistically unchanged, and SEM did not reveal any delamination or morphological changes to the devices. Hydrogen Peroxide plasma sterilization, however, resulted in severe damage of $\text{Ti}_3\text{C}_2\text{T}_x$ MXene films as confirmed by SEM, XRD, and Raman. Further, plasma sterilization significantly increased the recording impedance measurements and revealed a significant loss in conductivity. Ultimately, our findings indicate that EtO and Autoclave sterilization do not alter $\text{Ti}_3\text{C}_2\text{T}_x$ MXene devices and should be considered for all future MXene wearables and invasive implants.

3:45 PM NM04.10.07

MXenes-Mediated Photothermal Therapy on Reliable 3D Models of Breast Cancer [Ginevra Friggeri](#)¹, Giordano Perini¹, Valentina Palmieri², Massimiliano Papi¹ and Marco De Spirito¹; ¹Università Cattolica del Sacro Cuore, Italy; ²sistemi complessi, Italy

Breast cancer is the most commonly diagnosed invasive cancer among women globally. Current therapies (e.g. chemotherapy) show numerous limitations due to the lack of selectivity and the consistent side effects. This led to investigating novel approaches aimed at improving tumor-killing efficacy. We previously demonstrated the effect of new bioactive nanomaterials with promising photophysical properties, the MXenes, used to increase the efficiency of targeted breast cancer Photothermal Therapy (PTT). In this work, we investigated the effect of Few and Multi layers MXenes mediated-PTT on two different three-dimensional reliable models of breast cancer; conventional spheroids and bioprinted spheroids. We performed PTT on the two models of breast cancer by using a non-toxic concentration of MXenes ($50 \mu\text{g/mL}$). After PTT, a significant reduction in cell viability was observed along with a strong increase in reactive oxygen species (ROS). We furthermore investigated the effect of PTT on the migration of macrophages and endothelial cells towards cancer region in both 3D models. Our results indicate that PTT mediated by both Few and Multi layers MXenes significantly modulate tumor progression by inducing the cells death by increasing the temperature, particularly in the bioprinted model.

SESSION NM04.11: Virtual Session I: MXenes I
Session Chairs: Babak Anasori and Anupma Thakur
Tuesday Morning, December 6, 2022
NM04-virtual

8:00 AM NM04.11.02

Chemical Imaging of 2D Titanium Based MXenes During *In Situ* Annealing by Scanning Transmission X-Ray Microscopy [Faidra Amargianou](#)¹, Tianxiao Sun¹, Markus Weigand¹, Tyler Mathis², Yury Gogotsi² and Tristan Petit¹; ¹Helmholtz-Zentrum Berlin für Materialien und Energie GmbH, Germany; ²Drexel University, United States

MXenes include transition metal carbides/nitrides with intercalated cations, such as $\text{Li-Ti}_3\text{C}_2\text{T}_x$ and $\text{K-Ti}_3\text{C}_2\text{T}_x$, where T_x represents surface terminations (typically O, OH and F). They have shown promising performance for energy storage, which is highly dependent on the surface chemistry and the Ti oxidation state. Nevertheless, contributions of different oxygen bonds in the local chemistry of MXene flakes and interlayers are difficult to disentangle without high chemical and spatial sensitivity.

In this presentation, we will show that Scanning Transmission X-ray Microscopy (STXM) is well suited for chemical imaging on individual MXenes particles. This synchrotron-based method allows the recording of soft X-ray Absorption Spectra (sXAS) with $<60 \text{ nm}$ spatial resolution, hence enabling the characterization of single MXene particles with high chemical sensitivity to Ti oxidation state and oxygen bonding, as well as bulk sensitivity. We will present here the first STXM characterization of $\text{Ti}_3\text{C}_2\text{T}_x$, $\text{Li-Ti}_3\text{C}_2\text{T}_x$, and $\text{K-Ti}_3\text{C}_2\text{T}_x$ MXenes at the Ti L-, C K- and O K-edges. The data analysis with unsupervised machine learning algorithms of STXM measurements for intercalated MXenes achieved the identification of different oxygen-containing compounds. Moreover, STXM measurements in transmission and total electron yield detection mode at Ti L- and O K-edge allowed the comparison between surface and bulk properties for $\text{Ti}_3\text{C}_2\text{T}_x$ MXene.

A decisive step towards understanding the migration of oxygen as a termination and water species was also achieved with *in situ* temperature-dependent

STXM measurements for these MXenes. The local behaviour of oxygen during annealing up to 650°C was mapped at the Ti L- and O K-edge. These are the first bulk-sensitive measurements able to map oxygen redistribution inside MXene interlayer during annealing. The aforementioned experimental results advocate for the importance of spaces between MXene layers and overlapping flakes in the formation and control of oxygen-containing species in MXenes.

8:15 AM *NM04.11.03

2D Molybdenum Carbide (MXene) for CO₂ Hydrogenation Hui Zhou; Tsinghua University, China

Currently, the conversion of captured CO₂ into value-added chemicals or fuels is considered a key strategy to mitigate the yet increasing anthropogenic CO₂ emissions, in particular when combined with H₂ obtained using renewable energy. Depending on the catalyst and the reaction conditions used, thermocatalytic CO₂ hydrogenation can give CO, methanol, dimethyl ether (DME), methane, or heavier hydrocarbons. MXene materials, that is, a family of two-dimensional (2D) carbides, nitrides and carbonitrides with the general formula of M_n+1X_nT_x (where M is an early transition metal, n = 1, 2, 3, X is C and/or N and T are surface -O-, -OH and/or -F groups), are currently emerging in thermocatalytic applications as catalysts or supports with reactive metal-support interactions. Enabled by the scalable synthesis of MXenes, we report a gram-scale synthesis of a phase-pure multilayered hexagonal 2D-Mo₂C material with only Mo-terminated basal planes. 2D-Mo₂C is by a factor of six per mass of catalyst more active for CO formation than the reference β-Mo₂C catalyst and shows no deactivation on stream for more than 100 h. We also report that silica-supported, dispersed, reducible nanosheets of a delaminated molybdenum MXene, Mo₂CT_x, can be used to engineer a Cu/Mo₂CT_x interface that shows an at least six times increased intrinsic formation rate of methanol by the direct hydrogenation of CO₂ compared to Cu/SiO₂.

8:45 AM NM04.11.04

Probing the Hydration Shell of Cations Intercalated Between Two-Dimensional Ti₃C₂T_x MXene Layers Using Infrared Spectroscopy Mailis Lounasvuori¹, Tyler Mathis², Yury Gogotsi² and Tristan Petit¹; ¹Helmholtz-Zentrum Berlin, Germany; ²A.J. Drexel Nanomaterials Institute, United States

MXenes are a large family of 2D materials [1] with excellent potential for energy storage applications [2]. Ti₃C₂T_x (where T_x refers to surface terminations -O, -OH, -F, etc. present in varying amounts depending on synthesis conditions) is one of the most studied MXenes to date. Due to hydrophilic surfaces and weak attractive forces between the negatively charged layers, MXenes can retain significant amounts of water between the layers, and they can be intercalated with a variety of cations and molecules [3]. Understanding the structure and dynamics of intercalated species within MXene electrodes is important for the development of practical energy storage devices. Infrared spectroscopy is sensitive to the hydrogen bonding environment of water molecules and thus well suited for the study of water structures [4]. We have recently demonstrated that this method can be applied to probe proton intercalation into the MXene interlayer space [5].

Here, we use infrared spectroscopy in the attenuated reflectance mode to probe confined water between Ti₃C₂T_x MXene layers as a function of relative humidity. The MXene was intercalated with various cations (Li, Na, K, Cs, ...) or treated with an acidic solution to remove all intercalants [6]. Clear changes in the amount and hydrogen-bonding structure of the confined water are observed depending on the identity of the intercalated cation as well as the relative humidity. Because anions do not intercalate into MXenes [7], we are able to study the hydration shell of the cation without interference of anions or contact ion pairs. This work provides new understanding on the solvation of cations confined between MXene layers.

References

- [1] Naguib et al. Two-dimensional nanocrystals produced by exfoliation of Ti₃AlC₂. *Adv. Mater.* 2011, 23, 4248–4253
- [2] Jun et al. Review of MXenes as new nanomaterials for energy storage/delivery and selected environmental applications. *Nano Res.* 2019, 12, 471–487
- [3] Osti et al. Effect of metal ion intercalation on the structure of MXene and water dynamics on its internal surfaces. *ACS Appl. Mater. Interfaces* 2016, 8, 8859–8863
- [4] Ohno et al. The effect of cooperative hydrogen bonding on the OH stretching-band shift for water clusters studied by matrix-isolation infrared spectroscopy and density functional theory. *Phys. Chem. Chem. Phys.* 2005, 7, 3005–3014
- [5] Lounasvuori et al. Vibrational signature of hydrated protons confined in MXene interlayers. Under review 2022
- [6] Chen et al. Pristine Titanium Carbide MXene Films with Environmentally Stable Conductivity and Superior Mechanical Strength. *Adv. Funct. Mater.* 2020, 30, 1906996
- [7] Shpigel et al. Can Anions Be Inserted into MXene? *J. Am. Chem. Soc.* 2021, 143, 32, 12552–12559

9:00 AM DISCUSSION TIME

SESSION NM04.12: Virtual Session II: MXenes II
Session Chairs: Kartik Nemani and Brian Wyatt
Tuesday Morning, December 6, 2022
NM04-virtual

10:30 AM *NM04.12.01

Cation Intercalation and Its Role in Designing Electrochemical Response of MXenes Maria Lukatskaya; ETH Zurich, Switzerland

As electronic technology advances, the need in safe and long-lasting energy storage devices that occupy minimum volume arises. Short charging times of several seconds to minutes, with energy densities comparable to those of batteries, can be achieved in pseudocapacitors. These are sub-class of supercapacitors, where capacitance is mediated by fast redox reactions and can enable at least an order of magnitude more energy to be stored than in typical electrical double layer capacitors. Transition metal oxides (e.g. RuO₂, MnO₂) and conducting polymers (e.g. polyaniline) serve as typical examples. However, these materials are often high in cost and/or suffer from low cycling stability. As a result, the search for new pseudocapacitive materials constitutes an important direction today.

In this talk, I will discuss how the key performance metrics of pseudocapacitors – capacitance and charging rates – can be pushed to the limits in the materials that combine good electrical and ionic conductivities (ensuring fast charge transfer and hence charging rates) with high density of redox-active and ionically accessible sites (enabling high capacitance and charging rates). In particular, the electrochemistry of 2D transition metal carbides (MXenes), with an emphasis on the mechanism of charge storage and factors affecting the overall capacitive response in these materials will be discussed. Moreover, the role of the cation intercalation in layered MXenes as means to manipulate its electrochemical response are examined.

11:00 AM NM04.12.03

Ti₃C₂T_x MXene with High Mass Loading as a Binder Free Electrode for Supercapacitor [Anamika Ashok](#)¹, Niranjana M¹, Swathy B Saseendran¹ and Asha A S^{1,2,2}, ¹Cochin University of Science and Technology, Department of Physics, India; ²CUSAT, India

Titanium carbide MXene being the most studied member of the 2D transition metal carbides/nitrides (MXene) family, has found applications in the field of energy storage and energy generation, due to its dynamic but tunable surface chemistry, good hydrophilicity and electrical conductivity. Conductive and clay like, in situ HF etched titanium carbide MXene can be used as supercapacitor electrodes and are prospective candidates in flexible electronics for commercial supercapacitor application. Commercial supercapacitors also require high energy storage capability, for which a high mass loading is necessary. Herein a high mass loading electrode with high areal capacitance has been fabricated using a simple brush coating of clay like titanium carbide MXene on carbon cloth. A controlled alkalization of titanium carbide using a weak base, ammonium hydroxide has been carried out in the synthesis of titanium carbide MXene. The in situ alkalization process reduces the time of synthesis and causes an inherent expansion of the interlayer spacing, making the diffusion of ions easier. The structural, morphological, optical, and electronic properties have been studied using X-ray diffraction, scanning electron microscope, UV visible absorption spectroscopy, X-ray photoelectron spectroscopy analysis and Fourier transform infrared spectroscopy analysis. The prepared MXene has the characteristic (002) diffraction peak and a layered morphology, similar to the open accordion morphology of HF etched MXene. The optical studies indicated ease of delamination from the evolution of the plasmonic peak in the NIR region. XPS and FTIR studies indicated presence of -O, -F and -OH functional groups. Titanium carbide MXene electrode on glassy carbon and on carbon cloth were fabricated. Nafion-assisted coating in glassy carbon electrode was replaced by binder free coating of MXene clay, while using carbon cloth. A simple brush coating onto pre-heated carbon cloth produced uniform films, with good electrochemical performance. The prepared electrode exhibited good gravimetric capacitance of 109 F/g at a current density of 0.5 A/g and areal capacitance of 2500 mF/cm² at a current density of 11 mA/cm². High mass loading combined with high areal capacitance make the prepared electrode a potential candidate for commercial applications.

11:15 AM NM04.12.04

Two-Dimensional Titanium Carbide with Interlayer Spacing as Electrode Material for Supercapacitors [Meenu Sharma](#) and Atul Bhargav; Indian Institute of Technology Gandhinagar, India

It is essential to investigate novel electrode materials to advance the development of supercapacitors and their implementations in electronic applications. A group of two-dimensional (2D) transition metal carbides and nitrides known as MXenes (Ti₃C₂T_x) have earned more attention as electrode materials for industrial supercapacitors. It has the distinctive features that bulk materials lack, such as a large specific surface area, thermal resistive properties, a low energy barrier for electron transport, and a short ion diffusion path, which make desirable electrodes for energy storage devices. Titanium Carbide (Ti₃C₂T_x) is synthesized in this study using a relatively simple chemical method to develop low defects and high-quality MXene while keeping the stacking and interlayer spacers intact. The crystalline structure and surface morphology are investigated by XRD, SEM, TEM and BET analyses. An electrode is fabricated using a synthesized Ti₃C₂T_x as an active electrode material and Ni-foil as a current collector. The layered morphology is confirmed using a field emission scanning electron microscope, and the presence of the elements of the synthesized MXene is verified using energy-dispersive spectroscopy analysis. The specific surface area of MXene is estimated to be 38 m²g⁻¹ using the BET measurement by nitrogen adsorption and desorption isotherm, with a pore volume of 0.4029 cm³g⁻¹ and average pore size of 4 nm. The electrochemical performance of a Ti₃C₂T_x electrode is tested using cyclic voltammetry with a 6M KOH electrolyte. When used as an electrode for supercapacitors, Ti₃C₂T_x MXene demonstrated an exceptional specific capacitance of 831 Fg⁻¹ at a 2 mVs⁻¹ scan rate in the voltage window of 0.0-0.6 V. The layered structures of MXene improve electrolyte ion transport while also providing transition metal active redox sites on the surface. The electrode has remarkable cyclic stability of 97% over 10000 continuous cycles at 50 mV s⁻¹. The findings suggest an appealing strategy for producing two-dimensional nanomaterials-based electrodes and composites for improved implementation and innovative supercapacitor designs.

Keywords: MXene, Energy Storage, 2D materials

References:

- R. Li, L.Zhang, L. Shi, and P. Wang, MXene Ti₃C₂: an effective 2D light-to-heat conversion material, *ACS nano.*, 2017, **11**, 3752-3759.
S. Nam, J.N. Kim, S. Oh, J. Kim, C.W. Ahn, and I.K. Oh, Ti₃C₂T_x MXene for wearable energy devices: Supercapacitors and triboelectric nanogenerators, *APL Material.*, 2020, **8**, 110701.
B. Anasori, M.R. Lukatskaya, and Y. Gogotsi, 2D metal carbides and nitrides (MXenes) for energy storage, *Nature Reviews Materials.*, 2017, **2**,1-17.
X.Wang, Y. Li, S. Wang, F. Zhou, P. Das, C. Sun, S. Zheng and Z.S. Wu, MXene for energy storage: present status and future perspectives, *Journal of Physics: Energy.*, 2020, **2**, 032004.

11:30 AM NM04.12.05

Investigation of Structural and Morphological Properties of Two-Dimensional V₂CT_x (T_x=-OH,-F, Cl) MXene and Its Photocatalytic Activity [Monidipa Pramanik](#), Mukta V. Limaye and Shashi B. Singh; IISER BERHAMPUR, India

Photocatalytic dye degradation is a most promising and cost-effective way to remove organic pollutants from water in various industries. MXene, a new group of two-dimensional materials, has recently gained tremendous attention as a photocatalyst due to its unique surface functionalities, chemical composition, and physicochemical and visible light absorption properties. These properties make MXene a promising catalyst for the photodegradation of organic molecules. In this work, we have synthesized V₂CT_x (T_x = -OH, -F, Cl) MXene by acid etching method and have been characterized by X-ray diffraction, Raman spectroscopy, and scanning electron microscopy to confirm its structural and surface morphological properties. The chemical composition of catalysts was studied by X-ray photoelectron spectroscopy(XPS). The potentiality of photocatalytic degradation of V₂CT_x MXene was studied by UV-Visible spectroscopy using methylene blue (MB) and crystal violet(CV) under visible light irradiation. The degradation performance for 0.01 M MB dye is 97.9% in 45 minutes and for 0.25 M CV is 93% in 60 min under visible light. This work opens a path for studying the catalytic property of V₂CT_x MXene.

11:45 AM *NM04.12.06

Building 3D Architectures from 2D MXenes [Suelen Barg](#)^{1,2}; ¹University of Augsburg, Germany; ²The University of Manchester, United Kingdom

2D Materials-based 3D architectures are promising materials for advanced systems of future technologies. Among 2D materials, MXenes (especially their most studied member, Ti₃C₂T_x) present a unique opportunity for application via colloidal processing, as they are electrically conductive and chemically active, whilst still being easily dispersed in water. This talk will present an overview of the progress on the development of colloidal approaches towards 3D architectures of tuned microstructures built from 2D MXenes, with emphasis on ice-templating and extrusion-based additive manufacturing (AM) methods. The potential of these methods and materials will be exemplified in specific applications such as in the development of vertically aligned MXene and multi-material architectures for high-rate performance supercapacitors and the development of advanced composites for electrothermal heating.

12:15 PM DISCUSSION TIME

SESSION NM04.13: Virtual Session III: MXenes III
Session Chairs: Pooi See Lee and Kartik Nemani
Tuesday Afternoon, December 6, 2022
NM04-virtual

9:00 PM *NM04.13.01

MXenes as Electrode Materials for High Performance Rechargeable Batteries and Highly Efficient Electrocatalysis Guoxiu Wang and Xin Guo; University of Technology Sydney, Australia

The ever-increasing demand for renewable energy has urged the development of new materials for the new-generation energy storage and conversion. Among all the candidature materials, 2D transition metal carbides, carbonitrides and nitrides (often referred to as MXene) have drawn intensive attention owing to their excellent electrical conductivity and unique chemical and physical properties. Our research shows that MXene can be applied as host materials for anchoring single atoms to be used in electrochemical hydrogen generation [1] and carbon dioxide conversion [2], as well as composite materials for the application in new-generation batteries with excellent electrochemical performance such as in lithium-sulfur batteries [3, 4], lithium-iodine batteries [5], lithium/sodium-selenium batteries [6], sodium-ion batteries [7], sodium-sulfur batteries [8], and potassium-sulfur batteries [9]. Moreover, the careful design of the material architecture of MXenes has endowed the application for the desalination of saline water [10]. The excellent performances indicate that the MXene-based materials are the promising materials for the applications in the field of energy conversion and storage.

References:

- [1] J. Zhang, Y. Zhao, X. Guo, C. Chen, C.-L. Dong, R.-S. Liu, C.-P. Han, Y. Li, Y. Gogotsi, G.X. Wang, *Nature Catalysis*, 1 (2018) 985.
- [2] D. Zhao, Z. Chen, W. Yang, S. Liu, X. Zhang, Y. Yu, W.-C. Cheong, L. Zheng, F. Ren, G. Ying, X. Cao, D. Wang, Q. Peng, G.X. Wang, C. Chen, *J. Am. Chem. Soc.*, 141 (2019) 4086.
- [3] W. Bao, D. Su, W. Zhang, X. Guo, G.X. Wang, *Adv. Funct. Mater.*, 26 (2016) 8746-8756.
- [4] W. Bao, L. Liu, C. Wang, S. Choi, D. Wang, G.X. Wang, *Adv. Energy Mater.*, 8 (2018) 1702485.
- [5] X. Tang, D. Zhou, P. Li, X. Guo, C. Wang, F. Kang, B. Li, G. Wang, *ACS Cent. Sci.*, 5 (2019) 365.
- [6] F. Zhang, X. Guo, P. Xiong, J. Zhang, J. Song, K. Yan, X. Gao, H. Liu, G. Wang, *Adv. Energy Mater.*, 10 (2020) 2000446.
- [7] X. Guo, W. Zhang, J. Zhang, D. Zhou, X. Tang, X. Xu, B. Li, H. Liu, G. Wang, *ACS Nano*, 14 (2020) 3651-3659.
- [8] W. Bao, C. E. Shuck, W. Zhang, X. Guo, Y. Gogotsi, G. Wang, *ACS Nano*, 13 (2019) 11500-11509.
- [9] X. Tang, D. Zhou, P. Li, X. Guo, B. Sun, H. Liu, K. Yan, Y. Gogotsi, G. Wang, *Adv. Mater.*, 32 (2020) e1906739.
- [10] W. Bao, X. Tang, X. Guo, S. Choi, C. Wang, Y. Gogotsi, G. Wang, *Joule*, 2 (2018) 778-787.

9:30 PM NM04.13.02

Molecular-Level Methylcellulose/MXene Hybrids for Low-Voltage Electrochemical Actuators Shaohua Chen, Jing-Hao Ciou, Fei Yu, Jian Chen, Jian Lyu and Pooi See Lee; Nanyang Technological University, Singapore

Electrochemical actuators (ECAs) can generate deformation and force under very low input voltages, and are promising for various applications such as artificial muscles and soft robotics. $Ti_3C_2T_x$ MXene is a potential active material for ECAs due to its large volumetric capacitance and high electrical conductivity. However, MXene film suffers from unfavorable in-plane actuation performance in aqueous electrolytes because of the high in-plane alignment of MXene sheets and poor wet strength. Here, we fabricated molecular-level methylcellulose/MXene hybrid films with enlarged layer distances by a simple mixing and vacuum filtration process. The hybrid films show improved ambient stability and wet strength in 1 M aqueous Li_2SO_4 . Though the charge storage capacity was improved slightly, the hybrid films generated significantly higher in-plane actuation displacements in the aqueous electrolyte. Based on the direct strain monitoring as well as in-situ XRD and ex-situ XPS investigations, the enhanced actuation is ascribed to the enlarged interlayer distance allowing more ions/water to be intercalated/deintercalated and more importantly the large sliding of MXene sheets induced by methylcellulose during the charge/discharge. The assembled soft ECA has a high Young's modulus of 1.93 GPa and generated a peak-to-peak strain difference up to 0.541% and a blocking force of 4.7 times its gravity under 1-V triangular and DC voltages, respectively. The significant actuation enhancement induced by the insulating methylcellulose can inspire the rational design of high performance ECAs based on other nanomaterials.

Reference

Chen S., Ciou J.-H., Yu F., Chen J., Lv J., Lee P. S. Molecular-Level Methylcellulose/MXene Hybrids with Greatly Enhanced Electrochemical Actuation. *Advanced Materials*. 2022, 2200660.

9:45 PM *NM04.13.03

Pseudocapacitance Through MXene/Solid Electrolyte Interface Masashi Okubo; Waseda University, Japan

All-solid-state energy storage devices with non-flammable inorganic solid electrolytes are a key technology for addressing the safety issues of lithium-ion batteries with flammable organic liquid electrolytes. However, conventional electrode materials suffer from substantial volume change during lithium-ion (de)intercalation, leading to the failure of the interface between the electrode materials and solid electrolytes and then severe performance degradation. In this work, we report pseudocapacitance through a strain-free interface between a solid electrolyte and a transition-metal carbide nanosheet (MXene), where MXene electrodes show negligible structural changes during lithium-ion (de)intercalation. As a proof of concept, we demonstrate the stable operation of an all-solid-state hybrid capacitor ($Ti_3C_2T_x|Li_3PS_4$ glass/ $LiCoO_2$).

SESSION NM04.14: Virtual Session IV MXenes IV
Session Chairs: Babak Anasori and Anupma Thakur
Tuesday Afternoon, December 6, 2022
NM04-virtual

1:00 PM NM04.14.01

Effect of Alkali Metal Cations on the High Temperature Stability of $Ti_3C_2T_x$ and $Mo_2TiC_2T_x$ MXenes Brian Wyatt¹, Kartik Nemani¹, Matthew Boebinger², Zachary Hood³, Shiba Adhikari³, Annabelle Harding¹, Wyatt Highland¹, Raymond Unocic² and Babak Anasori¹; ¹Indiana University - Purdue University of Indianapolis, United States; ²Oak Ridge National Laboratory, United States; ³Argonne National Laboratory, United States

Two-dimensional transition metal carbides, known as MXenes, have found wide use in energy storage and catalysis applications. Although MXenes have been used in these applications, few studies have investigated the use of MXenes' interior transition metal carbide/nitride core and abundant surface groups as nanosized building blocks toward extreme environment nanoceramics. In this presentation, we illustrate the high-temperature behavior of $Ti_3C_2T_x$ and $Mo_2TiC_2T_x$ MXenes up to 2,000 °C. In addition, we exhibit the role of surface-adsorbed alkali metal cations (Na^+ , K^+ , Ca^{2+}) on improving the phase stability and controlling the phase transformation of these MXenes using *in situ* two-dimensional x-ray diffraction (XRD²) up to 1,100 °C using and *ex situ* XRD² up to 2,000 °C. We also present the changes in phase transformation of non-decorated and alkali metal cation decorated $Mo_2TiC_2T_x$ MXenes using *in situ* scanning transmission electron microscopy (STEM) up to 800 °C. The combination of *in situ* XRD² and STEM methods with *ex situ* XRD², x-ray photoelectron spectroscopy, and thermogravimetric analysis demonstrate the effect of alkali metal cations on improving the phase stability and controlling the phase transformation of MXenes. This presentation assists in furthering development of MXenes as a diverse and tunable family of nanoceramics for ultra-high temperature applications.

1:15 PM NM04.14.02

$Ti_3C_2T_x$ MXene-Derived Carbides as Additive Materials for Ultra-High Temperature Ceramics (UHTCs) Kartik Nemani^{1,2}, Yooran Im^{1,3} and Babak Anasori^{2,1}; ¹Purdue University, United States; ²Integrated Nanosystems Development Institute, United States; ³Indiana University Purdue University, United States

Zirconium diboride (ZrB₂) is one of the ultra-high temperature ceramics (UHTC), which are used for applications at temperatures above 2000 C. However, a significant drawback is its poor mechanical properties such as fracture toughness, poor densification behavior and oxidation resistance since monolithic boride is prone to the formation of volatile oxides (such as B₂O₃) at temperatures above 1100 C. In this project, we have investigated a one-pot, surfactant-free, aqueous mixing method to develop homogeneous ZrB₂- $Ti_3C_2T_x$ MXene green bodies and evaluated their sintering behavior. We present the phase transformation of $Ti_3C_2T_x$ MXene to TiC_n at the grain boundaries, the interface interactions between the ZrB₂- TiC_n grains and their densification mechanism. A nominal relative density of 96% is achieved with the addition of 0.5 wt% of MXene to ZrB₂ and sintering of the resulting powder mixture at 1900 C with 50 MPa pressure under vacuum. We discuss a fundamental understanding of the intermediate phase formation and evolution, and their effect on the mechanical properties of the resulting UHTC. This study lays the groundwork for 2D MXenes as compatible materials for UHTC applications that can be used as precursors for carbides in ultra-high temperature applications such as hypersonics, nuclear, and extraterrestrial travel.

1:30 PM NM04.14.03

Hybrid MXene Electrodes with Anomalous Electrochemical Response Armin VahidMohammadi, Kyle Matthews, Teng Zhang and Yury Gogotsi; Drexel University, United States

MXenes are a family of two-dimensional (2D) transition metal carbonitrides, with a general structure of $M_{n+1}X_nT_x$, where M is the transition metal, X is carbon or nitrogen, and T represents the surface terminations (F, O, OH) and $n = 1-4$ indicates to the number of atomic layers in their structure. Since their discovery, MXenes have shown promising properties for electrochemical charge storage applications and various MXene compositions have been tested in different electrochemical systems, both in their multilayered and delaminated forms. However, usually these materials show capacitive-like response in aqueous electrolytes with the exception of protic electrolytes such as H₂SO₄ where redox peaks and a pseudocapacitive behavior is observed. Particularly, MXenes tested in aqueous neutral electrolytes exhibit quasi-rectangular cyclic voltammograms. In this presentation, we demonstrate that through changing MXenes' electrode structure by hybridizing them with conducting large modifiers, these materials can show anomalous electrochemical response with distinct redox couples in neutral aqueous electrolytes. We primarily show this behavior on hybrid V_2CT_x electrodes, where the free-standing films exhibit a distinct cyclic voltammograms in various alkali cation containing electrolytes with broad cathodic and anodic peaks, unlike pristine V_2CT_x which has a capacitive response. The observed phenomena in hybrid structures indicates a different charge storage mechanism in these electrodes while maintaining the overall amount of the charge that can be stored. Our results open new avenues in understanding the charge storage mechanism in MXene electrodes which can be used to tailor the desired electrochemical response of these materials in different electrolyte systems.

1:45 PM NM04.14.04

MXene-MoS₂ Composite Coatings for Enhanced Solid Lubrication Dario Zambrano, Jose Y. Aguilar Hurtado and Andreas Rosenkranz; Universidad de Chile, Chile

Friction and wear occur in all moving mechanical systems thus greatly contributing towards energy losses and downgraded efficiencies. These aspects together with global warming, diminishing material and raw oil resources as well as more stringent restrictions for the use of certain additives in lubricating oils urgently ask for advanced lubrication concepts. In this regard, solid lubrication has emerged as a promising strategy to tackle these challenges. Very recently, MXene solid lubricant coatings have shown an outstanding wear performance and durability with the potential to outperform all state-of-the-art solid lubricants including graphene and MoS₂. Although showing an excellent wear performance, MXene solid lubricant coatings still demonstrate a rather poor frictional performance, which needs further optimization and improvement.

Therefore, we aim at fabricating innovative sandwich-like composite coatings consisting of two different 2D nano-materials ($Ti_3C_2T_x$ and MoS₂) on stainless steel substrates for solid lubrication purposes. As an additional variable, we vary the respective order of the different coating layers ($Ti_3C_2T_x/MoS_2$ and $MoS_2/Ti_3C_2T_x$). We envision that these sandwich-like composite coatings exhibit enhanced mechanical properties as well as good friction and wear properties at the same time due to the designed sandwich-like structure and synergetic effects originating from individual nano-sheets.

As a first step, single-material solid lubricant coatings (either only $Ti_3C_2T_x$ or MoS₂) with a thicknesses of 600 nm are spray-coated on stainless steel substrates with a particular emphasis on the coatings' homogeneity. Subsequently, the as-deposited coatings are holistically studied regarding their overall quality (roughness and thickness), physicochemical properties (surface chemistry) by complementary materials characterization. Afterwards, the effect of the material ($Ti_3C_2T_x$ or MoS₂) on friction and wear under dry sliding conditions is evaluated in short- (running-in) and long-term experiments (durability). Particular emphasis is laid on the underlying energy-dissipating friction and wear mechanisms. In this regard, the worn surfaces (coatings and counter-bodies) will be fully characterized by complementary characterization to elucidate the formation of potential tribolayers.

After having studied the effect of the underlying material, sandwich-like composite coatings combining $Ti_3C_2T_x$ and MoS₂ are spray-coated on stainless steel substrates. Regarding deposition, concentrations of 4 mgmL⁻¹ for MoS₂ and 5 mgmL⁻¹ for $Ti_3C_2T_x$ were used, modifying the applied volume to ensure the fabrication of high-quality, thickness and homogeneous sandwich-like composite coatings. To allow for a fair and direct comparison, the sandwich-like composite coatings will be evaluated using the same experimental conditions (materials characterization and tribological testing conditions). The worn composite coatings will be studied by advanced, complementary materials characterization to elucidate the underlying friction and wear mechanisms as well as potential synergetic effects stemming from the different 2D nano-sheets.

Summarizing, sandwich-like composite coatings (MoS₂/ $Ti_3C_2T_x$ and $Ti_3C_2T_x/MoS_2$) are expected to improve the interfacial properties and enhance the system's mechanical properties. This is hypothesized to induce synergetic tribological properties thus creating solid lubrication coatings with an enhanced

friction and wear performance at the same time.

2:00 PM DISCUSSION TIME

SYMPOSIUM NM05

Challenges and Opportunities in Solution Synthesis of Functional Nanomaterials
November 28 - December 7, 2022

Symposium Organizers

Nikolai Gaponik, TU Dresden
Andrey Rogach, City University of Hong Kong
Elena Shevchenko, Argonne National Laboratory
Dmitri Talapin, University of Chicago

Symposium Support

Bronze
Nanoscale

* Invited Paper
+ Distinguished Invited

SESSION NM05.01: Fundamentals of Nanomaterial Synthesis I
Session Chairs: Alexander Eychmueller and Dmitri Talapin
Monday Morning, November 28, 2022
Hynes, Level 2, Room 202

10:30 AM *NM05.01.01

Synthesis, Properties and Applications of Nanocrystals in Materials and Life Sciences Horst Weller^{1,2}; ¹Hamburg Univ, Germany; ²Fraunhofer CAN, Germany

Although colloidal nanocrystals of many different materials can be synthesized in high quality in respect of size, shape and crystallinity, our understanding of their formation and the involved chemical reactions is still rather poor. We will present detailed studies on nucleation and growth as well as ion exchange processes in nanocrystals. These include mass spectrometric, optical, electron microscopic and x-ray synchrotron experiments. Almost all applications of nanocrystals require the control of surface properties in respect of solubility, miscibility, biocompatibility, passivation of surface states as well as electronic and magnetic interaction with the environment. We will show various examples for ligand exchange and encapsulation of quantum dots, plasmonic and magnetic nanocrystals and will report on applications as high-performance ceramics, for display and lighting, electrocatalysis as well as for biolabeling and drug delivery.

11:00 AM *NM05.01.02

Highly Luminescent Lead Halide Perovskite Nanocrystals—Revisiting Their Synthesis and Tailoring Their Surface Chemistry Maksym V. Kovalenko^{1,2}; ¹ETH Zurich, Switzerland; ²Empa—Swiss Federal Laboratories for Materials Science and Technology, Switzerland

Colloidal lead halide perovskite (LHP) nanocrystals (NCs), with bright and spectrally narrow photoluminescence (PL) tunable over the entire visible spectral range, are of immense interest as classical and quantum light sources. Severe challenges LHP NCs form by sub-second fast and hence hard-to-control ionic metathesis reactions, which severely limits the access to size-uniform and shape-regular NCs in the sub-10 nm range. We show that a synthesis path comprising an intricate equilibrium between the precursor (TOPO-PbBr₂ complex) and the [PbBr₃⁻] solute for the NC nucleation may circumvent this challenge [1]. This results in a scalable, room-temperature synthesis of monodisperse and isolable CsPbBr₃ NCs, size-tunable in the 3-13 nm range. The kinetics of both nucleation and therefrom temporally separated growth are drastically slowed, resulting in total reaction times of up to 30 minutes. The methodology is then extended to FAPbBr₃ (FA = formamidinium) and MAPbBr₃ (MA = methylammonium), allowing for thorough experimental comparison and modeling of their physical properties under intermediate quantum confinement. In particular, NCs of all these compositions exhibit up to four excitonic transitions in their linear absorption spectra, and we demonstrate that the size-dependent confinement energy for all transitions is independent of the A-site cation.

We then show that this synthesis – relying on the labile ligand capping with TOPO-phosphinic acid mixture – makes for a convenient platform for the subsequent surface functionalization with diverse capping ligands [2]. Robust surface functionalization of highly ionic surfaces, as is the case of LHP NCs, has remained a formidable challenge due to the inherently non-covalent weak surface bonding. Leveraging the vast and facile molecular engineering of phospholipids, we present their efficacy as surface capping ligands for LHP NCs. Molecular dynamics simulations and solid-state NMR confirm that the surface affinity of these zwitterionic molecules is primarily governed by the geometric fitness of their anionic and cationic moieties. Judicious selection of the ligands yielded colloiddally robust FAPbBr₃ and MAPbBr₃ NCs and enabled colloids in a variety of solvents, from n-hexane to acetone. Robustness of the surface capping is also reflected in optical properties: NCs exhibit PL quantum yield (QY) above 96% after numerous purifications. NCs are essentially blinking-free at a single particle level.

Q. Akkerman *et al.* submitted
V. Morad *et al.* submitted

11:30 AM NM05.01.03

Symmetry Breaking in Chiral Lanthanide-Based Nanocrystals—A Model System to Study Nucleation and Growth [Gil Markovich](#), Gal Schwartz and Uri Hananel; Tel Aviv University, Israel

Many inorganic compounds crystallize in chiral space groups, such as quartz, for example. Our group has been studying the breaking of left-right symmetry in the formation of nanocrystals of such compounds. We have shown, that using small chiral bio-molecules, which interact with the crystals' building blocks, it is possible to achieve such a symmetry break. In particular, we have been working with the chiral $\text{TbPO}_4 \bullet \text{H}_2\text{O}$ nanocrystals, and have shown that their handedness can be controlled by preparing the nanocrystals in the presence of certain natural chiral molecules, such as tartaric acid.¹ We used circularly polarized luminescence measurements of Eu^{3+} dopant ions in the nanocrystals to follow the handedness and enantiomeric purity of the produced nanocrystals. Using single particle circularly polarized luminescence microscopy we were able to determine the handedness of individual nanocrystals and confirmed that we obtain a single enantiomer of the terbium phosphate nanocrystals when prepared with tartaric acid molecules.² This system exhibits ultra-high chirality amplification and can completely break symmetry on seeding with minute amounts of enantiomerically-pure seed particles. Such effects are typically attributed to autocatalytic effects also termed secondary nucleation. We study the nature of these effects through comparison of symmetry breaking by chiral ligands vs. addition of chiral seed particles. We also obtain important mechanistic information by following the nanocrystals' formation kinetics by in-situ monitoring total luminescence and circularly polarized luminescence over time.³ We believe that further studies of this model system might shed more light on the nature of nucleation in general and secondary-nucleation in particular.

¹ U. Hananel, A. Ben-Moshe, H. Diamant, G. Markovich, "Spontaneous and directed symmetry breaking in the formation of chiral nanocrystals", *Proc. Natl. Acad. Sci. USA* **116**, 11159-11164 (2019).

² E. Vinegrad, U. Hananel, G. Markovich, O. Cheshnovsky, "Determination of Handedness in a Single Chiral Nanocrystal via Circularly Polarized Luminescence", *ACS Nano* **13**, 601–608 (2019).

³ G. Schwartz, U. Hananel, L. Avram, A. Goldbourt, G. Markovich, "A Kinetic Isotope Effect in the Formation of Lanthanide Phosphate Nanocrystals", *J. Am. Chem. Soc.* **144**, 9451-9457 (2022).

11:45 AM NM05.01.04

Non-Hydrolytic Sol-Gel Chemistry to Functional Hybrid Materials [Nicola Pinna](#); Humboldt-Universitat Berlin, Germany

The current trend in various energy applications, ranging from lighting to batteries and electrolyzers, lays in the control of structural, physicochemical and morphological properties of materials and their interfaces.

During this presentation, recent strategies for nanostructured materials synthesis, targeting energy and environmental applications will be discussed. Especially, we will focus on one-pot strategies for the fabrication of hybrid and complex nanomaterials focusing on the importance of the organic-inorganic and inorganic-inorganic interfaces.

Among the examples presented, we will discuss the synthesis of complex nanostructures and the stabilization of metastable phases for applications in energy storage and conversion.

We will see that nowadays the available strategies allow a control in terms of composition, crystalline structure, morphology and nanostructure that would have been unimaginable just few years ago.

Finally, the open challenges the field is currently facing and possible further developments which are needed to meet the always growing demand for high performing materials will be also discussed.

SESSION NM05.02: Advanced Synthesis and Characterization Methods

Session Chairs: María Ibáñez and Elena Shevchenko

Monday Afternoon, November 28, 2022

Hynes, Level 2, Room 202

1:30 PM *NM05.02.01

Localizing Ligands on Nanocrystal Surfaces Kim Dümbgen¹, Ivan Infante² and [Zeger Hens](#)¹; ¹Ghent University, Belgium; ²Istituto Italiano di Tecnologia, Italy

Colloidal nanocrystals synthesized in apolar media are organic/inorganic hybrids that consist of a crystalline core and a surface capping of organic ligands. While the physical properties of individual nanocrystals are mostly determined by the inorganic core, the role of the organic ligand shell cannot be underestimated. Examples range from synthetic aspects to properties of single nanocrystals and nanocrystal assemblies, such as precursor conversion and nucleation and growth kinetics, the passivation of electronic trap states or the realization of high charge carrier mobility. As a result, the question as to how ligands bind and pack to the nanocrystal surface has been central to nanocrystal research for many years. Extensive insight was obtained by introducing innovative experimental methods to identify surface-bound ligands and, more recently, computational approaches to calculate properties of these ligands. An experimental method that stands out for the analysis of ligand binding is nuclear magnetic resonance (NMR) spectroscopy, due to its capability of identifying and quantifying nanocrystal-bound moieties through diffusion-ordered spectroscopy (DOSY) or nuclear Overhauser effect spectroscopy (NOESY). However, while in-situ NMR analysis of ligand exchange gives experimental insight in ligand binding - often formalized through the L-, X- or Z-type classification borrowed from coordination chemistry - understanding ligand packing from NMR data proved more difficult.

In this talk, we discuss recent progress on the interpretation of the NMR lineshape in terms of ligand packing on nanocrystal surfaces. We take InP nanocrystals synthesized by reacting InCl_3 and tris-diethylaminophosphine in oleylamine as a model system. After showing that the resulting nanocrystals have a mixed ligand shell consisting of chloride and oleylamine, we use spectral hole burning to show that the oleylamine ^1H NMR resonances are heterogeneously broadened. Moreover, by recording the relaxation dynamics of spectral holes, we show that the heterogeneous set of bound ligands consists of at least 2 pools that are not in close proximity, are not involved in chemical exchange and feature a different solvation. In practice, when using aromatic solvents, the more solvated pool is retrieved at the upfield side of the resonance, while the less solvated pool at the downfield side. Using molecular dynamics simulations based on a realistic, atomically precise InP model nanocrystal, we identify the most and least solvated pool as ligands bound to edges and facets, respectively. Interestingly, changes of NMR lineshape following partial ligand exchange reactions indicate that the pool of edge-localized ligands can be selectively removed, a result in line with the predicted weaker binding of ligands at those sites.

To conclude, we highlight that ligands may pack in different, static or dynamic ways to nanocrystal surfaces. Since each of these modes will have a different effect on the heterogeneous broadening of NMR resonances of bound ligands, more is to be learned from spectral hole burning and spectral hole burning relaxation than discussed in this talk.

2:00 PM NM05.02.02

Towards Endogenous DNP-NMR in Semiconducting Nanoparticles Ran Eitan Abutbul, Daniel Jardon-Alvarez and Michal Leskes; Weizmann Institute of Science, Israel

Many physical and chemical properties of nanomaterials are dominated by the properties of their surfaces. The importance of surfaces stems from the large surface-to-volume ratio of nanomaterials. These materials are synthesized and processed using ligand molecules, which bind and alter the properties of nanomaterials surfaces. Understanding the role of ligands in the rational design of functional nanomaterials is one of the main challenges in this field. The structure and properties characterization of these nanomaterials requires techniques such as TEM, FTIR UV-Vis-IR, and more. Information acquired from these techniques is invaluable, yet it is limited when attempting to probe a ligand-inorganic interface from a collective of nanostructured materials. Solid-state nuclear magnetic resonance (ssNMR) spectroscopy is a powerful tool for probing local structures at the atomic scale. The inherently low sensitivity of NMR could be overcome with dynamic nuclear polarization (DNP). Typically, organic radicals are added as polarizing agents (PA) to the sample in the exogenous approach. Polarization transfer from electron spin to the nuclear spin occurs upon microwave irradiation, thus enhancing the NMR signal. However, when dealing with ligand-coated nanomaterials, the presence of radicals can dramatically affect the interface under investigation and interfere with its characterization.

This work demonstrates the endogenous DNP approach in nanoparticles for the first time. Where the PAs are transition metal ions with unpaired electrons incorporated in the inorganic lattice. Mn-doped CdS nanoparticles were synthesized using the standard hot-injections technique and characterized using TEM, EPR, and ICP-MS. In addition to a significant DNP enhancement for ^{113}Cd nuclei, surface and core moieties were observed. This approach potentially paves the way for advanced characterization of the ligand-inorganic interface for surfactant-coated nanoparticles.

2:15 PM NM05.02.03

Improving Electron Pair Distribution Function (ePDF) for Nanomaterials—The Case of Iron Oxide Nanoparticles Naga Vishnu V. Mogili¹, Juliana T. Carvalho¹, Murillo H. Rodrigues^{1,2}, Jefferson Bettini¹, Edson R. Leite^{1,2} and João B. Souza Junior^{1,3}; ¹Brazilian Center for Research in Energy and Materials (CNPEM), Brazil; ²Universidade Federal de São Carlos (UFSCar), Brazil; ³Universidade Estadual de Campinas (UNICAMP), Brazil

Nanomaterials' properties are strongly related to their crystallographic atomic arrangement. Methods to characterize their atomic structure are fundamental to understanding materials' properties and, consequently, controlling their properties and achieving their full performance. However, classical X-ray diffraction (XRD) methods fail to elucidate the nanostructures due to the elevated peak broadening, a challenge that is known as the nanostructure problem. Pair Distribution Function (PDF) analysis obtained by neutrons and X-ray scattering (synchrotron) have been used to study nanomaterials with outstanding performance, but the access to synchrotron data is limited to the general nanoscience researchers. Electrons have become an alternative source as, nowadays, a transmission electron microscope (TEM) is certainly more accessible compared to synchrotrons. Electrons also have higher scattering power offering the advantage of using a small amount of sample, time-efficient data acquisition, and lower costs.¹ On the opposite side, electrons have a higher probability of multiple scattering and inelastic scattering leading to a harder data processing to collect the total scattering in the kinematical regime. Then, advances in implementing the PDF analysis using electron diffraction (ePDF) would be of great importance.¹ ePDF is a technique capable of analyzing materials structure directly in the real space with the $G(r)$ profile leading to the probability of occurrence of any pair of atoms within the material by their interatomic distances r .¹ Also, ePDF can reveal all nanostructure features, including bulk crystalline region to the surface, which frequently possesses higher atomic disorder.² In this work, methods to improve ePDF $G(r)$ profile were implemented by comparing the experimental scattering profile $I(Q)_{\text{exp}}$, structure factor $S(Q)_{\text{exp}}$, and the PDF $G(r)_{\text{exp}}$ with calculated $I(Q)_{\text{calc}}$, $S(Q)_{\text{calc}}$, and $G(r)_{\text{calc}}$ for spherical nanoparticles. Size-controlled iron oxide nanoparticles were synthesized to be used as a case study for ePDF data acquisition and processing toward quantitative $G(r)$ data analysis. The electron diffraction data acquisition was optimized by collecting the scattering of a self-sustained nanoparticle superlattice membrane to avoid a carbon background. The scattering from the organic ligands (oleic acid) was also removed from the $I(Q)_{\text{exp}}$ to acquire only the electron scattering from the nanomaterial. By applying a frequency filter, the contribution of possible multiple and inelastic scattering background on $S(Q)_{\text{exp}}$ was removed. Finally, the $G(r)_{\text{exp}}$ was multiplied by a constant to achieve approximate the signal with the $G(r)_{\text{calc}}$. The final ePDF $G(r)$ was compared to a nanostructure model using a structure refinement method in PDFgui software. Several iron oxide nanoparticles were used to test the proposed method, from the as-synthesized magnetite to oxidized maghemite nanoparticles. Excellent structure refinement was achieved with R_w below 14% showing that our new method of ePDF data acquisition and processing can be used as a quantitative atomic structure method for the short-range atomic ordering and the medium-range ordering (< 10 nm) present in nanoparticles. combining regular TEM analysis like morphology (size, size distribution, and shape), high-resolution, and chemical mapping, the ePDF atomic structure analysis adds to TEM a perfect crystallographic characterization tool to solve the nanostructure problem.

The authors would like to acknowledge FAPESP (Grants 2018/05159-1, 2021/03321-9) and CNPq (409787/2021-3).

[1] Souza Junior, J.B. et al. **Matter**. 2021, 4 (2), 441-460.

[2] Souza Junior, J.B. et al. **J. Phys. Chem. Lett.** 2020, 11 (4), 1564-1569.

2:30 PM NM05.02.04

High-throughput Materials Synthesis Strategies Towards Accelerated Discovery of Novel Functional Nanomaterials for Green Energy Production Ali Abdelhafiz, Zhichu Ren and Ju Li; Massachusetts Institute of Technology, United States

It has been challenging over the past three decades to find viable energy alternatives with higher efficiency and lower cost to beat the non-friendly and commercially dominant hydrocarbon energy sources. Hydrogen is deemed to be one of the most prominent candidates, as a green fuel. Hydrogen can be generated in abundance from water splitting. Utilization of hydrogen in fuel cells, with no doubt, produces no harmful gases. Nevertheless, the two parts of the technology: hydrogen production and reduction are cumbersome. Both processes rely on kinetically sluggish electrocatalytic reactions. Enormous research efforts have been spent, with thousands of studies presented in literature, despite the technology left with a dim light shed on from commercial and practical point of views. Many materials-related challenges are hindering the flourishing of green hydrogen technology, where poor catalyst durability is a major challenge, despite being made from very expensive elements (e.g., Ir, Ru or Pt). Therefore, gigantic effort of research has been devoted to find inexpensive alternatives. Transition metals showed interesting performance towards water splitting (e.g., oxygen evolution (OER)). Recent research showed that electrocatalysts designed by alloying two or more elements (e.g., transition metals) showed promising enhancement in catalytic activity and durability due to synergistic effects from alloying, such as strain engineering or electron exchange. The potential of the alloying approach is constrained by standard synthesis methods (e.g., wet chemistry and thermal decomposition techniques) due to the governing thermodynamics rules (e.g., miscibility of the different alloying elements). That renders the synthesis of high entropy alloys (HEA), with more than 3 elements, to be complicated and tedious to achieve by those conventional methods.

In the presented talk we are presenting different strategies to synthesize metastable high entropy alloys (HEA) and their outstanding catalytic performance towards OER, in correlation to their unique chemistries and structures. Rapid cycling of temperature from room 25 °C to highly elevated levels (1700 °C),

in conjunction with ultra-rapid cooling, within milli-second range have been demonstrated by different methods including rapid Joule heating, Intense light flashing, and microwave plasma shock. Our results show successful synthesis of non-noble metals HEA NPs, possessing higher catalytic activity than IrO₂ catalyst for OER. The nature of the alloying elements dictates OER activity by promoting different oxidation states of the catalytically active transition metals (e.g., Fe, Ni and Co). In addition, a phenomenal in-situ chemical welding of HEA NP to carbon support, yielded HEA catalysts with two orders of magnitude longer durability than IrO₂. Our developed techniques resulted in formation of super-strong metal-carbide bonds “chemically welding” HEA NP to the catalyst support.

Synthesis of various HEA catalyst and their electrocatalytic performance screening has been carried out by using liquid handler robots and multi-axes robotic arm systems. Moreover, to optimize the design of materials (structure and chemistry), we are using active learning techniques to evaluate the achieved performance results by applying Gaussian process, followed by applying Bayesian Optimization techniques to propose novel chemistries and structures with a higher probability to achieve further improved performances. The presented study does not open the door only towards developing novel catalysts for energy production. However, it presents a strategy with multiple successfully demonstrated platforms towards accelerated discovery of novel materials. The high-throughput nature of the synthesis protocols presented in this talk can produce tens of thousands of different novel chemistries, at the same time taken by conventional methods to synthesize just a few, at a minimal energy consumption, cost, and manpower.

2:45 PM BREAK

3:15 PM *NM05.02.05

Structural and Compositional Engineering of Superlattices Comprising Halide Perovskite Nanocubes [Maryna Bodnarchuk](#)^{1,2}, Ihor Cherniukh^{1,2}, Taras V. Sekh^{1,2}, Alex Travasset³, Rainer F. Mahr⁴, Thilo Stoeferle⁴, Mariia Svyrydenko^{1,2}, Viktoria Morad^{2,1}, Gabriele Raino^{2,1}, Rolf Erni¹ and Maksym V. Kovalenko^{2,1}; ¹Empa-Swiss Federal Laboratories for Materials Science and Technology, Switzerland; ²ETH Zürich, Switzerland; ³Iowa State University of Science and Technology, United States; ⁴IBM Zurich, Switzerland

Colloidal lead halide perovskite nanocrystals (LHP NCs, NCs, A=C⁺, FA⁺, FA=formamidinium; X=Cl, Br, I) have become a research spotlight owing to their spectrally narrow (<100 meV) fluorescence, tunable over the entire visible spectral region of 400-800 nm, as well as facile colloidal synthesis. These NCs are attractive single-photon emitters as well as make for an attractive building block for creating controlled, aggregated states exhibiting collective luminescence phenomena. Attaining such states through spontaneous self-assembly into long-range ordered superlattices (SLs) is a particularly attractive avenue. In this regard also the atomically flat, sharp cuboic shape of LHP NCs is of interest because the vast majority of prior work had invoked NCs of rather spherical shape. Long-range ordered SLs with the simple cubic packing of cubic perovskite NCs exhibit sharp red-shifted lines in their emission spectra and superfluorescence (a fast collective emission resulting from coherent multi-NCs excited states).

When CsPbBr₃ NCs are combined with spherical dielectric NCs, perovskite-type ABO₃ binary NC SLs form, wherein CsPbBr₃ nanocubes occupy B- and/or O-sites, while spherical dielectric Fe₃O₄ or NaGdF₄ NCs reside on A-sites. When truncated-cuboid PbS NCs are added to these systems, ternary ABO₃-phase form (PbS NCs occupy B-sites). Such ABO₃ SLs, as well as other newly obtained SL structures (binary NaCl, AlB₂- and ABO₆ types, columnar assemblies with disks, etc.), exhibit a high degree of orientational ordering of CsPbBr₃ nanocubes. These mesostructures exhibit superfluorescence as well, characterized, at high excitation density, by emission pulses with ultrafast (22 ps) radiative decay and Burnham-Chiao ringing behavior with a strongly accelerated build-up time. Combining CsPbBr₃ nanocubes with large and thick NaGdF₄ nanodisks results in the orthorhombic SL resembling CaC₂ structure with pairs of CsPbBr₃ NCs on one lattice site. We also implement two substrate-free methods of SL formation. Oil-in-oil templated assembly and self-assembly at the liquid-air interface result in the formation of binary supraparticles.

3:45 PM NM05.02.06

Controlling the Nucleation and Growth Kinetics of Spheroidal Lead Halide Perovskite Quantum Dots [Quinten A. Akkerman](#)¹, Anja Barfüßer^{1,2}, Maksym V. Kovalenko³ and Jochen Feldmann¹; ¹Ludwig-Maximilians-Universität (LMU), Germany; ²Empa-Swiss Federal Laboratories for Materials Science and Technology, Switzerland; ³ETH Zürich, Switzerland

Colloidal lead halide perovskites LHP (LHP) nanocrystals (NCs) have recently become popular light-emissive materials, of practical interest for LEDs, LCDs, lasers, as well as single photon light sources.^{1,2} Most studies on LHP NCs focus on relatively large cuboidal NC exceeding 10 nm in size, pointing out the inherent challenge of producing small (sub 10 nm), stable and monodisperse LHP quantum dots (QDs). This problem directly originates from the highly ionic lattice of LHPs, generally resulting in sub second reaction dynamics, making it very challenging to control their growth on an atomic level. Consequently, the current generation of LHP QDs (especially the hybrid organic-inorganic ones) show significantly less excitonic absorption landscapes compared to conventional QDs such as CdSe, even though LHPs have more simplistic band structure. This thus hinders studies into the size-quantization of excitons in LHPs (and possible practical use) as well as understanding of the mechanism of LHP QD formation, which still significantly lacks behind compared to conventional CdSe and PbS QDs.

<!--[endif]---->
<!--[endif]---->To solve this, we developed a room-temperature synthesis, in which the overall QD formation occurred on a time scale of up to 30 min, slowing down the reaction kinetics by several orders of magnitudes compared conventional LHP QD syntheses.³ The size of these QDs were tunable between 3 and 13 nm range and exhibited a rhombicuboctahedral (spheroidal) shape. These CsPbBr₃ QDs, as well as FAPbBr₃ and MAPbBr₃ exhibited up to four well-resolved excitonic transitions, finally bringing them on par with the highly excitonic absorption landscapes of CdSe and PbS QDs. This slow growth method also allowed for the first time to direct in-situ study the illusive reaction mechanism of LHP QDs, demonstrating the effective separation of the nucleation and growth stages due to the self-limiting formation of an Cs[PbBr₃] intermediate precursors. The slow growth approach was further extended by using an additional in-situ anion exchange step, resulting also in spheroidal CsPb(Cl:Br)₃ QDs with any Cl:Br ration and sizes from 4-10 nm.^{3,4} These quaternary QDs still exhibited up to five sharp excitonic absorption transitions, further demonstrating the versatility of the slow growth method. Finally, we used such spheroidal 6 nm CsPbBr₃ QDs to demonstrate that their respective excitons are confined with respect to their center-of-mass motion. Optical pumping of the lowest confined exciton transition with femtosecond laser pulses therefore not only bleaches all exciton resonances as measured with transient absorption spectroscopy, but also reveals a series exciton-to-biexciton transitions, which is further supported by their temporal dynamics.

References:

1. Protesescu, L. *et al.* Nanocrystals of Cesium Lead Halide Perovskites (CsPbX₃, X = Cl, Br, and I): Novel Optoelectronic Materials Showing Bright Emission with Wide Color Gamut. *Nano Lett.* **15**, 3692-3696 (2015).
2. Akkerman, Q. A., Rainò, G., Kovalenko, M. V. & Manna, L. Genesis, Challenges and Opportunities for Colloidal Lead Halide Perovskite Nanocrystals. *Nat. Mater.* **17**, 394-405 (2018).
3. Akkerman, Q. A. *et al.* Taming the Nucleation and Growth Kinetics of Lead Halide Perovskite Quantum Dots. *Research Square Preprint*, <https://doi.org/10.21203/rs.21203.rs-1236393/v1236391> (2022).
4. Akkerman, Q. A. Monodisperse Spheroidal Cesium Lead Chloride Bromide Quantum Dots, and a Fast Determination of Their Size and Halide Content. **Submitted**.
5. Barfüßer, A. *et al.* Confined Excitons in Spherical-like Halide Perovskite Quantum Dots. **Submitted**.

4:00 PM NM05.02.07

Machine Learning-Driven Synthesis Optimizations in Thin Films and Nanoparticles Lena Pilz, Carsten Natzeck, Jonas Wohlgemuth, Peter Weidler, Christof Wöll and Manuel Tsotsalas; KIT, Germany

Metal-Organic Frameworks (MOFs) have attracted much attention in the materials science community due to their high variability combined with well-defined structure. They are constructed from metal nodes and organic linker molecules to form regular, porous networks. [1]

Their preparation is influenced by several interdependent variables (e.g., metal and linker sources, concentration, solvent, modulators, reaction time and temperature, among others). But unfortunately, their pronounced influence, especially on nucleation, crystallisation processes and the resulting porous crystalline structure, is not yet understood. [2] In the last decade, machine learning (ML) methods have proven to be target-oriented and efficient for solving complex problems that cannot be solved with conventional approaches, such as the discovery and optimisation of synthetic parameter spaces for the production of specific MOFs. [3][4]

The idea of this research project is to use machine learning to establish the development of optimised synthesis processes and parameters. In the first part we will demonstrate the feasibility of ML optimization for several nanoparticle systems with the aim to achieve very small particle sizes with low distribution. The second, much more complex optimization is dedicated to the targeted setting of a specific orientation of a thin film with high crystallinity. This involves a great deal of understanding about the influences on the system as well as highlighting the supporting features of automated synthesis. Since it is usually too difficult for humans to vary more than one parameter at a time, machine learning algorithms are the perfect choice here to simultaneously optimize a variety of synthesis parameters that are changed simultaneously.

For this purpose, ranges must first be defined for the synthesis parameters within which they are to be varied. In the first instance the parameters are statistically spread for a defined number of experiments. After the execution and characterisation of each experimental result, new parameters are generated by a genetic algorithm, which recombines the previous parameters based on the evaluation of the results.

This step can be repeated as often as desired until the results are close enough to the desired goal. In the final step, all generated data is evaluated for relevance of the parameters again using a machine learning tool. This provides a lot of information both for biasing variables for similar systems and to understand the influences of the variables on the system.

Since the simultaneous variation of several parameters is possible, the time and money saved cannot be dismissed as an advantage. In addition, mathematically sound data are created at the end, which can be referred to for further experiments. And last but not least, if the possibility existed within the chosen parameters, a system optimised to the desired parameters emerged from this method.

References and acknowledgements

- [1] Kitagawa, S.; Kitaura, R.; Noro, S. Functional Porous Coordination Polymers. *Angewandte Chemie International Edition* 2004, 43 (18), 2334–2375.
- [2] Moosavi, S. M.; Chidambaram, A.; Talirz, L.; Haranczyk, M.; Stylianou, K. C.; Smit, B. Capturing Chemical Intuition in Synthesis of Metal-Organic Frameworks. *Nature Communications* 2019, 10 (1), 539.
- [3] Maik Jablonka, K.; Ongari, D.; Mohamad Moosavi, S.; Smit, B. Big-Data Science in Porous Materials: Materials Genomics and Machine Learning arXiv e-prints [Online], 2020.
- [4] Moliner, M.; Román-Leshkov, Y.; Corma, A., Machine Learning Applied to Zeolite Synthesis: The Missing Link for Realizing High-Throughput Discovery. *Acc. Chem. Res.* 2019, 52 (10), 2971-2980.

4:15 PM NM05.02.08

Data-Driven Insights from AuNP Synthesis Recipes Sanghoon Lee^{1,2}, Kevin Cruse¹, Samuel P. Gleason¹, Paul Alivisatos¹, Gerbrand Ceder^{1,2} and Anubhav Jain²; ¹UC Berkeley, United States; ²Lawrence Berkeley National Laboratory, United States

Gold nanoparticles are widely used in various applications because their properties are tunable depending on their shapes and sizes. Shape and size control of the AuNPs have been studied, however, the mechanisms of these syntheses are still unclear. In fact, not only are such studies limited in the number of factors and their levels considering the high dimensions of the synthesis space, but the syntheses are not always reproducible, and sometimes different synthesis outcomes are reported with the same recipe. This implies that some “missing factors” contribute to the synthesis outcomes in which are not always controlled nor reported. Therefore, it is crucial to collect a large synthesis dataset to identify i) regions that are easily reproducible through reported recipes, ii) regions with scarce data that need further exploration, iii) regions with conflicting results that in-depth studies to find missing factors are necessary.

In this work, we deliver three things. First, we developed a rule-based parser to extract the precursors and their amounts in the recipes and the resulting AuNP morphology and size, which could be used or easily adapted to not only other nanoparticle syntheses but also solution-based recipes parsing in general. Second, we provide the parsed AuNP synthesis dataset, along with the uncertainty measure for a given point in the synthesis space calculated from the neighboring data points, which one can use as a “map” for synthesis guidance. Lastly, we trained interpretable statistical models from the parsed dataset, which provide data-driven intuitions for the nucleation and growth process of the AuNPs.

4:30 PM NM05.02.09

Detection and Classification of Chiral Self-Assembled Nanostructured Helices in Electron Microscopy Images Using Generalizable Deep Learning Algorithms Anastasia Visheratina¹, Alexander Visheratin², Prashant Kumar¹, Michael Veksler¹ and Nicholas A. Kotov¹; ¹University of Michigan–Ann Arbor, United States; ²Beehive AI, United States

A chiral object has two mirror-image forms that are non-superimposable in three dimensions. Chirality plays a crucial role in chemistry, biology, and pharmacology, as most of the important biomolecules are chiral (amino acids, proteins, DNA). In 1998, it was discovered that chiral nanostructures could be chiral. Chiral inorganic nanostructures have distinct fundamental importance and are essential for further developing chemical, pharmaceutical, environmental, and biomedical technologies. To date, many researchers are focused on the establishment of the correlations between chiroptical and morphological properties of these materials by using circular dichroism and electron microscopies. A thorough investigation of electron microscopy images requires accumulating many images with their in-depth analysis, which is tedious and the 'manual' image processing is subject to experimentalist bias. Currently, there is a need for novel methods for the structural characterization of chiral nano- and micron-scale inorganic structures.

Here we developed an approach for synthesizing large sets of realistic scanning electron microscopy (SEM) images of chiral self-assembled nanostructured micro-helices of bowtie shape based on very small original SEM image sets (~200 SEM images). We used SEM images of a diverse pool of bowties, which allowed the training of state-of-the-art neural network models with the ability to detect morphological properties of chiral structures of various sizes. We tested the method by generating 10,000 images of bowtie-shaped particles with different chirality and training the YOLOv5 model to differentiate between right and left structures. As a result, this algorithm can reliably identify and classify chiral bowtie-shaped particles with accuracy as high as 94.4%. Furthermore, after training on bowtie particles, this model can successfully recognize *other* chiral shapes with different geometries without re-training. These findings indicate that deep learning techniques can potentially replicate the visual analysis of chiral objects, which opens up a path to other

computational methods capable of accurate automated analysis of a wide range of chiral features at different scales and their implementation in materials discovery for photonics and medicine.

SESSION NM05.03: Semiconductor Nanomaterials
Session Chairs: Jong-Soo Lee and Jose Souza
Tuesday Morning, November 29, 2022
Hynes, Level 2, Room 202

8:30 AM NM05.03.01

Co-Operative Cation Exchange Reaction in CdS Magic Size Cluster Yuan Yao; Cornell University, United States

Cation exchange has been developed as a post-synthetic method to explore a wide range of nanoparticle composition, phase, and morphology. Traditionally, the cation exchange reaction is explained by the reaction zone theory where the substitutional cations diffuse into the nanoparticle and form a reaction zone "shell" within the nanoparticle. Reaction zone theory implies the cation exchange is diffusion-controlled and the extent of cation exchange reaction is thus controlled by the propagation of the diffusion zone. However, several recent studies in nanoclusters (size <2 nm) find that cation exchange reactions take on discrete transformation steps. For example, the CdSe/Cu cation exchange shows a two steps mechanism, starting with the slow exchange of 1-3 Cu atoms and follow by an avalanche reaction which forms completely exchanged Cu₂Se nanoclusters. Using the CdS magic size cluster (MSC) as a model system, we investigated the cation exchange reaction mechanism in nanoclusters. The MSC cation exchange with Ag ions reveals a similar two steps reaction mechanism. The cation exchange reaction initiates with 1 to 2 Ag atoms incorporated into the MSC. Once the Ag concentration reaches the critical concentration (~10% Ag), a rapid increase of Ag content is observed followed by a complete phase transformation to Ag₂S. Using MALDI-TOF spectroscopy, we successfully identified two Ag exchanged reaction intermediates (Ag₂Cd₃₂S₃₃, Ag₁Cd₃₃S₃₃) as well as the fully exchanged nanocluster. X-ray diffraction and X-ray photoelectron spectroscopy also demonstrated a sudden change in crystal structure and electronic structure at the critical Ag concentration and corroborate the MALDI-TOF results. More interestingly, we found the Ag exchanged reaction intermediate has a low energy barrier for further cation exchange with other elements which were difficult to cation exchange. As a result, we used knowledge of this cluster exchange mechanism to successfully exchange Mn into AgCd₃₃S₃₃, to introduce interesting optomagnetic properties.

8:45 AM *NM05.03.02

Reaction Intermediates in the Synthesis of Colloidal Nanocrystals Raffaella Buonsanti; Ecole Polytechnique Federale de Lausanne, Switzerland

Over the past 40 years, scientists have learned to synthesize colloidal nanocrystals of different composition with tunable size and shape. These features dictate the properties of these nanomaterials. Thus, their control is crucial for the discovery of phenomena, many of which contribute to technological advances. One example of the societal impact of this class of materials is the use of semiconductor nanocrystals as the active component in displays with the best color purity on the market. A second example is their use as materials platforms to advance catalyst development. Yet, the synthesis of colloidal nanocrystals still proceeds by trial and error. The search for the reaction conditions to obtain the nanocrystals with the desired composition, size and shape is time consuming and can fail in delivering the target product.

In this talk, I will highlight the importance of identifying the reaction intermediates during the formation of colloidal nanocrystals for the development of a more predictive synthesis to these nanomaterials. By discussing specific examples, I will illustrate that the chemical nature of these intermediates is diverse and that state-of-the-art in-situ techniques combined with theory are often needed to capture those transient species during the synthesis of nanocrystals. Nevertheless, I will use concrete examples to demonstrate that such efforts are worth it as the discovered mechanistic pathways pinpoint the critical steps to enhance the tunability of existing materials and to accelerate the discover of new ones.

9:15 AM NM05.03.04

N-Heterocyclic Carbene-Based Polymer Coating of Gold Nanoparticles and Luminescent Quantum Dots Neda A. Nosratabad, Zhicheng Jin and Hedi M. Mattoussi; Florida State Univ, United States

Since they were first synthesized by Arduengo and coworkers in 1991, N-heterocyclic carbenes (NHCs) have generated much interest for use as versatile metal-coordinating groups. NHC-presenting molecules exhibit strong coordination interactions with transition metal ions and surfaces by sharing their non-bonding electron pairs with the σ -accepting orbitals of the metal ions. NHC-appended molecules have recently been actively exploited as potentially effective ligands for the surface passivation of various colloidal nanomaterials.

We characterize the coordination interactions between a few representative colloidal nanocrystals, including gold nanoparticles (AuNPs) and luminescent quantum dots (QDs), and one NHC-based polymer ligand. The latter presents multiple NHC groups and several short poly (ethylene glycol), PEG, chains as solubilizing blocks. We find that our NHC-decorated ligands rapidly coordinate onto both sets of nanocrystals, requiring ~ 5-10 min for complete ligand substitution and phase transfer. These Lewis base groups ideally match the soft Lewis acid character of transition metal colloids, promoting strong coordination bonding through soft-to-soft interactions. We combine NMR spectroscopy, fluorescence spectroscopy, high-resolution transmission electron microscopy supplemented with dynamic light scattering to characterize the nature of the binding interactions. Furthermore, the long-term stability of the NHC-stabilized nanocolloids have been tested after phase transfer to water, a highly challenging chemical venue for such groups, due to the moisture sensitive nature of NHC molecules. Data show that our NHC-stabilized nanocolloids exhibit long-term colloidal stability in buffer media while preserving their optical and fluorescing properties for at least one year of storage. We will discuss the ligand design and characterization of the polymer-stabilized nanocrystals under various conditions, with a particular focus on the beneficial effects of multi-coordination interactions.

9:30 AM BREAK

SESSION NM05.04: Fundamentals of Nanomaterial Synthesis II
Session Chairs: Nikolai Gaponik and Hedi Mattoussi
Tuesday Morning, November 29, 2022
Hynes, Level 2, Room 202

10:30 AM *NM05.04.01

Nanoparticle-Based Functional Nano-Materials—Modern Inorganic Aerogels Alexander Eychmüller, TU Dresden, Germany

The focus of my talk will be laid on non-ordered superstructures made from nanocrystals. Here, gels and aerogels manufactured from a variety of different nanoparticles have recently proven to provide an opportunity to marry the nanoscale world with that of materials of macro dimensions which can be easily manipulated and processed, whilst maintaining some of the nanoscale properties. This is best demonstrated when using size-quantized semiconductor nanocrystals for the aerogel formation: 3.5 nm sized CdTe nanocrystals display an orange colour (while bulk CdTe is black) which is maintained in a 1 cm³ aerogel and so is also the emission.¹ In terms of applications, however, gels formed from metal nanocrystals provide a wider field, particularly in electrocatalysis.² For this we concentrated our work on the amelioration of the building blocks as a plausible approach to graft aerogels with distinguished properties while preserving the aerogel superiority.³ In a further study, we prepared and analyzed a new class of hierarchical aerogels composed of multimetallic Ni-Pd_xPt_y nanoparticle building blocks with continuously engineered shape and compositions. This approach results in aerogels with hierarchical structures organizing the nanoscale regulated architecture and macroscale three-dimensional network structure. For gaining highest performance of these catalysts the surface chemistry as well as the formation mechanisms have to be studied and tuned.^{4,5} I will conclude my presentation with remarks on a set of more recent findings such as self-healing of metal gels and the formation of 2D-metal meshes.⁶ The latter display ligament sizes of 4 – 9 nm which is also the thickness of the meshes, surface coverages between 0.25 and 0.5, and fractal dimensions of 1.4 – 1.7. Those structures hold promise in various fields like sensors, electrodes, electrocatalysis, neural implants (stretchable electrodes), and fractal antennas.

References

- [1] N. Gaponik, A. Wolf, R. Marx, V. Lesnyak, K. Schilling, A. Eychmüller, *Adv. Mater.* 20, 4257 (2008).
- [2] a) N.C. Bigall, A.K. Herrmann, M. Vogel, M. Rose, P. Simon, W. Carrillo- Cabrera, D. Dorfs, S. Kaskel, N. Gaponik, A. Eychmüller, *Angew. Chem. Int. Ed.* 48, 9731 (2009), b) W. Liu, A.-K. Herrmann, N.C. Bigall, P. Rodriguez, D. Wen, M. Oezaslan, T.J. Schmidt, N. Gaponik and A. Eychmüller, *Acc. Chem. Res.* 48, 154 (2015).
- [3] a) B. Cai, A. Dianat, R. Hübner, W. Liu, D. Wen, A. Benad, L. Sonntag, T. Gemming, G. Cuniberti, A. Eychmüller, *Adv. Mater.* 29, 1605254 (2017), b) B. Cai, R. Hübner, K. Sasaki, Y. Zhang, D. Su, C. Ziegler, M.B. Vukmirovic, B. Rellinghaus, R.R. Adzic, A. Eychmüller, *Angew. Chem. Int. Ed.* 57, 2963 (2018). c) B. Cai, V. Sayevich, N. Gaponik, A. Eychmüller, *Adv. Mater.* 30, 1707518 (2018).
- [4] R. Du, J. Wang, R. Hübner, X. Fan, I. Senkowska, Y. Hu, S. Kaskel, A. Eychmüller, *Nat. Comm.* 11, 1590 (2020).
- [5] a) H. Ishikawa, S. Henning, J. Herranz, A. Eychmüller, M. Uchida, T.J. Schmidt, *J. Electrochem. Soc.* 165, F2 (2018), b) S. Jungblut, J.-O. Joswig, A. Eychmüller, *J. Phys. Chem. C* 123, 950 (2019), c) S. Jungblut, J.-O. Joswig, A. Eychmüller, *Phys. Chem. Chem. Phys.* 21, 5723 (2019), d) R. Du, Y. Hu, R. Hübner, J.-O. Joswig, X. Fan, K. Schneider, A. Eychmüller, *Science Advances* 5, 4590 (2019), e) P. Chauhan, K. Hiekel, J.S. Diercks, J. Herranz, V.A. Saveleva, P. Kavlyuk, A. Eychmüller, T.S. Schmidt, *ACS Mater. Au* 2, 278 (2022).
- [6] K. Hiekel, S. Jungblut, M. Georgi, A. Eychmüller, *Angew. Chem. Int. Ed.* 59, 12148 (2020).

11:00 AM NM05.04.02

Amalgamation Synthesis of Intermetallic Nanocrystals Jasper Clarysse, Annina Moser, Olesya Yarema, Vanessa Wood and Maksym Yarema; ETH Zurich, Switzerland

Bimetallic compounds are a vast family of materials with >20000 unique members and record-high performance in plasmonic, catalytic, magnetic, and energy storage applications. In strong dissonance, universal synthesis for polymetallic nanocrystals is missing, due to challenges to combine two dissimilar metals at the nanoscale. We overcome this limitation by the amalgamation reaction at the surface of nanocrystals, [1] thus unlocking up to a 1000 of new intermetallic nanocrystals with unprecedented quality for size uniformity, composition control, and phase purity. We show the universality of our amalgamation approach and achieve a row of crystalline and compositionally uniform intermetallic nanocrystals of Au-Ga, Ag-Ga, Cu-Ga, Ni-Ga, Pd-Ga, Pd-In and Pd-Zn compounds. Furthermore, we demonstrate a compositional tunability across phase diagrams (e.g., AuGa₂, AuGa, Au₇Ga₂, and Ga-doped Au nanocrystals for the bimetallic Au-Ga system), while each phase can be prepared with accurate size control and excellent size uniformity. Our new synthetic method is simple, predictive, and generalizable, giving access to a large family of intermetallic nanocrystals with unprecedented quality and flexibility of materials design, thus unlocking a multitude of possibilities for these materials.

- [1] J. Clarysse, A. Moser, O. Yarema, V. Wood, and M. Yarema, *Science Advances*, 2021, 7, eabg1934.

11:15 AM NM05.04.04

Salt-Templated Metal and Metal Oxide Porous Materials John Burpo¹, Felita W. Zhang¹, Veronica M. Lucian¹, Alexa Zammit¹, Edward M. Tang¹, Rosemary L. Calabro^{1,2}, Enoch A. Nagelli¹, Stephen F. Bartolucci² and Joshua A. Maurer²; ¹United States Military Academy, United States; ²U.S. Army Combat Capabilities Development Command-Armaments Center, United States

Pure metal, multi-metallic and alloy nanomaterials enable a broad range of catalytic applications with high surface area and tunable reaction specificity through the variation of metal composition. Synthesizing these materials as three-dimensional porous nanostructures enables control of surface area, pore size and mass transfer properties, electronic conductivity, and ultimately device integration. Discrete and aggregated nanoparticles offer tremendous design flexibility, yet methods to assemble them into extended 3-dimensional structures suffer from several limitations, especially aggregation and diffusion times. Insoluble salts offer a template approach to synthesize a range of porous noble and transition metal structures and monoliths. Chemical reduction of insoluble Magnus and Vauquelin salt needles formed from the combination of oppositely charged square planar platinum, palladium, gold, and copper ions have been previously demonstrated as templates for mesoporous macrobeam and macrotubes 10's to 100's of micrometers long with square cross-sections ranging from approximately 100 nm to 3 μm.¹⁻⁴ The use of insoluble noble metal salt templates was extended to the chemical reduction of copper and nickel transition metal poly-crystalline salts. After chemical reduction, metal gels were rinsed, solvent exchanged in ethanol, and supercritical dried in CO₂ to form aerogels. Metal and metal oxide phase composition varied depending on the sulfate, acetate, and chloride salt template anion. Aerogels were characterized using scanning electron microscopy, energy dispersive x-ray spectroscopy, x-ray diffractometry, nitrogen gas adsorption-desorption with and Brunauer-Emmett-Teller surface area analysis, vibrating-sample magnetometry, magnetic force microscopy, and nanoindentation. Electrochemical performance of copper and nickel oxide aerogels as pseudocapacitors was determined with electrochemical impedance spectroscopy and cyclic voltammetry. The use of salt precursors is envisioned as a synthesis route to a wide range of metal and multi-metallic nanostructures for catalytic, energy storage, and sensing applications.

References

- Burpo, F.J., Nagelli, E., Winter, S., McClure, J., Bartolucci, S., Burns, A., O'Brien, S. "Salt-Templated Hierarchically Porous Platinum Macrotube Synthesis." *ChemistrySelect*. 2018, 3, 4542-4546.
- Burpo, F.J., Nagelli, E., Morris, L., Woronowicz, K., Mitropoulos, A. "Salt-Mediated Au-Cu Nanofoam and Au-Cu-Pd Porous Macrobeam Synthesis." *Molecules*. 2018, 23, 1701-1715.

Burpo, F.J., Nagelli, E., Bartolucci, S., Mitropoulos, A., McClure, J., Baker, D., Losch, A., Chu, D. "Salt-Templated Platinum-Palladium Porous Macrobeam Synthesis." *MRS Communications*, 2019, 9(1), 280-287.

Burpo, F.J., Nagelli, E.A., Losch, A.R., Bui, J., Forcherio, G.T., Baker, D.R., McClure, J.P., Bartolucci, S.F., Chu, D.D. Salt-Templated Platinum-Copper Porous Macrobeams for Ethanol Oxidation. *Catalysts*, 2019, 9(8), 662.

11:30 AM NM05.04.05

Polyoxometalates—A Novel Surface Stabilizer for Optically Tunable 2D Systems Ali Jawaid and Richard A. Vaia; Air Force Research Laboratory, United States

2D van der Waals systems have attracted significant interest across multi-disciplinary fields ranging from sensors, optical filters, and structurally responsive composites. Access to these materials is paramount for technology development. Technologies that facilitate and expand methods to stabilize monolayers, disperse them into a wide array of matrices (i.e. solvents, polymers) is desirable for facile integration into current bulk manufacturing methods. Despite the advances made in the last decade, access to many systems is limited by liquid phase exfoliation techniques (i.e. H₂O/Surfactant) where surface corrosion, oxidation, hydrolysis are common challenges. In this regard, we demonstrate that polyoxometalates (POMs) can meet exfoliation and stabilization challenges for layered van der Waals heterostructures. This is exemplified in their ubiquitous ability to stabilize and exfoliate layered transition metal dichalcogenides (LTMDs); surface adsorption of POMs provide coulombic repulsion between individual layers in bulk crystallites and facilitate gentle delamination without the use of mechanical forces, minimizing surface defects and crystallite scission. POMs can further impart charge transfer to the LTMD surface resulting in tunable absorption edges for modular optics; this is further demonstrated via tuning the affinity of the POM to the LTMD surface to allow adaptive optical responses. The mechanism of surface adsorption, exfoliation, and stabilization can be transferred to colloidal systems outside of LTMDs (graphene, CIPs, MXenes) creating a general exfoliant for robust colloidal 2D systems.

SESSION NM05.05: Perovskite Nanomaterials
Session Chairs: Jong Soo Lee and Anghuman Nag
Tuesday Afternoon, November 29, 2022
Hynes, Level 2, Room 202

1:30 PM *NM05.05.01

Lead-Free Heterometallic Halide Layered Double Perovskite Nanocrystals Ou Chen; Brown University, United States

Halide perovskite nanocrystals have attracted a great amount of research attention due to their unique optoelectronic properties, leading to a range of potential applications including light emitters, displays, X-ray imaging and solar energy harvesting. In this context, lead-free halide perovskite and perovskite-analogue nanocrystals have emerged as a new category of materials that hold the potential for overcoming the instability and toxicity issues of lead-based counterparts. In this talk, I will discuss some of our recent studies about synthesis, characterization and application of different lead-free halide perovskite and perovskite-analogue nanocrystals. I will focus my talk on crystal phase control, composition and structure tuning, and applications of this special category of materials. Both experimental data and first-principal Density Functional Theory calculation results will be included in the talk.

2:00 PM *NM05.05.02

Engineering Colloidally Stable Blue-Emitting CsPbBr₃ Nanoplatelets Using Polysalt/PbBr₂ Ligands Sisi Wang, Wentao Wang, Selin Donmez and Hedi M. Mattoussi; Florida State Univ, United States

With their large exciton binding energy and precisely controlled thickness, two-dimensional colloidal perovskite nanoplatelets (NPLs) have attracted attention as promising blue-emitting materials. However, they tend to lose their optical, morphological and colloidal integrity with storage following growth.

Herein, we introduce a strategy using PbBr₂-complexed polymers as coating ligands that impart morphological and colloidal stability, while enhancing the photoluminescence quantum yield of the NPLs. The polymers present several ammonium (or imidazolium) bromide anchoring groups and alkyl chains with different length as solubilizing blocks. The presence of the quaternary ammonium salts facilitates the dissolution of PbBr₂ in organic solutions, forming polysalt-[Pb_xBr_y]^{2x-y} complexes that strongly interact with the NPL surfaces. We find that these complexes eliminate surface defects, compared to the as-grown materials, and improve their structural and morphological stability. This strategy has yielded blue-emitting samples that maintain color purity with narrow profiles at ~460 nm and with PLQY up to 80%. Additionally, significantly enhanced long term stability of the nanoplatelets under several challenging conditions, including UV irradiation and highly diluted conditions, has been achieved.

2:30 PM *NM05.05.03

Solution-Synthesized and Solution-Processed Infrared Photodetectors – Advancing the Limits of Spectrum and of Speed Edward H. Sargent^{1,2}; ¹University of Toronto, Canada; ²Northwestern University, United States

Both colloidal quantum dots and perovskites show promise as solution-synthesized and liquid-processed materials for optoelectronics. I will review the design, synthesis, processing, and device physics of such materials in light sensing, focusing especially on NIR, SWIR, and the path to the MWIR.

3:00 PM BREAK

SESSION NM05.06: Colloidal Self-Assembly
Session Chairs: Raffaella Buonsanti and Maksym Kovalenko
Tuesday Afternoon, November 29, 2022
Hynes, Level 2, Room 202

3:30 PM *NM05.06.01

Tuning Interparticle Interaction Inside Nanocrystal Superlattices by Solvent Vapor Exposure and Pressure Process Yasutaka Nagaoka and Ou Chen; Brown University, United States

My poster presentation discusses interparticle interactions between nanocrystals in superlattices and superparticles. Especially, recent results on in-situ small-angle X-ray scattering (SAXS) measurements during structural transformation upon solvent exposure, synthesis of superparticles, and the response to high pressure are presented.

Upon evaporating the solvent, superlattices and superparticles are spontaneously formed through nucleation and growth processes. The formation process is influenced by many structural factors of nanocrystals, including their shape, surface, and how the surfactant molecules interact with solvent molecules.

The mechanisms are highly complex, involving both kinetic pathways and thermodynamic stabilization. A clear demonstration of the interparticle interactions will be necessary to understand the formation processes. The clarification of the mechanism is especially crucial since current research indicates that the architectures and molecular structures inside nanocrystalline superlattices drastically influence the physical properties such as mechanical and optical properties of the resulting materials, resulting in new structured materials and metamaterials.

In order to better understand the nature of nanocrystal interparticle interactions, we conducted several in-situ experiments monitoring nanocrystal superlattices and superparticles under external stimuli such as solvent vapor exposure and mechanical pressure. Our experiments on solvent vapor exposure examined how cluster-based nanocrystal superlattices respond to different solvent molecules. In our experiments, we demonstrated molecular interactions between surfactant molecules and incoming solvent molecules within nanocrystal superlattices after exposure to solvent vapor, causing a change in the molecular shape of the surfactants. Subsequently, the molecular change triggered superstructural phase transitions and their mechanical properties changed accordingly. We have shown that the post-treatment of the nanocrystal superlattices with solvent vapors can induce orchestrated structural changes from the molecular structure to the superstructure. During our high-pressure experiments, we created a series of superparticles, superstructured nanocrystals with colloidal morphologies, and studied their behavior under pressure. Interparticle interactions under high pressure exhibit a different landscape than those under ambient conditions, leading to many interesting chemical/physical reactions. We present pressure-driven sintering processes in nanocrystal assemblies with different surface states under varied pressure ranges.

4:00 PM NM05.06.02

Monodisperse Nanocrystal Superparticles Through a Source–Sink Emulsion System [Emanuele Marino](#)¹, Sjoerd van Dongen¹, Steven J. Neuhaus¹, Weixingye Li¹, Austin W. Keller¹, Cherie R. Kagan¹, Thomas E. Kodger² and Christopher B. Murray¹; ¹University of Pennsylvania, United States; ²Wageningen University & Research, Netherlands

Superparticles made from colloidal nanocrystals have recently shown great promise in bridging the nanoscale and mesoscale, building artificial materials with properties designed from the bottom-up. As these properties depend on the dimension of the superparticle, there is a need for a general method to produce monodisperse nanocrystal superparticles. Here, we demonstrate an approach that readily yields spherical nanocrystal superparticles with a polydispersity as low as 2%. This method relies on the controlled densification of the nanocrystal-containing “source” emulsion by the swelling of a secondary “sink” emulsion. We show that this strategy is general and rapid, yielding monodisperse superparticles with controllable sizes and morphologies, including core/shell structures, within a few minutes. The superparticles show a high optical quality that results in lasing through the whispering gallery modes of the spherical structure, with an average quality factor of 1600. Assembling superparticles into small clusters selects the wavelength of the lasing modes, demonstrating an example of collective photonic behavior of these artificial solids.

Reference: E. Marino et al., *Chemistry of materials* 34 (6), 2779-2789, 2022.

4:15 PM NM05.06.03

Reversible Diffusionless Phase Transitions in 3D Nanoparticle Superlattices [Daryl W. Yee](#), Margaret S. Lee, Joyce An and Robert J. Macfarlane; Massachusetts Institute of Technology, United States

Natural materials often exhibit complex material properties due to hierarchically organized structural motifs at the molecular, nano, micro, and macroscopic size regimes. They have inspired a whole generation of advanced multifunctional synthetic materials that utilize structural hierarchy to reach new property spaces. Self-assembly approaches have been heavily utilized to fabricate these hierarchical materials as its ability to build materials via weak, dynamic interactions between nanometer-sized build blocks provides great control over material structure from the molecular to the micro-scale.

In particular, self-assembled nanoparticle superlattices (NPSLs) — three-dimensional ordered arrays of nanoparticles — have been the subject of significant interest due to their emergent properties that arise from the ordering of their nanoparticle building blocks. As a result, these nanoparticles superlattices are promising materials for a variety of applications, from optoelectronics to energy storage. Multiple methods have been developed to assemble NPSLs, and these crystallization processes have often been guided by chemical intuition derived from the formation of traditional bulk or atomic crystals. Chemical concepts like bond valency or packing factors can be directly analogized to structural features and phenomena observed in NPSLs, suggesting that more complex behaviors like microstructure formation or phase transitions could also be induced. Given that the properties of NPSLs are often governed by their crystal symmetry and lattice parameters, the ability to induce a phase transition to reversibly tune the crystal structure has the potential to lead to dynamic materials with switchable properties for a variety of applications, including optoelectronics, plasmonics, mechanics, and catalysis. As such, there has been significant interest in engineering NPSLs that are able to exhibit reversible polymorphic phase transitions.

Here, we report the assembly of nanocomposite tectons (NCTs), polymer grafted nanoparticles that have supramolecular recognition groups at the chain ends, into unary NPSLs that are capable of exhibiting a martensitic phase transition between a face-centered cubic (FCC) and a body-centered cubic (BCC) structure when the solvent quality is changed. The phase transition is rapid, reversible, and appears to proceed through an order-to-order crystal transition. We show the impact that NCT composition has on the phase transition behavior and discuss the potential mechanisms behind it. Importantly, we demonstrate that the phase transition can be kinetically arrested, allowing both polymorphs to be obtained in the solid form and examined. The BCC phase was observed to maintain the same crystal habit as the parent FCC phase but exhibited significant twinning, analogous to those observed in martensitic transformations. We discuss the impact that twinning has on the mechanical properties of these colloidal crystals, and highlight how these twinned crystals can be used to engineer macrostructures with twinned microstructures. Given the importance of phase transitions and twinning in atomic materials, the ability to replicate them in NPSLs represents a step forward in engineering hierarchically complex materials that can utilize them to augment their properties.

4:30 PM NM05.06.04

Design and Synthesis of Functional Nanostructured Materials via Colloidal Crystallization [Yuanwei Li](#), Wenjie Zhou, Ibrahim Tanriover, Hanxun Jin, Horacio Espinosa, Koray Aydin and Chad A. Mirkin; Northwestern University, United States

Controlling nanomaterial architecture is a versatile way to create materials with tailored properties. Colloidal crystal engineering has emerged as a powerful approach to precisely synthesizing materials with nanoscale architectures. For example, porous crystals are a class of materials with extraordinary properties. Multicomponent crystals provide a promising path forward for the creation of materials with synergistic physical and chemical properties. However, it is still remarkably difficult to synthesize designer multicomponent and porous crystals; moreover, their structure-function relationships remain elusive. Here, we take a materials-by-design approach that takes advantage of programmable DNA interactions to assemble monodispersed nanoparticles

of various shapes into (1) multicomponent co-crystals and (2) porous colloidal crystals, each with targeted chemical, optical, or mechanical properties. We further explore the structure-function relationships among these new materials.

To achieve designer multicomponent colloidal crystals, we have developed a series of polyethylene glycol-DNA ligands that enables the co-assembly of polyhedral nanoparticles and spherical nanoparticles into ordered co-crystals. Specifically, polyhedra of different sizes and shapes (e.g., octahedra, tetrahedra, decahedra, and bi-tetrahedra) are co-assembled based on geometry-inspired designs. Furthermore, polyhedral and spherical nanoparticles of different sizes are co-assembled into a series of novel hierarchical structures, where anisotropic nanoparticles are ordered, while spheres are disordered in the lattices. Using these design strategies, we have discovered eight new co-crystals in the DNA-engineered colloidal crystal family. These results highlight the potential of shape-complementarity design strategies for creating new and unusual colloidal co-crystals.

Utilizing our universal synthetic strategy for directing the site-specific growth of anisotropic seeds into exotic nanoparticle shapes and compositions provides a general pathway to design and synthesize an array of metal hollow nanoparticles that are promising building blocks for the assembly of porous colloidal crystals. These hollow nanoparticles, including nanoframes and nanocages, are subsequently assembled using DNA into open channel superlattices with a range of pore shapes and sizes (i.e., 10–1000 nm). We show that the assembly of hollow nanoparticle superlattices is driven by edge-to-edge DNA interactions. The edge-based assembly design rules that emerged from these studies were used to synthesize 12 open channel superlattices with control over crystal symmetry, channel geometry, and topology. We further show that by controlling the geometry and topology of pores, these superlattices can be used for encapsulating and immobilizing guest species within the host open channel structures, and incorporating inorganic or organic guests with spatial specificity into these porous crystals generates a new kind of host-guest structured material. Indeed, the controllable and tunable porosities and periodicities of open channel superlattices make them promising candidates to realize optical phenomena that are not observed in natural materials. For example, the effective refractivity of a porous Au-Pt cubic-close-packed crystal was found to be negative over a wide spectral range (1050–2000 nm). Finally, we found that porous metallic crystals have higher specific strength and stiffness compared to their solid counterparts, which provides new insights into the design and development of materials that are light but strong. These properties of open channel superlattices represent a new class of mechanical metamaterials, due to their porous, low-density structures and diverse crystal topologies. Overall, our work has made important steps toward the rational synthesis of functional co-crystals and porous crystals with significant implications in optics, catalysis, electronics, biology, and mechanics.

4:45 PM NM05.06.05

Spontaneous Assembly of Magnetic Nanochains Induced by Magnetic Dipole Interactions [Yulan Chen](#) and Amal El-Ghazaly; Cornell University, United States

Anisotropically-ordered magnetic nanoparticles (NPs) possess unique physicochemical properties and are important to various applications ranging from data storage to medical technologies. One-dimensional (1D) magnetic nanochain structures have often been produced by applying an external magnetic field during synthesis, where the discrete NPs are aligned into chains. However, this method is severely limited in its ability to scale up in manufacturing for use in practical applications since the reaction vessel size is limited by the magnetic field strength, i.e. size of the electromagnetic coils or magnet. Here, we demonstrate that it is possible to forgo the external magnetic field and only utilize the intrinsic dipole forces of the iron cobalt (FeCo) nanoparticles themselves in the reaction media to assemble them into nanochains during the synthesis process.

A challenging issue in magnetic assembly of dipolar colloids is that the dipolar interactions between individual building blocks are only possible in the near field. As a result, self-assembly of anisotropic nanostructures like chains is difficult to promote in the absence of externally-applied fields or other stimuli. In this work, we establish a method for the self-assembly of magnetic nanochains by investigating the usage of magnetic dipolar interactions between neighboring FeCo NPs in highly-concentrated reaction conditions. The small interparticle distance in this highly-concentrated regime drastically enhances dipole-dipole coupling and enables the large-scale synthesis of magnetic FeCo nanochains without using any templates, surfactants, or external magnetic fields.

The growth mechanism and resulting morphology of these self-assembled 1D nanochains were found to be strongly influenced by the reaction concentration, and analogously the relative strengths of the magnetic dipolar interactions. Magnetic dipolar interactions between NPs depend on particle size, interparticle distance, and their flow velocity in the reaction fluid. We experimentally show how the synergistic effect of the dipole-dipole attractive force and the fluid drag counteractive force is modified through changes to the synthesis conditions, including precursor ratios, total precursor quantity, and spinner rotation speed. Furthermore, through simulation, we illustrate the magnetic and fluid dynamic force landscapes of a single particle to provide insight into the range of reaction concentrations useful for yielding nanochains as opposed to isolated nanoparticles. Future research can take advantage of these intrinsic magnetic dipole forces, in conjunction with other ligand-mediated interparticle interactions, to self-assemble strongly-adhered, 1D anisotropic magnetic nanostructures with additional functionalities, or to fabricate even more complex three-dimensional geometrical arrangements at a commercial scale.

SESSION NM05.07: Poster Session
Session Chairs: Nikolai Gaponik and Dmitri Talapin
Tuesday Afternoon, November 29, 2022
8:00 PM - 10:00 PM
Hynes, Level 1, Hall A

NM05.07.01

Effect of Inter-Particle Distance in Liquid Phase Benzaldehyde Hydrogenation via Raspberry-Colloid Templated PdAu/SiO₂ Inverse Opals [Kang Rui Garrick Lim](#), Selina K. Kaiser, Sadhya Garg and Joanna Aizenberg; Harvard University, United States

The collective ensemble properties of nanoparticles (NPs) deposited on supported catalysts, defined by design parameters such as NP loading, dispersion, and inter-NP distance, have a pronounced impact on catalytic activity, selectivity, and stability. Traditional preparative methods of precipitation or impregnation entail nucleating NPs on the support. Thereby, a higher metal precursor concentration increases the NP loading but also yields larger NPs, which disguises the direct effects of NP size and inter-NP distance on catalysis. Herein, we use raspberry-colloid templating (RCT) to partially embed pre-formed dilute Pd-in-Au NPs within a macroporous SiO₂ support, ensuring a preserved NP size distribution during preparation and catalysis. By varying the NP loading in the RCT fabrication process, the average inter-NP distance can be altered without modifying the NP size distribution. This enables the independent investigation of the effect of inter-NP distance in liquid phase catalysis.

NM05.07.02

Chiroptically Active Copper Oxide Microstructures via Post-Synthetic Treatment of Copper-Aluminium Layered Double Hydroxides [Áine](#)

Coogan¹, Finn Purcell-Milton^{1,2}, Seán Cardiff^{1,1} and Yurii K. Gun'ko¹; ¹Trinity College Dublin, The University of Dublin, Ireland; ²Technological University Dublin, Ireland

In recent years, much research has focused on the development of new chiral inorganic nanostructures, including a wide variety of materials, such as nanosheets, nanowires, and tetrapods, among others.¹⁻³ Layered double hydroxides (LDHs) are a class of ionic 2D nanomaterials that are known for their porous laminar structures and anion-exchange properties. As such, they can host a wide variety of species in their interlayer – including chiral molecules.⁴ However, despite this unique property, to the best of our knowledge there are no reports on the development of chiral and chiroptically active LDHs nanostructures with chiral ligands.

In this work, we report the synthesis and investigation of carbonate-intercalated copper-aluminium (CuAl-CO₃) LDH nanosheets. The initial LDH nanomaterials have been synthesised by an easy scalable co-precipitation procedure. Then, the resultant 2D nanomaterials were treated with L- and D-Phenylalanine at room temperature in aqueous conditions, resulting in materials with strong chiroptical activity in the visible region, far beyond the onset of the CD signal from the original ligand. Time-dependent CD and powder X-Ray diffraction (pXRD) studies demonstrate a gradual transformation from achiral LDH nanosheets, to chiral copper (II) oxide (CuO) microstructural materials, exhibiting g-factors of up to 0.0035. We expect that these materials could have potential future applications in enantiomeric separation and asymmetric catalysis.

References:

- 1 - F. Purcell-Milton, R. McKenna, L. J. Brennan, C. P. Cullen, L. Guillemeney, N. V. Tepliakov, A. S. Baimuratov, I. D. Rukhlenko, T. S. Perova, G. S. Duesberg, A. V. Baranov, A. V. Fedorov and Y. K. Gun'ko, *ACS Nano*, 2018, **12**, 954–964.
- 2 - D. Kehoe, E. Mates-Torres, P. Samokhvalov, M. Garcia-Melchor and Y. K. Gun'ko, *J. Phys. Chem. C*, 2022, **126**, 434–443.
- 3 - J. E. Govan, E. Jan, A. Querejeta, N. A. Kotov and Y. K. Gun'ko, *Chem. Commun.*, 2010, **46**, 6072– 6074.
- 4 - S. Mallakpour and M. Dinari, *J. Therm. Anal. Calorim.*, 2015, **119**, 1123–1130.

NM05.07.03

Synthesis of Gold Nanowires for Stretchable Electronics [Laura Seufert](#)¹, Samuel Lienemann¹, Ulrika Linderhed^{1,2}, Mohammed Elmahmoudy¹, Mary J. Donahue¹ and Klas Tybrandt¹; ¹Linköping University, Sweden; ²RISE, Research Institute of Sweden, Sweden

Electrical stimulation in direct proximity to neural tissue is investigated to treat neurological disorders like Parkinson's disease and epilepsy. One major challenge for neural interfaces is the huge mechanical mismatch between the electronics and the tissue. This can be addressed by developing soft and stretchable devices. High performance stretchable conductors can be made from nanowires (NWs) embedded in elastomers like polydimethylsiloxane (PDMS). Silver nanowires (AgNWs) are commercially available in controlled dimensions and have been widely used for stretchable conductors. For biomedical applications, however, AuNWs are needed, and to date there exists no robust method of synthesizing large amounts of high aspect ratio AuNWs. In this work we present a novel synthesis of high aspect ratio AuNWs with smooth surface structure and selective control of the diameter of the nanowires in solution. We investigate how changes to the parameters of the reaction like temperature and concentration influence the material and characterize the nanowires using various imaging and analysis tools. Furthermore, we show the stable performance under cyclic stretching measurements of conductors produced by embedding the novel AuNWs in PDMS and other elastomers. The good performance and biocompatibility of the new material allowed for application in a stimulation experiment as a stretchable conductor.

NM05.07.04

Salt-Templated Nickel and Nickel Oxide Bacterial Cellulose Composite Electrodes for Pseudocapacitor Applications [Alexa Zammit](#)¹, Paul Trackey¹, Edward M. Tang¹, Jessica Liba², Galen Mandes¹, Rosemary L. Calabro^{1,3}, Enoch A. Nagelli¹, Stephen F. Bartolucci³, Joshua A. Maurer³ and John Burpo¹; ¹United States Military Academy, United States; ²U.S. Army Research Laboratory, United States; ³U.S. Army Combat Capabilities Development Command-Armaments Center, United States

To address the need for low-cost, transition metal porous nanomaterials for energy storage applications, one strategy is to use naturally occurring cellulose-based templates to better tune material properties such as feature size, pore structure, conductivity, material phase, and mechanical strength. Examples of this approach to control nanostructure and functionality include bacterial cellulose-ferromagnetic cobalt ferrite magnetic aerogels and cellulose nanofiber-palladium aerogels.^{1,2} Here, cellulose nanofibers derived from bacteria provide templates to synthesize lightweight, porous, and conductive nickel and nickel oxide aerogels for use as pseudocapacitors. These aerogels were synthesized through NaBH₄ chemical reduction of nickel sulfate equilibrated tempo-oxidized bacterial cellulose mats. Supercritically dried aerogels were thermally annealed in air to control the degree of nickel oxide material phase. Aerogels were characterized using scanning electron microscopy, energy dispersive x-ray spectroscopy, x-ray diffractometry, nitrogen gas adsorption-desorption with and Brunauer-Emmett-Teller surface area analysis, vibrating-sample magnetometry, magnetic force microscopy, and nanoindentation. Electrochemical performance was determined with electrochemical impedance spectroscopy and cyclic voltammetry. Due to the low-cost synthesis and tunable properties, these composite cellulose-metal/metal oxide aerogels are expected to provide material solutions to a wide range of energy storage, catalytic, and fuel-cell applications.

References

- ¹Olsson, R., Azizi Samir, M., Salazar-Alvarez, G. et al. Making flexible magnetic aerogels and stiff magnetic nanopaper using cellulose nanofibrils as templates. *Nature Nanotech* 5, 584–588 (2010).
- ²Burpo, F. J.; Nagelli, E. A.; Morris, L. A.; McClure, J. P.; Ryu, M. Y.; Palmer, J. L., Direct solution-based reduction synthesis of Au, Pd, and Pt aerogels. *J. Mater. Res.* **2017**, *32* (22), 4153–4165.

NM05.07.06

Tuning Morphology of Colloidally-Synthesized, Plasmonic Tungsten Oxide Nanostructures for Hydrogen Evolution Activity [Gregory Davis](#)¹, Xun Zhan² and Rajesh Sardar¹; ¹IUPUI, United States; ²Indiana University Bloomington, United States

An energy dense fuel source to replace the reliance of fossil fuels by our society the utmost importance for future generations. Solving this pressing issue by finding a solution which has a low environmental cost to our planet, should be the target of cutting-edge science. The hydrogen evolution reaction (HER) is of great interest due to the energy dense product H₂ gas. Metal oxide nanostructures show tremendous promises as a heterogeneous HER catalyst because of their unique optical and electronic properties which are only prevalent at the nanoscale size. Additionally, these materials offer tunable reactivity and serve as a support and the catalyst simultaneously; this allows for increased simplicity in catalytic systems. Most importantly, nanostructured metal-oxides can be synthesized from earth abundant transition metals, making the process economically more viable as compared to utilizing more expensive noble metals. However, current research does not elucidate a full understanding of morphology on catalytic activity towards the HER.

Specifically relating the crystalline (*hkl*) facets to the optimal HER performance. Herein, we present how shape of colloiddally-synthesized plasmonic tungsten oxide nanostructures influence the electrocatalytic HER activity as a function of morphology. The HER activities have been investigated by examining the optical, electrical properties, and crystalline facets of different morphologies such as one-dimensional rods and wires and two dimensional platelets. We determined that the two-dimensional platelets have a tafel slope of approximately 55 to 60 mV/dec and the wires gave a tafel slope of 205 to 215 mV/dec. The overpotential of these two nanostructures was found to be between -0.2V to -0.3V and -0.5V to -0.6V for platelets and wires respectively. This finding presents a distinct difference in electrochemical behavior which is based only on morphology. The ratio of the (*hkl*) facets to HER activity have revealed that the morphology is an important feature which must be addressed when optimizing a metal-oxide catalyst for the HER. As the platelets provide the largest surface to volume ratio of the most catalytic facet while also forming an effective support system owing to the stability of meta-oxide materials. The current work focusing on morphology dependent HER activity would prove interesting to open the door for an efficient and robust HER catalyst for the renewable energy production.

NM05.07.07

***p*-Block Metal-*d*-Block Metal High-Entropy Alloy Nanoparticles and Their Properties** Masashi Nakamura¹, Dongshuang Wu¹, Megumi Mukoyoshi¹, Kohei Kusada¹, Takaaki Toriyama², Tomokazu Yamamoto², Syo Matsumura², Yasukazu Murakami², Yoshiaki Kubota³, Shogo Kawaguchi⁴, Toshiaki Ina⁴ and Hiroshi Kitagawa¹; ¹Kyoto University, Japan; ²Kyushu University, Japan; ³Osaka Metropolitan University, Japan; ⁴JASRI/SPring-8, Japan

High-entropy alloy (HEA) is multiple-element alloy characterized by its large configurational entropy. Its complex physics yields appealing properties distinct from conventional alloy. Thanks to the vast compositional and configurational space, this class of material has greatly enriched the diversity of bulk materials library for more than 15 years.¹ Not like the bulk, however, the development of small-sized HEA nanoparticles (HEA NPs) is still in its dawn stage,² and only a few combinations of elements are explored so far.

We have focused on the combination of *p*-block metals (*p*Ms: In, Sn, Bi, etc.) and *d*-block metals (*d*Ms: platinum-group metals (PGMs), etc.) in HEA NPs (denoted as *pM-dM* HEA NPs). These 2 groups of elements have contrasting features in electronic structure or thermodynamic properties such as melting points, which should afford uniqueness of *pM-dM* system. However, *pM-dM* system has been poorly investigated even in binary NPs and much less in more complicated HEA NPs, partly due to difficulty in their synthesis. Here, we first report the synthesis of *pM-dM* HEA NPs using a facile wet-chemistry method. The successful formation of the HEA NPs was confirmed by revealing their crystal structure and electronic structure with a series of X-ray based spectroscopies and electron microscopy. The properties of the obtained NPs are also discussed.

1) a) J. W. Yeh *et al.*, *Adv. Eng. Mater.*, **2004**, *6*, 299-303. b) D. B. Miracle *et al.*, *Acta Mater.*, **2017**, *122*, 448-511. 2) Y. Yao *et al.*, *Science*, **2018**, *359*, 1489-1494.

NM05.07.08

Continuous-Flow Synthesis for Extremely Small IrPdPtRhRu High-Entropy Alloy Nanoparticles and Investigation of Their Hydrogen Evolution Catalytic Activity Hiroki Minamihara¹, Kohei Kusada^{1,2,3}, Dongshuang Wu¹, Tomokazu Yamamoto⁴, Takaaki Toriyama⁵, Syo Matsumura⁶, Loku S. Kumara⁵, Osami Sakata⁵, Shogo Kawaguchi⁵, Yoshiaki Kubota⁶ and Hiroshi Kitagawa¹; ¹Kyoto University, Japan; ²HAKUBI Center, Japan; ³JST-PRESTO, Japan; ⁴Kyushu University, Japan; ⁵JASRI SPring-8, Japan; ⁶Osaka Prefecture University, Japan

High-entropy alloy nanoparticles (HEA NPs) are of interest in various fields such as energy conversion catalysis.^[1] For example, IrPdPtRhRu HEA NPs showed remarkably high hydrogen evolution reaction (HER) activity compared with commercial Pt.^[2] Although the smaller HEA NPs are desired for catalytic use, most of the reported synthesis techniques of HEA NPs provide over 10-nm particle size because they stabilize the solid-solution phase under extreme conditions such as high temperature accelerating the atomic diffusion and particle growth.^[3,4] In this study, we first synthesized 1.3-nm IrPdPtRhRu HEA NPs, the smallest size of HEA NPs, by a liquid-phase reduction method at room temperature using an originally developed continuous flow reactor enabling inert synthesis conditions. The obtained NPs were characterized by scanning transmission electron microscopy (STEM) and Pair distribution function (PDF) analysis. Elemental maps suggested the successful mixing of five elements at the atomic level. PDF analysis for the obtained NPs indicated an fcc structure with ultrasmall particle size. Moreover, we investigated HER catalytic activity which plays an important role in energy conversion for the development of hydrogen-based energy resources. The 1.3-nm HEA NPs showed 8-times higher activity than commercial Pt which is a benchmark catalyst for HER, which is one of the best HER activities among reported highly active platinum group metal-based catalysts.

[1] Wu, D. *et al.*, *Chem. Sci.* **2020**, *11* (47), 12731–12736. [2] Amiri, A. *et al.*, *J. Mater. Chem. A* **2021**, *9* (2), 782–823. [3] S. Gao *et al.*, *Nat. Commun.* **2020**, *11*(1), 2016. [4] Yao, Y. *et al.*, *Science* **2018**, *359*(6383), 1489-1494.

NM05.07.09

Slot-Die Deposition of ZnO:Al Thin Films for Sustainable Optoelectronic Applications Ewan D. Matheson¹, Xinya Xu², Yongtao Qu¹, Pietro Maiello¹, Guillaume Zoppi¹ and Neil Beattie¹; ¹Northumbria University, United Kingdom; ²WaveOptics, United Kingdom

Slot-die coating is a solution-based method for forming thin films for optoelectronic devices and belongs to a family of coating methods known as pre-metered coating [1]. More traditional techniques such as vacuum-based physical vapour deposition (PVD), involves expensive equipment and is inefficient both in terms of material usage and energy [2]. In contrast, slot-die coating offers room temperature deposition with near 100% material usage efficiency. For thin film electronics, indium tin oxide (ITO) is currently favourite in the transparent conducting oxide (TCO) market, however it is expensive relative to other TCO's [3] and therefore a cheaper alternative is required to reduce the cost of optoelectronic devices. One candidate is ZnO:Al (AZO) which offers similar performance characteristics such as high band gap (3.5 eV), optical transmittance (~80 %) and low resistivity (10⁻⁴ Ωcm) [4,5].

In this study, slot-die coating was used to deposit AZO nanoparticles on glass. Scanning electron microscopy indicates that the films are homogeneous and densely packed with nanoparticle diameters ranging from 10 – 30 nm. Furthermore, the film thickness was found to be uniform across the substrate and could be controlled within a 30 nm range by adjusting key slot die parameters. X-ray diffraction measurements demonstrate crystallographic reflections from the nanoparticles that correlate with a ZnO reference and exhibit planar orientation. Annealing in an Ar atmosphere from 300 – 500 °C, was shown to increase the crystallinity. UV-Vis spectroscopy showed that the films exhibit a blue shift in the optical band gap (4.37 eV) which may be due to quantum confinement. Four-point probe electrical measurements revealed the nanoparticle film to have high sheet resistance due to the high number of interfaces introduced by the nanoparticles, however on a conductive ITO substrate, the cross-section resistivity was observed to be ~4×10⁻² Ωcm.

Compared to the slot-die deposited nanoparticle film, the PVD AZO film exhibits a larger grain size and a correspondingly lower energy band gap. Typically, PVD AZO film thicknesses range between 100 - 500 nm for optoelectronic devices however the films in this study are relatively thick at 1 μm [6]. X-ray diffraction also indicates correlation with the ZnO reference with sharper and more intense features compared to the nanoparticles, as well as orthogonal orientation. Four-point probe measurements indicates a resistivity of ~7×10⁻⁴ Ωcm which is significantly lower than the cross sectional resistivity of the nanoparticles.

In summary, slot-die deposited AZO nanoparticles for application in the manufacturing of high-throughput, low-cost optoelectronic devices, yielded uniform thin films with good optical properties and low materials wastage. Due to the substantial number of grain boundaries introduced by the

nanoparticles, conductivity was reduced compared to the PVD AZO sample. Further investigations will focus on potential approaches to improving the electrical properties of the slot-die films, such as incorporating metal nanoparticles in the film, as well as hydrothermal growth of ZnO nanowires using the slot-die nanoparticle thin film as a seed layer.

- [1] Carvalho, M. S., Khesghi, H. S. (2000). *AIChE Journal*, 46(10), 1907–1917.
- [2] Baptista, A., Silva, F., Porteiro, J., Míguez, J., Pinto, G. (2018). *Coatings*, 8(11).
- [3] Hartner, S., Ali, M., Schulz, C., Winterer, M., Wiggers, H. (2009). *Nanotechnology*, 20(44).
- [4] Zhang, Z., Bao, C., Ma, S., Hou, S. (2011). *Applied Surface Science*, 257(17), 7893–7899.
- [5] Gabás, M., Torelli, P., Barrett, N. T., Sacchi, M., Ramos Barrado, J. R. (2014). *APL Materials*, 2(1).
- [6] Subramanyam, T. K., Goutham, P., Pavan Kumar, S., Yaduraj, S. R., & Geetha, K. S. (2018). *Materials Today: Proceedings*, 5(4), 10851–10859.

NM05.07.10

One-Pot Synthesis Method of Hyaluronic Acid-Coated Gold Nanoparticles for Controlled Drug Release System [Junghun Park](#) and Hyoung-Mi Kim; Korea Institute of Industrial Technology, Korea (the Republic of)

Hyaluronic acid (HA) is a natural linear polysaccharide formed by repeating units of d-glucuronic acid and N-acetyl-d-glucosamine disaccharide. Since HA possesses excellent properties of biocompatibility, biodegradation, non-toxicity, and non-immunogenicity, it has been widely used for cosmetics and pharmaceuticals including drug delivery system. In this study, we newly studied one-pot synthesis of HA-coated gold nanoparticle (HA-AuNP) as drug delivery system. Various types of HA-AuNPs were synthesized using electron-beam irradiated HA, which makes the low molecular weight of HA. Sulfasalazine (SSZ) was used to demonstrate efficiency of drug delivery and controlled release of the HA-AuNP. We first characterized SSZ-HA-AuNP by TEM, UV-vis, DLS, and zeta-potential analysis. As the molecular weight of HA decreased, drug loading capacity and encapsulation efficiency of SSZ increased. Next, we tested time-dependent SSZ release profile at simulated gastric fluids and intestinal fluids. Controlled drug release in simulated intestinal condition over 24 h was observed by anomalous (non-Fickian) drug transport following Korsmeyer-Peppas model. This suggests that HA-AuNP can be used for a stomach dependent-sustain drug delivery system.

NM05.07.11

Rational Design of Dimensionally Stable Anodes for Active Chlorine Generation [Hyunwoo Lim](#)¹, Deok Ki Cho¹, Joo Ho Yoon¹, Chan Woo Lee² and Jin Young Kim¹; ¹Seoul National University, Korea (the Republic of); ²Kookmin University, Korea (the Republic of)

Chlor-alkali electrolysis, which contains chlorine evolution reaction (CER) and hydrogen evolution reaction (HER) as an anodic and cathodic reaction, is a critical industrial process for the production of chlorine gas, caustic soda, and hydrogen fuel. Dimensionally stable anode (DSA) has been exploited as the commercial electrode for CER because of its durable catalytic activity. However, the high precious metal contents of DSA (15 mol% of RuO₂ and 15 mol% of IrO₂) and the anodic corrosion of RuO₂ during the oxygen evolution reaction (OER), which is a side reaction of CER, remain fundamental challenges that must be addressed. Here, we demonstrate that low-temperature annealing of RuO₂ nanoparticles (~1.7 nm) supported on conductive Nb-doped TiO₂ (abbreviated as RuO₂/Nb:TiO₂-A200 NPs) leads to the formation of durable active sites with superior electrocatalytic activity and product selectivity toward chlorine generation (10 and 100 mA cm⁻² at 22 and 55 mV overpotential with a Faradaic efficiency of 97.3% in 0.6 M NaCl, which is much better than those of commercial DSA). The Nb doping not only enhances the electronic conductivity and suppresses the reactivity related to undesirable water oxidation of the TiO₂ support, but also enables thermal diffusion of Ti atoms into the RuO₂ lattice at the temperature of 200 °C, thereby forming ultrafine solid-solution nanoparticles having an ultrathin TiO₂ surface as a protective layer. This work provides a cost-effective fabrication strategy of stable RuO₂-based electrocatalysts for anodic reactions, as well as additional electrode structural insights into the design principle of DSA.

NM05.07.12

Dynamic Surface Modifications of MOF Nanoparticles via Alkoxyamine Functional Groups [Simon Spiegel](#)¹, Ilona Wagner¹, Salma Begum², Matthias Schwotzer¹, Isabelle Wessely², Stefan Bräse² and Manuel Tsotsalas¹; ¹Karlsruhe Institute for Technology (KIT)/Campus Nord, Germany; ²Karlsruhe Institute of Technology (KIT), Germany

Metal-organic frameworks (MOFs) have become one of the most popular class of materials, due to their outstanding versatility in composition and functionality, combined with their well-defined crystalline structures. MOFs show promise for diverse applications, ranging from catalysis, organic electronics, gas storage and separation, to biology and medicine. In many of these applications, surface chemistry is a crucial factor for the performance of MOFs. Therefore, the external surface engineering of metal-organic frameworks (MOFs) is an important design strategy, providing access to optimized chemical and colloidal stability. Common strategies for MOF surface modifications include either physical adsorption or chemical association of small molecules or (preformed)-polymers. However, most of the currently employed approaches lack precise control of the polymer density and are unable to dynamically modify the surface on demand.

We introduce alkoxyamines as versatile tool for the surface modification of MOF nanoparticles (NPs). These alkoxyamines can serve as an initiator in nitroxide mediated polymerization (NMP), hence they enable polymerization from the MOF surface. Furthermore, alkoxyamines provide the possibility to dynamically exchange of small molecules via nitroxide exchange reaction (NER).

In our studies we used UiO-66-NH₂ as a standard MOF template. The success of surface modification and successive surface polymerization was confirmed via various characterization methods, including time-of-flight secondary ion mass spectrometry (ToF-SIMS), size exclusion chromatography (SEC), attenuated total reflection infrared spectroscopy (ATR-IR) and nuclear magnetic resonance (NMR) spectroscopy.

NM05.07.13

Effect of Acid-Base Modulators on the Crystal Morphology of Zr-UiO-66 Metal-Organic Framework Nanoparticles [Burcu Akata Kurc](#) and Saeed A. Khan; Middle East Technical University, Turkey

Metal-organic frameworks (MOFs) are an emerging class of hybrid crystalline porous materials that consist of metal clusters (nodes) connected by organic linkers (struts) to form a three-dimensional molecular framework. MOFs have attracted considerable attention in recent years owing to their exceptional properties. Due to their remarkable design flexibility, ultra-high porosity, large specific surface area, and tunable properties, MOFs are indispensable for potential applications in clean energy, gas adsorption, and catalysis. Zr-UiO-66 is one of the archetypal MOFs with high surface area and chemical and thermal stability. Tuning the surface morphology of Zr-UiO-66 MOF crystals can significantly enhance their catalytic, gas adsorption, and gas sensing properties.

Conventionally, the solvothermal method is used for the synthesis of Zr-UiO-66. Various modifications have been made in the solvothermal route to tailor the morphology of Zr-MOF crystals and reduce the synthesis time. Zr-UiO-66 can be synthesized using different modulators like HCl, HF, acetic acid, and

TEA. This route allows one to speed up the synthesis reaction or induce a desired property, such as creating defects or tailoring crystal morphology.

In this study, UiO-66 was synthesized without and with the presence of acid-base modulators (acetic acid and TEA base). The synthesis of Zr-UiO-66 without a modulator at 80°C resulted in cubic crystals with an average particle size of 125 nm; however, no crystal morphology was observed at a reaction temperature of 120°C. It was interesting to see that octahedral-shaped crystals were obtained for UiO-66 at 120°C in 6 hours when acetic acid (2.4 M) and TEA (2 mM) were introduced into the reacting solution as modulators. SEM images showed discrete octahedral Zr-UiO-66 MOF crystals for acid-base co-modulated synthesis. The role of acetic acid is to engineer the crystal's shape by stopping the crystal's growth in particular directions, thus resulting in octahedral morphologies. TEA plays a role in the nucleation and mono-dispersity of the crystals. TEA also helps in reducing the time of crystal nucleation. The size of the octahedral crystal increased with the concentration of TEA in reacting solution. When the concentration of TEA was increased from 2 mM to 12 mM in the reaction solution, the mean crystal size of Zr-UiO-66 increased. At 12 mM TEA concentration in the precursor solution, the largest average crystal size of 1.02 μm was observed. The crystal size started to decrease as the TEA concentration was increased further. It can be hypothesized that the fast nucleation effect of TEA was dominant and could be the reason for relatively more polydispersity of crystals sizes. However, for 16 mM and 19 mM TEA concentrations, TEA helps obtain monodisperse crystal sizes by creating more and more nucleation points.

The project leading to these results has received funding from the Scientific and Technological Research Council of Turkey (TÜBİTAK) under grant agreement 220M002.

NM05.07.15

The High-Entropy Oxide Nanoparticles Consisting of All 3D Elements Ryohei Kanda¹, Kohei Kusada^{1,2,3}, Takaaki Toriyama⁴, Tomokazu Yamamoto⁴, Yasukazu Murakami^{4,5}, Syo Matsumura^{4,5}, Shogo Kawaguchi⁶, Yoshiaki Kubota⁷ and Hiroshi Kitagawa¹; ¹Kyoto University, Japan; ²The Hakubi Center Kyoto Univ., Japan; ³JST-PREST, Japan; ⁴URC Kyusyu University, Japan; ⁵Department of Applied Quantum Physics and Nuclear Engineering, Kyushu Univ., Japan; ⁶Japan Synchrotron Radiation Research Institute/SPring-8, Japan; ⁷Osaka Metropolitan Univ., Japan

High-entropy oxides (HEOs), which are complex oxides containing five or more metal cations at around the same molar ratio in a single phase, have attracted much attention because of their unique chemical and physical properties, for example, thermoelectric property^[1] and Li-ion conductivity^[2]. Following the first report in 2019^[3], lots kinds of HEO nanoparticle (NP) have been reported. For example, they consist of only five 3d transition elements or of homologous elements. HEO NPs are considered to be a new class of materials such as catalysts, but the syntheses of them have not been well developed because it is difficult to homogeneously mix diverse elements in nano-sized crystals.

Here, we succeeded for the first time in synthesizing HEO NPs consisting of all 3d transition elements (Sc, Ti, V, Cr, Mn, Fe, Co, Ni, Cu, and Zn) by a flow reactor with supercritical water. The formation of a single phase of the HEO NPs homogeneously consisting of all the ten 3d elements was confirmed by scanning transmission electron microscopy (STEM) and energy dispersive X-ray spectroscopy (EDS). X-ray diffraction (XRD) analysis revealed that all the ten 3d transition metals formed a solid-solution spinel oxide (Sc, Ti, V, Cr, Mn, Fe, Co, Ni, Cu, Zn)₂O₄, which is the same crystal structure as Fe₃O₄. The radial distributions calculated by Fourier transformation from X-ray absorption fine structure (XAFS) data revealed that all 3d elements are randomly located at tetrahedral and octahedral sites in spinel structure.

[1] J. L. Braun *et al.*, *Adv. Mater.*, **30**(51), 1805004 (2018), [2] D. Bérardan *et al.*, *J. Mater. Chem. A*, **4**, 9536-9541 (2016), [3] D. Wang *et al.*, *J. Mater. Chem. A*, **7**, 24211-24216 (2019)

NM05.07.16

Compositional Dependence of Structures and Activity for Hydrogen Evolution Reaction of Platinum-Group-Metal Quinary Alloy Nanoparticles Yuto Maruta¹, Kohei Kusada^{1,2,3}, Dongshuang Wu¹, Tomokazu Yamamoto⁴, Takaaki Toriyama⁴, Syo Matsumura^{4,5}, Okkyun Seo⁶, Satoshi Yasuno⁶, Shogo Kawaguchi⁶, Osami Sakata⁶, Yoshiaki Kubota⁷ and Hiroshi Kitagawa¹; ¹Kyoto University, Japan; ²HAKUBI Centre, Kyoto Univ, Japan; ³JST-PRESTO, Japan; ⁴URC, Kyushu Univ., Japan; ⁵Grad. Sch. Eng., Kyushu Univ., Japan; ⁶JASRI-SPring-8, Japan; ⁷Osaka Metropolitan Univ., Japan

Multi-element solid-solution alloy nanoparticles (NPs) have attracted much attention as a new class of catalysts because they have both high activities and stabilities for many kinds of reactions¹⁻³. For example, equimolar platinum-group metal (PGM) quinary alloy NPs show an extremely high catalytic activity for hydrogen evolution reaction (HER)³. Despite very high compositional designability of multi element alloy NPs, the composition dependence of their crystal and electronic structures, and properties have not been well investigated.

We synthesized PGM quinary alloy NPs with several compositions directly supported on carbon to investigate their compositional dependence of structures and catalytic activity for HER. The compositions of the obtained NPs were analyzed by X-ray fluorescence (XRF). They were also characterized by scanning transmission electron microscopy (STEM) coupled with energy-dispersive X-ray spectroscopy (EDX). The EDX maps confirmed the formation of homogeneous solid solutions. Their crystal structures were analyzed by synchrotron powder X-ray diffraction (PXRD), and their valence-band electronic structures were investigated by hard X-ray photoelectron spectroscopy (HAXPES). In addition, HER was selected as the target reaction and measured by a three-electrode electrochemical measurement. Their compositional dependences of lattice constants, *d*-band centers, and catalytic activities of HER were investigated. We found their lattice constants can be represented by simple linear combination formula, indicating multi-element alloy NPs follows Vegard⁴ law as binary alloy NPs⁴. In contrast, their *d*-band centers change nonlinearly with compositions, mainly because of the complex hybridization of the five constituent elements. Their catalytic activities are not simply correlated with compositions, suggesting different interpretations of the reaction mechanism such as a combination of multiple factors are needed for multi-element alloy NPs.

1) D. Wu, et al., *J. Am. Chem. Soc.*, 2020, 142, 32, 13833–13838. 2) D. Wu, et al., *J. Am. Chem. Soc.*, 2022, 144, 3365–3369. 3) D. Wu, et al., *Chem. Sci.*, 2020, 11, 12731–12736. 4) Y. Maruta, et al., *Chem Commun.*, 2022, 58, 6421-6424.

NM05.07.18

Improving Electron Pair Distribution Function (ePDF) for Nanomaterials—The Semiconductor CdSe Quantum Dot Case Olavo F. Verruma^{1,2}, Naga Vishnu V. Mogili¹, Isabela J. Vieira¹, Jefferson Bettini¹ and João B. Souza Junior¹; ¹National Center for Research in Energy and Materials, Brazil; ²University of São Paulo State–UNESP, Brazil

Quantum Dots (QDs) are nanometric semiconductor materials under massive study due to their optical and electronic properties controlled by quantum confinement. Cadmium Selenide (CdSe) is being tested in different applications¹, however, nanoparticle crystallographic structure can hinder the efficiency of QDs applications, mostly due to the concentration of defects such as grain boundaries, stacking faults, and vacancies. Besides the core-related defects, the surface of nanomaterials, which behave like a skin that is exposed to the environment, presents a higher concentration of defects created by the lower atomic coordination from atoms at the surface. The small nanoparticle size of QDs makes it more difficult to characterize the crystallographic structure by standard techniques like X-ray Diffraction. Elevated peak broadening and lower intensity of coherent scattering by nanomaterials create broad diffraction peaks almost convoluted with the diffusion scattering. Then, the Pair Distribution Function (PDF) analysis of the total scattering data has been raised as an alternative method to suppress those problems and solve the atomic arrangement structure for nanomaterials². Alternatively, the PDF from electron

diffraction (ePDF) presents itself as an optimal possibility to characterize nanoparticles as the strong electron matter interaction enables the acquiring of diffraction patterns for a known ensemble of nanoparticles, i.e. TEM equipment can collect diffraction by a precise nanoparticle region matching images and elemental composition analysis (EELS and EDS) with ePDF analysis. In this work, CdSe QDs were synthesized using cadmium oxide (CdO), selenium (Se), trioctylphosphine, oleic acid (OA), oleylamine (OAm), 1,2-hexadecanediol (HDD) and 1-octadecene as solvent. CdO was added to a three-neck round-bottom flask with OA and solvent. This mixture was heated to 100 °C (10 °C min⁻¹), and kept under a vacuum for 30 minutes, and then heated to 200 °C (10 °C min⁻¹) under a N₂ atmosphere, until the solution becomes translucent. The system was cooled to 100 °C, after that, HDD and OAm were added. The reaction was kept under a vacuum for 30 minutes. Subsequently, the reaction medium was heated at 300 °C (10 °C min⁻¹), under a N₂ atmosphere, and the Se precursor was injected. After injection, instantaneous formation of CdSe was observed and 30 minutes until the temperature began to drop spontaneously. CdSe QDs from 1.9 nm to 4.0 nm were synthesized by modifying the above process and changing precursors/ligands ratio, reaction time, and temperature. Then, using a holey carbon TEM grid a self-sustained QDs membrane was deposited in the TEM grid and the total electron scattering pattern was acquired in a Cs-corrected TEM (Titan Themis). Then, a modified code of eRDF Analyzer software was used to calculate the structure factor $S(Q)$ by normalizing the intensity scattering profile $I(Q)$ with the expected atomic scattering factors. The Reduced ePDF $G(r)$ was obtained by the Fourier Transform of $S(Q)$. Simulated $I(Q)$, $S(Q)$, and $G(r)$ for spherical z-CdSe (zinc blend, cubic structure) nanoparticles were introduced in the eRDF code to guide the data treatment and extraction of the final $G(r)$. The optical properties of CdSe QDs with different sizes were compared with the obtained crystallite size from ePDF $G(r)$ structural refinement using PDFGui software. We have seen that $G(r)$ results lead to smaller crystallite size compared to TEM morphological diameter and the size obtained from the position of the first excitonic peak. The presence of stacking faults is directly related to the lower crystallographic size and the loss of long-range atomic ordering in CdSe QDs. Concluding, ePDF $G(r)$ showed to be a good crystallographic tool for semiconductor CdSe QDs analysis, demonstrating the technique can be used to analyze the atomic structure of small nanoparticles.

[1] García de Arquer *et al.*, *Science* 373, 640, 2021

[2] *Matter* 4, 441–460, 3, 2021

NM05.07.20

A Comprehensive Study of Thiolation on Bare Gold Nanoparticles Produced by Laser Ablation in Liquids Jean Y. Tovar Sanchez¹, Maria B. De la Mora Mojica², Tupak García-Fernández³ and Mayo Villagrán-Muniz¹; ¹Instituto de Ciencias Aplicadas y Tecnología, Universidad Nacional Autónoma de México, Mexico; ²CONACyT Fellow-ICAT, Universidad Nacional Autónoma de México, Mexico; ³Universidad Autónoma de la Ciudad de México, Mexico

Gold nanoparticles (Au NPs) have several applications in optoelectronics, catalysis, biosensing, probing and medical therapy. The latter applications require an adequate coupling between the NP and the analyte to optimize its performance: a functionalization. To carry out the functionalization of Au NPs, one of the most used functional groups are thiols, in which functionalization is assumed through the chemical affinity between gold and sulfur. However, the efficiency of this thiolation depends on the properties of the Au NPs surface and the synthesis method. Most of the scientific research oriented to understand and optimize functionalization by different compounds that include thiols is focused on Au NPs obtained by chemical or biological methods, commonly capped with surfactants or in presence of other residuals from the synthesis. This implies another interaction of a layer surrounding the Au NPs with the thiolate compound. Here we study the thiolation mechanism and its consequences in bare Au NPs obtained by laser ablation in liquids (LAL). LAL is a green technique that allow us to obtain Au NPs with high purity. Since the Au NPs surface is not capped, this system let us study the direct interaction between the surface of Au NPs and thiolate compounds, as well as the influence of the surrounding media.

Au NPs thiolated with mercaptopropionic acid at different concentrations were studied by UV-vis-NIR absorbance, Dynamic Light Scattering spectroscopy, Zeta Potential, X-ray Photoelectron Spectroscopy and Transmission Electron Microscopy. The influence of the thiolation in the stability of the colloids is also addressed. A red shift in the absorption band is in general observed due to the presence of thiols. We observed that the Au NPs obtained by LAL are more sensitive to smaller amounts of thiols than their counterparts obtained by chemical methods. Also, we propose a fast and effective method based on Ellman colorimetric assay to optimize the amount of thiol used for functionalization for AuNPs obtained by LAL.

NM05.07.21

Organosilane-Based Control Over Chemical and Electronic State on 1D Anatase-Like Quat-Derived Nanomaterials Julia Martin¹, Rebecca Ramthun¹, Michelle Frasch¹, Erika Colin-Ulloa¹, Hussein Badr², Michel W. Barsoum², Lyubov Titova¹ and Ronald L. Grimm¹; ¹Worcester Polytechnic Institute, United States; ²Drexel University, United States

Recently discovered quaternary-derived nanomaterials (QDNs) possess a highly anisotropic 1D anatase-like (1DA) structure. While they demonstrate high oxidative stability and catalytic properties, little information exists on interfacial chemistry and electronic properties. We synthesized titanium-based QDNs and utilized ultraviolet photoelectron spectroscopy (UPS) to quantify valence band and Fermi energies as a function of surface treatments. Treatments included rinsing in LiCl as well as organosilane-based derivitization to change local electron density based on the inclusion of electron-withdrawing or electron-donating organic groups. UP spectra reveal moderate n-type doping as well as up to 1 eV shifts in band-edge positioning based on interfacial dipoles resulting from organosilane attachment. We discuss the results in the context of electromagnetic shielding, chemical sensing, catalytic, and photocatalytic applications.

NM05.07.22

Photothermal Study and Stability of Gold Nanoparticles with Different Morphology María F. Amézaga González and Perla E. García Casillas; UACJ, Mexico

Over recent years, some research utilizing gold nanoparticles physicochemical properties for photothermal applications has been conducted and published. The objective of this research is to obtain different morphologies of gold nanoparticles (sphere, roller, and star) to study and compare the colloidal stability and photothermal properties depending on the pH of each nanostructure by activating its resonance plasmon externally with a laser. The three morphologies of gold nanoparticles were synthesized by using and modifying the Turkevich method, the spheres were coated with the polymer polyethylene glycol (PEG) with the help of fluorescein (Fl). The characterization techniques that were used are: 1) Scanning electron microscopy (SEM) that was extracted to characterize the morphology and size of the nanostructures obtained. To obtain a better view of the nanoparticles and their diffraction pattern, it was necessary to use 2) transmission electron microscopy (TEM). 3) Ultraviolet-visible spectroscopy (UV-Vis) allowed obtaining the characteristic absorption spectrum of each gold nanostructure. 4) In Fourier transform infrared spectroscopy (FT-IR), the interactions of the PEG functional groups with the gold nanospheres were observed. Finally, the colloidal stability index (TSI) was evaluated by varying the pH of the regular medium (7) with PBS 1X (pH 7.2 and 7.4) and the photothermal properties were determined with the help of a laser (535 nm) and post-thermal properties of each of the gold nanostructures and the different media (pH). It is important to point out that, adding the polymer polyethylene glycol (PEG) and fluorescein to the gold nanospheres (AuNPs-Fl-PEG), helped to potentiate their colloidal stability at different pH (7.2 and 7.4), being the complex with the TSI more stable in 48 hours. It will also be developed that gold nanorods (AuNRs) are the best option for thermal applications. In closing that the morphology and coating of gold nanoparticles with PEG influence their colloidal stability and their photothermal properties (plasmon resonance) as a function of pH when stimulated with a laser (523 nm).

NM05.07.23

Synergistic Effect Between Single Au Atoms and Tensile-Strained Pd for Highly Efficient Electroreduction of CO₂ to Formate [Jinsol Bok](#)^{1,2} and Taeghwan Hyeon^{1,2}; ¹Seoul National University, Korea (the Republic of); ²Institute for Basic Science, Korea (the Republic of)

Among various metal catalysts, Pd is one of the most effective catalysts for the electrochemical reduction of CO₂ to formate, a valuable liquid product, at low overpotential. However, Pd metal has intrinsically high CO affinity which makes the metal surface vulnerable to CO poisoning, resulting in rapid deactivation toward CO₂ electroreduction. Herein, we design novel catalyst utilizing the interaction between metals and metal-organic frameworks. Atomically dispersed Au on tensile-strained Pd nanoparticles shows significantly improved formate production activity, selectivity, and stability with high CO poisoning tolerance. Moreover, we found that the tensile strain stabilizes all reaction intermediates on the Pd surface, whereas the atomically dispersed Au selectively destabilizes CO* without affecting other adsorbates. As a result, the conventional COOH* versus CO* scaling relation is broken, and our catalyst exhibits about 30-fold enhancement in partial current density and mass activity toward electrocatalytic formate production with over 99% faradaic efficiency, compared to Pd/C at -0.25 V versus RHE.

NM05.07.24

Microfluidics-Assisted Synthesis of Hyper-Branched Nanocrystals with Multi-Steps for the Electrochemical CO₂ Reduction [Minki Jun](#) and Kwangyeol Lee; Korea University, Korea (the Republic of)

Flow chemistry, based on microfluidics, has been considered a powerful synthetic method due to precise reaction control, high surface area per reactor volume, and high reproducibility. Also, extremely fast mixing time in flow chemistry can generate unstable reaction intermediates in high concentrations. Herein, we synthesized the hyper-branched hierarchical Cu₂O nanocrystals with numerous steps (h-Cu₂O ONSs) by microfluidics-based ultra-fast mixing of precursor solutions to obtain a very high concentration of CuOH intermediates. Furthermore, computational fluid dynamics (CFD) simulation and analysis were performed to understand the effect of mixing in a flow microreactor on the synthesis of h-Cu₂O ONSs. The prepared h-Cu₂O ONSs exhibited excellent selectivity toward C₂ products during electrochemical CO₂ reduction because of the numerous heterointerfaces between Cu₂O and Cu phases derived from rapid surface reconstruction at stepped structures.

NM05.07.25

Composite Cellulose Nanofiber-Alginate Biotemplated Cobalt Aerogels for Energy Storage and Catalytic Electrodes [Felita W. Zhang](#)¹, Paul Trackey¹, Alexa Zammit¹, Galen Mandes¹, Edward M. Tang¹, Rosemary L. Calabro^{1,2}, Enoch A. Nagelli¹, Stephen F. Bartolucci², Joshua A. Maurer² and John Burpo¹; ¹United States Military Academy, United States; ²U.S. Army Combat Capabilities Development Command-Armaments Center, United States

Biotemplated transition metal aerogels enable tunable porous composite materials to control metal/metal oxide functionalization, conductivity, pore structure, electrolyte mass transport, mechanical strength, specific surface area, and magneto-responsiveness. To demonstrate a solution-based synthesis method to develop cobalt and cobalt oxide aerogels for energy storage and catalytic electrodes, carboxymethyl cellulose nanofibers (CNF) and alginate were mixed to form a composite biopolymer hydrogel that served as a template for cobalt nanoparticle formation via chemical reduction of cobalt salt solutions. The CNF-alginate mixed to form a physically entangled, interpenetrating hydrogel requiring no covalent chemical crosslinking. The hydrogels combine the properties of both biopolymers to exhibit stiffness, flexibility, ease of gel formation, as well as abundant carboxyl groups that bind metal ions to facilitate biotemplating. CNF-alginate hydrogels at different biopolymer weight percents were equilibrated in CoCl₂ salt solutions, chemically reduced with NaBH₄, rinsed, solvent exchanged in ethanol, and supercritical dried with CO₂. The resulting aerogels were pyrolyzed in N₂ gas and thermally annealed in air to form either Co or Co₃O₄ porous composite electrodes. Aerogels were characterized using scanning electron microscopy, energy dispersive x-ray spectroscopy, x-ray diffractometry, thermogravimetric analysis, nitrogen gas adsorption-desorption with Brunauer-Emmett-Teller surface area analysis, vibrating-sample magnetometry, magnetic force microscopy, nanoindentation, and force-extension modulus testing. Electrochemical performance of cobalt catalysis of the oxygen reduction reaction and Co₃O₄ supercapacitance was determined with electrochemical impedance spectroscopy, cyclic voltammetry, and linear sweep voltammetry. The rapidly synthesized, low cost composite hydrogel solution-based transition metal synthesis approach is envisioned as an approach for a wide range of non-precious metal porous catalytic electrodes to address energy storage, catalysis, and sensing applications.

NM05.07.26

Synthesis of Single-Phase Spinel High Entropy Oxides Nanoparticles with Electrospinning [Xiao Han](#), Vijayaraghavan Sankaranarayanan Nair, Lin Li and Feng Yan; The University of Alabama, United States

High entropy oxides nanoparticles (HEO NPs) exhibit excellent performance in catalysis, energy storage, magnets, and biosensors due to their unique entropy stabilization mechanisms. However, the synthesis of HEO NPs containing five or more immiscible elements with a single-phase structure is still challenging. In this work, we present a new synthesis method to process single-phase HEO NPs including up to eight metal elements by electrospinning and low-temperature annealing in air condition. To mix the incorporated elements uniformly, the nitrate salts are used as precursors in the solution, which is applied to the electrospinning to generate nanofibers. The cations are enveloped in the nanofibers during the electrospinning process. With the following annealing in air at a low temperature, the single-phase spinel HEO NPs can be obtained. The single-phase spinel structure is confirmed by X-ray diffraction (XRD), selected area electron diffraction (SAED), and high-resolution transmission electron microscopy (HRTEM). X-ray photoelectron spectroscopy (XPS) provides the analysis of the oxidation state of the individual elements. In addition, the synthesized HEO NPs exhibit magnetic properties with the highest saturation magnetization with 9.588 emu/g and the highest coercivity with 147.175 Oe.

NM05.07.27

Effective Separation of Inorganic Nanoparticles via a Modified Centrifugation Model [Edan Marcial](#), Silas Wieland, Hannah Brodsky, Krista Dizon and Yiliang Luan; Binghamton University, The State University of New York, United States

Despite the broad use of centrifugation in materials research, the speed and time parameters for the centrifugation of dense nanoparticles (NPs) have been left to be determined by individual labs. Various models have been developed to identify the parameters for separation but have yet to be verified experimentally. Herein, this work presents a modified model for the effective centrifugation of inorganic NPs. To identify the required centrifuge speed and time for effective separation of NPs in nonpolar colloidal suspensions, a model relating the time for centrifugation to the NP's distance from the centrifuge's axis of rotation was derived. This model was first verified by separating half of a perovskite quantum dots raw suspension without agglomeration under the predicted conditions generated from the model. The results were confirmed using UV-Vis and photoluminescence spectroscopy. The effectiveness of the derived model for separating different NPs of varying sizes and densities will also be reported. This research gives a more accessible way to use centrifuges in all labs to separate NPs effectively.

NM05.07.28

Combined Application of Scherrer and Guinier Formulas for Proper X-Ray Determination of Size and Size Distribution in Systems of Monocrystalline Nanoparticles—Case Study CeO₂ Nanocubes Adriana Valério¹, Fabiane J. Trindade², Rafaela F. Penacchio¹, Maurício B. Estradiote¹, Cristiane B. Rodella³, André S. Ferlauto², Stefan Kycia⁴ and Sergio L. Morelhaio¹; ¹University of São Paulo, Brazil; ²Federal University of ABC, Brazil; ³Brazilian Synchrotron Light Laboratory (LNLS/CNPEM), Brazil; ⁴University of Guelph, Canada

X-ray diffraction and scattering phenomena are widely used as analytical tools in the optimization and control of nanomaterial synthesizing processes. In systems of monocrystalline nanoparticles with size distribution, the physical meaning of size values as determined by using X-ray methods is still controversial. To answer such fundamental issue, a series of virtual nanoparticles with sizes ranging from 1 nm to 90 nm were generated and their exact scattering power computed via pair distance distribution function. Calculated X-ray diffraction and scattering patterns from systems of virtual nanoparticles demonstrated that diffraction and scattering phenomena obtain matching results for monodisperse sizes. When a finite size distribution is introduced, the two methods produce differing results. The root of the problem is the different weighting by which each method interprets the size distribution. Once understood, the deviation in resulting size values from scattering and diffraction can be used as input to a simple formula that provides the size dispersion around the system most probable size value. To illustrate this effect and the data analysis procedure, X-ray diffraction and small-angle scattering experiments were applied to solve the size distributions in a series of samples of cubic ceria nanoparticles, revealing systematic changes in the size distribution as a function of synthesis parameters.

NM05.07.29

Size-Controlled Synthesis of Very High Aspect Ratio Cu_{2-x}Se_y Nanosheets Esra B. Karatas Ozkaraca, Rana Ucuncuoglu, Abdelhakim Elmhamdi, Elif S. Gur, Ceren Egemen and Mahmut Aksit; Gebze Technical University, Turkey

Unprecedentedly high aspect ratio nanosheets of Cu_{2-x}Se_y are synthesized by a novel technique based on the modification of previously known co-precipitation methods by hot injection of the Cu precursor. The novel surfactant-free method can produce Cu_{2-x}Se_y nanosheets with up to > 20 μm lateral length and ~10 nm average thickness, resulting in a very high aspect ratio of more than 1000:1. The nanosheet size and aspect ratio strongly vary with Cu:Se atomic ratio in the reactor. Powder X-Ray Diffraction (XRD) patterns obtained from the nanosheet powders have indicated different crystalline phases and/or dramatically different peak intensities depending on the temperature and volumetric ratio of the hot injected Cu precursor solution, whereas such alterations in the hot injection process do not cause noticeable variation in nanosheet size and morphology according to Scanning Electron Microscope (SEM) images. Time-dependent crystal phase and size evolutions of the nanosheets during the reaction are studied by ex-situ XRD and SEM characterization. Low-temperature thermoelectric measurements are performed on rectangular pellets prepared from the produced nanosheet powders. The photocatalytic performance of the synthesized Cu_{2-x}Se_y nanosheets is also evaluated by observing the time-dependent degradation of methylene blue under halogen light in solutions containing known concentrations of the Cu_{2-x}Se_y nanosheets.

NM05.07.30

Controlled Synthesis of Lead and Tin Halide Perovskite Nanocrystals Yasuhiro Tachibana^{1,2}; ¹RMIT University, Australia; ²Osaka University, Japan

Low dimensional colloidal halide perovskite nanocrystals from zero- to two-dimension have recently received extensive attention because of their facile synthesis and the outstanding size-tunable optoelectronic properties. However, iodide-based perovskite nanocrystals that are considered as a light harvester generally show lower photoluminescence quantum yield and poorer stability compared to those of bromide- or chloride-based counterparts. Here, we propose a new synthetic route, namely a two-step injection process, to successfully control CH₃NH₃PbI₃ (MAPbI₃) nanostructures with a high photoluminescence quantum yield of nearly 100%. Influence of three parameters, (1) the ligand concentration ratio, (2) reaction temperature and (3) precursor ratio, on perovskite morphology and optical property, were systematically investigated. We have found that the ligand concentration ratio drastically changes the morphology and photoluminescence quantum yield/lifetime. The nanoplatelets formed in non-polar solvent (diphenyl ether) show a good stability over 30 days. The formation mechanism of MAPbI₃ NCs is proposed by combining the experimental results with a saturation kinetics model.

Lead-free Sn(II) based, CsSn₂Br₅, perovskite nanocubes were synthesized using a modified hot-injection method by tuning the injection temperature and reaction conditions. The formation of Sn(IV) based, Cs₂SnBr₆, perovskite nanocrystals (PNCs) from CsSn₂Br₅ perovskite nanocubes was observed. X-ray diffraction measurements revealed that oxygen or water molecules in air gradually react with CsSn₂Br₅ perovskite nanocubes to form Cs₂SnBr₆ NCs. The stability of Cs₂SnBr₆ NCs was monitored by time-dependent absorption measurements. Both oxygen and water molecules react with the Cs₂SnBr₆ NCs to degrade, however water molecules appear largely to react with the NCs. The stability has been improved by dispersing the Cs₂SnBr₆ NCs in degassed anhydrous solvent.[1]

This work was partly supported by JSPS KAKENHI Grant (19H02813) and (22H02182), and the Collaborative Research Program of Institute for Chemical Research, Kyoto University (grant number 2021-78 and 2022-99), Japan. We would like to acknowledge supports from the Australia-Japan Foundation for the collaborative project between RMIT University and Kyoto University. We also acknowledge supports from ARC DP fund (DP180103815) and ARC LIEF fund (LE200100051), Australia, and Forefront Research Center, Faculty of Science at Osaka University.

References

[1] Y. Tachibana, et al. *J. Photopolym. Sci. Technol.*, submitted (2022).

NM05.07.31

Engineering ZnO Nanoparticles as a Substrate for Surface-Enhanced Raman Scattering Samuel O. Adesoye and Kristen Dellinger; North Carolina A & T UNIVERSITY, United States

Surface-enhanced Raman spectroscopy (SERS) is an emerging technology that has the potential to become a clinical diagnostic tool; however, there are some shortcomings that limit its widespread use. One such limitation is the substrate that is used to enhance the signal. The commonly used plasmonic substrates like gold and silver often result in aggregation, instability, and off-target effects. Semiconductor nanostructures, on the other hand, could overcome these problems; however, they provide a low signal enhancement. By engineering these semiconductor nanostructures, it is possible to increase their signal enhancement. To achieve this goal, we are developing innovative ways to improve Raman signal enhancement in metal oxides, which include tuning the band gap by substitutional doping and exploring coating with plasmonic materials to create hybrid SERS substrates. In this work, zinc oxide (ZnO) was synthesized by using a co-precipitation method and was doped with magnesium (Mg) with concentrations ranging from 2-10%. To characterize these substrates, the morphology and size distribution of the nanoparticles were obtained using the AURIGA field emission scanning electron microscope (FE-SEM) and dynamic light scattering. X-ray photoelectron spectroscopy (XPS) was used to determine the elemental composition. Optical properties were obtained with a UV-Vis spectrophotometer, while iRaman Prime portable Raman spectrometer (B&W Tek, Newark, DE) was used to acquire the Raman signal. The absorption edge of the Mg-doped ZnO nanoparticles was red-shifted compared to pure ZnO nanoparticles, and the band gap estimated using Tauc's plot also showed a decrease with increasing Mg doping. When 5,5'-dithiobis(2-nitrobenzoic acid) (DTNB) molecule was observed with the various nanoparticle substrates, an enhanced signal was observed for the doped substrates with the 2% doping giving the highest peak. Overall, we

anticipate this work to serve as a platform for improving the use of SERS substrates in molecular sensing and bio-detection applications.

NM05.07.35

Synthesis of Multilayered Fe₃O₄@SnO₂@C Nanocomposites via Amino-Functionalization [Gye Sek An](#), Jae Uk Hur, Jae Rok Shin, Jin Soon Han, Ji Hun Jeong, Su Young Kang, Jong Hun Kim, Jee In Kim and Jiwan Kim; Kyonggi University, Korea (the Republic of)

Nanocomposites composed of different materials can realize original physicochemical and electrical properties that will be fundamental for future technologies. Magnetite (Fe₃O₄) nanoparticles, with unique magnetic and electrochemical properties, have attracted significant attention in many fields, including recording material, bio, electromagnetic interference shielding, and secondary batteries. In particular, tin dioxide (SnO₂), an n-type semiconductor, has a high synergistic effect with Fe₃O₄, so many researchers have tried to combine these two materials. Nevertheless, composite materials composed of only oxide have low electrical conductivity and poor performance, so the help of high-conductivity materials is sometimes required. In this study, a systematic method for fabricating multilayered Fe₃O₄@SnO₂@C nanocomposites via surface treatment/modification and carbonization was proposed. Silane/polymer-based amino-functionalization has been introduced to coat carbon. Also, the carbon layer was formed on the surface of Fe₃O₄@SnO₂ nanoparticles through the dehydration of the carbon precursor using sulfuric acid at atmospheric pressure. Finally, the synthesized nanocomposite's structure, surface properties, dispersibility, and magnetism were evaluated.

NM05.07.37

In Situ Formation of PbTe-PbS Core-Shell Nanocrystal 3D Superlattices [Seungho Lee](#), Mariano Calcabrini, Sharona Horta, Tobias Kleinmanns, Daniel Balazs and Maria Ibáñez; Institute of Science and Technology Austria (ISTA), Austria

Nanocrystals can be arranged into long-range order structures. Common strategies for inducing nanocrystal self-assembly are controlled solvent evaporation and colloid destabilization with anti-solvents. In both cases, purifying the particles and adding controlled amounts of ligands are necessary before inducing the self-assembly process.

Here, we show a method that allows the simultaneous formation of PbTe-PbS core-shell nanocrystals and their assembly into three-dimensional superlattices, all in-situ, during the nanocrystal synthesis. We first provide evidence of the shell formation through powder X-ray diffraction and high-resolution transmission electron microscopy. Additionally, the ordering of the core-shell nanocrystals is observed by in situ small-angle x-ray scattering (SAXS) measurements. We further confirmed that the size of the core PbTe nanocrystals play a pivotal role in the 3D superlattice formation. The methodology present here is simple and may be extended to other material systems.

NM05.07.40

Bioinspired Synthesis of Crystalline Nanomaterials Through Peptoid-Based Approaches [Chun-Long Chen](#); Pacific Northwest National Laboratory, United States

In nature, biominerals (e.g. bones and teeth) are excellent examples of hierarchical materials whose formation and functions are controlled over multiple length scales by high information content biomacromolecules. Inspired by nature, many biomimetic approaches have been developed for the design and synthesis of crystalline nanomaterials. These approaches are attractive because they generate complex, functional materials under mild aqueous synthetic conditions. Despite the advances in developing new approaches for bioinspired materials synthesis, the rules of designing sequence-defined synthetic polymers that lead to the predictable synthesis of crystalline nanomaterials remain unclear.

As one of the most advanced classes of sequence-defined protein-mimetics, peptoids offer tremendous opportunities for bioinspired materials synthesis because tuning peptoid-peptoid and peptoid-particle interactions can be done solely by varying side-chain chemistry. In this presentation, two peptoid-based approaches will be discussed for controlled synthesis of crystalline nanomaterials. **The first** involves the design and synthesis of surfactant-like peptoids for controlling formation and morphogenesis of inorganic nanomaterials. **The second** approach exploits self-assembling peptoids for controlled synthesis of hierarchically structured hybrid materials. A combination of *in situ* imaging (e.g. *in situ* TEM) and molecular simulations are used to elucidate the important roles of particle attachments during the peptoid-directed formation of crystalline nanomaterials.

NM05.07.41

Ultrasonic Spray Deposited Co-MOF for Wearable Supercapacitors Oyku Cetin, Tufan Bolukbasi, Mete Batuhan Durukan, Gozde Ozturk and [Husnu E. Unalan](#); Middle East Technical University, Turkey

Supercapacitors are gaining more attention for wearable electronics because of their key properties such as flexibility, reversibility in continuous cycling, high power output. The textile-based flexible supercapacitors are potentially key devices for wearable electronics with their mechanical properties and charge storage capabilities. Herein, high-performance all-solid-state wearable asymmetric supercapacitors (ASCs) are prepared based on ultrasonic spray deposited cobalt metal-organic frameworks (Co-MOF) and iron sulphide/graphene nanocomposites (Fe_xS_y-G NCs) on carbon textiles as the positive and negative electrodes, respectively. Owing to the obtained unique structure of Co-MOF, high reversibility coupled with high specific capacitance of 396 mF.cm⁻² is achieved. Additional electrochemical data with assemble strategies for long-lasting devices will be correlatively presented.

This work was supported by The Scientific and Technological Research Council of Turkey (TUBITAK) under Grant No:119N344.

NM05.07.42

Gear-Meshing-Type Colloidal Crystallization of Concave Polyhedra [Wenjie Zhou](#), Yuanwei Li and Chad A. Mirkin; Northwestern University, United States

Colloidal crystallization of nanoscale building blocks represents chemists' attempt to mimic, modify, and ultimately recreate highly ordered structures based on what is found in nature. Despite the rising of colloidal crystals over the past decade, the majority of symmetries among which are cubic, tetragonal, or hexagonal. Constrained by the poor understanding of the structure-unit relationship, deliberately constructing colloidal superlattices with low symmetry, especially from highly symmetrical building blocks, still remains an outstanding challenge. Leveraging the DNA-mediated assembly of concave polyhedral nanocrystals, we report a series of rational symmetry reductions through steric hindrance engineering, the *gear-meshing* type colloidal crystallization. Through programming the DNA interactions as well as ligand occupation ratio, we show four types of gear-meshing mode, identified and investigated from in situ and ex situ experiments. This study opens up new opportunities for synthesizing plasmonic metamaterials with close arrangements and low symmetries.

NM05.07.43

UiO-66 and Silane-Based Capping Molecule Have Covalent Attachment [Abigail Berube](#), Nathaniel Keyes, Rebecca Dawley, Shawn Burdette and Ronald L. Grimm; Worcester Polytechnic Institute, United States

An emerging group of nanocontainers, metal-organic frameworks (MOFs), have highly stable and porous structures, thus making them excellent for trap and release of other molecules. Even though this structure is highly favorable, not much is known about their surface chemistry. We have synthesized a zirconium oxide-based MOF verified through powder x-ray diffraction (pXRD) and x-ray photoelectron spectroscopy (XPS) to quantify the surface of the structures to understand what can be placed on or used to 'cap' the porous structures. Silane-based molecules in solution were used to attempt to find a successful monolayered cap for the MOF, verified through XPS sputtering. Temperature programmed desorption (TPD) was used to understand the strength of the bonds between MOF and cap to further understand the surface of the MOF.

NM05.07.44

Microwave Synthesis of Single-Phase Nanoparticles Made of Multiprincipal Element Alloys Siyu Wu¹, Yuzi Liu², Yang Ren² and Yugang Sun¹; ¹Temple University, United States; ²Argonne National Laboratory, United States

Metal nanoparticles of multi-principal element alloys (MPEA) with a single crystalline phase have been synthesized by flash heating/cooling of nanosized metals encapsulated in micelle vesicles dispersed in an oil phase (e.g., cyclohexane). Flash heating is realized by selective absorption of a microwave pulse in metals to rapidly heat metals into uniform melts. The oil phase barely absorbs microwave and maintains the low temperature, which can rapidly quench the high-temperature metal melts to enable the flash cooling process. The precursor ions of four metals, including Au, Pt, Pd, and Cu, can be simultaneously reduced by hydrazine in the aqueous solution encapsulated in the micelle vesicles. The resulting metals efficiently absorb microwave energy to locally reach a temperature high enough to melt themselves into a uniform mixture. The duration of microwave pulse is crucial to ensure the reduced metals mix uniformly, while the temperature of oil phase is still low to rapidly quench the metals and freeze the single-phase crystalline lattices in alloy nanoparticles. The microwave-enabled flash heating/cooling provides a new method to synthesize single-phase MPEA nanoparticles of many metal combinations when the appropriate water-in-oil micelle systems and the appropriate reduction reactions of metal precursors are available.

NM05.07.45

Scalable, Inexpensive, One-Pot, Facile Synthesis of Crystalline Two-Dimensional Birnessite Flakes Hussein Badr and Michel W. Barsoum; Drexel University, United States

Synthesis of two-dimensional (2D) materials that is readily scalable, cost-effective, and eco-friendly is important from both scientific and industrial viewpoints. Currently, these 2D materials are synthesized either by selective etching of relatively expensive layered solids, viz. using a top-down approach, or by autoclaving metal salts/organic compounds. Herein, we describe a near-ambient, one-pot, inexpensive, scalable pathway to convert—through a bottom-up approach—5 different water-insoluble Mn-bearing precursors, viz. Mn₃O₄, Mn₂O₃, MnB, Mn₅SiB₂, and Mn₂AlB₂, into birnessite-based 2D flakes that, in some cases, are remarkably crystalline. The precursor powders are immersed in 25 wt % tetramethylammonium hydroxide aqueous solutions at 50°C to 80°C for 2 to 4 days. The structures, compositions, oxidation states, and morphologies of the synthesized flakes are determined using a battery of characterization techniques. The synthesized 2D sheets demonstrate reversible O₂ electrocatalysis with activities comparable with those of a commercial Pt/C catalyst.

NM05.07.48

Synthesis of Copper (Hydro-) Oxide Modified Nanoceria and Electroanalytical Studies of Performance in a Peroxide Decomposition Reaction Craig J. Neal, Elayaraja Kolanthai, Yifei Fu, Chaimae El Ghazouai, Samantha Stoltz and Sudipta Seal; University of Central Florida, United States

Cerium oxide has been a staple material within catalysis science and has found substantial use in biomedical applications in its nanoscale form. The utility of nanoscale cerium oxide (nanoceria) stems from its ability to undergo surface-mediated redox reactions at defect sites through inter-conversion between reduced (Ce³⁺) and oxidized (Ce⁴⁺) states. Often, ceria is used as a catalytic material or as an active substrate: undergoing redox reactions and donating/accepting oxygen via formation/destruction of oxygen vacancies at the material (near-) surface. In the presented study, nanoceria is synthesized through a simple alkaline forced hydrolysis reaction in presence of 20 mol% aqueous copper nitrate, resulting in formation of copper oxide/hydroxide surface phases on nanoceria. These surface phases are found to be redox-active: producing substantial (catalase) enzyme-mimetic activity and a consequent redox cycling of Cu(OH)/Cu(OH)₂. Enzyme-mimetic activity is demonstrated in chemical assay and reflected in results from UV-Vis spectrophotometry measurements. X-ray photoelectron studies confirm presence of these active hydroxide phases, while electroanalytical voltammetry studies provide insight into the phases' stability in presence of hydrogen peroxide. Tafel analysis and electrochemical impedance spectroscopy were performed to elucidate the observed electron transfer processes. Peroxide decomposition reactions suggest material utility as a therapeutic nanozyme for potential biomedical applications through the scavenging of pathogenic reactive oxygen species.

SESSION NM05.08: Nanoscale Chirality
Session Chairs: Gil Markovich and Anastasia Vishneratna
Wednesday Morning, November 30, 2022
Hynes, Level 2, Room 202

8:30 AM *NM05.08.01

Chirality and Complexity of Photonically Active Nanostructures Nicholas A. Kotov; University of Michigan, United States

Nanoscale chirality is a rapidly emerging field in science and engineering. The early observation of strong circular dichroism for individual nanoparticles (NPs) and their assemblies have developed into a rapidly expanding research area on chiral inorganic nanostructures. They encompass a large family of mirror-asymmetric constructs from metals, semiconductors, ceramics, and nanocarbons with multiple chiral geometries with characteristic scales from Ångströms to microns. Versatility in, scales, dimensions and polarizability of the inorganic materials enables their multiscale engineering to attain a broad range of optical and chemical properties. These capabilities as chiral materials enabled their fast technological translation for biosensing and optoelectronics, which, in turn, opened new venues for scientific inquiry into the unifying role chirality at the interface of materials science, biology, chemistry, and physics.

Some of the latest directions in this field is understanding the fascinating relationships between multiscale chirality and structural/functional complexity of biomimetic nanomaterials forming from the spontaneous hierarchical ordering of inorganic building blocks over multiple scales. Empirical observations of complex nanoassemblies are abundant, but physicochemical mechanisms leading to their geometrical complexity remain puzzling, especially for non-uniformly sized components. These mechanisms are discussed in this talk taking an example of hierarchically organized particles with twisted spikes and other morphologies from polydisperse Au-Cys nanoplatelets [1]. The complexity of these supraparticles is higher than biological counterparts or other

complex particles as enumerated by graph theory (GT). Complexity Index (C) and other GT parameters are applied to a variety of different nanoscale materials to assess their structural organization. As the result of this analysis, we determined that intricate organization Au-Cys supraparticles emerges from competing chirality-dependent assembly restrictions that render assembly pathways primarily dependent on nanoparticle symmetry rather than size. These findings open a pathway to a large family of colloids with complex architectures and unusual chiroptical and chemical properties. The design principles elaborated for nanoplatelets have been extended to engineering of other complex nanoassemblies. They include polarization-based drug discovery platforms for Alzheimer syndrome,[2] materials for chiral photonics,[3] biomimetic composites for energy and robotics, CO₂-dispersible catalysis,[4] chiral antiviral vaccines[5] and pharmaceutical quality control [6].

References

- [1] W. Jiang, Z.-B. et al, Emergence of Complexity in Hierarchically Organized Chiral Particles, *Science*, **2020**, 368, 6491, 642-648.
- [2] Jun Lu, et al, Enhanced optical asymmetry in supramolecular chiroplasmonic assemblies with long-range order, *Science*, **2021**, 371, 6536, 1368.
- [3] L. Ohnoutek, et al, Third Harmonic Mie Scattering From Semiconductor Nanohelices, *Nature Photonics*, **2022**, 16, 126–133.
- [4] L. Tang et al. Self-Assembly Mechanism of Complex Corrugated Particles" *JACS*, **2021** 143, 47, 19655–19667.
- [5] L. Xu, et al, Enantiomer-Dependent Immunological Response to Chiral Nanoparticles, *Nature*, **2022**, 601, 366–373.
- [6] Choi W. et al, Chiral Phonons in Microcrystals and Nanofibrils of Biomolecules, *Nature Photonics*, **2022** 16, 366–373.

9:00 AM NM05.08.02

Auger Recombination in Colloidal, Two-Dimensional Semiconductor Nanocrystals [Alexandra Brumberg](#)¹, John P. Philbin², Benjamin Diroll³, Eran Rabani² and Richard Schaller^{1,3}; ¹Northwestern University, United States; ²University of California, Berkeley, United States; ³Argonne National Laboratory, United States

Auger recombination (AR), a nonradiative recombination process in which an electron and a hole recombine and transfer its excess energy to a third carrier, negatively impacts the efficiencies of devices made from colloidal semiconductor nanocrystals (NCs) because of fast AR rates. Colloidal, two-dimensional semiconductor nanoplatelets (NPLs) offer a solution to the problem of fast AR rates in colloidal NCs while preserving other benefits of NCs such as band gap tunability and high photoluminescence efficiency. In NPLs, AR rates are reduced owing to quantum confinement in only one dimension with bulk-like lateral dimensions. However, the mix of quantum-confined and bulk-like dimensions in NPLs along the thickness and lateral axes, respectively, makes it difficult to predict their photophysical behaviors. I will discuss our investigations into two aspects of AR in two-dimensional NPLs: (1) the scaling of AR rates with NPL area and volume, and (2) the temperature dependence of AR rates.

1: Both zero- and one-dimensional NCs have been shown to follow a “universal volume scaling” relationship for AR rates as a function of volume. However, both experimental and theoretical efforts have yet to agree on the relationship between AR rate and NPL area and volume. We combine experiment with a new theoretical model to ultimately convey that AR rates scale with NPL area but not volume.

2: Conceptually, AR is expected to transition from temperature-dependent behavior in bulk semiconductors to temperature-independent behavior in QDs as a result of flattened band structure in the latter that facilitates satisfaction of linear momentum conservation. In NPLs, the expected behavior is unknown, and AR as a function of temperature has never been studied. We investigate the temperature dependence of biexciton lifetime and fluence-dependent emission in colloidal CdSe NPLs and compare the behavior to that observed with QDs. For NPLs, upon temperature reduction, biexciton lifetime surprisingly decreases and emission intensity increases nearly linearly with fluence rather than saturating, consistent with dominant radiative recombination rather than nonradiative AR. Notably, this suggests that NPLs differ fundamentally from isotropic NCs, and that AR cannot be assumed to be the dominant recombination mechanism for all NCs across all temperatures.

9:15 AM NM05.08.03

Morphological Growth Pathways of Peptide-Directed Chiral Gold Nanoparticles [Sang Won Im](#), Dongsu Zhang, Young Min Kim and Ki Tae Nam; Seoul National University, Korea (the Republic of)

Chirality is a ubiquitous property of nature and can be transferred from organic molecules to inorganic crystals by enantiospecific interactions. A representative example is peptide-directed chiral morphology evolution on gold nanoparticle that exhibits chiroptical properties applicable to light polarization control, sensing, and metamaterials. The mechanism of chirality transfer has been revealed, whereby enantiospecific interactions between R/S high-Miller-index plane and L/D peptides breaks mirror symmetry inherent in FCC lattice and induce 432-symmetric geometry. However, understanding the complex morphogenesis starting from achiral seed to final helicoid morphology dependent on the peptide sequences and growth conditions remained a challenge. Here, we defined the growth pathways of helicoid nanoparticles based on both crystallographic analysis and computational modelling. The key of understanding morphological evolution is the relationship between surface Miller indices and morphological change, which appear as 2D trajectories on crystallographic stereographic projection. We discovered that the growth pathways of 432 helicoids determine the formation of high-Miller-index-enclosed intermediated morphologies, and thus are coupled with chiral morphology formation. Further, we confirmed and extended our finding by modelling the chirality evolution by cellular automata and learning the morphogenesis rule. This study provides a comprehensive understanding of chirality evolution on nanoparticles that can be further extended to functional chiral inorganic crystals.

9:30 AM NM05.08.04

Light-Induced Printing of Helical Arrays on Solid Substrates [Ji-Young Kim](#), Connor McGlothlin, Minjeong Cha, Zechariah Pfaffenberger, Emine Turali-Emre, Wonjin Choi, Julie S. Biteen and Nicholas A. Kotov; University of Michigan, United States

Chemical structures with helical geometries aligned perpendicularly to the substrate display unique optical, biosensing, catalytic, and mechanical properties but are difficult to produce. At the molecular scale, self-alignment of helices along the surface normal was accomplished for biopolymers with thiol anchors. However, the helical segments had to be pre-assembled and orientational defects were frequent. At the nanoscale, the difficulties are exacerbated because the out-of-plane alignment of nanoscale structures is associated with prohibitively high energy costs. Overcoming the unfavorable thermodynamics by light-guided formation of silver nanocrystallites, the stand-up arrays of homochiral helicoids are produced by illumination with circularly polarized light (CPL). The handedness of the silver helicoids and their polarization spectrum are controlled by the ellipticity and wavelength of the incident photons. CPL-induced printing of centimeter-scale metasurfaces with on-the-fly control of polarization effects was demonstrated using a programmable motorized stage. Substrate versatility and high efficiency of light-to-matter chirality transfer enable rapid engineering of metamaterials with chiral patterns for multiple technologies.

9:45 AM BREAK

10:30 AM NM05.09.03

Liquid-Phase Synthesis of Functional Base-Metal Nanoparticles Andreas Reiß, Daniel Bartenbach, Lara-Pauline Faden, Sven Riegsinger and Claus Feldmann; Karlsruhe Institute of Technology, Germany

Nanoparticles of zerovalent transition metals, main-group metals and rare-earth metals can be used for a wide range of applications, including catalysis, hydrogen storage or high-energy materials. Moreover, base-metal nanoparticles can be utilized as highly-reactive starting materials to obtain novel metal compounds.^{1,2} To apply base-metal nanoparticles, first of all, they must be made available with high quality and purity. To this concern, we have established a naphthalenide-driven reduction of simple metal halides in THF, DME or pyridine, which we use to prepare nanoparticles of all transition metals, rare-earths and many main-group metals for the first time.³⁻⁵ The reduction instantaneously results in the nucleation of small sized (1-3 nm) base-metal nanoparticles with narrow size distribution (± 0.2 nm). The surfaces of the zerovalent metal nanoparticles are solely functionalised by the solvent (THF/DME) (so-called quasi-naked nanoparticles). Additional surfactants such as long-chained, high-molecular-weight amines or polymers are not needed. The obtained metal nanoparticles are stable in suspension under inert conditions but highly reactive when in contact with air or water. Therefore, they must be handled with great care under strict exclusion of air and moisture.³⁻⁵ Many of these base metal nanoparticles (e.g. Nb, Ta, rare earth) are now available for the first time. We will show the synthesis strategy, purification, and properties and application of the base-metal nanoparticles.^{4,6,7}

References

- [1] S. Riegsinger, R. Popescu, D. Gerthsen, C. Feldmann, *Chem. Commun.* **2022**, 10.1039/d2cc01846b.
- [2] A. Reiß, C. Donsbach, C. Feldmann, *Dalton Trans.* **2021**, 50, 16343 - 16352.
- [3] C. Schöttle, P. Bockstaller, R. Popescu, D. Gerthsen, C. Feldmann, *Angew. Chem. Int. Ed.* **2015**, 54, 9866 - 9870.
- [4] D. Bartenbach, O. Wenzel, R. Popescu, L.-P. Faden, A. Reiß, M. Kaiser, A. Zimina, J.-D. Grunwaldt, D. Gerthsen, C. Feldmann, *Angew. Chem. Int. Ed.* **2021**, 60, 17373 - 17377.
- [5] A. Egeberg, T. Block, O. Janka, O. Wenzel, D. Gerthsen, R. Pöttgen, C. Feldmann, *Small* **2019**, 15, 1902321.
- [6] A. Reiß, R. Popescu, D. Gerthsen, C. Feldmann, **2022**, in preparation.
- [7] L.-P. Faden, A. Reiß, R. Popescu, D. Gerthsen, C. Feldmann, **2022**, in preparation.

10:45 AM NM05.09.04

Activated Elemental Se—A Viable Synthetic Precursor for a Variety of Targets Kirill Kovnir; Iowa State University, United States

Se-containing nanomaterials often synthesized from toxic and expensive organo-Se precursors. We are reporting a facile alternative utilizing elemental Se which is cheap and non-toxic. Elemental Se reagent has a drawback of low solubility and reactivity resulting in sluggish kinetics at low temperatures. A process of elemental Se activation was developed resulting in stable solution of multiple Se species confirmed with ⁷⁷Se NMR studies, including R-Se-Se-R and never detected before “naked” Se₂²⁻. Dynamic equilibrium between the produced Se species allow to perform reactions at wide temperature ranges including room temperature. We have demonstrated the applicability of such activated Se for different targets ranging from few nm CdSe nanocrystals to large 100 nm sized crystals of superconducting FeSe.

11:00 AM NM05.09.05

Engineering of Sub-Nanometer Oxide Shell on Gold Nanoparticles Jean-Marc von Mentlen¹, Jasper Clarysse¹, Annina Moser¹, Dhananjaya Kumar¹, Olesya Yarema¹, Takumi Sannomiya², Maksym Yarema¹ and Vanessa Wood¹; ¹ETH Zürich, Switzerland; ²Tokyo Institute of Technology, Japan

Metal oxide shells fully or partially covering gold nanoparticles are intensively studied for a wide range of applications in the fields of catalysis and plasmonics. When carefully designed, these coatings enhance the functionality and stability of the nanoparticles. Yet, facile and well controlled fabrication methods of thin metal oxide layers on metal nanoparticles are still lacking. Currently used methods struggle to produce uniform layers below 1 nm. In this work, we show an easy fabrication process to reliably engineer uniform Ga₂O₃ shells on Au nanoparticles with a thickness ranging from sub- to several monolayers. These thin shells are obtained by a liquid-phase chemical oxidation of alloyed Au-Ga nanoparticles. We demonstrate how the plasmonic properties of the nanoparticles can be used to understand the reaction process and quantitatively monitor the Ga₂O₃ shell growth. Finally, we show as a practical application that the Ga₂O₃ coating prevents the sintering of the Au nanoparticles, ensuring thermal stability up to at least 250°C. Dealloying of bimetallic nanoparticles by in-solution oxidation is a promising approach to obtain controlled metal-metal oxide core-shell nanoparticles.

11:15 AM NM05.09.06

Formation of 3D Magnetic Nanowire Arrays by Cooperative Lateral Growth Fei Chen, Zihao Yang, Ruwen Peng and Mu Wang; Nanjing University, China

Nanowires typically grow along their longitudinal axis, and the long-range order among wires sustains only when a template exists. Here, we report an unprecedented electrochemical growth of ordered metallic nanowire arrays from an ultrathin electrolyte layer, which is achieved by solidifying the electrolyte solution below the freezing temperature. The thickness of the electrodeposit is instantaneously tunable by the applied electric pulses, leading to parallel ridges on webbed film without using any template. An array of metallic nanowires with desired separation and width determined by the applied pulses is formed on the substrate with arbitrary surface patterns by etching away the webbed film thereafter. This work demonstrates a previously unrecognized fabrication strategy that bridges the gap of top-down lithography and bottom-up self-organization in making ordered metallic nanowire arrays over a large area with low cost.

References:

- [1]. F. Chen, Z. Yang, J.-N. Li, F. Jia, F. Wang, D. Zhao, R.-W. Peng, M. Wang, *Science Advances.*, Vol 8, p. eabk0180 (2022)
- [2]. F. Chen, J. Li, F. Yu, D. Zhao, F. Wang, Y. Chen, R.-W. Peng, M. Wang, *Advanced Materials.*, Vol 28, p. 7193 (2016)

SESSION NM05.10: Mechanistic Studies and Surface Science of Nanomaterials Synthesis
Session Chairs: Maryna Bodnarchuk and Zeger Hens
Wednesday Afternoon, November 30, 2022
Hynes, Level 2, Room 202

1:30 PM *NM05.10.01

Advances and Challenges Toward High Efficient Colloidal InP Core-Shell Quantum Dots—Synthesis, Surface Chemistry and Their Applications
Derrick Allan Taylor, Justice Agbeshie Teku and Jong-Soo Lee; Daegu Gyeongbuk Institute of Science and Technology, Korea (the Republic of)

Semiconductor colloidal quantum dots (CQDs) have made remarkable progress due to their attractive size-tunable electronic and optical properties, low-cost production, high efficiency, and high stability. In particular, Indium phosphide (InP) quantum dots (QDs) have attracted a great deal of attention in next-generation display technologies, owing to their low intrinsic toxicity and tunable emission from visible to near-infrared region. Despite recent progress in improving the optical properties of InP-based QDs, current synthesis methods have often failed to produce InP QDs with high quantum yield and narrow size distributions, a prerequisite for realizing high color pure emissions. Recently, our group report the importance of precisely controlling the reaction kinetics of InP QDs by a two-step growth process to achieve the narrowest size distribution, engineering the shell coating to reduce interfacial defects for high photoluminescence yield quantum yield (PLQY). In this talk, I will introduce the great synthetic progress of InP core-shell QDs, based on the surface chemistry and the interfacial engineering of InP QDs. By optimizing synthesis conditions, the as-synthesized InP QDs core-multishell exhibited a bright green and red emission with a very high quantum yield and the narrowest emission linewidth of more than 90% and less than 33 nm, respectively. Finally, I will discuss the challenges related to the recent developments of InP QLED applications and the challenges for achieving high-performance devices.

2:30 PM BREAK

SESSION NM05.11: Synthesis of Oxide Nanomaterials
Session Chair: Nicola Pinna
Wednesday Afternoon, November 30, 2022
Hynes, Level 2, Room 202

3:30 PM NM05.11.02

Atomically Flat {011} Facets and Phase Tunability of HfO₂ Nanocrystals via an Anhydrous Wet-Chemical Approach Thorsten Ohlerth^{1,2}, Hongchu Du^{2,3}, Niclas Schmidt^{2,4}, Sonam Maiti^{2,4}, Silvia Karthäuser^{2,4}, Joachim Mayer^{2,3,5}, Rainer Waser^{2,4} and Ulrich Simon^{1,2}; ¹Institute of Inorganic Chemistry, RWTH Aachen University, Germany; ²JARA – Fundamentals of Future Information Technologies, Forschungszentrum Jülich GmbH, Germany; ³Ernst Ruska-Centre (ER-C-2), Forschungszentrum Jülich GmbH, Germany; ⁴Peter Grünberg Institute (PGI-7), Forschungszentrum Jülich GmbH, Germany; ⁵Central Facility for Electron Microscopy (GFE), RWTH Aachen University, Germany

The development of new nanomaterials in industry is driven by the everchanging socioeconomic trends in recent history. As for the IT sector, HfO₂ was introduced in 2007 as gate material in complementary metal oxide semiconductors (CMOS) and still is one of the state-of-the-art materials as of today. As high-κ-dielectric, hafnia has also risen awareness when Müller et al. found that it exhibits ferroelectric behaviour in thin films with a thickness of about 10 nm.[1] While nanocrystalline HfO₂ is usually processed via thin-film deposition techniques like atomic layer deposition (ALD) and chemical vapor deposition (CVD), wet-chemical syntheses in solution envisage three-dimensionally confined nanostructures that are not yet accessible for thin-films. Accordingly, we put our efforts in rationalizing the synthesis HfO₂ nanocrystals (HfO₂-NC) in order to obtain novel hafnia material classes. Prior to our work, the scientific community developed numerous synthesis protocols for colloidal hafnia.[2] The results of Tang et al. stand out among them, due to the astonishingly monodisperse HfO₂-NCs with sizes below 5 nm in diameter. This sol-gel synthesis approach served as base for subsequent studies, specifically in terms of size effects and crystal twinning behavior. Still, the results of different groups were inconsistent regarding isotropically shaped nanocrystals with the metastable tetragonal (*P4₂/nmc*, 137) crystal structure and anisotropically grown monoclinic (space group *P2₁/c*, 14) nanorods, that were seemingly obtained under similar conditions. In our work, we resolve these ambiguities by showing that specific heating techniques are crucial for the crystal growth dynamics. Furthermore, we extended the scope of the synthesis by the formation of anisotropic nanoprisms with atomically well defined {011} facets. We present that these nanoprisms tend towards self-assembly alongside their preferred growing direction, which is perpendicular to the aforementioned {011} crystal planes. Contrary to the well-investigated HfO₂ nanorods, these particles showcase no twinning alongside their long-axis dimension, which makes them perfect single orientated nanocrystals with only small size deviations. The particle size distribution, morphology and crystallinity of our HfO₂-NCs was predominantly investigated by means of transmission electron microscopy (TEM), while the role of molecular capping agents was analyzed via X-ray photoelectron spectroscopy (XPS) and thermogravimetric analysis (TGA). Our findings elucidate the nature for morphology selective growth and phase formation of the well-established sol-gel synthesis. We strive to extend our findings towards other transition metal oxides, premised on the opportunities that our approach for HfO₂ provides.

[1] J. Muller, T. S. Boscke, U. Schroder, S. Mueller, D. Brauhaus, U. Botzger, L. Frey and T. Mikołajick, *Nano lett.*, **2012**, 12, 4318–4323.

[2] J. Tang, J. Fabbri, R. D. Robinson, Y. Zhu, I. P. Herman, M. L. Steigerwald and L. E. Brus, *Chem. Mater.*, **2004**, 16, 1336–1342.

3:45 PM NM05.11.03

W/VO₂ Nanoparticles for Thermo-chromic Polymer Films—A Comparative Study Between Bead Milling of Powders and Hydrothermal Synthesis Pascal Buskens^{1,2,3}, Lavinia Calvi^{2,4}, Ryan Van Zandvoort^{1,3}, Janique Huppertz^{1,3}, Luc Leufkens^{1,3}, Roberto Habets^{1,3}, Daniel Mann^{1,3}, Nicole Meulendijks^{1,3}, Kimberly Timmers^{1,3}, Ken Elen^{2,4}, An Hardy^{2,4}, Marlies K. Van Bael^{2,4}, Ioannis Papakonstantinou⁵, Gurunatha Kargal Laxminarayana⁵, Ivan P. Parkin⁵, Romy Van Geijn^{1,3} and Roland Valckenborg¹; ¹TNO, Netherlands; ²Hasselt University, Belgium; ³Brightlands Materials Center, Netherlands; ⁴IMEC vzw, IMOMECA Associated Laboratory, Belgium; ⁵University College London, United Kingdom

Vanadium dioxide displays a structural phase transition (SPT) from monoclinic VO₂ (M) to rutile VO₂ (R) at 68°C, which is reversible [1]. This SPT is accompanied by a metal-insulator transition, which makes this material interesting for application in energy efficient windows. VO₂ (M) is an insulator and transmits solar infrared (s-IR) radiation, VO₂ (R) is metallic and reflects and/or absorbs s-IR light. For application in energy efficient windows, the switching temperature needs to be lowered from 68°C to 15-25°C, which is typically achieved by doping with metal ions such as W⁶⁺. To introduce thermo-chromic W/VO₂ in windows, we aimed at preparing thermo-chromic PVB polymer films comprising W/VO₂ nanoparticles of a size below 100 nm to

avoid scattering of visible light. These should then be incorporated into PVB via a masterbatch, and the resulting nanocomposite polymer films should be applied to laminate glass and produce insulating glass units with a laminated outboard. Based on the temperature of the outer glass pane and the nanocomposite film, the resulting window should then switch from a s-IR transmissive to a blocking state and *vice versa*. This contributes to a reduction in energy consumption and costs for heating and cooling of buildings in intermediate climates.

To prepare VO₂ and W/VO₂ nanoparticles, we selected two different routes: a hydrothermal synthesis starting from a mixture of organometallic V(IV) and W(VI) complexes, and a top-down processing route based on bead milling of VO₂ and W/VO₂ powders. We successfully prepared thermochromic VO₂ and W/VO₂ nanoparticles using both routes. We characterized their composition, size and shape using X-ray diffraction, laser diffraction, dynamic light scattering, scanning and transmission electron microscopy. Furthermore, we comparatively studied their functional performance focusing on the thermodynamics and kinetics of the SPT [2]. For that purpose, we performed differential scanning calorimetry at various heating and cooling rates. The switching kinetics were determined using Friedman's differential isoconversional method. For undoped VO₂ (M), we found that the activation energy (E_A) of the SPT decreases with increasing difference between the actual temperature of the material and its switching temperature. Furthermore, the activation energy decreases with progressive milling, and kinetic asymmetry is induced. For milled particulate materials, E_A is lower for the switch from VO₂ (R) to VO₂ (M) than for the opposite switch. For hydrothermally synthesized nanoparticles, E_A is in the same order of magnitude, albeit with inverse switching asymmetry. Latter may result from different defects that are introduced during both preparation techniques.

W/VO₂ nanoparticles obtained by bead milling were successfully introduced into PVB via a masterbatch, and the resulting nanocomposite polymer material was processed into films. These were then applied for lamination of glass plates up to 1 square meter in size. Subsequently, pilot scale windows were prepared comprising these laminated glass plates. We started testing these in demo houses to gather information on the performance of the innovative energy efficient window in real environment. Initial results show that the smart window transitions from an s-IR transparent to blocking state as soon as direct sunlight hits the window and ambient temperatures are above 20°C. The transition back to the s-IR transparent state usually happens over night when the glass surface cools down. The window is optimized to reduce energy consumption in moderate climates with cold winters and warm summers, such as in the Netherlands, which can lead to additional energy and cost savings of up to 8% and 23.70 € per square meter per year when compared to state of the art HR++ windows.

[1] L. Calvi *et al.*, *Solar Energy Materials & Solar Cells* **2021**, 224, 110977.

[2] L. Calvi *et al.*, *Solar Energy Materials & Solar Cells* **2022**, 242, 111738.

4:00 PM NM05.11.04

Hydrothermal Synthesis of Zinc Gallate Nanoparticles—A Reaction Kinetics Study David Beke^{1,2}, Mátyás M. Rudolf¹, Bence Márkus² and Adam Gali¹; ¹MTA Wigner RCP, Hungary; ²University of Notre Dame, United States

Zinc gallate (ZnGa₂O₄) has attracted increased attention for broad optical applications owing to its excellent thermal and chemical stability and its wide bandgap (≈4.4 – 5.2 eV). It is known to act as a phosphor host, with one example being chromium doping of the crystal lattice, which displays a red-infrared luminescence at around 700 nm under a wide UV-Visible or even X-ray excitation. The photon emission process can be prolonged from milliseconds to hours by introducing exciton traps. Such properties make this material a promising candidate for background-free bioimaging. These emitters may be used as a light source to trigger photodynamic or photo-induced therapy deep in the body, where these therapeutic approaches have not yet been accessible. Indeed, optical imaging could be advantageously carried out using a phosphor as a luminescent probe, emitting in the red-infrared part of the spectrum upon X-ray excitation. By using persistent luminescent nanoparticles or the capability of X-ray excitation to cross through the body, the autofluorescence and the absorption of tissue can be avoided. However, the optical properties of the hydrothermally synthesized nanoparticles are strongly influenced by the synthesis parameters.

The most accepted method to synthesize ZnGa₂O₄ NPs is the transformation of the oxides or hydroxides of the elements into crystalline spinel oxide. This can be accomplished by applying solvothermal methods at moderate temperatures. However, the reaction mechanism of hydrothermal synthesis of ZnGa₂O₄ has not been fully understood. Even though ZnGa₂O₄ synthesis is described as the hydroxide phase transforming into the corresponding oxide phase via an endothermic dehydration reaction, we found that the spinel oxide can form without hydroxide precipitation. We studied the reaction kinetics of the crystal growth with and without ultrasmall silicon carbide seeds, and we found a good correlation with the LSW model. More on that. We suggest a temperature-triggered and separated nucleation and crystallization process during the hydrothermal reaction. Reaction-limited nucleation creates an amorphous oxide that crystallizes during the second synthesis step.

Beke, D.; Nardi, M. V.; Bortel, G.; Timpel, M.; Czirány, Z.; Pasquali, L.; Chiappini, A.; Bais, G.; Rudolf, M.; Zalka, D.; Bigi, F.; Rossi, F.; Bencs, L.; Pekker, A.; Márkus, B. G.; Salviati, G.; Sadow, S. E.; Kamarás, K.; Simon, F.; Gali, A. Enhancement of X-Ray-Excited Red Luminescence of Chromium-Doped Zinc Gallate via Ultrasmall Silicon Carbide Nanocrystals. *Chem. Mater.* **2021**, 33 (7), 2457–2465. <https://doi.org/10.1021/acs.chemmater.0c04671>.

4:15 PM NM05.11.05

Possible Continuous (Successive) Fabrication of Nano-Structured Inorganic Materials via Soft, Solution Processing without Firing of Powders Masahiro Yoshimura; National Cheng Kung University, Taiwan

Practical devices would be better to be fabricated via continuous and/or successive Processes. Presently, however, they have generally been fabricated artificially and/or industrially by so-called high-technology, where high temperature, high pressure, vacuum, molecule, atom, ion, plasma, etc. using expensive equipments thus they consumed huge amount of resources and energies thus exhausted huge amounts of wastes: materials, heats and entropy. The major reasons might be 1) The reactants should be nano-sized species, 2) high-energy reaction might be required, thus 3) They cost economically and environmentally. To save this tragedy, a) we must consider “Cascade use of Heats”, and b) “Low energy Production of advanced materials via solution-based technologies.” c) Continuous(Successive) Fabrication will be possible in solution process(es).

We proposed in 1995 an innovative concept and technology, “Soft Processing” or “Soft Solution Processing,” which aims low energetic (=environmentally friendly) fabrication of shaped, sized, located, and oriented inorganic materials in/from solutions. When we have activated/stimulated interfacial reactions locally and/or moved the reaction point dynamically, we can get patterned ceramic films directly in solution without any firing, masking nor etching. Direct Patterning of CdS, PbS and CaWO₄ on papers by Ink-Jet Reaction method. Furthermore, we have succeeded to fabricate BaTiO₃ patterns on Ti by a laser beam scanning and carbon patterns on Si by plasma using a needle electrode scanning directly in solutions. Successes in TiO₂ and CeO₂ patterns by Ink-Jet Deposition, where nano-particles are nucleated and grown successively on the surface of substrate thus become dense even below 300 C will be presented. Nano-structured films of BaTiO₃ and direct carbon patterning in solution will be also talked ¹⁻³⁾ They are rather contrasting with recent General Solution Studies :3D Printing and Additive Engineering based upon Firing of Powders after Printing. I may talk about nanocarbon and graphene ⁴⁻⁵⁾.

MRS Bulletin, 25, Sept. issue 2000, special issue for Soft Processing of Advanced Inorganic Materials, Guest Editor: M. Yoshimura and J. Livage.

Yoshimura, M., *J. Mater. Sci.*, 41, 1299-1306 (2006).

Yoshimura, M., *Procedia Engineering*, 171, 40-52 (2017).

Yoshimura, M., *et al* *The Journal of Physical Chemistry C* 121, 19983-19988 (2017).

M Yoshimura, J Sentilnathan, *Chat. 9* in “Lithium-Ion Batteries and Solar Cells”, CRC (2021).

4:30 PM NM05.11.06

Chemically Exfoliated Thin Sheets of β -Bi₂O₃ Brianna L. Hoff, Guangming Cheng, Graciela Villalpando, Fang Yuan, Nan Yao and Leslie Schoop; Princeton University, United States

Exploring two dimensional (2D) materials is important for further developing the field of quantum materials. However, progress in 2D material development is limited by the ability to make them. Specifically, freestanding 2D materials with bulk non-layered structures remain particularly challenging to prepare. Traditionally, chemical or mechanical exfoliation is employed for obtaining freestanding 2D materials, but these methods typically require layered starting materials. Here we put forth a method for obtaining thin layers of β -Bi₂O₃, which has a three-dimensional covalent structure, by using chemical exfoliation. In this research, Na₃Ni₂BiO₆ was exfoliated with acid and water to obtain β Bi₂O₃, less than 10 nm in height and over one μ m in lateral size. Our results open the possibility for further exploring β -Bi₂O₃ nanosheets to determine whether their properties change from the bulk to the nanoscale. Furthermore, this research may facilitate further progress in obtaining nanosheets of non-layered bulk materials using chemical exfoliation.

SESSION NM05.12: Nanomaterials for Catalysis and Electrocatalysis

Session Chairs: Pascal Buskens and Ou Chen

Thursday Morning, December 1, 2022

Hynes, Level 2, Room 202

8:30 AM NM05.12.01

Elucidating Dopant Structure in Single-Atom Doped Transition Metal Dichalcogenides for Catalytic Hydrotreatment Steven L. Farrell¹, Ingrid J. Paredes², Srinivas Rangarajan², Anatoly Frenkel^{3,4} and Ayaskanta Sahu¹; ¹New York University, United States; ²Lehigh University, United States; ³Stony Brook University, The State University of New York, United States; ⁴Brookhaven National Laboratory, United States

Tailoring highly efficient catalysts to targeted applications is vital to reduce the carbon footprints of industrial processes; however, understanding and controlling nanostructure influence in catalyst design has proven difficult. Transition metal dichalcogenides, such as molybdenum sulfide (MoS₂), are important commercial catalysts employed in hydrodesulfurization (HDS) and hydrodeoxygenation (HDO) for crude oil and biomass valorization, respectively, due to their widespread availability and sulfur poisoning resistance. Nanoscale MoS₂ forms stable two-dimensional nanosheets with impressive catalytic activity along the nanosheet edge sites. Conversely, most of the non-edge atoms of the basal plane are inert. Thus, there is a strong impetus towards modifying 2D MoS₂ to activate the basal plane. Decorating the surface with singular dopant atoms, such as cobalt, has been shown to enhance catalytic properties of MoS₂ for hydrogenation, especially hydrotreating. However, little is understood about the location of the dopants and their subsequent influence on catalyst behavior. To investigate this gap in knowledge, we study the impact of Co-dopants in MoS₂ on hydrotreating reactions through strictly controlled, tunable in-situ Co doping of MoS₂ nanosheets grown via a bottom-up colloidal hot-injection method. Various Co loadings were studied for HDS of thiophene and HDO of p-cresol, probing the effects of dopant concentration and local structure of single Co atoms using x-ray absorption spectroscopy and density functional theory. We show that the relationship between dopant concentration, location and activity is interrelated, reaction-specific, and non-monotonous with performance peaking at 25% Co. We highlight the specific mechanisms that dictate how and where Co attaches to the surface and its influence on the catalytic performance. Understanding these mechanisms is critical for tailoring future catalysts to specific applications.

8:45 AM NM05.12.02

Nonequilibrium Flow-Synthesis of Immiscible Binary and High-Entropy Alloy Nanoparticles and Investigation of Their Catalytic Properties and Electronic Structures Kohei Kusada^{1,2}, Dongshuang Wu¹, Tomokazu Yamamoto³, Takaaki Toriyama³, Syo Matsumura³, Yusuke Nanba⁴, Michihisa Koyama⁴, Okkyun Seo⁵, Osami Sakata⁵ and Hiroshi Kitagawa¹; ¹Kyoto University, Japan; ²JST-PRESTO, Japan; ³Kyushu University, Japan; ⁴Shinshu University, Japan; ⁵JASRI, Japan

Solid-solution alloy nanoparticles (NPs), where the constituents mix at the atomic level, show a variety of attractive properties due to their tunable electronic structures. However, the majority of bulk alloy systems are phase-separated types under ambient conditions. We have demonstrated that the nanosize effect offers a chance to find a way out of this metallurgical difficulty; that is, we can obtain metal NPs having new phases that do not exist in bulk states¹⁻⁹. As one of the examples, we successfully synthesized PdRu solid-solution alloy NPs, although Ru and Pd are immiscible elements. The Pd_{0.5}Ru_{0.5} NPs having a similar electronic structure to Rh exhibit comparable NO_x reduction activity, even though monometallic Ru or Pd NPs do not show high activity.^{4, 8} Also, very recently we first synthesized high-entropy alloy NPs composed of all eight noble-metal-group elements (NM-HEA NPs) and revealed that the local density of states (LDOS) of every surface atom in NM-HEA are different.⁹ Some atoms of the same constituent element in HEA NPs have different LDOS profiles, whereas atoms of other elements can have similar LDOS profiles. In other words, one atom in HEA loses its elemental identity and it may be possible to create an ideal LDOS by adjusting the neighboring atoms. The NM-HEA NPs showed 10.8-times higher activity for hydrogen evolution reaction than commercial Pt/C, which is one of the best catalysts. However, it is still difficult to stably synthesize solid-solution alloy NPs, particularly nonequilibrium alloys that consist of combinations immiscible in the bulk.

We first developed a continuous-flow reactor providing high productivity with high reproducibility of solid-solution alloy NPs composed of immiscible combinations and multi-elements.⁹ The designed solvothermal flow reactor enabled us to use lower alcohol as a reductant that cannot be applied in a batch synthesis for these NPs.

1) K. Kusada, H. Kitagawa. *Adv. Mater.*, **2016**, 28, 1129. 2) K. Kusada, et al. *J. Am. Chem. Soc.*, **2010**, 132, 15896. 3) K. Kusada, et al. *J. Am. Chem. Soc.*, **2013**, 135, 5403. 4) K. Kusada, et al. *J. Am. Chem. Soc.*, **2014**, 136, 1864. 5) Q. Zhang et al., *Nat. Commun.*, **2018**, 9, 510. 6) K. Kusada et al., *Chem. Sci.*, **2019**, 10, 652. 7) D. Wu, et al. *J. Am. Chem. Soc.*, **2020**, 142, 13833. 8) K. Kusada, et al., *Adv. Mater.*, **2021**, 33, 2005206. 9) D. Wu, et al. *J. Am. Chem. Soc.*, **2022**, 144, 3365. 10) K. Kusada, et al., *J. Phys. Chem. C*, **2021**, 125, 458.

9:00 AM NM05.12.03

Silicon Nanoparticles as Solid-State Inhibitors for Methacrylic Autopolymerization Pooria Golvari, Khaled Alkameh and Stephen M. Kuebler; University of Central Florida, United States

Polymerization inhibitors are added to methacrylic monomers to extend their shelf life and often need to be removed prior to use by means of tedious procedures. We report that hydrogen terminated silicon nanoparticles (H-SiNPs) inhibit thermal polymerization of methyl methacrylate (MMA) and allyl methacrylate (AMA) at temperatures as high as 100 °C [1]. As *solid-state* inhibitors, H-SiNPs are advantageous because they can be readily separated from the monomer by centrifugation and/or filtration. The reaction MMA and AMA in the presence and absence of H-SiNPs at various temperatures were

explored using NMR and FTIR spectroscopy. In the presence of Si-H surface groups, methacrylic dimers form as a by-product of inhibition. Additionally, monomers attach to the surface of SiNPs through hydrosilylation of the methacrylic group, forming robust Si-C linkages that are resistant to hydrolysis. In the case of AMA, thermal hydrosilylation enables facile synthesis of free-standing vinyl terminated SiNPs. Catalytic hydrosilylation of H-SiNPs with AMA is being investigated using Kardstedt's catalyst (KC). Whereas KC has been extensively utilized for cross-linking of polysiloxanes [2], its effectiveness in facilitating hydrosilylation of olefins with H-SiNPs has not been methodically studied. Preliminary data show that MMA and AMA undergo hydrosilylation through the methacrylic group when high loadings of KC are used, in neat monomer or with toluene as solvent. The effect of solvent is being explored as a means to bias hydrosilylation selectively towards the vinyl group of AMA. This would enable methacrylate-capped free-standing SiNPs with potential applications in photocrosslinkable silicon formulations.

1. Golvari, P., K. Alkameh, and S.M. Kuebler, *Si-H Surface Groups Inhibit Methacrylic Polymerization: Thermal Hydrosilylation of Allyl Methacrylate with Silicon Nanoparticles*. Langmuir, 2022, in press.
2. Hofmann, R.J., M. Vlatković, and F. Wiesbrock, *Fifty years of hydrosilylation in polymer science: a review of current trends of low-cost transition-metal and metal-free catalysts, non-thermally triggered hydrosilylation reactions, and industrial applications*. Polymers, 2017. 9(10): p. 534.

9:15 AM NM05.12.04

3D Atomic Structure of Pt Nanocrystals Related to Their Catalytic Activity and Surface Ligand Adsorption [Sungin Kim](#)¹, Dohun Kang^{1,2}, Jimin Kwag¹, Dongjun Kim¹, Junyoung Heo¹ and Jungwon Park¹; ¹Seoul National University, Korea (the Republic of); ²Northwestern University, United States

The surface structure of nanocrystals determines catalytic activities and ligand adsorption behavior. However, it is challenging to precisely investigate the physicochemical behavior because the surface structure of synthesized nanocrystals consists of intricate and low-symmetry surface structures. Here, we revealed 3D atomic structure of sub 3-nm Pt nanocrystals and analyzed surface-related characteristics of the synthesized nanocrystals. First, we constructed 3D maps of the coordination number (CN) and generalized CN (GCN) for individual surface atoms to directly correlate types of constituent surface structures and catalytic activities, respectively. The results reveal that the synthesized Pt nanocrystals are enclosed by islands with nonuniform shapes that lead to complex surface structures, including a high ratio of low-coordinated surface atoms, reduced domain size of low-index facets, and various types of high-index facets. In addition, these intricate surface structures give rise to a wide range of GCN meaning various active sites, which explains the origin of high catalytic performance of small Pt nanocrystals in important reactions such as oxygen reduction reaction. Second, we applied a machine-learning-accelerated ab-initio calculation into the 3D atomic structures of Pt nanoparticles to analyze the complex adsorption behavior of polyvinylpyrrolidone (PVP) ligands on synthesized nanoparticles. Different angular configurations of the large-sized ligands on low-symmetry surfaces are thoroughly investigated. It is revealed that two components of binding affinity, short-range direct bonding and long-range van der Waals interaction, of PVP on synthesized Pt nanoparticles are differently affected by the coordination number of the binding atomic site and surface-exposed local geometry surrounding it. In addition, the adsorption directions of the large-sized ligand have a tendency depending on the types of adsorption centers, despite the low-symmetry surfaces. The results highlight the important contribution of vdW interactions to adsorption behavior of large-sized ligands on nanoparticle surfaces.

9:30 AM NM05.12.05

Water-Soluble Copper (I) Hydroxide Catalysts in Ligand-Free Suzuki-Miyaura Cross-Coupling Reactions [Priya Karna](#)¹, Debora Motta Meira², Zou Finrock² and Dong-Sheng Yang¹; ¹University of Kentucky, United States; ²Argonne National Laboratory, United States

Transition-metal catalyzed Suzuki-Miyaura (SM) cross-coupling is a powerful technique for constructing C-C bonds and has been widely used in the pharmaceutical, agricultural, and natural product syntheses. Although Pd has been used as the major catalyst for SM reactions, Cu has recently emerged as an alternative to Pd because Cu is inexpensive, less toxic, and easily available. A survey of the literature shows that most Cu-catalyzed SM reactions were carried with organic ligand-stabilized Cu catalysts. For ligand-free reactions, reaction phases and active species of Cu catalysts remain under debate. In this work, we report findings of ligand-free Cu-catalyzed-SM reactions using CuI as a precatalyst and benzene iodide and phenylboronic acid as coupling agents in the presence of potassium hydroxide, water, and polyethylene glycol 300. The catalyst is water-soluble copper (I) hydroxide (CuOH) species in their singlet electronic states as identified by UV-Vis absorption spectroscopy and x-ray photoelectron spectroscopy. It is formed by leaching of Cu(I) nanoparticles, which serve as the reservoir of the Cu(I) catalyst. The Cu(I) nanoparticles are characterized using transmission electron microscopy and extended x-ray absorption fine structure spectroscopy. Catalytically active CuOH catalyst is in the solution rather than on the surface of the Cu precipitate. The soluble Cu(I) species is stable for at least four weeks under ambient conditions, a desirable feature for any catalyst.

9:45 AM BREAK

10:15 AM NM05.12.06

Colloidal Synthesis of Size and Composition Controlled Alloy Nanocrystals as Selective Alkyne Semihydrogenation Catalysts [Jasper Clarysse](#), Jordan D. Silva, Seraphine Zhang, Scott Docherty, Maksym Yarema, Christophe Copéret and Vanessa Wood; ETH Zürich, Switzerland

The selective hydrogenation of alkynes to alkenes is an important transformation with applications in both the fine chemical industry (synthesis of vitamins and natural products) and polymer industry (selective removal of acetylene), where alloys are often employed as heterogeneous catalysts. Yet, advances in catalyst formulations that feature high activity, selectivity, durability and broad functional group tolerance and where both noble metals (e.g. Pd, Pt) and metals of environmental concern (e.g. Cd, Pb) are replaced by earth abundant and non-toxic metals are highly desirable. Here, we present the synthesis of uniform Ni-alloy nanocrystals (NCs), which are 3-4 nm in size and feature narrow size dispersions [1]. The nanocrystals are synthesized via an amalgamation seeded growth procedure [2], a generalized colloidal synthesis method developed by us for size and composition controlled nanocrystals of a wide range of alloys. The resulting catalysts are pristine, capped with non-poisoning oleylamine ligands and work as dispersions which are at the interface of homogeneous and heterogeneous catalysis. We find that Ni₃Zn NCs are particularly active and selective for the liquid-phase semi-hydrogenation of alkynes in batch, operating under mild reaction conditions. Furthermore, Ni₃Zn NCs are tolerant to a wide range of functional-groups, allowing the selective conversion of a broad scope of alkynes as studied with high-throughput experimentation. In addition, we show that the investigated substrate scope covers the chemical space of commercial alkynes to a large extent, as evaluated with data science techniques [1].

[1] J. Clarysse*, J. S. J. Silva*, S. Zhang, S. Docherty, M. Yarema, V. Wood, C. Copéret. *In progress* ...

[2] J. Clarysse*, A. Moser, O. Yarema, V. Wood, M. Yarema. *Sci Adv* 2021, 7 (31)

10:30 AM NM05.12.07

Supercritical Hydrothermal Synthesis of High Entropy Spinel Oxide Nanoparticles as Oxygen Evolution Electrocatalysts [Kazuyuki Iwase](#) and Itaru Honma; Institute of Multidisciplinary Research for Advanced Materials, Tohoku University, Japan

Hydrogen production via electrochemical water splitting using renewable energies has attracted attention to realize a sustainable society. The electrochemical oxygen evolution reaction (OER) is an important anode reaction in water splitting. To date, non-noble metal oxides composed only of

abundant elements have been extensively studied as OER catalysts since they can function as OER catalysts in alkaline solutions. Among metal oxides, spinel oxides have been widely studied as OER catalysts, as the composition and site occupancies of metal ions can be modulated by the choice of metal precursor and synthesis method to enhance OER activity. However, further enhancement of OER activity is needed. Recently, high entropy compounds, such as high entropy alloys (HEAs) and high entropy oxides (HEOs), which are solid solutions composed of multiple metal elements (usually more than 5), have also attracted attention as new catalyst platforms. It has been reported that HEAs and HEOs have specific electronic structures due to electronic interactions among constituent metal elements. The electronic structure of catalysts is one of the important determining parameters for the adsorption energies of reaction intermediates and catalytic activities for various electrocatalytic reactions. Therefore, as discussed above, high entropy spinel oxides (HE-SOs) are attractive as OER catalysts. In previous reports, HE-SOs have typically been synthesized by heat treatment of the metal precursors under high temperature, which results in highly crystallized particle formation. On the other hand, a two-step processing using heat treatment of the metal precursor obtained via hydrothermal synthesis can obtain HE-SO nanoparticles. While particle size is one of the important parameters for catalysts, the method for a simple one-step synthesis of HE-SO nanoparticles has been limited. Herein, we developed a simple one-pot solution synthesis process of HE-SO nanoparticles using a supercritical fluid as a reaction field. The supercritical fluids are attractive as a reaction field to synthesize various kinds of catalysts composed of nanoparticles or nanosheets[1]. In the present work, we have synthesized HE-SOs composed of five transition metals (Mn, Fe, Co, Ni, Zn). Briefly, metal precursor solutions and sodium hydroxide (NaOH) solutions were mixed and transferred into Hastelloy reactors, followed by a heat-treatment at 400 °C for 15 min. Cubic spinel nanoparticles with an average diameter of 18.6 nm in solid solutions were obtained. The valence states and coordination environment (e.g., site occupancies) were analyzed by X-ray absorption fine structure (XAFS). Co, Ni and Zn atoms existed as divalent ions, whereas Mn and Fe atoms existed as trivalent ions. In addition, Mn and Ni atoms selectively existed at octahedral 16d sites, whereas Co and Zn existed at tetrahedral 8a sites. The OER activities of HE-SOs were evaluated by cyclic voltammetry (CV) in O₂-saturated 1M KOH solutions using rotating disk electrode. The onset potential and Tafel slope values were 1.56 V vs. reversible hydrogen electrode (RHE) and 36.7 mV/dec, respectively. The onset potential of the synthesized HE-SO was similar to that of the reported spinel oxides-based catalysts with high OER activity, and the Tafel slope value of the HE-SO was lower than that of the reported spinel oxides. This result indicated that HE-SO functions as an efficient catalyst for OER. To our knowledge, this is the first demonstration of the synthesis of HE-SO nanoparticles by supercritical fluid processing [2]. Further detail of structure analysis and electrochemical characterizations will be discussed in the presentation.

[1] Y. Takahashi, Y. Nakayasu, **K. Iwase** *et al.*, *Dalton Trans.*, 2020, 49, 27, 9377-9384.

[2] **K. Iwase** *et al.*, *submitted*.

10:45 AM NM05.12.08

Developments of Highly Efficient Electrocatalytic 2D Nonlayered Materials via Ionic Layer Epitaxy Strategy *Ziyi Zhang, Yunhe Zhao, Guangyuan Yan, Xin Yin and Xudong Wang*; University of Wisconsin - Madison, United States

Many traditional high-performance electrocatalysts, such as precious metals (e.g., Pt, Pb) and metal oxides (e.g., RuO₂, IrO₂), have a nonlayered crystal structure with intrinsic isotropic chemical bonds in three dimensions. Creating 2D morphology from these nonlayered catalytic materials may offer higher impacts on catalyst design by exposing massive surface dangling bonds and active defects. However, compared with van der Waals solids, 2D nonlayered materials synthesis requires the control of kinetics to break the crystal symmetry fostering 2D anisotropy in crystal growth and stabilizing the structures far away from thermodynamic equilibrium. Here, we introduce a solution-based 2D nonlayered materials synthesis technology that distinguishes itself from others with the capability of unit-cell-level thickness control called the ionic layer epitaxy (ILE) technique. In this technology, an ionic surfactant monolayer is used as a soft template at the air-water interface to guide the growth of 2D materials; here, it was found that the control of the surfactant type and packing density in the monolayer brings up a new capability for the unit-cell-level precision thickness control and vacancy concentration tuning of 2D nonlayered material in ILE synthesis, which may enable a more comprehensively quantitative study on 2D electrocatalysis. ILE was recently developed as an effective strategy to synthesize 2D nonlayered materials, such as Pd, La₂O₃, and CoO, and we demonstrated that these are promising electrocatalysts. Owing to the ultrasmall thickness, high crystallinity, and exposure of highly active FCC (100) crystal facets, the 2 nm quasi-square shaped Pd nanosheets (NSs) exhibited a mass oxidation current as high as 1132.6 mA/mg which is more than 30 times higher catalytic activity in formic acid oxidation compared to the commercial Pd black.¹ This offered a promising approach toward rational design and synthesis of ultrathin metallic 2D NSs with enhanced functionality. The ultrathin rare-earth metal-based oxide, La₂O₃ NSs demonstrated a significantly improved oxygen evolution reactions (OER) performance.² Due to the ultrasmall thickness, the as-synthesized 2.27 nm La₂O₃ NS exhibits a current density of 10 mA cm⁻² and a mass activity as high as 6666.7 A g⁻¹ at an overpotential of 310 mV, which is three orders of magnitude higher than benchmark OER electrocatalysts, such as commercial IrO₂ and RuO₂. This presents a sustainable way for the development of highly efficient electrocatalysts with largely reduced mass loading of precious elements. Furthermore, 2.5 nm quadrangle-shaped bimetallic Co-Mo-O NSs with a 2:1 Co-to-Mo ratio exhibited an enhanced OER catalytic activity with 3 orders of magnitude higher mass activity compared to commercial IrO₂ and RuO₂ in an alkaline environment, delivered an even lower overpotential of 273 mV at 10 mA cm⁻², with a mass activity of 5472 A g⁻¹ and a superior turnover frequency of 1.47 s⁻¹ ($\eta = 330$ mV) due to its ultrasmall thickness. The ultrathin NSs synthesized via ILE techniques demonstrated a promising strategy for the development of substantial highly efficient 2D electrocatalyst materials that the remarkable mass activity associated with the unique ultrathin structure is particularly valuable for preserving rare and precious catalyst elements that have high costs and low supplies.

REFERENCES

1. Yin, X. *et al.* *Chemistry of Materials* **30**, 3308-3314, doi:10.1021/acs.chemmater.8b00575 (2018).
2. Yan, G. *et al.* *Nano-Micro Letters* **12**, 49, doi:10.1007/s40820-020-0387-5 (2020).
3. Zhao, Y. *et al.* *ACS Energy Letters* **6**, 3367-3375, doi:10.1021/acsenenergylett.1c01302 (2021).

11:00 AM NM05.12.09

Nanoconfinement and Mass Transport in Hollow Structured Pt-Rh Electrocatalysts Towards Efficient and Durable Ethanol Electrooxidation *Kyeong-Ho Kim and Betar Gallant*; Massachusetts Institute of Technology, United States

A major challenge of ethanol utilization in fuel cells relates to full oxidation of ethanol to CO₂, which comprises a 12-electron transfer reaction, with the obtained extent of this reaction at room temperature significantly lower due to unique thermodynamic and kinetic challenges of ethanol's C-C bond cleavage step. Consequently, in practice, the Faradaic efficiency (FE) of full oxidation of ethanol to CO₂ is often limited to <20%, with the majority of byproducts being C₂ intermediates in which C-C bonds persist: acetaldehyde (H₃C-COH) or acetic acid (H₃C-COOH), which generate only 2 and 4 electrons rather than 12 electrons.

In the ethanol oxidation reaction (EOR) mechanism, the surface coverage of OH functional groups affects reaction selectivity of the C-C bond cleavage step owing to competitive adsorption on the active sites between OH functional groups and each of the two carbons in ethanol for successful C-C bond splitting. While the optimized surface coverage of OH for high EOR selectivity can be achieved by reducing the pH of the alkaline electrolyte, the low concentration of OH⁻ in bulk solution may lead to undesired decreases in ionic conductivity. Therefore, it is compelling to examine methodologies that allow for decoupling of near-surface vs. bulk electrolyte composition and properties. Hence, to manipulate the surface coverage of OH without modulating the pH of bulk solution, we exploited the high generation rate of H⁺ released during EOR, which can create a local acidic environment near the

electrocatalyst surface.

In this study, the critical role of the electrode architecture affecting the EOR selectivity was investigated by controlling the extent of local pH swing manipulated by the different degree of electrode porosity that governs the mass transport of OH^- near the electrocatalyst surface. To modulate the degree of electrode porosity, binary $\text{Pt}_{1-x}\text{Rh}_x$ electrocatalysts were synthesized into hollow sphere morphologies with different particle sizes (250 and 350 nm) and compositions ($x=0.0, 0.4, 0.5, 0.6,$ and 0.66). The FE of full oxidation of ethanol to CO_2 was systematically compared in terms of different particle size and mass loading of hollow spheres in the electrodes by quantifying the EOR products using NMR and gas chromatography. The higher FE of CO_2 could be achieved by a more acidic environment of the more porous electrode structure with a smaller particle size and higher mass loading of electrocatalysts, suggesting the potential to control the EOR outcomes via electrode structural engineering.

11:15 AM NM05.12.10

Spin Selective Charge Transport Through Cysteine Capped Iridium Nanoparticles and Its Effect on the Electrochemical Catalytic Activity Carlos Mingo; Queen Mary University of London, United Kingdom

Highly efficient processes for energy conversion are a necessity to keep up with the growing demand for energy and a sustainable future. Electrocatalysts play a crucial role in this goal and so overcoming their shortcomings are essential. In this study, chiral iridium nanoparticles produced by way of functionalising iridium nanoparticles with L-cysteine in a two step synthesis process, demonstrates the ability to boost catalytic oxygen evolution reaction (OER) through an electron spin polarisation mechanism. As a result of the spin selective nature of the mechanism, potential parasitic species formation such as hydrogen peroxide is hindered, which can lead to prolonged catalyst life-time.

11:30 AM NM05.12.11

Tuning Electronic Structure and Composition of FeNi Nanoalloys for Enhanced Oxygen Evolution Electrocatalysis via a General Synthesis Strategy Yong Wang; Nanyang Technological University, Singapore

Developing low-cost and efficient oxygen evolution electrocatalysts is key to decarbonization. A novel, facile, surfactant-free and gram-level biomass-assisted fast heating and cooling synthesis method is reported for synthesizing a series of carbon-encapsulated dense and uniform FeNi nanoalloys with a single-phase face-centered cubic solid-solution crystalline structure and an average particle size of sub-5 nm. This method also enables precise control of both size and composition. Electrochemical measurements show that among $\text{Fe}_x\text{Ni}_{(1-x)}$ nanoalloys, $\text{Fe}_{0.5}\text{Ni}_{0.5}$ has the best performance. DFT calculations support the experimental findings and reveal that the optimally positioned d -band center of O-covered $\text{Fe}_{0.5}\text{Ni}_{0.5}$ renders a half-filled anti-bonding state, resulting in moderate binding energies of key reaction intermediates. By increasing the total metal content from 25 to 60 wt%, the 60% $\text{Fe}_{0.5}\text{Ni}_{0.5}/40\%$ C shows an extraordinarily low overpotential of 219 mV at 10 mA cm^{-2} with a small Tafel slope of 23.2 mV dec^{-1} for OER, which are much lower than most other FeNi-based electrocatalysts and even the state-of-the-art RuO_2 . It also shows robust durability in an alkaline environment for at least 50 h. The gram-level fast heating and cooling synthesis method is extendable to a wide range of binary, ternary, quaternary nanoalloys, as well as quinary and denary high-entropy-alloy nanoparticles.

11:45 AM NM05.12.12

Scalable, Near Ambient Conditions, One-Pot, Facile Synthesis of Carbon-Doped TiO_2 -Based Nanofilaments and 2D Flakes, Their Properties, and Potential Applications Hussein Badr and Michel W. Barsoum; Drexel University, United States

Two-dimensional (2D) materials, which possess atomic or nanometer thickness and infinite planar dimensions, thrive on the rich variety of features and properties that are vastly distinctive from their bulk counterparts. Conventionally, bulk synthesis of 2D materials has predominantly been through selective etching of layered solids. Herein and for the first time, we convert – near ambient conditions – a dozen of commercial, cheap precursors into one-dimensional (1D) nanofilaments that self-assemble into 2D flakes. In that, the precursor is simply stirred in tetramethylammonium hydroxide aqueous solution at 50–80 °C for tens of hours. The structure, composition, oxidation state, and morphology of the resulting sheets are resolved by density functional theory, X-ray diffraction, X-ray photoelectron, electron energy loss, Raman, X-ray absorption near edge structure spectroscopies, atomic force microscope, scanning, transmission and high-resolution transmission electron microscopies and selected area diffraction. The resulting flakes showed enhanced electrochemical performance as cathodes in both Li-ion battery and Li-S battery. They also found to be biocompatible to human cells and fatal to some types of cancer cells, thus showing potential in biomedical applications. The developed synthesis protocol of 1D and 2D materials in bulk-scale at near ambient conditions is paradigm shifting and will undoubtedly open new and exciting avenues of research and applications.

SESSION NM05.13: Applications-Driven Synthesis of Nanomaterials

Session Chairs: Artsiom Antanovich and Thorsten Ohlerth

Thursday Afternoon, December 1, 2022

Hynes, Level 2, Room 202

1:30 PM NM05.13.01

Thermochromic Solar Control Coatings on SiO_2 -Coated Float Glass for Energy-Efficient Smart Windows Roberto Habets^{1,2}, Cindy Yeung^{1,2}, Luc Leufkens^{1,2}, Fallon Colberts³, Kathleen Stout³, Marcel Verheijen^{4,5}, Zeger Vroon^{1,2,3}, Daniel Mann^{1,2} and Pascal Buskens^{1,2,6}; ¹The Netherlands Organisation for Applied Scientific Research (TNO), Netherlands; ²Brightlands Materials Center, Netherlands; ³Zuyd University of applied sciences, Netherlands; ⁴Eindhoven University of Technology, Netherlands; ⁵Eurofins Materials Science, Netherlands; ⁶Hasselt University (UHasselt), Belgium

Considering the fact that energy usage for heating and cooling of buildings is a major contributor to the energy consumption of the built environment, there is a clear need for energy-efficient windows. For intermediate climates with hot summers and cold winters, smart windows with switchable solar control properties are ideal.^[1] Thermochromic materials are of interest for application in smart windows since their optical properties change based on changing outdoor temperature. In our study, we used VO_2 as thermochromic material because of its reversible structural phase transition from a semiconductive monoclinic to a conductive rutile structure at a defined switching temperature of 68°C. Dopants, such as W, can reduce the switching temperature to values between 15°C and 30°C, which is required for smart windows.^[1]

Here, we report a nanocomposite single-layer coating comprising VO_2 and SiO_2 , and yielding unrivalled optical properties.^[2] We prepared these coatings by dip coating of a SiO_2 -coated float glass in an alcoholic solution of a vanadium(IV) oxalate complex and pre-oligomerized tetraethoxysilane, and thermally annealed the dried xerocoat in a two-step process. During thermal anneal of the xerocoat, phase separation occurred which resulted in Si and V rich domains. This process was studied in detail for a series of coatings with varying VO_2/SiO_2 ratio and varying coating thickness using high resolution transmission electron microscopy. We obtained non-scattering coatings with low surface roughness and randomly distributed VO_2 nanodomains,

incorporated in a SiO₂ matrix. They displayed unrivalled optical properties combining $T_{vis} > 60\%$ with $\Delta T_{sol} \geq 10\%$. Additionally, we demonstrate that with a pencil hardness $\geq 4H$ and a stability in ambient environment of at least 11 months, the coatings are suitable for industrial processing into insulating glass units. With building energy simulations on a typical Dutch building, we demonstrated that the use of smart windows with our thermochromic coatings can lead to energy savings of 24%, which equals annual cost savings of up to 470 € per household.^[2]

1:45 PM NM05.13.02

Tuning of Magnetic Nanowire Aerogel Aspect Ratio and Orientation Through Magnetic Field Assisted Synthesis Rosemary L. Calabro^{1,2}, Malina Hatton¹, Alexa Zammit¹, Felita W. Zhang¹, Edward M. Tang¹, Zachary T. Bone¹, Olivia S. Raykhman¹, Grant Lee¹, Veronica M. Lucian¹, Robert J. Wilson¹, Enoch A. Nagelli^{1,1}, Peter H. Chapman¹, Stephen F. Bartolucci², Joshua A. Maurer² and John Burpo^{1,1}; ¹United States Military Academy, United States; ²U.S. Army DEVCOM Armaments Center, United States

Three-dimensional porous transition metal nanostructures offer many desirable properties due to their high surface area, lightweight nature, and reaction tunability through variation of metal composition making them desirable candidates for catalytic and electrochemical applications. However, synthesis of these materials with control over micro and nanostructure, pore size, and phase composition presents limitations due to aggregation, reactant diffusion times, and a need for templates. Magnetic field assisted nanowire aerogel synthesis is a promising alternative to produce structures from ferromagnetic ion precursors that offers advantages such as rapid nanowire growth and control over nanowire aspect ratio and nanowire orientation through tuning of the applied magnetic field strength. This magnetic field assisted synthesis strategy was applied to produce both iron and cobalt aerogels using metal chloride precursors reduced with sodium borohydride in magnetic fields ranging from 0 mT to 160 mT. For the iron nanowire gels, increasing the magnetic field strength resulted in increased nanowire aspect ratios and a higher orientation order parameter (OOP) as determined from image analysis of scanning electron micrographs. At maximum field strengths, nanowire lengths exceeding 50 μm with average diameters of about 70 nm were achieved. For cobalt, the samples prepared in the absence of a magnetic field consisted of irregular spherical particles and as the magnetic field strength increased, the formation of elongated wire-like structures was favored. The magnetic properties of these magnetic gels were analyzed via vibrating sample magnetometry (VSM) and showed that the magnetic field strength used for synthesis influenced the measured coercivities and saturation magnetizations of the gels. These metal gels can be supercritically dried with CO₂ to form aerogels or be pressed into conformal thin films with ambient drying. These nanowires were further used as a sacrificial template for galvanic displacement with noble metals salts such as platinum which allowed for dissolution of the iron nanowires and formation of high surface area platinum nanotubes and electrochemical impedance spectroscopy (EIS) and cyclic voltammetry (CV) indicate high electrochemical accessible surface areas for catalytic applications. This galvanic displacement may be expanded to prepare numerous metallic and multi-metallic nanostructures while maintaining a similar overall orientation and structure as the sacrificial aerogel template, and we expect this magnetic field assisted nanowire aerogel synthetic method to be able to be expanded to multi-metallic and alloy ferromagnetic materials which will allow further tuning of the electrochemical and magnetic properties for a wide range of applications.

2:00 PM NM05.13.03

Metallization of Specific Protein Assemblies via Antibody-Guide in Mammalian Cells and Ex Vivo Tissues Chang Woo Song, Dae-Hyeon Song, Dong Gyu Kang, Ki Hyun Park, Chan E Park, Hyunwoo Kim, Yoon Sung Nam, Jihyeon Yeom, Seung Min J. Han and Jae-Byum Chang; Korea Advanced Institute of Science and Technology, Korea (the Republic of)

Constantly evolved organisms have hierarchical protein structures that are tailored to be suitable for certain functions. As a biotemplating approach, the mineralization of such biostructures has gained popularity in recent decades. Nevertheless, the use of specific proteins as templates has only been proved in very basic organisms, such as viruses and yeasts, and not in multicellular organisms having more complex protein structures. In this study, we propose a method for synthesizing metallic structures that mimic particular protein assemblies in mammalian cells and ex vivo tissues. To enable protein-specific growth of metals, target proteins are labeled with antibodies, which subsequently provide nucleation sites for metal particle growth. Various metal particles, including Au, Ag, Au@Pt (core@shell), and Au@Pd, are synthesized by using microtubules within the cells as templates. The synthesized cells exhibit significantly enhanced mechanical strength and catalytic activity for liquid-phase reactions. In addition, we demonstrate that by employing multiple proteins as templates for metal particle growth in the same cell, greater catalytic activity can be attained. Finally, we expand this method's application to mouse brain, kidney, and heart slices and imitate the unique protein assemblies inside these organs. We believe this technique can promote the transformation of certain protein structures into metallic frameworks in multicellular animals.

2:15 PM NM05.13.04

Surface and Interface Controlled Zero-Dimensional Nanomaterials for Advanced Printed Electronics Jisun Im¹, Gustavo Trindade², Richard Hague¹ and Christopher Tuck¹; ¹University of Nottingham, United Kingdom; ²National Physical Laboratory, United Kingdom

Inkjet printing of nanomaterials has been demonstrated to fabricate advanced electronic devices such as flexible and wearable electronics, optoelectronics and sensors by allowing the creation of customized device geometry. In particular, zero-dimensional (0D) nanomaterials, most commonly nanoparticles, have shown great potential for printed electronics since they provide unprecedented and desirable material properties due to their high surface area-to-volume ratio and quantum confinement properties.

Here we demonstrate the successful integration of 0D nanomaterials, such as novel metal nanoparticles (silver and gold) and silicon carbide nanoparticles, into Additive Manufacturing (AM) processes to produce flexible electronics with sensing capabilities. The surface and interface engineering of nanoparticles yields not only a dispersion compatible with various types of AM techniques but also tailorable functional properties. We demonstrate high electrical performance stability of inkjet-printed flexible gold electrodes in response to mechanical bending deformation by using gold nanoparticle functionalized with cohesion enhancer. Complex three-dimensional nanocomposite structures have been fabricated using two photon polymerization by modulating the interaction between the surface of plasmonic nanoparticles and the functional groups of polymers for optoelectronics application. Our advanced compositional (XPS and Orbi-SIMS) and morphological analysis (FIB-SEM and TEM) provides an insight into the effect of tailored surface and interface of nanoparticles on 3D printed structures and device performance.

2:30 PM NM05.13.05

Magnetic Nanosheets via Chemical Exfoliation of K₂Mn_xSn_{1-x}S₂ Fang Yuan¹, Leslie Schoop¹, Xiaoyu Song¹, Guangming Cheng¹, Nan Yao¹ and Yuriy Mozharivskiy²; ¹Princeton University, United States; ²McMaster University, Canada

We report two chemical routes to prepare new magnetically doped two-dimensional (2D) tin sulfides, i.e., Mn_xSn_{1-x}S₂ ($x = 0.1-0.2$), as derivatives of K₂Mn_xSn_{1-x}S₂. Initial codoping with K ensures high Mn doping in the nanosheets and is additionally aiding exfoliation. In chemical route 1, the parent compound is first reacted with a diluted HCl solution, which dissolves all K and half the Mn atoms, followed by treatment with TEOH/methanol, which results in exfoliation. In chemical route 2, K₂Mn_xSn_{1-x}S₂ treated with I₂ in acetonitrile, leading to the removal of almost all K atoms, followed by dispersing the product in dimethylformamide, which results in partial exfoliation. The composition and structures are characterized using scanning electron microscopy, high-resolution scanning transmission electron microscopy, and selected area electron diffraction. After K removal and before exfoliation, the structure is trigonal (*P-3m*) featuring hexagonal slabs with AA stacking and appropriate interlayer space along the c axis. Upon shaking, both

Mn_xSn_{1-x}S₂ (x = 0.1–0.2) phases can be exfoliated into thinner flakes, but nanosheets with a thickness of 2.5 nm can only be achieved via chemical route 1. Magnetic susceptibility measurements of the parent, intermediate, and restacked exfoliated products reveal that the manganese magnetic moment saturates at a moderate field, only in the exfoliated material. Mn_xSn_{1-x}S₂ nanosheets can be viewed as a magnetically doped derivative of SnS₂, a material that is used as a high on/off ratio transistor, photocatalyst, and electrode material. Therefore, the new layered metal sulfides obtained here may have diverse applications in 2D magnetism, catalysis, or batteries.

SESSION NM05.14: Virtual Session I
Session Chairs: Elena Shevchenko and Dmitri Talapin
Tuesday Afternoon, December 6, 2022
NM05-virtual

2:00 PM NM05.14.02

Wet Chemical Synthesis of Patterned Bismuth Ferrite Thin Films by Direct Writing (printing) and Characterization Using Printed Electrodes Sanjeev Patil¹ and Parasuraman Swaminathan^{1,2}; ¹IIT Madras, India; ²Indian Institute of Technology (IIT) Madras, India

BiFeO₃ (BFO) is the only naturally occurring room-temperature multiferroic with high Neel (643 K) and Curie (1103 K) temperatures enabling effective magnetic-ferroelectric coupling, thus opening avenues of non-volatile FRAM (ferroelectric random access memory), spintronics, MEMS and one of three realistic candidates to replace lead zirconate titanate (PZT) in ferroelectric and piezoelectric applications. Owing to lead's toxicity, safety, and disposal hazards, PZT is being phased out, and BFO leads over potassium sodium niobate (KNN) and NBT possess severe volatility and non-stoichiometric defects as well as a narrower operating temperature range due to lower Curie temperatures even after significant doping.

Wet chemical routes proffer the distinct advantage of large-scale production with lower temperatures compared to conventional solid-state reaction and lack of high vacuum requirements as in physical vapor deposition techniques. Of the routes available, sol-gel was chosen due to the flexibility in the choice of nanostructures that could be obtained- from thin films to nanoparticles.

In this work, BFO coatings were deposited on fluorine-doped tin oxide (FTO), indium-doped tin oxide (ITO), and quartz substrates via direct writing using a customized with optimized printing and extrusion parameters. A precursor-based ink was developed that remains stable in dispersion form for up to 9 months without aggregation or any phase separation. Choice of solvent, precursor, solvent-precursor ratio, chelating agent, and temperature were critical, which aided in achieving phase pure BFO at a low sintering temperature of 500 °C for 1 hour. Phase purity was ascertained by structural characterization- XRD, SEM-EDS, Raman spectroscopy, and UV-vis spectroscopy, while the BFO ink characteristics were optimized for printability using contact angle (wettability) and viscosity tests. Optical profilometry confirmed the thickness of films deposited, while UV-vis spectroscopy also indicated optical bandgap in the range of 2.6 to 2.9 eV using Tauc plots.

Traditionally, top and bottom electrodes were deposited by evaporation or sputtering, which necessitated high vacuum and expensive pure gold targets. This work utilized direct writing to print silver nanoparticles as electrodes to get Ag/BFO/ITO, Ag/BFO/FTO, and Ag/BFO/quartz heterostructures to frugally obtain contacts required for electrical characterization. By optimizing extrusion and nozzle parameters during printing, the significantly expensive material loss during sputtering/evaporation was bypassed, while flexibility with the printer allowed for choice of electrode shape (square/circular) and dimension without the need for a mask.

References:

- [1] H Liu, J Liu, H Zhu, Y Wang, J Ouyang, *Materials Letters*, 320, 132387 (2022)
- [2] N Spaldin, R Ramesh, *Nature Materials*, 18, 203 (2019)

2:05 PM NM05.14.03

Visible-Light-Active Organic Dye/Alumina-Silicate Nanocomposites for Photobiocidal-Triboelectric Fabric Coating Dong Uk Lee¹, Sang Bin Jeong², Ki Joon Heo³, Byeong Jin Lee¹, Se Kye Park¹, Jae Hak Shin², Jae Hee Jung² and Dong Yun Choi¹; ¹Korea institute of industrial technology, Korea (the Republic of); ²Sejong University, Korea (the Republic of); ³University College London, United Kingdom

Controlling airborne microorganisms (called bioaerosols) is vital for protecting public health. In the 21st century, bioaerosols have threatened public health in various forms, from severe acute respiratory syndrome in 2002, to pandemic influenza A in 2009, to Middle East respiratory syndrome coronavirus in 2012 and COVID-19 in 2019 [1]. COVID-19 is still an ongoing threat, with more than 536 million infections and 6.31 million deaths worldwide (as of 15 June 2022) [2]. Therefore, there is a need to develop innovative bioaerosol-inactivating materials. Various fiber-based filters composed of organic or inorganic antimicrobial materials, such as copper, silver nanoparticles, chitosan, and natural products, have been developed to filter against bioaerosols [3]. However, these air filters effectively inactivate only microorganisms in direct contact with antimicrobial agents; therefore, their effectiveness gradually decreases as dust accumulates over the antimicrobial material. In addition, conventional filter disinfection technologies based on ultraviolet (UV) irradiation, plasma, and thermal energy have been developed; however, these technologies require additional energy and devices [4].

Recently, visible-light-driven (VLD) biocidal technologies, based on sunlight or indoor light energy, have been a focus of research in the field of photocatalysis [5]. VLD biocidal surfaces or air filters have been prepared using photosensitizing dyes such as triarylmethane, phenothiazine, and xanthene derivatives [6]. The photosensitizing dyes are inexpensive and have various applications; however, because of their high affinity to water, they easily leach into the environment when they come into contact with moisture [7]. To become incorporated into polymer fibers, the dyes need to be firmly immobilized to guarantee the durability and washability of the fibers.

We introduce a novel fiber functionalization method that uses silica-alumina sol-gel (SAS) to endow a fibrous membrane with photocatalytic biocidal activity and reusability. The transparent SAS matrix immobilizes crystal violet (CV) photosensitizer dye and binds electronegative 1H, 1H, 2H, 2H-perfluorooctyltriethoxysilane (PFOTES) molecules to its surface [8]. Moreover, the SAS matrix enhances the dispersity of the photosensitizers (suppressing self-quenching) and protects them from degradation by ROS, enhancing the photodurability. The SAS/PFOTES-CV (SAPC) nanolayer produced more ROS via enhanced redox reaction and showed excellent photobiocidal efficiency (~99.99% for bacteria and a virus) under visible light irradiation (3 h, 7.2 mW cm⁻²) and photodurability (~83% reduction in bactericidal efficiency for the CV alone but ~0.34% for the SAPC filter after 3 days of light irradiation). Moreover, PFOTES bonded to the SAS thin film increased water resistance and triboelectrification ability of the filter. The SAPC filter maintained its filtration and antimicrobial properties after cyclic washing tests, which demonstrates that the excellent reusability. Our SPAC-based nanolayer coating technology is applicable to various textiles of face masks and protective clothing and can control the spread of COVID-19 and other airborne contagious diseases.

References

- [1] A. Nalbandian, *et al.*, *Nat. Med.* 27 (2021) 601–615.
- [2] “COVID-19 Dashboard.” The Center for Systems and Engineering (CSSE) at Johns Hopkins University.

- [3] S. Kumar, *et al.*, *Nano Lett.* 21 (2021) 337–343.
 [4] R. K. Campos, *et al.*, *ACS Nano* 14 (2020) 14017–14025.
 [5] P. Li *et al.*, *Nat. Commun.* 10 (2019) 2177.
 [6] P. Tang *et al.*, *ACS Appl. Mater. Interfaces* 12 (2020) 49442–49451.
 [7] K. J. Heo, *et al.*, *Nano Lett.* 21 (2021) 1576–1583.
 [8] S. B. Jeong *et al.*, *Chem. Eng. J.* 440 (2022) 135830.

Acknowledgement

This work was supported by the National Research Foundation of Korea(NRF) grant funded by the Korea government(MSIT) (No. 2022R1F1A1074255).

*Corresponding Author: D. Y. Choi; E-mail: dychoi311@kitech.re.kr

2:15 PM DISCUSSION TIME

SESSION NM05.15: Virtual Session II
 Session Chairs: Jun Hyuk Chang and Dmitri Talapin
 Wednesday Afternoon, December 7, 2022
 NM05-virtual

1:00 PM *NM05.15.01

Halide Perovskite and Perovskite-Related Nanocrystals—Synthesis and Optical Properties [Liberato Manna](#); Istituto Italiano di Tecnologia, Italy

Halide perovskite semiconductors can merge the highly efficient operational principles of conventional inorganic semiconductors with the low temperature solution processability of emerging organic and hybrid materials, offering a promising route towards cheaply generating electricity as well as light. Following a surge of interest in this class of materials, research on halide perovskite nanocrystals (NCs) as well has gathered momentum in the last years. While most of the emphasis has been put on CsPbX₃ perovskite NCs, more recently the so-called double perovskite NCs, having chemical formula A⁺₂B⁺B³⁺X₆, have been identified as possible alternative materials, together with various other metal halides structures and compositions, often doped with various other elements. This talk will also discuss the research efforts of our group on these materials. We will highlight how for example halide double perovskite NCs are less surface tolerant than the corresponding Pb-based perovskite NCs and that alternative surface passivation strategies need be devised in order to further optimize their optical performance. Other topics that will be covered are doping and the role of surface ligands on stabilizing the NCs, including those with alloy compositions, and doping of cesium manganese bromide nanocrystals with rare earths to elicit emission in the NIR region of the spectrum.

1:30 PM *NM05.15.02

Design of NPLs from the Inorganic Core to the Surface Chemistry Corentin Dabard¹, Hong Po¹, Thierry Barisien², Benjamin Diroll³, Juan Climente⁴, Benoit Roman⁵, Etienne Reyssat⁵, José Bico⁵, Emmanuel Lhuillier² and [Sandrine Ithurria](#)¹; ¹Sorbonne Université, France; ²Sorbonne Université, CNRS, Institut des NanoSciences de Paris, France; ³Argonne National Laboratory, United States; ⁴Universitat Jaume I, Spain; ⁵Université de Paris, France

II-VI semiconductor nanoplatelets are colloidal nanoparticles confined in one dimension which gives them exceptionally narrow optical properties. We are showing that through the design of core/crown/crown heterostructures, it is possible to synthesize nanoplatelets with green and red emissions from a single population. In the CdSe/CdTe/CdSe core/crown/crown NPLs, the exciton either recombine at the interface between 2 semiconductors due to the type II band alignment or in the CdSe area. The ratio of the two emissions can be tuned by the incident power. With increased power, the red emission saturates due to non-radiative Auger recombination thus affecting its emission much stronger than the green one. These NPLs can be introduced in LED. So, the design of the NPLs inorganic core enables to tune their optical properties but their shape can be further modified through the surface chemistry. NPLs with their large lateral dimensions can be considered as flexible substrate for the self-assembly of ligands which originally ensure the colloidal stability of NPLs. The stress brought by surface ligands and the specific zinc blende crystal structure of the NPLs induce a folding of NPLs as helices or twists. We show that an exchange from carboxylate ligands to halides ligands and thiolate ligands enable to unfold CdSe NPLs and to invert the chirality of the helices.

2:00 PM NM05.15.03

Lead Chalcohalides Nanocrystals and Chalcohalide-Perovskite Heterostructures [Stefano Toso](#)^{1,2}, Muhammad Imran¹, Quinten A. Akkerman¹, Beatriz Martín-García¹ and [Liberato Manna](#)¹; ¹Istituto Italiano di Tecnologia, Italy; ²Università Cattolica del Sacro Cuore, Italy

Lead-based colloidal semiconductors, in the form of lead chalcogenide and lead-halide perovskite nanocrystals, are extensively studied for applications in the infrared and visible spectral ranges respectively. Yet, these materials suffer from limitations, motivating the search for alternatives: lead-halide perovskites quickly degrade *in operando* conditions, and the more robust lead chalcogenides can be hardly pushed in the visible range due to the small band gaps. However, there is a class of materials that bridge between lead chalcogenides and perovskites, which has been little studied so far and may hold promises for optoelectronic applications. They are the lead chalcohalides, ternary compounds with general formula Pb₄E_bX_c (E = S, Se, Te; X = F, Cl, Br, I).

In an attempt to investigate these materials, we synthesized and solved the structure of two lead sulfohalides unknown to date (Pb₄S₃Br₂ and Pb₄S₂Cl₂), which proved to be indirect band gap semiconductors. When tested in photodetectors and solar cells, Pb₄S₃Br₂ demonstrated a photoresponse that, albeit modest, encouraged deeper investigations into this class of compounds. Further experiments led us to the synthesis of lead chalcohalide/perovskite heterostructures, that are nanoparticles composed of two connected crystalline domains. Their interface represents the first reported epitaxial connection of lead-halide perovskites with a phase outside the family of cesium lead halides, and is made possible by the intimate structural similarities that Pb₄S₃X₂ shares with some of the Cs-Pb-X compounds.

The formation of lead chalcohalide/lead perovskite heterostructures has a strong impact on the behavior of both materials. On the one hand, it quenches the otherwise bright photoluminescence of the perovskite, suggesting a delocalization of carriers on the chalcohalide domain that might be exploited for photo-harvesting. Moreover, the Pb₄S₃Br₂-CsPbI₃ epitaxial interface stabilizes the labile CsPbI₃ perovskite, potentially solving a well-known of perovskite-based photovoltaics. On the other hand, the perovskite exerts a strong templating effect on the chalcohalide domain, producing a complete phase selectivity for the case of lead sulfochlorides: Pb₄S₂Cl₂ nanocrystals forms when the perovskite is absent, while Pb₄S₃Cl₂/CsPbCl₃ heterostructures when it is present

(note the different stoichiometry). This approach could be pushed a step further, as we discovered how to selectively etch the perovskite domain of the heterostructures, hence obtaining phase-pure $\text{Pb}_4\text{S}_3\text{Cl}_2$ nanocrystals that could not be obtained by direct synthesis due to the competitive nucleation of $\text{Pb}_3\text{S}_2\text{Cl}_2$.

These results motivate further research on lead chalcogenides, and pave the road for the advanced control over the synthesis of colloidal inorganic nanomaterials through epitaxial templating.

2:15 PM NM05.15.04

Synthesis of MIL-Modified BiFeO_3 Nanocrystals for Enhancement of the Photoinduced Antibacterial Activity Under Visible Sunlight Irradiation Luca Pulvirenti, Cinzia Lombardo, Mario Salmeri, Maria Teresa Cambria and Guglielmo G. Condorelli; University of Catania, Italy

Antibiotic resistance is a critical challenge for modern medicine, although several approaches have been developed to address this serious global problem. Among these, one of the most promising systems involves the use of light-activated antibacterial agents, which, to be effective, must be irradiated with very intense visible light sources or UV radiation. However, this condition is not always easy to recreate.

Against this background, we research discusses a nanometer hybrid material consisting of nanoparticles of bismuth multiferroic ferrite (BFO) modified through the growth of Metal-organic frameworks of the MIL (Materials Institute Lavoisier), which can be activated by natural sunlight irradiation. The obtained system retains both nanometric dimensions and the intrinsic photo degradative properties of BFO that are increased by the presence of Fe-based MIL.

In our paper we argue that the chemical characterization conducted through various complementary techniques (X-ray-diffraction, thermogravimetric analysis, FT-IR and X-ray photoelectron spectroscopies) confirmed the anchorage of the organic component.

The antibacterial activity was carried out on both Gram-positive and Gram-negative species with the method of the microdilutions in liquid medium, setting up serial dilutions to the doubling of each nanocompound in the range of [100 - 0,20 $\mu\text{g/ml}$]. Our experiments demonstrate that when incubated in the dark or after pre-illumination with UV-C, the nanoparticles did not exhibit any bacteriostatic or bactericidal activity even at the highest concentration tested (100 $\mu\text{g/ml}$). The antibacterial activity of the BFO@MIL against the Gram-positive species shows a significant increase in MIC (Minimum Inhibitory Concentration) and MBC (Minimum Bactericidal Concentration) values compared to BFO, confirming the photoactivating efficacy of this material following exposure to natural sunlight.

In particular, the BFO@MIL shows a reduction in MBC value (>100 to 0.39 $\mu\text{g/ml}$ and >100 to 0.20 $\mu\text{g/ml}$) on two tested strains of Staphylococcus (*S. Haemolyticus* ATCC 29970 and *S. Aureus* ATCC 25923 respectively). Therefore, BFO@MIL tested on another strain of Staphylococcus (*S. Haemolyticus* ATCC 31874) shows different MIC and MBC values (0,39 to 0,20 and >100 to 0,39 $\mu\text{g/ml}$ respectively)

In addition, the most relevant aspect for this material is the ability to inhibit the growth of four *E. Coli* strains (more resistant), although at the maximum concentration tested (100 $\mu\text{g/ml}$).

These results suggest that the new nanocomposite BFO@MIL has been successfully developed and has been an effective antibacterial agent against a wide range of microorganisms.

2:30 PM NM05.15.05

Enabling Applied Process Control of Solution Deposition of Hydroxyapatite Using JMP® Software Brid Murphy^{1,2} and Mick A. Morris^{1,2}; ¹Trinity College Dublin, Ireland; ²SFI Centre for Advanced Materials and BioEngineering Research, Ireland

Authors:

Brid Murphy^{1,2} and Michael A. Morris^{1,2}

AMBER Research Centre, CRANN Institute, Trinity College Dublin, Dublin 2, Ireland

School of Chemistry, Trinity College Dublin, Dublin 2, Ireland

Abstract:

In any novel coating technique, there are various dependencies pertaining to process and coating outcome. This results in complex dependencies on a range of interacting variables which can be extremely challenging to understand. Achieving such an understanding for solution deposited hydroxyapatite would facilitate ramping up of a lab-based system to an industrial scale system with controlled repeatability.

This work shows how automated computational models of raw data can be used to generate applied process controls for solution deposition of hydroxyapatite.

JMP® statistical software is used to build a design of experiments with process parameters as factors and characterisation data as responses. The visualisation of this data through multivariate analysis and regression modelling shows links within and between factors and responses. The DOE yielded a model for the complex solution deposited HA process which is subsequently automated using JMP Scripting language.

Some findings from the model include: (i) how initial substrate roughness influences oxygen atomic percentage of the films, (ii) how substrate roughness affects the proportionality between indicative spectroscopic peaks and (iii) how initial solution pH affects the weight of coating formed whereas temperature has little effect.

An industrial scale system could use the findings of this model to apply control limits to processing parameters leading to repeatability of coatings across separate batches. Separately, findings of this model highlight links that would be scientifically significant and worth pursuing in further research.

2:45 PM DISCUSSION TIME

SESSION NM05.16: Virtual Session III
Session Chairs: Justin Ondry and Elena Shevchenko
Wednesday Afternoon, December 7, 2022
NM05-virtual

6:30 PM NM05.16.01

Seedless One-Pot Synthesis of Gold Nanotriangles by Non-Thermal Liquid Phase Reduction Method Mao Hamamoto, Tomoki Yasu, Asahi Kimura, Haruki Toya and Hiromasa Yagyu; Kanto Gakuin University, Japan

Gold nanotriangles (GNTs) with edge lengths of hundreds nanometer exhibits a strong absorption peak at the wavelength of approximately 600 nm due to localized surface plasmon resonance of nanoparticles. Since the peak wavelength of GNTs lied in long wavelength in comparison with spherical GNPs and the transmitted color of solution is blue, GNTs shows an improved detection on immunochromatography.

GNTs can be synthesized by the seed-growth method [1] and non-seed method [2]. In the seed method, GNPs with a few nanometer particle sizes are pre-synthesized as a seed material and the seed are grown by adding gold ion solution, capping agent, and reducing agent. In the non-seed method, GNTs can be synthesized by one pot using thermal liquid-phase reduction with citrate acid. However, since thermal reduction requires precise temperature control of the solution and the reduction rate of gold ions affects to the edge lengths of GNTs, the non-seed method is difficult to realizing a stable synthesis of GNTs with edge lengths of hundreds of nanometer. In order to stably synthesize GNTs by non-seed and non-thermal liquid-phase reduction method, we demonstrated the synthesis method using reducing agent with composition of citrate acid and tannin acid.

Solution-A was a mixture of 0.21 mL hydrogen tetrachloroaurate tetrahydrate aqueous solution (29.7 mM) and 4.8 mL cetyltrimethyl ammonium bromide (CTAB) aqueous solution (9.15 mM). Solution-B was a mixture of 128 μ L sodium citrate acid solution (100 mM), 0.1 to 0.5 mL tannin acid solution (5.88 mM), and 7.5 mL distilled water. Solution-A and solution-B were mixed for 10 min in the 100 mL glass beaker with the mixing speed 700 rpm. In this experiment, the volume of sodium citrate acid solution was fixed, and the volume of tannin acid solution changed 0.1 to 0.5 mL. Following 3 days of stasis post synthesis at room temperature (23°C), the visible light absorption spectrum of the as-synthesized GNTs was recorded to analyze the peak wavelength. The edge lengths and yield of triangles (number of GNTs/total number of particles) of the as-synthesized solution after 3 days was evaluated by TEM observation.

From UV-visible absorbance spectra of solution, the solution with 0.1 mL of tannin acid solution exhibited purple color and the absorption peak at the wavelength of approximately 584 nm. The solution with 0.2 mL of tannin acid solution showed blue color and the strong absorption peak at the wavelength of approximately 619 nm. The solution with 0.3 to 0.5 mL of tannin acid solution indicated dark brown color and weak absorption peak. Moreover, the same color solution was obtained even if it was synthesized three times under the same conditions. From TEM observation, the synthesized solution confirmed that GNTs were observed in all solutions. The average edge length depends on volume of tannin acid solution and showed 127 nm with coefficient of variation of 0.74 for the solution with 0.2 mL of tannin acid solution. The yield of the triangles was 40.1 % for 0.1 mL tannin acid, 41.7 % for 0.2 mL tannin acid, 48.5 % for 0.3 mL tannin acid, and 24.8 % for 0.5 mL tannin acid. In thermal reduction method without tannin acid solution, the success rate of synthesis GNTs was 5 % and yield of the triangle was 30 %. These results confirmed that GNTs can be stably synthesized by seedless and non-thermal liquid-phase reduction method using tannin acid solution.

[1] X. Fan, Z. R. Guo, J. M. Hong, Y. Zhang, J. N. Zhang, and N. Gu, "Size-controlled growth of colloidal gold nanoplates and their high-purity acquisition", *Nanotechnology*, 21, 105602 (2010).

[2] D. V. R. Kumar, A. A. Kulkarni, and B. L. V. Prasad, "Synthesis of triangular gold nanoplates: Role of bromide ion and temperature", *Colloids and Surfaces A: Physicochem. Eng. Aspects*, 422, pp. 181-190 (2013).

6:45 PM NM05.16.02

Direct Patterning of Functional Ceramics on Conducting Substrates by Local Activated via Electro-Discharge Soft Solution Processing Sumanta Kumar Sahoo¹, Yu-Cyuan Hou¹, You-Yu Chen¹, Kripasindhu Sardar¹, Satoru Kaneko², Kou-Shuo Chang¹ and Masahiro Yoshimura¹; ¹National Cheng Kung University, Taiwan; ²Kanagawa Institute of Industrial Science and Technology (KISTEC), Taiwan

The modern electronic, ionic, and energy devices fabrication industry has been involved in the patterning of a wide range of ceramic nanostructures by various sophisticated methods, such as physical vapor deposition, chemical vapor deposition, advanced lithographic techniques, ink-jet printing, spin-coating, etc. on conducting substrates. These techniques were either requiring a vacuum system, immature material processing, non-ambient atmosphere conditions, or multiple steps of batch processing in the semiconductor industry. Mostly, vacuum-based fabrication involves solid-gas-solid materials transformation, which involves significantly high thermodynamical energies than real activation energies needed in materials processing. Again, the simplified fabrication process such as ink-jet printing, 3D printing, spin coating, etc., were involved in multi-step processes, and heating. This powder dispersion material process is not efficient in fabrication technology due to immature materials synthesis techniques. Therefore, most of today's synthesis as well as fabrication techniques are not environment friendly, as well as economically viable, which is a severe concern for a future sustainable society. Herewith, we are proposing a single-step soft solution processing for direct patterning of various functional ceramics (TiO₂, BaTiO₃, Al₂O₃, ZrO₂, ZrTiO₄, etc.) nanostructures onto a conducting substrate(s). A modified Pechini's process has been adopted for cationic metal(s) polymer complex solution, which is used as an electrolyte. These electrolytes have been locally activated by using a strong electric field by a high precision automated three-dimensional motorized sharp metal probe and are directly micropatterned on various conducting substrates (silicon, stainless steel, aluminum foil, transparent conductive films, etc.). The localized in-situ plasma formation, as well as redox reactions of metal(s) ion enabling in forming thin-films of various ceramic nanostructures. This one-step fabrication process of direct patterning is very cost-effective and environmentally benign because of the copious amount of materials used and no use of pre/post-processing materials techniques in various printing. Various physicochemical analyses were carried out on the micro-patterned functional ceramic nanostructures. Furthermore, mechanical, and electro-analytical studies were performed to explore the functional behavior of the micropatterns.

7:00 PM *NM05.16.03

Chirality, Stability and Optoelectronics from Nanoscale Interface of Hybrid Perovskites Angshuman Nag; Indian Institute of Science Education and Research (ISSER) Pune, India

Colloidal nanocrystals show surface-related phenomena owing to the small size of the crystal. In difference, hybrid perovskites like (C₄H₉NH₃)₂PbI₄ have layered crystal structure with periodic nanoscale interfaces between the inorganic {PbI₄}²⁻ and organic C₄H₉NH₃⁺ layers. Chemical compositions of such nanoscale interfaces can be designed in numerous ways yielding novel functionalities.^{1,2} For example, chirality can be induced from the organic sublattice to the inorganic one through such nanoscale interfaces. Consequently, the optical and optoelectronic properties, that mainly contributed by the inorganic sublattice, also attains chirality.³ In this talk, I will discuss about the composition-structure-chiroptic property relationships in a series of chiral 2D, 1D, and 0D hybrid perovskite derivative systems. The non-centrosymmetric crystal structure also leads to reasonably strong optical nonlinearity and has potential for bulk photovoltaics. I will also discuss about how non-covalent interactions (cation-p or halogen-halogen) can make such low-dimensional hybrid metal halides completely water-stable for years.^{4,5} It is to be noted here that the nanoscale physical and chemical properties mentioned here is governed by low-dimensional crystal structure of the hybrid system, and not by the size of the crystal.

1. Sheikh, T.; Nawale, V.; Pathoor, N.; Phadnis, C.; Chowdhury, A.; Nag, A. *Angew. Chem. Int. Ed.* **2020**, *59*, 11653.

2. Nag, A. "Plenty of Room" at the Interface of Hybrid Metal Halide Perovskite Single Crystals. *Nano Lett.* **2021**, *21*, 8529.

3. Sheikh, T.; Maqbool, S.; Rajput, P. R.; Mandal, P.; Nag, A. Effect of Chirality on the Optical Properties of Layered Hybrid Perovskite R- and S-methylbenzylammonium lead iodide. *Chem. Commun.* **2022**, *58*, 7650.

4. Sheikh, T.; Maqbool, S.; Mandal, P.; Nag, A. Introducing Intermolecular Cation-p Interactions for Water-Stable Low Dimensional Hybrid Lead Halide Perovskites. *Angew. Chem. Int. Ed.* **2021**, *60*, 18265.

5. Chakraborty, R.; Sheikh, T.; Nag, A. Iodine-Iodine Interactions Suppressing Phase Transitions of 2D Layered Hybrid (I-(CH₂)_n-NH₃)₂PbI₄ (n = 2-6) Perovskites. *Chem. Mater.* **2022**, *34*, 288.

7:30 PM NM05.16.04

Pathways of Formation of Colloidal Semiconductor Magic-Size Clusters and Quantum Dots Kui Yu; Sichuan University, China

Colloidal semiconductor binary II-VI metal (M) chalcogenide (E) quantum dots (QDs) have been produced together with magic-size clusters (MSCs), sometimes. For the past 40 years, the QD synthesis has been carried out largely as an empirical art, with limited knowledge about the pre-nucleation stage. Recently, we proposed a two-pathway model to explain the co-production of QDs and MSCs. The LaMer model of the classical nucleation theory (CNT) can be used to understand one pathway, which involves the formation of monomers (Mo) and fragments (Fr) that lead to the nucleation and growth of QDs. The other pathway is multi-step based, which involves the self-assembly of M and E precursors, followed by the M-E covalent bond formation inside each assembly that results in the precursor compound (PC) of MSCs. The PC can transform to ultra-small QDs with enhanced particle yield, binary MSCs, and alloy MSCs. Our studies bring an in-depth understanding of the coproduction of QDs and MSCs and of the prenucleation stage of QDs, contributing to the promotion of the solution synthesis of functional nanomaterials from an empirical art to a science.

References

1. Yu, K. et al Transformations Among Colloidal Semiconductor Magic-Size Clusters. *Acc. Chem. Res.* **2021**, *54*, 776–786.
2. Yu, K. et al A Two-pathway model for the evolution of colloidal compound semiconductor quantum dots and magic-size clusters. *Adv. Mater.* **2022**, *34*, e2107940.

7:45 PM NM05.16.05

Structural and Magnetic Characterization of Transition Metals-Substituted Cobalt Ferrite Nanocrystals Alondra Cartagena Toledo, Charielice M. Bonilla Pérez and Yarilyn Cedeno-Mattei; University of Puerto Rico at Ponce, Puerto Rico

Cobalt ferrite is a versatile nanomaterial that has been explored due to its wide range of potential applications (technological, biomedical, environmental, among others). It can be synthesized using different methods such as hydrothermal, sol-gel, and coprecipitation. Ferrites at the nanoscale can be optimized by tuning characteristics such as: crystal size, composition, cationic distribution, and shape. The cationic distribution and interaction between them will affect and modify the magnetic properties of ferrites. Accordingly, transition metal (TM) ions were used to substitute Co ions according to $TM_xCo_{1-x}Fe_2O_4$, where 'x' corresponds to the atomic fraction of transition metal. Ni^{2+} and Mn^{2+} were selected as Co substituting species based on the similitude between the ionic radius of Co^{2+} (0.82 Å), Ni^{2+} (0.78 Å), and Mn^{2+} (0.91 Å). In addition to the ionic radii, the coordination number and magnetic nature of Mn and Ni species were considered. All ferrite samples were prepared by the conventional coprecipitation method. Mn and Ni atomic fractions, 'x', between 0.0 and 1.0 were evaluated.

Introducing foreign ions into the spinel structure will cause a change into the superexchange interaction (occurs via intermediate atoms or ions, in this case, oxygen). It is a type of inter-particle interaction that allows the magnetic moments in a solid to interact with each other. This interaction will vary depending on the element causing changes into the magnetic properties (coercivity and saturation magnetization) due to different electronic configuration. X-Ray Diffraction (XRD) and Vibrating Sample Magnetometry (VSM) results confirmed the strong influence of crystal size, ferrite composition, and lattice distortion on the corresponding magnetic properties at the nanoscale. XRD results suggest there was no remarkable crystal growth by increasing the incorporation of Mn ions. The substitution of Co^{2+} by Mn^{2+} caused an increment in the cubic lattice parameter, 'a', attributed to the slightly larger ionic radius of Mn respect to Co. In contrast, the incorporation of Ni ions systematically increased the average crystallite size from 11 nm to 18 nm. A decrease in lattice parameter was observed as the Ni atomic fraction increased. It is attributed to the smaller ionic radius of Ni respect to Co. VSM results show a tail in coercivity and saturation magnetization. Coercivity values between 14 and 2583 Oe, as well as saturation magnetization values ranging between 10 and 67 emu/g were obtained.

8:00 PM DISCUSSION TIME

SYMPOSIUM NM06

2D Layered Materials and Heterostructures—Ubiquitous Electronics, Sensors, Multifunctional Coatings and More
November 28 - December 7, 2022

Symposium Organizers

Aida Ebrahimi, The Pennsylvania State University
Nicholas Glavin, Air Force Research Laboratory
SungWoo Nam, University of California, Irvine
Won Il Park, Hanyang University

Symposium Support

Bronze
MilliporeSigma

* Invited Paper
+ Distinguished Invited

SESSION NM06.01: Synthesis of 2D Materials and Heterostructures I
Session Chairs: Nicholas Glavin and David Moore
Monday Morning, November 28, 2022
Hynes, Level 2, Room 207

10:30 AM NM06.01.01

Scalable Synthesis of Large 2D Transition Metal Layered Hydroxides Lu Ping, Gillian E. Minarik, Hongze Gao and Xi Ling; Boston University, United States

The first successful exfoliation of graphene¹ in 2004 sparked a dramatic increase in 2D materials research and the repertoire of 2D materials family has since expanded. 2D crystals composed of single or few atomic layers display unique chemical, optical, and electronic properties compared with their bulk 3D counterparts due to the quantum confinement effect at the 2D limit². Two-dimensional (2D) transition metal layered hydroxides (TM-LHs), a class of materials composed of transition metal centers sandwiched between layers of coordinating hydroxide anions have attracted considerable interest for their potential in developing clean energy source^{3,4} and storage technologies^{5,6}. However, 2D TM-LHs with desired large domain size for electronic devices are not achieved yet, owing to challenges in reproducibility of 2D morphology and long-range crystallinity, limiting the domain size of previously reported samples (<5 μm)^{7,8}. Here, we report repeatable synthesis of 2D α -Ni(OH)₂ crystals of lateral size $\sim 20 \mu\text{m}$ with ~ 8 atomic layers derived from a condition-controlled hydrothermal process. A detailed investigation on the influence of the most critical synthetic conditions, including soaking temperature, starting pH, and cooling rate, on the domain size, crystal phase, and morphology was performed, providing mechanistic insights into the formation of 2D α -Ni(OH)₂ under hydrothermal reaction conditions. Moreover, the optical band gap energy of the synthesized 2D Ni(OH)₂ flakes is extrapolated as 2.55 eV from optical absorption measurements, suggesting the insulating nature. Electrical measurements further confirmed the insulating nature of the synthesized flakes, and a dielectric strength of up to 3.2 MV/cm was collected on a 4.9 nm flake (~ 6 atomic layers), which makes it a promising candidate for gate dielectric materials for 2D FETs devices. Furthermore, the crystal fields and orientations of 3d transition metals were compared and analyzed to evaluate the applicability of this method to other 3d first-row TM-LHs. 2D Co(OH)₂ was successfully synthesized following the same pathway, promoting the hydrothermal method as a facile, generalizable method for large-scale preparation of 2D TM-LHs. This work demonstrates a scalable pathway to synthesize large 2D TM-LHs flakes from simple methods and paves the way for the fundamental physical properties study and device applications of the 2D TM-LHs.

Reference

1. Novoselov, K. S. *et al.* Two-dimensional atomic crystals. *Proc. Natl. Acad. Sci. U. S. A.* **102**, 10451–10453 (2005).
2. Tan, J., Li, S., Liu, B. & Cheng, H.-M. Structure, Preparation, and Applications of 2D Material-Based Metal–Semiconductor Heterostructures. *Small Struct.* **2**, 2000093 (2021).
3. Deng, J., Wu, F., Gao, S., Dionysiou, D. D. & Huang, L.-Z. Self-activated Ni(OH)₂ Cathode for Complete Electrochemical Reduction of Trichloroethylene to Ethane in Low-conductivity Groundwater. *Appl. Catal. B Environ.* **309**, 121258 (2022).
4. Patil, S. J. *et al.* Fluorine Engineered Self-Supported Ultrathin 2D Nickel Hydroxide Nanosheets as Highly Robust and Stable Bifunctional Electrocatalysts for Oxygen Evolution and Urea Oxidation Reactions. *Small* **18**, (2022).
5. Huang, Z. H. *et al.* An electro-activated bimetallic zinc-nickel hydroxide cathode for supercapacitor with super-long 140,000 cycle durability. *Nano Energy* **82**, 105727 (2021).
6. Wu, Y. *et al.* Rational design of cobalt–nickel double hydroxides for flexible asymmetric supercapacitor with improved electrochemical performance. *J. Colloid Interface Sci.* **581**, 455–464 (2021).
7. Yuan, S. *et al.* Tunable metal hydroxide–organic frameworks for catalysing oxygen evolution. *Nat. Mater.* **21**, (2022).
8. Liu, C., Bai, Y., Wang, J., Qiu, Z. & Pang, H. Controllable synthesis of ultrathin layered transition metal hydroxide/zeolitic imidazolate framework-67 hybrid nanosheets for high-performance supercapacitors. *J. Mater. Chem. A* **9**, 11201–11209 (2021).

10:45 AM NM06.01.03

Epitaxial Growth of Single-Crystal Hexagonal Boron Nitride Multilayers on Ni(111) Kyung Yeol Ma^{1,2}, Leining Zhang^{2,1}, Rodney S. Ruoff^{1,2,1}, Manish Chhowalla³, Feng Ding^{2,1} and Hyeon Suk Shin^{1,2}; ¹Ulsan National Institute of Science and Technology, Korea (the Republic of); ²Institute of Basic Science (IBS), Korea (the Republic of); ³University of Cambridge, United Kingdom

Large-area single-crystal monolayers of two-dimensional (2D) materials such as graphene, hexagonal boron nitride (hBN) and transition metal dichalcogenides have been grown. hBN is considered to be the ‘ideal’ dielectric for 2D-materials-based field-effect transistors (FETs), offering the potential for extending Moore’s law. Although hBN thicker than a monolayer is more desirable as substrate for 2D semiconductors, highly uniform and single-crystal multilayer hBN growth has yet to be demonstrated. Here we report the epitaxial growth of wafer-scale single-crystal trilayer hBN by a chemical vapour deposition (CVD) method. Uniformly aligned hBN islands are found to grow on single-crystal Ni(111) at early stage and finally to coalesce into a single-crystal film. Cross-sectional transmission electron microscopy (TEM) results show that a Ni₂₃B₆ interlayer is formed (during cooling) between the single-crystal hBN film and Ni substrate by boron dissolution in Ni. There are epitaxial relationships between hBN and Ni₂₃B₆ and between Ni₂₃B₆ and Ni. We also find that the hBN film acts as a protective layer that remains intact during catalytic evolution of hydrogen, suggesting continuous single-crystal hBN. This hBN transferred onto the SiO₂ (300 nm)/Si wafer acts as a dielectric layer to reduce electron doping from the SiO₂ substrate in MoS₂ FETs. Our results demonstrate high-quality single-crystal multilayered hBN over large areas, which should open up new pathways for making it a ubiquitous substrate for 2D semiconductors.

11:00 AM NM06.01.04

First Observation of Suspended AA-Stacked Hexagonal Boron Nitride Grown on GaN Substrate by Metal-Organic Chemical Vapor Deposition Seokho Moon¹, Adrien Rousseau², Francis N. Odongo¹, Youngjae Kim^{3,4}, Yunjae Park^{5,6}, Jiye Kim¹, Jaewon Kim⁷, Pierre Valvin², Jaehye Cho⁸, Feng Ding^{5,6}, Jaedong Lee³, Si-Young Choi¹, Bernard Gil², Guillaume Cassabois² and Jong kyu Kim¹; ¹Pohang University of Science and Technology, Korea (the Republic of); ²CNRS-Universite de Montpellier, France; ³Daegu Gyeongbuk Institute of Science and Technology, Korea (the Republic of); ⁴Korea Institute for Advanced Study (KIAS), Korea (the Republic of); ⁵Ulsan National Institute of Science and Technology, Korea (the Republic of); ⁶Institute for Basic Science, Korea (the Republic of); ⁷Samsung Advanced Institute of Technology, Korea (the Republic of); ⁸Jeonbuk National University, Korea (the Republic of)

Hexagonal boron nitride (h-BN), an insulating two-dimensional layered material, has attracted great attention due to its fascinating properties and promising applications across the fields of photonics, quantum optics, and electronics. Given the layered structure of h-BN, various polytypes exist with high-symmetry stacking sequences where successive layers are rotated or translated, leading to a variety of physical properties. Almost all h-BN layers, either synthesized by various growth techniques or exfoliated from h-BN crystal, exhibit the AA’-stacking sequence, in which neighboring layers are arranged such that B and N atoms alternate along the c-axis,^[1–3] due to its thermodynamic stability.^[4,5] Although theoretical and experimental research on other h-BN polytypes including Bernal (AB) BN^[5,6] and rhombohedral BN^[7] were carried out, there is virtually no experimental observation of the h-BN with AA stacking where individual layers are periodically aligned along the c-axis without translation or rotation, because it is not likely to be formed in thermodynamic point of view.

Here, we report the growth of few-layer AA-stacked h-BN on a 2-inch epitaxial gallium nitride (GaN) wafer by using metal-organic chemical vapor

deposition (MOCVD). The h-BN has a very unique feature, in which 6–7-layer h-BN with AA stacking sequence is suspended on GaN nanoneedles. The formation of the AA-stacked h-BN is confirmed by the fifth-order aberration-corrected scanning transmission electron microscopy (Cs-STEM), unique deep ultraviolet photoluminescence (PL) spectra, and density-functional theory (DFT) calculation. A triangular configuration irrespective of layer number in Low-angle annular dark-field (LAADF)-STEM image and the interlayer distance slightly larger than that of exfoliated AA' stacked h-BN in cross-sectional bright field (BF)-STEM image of the suspended h-BN film clearly show the AA stacking configuration. In addition, The band-edge phonon-assisted recombination PL spectra at 4 K reveal key fingerprints brought by the AA-stacked h-BN including the vertical translation of the bandgap, different lineshape and scattering amplitude of phonon replica, and the absence of typical defect-related emission below 5.6 eV compared to exfoliated AA' stacked h-BN, which is consistent with DFT calculations. The mechanism of the formation of such unique and unprecedented atomic stacking will be discussed with nanoscopic optical and structural characterizations and theoretical calculations.

- [1] K. Y. Ma, L. Zhang, S. Jin, Y. Wang, S. I. Yoon, H. Hwang, J. Oh, D. S. Jeong, M. Wang, S. Chatterjee, G. Kim, A.-R. Jang, J. Yang, S. Ryu, H. Y. Jeong, R. S. Ruoff, M. Chhowalla, F. Ding, H. S. Shin, *Nature* **2022**, *606*, 88.
- [2] S. M. Kim, A. Hsu, M. H. Park, S. H. Chae, S. J. Yun, J. S. Lee, D.-H. Cho, W. Fang, C. Lee, T. Palacios, M. Dresselhaus, K. K. Kim, Y. H. Lee, J. Kong, *Nat Commun* **2015**, *6*, 8662.
- [3] A.-R. Jang, S. Hong, C. Hyun, S. I. Yoon, G. Kim, H. Y. Jeong, T. J. Shin, S. O. Park, K. Wong, S. K. Kwak, N. Park, K. Yu, E. Choi, A. Mishchenko, F. Withers, K. S. Novoselov, H. Lim, H. S. Shin, *Nano Lett.* **2016**, *16*, 3360.
- [4] N. Alem, R. Erni, C. Kisielowski, M. D. Rossell, W. Gannett, A. Zettl, *Phys. Rev. B* **2009**, *80*, 155425.
- [5] S. M. Gilbert, T. Pham, M. Dogan, S. Oh, B. Shevitski, G. Schumm, S. Liu, P. Ercius, S. Aloni, M. L. Cohen, A. Zettl, *2D Mater.* **2019**, *6*, 021006.
- [6] A. Rousseau, P. Valvin, W. Desrat, L. Xue, J. Li, J. H. Edgar, G. Cassabois, B. Gil, *ACS Nano* **2022**, *16*, 2756.
- [7] M. Chubarov, H. Pedersen, H. Högberg, Z. Czigány, M. Garbrecht, A. Henry, *Chem. Mater.* **2015**, *27*, 1640.

11:15 AM NM06.01.05

MOCVD Growth of Large-Scale TMDCs and Heterostructures Suhee Jang, Wonjun Chang and Won Il Park; Hanyang University, Korea (the Republic of)

Heterostructures (HSs) based on atomically thin two-dimensional transition metal chalcogenides (TMDCs) have gained increasing attention due to their chemical stability and unique interactions between materials, together with the applications in many fields such as electronics and optics. Despite the advances in the fabrication of vertical HSs through multiple steps of mechanical exfoliation and transfer, this approach suffers from fabricating 2D HSs on a large scale and precise control of the size, position, and the number of layers. In this study, we studied the large-area direct growth of TMDCs and their HSs (e.g., graphene/TMDC and TMDC/TMDC) using metal-organic chemical vapor deposition. We found that two mechanisms appear in the formation of heterogeneous structures: (1) epitaxial growth within the grain and (2) selective growth on defects. The formation of a two-dimensional heterogeneous structure with unique characteristics was verified by analyzing the structural, bonding, and interaction characteristics between various types of graphene/TMDCs and TMDC/TMDC HSs. We confirmed that the 2D HSs with abrupt heterointerface were uniformly grown over large-area using SEM, TEM, Raman, and PL analysis. By analyzing how the crystallinity of TMDC grown directly on the graphene changes depending on the crystalline direction of the graphene, we confirmed the epitaxial growth tendency in the process of forming heterogeneous structures. In particular, the TMDC HSs selectively grown on graphene defects possess ion channels comprising (i) van der Waals interlayer gaps for optimal Li⁺ extraction and (ii) negatively charged vertical inlets for cation attraction.

11:30 AM NM06.01.06

Two-Dimensional Indium Nitride Realized via Confinement Heteroepitaxy Furkan Turker¹, Chengye Dong¹, Zachary Trdinich¹ and Joshua A. Robinson^{1,1,2}; ¹The Pennsylvania State University, United States; ²Two-Dimensional Crystal Consortium, United States

Novel confinement techniques facilitate the formation of non-layered two-dimensional (2D) III-V semiconductors, e.g. GaN, with thickness-dependent optoelectronic properties. However, a gap lies in the experimental demonstration of 2D InN with its true atomic structure. Here, we demonstrate the formation of highly crystalline bilayer InN, at the bilayer quasi-free-standing epitaxial graphene (QFEG)/SiC (0001) interface via intercalation of metallic In and subsequent nitridation. Our scanning transmission electron microscopy (STEM) studies show that 2D InN is epitaxial to the underlying SiC (0001) with R3M space group, verified via Density Functional Theory. Furthermore, vertical transport studies on QFEG/2D InN/n-SiC demonstrate that the ohmic behavior of the QFEG/SiC transforms into tunneling junction via 2D InN intercalation. Importantly, electron energy loss spectroscopy (EELS) and transport analyses demonstrate that the band gap of 2D InN is ~2 eV, which is significantly larger than the one of bulk InN (0.7 eV). These results suggest strong quantum confinement effects for the InN in 2D limit.

SESSION NM06.02: Synthesis of 2D Materials and Heterostructures II

Session Chairs: Nicholas Glavin and SungWoo Nam

Monday Afternoon, November 28, 2022

Hynes, Level 2, Room 207

1:30 PM *NM06.02.01

Wafer-Scale Growth and Integration of Two-Dimensional Transition Metal Dichalcogenides Minsu Seol, Min Seok Yoo, Junyoung Kwon, Sang Won Kim and Kyung-Eun Byun; SAIT, Samsung Electronics, Korea (the Republic of)

So far, two-dimensional (2D) transition metal dichalcogenides (TMDs) have received great attention for their use as channels in electronic devices. The confined charges in atomically thin channels allow improved electrostatic gate control and reduced short-channel effects, which could facilitate continued transistor scaling. However, the integration of 2D TMDs with Si CMOS platforms has been a great challenge owing to the lack of high-throughput and large-scale production, proper characterization and integration processes for TMDs.

In this talk, we present our works on the growth, characterization, and integration of 2D TMDs. First, we demonstrate high-throughput production of 6–8-inch wafer-scale monolayer MoS₂ and WS₂ via a pulsed metalorganic chemical vapor deposition technique, using Mo(CO)₆, W(CO)₆, and (C₂H₅)₂S₂ as precursors. Periodic interruption of the precursor supply allowed successful regulation of secondary nucleation even under high growth rates, and as a result, wafer-scale monolayer MoS₂ and WS₂ were obtained within 12 min. Second, we present non-destructive characterization of wafer-scale TMDs. In particular, we used spectroscopic ellipsometry for analyzing both TMD and the dielectric thin film deposited on TMD at the same time. Third, we exhibit integration of TMDs as a channel of the field-effect transistor (FET). Thanks to the well-stitched continuous structure over the whole wafer, the as-grown TMDs can be transferred onto any desired substrate with minimal degradation via reliable wafer-scale de-bonding and bonding processes. On the basis of

our transferred TMD films, we demonstrate 8-inch wafer-scale batch fabrication of FETs via standard photolithography, and they showed uniform electrical performance with > 90% yield. Additional challenges on materials growth and device fabrication will also be discussed.

2:00 PM NM06.02.02

Wafer-Scale Synthesis of Monolayer 2D Polymers for Ultrathin Membranes and Heterostructures [Yu Zhong](#)¹, Baorui Cheng² and Jiwoong Park²; ¹Cornell University, United States; ²The University of Chicago, United States

2D polymers are made by cross-linking molecules into a 2D network which can be viewed as organic analogs of 2D atomic crystals. They are not only a new library of 2D building blocks for making vdW heterostructures but also offer unlimited structural tunability on the molecular level. In this talk, I will introduce a synthetic approach to synthesizing monolayer 2D polymers on a large scale. This approach incorporates key features necessary for scalable and facile processing, including large-area synthesis, ambient growth conditions, and compatibility with established patterning and integration methods. The 2D polymer films can serve as the thinnest semipermeable membranes, which deliver a record high osmotic power generation density. Furthermore, I will show the programmed assembly of hybrid organic-inorganic 2D heterostructures with monolayer precision. This approach allows for integrating versatile molecular building blocks into layered nanomaterials to develop ultrathin electronic devices.

Ref. *Science* **2019**, *366*, 1379-1384

2:15 PM *NM06.02.03

Synthesis and Application of Multifunctional Two-Dimensional Materials [Jun Lou](#); Rice University, United States

Two-dimensional (2D) materials, such as Graphene, h-BN and MoS₂, are promising candidates in a number of advanced functional and structural applications, owing to their exceptional electrical, optical, electrochemical and mechanical properties. Scalable growth of high quality 2D materials is crucial for their adoption in technological applications the same way the arrival of high-quality silicon single crystals was to the semiconductor industry. While CVD growth of wafer-scale monolayer graphene and TMDs has been demonstrated, considerable challenges still remain. In this talk, we first demonstrate the importance of real-time monitoring 2D crystal growth morphology as an underpinning for understanding, diagnosing and controlling the CVD process and environment for 2D material growth [1]. Using a micro-CVD setup facilitated by machine learning algorithms, the mapping of MoS₂ crystal shapes in the growth parameter space “encodes” a wealth of information, the deciphering of which led to better understanding of the fundamental CVD growth mechanism of 2D TMDs.

Next, we show that high quality ultrathin h-BN films are impervious to oxygen diffusion even at high temperatures and can serve as high-performance oxidation resistant coatings for nickel up to 1100°C in oxidizing atmospheres. The corrosion passivation performance in Na₂SO₄ solution of bare and h-BN coated copper indicates that such h-BN films could effectively suppress the anodic dissolution of copper. Inspired by these successes, we demonstrate the

[1] J. Zhang, F. Wang, V. Shenoy, M. Tang, J. Lou, *Towards Controlled Synthesis of 2D Crystals by Chemical Vapor Deposition (CVD)*, *Materials Today*, Vol. 40, 132-139, 2020.

[2] K. Zuo, W. Wang, A. Deshmukh, S. Jia, H. Guo, R. Xin, M. Elimelech, P.M. Ajayan, J. Lou, Q. Li, *Multifunctional Nanocoated Membranes for High-rate Electrothermal Desalination of Hypersaline Waters*, *Nature Nanotechnology*, Vol. 15, 1025-1032, 2020.

2:45 PM BREAK

3:15 PM NM06.02.04

2D Molybdenum Dichalcogenides by Atomic Layer Deposition [Raul Zazpe](#)^{1,2}, Jaroslav Charvot¹, Ludek Hromadko^{1,2}, Hanna Sopha^{1,2}, Jhonatan Rodriguez-Pereira^{1,2}, Filip Bures¹ and Jan Macak^{1,2}; ¹University Pardubice, Czechia; ²Central European Institute of Technology, Czechia

2D semiconductor transition metal dichalcogenides have attracted considerable attention due to their layered structure, suitable band gap, electrochemically active unsaturated edges and relatively good stability against photocorrosion. These properties result promising for different applications including, Li-ion batteries, photocatalysis and hydrogen evolution reaction (HER). Apart from the widely studied 2D MoS₂, 2D selenide and telluride equivalents, MoSe₂ and MoTe₂, have recently gained considerable interest due to their higher electrical conductivity, wider inter-layer distance and narrower bandgap as compared to MoS₂, high surface area and close to zero Gibbs free energy edges for hydrogen adsorption.

Unlike sulfide dichalcogenides, the lack of Se and Te precursors have prevented the synthesis of selenide and telluride dichalcogenides by ALD. In order to surpass such impediment, we present a set of novel in-house synthesized Se and Te compounds, which were successfully combined with commercial Mo precursor to synthesize MoSe₂ and MoTe₂ by ALD [1-5]. The as-deposited ALD MoSe₂ and MoTe₂ on substrates of different nature were extensively characterized by different techniques, which confirmed the chemical composition and revealed the growth of 2D flaky nano-crystalline MoSe₂ and MoTe₂. In parallel, MoSe₂ and MoTe₂@TiO₂ nanotube layers (TNTs) heterostructures were fabricated in a simple and fast fashion to explore and exploit the MoSe₂ and MoTe₂ photo- and electrocatalytic properties. TNTs act as excellent photoactive supporting material providing a high surface area, unique directionality for charge separation, and highly effective charge collection.

The presentation will introduce and describe the synthesis of the 2D Mo dichalcogenides, the corresponding physical and electrochemical characterization and encouraging results obtained in HER [4,5], photocatalysis [4-6] and Li-ion batteries [7].

[1] R. Zazpe et al, *FlatChem* (2020) 21 100166

[2] J. Charvot et al, *Chempluschem* (2020) 85 576

[3] J. Charvot et al, *RSC Adv.* (2021) 11 22140

[4] R. Zazpe et al, *ACS Appl. Nano Mater.* (2021) 3 12 12034

[5] R. Zazpe et al, *Appl. Mater. Today* (2021) 23 101017

[6] M. Motola et al, *Nanoscale* (2019) 11 23126

[7] H. Sopha et al *FlatChem* (2019) 17 100130

3:30 PM *NM06.02.05

Bio-Inspired Curved Artificial Vision Using Ultrathin Layered Materials [Dae-Hyeong Kim](#)^{1,2}; ¹Institute for Basic Science, Korea (the Republic of); ²Seoul National University, Korea (the Republic of)

Although recent efforts in device designs and fabrication strategies have resulted in meaningful progresses to the goal of the high-performance artificial vision, significant challenges still exist in developing a miniaturized and highly-sensitive artificial vision that enables the wide field-of-view (FoV) and/or

amphibious imaging. This is mainly due to bulky, heavy, and multiple lenses employed in the conventional wide-angle imaging devices. In this talk, inspired by structural and functional features of the natural visions, novel wide FoV artificial visions using curved ultrathin image sensor arrays are introduced. The bio-inspired artificial visions offer the wide FoV, a miniaturized module size, minimal optical aberrations, a deep depth-of-field, an enhanced light sensitivity, and an amphibious imaging capability in a simple integrated device format. Theoretical analyses in conjunction with imaging demonstrations have corroborated the validity of the proposed concept. These bio-inspired artificial visions are expected to provide new opportunities for the advanced electronics and robotics.

4:00 PM NM06.02.06

CVD Synthesis and Properties of Monolayer Lateral Heterostructures and Janus TMDs [Andrey Turchanin](#); Friedrich Schiller University Jena, Germany

Lateral heterostructures (LH) of monolayer transition metal dichalcogenides (TMDs), as well as Janus TMDs, open broad avenues for the engineering of novel nanomaterials for both basic research and applications. In this presentation, I will give an overview of our recent progress on the one-pot synthesis based on chemical vapor deposition, characterization of the basic properties, and device applications of these 2D materials including such systems as LH MoSe₂-WSe₂ and Janus SeMoS, and other related systems. A particular focus will be placed on the correlation between their structural and electronic/photonic properties. It will be also demonstrated how these advanced 2D materials can be employed in a variety of devices including phototransistors, rectifiers, photodetectors, ambipolar and anti-ambipolar transistors, electroluminescent light emitters, etc.

- [1] E. Najafidehaghani, Z. Gan, A. George, U. Kaiser, F. Eilenberger, A. Turchanin et al., "1D p-n junction electronic and optoelectronic devices from transition metal dichalcogenide lateral heterostructures grown by one-pot chemical vapor deposition synthesis", *Adv. Funct. Mater.* 31 (2021) 2101086.
- [2] D. Beret, I. Paradisanos, Z. Gan, A. George, J. Biskupek, U. Kaiser, A. Turchanin, B. Urbaszek et al., "Exciton spectroscopy and diffusion in MoSe₂-WSe₂ lateral heterostructures encapsulated in hexagonal boron nitride", *arXiv* (2022) 2204.07351.
- [3] Z. Gan, I. Paradisanos, Johannes Biskupek, Ute Kaiser, A. V. Krashennikov, B. Urbaszek, A. George, A. Turchanin et al., "Chemical vapor deposition of high optical quality large area monolayer Janus transition metal dichalcogenides", *arXiv* (2022) 2205.04751.

4:15 PM NM06.02.09

High Yield, Bottom-Up/Top-Down CVD Synthesis of 2D Layered Metal Selenides—A Promising Class of Materials for Applications in Electronics and Electrochemistry [Gilbert D. Nessim](#); Bar Ilan University, Israel

Since the excitement about graphene, a monolayer of graphite, with its 2010 Nobel Prize, there has been extensive research in the synthesis of other non-carbon few/mono-layers exhibiting a variety of bandgaps and semiconducting properties (e.g., n or p type). The main approaches to deposit few/monolayers on a substrate are: (a) bottom-up synthesis from precursors using chemical vapor deposition (CVD) or (b) top-down exfoliation (liquid or mechanical) of bulk layered material.

Here we show a combined bottom-up and top-down approach where (a) we synthesize in one step high yields of bulk layered materials by annealing a metal in the presence of a gas precursor (sublimated selenium from selenium powder) using chemical vapor deposition (CVD) and (b) we exfoliate and deposited (dropcast or Langmuir Blodgett) few/mono-layers on a substrate from a sonicated mixture of our material in a specific solvent. It is interesting to note that, besides the structure being 2D layered, the properties of the nanomaterials synthesized slightly differ from the materials with the same stoichiometry synthesized using conventional chemical methods (e.g., solvothermal).

In this talk, we will discuss the chemical synthesis, the very extensive characterizations, and the lessons we learned in making multiple metal selenides (Ag-Se, Cu-Se, W-Se, Mo-Se, etc.). We will see how we integrated these new materials into sensors, as functional coatings, and into electrochemical devices (see selected published papers below).

R. Konar and G.D. Nessim*

A Mini-Review Focusing on Ambient-Pressure Chemical Vapor Deposition (AP-CVD) Based Synthesis of Layered Transition Metal Selenides for Energy Storage Applications

Materials Advances, Vol. 3, 4471-4488, April 2022

M. Sadipani, R. Konar, H. Sclar, J. Grinblat, M. Talianker, M. Tkachev, X. Wu, A. Kondrakov, G.D. Nessim, and D. Aurbach*

Stabilizing High-Voltage Lithium-Ion Battery Cathodes Using Functional Coatings of 2D Tungsten Diselenide

ACS Energy Letters, 7, 1383-1391, March 2022

A. Moumen, R. Konar, D. Zappa, E. Teblum, I. Perelshtein, R. Lavi, S. Ruthstein, G.D. Nessim*, and E. Comini*

Robust Room-Temperature NO₂ Sensors from Exfoliated 2D Few-Layered CVD-Grown Bulk Tungsten Di-selenide (2H-WSe₂)

ACS Applied Materials and Interfaces, 13, 3, 4316-4329, Jan. 2021

R. Konar, S. Das, E. Teblum, A. Modak, I. Perelshtein, J.J. Richter, A. Schechter*, and G.D. Nessim*

Facile and Scalable Ambient Pressure Chemical Vapor Deposition-Assisted Synthesis of Layered Silver Selenide (β-Ag₂Se) on Ag foil as an Oxygen Reduction Catalyst in Alkaline Medium

Electrochimica Acta, 370, 137709, Jan. 2021

SESSION NM06.03: 2D Material Electronics and Photonics I

Session Chairs: Kiyoung Jo and Won Il Park

Tuesday Morning, November 29, 2022

Hynes, Level 2, Room 207

8:00 AM NM06.03.01

Van der Waals Contact Interface and Band Alignments Study of Bi Contacts on Variable Transition Metal Dichalcogenides [Seong Yeoul Kim](#), Xinglu Wang, Roy Joy and Robert M. Wallace; The University of Texas at Dallas, United States

The issue of high contact resistance (R_c) has remained an unsolved issue for transition metal dichalcogenides (TMDs) and it became more significant in sub-nano channel lengths. While the recent findings on bismuth (Bi) metal contacts on MoS₂ have reported remarkably low contact resistance and high on-current density, these results are not yet fully established.[1] It is necessary to first understand the interfacial chemistry and the band alignment between Bi and TMDs because the Fermi level may vary depending on the interfacial properties.[2]

In this work, the interface properties of Bi/TMDs (MoS₂, MoSe₂, WS₂, and WSe₂) are investigated by utilizing an *in-situ* ultrahigh vacuum (UHV) cluster

system including X-ray photoelectron spectroscopy (XPS) and an e-beam evaporator.[3] Metallization and interface analysis was conducted within UHV conditions to allow the precise investigation of the Bi/TMDs interface made possible by suppressing the effect of contamination from the ambient. Band alignments were investigated by using XPS core-level shift and valence band maximum spectra of the Bi/TMDs interface. The Fermi levels of the Bi/TMD interfaces are formed close to the conduction band minimum for all investigated TMDs after Bi deposition. Additionally, it was found that bonding associated with interfacial reaction of Bi/TMDs was below the limit of XPS detection (< 1 at. %). Based on the atomic force microscopy (AFM), Bi metal follows a Volmer-Weber (VM) growth mode consistent with a lack of interaction between Bi and TMDs. Ultimately, these results show that Bi forms van der Waals (vdW) interface with n-type contact properties on variable TMDs semiconductor materials.

Add acknowledgment for NEWLIMITS and NSF project: "This work was supported in part by NEWLIMITS, a center in nCORE, a Semiconductor Research Corporation (SRC) program sponsored by NIST through award number 70NANB17H041, and the National Science Foundation (DMR 2002741).

[1] Shen et al. *Nature* **2021**, 593 (7858), 211–217.

[2] Wang et al. *ACS Appl. Mater. Interfaces* **2021**, 13 (13), 15802–15810.

[3] Wallace, R.M. *ECS. Trans.* **2008**, 16 (5) 255-271.

8:15 AM NM06.03.02

Strain-Resilient Field-Effect Transistors Based on Wrinkled Graphene/MoS₂ Heterostructures [Hyunchul Kim](#), Kevin Zhao and Arend M. van der Zande; University of Illinois at Urbana-Champaign, United States

Realizing stretchable field-effect transistors (FETs) and integrated circuitry requires new materials that are simultaneously strain resilient yet have high electronic mobility. Two-dimensional (2D) materials are one of the most promising materials for flexible and stretchable FETs because of their extraordinary mechanical, electrical, and optical properties. For example, transistors from 2D heterostructures or with ALD grown gates on flexible substrates have been shown to accommodate strains of up to 1.5% and have device mobilities of 233 cm²/Vs^{1.2}. Meanwhile, leveraging principles of wrinkling, crumpling or kirigami have all been used to impart stretchability of well above 100% by leveraging the ultra-low bending modulus of 2D materials to minimize strain through 3D deformation³. These strategies have been used to demonstrate stretchable devices like electrodes, photodetectors, or strain sensors. The next step with enormous potential for high mobility yet stretchable integrated circuitry is to bring the 3D deformation with 2D heterostructures together to demonstrate stretchable FETs which leverage all the strengths of 2D materials.

In this work, we fabricated stretchable FETs on a soft substrate where 2D materials formed all the active electronic layers. Patterned graphene forms the electrodes and local gate, while MoS₂ serves as the transistor channel. ALD HfO₂ is the dielectric layer and also serves as the mechanical support. The entire structure is less than 15 nm thick, so it has a very low bending modulus, enabling easy 3D deformations that minimize strain. To achieve stretchability, we leveraged the principles of self-assembled wrinkling and kirigami. Transferring the device onto the pre-strained elastomer and releasing the strain induces wrinkling of the devices with wavelengths of 7.7 microns, smaller than the transistor channel. We patterned kirigami cuts onto the electrodes and between devices, which serve to help relieve strain and guide the wrinkling patterns. We examined the electrical properties of the FETs under compression and stretching. The initial experimental data shows that before applying strain, the FET on current was 0.14 μA, while the on/off current ratio was ~10³. The current device performance is limited by high contact resistance, which has been shown can be much lower in graphene-contacted MoS₂ devices on hard substrates, and can likely be improved. As a very promising sign, the electrical performance did not change for up to 21% compression.

This work provides a new strategy of strain-resilient 2D heterostructure FETs, which opens up new applications like strain-resilient integrated circuits, as well as fundamental investigations of how heterogeneous strain will affect electron transport.

References

1. Lee, G. H. *et al.* Flexible and transparent MoS₂ field-effect transistors on hexagonal boron nitride-graphene heterostructures. *ACS Nano* **7**, 7931–7936 (2013).

2. Zhu, W. *et al.* Black Phosphorus Flexible Thin Film Transistors at Gighertz Frequencies. *Nano Lett.* **16**, 2301–2306 (2016).

3. Zhang, Z., Tian, Z., Mei, Y. & Di, Z. Shaping and structuring 2D materials via kirigami and origami. *Mater. Sci. Eng. R Reports* **145**, 100621 (2021).

8:30 AM *NM06.03.03

Highly Stretchable van der Waals Thin Films for Adaptable and Breathable Electronics [Xiangfeng Duan](#); University of California-Los Angeles, United States

The integration of electronic systems with irregular, soft objects is of increasing interest for many emerging electronic applications including ubiquitous electronics for internet of things and bioelectronics intimately interacting with living organisms. The conventional electronics are typically made from hard inorganic materials cannot be easily integrated with soft biological structures due to the intrinsic mismatch in mechanical properties, permeability and environmental adaptability. Although the hard inorganic materials can be made flexible in the ultrathin membrane format, they are hardly stretchable and fundamentally incapable of forming conformal interface with irregular geometries with non-zero Gaussian curvatures due to the topological limitations. Here we will discuss a unique design of highly stretchable van der Waals thin films (VDWTFs) for microscopically adaptable membrane electronics. Assembled from solution-processable two-dimensional (2D) nanosheets, the VDWTFs feature bond-free vdW interactions among the staggered nanosheets, with a sliding and rotation degree of freedom between neighbouring nanosheets to ensure extraordinary mechanical flexibility, stretchability, malleability and adaptability to irregular surface topographies. Additionally, the staggered nanosheet architecture features a highly interconnected percolation network of nanometre-scale channels with an excellent permeability. The freestanding VDWTFs show an excellent mechanical match with soft biological tissues, naturally adapting to microscopic topographies and directly merging with dynamically changing organisms with highly conformal interfaces, endowing living organisms with electronic functions, including leaf-gate and skin-gate VDWTF transistors. With excellent conformability and adaptability to skin textures, the skin transistors allow for high fidelity monitoring skin potentials and electrophysiological signals with excellent signal-to-noise ratio and superior immunity to motion artifacts. The VDWTFs thus define a new platform of electronic membranes readily adaptable to different form factors, and can open up exciting opportunities for many emerging electronic applications.

9:00 AM NM06.03.04

Insertion of a Layered Electride for Low-Resistivity 2D Semiconductor Contacts Fouad Kaadou, Mohammad Rafiee Diznab, Ethan Gysbertsen, Adrian Rumson, Erin Johnson and [Jesse Maassen](#); Dalhousie University, Canada

A major challenge for 2D semiconductor-based devices is achieving low-resistance, barrier-free metal contacts. Parasitic contact resistance can significantly degrade device performance, including switching speed and power consumption. Some of the issues hindering the formation of ohmic contacts to 2D semiconductors include: weak van der Waals bonding to many metals leading to tunneling barriers, strong chemical bonding to metals that significantly alter the electronic states of the atomically-thin semiconductor, and Fermi-level pinning. New strategies to form low-resistivity ohmic contacts that eliminate Schottky/tunneling barriers are needed, such as phase engineering [1], Fermi-level depinning [2] and semimetal contacts [3].

In this talk, we focus on the insertion of a 2D electride between the metal and the 2D semiconductor, to promote charge transfer and eliminate the potential barrier to facilitate electron transport [4]. Layered electrides are ionic solids with loosely-bound conducting electrons located in the interstitial regions between the atomic layers, and on their surfaces when exfoliated to form 2D electrides. Using density-functional theory we explore the electronic properties of semiconductor-electride-metal heterojunctions, with an emphasis on monolayer MoS₂ as the 2D semiconductor, Ca₂N as the 2D electride and gold as the metal. An analysis of the charge transfer, exfoliation energy, band structure and electrostatic potential demonstrates that Ca₂N donates nearly all of its surface charge resulting in the metallization of the MoS₂ and a barrier-free contact. By comparison, the electride-free MoS₂-Au contact displays a large tunneling barrier and Fermi-level pinning. These findings suggest that introducing a layered electride in the 2D semiconductor-metal interface is a promising strategy towards achieving ultralow-resistivity, ohmic contacts.

- [1] Kappera, Voiry, Yalcin, et al., Nat. Mater. **13**, 1128 (2014).
- [2] Farmanbar and Brocks, Phys. Rev. B **91**, 161304 (2015).
- [3] Shen, Su, Lin, et al., Nature **593**, 211 (2021).
- [4] Kaadou, Maassen, and Johnson, J. Phys. Chem. C **125**, 11656 (2021).

Acknowledgements: this research is supported by NSERC, SRC and Compute Canada.

9:15 AM NM06.03.05

Hydroxide Vapor Phase Deposition for Low-Defect-Density 2D TMDs Growth Yi Wan and Li Lain-Jong; The University of Hong Kong, Hong Kong

Two-dimensional (2D) semiconducting monolayer materials such as transition metal dichalcogenides (TMDs) MX₂ (M=Mo, W; X=S, Se) are considered promising as channel materials to extend the Moore's Law in the post-Si era. Recently, wafer-scale single-crystal TMD monolayers have been demonstrated by chemical vapor deposition (CVD), which shows homogeneous electrical performance due to the decreased grain boundaries. Nevertheless, the abundant point defects in TMD monolayers like vacancies and impurities introduced during the synthetic processes limit their electrical quality. Thus, innovative endeavors on growth reactions to realize low-defect-density growth are urgently needed. Here, we reported that adopting extremely pure metal precursor in combination with hydroxide vapor phase deposition (OHVPD) enables the growth of low-defect-density TMD monolayers. The PL spectra show the superior optical quality of OHVPD-TMD monolayers (i.e., WS₂ and MoS₂) with higher peak energies and narrower FWHM compared to conventional CVD samples. The scanning tunneling microscopy (STM) images show that the transferred OHVPD-TMD monolayers have one order of magnitude lower defect density compared to samples prepared by the CVD method. The field effect transistor (FET) devices based on OHVPD-WS₂ monolayers reach a peak electron mobility of ~200 cm²/Vs at room temperature, and ~800 cm²/Vs at 15K. The on-state current of short-channel-length devices (100 nm) reaches a value of ~400 mA/mm. Based on STM and device measurements, the as-grown high-quality TMD monolayer films are less susceptible to subsequent film transferring and device fabricating processes.

9:30 AM BREAK

10:00 AM NM06.03.06

Electrical Transparency of Tungsten Disulphide-Graphene Heterostructures Sayanti Samaddar, Olga Kazakova, Alexander Tzalenchuk and Cristina E. Giusca; National Physical Laboratory, United Kingdom

Vertical heterostructures of tungsten disulphide on graphene (WS₂/graphene) are relevant for optoelectronic, spintronic, and valleytronic devices, all requiring detailed knowledge of the electronic interface properties.

We investigated the electrical nature of such interfaces without conventional device integration and associated fabrication that is often detrimental to the structural integrity of monolayer materials, by using a four-probe scanning tunnelling microscope. The measurements provided important insights into the electrical transport properties of monolayer WS₂ synthesized by chemical vapour transport on epitaxial graphene, featuring a Schottky-type contact between the metallic probe and WS₂, but Ohmic transport in the WS₂/graphene heterostructure, and a highly transparent interface evidenced by the measured four-probe resistances.

The electrical transparency of the WS₂/graphene interface is of considerable significance to a range of applications related to ultrathin electronics and optoelectronics seeking to overcome challenges associated with achieving optimized and reliable contacts to atomically thin materials.

10:15 AM NM06.03.07

Intrinsic High-Order Ionic Layered Superlattices in 2D DJ-Phase Oxide Perovskites Kyungjune Cho¹, Haena Yim¹, Takhee Lee², Ji-Won Choi¹ and Seungjun Chung¹; ¹Korea Institute of Science and Technology, Korea (the Republic of); ²Seoul National University, Korea (the Republic of)

2D layered materials have emerged as promising materials due to their attractive physical properties[1]. In addition, the vast variety of promising 2D material candidates, including graphene, h-BN, TMCs, MAXenes, and nanosheet family, and the ability to realize heterostructures with a high degree of freedom provides us huge opportunities freeing up the structural design of functional devices and their material combinations. These attractive properties offer tremendous possibilities to expand the functionalities of 2D material-based devices for various future applications.[1]

In this sense, novel 2D layered materials are always welcome. Recently, layered oxide perovskites have gained huge attention by means of their high stability and tunability. Additionally, an oxide perovskite monolayer was successfully exfoliated by ion-exchange methods from Dion-Jacobson (DJ) phase (A_{n-1}B_nX_{3n+1}) bulk perovskite crystals, immersing themselves into the world of 2D materials. Innately, perovskite materials are highly tunable in their compositions. Not only that, as well as other 2D layered materials, low-dimensional perovskite layers are expected to exhibit novel physics, which means that exploring their intrinsic material properties is highly demanded.[2]

In this presentation, we will introduce unprecedented intrinsic high-order ionic layered superlattices in 2D DJ-phase oxide perovskites. We have confirmed that these exfoliated 2D DJ perovskite layers are compatible with the conventional 2D vdW platform by successfully picking them up with the PDMS stamp which has been conventionally used in the field of 2D vdW materials. Owing to the design freedom of the vdW platform, we could fabricate vertical junction devices with 2D DJ-phase oxide perovskite Sr₂Nb₃O₁₀ flakes employing graphene (Gr) electrodes which are known to be suitable for investigating intrinsic properties of materials due to their passive nature. From the systematic measurement of electronic properties of the vertical junction devices, the intrinsic high-order ionic layered superlattices in few-layer SNO flakes could be found. During the ion-exchange process for exfoliation, there will always be few-layer flakes that are not fully exfoliated. Thus, this a few-layer SNO flake (HSNO) has alternative layers composed of positively charged proton layers (H⁺) and negatively charged SNO layers (Sr₂Nb₃O₁₀) forming ionic layered superlattices. These superlattices can introduce quantum wells along the z-axis, resulting in the resonance tunneling through the quantum wells formed through the vertical junction and huge charge trapping in the energy well structures. Additionally, unprecedented memristor devices and artificial synaptic devices will be shown as potential applications by virtue of quantum wells and their charge trapping behavior from the intrinsic ionic superlattices. We believe that our results pave the way for understanding emerging 2D layered DJ oxide perovskite materials.

Ref

[1] K. Cho et al. ACS Nano, 13, 9, 9713-9734

[2] A. C. Ricciardulli et al. Nat. Mater. 2021, 20, 1325-1336

10:30 AM NM06.03.08

Graphene Heterostructure Field Effect Transistors Encapsulated by Isotopically Pure Hexagonal Boron Nitride Aroop K. Behera¹, Ayaz Ali^{2,3}, C. Thomas Harris^{4,4}, Douglas V. Pete^{4,4}, Eli Janzen¹, Ozhan Koybasi², James H. Edgar¹, Branson D. Belle⁵ and Suprem R. Das^{1,1}; ¹Kansas State University, United States; ²SINTEF DIGITAL, Norway; ³University of Sindh, Pakistan; ⁴Sandia National Laboratories, United States; ⁵SINTEF, Norway

Graphene, an atomically layered 2D semimetal has been a prime focus of study in the last two decades for its use as a channel material in field effect transistors (FETs) due to its high carrier mobility originating from graphene's linear band dispersion. Recent studies have also shown that enhanced electrical mobility, low contact resistance and ballistic transport can be achieved in graphene by fabricating one-dimensional edge contacts in a graphene channel encapsulated by hexagonal boron nitride (hBN)¹. Furthermore, low frequency noise (LFN) studies on such hBN encapsulated graphene heterostructure field effect transistors (HFETs) have shown ultra-low noise in carrier rich regions². However, most of the studies on graphene-based HFETs incorporate hexagonal boron-nitride with naturally occurring boron isotopic concentration. Boron, a constituent element in hBN, has two isotopes, ¹⁰B and ¹¹B. Naturally occurring hBN has a boron constituent ratio of 20% ¹⁰B and 80% ¹¹B. In this presentation we will discuss a comparative study that we performed on both the temperature dependent transport and LFN of single layer graphene (SLG) HFETs encapsulated in natural and isotopically pure hBN. Understanding the carrier physics of SLG in different isotopically pure encapsulated geometries will aid us in engineering low-noise graphene-based FETs for future digital electronics.

1. Wang, Lei, et al. "One-dimensional electrical contact to a two-dimensional material." *Science* 342.6158 (2013): 614-617.

2. Behera, Aroop K., et al. "High-Performance and Ultralow-Noise Two-Dimensional Heterostructure Field-Effect Transistors with One-Dimensional Electrical Contacts." *ACS Applied Electronic Materials* 3.9 (2021): 4126-4134.

10:45 AM *NM06.03.09

Synthesis of 2D Crystals and Structures for Electronic Devices Xi Ling and Kyungjune Cho; Boston University, United States

Developing new type of 2D materials remains highly desirable given their versatile properties and applications in electronic nanodevices. Conventional 2D materials such as graphene and transition metal dichalcogenides, whose bulks are van der Waals layered materials, have been realized through top-down mechanical exfoliation and self-limited in plane growth using chemical vapor deposition (CVD), thanks to the weak binding among layers in their bulks. Consequently, unprecedented properties have been observed in the monolayers compared to the bulk. However, the majority materials in nature, are atomically bonded in three-dimensional mode. Synthesizing atomically thin 2D crystals of these materials using the conventional synthetic strategies remains a great challenge. In addition, although progress has been made in successful synthesis of a library of van der Waals 2D materials such as graphene and transition metal dichalcogenides, there are still a lot of members in the family underexplored. Driven by the need of high crystallinity and scalable 2D materials for electronic devices, as well as a low thermal budget growth condition enabling the 3D monolithic integration, our group focuses on developing effective synthesis strategies for various 2D crystals with diverse electronic properties. In this talk, I will first introduce the atomic substitution method where we chemically convert layered metal chalcogenides such as MoS₂, WS₂ and GaS, to ultrathin metal nitrides such as MoN_x, WN_x, and GaN. The thickness of the obtained nitrides can be tuned by using different number of layers of metal chalcogenides, providing a platform for the study of their fundamental properties at quantum region and for the application in nanoelectronics devices. Moreover, the conversion process is investigated using transmission electron microscope, where edge and surface conversion are observed, leading to the formation of lateral and vertical heterostructures. Particularly, a mask-assisted method is used to obtain the MoS₂-MoN_x-MoS₂ lateral junction, where metallic MoN_x serves as the electrode for semiconducting MoS₂ field-effect transistors (FET). Second, I will introduce our recent work on realizing ultrathin 3d metal hydroxides with long-range ordering. The UV-vis. spectra bandgap and electrical measurements show the semiconductor behavior of the materials.

11:15 AM *NM06.03.10

Two-Dimensional and Layered Material Inks for Additive Electronics Manufacturing David Estrada^{1,2}; ¹Boise State University, United States; ²Idaho National Laboratory, United States

This talk will describe recent progress in formation of 2D and layered nanomaterial inks for additive electronics manufacturing using various material jetting printers such as inkjet, aerosol jet, and plasma jet printers.

SESSION NM06.04: 2D Material Electronics and Photonics II

Session Chairs: Nicholas Glavin and SungWoo Nam

Tuesday Afternoon, November 29, 2022

Hynes, Level 2, Room 207

1:30 PM NM06.04.01

Giant Intrinsic Spin-Orbit Torque and Device Applications Based on Topological van-der-Waals Ferromagnetic Metal Fe₃GeTe₂ Kaixuan Zhang¹, Jingyuan Cui¹, Hyun-Woo Lee² and Je-Geun Park¹; ¹Seoul National University, Korea (the Republic of); ²Pohang University of Science and Technology, Korea (the Republic of)

Electrical control of magnetic states triggers a new era of spintronic applications and device functionalization. Compared to conventional purely magnetic-field-controlled information switching, the current-controlled device in principle allows much lower power consumption, larger memory density, and higher speed. Current-driven spin-orbit torque is an emergent key player for the so-called spin-orbit-torque-Magnetic-Random-Access-Memory (SOT-MRAM), which is the most promising commercial on-chip magnetic-RAM in the near future¹. Unfortunately, the switching current density and power dissipation remain too high for conventional magnet/heavy-metal based SOT-MRAM¹, stimulating us to exploit new systems with large SOT.

We thus turn attention to the van-der-Waals (vdW) magnetic materials, which have rapidly flourished to become star members in the field of two-dimensional materials and device physics recently²⁻⁷. Among all the magnetic vdW materials, Fe₃GeTe₂ is special as the only topological ferromagnetic vdW metal⁸, exhibiting well-behaved ferromagnet behavior with a coercivity of several kOe, and prominent anomalous Hall effect with large Berry curvature. Spin-orbit torque and anomalous Hall effect share similar physical scenarios associated with spin-orbit coupling, rendering Fe₃GeTe₂ an ideal

testbed for large intrinsic spin-orbit torque.

Here we discover^[9] that an in-plane current can tune the hard ferromagnet state to a soft one in the nanoscale Fe₃GeTe₂ devices, through a substantial reduction of coercive field. This surprising finding is possible because the in-plane current produces a highly unusual type of gigantic spin-orbit torque for single Fe₃GeTe₂ itself without an additional heavy-metal layer. Such spin-orbit torque is directly related to the large Berry curvature and so its band topology. Furthermore, we demonstrate a working model of new magnetic memory based on the principle of our discovery in Fe₃GeTe₂, where highly efficient nonvolatile switching and multi-level states by the tiny current are achieved^[10]. Taking one more step forward, we develop this memory model to an all-vdW classic three-terminal SOT device, where the magnetic information can be written by spin-orbit torque and read by tunneling magnetoresistance separately. Our surprising discovery and systematic investigation depict a prototypical route from fundamentally important physics to practical device applications, and also bring the exciting magnetic vdW materials to sharpen spintronics.

[1] M. Cubukcu, O. Boulle, M. Drouard, K. Garello, C. O. Avci, I. M. Miron, J. Langer, B. Ocker, P. Gambardella, G. Gaudin, *Appl. Phys. Lett.* **2014**, *104*, 042406.

[2] J. G. Park, *J. Phys. Condens. Matter* **2016**, *28*, 301001.

[3] J. U. Lee, et. al., *Nano Lett.* **2016**, *16*, 7433.

[4] B. Huang, G. Clark, E. Navarro-Moratalla, D. R. Klein, R. Cheng, K. L. Seyler, D. Zhong, E. Schmidgall, M. A. McGuire, D. H. Cobden, W. Yao, D. Xiao, P. Jarillo-Herrero, X. Xu, *Nature* **2017**, *546*, 270.

[5] C. Gong, L. Li, Z. Li, H. Ji, A. Stern, Y. Xia, T. Cao, W. Bao, C. Wang, Y. Wang, Z. Q. Qiu, R. J. Cava, S. G. Louie, J. Xia, X. Zhang, *Nature* **2017**, *546*, 265.

[6] K. S. Burch, D. Mandrus, J. G. Park, *Nature* **2018**, *563*, 47.

[7] S. Kang, K. Kim, B. H. Kim, J. Kim, K. I. Sim, J.-U. Lee, S. Lee, K. Park, S. Yun, T. Kim, A. Nag, A. Walters, M. Garcia-Fernandez, J. Li, L. Chapon, K.-J. Zhou, Y.-W. Son, J. H. Kim, H. Cheong, J.-G. Park, *Nature* **2020**, *583*, 785.

[8] K. Kim, J. Seo, E. Lee, K. T. Ko, B. S. Kim, B. G. Jang, J. M. Ok, J. Lee, Y. J. Jo, W. Kang, J. H. Shim, C. Kim, H. W. Yeom, B. Il Min, B. J. Yang, J. S. Kim, *Nat. Mater.* **2018**, *17*, 794.

[9] K. Zhang, S. Han, Y. Lee, M. J. Coak, J. Kim, I. Hwang, S. Son, J. Shin, M. Lim, D. Jo, K. Kim, D. Kim, H.-W. Lee, J.-G. Park, *Adv. Mater.* **2021**, *33*, 2004110.

[10] K. Zhang, Y. Lee, M. J. Coak, J. Kim, S. Son, I. Hwang, D. S. Ko, Y. Oh, I. Jeon, D. Kim, C. Zeng, H.-W. Lee, J.-G. Park, *Adv. Funct. Mater.* **2021**, *31*, 2105992.

1:45 PM NM06.04.02

Spin Selective Robust Layered Heterostructure in Oxygen Evolution Reaction Yang Li^{1,1}, Yan Wang¹, Andrew F. May², Jong Chan Kim³, Hu Young Jeong³, Jieun Yang⁴ and Manish Chhowalla¹; ¹University of Cambridge, United Kingdom; ²Oak Ridge National Laboratory, United States; ³Ulsan National Institute of Science and Engineering, Korea (the Republic of); ⁴Kyung Hee University, Korea (the Republic of)

Quantum phenomena such as spin polarization and topological protected states have been widely studied for electronics. Spin polarized, and topological protected active sites also offer opportunities for reducing thermodynamic potential and kinetics of reactions as well as increasing the lifetimes of catalysts. However, quantum effects have yet to be widely exploited in catalysis because the electrochemical environment in which reactions are performed destroys quantum coherence. Thus, catalytically active quantum materials that are protected by electrochemically and quantum mechanically transparent layers are required. Here we show two-fold enhancement in the oxygen evolution reaction (OER) current (at 1.7 V versus reversible hydrogen electrode) through spin selective catalysis using two dimensional Fe_{3-x}GeTe₂ (FGT) as the catalyst and graphene or hexagonal boron nitride (hBN) as the quantum coherent protective layer. FGT is typically highly unstable in air and electrolytes used for OER, but our experiments show that the reaction can be performed when protected by catalytically inactive graphene or hBN layers. Our results show that spins in FGT can be polarized in the presence of a magnetic field at room temperature, and spin information at active sites can be transmitted through graphene and hBN with thicknesses of up to 6 nm. This electrochemical and spin information transparency of graphene and hBN allows the reaction to proceed in a kinetically enhanced manner on the surface of these layers – even though they are not catalytically active for the OER reaction. Our results provide new insight into spin selective catalysis and on the electrochemical and quantum transparency of graphene and hBN, which could lead to integration of quantum materials for catalysis.

2:00 PM NM06.04.03

Printable Memristive Neurons from Solution-Processed Hexagonal Boron Nitride Lckai Song¹, Pengyu Liu¹, Jingfang Pei¹, Songwei Liu¹, Yang Liu¹, Shuo Gao² and Guohua Hu¹; ¹The Chinese University of Hong Kong, China; ²School of Instrumentation Science and Optoelectronics, Beihang University, China

Biological neurons capable of performing complex non-linear operations with high efficiency inspire recent rapid progress in neuromorphic computing. The realization of artificial neurons is key to enabling neuromorphic electronics and systems. Current approaches may, however, lead to complicated device and circuitry designs as well as switching operations. Herein we demonstrate simplified leaky integrate-and-fire (LIF) neurons with printable volatile threshold switching memristors from solution-processed hexagonal boron nitride (hBN).

We start with hBN exfoliation via liquid-phase exfoliation, followed by ink formulation in isopropanol/2-butanol. The ink is finely tuned to suit versatile printing techniques, such as maskless inkjet printing and high-speed slot-die coating. The memristors are then printed by sandwiching the hBN as the switching medium between silver electrodes. We note that this approach can allow wafer-scale memristor array printing at high speed. The printed hBN memristors exhibit a volatile threshold switching with a threshold voltage of ~1 V, an on/off ratio of >10⁶, and a switching speed of <1 μs, arising from the ultrafast formation and disruption of silver ion filaments in the hBN switching medium. With such an ultrafast volatile threshold switching characteristic, the memristors are then integrated into a simple resistor-capacitor (RC) charging circuit to construct artificial LIF neurons. Notably, the forming-free nature of the memristors endows the simple circuit design, while the high switching ratio eases the peripheral circuit burden to distinguish the conductance change. When fed with electrical spikes of variable frequencies, the capacitor would charge and accumulate the spikes to a membrane potential beyond the threshold voltage of the memristor and lead the memristor to switch and “fire” an electrical spike. After the firing, the memristor would spontaneously reset due to a potential drop, preparing for subsequent firings. Besides, the LIF neurons can perform spatial summation of multiple temporal inputs, allowing us to implement logic operations of the spikes. The leaky integrate-and-fire and spatiotemporal behaviours successfully mimic the biological neurons and, importantly, fit well into activation functions that could be exploited as non-linearity to artificial neural networks to solve non-linear problems. As such, we integrate our LIF neurons into a three-layer spiking neural network by simulation, and after training, achieve classification of MNIST hand-written digits with an accuracy of >95%.

Our approach can be scaled to wafer-scale manufacturing, and the printed volatile threshold switching memristors can be conveniently integrated as simplified artificial neurons for neuromorphic computing. The printing method can also be potentially integrated into advanced CMOS and MEMS

technologies for neuromorphic circuits with high-level integration and complexity. We believe our neurons provide various possibilities for neuromorphic technology development, from intelligent microprocessors and system-on-plastic to biomimetic electronics, sensors, and even brain-computer interfaces.

2:15 PM *NM06.04.04

2D/3D Heterostructures for Low-Power Logic and Memory Devices [Deep M. Jariwala](#); University of Pennsylvania, United States

The isolation of a growing number of two-dimensional (2D) materials has inspired worldwide efforts to integrate distinct 2D materials into van der Waals (vdW) heterostructures. While a tremendous amount of research activity has occurred in assembling disparate 2D materials into “all-2D” van der Waals heterostructures and making outstanding progress on fundamental studies, practical applications of 2D materials will require a broader integration strategy. I will present our ongoing and recent work on integration of 2D materials with 3D electronic materials to realize logic switches and memory devices with novel functionality that can potentially augment the performance and functionality of Silicon technology. First, I will present our recent work on gate-tunable diode¹ and tunnel junction devices² based on integration of 2D chalcogenides with Si and GaN. Following this I will present our recent work on non-volatile memories based on Ferroelectric Field Effect Transistors (FE-FETs) made using a heterostructure of MoS₂/AlScN^{3,4} and I also will present our work on Ferroelectric Diode devices also based on thin AlScN.⁵

References:

1. Miao, J.; et al. Jariwala, D., *Nano Letters* **2020**, *20* (4), 2907-2915.
2. Miao, J.; et al. Jariwala, D., *arXiv preprint arXiv:2111.06396* **2021**.
3. Liu, X.; et al. Jariwala, D., *Nano Letters* **2021**, *21* (9), 3753-3761.
4. Kim, K.-H.; et al. Jariwala, D., *arXiv preprint arXiv:2201.02153* **2022**.
5. Liu, X.; et al. Jariwala, D., *Applied Physics Letters* **2021**, *118* (20), 202901.

2:45 PM NM06.04.05

Two-Dimensional Violet Phosphorus—A p-Type Semiconductor for (Opto)Electronics [Antonio Gaetano Ricciardulli](#)¹, Ye Wang¹, Sheng Yang² and Paolo Samori¹; ¹University of Strasbourg, France; ²Max Planck Institute for Solid State Research, Germany

The surge of two-dimensional (2D) materials overwhelmed the field of conventional semiconductors for (opto)electronics, owing to their unique electrical and optical features, condensed in the atomic limit.¹ In this framework, novel paradigms in fundamental and applied research have been unveiled by the assembly of 2D *p-n* junctions. However, the landscape of 2D semiconductors is currently dominated by *n*-type materials. In contrast, only few *p*-type 2D species have been reported so far. As a result, the lack of diversity severely hinders the full exploitation of 2D systems beyond the state-of-the-art. To respond to the demanding quest for novel 2D materials endowed with *p*-type characteristics, we have synthesized high-quality *p*-type 2D violet phosphorus (VP) in a feasible fashion.³ First, a strategy to grow pure VP crystals on the centimeter-scale was designed. Then, thin VP sheets were delaminated via sonication-assisted liquid-phase exfoliation. The yielded flakes exhibited thicknesses down to the monolayer limit and large lateral size up to 2 μm. Our method enabled the successful development of VP-based thin-film electronics. Field-effect transistors (FETs) exhibit distinct *p*-type transport characteristics with air stable hole mobilities up to 2.25 cm² V⁻¹ s⁻¹ and a high *I*_{on}/*I*_{off} ratio of 10⁴ at room temperature, exceeding most of the reported thin-film 2D materials. Proof-of-concept photodetectors displayed a photoresponsivity of 10 mA W⁻¹ and a response time down to 0.16 s. Finally, VP was integrated as PMOS working material in a complementary metal oxide semiconductor (CMOS) logic circuit, which output an outstanding voltage gain of ~17. Our work predestines VP as an enticing and versatile *p*-type candidate for next-generation more-than-Moore (opto)electronics.

¹A. G. Ricciardulli et al., *Nat. Mater.* **2021**, *20*, 1325

²Q. He et al., *ACS Nano* **2019**, *13*, 12294

³A. G. Ricciardulli et al., *J. Am. Chem. Soc.* **2022**, *144*, 3660

3:00 PM BREAK

3:30 PM NM06.04.06

Observation of Intrinsic Avalanche Multiplication in Ambipolar WSe₂ and its Application to Low-Subthreshold Swing Impact Ionization Transistors [Jaeyoung Kim](#)¹, Kyunjune Cho², Keehoon Kang¹ and Takhee Lee¹; ¹Seoul National University, Korea (the Republic of); ²Korea Institute of Science and Technology, Korea (the Republic of)

Recently there has been a growing number of studies that have incorporated the merits of avalanche multiplication with two-dimensional (2D) materials in the form of avalanche photodetectors and transistors [1,2]. Previous studies have mainly focused on developing high-performance devices with unipolar semiconductor as the active material. However, fundamental understanding of the multiplication process in ambipolar materials is required for optimizing material selection, as well as establishing novel architectures. In ambipolar WSe₂ field-effect transistors (FETs), two distinct phenomena of ambipolar transport and avalanche multiplication can occur, and both exhibit secondary rise of output current at high lateral voltage. We distinguished between these two competing phenomena using the method of channel length modulation [3]. In long channel length devices, minority charge carriers are accumulated near the drain side of the channel, and the critical voltage is modulated in equal amounts as the gate voltage. In contrast, short channel length devices undergo carrier multiplication at high lateral voltages, and the breakdown voltage is insensitive to change in the gate voltage. Through the use of electrostatic gating, we extracted multiplication characteristics from both electron- and hole-induced avalanche multiplication in WSe₂ and compared the results with conventional semiconductors. Furthermore, we demonstrate the implementation of intrinsic multiplication process into device application of impact ionization transistor through selective channel gating, which enables low subthreshold swing to overcome the thermionic limitation of transistors. Our study provides a simple and robust method to examine carrier multiplication in ambipolar materials and will foster the development of novel, atomically thin electronic devices utilizing avalanche multiplication.

[1] J. Seo et al., *Adv. Sci.* **8**, 2102437 (2021).

[2] A. Gao et al., *Nature Nanotech.* **14**, 217 (2019).

[3] J. Kim et al., *ACS Nano*, **16**, 5376 (2022).

3:45 PM NM06.04.07

Switchable Operation Mode and Deterministic Light-to-Voltage Conversion in a Two-Dimensional Semiconductor/Metal Heterostructure [Mingde Du](#), Xiaopi Cui, Luojun Du, Bin Zhang and Zhipei Sun; Aalto University, Finland

van der Waals (vdW) heterostructures based on two-dimensional (2D) materials have been extensively studied for optoelectronic applications, and most of the reported devices work with a sole mechanism. The emerging metallic 2D materials provide us with new options for building functional vdW heterostructures via rational band engineering design. Here we investigate a vdW semiconductor/metal heterostructure, in which the electron affinity of the semiconductor and the work function of the metal are elaborately selected. Electrical characterization verifies the exceptional rectifying effect of the

heterostructure diode. Further photocurrent mapping indicates that the photoresponse mechanism is switchable between photovoltaic device and phototransistor, or in another word, the metal plays an alternative role. Specifically, this device works in a photovoltaic manner under reverse bias, whereas it turns to a phototransistor under forward bias. Interestingly, the open-circuit voltage (V_{oc}) generated under photovoltaic operation is independent of gate voltage (V_{gate}), indicating that the metallic 2D material on the bottom plays a role of effective dielectric screening. This V_{gate} -independent photovoltage is quite useful for an on-chip light-to-voltage conversion, where a deterministic voltage is expected under constant light illumination. Our results demonstrate the valuable application of 2D metals in functional devices, as well as switchable operation mode and deterministic light-to-voltage conversion with 2D semiconductor/metal heterostructure.

4:00 PM *NM06.04.08

Designing Novel Electronic and Optoelectronic Properties in 2D Layered Materials by Strain and Plasmonic Engineering [Nai-Chang Yeh](#), Duxing Hao, Wei-Hsiang Lin and Daniel Anderson; California Institute of Technology, United States

In this talk we will show that valley-Hall transistors based on nanoscale strain-engineered monolayer graphene can exhibit quantum oscillations as well as quantum valley-Hall and quantum anomalous Hall effects (QVHE and QAHE) in the absence of any external magnetic fields. These findings associated with strain-induced giant pseudo-magnetic fields (PMFs) can pave the way towards realizing low-dissipative topological electronics, spintronics and optoelectronics in graphene with controlled strain superlattices. We will also demonstrate that the use of plasmonic vortices and backgate voltages can dramatically enhance the photoluminescence intensity and the degree of valley polarization in monolayer transition-metal dichalcogenide (TMD) WS_2 at room temperature. This approach can be further employed to develop novel opto-valleytronic/spintronic devices for topological photonic applications. Finally, we will describe new strategies to optimize the electronic and photonic properties of monolayer TMDs by post-CVD processing.

4:30 PM NM06.04.09

Complex Strain Profiles and Electronic Mobility Enhancement in Two-Dimensional Monolayers Using Patterned Stressor Layers [Yue Zhang](#)¹, Mohammad A. Hossain¹, Kelly Hwang¹, Joe Maduzia¹, Paolo Ferrari¹, Tara Pena², Stephen M. Wu^{2,2} and Arend M. van der Zande^{1,3}; ¹University of Illinois Urbana Champaign, United States; ²University of Rochester, United States; ³University of Illinois at Urbana-Champaign, United States

Recently, strain has emerged as a means to control material properties on an unprecedented scale. Two-dimensional materials (graphene and other van der Waals materials) are ideal “ultrastrength” materials systems for tuning properties via strain: they host rich quantum behavior, offer exquisite access to strain manipulation in individual atomic layers, and sustain enormous strains. Yet, most techniques for generating strains, like templated substrates, nanoscale bubbles, microscale wrinkling, or nanoindentation can apply large or localized strains, but are difficult to pattern or design. Moreover, many applications of strain engineering, such as mobility enhancement and directed exciton diffusion are limited due to the specialized substrates used in most of these methods. A recent promising trend borrows from the decades old techniques from the semiconductor industry using deposited stressor layers to generate tensile or compressive bi-axial strain on 2D materials on hard substrates[1], enabling new methods of 2D strain engineering that are compatible with device engineering and CMOS technology.

Here we explore the mechanical boundary conditions and shape affect the strain induced in the 2D material by deposited stressors, and how the induced inhomogeneous strains affect the optical and electronic properties of the material. First, we used e-beam lithography to deposit patterned oxide stressors (30 to 80 nm thick MgO) on top of large, continuous exfoliated monolayer molybdenum disulfide (MoS_2). We explored different shapes (squares, triangles, circles, etc.) of the stressors and out-of-plane boundary conditions, with smallest feature down to sub-50 nm. We employed hyperspectral Raman mapping to get spatial maps of the characteristic in-plane and out-of-plane phonon modes of MoS_2 , then measured the position dependent peak shifts to extract the local strain and doping profile of the MoS_2 near localized strains. The MgO stressor induces tensile strain in the MoS_2 monolayer of up to 0.8%, and we observed a large, shape dependent strain gradients of $> 0.2\%/\mu m$ near the edge of stressor, leading to complex strain profiles under and near the stressors. Using photoluminescence mapping, we found that the patterned tensile strain induces position dependent shifts in the bandgap of > 60 meV, with the bandgap closely following the patterned strain profile. Using finite element analysis (FEA) simulations, we explored how interfacial boundary conditions and stressor shape determine the resulting strain profiles, giving the potential for designable strain profiles.

Next, inspired by the strain-based mobility enhancement in silicon transistors, we investigated how strain engineering with the stressors to improve the performance in monolayer MoS_2 -based field effect transistors (FETs). Preliminary data shows significant mobility enhancements of $> 2x$, though we are still working to deconvolve the relative contributions from strain, doping and dielectric screening created by the stressor layers. These results point to a promising strategy new strategy device-compatible strain engineering of electronic and quantum properties in 2D materials.

Reference

- [1] Azizmanesh, Ahmad, et al. "Uniaxial and biaxial strain engineering in 2D MoS_2 with lithographically patterned thin film stressors." *Applied Physics Letters* 118.21 (2021): 213104.
- [2]. Michail, Antonios, et al. "Optical detection of strain and doping inhomogeneities in single layer MoS_2 ." *Applied Physics Letters* 108.17 (2016): 173102.

4:45 PM NM06.04.10

Large-Scale Characterization of 2D Material Flakes—Automation, Shape Parameters and a Route to Standardization Thales Fernandes¹, Helio Chacham¹, Joyce Santos¹, Mariana Prado², Elisangela Silva-Pinto³, Luiz Cancado¹ and [Bernardo R. Neves](#)¹; ¹University Federal-Minas Gerais, Brazil; ²UFOP, Brazil; ³IFMG, Brazil

The imminent 2D materials revolution will require industrial-scale quantities of well characterized flakes, which are the preferred morphology for many applications such as smart paints, composites, cements and others. The large-scale production of such flakes is a rapidly evolving field, with remarkable improvements in several comminution processes like liquid-phase exfoliation. However, massive production also requires massive characterization, which, unfortunately, has advanced in a much slower pace, creating a bottleneck for widespread industrial applications. In the present work, we bring a new methodology based on measurement automation and well-defined shape parameters that efficiently characterizes statistically-relevant 2D material quantities ($> 10,000$ flakes) and brings meaningful information about their representative morphology, including the effects of several production parameters with the use of an intuitive representation system [1-3]. More specifically, using graphene and talc as representative 2D materials, we demonstrate a semi-automated atomic force microscopy (AFM) protocol that rapidly reveals the precise morphology of tens of thousands of flakes [1]. In addition to conventional size parameters (flake area, volume and thickness), we propose a set of dimensionless shape parameters that correctly map to actual and relevant flake dimensions: three pertinent size parameters (thickness, maximum and minimum calipers) normalized by the cube root of flake volume [2, 3]. The statistical distributions of all parameters are thoroughly analyzed, unveiling the effects of typical production steps (centrifugation and different comminution processes) [2,3]. For example, flake thickness-wise, centrifugation leads to more symmetrical shapes, but, unexpectedly, it also leads to more asymmetrical length-wise shapes [2, 3]. Finally, we also propose a three-dimensional representation system – topological vectors – that enable a straightforward, yet precise, visualization and comparison of any set of parameters for different samples [3]. More important than their specific findings for each 2D system investigated in these three studies [1-3], it is their demonstration of a general and robust analysis framework that stands out as their most relevant contribution. The easiness of implementation of the automated AFM protocol coupled with the

breadth of the proposed shape parameters and the topological vectors representation system create a simple, yet powerful, characterization path for thorough and straightforward representation and comparison of any 2D material flake system. In other words, these three works [1-3] pave the way to a feasible route towards standardization of the morphological characterization of 2D material flakes.

References:

- [1] Thales F. D. Fernandes *et al.*, A semi-automated general statistical treatment of graphene systems, *2D Mater.* **7** 025045 (2020).
- [2] Helio Chacham *et al.*, Controlling the morphology of nanoflakes obtained by Liquid-Phase Exfoliation: implications for the mass production of 2D Materials, *ACS Appl. Nano Mater.* **3** 12095–12105 (2020).
- [3] Joyce C. C. Santos *et al.* Topological vectors as a fingerprinting system for 2D-material flake distributions, *npj 2D Materials and Applications* **5** 51 (2021).

SESSION NM06.05: Poster Session I: 2D Layered Materials and Heterostructures

Session Chairs: Nicholas Glavin and Won Il Park

Tuesday Afternoon, November 29, 2022

8:00 PM - 10:00 PM

Hynes, Level 1, Hall A

NM06.05.01

Metal-Graphene Interface in Evaporative-Deposition Growth of Various Metals on Graphene Zhien Wang, Haozhe Wang, Jiadi Zhu, Xudong Zheng and Jing Kong; Massachusetts Institute of Technology, United States

Graphene, the first member in 2D materials family, has very unique electrical, optical and mechanical properties, which opens up vast opportunities for applications. The understanding of metal-graphene interface is crucial for many research and applications, but hasn't been understood thoroughly due to the difficulty in characterization. Here we observed that when depositing 8-15 nanometers metal onto CVD (chemical vapor deposition) grown graphene, for certain types of metal there is a change in optical contrast compared to the area without graphene underneath, but for others such change is not noticeable. In this work we carried out various investigations to understand the reasons behind the phenomena and explored their potential applications.

NM06.05.02

Infrared Photodetectors Based on van der Waals Materials Wei Yan¹, Brett C. Johnson^{2,3}, Kenneth Crozier² and James Bullock²; ¹The University of Melbourne, Australia; ²MELBOURNE UNIVERSITY, Australia; ³RMIT University, Australia

Optoelectronic devices that collect or emit photons in the short-wave infrared (SWIR, 1.4–3 μm) band are used in fields such as imaging, thermophotovoltaics, and optical communication. Presently, these application spaces are dominated by materials such as $\text{In}_x\text{Ga}_{1-x}\text{As}$ and $\text{Hg}_{1-x}\text{Cd}_x\text{Te}$, which have been engineered over decades to provide near-unity quantum efficiencies. Despite the maturity of these technologies, there are still fundamental roadblocks intrinsically associated with the use of three-dimensional (3D) semiconductors. In SWIR photodetectors, these limitations impose tradeoffs between sensitivity and cost or size. As such, there is significant interest in the exploration of alternative materials with the potential to overcome such limitations. Recently, a suite of two-dimensional (2D) van der Waals materials with bandgaps in the short-, mid- and long-wave IR regions have demonstrated surprisingly high figures-of-merit for photodetection.

The self-terminated, layered structure of van der Waals materials introduces fundamental advantages for IR optoelectronic devices. These are mainly associated with the potential for low noise while maintaining high internal quantum efficiency when reducing IR absorber thicknesses. In this study, we introduce a new van der Waals material candidate, zirconium germanium telluride (ZrGeTe_4), to a growing family of promising IR van der Waals materials.

We find the bulk form ZrGeTe_4 has an indirect band edge around ~ 0.5 eV, in close agreement with previous theoretical predictions. This material is found to be stable up to 140 $^\circ\text{C}$ and shows minimal compositional variation even after >30 days of storage in the humid air.

We demonstrate a simple proof-of-concept broad spectrum photodetectors with responsivities $R(\lambda)$ above 0.1 AW^{-1} across both the visible and short-wave infrared wavelengths. This corresponds to a specific detectivity D^* of $\sim 10^9 \text{ cm Hz}^{1/2} \text{ W}^{-1}$ at $\lambda = 1.4 \mu\text{m}$ at room temperature ($V_{\text{SD}} > \pm 0.5 \text{ V}$, $V_{\text{G}} = 0 \text{ V}$). These values are remarkably high, especially considering the infancy of this material's exploration. These devices show a linear photoresponse vs illumination intensity relationship over ~ 4 orders of magnitude, and fast rise/fall times of ~ 50 ns, also verified by a 3 dB roll-off frequency of 5.9 MHz. Laser beam induced current (LBIC) analysis reveals that the device behaves as a set of two opposing photodiodes, whereby current can be collected at either side of the device by choosing the V_{SD} bias direction.

As the first demonstration of photodetection using ZrGeTe_4 , these characteristics measured on a simple proof-of-concept device show the exciting potential of the ZrGeTe_4 for room temperature IR optoelectronic applications.

NM06.05.03

Detection of Odor Molecule Gas Using Graphene Field-Effect Transistor Modified by Self-Assembling Peptide Yui Yamazaki¹, Tatsuru Hitomi¹, Kou Yamada², Yoshiaki Sugizaki², Atsunobu Isobayashi², Hideyuki Tomizawa² and Yuhei Hayamizu¹; ¹Tokyo Institute of Technology, Japan; ²Toshiba Corporation, Japan

Detection of agricultural products and foods at an airport is vital for quarantine. In this sense, sensing volatile organic compounds (VOCs) is gaining more interest in continuously monitoring the prohibited materials brought into a country. Commercial VOC sensors are inexpensive and can be mass-produced, but they detect various odors and are not selective. Therefore, it is crucial to develop a sensing system for VOC gas with high sensitivity and selectivity. Graphene, a typical two-dimensional material, has been expected to be applied to biosensors because of its excellent electronic properties and high specific surface area. Many studies have been conducted on VOC sensors based on graphene field-effect transistors (GFETs), such as a NO_2 gas sensor with ppm-order sensitivity [1]. Furthermore, polymer-functionalized graphene surface increased the sensitivity to specific gasses [2]. Despite the progress of the VOC sensors based on graphene FETs, it is still necessary to improve their selectivity and sensitivity simultaneously. We attempted to detect odor molecules using self-assembled peptides selectively. It is known that some engineered peptides form a uniform self-assembled film on a two-dimensional material [2]. These peptides physically adsorb onto surfaces and modify the surface without compromising graphene's intrinsic electronic properties, indicating that self-assembled peptides are promising to functionalize GFET biosensors. In the experiments, we developed multiple kinds of peptides with unique amino-acid sequences and investigated the electrical response of GFETs functionalized by these peptides. After self-assembling peptides on the surface of GFETs, we tested GFET response against several types of odor molecules such as methyl salicylate, methyl propionate, and limonene. The conductivity change was found to increase for all odor molecules as the concentration of odor molecules in carrier gas increased. The principal component analysis (PCA) successfully classified the difference in GFET responses depending on odor molecules and peptide sequences. We believe that the designability of the

peptide sequence allows us to produce highly sensitive and selective detection of molecules in gasses for a variety of other molecules. This work was supported by the Cabinet Office (CAO), Cross-ministerial Strategic Innovation Promotion Program (SIP), “An intelligent knowledge processing infrastructure, integrating physical and virtual domains” (funding agency: NEDO).

[Reference]

[1] F. Schedin, A. Geim, S. Morozov, et al. *Nature Mater* 6, 652–655 (2007).

[2] D. Khatayevich, T. Page, C. Gresswell, et al. *Small*, 10, 8, 1505-1513 (2014).

NM06.05.04

Van der Waals Schottky Gated MoS₂ Metal-Semiconductor Field-Effect Transistor at the Schottky-Mott Limit Yeon Ho Kim¹, Wei Jiang², Donghun Lee¹, Yeonsu Jeong³, Jong Chan Kim⁴, Woong Huh¹, Tae Soo Kim⁵, Jae-Pil So¹, Hong Gyu Park^{1,1}, Kibum Kang⁵, Hu Young Jeong⁴, Seongil Im³, Tony Low² and Chul-Ho Lee^{1,1}; ¹Korea University, Korea (the Republic of); ²University of Minnesota, United States; ³Yonsei University, Korea (the Republic of); ⁴Ulsan National Institute of Science and Technology, Korea (the Republic of); ⁵Korea Advanced Institute of Science and Technology, Korea (the Republic of)

Van der Waals (*vdW*) semiconductors such as transition metal dichalcogenides (TMDs) have emerged as a promising material for next-generation electronics due to excellent gate coupling and immunity to short channel effects even at the ultimate scaling. To achieve a high-performance electronic device, the gate stack that enables the effective electrostatic control of the TMD channel is necessary. In this regard, the metal-semiconductor junction can be a promising alternative to a conventional metal-oxide-semiconductor structure. Nevertheless, control of the metal-*vdW* semiconductor junction is still challenging because of the unavoidable Fermi-level (E_F) pinning effect induced by numerous gap states. Here, we propose a new device architecture of *vdW* metal-semiconductor field-effect transistors (MESFETs) using a Schottky gate junction between the TMD and the surface-oxidized metal. The *vdW* MESFETs exhibit the sub-1V operation with the subthreshold swing of ~60 mV/dec and negligible hysteresis. These intrinsic Boltzmann-limited FET characteristics are attributed to forming the E_F pinning-free gate stack at the Schottky-Mott limit. Furthermore, we experimentally and theoretically confirm that E_F depinning can be achieved by suppressing metal-induced gap states at the interface between the oxidized metal and the transferred TMD channel.

NM06.05.05

Toward Wafer-Scale Growth of Sb₂Te₃ Films via Low-Temperature ALD for Self-Powered Broadband Photodetector Jun Yang^{1,2}, Samik Mukherjee¹ and Kornelius Nielsch^{1,2}; ¹Leibniz Institute for Solid State and Materials Research Dresden, Germany; ²Technische Universität Dresden, Germany

P-type Sb₂Te₃ thin film was deposited on a wafer-scale by atomic layer deposition (ALD) at 80 °C using (Et₃Si)₂Te and SbCl₃ as precursors. The good crystal quality, low defect, and excellent uniformity of low-temperature ALD processed Sb₂Te₃ was supported by Raman, Transmission Electron Microscopy (TEM), and X-ray photoelectron spectroscopy (XPS) measurements. Furthermore, high-performance self-powered broadband photodetectors based on Sb₂Te₃/Si heterostructure were fabricated. The photodetector has a wide detection range of visible (405 nm) to near-infrared (1550 nm). Meanwhile, a high responsivity of 4287 mA/W at 405 nm, and a quick rise time of 98 μs (t_{rise}) were obtained under 0 bias voltage. The rapid response speed is benefited from enhanced photogenerated carriers' separation by a strong built-in electric field[YJ1] between p-type Sb₂Te₃ thin film and n-type Si heterostructure. The temperature-dependent performance of Sb₂Te₃/Si photodetector was thoroughly examined. The photodetector exhibits steady ON/OFF behavior even at a high temperature of 473 K, confirming the suitability of our photodetector device for logic circuit application under a harsh environment. The Sb₂Te₃/Si heterostructure self-powered photodetector with excellent performance based on the ALD process shows the great potential application in optoelectronic devices.

NM06.05.06

Heterogeneously Integrated 2D-Silicon Heterostructures for Bioresorbable, Wireless Neurochemical System Jaehyung Shim¹, Seung Min Yang¹, Hyun-U Cho², Tae-Min Jang¹, Gwan-Jin Ko¹, Jeongeun Shim², Tae Hee Kim³, Jia Zhu⁴, Sangun Park³, Yoon Seok Kim¹, Su-Yeon Joung¹, Jong Chan Choe¹, Jeong-Woong Shin¹, Joong Hoon Lee¹, Yu Min Kang², Huanyu Cheng⁴, Youngmee Jung³, Dong Pyo Jang², Suk-Won Hwang¹ and Chul-Ho Lee¹; ¹Korea University, Korea (the Republic of); ²Hanyang University, Korea (the Republic of); ³Korea Institute of Science and Technology, Korea (the Republic of); ⁴The Pennsylvania State University, United States

Although evaluation of degenerative brain diseases and regulation of essential functions in the body are closely related to neurotransmitters, many studies have been conducted to indirectly observe these biochemical messengers by monitoring physical, mechanical, and electrophysiological parameters rather than direct observation. Here, we report a heterogeneous integration of bioresorbable 2D transition metal dichalcogenides and silicon-based neurochemical analyzer for implementing a fully implantable brain-integrated system that enables simultaneous wireless monitoring of the temporal-dynamic behavior of dopamine and related parameters. Extensive investigation of molybdenum/tungsten disulfide (MoS₂/WS₂) nanosheets and catalytic iron nanoparticles (Fe NPs), along with theoretical modeling tools, highlights the underlying mechanisms of robust chemical and target-specific responses to the neurotransmitters. Systematic characterization demonstrates the reversibility, stability, and long-term operating performance of degradable bioelectronics, and the sensitivity and selectivity of degradable bioelectronics are superior to those of non-degradable materials. A complete in vivo experimental comparison, including the case with carbon fiber electrodes, demonstrates its potential as a clinically accessible tool for related neurodegenerative diseases.

NM06.05.07

Graphene-based Field Effect Transistor Array for Detection of Gaseous Disease Biomarkers Through Impedance Measurements Dominic J. Wales, Bruno Gil Rosa, Haijie Tan and Eric Yeatman; Imperial College London, United Kingdom

For biomarker sensing applications, in the solution and gas phases, functionalized graphene field-effect transistors (gFET) have been employed as sensors for selective detection of biomarkers due to graphene's high sensitivity towards immobilized molecules.^{1,2} However, a drawback of this approach is potentially poor sensor repeatability and/or shelf life due to degradation of the functionalisation.²⁻⁴ However, the alternative of using pristine graphene is not suited for discriminative detection of vapour biomarkers due to low sensitivity.⁵

Therefore, to overcome these drawbacks of both functionalised and pristine graphene gas sensors, we present the use of an AC impedance unfunctionalized gFET biosensor for gaseous biomarker sensing toward breathomics application. Our novel approach builds on the enhanced sensing capabilities demonstrated in our earlier AC impedance gFET sensor work,⁶ builds on the work of Liu *et al.*,⁷ and incorporates a quantitative structure-property relationship (QSPR) approach for development of predictive discriminative sensor response models.⁸ In addition, we also explore the incorporation of the low-frequency spectral noise modality to further enhance discriminative sensing.⁹

1. L. Xu, S. Ramadan, B. G. Rosa, Y. Zhang, T. Yin, E. Torres, O. Shafarost, A. Panagiotopoulos, B. Li, G. Kerherve, D. K. Kim, C. Mattevi, L. Jiao, P. Petrov, N. Klein, *Sensors & Diagnostics* (2022), doi:10.1039/D2SD00076H.

2. A. Béraud, M. Sauvage, C. M. Bazán, M. Tie, A. Bencherif, D. Bouilly, *Analyst*, **146**, 403–428 (2021).

3. N. Bhalla, P. Jolly, N. Formisano, P. Estrela, *Essays Biochem.* **60**, 1–8 (2016).
4. S. A. Spring, S. Goggins, C. G. Frost, C. Sedgwick, R. B. P. Elmes, P. Harvey, X.-P. He, *Molecules.* **26**, 2130 (2021).
5. Y. Dan, Y. Lu, N. J. Kybert, Z. Luo, A. T. C. Johnson, *Nano Lett.* **9**, 1472–1475 (2009).
6. B. Gil, S. Anastasova, B. Lo, *Carbon N. Y.* **193**, 394–403 (2022).
7. H. Liu, Y. Liu, Y. Chu, T. Hayasaka, N. Joshi, Y. Cui, X. Wang, Z. You, L. Lin, *Sensors Actuators B Chem.* **263**, 94–102 (2018).
8. D. J. Wales, R. M. Parker, P. Quainoo, P. A. Cooper, J. C. Gates, M. C. Grossel, P. G. R. Smith, *Sensors Actuators B Chem.* **232**, 595–604 (2016).
9. S. Rummyantsev, G. Liu, M. S. Shur, R. A. Potyralo, A. A. Balandin, *Nano Lett.* **12**, 2294–2298 (2012).

NM06.05.08

Effect of a Graphene/MoS₂ Heterointerface on the Phase Transition Induced by Lithium Intercalation Maria Bambrick-Santoyo, Mengjing Wang, Joshua Pondick, Natalie Williams, Serrae Reed and Judy Cha; Yale University, United States

Two-dimensional transition metal dichalcogenides (2D TMDCs) are promising for a wide range of energy and electronic applications including batteries, photovoltaics, catalysis, sensing, and memory. One method of modifying the properties of 2D TMDCs is through electrochemical intercalation—as Li ions are inserted into the interlayer gaps of the host material, a structural and electronic phase change is induced. Recent Li intercalation studies of molybdenum disulfide (MoS₂) indicate that a 2D heterointerface, such as graphene above MoS₂, suppresses the intercalation-induced phase transition from the semiconducting 2H phase to the metallic 1T' phase by as much as 0.6 V extra electrochemical voltage compared to bare MoS₂ [1, 2]. Such a delay presents an opportunity to design a novel device architecture in which the electrochemical intercalation is used as a knob to turn on and off a switching device. To test this, we studied a new geometry of MoS₂ / graphene heterostructures: a flake of MoS₂ with a narrow strip of graphene placed on top across the middle of MoS₂. We used *in situ* Raman spectroscopy and optical characterization to monitor the phase transition in these heterostructures. This design was expected to yield a flake with the central graphene-covered region remaining 2H while the neighboring uncovered regions transformed into 1T' at the phase transition voltage of MoS₂, creating a metallic (1T') / semiconducting (2H) / metallic (1T') pattern. Surprisingly, however, the graphene-covered region of MoS₂ did not require additional voltage to transition from the 2H to the 1T' phase, in contrast to our previous observations. This surprising result might come from a difference in device architecture: Pondick *et al.* performed intercalation experiments with electrodes contacting both MoS₂ and graphene, whereas our electrodes only contacted MoS₂. We hypothesize that the voltage supplied indirectly to graphene through contact with an MoS₂ flake may not be sufficient to intercalate Li into graphene, essentially eliminating graphene's effect on the phase transition. To test this hypothesis, we have designed a device with electrodes directly contacting both MoS₂ and graphene. In this study, we thus show that the graphene / MoS₂ heterostructure has wide applications—for example, it could yield the design for a transistor with a changeable channel length based on the electrochemical voltage applied.

- [1] J. V. Pondick, A. Kumar, M. Wang, S. Yazdani, J. M. Woods, D. Y. Qiu, and J. J. Cha. *ACS Applied Nano Materials* 2021, 4, 12, 14105–14114.
 [2] S. Yazdani, J. V. Pondick, A. Kumar, M. Yarali, J. M. Woods, D. J. Hynek, D. Y. Qiu, and J. J. Cha. *ACS Applied Materials & Interfaces* 2021, 13, 10603–10611.

NM06.05.09

Tunable Synthesis of Large 2D α -Ni(OH)₂ with Mechanistic Insights for Intra-Plane Growth of 2D Transition Metal Layered Hydroxides Gillian E. Minarik, Lu Ping and Xi Ling; Boston University, United States

As a long-used electroactive material in rechargeable batteries,^{1,2} nickel hydroxide (Ni(OH)₂) has an ongoing history of addressing critical applications in clean energy production and storage.^{3,4,5} Ni(OH)₂ belongs to the family of transition metal layered hydroxides (TM-LHs), an isostructural class of materials in which six-coordinate transition metal centers occupy a trigonal lattice, held in the vertical dimension by weak dispersion forces. The weak, non-covalent interactions in the *c*-direction give rise to sheet-like layers which stack to form bulk material, with pure and intercalated forms designated α - and β - phases respectively.² In a manner analogous to van der Waals (VdW) crystals, pioneers in the recent advent of two-dimensional (2D) materials research,^{6,7} the relatively weak interlayer interactions pose TM-LHs as logical candidates to be isolated with mono- and few-atom thickness. However, while Ni(OH)₂ boasts an extensive repertoire of syntheses, its 2D form remains largely unstudied due to challenges in reproducing sufficient domain size (>5 μ m) and long-range crystallinity.^{4, 8, 9, 10} Here, we report repeatable growth of round single-crystalline 2D α -Ni(OH)₂ nanosheets (thinnest ~6 atomic layers) with unprecedented lateral domain size (average ~20 μ m) by mixed treatment under hydrothermal conditions and urea hydrolysis. The morphology, structure and quantum properties were examined and determined by Optical Microscopy (OM), Scanning Electron Microscopy (SEM), Atomic Force Microscopy (AFM), Powder X-Ray Diffraction (PXRD), Transmission Electron Microscopy (TEM) and Ultraviolet-visible Spectroscopy (UV-Vis). Our study also involves systematic control of parameters including precursor ratio, starting pH, soaking temperature, and cooling rate to elucidate the dominating factors for crystal growth, with emphasis on promoting *ab* in-plane isotropy. Resulting crystals were characterized by OM and PXRD, illustrating α - β phase transition at higher pH and reaction temperature with controlled adjustment of unit cell dimensions, owing to varying degrees of hydration and foreign-ion intercalation. Using a heterogeneous precipitation model, we harness these condition-dependent results to propose in-plane versus out-of-plane growth mechanisms based on edge-on substitution of hexaaquanickel(II) species in solution. Furthermore, we provide general guidelines for tuning the domain size, thickness, phase-dependence, and morphology of 2D Ni(OH)₂ crystals through adjustment of key parameters, illustrating the great synthetic flexibility afforded by the urea-hydrothermal approach. We further applied our understanding to the synthesis of other 2D TM-LHs such as Co(OH)₂. Our detailed synthetic investigation introduces a tunable and scalable pathway to synthesize large 2D TM-LHs flakes from simple methods and opens the 2D TM-LHs as an exciting addition to 2D materials research for future studies on the opto-electronic device applications.

References

1. Oliva, P. *et al. J. Power Sources* 1982, **8**, 229-255.
2. Hall, D. S., *et al. Proc. R. Soc. A.* 2015, **471**(2174).
3. Patel, R. *et al. J. of Mater. Chem.* 2018, **6**(1), 12-19.
4. Patil, S. J. *et al. Small* 2022, **18**(7), 2103326.
5. Deng, J.; Wu, F., Gao, S.; Dionysiou, D. D.; & Huang, L.-Z. *Appl. Catal. B Environ.* 2022, **309**, 121258.
6. Novoselov, K. S. *Proc. Natl. Acad. Sci. U. S. A.* 2005, **102**, 10451–10453.
7. Mas-Balleste, R., *et al. Nanoscale*, 2010, **3**, 10-20.
8. Su, C., *et al. J. Mater. Chem. C.* 2020, **8**(9), 3010-3016.
9. Yuan, S. *et al. Nat. Mater.* 2022, **21**(6), 673-680.
10. Liu, C.; Bai, Y.; Wang, J.; Qiu, Z.; & Pang, H. *J. Mater. Chem. A.* 2021, **9**(18), 11201–11209.

NM06.05.10

High Mobility Patterned MoS₂ Semiconductor Using Jet-Printing on a High-K Gate Dielectric in Thin-Film Transistor Woon-Scop Choi and Thi Thu Thuy Can; Hoseo University, Korea (the Republic of)

Recently, transition-metal dichalcogenides (TMDs) have attracted much attention as new materials for electronics devices, electrocatalysts, photocatalysts,

sensors, batteries, and bio-applications. Most TMDs are two-dimensional (2D) materials with a single layer. Bonds between each layer are made up of Van der Waals bonds, while intra-layer atoms bind together as covalent bonds.

Chemical vapor deposition (CVD) with sulfur gas is the most popular method for synthesizing large-scale 2D materials with high quality. Various MoS₂ can be obtained from this method using various precursors with different properties, process temperatures, and substrate materials. Solution process methods show advantages for preparing films with large size, high throughput, low cost, thickness control, and an environmentally friendly process. Even though there is sulfur in the precursors of the solution-process synthesis methods, supplementing the sulfur that is lost in the high-temperature CVD process is unavoidable.

Solution synthesis of MoS₂ precursor followed by direct printing could be an effective way to make printed electronic devices. A linear MoS₂ pattern was obtained by an electrohydrodynamic (EHD)-jet printer with a sol-gel system without chemical vapor deposition. The morphology of the MoS₂ after a transfer process was maintained without wrinkles or cracking, resulting in a smooth surface compared with that of spin-coated films. EHD-jet printed MoS₂ was transferred onto high-k dielectric Al₂O₃ and used as a semiconductor layer in thin film transistor (TFT) devices. The printed MoS₂ TFT has relatively good electrical characteristics, such as a linear field effect mobility, current ratio, and low subthreshold swing of 50 cm² V⁻¹ s⁻¹, 7.39×10⁶, and 0.7 V decade⁻¹, respectively. This new methodology can be applied to multifarious devices and has the potential for scalability in 2D materials.

NM06.05.11

Two-Dimensional Manganese at the Epitaxial Graphene/6H-SiC Interface [Chengye Dong](#), Furkan Turker, Alexander Vera, Ke Wang and Joshua A. Robinson; The Pennsylvania State University, United States

Two-dimensional (2D) metals are of interest due to unique properties, including superconductivity, enhanced charge-density-wave order, and magnetism¹. However, synthesizing these materials and environmental sensitivity are continued bottlenecks toward exploring these materials in ambient, and including them in a range of applications. Recent advances in intercalating metals at the epitaxial graphene (EG) – silicon carbide (SiC) interface inspired our recent works, dubbed “confinement heteroepitaxy (CHet)”, to synthesize scalable, environmentally stable 2D metals that exhibit distinct properties from their bulk counterparts^{2,3}. For example, 2D Ag confined between EG and SiC is a 2D semiconductor with 1 eV band gap².

Here, we will discuss our advances toward realizing large-area, atomically thin manganese (Mn). 2D Mn between EG and SiC is predicted to be magnetic, and a Dirac half metal enabling the quantum anomalous Hall effect^{4,5}. Therefore, experimental realization of 2D Mn will be beneficial for exploring and understanding its structures, properties and potential applications in information storage and quantum devices. Herein, the effect of parameters, such as temperature, time and pressure, on intercalation efficiency are discussed. Ideal conditions for Mn intercalation at the EG and quasi-freestanding EG (QFEG) on 6H SiC is identified to be near-atmosphere pressure argon at 1000 °C for 2 hours. X-ray photoelectron spectroscopy (XPS) results confirm that Mn-Mn and Mn-Si bonding exist, and high-resolution transition electron microscopy indicates that monolayer Mn can form at the EG/SiC interface. However, we also find Mn diffuses into the top 2-3 SiC layers for QFEG. Since the SiC surface of QFEG is passivated by H atoms which likely de-intercalate from interface, leaving Si dangling bonding during the CHet process, such dangling bonds may accelerate Mn diffusion into SiC. In addition, DFT calculations are conducted to corroborate and aid in proposing a mechanism of our observations. We will also discuss magneto-optical Kerr effect microscopy and magnetic force microscopy related to magnetic properties of 2D Mn.

1. Ma, Yang, et al., *Materials Chemistry Frontiers* 2, no. 3 (2018): 456-467.
2. Lee, Woojoo, et al., *arXiv preprint arXiv:2201.01701* (2022).
3. N. Briggs, et al., *Nature Materials* 19, 637-643 (2020).
4. Jayasekera, Thushari, et al., *Physical review letters* 104, no. 14 (2010): 146801.
5. Li, Yuanchang, et al., *Physical Review B* 92, no. 20 (2015): 201403.

NM06.05.12

Copper-Aluminum Layered Double Hydroxides with Different Morphologies and Compositions as CO₂ Reduction Electrocatalysts [Tomo Hirano](#), Kazuyuki Iwase and Itaru Honma; Institute of Multidisciplinary Research for Advanced Materials, Tohoku University, Japan

Electrochemical CO₂ reduction reaction (CO₂RR) has attracted attention as a reaction that can convert CO₂ to value-added products, such as carbon monoxide (CO) or hydrocarbons, under ambient conditions (i.e., room temperature and atmospheric pressure). For CO₂RR catalysts, improving the selectivity of the desired CO₂RR products and suppressing the competitive electrochemical hydrogen evolution reaction (HER) are important. Copper (Cu) is the only material that produces various kinds of products, such as carbon monoxide (CO), formate (HCOO⁻), methane (CH₄), and ethylene (C₂H₄). Previously, alloyed Cu-aluminum (Al) catalysts are suggested to show high CO₂RR activity.^[1] In addition, it was also reported that Cu-based oxides could catalyze CO₂RR in high efficiencies.^[2] Therefore, in the present work, we focused on Cu-Al based layered double hydroxides (Cu-Al/LDH) which is Cu and Al based oxide materials with two dimensional structure. We designed various Cu-Al/LDHs with different sizes and morphologies by changing the synthesis conditions and evaluated the CO₂RR activity.

Cu-Al/LDHs with different compositions and morphologies were synthesized by controlling the synthesis condition by modifying the reported coprecipitation method.^[3] The Cu-Al nitrate solutions (Cu/Al molar ratio of 3.0) were added dropwise to the sodium carbonate solutions at the desired temperature (e.g., 30 ~ 150°C) and solution pH (e.g., 4 or 8). The CO₂RR activities were evaluated with a custom-made gas-diffusion electrode (GDE) setup using 1 M KHCO₃ solution as an electrolyte with continuous CO₂ flow.

First, Cu-Al/LDHs were characterized by powder X-ray diffraction (XRD) pattern. For all samples, peaks assignable to the LDH structures were observed at 10.2° or 11.7°, though (003) peaks position shifted when the solution pH changed. Although the small peaks corresponding to malachite [Cu²⁺₂(CO₃)(OH)₂] were observed as byproducts, no clear peaks ascribed to Cu or Al-based oxides were observed. These results indicated that Cu-Al/LDHs were successfully synthesized. As the temperature and solution pH of LDH synthesis increased, the full width at half maximum (FWHM) for the (003) peaks of LDH decreased. This result indicated that LDH synthesized under high temperature possessed larger sheet size, which were also confirmed by transmission electron microscope (TEM) images. X-ray photoelectron spectroscopy (XPS) measurements suggested that interlayer anions of LDH changed from NO₃⁻ to CO₃²⁻ as pH of the solution increased. This result showed good agreement with the peak shift of the (003) of the XRD measurements.

Next, CO₂RR activities were investigated. CO and HCOO⁻ were detected as major CO₂RR products. H₂ was also detected as a HER product. Cu-Al/LDH synthesized under high temperature with a larger sheet size showed a faradic efficiency for CO generation of 42% and that for HCOO⁻ of 22% at 50 mA.^[4] In addition, the Cu-Al/LDHs with larger sheet sizes tend to show higher faradaic efficiencies for CO₂RR. Based on previous reports, low-coordinated Cu sites (i.e., edge Cu atoms in Cu nanoparticles) are considered active sites for HER. This result suggested that the basal plane of LDHs functioned as active sites for CO₂RR and sheet size of LDHs is an important determining parameter of CO₂RR for Cu-Al/LDHs.

References: [1] Miao Z. *et al.*, *Nature*, **581**, 178-183(2020). [2] Christina W. *et al.*, *Nature*, **508**, 504-507(2014). [3] F. Wang *et al.*, *Sens. Actuators B*, **273**, 41-47(2018). [4] [T. Hirano](#) *et al.*, *ChemSusChem*, **15**, e202102340(2022).

NM06.05.13

Photovoltaic and Photo-Capacitance Effects of WSe₂ Thin Films [Donghyeon Lee](#) and Sanghan Lee; Gwangju Institute of Science and Technology, Korea (the Republic of)

The layer number dependent bandgap reported in two-dimensional (2D) materials provide an extra degree of freedom to tune the optical properties of photodetectors. 2D transition metal dichalcogenides (TMDs) have been considered as the appealing candidates for photodetection owing to their strong light-matter interactions and the layer number dependent electrical and optical properties. Among them, tungsten diselenide (WSe₂) attracted significant research interest for its high quantum efficiency and reasonably high carrier mobility. Recent study of WSe₂ photodetector is mainly focused on enhancing photocurrent generation by manipulating the metal-semiconductor contacts due to Schottky barrier formation of WSe₂ with most metal contacts. However, there is lack of study of photo-induced electrical properties of WSe₂ other than photocurrent generation, such as photo-capacitance, photo-impedance, etc. Revealing the mechanisms of the photo-induced electrical properties of TMDs other than photocurrent is crucial to understand the fundamentals of the light-matter interactions in TMDs.

Here, we investigate the photo-induced effects of WSe₂ film deposited by pulsed laser deposition technique on Si substrate with top ITO electrode. We observed the photo-capacitance effect on the fabricated film with as large as ~75% enhancement in capacitance under the white light illumination, accompanied by photocurrent. These effects will give an additional dimension to the application potential of WSe₂ in fields such as photoelectric memory devices, which employs the capacitance change stimulated by light.

NM06.05.14

First-Principles Study of H₂ Adsorption Mechanism on Defective MoSe₂/Graphene Heterostructures Wadha K. AlFalasi and Nacir Tit; United Arab Emirates University, United Arab Emirates

Transition metal di-chalcogenide monolayers (TMD-MLs), a novel class of the 2D materials, exhibit tremendous properties such as their tuneable band gap, high surface to volume ratio, appropriate carrier mobility, large spin-orbit coupling and thermal stability which make this class of 2D-materials a promising leading candidate for many applications. In gas-sensing field, the TMD-graphene hetero-structure provides adsorption sites with excellent interaction with gas molecules. Moreover, our recent studies have shown that magnetization is easily triggered/induced in MoSe₂ MLs through either metal vacancies or TM-substitutional doping. The chemisorption of molecules on such sites would affect the magnetisation, which further enhances the gas response. In the present work, the spin-polarised density-functional theory (DFT) is applied to investigate the adsorption of hydrogen-gas molecules on 4 different adsorbent monolayer and hetero-structures: (1) MoSe₂ ML with single vacancy of Mo "MoSe₂:V_{Mo} ML"; (2) Mn-doped MoSe₂ ML "MoSe₂:Mn ML"; (3) MoSe₂:V_{Mo}/graphene hetero-structure; and (4) MoSe₂:Mn/graphene hetero-structure. The results of phonon spectra, adsorption energy, spin-polarised band structures, magnetisation, charge exchange using Bader analysis will be presented. Furthermore, benchmarking with experimental and theoretical data existing in literature will be presented. The results should contribute in improving the performance of hydrogen gas-sensors and energy-storage applications.

NM06.05.15

Graphene-Based Closed-Loop Neurotechnology for Treatment of Movement Disorders Nicola Ria^{1,2}; ¹ICN2, Spain; ²The University of Manchester, United Kingdom

Neural activity in the central nervous system is governed by neural oscillations. The anomaly in the frequency bands of the oscillations can lead to pathological conditions of the nervous system due to impaired cognitive functions and memory. In particular, in Parkinson's disease (PD), an increase in the power of beta oscillations in the subthalamic nucleus (STN) is observed, and in previous studies it has been proposed as a potential biomarker. Stimulation with electrodes implanted in the STN (deep brain stimulation - DBS) can alter the power of beta oscillations, thus aiding in the treatment of the disease.

For this reason, I have designed and fabricated neural probes with a new generation of graphene oxide electrodes called EGNITE. The porosity of this material increases the active surface of the electrodes and this allows to inject a very high density current compared to traditional platinum electrodes. An activation process is required to exploit the entire surface also contained within the pores. The electrochemical characterization highlights high performance in terms of charge injection limit, impedance and stability. This neural probe also has the ability to record brain activity and even detect single peaks due to the small size of the electrodes (25 μm) and the high signal-to-noise ratio. The ultimate goal will be to develop a closed-loop system for recording and pacing precisely when it is necessary to effectively treat PD symptoms such as tremor.

The structure of the device consists of a very thin layer of polyamide which makes the device very flexible. The flexibility improves biocompatibility and allows the use of the device for longer periods with better performance in terms of measured signal quality and stimulation efficacy. The flexibility of the device requires the use of a silicon shuttle as a rigid support to penetrate the brain. The attachment is made with biocompatible and soluble glue like hydrogels or polyethylene glycol to be able to detach the shuttle once insertion is complete.

We performed some acute experiments on rats in the University of Manchester (nanomedicine laboratory) with some very good initial results. The applied stimulation protocol can temporarily suppress beta oscillations which are biomarkers of Parkinson's disease.

The objectives of the project are very ambitious;

We want to improve the efficacy of therapy by providing personalized treatment with closed loop technology (CLT) that makes parameter setting automatic and adaptive. While traditional DBS systems continuously provide pulsed pacing at a high rate, CLT incorporates pacing feedback control based on measures of pathological brain activity. This strategy has the advantage of stimulating only when needed, potentially reducing the negative side effects associated with continuous stimulation.

Another important goal is the understanding of the PD biomarkers available to close the feedback loop and provide control strategies for stimulation. Specifically for the stimulation parameters, we will study the effects of the temporal spacing or distribution of the stimulation pulses. The temporal pattern is an important parameter for the optimization of the response to DBS because its modulation can alter the encoding of the speed of the neural response.

NM06.05.16

Direct Growth of Hexagonal Boron Nitride for Silicon-Based Resistive Switching Memory Jiye Kim¹, Seokho Moon¹, Hokyong Jeong^{2,1}, Jaewon Kim^{3,1}, Chang-Won Choi¹, Inyong Hwang¹, Jaesub Song¹ and Jong kyu Kim¹; ¹Pohang University of Science and Technology, Korea (the Republic of); ²Samsung Electronics Memory Division, Korea (the Republic of); ³Samsung Advanced Institute of Technology, Korea (the Republic of)

Hexagonal boron nitride (h-BN) has been regarded as a promising material for next-generation energy-efficient resistive switching (RS) memories due to its excellent thermal conductivity, reliability, and stability. CVD-grown h-BN films on metal foil substrates have been widely studied for RS memories. However, the transfer of such CVD-grown h-BN films onto a target substrate is necessary for device fabrication, which accompanies various deformation

of h-BN films such as tears, wrinkles, and other impurities, degrading the performance of devices. Here, we present the direct growth of h-BN on 2-inch highly doped silicon (Si) substrate by metal-organic chemical vapor deposition (MOCVD) for realizing a transfer-free h-BN-based RS memory. The few-layer h-BN grown on Si act as the RS medium in a metal-insulator-semiconductor (MIS) structure, exhibiting both unipolar and bipolar resistive switching behaviors depending on metal electrodes. The transfer-free, direct-grown h-BN-based RS memory shows excellent reliability and low variability. The switching mechanism of h-BN-based RS memories will be discussed with various h-BN active media having various defects characteristics which were controlled by modulating MOCVD growth parameters.

NM06.05.17

High Performance and Broadband Photodetector Based on Transition Metal Dichalcogenides van der Waals Heterostructures Ahmed R. Elbanna^{1,2}, Zeng Wang¹, Yuanda Liu¹, Qing yang Steve Wu¹, Zi En Ooi¹, Mengting Jiang¹, Jisheng Pan¹, Ze Xiang Shen^{2,2,2} and Jinghua Teng¹; ¹Institute of Materials Research and Engineering, Agency for Science, Technology and Research (A*STAR), Singapore; ²Nanyang Technological University, Singapore

Photodetectors (PDs) are used in various applications, such as pollution detection, imaging, defence, optical communication and chemical analysis, determined by their detection bands. The emerging two-dimensional materials and their hybrid systems have great potential for PDs thanks to their unique optoelectronic properties. The semi-metallic graphene has a broadband absorption from UV to terahertz. However, graphene-based PDs suffer from low absorption (2.3 % for monolayer) and high dark current, which is not favourable for PDs. The semi-insulating hexagonal boron nitride is only used for photodetection in the UV band due to its large bandgap. Meanwhile, the transition metal dichalcogenides (TMDs) semiconductors show higher absorption than graphene. However, their operational wavelength is limited by the bandgap of the material (in the visible range for most of the TMDs). The band energy of van der Waals heterostructures can be engineered by using different TMDs with the appropriate band alignment. Here, we report SnSe₂/MoS₂ heterostructure PD operating in the wavelength range from deep UV to IR. Our heterostructure PD not only shows broadband detection but also a higher performance than the parent materials and other reported PDs.

NM06.05.18

Layer Controlled MoS₂ Synthesis Using Multi-Step Metal Organic Chemical Vapor Deposition Hyun-geun Oh, Donghoon Moon and Gwan-Hyong Lee; Seoul National University, Korea, Korea (the Republic of)

The large-scale growth of semiconducting transition metal dichalcogenides (TMDs) thin film is the basis of commercialization of two-dimensional materials. For this, metal organic chemical vapor deposition (MOCVD), which can supply precursors in gas phase, provides synthesis process of uniform wafer-scale TMDs monolayer film. In addition, it is necessary to control the number of layers of TMDs to provide various device fabrication and usability. Here we report the layer controlled MoS₂ synthesis using multi-step MOCVD process. Multi-step consists of nucleation step and lateral growth step. One cycle can synthesize monolayer. Therefore, we can synthesize the desired number of layers of MoS₂ through cycle iteration. The as-grown MoS₂ samples were characterized with raman spectroscopy, photoluminescence (PL), transmission electron microscope (TEM) and atomic force microscopy (AFM). Our work will be a step towards the revelation of mechanism of TMDs growth and the synthesis of high quality MoS₂ film.

NM06.05.19

Atomic Layer Deposited Elemental Chalcogen Thin Films, Two-Dimensional Tellurium Changhwan Kim¹, Namwook Hur¹, Jiho Yang², Saeyoung Oh¹, Hu Young Jeong¹, Bonggeun Shong² and Joonki Suh^{1,1}; ¹Ulsan National Institute of Science and Technology, Korea (the Republic of); ²Hongik University, Korea (the Republic of)

Tellurium, an emerging van der Waals solid, has been spotlighted in electronics, optoelectronics, and spintronics owing to its physico-chemical properties such as robust chirality, intrinsic in-plane anisotropy, superior field-effect hole mobility and fast resistive switching. To fully implement such potentials into real-world applications, atomic layer deposition can be an ideally suited process compared to other vapor-phase synthetic methods thanks to its deposition mechanism and self-limiting surface reaction. Herein, we demonstrate wafer-scale tellurium thin films with exceptional homogeneity and controllability of thickness through the newly developed low-temperature ALD process. It is enabled by (i) introducing the co-reactant to alleviate the size effect of ligands and (ii) repeating the identical pulses to minimize the spatial blocking originating from inhibitors such as by-products and physisorbed molecules. With our synergistically designed process, film morphologies (*e.g.*, surface coverage and roughness) were remarkably improved and as-deposited poly-crystalline film exhibited the high crystallinity on the SiO₂/Si substrate despite the low deposition temperature (~50 °C). Our work can extend the options for tellurium films with conformality, scalability and crystallinity at low temperature.

NM06.05.21

Gas Sensitivity Changes by Defect Kind on Graphene Gas Sensors Sunmog Yeo, Young Jun Yoon, Jun Mok Ha and Chang-Goo Kang; Korea Atomic Energy Research Institute, Korea (the Republic of)

Generally speaking, defects generate negative effects on the materials or devices so that researchers try to fabricate more perfect materials or devices. However, well controlled defects give rise to various effects on the materials including optical, electrical, and magnetic effects. By tailoring these effects, many useful performances have been enhanced in photo detector, chemical sensor, catalyst and biomedical areas. On the other hands, because graphene consists of carbon atoms with sp² hybridizations, defects in graphene generate more dangling bonds on graphene. This means that there are more possibilities for gas molecules to adsorb on graphene. In fact, a DFT calculation shows that the defected graphene has more adsorption energy, meaning that a graphene gas sensor with defects has more sensitivity. In this paper, we present that the sensitivity of the graphene gas sensor depends on the defect kind. We produce defects on graphene using ion bombardment with various ion sizes such as H⁺ and N⁺. In addition, we compare the amount of defects by Raman spectroscopy and measure the sensitivities of the graphene gas sensors which have the similar amount of defects produced by different ions. We discuss the sensitivity changes by defect kind for the graphene gas sensors.

NM06.05.22

20 nm Nanogap Gas Sensors with Fast Response and Fast Recovery Yutaka Majima and Yexiao Sun; Tokyo Institute of Technology, Japan

Pt-based nanogap electrodes with a gap separation of 20 nm were fabricated by electron beam lithography (EBL). Using these electrodes, nanogap gas sensors were fabricated by combining sensing materials. A bottom-contact and top-contact nanogap gas sensor was fabricated. The response and recovery of the gas sensor were found to be strongly dependent on the gap separation. With the nanogap gas sensor, a large electric field equivalent to the breakdown voltage of the sensing material can be applied with the application of a few volts. The proposed method of fabricating robust ultrafine nanogap electrodes opens the possibility of developing various nanogap gas sensors with fast response and fast recovery.

NM06.05.23

Physical Vapor Deposition of Conductive Two-Dimensional Metal-Organic Framework Thin Film Seoungmin Chon¹, Ryo Nakayama¹, Shunta

Iwamoto¹, Shigeru Kobayashi¹, Ryota Shimizu¹ and Taro Hitosugi^{2,1}; ¹Tokyo Institute of Technology, Japan; ²The University of Tokyo, Japan

Metal–organic frameworks (MOFs) are porous materials that consist of coordinated metal ions and organic ligands. Among various MOFs, two-dimensional (2D) electrically conductive MOFs attract considerable attention owing to diverse applications such as electrocatalysts, energy storage devices, and chemiresistive sensors [1]. For such device applications, the fabrication of the conducting MOF thin films is desired using physical vapor deposition (PVD), which is a solvent-free process different from the conventional wet processes. So far, a few papers reported a conductive MOF monolayer on metallic substrates by PVD [2,3]. However, conductive MOF thin films have never been fabricated on insulating substrates by PVD. In this study, we utilize infrared-pulsed laser deposition (IR-PLD) as a physical vapor deposition method and fabricate a conductive 2D MOF thin film, Cu₃(HHTP)₂ (HHTP = 2,3,6,7,10,11-hexahydroxytriphenylene) on an insulating Al₂O₃ substrate.

Cu₃(HHTP)₂ thin films were deposited on Al₂O₃ (0001) substrate (3 mm × 5 mm) using IR-PLD [4,5]. Cu(OAc)₂ (copper acetate anhydrate) and HHTP were used as precursors for a metal ion and a ligand. Each powder is mixed with IR absorbing agent (Si powder) and then, pelletized in the Ar-filled glovebox. The pellets are transferred to the IR-PLD chamber with no exposure to air to prevent degradation. The thin film is deposited in a multilayer form: alternate deposition of HHTP and Cu(OAc)₂ is repeated 5 times. Each thickness of the HHTP and Cu(OAc)₂ layers is fixed to 10 nm and 8 nm, respectively, to satisfy the stoichiometric molar ratio of Cu₃(HHTP)₂. The substrate temperature is 150 °C and post-deposition annealing is continuously performed in the deposition chamber at 150 °C for 30 min. After the post-deposition annealing, the black film with the thickness of ~90 nm is obtained. The fabricated thin films were characterized by IR spectroscopy, and ultraviolet-visible (UV–vis) optical transmittance spectroscopy. The electrical conductivity of thin films is measured by the four-terminal method.

An IR spectrum of the film indicates the formation of Cu₃(HHTP)₂ from HHTP and Cu(OAc)₂ precursors. Precursor-derived peaks disappeared: neither the O–H band of HHTP (3,200–3,500 cm⁻¹) nor C=O band of Cu(OAc)₂ (~1,580 cm⁻¹) are observed. Instead, C–O stretching (1,174 cm⁻¹) and C–H scissoring vibration (1,421 cm⁻¹) appeared, which are similar to bulk Cu₃(HHTP)₂ [6]. Thus, we confirm that alternate layers of HHTP and Cu(OAc)₂ precursors are reacted to form Cu₃(HHTP)₂. Next, UV-vis optical transmittance spectra show a decrease in transmittance at 600–650 nm, which can be attributed to the ligand-to-metal charge transfer absorption band of Cu₃(HHTP)₂ [7]. The electrical conductivity of the fabricated Cu₃(HHTP)₂ thin film is 1.1 × 10⁻¹ S cm⁻¹. This is comparable to those of Cu₃(HHTP)₂ thin films prepared by wet processes (1.0 × 10⁻³ to 2.9 × 10⁻¹ S cm⁻¹) [8,9]. These results show that electrically conducting 2D Cu₃(HHTP)₂ thin film is successfully fabricated on the insulating Al₂O₃ substrate by IR-PLD.

[1] L. Xie *et al.*, *Chem. Rev.*, **16**, 8536 (2020).

[2] Z. Gao *et al.*, *Nanoscale*, **11**, 878 (2019).

[3] R. Zhang *et al.*, *Angew. Chem. Int. Ed.*, **59**, 2669, (2019).

[4] S. Maruyama *et al.*, *ACS Nano*, **4**, 5946 (2010).

[5] H. Oguchi *et al.*, *ACS Appl. Electron. Mater.*, **1**, 1792, (2019).

[6] W. Koo *et al.*, *Adv. Sci.*, **6**, 1900250, (2019).

[7] W. Zhao *et al.*, *Adv. Mater. Interfaces*, **8**, 2100308, (2021).

[8] X. Song *et al.*, *Angew. Chem., Int. Ed.*, **59**, 1118, (2020).

[9] V. Rubio-Giménez *et al.*, *Adv. Mater.*, **30**, 1704291, (2018).

NM06.05.24

High Yield Shear Exfoliation of MoS₂ Nanosheets by Green Chemistry Esra B. Karatas Ozkaraca, Abdelhakim Elmhamdi, Rana Ucuncuoglu, Naim Kurtuldu and Mahmut Aksit; Gebze Technical University, Turkey

Exfoliation of layered materials offers a diversified supply of 2D crystals with features beneficial in applications ranging from electronics and energy storage to photocatalysis. Here we report scalable, high yield, and simple liquid shear exfoliation of molybdenum disulfide (MoS₂) nanosheets from the commercially available bulk powder using several different, naturally available, and biodegradable long-chain hydrocarbons (LHCs). The exfoliated nanosheets can be isolated from the LHCs by centrifuging and washing with acetone or simply by evaporation of the LHCs by heat treatment upon centrifuging. The exfoliated nanosheets can be size separated by varying the centrifuge rotation speed with different corresponding yields. Liquid shear exfoliation parameters such as liquid mixing speed and time significantly affect the nanosheet production yield values depending on the nanosheet thickness. The nanosheet thicknesses are evaluated by XRD-Scherrer Broadening crystal size analysis that is corrected for instrumental broadening. After 4 hours of liquid shear exfoliation at maximum liquid mixing speed, 8% of the final product consists of MoS₂ nanosheets with an average thickness of 51 nm, whereas 32% of the final product has an average thickness of 105 nm. Specific surface areas of the final products are measured by the Brunauer-Emmett-Teller (BET) method for comparative analysis of the nanosheet thicknesses. Raman Spectroscopy is also performed on the nanosheet products to evaluate Raman peak shifts associated with nanosheet thickness.

NM06.05.26

Metal Cocatalyst Dictates Electron Transfer in Ag-Decorated MoS₂ Nanosheets Bo-An Chen, Sylwia Ptasinska and Prashant Kamat; University of Notre Dame, United States

Two-dimensional transition metal dichalcogenides such as atomically thin MoS₂ nanosheets are useful as low-cost solar energy conversion materials. Colloidally stable few- and monolayer MoS₂ nanosheets in dimethylformamide were prepared via an electrochemically-assisted liquid phase exfoliation approach. These nanosheets were further modified with Ag nanoparticles using photocatalytic reduction of Ag⁺ ions. A methyl viologen redox couple was employed as a probe to determine the rate constants of photoinduced forward electron transfer (k_f) and dark back electron transfer (k_b) processes to establish the role of Ag cocatalyst in promoting photocatalytic reduction. The competition between these two processes dictates the buildup of a steady-state concentration of the reduction product (methyl viologen radical) under visible light irradiation. The k_f and k_b rate constants increase with increasing Ag nanoparticle loading but with different dependencies, yielding a maximum reduction efficiency of 4.4%. At higher Ag loadings, the reduction yield decreases as back electron transfer dominates over the forward electron transfer process. Establishing the role of noble metal cocatalyst in the photoinduced charge transfer processes of Ag-MoS₂ hybrid composites offers design strategies to maximize the photocatalytic performance of semiconductor-metal heterostructures.

NM06.05.27

Star-Shaped WS₂ Monolayers with Twin Grain Boundaries Promoted by Molybdenum Atoms Na Zhang^{1,1,1}, David Sanchez¹, Nadire Nayir^{1,1,2}, Yanzhou Ji¹, Tianyi Zhang³, Ke Wang¹, Da Zhou¹, Mingzu Liu¹, Zhuohang Yu¹, Adri C.T. van Duin^{1,1} and Mauricio Terrones^{1,1,1}; ¹The Pennsylvania State University, United States; ²Karamanoglu Mehmetbey University, Turkey; ³Massachusetts Institute of Technology, United States

Monolayers of transition-metal dichalcogenides (TMDs) exhibit fascinating properties that make them attractive in optics, electronics¹, spintronics, and valleytronics², and it is of vital importance to understand and control their morphology to tune their physical properties³. However, the origin of their

morphology evolution is still highly elusive, which hinders the synthesis of desired morphologies for specific applications. Herein, we report the controllable synthesis and formation mechanism of star-shaped WS₂ monolayers by artificially adding trace concentrations of molybdenum using a liquid-phase precursor-assisted approach. Fluorescence imaging and photoluminescence (PL) mapping of six-arm stars revealed bright lines between adjacent arms. To correlate the morphology and optical properties with the microstructure, dark-field transmission electron microscopy (DF-TEM) was implemented to confirm the presence of polycrystal domains with a 60° lattice misorientation and a mirror twin grain boundary. Detailed analysis of the grain boundary and molybdenum atom distribution was assessed using high-resolution, high angle annular dark-field scanning transmission electron microscopy (HAADF-STEM). The relationship of the growth morphology of WS₂ stars and the molybdenum to tungsten ratio of the precursor was also carefully investigated. In corroboration with the experimental results, we further developed a multiscale model which combines density functional theory and the Wulff construction, for the observed morphology evolution of WMoS₂ domains as a function of local chemical environment during growth. Our study provides further insights into controlling the morphology of crystalline TMD monolayers.

References:

1. Wang, Q. H., Kalantar-Zadeh, K., Kis, A., Coleman, J. N., & Strano, M. S. (2012). *Nature nanotechnology*, 7(11), 699-712.
2. Tong, W. Y., Gong, S. J., Wan, X., & Duan, C. G. (2016). *Nature communications*, 7(1), 1-7.
3. Dong, J., Liu, Y., & Ding, F. (2022). *NPJ Computational Materials*, 8(1), 1-11.

NM06.05.28

Investigating Substrate Effects on WTe₂ Thin-Film Growth David Hynck¹, Elifnaz Onder¹, James L. Hart², Gangtae Jin², Mengjing Wang² and Judy Cha²; ¹Yale University, United States; ²Cornell University, United States

WTe₂ is a 2D transition metal dichalcogenide, which exhibits large magnetoresistance, superconductivity, and quantum spin Hall states, and is a predicted type-II Weyl semi-metal, making it an ideal candidate material to study for next-generation electronic and spintronic devices. Currently, wafer-scale growth of 2D transition metal tellurides such as WTe₂ remains difficult to achieve due to the lack of stable Te precursors for processes such as atomic layer deposition (ALD) and metal-organic chemical vapor deposition (MOCVD), and an incomplete understanding of the growth dynamics such as the effects of substrate interactions during growth. For scalable and reproducible synthesis to be achieved, more mechanistic studies are needed.

Here, we investigate the role of the growth substrate (sapphire and SiO₂) on the direct synthesis of WTe₂ thin films. Previously, we showed that the choice of growth substrate impacts the phase stability and large-scale uniformity for transition metal ditelluride films such as MoTe₂ (*CrystEngComm* **2021**, 23, 7963–7969). WTe₂ thin films are synthesized using methods previously developed by our group for the large-scale growth of MoTe₂ (*ACS Nano* **2021**, 15, 410–418) where ALD grown WO₃ precursor thin films are converted to WTe₂ by annealing at high temperatures in a tellurium-rich environment. Using a range of characterization techniques such as Raman spectroscopy, transmission electron microscopy, and x-ray photoelectron spectroscopy, we find that there are impacts from the substrate on the growth dynamics of WTe₂ thin films that range from changes in optimal growth time to differences in morphology for films with the same starting oxide precursor thickness on sapphire vs SiO₂.

NM06.05.29

Ultrasonic Spray Deposited 1T-MoS₂ for In-Plane Microsupercapacitors Deniz Keskin, Mustafa C. Gorur, Mete Batuhan Durukan and Husnu E. Unalan; Middle East Technical University, Turkey

The rapid growth of portable, flexible and wearable small devices and integrated electronics has increased the need for on-chip and small-scale energy storage devices such as micro-supercapacitors. Micro-supercapacitors can be integrated into series or parallel with miniature electronic devices and provide long life and fast charge/discharge rate. Moreover, by using the interconnected coplanar electrode architecture, rate capacity and power density can be further increased as the structure provides a high active surface area. Molybdenum disulfide (MoS₂) attracted lots of interest with successful demonstrations in applications such as electrocatalysts, transistors, and especially energy storage devices. 1T-MoS₂ is metallic and has favorable electrochemical properties owing to the layers' ability to expand and intercalate ions with high electrical conductivity. In this work, the ultrasonic spray coating method was used for the deposition of 1T-MoS₂ thin films on desired substrates. Firstly, a result of 264 F/g specific capacitance was obtained through cyclic voltammetry with a 5 mV/s scan rate in a three-electrode setup with a KOH electrolyte. Then, a simple laser ablation method was utilized to fabricate interdigitated finger electrodes to obtain 1T-MoS₂ micro-supercapacitors. The capacitive behavior of 1T-MoS₂ was investigated through cyclic voltammetry, galvanostatic charge-discharge, and impedance spectroscopy. Detailed analysis of the capacitive behavior will be presented with the comparison of patterning and amount/thickness of the active material. With the integration of micro-supercapacitors, many forward-looking flexible, wearable and portable devices in various applications can be developed.

This work was supported by The Scientific and Technological Research Council of Turkey (TUBITAK) under Grant No:220M003.

NM06.05.31

Phase-Selective Heteroepitaxy of Tetravalent-Doped Ruddlesden-Popper Structure La_{n+1}Ni_nO_{3n+1} Thin Films Akifumi Matsuda¹, Yuki Goto¹, Kazuya Kawamura¹, Kenta Kaneko¹, Satoru Kaneko^{2,1} and Mamoru Yoshimoto¹; ¹Tokyo Institute of Technology, Japan; ²Kanagawa Institute of Industrial Science and Technology, Japan

Ruddlesden-Popper phase nickelates with formula A_{n+1}Ni_nO_{2n+1} also exhibit noteworthy electronic properties based on their 2D-layered perovskite structure and mixed valence state of Ni ions^[1]. Recently, Nd_{1-x}Sr_xNiO₂ and La_{1-x}Ca_xNiO₂ thin film was reported to reveal superconductivity, which material is composed of NiO₂ layers with square-planar coordination reduced from the Ruddlesden-Popper structure of NdNiO₃ and LaNiO₃^[2,3]. The layer number "n" in Ruddlesden-Popper phase La_{n+1}Ni_nO_{3n+1} has an impact on physical properties such as conductivity via modification of Ni-ion valence. Thus, phase-selective epitaxial growth of La_{n+1}Ni_nO_{3n+1} thin films is of importance. In addition, property control of La_{n+1}Ni_nO_{3n+1} by doping divalent impurities to substitute La³⁺ has been studied as mentioned above. Obtaining further knowledge of the effect of aliovalent doping to epitaxial lanthanum nickelate films on their crystal growth and structure would advance understanding and control of properties in 2D-layered nickelates. In this study, phase-selective epitaxial formation of Ruddlesden-Popper structure La_{n+1}Ni_nO_{3n+1} (n=2, 3, ∞) was obtained by control of growth rate and O₂ pressure. In addition, the effect of tetravalent doping on structure and property was also investigated.

The thin films were grown by pulsed laser deposition (PLD) technique equipped with a KrF excimer laser (λ=248 nm). Sintered target of Sn⁴⁺ and Hf⁴⁺ doped (0.625 at% for each) La₄Ni₃O₁₀ was used as well as the pure one. Single crystal LaAlO₃ (100) and NdGaO₃ (100) substrates were used with respect to their small planar lattice mismatch of 1.94% and 0.34% with La_{n+1}Ni_nO_{3n+1} (001), respectively. Laser fluence was fixed at ~1.2 J/cm², and repetition was varied from 2 to 10 Hz. The growth took place in partial O₂ pressure (pO₂) of 0.1–50 Pa at substrate temperature up to 750°C. According to the XRD measurement, epitaxial growth of La₃Ni₂O₇ (n=2) in which crystal Ni²⁺ and Ni³⁺ contents are balanced and LaNiO₃ (n=∞) comprising only Ni³⁺ was obtained on LaAlO₃ (100) by PLD at 680°C in pO₂ of 10 and 50 Pa, respectively. La₄Ni₃O₁₀ (n=3) film was epitaxial on NdGaO₃ (100) by PLD at 700°C in pO₂ of 10 Pa and subsequent O₂-annealing at 950°C; the imbalance of Ni²⁺ and Ni³⁺ required more controlled oxidizing condition in the crystal growth. The epitaxial relationships were as follows; La₃Ni₂O₇ (001)<110>//LaAlO₃ (100)<001>, LaNiO₃ (001)<110>//LaAlO₃ (100)<001>, and La₄Ni₃O₁₀ (001)<110>//NdGaO₃ (110)<001>. Thus, phase-selective epitaxy of tetravalent-doped Ruddlesden-Popper structure La_{n+1}Ni_nO_{3n+1} (n=2, 3, and ∞) films

was obtained. The dopants in the films slightly shifted diffraction peaks to lower angle, that substitution of Ni-ions with ratio smaller than La^{3+} was suggested. The Sn and Hf doped $\text{La}_3\text{Ni}_2\text{O}_7$, $\text{La}_4\text{Ni}_3\text{O}_{10}$, and LaNiO_3 epitaxial thin films in this study demonstrated increasing resistivity along decrease of measurement temperature. The resistivity of above mentioned epitaxial thin films were 1.2×10^{-3} , 1.1×10^{-3} , and $5.4 \times 10^{-4} \Omega\text{cm}$, respectively at room temperature, which was improved compared to previously reported bulk materials. The results of detailed structural analyses and property measurement, as well as the effect of post-depositional thermal treatment would also be discussed.

[1] S. N. Ruddlesden and P. Popper, *Acta Crystallogr.*, 11 (1958) 54–55.

[2] D. Li et al., *Nature*, 572 (2019) 624–628.

[3] S. Zeng et al., *Sci. Adv.*, 8 (2022) eabl9927.

NM06.05.32

Atomistic Synapse Networks on Atomically Thin van der Waals Photo-Memtransistors Geonho Mun^{1,2}, Seok Young Min^{1,2}, Seung-Young Seo^{1,2}, Cheolhee Han^{1,2}, Suk-Ho Lee^{1,2}, Heonsu Ahn^{1,2}, Feng Ding², Seyoung Kim¹ and Moon-Ho Jo^{1,2}; ¹Pohang University of Science and Technology, Korea (the Republic of); ²Institute for Basic Science, Korea (the Republic of)

We report a new type of atomistic synaptic networks on an atomically thin van der Waals (vdW) heterostructure, where the two-dimensional (2D) tungsten disulfide (WS₂) semiconductor serves as a gate-tunable photoactive layer between a pair of single-layer graphene electrodes, as we dubbed a photo-memtransistor. A train of ultraviolet (UV) pulses on to the WS₂ memristor generate dopants in atomic-level precision, enabling reconfigurable modulation of the channel conductance. Such photo-induced conductance modulation can be explained by a parallel resistor network model, enabling the accurate operation of the synaptic dynamics of the memristor. In addition, we show that such device operation is not only limited to WS₂, but generally realized in other 2D vdW semiconductors. In this work, demonstration of atomically thin photo-memtransistor arrays, where the synaptic weights can be tuned in atomistic precision, provides implications for a new type of artificial neural networks for parallel matrix computations with a high integration density.

NM06.05.33

Large-Scale Heteroepitaxial Growth of 2D Single-Crystalline WSe₂/WS₂ Suk-Ho Lee^{1,2}, Cheolhee Han^{1,2} and Moon-Ho Jo^{1,2}; ¹IBS, Korea (the Republic of); ²POSTECH, Korea (the Republic of)

We report atomic layer-by-layer growth of epitaxial van der Waals (vdW) semiconductor WSe₂/WS₂ superlattices (SLs). Metal-organic chemical vapor deposition (MOCVD) enables vertically stacking of atomically thin semiconductors with programmable stacking periodicities. Moreover, single-crystalline vdW semiconductor growth was achieved on stepped substrate. Systematic studies for single-crystalline homoepitaxial stacking will be discussed. VdW epitaxy was kinetically controlled to achieve anisotropic two-dimensional growth without interlayer atomic mixing, resulting in the tunable two-dimensional (2D) vdW electronic systems. Each monolayer stacking was verified by transmission electron microscope (TEM) studies & optical characterization (photoluminescence, absorbance). Finally, we show electronic & optoelectronic property of our WSe₂/WS₂ vdW superlattices. Our work suggests on synthetic material platform of 2D vertical p,n junction devices & multiple quantum well devices.

NM06.05.34

Designing Carbon Cluster for Graphene Growth by Molecular Dynamics—Selection of Substrate Material, Crystal Orientation Satoru Kaneko^{1,2,3}, Manabu Yasui¹, Masahito Kurouchi¹, Chihiro Kato¹, Satomi Tanaka¹, Takashi Tokumasu⁴, Shigeo Yasuhara⁵, Tamio Endo⁵, Musa Can⁶, Rwei-Sung Yu⁷, Kripasindhu Sardar², Sumanta Sahoo², Masahiro Yoshimura², Akifumi Matsuda³ and Mamoru Yoshimoto³; ¹KISTEC, Japan; ²National Cheng Kung University, Taiwan; ³Tokyo Institute of Technology, Japan; ⁴Tohoku University, Japan; ⁵Japan Advanced Chemicals, Japan; ⁶Istanbul University, Turkey; ⁷Asian University, Taiwan

The stability of amorphous carbon in the CVD condition causes co-existence of graphene and intrinsic contamination on the surface of the CVD graphene. However, carbon dioxide as a gentle oxidant selectively eliminates intrinsic contamination to form *superflat* surface of a chemical vapor deposition (CVD) graphene as post annealing process[1]. Pulsed laser deposition (PLD) is one of popular physical vapor deposition (PVD) methods with much wider atmospheric environment compared to the CVD. Carbon clusters are generated in a plume by PLD, however, with suitable substrate and crystal orientation, graphitic clusters can be designed to reach and flatly cover the surface of substrates. Molecular dynamics was employed to select suitable substrate of candidates, and graphene was experimentally deposited on the candidate substrates in carbon dioxide atmosphere.

In order to select suitable substrate with suitable crystal orientation for graphene growth, absorptive stability was estimated on carbon cluster designed on candidate substrates; Si(001), Si(111), MgO(100), Al₂O₃ and SrTiO₃. Absorptive stability was evaluated by absorption energy between carbon cluster and candidate substrate. Absorption energy was evaluated to be

$$E_{\text{tot_sub}} + E_{\text{tot_cluster}} - E_{\text{tot_supercell}},$$

where $E_{\text{tot_sub}}$ and $E_{\text{tot_cluster}}$ were total energy of subs and graphitic cluster, and $E_{\text{tot_supercell}}$ was total energy of supercell consisting of cluster placed on candidate substrate. The details of estimation of absorption energy was found in elsewhere[2]. As carbon clusters, a carbon atom, six membered ring (6-ring), and 6 six membered rings (nano graphene) were placed on candidate substrates.

The absorption energy of graphene on SrTiO₃(001) and Si(001) were estimated to be 570 and 550 kJ/mol, respectively. Although graphene grew on SrTiO₃ substrate while DLC related materials grew on Si(001), there was not much difference in absorption energy between SrTiO₃ and Si substrates. However form of six-ring on each substrates was remarkably different after optimal structure in supercell. After optimizing supercell of six ring placed on Si(001), the six ring did not lie on silicon substrate flatly but it stood up vertically on the substrate while a six ring flatly lied on SrTiO₃ substrate. Actually in our experiment, AFM image revealed the growth of nano balls on the surface of silicon substrate while graphene grew with “layer by layer growth” on SrTiO₃ substrate[3]. Among candidate substrate, Si(001), Si(111), MgO(100), Al₂O₃(001) and SrTiO₃, molecular dynamics showed 6-ring and nanographene flatly cover the surface on only SrTiO₃ substrate. AFM images on Si, Al₂O₃ and MgO showed rough surface with Sa ~4.34, 5.63, 4.1 nm, respectively. For graphene growth on SrTiO₃ substrate showed Sa ~63 pm.

In order to select suitable substrate, evaluation of absorptive stability can be good guideline not only for graphene but other functioning materials on variety of substrates. Evaluation of variety of combination of carbon materials and substrates is in progress.

[1] J. Zhang et al., *Angew. Chem. Int. Ed.* 58, 14446 (2019).

[2] S. Kaneko et. Al. *Appl. Surf. Sci.* 586, 152776 (2022).

[3] S. Kaneko et. al. *ACS Omega* 2, 1523 (2017).

NM06.05.35

Switchable Bulk Photovoltaic Effect in Rhombohedral Transition Metal Dichalcogenides Homobilayers Ji-Hwan Baek¹, Seong Chul Hong¹, Yeon Ho Kim², Yeonjoon Jung¹, Chul-Ho Lee² and Gwan-Hyong Lee¹; ¹Seoul National University, Korea (the Republic of); ²Korea University, Korea (the Republic of)

Recently, the ferroelectric property in bilayer rhombohedral phase (3R) transition metal dichalcogenides (TMDs) bilayers was reported both theoretically and experimentally due to the inversion symmetry breaking, while the net electrical polarization in the 2H phase is zero due to the presence of the inversion symmetry. The spontaneous electrical polarization direction of 3R-TMDs is determined by a stacking sequence of metal (M) and chalcogen (X) atoms, XM- or MX- stacking, where every X atom on the top layer is located over the M atoms on the bottom layer in the XM stacking and vice versa. Not only the ferroelectricity but a bulk photovoltaic effect can be induced from this intrinsic polarization in 3R TMDs bilayers without built-in potential. Here we fabricated 3R TMDs bilayers devices with near-zero twist angle which have triangular domains of the XM and MX stacking are formed alternately, and an area of those domains can be modulated by applying external out-of-plane electric field, because the stacking sequence of M and X atoms are aligned along the direction of the external electric field. As a result, the opposite direction of photocurrent was obtained by changing the sign of the applied gate voltage.

NM06.05.36

Comparison of Pt Nanosheet and Pt Nanoparticles-Decorated Graphene in Aliphatic Alcohol Sensing Properties Yusuke Hamanaka, Takahisa Tanaka and Ken Uchida; The University of Tokyo, Japan

1. Introduction

Detection of aliphatic alcohols in air is important due to its potential application to human health monitoring or safety management in industrial processes. As the material of chemiresistive sensors for aliphatic alcohols such as methanol or ethanol, Pt has attracted a lot of attention because it facilitates the oxidation reaction. In fact, Pt has been utilized for gas sensor applications in the form of nanosheets or nanoparticles [1][2]. However, it has not been fully investigated how the structures, such as nanosheets and nanoparticles, of Pt affect the sensor performance and sensing mechanisms. In this study, we fabricated two different Pt-based aliphatic alcohol resistive sensors. One is Pt nanosheet, and the other is Pt nanoparticles-decorated graphene field effect transistor (Pt-GFET). We evaluated and compared the performance of these two kinds of Pt-based sensors against aliphatic alcohols: ethanol and heptanol.

2. Method

2.1. Fabrication of Pt nanosheet

3-nm-thick Pt was deposited on 90-nm-thick SiO₂ layers above bulk Si substrate by electron beam deposition. The length and width of the nanosheet were 3400 μm and 200 μm, respectively. Then, Cr and Au were also deposited as electrodes in the same manner.

2.2. Fabrication of Pt-GFET

Graphene transistors with the channel of 200-μm length and 50-μm width were fabricated using a monolayer graphene grown by chemical vapor deposition. Then 0.5-nm-thick Pt was deposited by electron beam deposition and annealed at 250 °C in N₂ atmosphere for 30 min to agglomerate it.

2.3. Alcohol sensing measurement

The sensing measurements were performed by measuring the resistance change of the sensors as the sensor responses during continuous exposure to dry air, 100-ppm ethanol or 100-ppm heptanol in dry air. Sensor outputs, namely the resistance change of the sensors, were measured at 200 °C using a Keithley 2636A source meter at constant biases. The constant biases were 0.1 V and 0.05 V for Pt nanosheets and Pt-GFETs, respectively.

3. Results and Discussion

Pt nanosheets and Pt-GFETs showed the resistance change under ethanol and heptanol atmospheres, demonstrating that both the devices worked as aliphatic alcohol sensors. Pt nanosheet showed the greater responses than Pt-GFET for both the alcohols. Although the magnitude of the response was small, Pt-GFET showed a larger response to heptanol than to ethanol, which differs from the fact that the responses of Pt nanosheet to these alcohols were almost the same. This may arise from the attractive interactions between graphene and the analytes. Graphene attracts aliphatic alcohols through CH/π interaction [3], and the interaction would be stronger as alkyl chain length increases. Therefore, the stronger adsorption of heptanol on graphene may facilitate the reaction of heptanol with Pt. This indicates that in designing gas sensors using Pt nanoparticles, the interaction between the supporting material and the analyte may have a significant influence on the sensor performance. In the same manner, it may be possible to enhance the sensitivity of Pt nanosheet sensor by choosing the substrate material that has a stronger interaction with the analyte.

4. Conclusion

In this study, we evaluated the sensor performance of Pt nanosheet and Pt-GFET against ethanol and heptanol. While the Pt nanosheet sensor showed almost the same response to these alcohols, Pt-GFET sensor showed a greater response to heptanol with a longer alkyl chain. We plan to further investigate the effect of substrate material on sensor performance of Pt nanosheet. In addition, we will compare the response and recovery speed to elucidate the reaction mechanisms.

Acknowledgement

This work was partly supported by JST CREST Grant Number JPMJCR1912 and JSPS KAKENHI Grant Number 19H00756, 18H05423.

References

- [1] T. Tanaka *et al.*, *Sens. Actuators B Chem.*, **258**, 913 (2018).
- [2] J. Wang *et al.*, *Sens. Actuators B Chem.*, **220**, 755 (2015).
- [3] X. Wang *et al.*, *J. Mater. Des.*, **139**, 372 (2018).

NM06.05.37

Towards Recyclable Nanofiltration Membranes—Oxidised Boron Nitride-Layered Double Hydroxide Hybrid Membranes for Water Purification and Photocatalysis Aine Coogan¹, Natalia Garcia Doménech¹, Quentin Fedix², Amy Donlan¹, Finn Purcell-Milton^{1,3} and Yurii K. Gun'ko¹; ¹Trinity College Dublin, The University of Dublin, Ireland; ²Institut universitaire de technologie Clermont-Auvergne, France; ³Technological University Dublin, Ireland

Access to clean water has becoming increasingly scarce in recent years due to various factors, such as increasing population density, urbanisation, climate change and inequality, among others. The development of new, inexpensive, and reliable methods of the removal of various pollutants and toxins from water is vitally important. In recent years, the emergence of 2D nanomaterial-based nanofiltration (NF) membranes has become an exciting prospect for water purification.¹ In particular, boron nitride (BN)-based membranes have been shown to be very effective in the removal of various dyes from water, that are often leached into wastewater by the textile industry.² While these membranes show excellent performances for the removal of the dyes, they suffer from one major drawback – normally they are not reusable. The interest in layered double hydroxides (LDHs) has experienced a resurgence in recent years,

due to their ease of synthesis and tunability, which gives rise to a vast number of applications, ranging from biomedical, to electronic, to catalytic.³⁻⁶

Here we report a variety of LDHs (including Cu- and Cr- containing LDHs) which have been synthesised by co-precipitation techniques. These LDHs were used as components for production of hybrid NF membranes with oxidised BN (BNOx). These membranes have been prepared by exfoliation and vacuum filtration. The novel, hybrid BNOx-LDH membranes exhibited retentions of up to > 99% for methyl orange (MO) dye. These membranes also demonstrated photodegradation of the dye under UV and visible light conditions. By observation of the colour change of different MO-loaded membranes over time, as well as kinetic studies, we show that the strong photocatalytic properties of these membranes are as a result of the presence of LDHs. We believe this work represents a significant step towards achieving the goal of high-performance, recyclable, and cost-effective nanofiltration membranes.

References:

- 1 - N. García Doménech, F. Purcell-Milton and Y. K. Gun'ko, *Mater. Today Commun.*, 2020, **23**, 100888.
- 2 - N. García Doménech, F. Purcell-Milton, A. S. Arjona, M.-L. C. García, M. Ward, M. B. Cabré, A. Rafferty, K. McKelvey, P. Dunne and Y. K. Gun'ko, *Nanomater.* 2022, **12**, 473.
- 3 - S. Berner, P. Araya, J. Govan and H. Palza, *J. Ind. Eng. Chem.*, 2018, **59**, 134–140.
- 4 - J. Li, S. Zhang, Y. Chen, T. Liu, C. Liu, X. Zhang, M. Yi, Z. Chu and X. Han, *RSC Adv.*, 2017, **7**, 29051–29057.
- 5 - K. Abderrazek, N. F. Srasra and E. Srasra, *Clay Miner.*, 2017, **52**, 203–215.
- 6 - N. Baliarsingh, K. M. Parida and G. C. Pradhan, *Ind. Eng. Chem. Res.*, 2014, **53**, 3834–3841.

NM06.05.38

Numerical Study of a Capacitive Graphene Oxide Humidity Sensor with Etched Configuration Meriam Mohammedure; TII, United Arab Emirates

The geometrical dependence of humidity sensors on sensing performance has not been quantitatively outlined. Furthermore, the etching effect on humidity sensors is still elusive due to the difficulty in separating the effects of the geometrical change and etching-induced porosity on the overall performance. Here, we use COMSOL Multiphysics to perform a numerical study of a capacitive graphene oxide (GO) humidity sensor, with emphasis on the dimensions and etching effect on their sensing performance. GO is a useful and promising material in detecting humidity because of its selective superpermeability to water molecules. The mechanism of improved sensing performance of the etched humidity sensors is discussed in terms of the morphological profile and the effective permittivity including the etching-induced porosity effect. Our study shows that as compared to the unetched sensors, isotropic etching achieves the lowest response time of 1.011 s at 15.75% porosity, while vertical etching achieves the highest capacitance sensitivity of 0.106 fF/RH %.

NM06.05.39

Thermal Sculpting of 2D TMDs Nanocircuits for Large-Scale Nanoelectronics Giorgio Zambito, Maria Caterina Giordano, Matteo Gardella and Francesco Buatier de Mongeot; University of Genoa, Italy

Two-dimensional (2D) Transition Metal Dichalcogenide semiconductors (TMDs) have recently gained lots of interest as promising platforms for new-generation electronic and optoelectronic devices [1-5]. In most cases, proof-of-concept devices have been fabricated by exploiting mechanically exfoliated flakes, which suffer from stochastic positioning and shape, along with limited size at the microscale. Also, the re-shaping of 2D materials represents an interesting possibility for tailoring optoelectronic properties of 2D TMDs, as well as enabling the fabrication of devices with controlled geometries. One way to achieve such re-shaping of exfoliated microflakes is based on state-of-the-art lithography combined with chemical etching (i.e., subtractive approach) which introduces contaminations of the 2D material and, although effective for proof-of-concept device, is not suitable for scalable devices. In this work we show a novel additive nanofabrication approach for creating deterministic TMDs nano-circuits based on few-layer MoS₂, through the combination of large-area Ion Beam Sputtering growth and thermal-Scanning Probe Lithography (t-SPL) [6]. This latter technique enables the control of a hot silicon nanoprobe (radius ~ 10nm) which can be transiently heated by Joule effect and employed as a high-resolution lithographic tool. Indeed, we exploit t-SPL to write deterministic nanopaths onto a sacrificial polymer layer. These nanopatterns spread over a large-area substrate are homogeneously coated by a few-layer MoS₂ film via a custom-made physical deposition system based on the Ion Beam Sputtering of a MoS₂ target. This additive approach allows us to fabricate well-defined few-layer MoS₂ nanopaths with sharp-edges, that are deterministically located over large-scale substrates. After high temperature recrystallization the few-layer TMDs nanopatterns show clear Raman spectroscopy features and optoelectronic response characteristic of the few-layer 2H-MoS₂ semiconducting phase.

We finally engineered high-resolution 2D TMDs nanodevices to investigate the electronic transport properties of these layers via Kelvin Probe microscopy and conductive – AFM imaging. The high-resolution imaging of the local electronic response demonstrates that these few-layer MoS₂ nanocircuits are endowed with competitive transport properties and represent a suitable platform for ultra-thin semiconducting interconnections in integrated electronic and optoelectronic devices.

In conclusion, we demonstrate a novel route for large-area growth and deterministic nanopatterning of few-layer TMDs, which represents an enabling technology for the future fabrication of in-series devices based on 2D semiconducting Van der Waals materials.

- [1] Wang, Q. et al., *Nature Nanotech.* 7, 699–712 (2012).
- [2] C. Martella et al., *Adv. Mater.*, 2018, 30, 1705615.
- [3] M. Bhatnagar et al., *Nanoscale*, 2020, 12, 24385–24393.
- [4] M. Bhatnagar et al. *ACS Appl. Mater. Interfaces* 2021, 13, 11, 13508–13516
- [5] C. Mennucci et al. *Adv. Optical Mater.* 2021, 9, 2001408.
- [6] M.C. Giordano et al, “Deterministic Thermal Sculpting of Large-Scale 2D Semiconductor Nanocircuits”, under review, Department of Physics, University of Genova, 2022.

NM06.05.40

Nanostructuring of WS₂, MoS₂ and PdS by Salt-Assisted Milling in NaCl and KCl Tabbetha A. Dobbins and Denise Omoruyi; Rowan Univ, United States

Salt-assisted milling has been reported in the literature to yield individual, exfoliated, layers of transition metal dichalcogenide (TMDs). TMDs are commonly used as catalysts in methane conversion to liquid fuels and for hydrotreatment to reduce sulfides, nitrides, and aromatics yielding. Bond strength is a key parameter for catalytic efficiency. Bond strength scales inversely with bond length (in many materials). In this work, XAFS is used to quantify bond length. Nanoconfinement will improve efficiency of reaction by permitting longer times for methane interaction with the catalyst. USAXS is used to measure catalyst size. This project measures bond length, electronic structure, and particle sizes for the nanostructured transition metal dichalcogenide (TMD) catalysts MoS₂, PdS and WS₂. Published literature gives a mechanism for the effectiveness of salt-assisted milling based on mechanical interactions with no data reported on Na/K-M, Na/K-S (where M = Mo, Ti, or W) chemical interactions.[1] Results gained will yield new insights to the literature. If M-S bond lengthening is observed, it could explain the hierarchy of catalytic efficiency among the TMDs.

[1] Han, C. et al. High-Yield Production of MoS₂ and WS₂ Quantum Sheets from Their Bulk Materials. *Nano Lett.* 17, 7767–7772 (2017).

NM06.05.41

Size and Quality Enhancement of 2D Semiconducting Metal–Organic Chalcogenolates by Amine Addition [Watcharaphol Paritmongkol](#), Tomoaki Sakurada, Woo Seok Lee, Ruomeng Wan, Peter Müller and William Tisdale; Massachusetts Institute of Technology, United States

The use of two-dimensional (2D) materials in next-generation technologies is often limited by small lateral size and/or crystal defects. Here, we introduce a simple chemical strategy to improve the size and overall quality of 2D metal–organic chalcogenolates (MOCs), a new class of hybrid organic–inorganic 2D semiconductors that can exhibit in-plane anisotropy and blue luminescence. By inducing the formation of silver–amine complexes during a solution growth method, we increase the average size of silver phenylselenolate (AgSePh) microcrystals from <5 μm to >1 μm, while simultaneously extending the photoluminescence lifetime and suppressing mid-gap emission. Mechanistic studies using ⁷⁷Se NMR suggest dual roles for the amine in promoting the formation of a key reactive intermediate and slowing down the final conversion to AgSePh. Finally, we show that amine addition is generalizable to the synthesis of other 2D MOCs, as demonstrated by the growth of single crystals of silver 4-methylphenylselenolate (AgSePhMe), a novel member of the 2D MOC family.

NM06.05.42

TiO₂-Based 1D Nanofilaments and 2D Flakes—Bottom-up, Scalable Synthesis and Their Electronic Structures Revealed by Transient and Steady-State Optical Absorption and Photoelectron Spectroscopy [Hussein Badr](#)¹, Erika Colin-Ulloa², Julia Martin², Ryan Hanna², Michelle Frasch², Rebecca R. Ramthun², Michel W. Barsoum¹, Ronald L. Grimm² and Lyubov Titova²; ¹Drexel University, United States; ²Worcester Polytechnic Institute, United States

We recently demonstrated scalable, one-pot synthesis of TiO₂-based one-dimensional, 1D, nanofilaments that self-assemble in two-dimensional flakes, 2D. Simply, we immerse a dozen of cheap, earth-abundant, non-toxic, water-insoluble, precursors such including TiC, TiN, TiSi₂ in tetramethylammonium hydroxide aqueous solution at 50–80 °C for tens of hours. The resulting structures, morphologies, chemical compositions were characterized using a battery of characterization techniques. That study revealed a large band gap energy, $E_g \approx 4.0$ eV, and the presence of intra-gap defect states based on Tauc plots of UV-Vis absorbance data. Here we probe the electronic structure with a combination of transient absorption (TA) spectroscopy with sub-band-gap, visible-light illumination as well as ultraviolet photoelectron spectroscopy (UPS). UPS spectra demonstrate a work function of 4.0 ± 0.3 eV vs vacuum and a Fermi energy of 3.8 ± 0.1 eV with respect to the valence band edge. Sub-gap optical excitation in 1D/2D nanostructures synthesized from TiC results in photoexcitations with lifetimes in excess of nanoseconds. In combination with the established oxidative stability, long-lived visible photoexcitations and optical emission bring forward possible applications of 1D/2D nanostructures in photocatalysis and optoelectronic applications.

NM06.05.43

Solution-Processable Fabrication of Nanoporous Ag Structures and Patterns by Coating, Printing and Imprinting of Ionic Ag Ink Layers Toward Functional Electronic, Photonic and Sensing Applications [Minwook Kim](#), Kwangjun Kim and Jong G. Ok; Seoul National University of Science and Technology, Korea (the Republic of)

Silver films possess excellent thermal and electrical conductivity and form unique nanoporous morphology based on high surface tension when melting, spurring many applications in flexible electrodes, optics, and sensors. However, the conventional vacuum deposition process for forming a silver thin film entails limitations in substrate material and area, low productivity, and high process cost. Addressing these issues, we demonstrate cost-effective and scalable solution-processable manufacturing of nanoporous silver thin films based on the coating of ionic Ag ink and its mild thermal annealing for Ag reduction [1]. The process can be implemented through spin coating of ionic Ag ink and heat treatment (~180 °C) on various substrates such as silicon, glass, and polymer films. By tuning ink concentration, coating speed, and annealing temperature, the thin film's surface morphology (porosity) and thickness can be quantitatively controlled. This also leads to facile control of optical transmittance and electrical conductivity of the nanoporous silver thin film. Moving forward, we can create the patterned Ag structures by adopting various lithography techniques involving photolithography and nanoimprint lithography. For instance, a polydimethylsiloxane (PDMS)-made mold can be used for transfer printing and soft contact nanoimprinting of solution-processable nanoporous silver thin films [2]. Controlling the strain of a PDMS mold at contact further enables the modulation of printed/imprinted silver patterns for specific uses (e.g., tuning of resonance wavelength). Another useful function of the nanoporous Ag film is that it can be used as a seed layer for hydrothermal synthesis of zinc oxide nanowires (ZNWs) [3]. Practically utilizing this method to developing flexible and transparent sensors, ZNWs can be selectively grown on photolithography-patterned Ag mesh or interdigitated electrodes. Many diverse devices and systems can benefit from this work, including but not limited to sensors, electronics, photonics, and energy harvesters, some of which are in progress for future reports.

Acknowledgment

This work was supported by the National Research Foundation of Korea (NRF) grants (No. 2020R1F1A1073760, No. 2021M3H4A3A02099204, and 2022M3C1A3090850 (Ministry of Science and ICT) and No. 2022R111A2073224 (Ministry of Education)) funded by the Korean Government.

References

1. J. D. Kim*, H. Choi*, K. Kim*, H. Chae*, H. Yi, M. H. Jeong, N. Lee, M. Lee, M. C. Kim, J. W. Suk, K.-T. Lee, H. E. Jeong, and J. G. Ok (*equal contributions), Ionic solution-processable Ag nanostructures with tunable optical and electrical properties and strong adhesion to general substrates, *Applied Materials Today* 27, 101475 (Jun 2022). <https://doi.org/10.1016/j.apmt.2022.101475>
2. M. Kim*, D. K. Oh*, J. D. Kim*, M. Jeong, H. Kim, C. Jung, J. Song, W. Lee, J. Rho, and J. G. Ok (*equal contributions), Facile fabrication of stretchable photonic Ag nanostructures by soft-contact patterning of ionic Ag solution coatings, *Nanophotonics* 11 (11), 2693–2700 (Jun 2022). <https://doi.org/10.1515/nanoph-2021-0812>
3. H. Choi*, K. Kim*, M. Kim*, J. D. Kim, I. Cho, I. Kim, H. Chae, I. Han, H. Kim, J. H. Seo, H. W. Baac, I. Park, and J. G. Ok (*equal contributions), Solution-processable Ag-mediated ZnO nanowires for scalable low-temperature fabrication of flexible devices, *ACS Applied Electronic Materials* 4 (3), 910–916 (Mar 2022). <https://doi.org/10.1021/acsaelm.2c00035>

NM06.05.44

Fast and Efficient Electrochemical Thinning of Ultra-Large Supported and Free-Standing Molybdenum Disulfide Layers on Gold Surfaces Nicollí Freitas¹, Bianca Rocha Florindo¹, Vitória M. Freitas¹, Maria H. Piazzetta¹, Carlos A. Ospina¹, Jefferson Bettini¹, Mathias Strauss¹, Edson R. Leite¹, Angelo L. Gobbi¹, Renato S. Lima¹ and [Murilo Santhiago](#)^{1,2}; ¹Brazilian Nanotechnology National Laboratory, Brazil; ²Universidade Federal do ABC, Brazil

Molybdenum disulfide (MoS₂) is a very promising layered material for electrical, optical and electrochemical applications. Among different preparation routes, electrochemistry has gain interest due to its simple, fast, scalable and simple instrumentation. However, obtaining large-area monolayer MoS₂ that will enable the fabrication of novel electronic and electrochemical devices on the basal plane is still challenging. In this work, we explored the high affinity

of MoS₂ by gold surfaces and reported a fast electrochemical method that promotes the thinning of bulk MoS₂ down to a monolayer. By selecting a proper applied potential, more than 90% of the bulk regions can be removed from large-area MoS₂ crystals while preserving the first layer attached to the electrode. The thinning process was confirmed by optical microscopy, atomic force microscopy, photoluminescence, and Raman spectroscopy. The hyphenation of electrochemistry and optical microscopy revealed that the thinning process starts at the edges and moves in the direction of the center of the flake and it was used to estimate the thinning area and thinning rate. Finally, we will demonstrate the preparation of large-area and free-standing MoS₂ monolayers using microfabricated microhole-structured Ni/Au meshes [1].

References:

[1] Freitas, N.; Florindo, B. R.; Freitas, V. M. S.; Piazzetta, M. H. O.; Ospina, C. A.; Bettini, J.; Strauss, M.; Leite, E. R.; Gobbi, A. L.; Lima, R. S.; Santiago, M.; *Nanoscale*, 2022, 14, 6811-6821

NM06.05.46

Magnetic Property Transition of Layered Antiferromagnet MnPS₃ via Organic Ion Intercalation Min-kyung Jo^{1,2}, Seorin Cho¹, Jun Woo Choi³, Gichang Noh^{3,1}, Eoram Moon¹, Jeongtae Kim², Kibum Kang¹ and Seungwoo Song²; ¹Korea Advanced Institute of Science and Technology, Korea (the Republic of); ²Korea Research Institute of Standards and Science, Korea (the Republic of); ³Korea Institute of Science and Technology, Korea (the Republic of)

Since the discovery of the intrinsic vdW magnets with atomic thickness in 2017, they have gained much attention as potential materials for high-speed and low-power spintronic devices. The intercalation is an effective property tuning method of vdW materials in that it leads to a high amount of charge doping, or the vacancy formation in the lattice depending on the intercalation mechanism, and interlayer expansion. Because these parameters are highly related to the exchange interaction between magnetic atoms, intercalation could result in the magnetic property change of 2D materials. In this study, we tuned the magnetic properties of a layered Heisenberg antiferromagnet MnPS₃ via the facile intercalation method of the TMA⁺ (tetramethylammonium) ion. After intercalation, MnPS₃ showed a ferrimagnetic behavior with Curie temperature at ~35 K in contrast to the pristine antiferromagnetic behavior with Neel temperature at ~78 K. The drastic change in magnetic property was attributed to the formation of Mn²⁺ vacancies in exchange for the insertion of TMA⁺ ions. The corresponding magnetic-phonon coupling effect was compared between the pristine and intercalated MnPS₃ by analyzing the temperature-dependent Raman spectrums.

NM06.05.47

Near-Unity Valley Polarized State in Gd-Doped WSe₂ Monolayers Byeong Wook Cho^{1,2}, Seong-Gon Kim³ and Young Hee Lee²; ¹Sungkyunkwan University, Korea (the Republic of); ²Center for Integrated Nanostructure and Physics, Korea (the Republic of); ³Mississippi State University, United States

Abstract: Monolayer transition metal dichalcogenides (TMDs) have been regarded as an ideal platform to utilize valley degree of freedom with their inherent spin-valley locking. However, a robust valley polarization, which is essential for potential valleytronic devices, has been only accessible by complicated device structure or external field. Here, we observe near-unity valley polarization in WSe₂ monolayers substitutionally doped with rare-earth Gd atoms synthesized by chemical vapor deposition. The emission from strongly valley polarized state persists up to ~100K, maintaining its high polarizability. It is expected that the emissions are originated from spin up (down) Gd band coupled with conduction band edge at K (K') valley. This finding paves a new way to manipulate valley degree of freedom in monolayer TMDs by means of substitutional doping.

NM06.05.48

The nanoscale thermal properties of isotopically enriched hexagonal boron nitride William D. Hutchins and Patrick E. Hopkins; University of Virginia, United States

In the manufacturing process of semiconductors it is important to catalogue the changes made to a material at all stages of production due to the precise nature of their applications. Titanium Dioxide (TiO₂) is among the most useful semiconductors due to its uses in a variety of applications ranging from pigments to photocatalysis. A major step in the synthesis of thin TiO₂ films is the annealing process which increases crystallinity and forms a homogeneous structure. Thus it is important to study the effects of annealing temperature, and holding time to produce higher quality films. Recent works in thin TiO₂ films focus on crystallography and morphological and optical band-gap phenomena using X-ray diffraction, optical transmission spectroscopy, and electron microscopy, etc. In this work, we use ultrafast pump-probe techniques to study the electron-phonon interactions of un-annealed and annealed TiO₂ films. We find a correlation between these thermal properties and crystal structure.

We use time-domain and steady-state thermoreflectance techniques to map the grain structure and measure the thermal conductivity trends. To study the electron-phonon response a multi-frequency infrared pump probe technique is used. Investigating the ultrafast thermal dynamics of TiO₂ with different annealing parameters allow us to build out a database for how the morphological structure changes, how this structure effects the thermal and optical phonon space, and the dynamic changes caused by an absorption process: the electron-phonon re-normalization. Our findings open a potential window for future investigations about using thermal characterization for annealed semiconductor.

SESSION NM06.06: 2D Material Sensors I
Session Chairs: Lucas Beagle and SungWoo Nam
Wednesday Morning, November 30, 2022
Hynes, Level 2, Room 207

8:00 AM NM06.06.01

SnS₂ Quantum Dots Decorated on Monolayer MoS₂ for High Performance Broadband Photodetector Chandra S. Koll^{1,2}, Venkatarao Selamneni¹, Bárbara Alejandra Muñoz Martínez², Andres De Luna Bugallo³ and Parikshit Sahatiya¹; ¹Birla Institute of Technology & Science Pilani, Hyderabad Campus, India; ²Centro de Investigación y de Estudios Avanzados del Instituto Politécnico Nacional, Mexico; ³Universidad Nacional Autónoma de México, Mexico

Two-dimensional (2D) materials have great optical and electronic properties, which make them excellent for photodetectors and give them a lot of potential uses. Even if there are several approaches to increase the photodetector's responsivity, the electromagnetic spectrum's limited photodetection spectral range is the primary issue limiting the performance of photodetectors. Quantum dots (QDs) of tin sulfide (SnS₂) are wide band gap semiconductors in the ultraviolet and visible spectrums; they display a high optical absorption coefficient and considerable photoconductivity. In addition, recent research reveals

that due to their surface effects and quantum confinement, QDs have excellent local photon trapping capabilities, making them ideal light absorbers that increase the performance of photodetectors combining with them 2D materials. In this study, a 0D/2D SnS₂-QDs/monolayer MoS₂ hybrid for high-performing and wideband (UV, VIS, and NIR) photodetection is created. Utilizing chemical vapor deposition (CVD), monolayer MoS₂ is formed on SiO₂/Si, and SnS₂-QDs are spin-coated processes made using an inexpensive solution process. The increasing 0D/2D MoS₂-SnS₂ photodetector device performance may be attributed to the band bending and built-in potential formed at the junction of SnS₂-QDs and MoS₂, which increases the booster and parting efficacy of the photoexcited charge carriers. The mixed-dimensional construction also reduces the photodetector's dark current. The decorated SnS₂-QDs on monolayer MoS₂ not only enhance the device's performance but also expand its spectral range into the ultraviolet zone. The UV, Visible, and NIR photoresponsivity of the device are 280 A/W, 450 A/W, and 180 A/W, respectively. Due to the high absorbance of a single layer of MoS₂, the devices' highest responsivity was seen in the visible spectrum. The measured reaction time of the fabricated device is 80 milliseconds fast response time. The implementation of the 0D–2D mixed-dimensional heterostructures presented here will expand the design space for next-generation optoelectronic applications, as demonstrated by our results.

8:15 AM NM06.06.02

Printed Graphene FET Biosensors for Multi-Analyte Detection Benji Fenech Salerno, Martin Holicky, Chengning Yao and Felice Torrisi; Imperial College London, United Kingdom

The rise of point-of-care (PoC) diagnostic technology has been insistent and clear. Accelerated by the COVID-19 pandemic, the healthcare industry is transitioning to a future of increased diagnostic digitisation, democratisation, and decentralisation.[1] The World Health Organisation (WHO) set out seven key criteria for PoC devices in the early 2000s.[2] For maximum impact, tests had to be Affordable, Sensitive, Specific, User friendly, Rapid and robust, Equipment-free and Deliverable to end-user, or ASSURED in short. These criteria were revised in 2019 to REASSURED, emphasising the need for Real-time connectivity and Ease of sample collection as well.[3]

Within this context, graphene is an ideal material to develop biosensors as it can be made in a stable, biocompatible manner which supplemented by its high-mobility, semi-metallic electronic properties make it well suited for sensing of biologically relevant analytes.[4] Moreover, graphene can be dispersed as inks, which in combination with other 2D materials (conducting, insulating and semiconducting) offers a route for economical, flexible printed electronics devices on a wearable platform.[5], [6]

In this work, we demonstrate printed graphene field effect transistor (GFET) biosensors for the detection of multiple analytes. Using liquid phase exfoliation (LPE), we optimised an environmentally sustainable graphene-polymer ink. Inks can be tailored to shown concentrations of 0.1 mg/mL to > 10 mg/mL, to allow for variable deposition techniques. Raman spectroscopy indicated that the inks comprised of electronically decoupled layers of graphene. The lateral flake size was characterized by AFM, SEM and TEM, with a likely modal average of 200 nm within a range of flakes extending to 500 nm and mean flake thickness of < 5 nm. The high-quality inks were printed to fabricate transistor devices with reliable and replicable manufacturing, with intra-batch variation of FET electronic properties of < 5 %. The GFETs were subsequently optimised pH detection (resolution of < 0.05 pH), Na⁺ (detection limit < 1 μmol/L) and enzymatic substrates.

References

- [1] A. Bose, "Next-generation Diagnostics Outlook, 2022. Recovery in Routine Testing and Focus on Personalised Diagnostics to Propel Growth," 2022.
- [2] D. Mabey, R. W. Peeling, A. Ustianowski, and M. D. Perkins, "Diagnostics for the developing world," *Nat. Rev. Microbiol.*, vol. 2, pp. 231–240, 2004, doi: 10.1038/nrmicro841.
- [3] K. J. Land, D. I. Boeras, X. S. Chen, A. R. Ramsay, and R. W. Peeling, "REASSURED diagnostics to inform disease control strategies, strengthen health systems and improve patient outcomes," *Nat. Microbiol.*, vol. 4, no. 1, pp. 46–54, 2019, doi: 10.1038/s41564-018-0295-3.
- [4] W. Wen *et al.*, "Recent advances in emerging 2D nanomaterials for biosensing and bioimaging applications," *Mater. Today*, vol. 21, no. 2, pp. 164–177, 2018, doi: 10.1016/j.mattod.2017.09.001.
- [5] T. Carey *et al.*, "Fully inkjet-printed two-dimensional material field-effect heterojunctions for wearable and textile electronics," *Nat. Commun.*, vol. 8, p. 1202, 2017, doi: 10.1038/s41467-017-01210-2.
- [6] S. Qiang, T. Carey, A. Arbab, W. Song, C. Wang, and F. Torrisi, "Wearable solid-state capacitors based on two-dimensional material all-textile heterostructures," *Nanoscale*, vol. 11, pp. 9912–9919, 2019, doi: 10.1039/c9nr00463g.

8:30 AM *NM06.06.03

Graphene Bioimpedance Tattoos for Blood Pressure Monitoring Dmitry Kireev¹, Kaan Sel², Bassem Ibrahim², Roozbeh Jafari² and Deji Akinwande¹; ¹The University of Texas at Austin, United States; ²Texas A&M University, United States

Monitoring complex health-related electrophysiological signals such as arterial blood pressure (BP) in ambulatory settings is essential for a proper understanding of health conditions, predominantly cardiovascular diseases. Moreover, continuous long-term monitoring of BP for patients with sleep apnea, stroke, or hypertension is essential to understand their health risk factors and build preventative care routines. While conventional ambulatory BP monitoring devices exist, they are uncomfortable, bulky, and intrusive. The common drawbacks of all these systems are their bulkiness and incompatibility with skin's elastic properties, causing sensor's displacement during usage, consequently requiring frequent system re-calibration. Here, we present a unique wearable BP monitoring platform that leverages imperceptible atomically-thin and electrically conductive graphene electronic tattoos (GETs) as the main building block. The GETs are placed over the radial and ulnar arteries on the wrist and subsequently used as current injection and voltage sensing electrodes, measuring arterial bioimpedance. In contrast to any other wearable system, the atomically thin, lightweight, and skin-conformable GETs do not apply any external tension onto the skin during the operation, and able to perform long-term and nocturnal measurements without discomforting the subjects. Using bioimpedance modality allows us to disregard the tattoo-skin interface, which is typically 2-4 orders of magnitude larger compared to tissue impedance, and record only from the areas of interest. Employing a machine learning regression model on the recorded bioimpedance value, we yield effective beat-to-beat detection of diastolic and systolic BP values with IEEE grade-A accuracy. Besides BP, we show that the same Bio-Z signal can be post-processed to estimate person's RR in an entirely wearable and non-invasive manner.

9:00 AM NM06.06.04

3D Printing of Polyvinylidene Fluoride and Layered MoS₂ Composites for Piezoelectric Sensing Md Nurul Islam¹, Rifat Hasan Rupom¹, Aqsa Nazir¹, Rigoberto C. Advincula^{2,3}, Narendra Dahotre¹, Wobong Choi^{1,1} and Yijie Jiang¹; ¹University of North Texas, United States; ²The University of Tennessee, Knoxville, United States; ³Oak Ridge National Laboratory, United States

Flexible and stretchable piezoelectric sensors have numerous applications in wearable electronics, healthcare, and structural health monitoring. Most of them are made from piezoelectric polymer materials such as polyvinylidene fluoride (PVDF) and its copolymers that have limited piezoelectric response. Recent discoveries in two-dimensional materials as high-performance piezoelectric materials provide a promising route to formulating novel composites for sensors and actuators. Here, we develop nanocomposites using PVDF and layered molybdenum disulfide (MoS₂) into 3D printable, stretchable, and

flexible piezoelectric sensors. Ink is formulated by distributing layered MoS₂ into PVDF by high-power vacuum mixing to achieve desired rheological properties for direct ink writing (DIW) 3D printing. We harness the shear stress-induced PVDF dipole mechanical poling and nanomaterial alignment during DIW printing for piezoelectric sensitivity enhancement. A remarkable 87.5% improvement in piezoelectric coefficient is achieved in 3D printed PVDF compared with casted samples. Furthermore, we observe enhancement up to 8.1 and 4.3 times increment in the piezoelectric coefficient for nanocomposites with 8 wt% MoS₂ loading over casted and 3D printed neat PVDF. We thoroughly examine the piezoelectric response enhancement of PVDF by β phase enhancement mechanism as a function of MoS₂ fraction as well as the heterogeneous strain distribution in PVDF-MoS₂ nanocomposite via numerical simulations. In this presentation, we will discuss the experimental analysis and its mechanistic study along with the piezo sensor performance from 3D printed MoS₂-PVDF composite.

9:15 AM NM06.06.05

Implantable Aptamer-Graphene Microtransistors for Real-Time Monitoring of Neurochemical Release *In Vivo* Guangfu Wu and Yi Zhang; University of Connecticut, United States

The real-time monitoring of neurochemical release *in vivo* plays a critical role in understanding the biochemical process of the complex nervous system. Current technologies for such applications, including microdialysis and fast-scan cyclic voltammetry, suffer from limited spatiotemporal resolution or poor selectivity. Here, we report a soft implantable aptamer-graphene microtransistor probe for real-time monitoring of neurochemical release. As a demonstration, we show the monitoring of dopamine with nearly cellular-scale spatial resolution, high selectivity (dopamine sensor >19-fold over norepinephrine), and picomolar sensitivity, simultaneously. Systematic benchtop evaluations, *ex vivo* experiments, and *in vivo* studies in mice models highlight the key features and demonstrate the capability of capturing the dopamine release dynamics evoked by pharmacological stimulation, suggesting the potential applications in basic neuroscience studies and studying neurological disease-related processes. The developed system can be easily adapted for monitoring other neurochemicals and drugs by simply replacing the aptamers functionalized on the graphene microtransistors.

9:30 AM BREAK

10:00 AM *NM06.06.06

Graphene E-Tattoos for Wireless and Mobile Electrodermal Activity Sensing Enabled by Heterogenous Serpentine Ribbons Nanshu Lu; The University of Texas at Austin, United States

Electrodermal activity (EDA) is a skin conductance change that indicates psychological or physiological arousal and has been used as a quantitative index of mental stress levels for decades. State-of-the-art EDA devices suffer from short-term wearability when mounted on the palm or low signal fidelity when measured off palm. Our previous innovation of sub-micron-thick, transparent graphene e-tattoos (GET) [<http://dx.doi.org/10.1021/acsnano.7b02182>, <http://dx.doi.org/10.1038/s41699-018-0064-4>] is ideal for long-term unobstructive and imperceptible EDA sensing on the palm. The filamentary-serpentine-shaped GET is so thin and so soft that it is imperceptible optically and mechanically. However, there still lacks mechanically robust electrical connection to interface GET with rigid circuit boards [<http://dx.doi.org/10.1088/2053-1583/ab4c0f>]. To overcome the orders of magnitude mismatch of stiffness between them, we introduce a novel interface design of heterogeneous serpentine ribbons (HSPR), which refer to serpentine GET overlapping with a serpentine gold ribbon. In comparison with heterogeneous straight ribbons (HSTR), a maximum of 50 folds of strain reduction in GET using HSPR have been confirmed. When the HSPR is clamped end-to-end and subjected to uniaxial tension, its resistance only doubles after 42% of applied strain, which is determined as the stretchability. We also provide a guideline to predict the stretchability of HSPR based on FEM. Furthermore, to prevent the damage of the gold ribbon to contact with the rigid circuit board, a reusable conductive soft interlayer is employed and works both as a vertical via and a mechanical buffer layer which could isolate the mechanical scrubbing from the rigid watch. Finally, the combination of HSPR and a conductive soft interlayer between the GET and a rigid EDA watch enables ~15 hrs of continuous and ambulatory EDA monitoring. This method offers a remedy for the long-standing interconnect challenges between ultrathin e-tattoos and rigid electronics, which could significantly enhance the practical use of e-tattoos.

10:30 AM *NM06.06.08

Graphene-Based Wearable Sensor for Healthcare Monitoring Jong-Hyun Ahn; Yonsei University, Korea (the Republic of)

Biosignals, such as skin temperature, EEG, and ECG, provide information regarding the general condition of the human body and facilitate the diagnosis of various diseases. In this talk, we present a wearable thermal patch with dual functions of continuous skin temperature sensing and thermotherapy for effective self-care treatment and an EEG/EKG sensor with clinical diagnostic function to monitor for abnormal brain and cardiac rhythms in patients. The thermal patch consists of a graphene-based capacitive sensor, a graphene thermal pad, and a flexible read-out board with a wireless communication module. The wearable sensor continuously monitors the temperature variation over a large area of skin area with high resolution and sensitivity and performs thermotherapy via the graphene-based heater mounted at the bottom of the device. Animal studies prove that the proposed system can be used to diagnose various diseases. In addition, EEG/ECG sensor consists of graphene electrodes and read-out circuits with a wireless communication module. The sensor attached to the skin of the head and chest continuously monitors EEG and ECG from the brain and heart. This technology could be useful in the development of convenient and wearable healthcare devices.

11:00 AM NM06.06.10

Covalent Organic Frameworks as Selective AC-Impedimetric Sensor Materials David Moore^{1,2}, Nicholas Glavin¹, Lucas K. Beagle^{2,1} and Ly Tran^{2,1}; ¹Air Force Research Laboratory, United States; ²UES, Inc., United States

Covalent Organic Frameworks (COFs) films hold much promise in material research due to the breadth of properties they possess. They are inherently porous, and clever synthesis can construct nanosheets of almost any pore size or functionalization. Consequently, they have the inherent ability to be species-selective in several ways, such as size, chemical affinity, and tunable physisorption. This is excellent for sensing, but most COFs have the drawback of being insulative, thus making it challenging to form them into direct sensors. Various approaches have been used in literature, but in this talk we will discuss building upon a novel real-time impedance spectroscopy approach that can be sensitive to femtofarad level changes in capacitance to observe changes in permittivity of the COF film as analytes adsorb to the COF directly. Practical challenges and limitations as well as comparisons to other techniques will be discussed.

1:30 PM *NM06.07.01

Additive Manufacturing of Two-Dimensional Material Inks for Ubiquitous Sensors [Mark C. Hersam](#); Northwestern University, United States

Two-dimensional (2D) materials have emerged as promising candidates for next-generation electronic [1], quantum [2], and sensing technologies [3]. With properties ranging from insulating (e.g., hexagonal boron nitride) to semiconducting (e.g., transition metal dichalcogenides) to conducting (e.g., graphene), nearly any electronic device can be fabricated by properly assembling 2D materials into heterostructures [4]. While device prototypes have been demonstrated on idealized research-scale samples, scalable manufacturing remains a challenge for 2D materials. In parallel, the field of printed electronics has made significant progress towards roll-to-roll additive manufacturing based on organic and nanoparticle inks. This talk will explore recent work aimed at uniting these efforts by designing electronic inks that combine the superlative electronic properties of 2D materials with the scalable manufacturing of printed electronics. To achieve this objective, multiple design goals have been concurrently pursued including exfoliation (i.e., optimizing yield, throughput, and flake size), ink formulation (i.e., engineering solvents and stabilizing surfactants and polymers for aerosol, inkjet, gravure, screen, and 3D printing), printed structure morphology (i.e., controlling film morphology and microstructure following printing via solvent evaporation, solvent additives, and curing conditions), and control of interfacial properties (i.e., minimizing interfacial resistance in conductive inks, maximizing capacitance in dielectric inks, and maximizing mobility for semiconductor inks). By achieving high levels of 2D material ink homogeneity and printing fidelity, a variety of high-performance applications have been achieved including electronics, photodetectors, supercapacitors, batteries, and sensors [4-9].

[1] V. K. Sangwan and M. C. Hersam, *Nature Nanotechnology*, **15**, 517 (2020).

[2] X. Liu and M. C. Hersam, *Nature Reviews Materials*, **4**, 669 (2019).

[3] X. Sui, *et al.*, *Materials Today*, **48**, 135 (2021).

[4] M. E. Beck and M. C. Hersam, *ACS Nano*, **14**, 6498 (2020).

[5] V. K. Sangwan, *et al.*, *Advanced Functional Materials*, **31**, 2107385 (2021).

[6] J.-W. T. Seo, *et al.*, *ACS Appl. Mater. Interfaces*, **11**, 5675 (2019).

[7] C. M. Thomas, *et al.*, *ACS Energy Letters*, **7**, 1558 (2022).

[8] K.-Y. Park, *et al.*, *Advanced Materials*, **34**, 2106402 (2022).

[9] C. C. Pola, *et al.*, *2D Materials*, **9**, 035016 (2022).

2:00 PM NM06.07.02

Amplification-Free Detection of SARS-CoV-2 and Respiratory Syncytial Virus Using CRISPR Cas13a and Graphene Field-Effect Transistors [Huijie Li](#), Guangfu Wu, Zhengyan Weng and Yi Zhang; University of Connecticut, United States

The clustered regularly interspaced short palindromic repeats (CRISPR)/CRISPR-associated (Cas) systems have recently received notable attention for their applications in nucleic acid detection. Despite many attempts, most current CRISPR-based biosensors in infectious respiratory disease diagnostic applications still require target preamplifications. This study reports a new biosensor for amplification-free nucleic acid detection via harnessing the trans-cleavage mechanism of Cas13a and ultrasensitive graphene field-effect transistors (gFETs). CRISPR Cas13a-gFET achieves the detection of SARS-CoV-2 and respiratory syncytial virus (RSV) genome down to 1 attomolar without target preamplifications. Additionally, we validate the detection performance using clinical SARS-CoV-2 samples, including those with low viral loads (Ct value > 30). Overall, these findings establish our CRISPR Cas13a-gFET among the most sensitive amplification-free nucleic acid diagnostic platforms to date.

2:15 PM NM06.07.03

Inkjet Printed Graphene Sensors for Electrochemical Detection of Phosphates [Rajavel Krishnamoorthy](#), Thiba Nagaraja and Suprem R. Das; Kansas State University, United States

Phosphate is an essential element in our eco-systems, regulating biochemical reactions starting from living matter/biological cells to environmental presence such as in soils. Both limitation as well as over exposure of phosphates can cause detrimental consequences. As such, continuous monitoring of electrochemically inactive phosphates in real samples is crucial for studying number of applications, such as soil health to human health. The present study aimed at developing graphene-based inkjet printed electrochemical sensors to identify different phosphate ions. Large scale exfoliation of few-layer graphene material was synthesized by liquid phase exfoliation from bulk stacked graphite samples, with an effort to achieve highly conductive graphene inks. Defined patterns of sensing electrodes were fabricated using additively manufactured graphene inks with aid of inkjet printing method. The few-layers of exfoliated graphene was uniformly patterned onto the flexible substrate and forms low resistive conducting network. Structural and morphological characterizations are provided to aid large charge transfer in electrochemical cell. Molybdenum based redox electrochemical species on printed graphene electrodes was applied for wide concentration range detection of phosphates using cyclic voltammetry and amperometry. The performance of inkjet printed electrodes was validated with commercial electrodes by different electrochemical sensor characterization parameters such as sensitivity and limit of detection which showed superior results. The additive manufacturing and phosphate sensing performance of graphene based inkjet printed electrodes could be further utilized for monitoring real-time phosphate sensing using a portable hand held potentiostat.

2:30 PM *NM06.07.04

Integrated Biosensor Platform Based on Graphene Transistor Arrays for Real-Time High-Accuracy Ion Sensing [Mantian Xue](#)¹, Charles Mackin², Wei-Hung Weng¹, Jiadi Zhu¹, Yiyue Luo¹, Shao-Xiong Lennon Luo¹, Ang-Yu Lu¹, Marek Hempel¹, Elaine McVay¹, Jing Kong¹ and Tomas Palacios¹; ¹Massachusetts Institute of Technology, United States; ²IBM Almaden Research Center, United States

Smart sensors, such as sweat sensors, targeting various physiologically relevant biomarkers in biofluids have recently demonstrated great potential for health-tracking and medical diagnosis. Two-dimensional (2D) materials are particularly promising in biochemical sensing applications thanks to their large-surface-to-volume ratio, which allows the sensor channel to be readily modulated upon chemical changes near the surface, translating chemical signals into the electrical or optical domain with enhanced sensitivity. Graphene is the most widely studied material among all 2D materials. It has the largest surface-to-volume ratio and exhibits a number of promising characteristics. Despite advances in material synthesis, large-area integration of devices based on graphene and other novel materials still suffer from strong device-to-device variability caused by intrinsic defects, gate oxide nonuniformities, and parasitic effects. Device fabrication also introduces additional variability in sensor response from batch to batch. Here we demonstrate an approach to overcome the challenges in 2D material-based sensing devices and achieve high performance and enhanced functionality. Rather than focusing on the improvement of intrinsic material quality, fabrication uniformity and surface functionalization, we develop a high-density graphene-based sensor array platform to overcome the large degree of variability of advanced materials. We fabricate arrays (16×16) of graphene devices to provide more than 200 working sensing units for each chip, and configure them into multi-ion sensors by functionalizing the surface with three different ion-selective membranes (ISMs). Ionized calcium, potassium, and sodium were chosen as analytes of interest due to their commonplace in diagnostic tests and their physiological importance in blood, urine, and sweat. We demonstrate near-ideal sensitivity, excellent reversibility, and large detection range for each type of sensor

despite non-uniformity in individual devices. The variations and imperfections in material synthesis and device fabrication can be leveraged by statistical analysis and machine learning algorithms. A profile-matching calibration method utilizing sensor non-uniformity and redundancy is introduced to eliminate the need for multiple calibration solutions, which is especially useful for sensing applications targeting portability and field use. A Random Forest algorithm is used to quantify analyte concentrations in the presence of multiple-ions. The abundance ($N > 200$) and multiplexity of sensors and sensor types are shown beneficial for improving model accuracy. We demonstrate that system-level co-design of sensing arrays and algorithms significantly improves sensor performance thus enabling rapid prototyping and in-depth data analysis in spite of the limitations present in graphene and other advanced 2D materials.

3:00 PM BREAK

4:00 PM *NM06.07.06

Roll-to-Roll Production of Two-Dimensional Electronic Pathogen Sensors Christopher Muratore; University of Dayton, United States

Materials with high surface-to-volume ratios demonstrate exquisite sensitivity and detection limits in diverse molecular sensing applications. Integration of nanowires, nanotubes, and two-dimensional (2D) semiconductors into sensing devices, however, presents challenges inhibiting product development. For example, thousands of trials are required to obtain government approval for point of care diagnostics, yet producing a suitable number of 2D devices via conventional synthesis and fabrication techniques to meet this is not feasible. To realize applications of 2D transducers in ubiquitous low-cost diagnostic devices, new fabrication approaches are required. Processes for high-rate ($> 10^6$ per day) mass-production of low-cost two-dimensional electronic medical diagnostic devices with limits of detection rivaling PCR will be presented. Rapid and inexpensive sensor chip fabrication relies upon laser patterning and crystallization processes in a roll-to-roll physical vapor deposition system. In addition to electronic properties responsive to molecular attachment, the composition of 2D MoS₂ or other transition metal dichalcogenides with tunable sulfur vacancy density facilitates direct functionalization for highly selective analyte binding with antibody fragments or even smaller molecules for enhanced sensitivity. A large supply of unfunctionalized diagnostic devices may therefore be stored to be functionalized with any selective binding agent on-demand to immediately reduce the impact of future disease outbreaks. Materials for large-scale device fabrication were selected to ensure recyclability of the devices for reduced waste stream impact in anticipation of large numbers of devices are consumed daily. A combination of fundamental studies to highlight the role of defects in 2D MoS₂ on the sensitivity and dynamic range of the 2D devices is shown via extensive testing of thousands of mass-produced device measurements of biologically significant concentrations as low as 10 fg/mL of viral proteins and/or other biomarkers as low 10 fg/mL in the presence of interference protein concentrations $> 10^{12}$ times higher than those of the target analytes. Response times for most analytes are 2 minutes or less. Detection of multiple analytes on an array of sensors fabricated on a single flexible chip is straightforward as the laser patterning steps dictating device architecture are adjustable by directing the automated patterning laser with a modified electronic drawing possessing the desired features. Integration of other processes to facilitate production exceeding a million devices daily, such as *in situ* device quality control via high throughput Raman spectroscopy and chip singulation tools is shown for high-yield, low-cost production of devices performance meeting stringent requirements for quantitative analysis of biological samples.

4:30 PM NM06.07.07

Chemiresistive 2D Materials Decorated Angstrom-Level Porous Graphene Oxide for Exceptional Surface Activity Ji-Soo Jang; Korea Institute of Science and Technology, Korea (the Republic of)

Recently, intrinsically metallic two-dimensional (2D) materials have gained major recognition as surface active layers, taking advantage of the abundant highly active adsorption sites and fast charge transfer even at room temperature (RT)¹. Of such materials, black phosphorous (BP) has a puckered orthorhombic 2D atomic structure with extremely high hole mobility ($10,000 \text{ cm}^2 \text{ V}^{-1} \text{ s}^{-1}$) and large surface area²⁻³. 2D MXene is another promising candidate for surface reactors, offering a significantly high electrical conductivity, chemical versatility via surface functionalization, and favorable signal-to-noise ratio (SNR) during operation⁴. Therefore, 2D BP and MXene have triggered enormous research interests in catalysis, energy storage, and chemical sensing. However, unfortunately, low stability of these 2D materials under practical operating conditions remains a critical bottleneck, particularly as they are prone to oxidization under moisture⁵⁻⁶.

In order to guarantee minimal oxidation/deterioration of such BP or MXene required for reliable performances, various encapsulation/protection methodologies have been introduced recently. Nonetheless, adding specific passivation layers was found to prohibit the efficient permeation of any desired molecules to the underlying 2D materials, thus greatly hampering the desired surface activities. Till date, there seems to be an inevitable tradeoff between material performance and chemical stability for the 2D active materials.

Here, we present ultra-stable 2D heterostructures obtained from decorating BP and MXene with few-layer holey graphene oxide (FHGO) membranes. In the resulting system, FHGO serves as a multifunctional passivation layer that shields BP or MXene from oxidative degradation, while allowing the selective diffusion of target gas molecules through its micropores and towards the underlying 2D material. Through a case study of dilute NO₂ sensing, we demonstrate that our hetero-2D structures show greatly enhanced sensing performance under humid conditions, where exceptionally fast sensing speed and response are consistently observed, and high stability is impressively retained upon repetitive sensing cycles for 1,000 min. These results corroborate the efficacy of material decoration with porous FHGO membrane, and suggest this to be a generalizable strategy towards reliable high-performance applications of 2D conductive materials.

SESSION NM06.08: Poster Session II: 2D Layered Materials and Heterostructures

Session Chairs: Nicholas Glavin and SungWoo Nam

Wednesday Afternoon, November 30, 2022

8:00 PM - 10:00 PM

Hynes, Level 1, Hall A

NM06.08.01

Graphene via Contact Architecture for Vertical Integration of vdW Heterostructure Devices Yongjun Shin¹, Junyoung Kwon² and Gwan-Hyong Lee¹; ¹Seoul National University, Korea (the Republic of); ²Yonsei University, Korea (the Republic of)

Two-dimensional (2D) devices and their van der Waals (vdW) heterostructures attract considerable attention owing to their potential for next-generation logic and memory applications. In addition, 2D devices are projected to have high integration capabilities, while maintaining nanoscale thickness. However, the fabrication of 2D devices and their circuits is challenging because of the high precision required to etch and pattern ultrathin 2D materials for

integration. Here, the fabrication of a graphene via contact architecture to electrically connect graphene electrodes (or leads) embedded in vdW heterostructures is demonstrated. Graphene via contacts comprising of edge and fluorinated graphene (FG) electrodes is fabricated by successive fluorination and plasma etching processes. A one-step fabrication process that utilizes the graphene contacts is developed for a vertically integrated complementary inverter based on n- and p-type 2D field-effect transistors (FETs). This study provides a promising method to fabricate vertically integrated 2D devices, which are essential in 2D material-based devices and circuits.

NM06.08.02

Wafer-Scale Growth of Ultra-Thin SnSe_x (x=1,2) by Low-Temperature MOCVD [Sungyeon Kim](#)¹, Hoyeon Cho¹, Seonhwa Jeon², Jaewon Kim¹, Kyungmin Ko¹, Swati Singh¹, Sungkyu Kim³ and Joonki Suh^{1,2}; ¹Ulsan National Institute of Science and Technology (UNIST), Korea (the Republic of); ²Ulsan National Institute of Science and Technology, Korea (the Republic of); ³Sejong University, Korea (the Republic of)

Two-dimensional van der Waals (vdW) crystals are a recently emerging class of electronic materials, and among them, Mo-, W-based transition-metal dichalcogenides (TMDs) have been successfully synthesized in the form of wafer-scale thin films until now. On the other hand, the group IV metal chalcogenides including Sn-based compounds have been limited in their applications with small flakes or thick films despite their promising properties. The reason is that the absence of suitable precursors and low growth temperature made it difficult for the materials to diffuse on the substrate and grow into a large-area thin film. In this work, we demonstrate gas-phase synthesis ultra-thin SnSe_x (x=1 and 2) films with high crystallinity and wafer-scale homogeneity. It is enabled by low-temperature metal-organic chemical vapor deposition (MOCVD) in which relatively compact and non-toxic methyl ligand precursors are used. Also, we overcome the temperature mismatch between high precursor decomposition temperature (~650°C) and low growth temperature (~200°C) by designing the separate functional zones with independent thermal control. Through this preferable growth condition, SnSe₂ ultra-thin film (3–5 nm) can be ultimately synthesized in wafer-scale. Afterward, n-type SnSe₂ thin film can be polarity change to p-type SnSe by thermally induced phase transition in inert and stable condition. SnSe thin film can also keep high crystallinity and homogeneity across the wafer despite the crystal structure change. Both n-type SnSe₂ and p-type SnSe thin films can be applied as p-n junction channel array with type II band alignment. This study will serve as a stepping stone to accelerate the electronic and thermoelectric device applications of high quality SnSe_x (x=1,2) thin film in the wafer-scale.

NM06.08.03

Epitaxial Single-Crystal Growth of Transition Metal Dichalcogenide Monolayers via Atomic Sawtooth Au Surface [Jina Lee](#)¹, Soo Ho Choi¹, Soo Min Kim², Ki Kang Kim¹ and Young Hee Lee¹; ¹Sungkyunkwan University, Korea (the Republic of); ²Sookmyung Women's University, Korea (the Republic of)

Two-dimensional (2D) layered materials such as graphene, transition metal dichalcogenides (TMDs), and hexagonal boron nitride have attracted attention due to their distinctive physical and chemical properties. Therefore, many applications such as high-performance field-effect transistors, atomically thin pn diodes, and Coulomb drag transistors have been investigated. However, such applications are currently only available with a lateral size of up to a few tens of micrometers. Therefore, the growth of single-crystal 2D materials is highly desired to manifest intrinsic physical and chemical properties over the whole region. While wafer-scale single-crystal hexagonal boron nitride film has been successfully grown on liquid Au and vicinal Cu surfaces, an ideal growth platform for diatomic transition metal dichalcogenides has not been established to date. Here, we report the single-crystal growth of monolayer TMD films on atomic sawtooth Au substrates. The atomic sawtooth Au surface, which has periodic atomic step-edges and terraces, is simply prepared by one-step solidification of liquid Au. The atomic step-edges provoke the anisotropic adsorption energy of the TMD cluster, eventually leading to the growth of coherently aligned TMD grains over the whole region. The aligned TMD grains are merged without producing grain boundaries and form the single-crystal TMD films. Furthermore, the growth of several TMD monolayer films, including WS₂, WSe₂, MoS₂, the MoSe₂/WSe₂ heterostructure, and W_{1-x}Mo_xS₂ alloys is demonstrated, indicating that the atomic sawtooth surface could be employed as a universal growth template. This strategy provides a general avenue for the single-crystal growth of diatomic van der Waals heterostructures on a wafer scale, to further facilitate the applications of TMDs in post-silicon technology.

NM06.08.04

Synthesis of High-Quality, Large Violet Phosphorus Crystals by Mixed Metal Flux [Jiwon Kim](#), Soo Ho Choi, Junseong Song, Ki Kang Kim and Young Hee Lee; Sungkyunkwan University, Korea (the Republic of)

Among diverse phosphorus allotropes, black phosphorus has been attracting significant attention due to the van der Waals layered structure, anisotropic property, Si-like bandgap, and high carrier mobility. However, it is difficult to apply black phosphorus to practical applications due to its poor ambient stability. Recently, violet phosphorus (VP) has newly emerged as the most stable phosphorus allotropes with similar properties. However, current chemical vapor transport (CVT) technology has limitations of small crystal sizes up to 0.5 mm and low crystal quality. In addition, black phosphorus always exists as a side product in the CVT synthesis of VP. Therefore, the synthesis of pure VP is still challenging owing to the absence of a new synthesis method. Here, we report a mixed metal flux method to synthesize high-quality, large VP crystals. VP crystals up to 5 mm in lateral size are synthesized by mixed tin and bismuth flux at high temperatures, whereas tiny black phosphorus crystals are obtained at low temperatures. It implies that the growth temperature is a key parameter to determine the phase of phosphorus. The full width at half maximum of ~0.14° is observed in X-ray diffraction, indicating the high crystal quality of the VP crystal. Furthermore, the crystal size can be simply controlled by adjusting the cooling rate in the synthesis process.

NM06.08.05

Self-Wrinkling Insulating Nanosheets as Substrates for Wrinkling of Graphene, Graphene Oxide and Other 2D Materials [Barbara Pacakova](#)¹, Paulo H. Michels Brito¹, Josef Breu², Koiti Araki³ and Jon Otto Fossum¹; ¹Norwegian University of Science and Technology, Norway; ²University of Bayreuth, Germany; ³USP Sao Paulo, Brazil

Material properties of graphene¹⁻³, such as mechanical, electronic, optical, and chemical, can be altered by changing its topography⁴⁻⁶. Many applications based on the capture of gases and molecules, such as graphene sensors⁷, require enhancement of chemical reactivity and subsequent functionalization of graphene. However, planar structure of graphene is disadvantageous for this purpose as in general, graphene carbon atoms located within the plane are almost inert compared to C atoms on defects and edges that are more reactive.

Enhanced chemical reactivity can be achieved by increasing the curvature of topographical features^{4,6} – by wrinkling, rippling and crumpling⁸, as curved parts are more reactive than planar regions.

Here we report unique wide band gap insulating single layers of high aspect ratio, that wrinkle spontaneously after deposition on a substrate – 1 nm thin clay mineral sheets decorated with nanoparticles. As these nanosheets readily disperse in water, this approach of formation of self-wrinkled substrates allows creation of self-assembled wrinkled 2D heterostructures, including graphene.

References:

1. K., G. A. & S., N. K. The rise of graphene. *Nat. Mater.* **6**, 183–191 (2007).
2. Katsnelson, M. I. Graphene: carbon in two dimensions. *Mater. Today* **10**, 20–27 (2007).
3. Castro Neto, A. H., Peres, N. M. R., Novoselov, K. S. & Geim, A. K. The electronic properties of graphene. *Rev. Mod. Phys.* **81**, 109–162 (2009).

4. Deng, S. & Berry, V. Wrinkled, rippled and crumpled graphene: An overview of formation mechanism, electronic properties, and applications. *Mater. Today* **19**, 197–212 (2016).
5. Pacheco Sanjuan, A. A., Mehboudi, M., Harriss, E. O., Terrones, H. & Barraza-Lopez, S. Quantitative chemistry and the discrete geometry of conformal atom-thin crystals. *ACS Nano* **8**, 1136–1146 (2014).
6. Deng, S. *et al.* Graphene Wrinkles Enable Spatially Defined Chemistry. *Nano Lett.* **19**, 5640–5646 (2019).
7. Tian, W., Liu, X. & Yu, W. Research progress of gas sensor based on graphene and its derivatives: A review. *Appl. Sci.* **8**, (2018).
8. Boukhalov, D. W. & Katsnelson, M. I. Enhancement of chemical activity in corrugated graphene. *J. Phys. Chem. C* **113**, 14176–14178 (2009).

NM06.08.07

Multifunctional Nanosheets for Electromagnetic Interference Shielding and Infrared Detection Emma J. Renteria¹, Grant D. Heileman¹, Sadvikas J. Addamane², Thomas J. Rotter¹, Ganesh Balakrishnan^{1,1}, Christos Christodoulou¹ and Francesca Cavallo^{1,1}; ¹University of New Mexico, United States; ²Sandia National Laboratories, United States

We report our recent results on developing multi-functional materials for electromagnetic interference (EMI) shielding and infrared detection. The work is motivated by the increasing use of devices that saturate the environment with radio-frequency (RF) electromagnetic radiation. RF radiation can disrupt the operation of electronic components, including sources and detectors of infrared (IR) radiation that are widely used in communication systems and night-vision cameras. Our work focuses on integrating a front-end shield of radio waves with an optoelectronic IR detector in a sheet that can conform to non-planar surfaces, such as windows on an aircraft and domes in IR cameras. In our design, a single-crystalline and highly doped III-As nanomembrane (NM) serves as the IR-transparent shield of EMI. The optoelectronic IR detector is based on black phosphorous (bP). Here, we present our effort in the characterization of IR transmittance and shielding effectiveness of III-As NMs. In addition, we show preliminary results on the integration of bP IR absorbers with III-As NMs. We fabricate III-As NMs with a thickness of a few hundred nanometers and a nominal doping level ranging between 10^{19} and 10^{20} cm⁻³. The NMs are grown by molecular beam epitaxy onto GaAs substrates coated with lattice-matched sacrificial layers or etch stop layers (e.g., AlAs or AlGaAs). Freestanding NMs are isolated either by selective etching of the sacrificial layer or by removal of the growth substrate and etch-stop layer. After transfer to a new host (e.g., Kapton film), we measure the optical transmittance of the NMs above 1 μm. We extract the shielding effectiveness of the NM from measured s-parameters of frequencies ranging from 60 to 90 GHz. The extracted shield effectiveness is benchmarked against theoretical calculations to identify shielding mechanisms in the NM. Theoretical calculations use measured DC conductivities of the released NMs. We identify primary reflection (i.e., reflection of the RF radiation by the front surface of the NMs) as the dominant shielding mechanism in NMs. In addition, we quantify the effect of multiple internal reflections on shielding effectiveness.

This research was supported by an appointment to the Intelligence Community Postdoctoral Research Fellowship Program at University of New Mexico administered by Oak Ridge Institute for Science and Education (ORISE) through an interagency agreement between the U.S. Department of Energy and the Office of the Director of National Intelligence (ODNI). This work was performed, in part, at the Center for Integrated Nanotechnologies, an Office of Science User Facility operated for the US Department of Energy (DOE) Office of Science by Los Alamos National Laboratory (Contract 89233218CNA000001) and Sandia National Laboratories (Contract DE-NA-0003525).

NM06.08.08

Ultrafast Carrier Dynamics In 2D GeS—Role of Valley Polarization Sepideh Khanmohammadi¹, Catherine Tran², Erika Colin-Ulloa³, Kateryna Kushnir¹, Kristie Koski² and Lyubov Titova¹; ¹Worcester Polytechnic Institute, United States; ²University of California, Davis, United States; ³worcester polytechnic institute, United States

Germanium sulfide (GeS) is a 2D semiconductor with high carrier mobility, a moderate band gap of about 1.5 eV, and highly anisotropic optical properties. In-plane anisotropy and a large in-plane spontaneous electric polarization in GeS have been predicted to result in a shift current in response to above-the-gap excitation. In our recent work, we have demonstrated shift current generation in GeS using THz emission spectroscopy. Here, we use time-resolved THz spectroscopy to investigate the dynamics and lifetimes of photoexcited carriers. We find that excitation with 1.55 eV vs 3.1 eV optical pulses results in drastically different photoconductivity response. Photoconductivity builds up slowly, over ~ ten picoseconds and persists for nanoseconds when excited with 1.55 eV. On the other hand, photoconductivity rise time is short and photoexcited carrier lifetime is on the order of hundreds of picoseconds for 3.1 eV excitation. We discuss these differences in terms of intervalley scattering effects. We also investigate in-plane anisotropy of photoconductivity.

NM06.08.10

Single-Crystal WS₂ Growth on High Miscut Angle Substrate Hyun Je Cho^{1,2}, Jong Yun Choi^{1,2}, Heonsu Ahn^{1,2}, Geonho Mun^{1,2}, Jaeyoung Kim², Hyunjin Jung² and Moon-Ho Jo^{1,2}; ¹POSTECH, Korea (the Republic of); ²Institute for Basic Science, Korea (the Republic of)

We report single crystalline monolayer tungsten disulfide (WS₂) growth on high miscut angle c-plane sapphire substrate. Unlike other step-edge-guided growth, we use high miscut angle substrate to initiate uni-directional nucleation. Since the high miscut angle substrate containing high portion of step-edge, terrace nucleation had successively suppressed, leading to high quality single crystalline monolayer film can be acquired. Single crystalline texture is verified by microscopies and transmission electron microscope studies. Moreover, low energy electron diffraction measurements at different points perfectly exhibit 3-fold symmetry without any angle deviation. We also synthesize monolayer WS₂ nanoribbon by controlling the anisotropic growth. Finally, we show electronic and optoelectronic properties of our single crystal WS₂ film and WS₂ nanoribbon. Our method not only offers a universal and scalable growth strategy to produce TMDC single crystals for future electronics, but also gives perfect platform for studying large scale moiré physics.

References

1. L. Wang *et al.* Epitaxial growth of a 100-square-centimetre single-crystal hexagonal boron nitride monolayer on copper. *Nature* **570**, 91 (2019)
2. K. V. Bets *et al.* How the complementarity at vicinal steps enables growth of 2D monocrystals. *Nano Lett.* **19**, 2027–2031 (2019).

NM06.08.12

Superior Mechanical Properties of Multi-Layer Covalent-Organic-Frameworks Enabled by Rationally Tuning Molecular Interlayer Interactions Qiyi Fang¹, Zhengqian Pang², Qing Ai¹, Yifeng Liu¹, Tianshu Zhai¹, Guanhuai Gao¹, Yifan Zhu¹, Teng Li² and Jun Lou¹; ¹Rice University, United States; ²University of Maryland College Park, United States

Two-dimensional covalent-organic-frameworks (2D COFs) is a class of porous 2D polymer with periodic structure and ordered skeleton assembled from covalent bonds. 2D COFs distinct from 2D inorganic analogue by their high designability, which make them potential platform for mechanistic studies of mechanical behavior at 2D limit. In this talk, we will present the systematical study of the structure-mechanical properties relation by designing the structure of 2D COFs. With optimized Langmuir-Blodgett method, we successfully prepared layer-controlled 2D COFs, and measured their mechanical properties by nanoindentation. Our result showed that the interlayer hydrogen bonds in COFs provide enhanced interlayer interaction, leading to layer-independent mechanical properties, in sharp contrast with 2D COFs without interlayer hydrogen bonds, in which the mechanical properties significantly

decreased as layer number increased. DFT calculation showed that the layer-independent mechanical properties are attributed to higher energy barriers against interlayer sliding due to the presence of interlayer hydrogen bonds. These results indicate that COFs can be a very promising platform for the preparation high-performance 2D polymeric materials by precise molecular design.

NM06.08.13

MoS₂—Carbon Materials Composite with Dual Phase of MoS₂ and Their Application for Energy Storage System Kyu Yeon Jang^{1,2}, Yeong A. Lee^{1,3} and Hana Yoon¹; ¹Korea Institute of Energy Research (KIER), Korea (the Republic of); ²University of Science and Technology (UST), Korea (the Republic of); ³Chungnam National University, Korea (the Republic of)

Graphite and graphene are known to be very good anode materials for lithium ion batteries due to their excellent stability, but have a low theoretical capacity of 372 mAh/g.¹ Electric vehicles and various electronic devices require a battery with a higher capacity than the current capacity, and it is essential to develop an anode material with a higher capacity.² Therefore, anode materials using Si are in the spotlight, but Si has a higher capacity (~4200mAh/g) than conventional graphite materials, but there is a problem of volume expansion when the cycle is performed, so it has a bottleneck in terms of stability.³ Transition metal dichalcogenides (TMD) materials are attracting a lot of attention because of their structural properties, excellent stability, low cost and high storage capacity.⁴ The theoretical capacity of MoS₂, one of the TMD materials, is known to be 670 mAh/g, making it a promising material for a new LIB anode material.⁵ In particular, it is very advantageous to make a single layer of MoS₂ because their layered structure is combined with a weak van der Waals force.⁶ It is typically known to have 1T and 2H structures. The 1T phase of MoS₂ has the properties of a conductor and therefore has excellent conductivity as a LIB anode material. 1T structures can be produced when a single layer is made through exfoliation. However, due to its metastable structure, it is easily converted to the 2H phase as the most stable phase.⁷

In this study, a composite of MoS₂ and graphene was prepared by a chemical exfoliation method, and through this, a stable and high-capacity anode material was realized using the high energy storage capacity of MoS₂ and the stability of graphene. In addition, a mixed phase of 1T and 2H structures was generated through the post-treatment process, and it was confirmed that the 1T phase was stably present. Through this, the diffusion of Li⁺ was facilitated by securing wide interface spacing and high conductivity of the 1T structure, and as a result, superior conductivity and high capacity were stably maintained compared to the single-phase material of the 2H structure.

(1) Nishi, Y. Lithium Ion Secondary Batteries; Past 10 Years and the Future. *J. Power Sources* **2001**, *100* (1–2), 101–106.

(2) Armand M., Tarascon -M. J. Building better batteries. *Nature* **2008**, *451*, 652-657.

(3) Casimir, A.; Zhang, H.; Ogoke, O.; Amine, J. C.; Lu, J.; Wu, G. Silicon-Based Anodes for Lithium-Ion Batteries: Effectiveness of Materials Synthesis and Electrode Preparation. *Nano Energy* **2016**, *27*, 359–376.

(4) Choi, W.; Choudhary, N.; Han, G. H.; Park, J.; Akinwande, D.; Lee, Y. H. Recent Development of Two-Dimensional Transition Metal Dichalcogenides and Their Applications. *Mater. Today* **2017**, *20* (3), 116–130.

(5) Stephenson, T.; Li, Z.; Olsen, B.; Mitlin, D. Lithium Ion Battery Applications of Molybdenum Disulfide (MoS₂) Nanocomposites. *Energy Environ. Sci.* **2014**, *7* (1), 209–231.

(6) Li, H.; Wu, J. Bin; Ran, F.; Lin, M. L.; Liu, X. L.; Zhao, Y.; Lu, X.; Xiong, Q.; Zhang, J.; Huang, W.; et al. Interfacial Interactions in van Der Waals Heterostructures of MoS₂ and Graphene. *ACS Nano* **2017**, *11* (11), 11714–11723.

(7) Lei, Z.; Zhan, J.; Tang, L.; Zhang, Y.; Wang, Y. Recent Development of Metallic (1T) Phase of Molybdenum Disulfide for Energy Conversion and Storage. *Adv. Energy Mater.* **2018**, *8* (19), 1–29.

NM06.08.15

Direct Patterning of Multi-Functional Photo-Reduced Graphene Oxide Fabrics (rGOF) on the Liquid Surface HaoTian H. Shi^{1,2,3}, Sung Hwa Hong² and Hani E. Naguib^{2,2}; ¹Western University, Canada; ²University of Toronto, Canada; ³University of Cambridge, United Kingdom

A multi-functional photo-reduced graphene oxide fabric (rGOF) has been successfully created through an accessible laser direct-write technique at the liquid-air interface. Without the need for any substrate, patternable and porous rGOF can be readily created at the liquid surface through the photoreduction of self-assembled surface graphene oxides (GO). Processing parameters, such as the laser power, printing speed, laser focus, and inclusion of post-processing steps, can lead to tailorable rGOF morphologies. rGOF layering can also lead to the creation of 3-dimensional rGO stacking, further enhancing its functional performance. The as-printed rGOF can be transfer-printed onto any desirable substrates and has demonstrated tremendous potential in energy storage, Joule heating, temperature sensing, humidity sensing, tactile sensing, and ammonia sensing applications.

NM06.08.16

Laser-Assisted Zone Crystallization in Superscalable, Contactless Wet Coating of Ultrathin Films for Flexible Piezoelectrics and Electronics Adam Kiersnowski, Paulina Budzicka, Maciej Frankowski, Michal Wyskiel and Krzysztof Janus; Wroclaw University of Science and Technology, Poland

Fabrication of elastic piezoelectric generators, polymer-based pressure or vibration sensors, as well as flexible thin-film-based electronic devices, represent examples of a growing number of material technologies that require large-scale thin functional films deposition. There are several technologically-proven deposition solutions available such as roll-to-roll (rotogravure/doctor blade coating, spray coating, or inkjet printing). Application of a particular deposition method depends on surface properties and deposited material. Quite often, however, implementation of a particular thin film technology is limited by scalability of the deposition method. The scalability is important, since deposition method have a key influence on e.g. wetting dynamics, solidification, crystallization and other factors critically affecting e.g. crystal size and orientation. The other challenge today is coating films on wavy, dimpled or other non-flat surfaces. Contact methods, such as listed above, typically fail in film deposition on non-flat surfaces.

In our report, we demonstrate a contactless wet film deposition method that addresses the scalability issues and enables wet, ink-based fabrication of films on flat and curved surfaces. In our approach we used specifically tuned laser beam to induce thermal gradients of substrate surface free energy and ink viscosity. The gradients induce local, internal flow in the ink causing formation of an ink bulge close to the laser spot. The bulge can be moved on the surface by moving the laser-heated spot over the substrate. The moving ink bulge is followed by a local solvent evaporation that causes deposition of a film. The footprint profile of the liquid bulge can be controlled by the laser focus. Using the line-focused laser enables deposition of the solid film in the way analogical to the doctor blade, but without any physical contact of the coating tool with the solution – the laser beam acts as a coating blade. The length of the focal line defines the coated area. Because of the working principle, we call the method laser-assisted zone crystallization (LAZEC).

We tested the LAZEC in fabrication of polymer and molecular films with thickness ranging from 3 to 100 nm and specific electronic properties. X-ray diffraction revealed high degrees of structural order and spatial orientation of the films. The ordered nature of the sample stems from, inter alia, controlled thermal conditions of the solidification process. Structure control in the LAZEC permits e.g. fabrication of organic semiconductor films revealing highly anisotropic charge transport properties. In our study we have also tested fabrication of piezoelectric polymer films. Imparting piezoelectricity to a polymer requires uniaxially, homogeneously and permanently oriented dipole moments in specific crystal polymorphs. Since the LAZEC inherently enables control over crystallization thermal conditions, it also permits a wide range control over a polymorphism. A control over the orientation of dipole moments was achieved by using external electric field. Using poly(vinylidene fluoride) (PVDF) and its copolymers as examples we demonstrate deposition of 100-nm thin piezoelectric films revealing d_{33} piezoelectric moduli comparable to their conventionally fabricated free standing film counterparts. During the

fabrication of the piezoelectric films we used external electric fields to pole the samples. Noteworthy, the poling in LAZEC deposition required electric field several orders of magnitude weaker than the field used in conventional techniques (e.g. corona poling) and films required no mechanical treatment after the deposition. Voltages lower than 1 kV were enough to render PVDF film piezoelectric. In addition to the above experiments the presentation is aimed at showcasing deposition of functional organic films on curved parts of optical lenses.

The work was supported by National Science Centre Poland (NCN) through the grant UMO-2017/25/B/ST5/02869

NM06.08.17

2D Amorphous Carbon Dielectric for Nanoelectronics Congjun Wang; National Energy Technology Laboratory, United States

Two-dimensional (2D) semiconductors and semimetals could enable performance and scaling of solid-state electronic devices beyond the limits of those built on their conventional bulk counterparts. However, their suitable accompanying 2D dielectric, ideally in the highly disordered amorphous form similar to SiO₂ for silicon, has not been identified, which prevents nanoelectronic devices based on low-dimensional nanomaterials from fulfilling their potential. The synthesis of 2D amorphous dielectrics and their integration into electronic devices are challenging due to the metastable nature of amorphous phases. Here we discuss the synthesis of a solution processible precursor to enable a scalable and solution-based strategy to prepare large-area and freestanding 2D amorphous carbon monolayers and multilayers as novel dielectrics. The synthesis and characterization of the carbon precursor and the 2D amorphous carbon film will be described. To demonstrate the effectiveness of the 2D amorphous carbon as dielectric materials, carbon nanoelectronic devices are fabricated and evaluated.

NM06.08.18

Remote Epitaxy of Electrodeposited Zn and Cu on Graphene Salem C. Wright, Sonakshi Saini, Tejas Raman, Mengkun Tian, Pralav P. Shetty and Matthew T. McDowell; Georgia Institute of Technology, United States

Control over the growth of metals on 2D materials is important for creating electrical contacts to 2D-material-based electronic devices, as well as for energy storage devices such as batteries in which 2D materials are used. Recently, it has been shown that graphene and other 2D materials allow for an underlying substrate to exert a structural influence on semiconductors grown onto the 2D material through “remote epitaxy.”^[1] Remote epitaxy has been observed primarily for semiconductors grown by vacuum deposition methods, and it represents an appealing method for versatile control over the orientation of deposited materials. However, it is unclear if remote epitaxy plays a role in the deposition of metals through methods such as electrodeposition. Here, we show that remote epitaxy acts to determine the growth characteristics of Zn and Cu electrodeposited on graphene/Cu substrates. Through a combination of three-electrode electrochemical experiments and extensive electron backscattered diffraction (EBSD) analysis, we show that the crystallographic orientation of the Cu grain below graphene determines the orientation of the electrodeposited metal, with the close-packed planes of the varying materials exhibiting epitaxial relationships. Transmission electron microscopy (TEM) is used to confirm the orientation relationship between the Cu substrate and the deposit through the graphene layer, providing atomic-scale information regarding the interface revealing that misfit strain is accommodated through edge dislocations. The graphene not only acts as a window layer, but also protects the underlying metal from oxidation to enable structurally continuous growth of the electrodeposit. These findings are important since they show that remote epitaxy can be achieved without vacuum methods using aqueous electrodeposition. Our results suggest that graphene coatings could be an effective way to enable controlled electrodeposition of a variety of metals, including those relevant to high-energy batteries (lithium, sodium).

[1] Y. Kim, S. S. Cruz, K. Lee, B. O. Alawode, C. Choi, Y. Song, J. M. Johnson, C. Heidelberger, W. Kong, S. Choi, K. Qiao, I. Almansouri, E. A. Fitzgerald, J. Kong, A. M. Kolpak, J. Hwang, J. Kim, *Nature* **2017**, *544*, DOI 10.1038/nature22053.

NM06.08.20

Biotene—A New 2D Natural Oxide from Biotite Preeti L. Mahapatra¹, Raphael Tromer², Prafull Pandey³, Gelu Costin⁴, Basudev Iahiri¹, Kamanio Chattopadhyay³, Pulickel Ajayan⁴, Ajit K. Roy⁵, Douglas S. Galvao², Partha Kumbhakar¹ and Chandra Sekhar Tiwary¹; ¹IIT Kharagpur, India; ²State University of Campinas, Brazil; ³Indian Institute of Science, India; ⁴Rice University, United States; ⁵Air Force Research Laboratory, United States

In this work, we employed liquid-phase exfoliation from naturally abundant biotite to demonstrate the synthesis and characterization of ultrathin metal oxide termed biotene. To gather energy, the flexoelectric response of the atomically thin biotene during sequential bending has been used. The effective flexoelectric response was improved due to the presence of surface charges, and the voltage increased up to 8 V, with a high mechano-sensitivity of 0.79 Vn⁻¹ for force applied. The flexoelectric response was verified using density functional theory (DFT) simulations. In the atomically thin biotene, the magnetic field and thermal heating suggest increased sensitivity. The development of two-dimensional (2D) metal-oxide biotene for energy generation and harvesting indicates a multitude of potential 2D-oxide materials for energy generation and harvesting.

NM06.08.22

Formation of Monolayer Metal Oxides via Room Temperature Conversion from Two-Dimensional Transitional Metal Dichalcogenides Xudong Zheng¹, Zhien Wang¹, Tianyi Zhang¹, Benjia Dou¹, Jiangtao Wang¹, Ji-Hoon Park¹, Saïen Xie², Darrell Schlom³ and Jing Kong¹; ¹Massachusetts Institute of Technology, United States; ²Princeton University, United States; ³Cornell University, United States

Two-dimensional (2D) materials have attracted significant interest due to their ultra-thin thickness and quantum confinement effect. Despite the rich and diverse library of discovered 2D materials, the study of metal oxides as atomically thin films have been limited. Here, by using 2D transitional metal dichalcogenides (TMDs) as starting templates for conversion, we show that monolayer metal oxides can be directly formed at room temperature. In this work we characterized the structural, optical and electrical properties of as-synthesized monolayer metal oxides and compared with their original template material. This strategy should be easily extended to a variety of metal oxides, enabling the study of monolayer metal oxides for the future.

NM06.08.23

Solution-Gated Ultrathin Channel Indium Tin Oxide-Based Field-Effect Transistor Fabricated by a One-Step Procedure and Effect of Surface Modification on SARS-CoV-2 Detection Ritsu Katayama and Toshiya Sakata; The University of Tokyo, Japan

Introduction

Recently, indium tin oxide (ITO) has been widely used as an electrode material for flat panel displays owing to its transparency and conductivity. In our laboratory, we have found that a solution-gated ultrathin channel ITO-based field-effect transistor (FET) can be fabricated for biosensing in a single step by sputtering ITO using a shadow mask with controlled thickness, thus providing an “all-by-ITO” technology [1].

Solution-gated FETs with silicon or other semiconductive materials as channels can specifically and selectively detect ions and biomolecules related to biological functions by chemically modifying the gate electrode surface, and these are known as biologically coupled FETs (Bio-FETs) [2]. Since Bio-FETs can directly detect the charges of ions and biomolecules, they do not require to label fluorescent dyes and to induce redox reactions based on

enzymes. Therefore, Bio-FETs are expected to be used as *in vitro* diagnostic devices for a label-free monitoring of health conditions in daily life. In this study, we investigated the electrical properties of the solution-gated ultrathin channel ITO-based FET (ultrathin channel ITO-based FET), which was fabricated in a single step, with a thin ITO channel (<30–40 nm) and thick ITO source/drain electrodes (ca. 100 nm), and performed the chemical modification of the thin ITO channel for its application in biosensors.

2. Methods

First, the ultrathin channel ITO-based FET was fabricated on a glass substrate by sputtering using a shadow mask with controlled thickness. The ultrathin channel ITO-based FET were then modified with 4-Nitrobenzenediazonium tetrafluoroborate (NBD). NBD thin film was electrochemically deposited on the channel surface using a cyclic voltammetry (CV) method with 1 mM of NBD, 25 mM of tetrabutylammonium hexafluorophosphate, and 2mM of 2,2-diphenyl-1-picrylhydrazil. Furthermore, nitro groups in the NBD thin film were reduced to amino groups by the CV method. The channel surface was then immersed in a solvent containing 1 mM N-succinimidyl 3-maleimidobenzonate for 1 hour, washed with deionized water, and reacted with 5 M thiolated SARS-CoV-2 aptamer overnight to chemically modify the channel surface. A semiconductor parameter analyzer was used to measure the fundamental properties such as drain current (I_d) – gate voltage (V_g) transfer characteristics and to detect inactivated SARS-CoV-2 viruses in real time. An elemental analysis of the channel surface before and after the surface modifications was performed by Auger electron spectrometer (AES).

3. Results and Discussion

Even after the NBD modification onto the ITO channel by the CV method, not only was the pH responsivity of the ultrathin channel ITO-based FET maintained, showing the Nernstian response, but the fundamental characteristics such as subthreshold slope (SS) in the V_g - I_d transfer characteristic were also hardly deteriorated. Thus, we confirmed that the surface modification of the ITO channel by the CV method is useful for the immobilization of aptamer molecules to recognize targets such as viruses using the ultrathin channel ITO-based FET.

Furthermore, we demonstrated the detection of inactivated SARS-CoV-2 viruses with high sensitivity using the ultrathin channel ITO-based FET chemically modified with the SARS-CoV-2 aptamer. The elemental analysis of the ITO channel surface by AES before and after the surface modification showed the presence of N from the NBD, O and P from phosphate backbone of the aptamer molecule. It also indicated the validity of the surface modification for the SARS-CoV-2 measurements.

References

1. Toshiya Sakata, Shoichi Nishitani, Akiko Saito, and Yuta Fukasawa, *ACS Appl. Mater. Interfaces* 2021, 13, 32, 38569–38578.
2. Toshiya Sakata, *ACS Omega* 2019, 4, 7, 11852–11862.

NM06.08.25

CVD-Synthesized 2D Graphdiyne-Based Nanofilms for Ultrathin Compliant on-Skin Sensors Yichen Cai and Vincent Tung; King Abdullah University of Science and Technology (KAUST), Saudi Arabia

Thin-film electronics plably laminated onto epidermis for noninvasive, specific, and multifunctional sensing are ideal wearable systems for health-monitoring and information technologies.¹⁻³ However, it remains a critical challenge to fabricate ultrathin and compliant skin-like sensors with high imperceptibility and sensitivities.⁴ Graphdiyne (GDY) and its derivatives are emerging two-dimensional (2D) materials comprised of sp- and sp²-hybridized carbon atoms with excellent chemical, mechanical, thermal properties, and electrical conductivity, making them attractive candidates for ultrathin e-skin. Especially, compared with other common 2D materials, such as graphene, MoS₂, and MXene, hydrogen substituted graphdiyne (HsGDY) that we will show in this work, shows inherent softness to better match the skin interface. However, the implementation of HsGDY into e-skin, while promising and has long been touted by theorists, has yet to be experimentally demonstrated.

In this work, we present a multifunctional on-skin sensing system with high imperceptibility that couples a rationally designed conductive 2D HsGDY nanofilms with transparent flexible polyethylene terephthalate (PET) substrates. The large-area uniform HsGDY ultrathin films (thickness ~18 nm) are accomplished by a facile chemical vapor deposition (CVD) approach using ultra-flat (Cu 111) as substrates and 1,3,5-triethynyl benzene (TEB) as the building blocks, currently unachievable by solution-phase synthetic chemistry. Importantly, it demonstrates uniformly distributed in-plane pores and inherent softness for on-skin sensing can better match the curved skin interface with improved mechanical compliance when compared with other rigid 2D materials. Then, dominated by the subtle deformation-induced changes in the inter-domain tunneling conductance, the engineered HsGDY based on-skin sensors can show continuous, accurate, and real-time non-invasive spatial mapping of dynamic/static strains in both tensile/compressive directions, monitor various body motions with high sensitivity (GF~22.6, under 2% strain), fast response (~60 ms), and long-term durability (~5000 cycles). Moreover, such devices can dynamically distinguish between the temperature difference (extremely tiny deformation) and frequency of air inhaled and exhaled through the nostril, revealing quantitative assessment on the movement/health of the human body. The proof-of-concept strategy provides a new general route for the design of next-generation wearable organic bioelectronics with multiple electronic functionalities.

References:

1. Xu et al., *Nature* 2019, 571, 319-321.
2. Won et al., *Adv. Mater.* 2021, 33, 2002397.
3. Li et al., *Nat. Electron.* 2021, 4, 134.
4. Kim et al., *Nat. Commun.* 2019, 10, 1.

NM06.08.28

The Metastable Pressure-Induced Transformation of Raman Scattering Spectrum of Bulk HfS₂ Igor Antoniazzi¹, Magda Grzeszczyk², Jakub Gawraczynski¹, Tomasz Wozniak³, Jordi Ibanez⁴, Zahir Muhammad⁵, Weisheng Zhao⁵, Maciej R. Molas¹ and Adam Babinski¹; ¹University of Warsaw, Poland; ²National University of Singapore, Singapore; ³Wroclaw University of Science and Technology, Poland; ⁴Geosciences Barcelona (GEO3BCN), CSIC, Spain; ⁵Hefei Innovation Research Institute, China

The effect of hydrostatic pressure on the lattice dynamics of bulk hafnium disulphide (HfS₂) grown by chemical vapour transport method is investigated. The pattern of powder X-Ray diffraction of the investigated material was found to be in perfect agreement with that of the octahedral 1T phase of HfS₂. The Raman scattering has been studied at room temperature in diamond anvil cells in hydrostatic pressure up to 13.7 GPa.

There are four Raman modes observed at ambient pressure, which is consistent with previous studies.

There is an agreement in literature on the attribution of peaks at 266 cm⁻¹ and 344 cm⁻¹ to in-plane E_g and out-of-plane A_{1g} Raman-active modes, respectively. The peak at 325 cm⁻¹ is attributed to the infrared-active E_u (LO) or A_{2u}(LO) alike mode.

Not clear is also the assignment of the weak feature at 141 cm⁻¹. Its attribution to a second-order difference processes was suggested, as such peaks can be observed in Raman scattering spectra of some transition metal dichalcogenides (TMDs) however the E_u (TO) was also suggested as the signature of the mode.

The Raman scattering modes blueshift with increasing hydrostatic pressure with the pressure rates from 1.6 cm⁻¹/GPa to 4.4 cm⁻¹/GPa, which is similar to the values reported before.

The lineshape of the Raman scattering spectrum does not significantly change with increasing hydrostatic pressure up to 5.7 GPa, however a substantial enhancement of the A_{1g} peak intensity can be noticed under the highest pressure.

A change in the Raman scattering spectrum is observed in hydrostatic pressure between 6.2 GPa and 7.2 GPa.

Seven vibrational modes can be observed in the spectrum above the transformation, as compared to four modes before the transformation. The frequencies of the Raman scattering modes observed change linearly with pressure coefficients up to 2.6 cm⁻¹/GPa. A negative pressure coefficient (-0.13 cm⁻¹/GPa) of the Raman peak observed at the lowest energy (approx 95 cm⁻¹) can also be noticed. The overall lineshape of spectrum above the transformation does not change under pressure up to 13.7 GPa during compression. Surprisingly, the seven Raman modes can be observed under hydrostatic pressure down to 1.5 GPa during decompression. The apparent hysteresis of the Raman spectrum must reflect a metastable change in the sample structure. We analyse the effect in the context of iodine (I₂) molecules, which are found to be present in van der Waals gaps between the HfS₂ layers in the investigated structure. Possible scenarios leading to the observed metastability are proposed.

NM06.08.29

Activate N₂-Selective Pathways for Electrochemical Ammonia Oxidation—Dual Active Site Tandem Catalysis in 2D Layered Nanospace [Asuka Morinaga](#)^{1,2}, Keisuke Shirai¹, Hiromori Tsutsumi¹, Masaharu Nakayama¹ and Yu Katayama²; ¹Yamaguchi University, Japan; ²Osaka University, Japan

Ammonia oxidation reaction (AOR) plays a vital role in various applications including hydrogen production, direct ammonia fuel cell, and removal of ammonia-containing wastewater. During ideal AOR in an aqueous electrolyte, NH₃ undergoes dehydrogenation to form NH_x (x = 1 or 2), followed by the catalytical dimerization and electrochemical dehydrogenation to produce N₂.¹ However, most of the reported AOR catalysts, such as Pt² and NiCu alloys³, suffer from its low N₂ selectivity (undesired nitrogen oxides (NO_x) formation) and/or low long-term stability (catalyst poisoning from N_{ad} species). In this study, we introduce 2D layered MnO₂ composites co-intercalated with a dual active site, that is, hydrated Ni^{II} and Cu^{II} ions, for N₂-selective and stable AOR catalyst. Co-intercalated hydrated Ni^{II} and Cu^{II} ions are expected to accelerate the key (electro)chemical process, dehydrogenation and dimerization process, respectively, to achieve high N₂ selectivity.

Various spectroscopic methods such as X-ray diffraction, X-ray photoelectron spectroscopy, and high-energy X-ray total scattering were performed to clarify the electron and structural states of Ni^{II} and Cu^{II} within the layers. The result confirms that co-intercalated Ni^{II} and Cu^{II} coexist closely with a single ion state with negligible interaction, which is ideal for dual active site catalysis. Linear sweep voltammogram and gas chromatography analysis confirm the significant improvement in N₂-selectivity for Ni^{II}-Cu^{II} co-intercalated catalyst compared with single active site (Ni^{II} and Cu^{II}) counterparts. Furthermore, the role of Ni^{II} and Cu^{II} active sites for N₂-selective AOR was revealed by *operando* surface-enhanced infrared absorption spectroscopy. The result confirms that NH₃ was dehydrogenated in the vicinity of Ni^{II} site, and subsequent oxidation of Ni^{II} triggers the hand-over process of NH_x to Cu^{II} site, followed by the dimerization/dehydrogenation process in the vicinity of Cu^{II} to selectively produce N₂. This work revealed that the unique catalytic activity can be evoked by introducing multiple isolated metal complexes into 2D nano-spaces, providing a novel strategy for designing electrocatalysts with ideal efficiency and selectivity.

1 Gerischer, H. *et al.*, *J. Electroanal. Chem.* **1970**, 25, 421–433.

2 Matsui, T. *et al.*, *Langmuir* **2015**, 31, 11717–11723.

3 Adli, N. M. *et al.*, *J. Electrochem. Soc.* **2018**, 165, J3130.

NM06.08.30

Optimization of 2D Transition Metal Dichalcogenides Using Electronic Structure and Thermoelectric Coefficient Calculations [Isaiah Chen](#) and Paulette Clancy; Johns Hopkins University, United States

Transition metal dichalcogenides (TMDs) and doped layered compounds are emerging classes of two-dimensional (2D) materials with technological potential for their use in photovoltaic devices. These materials exhibit useful electronic, optical, and thermal properties with tunable direct bandgaps. However, there is a need to develop novel nanostructure design strategies to improve the thermoelectric performance and *p*-type characteristics of these materials. Computational materials design can assist in these efforts and accelerate materials development. To address this need, we have performed plane-wave density functional theory (DFT) calculations for a series of transition metal dichalcogenide thin films (MoTe₂, WTe₂) and bismuth-antimony alloys (BiSb, BiTe). In particular, we are focusing on TMDs that contain telluride, given their particular importance for device studies. We used DFT to focus on the tolerance of the properties of these materials to variations in polymorph, composition, and defect type. We have validated the DFT predictions against experimental and published computational work. We will also present the predictions of DFT-generated thermoelectric coefficients using the open-source BoltzTraP2 codebase, based on the Boltzmann transport equation. These coefficients include electrical conductivity, thermal conductivity, Seebeck coefficient, power factor, and figure of merit. We will show how variation of the band gap and density of states (DOS) in all structures will cover both semiconductors and metals with thermoelectric properties in the expected ranges of previous observations. Our goal is to use these calculated thermoelectric properties to gauge which materials are preferable for use in device fabrication and assist with optimizing the performance of these 2D materials. We will use a Bayesian optimization machine learning algorithm (Physical Analytics Pipeline) to search the large combinatorial space comprised of different compositional alloys and determine which combinations yield particularly noteworthy *p*-type characteristics.

NM06.08.31

Mo/MoSe₂/Ag Memories with *In Situ* Formation of Mo/MoSe₂ Heterostructures via Selective Diffusion of Se in Mo [So ByungJun](#); SungKyunKwan university, Korea (the Republic of)

Two-dimensional metal chalcogenides (TMDCs) are favorable candidates for high-density memristor crossbar arrays due to their ultrathin scaling limit, controllable interfacial properties, and potentiality in fabricating large-area electronics. However, the fabrication of large area crossbar arrays applied TMDCs has limitations by their high synthesis temperature and difficulty of mechanical transferring on the bottom electrode. The mechanical transfer can induce damages, such as cracks, wrinkles, and impurity residues between the electrode and active layer interface, which could degrade the device performance and uniformity over a large area. In this perspective, the present research involves the fabrication of crossbar array memristor using selectively diffusing selenium (Se) in pre-deposited molybdenum (Mo) to form Mo/MoSe₂ stack *in-situ*. This effortless way of forming the heterostructures of metal/TMDCs is not limited to Mo/MoSe₂ but can be generalized to a large spectrum of known TMDCs. This *in-situ* technique introduces an innovative way of forming a continuous mass of Mo/MoSe₂ with good quality interface leading to enhanced performance. Additionally, one-processing step reduction in a large number of sub-processes is introduced in this technique for the first time resulting in a fast and economical way of fabrication of two-terminal resistive memories. The present memories have been operated with small switching voltage (~ 1.1 V), high endurance (> 250 cycles), excellent retention (> 15000 s), minimum cycle-to-cycle and device-to-device variation. This implies that the present technique suggests the way toward non-destructive and easy fabrication of high-performance memristors.

NM06.08.32

Multi-Biomarker Thread-Based Biosensors for Monitoring Acute Compartment Syndrome [Atul Sharma](#)¹, Mossab K. Alsaedi¹, Junfei Xia¹, Giorgio Giatsidis² and Sameer R. Sonkusale¹; ¹Tufts University, United States; ²University of Massachusetts Chan Medical School, United States

Acute compartment syndrome (ACS) is a serious condition arising from pressure buildup due to swelling or internal bleeding of tissue, mostly as a result of

trauma [1]. ACS is prevalent in combat settings in military personnel as it could result from polytraumatic, blunt, or crushing accidents from explosions and the application of tourniquets [2]. Extreme trauma frequently results in ischemia, which can have long-term consequences like limb loss and death. Our overarching hypothesis is that early diagnosis of ACS may be possible through continuous and real-time assessment of physiological indicators, such as intramuscular oxygen, lactate, pH, and glucose [1,3]. Towards that goal, we propose the design of label-free thread-based electrochemical sensors for in-vivo measurement of these biomarkers inside the muscle tissue to capture physiological indicators for compartment syndrome detection. Compared to other flexible platforms, threads provide the most flexibility for tissue-embedded sensors, microfluidics, and bioelectronics [4-5]. For the enzymatic sensor (glucose and lactate), an amperometric method uses a two-electrode electrochemical set-up. The working electrode (WE) is composed of a composite Glutaraldehyde- Bovine Serum Albumin- Glucose Oxidase- Prussian Blue- carbon coated-suture (GA/BSA/GOx/PB/C) for glucose and GA/BSA/LOx/PB/C-coated suture for lactate sensing. An Ag/AgCl-coated suture as reference (RE) and counter electrodes (CE) is used. To measure pH, a composite silver/silver chloride (Ag/AgCl)-coated suture was utilized as the RE to determine the open-circuit potential of a polyaniline-carbon (PANI-C) coated suture. Fabrication on sensors starts with the cleaning of the suture (5/0 Polysorb™ by COVIDIEN) in isopropyl alcohol (sonication 15 min), followed by plasma treatment (5 min) and carbon-ink deposition [4-5]. To create enzymatic (glucose and lactate) sensors, PB was electrochemically deposited on a carbon-coated suture in an electrolyte solution (0.10 M HCl and 0.10 M KCl) containing potassium ferricyanide and iron chloride for 90 seconds, followed by a cyclic voltammetric scan from -0.20 to 1.0 V at 0.10 V/sec vs Ag/AgCl electrode and washed with distilled water. To restrict the sensing region, a polyurethane (PU 5% w/v) layer is coated on the sensor leaving both ends of the sensor exposed. One end (carbon coated) is for the potentiostat connections and the other end is for further deposition of the enzyme matrix, which makes up the sensing region. PU/PB/C-suture was incubated in an enzyme solution containing BSA, and GA in 0.10 M phosphate-buffered saline (PBS, pH 7.4) then washed with PBS and dried. To fabricate the pH sensor, pH-sensitive dye polyaniline was electrochemically deposited at 0.80 V for 900 sec and washed with distilled water. The RE was fabricated by dip-coating a cleaned suture in conductive Ag/AgCl paste [5] and then baking at 60°C for 30 min. An amperometric response was noted on an Ag suture (as a cathode) for the oxygen sensor. To protect the enzyme layer from biofouling, an alginate-calcium hydrogel was drop cast on the sensing region, dried, then washed with PBS. For a demonstration of sensor performance, the electrochemical measurements were performed with cannulated sensors submerged in a phantom skin-gel environment (2.0 % agarose solution in 0.10 M PBS, pH 7.4). Under optimal experimental conditions, the devised pH sensor showed an excellent sensitivity of -28 ± 3 mV/pH. Dissolved oxygen exhibited a linear relationship with change in current and a sensitivity of $0.66 \mu\text{A}/\text{mgL}^{-1}$, whereas the glucose and lactate sensor sensitivity was considered adequate at $18.53 \mu\text{A}/\text{mM}$ and $30 \mu\text{A}/\text{mM}$, respectively. Our results demonstrate that the thread-based flexible platform is capable of detecting physiological biomarkers in skin-mimicking models and could be particularly useful for continuous and real-time monitoring of several key metabolites such as glucose, lactate, pH, and oxygen in tissue.

NM06.08.34

Flexible Tellurium Nanowires and Tellurium Dual-Channel Field-Effect Phototransistor Array with High Linear Photoresponsivity Rho H. Yeol, Muhammad Naqi, Yongin Cho, Hae Won Cho, Pavan Pujar, Uisik Jung and Sunkook Kim; SKKU, Korea (the Republic of)

By introducing the method of uniformly synthesizing the tellurium nanowire (TeNWs) and the Tellurium hybrid structure to a flexible field effect transistor array, excellent electrical, mechanical and optical properties were achieved. All fabrication processes are carried out in a simple manner with low thermal budget (< 100 °C). Scanning electron microscopy (SEM) and Raman spectroscopy are performed to compare the uniform hybrid channel structure with bare Te related film. The hybrid structure of TeNWs/Te-film FET showed high mobility of $5.35 \text{ cm}^2/\text{Vs}$ as with $\sim 10^4$ on/off ratio, and all array devices have uniform electrical properties. Stability tests such as positive bias stress, negative bias stress, long term stability response, mechanical bending stress test can confirm the good reliability of the suggested device performance. High-performance phototransistor array is proved by verifying threshold voltage shift, response, sensitivity, photocurrent, and detectivity as the optical properties. It is expected that the stable operation and excellent optical properties of the flexible hybrid channel FET array can be attributed to enabling a wide range of applications in the next generation.

NM06.08.35

Digital Light Processing (DLP) Printing of Polymer-Based Graphene Oxide Nanocomposite as an Efficient Antibacterial Coating for Surgical Implants Justin P. Edaughal^{1,1,2}, Emily Buckner^{1,1,2}, Mary K. Mitchell³, Erick L. Ribeiro^{1,1,2}, Melissa Ellermann³ and Rigoberto C. Advincula^{1,1,2}; ¹The University of Tennessee, Knoxville, United States; ²Oak Ridge National Laboratory, United States; ³University of South Carolina, United States

Bacterial infections are one of the major causes of surgical implant inefficiency and failure. In fact, such infections can lead to post-surgical complications, requiring antibiotic treatment and, in some cases, full surgical removal, increasing cost, recovery time, and risks to the patient's health. Up to date, various antibacterial wet coatings have been developed as an attempt to suppress bacterial growth, however, the implementation of these coatings on implant surfaces has been limited, owing to their poor mechanical integrity, along with their intrinsic low chemical and thermal stability. The precise patterning ability of three-dimensional (3D) printing technologies can be employed to accurately coat implants, avoid potential post-surgical complications arising from infections, and maintain high thermomechanical stability. Graphene Oxide (GO) has been reported as a biocompatible material with high toxicity to microorganisms and low mammalian cytotoxicity. Herein, we present a Nanocomposite (NC) produced by the addition of Poly(N-vinylcarbazole) – GO dispersion (PVK-GO), as a nanofiller to a commercial photopolymer acrylate resin (Elegoo translucent resin). More specifically, a series of NCs with different PVK-GO compositions were obtained by varying the ratios of GO from 0 to 0.5 wt% in the PVK-GO dispersion. The resulting NCs were printed as coatings *via* Digital Light Processing (DLP) technique and subsequently subjected to two distinct thermal annealing processes. Several characterizations of the final NC-based coatings, including Raman Spectroscopy, Fourier Transform Infrared Spectroscopy (FTIR), Tensile Strength (UTM), Thermogravimetric Analysis (TGA), X-Ray Diffraction (XRD), and Scanning Electron Microscopy (SEM) revealed the effects arising from the addition of different compositions of PVK-GO nanofillers to the resin. Moreover, results from various bioassays, including disk diffusion test, biofilm growth assay, and fluorescent imaging using gram-positive and gram-negative bacteria, confirmed the efficient antibacterial activity of the printed NC-based coatings. To that end, the present study demonstrates the fabrication and optimization of a PVK-GO-based NC with enhanced thermomechanical properties as well as elevated antibacterial activity and its potential utilization as a 3D-printable coating for biomedical applications.

SESSION NM06.09: Multifunctional 2D Coatings
Session Chairs: Nicholas Glavin and David Moore
Thursday Morning, December 1, 2022
Hynes, Level 2, Room 207

8:00 AM NM06.09.01

Identification of Proteinogenic Amino Acids Using MoS₂ Solid-State Nanopores Assisted by Machine Learning Andreina Urquiola Hernandez, Adrien Nicolai, Guyeux Christophe and Senet Patrick; Université de Bourgogne Franche Comté, France

Solid-State Nanopores (SSN) made of 2-D materials such as molybdenum disulfide (MoS_2) have emerged as one of the most versatile sensors for single-biomolecule detection, which is essential for early disease diagnosis (biomarker detection). One of the most promising applications of SSN is DNA and protein sequencing, at a low cost and faster than the current standard methods. The detection principle relies on measuring the relatively small variations of ionic current as charged biomolecules immersed in an electrolyte traverse the nanopore, in response to an external voltage applied across the membrane. The passage of a biomolecule through the pore yields information about its structure and chemical properties, as demonstrated experimentally particularly for DNA molecules. Indeed, protein sequencing using SSN remains highly challenging since the protein ensemble is far more complex than the DNA ensemble [1].

In this work, we performed extensive unbiased all-atom classical Molecular Dynamics simulations to produce data of translocation of biological peptides through single-layer MoS_2 nanopores ($D = 1.5$ nm). Peptide made of the 20 different amino acids from the different families (non polar/hydrophobic, polar/neutral, basic and acidic) were chemically linked to a short polycationic charge carrier [2]. First, ionic current time series were computed from MD and peptide-induced blockade events were extracted and characterized using structural break detection. Second, clustering (unsupervised learning) of ionic current drops and duration using Gaussian Mixture Model was applied. Using this technique, we demonstrate that each amino acid presents a large diversity of ionic current characteristics, however, charged amino acids were distinguished from the others. Finally, classification (supervised learning) was also implemented to identify residue motifs inside the pore, using XGBoost classifiers. We show that the addition of ionic current drops and duration to time series as input variables of the model greatly improve its performance, leading to the identification of the twentyproteinogenic amino acid. These promising findings may offer a route toward protein sequencing using MoS_2 solid-state nanopores.

References

- [1] **A. Nicolai** and P. Senet. Challenges in Protein Sequencing using MoS_2 Nanopores, 2022. In Bowen, W., Vollmer, F., Gordon, R. (eds) Single Molecule Sensing Beyond Fluorescence. Nanostructure Science and Technology. Springer, Cham. https://doi.org/10.1007/978-3-030-90339-8_11
- [2] M. D. Barrios Perez, **A. Nicolai**, P. Delarue, V. Meunier, M. Drndic, and P. Senet. Improved model of ionic transport in 2-D MoS_2 membranes with sub-5 nm pores. *Appl. Phys. Lett.*, 2019, 114(2):023107.
- [3] A. Urquiola Hernandez, **A. Nicolai**, C. Guyeux, and P. Senet. Identification of the twenty proteinogenic amino acids using MoS_2 nanopores assisted by Machine Learning. *In preparation*.

8:15 AM NM06.09.02

Cation Driven Assembly of Two-Dimensional Reduced Graphene Oxide/Bilayered Vanadium Oxide Heterostructures for Li-Ion Batteries **Ryan Andris**, Timofey Averianov and Ekaterina Pomerantseva; Drexel University, United States

Inorganic two-dimensional (2D) materials can be advantageous for applications that require efficient ionic conductivity and high redox activity. They offer open diffusion pathways for ion intercalation as well as strategies to potentially mitigate structural damage that can occur from the repeated expansion and contraction processes due to the reversible Li^+ ion intercalation during extended Li^+ ion battery cycling. 2D bilayered vanadium oxide (BVO or $\delta\text{-V}_2\text{O}_5 \cdot n\text{H}_2\text{O}$) is an especially promising material for electrochemical applications because it has an open structure with large interlayer spacing and vanadium's high oxidation state. These properties allow BVO to host a large number of charge carrying ions and undergo several reduction steps. However, the electrochemical performance of this bilayered phase is limited by its poor electronic conductivity and structural instability. In this work, we improved the cyclability and rate performance of BVO through an exfoliation process, the subsequent cation-driven assembly of exfoliated BVO and single-layer graphene oxide (GO) nanoflakes, and heat treatment processing to simultaneously reduce GO and partially dehydrate BVO.

Exfoliation followed by cation-driven assembly is a versatile technique that can be utilized for a variety of metal oxides and different conductive carbon precursors. The cations are used to maximize and stabilize the heterointerface formation between the BVO and GO by pulling these negatively charged nanoflakes together. As a proof of principle, exfoliated BVO and GO nanoflakes were assembled using a concentrated lithium chloride solution. The resulting flocculates were filtered, dried, and heat treated under vacuum at 210°C to form a 2D heterostructure comprised of $\delta\text{-V}_2\text{O}_5 \cdot n\text{H}_2\text{O}$ and partially reduced graphene oxide as evidenced by cross-sectional scanning electron microscopy images, energy dispersive X-ray spectroscopy, X-ray photoelectron spectroscopy, Raman spectroscopy, and thermogravimetric analysis. The heat treatment is used to reduce the interlayer water content of BVO for better long-term stability and obtain reduced GO (rGO) to increase its electronic conductivity. The characterization techniques were also used to determine that the graphitic content of the heterostructure could be controlled by changing the initial GO concentration prior to assembly. Moreover, we found that the amount of GO present affected the BVO phase stability and electrochemical behavior.

The electrochemical charge storage properties of heterostructures with 0, 10, 20, and 35 wt% rGO were evaluated in Li^+ ions cells with non-aqueous electrolyte and exhibited initial capacities of 245, 260, 180, and 150 mAh g^{-1} , respectively. However, BVO/rGO-0wt% retained only 10% of its initial capacity after 20 cycles at a 20 mA g^{-1} specific current. In contrast, the BVO/rGO-10wt%, BVO/rGO-20wt%, and BVO/rGO-35wt% materials retained 80%, 97%, and 100% of their initial capacities after 20 cycles at the same specific current. Further, the BVO/rGO-35% heterostructure retained 75% of its initial capacity (110 mAh g^{-1}) after increasing the specific current from 20 mA g^{-1} to 200 mA g^{-1} , while the BVO/rGO-10 wt% and BVO/rGO-20 wt% samples retained only 18% (50 mAh g^{-1}) and 67% (120 mAh g^{-1}) of their initial capacities under the same cycling conditions. The improved capacity retention and rate performance of the materials with higher GO content indicates that the presence of GO inhibits the structural degradation of BVO during cycling as well as improves the overall electronic conductivity of the heterostructure. In summary, the cation driven assembly approach uses Li^+ ions to induce and stabilize the formation of stacked 2D layers of GO and exfoliated BVO for applications in energy storage devices, and it can be applied in a variety of systems utilizing 2D materials with complementary properties.

8:30 AM NM06.09.03

Tuning the Properties of 2D Materials Using Organic Molecules Natalie Williams^{1,2}, Serrae Reed¹, Haotian Huang¹, Nilay Hazari¹, Judy Cha^{1,2} and James L. Hart²; ¹Yale University, United States; ²Cornell University, United States

Surface functionalization using organic molecules is an effective method to dope two-dimensional (2D) materials due to their high surface areas. Furthermore, by tuning the properties of the molecule on ordered 2D crystals, surface functionalization can be used to precisely control the electronic properties of 2D materials.¹ In previous studies, we investigated the doping power of novel organic electron donors (OEDs) based on 4,4'-bipyridine on monolayer MoS_2 using field effect transistor (FET) measurements before and after surface functionalization, as well as various spectroscopic characterizations. For example, using the reductant DMAP-OED, we demonstrated that both the surface coverage and reduction potential of the molecule are critically important for controlling the carrier concentration in MoS_2 . We experimentally estimated the doping power of DMAP-OED to be between 0.6 – 1.3 electrons per molecule, with good agreement with DFT results.¹ Our more recent study showed that a more compact reductant, Me-OED, is an even greater dopant, achieving record levels of electron donation on MoS_2 FETs.²

Here, I discuss the organic reductant tetrakis(dimethylamino)ethylene (TDAE), a molecular dopant which has never been studied before for 2D functionalization but could greatly impact the electrical properties of 2D FET devices based on criteria developed in our previous research. The relative position of the Fermi level of many 2D transition metal dichalcogenides (TMDCs), like MoS_2 , falls below the reduction potential of TDAE, resulting in

facile n-type doping to the 2D surface. More importantly, the small size and planar structure of TDAE molecules should allow for greater molecular surface coverage, and thus more electronic charge doping to surfaces. Our research is aided by spectroscopic and atomic force microscopic characterization. This project is conducted on MoS₂, but it can be expanded to other 2D TMCDs and materials. Our results highlight how the physical characteristics of a molecule are at least as important as their chemical affinity for charge donation, allowing us to realize unprecedented levels of doping to MoS₂.

[1] Yarali, M.; Zhong, Y.; Reed, S. N.; Wang, J.; Ulman, K. A.; Charboneau, D. J.; Curley, J. B.; Hynek, D. J.; Pondick, J. V.; Yazdani, S.; Hazari, N.; Quek, S. Y.; Wang, H.; Cha, J. J., Near-Unity Molecular Doping Efficiency in Monolayer MoS₂. *Advanced Electronic Materials* 2021, 7 (2), 2000873.

[2] Reed-Lingenfelter, S. N.; Chen, Y.; Yarali, M.; Charboneau, D. J.; Curley, J. B.; Hynek, D. J.; Wang, M.; Williams, N. L.; Hazari, N.; Quek, S. Y.; Cha, J. J., Compact Super Electron-Donor to Monolayer MoS₂. *Nano Lett.* 2022, 22 (11), 4501-4508.

8:45 AM *NM06.09.04

Polymer Grafted Layered Transition Metal Dichalcogenide Hybrids and NanoComposites Ali Jawaid¹, Nikolaos Chalmes², Emmanuel Giannelis² and Richard A. Vaia¹; ¹Air Force Research Laboratory, United States; ²Cornell University, United States

Molecular-level hybridization between polymers and layered transition metal dichalcogenides (LTMDs) result in emergent opto-electronic properties that are spurring development of low-cost, large-area technologies, from multi-functional sensors to optical coatings. The semi-conductive and semi-metallic character of few-to-monolayer LTMDs are tuned with surface-bound species, such as polymers, via orbital coupling and charge injection. However, balancing the requisite stoichiometric surface control with dispersability, processibility, and subsequent mechanical robustness is challenging. To meet these challenges, we utilize the redox exfoliation method to generate anhydrous LTMD dispersions, which enables direct functionalization of the LTMD surface, such as via Grignard coupling, derivitization with polymers, such as via RAFT / ATRP growth techniques, and nanometer control of morphology, such as via stoichiometric blending with polymers. The expanded formulation space supports design of opto-electronic performance via specific polymer-LTMD interactions, as well as bottom-up assembly of single-component mesostructured nanocomposites with improved mechanical toughness, for integration into a wide range of coatings, films, and monoliths.

9:15 AM BREAK

9:45 AM NM06.09.05

Stabilization and Manipulation of Silicene via Interface Engineering Daya Sagar Dhungana¹, Chiara Massetti^{1,2}, Eleonora Bonaventura^{1,2}, Carlo Grazianetti¹, Christian Martella¹ and Alessandro Molle¹; ¹Consiglio Nazionale delle Ricerche, Italy; ²Università degli Studi di Milano-Bicocca, Italy

Silicene is the thinnest form of silicon, a two-dimensional (2D) layer with a quasi-planar (buckled) structure [1]. It is produced by epitaxy on substrates like (111)-terminated Ag in ultra-high vacuum conditions. Silicene has a chemically fragile nature for it is unstable on both of its faces. It undergoes quick environmental degradation on its top face if not encapsulated, and on its bottom face when stripped off from its epitaxial substrate. To address these issues, here we will report on stabilization schemes based on dry or wet chemical delamination starting from a both-side encapsulated silicene and ending up with a stable and durable silicene foil on a tested timescale of weeks [2]. We show that both-side encapsulation is made possible by Al₂O₃ capping of the top face [3] and interface engineering through the realization of a silicene-on-stanene heterostructure (with stanene being the 2D counterpart of tin) [4]. The silicene-stanene heterostructure proves to be a suitable layout where to capture unprecedented silicene-related features like local heat dispersion in silicene and its contribution to the optical reflectance of silver [5]. Finally, we show how the silicene foils can be manipulated (e.g. stretched, bent, and transferred to secondary substrates) as desired therein displaying high mechanical flexibility and structural stability thus paving the way to their facile integration into diverse nanotechnology device platforms.

[1] A. Molle et al., *Chem. Soc. Rev.* (2018) 47, 6370.

[2] C. Martella, et al, *Adv. Funct. Mater.* (2020) 30, 2004546.

[3] A. Molle et al., *Faraday Discuss.* (2021) 227, 171.

[4] D. S. Dhungana, et al., *Adv. Funct. Mater.* (2021) 31, 2102797.

[5] E. Bonaventura et al., under review.

10:00 AM NM06.09.06

3D Printing of Hydrothermal Vanadium Disulfide Electrodes for Zinc-Ion Batteries Stefano Tagliaferri, Maria S. Sokolikova, Nagaraju Goli, Mauro Ochi, Haoyu Bai and Cecilia Mattevi; Imperial College London, United Kingdom

Aqueous Zinc Ion Batteries are receiving growing attention as beyond-lithium power sources for wearable electronics and sensors, owing to their high theoretical capacity, environmental friendliness and low cost. Vanadium disulfide is a layered Transition Metal Dichalcogenide (TMD) with great potential for zinc ion battery cathodes, owing to its large interlayer spacing, fast ionic diffusion and high conductivity. Despite these beneficial features, vanadium disulfide has mainly been investigated in coin-cell batteries, which are difficult to directly integrate in wearable electronics.

Here, we demonstrated the combination of an easily-scalable hydrothermal synthesis with a room-temperature 3D Printing process to fabricate vanadium disulfide electrodes with customized geometry. The hydrothermal vanadium disulfide was mixed with a polymeric binder and conductive additives to obtain a stable ink with optimal printability. The architecture of the VS₂ electrodes was rationally tailored *via* the printing process to facilitate the electrolyte penetration and promote fast charge transfer. Finally, the printed vanadium disulfide electrodes were coupled with zinc anodes to assemble aqueous zinc-ion batteries.

10:15 AM NM06.09.08

Mechanisms of Selective Ion Transport in Layered MoS₂ and Graphene Oxide Membranes Eli V. Hoenig, Mingzhan Wang and Chong Liu; University of Chicago, United States

Two dimensional materials such as MoS₂ and graphene are excellent scaffolds for nanometer and even angstrom scale fluidic channels. Unique chemical and physical phenomena arise in channels for which the size of the confined species has the same order as the confining dimensions. Here, we exploit the interlayer gallery of functionalized MoS₂ and graphene oxide to study the selective transport of ions through < 1 nm quasi two dimensional channels. In graphene oxide, we find that the permeance of Cu²⁺ is high relative to that of other divalent ions (Mg²⁺/Ca²⁺/Co²⁺). From the X-ray absorption spectra and pair distribution functions of saturated graphene oxide membranes, we determine that the enhanced flux of Cu²⁺ is a result of its strong coordination with carboxylic acid functional groups¹. In MoS₂, we find, surprisingly, that the relative adsorption of Pb²⁺ and Cu²⁺ reverses when MoS₂ is functionalized with

carboxylic acid groups (the membrane uptake of Pb^{2+} is higher when functionalized)². Infrared spectroscopy reveals that this reversal is a result of the unique bidentate binding of Pb^{2+} in the functionalized MoS_2 channels. Here, we also discuss our recent investigation of the ion transport through pores in few-layer MoS_2 .

[1] Wang, Mingzhan, et al. "Tuning transport in graphene oxide membrane with single-site copper (II) cations." *Iscience* 25.4 (2022): 104044.

[2] Wang, Mingzhan, et al. "Anomalous Ion Transport Across Angstrom-scale Channels Enabled by Surface Chemistry." Manuscript in preparation (2022).

10:30 AM *NM06.09.09

Unusual Effects of Thermal Conduction in Twisted 2D Materials Sorren Warkander^{1,2}, Yin Liu¹, Lei Jin¹, Jie Yao¹ and Junqiao Wu^{1,2}; ¹University of California, Berkeley, United States; ²Lawrence Berkeley National Laboratory, United States

2D materials offer opportunities to tune the lattice and phonon structures, some of which are not possible in bulk materials. The moire superlattices formed in twisted bilayers are found to host rich and new electronic effects; they are expected to also have strong influence on phonon dispersion and thermal conduction that is twist angle dependent. In this work, we measure and strive to understand thermal conduction physics in these twisted stacked 2D materials, including in-plane thermal conduction moire superlattices of transition metal dichalcogenides, and cross-plane thermal conduction in GeS nanowires with a single screw dislocation in the core.

11:00 AM NM06.09.10

Tunable Adsorption and Catalysis on Two Dimensional Ferroelectric Materials and Heterostructures Joshua Young and Mo Li; New Jersey Institute of Technology, United States

Two dimensional ferroelectric materials display a switchable spontaneous electric polarization in one or few monolayers. While they have been primarily proposed as components for ultrathin electronic devices, switching the polarization can change the surface properties, providing a route to overcoming the Sabatier principle on one material. We first show that the surface of the ferroelectric MXene Y_2CO_2 [1] with an O vacancy can preferentially adsorb CO_2 or CO depending on if the surface is poled up or poled down. We then extend that by investigating the reduction of CO_2 to CO, formic acid, and methane, and find that the stability of various intermediates as well as the final product can be also changed by switching the direction of the polarization. Second, we interface single transition metal atom and dimer (Cu and Fe) doped graphene with ferroelectric In_2Se_3 ; by switching the In_2Se_3 layer, the adsorptive properties of the metal-doped graphene layer can also be altered, leading to selective adsorption and catalysis. This is a unique route to preferential adsorption and product selectivity in catalysis.

[1] M Li, O Omisakin, J Young, *Nanoscale* 14 6970 (2022)

11:15 AM NM06.09.11

Transient Laser Photothermal Generation of 3D Graphene for Sensing and Energy Applications Pilgyu Kang^{1,1}, Byoung Gak Kim^{2,3}, Minsu Kim², Seung Min Lee^{1,1} and Shirin Movaghgharnezhad¹; ¹George Mason University, United States; ²Korea Research Institute of Chemical Technology, Korea (the Republic of); ³University of Science and Technology, Korea (the Republic of)

Nanomaterials have shown potential for high-performance functional materials especially in sensing and energy applications. Structuring of nanomaterials, including atomically-thin two-dimensional (2D) materials (e.g. graphene) and combining 2D materials with conventional materials such as metals and polymers can enable new functionalities and high performance by engineering exceptional and outstanding mechanical, electrical, and optical properties. We present a facile and rapid laser photothermal processing method to produce 3D porous graphene as well as a nanoassembly of 3D porous graphene and PdNPs from polymer films. Multi-dimensional hybrid nanomaterials combining 3D graphene and 1D metallic nanoparticles are produced in large scale with low production cost by transient laser photothermal processing. The films are photothermally processed using a laser to generate a nanohybrid via photo-induced thermal and chemical processes. The nanohybrid exhibits four-times-enhanced electrical conductivity compared to plain porous graphene, high crystallinity, and coherent covalent metal bonds with a homogeneous size and distribution of PdNPs in the hierarchical micro/meso/macro porous graphene structures, allowing high-performance hydrogen sensing (1 ppm) with outstanding mechanical reliability, flexibility, and durability upon bending and twisting. The nanoassembly is integrated with a wireless sensing platform and hydrogen leakage (1 ppm) is detected by a smartphone. This laser-based nanomanufacturing of the nanoassembly can potentially be applied to wearable detector production platforms in the military and industry. A facile, fast, and scalable laser-induced photothermal method was also used to achieve flexible monolithic bilayer sheets (MBS) of hierarchically porous graphitic carbon (HPGC) and polymeric foam for use in salt-resistant and flexible solar steam generators. The MBS-based self-floating solar steam generator shows outstanding solar desalination performance with a solar thermal efficiency of 83.2% under 1-sun illumination and a high salt-rejection ratio (99.9%). The all-in-one multi-functionalities of the MBS, including broad-spectrum solar light absorption, heat localization, and capillary action enabled efficient solar thermal energy transformation. Our laser-based photothermal method holds promise to achieve high-performance solar thermal systems with substantial cost reduction by scalable production of multiscale hierarchically structured materials from micro-structured polymers.

SESSION NM06.10: Theory and Simulation-Driven Studies in 2D Materials

Session Chairs: Xiwen Liu and SungWoo Nam

Thursday Afternoon, December 1, 2022

Hynes, Level 2, Room 207

1:30 PM NM06.10.01

Designing New 2D Nanomaterials with an Environmentally Friendly Synthesis Route—A DFT + Solvent-Ion-Model-Driven Study Mona Layegh and Joseph W. Bennett; University of Maryland Baltimore County, United States

The growing demand for designing and synthesis of stable new classes of layered and non-layered 2D nanomaterials with novel properties to open up new avenues toward a wide range of applications is not deniable. This is mainly due to their unique electronic, optical, chemical, and magnetic properties associated with size, structure and shape which originates from the quantum confinement effects in these materials. Having said that, we are developing a model to chemically manipulate known 3D bulk materials and their surfaces to create new functional nanomaterials by the chemical manipulation with a high stability using Density Functional Method (DFT) plus Thermodynamic analysis. As one of the main points of this model, using water as the aqueous

media to create this new 2D materials yields an ecofriendly synthesis approach. The study starts with narrowing down the choice of known *ABX* compounds on the basis of their valence electrons and magnetic interactions and cell crystalline structure. Then, the classes of collected compounds will be filtered through the Pourbaix diagram characteristics of their *A* element so that they can be exfoliated in environmentally friendly aqueous media like water. The final obtained results of bulk compounds are ready to be the subject of DFT calculations in terms of structural, electronic and band gap properties. Following that, we apply the surface slab model and the subsequent surface transformation thermodynamics to design 2D materials. The last step will be bridging between the dissolution and hydration in an atomistic level and the changes in the electronic structure, stability, and surface reactivities of the obtained 2D nanomaterials.

1:45 PM NM06.10.02

The Role of Interlayer Charge Compression Effects in the van der Waals Heterointerfaces of ReSe₂/graphene and ReSe₂/h-BN Demystified Jaehyeok Ko¹, Woosun Jang² and Aloysius Soon¹; ¹Yonsei University, Korea (the Republic of); ²Seoul National University, Korea (the Republic of)

Heterointerfaces of two-dimensional (2D) van der Waals (vdW) nanomaterials often exhibit unusual, “*non-textbook*” bonding mechanism that involves distinct (i.e., weak but non-negligible) orbital coupling within the compressed vdW gap [1]. This unique bonding mechanism is speculated to be quite different from the previously reported charge compression effect in ultrathin oxide films on metals [2]. To unravel this atypical bonding mechanism for 2D heterointerfaces, using vdW-corrected density-functional theory calculations, we examine the compressed charge redistribution in the heterostructures of ReSe₂/graphene and ReSe₂/h-BN. Here, we report the optimized atomic structures, electronic density-of-states, (integrated) planar-averaged electron density differences for these heterostructures, while focusing on the explicit contributions of the conductive graphene and insulating h-BN substrates to the interlayer confined charges. We demonstrate that this charge compression effect in the vdW gap is ubiquitous regardless of the nature of the substrates, and the magnitude of the confined charges can be modulated by atomic strain engineering. This study highlights the importance of understanding the interlayer charge compression effects by tailoring work function design for low-dimensional device applications [3].

[1] T. T. Ly, Y.-J. Lee, B. K. Choi, H. Lee, H. J. Kim, G. Duvjir, N. H. Lam, K. Jang, K. Palotás, Y. J. Chang, A. Soon, and J. Kim, *Appl. Surf. Sci.* **579**, 152187 (2022).

[2] L. Giordano, F. Cinquini, and G. Pacchioni, *Phys. Rev. B.* **73**, 045414 (2006).

[3] W. Jang, J. Lee, C. In, H. Choi, and A. Soon, *ACS Appl. Mater. Interfaces* **9**, 42050 (2017).

2:00 PM NM06.10.03

Theory of the Near-Field Electrostatic Effects in 2D Materials and van der Waals Heterostructures Qunfei Zhou¹, Michele Kotiuga² and Pierre Darancet³; ¹Northwestern University, United States; ²EPFL, Switzerland; ³Argonne National Laboratory, United States

Two-dimensional (2D) materials have demonstrated a wealth of intrinsic as well as exotic electronic properties arising from near-field electrostatic interactions between layers and from surface organic adsorbates, such as emergent ferroelectric order, excitonic energy landscape, and moiré superlattices. In this work, we derive an analytical theory for such near-field electrostatic effects, and validate it through first-principles calculations [1-2]. We demonstrate that superlattice potentials can be obtained in both 2D-2D and mixed-dimensional organic-2D heterostructures. We develop a classical electrostatic model of the superlattice potentials beyond the multipole expansion. Our theory quantitatively captures the out-of-plane decay and in-plane modulation, as well as elucidates the impacts of geometric effects, structural distortions, and material polarity on the electrostatic potentials. Finally, we demonstrate the applicability of this theory on efficient prediction of the material-/angle-specific moiré potentials with periodicities challenging for DFT calculations, and band structure engineering for 2D materials by the near-field electrostatic effects.

[1] Q. Zhou, A. Bukuru, S. Trevor, K. Michele, and P. Darancet. *arXiv:2109.09990* (2021).

[2] Q. Zhou, K. Michele, and P. Darancet. *arXiv:2205.04606* (2022).

2:15 PM BREAK

2:45 PM NM06.10.04

Designing 2D Chalcogenide Piezoelectrics Jonathan Chin¹, Maria Hulse², Derrick Shao Heng Liu², Sebastian Marini¹, Roman Engel-Herbert² and Lauren M. Garten¹; ¹Georgia Institute of Technology, United States; ²The Pennsylvania State University, United States

Tin selenide (SnSe) is centrosymmetric in bulk but can become piezoelectric when reduced to an odd number of layers near the monolayer limit. However, synthesizing a monolayer of SnSe is challenging because the interlayer bonding is stronger than most 2D materials, making controllable exfoliation difficult. This work focuses on developing routes to stabilize monolayer films of SnSe by molecular beam epitaxy (MBE).

The processing window for SnSe on MgO substrates fell between 250 – 300 °C for flux ratios of 1:3 – 1:5 (Sn:Se). The Raman modes present in thick films are consistent with the *Pnma* phase of SnSe with the mode at 185 cm⁻¹ appearing first. Once the phase formation conditions were identified then changes in the Raman spectroscopy with processing time were used to identify the onset of crystallization. These results were then used to estimate the timing necessary to grow a monolayer film. The thickness of the MBE films was directly measured by atomic force microscopy corroborating the layer timing determined from the Raman results. Then X-ray photoelectric spectroscopy was used to determine the surface stability of these 2D films against oxidation and degradation. The timing and processing conditions necessary to achieve 2D SnSe will be discussed in this talk. These results will provide insight into routes to control the layering and surface stability of SnSe that will be necessary for the development of 2D piezoelectric and electronic devices.

3:00 PM NM06.10.05

Machine Learning Aided Understanding of the Interaction in Borophene-Boride Hetero-Structures Luqing Wang^{1,2}, Qunfei Zhou^{1,2}, Qiucheng Li¹, Joshua T. Paul², Mark C. Hersam¹, Pierre Darancet^{2,1} and Maria K. Chan^{2,1}; ¹Northwestern University, United States; ²Argonne National Laboratory, United States

Borophene is unusual among two-dimensional (2D) materials for the lack of a bulk layered counterpart, resulting in novel properties which are not inherited and cannot be predicted from bulk boron, as well as polymorphic phases which enrich its properties. Also, its metallicity is unusual within the 2D materials family and enriches the diversity of available materials properties. However, the application of borophene is limited by the lack of achievement of freestanding borophene. It's difficult to lift borophene from the substrates due to the strong interaction between them. Thus it is important to search for optimal substrates for borophene synthesis and separation. Recently, it was reported that boride is formed through the reconstruction of the top metal layer mixed with boron during borophene synthesis on Al(111) [1]. Metal borides have the potential to be superior substrates, compared to metals, for borophene synthesis and separation. The understanding of the interaction in borophene-boride hetero-structures would assist the search of optimal substrates as well as reveal the synthesis mechanism. What borides surfaces are optimal substrates for borophene synthesis? What intrinsic properties of borides dominantly affect the interaction in borophene-boride hetero-structures? How does the charge transfer between borophene and borides affect the interaction? Here we

explore these questions through machine learning and density functional theory calculations of their structures, binding energies, and charge transfer. This work allows us to explore alternative routes of borophene synthesis.

Acknowledgements:

We acknowledge funding from the National Science Foundation MRSEC program under grant number DMR-1720139. Use of the Center for Nanoscale Materials, an Office of Science user facility, was supported by the U.S. Department of Energy, Office of Science, Office of Basic Energy Sciences, under Contract No. DE-AC02-06CH11357.

Reference:

[1] Alexei B. Preobrajenski, Andrey Lyalin, Tetsuya Taketsugu, Nikolay A. Vinogradov, and Alexander S. Vinogradov., "Honeycomb Boron on Al(111): From the Concept of Borophene to the Two-Dimensional Boride." *ACS Nano* 2021 15 (9), 15153-15165.

SESSION NM06.11: Synthesis of 2D Materials and Heterostructures III

Session Chairs: Xiwen Liu and SungWoo Nam

Thursday Afternoon, December 1, 2022

Hynes, Level 2, Room 207

3:45 PM NM06.11.01

Impact of Metal Solvent Composition on the Properties of hBN Crystals Grown from Molten Metal Solutions Eli Janzen¹, Bernard Gil², Guillaume Cassabois², Adrien Rousseau² and James H. Edgar¹; ¹Kansas State University, United States; ²CNRS-Université de Montpellier, France

Hexagonal boron nitride (hBN) is a wide energy bandgap (>6.0 eV) semiconductor with a layered graphite-like structure and a high internal quantum yield for deep ultraviolet luminescence. These properties make it a good candidate deep UV light emitters and detectors, single photon emitters, and in nanophotonics by forming strong phonon polaritons. [1] While many researchers have focused on the heteroepitaxy deposition of hBN, there are many advantages to its bulk crystal growth via the solution growth method. Atmospheric pressure solution growth of hBN crystals using molten metals as solvents can produce material with crystal quality (Raman E_{2g} FWHM < 8 cm^{-1} [2]) that is as good or better than material produced by high temperature high pressure solution growth. Furthermore, it is a scalable process that is more capable at growing much larger crystals (up to 4 cm^2 [3]) than the high pressure process.

Here we report on the effects of the metal solvent composition on the crystal growth process and the quality of crystals produced. We analyzed how the process is affected using four different solvents: iron, iron-vanadium, nickel-chromium, and cobalt-chromium. These solvents represent a large range of nitrogen solubilities, with Fe and Fe-V having low solubility (0.04-0.1 mass% N) and Co-Cr and Ni-Cr having high solubility (0.15-0.3 mass% N). Crystal growth experiments were conducted with each of these solvents with varying compositions, the results of which were analyzed with optical microscopy, surface profilometry, and photoluminescence spectroscopy.

Based these results, the solvent appears to primarily affect three different characteristics: crystal thickness, the prevalence of certain defects, and the morphology of the bulk crystals. Crystals grown from Ni-Cr and Co-Cr solvents were hexagonal shaped with large steps and thicker (10-100 μm as-grown) than those grown from other solvents. In contrast, crystals grown from Fe and Fe-V were triangular-shaped with many wrinkles and thinner (5-30 μm as-grown). Comparisons between the photoluminescence spectra are also made, but the trends are less clear, though most spectra showed a strong peak at 5.75 eV, indicating high quality crystals can be grown with any of these solvents. To better understand these effects, the properties of the solvent such as nitrogen solubility are correlated with these observations and a model for their cause is proposed.

These results demonstrate that solvent choice is an important factor for optimizing atmospheric pressure solution growth of hBN and suggests a potential avenue to tailor crystals for specific applications. For example, in devices where a thicker crystal would improve efficiency, the crystals could be grown from a Ni-Cr solvent, while for devices that function better with thin crystals, they could be grown from an Fe solvent instead. Furthermore, these results provide insights into the mechanisms that guide hBN solution growth that can be used to optimize the process in general.

References:

[1] J.D. Caldwell, I. Aharonovich, G. Cassabois, J.H. Edgar, B. Gil, and D. Basov, Photonics applications of hexagonal boron nitride, *Nature Rev. Mater.* 4 552-567 (2019).

[2] S. Liu, R. He, Z. Ye, X. Du, J. Y. Lin, H. X. Jiang, B. Liu and J. H. Edgar, "Large scale growth of high quality hexagonal boron nitride crystals at atmospheric pressure from an iron-chromium flux," *Crystal Growth & Design*, vol. 17, pp. 4932-4935, 2017.

[3] J. Li, J. Wang, X. Zhang, C. Elias, G. Ye, D. Evans, G. Eda, J. M. Redwing, G. Cassabois, B. Gil, P. Valvin, R. He, B. Liu and J. H. Edgar, "Hexagonal boron nitride crystal growth from iron, a single component flux," *ACS Nano*, vol. 15, pp. 7032-7039, 2021.

4:00 PM NM06.11.02

In-Plane TMDs Heterostructure Mesh Grown by Gap-Filling Chemical Vapor Deposition Hongwei Liu^{1,2}, Jing Kong² and Zhengtang Luo¹; ¹Hong Kong University of Science and Technology, Hong Kong; ²Massachusetts Institute of Technology, United States

Lateral superlattices have been a research focus due to the strain induced in their coherent structure, while the growth of large size heterostructure with high density of heterointerfaces remains challenging. In this work, we report a gap-filling approach to synthesize large scale lateral mesh heterostructures of WS_2 embedded in MoS_2 matrix. This synthesis method utilizes the uniformly distributed gaps in single crystalline MoS_2 made from by sulfur substitution-induced transformation of metastable- MoTe_2 as the growth pattern, for the second material growth. By finely controlling the growth kinetics, highly crystalline WS_2/MoS_2 lateral heterostructure mesh is successfully grown. Optical images and Raman mapping show a clear spatial distribution of WS_2 channels embedded in MoS_2 . The coherent epitaxial nature is further confirmed by scanning transmission electron microscopy, showing insignificant dislocation at the interfaces. Density function theory simulation suggests that growth of WS_2 starts from the edges of cracked MoS_2 .

4:15 PM NM06.11.03

Stable Black Phosphorus Nanoassembly Achieved Through Heterogeneous Hydrophobic Functionalization Yan-Lin Wang, Ying-Hao Pai, Karan Giri, I-Jung Wang, Yi-Chen Chen, Cheng-Ju Yang, Pei-Hsuan Cho, Yu-Chieh Shih, Chuan-Wen Wang, Ling-Chun Chao and Chun-Hua Chen; National Yang Ming Chiao Tung University, Taiwan

Black phosphorus (BP), a promising two-dimensional material, has sparked a research boom in various fields. BP possesses a tunable direct bandgap varying from 0.3 eV of bulk to 2.2 eV of the monolayer, which perfectly bridges the energy gap between graphene and transition metal dichalcogenides. Besides this, numerous extraordinary characteristics, including ultrahigh hole mobility of $\sim 10^3$ cm²/V s, current on-off ratios of $\sim 10^5$, current density, and high in-plane anisotropy of the optical, electrical, and vibrational properties, further expand the scope and possibilities in a variety of applications. However, its fatal atmospheric instability, which mainly originates from the continuous oxidation and hydration spontaneously beginning from the surface phosphorene atoms under the ambient atmosphere, seriously obstructs the progress of most practical applications.

In this work, the selective deposition of Al₂O₃ capping layers with either hydrophobic or hydrophilic surfaces has been successfully achieved on the top surface of the BP flake assemblies via tuning the layer structure and porosity. Dielectric Al₂O₃ is the best candidate, mainly due to its chemical stability and weaker response to most gases. The moisture resistance, lifetime, and the humidity sensing potential of the BP flakes assembled devices capped with hydrophilic dense Al₂O₃ layers, and hydrophobic porous Al₂O₃ nanoassemblies were evaluated by monitoring the overall resistance change under periodical exposure to high-humidity environments (RH = 85%). It was found that the pristine BP flake assembly completely loses its humidity sensing ability at RH = 85% after being stored at RH = 70% for three weeks. Remarkably, with the presence of hydrophobic Al₂O₃ capping layers, a 75% residual humidity sensing response is maintained after five weeks. In other words, the Al₂O₃ capping layers provide complete protection against severe and rapid degradation of the original BP, even in high humidity environments. The proposed functionalization strategy for the BP assemblies further opens the possibility of creating novel BP devices.

4:30 PM NM06.11.04

Target-Specific Synthesis of Monolayer Molybdenum Disulfide via Adaptive Experimental Design with Batch Bayesian Optimization Yujia Wang, Guoyan Li, Xiaoning Jin and Swastik Kar; Northeastern University, United States

Abstract

When it comes to the predictable synthesis of 2D transition metal dichalcogenides using chemical vapor deposition, the large number of design of experiments (DoE) parameters (such as temperature, pressure, flowrate, quantity and initial positioning of precursors, pressure etc.) and their and complex interdependencies is a well-recognized experimental challenge. Often, small changes in one of these parameters can lead to large variabilities in size, yield, and quality. Although literature is replete with information regarding growth conditions, they vary from system to system. Hence, a method that can reduce the inevitable risk of "trial and error" approaches and guide experimentalists systematically towards the most suitable outcome is important for accelerating research. Here, in order to increase the efficacy and accelerate development, we present a machine learning approach to experiment design providing an alternative data-enabled materials synthesis design to establish desired process-and-quality linkage within the target material quality space. The proposed approach uses a batch Bayesian optimization-based method that employs a batch acquisition strategy to adaptively guide the selection of the experimental parameters and iteratively find the most rapid path for reaching the optimized design of experiments for a target material quality. Using the synthesis of molybdenum disulfide (MoS₂) by thermal chemical vapor deposition as an example, we extracted five physically correlated experimental parameters (position of the sulfur precursor, position of MO₂ precursor, Ar gas flow rate, temperature ramp-up rate, maximum temperature holding time) and three physically correlated observational parameters (Raman peak height, Excitonic linewidth, Shape). We combine an efficient and predictive surrogate model for monolayer prediction with a batch Bayesian Optimization algorithm to adaptively explore and exploit the design space. We show the success of implementing this method in MoS₂ synthesis in which MoS₂ with target observational parameters is achieved within 3 batches of experiments (46 samples) and the optimal region of synthesis parameters need to make targeted materials are identified.

Acknowledgements

This research was supported by the Crystal Systems Innovations Fellowship to support Y.W. and partially supported by the Northeastern University TIER1 Seed Grant.

Y.W. and G.L. contributed equally

SESSION NM06.12: Advanced Characterization and Unique Phenomena in 2D Layered Materials

Session Chairs: Nicholas Glavin and Won Il Park

Friday Morning, December 2, 2022

Hynes, Level 2, Room 207

8:00 AM NM06.12.01

⁶⁰Co Gamma-Ray Irradiation Effects in Aerosol Jet Printed Two-Dimensional Multilayered Materials [Twinkle Pandhi](#)¹, Gregory P. Horne², Fahima Ouchen³, Timothy A. Prusnick³, Roberto S. Aga³ and Emily M. Heckman¹; ¹Sensors Directorate, Air Force Research Lab, United States; ²Idaho National Laboratory, United States; ³KBRwyle, United States

Recent advances in nuclear applications and the development of the US Space Force has led to an increased interest in radiation-detection and radiation hardness technologies.¹⁻³ Novel ionizing radiation-tolerant (X-rays, γ -rays, neutrons) materials and fabrication processes are needed to develop next-generation radiation-detection systems that meet size, weight, power consumption, and cost (SWaP-C) considerations.⁴⁻⁶ Inorganic semiconductor materials, such as silicon, cadmium, zinc telluride, or mercury iodide-based radiation detection systems are currently fabricated using a standard silicon-based lithography process.⁵ While this silicon-based electronic system enables high performance, it does have several drawbacks: its inability to conform to various structures, limited large-area processing, and relatively high cost.⁷

Two-dimensional (2D) materials offer unique electrical, optical, and mechanical properties that may make them advantageous for use in harsh nuclear or space environments.^{8,9} Mono to few layers of 2D materials such as graphene, hexagonal boron nitride, black phosphorus, and metal dichalcogenides have shown negligible change in performance after irradiation and are reported to exhibit high degrees of radiation hardness.^{10,11} Solution-based deposition techniques allow for a cost-effective approach for rapid prototyping of devices. Additive manufacturing technologies (direct-write, aerosol jet printing, inkjet printing, etc.) offer low-cost, high-throughput production of flexible electronics, with little material waste and a high degree of compatibility to most substrates of interest.¹²⁻¹⁴

Previous studies have reported on gamma irradiation for mechanically exfoliated, chemical vapor deposition (CVD), and epitaxial grown graphene-based devices.¹⁵⁻¹⁹ However, irradiation effects on printed 2D materials have yet to be reported. This work investigates the roles of microstructure and the substrate properties affected by gamma irradiation in aerosol-jet printed (AJP) 2D materials. The information gained from this study is expected to provide new fundamental insights that can guide the development of nuclear and space applications of printed 2D material devices.

Radiation effects from ⁶⁰Co gamma-ray radiation are reported for aerosol-jet printed 2D-materials (graphene, MoS₂, WS₂, and h-BN) on various substrates (Si/SiO₂, glass, sapphire, and kapton). Irradiated samples were characterized through Raman spectroscopy, SEM/EDX, XPS, and stylus profilometer.

Furthermore, we fabricated AJP h-BN capacitors to study the effects of gamma radiation on its electrical properties. The information gained from this study is expected to provide new fundamental insights that can guide the development of nuclear and space applications of printed 2D material devices.

References

- 1 Benton, E. R. *et al. Nucl. Instruments Methods Phys. Res. Sect. B Beam Interact. with Mater. Atoms* (2001)
- 2 Elgazzar, A. H. *et al. in The Pathophysiological Basis of Nuclear Medicine* (2015)
- 3 Stassinopoulos, E. G. *et al. Proc. IEEE* (1988)
- 4 Morosh, V. *et al. Radiat. Meas.* 143, (2021)
- 5 Maiello, M. L. *Health Phys.* (2008)
- 6 Posar, J. A. *et al. Flexible and Printed Electronics* 6, (2021)
- 7 Agosteo, S. in *Radiation Measurements* (2010)
- 8 Editorial. *Nat. Photonics* 10, 201–201 (2016)
- 9 Rao, C. N. R. *et al. ACS Appl. Mater. Interfaces* (2015)
- 10 Ochedowski, O. *et al. J. Appl. Phys.* (2013)
- 11 Krashennikov, A. V. *Nanoscale Horizons* 5, (2020)
- 12 Li, J. *et al. ChemPhysChem* 15, 3427–3434 (2014)
- 13 Xu, Y. *et al. Nanomaterials* (2018)
- 14 Seifert, T. *et al. Ind. Eng. Chem. Res.* 54, 769–779 (2015)
- 15 Walker, R. C. *et al. Phys. Status Solidi Appl. Mater. Sci.* (2016)
- 16 Kashid, R. V. *et al. Radiat. Eff. Defects Solids* 169, (2014)
- 17 Cazalas, E. *et al. Appl. Phys. Lett.* 115, (2019)
- 18 Isherwood, L. H. *et al. J. Phys. Chem. C* 125, 4211–4222 (2021)
- 19 Felix, J. F. *et al. Nanoscale Horizons* 5, 259–267 (2020)

8:15 AM NM06.12.02

A Path Toward Achieving Perfect Absorption in 2D Heterostructures Dongjea Seo¹, Seungjun Lee¹, Nezhueyotl Izquierdo¹, Sang Hyun Park¹, Eng Hock Lee¹, Rehan Younas², Guanyu Zhou², Christopher Hinkle², Tony Low¹ and Steven Koester¹; ¹University of Minnesota, United States; ²University of Notre Dame, United States

MoS₂ is a promising material for atomically thin perfect absorbers due to the high oscillator strength of its excitonic transitions and excellent band nesting. As MoS₂ is thinned from multilayer to monolayer, the magnitude and energy of its optical conductivity were exponential attenuation in magnitude and manifested by a gradual blueshift in energy with decreasing layer number due to interlayer orbital hybridization. The intrinsically poor light absorption of monolayer MoS₂, which varies by about 12 % in visible spectral range, induces the weak light-matter interaction. Although this absorption is surprising for the atomic thickness of MoS₂, these values must be increased to design MoS₂-based absorbers. Most approaches to improving the light-matter interaction of MoS₂ have been devoted to plasmonic nanostructure and photonic crystal. The photonic crystal slab with a perfect conductor mirror achieves near-unity absorption at 450 nm and average absorption of 51 % over the spectrum from 400 to 700 nm in the MoS₂ [1].

Here, we demonstrate a new approach to achieving perfect light absorption in MoS₂/graphene/MoS₂ (MGM) heterostructure. By putting graphene in the intermediate layer to reduce the interlayer interaction of MoS₂ with each other, the doubling effect of light absorption can be obtained. As a demonstration of the concept, we experimentally show the optical contrast of MGM heterostructure can be improved by ~28 % compared to the bilayer MoS₂ at $\lambda = 442$ nm near the band nesting region. This result is in excellent agreement with the density functional theory of absorbance of a freestanding MGM heterostructure. Based on this structure, we also demonstrate a method based on the insertion of a silver (Ag) mirror layer between the dielectric layer and the substrate to enhance the optical absorption, resulting from Fabry-Perot cavity reflection. The interband absorption of MGM heterostructure is maximized by the cavity resonance and can reach the near-perfect absorption for frequencies satisfying the cavity resonance condition. With various 2D materials and optimization strategies, we can realize ideal absorption over the wide frequency range from UV to IR. Our study points to a new opportunity to combine 2D heterostructure with cavity optics to enable novel device applications such as high-efficiency solar cells with nanometer-scale thickness.

References

- [1] J. Piper and S. Fan, *ACS Photonics* 3(4),(2016) 571–577

8:30 AM NM06.12.03

Two-Dimensional Janus GePAs Monolayer: Direct Band Gap Semiconductor with High and Anisotropic Mobility for Efficient Photocatalytic Water Splitting Dogukan Hazar Ozbey¹, Mehmet E. Kiliç² and Engin Durgun¹; ¹Bilkent University, Turkey; ²Korea Institute of Science and Technology, Korea (the Republic of)

Two-dimensional (2D) materials with suitable electronic and optical properties offer different possibilities for photocatalytic applications. Although various 2D materials have hitherto been specified as adequate candidates, materials with high photocatalytic efficiency for water splitting are still minimal. In this study, we predict a 2D Janus GePAs monolayer and examine its capability for photocatalytic water splitting by performing first-principles calculations. The GePAs monolayer is shown to possess robust dynamic and thermal stability. The direct electronic band gap in the visible region and band edge positions of the strain-free and strained monolayers are revealed to be convenient for redox reactions in wide pH ranges. The low recombination probability of charge carriers ensured by high and anisotropic carrier mobility enhances the material's photocatalytic potential. Optical response calculations, including many-body interactions, exhibit significant optical absorption capacity in the UV–visible range. Furthermore, low exciton binding energy facilitates dissociation into free electrons and holes, promoting photocatalytic reactions. Our study suggests GePAs monolayer is an ideal and remarkably promising material to be utilized in visible-light-driven photocatalytic applications.

8:45 AM NM06.12.04

Probing Sulfur Vacancies in MoS₂ by Photoluminescence Yiru Zhu¹, Yan Wang¹, Soumya Sarkar¹, Juhwan Lim¹, Zhepeng Zhang², Goki Eda², Robert Hoye³ and Manish Chhowalla¹; ¹University of Cambridge, United Kingdom; ²National University of Singapore, Singapore; ³Imperial College London, United Kingdom

Chalcogen vacancies can influence the electronic structure of 2D transition metal dichalcogenides (TMDs) by introducing mid-gap defect states. A relatively simple way to create chalcogen vacancies is by thermal annealing. The vacancy defects are optically active and can be probed by photoluminescence (PL) spectroscopy. In this study, we annealed mechanically exfoliated monolayer MoS₂ in different atmospheres and probed the sulfur vacancy states by PL. In nitrogen or argon atmosphere, room temperature defect emission is absent. However, annealing in hydrogen/argon (5% H₂) gives rise to room-temperature defect PL peak at 1.72 eV. Stronger defect PL signal at 10K is observed when annealing time is increased. We show that sulfur vacancies can be passivated by annealing in sulfur vapor. X-ray photoemission spectroscopy is used to confirm the creation and passivation of sulfur

vacancies. Our results suggest that defect states introduced by sulfur vacancies act as trapping centres for radiative recombination and can be passivated by annealing in sulfur vapor environment.

9:00 AM NM06.12.05

Direct Write, Read and Erase of a Graphene/Monolayer Electrolyte/h-BN Heterostructure via Electric Force Microscopy Huiran Wang¹, Shubham S. Awate¹, Ke Xu^{2,2} and Susan Fullerton^{1,1}; ¹University of Pittsburgh, United States; ²Rochester Institute of Technology, United States

A solid-state, non-volatile memory based on electric-double-layer (EDL) gating using a monolayer electrolyte (ME) has been developed in our lab. This ME consists of cobalt crown ether phthalocyanine (CoCrPc) and a lithium salt that forms an ordered array on the surface of 2D materials. Each crown ether solvates one cation that is stable in two states in the crown – one near the 2D material creating a low-resistance state and the other further away creating a high-resistance state. The location is set by an electric field via a backgated transistor architecture. Here, we investigate an approach to locally toggle the ions through the crown using an atomic-force microscopy (AFM) tip. Instead of a three-terminal transistor, here we use a two-terminal stack of graphene/ME/hexagonal boron-nitride (h-BN) on p-doped Si prepared by dry flake transfer. P-doped Si serves as one terminal, and the AFM tip/graphene as the second. AFM is used in electric force microscopy (EFM) mode to write, read, and erase the stacks. The AFM tip is brought into contact with the graphene surface to perform the local switching on the stack wherein the AFM tip acts like a charge source to locally inject charges to the graphene surface while the p-doped Si is grounded. The resulting electric field toggles the ion back and forth through the crown. By switching the location of the ions using a “write” voltage > 9 V, the differences of the electrostatic interaction between the tip and the written regions can be detected using a “read” voltage. In this non-contact reading mode, the tip is raised to lift height and biased ($V_{\text{read}} = \pm 3\text{V}$) to sense the local electric field of the sample surface. The read voltage is chosen so as not to disturb the state of the ions. These differences of tip-sample interaction appear as a change in the phase, indicating the tip is experiencing a repulsive or attractive force during the scan. When the ions are positioned closer to the graphene surface, graphene will be n-doped and the repulsion between the tip and the sample surface is increased. Our results show a continuously increasing phase shift (total ~ 0.7 degree) with increasing write voltages from 5 to 10 V, detected by a read voltage of 3 V (45 nm lift height). This trend suggests that lithium ions are switching through the crown, and that more of them are switching with increasing write voltage. A reverse “erase” bias is applied to the same region to push the ions away from the graphene, and the region is read with the same read voltage. The results show no increasing phase shift, suggesting a successful erase. The same procedure was also performed on control samples without the ME (i.e., graphene/h-BN), confirming that the origin of the phase shift is ME. We also confirm that the polymer residue from the dry flake transfer is not the origin of the phase shift. In addition, the magnitude of the phase shift as a function of tip bias provides a means to quantify the surface charge. We estimate the surface charge to be $5.44 \times 10^{12} \text{ cm}^{-2}$ for graphene alone (without the monolayer electrolyte), and the value for the monolayer electrolyte stack will be reported. This work is supported by the NSF under Grant # NSF-DMR-EPM CAREER: 1847808.

9:15 AM BREAK

9:45 AM NM06.12.06

Defect Engineering Graphene for Dynamic Reliability Boran Kumral¹, Teng Cui^{1,2}, Pedro Guerre Demingos¹, Nima Barri¹, Chandra V. Singh¹ and Tobin Filletter¹; ¹University of Toronto, Canada; ²Stanford University, United States

The ability to withstand high tensile strain as a result of strong in-plane sp^2 covalent bonding, low bending stiffness, and a wide variety of tunable electrical properties has led to wide interest in the development of 2D materials-based flexible devices such as flexible electronics, nanocomposites, and multifunctional coatings. Despite exceptional intrinsic mechanical, electrical, and optical properties, challenges remain in the realization of 2D materials in their functional device applications. The interface between 2D materials and soft stretchable substrates is a governing parameter in proposed 2D materials-based flexible devices. However, the same interface is dominated by van der Waals (vdW) forces and the mismatch in elastic constants between the contact materials leads to very low adhesion energy (also referred as interface toughness, work of separation, or work of adhesion). For example, the adhesion energy between monolayer graphene and silicon oxide is estimated to be $\sim 450 \text{ mJ.m}^{-2}$ (1), while the adhesion energy between monolayer graphene and polydimethylsiloxane (PDMS), a soft and stretchable elastomeric substrate, is estimated to be only $\sim 7 \text{ mJ.m}^{-2}$ (2). When the 2D material/stretchable substrate system is subjected to cyclic loading by applying continuous tension and compression, the low adhesion leads to decoupling, slippage, and extensive damage propagation in the 2D lattice (3). With only 10 cycles of cyclic loading of graphene on PDMS at $\epsilon = 20\%$ strain range, $\sim 30\%$ of a graphene flake's area is catastrophically damaged (3).

We reveal that through careful defect engineering of graphene, the contact interface between graphene and PDMS can be modified to increase the adhesion energy to $\sim 40 \text{ mJ.m}^{-2}$, which is characterized with an atomic force microscope (AFM) by employing buckling-based metrology (4). The defect engineering consists of exposing a single side of a graphene flake to controlled and mild oxygen plasma, and then placing the flake's functionalized side in direct contact with PDMS. The type and density of defects are characterized using X-ray photoelectron spectroscopy (XPS) and Raman spectroscopy. The defects present are revealed to be a low density of sp^3 -type defects, mainly oxygen functional groups. In situ micro tensile testing under an optical microscope and optical image processing reveals that the increased adhesion in defect engineered graphene/PDMS systems drastically inhibits damage propagation and improves fatigue life. Additionally, insight into the role of each functional group in relation to the change in adhesion is investigated using molecular dynamics (MD) simulations. This work could be extended to other 2D material/stretchable substrate systems and offers insight into achieving dynamically reliable contacts, which could facilitate the development of 2D materials-based flexible devices.

1. S. P. Koenig, N. G. Boddeti, M. L. Dunn, J. S. Bunch, Ultrastrong adhesion of graphene membranes. *Nature Nanotechnology*. **6**, 543–546 (2011).
2. S. Scharfenberg, D. Z. Rocklin, C. Chialvo, R. L. Weaver, P. M. Goldbart, N. Mason, Probing the mechanical properties of graphene using a corrugated elastic substrate. *Applied Physics Letters*. **98**, 1–4 (2011).
3. T. Cui, K. Yip, A. Hassan, G. Wang, X. Liu, Y. Sun, T. Filletter, Graphene fatigue through van der Waals interactions. *Science Advances*. **6** (2020), doi:10.1126/sciadv.abb1335.
4. C. J. Brennan, J. Nguyen, E. T. Yu, N. Lu, Interface Adhesion between 2D Materials and Elastomers Measured by Buckle Delaminations. *Advanced Materials Interfaces*. **2**, 1–7 (2015).

10:00 AM NM06.12.07

In Situ TEM Imaging of Novel Edge Reconstruction in Bilayer Phosphorene Sol Lee^{1,2}, Yangjin Lee^{1,2}, Li Ping Ding^{2,3}, Kihyun Lee¹, Feng Ding^{2,4} and Kwanpyo Kim^{1,2}; ¹Yonsei University, Korea (the Republic of); ²Institute for Basic Science, Korea (the Republic of); ³Shaanxi University of Science & Technology, China; ⁴Ulsan National Institute of Science and Technology, Korea (the Republic of)

Atomic-scale characterization of two-dimensional (2D) materials and their heterostructure is indispensable to understanding their physical, electrical, and chemical properties. In particular, atomic-scale configurations and morphology of 2D crystals' edges strongly influence properties including electronic, transport, and optical properties. Transmission electron microscopy (TEM) has been employed to observe the atomic-scale edge structure of various 2D materials. Moreover, via in-situ TEM capabilities, the controlled edge formation under various environments and stimuli has been achieved. On the other

hand, atomic-scale TEM imaging of crystalline edges of phosphorene has been quite challenging compared to other 2D crystals. The main obstacle is the sample's vulnerability to ambient exposure and the characterization process.

Here, we report the atomic scale TEM observation of ultra-stable self-passivated phosphorene edges in bilayer phosphorene. We use graphene as a supporting layer for phosphorene to suppress the electron-beam-induced radiolysis effect during TEM measurement. We prepare phosphorene/graphene vertical heterostructure samples on an in-situ heating chip by dry-transfer technique. Using in situ heating, the prepared phosphorene/graphene samples suffer from little residues and adsorbates. At elevated temperatures, the layer-by-layer etching of black phosphorus has been observed, which leads to the formation of monolayer and bilayer phosphorene. While etching of monolayer phosphorene under e-beam is pronounced, we observe that the edge of bilayer phosphorene with zigzag edge configuration shows high stability under the electron beam.

To investigate the detailed edge configuration of stable bilayer ZZ phosphorene edge, we perform TEM imaging at various defocus values as well as tilting configurations. Based on first-principles calculations and TEM image simulations, we confirm that the bilayer ZZ edge shows the reconstruction with the interlayer self-passivating covalent bonds. Our theoretical calculations also confirm the low formation energy of the observed edge configuration compared to other possible configurations. Our study demonstrates that atomic-scale reconstruction of phosphorus can be harnessed to fabricate stable phosphorene nanostructures with precisely controlled thickness and edge configuration.

10:15 AM NM06.12.08

Strain Fields at the Micro-Scale in Two-Dimensional Materials [Elena Blundo](#)¹, Cinzia Di Giorgio², Giorgio Pettinari³, Tanju Yildirim⁴, Alessandro Surrente⁵, Paulo Eduardo Faria Junior⁶, Mikhail Prosnikov⁷, Katarzyna Olkowska Pucko⁸, Maciej R. Molas⁸, Marco Felici¹, Adam Babinski⁸, Peter Christianen⁹, Fabrizio Bobba², Jaroslav Fabian⁶ and Antonio Polimeni¹; ¹Sapienza, University of Rome, Italy; ²Università di Salerno, Italy; ³Centro Nazionale Ricerche, Italy; ⁴National Institute for Materials Science, Japan; ⁵University of Wrocław, Poland; ⁶Universität Regensburg, Germany; ⁷IoFFE Institute, Russian Federation; ⁸University of Warsaw, Poland; ⁹High Field Magnet Laboratory, Netherlands

The variegated family of two-dimensional (2D) materials comprises crystals that have attracted great interest for their exceptional characteristics. Among them, hBN is a thermally stable and mechanically robust insulator, and semiconducting transition-metal dichalcogenides (TMDs) possess alluring optoelectronic and spin properties when reduced to the single layer. In particular, TMD monolayers are characterised by a direct bandgap, resulting in an efficient light emission in the visible/infrared range, which renders them appealing for optoelectronic devices. Furthermore, a strong spin-orbit coupling makes them interesting candidates for valley- and spin-tronics. Indeed, the inherent plane-confined nature of these materials -coupled to their exceptional mechanical flexibility and robustness- makes them highly sensitive to external stimuli. Methods to tailor their unique properties on demand have been thus sought after, and protocols based on controllable external perturbations such as mechanical deformations have shown promise in this respect.

Here, we explore new strategies to tune the peculiar properties of 2D TMDs and hBN by mechanical deformations.

We show how low-energy hydrogen-ion irradiation of bulk flakes can be exploited to engender localised strains. More specifically, the hydrogen ions penetrate through one or a few layers, leading to the production and accumulation of molecular hydrogen in the first interlayer region. The trapped gas coalesces, leading to a local blistering of the material, and thus to the formation of few-layer-thick micro/nano-bubbles [1,2].

The bubbles host complex strain fields that reach high values. Raman measurements allowed us to characterise experimentally the strain and its effect on the vibrational properties of the materials [2,3]. An analytical model allows us to calculate the strain distribution, in agreement with the experiments. The model further allows us to obtain precious information on the adhesion energy between the bubble and the substrate, and the bubbles can thus be exploited to measure the adhesion energy of a variety of van der Waals materials [3]. Furthermore, nano-indentation measurements permitted us to probe the elastic properties of the material and highlight their exceptional flexibility [4].

These bubbles are durable and incredibly robust, and in TMDs the bubble thickness is just one layer. In turn, TMD bubbles behave as efficient light emitters. The high fields they host cause dramatic changes in the TMD opto-electronic properties, and photoluminescence steady-state and time-resolved studies enabled the characterisation of the strain-induced band-structure modifications and revealed intriguing phenomena, such as a strain-induced direct-to-indirect bandgap crossover [5]. Our optical characterisation further allowed to pinpoint hybridization phenomena between direct and indirect excitons [6].

Our results unveil unprecedented information on the strain effects on TMDs and hBN, the understanding of which represents an essential step towards their integration into flexible electronic devices.

[1] D. Tedeschi, E. Blundo, et al., *Adv. Mater.* 31, 1903795 (2019).

[2] E. Blundo et al., *Nano Lett.* 22, 1525 (2022).

[3] E. Blundo et al., *Phys. Rev. Lett.* 124, 046101 (2021).

[4] C. Di Giorgio, E. Blundo et al., *ACS Appl. Mater. Interfaces* 13, 48228 (2021).

[5] E. Blundo et al., *Phys. Rev. Res.* 2, 012024 (2020).

[6] E. Blundo et al., *Phys. Rev. Lett.* (2022), in press.

10:30 AM NM06.12.09

In Situ Monitoring of Phase Transition of MoS₂ During Chemical Lithiation [Juhwan Lim](#), Jung-In Lee, Christoph Schnedermann, Manish Chhowalla and Akshay Rao; University of Cambridge, United Kingdom

Phase engineering of MoS₂, mainly between two crystallographic phases of octahedral (1T) phase and trigonal prismatic (2H) phase, has attracted attention for its ability to tailor different phases within a single flake and enhance the materials and device performances, such as higher hydrogen evolution efficiency and lower contact resistance. Many studies have used lithiation, both chemically and electrochemically, to change the phase of MoS₂, from the semiconducting 2H- to metallic 1T phase. It is understood that the intercalation of Li cations into the van der Waals gap of 2H-MoS₂ promotes the 2H/1T phase transition by electron donation. n-butyl lithium (n-BuLi) is the most widely used organolithium reagent for chemical lithiation of transition metal dichalcogenides (TMDs). However, a better understanding of this chemical lithiation reaction is required, not only to provide mechanistic insight, but also to enable more efficient phase engineering of transition metal dichalcogenides for electronic, optoelectronic, and energy applications. Recently, in-situ characterization techniques (ex, in-situ Raman, STEM/TEM, LCM-DIM) have been applied to monitor the phase transition of bulk or multilayer MoS₂ using electrochemical lithiation or direct contact of lithium metal. However, practical limitations on handling the highly pyrophoric n-BuLi, as well as the lack of optimized operando characterization techniques have curtailed the microscopic understanding of the lithiation and structural transition. Here, we captured in real-time the chemically-induced 2H to 1T phase transition of mechanically exfoliated mono-, bi-, and multilayer MoS₂ flakes in n-BuLi using in-situ optical reflectance interferometric contrast microscopy (RICM). By exploiting the different dielectric properties of 2H-MoS₂ and 1T-MoS₂, we directly quantified the phase transition dynamics in micrometer-sized MoS₂ flakes with diffraction-limited resolution (~200 nm) and

complemented the results with ex-situ Raman and Photoluminescence (PL) measurement to obtain detailed structural insights into this process. We reveal that the phase transition is charge-transfer limited in few-layer MoS₂, which gives rise to sharp phase fronts propagating from the edges of the flake inwards with constant velocity. Comparison to monolayer MoS₂ further highlights the importance of surface reactivity. Incorporating the result from the ex-situ measurement of flakes of the different number of layers, such as ground state A-exciton and low-energy PL emission, shifts or broadening of E_{2g} and A_{1g} Raman peaks, and arising of Raman J peaks, we suggest a systematic interpretation for this behavior. Critically, the phase transition dynamics appeared highly dependent on the illumination conditions, with mild above-bandgap illumination accelerating the transition and changing the underlying mechanism. We suggest possible applications to harness this effect open up new possibilities in phase engineering of MoS₂ and other TMDs.

10:45 AM NM06.12.11

Studies of 2D Materials by Scanning Tunneling Microscopy Associated with a Light Detector Ricardo Peña Román¹, Fábio J. Costa¹, Thiago G. Brito¹, Ingrid D. Barcelos² and Luiz F. Zagonel¹; ¹Campinas University, Brazil; ²Centro Nacional de Pesquisa em Energia e Materiais, Brazil

2D materials are been considered for several applications due to their new and promising mechanical, electronic and optical properties. Scanning Tunneling Microscopy (STM) is a great tool to investigate their morphology and electronic structure by means of imaging (which reaches atomic resolution) and spectroscopy. Adding a light detector to the STM provides access to the light emission that is triggered by the very local tunnel current (usually called STM induced light emission or luminescence, STML). We have developed a new light collection device compatible with an adapted low temperature UHV STM. [1] This device is based on an off axis parabolic mirror and it is designed to have high collection efficiency while keeping high spectral resolution. Using our STM equipped with such device, we studied WSe₂ mechanically transferred to gold, to HOPG, and to ITO. These conducting substrates affect this transition metal dichalcogenide (TMD) in different ways.[2] After the mechanical transfer, a water interlayer isolates the TMD from gold and from ITO, but such interfacial layer was not observed for HOPG. After an annealing, light is severely quenched on the TMD over gold while on ITO the TMD preserves its emission and becomes highly doped. The TMD on HOPG was not significantly doped but was also quenched. Another study used HOPG as a support to epitaxial growth of hexagonal boron nitride (h-BN). This substrate preserved h-BN properties and both the electronic gap and light emission from defects could be determined.[3]

References:

[1] Ricardo Javier Peña Román et al. Review of Scientific Instruments 93, 043704, 2022.

[2] Ricardo Javier Peña Román et al. Nanoscale, 12, 13460-13470, 2020.

[3] Ricardo Javier Peña Román et al. 2D Mater. 8 044001, 2021.

This work was supported by the Fundação de Amparo à Pesquisa do Estado de São Paulo (FAPESP) Projects 14/23399-9 and 2021/06893-3.

SESSION NM06.13: Advanced Synthesis, Processing and Characterization of 2D Materials

Session Chairs: Nicholas Glavin and SungWoo Nam

Friday Afternoon, December 2, 2022

Hynes, Level 2, Room 207

1:30 PM NM06.13.01

Colossal Photocurrents in Topological Janus Transition Metal Dichalcogenides Haowei Xu, Hua Wang, Yunfan Guo, Jing Kong and Ju Li; Massachusetts Institute of Technology, United States

Nonlinear optical properties such as bulk photovoltaic effects possess great potentials in energy harvesting, photodetection, rectification, etc. To enable efficient light-current conversion, materials with strong photo-responsivity are highly desirable. In this work, we predict that monolayer Janus transition metal dichalcogenides (JTMDs) in the 1T' phase possess colossal nonlinear photoconductivity owing to their topological band mixing, strong inversion symmetry breaking, and small electronic bandgap. 1T' JTMDs have inverted bandgaps on the order of 10 meV and are exceptionally responsive to light in the terahertz (THz) range. By first-principles calculations, we reveal that 1T' JTMDs possess shift current (SC) conductivity as large as 2300 nm μA V⁻², equivalent to a photo-responsivity of 2800 mA/W. The circular current (CC) conductivity of 1T' JTMDs is as large as 10⁴ nm μA V⁻². These remarkable photo-responsivities indicate that the 1T' JTMDs can serve as efficient photodetectors in the THz range. We also find that external stimuli such as the in-plane strain and out-of-plane electric field can induce topological phase transitions in 1T' JTMDs, and that the SC can abruptly flip their directions. The abrupt change of the nonlinear photocurrent can be used to characterize the topological transition, that has potential use in 2D optomechanics and nonlinear optoelectronics.

1:45 PM NM06.13.02

Effects of Electrostatic Interactions and Charge Transfer Mechanisms on Interlayer Excitons in van der Waals Heterostructures Jaehoon Ji and Jong Hyun Choi; Purdue University, United States

Atomically thin heterostructures from transition metal dichalcogenides (e.g., MoS₂/WSe₂) may exhibit interlayer excitons (IXs) due to strong light-matter interaction.¹ IXs are bound states of spatially separate electrons and holes in opposite 2D semiconducting heterolayers. The IXs show various unique properties, including large binding energy, long lifetime, diffusion length, and substantial dipolar interaction.² These characteristics may be exploited to develop diverse optoelectronics, including light emitting diodes, photodetectors, photovoltaics, and excitonic devices. Given the importance, several mechanisms have been explored for tailoring the formation and behavior of IXs such as external electrical field and doping.²

Despite the extensive studies, the effects of electrostatic interactions (e.g., dielectric screening and dipolar interaction of charges) and charge transfer pathways on the IX formation have not been fully understood. To elucidate them in this work, we have introduced a new approach of inserting an organic layer between MoS₂ and WSe₂ heterobilayers.³ The sandwiched organics, 1,3-bis(3,5-dipyrid-3-ylphenyl)benzene (B3PyPB) and eosin Y (EY), were chosen for their properties that may reduce the dielectric screening on the charges of IXs due to the smaller dielectric constants of the organic layers than those of TMDs. Additionally, the inserted layer may expand the separation distance of IXs. Given the reduced screening and the increased distance, the binding energy of IXs will be reduced. We estimated the change of the exciton binding energy by using a simple hydrogen-like particle model.⁴ The organic-inserted hybrid heterostructure had a smaller binding energy than the control, MoS₂/WSe₂ heterostructure by ~40 meV. This was confirmed by PL spectroscopy of the hetero-samples with and without organic layers. The B3PyPB-inserted MoS₂/WSe₂ sample showed a blueshifted IX emission compared to the TMD-only heterojunction, consistent with the binding energy theory.

Furthermore, we found that the charge transfer pathways can modulate the IX energy. The EY may develop type II energy level alignments that facilitate energetically favorable charge transfer. In contrast, B3PyPB creates a substantial energy barrier at the TMD/organic interface that only allows a tunneling

of charges. The PL measurements show that MoS₂/EY/WSe₂ exhibits an IX emission at ~1.62 eV, which is higher than the emission energy (~1.60 eV) from the B3PyPB-embedded heterojunction. Due to the energetically favorable transport, the EY-inserted hybrid may accommodate a greater extent of IXs than the other. Since the IXs are aligned in an out-of-plane direction within the ultrathin structure, they may behave as repulsive dipoles, leading to the further increase of IX energy. By adopting a model that correlates the emission energy and the dipole density, we found that MoS₂/EY/WSe₂ has a higher dipole density than the B3PyPB-inserted sample (by ~2.5x10¹² cm⁻²). The results strongly suggest that the IX properties can be tuned by varying the dielectric environments, the electrostatic interaction, and the charge transfer pathways. This work may pave a new way to control the IXs for future optoelectronics.

References

1. Hertzog, M., *et al.*, *Chemical Society Reviews* (2019) 48, 937
2. Kamban, H. C., *et al.*, *Scientific Reports* (2020) 10, 5537
3. Ji, J., *et al.*, *ACS Applied Electronic Materials* (2021) 3, 3052
4. Leavitt, R. P., *et al.*, *Physical Review B* (1990) 42, 11774

2:00 PM NM06.13.03

Controlled Synthesis of Large-Sized 2D Ultrathin SnSe Crystals with In-Plane Ferroelectricity Tianyi Zhang¹, Ming-Hui Chiu^{1,2}, Xiang Ji¹, Nannan Mao¹, Yue Luo³, Chuqiao Shi⁴, Yimo Han⁴, William L. Wilson³, Vincent Tung² and Jing Kong¹; ¹Massachusetts Institute of Technology, United States; ²King Abdullah University of Science and Technology, Saudi Arabia; ³Harvard University, United States; ⁴Rice University, United States

Tin (II) selenide (SnSe) is an emerging member of two-dimensional (2D) materials with many intriguing properties, such as record-high thermoelectric figure of merit (ZT), purely in-plane ferroelectricity, and excellent nonlinear optical properties. Moreover, as a semiconducting material that is structurally analogous to layered black phosphorus, a rising star for next-generation nanoelectronics, 2D SnSe is anticipated to possess attractive electronic and optoelectronic properties, such as thickness-dependent bandgap and high photoresponse. To facilitate the exploration of these functional properties and applications, it is important to develop controllable routes to synthesize ultrathin crystals of SnSe with large area and high quality. Physical vapor deposition (PVD) constitutes a reliable method to synthesize 2D SnSe with the scaling-up potential. Nevertheless, effects of various growth parameters have not yet been systematically investigated, and current PVD-synthesized SnSe flakes are often thick (> 10 nm) with small lateral sizes (< 10 μm). In this work, we demonstrate the growth of high-quality 2D SnSe crystals *via* a low-pressure PVD method, which display in-plane ferroelectric domains observed by polarization-dependent reflectivity spectroscopy. We further comprehensively studied roles of various parameters, including substrate pre-annealing, growth duration, temperature, and growth pressure, which enables us to rationally optimize the growth and obtain 2D SnSe crystals with lateral size up to ~23.0 μm and controllable thicknesses down to ~2.0 nm (3-4 layers). Our work takes an important step forward on the controlled growth of large-area 2D SnSe, facilitating the future exploration of its interesting multiferroic properties and applications with atomic thickness.

2:15 PM NM06.13.04

Continuous Liquid Metal Printed 2D TCO Superlattices Youxiong Ye, Andrew B. Hamlin, Md Saifur Rahman, Julia Huddy and William J. Scheideler; Dartmouth College, United States

Two-dimensional (2D) conducting metal oxides offer unprecedented control of thin film electrostatics at the nanoscale. We present a scalable, roller-based continuous liquid metal printing (CLMP) approach for fabricating large area (100 cm²) layered transparent conductive oxides (TCOs) via rapid low-temperature Cabrera-Mott oxidation of compliant liquid metals (Ga, In). We exploit repeating heterostructures of these 2D oxides (3 nm per layer) to produce TCOs at 180 °C with record conductivity while simultaneously raising visible range transmittance above 98%. HRTEM and XRD characterization reveal the unique 2D film morphology consisting of large grained cubic InO_x layered with amorphous GaO_x. To investigate the impact of modulation doping at the type I heterojunction between InO_x / GaO_x, we also present XPS, UV-Vis, and Hall characterization. Our rapid (6 m / min) low-temperature CLMP approach yields flexible TCOs that demonstrate 20X enhanced strain tolerance while requiring zero post-annealing and offering greater conductivity than low-temperature ITO, which is limited by poor dopant activation. These capabilities establish CLMP 2D TCOs as a promising set of transparent electrode materials for flexible optoelectronic devices such as photodetectors and displays.

2:30 PM NM06.13.05

Photoresist-Free and Large-Area Patterning Method for van der Waals Materials via Direct Optical Lithography Seong Rae Cho¹, Seonghun Ahn¹, Seung Hyung Lee¹, Heonhak Ha¹, Tae Soo Kim¹, Min-kyung Jo^{1,2}, Chanwoo Song¹, Tae Hong Im¹, Pragya Rani¹, Minseung Gyeon¹, Kiwon Cho¹, Seungwoo Song², Min Seok Jang¹, Yong-Hoon Cho¹, Keon Jae Lee¹ and Kibum Kang¹; ¹Korea Advanced Institute of Science and Technology, Korea (the Republic of); ²Korea Research Institute of Standards and Science, Korea (the Republic of)

Van der Waals (vdW) materials have attracted significant interest as new research platforms of next-era research since they exhibit novel properties with surface-dominant geometry. However, the properties of vdW materials are highly affected by the surface state of the materials owing to the geometrical feature of the materials and, therefore, the conventional photolithography technique accompanying undesired photoresist residues and solution process has negative effects on vdW materials. Several alternative patterning techniques have been reported to avoid the issue, but they suffer from low resolution, scalability, and low throughput.

In this work, we report a new patterning technique, the direct optical lithography technique, specialized for vdW materials. The direct optical lithography uses highly intensive photo illumination in a short pulse with a special photomask to follow the advantage of conventional photolithography without photoresists and solvents. We patterned various vdW materials (monolayer MoS₂, bilayer MoS₂, monolayer graphene, monolayer WSe₂, and two-dimensional metal-organic framework) in multiscale and desired shapes. Morphological characterization revealed that direct optical lithography did not cause photoresist residues unlike conventional photolithography and optical characterization exhibited critical differences between direct optical lithography and conventional photolithography. The finite element method (FEM) simulation results demonstrated that the photo source used in this work, the highly intensive light with a short pulse, was suitable for high-resolution patterning of vdW materials without degradation of patterned materials.

2:45 PM NM06.13.06

Humidity Controlled Composition and Morphology of 2D Material Nanobubbles Daniel Sanchez¹, Andrei Dolocan², Jinlong He³, Santiago Diaz-Arauzo², Eunbin Kim², Melanie Murillo², Jiaming He², Zhaohe Dai⁴, Ying Li³ and Nanshu Lu²; ¹University of Pennsylvania, United States; ²The University of Texas at Austin, United States; ³University of Connecticut, United States; ⁴Peking University, China

When two-dimensional (2D) materials are transferred onto a supporting substrate, matter trapped at the interface can spontaneously coalesce to form nanobubbles. These bubbles are emerging for novel nanoscale applications to strain engineer 2D materials and to explore chemical reactions under nanoscale confinement. Strategies to deterministically control the chemical content of these bubbles remain unclear, and current analyses of the contents of spontaneously formed bubbles offer limited chemical information about the trapped matter. We therefore develop a three-dimensional chemical analysis methodology combining cryo-ToF-SIMS (time-of-flight secondary ion mass spectrometry), atomic force microscopy (AFM), and computational modeling

to study the intricate structural chemical composition and the morphology of nanobubbles formed in various environments. By applying this methodology to nanobubbles produced in different relative humidities (RHs), we discover their rich chemical composition, consisting of phase-separated water, hydrocarbons, and substrate materials. Our technique can identify, locate and relatively quantify, with an unprecedented level of detail, the composing species of these nanobubbles, unambiguously proving their chemical inhomogeneity, which settles the long-standing debate concerning the co-existence of multiple chemical species within spontaneously formed nanobubbles under 2D materials. Importantly, we find that both the phase separation and the individual concentrations of the trapped chemicals vary with the RH of the fabrication environment. This methodology is generally applicable to stacked 2D materials to fundamentally understand their material properties and matter confined to their interfaces. Our work significantly deepens the current understanding of spontaneously formed nanobubbles and unveils new design avenues for their chemical tunability.

3:00 PM BREAK

SESSION NM06.14: 2D Magnetics and Ferroelectrics
Session Chairs: Nicholas Glavin and SungWoo Nam
Friday Afternoon, December 2, 2022
Hynes, Level 2, Room 207

3:30 PM NM06.14.01

Crystal Anisotropy Implications on the Intrinsic Magnetism in van der Waals FePS₃ Ellenor Geraffy; Technion Institute of Technology, Israel

Ultrathin 2-D van der Waals (vdW) semiconductor materials have procured scientific and technological interest since the discovery of single layered graphene in 2004. Similar to graphene, transition metal trichalcogenides, with the general chemical formula MPX₃ (M= 1st row transition metals, X = chalcogenides), possess fast electron transport and strong spin orbit coupling without the drawback of no bandgap. These vdW inorganic lamellar compounds are characterized by strong intralayer covalent bonding and weak vdW interaction between adjacent layers. Transition metal atoms endow these materials with magnetic (either ferromagnetic or antiferromagnetic Neel, zigzag or stripy) and magneto-optical properties which can be utilized for new generation 2D magnets and opto-spintronic devices. Yet, the fundamental understanding of these materials as well as the manipulation of their intrinsic magnetism via external stimuli remains to be an unexplored endeavor.

FePS₃ exhibits an overall zigzag antiferromagnetic ordering owing to its ferromagnetic Fe zigzag chains which are antiferromagnetically coupled to each other, resulting in a high linear dichroism dependency which is direction dependent. Additionally, the presence of crystallographic anisotropy is expected to yield significant impacts on its intrinsic magnetism and optical properties, particularly in the presence of external factors such as increasing temperature and external magnetic fields.

In this talk, the correlation between the crystallographic anisotropy and the optical and intrinsic magnetic properties in FePS₃ is shown using temperature dependent photoluminescence (PL) and magneto-PL measurements. Additionally, the presence of a metamagnetic phase transitions in FePS₃ upon inducing thermal and magnetic fluctuations using temperature dependent PL and linearly and circularly polarized magneto-PL.

3:45 PM NM06.14.02

Magnetic and Catalytic Properties of Two-Dimensional Cobalt Tellurides Raphael M. Tromer¹, Solomon D. Negedu², Saif Siddique², Femi E. Olu², Mithun Palit³, Ajit K. Roy⁴, Cristiano F. Woellner⁵, Prafull Pandey⁶, Douglas S. Galvao¹, Partha Kumbhakar² and Chandra Tiwar²; ¹universidade estadual de campinas, Brazil; ²Metallurgical and Materials Engineering, India; ³Defence Metallurgical Research Laboratory, India; ⁴Materials and Manufacturing Directorate, Air Force Research Laboratory, United States; ⁵Universidade Federal do Paraná, Brazil; ⁶Department of Materials Engineering, Indian Institute of Science, India

Recently, 2D cobalt telluride materials have attracted much attention due to their potential applications in memory devices, sensors, spintronics, and biomedical areas. [1-4]. In this work we investigated the magnetic and catalytic properties of synthesized 2D cobalt telluride (CoTe) from its bulk crystals using a simple liquid exfoliation method [1,4]. The results from the hysteresis curves show that the magnetic saturation value for 2D CoTe is ~400 times the corresponding values of their bulk counterpart. They exhibit good absorption in the high-energy region corresponding to the ultraviolet range. We also carried out density functional theory (DFT) [5] simulations to gain further insights on their structural and electronic properties. Our results suggest that the reduced coordination number of the surface atoms, anisotropy, and surface charge effects are responsible for the larger magnetism presented by 2D CoTe in comparison to their bulk structures. Moreover, the semiconducting nature and surface charges of 2D CoTe lead to a significant photocatalytic behavior. These results strongly support that 2D CoTe are promising materials for magnetic and catalytic applications.

[1] Saif Siddique, Chinmayee Chowde Gowda, Solomon Demiss, Raphael Tromer, Sourav Paul, Kishor Kumar

Sadasivuni, Emmanuel Femi Olu, Amreesh Chandra, Vidya Kochat, Douglas S. Galvão, Partha Kumbhakar, Rohan Mishra, Pulickel M. Ajayan and, Chandra Sekhar Tiwary., Mater. Today, 51, 402 (2021).

[2] T. Hu, X. Mei, Y. Wang, X. Weng, R. Liang, M. Wei, Sci. Bull. 64, 1707 (2019).

[3] S. Manzeli, D. Ovchinnikov, D. Pasquier, O.V. Yazyev, A. Kis, Nat. Rev. Mater. 2, 1 (2017).

[4] N. Sethulakshmi, A. Mishra, P.M. Ajayan, Y. Kawazoe, A.K. Roy, A.K. Singh, C.S. Tiwary, Mater. Today 27, 107 (2019).

4:00 PM NM06.14.03

Synthesis, Fabrication and Characterization of a Fe:MoS₂-Based Magnetic Tunneling Junction Siwei Chen, Zitao Tang, Mengqi Fang, Kyungnam Kang, Abdus Salam Sarkar, Na Liu, Yuze Zhang, Stefan Strauf, Grzegorz Hader and Eui-Hyeok Yang; Stevens Institute of Technology, United States

The discovery of ferromagnetism in 2D atomic layers, including chromium triiodide (CrI₃), chromium germanium telluride, and other van der Waals (vdW) materials, has enabled the exploration of vdW magnetism, opening new avenues for the next-generation spintronic. For example, 2D van der Waals magnets can be used to construct magnetic tunnel junctions (MTJs) toward spintronic memory systems such as magnetic random access memories (MRAM). A rapid current-induced magnetization switching (CIMS) is essential for high-speed and low-power next-generation spintronics [1-4], which may be achieved using 2D magnets. Recently, room temperature ferromagnetism was demonstrated in *in-situ* Fe-doped MoS₂ (Fe:MoS₂) and V-doped WSe₂ (V:WSe₂) via chemical vapor deposition (CVD) [5-7]. These 2D magnets can be used as electrodes or barriers in vdW MTJs.

Here, we present the synthesis, layer transfer, and characterization of a 2D magnet (*i.e.*, Fe:MoS₂ monolayer)-based MTJ, consisting of a thin film Fe, multilayered hBN and a Fe:MoS₂ monolayer.

The Fe:MoS₂ monolayers were synthesized via low-pressure chemical vapor deposition. The Fe:MoS₂/graphene was fabricated by directly transferring an exfoliated multilayer graphene onto CVD-grown Fe:MoS₂ via PDMS stamping. A Fe layer connected to Au/Cr electrodes as the bottom electrodes and a

multilayer hBN was transferred onto the Fe thin film via PDMS-stamping, followed by another transfer of the Fe:MoS₂/graphene junction onto Fe/hBN via a PMMA-based wet transfer. Here, hBN was used as the tunneling barrier, Fe:MoS₂ as the free layer, and Fe thin film as the fixed layer of the 2D MTJ. A probe station with Keithley 6487 pico amperometry was used to test the IV characteristics of the fabricated MTJ at room temperature. The MTJ junction showed a parabolic tunneling behavior under 0.3V source-drain voltage.

We will measure the tunneling magnetoresistance (TMR) inside an ultra-low vibration cryogen-free cooling closed-cycle cryostat at 4 K to measure the CIMS by applying short current pulses over the junction. (We will add these data in a week.)

KEYWORDS: magnetic tunnel junction, spin valve, van der Waals heterostructure

References:

- S. Ikeda, *Nature Materials*, 9(9), 721–724, (2010).
- Z. Fei, B. Huang, *Nature Materials*, 17 (9), 778–782, (2018).
- K. Shayan, *Nano Letters*, 19(10), 7301–7308, (2019).
- S. Jiang, *Nature Materials*, 17(5), 406–410, (2018).
- F. Zhang, *Advanced Science*, 7(24), 2001174, (2020).
- S. Fu, *Nature Communications*, 11(1), 2034, (2020).
- L. Na, *Nanoscale*, 2021,13, 832-841

4:15 PM NM06.14.04

Ferromagnetic Properties of Fe-Doped Tungsten Diselenide Monolayers Toward Diluted Magnetic Semiconductors Mengqi Fang¹, Siwei Chen¹, Kyungham Kang¹, Arunabh Mukherjee², A. Nick Vamvakas² and Eui-Hyeok Yang¹; ¹Stevens Institute of Technology, United States; ²University of Rochester, United States

Two-dimensional (2D) transition metal dichalcogenides (TMDs) possess interesting electronic, optical, and structural features, including a direct band gap in monolayers with a photoluminescence emission in the visible and near-infrared spectral range [1-2], which due to transition metal atoms fill non-bonded d-bands to a variety of levels [3]. With the superior 2D atomic thickness and tunable electronic band structure, TMDs, have become suitable candidates for studying high nonlinear optical susceptibilities, spin-orbit interactions, and novel valleytronics properties [4]. Doping is an efficient way to tune the properties of TMDs. These 2D TMD semiconductors doped with transition metal atoms (such as vanadium (V), Rhenium (Re), and iron (Fe)) link the properties of semiconductors and ferromagnets, creating new known as dilute magnetic semiconductors (DMS) [5]. These 2D DMS were synthesized via chemical vapor deposition (CVD), thereby opening the door toward utilizing novel modes of magneto-electronic and magneto-optical responses of 2D heterostructures [6-8].

Here we demonstrate an in situ substitutional doping of iron atoms into WSe₂ monolayers via low-pressure chemical vapor deposition (LPCVD). Fe₃O₄ particles as iron sources were cast onto the SiO₂/Si substrate, and a MoO₃-deposited substrate contacted the source substrate face-to-face. The furnace was then heated to 850 °C and held for 15 mins. During the heating process, selenium (Se) is provided via vaporizing Se powder placed in crucibles outside the central furnace area as the furnace temperature rises to 640 °C. Argon (Ar) gas was flown to the furnace at 200 °C, and hydrogen (H₂) gas was supplied at 660 °C. To verify the growth of monolayer Fe: WSe₂ domains, we first characterized the samples via Raman/PL spectroscopy and atomic force microscopy (AFM), confirming that the grown materials are Fe-doped WSe₂ monolayers. We plan to characterize the ferromagnetic domains of the grown materials using magnetic force microscopy (MFM) at our facility (new MFM equipment has been recently installed). Finally, the ferromagnetic nature of the grown Fe-doped WSe₂ monolayers will be confirmed using spatially resolving nitrogen-vacancy (NV⁻) center magnetometry (this characterization has been routinely performed by the authors' group [9]).

Reference:

- [1] A. K. Geim et al., *Science*, **324** (5934), 1530–1534, 2009.
- [2] Q. Fu et al., *Advanced Materials*, **33** (6), 1907818, (2021).
- [3] M. Chhowalla et al., *Nature Chemistry*, **5** (4), 263–275, (2013).
- [4] R. Lv et al., *Accounts of chemical research*, **48** (1), 56–64, (2015).
- [5] Furdyna et al., *Journal of Applied Physics*, **61** (8), 3526-3531, (1987).
- [6] S. Tiwari et al., *npj 2D Materials and Applications*, **5** (1), 1–7, (2021).
- [7] S. J. Yun et al., *Advanced Science*, **7** (9), 1903076, (2020).
- [8] Z. Jiang et al., *Nanoscale Horizons*, **3** (3), 335–341, (2018).
- [9] Fu, S et al., *Nature communications*, **11** (1), 1-8, (2020).

4:30 PM NM06.14.05

Giant Nonlinear Optical Response via Coherent Stacking of In-Plane Ferroelectric Layers Nannan Mao¹, Yue Luo², Ming-Hui Chiu¹, Chuqiao Shi³, William L. Wilson², Yimo Han³, William Tisdale¹ and Jing Kong¹; ¹Massachusetts Institute of Technology, United States; ²Harvard University, United States; ³Rice University, United States

Ferroelectric materials are essential components for various applications such as high-density non-volatile memories, nonlinear optics, electro-optical switches and sensors. Thin-film ferroelectric materials hold great promise on miniaturization and on-chip integration of related functional devices. Recently, a class of 2D materials called group-IV monochalcogenides have attracted extensive attentions due to robust in-plane ferroelectricity in atomically-thin layer (1-5). Besides ferroelectric property at room temperature, these materials were predicted with a range of fascinating properties, such as giant nonlinear optical effect (6, 7), large piezoelectric (8, 9) and thermoelectric coefficient (10), multiferroic (6, 11), spintronic properties (12) and promising bulk photovoltaic effect (13). Herein we demonstrate the in-plane ferroelectricity in thin flake of tin monoselenide. Giant second harmonic generation was observed due to parallel ferroelectric stacking structure. The measured nonlinear optical susceptibility is more than one order-of-magnitude larger than that of monolayer TMDs such MoS₂. Our findings open up exciting opportunities of the applications of group-IV monochalcogenides in ultrathin non-volatile memory and miniaturized nonlinear optical devices.

Reference

- 1. Chang, K. et al. Discovery of robust in-plane ferroelectricity in atomic-thick SnTe. *Science* **353**, 274-278 (2016).
- 2. Chang, K. et al. Microscopic Manipulation of Ferroelectric Domains in SnSe Monolayers at Room Temperature. *Nano Lett.* **20**, 6590-6597 (2020).
- 3. Higashitarumizu, N. et al. Purely in-plane ferroelectricity in monolayer SnS at room temperature. *Nat. Commun.* **11**, 2428 (2020).
- 4. Fei, R., Kang, W. & Yang, L. Ferroelectricity and Phase Transitions in Monolayer Group-IV Monochalcogenides. *Phys. Rev. Lett.* **117**, 097601 (2016).
- 5. Barraza-Lopez, S., Fregoso, B.M., Villanova, J.W., Parkin, S.S.P. & Chang, K. Colloquium: Physical properties of group-IV monochalcogenide monolayers. *Reviews of Modern Physics* **93**, 011001 (2021).
- 6. Wang, H. & Qian, X.F. Giant Optical Second Harmonic Generation in Two-Dimensional Multiferroics. *Nano Lett.* **17**, 5027-5034 (2017).
- 7. Raj Panday, S. & Fregoso, B.M. Strong second harmonic generation in two-dimensional ferroelectric IV-monochalcogenides. *J. Phys.: Condens. Matter* **29**, 43LT01 (2017).

8. Fei, R., Li, W., Li, J. & Yang, L. Giant piezoelectricity of monolayer group IV monochalcogenides: SnSe, SnS, GeSe, and GeS. *Appl. Phys. Lett.* **107**, 173104 (2015).
9. Gomes, L.C., Carvalho, A. & Castro Neto, A.H. Enhanced piezoelectricity and modified dielectric screening of two-dimensional group-IV monochalcogenides. *Phys. Rev. B* **92**, 214103 (2015).
10. Zhao, L.-D. et al. Ultralow thermal conductivity and high thermoelectric figure of merit in SnSe crystals. *Nature* **508**, 373-377 (2014).
11. Wang, H. & Qian, X. Two-dimensional multiferroics in monolayer group IV monochalcogenides. *2D Mater.* **4**, 015042 (2017).
12. Hanakata, P.Z., Carvalho, A., Campbell, D.K. & Park, H.S. Polarization and valley switching in monolayer group-IV monochalcogenides. *Phys. Rev. B* **94**, 035304 (2016).
13. Rangel, T. et al. Large Bulk Photovoltaic Effect and Spontaneous Polarization of Single-Layer Monochalcogenides. *Phys. Rev. Lett.* **119**, 067402 (2017).

SESSION NM06.15: Virtual Session: 2D Layered Materials and Heterostructures

Session Chairs: Nicholas Glavin and SungWoo Nam

Tuesday Afternoon, December 6, 2022

NM06-virtual

8:50 PM NM06.15.01

Engineering Interlayer Electron-Phonon Coupling in WS₂/h-BN Heterostructures Yi F. Li¹, Xiaowei Zhang¹, Jinhuan Wang¹, Xiaoli Ma², Jin-An Shi³, Xiangdong Guo⁴, Yonggang Zuo⁵, Ruijie Li¹, Hao Hong⁶, Ning Li⁶, Kai Xu³, Xinyu Huang⁷, Hui Feng Tian¹, Ying Yang⁸, Zhixin Yao^{1,9}, Xiao Li⁸, Junjie Guo⁹, Yuang Huang⁷, Peng Gao¹, Lifeng Wang², Xiaoxia Yang⁴, Qing Dai⁴, EnGe Wang¹, Kaihui Liu¹, Wu Zhou³, Xiaohui Yu², Liangbo Liang¹⁰, Ying Jiang¹, Xin-Zheng Li¹ and Lei Liu¹; ¹Peking University, China; ²Institute of Physics, Chinese Academy of Sciences, China; ³University of Chinese Academy of Sciences, China; ⁴National Center for Nanoscience and Technology, China; ⁵Kunming University of Science and Technology, China; ⁶School of Physics, Peking University, China; ⁷Beijing Institute of Technology, China; ⁸School of Physics and Technology, Nanjing Normal University, China; ⁹Taiyuan University of Technology, China; ¹⁰Oak Ridge National Laboratory, United States

The nonadiabatic electron-phonon coupling (EPC) is ubiquitous in condensed matter physics and materials science, and plays a critical role in areas of transport scattering, conventional superconductivity, optical properties, spintronics, and quantum information. Particularly in van der Waals (vdW) heterostructures, the non-local interlayer EPC, which bridges electrons and phonons belonging to different layers, provides one unique channel to engineer these elementary particles, realizing emergent quantum behaviors. However, in-depth exploration of interlayer EPC effects is limited by stringent conditions for occurrence, and the efficient engineering of the interlayer EPC strength has remained elusive. Here we report a multi-tier engineering approach of studying the interlayer EPC in WS₂/hexagonal boron nitride (h-BN) heterostructures, including the isotope enrichment of h-BN substrates (h-¹⁰BN and h-¹¹BN), temperature tuning, and application of high pressures. The hyperfine, robust isotope dependence of Raman intensities was unambiguously revealed in isotopically-engineered heterostructures. Combined with theoretical calculations, we anticipate that the WS₂/h-BN supercell could induce Brillouin-zone-folded phonons which contribute to the interlayer coupling, leading to complex nature of the broad Raman peaks at ~800 cm⁻¹. We further demonstrate the significance of a previously unexplored parameter, the interlayer spacing between WS₂ and h-BN. By varying temperature and applying high pressure, we can effectively manipulate the strength of the interlayer coupling with turn-on/off capabilities, indicating the critical thresholds of the layer-layer spacing for activating and strengthening the interlayer EPC. Our findings provide new opportunities to engineer van der Waals heterostructures with controlled interlayer coupling.

9:05 PM NM06.15.03

Additives and Post Treatments to Enhance Graphene Oxide Membrane Desalination Aaron Morelos-Gomez¹, Souya Terashima¹, Roque Sánchez-Salas², Rodolfo Cruz-Silva¹ and Morinobu Endo¹; ¹Shinshu University, Japan; ²University of Sussex, United Kingdom

Water is a natural source vital for a sustainable society. However, given climate change and population growth natural water source are being depleted. Therefore, seawater desalination may provide potable water. This can be performed by using membrane technology. Traditionally, these membranes are polymer-based. Unfortunately, they are prone to fouling and can exhibit low chemical stability, therefore, alternative membranes are needed. Graphene oxide (GO) is 2d-material that can be produced in large quantities and is easy to handle. We have developed an original method to make GO membranes by spray-coating. Over the course of six years, we have modified graphene oxide membranes by adding nanomaterials and surfactants, and with post treatments such as heating, plasma, divalent ion cross linking and solvent hydration. The data consists of a wide range of desalination performance from 40% to 90% NaCl rejection and permeate flux between 0.2 and 1 m³m⁻²day⁻¹, therefore GO membrane desalination is highly sensitive to the preparation method. In this work, we performed a statistical analysis on the obtained results to determine the most relevant factors for GO membrane desalination. For flux, the added nanomaterials and concentration exhibit the highest impact; and for salt rejection the GO concentration, number of coats and post treatment have the highest correlation. The identification of the most relevant parameters may serve as a guide to design GO membranes with higher desalination performance.

9:20 PM NM06.15.04

Room Temperature H₂S Gas Sensor Using One-Step CVD Grown MoS₂ and 2H - MoS₂/1T@ 2H - MoS₂ Heterostructure Swathy B. Saseendran¹, Anamika Ashok¹ and Asha A S^{1,2}; ¹Cochin University of Science and Technology, India; ²cochin university of science and technology, India

MoS₂; a 2D TMDC (Transition Metal Dichalcogenides) has attracted immense attention in energy storage devices, optoelectronic devices, optical switching devices, and gas sensors due to its unique physical and chemical properties. MoS₂ thin films and nanostructures can be synthesized by different physical and chemical growth mechanisms. CVD is one of the most effective methods to achieve large-area growth of atomically thin horizontal and vertical 2D TMDCs for device applications. The vertically aligned MoS₂ nanostructures are reported to have maximum edge sites, reactive dangling bonds, and high adsorption-desorption capacity, making them an attractive candidate for gas sensing. In CVD the growth conditions such as the temperature of the heating zone, growth duration, the pressure inside the tube, and the carrier gas flow rate can be tuned to change the alignment and number of layers of MoS₂ thin films. In this work growth parameters such as temperature, Mo:S ratio, sulfur-source to substrate position, and growth time have been optimized for synthesizing few-layered vertically aligned MoS₂ thin films through a one-step CVD process. The formation of MoS₂ thin film was confirmed by the presence of and peaks in the Raman spectra. The presence of an intense (002) peak in the XRD pattern further indicates the formation of c- axis oriented MoS₂ thin film. FESEM and TEM images show an obvious evolution from horizontal to vertical morphology of MoS₂ nanoflakes with the variation in growth condition. The vertical morphology, provides a high rate of adsorption and desorption processes and outstanding gas sensing properties due to the presence of dangling bonds and higher aspect ratio. Herein, few-layered vertically aligned MoS₂ nanoflakes were obtained directly on Si/SiO₂ substrate

supported with interdigital Au electrodes and were used for gas sensing measurement. The fabricated MoS₂ sensor shows response towards H₂S at room temperature. However, sensors fabricated from 2D TMDCs suffered sluggish response and recovery time. Therefore to prevent homogeneous restacking and to enlarge the active surface area 2D/2D heterostructure was developed by decorating MoS₂ thin films on Si/SiO₂ substrate with the hydrothermally synthesized 1T/2H MoS₂ nanostructures. These 2D / 2D heterostructure-based gas sensors showed enhanced response and sensitivity towards H₂S sensing at room temperature and the architecture can be considered for developing efficient gas sensors.

9:35 PM NM06.15.05

Argon Plasma Thinning of Bi₂O₂Se and the Impacts on Transistor Performance Ming Gao, Wei Wei, Zhe Zeng and Chunxiang Zhu; National University of Singapore, Singapore

The argon plasma etching is used to uniformly thin thickness of as-exfoliated 2D Bi₂O₂Se nanoflake, because the interlayer binding energy of Bi₂O₂Se (76.8 meV/Å²) is much larger than that of graphene (21.1 meV/Å²) or MoS₂ (26.3 meV/Å²) which makes it difficult to obtain ultra thin film. The clean surface morphology and good crystalline quality of Bi₂O₂Se nanoflakes after etching are obtained and characterized. The X-ray photoelectron spectroscopy results show that the O and Se vacancies on the top surface of Bi₂O₂Se nanoflakes are created during etching, which can be passivated by forming an ultrathin oxide layer with UV ozone treatment. The on-current/off-current (I_{on}/I_{off}) ratio of bottom gate Bi₂O₂Se FET increases with argon etching time, and is further improved by UV ozone treatment. Eventually the thickness-controlled Bi₂O₂Se FET obtains a high I_{on}/I_{off} ratio of $>5.0 \times 10^4$. Importantly, the variation trend of I_{on}/I_{off} ratio and the electronic transport properties for Bi₂O₂Se FETs are well described by parallel resistor model and corresponding energy band diagram. Moreover, the $I_{ds}-V_{gs}$ hysteresis and its inversion with UV irradiation are interpreted by charges trapping/detrapping and tunneling mechanism, respectively.

9:50 PM NM06.15.06

Novel Two-Dimensional-Based Materials as Effective Electrothermal Agents for Advanced-Imaging-Enhanced Combination Cancer Therapy Maria P. Meivita¹, Denise Lee¹, Natasa Bajalovic¹ and Desmond K. Loke^{1,2}; ¹Singapore University of Technology and Design, Singapore; ²Office of Innovation, Changi General Hospital, Singapore

In clinical studies, the utilization of electrothermal agent (ETA) in cancer electrothermal therapy has shown promising results. The safety concerns are addressed by the rapid degradation of ETAs, but the electrothermal stability required for efficacious treatment is limited. On the other hand, slow degradation occurs in ETAs with high electrothermal stability. Limited solutions exist to address the balance between the high electrothermal stability and rapid degradation of ETAs. Herein, we report that the assembly of novel two-dimensional (2D) material types can accelerate the degradation of 2D materials, while also maintaining high electrothermal stability. Moreover, by utilizing specified 2D materials archetypes, advanced imaging can be achieved for cancer monitoring. Thus, this work not only introduces an 'ideal' ETA that avoids the limitations of ETAs, but also provides the proof-of-concept application of 2D-based materials in advanced-imaging-facilitated combination cancer therapy.

10:05 PM NM06.15.07

A GO/CoMo₃S₁₃ Chalcogel Heterostructure with Rich Catalytic Mo–S–Co Bridge Sites for the Hydrogen Evolution Reaction Thanh Duy C. Ha¹, Huu Ha Do², Heehyeon Lee³, Thi Thu Ha Nguyen⁴, Youngtak Oh³, Soo Young Kim⁵ and Myung-Gil Kim¹; ¹Sungkyunkwan University, Korea (the Republic of); ²Chung-Ang University, Korea (the Republic of); ³Korea Institute of Science and Technology, Korea (the Republic of); ⁴Hanoi National University of Education, Viet Nam; ⁵Korea University, Korea (the Republic of)

Molybdenum disulfide (MoS₂)-based materials are extensively studied as promising hydrogen evolution reaction (HER) catalysts. In order to bring out the full potential of chalcogenide chemistry, precise control over the active sulfur sites and enhancement of electronic conductivity need to be achieved. This study develops a highly active HER catalyst with an optimized active site-controlled cobalt molybdenum sulfide (CoMo₃S₁₃) chalcogel/graphene oxide aerogel heterostructure. The highly active CoMo₃S₁₃ chalcogel catalyst was achieved by the synergetic catalytic sites of [Mo₃S₁₃]²⁻ and the Mo–S–Co bridge. The optimized GO/CoMo₃S₁₃ chalcogel heterostructure catalyst exhibited high catalytic HER performance with an overvoltage of 130 mV, a current density of 10 mA cm⁻², a small Tafel slope of 40.1 mV dec⁻¹, and remarkable stability after 12 h of testing. This study presents a successful example of a synergistic heterostructure exploiting both the appealing electrical functionality of GO and catalytically active [Mo₃S₁₃]²⁻ sites.

10:10 PM NM06.15.08

Threshold Voltage and On-Off Current Ratio Tuning of MoS₂ Transistor Fatemeh Khorramshahi; VTT Technical Research Center of Finland, Finland

Immunity to short channel effects and abrupt switching along with transparency and flexibility have made 2D molybdenum disulfide (MoS₂) transistors compelling to be used in digital logic circuits. However, difficulties in obtaining a positive threshold voltage (V_{th}) have hindered its application as in digital logics, an incorrect V_{th} can lead to large short-circuit power consumption during switching. Similarly, a poor ON/OFF current ratio (I_{on}/I_{off}) can cause impractically low output swings and high leakage.

In this work, we employed the strategy of tuning the work function of gate metal using an ALD-grown metal plus thinning the gate oxide dielectric in order to reduce the trap states to shift the threshold voltage towards the positive direction and increase I_{on}/I_{off} . To achieve that, two series of transistors were fabricated using a bottom gate structure on silicon substrates. The transistor's channel lengths varied from 1.5 μm to 40 μm and the channel widths varied from 10 μm to 160 μm. In one series of transistors, niobium was deposited as the gate metal and 35 nm aluminum oxide (Al₂O₃) was used as the gate dielectric. In the second series of transistors, titanium nitride (TiN) and 12 nm Al₂O₃ were used as the gate metal and the gate dielectric respectively. A CVD-grown multilayer MoS₂ was wet transferred to the structure and used as the gate channel.

The electrical characteristics of the transistors were measured in the ambient environment and under dark conditions. A virtual source (VS) model was used to fit a curve on the measured data. The extracted transistors parameters from the fitted curves for the two series of transistors were compared. It was observed that the device performance enhanced significantly when TiN and thinner Al₂O₃ were deposited as the gate metal and the gate dielectric. While as-fabricated devices with Nb and 35 nm Al₂O₃ showed a negative threshold voltage of ~ -3 V, the device threshold voltage shifted toward the negative direction over time and by keeping the sample in the ambient environment. The I_{on}/I_{off} of these devices did not exceed 10⁴.

The transistors using TiN gate metal and 12 nm Al₂O₃ with the W/L ratio of 160/10 showed the ON-OFF current ratio of 10⁶ with the ON current of 11.4 μA at V_{ds} of 1 V and V_{gs} of 5 V and the threshold voltage of 1.1 V. The average threshold voltage of the transistors fabricated using TiN gate metal and thin Al₂O₃ dielectric layer for different W/L ratios was 1.3 V. We were able to adjust the threshold voltage to the positive values and tune the on-off current ratio across 10⁴ to 10⁶. This study shows a comparably simple strategy for the fabrication of MoS₂ transistor for low power consumption logic circuits for industrial applications.

10:15 PM NM06.15.09

pH Sensing Performances of CVD Graphene-Based ISFETs with High Stability Zhe Zeng, Wei Wei, Ming Gao and Chunxiang Zhu; National University of Singapore, Singapore

This work aims to investigate the pH sensing performances of CVD graphene, develop highly stable graphene-based ISFETs with reduced drift and hysteresis effects and further improve the sensing performance by applying plasma treatments on graphene. The advantage of graphene is its robust honeycomb ring structure formed by tightly bonded sp^2 carbons, which makes it a super barrier against diffusion species like water. This property addresses the stability issues of ISFETs, which are mainly caused by the slow penetration of water and water-related species into the gate sensing oxide in traditional ISFET structures. As a result, graphene-based ISFETs exhibit low drift rates, normally below 1 mV/hr, and small hysteresis widths within 3 mV, which is competitive among most metal oxides. Besides, a fresh polycrystalline CVD-grown graphene with minor oxidation is less sensitive to pH with about 5 mV/pH, however, we could tune up the sensitivity by surface oxygen plasma treatments, resulting in as high as 40 mV/pH with high stability and reliability. Lastly, we have also demonstrated a reference-electrode-free ISFET that comprises two graphene sensing films with different sensitivities, exhibiting a drift rate as low as 0.38mV/hr, which can be an example of future development of graphene-based ISFETs.

10:20 PM NM06.15.10

Signatures of Rashba Effect in Angle Dependent Magnetoresistance Anshu Gupta and Suvankar Chakraverty; INST mohali, India

We have studied the angular dependence of the longitudinal and planar magnetoresistance at the conducting interface of $LaVO_3$ - $KTaO_3$ having strong spin-orbit coupling strength. The system exhibited negative longitudinal magnetoresistance, planar Hall effect and anisotropic magnetoresistance which are the signature of chiral anomaly. The observance of negative magnetoresistance for all in-plane angles is unusual feature. These features are of quantum origin arises from strong spin-orbit coupling and pave a path to engineer non-magnetic materials as sensors for vector magnetic fields.

10:25 PM NM06.15.11

Enhanced Photoresponsivity by Photovoltaic Effect in MoS_2/WSe_2 Heterostructure Seokwon Choi; Department of Electrical and Computer Engineering, Sungkyunkwan University, Korea (the Republic of)

There are various types of photosensors that can be classified according to sensing mechanisms such as photoelectric or photochemical effects, or various performance metrics such as spectral responses. Two-dimensional transition metal dichalcogenides (2D TMDs), such as MoS_2 and WS_2 , are widely known as photoabsorbent material in photodetectors. Most of the reported MoS_2 photodetectors has disadvantages of quantitative control due to their photo gating effect. These devices typically suffer from poor responsivity and response speed and low on/off ratio. To solve these shortcomings, van der Waals (vdW) heterostructures can be utilized. Van der Waals heterostructures provide a unique platform for next-generation optoelectronics with unique flexibility and high performance with two-dimensional materials integrated with a variety of functional materials

In our study, we demonstrated a high-response photodetector with MoS_2/WSe_2 heterostructure on Al_2O_3 insulator. While using single layer MoS_2 as a channel, a photodetector is fabricated by covering MoS_2/WSe_2 van der Waals (vdW) heterostructure, which facilitates efficient separation and transportation of photogenerated carriers based on photovoltaic effect. By fabricating MoS_2/WSe_2 heterostructure on top of Al_2O_3 insulator, the photodetector can get higher on-off ratio and high responsivity. It shows a high responsivity of 80 mA/W and 30 mA/W with a 638 nm laser, which is 20-times higher than traditional MoS_2 photodetectors, and it also demonstrates the advantage of an improvement in photocurrent ratio resulting from the enhancement of on-current by more than 10-times. This mechanism is expected to be applied to increase the efficiency of photodetectors as well as electric devices such as solar cells

10:30 PM NM06.15.12

Defect Engineered 2D Layered Double Hydroxide Electrocatalysts for Improved Water and Biomass Electro-Oxidation Muhammad Zubair and Nicholas Bedford; University of New South Wales, Australia

Layered double hydroxides (LDHs) are promising materials due to their ability to modulate metal chemistries within 2D lattice that allows an optimized structure and electronics for the limiting oxygen evolution reaction (OER) and alternative biomass electro-oxidation. Substantial efforts have been devoted in developing transition metal (double) hydroxide based electrocatalysts for oxygen evolution reaction (OER) in alkaline electrolyte. Still, the fundamental understanding of electrocatalytic structure and its influence on reactivity is limited, particularly in electrochemical biomass conversion reactions. The most common LDHs for electrochemical conversions employ a base structure of M^{2+}/M^{3+} hydroxides using Co, Fe, and/or Ni, where reaction performance can be improved with the inclusion of high valency metal dopants, modulation of the interlayer spacing/anion chemistry and heterostructuring onto various substrates (e.g., graphene, carbon nanotubes). Though relatively understudied, the incorporation of oxygen vacancies (V_O) have also shown the ability to greatly improve the electrochemical performance. From a fundamental prospective, the precise role of V_O is not well elucidated, leading to lack of atomic-scale insights needed for further electrocatalyst development for OER and biomass electro-oxidation. Here we report, an alternative approach to elucidate electrocatalytic structure and activity relationships in Cerium and lanthanum doped transition metal (such as Co, Ni, Fe) based layered (double) hydroxide electrocatalysts. High resolution TEM, EDX mapping and AFM revealed layered structure with uniform incorporation of Cerium/Lanthanum in layered structure. High Energy XRD derived pair distribution function (PDF) analysis described the long range crystalline nature of as synthesized LDH materials. The electrochemical performance tests revealed Cerium/Lanthanum doping is not only beneficial for OER but also synergetic to biomass conversion. The atomic level structural insights through in-situ X-ray absorption spectroscopy allows density functional theory (DFT) to predict synergetic role of Cerium. These atomic level structural attributes correlated with electrocatalyst activity are essential for rationally design low cost, able to generate high current density with low overpotential and long term stable electrocatalysts to meet practical requirements. Taken together, our work not only demonstrates the ease of V_O generation through Ce doping but provides further atomic scale insights needed to guide future LDH development for OER and other potential electrooxidation reactions.

SESSION NM06.16: Virtual Session: 2D Layered Materials and Heterostructures

Session Chairs: Nicholas Glavin and Won Il Park

Wednesday Morning, December 7, 2022

NM06-virtual

8:00 AM *NM06.16.01

Two-Dimensional Materials Based On-Skin-Wearable Electronics Shideh Kabiri; Queen's University, Canada

In the last two years we have witnessed the quick transition to remote and virtual life in various aspects such as education, work, healthcare and even entertainment. We have realized how reliable and high-performance wearables can influence the quality and accessibility of health care. Ideal and practical wearables can be imagined as accurate, multifunctional, low weight, comfortable to wear, affordable and even visually imperceptible to

offer privacy and mental comfort to users.

Conventional electronics made of rigid metal and semiconductors are performant and well-established but when it comes to sensing and functioning at the interface with soft tissues and body, they lack the mechanical compatibility results in poor sensing and electrical performance, irritation and in the case implantable devices creating scar tissue and triggering foreign body reaction.

Two-dimensional materials are a group of atomically thin materials with a wide range of electrical, optical and mechanical properties that make them excellent candidates for making on-skin wearable electronics and sensors.

Here, we present: 1) a group of skin-soft, ultrathin, stretchable and visually imperceptible on-skin-wearable sensors for physiological sensing that can conform to the microscopic features of skin; and 2) a methodology for fabricating two dimensional based ultrathin and stretchable electronics circuits, mechanically compatible with such skin-soft wearable sensors. Minimizing local strain in the vicinity of the electronic circuit's active devices using our strategy, results in stable operation of the circuits under various forms of deformation during daily activities. This platform paves the way for the fabrication of fully integrated ultrathin stretchable and visually imperceptible wearable sensor-circuits.

8:30 AM *NM06.16.02

Low-Power Artificial Neural Networks and Logic-in-Memory Circuits with Monolayer MoS₂ Andras Kis; Ecole Polytechnique Federale de Lausanne, Switzerland

Machine learning and signal processing on the edge are poised to influence our everyday lives with devices that will learn and infer from data generated by smart sensors and other devices for the Internet of Things. The next leap towards ubiquitous electronics requires increased energy-efficiency of processors for specialized data-driven applications. I will present here how we realised an in-memory processor fabricated using a two-dimensional materials platform can potentially outperform its silicon counterparts in both standard and non-traditional Von Neumann architectures for artificial neural networks. The circuits are based on a flash memory array with a two-dimensional channel using wafer-scale MoS₂. Simulations and experiments show that the device can be scaled down to sub- μm channel length without any significant impact on its memory performance.

9:00 AM NM06.16.03

Large Area Growth of Single Phase Transition Metal Tellurides Nanosheets Through Simulation Guided AP-CVD Tellurization Alessio Lamperti¹, Pinaka Pani Tummala^{1,2,3}, Sara Ghomi^{1,4}, Carlo S. Casari⁴, Christian Martella¹ and Alessandro Molle¹; ¹IMM-CNR Agrate Brianza, Italy; ²Università Cattolica del Sacro Cuore, Italy; ³KU Leuven, Belgium; ⁴Politecnico di Milano, Italy

Among transition metal dichalcogenides, transition metal mono- and di-tellurides (TMTs) are the subject of a significant attention due to their intriguing polymorphic nature from semiconductor to metal and topological Weyl semimetal. To date, considerable efforts have been devoted to synthesizing single phase TMTs nanosheets with superior quality and lateral extension suitable for device integration in nanotechnologies and fundamental investigations. Ambient pressure chemical vapor deposition (AP-CVD) is an easy and cost effective method for synthesizing TMTs nanosheets up to the centimeter scale, due to its high flexibility. Here we report on AP-CVD large area growth and selective phase tuning strategies combined with finite element simulations for obtaining single phase TMTs nanosheets by design via tellurization of a predeposited metallic thin film by e-beam evaporation. In particular, we demonstrate the capability to obtain MoTe₂ in pure 1T' and 2H phase, PtTe₂ in 1T phase and NiTe₂ in 1T phase. In all cases, the AP-CVD tellurization makes use of Te solid powder as source for the generation of Te vapors and Me (Me: Mo, Pt, Ni) thin films of variable nominal thickness from 4 to 10 nm, on SiO₂/Si substrates.

Considering MoTe₂ case as an example, we also show a detailed study of the heterogeneous vapor-solid reaction between the pre-deposited Mo film and Te vapor optimizing the scalability and quality of the MoTe₂ nanosheets. Specifically, with simulation based on finite element method, for a given growth temperature, we show MoTe₂ structure and morphology are kinetically dictated by the distribution of the Te concentration gradient on the reaction site with varying geometric configurations inside the CVD reactor. Further, the role of temperature and Te concentration is elucidated for the other cases to achieve PtTe₂ and NiTe₂ growth. We characterize the so-grown nanosheets by using several techniques, such as Raman visible spectroscopy, atomic force microscopy, X-ray diffraction and transmission electron microscopy. By combining the results we could retrieve the structure of the different TMTs nanosheets in terms of their crystalline phase and crystallinity, thickness (number of layers), morphology, RMS roughness and domain (grain) size. In synthesis, we obtain nanosheets in pure single phase, with a polycrystalline character related to the pristine metallic thin film, with RMS roughness limited to few nm and a grain size in the tenth to the hundreds nm range.

Our study elucidates a methodological approach that could be considered as an efficient, scalable, and relatively simple solution to enable the controlled growth and optimize the characteristics of TMTs, and in extension TMDs, over large areas, whenever a tellurization (chalcogenization) CVD based process is considered. Furthermore, this concept provides a pivot scheme for enabling scalable integration of TMTs exhibiting single phase in potential applications for novel micro- and nano-electronics, spintronics, photonics, and thermoelectric devices.

9:15 AM NM06.16.04

Molecular Layer Deposition Approach for Hybrid Metalorganic-Inorganic Systems— Thin Film Oxides Functionalized with a Luminescent Europium Complex Monolayer Anna L. Pellegrino^{1,2}, Adolfo Speghini^{3,4}, Guglielmo G. Condorelli^{1,2} and Graziella Malandrino^{1,2}; ¹Università degli Studi di Catania, Italy; ²INSTM UdR Catania, Italy; ³Nanomaterials Research Group, Department of Biotechnology, Italy; ⁴INSTM RU Verona, Italy

The organic-inorganic hybrid systems have attracted great attention because of their potential applications in several fields of material science such as sensors, dye sensitized solar cells (DSSCs), optoelectronic devices, and heterogeneous catalysis. In these systems, transition metal oxides thin films are the most promising inorganic materials, due to their wide spectrum of magnetic, electrical, and optical properties. Nickel oxide has been chosen as the inorganic component of the hybrid system due to its multifunctional properties such as high dielectric constant, low resistivity and UV optical transparency.

The most common functional organic moieties chosen for the hybrid approach are the molecules having silane, thiol and carboxylic functionalities as anchoring groups. Among these, the attention has been devoted to luminescent lanthanide complexes due to the exceptional photophysical properties such as high quantum yields and sharp emission profiles related to f-f electronic transitions. Eu(III) complexes have attracted growing interest as efficient downshifter and as a probe to sense the chemical environment.

For a variety of applications, the possibility of a fast, high efficiency and reproducible assembly method of molecules into nanostructured solid substrates is of great importance. Molecular layer deposition (MLD) is a solvent free method to create conformal coatings of organic molecules layers through self-limiting reactions on the surface and with an excellent molecular-level control of thickness and composition.

In the present work, we applied for the first time a full vapor phase approach based on the sequential steps of (i) Metal-Organic Chemical Vapor Deposition (MOCVD) of the inorganic NiO thin films, and (ii) MLD to link, in a covalent way, on the activated surface an Eu(β -diket)₃L complex, where β -diket is a β -diketone and L is a Lewis base. An accurate X-ray photoelectron characterization confirmed the optimal parameter conditions of the activation step and of the covalent anchoring of the luminescent europium(III) adduct on the NiO films. Emission spectroscopy of the hybrid NiO/Eu(III) system shows that an accurate control of the Eu(III) coordination sphere may tune the luminescence of the monolayers.

9:30 AM NM06.16.06

Schottky Barrier Variable Heterostructure Hydrogen Gas Detector through Electron Transfer between Pd NPs and Graphene Jihun Sim and Woojong Yu; Sungkyunkwan University, Korea (the Republic of)

Among future fuels that are in the spotlight, hydrogen has a dangerous side. The combustion rate and low flash point of hydrogen cause major explosion accidents. Therefore, leakage accidents are the most important issue in using hydrogen as a fuel. Therefore, a system that can detect hydrogen from very low concentrations is an essential problem.

Palladium (Pd) has the property of decomposing and bonding hydrogen molecules when exposed to hydrogen atmosphere. At this time, the volume changes at the same time as the bonding, and the energy structure of Pd also changes. Research on a system for sensing hydrogen using these properties of Pd has been conducted. In this study, we propose a hydrogen sensor attached to the surface of graphene by fabricating such Pd in the form of nanoparticles (NPs).

In the case of Pd NPs, it has a larger surface area than that of Pd sheet, minimizing the effect of volume increase and maximizing the contact area with hydrogen molecules. Pd NPs were fabricated through the annealing process and were confirmed using electrical characterization and Scanning Electron Microscope (SEM). When Pd NPs are attached to graphene, electrons are moved between graphene and Pd NPs when the energy structure is changed as the Pd NPs adsorb hydrogen. This results in changes in the energy structure and surface conductivity of graphene. This change occurs with the concentration of hydrogen.

We fabricated a device using a heterogeneous structure of Silicon (Si) and Graphene. The two materials have the characteristics of a semiconductor and a metalloid, forming a Schottky barrier. Then, Pd NPs are attached to the graphene surface of the device. When the device is exposed to hydrogen, the Pd NPs adsorb hydrogen, which changes the energy structure of graphene. As a result, the Schottky barrier between Si and graphene changes and the current flowing through the device changes.

Using this principle, the reactivity to hydrogen is electrically detected with a Si/graphene heterostructure device. As a result of the detection, it was confirmed that it was possible to detect low-concentration hydrogen gas at a level of 250 ppm.

9:35 AM NM06.16.07

Conductivity Modulation of Solution-Processed Two-Dimensional Materials for Printed Electronics Development Songwei Liu¹, Xiaoyue Fan², Pengyu Liu¹, Jingfang Pei¹, Yang Liu¹, Lekai Song¹, Yingyi Wen¹, Gang Wang² and Guohua Hu¹; ¹The Chinese University of Hong Kong, Hong Kong; ²Beijing Institute of Technology, China

Printing of two-dimensional (2D) materials is emerging as a promising approach for scalable electronics manufacturing. The state-of-art advances, however, show inferior device performance due to poor electrical conductivity as a result of the discrete nature of the printed 2D material networks. Methods such as modifying the connections and alignments between the 2D material nanoflakes show limited enhancements. Here we introduce a ferroelectric polarization effect to overcome the conductivity limitation of printed 2D material networks and exploit this mechanism in printed electronics developments.

We start printed electronics fabrication with solution processing of 2D materials. The yield 2D materials are in an irregular, nanoscale dimension. Using MoS₂ as the example, we show that printed thin films from such nanoflakes give an extensively high electrical resistance due to the poor inter-flake contacts and the carrier transport of the nanoflakes. This makes it impractical to fabricate functional printed electronics. To address this issue, we couple the printed MoS₂ with ferroelectrics and show significant electrical resistance tuning from a high resistive state to a low resistive state, with a ratio of >10³. We assume this arises from a complex mechanism of printed MoS₂ under the electric field. Our detailed density-functional theory calculations and spectroscopic characterisations suggest MoS₂ transition from a semiconducting state to a metallic state, driven by the localized electric field exerted by the nonlinear electric polarization of the ferroelectrics. The localized electric field can cause the electron cloud of MoS₂ to redistribute and form conductive electron gases on the surface or between the atomic planes. Such distortion in the electron cloud may deform the atomic structure of MoS₂, leading to a phase transition that can further promote the conductivity. Exploiting this transition, we demonstrate printed memristive electronics, for instance, ferroelectric tunnelling junctions, and show the possibility of implementing neuromorphic computing. Besides MoS₂, this transition mechanism may also be viable for other 2D materials (e.g. MoTe₂) and low-dimensional materials (e.g. CNTs).

Our approach to tune conductivity may serve as a universal strategy for modulating the properties of solution-processed low-dimensional material networks, and through printing, the approach can lead to scaled-up and even wafer-scale manufacturing of electronics that can find applications in, for instance, integrated and intelligent circuits, in-memory neuromorphic computing, and human-machine interfaces.

9:40 AM NM06.16.08

Bottom-up Assembly of Patterned Graphene/MoS₂ Heterostructures Xin Chen, Kathrin Knirsch and Andreas Hirsch; Friedrich-Alexander-Universität Erlangen-Nürnberg, Germany

Combining two-dimensional materials into one vertical stack has evolved as an appealing strategy to modify the materials' properties and enable functional integrity and complexity. Among the heterostructures investigated so far, graphene/MoS₂ (G/MoS₂) heterostructures have drawn particular attention owing to their extraordinary properties and great potential for the use in high-performance devices.^[1-2] The individual layers of such heterostructures are usually held together by van der Waals (vdW) forces. However, for most vdW interfaces, the structural disorders and contaminations induced by the integration steps are not rare, which are detrimental to the interface quality and would severely limit electronic communication and device efficacy. Here, we will present an efficient and facile approach to bottom-up construct covalently bridged G/MoS₂ heterostructures in a spatially defined manner. The formation of these patterned heterostructures was demonstrated by Raman and photoluminescence (PL) spectroscopies and Kelvin probe force microscopy (KPFM). Our approach enables the high throughput generation of covalent hetero-interfaces and precise transcription of spatial patterns from the bottom to the top layer of the heterostructures.^[3] This covalent assembly concept has great potential to be extended to the construction of a broad array of two-layer or multi-layered covalent heterostructures, which is of great importance for future material design and engineering.

References

- (1) Shih, C.-J.; Wang, Q. H.; Son, Y.; Jin, Z.; Blankschtein, D.; Strano, M. S., *ACS Nano* **2014**, *8* (6), 5790-5798.
- (2) Li, S.; Liu, Y.; Zhao, X.; Shen, Q.; Zhao, W.; Tan, Q.; Zhang, N.; Li, P.; Jiao, L.; Qu, X., *Adv. Mater.* **2021**, *33* (12), 2007480.
- (3) Chen, X.; Assebban, M.; Kohring, M.; Bao, L.; Weber, H. B.; Knirsch, K. C.; Hirsch, A., *J. Am. Chem. Soc.* **2022**, *144* (22), 9645-9650.

9:55 AM NM06.16.09

3D Printing of 0D-2D Material-Based Aerogels for High-Performance Room-Temperature Ammonia and Formaldehyde Sensing Zhuo Chen, Bingham Zhou and Tawfique Hasan; University of Cambridge, United Kingdom

Graphene-based aerogels are promising for gas sensing due to their high porosity, large surface area, and additive manufacturability of complex shapes through 3D printing. However, their performances are greatly hindered by graphene's intrinsically poor gas sensing capability and the lack of

understanding of the effect of aerogel morphology on mass transfer. We hybridize graphene with tin oxide quantum dots (QDs) and fabricate highly sensitive 3D-printed aerogel-based gas sensors. We quantitatively identify two factors that affect the gas sensing performance of the aerogels, namely cross-sectional area and surface porosity of the printed structures. Through Knudsen-diffusion-based modelling and empirical analysis, we show that filament-structured aerogel sensors with smaller cross-sectional area have response towards ammonia and formaldehyde which are significantly superior to widely demonstrated aerogel 'thin-film' sensors. Meanwhile, the gas sensing performance can be further improved by increasing the surface porosity of printed aerogels to enable more efficient gas diffusion. Our findings enable precise control of the morphology of printed aerogels for optimized gas diffusion and sensing. The proposed hybrid aerogel gas sensor shows ultrahigh response at room temperature to ammonia (14%, 1ppm) and formaldehyde (13.3%, 1ppm), the best for chemiresistive aerogel sensors. Our approach to hybridized QDs-graphene-based aerogels and printing-enabled morphological control provides a promising strategy to design high-performance room-temperature ammonia and volatile organic compounds (VOCs) gas sensors and beyond.

10:10 AM DISCUSSION TIME

SYMPOSIUM NM07

Mixed Dimensional Heterostructures—From Synthesis to Application
November 28 - December 8, 2022

Symposium Organizers

Sanghoon Bae, Washington University in Saint Louis
Deep Jariwala, University of Pennsylvania
Jeehwan Kim, Massachusetts Institute of Technology
Kysang Lee, University of Virginia

* Invited Paper
+ Distinguished Invited

SESSION NM07.01: Growth and Synthesis of Various Dimensional Materials and Heterostructures I
Session Chairs: Deep Jariwala and Hyunseok Kim
Monday Morning, November 28, 2022
Hynes, Level 2, Room 203

10:30 AM *NM07.01.01

Boron Nitride on Sapphire a Scalable and Versatile van der Waals Template for Growth and Lift-Off of Thin Films and Devices Michael Snure¹ and Eric Blanton²; ¹Air Force Research Laboratory, United States; ²KBR, United States

Van der Waals surfaces, such as graphene or hBN, offer a unique route to growth, lift-off, and transfer of a wide variety of thin film materials and devices. Specifically, sp² bonded BN is interesting due to its atomically flat and smooth surface, high temperature and chemical stability, excellent insulating and dielectric properties, and ability to be grown uniformly over large areas 4" by commercial techniques such as metal organic chemical vapor deposition. Here we will describe the use of boron nitride on sapphire templates for growth of a variety of electronic films including GaN, AlN, AlScN, and Ga₂O₃. Key challenges, including nucleation, template morphology, stability, and strain will be covered with the goal of achieving high quality films that can be easily lifted off and transferred. Mechanical lift-off techniques including both soft and spalling induced methods for transfer of full wafers, individual devices, and selectively defined areas will be discussed. Finally, we will cover bonding these thin layers to a variety of surfaces in order to create heterojunctions and integrate devices.

11:00 AM NM07.01.02

Graphene Nanopattern for Single-Crystal Film Growth, Defect Reduction and Layer Transfer Hyunseok Kim, Sangho Lee, Jiho Shin and Jeehwan Kim; Massachusetts Institute of Technology, United States

Thin film heterostructures are key building blocks for advanced electronic and optoelectronic devices. For this, direct heteroepitaxy has been pursued for decades, although it has been challenging to reduce crystal defects stemming from lattice mismatches and thermal mismatches between materials. The layer transfer method has been proposed as an alternative approach, wherein dissimilar materials are separately grown and then hetero-integrated. However, the applicability of layer transfer techniques is limited by several technical challenges, such as controllability, throughput, and damage to the substrate. Remote epitaxy, which is a recently developed method to produce single-crystalline membranes, is a promising approach but cannot be applied to elemental materials such as Si and Ge.

In this work, we report graphene nanopattern as a universal template for the growth of single-crystal thin films that can be exfoliated as a freestanding form. This is realized by the chemical inertness of graphene, which allows selective nucleation at the exposed region, followed by lateral overgrowth onto graphene to form a planarized thin film. By employing graphene nanopattern, both group IV and III-V materials are utilized as the substrate as well as the epilayer. The epilayer can be exfoliated at the graphene interface because partially covered graphene effectively weakens the interface, which is corroborated by theoretical analyses of spalling theory. We reveal that graphene nanopattern not only works as a weakened interface for exfoliation, but

also allows for dislocation reduction in heteroepitaxial films. This is because of the flexibility and the dangling-bond-free nature of graphene, which provides an additional path for strain relaxation. Therefore, these results represent a meaningful step toward production of high-quality single-crystal membranes that can be hetero-integrated.

11:15 AM NM07.01.03

Direct Writing of Graphene and Silicon Carbide Quantum Dots on an Elastomer by Laser-Induced Carbonization [Shuichiro Hayashi](#) and Mitsuhiro Terakawa; Keio University, Japan

Laser-induced carbonization has been emerging as a versatile method to simultaneously synthesize and pattern functional materials on polymers for the realization of bendable and stretchable devices. By simply irradiating a flexible polymer with a laser beam, the organic substrate can be modified into electrically conductive material, namely graphene, allowing for the rapid fabrication of flexible electronic devices. Recently, we have demonstrated the formation of fluorescent graphene quantum dots (GQDs) by the laser-induced carbonization of polydimethylsiloxane (PDMS), expanding the possibilities of laser-induced carbonization for the fabrication of, not just electronic, but optoelectronic devices. It has been well established that laser-induced carbonization of PDMS results in the formation of graphene and silicon carbide (SiC) crystals, and our results suggested that the formation mechanism of the GQDs was a top-down method based on the laser-induced pyrolysis of these materials. In this study, we demonstrate the selective formation of nanometer-sized SiC crystals by laser-induced carbonization of PDMS using a femtosecond laser. Laser pulses of varying energies were irradiated onto the PDMS surface to induce carbonization. Transmission electron microscopy (TEM) observations revealed that the fabricated structures were composed of few-layered graphene sheets containing SiC nanocrystals. The average size of the observed SiC nanocrystals varied depending on the energy per laser pulse used for fabrication, where larger SiC nanocrystals were observed for structures fabricated using higher energies. Moreover, photoluminescence (PL) spectra obtained from the structures indicated an emission peak distinctively different from that of GQDs, centered at ~450 nm (ex. 320 nm). Such emission peak has been commonly reported for SiC quantum dots. When electrical conductivity measurements were performed, the current increased linearly with applied voltage in the case of structures fabricated using relatively lower energies per laser pulse. Contrarily, the current increased exponentially with applied voltage in the case of structures fabricated using relatively higher energies per laser pulse, indicating semiconducting property. To the best of our knowledge, this is the first demonstration of the fabrication of structures exhibiting measurable semiconducting properties by laser-induced carbonization. For the ultrafast thermalization of materials due to ultrashort-pulse irradiation, the generated thermoacoustic stress waves can induce localized pressures in the MPa and GPa regime, particularly for shorter pulse durations and higher energies per laser pulse. Since high-pressure conditions are favorable for synthesizing SiC, it is inferred that SiC nanocrystals were more easily synthesized using femtosecond laser pulses with high energies per laser pulse.

SESSION NM07.02: Application of Various Dimensional Materials and Heterostructures I
Session Chairs: Deep Jariwala and Jiho Shin
Monday Afternoon, November 28, 2022
Hynes, Level 2, Room 203

1:30 PM *NM07.02.01

Power Generation Using Non-Equilibrium Electron Gas Thermodynamic Cycle [Mona Zebarjadi](#)¹, Farjana F. Tonni¹, Kazuaki Yazawa² and Ali Shakouri²; ¹University of Virginia, United States; ²Purdue University, United States

A thermal to electrical power generator is proposed recently that replicates the idea of the thermodynamic cycle of mechanical heat engines using an analogous electron gas.¹ The non-equilibrium electron gas is compressed using electrostatic gating, heated using a localized heat source, and released. The input heat power is converted to electrical power upon the electron gas expansion and cooling. The power is fully delivered to the load within a few picosecond time scales when electrons are relaxed and cooled down to the lattice temperature. The cycle is then repeated. We present a Monte Carlo simulation of power generation by such a non-equilibrium electron gas using GaAs-based heterostructures. Electrons are confined using an enforced one-dimensional potential well to form a 2D electron gas. The confined electrons' temperature is then raised to higher temperatures instantaneously, replicating a localized short heat pulse. The compressed hot electrons are then released and their positions are tracked via a Monte Carlo simulator coupled with a 1D Poisson solver. At room temperatures, we observe hot electrons are cooled to lattice temperature within 3 to 10 ps depending on the amount of their excess energy. A current-voltage pulse is delivered with about 0.4 ps delay (related to the device dimensions and drift velocity) to the load. The electrical energy delivered to the load increases quadratically with increasing temperature. The simulation results show that the proposed solid-state device is not limited by the Carnot efficiency due to its transient nature and can have more than 50% energy conversion efficiency.

(1) Yazawa, K.; Shakouri, A. Electrothermal Energy Conversion Using Electron Gas Volumetric Change inside Semiconductors. *Applied Physics Letters* **2016**, *109* (4). <https://doi.org/10.1063/1.4960022>.

2:00 PM NM07.02.02

Vertically Stacked Full Color Micro-LEDs via Two-Dimensional Material-Based Layer Transfer [Jiho Shin](#)¹, Hyunseok Kim¹, Junseok Jeong¹, Suresh Sundaram² and Jeehan Kim¹; ¹Massachusetts Institute of Technology, United States; ²Georgia Tech Lorraine, France

Full color micro-light emitting diode (μ LED) displays have been explored for augmented and virtual reality (AR/VR) applications that require extremely high pixels-per-inch (PPI). However, conventional manufacturing processes based on pick-and-place methods are slow and expensive, and their resolutions are insufficient to meet the required pixel densities. Recent demonstrations of vertical μ LED displays attempt to address these issues by stacking freestanding red, green, and blue (RGB) LED membranes and fabricating top-down, but the absence of lift-off techniques to produce ultrathin, readily released, and low-cost layers of LEDs has delayed essential technological progress. Here, we report full color, vertically stacked μ LED displays that achieve the highest pixel density (5100 PPI) and the smallest pixel size (4.5 μ m) reported to date, which is uniquely enabled by two-dimensional material-based layer transfer (2DLT) techniques. 2DLT allows the growth of RGB LEDs with near-submicron thickness on 2D material-coated substrates via remote epitaxy or van der Waals epitaxy, mechanical release of LEDs from 2D materials, stacking of LEDs via adhesion layers, and top-down fabrication to yield vertical RGB pixels. The smallest ever pixel height of ~9 μ m is the key enabler for μ LED arrays with record high PPI. Facile mechanical release process allows high-throughput manufacturing of μ LEDs, and the reusability of wafers reduces material cost. Wavelength-selective polyimide absorbers serve as adhesive interlayers as well as optical filters that prevent interference between LEDs, allowing further reduction in stack thicknesses. We also demonstrate a highly resolved transfer of μ LED chips to illustrate the versatility of 2DLT for constructing large-scale μ LED displays. These results not only establish routes to exceptionally high-pixel density full color μ LED displays for AR/VR, but also offer a generalizable platform for broader classes of 3D-integrated systems.

2:15 PM NM07.02.03

Development of Mixed-Dimensional QDs/MoS₂/TiO₂ Heterostructured Resistive Random Access Memory with Interfacial Analog Switching Characteristics for Potential Neuromorphic Computing [Shin-Yi Tang](#), Yu-Chuan Shih, Ying-Chun Shen, Ruci-Hong Cyu, Ling Lee and Yu-Lun Chueh; National Tsing Hua University, Taiwan

Resistive random access memory (RRAM) has been considered as one of the most promising candidates for next-generation nanoscale nonvolatile memory devices and neuromorphic computing applications. In this study, a novel mixed-dimensional design of heterostructured RRAM devices with the switching layer composed of 0D quantum-dots (QDs), 2D MoS₂ and TiO₂ is proposed and exhibited prominent interfacial switching behaviors. Continuous MoS₂ bilayer synthesized through the chemical vapor reduction (CVR) process is transferred on top of TiO₂/Pt, followed by the decoration of QDs and the deposition of ITO top electrodes, to realize the mixed-dimensional memory device. Compared to typical filamentary type RRAMs, the insertion of QDs/MoS₂ layer enables the bias-controllable interfacial resistive change during set and reset process without abrupt switching, resulting from the effective electron-hole pair separation upon excitation and the generation of a thin MoO_x layer due to the accumulation of oxygen ions at the interface between MoS₂ and TiO₂, which is also proven through HRTEM observations. In addition, the enhanced endurance, multilevel storage and analog synaptic characteristics with improved linearity in potentiation and depression are demonstrated to open up the opportunities of this heterostructured device for future neuromorphic applications.

2:30 PM BREAK

3:00 PM NM07.02.04

InAs QD Layer Homojunction Combined with Zinc Oxynitride to Fabricate Phototransistors for Near-Infrared Sensing Applications [Jong-Ho Kim](#), Byung Ku Jung, Su K. Kim, Kwang Ro Yun, Min-Gyu Jeon, Tae-Ju Lee, Soong Ju Oh and Tae-Yeon Seong; Korea University, Korea (the Republic of)

Amorphous metal-oxide semiconductor thin-film transistors (AOS-TFT) have been widely studied for applications in various fields, including display panel driving devices, biosensors, gas sensors, and optical sensors because of their scalability, low off-current, and high uniformity of performance. Recently, the integration of AOS-TFT with light-absorbing materials, such as colloidal quantum dots (CQDs), perovskite, and conjugated polymers, has been widely investigated to develop near-infrared (NIR) detection devices. CQDs are also actively studied for application in hybrid phototransistors because of their tunable bandgap and low exciton binding energy. However, the low mobility of QD layers and significant charge accumulation within the QD layer limit the performance of phototransistors. Further, AOS phototransistors have disadvantages such as limited detection wavelength (< 450 nm), modest field-effect mobility (~10 cm²/Vs), and high persistent photocurrent (PPC) effect. The PPC effect is caused by the ionization of oxygen vacancy (V_O) under illumination, increasing the time to return to the initial state. Meanwhile, zinc oxynitride (ZnON) can be an alternative to solve most of the problems of AOS and QD layers. In ZnON, the PPC effect is suppressed because N 2p orbital covers V_O states. Further, since ZnON has high mobility (> 50 cm²/Vs) owing to its low effective mass (0.19 m₀) and no potential fluctuations in conduction band minima, it can compensate for the low mobility of QD layers.

Thus, in this study, low toxicity and chemically stable InAs QD layers were combined with promising ZnON to fabricate a hybrid phototransistor. In particular, homojunction of InAs QD layers was for the first time applied to resolve the charge accumulation in QD layers. InCl₃ and 2-Mercaptoethanol (ME) were adopted as ligands for InAs QDs. To form the homojunction of QD layers, an InAs-InCl₃ layer was deposited over the InAs-ME layer. Three hybrid phototransistors (e.g., InAs-InCl₃/InAs-ME/ZnON, InAs-ME/ZnON, bare ZnON) were prepared and their performances were compared. The responsivity of InAs-InCl₃/InAs-ME/ZnON, InAs-ME/ZnON, InAs-ME/ZnON, and bare ZnON at the light intensity of 20 μW/cm² was 2.59 × 10⁴, 1.47 × 10⁴, and 1.43 × 10² A/W, respectively. The detectivity of the InAs-InCl₃/InAs-ME/ZnON, InAs-ME/ZnON, and bare ZnON at 20 μW/cm² was 4.86 × 10¹³, 2.84 × 10¹³, and 3.30 × 10¹¹ Jones, respectively. A comparison shows that the QD homojunction-based phototransistors exhibit much better performance than the other two samples. To understand the surface characteristics and hole blocking mechanism, the depth profile of ZnON was examined with time-of-flight secondary ion mass spectroscopy. Moreover, to confirm the formation of an InAs QD homojunction, the Fermi levels of InAs-InCl₃ and InAs-ME were measured and obtained to be 4.2 and 4.06 eV, respectively. They were found to have the same optical bandgap of 1.27 eV. Further, transmission electron microscope elemental mapping was used to confirm the uniform distribution and stacking of the InAs QD and ZnON layers. These results show that the integration of the InAs QD homojunction and ZnON could serve as an important component of phototransistors for the fabrication of high-performance NIR sensing devices.

3:15 PM NM07.02.06

Simultaneous Control of Nanowire Morphology and Doping in Mixed-Dimensional Heterostructures for Topological Quantum Computing [Chunyi Huang](#)¹, [Didem Dede](#)², [Martin Friedl](#)¹, [Christopher E. Mead](#)¹, [Anna Fontcuberta i Morral](#)^{2,2} and [Lincoln J. Lauhon](#)¹; ¹Northwestern University, United States; ²EPFL, Switzerland; ³Lumiphase Corporation, Switzerland

Templated networks of semiconductor nanowire networks^[1,2] are a promising route to quantum computing through the manipulation of Majorana zero modes. These structures are inherently mixed dimensional; connected nanomembranes of GaAs are grown via selected area epitaxy in openings of lithographically patterned oxide masks, and one-dimensional InGaAs nanowires assemble atop the nanomembranes to define one-dimensional channels for electrons. The temperature and ratio of group III to group V elements are the primary variables used to tune the diffusivity of adatoms and control the faceting of the growth interface, directing the nanowire formation. In prior work, remote doping of the InGaAs nanowires was demonstrated, but control over the Si doping profile was limited by surface segregation,^[2] and an ideal delta-doping profile was not achieved. In this talk, we report a new approach to the simultaneous control of nanowire morphology and dopant distribution using atom probe tomography to reconstruct buried growth interfaces and the distribution of dopants. InGaAs nanowires were again grown on GaAs membranes, but dilute Al marker layers were introduced at various stages to visualize buried growth interfaces, track the diffusion of dopants, design modified growth processes. After finding that Si segregates preferentially to different facets, we implemented a strategy in which dopants are trapped by dilute ternary layers (In_xGa_{1-x}As and Al_xGa_{1-x}As) via increases in bulk solubility and/or modifications of the partition coefficient. Deposition of trapping layers was followed by the growth of GaAs spacer to separate the dopants (ionized impurities) from the channel. Si is incorporated at the onset of the trapping layer as intended, forming a narrow doping band several nanometers below the nanowire. A simple empirical model that assumes a linear dependence of the bulk solubility on Al concentration captures the resulting dopant profile, validating the principle of dopant trapping for controlled remote doping of nanowires grown on faceted supports. Such an approach can be generalized to other mixed-dimensional III-V heterostructures.

References:

- [1] Friedl, M., et al. Template-assisted scalable nanowire networks. *Nano Letters* 2018, 18, 2666.
- [2] Friedl, M., Cerveny, K., et al. Remote doping of scalable nanowire branches. *Nano Letters* 2020, 20, 3577.

3:30 PM NM07.02.07

Nanostructured Manganese-Oxide/Reduced Graphene Oxide Hybrid Nanocomposites for Performance Enhancements of All-Printed Supercapacitor Devices Erick L. Ribeiro^{1,2,3}, Mahshid Mokhtarnejad¹, Dibyendu Mukherjee¹, Bamin Khomami¹ and Rigoberto C. Advincula^{1,2,3},
¹University of Tennessee, Knoxville, United States; ²The University of Tennessee, Knoxville, United States; ³Oak Ridge National Laboratory, United States

Supercapacitor devices (SCs) have emerged as a promising energy-storage alternative that could enable the efficient utilization of electrical energy while fulfilling most of the technical specifications commonly encountered in the field of electronics. Additionally, SCs are essential for applications requiring high-power outputs and can be easily integrated into many complex electronic architectures, including small chips and flexible substrates. Nonetheless, alterations in the structural design of modern electronic devices to facilitate transportation and portability, especially inspired by the rapid expansion of the Internet of Things (IoT), have created strict requirements in dictating their operating conditions, consequently demanding engineers and scientists to explore novel functional materials and manufacturing approaches that go beyond the limits of the commonly-used power-source technologies. Herein, we present the synthesis of Hybrid Nanocomposites (HNCs) based on nanostructured Manganese Oxide species interfaced with reduced Graphene Oxide (rGO) for the fabrication of electrochemical active electrodes components in all-printed supercapacitor devices. Comprehensive structural characterizations demonstrate that the active material is composed of MnOx/Mn₃O₄ nanorods and nanoparticles embedded in rGO nanosheets. The development of such novel structures is facilitated by the extreme synthesis conditions (high temperatures and pressures) of the liquid-confined plasma plume present in the Laser Ablation Synthesis in Solution (LASiS) technique. Specifically, functional characterizations demonstrate that the performance of the active layer is highly correlated with the MnOx/Mn₃O₄ to rGO ratio and the morphology of MnOx/Mn₃O₄ nanostructures in HNCs. To that end, active layer inks comprising HNC samples prepared under optimal laser ablation conditions were dispersed into a percolated conductive network of electronic grade Graphene and Carbon Nanofibers (CNFs), which were subsequently applied to yield functional electrodes in an all-printed supercapacitor device. Electrochemical characterizations unequivocally reveal that the electrode composed of the LASiS-synthesized MnOx/Mn₃O₄-rGO HNCs exhibits a significantly higher charge storage capacity (325 F/g) when compared to the devices composed of electrodes containing commercially available nanostructured Mn₃O₄-Graphene Nanocomposites (NCs) (189 F/g). Overall, the results presented here pave the way for use of LASiS as a facile methodology for the synthesis of functional nanostructured materials for applications in the additive manufacturing of next-generation energy-storage devices

3:45 PM *NM07.02.09

Heterostructural Metal-Halide Perovskites for Optoelectronic Applications Hobeom Kim; Gwangju Institute of Science and Technology (GIST), Korea (the Republic of)

Metal-halide perovskites are interesting optoelectronic material as their dimensionality can be tuned by a facile chemical synthetic process to build a hybrid dimensional heterostructure. Plus, optoelectronic devices such as solar cells and light-emitting diodes (LEDs) using 3D perovskites as a photo-active material have shown great achievement in terms of their device performance. However, the 3D perovskites fundamentally suffer from their internal defects in the bulk and at the surface. For example, the presence of defects can cause quenching of charge carriers via non-radiative recombination channels to degrade the optoelectronic performance of the devices. In addition, the defects migrate to lead to peculiar electronic and optical behavior of the devices such as current-voltage hysteresis and luminance overshooting, which can seriously impact the stability of the perovskite optoelectronic devices accelerating their degradation. Thus, various strategies for defect passivation by using different classes of materials have been presented. Among them, here, we demonstrate the incorporation of 2D perovskites into the 3D perovskites to build 3D-2D hybrid or 3D/2D heterostructural perovskites. The mixed-dimensional perovskites prove to be effective in terms of suppression of defect or trap formation, and ion migration. Thus, LEDs and solar cells employing the mixed-dimensional perovskites exhibit improved optoelectronic characteristics and operational stability.

[1] "Proton-transfer-induced 3D/2D hybrid perovskites suppress ion migration and reduce luminance overshoot" **H. Kim**†, J. S. Kim†, J.-M. Heo†, M. Pei, I.-H. Park, Z. Liu, H. J. Yun, M.-H. Park, S.-H. Jeong, Y.-H. Kim, J.-W. Park, E. Oveisi, S. Nagane, A. Sadhanala, L. Zhang, J. J. Kweon, S. K. Lee, H. Yang, H. M. Jang, R. H. Friend, K. P. Loh, M. K. Nazeeruddin, N.-G. Park, and T.-W. Lee*, *Nat. Commun.*, 11, 3378 (2020)

[2] "Employing 2D-perovskite as an electron blocking layer in highly efficient (18.5%) perovskite solar cells with printable low temperature carbon electrode" S. Zouhair†, S.-M. Yoo†, D. Bogachuk, J. P. Herterich, J. Lim, H. Kanda, B. Son, H. J. Yun, U. Würfel, A. Chahboun, M. K. Nazeeruddin, A. Hinsch, L. Wagner*, and **H. Kim*** *Adv. Energy Mater.*, 2200837 (2022)

[3] "Self Crystallized Multifunctional 2D Perovskite for Efficient and Stable Perovskite Solar Cells" **H. Kim**, M. Pei, Y. Lee, A. A. Sutanto, S. Paek, V. I. E. Queloz, A. J. Huckaba, K. T. Cho, H. J. Yun, H. Yang, and M. K. Nazeeruddin* *Adv. Funct. Mater.*, 30, 1910620 (2020)

[4] "Phase-Pure Quasi-2D Perovskite by Protonation of Neutral Amine" M. Dessimoz, S.-M. Yoo, H. Kanda, C. Igci, **H. Kim***, and M. K. Nazeeruddin* *J. Phys. Chem. Lett.* 12, 11323 (2021)

SESSION NM07.03: Poster Session I
Session Chairs: Sanghoon Bae and Vincent Tung
Monday Afternoon, November 28, 2022
8:00 PM - 10:00 PM
Hynes, Level 1, Hall A

NM07.03.01

Versatile and Cost-Effective High-Resolution Patterning of Carbon Nanotube Composite via Intaglio Contact Printing Seokwon Joo¹, Ju-Hyung Kim^{2,2} and Yoon-Kyu Song¹; ¹Seoul National University, Korea (the Republic of); ²Ajou University, Korea (the Republic of)

CNT is a promising material for next-generation electronics due to its unique properties such as mechanical strength, chemical stability, and environmental friendliness. Despite those superior characteristics, CNTs has been used to some limited applications due to a number of reasons – difficulty of patterning being the most critical among those. The traditional method for patterning CNT layers through photolithography provides high-quality CNT patterns, but has limitations in substrate, time, and cost. The solution process, which is a simple and cost-effective alternative, solves the limitation of the substrate as well, but has a disadvantage in dispersing CNTs in the solution that leads to films with non-uniform characteristics. In this work, we introduce a new method for printing high-resolution carbon nanotube (CNT) patterns on almost any type of substrates quickly and inexpensively. To solve this CNT patterning problem, we employed paraffin, an oligomer, in CNT films. Molten paraffin as a solvent facilitates dispersion of CNTs than

other solvents because the chains of paraffin molecules surround the CNTs and weaken the van der Waals force, thus forms a well-dispersed CNT in CNT/paraffin composites. Since this method does not require mono-disperse CNTs, mixing takes only a few seconds of simple stirring. The CNT/paraffin composite slurry is filled in the intaglio of the PDMS stamp (≥ 56 °C, which is the paraffin melting point) and then transferred to the substrate. In this case, as the composite slurry is hardened while being attached to the surface of the substrate (≤ 56 °C), the adhesive force between the composite and the substrate increases. Through this, we enable printing of the CNT composites on various substrates, such as leaves, clothes, and skin, as well as glasses and metals. The use of paraffin also provides improved physical properties, fast processing time, and low cost. We also measure various properties of the composite – e.g. electrical resistance of ~ 14.6 Ω cm, the minimum line width of 7 μm , bending stability up to 12,000 cycles, and self-healing properties by heating over 56 °C. Subsequently, high-resolution CNT composite patterns on various substrates have been applied to several applications. An interdigitated pattern of CNT composite is used to fabricate a capacitive touch sensor and a water drop energy harvesting device. As the line-width being decreased and the number of fingers increased, the performances of the two devices improve. In the capacitive touch sensor, the non-contact and contact sensing method are implemented, and the sensitivity is enhanced by reducing the line-width (50 μm). A noteworthy point in water drop harvesting device is the substrate. By printing on fluorinated ethylene propylene, a substrate that is difficult to coat due to its low surface energy, the polarization with water droplets is enhanced and the output value increases significantly. In addition, we print patterns on clothes and fabricated triboelectric nanogenerators in contact-separation mode, showing the potential for development into wearable energy harvesters or sensors. In conclusion, we introduce a method for printing CNTs on various substrates by mixing CNTs with paraffin. Through this method, it is possible to overcome the disadvantages of patterning CNTs via conventional methods. That is, high-resolution CNT printing is possible within a few minutes regardless of the substrate. It is also shown that patterned CNTs with the new method can be utilized in various applications. We anticipate this method will contribute to the development of patterning CNTs/CNT composites as well as the application of CNTs/CNT composites in the commercial domain.

NM07.03.02

Tetrazole-Based Metal-Organic Frameworks for Energetic Materials with Excellent Properties in Sensitivity Hae-Wook Yoo and Kuktae Kwon; Agency for Defense Development, Korea (the Republic of)

Metal-organic frameworks (MOFs) are a material with a great diversity of properties from diverse three-dimensional structures that can be achieved through the combination of various metals and organic materials, and are expected to be useful in a wide range of fields. In this study, MOFs structures with energy properties (eMOFs) were developed using tetrazole as an organic framework; 5-methyltetrazole (mtz) and 5-aminotetrazole (atz). Through combinations attempts with various metals, the eMOF-1 $[\text{Mn}_3(\text{mtz})_{6.1}(\text{atz})_{2.9}(\text{NO}_3)]$ and eMOF-2 $[\text{Cu}(\text{mtz})_2]$ were successfully synthesized. The heat of formation for these materials was obtained by measuring the heat of combustion through bomb calorimeter (BCA), and this was introduced into the Explo 5 program to calculate explosive properties such as detonation velocity and pressure. In addition, by directly measuring friction, impact, and electrostatic sensitivity, the characteristics as energy materials were confirmed in all directions. In case of eMOF-1, it represented higher detonation velocity than TNT, a representative explosive, and to show excellent insensitivity characteristics. In the development of energetic materials, improvement in sensitivity characteristics at similar performance is a very important factor, and it was expected that eMOF could develop into a new field of energetic material development through this study.

NM07.03.04

Multifunctional Electrospun Nanofiber Air Filters for Removing Particulate Matter and Sensing Formaldehyde Gas Simultaneously Jin Yeong Song and Sang Min Park; Pusan National University, Korea (the Republic of)

Particulate matter (PM) and volatile organic compounds (VOCs) in contaminated air have harmed human health and the global biosphere. PM is defined as particles smaller than 10 μm in size and composed of ionic, metal, and carbon components. VOCs are invisible gases made up of dangerous CO, NO₂, and HCHO (formaldehyde). Many filters for treating PMs and VOCs, which cause a variety of ailments, have been developed, but people are still becoming exposed to these contaminants.

Electrospinning has been explored with significant interest among many methods for fabricating air filters because of its unique ability to produce nanofibers with adjustable permeability and porosity. Various electrospun nanofiber filters with better PM removal performance and lower pressure drops than commercial filters have been developed. However, electrospun nanofiber filters were challenging to maintain their morphology due to weak mechanical properties and be uniformly deposited on non-conductive substrates by instability from the electrospinning process.

Removing VOCs with adsorption frameworks is generally ineffective compared to PM removal. Meanwhile, colorimetric nanofiber membranes have been demonstrated for their rapid color changes induced by VOC reactions without the need for expensive equipment or a controlled environment. Still, these nanofiber membranes or mats have been revealed in treating one type of air pollutants, such as PM or VOCs.

In this study, we proposed a fabrication process of electrospun nanofiber filters that remove PM while also detecting formaldehyde gas. By our methods, fabricated nanofiber filters were uniformly and directly deposited on non-conductive masks and showed self-assembled structures that could possess a high PM removal rate and moderate pressure drop compared to commercial filters. As a representative indoor VOC capable of causing underlying death even at low concentrations, formaldehyde was also colorimetrically detected by changing the color of nanofiber filters that can effectively remove PM. As a result, the fabrication of an electrospun nanofiber filter that can simultaneously perform PM capture and formaldehyde detection in complex air pollution was successfully demonstrated. We believed that this fabrication process is pioneering work for producing nanofiber filters for capturing PM and synchronously sensing VOCs and that it could provide new insight into the production of multifunctional electrospun nanofiber filters.

This work was supported by the National Research Foundation of Korea (NRF) grant funded by the Korea government (MSIT) (No.

2020R1C1C100944311) and BK21 FOUR Program by Pusan National University Research Grant, 2021. Jin Yeong Song is grateful for financial support from Hyundai Motor Chung Mong-Koo Foundation.

NM07.03.05

Heterointerfaces of Carbon Incorporated Ni₂P-Fe₂P Hollow Nanorods as Superior Electrocatalysts for Oxygen Evolution Reaction Siva Kumar Ramesh¹, Jihye Son¹, Vinoth Ganesan² and Jinkwon Kim¹; ¹Kongju National University, Korea (the Republic of); ²Kumoh National Institute of Technology, Korea (the Republic of)

The rational design of transition metal-based hollow nanostructures is critical for improving hydrogen production efficiency through water electrolysis and rechargeable metal-air batteries. In this study, a self-templating approach is reported to synthesize carbon-incorporated Ni₂P-Fe₂P hollow nanorods ((Ni,Fe)₂P/C HNRs) as efficient oxygen evolution reaction (OER) in alkaline solutions. First, a Ni₂(BDC)₂(DABCO)-MOF (Ni-MOF) is converted to NiFe-PBA hollow nanorods (HNRs) by anion ion exchange, followed by a subsequent phosphidation process to construct (Ni,Fe)₂P/C HNRs. Benefiting from the synergistic effect of heterostructure phosphide composition and unique hollow rod morphology, (Ni,Fe)₂P/C HNRs have a high specific surface area and superior electrocatalytic OER performance. The as-prepared (Ni,Fe)₂P/C HNRs exhibit OER performance with a small overpotential of 258 mV to reach a current density of 10 mA cm⁻², a small Tafel slope of 45.5 mV dec⁻¹, and long-term stability for 40 h, which significantly outperforms the (Ni,Fe)₂P/C NPs and commercial RuO₂. Post-XPS and SEM measurement of (Ni,Fe)₂P/C NPs indicates the robust nature of the catalyst.

NM07.03.06

2D Halide Perovskite Growth within Interlayer Spacings of van der Waals Substrates [Saloni Pendse](#) and Jian Shi; Rensselaer Polytechnic Institute, United States

Two-dimensional hybrid organic-inorganic perovskites (2D-HOIPs) have been extensively researched for use in solar cells as well as optoelectronic devices over the past few years. While various solution-based techniques have been explored and established for growth of 2D-HOIPs in polycrystalline and bulk form, studies of their growth in single-crystalline thin film forms have been limited. Here, we report a solution-based method for growth of 2D-HOIPs using muscovite mica as a van der Waals substrate that yields millimeter scale perovskite flakes. Interestingly, the grown 2D-HOIP flakes lie embedded within interlayer spacings of muscovite mica. We find that such 2D-HOIP flakes buried in mica demonstrate enhanced photostability in comparison to conventional 2D-HOIP flakes. Such liquid phase growth in the interlayer spacings of van der Waals substrates opens a new avenue for developing novel materials structure for designing high-performance optoelectronic devices.

NM07.03.07

An Experimental and Computational Approach to the Effective PEC Water Oxidation of Rh Deposited α -Fe₂O₃ [Young-Min Kim](#)¹, Ye-Rin Hong^{1,2} and Yun-Mo Sung¹; ¹Korea University, Korea (the Republic of); ²KIST, Korea (the Republic of)

Among water-splitting metal oxide materials, hematite (Fe₂O₃) has been well known for its facile synthesis, low toxicity, and significant chemical stability, while fast recombination rate and sluggish electron transfer kinetics highly limit the carrier transfer. Introducing noble metal catalysts on metal oxide photoelectrodes is a common strategy for enhancing various water-splitting materials' photoelectrochemical (PEC) performances. Although the effect of various noble metals such as Au, Ag and Pt on the performance of Fe₂O₃ has been extensively studied in the aspects of catalytic performances and electron injections, Rh has been less investigated for photocatalytic applications.

In this study, we propose Rh as a promising candidate for enhancing the PEC capability of Fe₂O₃ photoanodes. The PEC performances of the Rh/Fe₂O₃ photoanodes were analyzed in detail by both experimental and computational approaches. The Fe₂O₃ nanorods were first fabricated using a two-step hydrothermal synthesis and subsequently the 2 nm-sized Rh clusters were deposited onto the Fe₂O₃ nanorods using the facile UV-assisted solution casting method. The electrochemical analyses were done to discover distinct charge separation mechanisms of the Rh cluster catalysts. In detail, electronic circuits were constructed using EIS analysis and the donor densities were determined from Mott-Schottky plots. The resulting electronic properties of Rh/Fe₂O₃ revealed that the Rh cluster is highly responsible for charge separation and hole transport, leading to significantly enhanced PEC performance. Owing to enhanced carrier generation and hole transfer, the optimum Rh/Fe₂O₃ showed a photocurrent density of 0.81 mA/cm² at 1.23 V_{RHE}, which corresponds to the 100% increase compared to the pristine Fe₂O₃ nanorod electrode.

In addition, we confirmed the role of the Rh cluster on the OER process using DFT calculations. The bulk and surface slab models were constructed based on the fabricated Fe₂O₃, with a preferred growth orientation of (1 1 0). The calculated free energy changes on each reaction step of pristine Fe₂O₃ (1 1 0) well corresponded to previous studies, showing a high OER overpotential of 0.80 eV at the OH* → O* step. On the Rh/Fe₂O₃ (1 1 0), the rate-determining step moved to the O* → OOH* step, and the OER overpotential was significantly reduced to 0.58 eV, indicating the lowered energy barrier of the OER process due to the catalytic performance of the Rh clusters.

NM07.03.08

Next-Generation Passive Cooling Textile with Targeted Optical Performances [Kyuin Park](#) and Margaret Frey; Cornell University, United States

Smart thermal management is a key to conserving energy use. Ironically, high-tech, active methods to cool down are considered superior to passive solutions in the battle against climate change. In recent years, the studies of passive radiative cooling (RC) have generated notable results and contributed to a net-zero-energy future.^{1,2} These RC materials have heterostructures with mid-IR (MIR) ($\lambda=8\mu\text{m}\sim 14\mu\text{m}$) transparency that allow dissipation of heat from the surface. Another approach to cooling is to prevent heating by reflecting the NIR radiation ($\lambda=0.8\mu\text{m}\sim 2.5\mu\text{m}$) which accounts for 52% of the total solar irradiance. Recently, researchers have successfully improved the NIR reflectance and achieved 12 degrees Celsius cooling performance by incorporating nanofibers.³ Unlike coatings, films, and membranes in 0D or 2D structures for RC applications, 2D matrices composed of continuous 1D nanofiber highlighted intrinsic physical and optical properties and the potential to widen applications into wearables and other textile systems. Thus, in order to amplify the effectiveness of passive cooling and to utilize the intrinsic properties of textile, this study presents a fabrication method and quantitative results for a next-generation, passive cooling textile by creating a heterostructure that targets two different radiation spectrums, MIR and near-IR (NIR).

Combination of NIR and MIR optical optimizations into a textile structure is not only beneficial in performance, but also promising. First, this textile structure is ideal for wide applications, unlike a 2D non-breathable membrane or 0D particle coatings that require substrates. Though a textile and a porous membrane may have similar optical performance due to similar roughness and voids, a textile structure allows moisture and air to permeate through, which improves convection and evaporation. Secondly, the surface of fibers provides a dimension to introduce another hetero-interface. With the added dimension, we have incorporated porosity and nanoparticles on an electrospun bio-based polymer, polylactic acid (PLA). Fibers with uniform and non-uniform diameters, various average diameters, and varying porosities were successfully fabricated by electrospinning. Optical analysis of a 10g/m² electrospun fiber sample using UV-Vis-NIR with integrating spheres showed ~80% reflectance in NIR. Additionally, there was no significant change in NIR performances when highly porous fibers with a pore diameter of 0.1 μm were tested. With optimization of pores and nanoparticles, such as TiO₂, SiO₂, and Ag, we expect to observe significant effects in the full spectrum of radiation from UV to MIR. After optical evaluations, real-time outdoor thermal testing can be conducted to monitor the result with respect to time and temperature.

Further advancements in optical properties across the full spectrum of radiation have important implications in improving passive cooling methods. This study will strengthen the capability of passive thermoregulation methods for the human body and outdoor objects, such as buildings. Demonstrating fabrication methods and resultant prototypes would allow discussions among researchers in advancing heat regulation techniques, and furthermore, affect a wider scope of research and applications, such as solar absorber and aerogel-like barrier.

¹ Mandal, Jyotirmoy, et al. *Science*, **2018**, doi.org/10.1126/science.aat9513.

² Hsu, Po-Chun, et al. *Science*, **2016**, doi.org/10.1126/science.aaf5471.

³ Kim, Gunwoo, et al. *ACS Nano*, **2021**, doi.org/10.1021/acsnano.1c04104.

NM07.03.09

Photoelectrochemical CO₂ Reduction Toward Multicarbon Products with Silicon Nanowire Photocathodes Interfaced with Copper Nanoparticles [Inwhan Roh](#)^{1,2} and Peidong Yang^{1,2}; ¹University of California, Berkeley, United States; ²Lawrence Berkeley National Laboratory, United States

The development of photoelectrochemical systems for converting CO₂ into chemical feedstocks offers an attractive strategy for clean energy storage by directly utilizing solar energy, but selectivity and stability for these systems have thus been limited. A promising approach is to use a multicomponent system in which each individual component is optimized for a different aspect of the photoelectrochemical process. Here, we fabricate high aspect ratio

silicon nanowire (SiNW) arrays on a wafer scale to use as photocathodes for its favorable light absorption and charge separation properties and form a radial n⁺p junction for increased photovoltage and stability. We then interface these photocathodes with a copper nanoparticle (CuNP) ensemble through a facile dropcasting method to drive efficient photoelectrochemical CO₂ conversion to multicarbon products. This integrated system enables CO₂-to-C₂H₄ conversion with faradaic efficiency approaching 25% and partial current densities above 2.5 mA/cm² at -0.50 V vs RHE, while the nanowire photocathodes deliver 350 mV of photovoltage under 1 sun illumination. Under 50 h of continual bias and illumination, CuNP/SiNW can sustain stable photoelectrochemical CO₂ reduction. These results demonstrate the nanowire/catalyst system as a powerful modular platform to achieve stable photoelectrochemical CO₂ reduction and the feasibility to facilitate complex reactions toward multicarbon products using generated photocarriers.

NM07.03.10

Single-Atom Pt Stabilized on One-Dimensional Nanostructure Support via Carbon Nitride/SnO₂ Heterojunction Trapping Hamin Shin and Il-Doo Kim; Korea Advanced Institute of Science and Technology, Korea (the Republic of)

Catalysis with single-atom catalysts (SACs) exhibits outstanding reactivity and selectivity. However, fabrication of supports for the single atoms with structural versatility remains a challenge to be overcome, for further steps toward catalytic activity augmentation. Here, we demonstrate an effective synthetic approach for a Pt SAC stabilized on a controllable one-dimensional (1D) metal oxide nano-heterostructure support, by trapping the single atoms at heterojunctions of a carbon nitride/SnO₂ heterostructure. With the ultrahigh specific surface area (54.29 m² g⁻¹) of the nanostructure, we obtained maximized catalytic active sites, as well as further catalytic enhancement achieved with the heterojunction between carbon nitride and SnO₂. X-ray absorption fine structure analysis and HAADF-STEM analysis reveal a homogeneous atomic dispersion of Pt species between carbon nitride and SnO₂ nanograins. This Pt SAC system with the 1D nano-heterostructure support exhibits high sensitivity and selectivity toward detection of formaldehyde gas among state-of-the-art gas sensors. Further *ex situ* TEM analysis confirms excellent thermal stability and sinter resistance of the heterojunction-immobilized Pt single atoms.

NM07.03.11

Tuning Nanowire Lasers via Hybridization with Two-Dimensional Materials Edwin Eobaldt¹, Francesco Vitale¹, Maximilian Zapf¹, Margarita Lapteva¹, Tarlan Hamzayev¹, Christof Neumann², Ziyang Gan², Emad Najafidehaghani², Antony George², Andrey Turchanin^{2,3}, Giancarlo Soavi^{1,3} and Carsten Ronning^{1,3}; ¹Institute of Solid State Physics, University of Jena, Germany; ²Institute of Physical Chemistry, University of Jena, Germany; ³Abbe Center of Photonics, University of Jena, Germany

Semiconductor nanowires have attracted great scientific interest due to their remarkable waveguiding properties and their intrinsic capability to lase under sufficiently high excitation, thus, paving the way towards nanoscaled coherent light sources and the realization of all-optical circuits. The spectral and temporal characteristic of single nanowire lasers have been extensively studied in the past decade. Today's research focuses on their effective integration into functional and nanoscaled environments. In this regard, the hybridization of semiconductor nanowire lasers with two-dimensional materials could offer new knobs to control and modulate lasing at the nanoscale through carrier transport at the heterointerface. We focused on hybrid systems containing ZnO nanowires on top of MoS₂ monolayers. As a consequence of their high optical gain supplied by the formation of an electron hole plasma, ZnO nanowires provide robust ultraviolet lasing emission at room temperature. On the other hand, MoS₂ monolayers emit light in the visible range which, in turn, does not spectrally overlap with the nanowire lasing emission. Additionally, the lattice constants of these materials match almost perfectly, making them ideal candidates for hybrid 1D-2D heterostructures. Our findings show a significant blue-shift of the nanowire lasing modes after the hybridization. Supported by photoelectron spectroscopy measurements, this blue shift can be assigned to the formation of a type II band alignment at the heterointerface, leading to an effective separation and transfer of electrons from MoS₂ to ZnO. This results in an increase of the ZnO optical band gap induced by the carrier injection into the nanowire conduction band, known as the Moss-Burstein effect.

NM07.03.12

An Enhanced Gas Sensor Based on Zig-Zag TiO₂ Nanorods (1D)-BiVO₄ Nanosheet (2D) Heterojunction Yuk YeonJi and Sanghan Lee; Gwangju Institute of Science and Technology, Korea (the Republic of)

The detection of low-concentration gases and odors in fields such as healthcare, mobility, and indoor environment control is attracting tremendous attention. Among various gases, oxidizing gas can cause damage to the human respiratory tract even quite low concentration. At present, oxidizing gas can be tested by gas sensors of all types, including semiconductor metal oxide (SMO), electrochemical, organic compound, optical and carbon-based gas sensor. Within them, SMO gas sensor have been widely concerned due to their advantages, such as simple device structure and manufacturing process, easy integration and suitable for online measurement. Various nanostructures have been investigated for oxidizing gas sensing performance, primarily in single oxides, such ZnO, SnO, Fe₂O₃, TiO₂ and BiVO₄ combining with different modification skills including constructing of complex multi-dimensional structures, loading of noble metal catalysts and doping of MOSs, etc. However, there are still great challenges for constructing high-performance oxidizing gas sensors. Representatively, poor active surface area of nanostructure and large energy band gap of SMO resulting low detection limit. Recently, many researchers have attempted to overcome these issues. There are some strategies such as increasing active sites for adsorption of target gas and design of novel nanostructure via formation of heterojunction. Zigzag structure is one of the most effective structures that can expand the surface to volume ratio compared to other one-dimensional (1D) nanostructure like nanowires and nanorods. In addition, n-n heterojunction structure leads to energy band bending and high potential barrier at material interface, which improving resistance changes.

Herein, we demonstrated a gas sensor enhanced by fabricating heterojunction between 1D TiO₂ zigzag nanorod and two-dimensional (2D) BiVO₄ nanosheet on Si wafer. The 1D TiO₂ zigzag nanorods were realized on 2D BiVO₄ nanosheet by glancing angle deposition (GLAD) method using e-beam evaporation. Compared to the single TiO₂ zigzag nanorods, the TiO₂-BiVO₄ n-n heterostructures can induce a large quantifiable variation in resistance when the oxidizing gas adsorbed at the surface even at room temperature. This improvement is induced by increased depletion layer width at the surface and energy band bending between TiO₂ and BiVO₄ interface. Additionally, we performed the analysis about sensing properties including stability and response time at the room temperature.

We believe that our study will be a cornerstone for the application of functional nanoscale heterostructures based on SMO to gas sensor.

NM07.03.13

Hematite-Based Photoanodes Realized on Flexible YSZ Substrate for Photoelectrochemical Sensing of Hydrogen Peroxide Hwang Junbeom and Sanghan Lee; Gwangju Institute of Science and Technology, Korea (the Republic of)

One of important chemical, hydrogen peroxide (H₂O₂) is broadly utilized in the various field and it also considered as a kind of toxic chemical for living organisms. When H₂O₂ remains in overdoes in living organism can cause serious diseases, the fast and accurate monitoring of H₂O₂ is of great importance. At present, many methods have been developed successfully for the detection of H₂O₂ with high reliability and selectivity. Among them, photoelectrochemical (PEC) detection is a promising protocol owing to its high sensitivity, low background signal, easy operation and simple equipment. Among various semiconductor materials, hematite (α -Fe₂O₃) has been generally used in PEC application, due to its favorable band-gap (~2.1 eV), wide light harvest range, excellent chemical stability, elemental abundance, and low-cost. Recently, many studies have been reported to improve the sensitivity

of PEC H_2O_2 sensors and verify the reaction mechanism of detection of H_2O_2 with PEC sensors. Even so, owing to its intrinsic properties, $\alpha\text{-Fe}_2\text{O}_3$ based photoelectrodes still have great challenges to achieve high efficiency before practical application. In addition, the photoanodes, which are synthesized on rigid substrates, such as glass-based FTO or ITO are hardly applicable to human-body contact bio-sensor because of its physical property. However, due to the high synthesis temperature of hematite (800 °C), it is difficult to form high-efficiency hematite on polyethylene terephthalate or polyimide substrates, which are conventional flexible substrates. In order to overcome limitations above for practical application, yttria-stabilized zirconia (YSZ) substrate was adopted due to its intrinsic properties, such as superior thermal stability (~1450 °C) and flexibility.

Herein, we successfully synthesized the high-efficiency hematite nanostructure photoanodes on flexible yttria-stabilized zirconia (YSZ) substrate via simple hydrothermal method. For the growth of hematite nanostructure, first of all, platinum/titanium (Pt/Ti) layer was grown on YSZ substrate via electron-beam evaporator. Pt/Ti bottom electrode also performed as a function of growth buffer layer and metal ion doping. By using the novel $\text{Fe}_2\text{O}_3/\text{Pt}/\text{Ti}/\text{YSZ}$ (FPTY) photoanode, state-of-the-art PEC response toward H_2O_2 detection was achieved and also we evaluated the H_2O_2 sensitivity when the FPTY photoanode was bent and it was maintained as it is.

We expect that our study will open the way for the development of flexible H_2O_2 PEC sensor and be applied for the fabrication of next-generation electronic devices through follow-up studies.

NM07.03.15

Application of g- $\text{C}_3\text{N}_4/\text{Sn}_3\text{O}_4$ Heterostructure for Photoelectrochemical H_2 Generation Fernanda d. Romeiro, João A. Perini, [Marcelo O. Orlandi](#) and Maria Valnice B. Zanoni; UNESP, Brazil

The hydrogen gas (H_2) has attracted attention due to its environmentally friendly burn with no emission of greenhouse gases [1]. Among the nanostructured materials studied for this purpose, the n-type Sn_3O_4 has been recently applied for H_2 generation. To avoid rapid rate of charge carrier recombination and improve photoelectrochemical performance in Sn_3O_4 , the construction of heterojunctions can be generally employed to overcome charge recombination at the interfaces of two semiconductors.

Herein, Sn_3O_4 and g- $\text{C}_3\text{N}_4/\text{Sn}_3\text{O}_4$ heterostructures were synthesized via the microwave-assisted hydrothermal method, while g- C_3N_4 was obtained by the heating of melamine. The g- C_3N_4 , Sn_3O_4 and g- $\text{C}_3\text{N}_4/\text{Sn}_3\text{O}_4$ films for the working electrodes were prepared by spin coating. The photoelectrochemical tests for H_2 generation was performed using a solar simulator (300 W Xenon lamp) and a sealed photoelectrochemical reactor containing two compartments and equipped with a quartz window (electrolyte: 0.1 mol L^{-1} Na_2SO_4). The H_2 gas was identified and quantified using gas chromatography with a *thermal conductivity detector*.

The characterization of g- C_3N_4 by X-ray diffraction revealed peaks at $2\theta = 13.1^\circ$ and 27.4° corresponding to (100) and (002) hexagonal structure planes (JCPDS 87-1526), respectively; for the Sn_3O_4 and the g- $\text{C}_3\text{N}_4/\text{Sn}_3\text{O}_4$ materials, the diffraction patterns matched the triclinic structure (JCPDS 16-0737). The FTIR and Raman spectrum of the nanocomposites confirmed the obtaining of g- $\text{C}_3\text{N}_4/\text{Sn}_3\text{O}_4$ heterostructure. SEM and TEM images showed that g- C_3N_4 presented a two-dimensional structure consisting of micrometer-long wrinkled sheets (2D material), while the Sn_3O_4 3D nanomaterial is formed by petals-like morphology with nanometric thickness. In comparison to pure materials, the nanocomposite presented Sn_3O_4 nanopetals distributed over the g- C_3N_4 sheets, suggesting the effective formation of the g- $\text{C}_3\text{N}_4/\text{Sn}_3\text{O}_4$ heterostructure. The Sn_3O_4 presented a $E_{\text{gap}} = 2.9$ eV, while both g- C_3N_4 and g- $\text{C}_3\text{N}_4/\text{Sn}_3\text{O}_4$ possessed $E_{\text{gap}} = 2.7$ eV, indicating that all the photoelectrocatalysts showed promising application in the visible light region.

During photoelectrochemical tests the g- $\text{C}_3\text{N}_4/\text{Sn}_3\text{O}_4$ composite presented the highest photocurrent density of (1.2 $\text{mA}\cdot\text{cm}^{-2}$). Transient photocurrent curves showed that the g- $\text{C}_3\text{N}_4/\text{Sn}_3\text{O}_4$ nanocomposite showed a quick response in the presence of light and back to zero when the light was turned off, indicating that the nanomaterial is sensitive to the UV-vis irradiation and presents faster charge separation [2]. Constant potential electrolysis experiments were performed (at 0.8 V vs Ag/AgCl, under UV-vis irradiation) for all samples and indicated their high stability. Nyquist plots showed that g- $\text{C}_3\text{N}_4/\text{Sn}_3\text{O}_4$ has lower electron transport resistance than the g- C_3N_4 and Sn_3O_4 , indicating that its charge transfer is faster. The cumulative H_2 formation using all electrodes showed a stable production of H_2 for pure g- C_3N_4 and Sn_3O_4 materials within the investigated time period of 3 h, while for the g- $\text{C}_3\text{N}_4/\text{Sn}_3\text{O}_4$ a crescent generation of H_2 was observed until reach the maximum of 0.487 $\text{mmol}\cdot\text{L}^{-1}$. The H_2 production rate was nearly 4.4 and 4.8 times higher than the H_2 production using of g- C_3N_4 and Sn_3O_4 photoanode, respectively. This observation can be explained by the synergistic effect between Sn_3O_4 nanostructures and g- C_3N_4 nanosheets, in which the heterostructure exhibited efficient separation of photoexcited electron-hole pairs, which decreased the recombination rate and therefore promoted higher H_2 generation. Therefore, this study offers a promising strategy to synthesize effective and low cost photocatalyst for energy conversion applications, especially for H_2 generation.

NM07.03.16

Tailoring the Dielectric Contrast of Hierarchically Structured Photoelectrodes via Sol-Gel Synthesis of Ternary Metal Oxides [Joseph J. Muhanga](#) and Robert H. Coridan; University of Arkansas, United States

A common problem in photoelectrochemistry is that attractive thin film semiconductors for use as light absorbing photoelectrodes often have long characteristic absorption length and short minority carrier diffusion length. This is a particularly common combination of properties for chemically synthesized, nanoparticulate films formed via chemical synthesis. Strategies for increasing the incident photon-to-electron conversion efficiency (IPCE) in photoelectrodes often involve the use of multiscale porosity. The optical advantage of hierarchical nanostructure in these electrodes is that it induces light scattering to increase the effective path length in thin film light absorbers. More complex schemes induce modes of resonant light trapping (via photonic crystals, for example) to confine and concentrate incident light to small volumes of the electrode. The transition from a weak scattering structure to a strong one depends on the refractive index contrast between the electrode material and the surrounding electrolyte. The optical properties of these structures are predictable by electromagnetic simulations such as finite element methods. However, the continuously definable parameters in simulations do not directly translate to experimental systems due to the limitations of physically realizable materials. Here, we describe the experimental synthesis of ternary metal oxide composites (Ta-Ti-O, for example) via sol-gel synthesis as an experimental approach to tailor the refractive index contrast in hierarchically structured photonic glass electrodes. The difference in refractive index between TiO_2 ($n = 2.5$) and Ta_2O_5 ($n = 2.1$) or Ga_2O_3 ($n = 1.9$) enables nearly continuous control over the *effective* refractive index in that range. Sol gel infiltration in colloid-templated structure allows this control to be integrated into a three-dimensional electrode structure. We will show how simulation and experimental results can elucidate the connection between the synthesis and optical properties of thin film and three-dimensional structures. These materials can then serve as hierarchically structured transparent conductive oxide current collectors for photoelectrochemical and optoelectronic applications.

NM07.03.17

Machine Learning Methods for the Prediction of Solution Synthesis Parameters Stefan Wuttke¹, Manuel Tsotsalas² and [Pascal Friederich](#)²;

¹BCMaterials, Spain; ²Karlsruhe Institute of Technology, Germany

Despite rapid progress in predicting materials properties, the potential of using machine learning (ML) methods to predict optimal synthesis parameters is still untapped. In Luo et al. [1], we demonstrate how ML can be used for rationalization and acceleration of the discovery process of metal-organic frameworks (MOFs) by directly predicting the synthesis conditions of a MOF based on its crystal structure. Our approach is based on: i) establishing the first MOF synthesis database via automatic extraction of synthesis parameters from the literature, ii) training and optimizing ML models by employing the MOF database, and iii) predicting the synthesis conditions for new MOF structures. The ML models, even at an initial stage, exhibit a good prediction

performance, outperforming human expert predictions, obtained through a synthesis survey. The automated synthesis prediction is available via a web tool on <https://mof-synthesis.aimat.science>. The methods presented in this work are not application-specific, and thus can be transferred to other materials classes.

[1] Luo, Y., Bag, S., Zaremba, O., Cierpka, A., Andreo, J., Wuttke, S., Friederich, P. and Tsotsalas, M., 2022. MOF Synthesis Prediction Enabled by Automatic Data Mining and Machine Learning. *Angewandte Chemie International Edition*, 61(19), p.e202200242.

NM07.03.18

A Strategy to Enhance Humidity Robustness of P-Type Sensors for Breath Acetone Quantification [Dina N. Oosthuizen](#)¹, Ines C. Weber^{1,2} and Sotiris E. Pratsinis¹; ¹ETH Zurich, Switzerland; ²University Hospital Zurich, Switzerland

The compounds present in human breath can be exploited to give physiological information to indicate the early-stage development of diseases and assist in guiding their therapy [1]. Specifically, breath acetone is a promising biomarker for non-invasive fat metabolism monitoring [2]. Portable, low-cost, low-power gas sensors for non-invasive medical diagnostics [3] should have a low operating temperature (i.e., power consumption). However, only a few low-temperature semiconducting metal oxide (SMOx) sensors (Pt/Sb₂O₃-Fe₂O₃ [4] and BaSnO₃ [5]) so far, as most sensors have insufficient robustness to humidity (i.e., poor sensor stability), and, to our knowledge, none of these sensors could quantify acetone concentrations in breath.

Heterostructure materials have been proposed to effectively eliminate the humidity cross-sensitivity of SMOx sensors, specifically CeO₂ and either In₂O₃ [6] or SnO₂ [7], for the humidity-robust detection of acetone and trimethylamine. Flame spray pyrolysis (FSP) technology enables the production of sensors with unprecedented performance [8], with control over the composition and morphology of the sensing materials.

Here, we introduce a low-power sensor operated at 150 °C that detects acetone with high sensitivity (i.e., down to 50 ppb) at 90% relative humidity (RH). It consists of a Ce-doped CuO nanoparticle sensing film deposited directly by single-step flame spray pyrolysis (FSP), as determined by XRD and XPS analysis. Most remarkably, this sensor features excellent selectivity towards key inorganic breath interferents in gas mixtures even at orders of magnitude higher concentrations (i.e., up to 20 and 25 ppm of H₂ and CO). In addition, it showed increased humidity robustness to changes in humidity between 10 and 90% RH, which is likely due to the presence of CeO₂ nanoclusters [6]. Finally, this sensor accurately detected acetone concentrations in the exhaled breath of 16 volunteers ($r = 0.95$, bias and precision of 90 and 457 ppb) in a standardized setting (i.e., low breath ethanol concentrations (< 400 ppb)), despite the presence of various other breath components that typically interfere with acetone detection (e.g., isoprene). In addition, this sensor can detect even other organic volatiles such as ethanol, which may be interesting for other applications such as the automotive fuel industry [9]. In the case of breath acetone detection, where ethanol interference in the background is undesired, this can be circumvented by adding a filter upstream of the sensor [10]. As a result, this sensor is most appealing for integration into low-power and mobile health devices for continuous metabolic health monitoring.

[1] Musa-Veloso, K. et al. (2002) *Am. J. Clin. Nutr.*, **76**, 65. DOI: 10.1093/ajcn/76.1.65.

[2] Anderson, J.C. (2015) *Obesity*, **23**, 2327. DOI: 10.1002/oby.21242.

[3] Güntner, A.T. et al. (2019) *ACS Sensors*, **4**, 268–280. DOI: 10.1021/acssensors.8b00937.

[4] Sen, S. et al. (2021) *Microchem. J.*, **165**, 106111. DOI: <https://doi.org/10.1016/j.microc.2021.106111>.

[5] Verma, A. et al. (2022) *Sensors Actuators B Chem.*, **361**, 131708. DOI: <https://doi.org/10.1016/j.snb.2022.131708>.

[6] Yoon, J.-W. et al. (2016) *Small*, **12**, 4229. DOI: 10.1002/sml.201601507.

[7] Zhu, X. et al. (2022) *ACS Appl. Mater. Interfaces*, **14**, 25680–25692. DOI: 10.1021/acsmi.2c03575.

[8] Righettoni, M. et al. (2015) *Mater. Today*, **18**, 163. DOI: 10.1016/j.mattod.2014.08.017.

[9] Hansen, A.C. et al. (2005) *Bioresour. Technol.*, **96**, 277–285. DOI: <https://doi.org/10.1016/j.biortech.2004.04.007>.

[10] Weber, I.C. et al. (2022) *Sensors Actuators B Chem.*, **356**, 131346. DOI: 10.1016/j.snb.2021.131346.

NM07.03.20

Rational Discovery of Complex Chalcogenides Using Mixed Fluxes [Xiuquan Zhou](#)¹, Wenqian Xu¹, Maria K. Chan¹, Duck Young Chung¹ and Mercouri G. Kanatzidis^{1,2}; ¹Argonne National Laboratory, United States; ²Northwestern University, United States

Advancements in many modern technologies rely on the continuous discovery of novel materials. However, the design of synthesis routes leading to new and targeted solid-state materials requires understanding of reactivity patterns. The extent of control and predictability of synthetic outcomes for extended solids composed of more than three elements compared to that for many molecular compounds is low. Consequently, exploratory synthesis is an invaluable tool for materials discovery—as the pioneer in this field, John Corbett, described “It is always difficult to predict the unimaginable”. Due to the knowledge accumulating from exploratory synthesis and the progress made during the past decades, predictive synthesis, including identifying composition and structure that confer the desired properties and synthesizing the desired targets, may soon be within reach. However, this requires the ability to understand and predict viable reaction pathways. Therefore, novel synthetic strategies to reveal effective reaction pathways that can add a more “rational” component to exploratory synthesis are required to accelerate materials discovery and achieve the ultimate goal—synthesizable materials by design. Advances in synthesis science are necessary to increase efficiency and accelerate materials discovery. We present a highly effective methodology for the rational discovery of materials using high-temperature solutions or fluxes having tunable solubility. This methodology facilitates product selection by projecting the free energy landscape into real synthetic variables: temperature and flux ratio. We demonstrate the effectiveness of this technique by synthesizing the chalcogenide system of $A(\text{Ba})\text{-Cu-Q}(\text{O})$ ($Q = \text{S or Se}$, $A = \text{Na, K, or Rb}$) using mixed AOH/AX ($A = \text{Li, Na, K or Rb}$; $X = \text{Cl or I}$) fluxes. We present 30 novel compounds, including more than 10 unique structural types, by systematically varying the temperature and flux ratios without requiring changing the proportions of starting materials. In addition, we found that the structural dimensionality of the compounds decreases with increasing reactant solubility and temperature. Our methodology serves as an effective generic strategy for the rational discovery of inorganic solids.

<!--[endif]-->

NM07.03.21

Development of Flexible Super Hybrid Electrode for Auto-Defogging System for Windshields of Electric Cars [Woo-Seok Cheong](#)¹, Young-Hoi Kim¹ and Young-Shin Kim²; ¹ETRI, Korea (the Republic of); ²Daeki hitec, Korea (the Republic of)

Transparent heaters have been developed by using various types of transparent electrodes such as indium-tin oxide (ITO), carbon nano tube (CNT), graphene, metal nanowire, metal grid (mesh), including hybrid transparent electrode. However, windshield transparent heaters for defogging can't be realized by those transparent electrodes, because of high sheet resistance. Recently, we designed ‘super hybrid electrode (SHE)’, which could be made by combining metal grids with oxide/metal/oxide electrode based on a newly developed electroplating method [1]. In this work, we successfully developed ‘flexible-super hybrid electrode’ (F-SHE), using flexible substrate, high transparent photo-resist (PR) for realizing flexible transparent heaters. The highly transparent PR surrounding the metal grids could be bent due to the decrease of the mechanical stress, sustaining the good properties of the sheet resistance

and the transmittance. F-SHE film showed the extremely low sheet resistance ($0.2 \sim 0.6 \Omega$), high transmittance (over 80% at 550nm), and small critical bending radius ($\sim 3\text{mm}$), which can be applied for the auto-defogging system of automobile windshield heaters.

Ref[1] W.S.Cheong, et al, "High-performance transparent electrodes for automobile windshield heaters prepared by combining metal grids and oxide/metal/oxide transparent electrodes", *Adv. Mater. Technol.* 2019, 4, 1800550.

This work was supported by the R&D project of MOTIE/KEIT. [20019194, Development of auto defogging system for electric cars].

NM07.03.22

Flame-Made Nanoparticle Sensing Film Coupled with Catalytic Filter Detects Carcinogenic Benzene in Indoor Air Ines Weber and Sotiris E. Pratsinis; ETH Zurich, Switzerland

Metal oxide gas sensors comprising heterostructured sensing layers are most promising for detecting gases down to parts per billion (ppb).¹ However, these sensors typically lack sufficient selectivity in complex gas mixtures. To tackle this challenge, flame-made catalytic filters may be used upstream of the sensors.² These filters convert interfering species (e.g., ethanol³) to inert CO₂, while letting target analytes pass for detection by the sensor. Carefully tailoring the surface properties of such catalytic filters and nanoporous sensing layers allows to optimize their selectivity, as was demonstrated previously for the detection of acetone⁴ in breath during exercise⁵ and in diabetes⁶.

Nowadays, selective sensing systems are urgently needed to monitor indoor and environmental air and warn us from toxic pollutants. For example, benzene is a highly toxic and carcinogenic air pollutant that causes leukemia⁷. More than 1 million workers are exposed routinely to carcinogenic benzene contained in various consumer products (e.g., gasoline, rubbers, dyes) and released from combustion of organics (e.g., tobacco). Hence, it requires real-time monitoring to mitigate health risks.

Here, we introduce a compact WO₃ nano-catalyst filter made by flame aerosol technology and couple it to a similarly made Pd/SnO₂ sensing layer⁸. Both sensor and filter are integrated into a handheld device that is operated through a raspberry pi microcontroller, while a pump at the sensor outlet provides a continuous flow. Thereby, the catalytic filter effectively removes all interferents (including alcohols, ketones, inorganics, and aromatics) while the benzene passes and is detected by the downstream sensor. Most importantly, when tested on benzene-spiked indoor air this detector accurately ($R^2 = 0.98$) tracks its concentrations even below legal limits (i.e., 50 ppb) and in the presence of orders of magnitude higher toluene and *m*-xylene concentrations ($R^2 = 0.94$), in good agreement with mass spectrometry. Hence, this detector is promising for on-site and real-time monitoring to prevent harmful exposure.

References

1. Güntner, A. T., Abegg, A., Königstein, K., Gerber, P. A., Schmidt-Trucksäss, A., Pratsinis, S. E., Breath Sensors for Health Monitoring. *ACS Sens* 4, 268–280 (2019).
2. Weber, I. C. & Güntner, A. T. Catalytic filters for metal oxide gas sensors. *Sens Actuators B Chem* 356, 131346 (2022).
3. Güntner, A. T., Weber, I. C. & Pratsinis, S. E. Catalytic filter for continuous and selective ethanol removal prior to gas sensing. *ACS Sens* 5, 1058–1067 (2020).
4. Weber, I. C., Braun, H. P., Krumeich, F., Güntner, A. T. & Pratsinis, S. E. Superior Acetone Selectivity in Gas Mixtures by Catalyst Filtered Chemoresistive Sensors. *Advanced Science* 7, 2001503 (2020).
5. Weber, I. C., Derron, N., Königstein K., Gerber P. A., Güntner A. T., Sotiris S. E., Monitoring Lipolysis by Sensing Breath Acetone down to ppb. *Small Sci.* 1, 2100004 (2021).
6. Güntner, A. T., Weber, I. C., Schon, S., Pratsinis, S. E. & Gerber, P. A. Monitoring rapid metabolic changes in health and type-1 diabetes with breath acetone sensors. *Sens. Actuator B-Chem*. doi: 10.1016/j.snb.2022.132182 (2022).
7. Fiebelkorn, S. & Meredith, C. Estimation of the Leukemia Risk in Human Populations Exposed to Benzene from Tobacco Smoke Using Epidemiological Data. *Risk Analysis* 38, 1490–1501 (2018).
8. Weber, I. C., Rüedi, P., Sot, P., Güntner, A. T. & Pratsinis, S. E. Handheld device for selective benzene sensing over toluene and xylene. *Advanced Science* 9, 2103853 (2022).

NM07.03.23

Anisotropic van der Waals Epitaxy and Sliding of CsPbBr₃ Microplatelets on ReSe₂ Noya R. Itzhak, Ifat Kaplan-Ashiri, Hagai Cohen, Irit Rosenhek Goldian, Olga Brontvein, Katya Rechav and Ernesto Joselevich; Weizmann Institute of Science, Israel

The growth of highly crystalline semiconductor nanostructures with low defect concentration is essential for realizing their optoelectronic properties and for their efficient integration into functional nanodevices. Our group has shown that nanowires can grow on a single crystal or amorphous substrates using covalent epitaxy and graphoepitaxy to generate well-aligned and guided nanowires with controlled crystallographic orientation. However, covalent epitaxial relations often induce strain and stress in the nanocrystals, leading to dislocations and other defects, which affect the physical properties of semiconductor nanostructures. Substituting covalent substrates with 2D van der Waals (vdW) layered materials could relieve stress and strain issues, as weaker interactions are formed between the top layer of the vdW material and the formed nanostructure. Therefore, we suggest extending the guided growth approach by using vdW epitaxy on 2D materials. Here we present the vapor-solid growth of micro- and nano-platelets of well-ordered cubic CsPbBr₃ on 2D layered triclinic ReSe₂ substrate. X-ray photoelectron spectroscopy (XPS) and cathodoluminescence (CL) measurements revealed type I band alignment, with energy transfer from the CsPbBr₃ platelets to the ReSe₂ substrate. Such heterostructure could be integrated into an enhanced photodetector compared to ReSe₂ based photodetector. To further investigate the vdW epitaxial nature of the heterostructure, we characterized the heterostructure interface by applying lateral force and sliding the CsPbBr₃ platelets on the ReSe₂ using atomic force microscopy (AFM). Our results indicate that some sliding directions are preferable to others, which could be attributed to the in-plane anisotropy of the ReSe₂ surface. These results open a route for the ordered design of heterostructure devices with interesting energy transfer mechanisms and improved optical and electrical properties owing to the lower miss-match stresses induced by vdW vs. covalent epitaxy.

NM07.03.24

Unveiling Ultrafast Exciton Polariton Dynamics in Large-Area van der Waals Superlattices Tzu-Yu Peng^{1,2}, Jason Lynch³, Jing-Wei Yang^{1,2}, Yen-Yu Wang^{1,2}, Xing-Hao Lee^{1,2}, Deep M. Jariwala³ and Yu-Jung Lu^{1,2}; ¹Department of Physics, National Taiwan University, Taiwan; ²Research Center for Applied Sciences, Academia Sinica, Taiwan; ³Electrical and Systems Engineering, University of Pennsylvania, United States

The discovery and large-area synthesis of two-dimensional (2D) materials with controlled thickness, composition, and crystal quality open up a much wider range of possibilities for the hetero-integration of novel and multi-functional photonic platforms. In this work, we develop 2D chalcogenide materials, assemble them into superlattices with oxide materials, and investigate the strong light-matter interaction in this novel materials platform. The large-area superlattices were grown via artificial layering of the Al₂O₃ and monolayer WS₂.¹ The monolayer WS₂ can keep the direct bandgap properties to serve as an efficient emitter at a center wavelength of 611 nm. We performed the angle-dependent transient absorption spectroscopy (TAS) measurement to determine the carrier dynamics in the WS₂/Al₂O₃ superlattices (N= 5) coupled with a waveguide cavity. By using the femtosecond time-resolved pump-

probe TAS, we obtain the strong light-matter interaction induced upper (568 nm) and lower (629 nm) exciton-polaritons splitting in the designed $\text{WS}_2/\text{Al}_2\text{O}_3$ superlattices at a large incident angle of 80 degrees under TE polarized light. In addition, we observed ultrafast lifetime of upper exciton-polaritons reduced from 1 picosecond to 0.6 picosecond with an increase probe angle. Moreover, we found the quasiparticle competition behavior between the upper and lower exciton-polaritons, and there has a significant nonlinear effect can be observed. In the end, we will discuss the working mechanism of the carrier dynamics in large-area superlattices coupled with a waveguide cavity and the outlook for van der Waals superlattices.

1. Kumar, P. *et al.* Light-matter coupling in large-area van der Waals superlattices. *Nature Nanotechnology* **17**, 182-189, doi:10.1038/s41565-021-01023-x (2022).

NM07.03.25

Optical and Magneto-optical Effects of Epitaxial Grown Ce:YIG/YAG [Yuki Yoshihara](#)^{1,2}, Pang Boey Lim², Mitsuteru Inoue¹, Kazushi Ishiyama¹ and Taichi Goto¹; ¹Tohoku University, Japan; ²Toyohashi University of Technology, Japan

Magneto-optical effects can be applied to many dynamic optical/photonic applications, e.g., spatial light modulator [1] and optical Q-switch [2]. In these devices, the magneto-optical and light-emitting parts are usually separated. For instance, the magnetic film is separately placed in front of/behind the light sources. In these optical systems, all optical elements need to be aligned carefully to minimize the optical loss, preventing from miniaturization of the device and increasing the fabrication cost. Hence, integrating all-optical components into one chip provides a large advantage for developing optical applications. To demonstrate such an integration, we fabricated the cerium-substituted yttrium iron garnet (Ce:YIG) film on the yttrium aluminum garnet (YAG) substrate. Ce:YIG is widely known as a magneto-optical film showing a large Faraday rotation at the near-infrared wavelengths [3,4]. YAG doped with Nd is widely used as solid-state laser material. The Ce:YIG film was hetero epitaxially grown on YAG substrate using radio frequency ion beam sputtering. The Ce:YIG films were deposited onto double-side polished and (111) oriented YAG substrate. The temperature of the substrate was held at 850°C using the heater. The substrate size is 10 mm by 10 mm. The thickness of the grown film was about 2 micrometers.

The x-ray diffraction peak s at (444) and (888) were observed, and other peaks were not, showing a single crystalline garnet phase. The reciprocal space map of the Ce:YIG/YAG sample showed a relaxed crystalline state. The magnetic properties measured by vibrating sample magnetometer (VSM) showed a magnetization of 91 emu/cc. The Faraday rotation loop was measured using a magneto-optical measurement system at a wavelength of 1064 nm. The Faraday rotation angle of $-0.94^\circ/\mu\text{m}$ was obtained. The remanent and coercivity of Faraday rotation angle were $0.09^\circ/\mu\text{m}$ and 125 Oe. Therefore, these results showed the first integration of Ce:YIG on YAG substrate as an important milestone in developing magneto-optical elements combined with a light emitting system.

[1] H. Takagi, K. Nakamura, T. Goto, P. B. Lim, and M. Inoue, "Magneto-optic spatial light modulator with submicron-size magnetic pixels for wide-viewing-angle holographic displays," *Optics Letters*, **39**, 3344-3347 (2014).

[2] T. Goto, R. Morimoto, J. W. Pritchard, M. Mina, H. Takagi, Y. Nakamura, P. B. Lim, T. Taira, and M. Inoue, "Magneto-optical Q-switching using magnetic garnet film with micromagnetic domains," *Optics Express*, **24**, 17635-17643 (2016).

[3] Y. Yoshihara, T. Sugita, P. B. Lim, Y. Tamba, H. Inoue, K. Ishiyama, M. Inoue, C. A. Ross, and T. Goto, "Thickness-dependent magneto-optical properties of ion beam sputtered polycrystalline $\text{Ce}_1\text{Y}_2\text{Fe}_5\text{O}_{12}$ films," *Optical Materials*, (in press).

[4] T. Goto, M.C. Onbasli, D.H. Kim, V. Singh, M. Inoue, L.C. Kimerling, C.A. Ross, "A nonreciprocal racetrack resonator based on vacuum-annealed magneto-optical cerium-substituted yttrium iron garnet," *Optics Express*, **22**, 19047-19054, (2014).

NM07.03.26

Wafer-Scale Growth of Amorphous Boron Nitride Thin Films [Hyeongjoon Kim](#), Minsu Kim, Kyung Yeol Ma and Hyeon Suk Shin; UNIST, Korea (the Republic of)

Amorphous materials have been widely studied in many fields. Among them, amorphous boron nitride (aBN) has recently attracted attention because of its excellent electrical (dielectric constant of 1.89, high breakdown field of 7.3 MV/cm) and mechanical property (high hardness > 11 GPa)[1]. In particular, its ultralow dielectric constant showed the potential for use as an interlayer dielectric (ILD in integrated circuits). However, a limitation in aBN study is that it is difficult to grow pure aBN thin films. In this presentation, we demonstrate the growth of 6-inch wafer-scale aBN thin films by plasma enhanced chemical vapor deposition (PECVD) and their uniformity of thickness and dielectric constant. We found that the formation of hBN nano-crystallites in the aBN thin films results in the increase of dielectric constant as the thickness of the aBN thin films increases. Thus, we show the relationship of three parameters: the thickness of the aBN thin film, the amount of hBN nano-crystallites, and dielectric constant of the aBN thin film. In addition, we investigated the thermal stability and the diffusion barrier performance of the aBN thin films to see if they can be used as a capping layer or ILD in back end-of-line (BEOL). Lastly, we show the control of the density of the aBN thin films by changing the experimental parameters such as plasma power and flow rate of borazine as a precursor because their density is related to the mechanical property. These results pave the way for the practical application of aBN as an ultra-low dielectric material for electronic devices.

Refereces

[1] Hong, S. *et al.*, *Nature*, 2020, 582, 511.

NM07.03.27

Control of Degree of Structural Disorder in Amorphous Boron Nitride Film [Minsu Kim](#), Hyeongjoon Kim, Kyung Yeol Ma and Hyeon Suk Shin; Ulsan National Institute of Science and Technology, Korea (the Republic of)

As the size of the device decreases, the 'resistance and capacitance delay (RC delay)' determines the operating performance of the chip. In order to reduce the RC delay, it is necessary to reduce the dielectric constant of the material deposited between the metal electrodes in the downstream process of the integrated circuit. Existing low- κ Si-based materials have been studied to increase porosity so far. As a result, the dielectric constant is close to that of air, but its commercial use is limited due to the weakening of mechanical properties due to the high porosity.

Recently, amorphous boron nitride (aBN) has been considered as a next-generation ultra-low- κ material [1]. In this presentation, we demonstrate the change in dielectric constant of aBN according to its degree of structural disorder. The dielectric constant of aBN increases as boron and nitrogen atoms have an ordered structure which appears with the formation of hBN nano-crystallites in the aBN thin film. Thus, we show changes in the degree of structural disorder and the dielectric constant of the aBN thin film when carbon element is doped into it.

Tuesday Morning, November 29, 2022
Hynes, Level 2, Room 203

8:15 AM *NM07.04.01

Straining van der Waals Sheets via the Self-Rolled-up Membrane Platform Xiuling Li¹, Apratim Khandelwal² and Paul Froeter²; ¹The University of Texas at Austin, United States; ²University of Illinois at Urbana-Champaign, United States

It is well known strain can alter the bandstructures of semiconductors. Here we use the self-rolled-up membrane (S-RuM) platform for strain engineering and integration of 2D van der Waals sheets with stressed dielectric thin films to tailor the transport and optical properties.

8:45 AM NM07.04.02

Defect Seeded Remote Epitaxy of GaAs Films on Graphene Muhammad Zulqurnain, Oliver J Burton, Lucy E Goff, Mohamed Al-Hada, Stephan Hofmann and Louise C Hirst; University of Cambridge, United Kingdom

Remote epitaxy is an emerging semiconductor film deposition technique, first reported in 2017 (Kim, Nature) which offers low defect growth of single crystal films which can be readily exfoliated from a growth template using a monolayer graphene interface. This approach enables film integration with dissimilar materials for novel device architectures, along with reuse of growth substrates for reduced cost, addressing longstanding challenges for the technologically important III-V materials family. CVD growth of graphene and wet transfer to a III-V substrate with a polymer handle is a potentially scalable and low cost approach to producing the required growth surface for remote epitaxy of these materials. Previous authors have compared remote epitaxy of GaAs using wet and dry transfer techniques, concluding that the formation of an interface native oxide during wet transfer prohibited single crystal formation via this technique (Kim, ACS Nano, 2021).

In this work, we have shown that single crystal GaAs films can be grown on a wet transferred CVD graphene monolayer, with an underlying GaAs substrate, through the controlled introduction of nanoscale defects with an argon (Ar) ion beam. Prior to pinhole introduction the presence of an oxide layer at the graphene/substrate interface is confirmed by XPS. Following Ar ion-beam exposure the pinhole defects are identified by Raman spectroscopy with the onset of the D peak at 1350 cm⁻¹. A clear improvement in the crystalline quality of the epitaxial layer is observed in regions exposed to the Ar-ion beam. Single crystal GaAs films are formed in monolayer regions of the graphene exposed to Ar, confirmed by EBSD. The quality of the film is significantly improved in Ar-ion beam exposed regions with reduced roughness characterised by AFM, also reduced crystal misorientation and As antisite signatures are present in the Raman spectra of the GaAs film with increasing Ar-ion beam exposure time. A hybrid mechanism of seeded lateral overgrowth propagated by remote epitaxy on monolayer graphene is indicated, determined from the absence of wetting on multi-layer graphene, which screens the underlying crystal template. Furthermore, film exfoliation, as required for integration with off-wafer device architectures and substrate reuse, is still possible even with the presence of nanoscale defects in the graphene interface monolayer. The back side of the exfoliated epilayer revealed the occurrence of GaAs nucleation through defects in graphene in Ar-ion beam treated regions, confirmed by SEM showing equal spread of dark spots in monolayer graphene regions and further supported by mirrored features in SEM of the growth substrate after release of the GaAs film. Moreover, Raman spectra show that after film exfoliation the graphene is still attached to the substrate, and ready for subsequent growth without additional ion beam exposure.

The approach demonstrated here, circumvents the issue of additional screening from the interface native oxide formed under wet transferred CVD graphene, to allow remote epitaxial growth of GaAs using lower cost and scalable graphene process methods and therefore offers an alternative approach for the further development of remote epitaxy.

Kim et al. Nature 544.7650 (2017): 340-343, DOI: 10.1038/nature22053

Kim et al. ACS nano 15.6 (2021): 10587-10596, DOI: 10.1021/acsnano.1c03296

9:00 AM NM07.04.03

Remote Epitaxy for Freestanding GaN Membrane on Wafer-Scale 2D Materials Bo-In Park, Jekyung Kim, Yunpeng Liu, Hyunseok Kim and Jeehwan Kim; Massachusetts Institute of Technology, United States

Along with the rapid development of industries including communication, military, aviation, automobile, and high electric power, the demand for semiconductor technology is skyrocketing. In particular, GaN and SiC-based compound semiconductors for cutting edge optical and power devices are receiving highlights as the next-generation semiconductors that can change the world. The compound semiconductors are already being actively applied in the industries.

The principle of "Remote epitaxy" technology has been recently discovered. Researchers in the various fields relevant to epitaxy have begun to pay attention to the new scientific discoveries. Remote epitaxy, developed for the epitaxy of high-quality compound semiconductor materials, is realized by the unique surface and physical characteristics of several two-dimensional (2D) materials. Remote epitaxy is different from the existing epitaxy technology in way that it can produce freestanding membranes due to the easy separation and transfer from the substrate. We have demonstrated the feasibility of this technology over the past several years as well as developed scientific knowledge on the fabrication of various high-quality compound semiconductor materials.

In this study, remote epitaxy for the fabrication of freestanding, high-quality single crystalline GaN membrane is introduced. The manufacturing process of optimized 2D materials from various epitaxy processes is introduced and their characteristics are analyzed in detail. The development of defect-free 2D materials by remote epitaxy enabled the fabrication of high-quality single crystalline membrane at wafer scale.

9:15 AM NM07.04.04

Vapor-Liquid-Solid Growth of One-Dimensional van der Waals Nanowires and Their Heterostructures Thang Phan^{1,2}, Kate Reidy¹, Joachim D. Thomsen¹, Baoming Wang¹, Nishant Deshmukh³, Michael A. Filler³ and Frances M. Ross¹; ¹Massachusetts Institute of Technology, United States; ²Northwestern University, United States; ³Georgia Institute of Technology, United States

Transition metal trichalcogenides (TMTs) are one-dimensional (1D) layered materials containing trigonal prismatic chains of metals and chalcogens bonded via weak van der Waals (vdW) force. The materials host intriguing correlated physics in the bulk, such as charge density waves and superconductivity. However nanostructured forms of TMTs have been rarely explored due to the difficulty in nanomaterial synthesis and assembly. Niobium trisulfide (NbS₃) is one of the least studied members in the family of TMTs, in part because of obstacles in synthesizing the material with a pure phase and controlled composition.

Here we present a vapor-liquid-solid (VLS) growth of NbS₃ nanowires on several bulk and 2D vdW substrates, including graphene and hexagonal boron nitride. The growth employs an alloy of a metal (gold, Au) and an alkali metal halide (sodium chloride, NaCl) as a VLS catalyst. The materials show several distinct 1D morphologies, specifically wires, ribbons and walls; and two growth orientations, [010] and [100], in which the chain direction is parallel or perpendicular to the nanowire growth direction, respectively. We discuss the details of the growth mechanism based on the relationships we measure between dimensions and morphologies of NbS₃ and the catalyst volume, the growth time, and the growth substrate. We also compare the VLS

growth with uncatalyzed growth (e.g., vapor-solid) to explore the role of several synthesis parameters. Last but not least, we extend the VLS growth method to synthesize other TMTs, namely NbSe₃ and TiS₃. Our study introduces a new opportunity to expand the library of vdW materials towards emerging 1D materials and heterostructures.

9:30 AM NM07.04.05

MOCVD Process Development for Direct Synthesis of 2D-2D Heterostructures Songyao Tang¹, Annika Grundmann¹, Hleb Fiazdushkin¹, Amir Ghiami¹, Michael Heuken^{1,2}, Andrei Vescan¹ and Holger Kalisch¹; ¹RWTH Aachen University, Germany; ²AIXTRON SE, Germany

Favorable properties of 2D materials are recommending them as promising building blocks for future electronic devices. Recently, a variety of novel all-2D vertically-integrated devices have been demonstrated with superior performance. However, such delicate 2D vertical integration is commonly prepared through layer-by-layer stacking methods, the efficiency, reproducibility and scalability of which are severely hampered by the manual transfer and stacking procedures. On the other hand, metal-organic chemical vapor deposition (MOCVD) has been widely studied as a scalable and controllable technique to fabricate individual 2D layers, which also shows the potential of combining multiple processes to realize layer-by-layer deposition. Nevertheless, just a few publications regarding the successive growth of different 2D materials via MOCVD have been reported.

In this work, we report on the latest progress using MOCVD for the direct synthesis of 2D-2D heterostructures of transition metal dichalcogenide (TMDC) monolayers. A commercial AIXTRON CCS reactor with advanced ARGUS and LayTec in-situ monitoring systems is employed as the experimental platform. Tungsten/molybdenum hexacarbonyl (WCO/MCO), di-tert-butyl sulfide (DTBS) and di-iso-propyl selenide (DiPSe) were used as precursors with H₂ as carrier gas. 2" c-plane sapphire with a nominal 0.2° off-cut towards m-plane is chosen as substrate. A 30 min H₂ sapphire desorption (150 hPa, 1050 °C on wafer surface) was carried out before deposition. Scanning electron microscopy (SEM), atomic force microscopy (AFM), Raman as well as UV-vis and photoluminescence (PL) spectroscopy were used for characterization.

In order to obtain a clean and planar interface between two distinct layers, the lateral growth of the first underneath layer needs to be carefully controlled, which means that the monolayer should coalesce with minimal parasitic bilayer coverage formed. Previously, a two-stage migration-enhanced MOCVD process has been proposed by our group to serve this purpose in the case of WS₂ [1], with stage I being an optimized lower-temperature nucleation step. By ramping down the injection flux of WCO by -75% during the higher-temperature lateral-growth stage II in 144 min, the bilayer coverage of WS₂ is suppressed to <20% while the monolayer coverage exceeds 99%. Similar results could be achieved in the synthesis of WSe₂ monolayers. Although the nucleation density of WSe₂ (after stage I) is much lower than that of WS₂, fully-coalesced WSe₂ monolayers can still be achieved with <20% bilayer coverage via WCO ramp-down in 90 min. These two disparate processes are merged into one successive process to fabricate WS₂/WSe₂ heterostructures. The in-situ transient-reflectance data provide a real-time insight into the growth process. The detailed growth mechanism can be analyzed by comparing nanoscale morphology of (hetero)structures, revealing the difference between sapphire and the as-deposited WS₂ monolayer as the growth template for WSe₂. The distinct excitonic absorption peaks of WS₂ (near 600 nm) and WSe₂ (near 750 nm) can be read out from the absorbance spectra of heterostructures, which matches well with the PL emission spectra. The A peak of WS₂ is found to be red-shifted as WSe₂ gradually coalesces on top of WS₂. The formation of WS₂/WSe₂ heterostructures can also find support in Raman spectra. Further studies are ongoing to examine the quality of such layer-by-layer grown 2D-2D heterostructures.

In conclusion, based on two-stage migration-enhanced MOCVD processes, the direct synthesis of 2D-2D heterostructures can be realized in one MOCVD process without growth interruption. This work tends to draw more attention to the research field of direct synthesis of various 2D heterostructures as well as scalable fabrication towards all-2D devices.

[1] S. Tang *et al.*, Migration-Enhanced MOCVD of Fully-Coalesced WS₂ Monolayers, MRS Spring Meeting 2022, 8-13 May (manuscript in preparation)

9:45 AM BREAK

10:15 AM *NM07.04.06

Step-Edge Nucleation and Control of Domain Orientation in TMD Epitaxy on Sapphire Haoyue Zhu, Tanushree Choudhury, Nadire Nayir, Adri C.T. van Duin and Joan M. Redwing; The Pennsylvania State University, United States

Wafer-scale synthesis of semiconducting transition metal dichalcogenide (TMDs) monolayers is of significant interest for device applications to circumvent size limitations associated with the use of exfoliated flakes. Promising results have been demonstrated for epitaxial films deposited by vapor phase techniques such as CVD and MOCVD. However, the three-fold symmetry of TMDs such as MoS₂ and WSe₂, results in two energetically equivalent domain alignments, often referred to as 0° and 60° domains, when grown on flat high symmetry substrates such as c-plane sapphire and graphene. The oppositely oriented domains give rise to inversion domain boundaries (IDBs) upon coalescence which exhibit a metallic character and are generally undesirable. In this study, we demonstrate the epitaxial growth of unidirectional TMD monolayers on 2" diameter c-plane sapphire substrates with a significantly reduced density of inversion domains. Steps on the sapphire surface are shown to play a key role in TMD nucleation and impart a preferred orientation to the domains depending on the step edge structure and chemistry.

Metalorganic chemical vapor deposition (MOCVD) was used for the epitaxial growth of WSe₂ monolayers on c-plane sapphire in a cold-wall horizontal quartz-tube reactor. The as-received sapphire substrates, which are miscut ~0.2° toward the m-axis, consist of steps with sub-1 nm step height separated by 50-70 nm wide terraces. A three-step nucleation-ripening-lateral growth process, carried out at temperatures ranging from 850°C to 1000°C, was used to achieve epitaxial films using W(CO)₆ and H₂Se as precursors in a H₂ carrier gas. Density functional theory calculations demonstrate that the extent of Se passivation of the sapphire surface and the presence of oxygen remnants near the step edge are critical factors in determining the location of TMD nucleation on the step edge and the subsequent domain orientation relative to the underlying sapphire. Continued lateral growth for times ranging from 10-30 minutes results in fully coalesced TMD monolayers that are epitaxially oriented on the sapphire, as assessed by in-plane x-ray diffraction, with a reduced density of inversion domain boundaries (<15% areal coverage). The results demonstrate the important role of step structure and chemistry in nucleation and epitaxial growth of TMD monolayers.

10:45 AM NM07.04.07

Chemical Synthesis of Metal-Capped Semiconductor Nanowires Bo Shen, Liliang Huang and Chad Mirkin; Northwestern University, United States

Semiconductor nanowires (NWs) capped with metal nanoparticles (NPs) show multifunctional and synergistic properties, which are important for a diverse set of applications including catalysis, photonics, and electronics. Conventional colloidal synthesis for this class of hybrid structures requires complex and sequential seeded growth methods, and processes for preparing such wires are not universal. In this work, we present a new and general method for synthesizing metal-semiconductor nanohybrids based on particle catalysts prepared by scanning probe block copolymer lithography and chemical vapor deposition. By using metallic heterodimer NPs as catalysts for NW growth, semiconductor NWs capped with metallic particles (Au, Ag, Co, Ni) are formed. Importantly, these findings show that the growth processes for NWs on NPs are regioselective and controlled by the chemical composition of the metallic heterodimer. Studies show that the structures of multimetal-capped NWs are thermodynamically stable, and Density functional theory (DFT) simulations confirm that their spatial distributions are the most energetically favorable structures. Taken together, three different NW growth modes are postulated, including one without precedent: growth on a single metal domain, insertion between two metal domains, and growth at the interface of two metal domains. Consequently, this work provides a fundamental and general guide for the controllable synthesis of semiconductor NWs using

heterostructure catalysts, allowing one to make metal-semiconductor nanohybrids with high regioselectivity.

11:00 AM NM07.04.08

Substrate Role in the 0D Nanoparticle-Catalyzed Synthesis of 1D Epitaxial SnO₂ Nanostructures [Jasmin-Clara Bürger](#)¹, Sebastian Gutsch¹, Vanessa Wollersen^{2,2}, Di Wang^{2,2}, Christian Kübel^{2,2} and Margit Zacharias¹; ¹University of Freiburg, Germany; ²Karlsruhe Institute of Technology (KIT), Germany

The epitaxial planar growth of laterally aligned tin oxide (SnO₂) nanowires along the substrate surface is superior for the integration of 1D nanostructures in sensors and electronic circuits - but is also highly challenging by its small parameter window demanding precisely controlled growth settings. In this study, we varied the substrate material and alignment in 1D planar SnO₂ nanostructure synthesis. Here, we provided experimentally-confirmed thermodynamic considerations and combined these with advanced microscopic FIB preparation of TEM lamellae of longitudinal and cross-sectional cuts of the laterally aligned SnO₂ nanostructures.[1] Prerequisites for an appropriate substrate are not only the chemical stability at growth conditions but also a monocrystalline or structured surface for guiding the growth direction. TEM investigations revealed the heteroepitaxial contact between the SnO₂ crystal lattice and the growth substrate surface and allowed for strain location within the NW cross-section. The theoretical and experimental results gave unique insights into the initial steps of the epitaxial growth of planar 1D SnO₂ nanostructures on crystalline surfaces for promising heterostructure architectures between the 2D substrate, the planar 1D SnO₂ nanostructure and the 0D gold catalyst particle.

[1] J.-C. Bürger et al., *Cryst. Growth Des.* (2021), 21 (1), 191-199

11:15 AM *NM07.04.09

Tailoring Semiconductor Polytype Selection During Molecular-Beam Epitaxy [Rachel S. Goldman](#); University of Michigan, United States

Semiconductor polytype heterostructures, which consist of chemically homogeneous structures formed via an abrupt change in crystal structure, offer opportunities for performance exceeding those of composition-based semiconductor heterostructures. Of particular interest are heterostructures formed via an abrupt change in atomic plane stacking sequence, such as the transition from the wurtzite (WZ) polytype, with AB stacking, to the zincblende (ZB) polytype, with ABC stacking. At a fixed chemistry WZ/ZB heterojunction, the lattice mismatch and thermal expansion coefficient mismatch are typically < 0.1%, leading to a negligible interfacial defect concentration. Meanwhile, the WZ/ZB band offset and polarization discontinuity are expected to lead to the confinement of a two-dimensional electron gas (2DEG) at the interface, without the need for impurity doping and/or alloying. Depending on the type I (nested) vs. type II (staggered) band offset at the WZ/ZB polytype junction, such heterostructures would also be promising for high power electronics and single photon emitters. Recently, we discovered a metal-mediated growth process to nucleate the metastable ZB polytype during molecular-beam epitaxy of GaN [1]. Interestingly, for both nanowires and films, a transformation from the ZB to WZ polytype occurs after 1 hour of growth, at a thickness of 150 nm. Due to the consistency in the timing of the transformation, we hypothesize that the ZB-to-WZ transformation is not due to a random event but instead due to an extrinsic effect associated with the growth process. We will discuss the relative influences of effusion-cell-induced surface heating and electron beam-induced surface polarization on polytype selection and transformation, along with prospects for realization of GaN QDs-in-NWs single-photon emitters and lattice-matched polarization-doped WZ/ZB GaN high-electron mobility transistors.

[1] H. Lu, S. Moniri, C. Reese, S. Jeon, A. Katcher, T. Hill, H. Deng, and R.S. Goldman "Influence of gallium surface saturation on GaN nanowire polytype selection during molecular-beam epitaxy", *Appl. Phys. Lett.* 119, 031601 (2021).

SESSION NM07.05: Application of Various Dimensional Materials and Heterostructures II
Session Chairs: Jekyung Kim and Kyusang Lee
Tuesday Afternoon, November 29, 2022
Hynes, Level 2, Room 203

1:30 PM NM07.05.01

Commensurate Assembly of C₆₀ on Black Phosphorus for Vertical Transistor Applications [Tae Keun K. Yun](#), Yangjin Lee and Kwanpyo Kim; Yonsei University, Korea (the Republic of)

Two-dimensional (2D) layered materials have recently attracted enormous research interest as templates for fabrication of new van der Waals (vdW) heterostructures hosting other 2D materials, inorganic nanostructures, and organic molecules featuring unlimited combinations. Novel physical properties can emerge from the coherent interaction of components in various vdW heterostructures. Among various 2D materials, black phosphorus (BP) can function as a unique 2D template due to its anisotropic puckered atomic structure, which may lead to the strong epitaxial growth of organic molecules through well-controlled assembly. When the pristine surface of BP is preserved during the sample fabrication, the remarkable epitaxial assembly of C₆₀ on BP is indeed achieved. BP template induces aligned C₆₀ assembly with higher-order commensurism, which is confirmed by state-of-the-art transmission electron microscopy and theoretical analyses. We also fabricate the lateral and vertical devices with C₆₀/BP junction via lithography-free clean process and investigate the charge transfer in lateral devices and charge transport behaviors across C₆₀ and BP interface in vertical devices showing tunable barrier from 0.2 to 0.5 eV. Optoelectrical properties of vertical devices are also investigated under infrared and visible light illumination yielding high photo-responsivities up to ~100 A/W under visible light and showing fast response time.

1:45 PM NM07.05.02

Freestanding Single-Crystalline Oxide Membrane and Its Pyroelectric Application [Xinyuan Zhang](#)¹, Celesta S. Chang¹, Shane Lindemann², Owen Erickwen², Marx Akl³, Yunfeng Shi³, Chang-Beom Eom² and Jeehwan Kim¹; ¹Massachusetts Institute of Technology, United States; ²University of Wisconsin-Madison, United States; ³Rensselaer Polytechnic Institute, United States

Infrared (IR) imaging has significant demand in commercial, medical and military applications such as night vision, blood vessel surgery and gas sensing. Compared to photon detectors which requires complex cryogenic cooling and have limited spectral bandwidth, thermal detectors do not, and have the advantage of constant detectivity over the whole IR range, thus becoming the technology of choice. However, one crucial downside of thermal detectors is that the detectivity is several magnitudes of order lower than that of conventional HgCdTe photon detectors, preventing the production of high performance thermal IR detector. Recent development of various thin film lift-off methods offers new opportunity for realizing pyroelectric IR detector with high detectivity and fast response, but all of the previous methods have drawbacks, which are either time-consuming, not scalable, or produce film with nonuniform thickness. Consequently, it has been a big challenge to produce single-crystalline pyroelectric nanomembranes.

Pb(Mg_{1/3}Nb_{2/3})O₃-PbTiO₃ (PMN-PT) and LiTaO₃ (LT) are perovskites with high pyroelectric coefficients and figure-of-merits, which are potential candidates for developing infrared detectors. In this study, we show a new buffer-free technique that enables freestanding, high quality PMN-PT and LT

nanomembranes. Single-crystalline film epitaxially grown on substrate without any buffer layer can be directly exfoliated by a nickel stressor with 100% yield. We confirm that pyroelectric property is not degraded after exfoliation and transfer processes. Our work is expected to improve the pyroelectric thermal detectors to show much better performance than the current state-of-the-art ones, as the detectivity and response time can be significantly improved by achieving ultra-thin (nanometer scale) film. Also, freestanding film will enable fabrication of suspended structure with good thermal isolation, thus increasing responsivity of the IR detector.

2:00 PM NM07.05.03

Optimization of 1D Core-Shell Heterostructures for Gas Sensing [Nicola Pinna](#); Humboldt-Universität Berlin, Germany

Hierarchical core-shell heterostructures composed of p-, n-type and insulating metal oxide shells deposited onto carbon nanotubes (CNTs) were synthesized using atomic layer deposition. Precisely controlled films of alternating metal oxides were uniformly deposited onto the inner and outer walls of the CNTs. The morphological, microstructural and electrical characteristics of the as prepared core-shell heterostructures were thoroughly investigated. The electrical resistance measurements highlighted the large influence of the metal oxides thickness and charge carriers types on increasing of many order of magnitude the baseline resistance of the core-shell heterostructures with various thicknesses of the metal oxide shell layers, suggesting that the conductivity of the sensors is dominated by Schottky barrier junctions across the n-p interfaces.

The behavior of our sensors was investigated for low concentrations of volatile organic compounds and pollutants. The gas sensing response of the heterostructures showed a strong dependence on the thickness of the metal oxide shell layers and the type of heterostructures formed. On the basis of the morphological, microstructural and electrical characterization and sensing results, the sensing mechanism which accounts for the marked variation in the resistance during the interaction of the target gas molecules will be discussed.

2:15 PM BREAK

2:45 PM NM07.05.05

3D Mesoporous Networks of Linked Metal Chalcogenide Nanoparticles for Improved Photocatalytic Hydrogen Generation Activity [Ioannis Vamvasakis](#) and [Gerassimos S. Armatas](#); University of Crete, Greece

Photocatalytic hydrogen production through water splitting has recently gained significant attention for efficient solar-to-chemical energy conversion.¹ However, despite immense research efforts on semiconductor materials, key challenges of obtaining catalysts with high activity and long-term stability still remain. Recently, the synthesis of highly crystalline mesoporous semiconductors has been the focus in the field of electro- and photocatalysis. These materials combine the high reactivity of semiconductor nanoparticles with mesoporosity, offering new perspectives in designing novel catalysts with improved efficiency and reliability. Unlike to bulk-like microstructures and individual nanoparticles, 3D mesoporous networks of connected nanoparticles can benefit from the large and accessible surface area within the assembled structure and enhanced light-harvesting efficiency arising from multiple scattering of light inside the pores.

Herein, we present the synthesis of chemically stable and robust mesoporous networks of β -Ni(OH)₂-modified and CdS and Ni₂P-decorated CdS/ZnS nanocrystal (ca. 4–5 nm) assemblies (NCAs) that show high photocatalytic activity for hydrogen evolution under visible light irradiation.² We utilize polymer-assisted self-assembly of colloidal nanoparticles to assemble mesoporous CdS and ZnS nanoparticle-linked frameworks with high interstitial porosity. This method utilizes the nanoparticles as building block units and based on the coassembly of these nanoscopic units with organic structure-directing agents to construct 3D structures with open-pore morphology.³ The resulting materials feature a nanometer-sized framework perforated by uniform pores, which allows rapid mass transport and provides plenty of exposed surface-active sites available for reaction. Photocatalytic measurements coupled with UV-vis/NIR, TRPL and electrochemical spectroscopy studies suggest that the outstanding photocatalytic hydrogen production performance of these unique heterostructures mainly arises from the accessible 3D open-pore structure and the favorable band-alignment with the respective co-catalyst, which suppresses carrier recombination and promotes efficient charge-transport at the junction interfaces. As thus, the β -Ni(OH)₂/CdS catalyst containing 10 wt% Ni reached a photocatalytic H₂-evolution rate of 1.4 mmol/h with an apparent QY of 72% at 420 nm, while demonstrating excellent stability in alkaline (5M NaOH) ethanol solution (10% v/v). The results of these studies can offer new insights into the design and development of efficient photocatalysts for energy conversion and environmental remediation applications.

References

- (1) H. Ahmad, S.K. Kamarudin, L.J. Minggu, M. Kassim, *Renew. Sust. Energ. Rev.* **2015**, 43, 599.
- (2) a) I. Vamvasakis, I.T. Papadas, Th. Tzanoudakis, Ch. Drivas, S.A. Choulis, S. Kennou, G.S. Armatas, *ACS Catal.* **2018**, 8, 8726. b) I. Vamvasakis, K.S. Subrahmanyam, M.G. Kanatzidis, G.S. Armatas, *ACS Nano* **2015**, 9, 4419.
- (3) I.T. Papadas, I. Vamvasakis, I. Tamiolakis, G.S. Armatas, *Chem. Mater.* **2016**, 28, 2886.
- (4) We acknowledge support from the Hellenic Foundation for Research and Innovation (H.F.R.I.) under the “1st Call for H.F.R.I. Research Projects to support Faculty Members & Researchers and the Procurement of High-cost research equipment grant” (Project Number: 400).

3:00 PM NM07.05.06

Heterostructured Nanomaterial Sensors for the Selective Detection of Breath Markers [Ines Weber](#) and Sotiris E. Pratsinis; ETH Zurich, Switzerland

Chemo-resistive sensors bear huge potential in emerging applications such as breath analysis and air quality monitoring due to their low cost, high sensitivity and compact design. Despite decades of research and advancements in sensor material design (e.g., compositing with carbon nanotubes¹), such sensors can rarely be found in real-life applications due to their limited selectivity.

Here, we present a novel approach to design selective sensing systems for the detection of the breath marker acetone, a bio-marker for lipolysis². It is based on nanoparticle filters³ comprising mixed heterostructures of metal oxide materials fabricated by flame spray pyrolysis that pre-screen chemo-resistive sensors.⁴ These filters act as nano-catalysts and selectively convert undesired interferents to non-responsive species (e.g., ethanol⁵) while leaving the target analyte acetone intact. Moreover, such filters can be produced in a scalable and low-cost manner at room temperature⁶ using flame-spray pyrolysis. In fact, catalytic filters made of Pt/Al₂O₃ nanoparticles markedly enhanced the acetone selectivity of heterostructured Si/WO₃ sensors (>250) towards various interferents (e.g., alcohols, isoprene, ammonia, H₂, and CO).⁷ This enabled accurate acetone detection even in the presence of orders of magnitude higher interferent concentrations.

Therefore, this filter-sensor device was tested on real human breath to monitor acetone in various scenarios including dieting⁸, exercising⁹ and even to distinguish people in health from diabetes¹⁰. Due to the unique filter and sensor material design, this detector is capable of accurately detecting acetone concentrations in all three scenarios, in excellent agreement with bench-top proton transfer reaction time of flight mass spectrometry. Notably, this allowed to track acetone concentrations directly during exercise, giving information about cardio-respiratory fitness. Similarly, such sensors can be used to distinguish between healthy people and diabetes when following standardized protocols.¹⁰ Finally, it may assist in guiding dieting and weight-loss, as we are currently investigating in a randomized clinical trial on intermittent fasting diets with 75 volunteers. Hence, this heterostructured filter and sensor is most promising as mobile health device for routing personalized metabolic health monitoring.

1. Narjinary, M., Rana, P., Sen, A. & Pal, M. Enhanced and selective acetone sensing properties of SnO₂-MWCNT nanocomposites: Promising materials for diabetes sensor. *Mater. Des.* **115**, 158–164 (2017).
2. Anderson, J. C. Measuring Breath Acetone for Monitoring Fat Loss: Review. *Obesity* **23**, 2327–2334 (2015).
3. Van den Broek, J., Weber, I. C., Güntner, A. T. & Pratsinis, S. E. Highly selective gas sensing enabled by filters. *Mater. Horizons* **8**, 661–684 (2021).
4. Weber, I. C. & Güntner, A. T. Catalytic filters for metal oxide gas sensors. *Sensors Actuators B Chem.* **356**, 131346 (2022).
5. Güntner, A. T., Weber, I. C. & Pratsinis, S. E. Catalytic filter for continuous and selective ethanol removal prior to gas sensing. *ACS Sensors* **5**, 1058–1067 (2020).
6. Weber, I. C., Wang, C.-T. & Güntner, A. T. Room-temperature catalyst enables selective acetone sensing. *Materials*. **14**, 1839 (2021).
7. Weber, I. C., Braun, H. P., Krumeich, F., Güntner, A. T. & Pratsinis, S. E. Superior Acetone Selectivity in Gas Mixtures by Catalyst Filtered Chemoresistive Sensors. *Adv. Sci.* **7**, 2001503 (2020).
8. Güntner, A. T. *et al.* Noninvasive Body Fat Burn Monitoring from Exhaled Acetone with Si-doped WO₃-sensing Nanoparticles. *Anal. Chem.* **89**, 10578–10584 (2017).
9. Weber, I. C. *et al.* Monitoring Lipolysis by Sensing Breath Acetone down to ppb. *Small Sci.* **1**, 2100004 (2021).
10. Güntner, A. T., Weber, I. C., Schon, S., Pratsinis, S. E. & Gerber, P. A. Monitoring rapid metabolic changes in health and type-1 diabetes with breath acetone sensors. *Sens. Actuator B-Chem.* doi: 10.1016/j.snb.2022.132182 (2022).

3:15 PM NM07.05.07

Pseudo-Graphene on SiC for High-Quality GaN Membrane Jekyung Kim, Bo-In Park, Dusik Bae, Doyoon Lee, Junseok Jeong, Yunpeng Liu, Hyunseok Kim and Jeehwan Kim; Massachusetts Institute of Technology, United States

Free-standing membranes are building blocks for various electronic and photonic devices since they can provide a large degree of freedom for the platform. Besides, along with their extraordinary material properties, single-crystalline free-standing membranes can reduce material costs. In this regards, fabrication of free-standing membranes requires successful separation of active materials from various types of substrates. However, conventional approaches have exhibited challenges in the sense of poor interface quality, complexity in choice of materials, and such. Recently, remote epitaxy has arisen as a new technology that can overcome current limitations enabling both high crystal quality and simplicity in the materials. In remote epitaxy, electrostatic potential is not completely screened by 2D material (e.g. graphene) inserted as a releasing layer between the substrate and the active material. In other words, remote interaction between two materials results in the successful epitaxial growth of the active material such as GaAs or GaN. The quality of 2D material, therefore, is highly crucial in achieving high-quality single-crystalline free-standing membranes. In this study, we demonstrated a new 2D platform using graphene/SiC in remote epitaxy. We discovered that graphitized SiC has sp²-bonded graphene layer on the very top surface and sp³-bonded pseudo-graphene(pGr) between graphene and SiC. The graphene fully covers pGr providing sufficient van der Waals force above the epitaxial layer, enabling efficient transfer of free-standing membranes without any possible damage. This research includes systematic studies on pGr/SiC used as a releasing layer for free-standing GaAs/GaN membranes.

3:30 PM NM07.05.08

Enhanced Dielectric Strength and Capacitive Energy Density in Ultrathin 2D Glassy Polymer Films Maninderjeet Singh and Alamgir Karim; University of Houston, United States

Ultrathin polymer films present unique opportunities to understand the physics and properties of polymers at the nanoscale as the polymer films start to behave as 2D materials instead of their usual 3D behavior. Ultrathin polymer films have been shown to demonstrate differences in properties such as glass transition temperature, mechanical properties, polymer mobility, etc. as compared to their bulk counterparts. In this work, we demonstrate that ultrathin glassy polymer films (~100 nm) show an order of magnitude higher dielectric strength (E_{BD}) and two orders of magnitude higher capacitive energy density ($U_{max} \propto E_{BD}^2$) of ~100 J/cm³ in standard localized point-contact measurements, as compared to the bulk polymer films when used as dielectric capacitors. The dielectric capacitors demonstrate 3–4 order of magnitude higher power densities as compared to electrochemical energy storage devices such as batteries, thus making them useful as high-power density energy storage devices. We believe that the enhancement of the dielectric strength and capacitive energy density is due to the tighter chain packing of polymers, cast from a good solvent into thin films, dried under conditions of slow evaporation of the good solvent. We test the density of thin polymer films by optical measurements and observe that the ultrathin films show higher densities and thus lower free volume as compared to their bulk counterparts, which might be a governing factor for the enhancement of the dielectric strength. Furthermore, we observe that the dielectric strength of annealed ultrathin polymer films decreases as compared to the as-cast films, which might be attributed to the surface segregation of chain ends upon annealing, which act as defect sites for the dielectric breakdown of the polymer films. Moreover, the ultrathin films of polymers having sub-room temperature glass transition don't show ultra-high dielectric strength and capacitive energy density, which might be due to the presence of excess free volume in these polymer films that act as defect sites for breakdown. This enhancement of dielectric strength in ultrathin polymer films might help in increasing the understanding of polymer behavior in ultrathin films.

3:45 PM NM07.05.09

Potential of Joule Heating Method for the Synthesis of a Variety of MoO₃ and WO₃ Nanomaterials Beatriz Rodríguez Fernández¹, Teresa Cuberes², Pedro Hidalgo¹ and Bianchi Mendez¹; ¹University of Complutense, Spain; ²Universidad Castilla la Mancha, Spain

Crystalline structure and quality, and dimensionality in nanomaterials are quite affected by the synthesis route. This is of paramount relevance when it comes to oxide nanomaterials, which can occur with a variety of phases. Among them, transitional metal oxides are considered very promising candidates for multiple applications like electronic devices among others. In this work, we expose a rapid synthesis of metal oxide nano- and microstructures via the resistive heating of metallic wires, Mo and W, due to the flow of an electric current. The method is proved as an effective route to obtain van der Waals (vdW) and non-vdW bonded materials as MoO₃ and WO₃, respectively. The growth mechanism is discussed in terms of local oxidation of the surface of the wire as well as diffusion and electromigration processes [1,2]. The processes will be discussed in the framework of Multiphysics modelling and compared with experimental results.

The detailed morphological, structural and chemical analysis of the MoO₃ and WO₃ nanomaterials, carried out by scanning electron microscopy (SEM), Raman spectroscopy, X-ray diffraction (XRD), transmission electron microscopy (TEM) and X-ray photoelectron spectroscopy (XPS), reveal that several phases are simultaneously stabilized, which is of great interest. In the case of MoO₃, nanomembranes of alpha-phase and nanospheres of beta-phase are produced, while monoclinic I, monoclinic II and triclinic phases of WO₃ are produced by the resistive heating of W metallic wire. In addition, the MoO₃ and WO₃ nanostructures have been embedded in a poly(vinyl alcohol) matrix to achieve nanocomposite films, and their optical and mechanical properties have been explored. In summary, our results show that resistive heating is a simple and low energy method to synthesized transition metal oxide nanomembranes and nanostructures in a fast and low-cost way with promising applications.

[1] B. Rodríguez, P. Hidalgo, J. Piqueras and B. Méndez, *RSC Adv.*, **10**, 11892 (2020).

[2] S. K. Lin, Y. C. Liu, S. J. Chiu, Y. T. Liu and H. Y. Lee, *Sci. Rep.* **7**, 3082 (2017).

4:00 PM NM07.05.10

Portable Bulk-Water Disinfection by Electric Manipulating and Live Capturing Bacteria with Divergently Branched Porous Graphite Yifei Liu, Xianfu Luo, Weigu Li, Zexi Liang and Donglei (Emma) Fan; The University of Texas at Austin, United States

An easy access to clean water is pivotal for a sustainable modern society. Nevertheless, it remains arduous to develop efficient and low-cost portable water disinfection systems for point-of-use (POU) applications. The overcoming of this challenge is particularly imperative for the society's resilience. Here, we report an innovative POU disinfection scheme and device prototype for the capture and removal of pathogen in bulk water. The system is made of AC-electric-field-powered three-dimensional (3D) porous dendritic graphite foams (PDGF) integrated in a 3D-printed water-purification module. The device is simple, portable, and can reproducibly remove 99.997 % E-coli bacterial cells from bulk water using only a few voltages and among the lowest energy of 435.5 J L^{-1} . It successfully brings natural water in the Waller Creek at UT Austin to the safe level. The strategically fabricated PDGF materials are robust and low cost at only \$1.42 per piece and demonstrates at least 20 repeated uses without functional degradation. Brownian dynamics simulations are carried out to shed light to the disinfection mechanism. The innovative scheme, material, and device prototype for water disinfection reported in this work could inspire new paradigms for POU water treatment.

SESSION NM07.06: Application of Various Dimensional Materials and Heterostructures III

Session Chairs: Sanghoon Bae and Jinkyong Yoo

Wednesday Morning, November 30, 2022

Hynes, Level 2, Room 203

8:00 AM *NM07.06.01

MoS₂ Thin-Film Transistor Backplanes for Display and Imaging Jong-Hyun Ahn; Yonsei University, Korea (the Republic of)

Thin-Film Transistors (TFT) are being widely used as a backplane to drive emissive devices such as LCD, OLED, micro-LED, and image sensors such as optical and X-ray. Amorphous-Si, Poly-Si, and oxide semiconductors are commonly used in backplane TFT. High carrier mobility, high on/off ratio, and stability are important characteristics for backplane TFT. Two-dimensional semiconductors, especially MoS₂, are proposed as an alternative material to improve the mechanical flexibility of the resulting devices. In this talk, we present the fabrication of MoS₂-based backplane TFT to drive flexible display and image sensors. For this purpose, we synthesized high-quality monolayer MoS₂ through a modified metal-organic chemical vapor deposition (MOCVD) process and fabricated a TFT array using conventional photolithography and etching processes. The good mechanical properties of MoS₂ enable the development of various flexible devices that cannot be easily reproduced with conventional materials. Examples of devices include wearable OLED display and X-ray image sensor.

8:30 AM NM07.06.02

Fabrication of 3D Hierarchical ZnO/ZIF-8 Nanostructure for Highly Sensitive and Selective Room Temperature Gas Sensor Jinho Lee¹, Young-Seok Shim² and Seokwoo Jeon¹; ¹Korea advanced Institute of Science and Technology, Korea (the Republic of); ²Silla University, Korea (the Republic of)

Semiconductor metal oxide (SMO)-based gas sensors have been utilized as powerful sensing material for high performance gas sensor, however, low gas selectivity still remains as a crucial problem for SMO-based gas sensor. Recently, a new method has been proposed to enhance gas selectivity, which employ nanoporous materials such as metal-organic frameworks (MOF) as a gas filter to physically modulate gas diffusion. However, the usage of MOF as a gas filter for metal oxide gas sensor still have issues on degradation of gas responses with diffusion process. Herein, we introduce a 3D hierarchical nanostructure with highly ordered 3D ZnO scaffold and zeolitic imidazolate framework (ZIF-8) were fabricated for room temperature gas sensing to enhance both the gas sensitivity and gas selectivity. The highly ordered and periodic porous nanostructure of ZnO enlarge the gas sensitivity with large surface area, good gas diffusion and enhanced light absorption. The ZIF-8 nanofilm were decorated on the surface of 3D ZnO nanostructure with the controlled film thickness. With the exquisite decoration process, the resulted hierarchical nanostructure shows highly ordered and periodic nanostructure, which can offer the advance in gas sensitivity. The 3D hierarchical ZnO/ZIF-8 nanostructure exhibit improved gas selectivity to NO₂ gas, which molecular size are compatible to pore size of ZIF-8. The gas response to relatively large gas molecules such as toluene and acetone are clearly suppressed compared to 3D pristine ZnO nanostructure, which is attributed to gas filter effects of nanoporous ZIF-8. Especially, 3D hierarchical ZnO/ZIF-8 nanostructure show enhanced NO₂ gas responses compared with 3D pristine ZnO nanostructure (22.8-fold improvement @ 0.1 ppm), which demonstrates the dual role of ZIF-8 film that gas filter effects and catalytic effects for enhance gas sensitivity. The rational design and realization of 3D hierarchical nanostructure for high performance gas sensor at room temperature suggests future perspective for target-purpose gas sensor based on nanostructured material.

8:45 AM NM07.06.03

Morphology-Dependent Zinc Oxide Structures and Their Applications to Negative Differential Resistance Behaviors in Mixed-Dimensional 0D/3D Zinc Oxide Quantum Dots/p-Si Heterostructure Devices Somi Kim¹, Taehyun Park¹, Hyung Joong Yun² and Hocheon Yoo¹; ¹Gachon University, Korea (the Republic of); ²Korea Basic Science Institute (KBSI), Korea (the Republic of)

Negative differential resistance (NDR) behavior has considerably been the focus of attention due to its novel switching properties, which exhibit an *n*-shaped current-voltage characteristic without a monolithic increase of current as the applied voltage bias increases. This study presents the findings of morphology-dependent NDR behavior in which three types of zinc oxide (ZnO) build a junction with *p*-Si in the form of quantum dots (QDs), nanoparticles (NPs), and sol-gel-derived films (hereinafter referred to as Film) with grain sizes of 10.14 nm, 39.91 nm, and 99.60 nm, respectively. The operation principle of NDR behavior and control of peak-to-valley ratio (PVCr) were elucidated through a comprehensive study, including an analysis of the energy band structure, morphological investigation, chemical structure, and electrical characterization, according to the ZnO morphology and dimension. The peak current of three types ZnO increased in the order of Film, NPs, and QDs, and it is emphasized that the maximum PVCr of 4.96 A/A was obtained in the mixed-dimensional 0D QDs/3D *p*-Si heterostructure devices. The differential resistance (R_{diff}) of the mixed-dimensional QDs/*p*-Si heterostructure devices was 0.3 mΩ, which was significantly larger than reported values in previous studies. As a result, the NDR properties including the peak and valley current of PVCr, can be accordingly controllable through the proposed morphological control scheme with the same ZnO material. It is worth noting that the mixed-dimensional QDs/*p*-Si heterostructure devices in this study exhibited the NDR behavior achieving 100% yield and high uniformity without external stimuli such as photo-induced or controlled atmosphere such as high vacuum and cryogenic environment. This is the result of experimentally demonstration that the NDR can be stably implemented in ambient environment, not under specific conditions, which enabling the development of further practical applications, such as the study of multi-value logic circuits with two threshold voltage (V_{TH}) characteristics using NDR behavior.

9:00 AM *NM07.06.04

Plasmon-Enhanced Photodetection in a Monolayer MoS₂ Phototransistor with Ultrahigh Photoresponsivity Yu-Jung Lu^{1,2}; ¹Academia Sinica, Taiwan; ²National Taiwan University, Taiwan

Monolayer transition metal dichalcogenides (TMDs) with an atomically thin nature are promising materials for electronics and photonics, especially at highly scaled lateral dimensions. However, the characteristically low total absorption of photons in the monolayer TMD has become a challenge in the access to and realization of monolayer TMD-based high-performance optoelectronic functionalities and devices. Here, we report gate-tunable plasmonic phototransistors (photoFETs) that consist of monolayer molybdenum disulfide (MoS₂) photoFETs integrated with the two-dimensional plasmonic crystals (Ag, HfN, TiN). The plasmonic photoFET has giant enhancement in the photocurrent compared to pristine 2D material-based photoFETs. The achievement is based on the breakthrough of the realization and characterization of a gate-tunable atomistically-thin phototransistor device consisting of a monolayer MoS₂ photoFET integrated with a two-dimensional (2D) plasmonic crystal to enhance the light absorption rate, photo-carrier generation rate, photo-gating, and hot-carrier transfer rate. Moreover, this talk will describe different design of plasmonic phototransistors that is extensible to other types of 2D materials for ultrathin high-performance optoelectronic devices at highly scaled dimensions. Finally, we will discuss prospects for next-generation ultra-compact optoelectronic devices in the trans-Moore era.

9:30 AM BREAK

10:00 AM NM07.06.05

Fabrication of Microcavity and Quantum Wells Composed of Two-Dimensional and Three-Dimensional Materials Xuejing Wang¹, Yeonhoo Kim¹, Benjamin K. Derby¹, Xuedan Ma², Towfiq Ahmed¹, Suhyun Kim³, Kibum Kang³, Ting S. Luk⁴, Young Joon Hong⁵, Aiping Chen¹ and Jinkyoun Yoo¹; ¹Los Alamos National Laboratory, United States; ²Argonne National Laboratory, United States; ³Korea Advanced Institute of Science and Technology, Korea (the Republic of); ⁴Sandia National Laboratories, United States; ⁵Sejong University, Korea (the Republic of)

Emerging nanomaterials have attracted much attention due to their novel functionalities, but have also been hindered by lack of scalable synthesis and of ways of controlling characteristics. Atomically thin two-dimensional (2D) materials are good examples of novel materials set promising exotic properties and requiring established manufacturing approaches for practical applications. Heterostructuring is a powerful and general strategy to control physical properties of materials. Moreover, heterostructuring can offer novel characteristics differentiating the heterostructure from individual component in a structure. Recently, 2D/2D heterostructures prepared by stacking are being explored to observe quantum phenomena. Besides the 2D/2D heterostructures, heterostructuring with 2D and conventional materials in other dimensions (e.g. bulk-like structure for 3D and nanowires for 1D) has shown great potential for multi-dimensional heterostructures.

In this presentation I'll discuss how to prepare multi-dimensional heterostructures composed of 2D and conventional semiconducting materials. The experimental approach is remote epitaxial growth ZnO on 2D materials including graphene, hexagonal boron nitride, transition metal dichalcogenides. Hydrothermal synthesis, metalorganic chemical vapor deposition, and pulsed laser deposition were employed to fabricate microcavities and quantum wells embedding monolayer molybdenum disulfide layers. Cross-sectional transmission electron microscopy, microphotoluminescence, cathodoluminescence, and electron beam induced current microscopy measurements were utilized to investigate the interfacial structures and functional properties of the heterostructures with high spatial resolution.

10:15 AM NM07.06.06

Multiplication of Freestanding Compound Semiconductor Membranes from a Single Wafer by Alternating Growth with 2D Materials Ne Myo Han, Hyunseok Kim, Yunpeng Liu, Kuangye Lu, Celesta S. Chang and Jeehwan Kim; Massachusetts Institute of Technology, United States

Single-crystal compound semiconductors, such as III-N and III-V, are important building blocks for functional devices due to their high electron mobilities, wide range of bandgaps, and excellent optoelectronic properties. However, current methods to produce their freestanding membranes for heterointegration suffer from slow processes or poor material quality. Here, we demonstrate an approach to grow and harvest multiple wafer-scale single-crystal membranes with high throughput by introducing weak van der Waals interfaces between epitaxial layers. This is achieved by directly growing two-dimensional (2D) materials on compound semiconductors in their native deposition systems, which enables alternating growth of 2D material and compound semiconductor epitaxial layers in a single run. Each epilayer in the multi-stack structure is then sequentially harvested by mechanical exfoliation, producing multiple freestanding single-crystal membranes with extremely high throughput from a single wafer, primed for integration in mixed-dimensional heterostructures.

10:30 AM NM07.06.07

Reconfigurable Source-Gated Transistor Based on 2D Ferroelectric Heterostructure Joonseok Kim, Ting-Ching Chu, Hyeonseon Choi, Zhehao Zhu and Lincoln J. Lauhon; Northwestern University, United States

The integration of ferroelectric materials into conventional field-effect transistors (FETs) and optoelectronic devices creates new opportunities for low-power and non-volatile devices of relevance to neuromorphic computing. The remnant polarization can be used to modulate carrier concentration when ferroelectrics are employed as a dielectric or the Schottky barrier height if employed as the semiconducting channel, and the reduced screening in two-dimensional (2D) layered materials can enhance these effects. While 2D FETs with non-volatile output characteristics have been demonstrated, it can be challenging to achieve stable output current saturation in conventional thin-film transistors in which pinch-off occurs at the drain. In contrast, source-gated transistors (SGTs) produce pinch-off at the source electrode where the large Schottky barrier depletes the semiconductor. Pinch-off can be realized at low drain voltages and is independent of channel length. Furthermore, SGTs allow for reduced power consumption compared to conventional FETs with similar dimensions and geometries.

We have integrated the ferroelectric semiconductor In₂Se₃ into the source contact of monolayer (1L-) MoS₂ transistors to realize non-volatile mixed-dimensional SGTs with robust and tunable current saturation. Au is used as the drain electrode of the 1L-MoS₂ FET and the source contact is Ti. In this scheme, the remnant polarization of In₂Se₃ modulates the Schottky barrier at the Ti/In₂Se₃ metal-semiconductor interface and hence the resulting depletion of the MoS₂ channel beneath the contact and extending into the channel. When positive drain bias is applied, the output characteristics show strong current saturation. In contrast, a negative drain bias produces a linear response in the output, suggesting that the Ti/In₂Se₃ injection is responsible for the current saturation. The output impedance at positive drain bias above $V_{d,sat}$ reaches 8 G Ω , which is more than two orders of magnitude larger than the output impedance under negative drain bias. Transfer characteristics show a clear hysteresis loop at positive V_D , stemming from ferroelectric switching of the In₂Se₃. The ferroelectric hysteresis induces non-volatile reconfiguration of the saturation current by more than an order of magnitude dependent on gate bias history. Analysis of temperature-dependent I-V characteristics was used to estimate that the Schottky barrier is modulated by ~45 mV by the gate polarization. *In operando* Kelvin probe force microscopy (KPFM) under saturating drain bias confirms that the potential drops primarily at the source contact, consistent with expectations for an SGT. In summary, we have demonstrated the integration of a 2D ferroelectric interlayer into the vertical contact of a lateral MoS₂ transistor resulting in a novel non-volatile SGT with the potential to reduce the power consumption of reconfigurable devices and enable cascading neuromorphic circuits.

10:45 AM NM07.06.08

Scalable Preparation of Vanadium-Based Carbon Nanostructures for Hybrid Supercapacitor Applications [Sunil P. Lonkar](#) and Chiara Busa; Technology Innovation Institute, United Arab Emirates

The ever-growing demands and rapid development of energy storage devices and systems pressed the need for low-cost yet highly performing electrode materials. The transition metal oxide and sulfide-based hybrids holds great promise as the active electrode materials in supercapacitors, due to their large surface area and variable oxidation states. These properties enable significantly high energy storage *via* electrical double layer and pseudocapacitive charge storage mechanisms. Herein, we discuss a facile, scalable, and environment-friendly preparation process to produce transition metal sulfide and oxides based on resource rich metals such as Mn, Fe, V etc. and their hybrids with carbonaceous materials, such as carbon nanotubes and graphene. This strategy encompasses solvent-less mixing of a metal salt, surfeit yet non-toxic abundant elemental sulfur and carbon precursor under continuous ball milling and thermo-annealing. The resulting nano hybrids were thoroughly investigated by means of several techniques. XRD, HRTEM, SEM, Raman and BET could gather insights on the morphology and the fine material structure, as well as on the spectroscopic properties. Finally, the electrochemical properties as supercapacitor components were investigated in regards with varyingly increasing carbon content. The nano hybrids were tested in both aqueous and organic electrolytes for better energy and power performances. Charge storage performances and components stability in both symmetric and asymmetric devices were assessed via CV, GCD, EIS.

11:00 AM NM07.06.09

Structurally Intact Hydrophilic Carbon Fiber Paper – Nanoparticle Assemblies for CO₂ Reduction [Connor Cox](#), Madeleine Wilsey, Kendra Watson, Omolade Fasusi, Brian Yegela, Ryland C. Forsythe and Astrid M. Müller; University of Rochester, United States

We report a green chemical approach to render carbon fiber paper hydrophilic for an unprecedentedly long time. Selective hydroxylation of carbon surfaces preserved the carbon fiber network, while imparting hydrophilicity that was sustained for more than 10 months, far longer than reported hydrophilization techniques, which are often much harsher and more destructive to the carbon fiber paper mesostructure. Our technology offers an environmentally friendly, scalable, and rapid process to obtain hydrophilic carbon fiber paper, opening the door for new applications, such as aqueous electrochemistry. With its high surface area, electrical conductivity, robustness, chemical inertness, and low-cost, carbon fiber paper is an ideal support for nanomaterial catalysts. However, the native hydrophobicity of carbon fibers has limited adoption in aqueous electrocatalysis thus far. Existing processes for carbon fiber paper hydrophilization include plasma or chemical etching techniques, ozone treatments, or thermal treatments; these all suffer serious disadvantages. Plasma etches are difficult to scale, and both plasma and ozone treatments require major capital expense. These plasma and ozone treatments, alongside chemical etching or thermal processing, significantly damage and embrittle the material, compromising carefully engineered carbon fiber networks. Our acid-free hydrophilization method allows for selective hydroxylation of carbon fiber surfaces without overoxidation, while preserving the mesostructure of the material. Systematic design and evaluation of thirteen unique chemical treatments allowed us to identify that hydroxyl, rather than carboxyl, surface functional groups imparted long-lasting hydrophilicity to carbon fibers. The rapid loss of hydrophilicity observed with harsher treatments, such as strong acids or high temperatures, was likely caused by overoxidation of carbon surfaces to aldehydes and carboxyls. Furthermore, the rapidity of less than 30 minutes and solution-processable nature of our process set it apart from previously published approaches for carbon fiber paper hydrophilization.

With this technology in hand, we were able to capitalize on the hydrophilicity of our treated carbon fiber paper to conduct aqueous electrochemical CO₂ reduction. After rendering carbon fiber paper hydrophilic, the properties which make carbon fiber paper an ideal nanoparticulate support can now be taken advantage of in an aqueous environment. Gold nanoparticles were uniformly distributed throughout the carbon fiber network to form carbon fiber paper – nanoparticles cathodes, which electrochemically reduced CO₂ to syngas with tunable CO:H₂ ratios. Generation of syngas through electrochemical CO₂ reduction can be paired with renewable energy sources to produce this important chemical feedstock without fossil fuels. The incorporation of our rapid green-chemical approach to hydrophilizing carbon fiber paper for the preparation of carbon fiber paper – nanoparticle assemblies with long durability is an important step toward the realization of electrocatalytic successor technologies.

SESSION NM07.07: Physics of Various Dimensional Materials and Heterostructures

Session Chairs: Sanghoon Bae and Jian Shi

Wednesday Afternoon, November 30, 2022

Hynes, Level 2, Room 203

1:30 PM *NM07.07.01

Strain Control of Phase Transitions in Freestanding Oxide Membranes [Harold Y. Hwang](#)^{1,2}; ¹Stanford University, United States; ²SLAC National Accelerator Laboratory, United States

The ability to create and manipulate materials in two-dimensional (2D) form has repeatedly had transformative impact on science and technology. In parallel with the exfoliation and stacking of intrinsically layered crystals, the atomic-scale thin film growth of complex materials has enabled the creation of artificial 2D heterostructures with novel functionality and emergent phenomena, as seen in perovskite oxides. We present a general method to create freestanding complex oxide membranes and heterostructures using epitaxial water-soluble buffer layers, with millimeter-scale lateral dimensions and nanometer-scale thickness. This facilitates many new opportunities we are beginning to explore; here we will focus on the strain control of ferroelectric, magnetic, and other phase transitions in oxide membranes.

2:00 PM NM07.07.02

Atomic Scale Design of the 2D/3D Interface [Kate Reidy](#)¹, Joachim D. Thomsen¹, Andrea Konečná², Benedikt Haas³, Baoming Wang¹, Eugene Park¹, Julian Klein¹, Prineha Narang⁴, Christoph T. Koch⁵, Juan Carlos Idrobo⁵ and Frances M. Ross¹; ¹Massachusetts Institute of Technology, United States; ²Brno University of Technology, Czechia; ³Humboldt-Universität zu Berlin, Germany; ⁴UCLA, United States; ⁵University of Washington, United States

A fundamental understanding of the interface between three-dimensional (3D) metals and two-dimensional (2D) van der Waals materials is crucial for the integration of nanoscale devices into mainstream technologies.¹ The reasons for this are twofold: (1) since bulk metallic contacts, such as Ti or Au, are crucial for existing 2D device fabrication, for example in electronic gating, control, and readout; and (2) since ‘mixed dimensional’ 2D/3D heterointegration² allows novel functionalities that cannot be obtained by either material alone – for example exciton-plasmonic coupling, integrated spintronic circuits, and tunnel barriers in superconducting qubits. In all of these cases, the atomic structure at the interface between the metal and the 2D material (2D/3D interface) directly affects the device performance.³

Here, we explore the local electronic, optical and structural properties of well-controlled device-relevant 2D/3D interfaces using a combination of monochromated high-energy resolution electron energy-loss spectroscopy (EELS), atomic resolution STEM and *in situ* ultra-high vacuum (UHV) TEM. First, we demonstrate ultra-low defect-density 2D/3D interfaces using slow metal evaporation rates onto clean suspended 2D materials in UHV.⁴ Focusing initially on the MoS₂/Au heterostructure, we investigate epitaxial Au nanoisland growth in its equilibrium Winterbottom shape, providing a quantitative estimate for 2D/3D interface energy through thermodynamic modelling. We use these well-defined interfaces to elucidate the effect of 2D/3D integration on electronic properties. Here, monochromated STEM-EELS allows us to map local changes of plasmonic and excitonic spectra of a MoS₂/Au heterostructure on the nanometer scale. We extend our analysis to the technologically relevant metals Ti and Nb and show that suspended 2D materials enable the formation of metal/2D/metal (3D/2D/3D) heterostructures. Such understanding of the structure-property relationship allows versatile design of 2D/3D heterostructures for next generation nanoscale devices, and we discuss mechanisms by which optimizing this 2D/3D interface is crucial for improving existing devices as well as generating novel 'mixed-dimensional' 2D/3D heterostructures.

1. Bae, S.-H., et al. *Nat. Mater.* **18**, 550–560 (2019).
2. Jariwala, D., Marks, T. J. & Hersam, M. C. *Nat. Mater.* **16**, 170–181 (2017).
3. Liu, Y., Huang, Y. & Duan, X. *Nature* **567**, 323 (2019).
4. Reidy, K.* , Varnavides, G.* et al. *Nature Comm.* **12**, 1290 (2021).

2:15 PM NM07.07.03

Machine-Learning Assisted High-Throughput Computational Identification of Mixed-Dimensional Materials Joshua T. Paul^{1,2}, Nina Andrejevic², Lincoln J. Lauhon¹, Pierre Darancet^{2,1} and Maria K. Chan^{2,1}; ¹Northwestern University, United States; ²Argonne National Laboratory, United States

The nano revolution started with the discovery of graphene and has led to a great deal of research into low-dimensional systems. These systems range from 0D nanoparticles to 1D nanowires and nanoribbons to 2D monolayers, all of which experience quantum confinement that can give rise to unique properties. More recently, mixed dimensional materials have received increasing attention due to the potential for synergistic and emergent properties in combinations of 2D, 1D, and 0D systems. These investigations have used intentionally synthesized mixed dimensional systems, but the question of what mixed dimensional materials occur in nature has yet to be tackled. In this work, we search the MaterialsProject database for crystals that contain sub-networks of atoms with differing dimensionalities (e.g., 1D nanowires between 2D layers). We perform this search with the Topological Scaling Algorithm, using atomic radii as a first pass and the CrystallNN algorithm as a second. We follow by using the Electron Localization Function to train an ensemble of neural network classifiers to distinguish bonds with a set of well-chosen materials examples. Subsequently, we apply the trained models to classify bond types and identify candidate mixed-dimensional heterostructures from a broad range of materials systems as a third pass. From these searches, we identify several mixed-dimensional crystal structures, which we then relax using Density Functional Theory while accounting for van der Waals forces. Finally, we calculate various properties in these crystals, including the electronic structure and thermodynamic stability.

2:30 PM BREAK

3:30 PM NM07.07.04

Study of How Remote Epitaxy is Truly Remote Celesta S. Chang¹, Bo-In Park¹, Junseok Jeong¹, Kiseok Kim¹, Hyunseok Kim¹, Matthew Baron², Hyunjun Sim², Sangho Lee¹, Xinyuan Zhang¹, Young Joon Hong³, Darrell Schlom² and Jeehwan Kim¹; ¹Massachusetts Institute of Technology, United States; ²Cornell University, United States; ³Sejong University, Korea (the Republic of)

Growth of single-crystalline films by remote epitaxy has been studied for the past few years, however the underlying physics and mechanism of remote nucleation and growth have not yet been fully understood. As a result, remote epitaxy may be confused with van der Waals epitaxy, or especially through-hole epitaxy that also involves the use of 2D layers.

Since 2D layers are atomically thin and therefore easy to damage, preparation of 2D-layer coated substrates for remote epitaxy can suffer from tearing, wrinkles, and pinholes of the 2D layer during transfer. This brings up the question whether remote epitaxy is actually happening remote, or whether through-hole epitaxy is dominating such that nucleation from direct epitaxy through pinholes eventually coalesce to form the epilayer.

One example of widely used through-hole epitaxy, is epitaxial lateral overgrowth, where growth takes place on a periodic mask covering the substrate. This method has been widely utilized for semiconductor materials to block dislocations threading from the substrate. However, it can only be applied to certain materials such as III-V, III-N materials like GaN or InGaAs that exhibit lateral growth mode. On the other hand, same methods for oxides would be impossible as they are known to be dominated by vertical growth mode. Also, as remote epitaxy is completed only when the epilayer is both single-crystalline and possible to be peeled off, for through-hole epitaxy to behave like remote epitaxy, stringent requirement for periods and widths of the mask should be imposed for clean exfoliation to take place.

In this talk, we first mimic through-hole epitaxy via graphene mask, where we intentionally nanopattern the graphene to have various widths and periods. Growth of BaTiO₃ on SrTiO₃ covered with graphene masks show that oxides exhibit a strong vertical growth mode such that a fully merged film is impossible to achieve with through-hole epitaxy. Second, by growing GaN on different thicknesses of graphene-coated GaN, we discuss the different nucleation behavior on graphene. Through our fundamental study, we hope to understand remote epitaxy better to provide building blocks for heterogeneous materials platforms for future cutting-edge applications.

3:45 PM NM07.07.05

Atomic-Scale Characterization of Engineered Strain Gradients in Free-Standing Oxide Membranes Harikrishnan Kunhikrishnan Premakumari¹, Varun Harbola², Jaehong Choi¹, Kevin J. Crust², Yonghun Lee², Yu-Tsun Shao¹, Gregory D. Fuchs¹, Harold Y. Hwang² and David A. Muller¹; ¹Cornell University, United States; ²Stanford University, United States

Due to the inherent difficulty of stabilizing large strain gradients in thin films or bulk materials, the study of flexoelectric effects has largely been limited to dislocations, cracks, or other defect sites. However, with the recent advances in lift-off techniques for producing freestanding membranes, it has become possible to engineer and study large strain gradients in nanostructures. Here, using a platform of lifted-off strontium titanate (STO) membranes transferred onto a nanofabricated array of silicon dioxide (SiO₂) nanopillars, we measure large strain gradients ($> 10^6 \text{ m}^{-1}$) near the apex of the resulting folds in the STO membranes using scanning transmission electron microscopy. Through the flexoelectric effect, such high strain gradients induce a polarization of around 25 $\mu\text{C}/\text{cm}^2$, comparable to that in ferroelectric materials. Further, using electron energy loss spectroscopy (EELS), we track the energy shifts in the titanium L_{2,3} edge and observe a monotonic increase of about 0.1 eV in the crystal field splitting energy as we move from a region of positive to negative strain.

4:00 PM *NM07.07.06

Two-Dimensional Crystals and Nanomembranes with In-Plane Dipoles for Energy Conversion and Spintronics [Jian Shi](#); Rensselaer Polytechnic Institute, United States

In the design of high-performance spintronic or energy conversion devices, it has been recognized that in-plane electric dipoles in van der Waals crystals or two-dimensional quantum membranes could provide a plethora of opportunities. For example, it has been widely recently formulated that in-plane ferroelectric polarization in quantum well crystal could produce a unidirectional effective magnetic field through the Rashba-Dresselhaus effect leading to the creation of persistent spin helix. Further, the flexibility in the design of the phononic boundary conditions of low-dimensional crystals allows the possibility for the engineering of phonon dynamics-determined dipole-related physical properties. In this talk, I will present our recent progresses of understanding the relationships between physical properties and in-plane dipole dynamics in two-dimensional crystals and nanomembranes.

4:30 PM NM07.07.07

A Route to Fabricate Mixed Dimensional, Ultrathin Molybdenum Carbide/Selenide Heterostructures [David Sanchez](#), Alexander J. Sredensckek, Da Zhou, Jiayang Wang, Daniel Cintron Figueroa, Andres Fest, Susan B. Sinnott, Joshua A. Robinson and Mauricio Terrones; The Pennsylvania State University, United States

The non-layered, superconducting group VI transition metal carbide (TMC) and layered, semiconducting group VI transition metal dichalcogenide (TMD) families have individually received much attention over the last century with recent advancements in the capability to fabricate ultrathin crystals for nanoelectronics. Tuning the electronic properties of these materials typically involves modifying the transition metal atom; however, we found that manipulating the nonmetal atom also yields significant differences in the physicochemical properties. A previous study by our group demonstrated that post-growth heat treatment of molybdenum carbide (α -Mo₂C) with hydrogen sulfide gas can be used to fabricate an ultrathin, molybdenum carbide/molybdenum disulfide (α -Mo₂C/MoS₂) heterostructure with enhanced superconducting properties [1]. In the present work, we extend the heat treatment process to selenium and successfully formed a non-layered/layered molybdenum carbide/molybdenum diselenide (α -Mo₂C/MoSe₂) heterostructure. We further describe the structure and property relationships of this heterostructure and highlight the differences between the selenization and sulfurization processes. We demonstrated the synthesis of ultrathin, single crystal α -Mo₂C nanoplatelets using a previously reported chemical vapor deposition approach [2]. We studied and identified that the type of selenium precursor and temperature used in the post-growth heat treatment have a significant impact on the resulting α -Mo₂C/MoSe₂ heterostructure. To corroborate the effects of these parameters on the formation of the heterostructure, we implemented structural techniques such as Raman spectroscopy, scanning electron microscopy (SEM), X-ray diffraction (XRD), and planar/cross-sectional scanning/transmission electron microscopy (S/TEM). Electronic transport measurements in a four-point probe arrangement were undertaken to study the changes to the superconductivity of α -Mo₂C and elucidate the transport behavior in the α -Mo₂C/MoSe₂ heterostructure. First-principles calculations were also performed to study the energetic and electronic characteristics of the interface. Finally, we propose a general conversion mechanism and highlight key synthesis aspects to fabricate ultrathin, atomically-sharp TMC/TMD heterostructures which are critical to applying these novel materials to nanoelectronics.

1. F. Zhang, et al., PNAS, 2020, 117 (33), 19685-19693.
2. C. Xu, et al., Nat Mater, 2015, 14 (11), 1135-1141.

SESSION NM07.08: Poster Session II
Session Chairs: Kyusang Lee and Yu-Jung Lu
Wednesday Afternoon, November 30, 2022
8:00 PM - 10:00 PM
Hynes, Level 1, Hall A

NM07.08.01

New Metallic Aerogels from 1D to 3D Structures—Electrical, Mechanical and Electrochemical Properties [Caroline Celle](#), Jean-Pierre Simonato and Maribel Touron; CEA Grenoble, France

Intensive research is carried out on new emerging highly porous materials with high electrical conductivity and very low densities. Silver nanowires (AgNWs) are a dimension-wise building block material for conductive 3D-percolated networks. These materials, due to their spatial organization, are of interest for negative electrode of Lithium batteries.

S. S. Kistler discovered a new class of ultralight materials with remarkable properties in 1931 : the aerogels. since then, a wide range of composition has been studied to obtain unique properties such as lightweight or electrical conductivity. This research work focuses on new aerogels made from silver nanowires and polymers.

Cryogels are obtained by freeze-drying concentrated suspensions. As the solid components are freeze-templated, cryoprotectants, freezing rates and directions tune the final structure and thus the properties. Pure AgNWs networks lack stability. most binding agents for mechanical properties improvements cause drastic losses in electrical conductivity.

This research work focuses on new aerogels made from silver nanowires and polymers.

The synthesis principle used in this work is based on the assembly of one-dimensional nanowires to form a three-dimensional (3D) network. The organization in space of the solid elements of the aerogel is due to the freeze-drying process. Cryogels are obtained by freeze-drying concentrated suspensions. Variable freezing directions and rates are used to modify the ice-template and thus the final structure and properties. Pure AgNWs networks lack stability. Most of the binders used to improve the mechanical properties cause considerable losses in electrical conductivity.

In this work, we have synthesized new hybrid cryogels with controlled dimensions and good synergistic behaviour. The morphological, electrical and mechanical properties of these aerogels are characterized to provide a better understanding of the relationship between synthesis parameters and final properties. The electrical and mechanical properties as well as the electrochemical stability have been investigated and will be discussed. The unique structures obtained present a very high porosity (higher than 98 percent), a very low density (a few mg.cm⁻³) as well as a high electrical conductivity (hundreds of S.m⁻¹) for a high mechanical strength (higher than ten of kPa) in spite of the high porosity. The applicative interest of these materials is explored. On the one hand, electromechanical characterizations of aerogels are studied in order to develop a piezoresistive sensor (electrical resistance variations of 20 percent for deformations of 50 percent are maintained over a hundred cycles). On the other hand, electrochemical characterizations are carried out in order to use the synthesized aerogels as anodes of lithium metal batteries. A first demonstration as an electrode has been performed in view of a future integration in solid state batteries.

NM07.08.02

Nucleation and Growth of Monolayer MoS₂ by Sulfurization of Faceted MoO₂ Crystals Yeonjoon Jung, Huijie Ryu, Hangyel Kim, Jaewoong Joo, Seong Chul Hong and Gwan-Hyong Lee; Seoul National University, Korea (the Republic of)

Fabrication of stable and clean van der Waals heterostructures has been required to develop 2D materials-based devices with high performance. Even though the vdW heterostructures have been demonstrated by stacking 2D materials, direct growth of 2D materials on other 2D or 3D materials is critical because the interfacial properties are determined by defects, crystallinity, and crystalline rotation angle at the heterointerface. Here, we synthesized highly crystalline monolayer MoS₂ by using a faceted MoO₂ crystals as a growth seed. A seamless heterostructure of metallic MoO₂ and semiconducting MoS₂ was fabricated. We explored how nucleation and growth of the MoS₂ occur on the surface and terraces of the faceted MoO₂ crystals. Although the multilayer are nucleated at different terraces of MoO₂, highly crystalline monolayer MoS₂ with superior optical and electrical properties can be grown on the SiO₂ substrate around edge of the MoO₂ due to different diffusivity on the SiO₂ and MoO₂. We also observed a strong charge transfer between the metallic MoO₂ and semiconducting MoS₂, leading to strong quenching of photoluminescence. Our study provides deeper understanding in growth of 2D materials on the bulky seeds and shows probability to grow high quality 2D materials by controlling nucleation sites and diffusivity of source materials on the target substrate.

NM07.08.04

Strain Modulated Charge Transfer of (0D–2D) ZnS/ZnIn₂S₄ Heterostructure Through a Facile *In Situ* Synthesis for Efficient Solar to Fuel Conversion Amr Sabbah¹, Indrajit Shown², Mohammad Qorbani³, Li-Chyong Chen³ and Kuei-Hsien Chen¹; ¹Academia Sinica, Taiwan; ²Hindustan Institute of Technology and Science, India; ³National Taiwan University, Taiwan

Forming an intermediate electric field at the interface of two semiconductors to facilitate charge transfer and isolate redox reactions is still challenging for catalysis applications. However, great progress has been achieved regarding the rational design of different dimensional semiconductors, the in-situ growth of the heterostructure is considered the best choice to achieve a high-quality interface. In this study, we fabricate a ZnS/ZnIn₂S₄ (0D–2D) heterostructure catalyst, where cubic ZnS crystals are decorating a hexagonal ZnIn₂S₄ (ZIS) layer structured with a high difference in the solubility product constant K_{sp} , using a single pot hydrothermal approach. We used XRD, HRTEM, and band alignment studies to determine the origin of the interfacial charge transfer mechanism, which is based on lattice mismatch and related interfacial microstrain. The structural strain at the interface was caused by lattice mismatch in the composites caused by heterostructuring between two lattices due to the interatomic distances and different crystal symmetries. In addition, this interfacial mismatch strain can induce mid-gap states at the interface that facilitate electron and hole recombination forming a Z-scheme configuration. The low-temperature photoluminescence study was studied to reveal the nature of the defect state at the interface and to provide a clear explanation for the charge carriers' mechanism. The microstructure and spectroscopy analysis both disclose that the optimum ratio of ZnS and ZIS with this (0D–2D) catalyst exhibits improved charge carrier separation and shows significantly enhanced photochemical CO₂ reduction and hydrogen evolution.

NM07.08.05

Flexible and Transparent Nanocomposites with 3D Heterogenous Interfaces for Attachable Optics with Superior UV Protection Junyong Ahn, Seohan Yun, Taehyun Ryu and Junyong Park; Kumoh National Institute of Technology, Korea (the Republic of)

Ultraviolet (UV) rays caused by various electronic devices such as mobile phones and tablets can be harmful to the human body when continuously exposed, so interest in and demand for UV blocking materials and technologies are increasing. In the meantime, many cream-type products containing TiO₂ or ZnO nanopowders have been developed to block sunlight, but the library of film-type transparent materials that can be applied to optoelectronic devices is still not diverse. In this presentation, we present a flexible and transparent nanocomposite embedded with 3D networked ultrathin (< 60 nm) ZnO. Compared with typical 2D thin film materials, 3D networked ZnO has much more scattering and absorption interfaces in the vertical direction, resulting in higher UV blocking efficiency, assuming the same footprint. The morphology of the 3D network is determined by the sacrificial nanoporous template used, and the ZnO content of the nanocomposite is precisely controlled through the process parameters of atomic layer deposition. By optimizing the morphology of the 3D network and the ZnO content, we have successfully realized a flexible nanocomposite film that exhibits both visible transparency (> 60%) and excellent blocking efficiency (> 99%) in the UVB region. The usefulness of the developed nanocomposite film can be further enhanced through additional surface texturing to improve its adhesion function. We plan to present the UV blocking performance of the accessory-type nanocomposite film by attaching it to portable electronic devices and human skin.

NM07.08.06

Readily Transferrable Growth of Crystallographically Aligned GaN Thin Film on Multilayer Graphene Transferred onto Sapphire Substrates by Thru-Hole Epitaxy Hyunkyu Lee and Chinkyoo Kim; Kyung Hee Univ, Korea (the Republic of)

We heteroepitaxially grew GaN films on multilayer graphene transferred onto r-sapphire substrates. XRD measurement and analysis revealed that GaN films, grown on multilayer graphene transferred onto r-sapphire substrates, were crystallographically aligned with an underlying substrate. Despite well-established crystallographic alignment with the underlying substrate, the GaN films were easily detached from the graphene/sapphire template by using a thermal release tape. Due to the usage of thick graphene multilayers, the GaN films were not grown by remote epitaxy. Extensive TEM analysis across the interfacial regions showed that small holes in the nanometer scale played a major role in establishing both crystallographic alignment and easy detachability. In contrast with remote epitaxy, no strict conditions on the number of a layer or defect-free high quality for graphene were required for our growth method, thru-hole epitaxy.

NM07.08.10

Evidence For a Giant Magneto-Electric Coupling in Composites of Coaxial Nanofibers of Nickel Zinc Ferrite and PZT Bingfeng Ge^{1,2}, Jiahui Liu^{1,2}, Jitao Zhang² and Gopalan Srinivasan¹; ¹Oakland University, United States; ²Zhengzhou University of Light Industry, China

Ferromagnetic-ferroelectric composites are of interests for studies on the nature of magneto-electric (ME) interactions between the two phases and for applications in useful technologies. The interactions are aided by mechanical forces, i.e., magnetostriction in the ferromagnet in a magnetic field and piezoelectric deformation in the ferroelectric in an electric field and the strength of ME coupling depends on efficient transfer of strain from one phase to the other. A significant enhancement in the coupling strength can be accomplished in a nanocomposite in which the ratio of surface area-to-volume is orders of magnitude higher than in bulk or thick film composites [1,2].

This work is on the synthesis of nanofibers of nickel zinc ferrite, Ni(1-x)Zn_xFe₂O₄ (x = 0.5-0.9) (NZFO) and lead zirconate titanate (PZT) by electrospinning and measurements of strengths of ME interactions in discs made of the nanofibers. Two types of fibers were made: (i) Core-shell nanofibers with either ferrite or PZT core and (ii) Composites fibers of ferrite and PZT. In electrospinning of core-shell fibers sol-gels of the ferrite and ferroelectrics were dispensed through a dual chamber needle. For composite fibers sols of equal volumes of ferrite and PZT were mixed and dispensed through a single needle. Electric fields, 1.5 – 2 kV/cm, was applied between the needle and a collector made of a rotating aluminum drum. Fibers are formed when the electrostatic forces overcome the surface tension. Core-shell fibers and composite fibers with an average diameter of 200-500 nm were prepared. Fibers were annealed at 700-900 C and characterized in terms of structure by electron microscopy, X-ray diffraction, and scanning probe

microscopy (SPM). Fibers were free of impurities, ferromagnetic parameters for the fibers compared favorably with parameters for bulk NZFO, but the saturation ferroelectric polarization was two orders of magnitude smaller than for bulk samples.

The fibers were pressed into discs for measurements of strength of ME coupling by static magnetic field H induced polarization and low-frequency ME voltage coefficients (MEVC). The fractional change in the remnant polarization dPr/Pr measured as a function of $H=0-7$ kOe and a giant ME coupling was evident in discs made of core-shell fibers. The maximum change in dPr/Pr increased with increase in Zn concentration, from -3% for $x=0.1$ to 82% for $x=0.3$ and then decreased with increase in Zn concentration to -1% for $x=0.5$. A hysteresis in dPr/Pr vs H was measured for all of the discs. Discs of composite fibers, however, had much smaller dPr/Pr -values of -1 to -3%. Data on MEVC vs bias field H obtained by applying a static field H and an ac magnetic field h at 30 Hz, both fields parallel to each other and parallel to the plane of a disk of fibers. Discs of core-shell fibers showed a large ME response at $H=0$ and was indicative of a built-in magnetic field likely due to anisotropy in the fibers. With increase in H , MEVC increased to values as high as 17 mV/cm Oe and then with increase in H decreased to near-zero value. The maximum MEVC for discs of NZFO-PZT composite fibers was small, on the order of 2-3 mV/cm Oe. Thus the results of this study showing a giant ME coupling in discs of core-shell fibers are indicative of their potential use for sensors and energy harvesting applications.

The research at Oakland University was supported by a grant from AFOSR and the National Science Foundation (DMR- 1808892).

References

1. Ying Liu, et.al., MRS Communications 2020, 10, 230.
2. Ying Liu, et.al., J. Compos.Sci. 2021, 5, 268.

NM07.08.11

2D Magnetic Nanosheets Made in Aqueous Suspension Paulo H. Michels Brito¹, Barbara Pacakova¹, Leander Michels¹, Sergio H. Toma², Koiti Araki², Josef Breu³, Kenneth D. Knudsen^{4,1} and Jon Otto Fossum¹; ¹Norwegian University of Science and Technology, Norway; ²University of São Paulo, Brazil; ³Universität Bayreuth, Germany; ⁴Institute for Energy Technology, Norway

The development of 2D nanosheets in stable suspension that respond rapidly to and can be manipulated by applied magnetic fields may become highly desired, for instance extractions. Here we report the efficient and unique approach of decoration of 2D clay nanosheets in liquid suspension with magnetic nanoparticles only in one side. Superparamagnetic iron oxide nanoparticles were used to functionalize insulating transparent synthetic sodium fluorohectorite clay nanosheets with aspect ratio of about 20,000. The nanoparticle density on the nanosheets are tuned to different coverage fractions. Small Angle X-ray Scattering (SAXS), spectroscopy (FTIR, UV-VIS), microscopy techniques (SEM and AFM), and magnetic properties were used to characterize the magnetic nanosheets. This new material opens new possibilities of scalable applications.

NM07.08.13

Selected Area Chemical Vapor Deposition of Three Dimensional Nanoarchitectures John Lasseter¹, Steven Randolph² and Philip Rack¹; ¹University of Tennessee, United States; ²Oak Ridge National Laboratory, United States

We showcase selected area chemical vapor deposition (CVD) on 3D nanostructures by taking advantage of photothermal heat transport, which is intrinsic to the nanostructure and not limited to a specific substrate. Nanostructure templates are deposited through lithographic, direct write and other nanofabrication methods and results indicate the ability to initiate the process below the diffraction limit. Focused Electron Beam Induced Deposition (FEBID) is featured as a high-resolution nanofabrication method with short iteration times. The nanostructures are then irradiated under a focused, unpolarized laser with gas precursor flow and no electron beam to induce photothermal CVD. PtC_x FEBID deposits were systematically investigated to show the effects of laser pulse width, power, and repetition rate on growth rates. Finite element thermal simulations were performed and corroborate experiment - evidence points towards a deposition process dominated by the nanostructure thermal conductivity and geometry, but substrate thermal conductivity and the nanostructure optical absorbance still have some effect. Efforts to create functional nanostructures by utilizing magnetic (Co₂(CO)₈), plasmonic (dimethylgold(III) acetylacetonate) and O₂/H₂O gas coflows for material purification are presented, as well as the ability to modify FEBID deposits in parallel.

NM07.08.14

Emergence of Ferromagnetism in Aluminum/Silver Nanoparticle Composites Ken Hakamata¹, Taku Saiki², Akira Matsuo³, Mahito Yamamoto¹ and Mitsuru Inada¹; ¹Kansai University, Japan; ²kansai University, Japan; ³The University of Tokyo, Japan

The highlight of this study is that the magnetic properties of a composite of superparamagnetic aluminum nanoparticles (Al NPs) and diamagnetic silver nanoparticles (Ag NPs) exhibited ferromagnetism. In addition, temperature-independent paramagnetic components were observed in the composites that were not observed in both Al and Ag NPs alone. These results indicate the induction of unique magnetic moments in the nanoparticle composite and the presence of magnetic exchange interactions within the composites.

Al NPs were prepared by pulsed laser ablation of α -alumina powder in pure water. Scanning Electron microscopy and X-ray diffraction measurements showed that the Al NPs were polycrystalline with an average particle size of 19 nm. The magnetic properties of the Al NPs were measured by MPMS. The M-H curves showed superparamagnetism, but no temperature-independent Pauli paramagnetic component was found. Based on the electron spin resonance measurements, the origin of the magnetic moment seems to be the oxygen defects in the surface oxide layer of the Al NPs.

We prepared (Al NP)_x/(Ag NP)_{1-x} composites by mixing the Al NPs and Ag NP paste, and investigated their magnetic properties by MPMS. It should be noted that the Ag NPs were weakly diamagnetic. With increasing x , the composites showed superparamagnetism, but the increase in saturation magnetization was not monotonic. The $x=0.6-0.8$ composites showed hysteresis in the M-H curves, indicating that the composites were ferromagnetic. In addition, for these composites, a temperature-independent paramagnetic component was observed in the M-T curves. Although the origin and mechanisms of the magnetic properties are under investigation, the experimental results show that the unique magnetic moment is induced in the composites, and the existence of the magnetic exchange interactions inside and/or interface of the composites.

NM07.08.15

Ni-Catalyzed GaP Nanowires and Nanosheets with Crystallographic Phase Control—Implications for Single-Material Heterostructures Bruno C. Silva^{1,2}, Lucas M. Nascimento¹, Helio T. Obata¹, Antonio A. von Zuben¹, Arandi G. Bezerra Jr.³, Wido H. Schreiner⁴, Fernando Iikawa¹, Martien Den-Hertog², Odilon D. Couto Jr.¹ and Monica A. Cotta¹; ¹UNICAMP, Brazil; ²Institut Néel, France; ³Universidade Tecnológica Federal do Paraná, Brazil; ⁴Universidade Federal do Paraná, Brazil

III-V semiconductor nanostructures have been considered for several applications, ranging from quantum computing to optoelectronics and energy conversion [1-3]. In particular, wurtzite Gallium Phosphide nanowires work as a substrate to direct band gap hexagonal Si and SiGe alloys [4]. However, the ability to change morphologies, from nanowires to nanosheets, provides a tool to better adapt the nanostructures to the intended applications. Two-dimensional GaP materials, which have not been explored so far, would make easier their integration into device fabrication processes, and controlling

crystallographic phase transition from zincblende to wurtzite provides the opportunity of creating heterostructures in a single material. Here, we explore these possibilities and report the growth of GaP nanostructures by Chemical Beam Epitaxy, catalyzed by Ni nanoparticles formed from thermal deposition of a thin Ni layer. Samples were obtained under different growth conditions, with temperatures in the range 530-590°C and TEG and thermally-cracked PH₃ as group III and V precursors, respectively. Electron microscopy analysis of the samples shows both nanowires and nanosheets, with the nanosheet population increasing with temperature. High resolution transmission electron microscopy reveals that nanosheets are primarily zincblende, while nanowires present a mixture of zincblende and wurtzite phases. The observed growth rates indicate that Ni serves as a better catalyst for Ga-based nanowires than Au. Atomic force microscopy of the nanosheets reveals width and length values up to 2 and 10 µm, respectively, with 50 to 100 nm thickness. Photoluminescence at low temperatures of the as-grown samples shows characteristic signal from wurtzite GaP crystal structure, with typical defect luminescence as well as optical emissions in the green spectral range at 2.16 eV and 2.20 eV with linewidths ~ 30 meV. These results indicate the feasibility of our approach to grow different types of GaP semiconductor nanostructures using Ni catalysts, and provide new possibilities of heterostructures for this single optoelectronic material. Acknowledgements: FAPESP, CNPq, CAPES

References:

[1] De La Mata M et. al. Nano Lett. 16, 825–33, 2016.

[2] Kelrich A. et. al. Nano Lett. 16, 2837–33, 2016.

[3] Sung, M. et al. Adv. Ener. Mat. 6, 1600087, 2016

[4] Hauge H. I. T. et. al. Nano Lett. 15, 5855–60, 2015.

NM07.08.16

Low Thermal Budget Photonic Curing as a Rapid and Facile Method for the Preparation of Nickel Oxide/Carbon Composites Binod Subedi, Najma Khatoun and Douglas B. Chrisey; Tulane University, United States

Low thermal budget photonic curing technique can process metal organic precursors and convert them into nanocomposites in short period of time (few seconds). In this work, we demonstrate that nickel acetylacetonate (Ni(acac)) can be converted into nanocomposite thin films of nickel oxide and reduced graphitic oxide (NiO-rGO) using this technique. Systematic investigation of morphology, structure, and electrochemical properties of films prepared using different bank voltages of photonic curing (500V, 600V, and 700V) is performed. During photonic curing at these voltages, samples are processed using light energy with peak power per unit area 8.2 kW/cm², 14 kW/cm², and 22 kW/cm² respectively. The total energy irradiated per unit area is kept constant at 43J/cm² for all films by varying the number of pulses. As the peak power used to process the sample increases, maximum temperature of the film also increases, which in turn affects the porosity, quality of crystallinity, and elemental composition in the composites. We studied these films using SEM, TEM, Raman Spectroscopy, and EDXS. We also used films prepared at 700V to construct a hybrid capacitor device with activated carbon as negative electrode and NiO-rGO as positive electrode. CV, GCD and EIS measurements were performed to study the energy storage properties of the films. Thermal profiles of films are also estimated using simulations based on physical properties of the precursor molecules and processing parameters used during photonic curing. Analysis of simulations and experimental results indicate that, to understand and optimize the resulting nanostructures, photochemical reactions also need to be taken into consideration. The study also sheds light into the importance of using higher power as opposed to processing over longer period.

NM07.08.17

Shape-Selective Filtration Using Lamellar Block Copolymer-Based 1D Slit Membranes Maninderjeet Singh and Alamgir Karim; University of Houston, United States

The growing need for highly efficient water purification and bioseparations necessitates innovations in ultra-filtration membranes. Block copolymer (BCP) membranes have emerged as a promising player for efficient ultra-filtration due to their uniform pore sizes and sharp cut-offs. Most of the work in BCP membranes has focused on using cylindrical pores. In this work, we demonstrate novel slit-based membranes using lamellar block copolymers. The lamellar BCPs are vertically oriented in one step film casting process by neutral solvent design. The vertically oriented BCPs are converted to slit membranes using a wet etching process. These slit-shaped membranes demonstrate sharp cut-offs for solute filtration. Furthermore, we demonstrate the first example of enhanced separation of 1-D nanomaterials (nanorods) as compared to the 0-D nanomaterials (nanoparticles) using these slit-based membranes, which is facilitated by the shape similarity of 1-D nanomaterials with the nano-slits. Additionally, we show that these slit-shaped membranes show permeability of similar-sized Lysozyme and BSA proteins while retaining the IgG antibodies, thus making them highly useful for bioseparations. We believe that these slit-shaped membranes will be useful for shape-selective filtrations across a spectrum of applications.

NM07.08.18

Charge Carrier Transfer Dynamics in 0D-2D Heterostructures Studied by Pump-Probe Transient Optical Method Mircea Cotlet; Brookhaven National Laboratory, United States

Mixed dimensional heterostructures present recent interest because they can add in optical, electronic and magnetic properties with respect to the elements used to make the mix. Emerging properties can be expected to occur or improved behavior of existing properties can be obtained rather than the added properties expected by the summation of individual properties. Improved or directed behavior can be achieved for example by understanding interfacial interactions between components which are part of the mix. For example carrier transport at the interface can be regulated if one understands the behavior of this process at the interface. Here we present femtosecond transient optical studies of charge carriers in lead sulphide quantum dot-layered molybdenum sulphide mixed heterostructures and describe the role of nanoparticle size and layer number of the 2D material on the kinetics of charge transport.

NM07.08.19

Direct Growth of Clean-Surfaced Monolayer Graphene on SrTiO₃ Substrates via Metal-Catalyst-Free Chemical Vapor Deposition Mingi Moon¹, Celesta S. Chang², Doyoon Lee², Yun Seog Lee¹ and Jeehwan Kim²; ¹Seoul National University, Korea (the Republic of); ²Massachusetts Institute of Technology, United States

Graphene has been used as a major buffer layer in remote epitaxy, due to its thin, flexible, and sheer nature that allows the strong crystal potential of the substrate to easily penetrate and influence the nucleation of the epilayer. Thanks to the weak van der Waals force of graphene, exfoliation of materials ranging from III-V, III-N to complex oxides has been demonstrated over the past few years. In the beginning, the quality of the obtained freestanding films - smoothness of the surface, percentage of the exfoliated area, or defect density - suffered largely from the quality of graphene as graphene had to be transferred to the host substrate by wet/dry transfer method. These methods are likely to create pinholes, wrinkles and polymer residues on the graphene surface that would highly affect the nucleation. In the efforts of developing direct growth of graphene and other 2D materials on III-V, III-N platforms, wafer-scale exfoliation with high crystallinity has become possible.

As complex oxides host a myriad of different physical properties such as ferroelectricity, piezoelectricity and ferromagnetism, the demand for obtaining wafer-scale with high crystallinity has been increasing. Similarly for complex oxides, several methods have been developed to grow monolayer graphene

on substrates such as MgO, SiO₂, and Al₂O₃ with the aid of metal catalysts. However, the use of metal catalyst itself can degrade the graphene quality during the synthesis of graphene. For example, once Cu catalyst is deposited or scattered on substrates, the following growth process involves evaporation of metal which leads to the creation of pinholes and voids at the graphene surface. Thus, the synthesis of clean-surfaced single layered graphene on oxide substrates has been challenging.

In this study, we demonstrate the method of growing clean-surfaced monolayer graphene on electrically insulating SrTiO₃ (STO) substrates using metal-catalyst-free chemical vapor deposition (CVD). Any potential of contamination was blocked in advance by the treatment of STO substrates with buffered oxide etchant (BOE) and annealing at 1000 °C. The CVD chamber was maintained at ultra-high vacuum (~10⁻⁶ Torr) before growth. Monolayer graphene was formed with the mixture of gas (Ar, H₂, and CH₄) at the atmospheric pressure followed by H₂ etching process to clean the surface of graphene. Quantitative evaluation of the number of graphene layers was carried out using Raman spectroscopy by transferring the graphene on SiO₂ wafer. The quality of as-grown graphene was determined by scanning electron microscopy (SEM) and transmission electron microscopy (TEM) confirming the clean surface and the thickness of as-grown graphene respectively. The change in lattice parameter of STO substrates before and after graphene formation due to carbon absorption was measured by X-ray diffraction (XRD) to estimate the lattice mismatch with the desired epilayer via remote epitaxy. Our growth of clean-surfaced monolayer graphene on STO substrates will provide a platform for remote epitaxy of perovskite-type complex oxides, which will drastically improve the quality of freestanding oxide films and eventually enable the demonstration of wafer-scale exfoliation that has been extremely limited.

NM07.08.22

Unconventional Behavior in Low-Resistance Metal Contacts to High-Purity, hBN-Encapsulated Monolayer Semiconductors [Yang Liu](#), Song Liu and James Hone; Columbia University, United States

Two-dimensional (2D) monolayer semiconductors such as transition metal dichalcogenides (TMDs) have attracted intense attention in electronics and optoelectronics due to properties such as high mobility, direct optical bandgap, and mechanical flexibility. For most applications, optimum performance is attained using high-purity TMDs encapsulated with hexagonal boron nitride (hBN) to minimize extrinsic disorder. However, achieving high-quality contacts to hBN-encapsulated ultrapure monolayer TMDs remains challenging. Here we first report a well-developed flux growth strategy that could produce a series of centimeter-sized single-crystal TMDs with record low defect densities of ~10⁹-10¹⁰ cm⁻², including 2H-WSe₂, 2H-MoSe₂, Td-WTe₂, 2H-MoTe₂ and 1T'-MoTe₂. Next, taking the ultraclean semiconductor WSe₂ as an example, we demonstrate a process for mechanical transfer of metal contacts embedded within hBN onto ultraclean monolayer TMDs that minimizes doping, strain, and interfacial roughness. Using this process, we further show efficient contacts to hBN-encapsulated ultrapure monolayer WSe₂. This method achieves excellent electric performance with room temperature contact resistance R_c near 5 Ω , and enables hysteresis-free transistors with record-high mobility of 655 cm²/Vs at room temperature. Furthermore, these contacts show an ultralong transfer length of 1 μ m, placing them in a regime distinct from previous reports for contacts to TMDs and bulk semiconductors. This work provides a general method of making strain- and doping-free hBN-encapsulated vdW contacts and highlights critical challenges for device applications.

NM07.08.23

Direct Synthesis of Vertically Oriented π -Conjugated Metal-Organic Frameworks on Conductive Substrates [Sun Hae Ra Shin](#), Jinhui Tao, Maria Sushko, Nathan Canfield, Mark Bowden and Praveen Thallapally; Pacific Northwest National Laboratory, United States

The π -conjugated metal-organic frameworks (MOFs) are a new class of MOFs with strong in-plane π -conjugation and weak out-of-plane π - π stacking. The π -conjugated MOFs exhibit notable properties such as intrinsic porosity, crystallinity as well as excellent electrical conductivity mediated by delocalized π -electrons. These unique features have motivated increasing effort to explore the π -conjugated MOFs for promising device applications in optoelectronics, catalysis, and energy that require the π -conjugated MOFs in the form of thin film or coating. In this study, vertically aligned triphenylene catecholate-based MOFs were directly grown on conductive substrates by a simple hydrothermal method. Effects of substrate identity such as surface chemistry and roughness on crystal growth behavior such as nucleation density, orientation, and growth kinetics were investigated.

NM07.08.24

Three-Dimensional Nanofabrication with Sub-20 nm Resolution and Eight-Inch Wafer Scalability via Thermally Assisted Nanotransfer Printing [Tae Wan Park](#), Young Lim Kang and Woon Ik Park; Pukyong National University, Korea (the Republic of)

Nanotransfer printing (nTP) is one of the promising nanofabrication methods due to its process simplicity, cost-effectiveness, and scalability for two-/three-dimensional nanostructures. However, various nTP techniques still have critical challenges for realizing sub-50 nm high-resolution pattern formation at wafer-scale. Here, we introduce a simple and practical thermally assisted nanotransfer printing (T-nTP) process that can effectively produce well-ordered sub-20 nm nanostructures over an 8-inch wafer by the use of a heat-rolling-press system that can provide uniform heat and pressure. The T-nTP process enables reliable pattern formation of metallic (Pt, Pd, Ag) and semiconducting (NiO, WO₃, Ge_xSb_yTe_z) materials with functionalities on diverse substrates including rigid Si, flexible polyethylene terephthalate (PET), and slippery glass. Furthermore, we show the formation of ultrafine (≤ 20 nm) 3D hierarchical nanostructures via the combined method of T-nTP and directed self-assembly (DSA) of block copolymers (BCPs). Moreover, we also demonstrate how to obtain a high-density NiO/Pt memristive crossbar nanoscale pattern with a width of 14 nm, showing excellent unipolar resistive switching behavior. We expect that the proposed novel T-nTP method will be applicable to high-throughput nanofabrication combined with other patterning techniques.

NM07.08.25

Reliable Pattern Transfer Printing from Nanoscale to Sub-Micron Feature Size Using Various Polymeric Replica Materials [Young Lim Kang](#), Tae Wan Park and Woon Ik Park; Pukyong National University, Korea (the Republic of)

Nanotransfer printing (nTP) technology provides good reliability and compatibility with other lithography technologies in the fabrication of high-performance memory devices, wearable displays, and photovoltaics. To obtain various nanoscale to microscale patterns in nTP, the selection of replica materials is very important because of patternability from the contact effect between the target materials and desirable substrates. Here, we show a useful and practical thermally assisted nanotransfer printing (T-nTP) method to generate defect-free nano-/micro-structures on substrates using several polymeric replica materials as transfer-printing media. Specifically, we introduce several candidates for reliable pattern replication from Si master mold with various nano-to-micro patterns, such as poly(methyl methacrylate) (PMMA), polystyrene (PS), and poly(4-vinylpyridine) (P4VP). Furthermore, the realization of highly ordered patterns of metal (Pt) and oxide (NiO, Li₂CO₃) on arbitrary substrate can be achieved by using duplicated soft materials through angled deposition and transfer-printing process. Moreover, we show well-defined nanostructures on the diverse surfaces including Cu foil, slippery glass, flexible PET, and curved surface of goggle. We expect that this pattern formation method using soft materials will be applied to advanced emerging devices with complex patterns.

8:00 AM NM07.09.02

Optical Properties of Xene Heterostructures Grown by MBE Eleonora Bonaventura^{1,2}, Daya Sagar Dhungana¹, Christian Martella¹, Salvatore Macis³, Stefano Lupi³, Emiliano Bonera², Carlo Grazianetti¹ and Alessandro Molle¹; ¹Consiglio Nazionale delle Ricerche, Italy; ²Università degli Studi di Milano-Bicocca, Italy; ³Sapienza - Università di Roma, Italy

The dimensional reduction brought by the advent of two-dimensional (2D) materials opened new routes for nanoelectronics and photonics applications. In this framework, the Xenes (artificial graphene-like mono-elemental lattices) represented a new forefront because of their peculiarities [1]. Unfortunately, the high chemical reactivity and the strong hybridization effects with the native substrates limited their use to date: silicene on silver and tin on sapphire are two of the most striking examples in this respect. Despite the different nature of the above-mentioned substrates - metallic silver and insulating sapphire - their effect on the properties of Xenes is an intriguing framework where the epitaxial growth of the Xenes can be engineered by *ad hoc* processes. While the hybridization between the electronic states of silicene and the underlying silver are predominant in the former case [2], oxidation effects occur in the latter due to the reactivity of tin [3]. For these reasons, the Xene-based heterostructure concept takes on a certain relevance [4]. Vertical stacks of different layers of atomically thin crystals enable to create novel structures and in turn to control their electronic properties. Such stacks, in a close analogy to the van der Waals heterostructures, could offer an unprecedented degree of freedom in discovering new functionalities. Here, we report on the optical properties of new Xenes-based configurations, i.e. silicene-stanene on Ag(111) and stanene-graphene on Al₂O₃(0001), made accessible by spectroscopic measurements in the MIR-UV spectral range (from 0.12 to 6.5 eV) and Raman spectroscopy measurements. Our results highlight the role of the inter-layer in electronically and chemically decoupling the on top Xene from the native substrate, resulting in a different response when two layers are combined. The decoupling effect for silicene on stanene is studied in terms of the photo-thermal Raman response, revealing stark differences in the heat transport properties of single layer epitaxial Xenes and heterostructures [5]. In the case of stanene on graphene, X-ray photoelectron spectroscopy shows an effective role of graphene to avoid tin oxidation, whereas the optical analysis discloses an intriguing response from the tin layer different from that grown directly in contact with the Al₂O₃(0001) substrate. Finally, our findings support the possibility of tuning the well-known plasmonic response of either silver or graphene by combining different atomically thin layers on their surface.

[1] A. Molle, J. Goldberger, M. Houssa, Y. Xu, S.-C. Zhang and D. Akinwande, *Nat. Mater.*, 2017, 16, 163–169.

[2] E. Cinquanta, G. Fratesi, S. Dal Conte, C. Grazianetti, F. Scotognella, S. Stagira, C. Vozzi, G. Onida and A. Molle, *Phys. Rev. B - Condens. Matter Phys.*, 2015, 92, 165427.

[3] C. Grazianetti, E. Bonaventura, C. Martella, A. Molle and S. Lupi, *ACS Appl. Nano Mater.*, 2021, 4, 2351–2356.

[4] D. S. Dhungana, C. Grazianetti, C. Martella, S. Achilli, G. Fratesi and A. Molle, *Adv. Funct. Mater.*, 2021, 31, 2102797.

[5] E. Bonaventura, D. S. Dhungana, C. Martella, C. Grazianetti, S. Macis, S. Lupi, E. Bonera, A. Molle, submitted.

8:15 AM NM07.09.03

Two-Step Annealing and Diffusion-Driven Exfoliation of Cerium-Doped Terbium Iron Garnet on Silicon Substrates Pang-Hsiao Liu¹ and Karthik Srinivasan^{1,2}; ¹University of Minnesota Twin Cities, United States; ²Cornell University, United States

Thin-film rare-earth iron garnets are very promising non-reciprocal materials for isolators or circulators in photonic devices due to large Faraday rotation and low optical absorption. However, integration of these garnets as thin films in photonic systems faces some challenges, including reduced magneto-optical properties due to poor crystallinity in as-deposited films and limited acceptable annealing of semiconductor devices. To solve these problems, cerium-doped terbium iron garnet (CeTbIG) thin films have been deposited on silicon wafers in this work by sputtering followed by various two-step annealing. During deposition, the Ce content was controlled using the bias voltage of the Ce-target for reproducible CeTbIG. A systematic study of annealing was conducted, involving a first low temperature anneal and a second crystallization treatment to determine when exfoliation will occur. Specifically, a 400°C anneal for 3 minutes followed by a set of high-temperature treatments (950°C for 30 seconds then 900°C for 5 minutes) shows excellent crystallinity without the formation of any undesired phases. This is an improvement compared to traditional single-temperature anneals. Also, the high-temperature sequence caused vacancy diffusion, leading to the formation of a gap just inside the CeTbIG thin film at the substrate interface. This gap enables easy exfoliation. By analysis of diffusivities of iron and rare-earth cations from strain rate-stress data, it was determined that the diffusion mechanism may be related to Nabarro-Herring (lattice diffusion) model. The saturation magnetization and Faraday rotation of the exfoliated CeTbIG film were measured and found comparable to those of the CeTbIG film on the silicon substrate. By applying the two-step annealing an optimized CeTbIG exfoliated films were obtained. These films were transferred onto commercially integrated Si-waveguides for characterization of the magneto-optical properties.

8:30 AM BREAK

9:00 AM NM07.09.04

Low-Temperature Growth of 3D Semiconductors with Improved-Quality Using Remote Epitaxy Guanyu Zhou, Rehan Younas, Tian Sun, Galen Harden, Yansong Li, Anthony Hoffman and Christopher Hinkle; University of Notre Dame, United States

Advanced semiconductor technologies such as three-dimensional (3D) monolithic integration and flexible electronics require low-temperature growth of materials that support high-performance devices. However, a big challenge of low-temperature growth is that insufficient atomic diffusion directly leads to poor film quality and consequently poor device performance. Conventional methods to improve growth quality, such as using surfactants, introduce unwanted impurities. Here, using remote epitaxy¹, we show that the quality of low-temperature grown 3D semiconductors are significantly improved on atomically-thin two-dimensional (2D) materials. This is because, from a growth kinetics point of view, atomic diffusion D , which significantly affects film growth quality², is exponentially dependent on substrate temperature T and potential-energy barrier for adatom diffusion V_s : $D \propto \exp(-V_s/k_B T)$. Using remote epitaxy methods, the adatom-substrate interactions are actually attenuated due to the spatial separation by the 2D interlayer, decreasing V_s and improving the growth quality at low temperatures³. Moreover, the surfaces of 2D materials are relatively dangling bond free, providing greatly enhanced adatom diffusion and offering a new route toward improving overlayer growth quality at low-temperature. We demonstrate that, as model systems, GaN and ZnSe grown using WSe₂ and graphene exhibit superior quality with temperatures lower by >200 °C compared to direct growth as characterized by X-ray diffraction and Hall measurements. We also study the growth quality of GaN and ZnSe through tuning the adatom-substrate ionic interactions and the atomic diffusion by changing the thickness and the grain size of the WSe₂ layers, respectively, and find that the growth quality maximizes at an optimized thickness of WSe₂, whereas monotonously increases with larger WSe₂ grain size.

In addition to growth improvement, we further demonstrate an improved method to precisely obtain the band alignment of the ZnSe/WSe₂ heterostructure using X-ray photoelectron spectroscopy, taking advantage of the easy exfoliation of the grown 2D/3D heterostructure off of the substrates. This method

eliminates any concern from electronic structure changes due to quantum confinement caused by needing to use thin overlayers to remain photoelectron transparent in the conventional method.

Our results reveal the *benefits* of a reduced potential field through remote epitaxy, showing significant promise for reducing the growth temperature of 3D semiconductors and other materials as a solution to severe thermal budget constraints. The realization of low-temperature grown, high-performance materials through remote epitaxy can enable transformative new technologies that are greatly limited by severe thermal budget restrictions. Moreover, the 2D/3D heterostructures could also enable promising new heterostructures for novel device designs.

This work was supported in part by NEWLIMITS, a center in nCORE, a Semiconductor Research Corporation (SRC) program sponsored by NIST through award number 70NANB17H041. This work was also supported in part by the SRC through the Global Research Consortium (GRC) program.

1. Kim, Y. *et al. Nature* **544**, 340–343 (2017).
2. Zhang, Z. & Lagally, M. G. *Science* **276**, 377–383 (1997).
3. Brenner, D. W. *Phys. status solidi* **217**, 23–40 (2000).

9:15 AM NM07.09.05

Atomically Clean van der Waals Interfaces for Reliable Remote Epitaxy of Complex-Oxide Membranes Sangho Lee¹, Kiseok Kim¹, Celesta S. Chang¹, Xinyuan Zhang¹, Min-Kyu Song¹, Mingi Moon^{2,1} and Jeehwan Kim¹; ¹Massachusetts Institute of Technology, United States; ²Seoul National University, Korea (the Republic of)

Recent developments in graphene-based remote epitaxy and layer transfer techniques allow for generating a wide range of freestanding complex-oxide membranes with high-crystallinity including perovskite, spinel, and garnet. Such single-crystalline complex-oxide membranes can be easily stacked to form unique material systems, where structurally and chemically incompatible materials are interfaced with each other. Thus, material spectrum can be greatly expanded to explore new physical phenomena by creating the artificial heterostructures as well as to enhance material properties by avoiding the substrate clamping effect. However, graphene transfer – a typical graphene formation process on the growth substrates – inevitably introduces a significant number of unwanted defects such as wrinkles, holes, process residues, and interfacial contamination, which could disturb remote interaction between the substrate and epitaxial layer through graphene and thereby reduce crystal quality and exfoliation yield of membranes. Here, we propose a direct synthesis of two-dimensional (2D) material on the epitaxial substrates of complex-oxides including MgAl₂O₄ (MAO) and Gd₃Ga₅O₁₂ (GGG) to demonstrate reliable remote epitaxy of spinel CoFe₂O₄ (CFO) and garnet Y₃Fe₅O₁₂ (YIG) respectively via defect-free 2D interlayer. Atomically clean van der Waals (vdW) interfaces created by a direct growth of 2D material onto growth substrates offer an ideal platform for high-throughput production of single-crystalline complex-oxide membranes and efficient manipulation of physical properties at well-defined heterointerfaces.

9:30 AM NM07.09.06

Nucleation of Hexagonal Germanium Grains on Defect Engineered MoS₂ Monolayers Xuejing Wang¹, Ryan Kaufmann², Renjie Chen³, Towfiq Ahmed⁴, Michael T. Pettes¹, Paul G. Kotula⁵, Ismail Bilgin⁶, Swastik Kar⁷ and Jinkyong Yoo¹; ¹Los Alamos National Laboratory, United States; ²The University of British Columbia, Canada; ³University of California San Diego, United States; ⁴Pacific Northwest National Laboratory, United States; ⁵Sandia National Laboratories, United States; ⁶Ludwig-Maximilians-Universität München, Germany; ⁷Northeastern University, United States

Hexagonal group IV semiconductors have shown great potential for optoelectronic devices as they possess direct electronic band gaps. However, challenges exist in reliable synthesis, which has been majorly limited to structural transfer in order to maintain the hexagonal in-plane lattices. In this work, we demonstrate the formation of hexagonal germanium (Ge) using molybdenum disulfide (MoS₂) monolayer substrates. Suggested by quantum molecular dynamics calculation, the hexagonal Ge is thermodynamically preferable to cubic Ge on monolayer MoS₂ with sulfur vacancies in certain temperature ranges, which is verified experimentally by transmission electron microscopy analyses. Structural characterization and Raman measurements have revealed that strain at Ge grain boundaries can facilitate nucleation of hexagonal Ge phase. Our reported approach to nucleate hexagonal Ge paves the way to accomplishing continuous thin films of hexagonal group IV semiconductors. Moreover, this study provides understanding on the formation mechanisms of heterostructures composed of two-dimensional materials and conventional three-dimensional semiconductors.

9:45 AM *NM07.09.07

Controlling the Location and Morphology of 3D Nanostructures During van der Waals Epitaxy Frances M. Ross; Massachusetts Institute of Technology, United States

van der Waals epitaxy enables the integration of 2D and 3D materials, optimally creating well-ordered 2D/3D interfaces with properties suitable for electronic devices. Critical aspects of the deposited 3D material, such as the density and location of nucleation sites and the morphology of epitaxial islands, depend globally on growth and materials parameters but locally on the condition of the initial van der Waals surface. Here we discuss how the 2D surface can be patterned before growing the 3D material so that a spatially inhomogeneous deposit results. We first discuss the importance of the substrate on which the 2D layer is supported. We demonstrate that freestanding regions of graphene show orders of magnitude lower nucleation density for Au, compared to the surrounding supported areas. This phenomenon, which we attribute to the effect of roughness on diffusion parameters, represents a method of patterning the deposited material that does not involve lithography of the top surface of the 2D layer. We next discuss the use of defects and step edges to modify nucleation sites, and consider the use of strain transfer across freestanding regions of the 2D material to control island shape and create stacked self-assembled structures. We finally describe nucleation and morphology control through heterogeneous sites, which may be catalytic nanomaterials or structures that modify surface energy locally. By combining these strategies, we suggest that modification of a 2D layer followed by van der Waals epitaxy presents versatile opportunities to form mixed dimensional structures that combine 3D materials on 2D surfaces.

10:15 AM NM07.09.08

Micro- and Nanowires of Ni and Mn Oxides and Their Heterostructures Synthesized by a One-Step Vapor Solid Method Javier Garcia-Alonso, David Maestre and Ana Cremades; Universidad Complutense de Madrid, Spain

The synthesis of transition metal oxide micro- and nanostructures with controlled dimensions, morphology and composition have gained increasing relevance in recent years due to their wide range of applications in many fields of research such as photocatalysis, spintronics, optoelectronics, and energy storage [1]. The achievement of controlled doping and the fabrication of heterostructures based on these oxides at the micro- and nanoscale are go-to topics that can broaden the field of applications of these materials. Different synthesis processes have been explored so far to obtain elongated structures of Mn and Ni oxides with controlled morphology, composition and structural properties, however in most cases the growth of heterostructures formed by these oxides require of more complex synthesis routes with different steps.

In this work, we present the synthesis and characterization of Mn and Ni oxides in form of elongated microstructures, nanowires, and hierarchical structures. Combination of NiO with metallic Mn and Ni powders were used as precursors. After thermal treatments at 1000 – 1500°C under a controlled Ar flow the growth of high yield of elongated micro- and nanostructures through a one-step vapor – solid method is promoted. The elongated microstructures present a square base with dimensions usually in the range of tenths of microns and lengths up to hundreds of microns. Most of these elongated microstructures show the growth of nanowires with lower dimensions at their apex, leading to brush-like morphologies, as confirmed by electron

microscopy. These nanowires, in some cases following hierarchical growths, show diameters from tens to hundreds of nanometers and tend to grow from nucleation points related to variations in the Ni/Mn composition. The bigger microrods show Mn-rich areas mainly related to Mn_3O_4 while the bunch of nanowires at the apex is associated with Ni-rich areas mostly formed by NiO and diverse Mn-oxides, as demonstrated by XRD and micro-Raman spectroscopy. Considering that NiO is one of the few p-type oxides, this one-step growth can lead to the formation of p-n heterostructures at the micro- and nanoscale. Moreover, Ni doped Mn_2O_3 and Mn doped NiO are also promoted during the growth, as confirmed by energy dispersive x-ray spectroscopy (EDS).

X-ray photoelectron spectroscopy (XPS) spectra confirm variation mainly in the Mn(2p) and O(1s) core levels as a function of the probed regions along the elongated structures. Finally, photoluminescence acquired with a 325 nm laser indicates the presence of a broad visible emission centered around 500 nm at the region with nanowires, which can be related to the presence of Ni vacancies in the NiO areas.

The achievement of low dimensional elongated structures presenting a hierarchical growth based on transition metal oxides will improve the applicability of these materials in diverse fields of technological research.

[1] J. García-Alonso, D. Maestre, E. Nogales, A. Cremades, B. Mendez. "Study of NiGa2O4 microneedles grown by a thermal-evaporation method". J. García-Alonso, D. Maestre, E. Nogales, A. Cremades, B. Méndez. *Journal of Alloys and Compounds*, 919 (2022), 165718

10:30 AM NM07.09.09

In Situ X-Ray Studies of Remote Epitaxy of Perovskite Oxides on Graphene [Hua Zhou](#), Xi Yan, Hui Cao, Yan Li, Hawoong Hong, Nathan Guisinger and Dillon D. Fong; Argonne National Laboratory, United States

Remote epitaxy is a novel synthesis technique that allows for the fabrication of thin, freestanding single crystals and nanomembranes. It relies on a sacrificial graphene layer between a thin film and a single-crystalline substrate: during film deposition, the electronic interactions across the graphene are strong enough to enable epitaxial growth but weak enough to allow mechanical release of the film. Others have demonstrated methods for the fabrication of freestanding structures, but the procedures are often materials-specific in terms of the interlayer permitting epitaxial growth. Use of a more universal interlayer can facilitate the development of "stacktronics", where a variety of single crystalline materials can be laid atop each other at low to moderate temperatures, leading to the synthesis of complex van der Waals heterostructures. Details regarding nucleation and growth via remote epitaxy remain unknown, however, due to the many difficulties in studying synthesis in the growth environment with atomic-scale resolution. Thus, advances in stacktronics require improved understanding of remote epitaxy and insight into the impact of interlayer thickness and deposition conditions on the nucleation and growth of thin films. This necessitates *in situ* studies sensitive to the atomic-level structure conducted in the growth environment. *In situ* measurements are particularly important for the synthesis of complex oxides such as perovskite oxides, where small changes to the degree of oxygen incorporation can impact the properties of the film / interface as well as degrade the graphene interlayer.

In this talk, we will demonstrate a set of *in situ* studies of perovskite oxide thin film synthesis on polycrystalline graphene few layers, using synchrotron X-ray scattering to investigate the deposition of $SrTiO_3$ (STO) and $LaNiO_3$ (LNO) by molecular beam epitaxy (MBE) onto graphene-coated STO (001) substrates. X-ray phase retrieval methods are used to reconstruct the electron density profiles from X-ray crystal truncation rods measured under different growth conditions. Our *in situ* observations combined with post-growth spectroscopy provide a number of key insights regarding graphene in the synthesis environment and the resulting effects on the complex oxide / graphene heterostructure. We observe the effect of oxygen partial pressure on graphene-coated STO, finding that most of the graphene is removed at $pO_2 = 2 \times 10^{-4}$ Torr at 760°C. Lower oxygen partial pressures can be used for the growth of $SrTiO_3$ on graphene, which was confirmed by the deposition of 12UC STO on 1ML G. The crystallinity of the film, however, depends on both its thickness and the thickness of the interlayer: for example, 12UC STO is epitaxial when grown on 1ML G but polycrystalline when grown on 2ML G; 3UC STO is epitaxial on 4ML G but becomes more polycrystalline with increasing film thickness. The crystal quality appears to depend on the additional electron density lying above the topmost graphene layer ($> 9 \text{ \AA}$), as nuclei formed on these regions may have poor interaction with the underlying crystal substrate. We also find the etching of graphene in an ozone environment for LNO remote epitaxy even with the presence of an STO buffer layer on graphene interlayers. So, thicker oxide buffer layers and the use of single crystalline graphene may be necessary for the synthesis of nickelate heterostructures on graphene.

SESSION NM07.10: Growth and Application of Various Dimensional Materials and Heterostructures

Session Chair: Rachael Myers-Ward

Thursday Afternoon, December 1, 2022

Hynes, Level 2, Room 203

1:30 PM *NM07.10.01

Hydride Vapor Phase Epitaxy as a Platform for Materials Integration [Aaron Ptak](#); National Renewable Energy Lab, United States

Hydride vapor phase epitaxy (HVPE) is an epitaxial growth technique developed many decades ago that has seen a resurgence in recent years. HVPE is well-known for producing very pure material at very high growth rates. This led to the development of, for example, high-quality GaN templates on sapphire substrates that enabled nitride devices grown by other techniques. In recent years, however, HVPE has moved into producing nitride and oxide devices on its own, and has now branched into arsenide and phosphide devices as well due to the advent of the Dynamic-HVPE technique. In Dynamic-HVPE, the substrate moves between adjacent growth chambers to create chemically- and structurally-abrupt heterointerfaces, which was not possible using more traditional HVPE methods.

Another beneficial property of HVPE is the ability to tune the kinetics of growth on different surfaces, leading to the ability to create useful surface features. These include peak-and-valley morphologies and other surfaces with stable facets that can be used to create, for example, quantum wires. HVPE growth parameters can also be tuned to planarize surface features when desired. This latter feature may enable simple substrate reuse by planarizing rough morphology resultant from reusing a substrate many times after device exfoliation. This talk will describe different aspects of the HVPE growth technique and how they can be used to develop materials with useful morphology.

2:00 PM NM07.10.02

Reconfigurable Heterointegration of Artificial Intelligence Chips Using GaAs/InGaP-Based Optoelectronic Devices Chanyeol Choi¹, [Min-Kyu Song](#)¹, Hyunseok Kim¹, Jihoon Kang¹, Hanwool Yeon², Celesta S. Chang¹, Jun Min Suh¹, Jiho Shin¹, Huaqiang Wu³, Peng Lin⁴ and Jeehwan Kim¹;

¹Massachusetts Institute of Technology, United States; ²Gwangju Institute of Science and Technology, Korea (the Republic of); ³Tsinghua University, China; ⁴Zhejiang University, China

The deployment of conventional integration technologies still faces the issues including material degradation due to intimate contact between chips, fixed modality due to fixed connection to one single sensor, and limited data processing due to constraint for addition of processors in varying computing situation. In this work, we developed a novel reconfigurable 3D heterogeneous integration platform using optoelectronic devices for chip-to-chip communication. Freestanding GaAs/InGaP membrane was integrated into each chip by epitaxial lift-off (ELO) process. Chip-to-chip communication was enabled by optical transmission between GaAs LEDs and InGaP photodiodes. Optical communication without any electrical interconnect resulted not only in elimination of interference from physical contact, but also in great reconfigurability of the chips. Furthermore, the neuromorphic computing layers were embedded in each stackable chip as AI hardware accelerators for extremely efficient processing. This technique will solve the shortcomings of previous conventional 3D heterogeneous integration methods. With the Lego-like 3D heterointegration method based on the GaAs/InGaP stack, the sensor-computing systems can provide unlimited modality, highly efficient computing and adaptability to varying computing tasks.

2:15 PM NM07.10.03

High Indium Content InGaN Strain Relaxation [Yunpeng Liu](#) and Jeehwan Kim; Massachusetts Institute of Technology, United States

Light-emitting diode (LED) is the most popular light source in the modern world. Because LED owns higher efficiency and brightness compared with conventional light sources, it is widely used in the illumination and the display of numerous devices. Due to its tunable bandgap, indium gallium nitride (InGaN) has been used as the material to make blue and green LEDs. However, in order to decrease the band gap of InGaN, more indium has to be incorporated into the material, which leads to a high lattice mismatch between the InGaN layer and the GaN substrate. This mismatch causes the low quality of high indium content InGaN, which obstacles the approach to use InGaN as the base material for RGB (red, green and blue) pixels. Here, we propose a method to fabricate high quality LED based on InGaN with high indium content using remote epitaxy. Conventionally, when an epilayer is grown on the substrate using epitaxy methods such as molecular beam epitaxy (MBE) and metal organic chemical vapor deposition (MOCVD), the lattice structure of the epilayer always perfectly follows the lattice structure of the substrate. Therefore, the epitaxial InGaN layer is always strained on the substrate because they are connected by strong covalent bonds.

Remote epitaxy provides a way to avoid this constraint. When a layer of 2D material is deposited prior to the epilayer, the epilayer grown on the top of the 2D material still follows the crystalline structure of the substrate under the influence of the penetrated potential field from the substrate. However, unlike normal epitaxy methods, the epilayer of remote epitaxy spontaneously relaxes due to the slippery surface of the 2D material. The Van der Waal force on the 2D material doesn't limit the relaxation like the covalent bond. Therefore, high quality InGaN can be obtained with this method. We have demonstrated the remote epitaxy based on in-situ MBE grown amorphous boron nitride (aBN). By doing the in-situ remote epitaxy, contaminations are avoided, and epitaxial membrane quality is improved compared with the previous transferred graphene method. High quality single-crystalline GaN is obtained with this method. These results show that aBN can be a good candidate for the InGaN remote epitaxy and build the foundation for this work. By depositing InGaN on 2D/GaN substrate, the misfit strain can be relaxed from the beginning of the growth regardless of the indium composition. By avoiding the strain-relaxation process, most of the dislocations can be eliminated. Similarly, the relaxed film also helps alleviate the quantum-confined Stark effect.

2:30 PM BREAK

3:00 PM *NM07.10.04

High-Quality SiC Remote Epitaxy for Stackable Electronics [Rachael Myers-Ward](#), D. Pennachio, Jenifer Hajzus, Andrew Lang and R Stroud; Naval Research Laboratory, United States

Remote epitaxy (RE) is a growth process performed on a graphene-covered substrate where the adatom registry is guided by the electrostatic fields penetrating through the graphene from the underlying substrate rather than interactions with the graphene lattice. The remote epitaxy is easily exfoliated from the substrate due to weak van der Waals bonding of the graphene to the substrate, enabling transfer to desired substrates and thus allowing heterostructures that typically cannot be created with current methods. This technique has the possibility of impacting several research areas including SiC and GaN SMART power, integration of opto- and electronic devices, improving HEMT performance by transferring to higher thermal conductivity substrate, flexible electronics and quantum sciences.

In this work, we focus on the RE of SiC grown on graphene on SiC (0001) using a hot-wall chemical vapor deposition reactor. Controlling the thickness of graphene is achieved using off-axis substrates, where 1 – 5 monolayers is possible. To maintain the graphene during SiC remote epitaxy, a study of the Ar/H₂ flow ratio during remote epitaxial growth was conducted. Single crystalline material was achieved for both the on- and off-axis substrates when a low C/Si ratio was used. This growth condition resulted in a stepped film morphology for the on-axis substrate while the off-axis substrate produced intermittent step bunching, consistent with typical off-axis growth at low C/Si ratios. Films were characterized using Nomarski microscopy, scanning electron microscopy, transmission electron microscopy and electron backscattering detection. In summary, the growth of high quality SiC RE is shown to result from both on- and off-axis SiC substrates and has the possibility to be used for power electronics and quantum sciences applications.

Research at NRL was supported by the Office of Naval Research.

3:30 PM NM07.10.05

DFT Atomic-Scale Modeling and Simulation of Ultrawide Bandgap (UWBG) Heterostructured Materials [Ugonna C. Ohiri](#), Stephen Van Campen, Robert Howell and Josephine Chang; Northrop Grumman Corporation, United States

Ultra-wide bandgap (UWBG) materials (i.e., $E_g > 3.4$ eV) possess superior material properties for enabling the next-generation of high-power density and high-performance radio-frequency (RF) monolithic microwave integrated circuit (MMIC) devices. There has been recent major interest in developing high-performance diamond electronics, but there are still some challenges which exist for diamond as a material, such as incomplete ionization for highly n+ doped epilayer films and weak electron mobility at high operating temperatures.

Here, we report on a deep dive exploration into various UWBG materials (e.g., Diamond, Ga₂O₃, AlN, cubic boron nitride, hexagonal boron nitride, etc.), and understanding how these UWBG materials form intriguing heterogeneous interfaces with each other. High-throughput density functional theory (DFT) atomic-scale modeling and simulation studies will be presented on these various UWBG materials and a combination of UWBG heterointerfaces. Simulated electronic material parameters such as electronic band-structures, projected density of states (PDOS), electron/hole mobility, thermal conductivity, and Raman will be presented. For example, cubic boron nitride (c-BN) is strongly lattice matched to diamond, is iso-electronic with diamond, and is a strong candidate for enabling diamond/c-BN based two-dimensional electron- and hole gas (i.e., 2DEG and 2DHG) based field effect transistors and other interesting high-power device configurations. This presentation will highlight and also take a deeper exploration into various undoped and doped diamond/c-BN heterointerfaces.

Overall, the presented DFT modeling and simulation results will shed light into what combination of UWBG materials are within the physical design space

and will lay a general pathway for physically realizing high-power density and high-performance RF MMIC devices.

3:45 PM NM07.10.06

Amorphous 2D Materials – A Novel Platform for Remote Epitaxy and Nanopatterned Epitaxy of III-V Semiconductors with Low Decomposition Temperatures [Kuangye Lu](#), Hyunseok Kim, Sangho Lee, Ne Myo Han, Yunpeng Liu and Jechwan Kim; Massachusetts Institute of Technology, United States

III-V semiconductor materials such as indium phosphide (InP) offer outstanding photonic properties that outperforms silicon, but the cost of these wafers is extremely expensive. Although reusing original wafers can effectively minimize the cost, current techniques for wafer recycling of these substrates add significant costs in fabrication, nullifying the cost savings by reusing the wafers. Besides, unlike other III-V materials such as gallium arsenide (GaAs), commonly used epitaxial lift-off method for wafer recycling is not well studied for materials like InP due to lack of lattice-matched sacrificial layers, which makes reusing these wafers more difficult. Remote epitaxy and nanopatterned epitaxy are newly discovered methods that enable single-crystal growth of III-V semiconductor thin films and easy exfoliation of these grown films, thus promising for a new cost-effective pathway of reusing wafers. However, previous methods of transferring two-dimensional (2D) materials, which use polymethyl methacrylate (PMMA) or metal stressor layers to transfer 2D materials grown on foreign substrates like copper (Cu) or silicon carbide (SiC), introduce defects and damages on the 2D layer and/or substrates during the transfer process. Remote epitaxial and nanopatterned epitaxial films grown on the damaged 2D layer/substrate suffer from lower crystal quality and imperfect exfoliation, which undermines wafer reusability and device performance.

Here we report the MBE growth of amorphous boron nitride (a-BN) on InP wafers at low temperature that enabled improved quality of remote epitaxial and nanopatterned epitaxial films and their perfect exfoliation. We show fully covered a-BN on InP substrates despite their low decomposition temperatures. The surface of a-BN coated InP substrate remains smooth with a RMS roughness of around 3Å. We also demonstrate 100% coverage of single-crystal InP thin films grown on a-BN, with the film's quality significantly improved compared to the case of transferred 2D materials. In addition, the growth and exfoliation were successfully repeated multiple times, proving the feasibility for InP wafer recycling. Through this low temperature MBE growth approach with remote epitaxy and nanopatterned epitaxy, we successfully demonstrate large-scale flexible thin film exfoliation and recycling of InP substrates, which will lead to new opportunities in InP thin film-based photonics and novel heterostructures with significantly reduced cost.

4:00 PM *NM07.10.07

From III-Vs to Si: Thin Film Electronics for Imaging and Energy [Stephen R. Forrest](#), Rebecca Lentz, Byungjun Lee, jihun lim, Dejiu Fan, Bosun Roy-Layinde, Tobias Burger and Andrej Lenert; University of Michigan, United States

The combination of non-destructive epitaxial liftoff and cold weld bonding of III-V materials developed in our laboratory has opened the way to realizing a variety of thin film inorganic semiconductor devices that can serve applications that have heretofore not been accessible to conventional semiconductors. (Lee et al., 2014) For example, we have demonstrated devices as diverse as cylindrical and hemispherical imagers (the latter of which that undergo a topological transformation during fabrication), (Fan et al., 2019) and more recently, extremely high efficiency thermal photovoltaics that employ exceptionally long air-bridges where the very thin active semiconductor is suspended between gold pillars. (Fan et al., 2020) More recently, we have demonstrated air-bridge TPVs in Si to obtain more favorable economics for this important renewable energy storage application. In this talk we will discuss advances and state of the art in thin film electronics, considering current applications and prospects for the future.

Fan, D., Burger, T., McSherry, S., Lee, B., Lenert, A. J. & Forrest, S. R. 2020. Nearly perfect photon utilization in an air-bridge thermophotovoltaic cell. *Nature*, 586, 237.

Fan, D., Lee, B., Coburn, C. & Forrest, S. R. 2019. From 2D to 3D: Strain-and elongation-free topological transformations of optoelectronic circuits. *Proc. National Academy of Sciences*, 201813001.

Lee, K., Zimmerman, J. D., Hughes, T. W. & Forrest, S. R. 2014. Non-Destructive Wafer Recycling for Low-Cost Thin-Film Flexible Optoelectronics. *Adv. Functional Mater.*, 24, 4284.

4:30 PM NM07.10.08

van der Waals Epitaxy of Oxide Thin Films on Flexible Synthetic Mica for Modulation of Physical Properties by Bending Stress [Yuta Arata](#), Hiroyuki Nishinaka, Minoru Takeda and Masahiro Yoshimoto; Kyoto Institute of Technology, Japan

Modulations of the physical properties of materials by doping, alloying, and straining play an important role in electronics and optoelectronics. Recently, it has been demonstrated that the various properties of single nanowires were modulated by strain [1, 2]. However, the difficulty of bending a single nanowire is a significant barrier to applying devices. On the other hand, thin films deposited on flexible substrates can be simply bent. However, conventional flexible substrates, amorphous organic compounds such as polyimide (PI) and polyethylene terephthalate (PET), do not allow epitaxial growth of single-crystal thin films. It has been demonstrated to transfer the thin films to the flexible substrates; however, complicated processes such as epitaxial lift-off and sacrificial layer etching were required [3, 4]. We utilized synthetic mica substrates to directly grow epitaxial oxide thin films via van der Waals epitaxy [5]. The synthetic mica substrates can be thinned and bent easily by cleaving. We used the cleaved synthetic mica to bend the thin film and the strain applied by bending to modulate the properties.

We grew ZnO thin films on the synthetic mica substrates and demonstrated the modulation of optical properties by bending strain. ZnO thin films were grown by mist chemical vapor deposition (CVD) using a solution of zinc acetylacetonate ($Zn(C_5H_7O_2)_2$) dissolved in a mixture of methanol and de-ionized water as a precursor. Epitaxial ZnO thin film was grown on synthetic mica at a growth temperature of 400 °C. To investigate the impact on the optical properties by strain, we measured photoluminescence (PL) of the ZnO thin film with and without bending. By bending with a radius of curvature of 5 mm, the peak energy was red-shifted to 0.02 eV compared with an unbent state. Thus, we have successfully modulated the PL peak of the ZnO thin film with the bending strain.

In addition, we grew epitaxial VO₂ thin film on the synthetic mica and demonstrated modulation of the metal-insulator transition temperature by the bending strain. We utilized SnO₂ buffer layers to grow epitaxially VO₂ thin films. VO₂ and SnO₂ layers were grown by mist CVD using vanadyl acetylacetonate ($VO(C_5H_7O_2)_2$) and tin chloride pentahydrate ($SnCl_4 \cdot 5H_2O$) as precursors, respectively. Epitaxial VO₂ thin film were grown on the SnO₂ buffer layer on the synthetic mica at a growth temperature of 500 °C. Using the epitaxial VO₂ thin film with bendable, we measured the electrical resistance as a function of temperature with and without bending. VO₂ thin film exhibited metal-insulator transitions both with and without bending. By bending with a radius of curvature of 5 mm, the metal-insulator transition temperature increased by 2.5 °C compared to the unbent state.

In the symposium, we will discuss the magnitude of strain with bending and detailed measurements of PL and metal-insulator transition characteristics.

[1] B. Wei *et al.*, *Nano Lett.*, **12**, 4595 (2012). [2] M. Zapf *et al.*, *Nano Lett.*, **17**, 6637 (2017). [3] L. Shen *et al.*, *Adv. Mater.*, **29**, 1702411 (2017). [4] W. H. Dong *et al.*, *ACS Appl. Mater. Interfaces*, **11**, 30477 (2019). [5] Y. Bitla and Y. -H. Chu, *Nanoscale*, **12**, 18523 (2020).

1:30 PM *NM07.11.01

Heterogeneous Integration of Complex-Oxide Membranes [Hyunseong Kum](#); Yonsei University, Korea (the Republic of)

We will discuss our recent results in producing thin complex-oxide membranes, as well as applications integrating complex-oxides onto conventional semiconductor devices. Detailed characterization of the transferred complex-oxide/semiconductor interface will be presented.

2:00 PM NM07.11.02

Controlling Exciton Dynamics at Organic/2D Interfaces with Nanoscale Molecular Patterns Kushal Rijal, Stephanie Amos, Pavel Valencia-Acuna, Fatimah Rudayni, Neno Fuller, Hui Zhao, Hartwin Peelaers and [Wai-Lun Chan](#); University of Kansas, United States

Recently, the moiré pattern formed at 2D transition metal dichalcogenide (TMD) heterostructures has been used to control the dynamics of interlayer excitons (IX) at the TMD/TMD interface. At organic/TMD interfaces, similar periodic potentials can be created by controlling the nanoscale molecular pattern on top of the 2D layer. In this work, two molecules, PTCDI and PTCDA, which possess similar properties but form different molecular patterns on a MoS₂ surface, are investigated. Using photoemission spectroscopy, a large HOMO energy level splitting is observed in PTCDI on MoS₂, but not in PTCDA on MoS₂. Density functional theory calculation shows that the splitting originates from the different molecular patterns. The energy splitting causes very different IX's dynamics for the two heterostructures, which are studied by time-resolved photoemission spectroscopy. For PTCDI/MoS₂, the electron within the IX is spatially localized near the interface. On the other hand, for PTCDA/MoS₂, the electron within the IX is delocalized across the molecular film. Because of the spatial localization, the IX at PTCDI/MoS₂ shows an order of magnitude stronger photoluminescence intensity as compared to the IX at PTCDA/MoS₂. On the other hand, the IX at PTCDA/MoS₂ is more likely to dissociate into free carriers because of the electron delocalization within the IX. This work is supported by NSF grant DMR-2109979.

2:15 PM NM07.11.04

Growth of Thin-Film WS₂ for Solar Cell and Photodetector Applications [Mohd Samim Reza](#), Tejveer S. Anand, Henam S. Devi and Madhusudan Singh; Indian Institute of Technology Delhi, India

Tungsten disulfide, a transition metal dichalcogenide (TMDs) semiconductor, has a bulk phase bandgap of 1.35 eV, very close to the Shockley-Queisser limit for two-level systems at AM1.5G solar spectrum, making it a compelling material for solar photovoltaic applications[1]. Its applications in photovoltaics are still in their inception due to the difficulty of obtaining a uniform, pin-hole-free WS₂ thin film with good adhesion [2,3]. This work reports on a two-step process involving sulfurization to grow a WS₂ thin film on a SiO₂ substrate (University Wafers) using a custom-built 12-zone horizontal split furnace (Quazar Technologies) for possible solar cell and photodetector applications. A thin film (~10 nm) of tungsten was deposited on a SiO₂ substrate at a rate of ~0.6 Å using DC sputtering system (Angstrom Engineering). This thin film was subsequently heated to 800-1100°C under 0-300 sccm of Ar flow in the furnace in presence of elemental sulfur for sulfurization. X-ray diffraction (Rigaku Ultima IV, Copper K α = 1.54 Å) scans of the film revealed a sharp and intense peak at 14.12° (2H-WS₂ nanosheet: JCPDS 08-0237), corresponding to (002) growth with a = 3.154 Å and c = 12.362 Å. The other peaks at 28.12° and 43.20° are inferred to correspond to (004) and (006) crystal planes. Further, Raman spectra (Renishaw inVia confocal microscope-based Raman spectrometer) of the sample reveal in-plane (E_{12g}) and out-of-plane (A_{1g}) vibrational modes at wavenumbers 348.25/cm and 412.90/cm, confirming the WS₂ growth. The wavenumber difference and intensity ratio of E_{12g} and A_{1g} vibrational mode peaks are estimated to be 64.65 and 1.03, respectively, confirming the multilayer growth. Raman mapping over an area of 5.1 x 5.1 μ m with a step size of 300 nm suggests consistent growth free of directional bias in the sulfurization process. The peak differences range from 64.65/cm to 70.72/cm, with an average of 68.34/cm[4], while the intensity ratio ranges from 0.88 to 1.13, with an average of 1.03, again confirming the uniform multilayer growth. Field-emission scanning electron microscope (FESEM, JEOL JSM-7800F Prime) scans indicate formation of nanoflakes. Surface photovoltage spectroscopy (KP Technology KP020+SPS040) was used to measure the work function (-4.613 eV). Atomic force microscopy scans (Asylum Research MFP3D-BIO) were used to estimate the surface roughness of the grown WS₂ layer to be 62.33 nm, while the underlying tungsten layer had a surface roughness of 72.99 nm. This suggests that the process of bulk incorporation of sulfur leads to significant increase in surface roughness. As we expected to fabricate heterojunctions of WS₂ with a variety of solution-phase p-type materials in ongoing work, the resulting increase in surface contact area of the heterojunction is expected to provide a larger number of exciton dissociation sites expected to increase the short circuit current, and to reduce optical reflection of the device[5,6].

References :

1. Physica status solidi (a) 214, no. 12 (2017): 1700218
2. Scientific reports 10, no. 1 (2020): 1-11
3. Materials Today Advances 8 (2020): 100098
4. Scientific Reports 3 (2013): 1755
5. Micromachines 10, no. 9 (2019): 619
6. Progress in Photovoltaics: Research and Applications 30, no. 6 (2022): 622-631

2:20 PM NM07.11.05

Chip-less Battery-less Wireless Electronic Skin by Single Crystalline Freestanding Membranes Yeongin Kim^{1,2}, [Jun Min Suh](#)¹, Jiho Shin¹, Yunpeng Liu¹, Hanwool Yeon³, Kuan Qiao¹, Jiyeon Han⁴ and Jeehwan Kim¹; ¹Massachusetts Institute of Technology, United States; ²University of Cincinnati, United States; ³Gwangju Institute of Science and Technology, Korea (the Republic of); ⁴Amorepacific, Korea (the Republic of)

Electronic skin (e-skin) has been developed to obtain a non-invasive human health monitoring electronic system with its imperceptibility. So far, one of the major shortcomings in this field is the bulky wireless communication system that severely affects its wearability. We introduce a single-crystalline non-Si-based e-skin system where fully conformable, ultrathin, piezoelectric, compound semiconductor membranes are incorporated as power-efficient wireless communication modules and extremely high sensitivity sensors without needing bulky chips and batteries. The developed GaN surface acoustic wave-based device successfully measured three different inputs wirelessly. The consistency and accuracy of the measured heart rate and pulse waveforms over a 7-day period strongly demonstrate the reusability and long-term wearability of our device. This study will change the paradigm of e-skins by providing versatile wireless platforms for fully imperceptible e-skins with very high sensitivity and low power consumption.

2:35 PM DISCUSSION TIME

10:00 AM *NM07.12.01

Mixed-Dimensional Heterostructures via Confinement Heteroepitaxy [Joshua A. Robinson](#); The Pennsylvania State University, United States

The last decade has seen an exponential growth in the science and technology of two-dimensional materials (2D), with emphasis on next-generation electronics due to their atomically thin nature and properties ranging from metallic to insulator. In this talk, I will discuss recent breakthroughs in two-dimensional atomic layer synthesis and properties, including novel confinement techniques to facilitate the formation of non-layered 2D metals, semiconductors, and insulators. In particular, I will discuss the utilization of confinement heteroepitaxy (CHet) as a platform to create novel heterostructures that are the foundation for a range of phenomena, from topological superconductivity to ultra-high frequency devices. By shrinking traditional metals and oxides to atomically thin structures, we find that their properties are completely different than their bulk counterparts, lending themselves to unique quantum, electronic, and optical applications not possible before.

10:30 AM *NM07.12.03

Fabricating Clean Two-Dimensional Material Devices in Ultra-High Vacuum [Yuanbo Zhang](#); Fudan University, China

In this talk, I will describe our recent effort on the construction of a UHV system for fabricating clean two-dimensional material devices.

11:00 AM NM07.12.04

Silver Functionalized Cellulose /CNT Composites for Phthalates Detection—A Sensitivity Enhancement [Panchali Anuchani](#), Hansini Abeysinghe and Thusitha N. Etampawala; Faculty of Applied Sciences, University of Sri Jayewardenepura, Sri Lanka

Phthalates are widely known plasticizer types used in the production of flexible plastic products. However, these do not form chemical bonds with the matrix material, such that they can easily leach into the environment over time. Exposure to certain phthalates causes adverse health and environmental impacts. Therefore, some countries have already banned the use of some phthalates in consumer products. Despite these adverse effects, many countries are still using phthalates in plastic processing. Therefore, rapid and easy monitoring of the presence of phthalates in different environments is crucial. Recently our research team has introduced a novel phthalate adsorbing cellulose/carbon nanotube (CNT) composite material that can be coupled with Electrochemical Impedance Spectroscopy or Four-Probe conductivity measurement techniques to identify the phthalates in solutions, which shows potential for overcoming the limitations of already existing phthalate detecting methods. Adsorption of dielectric phthalate molecules with bulky side groups onto the highly electrically conductive CNTs present inside the cellulose matrix would increase the electron tunneling distances between the CNTs, resulting in a conductivity decrease. This conductivity decrease of the composite after phthalate adsorption was detected by performing three-electrode Electrochemical Impedance Spectroscopy (EIS) using a potentiostat. However, the developed composite was only sensitive down to 1000 (v/v) ppm concentrated phthalates in methanol solution at room temperature. Therefore, in this study, we introduced a method of enhancing the sensitivity of this developed composite material by following the approach of using heterogeneous integration of mixed dimensional fillers that has high affinity to phthalates. Specifically, the cellulose matrix was functionalized with Ag nanoparticles. The impregnation of Ag nanoparticles was primarily confirmed by Raman Spectroscopy. Further experiments are in progress to confirm the presence and the distribution of Ag nanoparticles in the cellulose matrix. This impregnation would modify the hydroxyl groups of cellulose molecules by forming $O^- Ag^+$ ionic bonds. These $Ag^+ O^-$ groups show the potential to create intermolecular interactions, including hydrogen bonds, ion-dipolar interactions, and van der Waals interactions with the phthalates. Since the incorporation of Ag onto cellulose promotes phthalate absorption along with the CNTs, which adsorb phthalates via the formation of $\pi-\pi$ electron donor-acceptor interactions, seems to be the reason behind the enhanced sensitivity limit of the newly developed material compared to CNT/cellulose composite. The Ag nanoparticle functionalized cellulose/CNT composite paper successfully detected DNOP and DPHP with concentrations down to 1 ppm (v/v) in methanol solution at room temperature. Moreover, all these conductivity reductions after phthalate absorption were able to detect using a four-probe conductivity meter, which is much less sensitive than the potentiostat. Here, the current change variation of the composite paper before and after the absorption of phthalates was observed. High sensitivity, easy tunability of sensitivity based on the composition of integrated mixed dimensional materials, and the ability to directly test the phthalates without any other materials unlike with the potentiostat are some of the advantages observed with the use of mixed dimensional fillers (0D Ag nanoparticles and 1D CNTs) incorporated to the matrix (cellulose) of the phthalate sensing paper. This newly developed material shows more potential for developing into a portable, real-time, and in-situ phthalate-detecting sensor.

11:15 AM *NM07.12.05

2D van der Waals Heterostructures for Neuromorphic Applications [Feng Miao](#); Nanjing University, China

Van der Waals (vdW) heterostructures are formed by stacking layers of different 2D materials and offer possibilities to design new structures with atomic-level precision. In this talk, I will show how these heterostructures provide unprecedented opportunities to realize emerging device applications, especially in the fields of neuromorphic electronics and optoelectronics.

I will first show that highly robust memristors with good thermal stability, which is lacking in traditional memristors, can be created from a vdW heterostructure composed of graphene/MoS_{2-x}O_x/graphene. With the help of *in situ* electron microscopy, we revealed the origin of good thermal stability and a possible switching mechanism.^[1] We also demonstrated that artificial neuron devices and reconfigurable synaptic devices can be realized based on unique tuneable properties of various 2D materials.^[2]

vdW vertical heterostructures can also be exploited to realize neuromorphic optoelectronic applications. We demonstrated a prototype reconfigurable neural network vision sensor that operates via the gate-tunable positive and negative photoresponses of a WSe₂/BN heterostructure, and in-sensor broadband convolutional processing using a band-alignment-tuneable PdSe₂/MoTe₂ heterostructure.^[3-4] A neuromorphic vision system with brain-inspired visual perception can be further realized by networking such retinomorphic sensors with a memristive crossbar array.^[5]

In the last part of my talk, our latest results on a scalable massively parallel computing scheme using continuous-time data representation in crossbar arrays^[6] will be presented.

References:

[1] M. Wang, S. Cai, C. Pan, C. Wang, X. Lian, Y. Zhuo, K. Xu, T. Cao, X. Pan, B. Wang, S. Liang, J. Yang*, P. Wang*, F. Miao*, *Nature Electronics* **1**,

130 (2018).

[2] C. Pan, C. Wang, S.-J Liang*, Y. Wang, T. Cao, P. Wang, C. Wang, S. Wang, B. Cheng, A. Gao, E. Liu, K. Watanabe, T. Taniguchi, F. Miao*, *Nature Electronics* **3**, 383 (2020).

[3] C. Wang, S.-J Liang, S. Wang, P. Wang, Z. Li, Z. Wang, A. Gao, C. Pan, C. Liu, J. Liu, H. Yang, X. Liu, W. Song, C. Wang, B. Cheng, X. Wang, K. Chen, Z. Wang, K. Watanabe, T. Taniguchi, J. Yang*, F. Miao*, *Science Advances* **6**, eaba6173 (2020).

[4] L. Pi, P. Wang, S. Liang, Peng Luo, Haoyun Wang, Dongyan Li, Zexin Li, Ping Chen, Xing Zhou*, F. Miao*, Tianyou Zhai*, *Nature Electronics* **5**, 248 (2022).

[5] S. Wang, C. Wang, P. Wang, C. Wang, Z. Li, C. Pan, Y. Dai, A. Gao, C. Liu, J. Liu, H. Yang, X. Liu, B. Cheng, K. Chen, Z. Wang, K. Watanabe, T. Taniguchi, S.-J Liang*, F. Miao*, *National Science Review* **8**, nwaal72 (2021).

[6] C. Wang, S.-J Liang, C. Wang, Z. Yang, Y. Ge, C. Pan, X. Shen, W. Wei, Z. Zhang, B. Cheng, C. Zhang, F. Miao*, *Nature Nanotechnology* **16**, 1079 (2021).

11:45 AM DISCUSSION TIME

SESSION NM07.13: On-Demand Presentation
Thursday Morning, December 8, 2022
NM07-virtual

7:00 AM

New Insights into the Influence of Metal Sulfides Precursor on SO₂ Resistance Property for NH₃-SCR Catalyst Bora Ye¹, Bora Jeong¹, Myeung-Jin Lee^{1,2}, Kyung-yo Park^{1,3}, Donghyeok Kim^{1,2}, Jae il Jung^{1,4} and Hong-Dae Kim¹; ¹Korea Institute of Industrial Technology, Korea (the Republic of); ²Ulsan National Institute of Science and Technology, Korea (the Republic of); ³Pusan National University, Korea (the Republic of); ⁴Hanyang University, Kuwait

As emissions regulation of Nitrogen oxides (NO_x) are tightened around the world, many industrial applications such as power plant, steel mill, and cement plants are demanding higher NO_x removal efficiency. The selective catalytic reduction with NH₃ catalysts are mainly used for NO_x removal technology based on its high efficiency in the temperature range of 350 to 400°C [1]. But in many flue gases, the presence of SO₂ causes decreased the catalyst activity at temperature lower than 250 °C.

In order to solve this problem, research on changing the surface acidity by exposing to SO₂ atmosphere or injecting sulfur to the catalyst has been conducted [2]. Therefore, in this study, metal sulphides (MS₂) precursor was used to make a catalyst that partially contains sulfur, has sulfur resistance, and can even act as a support. WS₂ and MoS₂, which are transition metal dichalcogenides (TMDs) materials containing W and Mo, which are mainly used as main catalysts of SCR catalysts, were applied to increase catalytic activity. In general, metal sulfides are converted to oxide form when exposed to high-temperature oxygen atmosphere, and because of their two-dimensional structure, they applied to inhibit aggregation by dispersing active materials. Since the main reaction takes place in a small amount of vanadium, dispersing it on a support with a high specific surface area without aggregation is the main way to increase catalytic activity. By confirming the thermal decomposition behavior of MS₂, the optimal coexistence form of sulfides and oxides was found by optimizing the catalyst calcination temperature, and as a result, an optimal catalyst with resistance to SO₂ was prepared.

SYMPOSIUM SB01

Responsive Nanomaterials for Theranostics and Tissue Engineering
November 28 - December 7, 2022

Symposium Organizers

Herdeline Ardoña, University of California, Irvine

Juan Beltran-Huarac, East Carolina University

Jennifer Carpena-Núñez, UES Inc./Air Force Research Laboratory

Georgios Sotiriou, Karolinska Institutet

Symposium Support

Bronze

JACS Au

MilliporeSigma

* Invited Paper

+ Distinguished Invited

SESSION SB01.01: Nano-Biomaterials
Session Chairs: Herdeline Ardoña and Juan Beltran-Huarac

11:00 AM SB01.01.02

Peptide-Functionalized Layer-by-Layer Nanoparticles with Improved Blood Brain Barrier Permeability for Glioblastoma Treatment Priva Ganesh, Nicholas Lamson and Paula T. Hammond; Massachusetts Institute of Technology, United States

Glioblastoma is an aggressive brain tumor that accounts for almost 50% of all brain and central nervous system tumors, but the current standard of care gives a median survival of only 15 months. The greatest obstacle in the treatment of glioblastomas is the blood-brain barrier (BBB), the endothelial cells that line the vessels of the brain and are stitched together into a barrier by tight junction complexes. The BBB is designed to prevent pathogens from entering the brain, but its inability to distinguish between harmful substances and therapeutics leads to a fundamental problem in brain drug delivery. One approach to overcoming this barrier is encapsulating drugs in nanoparticles whose surfaces are engineered (usually, with the addition of ligands) to promote binding to various receptors of the BBB, thus triggering transcytosis and allowing the nanoparticle and its drug contents to cross the BBB.

Previous research has shown that electrostatic absorption (as opposed to covalent functionalization) is a quick and effective method for attaching cationic, tumor-penetrating peptides to anionic nanoparticles synthesized through an iterative layer-by-layer (LbL) approach [1]. Here, we demonstrate that LbL nanoparticles functionalized with BBB-targeting peptides, including Angiopep-2 and RAP12, can penetrate the BBB to deliver their contents to the brain. We probe how different characteristics of the nanoparticles (e.g. polyanion used to present surface chemistry in the outermost layer) and peptides (e.g. charge, size) affect stability of the LbL nanoparticles in a variety of salt and temperature conditions. Particles that exhibited the highest stability were screened through cell culture and mouse models of the BBB, and certain peptides lead to increased uptake both *in vitro* and *in vivo* in the mouse brain. Ongoing work includes molecular dynamics simulations to understand interactions between the BBB-targeting peptides and the outermost polymeric layer of the nanoparticles, with a focus on matching *in silico* conformation results with outcomes from biological experiments to enable future prediction of the effectiveness of various peptide-outer layer combinations.

1. N. Boehnke, K.J. Dolph, V.M. Juarez, J.M. Lanoha, and P.T. Hammond, *Bioconjug. Chem.* 31(9) 2211-2219 (2020)

11:15 AM SB01.01.03

Leveraging Inverse-Opal Nanomaterials for Ultra-Sensitive and High-Throughput EV Subpopulation Isolation in Clinical Samples Andrew A. Lin, Zhimin Jiang, James Pikul and David Issadore; University of Pennsylvania, United States

Extracellular vesicles contain multiple protein and nucleic acid cargoes from their cells of origin which circulate peripherally in bodily fluids such as blood, saliva, and urine; as a result, clinicians and scientists have sought to leverage EV-derived biomarkers to diagnose, stage, and manage cancer. However, the nanoscale size (30-300 nm diameter) and high background in clinical samples (10^{12} EVs/mL in serum) of EVs makes the isolation of EV subpopulations especially challenging.

In response to this challenge, we have developed a new approach to EV isolation which leverages inverse-opal nanomaterials to perform precise and high-throughput EV sorting directly from clinical samples via billions of nanomagnetic sorters operating in parallel. IOs have previously shown multiple favorable material properties including high mechanical strength and large surface areas. The chips leverage these advantages via our fabrication process, which involves the electrodeposition of ferromagnetic nickel followed by a gold passivation layer onto a self-assembled microlattice whose thickness can be tuned from 20 to 50 μm and with internal trap sizes tunable from 400 to 650 nm. This yields $>10^9$ nanoscale magnetophoretic sorting devices in a postage-stamp-sized three-dimensional lattice without the requirement for capital-intensive nanolithography. With this large-scale parallelization of traps in three dimensions, we demonstrate via finite-element simulations as well as experiments with magnetic nanoparticles that our device can isolate 50 nm magnetic nanoparticles from suspension at flow rates in excess of 50 mL/hr.

To demonstrate the viability of this platform for the isolation of EVs, we proceeded to isolate immunomagnetically-labeled EVs in a model system of pancreatic cancer. We isolated EVs whose sizes, surface proteins, and internal cargoes all matched those isolated via conventional methods while achieving a ~100% increase in yield. We demonstrate the ability to isolate EVs directly from human plasma via multiple antibody panels including a preliminary tumor-specific panel. By expanding on the proof-of-concept device characterization and initial testing shown here, this new approach can enable low-cost, rapid, and precise sorting of EV subpopulations for clinical questions.

11:30 AM SB01.01.04

Biomimetic Virus-Based De Novo Niche for Soft Tissue Engineering So Young Yoo; Pusan National University, Korea (the Republic of)

Extracellular niches play a crucial role in overcoming the surrounding harsh pathological environments as well as for stem cell differentiation and other important functions. Nanofibrous arginine-glycine-aspartic acid-engineered M13 phage has recently been considered as an extracellular matrix-mimicking bioinspired nanofiber that serves as an instructive tissue engineering material, providing a vascular niche and cytoprotective function at injured sites, which is an essential option for stem cell therapy. Herein, the novel and essential therapeutic cues provided by an engineered phage are exploited, contributing to de novo

soft tissue niche engineering, where the interplay of biomimetic phage cues with surrounding organ tissues is identified and cells are implanted between tissues to achieve an appropriate soft tissue niche that enables the proper functioning of the implanted stem cells at the injured site. These biomimetic phage nanofiber cues are considerably supportive for cell therapy, as they establish promising therapeutic extracellular de novo soft tissue niches for curing ischemic diseases.

11:45 AM SB01.01.05

Magnetic Control of the Endothelium Permeability via Magneto-Mechanical Actuation Using Iron Oxide Nanoparticles Mohammad Kanber, Homeira Faridnejad, Obum Umerah and Juan Beltran-Huarez; East Carolina University, United States

Cancer treatment is one of the major health problems that burdens our society. According to the latest publication of the American Cancer Society, the cancer mortality rate has reached 32% in 2021. Tumor hypoxia is one of the main cancer complications, wherein solid tumors grow as they develop larger resistance to current therapies due to the extracellular matrix remodeling of cancer cells. Extracellular remodeling involves the development of abnormal vasculature that can be twisted leading to a dead end and subsequent back blood pressure flow. This imposes certain limitations on drug therapy due to the heterogeneous tumor hypoxic microenvironment. One way to overcome this problem is to disrupt the vascular endothelial-cadherin (VE-cadherin) junctions, using superparamagnetic iron oxide nanoparticles (SPIONs). Direct treatment of SPIONs can cause uncontrolled leakiness and subsequent tumor migration, thus prompting the appearance of new metastatic sites. In this project, we use an indirect approach to internalize ND-PEG SPIONs into human

umbilical vein endothelial cells (HUVECs). Then these particles are magnetically activated to induce leakiness on HUVEC monolayers. We control the magnetic activity of ND-PEG SPIONs using non-heating AC magnetic fields. Intracellular ND-PEG SPIONs can assemble near the cytoskeleton and induce hypotension, which can affect cellular integration and VE-Cadherin proteins and in turn the adherens junctions. Our findings indicate that the controlled mechanical motion induced over ND-PEG SPIONs by magnetic torques can disrupt these junctions and enable the passage of therapeutic drugs. This approach can also have the potential to avert cancer migration. This innovative magnetic control provides an effective remotely-controlled drug delivery method harnessing the physics and biology of endothelial adherens junctions. This approach can open a new avenue for targeted drug delivery to specific anatomic regions within the body for a broad range of disease interventions.

SESSION SB01.02: Immuno-Materials/ Drug Delivery
Session Chairs: Jennifer Carpena-Núñez and Georgios Sotiriou
Monday Afternoon, November 28, 2022
Hynes, Level 1, Room 104

2:00 PM SB01.02.02

Ultrahigh Drug-Loaded Micelles for the Treatment of Triple-Negative Breast Cancer and Their Bone Metastases Richard d'Arcy¹, Patrick Gerber¹, Rebecca Cook¹, Julie Rhoades (Sterling)² and Craig Duvall¹; ¹Vanderbilt University, United States; ²Vanderbilt University Medical Center, United States

Triple-negative breast cancer (TNBC) is responsible for 15-20% of breast cancers and are unresponsive to therapies targeting estrogen, progesterone and HER2. Conventional chemotherapeutics are front-line for TNBC but resistance to these drugs make it a particularly challenging cancer to treat. Nanomedicine offers an exciting modality to better target, treat and potentially prevent resistance, e.g. by significantly increasing the maximum tolerated doses (MTD) of drug and consequently increasing the overall tumoral drug concentration. This effect is dependent on having a high drug loading capacity (LC), with 'ultra' high drug loading (LC = 35%) observed to give the highest potential MTDs.

Herein, we have rationally designed through carefully tailoring pi-interacting and hydrogen-bond donating co-monomer ratios a polymeric nanocarrier library capable of loading paclitaxel with an LC in the 'ultra' high range, and which also possess a tunable, Reactive Oxygen Species (ROS)-triggered release mechanism. These particles were found to have field-leading MTDs for paclitaxel (150 mg/kg, dosed 2-times per week for 2 weeks). We further investigated the difference between fast or slow drug release formulations in a xenograft mammary fat pad model of TNBC (MDA-MB-231s). Using only a single dose of ultrahigh paclitaxel-loaded micelles at their MTD (150 mg/kg), the Slow-release group displayed a significantly longer median survival than the Fast-release (59.5* v 47.5 days); both were significantly better than conventional paclitaxel treatment, Taxol and the saline control (only 34 and 26.5 days respectively).

With this slow release formulation we further evaluated their ability to treat an aggressive bone metastasis model in mice intratibially inoculated with 4T1-bone-cloned cells. When treated 2x/week over 3 weeks we found significant reduction in bone lesions and tumor burden, and with complete tumor eradication in 2/7 mice when treated at 75 mg/kg paclitaxel or 5/8 when treated at 150 mg/kg.

This study therefore highlights the importance of controlling the release rate from nanomedicines as well as the importance of ultrahigh loading of nanoparticles. Together, these factors maximize the overall drug dose as well as its retention time in the tumor, ultimately improving therapeutic outcomes.

2:15 PM SB01.02.03

Cross Linked Cyclodextrin Nanoparticles Enable Effective Delivery of Immunostimulatory Agents to Glioblastoma Associated Myeloid Cells Elias A. Halabi Rosillo, Sophie Lugani, Juhyun Oh, Rainer Kohler, Hannah Peterson, Christopher Garris and Ralph Weissleder; Harvard Medical School, United States

Myeloid cells create a highly immunosuppressive environment in glioblastoma multiforme (GBM) and contribute to poor immunotherapy responses. Based on the hypothesis that small molecules can be used to stimulate myeloid cells for more efficient effector functions, we developed a cyclodextrin nanoparticle (CDNP) approach to deliver dual NFκB pathway-inducing agents into these cells. Using fluorescently labeled CDNP analogs we were able to visualize the accumulation of the particles in live mice implanted with GBM to show that CDNPs have a high affinity to myeloid cells (primarily tumor associated dendritic cells and macrophages). When CDNPs were loaded with a TLR8 agonist (R848) and a cIAP inhibitor (LCL-161) we were able to show that interleukin (IL)-12 production could be jumpstarted in these cells. Herein show that CDNP-mediated myeloid re-education through TLR and non-canonical NFκB signaling can drive anti-tumor immunity in GBM.

2:30 PM SB01.02.04

Rational Design of Next-Generation mRNA Nanovaccines for Immunization Against Respiratory Syncytial Virus Afsaneh Radmand and James Dahlman; Georgia Institute of Technology, United States

mRNA-based lipid nanoparticle (LNP) vaccines (nanovaccines) have shown their safety and efficacy against COVID-19 in clinics. Along with this major clinical advancement, the high throughput *in vivo* screening platforms has advanced to bring about the full potential of nanovaccines. Such systems allow a more comprehensive understanding of the factors affecting biological responses and their clinical relevance with minimal sacrifice of animals. Here in this work, we used high throughput *in vivo* LNP screening system, to quantify the functional mRNA delivery (mRNA turn into protein) of hundreds of lipid nanoparticles in the same animal. By leveraging this system, we discovered next-generation nanovaccines against the respiratory syncytial virus (RSV). RSV is an RNA virus that encodes for 11 proteins and two of which (F & G) are capable of inducing neutralized antibodies. In particular, we focused on RSV-F for the following two reasons. First, it is well-conserved across viral serotypes and antigenic subgroups (A & B). Second, most of the neutralizing antibodies produced by natural RSV infection predominantly target RSV-F.

For the screening, we designed 100 LNPs with distinct chemical compositions. Then we barcoded each LNP in the microfluidic formulation. Followed by characterization as material quality control, barcoded LNPs that meet criteria (monodisperse; < 200 nm) were pooled as libraries and administered intramuscularly. Then, by next-generation sequencing on barcoded LNPs in the harvested tissue, we identified the nanovaccines (RSV1 and RSV2) that deliver the target mRNA to antigen-presenting cells in lymph nodes and muscle at levels comparable to Moderna and Pfizer-BioNTech lipid nanoparticles. We, therefore, further explored RSV1 and RSV2 with RSV-F mRNA. Next, we immunized mice with these LNPs varying doses of RSV-F mRNA and quantified the antibody response in serum following prime and a boost. We found that RSV1 and RSV2 led to similar antibody responses at high doses compared to Moderna LNP used as a positive control. But at a low dose, RSV1 and 2 led to a lower antibody response, suggesting that protein expression is necessary but not sufficient criteria during vaccine development at a preclinical stage in mice.

To enhance the immunogenicity of these LNPs at low doses, we hypothesized we could provide the LNPs with self-adjuvanting properties by modulating the mass of ionizable lipid mass (one of the essential components of lipid nanoparticle) per mass of mRNA in lipid nanoparticle formulation. As a result, we found an enhancement in RSV1 and RSV2 vaccine efficacy both in terms of protein expression and antibody response with the increased lipid:RNA ratio. We hypothesized that this effect could be due to two reasons. First, increasing the protein expression leads to an enhanced antibody response. Second, the increased mass of ionizable lipids serves as an adjuvant to stimulate the innate immune response. If the second hypothesis is true, stimulating the innate immune response would further enhance the adaptive immune response. Therefore, we included a TLR7 adjuvant into our LNP formulation, an endosomal single-stranded RNA agonist, and investigated the humoral and cellular response. We found that TLR7 adjuvant further enhanced the quality of produced anti-RSV F antibodies but did not enhance the cellular response.

In summary, we discovered two LNP vaccine candidates by *in vivo* high throughput LNP screening system. We also investigated factors affecting their response, and rationally enhanced their immunogenicity for immunizing against RSV at a preclinical stage in mice. We envision this study will guide scientists to design more effective nanovaccines for immunization against viruses and help accelerate mRNA-based vaccines.

2:45 PM BREAK

3:15 PM *SB01.02.05

Peptide Assemblies as Active Immunotherapies to Treat Chronic Inflammatory Diseases Elizabeth J. Curvino, Shamitha Shetty, Emily F. Roe, Yaoying Wu and Joel Collier; Duke University, United States

Chronic inflammatory diseases such as rheumatoid arthritis, psoriasis, and inflammatory bowel disease are currently treated using monoclonal antibodies and other biologics that neutralize key inflammatory mediators such as cytokines. Although beneficial for many, a large proportion of patients do not respond to them or stop responding as they develop anti-drug antibodies against the repeated injections. Anti-cytokine biologics also are expensive and have stringent storage requirements, limiting access to only the most well-resourced areas of the globe. Active immunotherapies, where therapeutic B-cell or T-cell responses are generated in the patient against selected targets, may provide alternatives with fewer dosing requirements, better shelf stability, and lower non-response rates. However, platforms for safely and predictably generating therapeutic anti-inflammatory adaptive immune responses have yet to be developed clinically. In this talk, active immunotherapies against several targets, including TNF, IL-1 β , IL-17, phosphorylcholine, and complement proteins will be described, based on supramolecular peptide and protein assemblies. Design rules for eliciting predictable B-cell and T-cell responses against chosen targets using supramolecular peptide assemblies will be discussed, along with strategies for raising therapeutic responses in tissues of interest, including the gut. In preclinical mouse models of psoriasis, acute septic shock, inflammatory bowel disease, and rheumatoid arthritis, supramolecular active immunotherapies have exhibited considerable therapeutic efficacy, and these results will be highlighted.

3:45 PM SB01.02.06

Observation of Immune Activation Through Simultaneous Cell Receptor Monitoring Using Lanthanide Doped Upconverting Nanoparticles Ariel Siber, Jason Casar, Chris Siefe, Vincent van Unen, Mark Davis and Jennifer A. Dionne; Stanford University, United States

Immune synapse (IS) formation, maintenance, and communication are conducted through the bonding of cell receptors. Long-duration cell receptor tracking throughout the synaptic activation process is difficult with current organic and inorganic fluorophores and quantum dots due to issues of biocompatibility, quenching, and photobleaching. Lanthanide doped upconverting nanoparticles (UCNP) are photostable over hours, and have the ability to convert incident photons to a higher frequency allowing for biologically transparent Near-IR (NIR) excitation and visible emission. Here, we show how UCNP can be used as *in-situ* optical emitters to simultaneously observe multiple cell receptors throughout the stages of immune activation during a 6-8 hour IS interaction.

We colloiddally synthesize 15 nm diameter hexagonal phase NaYF₄ nanoparticles, each doped with a different Lanthanide emitter — 2% Er, 0.5% Tm, or 2% Ho as well as the sensitizer Yb at 20%. The nanoparticles are shelled with inert, 4 nm thick NaYF₄ to minimize quenching. To disperse these UCNP in aqueous solutions, we wrap them in poly(maleic anhydride-alt-1-octadecene) (PMAO) hydrolyzed with 4-Dimethylaminopyridine (DMAP). Upon illumination at 980 nm these particles upconvert to visible light in the red, blue, and green. To target immune cells, we use a carbodiimide crosslinker to functionalize each nanoparticle with one of three antibodies targeting the cell receptors — CD69 (early activation marker), ICOS (co-stimulatory), and PD1 (co-inhibitory) — through neutravidin-biotin linkages. We confirm the functionalization of these nanoparticles using TEM, FTIR, UV-Vis, and fluorescence characterization methods. Live-dead assays with cloned cytotoxic T lymphocyte (CTL) cells that recognize cytomegalovirus (CMV) confirm the nanoparticles lack of cytotoxicity. We then image these nanoparticles on immune cells using scanning confocal microscopy. We demonstrate the ability to simultaneously track cell receptor expression through the stages of immune cell activation over the course of 8 hours without signal instability. As a control we parallelly track these activation factors using Fluorescent Activated Cell Sorting (FACS). Additionally, we demonstrate the ability of UCNP to dynamically observe receptor binding kinetics in response to temperatures ranging between 20 and 40°C, as well as binding kinetics of the cytokine immunotherapy, Aldesleukin or IL2. Our work lays the foundation for future *in-situ* studies of simultaneous cell receptor tracking using a larger assortment of UCNP with a functionalization platform that can be generalized to a variety of proteins and cell types.

4:00 PM SB01.02.07

Spatiotemporally Resolved Stimuli-Responsive Sequential Drug Delivery System to Curb Antibiotic Resistance Development Meera Patel, Alexander Corbett, Nesha Andoy and Ruby Sullan; University of Toronto, Canada

The emergence of antibiotic resistance has become a major public health threat. To slow down the development of antibiotic resistance, our group is developing a smart hydrogel drug delivery system to efficiently inhibit growth of Gram-negative bacteria. Although the target for many available antibiotics for Gram-positives can also be found in Gram-negative bacteria, the outer membrane permeability barrier limits drug efficacy to small hydrophilic antibiotics only. To overcome this limitation, we develop a laser-responsive drug delivery platform that can sequentially deliver a membrane potentiator, Ethylenediaminetetraacetic acid (EDTA), followed by a large hydrophobic antibiotic, rifampicin. For this, we leverage on the photoactivity of polydopamine nanospheres (PDNS), the temperature-dependent properties of liposomal carriers, and the flexibility afforded by hybrid hydrogel systems. The different phase transition temperatures (T_m) of phospholipids facilitated creation of liposomal drug nanocarriers that would release the loaded cargo at different temperatures. Membrane-disrupting molecules will be released first to prime the outer membrane of Gram-negatives, hence rendering the bacteria more susceptible to the hydrophobic antibiotic that will only be released after the pathogens have been exposed to the membrane permeabilizer. Having the ability to prime Gram-negative bacteria to the otherwise active “Gram-positive antibiotics” will broaden the repertoire of drugs that can be used for any type of bacterial infections. Furthermore, due to the photothermal activity of PDNS, an externally controlled laser can be used to trigger this sequential release of antimicrobials. Having drug delivery systems that can respond to an external stimulus and have that spatial and temporal control over drug bioavailability is a significant step towards preventing the unnecessary exposure of other microorganisms to antibiotics, helping mitigate antibiotic resistance development.

4:15 PM SB01.02.08

Novel Therapeutic Modalities Using Nanofiber-Based “Intelligent” Drug Delivery Daewoo Han¹, Serdar Tort² and Andrew J. Steckl¹; ¹University of Cincinnati, United States; ²Gazi University, Turkey

Development of novel materials platforms for controlled (“intelligent”) release of functional molecules has emerged in materials research for medical applications. Controlled release of functional molecules in response to external stimuli is the key for intelligent release. Coaxial electrospinning technique¹ is a versatile method to integrate multiple functional materials into novel delivery systems, producing core-sheath fibers with advanced features: (a) combination of multiple functional materials; (b) encapsulation of functional molecules (drug, proteins, etc.) with controlled release kinetics; (c) protection of encapsulated molecules from outer environment. Intrinsic properties of nanofiber membranes (high surface-to-volume ratio and porosity) enable much quicker response to external stimuli compared to equivalent solid films. Complex nanofibers produced by coaxial electrospinning have been used in various advanced platforms for chem/bio/medical applications.

To obtain release triggered by external stimuli, self-immolative polymer (SIP) has been incorporated into the outer sheath layer encapsulating the releasing core materials.² As SIP is depolymerized (“unzip”) upon cleavage of the head-molecule by specific target, stimuli drug molecules are released. A multi-phased controlled release was developed by integrating two different pH-responsive polymers into core-sheath fibers.³ Fibers with Eudragit L100 core and S100 sheath provide 3-phase response within physiological pH range: pH < 5, no release is observed from either core or sheath layer; pH=5-6, sustained release from the core is obtained with different release kinetics; pH > 6, both core and sheath materials are quickly dissolved. This approach is very promising for targeted oral drug delivery because human organs have different pH values.

Other methodologies utilizing electrospun fibers include transdermal patches of parylene coated PCL fibers containing the drug pramipexole. These patches have demonstrated long-term drug delivery, ease-of-use, and no first-pass effect. Without parylene, 100% pramipexole load is released within 12 h, while parylene coating provided only 52% release over 10 days.⁴ Microneedles loaded with electrosprayed nanoparticles for painless drug delivery via skin penetration were also demonstrated. Extremely small needles caused least pain to the host while directly delivering the loaded drug into the blood or interstitial fluid streams.⁵ While patches and microneedles were developed to minimize physical disruption, implantation into the body is needed for certain cases. We developed a nanofibrous implant for localized chemotherapy against brain cancers. To circumvent the blood-brain-barrier, implanting the drug delivery device after tumor resection provides highly effective drug delivery to the targeted area. Our implantable device provides continuous drug release up to 160 days, significant increase of median survival and long-term survival rates of 50%.⁶

1. Han, D.; Steckl, A. J., Coaxial Electrospinning Formation of Complex Polymer Fibers and their Applications. *ChemPlusChem* **2019**, *84*, 1453.

2. Han, D. et. al, Stimuli-Responsive Self-Immolative Polymer Nanofiber Membranes Formed by Coaxial Electrospinning. *ACS Appl. Mater. Interfaces* **2016**, *9*, 11858.

3. Han, D. Steckl, A. J., Selective pH-Responsive Core–Sheath Nanofiber Membranes for Chem/Bio/Med Applications: Targeted Delivery of Functional Molecules. *ACS Appl. Mater. Interfaces* **2017**, *9*, 42653.

4. Tort, S. et. al, Controlled drug release of parylene-coated pramipexole nanofibers for transdermal applications. *Surface and Coatings Technology* **2021**, *409*, 126831.

5. Tort, S. et. al, In vitro and in vivo evaluation of microneedles coated with electrosprayed micro/nanoparticles for medical skin treatments. *J Microencapsul* **2020**, *37*, 517.

6. Han, D. et. al, Multi-layered core-sheath fiber membranes for controlled drug release in the local treatment of brain tumor. *Scientific Reports* **2019**, *9*, 17936.

4:30 PM SB01.02.09

Modeling Coronavirus Spike Protein Dynamics—Implications for Immunogenicity and Immune Escape Genevieve Kunkel, Mohammad Madani, Simon White, Paulo Verardi and Anna Tarakanova; University of Connecticut, United States

The ongoing COVID-19 pandemic is a global public health emergency requiring urgent development of efficacious vaccines. With continual waves of COVID-19 outbreaks since 2019, in addition to the outbreaks associated with SARS-CoV and MERS-CoV over the last two decades, the threat presented by coronaviruses is everchanging and long-term. This provides reason to develop more targeted, 2nd generation vaccines for continual treatment as new variants emerge. The SARS-CoV-2 surface Spike (S) glycoprotein represents a prime target for vaccine development because antibodies that block viral attachment and entry, i.e. neutralizing antibodies, bind almost exclusively to the receptor binding domain (RBD). Here, we develop computational models for a large subset of S proteins associated with SARS-CoV-2—including Delta, and Omicron variants—implemented through coarse-grained elastic network models and normal mode analysis. We then analyze local protein domain dynamics of the S protein systems and their predicted thermal stability to characterize structural and dynamical variability among them. Our results are compared against existing experimental data and used to elucidate the impact and mechanisms of SARS-CoV-2 S protein mutations and their associated antibody binding behavior. We construct a SARS-CoV-2 antigenic map to highlight the location and accessibility of antibody binding domains in SARS-CoV-2 S proteins. We then offer predictions about the neutralization capabilities of antibody and S mutant combinations based on protein dynamic signatures. SARS-CoV-2 S protein dynamics are compared to SARS-CoV and MERS-CoV S proteins to investigate differing antibody binding and cellular fusion mechanisms that may explain the high transmissibility of SARS-CoV-2. Our results provide insights into the dynamics-driven mechanisms of immunogenicity associated with coronavirus S proteins and present a new approach to characterize and screen potential mutant candidates for immunogen design, as well as to characterize emerging natural variants that may escape vaccine-induced antibody responses.

SESSION SB01.03: Poster Session I
Session Chairs: Juan Beltran-Huarac and Georgios Sotiriou
Monday Afternoon, November 28, 2022
8:00 PM - 10:00 PM
Hynes, Level 1, Hall A

SB01.03.01

Protein-Adjuvant Co-Delivery via Encapsulation in Lipid Nanovesicles for Enhanced Vaccine Immune Responses Dong Jae Lee, Bon Il Koo and Yoon Sung Nam; Korea Advanced Institute of Science and Technology, Korea (the Republic of)

After more than two years, the coronavirus pandemic is finally coming to an end. Many countries around the world have lifted mask mandates, people are returning to their daily lives, and international travel levels are slowly reaching pre-pandemic numbers. While each country took different approaches to combat the coronavirus pandemic, one thing was common among all countries: encouraging the public to get vaccinated. Traditional vaccines consist of antigenic proteins mixed with adjuvants which increase the immune responses. Although a simple mixture may be enough in several cases, separated delivery of the antigen and adjuvants leads to lower immune responses. Co-delivery of the antigen and adjuvant results in more efficient cross-presentation

and higher immune responses.

Here, we report on enhanced vaccine immune response from the co-delivery of protein antigen-nucleic acid adjuvant mixture encapsulated in lipid nanoparticles. The antigen and adjuvant were encapsulated in multilamellar lipid nanovesicles coated with hyaluronic acid for enhanced antigen cross-presentation. Compared to the unencapsulated mixture, encapsulation of the antigenic protein and the nucleic acid adjuvant increased the delivery efficiency to the immune cells and the resulting immune responses. Delivery efficiency was confirmed using confocal microscopy, and the immune responses were analyzed using flow cytometry. Analyses of the immune responses from the bone marrow-derived dendritic cells (*in vitro*) and splenocytes (*in vivo*) of C57BL/6 mice showed increased levels of anti-antigen antibody (immunoglobulin G), cytokines (interferon gamma) and expression of surface markers (CD40, CD80, CD86) with encapsulated vaccine samples compared to unencapsulated control groups. Our results show that encapsulation of the protein antigen-nucleic acid adjuvant co-delivery mixture in lipid nanovesicles is a promising and effective method for vaccine immunization.

Acknowledgement: This work was supported by a grant of the Korea Health Technology R&D Project through the Korea Health Industry Development Institute (KHIDI), funded by the Ministry of Health & Welfare, Republic of Korea (HV22C0209).

[1] Bon Il Koo, Seon-Mi Jin, Hayeon Kim, Dong Jae Lee, Eunji Lee, and Yoon Sung Nam, Conjugation-free Multilamellar Protein-lipid Hybrid Vesicles for Multifaceted Immune Responses, *Advanced Healthcare Materials* (2021) 2101239.

SB01.03.02

Luminal Coating of the Intestine for Oral Peptide Delivery Gillian Audia^{1,2}, Yuhan Lee² and Jeffrey M. Karp²; ¹Northeastern University, United States; ²Brigham and Women's Hospital, United States

Though oral drug delivery is the patient-preferred route of administration, oral protein delivery remains evasive due to the challenges of navigating the low pH environment and digestive enzymes present in the gastrointestinal tract. Ultimately, these challenges result in low bioavailability of orally delivered protein drugs that preclude the translation of oral formulations to the clinic. Here we develop an orally administered gut-coating formulation that provides a transient coating of the bowel that can be used to protect protein drug cargo and direct it to the tissue wall. We identified a sucrose octasulfate aluminium complex and further engineered the pH-dependent material into a complex coacervate formulation linked via pH-independent electrostatic interaction, which allowed an effective transient physical coating on the gastrointestinal mucosa, independent of gastric acid exposure. The formulation protected biological agents from gastric acid exposure and degradation, which enabled oral delivery to the small bowel mucosa. Horseradish peroxidase (HRP) loaded into the gut coating material maintained activity before and after exposure to simulated gastric fluid (pH=1), while naked HRP showed complete loss of activity. HRP is released from LuCl gradually, with 62% of cargo released in the first four hours, and another 10% of cargo released over 24 hours. This technology will have the potential to enable oral delivery of protein therapeutics while protecting them from degradation from the gastric environment.

SB01.03.03

Chiral Plasmonic Hybrid Nanostructure Based Cascade Enzymatic Reaction for Enhanced Photodynamic Cancer Therapy Haeun Kang¹, Subin Yu¹, Ryeong Myeong Kim², Ki Tae Nam², Sehoon Kim³ and Dong Ha Kim¹; ¹Ewha Womans University, Korea (the Republic of); ²Seoul National University, Korea (the Republic of); ³Korea Institute of Science and Technology, Korea (the Republic of)

Nanozymes, which are defined for nanomaterials with enzyme-like properties, have attracted significant attraction as promising alternatives for natural enzymes due to its attractive features. Compared with natural enzymes, nanozymes possess the advantages of facile synthesis, high stability, low cost, and easy for mass-production. Despite these advantages, nanozyme's low catalytic efficiency as a result of limited selectivity for substrate and its intrinsic low performance have still remained challenges.¹ To overcome these drawbacks, in this study, chiral plasmonic hybrid nanozymes were introduced to maximize interaction with circularly polarized light (CPL) and cascade enzymatic reactions were designed for photodynamic cancer therapy. Glucose oxidase (GOD)-like activity of chiral gold nanoparticle (D-Au NP) showed significant enhanced enzymatic performance with right-handed circularly polarized light (RCP), while peroxidase (POD)-like activity of palladium deposited chiral gold nanoparticles (L-Au NP@Pd) increased with left-handed circularly polarized light (LCP). In addition, D-glucose, the substrate for GOD-like activity showed significantly enhanced catalytic effect with D-Au NP rather than L-Au NP. These results show that chirality of nanozymes play a key role in the enzymatic performance with CPL. Also, introduction of chiral hybrid nanozymes in this cascade enzymatic reaction platform increased the overall therapeutic effects for photodynamic cancer therapy. When D-Au NP and L-Au NP@Pd were localized in the tumor site via EPR effect², RCP was irradiated to generate H₂O₂ from D-glucose through GOD-like activity of D-Au NP. Then, LCP was irradiated to generate hydroxyl radical through POD-like activity of Pd.³ Under 808nm-CPL light irradiation, *in vitro* phototherapy effect was investigated on Hela cells. Interestingly, cancer cell viability was significantly decreased when LCP and RCP were irradiated sequentially, suggesting that enhanced amount of hydroxyl radicals were generated. Therefore, endowing the chirality to nanozymes, the chiral hybrid nanozymes herein introduced can open up new horizons for diagnosis, treatment, and theranostics as advanced nanozymes candidates.

References

- (1) Wei, H.; Wang, E. Nanomaterials with enzyme-like characteristics (nanozymes): next-generation artificial enzymes. *Chem. Soc. Rev.*, 42, 6060 (2013)
- (2) Kalyane, D.; Raval, N.; Maheshwari, R.; Tambe, V.; Kalia, K.; Tekade, Rakesh K. Employment of enhanced permeability and retention effect (EPR): Nanoparticle-based precision tools for targeting of therapeutic and diagnostic agent in cancer. *Materials Science & Engineering C.*, 98, 1252 (2019)
- (3) Gao, S.; Lin, H.; Zhang, H.; Yao, H.; Chen, Y.; Shi, J. Nanocatalytic Tumor Therapy by Biomimetic Dual Inorganic Nanozyme-Catalyzed Cascade Reaction. *Adv. Sci.*, 6, 1801733 (2019)

SB01.03.04

Hybrid Nanotubes (HyNTs)—Iontophoretic Molecular Delivery System Bowen Zhang, Kazuhiro Oyama, Yuiko Mizuguchi and Takeo Miyake; Waseda University, Japan

Delivering biomolecules into living cells and tissues has become an important challenge in medical and biological fields. Conventional techniques such as virus vector and electroporation are utilized commonly for small molecule delivery, but still remain several problems of low efficiency and low viability for large molecules such as biological proteins and organelles. To overcome this problem, we demonstrate the macromolecular delivery into adhesive cells with hybrid nanotubes (Au nanotube/conductive polymer) that promotes the flow of ions at an applied voltage (about 50 mV) below the cell membrane potential [1-2]. As a result, we have succeeded in developing an electric nanoinjector that delivers macromolecules such as green fluorescent protein (GFP) and DNA plasmid into cells.

[1] Miyake, et.al. "Nanostraw membrane stamping for direct delivery of molecules into adhesive cells", *Scientific Reports*, 9, 6806, 2019.

[2] Miyake, et.al. "High-Efficient and Dosage-Controllable Intracellular Cargo Delivery through Electrochemical Metal-Organic Hybrid Nanogates", *Small Science*, 10, 1002, 2021.

SB01.03.05

Unveiling the Behaviour of MOF Drug Nanocarriers with Nanoscale Multimodal Spectromicroscopy Maeva Chaudard^{1,2}, Ruxandra Gref² and Marta de Frutos¹; ¹Laboratoire de Physique des Solides, France; ²Institut des Sciences Moléculaires d'Orsay, France

The current sanitary crisis has demonstrated the constant need for new technologies in health care. For decades, nanotechnologies have been gaining interest as efficient tools for health improvement. Among them, drug delivery systems are designed as smart vessels to provide slow and controlled release of drugs targeting the diseased organs or tissues. For more than 15 years, metal-organic framework nanoparticles (nanoMOFs) have been studied as promising drug nanocarriers.¹ They are currently viewed as potential candidates for cancer or infection therapies.² NanoMOFs are porous nanoparticles created by the self-assembly of metal clusters and organic linkers. They exhibit a high drug payload that reaches about 30 wt%.³ In addition, their versatile composition allows their properties to be tuned to the therapy. A careful selection of building blocks can lead to biocompatibility, biodegradability, an amphiphilic inner environment to load hydrophilic drugs, or synergetic bioactivity of both linkers and metals. Among the many assembly possibilities, iron trimesate nanoMOFs have gained interest for their additional theranostic capacities.⁴ Furthermore, a polymer corona can be coated onto the nanoMOF's surface to convey additional properties to the nanosystem. Recent studies have highlighted the use of cyclodextrin and mannose grafting to provide stealth and tissue targeting.⁵ Others have also shown the possibility of pH-responsivity using cyclodextrins.⁶ Nonetheless, many questions remain about these complex nanosystems regarding their drug distribution and interaction with biological matter. Although phosphate molecules were shown to be involved in the biodegradation of iron trimesate,^{3,7} the degradation mechanism is still not fully unravelled. Besides, an in-depth understanding of their cellular fate is needed to develop biomedical applications. Here, we present a label-free approach for studying individual nanoMOFs at the nanoscale, which could also be applied in the analysis of their interaction with cells. We demonstrate that spectromicroscopy could be the key to unravelling the drug distribution and biodegradation mechanisms. Indeed, using STEM-EELS (Scanning Transmission Electron Microscopy coupled with Electron Energy Loss Spectroscopy), we simultaneously image and analyse iron trimesate nanoMOFs with a spatial resolution below 10 nm. First, with a multimodal approach, we studied the infrared, UV-vis and soft X-ray spectral ranges to perform a fine structure analysis of both the organic and inorganic parts. Secondly, we acquired chemical maps to determine the distribution of each component throughout the specimen. Finally, we highlight the possibilities of characterizing each step of the nanosystem's development: from the framework synthesis and its interaction with drugs to the degradation mechanism and the biological evaluations.

1. Horcajada, P. *et al. Angewandte Chemie* **118**, 6120–6124 (2006).
2. He, S. *et al. Acta Pharmaceutica Sinica B* (2021) doi:10.1016/j.apsb.2021.03.019.
3. Rodriguez-Ruiz, V. *et al. Journal of Drug Targeting* **23**, 759–767 (2015).
4. Horcajada, P. *et al. Nature Materials* **9**, 172–178 (2010).
5. Agostoni, V. *et al. Sci Rep* **5**, 7925 (2015).
6. Lajevardi, A., Sadr, M. H., Yarak, M. T., Badiei, A. & Armaghan, M. *New J. Chem.* **42**, 9690–9701 (2018).
7. Li, X. *et al. Scientific Reports* **7**, 13142 (2017).

SB01.03.06

Si-SiO₂ Core-Shell Nanoelectrode Arrays for Intracellular Sensing and Stimulation Yiming Wang, Daniel Loh and Daniel Nocera; Harvard University, United States

Intracellular electrochemical analysis is a powerful tool for detecting cellular metabolites and understanding cellular processes. However, it is challenging to make submicrometer sized electrodes and modify them with desired sensing modules. It is essential to develop methodologies to fabricate and modify nanoelectrodes with reproducibility and scalability. Taking advantage of well-established nanofabrication technologies in semiconductor industry, our group developed techniques to produce high aspect ratio silicon nanowires in a wafer scale. In the current work, we manufactured high aspect ratio Si-SiO₂ core-shell nanoelectrode arrays with electrode area compatible with conventional nanoelectrodes, but with great scalability and reproducibility. We further developed a general modification method for the nanoelectrode arrays for parallel intracellular sensing and stimulation.

SB01.03.07

Characterizing Nano-Bio Interactions on Hematopoietic Stem Cell Targeting Layer-by-Layer Nanoparticles for Gene Therapy Bhuvna Murthy, Tamara Dacoba, Simone A. Douglas-Green and Paula T. Hammond; Massachusetts Institute of Technology, United States

Sickle cell disease (SCD) is the most commonly inherited blood disorder in the United States that affects ~100,000 people. This autosomal genetic disorder is caused by a single mutation on hemoglobin found on red blood cells (RBCs). In deoxygenated conditions, the mutated hemoglobin causes RBCs to sickle. Gene therapy is a potential cure, where hematopoietic stem cells (HSCs), precursors to RBCs, could be targeted to correct the mutation. We will use the layer-by-layer (LbL) technique, to develop a library of nanoparticles functionalized with HSC targeting antibodies to deliver therapeutics. Nanoparticles are layered with negatively charged polymers including hyaluronate, which has increased circulation times in vivo, as well as polyacrylate and poly-L-glutamate, which have decreased clearance by immune surveillance cells. When nanoparticles enter biological fluids, nano-bio interactions occur, where proteins adsorb to their surface, forming a “fluid biological barrier” known as the protein corona (PC). PC affects nanoparticle circulation times, immunologic toxicity, and colloidal stability; it can be used to tune targeting of nanoparticles as its properties vary based on surrounding biological fluid and tissues. Here, we characterize properties of the PC on HSC-targeting LbL nanoparticles for gene therapeutic delivery in SCD and assess how these interactions affect uptake into cells.

To characterize the PC, our library of nanoparticles were incubated with varying concentrations of fetal bovine serum (FBS) at physiological temperature (37C) for 30 minutes. Incubations were performed at high and low volume ratios of nanoparticles to FBS to assess the effect of varying amounts of protein. To remove unbound protein, nanoparticles were centrifuged, and the pellet was washed and resuspended in water. Protein-coated nanoparticles were assessed for size and surface charge using dynamic light scattering and laser Doppler velocimetry. Protein concentration was quantified using a Bicinchoninic acid assay and protein composition was observed using SDS-PAGE. Effects of PC on nanoparticle uptake in cells were also measured; protein-coated nanoparticles were prepared, as previously described, before incubating with EL4 cells, which have the CD45 marker characteristic of HSC-derived cells. Uptake of Cy5-labeled nanoparticles was analyzed using fluorescence activated cell sorting.

We determined nanoparticles maintain colloidal stability through protein interaction based on consistent size and surface charge measurement. SDS-PAGE showed distinct band patterns, indicating proteins of varying molecular weight, for each outer layer polymer of the nanoparticles, which suggests surface chemistry and charge affects PC composition. Analysis of nanoparticle uptake demonstrated that outer layer chemistry affects nano-bio interactions as hyaluronate and polyacrylate outer layers did not have significant changes in uptake in EL4 cells, while poly-L-glutamate nanoparticles showed an increase in uptake. Most notably, nanoparticle uptake was highest at incubation in biologically relevant conditions, with 10% FBS at a nanoparticle to FBS ratio of 1:10. Incubation with 100% FBS at the same ratio resulted in lower uptake in all nanoparticles, suggesting higher protein content interferes with uptake.

Overall, it was determined that outer surface chemistry of nanoparticles affects properties of protein corona as well as uptake in cells. It was also determined that varying protein concentration and volume ratio of nanoparticles to protein are effective methods of assessing PC for nanoparticles. PC

characterization in these HSC-targeting nanoparticles is essential to tuning specificity of targeting and can significantly affect immunological clearance and circulation times, causing non-specific uptake. Understanding its role in nano-bio interactions is integral in nanoparticle targeting and in creating an effective nanoparticle for gene therapeutic delivery.

SB01.03.08

H₂O₂-Activatable Antioxidant Polymeric Prodrug Nanoparticles as Therapeutics for Renal Ischemia/Reperfusion Injury Hyunbin Shin, Sooyeon Kim, Nanhee Song, Hayoung Jun, Hanui Jo and Dongwon Lee; Jeonbuk National University, Korea (the Republic of)

During organ transplantation, blood vessels are temporarily tied to prevent bleeding and organs which do not receive sufficient oxygen and nutrients undergo ischemic damages. To prevent damages to these organs, blood must be rapidly re-supplied. Paradoxically, however, blood resupply induces greater organ damages which is called ischemia-reperfusion (IR) injury. Renal IR injury is an inevitable complication in various clinical settings including kidney transplantation and major vascular surgeries. Renal IR injury contributes to the development of acute kidney injury which still remains a major clinical challenge. One of major culprits of renal IR injury is the massive production of reactive oxygen species (ROS) including hydrogen peroxide (H₂O₂) that initiate inflammatory signaling pathways, leading to renal cell death. It can be also hypothesized that effective elimination of overproduced H₂O₂ provides a promising strategy to prevent renal IR injury.

Vanillyl alcohol (VA) is an herbal agent in oriental medicine and has been used for the treatment of ischemic brain injury and coronary arterial diseases due to its potent antioxidant and anti-inflammatory activities. Ursodeoxycholic acid (UDCA) is one of bile acids and has been well known to inhibit the generation of intracellular ROS and suppresses the production of pro-inflammatory cytokines. However, UDCA and VA alone cannot be used for the prevention of renal IR injury due to their insufficient therapeutic activity and the lack of H₂O₂ scavenging ability. It can be therefore postulated that therapeutics that are able to not only scavenge H₂O₂ rapidly but also deliver both VA and UDCA concurrently to the target site have great potential for the prevention of renal IR injury. To realize the concurrent delivery of sufficient amount of both VA and UDCA and H₂O₂ scavenging with single nanoparticles, we developed H₂O₂-activatable antioxidant and anti-inflammatory polymer, PVU73 by exploiting the concept of polymeric prodrug that incorporates bioactive compounds (VA and UDCA) in the backbone and releases them during degradation. As a polymeric prodrug of VA and UDCA, PVU73 was developed to covalently incorporate VA and UDCA in its backbone through a peroxalate linkage that can be readily cleaved by H₂O₂ and also scavenge H₂O₂. PVU73 could be formulated into nanoparticles of a mean diameter of ~220 nm by a conventional single emulsion method. For preferential targeting to kidney with IR injury, PVU73 nanoparticles were coated with fucoidan that has high affinity to p-selectin which is an adhesion molecule overexpressed on the endothelium in the inflammatory site. The translational therapeutic potential of fucoidan-coated PVU73 (Fu-PVU73) nanoparticles was evaluated using a mouse model of renal IR injury. The results revealed that Fu-PVU73 nanoparticles hold great potential as therapeutic agents for renal IR injury due to their H₂O₂ scavenging ability and potent anti-inflammatory activities. We anticipate that Fu-PVU73 nanoparticles have tremendous therapeutic potentials for not only renal IR injury but also various ROS-associated inflammatory diseases.

SB01.03.09

Tumor-Targeting Oxidative Stress Nanoamplifiers as Immunogenic Cell Death-Inducing Anticancer Nanomedicine Nanhee Song, Nuri Kim, Manseok Yang, Gayoung kwon, Soonyoung Kwon and Dongwon Lee; Jeonbuk National University, Korea (the Republic of)

Compared to normal cells, cancer cells are under oxidative stress associated with a high level of reactive oxygen species (ROS) and are also more susceptible to insults of pro-oxidants that generate ROS or scavenge antioxidants such as glutathione (GSH). Cancer cells employ a variety of adaptation mechanisms in response to excessive oxidative stress. In order to maintain redox balance, increased oxidative stress leads to up-regulation of antioxidant system activity. Among endogenous antioxidants, GSH is a major ROS-scavenger and plays fundamental roles in sustaining cellular redox homeostasis. It has been reported that quinone methide (QM) intermediate generated from the hydrolysis of phenyl ester instantaneously depletes intracellular antioxidant GSH, leading to mitochondria-dependent apoptosis. The combination of ROS generation with GSH depletion has been suggested to cooperatively accumulate ROS to amplify oxidative stress, leading to enhanced cell death. Additionally, it has been also reported that a ROS level above a cytotoxic threshold level elicits the immunogenicity of dying cancer cells. Elevated oxidative stress elicits immunogenic cell death (ICD) that is a type of apoptotic cell demise and boosts anticancer immunity.

In this study, we developed disulfide-bridged phenylene benzoate (ssPB) to exert therapeutic effects of GSH-depleting prooxidants. ssPB was rationally designed to fulfill the requirements for not only QM generation but also self-assembling behaviors. ssPB was expected to form self-assembled nanoconstructs and undergo esterase-catalyzed hydrolysis of phenolic ester to produce two QM intermediates that deplete intracellular antioxidant GSH, leading to enhanced intracellular ROS accumulation that can result in cancer cell death. 2'-Benzoyloxy-cinnamaldehyde (BCA) is a derivative of cinnamaldehyde that is a major component of cinnamon and exerts potent anticancer and antiproliferative activities by including ROS generation. On the basis of assumption that the convergence of GSH depletion with ROS elevation cooperatively amplifies oxidative stress and induces immunogenic apoptosis, we designed F-ssPBCA nanoparticles as a tumor-targeted oxidative stress amplifier as well as ICD inducing anticancer nanomedicine, composed of ssPB, BCA and tumor-targeting fucoidan. Under the tumor condition, F-ssPBCA nanoparticles significantly elevate oxidative stress to kill cancer cells and also evoke ICD featured by the release of CRT (Calreticulin), HMGB-1 (high mobility group box-1), and adenosine triphosphate (ATP). While ssPB and BCA alone are insufficient to boost ICD individually, their cooperative therapeutic activities significantly amplify oxidative stress in cancer cells, leading to ICD. To test this concept, the biophysical properties of F-ssPBCA nanoparticles were extensively examined and their anticancer therapeutic activities were also examined using cell culture models and xenograft mouse models. The results in this study demonstrate that prooxidant-mediated massive ROS accumulation is a highly effect strategy to kill cancer cells selectively and even evoke ICD. We therefore anticipate that oxidative stress amplifying F-ssPBCA nanoparticles hold tremendous translational potential as tumor-targeting anticancer nanomedicine with immunostimulating activities.

SB01.03.11

Iridium Oxide-Protein Hybrid Film for Neural Interfaces Application with Enhanced Electroactivity and Bioactivity Enable Electrically-Manipulatable Physical and Chemical Neuronal Activation Guan Xun Lee and Pochun Chen; National Taipei University of Technology, Taiwan

Iridium oxide (IrO_x) is a promising electrode material of implantable neural therapeutic devices owing to the remarkable performance on neural stimulation. However, the current IrO_x electrode lacks biocompatibility and bioactive interactions with nerve tissues. Even the commonly-used polymeric surface coating results in the weak physical adhesion between organic/inorganic interfaces, limiting the chronic application. Accordingly, we proposed a smart iridium oxide- plasma protein (IrO_x-PP) electrode with enhanced electroactivity, electrochemical stability, biocompatibility, and bioactivity that can permit controllable topographical, electrical, and chemical stimuli to enhance neuronal activity. Electrochemical deposition facilitated the formation of inorganic/organic nanoparticle (NP)-protein corona structures in which the soft NP-corona allowed a repeatable burst-to-zero-to-burst PP release and the hard NP-corona with an order atomic structure that enabled enhanced electrochemical stability and bioactivity. The incorporated PP contributed to nanorough surface structures that led to higher current storage capacity, lower impedance, better cell growth and more significant neurite outgrowth than that of pristine IrO_x. Electrical stimulation (ES) on IrO_x-PP permitted synchronous neuromodulation, on-demand PP release and cell uptake, leading to 2.5-fold higher cell density and more significant neurite outgrowth than that on IrO_x. Such bioactive inorganic-organic hybrid electrode with synergistic effect of physical and chemical neuromodulation is expected to be a revolutionary platform to provide more efficient and biocompatible implanted neural

therapies.

SB01.03.12

A ROS-Scavenging ‘Stealth’ Polymer, Poly(thioglycidyl glycerol)(PTGG), Outperforms PEG in Protein Conjugates and Enhances Protein Stability to Environmental and Biological Stressors Richard d’Arcy¹, Farah El Mohtadi², Nora Francini¹ and Nicola Tirelli³; ¹Vanderbilt University, United States; ²University of Portsmouth, United Kingdom; ³Istituto Italiano di Tecnologia, Italy

Poly(ethylene glycol)(PEG) is a low-fouling polymer commonly used for extending plasma half-lives of biologics but does suffer significant drawbacks; for example, PEGylation offers no protection from denaturation (e.g. via lyophilization, storage or oxidation). Furthermore, a growing incidences of PEG immunogenicity has put into question its biological inertness, and already led to the market withdrawal of peginesatide (Omontys), pegloticase (Krystexxa) and the cessation of pegnivacogin (Revolixys) trials, while dozens of other PEGylated formulations present antiPEG antibodies, accelerated blood clearance, infusion reactions and reduced efficacy overtime, thus highlighting a clear need for next-generation ‘stealth’ technologies.

Accordingly, we identified the lack of (pharmacological) activity as a missed opportunity as PEG offers no inherent protection from environmental stressors, but proteins are readily susceptible to chemical changes that can arise along the manufacturing line (production, sterilization, lyophilization), as well as in vivo after administration. The addition of excipients (antioxidants, cryo/lyoprotectants) only partially address the issue as they are not chemically bound to the protein, so their protective function ceases after administration.

We have thus rationally designed a new ‘active-stealth’ polymer, poly(thioglycidyl glycerol)(PTGG), composed of a cryo/lyoprotective glycerol-derived side-chain and an antioxidant polysulfide backbone. In human plasma, PTGG was significantly less immunogenic than PEG (up to 35% less complement activation), but also features a potent ROS-scavenging and anti-inflammatory action (~50% reduction of TNF- α in LPS-stimulated macrophages at only 0.1 mg/mL). PTGG was efficiently conjugated to proteins via a one-pot processes; molar mass- and grafting density-matched PTGG-lysozyme conjugates demonstrated superiority to their PEG analogs in terms of both enzyme activity, and stability against freeze-drying or oxidation. In rats, PTGG-ovalbumin conjugates (used as a model immunogenic protein) displayed a considerably longer circulation than PEG-ovalbumin ($t_{1/2} = 28.2$ vs 14.1 hours, 1.4-fold higher AUC on first dose) without an associated ABC effect ($t_{1/2} = 26.3$ vs 10.7, second dose). These findings, and in particular its double ‘active-stealth’ character, position PTGG as a promising alternative to PEG for conjugation to biologics.

SB01.03.13

Magnetic Properties of Iron Oxide Nanoparticles with Different Geometries Alexis G. Lavin, Nataniel Medina, Wenny Pantoja and Gerardo Morell; Universidad de Puerto Rico, United States

The functional hybrids based on iron oxide nanoparticles are interesting for multimode imaging and synergistic cancer therapies. In this research, we optimized morphologies as hexagonal, cubic, spherical, and star-shaped. We synthesized them using a thermal decomposition process, optimizing parameters as organic solvents batch time residence and different temperatures. The HR-TEM images show homogeneous and dispersed nanoparticles with sizes between 10 and 120 nm. The XRD patterns contain peaks associated with the spinel structure type (Fd3m) characteristic of Fe₃O₄ (magnetite, JCPDS File No. 19-0629). Magnetic studies were performed at different temperatures, finding the highest saturation magnetization (Ms) 68.24 emu/g at 300K by the star-shaped geometry. The relaxivity studies indicate that they induce T₂ responses according to their size and morphology. We propose specific geometries and surface coordination with various moieties to increase the response for biomedical applications

SESSION SB01.04: Responsive Nanomaterials Development
Session Chairs: Herdeline Ardoña and Juan Beltran-Huarac
Tuesday Morning, November 29, 2022
Hynes, Level 1, Room 104

8:15 AM SB01.04.01

Supramolecular-Assembly-Enabled Synthetic mRNA Switch for Efficient and Accurate Cell Fate Control Yaxin Hu, Qiuyu Lu, Cheuk Yin Li and Yi Kuang; Hong Kong University of Science and Technology, China

Synthetic mRNA switches are promising tools capable of regulating target protein levels (output) in response to specific molecular signals (input). Conventional synthetic mRNA switch commonly consists of two domains: an input sensing module and a output coding module. The sensing domain interacts with input via noncovalent interactions to repress output production. Leaky expression of output signal is an innate limitation of conventional synthetic mRNA switch. Here, we engineered a novel readout control module to alleviate the signal noise generated by leaky output expression. This readout control module is based on aptamer-protein interaction. An array of aptamers is used as scaffolding to assemble inactive output protein. Only in the absence of input, ample amount of output protein can saturate the aptamer array to form functional protein assemblies. While in the presence of input, the leaky output protein production is insufficient to trigger assembly formation. Synthetic mRNA switches carrying this readout control module can sense different input with higher signal-to-noise ratio, offering efficient and accurate output signal production. This novel design combines chemistry and synthetic biology principles to offer a generally applicable synthetic mRNA switch model, featuring the near-complete sequestering of output signal noise, stronger input sensitivity, and a wider output operation range. With these prominent properties, we believe this novel switch model can efficient and accurate orthogonal control of cell fate, bringing enormous potentials in building complex synthetic mRNA circuits for next-generation diagnostic and therapeutic purposes.

8:30 AM SB01.04.02

Tuneable Glycosylated Polypeptide Nanoparticles by N-Carboxyanhydride Emulsion Polymerisation Nicola Judge¹, Ruairi Brannigan^{1,2} and Andreas Heise¹; ¹Royal College of Surgeons in Ireland, Ireland; ²Dublin City University, Ireland

Biodegradable nanoparticles produced by emulsion polymerisation find applications in many fields such as nutraceutical, agriculture, and medicine. Crucial aspects of tuneability have recently focused on the shape, size and core composition as a way to control the drug loading, biodistribution and targeting capabilities within medicinal drug delivery applications. Consequently, glycosylated nanoparticles have received increased interest in the field as the tuneable nature of the emulsion process combined with the well documented targeting ability of glycans has the potential to create libraries of well-designed delivery vehicles.

Our interests lie in a new class of nanoparticles fully based on synthetic polypeptides which allow for a premeditated surface through the utilisation of a high molecular weight surfactant remaining adsorbed onto the surface. Therefore we have recently developed a novel route for the synthesis of

glycosylated degradable nanoparticles composed of a polypeptide core and a glycopeptide shell. Herein, the synthesis and analysis of a series of degradable glycosylated polypeptide nanoparticles (GlycoPep NPs) is described. GlycoPep NPs were synthesised by miniemulsion ring-opening polymerisation (ROP) of *N*-carboxyanhydrides (NCA) in aqueous conditions; during which varying glycopolypeptides were utilised as surfactants. The size of the GlycoPep NP's could be tailored based on the core and surfactant polypeptide composition and the concentration ratio. Dynamic light scattering (DLS), Nanoparticle Tracking Analysis (NTA), Transmission Electron Microscopy (TEM) and Asymmetric Field Flow Fractionation (AF4) confirmed the highly stable and reproducible nature of the particles produced. The nanoparticles could be lyophilised and resuspended in water and buffer solutions, enhancing their bio-applicability. We will look to elucidate their binding interactions by utilising the pendant sugar within the surfactant as the system is only composed of bio-relevant materials. This methodology therefore opens up a library of bio-inspired glycosylated polypeptide nanoparticles which can be highly tuned giving them significant potential for the delivery of therapeutic agents.

8:45 AM SB01.04.03

Cyclodextrin-Based Metal-Organic Frameworks as Nano Platforms for Biomedical Applications Min Peng, Anna M. Kaczmarek and Kristof Van Hecke; Ghent University, Belgium

Cyclodextrins (CDs) form a family of naturally abundant, inexpensive, cyclic oligosaccharides, consisting of truncated cone-shaped molecules, with a hydrophobic cavity and a hydrophilic surface. Through the coordination of CDs with alkali metal ions (Cs^+ , K^+ , ...), biocompatible, carbohydrate CD-based, porous metal-organic frameworks (CD-MOFs) can be obtained. These CD-MOFs are attractive materials for practical applications as they can be considered as biocompatible, biodegradable and sustainable nanoporous MOF alternatives. Hence, CD-MOFs have already found a wide range of applications, such as molecular adsorption, separation and recognition, drug delivery, as host template for nanoparticle synthesis, and light emission and sensing.

In this work, we first designed macro- and nanosized core, as well as core-shell, γ -cyclodextrin metal-organic frameworks (γ -CD-MOFs) and used them as platforms for the encapsulation of dye molecules to develop the first CD-MOF-based ratiometric optical thermometer materials. A novel dye combination was employed for this purpose, i.e., the duo rhodamine B (RhB) and fluorescein (FL). RhB is highly temperature-sensitive, whereas FL is less temperature-sensitive, and its luminescence emission peak is used as a reference. Promising results in terms of thermometric properties were obtained for a whole series of dye-encapsulated γ -CD-MOF materials based on this dye combination, with high relative sensitivities, even up to $5\% \text{K}^{-1}$, for the dye-encapsulated 75%RhB-25%FL nanosized γ -CD-MOF, among the highest performance values reported so far for luminescent dual thermometers. In our study, we have additionally developed a simple yet effective preparation method for core-shell γ -CD MOFs, allowing effective manipulation of the γ -CD-MOF shell growth. The proposed method allows incorporation of the FL and RhB dyes in the γ -CD-MOFs in a more controlled manner, enhancing the efficiency of the developed ratiometric (macro) γ -CD-MOF thermometers.

In recent years, the incorporation of metal or metal oxide nanoparticles (NPs) into porous MOFs to form NP-MOF structures has attracted great interest. Although procedures for the deposition of Ag and/or Au NPs (AgNPs, AuNPs) in MOFs have already been reported, their application with CD-MOFs has not been investigated thoroughly yet. Both AgNPs and AuNPs are plasmonic, which means they could be exploited to concentrate light at a certain wavelength, providing local heating and, thus, be employed for photothermal therapy and can play a beneficial role when it comes to CD-MOFs used as drug delivery systems, as local heating can speed up the drug release.

In this work, we therefore investigated different routes of depositing AuNPs and AgNPs in a convenient manner into nanosized CD-MOFs. The loading of the NPs can be easily steered by increasing or decreasing the amount of used metal precursors. The NPs can be synthesized at low temperatures which do not affect the structure nor crystallinity of the nano CD-MOFs. We could also show that small and very uniform AuNPs and AgNPs can be obtained upon dissolving the CD-MOF template. Therefore, this is an ideal route to yield well water-dispersible metal nanoparticles without the use of any ligands or surfactants. Analogously to the first employed dye combination of RhB and FL, the thermometry properties of the nano CD-MOFs, with deposited AuNPs and AgNPs, were obtained upon embedding a mixture of a different dye combination, i.e. the RhB and rhodamine 110 (Rh110) pair in the pores of the CD-MOFs.

This is the first work where CD-MOFs are proposed for the development of luminescent thermometric materials, and in combination with plasmonic AuNPs and AgNPs. By employing this approach, various fluorescent dyes can be combined, which opens new possibilities toward the future development of a wide range of ratiometric biological (plasmonic) nanothermometers.

9:00 AM SB01.04.04

Investigation of Nanoscale Distance-Dependent Antibody-Antigen Binding for Mast Cell Activation Leonie Schneider, Carmen Martínez-Domínguez, Kersten S. Rabe and Christof M. Niemeyer; Karlsruhe Institute of Technology, Germany

Cellular immune responses in mast cells are regulated in the early stages of cell signalling and play a pivotal role in the initiation and development of type I hypersensitivity reaction. The spatial organization of IgE's high-affinity transmembrane receptor, FcεRI, into molecular clusters stimulates inflammatory mediator degranulation, cytokine production and phospholipid production.^[1] Receptor-clustering is mediated by multivalent antigen binding of the IgE antigen binding fragments (Fab) of receptor-bound antibodies on the cell surface. Here, the spatial tolerance of Fabs towards repetitive nanopatterns of antigens is crucial for initiation or inhibition of an immune response.^[2] To investigate structural constraints of antibodies binding to multivalent antigens to initiate effector functions and cell activation, we utilize supramolecular DNA architectures decorated with small hapten molecules and present them to the cell membrane. This Multiscale-Origami Structures as Interfaces for Cells (MOSAIC) technology allows precise control over the number, stoichiometry and arrangement of the signalling molecules on the nanometer scale, imitating the ultrastructural features of biomolecular assemblies.^[3]

In this contribution we report on hapten-decorated DNA origami nanostructures (DON) to investigate the spatial tolerance of free and membrane-associated antibodies on the nanoscale regarding antigen-mediated effects on mast cell activation. We designed distinctive nanoscale arrangements of haptens to induce receptor clustering and for the first time investigated the relation between antigen-binding affinity and mast cell signalling, an important feature for tailoring next generation monoclonal antibodies (mAb) for immunotherapy. We synthesized rectangular DON with a size of $70 \times 100 \text{ nm}^2$ as molecular pegboards and incorporated protruding oligonucleotides for DNA-directed immobilization on solid surfaces and dinitrophenol (DNP)-ligands with precisely defined distances. We investigated the interaction kinetics of anti-DNP IgE and anti-DNP IgG to these DNP-decorated DON with distinct DNP-distances of 6 – 30 nm aiming for a better understanding of the native structure and Fab flexibility of antibodies. We also investigated the binding kinetics of DNP-decorated DON and FcεRI-receptor-bound anti-DNP IgE antibodies on the surface of rat basophilic leukemia (RBL)-2H3 cells, a model for mast cells, using LigandTracer technology.^[4] To put our results in a biological context, we performed cell signalling assays to study the effect of antigen-antibody binding affinity and receptor-clustering on cellular activation.^[5] To the best of our knowledge, these studies are the first to investigate the distance dependence of free and receptor-bound IgE antibodies using surface-immobilized hapten-decorated DNA origami to elucidate fundamental biological principles of mast cell activation.

- [1] D. Sil, J. B. Lee, D. Luo, D. Holowka, B. Baird, *ACS Chemical Biology* **2007**, *2*, 674-684.
 [2] A. Shaw, I. T. Hoffecker, I. Smyrlaki, J. Rosa, A. Grevys, D. Bratlie, I. Sandlie, T. E. Michaelsen, J. T. Andersen, B. Hogberg, *Nat Nanotechnol* **2019**, *14*, 184-190.
 [3] A. Angelin, S. Weigel, R. Garrecht, R. Meyer, J. Bauer, R. K. Kumar, M. Hirtz, C. M. Niemeyer, *Angew Chem Int Ed Engl* **2015**, *54*, 15813-15817.
 [4] S. Bondza, A. Marosan, S. Kara, J. Lösing, M. Peipp, F. Nimmerjahn, J. Buijs, A. Lux, *Front Immunol* **2021**, *11*, 609941-609941.
 [5] L. Schneider, C. Martínez-Domínguez, K. S. Rabe, C. M. Niemeyer, **2022**, in preparation.

9:15 AM SB01.04.05

AI-Enhanced ND Biosensor Automates Sensitivity Prediction to OXPPOS Inhibitors [Jingru Xu](#)¹, Mengjia Zheng², Chenjie Xu² and Edward Chow¹;
¹National University of Singapore, Singapore; ²City University of Hong Kong, China

Hepatocellular carcinoma (HCC) is the one of leading causes of cancer-related mortality worldwide. Spalt-like transcription factor 4 (SALL4) is an oncofetal protein in HCC, and high SALL4 expression level is correlated to poor prognosis. However, SALL4 lacks well-structured small molecule binding pockets, making it difficult to design targeted inhibitors. There was a therapeutic strategy based on the increased oxidative phosphorylation (OXPHOS) in SALL4^{hi} HCC cells. SALL4-induced high expression level of OXPPOS serves as a therapeutically targetable vulnerability in HCC that specific OXPPOS inhibitors can be applied.

Here, we developed a workflow that utilized molecular beacon, a nucleic-acid-based, activatable sensor with high specificity to the target mRNA, delivered by nanodiamond, to establish an artificial intelligence (AI)-based platform for rapid evaluation of patient-specific drug sensitivity. Specifically, when the HCC cells were treated with the nanodiamond-mediated OXPPOS biosensor, high sensitivity and specificity of the sensor allowed the identification of OXPPOS expression in cells. Assisted by a trained convolutional neural network, drug sensitivity of cells towards an OXPPOS inhibitor, IACS-010759, can be accurately predicted. The whole assessment could be accomplished within two days, enabling rapid and efficient clinical decision support for HCC treatment.

9:30 AM *SB01.04.06

Nanomaterials as Building Blocks in Functional Biomaterials Design [Mark W. Tibbitt](#); ETH Zürich, Switzerland

Engineering responsive biomaterials from reversible interactions enables the design of injectable drug delivery platforms and materials for 3D bioprinting. Among the emerging motifs to assemble these materials, polymer-nanoparticle interactions have been introduced as a useful strategy to assemble polymer-nanoparticle materials. In this approach, engineered nanoparticles are used as constituent building blocks in the material design, allowing for a broad range of functionality in biomaterials design. In this presentation, we will describe our efforts in the design of polymer-nanoparticle hydrogels as bioinks for 3D printing. We designed a universal carrier ink composed of PEGylated polymer nanoparticles, cellulose derivatives, and a range of secondary polymers. The rheology enables extrusion-based printing, and the inclusion of secondary polymers provides a strategy for stabilization of the printed constructs. This strategy has been applied in the design of printed constructs for tissue engineering and multimodal drug delivery. In addition, we have advanced this platform by including a supramolecular binding motif based on polypseudorotaxane formation of alpha-cyclodextrin (αCD) on the surface of the PEGylated nanoparticles. This approach enabled tunable mechanical properties as well as modular design of polymer-nanoparticle hydrogels via exchange of the nanoparticles and polymers. Supramolecular reinforcement of polymer-nanoparticles further expanded the scope of applications, including the design of injectable materials for sustained biomolecule release.

10:00 AM BREAK

10:30 AM *SB01.04.07

Enzymatic Responsive Supramolecular Assemblies for Targeting Subcellular Organelles Weiyi Tan, Meihui Yi, Jiaqi Guo, Qiuxin Zhang, Adrianna Shy, Yuchen Qiao and [Bing Xu](#); Brandeis University, United States

Subcellular compartmentalization is a key feature of eukaryotic cells. Selectively targeting subcellular compartments, though holding many exciting opportunities for biomedicine, remains rather underdeveloped. Enzyme-instructed self-assembly (EISA), an approach that integrate enzymatic reactions and self-assembly, provides a new way for subcellular targeting. In this talk, we briefly introduce the development of supramolecular self-assemblies for targeting mitochondria, endoplasmic reticulum, Golgi apparatus, nucleus, and cell membrane. We mainly focus on the use EISA of peptide assemblies, which spatiotemporally controls the formation of supramolecular nanofibers, for subcellular targeting and its applications, such as developing novel cancer therapeutics.

11:00 AM SB01.04.08

Synthesis of NIR-II Absorbing Gelatin Stabilized Gold Nanorods and Its Photothermal Therapy Application Against Fibroblast Histiocytoma Cells [Samuel O. Oluwafemi](#); University of Johannesburg, South Africa

The excellent photothermal properties of gold nanorods (Au-NRs) make them one of the most researched plasmonic photothermal nanomaterials. However, their biological applications have been hampered greatly due to surfactant-induced cytotoxicity. We herein report a simple synthesis of highly biocompatible gelatin stabilized Au-NRs (gelatin@Au-NRs) to address this issue. The optical and structural properties of the as-synthesized gelatin@Au-NRs were investigated by Zetasizer, Ultraviolet-Visible-Near Infrared (UV-Vis-NIR) spectroscopy, high-resolution transmission electron microscopy (HR-TEM), and Fourier transform infrared spectroscopy (FTIR). The as-synthesized gelatin@Au-NRs were highly crystalline and rod-like in shape with an average length and diameter of 66.2 ± 2.3 nm and 10 ± 1.6 nm, respectively. The as-synthesized gelatin@Au-NRs showed high stability in common biological media (phosphate buffer saline and Dulbecco's Modified Eagle's Medium) compared to CTAB capped Au-NRs. Similarly, the gelatin@Au-NRs showed an improved heat production and outstanding cell viability against two different cancer cell lines; KM-Luc/GFP (mouse fibroblast histiocytoma cell line) and FM3A-Luc (breast carcinoma cell line) compared to CTAB capped Au-NRs and PEG@Au-NRs. An in vitro photothermal therapy study against KMLuc/ GFP showed that gelatin@Au-NRs effectively destroy the cancer cells.

11:15 AM SB01.04.09

Manufacturing of Halloysite Nanotubes/Barium Titanate Nanoparticles Reinforced Functional Hydrogels for Bone Tissue Repair [Anuj Kumar](#), Ankur Sood, Ritu Singhmar and Sung Soo Han; Yeungnam University, Korea (the Republic of)

Bone defects caused by fractures, diseases, hereditary deformations, and surgical reconstructions are serious clinical challenges, wherein the self-healing of large bone defects is not able to bridge the gap and requires a biomaterial-based scaffold to facilitate bone repair under a native-like three-dimensional (3D) microenvironment. However, the design and fabrication of an appropriate scaffold is a great challenge for efficient cellular responses to develop new bone tissue. Therefore, the search for developing a suitable scaffold for bone repair is still unaccomplished. Herein, hydrogel as a 3D polymeric network provides the most suitable dynamic microenvironment to repair damaged bone tissues. The efficiency of hydrogels in repairing bone tissue is limited due to

their low mechanical properties and bioactivity, which presents challenges in designing effective hydrogels with robust mechanical attributes and acceptable bioactivity. In our study, we synthesized functional hybrid hydrogels by incorporating halloysite nanotubes and barium titanate nanoparticles, and as-obtained hydrogels showed promising porous and surface characteristics (i.e. microstructure and roughness), improved mechanical properties, enhanced *in-vitro* bioactivity, and satisfactory cytocompatibility (*in-vitro*).

11:30 AM SB01.04.10

Monitoring Nanoparticle Dissolution via a Fluorescence-Color Shift Christian Ritschel¹, Joanna Napp^{2,3}, Frauke Alves^{2,3} and Claus Feldmann¹;

¹Karlsruhe Institute of Technology (KIT), Germany; ²University Medical Center Goettingen (UMG), Germany; ³Max Planck Institute for Multidisciplinary Sciences, Germany

Optical imaging (OI) has emerged as a cost-effective, versatile method for biomedical monitoring and is used to visualize and distinguish cellular compartments and tissues as well as to study active cellular processes.¹ Specific markers with suitable fluorescence characteristics, sufficient physiological and photochemical stability, as well as high biocompatibility are essential for the success of OI.

For this purpose, a variety of molecular fluorescent dyes has been suggested and was attached in different ways to carrier molecules or carrier structures.² Alternatively, fluorescent nanoparticles, such as quantum dots, plasmonic metal nanoparticles, or up-converting nanoparticles have been widely used and are typically characterized by higher chemical and photochemical stability as compared to molecular fluorescent dyes.³

Aiming at theranostic nanoparticles, we have developed the concept of inorganic-organic hybrid nanoparticles (IOH-NPs).⁴ These IOH-NPs are characterized by a saline composition with an inorganic cation and a functional organic anion. The functional organic anion can be a fluorescent dye and/or a pharmaceutical drug, which contains a phosphate, sulfonate, or carboxylate group. Together with a suitable inorganic cation, the functional organic anion forms insoluble saline nanoparticles in water.

The optical detection of nanoparticles is usually related to a change in intensity, not a change of the wavelength. In some cases, the change of the fluorescence intensity was used to the point of an on-off or off-on behavior. Such fluorescent nanoparticles were exploited, for example, to study cellular uptake, drug delivery, drug release, and all kinds of sensing effects, which can be partly performed in real-time. However, a change of the emission intensity has the disadvantage of being concentration-dependent, which either requires a distinct on-off/off-on emission characteristics or a normalization of the emission intensity on a suitable reference. In this regard, a wavelength change of the emission as a response of a certain effect would be more effective. However, a wavelength shift is more complex in regard of the selection of the fluorescence markers and has only been reported in a few cases until now.⁵

Aiming at a fluorescence-based monitoring of the dissolution of nanoparticles and specifically the differentiation of the intact solid nanoparticles and the homogeneous solution after the nanoparticle dissolution, we have examined different strategies involving two different fluorescent dyes. We were successful with a mixture of $[\text{La}(\text{OH})_2]^{2+}[\text{ICG}]_2^-$ and $[\text{La}(\text{OH})_2]^{2+}[\text{PTC}]_4^-$ inorganic-organic hybrid nanoparticles (IOH-NPs) (ICG: indocyanine green, PTC: perylene-3,4,9,10-tetracarboxylate), which show an emission shift from red (intact nanoparticles in aqueous suspension) to green (aqueous solution after dissolution). Special advantages of the IOH-NPs comprise an aqueous synthesis, a simple material composition, an unprecedented high dye load (70-85 wt-% of total nanoparticle weight).⁶

This novel system of fluorescence markers – including synthesis, nanoparticle characterization, and first *in vitro* studies – will be presented with this contribution.

1. S. Kunjachan, J. Ehling, G. Storm, F. Kiessling and T. Lammers, *Chem. Rev.*, **2015**, *115*, 10907-937.

2. O. S. Wolfbeis, *Chem. Soc. Rev.*, **2015**, *44*, 4743-4768.

3. K. D. Wegner and N. Hildebrandt, *Chem. Soc. Rev.*, **2015**, *44*, 4792-4834.

4. a) M. Poß, E. Zittel, C. Seidl, A. Meschkov, L. Muñoz, U. Schepers and C. Feldmann, *Adv. Funct. Mater.*, **2018**, *28*, 1801074(1-8). b) M. Poß, R. J. Tower, J. Napp, L. C. Appold, T. Lammers, F. Alves, C.-C. Glüer, S. Boretius and C. Feldmann, *Chem. Mater.*, **2017**, *29*, 3547-3554.

5. a) W. Zhao, Y. Zhao, Q. Wang, T. Liu, J. Sun and R. Zhang, *Small*, **2019**, *15*, 1903060. b) G. Shim, S. Ko, D. Kim, Q.-V. Le, G. T. Park, J. Lee, T. Kwon, H.-G. Choi, Y. B. Kim and Y.-K. Oh, *J. Contr. Rel.*, **2017**, *267*, 67-79.

6. C. Ritschel, J. Napp, F. Alves, C. Feldmann, **2022**, *submitted*.

11:45 AM SB01.04.11

Design and Fabrication of a Highly Sensitive and Selective Non-Enzymatic Glucose Sensor by a Nafion-Modified Nanoporous Platinum Electrode Yu-Lin Lee, Yun-Yang Sun and Pochun Chen; National Taipei University of Technology, Taiwan

Alzheimer's disease has been reported to be related to the level of glucose concentration in the brain. This study develops a non-enzymatic glucose sensor using a nanoporous platinum electrode. First, we decorate nanoporous platinum on a commercial gold electrode by cyclic voltammetry electrodeposition. Then, we further modified Nafion on the surface of nanoporous platinum to improve the selectivity of the glucose sensor. We characterize the Nafion-modified nanoporous platinum electrode's morphology, crystallinity, and composition by SEM, XRD, and FTIR, respectively. We evaluate the glucose sensor by electrochemical methods, including cyclic voltammetry, chronoamperometry, and electrochemical impedance spectrum in an artificial cerebrospinal fluid (ACSF). The nanoporous platinum and Nafion-modified nanoporous platinum show their sensitivities of $38.31 \mu\text{Acm}^{-2}\text{mM}^{-1}$ and $27.42 \mu\text{Acm}^{-2}\text{mM}^{-1}$ in ACSF, respectively. Additionally, the Nafion-modified nanoporous platinum remains desirable sensitivity and presents excellent selectivity to interferences, including dopamine (DA), ascorbic acid (AA), fructose, and lactose.

SESSION SB01.05: Nanomaterials for Imaging, Sensing and Theranostics I

Session Chairs: Jennifer Carpena-Núñez and Georgios Sotiriou

Tuesday Afternoon, November 29, 2022

Hynes, Level 1, Room 104

1:30 PM *SB01.05.00

Designing Biomaterials to Heal the Body Molly Stevens; Imperial College London, United Kingdom

Bio-responsive hybrid materials are of growing importance with potential applications in therapeutic delivery and tissue engineering. In this talk, I will provide an overview of our recent developments in the design of biointerfaces with interesting features such as the incorporation of biological and topographical cues to enhance tissue regeneration, wound healing and cell differentiation [1]. I will show how we are using remote fields for *in vivo* remote-triggered hydrogelation of lipid based nanocarriers for controlled drug delivery [2] and advanced manufacturing strategies to engineer complex 3D architectures that mimic anisotropic multiscale tissue structures and to generate spatially arranged bioinstructive cues [3]. I will discuss the multi-scale

approach that we use to inform the design of smart biomaterials - from molecular dynamics simulation that help us understand self-assembly and organisation at the nanoscale [4], to Raman-based techniques used to visualise the molecular composition of living tissues [5] and to characterise single nanoparticles in a high-throughput label-free manner using our patented SPARTA™ technology [6]. SPARTA™ has become an integral tool for the design of nanotherapeutics, with recent examples including DOPC-containing lipid nanoparticles for nucleic acid delivery and dendrimer-based systems for controlled delivery of antibacterial drugs, and for profiling extracellular vesicles (EVs) for detection of breast cancer through a minimally invasive liquid biopsy. Finally, I will discuss how we are establishing effective translational pipelines to drive our innovations to clinical application.

[1] T. von Erlach, ... M. M. Stevens. "Cell geometry dependent changes in plasma membrane order direct stem cell signalling and fate." *Nature Materials*. 2018. 17: 237-242.

[2] V. Nele, ... M. M. Stevens. "Ultrasound triggered enzymatic gelation." *Advanced Materials*. 2020. 32(7):1905914.

[3] L. Ouyang, ... M. M. Stevens. "Expanding and optimizing 3D bioprinting capabilities using complementary network bioinks." *Science Advances*. 2020. 6(38): eabc5529.

[4] A. Belessiotis-Richards, ... M. M. Stevens. "Coarse grained simulations suggest the epsin N-terminal homology domain can sense membrane curvature without its terminal amphipathic helix." *ACS Nano*. 2020. 14(12):16919-16928.

[5] H. Hogset... M. M. Stevens. "In vivo biomolecular imaging of zebrafish embryos using confocal Raman spectroscopy." *Nature Communications*. 2020. 11:6172.

[6] J. Penders... M. Stevens. "Single particle automated Raman trapping analysis." *Nature Communications*. 2018, 9: 4256

2:00 PM SB01.05.01

Stimuli-Responsive Surface Coating Properties of T₂ MRI Contrast Agents Dylan M. Ines, Jake Villanova and Vicki L. Colvin; Brown University, United States

Iron oxide nanocrystals (IONCs) are FDA approved Magnetic Resonance Imaging (MRI) contrast agents with high biocompatibility, hepatobiliary clearance, and contrast performance. It has been demonstrated that polymeric nanocrystal surface coatings have a significant impact on T₂ contrast performance (relaxivity). These non-magnetic polymers at IONC interfaces can influence the diffusion of bulk water within the local magnetic field of the nanocrystal core – thus impacting relaxation dynamics. Specific environmental or molecular stimuli can induce changes in contrast performance, increasing signal-to-noise and highlighting pathological areas of interest. The result is a "smart" molecular imaging contrast agent that exhibits stimuli-responsive contrast changes. "Smart" T₂ contrast agents currently rely on *interparticle* clustering effects to increase relaxivity. Compared to an individual IONC, clusters increase their effective diameter and generate greater magnetic field inhomogeneities and promote T₂ relaxation. However, clustering is clinically problematic due to aggregation and toxicity concerns. Thus, "smart" T₂ contrast agents that exhibit *intraparticle* changes in surface coating to modulate relaxivity are promising candidates for clinical applications. For example, IONCs that can decrease their hydrodynamic diameter or polymeric grafting density in the presence of environmental or molecular stimuli can improve their relaxometric properties and display higher signal-to-noise. Particularly when cleavable peptide sequences are incorporated into IONC surfaces, the coatings can undergo substantial changes when in the presence of certain proteases which are established biomarkers of cancer, traumatic brain injury, or other pathologies. Proteases cleave a target portion of the IONC surface coating, directly modulating its thickness, stability, and/or grafting density.

Here, we highlight a shift in optimizing contrast performance by modulating surface coating properties instead of magnetic core properties. Additionally, a novel framework for conceptualizing the impact of surface coatings on water diffusion and resulting contrast performance was developed. This framework provides a more detailed explanation for contrast performance trends found in the literature and informs the rational design of high-performance contrast agents. The effects of grafting density and thickness on relaxivity were measured for various surface coatings. The impacts of physiologically relevant pH ranges and metal cation concentrations on contrast performance were evaluated for a range of surface coatings. Contrast performance was also evaluated upon IONC conjugation to a target peptide sequence. Stimulus-responsiveness was probed by introducing clinically relevant proteases to the conjugated IONC system and measuring changes in relaxivity.

2:15 PM SB01.05.02

X-Ray Nano-Contrast Agents with Targeting Specificity for Breast Cancer Detection Manos Gkikas¹, Kalyan Ramesh¹, Alice Truong² and Mary Rusckowski²; ¹University of Massachusetts--Lowell, United States; ²University of Massachusetts Medical School, United States

X-ray-computed tomography (CT) is considered one of the powerful diagnostic techniques for preclinical and clinical studies due to deep tissue penetration, high resolution, cost effectiveness, rapid scan times and patient comfort. Non-invasive disease detection with pronounced signal enhancement at the site of injury is a great challenge in medicine and allows for detection in early stages. Designing polymer-stabilized metallic nanoparticle (NP) X-ray contrast probes for spectral CT imaging that can be statistically discriminated from biological fluids, tissue, and bone (a property that is impossible to achieve with conventional CT), and are empowered by molecular recognition, aligns towards that direction. Although X-ray contrast with high-Z metals has been successfully shown in cells and small animals, the probes usually focus on intravenous imaging and NP fate, while there are only few cases reporting disease-targeting NPs with prolonged imaging capabilities. We have established a Team (UML/UMMS) to develop ligand-specific X-ray contrast probes for breast cancer cells, aiming to achieve early disease diagnosis at low NP dosages and enhanced detection. Our approach combines targeting specificity with dual-energy CT (DE-CT) or photon-counting spectral CT (PCD-CT), a state-of-the-art form of CT that allows for visualization of tissue composition based on intensity of signal, which is dictated by atomic number and density of contrast materials, and thus is enhanced by metallic NPs. Au offers significant advantages towards materials differentiation since its K-edge is 81 vs. 4 keV of Ca, while its density is 19.6 vs. 1.6 g/mL of Ca. Since X-ray absorption is highly dependent on K-edge and density of materials, we synthesize Au-based nano-contrast agents with high affinity for breast cancer cells and enhanced retention, and CT contrast comparable to FDA-approved iodinated molecules. Our materials are tested in vitro as well as in vivo using a breast cancer animal model. Among our recent findings is the ability to detect breast tumors for up to 21 days using only 0.5 mg Au. Future directions include theranostic materials, combining our enhanced prolonged diagnosis with radiation therapy or chemo/immuno drugs.

2:30 PM *SB01.05.03

Point of Care Diagnostic Ammonia Sensing by Responsive Silver Nanoparticles Padryk Merkl and Georgios Sotiriou; Karolinska Institutet, Sweden

Ammonia is produced and consumed in the human body as a normal part of homeostasis, with the urease activity of intestinal bacteria thought to contribute significantly to blood ammonia levels. The ammonia found in blood is largely dominated by the ionised (NH₄⁺) form although to a lesser extent the unionised NH₃ form can be found. Here ammonia levels are used to refer to the total ammonia content of both ionised and unionised ammonia. The liver plays a critical role in maintaining blood ammonia levels below the threshold considered to be hyperammonaemia (>50 μM) in adult humans. Elevated blood ammonia levels can give rise to diffuse symptoms ranging from minor cognitive or behavioural changes to coma. In well-equipped hospital diagnostic labs ammonia levels are routinely analysed by enzymatic assays, however, due to the specialised equipment and cold-chain requirements their application in resource limited settings can be challenging. An alternative analytical method for determination of ammonia levels is the Berthelot reaction and its subsequent derivatives. This relies on the reaction of ammonia with the hypochlorite ion to cause conversion of phenol to the strongly blue coloured

indophenol. A similar reaction scheme is exploited in this study, whereby the reaction of the hypochlorite ion with silver nanoparticles is exploited to derive ammonia sensitivity. Silver nanoparticles are produced by flame spray pyrolysis as either a powder or deposited on porous glass-fibre filter paper. The addition of hypochlorite to the silver nanoparticles causes their oxidative dissolution and therefore a strong decrease in the plasmonic absorbance. However, in the presence of ammonia the hypochlorite can be neutralised preserving the plasmonic properties of the silver nanoparticles and therefore also their colour. A thin silica coating was applied to the silver nanoparticles and optimised to provide stable ammonia determination in isotonic solutions down to physiologically relevant ammonia concentrations. Measurements were also demonstrated from simulated serum by applying a perfluorosulfonic acid polymer (Nafion™), which displays selective transport of small positively charged species. Furthermore, the silver nanoparticles directly deposited onto filter paper were used for ammonia concentration determination in a paper-based point of care naked eye format. This project has received funding from the European Research Council (ERC) under the European Union's Horizon 2020 research and innovation program (ERC Grant agreement # 758705). Funding from the Karolinska Institutet, the Swedish Research Council (2021-05494), and the Swedish Foundation for Strategic Research (FFL18-0043) is kindly acknowledged.

3:00 PM BREAK

3:30 PM *SB01.05.04

Biodegradable Piezoelectric Nanofibers for Tissue Regenerative Engineering Yang Liu, Thanh Le and [Thanh D. Nguyen](#); University of Connecticut, United States

Every year, millions of Americans suffer from bone and cartilage diseases like osteoarthritis. Artificial “engineered” bone and cartilage grafts constructed *in vitro* by using synthetic biomaterial scaffolds – have received considerable attentions. Yet, the constructed tissues often rely on potentially toxic growth factors and/or seeded stem cells which pose risks of immune rejection, limited supplies and undesired cell differentiation into cancers. Alternative to the biochemical factors, electrical cues can be used as a safe and effective stimulation for tissue regeneration. Herein, for the first time, we present a cell-free and growth factor-free biodegradable piezoelectric (poly (L-lactic acid)) (PLLA) nanofiber scaffold which under applied force can act as a battery-less electrical stimulator to promote chondrogenesis and cartilage regeneration. We have reported the piezoelectric tissue scaffold and the piezoelectric PLLA in several journals of Science Translational Medicine, PNAS and Nano Energy (Science Transl. Med. 14, (627), eabi7282, 2022; PNAS 117.1 (2020): 214-220, PNAS 115.5 (2018): 909-914, and Nano Energy 76 (2020): 105028.). The PLLA scaffold with applied force can generate piezoelectric charge to significantly improve chondrogenic effect of adipose stem cells *in vitro*. Rabbits conditioned with critical-sized osteochondral defects and receiving piezoelectric scaffold + exercise treatment showed a significant hyaline-cartilage regeneration with completely healed cartilages that exhibit abundant chondrocytes and collagen type II. The hybrid biodegradable piezoelectric scaffold/stimulator system, presented herein, could be used to not only heal cartilage but also bone, nerve, muscle etc. without the need of invasive removal process, offering a significant impact on the field of tissue regenerative engineering.

4:00 PM SB01.05.05

In Situ Upconverting Nanoparticle-Based Force Sensors for Gastrointestinal Imaging [Cindy Shi](#), Jason Casar, Chris Siefe, Beatriz Robinson, Mia Cano, Julia Kaltschmidt and Jennifer A. Dionne; Stanford University, United States

Mechanical forces play a fundamental role in a myriad of biological processes such as stem cell differentiation, cardiovascular health, cancer progression, and digestion. The enteric nervous system is of particular interest for its neuromuscular complexity and bi-directional communication with the central nervous system, playing a significant role in neurodegenerative pathology. Quantifying colonic mechanical forces is important for understanding disease development, but current biological force measurement techniques are limited: *ex vivo* techniques such as atomic force microscopy and traction force microscopy do not measure forces in accurate physiological conditions, while *in vivo* measurement techniques like stents and catheters cause uncomfortable colon distension and risk damage or rupture. Nanoscale markers such as resonant energy transfer-based molecular tethers, oil droplets, and quantum dots also lack the robust signal to overcome a rapidly changing biological environment. Here, we demonstrate upconverting nanoparticles (UCNPs) as minimally invasive optical force sensors, delivered in polydimethylsiloxane (PDMS) pellets for *in vivo* gastro-intestinal tract imaging. UCNPs change their color via a ratiometric change in their two emission peaks in a linear fashion with externally applied pressure. Furthermore, they are photostable, absorb in the near-infrared tissue transparency region, can be functionalized to target specific biological structures, and do not require toxic heavy metals like cadmium for synthesis. We synthesize monodisperse 13-nm diameter cubic phase SrLuF:Yb, Er, Mn@SrLuF UCNPs, then use dual confocal-AFM microscopy to exert forces on these particles and determine their dynamic range of mechanosensitivity in the nanoNewton to microNewton force regime. We vary the Mn dopants concentration from 0% to 10% and optimize the Mn concentration to maximize color change and mechano-sensitivity. Next, we embed the UCNPs in PDMS mimics of mouse fecal pellets to create a colonic probe. We calibrate the spectral response of the UCNPs embedded in PDMS using dual confocal-AFM, demonstrating that red-to-green emission ratio changes repeatedly over multiple compression and decompression cycles from 0 to 100 nanoNewtons. Finally, we deploy these pellet probes in excised mouse colons from both wild type and ETV-/- knockout mice to image and quantify forces in healthy colon pumping and irregular colon pumping, respectively. We compare the time-averaged force and location-dependent force exerted by the colons, as well as total time for pellet transition to demonstrate that our UCNP mechanosensor is able to distinguish between biological phenotypes with bright, robust optical signal that can penetrate colon wall tissue without damaging it. This platform provides a straightforward method for imaging intraluminal force dynamics in the colon and can be extended a range of other hollow neuromuscular organ systems, such as the stomach or heart cavities.

4:15 PM SB01.05.06

In Vivo Tracking of Long Circulating Bimodal PEGylated Au@SiO₂ Nanoparticles (NPs) Combining Near Infrared (NIR) Optical Imaging (OI) and μ -Computed Tomography (μ CT) [Megi Bejko](#)^{1,2}, [Clement Vecco-Garda](#)², [Coralie Genevois](#)³, [Nestor Pallares-Lupon](#)⁴, [Richard Walton](#)⁴, [Franck Couillaud](#)³, [Olivier Sandre](#)¹ and [Stéphane Mornet](#)²; ¹Laboratoire de Chimie des Polymères Organiques, France; ²Institut de Chimie de la Matière Condensée de Bordeaux, France; ³Bordeaux Research Institute On Cancer, France; ⁴L'institut de Rythmologie et Modélisation Cardiaque, France

Thanks to their physicochemical features, Au NPs present a broad scope for innovative treatments in oncology with applications ranging from imaging to drug delivery, and photo-induced therapy.¹ One of the particularities of this element is the high atomic number and thus high X-ray absorption coefficient, endowing them with substantial contrast enhancement in X-Ray CT scans. These properties combined with the biocompatibility and tunable surface chemistry, has encouraged the use of Au NPs for μ CT imaging in vascular, cardiac and cancer fields.² The high spatial resolution (1 μ m) afforded by μ CT imaging, allows non-invasive quantification of local accumulated Au in zones of interest. This enables robust full body evaluation of the *in vivo* fate of Au NPs in rodents, which is beneficial in a preclinical setting. However, studies regarding the *in vivo* fate of Au NPs for μ CT imaging rely on injecting large amounts (up to 1.1 g Au/kg) to promote sufficient local concentration, necessary to enhance contrast of tumors at high-resolution.³ This is done to counteract the poor pharmacokinetics (PK) of the NP as well as the low sensitivity of μ CT. Herein, we propose to combine two complementary imaging techniques: μ CT with classic NIR OI. Thereby, bimodal core-shell NPs with an Au core and fluorescent SiO₂ shell is designed to associate high spatial resolution and non-invasive quantitative analysis of μ CT with the high sensitivity of NIR OI. Combining these two imaging modalities enables full tracking of the *in vivo* fate of the NPs. In addition, physicochemical features of the NPs are adjusted to promote long blood circulation times and prevent injection of

clinically irrelevant doses.

For this, fluorescent SiO₂ is grown on 15 nm Au NPs following known sol-gel protocols.⁴ The SiO₂ shell reduces the high attraction potential of the Au surface, which has a Hamaker constant 50x higher than amorphous SiO₂.^{5,6} This surface modification is a first step towards long circulating NPs by minimizing plasma protein adsorption. The second step consists on the covalent grafting of polyethylene glycol (PEG) (M_w=4 kDa) on to the SiO₂ shell in a dense brush conformational regime giving an R_p/D (R_p: Flory radius, D: distance between two anchoring sites) value of 5. This value is higher than the threshold R_p/D = 4.0, above which NPs possess prolonged blood circulation times as reported for SiO₂ NPs by our team.⁷ A final neutral NP surface charge (+3 mV, pH=7.4) is purposely generated as reports show better PK when compared to their positive counterparts.⁸ A low quantity of Au (0.06 g Au/kg) is then *i.v.* injected in mice (N=9) possessing subcutaneous prostate cancer (RM1), genetically modified to overexpress the luciferase firefly enzyme. The PK of the NPs is evaluated by OI where the maximal tumor accumulation is observed 24h post injection and NP circulation persisted up to 72h post-injection. μ CT imaging is then acquired on anesthetized mice (N=6) 24h post-injection. The images reveal micro-distributions of Au in organs of interest (*i.e.* liver, spleen) and tumor periphery at a higher spatial resolution than OI. Thanks to prior calibration of μ CT signal, the 3D distribution and quantity of accumulated Au with respect to the quantity of NPs injected is determined in peripheral tumors and key organs.

In conclusion, two complementary imaging techniques are combined, allowing a full non-invasive tracking of bimodal NPs using realistic administered doses (reduced by a factor 20): OI provided PK and biodistribution of circulating NPs and μ CT quantitatively evaluated 3D distribution within organs and tumors.

References:

1. Bansal, S. A. et al., *Nanoscale Adv.* **2020**
2. Ashton, J. R. et al., *Front. Pharmacol.* **2015**
3. Hainfeld, J. F. et al., *Br. J. Radiol.* **2011**
4. Fernández-López, C. et al., *Langmuir* **2009**
5. Bergstrom, L., *Adv. Colloid Interface Sci.* **1997**
6. Biggs, S. et al., *J. Chem. Phys.* **1994**
7. Adumeau, L. et al., *Biochim. Biophys. Acta BBA.* **2017**
8. Sakulkhu, U. et al., *Nanoscale* **2014**

4:30 PM SB01.05.07

A Quantitative Analysis of the Tissue Digestion Procedure Required for the Uniform 4-fold Expansion of the Whole Mouse Embryos [Jueun Sim](#)¹, Chan E Park¹, In Cho¹, Kyeongbae Min², Minho Eom¹, Seungjae Han¹, Hyungju Jeon³, Hyung-Ju Cho⁴, Eun-Seo Cho¹, Ajeet Kumar¹, Yosep Chong⁵, Jeong Seuk Kang⁶, Kiryl D. Piatkevich⁷, Erica E. Jung⁸, Du-Seock Kang¹, Seok-Kyu Kwon³, Jinhyun Kim³, Ki-Jun Yoon¹, Jeongsoo Lee⁴, Edward S. Boyden⁹, Yong-Gyu Yoon¹ and Jae-Byum Chang¹; ¹Korea Advanced Institute of Science and Technology, Korea (the Republic of); ²Sungkyunkwan University, Korea (the Republic of); ³Korea Institute of Science and Technology, Korea (the Republic of); ⁴Korea Research Institute of Bioscience & BioTechnology, Korea (the Republic of); ⁵Catholic University Seoul St.Mary, Korea (the Republic of); ⁶Harvard University, United States; ⁷Westlake University, China; ⁸University of Illinois at Chicago, United States; ⁹Massachusetts Institute of Technology, United States

The outstanding functions of living organisms are the result of a diverse range of biomolecules and their hierarchical architectures, which in some cases have still not been discovered. To fully investigate and exploit such inspiring structures and design principles, a comprehensive visualization of the entire, intact organism at sub-cellular resolution is required. For example, in the study of structure-function relationships in skeletal muscles, high spatial resolution is required to elucidate morphological details of single myofibrils, whereas full spatial coverage is required to understand how different parts of muscles are distributed and associated together throughout the entire body. Several imaging techniques, such as tissue clearing, computed tomography, and electron microscopy, have been used for studying biological systems. However, none of these approaches solely provides nanometer resolution beyond centimeter-scales with sufficiently high contrast and throughput. Expansion microscopy (ExM) combined with the labeling of functional groups of proteins with fluorophores would be an appealing candidate for achieving such a goal. By physically expanding the specimens, ExM can image the microstructure inside the biological systems with a lateral resolution of 60 nm. Once a swellable hydrogel is synthesized inside the biological specimens, the hydrogel-organism hybrids can expand fourfolds in water, and the nanostructures smaller than the diffraction limit of light can be resolved under a diffraction-limited optical microscope. However, the application of ExM has been limited to relatively simple specimens, such as cultured cells, tissue slices, and small organisms, such as bacteria. The ExM imaging of more vertebrate bodies, which contain a great number of highly sophisticated nanostructures, has not yet been demonstrated due to the difficulty of expanding mechanically tough body parts. Recently, we reported whole-body ExM, which enables the expansion of whole mouse embryos. Whole-body ExM requires the digestion of the whole mouse embryos with a mixture of collagenase and post-gel ethylenediaminetetraacetic acid (EDTA) treatment. However, whole-body ExM relies on prolonged and harsh enzyme treatment, and the minimum digestion time required for the uniform expansion of the whole mouse embryo has not been quantified. In this study, the effect of digestion duration and digestion conditions on the expansion uniformity of the whole mouse embryo is investigated. This study presents an enhanced digestion strategy that guarantees the uniform expansion of the whole mouse embryo despite the shortest possible digestion period. Using the optimized methodology, we visualize the nanoscale features of several organs throughout the whole mouse embryo with a 60-nm resolution.

4:45 PM SB01.05.08

Novel Single-Molecule Electrical Detection Method with Applications in Cancer and Covid19 Detection [Keshani G. Pattiya Arachchilage](#), Subrata Chandra and Juan M. Artes Vivancos; University of Massachusetts, Lowell, United States

Cancer is one of the most frequent causes of death globally.^[1] Blood samples, or other body fluids, can contain cancer biomarkers such as circulating free tumor nucleic acids (ctNA), which are promising for early cancer detection in liquid biopsies.^{[2][3]} Detecting ctNA in the blood is challenging because of the low ctNA concentration and the low frequency of mutations compared to wild-type sequences.^[2] Nanotechnology bioelectronics methods can help to address this challenge. In particular, the Scanning Tunneling Microscopic (STM)-assisted break junctions method (STM-BJ)^[4] has recently allowed the first demonstration of detection and identification of RNA from *E. coli* via single-molecule conductance.^[5] This is an ideal emerging technique for liquid biopsy bioelectronics since it is extremely sensitive, specific, and non-invasive.

This work focuses on characterizing ctNAs using the STM-BJ to investigate an effective method for their ultra-sensitive detection in complex samples. The study's central hypothesis is that the sequences of ctNAs can be used to detect cancers by finding their unique electronic fingerprints. We focus the study on KRAS, BRAF, and NRAS as effective cancer biomarkers in agreement with data from the Pan-Cancer Analysis of Whole Genomes (PCAWG) Consortium of the International Cancer Genome Consortium (ICGC) and The Cancer Genome Atlas (TCGA).^{[6][7]} We have already obtained preliminary data for wild-type and mutated RNA sequences for a few candidate cancer biomarkers (Ex: KRAS Exon 2 Wild type, G12V, and G12C mutations). We expect to understand the bioelectronics interface between genetic material and nanostructured electrodes. Our initial analysis and the results pave the way for the early detection of bioelectronics fingerprints from biomarkers through liquid biopsy using nanotechnology. The same idea can be applied to other applications such as covid detection. We conducted a comprehensive literature survey and bioinformatics analysis to identify the most appropriate candidate nucleic acid sequences for all human coronaviruses, SARS-Cov2, and other SARS-Cov2 variants such as Delta, Omicron, etc and obtained some preliminary single-molecule conductance data. This emerging method may allow beginning treatments early, potentially saving many lives from cancer and covid patients in the future.

References

1. Campbell PJ, Getz G, Korbel JO, *et al.* Pan-cancer analysis of whole genomes. *Nature* 2020;578:82–93. DOI:10.1038/s41586-020-1969-6.
2. Das J, Kelley SO. High-Performance Nucleic Acid Sensors for Liquid Biopsy Applications. *Angew Chemie - Int Ed* 2019. DOI:10.1002/anie.201905005.
3. Henry NL, Hayes DF. Cancer biomarkers. *Mol Oncol* 2012;6:140–6. DOI:10.1016/j.molonc.2012.01.010.
4. Xu B, Tao NJ. Measurement of single-molecule resistance by repeated formation of molecular junctions. *Science* (80-) 2003;301:1221–3. DOI:10.1126/science.1087481.
5. Li Y, Artés JM, Demir B, *et al.* Detection and identification of genetic material via single-molecule conductance. *Nat Nanotechnol* 2018;13:1167–73. DOI:10.1038/s41565-018-0285-x.
6. Rheinbay E, Nielsen MM, Abascal F, *et al.* Analyses of non-coding somatic drivers in 2,658 cancer whole genomes. *Nature* 2020;578:102–11. DOI:10.1038/s41586-020-1965-x.
7. Sapio MR, Posca D, Troncone G, *et al.* Detection of BRAF mutation in thyroid papillary carcinomas by mutant allele-specific PCR amplification (MASA). *Eur J Endocrinol* 2006;154:341–8. DOI:10.1530/EJE.1.02072.

SESSION SB01.06: Poster Session II
Session Chairs: Herdeline Ardoña and Jennifer Carpena-Núñez
Tuesday Afternoon, November 29, 2022
8:00 PM - 10:00 PM
Hynes, Level 1, Hall A

SB01.06.01

Enzyme Responsive Peptides for Endocytosis and Targeting Golgi Apparatus Weiyi Tan and Bing Xu; Brandeis University, United States

Golgi apparatus (GA) is the hub of intracellular trafficking, but selectively targeting GA by synthetic molecules remains a challenge. Here we show that an unconventional type of peptide, as substrates of enzymes (e.g., alkaline phosphatase, thioesterase), for instantly targeting GA of cells. Preliminary mechanistic studies indicate that the peptides, above or below their critical micelle concentrations, enter cells mainly via caveolin-mediated endocytosis or macropinocytosis, respectively. The peptides, at about 5-10 times of the imaging concentrations, buildup in ER and GA, disrupt protein trafficking, thus lead to cell death via multiple pathways. This work illustrates the first example of an enzyme responsive and redox active molecular platform for targeting GA and controlling cell fates.

SB01.06.02

Low Impedance Stretchable Epicardial Electrodes for Treating Cardiac Diseases Sung-Hyuk Sunwoo^{1,2}; ¹Seoul National University Hospital, Korea (the Republic of); ²Seoul National University, Korea (the Republic of)

Conventional cardiac implants, including cardiac resynchronization therapy (CRT) systems and implantable cardioverter defibrillators (ICDs), have modulated cardiac conduction and following contraction process in heart failure patients. However, the transvenous lead implantation is incompatible with large-area electrophysiological mapping and selective multi-channel stimulations. Moreover, there are several lead-related drawbacks in conventional CRTs and ICDs. Several reports point to the rigid metal leads as the cause of post-implant issues, such as intravascular thrombosis, lead infection, myocardial damage, and even myocardial perforation. Here, this poster presentation introduces fabrication of soft and conductive epicardial mesh electrodes using a stretchable low-impedance nanocomposite comprising silver-gold core-shell nanowires (Ag-Au NWs) with platinum black (Pt black) in an elastomeric matrix. The soft and conductive epicardial mesh electrodes with low impedance presented a potential solution to the abovementioned issues. The high stretchability, conductivity, biocompatibility, and electrochemical properties of the elastomeric nanocomposite enable excellent quality of electrogram recording and electric stimulations on the animal heart. The various cardiac arrhythmias, such as ventricular bradycardia and ventricular fibrillation, can be monitored and successfully treated with pacing. Electrical pacing using epicardial mesh electrodes supported not only treating arrhythmias but also the effective contraction of the heart.

SB01.06.04

Light-Responsive Unique Plasmonic Nanomaterials Conjugated with Bioorthogonal Catalysts for Theragnostics Subin Yu¹, Dohyub Jang², Haeun Kang¹, Wen-Tse Huang³, Minju Kim¹, Ru Shi Liu³, Sehoon Kim² and Dong Ha Kim¹; ¹Ewha Womans University, Korea (the Republic of); ²Korea Institute of Science and Technology, Korea (the Republic of); ³National Taiwan University, Taiwan

Any chemical reaction which occurs inside the living system without interference from the biochemical reaction, so-called a bioorthogonal reaction, can be a new powerful strategy to manipulate the biological system.¹ To achieve the bioorthogonal reaction, the selection of bioorthogonal catalyst is important, which provide a platform for the changing of substrates to activated species, such as drug, photosensitizers, and fluorescent.¹ Especially, palladium (Pd) is the highly efficient catalyst for the bioorthogonal reaction of prodrugs and pro-fluorophores, however, the intrinsically insufficient catalytic activities have restricted their biological *in vivo* application.² Herein, we introduced the unique light-responsive plasmonic nanomaterials conjugated with the palladium as bioorthogonal nanocatalysts for combinatorial photothermal and photodynamic cancer treatment along with tumor imaging. The light can modulate the catalytic performance of these bioorthogonal nanocatalysts in terms of LSPR induced hot carrier generation, local field enhancement, and heat, which in return, would enhance the bioorthogonal nanocatalysts activities for cleavage reaction, and generate more activated photosensitizer from pro-photosensitizer at the given condition. The pro-photosensitizer conversion experiments with our hybrid bioorthogonal nanocatalysts under light illumination showcased the significant enhancement of conversion efficiency, confirming the enhancement of bioorthogonal reaction efficiency by using plasmonic features. In addition, the photothermal effect was incorporated to achieve synergistic photothermal and photodynamic therapy. Taken together, our bioorthogonal nanocatalysts open up a new paradigm to achieve an efficient bioorthogonal reaction to treat cancer.

References

- [1] E. Latocheski; G.M. D. Forno; T. M. Ferreira; B. L. Oliveira; G. J. L. Bernardes and J. B. Domingos, *Chem. Soc. Rev.*, **2020**, *49*, 7710-7729.
- [2] M. A. Miller; B. Askevold; H. Mikula; R. H. Kohler; D. Pirovich and R. Weissleder, *Nat. Commun.*, **2017**, *8*, 15906.

KEYWORDS: bioorthogonal catalyst, deallylation, plasmonic effect, photodynamic therapy, photothermal therapy

SB01.06.05

Hyaluronate Based Upconverting Nanoparticles for Transdermal Delivery Hye Eun Choi, Mina Kwon and Ki Su Kim; Pusan National University, Korea (the Republic of)

Photomedicine has garnered widespread scientific interest since it utilizes photons for direct or indirect stimulation of therapeutic effects. In the visible light spectrum, short-wavelength blue light is highly advantageous in photomedicine since it carries more energy than red or green light. However, the limitations of blue light illumination sources are poor tissue penetration and the potential threat of damaging healthy cells. For overcoming these technical limitations, the anti-stokes upconversion (UC) process has been actively investigated which allows producing visible illumination deep inside the tissue by converting two or more red photons of low frequency into a single photon with a higher frequency. In particular, the UC could be realized through the triplet-triplet annihilation (TTA) process in which the photon energy is absorbed by a sensitizer chromophore and subsequently transferred to an acceptor chromophore through triplet-triplet energy transfer. As a result, two excited acceptor molecules undergo the TTA process producing singlet fluorescence of higher frequency. Thus, transdermal delivery of the light source can be implemented by loading the UC chromophore on biocompatible polymeric nanoparticles, such as hyaluronic acid (HA) and poly(ϵ -caprolactone) (PCL).

In this study, we encapsulated palladium(II) tetraphenyl tetrabenzoporphyrin (PdTPBP, λ_{ex} =635 nm) as a photosensitizer and perylene (λ_{em} =470 nm) as an acceptor based red-to-blue UC chromophores into polycaprolactone grafted hyaluronic acid nanoparticles (HA-PCL/UC NPs), which can serve as the transdermal delivery carrier of the blue light source that can be activated using red light illumination. We have successfully synthesized HA-PCL NPs through the oil-in-water (O/W) emulsion method by conjugating HA and PCL using 1,4-diaminobutane as a linker, which was confirmed by ¹H NMR and FTIR. The TEM and DLS characterization revealed HA-PCL NPs are of spherical shape and nanoscale size range suitable for efficient deep penetration into the skin tissue. The permeation of HA-PCL/UC NPs was measured through porcine skin tissue over 24 hours and showed the applicability of our NPs in real skin tissue. The low cytotoxicity and enhanced cellular uptake in HA-PCL/UC NPs were confirmed through in vitro experiments. For optical properties, HA-PCL/UC NPs that steady emitted blue light showed outstanding UC quantum yield in a water environment under 635 nm laser irradiation. In conclusion, our results suggest that the developed HA-based red-to-blue upconverting NPs can be utilized as transdermal light delivery in a variety of biomedical applications, such as drug delivery, antibacterial therapy, bioimaging, and diagnostic imaging.

SB01.06.06

Superhydrophobic Hybrid Nanoparticle Coatings Against Biofilm Growth Stefanie . Dietl, Padryk Merkl and Georgios Sotiriou; Karolinska Institutet, Sweden

Device-related infections are a major burden both to the patients and the healthcare system. These infections often occur due to biofilm formation. Biofilms are dense microcolonies of bacteria adherent to a surface that secrete a glue-like matrix of extracellular polymeric substances. Since biofilms are often resistant to conventional antimicrobial interventions, their formation can lead to severe and persistent infections. They often require the removal of the device and can lead to severe complications. These biofilm-based infections urgently call for the development of new therapeutic or preventative strategies.¹

An attractive approach to prevent biofilm formation is the physicochemical modification of the surface. Such a modification can prevent the initial attachment of bacteria and therefore prevents the formation of the microcolonies, which could become a biofilm. Surface charge, surface hydrophobicity, and surface composition significantly impact the bacteria's attachment. This has been successfully applied to design hydrophobic and superhydrophobic surfaces that can reduce the colonization and adhesion of bacteria and prevent biofilm formation. Rare earth oxides have been successfully applied for the development of hydrophobic and superhydrophobic surfaces due to the adsorption of gaseous organic compounds. However, a thorough characterization of the antibiofilm properties and comparison with other metal oxides is lacking.^{1,2}

Flame spray pyrolysis was used here to produce hydrophobic and hydrophilic nanoparticle coatings of rare earth oxides and other metal oxides to investigate the dependence of biofilm formation on surface hydrophobicity and composition. Nanoparticles were deposited directly on substrates by flame spray pyrolysis in a single step. In this technique, a combustible liquid precursor solution containing the metal of choice is atomized and subsequently ignited.³ The coatings were fabricated by depositing highly porous metal oxide nanoparticle coatings onto a water-cooled substrate.

The initial hydrophilic coating was converted to a hydrophobic coating by the adsorption or infusion of silicone oil. By tuning the metal oxide coating and silicone oil a range of stable hydrophobic and hydrophilic coatings were prepared and their effect on biofilm formation investigated.

The affinity of metal oxide and rare earth oxide nanoparticle coatings to adsorb volatile organic compounds and the subsequent wettability of the coatings was investigated. The coatings were applied and assessed for the inhibition of biofilm formation by clinically relevant pathogens on medical device mimicking surfaces.

This project has received funding from the European Research Council (ERC) under the European Union's Horizon 2020 research and innovation programme (ERC Grant agreement n 758705). Funding from the Karolinska Institutet, the Swedish Research Council (2021-05494) and the Swedish Foundation for Strategic Research (SSF) (FFL18-0043) is kindly acknowledged.

1. Chan Y, Wu XH, Chieng BW, Ibrahim NA, Then YY. *Nanomaterials*. 2021;11(4):1046

2. Oh J, Orejon D, Park W, et al. *iScience*. 2022;25(1):103691.

3. Meierhofer F, Mädler L, Fritsching U. *AIChE Journal*. 2020;66(2):e16885.

SB01.06.07

Piezoelectric Accelerated Tissue Engineering Using HA Nanoparticle Embedded Nature Protein-Based Coaxial Nanomembrane Ji Yeon Lee¹, Chan Hee Park² and Cheol Sang Kim²; ¹Korea Advanced Institute of Science and Technology, Korea (the Republic of); ²Jeonbuk National University, Korea (the Republic of)

Amidst problems associated with the aging population, addressing fracture patients with poor bone quality associated with the loss and deformation of cellular matrix proteins has been a major challenge. Recently, nanofibers have attracted significant attention as substrates that mimic the structural microenvironment of the native extracellular matrix. Despite their morphological advantages, nanofiber-based tissue engineering therapies limit electric signaling pathways that control cell-to-cell physiological interactions. Here, we exploit piezoelectric protein-based coaxial nanofibers enhanced by the alpha-helix to beta-sheet transition to produce appropriate bioelectrical signals, which provide electroactivity for matrix production *via* cell growth and proliferation. The coaxial nanofiber is composed of a hydroxyapatite (HA) nanoparticles-embedded piezo-protein shell and a polycaprolactone (PCL) core with simvastatin (SIM). Gradual biodegradation of the protein reveals HA nanoparticles, which support adhesion of proteins and involvement in cell differentiation with mineralization, while continuous release of SIM assists the rapid growth of HA. The designed beta-sheet protein shell/PCL core nanofibers are promising candidates for tissue engineering and mechano-electrical transduction platform due to their phased functionality in electrophysiological activity, biodegradability, HA nucleation, and mineralization. Overall, the proposed strategy has the potential to meet the challenging requirements in inducing rapid tissue function reconstruction. This work was supported by the National Research Foundation of Korea (NRF) grant funded by the Korea government (MSIT) (No. 2021R1C1C2011542) and NRF-2017-Fostering Core Leaders of the Future Basic Science Program/Global Ph.D. Fellowship Program.

SB01.06.09

Biofilm Eradication by Photothermal Near-Infrared Activated Spherical Silver Nanoaggregates Padryk Merkl¹, Shuzhi Zhou¹, Apostolos

Zaganiaris¹, Mariam Shahata¹, Athina Eleftheraki¹, Thomas Thersleff² and Georgios Sotiriou¹; ¹Karolinska Institutet, Sweden; ²Stockholm University, Sweden

Near-infrared (NIR) light finds many important applications in biomedicine due to the ability of NIR light to penetrate tissue which provides allows for minimally invasive therapeutic and diagnostic devices in-vivo. Typical NIR extinction optimisation strategies rely on plasmonic nanostructures with complex, non-spherical geometries with typically difficult synthetic routes. This provides an immediate limitation for the translation of derived technologies to commercial therapeutic products. The photothermal effect, whereby the absorbed light is converted into heat due to non-radiative decay processes, is often applied to derive biomedical treatments. The temperature increases which can be produced can be harnessed to kill cancerous or infected tissue. Biofilms are a highly resistant form of bacterial infections often found in-vivo on infected implanted medical devices such as catheters. Biofilms form a dense and inhomogeneous structure and their treatment by typical strategies such as antibiotics is challenging. This study presents the single-step aerosol self-assembly of plasmonic fractal-like nanoaggregates by flame spray pyrolysis that are formed of spherical silver nanoparticles with tuneable extinction from the visible to NIR wavelengths. The extinction spectrum of the nanoaggregates was tuned by introducing a SiO₂ spacer during flame aerosol synthesis allowing optimisation of NIR extinction at the readily available laser line at 808 nm. Simulations of the optical properties of such fractal nanoaggregates were performed using the coupled dipole approximation to further elucidate the origin of the optical performance. Aerosol self-assembly of particle films was performed on polydimethylsiloxane coated substrates directly from the flame synthesis and further encased with a top polymer layer, forming plasmonic photothermal nanocomposite films. These photothermal nanocomposites were applied to eradicate established biofilms of clinically-relevant *E. coli* and *S. aureus* strains using 808 nm NIR irradiation. This project has received funding from the European Research Council (ERC) under the European Union's Horizon 2020 research and innovation program (ERC Grant agreement # 758705). Funding from the Karolinska Institutet Faculty Board, the Swedish Research Council (2016-03471), the Torsten Söderberg Foundation (M87/18), and the Swedish Foundation for Strategic Research (FFL18-0043) is kindly acknowledged.

SB01.06.10

Nanoparticles 'Clicked' onto Nanofibrous Scaffolds for Meniscal Repair Emily Sharp^{1,1}, Ryan C. Locke^{1,2}, Bian Jang¹, Tao Gui¹, Su Jin Heo¹, Nathaniel Dymant¹, Zhiliang Cheng¹, Ling Qin¹ and Robert L. Mauck^{1,1,2}; ¹University of Pennsylvania, United States; ²Philadelphia VA Medical Center, United States

Click chemistry is a class of reactions wherein molecular pieces are easily joined together, like buckling two pieces of a seat belt [1]. In the context of tissue engineering, click chemistry can serve to fabricate innovative delivery mechanisms capable of regenerating damaged or diseased tissues via spatiotemporal-controlled release. Dense connective tissues, such as knee menisci, sustain demanding load-bearing functions via a complex arrangement of extracellular matrix proteins that surrounds and protects tissue specific cell types. Following injury, endogenous cells within these tissues are unable to promote tissue regeneration and instead form less functional scar tissue. Thus, therapies that activate and recruit endogenous cells to promote tissue regeneration may significantly improve treatment and quality of life for millions of patients annually. Click chemistry-based delivery systems present a novel way of achieving these therapeutics. We previously showed that activation of Hedgehog signaling via a small molecule agonist, Purmorphamine (Pur), accelerated wound closure and attenuated cartilage erosion that results from meniscus injury [2]. **Here, we overcome challenges to Pur delivery, such as rapid clearance and off-target toxicity, via delivery from polymeric nanoparticles (NPs) localized to the injury site by immobilizing NPs on a nanofibrous repair scaffold via click chemistry.**

Rather than employing copper-catalyzed azide-alkyne cycloaddition as done by Lancuski et. al. [3], we utilized strain-promoted azide-alkyne cycloaddition (SPAAC) to functionalize electrospun polycaprolactone (PCL) nanofibrous scaffolds with azide groups that click with PEG-PCL NPs (prepared via oil-in-water emulsion) containing the alkyne counterpart (DBCO). These azide-modified scaffolds, when compared to electrospun PCL controls lacking azide groups, selectively reacted with DBCO-conjugated fluorophores, validating the successful fabrication of a 'clickable' scaffold. Scratch assays using murine and porcine meniscus fibrochondrocytes revealed that Pur-loaded, DBCO-conjugated NPs increased the migration of meniscus fibrochondrocytes compared to free Pur delivery. We then implanted NP-conjugated scaffolds *in vivo* using a nude rat xenotransplant model. For this, adult porcine meniscal explants were incised to create a horizontal defect that was either left unfilled or filled with NP-conjugated scaffolds (Pur-loaded and empty). All groups were evaluated at 3 and 14 days and analyzed for cell invasion via staining of nuclei and matrix deposition with H&E. We observed increased cell infiltration from day 3 to 14. More notably, there was a marked increase in cell number with implantation of Pur-loaded NPs compared to empty controls. This study validates a new approach to produce nanofibrous azide-functionalized PCL scaffolds via SPAAC click chemistry. The reaction between azide-modified PCL nanofibers and fluorophore-DBCO was highly specific, fast, repeatable, and stable over the long-term after repeated washes. This indicates that azide-modified PCL scaffolds may be used to immobilize DBCO-modified NPs. When tested *in vivo*, Pur delivery via NP-conjugated scaffolds accelerated meniscal repair via increased cell infiltration. These data support the novel use of click chemistry-based approaches for sustained and localized delivery of small molecule drugs for dense connective tissue repair. Clinically, this delivery method has the potential to overcome many challenges in musculoskeletal tissue repair by providing sustained and local release. More generally, this study demonstrates the applicability of click chemistry-based mechanisms in biomedical therapeutics.

References: [1] TCI Chemicals. "Click Chemistry." [2] Wei+ eLife 2021. [3] Lancuski+ ACS Appl Mater Inter 2012.

Acknowledgements: This work was supported by the Department of Veterans' Affairs (I01 RX003375) and NIH/NIAMS (R01 AR071340, T32-AR-05346, P30 AR069619).

SB01.06.13

Implantable Drug Delivery Vehicle Using Bipolar Membrane Sung-Geun Choi, Ji-Eun Han, Myung-Gyun Choi and Seung-Kyun Kang; Seoul National University, Korea (the Republic of)

Implantable drug delivery can localize drug effect only on diseases region, resulting in the minimization of the amount of mis-delivered drug and its side effect as well as the maximization of drug efficacy. The previous implantable drug delivery systems use convection of drug solution or, diffusion of drug solute for drug effect localization onto legion. However, each method has clear limitation; convection method causes mis-delivery to normal tissue due to drug solution flow and diffusion method is impossible to control drug release rate. In addition, these methods focus on exposing drug only to the surface of disease region, and therefore it is hard to target drug to lesion located in deep tissue. The bipolar membrane under electric field according to bias direction and amplitude can control drug release rate. Under forward bias, bipolar membrane has ionic conduction and release ionized drug while under reverse bias, it inhibitions drug from leakage due to ionic depletion zone. The strength of applied voltage can decide drug release rate. This drug release type by electrophoresis can focus drug on legion. Furthermore, electric field passing through the legion, called iontophoresis, can guide drug to reach for the deep legion, resulting in increase in the biodistribution of drug.

SB01.06.15

Investigating The Effect of A Dynamic Magnetic Field on The Rate of DPSC Neuronal Differentiation Alexander C. Wang¹, Sahil Sood², Rebecca Sullivan³, Hillel Schein⁴, Nikhita Srivinas⁵, Oran Goodman⁶, Adam Hansen⁷ and Miriam Rafailovich¹; ¹Sewickley Academy Senior School, United States; ²Lambert High School, United States; ³Yeshiva University High School for Girls, United States; ⁴Davis Renov Stahler Yeshiva High School for Boys, United States; ⁵Lausanne Collegiate School, United States; ⁶The Frisch School, United States; ⁷Stony Brook University, The State University of New York,

Neurodegenerative diseases pose a major health risk, as neurons are unable to repair themselves. Previous research at our lab has shown an increase in the differentiation rate of dental pulp stem cells (DPSCs) into neurons via plating on Poly-lactic Acid (PLA) and 20% resorcinol diphenyl phosphate (RDP) clay polymer blends. Furthermore, there is evidence that the usage of a spinning, dynamic magnetic field (MF) successfully stimulates superparamagnetic iron-oxide nanoparticles (NP) to attach to neuron cell surfaces and induced axon regeneration in mature neurons. Therefore, we were interested in whether a PLA+20% RDP clay surface in combination with NP and MF treatment will further promote neuronal differentiation. Preliminary results have shown a significantly higher neuronal differentiation rate in cells with all four elements present.

We spin casted silicon wafers with either pure PLA or PLA+20% RDP chloroform-based solutions to create thin polymer films and two initial experimental groups based on surface chemistry. Following, DPSCs were plated onto wafers, which were placed in cell plates, and cultured in DPSC media for three days. On day 3, DPSC media was exchanged for neuronal media. On the following day, the 24 wafers designated as NP+ were treated with iron-oxide nanoparticles. For the next six days, every other day, 12 cell plates, all of which contained NPs, were placed in the MF for 30 minutes each. The MF stimulated NPs by rotating multiple magnets above the cell plate. The rotation speed was programmed to be one Hz in C++. The DC motor that rotated the magnetic ring was connected to an Arduino board and received program input from a laptop. At this point, four total experimental groups were established, PLA NP+ MF-, PLA+20% RDP clay NP+ MF-, PLA NP+ MF+, and PLA+20% RDP NP+ MF+.

Before DPSC media was changed to neuronal media on day 3, we tested cell modulus rigidity on an atomic force microscope, with lower values indicating softer, neuron-like cells. PLA NP- MF- and PLA+20% RDP clay NP- MF- cells displayed an average relative modulus value of 0.54 and 0.55, respectively. Day 9 modulus testing showed that PLA NP+ MF- cells displayed an average relative modulus of 0.54, PLA NP+ MF+ 0.48, PLA+20% RDP clay NP+ MF- 0.62, and PLA+20% RDP clay NP+ MF+ 0.51. Cells with MF treatment all had lower modulus values than their non-MF treatment counterparts, indicating higher neurogenic rates. We attribute the rigidity added by the NPs to higher modulus values in day 9 cells compared to day 3 cells. Furthermore, the rigidity of RDP clay increases the modulus values of PLA+20% RDP clay cells.

We performed EVOS imaging on each sample to provide comparative data on morphology. Three cells on each image had their aspect ratios (cell length/width) calculated via ImageJ, allowing us to quantifiably compare morphology, as neurons display higher aspect ratios than DPSCs.

EVOS testing on day 3 (pre-neuronal media) provided baseline morphology of DPSCs. The cells had unbranched cell bodies, with a relatively low 3.56 aspect ratio. In day 11 images, axon and dendritic development were largely visible in PLA NP+ MF+ and PLA+20% RDP clay NP+ MF+ cells, showing an average aspect ratio of 15.00 and 18.78, respectively. However, aspect ratios of PLA NP+ MF- were only 6.85, meaning that the average aspect ratio of PLA NP+ MF+ cells and PLA+20% NP+ MF+ cells were 119% and 174% higher than the NP+ MF- control, respectively.

As a final confirmational test, RT-PCR gene analysis will be performed on day 28 to compare the expression of the NES, TUBB 3, and NEFM genetic markers. NES and TUBB 3 are early-stage neuronal developmental markers, and NEFM is a late-stage neuronal development marker. We hypothesize that during RT-PCR testing, the NEFM gene will be upregulated in MF+ cells and that the NES and TUBB 3 genes will be downregulated in MF+ cells, correlating with neuronal development.

SB01.06.16

Impact of Titanium Dioxide (TiO₂) Nanoparticles on the Formation of a Living Skin Equivalent Sarah Yim¹, Annie Hu², Jeffrey Zhang³, Matthew Sharin⁴, Navya Gautam⁵, Harsha Rajkumar⁶, Darshini Podder⁷, Sherlyn Wu⁸, Diya Rai-Gersappe⁹, Noah Kim¹⁰, Shi Fu¹⁰, Miriam Rafailovich¹⁰, Marcia Simon¹⁰, Ian Lau¹¹, Nicole Niculescu¹⁰ and Christopher Gazis¹⁰; ¹Seoul International School, Korea (the Republic of); ²Great Oak High School, United States; ³Shenzhen Middle School, China; ⁴Lawrence High School, United States; ⁵Hauppauge High School, United States; ⁶Fremont Christian High School, United States; ⁷Jericho High School, United States; ⁸Stuyvesant High School, United States; ⁹Vassar College, United States; ¹⁰Stony Brook University, The State University of New York, United States; ¹¹Tufts University, United States

Titanium dioxide (TiO₂) is used in many commercial products due to its ability to absorb UV rays and achieve a highly white color [1]. While nanoparticles of TiO₂ do not penetrate the stratum corneum easily, if they are ingested or used in wound healing products, they come in contact with viable tissue and can easily be absorbed. Cells containing low concentrations of nanoparticles are still viable, but the particles can interfere with executing their normal functions. Skin is one of the few functional organs that can be manufactured in vitro. Organotypics can then be used to probe the impact of different substances on cell assembly and functionality. Here we investigate the impact of exposure to rutile TiO₂ nanoparticles for keratinocytes and fibroblasts, which are then used to self assemble into a viable skin construct. Dermal fibroblasts and keratinocytes were exposed separately in culture to 0.4 and 0.8 mg/ml of TiO₂ nanoparticles for 24 hours. Visual analysis of Alexa Fluor 488 – phalloidin stained fibroblasts showed that actin filaments remained straight after TiO₂ treatment, indicating a healthy cytoskeleton. From the flow cytometry of treated keratinocytes and fibroblasts, showing that initial TiO₂ association in fibroblasts was significantly greater (almost 100% compared to 50% in keratinocytes), and this number remained near 100% for several days. Next, we evaluated fibroblasts cell proliferation rates for 5 days with the treatment concentration of 0, 0.2, 0.4, 0.8, and 1.2 mg/mL respectively; keratinocyte proliferation rate comparisons were conducted by evaluating colony formation efficiency (CFE). Results demonstrated that presence of TiO₂ nanoparticles did not significantly impact cell proliferation which occurred at the same rate as the control for either cell type. We then examined the impact of TiO₂ on cell modulus, which increased with increasing concentration, indicating increased stiffness. Lastly, we examined fibroblasts' ability to contract collagen gels and in this case as well no difference in the ability to contract was observed.

On the other hand, when these cells were used to create four types of constructs, large disruption of the skin structure was observed. Four types of constructs were assembled, a control with no TiO₂, two constructs where TiO₂ was only in either the keratinocyte (epidermal) layer or the fibroblast layer and one where the particles were in both layers [2]. While histological analysis showed that TiO₂ treated fibroblasts did not adversely impact the formation of the dermal layer in any of the constructs, the presence of the particles in the keratinocytes layer showed much more dramatic effects. At a concentration of 0.4 mg/ml a functional skin construct was created, but large TiO₂ aggregates were observed at the surface of the stratum corneum, which appeared almost as if the TiO₂ in the cells had been secreted, aggregated, and removed from the construct. Higher concentrations, 0.8 mg/ml showed far more large aggregates. In this case, though, large regions without stratum corneum formation were observed, strongly disrupting the tissue. Reduced expression of filaggrin was observed in these layers indicating incomplete differentiation of the keratinocytes disrupting stratum corneum formation.

[1] Dréno, B., Alexis, A., Chuberre, B. and Marinovich, M. (2019), Safety of titanium dioxide nanoparticles in cosmetics. *J Eur Acad Dermatol Venereol*, 33: 34-46. <https://doi.org/10.1111/jdv.15943>

[2] Li, J, Fu, S, Lu, KW, et al. Engineering functional skin constructs: A quantitative comparison of three-dimensional bioprinting with traditional methods. *Exp Dermatol*. 2022; 31: 516– 527. <https://doi.org/10.1111/exd.14488>

SB01.06.17

Impact of TiO₂ on HUVEC Angiogenesis and Bacterial Infection Sarah Yim¹, Annie Hu², Jeffrey Zhang³, Matthew Sharin⁴, Navya Gautam⁵, Harsha Rajkumar⁶, Darshini Podder⁷, Sherlyn Wu⁸, Diya Rai-Gersappe⁹, Noah Kim¹⁰, Shi Fu¹⁰, Miriam Rafailovich¹⁰, Marcia Simon¹⁰, Ian Lau¹¹, Nicole Niculescu¹⁰ and Christopher Gazis¹⁰; ¹Seoul International School, Korea (the Republic of); ²Great Oak High School, United States; ³Shenzhen Middle School, China; ⁴Lawrence High School, United States; ⁵Hauppauge High School, United States; ⁶Fremont Christian High School, United States; ⁷Jericho High School, United States; ⁸Stuyvesant High School, United States; ⁹Vassar College, United States; ¹⁰Stony Brook University, The State University of

New York, United States; ¹¹Tufts University, United States

Exposure to TiO₂ has been shown to have detrimental effects on different types of tissue. We had previously shown that exposure of HeLa cells to TiO₂ rutile nanoparticles increased their susceptibility to bacterial infection, which was attributed to upregulation of enzymes which disrupt the inner and outer balance of membrane cholesterol [1]. Here we explore its impact on endothelial cells which comprise the tissue used to form vasculature. Bacterial infection of veins or arteries can be very serious as the bacteria is then spread systemically through the blood. We first exposed HUVEC cells to 0.1 and 0.2 mg/ml of rutile TiO₂ nanoparticles for 24 hours and then exposed the cells to staph aureus for 90 minutes. The cells were then lysed and the bacterial colonies were counted. Surprisingly, in this case, exposure to TiO₂ reduced the infection by 27% and 40% for the two concentrations, respectively. Since the cells were incubated without external illumination, this antibacterial action was not caused by electron emission from the particles. This was further confirmed when no effect on bacterial survival was measured when the bacteria were cultured with just TiO₂ in the media. RT-PCR indicated upregulation of ABCA1 but downregulation of ABCG1. Further work is in progress to quantify the impact on cholesterol generation.

HUVEC cells are also involved in angiogenesis when plated on a matrigel (10 mg/mL) matrix. HUVEC cells were incubated with TiO₂ at concentrations of 0, 0.1, 0.15, 0.2 mg/mL and the formation of the angiogenesis network was continuously imaged over a period of 16 hours. To track the gel mechanics during the network formation process, red fluorescent microbeads with the size of 1 μ m were mixed with Matrigel. Over the 16-hour period, time lapse imaging was performed every 20 minutes to record both the network development and microbeads displacement. The HUVEC networks were then quantified by the following attributes as the function of time: the amount of the nodes, total length of the tubes, clustered area size, amount of the tubes and branches of the network. Meanwhile, each single microbead's displacement was computed via OpenCV's digital image speckle correlation (DISC) algorithm in comparing the consecutive time frames. The results showed that in each case network formation was initiated roughly 4 hours earlier in the cells exposed to TiO₂, but the average length of the tubes was significantly shorter and the number of nodes formed by cells not participating in angiogenesis was greater. The network splines are composed of single cells stretched between nodes, where increased flexibility translates into longer tube length. DISC analysis indicated that the traction forces on the matrigel exerted by cells exposed to TiO₂ were smaller than those exerted by the unexposed cells, consistent with decreased ability to stretch between nodes. The modulus of the cells were also measured using atomic force microscopy, and the data showed that the cells exposed to the nanoparticles were stiffer which is also consistent with decreased ability to stretch. Taken together, these results indicate that exposure to TiO₂ increases the rate of angiogenesis, while decreasing the network lattice parameter and the forces exerted on the matrigel support.

[1] Fan Yang, Shu-Lin Liu, Yan Xu, Stephen G. Walker, Wonhwa Cho, Tatsiana Mironava, Miriam Rafailovich, The impact of TiO₂ nanoparticle exposure on transmembrane cholesterol transport and enhanced bacterial infectivity in HeLa cells, *Acta Biomaterialia*, Volume 135, 2021, Pages 606-616, ISSN 1742-7061, <https://doi.org/10.1016/j.actbio.2021.08.012>

SB01.06.18

Evaluating the Effect of Resorcinol Diphenyl Phosphate (RDP) Concentrations in Clay on the Neurogenic Differentiation of Human Dental Pulp Stem Cells (hDPSCs) [Rebecca Sullivan](#), Hillel Schein, Nikhita Srinivas, Oran Goodman, Alex C. Wang, Sahil Sood, Adam Hansen, Miriam Rafailovich, Anna Cho and Kuan-Che Feng; Stony Brook University, The State University of New York, United States

Neurons are used to communicate information between the human body and the brain. Currently, there is no cure for neurological diseases, however, clinical trials have shown stem cell differentiation to be a promising treatment for these conditions. In this experiment, hDPSCs were plated onto coated silicon wafers. Several properties of the substrate's surface may affect cell differentiation including surface mechanics, surface chemistry, and surface topography. This project examined the effect of surface chemistry on cell differentiation by adding varying concentrations of RDP-Clay to the silicon wafer coating and comparing the results. RDP consists of one phosphate and two phenyl groups that are toxic to cells, but the RDP was mixed with clay so the phosphate groups would be adsorbed into the clay, thereby releasing the phenyl groups, thereby eliminating RDP's toxicity and enabling the phosphates to allow for cell growth. Solutions of RDP-Clay and PLA were made in chloroform and spun cast onto HF etched Si wafers. In order to probe the role of the phosphate as opposed to simply a nucleation site for the PLA, 20% 30B Clay was also used in combination with PLA. Differentiation of DPSC on tissue culture plastic (TCP) has already been reported [1] and here we compare the effect of the PLA and PLA/Clay substrates. Pure PLA, PLA with 20% RDP-Clay, PLA with 30% RDP-Clay, and PLA with 20% 30B clay were spun cast out of the chloroform solution onto HF etched and polished silicon wafers, annealed overnight in vacuum of 10⁻³ Torr, T=180 C, to remove solvent and sterilize. The surfaces of the coated silicon wafers were analyzed using an atomic force microscope. Pure PLA had the flattest surface of 7.282 nm, 20% RDP-Clay had a surface roughness of 67.6 nm, 30% RDP-Clay had a surface roughness of 87.1 nm, and 20% 30B Clay had the roughest surface of 91.442 nm. In all cases, the substrates nucleated with greater crystallinity and hence, roughness. Substrates were then coated with laminin and the cells were plated directly. The moduli of the cells on the different substrates were measured on day 5, before changing to neurogenic media and 9 days after differentiation. Late stage differentiation will be confirmed and compared between the different substrates via RT-PCR. Preliminary Results indicate that in all cases the modulus of the cells decreased on day 14 relative to day 5, consistent with eventual differentiation. Additionally, as cells differentiate into neurons, their shapes become longer and thinner, creating a larger aspect ratio. The days 5, before changing to neural media, and day 14, after having been in neural media for 9 days, EVOS images show that as time progressed, the aspect ratio increased. Between days 5 and 14, PLA control had an aspect ratio increase of 40%, and TCP had an aspect ratio increase of 110%. Compared to PLA, TCP was 58.57% greater, 20% 30B was 26.73% greater, 30% RDP-Clay was 26.83% greater. 20% RDP-Clay had the highest aspect ratio which was 42.81% greater than PLA. RT-PCR will be performed at day 28 of culture, which will determine the preferred substrate for differentiation.

Work Supported by the Morin Charitable Trust

[1] Chang CC, Chang KC, Tsai SJ, Chang HH, Lin CP. Neurogenic differentiation of dental pulp stem cells to neuron-like cells in dopaminergic and motor neuronal inductive media. *J Formos Med Assoc.* 2014 Dec;113(12):956-65. doi: 10.1016/j.jfma.2014.09.003. Epub 2014 Nov 12. PMID: 25438878.

Acknowledgement

SESSION SB01.07: Nanomaterials for Imaging, Sensing and Theranostics II
Session Chairs: Herdeline Ardoña and Jennifer Carpena-Núñez
Wednesday Morning, November 30, 2022
Hynes, Level 1, Room 104

8:30 AM SB01.07.02

Combining Optical Thermometry and Drug Delivery in Novel Hybrid Nanomaterials for Theranostics [Anna M. Kaczmarek](#); Ghent University, Belgium

The design and development of non-contact luminescence nanothermometers is important for many applications, including the biomedical field. This discipline has advanced tremendously in the last decade, however still showing a lot of room for improvements, especially when it comes to combining multiple functionalities in just one nano-sized material.

One of our goals has been combining thermometry with drug delivery through the design of various advanced (hybrid) architectures. We aim at materials which can be used for diagnostic purposes based on very precise temperature readings and deliver the desired therapeutic on demand (pH change, near infrared laser irradiation, etc). We push our efforts further to design materials which would be decomposable after a certain period of time in the human body, eliminating the risk of nanoparticle accumulation, which is one of the current concerns of using nanoparticles in biomedical applications.

In this presentation we will overview our current successes in this field as well as highlight the challenges and potential ahead.

8:45 AM SB01.07.03

Inorganic-Organic Hybrid Nanoparticles—High-Load Drug Carriers with Theranostic Features Claus Feldmann¹, Frauke Alves² and Joanna Napp²; ¹Karlsruhe Institute of Technology, Germany; ²Max Planck Institute for Multidisciplinary Sciences, Germany

Inorganic-organic hybrid nanoparticles (IOH-NPs) basically have a composition $[M]^{2+}[R_{Drug}OPO_3]^{2-}$ and contain a drug anion $[R_{Drug}OPO_3]^{2-}$ and an inorganic cation (e.g., $[ZrO]^{2+}$, $[La(OH)]^{2+}$, $[GdO]^{+}$, $[Bi(OH)]^{2+}$).¹ The inorganic cation guarantees the insolubility of the IOH-NPs in water and allows the nucleation of nanoparticles with high colloidal stability in aqueous suspensions. Due to the saline composition with equimolar amounts of drug anion and inorganic cation, IOH-NPs exhibit unprecedented high drug loads of 70-90% of the total nanoparticle mass.^{1,2} Specific examples are $[ZrO]^{2+}[BMP]^{2-}$, $[ZrO]^{2+}[CLP]^{2-}$ or $[ZrO]^{2+}[FdUMP]^{2-}$ with the anti-inflammatory agent betamethason phosphate (BMP) (81 wt-% per nanoparticle), the last-line antibiotic clindamycin phosphate (CLP) (82 wt-% per nanoparticle), or the cytostatic agent 5'-fluoro-2'-deoxyuridine 5'-monophosphate (FdUMP) (75 wt-% per nanoparticle). *In vitro* and *in vivo* studies show high uptake as well as excellent biocompatibility and activity. The IOH-NP concept has been transferred to >50 different nanoparticles and drugs, and offers widespread advantages:^{1,2}

- New patented class of materials
- Easy synthesis in water
- Extremely high drug load (70-90 % of total nanoparticle mass)
- Platform concept with flexible composition
- Realization of drug cocktails, optionally with chemotherapeutic, antibiotic, antiviral or anti-inflammatory agents in one nanoparticle
- Higher efficacy and/or significantly lower side effects due to targeted transport of the chemotherapeutic cocktail into the tumor
- Transport of active agent (instead of prodrugs)
- Simultaneous release (in time and in place) of drug cocktail for effective reduction of resistances (in general) and metastases (cancer)

Localization and tracking of drug release by imaging methods (OI, PAI, MRI, PET)

With this contribution, we present the current status and perspectives of the IOH-NPs with drug cocktails.

References

- [1] J. G. Heck, J. Napp, S. Simonato, J. Möllmer, M. Lange, H. R. Reichardt, R. Staudt, F. Alves, C. Feldmann, *J. Am. Chem. Soc.* **2015**, *137*, 7329-7336.
[2] (a) C. Ritschel, J. Napp, F. Alves, C. Feldmann, **2022**, *submitted*. (b) K. Sabljo, J. Napp, F. Alves, C. Feldmann, *Chem. Commun.* **2022**, *in revision*. (c) B. L. Neumeier, J. G. Heck, C. Feldmann, *J. Mater. Chem. C* **2019**, *7*, 3543-3552. (d) J. Napp, M. A. Markus, J. G. Heck, C. Dullin, W. Möbius, D. Gorpas, C. Feldmann, F. Alves, *Theranost.* **2018**, *8*, 6367-6368. (e) M. Poß, E. Zittel, C. Seidl, A. Meschkov, L. Muñoz, U. Schepers, C. Feldmann, *Adv. Funct. Mater.* **2018**, *28*, 1801074(1-8). (f) M. Poß, R. J. Tower, J. Napp, L. C. Appold, T. Lammers, F. Alves, C.-C. Glüer, S. Boretius, C. Feldmann, *Chem. Mater.* **2017**, *29*, 3547-3554.

9:00 AM SB01.07.04

Protein Cages with Functional Surface Loops for Theranostics Jeroen Cornelissen and Sandra Michel-Souzy; University of Twente, Netherlands

Different types of protein cages are nowadays studied in the fields of nano- and materials science, because of their well-defined size and structure in the nanometer regime. Compared to more traditional polymer-based nanoparticles, these – often – virus-based materials are extremely uniform, and the position of functional groups is precisely defined. Encapsulins are protein cages found in bacteria that have interesting properties with respect to (thermal) stability and cargo loading. In the past we and others have studied the application of encapsulins, but so far, their preparation, durability and functionalization are restricted to fundamental studies.¹

Here, we report the design of encapsulins from two different origins (e.g., *T. maritima* and *B. linens*) with functional loops on its surface.² This allows for site specific genetic or chemical modification to combine targeting and detection moieties on both the surface and the protein cage interior. We, furthermore, optimized the cages' production and showed that, under the selected conditions, these are stable over time periods of at least a year. The research presented in the contribution, therefore, paves the way for further straight forward engineering and production of the encapsulins, for therapeutics, diagnostics or vaccine development.

References

1. R. Putri, *et al. ACS Nano* 2017 *11*, 12796-12804.
2. S. Michel-Souzy, *et al. Biomacromolecules* 2021, *22*, 5234–5242.

9:15 AM SB01.07.05

Ultrasmall SiO₂@Au Nanoshells for Photothermal Nano-Theranostic and -Therapeutic Applications Luis Manuel¹, Vinoin D. Vincely², Caroyln L. Bayer² and Kevin M. McPeak¹; ¹Louisiana State University, United States; ²Tulane University, United States

Nanoshells made of thin Au layers on SiO₂ cores exhibit strong resonances in the biological transmission window. Several examples in the literature show the use of these particles in biomedical applications, such as the photothermal ablation of cancer cells. However, many photothermal-based approaches rely on nanoshells with resonances primarily due to scattering effects but nanoparticles with absorption-dominant resonances better suit such approaches.

Ultrasmall nanoshells that exhibit absorption-dominant resonances are ideal biological agents due to their low surface-to-volume ratio, ease of clearance, and cellular uptake rates but have not been developed due to synthetic challenges.

Herein, we decrease the size of nanoshells beyond previous limitations (i.e., sub 100 nm), making them better suited for absorption-based applications. As a case study, we compare absorption-dominant to scattering-dominant nanoshells as contrast agents in photoacoustic imaging, highlighting the role of the nanoshells' optical properties and the implications for absorption-based biomedical applications. Additionally, we tailor nanoshells further for photoacoustic imaging by considering heat transfer effects on the surrounding medium. Optimum nanoshells have 50 nm SiO₂ and 6.8 nm Au shells. The dominant extinction phenomenon is confirmed using an integrating sphere to separate light absorption from scattering, which is not typical of studies on colloidal samples.

9:30 AM *SB01.07.01

Carbon Nanotube Technology—An Efficient Platform for Virus Enrichment and Detection Mauricio Terrones^{1,2} and Nestor P. Lopez¹; ¹The Pennsylvania State University, United States; ²Shinshu University, Japan

The global COVID-19 pandemic is exerting devastating impacts on individual livelihoods, local communities, and the global economy. Accurate, real-time, and widespread testing is needed in order to track the disease, prevent further infections, and gain basic fundamental understanding of the disease, such as the number of infections, infection rate, etc. This talk will discuss the design and fabrication of disposable cartridges using a label-free virus enrichment platform consisting of microarrays of aligned carbon nanotubes (CNTs) in conjunction with gold metal nanoparticles. These trapped viruses are detected and identified using Raman spectroscopy in conjunction with Machine Learning models. More importantly, after viral capture, these viruses remain viable permitting subsequent in-depth characterizations by various conventional methods. This technology successfully enriched rhinovirus, influenza virus, coronavirus and parainfluenza viruses, and maintained the stoichiometric viral proportions when the samples contained more than one type of virus, thus emulating coinfection. Viral capture and detection took only a few minutes with a 70-fold enrichment enhancement; detection could be achieved with as little as 102 EID50/mL, with a virus specificity > 95%. This enrichment method coupled to Raman virus identification constitutes an innovative system that could be used to quickly track and monitor viral outbreaks in real-time.

References

- [1] Y. Yeh, M. Terrones, *et al.*, *Science Advances*, **2016**, 2, e1601026.
- [2] Y. Yeh, M. Terrones, *et al.*, *PNAS*, **2020**, 117, 895-901.
- [3] J. Ye, Y. Yeh, M. Terrones, *et al.*, *PNAS*, **2022**, *in press*
- [4] A.L. Elías, M. Terrones, *et al.*, *Small*, **2007**, 3, 1723-1729
- [5] Y. Yeh, M. Terrones, *et al.*, *Adv. Mater.*, **2018**, doi.org/10.1002/adma.201703321

10:00 AM BREAK

SESSION SB01.08: Adaptive Nano-Bio Interfaces
Session Chairs: Herdeline Ardoña and Vasiliki Tsikourkitoudi
Wednesday Morning, November 30, 2022
Hynes, Level 1, Room 104

10:30 AM *SB01.08.01

Dynamic Structures and Machines That Feed Living Systems Leila Deravi; Northeastern University, United States

We are developing bio-inspired systems, structures, and machines that can perform complex tasks in response to controlled stimuli. A molecular-level approach to building these materials that can produce programmable transformations in response to specific chemical inputs will be discussed for applications ranging from sensors to supplements.

11:00 AM SB01.08.02

Externally-Triggerable Liposomes for Personalized, Non-Invasive Control of Local Anesthesia Alina Rweji; TU Delft, Netherlands

Pain has a major impact on quality of life and affects billions of people worldwide. Yet, current treatments are either associated with significant side effects (i.e., opioids), suffer from insufficient durations of action (i.e., local anesthetics), or inability to provide adequate treatment with the patient's changing physical conditions and pain states. Here we present externally-triggerable liposomes as a vehicle to provide spatio-temporal control of pain relief, enabling non-invasive control of the duration, intensity and timing of pain relief via external triggers, such as light and ultrasound. Inspired by the natural lipid degradation process via peroxidation, we have engineered near-infrared-light- and ultrasound-triggerable liposomes that encapsulate the local anesthetic tetrodotoxin. Our results show significant triggering of lipid peroxidation upon exposure to external energy, leading to the effective activation of drug release events. The drug release can be activated repeatedly upon exposure to the external trigger. *In vivo* results show successful generation of nerve block upon exposure to a low- and biocompatible dosage of near infrared light and/or ultrasound. These results demonstrate the promising potential of utilizing such systems for personalized pain therapy, in which patients can control the intensity, duration, and timing of therapy via light and/or ultrasound.

11:15 AM SB01.08.03

Magneto-thermal Control of Nerve Growth Dekel Rosenfeld; Tel Aviv University, Israel

Nerve injuries are common with lifelong consequences. Despite their ability to regenerate, the full recovery of peripheral nerves is limited, and determined by several factors including the severity of the injury, patient age, medical history, onset of intervention post-injury and the slow rate of axonal growth. While chemical factors can accelerate the axonal growth process, recent studies have demonstrated that it can also be achieved via electrical and optogenetic stimulation. However, the governing mechanisms of those approaches require further investigation. In this project, we trigger calcium influx via activation of heat sensitive ion channels to achieve calcium-dependent accelerated nerve growth. To this end, we use the magneto-thermal approach that relies on heat dissipation from functionalized magnetic nanoparticles with diameter of 20-22 nm, exposed to weak alternating magnetic fields. We triggered the opening of the transient receptor potential vanilloid 1 heat sensitive ion channel (TRPV1), a calcium permeable non-selective cation channel. We demonstrate accelerated axonal growth followed TRPV1 activation in a dorsal root ganglion explant model, quantified via neurofilament elongation and Schwann cell migration.

Our method presents a novel approach to use magnetic materials and magnetic nanocomposites for nerve regeneration in a calcium-dependent process. Considering the limited regeneration capabilities of the nervous system, we present a strategy to overcome this limitation via remote stimulation and uncover new mechanism focusing on the role of TRPV1 in mediating axonal growth.

11:30 AM SB01.08.04

Seeing the Sound—Ultrasound and Infrared Responsive Nanomaterials for Non-Invasive Neuromodulation Xiang Wu and Guosong Hong; Stanford University, United States

Understanding complex neural circuitry and its correlation with specific behaviors requires spatially and temporally precise modulation of neuron subtypes in certain brain regions. For decades, neural stimulation has been predominantly achieved with traditional electrical stimulation. More recently, optogenetics has gained great popularity due to its rapid control of neural activities with visible light and its dissection of neural circuitry by selectively

modulating specific neuron subtypes. However, deep-brain neural modulation usually involves invasive implantation of stimulation electrodes and optical fibers due to the limited penetration of electric fields and visible light in the brain tissue. These brain implants lead to acute damage and chronic gliosis in the brain tissue, while tethering the animal to an electrical wire or an optical fiber interferes with naturalistic behaviors of freely moving subjects. To address these challenges, we developed ultrasound and second near-infrared (NIR-II, 1000-1700 nm) responsive nanomaterials for non-invasive neuromodulation. First, we developed ultrasound-mediated nanoscopic light sources—mechanoluminescent nanomaterials for non-invasive optogenetics. These nanomaterials can be delivered via the endogenous circulatory system and provide millisecond timescale switching of local light emission upon deep-penetrating focused ultrasound stimulation. We demonstrated that the ultrasound-mediated light emission from the nanomaterials circulating in the blood was sufficient to activate channelrhodopsin-2 (ChR2)-expressing neurons in the brain and trigger behavioral response in live mice in a non-invasive manner, a technique which we termed “sono-optogenetics”. We envisage that sono-optogenetics provides a unique tool of rapid screening of different target regions in the brain for optogenetic neuromodulation, owing to the ease of changing the location of ultrasound focus in the brain by eliminating fiber optic implantation. **This work was published in PNAS (Wu, X. et al. Sono-optogenetics facilitated by a circulation-delivered rechargeable light source for minimally invasive optogenetics. *Proc. Natl. Acad. Sci. USA* 116, 26332–26342 (2019)) and was awarded the Science and PINS Prize for Neuromodulation in 2020.**

Second, to afford non-invasive, remote neuromodulation in freely behaving animals, we developed polymeric nanomaterials termed MINDS (macromolecular infrared nanotransducers for deep-brain stimulation). MINDS can efficiently absorb light in one of the biological transparency windows, the NIR-II window, modulating neural activity via temperature-sensitive transient receptor potential (TRP) channels. MINDS have a photothermal conversion efficiency of 71% at 1064 nm, the wavelength at which light attenuation by brain tissue is minimized. As a result, through-scalp wide-field NIR-II illumination can activate TRP channels sensitized by MINDS up to a depth of 5 mm in the mouse brain, leveraging a bioinspired mechanism underlying infrared sensitivity in rattlesnakes (as demonstrated by the Nobel Laureate David Julius). Specifically, MINDS act as an NIR-II sensitizer to activate TRP-expressing neurons in the hippocampus, motor cortex and ventral tegmental area of mice with minimal tissue damage under wide-field NIR-II illumination, resulting in substantial behavioral and electrophysiological changes. Due to its non-invasive and tether-free interface, our NIR-II neuromodulation technique enables the study of animal behavior in its most natural state and is particularly suitable for modulating neural activities in socially interacting experiments involving multiple subjects, such as in the IntelliCage, in the future. **This work was recently published in *Nat. Biomed. Eng.* (Wu, X. et al. Tether-free photothermal deep-brain stimulation in freely behaving mice via wide-field illumination in the near-infrared-II window. *Nat. Biomed. Eng.* <https://doi.org/10.1038/s41551-022-00862-w> (2022)).**

SESSION SB01.09: Antimicrobial and Anti-Pathogenic Nanomaterials I

Session Chairs: Herdeline Ardoña and Xiaoyuan Chen

Wednesday Afternoon, November 30, 2022

Hynes, Level 1, Room 104

1:30 PM *SB01.09.01

Nanostructured Nanomaterials in Biomedical Applications—From Graphene to Virus Assemblies Rigoberto C. Advincula^{1,2,3}; ¹Case Western Reserve University, United States; ²The University of Tennessee, Knoxville, United States; ³Oak Ridge National Laboratory, United States

Nanostructuring interfaces and colloidal assemblies enable the convergence of processing methods and functions with high correspondence at the nanoscale. There is high interest in the electrical and thermal conductivity properties of graphene. However, they play a key role in mediating redox function and the generation of radical oxygen species in biological applications. Their application as anti-pathogenic agents is only now being appreciated and deemed scalable. This talk will focus on graphene (G) and graphene oxide(GO) nanomaterials as ultrathin films to result in anti-microbial properties. We also describe the preparation of very stable colloidal templates of graphene with anti-microbial properties. Interestingly, these colloidal particle templates can be used to prepare virus nanoparticles that can have theranostic applications. Lastly, we demonstrate their use as 3D printed devices with low toxicity for biomedical applications.

2:00 PM *SB01.09.02

Antibacterial and Antiviral Materials for the Prevention of Transmission of Hospital Acquired Infections Raechelle D'Sa and Jenny Aveyard; University of Liverpool, United Kingdom

Many infectious diseases can be spread through the viral or bacterial aerosols or contaminated surfaces. Bacterial diseases that are caused by multi-drug resistant bacteria such as methicillin-resistant *Staphylococcus aureus* (MRSA) and *Pseudomonas aeruginosa* are especially challenging to treat. Both of these organisms can reside on surfaces for weeks and are in the top 12 list of the World Health organisation of priority pathogens. Developing materials that can eradicate the bacteria on contact is essential to prevent the transmission of these infections. In the current COVID19 pandemic, although direct inhalation of infectious aerosols is the main mechanism of transmission, surfaces have also been shown to play a role in transmission. Nitric oxide is a well document antibacterial and antiviral molecule that has broad spectrum activity. In this study, nitric oxide donor molecules were embedded into polymeric surfaces/matrices for a sustained and controlled release of the molecule for over 72 hours. The kinetics and concentration of release was studied by chemiluminescence. The antibacterial efficacy was tested against planktonic and biofilm adhered bacteria and optimal material demonstrated a 4 log reduction for MRSA and 2 log for P. aeruginosa. Antiviral efficacy was measured against the Delta and Omicron variants of the SARS-CoV-2 virus. Time course studies demonstrated a faster kill rate with the Delta variant. Cytocompatibility studies demonstrated at antibacterial and antiviral concentrations, the materials were not cytotoxic. Therefore these materials should good promise for the prevention of bacterial and viral infections from surfaces.

2:30 PM BREAK

3:30 PM SB01.09.03

Lipid Core Nanocapsules for Antimicrobials Drug Delivery Janaina Artem Ataide¹, Angela F. Jozala² and Priscila G. Mazzola¹; ¹UNICAMP, Brazil; ²UNISO, Brazil

Over the past years, the development of biodegradable nanoparticulate systems for drug delivery has aroused great interest. Substantial advances happened in the development of functional nanomaterials towards biomedical materials, mainly for targeted therapies and drug delivery. Lipid core nanocapsules (LCN), a class of nanocapsules in which a polymeric shell is arranged around an inner core and is formed by a dispersion of a liquid lipid and a solid lipid, have gained attention since they can vehicle actives soluble in their lipidic core or polymeric shell. PCL (poly-E-caprolactone), a biocompatible and biodegradable polymer, has been used to encapsulate a wide range of drugs, achieving targeted and controlled drug delivery. Fluconazole, a bis-triazole antifungal, and rifamycin SV, an ansamycin antibiotic, could benefit from encapsulation. Our objective was to encapsulate fluconazole and rifamycin SV in

LCN, aiming to improve existing treatments by controlling their release. Empty-LCN (unloaded), Flu-LCN (LCN loaded with fluconazole) and Rif-LCN (LCN loaded with rifamycin SV) were prepared as previously described. Empty-LCN presented mean diameter of 220 nm, with PDI around 0.13 and zeta potential of -27 mV, while Flu-LCN and Rif-LCN presented around 230 nm diameter, PDI 0.15 and -28 mV zeta potential, determined by DLS in ZetaSizer Nano ZS equipment. Total drug concentration was determined by HPLC/UV, as well as encapsulation efficiency after separating non-encapsulated drug by ultrafiltration-centrifugation. Fluconazole presented a type II distribution in LCN, with encapsulation efficiency calculated as 8.0%, drug content of 798 µg/mL and drug loading of 0.17%. On the other hand, rifamycin SV presented a type III distribution, with encapsulation efficiency of 66.2%, drug content of 743 µg/mL and drug loading of 1.28%. Profile of drug release from LCN was determined by *in vitro* Franz-cell diffusion. Around 53% of fluconazole was released in the first 7h, reaching 77% in 48h; while less than 5% of rifamycin SV was released in the first 8h, reaching 21% in 48h. *In vitro* antimicrobial activity of free drugs and LCN formulations was determined using minimal inhibitory concentration (MIC) method against *S. aureus*, *P. aeruginosa* and *C. albicans* microorganisms. Empty-LCN did not show any antimicrobial activity. Free-Flu and Flu-LCN did not showed activity in the tested concentrations for *S. aureus* and *P. aeruginosa*, and a MIC of 0.39 µg/mL for *C. albicans*. Free-Rif and Rif-LCN showed MIC of 3.1×10^{-3} µg/mL for *S. aureus*, 100 µg/mL for *P. aeruginosa*, and no activity against *C. albicans*. LCN formulations with fluconazole and rifamycin SV were successfully produced. Depending on drug characteristics, higher encapsulation efficiency and drug loading was achieved, with a more prolonged release. Antimicrobial activity of fluconazole and rifamycin SV was maintained after encapsulation in LCN formulations, and no activity was reported for empty-LCN.

3:45 PM SB01.09.04

Antimicrobial Potential of High-Drug Loaded Calcium Phosphate Nanoparticles Engineered by Flame Spray Pyrolysis Vasiliki Tsikourkitoudi and Georgios Sotiriou; Karolinska Institutet, Sweden

Infectious diseases resulting from pathogenic microorganisms are one of the most significant global health threats, while overuse of antimicrobial drugs has caused an emergence of antimicrobial resistance. Thus, novel approaches are needed to address the unmet medical need for eradication and prevention of infections caused by antimicrobial resistant bacteria.

Recent advances in nanomedicine have shown the potential of nanoparticles as carriers for antimicrobial drugs, such as antimicrobial peptides, in improving the treatment of infectious diseases. Their large surface-to-volume ratio renders them unique antimicrobial agents with high drug loading capacity.

In this regard, here, we propose a novel antimicrobial drug delivery platform based on calcium phosphate (CaP) nanoparticles. We fabricated CaP nanoparticles by flame spray pyrolysis (FSP), an intrinsically scalable and reproducible nanomanufacturing process. We exploited the versatility of this method for the synthesis of CaP nanocarriers with tailored properties. We further established an experimental protocol for loading biologics by physisorption on flame-made CaP nanoparticles. More precisely, we loaded bovine serum albumin (BSA) and bradykinin as model protein and peptide, respectively, and investigated the effect of their concentration and incubation time on loading efficiency. We implemented the established protocol by loading antimicrobial peptides (LL37 and a mannose receptor-derived one, MRC-1) on CaP and assessed their stability against proteolytic degradation and their therapeutic potential against bacterial infections both *in vitro* and *in vivo*.

High loading values, reaching 350 mg/g and 600 mg/g of CaP for BSA and bradykinin, respectively, were obtained, whereas maximum LL37 loading (~800 mg/g) outperformed all loading values found in the literature. High loading values were attributed to typical fractal-like structure of flame-made agglomerates/aggregates. The protective potential of CaP nanocarriers against enzymatic degradation of LL37 was evaluated by gel electrophoresis in a degradation assay using Proteinase K. LL37 loading on CaP nanoparticles kept LL37 intact, as the peptide resisted degradation up to 240 min.

To verify if LL37 also retained its antimicrobial function after being physisorbed onto CaP nanoparticles, we studied its antimicrobial activity against both Gram-positive (*Streptococcus pneumoniae*) and Gram-negative (*Escherichia coli*) pathogens by monitoring the bacterial growth under incubation with different concentrations of LL37, either free or loaded on CaP nanoparticles. Similar antimicrobial activity for free LL37 and LL37-loaded CaP was observed for *S. pneumoniae*, whereas for *E. coli*, LL37-loaded CaP exhibited better antimicrobial performance than free peptide.

Finally, we explored the *in vivo* antimicrobial efficacy of the flame-made CaP nanoparticles after loading MRC-1 peptide. We first visualized the biodistribution of MRC-1-loaded nanoparticles in mice by administering fluorescently labelled peptide-loaded particles and imaging using an IVIS Spectrum-CT imaging system and verified that the peptide loaded particles reached the lungs. Then, MRC-1 peptide loaded CaP nanoparticles were administered intranasally to mice previously infected by *S. pneumoniae*. The administration of MRC-1 peptide loaded CaP nanoparticles was shown to reduce development of pneumococcal disease *in vivo* enhancing mice survival.

In a nutshell, we present synthesis of a biocompatible/biodegradable nanocarrier by an intrinsically scalable and reproducible synthesis method. Typical fractal-like structure of flame-made nanoparticles promoted high drug loading efficiency and enabled protection of antimicrobial peptides from enzymatic degradation, enabling their safe delivery. High loading values achieved along with the *in vitro* and *in vivo* protective effect of the nanoparticles facilitate clinical translation of flame-made CaP nanoparticles as drug carriers.

SESSION SB01.10: Biomimetic Nanotherapeutics
Session Chairs: Juan Beltran-Huarac and Georgios Sotiriou
Thursday Morning, December 1, 2022
Hynes, Level 1, Room 104

9:00 AM SB01.10.01

Novel Nanozymes to Replace Natural Enzyme in Biosensing and Beyond Moon Il Kim; Gachon University, Korea (the Republic of)

Recently, nanozymes have been intensively studied due to their superior qualities such as extremely high stability with robustness even under stringent conditions, tunable catalytic activity and specificity, and ability to be synthesized on a large-scale at low costs. In this presentation, I will discuss our current progresses how to develop novel nanozymes and their representative applications in biosensing technology. First, I will describe a new and simple colorimetric strategy for the detection of nucleic acids, which relies on target DNA-induced shielding action against the peroxidase mimicking activity of magnetic nanoparticles (MNPs) or oxidase mimicking activity of cerium oxide nanoparticles (CeO₂ NPs). Second, I will discuss a nanostructured multi-catalyst system consisting of MNPs and an oxidative enzyme entrapped in large pore sized mesoporous silica for convenient detection of biologically important target molecules. The oxidative enzyme in the multi-catalyst system generates H₂O₂ through its catalytic action for a target molecule, which subsequently activates MNPs to convert a selected substrate into a colored product. Besides, I will introduce highly efficient electrochemical biosensing system by employing conductive nanocomposite and ultrafast colorimetric immunoassay system by employing a nanocomposite entrapping magnetic and platinum nanoparticles. Finally, I will also describe biosensors based on new nanozymes including Fe-aminoclay, Cu-nanoflower, N & B-doped graphene, and Fe-N₄-graphene, as well as nanozyme-mediated paper-based analytical devices. These achievements should accelerate and widen the utility of nanozymes as next-generation alternatives to natural enzymes in biosensing and beyond.

9:15 AM SB01.10.02**Multimodal Lipid Nanoparticle Imaging for Assessing Tumor Biodistribution Across Multiple Scales** Jeremy M. Quintana, Thomas S. Ng, Huiyu Hu, Ralph Weissleder and Miles Miller; Massachusetts General Hospital, United States

Covid-19 vaccines based on mRNA delivery via lipid nanoparticles (LNP) have provided evidence of the therapeutic potential of this platform, and expanded efforts are underway to develop LNP for delivering immunomodulatory nucleic acid payloads to treat various solid cancers. While a variety of studies have explored new combinations of lipid and therapeutic components, there is relatively little data on how LNP behave spatially within solid tumors, particularly at dynamic and single-cell levels. To better examine how LNP transport within the tumor microenvironment, we have developed a strategy to track their quantitative biodistribution by positron emission tomography (PET). Combination of LNP-PET with magnetic resonance imaging (MRI) supports soft-tissue anatomical and functional context of LNP distribution, while LNP labeling with lipid-conjugated fluorophore supports microscopy evaluation at subcellular resolution. As a proof of principle, we based our model LNP on clinical formulations and used derivatives of 1, 2-distearoyl-sn-glycero-3-phosphoethanolamine-poly(ethylene glycol), which were synthesized to incorporate fluorophore and PET radionuclide chelator into the lipid interface. Modified LNP were formed with average diameters in the range of 80-150 nm, and were evaluated in the 4T1 murine model of metastatic breast cancer, a disease where LNP are being clinically tested. We hypothesize these functionalized lipid nanoparticles will allow us to more closely study rate-limiting factors related to efficacy and off-target toxicity, especially in the context of metastatic disease in breast cancers.

9:30 AM BREAK**10:00 AM SB01.10.04****Graphene Oxide and Healthcare Applications—Nets, Crowded Body Fluids, Cell Highways** Valentina Palmieri^{1,2}, Giordano Perini², Alberto Augello², Marco De Spirito² and Massimiliano Papi²; ¹National Research Council, Italy; ²Catholic University of Sacred Heart, Italy

Around ten years ago, graphene oxide has attracted a wide scientific community interest for applications in healthcare as new antibiotics safe for eukaryotic cells. However controversy emerged and subsequent biophysical studies elucidated the instability of this nanomaterial in body fluids rich in electrolytes, proteins, and more. With the formation of nets and the adsorption of soluble factors on its surface, cells and microorganisms do not interact with single bidimensional flakes but with large aggregates. Here we discuss how the adsorption of ions and molecules on nanomaterials surface can be exploited to modulate graphene oxide antimicrobial activity. Furthermore, the formation of the so-called protein corona on graphene oxide will be discussed in light of drug delivery, and diagnostic applications. The protein corona layer on tridimensional graphene scaffolds will be also debated for the future improvement of graphene oxide bioactivity in 2D and 3D.

10:15 AM SB01.10.06**Enhancing Osteogenic Possibilities Through Bone Tissue Engineering** Kalpna Katti, Krishna C. Kundu, Sharad V. Jaswandkar and Dinesh R. Katti; North Dakota State University, United States

Current clinical therapeutic approaches for critical size bone defects regeneration suffer from severe limitations such as limited availability, increased risk of infection, donor site morbidity, and insufficient transplant integration. These limitations necessitate scaffolds with accelerated bone defect repair. We report the use of a unique interlocking polymer clay nanocomposite scaffold system incorporated with bone morphogenic proteins 2 and 7 (BMP-2 and BMP-7). In addition coculturing the porous polymer clay scaffolds with osteoblast cells (hFOB) and mesenchymal stem cells (MSCs) is used to evaluate the long-term effect of BMPs on bone regeneration for a period of 9 weeks. The total release of BMP-2 and BMP-7 was observed from the scaffolds by day 16. We observed improved cell proliferation, viability, and osteogenic differentiation of the cells with the BMPs incorporated scaffolds. Gene expression studies indicate a significant increase in the bone-related proteins, osteogenesis-related proteins, and Wnt-factors-related proteins with BMPs coated samples compared with uncoated samples, indicating that BMPs played a crucial role in initial osteogenesis and ECM formation. In addition, Alizarin Red S staining and scanning electron microscopy images show a significant increase in the mineralized bone nodule formation with BMPs coated samples compared with uncoated samples suggesting BMPs played a decisive role in bone regeneration. Furthermore, at 9 weeks, nanoindentation experiments on BMP-2/BMP-7 coated scaffolds showed a 120% increase in the elastic modulus, indicating enhanced ECM formation. Thus, BMPs play a crucial role in osteogenesis at the initial stages well beyond the time period of total release of BMPs. This study provides valuable insight into the mechanisms of the BMPs association in bone regeneration and demonstrates the feasibility of the interlocking scaffold system as a bone graft for critical size bone defects repair application. Induction of osteogenesis using the nanoclay materials as well as enhanced osteogenesis is enabled in the unique scaffold block interlocked system.

SESSION SB01.11: Virtual Session: Responsive Nanomaterials Development II

Session Chairs: Herdeline Ardoña and Juan Beltran-Huarac

Tuesday Morning, December 6, 2022

SB01-virtual

10:30 AM *SB01.11.01**Understanding Structural, Chemical and Physical Variations in Lipid Nanoparticles** Georgios Pyrgiotakis, Charles Dahlheim, Donald Johnson, Linda Obenauer-Kutner, Raquel Feliz, Denette Murphy and Erinc Sahin; Bristol-Myers Squibb, United States

Lipid Nanoparticles have been around since the early nineties and have been successfully commercialized in the drug delivery space over the last two decades. Recently, the successful development of the SARS-Cov-2 vaccines established them as a promising technology for the targeted delivery of genes, DNA/RNA, and pharmaceutical products. Further they can be decorated with moieties that hold potential to tissue-specific delivery. Their manufacturing has unique challenges, as complex nanoscale physicochemical phenomena can impact their quality attributes such as size, drug loading, targeting agent availability, and particle morphology. Here, we present approaches that can help shed light to some of these nanoscale phenomena and enable study of 1) particle size and structure variations via Asymmetric Flow Field Flow Fractionation (A4F), 2) drug and targeting agent loading distribution via fractionation with size exclusion chromatography, and 3) real-time particle size measurement during manufacturing via Spatially Resolved Dynamic Light Scattering (SR-DLS). Our data show detection and quantitation of structural and compositional variability within LNPs. We also demonstrate the potential of the SR-DLS as a process analytical technology for real-time, in-line measurement of particle size integrated within manufacturing.

11:00 AM SB01.11.02

2D Nanohybrid Artificial Antibody for Diagnosis and Therapy of Pathogen Infection [Sin Lee¹](#), Yoonhee So¹, Hyunji Lee¹, Yesol Myeong¹, Chul-Su Yang¹, Hwanky Lee² and Jong-Ho Kim¹; ¹Hanyang University, Korea (the Republic of); ²Dankook University, Korea (the Republic of)

For the selective recognition of diverse targets ranging from pathogens to small analytes, antibodies have been widely used due to their high binding affinity and specificity. However, antibodies have several limitations of low stability, long production time, short shelf-life, and high cost. Therefore, it is of great significance to develop artificial antibodies that can circumvent the shortcomings of antibodies for sensing and therapy. Herein, we report a facile strategy for the synthesis of artificial antibodies consisting of luminescent transition metal dichalcogenide (TMD) nanosheets and nonbiological polymeric recognition phases for the selective detection of the target pathogens, *Escherichia coli* O157:H7 (*E. coli* O157:H7) and *Staphylococcus aureus* (*S. aureus*). The TMD nanosheets with a neutral dextran phase at their interface selectively recognized *S. aureus*, whereas the nanosheets bearing a carboxymethylated dextran phase selectively recognized *E. coli* O157:H7 with high binding affinity. The mechanism responsible for the selective recognition of the artificial antibodies against the specific bacteria was thoroughly identified by experiments and molecular dynamics simulations. The WS₂ artificial antibody could selectively detect the target bacteria at the concentration as low as a single copy of bacterium from human serum based on the strong Raman signal of WS₂. In addition, the MoSe₂ artificial antibodies selectively killed the pathogenic bacteria under near-infrared (NIR) irradiation. Finally, the MoSe₂ artificial antibodies were successfully applied for the selective detection and killing of the pathogenic bacteria in the wounds of infected mice under NIR irradiation. This new artificial antibody approach can be extended for recognition of a variety of biomolecules for selective sensing and therapy.

11:15 AM SB01.11.03

The Effect of Microsphere Growth and Static Magnetic Field on Osteogenic Differentiation of Dental Pulp Stem Cells [Angeline Sun¹](#), Kuan-Cheng Feng², Emir Mulic², Sooraj Shah², Yiwei Fang², Yu-Chung Lin², Marcia Simon² and Miriam Rafailovich²; ¹Taipei American School, Taiwan; ²Stony Brook University, The State University of New York, United States

Dental pulp stem cells (DPSCs) have great potential in regenerative medicine due to their noninvasive extraction, low immunogenicity, and multipotency [1]. Previous research revealed that under the influence of chemical stimuli, DPSCs can differentiate into functional osteoblasts that secrete extracellular matrix (ECM) [1, 2]. The osteogenic potential of DPSCs is of great importance due to its therapeutic applications in bone mineralization and reconstruction [3]. Through careful modifications of the cell microenvironment such as three-dimensional culture methods [4] and magneto-mechanical stimulations [5], the osteogenic differentiation of DPSCs can be enhanced significantly. This study aims to investigate the effect of microsphere formation and static magnetic fields on osteogenic differentiation.

After trypsinization after passage four of DPSCs, cells were placed in U-bottom non-adhesive suspension wells or flat-bottom wells covered with 50, 100, and 150 μ L 2% agarose to induce microsphere formation. Different volumes of agarose produce different degrees of curvature, thereby influencing the compactness of the microspheres. Through EVOS imaging, we observed that agarose wells were better at forming dense aggregates compared to suspension wells. At different timepoints after microsphere growth (5 and 7 days in wells), the cells were plated onto 6-well tissue culture plates. After 7 days of plating, ascorbic acid and β -glycerophosphate were added into the medium to induce osteogenic differentiation. After 28 days of plating, PCR was performed to quantify mRNA of osteocalcin (OCN) and dentin sialophosphoprotein (DSPP). All results were normalized with the housekeeping gene GAPDH related to Day 0. The results confirmed the observations from EVOS that agarose wells induced greater osteogenic potential. DPSCs in 100 μ L agarose wells plated 5 days after growth expressed the greatest level of OCN. Unexpectedly, suspension wells seem to induce greater odontoblastic potential than agarose wells. The expression of DSPP was highest in suspension wells plated 5 days and 7 days after growth.

The synergistic effect of magnetic fields and magnetic scaffolds has been proposed to enhance osteogenesis through activating signaling pathways [5]. For the magneto-mechanical stimuli, cells were plated onto different scaffolds and incubated in the presence or absence of magnetic fields. The three types of compression-molded scaffolds were pure polylactic acid (PLA), a biodegradable polyester frequently used in tissue engineering [6], 95% PLA and 5% RDP clay, and 90% PLA and 10% magnetic iron oxide microparticles. Using atomic force microscopy (AFM) to characterize surface topology, we found that all three scaffolds were of nanoscale roughness, with the scaffolds containing iron oxide being the roughest. After 28 days of incubation, EVOS was used to image cell morphology and biomineralization. Cells were stained with Alexa Fluor 488, DAPI, and Xylenol Orange to visualize actin, DNA, and calcium deposition respectively. We observed calcium deposition between the DPSCs. PCR results of the osteogenic-related genes confirmed the synergistic effect as the expression level of DSPP and OCN in cells grown in presence of magnets on iron oxide scaffolds were significantly higher than cells grown on pure PLA with magnets present and cells grown on iron oxide scaffolds without magnets. SEM will be used to determine the conformation of extracellular matrix proteins deposited on the different scaffolds and their ability to template the mineralized deposits. Raman spectroscopy will be used to determine the nature of the mineralized tissue.

11:30 AM SB01.11.04

Design and Production of Multifunctional Implantable Patches Combined with Drug-Loaded Nanoparticles for Treatment of Breast Cancer [Beril Ustunkaya¹](#), Eda Güneç¹, Eric M. Tan^{2,1}, Ozlem Kutlu² and Gozde O. Ince^{1,2}; ¹Sabancı University, Turkey; ²Sabancı University Nanotechnology Research and Application Center (SUNUM), Turkey

Breast cancer is the second most common cancer type worldwide [1]. Human Epidermal Growth Factor Receptor 2 positive (HER2+), Hormone Receptor positive (HR+) and triple-negative being three different subtypes of breast cancer, research has been dedicated to exploit their molecular mechanism, treatments, and recurrence [2]. Herein, we propose a novel implantable multifunctional patch design that will provide the tumor treatment for different subtypes of breast cancer, and will trigger immune response to prevent the recurrence in the long run. The multifunctional patch carries a nanoparticle system that enables combined photothermal and photodynamic therapy for cancer treatment, and also biomolecules that will activate the immune system against the possible recurrence. The nanoparticle system is comprised of three functional subunits one of which enables site-specific delivery as it includes specific proteins to the different breast cancer subtypes, and the others provide treatment by photothermal, and photodynamic therapies. These functional nanoparticles will be excited by two different Near Infrared (NIR) lasers which are of 808 nm and 1060 nm to trigger the treatment at the intended site. The activation of the immune system will be achieved by the biomolecules as they are released from the blow-spun patches. The chemical compositions and the morphologies of both the nanoparticles and the blow-spun patches will be investigated by Fourier transform infrared spectroscopy (FTIR), and Scanning Electron Microscopy (SEM), respectively. The sizes and the zeta potential of the fabricated nanoparticles will be characterized by the Dynamic Light Scattering (DLS) method. The degradation performances of the blow-spun patches will be examined in phosphate buffered saline (PBS) and lysosome-mimicking solution (LMS), and enzyme-linked immunosorbent assay (ELISA) will be used to study the release of biomolecules from the patches. While the cellular uptake of the nanoparticles and their success in the phototherapy will be investigated by microscopic technique, the success of the patches in the stimulation of the immune system will be studied in vitro on T helper cells and B cells with dendritic cell morphology (BDCM). This novel multifunctional patch design will offer both the specific treatment for breast cancer subtypes and the long-term preventative effect against the possible recurrence.

References

[1] Zubair, M., Wang, S., & Ali, N. (2021). Advanced Approaches to Breast Cancer Classification and Diagnosis. In *Frontiers in Pharmacology* (Vol. 11).

11:45 AM SB01.11.05

Photo-Initiated Chemical Vapor Deposition of Polymer Thin Films onto Electrospun Nanofibers for Controlled Drug Release [Eda Güney](#)¹, Abdurrahim Can Egil¹, Faruk Can² and Gozde O. Ince^{1,2}; ¹Sabancı University, Turkey; ²Sabancı University Nanotechnology Research and Application Center (SUNUM), Turkey

Drug release kinetics highly depend on the surface chemistry of the scaffolds. Surface modifications can be performed by different techniques to alter the surface properties of the scaffolds and thus to provide controlled drug release. However, the conventional modification techniques have several disadvantages such as non-uniformity on the surface, lack of precise process control, weak stability, and possibility of the fiber destruction [1]. In this study, we propose a novel technique to coat the surface of the drug-loaded electrospun nanofiber scaffolds for controlled drug release applications without causing any damage to the fibers and the drug which is being encapsulated. The surface modification will be carried out by photo-initiated chemical vapor deposition (piCVD) technique, which will allow the material to maintain its own properties and also to provide controlled drug release. First, the drug-loaded scaffolds will be produced using biocompatible and biodegradable polymers by electrospinning process. Then, the surface of the fabricated scaffolds will be coated with polymer thin films by the piCVD technique. The piCVD technique will involve photopolymerization of one or more vapor-phase monomers using an initiator and their deposition on the scaffold surface to produce the desired thin films. The photopolymerization will be carried out by short-wavelength emission of UV-light at 254 nm under mild deposition conditions. A kinetic study will be conducted to determine the optimal deposition conditions. The drug release performances of the uncoated and polymer-coated nanofiber scaffolds will be examined comparatively. While the changes in fiber structure after the coating will be examined by scanning electron microscopy (SEM), the chemical characterization of the scaffolds will be performed by Fourier transform infrared spectroscopy (FTIR). The proposed surface modification approach seems to be a promising avenue of research for controlled drug release applications.

References

[1] Biazar, Esmacil, Mahshad Kamalvand, and Farzaneh Avani. "Recent advances in surface modification of biopolymeric nanofibrous scaffolds." *International Journal of Polymeric Materials and Polymeric Biomaterials* 71.7 (2022): 493-512.

12:00 PM SB01.11.06

Nanotoxicological Assessment and Cell Internalization for Cancer Cells of Luminescent Nanoparticles [Dalia H. Chavez](#)^{1,2}, Karla O. Chavez Garcia³ and Gustavo Hirata³; ¹Instituto Educativo del Noroeste AC, Mexico; ²Centro de Enseñanza Técnica y Superior, Mexico; ³Centro de Nanociencias y Nanotecnología, Mexico

The detection of cancer cells by bioimaging with luminescent nanoparticles instead of usual dyes is being eagerly investigated. In this study we prepared upconversion (UCNPs) and downconversion (DCNPs) nanoparticles (NPs) by sol-gel method. The UCNPs uses a near infrared beam (NIR $\lambda=980$ nm) as the excitation source to upconvert the energy into light in the visible region. The present study used UCNPs: $Y_2O_3/Gd_2O_3:Yb^{3+}/Er^{3+}$ capable of emitting red or green photons of 660 nm and 550 nm wavelength. The DCNPs were: $Y_2O_3:Eu^{3+}$ and Eu^{3+}/Bi^{3+} excited at $\lambda=250$ nm and 330 nm with red emission at 660 nm. The functionalization was done by aminosilanes and folic acid (FA-UCNPs and FA-DCNPs). Folic acid binds to the folate receptor on the surface of certain types of cancer cells, and this binding promotes internalization of the NPs via endocytosis. The NPs were characterized by TEM, EDS, and FTIR. Cytotoxicity was also analyzed using the MTT (methyl-134 thiazolyltetrazolium) colorimetric assay. Finally, cellular uptake of FA-UCNPs was determined using flow cytometry and epifluorescence microscopy; we also did a comparison between cellular uptake of spheroidal NPs and two-dimensional (2D) cell culture models, also known as monolayers, finding that the architectural arrangement of 3D cell cultures allowed up to 20% more internalization of FA-UCNPs than in 2D cell arrangements.

12:15 PM SB01.11.07

Tuning Size and Spacing of Liganded Gold Nanoparticle Arrays for Macrophage Modulation [Thomas Myeongseok Koo](#)¹, Yuri Kim¹, Ramar Thangam¹, Myeong Soo Kim¹, Woo Young Jang¹, Nayeon Kang¹, Sunhong Min¹, Seong Yeol Kim¹, Letao Yang², Hyunsik Hong¹, Hee Joon Jung³, Eui Kwan Koh⁴, Kapil D. Patel¹, Sungkyu Lee¹, Hong En Fu¹, Yoo Sang Jeon¹, Bum Chul Park¹, Soo Young Kim¹, Steve Park⁵, Junmin Lee⁶, Luo Gu⁷, Dong-Hyun Kim³, Tae-Hyung Kim⁸, Ki-Bum Lee², Woong Kyo Jeong¹, Ramasamy Paulmurugan⁹, Young Keun Kim¹ and Heemin Kang¹; ¹Korea University, Korea (the Republic of); ²Rutgers, The State University of New Jersey, United States; ³Northwestern University, United States; ⁴Korea Basic Science Institute, Korea (the Republic of); ⁵Korea Advanced Institute of Science and Technology, Korea (the Republic of); ⁶Pohang University of Science and Technology, Korea (the Republic of); ⁷Johns Hopkins University, United States; ⁸Chung-Ang University, Korea (the Republic of); ⁹Stanford University, United States

Fibronectin (FN), one of the proteins organizing the extracellular matrix (ECM), plays an important role in the cell adhesion process. Especially, differently distributed FN of the ECM can determine inflammatory M1 polarization or pro-healing M2 polarization of macrophages, which modulate inflammation or wound healing, respectively [1]. This action occurs when the integrin of a cell recognizes and ligates to the tripeptide amino acid sequence of Arg-Gly-Asp (RGD) presented by FN. In addition, it has been studied that the polarization of macrophages can be controlled by modulating the array of liganded nanostructures [2].

Here, we report the submolecular-level-controlled size and spacing of liganded nanoparticle arrays for dynamic macrophage modulation. The size and spacing of liganded gold nanoparticles (GNP) assembled on a nano-sized magnetite template are precisely tuned from 3 to 20 nm via various seed-mediated growth. The liganded GNP-magnetite nanoassemblies are bound to the substrate via the flexible polymer linkers, which can shrink by in situ magnetic fields. When the space of liganded GNP is about 3 nm compared to the case of 13 nm or 20 nm, integrin binding to RGD ligand is promoted, and pro-healing polarization is stimulated. As the size of the liganded GNP increases from 13 nm to 20 nm, integrin binding improves, and anchoring the liganded GNP-magnetite nanoassemblies to the substrate using a permanent magnet promotes macrophage adhesion as much as 3 nm-spaced liganded GNPs. Increasing the spacing of liganded GNPs from 3 nm to 17 nm prevents integrin binding; therefore, inflammatory polarization appears. The results of this research are confirmed both in vitro and in vivo.

[1] W. J. Kao and D. Lee, *Biomaterials* 22, 2901-2909 (2001)

[2] S. Min *et al.*, *Nano Letters* 20, 7272-7280 (2020)

12:30 PM SB01.11.08

Detection of Circulating Tumor Cells from Clinical Blood by Electrically Charged Fe₃O₄ Nanoparticles [Yuxin Wang](#), Zicheng Deng, Jiajie Diao and Donglu Shi; University of Cincinnati, United States

Tumor metastasis has been found to be associated with circulating tumor cells (CTCs) that shed from the primary tumor and enter the circulation. The

characteristics of CTCs offer highly valuable information in assessing tumor aggressiveness and predicting the subsequent growth at distant organs. Therefore, detection and isolation of CTCs can serve as an effective tool in cancer diagnosis and prognosis through liquid biopsy. As a result of extreme rarity of CTCs, however, it has been extremely challenging to sensitively detect, effectively capture, and accurately identify CTCs from clinical blood. Current CTCs detection technologies mainly rely up on either the biomarker-conjugated magnetic beads or size-sensitive microfiltration membrane with certain limitations in sensitivity. In this presentation, we report an alternative but more sensitive CTC detection approach based on the cancer cell surface charge which is metabolically regulated by glycolysis without any conventional biomarkers. Based on the well-known Warburg effect, the cross-membrane movement of lactate inevitably removes labile inorganic cations, resulting in a net of negative charge on the cancer cell surfaces. A positively charged nanoprobe is designed and engineered to bind electrostatically onto the negatively charged cancer cells for capture and isolation. Since high glycolysis capacity is a hallmark characteristic of all cancer cells, the charge-based CTC detection can apply to different cancers regardless of their phenotypes. Our preliminary results show strong binding of the positively-charged nanoprobe on the cell surfaces of multitude of cancer types while insignificant binding is observed for the negatively charged nanoprobe counterpart. Also discussed is the relationship between the cancer cell surface charge and the glycolysis capacity which is the key that dictates the CTC detection sensitivity.

SESSION SB01.12: Virtual Session II
Session Chairs: Padryk Merkl and Vasiliki Tsikourkitoudi
Wednesday Afternoon, December 7, 2022
SB01-virtual

1:00 PM *SB01.12.01

Protein Engineered Biomaterials for MRI-Traceable Drug Encapsulation Dustin Britton, Lindsay Hill, Michael Meleties and [Jin Montclare](#); New York Univ, United States

Inspired by nature's biopolymers, we engineer artificial protein materials on the genetic and chemical level leading to new properties, specifically traceability. We employ synthetic and chemical biology to construct our materials and endow them with theranostic ability. In particular, we have fabricated protein-derived nanomaterials: coiled-coil fibers and helix-elastin block polymers. We investigate the fundamental self-assembly and molecular recognition capabilities of these systems. More importantly, we are able to harness these structure as well as others to interface with small molecule therapeutics and cells. Our studies lead to insights in how we can program self-assembling protein biomaterials to be visualized and deliver therapeutics.

1:30 PM SB01.12.04

Reconstructing Bone Defects Using *In Vivo* Nanocomposite Scaffold Printing [Adnan Memic](#); King AbdulAziz University, Saudi Arabia

Critically sized bovine defects commonly caused by traumatic injuries and tumor removal can overwhelm the regenerative capacity of the native tissue. Reparative strategies such as auto, xeno, and allografts are clinically insufficient to treat such defects. For the first time, we introduce the use of handheld melt spun three dimensional printers that can deposit materials directly within the defect site to properly fill the cavity and form free-standing scaffolds. Our 3D nanocomposite filaments can be deposited using low-temperature printing to avoid overheating of the surrounding tissues. The *in situ or in vivo* printed scaffolds have moderate adhesion to wet bone tissue, which can prevent scaffold dislocation. The printed scaffolds showed a high level of biocompatibility and were osteoconductive supporting the osteodifferentiation of mesenchymal stem cells.

1:45 PM SB01.12.05

Fast Growth of AgMOF—Micro and Nano Crystals as Antibacterial Coating for Ti-Based Implants [Vincenzo Paratore](#)¹, [Domenico Franco](#)^{2,3}, [Giovanna Calabrese](#)², [Salvatore Guglielmino](#)², [Sabrina Conoci](#)^{2,3} and [Guglielmo G. Condorelli](#)¹; ¹Università degli Studi di Catania, Italy; ²Università degli studi di Messina, Italy; ³IBMTech s.r.l., Italy

Bacterial infections are quite common in post-operative recovery for prosthetic bone replacements due to the bacteria capability of adapting to commonly used drugs. This leads to rejection of the prostheses and a subsequent return to the operating room for the replacement of the prosthesis. The study of new antibacterial materials and of their anchoring on implants surfaces has, therefore, a key role in scientific research. Various inorganic and organic materials have been used for this purpose, and, among them, MOF (Metal Organic Framework) possess great potentiality. They are composed by organic ligands and metallic subunits, bond together to obtain a framework. They present a series of active sites, micro and nano porous structures and highly modulable surface areas. Silver-based inorganic materials gained interests in biomedical applications thanks to Ag⁺ ions antibacterial properties.

We synthesized a silver-based MOF using a new synthetic method through which less toxic solvents, lower temperatures, and much shorter times are involved compared to commonly used approaches. We chose 1,4-benzene dicarboxylic acid as ligand because of its low toxicity and the weak bond with Ag⁺ that allow slow release of Ag⁺ ions in solution. The developed approach makes it possible to control the growth of specific crystalline phases in solution and on the implant surface as well.

We developed a fast low temperature synthetic method using dimethyl sulfoxide as solvent. Starting from AgNO₃, and using ammonia to stabilize Ag⁺ ions, we obtained a mixed crystalline phase in 3h and the pure product in 5h at 70°C. To reduce synthesis times, we used two modulators (KCl and benzoic acid). In these conditions, the pure product was obtained in 3h with both modulators at 70°C. The silver ions release has been studied in water solution in neutral conditions and at different pH levels to verify a possible increased release during infections, in which pH values drop. Antibacterial properties were then evaluated to obtain the Minimum Inhibiting Concentration (MIC) and the Minimum Bactericidal Concentration (MBC). For gram-negative MIC and MBC were observed at 7.8 µg/ml and for gram-positive MIC and MBC were observed at 31.3 µg/ml and 62.5 µg/ml respectively.

We also grow this material on a classic titanium scaffold for bone transplantation. To achieve surface growth, we treated titanium scaffolds and functionalized its surface with organic ligands like p-phosphono benzoic acid. By immersing the scaffold in an Ag⁺ ion solution it was possible to obtain preferential crystallization sites for the MOF. Using similar synthesis methods, we obtained a continuous coverage of the Ti substrate.

2:00 PM SB01.12.06

Surface-Enhanced Raman Scattering Sensing of Various Analytes Based on the Polymer-Metal Composite Sensor Particles [Nikunj Kumar Visaveliya](#); The City College of New York, United States

Surface-enhanced Raman scattering (SERS) spectroscopy is one of the most powerful analytical techniques to detect trace amounts of various analytes, in which significant field enhancement can be realized upon adsorption of molecules (analytes) on the surface of metal nanostructure. A key component for better results and analysis through this method is the SERS substrate that needs to be equipped with plenty of hotspots as well as metallic-rich and relatively roughened surfaces. Despite a large number of SERS substrates being routinely utilized, there is still room and hence search is continuing for the

dynamic substrates that reveal the extraordinary sensing outcomes. Particle-based SERS substrates based on polymer-metal composite particles in which polymer as support can provide the platform to meet such requirements by systematically depositing metal nanostructures at the surface of polymer particles. The characteristics of the polymers such as biocompatibility, swellability, porosity, transparency, metal loading ability, and high surface area are particularly useful in the formation of the efficient particle-based substrate. Microfluidics is a promising technique for the fabrication of polymer-supported sensor particles of nanoscale and microscale with uniformity because of their advantages over the batch platform. For nanoscale sensor particles, the metal nanoparticles can be incorporated and anchored at the surface of polymer nanoparticles electrostatically in the swellable shell layer, and a ligand-free metal layer can be deposited by a metal-catalyzed metal enforcement process. Here, the development of the polymer-metal composite particles at nanometer and micrometer length scales, and their applications as sensor particles for SERS sensing are presented. Microfluidic techniques were utilized for the generation of uniform sensor particles of micrometer length scale with the precise distribution of metal nanoparticles in the interior and at the surface. Furthermore, metal-catalyzed metal enforcement approaches initiated for achieving a ligand-free metal surface for direct analyte interactions because of the availability of a large number of hotspots in roughened metallic surface, and experimental demonstration of sequential SERS analysis of multiple analytes through microfluidics has been established that is demonstrated in this work.

2:15 PM SB01.12.07

3D Nano-Biohybrid Carbon Nanotube Forest for Cardiac Tissue Engineering Roya Bagheri, Masoud Kasraie, Xinqian Chen, Zhiying Shan and Parisa Abadi; Michigan Technological University, United States

Biohybrid cell-material structures have applications in tissue engineering, disease modeling, biorobotics, etc. Conductive materials, in particular, are useful in applications such as bioelectronics and pacing. The scaffolds that are used for making biohybrid structures have so far been limited to those with low electrical conductivities. Carbon nanotube forests have high electrical conductivity as well as mechanical compliance and stability, which are not offered by other commonly used cell scaffolds. Here, we developed a new 3D biohybrid structure using CNT forests and cardiomyocytes. The CNT Forest was fabricated on a silicon wafer by a chemical vapor deposition technique under atmospheric pressure. The sterilization procedure of CNT forests started with soaking the samples in 70% ethanol, followed by UV light exposure overnight. After sterilization, samples were coated with 1 wt.% gelatin. Physical characterization of the scaffolds was performed by scanning electron microscopy (SEM), four-point probe conductivity measurement, and electrochemical impedance measurement. The cardiomyocytes were isolated from 1-3 day old neonatal rat hearts and cultured on the CNT forest - gelatin scaffold for 19 days. All animal protocols were approved by the Michigan Technological University Institutional Animal Care and Use Committee. The cytocompatibility of the CNT forest - gelatin scaffold was assessed through the live/dead assay on day 2, and PrestoBlue assay on days 2, 8, and 11 from the start of culturing. The performance of cardiomyocytes on the scaffold was investigated using immunofluorescence cardiomyocyte labeling (Alpha actinin and Troponin T) and SEM imaging. The morphology and microstructure of the CNT forest - gelatin scaffolds were studied with SEM imaging. The CNT Forest had wavy and entangled CNTs with an average height of ~200 microns. The SEM images of CNTs before and after coating demonstrated that the CNTs were bent and formed micron-scale islands due to electrocapillary forces produced by gelatin. The electrical characterization of the scaffold showed that the coated CNT scaffold is conductive in liquid, and the impedance decreases due to the presence of gelatin. The live-dead assay indicated 89% viability on day 3 for the CNT forest-gelatin scaffold, which was in the range with the control. The PrestoBlue assay, which quantifies absorbance by dead cells, showed no toxicity for the scaffolds. The SEM images of cardiomyocytes on the scaffold showed the cells were spread and well-adhered to the structure on top and along with the height of CNT forests forming a 3D network. The cells expressed mature cardiomyocyte markers for alpha-actinin (actin-binding proteins cardiac marker) and troponin T (cytoskeletal organization cardiac marker) in fluorescence imaging. The cardiomyocyte cells were well-adhered to the CNT forest-gelatin scaffolds with no sign of toxicity for 11 days of culturing. They formed a 3D network and showed markers of mature cardiomyocytes. Our results indicate that the unique multi-scale structure of the CNT forest scaffolds makes them ideal for a highly conductive scaffold for biohybrid material-cardiomyocyte structures.

2:30 PM SB01.12.08

Engineered Implants with Smart and Sustained Release of Antimicrobial Agents Hessah Alotaibi^{1,2}, Etelka Chung³, Vikaramjeet Singh¹, Guogang Ren³ and Jie Huang¹; ¹University College London, United Kingdom; ²King Faisal University, Saudi Arabia; ³University of Hertfordshire, United Kingdom

Infections caused by microorganisms during implant-mediated tissues regeneration therapy can lead to further complications and ultimate failure of the healing process. Therefore, an implant empowered with controlled and sustained release of antimicrobial agents is highly desired for tissue engineering applications. Here, we present a novel antibacterial film for wound healing applications constructed from metal organic frameworks (MOFs) and polymers for a sustained release of antimicrobial agents. Cyclodextrin metal organic frameworks (CD-MOFs) are embedded into biodegradable and biocompatible polymers, polycaprolactone (PCL) and polyethylene oxide (PEO). The concentration of polymers and MOFs was carefully optimized to obtain a highly flexible and strong film with a thickness of about 500 μm . The γ -CD-MOFs have been extensively exploited for their applications in biomedicine due to the biocompatible nature of its building blocks, i.e. γ -cyclodextrin and potassium ions. CD-MOFs possess two types of highly organised channels, hydrophilic (1.7 nm) pores resulted from CD coordination with potassium and inherent hydrophobic cavities (0.9 nm) of CD itself. However, their real potential in pharmaceutical sector is compromised due to their susceptible nature to water and poor processability of CD-MOF powder. In this work, cavities of CD-MOFs were utilised by *in situ* synthesis of ultra-small silver nanoparticles (AgNPs) with an average size of 2-5 nm. CD-MOFs. The optimised maximum concentration of CD-MOFs in the resulted film is 10% (w/w) with homogenous distribution of CD-MOFs nanoparticles. The CD-MOFs film shows a moisture triggered sustained release of AgNPs for more than 72 hr. The antimicrobial efficacy of the film was tested against *E. Coli*, *S. aureus*, and, and fungi *Candida* using zone of inhibition diameters (ZOI) and the results were 0.87 ± 0.06 , 1 ± 0.1 and 0.97 ± 0.15 cm. The novel CD-MOFs film shows a great potential to be used as an antimicrobial film for the sustained release of antimicrobial agents in biomedical applications.

2:35 PM DISCUSSION TIME

SYMPOSIUM SB02

Symposium Organizers

Liangbing Hu, University of Maryland
Sang-Young Lee, Yonsei University
Yuanyuan Li, KTH Royal Institute of Technology
Orlando Rojas, University of British Columbia

* Invited Paper
+ Distinguished Invited

SESSION SB02.01: Lignocellulose Processing and Understanding I
Session Chairs: Alireza Hajian and Kai Zhang
Monday Morning, November 28, 2022
Hynes, Level 1, Room 109

10:30 AM INTRODUCTORY REMARK

10:45 AM *SB02.01.01

Advanced and Functional Lightweight Composite Components from Nanocellulose [Daniel Soderberg](#); KTH Royal Institute of Technology, Sweden

For almost a decade, significant efforts have been made to fabricate material concepts from nanocellulose, e.g. barriers, films, foams, and fibres (filaments). As a result of combined knowledge of fibre suspension hydrodynamics, fibre technology and nanoscale interactions it has been shown to be possible to spin continuous filaments from a 100% nanocellulose dispersion with good mechanical performance and a possibility for functionalization e.g. conductivity or piezo resistivity. As a continued effort the technology has been further developed to allow scalable manufacturing in larger volumes, which allows research on applications that uses these filaments. Given the nature of the filaments, it is shown that it is possible to achieve components with transparency, mechanical performance and a possibility to serve as a basis for further functionalisation.

11:15 AM SB02.01.02

Solid Biofoams like Wood [Mikko Alava](#), Juha Koivisto, Luisa Jannuzzi, Leevi Viitanen and Tero Mäkinen; Aalto University, Finland

Mimicking natural biological structures allows us to exploit tried design concepts for advanced material solutions. Wood is an example of an interesting natural material to replicate, as it exhibits excellent anisotropic mechanical properties and also performs well as a thermal insulator. We demonstrate a process of creating a cellular structure similar to natural wood -- a solid foam -- from forest-derived bio-constituents (M. Reichler et al., Sci. Reports 11,1 (2021)). As such, the resulting material has anisotropic mechanical properties such as elastic modulus and yield stress and exhibits complex mechanical response similar to natural wood. The heat conductivity is low due to the low density and closed pore structure. This novel paper recyclable material can be used as a substitute for oil-based packaging and insulation foams such as expanded polystyrene or polyurethane.

11:30 AM SB02.01.03

Association of Bacterial Nanocellulose with Fibroin to Develop a Wound Healing Bioproduct [Priscila G. Mazzola](#)¹, Carolina Talarico², Janaina Artem Ataide¹, Norberto Aranha² and Angela F. Jozala²; ¹UNICAMP, Brazil; ²UNISO, Brazil

Bacterial nanocellulose (BC) is an extracellular polysaccharide secreted mainly by bacteria of genera *Gluconacetobacter*. Different from vegetable cellulose, BC is produced in pure form, free from other polymers. Previous studies have already reported the potential of BC in medical applications. A promising and innovative alternative to optimize the benefits attributed to BC would be its association with polymeric composites, such as fibroin; with the aim of overcoming its limitations and increasing the field of its applications. Thus, we aimed the development of bioproduct for healing by associating BC and fibroin (BC-FB). The incorporation of nanocellulose into fibroin was carried out by immersion at 25 °C, followed by its characterization by Fourier transform infrared spectroscopy (FTIR-ATR), scanning electron microscopy (SEM) coupled with energy dispersive spectroscopy (EDS), and mucoadhesion were performed. FTIR-ATR showed the presence of characteristic groups from BNC and fibroin in the final bioproduct, as well in EDS analysis. Based on SEM images, it was possible to note a similarity in formed network between BC and BC-FB, and a reduction in pores in the second sample. During mucoadhesion assay, the force necessary to remove BC-FB was lower than the force for only BC (0.456 N and 0.493 N, respectively). There was also a decrease in the mucoadhesive strength after incorporation of fibroin (from 1.656 N to 1.276 N). Once the structure is essential for materials, the BC-FB membrane could be explored in other research, such as filter membrane or bone regeneration. Additionally, the membrane production by immersion did not use hazardous substances, promoting environmental-friendly practices and reducing costs.

11:45 AM SB02.01.04

Cellulose Functional Materials for Fiber-Based Energy Harvesting and Storage Devices Jose Tiago Carvalho¹, Raquel Barras¹, Rodrigo F. Martins¹, Diana Gaspar² and [Luis Pereira](#)^{2,1}; ¹FCT NOVA, Portugal; ²Almascience Colab, Portugal

Developing sustainable options for energy conversion and storage in textiles is needed to power future wearable "Internet of Things" (IoT) electronics. This process must consider new possible alternatives that address questions of sustainability, reuse, repair, or even a second life application. Herein, we pair stretch-broken carbon fiber yarns (SBCFYs), as current collectors, and an in-situ regenerated cellulose-based ionic hydrogel (RCIHs) as an electrolyte, to fabricate 1D fiber-shaped supercapacitors (FSCs). The areal specific capacitance reaches 433.02 $\mu\text{F cm}^{-2}$ at 5 $\mu\text{A cm}^{-2}$, while the specific energy density is 1.73 $\times 10^{-2}$ $\mu\text{Wh cm}^{-2}$. The maximum achieved specific power density is 5.33 $\times 10^{-1}$ mW cm^{-2} , at 1 mA cm^{-2} . The 1D FSCs possess a long-life cycle, 92 % capacitance retention after 10000 consecutive cyclic voltammetry cycles, higher than similar ones using reference PVA/H₃PO₄ gel electrolyte. We also propose Triboelectric Generator Yarns (TEG yarns) using a new method for depositing PDMS directly onto conductive carbon yarns. The in-situ PDMS curing method described in this study allows the fast formation of a uniform thick coating over conductive surfaces regardless of their roughness. Single-electrode configuration TEG yarns are developed, and their electrical output is optimized by precisely adjusting the PDMS layer thickness and by changing the chemical and physical nature of the SBCFYs surface, reaching a power density of 74.1 $\mu\text{W cm}^{-2}$. We demonstrate that asymmetric electrophoretic deposition of nanocrystalline cellulose films results in increase of 100% of the TEGs electrical output to around 142.7 $\mu\text{W cm}^{-2}$.

SESSION SB02.02: Lignocellulose Processing and Understanding II
Session Chairs: Mahiar Hamed and Amir Sheikhi
Monday Afternoon, November 28, 2022
Hynes, Level 1, Room 109

1:30 PM *SB02.02.01

Nanopolysaccharide Interaction with Bacteria—Effect of Surface Functionality Aji Mathew, Andrea A. Sanchez, Jing Li and Edouard Pesquet; Stockholm University, Sweden

The interaction between different nanopolysaccharides and *E. coli* was evaluated by exposing *E. coli* to cellulose nanocrystals (CNC), TEMPO-oxidized cellulose nanofibrils (T-CNF) and ligno-cellulose nanocrystals (L-CNC). The observations of the bacteria cultures showed that none of the films had a cytotoxic effect over the *E. coli* when in indirect contact. Nevertheless, T-CNF and L-CNC, showed cytostatic effect on the growth of the cells, with T-CNF being the most prominent. The nanomechanical properties and interacting forces between the nanopolysaccharide film surfaces and the *E. coli* were studied using in situ PeakForce quantitative nanomechanical mapping (PFQNM). The PFQNM results demonstrated that the different types of nanopolysaccharides affect in site selectivity of the films against cell adhesion, and that all the studied samples altered the nanomechanical properties of cell envelopes in different ways. The surface morphology of *E. coli* cells was affected when in direct contact with the nanopolysaccharide films during incubation, except for *E. coli* cells attached to the CNC films. For all the cases, a stiffening effect was observed on the cell walls (based on the DMT modulus) after exposure to the nanopolysaccharide surfaces; being lowest for CNC compared to T-CNF and L-CNC. It was not possible to determine any obvious effect on the bacterial cells exposed to CNC films, but in the case of T-CNF and L-CNC substantially decreased cell growth and reduced the adhesion force, corroborating the great potential as antibiofouling material and capacity to interact with cytoplasm leading to cell leakage and possibly cell death. Overall, these studies pave the path for understanding how different types of nanocellulose and nanochitin can be used to tailor bacterial inhibition/proliferation properties on different materials.

2:00 PM SB02.02.02

The Interaction Between CO₂ and NaOH-Dissolved Cellulose as a Potential in Cellulose Technology Aleksandra M. Kozlowski and Merima Hasani; Chalmers University of Technology, Sweden

The growing awareness of consumers, governments, and industries on their influence on the environment generated the world trend to search for solutions to mitigating climate change. Perhaps the most popular subject refers to carbon dioxide capture and applications of green resources for this reason. From the perspective of renewable and sustainable materials, it is hard to think about better candidates than biopolymers. Over the past few years, a lot of attention has been given to understanding the mechanism of action between various saccharides and CO₂; yet the most abundant of them all, cellulose, remained in the shadow of investigations. The reason behind this low interest could be the perception of cellulose as a difficult to process, with applications more related to the paper, textile, or packaging industry. However, in our study, we present that cellulose exhibit a strong affinity for alkali-dissolved CO₂ that leads to coagulation of polymer and formation of novel material with a perspective for industrial applications. Here, we take the control over the gas delivery and conclusively study the effect of CO₂ on cellulose dissolved in NaOH at two different temperatures (25 and 5 °C). The *in-situ* analysis gives an insight to carbonation (cellulose vs inorganic species), changes in temperature and pH. It allows hypothesising on the initial mechanism of interaction between cellulose and CO₂ that results in polymer coagulant. Furthermore, the created coagulants, analysed from the perspective of structural and crystallinity changes, prove competitive to alcohol precipitates. This opens for the employment of CO₂ in the process of cellulose regeneration. Our findings are presented with the implication for cellulose processability, in the context of cellulose derivatives and regenerated fibres production, as well as effective exploitation of CO₂ gas.

2:15 PM SB02.02.03

Targeted Functional Methylcellulose-Nanocomposite Materials via Self-Limiting Electrospray Deposition Michael Grzenda¹, Maria Atzampou¹, Jonathan M. Blisko², Rachel Vladimirovsky¹, Kelly Hughes¹, Christopher E. Shuck³, Xin Yong², Jeffrey Zahn¹ and Jonathan P. Singer¹; ¹Rutgers, the State University of New Jersey, United States; ²Binghamton University, The State University of New York, United States; ³Drexel University, United States

Electrospray deposition (ESD) uses strong electric fields to produce generations of monodisperse droplets from solutions/dispersions that are driven towards grounded targets. Self-limiting electrospray deposition (SLED) is a phenomenon recently discovered by our group in which targeted, 3D coatings can be achieved by spraying insulating polymers below their glass transition temperatures, which trap charge and repel incoming spray droplets. Recent work from our group has shown that methylcellulose (MC) exhibits self-limiting behavior when sprayed from water/ethanol solutions and is also capable of forming nanowire morphologies. This unique spray regime is an intermediate between the electrospinning of wire mats and particle sprays. As part of this prior work, it was demonstrated that because MC forms fibril gels, the shear of spray leads to shear thickening and homogenous gelation of the MC that allows for nanowire particles to form, eventually forming a forest as deposition continues. However, when conductive particles are added to SLED sprays, the buildup of charge required to repel incoming material becomes disrupted as particle loading increases. As would be expected, this relationship is not dependent solely on concentration. Here, we are able to show that an interaction exists between particle morphology and the formation of the MC nanowire in composite sprays. While larger spherical particles, 200 nm and above, will disrupt nanowire formation, smaller particles, 50 nm and below, become incorporated in the nanowire. Furthermore, the concentration of smaller particles changes the length of the nanowire. We take advantage of these phenomena to use MC nanowires to prevent and reduce the percolation of conductive particles during spray which allows for highly controlled deposition. For conductive particles, we use 2D Ti₃C₂ MXene of two different sizes as well as spherical ITO which all have similar sheet resistances. To quantify the growth of these materials and examine the dynamic interaction of composition, particle properties, and feature geometry, photolithography patterned chips with gratings of varying widths and spacings were designed. These chips were sprayed with composite materials of varying concentration, and the widths of the features after spray were measured. Scanning electron microscopy shows these deposited materials are able to maintain unique low-density morphologies. Using these findings, it was possible to design highly controlled, optimally loaded, functional targeted sprays of MC containing either MXene or ITO. As a demonstration, MXene containing spray was used to functionalize interdigitated electrodes with features and spacings as low as 50 microns and a substantial increase in capacitance was measured. Upgraded patterns on polyimide substrates demonstrate the compatibility of this process with flexible electronics.

2:30 PM SB02.02.04

Elucidating Emergent Properties of Lignocellulosic Biopolymer Assemblies Through Macromolecular Modeling Peter Ciesielski, Lintao Bu, Meagan Crowley, Vivek Bharadwaj, Bennett Addison, Braden Pierce, Yannick Bomble and Michael Crowley; National Renewable Energy Laboratory,

United States

Lignocellulosic materials are a class an incredibly complex, highly diverse, and multifunctional polymer nanocomposites. Even within a cell wall, the biopolymer structure and composition vary locally to provide different properties and functionalities to each tissue type. For example, the secondary cell walls found in xylem tissue contain large bundles elementary cellulose fibrils, decorated with hemicellulose and lignin, to impart mechanical integrity. In contrast, the compound middle lamella found between adjoining cells contains little or no cellulose but is rich in lignin and pectin to provide adhesive properties. Aside from differing biopolymer compositions, modifications to monomer composition (such as the ratio of syringyl to guaiacyl units in lignin) and backbone decoration (such as acetylation of xylan) are also used by plants to impart specialized functionality to lignocellulosic assemblies. Furthermore, process-induced modification, such as lignin extraction and enzymatic hydrolysis, impart additional changes that alter the properties of the material. In this presentation, I will overview molecular modeling methods used by our group to identify structure/property/function relationships in lignocellulosic biopolymer assemblies. First, I will describe the construction of macromolecular models of secondary cell walls containing cellulose, hemicellulose, and lignin using best available experimental data to assign their spatial proximity and nanoscale arrangement. Variations of these models are employed in simulations of mechanical deformation to investigate the impacts of polymer composition and macromolecular architecture. We find that alterations in lignin monomer ratio impacts mechanical moduli and propensity to form defects in cellulose fibrils during mechanical deformation. Next, I will present our recent molecular models for the compound middle lamella tissue, which has been identified as the primary location of failure during chemo-mechanical deconstruction. Variations in biopolymer composition and moisture content produce large changes in the mechanical properties of this tissue type, which have practical implications for biorefining and bio-based material design strategies.

2:45 PM SB02.02.05

Tunable Hydrogels of Cellulose Nanocrystals Cross-Linked with Water Soluble Polysaccharides [Teemu Suutari](#)¹, Ville Rissanen², Suvi Arola², Tekla Tammelin² and Eero Kontturi¹; ¹Aalto University, Finland; ²VTT Technical Research Centre of Finland Ltd, Finland

Hydrogels based on nanosized cellulose have potential in a wide range of different applications. Often, cellulose nanofibers (CNFs) are used for hydrogel preparation, as the highly flexible CNF fibrils have an inherent tendency to entangle, forming gels already at very low concentrations. Cellulose nanocrystals (CNCs), on the other hand, are highly crystalline structures and as such do not exhibit similar gelling properties and are therefore utilized in hydrogels to lesser extent. However, the gelling property can be a limiting factor for easy CNF manipulation, while the more fluid-like CNC can be utilized at broader concentration ranges, allowing hydrogel tunability at much wider parameter space.

In this work we have investigated different water-soluble polysaccharides in their ability to function as cross-linkers and facilitate CNC hydrogel formation. For this, we have tested 15 different water-soluble polysaccharides, such as xanthan, hydroxypropyl cellulose, carboxymethyl cellulose (CMC), hydroxyethyl cellulose (HEC) xylan, guar, and three types of mixed linkage glucans (MLGs), among others. CNCs from different sources were used, including bacterial cellulose and cellulose from bleached softwood pulp both treated with HCl gas hydrolysis and 2,2,6,6-tetramethylpiperidine-1-oxyl (TEMPO) radical-mediated oxidation. The CNCs and polysaccharides were mixed at different ratios and the performance of the formed hydrogels were tested in their rheological properties and their porosity was investigated using thermoporosimetry.

One possible application for hydrogels includes immobilization of photosynthetic cells. Photosynthetic cells can be utilized as a renewable, sustainable, and economical method for biofuel, food, and medicinal compounds production. Thus far, these cell factories have been mostly maintained in suspension cultures. For improved efficacy of light utilization, energy loss and water consumption, cells can be immobilized in different structures, such as alginate. However, capturing cells in these structures can inhibit the transfer of substrates and the produced chemicals, while still facilitating undesired cell division. Hydrogels made from nanocellulose offer a great alternative for cell immobilization, as cellulose is abundantly available, biocompatible, and biodegradable. Also, nanocellulose hydrogels provide controllable transparency, good gas barrier properties and can be tuned in their permeability and wet strength. Furthermore, they offer good mechanical stability and high porosity, both which are beneficial for a long-term cell survival and efficient production of desired chemicals. Therefore, the prepared nanocellulose hydrogels were evaluated in their suitability for cellular immobilization, biocompatibility, and long-term cell viability by entrapping a wild-type cyanobacterial strain *Synechocystis* sp. PCC6803 within the gels and monitoring the long-term photosynthetic activity. The most promising cross-linkers in terms of good hydrogel formation, mechanical properties, biocompatibility, and long-term cyanobacteria performance were found out to be HEC, CMC, and all three MLGs.

To further finetune the properties and to optimize the hydrogel performance, the fundamental interactions of the hydrogel components were studied using a CNC model films in surface plasmon resonance and quartz crystal microbalance. These interaction studies revealed that e.g., the binding of MLGs on CNCs was concentration dependent, but the extent of binding was not affected by the molecular weight of MLG, implying that any MLG type is suitable for robust construction of hydrogels from CNCs. The polysaccharide-CNC thin films were further characterized using atomic force microscopy and ellipsometry.

3:00 PM BREAK

3:30 PM DISCUSSION TIME

4:00 PM SB02.02.07

Studying Wood-Water Relationships with Molecular Dynamics—How Far We Are Now? [Dominique Derome](#)¹, Wenqiang Liu¹, Ali Shomali², Chi Zhang², Benoit Coasne³ and Jan Carmeliet²; ¹Université de Sherbrooke, Canada; ²ETH Zurich, Switzerland; ³Univ Grenoble Alpes, France

Wood is an orthotropic cellular biomaterial. As a plant and as a building material, water impacts the behavior of wood. Wood is also a hierarchical material. At the base of this hierarchy lies the cell wall material. As water molecules are adsorbed by the hydrophilic matrix that make up the cell walls, the induced fluid-solid interaction forces result in swelling of these cell walls. Thus, this process, at the origin of wood-moisture relationships, lies at the nanoporous material scale.

The layer S2 of the wood cell wall is actually a composite polymeric material. Stiff crystalline cellulose bundles to form fibrils that are embedded by a profoundly organized matrix of different hemicelluloses, galactoglucomannan and glucuronoarabinoxylan, and of two states of guaiacyl lignin, non-condensed and condensed, considering here coniferous species. We have reproduced these assemblies and subjected them to different in-silico experiments. Using grand canonical Monte-Carlo and molecular dynamics, we have obtained adsorption and desorption isotherms of different polymeric systems. Water is known to rearrange the internal structure of the material of the S2 cell wall. The in-silico systems obtained at different moisture content can be probed to provide insights on the extent of this rearrangement in terms of configuration and in terms on its influence on the physical properties of the material.

Atomistic simulations used to mimic water adsorption and desorption in amorphous polymers, allow observations on mechanical behavior like swelling and shrinking, mechanical softening in compression and shear, and on the stick-slip behavior of the stiff fibrils pulled out of the matrix. We observed

hysteresis not only in water sorption but also in mechanical properties. This hygro-mechanical behavior can also be observed in particular from the breaking and reforming of hydrogen bonds.

Atomistic modeling is an insightful tool for the in-depth study of the coupled effects of water sorption on hygro and mechanical properties of different polymeric components. Molecular modeling can contribute to support and complement experimental methods which yield, most frequently, indirect structural information. With molecular modeling, there is a freedom of investigating unlimited possibilities of configurations, ranging from individual wood polymer materials to composite structure resembling subunits of wood S2 cell wall. This presentation will cover recent methodological developments towards good practices for such simulations and the recent insights on wood cell wall S2 layer hygro-mechanical behavior.

4:15 PM SB02.02.08

Examining the Development of Secondary Cell Walls in Arabidopsis Inflorescence Stem Using Hard and Soft X-Ray Scattering Joshua T. Del Mundo¹, Sarah Pfaff¹, Liza Wilson¹, Masoud Ghasemi¹, Guillaume Freychet², Mikhail Zhernenkov², Eliot Gann³, Daniel Cosgrove¹, Esther Gomez^{1,1} and Enrique Gomez^{1,1,1}; ¹The Pennsylvania State University, United States; ²Brookhaven National Laboratory, United States; ³National Institute of Standards and Technology, United States

The durable secondary cell wall gives vascular plants the structural foundation needed to grow upwards. Fundamental research of the synthesis and material properties of secondary cell wall is the first step to developing new bio-derived materials and the utilization of lignocellulosic biomass as a renewable energy source. It is a composite material composed of cellulose microfibrils, hemicellulose, and lignin. The process of how these components come together to form the secondary cell wall in the plant is currently poorly understood. To track the development of secondary cell wall formation at different stages, we use the base of *Arabidopsis thaliana* inflorescence stems harvested at different heights. The total inflorescence stem height is proportional to the progress of secondary cell wall development in the interfascicular fiber (IFF) cells in the stem base. At lower stem heights (5 cm), we see little secondary cell wall in the IFFs and at higher stem heights (34 cm), we see full lignification of IFFs. Small-angle X-ray scattering (SAXS) tracks the changes in cellulose microfibril spacing and microfibril angle distribution. Wide-angle X-ray scattering (WAXS) tracks the relative crystalline cellulose content, chain packing, and coherence length. To investigate the effects of the content and structure of xylan, a principal hemicellulose, on secondary cell wall formation, we examined the stems of *irx14* mutants. We found that compared to the wild type, the *irx14* mutants had altered cellulose microfibril angle distribution and coherence length, but not individual cellulose chain packing distribution. To determine the spacing of lignin domains in secondary cell wall, we applied resonant soft X-ray scattering (RSOXS). Lignin is unique from other cell wall components in that it is highly aromatic, to which the secondary cell wall owes its hydrophobicity and resistance to degradation. RSOXS probes the sample with an X-ray beam tuned around the carbon absorption edge, increasing the contrast between lignin and other cell wall components without the need for labelling. At energies where the contrast between cellulose and lignin is enhanced, we see a broad nanometer-scale feature at high stem height, but not low stem height.

4:30 PM SB02.02.10

Cellulose-Based Biosensing Platforms—Fabrication and Detection Strategies Rodrigo F. Martins^{1,2} and Elvira Fortunato^{1,2}; ¹FCT UNL, Portugal; ²UNINOVA, Portugal

The development of accurate, reliable, and inexpensive analytical platforms is of utmost relevance to several fields from clinical diagnosis to environmental screening. Moreover, the use of inexpensive materials and cost-effective manufacturing processes for production of such devices is very attractive and must be aligned with the European Green Deal and the United Nation's Sustainable Development Goals. In that sense, cellulosic materials are appealing candidates to be used as low-cost disposable materials for biosensing platforms, with great emphasis in point-of-care (POC) settings, particularly in resource-poor countries. Here, we show the use of cellulose-based substrates with both passive and active roles in biosensing platforms allied with cost-effective, energy-efficient and scalable fabrication routes. These biosensors were developed with both optical and electrochemical mechanisms, due to their meritorious ability to offer high selectivity and sensitivity, ease of fabrication and usage, easy miniaturization, low cost and versatility. Specifically, we present examples of (i) cellulose-based colourimetric biosensors using wax printing technology combined with colourimetric detection using both natural and biomimetic receptors for a multitude of applications, ranging from bacteria detection to diabetes control [1]; (ii) cellulose-based Surface-Enhanced Raman Scattering platforms, produced using both physical and chemical routes, for the detection of antibiotics, cancer biomarkers and spike protein from SARS-CoV-2 virus, where the influence of different types of cellulosic materials is demonstrated [2,3,4]; (iii) cellulose-based electrochemical biosensors, using laser-induced graphene electrodes with tailored conductive and electrochemical properties, applied for amperometric, enzymatic biosensing schemes for glucose detection and with potential for sensing of other metabolites [5]. In conclusion, the biosensing concepts explored herein pave the way toward developing robust analytical devices with the potential to be integrated with stand-alone multifunctional platforms to be used in POC settings.

[1] Pinheiro, T., et al, ACS Appl. Mater. Interfaces, 13, 2021.

[2] Marques, A.C., et al, Scientific Reports, 9, 2019.

[3] Ferreira, N. et al, ACS Sensors, 4, 2019.

[4] Marques, A.C., et al, Applied Surface Science, 561, 2021.

[5] Pinheiro, T., et al, Adv. Mater. Interfaces, 8, 2021.

National funds from FCT financed this work - Fundação para a Ciência e a Tecnologia, I.P., in the scope of the projects LA/P/0037/2020, UIDP/50025/2020 UIDB/50025/2020 of the Associate Laboratory Institute of Nanostructures, Nanomodelling and Nanofabrication – i3N. The authors also acknowledge funding from the European Research Council (ERC) ref 787410 -DIGISMART and from BEST project, ALT20-03-0247-FEDER-113469/LISBOA-01-0247-FEDER-113469. T. P. also acknowledge the funding from National Foundation for Science and Technology, through the PhD Grant 2020.08606.BD.

SESSION SB02.03: Poster Session: Lignocellulose
Session Chairs: Alireza Hajian and Yuanyuan Li
Monday Afternoon, November 28, 2022
8:00 PM - 10:00 PM
Hynes, Level 1, Hall A

SB02.03.01

Physical Properties of Polypropylene Plastic Resins Composite with Natural Derived Cellulose Fibers Mikyung Kim and Songhyun Yoon; DYETEC

Institute, Korea (the Republic of)

Recently, an eco-friendly industry that is carbon-neutral has become important, and active application of eco-friendly materials with increased biomass content is required for plastic products applied to automobiles. As eco-friendly materials for automobiles, plastic composites using natural fibers such as wood powder, kenaf, and hemp as reinforcing materials are being applied as interior materials for automobiles such as door trims. However, wood powder or plant fiber combined in plastic resin as a reinforcing material for improving biomass content and improving plastic properties contains impurities such as sugar, pectin, and hemicellulose in addition to cellulose components, which may cause unique odor problems and durability degradation.

This research attempted to apply regenerated cellulose fibers such as tencel and rayon, which are generally used in the textile industry, as a plastic resin reinforcement for automobiles. Since the regenerated cellulose fiber is a purified cellulose fiber in which impurities have been removed in a manufacturing process, it was determined that the application to a plastic composite is better than plant fibers such as wood powder, kenaf, and hemp. Therefore, in order to improve the biomass content of automotive plastic materials and the durable properties of plastic composites, mixing and composite properties with polypropylene resin were investigated using naturally derived regenerated cellulose fibers such as tencel and rayon. Tencel and rayon fibers are cellulose-based fibers and are hydrophilic, so their compatibility with industrial resins such as polypropylene is low. In this work, by silanizing and surface modification of the regenerated cellulose fiber to impart hydrophobic properties, compatibility with the polypropylene resin is improved and the physical properties of the composite are expected.

SB02.03.02

Hydrogel Supercapacitor Fabricated by Lignin-Mediated Laser-Induced Graphitization Rikuto Miyakoshi, Shuichiro Hayashi and Mitsuhiro Terakawa; Keio University, Japan

Supercapacitors have drawn remarkable attention among energy storage devices due to their fast storage capability and enhanced cyclic stability. Hydrogels are one of the promising materials to be used for supercapacitors since they can easily absorb and retain liquid electrolytes. If conductive structures can be directly patterned on hydrogels, the hydrogel can fulfill both roles as an electrolyte retainer and supporting material. Laser-induced graphitization is a compelling technique to directly pattern electrically conductive graphitic carbon on a polymer by simply irradiating a laser beam. To the best of our knowledge, the one-step fabrication of electrically conductive structures on hydrogels by laser-induced graphitization has yet to be demonstrated. In this study, we demonstrated the direct fabrication of electrically conductive graphitic structures on hydrogels by laser-induced graphitization using lignin. Agarose hydrogel containing lignin, both biomass materials, were chosen as a precursor material for realizing the fabrication of a fully-biomass supercapacitor. The irradiation of 522-nm femtosecond laser pulses modified the surface of the hydrogel to a visibly-black colored structure that exhibit electrical conductivity. The Raman spectrum obtained from the structure showed peaks that correspond to D, G, and 2D bands, suggesting the formation of graphitic carbon. The fabricated structures exhibited a higher conductivity for higher lignin concentrations. No visible modification was observed after laser irradiation when no lignin was added to the agarose hydrogel. It should be noted that lignin is an organic material that exhibits high optical absorbance of 522-nm light. Therefore, the addition of lignin into the agarose hydrogel increases the absorbed energy, as well as the carbon content, which may lead to the facilitation of graphitization. To investigate the capability of the fabricated structures for supercapacitors, a pair of structures to be used as electrodes were fabricated on agarose/lignin hydrogels containing NaCl. Capacitance behavior was confirmed from the structures, demonstrating the one-stepped fabrication of hydrogel-based supercapacitors. The prepared hydrogel acts as the electrolyte retainer and supporting material of the fabricated supercapacitor. The proposed method offers a facile fabrication of a hydrogel-based supercapacitor.

SB02.03.03

Vertical Integration of Multi-Electrodes into a Single Sheet Of Paper and the Control of the Equivalent Circuit for a High-Density Flexible Supercapacitor Yeon Woo Kim, In Hyeok Oh, Jung Hyeon Jin, Seung Deok Seo and Suk Tai Chang; Chung-Ang University, Korea (the Republic of)

Paper is an excellent substrate for flexible devices due to its various advantages such as flexibility, porosity, lightness, thinness, and low cost. Its inherent characteristics can be also exploited to overcome the limitations of conventional substrates, such as weak adhesion and large mass densities. Here, we propose a facile method for fabricating vertically integrated multi-electrodes into only a single sheet of paper. Despite the randomly distributed fibrous networks in a paper, the multi-layered electrodes were uniformly formed and completely separated by applying a removable hydrophobic wax barrier confinement inside a single sheet of paper. The integrated multi-layer electrodes can be used as ultra-thin supercapacitor paper with flexible circuit diversion. Using multi-layered electrodes, we demonstrated the control of the equivalent circuits in the supercapacitor paper by simply changing the contact pad grounding. By changing the circuit structures, the multi-layer electrodes exhibited excellent electrochemical properties without device volume changes and additional components. The single incorporated electrode inside the paper with electrodeposited MnO_2 exhibited a high areal capacitance of 711 mF cm^{-2} . Moreover, the single sheet of supercapacitor paper with integrated multi-electrodes exhibited greater energy and power densities than a single electrode with the same area by factors of 3.8 and 1.75, respectively, based on the control of the equivalent circuit.

This research was funded and conducted under the Competency Development Program for Industry Specialists of the Korean Ministry of Trade, Industry and Energy(MOTIE), operated by Korea Institute for Advancement of Technology (KIAT). (No. P0012453, Next-generation Display Expert Training project for Innovation Process and Equipment, Materials Engineers), and supported by a National Research Foundation of Korea (NRF) grant funded by the Korean government (MSIT) (2022R1A2C1005739)

SB02.03.04

Reinforced Ferromagnetic Properties in $\text{CNC@CoFe}_2\text{O}_4/\text{P(VDF-TrFE)}$ Nanofiber Composites for Magnetic Energy Harvester Su-Chul Yang and Manseong Song; Dong-A University, Korea (the Republic of)

After the fourth industrial revolution, the worldwide commercialization of electronic devices has been proceeding. According to the rising demand for electronic devices, demands for energy sources have also been increasing. To satisfy it, energy harvesters which can scavenge energy from ambient circumstances have been developed. Despite the diverse ways to convert energy obtained from the environment to a practical energy source, there are several limits to its application into daily life. The energy harvesters working under contact mode, in particular, would be exposed by performance degradation due to the continued contact or restricted in specific areas where the physical contact is not permitted. In this respect, the issues mentioned above could be solved by introducing the magneto-mechano-electric (MME) materials. The MME effect is defined as the electrical polarization in the ferroelectric piezoelectric (FP) phase induced by strain originated from physically adjacent ferromagnetic magnetostrictive (FM) phase under external magnetic field, and it is basically based on the non-contact mode. When it comes to polymer-based MME composites, representatively, it has been drawn attention from many research groups because of its advantages including generated voltage which is sufficient enough to operate the low voltage device, high cost-efficiency, and versatility of applicable structure due to the high flexibility. The reported method in general to achieve high output voltage from this type of MME composites so far was the surface or composition modification for FM phase material which is responsible for stress causing the polarization of the FP phase. Many researchers have tried to treat the FM phase materials by adding a coating agent to control the morphological character or regulating the chemical composition via post-treatment. In consequence, the overall process was getting longer due to the additional treatment, moreover, the ferromagnetism related to MME properties in direct, fundamentally, was diminished ascribed to the lower actual weight fraction of FM

phase compared to the pure state.

In this research, the new way to reinforce the ferromagnetism, which is in proportional to MME properties, in magnetic filler was suggested. To be specific, the cellulose nanocrystal(CNC) was incorporated into the reaction for the synthesis of the CNC@CoFe₂O₄(CFO) nano hybrid filler. The prepared fillers exhibit higher overall ferromagnetic properties including maximal saturation magnetization (M_s) of 71.8 emu/g and remnant magnetization (M_r) of 32.9 emu/g increased by 22.5% and 24.2%, respectively, in comparison with conventionally synthesized pure CFO nanoparticles even without any further treatment. To interpret the origin of the results, the morphological, surface chemical structural, crystallographic, and ferromagnetic analysis were performed. Through the investigation, it was found that the reinforced magnetic properties were largely due to the expanded crystallite size attributed to the nucleation site provided by introduction of CNC. Thereafter, to investigate the influence from reinforced ferromagnetism of hybrid fillers to the MME properties in composites, the CNC@CFO/P(VDF-TrFE) nanofiber composites was designed. It was observed that the ferromagnetism in composites with hybrid filler was enhanced, manifesting M_s of 4.17 emu/g and M_r of 2.03 emu/g increased by 36.8% and 51.5%, respectively, compared to composites prepared with equal contents of CFO without CNC. Finally, the MME composites were subjected under cyclic magnetic driven voltage measurement based on the bending motion. As a result, it was confirmed that the output voltage generated from the MME composites with CNC was 219.7 mV which is as higher as 72% than the composites prepared without CNC. On the basis of these results, it was concluded that the prepared MME composites with CNC are of the potential for non-contact energy harvesting application.

SB02.03.05

Photocatalytic Degradation of Lignin Model Compounds Using 2D-MoO₃/Noble Metal Nanoparticles Hybrid Nanostructures [Jihoon Park](#) and Youngsoo Kim; Yeungnam University, Korea (the Republic of)

Hybrid nanostructures that consist of two-dimensional nanomaterials and plasmonic nanoparticles have been receiving great interest in the academic and industrial fields. The hybrid nanostructures exhibit unique optical characteristics in combination with the physicochemical properties of 2D nanomaterial and the plasmonic optical effects. Thus, hybrid nanostructures have been widely investigated for optical sensors, solar cells, and electronic devices. In addition, the 2D/plasmonic nanoparticles hybrid nanostructures enable improved photocatalytic performance owing to enhanced charge carrier generation and efficient charge transfer. Lignin, which is a natural bio-polymer, is composed of a number of aromatic rings with diverse functional groups such as carbonyl, hydroxy, and methoxy groups. Therefore, it can be expected that the efficient decomposition of lignin is able to alternate various polymeric materials that came from fossil fuels. In this research, we employed MoO₃/metal nanoparticle hybrid nanostructure to drive photocatalytic degradation of the lignin model compound. We prepared a hybrid nanostructure through the exfoliation of bulk MoO₃ and photoelectrochemical deposition of noble metal nanoparticles such as Au, Ag, Pd, and Pt on the exfoliated MoO₃ nanosheet. Furthermore, we compared the photocatalytic degradation efficiency of the lignin compound with respect to the type of metal nanoparticles and performed a mechanism study of the degradation. The hybrid nanostructures were characterized by UV-Vis spectrophotometer, TEM, and XRD. As well as, qualitative and quantitative analyses for the lignin compound and the products after degradation were carried out using UV-Vis spectrophotometer, HPLC, and NMR.

SB02.03.06

Bouligand Multilayers—Artificially Constructed Cellulose Nanocrystals Chiral Films [Daria Bukharina](#), Lindsay Southard, Saewon Kang, Peng Min and Vladimir Tsukruk; Georgia Institute of Technology, United States

Natural photonic crystals, such as cellulose nanocrystals, have the ability to self-assemble into complex hierarchical structures, however, because of the homochirality in nature they can only assemble into left-handed chiral structures. Here, we will demonstrate bottom-up approach to assemble cellulose nanocrystals thin films of both handednesses. First, we assembled linearly oriented CNC monolayer via shear-induced alignment. Then, artificial chiral Bouligand nanostructures were constructed via Layer-by-Layer (LbL) deposition technique by depositing each next layer in clockwise and counter-clockwise fashion rotating the substrate at a fixed angle. The chiroptical properties measurements of the obtained thin films resulted in mirror-imaged circular dichroism (CD) spectra, indicating successful construction of both left- and right-handed CNC films. Those chiroptical properties and films' anisotropy will be controlled by changing the rotation angle and the number of deposited layers, i.e., film's thickness. Our fabrication strategy has several advantages. First, doctor blade deposition technique allows to produce large-area films. Second, LbL deposition guarantees precise control of the rotation angle and direction. Atomic force microscopy will confirm the alignment of the monolayers deposited, as well as their thickness in conjunction with ellipsometry. CD and UV-vis studies will reveal chiral optical activity of the deposited films. Lastly, effectiveness of artificially obtained chiral photonic CNC films will be confirmed by the g-factor, dimensionless factor characterizing the efficiency of the light-passing-through-the-film polarization and will be presented. Such control of the CD response with respect to the peak sign, position and intensity is unique for CNC films.

SB02.03.07

Wood-Derived Lignocellulosic Nanofibrils Based Triboelectric Nanogenerator for Electronic Integration [Asif Abdullah Khan](#)¹, [Md. Masud Rana](#)¹, [Nicolas R Tanguy](#)², [Xiao Zhang](#)², [Nicole Tratnik](#)², [Heyu Chen](#)², [Dayan Ban](#)¹ and [Ning Yan](#)²; ¹University of Waterloo, Canada; ²University of Toronto, Canada

Triboelectric nanogenerators (TENGs) are a transformative energy harvesting technology owing to their high-power output, simple architecture, small size, and low cost. They are highly promising to provide embedded powering capabilities to next-generation of disposable wearable electronics (i.e. as part of glasses, shoes, or fabrics) that are completely autonomous. TENGs generate electrical energy by harvesting chaotic and low frequency mechanical energy from environmental or human motions (i.e. waves, wind, walking, running) through the coupling of triboelectric effect and electrostatic induction. To date, PTFE and other fluorinated polymers accounted for negative tribolayers in more than 50% of reported TENGs in the literature. However, there are growing global interests in replacing petroleum-based non-biodegradable plastics by green natural materials to attain a higher sustainability and a lower environmental impact. As a result, (ligno)cellulose, ubiquitous as a low-cost, renewable, biocompatible, and biodegradable material, has attracted significant attentions. Previous studies demonstrated the potential of using renewable lignocellulosic materials as the tribopositive layer replacing other common tribopositive substrates (such as metals, metal oxides, and petroleum-based polymers). Here, we report the discovery of a natural tribonegative material, LCNFs, wherein the lignin bound on the surface of the cellulose nanofibrils possess strong tribonegative properties by acting as an electron-withdrawing component. Specifically, we demonstrated that LCNF nanopaper performed as a highly tribonegative layer in TENGs, outperforming PTFE and conventional petroleum-based plastic tribonegative materials. When LCNF nanopaper was combined as a tribonegative layer with aluminum as a tribopositive one in a zigzag structure to form a cascade type of TENG, it could be used as a power source to run a wireless communication node, which had never been achieved before by any reported TENGs containing a natural material as the tribonegative layer. Our results illustrated the excellent promise of using lignocellulosic materials as green alternatives to fluorine-containing polymers in high power output TENGs for developing green self-powering wireless disposable electronics. We report for the first time a natural wood-derived lignocellulosic nanofibrils (LCNF) tribolayer that could replace fluorine-containing petroleum-based polymers as a tribonegative material for TENGs. The high tribonegativity was due to the presence of natural lignin on the surface of LCNF. The LCNF nanopaper-based TENGs produced significantly higher voltage (~160%) and current (~120%) than TENGs with PTFE as the tribonegative material when paired with various polymeric/metallic tribolayers. Furthermore, assembling LCNF nanopaper tribolayer into a cascade TENG generated an output sufficient for powering a wireless communication node, capable of sending a radio-frequency signal to a smartphone every 3 minutes. This study demonstrates the excellent promises of using LCNF to make high-

performance and more environmentally friendly wireless self-powered electronics; and thus pinpoints a new approach for fabricating sustainable triboelectric nanogenerators using natural lignocellulosic materials instead of conventional fluorine-containing petroleum-based polymers as

SB02.03.08

Edible, Strong and Water-Repellent of Bacterial Cellulose by Biosynthesis/Physical Modification and Its Potential Application on Food Packaging Ka Man Cheung and To Ngai; The Chinese University of Hong Kong, China

The ubiquitous petrochemical-based plastics have caused serious waste pollution in the environment. In the last few decades, scientists have tried to exploit a variety of degradable bio-based polymers to replace plastics and take effort for improving their properties. Bacterial cellulose (BC) has been a spotlight on food packaging, including green route of biosynthesis, low energy purification process and high quality of product with strong mechanical properties¹. However, the high hygroscopicity of such material becomes its major obstacle to be used as food packaging.

Herein, a new strategy for fabricating the edible, strong, translucent, water-repellent, and biodegradable BC-based composite packaging was proposed via biosynthesis, with the help of organic-biobased additive in the culture medium and the alginate-polyol composite as the physical coating. After the modification, a completely edible, non-toxic film with steady, strong mechanical properties in both dry and humid environments can be achieved, further displaying the advancement including large-scale production and simple reaction with low energy-efficient process. All in all, this composite material demonstrates a high potential in contributing to a more environmentally friendly kind of food packaging material and reduces the reliance on the use of plastics.

Reference:

Azeredo, H. M. C., Barud, H., Farinas, C. S., Vasconcellos, V. M., & Claro, A. M. (2019). *Frontiers in Sustainable Food Systems*, 3.

SB02.03.10

Low Poisson's Ratio Stretchable Films Prepared by Hydrogel Temperature Responsiveness Jisu Shin and Jonghwi Lee; Chung-Ang University, Korea (the Republic of)

In the research on stretchable films such as wearable display elements or sensors that can be attached to the skin, shrinkage of the film width due to the positive Poisson's ratio has been a problem. Recently, research on auxetic structures with negative Poisson's ratio is being conducted as a solution, but there are limitations in the application because it is 3D-printing structure form which is not a film. Herein, we conducted a study on a film with a low Poisson's ratio by using cellulose nanocrystal (CNC), poly(N-isopropylacrylamide) (PNIPAm), and hydroxypropyl cellulose (HPC) as fillers and using the alignment of fillers and the shrinkage characteristics of the hydrogels. The composite film was aligned with fillers using directional melt crystallization (DMC) method. DMC is a method for obtaining a porous structure by controlling the three-dimensional temperature gradient. Through the DMC, porous structure with CNC, PNIPAm, and HPC can be obtained, and this is confirmed through SEM. In the case of PNIPAm and HPC, it can be observed through SEM that the existing pores are formed into a re-entrant structure due to hydrogel shrinkage. This re-entrant structure makes low Poisson's ratio. After shrinking process, stretchable films are manufactured by infiltration of polydimethylsiloxane (PDMS), and polyurethane (PU) to the aligned foam. For CNC film, the Poisson's ratio is 0.103, and for CNC with PNIPAm film's Poisson's ratio is 0.043. This is significantly lower than the PDMS Poisson's ratio of 0.5, and as the concentration of fillers increases, the Poisson's ratio tends to decrease. In the case of the CNC and PU film, which is more stretchable than PDMS, the Poisson's ratio is 0.102 and the strain and young's modulus values are 500% and 1.28 MPa respectively, which is higher than the CNC with PDMS films. The areal strain ratio of CNC with PNIPAm is 6% and in order to further enhance the effect of the re-entrant structure, it was manufactured by replacing with HPC, and this film of areal strain ratio is 19%. The maximum transmittance of the films in this study reached up to 80% by UV-vis. Through transparency and complementation of physical properties, this film research can be applied to more diverse future material applications.

SB02.03.11

Preparation of Ionically Modified Self-Assembled Films Based on Cellulose Nanocrystals Diana Gaspar^{1,2}, Paul Grey², Bruno Mendes², Madalena Roque², Rodrigo F. Martins² and Luis Pereira^{1,2}; ¹AlmaScience, Portugal; ²FCT-NOVA, Portugal

Many approaches exist in the quest for efficient, abundant, cheap and eco-friendly photonics that can be easily integrated with other platforms for practical applications.

Approaches using 3D metamaterials, mesoporous semiconductors or plasmonic are promising. However, they tend to be complex in fabrication involving methods that require high energy input (such as vacuum and physical vapour deposition) for the deposition of materials, and in many cases not so green materials, nor sustainable, are expensive and colour limited.

Currently, we are facing a never-increasing interest to move to more sustainable materials that can achieve equivalent results for less energy input, and Nature is a privileged source of inspiration for the greatest technological advances. The steady and long optimization over millennia of periodic structures as the ones present in chameleons or iridescence mechanisms in beetles or butterflies, attract a lot of attention to natural micro and nanostructures. One attempt to mimic those assemblies is being pursued using cellulose nanocrystals (CNCs) that are able to self-organize into a chiral nematic liquid crystalline phase in aqueous suspensions. When the solvent is dried the chiral arrangement is retained and solid films are obtained that behave like 1D photonic crystals with iridescent colours. The intrinsic left-handedness of such structures is capable of interacting selectively with left and right-circular polarized light (LCPL and RCPL).

The manipulation of the pitch and therefore the reflected colour is particularly interesting and one of the topics that catch the attention in this field.

Approaches to manipulating the self-assembly of the CNC by either using external stimuli such as magnetic and electric fields, drying process with different interfaces or playing with the chemistry behind the acid hydrolysis are examples of solutions to shift the photonic bandgap throughout the visible and infra-red spectrum.

With this work, we demonstrate that CNC suspensions low concentrations (~4-wt.%) with proper evaporation-induced self-assembly conditions lead to the formation of films with interesting photonic properties with a left-handed twisted arrangement. The novelty of this is the use of strong acid cation resins to mediate the counterion exchange on commercial CNCs. It was observed that the addition of different concentrations of alkali salts to the CNCs suspension leads to a blue shift of the photonic bandgap with higher salt concentrations. Also, it was observed that the ageing of the suspensions can enhance the distinction between LCPL and RCPL (initial $\Delta\text{CPL} \approx 42\%$ to an $\Delta\text{CPL} \approx 60\%$), while the photonic bandgap remains nearly unchanged. Combining the photonic character of the tailored CNC films, whose photonic bandgap can be match with the bandgap of light sensitivity of semiconductor materials based on ZnO, it will be possible to create devices capable of discrimination between LCPL and RCPL signals in the blue region.

SB02.03.12

Paper Transistors for Logic and Analogic Applications Rodrigo F. Martins^{1,2}; ¹UNINOVA, Portugal; ²FCT UNL, Portugal

The aim of this presentation is to report the physics and electronics behaviour of a dual gate paper transistor where paper is simultaneously the substrate and the dielectric, while a metal-oxide-semiconductor (IGZO) is used as the active channel, and a back floating electrode is used, able to present logic

functionalities simply by varying the amplitude and frequency of the input gate signals. These transistors operate at drain voltages of 1 V with low power, exhibiting $I_{ON}/I_{OFF} > 10^4$ and mobility $\approx 2 \text{ cm}^2\text{V}^{-1}\text{s}^{-1}$, serving the specifications for a broad range of smart disposable low-power electronics. To sustain all this, an analytical compact model was developed able to precisely reproduce the response of paper-based dual-gate FETs and provide a full understanding of their unique and innovative operational characteristics.

References

Rodrigo Martins, Diana Gaspar, Manuel J. Mendes, Luis Pereira, Jorge Martins, Pydi Bahubalindrani, Pedro Barquinha, Elvira Fortunato, Papertronics: Multigate paper transistor for multifunction applications, *Applied Materials Today* 12, (2018) pp. 402–414.
D. Gaspar, J. Martins, P. Bahubalindrani, L. Pereira, E. Fortunato, R. Martins, Planar Dual-Gate Paper/Oxide Field Effect Transistors as Universal Logic Gates, *Advanced Electronics Materials*, Vol. 4 (12), (2018), 1800423. DOI: 10.1002/aelm.201800423

SB02.03.15

Environmentally-Friendly Chemical and Physical Methods for Deweaving and Functionalization of Waste Cotton Fabric Ivan J. Yuan¹, Hannah Tao², Andrew Yuen³, Elizabeth Zhang⁴, Aleena Sheikh⁵, Michael Cui⁶ and Miriam Rafailovich⁶; ¹Shanghai High School International Division, China; ²Academy for Information Technology, United States; ³Jericho High School, United States; ⁴Massachusetts Institute of Technology, United States; ⁵MDQ Academy, United States; ⁶Stony Brook University, The State University of New York, United States

As the demand for cellulosic fibers increases, the amount of cotton fabric waste produced also increases. Many methods currently available for recycling cellulose involve costly and potentially hazardous reagents such as ionic liquids and N-methylmorpholine-N-oxide [1]. We will show that mild physical and chemical treatments can deweave cotton fabric into fibers that can then be re-woven or repurposed for many applications.

Diagonally-cut cotton muslin fabric pieces of around 0.25 g were deweaved using a 40 mL solution of 0.5 M citric acid, 0.5 M sodium nitrate, or a 3:1 mixture of the two aforementioned solutions, being stirred at 600 rpm and 50°C. Samples were subsequently washed, with multiple rinses of vacuum filtration with deionized water ($>18\text{m}\Omega/\text{cm}$), and then vacuum dried. The solution was shown to successfully deweave material, however significant decreases in solution volume, pH, and fiber bleaching imply that the solution requires replenishment by adding fresh stock solution with each reuse. Around 93% of the mass of the untreated fabric was retained after deweaving, and suspended microfibers could be observed in the final solution.

The untreated fabric and deweaved fibers were examined using Fourier-transform infrared (FTIR) spectroscopy, which indicates preservation of the β -glycosidic linkage (898 cm^{-1}) in cellulose as well as other peaks characteristic of cellulose. Comparison of the peak associated with the C=O stretching vibration (1727 cm^{-1}) shows that this peak is insignificant for the untreated cotton fabric and the fibers deweaved with sodium nitrate, but is clearly seen in the fibers deweaved with the 3:1 mixture and is even higher in the fibers deweaved with citric acid, suggesting that esterification between citric acid and cellulose occurred. This is supported by the results of a back titration experiment, using sodium hydroxide and then hydrochloric acid, performed on the citric acid-deweaved sample. After titration, the fiber surface exhibited a color change to that of the indicator's acidic form, which could result from citrate groups added during esterification.

Tensile strength tests were conducted on individual fibers to characterize mechanical changes after deweaving. Compared to fibers from the untreated fabric, fibers deweaved with citric acid have a lower ultimate tensile strength (175 MPa compared to 404 MPa) but a greater elongation at rupture (5.8% compared to 4.6%). However, the untreated fibers snapped upon reaching the ultimate tensile strength, while the fiber strands within the deweaved fibers were gradually pulled apart, pointing to the decrease in friction between fiber strands. This is supported by previous results from X-ray computed tomography and scanning electron microscopy, which show that the fiber bundle is less tightly packed after deweaving. Negative zeta potential values (-3 to -6 mV) on the solution with suspended microfibers may be due to dissociation of carboxylic acid groups from esterification, further indicating the presence of interfiber repulsion that can increase the spacing between fibers. The arrangement of cellulose polymers within the strands of fibers, and thus the strength of individual strands, is likely preserved as the total crystallinity index and the lateral order index computed with FTIR peak heights [2] show no substantial changes. Therefore, the decrease in fiber strength is likely due to physical, rather than chemical, changes.

Preliminary tests demonstrate the possibility of scaling up the deweaving procedure by using larger parallelogram-shaped pieces of fabric. Experiments are being conducted to quantify the degree of esterification, clarify the chemical basis for deweaving, retain and analyze the produced microfibers, and scale up the process.

[1] El Seoud, O. A., et. al, *Macromol. Mater. Eng.*, **2020**, 305, 1900832

[2] Nelson, M. L. and O'Connor, R. T., *J. Appl. Polym. Sci.*, **1964**, 8, 1325

We would like to thank the Morin Charitable Trust for funding.

SB02.03.16

Binary Cooperative Thermal Treatment of Cellulose and MoS₂ for Preparation of Sustainable Paper-Based Electrochemical Devices for Hydrogen Evolution Leonardo H. Hasimoto^{1,2}, Jefferson Bettini¹, Edson R. Leite¹, Renato S. Lima^{1,2}, Lifeng Liu³ and Murilo Santhiago^{1,2}; ¹Brazilian Nanotechnology National Laboratory, Brazil; ²Universidade Federal do ABC, Brazil; ³International Iberian Nanotechnology Laboratory (INL), Portugal

The simple, fast, scalable, and integrative preparation of sustainable electrodes using earth-abundant materials toward energy applications is a long-standing challenge. In this work, we attempted to achieve such features by developing a binary cooperative thermal process using cellulose sheets and molybdenum disulfide (MoS₂) toward hydrogen evolution reaction (HER). The thermal process converts cellulose into a highly conductive hydrophobic carbon-based material while generating chemical defects on MoS₂. The latter is of fundamental importance to improve the catalytic activity for HER through activating the well-known inert MoS₂ basal planes. Thermal desulfurization was confirmed by X-ray photoelectron spectroscopy, Kelvin probe force microscopy, Raman spectroscopy and energy-dispersive X-ray spectroscopy. Interestingly, a desulfurization gradient was observed at the MoS₂ particles, where the edges are more defective than the basal planes. The resulting defect-like MoS₂ particles are highly active toward HER. In addition, the porosity of paper enables simple filtration of catalysts and the possibility to tune electrochemically active surface area by simply adding isopropanol before the electrolysis. Finally, we showed an ultrafast coating method using a commercial MoS₂ spray on sheets of paper that enables H₂ bubble generation at specific regions of the electrode. The overpotential (η) positively shifted more than 300 mV when compared with non-treated MoS₂, reaching $\eta = 240 \text{ mV}$ to obtain 10 mA cm^{-2} of HER current density.

SESSION SB02.06: Lignocellulose Processing and Application I

Session Chairs: Tian Li and Lars Wagberg

Wednesday Morning, November 30, 2022

Hynes, Level 1, Room 109

8:45 AM *SB02.06.01**Modification of Lignocellulose at Diverse Dimensions for Tuning Functionalities of Materials** Kai Zhang; University of Göttingen, Germany

In order to modify lignocellulose and convert it into functional materials for various scenarios in an environmentally friendly way, the development of corresponding chemical and also accompanying engineering methods is often required. Chemical modifications of lignocellulose demonstrate a promising strategy for endow it with various functionalities, while distinct challenges exist for the lignocellulose at various dimensions ranging from molecular to nanoscale. Herein, own advances regarding modifications of lignocellulose at diverse dimensions, either as polymers or as nanostructures, for functional materials will be presented. The introduction of diverse pending functional groups either along the cellulose chains or on nanocellulose surface will affect the structure formation and the exposure of the functionalities in the functional materials. By addressing the chemical modifications for tuning the functionalities in the final material design, further potential solutions will be opened for sustainable development to boost the use of this renewable, biobased material.

9:15 AM *SB02.06.02**Development of Low-Cost Bio-Filled Additive Manufacturing Composite Feedstocks** Xianhui Zhao¹, Halil Tekinalp¹, Erin Webb¹, Hongli Zhu² and Soydan Ozcan¹; ¹Oak Ridge National Laboratory, United States; ²Northeastern University, United States

Biomass fibers have been commonly used for reinforcing polymers (e.g., polylactic acid [PLA]) because of their low density, low cost, renewable nature, biodegradability, and abundance. In this study, pine/PLA composites were produced with a high loading (40 wt%) of pine fibers to reduce the composite feedstock cost for the additive manufacturing application. To improve composite performance, low-cost aspartic acid was incorporated. The aspartic acid loading was optimized, and the composites prepared were characterized to understand the effect of aspartic acid content on different composite properties using tensile testing, dynamic mechanical analysis (DMA), thermogravimetric analysis (TGA), gel permeation chromatography (GPC), differential scanning calorimetry (DSC), scanning electron microscopy (SEM), and rheological testing. Results show that the Young's modulus of the composites was improved by 30% with the addition of a small amount of aspartic acid (0.7 wt%). The coupling agent was found to be effective in tuning the properties of the composites for specific applications.

9:45 AM SB02.06.03**Laser-Induced Carbonization of Sodium Chloride-Impregnated Cellulose Nanofiber Films for Efficient Moisture-Electric Energy Transformation** Jakyung Eun, Seonghye Ha, Jaehyun Na and Sangmin Jeon; Pohang University of Science and Technology, Korea (the Republic of)

We developed high-performance moisture-driven power generators (MPGs) using sodium chloride (NaCl) impregnated cellulose nanofiber films (CNFs). CNFs impregnated with different amounts of NaCl were obtained by immersing CNFs in NaCl solutions of various concentrations. An infrared laser was employed to photothermally convert the CNFs to porous graphitic carbon films (GCFs) under ambient conditions. By focusing the laser beam on the top surface of the CNF, the laser intensity was the highest on the top surface and gradually decreased toward the bottom surface. Since the focal temperature of the laser beam (~2000 °C) was higher than the boiling point of NaCl, the NaCl particles near the top surface evaporated more rapidly, creating a NaCl concentration gradient along the thickness direction. In addition, the top surface became more graphitized than the bottom surface, producing a more porous structure on the top surface. When the GCF was exposed to moisture, the dissociated sodium ions migrated along the preformed concentration gradient, producing electricity. The maximum voltage and current outputs were 0.65 V and 550 $\mu\text{A}/\text{cm}^2$, respectively, at 90% relative humidity (RH). In particular, the current density output was produced continuously rather than pulsed, and was the highest current reported so far. Such a high current density was obtained by impregnating excess ions and implementing a high NaCl concentration gradient using LIG along the thickness direction of the extremely thin GCF. Furthermore, the porous structure of the GCF was found to produce higher performance than the graphene oxide-cellulose nanofiber composites (GO-CNF) with NaCl due to the presence of more water pathways for ion transport between electrodes. The developed device demonstrated its applicability by turning on four green light-emitting diodes (LEDs) operating at an onset potential of 2 V for 48h using six GCFs (each 3 mm \times 3 mm \times 240 μm in size) connected in series without a separate rectifier circuit and capacitor. Since moisture is ubiquitous, it has great potential for a wide range of applications such as sweat-powered wearable devices and remote environmental sensors.

10:00 AM SB02.06.04**Hybrid Materials from Cellulose Nanofibrils and Charged Core-Shell Nanolatexes** Asa Jerlhagen^{1,2}, Alexandros E. Alexakis¹, Rosella Telaretti Leggieri¹, Adrian Eliasson^{1,2} and Eva Malmström^{1,2}; ¹KTH, Sweden; ²FibRe; A Vinnova Competence Centre, Sweden

Cellulose nanofibrils (CNFs) are one of the most promising lignocellulosic feedstocks for the design of sustainable and advanced materials to meet the challenges of the future. CNFs are produced as aqueous colloidal dispersions of fibrils with diameters of a few nanometers and aspect ratios of several hundred. These dispersions can be dewatered in different processes to give foams, membranes, nanopapers, and nano-reinforcements, to name a few. The mechanisms for dewatering, and the impact of additives upon the assembly of nanofibrils, remains a challenging topic with great potential for tailoring the material to new properties and applications.

The exploration of core-shell polymeric nanolatexes as CNF additives is still just in its infancy. In this project we combine CNFs with a nanolatex synthesized through reversible addition-fragmentation chain-transfer (RAFT)-mediated polymerization-induced self-assembly (PISA) in water. The PISA process makes for a flexible platform in the synthesis of functional nanolatex with tunable size, surface charge and functionality. These nanoparticles have already shown great promise as compatibilizers when adsorbed to CNFs [1], and early work has indicated the introduction of interesting mechanical behavior to CNF materials [2].

In this project we investigate structures formed between anionic CNFs and small additives of a cationic nanolatex. We look at the impact of nanolatex charge and size as nanolatex is adsorbed to CNFs in dispersion and dewatered to give hybrid structures. The addition of nanolatex affects the mechanical properties, water sensitivity and response to heat treatment of these materials. The current work is an indication that nanolatexes can act as efficient compatibilisers for CNF networks, and that these hybrid structures deserve further systematic investigation.

[1] Alexakis, A. E., et al. (2021). "Modification of cellulose through physisorption of cationic bio-based nanolatexes – comparing emulsion polymerization and RAFT-mediated polymerization-induced self-assembly." *Green Chemistry*.

[2] Engström, J., et al. (2017). "Soft and rigid core latex nanoparticles prepared by RAFT-mediated surfactant-free emulsion polymerization for cellulose modification – a comparative study." *Polymer Chemistry* 8(6): 1061-1073.

10:15 AM BREAK**10:45 AM *SB02.06.05****Molecular Engineering of Biorefining Lignin Waste for Solid-State Electrolyte** Hongli Zhu; Northeastern University, United States

Current global energy sector is still dominated by the fossil-based energy. Renewable energies, especially these derived from Nature have been extensively sought after as a sustainable solution for emerging energy needs. Among them, wood-derived energy and energy storage devices come of the age in recent years. However, current conversion of wood and other plant as well into energy, either the energy storage devices or biofuel production, heavily depends on the delignification, which is a process to remove the lignin polymer existed in plant cell wall. In fact, lignin is the second most abundant biopolymer on earth next to cellulose but a massive industrial waste produced both in paper industry and biofuel manufacturing. Our concept in this research is to convert this industrial lignin waste from biofuel production (also known as biorefining) into solid-state electrolyte (SSE) to enable its application in next generation lithium battery.

The rationale of our experimental design lies in the abundant hydroxyl groups in the lignin polymer, which provides grafting sites for bonding polyethylene glycol (PEG), a most efficient polymer for the SSE of the ASSLBs. Moreover, lignin polymer itself contains plentiful aromatic rings and rich electron-donor groups such as ether type linkages, methoxyl groups (-OCH₃), and aromatic and aliphatic hydroxyl groups. These chemical structures of lignin facilitate its interactions with Li salt and improve ion conduction at the interface when ceramics were added into the SSE. We prepared two types of SSE by using the synthesized PEG-g-lignin. The first one was solid polymer electrolyte (SPE), which was prepared by mixing PEG-g-lignin with poly(vinylidene fluoride)-co-hexafluoropropylene (PVDF-HFP) and lithium bis(trifluoromethanesulfonyl)imide (LiTFSI). The resultant SPE had an ionic conductivity of 2.5×10^{-5} S cm⁻¹ at 25°C. The second one was composite polymer electrolyte (CPE), which was prepared by adding Li_{6.4}La₃Ga_{0.2}Zr₂O₁₂ (LLGZO) into the PEG-g-lignin and PVDF-HFP composite. The ionic conductivity of the resultant CPE was further enhanced to 6.5×10^{-5} S cm⁻¹. This ionic conductivity represents 2.6×10⁵-fold and 2.8×10³-fold higher than that of pure PVDF-HFP (9.7×10^{-11} S cm⁻¹) and pure PEO (9.0×10^{-9} S cm⁻¹) based SSE, respectively. Mechanistic study by using 2D HSQC NMR revealed that PEG-g-lignin has increased ether type β-O-4 linkages that can promote the interchain hopping of Li⁺ between lignin polymer chains, and 31P NMR revealed that lignin phenolic end can be associated by Li⁺.

The research has both significant novelty and broad impact. 1). The study converted a largely overlooked biorefining waste into the solid-state electrolyte, which opened up a new avenue for industrial waste valorization toward a thriving billion dollars market of next generation lithium battery. 2). By substituting petroleum-derived PEO and other synthetic polymers for SSE, plant-derived lignin polymer will indeed transform the sustainability of current ASSLBs. 3). The study also informed a broader research community and opened new avenues for building up a holistic bio-based energy system. The integration of a sustainable energy storage manufacturing with biofuel production platform will transform current energy sector by simultaneously enhancing biofuel production and promoting the biopolymers from Nature into high energy density, high cycling performance and safe ASSLBs.

11:15 AM SB02.06.06

Injectable Lignin Based Cryogels with Antioxidant and Antibacterial Properties for Biomedical Applications Adnan Memic¹, Turdimuhammed Abdullah¹, Thibault Colombani² and Sidi A. Bencherif²; ¹King AbdulAziz University, Saudi Arabia; ²Northeastern University, United States

Hydrogel-based biomaterials, especially those derived from natural polymers, have been regarded as one of the most promising scaffolds for biomedical research. These multifunctional scaffolds can exhibit high water adsorption capacity, biocompatibility, and biomechanical properties that can match native tissues. Cryogels are a special type of hydrogels in which polymers are cross-linked around ice crystals. As a result, cryogels exhibit unique physical features, including a macroporous and interconnected network, flexibility, shape-memory properties, and syringe injectability. Herein, we developed a multifunctional, i.e., antibacterial, antioxidant, and injectable cryogel by combining lignin with gelatin. The cryogel with 0.2% lignin showed a compressive modulus of 25 kPa and a compressive stress of 140 kPa at 80% strain, which is, respectively, 1.8 and 7 times higher than those of the pure gelatin cryogels. Meanwhile, such a cryogel formulation could completely recover its shape after compression up to 90% and was needle-injectable. Additionally, the lignin-co-gelatin cryogel inhibited the most common surgical site infection-associated pathogenic bacteria. Furthermore, lignin-co-gelatin cryogel was found to scavenge free radicals and have good cytocompatibility, and the cryogels with up to 0.2% lignin minimally activate naïve mouse bone marrow-derived dendritic cells. Overall, the current approach shows great promise for the design of bioresource-based multifunctional cryogels for a wide range of biomedical applications.

11:30 AM SB02.06.07

Utilization of Ultrasonication and Plasticizers to Increase the Thermo-Processability of Lignocellulose Adrian Eliasson^{1,2}, Eva Malmström^{1,2}, Lars Wagberg^{1,2}, Mikael Hedenqvist^{1,2} and Anette Larsson^{3,2}; ¹KTH The royal institute of technology, Sweden; ²FibRe Lignocellulose-based Thermoplastics A VINNOVA Competence centre, Sweden; ³Chalmers University of Technology, Sweden

Polymeric materials are essential in today's modern society and their production has increased exponentially since their commercialization in the 1940s. One of the largest industrial sectors is packaging, estimated to 146 million tons in 2015 [1]. A large fraction of the packaging material is single use and ends up in landfill or is incinerated, as most plastics used are non-degradable and recycling is still challenging in large parts of the world. Material research has focused on decreasing the environmental impact of these kinds of materials by reducing and replacing them with, for example cellulose-based materials like cardboard, but also more innovative materials like bio-based foams. Cellulose is an abundant biopolymer already widely used, while also being bio-degradable and recyclable. One limiting factor for conventional cellulose-based materials is the limitations when shaping cardboard and paper-based materials. Although cellulose is a polymer it does not show typical polymeric behaviors such as thermo-processability which most synthetic polymers do. Our approach, inspired by plasticization of gluten [2], is to incorporate a small amount of plasticizer into the lignocellulose matrix. Our hypothesis is that the small plasticizing molecules will reduce the strong intermolecular interactions within cellulose and enhance the molecular mobility. Successful implementation will increase the lignocellulose's thermo-processability and yield a material which can be processed through conventional thermo-processing such as extrusion or injection moulding allowing more advanced shaping opportunities than existing methods.

A step on the way has been the incorporation of different bio-based plasticizers through ultrasonication as a means to open up the fibers, aiding the sorption of glycerol, urea, and citric acid. The formed materials have been evaluated in regard to plasticizer content, thermal behavior, mechanical properties, degree of crystallinity and interaction with water. In this work, the primary focus was to understand the effect of ultrasonication on plasticizer sorption and its correlation to the highly improved physical properties of the formed materials. The sonication itself, a high energy treatment, peels off fibrils from the fiber surface, breaks down the crystal region and exposes hydroxyl groups which in turn increase the ductility and ultimate strength compared to the reference material [3]. The combination of plasticizer and sonication aids the sorption of urea and glycerol which leads to an increase in the ductility and ultimate strength further. As a result, a 100% bio-based material consisting of more than 75 % lignocellulose is under evaluation as an extrudable material for packaging applications with the potential to be bio-degradable and/or recyclable.

Using renewable resources to produce a thermo-processable lignocellulosic material as a potential alternative to single use plastics in the packaging industry has the potential to reduce our need for fossil-based materials, promote circular materials and reduce CO₂ emissions. This in turn contributes towards the fulfillment of circular bioeconomic principles and the United Nations Sustainable Development Goals 2030.

1. Geyer, R., Jambeck, J. R., & Law, K. L. (2017). Production, use, and fate of all plastics ever made. *Science Advances*, 3(7), e1700782.
2. Özeren HD, Wei X-F, Nilsson F, Olsson RT, Hedenqvist MS. Role of hydrogen bonding in wheat gluten protein systems plasticized with glycerol and

water. *Polymer* (Guilford). **2021**, 232, 124149.

3. An X, Liu J, Liu L, Zhang H, Nie S, Cao H, et al. Improving the flexibility of bamboo mechanical pulp fibers for production of high soft tissue handsheets. *Industrial Crops and Products*. 2020;150:112410

11:45 AM SB02.06.08

Pharmaceutical Manufacturing on Reconfigurable Paperfluidics Josselyn Mata-Calidonio¹, Jose Gomez-Marquez² and [Kimberly Hamad-Schifferli](#)¹;

¹University of Massachusetts Boston, United States; ²PopUp Labs, United States

We discuss the use of paperfluidic devices for the synthesis of molecules and nanoparticles using Asynchronous Modular Paperfluidic Linear Instrument-free (Ampli) blocks, which are paper membranes on blocks that can be interlocked together in different configurations. Reagents are embedded into the paper membranes of each block, and blocks are snapped together in a desired sequence for a chemical reaction. The reaction is initiated by adding solvent to the first block, which allows the reagents to flow from one block to the next. We synthesized both gold nanoparticles and pharmaceutically relevant small molecules. Extracted reaction products were characterized using Raman, optical absorption, and dynamic light scattering spectroscopies. Kinetics of reactions and parameters for reaction optimization will be discussed. Ampli blocks allow small scale, on-demand synthesis of molecules and thus can potentially enable de-centralized chemical production, which has the potential to address the challenges associated with supply chains in pharmaceutical distribution. Furthermore, because Ampli blocks can be easily reconfigurable by the enduser, it can be deployed in extreme environments by non-trained experts.

SESSION SB02.07: Lignocellulose Processing and Application II

Session Chairs: Qi Dong and Daniel Soderberg

Wednesday Afternoon, November 30, 2022

Hynes, Level 1, Room 109

1:30 PM *SB02.07.01

Cellulose Based High Performance Ambient Water Harvesting [Tian Li](#); Purdue University, United States

Emerging atmospheric water harvesting (AWH) technologies promise water supply to underdeveloped regions that have no access to liquid water resources. The prevailing AWH systems, including condensation- or sorption-based, mostly rely on a single mechanism and thus have a limited range of working conditions and inferior performance. We synergistically integrate multiple mechanisms, including thermosorption effect, radiative cooling, and multiscale cellulose-water interactions, and demonstrate a low-cost (~ 4 USD kg⁻¹) and high performance (up to 6.75 L kg⁻¹ day⁻¹ in field tests) AWH system requiring zero active energy input. The proposed system consists of a highly scalable and sustainable cellulose scaffold impregnated with hygroscopic deliquescent lithium chloride (LiCl) salt. Cellulose scaffold and coated LiCl synergistically interact with water at different scales from molecular, to nanometer, and micrometer scales, providing a fast harvesting rate and high yield over a wide operation range. Iterating radiative cooling and solar heating workflow achieves simultaneous enhancement of water capture and release through the so-called temperature-swing strategy. The captured water in return facilitates radiative cooling due to the intrinsically high infrared (IR) emissivity of the LiCl-cellulose composite. With our simple yet effective material design, the AWH working range extends to lower than ~ 10% relative humidity (RH), and the water uptake in the controlled lab test reaches 16 kg kg⁻¹ at 90% RH (sample at 19°C, i.e. 6°C below 25°C ambient temperature). In addition, we propose a theoretical model capable of elucidating the experimental water uptake curves and demonstrating the synergy among cellulose-LiCl-water-energy interaction. The promising performance emphasizes the potential of involving multiple AWH mechanisms and points to an alternative pathway to stimulate future improvement.

2:00 PM SB02.07.02

Chitosan-Based N-, S-Doped Nanostructured Carbon/Graphene Oxide Composite as a Sulphur Host in the Lithium-Sulphur Batteries [Kirill Murashko](#), Sara-Maaria Mesceriakove, Anna Lähde and Jorma Jokiniemi; University of Eastern Finland, Finland

Among the all next-generation batteries the lithium-sulphur battery, which uses extremely cheap sulphur as the positive electrode and the ultra-high-capacity lithium metal as the negative electrode, is at the forefront of emerging battery technologies by offering higher specific energy, at a lower price and lower CO₂ footprint compared to today's lithium-ion (Li-ion) batteries. Because of the complex, multi-electron chemical reaction the theoretical gravimetric energy density of the Li-S batteries is 2 567 Wh/ kg, which is 4.5-fold higher than the conventional lithium-ion technologies have. However, the instability of the sulphur cathode and lithium metal anode, which results in the poor cycling stability of the battery are the main factors that have limited the successful commercialization of this technology. In Li-S batteries, the liquid electrolyte and the sulphur cathode act like a couple to form the highly soluble lithium polysulfides (LiPS), which causes the well-known "shuttle effect" and lead to the loss of active material, Li metal anode corrosion, and low coulombic efficiency during interaction of the LiPS with Li metal anode. Moreover, the sulphur by itself has a high-volume change over the cycling and low conductivity that also have a negative effect on the electrochemical performances of Li-S batteries. Currently, the most perspective solution to address the above drawbacks is incorporating sulphur with a porous carbon host, which will tolerate sulphur volume expansion, improve the conductivity of the electrode, prevent the shuttle effect and allow reversible lithium-ion migration during charging and discharging. The high conductive carbon materials such as graphene and graphene oxide were suggested as one of the best options as hosts for sulphur in the Li-S battery cathode. These materials not only have a high electrical conductivity but may be doped with different functional groups, which improve the electrochemical properties of the Li-S battery cathodes. However, the currently available synthesis methods for these materials are complex, expensive, and usually require using of the highly toxic chemical. Moreover, the sulphur loading in such a host is limited by the material porosity and restacking possibility of the graphene or graphene oxide sheets. In our current work, we investigated the possibility to decrease the amount of graphene oxide during the creation of the sulphur-graphene oxide composite material. We proposed a one-step carbonization method to prepare 3D nanostructured porous nitrogen and sulphur doped carbon materials where graphene oxide is used as the conductive support for the carbon. Such 3D nanostructured carbon materials were created by using chitosan hydrogel as the main carbon source. Chitosan is mainly produced by the deacetylation of chitin which is the second most abundant and renewable biopolymer after cellulose. The chitosan has large amounts of amino groups, which leads to the creation of the self-nitrogen-doped carbon after the pyrolysis process. In addition, thiourea and potassium carbonate are introduced into the chitosan hydrogel and play key roles in optimizing the structure of the carbon material. Thiourea not only generates gas through pyrolysis to form pores, but its own rich nitrogen and sulphur elements can be partially retained in the finally obtained carbon material. The structural, compositional, and morphological properties of the created material were investigated using SEM, EDS, Raman spectroscopy, FTIR and TGA techniques. The produced N,S-doped nanostructured materials have a high surface area of up to 1500 m²/g and because of the heteroatom doping allow to improve the electrochemical performance of the Li-S battery cathode, when the developed material is used as the sulphur host.

2:15 PM SB02.07.03

The Secret Ingredient, Cellulose—Exploring Its Potential in Desalination Membranes [Raed Hashaikheh](#); New York University Abu Dhabi, United Arab Emirates

Seawater desalination by utilizing a membrane-based technology is a crucial step to overcome the freshwater shortage in some regions of the world. However, the durability and performance of membranes rely on the type of materials and fillers utilized for the fabrication of the membrane. In the efforts towards sustainable, biocompatible, low cost and economical materials, cellulose-based materials or derivatives are the main focus to develop membranes for water desalination. Herein, cellulose is explored as:

Novel material with unique structure to control swelling of reverse osmosis membranes.

Innovative entrapping media for better electrically conductive desalination membranes.

Coating layer to create hydrophilic surface for better desalination of oily wastewater.

Anti-swelling desalination membranes. Novel networked cellulose (NC) material is prepared via combination of controlled sulfuric acid hydrolysis and calculated ethanol regeneration of microcrystalline cellulose (MCC). While acid concentration was kept constant at 70%, factors such as hydrolysis time and temperature were varied to obtain the unique structure. The high-yield material has interesting mechanical integrity with tangled networked fibers that make it suitable for improving materials properties. NC was employed as an anti-swelling material that improved the performance of polyvinyl alcohol (PVA) reverse osmosis (RO) membranes. The open structure of NC entraps the PVA polymer inside and restrict PVA from expanding. This in turn imparts it stability against swelling. In addition, the hydrogen bonding formed provides a compact structure and thus prevents the membrane from swelling. The swelling capacity of PVA was reduced from 340% to 150% without compromising desalination performance. In addition, the tensile strength of wet PVA improved 1520% and the elastic modulus improved 1400% upon blending with NC.

Electrically enhanced fouling control nanofiltration/RO membranes. Electrically conductive membranes based on NC and carbon nanostructures (CNS) were fabricated via vacuum filtration. The hydrolysis process of cellulose was exploited to better incorporate and entrap CNS within the NC structure. High surface area multi-walled CNTs become trapped in the structure of networked cellulose. Membranes were tested and analyzed for their electrocatalytic activity and explored for their potential in fighting fouling issue. Furthermore, the compaction of pores via incorporation of NC resulted in promising results with respect to nanofiltration of divalent ions, with a rejection of 60% for $MgSO_4$ and 47% for $CaCl_2$, while maintaining a high flux of $\geq 100 L m^{-2} h^{-1}$. Furthermore, NC/CNS/PVA membranes demonstrated enhanced electrocatalytic activity. The RO membranes were tested with 25,000 ppm NaCl as feed, and exhibited 99.8% salt rejection with 93% increase in flux compared to PVA-NC with no CNS implying homogeneously mixed CNS. The membrane surface was recovered after fouling via electrolytic cleaning where the membrane was used as the cathode and a potential of $-5 V$ was applied for 20 min.

Improved distillation membranes (MD). A novel concept of stacking two membranes with different wettabilities to obtain a dual-layered membrane was developed. The hydrophilic top layer composed of electrospun PVDF-HFP impregnated with regenerated MCC cellulose while the bottom layer kept hydrophobic. Top layer acted as a hydrophilic barrier preventing oil from passing to the hydrophobic bottom layer during MD process. When tested with saline feed containing 1000 ppm of oil, the stacked dual-layered membrane yielded fresh water flux up to $12.8 kg m^{-2} h^{-1}$ with complete salt rejection revealing a simple and scalable method for oily wastewater treatment using relatively inexpensive, abundant and ecofriendly materials.

2:30 PM BREAK

3:30 PM *SB02.07.04

Molecular Engineering of Cellulose-Based Materials for Advanced Applications [Qi Dong](#) and Liangbing Hu; University of Maryland, United States

The natural abundancy, sustainability, and hierarchical structure of cellulose-based materials make them a promising platform for developing new functionalities. In particular, molecular engineering of cellulose-based materials holds great promise in constructing tailored nanoscale structures and therefore unique properties. In this talk, we will first introduce a general design strategy for achieving one-dimensional (1D), high-performance ion conductors through molecular engineering of cellulose nanofibrils by Cu^{2+} -coordination. The cellulose nanofibrils by themselves are not ionic conductive; however, by opening the molecular channels between the cellulose chains through Cu^{2+} coordination we are able to achieve high ionic conductivities. This enhanced ion transport is enabled by a unique cation hopping mechanism that is decoupled from the polymer segmental motion. As a proof-of-concept demonstration, we show that such decoupling gives rise to multiple advantages of the cellulose-based Li-ion conductor, including a high transference number (0.78 vs. 0.2–0.5 in other polymers), low activation energy (0.19 eV), and a wide electrochemical stability window (4.5 V) that accommodate both Li metal anode and high-voltage cathodes. We further demonstrate this 1D ion conductor not only as a thin, high-conductivity solid-state electrolyte but also as an effective ion-conducting additive for the solid cathode, providing continuous ion transport pathways with a low percolation threshold, which allows us to enable the thickest $LiFePO_4$ solid-state cathode ever reported for high energy density.

In a separate topic, we will discuss a Cu^{2+} -crosslinked chitosan (chitosan-Cu) material as a stable and high-performance hydroxide exchange membrane. Similar to the structure of the Cu^{2+} coordinated cellulose, the Cu^{2+} ions are coordinated with the amino and hydroxyl groups of chitosan to crosslink the chitosan chains, forming hexagonal nanochannels (~1 nm in diameter) that can accommodate water diffusion and facilitate fast ion transport. The chitosan-Cu exhibits a high hydroxide conductivity of $67 mS cm^{-1}$ at room temperature, which is among the highest compared to other hydroxide exchange membranes. In addition, the Cu^{2+} coordination also enhances the mechanical strength of the membrane, reduces its permeability, and most importantly, improves its stability in alkaline solution. These advantages make chitosan-Cu an outstanding hydroxide exchange membrane candidate for fuel cells and electrolyzer, which we demonstrate in a direct methanol fuel cell that achieves a high power density of $305 mW cm^{-2}$.

4:00 PM SB02.07.05

Direct Laser Writing of Laser-Induced-Graphene (LIG) on Recycled Wood for Smart Furniture Applications [Han Ku Nam](#)¹, [Dongwook Yang](#)¹, [Truong-Son D. Le](#)¹, [Younggeun Lee](#)¹, [Byunggi Kim](#)², [Young-Ryeul Kim](#)¹, [Seung-Woo Kim](#)¹ and [Young-Jin Kim](#)¹; ¹KAIST, Korea (the Republic of); ²The University of Tokyo, Japan

About 30% of the earth's land is covered by forests, which are mostly composed of trees. As such, wood is naturally abundant and inexpensive; thus, it has been used for a variety of purposes, including furniture, paper, buildings, and vehicles for thousands of years. Today, it is mainly utilized in thermal power plants as a fuel material. Recently, strong interest in green technology has risen around the world, so extensive studies are being conducted on transparent wood formation and wood-based carbonization filter production. Since recycling is more spotlighted for carbon naturalization to save the earth, the global wood recycling market also keeps expanding. However, the key applications of recycled wooden biomass or waste woods have been limited to manufacturing the packaging boxes, fuel biochips for cogeneration plants, fertilizers, and synthetic woods. Biochip production is the largest portion of the wood recycling market, but substitute renewable energy sources, such as solar power, wind power, and tidal power technologies are being actively developed. Therefore, more attractive wood recycling technology needs to be developed. Direct laser writing of Laser-Induced-Graphene (LIG) is considered as one of the technology candidates for taking eco-friendly and economical benefits of waste woods into new markets. Our group reported that high-quality three-dimensional porous multilayer graphene can be formed by illuminating femtosecond laser pulses in ambient air without additional fire-retardant treatment or an inert gas environment. Here, we report femtosecond-laser-direct-writing (FsLDW) of LIGs on recycled waste wood for realizing smart furniture. We tested the LIG formation on particleboards, medium-density fiberboards, and oriented strand boards, as the recycled wood examples.

Ytterbium-doped fiber femtosecond laser with a 250-fs pulse duration, a 1040 nm center wavelength, and a 200 kHz repetition rate was used as the light source with a beam-scanning Galvano scanner with a maximum scanning speed of 2.0 m/s. Various combinations of laser power, wavelength, and beam scanning speeds were delivered onto the recycled wood samples for optimizing the LIG quality then monitored the resulting chemical composition and electrical conductivity. A low sheet resistance of 5.8 Ω /sq was attained on a medium density fiberboard; this is the best value to our best knowledge. A series of chemical composition tests, including SEM (Scanning Electron Microscope), TGA (Thermogravimetric analysis), XRD (X-ray diffraction), XPS (X-ray Photoelectron Spectroscopy), and Raman spectroscopy were performed, which confirmed the successful graphene formation. This LIG electrode will be applied to a joule heating-based heater for a stove warmer on a dining table application, a pulse sensor installed on chair armrests, and power switches without electrical metal-wire interconnects for green and smart furniture applications

4:15 PM SB02.07.07

Multifunctional Composite Paper Adaptable to Industrial Papermaking [Alireza Hajian](#); MIT, United States

Paper lacks functions such as heat, electrical or ion conductance required for various engineering applications. For this reason, various approaches have been used to add such functions in the form of inks, nanoparticles, or biopolymers onto a prefabricated paper. These processes include screen or digital printing, and roll-to-roll press, resulting in two main categories of multifunctional paper: Printed electronics and paper microfluids analytical systems. In either of these, pulp fibers are in dry state and full-exploitation of the fiber adsorption is not possible, furthermore, it requires an added step/cost in the paper industry and devices that are coated/fabricated onto the paper, and makes the recycling process more complex.

We hereby advance papermaking by an industrially scalable chemical modification of pulp that can subsequently adsorb numerous functional materials ranging from conducting polymers to nanoparticles to turn the wet pulp into functional pulp. The functionalized pulps can then be used alone or in mixtures in industrial paper-making to form a fundamentally new form of functional paper at scale. As an example, we show a paper battery that is stable more than 1400 charge-discharge cycles.

4:30 PM SB02.07.08

Porous Silicon Nano-Quill Anodes for Lithium-Ion Batteries [Nancy Chen](#)¹, [Morteza Sabet](#)¹, [Nawraj Sapkota](#)¹, [Shailendra Chiluwal](#)¹, [Craig M. Clemons](#)^{2,1}, [Apparao M. Rao](#)¹ and [Srikanth Pilla](#)¹; ¹Clemson University, United States; ²Forest Products Laboratory, United States

The growing population and increasing energy demands are overwhelming our fossil fuel supply and limiting future generations' availability. With the rapid electrification of the transportation sector, rechargeable lithium-ion batteries (LIBs) are emerging to replace conventional fuel-based technologies. LIBs continuously evolve due to demands for higher energy density and long cycling life. Among the recent developments in anode electrode materials, silicon (Si) is regarded as the most promising replacement for graphite due to its high theoretical specific capacity (~4200 mAh g⁻¹), which is over 10 times greater than that of graphite anodes (~372 mAh g⁻¹). Despite the advancements, persisting challenges hinder the commercialization of Si for LIB anodes. Si-based electrodes are susceptible to rapid degradation due to the large volume change (approx. 400%) of Si particles during lithium insertion and extraction. The repeated volume change leads to the pulverization of the Si material, ultimately leading to decreased cycling stability from the loss of contact with the current collector. To overcome this obstacle, 3-dimensional (3D) porous and hollow nanostructures have been employed to provide sufficient void space to accommodate the volume change during electrochemical cycling. However, with the demands for material cost-reduction from industry, Si structures' strategic engineering must be cost-effective for commercial viability.

Our team has developed a patent-pending methodology for utilizing bio-renewable templates to synthesize a 3D Si architecture called Si nano-quills (SiNQs). We innovated a two-step, cost-effective process that yields SiNQs with a porous morphology and hollow interior structure. First, in a scalable sol-gel process, silica gel particles were prepared using low-cost chemicals. A unique mesoporous morphology was engineered using surfactant-modified cellulose nanocrystals as a sacrificial template. The templates were removed via thermal treatment to form silica nano-quills (SilicaNQs), which possess a 3D bulk structure comprised of hollow quill-like arms and a high degree of porosity. In the second step, we employed a low-temperature magnesiothermic reduction method to convert SilicaNQs into SiNQs with a relatively large surface area. A water-based slurry was prepared using a combination of SiNQ and graphite as the active materials. The slurry with 73 wt% MCMB graphite, 15 wt% SiNQ, 2 wt% carbon black, and 10 wt% LiPAA binder was cast onto the commercial copper foil. After room-temperature drying, the electrode was calendared, and vacuum dried. We also prepared batteries using commercial Si nanoparticles (100nm, spherical) with the same slurry composition. The 2032-type coin half cells were assembled for battery testing using SiNQ-graphite and Si-graphite electrodes (with an active mass loading of 3 mg cm⁻²). The coin cells underwent a formation cycle at a current rate of 0.05C, followed by continuous cycling at a current rate of 0.1C (90 mA g⁻¹) over the potential range of 0.005 – 1.5 V at room temperature. The SiNQ-graphite anode offered an initial reversible capacity of 587 mAh g⁻¹ and superior capacity retention of 91% after 90 cycles. In comparison, the commercial Si-graphite battery exhibited an initial capacity of 375 mAh g⁻¹ and capacity retention of 61% after 90 cycles. The SiNQs possess a BET surface area of 399 m² g⁻¹, and a total pore volume of 0.64 cm³ g⁻¹. The superior performance of SiNQs is due to their unique morphology that offers high surface area and porosity for effective diffusion of lithium ions and their electrochemical interactions with NQs, leading to a higher reversible capacity. Moreover, the porous architecture of SiNQs can effectively mitigate the volume change during lithiation and delithiation, thus providing a good cycling performance.

SESSION SB02.08: Virtual Session I: Lignocellulose Understanding, Processing and Application
Session Chairs: [Chaoji Chen](#) and [Yuan Yao](#)
Tuesday Morning, December 6, 2022
SB02-virtual

8:00 AM *SB02.08.02

Functional Wood Materials [Ingo Burgert](#)^{1,2} and [Guido Panzarasa](#)¹; ¹ETH Zurich, Switzerland; ²Empa–Swiss Federal Laboratories for Materials Science and Technology, Switzerland

The lecture reports on new developments in the field of functional wood materials. The sophisticated and highly porous hierarchical structure of wood provides a versatile scaffold for functionalization treatments, and the mechanical properties, outstanding in view of its low density, make wood a biomaterial of choice to develop high-performance hybrid materials and composites. Structure-retaining modification and functionalization in top-down approaches allows to profit from these intrinsic features of the wood structure. Moreover, the CO₂-storing capacity and the renewable nature of wood are highly beneficial characteristics, but the potential of functional wood materials to substitute less eco-friendly engineering materials for a transition toward circular economy highly depends on processing conditions and achievable performances. In this talk, various approaches to utilize the hierarchical wood structure will be discussed along with strategies to address essential remaining challenges, including large-scale production and adherence to green chemistry principles.

8:30 AM *SB02.08.04

Supramolecular Engineering of Cellulosic Materials [Chaoji Chen](#); Wuhan University, China

Natural polymers derived from biomass such as cellulose have emerged as a sustainable group of materials widely used in consumer products and functional devices. The renewable and sustainable features of cellulose have made it extremely attractive when competing with the petrochemical-based counterparts. Through engineering cellulosic materials at the supramolecular scale, we are able to regulate their supramolecular structure, configuration and their mechanical, electronic, ionic, fluidic, optical and thermal properties, imparting them with improved or even new functions for potential uses in multiple sustainable devices. In this talk, I will discuss the supramolecular engineering strategies of cellulosic materials and their potential uses in various sustainable devices.

9:00 AM SB02.08.05

Carbon Spheres Incorporated Cellulosic Sensing Paper for Detection of Phthalic Acid Esters in Solutions [Hansini Abeysinghe](#)^{1,2}, Thusitha N. Etampawala^{1,1,2}, Niluka Sewwandi¹, Panchali Anuchani¹ and Asurasinghe Rajamanthrilage Kumarasinghe¹; ¹Faculty of Applied Sciences, University of Sri Jayawardenepura, Sri Lanka; ²Faculty of Applied Science, University of Sri Jayawardenepura, Sri Lanka

Phthalic acid esters (PAEs) or phthalates are one of the ubiquitous environmental pollutants that seem to have a considerable impact on human and biological bodies. After discovering their potential to cause health disorders like endocrine disruption, various PAE detection techniques were developed. Most of them rely on sophisticated instruments and lengthy laboratory procedures. The lack of simple, rapid, in-situ, and real-time techniques to monitor the presence of PAEs seems to be a significant issue, with more attention placed on energy saving, sustainability, and green chemistry. Therefore, this study focuses on developing a quick and easy PAE detection technique that facilitates low energy and low time consumption while promoting green chemistry. Specifically, a novel carbon sphere (CS) incorporated cellulose composite was developed as a PAE sensing paper, where the presence of PAEs in a solution was directly detected based on the conductivity reduction of the composite paper. Though a similar concept of detecting PAEs using the conductivity reduction of the sensing paper was tested using both Multi-Walled Carbon Nanotube (MWCNT) buckypaper and MWCNT/cellulose composite paper, their limited sensitivity remains a challenge. Therefore, in this study non-catalytic CSs synthesized using acetylene pyrolysis were used instead of MWCNTs with the intention of increasing the sensitivity limit past 1000 (v/v) ppm.

The CSs are highly electrically conductive due to a continuous π -electron cloud around the sphere-shaped network of aromatic carbon rings. CSs show potential at adsorbing PAE molecules by primarily forming π - π electron donor-acceptor interactions since both the donor and the acceptor have aromatic rings. However, the PAE molecules are dielectric since they have no continuous π -electron cloud across the molecules containing an aromatic ring with two ester-linked alkyl chains. It was assumed that the adsorption of dielectric PAE molecules with bulky side groups onto the CS would increase the tunneling distance between the CSs, resulting in a disruption in their conductivity network, which in turn reduces the conductivity of the composite. Therefore, a reduction in the overall conductivity of the sensing paper is expected if the PAE molecules are adsorbed from the sample solution. It cannot make a paper consisting of entirely CSs for many reasons.

Consequently, a suitable matrix is needed to support the assembly of CSs. The matrix should have high water absorptivity showing potential for creating passages through the material, such that the PAE molecules present in the solution could direct to the carbon spheres incorporated inside. Therefore, in this study, cellulose, a biologically originated, cheap, and easily accessible polymer, was chosen as the matrix over the other suitable fossil-originated synthetic polymers. The CS-Cellulose composite was developed by compressing the filter cake obtained by vacuum filtering a homogenized solution of carbon spheres in cellulose pulp. The specificity of this study is that the recycled cellulose papers obtained from the local market were used as the source of cellulose. Here, the conductivity variation of the cellulosic sensing paper was measured using a four-probe conductivity meter, where the supplied voltage was varied from 0 – 10V until the target current was achieved. The overall conductivity decrement of the cellulosic paper in the presence of adsorbed PAEs could be easily identified by observing the current variation change. This conductivity decrease could be quantitatively detected by considering the sheet resistance, resistivity, and conductivity values. Using this technique with novel 10% CS-cellulose sensing paper, the presence of DPHP (di(2-propylheptyl) phthalate) in a series of 100000 – 1 (v/v) ppm solutions was detected. The simplicity and easy-to-handle nature of the developed method show potential for developing a portable, in-situ, and real-time PAE monitoring system.

9:15 AM SB02.08.06

Nanoscale Insight in Moisture Adsorption in Lignin, Amorphous Cellulose, and Their Mixtures Investigated with Monte Carlo and Molecular Dynamics Simulation [Ali Shomali](#)¹, Chi Zhang¹, Wenqiang Liu², Benoit Coasne³, Eleanor J. Schofield⁴, Dominique Derome² and Jan Carmeliet¹; ¹ETH Zurich, Switzerland; ²Université de Sherbrooke, Canada; ³CNRS, LIPhy, France; ⁴HM Naval Base, United Kingdom

Second to cellulose, lignin is the most abundant renewable polymer on the planet. Majorly found in plant cell wall composite, cross-linked to hemicellulose, and acting as the cohesive matrix that surrounds the wood holocellulose and provides increased hydrophobicity and chemical stability to the composite, Lignin is an exceptional source for different monomers and novel materials, biofuel feedstock and chemicals. In addition, Due to its less susceptibility to biological attack and high compatibility with holocellulose, synthesized lignin-based oligomers and lignin nanoparticles have been considered as potential consolidation material for archaeological wood. Due to the highly heterogeneous structure of lignin and complications of its extraction and separation in experimental approaches, relatively little evidence exists on lignin and cellulose interaction and its response to water adsorption on the molecular level. In this study, a molecular model is used to investigate hygromechanical properties of lignocellulose mixtures and to provide insight into the role of lignin and its derivatives as consolidation agents in wood composites with the aim of finding a mixture model that accurately describes the behavior of lignocellulose mixtures. Molecular models studied include an amorphous cellulose model composed of cellobiose units, various models for lignin from linear lignin composed of guaiacyl (G-type) and syringyl (S-type) units together with more complex models of softwood (spruce) and hardwood (birch) built using a stochastic method to accommodate more complex arrangements of units and linkages and mixtures of amorphous cellulose and uncondensed G-type lignin of different mass ratio. Hydrated samples equilibrated at relative humidity ranging from fully dry to saturation pressure are prepared by employing an iterative hybrid all-atom molecular dynamics and grand canonical Monte-Carlo (GCMC) simulation. The hybrid GCMC/MD technique provides an excellent tool to capture the highly coupled nature of sorption-induced swelling in the lignocellulose mixture by enabling us to capture the sorption by applying relative humidity in GCMC and allowing the resultant swelling during relaxation in the MD stage of the simulation. By applying the mechanical tests to hydrated samples role of lignin in adsorption-induced mechanical softening in wood-polymer is also studied. MD results for different lignin components show linear G-type lignin as the least hygroscopic and the linear S-type lignin, with the higher number of methoxy group, as the most hygroscopic lignin model examined. Amorphous cellulose shows considerably higher adsorption and swelling compared to all lignin models due to its hygroscopic nature and the high number of hydroxyl groups hosting many sorption sites. Looking at mixtures of the two components, as the lignin content increase, The sorption isotherms, swelling curves and mechanical data reveal reduced moisture adsorption and swelling together with mechanical softening signifying the effect of the polymer interaction, which is further characterized by measuring porosity pore size distribution and hydrogen bonding network. The rule of mixture is introduced as an analysis tool to elicit the role of polymer interphase. Comparing the mixture rule to MD data reveals the mixture rule as an acceptable but overestimating approximation of moisture content and swelling, the difference is then taken into account as the properties of cellulose-lignin interphase. The underlying molecular mechanism describing the lignocellulose hygromechanical response is compared to what we learned in our recent studies regarding molecular phenomena involved in polyethylene glycol consolidation of wood in order to unravel molecular characteristics of an inspired wood cell wall consolidant. Although lignin induces less softening in a mixture with amorphous

cellulose, the moisture reduction and anti-swelling effects are less significant.

10:05 AM DISCUSSION TIME

SESSION SB02.09: Virtual Session II: Lignocellulose Understanding, Processing and Application
Session Chairs: Yuanyuan Li and Kai Zhang
Tuesday Morning, December 6, 2022
SB02-virtual

10:30 AM *SB02.09.01

Biomimetic Colour Engineering From Nature to Applications [Silvia Vignolini](#); University of Cambridge, United Kingdom

In a changing world, Nature must serve as a source of inspiration to develop more sustainable materials. For instance, plants' most brilliant and striking colours result from the helicoidal arrangement of cellulose nanofibrils. Interestingly, similar helicoidal architectures with analogous optical responses can be obtained in vitro by self-assembly of cellulose nanocrystals (CNCs) derived from biomass. CNCs are rod-like colloids capable of arranging into a liquid crystalline phase above a critical concentration in suspension, which upon complete removal of the solvent, lead to photonic films. So far, this process has been explored and studied only on a relatively small scale, neglecting the limitations and challenges posed by the use of large-scale and continuous processes which are required in any industrial context.

In this presentation, I will address these limitations by demonstrating how the self-assembly of CNCs can be controlled to produce meters-long films using a roll-to-roll (R2R) technique. Particularly, we demonstrated how the suspension properties, the casting parameters and drying conditions relate to the optical properties of the produced films.

To validate the use of this technique and material for pigment preparation, we developed a protocol to prepare coloured microparticles from R2R-cast CNC films. The optical properties of the CNC microparticles were then assessed in various environments and finally benchmarked against other commercial effect pigments and glitter. The prepared microparticles are compatible with a wide range of formulations, making them ideal to replace controversial mineral pigments based on mica and titanium dioxide as well as non-biodegradable glitters.

11:00 AM SB02.09.02

An Overview of Criteria of Lignocellulosic Waste and Residues for Packaging Production Leading to Circular Bioeconomy [Samantha Islam](#) and Jonathan M. Cullen; University of Cambridge, United Kingdom

Extensive use of petrochemical plastic packaging, coupled with the lack of systematic collection and disposal, leads to a major contamination in soils and aquatic environments. In response, widespread research is taking place to replace petrochemical plastics with biodegradable polymers i.e. substances capable of being decomposed avoiding environmental pollution. Lignocellulose (LC), the most abundant biomass composites from forest and agriculture, can produce cellulose nanofibrils (CNF), a biodegradable packaging material with significant mechanical, barrier and colloidal properties, low density and renewability. However, the cost of production and the negative environmental impact of agricultural expansion are two major obstacles for commercial upscaling of CNF production. Compared to primary resources, CNF extracted from lignocellulosic wastes and residues (LCW&R) e.g. primary forestry and agricultural residues, and municipal and industrial LC-based wastes, not only lowers the production cost but also removes the need for cropland expansion. Moreover, the use of LCW&R in CNF production, indicating material recovery and recycling in the Waste hierarchy (i.e. the ranking of waste management options), provides a more profitable, environment friendly biowaste treatment compared to incineration and landfilling. Various feedstock criteria influences the properties, performance, processing efficiency and production cost of CNFs. Understanding of how the feedstocks perform across these criteria is required for the optimal feedstock selection in commercial CNF production. However, a consolidated overview of criteria defining the suitability of LCW&R for optimal CNF production is absent in the literature. Therefore, this study performs an iterative literature review and presents an overview of the LCW&R characteristics to consider for the successful commercial production of CNF as a packaging material. The 14 criteria of LCW&Rs identified in this study are: availability; elemental composition; cellulose content; hemicellulose content; lignin content; ash content; cell wall thickness; price, seasonal variability; durability; bulk density; environmental impact; land impact; and biodiversity impact. The results of the study can be used to support decisions on managing lignocellulosic waste and producing bioplastic packaging that can enable circular bioeconomy.

11:15 AM SB02.09.03

Nanostructure and Interfacial Mechanical Properties of PEG-Treated Nanocomposites Studied with Molecular Dynamics Simulation [Wenqiang Liu](#)¹, [Ali Shomali](#)², [Chi Zhang](#)², [Benoit Coasne](#)³, [Jan Carmeliet](#)² and [Dominique Derome](#)¹; ¹Université de Sherbrooke, Canada; ²ETH Zurich, Switzerland; ³Univ. Grenoble Alpes, CNRS, LIPhy, France

Polyethylene glycol (PEG) is widely used in the treatment of archeological wood to reinforce the decayed wood structure[1]. Understanding the mechanisms that allow PEG to strengthen archeological wood can provide fundamental insights into wood hygromechanical behavior. Inspired by the structure and components of the wood S2 cell wall layer, the composites composed of crystalline cellulose and PEG-treated amorphous cellulose are used to study the interfacial mechanical behavior of the fiber-matrix with the aim to reveal the impact of PEG molecules on the stick-slip behavior. GROMACS package[2] and the OPLS force field[3] are used for the MD simulations. The composites in the dry state are composed of infinitely long crystalline cellulose fiber embedded in a PEG-impregnated amorphous cellulose matrix. Seven levels of PEG loading and eleven levels of moisture loading are constructed resulting in a total of 77 initial configurations. The pulling-out test simulations are carried out to study the interfacial mechanical properties of the composites while recording the shear stress and the displacement of the crystalline cellulose.

The initial densities of the dry systems range from 1.4 g/cm³ to 1.44 g/cm³ depending on the given PEG mass ratio. Three factors including, the atom number densities of the matrix atoms all exhibit peak values at certain distances to the surface of crystalline cellulose, a linear correlated relationship between the number density peak values of water atoms and hydrogen bond numbers between crystalline cellulose and water molecules with increasing the moisture content, and the chains of amorphous matrix near the fiber-matrix interface tends to be more aligned revealed by Herman orientation functions, all demonstrate that the ordered structure of crystalline cellulose has a significant impact on the distribution of matrix atoms. The pure amorphous cellulose swells linearly with PEG variation, which indicates that PEG molecules behave like integrated with the amorphous matrix. The swelling coefficients concerning the moisture content variation are found to be larger for the composites with a higher PEG mass ratio.

The maximum shear forces are extracted from the pulling-out simulations which span all PEG mass ratios and moisture content constructed. The shear force map shows that the maximum shear force appears at around 10%-15% PEG mass ratio and 3%-6% moisture content, which indicates the consolidation of the interfacial mechanical property at low moisture content.

- [1] R.J. Barbour, Treatments for Waterlogged and Dry Archaeological Wood, in: Archaeological Wood, American Chemical Society, 1989; pp. 177–192.
[2] M. Abraham, T. Murtola, R. Schulz, S. Páll, J.C. Smith, B. Hess, E. Lindahl, GROMACS: High performance molecular simulations through multi-level parallelism from laptops to supercomputers, (2015).
[3] M.J. Robertson, J. Tirado-Rives, W.L. Jorgensen, Improved Peptide and Protein Torsional Energetics with the OPLS-AA Force Field, J. Chem. Theory Comput. 11 (2015) 3499–3509.

11:30 AM SB02.09.04

Electrochemical Osmotic Hydrogel Actuators—A Fundamentally New Soft Material with Many Possibilities Mahiar M. Hamedj¹, Christoph Keplinger² and Tobias Bensefelt¹; ¹KTH, Sweden; ²Max Planck Institute for Intelligent Systems, Germany

Intelligent systems combine sensing, actuation, and computation to achieve complex tasks and functions. Soft electrically controlled multifunctional materials, especially hydrogels, are the most promising materials for such systems as they are as adaptable as biological systems yet compatible with advanced systems through electronics. There are however no reports on such soft multifunctional materials and not even hydrogel actuators with direct electric control.

We show an electroactive hydrogels fabricated from two components: a hydrophilic, ionically charged nanofibril (cellulose nanofibrils from trees), and carbon nanotubes. These nanoparticle composite networks are mechanically robust, yet they have an open mesoporous structure that can hold lots of water and be highly permeable to substances in their surroundings. The anisotropy of the network allows high expansion in one direction while maintaining high strength and electric conductivity in the other. These hydrogels are fundamentally different from polymer hydrogels, and their behavior is not described by classical polymer physics: e.g., polymer gels have entropy elastic deformation, while nanowire hydrogels deform plastically via a stick-slip-stick behavior. As a result, they show emergent properties not present in any previously known soft material. In particular, they possess two unique properties which are immediately suitable in the area of soft intelligent systems:

The electrochemical charge/discharge of the carbon nanotubes in the hydrogels controls the internal salt concentration and consequently their osmotic swelling. This allows direct electrically controlled actuation where around 700 water molecules expand/contract the structure for each ion/electron pair inserted/de-inserted at only ± 1 volt, resulting in up to 300% electroosmotic expansion. This mode of electronic actuation has not been shown before, and is a fundamental advancement for soft materials.

The coupling between expansion and electric resistance allows self-sensing and possible feedback to control and lock a particular expanded state. The relation between expansion and pore size further allows for electrically tunable membranes with a mesoporosity relevant for permeability to larger molecules. These tunable membranes are the first example of electrically controlled mesoporosity suitable for larger molecules such as drugs or proteins. No such active membrane has been presented before, and the best current tunable membranes are dense graphene or conducting polymer membranes for controlling the permeability of gases or water.

Our hydrogels are a new form of soft material and groundbreaking as they monolithically integrate actuation with other functions, not easily achieved with other material systems. They can further be made in any lab using available cheap bulk materials, and shaped into various forms ranging from sheets to fibers, to advanced 3D printed structures.

11:45 AM *SB02.09.05

Systems Modeling Approaches for Sustainable Material Development: Techno-Economic and Environmental Considerations Yuan Yao; Yale University, United States

Developing sustainable materials requires a comprehensive understanding of the potential environmental, economic, and societal implications of different material, process, and design strategies. Life Cycle Assessment (LCA) and Techno-Economic Analysis (TEA) have been widely used to assess the potential environmental impacts and economic feasibility of various materials. However, applying LCA and TEA to new materials is challenging due to the lack of large-scale data and limited knowledge of systems effects. Furthermore, the impacts of biomass utilization on ecosystems depend on many complex spatial and temporal factors (e.g., land management, climate and soil conditions), most of which are difficult to be considered in LCA for early-stage material development.

This talk will present several innovative systems modeling frameworks that we have been developing to address this challenge. Our frameworks integrate engineering simulations with advanced modeling approaches in different disciplines, such as LCA, TEA, machine learning, supply chain analysis, ecosystem modeling, and system dynamics. In addition, our frameworks help understand the potential environmental or economic implications of new biomass-derived materials at product-, process-, and industry-wide scales. By the crucial integration of those modeling techniques from engineering, industrial ecology, and data science, our research has demonstrated how interdisciplinary approaches can support sustainable material development.

Several examples will be presented to show how these integrated systems analyses can enhance engineering, process, supply chain, and policy design for sustainable biomass-based materials. The examples will focus on wood-based materials, including mass timber for large-scale building applications, as well as materials derived from forest residues (a waste, under-utilized resource) as carbon-negative technologies. These case studies will highlight the potential of lignocellulosic materials in mitigating climate change and other environmental impacts such as eutrophication, and identify the main process-, supply-chain, and socioeconomic factors determining these potentials. In addition, the presentation will discuss how material manufacturing and land management can be optimized simultaneously for maximum environmental benefits.

12:15 PM DISCUSSION TIME

SYMPOSIUM SB03

Materials and Designs for 3D Bioelectronic Interfaces
November 28 - December 6, 2022

Symposium Organizers

Alex Chortos, Purdue University
Jia Liu, Harvard University
Alina Rwei, TU Delft
Lizhi Xu, The University of Hong Kong

Symposium Support

Bronze
ChemComm
Journal of Materials Chemistry C
Science Robotics | AAAS

* Invited Paper
+ Distinguished Invited

SESSION SB03.01: Bioelectronic Materials and Structures I
Session Chairs: Alex Chortos, Jia Liu, Alina Rwei and Lizhi Xu
Monday Morning, November 28, 2022
Hynes, Level 1, Room 111

10:30 AM *SB03.01.01

Intrinsically-Soft Conductors for Conformal Tissue-Device Interfacing Dae-Hyeong Kim; Institute for Basic Science, Korea (the Republic of)

Recent advances in flexible and stretchable electronics have attracted great attention due to its potential applications in personalized bio-integrated healthcare devices. The mechanical mismatch between conventional rigid electronic devices and soft human tissues oftentimes causes various issues, such as a low signal-to-noise ratio of biosensors, inflammations on the tissue interfacing with the bioelectronics, skin irritations in the case of long-term wearing of the device, and ineffective electrical stimulations in feedback therapies. Ultra-flexible and stretchable bioelectronic devices have a low system modulus and intrinsic softness, and thereby have a potential to solve these issues. Nanomaterials and their composites with the elastomeric matrix are a particularly promising material candidate for realizing this soft bioelectronics concept. In this talk, the unique strategies in the synthesis of nanomaterials, processing as stretchable functional nanocomposites, seamless integration into soft bioelectronics, and their wearable and/or implantable device applications are presented. These efforts have combined recent breakthroughs in nanomaterials and soft electronics, and are expected to address unmet clinical challenges.

11:00 AM SB03.01.02

Reconfigurable 3D Microelectronic Interface via Deterministic Microfolding Wubin Bai; University of North Carolina at Chapel Hill, United States

DNA and proteins fold in three dimensions (3D) to enable functions that sustain life. Emulation of such reversible folding schemes for functional materials can create promising opportunities for advancing a wide range of technologies. In particular, morphing 3D mesostructures via multiple dimensions for high-performance materials including monocrystalline silicon can enable unconventional designs in sensory robotics, biomedical devices, microelectronics, and microelectromechanical systems. Existing approaches to morphing functional materials mostly rely on planar processes, which often complicates needed mechanisms for structural reconfiguration and limits the choice of materials composition and dimension. This presentation will introduce a bioinspired microfolding strategy to realize 3D reconfigurable microelectronic systems in freestanding forms with various advanced materials and complex architectures. The microfolding mechanism allows access to any transitional states of the folded 3D structures in a reversible fashion, to modulate functionalities on demand. Demonstrations on microantennas for telecommunication, wearable accelerometers for tremor monitoring, and epicardial bioelectronic probes for cardiac mapping, all of which are achieved via the microfolding strategy, further highlight the high potential for a broad range of applications in healthcare and communications industry.

11:15 AM *SB03.01.03

Bioadhesive Electronics and Ultrasound Xuanhe Zhao; Massachusetts Institute of Technology, United States

This talk will focus on two technologies developed at MIT Zhao Lab: 1. bioadhesive electronics that can adhere to diverse wet dynamic organs in the body without the formation of fibrotic encapsulation on the tissue-device interfaces, and 2. bioadhesive ultrasound capable of wearable imaging diverse internal organs continuously over days. I will first discuss a set of general principles for designing bioadhesive interfaces. I will illustrate the impacts of bioadhesive electronics and ultrasound on health and biology. I will conclude the talk with a vision of merging human-machine intelligence for a better world.

SESSION SB03.02: Bioelectronic Materials and Structures II
Session Chairs: Alex Chortos, Jia Liu, Alina Rwei and Lizhi Xu
Monday Afternoon, November 28, 2022
Hynes, Level 1, Room 111

1:30 PM SB03.02.02

Villi Inspired Elastomeric Interlocking Device for Intestinal Retentive Applications Durva A. Naik, Gaurav Balakrishnan and Christopher J. Bettinger;

Achieving prolonged retention of medical devices in the small intestine while mitigating tissue trauma remains a significant clinical challenge. Tissue-piercing microneedles harm intestinal epithelium inducing inflammation while reactive mucoadhesives are susceptible to fouling. Inspired by morphology of the intestinal villi, a mechanical interlocker laminated with high-aspect-ratio elastomeric microposts, that mimic dimensions of the villi, is investigated to develop intestinal retentive platforms. Effectiveness of the interlockers to resist peristalsis is characterized by performing mechanical simulations on Autodesk Fusion 360 and by determining the resistive force applied by villus when it collides with mobile micropost using Euler-Bernoulli beam theory for large deflections.

The interlocking properties are optimized by studying two simulation models that investigate the influence of device material properties ($50\text{kPa} < E_m < 1\text{GPa}$, Poisson's ratio = 0.49), micropost pitch (20,16,12,9 microposts per mm^2), arrangement (cubic/hexagonal) and tip geometry (round/cubic) on the resistive force as the microposts interaction with villi under peristaltic shear ($0.01\text{N}/\text{cm}^2$) and contraction (2666.45Pa). Digital Light Processing (DLP) 3D printing in tandem with a multi-step replica molding technique is used to fabricate the microposts and artificial villi ($E_v = 50\text{kPa}$). Dimensions of the microposts are optimized to address shrinkage post UV curing to achieve desired aspect ratio of $\sim 5:1$ (length = 1500 μm) and scanning electron microscopy is used to characterize the microposts (surface roughness = 20 μm). Work of interlocking between fabricated microposts and villi under varying preload and drag velocity is then evaluated through in vitro lap-shear tests performed on customized equipment to validate simulation results.

It is demonstrated that the ability of individual villus to resist movement of a mobile micropost is directly proportional to the elastic modulus of the micropost and preload (F_{sim} upto 812 μN , $E_m = 10\text{MPa}$). In vitro studies comply with simulation results permitting use of computational approach for future study of elastomeric mechanical interlocking systems ($F_{\text{sim}}/F_{\text{exp}} = 1.06$, $E_m = 2.05\text{MPa}$, degree of overlap = 95%). Additionally, interlockers seating 20 round tipped microposts per mm^2 arranged hexagonally can effortlessly consolidate within villi ($>95\%$ degree of overlap) through peristaltic contraction thereby eliminating the need for external stimulation and optimally resist peristaltic shear via mechanical interlocking (Experimental Work of Interlocking = 64 μJ per mm^2).

These interlockers present a compliant non-penetrative method to develop minimally invasive intestinal retentive platforms for applications in gut diagnostics by indwelling sensors, neuromodulation and oral drug delivery.

1:45 PM SB03.02.03

Mechanically Robust and Electrically Conductive Hydrogels with Hybrid Nanofibrous Network [Huimin He](#) and Lizhi Xu; The University of Hong Kong, China

Conductive hydrogels are promising candidate materials for the construction of soft bioelectronics. Their mechanical flexibility, water content, and porosity approach those of biological tissues, providing a compliant interface between the human body and electronic hardware. However, most of available conductive hydrogels exhibit poor mechanical properties, which hinders their application in durable bio-integrated systems. This presentation will highlight our recent works on aramid-nanofiber-based multifunctional hydrogels, which provide a combination of high strength, elasticity, and electrical conductivity. Highly branched aramid nanofibers afford a robust 3D framework resembling those in load-bearing soft tissues. When interlaced with polyvinyl alcohol and crosslinked with both non-covalent and covalent interactions, the nanofiber composites exhibit a high water content of $\sim 80\text{ wt}\%$, strength of $\sim 10\text{ MPa}$, ductility of $\sim 400\%$, and shape recovery of $\sim 99.5\%$ under 0.3 MPa of cyclic tensile stress. Mobile ions or conducting polymers infiltrated in the nanofibrous network impart a high electrical conductivity, enabling bioelectronic interfaces and large-strain sensors with stable operation. In addition, embedded silver nanoparticles could afford broad-spectrum antimicrobial activities, which is favorable for medical devices. The versatility of aramid-nanofiber-based composites suggests their further possibilities for functionalization and scalable fabrication toward sophisticated bioelectronic systems.

2:30 PM *SB03.02.05

Biocompatible Composites or Heterojunctions for Living Composites [Bozhi Tian](#); University of Chicago, United States

The use of biocompatible and biodegradable devices for the modulation of cells and tissues has many potential implications for medical and industrial technologies. This presentation will showcase several recent projects in this area. First, I will discuss the construction of a soil-like material from nanostructured minerals, starch granules, and liquid metals, designed to mimic immobile inorganic and organic materials and mobile phases in soil. This soil-like material is biocompatible and recyclable. It possesses chemical, optical, or mechanical responsiveness to yield write-erase electrical functions. Using soil-like materials, we demonstrate enhanced microbial metabolism and biofuel production in vitro. In addition, it can enrich gut bacterial diversity under pathological conditions and remedy bacterial dysbiosis in vivo. Afterwards, I will present a class of granule-enabled hydrogel composites that contain a range of biopolymers and synthetic hydrogels. The composites have many tissue-like properties, such as strain-stiffening behaviors. Using granular tissue-like materials, pneumatically actuated bioelectronic device applications have been developed, such as recording the electrocardiogram signal of the heart ex vivo. Additionally, I will present a recently developed nanoporous/non-porous heterojunction for improved actuation biointerfaces. At the end of my presentation, I will discuss future composite or heterojunction developments towards living machines.

2:30 PM BREAK

3:00 PM SB03.02.06

Fishbone Nanowires for In Vivo Intracellular Recording Across the Depth of an Intact Brain Youngbin Tchoc¹, [Jihwan Lee](#)¹, Karen Tonsfeldt^{1,1}, Guy Bouvier², Andrew Bourhis¹, Keundong Lee¹, Ritwik Vatsyayan¹, Samantha Russman¹, Grace Lykins¹, Massimo Scanziani² and Shadi Dayeh¹; ¹University of California, San Diego, United States; ²University of California, San Francisco, United States

Intracellular recordings have long been the gold standard for neurophysiological investigations, but their technical requirements have severely limited their scalability to large populations of neurons, especially in intact brains. Here, we developed fishbone intracellular nanowire electrode (FINE) that is composed of ultra-sharp tip nanowire electrode arrays integrated at a slanted angle on the sides of an implantable shank to record the intracellular potentials from ensembles of neurons *in vivo* across the depth of an intact brain.

FINE was designed to deliver ultrasharp nanowires into the depth of the brain that could subsequently form intracellular interface with individual neurons. To deliver the ultrasharp nanowires undamaged into the depth of the brain, the nanowires were designed to point backward at an angle from the insertion direction and sturdy polycrystalline platinum silicide (PtSi) was used for the body of the nanowires. Once the implantation was completed, sub-micron scale small retractions of FINE resulted in intracellular-like potentials. The mechanical retraction most likely caused the ultrasharp nanowires to push against or penetrate through the surrounding neurons' cell membrane, leading to intracellular-like nanowire-neuron interface. We also compared the distinctive recording characteristics of nanowire probes compared to the extracellular recording using the planar probes (30 μm) on FINE which were placed in close proximity to the nanowire probes. The FINE's capability of recording intracellular-like potentials from neural ensembles will potentially enable us to answer fundamental neuroscience questions.

3:15 PM SB03.02.07

Highly Flexible Thread-Based Eutectogel Organic Electrochemical Transistors [Rachel E. Owyung](#), Wenxin Zeng, Matthew Panzer and Sameer R. Sonkusale; Tufts University, United States

Electronic devices made from organic materials and polymer systems have attracted much attention across bioelectronic applications that interface closely with the human body, ranging from health monitoring devices to consumer wearables. Versus conventional silicon, organic transistors and electronics realized on flexible substrates can more closely resemble the mechanical properties of the underlying human skin, for improved comfort and accuracy when recording biosignals. Particularly, organic electrochemical transistors (OECTs) have emerged as promising bioelectronic active components, due to their biofriendly composition, facile processing, and high transconductance. Often aqueous electrolytes are used for gating through formation of electrolytic double layers. However, such transistors are volatile and prone to degradation from dehydration over time.

In this work, we utilize a two-prong approach to address this challenge. Firstly, the electrolyte used is a gelatin-supported deep eutectic solvent gel electrolyte or "eutectogel," rather than an archetypical aqueous electrolyte solution. The eutectogel, comprised of choline chloride and ethylene glycol supported by 20 wt.% gelatin, provides a nonvolatile electrolyte for long term device usage without further encapsulation, and the gel support scaffold provides mechanical stability (ie can act as the substrate itself) and leakproof operation of the device. The resulting OECT devices show excellent device performance and stability of transistor operation in ambient conditions without further coatings over several days or weeks. Further, experiments suggest excellent water vapor permeability, which would allow the gel to sit on-body and still allow for the underlying skin to breathe. The second factor in our design is an active channel fiber, which contains PEDOT:PSS between source and drain electrodes deposited via a novel cleanroom-free electroless deposition approach. The fiber adds additional geometric freedom, such that the active channel can be placed anywhere within the eutectogel for transistor action, for more conformal electronics.

The presented transistors operate at low voltage (within ~ 1 V), exhibit a maximum transconductance and ON/OFF ratio of 16 mS and 10^3 , respectively, for the champion device, and an average transconductance efficiency of $4.7 \pm 1.2 \text{ V}^{-1}$ at the applied biasing point of 0 V. A hydrogel equivalent OECT was fabricated and compared with the eutectogel OECT. The hydrogel OECT lost 75% volume over 72 hours and the max transconductance exhibited a 94% change after 24 hours. Conversely, the eutectogel OECT observed no measurable change in volume and only a 12% change in max transconductance over 7 days, likely due to the instability of PEDOT:PSS in ambient conditions itself. This novel device design and construction of 3D electronic circuits could lead to future implementations of smart wearables that better resemble the body it interfaces with.

3:30 PM SB03.02.08

3D Printing Piezoelectric Materials for Smart Tissue-Mimetic Bioelectronics [Jun Li](#); University of Wisconsin--Madison, United States

Piezoelectric materials are an ideal selection for advanced bioelectronic applications including human-machine interfacing, revolutionary therapeutic strategies, and self-sustainable energy solutions. Recent advances in additive manufacturing opened up the possibility of creating complex piezoelectric structures that can seamlessly integrate with bodies to modulate biological activities. Nevertheless, currently printed structures only has fair electromechanical couplings and poor mechanical properties. It demands long-time and energy-intensive post poling to enable piezoelectricity, which significantly increases fabrication time and limits structure designs. Therefore, concurrent 3D-printed piezoelectric materials could hardly meet practical requirements. We developed electric field-assisted 3D printing technologies that enable fast printing of complex and polarized ferroelectric materials with high fidelity and superb piezoelectric performance. Leveraging these technologies, we were capable of realizing smart artificial organs with build-in piezoelectricity and biomimetic properties.

We first directly printed a 3D sinusoidal artificial artery of biocompatible piezoelectric composites. The prints consisted of ferroelectric potassium sodium niobate (KNN) particles embedded within a ferroelectric polyvinylidene fluoride (PVDF) polymer matrix, which can be poled during printing within a few seconds. The synergistic effect from the KNN particles and the PVDF matrix yields a superb piezoelectric performance (bulk-scale $d_{33} > 12 \text{ pC N}^{-1}$). The sinusoidal architecture brings the mechanical modulus close to the level of blood vessels. The desired piezoelectric and mechanical properties of the artificial artery provide an excellent sensitivity to pressure change ($0.306 \text{ mV mmHg}^{-1}$, $R_2 > 0.99$) within the range of human blood pressure (11.25–225.00 mmHg). The high pressure sensitivity and the ability to detect subtle vessel motion pattern change enable early detection of partial occlusion, allowing for preventing grafts failure.

We further developed a 3D printed ferroelectric metamaterial that offers simultaneous ceramic-like high piezoelectric properties and bone-like high mechanical toughness. In this work, we adapted the nacre architecture in the design of a lamellar ferroelectric metamaterial to improve its mechanical toughness, where alternating soft ferroelectric and hard electrode layers are directly printed in bulk with an in situ poling function through low-voltage-assisted 3D printing. The principle for piezoelectricity enhancement was adapted from commercial piezo-stacks and enabled by the development of processable and printable ferroelectric and conductive composites. High-fidelity multilayered 3D ferroelectric metamaterial was printed and poled in one step at a constant low voltage. The as-printed material exhibited a significantly enhanced bulk-scale d_{33} of over 150 pC N^{-1} , as well as a superior mechanical toughness of $\sim 5.5 \text{ MPa m}^{1/2}$, more than three times higher than those of conventional piezo-ceramics. The excellent printability together with the combination of both high piezoelectric and mechanical behaviors allowed for the creation of artificial bone with tunable anisotropic piezoelectric responses and bone-comparable mechanical properties.

Reference:

- [1] Li, Jun, et al. *Advanced functional materials* 30.39 (2020): 2002868.
- [2] Li, Jun, et al. *ACS Nano* 15.9 (2021): 14903-14914.

SESSION SB03.03: Poster Session: Materials and Designs for 3D Bioelectronic Interfaces

Session Chairs: Alex Chortos, Jia Liu, Alina Rwei and Lizhi Xu

Monday Afternoon, November 28, 2022

8:00 PM - 10:00 PM

Hynes, Level 1, Hall A

SB03.03.01

Porosity-Permeability-Mechanics Relationship of Porous Silicone for Interface with Skin [Ruohan Xu](#) and Zhao Qin; Syracuse University, United States

Silicone is currently used in a variety of skin-related applications, including wearable electronic devices and medical devices such as aspirators, breast prostheses, and cosmetic fillers. Its low modulus and nonlinear mechanics make it suitable for making flexible devices that adapt well to the body and skin profiles and wear with comfort. However, a thick silicone layer has poor breathability, heat conductivity, and oxygen permeability, causing an immune response to the skin after a long-time wearing. The symptom becomes more serious with accumulated heat. Adding sacrificial particles, including salt and dissolvable polymers, can effectively make the material porous and more permeable to air, but the porosity-permeability-mechanics relationship of the material is not clear. In this study, we prepared porous silicone and tested it to find different porosity in the air permeability and oxygen passing rate of silicone. We found that the porous silicon is permeable to oxygen, which significantly increases the comfort to wear. Our study serves as a reference to reveal the trade-off between the permeability of silicone and its mechanical properties, making it rational to design flexible products that interface with different human tissues.

SB03.03.02

Flexible, Sticky and Biodegradable Wireless Device for Drug Delivery to Brain Tumors Gi Doo Cha¹, Seung Hong Choi¹ and Dae-Hyeong Kim²;

¹Seoul National University Hospital, Korea (the Republic of); ²Seoul National University, Korea (the Republic of)

Implantation of biodegradable wafers near the brain surgery site to deliver anti-cancer agents which target residual tumor cells by bypassing the blood-brain barrier has been a promising method for brain tumor treatment. However, further improvement in the prognosis is still necessary. We herein present novel materials and device technologies for drug delivery to brain tumors, i.e., a flexible, sticky, and biodegradable drug-loaded patch integrated with wireless electronics for controlled intracranial drug delivery through mild-thermic actuation. The flexible and bifacially-designed sticky/hydrophobic device allows conformal adhesion on the brain surgery site and provides spatially-controlled and temporarily-extended drug delivery to brain tumors while minimizing unintended drug leakage to the cerebrospinal fluid. Biodegradation of the entire device minimizes potential neurological side-effects. Application of the device to the mouse model confirms tumor volume suppression and improved survival rate. Demonstration in a large animal model (canine model) exhibited its potential for human application.

SB03.03.03

3D Protruded and Soft Cuff-type Electrode for Reliable Peripheral Neural Interface Electronics Hee-Jeong Jin¹, Yoo Na Kang² and Min-Ho Seo¹;

¹Pusan National University, Korea (the Republic of); ²Korea Institute of Machinery & Materials, Korea (the Republic of)

Cuff-type (or curvy-type, equivalently) electrodes have gained great interest in the field of the peripheral nerve systems, because their 3D cylindrical structure can make reasonably effective contact with peripheral nerve tissues without damage. Conventionally, the cuff-type neural interface electrodes have been developed using metals, such as gold and platinum, however, the rigid metal electrodes still suffer from the low signal-to-noise ratio (SNR) issue for recording since a tight cuff for achieving close contact to a nerve could cause eventual nerve damage during long-term implantation. To address the contact problem, various studies, for example, coating a conductive polymer or a nano-composite on the metal surface, have been actively performed, but there is a fundamental limitation to the metal-based cuff to reduce its mechanical stiffness. More recently, a hydrogel-based soft cuff type electrode has been developed, but the unacceptably high impedance of the electrode still limits its applications.

Here, we developed a mechanically soft cuff-type neural interface device that includes a 3D-protruded elastic electrode for reliable contact. The developed device is not only composed of a thin and small polydimethylsiloxane (PDMS) cuff (inner diameter \approx 1 mm), but also has \sim 100 μ m-thick carbon-black based conductive elastomeric electrodes in the cuff, realizing excellent electrical conductivity and low mechanical modulus. To demonstrate the proposed device, we developed advanced micro-fabrication, combining UV-laser ablation, screen printing, and pre-strain PDMS bonding technique. The fabricated device does not only show elastic stretchability and flexibility by $>30\%$ with a mechanical modulus (826.60 ± 2.23 kPa), similar to that of human peripheral nerve, but it also shows 99.84 ± 1.98 k Ω of impedance (@1 kHz) that is comparable to that of conventional metal electrodes. Moreover, the developed device shows a negligible mechanical modulus changes in the cyclic strain (ϵ) test (1.3%-change for 10000-cycle of $\epsilon=35\%$) and an insignificant resistance change for 7-day in PH7.4 phosphate buffer saline (PBS) solution (7.8%-change). Finally, we performed a bio-compatibility of the developed electrode using the dilution extraction method, and confirmed the $>80\%$ cell viability. From the conducted tests, we experimentally confirm that the developed cuff-type device unprecedentedly shows high mechanical softness, electrical conductivity, and bio-compatibility. Moreover, the shape and dimension of the electrodes can be easily changed owing to the high design-freedom of the developed fabrication method. Thus, we expect the proposed device can be widely used for various peripheral neural interface applications, such as neuro-modulation and pain-control.

SB03.03.04

1024-Channel, Ultra-Sharp, Individually Addressable Silicon-Based Nanowire Arrays for Natively Recording Intracellular Activity in Neuronal Networks Jihwan Lee¹, Youngbin Tchoe¹, Ren Liu², Deborah Pre³, Karen Tonsfeldt¹, Andrew Bourhis¹, Agnieszka D'Antonio-Chroska¹, Gaelle Robin³, Sang Heon Lee¹, Yun Goo Ro¹, M. Lisa Phipps⁴, Jinkyong Yoo⁴, John Nogan⁴, Jennifer Martinez⁵, Kelly Frazer¹, Anne G. Bang³ and Shadi Dayeh¹;

¹University of California, San Diego, United States; ²Harvard University, United States; ³Sanford Burnham Prebys Medical Discovery Institute, United States; ⁴Center for Integrated Nanotechnologies, Sandia National Laboratories, United States; ⁵Northern Arizona University, United States

Introduction

Intracellular access with high spatiotemporal resolution and minimal invasiveness is imperative in understanding how neurons regulate and orchestrate network activity, and how such activity can be influenced by pharmacology or other interventional methods. The gold standard technique to achieve high-fidelity intracellular recordings involves patch clamp electrophysiology, but it only permits short recording duration and can potentially damage cell health. Other research primarily focuses on vertical, nanoscale interfaces and often employ electroporation or optoporation to permeate the cell membrane and obtain intracellular potentials; however, such methods tend to lead to attenuation of recorded potentials. In our research, we report 1024-channel, vertical, ultra-sharp, silicon-based nanowire arrays to allow long-term, native recordings of intracellular potentials without any electroporation treatment.

Methods

Fabrication of these ultra-sharp tip nanowires were processed with techniques that could provide scalability up to 1024 channels to achieve simultaneous recordings over extended areas, with each single nanowire electrode individually addressed to each channel. We employed top-down etching and successive thermal oxidation on silicon substrate to realize sub-10 nm nanowires, which were subsequently coated with platinum for electrical connection. The nanowire arrays were passivated with dual layer of silicon oxide and plasma-treated parylene C to promote neuronal cell culture adhesion and prevent delamination of metal interconnects.

Results

Previously fabricated nanowires have shown stable amplitudes of intracellular potentials from 3D tissue-like networks of rat cortical neurons across long culture times up to 19 days *in vitro*. Sequential cross-sectional microscopy have revealed intimate nanowire and neuron soma interface. Modulation of electrophysiological activities are demonstrated clearly with pharmacological drugs (picrotoxin and tetrodotoxin) to either stimulate or inhibit neuronal activities. We detected graded membrane potentials prior to recorded action potential from neuronal recordings, exhibiting ability of our platform to record subthreshold potentials and observed synaptic network activities between neurons. Our experiments and simulations demonstrate that as the number of

nanowires per channel decreased, the peak-to-peak amplitude of intracellular signals increased, revealing the importance of individual addressability.

Conclusion

Individually addressable nanowire arrays with height exceeding ~6 μm can naturally permeate neurons and record intracellular potentials over extended durations of time. Overall, this study advances our understanding of and control over high-quality multi-channel intracellular recordings, and paves the way toward predictive and high-throughput electrophysiological drug screening platforms.

SB03.03.05

A Scalable, Rapidly Reconfigurable Microfluidic Platform Enables Dynamic Flow Conditions ‘On-Chip’ [Bryan Schellberg](#), Ryan Koppes and Abigail Koppes; Northeastern University, United States

Microfluidic devices, or “organ-chips”, are an emergent technology that bridges the gap between in-vitro and in-vivo models. With growing pressure from the EPA and other government agencies to reduce or eliminate the use of animals in research, microfluidics offer a robust alternative. However, the most common production method (soft lithography) is expensive and requires specialized equipment, preventing widespread use and adoption of this technology. With recent advances in three-dimensional (3D) printing technology, the chip fabrication process may be simplified considerably without sacrificing the micron-scale resolution required to simulate physiological environments in-vitro.

In this work, a scalable and rapidly reconfigurable chip platform is realized by interfacing our previously validated laser-cut and assembly-based method with 3D printing technology [1]. Laser-cut poly (methyl methacrylate) (PMMA) sheets are used to build the culture and flow compartments of the chip, and stereolithography (SLA) 3D printed resin “tops” provide the described functionality. The chip is built layer-by-layer with 1.6 mm PMMA sheets and a 4.8 mm resin upper layer. Each layer has uniform rectangular dimensions of 22 mm by 40 mm. 50 μm double-sided adhesive tape is sandwiched between each PMMA sheet to bond the lower layers together. Magnets compress a 0.4 mm thick fluoroelastomer rubber gasket at the resin-PMMA interface, forming a reversible seal for removal and re-use of chip tops. Leak tests conducted using water and a 1 mL syringe show complete sealing at pressures well above standard operating conditions.

The chip top features 3 mm by 10 mm dovetail style joints that interlock, like puzzle pieces, with up to four independent 3D printed “chip connectors”. Joints between tops and connectors fit together with a simple “push-to-fit” action, enabling rapid setup and reconfiguration of scalable chip arrays. Internal microchannels pass through the center plane of both the top and connector, allowing fluid flow from one chip to another via in/outlets at each of the joint faces. Fluoroelastomer O-rings embedded in the face of each top-connector joint reversibly seal, preventing leakage. Fluid flow within, and across, chips is directed using 3D printed hand-operated valves. The integrated valves enable flow path customization by simply redirecting or blocking off flow at set points on the chip top or connector. With all individual components prepared, an array of chips may be assembled, or rearranged from a previous configuration, in minutes. Overall, we propose a microfluidic platform that is scalable, modular, and enables dynamic control of microfluidic flow conditions on-chip without the need to adjust offline components such as syringe pumps or reservoirs. Ongoing work is focused on leveraging the current platform to include integrated characterization on-chip towards spatiotemporal data collection. Interfacing SLA 3D printing with established chip fabrication methods opens opportunities for full customization of in-vitro models to recapitulate physiologically relevant conditions on-chip.

[1] S. Hoscic *et al.*, ACS Biomater. Sci. Eng. 7, 2949-2963 (2021)

SB03.03.06

Development and Characterization of Directed Biosurface-Active Polymerizable Thiophenes [Quintin Baugh](#), Chun-Yuan Lo, Yuhang Wu, Junghyun Lee, Laure V. Kayser and David C. Martin; University of Delaware, United States

A promising new candidate for bio-electronic interfacing has been developed in the form of a hybrid 3,4-ethylenedioxythiophene/phospholipid monomer, EDOT-phospholipid. The hybrid nature of this molecule covalently fuses together the chemical functionality and specificity of biologically derived lipids to electrochemically active thiophenes in a manner that is intended to promote biological surface-directed electrochemistry. The thermal and electrochemical properties of EDOT-phospholipid have been investigated over biologically relevant conditions using a variety of methods. Thermogravimetric analysis (TGA) and differential scanning calorimetry (DSC) defined the melting point at 75.8 C with a degradation onset temperature of 180 C. The thermal stability and morphology have been investigated using hot-stage optical microscopy coupled with thermally controlled wide-angle x-ray diffraction (XRD) tuned to the thermal profiles determined by TGA/DSC. Diffusion couple experiments show the phases of EDOT-phospholipid across the full spectrum of aqueous concentrations, reinforced with surface infrared-mapping. The capacity for electrochemical polymerization was also investigated using electrochemical impedance spectroscopy (EIS) at varying aqueous concentrations and using alternate counterions. The biological interactions with human neural cells have also been investigated through the exposure of SH-SY5Y human neuroblastoma cell lines to EDOT-phospholipid and exposure to similar electrochemical conditions.

SB03.03.07

Conformal Esophageal Catheter Balloon with On-Surface Fully Printed Electronics Fabricated by Cylindrical Coordinate-Based Aerosol Jet Printing [Hansel A. Hobbie](#), Paolo Maccarini and Aaron D. Franklin; Duke University, United States

Barrett’s Esophagus (BE), a precursor to esophageal cancer (EsC), is a condition of the lower esophagus that causes the esophageal lining to inflame and thicken as the normal epithelial tissue is replaced with metaplastic intestinal tissue. BE is caused by stomach acid reflux into the esophagus, occurring as a complication of gastroesophageal reflux disease (GERD), which affects ~30 million people in North America. If left untreated, BE can continue to spread by causing more tissue erosion and the formation of precancerous lesions at both the epithelial surface and within the nonvisible mucosal layer. These lesions can then further deteriorate into adenocarcinomas, which have become the most common form of EsC with a 5-year survival rate of only 20%. Currently, the most prominent treatment for BE involves the use of an esophageal catheter to radiatively ablate affected tissue; however, this technique lacks precision in localized heating and control in terms of monitoring thermal impact on the tissue during treatment. These issues can easily lead to incomplete treatment of the BE lesions, especially those deep in the mucosal layer, requiring the endoscopic procedure to be repeated. Consequently, it is of great importance to develop an esophageal catheter that overcomes these deficiencies to provide precise ablation with tissue temperature dosimetry to ensure full treatment with minimum procedures.

In this work, we demonstrate the design, fabrication, and testing of an esophageal catheter system that is capable of high precision radiative heating and real-time temperature monitoring of surrounding material. These advanced capabilities are achieved by the design of a dual-mode antenna that can create localized heating when radiating and can measure thermal body radiation when receiving. By transmitting higher frequency microwave energy, as opposed to typical radio frequency-based ablaters, our device offers more precise heating due to the smaller resolution of the applied wavelength. This precision is then reciprocally utilized in the receiving mode of the antenna to accurately quantify the volume-averaged temperature of encompassing materials. To accomplish the fabrication of this antenna and accompanying sensors onto the complex 3D surface of our soft-material catheter, we developed a custom aerosol jet printer attachment for converting rectangular coordinate-based planar printing to a cylindrical coordinate-based printing approach. This

innovative mechanism enables material deposition onto nonplanar surfaces of revolution, thus providing a simple platform to manufacture and rapidly prototype the design of printed bioelectronics directly on the curved surface of our catheter. The main body of the catheter, which is made of polyurethane, is a balloon that inflates to the shape of the esophagus ensuring conformal contact with the esophageal lining. Using our cylindrical coordinate-based printing method, we print highly conductive silver nanowire and graphene inks onto the circumference of this balloon in an inflated state to fabricate a temperature sensor, a pressure sensor, and the ground plane for our dual-mode microwave antenna. Both sensors utilize the environmentally sensitive properties of graphene to individually monitor temperature on the tissue lining and pressure as the inflated balloon achieves contact with the esophagus. The printed ground plane, which wraps around the circumference of the balloon, operates in tandem with a coaxially mounted monopole in the center of the balloon as the dual-mode antenna. Then as a final step, these surface mounted bioelectronics are covered in a biocompatible encapsulation layer to protect the patient as well as the deposited material. Ultimately, with real-time quantification of tissue temperature and the ability to precisely tune ablation, our esophageal catheter system will enable innovative endoscopic treatment to treat BE fully from the epithelium down to the mucosal tissue layer.

SB03.03.08

Surface-Embedding of Microparticles for Biodegradable Fiber Electrodes in Implantable Electronics [Jinho Kim](#)¹, Seohyun Woo¹, Jaehong Lee¹, Congqi Yang² and Seongjun Park²; ¹Daegu Gyeongbuk Institute of Science and Technology, Korea (the Republic of); ²Korea Advanced Institute of Science and Technology, Korea (the Republic of)

Biodegradable materials, which can dissolve by body fluid after use, have been recently highlighted in the field of implantable sensors. The biodegradable sensors can monitor various biosignal and eliminate the need for surgical extraction of implanted sensors after their usage. However, previously reported biodegradable sensors are generally in planar structure that requires additional suturing for stable fixation of the sensors onto target organs or tissues in human body^{1,2}. The additional suturing can damage the sensors which mainly consist of soft materials. Although a few 1-dimensional (1D) implantable sensors have been developed to overcome this limitation, the 1D implantable sensors composed of biodegradable materials have been barely studied^{3,4}. To fabricate the biodegradable 1D sensor, the development of high-performance 1D electrodes is fundamentally essential^{5,6}.

In this work, we developed a biodegradable fiber electrode with high electrical and mechanical performance for implantable electronic devices. The biodegradable fiber electrode is composed of Polycaprolactone (PCL) core and conductive composite layer of PCL and Molybdenum (Mo) microparticles. The fabrication process for the biodegradable fiber consists of three steps: Melt-drawing⁷ and cold drawing of PCL fibers, and surface-embedding of Mo microparticles. The fabricated biodegradable fibers simultaneously showed outstanding electrical resistance (42 Ω /cm) based on dense electrical connections between the large number of Mo microparticles and high mechanical stability due to the intact PCL core. In addition, the fiber electrodes exhibited electrical stability and durability under repeated bending deformations (4000 cycles). The biocompatibility and biodegradable properties of the fiber electrode is also verified. We demonstrated that the developed biodegradable fibers could be applied to develop biodegradable fiber-based drug-release monitoring sensors, electrical stimulators, and interconnectors.

1. Boutry, C. M. *et al.* A stretchable and biodegradable strain and pressure sensor for orthopaedic application. *Nat. Electron.* **1**, 314–321 (2018).
2. Ouyang, H. *et al.* A Bioresorbable Dynamic Pressure Sensor for Cardiovascular Postoperative Care. *Adv. Mater.* **33**, 1–9 (2021).
3. Lee, J. *et al.* Stretchable and suturable fibre sensors for wireless monitoring of connective tissue strain. *Nat. Electron.* (2021) doi:10.1038/s41928-021-00557-1.
4. Kalidasan, V. *et al.* Wirelessly operated bioelectronic sutures for the monitoring of deep surgical wounds. *Nat. Biomed. Eng.* **5**, 1217–1227 (2021).
5. Kim, K. S. *et al.* Biodegradable Molybdenum/Polybutylene Adipate Terephthalate Conductive Paste for Flexible and Stretchable Transient Electronics. *Adv. Mater. Technol.* **2001297**, 1–12 (2021).
6. Koo, J. *et al.* Wireless bioresorbable electronic system enables sustained nonpharmacological neuroregenerative therapy. *Nat. Med.* **24**, 1830–1836 (2018).
7. Fu, R. *et al.* Implantable and Biodegradable Poly(L-lactic acid) Fibers for Optical Neural Interfaces. *Adv. Opt. Mater.* **6**, 1–8 (2018).

SB03.03.09

Universal Sustainable Adhesive Bioelectronics Enabled by Hierarchical Architectures [Da Wan Kim](#), Yeon Soo Lee, Seung Hwan Jeon, Dohyun Lim and Changhyun Pang; Sungkyunkwan University, Korea (the Republic of)

Recent studies on soft adhesives have sought to deeply understand how their chemical or mechanical structures interact strongly with living tissues. The aim is to optimally address the unmet needs of patients with acute or chronic diseases. Synergistic adhesion involving both mechanical interactions (capillarity-assisted suction stress) and electrostatic (hydrogen bonds) seems to be effective in overcoming the challenges associated with long-term unstable coupling to tissues. Here, we developed the electrostatically and mechanically synergistic mechanism of sustainable tissue adhesion with minimal residue by implementing hybrid multiscale architectures.^[1] By investigating various geometric parameters of microchannels on the adhesive surface, we develop a simple model to maximize adhesion strength via a time-dependent zig-zag profile and an arresting effect against crack propagation.^[2] In addition, a thermodynamic model based on a tailored multiscale combinatory adhesive was proposed. The model supported the experimental results that the thermodynamically controlled swelling of the porous hydrogel embedded in the hierarchical elastomeric structure enhances biofluid-insensitive sustainable in situ adhesion to diverse soft, slippery, and wet organ surfaces, as well as clean detachment in the peeling direction. Based on the robust tissue adhesion capability, we successfully demonstrated universal reliable measurements of electrophysiological signals generated by various tissues ranging from rodent sciatic nerve, the muscle, brain, and human skin.

[1] Da Wan Kim *et al.* *Adv. Mater.* 2022, 34(5), 2105338.

[2] Da Wan Kim *et al.* *Adv. Funct. Mater.* 2019, 29, 1807614.

SB03.03.10

Wireless, Battery-Free Push-Pull Microsystem for Membrane-Free Neurochemical Sampling in Freely Moving Animals [Guangfu Wu](#) and Yi Zhang; University of Connecticut, United States

Extensive studies in both animals and humans have demonstrated that high molecular weight neurochemicals, such as neuropeptides and other polypeptide neurochemicals, play critical roles in various neurological disorders. Despite many attempts, existing methods are constrained by detecting neuropeptide release in small animal models during behavior tasks, which leaves the molecular mechanisms underlying many neurological and psychological disorders unresolved. Here, we report a wireless, programmable push-pull microsystem for membrane-free neurochemical sampling with cellular spatial resolution in freely moving animals. In vitro studies demonstrate the sampling of various neurochemicals with high recovery (>80%). Open-field tests reveal that the device implantation does not affect the natural behavior of mice. The probe successfully captures the pharmacologically evoked release of neuropeptide Y in freely moving mice. This wireless push-pull microsystem creates opportunities for neuroscientists to understand where, when, and how the release of neuropeptides modulates diverse behavioral outputs of the brain.

SB03.03.11

Wearable Label-Free Electrochemical AMH Immunosensor Based on Flexible Conductive Fiber [Hyeji Ryu](#), Seohyun Woo, Minji Jeong and Jaehong

Lee; Daegu Gyeongbuk Institute of Science and Technology, Korea (the Republic of)

According to the World Health Organization, Infertility has affected the lives of 48 million couples of people globally. Early diagnosis of infertility can play a critical role in its successful and effective treatment. Menstrual blood is one of the biofluids which contains several biomarkers for monitoring female infertility patients. Among the menstrual blood biomarkers, Anti-Müllerian hormone (AMH), a glycoprotein hormone produced by the primordial follicles that can regulate the primordial follicle recruitment, is highly important for monitoring ovarian reserve in females [1]. To monitor the level of AMH in the body, Enzyme-linked immunosorbent assay (ELISA) has been typically used to detect serum AMH concentration. However, practical drawbacks of the ELISA include the need for blood-taking, long analysis time, labeling process, and bulky sensing instrument [2]. Wearable biosensor can be the powerful approach for the early diagnosis due to its advantages in terms of continuous real-time health monitoring, noninvasiveness, portability, and simplicity [3].

Here in, we developed a wearable electrochemical AMH immunosensor based on flexible conductive fibers for real-time AMH monitoring in menstrual blood sample. Polyurethane (PU)-coated polyethylene terephthalate (PET) fiber was used as a substrate to fabricate the flexible fiber electrode. Gold (Au) precursors were efficiently absorbed into the PU layer and then directly reduced to Au nanoparticles (AuNPs), forming a conductive composite of AuNPs and PU on the fiber. The AuNPs-based conductive fiber showed highly flexibility, stability against bending deformation (1000 repeated cycles), and excellent biocompatibility. Anti-AMH was immobilized on the AuNPs on the conductive fiber electrode by using 1-ethyl-3-(3-dimethylaminopropyl) carbodiimide (EDC) and N-hydroxysulfosuccinimide (NHS) coupling agents. Electrochemical characterization of the layer-by-layer assembly of the immunosensor was obtained by electrochemical impedance spectroscopy (EIS) and cyclic voltammetry (CV). To characterize the AMH detection, the performance of the sensor was investigated by using square wave voltammetry (SWV). In addition, we demonstrated that the fiber-based flexible AMH sensor can be successfully applied to textile-based wearable AMH sensors which monitor the AMH level in menstrual blood. This sensor can be appropriate to apply to integrate textile as a wearable electrochemical sensor for menstrual blood AMH.

[1] Rigon, C. et al. Association study of AMH and AMHR2 polymorphisms with unexplained infertility. *Fertility and sterility*, 94(4), 1244-1248 (2010). doi: 10.1016/j.fertnstert.2009.05.025

[2] Takaloo, S. et al. Wearable electrochemical flexible biosensors: With the focus on affinity biosensors. *Sensing and Bio-Sensing Research*, 32, 100403. (2021). doi: 10.1016/j.sbsr.2021.100403

[3] San Nah, J. et al. A wearable microfluidics-integrated impedimetric immunosensor based on Ti3C2Tx MXene incorporated laser-burned graphene for noninvasive sweat cortisol detection. *Sensors and Actuators B: Chemical*, 329, 129206. (2021). doi: 10.1016/j.snb.2020.129206

SB03.03.12

Use of Laser Induced Graphene (LIG) Electrodes for Hydration Status Monitoring in Artificial Urine Through Electrochemical Impedance Spectroscopy (EIS) Julio Fajardo¹, Andrea Lara¹, Andres Cazali¹, Marcelo Del Aguila¹, Victor Tzorin¹, Douglas Lira¹, Ariel Gonzalez¹, Maria Asplund^{2,2,3} and Jose A. Leal Ordonez^{2,2,1}, ¹Galileo University, Guatemala; ²University of Freiburg, Germany; ³Chalmers University of Technology, Sweden

Water is known as the source of life as it constitutes over 60% of cellular and body composition. It is fundamental for the proper functioning of all organs to keep a constant water content; otherwise, the risk of deterioration and sub-optimal performance increases. Under normal circumstances, a glass of water can reverse the effects of momentary dehydration, as well as a balanced diet, can ensure the correct electrolyte concentrations required for homeostatic maintenance in the body. However, this is not the case for several people in the world, which are at risk of sustained or even chronic dehydration. The latter can be due to poor access to water and food (e.g., developing or war-stricken countries), labor in harsh environments (e.g., field workers at coffee or sugar cane plantations, soldiers, construction workers), or as a result of the physiological aging process. Moreover, chronic dehydration is associated with several dangerous health conditions (e.g., hypertension, renal failure, diabetes, cancer, heart infarction, dementia, etc.) and should be prevented. Unfortunately, in most situations, the first signs of dehydration are mistaken or ignored by patients, which makes the early detection of this process of the utmost importance.

For people within the aforementioned risk groups, it is recommended to be aware of changes in the body throughout the day to recognize the early symptoms of dehydration such as thirst, loss of perspiration and darker-colored urine. Nonetheless, this can't be considered as a reliable, reproducible diagnostic tool, as it does not provide absolute water content and does not consider the loss of essential electrolytes. These people should have access to simple, cheap and reliable diagnostic tools to prevent any critical condition. Current laboratory based solutions like urine specific gravity and osmolality measurements provide clear insight into critical water and electrolyte concentrations and allow to take countermeasures when dehydration, hypo- or hyperkalemia, or -natremia are happening. Nevertheless, this is always a reactive solution to an ongoing problem and would not be feasible as a continuous preventive measure.

As an alternative, we propose the use of cost-effective laser-induced graphene (LIG) electrodes in combination with an AD5940 (Analog Devices, USA) impedance analyzer to perform electrochemical impedance spectroscopy (EIS) of urine samples. The data can then be analyzed through machine learning algorithms to determine the sample's relative water, sodium, and potassium concentration. With this approach, we can bring hydration monitoring to any place in the world.

Kapton sheets were pyrolyzed using a CO₂ laser to fabricate the LIG electrodes. These were then connected through 3D printed holders to the AD5940 impedance analyser and submerged in carefully prepared artificial urine solutions of varying water, sodium and potassium concentrations. The measurements were conducted with several electrodes and repeated until an appropriate set for machine learning training was obtained. During the experiments, the concentration changes could be measured as a change in the EIS spectrum of the solution, which could be then translated to the adequate proportion of water, sodium or potassium. We conclude that LIG electrodes and the AD5940 impedance analyzer are suitable for bioimpedance spectroscopy analysis. Furthermore, combination of these measurements with machine learning can be used for preliminary detection of dehydration in urine, and could be implemented in situations where constant monitoring with limited resources is necessary. Furthermore, the results obtained herein, pave the way for the use of LIG electrodes and EIS for the observation and quantification of biological processes in which bioimpedance plays a significant role such as wound healing monitoring, early cancer detection, live cell monitoring, impedance cardiography, impedance tomography, and many more.

SB03.03.13

Bioinspired Stretchable Water-Repellent Carbon Nanotube-Implanted Adhesive Electronics Patches Hyeonho Min^{1,2}, Gui Won Hwang¹, Jinhyung Kim¹ and Changhyun Pang¹; ¹Sungkyunkwan University, Korea (the Republic of); ²Korea Research Institute of Standards and Science, Korea (the Republic of)

For reliable real-time diagnosis of dynamic human body, wearable devices with adhesive interfaces for vertical/horizontal directions of dry/wet biological surfaces and water-repellent stretchable electrical performance are in high demand. Here, we present an electrically adhesive patch inspired by a diving beetle with a conductive multi-scale architecture, mechanical-stably implanted with nanowires that provides a skin-adaptable, isotropic stretchable interface for a multi-biometric signal monitoring device. Using a facile all-solution-based process, a hydrophobic, stretchable carbon-nanotube-implanted conductive

composite electrode on insect-like adhesive architectures is fabricated. The conductive adhesive patch with bioinspired wrinkled micro suction cups exhibits remarkable enhanced wet adhesion with sweat-drainability, as well as high stretchable electrical performance under tensile strain in dry and wet conditions. Furthermore, this unique structure exhibits multidirectional bonding (i.e. normal and shear directions) through enhanced horizontal bonding as well as conventional vertical bonding. Due to the high durability and softness of the biomimetic electro-adhesive patch, its performance is successfully maintained even after repeated attachments (<1000 cycles) and mechanical stretching. In order to demonstrate a multiplexed wearable device by minimizing discomfort and signal noise, ECG and temperature measurement on soft skin can be performed simultaneously in a dry and humid environment

SB03.03.14

An Intelligent Skin Patch with Bio-Inspired Architectures for Diagnostics and Treatment Jihyun Lee, Sangyul Baik, Hyoung-Ki Park and Changhyun Pang; Sungkyunkwan University, Korea (the Republic of)

Recent advances in bio-inspired architectures have received attention as promising approaches with which to implement smart skin-interfacial devices for personalized healthcare. In situ skin diagnosis requires adaptable skin adherence and rapid capture of clinical biofluids. Here, we report a simple, all-in-one device consisting of bio-inspired architectures and hydrogels that can rapidly capture biofluids and conformally attach to skin for stable, real-time monitoring of health. Inspired by the male diving beetle, the skin patch achieves repeatable, enhanced, and multidirectional adhesion to human skin in dry/wet environments, revealing the role of the cavities in these architectures. The hydrogels within the microplungers instantaneously absorb liquids from the epidermis for enhanced adhesiveness and reversibly change color for visual indication of skin pH levels. In addition, our hybrid skin patch system demonstrated reversible and directional adhesion to the complex skin surface, while allowing the drug-containing hydrogel to be in ultra-intimate contact with the non-flat skin with hierarchical roughness. With the aid of diving beetle-inspired adhesive, this extraordinary conformal hydrogel interface provides an efficient strategy for the diagnostics and treatment of skin diseases.

SB03.03.15

Mechanically Transformative Electronics Integrated with Soft, Stretchable Radiative Cooler for Reliable Rigidity- and Shape-Tuning in Hot Outdoors Sang-Hyuk Byun¹, Joo Ho Yun², Se-Yeon Heo², Chuanqian Shi³, Gil Ju Lee⁴, Karen-Christian Agno¹, Kyung-In Jang⁵, Jianliang Xiao³, Young Min Song² and Jae-Woong Jeong¹; ¹Korea Advanced Institute of Science and Technology, Korea (the Republic of); ²Gwangju Institute of Science and Technology, Korea (the Republic of); ³University of Colorado Boulder, United States; ⁴Pusan National University, Korea (the Republic of); ⁵Daegu Gyeongbuk Institute of Science and Technology, Korea (the Republic of)

The integration of a mechanically tunable gallium-based platform with soft electronics, referred to as a transformative electronic system (TES), provides an optimized mechanical interface of electronic devices intended for specific use. The stiff and flat interface of rigid electronics, such as smartphones and laptops, allows robust and convenient handling, while the compliant and deformable nature of soft electronics favors wearable and implantable applications. However, the mechanical properties of each electronics are fixed, restricting their applications beyond the original target use. The stiffness-tuning ability of TES can overcome the inherent constraints of both rigid and soft electronics owing to their fixed rigidity. Through the liquid-solid phase transition of gallium, the TES can exploit the key features of both rigid and soft electronics. While the low melting point of gallium (T_{melt} : 29.76 °C) makes the softened TES appealing for wearable and implantable applications, however, it can also inhibit the stable rigid-mode operation of TES, especially in a hot outdoor environment due to unwanted liquefaction of gallium. Therefore, proper thermal management is required for the gallium-based TES to prevent undesired softening during the rigid-mode operation. Previous approaches to managing excessive heat of electronics involve either enhancement of the device's thermal conductivity for effective heat dissipation or integration of an active cooling system (e.g., coolant circulator and thermoelectric device). However, these strategies are not suitable for TES in preventing unwanted softening due to insufficient cooling capability and high power consumption, respectively.

Here, we present an advanced design of TES that incorporates a stretchable radiative cooling system for a reliable rigid-mode operation in the hot outdoors. The stretchable radiative cooler provides enhanced reflectivity in the solar spectrum and thermal emissivity in the atmospheric window for zero-power cooling of TES. The outstanding optical characteristics are attributed to our unique design of the radiative cooler, which is a multi-layered structure of porous styrene-ethylene-butylene-styrene (SEBS) to maximize multiple Mie scattering, and provide sufficient cooling capability even under strong sunlight. Therefore, the integration of the radiative cooler with TES effectively prevents the undesired rigid-to-soft mode conversion in the hot outdoors. The radiative cooler shows sub-ambient cooling of ~4.5 °C under peak solar power of 927 W/m², maintaining the desired high rigidity of TES in a hot environment under sunlight. When the radiative-cooler-integrated TES is mounted on the skin (33–35 °C), the system becomes soft and available for use as a wearable device. Due to the flexible and stretchable properties of the radiative cooler, our proposed TES design allows 3-dimensional conformal integration on the skin with natural deformations. Furthermore, the proof-of-concept demonstration of the radiative-cooler-integrated TES, which can convert between a rigid handheld form and a soft wearable form, verifies the reliable rigid-mode operation in a hot outdoor environment when desired, suggesting that the radiative cooler is a highly favorable option for thermal management of a gallium-based TES owing to its zero-powered sub-ambient cooling capability.

SESSION SB03.04: Wearable and Implantable Devices I
Session Chairs: Alex Chortos, Jia Liu, Alina Rwei and Lizhi Xu
Tuesday Morning, November 29, 2022
Hynes, Level 1, Room 111

8:30 AM *SB03.04.01

Wearable Ultrasonic Technologies for Deep Tissue Sensing Sheng Xu; University of California, San Diego, United States

Wearable electronic devices that can noninvasively and continuously acquire vital signs from the human body represent an important trend for healthcare. Combined strategies of materials design and advanced microfabrication allow the integration of various components and devices on a soft wearable platform, resulting in functional systems with minimal constraints on the human body. Physiological signals in deep tissues are particularly valuable, because they have a stronger and faster correlation with the events in the human body than those signals on the skin surface. In this presentation, I will demonstrate a wearable ultrasonic technology that can noninvasively and continuously acquire dynamic information about our deep tissues and central organs. I will demonstrate use cases of this wearable ultrasonic technology in recording hemodynamics in central vessels, blood vessel distributions, cardiac chamber activities, and deep tissue biomechanics. The wearable ultrasonic technology represents a platform that holds profound implications for a wide range of applications in consumer electronics, defense medicine, and clinical practices.

9:00 AM SB03.04.02

Correlation Analysis between Blood Glucose and Tear Glucose in Animal Models Using Smart Contact Lenses [Wonjung Park](#), Byungjun Joo and Jang-ung Park; Yonsei University, Korea (the Republic of)

With the development of a healthcare system, studies regarding the diagnosis of diabetes non-invasively by monitoring the glucose level in various body fluids such as tear, saliva and ISF are ongoing. Among them, tear is emerging as the one of the most promising body fluids for monitoring health conditions and many studies are underway to measure the tear glucose level through various biomedical platforms including contact lenses. For these platforms to be reliable for diagnosing diabetes, it is essential to clarify the correlation between blood glucose and tear glucose which remains controversial. To address this controversial issue, studies that present the relationship between blood glucose and tear glucose using smart contact lenses were reported. However, previous smart contact lenses were operated only at specified time which is non-continuous and have failed to identify the exact correlation.

Herein, we present an in-depth investigation of the correlation between blood glucose and tear glucose. Our smart contact lenses are capable of continuous and long-term measurements at short time intervals which enables exact comparative analysis. The developed smart contact lenses were applied to normal and diabetic animal models for authentic clinical investigation of the correlation between blood glucose and tear glucose. This approach can offer unprecedented prospects for applications of the advanced biomedical platforms in further clinical trials.

9:15 AM SB03.04.03

Wireless Non-Invasive Monitoring of Cholesterol Using A Smart Contact Lens [Hayoung Song](#), Haein Shin and Jang-ung Park; Yonsei University, Korea (the Republic of)

Excessive cholesterol levels in the human body can cause an accumulation of plaques in an artery, which can induce hyperlipidemia. For diagnosing hyperlipidemia, it is important to continuously detect cholesterol levels. In recent years, the smart contact lens platform has emerged as a promising wearable healthcare device platform that measures non-invasive physiological signals in the human body. Herein, we present a soft smart contact lens that can detect cholesterol levels in tear fluids for monitoring hyperlipidemia patients using a smartphone. This smart contact lens incorporates an electrochemical biosensor for the detection of cholesterol concentrations, a stretchable antenna, and a near-field communication chip for wireless communication, which makes a smartphone the only device required to operate this smart contact lens wirelessly. The hyperlipidemia rabbit model was utilized to confirm the correlation between cholesterol levels in tear fluid and blood and to verify the feasibility of this smart contact lens for the diagnostic application of cholesterol-related diseases. Moreover, in-vivo studies with human subjects demonstrated high potential as a non-invasive healthcare device with good wearability and reliability as a non-invasive healthcare device.

9:30 AM *SB03.04.04

Designing Bioelectronic Materials for Regenerative Medicine and Biosensing [Molly Stevens](#); Imperial College London, United Kingdom

This talk will provide an overview of our work on chemical modification and functionalisation strategies to obtain designer materials for bioelectronic applications in regenerative medicine and biosensing. I will discuss how we introduce moieties to the polymer backbone to obtain tunable properties such as semi-conductivity [1], self-immolation [2] and light sensitivity [3]. We design, synthesise and fabricate conjugated polymer-based scaffolds presenting complex electrical and topographical cues to support neural stem cell adhesion, growth and differentiation [4]. I will also discuss the opportunities presented by organic bioelectronics that can be applied as powerful tools for disease diagnostics and cellular monitoring and interfacing [6]. Finally, I will talk about how we are establishing effective translational pipelines to drive our innovations to clinical application.

[1] A. Creamer... M. M. Stevens, M. Heeney. "Quantitative post-polymerisation functionalisation of conjugated polymer backbones and its application in multi-functionalised semiconducting polymer nanoparticles." *Nature Communications*. 2018. 9: 3237.

[2] D. A. Roberts... M. M. Stevens. "Dynamic pH responsivity of triazole-based self-immolative linkers." *Chemical Science*. 2020. 11:3713-3718.

[3] C. D. Spicer... M. M. Stevens. "Synthesis of hetero-bifunctional, end-capped oligo-EDOT derivatives." *Chem*. 2017. 2(1): 125-138.

[4] K. Ritzau-Reid... M. M. Stevens. "An electroactive oligo-EDOT platform for neural tissue engineering." *Advanced Functional Materials*. 2020. DOI: 10.1002/adfm.202003710.

[5] S. Higgins... M. M. Stevens. "Organic Bioelectronics: Using Highly Conjugated Polymers to Interface with Biomolecules, Cells and Tissues in the Human Body". *Advanced Materials Technologies*. 2020. DOI: 10.1002/admt.202000384.

10:00 AM BREAK

10:30 AM *SB03.04.05

Mechanics of Bio-Conformable Devices [Nanshu Lu](#); The University of Texas at Austin, United States

Noninvasive or invasive body-conformable devices include epidermal electronics, smart contact lenses, implantable artificial retina, integumentary cardiac membranes and so on. They provide functionalities from biometric sensing to therapeutics, from prosthesis to augmented capabilities. As human organs are soft and curvilinear but electronic devices are conventionally rigid and planar, it is important to understand their mismatch and develop mechanics models to guide the design of the material, structure and interface of body-conformable devices. This talk will present an overview of the field [1] and a few examples related to epidermal electronics [2, 3] and artificial retina [4]. Analytical and numerical models have been established and experimentally validated. In particular, a scaling law has been derived for non-stretchable circular sheets conforming to spherical surfaces with and without cuts [5].

1. Liu, S., et al., Strategies for body-conformable electronics. *Matter*, 2022. 5(4): p. 1104-1136.

2. Wang, L. and N. Lu, Conformability of a Thin Elastic Membrane Laminated on a Soft Substrate With Slightly Wavy Surface. *Journal of Applied Mechanics*, 2016. 83(4): p. 041007.

3. Wang, L., et al., A Thin Elastic Membrane Conformed to a Soft and Rough Substrate Subjected to Stretching/Compression. *Journal of Applied Mechanics*, 2017. 84(11): p. 111003.

4. Choi, C., et al., Human eye-inspired soft optoelectronic device using high-density MoS₂-graphene curved image sensor array. *Nature Communications*, 2017. 8: p. 1664.

5. Liu, S., et al., Cut-facilitated thin sheets conforming to spherical surfaces. to be submitted, 2022.

11:00 AM SB03.04.06

Multi-Variable Biosensing Platform Based on Aerosol Jet Printed Organic Electrochemical Transistors (OECTs) for Diabetic Wound Care [Paul Lavryshyn](#), Jiaxin Fan, Sheldon Parr, Matt Larouche, Michael Lanyon, Douglas Zochodne and Manisha Gupta; University of Alberta, Canada

Diabetic patients have an increased risk of developing chronic foot ulcers/wounds that may lead to severe consequences, including lower-extremity amputation and mortality. Studies have shown that specific parameters, such as pH, pressure, moisture, and temperature, are related to wound infection and healing phases [1]. However, in conventional wound management physicians have limited access to the real-time monitoring of these parameters and can

only assess wound status by removing the dressing, which often leads to patient discomfort and may disrupt the healing process [1]. Continuous monitoring of the wound environment with embedded wound dressing biosensors provides real-time wound status to physicians, which can aid wound care decision-making to reduce severe outcomes.

Here, we have developed a multi-variable biosensing platform to achieve *in situ* continuous monitoring of glucose and temperature levels on chronic diabetic mice wounds. Organic electrochemical transistors (OECTs) were selected for enzymatic glucose sensor development due to their high intrinsic signal amplification, low operation voltages, and compatibility with aqueous environments. We have previously reported functionalization optimization of aerosol jet printed glucose sensors[2]. In this work, the OECTs were fabricated using an Optomec Aerosol Jet 5X printer on flexible Kapton substrates with Au nanoparticle ink for the source and drain electrodes, Pt nanoparticle ink for the gate electrode, a PEDOT:PSS channel, and polyimide as the insulator. Glucose sensing was achieved by functionalizing the printed Pt gate with glucose oxidase, chitosan, and Nafion. The glucose sensor was first optimized in simulated wound fluid to achieve a desired detection range of 0.1mM – 50 mM with an average sensitivity of 0.17NR/dec.

The resistive temperature sensor was developed from a thermoplastic and carbon nanotube nanocomposite mixture. The nanocomposite was drop casted and annealed on printed Au traces and demonstrated a high linearity in its resistance change for the temperature range of 20°C to 55°C. Currently, the sensitivity is approximately 20 $\Omega/^\circ\text{C}$ with an average negative temperature coefficient of -0.001 K^{-1} . The ease of fabrication coupled with extremely high linearity ($R^2 > 0.999$) makes this an ideal candidate for temperature detection to include with our OECT devices on one substrate.

We developed a custom-designed circuit with signal processing hardware for data collection during *in vivo* wound monitoring. It includes low-noise biasing circuitry to enable OECT operation as well as a multi-channel analog to digital converter for the measurement of OECT voltage and current characteristics. Raw 32-bit data is logged to an on-board high-capacity SD card for long-term operation and further data processing is done off-board using a custom MATLAB program. Preliminary results of our glucose and temperature level measurements using our biosensing platform on healthy and diabetic mice animal model wounds will be presented.

Reference

- [1] Salvo, P., Calisi, N., Melai, B., Dini, V., Paoletti, C., Lomonaco, T., Pucci, A., di Francesco, F., Piaggese, A., & Romanelli, M, *Temperature- and pH-sensitive wearable materials for monitoring foot ulcers*. International Journal of Nanomedicine, 2017. 12: p. 949.
[2] Fan, J., A.A. Forero Pico, and M. Gupta, *A functionalization study of aerosol jet printed organic electrochemical transistors (OECTs) for glucose detection*. Materials Advances, 2021. 2(22): p. 7445-7455.

11:15 AM SB03.04.07

Optimization of Polyaniline based Flexible pH Sensor for Diabetic Wound Sensing Michelle Livojevic, Anoushka Ganguli and Manisha Gupta; University of Alberta, Canada

pH is a very important parameter for many different applications where the acidic or basic nature of the media can affect the outcomes. One such application is continuous real-time monitoring of the pH of a diabetic wound is of great importance along with other parameters like glucose, lactate etc. pH of the diabetic wound also provides the information about whether the wound is infected. In addition, the sensing of other parameters like glucose and lactate typically rely on enzymatic reactions which are affected by the pH of the wound exudate. Also, the pH of a wound can give an idea of how well it is healing. Thus, pH sensing is important by itself and also to calibrate the other readings of biosensors in the wound environment. The reliance on pH to determine the outcomes of processes and to establish baselines for sensors is the motivation behind the development of the flexible miniature pH sensor reported here. Due to the small size and flexibility of the pH sensor it can easily be integrated for use in many different situations.

In this work, an electrochemical pH sensor was developed using polyaniline (PANI) as the pH sensitive material. PANI was selected due to its ability to reversibly undergo protonation and deprotonation from its emeraldine base (EB) form to the emeraldine salt (ES) form and back, in the presence of acidic or basic media. This is utilized as the sensing mechanism as the EB form is less conductive than the ES form. Thus, based on the pH of the sample the conductivity of the PANI thin film will change. Another reason that PANI was chosen is that it is sensitive to the physiologically relevant pH range of 4 - 9.[1] One issue with PANI is that pristine PANI thin films are very fragile - therefore, polyvinyl alcohol (PVA) is added to increase the mechanical durability and flexibility of the pH sensor. The sensors were fabricated using an Optomec Aerosol Jet 5X printer to print gold electrodes on a flexible Kapton substrate, followed by a passivation layer of polyimide (PI) to prevent shorting of the device. Next the device was treated with oxygen plasma to enhance the adhesion of the PANI/PVA film to the Kapton substrate. Finally, a PANI/PVA thin film is spin coated on the device to create the pH sensitive film. Devices will be optimized by varying the geometry and composition. Results of pH measurements in different artificial buffers will be presented. To improve the signal to noise quality the developed PANI/PVA thin films will be used in organic electrochemical transistors (OECT) as the gate or channel material.

References

- [1] L. A. Schneider, A. Korber, S. Grabbe, and J. Dissemond, "Influence of pH on wound-healing: A new perspective for wound-therapy?," *Archives of Dermatological Research*, vol. 298, no. 9, pp. 413–420, Feb. 2007, doi: 10.1007/S00403-006-0713-X.

11:30 AM SB03.04.08

Rapid Meniscus-Guided Printing of Stable Semi-Solid-State Liquid Metal Microgranular-Particle for Soft Electronics Gun-Hee Lee; KAIST, Korea (the Republic of)

Liquid metal is being regarded as a promising material for soft electronics owing to its distinct combination of high electrical conductivity comparable to that of metals and exceptional deformability derived from its liquid state. However, the applicability of liquid metal is still limited due to the difficulty in simultaneously achieving its mechanical stability and initial conductivity. Furthermore, reliable and rapid patterning of stable liquid metal directly on various soft substrates at high-resolution remains a formidable challenge. In this work, meniscus-guided printing of ink containing polyelectrolyte-attached liquid metal microgranular-particle in an aqueous solvent to generate semi-solid-state liquid metal is presented. Our liquid metal microgranular-particle printed in the evaporative regime is mechanically stable, initially conductive, and patternable down to 50 μm on various substrates. Demonstrations of the ultrastretchable ($\sim 500\%$ strain) electrical circuit, customized e-skin, and zero-waste ECG sensor validate the simplicity, versatility, and reliability of this manufacturing strategy, enabling broad utility in the development of advanced soft electronics.

1:30 PM SB03.05.01

Conformable Microneedle Interstitial Fluid Accessing Platform for Biochemical Sensing Wonryung Lee; Korea Institute of Science and Technology, Korea (the Republic of)

Conformable sensing platforms are widely used as medical device platforms because of their ability to adapt well to complex biological structures. In particular, due to its flexibility and biocompatibility, it is used to measure bioelectrical signals in organs (eg brain, heart, muscle). In recent research, using this conformable sensing platform, many research groups are trying to access biofluids in various ways to measure biochemical signals as well as bioelectrical signals. As an example, there is a method using sweat to access biofluids. However, it has limitation to long-term monitoring of the disease, since it must be generated through electrical stimulation.

The microneedle platform is one candidate to access Interstitial fluid as penetration. To provide skin penetrability and conformability to skin simultaneously, the integrated substrate for this device must offer both a high Young's modulus microneedle ($10^2\sim 10^3$ μm) and a sub-micron-thick conformable substrate (~ 10 μm). A sub-micron-thick substrate can make high mechanical stress by wrinkling or crumpling, which causes damage to the interface between needle and substrate.

In the work reported here, we developed a novel multi-microneedle pH sensor array on soft substrates by integrating two siloxane-based polymers, each with a different Young's modulus. The device could have two advantages through these integrated substrates, including skin penetrability of low Young's modulus PDMS and conformability to the skin of high Young's modulus epoxy siloxane, respectively. The medical applicability of these conformable microneedle pH sensors was demonstrated by measuring the pH distribution on the dermal layer of a peripheral-vascular-disease rat model. Furthermore, glucose sensing was also demonstrated.

Wonryung Lee et al., "Conformable Microneedle pH Sensors via the Integration of two Different Siloxane Polymers for Mapping Peripheral Artery Disease" *Science Advances* (2021).

1:45 PM SB03.05.02

Gelatin-Based Ingestible Impedance Sensor for Diagnosing Eosinophilic Esophagitis Gaurav Balakrishnan, Durva Naik, Arnav Bhat, Julie Shin Kim, Sonu Marukyan, Aditya Khair and Christopher J. Bettinger; Carnegie Mellon University, United States

Eosinophilic esophagitis (EoE) is an allergen-induced esophageal inflammatory condition that affects over 200,000 patients in the United States, causing symptoms such as dysphagia, chest pain, and heart burn. With a lack of effective treatment options, early diagnosis and allergen identification is key in managing EoE. Current diagnostic protocols involve frequent endoscopies and tissue biopsies, creating an inconvenient and painful experience for patients. Research has shown that electrical impedance can be used to diagnose EoE because of intercellular dilation. Here, we design, fabricate, and test a gelatin-based ingestible impedance sensing capsule using both *in vitro* and *ex vivo* test beds.

Impedance sensing capsules were fabricated by integrating microfabricated thin-film electrodes with soft gelatin-based structural materials via a custom aqueous-phase transfer printing method. Through controlling the addition of a non-volatile solvent glycerol (50% v/v) and cross-linking agent genipin (10% crosslinking), the mechanical properties of the gelatin substrate were optimized ($E \sim 25\text{kPa}$, $\epsilon_{\text{max}} \sim 200\%$). The transferred devices on a 0.5 mm gelatin substrate demonstrate a low bending stiffness of 1.5×10^{-8} Nm^2 , allowing for the structures to be easily wrapped around a cylinder of 1 cm to form a capsule.

The microfabricated sensors were first tested using a synthetic electrochemical tissue phantom comprising varying volume fractions of 20 μm dielectric polystyrene (PS) microparticles dispersed in ionic agarose hydrogels to mimic changes in intercellular spacing. The impedance spectra show that composites with higher PS volume fractions display higher impedances and effective solution resistance values. Furthermore, normalized experimental impedance spectra show strong agreement with predicted spectra calculated using a Poisson-Nernst-Planck model of the composite system.

An *ex vivo* disease model was generated by treating porcine esophageal explants in 0.1 M HCl. Histology was performed to show that there is damage induced to the epithelial layer, causing an increased intercellular spacing. Microfabricated sensors interfaced with planar tissue section show that they are capable of distinguishing between the healthy and damaged tissues, with an over three-fold difference between the impedance of healthy and diseased tissue at 10kHz ($Z_{\text{healthy}} = 10\text{k}\Omega$, $Z_{\text{diseased}} = 3\text{k}\Omega$). Following this, 8-channel multiplexed impedance measurements were performed using the gelatin-based sensing capsules linearly translated through a porcine esophagus to obtain impedance heat maps. It is observed that the electrodes have sufficient contact with the epithelial tissue, with a significant increase in impedance on exit from the esophagus ($Z_{\text{in eso}} = 15\text{k}\Omega$, $Z_{\text{out eso}} = 200\text{k}\Omega$; @ 10kHz). Additionally, the sensors provide accurate impedance measurements through healthy and diseased esophagi at translation velocities similar to the rate of swallowing ($v = 8$ cm/s).

In conclusion, ingestible impedance sensors are a promising non-invasive and reliable platform to diagnose eosinophilic esophagitis. The presented transfer printing method is a versatile technique that can be useful in fabricating soft, hydrogel devices for a wide range of soft bioelectronic applications. Lastly, the *in vitro* synthetic model is a promising testbed for conditions that result in the impeded barrier function of epithelial tissues.

2:00 PM SB03.05.03

Bioelectronics Integrated on 3D Skin Surfaces via Kirigami-Structured Nanofibrous Membranes and Transfer-Printed Microsensors Hegeng Li, Liu Hongzhen, Sun Mingze and Lizhi Xu; The University of Hong Kong, Hong Kong

Skin-integrated soft electronics have attracted extensive research attention due to their potential utility for fitness monitoring, disease management, human-machine interfaces, and other applications. Although many materials and device components were explored for the construction of skin-integrated systems, achieving multifunctional sensor platform combined with good breathability, conformability and robustness on the skin remains difficult. Herein, two platforms were built for 3D interfaces between bioelectronics and the skin. Firstly, breathable and conformal electronic membranes (BCEMs) were manufactured with hybrid integration of microfabricated multifunctional sensors and kirigami-structured nanofibrous substrates. The resulting membrane devices exhibit tissue-like mechanical properties with high permeability for vapor transport. In addition, kirigami structures can be introduced into these membranes, providing high stretchability and 3D conformability for large-area integration on the skin. In the second scheme, tough and permeable aramid nanofiber- polyvinyl alcohol (ANF-PVA) membranes were introduced to build robust kirigami electronics. The nanofiber composite endows high fracture toughness of kirigami membranes, which can prevent failure of kirigami membranes upon stretching due to crack propagation. Energy release rate were calculated by finite element analysis (FEA) to evaluate the robustness of kirigami membranes. Microfabricated sensors and conductive polymers were employed to be the electronic components of kirigami electronics. The multifunctional sensors array from these two platforms allowed for spatiotemporal measurement of bioelectrical signals, temperature, skin hydration, and potentially many other physiological parameters. The robust performance and manufacturing scalability provided by these multifunctional skin electronics may create further opportunities for the development of advanced wearable

systems.

2:15 PM *SB03.05.04

Electronic and Tissue Interactions SuPing Lyu; Medtronic Incorporated, United States

Integration of medical devices into the patients is a must-pass step for the devices to function as intended. Obviously, it can be easier for devices that are intended to work for hours or days than those intended to function for years. Mechanical forms, fit and placement, electrical, chemical, and/or optical communications, and biological interactions are among the factors that need be considered. For certain devices and applications, the changes of devices over time are parts of the intended designs such as those with resorbable devices. More factors need be considered for them.

This talk is focused on how the tissues of the patients may impact the devices' placement and their functions. Specific examples would include how the patient tissues mechanically and biologically affect the electric and/or electronic devices, causing the functions to be different than observed in vitro. One example is electrodes of electrical stimulation devices such as cardiac pacemakers. The electrodes inserted in the tissues must have certain electric and chemical properties in order for them to deliver the electric signals to the tissues. Another example is implanted electronic devices that must be protected from being damaged by the body fluids of the patients. Water diffused into electronics can easily lead to loss of functions. This is one of the most critical questions that need be answered to make devices for long term implantable applications for the patients. Biocompatibility of devices will also be discussed briefly.

2:45 PM BREAK

3:15 PM *SB03.05.05

Soft Electronic Materials, Sensors and Integrated Systems for Biointerfaces Zhenan Bao; Stanford University, United States

In this talk, I will discuss our recent progress in soft conductive materials development, sensors for in vivo neurotransmitter sensing and integrated systems with multi-modal sensing and stimulation.

3:45 PM SB03.05.06

Bioadhesive Electronics for Atraumatic Cardiac Monitoring and Pacing *In Vivo* Jue Deng and Xuanhe Zhao; Massachusetts Institute of Technology, United States

Existing clinically-adopted bioelectronic implants mostly rely on surgical suturing or insertion of electrodes to the target tissue for diagnostic and therapeutic applications. However, these approaches can cause tissue trauma during the application and/or retrieval of the bioelectronic implants, potentially causing detrimental complications such as bleeding, tissue damage, and/or device failure. Here, we report a bioadhesive electronic device for atraumatic epicardial monitoring and pacing of the heart in vivo to overcome the limitations of existing bioelectronic implants. We use multi-material 3D printing to fabricate the bioadhesive electronic device, which offers rapid atraumatic application and retrieval as well as robust mechanical and electrical interfacing with the heart. We systematically validate the mechanical and electrical properties, biocompatibility, continuous epicardial monitoring and pacing capability, and rapid on-demand atraumatic application and removal of the bioadhesive electronics based on in vivo rat and porcine models. These findings may offer a promising platform for atraumatic bioelectronic diagnosis and treatment and inspire the future development of bioadhesive electronics.

4:00 PM SB03.05.07

Liquid 3D Bioelectronics for Diagnosis and Therapeutic Stimulation in Cardiovascular Disease Sumin Kim and Jang-ung Park; Yonsei University, Korea (the Republic of)

Accuracy in recording the electrocardiograms (ECGs) is essential for the diagnosis and treatment of cardiovascular diseases such as arrhythmia, bradycardia, or atrial fibrillation. Previous studies have been conducted for accurate monitoring of ECGs, but existing devices using planar, rigid materials with high moduli (>1 GPa) have a mechanical mismatch in interface with the biological tissues (~100 KPa). This causes various problems such as lowering the quality of ECGs, resulting in immune responses and damaging the tissue during long-term recording. Additionally, the epicardium layer of the heart adjoining the myocardium, where most planar devices are attached, restricts the clear recording of the ECGs. Therefore, for precise and long-term recording, the development of a tissue-like and injectable three-dimensional (3D) device that can reach the myocardium to reduce undesirable noise levels is important. Here, we demonstrate the liquid 3D bioelectronics based on microneedle structure for both functions of cardiac diagnosis and therapeutic stimulation, with their tattooable, injectable, and biocompatible properties. The fluidity of these liquid 3D microneedles is beneficial in preventing tissue injury by offering reliable operations. Through an in-vivo experiment with a rabbit model, we confirmed that the liquid 3D microneedles are capable of monitoring clearer signals compared to the conventional planar electrodes, and of transmitting electrical stimulus to a live heart for recovering from cardiac disorder to a normal rhythm.

SESSION SB03.06: Neural Interfaces I
Session Chairs: Alex Chortos, Jia Liu and Lizhi Xu
Wednesday Morning, November 30, 2022
Hynes, Level 1, Room 111

8:30 AM SB03.06.01

Implantable Bioelectronic Scaffolds Laden with Therapeutic Schwann Cells for Nerve Repair Ryan P. Trueman, Owein Guillemot-Legrès, Henry Lancashire, Alethea Tabor, Bob Schroeder and James B. Phillips; University College London, United Kingdom

Nerve injuries can occur following physical trauma and, in severe cases, the nerve is completely severed (full transection of the axons), creating a gap that requires surgical intervention to allow regeneration. The current gold standard of treatment for severe nerve injuries is to obtain nerve tissue from elsewhere in the patient's body and use it as a graft to bridge the gap. This presents various problems including loss of nerve function at the donor site, limited availability of donor tissue, and poor functional recovery. Electrical stimulation has shown promise in both direct applications to less severe nerve injuries¹ and to the cells responsible for nerve regeneration². This work aims to create a bioelectronic, cell laden construct that can be used to replace, and potentially surpass, the current gold standard autograft for treatment for nerve injuries.

The artificial bioelectronic scaffolds are comprised of a composite material of temperature controlled, templated oxidative polymerized polypyrrole (PPy)

nanoparticles combined with fibrillar collagen to create a homogenous hydrogel. These gels were then processed using a technique known as gel aspiration-ejection (GAE). GAE aligns the material within the hydrogel, whilst removing the bulk of the entrapped water. Furthermore, our work investigates Schwann cells, a therapeutic cell type for nerve regeneration, and the effect of electrical stimulation through gene analysis of key repair phenotype genes.

This results in dense, aligned conductive scaffolds suitable for implantation in cases of severe nerve injury. An advantage of the GAE technique is that during the manufacturing process, therapeutic cells, such as Schwann cells³, can be directly incorporated and distributed throughout the composite hydrogel, creating a cell laden, bioelectronic construct.

Monolayer Schwann cell cultures were investigated to detect gene expression changes caused by a single application of electrical stimulation. This experiment revealed significant upregulation of pro-regenerative gene expression due to the external stimulation, and importantly, a significant upregulation of c-Jun, often cited as the key transcription factor of Schwann cell repair phenotype⁴. Furthermore, upregulation in gene expression of neurotrophic factors was also shown following electrical stimulation. Our work has shown that it is possible to create these cell laden bioelectronic scaffolds. Therapeutic cells within the constructs do not have altered viability, indicating that the material is biocompatible, and the fabrication process is suitable.

By developing bioelectronic cell laden tissue engineered constructs for peripheral nerve repair, we aim to enhance both the therapeutic cells within the construct, and the body's endogenous nerve repair program. Through the process of implanting a bioelectronic scaffold, subsequent applications of electrical stimulation following surgical repair may be used throughout the regenerative process, to further augment the nerve regeneration process. Future work involves conducting the same gene analysis experiment on the therapeutic cell laden bioelectronic constructs to assess if conductive material augments the benefits shown within monolayer cultures.

1. Chan, K.M., Curran, M.W.T. & Gordon, T. The use of brief post-surgical low frequency electrical stimulation to enhance nerve regeneration in clinical practice. *J Physiol* **594**, 3553-3559 (2016).
2. Trueman, R.P., Ahlawat, A.S. & Phillips, J. A shock to the (nervous) system: Bioelectricity within peripheral nerve tissue engineering. *Tissue Eng Part B Rev* (2021).
3. Muangsanit, P. et al. Rapidly formed stable and aligned dense collagen gels seeded with Schwann cells support peripheral nerve regeneration. *J Neural Eng* **17**, 046036 (2020).
4. Wagstaff, L.J. et al. Failures of nerve regeneration caused by aging or chronic denervation are rescued by restoring Schwann cell c-Jun. *eLife* **10**, e62232 (2021).

8:45 AM SB03.06.02

Flexible Electronics Enable New Insight Into Neuronal Network Dysfunction That Progresses with Aging and Alzheimer's Disease [Theodore J. Zwanig](#)^{1,2}, Noah Pettit², Chris Harvey², Charles M. Lieber³ and Bradley T. Hyman^{1,2}; ¹Massachusetts General Hospital, United States; ²Harvard Medical School, United States; ³Harvard University, United States

A major challenge in studying aging processes is that they occur over long time scales and across brain regions, yet they involve changes in individual neurons with millisecond activity. Recent advances in the design of implantable flexible electronics allow them to study the same individual neurons and circuits over multiple months. These properties enable the study of functional changes in brain processes that occur over long periods of time, such as the onset of dementia associated with Alzheimer's disease pathology. In this presentation I will describe the design and use of flexible electronics implanted into the brains of mice that progressively accumulate Alzheimer's disease pathology with age. I will show how flexible electronics enable unique insight into cellular and circuit-level changes over long periods of time. Specifically, two flexible electrophysiology probes with neuron-like design were implanted into a single hemisphere of ThyTau22 or WT mice. One probe was targeted to the hippocampus, and the other to the medial entorhinal cortex. Recordings were made with each probe once per week over 6 months while mice run along a linear track in virtual reality. These data show the progression of an aging and tau-pathology correlated decrease in neuronal network integrity that occurs both within and between the hippocampus and entorhinal cortex at different rates.

9:00 AM SB03.06.03

A Bidirectional Neural Probe for Optical, Electrical and Chemical Probing of Neural Dynamics [Nicolette Driscoll](#), Marc-Joseph Antonini, Atharva Sahasrabudhe, Anthony Tabet and Polina Anikeeva; Massachusetts Institute of Technology, United States

Within the brain, billions of neurons communicate via diverse electrical and chemical signaling mechanisms. To begin to unravel how the function of specific neuronal subtypes within neural circuits gives rise to behavior, methods of recording and modulating neural activity across electrical, optical, and chemical modalities have been developed. Each technique has its own set of advantages and constraints, especially regarding spatial and temporal resolution, cell-type specificity, and the necessity of genetic manipulation. Combining multiple neural interfacing modalities into a single probe can leverage their unique advantages to reveal new insights into neural circuit dynamics. Here, we report a bidirectional, multifunctional neural probe that, for the first time, combines six modalities of neural interfacing: electrophysiology, electrical stimulation, fiber photometry, optogenetic stimulation, fast-scanning cyclic voltammetry (FSCV), and drug/gene delivery. We employed convergence thermal drawing to fabricate meters-long 300 μm diameter flexible fibers containing a polymer optical waveguide for fiber photometry and optogenetics, a microfluidic channel for drug/gene delivery, and carbon nanotube (CNT) electrodes for electrophysiology, electrical stimulation, and FSCV recording of a neurotransmitter dopamine (DA). Polymeric components with similar glass transition temperatures (T_g) were first machined into a macroscale preform containing the optical waveguide, a microfluidic channel, and hollow channels for CNT yarn electrodes. During the draw, the polymer preform was heated above its T_g and stretched such that the hollow channels shrank and converged around high T_g CNT yarns, which were thus integrated into the macroscale fiber. This resulted in a multimaterial macroscale fiber with conserved cross-sectional geometry compared to the preform. We demonstrate the use of our multimodal neural probe *in vivo* by implanting probes into the ventral tegmental area (VTA) and nucleus accumbens (NAc) of adult mice and investigating mesolimbic dopaminergic reward pathways. During implantation, the embedded microfluidic channel was used to deliver opsins (ChrimsonR) and optical reporters (dLight1.1) to the target brain regions. Following recovery, we performed combinations of electrical and optical stimulation, coupled with fiber photometry, electrophysiology, and FSCV recording to illustrate the utility of our multimodal probe for studying circuit level neural dynamics.

9:15 AM *SB03.06.04

Soft Subdural Electrode Arrays Tailored to Monitor Slow and Fast Neural Activity [Stephanie P. Lacour](#); Ecole Polytechnique Federale de Lausanne, Switzerland

Brain signals arising from neuropathologies can include both fast (e.g. fast ripples, up to 1kHz) and slower signals (e.g. spreading depolarization (SD) below 1Hz). Building interfaces that can monitor the full bandwidth of neural signals is thus crucial for a deeper understanding of the possible links

between the two electrophysiological signatures in brain diseases.

We report on our efforts to engineer soft subdural electrode arrays scaled to large animal models and chronic studies. Such translation requires high manufacturing reproducibility and performance stability of the soft device materials and devices. We verify the functional integrity and stability of the soft brain implants *in vivo* over time using *in-vivo* electrochemical spectroscopy measurements.

We implemented the soft neurotechnology to monitor seizure episodes and slow depolarization (SDs) in a middle cerebral and anterior artery occlusion (MCA and AA) pig model of ischemic stroke. The electrode array was designed to cover a large surface of the cortex (5.2 cm²) from 32 electrodes of 250 μm radius, in order to follow the spread of SDs over a large portion of the occluded hemisphere. Electrodes are coated with a soft platinum-based composite to guarantee low electrode impedance. We monitor continuously cortical activity using a wireless amplifier system at 1kHz sampling starting from the healthy cortex pre-occlusion, during the occlusion itself and post-occlusion over a timespan of 18 to 26 hours.

Slow patterns (SDs) and faster activity resembling focal seizures were successfully recorded in three animals indicating the soft electrode arrays are a promising interface to help decipher pathological activities for neurological diseases.

9:45 AM BREAK

10:15 AM *SB03.06.05

Peripheral Neural Interfaces to Restore Sensory, Motor and Autonomic Functions Silvestro Micera^{1,2}, Eugenio Redolfi Riva², Ciro Zinno², Alice Giannotti² and Melis Özkan¹; ¹Ecole Polytechnique Federale de Lausanne, Switzerland; ²Scuola Superiore Sant'Anna, Italy

Neuroengineering is a novel discipline combining engineering including micro and nanotechnology, electrical and mechanical, and computer science with cellular, molecular, and cognitive neuroscience to increase our basic knowledge of how the nervous system works and to develop systems able to restore functions in people affected by different types of neural disability.

Here we are going to present our recent activities to develop new and more effective peripheral interfaces for different applications. First, we are going to show how a new regenerative interface can allow to re-connect the vagus nerve with cardiac functions. Then, we are going to show how a three-dimensional intraneural interface can be used for recording and stimulation to restore bladder functions. Finally, we are going to show how new epineural interfaces can be developed for bidirectional prosthetic systems.

10:45 AM SB03.06.06

Printing of Soft Neural Interface Systems on the Cranium for Wireless Neural Recording Yong Won Kwon, Young-Geun Park, Dong Ha Lee and Jang-ung Park; Yonsei University, Korea (the Republic of)

Unveiling the mechanism of the functional connectivity of the brain can help reveal the treatments for brain dysfunction causing brain disorders and neurodegenerative diseases. Thus, long-term monitoring of brain activities with high-spatiotemporal resolution in natural conditions of subject is necessary. Moreover, current approaches for wireless neural recording based on battery-powered or battery-free systems, deteriorate integration to the biological system by requiring replacement of intermittent batteries and heavy batteries mounted on the head, or additional bulky stages for wireless power transfer and data acquisition system.

To overcome these limitations, we report a soft, conformable, and printable neural interface system on the cranium for wireless neural recording that can be conformally integrated within the subject's head, with the high-resolution printing of eutectic gallium-indium alloy (EGaIn; 75.5% gallium, 24.5% indium by weight), which is a representative gallium-based liquid metal. The printed neural interface system comprises soft neural probes, cranial circuits, and form factor-free batteries. First, liquid metal-based neural probes are fabricated structurally and mechanically similar to neurons (~ 5 μm), minimizing the formation of inflammation and immune responses. Second, liquid metal-based cranial circuits are directly printed on the surface of the cranium for electrical connection to neural probes, which are implanted in multiple brain regions of a single subject, with adaptable geometries. Third, liquid metal-based electrical interconnections with subsidiary electronics form miniaturized and conformal circuits on the cranium within the subject's head, which maximizes the integrity of electronics to biological systems, minimizing bulky head-mounted configurations. Furthermore, *in-vivo* recording using our device in freely moving mice demonstrated the simultaneous recording of local field potentials (LFPs) and single-unit spiking in multiple regions of the brain, as well as its biocompatibility and stability for the long term (~ 33 weeks), and these results suggest its broad and practical applications for various bioelectronics and neuroscience research.

11:00 AM SB03.06.07

Fully Injectable Tissue Engineered Bioelectronics for the Brain Alexander J. Boys, Alejandro Carnicer-Lombarte, Ana Fernandez-Villegas, Gabriele Kaminski Shierle, George G. Malliaras and Roisin Owens; University of Cambridge, United Kingdom

Stable, long-term integration between implanted devices and the brain remains a challenge. Properly interfaced neural implants provide the potential for recording brain activity, enabling the generation of neurally-driven prosthetics, treatment of neuroses, and a deeper understanding of brain function, among other applications. One of the major issues inhibiting long-term recordings of the brain is the lack of integration between an implant and surrounding tissue. This lack of integration often results in an inflammatory and subsequent scarring response driven by mechanical mismatches between the probe and adjacent tissue, as well as damage caused during implant placement. Tissue engineered implants provide a solution to this problem through their superior integrative capacity *in vivo* but traditionally lack any interactive components. To generate a tissue engineered neural probe, we have combined the recording capabilities of bioelectronic devices with the regenerative capacity of cellularized, tissue engineered implants to create a new implant system. Here, we developed a fully injectable bioelectronic, tissue engineered implant system for integration with the brain.

We constructed a bioelectronic device with a minimized cross-section and individually articulable leads (32 leads, each 8 x 4 μm in cross-section) to reduce the footprint of the device at the implantation site. We utilized a needle to place the device and to inject a tissue engineered matrix containing primary neurons to assist in implant placement and integration between the device and surrounding tissue. After 3 weeks, the tissue engineered insertion site was well-integrated into surrounding tissue with no clear boundary between the insertion site and brain. The interior of the implant site is entirely cellularized, primarily with neurons. A minimal microglial response was noted at the insertion site. Astrocytes were visible within the boundaries of the implant site as well. Astrocytes were also surrounding the implant site but not in conjunction with microglia, likely indicating remodeling of the insertion site. Conversely, in the control, a large boundary, consisting of astrocytes and microglia, is visible, and the interior of the implant site contained fragmented tissue.

We show the design and implementation of a fully injectable system for placing tissue engineered bioelectronic implants into the brain. This system allows for the placement of viable cell populations along with functional bioelectronic recording devices that integrate into surrounding tissue. We are now examining the long-term implications for this system and recording efficacy for neural signals over this period. Overall, we have generated a new, injectable implant system for placing bioelectronic tissue engineered brain implants. This system has potential to promote long-term recordings and integration, while causing minimal damage at the insertion site, and provides a means for new therapeutic approaches in the brain.

11:15 AM SB03.06.08

A Flexible and Scalable Neurophysiological Acquisition Array for High-Definition Brain Mapping [Andrew Bourhis](#), Ian Galton and Shadi Dayeh; University of California, San Diego, United States

For decades, neurophysiologists have relied on electrophysiological recording arrays to investigate cortical function. Electroencephalography (EEG) grid arrays are routinely placed on the cortical surface for mapping of functional and diseased cortical tissue and have improved patient outcomes. However, clinically used EEG arrays have low spatial resolution and have seen little innovation until recently. Owing in part to advances in materials science and semiconductor devices, the field of neural interface technology is now exploding, with different approaches demonstrating improvements in spatiotemporal resolution, coverage, implantability, and scalability towards higher channel counts. Despite these recent strides, many problems in this field remain unsolved. One of these challenges is the scalability of systems towards ultra-high channel counts where wiring within the arrays and toward the outside world remains a major bottleneck. Integrated circuits fabricated using conventional lithographic techniques can significantly simplify routing and reduce the number of connecting wires, but rigid and brittle silicon-based acquisition electronics are incompatible with soft neural tissue.

Toward this end, we have developed a flexible neural interface that incorporates dual-gate indium gallium zinc oxide (IGZO) thin-film transistors (TFT) as active amplifying and multiplexing elements for neurophysiological sensors. These TFTs are optimized for bio-interface applications, generating low heat densities during normal operation while maintaining high sensitivity, with electron mobilities up to $30\text{cm}^2/\text{Vs}$ and transconductance per unit drain current comparable to silicon technologies. The TFTs are built with a low-temperature monolithic fabrication process which is compatible with polymer substrates, incorporating a novel multi-layer ceramic-polymer hermetic sealing which acts to protect the system against fluids and charged ions. We have demonstrated that this strategy protects traces from undergoing any electrochemical reaction while immersed in phosphate-buffered saline for 24 hours and driving them with $\pm 6\text{V}$ amplitude square waves, and we plan on conducting accelerated aging tests with single TFT devices under various bias conditions. We have also fabricated 256-channel multiplexed EEG arrays and have fine-tuned the device characteristics and fabrication flow to be able to conduct benchtop experiments in PBS prior to conducting an in-vivo whisker-barrel stimulation experiment in a rat model.

11:30 AM SB03.06.09

Adaptable Liquid Metal Neural Probes for Neural Recording and Localized Stimulation [Dong Ha Lee](#), Yong Won Kwon, Young-Geun Park and Jang-ung Park; Yonsei University, Korea (the Republic of)

Monitoring neural activities and stimulating deep regions of the brain are the essential method to diagnose and treat neurological disorders such as Parkinson's disease, tremor, and dystonia. Recently, neural probes that can monitor neuronal signals and stimulate deep brain regions, have been researched as implantable bioelectronics for deep brain interface. However, current neural probes are based on solid metals or silicon, which cause inflammation and glial scars at tissue-electrode interfaces during micromovements of the brain with complicated nanofabrication methodologies. For long-term, stable recording and stimulation of the brain, which is essential for the neural probe as a device for the treatment of chronic neurological diseases, such bioelectronic devices require softness as a tissue, high conductivity, and long-term biostability. Gallium-based liquid metals have low Young's modulus compared to rigid metals while maintaining high conductivity and also show great biocompatibility, making them a potential applicant to neural probes.

Herein, we present the adaptable, facilely fabricated liquid-type neural probes applicable for both neural recording and electrical stimulation. The liquid form of our neural probe has comparable Young's modulus to the neural tissues compared to former neural probes using rigid metals, minimizing the formation of inflammation and glial scars on the brain tissues when implanted. A porous nanostructure was formed on the electrode-tissue interface, improving the electrochemical properties such as the impedance, charge storage capacity, and charge injection capacity for effective recording of neural signals and charge injection during electrical stimulation. Moreover, the liquid extrusion resulting from the electrical stimulation-induced current was effectively controlled, and biostability was improved due to this porous biocompatible nanostructure. We also demonstrate *in-vivo* tests for electrical stimulation and recording of neuronal signals from the rat's brain. Through electrical stimulation to the rat's brain, the rat's behaviors were controlled to a stable and manageable level, furthermore, significant changes in recorded neural signals were detected with different behavior conditions. These effective recording and stimulation results using our liquid-type neural probes are expected to play a role in the treatment of neurological disorders.

SESSION SB03.07: Neural Interfaces II
Session Chairs: Alex Chortos, Jia Liu and Lizhi Xu
Wednesday Afternoon, November 30, 2022
Hynes, Level 1, Room 111

1:30 PM SB03.07.01

Human Brain Mapping with Multi-Thousand Channel PtNRGrids Resolves Spatiotemporal Dynamics Youngbin Tchae¹, Andrew Bourhis¹, Daniel R. Cleary¹, Brittany Stedelin², [Jihwan Lee](#)¹, Karen Tonsfeldt^{1,4}, Erik C. Brown², Dominic Siler², Angélique C. Paulk³, Jimmy C. Yang³, Hongseok Oh¹, Yun Goo Ro¹, Keundong Lee¹, Samantha Russman¹, Mehran Ganji¹, Ian Galton¹, Sharona Ben-Haim¹, Ahmed M. Raslan² and Shadi Dayeh¹; ¹University of California, San Diego, United States; ²Oregon Health & Science University, United States; ³Massachusetts General Hospital, United States

Electrophysiological devices are critical for mapping eloquent and diseased brain regions and therapeutic neuromodulation in clinical settings and are extensively utilized for research in brain-machine interfaces. However, the existing devices are often limited in either spatial resolution or cortical coverage, even including those with thousands of channels used in animal experiments. Here, we developed scalable manufacturing processes and dense connectorization to achieve reconfigurable thin-film, multi-thousand channel neurophysiological recording grids using platinum-nanorods (PtNRGrids). With PtNRGrids, we have achieved a multi-thousand channel array of small ($30\ \mu\text{m}$) contacts with low impedance, providing unparalleled spatial and temporal resolution over a large cortical area. The 7° long cortical electrodes together with our sterilizable compact connector overcome challenges associated with the required large separation between the sterile surgical field and the non-sterile acquisition electronics enabling reliable intraoperative recordings from patients undergoing neurosurgical resections.

The spatiotemporal recording capability of the PtNRGrids is investigated first with anesthetized rat model undergoing whisker air-puff stimulations using high-density 32×32 array electrodes with $150\ \mu\text{m}$ pitch and $4.8\ \text{mm} \times 4.8\ \text{mm}$ coverage. The spatial mapping of stimulation evoked high gamma activity (HGA) measured from the electrode clearly distinguished functional boundaries of individual whisker barrels at $150\ \mu\text{m}$ resolution that captured the histochemically-demonstrated structure.

In the clinical setting, PtNRGrids resolved fine, complex temporal dynamics from the cortical surface in an awake human patient performing grasping tasks. HGA showed distinctive neural correlates of hand movements when compared to baseline. Furthermore, we recorded phase reversal boundaries during motor mapping to precisely localize the central sulcus in sub-mm scale resolution. These results with our high-density grids offer an unprecedented view of the functional organization and coordination of motor function over large brain regions in the human cortex. Additionally, the PtNRGrids

identified the spatial spread and dynamics of epileptic discharges in a patient undergoing epilepsy surgery at 1 mm spatial resolution, including activity induced by direct electrical stimulation. Collectively, these findings demonstrate the power of the PtNRGrids to transform clinical mapping and research with brain-machine interfaces and highlights a path toward novel therapeutics.

1:45 PM SB03.07.02

Direct-Print 3D Electrodes for High-Resolution and High-Multiplexity Neural Interfaces Pingyu Wang¹, Eric Wu¹, Hasan Ulsan², A.J. Phillips¹, Sasidhar Madugula¹, Ramandeep Vilku¹, Eric T. Zhao¹, Andreas Hierlemann², Guosong Hong¹, E.J. Chichilnisky^{1,1} and Nicholas Melosh¹; ¹Stanford University, United States; ²ETH Zürich, Switzerland

With advances in complementary metal-oxide-semiconductor (CMOS) technology, it is now possible to sense or modulate neural activity at an unprecedentedly large scale, through multiple modalities, and at a spatial resolution matching the neuron density. However, most planar and rigid CMOS devices have limited access to regions within neural tissue, limiting our ability to understand or modulate neural activity. To bridge this geometrical gap, researchers have investigated integrating penetrating electrodes onto CMOS devices, yet many critical challenges remain. For example, these penetrating electrodes have low spatial density and their fabrication processes can damage the CMOS electronics.

Here, we leveraged a high-resolution 3D printing technology to directly build high-density penetrating microelectrode arrays onto CMOS devices. We fabricated 6,600 electrodes with varying heights and pitched at 35µm. The highly versatile process allows customization of array shape and spatial density to tailor to different tissue shape or neuron density. We characterized the electrical and electrochemical properties of the electrode array, and showed that they can be easily customized. As a proof-of-principle demonstration, we recorded retinal ganglion cell activity *ex vivo*. With this technology, we hope to achieve neural interfacing at single-cell and single-cell-type resolution, which will be crucial for communicating with neural circuits using their natural neural codes.

2:00 PM SB03.07.03

Electrophoretic Devices for Brain Cancer Therapy Tobias Naegele¹, Johannes Gurke² and George G. Malliaras¹; ¹University of Cambridge, United Kingdom; ²University of Potsdam, Germany

A fundamental limitation for the success of chemotherapy in brain cancer therapies is the blood-brain-barrier which plays a pivotal role in protecting the central nervous system but also significantly reduces the amount of cancer drugs which can be delivered into a tumour [1]. Bad vascularisation of solid brain tumours further complicates delivery of therapeutically relevant drug doses [2]. Therefore, the off-target toxicity of many common chemotherapeutics places strong constraints on the amount of drugs which can be safely systemically administered.

Here, we present a novel implantable device which allows highly spatially selective delivery of charged drug molecules directly into brain tumours. Our device combines a microfluidic system for drug transport with embedded electrodes which facilitate electrophoretic transport of charged drug molecules into the target tissue. This allows delivery of drug molecules without transport of bulk solvent preventing issues arising from intracranial pressure gradients. We have investigated different electrode reactions in order to overcome limitations arising from limited electrode capacitances. The device is uniquely designed for cranial implantation ensuring minimal damage to healthy tissue when implanted. By employing stereolithographic 3D printing for the device fabrication, we allow easy modification of the design to adapt the device driven by individual tumour morphologies. Our device is not limited to specific drug molecules and can therefore easily be adapted to different cancer therapy schedules. While electrophoretic drug delivery was first described in the early 20th century and has been used since primarily for transdermal drug delivery, we believe that our approach is one of the first times this has been demonstrated for brain cancer therapy. Electrophoretic delivery will facilitate significantly higher drug concentrations in the tumour tissue than when systemically delivered while having minimal systemic impact.

[1] D. S. Hersh et al. 'Evolving Drug Delivery Strategies to Overcome the Blood Brain Barrier'. In: Current Pharmaceutical Design 22.9 (2016), pp. 1177–1193

[2] J. D. Byrne et al. 'Local iontophoretic administration of cytotoxic therapies to solid tumors'. In: Science Translational Medicine 7.273 (Feb. 2015), 273ra14–273ra14.

2:15 PM SB03.07.04

Multiplex Neurochemical Sensing via Electrografting-Enabled Site-Selective Functionalization of Graphene Field-Effect Transistors Yang Song, Zan Gao, Guangfu Wu and Yi Zhang; University of Connecticut, United States

Neurochemicals corelease has received much attention in understanding brain activity and cognition. Despite many attempts, the multiplex monitoring of coreleased neurochemicals with spatiotemporal precision and minimal crosstalk using existing methods is challenging. Here, we report a soft neural probe for multiplex neurochemical monitoring via electrografting-assisted site-selective functionalization of aptamers on graphene field-effect transistors (G-FETs). The neural probes possess excellent flexibility, ultralight mass (28 mg), and a nearly cellular-scale dimension of 50 µm × 50 µm for each G-FET. As a demonstration example, we show that G-FETs with electrochemically grafted molecular linkers (-COOH or -NH₂) and specific aptamers can be used to monitor serotonin and dopamine with high sensitivity (limit of detection: 10 pM) and selectivity (dopamine sensor > 22-fold over norepinephrine; serotonin sensor > 15-fold over dopamine). In addition, we demonstrate the feasibility for the simultaneous monitoring of dopamine and serotonin in a single neural probe with minimal crosstalk and interferences. The developed multiplex neural probes can be used to study the corelease of dopamine and serotonin in the brain, spinal cord and peripheral nerves, suggesting broad applications in neuroscience research. The developed multiplex methodology can also be adapted for monitoring other neurochemicals, such as other monoamines, amino acids and neuropeptides, by simply replacing the target aptamers functionalized on the G-FETs.

2:30 PM BREAK

3:30 PM *SB03.07.05

Miniature Battery-Free Bioelectronic Devices and Networks Jacob T. Robinson; Rice University, United States

Electronic devices that sense or manipulate biological signals have the potential to improve medical outcomes by directly acting on nerves, brain areas, and organs. However, despite the potential for these "bioelectronics devices" only a handful of implanted bioelectronic devices are currently the standard of care. One reason that implantable bioelectronics are not more widely used is that they typically require a relatively large battery pack roughly the size of a matchbox, and long wires that connect the battery pack to the sensing or stimulation target inside the body.

By creating bioelectronic devices that function without the need for batteries it would be possible to miniaturize these technologies to millimeter-scale dimensions that could easily be implanted with minimally invasive surgeries. This approach would further allow distributed networks of sensors and

actuators to measure and manipulate physiological activity throughout the body to enable precise and adaptive bioelectronic therapies with minimal risks or interference with daily activities. Magnetolectric materials offer a platform wireless power transfer technology particularly well suited for this goal of miniature bioelectronics.

Here we will discuss how magnetolectric materials function for wireless power transfer through the body and how they enable millimeter-sized devices that can be implanted through catheters and used to reach nerve targets via blood vessels. We go on to describe new opportunities for creating bioelectronic networks and how advances in magnetolectric materials can enable even smaller implantable bioelectronic interfaces.

4:00 PM SB03.07.06

Highly Sensitive and Tunable Organic Voltage Amplifiers Based on Inkjet-Printed Organic Electrochemical Transistors for *In Vivo* Recordings of Brain Activity [Yongwoo Lee](#)¹, Alejandro Carnicer-Lombarte², Sanggil Han², Ben Woodington², Seungjin Chai¹, Anastasios Polykravos², Santiago Velasco-Bosom², George G. Malliaras² and Sungjune Jung^{1,1}; ¹Pohang University of Science and Technology, Korea (the Republic of); ²University of Cambridge, United Kingdom

Organic electrochemical transistors (OECTs) exhibit great potential in electrophysiology signal-recording applications. Their mechanism of operation leverages mixed ionic/electronic conduction, and this makes them amplifying transducers that offer a high signal-to-noise ratio. However, the output of OECTs is current and this makes them incompatible with most electrophysiology data acquisition systems. To maximize their utilization, a circuit converting their output to the voltage without bulky back-end connectivity would be highly desirable. Here, we present inkjet-printed organic voltage amplifiers by integrating active and passive electrical components on a single, highly flexible substrate for *in vivo* brain activity recording. Drop-on-demand printing facilitates fine-tuning of the voltage amplification properties while monolithic integration of the printed circuit achieves significant noise reduction. Finally, we validate the conformable brain-integrated organic voltage amplifiers as electrocorticography devices in a rat *in vivo* model, showing their ability to record local field potentials in an experimental model of spontaneous and epileptiform activity in rats. Our results pave the way for the use of OECT-based circuits toward the seamless interface between biology and electronics.

4:15 PM SB03.07.07

A Lubricated Non-Immunogenic Neural Probe for Acute Insertion Trauma Minimization and Long-Term Signal Recording [Yeontaek Lee](#)¹, Hyogeun Shin², Il-Joo Cho² and Jungmok Seo¹; ¹Yonsei University, Korea (the Republic of); ²Korea Institute of Science and Technology, Korea (the Republic of)

Brain-machine interfaces (BMI) are being spotlighted as a tool to help people with extensive clinical disabilities. For example, neural signals recorded from the brain through chronically implanted electrodes can be decoded into a synthesized voice, controlling the movement of computer cursors and robotic limbs. Therefore, it is most essential to seamlessly integrate interfaces between the brain tissue and the implanted neural probe to record and control neurons over long periods of time. In recent decades, a myriad of neural probes with different shapes, materials, multiplexities, and functionalities has been developed for firm integration with brain tissue to record single action potentials stably from neurons. However, clinical BMI has not yet been widely adopted, largely because of the biological inflammatory responses on probe-tissue interfaces that arise from acute insertion trauma and chronic foreign body reaction. Intense insertion trauma not only causes an increase of acute neural loss but also accelerates the initial formation of the glial sheath around the implanted probe. Furthermore, the thickness of this glial sheath increases gradually due to the foreign body reaction, eventually driving neurons away from electrodes beyond effective recording range.

Here, we report a lubricated immune-stealth probe surface (LIPS), a neural probe electrode surface fully combined with a thin lubricant layer that displays frictionless and anti-biofouling properties *in vitro* and uncompromised electrode performance *in vivo*. The simple act of coating extends the lifetime of implantable devices by minimizing both the inflammatory response that arises from probe insertion trauma and the adhesion of inflammatory factors. LIPS can repel the adhesion of various body fluids (artificial cerebrospinal fluid; aCSF, simulated body fluid; SBF, and blood) and maintain its extraordinary anti-biofouling properties. Its exceptional anti-biofouling properties against plasma proteins and glial cells were confirmed *in vitro*, resulting in less than 1% attachment, whereas extensive adhesion occurred on bare probe surfaces. Also, our mechanical analysis confirmed that LIPS could reduce 86% of impulse from probe-tissue interface friction, shortening the acute inflammatory response that follows. Lastly, *in vivo* evaluation of the LIPS applied neural probe's electro-physiological performance was conducted. Compared to the bare probe, LIPS transiently doubled in the number of recording channels and displayed up to 9-fold improvement in signal-to-noise ratio (SNR). Long-term effects of LIPS formation included an electrode lifetime double that of the bare probe, as shown by their ability to record neuronal action potentials over a period of 4 months. This is consistent with the immunohistology results, which revealed minimal foreign body reaction on LIPS. Therefore, LIPS displays potential as a non-immunogenic surface for versatile use in BMI applications – even for the studies of deep brain electro-physiology that require insertion of rigid probes.

4:30 PM SB03.07.08

Miniaturized and Multifunctional Hydrogel Probes for Neuromodulation [Sizhe Huang](#)¹, Collin Maley², Kayla Felix¹, Weixuan Chen¹, Qianbin Wang¹ and Siyuan Rao¹; ¹University of Massachusetts Amherst, United States; ²Boston University, United States

Neural probe technologies have been used in the nervous system to modulate and record neural signaling via different modalities for understanding the mechanisms underlying neurological disorders, yet the long-term stability of such interfaces has been hindered due to the immune response caused by the mechanical mismatch between the tissues and devices. Also, the integration of different modalities within a biocompatible neural probe without increasing its rigidity and dimensions has been unachievable. Here, we report a multifunctional neural fiber probe based on soft and stretchable hydrogel materials (Polyvinyl Alcohol, PVA) via a one-step molding and extrusion method with controllable shrinking manners to address these challenges. The results have demonstrated that the PVA fiber probes can achieve a high shrinking ratio at hydrated states with a high refractive index, low absorbance, and low light loss. Additionally, a microfluidic channel has been integrated into a hydrogel optical core for pharmaceutical delivery via hydrogel shrinking manners. Furthermore, the hydrogel neural probe has been implanted into the social circuit-related brain region (Ventral tegmental area, VTA) of mice which permits chronically optogenetic stimulation, chemical intervention, and behavior studies of neural circuits in moving and socializing animals.

4:45 PM SB03.07.09

Supercapacitor RuO₂-Integrated Optoelectronic Neural Interface for Safe and Efficient Neurostimulation [Onuralp Karatum](#)¹, Erdost Yildiz¹, Humeyra Nur Kaleli¹, Afsun Sahin¹, Burak Ulgu² and Sedat Nizamoglu¹; ¹Koc University, Turkey; ²Bilkent University, Turkey

Fabrication of light-sensitive and safe optoelectronic biointerfaces that have high charge densities is important for non-invasive photostimulation of neurons with low light intensities. Photocapacitive biointerfaces offer a biocompatible charge injection mechanism, but their charge injection densities are mostly limited with the double-layer capacitance at the electrode-electrolyte interface. Here, we integrated supercapacitor ruthenium oxide (RuO₂) into an organic photocapacitive biointerface architecture to overcome the double-layer capacitance-limited charge injection. ¹RuO₂-integrated biointerfaces exhibit more than an-order-of-magnitude enhancement of photogenerated charge density because of high interfacial pseudocapacitance of RuO₂ that results from fast and reversible redox reactions. The improved photoresponse of the biointerfaces enabled light-induced activation of voltage-gated sodium channels

that led to repetitive and high success rate firing of action potentials in primary hippocampal neurons with light intensities below 1 mW mm⁻². The reversible faradaic reactions induced by RuO₂ provides a safe charge injection route at the device-electrolyte interface, which was supported via intracellular oxidative stress analysis. We verify the stability of RuO₂ biointerfaces with accelerated ageing and sterilization tests and confirm their *in vitro* biocompatibility via cytotoxicity analysis. Our findings show that flexible and all-solution-processed RuO₂ biointerfaces can be used for photomodulation of neurons with safe charge injection and low light intensities.

(1) Karatum, O.; Yildiz, E.; Kaleli, H. N.; Sahin, A.; Ulgut, B.; Nizamoglu, S. RuO₂ Supercapacitor Enabled Flexible, Safe, and Efficient Optoelectronic Neural Interface. *Advanced Functional Materials* **2022**, 2109365

SESSION SB03.08: Devices for Cells and Tissues I
Session Chairs: Alex Chortos, Jia Liu, Alina Rwei and Lizhi Xu
Thursday Morning, December 1, 2022
Hynes, Level 1, Room 111

8:30 AM SB03.08.01

Comparing a Conventional 2D with a 3D Bioelectronic Platform for Studying the Mechanism of Diet on Host-Microbiome Interactions in the Human Gut Verena Stoeger and Roisin Owens; University of Cambridge, United Kingdom

Increasing evidence demonstrates that the gut microbiome plays a significant role in human health and disease. Moreover, a strong association of the gut microbiome with the aetiology of non-communicable diseases such as type II diabetes or inflammatory bowel disease (IBD) exists.¹ Metabolites, synthesized by gut bacteria from the diet, are key for inducing beneficial health effects within host-microbiome interactions. The most prominent metabolites are short-chain fatty acids (SCFA), which are mainly acetate, propionate, and butyrate, predominantly produced by fermentation of dietary-derived fibre by bacteria like *F. prausnitzii*.² SCFAs have been shown to induce several favourable health effects in the mechanism of diabetes or obesity, but are also able to improve the functionality of the gut barrier in IBD. These effects induced by SCFAs are suggested to be mediated via activation of G-Protein coupled receptors (GPCR), especially the candidate GPR43, however, full mechanisms are not well understood yet.³ The most obvious reasons for that are the limited possibility to study non-invasively host-microbiome interactions in humans as well as a lack of access to human biopsies. Conventional 2D *in vitro* models are valuable tools for high-throughput screening and animal studies allow to get insights into cause-effect relationships, however, a translation to human physiology is still challenging.⁴ Thus, with the recently developed electronic 3D model of the human gut, we are aiming to generate predictions on host-microbiome interactions that are closer to the real human *in vivo* situation. The use of a soft and tissue-like electroactive scaffold (PEDOT: PSS) as a platform for cell hosting, allows to monitor in real-time non-invasively changes of the electrical resistance as a readout parameter of the gut barrier functionality (barrier integrity).⁵ Co-culturing of cell lines promotes cell-cell communications and thereby improves the expression of native cell receptor profiles as well as cell signalling processes.⁶ In addition, the integration of a bioelectronic sensor enables detection of the overall cell activity after activation of GPR43 by SCFAs instead of single pathway analysis, commonly done in conventional receptor assays.⁷ Currently, the effects of SCFAs on markers of the gut barrier integrity are compared in (i) traditional 2D Transwell inserts versus the 3D bioelectronic model of the human gut. Moreover, for getting a better understanding of the bioelectrical signature of the 3D platform, (ii) electrical readouts are deconvoluted using conventional molecular biological techniques like RT-qPCR.

References:

- [1] Finlay, B. B., CIFAR Humans, and Microbiome. "Are noncommunicable diseases communicable?" *Science* 367.6475 (2020): 250-251.
- [2] Parada Venegas, Daniela, et al. "Short-chain fatty acids (SCFAs)-mediated gut epithelial and immune regulation and its relevance for inflammatory bowel diseases." *Frontiers in immunology* (2019): 277.
- [3] Zhang, Zhilin, et al. "Regulatory role of short-chain fatty acids in inflammatory bowel disease." *Cell Communication and Signaling* 20.1 (2022): 1-10.
- [4] Leenaars, Cathalijn HC, et al. "Animal to human translation: A systematic scoping review of reported concordance rates." *Journal of translational medicine* 17.1 (2019): 1-22.
- [5] Pitsalidis, Charalampos, et al. "Organic bioelectronics for *in vitro* systems." *Chemical Reviews* (2021).
- [6] Edmondson, Rasheena, et al. "Three-dimensional cell culture systems and their applications in drug discovery and cell-based biosensors." *Assay and drug development technologies* 12.4 (2014): 207-218.
- [7] Hillger, Julia M., et al. "Whole-cell biosensor for label-free detection of GPCR-mediated drug responses in personal cell lines." *Biosensors and Bioelectronics* 74 (2015): 233-242.

8:45 AM SB03.08.02

3D Multifunctional Bioelectronics for Multimodal Charting of the Human Induced Pluripotent Stem Cell Derived Organoids Ren Liu, Qiang Li, Zuwan Lin, Xin Tang and Jia Liu; Harvard University, United States

Induced pluripotent stem cells (iPSCs) technology has created great opportunity for modelling human diseases and offers potential for application of personalized regenerative cell therapies. To fully understand and assess the function and maturation of stem cells-derived tissues and organoids, we need multimodal methods capable of long-term stably recording individual cell electrical activity with high spatiotemporal resolution across three-dimensional (3D) tissues, multiplexed profiling of a large number of genes in electrically recorded cells, and cross-modal computational analysis. However, none of existing technologies can fulfill these requirements. In this talk, I will first introduce the development of soft "tissue-like" stretchable mesh nanoelectronics, which match the physical and mechanical properties of soft tissue. I will also present how to integrate multifunctional sensors into the soft "tissue-like" nanoelectronics to map the multimodal tissue functions. Then I will discuss how to distribute the stretchable tissue-like bioelectronics across the entire 3D organoids by their organogenetic processes. I will discuss the seamless and noninvasive coupling of electrodes to cells, capable of providing long-term stable electrical contacts with progenitor or stem cell, captures the emergence of single-cell action potentials and enables long-term stable, continuous recording from 3D organoids during their development process. Third, I will introduce our efforts to combine the *in situ* single-cell RNA sequencing with soft bioelectronics as a method termed "*in situ* electro-seq". *In situ* electro-seq enables large-scale single-cell electrical recording and high-throughput single-cell sequencing to systematically and simultaneously investigate single-cell electrophysiology and gene expression across the intact iPSC-CMs organoids. Finally, the future perspective to apply these technologies to both *in vitro* and *in vivo* biosystems for stem cell therapies will be discussed.

9:00 AM *SB03.08.03

Controlled Small Molecule Transport in Nanofluidic Channels Aleksandr Noy^{1,2}; ¹Lawrence Livermore National Laboratory, United States;

²University of California, Merced, United States

The ability to control and direct specific ion transport across multiple scales is one of the fundamental challenges for bioelectronic applications. While researchers have traditionally focused on organic materials such as conductive polymers for these tasks, recent progress in materials science associated with development of 1D and 2D nanomaterials is beginning to offer some potential alternatives. Precise control over molecular confinement, readily achievable in these materials, provides additional unique opportunities to enhance their performance. I will discuss several examples of controlling ion and small molecule transport in highly confined channels with conductive walls. I will highlight some of the unusual mechanisms that enhance ion transport efficiency and ion transport selectivity in these systems, discuss the energy barriers for transport in these systems, and outline some challenges that we face in translating these unique transport properties into applications.

9:30 AM BREAK

10:00 AM *SB03.08.04

Materials for 3D Mesoscale Bioelectronic and Microfluidic Interface Technologies [John A. Rogers](#); Northwestern University, United States

Three-dimensional (3D), sub-millimeter-scale tissue constructs formed using human stem cells, ranging from spheroids and organoids to assembloids, are of rapidly growing interest due to their ability to reproduce essential features of vital organs in a patient specific manner. These miniaturized, fragile 3D living systems cannot, however, be examined easily using most conventional methods for sensing and manipulation, nor can they be grown to sizes larger than those that can be sustained by passive diffusion to and from surrounding media. This talk describes the essential materials and assembly aspects of a type of compliant, 3D technology framework that can be tailored with shapes, sizes and complex geometries to match those of spheroids, organoids and assembloids. Systematic studies demonstrate various electrical, fluidic, thermal, chemical and optical modes of operation that can be supported by these constructs. Examples include their use in monitoring electrophysiological behaviors and mechanical characteristics of cortical spheroids and in forming complex assembloids from dissimilar collections of spheroids.

10:30 AM SB03.08.05

Adaptive Fibre Organic Electrochemical Transistor for Volumetric Embedded Sensing in Organ-on-a-Chip [Yifei Pan](#), [Yaqi Sheng](#), [Yan Yan Shery Huang](#) and [Ruishan Liu](#); University of Cambridge, United Kingdom

Three-dimensional (3D) organ-on-a-chip models, which aim to recreate key *in vivo*, physio-pathological behaviours of organs on microfluidics, have become an important platform for fundamental research and for pharmaceutical testing. As these *in vitro* models increase in size and complexity, it is paramount to find means of monitoring the dynamics of tissue states in thick sections. Although various transistors and sensors have been developed to integrate with 3D cell cultures, their pre-set formats limit their adaptation and utilisation in a wide range of organ-on-a-chip contexts. Here, an ultra-flexible fibre organic electrochemical transistor (ufOECT) is fabricated to perform volumetric sensing in diverse formats of 3D cultures and organ-on-a-chips. With a diameter of ~30µm, and a length adjustable between millimetres to centimetres, the ufOECT can be twisted, curved, or straightened for embedding into a cell culture device for *in situ* monitoring of effective tissue matrix impedance. It is envisaged that ufOECT could be developed into a powerful tool for low-cost, scalable, label-free and sustainable monitoring organ-on-a-chip devices.

10:45 AM SB03.08.06

3D Bioelectronic Models of the Human Gut and Microbiome [Chrysanthi-Maria Moysidou](#)¹, [Douglas van Niekerk](#)¹, [Verena Stoeger](#)¹, [Lorraine Draper](#)², [Aimee Whitters](#)¹, [Colin Hill](#)² and [Roisin Owens](#)¹; ¹University of Cambridge, United Kingdom; ²University College Cork, Ireland

The implications of gut microbiome in various aspects of health and disease is now a well-established concept in modern biomedicine. Over the past decades, numerous studies have revealed links between host health and microbial activity, spanning from digestion and metabolism to autoimmune disorders and neuroinflammation. However, the exact mechanisms underlying the complex host-microbiome cross-talk remain still a mystery,^[1] mainly due to the lack of human clinical models and the challenges of translating data from animal models to human systems. Tissue-engineered constructs represent a highly promising alternative technology, apt for tackling these challenges. Such models have benefited from the use of inert gels and scaffolds as substrates for growing human cells within 3D biomimetic microenvironments, prompting tissue formation. However, monitoring technologies used to characterize cell status and activity, as well as to assess treatment effects are ill adapted to 3D biology.^[2]

Here, we report on the establishment of a 3D human intestinal model within e-Transmembranes (patent pending), a novel 3D bioelectronic platform recently developed by our group. We first describe the development of the 3D biological system, comprising intestinal and connective tissue cellular components, on the electroactive scaffolds of the e-Transmembranes, which act both as tissue substrates and as electrodes; tissue formation invokes changes on the scaffold conductivity, which is dynamically monitored via Electrochemical Impedance Spectroscopy. We then implement this bioelectronic tissue construct in a proof-of-concept study, looking at the impact of microbiota on the gut barrier integrity. More specifically, we compare the effect of a cohort of postbiotics (i.e., inanimate microorganisms and/or their components that confers a health benefit on the host)^[3], with well-known properties, on the morphology and functionality of the intestinal barrier with the respective effects of live bacterial strains (i.e., probiotics approach), also present in the postbiotic cohort. Thanks to real-time, high-content, comprehensive electrical readouts provided by our platform, we are able to closely follow both the evolution of tissue formation (~1 month) and the intimate interactions between host and microbes/microbial components during the postbiotic/probiotic interventions (~24hours). Optical and molecular biology assays at the end of the respective experimental period validate our findings, establishing the electrical signature i) of the complex tissue and its components and ii) of the impact of postbiotic and probiotic interventions on the 3D gut barrier model, thus revealing valuable information on the host-microbiome cross-talk with unprecedented time-resolution. Currently, we are working on interfacing our bioelectronic platform with more complex biological systems, such as intestinal organoids, immune cells and neurons, to further study host-microbe interactions within multi-tissue platforms. We anticipate that the unparalleled capabilities of our bioelectronic tools, combined with our tissue engineering strategy, will serve as a framework for further studies, including toxicology and drug screening/development applications.

Refs:

[1] J. F. Cryan, K. J. O'Riordan, K. Sandhu, V. Peterson, T. G. Dinan, *The Lancet Neurology* **2019**, *0*, DOI 10.1016/S1474-4422(19)30356-4.

[2] C. M. Moysidou, C. Barberio, R. M. Owens, *Frontiers in Bioengineering and Biotechnology* **2021**, *8*, 620962.

[3] S. Salminen, M. C. Collado, A. Endo, C. Hill, S. Lebeer, E. M. M. Quigley, M. E. Sanders, R. Shamir, J. R. Swann, H. Szajewska, et al., *Nature Reviews Gastroenterology & Hepatology* **2021**, *18*:9, 649.

11:00 AM SB03.08.07

Engineering Flexible Electronics for Monitoring Cellular Systems at the Air Liquid Interface (ALI), [Sarah L. Barron](#)^{1,2}, [Sophie Oldroyd](#)¹ and [Roisin Owens](#)¹; ¹University of Cambridge, United Kingdom; ²AstraZeneca, United Kingdom

Over the past decade there has been substantial growth in the field of flexible electronics for a wide range of applications including device displays, wearables and *in vivo* implants. However, their use in the pharmaceutical industry for the purpose of *in vitro* drug screening has been neglected, leaving gold standard electronic techniques outdated and unnameable to advanced biomimetic cell models. Air Liquid Interface (ALI) cultures, such as those

representative of the lung or skin, pose an additional challenge where the system can not be submerged in an electrolyte for electrode operation. To date, there is no commercially available sensor capable of continuously and non-invasively monitoring at ALI, meaning valuable mechanistic insights into barrier properties may yet be discovered.¹ Building on our previous work² and to address the above limitations, flexible microelectrode arrays have been fabricated using established photolithographic techniques.³ These devices display high conformability and biocompatibility with 21 day old human ALI culture and are capable of monitoring epithelial barrier formation and disruption in real-time, offering combined optical-electrical readouts. This platform provides new insights into barrier properties for improved understanding and pharmacological targeting of biological barrier systems in health and disease. Future directions including validation in other advanced ALI microsystems such as organoid, tissue engineered and lab-on-chip applications.

References

1. Barron S L. et al, (2021). *Advanced Biology*. 2000624.
2. Ferro A P. et al, (2018). *Advanced Biosystems*. 1800249
3. Khodagholy, D. et al, (2011). *Advanced Materials* 23, H268–H272

11:15 AM DISCUSSION TIME

11:30 AM SB03.08.09

Label-Free Optical Recording of Bioelectrical Signals Harnessing Bio-electrochromic Materials Interface. Yuecheng Peter Zhou¹, Erica Liu¹, Holger Müller^{2,3} and Bianxiao Cui¹; ¹Stanford University, United States; ²University of California, Berkeley, United States; ³Lawrence Berkeley National Laboratory, United States

Understanding how a network of neurons receive, store and process information in the human brain is a grand scientific challenge of our time. Neurons encode and communicate information through electrical signals. Traditional electrode-based recording methods such as patch clamp or multielectrode arrays are either highly invasive to cells or inflexible to sense electrical fields of cells at user-selected spatial positions with limited recording capacity. Existing optical methods, on the other hand, rely heavily on inserting voltage-sensitive fluorescent molecules into the cell membrane, which suffer from cell phototoxicity, limited recording duration and signal-to-noise ratio due to photobleaching.

Here, we introduce ElectroChromic Optical REcording (ECORE), a new electrophysiology method that optically reads out the electrical activity of electrogenic cells in a label-free and non-perturbative manner harnessing the unique properties of electrochromic polymers. The ECORE method fundamentally differs from any existing voltage recording approaches in that cell electrical signals are read out optically through voltage-sensitive optical absorption of electrochromic polymer thin films. Changes in optical reflection of the film, rather than fluorescence, are detected to probe cell electrical activities through a home-engineered optical system with a high signal-to-noise ratio. In this way, ECORE does not perturb the physiology of cells without the insertion of any molecular probes. It is also not limited by photobleaching or phototoxicity, making it a suitable tool for long-term recording of cell electrical signals over weeks or months. I will talk about single-color, dual-color, and multi-channel optical recording of electrical signals from heart muscle cells, heart tissue, neurons, and brain slices interfaced with different conjugated electrochromic polymers with high sensitivity and throughput.

SESSION SB03.09: Devices for Cells and Tissues II
Session Chairs: Alex Chortos, Jia Liu, Alina Rwei and Lizhi Xu
Thursday Afternoon, December 1, 2022
Hynes, Level 1, Room 111

1:45 PM SB03.09.01

Cyborg Engineering—Integration of Soft Nanoelectronics with hiPSC-Derived Three-dimensional Tissues and Organoids Qiang Li¹, Zuwan Lin¹, Ren Liu¹, Xin Tang¹, Xiao Wang^{2,3} and Jia Liu¹; ¹Harvard University, United States; ²Broad Institute of MIT and Harvard, United States; ³Massachusetts Institute of Technology, United States

Complex organs (e.g., heart and brain) rely on spatiotemporally orchestrated interaction of heterogeneous cells to maintain the whole-organ functions. Thus, understating the development, mechanisms, and diseases of these organs require system-level mapping of cellular activities across entire three-dimensional (3D) volumes. Simultaneously charting single-cell gene expression and electrophysiology in intact tissues across time and space is crucial to understand gene-to-function relationships. Such multimodal methods require stable and continuous recording of individual cell electrical activity, multiplexed profiling of a large number of genes in electrically recorded cells, and multi- and cross-modal computational analysis. In this talk, I will first introduce the cyborg organoid platform, which implanted and distributed soft stretchable nanoelectronics through 2D-to-3D organogenesis triggered by cell-cell interactions, enabling long-term stable and tissue-wide recording of cardiac and brain organoids at single-cell resolution throughout tissue development with minimal impact on growth and differentiation. Then, I will discuss our efforts to integrate cyborg organoid technology with *in situ* RNA sequencing as an *in situ* electro-sequencing (electro-seq) technology to stably map millisecond-timescale electrical activity and simultaneously profile single-cell transcriptomes across 3D tissues. We applied *in situ* electro-seq to human-induced pluripotent stem cell-derived cardiomyocyte (hiPSC-CM) patches, enabling multi-modal *in situ* analysis of CM electrophysiology with gene expression at the cellular level, jointly defining cell states and developmental trajectories. Using machine learning-based cross-modal analysis, *in situ* electro-seq identified gene-to-electrophysiology relationships across CM development and accurately reconstructed the evolution of gene expression profiles based on long-term stable electrical measurements. Finally, I will discuss the future directions to apply these technologies to 3D developing tissues and organoids, creating spatiotemporal multi-modal maps and predictive models to assess the functional and transcriptional maturation of the human organoids for cell therapies.

2:00 PM *SB03.09.02

Toward Multimodality Sense (and Actuate) of Three-Dimensional (3D) Tissues Tzahi Cohen-Karni; Carnegie Mellon University, United States

My team's efforts are focused on the development and engineering of nanomaterials-based platforms to interrogate and affect the electrical properties of tissue and cells such as cardiomyocytes, and neurons, with a specific goal to understand electrical signal transduction in complex 3D cellular assemblies, e.g., organoids or spheroids. Highly flexible bottom-up nanomaterials synthesis capabilities allow us to form unique hybrid-nanomaterials that can be used in various input/output bioelectrical interfaces, i.e., bioelectrical platforms for chemical and physical sensing and actuation. We developed a breakthrough bioelectrical interface, a 3D self-rolled biosensor arrays (3D-SR-BAs) of either active field effect transistors or passive microelectrodes to measure both cardiac and neural spheroids electrophysiology in 3D. This approach enables electrophysiological investigation and monitoring of the complex signal transduction in 3D cellular assemblies toward an organ-on-an-electronic-chip (organ-on-e-chip) platform for tissue maturation investigations and

development of drugs for disease treatment. Utilizing graphene, a two-dimensional (2D) atomically thin carbon allotrope, we can simultaneously record the intracellular electrical activity of multiple excitable cells with ultra-microelectrodes that can be as small as an axon (ca. 2 μ m). The outstanding electrochemical properties of the synthesized hybrid-nanomaterials allow us to develop highly efficient catalysts, and electrical sensors and actuators. We demonstrated sensors capable of exploring brain chemistry and sensors/actuators that are deployed in a 3D tissue models. Finally, using the unique optical properties of nanocarbons in the form of graphene-based hybrid-nanomaterials and 2D nanocarbidides (MXene), we have formed remote, non-genetic bioelectrical interfaces with excitable cells and modulated cellular and network activity with low needed energy and high precision. In summary, the exceptional synthetic control and flexible assembly of nanomaterials provide powerful tools for fundamental studies and applications in life science and potentially seamlessly merge nanomaterials-based platforms with cells and tissue, fusing nonliving and living systems together.

2:30 PM *SB03.09.03

Graphene-Based Autonomous Wearable Sweat Biosensors Wei Gao; California Institute of Technology, United States

Wearable and flexible non-invasive bioelectronics for the continuous monitoring of metabolites in sweat can detect a few analytes at sufficiently high concentrations, typically during vigorous exercise so as to generate sufficient quantity of the biofluid. Here, we report the design and performance of wearable electrochemical biosensors for the continuous analysis, in sweat during physical exercise and at rest, of trace levels of a variety of biomarkers including metabolites, amino acids, and vitamins. The wearable sensors consist of laser-engraved graphene electrodes, functionalized with target-specific receptors such as antibody-like molecularly imprinted polymers, and integrated with modules for iontophoresis-based sweat induction, microfluidic sweat sampling, signal processing and calibration, and wireless communication. The clinical value of our wearable sensors was evaluated through multiple human studies involving both healthy and patient populations toward physiological monitoring, nutritional monitoring, disease diagnosis, mental health assessment, and drug personalization. These wearable and flexible devices could open the door to a wide range of personalized monitoring, diagnostic, and therapeutic applications.

3:00 PM BREAK

3:30 PM SB03.09.04

Real-Time Pressure Mapping of Brain Organoids by Active-Matrix Array of Field-Effect Transistor Jakyoung Lee, Hunkyu Seo, Moohyun Kim and Jang-ung Park; Yonsei University, Korea (the Republic of)

Brain organoids are being studied for neurodegenerative disease modeling due to their intrinsic three-dimensional (3D) phenotypic characteristics. They are typically cultured for a long time, with their size growing as each day passes. Interestingly, at the end of their functional lifespan, their size does not change significantly, and necrosis starts from the core decreasing the central density of brain organoids. Therefore, it is important to inspect their core condition for characterization of their age. Generally, the cores of organoids are observed by using a confocal microscope. However, this method tends to be inaccurate as the optical characterization cannot thoroughly examine the inside of the organoid.

Herein, we developed a pressure sensor with an active-matrix array for the real-time monitoring of brain organoids. The sensor consists of an array of field-effect transistors (FET) based on Si channels. The channels are extremely small, 10 μ m x 10 μ m, capable to detect delicate weight of the brain organoids and represent high-resolution pressure sensing. Recording the pressure signal readouts detected from each channel allows 2D mapping that makes it possible to visualize the pressure distribution of the brain organoids. This distribution correlates to the core density which reflects the condition of the organoids, thus it provides the indicator of age characterization. In addition, the examination of their conditions in real-time is simultaneous with the cultivation of organoids due to the media well placed directly above the top gate of the device. Therefore, real-time monitoring through our active-matrix array sensor is expected to manage the brain organoids effectively and evaluate the unconventional mechano-physiological conditions even during the cultivation phase.

3:45 PM SB03.09.05

An Effective On-Demand Chronic Oxygen Delivery Strategy for Implanted Cells via Electrocatalytic Oxygen Evolution Reaction Inkyu Lee¹, Abhijith Surendran², Seonghan Jo¹, Samantha Fleury³, Abijeet S. Mehta², Ian Gimino¹, Georgios Nikifordis², Xudong Ji², Omid Veisheh³, Jonathan Rivnay² and Tzahi Cohen-Karni^{1,1}; ¹Carnegie Mellon University, United States; ²Northwestern University, United States; ³Rice University, United States

Immunoisolation device containing therapeutic cells has been regarded as a promising cell therapy technique, encapsulating the cells within size-exclusive immunobarrier without the use of immunosuppression. However, the barrier restricts the diffusion of nutrients for the cells. High cell density needed for minimizing device footprint resulting with innately large oxygen consumption further exacerbates local oxygen deficiency. Moreover, physiological oxygen tensions are insufficient to sustain such densely packed cells. Several approaches were developed to support the cells using exogenous oxygen, for example, periodic oxygen injection and embedding peroxide solids. Nevertheless, their capabilities are limited because of a lack of controllability and the exhaustion of oxygen-generating agents.

Here, we report a miniaturized and chronic on-demand electrochemical cell maintenance platform via electrocatalytic oxygen evolution reaction, employing iridium oxide as an electrocatalyst. The distribution of generated oxygen was manipulated by the geometries of catalytic arrays, supported by diffusion simulation. The actual oxygen-generating capabilities of the system were verified by using an oxygen-sensitive probe, and on-demand oxygen delivery was realized by fine-tuning the applied potential/current. We further demonstrated that our strategy does not produce detrimental side reactions. Importantly, our unique bioelectrical oxygenating system significantly improved cellular viability and functionality of cell capsules (60kcell/mm³) for up to 21 days in vitro under hypoxic conditions (1 % oxygen). By supporting high cell density, our effective and versatile bioelectronic system opens up broad bioengineering applications from organoid basic research to clinical opportunities for patients who are suffering from chronic endocrine disorders.

4:00 PM SB03.09.06

Monitoring of 3D-Printed Airway Model Integrity with an Printed Organic Electrochemical Transistor Seungjin Chai¹, Yunji Lee¹, Yongwoo Lee¹, Woojo Kim¹, Roisin Owens² and Sungjune Jung^{1,1}; ¹Pohang University of Science and Technology, Korea (the Republic of); ²University of Cambridge, United Kingdom

SARS-CoV-2 pandemic has drawn new attention to virus neutralization assay and neutralizing antibody quantification for drug testing preclinical testing and determining drug testing efficacy over time. Disruption of epithelial barriers is a key clinical turning point that differentiates patients who are likely to develop severe virus outcomes. However, convenient, fast and accurate barrier measurement remains a challenge. Organic electrochemical transistor(OECT) has shown a great potential particularly in capturing ionic signals, therefore extensively employed to probe local ion flux changes that are caused by paracellular flow of soluble molecules controlled by tight junctions. Here, we report inkjet printed PEDOT:PSS-based OECT for barrier measurement platform with inkjet printed 3D-printed airway model. We have developed a reliable printing process for fabricating OECT devices. Volumetric capacitance and transconductance of a device were significantly enhanced as the number of printed layered increased. Transient response in OECT could evaluate 3D-printed airway model. Finally, Influenza A virus infection was monitored in a 3D airway model with OECT. We could be detected barrier integrity with the advantages of a noninvasive process. Our platform show promise for use in vaccine evaluation.

4:15 PM SB03.09.07

A Miniature 3D Electrochemical Biosensor for the Detection of Collagenase Type I Grazielle M. Cruzado¹, Geraldine Merle¹ and Ashkan Koushanpour²; ¹Polytechnique Montreal, Canada; ²McGill University, Canada

Breast cancer can occur in women at any age after puberty, and according to WHO accounts for 685,000 deaths globally, in 2020. A variety of carcinogenesis processes are intimately related to the extracellular environment, and because collagenases play an important role in extracellular matrix remodeling, they are found to be commonly associated with cancer pathologies. It is known that collagenase type I is commonly associated with enhanced breast cancer growth and metastasis. The levels of collagenase I in a normal adult body are usually low (1.19 ± 0.7 ng/mL) and an elevated concentration is a predictive marker for future development of an invasive type of breast cancer. There's an urge for rapid and efficient tests to help the early diagnosis and consequently treatment of this type of cancer, so that the survival rates can significantly increase. Current technologies – liquid chromatography-mass spectroscopy, fluorescence resonance energy transfer, surface plasmon resonance and ELISA – are costly, complicated, labour intensive, and time-consuming. Additionally, since molecular diagnostic tests and instrumentation are complex, they require highly knowledgeable and expert scientists to establish benchmarks. Compared to these approaches, electrochemical techniques are simpler, faster, low-cost, and user-friendly.

Here we report a miniature 3D electrochemical biosensor for the detection of Collagenase I. A portable 3D electrochemical system was built using 3D printing. Given the hydrolysis ability of the collagenase, a short peptide sequence was chemically modified with a redox probe and attached to a gold electrode. Improving on the signal to noise ratio and sensitivity without affecting the volume of the electrode was achieved with Au nanospikes. Au nanospikes were first electrodeposited using Pb to guide the Au growth and to increase the deposition rate due to the cathodic depolarisation of the electrode surface. Given the presence of cysteine in the peptide, thiol chemistry was applied by simply immersing the Au surface of the 3D electrode. The successful grafting was well established by FT-IR, electrochemical analysis through cyclic voltammetry (CV) and square wave voltammetry (SWV) and SEM analysis. The cleavage of the peptide by the collagenase, was measured after only 10 minutes via the signal decrease due to the decrease in the tunneling current. The peptide loaded Au nanospike system performance was verified in collagenase type I solution (PBS, pH 7.4) exhibiting linear range of detection of 1 to 500 ng.mL⁻¹ and LOD of 0.07ng/ml The peptide loaded Au nanospikes on an unconventional 3D system showed as a desirable candidate to become an alternative to the conventional and complex assay for the detection of collagenase and can be deployed for mass testing in point-of-care settings.

4:30 PM SB03.09.08

Aerosol Jet Printed OECT-Based SARS-CoV-2 Spike Proteins Disposable Biosensors with n-type Naphthalene Diimide Small-Molecule OMIECs Seongdae Kang, Jiaxin Fan and Manisha Gupta; University of Alberta, Canada

COVID-19 pandemic is still an ongoing issue in our community. The battle against this disease still imposes a heavy burden on hospitals and the healthcare system. Screening asymptomatic and mild case patient is profoundly essential to abate this threat. The development of rapid, accurate, and predictable diagnosis methods will provide huge assistance to public health. The current sample collection method for the nasal antigen test is uncomfortable and has a higher risk of bleeding. Moreover, the South African researcher suggested that the saliva sample is preferred to the nasal one for detecting Omicron, the dominant variant.¹⁾

Here, we report all-printed organic electrochemical transistor (OECT)-based single-use disposable biosensors with n-type naphthalene diimide (NDI) small-molecule organic mixed ionic-electronic conductor (OMIEC) channel for SARS-COV-2 spike protein detection.

We developed an all-printed OECT biosensor using an Optomec Aerosol Jet 5X 3D printer onto a flexible polyimide substrate. Gold nanoparticle ink was used for printing the source/drain and gate electrode. The glycolated naphthalene diimide (gNDI-Br₂) small-molecule OMIEC is deposited to form the channel with a width of 600 μm, a length of 100 μm, and an optimized thickness of 2 μm. SARS-CoV-2 spike protein detection was achieved by the functionalization of the printed gold gate electrode with antibodies which are anchored via thiol-based self-assembled monolayers (SAMs).

The 3D printed p-type OMIECs have been applied for the OECT and published²⁾, but the n-type has not. We have previously presented the mixed ionic-electronic conduction behaviour of the gNDI-Br₂ n-type small-molecule OMIEC³⁾. In this work, we were able to fabricate all-printed OECT biosensors with NDI channel material because the gNDI-Br₂ is easily processable with common organic solvents that are suitable for printing. This is the first demonstration for the n-type gNDI-Br₂ OMIEC that can be utilized as the OECT channel material.

The SARS-CoV-2 antibodies functionalized OECT antigen biosensors showed a noticeable shift in their transfer characteristics before and after the antibody attachment. The biosensor was tested with different concentrations of SARS-CoV-2 S1 spike protein (1 pg/mL to 10 μg/mL) solution in 1X PBS with 5 min of incubation time. The transfer characteristics were collected after the incubation and demonstrated a clear trend with spike protein concentration. The threshold voltage, V_T , shifted to a higher value as the spike protein concentration increases. To the best of our knowledge, this NDI-based biosensor is the first n-type OECT-based immunosensor. By modifying the gate functionalization, the NDI biosensor can be used for detecting other bio-analytes such as different types of viruses or enzymes. We will present the biosensor geometry optimization, sensing with different SARS-CoV-2 spike protein variants, and preliminary results of detecting SARS-COV-2 spike protein in an artificial saliva buffer.

Reference

- 1) G. Marais, N. Hsiao, A. Iranzadeh, D. Doolabh, A. Enoch, C. Chu, C. Williamson, A. Brink, D. Hardie, medRxiv. (2021) <https://doi.org/10.1101/2021.12.22.21268246>
- 2) J. Fan, AAF. Pico, M. Gupta, Mater, Adv. (2021) <https://doi.org/10.1039/D1MA00479D>
- 3) S. Kang, J. Fan, J. Soares, M. Gupta, 2019 MRS Fall. (2019)

SESSION SB03.10: Virtual Session: Materials and Designs for 3D Bioelectronic Interfaces

Session Chairs: Alex Chortos, Jia Liu, Alina Rwei and Lizhi Xu

Tuesday Morning, December 6, 2022

SB03-virtual

8:00 AM *SB03.10.01

Silicon-Based Optoelectronic Interfaces for Biological Modulations Xing Sheng¹ and Yunxiang Huang²; ¹Tsinghua University, China; ²Dartmouth College, United States

The capability to selectively and precisely modulate biological activities represents a powerful tool for fundamental research and clinical therapeutics. Traditional electrical stimulations associate with bulky and tethered implants, and optogenetic methods rely on genetic modification for cell targeting. Here, we report an optoelectronic, non-genetic strategy for exciting and inhibiting biological activities, accomplished by bioresorbable, thin-film silicon

based 3D structures. Under illumination, these structures establish polarity-dependent, positive or negative voltages at the semiconductor/solution interface. Such photovoltaic signals enable deterministic depolarization and hyperpolarization of cultured neurons and stem cells, upregulating and downregulating intracellular calcium dynamics in vitro. Furthermore, flexible, thin-film Si based devices mounted on the animal tissue selectively activate and silence in vivo activities. We demonstrate that these Si structures can modulate the neural activities as well as the bone regeneration process. Finally, these Si membranes naturally dissolve within the animal body. Such a Si-based material and device platform offers broad potential for biomedical applications.

8:30 AM *SB03.10.02

Bioinspired Self-Adaptive Conformal Electronic Armor, Electronic Tattoo and iFlexSense Skin Yongan Huang and Shan Jiang; Huazhong Univ of Science & Technology, China

Conformability plays a ballast role in the final functionality and performance of flexible electronics since it is the basis of superior signal-to-noise ratio and large area mapping capability. It involves flexibility and stretchability, which depends on key factors such as geometry, material, and surface curvature.

The interfacial mechanics and adhesion strength at the interfaces determine the nature of this contact. However, conformable integration of flexible electronics on complex 3D surfaces remains to be challenging and costly both from a design and manufacturing perspective.

Bioinspiration has been proved powerful and effective to develop novel materials, devices, and structures from biological systems and biological evolution and refinement which has occurred over millions of years. Historically, many great ideas in science and technology often arise from studying nature.

Bioinspired flexible electronics have been widely investigated, the imitated objects range from plants to animals or human, from birds to reptiles, and from terrestrial species to marine species. This presentation mainly introduces bioinspired strategies to design the flexible electronics:

1) **Bioinspired Electronic Armor:** Bioinspired by freeform snakeskin composed of rigid scales and connective soft integument, we propose a novel rigid-structure-based electronic armor (E-armor) that reconciles the protectability and conformability while enables stable electronic functions. It can render the rigid, non-stretchable devices fully conformable to arbitrary 3D surfaces. Based on the unique soft-hinge Kirigami regime, it can make use of the supernormal mechanical advantages like auxetic stretchability and high fill factor but overcome the inherent buckling conflict, rendering the stiff, non-stretchable electronics fully conform to arbitrary 3D surfaces. Meanwhile, the conductivity of soft nodes endows the Kiri-MM with electrical connotation and innovative functionalities. The results establish new directions for applied and basic research in the fields of flexible electronics and soft robotics, with relevance to grant challenges in improving the survivability of flexible electronics in complex environments.

2) **Bioinspired Electronic Tattoo:** Bioinspired by the breathable human skin, we have successfully designed, fabricated, compensated, and applied a substrate-free tattoo-like electrode system for large-scale epidermal electrophysiology. Highly stretchable and high-area filling-factor electrodes are designed using Peano curves with transformable topology. The breathability of the substrate-free epidermal electrodes is quantified through thermal and hydration characterizations. Applications of these electrodes include multichannel ECG, accurate ASL recognition, and prostheses control, as well as mapping of neck activities. These low-cost but large-area and high-performance epidermal electrodes have paved the way for future large-area epidermal electronics necessary for personnel health/performance management, disease diagnosis, and human-machine interaction.

3) **Bioinspired iFlexSense Skin:** Bioinspired by the unprecedented sensing abilities (skin, synapse, immune system, and brain) of flying creatures, we innovatively propose an intelligent flexible sensing skin with multifunctional sensor array, data transmission, impact monitoring and artificial intelligence for aerodynamic measurement of complex surface. The skin-like mechanosensation system integrates with five kinds of flexible sensors, including capacitive sensors, piezoelectric sensors, hot-film sensors, temperature sensors, and strain sensors. The synapse-like encoding system is also directly integrated on the sensing skin to convert analog data to digital data to diminish the transmission noise. The brain-like intelligent algorithm is employed to for analyzing the data and making a judgment, such as identifying and localizing the impacts.

9:00 AM SB03.10.05

Novel Ultra-Sensitive Permeation-Measuring Methods for Ultra-High Barrier Encapsulations of Compliant Implantable Bioelectronics Massimo Mariello¹, Kangling Wu¹, Marion Von Allmen², Matthias Van Gompel², Stephanie P. Lacour¹ and Yves Letier¹; ¹Ecole Polytechnique Federale de Lausanne, Switzerland; ²Comelec SA, Switzerland

The next generation of implantable bioelectronic devices are soft, compliant and flexible/stretchable and they need to be protected from the body environment through high-barrier coatings. A critical challenge is the design, synthesis and integration of these coatings in order to guarantee simultaneously hermeticity, biocompatibility, flexibility, mechanical integrity, compatibility with microfabrication processes, long-term reliability and stability (at least longer than 5÷10 years in the body). Against standard barrier technologies based on macroscopic rigid capsules made in Titanium or ceramics, or on thick soft silicones, the next generation of barrier coatings relies on thin-film encapsulations (TFE). They can be manufactured through several deposition techniques (ALD, PECVD, thermal growth, etc.), based on organic/inorganic single-layers or hybrid multilayers. The accurate evaluation of their barrier performances is still a challenge, because standard measuring systems are characterized by too high sensitivity limits ($> 10^{-5}$ g/m²/day) which cannot detect the ultra-low permeation capabilities of the coatings. Hence, novel ultrasensitive (at least 10^{-7} g/m²/day) quantitative methods to assess the barrier hermeticity need to be engineered.

In this work, we introduce a comprehensive method to quantify ultra-low permeability of TFE engineered for bioelectronic micro-devices. The method relies on magnesium (Mg) thin-film sensors. Corrosion of Mg induced by water diffusion in the barrier coating is observed and analysed in terms of optical, electrical and electrochemical properties of Mg structures. The advantages of this approach are that Mg does not need a fully inert atmosphere and it can be easily integrated in the microfabrication processes of implantable bioelectronic devices. Different methods are presented based on the optical characterization of Mg thin films coated with some standard barriers, the monitoring of their electrical resistance during corrosion, or the analysis of the anticorrosive properties of the encapsulations through electrochemical measurements. Several testing conditions are selected, including exposure to wet air or soaking in a phosphate buffer saline (PBS) solution that mimics the body biofluids. High temperatures are chosen to perform accelerated tests whereas specific analytical/computational models are used to extract from the measurements the water-vapour transmission rates (WVTR) of the barriers. Rigid, flexible and stretchable substrates coated with TFE are used to evaluate the versatility of the measuring system. A record sensitivity of 3.3×10^{-8} g/m²/day was achieved, which is lower than the other current methods. The integration of this method into real active implants is also demonstrated.

The proposed characterization strategy answers a long-term need to assess thin film hermeticity, reveals tangible prospective applications for the development of thin hermetic customizable packaging for miniaturized implantable electronics, and promise quantitative evaluation of all types of conformal TFE for bioelectronic systems in a reliable way.

9:15 AM SB03.10.06

Surface Modulation of Conducting Polymers for Advanced Organic Neural Interfaces Michele Bianchi^{1,2}, Alice Lunghi^{1,3}, Sonia Guzzo^{1,3}, Anna De Salvo^{1,3}, Pierpaolo Greco³, Mauro Murgia^{1,4}, Michele Di Lauro¹, Luciano Fadiga^{1,3} and Fabio Biscarini^{1,2}; ¹Italian Institute of Technology, Italy; ²Università degli Studi di Modena e Reggio Emilia, Italy; ³Università di Ferrara, Italy; ⁴National Research Council, Italy

Surface modulation of conducting polymers (CPs) has attracted great interest in organic electronics due to the possibility of controlling the optical, electrical and electrochemical properties of devices through the introduction of preferential charge transport pathways or by increasing the active area of the material [1,2]. Micro- and nanopatterning techniques such as 3D printing, inkjet printing, plasma etching, nanosphere lithography and soft-lithography

have been exploited in a number of applications, including organic photovoltaic cells (OPVs), field effect transistors (OFETs) and light emitting diodes (OLEDs).

However, surface modulation of CPs for bio-related applications such as multi-electrode arrays (MEA), neural interfaces, neuromorphic devices and tissue engineering, is largely unexplored, despite the rapidly growing role of CPs in these fields [3,4]. At the Center for Translational Neurophysiology of Speech and Communication of the Italian Institute of Technology (IIT), we pursue the design and fabrication of micro- and nanopatterned/modulated CPs that can be easily integrated on flexible substrates in order to design advanced organic neural interfaces.

Multi-electrode arrays with 3D micropillars enable the recording of electrophysiological signals in vitro with higher accuracy and signal-to-noise ratio than planar arrays. I will present a simple approach for the fabrication of flexible interfaces featuring poly(3,4-ethylenedioxythiophene)-poly(styrenesulfonate) (PEDOT:PSS) micropillars on a technologically interesting flexible polydimethylsiloxane (PDMS) substrate [5]. Large-area, isotropic arrays of PEDOT:PSS micropillars with tailored geometric area, surface properties and electrochemical characteristics were fabricated by a combination of soft-lithography and electrodeposition methods. The 3D PEDOT:PSS micropillars were demonstrated to optimally support adhesion, growth and differentiation of SH-SY5Y cells and influence the direction of neurite outgrowth. I will also describe the integration of such micropillar arrays into ultra-flexible surface arrays for neural recording and stimulation.

I will then show the possibility of influencing neuronal polarization and accelerating neurite outgrowth during cell differentiation using PEDOT:PSS nanogrooves, with a potentially major impact in the field of neural tissue regeneration, where synergistic integration of electrical stimulation and topographical guidance is expected to accelerate axonal reconnection and regeneration of damaged tissue.

Organic electrochemical transistors (OECTs) can be integrated into neural interfaces to significantly increase the signal-to-noise ratio during recording [6]. In this context, I will show that the transconductance (a figure of merit of the device directly related to its ability to amplify electrophysiological signals) can be significantly increased by nanomodulating the surface of ultrathin PEDOT channel through a simple stamp-assisted soft-lithography approach.

[1] C. Park, J. Na, E. Kim, *ACS Appl. Mater. Interfaces* **2017**, 28802.

[2] V. Q. Nguyen, D. Schaming, P. Martin, J. C. Lacroix, *ACS Appl. Mater. Interfaces* **2015**, 7, 21673.

[3] M. Bianchi, A. De Salvo, M. Asplund, S. Carli, M. Di Lauro, A. Schulze-Bonhage, T. Stieglitz, L. Fadiga, F. Biscarini, *Adv. Sci.* **2022**, 2104701.

[4] G. Calandra Sebastianella, M. Di Lauro, M. Murgia, M. Bianchi, S. Carli, M. Zoli, L. Fadiga, F. Biscarini, *Adv. Electron. Mater.* **2021**, 2100755.

[5] A. Lunghi, A. Mariano, M. Bianchi, N.B. Dinger, M. Murgia, E. Rondanina, A. Toma, P. Greco, M. Di Lauro, F. Santoro, L. Fadiga, F. Biscarini, *Adv. Mater. Interfaces* **2022**, in press

[6] M. Di Lauro, E. Zucchini, A. De Salvo, E. Delfino, M. Bianchi, M. Murgia, S. Carli, F. Biscarini, L. Fadiga, *Adv. Mater. Interfaces* **2022**, 2101798.

9:45 AM DISCUSSION TIME

SYMPOSIUM SB04

Bioelectricity in Microbial-Based Living Materials
November 28 - December 7, 2022

Symposium Organizers

Guillermo Bazan, University of California, Santa Barbara
Giuseppe Paternò, Politecnico di Milano, Department of Physics
Teuta Pilizota, University of Edinburgh
Tanya Tschirhart, U.S. Naval Research Laboratory

* Invited Paper

+ Distinguished Invited

SESSION SB04.01: Biomaterials and Interfaces I

Session Chairs: Giuseppe Paternò and Teuta Pilizota

Monday Morning, November 28, 2022

Hynes, Level 3, Room 303

10:30 AM *SB04.01.01

Organic Semiconductor Nanoparticles Restore Vision in Blind Retinas [Guglielmo Lanzani](#)^{1,2}; ¹Italian Inst of Technology, Italy; ²Politecnico di Milano, Italy

Inherited retinal dystrophies and late-stage age-related macular degeneration, for which treatments remain limited, are among the most prevalent causes of legal blindness. Retinal prostheses have been developed to stimulate the inner retinal network; however, lack of sensitivity and resolution, and the need for wiring or external cameras, have limited their application. Here I report on the use of conjugated polymer nanoparticles (P3HT NPs), showing that they mediate light-evoked stimulation of retinal neurons and persistently rescue visual functions when subretinally injected in a rat model of retinitis pigmentosa. In particular I will report on recent results showing that the organic liquid prosthesis is effective also in retinas that have undergone a process of rewiring caused by the loss of photoreceptor function.

11:00 AM SB04.01.02

Optical Mirroring of Electrical Signals from Non-Electrogenic Cells Rosalia Moreddu¹, Alessio Boschi^{1,2}, Marta d'Amora^{1,3}, Giuseppina Iachetta¹, Michele Dipalo¹ and Francesco De Angelis¹; ¹Istituto Italiano di Tecnologia, Italy; ²University of Genoa, Italy; ³University of Pisa, Italy

Cell membrane potential is known to be an essential parameter to monitor the electrical activities of excitable cells, such as neurons and cardiac cells. However, recent data has revealed that it also plays a crucial role in non-excitable cells, such as epithelial cells. Electrical perturbations induce localized bioelectrical changes, which can trigger different cell responses, including migration, mitosis, and mutation.¹

The directional migration of cells under an electric field is known as galvanotaxis, and represents a dominant mechanism in guiding the behavior of multiple cell populations in mammals, fishes, amphibians, and plants.^{2,3} Wound healing is controlled by endogenous electric fields, generated by ion transport across the epithelium, which set a trans-epithelial potential difference (TCPD) of +40 mV in healthy conditions. At the wound, the TCPD falls to zero, but it is maintained at normal levels in its proximity (~0.5 mm) to drive epithelial cells to migrate and heal the wound.⁴ Bioelectrical cues are also involved in cellular mutation, responsible for the onset of multiple diseases. For example, cell electrical charges are the biophysical manifestation of metabolic patterns in cancer development and metastasis.⁵ Cancer cells exhibit the Warburg Effect, resulting in the secretion of lactate anions that produce a high concentration of negative surface charges.⁵ The membrane potential is also highly correlated with mitosis, DNA synthesis, cell cycle progression and overall cellular proliferation.⁶

Understanding these mechanisms is the key to unravel precision diagnostic and therapeutic strategies. However, this dynamic information is currently hard to access because existing technologies for electrophysiological recording of resting cell membrane potentials are invasive: they require physical access to the intracellular compartments, which implies the disruption of the cell membrane (known as electroporation).⁷ This makes it challenging to perform passive measurements and prolonged recordings under varying conditions.

A variety of alternative or complementary technologies based on optical methods were introduced in the past decades. However, the majority of them are designed to be implemented in electrogenic cells, which transport signals through action potentials (i.e., rapid polarization and depolarization of the cell membrane). Nevertheless, most of the cells in the human body do not fire action potentials, and their mechanisms of communication happen in a narrower signal range.

In this work, we present a novel approach in electrophysiological recording, based on optical mirroring of bioelectric charges. The feasibility of this method was previously demonstrated for the high throughput recording of action potentials in human-derived cardiomyocytes.⁷ In this context, the technology was refined and implemented in epithelial cells.

The nano-platform consisted of two chambers separated by a thin membrane. Pass-through electrodes enabled to mirror the cell membrane charge (top) all the way to the optical chamber (bottom), where dispersed fluorophores migrated to balance the charge, generating a dynamic fluorescent signal. Fluorescence was recorded with a camera, while exciting the fluorophores with incident light. Preliminary results on HEK cells yielded a fluorescence intensity increase of the 2.5% in presence of a cell on the microelectrode compared to reference microelectrodes. At present, this technology may be used to evaluate cell-substrate adhesion, monitor cell proliferation, and test novel biomaterials. In the near future, further investigations could allow extrapolating quantitative data on resting membrane potential in dynamic settings to perform cell/tissue studies on wound healing, cellular division, and cancer progression.

References:

- ¹ Huang, Y. J. et al. *Sci Rep* 2016, 6, 21583.
- ² Zhao, M. et al. *Nature* 2006, 442 (7101), 457-60.
- ³ McCaig, C. D. et al. *Physiol Rev* 2005, 85 (3), 943-78.
- ⁴ Song, B. et al. *Proc Natl Acad Sci U S A* 2002, 99 (21), 13577-82.
- ⁵ Vieira, A. C. et al. *PLoS One* 2011, 6 (2), e17411.
- ⁶ Kadir, L. et al. *Front Physiol* 2018, 9, 1661.
- ⁷ Barbaglia, A. et al. *Adv Mater* 2021, 33 (7), e2004234

11:15 AM SB04.01.03

Membrane-Targeted Molecules for Cell Optostimulation Arianna Magni^{1,2}, Matteo Moschetta², Giuseppe M. Paternò^{1,2}, Chiara Bertarelli^{1,2}, Luca Beverina³, Fabio Benfenati² and Guglielmo Lanzani^{2,1}; ¹Politecnico di Milano, Italy; ²Istituto Italiano di Tecnologia, Italy; ³Università degli Studi di Milano-Bicocca, Italy

Light-driven modulation of cellular activity with both high spatial and temporal resolution is becoming an increasingly active research area. Existing approaches, such as optogenetics, have shown promising results and, as an alternative, we envision the use of light-sensitive molecules that act as photo-actuators avoiding genetic manipulation.

We are interested in investigating the effects of different photo-actuators, such as azobenzene-based photochromic and donor-acceptor molecules. These compounds are designed to satisfy the following requirements: (i) absorb light in the visible or near-infrared window of the spectrum; (ii) spontaneously and efficiently partition into the lipid bilayers owing to their amphiphilicity, (iii) exhibit low toxicity in dark condition and preferentially also under illumination.

We combine the observation of the photoinduced effects on both HEK-293 cells and primary neurons, which are evaluated by exploiting electrophysiology, while steady-state and time-resolved optical spectroscopies reveal their photophysics and functioning mechanism.

Taken together, our data allows us to identify different light-driven mechanisms, responsible for the photoinduced effects observed on cells. These include, for instance, (i) the thinning or thickening of the membrane due to conformational changes in the molecules, (ii) the increase of the membrane permeabilization, and the formation of pore-like structures likely due to the lipid peroxidation following the photosensitization of singlet oxygen within the cell membrane, (iii) the rearrangement of the charges adsorbed to the membrane due to variations in the molecular dipole moment.

11:30 AM *SB04.01.04

Electron-Transporting Conjugated Polymers for Electronic Biohybrids Sahika Inal; King Abdullah University of Science and Technology, Saudi Arabia

Establishing close interactions between biological systems and synthetic materials is the key to forming biohybrid assemblies that find use in sensors, actuators, and robotics. In this work, I will present an electronic platform based on an n-type conjugated polymer that is tailored to form favorable interactions with catalytic enzymes.¹ When this biohybrid is applied in an enhancement mode organic electrochemical transistor (OECT), the device detects glucose and lactate in blood serum or saliva with excellent sensitivity and selectivity over six orders of magnitude wide detection range. The same biohybrid serves as the anode of a glucose fuel cell, extracting enough power from bodily fluids to drive the microscale OECT sensors. While showing the unique characteristics of these devices, I will discuss the possible pathways through which the polymer film generates charges as the enzyme reacts with its metabolites.² I will then show how these biohybrids are also responding to visible and NIR light by generating photocurrents in aqueous electrolytes.

¹ Ohayon et al *Nat. Mater.*, 2020, 19, 456.

² Druet et al *Adv. Electron. Mater.* 2022, 2200065.

1:30 PM *SB04.02.01

Programming Bioelectronic Bacteria as Real-Time and Multi-Channel Sensors Xu Zhang¹, Lin Su^{1,2}, Joshua Atkinson^{1,3} and Caroline Ajo-Franklin¹;
¹Rice University, United States; ²University of Cambridge, United Kingdom; ³University of Southern California, United States

Challenged by a changing climate, dwindling natural resources, and a growing global population, we need advanced renewable materials that meld the sustainability of biological materials with the functionality of conventional materials. To help address this need, my research group creates sustainable and environmentally-responsive living materials by seamlessly integrating conventional materials with living systems. One major effort in our group is to co-engineer microorganisms and microelectronics to serve as living bioelectronic sensors that can selectively sense a variety of complex molecules in real-time.

In my talk, I will first describe a collaborative project with the Silberg group at Rice to develop bioelectronic sensors that have minute detection times. We programmed *Escherichia coli* to produce current in response to specific chemicals using a modular, eight-component, synthetic electron transport chain. As designed, this strain produced electrical current upon exposure to thiosulfate, an anion that causes microbial blooms, in two minutes. By incorporating a protein switch into the synthetic pathway and encapsulating the bacteria with conductive nanomaterials, this amperometric sensor could be modified to detect an endocrine disruptor within two minutes in riverine water. Our results provide design rules to sense a variety of chemicals with mass transport-limited detection times and a new platform for miniature, low-power bioelectronic sensors that safeguard ecological and human health.

In the second part of my talk, I will describe how we have created bioelectronic sensors that convey multiple channels of information. Existing bioelectronic sensors can sense a variety of hazards to human and environmental health, however, these sensors transmit information through only a single electrochemical channel. This severely limits the amount of sensing information that can be transmitted. To increase this information content, we developed a multichannel bioelectronic sensor in which different chemicals modulate distinct extracellular electron transfer pathways in *E. coli*. To create an *E. coli* strain with two reporting channels, we introduced a riboflavin synthesis pathway from *Bacillus subtilis* alongside the metal reducing (Mtr) pathway from *Shewanella oneidensis*. We can distinguish whether one or both pathways are active in this strain using either chronoamperometry or a series of amperometric measurements at distinct redox potentials. To demonstrate multi-channel bioelectronic sensing, we regulated the Mtr and riboflavin pathways using arsenic and cadmium responsive promoters. With this strain, we used a series of amperometric measurements at distinct redox potentials to distinguish the presence of the different heavy metals *in situ*. These accomplishments provide a new platform for multichannel bioelectronic sensors that simultaneously detect and report multiple toxins.

2:00 PM SB04.02.02

Bioelectricity in Microalgae Cohorts Paulo R. Rocha¹ and Lode Vandamme²; ¹University of Coimbra, Portugal; ²Eindhoven University of Technology, Netherlands

Diatoms are early Jurassic microalgae, a photosynthetic group with a major environmental role on the planet due to the biogeochemical cycling of silica and global fixation of carbon. However, they can evolve into harmful blooms through a resourceful communication mechanism, not yet fully understood. Harmful algae blooms in water supply reservoirs must be eradicated due to unwanted toxin production and filter blocking at water treatment works. Until now there has been no efficient consensus that harmful microorganisms such as diatoms communicate with each other and no accurate and self-sustained tool to monitor such communication.

Here, we demonstrate the ability to electrically monitor a diatom cohort. The breakthrough is realized by means of a unique measurement setup based on low impedance electrodes that exploit the large Helmholtz-Gouy-Chapman double-layer capacitance. The sensing system comprises a transducer based on a metal/Si/SiO₂/Au electrode. Small extracellular voltages of diatoms adhered to the electrode induce a displacement current that is enhanced by a gain factor proportional to the double-layer capacitance.

The origin is paracrine signalling, which is a feedback, or survival, mechanism that counteracts changes in the physicochemical environment. The intracellular messenger could be related to Ca²⁺ ions since spatiotemporal changes in their concentration match the characteristics of the intercellular waves. Our conclusion is supported by using a Ca²⁺ channel inhibitor. The transport of Ca²⁺ ions through the membrane to the extracellular medium is blocked and the intercellular waves disappear. The translation of microalgae cooperative signalling paves the way for early detection and prevention of harmful blooms and an extensive range of stress-induced alterations in the aquatic ecosystem.

2:15 PM BREAK

2:45 PM *SB04.02.04

Strategies for Improving Extracellular Electron Transfer Between Microbes and Electrode Materials Shelley Minteer; University of Utah, United States

Over the last two decades, there has been a wealth of research in using microbially modified electrodes for various applications from microbial fuel cells to biosensing to electrosynthesis. The majority of these technologies are limited by slow extracellular electron transfer between the microbe and the electrode material. This talk will discuss chemical, materials, and biological strategies for improving extracellular electron transfer. It will start with a discussion of materials modification strategies for improving the surface area and biotic-abiotic interface to enhance current densities followed by a discussion of chemical strategies for mediating electron transfer. Finally, the use of synthetic biology to genetically engineer microbes to communicate directly with electrode surfaces will be discussed and the talk will compare and contrast the chemical, materials, and biological strategies for improving electron transfer and therefore performance of these bioelectrochemical systems.

3:15 PM SB04.02.05

Solar Power to Electricity—A Photovoltaic Perspective on the Plant Microbial Fuel Cell Thessa Van Limbergen¹, Robin Bonnét^{2,1}, Jeroen Hustings¹,

Roland Valcke¹, Sofie Thijs¹, Jaco Vangronsveld^{1,3} and Jean V. Manca¹; ¹Hasselt University, Belgium; ²Aarhus University, Denmark; ³Maria Curie-Sklodowska University, Poland

The keywords solar power and electricity combined evidently point our minds toward photovoltaics. However, plant microbial fuel cells (PMFCs) have a similar working principle. The technology – which emerged in 2008 – combines living plants and microorganisms in an *in situ* fuel cell configuration, also converting sunlight into electricity [1]. But how do these two technologies compare? In this study, PMFCs were approached from a photovoltaic perspective. A rough upper limit for the overall energy conversion efficiency was estimated and compared to various classes of photovoltaics. To this end, each intermediate step in the working principle of plant microbial fuel cells was investigated, and of each step, the maximum efficiency found in literature was used to calculate the maximum power conversion efficiency. This approach estimated the maximum efficiency to be around 1%, more than one order of magnitude lower than traditional and emerging photovoltaics [2].

Going from theory to practice, the corresponding maximum power density was compared to the historical evolution of reported power output values. However, no apparent increase through time could be seen since their emergence. The application of the technology may explain this as the plant microbial fuel cell has many dedicated niche applications ranging from sensing to remediation, where power output might not be of interest [3]. Even though various routes toward increased power output are still being proposed, it is clear that PMFCs are intrinsically limited and dwarfed in comparison to photovoltaics when looking at power output alone. Nonetheless, the various niche applications - together with certain advantages the technology has over photovoltaics, i.e., aesthetics, price, straightforwardness, etc. - provide an added value to the technology.

This critical discussion aids in placing the plant microbial fuel cells, their applications, and expectations in the world of green, and particularly of solar energy-related research.

[1] Strik D.P.B.T.B. et al., *Int. J. Energy Res.* **32** (2008)

[2] NREL - Best Research-Cell Efficiency Chart (2022)

[3] Ebrahimi A. et al., *J. Environ. Chem. Eng.* **9** (2021)

3:30 PM SB04.02.06

Improving the Photoelectron Transfer from Photosynthetic Proteins into TiO₂ Electrodes for Bio-Sensitized Solar Cell Application Christopher Espinoza-Araya^{1,1,1}, Jose Daniel Zelada-Ramírez^{1,1}, Dariana Aguilar^{1,1}, Alexandra Tames^{1,1}, Jesse Bergkamp², Ernesto Montero-Zeledón^{1,1}, Venkatesan Renugopalakrishnan^{3,4}, Barry Bruce^{5,5} and **Claudia C. Villarreal**^{1,1}; ¹Instituto Tecnológico de Costa Rica, Costa Rica; ²California State University, United States; ³Harvard Medical School, United States; ⁴Northeastern University, United States; ⁵University of Tennessee at Knoxville, United States

The bio-sensitized solar cell is the architecture with the highest power conversion efficiencies (PCE) amongst photovoltaic devices that integrate natural photosynthetic proteins (1-2%). In these devices, a nanostructured wide-bandgap semiconducting electrode is coated with the protein and used as the photoanode in an electrochemical cell. Our team studies two different biosensitizers that stand out as some of the best performing natural light absorbers in bio-photovoltaic devices: **bacteriorhodopsin** (bR), a light-driven proton pump from archaeobacteria, and **photosystem I** (PSI), a chlorophyll-protein complex from cyanobacteria and green plants that catalyzes photoactivated unidirectional electron transfer in oxygenic photosynthesis. Two factors that currently limit the **charge transfer efficiency** from the protein to the TiO₂ are the reduced contact area between the two materials and the non-specific orientation of the protein with respect to TiO₂. The proteins here studied are significantly larger than traditional synthetic dyes, which hinders their penetration into the pores of the TiO₂ nanoparticle layer during impregnation. The use of **TiO₂ nanorods doped with CNTs** is proposed to provide larger contact area where the protein can inject the photoelectrons into the semiconductor. In nature, electron transfer occurs in very specific electrical pathways that have evolved over millions of years, while simple dropcasting of a protein onto the electrode results in random orientations that may or may not connect these natural electrical wires with the electrode surface. Alternative techniques to promote an organized interface with **preferential orientation of the proteins** on the TiO₂ are here explored, so that the electron injection is directional according to the natural function of the biomolecule in the organism. *In situ* crystallization and structural modifications of the protein are proposed to drive a preferential orientation on the electrode. The effect of these variables in photovoltaic performance of devices is determined. The devices here proposed consist on the biosensitized TiO₂ photoanode and a PEDOT/CNT counter-electrode. A gel electrolyte is used to connect the two electrodes, containing the hydroquinone/benzoquinone pair or aqueous-soluble bipyridine cobalt(II/III) complexes as direct redox mediators for bR and PSI, respectively. These work intends to deepen the understanding of electron transfer in a bio-hybrid interface for photogeneration of bioelectricity.

SESSION SB04.03: Biomaterials and Interfaces II
Session Chairs: Guillermo Bazan and Teuta Pilizota
Tuesday Morning, November 29, 2022
Hynes, Level 3, Room 303

8:30 AM SB04.03.03

Externally Tunable, Low Power Electrostatic Control of Cell Adhesion with Nanometric High-k Dielectric Films **Victor Leon**, Baptiste Blanc, Sophia Sonert and Kripa Varanasi; Massachusetts Institute of Technology, United States

Biological systems are notoriously difficult to control. A major technical issue is controlling where and when bio-adhesion occurs on surfaces in engineered systems. Promoting bio-adhesion may be useful to pattern cells for tissue engineering. Preventing bio-adhesion is useful in micro-algal photobioreactors, where cleaning operations are costly and time consuming.

Current methods to promote or inhibit bio-adhesion depend on directly modifying the surface chemistry (e.g. hydrophobicity, molecular end groups). Here, we study the interaction between micro-algae cells (i.e. freshwater *Chlorella vulgaris* and saltwater *Nannochloropsis oculata*), and an engineered surface that can actively change its zeta potential based on the magnitude and polarity of applied voltage without changing its chemistry. Since the studied algae have negative zeta potentials, colloidal DLVO theory suggests that a surface with negative zeta potential should repel algae and a surface with positive zeta potential should attract algae. We observe that algae adhesion is inhibited at negative zeta potentials and enhanced at positive zeta potentials with a power draw of ~nW by applying +/- 1V. Using microfluidic experiments, we report the effect of varying voltage magnitude, voltage polarity, wall shear, algae species, and solution salinity on bio-adhesion. We also conduct longer term (4 week) bio-adhesion and patterning experiments to observe the effect on practical performance

8:45 AM SB04.03.04

Novel Approach for Precise Measurement of Bioelectronic Interface—Transfer Length Method-Based Interface Electrical Characterization

Jinpyeo Jeung¹, Inyeol Yun¹ and Yoonyoung Chung^{1,2}; ¹Pohang University of Science and Technology, Korea (the Republic of); ²Center of Semiconductor Technology Convergence, Korea (the Republic of)

Bioelectronic interfaces significantly affect the signal transmission between electronic devices and biomaterials. Therefore, the electrical characterization of bioelectronics interfaces is of paramount importance for designing various bioelectronic devices or biohybrid sensors. Conventionally, the characterization of bioelectronic interface impedance relies on estimation using electrochemical impedance spectroscopy (EIS) data. However, the conventional method possesses a critical limitation in that the results of the electrical characterization are not unique since different estimations can produce identical impedance results.¹ The limitation undermines the reliability of the measurements and can cause errors. Thus, the development of a method that can accurately distinguish and measure the impedance of the bioelectronic interface and bulk is necessary.

In this study, we propose a novel method that satisfies the necessity by applying the transfer length method in an electrode/electrolyte system. Transfer length method-based interface electrical characterization (TLM-IEC) obtains accurate bulk electrolyte impedance by measuring impedance between electrodes at various intervals, and then the interface impedance is obtained by removing the bulk electrolyte impedance from the total impedance. The validity of the TLM-IEC was confirmed, and the method exhibits a superior advantage over the conventional method since the impedances of the interface and bulk are measured, not estimated. The unique electrical characterization of bioelectronic interface by the TLM-IEC can facilitate the optimized design of bioelectronic devices and sensors, and can be utilized for various applications.

Reference

1. Y. Liu, Y. Bai, W. Jaegermann, R. Hausbrand, and B. X. Xu, "Impedance Modeling of Solid-State Electrolytes: Influence of the Contacted Space Charge Layer," ACS Appl. Mater. Interfaces, vol. 13, no. 4, pp. 5895-5906, Feb 3 2021.

9:00 AM *SB04.03.05

Controlling the Resting Membrane Potential of Bacteria—Decoupling Hyperpolarization, Reactive Oxygen Species Generation, Enzyme Activity and Membrane Permeabilization [Christine Payne](#); Duke University, United States

Cells generate a -10 mV to -100 mV electrical potential across the plasma membrane driven by an ion gradient. This resting membrane potential, in comparison to the action potentials of neurons and muscle cells, is present in all cells, including bacteria. A fundamental understanding of bacterial electrophysiology would lead to new methods for the control of engineered living materials, as well as significant advances in synthetic biology, cell growth in industrial bioreactors, and screening of anti-bacterial agents. Recent research in the Payne Lab is aimed at understanding bioelectricity in bacteria guided by questions of heterogeneity and cell growth with applications in materials science. The resting membrane potential of individual cells within a population is highly heterogeneous. In addition to cell-level heterogeneity, we also observe temporal heterogeneity with 2% of individual cells showing short bursts of hyperpolarization, referred to as “spiking.” We have developed methods to image and control resting membrane potential, simultaneously, on the single cell level to determine the underlying source of both the cellular and temporal heterogeneity. We use blue light, which can be patterned, to suppress cell growth in certain regions, creating patterned bacteria, in a way that is not possible using diffusible reagents that affect all cells equally. Blue light-mediated hyperpolarization is coupled with a range of cellular responses including generation of reactive oxygen species, altered enzymatic activity, and changes in membrane permeability, in addition to the inherent heterogeneity of this system. Our experiments are aimed at decoupling these cellular responses to determine what factors drive the associated decrease in cell growth. We hope these experiments will provide new insights in the growing field of bacterial electrophysiology.

SESSION SB04.04: Biomaterials and Interfaces III
Session Chairs: Giuseppe Paternò and Teuta Pilizota
Tuesday Afternoon, November 29, 2022
Hynes, Level 3, Room 303

1:45 PM *SB04.04.01

Generating Electricity from Ambient Water with Microbial Biofilms or Their Protein Nanowires [Jun Yao](#); University of Massachusetts Amherst, United States

Water sources in both gaseous and liquid forms are ubiquitous. The electrostatic and hydrokinetic energy associated with this water is a large reservoir that potentially could be transformed into a sustainable source of energy for powering electronics. We have found that useful amounts of electricity can be generated from water with microbial materials. For example, protein nanowires harvested from the microbe *Geobacter sulfurreducens* are the functional material in ‘Air-gen’ devices that continuously generate electricity from the ambient humidity that is available literally anywhere on earth. We also found that devices fabricated from microbial biofilms can generate electricity from evaporating liquid water, achieving energy densities higher than those possible with traditionally engineered materials. These two types of devices for generating electricity from water are complementary, closing the loop for broadly harvesting electricity from all distributed water forms on earth. We further demonstrate the practical application of both types of devices for continuous, sustainable powering of wearable electronic devices that monitor important human physiological functions.

2:15 PM SB04.04.02

Membrane-Targeted Photoswitch Induces Cardiac Cells and Tissue Optical Pacing [Vito Vurro](#)¹, [Carlotta Ronchi](#)¹, [Valentina Sesti](#)^{2,1}, [Silvia Crasto](#)^{3,4}, [Maria Rosa Antognazza](#)¹, [Chiara Bertarelli](#)^{2,1}, [Elisa Di Pasquale](#)^{3,4}, [Guglielmo Lanzani](#)^{1,2} and [Francesco Lodola](#)⁵; ¹Istituto Italiano di Tecnologia, Italy; ²Politecnico di Milano, Italy; ³National Research Council of Italy, Italy; ⁴Humanitas Clinical and Research Center, Italy; ⁵Università degli Studi di Milano-Bicocca, Italy

The study of human-machine interaction is an appealing research area where the developed interfaces find application in robotic,^{1,2} biological^{3,4} and medical areas.⁵ In particular, great interest is rising for the development of a contactless and wireless interaction. Within this context, light represents a clean and spatiotemporal precise tool to achieve such a goal.⁶ Conjugated molecules and polymers offer a promising platform to interface with cells and living organisms due to their high optical absorption/emission cross section, chemical synthesis’ easiness and relatively low toxicity.^{7,8} In this work, we focus on cardiomyocytes photopacing, which are interesting candidates to test the stimulation process due to their excitability, contraction ability and their electrical behaviour. Specifically, we present the use of an azobenzene-derivative that is able to trigger the signalling process in muscle cells at all the physiological levels of the contraction. We characterized the effect of the photostimulation on electrophysiology response, calcium wave generation and contraction activity. Moreover, we test this approach on *in vitro* micro-physiological systems controlling its macroscopic contraction activity.

This last step consists of the realization of a bio-hybrid photoresponsive smart tissue, which is crucial for moving towards a real translational application and achieve the ultimate goal of this project. This can be a breakthrough for future applications in robotics and pharmacology, as well as tissue regeneration.

References

1. Feinberg, A. W. Biological Soft Robotics. *Annu. Rev. Biomed. Eng.* **17**, 243–265 (2015).
2. Ricotti, L. *et al.* Biohybrid actuators for robotics: A review of devices actuated by living cells. *Sci. Robot.* **2**, eaaq0495 (2017).
3. Antognazza, M. R., Abdel Aziz, I. & Lodola, F. Use of Exogenous and Endogenous Photomediators as Efficient ROS Modulation Tools: Results and Perspectives for Therapeutic Purposes. *Oxid. Med. Cell. Longev.* **2019**, 1–14 (2019).
4. Colombo, E., Feyen, P., Antognazza, M. R., Lanzani, G. & Benfenati, F. Nanoparticles: A Challenging Vehicle for Neural Stimulation. *Front. Neurosci.* **10**, (2016).
5. Maya-Vetencourt, J. F. *et al.* A fully organic retinal prosthesis restores vision in a rat model of degenerative blindness. *Nat. Mater.* **16**, 681–689 (2017).
6. Vurro, V., Venturino, I. & Lanzani, G. A perspective on the use of light as a driving element for bio-hybrid actuation. *Appl. Phys. Lett.* **120**, 080502 (2022).
7. Di Maria, F., Lodola, F., Zucchetti, E., Benfenati, F. & Lanzani, G. The evolution of artificial light actuators in living systems: from planar to nanostructured interfaces. *Chem. Soc. Rev.* **47**, 4757–4780 (2018).
8. Hopkins, J. *et al.* Photoactive Organic Substrates for Cell Stimulation: Progress and Perspectives. *Adv. Mater. Technol.* **4**, 1800744 (2019).

2:30 PM BREAK

3:00 PM *SB04.04.03

Designing Bioelectronic Interfaces with Peptidic Assemblies [Herdeline Ardoña](#), Ze-Fan Yao, Yuyao Kuang and Sujeung Lim; University of California, Irvine, United States

Integration of synthetic electronic biomaterials with living systems has emerged as an approach for modulating or probing cellular behavior and tissue function that minimize the need for contact with traditional, bulky, and non-flexible inorganic electrodes. Bioelectronic materials have been demonstrated to effectively integrate with cells, in vitro tissue models, organoids, and even with small model organisms, but the long-term effects of these materials on living systems are rarely considered when designing a material. In this presentation, we present peptide-based structures functionalized with π -conjugated units as designer biomolecules that can be interfaced with excitable cells. We present herein structure-function relationships that demonstrate the dependence of assembly behavior on monomeric structure and assembly trigger used while in completely aqueous environments. First, we show that small molecule coupling agents that allow for anhydride formation generate peptidic π -conjugated conduits that are amenable to disassembly once the fuel is diminished and anhydride hydrolysis predominates. The compliance of a peptide-bearing quaterthiophene monomer to this process is highly dependent on the electrostatic nature of the peptide sequence used. On the other hand, peptide-polydiacetylene conjugates will also be discussed as π -conjugated assemblies that exhibit sequence-dependent photophysical and electrical properties. Our results show the differential impacts of amino acid size and polarity, and the degree that these molecular parameters can influence bulk properties based on the location of the residue substitution. Interestingly, we also show that the interaction of fibroblasts (as a model cell line) with the monomeric and polymeric equivalents of these peptide-polymer also sequence-dependence. Collectively, these findings shed light to the tunability of properties and assembly behavior of π -conjugated peptides under physiologically relevant environments. In the future, we will leverage these design principles for engineering biotic-abiotic interfaces that rely on the properties of these peptides functionalized with π -conjugated units.

3:30 PM *SB04.04.05

Healable, Stretchable and Flexible Bioelectronics [Fabio Cicoira](#); Polytechnique Montréal, Canada

The ability of certain materials to regenerate after damage has attracted a great deal of attention since the ancient times. For instance, self-healing concretes, able to resist earthquakes, aging, weather, and seawater have been known since the times of ancient Rome and are still the object of research. While the field of mechanically healable materials is relatively established, self-healing conductors are still rare, and are nowadays attracting enormous interest for applications in electronic skin for health monitoring, wearable and stretchable sensors, actuators, transistors, energy harvesting, and storage devices, such as batteries and supercapacitors. Self-healing can significantly enhance the lifetime of conducting materials, leading to the improved environmental sustainability and reduced costs.

Conducting polymers exhibit attractive properties, such as mixed ionic-electronic conductivity, leading to low interfacial impedance, tunability by chemical synthesis, ease of process via solution process and printing, and biomechanical compatibility with living tissues, which makes them ideal materials for bioelectronics and stretchable electronics. However, they show typically poor mechanical properties and are therefore not suitable as self-healing materials. Self-healing conductors can be achieved upon mixing with other polymers, such as poly(vinyl alcohol) (PVA) and poly(ethylene glycol) (PEG), which provide the mechanical characteristics leading to self-healing.

My talk will deal with processing and characterization of conducting polymer films and hydrogels and devices for healable, flexible, stretchable and electronics as well as for implantable electrodes. I will particularly focus on processing strategies to fabricate stretchable and self-healing conductors and their applications. [1-9]

References

1. Y. Li, X. Zhou, B. Sarkar, N. Gagnon-Lafrenais, and F. Cicoira, *Adv. Mater.* 2108932, 2022.
2. Y. Li, X. Li, S. Zhang, L. Liu, N. Hamad, S. R. Bobbara, D. Pasini, F. Cicoira, *Adv. Funct. Mater.*, 30, 2002853, 2020.
3. Y. Li, X. Li, R. N. Unnava Venkata, S. Zhang, F. Cicoira, *Flexible and Printed Electronics* 4, 044004, 2019.
4. N. Rossetti, P. Luthra, J. Hagler, A. H. J. Lee, C. Bodart, X. Li, G. Ducharme *et al.*, *ACS Appl. Bio Mater.* 2, 5154-5163, 2019.
5. C. Bodart, N. Rossetti, S. Schougaard, F. Amzica, F. Cicoira *et al.*, *ACS Appl. Mater. Interfaces*, 11, 17226-17233, 2019.
6. S. Zhang, Y. Li, G. Tomasello, M. Anthonisen, X. Li, M. Mazzeo, A. Genco, P. Grutter, F. Cicoira, *Adv. Electron. Mater.* 1900191, 2019.
7. S. Zhang, F. Cicoira, *Adv. Mater.* 29, 1703098, 2017.
8. X. Zhou, A. Rajeev, A. Subramanian, Y. Li, N. Rossetti, G. Natale, G. A. Lodygensky, and F. Cicoira, *Acta Biomaterialia*, 139, 296-306, 2022.

SESSION SB04.05: Poster Session
Session Chairs: Guillermo Bazan and Tanya Tschirhart
Tuesday Afternoon, November 29, 2022
8:00 PM - 10:00 PM
Hynes, Level 1, Hall A

SB04.05.01

Photosynthesis Re-Wired on the Pico-Second Timescale Tomi Baikie, Laura Wey, Christopher Howe, Christoph Schnedermann, Akshay Rao and Jenny Zhang; University of Cambridge, United Kingdom

Photosystems II and I (PSII and PSI) are the reaction centre complexes that drive the light reactions of photosynthesis. PSII performs light-driven water oxidation (quantum efficiencies and catalysis rates of up to 80% and 1000 e⁻s⁻¹, respectively) and PSI further photo-energises the harvested electrons (quantum efficiencies of ~100%). The impressive performance of the light harvesting components of photosynthesis has motivated extensive biological, artificial and biohybrid approaches to re-wire photosynthesis to enable higher efficiencies and new reaction pathways, such as H₂ evolution or alternative CO₂ fixation. To date these approaches have focussed on charge extraction at the terminal electron quinones of PSII and terminal iron-sulfur clusters of PSI. Ideally electron extraction would be possible immediately from the photoexcited reaction centres to enable the greatest thermodynamic gains. However, this was believed to be impossible because the reaction centres are buried around 4 nm within PSII and 5 nm within PSI from the cytoplasmic face. Here, we demonstrate using *in vivo* ultrafast transient absorption (TA) spectroscopy that it is possible to extract electrons directly from photoexcited PSI and PSII, using both live cyanobacterial cells and isolated photosystems, with the exogenous electron mediator 2,6-dichloro-1,4-benzoquinone (DCBQ). We postulate that DCBQ can oxidise peripheral chlorophyll pigments participating in highly delocalised charge transfer (CT) states after initial photoexcitation. Our results open new avenues to study and re-wire photosynthesis for bioenergy and semi-artificial photosynthesis.

SB04.05.02

Blue Light Patterning for Engineered Living Materials Xu Han and Christine Payne; Duke University, United States

Engineered living materials have many exciting properties such as self-healing, bioresponsivity, and the formation of composite materials with complex structures. One challenge in the advancement of engineered living materials is controlling the growth of single cells to form micro- and nano-scale patterns. We, and others, have reported the use of low intensity blue light to control the resting membrane potential of bacteria at the single cell level. We found that blue light (480 nm, <60 s) can slow the growth of *B. subtilis* and *E. coli* without damaging the cells. The growth rate of bacteria is inversely proportional to blue light exposure time. We have used this method to pattern bacteria by controlled cell growth. This use of blue light provides a low-cost, high-throughput method for patterning biofilms or the deposition of materials by bacteria, such as bacterial cellulose and calcium carbonate. Current research is aimed at characterizing the underlying mechanism for the slowed bacteria growth including hyperpolarization, generation of reactive oxygen species, and enzyme activity.

SB04.05.03

Self-Assembled Hybrid Structure of Natural Photosystems in Bio-Photovoltaic Cells for Enhanced Photoelectric Current Generation Nyeongbeen Jo and Yoon Sung Nam; Korea Advanced Institute of Science and Technology, Korea (the Republic of)

In the natural photosynthesis of plant or cyanobacteria, functional proteins and redox cofactors are sophisticatedly self-assembled in the thylakoid membrane, exhibiting nearly 100 % of light-harvesting quantum efficiency. Photosystem I (PSI) is an integrated membrane protein complex that catalyzes the transfer of electrons using light energy. The photon energy absorbed by PSI also provides a proton motive force used to produce organic compounds. This finding has inspired engineers to pursue biomimetic and bio-inspired designs for efficient light-harvesting and charge extraction. However, the efficiency of nano-bio hybrid photosystems is often limited by the poorly-oriented assembly of photosystems with nanomaterials. In this work, we assembled PSI with protonated-carbon nitride (PCN) nanosheets through balanced intermolecular interactions, resulting in linker-free PSI/PCN hybrid nanostructures that generate favorable electronic interfacial structures for charge transfer through a Z-scheme system. Surface-modified carbon nitrides can provide photocatalytic activity under visible light irradiation conditions and a new electron transfer path in the hybrid structure with PSI. Electrostatic hybridization between protonated sites on the PCN nanosheets and the partially negatively charged lumen side of PSs provides a favorable orientation for efficient electron transfer. The PSI/PCN hybrids exhibit a photocurrent density more than 28 times higher than randomly oriented PSI. We also show that when coupling the developed bio-photocathode with a PSII-based photoanode, a photocurrent of 7.7 $\mu\text{A cm}^{-2}$ under bias-free conditions and a cell power up to 0.9 $\mu\text{W cm}^{-2}$ can be achieved. This study provides a vital strategy to construct an efficient biochemical photoelectrode based on natural photosystems coupled with semiconductor carbon nanostructures through simple self-assembly in a favorable orientation for efficient and stable interfacial electron transfer. This work was supported by Nano-Material Technology Development Program through the National Research Foundation of Korea (NRF) funded by the Ministry of Science, ICT & Future Planning (NRF-2017M3A7B4052797).

SB04.05.04

Carbon Nanomaterials to Improve Charge Transfer at the Electrode Interface in Microbial Fuel Cell for Wastewater Treatment and Bioelectricity Generation Denisse P. Murillo, Daniela Zúñiga Rivera, Karina Tellería Chaves, Mónica Carmona Córdoba, Ricardo Esquivel-Isern and Claudia C. Villarreal; Instituto Tecnológico de Costa Rica, Costa Rica

At least 50% of the wastewater from human activities is discharged into the environment without treatment, a practice that compromises the human right to access clean water and sanitation. Microbial fuel cells (MFCs) are devices capable of converting chemical energy into electrical energy through electrochemical reactions, using the electrosynthesis of microorganisms. In this work, a device composed of two chambers is proposed. Biodigester effluent is used as an anolyte and oxidation of organic components is performed by bacteria at the electrode surface in the anodic chamber, while the reduction of heavy metals from industrial wastewater takes place in the cathodic chamber. The proposed MFC can simultaneously reduce the load of pollutants in agricultural and metallurgical wastewater and produce renewable energy. The objective of this study is to determine the effect of coating the graphite electrodes in the cathodic and anodic chamber with carbon nanomaterials, including graphene and a seamless hybrid of graphene and carbon nanotubes, both materials obtained by chemical vapour deposition. The nanostructured electrodes provide a larger surface area and increased electron transfer rates to improve the performance of bioelectricity generation. This work improves the comprehension of bioelectrochemical phenomena occurring in biofilm-based microbial devices and analyzes how the electrode surface structure can tune the charge transfer efficiency at the interface of living organism and carbon electrodes.

SB04.05.06

PEDOT:PSS Based Soft, Healable and Highly Adhesive Hydrogels for Monitoring Human Health Xin Zhou¹, Gregory A. Lodygensky^{2,3} and Fabio Cicoira¹; ¹Polytechnique of Montreal, Canada; ²Sainte-Justine University Hospital Research Center, Canada; ³University of Montreal, Canada

Flexible, soft, self-healing, and adhesive conductive materials with Young's modulus matching biological tissues (with a moduli of 0.5-500 KPa) are highly desired for applications in bioelectronics. Here, we report self-healing, stretchable, highly adhesive, and conductive hydrogels obtained by mixing polyvinyl alcohol (PVA), borax, and Poly(3,4-ethylenedioxythiophene) doped with polystyrene sulfonate (PEDOT:PSS) screen printing paste. The prepared hydrogels demonstrated remarkable compliance on skin, outstanding plastic stretchability (over 10000% strain), high adhesion on pig skin (1.96

N/cm²), a good strain sensitivity (gauge factor = 3.88 at 500 % strain), remarkable self-healing properties, and low compressive Young's modulus (~3.7 KPa). Our hydrogels were used to fabricate electrophysiological epidermal patch electrodes, which exhibited high-quality similar to commercial Ag/AgCl gel electrodes for recording of electrocardiography (ECG) and electromyography (EMG) signals.

SB04.05.07

Printable and Self-Adhesive Dry Epidermal Electrodes Using PEDOT:PSS and Polyurethane-Based Composite [Pierre Kateb](#)¹, Jinsil Kim¹, Xin Zhou¹, Gregory A. Lodyginsky² and Fabio Cicoira¹; ¹Polytechnique Montreal, Canada; ²Sainte-Justine Mother and Child University Hospital Center, Canada

Monitoring the vital signs of children born prematurely is of paramount importance for their health. Electrocardiography (ECG), electromyography (EMG), heart rate and respiration data are used to assess their well-being and development. These measurements require the placement of electrodes on the skin via an adhesive, which can lead to damage during its removal because the skin of premature infants does not have a protective outer layer. Therefore, alternative monitoring methods are needed to increase comfort and reduce the burden of preterm infants. This can be achieved with flexible, stretchable, and self-adhesive electrodes that can adapt to the shape and movements of the child while maintaining signal quality for a long-term use. Commonly used biomedical electrodes for on-skin electrophysiological measurements are hydrogel-based and suffer from water loss, therefore degrading and losing signal quality overtime. Long-term monitoring using gels is therefore hindered. On the other hand, electrodes using adhesives often adhere too strongly for sensitive skin and can only be used once. Herein, a conductive polymer, poly(3,4-ethylenedioxythiophene) polystyrene sulfonate (PEDOT:PSS), is mixed with a short chain polyurethane diol (PUD) and printed onto a thin thermoplastic polyurethane substrate to obtain a reusable, wearable and dry electrode for durable electrophysiological signal monitoring. Due to its light adhesivity, the dry electrode can conform to the skin and reduce noise during the signal acquisition without inducing pain during its removal. Furthermore, PUD/PEDOT:PSS electrodes showed stretchability and a Young's Modulus similar to skin, which demonstrates the durability of the electrodes and tolerance to repeated mechanical strains, while maintaining high conductivity. Strain-stress, cyclic stress, electrotensile as well as adhesion tests confirm this PUD/ PEDOT:PSS composite's excellent mechanical properties. Weeklong EMG and ECG measurements with the same electrodes also showed its capability for long-term usage. Such an electrode is more suitable for long-term health monitoring of patients with fragile skin, such as premature infants.

SB04.05.09

Electropolymerized PEDOT Coatings on Penetrating Neural Probes Improve Chronic In Vivo Electrochemical Stability [Jeeyeon Yeu](#)¹, Jo'Elen Hagler¹, Guillaume Ducharme², Bénédicte Amilhon^{2,3} and Fabio Cicoira¹; ¹Polytechnique Montreal, Canada; ²Université de Montréal, Canada; ³CHU Sainte-Justine Research Center, Canada

The conducting polymer poly(3,4-ethylenedioxythiophene) (PEDOT) is a promising material for improving the stimulation efficiency of neural microelectrodes due to its many advantageous characteristics, such as mechanical compliancy, electrochemical stability, and high conductivity. Studies on the long-term in vivo electrochemical stability of penetrating PEDOT-coated electrodes undergoing high-frequency stimulation are not extensively done and the immune response of the brain towards PEDOT-coated stimulating neural probes is not well investigated. In this study, electropolymerized PEDOT doped with tetrafluoroborate (PEDOT:BF₄) is selectively deposited on the electrodes of platinum iridium (PtIr) neural probes and implanted for 2 weeks and 2 months to evaluate the effect of implantation on the electrical performance, along with the foreign body response to the probes. Histological analysis after 8 weeks of implantation shows no difference in the degree of inflammation around PtIr and PEDOT probes. Furthermore, PEDOT and PtIr probes are implanted for 60 days, and subject to daily high frequency stimulation while being monitored for changes in electrochemical properties. Impedance measurements confirm an overall lower impedance for PEDOT probes. This study shows that PEDOT:BF₄ coatings can contribute to the electrochemical stability of neural interfacing devices for stimulation and recording.

SB04.05.10

Electrodeposition of PEDOT on Nickel-Plated Copper for Biomedical Electrodes [Kathel C. Dongnang Ngoula](#), Sara Ebrahimi, Sally Zhou and Fabio Cicoira; Polytechnique Montreal, Canada

Current approaches in the healthcare field use electrodes as biomedical devices at the interface of biological systems and electronics to either transmit electrical impulses or as sensors to record bioelectric signals. The main hindrance to these measures is the resistance to the flow of the electric signal from the living tissues, called the impedance. Recent advances are proposing organic conducting polymers, mainly poly(3,4-ethylenedioxythiophene) (PEDOT), to improve signal acquisition and lower the impedance at the electrode/tissue interface. In fact, PEDOT has been shown to have a low impedance, a high conductivity due to its mixed electronic ionic conduction, good electrochemical stability, and biocompatibility allowing its use in bioelectronic devices.¹ The present study proposes using PEDOT as a coating on Nickel plated copper (Ni-Cu) electrodes to design innovative devices with low impedance and high conductivity to record bio-signals for diagnosis, monitoring, and prevention of medical conditions. The nickel coating has been achieved through an electroless plating process in a nickel-plating bath.² Afterwards, the PEDOT coating has been achieved through cyclic voltammetry (CV) and a galvanostatic chronopotentiometry (CP) electropolymerization of the 3,4-ethylenedioxythiophene (EDOT) monomer. The bath contained the EDOT monomer and the dopant, lithium perchlorate (LiClO₄), dissolved in either water or acetonitrile (ACN). A variety of potential ranges were considered for cyclic voltammetry, but only cycling held constant between -1.0 V and +1.2 V produces the agglomeration of PEDOT on the substrate. The chronoamperometric method resulted in homogeneous/uniform PEDOT films, and by optimizing the electropolymerization conditions, we demonstrated the mechanical and electrochemical stability of PEDOT doped with LiClO₄ deposited on Ni-Cu electrodes. The coatings have been analyzed and characterized using electrochemical impedance spectroscopy (EIS) and CV in a phosphate-buffered saline solution (PBS), X-ray photoelectron spectroscopy (XPS), and scanning electron microscopy (SEM). As a result of PEDOT coating's potential electrocatalytic properties, an improvement in the electrode's electrochemical properties was achieved, resulting in reduced impedance and higher performance. Due to their high capacitance and low impedance, PEDOT Ni-Cu electrodes can be used as convenient electrodes for detecting biological signals, improving biomedical devices in the future.

References:

1. Rossetti, N., Luthra, P., Hagler, J. E., Jae Lee, A. H., Bodart, C., Li, X., ... & Cicoira, F. Poly (3,4-ethylenedioxythiophene)(PEDOT) coatings for high-quality electromyography recording. *ACS Applied Bio Materials*. **2019**, 2(11), 5154-5163.
2. Son, J., Hong, Y., Yavuz, C. T., & Han, J. I. Thiourea-based extraction and deposition of gold for electroless nickel immersion gold process. *Industrial & Engineering Chemistry Research*. **2020**, 59(16), 8086-8092.

SB04.05.11

All-Printed and Fully-Stretchable Organic Electrochemical Transistors Based on Hydrogel Electrolyte [Chi-hyeong Kim](#)¹, Mona Azimi¹, Harini Nagarajan² and Fabio Cicoira³; ¹Polytechnique Montréal, Canada; ²Madras Institute of Technology, India; ³Polytechnique Montreal, Canada

Solution-processable organic materials are desirable for functionalized wearable devices. To maximize that feature of organic polymers, printing is one of

the best methods to cast films or patterns. Herein, we fabricated fully-stretchable organic electrochemical transistors(OECTs) by a conventional PBC printer. To achieve the stretching of the whole body of the devices, a printed planar gate electrode and polyvinyl alcohol(PVA) hydrogel electrolyte were employed. The simplicity of the PCB printer made it possible to print a wide range of viscous inks, from an organic semiconductor to a hydrogel precursor. A Stretchable silver paste provided a soft feature to drain/source, gate and interconnect without any strategies to improve the stretchability of metallic components, such as pre-stretching methods and formation of stretchable patterns. Moreover, unlike reported studies of printed ion-gel electrolytes for transistors, a printed hydrogel electrolyte on OECTs has not been reported yet. The resulting OECTs showed decent performance comparable to ink-jet or screen-printed OECTs; the maximum transconductance and on/off ratio were 1.2mS and around 1400, respectively. The devices were stable in electromechanical behavior until 30% strain which is required for wearable electronics on the skin.

SESSION SB04.06: Emerging Applications—Biosensors
Session Chairs: Giuseppe Paternò and Tanya Tschirhart
Wednesday Morning, November 30, 2022
Hynes, Level 3, Room 303

10:00 AM *SB04.06.01

Redox-Linked Synthetic Biology and Electrogenetics Opens Lines of Communication William Bentley, Eric VanArsdale, Sally Wang, Chen-Yu Chen, Eunkyong Kim, Zhiling Zhao, Jinyang Li, Rahma Zakaria, Chen-Yu Tsao, Kayla Chun, Dana Motabar, Monica Chu and Gregory Payne; University of Maryland, United States

Microelectronics has transformed our lives. It has changed the way we collect, process, and transmit information. The intersection between microelectronics and biology has also been transformative – ionic currents that control cardiovascular and neural systems are detected and even corrected using electronics (e.g., EKG & defibrillators). Yet, the microelectronics world has barely “sampled” the vast repertoire of chemical information in our biological world. Take for example the human immune, endocrine, and gastrointestinal systems – they are largely opaque to the methods of electrical sensing and communication. In biology, information is often contained in the *structure of its molecules* – molecules that move from place to place and based on their structure, convey information and provoke a response.

We envision new processes and deployable products that open the dialogue between biology and microelectronics – that eavesdrop on and manipulate biological systems within their own settings and in ways that speed corrective actions. We view biofabrication and synthetic biology as integral technologies for achieving this vision. Synthetic biology, often visualized as an innovative means for “green” product synthesis through the genetic rearrangement of cells, can also provide a means to connect biological systems with microelectronic devices. Cells can be reprogrammed to close the communication gap that exists between the electrons and photons of devices and the molecules and ions of biology. This is enabled, in part, through redox mediators – biological carriers of electrons that transfer “packets” information to and from electronics. We have suggested the purposeful electronically actuated elicitation of gene expression is “electrogenetics”. Biofabrication, the assembly of biological components using biological means or mimics thereof, offers a means to close the fabrication gap – a gap that stems from the disparity between biological systems, assembled of labile components using built-in error correction, and devices, built of potentially toxic materials using error prevention and byproduct exclusion. Here, innovative materials, electronics, biomolecular and cellular engineering strategies can be developed to mediate “molecular” communication - information transfer to microelectronic systems and back. New systems and devices are continually emerging that integrate abiotic and biological components (e.g. animal-on-a-chip devices, chip based manufacturing systems, etc.) at a hierarchy of length scales. New systems may emerge that eavesdrop on and electronically guide cellular consortia, vastly expanding our synthetic biology repertoire while utilizing increasingly complex raw materials.

We suggest that a great many of our society’s grand challenges in sustainability, food, energy, and medicine may be addressed by developing tools that open lines of communication between the biological and electronics worlds.

10:30 AM SB04.06.02

Broad Bacteria Biosensing Based on Integration of 3D Organic Transistors in Fluid Flow Cells Jingchu Huang, Daewoo Han and Andrew J. Steckl; University of Cincinnati, United States

A novel approach for bacteria biosensing using organic electrochemical transistors (OECT)¹ has been demonstrated in the sensing of cells and metabolic products (carbohydrates, protein, and cations)². OECTs are attractive for bacteria biosensing due high sensitivity, fast diagnostics, and simpler bacteria handling. The use of OECT enables the detection of bacterial contamination in home-liquid-goods and provide potential real-time monitoring capabilities. Two main requirements for bacteria sensing in liquid products are: (a) non-specific detection (no capture agents) - there are hundreds of common bacteria strains present in daily living that are harmful to humans; (b) high sensitivity – for early detection of liquid goods contamination, at bacteria concentrations as low as a few hundred colony-forming units per mL (CFU/ml). OECTs can respond to bacteria attached to (or near) either the source-drain channel or the gate electrode. Here, we report on universal bacteria sensing using OECTs integrated within a microfluidic flow cell. A conductive microporous filter membrane in the flow cell device was utilized to accumulate the bacteria and serve as a gate electrode for OECT operation (“gate filter”). The device can detect ~ 10² CFU/ml bacteria in mixtures of household liquid products and common bacteria growth broths. This is the result of bacteria accumulation on the gate causing a shift in the OECT source-drain channel current (I_{ds}).

The overall sensor consists of a dual PEDOT: PSS gate OECT, a 3D-printed flow cell, and an Au-coated 0.4um PETE filter membrane as the gate electrode. The dual OECTs are integrated into the flow cell device and both channel sensing and gate sensing approaches are evaluated using *pseudomonas fluorescens*, a common Gram-negative bacterium. OECT channel sensing shows good discrimination between bacteria and sterile solutions, with higher bacteria concentration resulting in higher I_{ds} shift and increased peak transconductance (g_m). At $V_g = 0.3V$, compared to sterile solution a solution of 10⁵ CFU/ml bacteria results in ~ 43% and 100% increase in I_{ds} (2.51mA) and g_m (7.2mS), respectively. In the flow cell device operation, bacteria trapped on the gate filter results in additional gate-to-electrolyte potential drop on the effective gate voltage. Sterile and bacteria solutions of 10² and 10³ CFU/ml display the same I_{ds} starting point (4.6 mA) at $V_g = 0V$. As gate bias is applied, the higher bacteria concentration samples have a sharper I_{ds} reduction. At $V_g = 0.3V$, the channel current is reduced to 1.7 mA for the sterile solution, 1.3 mA for the 10² CFU/ml, and 0.5 mA for the 10³ CFU/ml bacteria solutions. The higher bacteria concentration results in a smaller voltage required to switch off the OECT of 0.5 and 0.7V for 10³ and 10² CFU/ml, respectively. With the OECT flow cell approach, bacteria detection resolution reached a low value of ~ 10² CFU/ml. For continuous real-time detection testing using OECT flow cells, the device maintains $I_{ds} = 3.5mA$ at $V_g = 0.3V$ when flowing sterile solution at 3ml/hr. Introducing 10³ CFU/ml bacteria solution results in the I_{ds} current decrease with a 1.5mA/hr rate. In summary, the 3D-printed flow cell incorporating OECTs has been used to sense low levels of bacteria present in commercial household liquid products within an hour without the need for amplification, providing a promising approach towards future biosensing

system.

Frantz, E., Han, D., & Steckl, A. *ECS Meeting Abstracts*, **2021**, May, No. 55, p. 1416.

Marks, A., Griggs, S., Gasparini, N., & Moser, M. *Advanced Materials Interfaces*, **2022**, 9(6), 2102039

10:45 AM SB04.06.03

Recording of Intracellular Action Potential of Cardiomyocytes by Means of Organic Electrochemical Transistors Silvia Conti, Rustamzhan Melikov, Giuseppina Iachetta, Michele Dipalo, Francesco Tantussi and Francesco De Angelis; Istituto Italiano di Tecnologia, Italy

The existence of an electronic coupling between electrogenic cells and electronic supports is the bases of any tailored system employed to study biology-driven phenomena. During real-time monitoring of electrophysiological signals (action potentials, APs), the communication typically occurs at the cell (neurons or cardiomyocytes)/transducer interface, whose optimization is fundamental to make the investigation of neurodegenerative and cardiac diseases effective. In the last 20 years, organic materials have been largely used for the fabrication of bioelectronic devices thanks to their biocompatibility, easy processability, tunability of physical properties, stimuli-responsiveness and high conformability¹.

Organic electrochemical transistors (OECTs) using Poly(3,4-ethylenedioxythiophene):poly(styrenesulfonate) PEDOT:PSS as active material, present features that make them perfectly suitable for the record of electrophysiological potentials: *i*) the biocompatibility, *ii*) the flexibility, and *iii*) the double ionic/electronic conductivity of the polymer. The cell/transducer interface is, in this case, represented by the active material that interfaces the biological system and dictates the transduction of the ionic transmembrane flows (able to dope/de-dope the polymer) into an electrical readout². Moreover, *iv*) the high source-drain current levels and *v*) the large transconductance values that characterized this type of devices, allow to keep low operating voltages and reduced heat generation, necessary for the system durability in aqueous biological environment³. Being a non-invasive measurement, it increases the vitality of the cells, allowing multiple and long-duration recordings, fundamental for chronic studies.

In this work, we report *in vitro* recordings of APs of human induced pluripotent stem cell-derived cardiomyocytes (hiPSC-CMs) by using planar OECTs with spin-coated PEDOT:PSS channel. hiPSCs-CMs were cultured directly on the polymeric surface. Extracellular potential recordings were obtained by simply turning on the transistors at their maximum transconductance and following the variation of both the drain-source and the gate-source currents. Extracellular signals present a typical and predominant negative phase (with amplitude around 0.3 mV) and an expected short duration of around 20 ms^{2,4}. Intracellular signals were recording adopting a cell optoporation protocol (large pulse, low current intensity) that enabled the measurement without stimulating the cells⁵. Amplitudes in the range of 3-4 mV were recorded, which is comparable to performance obtained with similar devices that use electroporation⁵. To improve the photocurrent response different formulations of PEDOT:PSS with the addition of gold nanoparticles are tested. Drug screening tests are performed to assess the ability of the devices to detect cardiotoxic effects; live/dead assay and immunofluorescence imaging to evaluate their biocompatibility. In future, additional electronics and biosensing elements could be complemented on the same device paving the way to multifunctional, reliable, and low-cost biosensors.

1. Ohayon, D. & Inal, S. Organic Bioelectronics: From Functional Materials to Next-Generation Devices and Power Sources. *Adv. Mater.* **32**, 2001439 (2020).

2. Gu, X. *et al.* Organic Electrochemical Transistor Arrays for In Vitro Electrophysiology Monitoring of 2D and 3D Cardiac Tissues. *Adv. Biosyst.* **3**, 1–8 (2019).

3. Jimbo, Y. *et al.* An organic transistor matrix for multipoint intracellular action potential recording. *Proc. Natl. Acad. Sci.* **118**, 1–8 (2021).

4. Liang, Y. *et al.* Tuning Channel Architecture of Interdigitated Organic Electrochemical Transistors for Recording the Action Potentials of Electrogenic Cells. *Adv. Funct. Mater.* **29**, (2019).

5. Abbott, J. *et al.* A nanoelectrode array for obtaining intracellular recordings from thousands of connected neurons. *Nat. Biomed. Eng.* **4**, 232–241 (2020).

11:00 AM SB04.06.04

Wireless Detection of Enzyme-Powered Hydrogel Motor for Autonomous Mobile Biosensors Shogo Himori and Toshiya Sakata; The University of Tokyo, Japan

Electrochemical detection methods are promising for accessible biosensors to all citizens because of their simple principle, and various types of electrochemical biosensors have been developed, including wearable sensors and implantable sensors [1]. However, these sensors cannot reach wide-area spatial information, although they can detect biological information near the electrodes. Therefore, we are proposing a new-type biosensor, an autonomous mobile biosensor that moves in solution and continuously tells us the biological information.

In the Marangoni motor system, the motor releases surfactant from its body, allowing it to move in solution while generating a surface tension gradient around itself [2]. Urease, one enzyme, catalyzes the production of ammonia molecules from the biomolecule urea, and the ammonia reduces surface tension [3]. It suggests that the urease-modified motor can generate driving force in urea containing bio-solution without external energy supply. In addition, conductive polymer hydrogels are suitable for the motor body material because of their conductivity, which mediates electrochemical information, and their porosity, which allows enzymes to be carried in the three-dimensional polymer network. Common electrochemical sensors use wires to connect the sensing electrodes with external measurement systems for the collection of electrical signals, but the wires inhibit the movement of the motors in the autonomous mobile biosensor. In this study, a wireless sensing system was developed to acquire biological signals from the self-propelled conductive hydrogel motor.

The conductive hydrogels were fabricated from a mixture of poly(3,4-ethylene dioxythiophene): poly (styrene sulfonate) (PEDOT: PSS) and dimethyl sulfoxide (DMSO) [4]. Enzyme-based motorization was investigated via modification of urease on a conductive hydrogel by physical cross-linking with glutaraldehyde. In developing wireless motor detection, we examined impedance sensing methods. Two parallel Au electrodes, called direct electrodes (DEs) were placed in PBS and connected to the electrochemical analyzer. In addition, four materials (Au, ITO; indium tin oxide, Gel; conductive hydrogel, glass), called bipolar electrodes (BPE) were placed between the DEs wirelessly, and the impedance changes depending on the material and placement of the BPEs were investigated.

As a result, the urease-modified hydrogel motor began moving in PBS including urea on the basics of the enzymatic reaction. It indicates that urease-modified gel can obtain driving energy from urea and move continuously in bio solution. In addition, the impedance change was studied depending on the wireless BPE material, and it was found that when conductive materials (Au, ITO, Gel) were put between the DEs, the impedance at high frequency become lower than when no material was put in the solution. In contrast, when glass, an insulator, is placed between the DEs, the impedance increases. It indicates that the conductivity of the BPE material alters the current flowing between the DEs. Besides, impedance change dependent on the wireless gel position was also investigated, and it was found that the impedance change became smaller as the gel moved away from the DEs. It indicates that the impedance measurement method provides information on the movement of the gel wirelessly. In the future, we will capture urea concentration-dependent changes in gel motion wirelessly and investigate potential applications in biosensing.

[References]

[1] S. Himori and T. Sakata, *RSC Adv.*, **12**, 5369–5373, (2022). [2] X. Arqu e *et al.*, *Nat. Commun.*, **10**, 2826, (2019). [3] Y. Xu *et al.*, *Chem. – An Asian J.*, **16**, 1762–1766, (2021). [4] B. Lu *et al.*, *Nat. Commun.*, **10**, 1043, (2019).

11:15 AM *SB04.06.05

A Living Electronic Biosensor for the Marine Environment Sarah M. Glaven¹, Lina Bird¹, Dasha Leary¹, Judson Hervey¹, Jaimee Compton¹ and Christopher A. Voigt²; ¹U.S. Naval Research Laboratory, United States; ²Massachusetts Institute of Technology, United States

Microbial extracellular electron transfer (EET) by electroactive bacteria can be reprogrammed using bioengineering to enhance existing technologies (e.g. microbial fuel cells) or create entirely new ones (living electronic sensors). A current bottleneck in engineering electroactive bacteria is the selection and development of chassis strains that can both host complex EET machinery and survive under conditions relevant to the application of interest. In this talk I will describe our efforts to develop *Marinobacter atlanticus*, a gram-negative marine bacterium, as an engineered electroactive bacterium for sense and respond in seawater. Genetically encoded sensors optimized for use in *E. coli* were used to control expression of the *Shewanella oneidensis* electron transfer pathway in planktonic and biofilm attached cells. Electrical current production could be induced during biofilm growth in artificial seawater when sensors controlling expression of different components of the pathway were activated by addition of 2,4-diacetylphloroglucinol (DAPG), isopropyl β -D-1-thiogalactopyranoside (IPTG), and tetracycline (Tc). Significant current production also required addition of menaquinone, which *M. atlanticus* does not produce, for electron transfer from the inner membrane to the expressed electron transfer pathway. Electron transfer was also reversible, indicating electron transfer into *M. atlanticus* could be controlled. These results show that an operationally relevant marine bacterium can be genetically engineered for environmental sensing and response using an electrical signal.

SESSION SB04.07: Emerging Applications
Session Chairs: Teuta Pilizota and Tanya Tschirhart
Wednesday Afternoon, November 30, 2022
Hynes, Level 3, Room 303

1:30 PM *SB04.07.01

Photosynthetic Microorganisms for Photoconversion Gianluca Maria Farinola¹, Rossella Labarile^{1,2}, Danilo Vona¹, Gabriella Buscemi¹, Matteo Grattieri¹, Roberta Ragni¹ and Massimo Trotta²; ¹Universita' degli Studi di Bari Aldo Moro, Italy; ²CNR, Italy

Photosynthetic microorganisms and their molecular components represent attractive functional elements for harvesting and conversion of solar energy in bioelectronic devices [1].

We have recently investigated several approaches for addressing the Reaction Center (RC) photoenzyme extracted from the purple non sulfur photosynthetic bacterium *Rhodobacter (R.) sphaeroides* in optoelectronic devices for conversion of solar energy into photocurrent.

We have used polydopamine (PDA) for immobilizing and interfacing RC on ITO electrodes, by simple polymerization of dopamine in aqueous media [2].

We also used polydopamine to directly integrate living cells of photosynthetic bacteria onto electrodes in bio-photoelectrochemical cells. Two different approaches were used for *R. sphaeroides* and its closely related strain *R. capsulatus*, respectively. The encapsulation of entire bacterial cells of *R. sphaeroides* in PDA conductive coating was obtained by addition of dopamine in bacterial growth medium [3]. In the case of the *R. capsulatus* a one-pot procedure was used, which was initiated by oxygenic polymerization followed by electrochemical polymerization of dopamine, including redox mediators [4].

We have also explored the possibility to directly interface photosynthetic microorganisms with electrodes without the use of an additional soft interfacing material. For this purpose, we used the unicellular diatom algae *Phaeodactylum tricoratum*, exploiting their spontaneous biofilm formation.

Our study discloses new concepts for the generation of bio-hybrid materials for sunlight photoconversion and for light-responsive bioelectronics from the combination of photosynthetic microorganisms with tailored functional materials.

[1] F. Milano, A. Punzi, R. Ragni, M. Trotta, G.M. Farinola, Adv. Funct. Mater., 29, 1805521, (2019).

[2] M. Lo Presti, M. M. Giangregorio, R. Ragni, L. Giotta, M. R. Guascito, R. Comparelli, E. Fanizza, R. R. Tangorra, A. Agostiano, M. Losurdo, G. M. Farinola, F. Milano, M. Trotta, Adv. Electron. Mater., 6, 2000140, (2020).

[3] D. Vona, G. Buscemi, R. Ragni, M. Cantore, S. Cicco, G.M. Farinola, M. Trotta, MRS Advances, 5(18-19): p. 957-963, (2020).

[4] G. Buscemi, D. Vona, P. Stufano, R. Labarile, P. Cosma, A. Agostiano, M. Trotta, G.M. Farinola, M. Grattieri, ACS Appl. Mater. Interfaces 14, 23, 26631–26641, (2022).

2:00 PM SB04.07.02

Machine-Learning-Based Inverse Design for Electrochemically Controlled Microscopic Gradients of O₂ and H₂O₂ Yi Chen, Jingyu Wang, Ben Hoar, Shengtao Lu and Chong Liu; University of California, Los Angeles, United States

A fundamental understanding of the extracellular microenvironments of O₂ and reactive oxygen species (ROS) such as H₂O₂, ubiquitous in microbiology, demands high-throughput methods of mimicking, controlling, and perturbing gradients of O₂ and H₂O₂ at microscopic scale with high spatiotemporal precision. However, there is a paucity for a high-throughput strategy of microenvironment design and it remains challenging to achieve O₂ and H₂O₂ heterogeneities with the microbiologically desirable spatiotemporal resolutions. Here we report the inverse design, based on machine learning (ML), of electrochemically generated microscopic O₂ and H₂O₂ profiles relevant for microbiology. Microwave arrays with suitably designed electrochemical catalysts enable the independent control of O₂ and H₂O₂ profiles with spatial resolution of $\sim 10^1$ μm and temporal resolution of $\sim 10^0$ sec. Neural networks aided by data augmentation inversely design the experimental conditions needed for targeted O₂ and H₂O₂ microenvironments while being order-of-magnitude faster. Interfacing ML-based inverse design with electrochemically controlled concentration heterogeneity creates a viable fast-response platform towards better understanding the extracellular space with desirable spatiotemporal control.

2:15 PM SB04.07.03

Enhancing Solar-Driven CO₂ Reduction to Multi-Carbon Products via Adapted Whole-Cell Catalysts and a Silicon Nanowire Photocathode Jimin Kim and Peidong Yang; UC Berkeley, United States

Due to the anthropogenic CO₂ emissions, the atmospheric concentration of CO₂ exceeded 413 ppm in 2020, sharply increasing from 270 ppm at the beginning of the industrial revolution. Dramatic climate changes, such as extreme heat waves, wildfires, and droughts, are affecting human societies and ecosystems at such alarming levels that their influence can no longer be ignored. Thus, developing alternatives to fossil fuels and mitigating CO₂ emissions at a necessary scale is more urgent than ever to establish a carbon-neutral society. Catalytic CO₂ conversion to renewable fuels has been the focus of intensive research with the goal of closing the carbon loop. Photosynthetic biohybrid systems (PBSs), in which a photoactive semiconductor directly

interfaces with nonphotosynthetic, CO₂-reducing bacteria, represent a promising approach for the renewable and sustainable production of fuels and chemicals. They combine the best features of semiconducting nanomaterials and biological whole-cell catalysts to power biocatalytic CO₂ conversion with light. Semiconducting nanomaterials can harvest solar energy efficiently. Nature's catalytic machinery enclosed in its cellular environment provides low activation energies and exquisite product selectivity through its cascade reactions. We demonstrate that by tuning the local chemical environment of a silicon nanowire – acetogen *Sporomusa ovata* (*S. ovata*) biohybrid, we can maximize the interfacial area between living cells and cathodes and boost the bioelectrochemical CO₂ reduction rate. In addition to optimizing the local environment, the rational design of biocatalysts in PBSs is imperative to reduce CO₂ into valuable chemicals effectively. We introduce a methanol adapted *S. ovata* to enhance the sluggish biocatalytic activity of wild-type microorganisms into our silicon nanowires (Si NWs) photocathodes for efficient solar-to-chemical conversion. Electrochemical impedance spectroscopy (EIS) is exploited to study the biohybrid system and the biofilm cathodes. We illustrate the fundamental charge transfer mechanisms at the biotic-abiotic interface between silicon nanowires and microorganisms. Using adapted *S. ovata* decreases the charge transfer resistance at the cathodes and facilitates charge transfer from directly interfaced solid electrodes. Finally, this new generation of biohybrids with adapted *S. ovata* enables an increase of solar CO₂ fixation under photoelectrochemical reducing environments on the Si NWs photocathode.

2:30 PM BREAK

3:30 PM SB04.07.04

Enzyme Bioanode with Electropolymerized Thiazine for Formic Acid/O₂ Biofuel Cells Motohiro Kosugi, Yuki Fujii, Ryoichi Tatara and Shinichi Komaba; Tokyo University of Science, Japan

An enzymatic biofuel cell (EBFC) is a type of power generating device where enzymes function as catalysts to oxidize biofuel (saccharides such as glucose or alcohols)^{[1]-[4]} and reduce oxygen molecules.^{[5]-[7]} It can be operated under mild conditions of neutral solution, room temperature and atmospheric pressure. The main advantage of an EBFC is the utilization of renewable energy sources through enzymatic reactions. Among the fuel sources currently available for EBFCs, formic acid is oxidized by formate dehydrogenase (FDH) at a low potential and is expected to high-voltage EBFCs. Most of the previously reported fuel cells with formic acid as the fuel utilize palladium or platinum as catalysts, and there are few reports of enzymes being used as catalysts. Using enzymes has the advantage of being relatively inexpensive compared to other catalysts in EBFCs. In this study, we focused on FDH with nicotinamide adenine dinucleotide (NAD) as the active site and prepared enzymatic bioanodes modified with three different electropolymerized thiazine dyes, methylene blue (MB), thionine (Th), and Azure A (AA), as electrocatalyst and investigated their electrochemical properties.

The bioanodes were prepared as follows: 1) carbon powders (carbon nanotube or sucrose-derived carbon) was dispersed in water with sodium polyglutamate as the binder and dropped on carbon-felt (CF) electrodes (thickness: 2 mm; diameter: 11 mm), then the carbon electrodes were modified with the three electropolymerized films, polyMB, polyTh, and polyAA, and 3) FDH solution was drop-cast on the electrodes. Electrochemical measurements were conducted at room temperature in the phosphate buffer solution (0.1 mol dm⁻³ PBS at pH = 7.0) containing NAD (10 mmol dm⁻³) and sodium formate (0.15 mmol dm⁻³).

At the prepared electrode, formate was anodically oxidized with FDH at the electropolymerized electrode, and the coenzyme NAD was simultaneously reduced to NADH. The oxidation of NADH by the electropolymerized thiazine was expected to proceed rapidly. We successfully observed an oxidation current at -0.05 V (vs. Ag/AgCl), generated by the anodic decomposition of formate ions, in the substrate solution. This confirms that the electrochemically deposited thiazine polymer can act as electrocatalyst for the series of above oxidation reaction as expected. Among three thiazine dyes, it was found that polyMB has the highest catalytic activity for NADH oxidation, yielding the highest oxidation current densities owing to the efficient electron transfer process. The comparison of the electrochemical properties of the bioanode prepared with CNT and pyrolytic sucrose-derived carbon will also be discussed in the presentation.

References

- [1] S. Komaba, et al., *Electrochemistry*, **76**, 55 (2008)
- [2] Y. Handa, S. Komaba, et al., *ChemPhysChem*, **15**, 2145 (2014).
- [3] R. Yasujima, S. Komaba, et al., *ChemElectroChem*, **5**, 2271, (2018).
- [4] R. Toda, S. Komaba et al., *ChemElectroChem*, **8**, 4199 (2021).
- [5] K. Yamagiwa, S. Komaba, et al., *J. Electrochem. Soc.*, **162**, F1425 (2015).
- [6] K. Yasueda, S. Komaba, et al., *J. Electrochem. Soc.*, **165**, F1369 (2018).
- [7] R. Tatara, S. Komaba, et al., *J. Electrochem. Soc.*, **168**, 074506 (2021)

3:45 PM SB04.07.05

Cable Bacteria—Electrifying Electronic Biological Materials with Record Intrinsic Electrical Properties—From Transistors to Billie Eilish Jean V. Manca¹, Robin Bonnè², Raghavendran Thiruvallur Eachembadi¹, Koen Wouters¹, Nico Franssaert¹, Roland Valcke¹ and Bart Cleuren¹; ¹University of Hasselt, Belgium; ²Aarhus University, Denmark

Cable bacteria, a group of filamentous electroactive bacteria, have developed a unique energy metabolism and parallel fibre structures demonstrating electron transport for conduction lengths up to 1 cm and with fibre conductivities exceeding 10 S/cm. Conduction measurements carried out in high vacuum excluded the possibility of ionic conduction, but the fundamental charge transport mechanisms remain unknown. The observed electron transport in cable bacteria over distances in the order of centimeters is remarkable in the biological world.

Cable bacteria as 'living electrical wires' are of fundamental interest to better understand the underlying biological processes, but are also potentially interesting as alternative organic electronic materials for the emerging field of bioelectronics as e.g. biocompatible electrical connections and circuits, conductive composite materials, (nano-) sensors, transistors.... In order to investigate the intrinsic electrical properties and underlying transport mechanisms, our approach is to study them with a range of macroscopic and nanoscale solid state electrical characterisation techniques, in combination with structural and analytical techniques ranging from SEM to ToF-SIMS.

The electrical circuitry in a single cable bacterium is visualized with nanoscopic resolution using conductive atomic force microscopy (C-AFM). Combined with perturbation experiments, it is demonstrated that electrical currents are conveyed through a parallel network of conductive fibers embedded in the cell envelope, which are electrically interconnected between adjacent cells. This structural organization provides a fail-safe electrical network for long-distance electron transport in these filamentous microorganisms.

Impedance spectroscopy provides an equivalent electrical circuit model, which demonstrates that dry cable bacteria filaments function as resistive biological wires. Temperature-dependent electrical characterization reveals that the conductivity can be described with an Arrhenius-type relation over a broad temperature range (-195°C to +50°C), demonstrating that charge transport is thermally activated with a low activation energy of 40-50 meV. Furthermore, cable bacterium filaments can be utilized as the channel in a field-effect transistor.

The measured intrinsic electrical properties result very similar to for instance organic semiconductors, situating them in the context of electrical functional materials between semiconductors and conductors. These electrifying 'bad guy' microorganisms – with from various perspectives behave as they are not supposed to – are attracting growing interest and in the long-term could open novel avenues in emerging domains such as bioelectronics, biodegradable electronics and electronic biological materials (e-biologics). As a proof-of-principle for electrical transmission capabilities through cable bacteria filaments, the music track "Bad Guy" of Billie Eilish is transported through them. Cable Bacteria are rock & roll.

4:00 PM SB04.07.06

Enabling Electron Injection for Microbial Electrosynthesis with n-Type Conjugated Polyelectrolytes [Glenn Quek](#), Ricardo J. Vázquez, Samantha R. Mccuskey and Guillermo Bazan; National University of Singapore, Singapore

Microbial electrosynthesis – using renewable electricity to stimulate microbial metabolism – holds the promise of sustainable chemical production. A key limitation hindering performance are slow electron transfer rates at biotic-abiotic interfaces. Here, we rationally design a water-processible n-type organic semiconducting polymer and demonstrate its use as a soft conductive material to encapsulate electroactive *Shewanella oneidensis* MR-1. The self-assembled three-dimensional living biocomposite amplifies current uptake from the electrode ≈ 674 -fold over controls with the same initial number of cells, thereby enabling continuous synthesis of succinate from fumarate. By demonstrating synergy between living cells with n-type organic semiconductor materials, these results provide new strategies for improving the performance of bioelectrosynthesis technologies.

4:15 PM SB04.07.07

The Impact of Oxygen on Mtr-expressing *Escherichia coli* [Xu Zhang](#) and Caroline Ajo-Franklin; Rice University, United States

In bioelectrochemical systems (BESs), anaerobic conditions are used to generate current from microorganisms because oxygen can compete with an electrode as a terminal electron acceptor. However, prior studies have shown that oxygen enhances current production from *Shewanella oneidensis* MR-1 by counterbalancing a modest decrease in current per cell with a substantial increase in the total biomass. This opens the possibility that BESs based on oxygen-tolerant microorganisms might not need anaerobic conditions for maximal current production. Here we investigated this question in the facultative anaerobe *Escherichia coli*, which has been engineered to produce current using the Mtr pathway from *Shewanella oneidensis* MR-1.

To investigate the effect of oxygen on the current production of *Escherichia coli*, we have introduced different oxygen levels to BESs containing Mtr-expressing *E. coli* and monitored current production, biomass, protein expression and metabolic products. Our results showed that oxygen exposure substantially boosted current up to 30-fold relative to anaerobic conditions. With increasing oxygen levels, both the current per cell and total biomass increase. Oxygen enhances the expression of the Mtr proteins relative to anaerobic conditions. Additionally, oxygen levels linearly increased the abundance of the first protein in the Mtr pathway, indicating that this protein is the limiting step in the current production. Additionally, oxygen increased energy flux and substrate utilization.

In summary, oxygen enhances the current production of Mtr-expressing *Escherichia coli*. This work challenges the prevailing paradigm that anaerobic conditions promote current production, suggesting that bioelectronic applications can be performed in oxygen-rich conditions.

SESSION SB04.08: Virtual Session
Session Chairs: Giuseppe Paternò and Tanya Tschirhart
Wednesday Morning, December 7, 2022
SB04-virtual

10:30 AM SB04.08.01

Electrolyte-Gated Transistors Biosensors for Healthcare Applications [Matteo Sensi](#)¹, [Marcello Berto](#)¹, [Carlo A. Bortolotti](#)¹ and [Fabio Biscarini](#)^{1,2}; ¹Università degli Studi di Modena e Reggio Emilia, Italy; ²Istituto Italiano di Tecnologia, Italy

Electrolyte-gated transistors (EGTs) based on organic semiconductors and graphene derivatives are emerging in the field of biosensing because they are ultrasensitive, label-free, can be fabricated on flexible substrates at low cost and interfaced with biological samples.^{1,2} We show some examples to demonstrate the possibility to use this technology to develop biosensors for different healthcare applications, by just selecting the most effective device architecture and material.

All the presented devices share a common transistor architecture, consisting of two interdigitated electrodes, source and drain, covered with an active material, in contact with a gate electrode through an electrolyte. The biosensing event takes place at the gate/electrolyte interface, by functionalization of the gold gate with a biorecognition moiety, and it is amplified by the active material channel thanks to the high-capacitance electrical double-layers formed at the gate/electrolyte and electrolyte/channel interfaces.

We fabricated EGTs biosensors for ultrasensitive detection of biomarkers by using different materials in the channel, namely ambipolar Reduced-Graphene Oxide, organic p-type semiconductor TIPS-Pentacene and poly(3,4-ethylenedioxythiophene)polystyrene sulfonate (PEDOT:PSS) polymer mixture.

Thanks to tailored gate bio-functionalization, we realized a disposable rGO-EGT immunosensor for the detection of anti-Infliximab antibodies, which are produced by patients upon treatment with the immunotherapeutic drug Infliximab and can make the therapy ineffective. Furthermore, we developed an Electrolyte-Gated Organic Field-Effect Transistor (EGOFET) immunosensor for the detection of anti-Nivolumab antibodies, based on the organic semiconductor TIPS-pentacene, showing fM theoretical Limit of Detection (LOD).³ We also successfully employed an organic electrochemical transistor (OECT) genosensor for the detection of oligonucleotides, thanks to a facile functionalization process based on polydopamine.⁴ Finally, we demonstrated the possibility to use EGOFET for the specific detection of transcription factors, by using the consensus DNA sequence as biorecognition element.

We conclude that EGTs biosensors show promising performances for the future application at the Point-of-Care but also for fundamental studies on macromolecules interactions.

References

- 1) Burtscher, B.; Manco Urbina, P. A.; Diacci, C.; *Advanced Healthcare Materials*. 2021, 10 (20), 2100955.
- 2) Torricelli, F.; *Nat. Rev. Methods Prim.* 2021, 1 (66).
- 3) Sensi, M.; *Chem. Commun.* 2021, 57 (3), 367–370.
- 4) Sensi, M.; *Macromol. Mater. Eng.* 2022, 307 (5), 2100880.

10:45 AM SB04.08.02

Enhancement of Bacteria Detection with an Extended-Gate Field-Effect Transistor (EGFET) by Dielectrophoretic Trapping of Bacteria Annalena Eckert¹, Lea Könemund¹, Tamina Kirkklies¹, Svenja Herdan¹, Laurie Neumann¹, Felix Hirschberg¹, Rebekka Biedendieck², Hans-Hermann Johannes^{1,3}, Dieter Jahn² and Wolfgang Kowalsky^{1,3}; ¹Technische Universität Braunschweig, Institut für Hochfrequenztechnik, Germany; ²Institute of Microbiology and Braunschweig Integrated Centre of Systems Biology (BRICS), Germany; ³Cluster of Excellence PhoenixD, Germany

Bacterial infections that do not respond to treatment are a leading cause of death worldwide and a major public health threat. For example, the O157:H7 strain of *Escherichia coli* (*E. coli*) is considered one of the most dangerous foodborne pathogens. It is crucial to detect pathogenic organisms at an early stage so that appropriate treatment and targeted use of antibiotics can be undertaken. Conventional detection techniques, such as enzyme-linked immunosorbent assay (ELISA) or polymerase chain reaction (PCR) are time-consuming, expensive, and require trained professionals. A method for rapid detection of bacteria that is inexpensive, provides a reliable result, and is easy to use is becoming increasingly important. The development of suitable electronic transducers that provide label-free, low-cost, rapid detection of bacteria is of great interest, as this approach could be extended to the development of handheld devices for point-of-care applications.

In previous work, a detection method based on an extended-gate field-effect transistor (EGFET) was developed for the detection of *E. coli* K12, a common well investigated apathogenic model strain. The sensing region of the EGFET was functionalized with modified porphyrins containing two different linkers: One linker connects the porphyrin to the electrode surface of the gate, and the other binds bacterial cells to the functional layer via a specific peptide chain. After applying a bacterial suspension onto the functional layer, the cells can thus bind to it. The negative charge on the surface of the cells changes the electrical potential at the electrode surface, which affects the electrical behavior of the EGFET. The presence of bound *E. coli* cells on the functionalized sensor surface has already been successfully detected¹.

The aim of this research is to concentrate bacteria specifically on the sensor surface of the EGFET by exerting a dielectrophoretic force on the cells in a combined system. The electrokinetic effect of dielectrophoresis (DEP) enables contactless manipulation of biological cells in fluids. DEP utilizes the geometry of electrodes to generate non-uniform high-frequency electric fields that exert an attractive or repulsive force on dielectric particles, inducing movement toward areas of maximum electric field gradient (positive-DEP) or minimum electric field gradient (negative-DEP). DEP is a flexible and versatile method for immobilizing, separating, and concentrating cells and has been successfully optimized for the fixation of bacteria on electrodes in previous work. It will be investigated to what extent the reliability and sensitivity of the sensor can be increased by dielectrophoretically trapping the bacteria on the transistor gate. Furthermore, it is possible to extend the functionality of the sensor with selectivity by combining it with DEP. DEP is capable of selectively separating biological particles by properties such as size, material, and shape, which allows selective detection of a bacterial species from a heterogeneous suspension.

Reference: 1. Könemund, L., Neumann, L., Hirschberg, F. *et al.* Functionalization of an extended-gate field-effect transistor (EGFET) for bacteria detection. *Sci Rep* **12**, 4397 (2022)

Key words: dielectrophoresis (DEP), biosensing, EGFET, porphyrin, *E. coli* immobilization

10:50 AM SB04.08.03

All Printed Vertical Organic Electrochemical Transistor Mona Azimi¹, Chi-hyeong Kim¹, Harini Nagarajan² and Fabio Cicoira¹; ¹Polytechnique Montreal, Canada; ²Madras Institute of Technology, India

Recently printing techniques attracted significant attention for the fabrication of electronic devices especially organic electrochemical transistors (OECTs). Printing method is a low-cost additive process with fast prototyping and compatibility with different flexible or stretchable substrates. Poly(3,4-ethylenedioxythiophene) (PEDOT:PSS) is a commonly used p-type material for OECTs due to its stability in aqueous media. Most of the reported OECTs to date have large channel lengths in tens of micrometers, which limits the transistor performance and transconductance. Downscaling the channel length is challenging by a common photolithography method. Here we used the printing technique to fabricate vertical configuration of OECTs where the channel length is defined by the thickness of printed active material (PEDOT:PSS), sandwiched between source and drain electrodes (silver electrodes). Printable semi-solid gel is used as an electrolyte for devices. We compared the planar configuration with vertical devices, and significantly higher transconductance is obtained for vertical configuration.

10:55 AM *SB04.08.04

Electrical Control of Immune Cell Function Ann M. Rajnicek; University of Aberdeen, United Kingdom

Bioelectrical signalling drives behaviour of cells at scales from single bacteria to multicellular tissues. Improved understanding of bioelectrical phenomena, including their influence on immune cell function, will lead to improved electroconductive materials relevant to repair of epithelial and tissue damage. When an epithelium is wounded an endogenous, steady electric field (EF) of ~100 mV/mm is driven through the neighbouring tissues (cathode at the centre) and the success of wound closure relates to the presence and magnitude of this wound EF. In part this is because the EF steers migration of epithelial cells toward the wound site to close the gap. But Immune cells, including monocytes and macrophages, are also important contributors to successful wound healing. For many years the stimuli driving their function were principally attributed to chemical signalling factors present within the wound microenvironment, with no regard given to bioelectrical signals.

We therefore studied the responses of cultures of primary human monocytes and macrophages exposed to physiologically relevant EFs. Time lapse observation of monocytes, which are macrophage precursors, showed that an EF of 150 mV/mm applied for 2h steered migration toward the cathode and increased the speed of migration compared to controls (no EF). This suggests that these 'first responders' would be guided toward the wound centre (cathode) by an endogenous EF.

However, human macrophages responded differently. Macrophages migrated preferentially toward the anode (opposite to monocytes) and their speed of migration was increased compared to controls. Impressively, the macrophages were exquisitely sensitive to the EF stimulus, responding with migration toward the anode at EFs as small as 5 mV/mm, well below the threshold of endogenous wound EFs. This suggests that macrophages arriving, later than the monocytes, migrate to the wound edges (anode) to clear debris and microbes.

Directed migration of macrophages was associated with elongation of the cells parallel to the EF axis and reorganisation of the actin cytoskeleton toward the leading edge. Since a key role of macrophages is phagocytic uptake of microbes and apoptotic cells in the wound environment, we tested whether the EF also enhanced phagocytosis. Macrophages were exposed to an EF for 2h then carboxylate beads, *Candida albicans*, or apoptotic neutrophils were added to the cultures and left without any EF for a further 2h. Phagocytosis increased significantly in each case, demonstrating that the EF 'priming' improved phagocytotic efficiency.

Mechanistically, these EF-induced functional changes are accompanied by clustering of phagocytic receptors toward the anode, enhanced PI3K and ERK activation, and mobilization of intracellular calcium. EFs also modulated cytokine production selectively and can augment some effects of conventional polarizing stimuli on cytokine secretion.

Human T cells, which are present in wounded epithelia (skin or airway), also displayed directed migration toward the cathode and activation upon

stimulation with physiological EFs (50 or 150 mV/mm). We showed for the first time that EF stimulation downregulated T cell activation following stimulation with antigen-activated APCs or anti-CD3/CD28 antibodies, as demonstrated by decreased IL-2 secretion and proliferation. Mechanistically, STAT3 modulation by the EF was implicated in the functional changes.

There are increasing efforts to use electrical stimulation to aid wound healing. This is especially important for recalcitrant or chronic wounds prone to infection, such as diabetic foot ulcers. Our work can inform design of electrical wound dressing materials seeking to target immune function and infection.

11:25 AM SB04.08.05

Enhanced Electron Transfer in Biophotovoltaic Devices Based on Self-Assembled Photosystem I Protein Complexes Nahid Torabi^{1,2}, Xinkai Qiu³, Sylvia Rousseva¹, Andreas Herrmann^{4,1} and Ryan Chiechi^{5,1}; ¹University Of Groningen, Netherlands; ²Zernike Institute for Advanced Materials, Netherlands; ³University of Cambridge, United Kingdom; ⁴RWTH Aachen University, Germany; ⁵North Carolina State University, United States

Biophotovoltaic (BPV) devices are a relatively new discipline in solar cells that utilize the components of natural photosynthetic proteins such as Photosystem I/II (PSI/II) from, for example, algae, plants, or cyanobacteria to effect photon-induced charge separation. The natural abundance and ease of isolation of these complexes, particularly PSI, make them ideal candidates for integration in biophotovoltaic devices. PSI converts photon energy into spatially separated electron/hole pairs. But does so with ~ 100% internal quantum efficiency by effectively building a precise, nano-scale junction into each protein complex. Our first work describes the fabrication of microfluidic devices with a focus on controlling the orientation of Photosystem I complexes, which directly affects the performance of biophotovoltaic devices by maximizing the efficiency of the extraction of electron/hole pairs from the complexes. The surface chemistry of the electrode on which the complexes assemble plays a critical role in their orientation. Recreating that self-assembly-driven precision and mimicking the replacement of degraded protein are two (of many) major challenges to the design of stable, high-efficiency devices. We addressed both of those problems with a simple device design that allows the circulation of fresh PSI through devices that use linkers to direct the equilibrium of a self-assembly process towards oriented, active complexes. The basic design of the BPV devices used to investigate the phenyl-C61-butyrac acid (PCBA) and a peptide (IQAc, sequence: IQAGKTEHLAPDC which a cysteine residue was attached to the C-terminus) linkers is a co-fabricated microfluidic channel that defines an electrode comprising the liquid metal eutectic Ga-In (EGaIn), which is in contact with the electrolytic medium. The floor of the microfluidic channel, which is perpendicular to the EGaIn electrode, supports a nanostructured gold electrode fabricated by shadow evaporation. The performance of devices fabricated using a fullerene, PCBA, was superior to that of a peptide, IQAc, as determined via the short circuit current, open circuit photovoltage, and power output. The PCBA linkers self-assemble onto nanopatterned gold electrodes, simultaneously directing the orientation of PSI and facilitating the collection of photogenerated electrons which show that fullerenes are well-known acceptor materials in organic photovoltaic devices, and facilitate the extraction of electrons from Photosystem I complexes without sacrificing control over the orientation of the complexes, highlighting this combination of traditional organic semiconductors with bio-molecules as a viable approach to co-opting natural photosynthetic systems for use in solar cells.

Also, to achieve continuous, optimal charge-transfer flux through multiple layers stacked on top of each other in solid-state BPV cells and to maximize their efficiency, the PSI complexes need to be kept properly aligned with respect to the hole/electron injection and structurally intact. In other work, we achieved a record efficiency of 0.64% for solid-state biophotovoltaic devices by tailoring the transport layers to maximize the extraction of charges from a layer of photosystem I. Specifically, we inserted complexes of gold nanoparticles into reduced graphene oxide to adjust the level alignment without sacrificing carrier mobility. We paired that layer with a polytyrosine-polyaniline hole-extraction layer. Our results demonstrate that the functionality of photosystem I in the non-natural environment of solid-state biophotovoltaic cells can be improved through the modification of electrodes with efficient charge-extraction layers. The decoration of graphene electrodes with gold nanoparticles is a generalizable approach for enhancing charge transport across interfaces, particularly when adjusting the levels of the active layer is not feasible, as is the case for photosystem I and other biological molecules.

11:40 AM DISCUSSION TIME

SYMPOSIUM SB05

Emergent Order and Mesoscale Structure Formation in Soft Condensed Matter
November 28 - December 8, 2022

Symposium Organizers

Julia Dshemuchadse, Cornell University
Chrisy Xiyu Du, Harvard University
Lucio Isa, ETH Zurich
Nicolas Vogel, University Erlangen-Nürnberg

Symposium Support

Bronze
ACS Omega

* Invited Paper
+ Distinguished Invited

SESSION SB05.01: Active Colloids
Session Chairs: Chrisy Xiyu Du and Metin Sitti

Monday Morning, November 28, 2022
Hynes, Level 1, Room 110

10:30 AM INTRODUCTORY REMARKS

11:00 AM SB05.01.02

Activity-Induced Polar Patterns of Filaments Gliding on a Sphere [Chiao-Peng Hsu](#), Alfredo Sciortino, Yu Alice du la Trobe and Andreas Bausch; Technische Universität München, Germany

Active matter systems feature the ability to form collective patterns as observed in a plethora of living systems, from schools of fish to swimming bacteria down to cytoskeletal structures. While many of these systems move in a wide, three-dimensional environment, several biological systems are confined by a curved topology. The role played by a non-Euclidean geometry on the self-organization of active systems is not yet fully understood, and few experimental systems are available to study it. Gliding assays, in which cytoskeletal filaments are driven by molecular motors grafted to a substrate, are an ideal candidate to address the microscopic mechanisms that underlie pattern formation in active systems. Here, we introduce an experimental setup in which actin filaments glide on the inner surface of a spherical lipid vesicle, thus embedding them in a curved geometry. We show that filaments self-assemble into polar, elongated structures and that, when these match the size of the spherical geometry, both confinement and topological constraints become relevant for the emergent patterns, leading to the formation of polar vortices and jammed states. These results experimentally demonstrate that activity-induced complex patterns can be shaped by spherical confinement and topology.

11:15 AM SB05.01.03

Light-Modulated Dynamic Assembly and Mode Switching of Semiconductor Nanorod Swarms in an Electric Field Zexi Liang and [Donglei \(Emma\) Fan](#); The University of Texas at Austin, United States

Collective behaviors are widely present in nature and artificial systems. The sizes of the constituting units range from nanometers to meters. Controllably tuning interactions among the constituting members in a swarm can result in complex assembling, structuring, and synchronous motion. Here, inspired by thermodynamic principles that govern phase transition in an equilibrium material system, we propose and explore a hypothesis for rationally creating various assembling modes in a non-equilibrium swarm made of semiconductor nanorods. Experimentally, we find the dense Si nanorods readily switch among three modes, *i.e.*, enhanced collective rotation, droplet-like clustering, and network formation by simply modulating visible light and applied electric field. Theoretical modeling considering light-controlled electrostatic interactions sheds light to the observation. This research presents a general approach for creating reconfigurable patterning and operation modes in a non-equilibrium swarm that points towards new opportunities for fundamental studies and applications.

11:30 AM *SB05.01.04

Optimally Transporting Active Drops [Suraj Shankar](#); Harvard University, United States

Transportation, in its broadest sense, is an important task in many fields, including engineering, physics, biology, and economics, and a great deal is known about optimal and efficient strategies to move matter, energy, and information around. But can we craft similar optimal protocols to transport autonomously moving (active) matter, such as self-propelled drops or migrating cells? I will discuss how we solve this inverse problem by using optimal control theory in the context of transporting a drop of an active fluid with minimal viscous dissipation by dynamically varying spatial active stresses within the drop. I will highlight natural strategies and characteristic trade-offs that emerge from the optimal policies, suggesting general principles for optimal transportation in synthetic and biological active systems.

SESSION SB05.02: Topology and Packing
Session Chairs: Julia Dshemuchadse and Prashant Kumar
Monday Afternoon, November 28, 2022
Hynes, Level 1, Room 110

1:30 PM SB05.02.02

Inferring Topological Transitions in Pattern-Forming Processes with Self-Supervised Learning Marcin Abram¹, Keith Burghardt¹, Greg Ver Steeg¹ and [Remi Dingreville](#)²; ¹University of Southern California, United States; ²Sandia National Laboratories, United States

The identification and classification of transitions in topological and microstructural regimes in pattern-forming processes is critical for understanding and fabricating microstructurally precise novel materials in many application domains. Unfortunately, relevant microstructure transitions may depend on process parameters in subtle and complex ways that are not captured by the classic theory of phase transition. While supervised machine learning methods may be useful for identifying transition regimes, they need labels which require prior knowledge of order parameters or relevant structures. Motivated by the universality principle for dynamical systems, we instead use a self-supervised approach to solve the inverse problem of predicting process parameters from observed microstructures using neural networks. This approach does not require labeled data about the target task of predicting microstructure transitions. We show that the difficulty of performing this prediction task is related to the goal of discovering microstructure regimes, because qualitative changes in microstructural patterns correspond to changes in uncertainty for our self-supervised prediction problem. We demonstrate the value of our approach by automatically discovering transitions in microstructural regimes in two distinct pattern-forming processes: the spinodal decomposition of a two-phase mixture and the formation of concentration modulations of binary alloys during physical vapor deposition of thin films. This approach opens a promising path forward for discovering and understanding unseen or hard-to-detect transition regimes, and ultimately for controlling complex pattern-forming processes. SNL is managed and operated by NTESS under DOE NNSA contract DE-NA0003525. SAND2022-3365 A

1:45 PM SB05.02.03

Templating and Nanostructuring of Hybrid Dendrimers, Knotty Polymers and Molecularly Imprinted Polymers (E-MIPS) [Rigoberto C. Advincula](#)^{1,2,3}; ¹Case Western Reserve University, United States; ²The University of Tennessee, Knoxville, United States; ³Oak Ridge National Laboratory, United States

There is high interest in new polymer synthesis routes, topologies, mechanisms, and templating (molecular and colloidal) for various applications.

Mesoscale and hierarchically inspired assemblies have their origin in the microstructure and composition in soft matter. The choices for synthesis go from linear, grafted, and hyperbranched systems to hybrid organic-inorganic systems. However, there are many other topologies that are of high interest because of their relevance to cyclic and supramolecular polymerization routes that have yet to be demonstrated. Molecular templating is utilized for building "cavities" that facilitate high-resolution sensing and selectivity. This talk will focus on three concepts of targeted assembly and templating: 1) Dendrimer topologies and hybrid nanoparticle electropolymerization, 2) Molecular imprinted polymer (MIP) using hybrid complexes, and 3) supramolecular polymer synthesis and assemblies in Knotty topologically inspired polymers. We also employ a number of macromolecular and surface characterization studies to define

successful synthesis strategies and assemblies. The end goal are to demonstrate the topologies and patterns to produce higher throughput synthetic methods: unlocking the utility for real applications.

2:00 PM SB05.02.04

Multiscale Hierarchical Structures from a Nanocluster Mesophase Richard Robinson and Yuan Yao; Cornell University, United States

The spontaneous self-organization of nanoscale materials into complex macroscopic architectures has intrigued scientists for decades, because it offers insight into how complex structures can emerge from primitive building blocks. Hierarchical self-assembled systems offer structural advantages that are absent in isolated constituent units. Nature is replete with fascinating examples of hierarchical assembly, such as proteins or DNA, and natural photonic structures as seen in butterfly wings or fish. Although synthetic materials that afford the same level of accuracy and complexity as biomolecules are currently beyond reach, research into the self-organization of artificial units has increased dramatically. Organic molecules and copolymers are among the most commonly used elementary units to form large-area patterning. More recently, advances in nanomaterial synthesis have provided access to a versatile library of nanoparticle building blocks with tunable composition, morphology and atomic structure that give rise to physiochemical properties unattainable in naturally occurring materials.

In this study, highly aligned structures are obtained from an organic-inorganic mesophase composed of 1.5 nm monodisperse Cd₃₇S₁₈ magic-size cluster building blocks. Impressively, structural alignment spans over seven orders of magnitude in length scale: nanoscale magic-size clusters arrange into a hexagonal geometry organized inside micrometer-sized filaments; self-assembly of these filaments leads to fibers that then organize into uniform arrays of centimeter-scale bands with well-defined surface periodicity. Enhanced patterning can be achieved by controlling processing conditions, resulting in bullseye and 'zigzag' stacking patterns with periodicity in two directions. The multiscale arrangement of MSC building blocks in filaments and striped films presents intriguing analogies to hierarchical assemblies in biological systems as well as the pervasive hierarchical structural organization throughout the natural world. Additionally, our thin films show strong circular dichroism response and reversible, chemically induced isomerization which triggers more intriguing scientific questions on the properties. Overall, our work demonstrates the ability of semiconductor nanomaterials to assemble into complex macroscopic structures, which provides a potential platform to realize advanced function.

2:15 PM SB05.02.05

Emergent Elastic Fields Induced by Topological Phase Transitions in a Chiral Molecular Crystal Kyohei Takae¹ and Takeshi Kawasaki²; ¹University of Tokyo, Japan; ²Nagoya University, Japan

Topological phase transitions into skyrmion and half-skyrmion phases are widely observed in condensed matter, such as chiral magnets and liquid crystals. They are utilized to design magnetoelectric, optical, and mechanoresponsive materials by controlling such topological phases. However, the role of the elastic field in nonuniform topological phases is elusive. To elucidate this problem, we construct a model describing chiral molecules and colloids in quasi-two-dimensional molecular crystals, which incorporates intermolecular chiral twisting and spheroidal steric interactions. We reveal that emergence of the elastic fields from the competition between steric anisotropy and intermolecular twisting is a key to control uniform, helical, and half-skyrmion structures. By utilizing the coupling between the spheroidal orientations and the elastic fields, these topological phases are switched by temperature, external electromagnetic fields, and anisotropic stresses, where a re-entrant phase transition between the helical and the half-skyrmion phases is discovered. Our results imply that controlling the emergent elastic fields is crucial for obtaining a fundamental physical principle for controlling topological phases using chiral molecular and colloidal crystals.

Reference:

K. Takae and T. Kawasaki, *Proc. Natl. Acad. Sci. U.S.A.* **119**, e2118492119 (2022).

2:30 PM BREAK

SESSION SB05.03: Computational Soft Matter

Session Chairs: Lucio Isa and Suraj Shankar

Monday Afternoon, November 28, 2022

Hynes, Level 1, Room 110

3:30 PM *SB05.03.01

Investigating Atomic-Scale Mechanisms of Crystallization Using Machine Learning Rodrigo Freitas; Massachusetts Institute of Technology, United States

Solid-liquid interfaces have notoriously haphazard atomic environments. While essentially amorphous, the liquid has short-range order and heterogeneous dynamics. The crystal, albeit ordered, contains a variety of defects ranging from adatoms to dislocation-created spiral steps. All these elements are of paramount importance in the crystal growth process, which makes the crystallization kinetics challenging to describe concisely in a single framework. In this talk I will present data-driven approaches to systematically detect, encode, and classify atomic-scale mechanisms of crystallization. It will also be shown how this approach naturally leads to a predictive kinetic model of crystallization that takes into account the entire zoo of microstructural elements present at solid-liquid interfaces. The result is an approach that blends prevailing scientific methods with data-science tools to produce physically-consistent models and novel conceptual knowledge

4:00 PM *SB05.03.02

Metallization of Colloid Crystals Monica Olvera de la Cruz, Yange Lin and Dingwen Qian; Northwestern University, United States

Numerous colloidal crystals have been designed and devised following via functionalization of nanoparticles. Size-asymmetric nanoparticle crystals are often stabilized by ionic-type bonding, where the smaller in size and/or charge component sits at fixed points within the lattice of the large nanoparticles. Here, we study the transition from ionic to metallic bonding, by which the lattice of the smaller component melts, yet the crystal of the large particles is preserved, as in metallic bonding. We discuss the physical properties of the system, including charge transport under an external field. Under a high external field, we find a transient state where the small particles condense into clusters. The resulting patterns are stabilized modifying the physical interactions.

4:30 PM SB05.03.03

Establishing Design Rules through Coarse-Grained Simulations of Metal–Organic Framework Synthesis Reum Scott, Julia Dshemuchadse and Phillip Milner; Cornell University, United States

The capabilities of coarse-grained simulations are applied to the modelling of two-dimensional Metal–Organic Framework (MOF) synthesis. The isoreticular chemistry of crystalline MOFs allows for modular and scalable reagents in synthesis, and furthermore, the simple nature of the synthesis allows for translation to coarse-grained simulations. The HOOMD-blue toolkit is used to construct the MOFs building blocks (metal nodes and organic linkers) from isotropic beads, retaining the basic symmetries of the molecular components. Lennard–Jones and Weeks–Chandler–Andersen pair potentials are used to model attractive and repulsive particle interactions, respectively. We analyze the crystallinity of the self-assembled products and explore the role of modulators—molecules that compete with the organic linkers in binding to the metal nodes to moderate the crystallization reaction—to explore the self-assembly mechanisms in defect-engineered MOFs.

4:45 PM SB05.03.04

Demystifying Complex Crystal Growth by Classifying Order in Local Environments Maya Martirosyan¹, Matthew Spellings², Hillary Pan¹ and Julia Dshemuchadse¹; ¹Cornell University, United States; ²Vector Institute of Artificial Intelligence, Canada

Understanding how order emerges via crystallization is necessary for controlling the growth of meso- and nanoscale materials or targeting desired material properties. While crystal growth is well understood for simple, close-packed structures, theoretical descriptions break down when applied to structures of higher complexity, where identical particles can occupy different local coordination environments. Developing generalizable rules of how crystal growth proceeds for complex structures requires a sophisticated description of particle environments to understand their evolution throughout the self-assembly process. We use a high-dimensional order parameter that represents local environments with spherical harmonics and utilizes unsupervised machine learning to classify particle environments not only into solid, liquid, and gas, but also into different Wyckoff positions in the same crystal structure, outperforming nearest neighbor analysis approaches. Applying this order parameter to molecular dynamics simulations of self-assembled complex structures allows us to track the emergence of crystalline order from the melt and to observe how identical particles choose their distinct “roles” in a structure as the crystal grows.

SESSION SB05.04: Confinement
Session Chairs: Michelle Driscoll and Lucio Isa
Tuesday Morning, November 29, 2022
Hynes, Level 1, Room 110

8:30 AM *SB05.04.01

Advanced Electron Tomography for Colloidal Self-Assemblies Sara Bals, Ajinkya Anil Kadu, Daniel Arenas Esteban, Adrián Pedrazo Tardajos, Safiyye Kavak, Nathalie Claes, Thomas Altantzis and Da Wang; University of Antwerp, Belgium

The controlled organization of nanoparticles (NPs) into assemblies has gained increasing scientific interest. By modifying e.g. the size and shape of the individual NPs, the inter-particle distances or the chemical composition of the building blocks, assemblies with various shapes and functionalities have been obtained. Since the properties of these nanostructures are inseparably connected to their three-dimensional (3D) structure and shape, a thorough structural and morphological characterization is of great importance.

Transmission Electron Microscopy (TEM) is an ideal technique to investigate materials at the nanometer level or even at the atomic scale. The technique has therefore been widely used in the study of nano-assemblies. However, TEM images only correspond to a two-dimensional (2D) projection of a 3D object. Therefore, electron tomography, a technique that derives a 3D reconstruction from a tilt series of 2D projection images, has become a standard technique to characterize nano-assemblies in 3D. When assemblies of metallic nanoparticles are investigated, acquisition of electron tomography series is usually performed in High Angle Annular Dark-Field Scanning TEM (HAADF-STEM) mode. In this manner, diffraction contrast present in Bright-Field TEM (BF-TEM) images is minimized, and the projection requirement for tomography is fulfilled. For relatively small (consisting of 100 particles or less) or loose assemblies, in which the distance between the composing building blocks is rather large, conventional electron tomography techniques enable one to determine the morphology and the inner structure of the assemblies. Moreover, a manual segmentation allows one to determine, e.g. the 3D stacking of the nanoparticles in a quantitative manner. On the other hand, when the size and density (atomic number Z) of the investigated assembly increases, several challenges appear that hamper a reliable interpretation of the structure.

In this contribution, we will discuss how acquisition, reconstruction and segmentation during an electron tomography experiment can be optimised to enable a quantitative analysis of the structure under investigation [1-4]. Another challenge is related to the investigation of assemblies of nanoparticles under realistic conditions. We will therefore discuss how to combine a 3D characterization of nanoparticle assemblies with in situ and cryo TEM studies [5,6].

[1] Altantzis T, Wang D, Kadu A, van Blaaderen A, Bals S, Journal of Physical Chemistry C 125, 26240 (2021).

[2] Zanaga D, Bleichrodt F, Altantzis T, Winckelmans N, Palenstijn WJ, Sijbers J, de Nijs B, van Huis MA, Sanchez-Iglesias A, Liz-Marzán LM, van Blaaderen A, Joost Batenburg K, Bals S, Van Tendeloo G, Nanoscale 8, 292 (2016).

[3] Wang D, van der Wee EB, Zanaga D, Altantzis T, Wu Y, Dasgupta T, Dijkstra M, Murray CB, Bals S, van Blaaderen A, Nature Communications 12, 3980 (2021).

[4] Wang D, Dasgupta T, van der Wee EB, Zanaga D, Altantzis T, Wu Y, Coli GM, Murray CB, Bals S, Dijkstra M, van Blaaderen A, Nature Physics, 17, 128 (2021).

[5] Kumar J, Eraña H, López-Martínez E, Claes N, Martín VF, Solís DM, Bals S, Cortajarena AL, Castilla J, Liz-Marzán LM, Proceedings of The National

Academy of Sciences of The United States Of America 115, 3225 (2018).

[6] Baginski M, Pedraza-Tardajos A, Altantzis T, Tupikowska M, Vetter A, Tomczyk E, Suryadharma RNS, Pawlak M, Andruszkiewicz A, Górecka E, Pocięcha D, Rockstuhl C, Bals S, Lewandowski W, ACS Nano 15, 4916 (2021).

9:00 AM *SB05.04.00

Packing Frustration and the Hidden Geometry of Bicontinuous Network Phases of Block Copolymers [Michael S. Dimitriyev](#), Abhiram Reddy and Gregory Grason; University of Massachusetts Amherst, United States

Block copolymers can self-assemble into a variety of ordered nanostructures, including the triply-periodic, bicontinuous double-gyroid (DG), double-diamond (DD), and double-primitive (DP) network phases. These phases consist of complex, intercatenated, labyrinthine domains, yet are supramolecular soft crystals with long-range order. Despite a history of experimental observations, as well as theoretical and computational studies, the formation and stability of these phases remains poorly understood and reliant on the vague notion of packing frustration. Here, we paint a picture of packing frustration -- an interplay between the thermodynamics governing interface geometry and chain stretching that is required by packing constraints of the polymer melt -- by turning to the strong segregation theory of block copolymers. The thermodynamic costs of satisfying this packing constraint is closely connected to the geometry of the terminal boundaries of each domain, i.e. the set of points defining the extent of chain stretching from the intermaterial dividing surfaces. We show that these terminal boundaries are well-approximated by a suitable set of medial surfaces, and that such medial geometry is essential to the stability of the network phases, resolving a long-standing puzzle of the stability of network phases in the strong segregation theory. Furthermore, we uncover new heuristics for polymer architectures that promote stability of the DG phase and explore how the medial geometry of the DG phase makes it more optimal than the competitor DD and DP phases. Finally, we introduce a map of packing frustration "hot spots" in each phase and illustrate how targeted infill of these hot spots can stabilize the DD and DP phases over the DG phase.

9:30 AM SB05.04.03

Controlling the Assembly of Anisotropic Particles *via* the Geometry of a Confining Interface [Rachael S. Skye](#)¹, Erin Teich² and Julia Dshemuchadse¹; ¹Cornell University, United States; ²Wellesley College, United States

Understanding the controlling factors for structure formation in colloids is highly complex and currently the subject of intense scientific study. As we learn to synthesize a diverse array of individual particles, with varying shapes and sizes, we also aim to understand how to assemble those particles into useful structures. This study uses computational methods to examine the assembly of a class of tetrahedrally shaped particles, with assembly controlled *via* confinement inside of a spherical container. These particles exhibit a variety of assembled structures depending on their vertex truncation; however, their assembly behavior in confinement has not previously been explored. We show how small spherical containers force assembly into concentric shells, whose high curvature favors a vertex-to-vertex motif. In larger containers, the particles' behavior changes to conform to a locally flat wall. This effect favors a vertex-to-midpoint motif, causing shapes near the phase boundary to modify their assembled local structure in order to better pack against this lower-curvature wall. We show how the geometry of the confining wall interacts with particle shape anisotropy to change the resultant structure, and we propose using these walls as a medium for enhancing the crystallinity of colloidal crystals. Further, we show how wall geometry can cause texture, biasing the structure to orient along certain crystal axes relative to the wall, thus allowing for reproducible and controllable growth. Through understanding the interactions of confinement geometry and crystal structure, we demonstrate a method for understanding and controlling the assembly of anisotropic particles.

9:45 AM SB05.04.04

Reconfigurable and Mesostructured Liquid-Shelled Capsules [Zhang Wu](#)¹, Joerg G. Werner² and David A. Weitz¹; ¹Harvard University, United States; ²Boston University, United States

Mesostructured microcapsules with a core-shell structure are good candidates for housing, protecting, delivering, and capturing biocargo. Mesostructured soft-matter shells made from benign materials such as polymers confine the encapsulant within a compatible environment as well as control its mass transport and exchange with the external environment. Synchronous communication of the encapsulants with the changeable external environment requires smart response of the capsule shells for desired molecular exchange. Reversibly stimuli-triggered responsive capsules could regulate the molecular diffusion across the shell by altering its molecular affinity and permeability. However, large property changes upon stimuli and the reversibility of the trigger-response of such dynamic capsules remain a challenge due to limitation of promising soft materials and their fabrication as mesoscaled architectures. Here we introduce reconfigurable and mesostructured liquid-shelled capsules with reversible stimuli-triggered changes of the shell phase composition and structure. Liquids in contrast to polymers offer fast dynamics and in combination with colloidal assemblies and large solid-liquid interfaces can undergo reversible changes of key property metrics without material degradation or fatigue. To this end, we employ microfluidics to template colloidosome microcapsules by introducing surface-functionalized particles in the shell of water-oil-water double emulsions. Upon self-assembly and crosslinking of the colloidal particles, we achieve a porous nearly close-packed particle framework in the liquid double emulsion shell. For colloidosome capsules with reversible stimuli-triggered property change, double emulsions with shell liquids composed of a dual oil system with temperature-dependent miscibility are fabricated. Upon temperature change, the shell undergoes liquid-liquid phase separation, therefore causing the reconfiguration of the double emulsion shell to a two-phase shell, a path towards controlled wetting-dewetting transitions of the porous colloidal shell framework to enable, for example, active closing and opening of the capsules to molecular and particle diffusion.

10:00 AM BREAK

SESSION SB05.05: Optical Properties
Session Chairs: Sara Bals and Lucio Isa
Tuesday Morning, November 29, 2022
Hynes, Level 1, Room 110

10:30 AM SB05.05.01

Shape and Interaction Decoupling for Colloidal Preassembly Lucia Baldauf¹, [Erin G. Teich](#)², Peter Schall³, Greg van Anders⁴ and Laura Rossi¹; ¹Delft University of Technology, Netherlands; ²Wellesley College, United States; ³University of Amsterdam, Netherlands; ⁴Queen's University, Canada

Creating materials with structure that is independently controllable at a range of scales requires breaking naturally occurring hierarchies. Breaking these hierarchies can be achieved via the decoupling of building block attributes from structure during assembly. Here, we demonstrate, through computer

simulations and experiments, that shape and interaction decoupling occur in colloidal cuboids suspended in evaporating emulsion droplets. The resulting colloidal clusters serve as "preassembled" mesoscale building blocks for larger-scale structures. We show that clusters of up to nine particles form mesoscale building blocks with geometries that are independent of the particles' degree of faceting and dipolar magnetic interactions. To highlight the potential of these superball clusters for hierarchical assembly, we demonstrate, using computer simulations, that clusters of six to nine particles can assemble into higher-order structures that differ from bulk self-assembly of individual particles. Our results suggest that preassembled building blocks present a viable route to hierarchical materials design.

10:45 AM SB05.05.02

Revealing the Emergence and Dynamics of Nanoparticle Moiré Patterns at the Nanoscale [Chang Liu](#), Lchan Yao, John Crockett, Chang Qian and Qian Chen; University of Illinois at Urbana-Champaign, United States

Moiré patterns from misaligned periodic structures can bring merit to not only artistic designs but to material properties, a salient example being magic angle graphene where superconducting phase can be observed. Here, with liquid-phase transmission electron microscope (TEM), we construct nanoparticle superlattices and obtain for the first time Moiré patterns at the nanoscale in real time and real space, where we investigate laws of order emergence and evolution from a dispersion of nanosized entities. To be specific, layers of hexagonal lattices are assembled from individual gold nanoparticles. Distinct from 2D materials where the interlayer and intralayer interactions are with limited control, we control the nanoparticle shape to manipulate the interlayer and intralayer interactions, which leads to different Moiré patterns. We apply neural network-based machine learning to investigate the structures and single particle dynamics with high spatiotemporal resolution, which further helps to reveal the interplay between the Moiré pattern and the grain boundary evolution. Furthermore, calculations based on pairwise interaction potential show distinct local position adjustment in different Moiré patterns both in plane and out of plan, resulting in normal, reduced order and disordered Moiré patterns. This work provides better understandings on nanoscale interactions, which can serve as a guideline for bottom-up material design and helps to study related optical properties.

11:00 AM SB05.05.03

Chiral Self-Assembly of Cellulose Nanocrystals—The Role of Composite Morphology [Thomas G. Parton](#), Richard M. Parker, Gea T. van de Kerkhof, Aurimas Narkevicius, Johannes S. Haataja, Bruno Frka-Petesic and Silvia Vignolini; Department of Chemistry, University of Cambridge, United Kingdom

Naturally-sourced cellulose nanocrystals (CNCs) are elongated nanoparticles that spontaneously form a left-handed cholesteric liquid crystal phase in aqueous suspension. This self-assembly process has been shown to be a promising way to create structurally colored films from sustainable materials (*Adv. Mater.* (2018) 30, 1704477), but the underlying mechanism by which chiral ordering emerges has remained unclear. Although the morphology of individual CNCs is believed to play an important role, most particles are not significantly twisted, and suspensions exhibit considerable polydispersity in both particle size and shape.

Here we will present an in-depth morphological analysis of sub-populations of individual CNCs, as imaged by transmission electron microscopy (TEM) and atomic force microscopy (AFM). We gradually tuned the size and shape of the CNCs using ultrasonication and correlated the morphology of individual particles with their ensemble behavior in suspension and in photonic films. This analysis revealed that CNC "bundles" (i.e. clusters of laterally-bound elementary crystallites) are essential for the formation of a cholesteric phase. These bundles act as chiral dopants, analogous to those used for molecular liquid crystals, and therefore explain how chirality is transferred across length-scales from the morphology of individual CNCs to the photonic nanostructure (*Nat. Commun.* (2022) 13, 2657).

11:15 AM SB05.05.04

Preparation of Pseudo-Single Grain Double Gyroid Thin Films for Advanced Optical Applications [Jinwoo Oh](#), Mahesh Mahanthappa and Christopher Ellison; University of Minnesota Twin Cities, United States

Materials with three-dimensional network structures (*Nets*) on sub-micron length scales are of great interest for their optical properties. The vivid colors of insect wing scales and bird feathers arise from naturally occurring *Nets* with spatial periodicities ranging 400 – 700 nm, which interact with visible light as photonic crystals. On the other hand, *Nets* with sub-wavelength scale periodicities (< 400 nm) have potential applications as optical metamaterials with exciting properties such as negative refraction and strong circular dichroisms. While *Nets* may be fabricated by top-down methods such as two-photon lithography, such methods are limited by their achievable lengthscales and the challenges associated with fabrication throughput. Bottom-up self-assembly of block copolymers provides a possible alternative for addressing these limitations. For example, Vignolini *et al.* prepared a gold single gyroid nanomaterial using a template based on ABC triblock terpolymer self-assembly and demonstrated its strong, orientation-dependent dichroic responses. Although these results suggest the promise of bottom-up self-assembly as means of accessing *Nets*, a significant challenge facing these approaches is the lack of control over *Net* grain sizes and their orientations relative to a substrate that are important in their optical applications. The self-assembly of block copolymers can be directed using chemical patterns or external fields, but few studies have applied these methods to block copolymers that form double gyroid (DG) *Nets*. Of these few examples, many rely on solvent annealing of block copolymer thin films sometimes in the presence of chemically or topographically patterned surfaces. In this study, we report a solvent-free, thermal processing method for producing pseudo-single grain DG thin films on silicon wafers bearing native oxide layers. Through top-down and cross-section scanning electron microscopy (SEM), we identify the well-defined orientation of the DG mesostructure with respect to the underlying substrate. These findings are corroborated using grazing-incidence small-angle X-ray scattering (GISAXS), and we use azimuthal angle-dependent GISAXS to investigate the degree of microstructural orientation. Thus, this thermal processing approach enables efficient unidirectional alignment of mesoscopic DG structures over large areas for future optical materials applications.

11:30 AM SB05.05.06

Hierarchical Self-Assembly of Bowtie Shaped Nanostructured Microparticles with Tunable Chiroptical Activity [Prashant Kumar](#)¹, Thi Vo¹, Minjeong Cha¹, Wenqian Xu², Anastasia Vishneratina¹, Ji-Young Kim¹, Wonjin Choi¹, Sharon Glotzer¹ and Nicholas A. Kotov¹; ¹University of Michigan—Ann Arbor, United States; ²Argonne National Laboratory, United States

Mathematical descriptors of mirror asymmetry are continuous, but chirality in chemical disciplines is often viewed as a binary characteristic of molecules and there was no known chemical structure with widely variable chirality measures. Here we show that sub-microscale nanostructured particles can be self-assembled from anisotropic building blocks with widely variable geometry, chirality measures and optical asymmetry while retaining consistent bowtie shapes. The self-limited self-organization of anisotropic building blocks [1] makes possible high synthetic reproducibility and computational predictability of their geometries for different concentrations of reagents, ionic components, enantiomeric compositions, media polarity and other parameters. The positive and negative chiroptical peaks observed from UV to IR parts of the spectrum originate from absorptive and scattering phenomena with contribution from both dipolar and quadrupolar modes characteristic of nanostructured particles with submicron scale chirality.[2] The dependence of geometrical chirality measures and chiroptical characteristics enable the predictive synthesis of bowties with desirable polarization rotation. Controllable pitch, length, width, and thickness leads to tunable chiroptical activity across from UV to IR, which can be used to print chiroptical metasurfaces for

photonic markers for machine vision devices.

References

1. Xia, Y. *et al.* Self-assembly of self-limiting monodisperse supraparticles from polydisperse nanoparticles. *Nature Nanotechnology* 6, 580–587 (2011).
2. Feng, W. *et al.* Assembly of mesoscale helices with near-unity enantiomeric excess and light-matter interactions for chiral semiconductors. *Science Advances* 3, (2017).

SESSION SB05.06: Data-Driven Materials Design
Session Chairs: Carl Goodrich and W. Benjamin Rogers
Tuesday Afternoon, November 29, 2022
Hynes, Level 1, Room 110

1:30 PM *SB05.06.01

Inverse Design for Learning in Soft Matter Systems [Andrea Liu](#)¹, Jason Rocks², Menachem Stern¹, Daniel Hexner³, Douglas Durian¹, Eleni Katifori¹ and Sidney Nagel⁴; ¹Univ of Pennsylvania, United States; ²Boston University, United States; ³Technion–Israel Institute of Technology, Israel; ⁴The University of Chicago, United States

Training an artificial neural network requires solving an inverse problem, so it is natural to apply concepts underlying machine learning to solve inverse design problems in soft matter systems. I will describe how global minimization of a loss function can be used to teach physical networks how to perform functions inspired by biology, such as the ability of proteins (e.g. hemoglobin) to change their conformations upon binding of an atom (oxygen) or molecule, or the ability of the brain's vascular network to send enhanced blood flow and oxygen to specific areas of the brain associated with a given task. Statistical physics teaches us that the ability to design ensembles of networks with the same function is crucial in order to understand the microscopic origins of collective phenomena. I will show how we apply persistent homology to such networks to learn how and what they learned. Finally, I will describe local learning methods that allow us to develop physical systems that can learn on their own, without requiring a processor or memory.

2:00 PM SB05.06.02

Targeted Discovery of Low-Coordinated Crystal Structures Using Highly Tunable Particle Interactions [Hillary Pan](#) and Julia Dshemuchadse; Cornell University, United States

Self-assembled soft-matter crystal structures have the potential to exhibit structural variety that vastly exceeds that of atomic-scale structures, mainly due to their highly tunable particle interactions. In simulation, particles interacting *via* simple, isotropic pair potentials have been shown to self-assemble into a wide range of crystal structures, yet how the shape of the interaction potential influences the resulting structure is still poorly understood. To search for new crystal structures, we have developed a new functional form for the interaction potential in which all energy wells and maxima can be tuned independently. Through targeted searches in a high-dimensional parameter space, we discover 20 new crystal structures, 14 of which are low-coordinated with average coordination environments ranging from 2 to 7 nearest neighbors. We will present specific characteristics of these structures, as well as general trends of the investigated systems. Our findings highlight the structural diversity of soft condensed matter that can potentially be used to design new soft materials with functional properties.

2:15 PM SB05.06.03

Towards the Data-Driven Design and Development of Materials Derived from Unstable Mixtures [Matthew Jones](#) and Nigel Clarke; University of Sheffield, United Kingdom

The field of polymer blending, which aims to combine the properties of polymers to create specialised materials, has the potential to play an important role in helping to tackle some of the major challenges that society faces in the 21st century. However, to realise this in a sustainable and time-effective manner, we must advance our knowledge of structure-property relationships and find ways to leverage these relationships in the design and development process of new materials. One obstacle to developing structure-property relationships is the challenge of characterising complex phase-separated microstructures using accessible experimental data. To overcome this, we recently proposed a method for succinctly describing such microstructures in terms of well-defined and quantifiable characteristics from scattering data using machine learning [1], namely Gaussian process regression. Our findings, which we obtained using numerical simulation data, suggest there is an opportunity for a more complete characterisation of experimental phase-separated microstructures using scattering data. Scattering is a powerful technique for monitoring phase separation in real-time. As such, the careful application of our method to future predictions of the scattering data could allow one to predict the future characteristics of the microstructure as it evolves. In the absence of a satisfactory nonlinear theory describing the time evolution of the scattering data during phase separation, we have demonstrated the ability of dynamic mode decomposition, a data-driven modelling method, to make accurate future predictions of numerical scattering data. We aim to combine these two works to develop a control system to manipulate phase separation to produce new materials with prescribed microstructures and, therefore, properties. We also aim to expand the scope of our work to systems other than polymer blends, for example, metallic alloys and ceramics.

[1] M. Jones and N. Clarke, Machine Learning Real Space Microstructure Characteristics from Scattering Data, *Soft Matter*, 14 (42) : 9689-9696, 2021

2:30 PM SB05.06.04

Machine Learning Augmented Computational Reverse-Engineering Analysis for Scattering Experiments of Assembled Mixtures of Nanoparticles Christian Heil¹, Anvay A. Patil², Ali Dhinojwala² and [Arthi Jayaraman](#)¹; ¹University of Delaware, United States; ²The University of Akron, United States

In the field of materials science and engineering, structural characterization is a critical step needed to link the materials' structure to its macroscopic properties. Small angle scattering (SAS) is a useful technique to characterize structure at multiple length scales. The output of SAS experiments is the averaged scattering intensity at various wave vectors, $I(q)$ vs. q , whose interpretation often relies on fitting with analytical models. The selection of analytical models can be a limitation for analyzing the scattering profile if and when appropriate analytical models exist for the material's structure of interest. In this talk, we will present a computational method we have developed called Computational Reverse Engineering Analysis of Scattering Experiments (CREASE) and show its application for analysis of spherical nanoparticle mixtures' assembled structure. We test the strengths and limitations of CREASE by using a variety of *in silico* $I(q)$ obtained from simulations of binary nanoparticle assemblies and nanoparticle solutions with varying mixture composition/concentration, nanoparticle size distribution, and degree of mixing/aggregation. We will also highlight the machine learning (ML) model used in CREASE that links features of the nanoparticle solutions (e.g., concentration, nanoparticles' tendency to aggregate) to computed scattering

profile; this ML model is applicable to different nanoparticle sizes without the need for additional data to retrain the model to be specific to the size of interest. Finally, we show how the nanoparticle structure reconstructed from scattering using CREASE can serve as input to optical modeling and achieve a computed reflectance spectrum that matches ones from the experimental systems.

2:45 PM SB05.06.05

Mesostructure Formation and Phase Transition of Imidazolium-Based Ionic Liquid Systems for Training Deep Neural Network Algorithm
Kyungtae Kim, Jacob LaNasa, Darrick Williams and Benjamin Nebgen; Los Alamos National Laboratory, United States

Quantitative small-angle and wide-angle X-ray scattering data of ionic liquid/water mixture systems were obtained and analyzed as training data sets for developing deep neural network (DNN) based computation architecture that can predict non-equilibrium, dynamical phenomena such as chemical reactions, self-assembly, and ionization. Quantum mechanics (QM) describes the physical laws that govern such processes, but the computational effort required to solve the equations given by QM makes predictive simulations of realistic systems practically impossible. Specialized DNN-based architectures have recently proved to be an accurate, general, and computationally efficient alternative to QM calculations for obtaining interatomic forces. While these DNN models have application potential in a wide range of chemical and materials discovery areas, they lack the ability to describe non-equilibrium processes such as the long-range transfer of electron charge and finite electron temperature effects. The research of probing mesoscale structures of ionic liquid/water mixtures provides quantitative information on mesoscale structures as well as cation-anion interactions to the DNN machine learning algorithm and serves as critical learning set to develop an efficient and accurate computational algorithm that can predict materials properties from molecular structure.

Ionic liquids are known to form various hierarchical, mesoscale ordered structures when mixed with water, similar to the phase behavior of lyotropic liquid crystals. The hierarchical self-assembly of soft materials including the ionic liquid systems is a complex phenomenon often not easily predictable by computation. Thus, the system of ionic liquid/water mixtures is an excellent platform to produce large data set to train the DNN algorithm. In addition, the ionic liquids are easy to synthesize yet they exhibit diverse possible ordered structures, which further justifies the use of the system in this study. Model systems of ionic liquids, consisting of a cation having linear hydrocarbon tail and simple anions such as thiocyanate or nitrate, were mixed with varying amounts of water to form microphase-separated, mesoscale ordered structures and subsequently measured by X-ray scattering. The obtained data were quantitatively analyzed by crystallographic methods and radial distribution function calculations.

3:00 PM BREAK

SESSION SB05.07: DNA/Tailored Assembly
Session Chairs: Xin Qi and Reum Scott
Tuesday Afternoon, November 29, 2022
Hynes, Level 1, Room 110

3:30 PM *SB05.07.01

Programming Self-Limited Assembly of Helical Tubules Using DNA Origami W. Benjamin Rogers, Daichi Hayakawa and Thomas E. Videback; Brandeis University, United States

Inspired by Nature's ability to make complex structures, self-assembly has emerged as a powerful technique for synthesizing nanoscale materials. While living systems are brimming with examples of functional nanomaterials that have one or more self-limited dimensions, such as virus capsids, cytoskeletal filaments, or complex molecular machines, most examples of synthetic self-assembly tend to produce periodic lattice structures with macroscopically uncontrolled dimensions. In this talk, I will explore the trade-offs between addressable assembly and self-closing assembly as routes to self-limitation using a specific class of self-limiting structure: helical tubules. We make triangular subunits using DNA origami that have specific, valence-limited interactions and designed binding angles, and study their assembly into tubules that have a self-limited width that is much larger than the size of an individual subunit. In the simplest case, the tubules are assembled from a single component by programming the dihedral angles between neighboring subunits. We show that the tubules can reach many micrometers in length and that their average width can be prescribed through the dihedral angles. However, we find that the same set of triangular subunits produces an ensemble of tubules with different widths and chirality---a fundamental limitation of using geometrical specificity alone to program self-limitation. The observed distribution is captured by a simple theoretical model that considers only the elastic bending energy of a curved sheet and the irreversibility of tubule closure. Finally, we demonstrate that the distributions of tubules can be further sculpted by increasing the number of subunit species, thereby increasing the assembly complexity. Rather than using a single type of triangular subunit, we use two species of triangles with distinct sets of specific interactions and show that even this simple binary mixture can eliminate half of the total number of off-target structures. Taken together, our findings highlight the complementary roles that programmed curvature and assembly complexity can play in self-limited assembly, which can be further generalized to the assembly of other complex, self-limited 3D geometries, such as helicoids, toroids, and crystalline frameworks.

4:00 PM *SB05.07.03

Assembling Biological Function Without Biology Carl Goodrich; Institute of Science and Technology Austria, Austria

Biology has discovered how to make exceedingly complex nano-machines — protein structures that consume energy to perform numerous functions, ranging from cargo transport to DNA replication. These machines are far more sophisticated than anything we can produce synthetically at this scale, limiting our ability to create new biological-like materials. Crucially, we lack a sufficient understanding of how such function can arise using simple synthetic building blocks. The past few decades have seen tremendous progress in synthesizing a variety of simple building blocks (e.g. DNA-coated colloids, de novo proteins, etc.) with controllable and specific interactions, and we are beginning to understand how to self-assemble complex structures out of them. However, biological nano-machines are more than just structure — they have kinetic and functional properties that cannot be inferred from their shape. I will show how differentiable programming enables us to design self-assembled nano-machines out of DNA-coated colloids. These machines have precisely controlled kinetics and can consume energy, drive themselves out of equilibrium without external input, and perform tasks. Finally, the simplicity of DNA-coated colloids as a model system enables us to learn general principles about functional self-assembly in non-biological settings.

4:30 PM SB05.07.04

Comprehensive View of Microscopic Interactions Between DNA-Coated Colloids for Colloidal Self-Assembly Fan Cui, Sophie Marbach, Jeana Zheng, Miranda Holmes-Cerfon and David Pine; New York University, United States

The self-assembly of colloidal particles into highly-ordered structures offers great promise for advanced optical materials. DNA has emerged as a most versatile tool to drive targeted structure formation due to its programmability, which enables specific attractive binding with controllable interaction strength and length scale. However, control of disorder, defects, melting, and crystal growth is hindered by the lack of a microscopic understanding of DNA-mediated colloidal interactions. Here we use total internal reflection microscopy to measure *in situ* the interaction potential between DNA-coated colloids with nanometer resolution and the macroscopic melting behavior. [1] The range and strength of the interaction are measured and linked to key material design parameters, including DNA sequence, polymer length, grafting density, and complementary fraction. We present a first-principles model that quantitatively reproduces our experimental data over a wide range of DNA ligand designs. Our theory identifies a subtle competition between DNA binding and steric repulsion and accurately predicts adhesion and melting at a molecular level. Combining experimental and theoretical results, our work provides a quantitative and predictive approach for guiding material design with DNA-nanotechnology and can be further extended to a diversity of colloidal and biological systems.

[1] Cui, F et. al., *Nat. Commun.* **2022**, *13*, 1.

SESSION SB05.08: Poster Session
Session Chairs: Julia Dshemuchadse and Chrisy Xiyu Du
Tuesday Afternoon, November 29, 2022
8:00 PM - 10:00 PM
Hynes, Level 1, Hall A

SB05.08.01

Novel Structures Found in Nanocrystal Self-Assemblies and the Thorough Characterization of the Superstructures and the Orientation of the Crystal Domains Yasutaka Nagaoka and Ou Chen; Brown University, United States

My poster presentation discusses novel structures found in nanocrystal self-assemblies and nanocrystal-based structured materials, as well as new synchrotron-based techniques to enable comprehensive structural characterization. The term "structural materials" refers to solid materials whose internal structures have been optimized to perform certain functions such as high mechanical properties, green and efficient catalysis, and optical properties for metamaterials and batteries. In the past few years, there has been a great deal of research dedicated to exploring further structures at the atomic and mesoscales of materials, and thanks to the efforts of scientists to enable large scale synthesis of nanocrystals with a variety of shapes, methods of processing, and the introduction of novel characterization techniques, the use of nanocrystals has gained a great deal of interest because of the expectation that nanostructured materials can address these functionality.

My poster presentation shows structures both at the atomic level and at the mesoscale, including amorphous, quasicrystals, and crystals, along with the characterization methods. We present a series of our works related to novel nanocrystal synthesis, self-assembly of superlattices, and a new method of creating bulk materials (high-pressure nanocrystal coining), which produces a variety of materials that could not otherwise be obtained. States like amorphous and quasicrystals, for instance, aren't often the most thermodynamically stable states, so they're not commonly observed in conventional structured materials. We demonstrated that Pd metal nanocrystals with appropriate surface states can contain ~98% amorphous states within their atomic arrangements, which could not be achieved by conventional methods. By compacting these nanocrystals into a solid, we have created the first amorphous pure metal possessing a centimeter-scale size. Another example is silver nanocrystals that form superstructures very sensitively based on the nanocrystals' morphologies. The polymorph of nanocrystal superlattices we present here contains structures that differ from predicted structures by simulation, proving nanocrystal self-assemblies as a very powerful methodology for creating novel structured materials. Furthermore, we present our characterization strategy to assess the structures thoroughly with respect to both the position of nanocrystals and the orientation of crystal domains. Combining rotational XRD measurements with TEM measurements, we constructed 3D structures in the superstructures and in the orientation of the crystal domains.

SB05.08.02

Simulating Pressure-Driven Solid-Solid Phase Transformations Across Crystal Structure Types Hongjin Du, Hillary Pan and Julia Dshemuchadse; Cornell University, United States

Pressure-induced phase transformations have been widely observed in many crystalline materials. Molecular dynamics simulations, in particular, have been used to understand high-pressure phase transitions—a typical example being the graphite-to-diamond transition. Here, we investigate the influence of pressure on the behavior of 16 known crystal structure types that have been shown to self-assemble in molecular dynamics simulations using isotropic, pairwise interaction potentials. We reproduce several experimentally-observed solid–solid phase transitions, and we discover two new crystal structures by running simulations under increasing pressure. A variety of other transformation behaviors as a function of pressure are also observed and analyzed to investigate the connection between different high-pressure behaviors and structural parameters such as coordination number, symmetry, and complexity. The results reveal that many simulated structures tend to approach an average coordination number of 12 at high pressure. Our work expands current knowledge of the relationship between structure and pressure, and it helps pave the way for the exploration of new materials.

SB05.08.03

Up-Conversion of Coherent Light Emission Inside of Polar Nematic Liquid Crystalline Media Daichi Okada, Hiroya Nishikawa and Fumito Araoka; RIKEN Center for Emergent Matter Science, Japan

Polar nematic liquid crystals (PNLCs) are kind of new types of fluid materials co-possessing fluidity and ferroelectricity. Since its discovery in 2017, it has attracted a lot of attention to the potential for novel applications such as flexible optical/optoelectrical devices. One of the most fascinating physical properties of PNLCs is efficient generation of optical second harmonics, which is ~100 times larger than quartz. Additionally, due to its fluidity, we can dope FNLCs with other functional molecules, enabling modification of their physical properties.

By taking such advantages of PNLCs, we herein demonstrate a flexible up-conversion system of coherent light emission. By doping fluorescent molecule into PNLCs and placing that into an optical cavity consisting of two dielectric mirrors with a distance around ~5 μ m, PNLCs layer can equip two functions for laser oscillation and second harmonic generation (SHG), simultaneously. We investigate their spontaneous SHG conversion process of lasing emission inside the optical cavity. Upon excitation of the doped fluorescent molecules by a pulsed laser light, clear and sharp emission peak with nonlinearity is confirmed beyond a certain excitation threshold. Under the lasing regime, additional emission peaks at the half wavelengths of lasing peaks are also detected, meaning intra-cavity wavelength conversion through the SHG process. The SHG intensity correlates the lasing emission intensity upon the excitation power change. Perhaps with the aid of the increase of the intracavity electric field at the resonance mode, the SHG efficiency of the intracavity conversion process is slightly higher than that of outside cavity without the laser oscillation process. Such a brand-new type of flexible up-conversion

device must be promising for future optical/optoelectric devices.

SB05.08.04

Predictive Design of Orientational Order in Confined Active Nematic Materials [Hiroki Miyazako](#), Kohei Tsuchiyama and Takaaki Nara; University of Tokyo, Japan

Elongated biological materials can be modeled as nematic liquid crystals which can actively move by energy consumption, known as “active nematics [1].” Recent studies have shown that such active nematic behaviors are observed in many biological systems, such as cytoskeleton-motor protein compounds and cell monolayers. In active nematic materials, the orientational order and the active behaviors are affected by topological defects, at which the orientation angle cannot be defined. Therefore, many studies have demonstrated spatial control of defect positions and movement by topographic guides or confinement to achieve the reproducible generation of targeted orientational patterns or defect movement. However, the geometrical effects of the guides or confinement have not been fully understood. For precise control of the orientational order, it is necessary to establish calculation methods to predict defect positions in various geometries.

To this end, this study aims to establish a calculation method for predicting and designing defect positions of confined active nematic materials. In our previous study [2], we derived an explicit formula of orientational angles and Frank elastic energy of nematic materials confined in a two-dimensional space. The formula was expressed by complex potentials defined on a unit disk and a conformal mapping from the unit disk to a simply-connected domain. Thus, the derived formula can be applied to any simply-connected domain, which is an advantage of the derived formula. However, our previous study cannot predict stochastic fluctuations of defect positions caused by random movement of the active nematic materials.

To quantify the stochasticity of the defect positions, we propose a numerical method to calculate equilibrium distributions of defects. By using the explicit formula of the Frank elastic energy described as a function of defect positions, the equilibrium distributions can be efficiently calculated based on Markov chain Monte Carlo methods. The computed distributions quantify spatial localization and stochastic fluctuations of defect positions in a confined space. Since the geometry of the confinement is expressed as a complex function in our approach, we can easily evaluate geometric effects on the spatial localization of the defects. Therefore, we can predict an optimal geometry for suppressing stochastic fluctuations of defects by tuning the parameters of the geometry.

The proposed method was experimentally verified by culturing mouse myoblast (C2C12) cells, which were used as a model of active nematic materials. The C2C12 cells were cultured on PDMS microgrooves whose geometries were parametrically expressed as $f(z)=z+az^3$. The cell alignment and the defects were observed by phase-contrast microscopy. The distributions of the defects were localized as the geometry became asymmetric, which were consistent with our proposed calculation method. The fluctuations of the defect positions were also evaluated from the experimental data by maximum likelihood methods. The evaluation suggested the spatial localization of the defects was mainly due to the geometric effects rather than the randomness of the cell migration and alignment. The proposed method will be applied to the high-reproducible and dependable fabrication of nematic orientational order in active nematic materials.

[1] A. Doostmohammadi *et al.*, *Nature Communications*, Vol. 9, 3246, 2018.

[2] H. Miyazako *et al.*, *Royal Society Open Science*, Vol.9, No.1, 211663, 2022.

SB05.08.05

Development of a Mesoscale Framework to Model Degradation of Polyolefins Under Temperature Gradients [Vaibhav A. Palkar](#) and Olga Kuksenok; Clemson University, United States

A major focus in the area of recycling plastics has been towards chemically selecting and producing monomers for low ceiling temperature polymers. However, controlled depolymerization of abundantly used polyolefins remains a major challenge. Microwave irradiation can be used to cause such depolymerization by introducing microwave absorbing nano sheets in the bulk of the polymer. Under microwave irradiation, local temperature gradients are introduced in the bulk of the polymer in the vicinity of the nano sheets. In this work, we develop a framework for modeling the thermal degradation of polyolefins under the action of such local temperature gradients. We use the mesoscale energy conserving dissipative particle dynamics (eDPD) approach along with the modified segmental repulsive potential (mSRP) to model linear polymer melts under a thermal gradient. We model bond breaking via a stochastic approach that simulates first order degradation reaction kinetics with a local temperature dependent reaction rate constant. We first simulate the depolymerization under constant temperature conditions and track evolution of dispersity, average molecular weights, and molecular weight distribution in the system. The time evolution of these properties follows previously known analytical trends. Under the action of a temperature gradient, faster depolymerization near the high temperature region results in formation of shorter polymer fragments with higher diffusivity compared to the longer chains in the low temperature region. We analyze the time scale of diffusion of various fragments after the temperature gradient is removed. The framework we propose in this work can be used to model controlled depolymerization of polyolefins under the action of pulsed microwave irradiation.

SB05.08.06

Fabrication of Hierarchically Converging Polymer Nanofibers via Liquid Crystal-Templated Chemical Vapor Polymerization and Their Growth Mechanisms [John Kim](#)¹, [Sangchul Roh](#)², [Soumyamouli Pal](#)², [Nicholas L. Abbott](#)² and [Joerg Lahann](#)¹; ¹University of Michigan, United States; ²Cornell University, United States

Hierarchical structures found in biological systems play essential roles (e.g., strong adhesion of gecko lizard, nutrition absorption of tree roots, and effective mass transport between neurons). Many attempts to artificially replicate these hierarchical structures were made by inducing stochastic turbulent flow to form dendritic polymer particles, chemically treating the aramid or cellulose fibers. Although these top-down hierarchies were successfully demonstrated, bottom-up hierarchy of end-attached nanofibers arrays have not yet been presented. Nanofibers with bottom-up hierarchy and long-range order of alignment can inspire us to mimic the properties of hairy structures of villi, lotus leaf, and gecko feet. Unlike the inorganic materials, it is challenging to fabricate structured polymer materials due to the intrinsic amorphous properties of polymer chains. Recently, chemical vapor polymerization (CVP) templated by liquid crystalline (LC) film overcame these challenges and allowed for engineering the polymer nanofibers arrays with controlled diameter, length, and 3-dimensional morphologies. However, nanofibers obtained from LC-templated CVP lacked of hierarchy and their growth mechanisms were not fully understood. Here, we report the method to synthesize bottom-up hierarchical nanofiber arrays by lowering the polymerization temperature and unveil the growth mechanism of the nanofibers. First, we demonstrate that the order of hierarchy can be controlled by varying the synthesis temperature. Second, we control the CVP time to observe intermediate growth phases and elucidate the growth mechanisms. Finally, we qualitatively test the adhesiveness of nanofibers to the substrates by attaching PDMS tape to the fibers and observing where fracture is occurring when taking off the tape.

SB05.08.07

Clathrate-Water Interface Control by 2D Janus Amphiphilic Peptide Nanosheets for Ice Recrystallization Inhibition [Ilhyung Choi](#), Nayeong Jeon and Eunji Lee; Gwangju Institute of Science and Technology, Korea (the Republic of)

: Ice-binding proteins (IBPs) in nature, which are known as the important components for preventing organisms from freezing damage, have been of significant interest for freezing point depression. Their ice recrystallization inhibition (IRI) capability has been investigated mainly at local atomic interactions between binding planes of ice crystals and ice-binding moieties. However, IBPs have a specific structure at the macroscale and the flat region on the protein surface binds to ice. We emulated the structural binding of IBPs to ice through the peptide assembly nanostructure. Amphiphilic peptides can be a versatile building block for the fabrication of hierarchical nanostructures based on a couple of non-covalent interactions of amino acids. We designed amphiphilic peptides with aromatic ring, alkyl chain, and negative charge to adjust mutual interaction between peptides. These peptides formed a β -sheet structure to further assemble a two-dimensional (2D) nanosheet with one side hydrophilic and the other side hydrophobic. The ice-binding moieties, coupled to one end of the peptide sequence, were located on the surface of the 2D nanosheet binding with water molecules on the ice crystal surface. The hydrophobic alkyl chains on the other side shielded ice crystal from water molecules which have the potential of becoming ice, thereby inducing IRI. This Janus 2D nanostructure served like a patch which is applied to the surface of the ice crystals, forming a depletion layer of water molecule between the ice crystals. Furthermore, we demonstrated that IRI ability is better when peptides with ice-binding moieties are formed into 2D morphology than into one-dimensional (1D) morphology via subtle modulation of peptide sequence because 2D morphology has a large contact area which can form bonds with water molecules.

SB05.08.08

Ice-Water Microcurvature Controllable MOF Cryopreservative with Lattice Matching of Hydrogen Bond Interactions [Nayeong Jeon](#)¹, In-ho Jeong², Eunyong Cho³, Jiyeon Lee¹, Ilhyung Choi¹, Eun Hee Han⁴, Hee Jung Lee³, Peter Chang-Whan Lee² and Eunji Lee¹; ¹Gwangju Institute of Science and Technology, Korea (the Republic of); ²University of Ulsan, Korea (the Republic of); ³Korea Institute of Materials Science, Korea (the Republic of); ⁴Korea Basic Science Institute, Korea (the Republic of)

The potential application of ice-binding proteins (IBPs) produced by some plants, insects, and fishes to survive in subzero environments has been of great interest as material candidates for the cryopreservation of drugs, cells, tissues, and foods. IBP adsorption to the ice surface can depress the water-freezing point and avoid ice-crystal growth, which is closely related to the presence of binding moieties complementary to the ice crystal plane. Inspired by the distinctive properties of IBPs, cryoprotectants adsorb to the ice, and hinder the growth, thus prohibiting the freeze damage to cells or tissue. Meanwhile, metal-organic framework (MOF) nanoparticles (NPs) can be a promising nanoscaffold that adopts the natural characteristics of IBPs, including the regular configuration and location of functional moieties affecting ice nucleation and growth at the molecular scale. Herein, MOF NPs with good biocompatibility were used as a cryoprotectant that is well dispersed and colloidal-stable in an aqueous solution. The interaction between the MOF NPs and the ice crystal planes was facilitated, by matching the distribution of hydroxyl groups that could be hydrogen bond donors or acceptors on the MOF NP crystal plane, and the spacing of hydroxyl groups on different ice crystal planes. The limited ice growth between MOF-801 NPs pinning on the ice surface increased the local curvature of ice, reducing the radius of these convex growth regions and making them thermodynamically unstable. The MOF-801 NP was size-controlled, that small NPs were adsorbed on the ice surface, and the concave growth zone of the ice narrowed, consequently increasing the curvature of the ice surface, and further enhancing the ice recrystallization inhibition (IRI) effect. The peptides acting as ice-binding moieties in natural IBPs, were incorporated into the surface of the MOF-801 NPs, further increasing the number of anchored clathrate water molecules and strengthening the IRI effects. The cryopreservation efficacy of these MOF NPs was measured on the nucleated cell line, and the MOF NPs having a high IRI effect due to the small size and introduction of peptides showed a good post-thaw cell recovery rate that can be a potential cryoprotectant. This research provided the favorable applicability of our developed MOF NPs in practical cellular cryopreservation and further, organ transplantation, cord blood storage, and vaccines/drugs.

SB05.08.10

Experimentally Informed Structure Optimization of Amorphous TiO₂ Films Grown by Atomic Layer Deposition [Jun Meng](#)¹, Mehrdad Abbasi², Yutao Dong¹, Corey Carlos¹, Xudong Wang¹, Jinwoo Hwang² and Dane Morgan¹; ¹University of Wisconsin-Madison, United States; ²The Ohio State University, United States

Amorphous TiO₂ (a-TiO₂) has been widely studied in recent years since it was reported as an effective coating material for protecting photoanodes from corrosion in Photoelectrochemical (PEC) systems, which is an innovative approach for hydrogen production through solar water-splitting. The stability and longevity of a-TiO₂ is strongly affected by its synthesis method, thickness, structural heterogeneity, etc., which implies that understanding of the structure-property relationship of a-TiO₂ is crucial for improving the performance through targeted materials design.

This study characterized the structural and electronic properties of Atomic Layer Deposition (ALD) grown a-TiO₂ thin films (~17nm) on Si. Fluctuation spectra $V(k)$ and angular correlation functions were determined with 4-dimensional scanning transmission electron microscopy (4D-STEM). The structural properties measured in this study and pair correlation function $G(r)$ from previous literatures were combined with an interatomic potential and used together to determine a realistic atomic model of a-TiO₂. This atomic model was found with the StructOpt code using a genetic algorithm that simultaneously minimizes energy and maximizes match to experimental short- and medium-range order, represented by $G(r)$ and $V(k)$, respectively. Compared with melt-quenched models, the StructOpt a-TiO₂ model presents an improved agreement with the medium-range ordering as represented by $V(k)$ and the k-space location of the dominant 2-fold angular correlations, although some minor higher order angular correlations are seen in the StructOpt structure that are not observed in the experiments. The electronic structure of the StructOpt a-TiO₂ model is studied by ab initio calculation and compared to experimental results on band gaps of crystalline and amorphous phases. This work provides a realistic a-TiO₂ structure model for further investigation of structure-property relationships and materials design and an updated StructOpt optimization package which optimizes against combined experimental and theoretical constraints to determine complex structures.

SB05.08.11

Effect of Plate Inclination on the Liquid Transfer between Nonparallel Plates [Hyeokgyun Moon](#)¹, Jinkee Lee^{1,2} and Gyoujin Cho²; ¹Sungkyunkwan university, Korea (the Republic of); ²Sungkyunkwan University, Korea (the Republic of)

With increasing demand for printed electronics, roll-to-roll printing has been garnering attention from researchers due to its cost-effectiveness and good scalability for mass production. In recent years, many researchers have focused on fabricating printed electronics that require high resolution using roll-to-roll printing. Few examples of such electronic devices include thin film transistors, sensors, and electronic circuits. For successful roll-to-roll printing, liquid transfer from pattern roll to target surface is of utmost importance, and the volume of liquid transferred divided by the total volume can be defined as transfer ratio. The desired liquid transfer can be achieved by precisely controlling the parameters that affect it such as physical properties of the liquid, volume, and surface wettability. Studies so far involving roll-to-roll printing have mainly focused on understanding the liquid transfer between two parallel plates by varying the parameters mentioned above. However, the actual roll-to-roll printing uses rolls instead of two parallel plates. In other words, the geometry is different for the two cases which results in change in the dynamics of the liquid transfer and hence the results of existing studies can no longer be applied. Therefore, in this study we replicate geometry closer to actual roll-to-roll printing system by using two nonparallel plates and we control their angle to study its effect on the transfer ratio of liquid between them. Additionally, we also vary the liquid viscosity, plate velocity and wettability to

understand the synergistic effect on the transfer ratio.

For our study, the mechanism of liquid transfer and diverse factors affecting the transfer ratio are investigated via both experiment and numerical simulation. The experiments are performed by varying parameters that affect liquid transfer (viscosity, plate velocity, plate wettability and plate angle) using the in-house asymmetric plate extensional rheometer. The process of liquid transfer is recorded using a high-speed camera and transfer dynamics is analyzed using MATLAB. The numerical simulation, based on the phase-field model and dynamic contact angle, facilitates reproducing the complex contact line motion such as slip and pinning which can help us understand and compare with experimental results. Based on the results, regardless of plate inclination, we could divide the transfer ratio into three regimes: quasi-static regime, transition regime and dynamic regime which showed dependence on the plate velocity¹. Overall, the transfer ratio on the inclined plate increases in comparison to the parallel plate, and this phenomenon is further enhanced in the dynamic regime. Additionally, the liquid viscosity and surface wettability were also observed to significantly affect the transfer ratio. Hence, in this study we intend on developing an engineering framework that can be used for controlling the liquid transfer and further be applied to optimize the roll-to-roll printing conditions.

1. Chen, H., T. Tang, and A. Amirfazli. "Effects of surface wettability on fast liquid transfer." *Physics of Fluids* 27.11 (2015)

Acknowledgement

This research was supported by Basic Science Research Program through the National Research Foundation of Korea (NRF) funded by the Ministry of Education (2021R1A6A1A03039696), the Ministry of Science, ICT & Future Planning (2020R1A2C3010568) and the Korea government (MIST) (2020R1A5A1019649).

SB05.08.12

Conducting Polymers as Dual Charge Conductors for Electrochemical Systems Gao Liu; Lawrence Berkeley National Lab, United States

Electrically conductive polymers are a class of polymers, which can conduct electricity. Conductive polymers have found niche applications such as anti-statics. The electrochemical energy storage devices, especially lithium-ion rechargeable batteries, has grown significantly in the past two decades. Recently multifunctional conductive polymers have been designed as dual ion and electron transport materials, and synthesized through a thermal process. These class of dual charge conducting polymers play a significant role as electrode binders for Silicon (Si) and Tin (Sn) alloy based anode electrode. Si is an attractive candidate for lithium-ion batteries because it delivers 10 times greater theoretical (~4200 mAh/g) specific capacity than that of a traditional graphite anode (~370 mAh/g). However, the widespread application of silicon materials has remained a significant challenge because of the large volume change during lithium insertion and extraction processes, disrupting both the Si electrode surface and electrode mechanical integrity. This large volume change causes electrode failure, leading to loss of the electrical contact and drastic capacity fading. Nanosizing the Si and Sn based anode materials provides better performance, but poses significant challenges to manufacturing of the electrode, including particle aggregation, and difficulties in maintaining constant electrical contacts to the nanoparticles, and excessive surface area. Conductive polymer binders can play multiple functions for Si electrode, including improved adhesion and connectivity, lithium ion compensation, better ion and electric conductivity as well as surface and interface modification. Organic and polymer chemistry has provided almost infinity possibilities to modify the polymeric binders to include the desired functionalities. This presentation will discuss the specific molecular design principles and synthetic steps to realize the structures and functionalities of the binders, how these binders interact with different alloy materials, and the electrochemical performances of the electrodes based on these binders.

SB05.08.13

Large-Area 2D Colloidal Microchannel Formation Under Non-Equilibrium Condition Ryan Dumont, Deepika Kakarla, Ashish Aphale and Bo Li; Kennesaw State University, United States

To face formidable challenges of future electronics with complex functionality and architecture, not only new materials but also new fabrication method need to be developed. However, topographical micropatterns (such as microchannels) are conventionally fabricated by complicated lithographic method, which are usually expensive and time-consuming, and not suitable for high throughput manufacture. Therefore, a low-cost, large-scale method for topographical template preparation needs to be developed. Recently, cracks formed in drying colloidal film have been demonstrated as ideal materials for microscale manufacturing. In this work, we first studied the key parameters that affect the dimensions of colloidal microchannel, such as channel-to-channel distance, channel width, and theoretical model is proposed to provide insights on colloidal microchannel formation. Then, the criteria for 2D microchannel formation (i.e., microchannel formed in both x and y direction) are investigated. The dimensions of 2D microchannel will be tuned by varying non-equilibrium condition, such as convective flux, temperature and evaporation rate. This work will provide a general strategy for generating of 2D microchannels, thereby offering a low-cost, large-area and lithography-free method for fabrication of patterns for printed electronics.

SB05.08.14

Pore-Size Dependent Adsorption Mechanism of Ammonia into MIL-101(Cr) Metal-Organic Framework Byeongryun Jeon and Jae Hyun Park; Gyeongsang National University, Korea (the Republic of)

Metal-organic frameworks (MOFs), nanoporous materials composed of metal nodes and organic ligands, are remarkably paid attention to as adsorption and storage medium for gases. A controllable pore-size nature of MOF enables species-specific adsorption for a particular purpose. However, the adsorption mechanism is not well understood yet. Among diverse gases, we focus on ammonia because it is popular for energy systems due to its nature of large vapor pressure and enthalpy of evaporation. The large vapor pressure can promote heat and mass transfer rate, and the large enthalpy of evaporation enables the reduction of the adsorption bed size.

Considering all the above, in this study, by employing extensive grand-canonical Monte Carlo (GCMC) simulations, we probe the adsorption mechanism of NH₃ into MIL-101(Cr) MOF depending on the pore sizes. The pore size is modulated by increasing the number of benzene rings in the ligand. Three different ligands with one (original), two, and three benzene rings are considered while the metal node remains unchanged. As a result, the original MOF without modification has 6.8 Å, 26.1 Å, and 33.6 Å -sized pores, the MOF with two benzene rings has 9.7 Å, 39.4 Å, and 49.9 Å -sized pores, and the MOF with three benzene ring has 12.7 Å, 52.5 Å, and 66.1 Å -sized pores. For each structure, the isotherm is calculated by varying the pressure from 1 to 9 bar. Interestingly, the results show that the original MOF with the shortest ligand absorbs the ammonia most rather than the other MOFs with the longer ligands except for the high pressure of 9 bar. When the pressure is sufficiently high, the MOFs with two ligands adsorb NH₃ most. Also, we observe that at a certain pressure, the NH₃ isotherm suddenly increases as the pore surface is closed (filled by gas completely) and the interior of the pore starts to be filled. At low pressure, the interaction between gas and MOF node governs the adsorption. However, at high pressure, the gas-gas interaction becomes dominant since all the nodes in a pore are occupied by the gas molecules already.

The potential energy analyses confirm the observations by GCMC simulations. Until the surface of the pore is fully occupied, the vicinity of the surface has the lowest energy sites. However, when the surface is closed by gas molecules and the pore interior starts to be filled, the NH₃-attractive sites are found in the middle of the pores. When an NH₃ molecule is adsorbed on the node, it creates additional favorable sites nearby for other NH₃ molecules. Therefore, the small pores have a NH₃ structure inside that is dominated by the shape of pore while the large pores permit regular NH₃ structure inside because the NH₃'s in the middle are adsorbed mostly on the site created by the other NH₃ molecules.

This work was supported by Korea Institute of Energy Technology Evaluation and Planning (KETEP), which is funded by the Korean government (MOTIE) (No. 20212050100010, Chemisorption heat pump system using electrochemical compressor).

SB05.08.15

In Situ Investigation of Low-Friction Tribofilm Formation in Transmission Fluids Matthew Flynn-Hepford¹, Arya Ahmadi¹, Holland Hysmith¹, Zixuan Li², Kerry Cogen² and Olga Ovchinnikova³; ¹University of Tennessee- Knoxville, United States; ²Infinium, United States; ³Oak Ridge National Laboratory, United States

On average, one third of the energy consumed by passenger cars is used to overcome friction in the system. About 15% of this total energy loss is converted to heat by friction in the transmission. In order to understand the mechanism of low-friction tribofilm formation in transmission fluids, Multimodal Atomic Force Microscopy (MM-AFM) was used to generate tribofilms and monitor their development on steel surfaces. This technique allows in situ nanoscale imaging of the tribofilm, combining Friction Force Microscopy (FFM) to monitor friction changes, with Nanoscale infrared spectroscopy (nano-IR) to monitor chemical changes on the surface. Several friction modifiers combined with phosphorus-based antiwear chemistry were analyzed as a function of contact pressure. Using MM-AFM to track frictional and chemical behaviors during tribofilm formation provides unique insight into the evolution of low-friction films while helping advance toward the goal of developing more efficient drivetrains.

SB05.08.16

Compositional Changes at Epoxy-resin/Inorganic Interfaces Revealed by 1-nm Resolution Electron Spectroscopy Tomohiro Miyata^{1,2,3}, Yohei Sato¹, Kaname Yoshida⁴, Hsin-Hui Huang⁴, Teruyasu Mizoguchi⁵, Katsumi Hagita⁶, Masashi Mizukami¹ and Hiroshi Jinnai¹; ¹Tohoku University, Japan; ²University of Maryland, United States; ³National Institute of Standards and Technology, United States; ⁴Japan Fine Ceramics Center, Japan; ⁵University of Tokyo, Japan; ⁶National Defence Academy, Japan

Epoxy resins are widely used in adhesives and fiber-reinforced plastics owing to their excellent adhesive and workable properties. The adhesive strength between the epoxy resin and inorganic surfaces directly affects the mechanical strength of composite materials. Therefore, understanding the origin of the adhesive properties has been anticipated. However, molecular-scale investigations on epoxy-resin/inorganic interfaces have little been performed due to the difficulty in measuring such “buried” interfaces. This study prepared the adhesive interfaces between an epoxy resin and two types of silicon substrates with different surface chemical states. Moreover, the compositional distributions in the vicinity of the epoxy-resin/silicon interfaces were analyzed with a 1-nm resolution using scanning transmission electron microscopy (STEM) and electron energy-loss spectroscopy (EELS).

Diglycidyl ether of bisphenol A (DGEBA) (Mitsubishi Chemical Co., Ltd., Japan) and *para*-diaminodicyclohexylmethane (PACM) (Tokyo Chemical Industry Co., Ltd., Japan) were used as the epoxy-resin prepolymer and curing agent. They were mixed so that the molar ratio of the epoxy groups to the active hydrogens of the amino groups becomes 1:1. (111) substrates of a silicon single crystal were prepared. The organic residue on the surface was removed with piranha solution. Subsequently, hydrogen (H)-terminated surfaces were prepared with 1.5 wt% hydrofluoric acid for 30 min. Some H-terminated surfaces were processed by water vapor plasma to be terminated with hydroxyl (OH) groups. The mixture of DGEBA and PACM was pasted on these silicon substrates and then cured at 100 °C for 90 min. Thin cross-sectional samples of the epoxy resin/silicon interfaces were fabricated using a Cryo Ion Slicer (JEOL Ltd., Japan). These samples were analyzed by annular dark-field STEM (ADF-STEM) and STEM-EELS using a transmission electron microscope JEM-ARM200F (JEOL Ltd., Japan).

ADF-STEM observation revealed that oxidized silicon layers with thicknesses of ~2 nm at both adhesive interfaces between the epoxy resin and H- or OH-terminated silicon substrates exist. In addition, C-K adsorption edge spectra, originating from the epoxy resin, were measured by EELS at 1 nm intervals in the vicinity of the adhesive interfaces. Because DGEBA contains aromatic rings in the molecular structure, a characteristic peak (π^* peak) appears in the C-K edge. However, PACM does not show the π^* peak in the C-K edge because it has no π bond in the molecular structure. The measured C-K edge spectra clarified that epoxy resin molecules infiltrated into the oxidized layers at the interfaces. Moreover, the π^* peak became smaller only at the interface of the OH-terminated silicon, suggesting that the compositional ratio of PACM to DGEBA became more significant at the interface of the OH-terminated silicon rather than that of the H-terminated silicon. Our study revealed that the compositional ratio of epoxy resins, which results in adhesive properties, changes in the vicinity of the epoxy-resin/inorganic interfaces under the influence of the surface chemical conditions of inorganic materials.

SB05.08.20

Charge-Transport Solution-State Seeding and Growth of Conjugated Polymers into Well-Defined Nanowire Yoon Junyeon, Junho Hwang and Eunji Lee; Gwangju Institute of Science and Technology, Korea (the Republic of)

Controlling the nanoscale morphology of the conjugated polymers (CPs) has been approaching an amount of interest due to its possibility of adjusting charge transfer property. In particular, one-dimensional nanostructures are ideal for charge transfer as they have effective carrier transport properties along the anisotropic stacking directions. Along this line, the pre-assembly of conjugated nanowires (NWs) in the solution state has drawn great interest as a potential replacement for the post-annealing process, securing roll-to-roll manufacturing with a large-area production and a significant cost decrease. The whisker method and the mixed solvent method are frequently utilized as typical solution processing techniques to provide additional driving forces for CPs assembly. Herein, in order to accomplish NW growth and doping without a physical driving force simultaneously, we have focused on charge transfer at the CPs and dopant contact, which can cause seeds-triggering growth of the CPs, rather than the doping procedure, which is often used to tune the electrical property of the CPs to induce the enhancement of the conductivity. Specifically, we will talk about the charge-transport driven CPs-crystal seeding and growth into NWs by adding dopant. Interestingly, it is clearly confirmed through in-situ liquid-cell TEM that controlling the concentration of the dopant or the molecular weight of the CP may have a strong effect on the formation of the NWs in the solution-state. This study might provide an innovative manufacturing strategy for mass production of high-efficiency doped organic semiconductor NWs for optoelectronic devices through solution-processing.

SB05.08.21

Biophysical Characteristics of amyloid- β Protein Aggregates Using a Molecular Structure-Specific Label-Free THz Spectroscopy for Alzheimer's Disease Chaejeong Heo^{1,2}, Taewoo Ha¹ and Young Hee Lee¹; ¹Sungkyunkwan University, Korea (the Republic of); ²Institute for Quantum Biophysics, Korea (the Republic of)

Alzheimer's pathology is correlated with structural conformation change of aggregated amyloid beta ($A\beta$) proteins. We identify the progressive aggregation stages of the $A\beta$ protein growth in a buffer solution using by the near-field THz spectroscopy and the newly defined biophysical marker based on real-time THz optical conductance. Here, we clearly detected and analyzed the $A\beta$ aggregation growth through solution-based label-free THz conductance measurement by precisely controlling the thickness of the protein sample in a buffer solution. Frequency-dependent conductance for $A\beta$ aggregates was obtained by measuring the differential transmittance of the time-domain spectroscopy in the THz range with a molar concentration of monomer, oligomer, and fibrillar forms. The monotonic decrease in the conductance at low frequency was dominated by a simple Drude component in the monomer with concentration and nonlinear conductance behaviors in the oligomer and fibril. By extracting the structural localization parameter, a dimensionless constant,

with the modified Drude–Smith model, we defined this to the biophysical value ($0 < DQ < 1$) as a structure-specific metric for a various A β aggregates at a low concentration of 0.1 $\mu\text{mol/L}$; $DQ = 1.0 \pm 0.002$ (fibril by full localization, mainly by Smith component), $DQ = 0.64 \pm 0.013$ (oligomer by intermixed localization), and $DQ = 0.0 \pm 0.000$ (monomer by Drude component). Furthermore, we can label-free monitor A β growth dynamics to identify various morphological phase transitions and steps during macro scale fibrils from monomers under physiological conditions. This suggests the new biophysical characteristics with intrinsic property of A β proteins for Alzheimer's disease.

SB05.08.22

Bulk Self-Assembly of Hybrid GO-clay Nanosheets Paulo H. Michels Brito¹, Barbara Pacakova¹, Martin Bygdas¹, Andrew N. Akanno¹, Veslemeløy Osmundsen¹, Josef Breu² and Jon Otto Fossum¹; ¹Norwegian University of Science and Technology, Norway; ²University of Bayreuth, Germany

Bulk self-assembly provides an efficient technique for large-scale production of materials which is often limited using the interfacial or deposition methods. One promising system in this context could be provided by functionalization of insulating nanosheets for the production of conductive/insulative heterostructures, for instance use in electronic devices. One such material is clay which completely delaminates in water to form insulating nanosheets, exhibiting one of the largest electron bandgaps known so far in 2D layers (1).

Here we present the self-assembly of graphene oxide (GO-) and synthetic fluorohectorite clay heterostructures in a bulk mixture of the two individual components in the presence of polyethyleneimine-ethyleneoxide (PEI-EO). The synthetic clay mineral used here is superior to other clays in terms of charge distribution, homogeneity, and crystalline perfection (2). This clay mineral delaminates in water to form nematic structures with cations present in the interlayer regions. Double layer clay nanosheets can be readily obtained via ordered stratification by partial interlayer cation exchange using ammonium cations (NH_4^+), providing bilayers with a net negative charge, and which can be double side coated with the polymer (2, 3). The GO is incorporated onto the clay surface via the polymer adhesion layer to form the complex GO-clay heterostructures. These 2D nanosheets have been investigated using SPM and XRD to determine their composition, mechanical and adhesion properties.

The results indicate that the synthesized GO-clay nanosheets presents interesting properties for possible applications in electronics and semiconductive devices. We are currently extending this work and attempting the cleavage of the double layer GO-clay nanosheets into single GO-clay layers to produce micrometer sized GO-clay Janus platelets.

Reference:

- (1) Pacakova B.; Vullum P.E.; Kirch A.; Breu J.; Miranda C.R.; Fossum J.O. Large Bandgap Insulating Superior Clay Nanosheets. MRS Bulletin. 2022, 47.
- (2) Stoter M.; Godrich S.; Feicht P.; Rosenfeldt S.; Thum H.; Neubauer J.W.; Seuss M.; Linder P.; Kalo H.; Moller M.; Fery A.; Forster S.; Papastavrou G.; Breu J. Controlled Exfoliation of Layered Silicate Heterostructures into Bilayers and their Conversion into Giant Janus Platelets. Angew. Chem. Int. Ed. 2016, 55, 7398-7402.
- (3) Michels-Brito P.H.; Malfatti-Gasperini A.; Mayr L.; Puentes-Martinez X.; Tenorio R.P.; Wagner D.R.; Knudsen K.D.; Araki K.; Oliveira R.G.; Breu J.; Cavalcanti L.P.; Fossum J.O. Unmodified Clay Nanosheets at the Air-Water Interface. Langmuir. 2021, 37, 1, 160-170.

SB05.08.23

Multiscale Structure and Properties Measurement of Soft Matter Using a Single Platform—Tribo-Rheology Chungman Kim^{1,2}, Jaewon Shim¹, Sangmin An³, David A. Weitz², Manhee Lee^{4,2} and Wonho Jhe^{1,2}; ¹Seoul National University, Korea (the Republic of); ²Harvard University, United States; ³Jeonbuk National University, Korea (the Republic of); ⁴Chungbuk National University, Korea (the Republic of)

Soft matter exhibits viscoelasticity, which is generally associated with the rheological structure of materials. To comprehensively understand the rheological structure and properties, it is, therefore, necessary to probe materials at the multiscale; materials should be measured with probes from bulk- to nano-scales, to fully reveal the internal structures of materials. However, conventional rheometers mostly limit the rheological measurements to the bulk scale. Here, we demonstrate multiscale measurement of structure and properties for polymer solutions, e.g., silicone oils, using a single platform: quartz tuning fork-based tribo-rheometer. This unique platform with different-sized probes allows to measure bulk rheological properties, molecularly ordered structures of polymers, and the tribo-rheological characteristics at solid interfaces. Our results offer a unified understanding of structures and properties relation for soft matter.

SB05.08.24

Phase Separation and Liquid Crystallinity in Mixtures of Rigid and Flexible Biopolymers Kimberly L. Weirich¹, Steven Huntley¹, Sam Rubin¹, Rui Zhang² and Juan de Pablo³; ¹Clemson University, United States; ²The Hong Kong University of Science and Technology, Hong Kong; ³University of Chicago, United States

Structured soft materials have internal order that give rise to unusual mechanical properties and emergent organization of inclusions and defects. Here we present a composite structured liquid formed from biopolymers of distinct rigidities. Biopolymer filaments, such as actin and microtubules, behave as rigid rods when much shorter than their persistence length. These short, rigid filaments are known to crowd into a thin fluid layer that can form a nematic liquid crystal, where filaments have orientational order but not positional order. Here we investigate the phase space in a mixture of short, rigid, nematic forming filaments with more flexible biopolymers, which are much longer than their persistence length. Using fluorescence microscopy, we investigate the domain and defect formation as the phase separated polymer mixture evolves. Using a continuum model of lyotropic liquid crystal, we extract material properties of the liquid crystal. Our results suggest a novel structured soft composite, which potentially informs physical mechanisms of controlling material properties in structured fluids and templating functional polymeric materials.

SESSION SB05.09: Crystal and Glasses
Session Chairs: Julia Dshemuchadse and Kyungtae Kim
Wednesday Morning, November 30, 2022
Hynes, Level 1, Room 110

8:30 AM *SB05.09.01

Pressure Processing of Nanocrystals and Nanocrystal Assemblies Ou Chen and Yasutaka Nagaoka; Brown University, United States

Pressure processing emerges as a fast and clean mechanical method to fabricate and transform novel nanomaterials without involvement of chemical reactions and post-purification processes. Recent studies have revealed that the pressure-treatment of nanomaterials is able, not only to induce structure transformation at the atomic level, but also to regulate translational alignment at nano-, meso- and even macro-scales. Exciting nanomaterials with unique structures and properties have been generated through a stress-driven “permanent-sintering” process. In this talk, I will discuss several of our recent studies about pressure processing of different types of nanocrystals and their ordered and non-ordered assemblies, including halide perovskite nanocrystals, metal nanoparticles, and quantum dot-metal heterostructure nanocrystals. In particular, I will focus on our new discovery of a novel method to produce tailored grain-boundary conditions with nanoscale precision from colloidal metal nanocrystals by a pressure-sintering process. The resulting bulk grain-boundary materials (which we call “nanocrystal coins”) possess a metal-like appearance, high conductivity and exceptional strength while inheriting the original domain features of the nanocrystal building blocks. Our studies may spur the development of new materials (through pressure-treatments) with functionalities crucially depends on the domain configuration at nanometer scale, such as superhard materials, thermoelectric generators, and functional electrodes.

9:00 AM SB05.09.02

The Onset of Glassy Dynamics in Two Dimensions as a Kosterlitz-Thouless Transition [Muhammad R. Hasyim](#)¹, Dimitrios Fraggedakis¹ and Kranthi K. Mandadapu^{1,2}; ¹The University of California, Berkeley, United States; ²Lawrence Berkeley National Laboratory, United States

The dynamics of glass formers exhibit dramatic slowdown below an onset temperature that delineates the high-temperature and supercooled regimes. For two-dimensional (2D) glass formers, we propose that the onset temperature can be described by a Kosterlitz-Thouless transition, driven by the elastic excitations underlying the relaxation mechanism for glassy dynamics. Analogous to dislocation-mediated melting in 2D crystals, the excitations exist as a bound dipole-dipole (or quadrupole) state in the supercooled regime and as free dipoles above the onset temperature. The Kosterlitz-Thouless scenario explains the emergent elastic behavior of 2D supercooled liquids at intermediate timescales, and thus the Mermin-Wagner fluctuations observed in experiments and simulations of 2D glass formers. The present work reveals the nature of 2D glass formers, where quasi-long-range order emerges in an analogous manner to 2D crystals at intermediate time scales, and is relevant to understanding colloidal films and other soft condensed matter systems under extreme confinement.

9:15 AM SB05.09.03

Depletion-Mediated Crystal Nucleation and Growth of Attractive Colloids [Sanghyuk Park](#)¹, Hyerim Hwang² and Shin-Hyun Kim¹; ¹Korea Advanced Institute of Science and Technology, Korea (the Republic of); ²Ewha Womans University, Korea (the Republic of)

Colloids are exquisite mimics of atoms or molecules in condensed matter. Since the particles are thermalized by the solvent, they form the same phases of atomic or molecular systems such as crystals, glasses, alloys, and liquids. Each particle mimics the behavior of an individual atom and their collective behavior mimics that of a condensed phase. Due to experimentally accessible time and length scales, they serve as an excellent model system to investigate a variety of phase behaviors that have not been accessible to experiment on the atomic level. Intensive studies have been done using hard-sphere or soft-sphere colloids to elucidate mechanisms underlying crystallization, melting, solid-solid transitions, and glass deformation, which provided new fundamental insights into the phenomena; structure, dynamics, and their time-dependent evolution are directly measured to find out key parameters that govern the processes. Progress in the synthesis of model colloids with controllable surface chemistry allows an alteration in the simplest interaction potentials, which, however, is still far behind from mimicking real atoms and molecules. In general, pair potentials of atoms and molecules are described using the Lennard-Jones potential, which represents one particular type of Mie potential. Therefore, it remains of great importance to design realistic colloidal systems with Mie potential that can more closely depict the phase behavior of atoms and molecules.

We employ the depletion interaction in aqueous suspensions of spherical colloids to formulate total pair potential to be comparable with that of atoms and molecules. Depletion force has been applied to modulate interparticle interactions in colloidal systems. Depletants in the suspension are excluded from the surfaces of colloids, which causes outward osmotic flow from the depletant-depleted interstitial region among colloids, exerting attractive force. This attractive interaction has been used to assemble colloidal particles into condensed phases. We suspend polystyrene particles with negative surface charges in water containing sodium chloride and depletant of poly(acrylamide-co-acrylic acid) (*p*(Am-co-AAc)) with a hydrodynamic radius of $r_h = 32.5$ nm. In the presence of the depletant, depletion attraction contributes to total pair potential in the range of separation smaller than the diameter of the depletant. Superposition of the depletion attraction with electrostatic repulsion and van der Waals attraction renders the particles to strongly repel in very short-range, gently attract in middle, and not interact in long-range, similarly with Mie potential.

With the pair potential, fluids, crystals, and glasses are respectively represented depending on the depth and slope of the pair potential. For example, the phase boundary between the fluids and crystals is roughly defined by the depth of the potential well, whereas that between the crystals and glasses is represented by the rate of colloidal assembly. For the crystalline phases, the nucleation rate is dictated by the depth and the growth is limited by slow colloidal diffusion. During growth, Ostwald ripening causes large crystallites to get larger while small ones shrink and disappear, in particular for large Laplace pressure gradient. The final morphology of crystals is either dendritic or polygonal, which is selected by whether or not the concentration gradient is maintained during the growth. The shape of the dendrites is determined by the crystal orientation, to be either six-fold or elongated X-shaped. These crystal growth behaviors are highly relevant to atomic and molecular systems. As the growth is dictated by the nucleation rate, the depth of potential energy well is the most important determinant that governs the overall pathway of nucleation and crystal growth.

9:30 AM SB05.09.04

Amorphous Calcium Phosphate (ACP) as a Precursor for Mineralization in Bone Tissue [Yongjae In](#), Urasawadee Amornkitbamrung and Hyunjung Shin; Sungkyunkwan University, Korea (the Republic of)

Bone mineralization refers to the crystallization of amorphous calcium phosphate in the extracellular matrix of all vertebrates. Human bones are composed of organic/inorganic mixture, and about 60% of inorganic components are hydroxyapatite (HAP), which is one of calcium phosphate. It is known that the crystallization of HAP does not follow classical nucleation theory. It has been found that the mineralization of HAP is achieved through a transient amorphous calcium phosphate (ACP) step both in vitro and in vivo. However, the proposed mechanisms of ACP transformation to HAP remained elusive for example, a dissolution-reprecipitation, the reconstruction of Posner's clusters, and a surface-mediated transformation. Therefore, the study of ACP-mediated HAP nucleation pathways and mechanisms is required and has profound implications for biomineralization. Synthetic ACPs were discovered by Betts and Posner's X-ray experiments in the 1970s to have a Ca:P molar ratio of ~1.5, a spherical feature, and a chemical structure of $\text{Ca}_9(\text{PO}_4)_6$. In human bone, it has been reported that Ca and P ions, which are constituents of HAP, are initiated from the mitochondria of osteoblast and are released in the form of ACP through the matrix vesicles (MV). After that, ACP crystallizes inside the collagen fibers to be crystalline hydroxyapatite platelets. So far, there are sufficient studies related to the properties of synthesized ACPs, but the analysis of crystallization of ACPs released from the cells into HAP is insufficient. In this study, the characteristics of ACPs secreted from cells and synthesized ACPs were analyzed, and collagen fibrils were mineralized using both ACPs. The Ca/P atomic ratio and chemical composition of ACPs were analyzed by Inductively Coupled Plasma and Transmission Electron Microscopy (TEM), and the phase of ACP was analyzed by powder X-ray diffraction. In the case of synthesized ACPs, spherical nucleation was observed in a solution containing Ca and P, and the Ca/P ratio in the process of becoming a ribbon was analyzed. The Ca/P ratio in the initial spherical state was about 0.9, but it increased with time. ACPs released by cells were obtained by ultrafiltration of matrix vesicles from osteoblasts and analyzed mainly by TEM. We

dispersed cell exosomes on a TEM grid by using ultrafiltration and finding the dark contrast due to the electron scattering by inorganic substances, Ca and P, in bright-field imaging, we also analyzed the mineral contents. Based on the study on the characteristics of ACP, mineralization in the collagen matrix was carried out to conduct a study on the synthesis of bone formation from the actual release of ACPs from osteoblasts to the mineralization of collagen. Therefore, the results presented in this study may better understand the mechanism of HAp mineralization in collagen fibrils and the actual bone formation process and ultimately help in the successful material design of tissue engineering.

9:45 AM SB05.09.05

Effects of Electrostatic Repulsion and Steric Exclusion on Single-Stranded DNA Attaching to the ZnS Surface of Quantum Dots Xingfei Wei and Rigoberto Hernandez; Johns Hopkins University, United States

DNA linked quantum dot (QD) assemblies have been applied in biological drug delivery, programmable materials, and photonics. The mechanism of a DNA chain attaching to the QD surface is very important to developing new DNA-QD nanostructures. In this work, we combine all-atom molecular dynamics simulations and experiments to reveal the mechanism of a single-stranded DNA (ssDNA) attaching to the ZnS surface of CdSe-ZnS (core-shell) QDs. We verified the ssDNA model chain conformation through agreement with experimental and theoretical conformations in the literature. We report the ssDNA chain conformation on a flat ZnS surface and on differently sized ZnS QD surfaces. They depend on the combined effects of electrostatic repulsion and steric exclusion from 3-mercaptopropionic acid (MPA) and O-(2-mercaptoethyl)-O'-methyl-hexa (ethylene glycol) (mPEG) capping on ZnS QDs. Both simulations and Förster Resonance Energy Transfer (FRET) experiments indicate that ssDNA tail is closer to the QD surface when the QD size is larger. In addition, we find through both simulations and Transmission Electron Microscopy (TEM) experiments that the maximum valence numbers are 1, 2 and 3 on QDs of 6, 9 and 14 nm in diameter, respectively. We emphasize the critical role of the electrostatic repulsion on the conformation and the number of attached ssDNA on the QD surface.

10:00 AM BREAK

SESSION SB05.10: Mechanics and Processing
Session Chairs: Ou Chen and Maya Martirosyan
Wednesday Morning, November 30, 2022
Hynes, Level 1, Room 110

10:30 AM SB05.10.01

Soft Material Assembly Assisted with Polymer Pen Nanolithography Jacob LaNasa and Kyungtae Kim; Los Alamos National Laboratory, United States

The intrinsic thermodynamics of polymeric and molecular materials can drive assembly into advantageous structures on the nanometer length scale. Specifically, block copolymers with two or more chemically distinct and covalently linked blocks that are enthalpically immiscible have the propensity to phase separate. These phase-separated regions can conform to many interesting structures that have been useful in areas including lithography, optics, and membrane design. Likewise, molecular aggregates are structures that readily assemble to a similar macromolecular length scale and can have unique interactions with visible light. In these assemblies, the long-range order is limited by uncontrolled nucleation and growth. Well-defined long-range order in these materials can strengthen photonic coherence and can make them intriguing candidates for visible-light integrated circuits. With state-of-the-art competencies at the Center for Integrated Nanotechnologies at Los Alamos National Laboratory, the structural assembly of soft materials can be assisted with polymer pen nanolithography. The polymer pen lithography technique is a novel approach to precise, high throughput application of soft materials onto a surface. In the case of polymeric assembly, strategic placement of defects can be used to predetermine nucleation sites and limit grain growth, effectively assisting the assembly process. In the case of molecular aggregates, printing of aggregate assemblies on the length scale of visible light can reduce the quantum incoherence of randomly assembled and multilayer grains. Here, a substrate can be pre-treated with a quasicrystalline-patterned poly(dimethylsiloxane) (PDMS) photoresist that is then photopolymerized to yield a durable and chemically selective defect architecture intended to influence the self-assembly of a poly(dimethylsiloxane)-*block*-poly(lactic acid) block copolymer. The structural and characteristics of the resulting assemblies are quantified using X-ray scattering and microscopy techniques.

10:45 AM SB05.10.02

Phase Separating Inks for the Additive Manufacturing of Porous Polymer Composites in Battery Applications Andrew L. Fassler^{1,2}, Ryan R. Kohlmeier^{1,2,3}, Gregory Horrocks¹, Luke A. Baldwin¹, Abigail Juhl¹ and Michael F. Durstock¹; ¹Air Force Research Laboratory, United States; ²UES, Inc, United States; ³Xerion, United States

The additive manufacturing of batteries offers great potential for the future of power integration in electronics, freeing up design space and enabling new device capabilities. This is especially true for thin film and flexible devices where current packaging (ex. coin cells, cylindrical cells, and pouches) prevents intimate incorporation of the battery into the device and must be designed around to maintain a device's flexibility. The ability to fabricate a cell directly onto the device itself can remove this restriction, as the shape and structure of the cell can be tailored to the device, fitting into unique form factors or even being designed to enable deformation. To achieve this, additive manufacturing approaches must be developed to deposit high performance battery component materials and to combine these materials to create high functioning galvanic cells.

One of the great challenges in the additive manufacturing of batteries is developing process compatible materials with the suitable composition and microstructure to enable appropriate performance, particularly porosity and pore structure. Electrodes must be porous to allow for electrolyte penetration and ion conductivity, highly loaded with active material to maximize energy density, and electrically conductive to transport energy to and from the active material. Likewise, separator membranes must be porous for electrolyte penetration and ion conductivity, but these features must be small enough and mechanically robust enough to prevent shorting and dendrite growth. In addition, the processing requirements for these materials must be straight forward to make techniques like 3D printing and coating possible.

We have developed an evaporation induced phase separation technique that utilizes a mixed solvent system to fabricate polymer materials and polymer-particle composites with controlled porous microstructures. The polymer is dissolved in a solvent solution composed of a good and poor solvent for the polymer, chosen such that the good solvent evaporates preferentially to the poor solvent. This leads to an instability in the ink upon drying, thereby causing phase separation into polymer poor and polymer rich phases and creating porosity upon solidification. We have used this process to develop a PVDF and Al₂O₃ composite that functions as a separator membrane for lithium ion batteries and can be deposited by multiple printing and casting techniques.

Additionally, we have demonstrated the ability to control the microstructures that form in these polymer-particle composites through the selection of particle size and loading, including creating both foam-like and granular morphologies. When combined with similar composite electrode materials, such as graphite or LiFePO₄ for lithium ion batteries, printed full cells can be achieved. Here, we explore approaches to how we can create fully printed batteries from these materials, as well as how to fabricate them on complex and non-planar substrates to enhance energy storage integration. Furthermore, we examine the challenges faced in controlling microstructure in multi-material and multi-layer additive manufacturing, particularly at the interfaces between different materials and how this can impact performance.

11:00 AM SB05.10.03

Large-Area Emerging Patterns by Thermally Engineered Template-Guided Self-Assembly Sung Bum Kang¹, Guanglong Huang², Gaurav Singhal¹, Dajie Xie¹, Daniel Hwai-En Hsieh¹, Youngmun Lee¹, Ashish A. Kulkarni³, Alexander J. Littlefield¹, John W. Smith¹, Qian Chen¹, Sanjiv Sinha¹, Katsuyo Thornton² and Paul Braun¹; ¹University of Illinois at Urbana-Champaign, United States; ²University of Michigan, United States; ³Brookhaven National Laboratory, United States

Template-directed self-assembly is a promising way of manipulating microstructure, enabling emergent functional properties including photonic, phononic, and mechanical. Moreover, the template can evolve microstructures that are distinct from initial starting structures, yielding ordered emerging patterns. However, instabilities at the interfaces between materials and templates hinder the formation of uniformly ordered emerging patterns in a long-range order, limiting practical applications. Here, we design low-thermal fluctuated templates which reduce instability of eutectic self-assembly materials at the interface, leading to a large area (~0.01 mm²), ordered checkerboard array of emerging patterns. The FDTD simulation suggests that the low thermal conductivity of the template can minimize temperature fluctuation, giving rise to uniformly ordered emerging patterns. In the serial sectioning of directionally self-assembled AgCl-KCl within the template, we note that microstructures are strongly influenced by the thermal conductivity of the template, and particularly large instability of microstructure at the interface between the template and material results in short-range order. The low thermal conductive template fabricated by porosification constrains thermal fluctuation caused by rapid thermal transport and produces a large-area emerging pattern. We also find that by using selective etching of self-assembled materials or templates, a variety of mesostructures are observed and can control optical properties, which reveal the promising potential for photonic and microscale-based applications.

11:15 AM SB05.10.04

Fabrication of Waterborne Polyurethane (WPU) Porous Layers Through Binary Particle Stabilized Pickering Foam Templating Zhenghao Shi and To Ngai; The Chinese University of Hong Kong, Hong Kong

As important raw materials utilized in fire-proof, sound insulation, thermal insulation, gas sorption, etc., the traditional solvent phase inversion methods to produce porous materials have resulted in air/water pollution and residual VOCs in the products, which have been restricted by many countries. Waterborne polymer products possess the superiority of being eco-friendly during manufacturing but are limited by foam stability. Pickering foam is an air-water mixture whose interface is stabilized by the particles without interfacial activity. Excess particle desorption energy from the air-water interface over surfactants ensures superior stability and potential templating porous material production. The classic view of Pickering foam requires specific particle wettability, explained through the maximum capillary pressure concept, which hinders its application in industry.

We have reported a new strategy to prepare ultra-stable aqueous foams from PVA-Silica binary component system¹. A series of Pickering aqueous foams were therefore achieved as the hydrophilic polymer and hydrophobic colloidal particles stabilized the Janus bilayer air-water interface in one step without massive particle wettability modification. The resulting Pickering foam afforded convincing stability over one month and templated the porous materials monolith. The work opened a new door for binary component Pickering foam and waterborne composite porous materials preparation.

In our recent work, the stabilization mechanism and kinetics of binary colloidal particles stabilized Pickering foam are under investigation. We are seeking for the potential to get the typical Pickering foam applied as a low-cost and eco-friendly scheme for porous materials industrial production. The Pickering aqueous foam systems, including hydrophilic-hydrophobic and hydrophilic-hydrophilic colloidal particles systems, are derived from waterborne polyurethane (WPU), hydrophobic silica particles (SP), and cellulose nanofibrils (NF) with typical wettability, surface charge, size distribution have been achieved.

Key Words: Porous material, Pickering foam, WPU, Silica particles, Cellulose nanofibrils

Reference

1. Y. Sheng, K. Lin, B. P. Binks and T. Ngai, *J Colloid Interface Sci*, 2020, 579, 628-636.

11:30 AM *SB05.10.05

Understanding and Controlling Tunable Organic-Inorganic Nanoparticle Self-Assembly Xin Qi; Dartmouth College, United States

Inspired by naturally occurring hierarchical materials, numerous beautiful and functional mesoscale architectures have been constructed in labs using solid-state nanoscale building blocks and bio- or biomimetic molecules via self-assembly. Their structures and assembly dynamics are tightly regulated by the system's convoluted energetics and entropic information, which may even respond to a minuscule change. For example, we recently reported a pH-regulated self-assembly of silica nanoparticles facilitated by an engineered bifunctional silica-binding protein sfGFP::Car9-Car9. The assembly and disassembly can be reversibly and cyclically modulated by alternating the solution pH between 7.5 and 8.5. In another study, we observed that an increment of the peptoid (i.e., the ligand) length by two monomers at a time would change the arrangement of a CdS quantum dot superlattice from close packing to square, further to monoclinic. However, the complexity of the nanoscale colloidal system often makes it difficult to probe the underlying physics via experimental means. Alternatively, we can construct suitable multi-scale theoretical toolkits by carefully selecting and combining theories and simulation algorithms from different levels (i.e., from ab initio to coarse-grained models) to connect the scales and gain physical insights into the assembly mechanisms. In this talk, I will elaborate on how we used multi-scale theoretical frameworks to reveal the key driving forces of self-assembly in these two cases. The knowledge we gained on the distinctive roles of organic ligands has further inspired new design principles in future studies.

1:30 PM *SB05.11.01**A Model Collective System Made of Spinning Micro-Disks—From Fundamentals to Microrobot Swarms** Gaurav Gardi and [Metin Sitti](#); Max Planck Institute for Intelligent Systems, Germany

Self-organization in colloidal systems has led to various fundamental studies on non-equilibrium systems and development of microrobot swarms. However, typical colloidal systems are limited in their behaviors and each system can only facilitate a few specialized studies. Therefore, developing a single model system that can controllably transition among diverse behaviors, would be very useful for various fundamental studies and for the development of microrobot swarms. We develop a collective system that utilizes the mutual interactions among its constituents, and its behaviors can be controlled via global stimuli. Our system consists magnetic micro-disks that interact via various physical interactions (magnetic dipole-dipole, hydrodynamic and capillary interactions) and the relative dominance of these interactions can be tuned by an external oscillating magnetic field. In this talk, we present various studies enabled by our system. First, we demonstrate that our system can form rotating collectives with varying degree of orientation order that can be controlled by a single control parameter: the rotation speed of the external magnetic field. These behaviors enable a fundamental study on development of a general-purpose order-parameter based on the information content of the self-assembled patterns. Next, we show that the mutual interactions among the micro-disks can be tuned to form various collective modes ranging from isotropic (rotating and static collectives) to anisotropic (chains) behaviors, and a gas-like behavior consisting self-propelling pairs. The mutual interactions are tuned by changing the profile of a 2D oscillating magnetic field, demonstrating that the external driving field and the mutual interactions can conjunctively generate transitions among behaviors and enable various controllable robotic functions. Last, we study the effect of heterogeneity in our system and demonstrate that our system can transition on-demand from a driven (following an external field) to an active (self-propelled) behavior or a mixture of both. Through these studies, we hope to convey that our system can act as a versatile model system facilitating fundamental studies that link driven and active behaviors, and also provide a step towards developing versatile and controllable microrobot collectives.

2:00 PM SB05.11.02**Self-Assembled and Nanostructured Triblock Terpolymer Organogels for Infusion Templating** [Yuanzhi Li](#) and Joerg G. Werner; Boston University, United States

Extended nanostructured materials are abundant in natural systems such as butterfly wings and beetle shells with high interior periodic order that produces splendid optical appearances and multifunctional mechanical and interfacial properties. Inspired by the versatility, durability, and functionality of natural materials, material scientists are seeking synthetic analogues of functional materials in bulk phase with highly ordered three-dimensional nanostructure for various applications in optics, catalysis, water purification, and energy storage. Herein, we introduce a versatile and scalable concept towards the fabrication of bulk nanostructured functional materials. We take advantage of the self-assembly of synthetic triblock terpolymers with chemically distinct blocks that self-assemble into ordered continuous nanostructures as bulk materials. Each of the three blocks serves a distinct purpose: One block within the self-assembled bulk material can be selectively crosslinked with tunable crosslink density which enables the formation of organo-gels with controllable swelling degrees in various kinds of organic solvents with retention of the periodicity of the ordered nanostructures. Another functional block is chemically tunable towards attracting and depositing reagents and nano-sized functional building blocks, while a chemically inert third block acts as a freely swollen gel phase that enables mass transport throughout the bulk structure. The size and symmetry of the nano-scaled features are tunable through the block fraction, the molecular weight of the polymer, crosslink density, and solvent quality. The monolithic triblock terpolymer organo-gels can serve as a versatile soft-template for the creation of various functional materials attribute to the unique physical and chemical properties of the triblock terpolymer. Specifically, the varied affinity of the building blocks to solvents and reagents, as well as the tunability of the functional groups facilitate the mass transfer and selective chemical reactions in infusion-deposition templating, respectively.

2:15 PM SB05.11.03**Using a Membrane to Impose Curvature and Alter the Morphologies of Growing Crystal** [Hao Wan](#)¹, [Geunwoong Jeon](#)², [Weiyue Xin](#)², [Gregory Grason](#)¹ and [Maria Santore](#)¹; ¹University of Massachusetts, Amherst, United States; ²University of Massachusetts Amherst, United States

Current understanding of two-dimensional crystal growth focuses on the interactions between flat substrates and flat growing crystals. By contrast, the understanding of the growth of curved crystals, especially those of non-zero Gaussian curvature of which limited examples exist, considers the stresses imposed by a curved template on a growing two-dimensional crystal, where molecular or colloidal units add to the growing crystal edges from above. In the current study, we demonstrate that when crystals grow within curved vesicle membranes, forces from the membrane and its bending, acting at the edges of the growing crystal, along with the impact of internal pressure, produce morphologies and scaling that run counter to expectations based on systems without the pulling of a growing crystal at its edges. In vesicle membranes, processing conditions, such as cooling rate and transport considerations cause variations in tension history, producing different interplays between bending energies and line tensions. The overall result, demonstrated in quantitative experiments and supported by modeling, is that flat compact solid domains grow reproducibly in small vesicles. However, despite more gradual curvature but higher membrane tension on larger vesicles, flower shaped domains are found and their shapes exhibit increasing complexity with increased vesicles size, tension and, ultimately, bending energy.

2:30 PM BREAK**3:30 PM SB05.11.04****Computational and Experimental Study Linking Polysulfamide Chain Design to the Hydrogen Bonding Induced Chain Aggregation** [Zijie Wu](#)¹, [Jiun Wei Wu](#)², [Quentin Michaudel](#)² and [Arthi Jayaraman](#)^{1,1}; ¹University of Delaware, United States; ²Texas A&M University, United States

Poly-N, N'-disubstituted sulfamides [Kulow et al. *Chem. Sci.*, 2020, **11**, 7807-7812], a new class of polymers structurally analogous to polyureas, are gaining attention in organocatalysis and medicinal chemistry. It is essential to have a fundamental understanding of poly-N, N'-disubstituted sulfamides to facilitate their wider commercial applications as replacements of polyureas. In this talk, we present a collaborative computational and experimental study of polysulfamide chains and their assembly driven by hydrogen bonding interactions between the sulfamide groups. We first share our newly developed coarse-grained (CG) model of polysulfamide that captures the directionality of inter-chain hydrogen bonds between sulfamide groups and allows us to study self-assembly of polysulfamide chains in molecular dynamics (MD) simulations. These simulations link the contour length, bulkiness, and flexibility of the N, N'-substituents on either side of the sulfamide groups to the morphology (e.g., positional and orientational order) of the polysulfamide assembly. We validate our CG model and simulation approaches by showing that the MD simulation results agree with the trend in assembly crystallinity for various aliphatic and aromatic N, N'-substituent chemistries measured by X-ray diffraction (XRD) and infrared (IR) in experiments. We then use the validated computational approach to explore new substituent chemistries and study the effects of substituent length and bulkiness on morphology of polysulfamide self-assembly, with the predictions tested against additional experimental syntheses and characterizations.

3:45 PM SB05.11.05

Calcium Ions Enable Intrinsically Disordered Phosphopeptides to Form Self-Oriented Filaments Jiaqi Guo¹, Fengbin Wang², Chen Liu³, Yimeng Huang¹, Weiyi Tan¹, Hongjian He¹, Meihui Yi¹, Xixiang Zhang³, Edward H. Egelman² and Bing Xu¹; ¹Brandeis University, United States; ²University of Virginia, United States; ³King Abdullah University of Science and Technology, Saudi Arabia

Biomimetic bone regeneration remains a major challenge because of limited understanding of protein-controlled biomineralization to form oriented architecture at molecular level. During the study of an intrinsically disordered peptide (IDP) containing phosphoserine and pyrene, we unexpectedly found that calcium ions transform the IDP from nanoparticles to self-oriented filaments via hierarchical self-assembly. HAADF confirms the interaction between strontium and phosphate in the filaments. Cryo-EM structure reveals that the hydrophobic pyrene forms the structured core and the IDP constitutes the flexible periphery of the helical nanofibers. These results indicate that calcium ions interact with flexible periphery of the nanoparticles to form fibrils and enhance interfibrillar interactions to form oriented filaments. To further understand the roles of the IDP for forming filaments, we synthesized analogs with controlled phosphorylation site, hydrophobic interactions, sequences, chirality, and mode of pairing to evaluate the significance in forming oriented filaments. The results confirm that noncovalent pairing, phosphoserine, and a proline residue prior to phosphoserine in the IDP are critical for the formation of the oriented filaments. Combining cryo-EM structural elucidation and molecular engineering, this work illustrates a useful model system based on strong hydrophobic interactions and IDPs for understanding and mimicking the initiation of phosphoprotein-controlled biomineralization.

4:00 PM SB05.11.06

Synthesis of Self-Supporting Porous Au Sponges Using Polymer Gel Templates Seohyeon Jang, Jihyeon Kang, Seyoung Choi, Ohhyun Kwon, Hojong Eom, Junhyeop Shin, Jongkwon Park and Inho Nam; Chung-Ang University, Korea (the Republic of)

Porous metal structures can be applicable in wide range of fields including electrochemical or acid-base catalyst, heat dissipation, and bio filtration. Porous template mediated metal structures have higher surface area ($1 \text{ m}^2\text{g}^{-1}$) than pure metal structures. Though the template method has been advanced rapidly using starch gel, dextran, pumice, and alumina, sacrificial template method has been seldom investigated. Here, sponge-like porous Au structures were synthesized using agarose gel, HAuCl₄, and NaBH₄ as sacrificial soft template, Au precursor, and reductant with simple heating method. First, agarose gel has a 3D cross-linked pore structure, which is easy to control the porosity, shape, and scale. This implies that the use of agarose as a soft sacrificial template enables synthesis of pure Au sponges with purposed porosity and shape. To synthesize the porous Au structure, agarose gel was formed by mixing agarose with water at elevated temperature around 95 °C. The Au precursor was penetrated into the agarose gel by a capillary force at room temperature for 18 h in a sealed container. The metal ions were easily soaked into the 3D pores of agarose gel, as it has hydrophilic characteristics, which supply high loading amount of metal. The metal ions in agarose gel was reduced by NaBH₄. The agarose is composed of many aldehyde groups, which promotes the reduction of metal ions and nucleation of metal clusters. Because of the reduction of Au ions in the pores of agarose, the agarose was getting darkened. The resulting Au-filled agarose gel was dried at room temperature and calcined for 5h at various temperatures to remove the agarose template and to form 3D Au structure. To understand the decomposition behavior during calcination step, thermal gravimetric analysis (TGA) was conducted. The weight loss observed from 200°C to 550°C by the decomposition of agarose template and the weight loss was around 80.5 wt %, which implies that the approximately 19.5 wt % of pure Au was formed in agarose gel. To investigate the structural change depending on the temperature, the Au-agarose bi-continuous structure was calcined at various temperatures of 200, 300, 500, 70, and 800 °C for 5 h. The porous Au showed continuous interconnected open-pore structure maintaining the intrinsic porous nature of the agarose matrix under 500 °C. In addition, the EDS showed that the synthesized Au had negligible impurities. However, the Au nanoparticles were aggregated showing dough-like structure without pore at the temperatures greater than 500 °C. The chemical states of the Au structure calcined at 200 °C are identical to that of pure Au crystal, demonstrating peak of Au (0) 4f_{7/2} and Au (0) 4f_{5/2} at 83.5 eV and 87.2 eV. The crystal structure of the Au sponge was also examined by XRD and Rietveld refinements. The measured lattice distance was 4.0705 Å, which is similar value to that of bulk Au (4.07 Å) calculated by DFT calculations. The chemical features at the interface between Au and carbon from agarose were investigated using TEM-EELS analysis. The EELS spectra of agarose template are identical to that of amorphous carbon with two peaks at 285 eV, and 290 eV, corresponding to the transition energy to the π^* and σ^* molecular orbitals of sp² bonds. Near the Au-carbon interface, slight peak shift of amorphous C signal was observed, indicating negligible interaction or bonding between Au and agarose template. In the Au region, the EELS spectra demonstrated strong localized electron energies. Based on the above results, the agarose template takes an excellent roll as a sacrificial template providing porous structure without interaction with Au nanoparticles and retaining the porous structures of Au sponges. In summary, the agarose is highly attractive material for the production of macroporous pure metal sponges with simple heating method. Furthermore, agarose gel is nature abundant, bio-degradable, and mechanically strong compared with other natural polymers.

4:15 PM SB05.11.07

Liquid Crystal Mesophase in Supercooled Liquid Gallium and Eutectic Gallium Indium Muhammad Yunusa¹, Alex Adaka², Amirreza Aghakhani¹, Hamed Shahsavani¹, Yubing Guo¹, Yunus Alapan¹, Antal Jákl² and Metin Sitti¹; ¹Max Planck Institute for Intelligent Systems, Germany; ²Kent State University, United States

The unusual structure and property of supercooled liquid metals have baffled scientists for decades. Unravelling the origin of the structural ordering in supercooled liquid gallium (Ga) has been a great scientific quest due to the recent emerging applications of liquid metals in soft electronics and sustainable energy. Hitherto, the liquid crystal (LC) properties of liquid gallium and eutectic gallium-indium have remained elusive. Here, reflective polarized optical microscopy on liquid Ga sandwiched between two glasses treated with rubbed polymers reveals the onset of an anisotropic reflection at 120 °C that increases on cooling and persists down to room temperature or below. The polymer rubbing usually aligns the director of thermotropic liquid crystals (LCs) parallel to the rubbing direction. On the other hand, when liquid Ga is sandwiched between substrates that align conventional LC molecules normal to the surface, the reflection is isotropic, but mechanical shear force induces anisotropic reflection that relaxes in seconds. The anisotropic response of the cell under the influence of mechanical force results in realignment of the aligned structure. Such alignment effects and shear-induced realignment are typical to conventional thermotropic LCs and indicate a LC structure behavior of liquid Ga.

Albeit, powder X-ray diffraction (PXRD) measurement conducted on the liquid gallium shows a downward shift of sharp peaks during heating above 70 °C in a glass capillary, the diffraction pattern cannot be indexed for any known gallium oxide or gallium hydroxide phase structure. Thus, the diffraction result could be attributed to a fluidic smectic behavior of the Ga clusters or plate-like structures in the supercooled liquid with layer arrangement. The characterization of the lamellar structure via atomic force microscopy was employed to measure the layer thickness of the nanometer-thick transparent films. We have exfoliated transparent lamellar films of tens of nanometer by the use of PDMS and clean glass surfaces at RT. The liquid-phase exfoliated transparent lamellar layers are obtained with thickness up to 120 nm, and parallel to the PDMS surface. Specifically, Ga textures obtained by atomic force and scanning electron microscopy reveal the existence of a lamellar structure corresponding to a smectic LC phase, where the nanometer-thin lamellar structure is transparent under transmission polarized optical microscopy. Counterintuitively, the molecular behavior of LC-Ga enabled electro-optics switching, where an anisotropically reflecting state was induced via the application of $1.8 \text{ V } \mu\text{m}^{-1}$ (DC) electric field at RT in between two ITO-coated glasses separated by 10 μm . Moreover, the homeotropic ITO cell was prepared by a polyimide (PI) polymer coating in which the electro-optical switching was realized by applying a square wave-alternating field (AC) of $1.9 \text{ V } \mu\text{m}^{-1}$ at 0.5 and 1 Hz across the cell.

Such spatial molecular arrangements may be attributed to dimer or plate-like molecular entities in the supercooled liquid Ga. The LC structure observation of electrically conductive liquid Ga can provide new opportunities in materials science, energy and LC applications.

4:30 PM *SB05.11.08**Microrollers Make Motifs—Emergent Structure in a Driven Colloidal Suspension** Michelle Driscoll; Northwestern University, United States

Does a rotating bead always spin in place? Not if that bead is small and near a surface: in this case, rotating leads to translational motion, as well as fast flows around the bead, even quite far away. These flows cause strong hydrodynamic coupling to nearby microrollers (rotating beads), which leads to a rich variety of collective effects. This system is experimentally realized by using magnetically actuated colloidal particles, and we find that these collective effects manifest as a wide array of emergent structure from shocks, to fingering patterns, to stable, hydrodynamically-bound clusters. We study these emergent structures using a variety of computational and experimental techniques, including Stokesian dynamics simulations and a coupled magnetic-optical imaging system. We find that in all cases, the scale of the emergent structures is set by a single geometric parameter: the height of the microroller above the surface. Recently, we have begun to study the interaction of microrollers with a structured environment, for example a forest of fixed obstacles or a sea of passive particles. In the case of fixed obstacles, we find a strong hydrodynamic trapping effect occurs in our experimental system, and we have used our simulation methods to characterize this trapping in detail. When the obstacles are free to move, we observe that the microrollers restructure the landscape around them, at length scales many times the size the roller.

SESSION SB05.12: Virtual Session
 Session Chairs: Julia Dshemuchadse and Junwei Wang
 Wednesday Morning, December 7, 2022
 SB05-virtual

8:00 AM *SB05.12.01**Studies of Surface Wetting Phenomena Using Colloidal Crystals and Glasses** Yilong Han; Hong Kong University of Science and Technology, Hong Kong

Colloids are outstanding model systems for the studies of phase transitions and related phenomena because Brownian motions of micrometer sized particles can be tracked by optical microscopy. Colloids with tunable attractions open the way to study solids' free surfaces. Here we experimentally observed three surface wetting phenomena at the single-particle level for the first time: premelting of crystal and glass, and pre-solid-solid transition. The latter two phenomena are proposed by us.

1. Crystal surface typically premelts into a thin liquid layer slightly before reaching the melting point. We find that the thickness of the premelted surface liquid diverges as a power law (i.e. complete premelting) for monolayer colloidal crystals, whereas saturates to a constant (i.e. blocked premelting) for bilayer and trilayer crystals [1]. Such behaviors are verified by simulation [2].
2. We propose that a crystal's surface can develop a thin layer of polymorphic crystal when the two crystals can form a coherent interface near their crystal-crystal transition point. We coin the word 'pre-solid-solid transition' because it is analogous to premelting or prefreezing with the same wetting mechanism: the total energy of the newly formed two interfaces is lower than the surface energy of the original solid. Although its mechanism is simple and should certainly hold, it is a blind spot in material science and can be viewed as the third type surface wetting precursor of phase transition. This phenomenon is confirmed by colloid experiments and simulations. The thickness of the surface crystal increases with the temperature as a power law, similar to premelting. It can also occur in nonequilibrium processes such as melting, crystallization and polycrystal annealing. We suggest several atomic and molecular crystals which may exhibit such phenomenon. Moreover, pre-solid-solid transition and premelting can coexist under thermal equilibrium when two triple points are close [3].
3. Glass melting has been poorly explored experimentally at the single-particle level. We assemble monolayer and multilayer colloidal glasses by vapor deposition such that they are sufficiently stable to melt from the surface. Structural and dynamic parameters reach their bulk values at different depths, which define a surface liquid layer and an intermediate glassy layer. The thicknesses of both layers increase in power laws upon approaching the glass transition point by slow heating, similar to crystal premelting. This circumvents the ambiguity in distinguishing supercooled liquid and glass. Such power-law behavior has been reported in polymer glass melting, but was not called as premelting. Moreover, melting is studied by rapidly changing temperature across the glass melting temperature, and the melting front behaviors are similar to crystal melting [4].

[1] B. Li, et al. Modes of surface premelting in attractive colloidal crystals, *Nature*, 531, 485 (2016).

[2] X. Wang, et al. Surface roughening, premelting and melting of monolayer and bilayer crystals, *Soft Matter*, 17, 688 (2021)

[3] X. Wang, et al. Polymorphic crystalline wetting layers on crystal surfaces, submitted, <https://doi.org/10.21203/rs.3.rs-910546/v1>

[4] Q. Zhang, et al. Surface premelting and melting of colloidal glasses, submitted, <https://doi.org/10.21203/rs.3.rs-1633832/v1>

8:30 AM SB05.12.02**Confinement-Induced Mechanical Phase Separation in Shear Thickening Suspensions** Qin Xu and Haitao Hu; Hong Kong University of Science and Technology, Hong Kong

We experimentally investigated the rheology of confined granular suspensions during shear-thickening transitions. When the shear dimensions are reduced to tens of particle diameters, the dense suspensions show unexpected flow behaviors across multiple length scales in response to the physical confinements. On macroscopic scales, the stress-controlled shear rheology was highly dependent on the measuring time for each applied shear stress, and S-shaped flow curves were observed at steady states. At microscopic levels, by using boundary stress microscopy (BSM), we observed sustained local stress oscillations with a time interval of approximately twice the global rotation period of the shear plate. The temporal fluctuations were also associated with a dynamically evolved phase separation, which indicated the migrations of high-stress regions involving locally jammed suspensions. We further show that the non-monotonic flow curves and local stress oscillations will simultaneously reduce as the system size increases. The study shows how boundary confinements can induce sustained mechanical phase separation in dense suspensions, and therefore controls their global rheological properties.

8:45 AM SB05.12.04**Function Follows Form—Semiconductor-Free Electronics from Morphology Controlled Metal Assemblies** Khalil ur Rehman^{1,2,1}, Yu-Ting Chiu³, Lu-Hsi Wang³, Radha Raman^{4,1,1}, Yuch-Yuan Li², Fang-Fei Chou³, Ya-Ping Hsieh^{1,1} and Mario Hofmann²; ¹Academia Sinica, Taiwan; ²National Taiwan University, Taiwan; ³Taipei First Girls' High School, Taiwan; ⁴National Central University, Taiwan

Current electronics are inextricably linked to the carrier transport properties of semiconducting materials. Novel requirements from wearable and ubiquitous computing applications, however, have highlighted the limitations of such materials in terms of scalable production, robustness, and achievable performance. We here demonstrate that complex electronic functionality can be achieved without the use of semiconductors. By controlling the connectivity ϕ between metallic particles, emergent structures can be realized that exhibit directed carrier transport – a hallmark of semiconductor devices. Experimental realization of this prediction was achieved in concentration gradients of percolative metal assemblies, where spatial changes in the number of neighbors produces distinct differences in conduction properties for carriers traveling with or against the direction of increasing concentration. This directed percolation process was observed in both aqueous particle dispersions and solid-state particle/polymer composites and yielded electronic devices with performances comparable to conventional semiconductor diodes. Connectivity-controlled assemblies provide attractive alternatives to semiconductors due to their robustness, high carrier mobility and tunability of fundamental device properties. The underlying ratchet-like rectification process unexpectedly imparts metallic assemblies with sensitive light detection abilities and opto-mechanical multifunctionality. Our advances not only open up a route towards the ultra-large-scale production of future electronics but shed light at a century-old question about the foundation of electronic functionality.

9:00 AM DISCUSSION TIME

SESSION SB05.13: Virtual Session II
Session Chairs: Chrisy Xiyu Du and Junwei Wang
Wednesday Morning, December 7, 2022
SB05-virtual

10:30 AM *SB05.13.01

Colour with a Twist [Silvia Vignolini](#); University of Cambridge, United Kingdom

The most brilliant colours in nature are obtained by structuring transparent materials on the scale of the wavelength of visible light. By designing the dimensions of such nanostructures, it is possible to achieve extremely intense colourations over the entire visible spectrum without using pigments or colorants. Colour obtained through structure, namely structural colour, is widespread in the animal and plant kingdom. Such natural photonic nanostructures are generally synthesised in ambient conditions using a limited range of biopolymers. Given these limitations, an amazing range of optical structures exists: from very ordered photonic structures, to partially disordered, to completely random ones. In this seminar, I will introduce some striking examples of natural photonic structures and share some insight on their development. Then I will review our recent advances to fabricate bio-mimetic photonic structures using the same material as nature. Developing biomimetic structures with cellulose enables us to fabricate novel photonic materials using low-cost polymers in ambient conditions. Importantly, it also allows us to understand the biological processes at work during the growth of these structures in plants.

11:00 AM DISCUSSION TIME

SESSION SB05.14: On-Demand Presentation
Thursday Morning, December 8, 2022
SB05-virtual

7:00 AM SB05.14.01

Ultrafast Crystallization of Ordered Mesoporous Metal Oxides and Carbon Structures in Seconds [Leyan Wang](#) and Kwan Wee Tan; Nanyang Technological University, Singapore

Ordered crystalline mesoporous metal oxides and carbon materials face risks of mesostructural collapse as a result of untamed atomic migration during crystallization at high temperatures and long hours. We introduce a facile approach combining block-copolymer-directed self-assembly with electric Joule heating (SNAP method) to realize ultrafast crystallization of various ordered nanocomposite systems, including Al_2O_3 -carbon, $\text{Al}_2\text{O}_3/\text{MgO}$ -carbon, TiO_2 -carbon, Fe_2O_3 -carbon and carbon structures. Removing the carbon matrix yields fully inorganic ordered Al_2O_3 and TiO_2 structures. SNAP-derived ordered oxide and oxide-carbon structures samples exhibit high CO_2 capture and efficient Li-ion battery performances than their furnace-treated counterparts. The SNAP method enables high energy efficiency and time savings and generalizability to other functional materials combinations that would appeal to a wide range of applications such as catalysis, sensing and clean energy generation.

SYMPOSIUM SB06

Structure-Function Relationships and Optoelectronic Processes in Organic and Organic/Inorganic Hybrid Materials for Flexible Electronics and Photovoltaics
November 28 - December 7, 2022

Symposium Organizers
Renaud Demadrille, CEA

Nicolas Leclerc, ICPEES-CNRS
Natalie Stingelin, Georgia Institute of Technology
Yana Vaynzof, Technical University Dresden

Symposium Support

Silver

Advanced Devices & Instrumentation, a Science Partner Journal

Bronze

1-Material, Inc.

Journal of Materials Chemistry C
Master of Chemical Sciences, Penn LPS

* Invited Paper
+ Distinguished Invited

SESSION SB06.01: Organic Semiconductors for Photovoltaics
Session Chairs: Renaud Demadrille and Nicolas Leclerc
Monday Morning, November 28, 2022
Hynes, Level 3, Room 312

10:30 AM *SB06.01.01

New Series of Electron Donor Conjugated Polymers Towards Improving the Performance and Stability of Organic Solar Cells [Christos Chochos](#)^{1,2};
¹Advent Technologies Inc, Greece; ²Institute of Chemical Biology/National Hellenic Research Foundation, Greece

It will be demonstrated the development of a series of conjugated polymers based on the donor-acceptor (D-A) approach consisting of benzodithiophene and quinoxaline derivatives as the electron rich and deficient building block that when employed as electron donor components at organic solar cells exhibit high performance and stability, simultaneously. Moreover, it will be shown how the highest occupied molecular orbital (HOMO) can be precisely control by only an atom change at the side substituents. This allowed for a detailed analysis when matching the energy levels of polymer donors and small molecule acceptors. Therefore, we were able to investigate organic solar cells with highest occupied molecular orbital energy level offsets (ΔE_{HOMO}) between 0 - 300 meV. It will be shown that exciton quenching at negligible ΔE_{HOMO} takes place on timescales approaching the intrinsic exciton lifetimes, drastically limiting external quantum efficiency. This finding it is quantitatively described via the Boltzmann steady-state equilibrium between charge transfer states and excitons and further reveal a long exciton lifetime as a decisive design criterion for maintaining efficient charge generation at negligible ΔE_{HOMO} . Moreover, the Boltzmann equilibrium quantitatively describes the major reduction in non-radiative voltage losses at very small ΔE_{HOMO} .

11:00 AM SB06.01.02

Development of Deuterated Non-Fullerene Acceptors for Use in Selective Tracking of Morphological Changes in Organic Photovoltaic Active Layer Blends [Matthew W. Bidwell](#)¹, [Zhengxing Peng](#)², [Andrej Classen](#)³, [Thomas Heumueller](#)³, [Christoph J. Brabec](#)³, [Harald Ade](#)² and [Iain McCulloch](#)^{4,1,5};
¹Imperial College London, United Kingdom; ²North Carolina State University, United States; ³Friedrich-Alexander-Universität Erlangen-Nürnberg, Germany; ⁴University of Oxford, United Kingdom; ⁵King Abdullah University of Science and Technology, Saudi Arabia

Organic semiconducting polymers and small molecules have shown a remarkable ability to act as photoactive components in organic photovoltaic (OPV) devices over the past decade, with widespread efficiencies of 18-19% for binary OPV systems which have rapidly approached the fabled 20% efficiency threshold needed for OPV technology commercialisation. Overall, there has been a paradigm shift in OPV device performance from 8% in 2012 to over 20% PCE in 2022.¹ This step-change has been propelled by the development of novel electron-accepting (n-type) materials, moving away from fullerene-based acceptors (PC₆₀BM/PC₇₀BM) to emerging third-generation OPV materials, known as non-fullerene acceptors (NFAs). These NFAs are typically composed of rigid electron-rich fused aromatic ladder-type cores with electron-deficient end groups such as ITIC and IDTBR, most notably with the recent emergence of a new family of high-performance Y6 NFA materials. However, the monumental increase in device efficiency has not been in lock-step with donor polymer:NFA solar cell device stability, which often show poor tolerance to oxygen, UV-light, thermal stimuli, and water which lead to photo-oxidative and chemical degradation, alongside thermodynamic instabilities in the photoactive blend, which remains a critical bottleneck towards real-world commercialisation of OPV technologies.²

This work presents a series of NFAs with deuterated side chains (d-NFAs), based on O-IDTBR and EH-IDTBR hydrogenated acceptors (h-NFAs), which share the same physical and optoelectronic properties as their hydrogenated counterparts and allow them to act as ideal proxies for accurately representing the h-NFAs within the chosen polymer:NFA blend morphologies. Understanding the morphological and chemical stability of donor polymer:NFA OPV blend systems is critical to optimising the delicate balance between the donor and acceptor blend mixing in devices, which is crucial for both long-term operational stability and high performance. With this in mind, the d-NFAs were selectively blended with the donor polymers Poly(3-hexylthiophene) (P3HT) and PffBT4T-2OD (PCE11) in OPV devices which were then sealed in degradation chambers under N₂ and placed under environmental stress, either via light soaking under AM 1.5 G or heating at 80 °C in the dark for 100-1300 hrs with continuous tracking of the device's J-V performance. This was done in order to decouple chemical and morphological changes in the active layer blend due to photo-degradation and thermal morphological demixing processes, which were then selectively investigated by ToF-SIMS (Time-of-Flight Secondary Ion Mass Spectrometry) and photoluminescence measurements.

Both sets of P3HT:d-IDTBR and PCE11:d-IDTBR active layer systems demonstrated excellent long-term thermal stability in the dark, with no significant losses in PCE, which was further corroborated through vertical and lateral ToF-SIMS measurements which showed no discernable phase separation of the d-NFAs from the donor polymers. Similarly for the light-aged devices, there were no notable losses in PCE which was further confirmed by ToF-SIMS measurements. The results suggest that overall P3HT:d-IDTBR and PCE11:d-IDTBR active layer blend systems are chemically and morphologically stable and that using deuterated NFAs is an effective methodology for probing blend morphologies of systems with polymers and NFAs that possess very similar chemical structures and heteroatoms. Future work would involve utilising d-NFAs as third components in ternary OPV blends with d-Y6 and similarly

tracking the morphological evolution of this component in active layer blends as a function of thermal and light aging conditions.

1. Zheng, Z. et al. Tandem Organic Solar Cell with 20.2% Efficiency. *Joule* 6, 171–184 (2022).
2. Speller, E. M. et al. From fullerene acceptors to non-fullerene acceptors: prospects and challenges in the stability of organic solar cells. *J. Mater. Chem. A* 7, 23361–23377 (2019).

11:15 AM SB06.01.03

Homoconjugated Non-Fullerene Acceptor Compounds with Very High Molar Extinction Coefficients Stefan Warrington and Iain A. Wright; Loughborough University, United Kingdom

Development of novel molecular and macromolecular materials for optoelectronic devices is an exciting field constantly evolving and motivated by an increasing understanding of the physical processes involved in how light and matter interact. The optoelectronic properties of organic semiconductor materials underpin their utility. This can be tuned and optimized using structural motifs and molecular design.

The development of new materials for organic solar cells (OSCs) has continued to expand rapidly in recent years driven by the emergence of non-fullerene acceptors as highly efficient components of these devices. Multi fused aromatic systems lead the way in high power conversion efficiency devices, most notably the non-fullerene acceptor Y6.^[1] These materials design motifs such as fused electron deficient cores with strongly electron accepting arms facilitate high extinction coefficients and efficient charge transport lending valuable design rules for developing new high-performance materials.

Homoconjugation across electron poor iptycene cores has been shown to induce an intramolecular charge transfer (ICT) state through a delocalized LUMO increasing the probability of transitions to and from this ICT state.^[2] This has been demonstrated to lead to super-additive enhancements in molar extinction coefficients and oscillator strength compared to non-homoconjugated chromophores and revealed a new approach to circumventing the energy gap law in low band gap delayed fluorescent emitters.^[3]

Here we present a new generation of homoconjugated ICT molecules designed for use as non-fullerene acceptors in OSC devices.

[1] Single-Junction Organic Solar Cell with over 15% Efficiency Using Fused-Ring Acceptor with Electron-Deficient Core, J. Yuan et al., *Joule* (2019); doi: 10.1016/j.joule.2019.01.004.

[2] Homoconjugation enhances the photophysical and electrochemical properties of a new 3D intramolecular charge transfer iptycene displaying deep blue emission, S. Montanaro et al., *J. Mater. Chem. C* (2019); doi: 10.1039/C9TC03255J

[3] Simultaneous enhancement of thermally activated delayed fluorescence and photoluminescence quantum yield via homoconjugation, S. Montanaro et al., *J. Mater. Chem. C* (2022); Submitted. Preprint at: <https://doi.org/10.33774/chemrxiv-2021-p3h9s-v2>

11:30 AM SB06.01.04

10.6% Organic Solar Cells Fabricated from Nanoparticle Dispersions Enabled by Electrical Doping Felix Manger, Philipp Marlow, Karen Fischer, Jonas Armleder, Christian Sprau and Alexander Colsmann; Karlsruhe Institute of Technology, Germany

Solution processing from nanoparticle dispersions allows the use of eco-friendly processing agents for the deposition of organic semiconductor thin-films for photovoltaic and other optoelectronic applications. Omitting surfactants to stabilize the dispersions is essential to not jeopardize the solar cell performance. So far, solar cells could only be fabricated from surfactant-free P3HT dispersions which show some intrinsic self-stabilization. In this work, the self-stabilization of P3HT nanoparticle dispersions is demystified, and electrostatic effects are identified as the origin of self-stabilization. By application of this gained knowledge, novel surfactant-free nanoparticle dispersions from other, high-performance organic semiconductors are synthesized by nanoprecipitation. Electrical doping warrants the electrostatic stabilization of the dispersions. For the first time, the corresponding solar cells achieved power conversion efficiencies of up to 10.6%, demonstrating the general feasibility of this alternate, all-eco-friendly processing route.

SESSION SB06.02: Device Physics and Engineering
Session Chairs: Thuc-Quyen Nguyen and Safa Shoaee
Monday Afternoon, November 28, 2022
Hynes, Level 3, Room 312

1:30 PM *SB06.02.01

Understanding Materials from the Device's Point of View and Vice Versa Sapir Bittons, Dan Liraz, Gil Sheleg and Nir Tessler; Technion-Israel Institute of Technology, Israel

Often one studies the chemical physics of materials with the goal to improve or understand their performance in a device, be it a solar cell or a field effect transistor. However, when we operate and measure the device performance, the device implements a very specific filter on the chemical or physical processes. The device structure and its operation conditions would decide on the relative importance of processes, and not less importantly on how the microscopic properties are being averaged to produce the device's output. I will demonstrate the above philosophy through examples like:

- 1) The standard FET operates with the current being a drift current. I will present a device structure where the current is determined by diffusion. Interestingly, the source operates as a pressure hose.
- 2) The exciton binding energy that organic bulk-heterojunction device "sees" is very different to what one would measure through careful (possibly irrelevant) measurements.
- 3) Mobility imbalance in solar cells was an important topic 20 years ago. It is time to move on.
- 4) Perovskite devices have rich electrochemistry. Trying to incorporate it into a device model tends to raise more questions than answers. Should we worry about it?

2:00 PM SB06.02.02

Device Physics of Dilute-Donor Narrow Band Gap Organic Solar Cells with Highly Transparent Active Layers Nora Schopp¹, Gulnur Akhtanova², Thuc-Quyen Nguyen¹ and Viktor Brus²; ¹University of California Santa Barbara, United States; ²Nazarbayev University, Kazakhstan

Organic Photovoltaics (OPVs) offer sustainable, solution-processable, and cost-effective energy harvesting solutions. While opaque devices underwent enormous progress in the past decade, it remains a challenge to meet the high transparency requirements for integrated semitransparent OPVs for windows, skylights, or greenhouses, and only a few examples with average visible transmittance (AVT) over 60% exist. Moreover, a systematic understanding of the photoelectronic processes in visibly transparent devices is still absent. In this work, we investigate the generation-recombination dynamics in three semitransparent blend systems with varied donor concentrations to understand their performance limitations. [1]

Specifically, we study charge generation, multi-mechanism recombination, and extraction in three OPV systems that are based on an ultra-narrow non-fullerene acceptor COTIC-4F and a polymer donor that absorbs in the visible range PCE10. The systematic reduction of the donor content from 40% to 30% and 20% leads to highly transparent active layers with blend AVTs of 64%, 70%, and 77%, respectively. Opaque devices in the optimized highly-reproducible device configuration comprising these transparent active layers lead to PCEs of 7.0%, 6.5%, and 4.1%. The investigation of these structures yields quantitative insights into changes in the charge generation profile, non-geminate recombination losses via the bimolecular, bulk and interface trap-assisted mechanisms, and extraction dynamics upon dilution of the donor. Lastly, we give an outlook for employing the highly transparent active layers in semitransparent OPV devices.

[1] N. Schopp, G. Akhtanova, P. Panoy, A. Arbut, S. Chae, A. Yi, J. Kim, V. Promarak, T.-Q. Nguyen and V.V. Brus, Unraveling Device Physics of Dilute-Donor Narrow Band Gap Organic Solar Cells with Highly Transparent Active Layers, *Advanced Materials* (2022) in press. DOI: 10.1002/adma.202203796

2:15 PM SB06.02.03

Hole Transport-Limited Electrochemical Doping in Conjugated Polymers Scott T. Keene¹, Joonatan Laulainen¹, Raj Pandya^{1,2}, Maximilian Moser³, Christoph Schnedermann¹, Paul Midgley¹, Iain McCulloch³, Akshay Rao¹ and George G. Malliaras¹; ¹University of Cambridge, United Kingdom; ²École Normale Supérieure, France; ³University of Oxford, United Kingdom

Organic mixed ionic electronic conductors (OMIECs) have recently risen as a promising material choice for bioelectronic devices due to their low impedance, soft mechanical properties, and ability to transduce ionic signals to electronic currents. These materials properties have enabled the development of high-performance devices for electrophysiological recordings, chemical sensing, cell monitoring, energy storage, and neuromorphic devices. The unique behaviour of OMIECs arises from ion intercalation through the bulk of the material which can modify the oxidation state, and therefore charge carrier concentration, of the conjugated polymer backbone. However, the current understanding of the dynamics of mixed charge transport remains limited.

The lack of mechanistic understanding of mixed transport hinders rational design of OMIECs, where assumptions must be made to assess their performance. For instance, in most semiconducting electrodes, mixed transport is assumed to be limited by ion motion due to their large effective mass compared to electrons/holes. Here, we show that this basic assumption does not hold for conjugated polymer electrodes. Using *operando* optical microscopy to differentiate between ionic and electronic transport, we reveal that, at low hole densities, electrochemical doping is limited by filling of low energy, low mobility hole sites. We show that the transition from hole- to ion-limited doping is determined by the degree of heterogeneous disorder in the polymer microstructure. Further doping leads to four orders of magnitude increase in hole mobility, resulting in an inversion from hole to ion-limited doping. This transition between hole and ion transport-limited doping results in much slower switching than expected for electrochemical devices employing otherwise high-performing materials. The results help inform the ideal microstructural features to optimize performance of electrochemical devices across their full range of operation.

2:30 PM SB06.02.04

Dual-Mode Organic Electrochemical Transistors Based on Self-Doped Conjugated Polyelectrolytes for Reconfigurable Electronics Tung Nguyen-Dang¹, Sangmin Chae¹, Jirat Chatsirisupachai^{2,1}, Vinich Promarak², Hiba Wakidi¹, Yon Visell¹ and Thuc-Quyen Nguyen¹; ¹University of California, Santa Barbara, United States; ²Vidyasirimedhi Institute of Science and Technology, Thailand

Dual mode transistors, the type of transistors that work in both depletion mode and enhancement mode, were reported more than 50 years ago using inorganic semiconductors (with silicon in 1963 and with III-V semiconductors in 1966). Thus far however, this type of devices has not been shown in organic electronics. In this talk, we report the dual mode organic transistors based on organic electrochemical transistors (OECTs) using self-doped conjugated polyelectrolytes as the active material. Via spectroelectrochemistry, we revealed a unique dual ionic transport property of these materials: they can be both doped and dedoped upon the interaction with anions and cations in an electrolyte. This property enables dual-mode functionality in OECTs, whose mode switching is accomplished by simply altering the polarity of the applied gate and drain voltages. Furthermore, we developed a device physics model which accurately describes the behavior of these transistors. We also demonstrated the utilization of dual-mode organic transistors in reconfigurable electronics by fabricating logic gates that could be switched between AND and NOR, and OR and NAND on the fly. Being simple, power efficient, and compatible with high throughput microfabrication techniques, dual mode OECTs are a promising candidate for the next generation of efficient computing systems and adaptive electronics.

Reference:

- (1) Nguyen-Dang, T.; Chae, S.; Visell, Y.; Nguyen, T.-Q.; et al. Dual-Mode Organic Electrochemical Transistors Based on Self-Doped Conjugated Polyelectrolytes for Reconfigurable Electronics. *Adv. Mater.* **2022**, *23* (34), 2200274.
- (2) Nguyen-Dang, T.; Chae, S.; Visell, Y.; Nguyen, T.-Q. et al. Efficient Fabrication of Organic Electrochemical Transistors via Wet Chemical Processing. *ACS Appl. Mater. Interfaces* **2022**, *14* (10), 12469–12478.
- (3) Lill, A. T.; Cao, D. X.; Nguyen-Dang, T.; Nguyen, T.-Q., et al. Organic Electrochemical Transistors Based on the Conjugated Polyelectrolyte PCPDTBT-SO3K (CPE-K). *Adv. Mater.* **2020**, *32* (33), 1908120.

2:45 PM BREAK

SESSION SB06.03: Structure, Charge Transport and Optoelectronic Processes in Organic Materials
Session Chairs: Viktor Brus and Nir Tessler
Monday Afternoon, November 28, 2022
Hynes, Level 3, Room 312

3:15 PM *SB06.03.01

Static Disorder, Dynamic Disorder, Wavefunction Delocalisation—Using Optical Spectroscopy to Assess Their Influence on Charge Transfer

States in Organic Solar Cell Materials Julian Kahle¹, Alexander Rudnick¹, Rishabh Saxena¹, R. Ammenhäuser², U. Scherf², Sergey Bagnich¹, Heinz Bässler³, S. Athanopoulos⁴ and Anna Köhler^{1,3,3}; ¹University of Bayreuth, Germany; ²Universität Wuppertal, Germany; ³Universität Bayreuth, Germany; ⁴Universidad Carlos III de Madrid, Spain

Charge transfers (CT) states play a key role in organic solar cells (OSC). In this presentation, I shall demonstrate how we can use time-dependent photoluminescence measurements to identify the contributions of static and dynamic disorder in charge transfer states and their spectra. Notably, from the temperature and time dependent linewidths of absorption, fluorescence, and CT emission, we infer the static and dynamic contributions to the total disorder. We discuss the role of spectral diffusion in this process. The impact of intermolecular interactions and excited state delocalisation will also be addressed.

3:45 PM SB06.03.02

Static and Dynamic Disorder in Thermal Vacuum Evaporated Organic Solar Cells Anna Jungbluth¹, Pascal Kaienburg¹, Andreas E. Lauritzen¹, Ming Zhu¹, Irfan Habib¹, Francis Otieno² and Moritz Riede¹; ¹University of Oxford, United Kingdom; ²University of the Witwatersrand, Johannesburg, South Africa

Organic solar cells (OSCs) have attracted interest over the last decades for their ease of processing and potential to generate inexpensive electricity for a growing population [1]. However, the commercial success of OSCs has long been hindered by their low power conversion efficiencies (PCEs). The main reasons for low PCEs are radiative and non-radiative energy losses of 100s meV that usually occur via charge transfer (CT) states at the interface between donor (D) and acceptor (A) molecules.

The origin of the CT state linewidth, and its influence on device performance, is still heavily debated [4]. Usually, broad spectral tails and large Stokes shifts between absorption and emission spectra are indicative of energetic disorder that negatively impacts charge transport, recombination, and the open-circuit voltage [4]. This energetic disorder can be classified into dynamic (temperature-dependent) and static (temperature-independent) contributions. While some work found negligible static disorder in OSCs [4], [6], other work observed the opposite and reported static disorder contributions of 50-150 meV [7], [8], [9].

In this work, we revisit the debate on dominant contributions to energetic disorder for small molecule OSCs. Using vacuum deposition techniques, we fabricate solar cells based on blends of C60 and donors like TAPC, α -Sexithiophene, DCV5T, CuPc, and Rubrene that show representative and comprehensive electronic and microstructural properties. By fabricating devices with 5 mol.% and 50 mol.% donor content, we study the impact of energetic disorder in dilute donor and intermixed D:A blends. We quantify energetic disorder by fitting temperature-dependent external quantum efficiency (EQE) spectra via semi-classical Marcus Levich Jortner theory.

We find that static disorder presents a dominant contribution to the CT state linewidth across our materials systems. In addition, by coupling our device data to grazing incidence wide-angle X-ray scattering (GIWAXS) measurements, we find larger energetic disorder for aggregating than for amorphous donors. Finally, we highlight the need for reducing energetic disorder to achieve lower voltage losses in both fullerene- and well-performing non-fullerene-based blends.

1. Riede M, et al. Organic solar cells—the path to commercial success. *Adv Energy Mater.* 2021;11: 2002653.
2. Jungbluth A, et al. Charge transfer state characterization and voltage losses of organic solar cells. *J Phys Mater.* 2021 [cited 23 Jan 2022]. doi:10.1088/2515-7639/ac44d9
3. Azzouzi M, et al. Factors Controlling Open-Circuit Voltage Losses in Organic Solar Cells. *Trends in Chemistry.* 2019;1: 49–62.
4. Tvingstedt K, et al. Temperature dependence of the spectral line-width of charge-transfer state emission in organic solar cells; static vs. dynamic disorder. *Mater Horiz.* 2020;7: 1888–1900.
5. Vandewal K, et al. Relating the open-circuit voltage to interface molecular properties of donor:acceptor bulk heterojunction solar cells. *Phys Rev B Condens Matter.* 2010;81: 125204.
6. Göhler C, et al. Temperature-Dependent Charge-Transfer-State Absorption and Emission Reveal the Dominant Role of Dynamic Disorder in Organic Solar Cells. *Phys Rev Applied.* 2021;15: 064009.
7. Burke TM, et al. Beyond Langevin recombination: How equilibrium between free carriers and charge transfer states determines the open-circuit voltage of organic solar cells. *Adv Energy Mater.* 2015;5: 1500123.
8. Kahle F-J, et al. How to interpret absorption and fluorescence spectra of charge transfer states in an organic solar cell. *Mater Horiz.* 2018;5: 837–848.
9. Linderl T, et al. Crystalline versus Amorphous Donor-Acceptor Blends: Influence of Layer Morphology on the Charge-Transfer Density of States. *Phys Rev Applied.* 2020;13: 024061.

4:00 PM SB06.03.03

Engineering an Injecting Layer for Light-Emitting Field Effect Transistors Lauren Miller and Mujeeb Chaudhry; Durham University, United Kingdom

Light-emitting field effect transistors (LEFETs) integrate transistor logic with the light emission of an organic light-emitting diode (OLED). Their dual functionality has the potential to simplify circuitry in several high-end applications, such as next generation displays. LEFETs incorporate a wide range of materials as the charge transporting and light-emitting layers within its complex device architecture. These include small molecules, polymers, single crystals, oxides and perovskites. However, LEFETs reported to-date suffer from poor external quantum efficiencies (EQEs), as balanced charge transport and injection into the light-emitting layer are difficult to realise.

Herein, we report an effective method for improving charge injection into hybrid LEFETs, comprising a n-type metal oxide layer for electron transport and a conjugated polymer for light emission. LEFETs exhibit charge carrier mobilities in the range of $10 \text{ cm}^2\text{V}^{-1}\text{s}^{-1}$, on/off ratios above 10^3 and low threshold voltages. Furthermore, a maximum EQE of 2 % was achieved at a brightness of 2500 cdm^{-2} . These devices show a significant improvement in key performance parameters and are a significant step towards the development of highly efficient LEFET technology.

4:15 PM *SB06.03.04

Functional Patterning of Graphene via an All-Supramolecular Strategy Quentin Ferez¹, Shiva Moradmand², Céline Fiorini-Debuisschert³, Fabrice Charra³, Imad Arfaoui² and Lydia Sosa Vargas¹; ¹Sorbonne Université -CNRS, France; ²Sorbonne Université-CNRS, France; ³Université Paris-Saclay, CEA-CNRS, France

Surface-confined, supramolecular self-assembly has been the focus of extensive research in the past decade[1]. A number of strategies have been developed and reported for surface patterning leading to novel applications in molecular electronics, photonics and nano-mechanical devices.[2] Despite

this, we are still at the early stages of exploiting them in viable, practical technologies since we are limited by their inability to form reproducible, ordered, integrated systems [3]. More specifically, in the case of graphene, we also have to overcome the strong charge transfer that occurs when electronically-active molecules are adsorbed on its surface.

To address this problem, we have developed a series of molecular dyads that can form ordered assemblies on graphene-like substrates and also bear an emissive component located out-of-the plane of the substrate. These dyads are held together via non-covalent interactions, which enable us to easily mix & match the components, resulting in a highly tunable system.

This relatively simple design allows us to control the orientation and distance of an emissive component above a graphene-like substrate through different supramolecular interactions and opens up an accessible route to electronically de-couple an optically-active molecule from graphene.[4]

[1] L. Sosa-Vargas, E. Kim, A.-J. Attias, *Mater. Horiz.* **2017**, *4*, 570-583.

[2] A. Ciesielski, C.-A. Palma, M. Bonini, P. Samori, *Adv. Mater.*, **2010**, *22*, 3506-3520; J. V. Barth, G. Constantini, K. Kern, *Nature*, **2005**, *437*, 671-679. S. Le Liepvre, P. Du, D. Kreher, F. Mathevet, A.-J. Attias, C. Fiorini-Debuisschert, L. Douillard, and F. Charra, *ACS Photonics*, **2016**, *3* (12), pp 2291–2296.

[3] K. Ariga, Q. Ji, J. P. Hill, Y. Bando, M. Aono, *NPG Asia Mater.*, **2012**, *4*, e17.

[4] Q. Fernez, S. Moradmand, M. Mattera, W. Djampa-Tapi, C. Fiorini-Debuisschert F. Charra, D. Kreher, F. Mathevet, I. Arfaoui, L. Sosa Vargas, (submitted).

4:45 PM SB06.03.05

Nanoscale Electrical Characterization of Organic and Hybrid Materials for Energy Applications Philippe E. Leclere, Van Dang Tran and Sy H. Pham; University of Mons, Belgium

The recent development of alternative sources of energy to fossil ones will play a crucial role in global electricity generation and should be one of the global strategies to reduce CO₂ emissions and stop climate change. To develop efficient and competitive modern electronics from semiconducting (organic, inorganic, or hybrid) materials for energy conversion and storage (flexible) devices, it is essential to understand the relationships between molecular architecture, supramolecular organization, microscopic morphologies, and optoelectronic properties in detail.

By using AFM-derived techniques (such as Conducting AFM, Kelvin Probe Force Microscopy – KPFM, and Scanning Microwave Impedance Microscopy - sMIM), electrical properties can be measured at the local scale (together with the morphological and mechanical characterization of the samples) helping the optimization of the device performances. For instance, for photovoltaic organic devices, we can spatially resolve by KPFM the surface photo-voltage in high-efficiency nanoscale phase segregated photovoltaic blends of conjugated polymers. We show on poly(thiophene)-based organic and hybrid systems how the lateral resolution in KPFM and in the photo(conducting) AFM can allow direct visualization of the carrier generation at the donor-acceptor interfaces and their transport through the percolation pathways in the nanometer range.

In fine, to fabricate flexible devices, we considered the high performances of flexible Transparent Conductive Electrodes (TCEs) based on silver nanowires (AgNWs) percolation networks. With optimized experimental conditions for the deposition, the AgNWs-based electrodes show low sheet resistance of 10 Ohm/sq combined to a high optical transmittance of 92.6% at $\lambda = 550$ nm. This leads to a valuable figure of merit as compared to other TCE's and the electrodes were successfully used for flexible organic and perovskite-based solar cells and light-emitting diodes.

5:00 PM *SB06.03.06

Probing Light-Matter Interactions in Hybrid Perovskites Marina S. Leite; University of California, Davis, United States

Metal halide hybrid organic-inorganic perovskites display near-optimal optical properties for optoelectronic devices, including photovoltaics and light-emitting diodes. Yet, this class of material has not been commercialized due to often-seen degradation. Overall, establishing the correlation between structure and optoelectronic performance is essential and requires the implementation of in situ characterization techniques that can assess material-light interactions. At the nanoscale, we realize atomic force microscopy (AFM) methods that enable us to resolve how grains and their boundaries are affected by photo-induced processes, such as ion migration. Through Kelvin-probe force microscopy we quantify spatial variations in photo-voltage. In the realm of material stability, we use high-throughput and automated optical measurements, such as steady-state photoluminescence (PL) and PL lifetime to monitor the effects of environmental stressors in hybrid perovskites. Here, we submit the material to distinct values of temperature and relative humidity and monitor, *in situ*, their optical response. We implement machine learning neural networks to forecast material behavior. The vast hyper-parameter space of hybrid perovskites' chemical composition is benefiting tremendously from artificial intelligence methods. To illustrate how one can gain understanding about the physical behavior of perovskites, we will showcase baseline models that apply machine learning, encompassing how to predict device power output as a function of temperature and how to find hidden correlations between property (electrical conductance) and dark-field optical images of material morphology.

SESSION SB06.04: Poster Session I
Session Chairs: Philippe Leclere and Caterina Soldano
Monday Afternoon, November 28, 2022
8:00 PM - 10:00 PM
Hynes, Level 1, Hall A

SB06.04.01

Chemical Synthesis of All-Peptide-Based Rotaxanes from Proline-Containing Cyclic Peptides. Taichi Kurita¹, Masahiro Higashi¹, Joan Gimenez-Dejoz², Seiya Fujita¹, Hirofumi Sato¹, Hirofumi Uji¹ and Keiji Numata^{1,2}; ¹Kyoto University, Japan; ²RIKEN CSRS, Japan

Mechanically interlocked molecules have a unique dynamic nature while permanently maintaining a spatial association between the components. This characteristic has been exploited to synthesize slide-ring materials [1] and molecular machines [2] with excellent properties that cannot be achieved with covalently bonded molecules. In the field of synthetic polymers, various mechanically interlocked molecules have been synthesized and applied in a wide range of fields. On the other hand, in the field of peptides and proteins, the synthesis of mechanically interlocked peptides is still difficult, although the construction of assemblies and host-guest chemistry, such as cation recognition, using cyclic peptides have been widely investigated [3,4]. Kimura et al. and Thomson et al. reported the synthesis of rotaxane using cyclic peptides [5,6]. However, all of them used synthetic polymers as the axis molecules, and there are no examples of chemical synthesis of all-peptide-based rotaxanes. This is because peptides do not have a strong mutual recognition motif. Recently, Leigh et al. reported that nucleophilic acyl substitution reactions between primary amines and electrophiles in the presence of crown ethers led to the synthesis of rotaxanes via axle-forming reactions inside the ring [7]. The characteristic feature of this method is that the crown ether forms a hydrogen

bond with the primary amine to enhance nucleophilicity, and the crown ether stabilizes the positive charge developing in the reaction intermediate on the axle-formation reaction, enabling the synthesis of rotaxane even with relatively weak interactions. In this study, we designed and synthesized cyclo[PGPGPGPC(StBu)], having an alternating sequence of proline and glycine, which is a cation recognition motif [4]. This cyclic peptide was mixed with a primary amine and a nucleophile. Electrospray ionization mass spectrum of the mixture showed a peak corresponding to rotaxane, suggesting that rotaxane was formed. The yield was calculated to be 0.19% by high-performance liquid chromatography. To estimate the reaction mechanism, ¹H NMR titration experiment was performed. The binding constant of cyclo[PGPGPGPC(StBu)] for primary amines was calculated to be $27 \pm 2 \text{ M}^{-1}$, which is not significantly different from the binding constant of 24-crown 8-ether for primary amines ($32 \pm 2 \text{ M}^{-1}$) [4]. This result suggests that the primary amine binds to the cyclic peptide via hydrogen bond in the initial state of the reaction. Although the nucleophilic acyl substitution reaction inside the cyclic peptide is considered sterically unfavorable, the rotaxane is presumably synthesized by two factors: hydrogen bonding to the cyclic peptide would enhance the nucleophilicity of the amine, and the cyclic peptide stabilizes the positive charge developing in the tetrahedral intermediate. In the current presentation, we will also present the influence of ring members and the solution structure of the cyclic peptide on the rotaxane-forming reaction.

- [1] Y. Okumura *et al. Adv. Mater.* **2001**, *13*, 485-487.
- [2] S. Cakmak *et al. Chem. Rev.* **2015**, *115*, 10081–10206.
- [3] T. Kurita *et al. Biomacromolecules* **2021**, *22*, 2815-2821.
- [4] V. Madison *et al. J. Am. Chem. Soc.* **1977**, *99*, 4788-4798.
- [5] S. Kimura *et al. Chem. Commun.* **2007** *10*, 1023-1025.
- [6] A. Thomson *et al. J. Am. Chem. Soc.* **2006**, *128*, 1784–1785.
- [7] D. Leigh *et al. J. Am. Chem. Soc.* **2018**, *140*, 6049–6052.

SB06.04.02

Donor-Acceptor Type Molecules for High Performance Green-Light-Selective Organic Photodiodes Younhee Lim¹, Sungyoung Yun¹, Daiki Minami², Taejin Choi¹, Hyeong-Ju Kim¹, Jisoo Shin¹, Chul-Joon Heo¹, Kyung-Bae Park¹ and Byoungki Choi¹; ¹Samsung Advanced Institute of Technology, Korea (the Republic of); ²Samsung Electronics, Korea (the Republic of)

The specific properties of organic semiconductors, such as the color tenability, mechanical flexibility, and low-cost process-ability, have attracted interest for future optoelectronic device applications. In particular, the dipolar donor (D)–acceptor (A) approach is a representative and powerful strategy to design the wavelength-selective organic absorbers, as the optical and electrical properties of the D–A type materials can be tuned using an appropriate combination of D and A moieties. Herein we report dipolar donor (D)- π -acceptor (A) molecules for application to green-light-selective organic photodiodes (OPDs). Novel p-type molecules combined with two types of fused heterocyclic donors and an electron-accepting unit has been synthesized and characterized. The molecules exhibit cyanine-like properties that are characterized by intense and sharp absorption. This molecular design leads to improved absorption properties, thermal stability, and higher photoelectric conversion compared to those of a molecular design based on a non-fused ring. A maximum external quantum efficiency of 66% ($\lambda_{\text{max}} = 550 \text{ nm}$) and high specific detectivity (D^*) of $8 \times 10^{13} \text{ cm Hz}^{1/2}/\text{W}$ are achieved in an OPD consisting of a bulk heterojunction blend of the p-type molecule and fullerene (C_{60}). Finally, the green-light-detection capability of the green-selective OPD is demonstrated by the optical simulation of a stacked-type organic-on-Si hybrid full-color photodetector comprising the green-light-selective OPD and a bottom Si photodiode with only blue and red color filters.

SB06.04.03

Development of High-Performance Near-Infrared Organic Phototransistors Using Diazapentalene-Containing Ultralow-Band-Gap Copolymers Doyoung Lee¹, Seoyoung Kim², Jungho Lee², Yongjoon Cho², So-Huei Kang², Wonbin Choi¹, Joonhak Oh¹ and Changduk Yang²; ¹Seoul National University, Korea (the Republic of); ²Ulsan National Institute of Science and Technology, Korea (the Republic of)

Absorbing near-infrared (NIR) range (760-1100nm) low-band-gap π -conjugated polymers are an interesting family of semiconductor materials and have opened up possibilities of being used in various functional optoelectronic applications, such as organic field-effect transistors (OFETs), organic photodetectors (OPTs), and electrochromic devices. Incorporating a quinoid structure into the polymer backbone is one of the powerful strategies for reducing the band gap, which has been verified by theoretical and experimental studies of the well-known poly(isothianaphthene) and poly-(thieno[3,4-b]pyrazine), which exhibit band gaps of less than 1.0 eV. However, such quinoid-type polymers typically have a very small band gap and poor stability toward oxidation, which renders them difficult to be employed in the aforementioned devices. Alternatively, utilizing donor-acceptor (D-A) interactions is recently widely employed in low-band-gap polymers, owing to its unique possibility of tuning the energy levels almost independently as well as their band gaps. But because of the limited availability of synthetic strategies and strong acceptor units, constructing new types of low-band-gap donor–acceptor-type copolymers for use in multiple functional applications remains a big challenge. Herein, we report the synthesis, characterization, and optoelectronic applications of a novel class of ultralow-band-gap copolymers (PDAP–Fu, PDAP–Th, and PDAP–Se) on the basis of the unique, interesting, yet rarely researched bicyclic 2,5-diazapentalene (DAP) strong acceptor in conjugation with chalcogenophene donors (furan (Fu), thiophene (Th), or selenophene (Se)). All of the copolymers exhibit broad NIR absorption and optical band gaps as low as $\sim 1.0 \text{ eV}$. The effects of the actual chalcogen atoms on the geometry, optical properties, energy levels, and film organization are carefully determined for OFET and OPT applications. Regarding the OFET studies, all of the copolymers show unipolar transport behavior in bottom-gate and top-contact OFETs, and PDAP–Se exhibits the highest hole mobility of $4.76 \times 10^{-1} \text{ cm}^2 \text{ V}^{-1} \text{ s}^{-1}$, with grazing-incidence X-ray diffraction (GIXD) data demonstrating a three-dimensional (3D) charge-conduction channel through the edge-on and face-on mixed large crystallites. Besides, investigations of the OPTs indicate that a high photoresponse is achieved for all of the copolymers at a wavelength of 1060 nm in the NIR spectral region combined with an excellent external quantum efficiency (η) and photodetectivity (D^*). This is particularly true for PDAP–Se ($\eta = 6.56 \times 104\%$ and $D^* = 1.80 \times 10^{12} \text{ Jones}$). It demonstrates that NIR light facilitates the photocurrent generation in DAP-based OPTs with good photochemical stability as shown by Fourier-transform infrared (FT-IR) and UV-vis-NIR spectra of the copolymer thin films before and after irradiation with 1060nm light for 24h. Thus, such ultralow-band-gap copolymers are promising candidates for use in integrated circuits and optoelectronic devices, ultimately realizing the potential benefits of the DAP-accepting unit as a conjugated backbone.

SB06.04.04

Paper-Based Wearable Ammonia Gas Sensor Using Iron(III)-Added PEDOT:PSS Hajime Fujita¹, Meiting Hao², Shinji Takeoka², Yuji Miyahara³, Tatsuro Goda³ and Toshinori Fujie¹; ¹Tokyo Institute of Technology, Japan; ²Waseda University, Japan; ³Tokyo Medical and Dental University, Japan; ⁴Toyo University, Japan

Paper electronics hold great potential that could replace conventional plastic electronics. Paper electronics are disposable and cost-effective, two distinct advantages for developing broadly accessible devices. However, the approach for functionalizing paper with electronic materials has not been sufficiently characterized from a chemical point of view. As a result, most paper-based electronic devices have an inferior electrical performance compared with plastic-based devices, which largely constrains their practical use. The design and fabrication of electronic materials on paper needs refinement to make

paper electronics a valid, practical option. Here, we report a high-performance, paper-based, wearable ammonia sensor comprising composite poly(3,4-ethylenedioxythiophene):poly(styrenesulfonate) (PEDOT:PSS) and iron(III) compounds. We combined different printing and coating methods to develop the ammonia-sensitive, composite substance PEDOT:PSS:Fe³⁺ on paper. Our sensor achieves 10-times smaller size than the conventional sensor on Kapton film and high tolerance for humidity without impairing practical sensor response. We demonstrate the utility of our device toward wearable ammonia-sensing in a facial mask and a nasal filter; wireless battery-free monitoring of food spoilage; and wireless battery-free monitoring of the ammonia level in a paper diaper. All the comprising materials—cellulose paper, PEDOT:PSS, and iron(III) compounds—are abundant and eco-friendly, a further benefit for applications in which biological tissues or disposable wearable products are eventually discarded with the sensor attached. Our approach may open the door to advanced healthcare based on ubiquitous wearable sensing.

SB06.04.05

Organic Devices for Solar Energy Conversion and Storage Fengling Zhang¹, Nannan Yao¹, LeiQiang Qin¹ and Yanfeng Liu^{1,2}; ¹Linköping University, Sweden; ²NingboTech University, China

Flexible organic solar cells (OSCs) made on plastic substrates with traditional printing techniques can be semitransparent and have broader applications than their inorganic counterparts. After the power conversion efficiencies (PCEs) of bulkheterojunction (BHJ) OSCs reached 19 % with non-fullerene acceptors (NFAs), a major challenge to further increase PCEs to >20% is how to reduce charge recombination in the BHJs. In the past 20 years, we have been working on optimizing processing of fullerene/non-fullerene OSCs and studying device physics to deepen understand on the mechanism of devices for enhancing the power conversion efficiency.

In my presentation, I will introduce our recent progress on organic devices for solar energy conversion and storage.

1. Monitor morphology formation of BHJ

To understand the BHJ morphology formation during solution processing, we studied three BHJ systems with the same donor PBDB-T and three different acceptors (PC₇₁BM; IT-M and N2200) via monitoring the morphology evolution during blade coating with a versatile in situ spectroscopy by recording photoluminescence (PL) and laser scattering (LS) signal, which indicated that the component with higher molecular weight dominates the blend film formation and the final morphology. (Liu et al., *Small Methods*, 2021, 2100585, <https://doi.org/10.1002/smt.202100585>)

2. Dilute donor NFA OSCs

The morphology and Donor/Acceptor ratio are crucial for PCEs of OSCs. In our recent work, we surprisingly found that the PCE is tolerant to PM6 contents ranging from 10 to 60 wt % in the OSCs based on PM6:Y6. Most surprisingly, a PCE over 10% was achieved in OSCs with only 10 wt% donor. The findings indicate low dependence of composition on charge generation, transport and extraction in NFA OSCs. (Yao et al., *J. Phys. Chem. Lett.* 2021, 12, 5039, <https://doi.org/10.1021/acsaelm.1c03017>) It's worth to note that even with large domains, the blends with low donor contents can still yield J_{sc} approaching 20 mA cm⁻². As the emerging NFAs have been demonstrated with long exciton diffusion length (Firdaus, Y. et al. *Nat. Commun.* 2020, 11, 5220), therefore, the charge generation process is more tolerant to the domain size. The findings are significant in the context of enabling large processing window, which is essential in a later scale-up stage, since it means lower sensitivity to compositional variations.

3. The Sunlight varies with time, season, and location on the earth. To extend the application of organic solar cells, storing electricity converted from the sunlight is necessary. Super-capacitors are components, which can store electricity. We developed hybrid super-capacitors based on MXene and polymers as well as integrating organic solar cells with super-capacitors (Photo-supercapacitors (PSCs)). Flexible semitransparent photovoltaic supercapacitors based on water-processed MXene electrodes were realized. The photovoltaic and storage performance of the PSC has potential applications as portable power units to charge low power consumption electronics/IoT. (L. Qin et al, *J. Mater. Chem. A*, 2020, 8, 5467, <https://doi.org/10.1039/d0ta00687d>)

SB06.04.06

Characterization of Organic Semiconducting Photoelectrodes for Electrically Floating Phototransduction Inside Biological Tissues Luca Bondi¹, Maria Rosa Antognazza², Edgar Gutierrez Fernandez^{3,4}, Beatrice Fraboni¹, Jaime Martín^{3,4}, Camilla Marzuoli^{2,5}, David Mecerreyes^{3,4}, Gabriele Tullii² and Tobias Cramer¹; ¹University of Bologna, Italy; ²Istituto Italiano di Tecnologia, Italy; ³University of the Basque Country, Spain; ⁴POLYMAT, Spain; ⁵Politecnico di Milano, Italy

Photoactive organic semiconductors are envisioned as a novel class of materials able to transduce light into stimulating signals inside biological cells or tissue [1]. These materials stand out due to their high optical absorbance coefficients, mechanical flexibility, ability to operate in a wet environment, and potential biocompatibility, enabling ultrathin and minimally invasive form factors not accessible with traditional inorganic materials. The chemical and physical nature of the interface between the semiconductor and the electrolyte gives rise to different, competing electrochemical phenomena. We addressed the problem considering polymeric as well as molecular organic materials in the form of both single-layer and p/n junction thin-films [2]. These are material systems that have been recently demonstrated to achieve the photomodulation of cardiac regeneration processes [3] or retinal neurons response [4]. The aim of our research is to unveil the fundamental processes that govern these photoactive devices and to develop both explicative and predictive models, which are necessary for the development of freestanding photoelectrodes, requiring no wiring or external bias, and which are stable in physiological conditions.

To decouple the intrinsic photovoltage generated by the material itself from the one generated at the semiconductor electrolyte interface, we compare photovoltage transients and spectra as observed both in presence and in absence of electrolyte. In addition, we compare photocurrent and photovoltage transients in presence and absence of oxygen to explore the processes leading to oxygen reduction reactions and ROS species generation in such interfaces. Quantitative determination of hydrogen peroxide generation with HRP-TMB assay permits to further determine the electrochemical conversion efficiencies for different materials. By combining the findings with electrochemical impedance spectroscopy, we develop simple equivalent circuit models to explain the observed photovoltage and its build-up dynamics in OSC floating photocathodes in contact with electrolyte. Circuitual modeling also allows to relate macroscopic as well as morphological features to physical properties, and to explore how utilization and ageing reflect on the device operativity performances. Applying different bias voltages, we explore the photoelectrical behavior of the system, determining how faradaic and capacitive contributions follow the variation. By modelling such dynamics, we obtain a quantitative description of the photovoltage transients and charging behaviour of floating photoelectrodes.

[1] J. Hopkins et al., *Photoactive Organic Substrates for Cell Stimulation: Progress and Perspectives*, *Adv. Mater. Technol.*, vol. 4, no. 5, pp. 1-10, 2019.

[2] T. Paltrinieri et al., *Understanding Photocapacitive and Photofaradaic Processes in Organic Semiconductor Photoelectrodes for Optobioelectronics*, *Adv. Funct. Mater.*, vol. 2010116, 2021.

[3] F. Lodola et al., *Conjugated polymers optically regulate the fate of endothelial colony-forming cells*, *Sci. Adv.*, vol. 5, no. 9, 2019.

[4] D. Rand et al., *Direct Electrical Neurostimulation with Organic Pigment Photocapacitors*, *Adv. Mater.*, vol. 30, no. 25, pp. 1-11, 2018.

SB06.04.07

A Chemically Doped Phenylene Vinylene Polymer with High Electron Conductivity Marc-Antoine Stoeckel¹, Han-Yan Wu¹, Chi-Yuan Yang¹, Yang

Lu², Ziang Wu³, Han Y. Woo³, Jian Pei², Magnus Berggren¹ and Simone Fabiano¹; ¹Linköping University, Sweden; ²Peking University, China; ³Korea University, Korea (the Republic of)

High-performing organic materials are required for efficient opto-, bioelectronic and thermoelectric applications. Among these materials, (semi-)conducting polymers are particularly appealing for these technologies, as they benefit from unique optoelectronic properties, low-cost production and their solution processability make them fully compatible with large-scale deposition methods. The most common way to reach high electrical conductivities with this class of materials is to dope the polymers through the addition of a heterogeneous doping entities to the system.

With the goal to produce highly-performing materials, huge efforts have been provided by the scientific community, notably through molecular design adjustments of these active materials. A current strategy towards this end is the planification and the rigidification of the polymer backbone, leading to a higher degree of order through a favorable molecular packing while decreasing the energetic disorder. This is the case, for example, for poly(p-phenylene vinylene) derivatives that benefit from both carbon-carbon double bonds between polymer units and intramolecular hydrogen bonds.

Another way of enhancing the performances of (semi)conducting polymers is to increase the microscopic order and then the crystallinity of the polymeric assembly by adjusting the processing of deposition. One way to do so is to use Langmuir-Schaefer (LS) technique that relies on the assembly of the polymer chains at the air/water interface when compressed between two moving barriers. The assembled film composed by a monolayer of polymers with a low degree of defect is then transferred onto a substrate integrating electrodes to make a fully functional device.

Here we report on LS films that are highly ordered and oriented at the monolayer limit. This describes a microscopic structure that is optimized for the transport of charges with strong anisotropic properties of electron conduction. Through a systematic analysis including scanning probe microscopy, optical spectroscopy, GIWAXS, and electrical measurements, we characterized the system in terms of structure, packing, energetics, and thermoelectric properties. We further optimized the electrical performances of the film when doping it with different molecular entities through secondary doping mechanisms, reaching n-type conductivities up to 4 S cm⁻¹, and a power factor of 1.5 μW m⁻¹ K⁻². Finally, we integrated this system as active material in organic electrochemical transistors (OECT) to study the penetration of ions within this structured thin-film to optimize the transconductance of these devices.

SB06.04.09

Exploring Ultrafast Symmetry-Breaking Photoinduced Charge Separation in Optoelectronic Materials George C. Fish¹, Frank Nüesch^{1,2} and Jacques-E. Moser¹; ¹École Polytechnique Fédérale de Lausanne, Switzerland; ²Empa–Swiss Federal Laboratories for Materials Science and Technology, Switzerland

In organic photovoltaics (OPVs), it is widely accepted that the open circuit voltage (V_{OC}) is predominantly determined by the energy level offset between the donor and acceptor material. A consequence of this is that increasing the driving force for charge separation negatively impacts upon the V_{OC} .

Recently, symmetry breaking photoinduced charge separation (SB-CS) has become an attractive topic in the field as it would allow for charges to be separated in systems with no energetic offset between the donor and acceptor material, thus increasing the V_{OC} and device efficiency.¹

Here, we use ultrafast transient absorption spectroscopy to probe photoinduced charge generation in cyanine and squaraine dyes, both classes of materials with a storied history in the OPV field. The high extinction coefficients of cyanine dyes have led to them being used extensively alongside fullerene acceptors in planar heterojunction devices, as well as being used as model systems to study the dissociation of charge transfer states.^{2,3}

In this work, we build upon results that demonstrated the possibility of pristine pentamethine cyanine (Cy5) thin films to undergo intrinsic charge generation.⁴ We demonstrate that SB-CS takes place in pristine Cy5 thin films and proceeds with a quantum yield of 86%, providing the first direct proof of high-efficiency intrinsic photoinduced charge generation in organic salt semiconductors. The driving force for the SB-CS process was determined to be, in part, due to local electric fields arising from the anions being located outside of H-aggregated cationic chromophore stacks. Furthermore, the counterion of the cyanine dye was varied in order to establish that the degree of aggregation plays a vital role in determining the efficiency of the charge separation process.⁵

Comparatively, our ultrafast studies on dicyanomethylene substituted squaraine dyes, which are promising materials for short wave infrared photodetectors⁶, revealed that an intrinsic SB-CS process does not occur. An absence of counterions resulted in there being no local electric fields to provide the driving force for the charge separation to take place.

1 E. Sebastian and M. Hariharan, *ACS Energy Lett.* 2022, 7, 696–711.

2 M. Bates and R. R. Lunt, *Sustain. Energy Fuels*, 2017, 1, 955–968.

3 A. Devizis, J. de Jonghe-Risse, R. Hany, F. Nüesch, S. Jenatsch, V. Gulbinas and J. E. Moser, *J. Am. Chem. Soc.* 2015, 137, 8192–8198.

4 L. Wang, S. Jenatsch, B. Ruhstaller, C. Hinderling, D. Gesevičius, R. Hany and F. Nüesch, *Adv. Func. Mater.* 2018, 28, 1–8.

5 G. C. Fish, J. M. Moreno-Naranjo, A. Billion, D. Kratzert, E. Hack, I. Krossing, F. Nüesch and J. E. Moser, *Phys. Chem. Chem. Phys.* 2021, 23, 23886–23895.

6 K. Strassel, W. H. Hu, S. Osbild, D. Padula, D. Rentsch, S. Yakunin, Y. Shynkarenko, M. Kovalenko, F. Nüesch, R. Hany and M. Bauer, *Sci. Technol. Adv. Mater.* 2021, 22, 194–204.

SB06.04.12

Shape Morphing Technology Based on a Plastic-Elastomer Framework for 3D Electronics Dukkyu Park, Jung Il Yoo and Heungcho Ko; Gwang-ju Institute of Science and Technology, Korea (the Republic of)

Three-dimensional electronics provide a strong advantage in the omnidirectional capability in sensing, displaying, communicating, and others. When direct device fabrication on 3D structures is extremely difficult, three-dimensional transformation technology based on a supporting substrate that mounts the planar membrane-type electronics becomes an excellent indirect method. When plastics are used for an additional substrate, the materials guarantee overall mechanical stability but allow only a small strain range. On the other hand, elastomers allow a large amount of strain but seem to be very soft mechanically. This study demonstrates a means of developing a plastic-elastomeric framework to achieve three-dimensional (3D) electronics with non-zero Gaussian curvature without losing mechanical stability. When using two controversial materials, it is important to guarantee the interfacial adhesion between the two materials and the possibility of controlling the shape transformation. To address the first issue, we used a self-assembled monolayer assembly that chemically bonds the two materials to guarantee strong interfacial adhesion. Regarding the second issue, we used shear-printed plastic lines to provide a driving force for automatic 3D transformation during thermal relaxation above the glass transition temperature and the elastomeric films to provide a basis for mounting the membrane electronics and allow a large amount of strain for complex 3D shapes. In a detailed study, we examined the shape morphing based on geometrical and mechanical parameters such as annealing temperature, annealing time, and other control parameters, including shear rate, line pitch, and relative thickness of plastic/elastomeric structure. In particular, we have successfully developed unusual 3D shapes such as cone, dome, and saddle shapes, among shapes predicted through mechanical finite element method simulation. To validate the feasibility of this strategy in 3D electronics, semiconductor-processed electrodes and indium-gallium-zinc-oxide transistor arrays were mounted on a plastic-elastomeric framework to

demonstrate a 3D-shaped membrane electronics device.

SB06.04.13

Microgravity as a Tool for a Molecular Understanding of the Active Layer Formation in Organic Solar Cells [Leif K. Ericsson](#), Ishita Jalan, Jan van Stam and Ellen Moons; Karlstad University, Sweden

Solution-processed organic photovoltaic (OPV) devices have gained serious attention during the last decade.¹ The active layer of an OPV solar cell consists of a thin solid film of an electron donor blended with an electron acceptor. One important factor for the performance is the nanostructured morphology of the active layer. It is known that molecular interactions govern the morphology formation process, whether it is a polymer-polymer system or a polymer-small molecule system.² Understanding the factors determining this structure formation on a molecular level enables not only morphology control, but also the prediction of suitable and more environmentally friendly solvents for a greener processing of OPV.

One way to enable a detailed study of the initial stage of the phase separation and hence the influence of molecular interactions, is to slow down the phase-separation process. Minimizing the influence from gravity on the film formation is known to slow down this process during the film formation.^{3,4} In this work we have prepared active layers under microgravity conditions at parabolic flights.⁵ For this purpose, we have designed a custom-built experiment setup for dip-coating from volatile solutions under microgravity conditions, meeting the security measures for parabolic flights.⁶ The resulting thin blend films are characterized using AFM and AFM-IR, the latter combining the high resolution of AFM with the chemical fingerprint of infrared spectroscopy. It is shown that the morphology is similar to films prepared at 1g conditions, but with differences that can be related to the absence of a gravitational field during the drying of the applied liquid coating. Film thickness as well as the size of structures due to phase-separation are shown to depend on the level of gravity during the drying of the films.

In parabolic flights, the microgravity phase lasts for 20–25 seconds, which is too short to ensure complete evaporation of the solvents. To guarantee complete evaporation under microgravity conditions, sounding rocket experiments with 6 minutes of microgravity will be performed in the autumn 2023. The construction of the equipment for sounding rocket flights is ongoing and the design concept will be described.

References:

1. Brabec, C. J. et al. Polymer-Fullerene Bulk-Heterojunction Solar Cells. *Adv. Mater.* 22, 3839–3856 (2010).
2. Ye, L. et al. Quantitative relations between interaction parameter, miscibility and function in organic solar cells. *Nat. Mater.* 17, 253–260 (2018).
3. Bamberger, S. et al. in *Separations Using Aqueous Phase Systems*, edited by D. Fisher and I. A. Sutherland (Springer, Boston, MA, 1989), pp. 281–286.
4. Bailey, A.E. et al. Spinodal Decomposition in a Model Colloid-Polymer Mixture in Microgravity. *Phys. Rev. Lett.* 99(20), 205701 (2007).
5. 70th ESA Parabolic Flight Campaign (2018) and 78th ESA Parabolic Flight Campaign (2022).
6. Ericsson, L.K.E. et al. An experimental setup for dip-coating of thin films for organic solar cells under microgravity conditions. *Rev. Sci. Instrum.* 92, 015108 (2021).

SB06.04.15

Deformable Polymer Semiconductor Thin-Film Crosslinked with Flexible Azide Photo-Crosslinker [Sein Chung](#) and Kilwon Cho; Pohang University of Science and Technology, Korea (the Republic of)

Stretchable transistors that use intrinsically deformable semiconducting conjugated polymers (CPs) as active layers are emerging as the next-generation key of electronics technology. To impart high deformability to a semiconducting polymer, a photo-initiated crosslinking approach has been reported with nitrene chemistry of azide-incorporated molecular additive. In this study, we elaborately investigated the complicated effects of azide photo-crosslinker's molecular length on various physicochemical characteristics and resultant deformability of photo-crosslinked conjugated polymer films.

For a systematic comparison, we newly synthesize a series of nitrene-induced photo-crosslinkers (*n*-NIPs) with different numeric ethylene glycol units (*n* = 1, 4, 8, and 13) that bridge two tetrafluoro-aryl azide end groups. A benchmark near-amorphous conjugated polymer, IDTBT, is co-processed with *n*-NIPs and crosslinked by brief exposure to UV light with 254 nm. We found that the length of ethylene glycol unit in *n*-NIPs affects the deformability of crosslinked IDTBT films, and the improvement is achieved not with semi-crystalline conjugated polymers such as DPPDTT or RR-P3HT but only with near-amorphous polymers such as IDTBT or RA-P3HT. Based on the systematic studies, we suggest that crosslinking density in an amorphous regime is significant in the improvement of thin-film deformability. We believe that these results will provide valuable insight into establishing a design principle of azide-based photo-crosslinkers for deformable polymer semiconductors with conjugation.

SB06.04.16

Organic Semiconductors with DNA Induced Chirality and Optoelectrical Functionalities [Moon Jong Han](#)¹, Hee Seong Yun², Yongjoon Cho³, Minkyu Kim¹, Changduk Yang³, Vladimir Tsukruk¹ and Dong Ki Yoon²; ¹Gerogia Institute of Technology, United States; ²Korea Advanced Institute of Science and Technology, Korea (the Republic of); ³Ulsan National Institute of Science and Technology, Korea (the Republic of)

We fabricate highly organized patterned thin films of DNA-templated perylene diimides (PDIs), which can realize the bio-organic field-effect transistor (BOFET) that has chiroptical and electrical functionalities. Shear-oriented PDI/DNA complex films show how periodic molecular orientation and charge transport are related, resulting in drastically different electro-optical properties at each condition, in which DNA is used as the chirality-inducing scaffold and charge-injection layer. BOFET shows a well-ordered supramolecular structure with high electron mobility, photoresponsivity, and photosensitivity, reaching $3.97 \text{ cm}^2 \text{ V}^{-1} \text{ s}^{-1}$, 1.18 A W^{-1} , and 7.76×10^3 , respectively. Interestingly, the resultant BOFET enables the definitive response to the handedness of circularly polarized light. We believe our work can be a cornerstone for the natural chirality of DNA and the electron conductivity of organic semiconducting molecules to be mutually used in the unique chiro-electro-optical functions.

SB06.04.18

Electrochemical Fabrication and Characterization of Organic Electrochemical Transistors (OECTs) Using poly(3,4-ethylenedioxythiophene (PEDOT)) [Jungghyun Lee](#), Shirang S. Chhatre, Peter Sitarik, Yuhang Wu, Quintin Baugh and David C. Martin; University of Delaware, United States

Organic electrochemical transistors (OECTs) with conductive polymers (CPs) as the active materials are one of the devices getting particular attention for bioelectronics due to their special properties such as low operating voltage and mixed ionic-electronic conductivity. Among various CPs, commercially available poly(3,4-ethylenedioxythiophene):poly(styrene sulfonate) (PEDOT:PSS) dispersions in the aqueous solutions have been widely used because they have high conductivity and biocompatibility. However, it has been difficult to modify the chemistry of PEDOT:PSS to control and functionalize device characteristics because of its high chemical stability. In this work, EDOT was electrochemically polymerized as the active material of OECTs with commonly used counterions of lithium perchlorate (LiClO_4), sodium *p*-toluene sulfonate (*p*TS), and poly(sodium 4-styrene sulfonate) (PSS). Commercially available gold interdigitated electrodes were used as the substrate and PEDOT served as the active channel material by filling the gaps between interdigitated electrodes during the electrochemical polymerization process. The electrochemically polymerized PEDOT films with large sized counterions (PSS), showed smooth and regular surfaces, while PEDOT films with relatively small sized counterions (LiClO_4 and *p*TS) showed much rougher and bumpy surfaces. PEDOT films with either *p*TS or PSS showed much better surface coverage ability for filling gaps between interdigitated electrodes rather

than with LiClO₄. OECTs were successfully fabricated with PEDOT and various counterions by the electrochemical polymerization process. The maximum transconductance, g_m , of a PEDOT OECT was 46 mS with the highest on-current level (> 10 mA) using *p*TS as the counterion. These results provide a relatively simple and efficient way to fabricate high performance OECTs with various monomers, counterions, and additives as active materials in order to modify and control the device characteristics for various applications.

SB06.04.19

Template Induced Highly Ordered Aggregates of Merocyanines for the Tuning of Optical Properties [Anna J. Kny](#)¹, Max Reimer², Noah Al-Shamery¹, Ritu Tomar¹, Thomas Bredow¹, Selina Olthof² and Moritz Sokolowski¹; ¹University of Bonn, Germany; ²University of Cologne, Germany

Merocyanines are widely investigated molecules with large dipole moments, adjustable optical bandgaps, and high absorption coefficients. They are of interest for the use in optoelectronic devices, in particular, for the application in organic solar cells [1]. By controlling the molecular packing, either via template mediated film growth on crystalline surfaces or by modification of the molecular structure such as a variation of the peripheral substituents, the optical properties can be tuned by the formation of J- or H-aggregates [2].

Here, we present a study on the adsorption and molecular ordering of the prototype merocyanine 2-[5-(5-dibutylamino-thiophen-2-yl-methylene)-4-*tert*-butyl-5*H*-thiazol-2-ylidene]-malononitrile (HB238) and its derivatives on single crystalline Ag(100) and KCl(100) surfaces. Measurements were performed on ultrathin films (range of about one monolayer) by a variety of surface sensitive techniques such as high resolution low energy electron diffraction (SPA-LEED), scanning tunneling microscopy (STM), and photoelectron spectroscopy (XPS, UPS). The results are complemented by density-functional theory (DFT) calculations.

Remarkably, the thermodynamically preferred phase of HB238 on the Ag(100) surface at room temperature is a commensurate superstructure which is considerably different from known bulk structures [3]. We observe domains of several hundreds of Angstroms in diameter composed of homochiral aggregates of four molecules which are arranged in a nearly circular manner. Hence, properties of J-aggregates are expected for this phase. This structure is stabilized mainly by hydrogen bonds between donor and acceptor groups of neighboring molecules. Interestingly, the molecular packing between the above described homochiral aggregates can be affected by a change of the sterically demanding peripheral substituents. We will demonstrate this by comparing the structure formation of HB238 to that of derivatives on the Ag(100) surface.

Finally, the question arises if similar structures can be prepared on different template surfaces, for example those of insulating layers that are needed to investigate the resulting optical properties. To answer this question it is important to understand how the structure formation on the Ag(100) surface depends on the interfacial bonding. For this purpose, we discuss the role of the functional groups on the interfacial bonding and compare the structure formation of HB238 on Ag(100) to its structure formation on a thin insulating layer of KCl(100) epitaxially grown on Ag(100). On the basis of these results we discuss the interplay of intermolecular and interfacial bonds essential for the film formation and hence most important for the tuning of the optical properties.

MCs were kindly provided by the group of Prof. K. Meerholz (Cologne). Supported by the DFG through the research training group 2591.

[1] A. Arjona-Esteban et al., JACS 137 (2015) 13524. [2] A. Liess et al., Adv. Funct. Mater. 29 (2019) 1805058. [3] N. Gildemeister et al., J. Mater. Chem. C 9 (2021) 10851-10864.

SB06.04.20

High Performance Organic Thermoelectrics Enabled by Controlling Counter-Ion-Induced Disorder in Highly Doped Conjugated Polymers [Jimin Kim](#), Duckhyun Ju and Kilwon Cho; Pohang University of Science and Technology (POSTECH), Korea (the Republic of)

The degree of structural and energetic disorder in conjugated polymers governs how effectively the charge carriers are transported as it impinges on the molecular geometry or π -orbital overlap. Thus, how the counter-ion-induced disorder affects the charge transport in highly doped conjugated polymer systems should be investigated to achieve high thermoelectric (TE) performance. However, experimentally controlling the disorder caused by the Coulomb interaction between the polymer and the dopant is difficult due to the limitations of dopant engineering. Herein, we systematically control the counter-ion-induced disorder and investigate the effect of disorder on the TE transport properties in poly(3,4-ethylenedioxythiophene) (PEDOT) by using anion exchange method. Multi-cyano-functionalized counter-ions, which exhibit different Coulomb interaction with PEDOT, change the structural and energetic disorder in PEDOT. To quantify the counter-ion-induced disorder, the degree of disorder is evaluated in several microscopic aspects: molecular ordering, density of states (DOS), and polaron behaviors. The low extent of counter-ion-induced disorder increases the planarity of the PEDOT chains and simultaneously narrows the DOS of PEDOT. In addition, an analysis of the number of unpaired polarons derived from the Curie susceptibility shows how the charge carriers are localized by the counter-ion-induced disorder. Consequently, these changes result in the opposite behaviors of the electrical conductivity and the Seebeck coefficient depending on the extent of disorder and thereby produce a remarkable power factor of 630.6 $\mu\text{W m}^{-1} \text{K}^{-2}$ and figure-of-merit ZT of 0.21 with the lowest degree of disorder. This work would provide a comprehensive understanding of counter-ion-induced disorder effect on charge transport in terms of optimizing TE performance.

SB06.04.21

Large Area Flexible Radiation Dosimeters for Radiation Therapy [Derek Dremann](#)¹, James Ververs², Daniel Bourland², John Anthony³, Karl Thorley³ and Oana D. Jurchescu¹; ¹Wake Forest University and Center for Functional Materials (CFM), United States; ²Wake Forest School of Medicine, United States; ³University of Kentucky Center for Applied Energy Research, United States

Cancer is one of the leading causes of death globally. Radiation therapy represents an important and popular treatment technique for many types of cancer. However, the effectiveness of radiation therapy is critically dependent on the accurate administration of the correct radiation dose to the target cancer cells. Another challenge is the risk presented by the radiation to surrounding healthy, non-cancerous cells. Therefore, knowing the exact radiation dosage a patient receives and the spatial distribution of that dosage is important for minimizing the damage to surrounding cells while ensuring enough radiation is delivered to treat the cancer. Well-established dosimetry techniques currently used in clinical settings are limited to single point-based measurements to determine the absolute radiation dose a patient receives, and accurately measuring the radiation dose over a large area remains a challenge.

Radiation detectors based on organic field-effect transistors (RAD-OFETs) offer a solution for flexible, conformal, large area, and high-resolution *in vivo* dosimetry at the skin surface. In this research, samples consisting of an array of 12 rows and 8 columns of organic field-effect transistors covering an active area of approx. 1.5 cm² were slot-die coated using 2,8-Difluoro-5,11-bis(triethylsilylethynyl)anthradithiophene (dif-TES ADT) or 5,11-bis(triethylgermylethynyl)anthradithiophene (dif-TEG ADT) blended with Poly(alpha-Methylstyrene) (PαMS) in a 1:1 W/W ratio providing a spatial resolution of 1.5 ± 0.02 mm². Samples of each blend received a 200 cGy dose of radiation with a source-to-surface distance of 100 cm using a 6 MV radiation source. Additionally, for one sample from each type we inserted a solid water bolus between the source and the RAD-OFETs. The bolus acts as a

tissue equivalent material shifting the peak radiation dose received closer to the surface of a patient. The shift in the threshold voltage before and after exposure to radiation was used to compare the variation in the radiation dose across the array of RAD-OFETS, while the sensitivity was observed to be constant across the devices, $S = 1.8 \pm 0.9 \times 10^{11} \mu\text{C Gy}^{-1} \text{cm}^{-3}$, with no significant difference being observed between samples. 2D-mapping the spatial distribution of the threshold voltage shift revealed that the samples with bolus overtop experienced greater variations in the threshold voltage, with hotspots near the center beam placement. These observations indicate that the presence of the bolus slab alters the radiation profile, and, in turn, the dose received by the patient. Our results are important because they provide for the first time the much-needed tools that can generate the information on the variations in the radiation dose over a large area, relevant to cancer therapy in a clinical setting.

SB06.04.22

Optimization of Porous TiO₂ Electron Transport Layer in Carbon-Based Perovskite Solar Cells [Takaya Shioki](#), Ryuki Tsuji, Kouta Oishi and Seigo Ito; University of Hyogo, Japan

Carbon-based multi-porous-layered-electrode perovskite solar cells (MPLE-PSCs) are the most promising for the general PV market due to their simple fabrication process with full printing and extremely high durability. However, the low photoelectric conversion efficiency (PCE) of MPLE-PSCs (less than 20% PCE) has been cited as an issue for practical use. In this study, we focused on the porous TiO₂ layer used as the electron transport layer in MPLE-PSCs and aimed to improve the device performance by optimizing the TiO₂ particle size.

The MPLE-PSC devices were fabricated as follows. Materials were stacked on an FTO glass substrate: a compact TiO₂ layer (as a blocking layer), a mesoporous TiO₂ layer (as an electron transport layer), a mesoporous ZrO₂ layer (as an insulating layer to prevent short circuit), and a mesoporous carbon layer (as a hole transport layer and back electrode) [1-2]. After that, a perovskite precursor solution was dropped on the electrode, and it was crystallized by annealing process.

In this study, six types of TiO₂ particle sizes of 98, 52, 43, 26, 18, and 14 nm were used for the mesoporous electron transport layer, and the performance of these six types of MPLE-PSCs was evaluated. As a result, the MPLE-PSCs using 43-nm TiO₂ showed the highest photoelectric conversion efficiency (PCE). In addition, it was confirmed that the short-circuit current density (J_{sc}) of the MPLE-PSCs changed for each TiO₂ particle size. This is thought to be due to the influence of the light absorption rate of the device. In this presentation, we will report the results of detailed analysis in the conference.

References

- [1] A. Mei, et al., Science 345, 295 (2014).
- [2] S. Ito, et al., Nano 9, 1440010 (2014).

SB06.04.23

100% Yield, 4-Inch Wafer-Scale Non-Volatile Optically-Guided Organic-Inorganic Heterostructure Memory Array with Simultaneous Detection and Storage of Text Image [Seongjae Kim](#)¹, Juhyung Seo¹, Taehyun Park² and Hocheon Yoo¹; ¹Gachon University, Korea (the Republic of); ²Chemical and Biological Engineering, Korea (the Republic of)

Photoreactive optically-guided memory allows photodetector and memory functions to be combined in a single device. Accordingly, the above-mentioned memory device reduces unnecessary signal delay by reducing the metal wiring between the photodetector and the memory device, and the detection and storage functions of two different devices can be available with one device, thereby reducing the overall system size [1-2]. Due to these advantages, an optically-guided memory is considered significantly promising as a potential thin-film transistor memory for next-generation applications, where image sensing and processing capabilities are simultaneously required. In this light, this talk presents an organic/inorganic heterogeneously stacked optically-guided memory. In the proposed memory devices, the number of electrons formed in the channel layer is modulated by the intensity of incident light, and thereby the excited electron/hole pairs change the degree of electron carriers trapped in the floating gate. Based on the proposed heterogeneous memory structure, this work also implements a 4-inch wafer-scale 12×12 memory transistor array consisting of 144 devices enabling image detection with 100% yield. This study also demonstrates a text image detection with non-volatile memory characteristics depending on the presence or absence of light irradiation during the programming operation.

References

1. Hong, Seongin, et al. "Multifunctional molybdenum disulfide flash memory using a PEDOT: PSS floating gate." NPG Asia Materials 13.1 (2021): 1-11.
2. Yang, Wei-Chen, et al. "Comprehensive non-volatile photo-programming transistor memory via a dual-functional perovskite-based floating gate." ACS Applied Materials & Interfaces 13.17 (2021): 20417-20426.

SB06.04.24

Nanoimprint Formation of the Atomically Ultra-Smooth Surface of the PEDOT: PSS Conducting Polymer Thin Film for Flexible Optoelectronic Devices [Yuto Maeda](#)¹, Naho Kaneko¹, Tomoaki Oga¹, Satoru Kaneko^{2,1}, Akifumi Matsuda¹ and Mamoru Yoshimoto¹; ¹Tokyo Institute of Technology, Japan; ²Kanagawa Institute of Industrial Science and Technology, Japan

Conductive polymer materials such as PEDOT: PSS with features of light weight and large area have become increasingly important in flexible electronics of organic thin-film solar cells or other optoelectronic devices [1]. In the construction of electronic devices on these polymer thin film electrodes, surface flatness and atomic- and/or nano-level surface control of conductive polymer thin films are essential for formation of fine and highly integrated devices. So far, by using the ultra-smooth sapphire (α -Al₂O₃ single crystal) wafers with self-organized approx. 0.3-nm high atomic-step straight nanopatterns as nanoimprinting molds [2], we had reported on the fabrication of surface ultra-smooth substrates by transferring their nanoscale patterns onto the surfaces of oxide glasses and thermoplastic polymers [3-5]. On the other hand, as for nanopatterning of PEDOT: PSS having no thermo-plasticity, there were only a few reports on stripe surface patterning (10nm depth and 700nm period) onto the thin film for increase of the organic photovoltaic device efficiency [6]. In this study, for formation of the atomically smooth surface on the PEDOT: PSS thin film, we investigated transcription of 0.3nm-high atomic-step and atomically flat terrace pattern of the sapphire mold onto the spin-coated PEDOT: PSS thin film surface via thermal nanoimprinting. We also characterized electric properties as well as the thermal or UV-light durability of the nanoimprinted pattern on the sample surfaces.

A flexible transparent polyimide sheet (PI; t~20 μm , ECRIO® VICT-Bnp, Mitsui Chemicals Co., Japan) was used as a polymer substrate for thin film deposition. PEDOT: PSS thin films were prepared by spin-coating PEDOT: PSS aqueous dispersion and drying at 170°C for 60 min. Thermal nanoimprinting was then performed at 200-270°C and 15 MPa for 40 min in vacuum on the PEDOT: PSS thin film surface using the sapphire mold with an atomic step and terrace width of about 600 nm. As a result, it was confirmed that an atomic step and terrace pattern corresponding to the sapphire mold could be transferred accurately onto the PEDOT: PSS thin film on the polyimide sheet in case of nanoimprinting at 260°C. The successful transfer was achieved under conditions near the glass transition temperature (about 265°C) of the polyimide substrate, suggesting that the nanopattern transfer onto the

PEDOT: PSS thin film might be related to softening phenomena of the substrate.

- [1] A. Radivo et al., *RSC Adv.*, **4**, 34014 (2014).
- [2] M. Yoshimoto et al., *Appl. Phys. Lett.* **67**, 2615 (1995).
- [3] K. Shimada et al., *Jpn. J. Appl. Phys.*, **55**, 098002 (2016).
- [4] G. Tan et al., *Appl. Phys. Express.*, **7**, 055202 (2014).
- [5] Y. Miyake et al., *Jpn. J. Appl. Phys.*, **50**, 078002 (2011).
- [6] J. B. Emah et al., *Appl. Phys. Lett.* **93**, 103301 (2008).

SB06.04.26

Effects of Post-treatment on the Transport Properties of Te/PEDOT:PSS and Ag₂Te/PEDOT:PSS Hybrid Thermoelectric Thin Films Rodrigo Rubio^{1,2}, Roberto Félix¹, Regan G. Wilks¹, Marcus Baer^{1,3,4} and Katherine A. Mazzio^{1,2}; ¹Helmholtz-Zentrum Berlin für Materialien und Energie GmbH, Germany; ²Humboldt-Universität zu Berlin, Germany; ³Friedrich-Alexander-Universität Erlangen-Nürnberg, Germany; ⁴Helmholtz-Institute Erlangen-Nürnberg for Renewable Energy, Germany

Hybrid organic/inorganic materials composed of tellurium (Te) nanowires (NWs) embedded into poly(3,4-ethylenedioxythiophene):poly(styrene sulfonate) (PEDOT:PSS) have been prominently studied after it was reported that their transport properties could be tuned by varying the length of the NWs and modulating the amount of PEDOT:PSS incorporated into the system.[1] Nevertheless, the influence of each constituent on the observed transport properties was not fully understood. Recently, based on molecular dynamics simulations and density functional theory calculations, it was proposed that the templating effect of PEDOT over the Te NWs surface is responsible for the enhanced transport properties of Te/PEDOT:PSS hybrids, and it was later experimentally demonstrated that the electronic transport occurs predominantly through the organic portion of the hybrid.[2,3] However, no direct experimental evidence of the existence of the templating effect was given.

It is well known that the electrical conductivity of conducting polymers (CPs) can be considerably enhanced when subjected to post-treatment processes, such as primary (i.e. charge transfer or acid-base processes) or secondary (morphological rearrangement that only impacts mobility and not oxidation level) doping. The transport properties strongly depend on the creation of polaron/bipolaron clusters dispersed through the polymer matrix, so their concentration and mobility are dependent on the oxidation level and the degree of crystalline domains.

In this work, we investigate the effects of tetrakis(dimethylamino)ethylene, sulfuric acid, and ethylene glycol post-treatments on the thermoelectric performance of p-type Te/PEDOT:PSS and n-type Ag₂Te/PEDOT:PSS hybrid materials. By analyzing the materials with X-ray diffraction, Raman spectroscopy, hard X-ray photoelectron spectroscopy, and Hall measurements, we find that variations of the thermoelectric performance are related to modifications in the morphological and chemical structure of PEDOT:PSS that is reflected in changes to the charge carrier density and mobility. Additionally, we present experimental evidence that strongly supports the templating effect causing the planar alignment of the first few layers of PEDOT over the NWs surface.

- [1] Yee, S., *Phys. Chem. Chem. Phys.*, 2013, 15, 4024-4032.
- [2] Kumar, P., *Nat. Commun.*, 2018, 9, 5347.
- [3] Yang, L., *Sci. Adv.*, 2021, 7, eabe6000.

SESSION SB06.05: Structure Properties Relationships, Organic Solar Cells and Photonic Devices
Session Chairs: Thomas Anthopoulos and Christos Chocho
Tuesday Morning, November 29, 2022
Hynes, Level 3, Room 312

8:30 AM *SB06.05.01

Organic Optoelectronic Devices Processed from Green Solvents Zhifang Du¹, Hoang Luong¹, Sina Sabury², Austin Jones², Manjunatha Reddy³, John Reynolds² and Thuc-Quyen Nguyen¹; ¹University of California, Santa Barbara, United States; ²Georgia Institute of Technology, United States; ³University of Lille, CNRS, Centrale Lille Institut, Univ. Artois, UMR 8181, France

Organic semiconductors (OSCs) comprise small molecules or polymers are attractive candidates for the fabrication of a range of technologies including large area and flexible plastic solar cells, photodetectors, organic thin film field-effect transistors (OFETs), and organic light-emitting diodes (OLEDs) for displays and lighting applications. New opportunities that integrate soft semiconductors are also emerging, including thermoelectric devices, bioelectronic monitoring devices, and hybrid soft/hard electronic materials. To accelerate the mass fabrication of OSCs, green solvent processing is crucial to reducing the environmentally hazardous effects of halogenated solvents. However, there are only a limited number of studies that focus on the improvement of device performance using green-solvent processing, and the connection between the green-solvent processing, morphology, and performance is still poorly understood. In this talk, I will discuss the design, synthesis, and performance of organic semiconductors processed from green solvents such as xylene and 2-methyltetrahydrofuran (2-MeTHF). 2-MeTHF is a biomass-derived (furfural or levulinic acid) and environmentally friendly solvent that is widely used in organic synthesis, which can be produced from low-cost and renewable agriculture feedstock. A combination of characterization methods were employed to gain insight into the film morphology and solar cell and photodetector performance.

9:00 AM SB06.05.02

The Morphological Stability of “Burn-Up” Non-Fullerene-Acceptor Organic Solar Cells Rachel Kilbride¹, Matthew Bidwell², Emma Spooner¹, Robert Dalglish³, Philipp Gutfreund⁴, James Tellam³, Nicola Gasparini², Iain McCulloch⁵, David Lidzey¹, Richard Jones⁶ and Andrew Parnell¹; ¹University of Sheffield, United Kingdom; ²Imperial College London, United Kingdom; ³ISIS Pulsed Neutron and Muon Source, United Kingdom; ⁴Institut Laue-Langevin, United Kingdom; ⁵University of Oxford, United Kingdom; ⁶The University of Manchester, United Kingdom

Over the past decade, the development of small molecule non-fullerene acceptors (NFAs) as the photoactive components in organic photovoltaic (OPV) devices has pushed efficiencies close to the fabled 20%^[1,2], an efficiency threshold considered essential for commercially viable OPV technologies. Unfortunately, increases in OPV device efficiency have not been in step with increased long-term operational stability and devices typically demonstrate an initial ‘burn-in’ period of rapid performance loss. The origin of this performance loss remains poorly understood and mitigation strategies are yet to be developed. In this work, the stability of a well-studied polymer : fullerene system (PTB7-Th : PC₇₁BM) is compared with a series of polymer : NFA systems based on PTB7-Th and the IDTBR family of NFAs. Polymer : IDTBR systems demonstrate superior stability, characterised by an unusual fill-

factor-driven efficiency enhancement or 'burn-up' improvement period within 24h of fabrication. The morphological origins of this phenomenon are explored across a broad range of length scales (\AA – nm – μm) using grazing incidence wide angle scattering (GIWAXS), small angle neutron scattering (SANS) and neutron reflectivity. Neutron scattering measurements of polymer : NFA blend films are made possible by the synthesis of deuterium-labelled NFA analogues (d-NFAs), providing unparalleled sensitivity and insight into the morphological stability and phase separation of the bulk-heterojunction photoactive blend. It is found that subtle changes in the degree of phase separation and NFA crystallinity during device ageing under inert conditions are closely linked to changes in PV efficiency. The findings described here provide a more thorough understanding of the morphological stability of the bulk heterojunction blend, essential for improving the operational lifetime and commercial viability of OPV technologies.

[1] L. Hong, H. Yao, Z. Wu, Y. Cui, T. Zhang, Y. Xu, R. Yu, Q. Liao, B. Gao, K. Xian, H. Y. Woo, Z. Ge, J. Hou, *Adv. Mater.* **2019**, *31*, 1903441.
[2] P. Bi, S. Zhang, Z. Chen, Y. Xu, Y. Cui, T. Zhang, J. Ren, J. Qin, L. Hong, X. Hao, J. Hou, *Joule* **2021**, *5*, 2408.

9:15 AM *SB06.05.03

Synthesis and Structure-Function Relationships in Fused Aromatics for Electronic and Photonic Applications [John Anthony](#); University of Kentucky, United States

In thin film devices, the precise nature of the interaction between chromophores is critical to the performance of any device. In acenes, we long ago developed a method to induce crystalline order that yields excellent performance in applications requiring efficient charge transport, such as organic transistors. Much more recently, we have begun to address the impact of dynamic disorder - disruptive phonon modes - to improve both the performance and reproducibility of our materials in organic transistors. Here, I will discuss three approaches we have explored to alter disruptive phonon modes through systematic structural variations, and will describe the approach and impact of each of these structural changes. The production of these structurally modified materials also required the development of new synthetic methods for the preparation of fused aromatic compounds, which will also be presented.

9:45 AM SB06.05.04

Green Emissive Blends in the Limit of Field-Effect Transport in Organic Light-Emitting Transistors [Caterina Soldano](#), [Ornella Laouadi](#) and [Katherine Gallegos-Rosas](#); Aalto University, Finland

Organic light-emitting transistors are photonic devices combining the function of an electrical switch with the capability of generating light under appropriate bias conditions. Achieving high-performance light-emitting transistors requires high mobility organic semiconductors, optimized device structures and highly efficient emissive layers.

Here, we studied the opto-electronic response of TCTA:Ir(ppy)₃ blends with varying doping concentration in the limit of field-effect within a transistor configuration. Increasing the dye concentration within the blend leads to a quenching of the photoluminescence signal; however, when implemented in the vertical stack in the transistor, we observed an approximate 5-fold improvement in the light output for a 10% Ir(ppy)₃ doping blend. We analyzed our results in terms of balanced charge transport in the emissive layer, which, in the limit of field-effect transport, leads to an improved exciton formation and decay process.

While the efficiency of our devices is yet to achieve state-of-the-art diode counterpart, this work demonstrates that engineering the emissive layer is a promising approach to enhance the light emission in field-effect devices. This opens the way for a broader exploitation of organic light-emitting transistors as alternative photonic devices in fields ranging from display technology to flexible and wearable electronics.

10:00 AM BREAK

SESSION SB06.06: Exciton Manipulation and Optoelectronic Processes

Session Chairs: John Anthony and Julie Euvrard

Tuesday Morning, November 29, 2022

Hynes, Level 3, Room 312

10:30 AM *SB06.06.01

The Interplay Between CT and Singlet Exciton Emission and Its Impact on Organic Solar Cells [Safa Shoaee](#); University of Potsdam, United States

Organic solar cells (OSCs) have rapidly advanced, reaching state-of-the-art efficiencies of above 19 % for single-junction solar cells [1]. Yet, these cells suffer from non-radiative recombination, which limits their FF and VOC. It is generally believed that free charge carrier recombination in OSCs proceeds primarily via reformation and decay of charge transfer (CT) states, involving radiative and non-radiative pathways. The latter typically dominates the decay rate and is, therefore, responsible for the VOC loss. The situation becomes more complex when the energy of the CT state, ECT, approaches the energy of the lowest singlet exciton, the local exciton of the component dominating the optical gap. In this case, reformation of the singlet exciton from the CT state becomes more likely, documented e.g. by an increased singlet exciton emission intensity in electroluminescence (EL) [2]. As singlet excitons are generally more emissive than CT states, this causes a significant reduction of the non-radiative voltage loss. It has, therefore, been proposed that OSCs benefit from a strongly-emitting singlet exciton [3]. In contrast, we have recently shown for the prototypical PM6:Y6 blend, that predominant emission from the S₁ state does not automatically mean that free charge recombination proceeds through this state [4]. Understanding the interplay between these two states and how they determine the voltage losses in relation to $\Delta E(S_1-CT)$ is therefore of great interest.

We combine PM6 with three different acceptors which have similarly low offsets while leaving the S₁ energy of the polymer unaffected. We show that the emission of the blends becomes dominated by the S₁ of the acceptor in all cases, but that the CT state properties determine the non-radiative processes and the VOC in all devices. Importantly, the high oscillator strength of the singlet exciton reduces the non-radiative voltage loss not because it is more emissive, but because its higher absorption as compared to the CT state lowers the radiative VOC limit. We suggest that it's only for very low CT state oscillator strengths and a fairly high radiative efficiency of the CT state that the VOC benefits from the radiative properties of the singlet excitons.

11:00 AM SB06.06.02

Direct Exciton Harvesting from a Bound Triplet Pair [Guiying He](#)¹, [Kaia R. Parenti](#)², [Luis M. Campos](#)² and [Matthew Sfeir](#)¹; ¹Advanced Science Research Center, City University of New York, United States; ²Columbia University, United States

Singlet fission is commonly defined as the generation of two triplet excitons from a single absorbed photon, which has received considerable attention because of its potential to overcome the Shockley-Queisser limit on the power conversion efficiency (PCE) of solar cells. However, ambiguities within this definition arise due to the complexity of the various double triplet states that exist in SF chromophores and corresponding interconversion processes. To

clarify this process, singlet fission is frequently depicted as sequential two-step conversion in which a singlet exciton decays into a bound triplet pair biexciton state which dissociates into two “free” triplet excitons. However, this model discounts the potential for direct harvesting from the coupled biexciton state. Using intramolecular SF dimers, we demonstrate that individual triplet excitons can be extracted directly from a bound triplet pair state prior to dissociation. These compounds have well-defined electronic interactions that allowing for detailed studies of multiexciton state and its dynamics. We show that due to the requirement for geminate triplet-triplet annihilation in these compounds, unique spectral and kinetic signatures can be used to quantify triplet pair harvesting yields. We achieve an internal quantum efficiency for triplet exciton transfer from the triplet pair of greater than 50%, limited only by the solubility of the compounds. The harvesting process is not dependent on the net multiplicity of the triplet pair state, suggesting that an explicit dissociation step is not a requirement for using triplet pairs to do chemical or electrical work.

11:15 AM SB06.06.03

Large Magnetic Field Sensitivity in a High Spin Ground-State Donor-Acceptor Conjugated Polymer Hamas U. Tahir¹, Naresh Eedugurala², Sheng-Ning Hsu¹, Daniel Adams², Jason D. Azoulay², Brett M. Savoie¹ and Bryan W. Boudouris¹; ¹Purdue University, United States; ²The University of Southern Mississippi, United States

Open-shell macromolecules are an emerging class of materials that have the potential to be implemented in multiple applications (e.g., energy storage devices and electronic systems). The presence of unpaired electrons endows these materials with unique properties that are difficult to achieve with conventional organic semiconductors, such as extremely long spin relaxation times. In addition to exhibiting weak spin-orbit coupling and hyperfine interactions, these polymers are paramagnetic due to their unpaired spins. This added functionality, which is not available in well-studied closed-shell organic semiconductors, make these materials suitable for spintronics applications. It is because radicals retain their magnetic moment in solid state electronic devices, thus enabling facile coupling with an external magnetic field. However, the utilization of open-shell macromolecules that could favor spin polarization and spin conservation during transport have been less studied. Here, we evaluate the magnetic behavior of poly(4-(4-(3,5-didodecylbenzylidene)-4H-cyclopenta[2,1-b:3,4-b']dithiophen-2-yl)-6,7-dimethyl-[1,2,5]-thiadiazolo[3,4-g]quinoxaline), a high spin donor acceptor conjugated diradical polymer that has a low bandgap and triplet ground state. We confirmed the high spin behavior with a series of temperature-dependent electron paramagnetic resonance and superconducting quantum interference device (SQUID) experiments. We also observe that, for $T < 180$ K, this polymer exhibits giant negative magnetoresistance (i.e., -95% at $T = 10$ K), which is largest negative magnetoresistance observed for organic molecules up to date. As the temperature increases, the thermal population of triplet state decreases and hence magnetoresistance decreases as well. Moreover, for $T > 180$ K, the magnetoresistance becomes positive, and relatively large positive magnetoresistance ($+13\%$) is observed at room temperature. These tunable magnetoresistance results suggest the indispensable correlation between diradical character and large magnetoresistance due to spin-spin interactions. Our results indicate that donor-acceptor conjugated diradical polymers with thermally accessible triplet state have potential for spintronic applications.

11:30 AM SB06.06.04

Efficient Single-Layer Inverted Organic Light-Emitting Diodes Based on TADF Emitters Xiao Tan, Paul Blom and Gert-Jan Wetzelaer; Max Planck Institute for Polymer Research, Germany

Recently, a yellow organic light-emitting diode (OLED) based on a single layer of a neat thermally activated delayed fluorescence (TADF) emitter sandwiched between two ohmic contacts has been demonstrated to achieve similar efficiency and longer lifetime compared to more complex multilayer architectures.^[1] For blue emitters, however, the required energy gap of ~ 3 eV, will often lead to trap-limited charge transport for either electrons or holes^[2], leading to severe charge imbalance in an OLED. Since for most organic blue emitters the electron affinity is lower than 3.6 eV, electron transport is frequently impaired. As a result, in a single-layer OLED, the emission zone will be situated close to the metallic cathode, leading to severe light-outcoupling losses. Here, this issue is solved by the design of inverted single-layer OLEDs. Despite the severely imbalanced transport of the used emitters, high external quantum efficiencies up to 19% are achieved even for blue TADF emitters. The high efficiencies are the result of the emission zone being shifted away from the metallic top electrode, due to a combination of using an inverted device structure and taking advantage of the superior hole transport through the emitters. This new device strategy bypasses the severe limitations of imbalanced and trap-limited transport inherent to blue emitters, which leads to improved performance in blue OLEDs.

1. *Nature Photonics*, 2019, 13(11): 765-769.

2. *Nature Materials*, 2019, 18(11): 1182-1186.

SESSION SB06.07: Structure-Properties in Organic Semiconductors

Session Chairs: Ryan Chiechi and Alberto Salleo

Tuesday Afternoon, November 29, 2022

Hynes, Level 3, Room 312

1:30 PM *SB06.07.01

Characterizing the Microstructure in Donor-Acceptor Blends and Linking It to Device Properties Alberto Salleo; Stanford University, United States

Donor-acceptor blends for organic photovoltaics have intricate microstructures with several characteristic lengthscales that all affect different aspects of the active layer performance, whether it's charge transport, charge splitting efficiency or photovoltage. I will describe how the microstructure of the high-performance PM6:Y6 blend changes with composition using semi-quantitative x-ray diffraction and high-sensitivity EQE measurements. I will show that transport and photovoltage are maximized at different compositions leading to a fundamental trade-off.

Spatially resolving the microstructure at the donor-acceptor interface can also lead to interesting insights. In this respect I will show a quantitative TEM study of a polymer-polymer blend to show that donor and acceptor exhibit a preferential relative orientation, suggesting a form of soft epitaxy. The effect of additives will also be examined quantitatively and linked to photovoltaic performance.

2:00 PM SB06.07.02

From Amorphous to Polycrystalline Rubrene—Charge Transport in Organic Semiconductors Paralleled with Silicon Julie Euvrard^{1,1}, Oki Gunawan², Antoine Kahn¹ and Barry P. Rand^{1,1}; ¹Princeton University, United States; ²IBM T. J. Watson Research Center, United States

While progress has been made in the design of new organic semiconductors (OSCs) with improved transport properties (i.e., high mobilities), our understanding of the mechanisms involved is still limited and hinders further development, due in large part to the inherent difficulty when comparing OSCs with different molecular structure and morphologies. For silicon, enhanced understanding finally came once comparisons could be made with

variations in morphology from single crystals to fully amorphous films. In this work, we achieve a similar feat in one single organic molecular system. In particular, rubrene is employed as the OSC as it spans transport mechanisms from thermally activated hopping in its amorphous form to band-like transport in highly ordered crystals. Various transport characterizations including variable temperature conductivity, advanced Hall effect and magnetoresistance measurements are performed on rubrene films with varying levels of order (polycrystalline vs amorphous), crystal phase (orthorhombic vs triclinic) and morphologies (platelet-like vs spherulitic grains). We find that conductivity can be tuned over four orders of magnitude when changing the level of order in the film from fully amorphous to polycrystalline with a few high-quality grains. Our results show that transport in polycrystalline orthorhombic films is limited by grain boundaries, as observed in polycrystalline silicon. The use of advanced Hall measurement, for the first time performed on OSC thin films without the use of “gating” (gate voltage applied through addition of a dielectric and gate electrode), provides access to the intrinsic properties of the semiconductor. Despite the very high resistivity of amorphous and triclinic rubrene, we are able to probe a Hall signal, pointing to the existence of a marginal density of delocalized carriers. Overall, our Hall and magnetoresistance measurements suggest a gradual transition from predominantly hopping transport to predominantly band-like transport as order is increased and crystal phase optimized. In summary, through this work we provide a comprehensive understanding of the interplay between order, molecular packing, morphology and charge transport in OSCs, akin to research on silicon decades ago. Our results point toward the application of a unified transport model with varying contributions of delocalized and localized carriers. More importantly, our study highlights that order alone is insufficient whereas intermolecular coupling is paramount for optimal transport, providing guidelines for the design of new molecules.

2:15 PM SB06.07.03

Supramolecular Self-Assembly as a Tool to Preserve Electronic Purity in Perylene-dimide Chromophores [Sascha Feldmann](#); Harvard University, United States

Organic chromophores are promising for the next generation of molecular electronic devices owing to their inherently flexible mechanical properties and the fact that the desired optoelectronic properties can be tailored through chemical design. Perylene-dimide (PDI) is such a candidate for molecular electronics but, like most, also shows strong excited-state quenching upon aggregation or upon chemical functionalization for better processing, hindering its use in future device applications. Here, we employ supramolecular self-assembly as a precise tool for preventing these undesired and performance-limiting effects. We form a supramolecular pseudo-cube based on functionalized PDI molecules and demonstrate that the rigidity provided by the cage framework allows us to retain the electronic purity of its individual PDI subcomponents that is typically lost upon aggregation, while also suppressing vibronic losses observed in the free ligand. This rigidity extends even to the solid state upon thin film formation. We demonstrate a rare case of benign inter-chromophore interactions in a cage and confirm delayed and enhanced fluorescence, mediated through both an excited multimer and a triplet reservoir. Supramolecular coordination thus provides an attractive route for controlling multi-chromophore interactions to fully enable device integration.

2:30 PM BREAK

SESSION SB06.08: Organic Electrochemical Transistors

Session Chairs: Sahika Inal and Natalie Stingelin

Tuesday Afternoon, November 29, 2022

Hynes, Level 3, Room 312

3:00 PM *SB06.08.01

Ambipolar Blend-Based Organic Electrochemical Transistors and Inverters [Gitti L. Frey](#); Technion--Israel Institute of Technology, Israel

Bioelectronic circuits translate biological to electric signals using organic electrochemical transistors (OECTs) based on organic mixed ionic-electronic conductors (OMIEC) in CMOS-like circuit architectures. Ambipolar OECTs, i.e. devices that can act as both p-type and n-type, can therefore reduce the complexity of circuit fabrication and increase device density. Ambipolarity in bioelectronics has another major advantage, the simultaneous detection of both cations and anions in one device, which further expands the prospects for diagnosis and sensing. Ambipolar OMIECs however, are scarce, limited by intricate material design and complex synthesis. We recently demonstrated that blending p-type and n-type OMIEC materials offers a simple and tunable approach for the fabrication of ambipolar OECTs and corresponding circuits. Building on the processing-morphology-performance relationships in organic solar cells, we implemented blends of polymers and small molecules where the morphology of the active layers can be controlled by materials selection, blend composition and processing conditions. We will present two families of blends: n-type polymer and p-type small molecules, or p-type polymer and n-type small molecules, confirming the generality and versatility of the approach. We will also discuss how the molecular design of the materials, with respect to energy level alignment and solubility, affect device performance. Finally, we will show that the ambipolar OECTs can be used as building blocks for CMOS-like circuits, more specifically, inverters made of two identical ambipolar OECTs. These inverters show high current and voltage amplification factors and excellent stability over multiple alternating polarity cycles with ON/OFF ratios exceeding 10^3 on both polarities and high gain. This work presents a simple and versatile new paradigm for the fabrication of ambipolar OMIECs and corresponding circuits with little constraints on materials design and synthesis and numerous possibilities for tunability and optimization towards higher performing bioelectronic applications.

3:30 PM SB06.08.02

Toward Stable p-type Organic Electrochemical Transistors [Silan Zhang](#)¹, [Penghui Ding](#)¹, [Mikhail Vagin](#)¹, [Marc-Antoine Stoeckel](#)¹, [Tero-Petri Ruoko](#)², [Xianjie Liu](#)¹, [Mats Fahlman](#)¹, [Magnus Berggren](#)¹, [Renee Kroon](#)¹ and [Simone Fabiano](#)¹; ¹Linköping University, Sweden; ²Tampere University, Finland

Organic electrochemical transistors (OECTs) have shown great promise in various applications ranging from digital logic circuits to biosensors and neuromorphic devices. Achieving high operational stability is paramount to enabling their broad commercial implementation into products. However, undesired electrochemical side reactions, such as the oxygen reduction reaction (ORR), affect the stability of both p-type and n-type OECTs. While several strategies have been proposed to mitigate ORR in OECTs, a deeper understanding of the relationship between ORR and material degradation is required to drive the design and synthesis of new high-performance materials. Here, we will elucidate the impact of ORR on the stability and degradation mechanisms of thiophene-based OECTs. We will also present a strategy to suppress ORR, thus boosting the OECT stability dramatically without sacrificing device performance.

3:45 PM SB06.08.03

Uniaxial Alignment of Polymer Chains—A Versatile Strategy to Achieve Faster Switching and Higher Performing Organic Electrochemical Transistors [Olivier Bardagot](#)¹, [Pablo Durand](#)², [Shubhradip Guchait](#)³, [Gonzague Rebetz](#)¹, [Martin Brinkmann](#)³, [Nicolas Leclerc](#)² and [Natalie Banerji](#)¹; ¹University of Bern, Switzerland; ²ICPEES-CNRS, France; ³ICS-CNRS, France

Organic electrochemical transistors (OECTs) are the cornerstone of emerging bioelectronic devices such as artificial synapses^[1] and electrophysiological signal amplifiers^[2]. To boost their development, two key parameters must be improved: (i) the signal amplification (to maximize device sensitivity), and (ii) the OECT response time (to detect sub-ms scale signals).

In parallel to polar side-chain engineering that proved to be an efficient strategy to improve concomitantly OECT response time and electronic performance^[3], we herein present a complementary strategy relying on uniaxial alignment of polymer chains between the source and the drain of the transistor. Using high temperature mechanical rubbing, Durand *et al.* demonstrated metal-like conductivity up to 50 000 S cm⁻¹ along the alignment direction for a chemically doped films of poly(2-(4,4'-bis(7-butoxyheptyl)-[2,2'-bithiophen]-5-yl)thieno[3,2-b]thiophene) (PBTTT-⁸O), a PBTTT polymer with a polar single ether side chain.^[4] In this presentation, we extend the potential of aligned PBTTT-⁸O to aqueous OECT-based applications.

First, the signal amplification was estimated through the product [μC^*] of electronic charge carrier mobility (μ) and volumetric capacitance (C^*), extracted for transistors of varying channel volumes. The isotropic, non-aligned, PBTTT-⁸O-based OECTs demonstrated state-of-the-art values over 600 F cm⁻¹ V⁻¹ s⁻¹ confirming the potential of single ether side chains.^[5] Interestingly, uniaxial alignment of PBTTT-⁸O led to a thirtyfold enhancement up to 20 000 F cm⁻¹ V⁻¹ s⁻¹, opening doors to unprecedented device sensitivity. Such increase is attributed to higher inter/intramolecular interactions in the probed direction resulting from the polymer chain alignment. Using chronoamperometry to evaluate C^* , a hole mobility of over 30 cm² V⁻¹ s⁻¹ was found.

Second, the response times of aligned and non-aligned PBTTT-⁸O-based OECTs were quantified by combining spectroelectrochemistry and multivariate curve resolution (MCR) analysis. We found that neutral species in aligned OECTs (i) dope about twice faster and (ii) dedope more than four times faster than non-aligned OECTs. These significant improvements are tentatively ascribed to faster ion injection/expulsion due to higher surface-to-volume ratio^[6] and faster charge injection/extraction due to higher hole mobility.

To summarize, we demonstrate not only that single ether side chains is an efficient molecular engineering strategy, but more importantly that uniaxial alignment of polymer chains between the source and the drain of OECTs is an effective strategy to concomitantly boost signal amplification and device response time. In particular, high temperature mechanical rubbing is a versatile and easily implementable method compatible with roll-to-roll processing. This work promises a bright future for highly structured OECT channels for fast and high performance bioelectronic devices.

[1] X. Ji, B. D. Paulsen, G. K. K. Chik, R. Wu, Y. Yin, P. K. L. Chan, J. Rivnay, *Nature Communications* **2021**, *12*, 2480.

[2] S. Bontapalle, M. Na, H. Park, K. Sim, *Chemical Communications* **2022**, DOI 10.1039/D1CC04884H.

[3] A. Savva, R. Hallani, C. Cendra, J. Sargailis, T. C. Hidalgo, S. Wustoni, R. Sheelamantula, X. Chen, M. Kirkus, A. Giovannitti, A. Salleo, I. McCulloch, S. Inal, *Advanced Functional Materials* **2020**, *30*, 1907657.

[4] P. Durand, H. Zeng, T. Biskup, V. Vijayakumar, V. Untilova, C. Kiefer, B. Heinrich, L. Herrmann, M. Brinkmann, N. Leclerc, *Advanced Energy Materials* **2021**, 2103049.

[5] S. E. Chen, L. Q. Flagg, J. W. Onorato, L. J. Richter, J. Guo, C. K. Luscombe, D. S. Ginger, *Journal of Materials Chemistry A* **2022**, DOI 10.1039/D2TA00683A.

[6] R. Giridharagopal, J. Guo, J. Kong, D. S. Ginger, *ACS Appl. Mater. Interfaces* **2021**, *13*, 34616–34624.

4:00 PM SB06.08.04

Separating the Double Layer from the Faradaic Processes at Conducting Polymer/Electrolyte Interfaces Using Electrochemical and Color Impedance Spectroscopies [Zhiting Chen](#) and Erin L. Ratcliff; University of Arizona, United States

The hybrid electrical-ionic transport properties of π -conjugated polymers offer a number of promising energy conversion and storage and biosensing applications for soft material semiconductors. Current studies focus predominantly on either electronic transport or ionic transport characteristics and structure-property relationships. As the electronic and ionic transports are highly coupled in electrochemical devices, it is a challenge to differentiate a redox process of the conjugated backbone (Faradaic) from the complementary intercalation of supporting electrolyte (non-Faradaic) at polymer/electrolyte interfaces with both energy and frequency resolution.

Spectroelectrochemical approaches offer enhanced sensitivity to particular reactions of interest; in particular, polaronic motion can be monitored at various time scales upon doping using the electrochromic properties of π -conjugated systems. Herein we use color impedance spectroscopy (CIS) to resolve the dynamic responses of a prototypical system, poly(3-hexylthiophene), thus separating out contributions from non-polaronic processes – specifically ion intercalation and solvation effects – from Faradaic processes.

Using CIS, we observe that higher doping potentials show a greater motion of polarons above the DC-bias baseline concentration, while all potentials considered demonstrates a critical frequency at which polaronic motion is frozen. This critical frequency offers a unique figure of merit, measured independent of complicated electrochemical impedance spectroscopy (EIS) analysis, by which to compare across polymer/electrolyte interfaces, including the role of charge-supporting electrolyte, solvent, and alternative Faradaic processes (ex. electrocatalysis).

SESSION SB06.09: Poster Session II
Session Chairs: Alexander Colsmann and Safa Shoaee
Tuesday Afternoon, November 29, 2022
8:00 PM - 10:00 PM
Hynes, Level 1, Hall A

SB06.09.01

Elimination of Charge-Carrier Trapping by Molecular Design [Oskar Sachnik](#), Jasper Michels, Gert-Jan Wetzelaer and Paul Blom; Max Planck Institute for Polymer Research, Germany

Most organic semiconductors suffer from an unbalanced charge transport, which is caused by trapping of holes and/or electrons by contaminants, such as water or oxygen. Devices that benefit from a balanced charge transport, such as organic light emitting diodes, organic solar cells and organic ambipolar transistors, ideally make use of organic semiconductors that possess energy levels within an energetic trap-free window with a width of 2.5 eV, for which charge trapping is near absent. However, for blue-emitting OLEDs, which require materials with a band gap larger than this window, removing or disabling charge traps poses a significant challenge. In this work, we demonstrate a strategy to design organic semiconductors, of which the HOMO and LUMO orbitals are spatially separated on different parts of the molecule. By modification of the chemical structure the molecular stacking can be tuned in a way

that the LUMO orbitals are protected from impurities that cause electron trapping, increasing the electron current by orders of magnitude. This illustrates a path towards large band gap organic semiconductors with balanced charge transport.

SB06.09.02

N-Type Small-Molecule Semiconductors for Bioelectronic Applications Simiao Yu¹, Christina J. Kousseff¹, William Neal¹, Han-Yan Wu², Simone Fabiano² and Christian Nielsen¹; ¹Queen Mary University of London, United Kingdom; ²Linköping University, Sweden

Organic electrochemical transistors (OECTs) have drawn tremendous attention in research communities all over the world due to their biocompatibility and synthetic tunability. In the last few years, molecular design has been playing an essential role in developing organic semiconductors for OECT devices. Previous research was mainly concentrated on the design of p-type materials for OECTs. Ever since a novel polymer comprising the naphthalene diimide (NDI) monomer was successfully designed and synthesized in 2016, considerable efforts have been devoted to developing novel n-type channel materials. The quick development of this field during the past few years can be attributed to the synthetic methods, various materials design strategies and device engineering protocols. With the emergence of novel molecules, detailed structure-property relationships of channel materials and reasons for their excellent performance should be explored further.

The work I will present is about a series of n-type small-molecule semiconductors based on naphthalene diimide (NDI) and perylene diimide (PDI) building blocks. When functionalized with different ion-transporting groups at the imide nitrogen positions, such as different length linear and cyclic ethylene glycol motifs, mixed ionic-electronic conduction properties were observed for thin films in aqueous environment. The solubility and aggregation behavior of these organic mixed conductors can be modified without changing the optical and electrochemical properties of the π -systems. Besides, PDI functionalized with an ion-selective ethylene glycol moiety exhibited good ion doping of the thin film with markedly different behavior in sodium chloride and potassium chloride solution, which paves the way for ion-selective mixed conductors as promising materials in organic electrochemical transistors and biosensors.

SB06.09.03

Understanding Interfacial Recombination Processes in Narrow-Band-Gap Organic Solar Cells Nora Schopp¹, Hoang Luong¹, Benjamin Luginbuhl¹, Patchareepond Panoy^{2,1}, Vinich Promarak², Viktor Brus³ and Thuc-Quyen Nguyen¹; ¹UC Santa Barbara, United States; ²Vistec, Thailand; ³Nazarbayev University, Kazakhstan

Recombination losses in organic photovoltaics (OPVs) remain a performance-limiting factor, including bulk trap-assisted recombination and interfacial recombination at the electrode:active layer interface. In this talk, we demonstrate the role of the front electrode:active layer interface in a narrow-band-gap system, **PCE10:COTIC-4F**, a promising candidate for semitransparent organic photovoltaics. Charge generation, recombination, and extraction are addressed, with a focus on interfacial recombination via surface traps by a comparison of four device structures with electrodes based on ZnO, ZnO/PFN-Br, PEDOT:PSS, and a self-doped conjugated polyelectrolyte (CPE-K). The amount of interfacial recombination is affected significantly by the electrode choice, while similar levels of bulk recombination are maintained. For the studied blend, we identify ZnO as a suitable choice, pairing low surface recombination rates with beneficial charge carrier generation, favorable energy level alignment, and efficient extraction. In contrast, PEDOT:PSS-based devices suffer from interfacial recombination, which can be suppressed when CPE-K is used instead.

SB06.09.04

Impact of Molecular Weight on Mixed Conduction—The Unexpected Role of Electrolyte Choice Dilara Meli¹, Joshua Tropp¹, Ruiheng Wu¹, Bryan D. Paulsen¹, Christopher J. Takacs² and Jonathan Rivnay^{1,1}; ¹Northwestern University, United States; ²SLAC National Accelerator Laboratory, United States

Organic mixed ionic electronic conductors (OMIECs) have shown promise in applications such as sensing of biological signals, organic inverters, and neuromorphics. OMIECs are particularly desirable due to their synthetic tunability, though this requires thorough understanding of structure-property relations in these materials. One such tunable parameter is the polymer molecular weight (Mn). While the effect of molecular weight on conjugated polymers for organic thin film transistor (OTFT) applications has been well studied, its effect on mixed conduction remains largely unknown. Shedding light on this relationship is important, not just to optimize performance of known polymer systems, but to improve understanding of mixed charge transport in OMIECs.

To elucidate the effect of molecular weight on mixed transport, a series of glycolated thiophene based polymers were synthesized via Kumada catalyst transfer polymerization to obtain polymers with molecular weights ranging from 13.9 to 32.5 kg/mol. This range had previously been found to contain the entanglement threshold of P3HT molecular weights in OTFTs. Organic electrochemical transistors (OECTs), a common test bed for OMIECs, were tested in both aqueous NaCl and KTFSI electrolytes, which are the most ubiquitous salts in aqueous metal halide electrolytes as well as ionic liquids and battery electrolytes, respectively. To help explain origins of observed differences in electronic performance, we performed operando grazing-incidence wide angle x-ray scattering (GIWAXS) and electrochemical quartz crystal microbalance (EQCM) experiments.

OECT measurements in NaCl show little differences in mobility (μ), volumetric capacitance (C^*), nor their product (μC^*) across the range of molecular weights. However, when tested in KTFSI, we observed a significant increase in μC^* due to an increase in μ between 18.2 and 22.4 kg/mol, which persisted across all higher Mn. GIWAXS data on both systems show similar passive swelling in both electrolytes as assessed from shifting of the lamellar peak after electrolyte exposure. Upon doping via application of a gate bias, polymers in KTFSI show a lamellar contraction in real space, whereas polymers in NaCl show an expansion, regardless of Mn. This suggests that in order to compensate for the positive electronic charges in the polymer, polymers in KTFSI expel K^+ ions and polymers in NaCl take up additional Cl^- ions. The relative shift in d-spacing is much smaller for the KTFSI than the NaCl, however, indicating that the polymer microstructure is much more stable against perturbations in KTFSI. This could, in part, be due to the affinity of the TFSI for the polymer, which could stabilize the microstructure.

In this work, we discovered a mobility threshold around 20 kg/mol when OECTs were operated in KTFSI, which is absent in devices operated in NaCl. Leveraging operando characterization techniques, we found that this absence could be explained by a more unstable microstructure of the material in NaCl, as observed via larger modulation of the lamellar spacing during doping and dedoping. In conclusion, percolation thresholds in OMIECs may only be accessible in suitable electrolytes, which can help guide materials choices given target applications.

SB06.09.05

Flexible Covalent Organic Framework Films Sandwiched with Ferroelectric Polymers for Electrostatic Energy Storage He Li, Chongqing Yang and Yi Liu; Lawrence Berkeley National Laboratory, United States

With the rapid development of science and technology, ever-increasing demand has been directed towards high-performing energy storage devices. Among the various electrical energy storage devices, dielectric film capacitors store charges electrostatically and thus have the fastest discharging rate compared to

batteries and supercapacitors. In addition, polymer-based electrostatic film capacitors exhibit intrinsic merits such as greater processability, flexibility, lightweight and voltage tolerance capability with respect to inorganic dielectric ceramics. Because film capacitors account for more than 25% of the volume and weight of electric power systems, the enhancement in energy density of film capacitors will help to reduce the volume, weight, and cost of electrified systems such as electrical vehicles and aircrafts. While the industrial benchmark capacitor film represented by biaxially oriented polypropylene (BOPP) exhibits high dielectric breakdown strength and charge-discharge efficiency, the energy density has been largely limited by its low dielectric constant (~ 2.25 at 1 kHz, 25 °C), which is smaller than 5 J/cm³ at its breakdown strength limit. It is therefore imperative to develop polymer dielectric materials with concurrent high dielectric constant and breakdown strength to achieve high energy densities.

Herein, we demonstrate an approach to high energy density devices by incorporating a layer of covalent organic framework (COF) within two layers of ferroelectric poly(vinylidene fluoride-*ter*-trifluoroethylene-*ter*-chlorofluoroethylene) P(VDF-TrFE-CFE) polymer. The imine-based COF films were synthesized using 2,5-dimethoxyterephthalaldehyde and 1,3,5-tri-(4-aminophenyl)benzene precursors at room temperature. The sandwich-structured ferroelectric polymer/COF films are prepared through a facile layer-by-layer solution casting method, which possess the largest k values (>35 at 1 kHz, 25 °C) amongst known polymer dielectrics. In addition, the combination of crystalline COF layer and soft ferroelectric polymer layers incurs excellent mechanical flexibility while retaining high mechanical strength (Young's modulus) of the COF film. More importantly, due to their all-organic nature, COFs exhibit desirable compatibility with polymers, circumventing issues caused by defects at the organic-inorganic interface in traditional dielectric polymer composites. The corresponding sandwich-structured film capacitors display high breakdown strength (>600 MV/m), and high discharged energy density of ~ 25 J/cm³, which is 5 times higher than the state-of-the-art BOPP film capacitor and 3 times higher than the pure P(VDF-TrFE-CFE) polymer. Furthermore, successive charging/discharging cyclic tests validate that the developed dielectric film capacitors show excellent operational stability under high-electric-field electrification conditions.

SB06.09.06

A Conjoint Theoretical and Experimental Approach for Structure-Relationship Comparison Between ITIC and Y Family Acceptors—From Molecules to Devices [Antoine Rillaerts](#), Florian Regnier, Jerome N. Cornil and Pascal Viville; UMons, Belgium

Since NFA molecules have made it possible to achieve nearly 20% yield, a lot of studies has been made on fine tuning to rise the record. In this work we have focused on structure-relationship properties of two important families of compound: ITIC, Y5 and their respective derivatives. The main goal is to give a better understanding behind this recent breakthrough in OPV. The theoretical part which consists of quantum-chemical calculations of electronic, optical and packing properties to have a closer look of structural changes on the electronic level energies, optical absorption coverage and modifications on the charge transport capabilities, considering the acceptor only. Calculations were made considering different solvent. The halogenation of both acceptors shows an electronic level energy lowering without impacting the optical absorption which make it possible to tune easily the V_{OC} . Regarding the crystal structures of each compound, halogenation change the way molecule are packed together and can modify charge carrier transport. About the experimental part, we carried out optical absorption, morphological and electrical properties analysis for each acceptor and blends with PM7 polymer donor. Absorption spectra gives us information about optical coverage and molecule behaviour transition between low-density system in solution and high-density system in films. The red shift that results from solution to film transition is more important for the Y molecules than ITIC series. In terms of morphology, AFM analysis demonstrated different solubility behaviours in function of the solvent used to spin-coat films and the structural changes like halogenation and side-chains length. Charge carrier mobility was analysed using impedance spectroscopy on MIS devices to probe vertical transport. Particularity of this acceptor generation is to accumulate both charge carrier and tend to be ambipolar. At the end, devices were built to make a correlation between all these characteristics and photovoltaic parameters.

SB06.09.07

Influence of Inter-Tube Junctions on the Charge Transport and the Thermoelectric Properties of Conjugate Polymer/Carbon Nanotube Composites [Seong Hyeon Kim](#) and Kilwon Cho; Pohang University of Science and Technology, Korea (the Republic of)

Conjugated polymer (CP)/carbon nanotube (CNT) composites have a variety of advantages as next-generation thermoelectric materials such as lightweight, flexibility, and biocompatibility. Thermoelectric performance of CP/CNT composites has been substantially enhanced compared with that of the individual components over decades. However, the origin and strategy for the performance improvement remains vague, without clear explanations at the molecular level. By complementarily using experimental methods with molecular dynamics simulations, we reveal the function of the CPs' structure to the thermoelectric properties at inter-tube junctions between adjacent CNTs. Indacenodithiophene-*co*-benzothiadiazole (IDTBT), which has a highly planar backbone chain and does not aggregate at inter-tube junctions, can facilitate intramolecular charge transport along backbone chains between adjacent CNTs than poly[2,5-bis(3-tetradecylthiophene-2-yl)thieno[3,2-*b*]thiophene] (PBTTT). The continuous distribution of IDTBT backbone chains spread out radially from CNTs enables both holes and phonons to be transported effectively at inter-tube junctions, which significantly increases electrical conductivity but also increases thermal conductivity somewhat. Nevertheless, IDTBT/CNT composites yield the highest thermoelectric power factor among CP/CNT composites not subjected to the chemical doping. The structure-performance relationships revealed in this study may contribute CP/CNT composites to be developed into commercially available thermoelectric materials.

SB06.09.08

Designs of Flexible Transparent Electrodes with Antireflection Coatings for High Performance Flexible Perovskite Solar Cells [Eunmi Cho](#)^{1,2}, Jin-Seong Park² and Sang-Jin Lee¹; ¹Korea Research Institute of Chemical Technology (KRICT), Korea (the Republic of); ²Hanyang University, Korea (the Republic of)

Flexible perovskite solar cells (F-PSCs) are of great interest because of their flexibility, light weight, portability, and compatibility with various form factors including curved surface, and low fabrication cost. Despite of enormous potential in applications, F-PSCs still suffer from low power conversion efficiency (PCE) compared to rigid PSCs largely because of the reduced photocurrent driven by low transmittance of their flexible substrate and transparent electrode. In this regard, we propose a newly developed plasma-polymerized-fluorocarbon (PPFC) thin film as an antireflection (AR) coating material for enhancing the efficiency of F-PSCs. The PPFC is a thin film with an amorphous structure produced by sputtering a composite target made by mixing PTFE and carbon nanotubes. The PPFC thin films have excellent AR effect due to low refractive index (~ 1.38), good adhesion to the substrate, uniformity of nanometer-level thickness and water repellency. When PPFC AR coating are deposited on the flexible polyethylene terephthalate (PET) substrates, the average difference in the transmittance of PPFC/PET increases by 3.23%, and the average difference in reflection decreases by 3.23%. After coating the PET/ITO with 100 nm PPFC film, the average difference in the reflectance decreases by 2.22%, and the average difference in transmittance increases by 1.40% in the visible region, resulting in maximum light transmittance due to the AR effect. The PPFC thin film is employed to improve the efficiency of F-PSCs, thereby increasing light absorption in the perovskite layer, and finally enhances the photocurrent in the F-PSCs. The enhanced photocurrent in the F-PSCs with the PPFC thin film is also verified by measuring the external quantum efficiency (EQE) spectra of F-PSCs without and with the PPFC thin film. All the F-PSCs with the PPFC thin film shows increased EQE in the entire visible range. The optimized F-PSCs with the 100 nm PPFC thin film greatly improves the PCE of F-PSCs from 18.6% to 20.4%. In addition, PPFC thin film have a hydrophobic surface and very flexible, its properties is enhanced the device stability against under harsh environmental conditions. These PPFC thin films are expected to be useful not only for F-PSCs but also for flexible

electronic devices in general, considering their excellent broadband light enhancement properties, self-cleaning surface, environmental stability and flexibility.

SB06.09.09

Correlating Charge Transport with Intrinsic Energetic Disorder, Paracrystallinity and Carrier-Dopant Distance in Doped Conjugated Polymers Michael Lu-Díaz¹, Muhamed Duhandzic², Zlatan Aksamija² and Dhandapani Venkataraman¹; ¹University of Massachusetts Amherst, United States; ²The University of Utah, United States

High-performing organic electronics rely on organic materials with efficient charge transport. Recent advances in understanding the effects of dopants in polymers pushed the field towards a deeper understanding of dopant-induced energetic disorder. Yet, the interaction between intrinsic energetic disorder, caused by polymer morphology, and extrinsic energetic disorder, caused by Coulomb interactions with dopant ions, has not been fully established. Here we investigate the role of repeat unit connectivity and long-range order of thiophene-based polymers on dopant-induced energetic disorder. The charge transport properties were obtained by measuring Seebeck coefficient and electrical conductivity using a vapor doping-de-doping procedure. The thin film structures were studied using UV-Vis spectroscopy, X-ray scattering, and atomic force microscopy. A phonon-assisted hopping model was used to simulate charge transport and fit to experimental data. This experimental-computational study shows that polymers with shorter polaron-counterion distances lead to increased extrinsic dopant-induced disorder due to additional Coulomb interactions. Our work shows a need for an integrated molecular design that requires both low intrinsic disorder and extrinsic dopant-induced energetic disorder for efficient charge transport.

SB06.09.10

Flexible Smart Labels for Mobile Authentication Using Photonic Physical Unclonable Functions Lilia Dias¹, Tiago Silvério², Lianshe Fu¹, Paulo Andre² and Maria Rute Ferreira Andre¹; ¹CICECO, Portugal; ²Instituto de Telecomunicações, Portugal

The Internet of Things (IoT) is a network of connected objects, interacting in real-time, without human supervision. However, the large-scale dissemination and the development of digital ecosystems requires mobile applications with fast and reliable methods to generate secure cryptographic keys, such as Physical Unclonable Functions (PUFs). In this work, functional operating photonic PUFs based on flexible tokens were produced at low-cost, energy-efficient, and scalable methods, using an organic-inorganic hybrid doped with lanthanide ions ($\text{Ln}^{3+}=\text{Eu}^{3+}$), displaying unique challenge-response pairs for two-factor authentication. Under laser irradiation, a speckle pattern is attained, and under UV light-emitting diodes, it displays a random luminescent intensity-based pattern, ensuring the two-factor authentication precision and recall values around 100%. Moreover, the two-factor authentication possibility enables this system to be used as a conventional PUF encryption proving a new paradigm of cryptographic key generation by featuring perceptual hash key extraction with images taken from a smartphone which can provide easy and fast remote authentication.

Acknowledgements: CICECO-Aveiro Institute of Materials (UIDB/50011/2020, UIDP/50011/2020, LA/P/0006/2020), Instituto de Telecomunicações (UIDB/50008/2020, UIDP/50008/2020); FCT/MEC, FEDER, PT2020. LMS Dias was supported by 2020.05802.BD.

SB06.09.11

Effect of pH-Controlled Dye Solution on Improving the Performance and Stability in Organic Solar Cells Nara Han and Dong-Yu Kim; Gwangju Institute of Science and Technology, Korea (the Republic of)

In bulk-heterojunction of organic solar cells (OSCs), the morphology of photoactive layer can be controlled through various chemical and physical treatment methods including alcohol treatment, anti-solvent method, and layer-by-layer deposition technique. In particular, it is meaningful that the appropriate film morphology for better charge generation, transport, and extraction is achieved by a simple and accessible process. Our group recently reported 'water treatment' with a small amount of water introduced in the preparation process of the active solution to give a physical impact that induces vortex agitation. In this work, we study the effect of pH-controlled dye solution on enhancing the device performance and stability in OSCs. We employed structure-changeable dye molecules within a variety of pH ranges (1-13) as an additive in the process. This strategy makes it possible to obtain more clear phase separation in the thin films treated under high pH conditions. More crucially, by applying this treatment under the basic condition with NaOH as a pH controller, the chemical reaction between the active solvent and additive was generated, thus resulting in enhanced short circuit current densities and fill factors. As a result, an improved efficiency (13.98%) of the device treated with pH-controlled dye solution was achieved compared with the efficiency (13.35%) of PM6:Y6 cells. All these results demonstrated that the treatment using pH-controlled dye solutions is a feasible and promising strategy to construct efficient and eco-friendly OSCs.

SB06.09.12

Highly Flexible Polymer Solar Cells Made with Uniform Silver Nanowire Patterned Electrodes on Robust PEN Substrate Su Hong Park, Na Yeon Kwon, Hyeonduo Je, Jin Young Park, Min Ju Cho and Dong Hoon Choi; Korea University, Korea (the Republic of)

The polymer solar cells (PSCs) have been extensively researched in recent years, and have the advantage that they can be applied to flexible devices. Although the brittle indium-tin-oxide (ITO) electrode was employed for flat-panel device, flexible transparent conductive electrodes should apply for the flexible and stretchable next-generation device, exhibiting low sheet resistance, high optical transmittance, low surface roughness, and increased flexibility. Various flexible transparent conductive electrodes, such as conducting polymers, graphene, metal nanowires, and hybrid types, have been proposed to replace ITO, and many studies have been conducted to demonstrate the excellent properties of electrodes using the above materials.

Generally, AgNWs were dispersed with the solvent of isopropanol, it is hard to spread uniformly on the hydrophobic plastic substrate because of the surface tension and its wettability. To overcome this problem, a few groups have attempted to confer hydrophilicity to the substrate by using PVA and PEDOT: PSS. However, the aqueous solution of the above polymers disadvantageously forms a non-uniform thin film; thus, the AgNW layer applied to the upper layer tends to be non-uniform. Therefore, it is necessary to study new coating materials that can change the surface properties of PET and PEN. However, all these methods only improve the adhesion between the AgNWs network and the substrate and are not ideal in terms of the overall uniform patterning process owing to the unsolved issue of random AgNWs distribution.

In this study, we successfully fabricate a patterned AgNW-based electrode on a flexible PEN substrate after the UV irradiation/washing of an overcoat layer composed of PEDOT: PSS and a UV sensitizer. To increase the wettability between the PEN substrate and the AgNWs, a stable, optically transparent, hydrophilic poly(2-hydroxyethyl methacrylate) (PHEMA) film is coated as an underlayer for the AgNWs. Furthermore, the conductivity and transmittance of the AgNW layer are optimized by varying the concentration of the AgNW solution. The patterned AgNW electrode achieves a low sheet resistance (R_{sh}) of 22.6 Ω/square and high transmittance of 92.35% at 550 nm. A polymer solar cell (PSC) was fabricated to evaluate the characteristics of the device employing the flexible electrodes. This PSC not only showed a high power conversion efficiency of 11.20%, similar to that of ITO-based devices, but also excellent mechanical stability, which is difficult to achieve in ITO-based flexible devices.

SB06.09.13

Crosslinkable Conjugated Polymers for Improvement in the Stability of Flexible Polymer Solar Cells Na Yeon Kwon, Su Hong Park, Hong Diem

Chau, Sung Hoon Jung, Min Ji Kang, Min Ju Cho and Dong Hoon Choi; Korea University, Korea (the Republic of)

The polymer solar cells (PSCs) have been extensively researched in recent years, and have the advantage that they can be applied to flexible devices. Although PSCs with bulk-heterojunction (BHJ) systems are composed of an active layer with binary blends of polymer donors and polymer acceptors and display high performance, the device stability is still challengeable. Even in well-mixed polymer blend films, long-term high-temperature conditions can induce phase separation in the films. Therefore, the shelf-life and operational stability of the PSCs in ambient and high-temperature environments should be carefully considered for the practical application of all-PSCs. Among the several strategies reported for improving the high-temperature stability of all-PSCs, the crosslinking reaction has emerged as an effective method for improving the stability and functions of the polymer films. On the other hand, single-component polymers via conjugated donor-acceptor block copolymers (CDABPs) have been proposed for use in many strategies to overcome the drawback of BHJ. These polymers can suppress phase separation and exhibit inert internal morphologies compared to the polymer blends; however, their thermal stability remains an issue to be addressed.

In this study, we demonstrated a novel crosslinkable polymer system: extrinsic single component system (PBDBT-BV₂₀ and N2200-TV₁₀) and intrinsic single component system (P(OXBTT-co-NDI2T)). First, random terpolymers were successfully synthesized by introducing thiophene-based monomers bearing vinyl functional groups in the side-chain. The physical properties of the blend films of PBDBT-BV₂₀ and N2200-TV₁₀ before and after thermal crosslinking were extensively investigated and compared to those of the homogeneous individual polymer films. In addition, the PSCs with the crosslinked blend film exhibited an excellent shelf-life of over 1200 h and a thermally stable power conversion efficiency (PCE). Furthermore, the crosslinked blend film exhibited excellent mechanical stability under bending stress in flexible PSCs using plastic substrates. After all, we synthesized a new CDABP (P(OXBTT-co-NDI2T)) bearing crosslinking groups to minimize phase separation and secure thermal stability of the internal morphology. The P(OXBTT-co-NDI2T) film exhibited a relatively high PCE and excellent thermal stability compared to the all-PSC device based on the P(OXBTT):P(NDI2T) blend film. The results of these studies indicate the promising potential of PSCs with crosslinkable conjugated polymers for future PSCs that require a long shelf-life, thermal and mechanical stability, and high performance.

SB06.09.16

Counterion Influence on Thermoelectric Properties of Electrochemically Doped Regioregular and Regiorandom poly(3-hexylthiophene) Kyle N. Bauster¹, Augustine Yusuf¹, Joel Bombile¹, Ahmed Ayyash¹, Ashkan Abtahi², Chad Risko¹ and Kenneth R. Graham¹; ¹University of Kentucky, United States; ²Purdue, United States

Doping of π -conjugated polymers is critical for tuning their properties and making them operable in many organic electronic devices including organic light emitting diodes, organic thermoelectrics, and organic electrochemical transistors. In both chemical doping and electrochemical doping an ionized dopant or counterion is required to balance the newly acquired charge on the doped π -conjugated polymer. The characteristics of this dopant or counterion, such as size, shape, and relative polarity, can significantly impact the optical, electronic, and thermoelectric properties of the resulting material. Here, we investigate how the counterion structure impacts the electrochemical doping ability, oxidation potential, ionization energy, and polaron absorbance of regioregular (rr) and regiorandom (rra) P3HT. We also probe how electrochemical doping with these different counterions leads to changes in conductivity and Seebeck coefficients influencing thermoelectric performance. The most prominent change in the polymer oxidation potential is observed for rr-P3HT with the large tetrakis[3,5-bis(trifluoromethyl)phenyl]borate anion. We propose that this large anion is excluded from the tightly packed crystalline regions and thus the oxidation potential is closer to that of the mostly amorphous rra-P3HT. The anions also result in significant differences in polaron absorbance and ionization energies as well as notable changes in peak broadening in epr spectra with increased doping. These results emphasize the important role that the counterion has in influencing the optical and electronic properties of doped π -conjugated polymers.

SB06.09.17

Large-Scale Anisotropy of Charge Transport in Molecular Ultrathin Film-Based OFETs Fabricated with Laser-Assisted Zone Crystallization Method Krzysztof Janus and Adam Kiersnowski; Wroclaw University of Science and Technology, Poland

Control of the crystallinity, crystal perfection, sizes and orientation of crystal domains in organic semiconductors (OSc) is essential for developing efficient electronic devices based on organic thin films. One of the key issues to be addressed is a control over anisotropy and size of crystal domains in the active layer of a device, as they both affect the overall device performance. The crystal anisotropy can cause locally directional charge carrier transport and, consequently, may lead to an inhomogeneous operation of devices, especially in an array. A broad distribution of size or a mismatch between ordered domains size and a device scale may as well cause issues with homogeneous operation devices in arrays. That is why formation of ordered, oriented domains is of importance. Growth of these domains is related to kinetic conditions and direction of the mass transport during solidification (crystallization) of the film. This is the reason why crystal structure and morphology of the OSc films are fabrication method-sensitive. Moreover, scalability of a fabrication method is a key in successful transferring laboratory results up to the industry scale.

In this contribution we therefore demonstrate a potential of laser-assisted zone crystallization (LAZEC) method in freely scalable fabrication of ultrathin films of organic semiconductors. The working principle of the LAZEC consists in scanning the surface with a laser beam in order to induce thermal gradients of surface free energy and ink viscosity. The gradients cause a flow-induced motion of the ink on the surface whereas a controlled evaporation of the solvent, as the laser is moving, causes solidification of non-volatile ink components on the surface to form a film. The gradients can be precisely controlled by adjusting the laser parameters (power, scanning speed) depending on the substrate and ink properties. The substrate temperature additionally controls the crystal growth temperature and hence further control over formation of crystal domains in the film.

In this contribution we demonstrate potential of the LAZEC by showcasing processing of small-molecular or polymer inks. The inks were chloroform, toluene or dichlorobenzene solutions of poly(hexylthiophene-co-thiophene) (P3HTT) or TIPS-pentacene (TP). We used TP and P3HTT to fabricate films with 20 nm thickness using different coating parameters. Morphology of the films was studied with optical and atomic-force microscopy. The crystal anisotropy was studied with synchrotron wide-angle X-ray diffraction (WAXD). In order to probe the charge carrier transport anisotropy and homogeneity we coated the films on arrays of top-gate, bottom-contact field effect transistors (OFETs). The film coating axis was oriented at variable angle with respect to source-drain electrode axis (i.e. the transistor channel axis). The WAXD studies revealed that the LAZEC coating can produce the films with crystal domains almost uniaxially oriented along the coating direction. Fine tuning of laser parameters and scanning speed enabled formation of films where the crystal domains revealed only just ± 10 deg. deviation from the director (coating) axis over the whole sample. The size of crystal domains was controlled with the laser speed and power. In line with morphological findings, OFET testing revealed several-fold difference between charge carrier mobility measured along and transverse to the coating direction. The morphology control in the LAZEC process enabled efficient, freely scalable fabrication of high-performance ultrathin films. For instance, the maximum p-type charge carrier field mobility recorded for 20-nm TP reached almost $0.1 \text{ cm}^2(\text{Vs})^{-1}$ whereas the maximum reported charge carrier mobility for bulk TP was a few $\text{cm}^2(\text{Vs})^{-1}$. Qualitatively similar observations were made for P3HTT films.

The work was supported by National Science Centre Poland (NCN) through the grants UMO-2017/25/B/ST5/02869 and UMO-2016/22/E/ST5/00472

SB06.09.18

Photonic Processing of Printable Optoelectronic Device Materials for Flexible Hybrid Electronics (FHE) Applications Charles Trudeau¹, Bilge Altay², Patrick Beaupre¹, Arjun Wadhwa³, Sylvain G. Cloutier³ and Martin Bolduc⁴; ¹INO - Institut National d'Optique, Canada; ²Rochester Institute of

Technology, United States; ³École de Technologie Supérieure, Canada; ⁴Université du Québec à Trois-Rivières, Canada

In this work, we present our recent progress on rapid photonic processing in the fabrication of printable and flexible hybrid electronic (FHE) devices and circuits. The pulsed photonic irradiation utilizes microseconds to milliseconds processing time onto thin flexible polymer or paper-based substrates, which suffer from low glass-transition temperatures. These new processing technologies show great promise in maintaining the integrity of the substrates without structural degradation due to shrinkage, charring or decomposition.

We will present flash-lamp [1-2] and laser [3] sintering experiments that show optimized sheet resistance values for silver and copper inks printed onto PET and SBS paper obtained at very high speed and spatial precision in comparison with conventional oven annealing. In addition, the results will show how these techniques can provide a greater control over the optoelectronic material properties in the fabrication of perovskite-based devices [4].

[1] B.N. Altay, B. Aksoy, D. Banerjee, D. Maddipatla, P.D. Fleming, M. Bolduc, S.G. Cloutier, and M. Demir, Lignin-Derived Carbon-Coated Functional Paper for Printed Electronics, *ACS Applied Electronic Materials* 3 (2021) 3904.

[2] B.N. Altay, V.S. Turkani, A.P. Pekarovicova, P.D. Fleming, M.Z. Atashbar, M. Bolduc, S.G. Cloutier, "One-step photonic curing of screen-printed conductive Ni flake electrodes for flexible electronics", *Scientific Reports* 11 (2021) 3393.

[3] M. Bolduc, C. Trudeau, P. Beaupré, S.G. Cloutier and P. Galarneau, "Thermal Dynamic Effects using Pulse-Shaping Laser Sintering of Printed Silver Inks", *Scientific Report* 8 (2018) 1418.

[4] C. Trudeau, P. Beaupré, M. Bolduc, and S.G. Cloutier, All inkjet-printed perovskite-based bolometers, *NPJ Flexible Electronics* 4 (2021) 34.

SB06.09.20

Solid-Solvent Hybrid Additive for the Simultaneous Control of the Macro- and Micro-Morphology in Non-Fullerene-Based Organic Solar Cells Dachwan Lee and Taiho Park; Pohang University of Science and Technology, Korea (the Republic of)

Most organic solar cells based on a bulk-heterojunction active layer are fabricated with the assistance of high boiling point solvent additives to optimize the phase separation of the donor and acceptor. The macroscopic phase separation can be controlled by this solvent additive. However, the control of the microscopic morphology (e.g., π - π stacking, orientation) of the inside phase is still dependent on the interaction and self-assembly characteristics of each donor and acceptor. In this work, we introduce a solid-solvent hybrid additive on PM6:Y6 solar cells to optimize both the macroscopic phase separation and the microscopic morphology at the same time. For the solvent additive, the well-known 1-CN solvent additive was used. For the solid additive, newly synthesized 3D star-shaped solid additives (Star-A and Star-F), which were delicately designed to achieve adequate electrical properties, electrostatic potential, and geometrical structure, were used to further optimize the microscopic morphology. Grazing-incidence small-angle X-ray scattering (GISAXS) and grazing-incidence wide-angle X-ray scattering (GIWAXS) measurements showed that the star additives not only induce the dense and enhanced microscopic intermolecular π - π stacking within the phase, but also further optimize the phase separation. By adding only 1% star-series solid additives, a significantly enhanced efficiency was achieved from PM6:Y6 solar cells.

SB06.09.21

Covalently Tethered, Semiconductor-Insulator-Conductor Polymer Networks for High-Reliability Foldable Transistors Seokran Choi, Hyukmin Kweon, Ukjin Jeong, Borina Ha, Jiyeon Ha and Do Hwan Kim; Hanyang University, Korea (the Republic of)

Polymer-based foldable electronics have gained significant attention as next-generation devices in the field of display and sensor technologies because of the flexible nature of polymers. Generally, the devices possess a heterogeneously multi-layered structure, indicating that mechanical stress derived from repeated folding and unfolding conditions can propagate both bulk and interfacial regimes of each component layer. This can cause not only cohesive failure of the bulk but also interfacial delamination between the layers. Therefore, to demonstrate foldable devices with high resistance to repetitive folding-unfolding stress, it is essential to secure excellent mechanical stability at both failure points. However, most approaches only focused on either enhancing deformability of component layers or improving interface stability by utilizing physical or chemical crosslinking between layers, resulting in insufficient mechanical stability against continuous folding stress. This strongly indicates that a practical strategy to simultaneously prevent cohesive and interfacial failures is sought after for the realization of high-performance foldable electronics against severe mechanical stress. Herein, we present a novel molecular design approach of deformable and covalently attachable interpenetrating polymer networks (DcA-IPNs) in which a ladder-like polysiloxane network is physically entangled with polymer matrix (conductor, semiconductor, and insulator). The interpenetrated polysiloxane network can induce short-range aggregation of polymer and restrain fragmentation of deformed chains so that mechanical energy dissipation in the bulk regime of layers can be efficiently proceeding. Moreover, DcA-IPNs possess unreacted silanol (Si-OH) groups at their surface regimes, which is capable of the formation of covalent bonds between adjacent layers for enhanced interfacial adhesion property. Based on this, we fabricated DcA-IPNs-based foldable transistors showing high operational stability against repeated folding-unfolding stresses without degradation of their electrical performance. We believe our novel approach will provide new insights into foldable electronics.

SB06.09.22

Thickness Tuned Ultra-Strong Light-Matter Coupling and Self-Grouping of Exciton-Ensemble in Single Crystals of Metal-Organic Framework Dileep Kottilil and Wei Ji; National University of Singapore, Singapore

Exciton-polaritons are coupled particles resulting from a strong interaction between electron-hole pairs (excitons) inside material and photonic modes of a microcavity. The unique features of these particles can be engineered for new technological applications such as inversionless lasers, all-optical logic gates and others. Recently researchers have been exploring ultra-strong coupling (USC) which is a new light-matter interaction regime that exceeds both weak and strong coupling schemes. Here, we introduce a solid-state organic polariton light source, for the first time, based on pristine and single-crystalline microplates of a dye-coordinated Metal-Organic Framework (MOF) operating under the USC regime. From optical measurements, we extract a record-high Rabi splitting value of 1.15 eV, which is 51% of the molecular transition energy. Further, the percentage of virtual photons in the polariton ground state is determined to be 1.79 %, indicating MOF as a promising platform for vacuum emission. A miniaturized form of such light sources has a wide variety of applications in science, technology and medicine. More importantly, we propose a novel physical mechanism for the first time, named 'self-grouping of exciton-ensemble', to explain the anomalous thickness dependence of multimode Rabi splitting. All the experimental results can only be explained using the correction factor introduced by this new mechanism.

An ultra-low threshold and a high degree of emission polarization have been achieved by stimulated polariton scattering occurred in single-crystallites of as-synthesized MOF microplates. With combined experiments and theoretical modelling, we found that the exciton-polaritons are formed at room temperature because of the strong coupling between Fabry-Perot cavity modes inherently formed by two parallel surfaces of a microplate and Frenkel excitons provided by the 2D layers of the dye linkers in the MOF. Such a cost-effective exciton-polariton cavity is realized at room temperature, without the support of any external mirrors made by metal coatings, or distributed Bragg reflectors (DBRs). Our findings confirm that MOFs, which can be synthesized readily from easily available materials under relatively mild conditions, are the potential candidates to unveil the previously unexplored fundamental physics and advanced applications of the USC regime without needing any complicated material fabrication procedures.

SB06.09.23

Towards a Comprehensive Theory of Organic Electrochemical Materials and Interfaces Loren G. Kaake; Simon Fraser University, Canada

The relationship between electrochemistry and organic electronic materials is over forty years old. Despite this long history, and the widespread use of electrochemical methods to characterize the electronic structure of pi-conjugated materials, the field has failed to reach consensus on many important questions. It is generally agreed that upon the application of potential, ions move into the bulk of an organic electronic material, doping p-type materials with holes by the inclusion of anions. However, this is not always the case, as demonstrated in the field of organic electrolyte gated field effect transistors. It has long been known that the same material combination can exhibit a transition from one mode of operation at a threshold voltage³ What determines the stability of the electrified interface between an ion conducting medium and a polymer semiconductor? This behavior can be described as a special case of mixing thermodynamics using a voltage dependent enthalpy of solvation. In the case where the free energy of mixing is negative, ions and their counterbalancing charge carriers move into the film. Because the film bulk is charge neutral, this process can be understood, to a first approximation, as diffusion according to Fick's law. More recently, the expression for Fickian diffusion in a thin film can be used to describe both in-operando infrared measurements, as well as the scan rate dependence of traditional cyclic voltammetry experiments. It is important to point out that the expression of Fick's law is a slowly converging series of exponential functions, presenting a dangerous dead-end for those fitting ion transport in terms of empirical models based on RC circuits and other ad-hoc exponential corrections. With respect to the structure-property relationship that governs the ion diffusion constant, the enthalpy of mixing presents a key inroad. The Vogel-Tammann-Fulcher equation, popular for aliphatic ion conductors, can be extended to describe the voltage dependence of the diffusion constant, as well as the seemingly paradoxical result that larger ions can sometimes move more quickly in organic semiconductors. This expression is also useful to understand the stability of organic solar cells. Ade and co-workers showed that the stability of organic solar cells can be understood in terms of molecular diffusion, the rate of which was influenced by solubility interactions. Importantly, the VTF equation contains a term related to the volume of mixing, providing a key parameter from which to understand the relationship between polymer crystallinity and ion diffusivity. The utility of the solvation enthalpy will also be demonstrated in understanding polymer swelling during electrochemical doping. However, it must be pointed out that a simple one-component diffusion model, even one which including enthalpy considerations is insufficient to describe the entire diversity of organic electrochemical materials. However, a two-component model which allows for the interconversion between species of different diffusivities is considerably more flexible. The ability of this model to describe charge trapping, and apparent non-Fickian diffusion will be described, with the aim of providing a description of ion transport phenomena in organic electronic that provides much-needed context for the detailed morphological understanding that has, and continues, to emerge.

SESSION SB06.10: Photodetectors, Phototransistors, Up-Conversion Processes
Session Chairs: Hoang Luong and Koen Vandewal
Wednesday Morning, November 30, 2022
Hynes, Level 3, Room 312

8:45 AM *SB06.10.01

Designs for Upconversion and Photomultiplication in Organic Shortwave Infrared Detectors Tse Nga Ng; University of California, San Diego, United States

Upconversion imagers that combine photosensing and display in a compact structure are attractive since they avoid the costly and complex process of pixilation. This talk will present the designs of polymeric upconversion imagers that combine photo-sensing and display in a compact structure, to enable visualization to 1300 nm (*Adv. Func. Mater.* 2021, 31, 210056). This shortwave infrared spectral region is particularly powerful for a variety of applications including environmental monitoring and medical diagnosis, enabling greater penetration depth and improved resolution in comparison to visible light.

The organic photodetectors are further improved by incorporating a new heterojunction interlayer to trigger trap-assisted photomultiplication. Previous approaches to induce photomultiplication in organic diodes have increased the photosignal but lacked control over reducing background noise. This work presents a new interlayer design based on a heterojunction bilayer that concurrently enables photomultiplication and suppresses the dark current in organic shortwave infrared detectors to improve the overall detectivity (*Mater. Horiz.* 2022, accepted). The heterojunction bilayer is consisted of a hole-transporting material copper thiocyanate and an electron-transporting material tin oxide. This combination serves to suppress the dark current and enhance the photoresponse, leading to an external quantum efficiency up to 560% and a detectivity of 3.5×10^9 Jones. The upconversion efficiency of the imager is doubled with 1.7 fold improvement in contrast compared to the imager without the heterojunction interlayer. The new interlayer design is generalizable to work with different organic semiconductors, making it attractive and easy to integrate with emerging organic infrared systems.

9:15 AM SB06.10.02

Synthesis and Characterization of Novel Chiroptical Low Bandgap π -Conjugated Polymers for Circularly Polarized Near-Infrared-Sensing Organic Thin-Film Phototransistors Hyemi Han, Jongtae Ahn, Do Kyung Hwang and Jung Ah Lim; Korea Institute of Science and Technology, Korea (the Republic of)

Chiral optoelectronics manipulating the circularly polarized (CP) light has received extensive attention over the past decades due to its promising opportunities in next-generation optoelectronics such as quantum computation, optical spintronics, encryption, and 3D displays. For achieving technological advances in such fields, various chiral organic semiconducting materials, that differentially absorb CP light according to the polarization direction, have been developed, but the chiroptoelectronic devices using them have not been rarely explored, which is still at a very early stage. Particularly, chiral semiconducting materials with optical activity in near-infrared (NIR, 700~1700 nm) spectral region have become increasingly important because it can fully extend their applicability including long-distance optical communication. Recently, in order to develop chiral material applicable to the chiroptical organic optoelectronic devices operating in NIR region, we synthesized novel chiral low bandgap π -conjugated polymers through four-step chemical reaction procedure, in which the chirality is induced by incorporating enantiopure (*R*-) or (*S*-) side chain substituents into donor-acceptor type polymer backbone showing excellent charge transport and NIR absorption properties. In spin-coated thin films, intrinsically chiral sidechain polymers brought about distinct circular dichroism in the NIR region at the local/molecular level, which was amplified by long-range structural chirality of polymer chains depending on the film thickness increment to 200 nm. We pursued to understand the origin of such chiroptical phenomenon of chiral sidechain polymer thin films by using a combination of molecular/spectroscopic analysis and peculiar morphological stacking features of supramolecular self-assemblies of chiral polymers. Based on this, we applied the chiral π -conjugated polymer thin films to circularly polarized NIR-sensing photoactive channel layer in organic thin-film phototransistors for direct detection of CP light and efficient amplification of photosignals, and optimized their thickness for a

high CP NIR-sensing efficiency. As a result, by distinguishing the left or right handedness of incident CP NIR lights with wavelength of 830 and 920 nm, they achieved excellent photoresponsivity of 31.6 and 26.1 A/W for each wavelength, along with a high photocurrent dissymmetry (g -factors > 1) as well as a fast optical response time (< 100 ms) at film thickness below 100 nm. This presentation provides new approaches for the design of chiroptical organic semiconducting materials and devices that can pave the way to high-performance chiral optoelectronic applications.

9:30 AM SB06.10.03

Acceptor-Substituted Squaraine Dyes for Organic Optical Upconversion Devices Michael Bauer¹, Wei-Hsu Hu¹, Frank Nüesch^{1,2} and Roland Hany¹; ¹Empa–Swiss Federal Laboratories for Materials Science and Technology, Switzerland; ²École Polytechnique Fédérale de Lausanne, Switzerland

Near infrared optical sensing and imaging are essential to an increasing number of next-generation photodetector applications in communications, process control or medical imaging. Recently, 1,3-squaraine dyes have been established as near-infrared absorbing or emitting dyes for these type of applications. However, most squaraine dyes show peak absorptions well below 1000 nm, a threshold wavelength below which organic photodetectors can hardly compete with the current inorganic silicon-based photodetector technology. Here, we show an approach to shift the peak absorption wavelength of squaraine dyes above 1000 nm through substitution on the central squaric acid core. The acceptor strength of this central moiety is enhanced by incorporation of dicyano- and rhodanine electron accepting groups. In addition, the central squaraine core is flanked by two benz[*cd*]indoles to generate a pronounced donor-acceptor-donor π -system. The feasibility of these core-substituted squaraine dyes for NIR detection above 1000 nm is demonstrated by integration in all-organic upconverter devices. These devices consist of an organic NIR sensitive photodetector and an organic light-emitting diode, connected in series. Organic upconverters convert NIR photons to visible photons and allow for pixel-free direct NIR imaging. Our NIR squaraine-based upconverters show a response well below the band gap edge of silicon and provide a low-cost opportunity for novel consumer and low-end imaging applications far into the shortwave infrared range.

[1] K. Strassel, W. Hu, S. Osbild, D. Padula, D. Rentsch, S. Yakunin, Y. Shynkarenko, M. Kovalenko, F. Nüesch, R. Hany, M. Bauer, *Sci. Technol. Adv. Mater.*, 2021, 22, 194-204.

[2] K. Strassel, A. Kaiser, S. Jenatsch, A. C. Véron, S. B. Anantharaman, E. Hack, M. Diethelm, F. Nüesch, R. Aderne, C. Legnani, S. Yakunin, M. Cremona, R. Hany, *ACS Appl. Mater. Interfaces* 2018, 10, 11063–11069

9:45 AM SB06.10.04

Bulk Heterojunction for Improved Solid-State Upconversion with Non-Fullerene Acceptors Emma Belliveau, Manchen Hu and Daniel Congreve; Stanford University, United States

Solid-state upconversion, a process whereby two lower energy photons are converted to one higher energy photon, is promising for a variety of applications, including photovoltaics, bioimaging, and night vision. For upconversion to be useful in these and other applications, a high external quantum efficiency (EQE) is required to generate sufficient quantities of upconverted light. Typical solid-state upconversion systems, based on intersystem crossing (ISC) in a sensitizer and subsequent triplet-triplet annihilation (TTA) in an annihilator, use dilute mixtures or very thin films of sensitizer, which results in minimal absorption of the low energy light to be upconverted, and hence low EQEs. Recent work from Izawa and Hiramoto [1] uses non-fullerene acceptors (NFAs) as sensitizers, which are paired with a donor-annihilator in a bilayer structure to generate triplets at an interface without the need for ISC or triplet diffusion in the sensitizer - significant loss mechanisms in solid-state upconversion systems. With this method, they achieve record near infrared (NIR)-to-visible EQEs of up to 2.3%. Our work builds upon this concept, inspired by organic photovoltaic (OPV) architectures, to create a bulk heterojunction (BHJ) upconversion film where the sensitizer and annihilator are combined in one solution-processed layer. This results in superior EQEs than their bilayer counterparts, due to the increased surface area between the two materials resulting in improved triplet generation. The benefits and applicability of this optimized BHJ upconversion system are then demonstrated with a NIR-to-visible imaging system.

References:

[1] Izawa, S., Hiramoto, M. Efficient solid-state photon upconversion enabled by triplet formation at an organic semiconductor interface. *Nat. Photon.* **15**, 895–900 (2021). <https://doi.org/10.1038/s41566-021-00904-w>

10:00 AM BREAK

SESSION SB06.11: Doping of Organic Semiconductors
Session Chairs: Nicolas Leclerc and Lydia Sosa Vargas
Wednesday Morning, November 30, 2022
Hynes, Level 3, Room 312

10:30 AM SB06.11.01

Controlling and Tracking Dopant Distributions and Morphologies in Molecularly-Doped n-Type Conjugated Polymers via Pendant Group Modification Ryan Chiechi^{1,2} and Lambert Jan Anton Kosters²; ¹North Carolina State University, United States; ²University of Groningen, Netherlands

The structural diversity of n-type conjugated polymers is somewhat lacking compared to their p-type equivalents, which have benefited considerably from nearly three decades of research in polymer-fullerene photovoltaic cells. However, n-type materials are finding applications in their doped form, which presents different synthetic design challenges than the aforementioned p-type semiconductor paradigm. In this contribution I will present some of our recent work on the versatile naphthalenediimide-bithiophene (PNDI2) framework and its performance as a thermoelectric material.

Charged dopants will phase-separate from conjugated polymers with non-polar pendant groups, hence the now-common use of polar (typically ether-containing) pendant groups. Using the PNDI2 backbone doped with n-DMBI, we investigated three different pendant groups: 1) branched alkyl (non-polar); glycol ether (polar); and alkyl-glycol-ether (non-polar and polar). We varied the regiochemistry of these chains such that the naphthalenediimide and bithiophene units had (mis)matching pairs of the various combinations of polar, non-polar and mixed pendant groups.

Counter-intuitively, the PNDI2 derivative with all polar pendant groups did not give the best performance. Rather, two polymers stood out. The highest doping efficiency (40 fold compared to the benchmark) correlated to both the regiochemistry and identity of the groups, while the highest power factor (5 fold compared to the benchmark) correlated to pendant groups with alkyl spacers between the backbone and the glycol ether functionality.

We ascribe these observations to the ability of the pendant groups to direct the charged dopant molecules, which is supported by spatially resolved absorbance spectroscopy. A central problem with doped, n-type polymers is that the polarons tend to localize more easily than in their p-type counterparts. This localization is exacerbated by coulomb interactions with the ionized dopant. Thus, pendant groups that place a polar phase far from the backbone and, importantly, farther from the acceptor units than the donor units in the backbone achieve morphologies that mitigate phase separation while achieving high

charge-carrier mobilities by avoiding the localization of carriers via nearby dopants. The use of spatially resolved absorbance spectroscopy allowed us to correlate topographical features from AFM to the intensity of absorption bands associated with doped polymer, linking morphological and electronic features to figures of merit.

Macromolecules **2021**, *54*, 3886-3896

Adv. Mater. **2021**, *33*, 2006694

10:45 AM SB06.11.02

Double Doping of a Low-Ionization-Energy Polythiophene with a Molybdenum Dithiolenene Complex Emmy N. Järsvall¹, Till Biskup², Yadong Zhang³, Renee Kroon^{1,4}, Stephen Barlow^{3,5}, Seth R. Marder^{3,5} and Christian Müller¹; ¹Chalmers University of Technology, Sweden; ²University of Saarland, Germany; ³Georgia Institute of Technology, United States; ⁴Linköping University, Sweden; ⁵University of Colorado Boulder, United States

Doping of organic semiconductors is crucial for tuning the charge-carrier density of conjugated polymers. The exchange of more than one electron between a monomeric dopant and an organic semiconductor allows the polaron density to be increased relative to the number of counterions that are introduced into the host matrix. Here, a molybdenum dithiolenene complex with a high electron affinity of 5.5 eV is shown to accept two electrons from a polythiophene that has a low ionization energy of 4.7 eV. Double p-doping is consistent with the ability of the monoanion salt of the molybdenum dithiolenene complex to dope the polymer. The transfer of two electrons to the neutral dopant was also confirmed by electron paramagnetic resonance spectroscopy since the monoanion, but not the dianion, of the molybdenum dithiolenene complex features an unpaired electron. Double doping allowed an ionization efficiency of 200% to be reached, which facilitates the design of strongly doped semiconductors while lessening any counterion-induced disruption of the nanostructure.

SESSION SB06.12: Modeling, Optoelectronic Properties in Organic Semiconductors

Session Chairs: Joel Bombile and Jerome Cornil

Wednesday Afternoon, November 30, 2022

Hynes, Level 3, Room 312

1:30 PM *SB06.12.01

Atomistic-Level Considerations of the Multitude of Factors to Engineer Crystalline Organic Semiconductors Chad Risko; University of Kentucky, United States

Organic semiconductors derived from π -conjugated molecules are of broad interest across a range of electronic and optical technologies. How molecular design and processing merge to result in semiconducting materials with optimal performance remains a mixture of art and science. Here we will discuss atomistic-scale simulations that explore how molecular chemistry and topology and processing conditions can provide insights into the development of crystalline organic semiconductors. We will also discuss data-driven approaches to explore molecular and materials properties of relevance for organic semiconductors.

2:00 PM SB06.12.02

Unraveling the Absorption Spectra and Relaxation Energy of NF-SMAs Using Multiparameter Franck Condon Models—A Structure-Function Study Somayeh Kashani^{1,1}, Zhen Wang^{1,1}, Chad Risko^{2,2} and Harald Ade^{1,1}; ¹North Carolina State University, United States; ²University of Kentucky, United States

Understanding correlations among the molecular structure, conformational diversity, and relaxation energy of a nonfullerene small molecule acceptor (NF-SMA) used in organic solar cells (OSCs) and their functional, optoelectronic properties is important to rationally design new materials with controlled properties. Although, correlations among molecular structure, optical and electronic gaps, and electron affinity of NF-SMAs have been studied extensively, an analysis of absorption spectra that classifies the NF-SMAs based on their electronic and vibrational finestructure is still missing. Here, we study the absorption spectra of 10 high-performing NF-SMAs in dilute solutions at room temperature, the most common tool utilized to uncover structure-spectra relations. Utilizing multiparameter Franck Condon (FC) analysis and quantum-chemical calculations, we show that the absorption spectra of NF-SMAs can be categorized into three types based on the molecular structures-spectra correlation: 1) The absorption spectrum of a linear ITIC-like molecular structure can be described by a single vibrational progression with one electronic transition and one effective vibrational mode. 2) The absorption spectra of curved, Y6-like structures can be described using a multiparameter FC model with two electronic transitions and two effective vibrational modes. Our results show that Y6 exhibits a highest conformation uniformity and the smallest intra-molecular relaxation energy, characteristics that may contribute to the Y6 success in state-of-the-art OSCs. 3) In contrast, structures like EH-IDTBR with π -bridges between the core and end groups have broader absorption spectra. The result of FC analysis and quantum-chemical calculations confirm the coexistence of different conformations and larger intra-molecular relaxation energies for these systems when compared to the other NF-SMAs in this study. These results provide insights for the design of new NF-SMAs, in particular a need for a simultaneously small number of molecular conformations and energetic disorder, and small relaxation energies, critical parameters that if controlled should improve the efficiency of organic photovoltaics or organic devices in general. The results clearly demonstrate that DFT calculations are able to provide excellent relative relaxation energies that can be utilized to assess molecules prior to synthesis.

2:15 PM SB06.12.03

A Quantum Mechanics/Molecular Mechanics Simulation Approach to Access the Charge Photo-Generation Properties in Organic Photovoltaic Materials Leandro R. Franco¹, Cleber Marchiori¹, Ellen Moons¹ and Moyses Araujo^{1,2}; ¹Karlstad University, Sweden; ²Uppsala University, Sweden

The development of new organic photovoltaic materials based on non-fullerene acceptors (NFAs) has led to a significant increase in the power conversion efficiency of organic photovoltaics (OPV) in the last years[1]. However, the fundamental understanding of the charge photogeneration mechanism at the molecular level is still lacking, a scientific challenge whose solution could be the watershed in the discovery of novel OPV materials. To contribute to this end, we are developing a multi-scale method that combines Quantum Mechanics (QM) calculations and Molecular Dynamics (MD) simulations within the scope of a sequential-QM/MD approach [2] to assess the charge photo-generation properties in organic photovoltaic materials. Despite being a well-established method to study small molecules in solution, it has not yet been developed to investigate polymer (and small organic molecule) films cast from solution. Our methodology starts with the simulation of film formation through solvent molecules evaporation using classical molecular dynamics simulations. Then additional MD simulations are carried out on the obtained film to generate uncorrelated configurations to be used on the properties' calculations. The latter is assessed through an electronic embedding scheme where a pre-defined molecular region, of the generated configuration, is treated at the QM level, incorporating explicit effects of the environment. For the QM calculations, density functional theory (DFT) and time-dependent DFT have

been employed. The quality of the force field parameters adopted in the MD simulations have been carefully analyzed. A set of representative NFAs small molecules and polymers have been studied, e.g. Y5, Y6, and PF5-Y5 polymer. Given the flexibility of the computational approach, we have been able to study these systems both in solution (chlorobenzene) and film. First, we have analyzed the structure of the films with focus, for instance, on the tendency to stabilize pi-pi stacking conformations. Then, the dynamics and molecular environment effects on the electronic transitions have been quantified with an improved description of the optical absorption. Finally, through the calculation of the fundamental and optical gaps the exciton binding energies have been estimated. Here, we have considered both the singlet and triplet excitons. The comparisons with experimental results confirm the suitability of the developed s-QM/MD approach, highlighting the importance of properly describing the dynamics and molecular environment effects in the modeling of the electronic properties of OPV materials.

References:

1. Armin, Ardalán, *et al.* *Advanced Energy Materials* **11**, 2003570 (2021).
2. Coutinho, Kaline, *et al.* Springer, Dordrecht, 2008. 159-189.

2:30 PM BREAK

SESSION SB06.13: Modeling, Doping of Organic Semiconductors
Session Chairs: Moyses Araujo and Chad Risko
Wednesday Afternoon, November 30, 2022
Hynes, Level 3, Room 312

3:30 PM *SB06.13.01

Impact of Phonons on Charge and Heat Transport in Organic Semiconductors Nemo McIntosh¹, Alexandre Vercouter¹, Marco Bardini¹, Samuele Giannini¹, Claudio Melis², David Beljonne¹ and Jerome N. Cornil¹; ¹University of Mons, Belgium; ²University of Cagliari, Italy

Charge transport in molecular crystals is reduced by the dynamic disorder induced by thermal fluctuations. This implies that the key parameters controlling charge transport at the molecular level (in particular the electronic couplings also referred to as transfer integrals) strongly fluctuate over time under the influence of intermolecular vibrations (phonons). Such thermal effects can be grasped from molecular dynamics simulations by extracting snapshots along the trajectory and by tracking the time evolution of relevant parameters. Nevertheless, such simulations do not tell us about the nature of the phonons contributing the most to the fluctuations of the transfer integrals, which would be of prime interest to design new strategies to freeze such detrimental degrees of freedom. In this context, I will first describe in this talk our recent efforts in this direction aiming at assessing the individual role of phonons as well as the possible impact of phonon dispersion. Interestingly, the same phonons are involved in heat transport so that their impact on the thermal conductivity can be also inferred. This is of high relevance to the field of organic thermoelectrics requiring strategies to minimize the thermal conductivity. The second part of the talk will describe some recent simulations of heat transport in molecular crystals, pointing to strong anharmonic effects for some structures leading to strongly localized phonons.

4:00 PM SB06.13.02

Bipolaron Formation Mechanism in Doped Conjugated Polymers Joel H. Bobile and Chad Risko; University of Kentucky, United States

Chemical doping is a powerful strategy for tuning the electronic properties of organic semiconducting materials based on π -conjugated polymers (CP), enhancing the performance of several organic electronic devices such as thin film transistors, light emitting diodes, photovoltaics, and thermoelectric generators. Large dopant concentrations are often necessary to achieve large electrical conductivities. As the dopant concentration increases, the natures of the charge carriers in doped CP's can change from polarons, singly charged quasi-particles with a spin, to bipolarons, which are doubly charged quasi-particles without a spin. Bipolaron formation can lead to improved electrical conductivity. Understanding the mechanism of their formation could provide an avenue to further optimize charge-carrier transport in doped CP's. We use first-principles calculations based on density functional theory (DFT) and time-dependent Density Functional theory (TD-DFT) with an optimally tuned hybrid functional to examine bipolaron formation in CP's. We perform calculations on charged oligomers in spin configurations corresponding to a bipolaron (singlet) or two polarons (triplet), with and without dopant counterions. We find that the effective attraction between two polarons by sharing the same distortion of nuclei or polarizable medium is not strong enough to overcome their repulsive coulomb interaction. However, when the polarons are forced to be sufficiently close to one another, as is the case in highly doped CP chains, the short-range attractive exchange coulomb interaction, working in synergy with the shared distortion of the surrounding medium, can make bipolarons more stable than polarons.

SESSION SB06.14: Poster Session III
Session Chairs: Emanuele Orgiu and Carmen Ruiz Herrero
Wednesday Afternoon, November 30, 2022
8:00 PM - 10:00 PM
Hynes, Level 1, Hall A

SB06.14.01

Screen Printed CO₂ Sensors Enabled by Functionalized Carbon Nanotubes Tianyi Liu, Rebekah Baggett, Zun (Cathy) Chen, Christopher Landorf, Vijaya Kayastha, Daniel Padilla, Marriana Nelson, Louis McCarthy and Jiadeng Zhu; Brewer Science, United States

The demand for CO₂ detection steadily increases mainly due to the greenhouse effect caused by CO₂ emission. Herein, we have demonstrated a low-cost and effective CO₂ sensor based on composite materials of polyethyleneimine (PEI) along with functionalized carbon nanotubes (f-CNTs). In this design, CNTs, which were modified for a better adhesion and a more evenly distribution, served as an adsorbent and a conductive component. PEI, which have reactive amine groups, served as the responsive materials for the sensor. The sensors were finally fabricated by screen printing using the f-CNTs/PEI composite ink with a proper viscosity, which showed excellent sensitivity and good stability. Effects of environmental chamber temperatures, humidity, and material topologies on the performance have been further explored. Besides material design, devices for sensor setup and a testing system have been demonstrated in this study.

SB06.14.02

First-Principles Study of Cyanine Analogues for Photon Upconversion Natalia P. Neme, Remco W. Havenith and Thomas la Cour Jansen; University of Groningen, Netherlands

Solar energy is the most promising renewable energy source, and therefore, solar cell power conversion efficiency (PCE) is a primary concern. The theoretical maximum conversion efficiency for solar cells is known as the Shockley-Queisser limit, and to go beyond it is crucial to improve the PCE. One approach to surpass this limit is by upconversion performed by a lanthanide-based inorganic-organic system. The strategy consists of attaching an antenna to a nanoparticle doped with lanthanides [1]. The antenna absorbs near infrared light, and subsequently the energy is transferred to the nanoparticle that ultimately will perform the upconversion.

The aim of this study is to investigate the photophysical properties of a cyanine dye analogue to be used as antenna, by performing first-principles calculations based on Density Functional Theory (DFT) and Time Dependent-DFT. Our goal is to investigate dyes that absorb in Near Infrared and cyanine ones are versatile compounds that by modifying their end groups and chain's length we influence their photophysical properties. The vinylene shift is experimentally known for these molecules, and it consists of a bathochromic shift of approximately 100 nm of the 0-0 vibronic transition when a vinyl group is added to the polymethine chain [2,3]. Our study showed that the saturated moiety of the ring in the methine bridge can interact with the conjugated pi-system. We showed here the origin of this interaction and how it can be used to fine tune the absorption energy of this class of dyes.

[1] Zou, W.; Visser, C.; Maduro, J. A.; Pshenichnikov, M. S.; Hummelen, J. C. *Nature Photonics* 2012, 6, 560–564.

[2] Mustroph, H. *Physical Sciences Reviews* 2020, 5.

[3] Kachkovski, A.; Kovalenko, N. *Dyes and pigments* 1997, 35, 131–148.

SB06.14.03

Polarized Light Microscopy as a Rapid, Non-Destructive Evaluation Method for Qualitative Evaluation of Morphology in Organic Semiconductor Thin-Films Christopher E. Petoukhoff¹ and Deirdre M. O'Carroll^{2,2}; ¹King Abdullah University of Science & Technology (KAUST), Saudi Arabia; ²Rutgers, The State University of New Jersey, United States

While preparation of thin-films of organic semiconductors *via* solution-based processing techniques is relatively straight-forward, understanding the morphology of these thin-films at different length scales, from micro- to nano-, which is critical in designing high-efficiency devices, can be fairly complex. High-efficiency organic photovoltaics (OPVs) are fabricated from blending two or more organic semiconductor components. This mixing process must be fine-tuned based on the ratio of different components, solvents utilized, and morphology-controlling additives, to obtain uniform thin-films at micro- and nano-scales. To characterize the uniformity, researchers must often turn to time-consuming or destructive techniques, such as atomic force microscopy (AFM) or scanning electron microscopy (SEM), which are not amenable to high-throughput, automated device fabrication facilities.

Polarized light microscopy (PLM) is a relatively unexplored technique for the characterization of organic semiconductor thin-films. PLM uses a set of orthogonal polarizers in the excitation and collection paths. As such, most of the incident light is filtered out from the image, and only the local optical birefringence is imaged, providing enhanced contrast compared to standard bright-field light microscopy. Organic semiconductors tend to have high degrees of anisotropy based on their molecular orientations and local degrees of crystallinity. Thus, PLM is a powerful imaging technique to qualitatively evaluate the morphology of organic semiconducting thin-films. Because it is a form of light microscopy, it is non-destructive, has a wide-field of view, and has potential to be employed in automated device fabrication facilities.

In this work, we employ PLM to evaluate the quality of thin-films of the stable conjugated polymer, PCDTBT. PCDTBT thin-films are an example of polymer thin-films that are challenging to prepare due to the neat polymer's poor solubility in typical organic solvents, its high viscosity, and its ease of aggregation. We optimized PCDTBT thin-films by varying the solvent, molecular weight, heating times and temperatures, and filtering conditions. Using PLM, we rapidly evaluated the quality of PCDTBT thin-films with various preparation conditions to find optimal conditions for uniform thin-films with low degrees of aggregation. Based on these optimal conditions, we fabricated PCDTBT hole-only devices in a metal-insulator-metal Schottky photodiode geometry for thick (200 nm) and thin (80 nm) PCDTBT layers. We extracted the Schottky barrier height and hole mobility of PCDTBT from current-voltage measurements and drift-diffusion simulations, respectively.

We will discuss the potential of PLM to interpret the nanoscale morphology and crystallinity of several other common organic donor-acceptor blends.

SB06.14.04

Controlling Anisotropic Properties Through Manipulation of Chiral Small Molecule Orientation Jessica Wade¹, Francesco Salerno¹, Rachel Kilbride², Dong Kuk Kim¹, Julia Schmidt¹, Joel Smith³, Luc LeBlanc⁴, Emma Wolpert¹, Adebayo Adeleke⁴, Erin Johnson⁴, Jenny Nelson¹, Tadashi Mori⁵, Kim E. Jeffs¹, Sandrine Heutz¹ and Matthew Fuchter¹; ¹Imperial College London, United Kingdom; ²University of Sheffield, United Kingdom; ³University of Oxford, United Kingdom; ⁴Dalhousie University, Canada; ⁵Osaka University, Japan

Chiral π -conjugated molecules offer new functionality to thin film technologies and represent a highly exciting and rapidly expanding area of scientific research. Due to the anisotropic functional properties of such materials such as the absorption and emission of circularly polarised light or the transport of spin-polarised electrons, the functionality, performance, and efficiency of chiral devices is critically dependent on the orientation of chiral molecules in thin films. Despite this, broadly applicable, simple methods to control molecular orientation of chiral materials in the bulk are yet to be developed. Here a novel approach is presented to control the orientation of a chiral small molecule (2,2'-dicyano[6]helicene, **CN6H**) in thin films: the use of organic (3,4,9,10-perylenetetracarboxylic dianhydride, PTCD) and inorganic (copper(I) iodide, CuI) templating layers. All **CN6H** and templating layers were grown via organic molecular beam deposition (OMBD), ensuring good film quality and reproducibility. Using grazing incidence wide angle X-ray scattering (GIWAXS) measurements, it is shown that using 3,4,9,10-PTCD templating layers, **CN6H** molecules adopt a 'face-on' orientation and self-assemble into upright supramolecular columns oriented with their helical axis perpendicular to the substrate. Alternatively, copper(I) iodide (CuI) templating induces the formation of supramolecular columns in an 'edge-on' orientation with their helical axis lying parallel to the substrate. Structural templating is further verified by 2D GIWAXS simulations of the **CN6H** crystal structure in face-on and edge-on orientations, demonstrating excellent agreement with experimental results. Through such control of orientation, it is shown that low- and high-energy chiroptical responses can be independently 'turned on' or 'turned off' as a function of molecular orientation. As such, the templating methodologies described here provide a simple way to engineer orientational control, and by association, anisotropic functional properties of chiral molecular systems for a range of emerging technologies.

SB06.14.06

Chiroptical Conjugated Polymer/Chiral Small Molecule Hybrid Thin-Films Based on Chirality Transfer Phenomenon Jung Ah Lim; Korea Institute of Science and Technology, Korea (the Republic of)

Chiral optoelectronics based on circularly polarized light (CP light) has recently garnered significant interest in various fields, including biosensing, 3D displays, cryptography, and quantum optics. CP light, continuously rotating at a steady-state along the propagation axis, enables structural chirality and quantum spin directions to be used as the main information vector. One forefront for the realization of chiral optoelectronic systems is the development of semiconducting materials with strong chiroptical activity and excellent electrical properties. π -Conjugated molecules (i.e. organic semiconductor) are one of the most promising chiroptical semiconductor materials because their optical rotation properties can be modulated by intentional designing of structural asymmetry. Considering that the performance of chiroptical electronic devices is determined by the photophysical, electrical, and morphological properties of the conjugated molecules, a new strategy for obtaining organic semiconductor thin-films with not only strong chiroptical activity but also good charge transport properties that can be directly applicable to the optoelectronic devices, is needed. In this presentation, we will suggest an effective way to obtain chiroptically active semiconductor thin films by blending of achiral conjugated polymer with excellent charge transport properties and versatile small molecules with strong chiroptical activity. We found that controlled phase separation and crystallization of these hybrid films resulted in a unique heterojunction bilayer structure that consisted of small chiral molecules at the top and a conjugated polymer-dominant mixed layer at the bottom. A photodiode based on this chirocentric hybrid film has demonstrated the ability to detect left- and right-handed circular polarization. In addition, a fundamental understanding on the crystalline structure of the hybrid film and the effect of intermolecular interactions on the chiroptical properties of the hybrid film will be discussed.

SB06.14.07

Silicone-Integrated Hole Transport Networks for High-Performance and High-Resolution OLED Microdisplay Borina Ha¹, Hyukmin Kweon¹, Seonkwon Kim², Ukjin Jeong¹, Seunghan Lee³, Moon Sung Kang³, Jeong Ho Cho² and Do Hwan Kim¹; ¹Hanyang University, Korea (the Republic of); ²Yonsei University, Korea (the Republic of); ³Sogang University, Korea (the Republic of)

Organic light-emitting diodes (OLEDs) have attracted great attention due to their unprecedented color purity, thin form factor, superior response time, and expanded color gamut. OLEDs are one of a major display technology exerting strong influence from commercialized display to microdisplay for virtual, augmented, mutual, and extended reality (VR/AR/MR/XR) devices. As the applicable scope of OLEDs has been expanded, high pixel densities over 1,000 pixels per inch (PPI) are strongly sought after. However, reduction of inter-pixel distance can induce pixel crosstalk which is resulting in deterioration of color gamut area and color purity, even though emission layers are completely separated. This is derived from parasitic currents flowing through common hole transport layers (HTLs) between adjacent pixels, indicating that for prevention of the crosstalk phenomenon, the HTLs must be pixelated with micro-scales in conjunction with emission layers. Practically, photolithographic patterning is the best candidate to effortlessly achieve precise micropatterns of the HTLs; however, it is not adaptable to organic hole transport materials because of their low chemical and physical endurance.

Herein, for realization of fine pixelated HTLs, we demonstrate silicone-integrated hole transport network (SI-HTN) in which silicone binder are homogeneously crosslinked with small molecule hole transport materials. Due to the embedded silicone moieties, the SI-HTN exhibited exceptional physico-chemical robustness, so that reactive ion etching (RIE)-coupled photolithography patterning can be utilized for realization of high-resolution pattern. On the basis of this, ultra-fine patterns of the SI-HTN (down to 1 μ m) was demonstrated based on the photolithography process. Furthermore, the SI-HTN showed improved hole injection capability compared to the neat HTL, thus, solution-processed high efficient OLEDs can be achieved. This indicates that the SI-HTN can simultaneously obtain not only high-resolution patterns, but also enhanced light-emitting performance of the OLEDs. We believe that our approach will provide guidance for next-generation of high-resolution OLEDs.

SB06.14.11

Using Density Functional Theory and Fukui Function to Analyze the Reaction Site of Hemoglobin to CO, O₂ and NO Wei Chen¹, Chi Hua Yu¹, Xiao Ru Wang¹ and Francisco Martin-Martinez²; ¹National Cheng Kung University, Taiwan; ²Swansea University, United Kingdom

Carbon monoxide poisoning is the most common cause of death from gas poisoning worldwide. About 6,600 people suffer long-term cognitive sequelae from carbon monoxide poisoning each year, with a total cost of about \$925 million. Carbon monoxide poisoning has always been a very important problem, but there are many environmental limitations in existing treatment methods, and the effect of treatment often causes sequelae. When a large amount of carbon monoxide enters the human system, it will quickly combine with hemoglobin to form carbon monoxide hemoglobin (COHb). The affinity of carbon monoxide to hemoglobin (Hb) is 200 to 200 times that of oxygen to carbon monoxide hemoglobin. Heme dissociates about 3,600 times faster than oxyhemoglobin, so heme transports oxygen poorly, leading to carbon monoxide poisoning. In biology, the dissociation and binding of CO, O₂, and NO to hemoglobin are very important. In this study, we performed density functional theory (DFT) and computed the Fukui function to analyze the reaction site of heme with CO, O₂, and NO. By comparing the calculations results for heme and different oxygen-containing molecules such as CO, O₂, and NO, we found the specific reaction sites of ferrous ions and carbon atoms in carbon monoxide molecules. This finding can help us to understand the binding mechanism of COHb. We can further extend the research to design an antidote that can break the carbon monoxide-heme bond quickly. The antidote for carbon monoxide poisoning can achieve the fastest therapeutic effect. Our work can be applied to develop an effective antidote and bring great benefits to the treatment of carbon monoxide poisoning.

SB06.14.12

Fabrication of Bulk Heterojunction Donor Polymer—Non-Fullerene Acceptor Nanoparticles for Use in Photocatalytic H₂ Evolution from Water Matthew W. Bidwell¹, Jan Kosco², Hyojung Cha¹, Calvin Howells², Michael Sachs¹, James R. Durrant¹ and Iain McCulloch^{3,1,2}; ¹Imperial College London, United Kingdom; ²King Abdullah University of Science and Technology, Saudi Arabia; ³University of Oxford, United Kingdom

As the global energy demand increases, finding cheap and sustainable sources of energy is increasingly important, with an urgent need to develop new materials and technologies capable of providing clean and fossil-fuel free energy on a Terrawatt scale worldwide. The use of fossil fuels has led to unprecedented levels of atmospheric CO₂, causing devastating anthropogenic climate change and has driven the search for alternative sources of energy. The past decade has witnessed a renaissance in photovoltaic (sunlight to electrical conversion) technologies with remarkable increases in performance and stability, establishing solar energy as a viable source of renewable energy worldwide.

A major obstacle to utilising the full potential of solar energy is the challenge of storing it for future use. Solar intensity and availability are intermittent and often mismatch with high consumer electricity demand, which regularly peaks after sunset. One way to address this issue is to store sunlight in the form of chemical bonds, known as “solar fuels”. The simplest solar fuel is H₂ which can be generated from the electrochemical splitting of water, using H₂ evolution photocatalysts (HEPs). This H₂ can then be further stored and used by consumers on-demand with the advantage of water being the only combustion by-product, free of any CO₂ emissions. Currently, most HEPs consist of single component inorganic semiconductors which are well established and have been used prominently in the field of photocatalysis. However, these materials also suffer inherent drawbacks. These include limited visible light absorption, high materials cost, and limited chemical tuneability, which severely hinder H₂ production efficiency. In contrast, organic semiconductors such as conjugated donor polymers and non-fullerene acceptors (NFAs) have been explored as alternatives to these inorganic systems and have the advantages of strong optical absorption properties, facile synthetic modification, low cost, and easily tuneable optoelectronic properties.

Amongst the numerous strategies for photoelectrochemical energy conversion of sunlight to solar fuels, the use of a one-pot particulate-based photocatalytic system, in which semiconductor photocatalysts are dispersed directly into water, is regarded as a cheap and economical approach toward industrial-scale solar hydrogen production. This is in part due to the intrinsic simplicity of the methodology, which forgoes the use of any electrical circuitry or device fabrication, requires a low initial investment of capital, and has the potential for sustainable scaling of the technology with the possibility of H₂ being directly collected from large batch flow photoreactors irradiated by the Sun.

With this in mind, the donor polymer PCE10 and NFA EH-IDTBR were investigated as HEPs in blended two-component nanoparticle systems with ascorbic acid as the sacrificial electron donor.¹ Through the synthesis and implementation of novel conjugated surfactants, as well as fine-tuning of NP fabrication conditions, it was possible to control the internal structure of the HEPs and transform them from a prototypical core-shell structure into a highly intermixed bulk heterojunction two-component system. Through this enhancement in internal morphology, improved nanoparticle surface charge extraction was realized, which led to stable HEPs for over 35 hrs. This change in morphology was elucidated through the use of cryogenic transmission electron microscopy and small-angle neutron scattering of deuterated EH-IDTBR and led to a ten-fold increase in H₂ efficiency and to an unprecedentedly high H₂ evolution rate of over 60 mmol h⁻¹ g⁻¹, with EQEs exceeding 5.6% across 660 - 700 nm in the visible spectrum, which is one of the highest for organic HEPs reported to date.

1. Kosco, J.*, Bidwell, M.* et al. Enhanced photocatalytic hydrogen evolution from organic semiconductor heterojunction nanoparticles. *Nature Materials* 19, 559–565 (2020).

SB06.14.13

Design Redox-active Semiconducting Polymers with High Stretchability and Mixed Ionic/Electronic Conductivity for Stretchable Organic Electrochemical Transistors Yahao Dai, Shilei Dai and Sihong Wang; University of Chicago, United States

Organic electrochemical transistor (OECT) is an emerging device platform for next-generation human-integrated bioelectronics owing to its high amplification and sensitivity to biological signals, and non-volatile signal retention for memory and computing applications. However, owing to the lack of stretchable redox-active semiconducting polymers, skin-like softness and stretchability have not yet been realized in high-performance OECTs for achieving seamless tissue-electronics interfaces. Here, through the molecular engineering approach, we report two stretchable redox-active semiconductors for OECT devices, namely poly(2-(3,3'-bis(2-(2-(2-methoxyethoxy)ethoxy)ethoxy)-[2,2'-bithiophen]-5)yl thiophene) (p(g2T-T)) and poly-[3,3'-bis(2-(2-(2-methoxyethoxy)ethoxy)ethoxy)-2,2'-bithiophene] (p(gT2)), which give exceptional stretchability over 200% strain and 100 stretching cycles, together with the OECT performance on par with the state of the art. Validated by the systematic structural characterization, sufficient chain alignment during stretching for stress dissipation is determined as the key enabler of high stretchability. By controlling the symmetry and chain length of polymer semiconductors, the key structural features for enabling the combination of high stretchability and high OECT performance are determined as non-linear backbone architecture, moderate side-chain density, and sufficiently high molecular weight. Using those highly stretchable polymer semiconductors, we fabricated an intrinsically stretchable OECT with the high normalized transconductance (~223 S cm⁻¹) and biaxial stretchability up to 100% strain, which has been further demonstrated as an ideal device platform for building stretchable electrocardiogram sensors and neuromorphic transistors.

SB06.14.14

Pyrrolic Small Molecule Chromophores for Applications in Electrochromic Materials Tiffany Q. Chen and Timothy Swager; Massachusetts Institute of Technology, United States

Electrochromic materials (EC) provide functional solutions for a variety of applications, including smart windows and optical display technologies. The use of organic materials provides advantages over inorganic materials in electrochromic devices. The ability to readily tune structure in organic materials through synthetic methods affords precision in controlling redox, optoelectronic, mechanical, and processing properties. As superior light-absorbing materials to inorganic materials, organic materials enable high optical contrast, allowing for the use of thinner films. In addition, the solution-processability of organic materials and their relatively low cost allow the use of coating methods to form functional, reproducible thin films that can be layered on a substrate.

Although organic electroactive polymers are promising candidates in this realm, these materials have distinct drawbacks, including inherent structural disorder resulting in spectral diffusion, limited modularity in structure and bandgaps, depletion of absorption at long wavelengths, and diminished performance with material deformation. In contrast, electrochromic small molecules with highly delocalized structures such as fused ring systems are promising chromophores that have received less attention in this field. Recent research in using small molecules has been motivated by their well-defined and rationally tunable structures, enhanced stability toward oxidative degradation, and batch-to-batch reproducibility. We report the development of a new class of symmetric small molecule chromophores based on pyrrolic scaffolds to address these current limitations in the field of electrochromic materials.

Program Acknowledgment: This research was supported by an appointment to the Intelligence Community Postdoctoral Research Fellowship Program at Massachusetts Institute of Technology administered by Oak Ridge Institute for Science and Education (ORISE) through an interagency agreement between the U.S. Department of Energy and the Office of the Director of National Intelligence (ODNI).

SB06.14.15

Accelerated Photodegradation Study of Multi-Component Organic Photovoltaic Materials with Robotic Micro-Experimentation Jacob Mauthe, Mihirsinh Chauhan, Ambika Pathak, Tonghui Wang, Samuel Shepard, Xingao Zhang, Benjamin Hines, Felix Castellano, Harald Ade and Aram Amassian; North Carolina State University, United States

With the advent of non-fullerene acceptors (NFA), the efficiency of organic photovoltaics (OPVs) has broken previous records and currently stands at a certified power conversion efficiency (PCE) of 19% [1]. Multi-component OPV blends have been increasingly used to improve the performance and stability of devices [2]. However, there is a lack of understanding of the fundamental mechanisms behind improvements in performance and even less so how these blends stabilize devices. Investigating photodegradation of a vast library of materials and their multi-component combinations is a demanding problem that currently requires considerable effort in terms of time and resources. We take the view that workflow automation combined with micro-experimentation and data-driven and machine learning-guided sample selection allowing for (semi-)autonomous workflows can significantly accelerate photodegradation investigations as well as multiparameter optimization. In this work, we describe a robotic platform, the RoboMapper, which formulates and prints miniature OPV active layer areas on transparent substrates and enables rapid evaluation of photodegradation in inert atmosphere under 4 to 40 suns. Printing on a scale 1/10th to 1/20th of the size of traditional samples consumes a fraction of materials, whereas robotic micro-UV-Vis characterization enables high throughput evaluation of photobleaching of all materials printed on chip. Using the RoboMapper, we conducted photodegradation campaigns on neat donor and acceptor materials [AA1], PM6, PTQ10, Y6, IT-4F, and PC₇₁BM, their binary, and multi-component blends. The performed photodegradation analysis of the vast library of materials showed that all acceptors and donors have different degradation behavior in neat films and blends as compared with different donor-acceptor combinations. Additionally, the data allows us to select the right donor-acceptor combinations for optimal

photostability in binary and ternary systems. Our study shows that approaches like the RoboMapper can be powerful for collection of big data equivalent to years of work in just a few weeks or months. The ability to prepare multiple samples simultaneously from a small amount of stock materials also considerably reduces the waste generated for the same quantity and quality of data.

1. Zhu, L., Zhang, M., Xu, J. et al. *Nat. Mater.* 21, 656–663 (2022).
2. Lingling, Z., Li, S. et al. *Energy Environ. Sci.* 13, 635–645 (2020).

SB06.14.16

Controlling Interlayers in Organic Semiconductor Devices towards Photo-Stimulated Bio Interfaces Maxim Shkunov, Leslie Askew and Aimee R. Sweeney; University of Surrey, United Kingdom

Photosensitive organic semiconductor materials designed as active layers in bioelectronic devices provide an effective mean to stimulate cells using optical excitation. Such devices are entirely self-powered, fully compatible with operation in bio-electrolyte environment, and can stimulate a variety of cells from peripheral neurons to retinal neurons. The nature of the excitation mechanism is expected to be mostly due to induced photo-voltage changes as well as photocurrent at the cell membrane. Device efficiency is hugely dependant on the interfaces, including organic semiconductor/electrolyte, semiconductor/electrode, and any heterojunction interfaces present in the device structure. Here, we present a study involving charge blocking/charge transport interlayers that are used to control both the polarity at the active interface, and the optoelectronic transduction process between the active layer and the electrolyte, be it Faradaic or capacitive. Donor-acceptor small molecules as well as conjugated polymers with various bandgaps are used to i) provide selective colour response of the devices to resemble the photoresponse of human cones and rods in the retina, and ii) target human tissue transparency window in the red part of spectrum towards peripheral nerves excitation. The results demonstrate that the addition of interlayers can control the charge species at the working electrode and substantially enhance photocurrent magnitude, whereas bulk-heterojunction interfaces provide further increase in both photovoltage and photocurrent.

We further discuss the suitability of organic semiconductors for potential medical applications as retinal bio-engineered prosthesis for the restoration of human vision, and peripheral nerves opto-stimulation, as well devices fabrication strategies via pixelation using ink-jet printing approaches on flexible substrates.

SB06.14.17

Accurate Threshold Voltage and Field-Effect Mobility Estimation for Thin-Film Transistors with Gate Voltage-Dependent Mobility in Linear Region Yuchen Zhou, Xiao Wang and Ananth Dodabalapur; University of Texas at Austin, United States

Carrier mobility is an essential figure of merit for transistors used in various electronic applications. High mobilities are generally desired for thin-film transistors (TFTs) with amorphous metal oxide and organic/polymer semiconducting channel materials, as it enables faster operating speeds for various applications including displays, RFID tags, and integrated circuits. Saturation mobility in TFTs will be inaccurate due to the dependence on carrier concentration in the gradual channel approximation. However, the reported linear mobility calculations are often inaccurate. This results in an overestimation of mobility under the gradual channel approximation, which is a direct consequence of the mobility being gate voltage-dependent instead of any artifact in the measurements.

The gradual channel approximation assumes a constant mobility independent of carrier density, which is often not the case for TFTs. Here we propose a calculation procedure that differs from the conventional field effect mobility calculation by explicitly considering the gate voltage-dependence of the mobility. The resulting equation consists of three terms: the transconductance term on the left-hand side, the differential mobility term with respect to gate voltage, and the modified field effect mobility on the right-hand side. The inclusion of the second term or the differential mobility term often results in calculated mobility values larger by a factor of between one and two.

Accurate threshold voltage values must also be considered for an improved mobility extraction. Previous literature demonstrated threshold voltage extraction using the linear extrapolation method on the drain current as a function of gate voltage, which often leads to a gate bias-dependent threshold voltage. The onset voltage V_{on} where the conduction starts increasing has been proposed to be used for mobility calculation. Another proposed method of calculating threshold voltage suggests that the voltage at which the gate voltage-dependence transitions into a power law dependence in the drain current can be used as the threshold voltage for TFTs. This definition considers that the exponential increase in drain current corresponds to the diffusion-limited subthreshold region but not the drift-limited subthreshold region. Corrected field effect mobility calculated using the conventional threshold voltage, corrected threshold voltage, and the onset voltage will be compared.

Amorphous indium-gallium-zinc-oxide (a-IGZO) TFTs and organic TFTs are used to illustrate the corrected field effect mobility and threshold voltage calculation process. In one sample TFT, the conventional field effect mobility calculation yields a value of $2 \text{ cm}^2/\text{V}\cdot\text{sec}$ while the corrected field effect mobility is approximately $1.2 \text{ cm}^2/\text{V}\cdot\text{sec}$, resulting in at least an overestimation of $\sim 67\%$.

This mobility calculation process can be applied to transistors with any semiconducting materials with non-constant mobilities in the linear region. It is a robust tool when it comes to accurately characterizing the device performance of thin-film transistors in the linear region.

SB06.14.18

Ultrafast Photochemistry of Melanin and Organic-Inorganic Melanin-Based Heterostructures Using Modern Ultrafast Pump-probe Microscopy and Spectroscopy Max DeMarco, Farnoush Nourigheimasi, Mathew Ballard, Lillian Getter and Elham Ghadiri; Wake Forest University, United States

Using melanin as organic biopolymer for optoelectronic or bioelectronic is intriguing. Melanin family are organic ubiquitous pigments found in human skin, hair, eyes, and the brain and almost in every higher-level organism in different forms. The functionality of melanin as a natural pigment is defined (although not fully understood) by its physical and chemical properties, such as its featureless broad UV-NIR optical absorption, antioxidant properties, temperature-dependent photoconductivity, and free radical scavenging behavior, chemical signatures that can support reversible cation binding. Many physical properties (such as dark current and photoconductivity) are dramatically affected by hydration and doping. Little has been understood so far about the nature of conductivity in melanin.

In this work, we integrate state of the art pump-probe transient absorption microscopy (PP-TAM) and pump-probe transient absorption spectroscopy (pp-TAS) to localize and investigate photochemical processes in melanin and melanin-based organic-inorganic and organic-organic heterostructures. The technique uniquely enables to visualize the photoexcited processes in few hundred nanometer spatial resolution and femtosecond time-resolution.

Through chemical synthesis, we have prepared melanin nanoparticles with controlled sizes (70 nm, 100 nm, and 250 nm) and chemical structures of dopamelanin and eumelanin. The active thin-film layer of melanin nanoparticles are prepared using inkjet printing and spin coating. To achieve multifunctional melanin-based nanostructures, we synthesized and fabricated donor-acceptor bilayers of melanin nanoparticles. The photochemical characteristics of the donor-acceptor melanin-based constructs are studied by photocatalytic degradation of methylene blue dye under selective UV-NIR and Vis-NIR irradiation condition. The melanin-TiO₂ nanostructured films and Melanin-PEDOT:SS films exhibit enhanced photocatalytic characteristics compared to pristine melanin upon both UV-NIR and Vis-NIR irradiation condition. The enhanced photocatalytic characteristics of the melanin-based heterostructures motivate to investigate the fundamental processes involved using ultrafast spectroscopy and microscopy. Using ultrafast broadband

measurements, we identified the spectral characteristics of excited state, and excited state relaxation dynamic in pristine melanin and melanin heterostructures. The ultrafast photochemical studies are remarkable in the sense that they shed light on the unknown photophysical characteristics of melanin, rationalize the enhanced photocatalytic activities, and identify melanin based heterostructures as a viable photochemical material for broad applications.

SB06.14.19

Self-Assembled Microbead Lasers Using Organic and Organic/Inorganic Hybrid Gain Materials for Multiplexed Bio-Imaging Kwon-Hyeon Kim^{1,2} and Seok-Hyun A. Yun^{1,2}; ¹Harvard Medical School, United States; ²Massachusetts General Hospital, United States

Fluorescent microbeads are widely used for applications in life sciences and medical diagnosis. The spectral contrast and sharpness of photoluminescence are critical in the utilities of microbeads for bio-imaging and multiplexing. Recently, there has been growing interest in using microbead lasers capable of generating ~100 times narrower emission linewidth than conventional fluorescence. Stimulated emission of microbead enhances spectral brightness and multiplexing capability. Here, we demonstrate novel types of microbeads that exhibit compact size and sub-nanometer linewidth using two types of gain material: Colloidal quantum dots and aggregation-induced emission (AIE) dyes. Self-assembled microbeads are fabricated by microfluidic chip using the oil-in-water emulsion method. Their high optical gain and refractive index allow lasing with a size less than 2 μm in the air. The feasibility of intracellular tagging and multi-color imaging *in vivo* is demonstrated. Multicolor imaging with proposed microbeads shows greatly enhanced spectral density and color-multiplexing capability compared to conventional fluorescence imaging.

SB06.14.20

All-Solution-Processed and Intrinsically Flexible Multicolor Perovskite Light-Emitting Diodes and Photodetectors on Textile and Paper Substrates Junyi Zhao; Washington University in St. Louis, United States

Solution-processable optoelectronic devices hold great potential for emerging low-cost and scalable fabrications of flexible electronics. Textiles and papers, made of percolation yarn- and fiber- networks that are commonly used in our daily life, are becoming novel platforms for next-generation wearable and health-monitoring electronics. In this work, we report a versatile and ultra-fast mask-free fabrication strategy that enables printing, even direct-handwriting, of all-solution-processed optoelectronic devices onto papers, textiles (cotton, polyester, and nylon), and other unconventional substrates including metal foil, plastic film, rubber, vinyl glove, and even 3-dimensional surfaces such as glass vial and spheres. Compared with existing microfabrication and printing processes, handwriting allows high-performance optoelectronics to be fabricated by untrained individuals in a time-efficient (a batch of devices could be made within a few minutes) and cost-effective manner. The handwriting technique is especially meaningful for early-stage demonstration or large-area applications with less stringent requirements on resolution such as E-Textiles, E-Packaging, and E-Papers. More specifically, we have formulated universal electronic inks that could either be used in printing/coating machines or loaded into ballpoint pens for direct handwriting on target substrates. These electronic inks include poly(3,4-ethylenedioxythiophene) polystyrene sulfonate (PEDOT:PSS) and poly(ethylene oxide) (PEO) composite ink for transparent anodes, halide perovskite (MAPbX_3) and polystyrene (PS)/ poly(methyl methacrylate) (PMMA) composite ink for the photoactive layer, polyethylenimine (PEI) ink for the electron transporting layer, and silver nanowires ink for semi-transparent cathodes. The PEO component blended in the PEDOT:PSS conducting ink not only helped planarize the rough percolating yarn/fiber substrates, but also improved the conductivity and conformability of conducting film, thus leading to improved device performance and stability. High-performance multicolor light-emitting diodes (LEDs) with emissions covering the entire visible spectrum and photodetectors (PDs) in both a vertical photodiode configuration and a lateral photoconductor configuration were obtained on paper substrate: LEDs exhibited a brightness up to 15,225 cd m^{-2} , a turn-on voltage of 2.4V, and current efficiency over 6.65%; PDs showed an on-off ratio over 10^4 with a response time of less than 15 ms. Owing to the intrinsic flexibility and stability of each functional layer, the hand-drawn LEDs could be bent to a 1 mm extreme curvature radius for over 5000 cycles without decay in performance. Overall, such low-cost and eco-friendly textile/paper-based LEDs and PDs via printing and handwriting could pave a way for the integration of optoelectronic devices with lightweight and human-machine interactive applications.

SB06.14.21

Transition Metal-Based NIR Material with Heteroleptic Structure for Bio-Medical Application Yongjin Park¹, Gyeong S. Lee², Hye R. Choi³, Chang H. Huh³, Yun H. Kim² and Kyung C. Choi¹; ¹Korea Advanced Institute of Science and Technology, Korea (the Republic of); ²Gyeongsang National University, Korea (the Republic of); ³Seoul National University Bundang Hospital, Korea (the Republic of)

Among the near-infrared (NIR) ranges, the area between 700 nm and 1000 nm, called the optical tissue window, is widely used in the bio-medical field because it has less scatter with skin cells and can penetrate deep into the skin to promote cell metabolism. However, it is very challenging to develop a low-gap organic material that emits light in the NIR region due to the increased proportion of non-radiative decay rate by the energy gap law. In order to overcome this hurdle, various types of development methods are being studied such as the use of thermally activated delayed fluorescence (TADF) and transition metal-based phosphorescent materials.

In this study, a novel Ir(III) complex was synthesized and designed using a thienothiophene moiety. This material is composed of a fused thiophene structure, and thus is exceedingly rigid and has an extended construction length, thereby reducing the energy gap. In addition, since it has a high electron density structure, the covalent bond between the ligand and iridium can be strengthened to provide stability to the device. Moreover, dipole moments are more likely to be horizontally oriented in heteroleptic structures than in homogeneous structures, thus boosting the performance of the device. Notably, it has a lower non-radiative decay rate than other reported Ir(III)-based NIR emitters. The radiative lifetime is 660 ns, allowing for efficient luminescence with a narrow energy gap. To demonstrate the properties of this novel material, a NIR OLED was fabricated with an emission peak of 700 nm. This optoelectronic device has a very high radiant emittance and a stable operation lifetime with a Lambertian light distribution. It exhibits excellent electrical and optical properties compared to previously reported Ir(III)-based NIR OLEDs. Furthermore, significant proliferation results were verified compared to the control group in fibroblast cell experiments.

SB06.14.22

Coarsening-Induced Hierarchically Interconnected Porous Carbon Polyhedrons Derived from Metal-Organic Frameworks for Stretchable Ionogel-Based Supercapacitors Incheol Heo, Chanyoung Lee and Won Cheol Yoo; Hanyang University, Korea (the Republic of)

For ultrahigh-energy-density supercapacitors (SCs), hierarchically interconnected micro-/meso-/macroporous carbons (HICs) are desirable for both effective ion polarization and transport, especially when electrochemically stable but dynamically sluggish ionic liquids are employed as the electrolytes. In this presentation, we develop an effective strategy for preparing HICs with well-developed all-pore regimes for ultrahigh-energy-density SCs using electrochemically stable ionic liquid (IL) electrolytes. The HICs are synthesized *via* coarsening of the Cu nanoparticles (NPs) within carbon polyhedrons derived from the polymer-infiltrated metal-organic framework (MOF). During thermolysis process, the coarsening process of Cu NPs occurs, in which the locations vacated by the Cu NPs are left as large meso/macropores. HIC polyhedron presents an ultrahigh specific surface area (SSA, 3064 $\text{m}^2 \text{g}^{-1}$) and the HIC-based SCs exhibit an outstanding capacitance of 268.4 F g^{-1} with an ultrahigh energy density of 149 Wh kg^{-1} , which are comparable to the best values

reported to date, indicating that expedited ion-transport via hierarchically interconnected large meso/macropores affords maximum utilization of the micropores of the carbon electrodes. Furthermore, stretchable all-solid-state SCs operating at 120% strain with a very high areal capacitance of 33 mF cm⁻² and an energy density of 0.041 mWh cm⁻² are also demonstrated. These results provide a ubiquitous strategy for developing MOF-based hierarchically interconnected carbonaceous materials with ultrahigh SSA for high-performance SCs compatible with stretchable and wearable electronic devices.

SB06.14.23

Selective Plasticization and Three-Dimensional Transformation Based on Membrane-Type Electronics and Supportive Plastic Framework Jiun Cha^{1,2}, Gi-Gwan Kim^{1,2}, Seunghyun Kim^{1,2} and Heungcho Ko^{1,2}; ¹National Research Foundation of Korea, Korea (the Republic of); ²Gwangju Institute of Science and Technology, Korea (the Republic of)

Three-dimensional(3D) transformation of planar-type electronics has been widely studied in various devices such as solar cells, batteries, antennas, photodetectors, image sensors, and displays for superior electrical and mechanical properties to overcome the two-dimensional limitation. The shape transformation method seems promising when direct device fabrication on 3D structures is extremely difficult. Here, we demonstrate a straightforward electronics-level 3D transformation method by creating supportive substrates containing microfluidic channels that can insert a liquid plasticizer for hard-to-soft transition and allow bending under mild manners in the plasticized regions. In particular, spatially designed microfluidic channels allow the control of the plasticizer's flow direction and the confinement of a specific amount of plasticizer to diffuse around the channels. For example, small microfluidic channels allow the plasticizer's flow to adjacent channels without losing mechanical strength, whereas large size allows extreme bending up to a 180° bending angle without electrical failure of the device layer. Using this method, an extreme case of bending metal electrodes and indium gallium zinc oxide (IGZO) thin-film transistors is possible without device failure. Finally, a truncated octahedral LED array is also developed to demonstrate the capability of this method for complex three-dimensional electronics.

SB06.14.24

Spectral Selective Solar Harvesting and Energy Generation via Porphyrin-Based Hybrid Films Jou Lin and Donglu Shi; University of Cincinnati, United States

The conventional solar harvesting relies on natural spectrum of sunlight from UV to IR which is not efficient for energy applications including photovoltaic due to incompatible photon energies with the bandgaps of semiconductors. Spectral selective solar harvest can address this critical issue by structurally tailoring the materials to absorb photon energies in the specified and desired regions. We have designed and synthesized transparent porphyrin-based hybrid thin films that characteristically exhibit absorption peaks near 400 nm (blue-violet) and 700 nm (NIR) with a high average visible transmittance (AVT). To be able to tune the absorptions, a unique porphyrin-based hybrid is developed with systematic additions of phthalocyanine and Fe₃O₄@Cu_{2-x}S with much stronger NIR absorptions. Phthalocyanine has more pronounced UV and NIR absorptions, but a narrower "optical window" than that of chlorophyllin. Fe₃O₄@Cu_{2-x}S is known for broad and strong IR absorptions around 1200 nm. UV-Vis and Raman spectroscopy experiments have been carried out to characterize the porphyrin-based hybrids. We have found congruent mixtures between chlorophyllin and Fe₃O₄@Cu_{2-x}S resulting in even broader NIR absorptions while maintaining the optical window between 400 and 650 nm for high AVTs. This will provide an ideal spectrum for a transparent but strongly UV/NIR absorbing characteristic for photothermal energy generation. Also discussed are the operating mechanisms underlying the thermal-photonic behaviors associated with the hybrid structures.

SB06.14.25

On the Formation of Halogen Bonds to Boost the Charge Carrier Mobility in NDI Semiconductors Tero-Petri Ruoko¹, Marc-Antoine Stoeckel², Rakesh Puttreddy¹, Chi-Yuan Yang², Ziang Wu³, Nuno Candeias⁴, Han Y. Woo³, Simone Fabiano² and Arri Priimägi¹; ¹Tampere University, Finland; ²Linköping University, Sweden; ³Korea University, Korea (the Republic of); ⁴University of Aveiro, Portugal

Organic semiconductors with a high charge carrier mobility are essential to ensure efficient electronic devices, such as field-effect transistors (FETs), solar cells, and light-emitting diodes. The charge carrier mobility in these organic materials is the consequence of the interplay between a complex set of physical parameters related to morphology, energetic and structural disorder, and defects, which ultimately are related to the molecular chemical structure. Therefore, one strategy to improve the performances of semiconducting small molecule is to promote a defect-free packing. This can be achieved through processes that lead to different qualities of materials, via the formation of molecular single crystals. Another approach consists of attaching certain functionalities to the semiconducting backbone that will improve the packing through specific interactions. This approach, however, can result in a deterioration of the initial performances of the semiconductor, as it can strongly affect its properties (different packing, energy levels and orbitals, ...). An under-explored strategy to enhance the performances of molecular semiconductors in OFETs is to enhance the crystallinity of the thin film by using a blend of a semiconductor and an ad hoc molecule that will selectively bind to it and impose a molecular packing with superior performances. To this end, we employed here an NDI molecule bearing a pyridine group in the 2, 6 positions. Upon the addition of an aromatic halogenated molecules, the nitrogen of the pyridine is able to form a bond with this aromatic molecule through the formation of a halogen bond. Upon the formation of this bond, the as-cast film not only present a higher crystallinity, but also larger crystalline domains. This is therefore reflected in the electron mobility that increases by almost two orders of magnitude for the blend compared to the pristine molecule. Through a systematic study of the electrical performances of these materials, and supported by AFM, GIWAXS, Raman spectroscopy and simulations, we were able to rationalize the underlying mechanism to interpret the higher performances observed with OFETs.

SB06.14.26

Twisting Organic Semiconductors Crystals for Orientation Control to Improve the Charge Injection and Photoconductivity Sehee Jeong, Alexander Shtukenberg, Bart Kahr and Stephanie Lee; New York University, United States

Orientation control in organic semiconductors has been at the forefront of organic electronics research over the past few decades, with up to orders of magnitude variations in charge mobilities, absorption coefficients, photoluminescence intensities along different crystallographic directions. In this work, we demonstrate a generalizable strategy to introduce periodic variations in the out-of-plane orientations of small molecule 5,11-bis(triisopropylsilyl)ethynyl)anthradithiophene (TIPS ADT) crystals via twisting. TIPS ADT crystallized from the melt in the presence of 16 wt % polyethylene (PE) forms banded spherulites of crystalline fibrils that twist in concert with one another about the radial growth direction. One full rotation in crystal orientation occurs over a distance of 40 – 400 nm depending on the crystallization temperature, introducing periodic variations to the absorption, photoluminescence and Raman spectra on a commensurate length scale. Although TIPS ADT molecules and straight crystals are not optically active, Mueller Matrix imaging revealed strong circular dichroism (CD) of twisted crystals, with TIPS ADT banded spherulites exhibiting domains of positive or negative CD signal depending on the crystal twisting sense. The introduction to continuously varying out-of-plane orientations from spontaneous crystal twisting further resulted in significant improvements in both the conductivity and photoconductivity in twisted TIPS ADT crystals compared to straight TIPS ADT crystals. Local conductive atomic force microscopy mapping revealed enhanced charge injection and extraction in films of twisted TIPS ADT crystals compared to those comprising straight TIPS ADT crystals. The photocurrent and external quantum efficiency of twisted TIPS ADT photodetectors were measured to be 3.2 and 11.6 times larger, respectively, than those measured for photodetectors comprising straight TIPS ADT crystals. These

improvements are a direct consequence of twisted TIPS ADT crystals possessing out-of-plane orientations that present smaller barriers to charge transport compared to straight TIPS ADT crystals.

SB06.14.27

All-time Operation Hybrid Energy Harvesting System through Non-fullerene-based Organic Photovoltaics and Triboelectric Nanogenerator Hyojeong Choi¹, Yongju Lee¹, Selim Han^{1,2}, Swarup Biswas¹ and Hyeok Kim¹; ¹University of Seoul, Korea (the Republic of); ²Korea Institute of Industrial Technology(KITECH), Korea (the Republic of)

With the rapid development of the Internet of Things (IoT), the number of sensors used in IoT is expected to exceed 200 billion by 2025. Therefore, research on creating a sustainable energy source with the stimuli that can be obtained is becoming crucially indispensable. Among various energy harvesters, Organic Photovoltaic (OPV), which produces energy through light absorption, is easy to be fabricated due to the solution process and can be manufactured in a large area. However, since OPV is greatly affected by the surrounding environment, it is difficult to harvest energy that can be always operated, and many studies are being conducted to solve this problem. Accordingly, by incorporating a Triboelectric Nanogenerator (TENG) to the system, we have developed an OPV-TENG hybrid energy harvesting system that harvests electrical energy from wasted mechanical energy in the surrounding environment, while simultaneously producing low-illuminance energy through bandgap matching. In addition, we developed TENG with newly synthesized Deco-flex[®] with good elasticity and output characteristics using an eco-friendly elastomer, which has a high resolution of 0.4 kPa and is sensitive enough to obtain a maximum output of 5 V and 1.03 μ A. This was combined with OPV in series and measured at low illumination (LED 1000 lux: 0.32 mW/cm²). As a result, the output voltage and current of about 10.5 V and 1.3 μ A were come out, respectively. It was confirmed that it increased about 4.6 times compared to when measured with a single OPV and increased by 1.03 times compared to when measured with a single TENG. Through this, the OPV-TENG hybrid energy harvesting system can harvest energy not only under 1-Sun (AM 1.5: 100 mW/cm²) and low light (LED 1000 lux: 0.32 mW/cm², Halogen 1000 lux: 4.98 mW/cm²) light sources but also under various climatic environments. Moreover, it is expected to supply sustainable power by supplementing the low open circuit voltage (V_{OC}) of OPV through TENG, thus complement the limit of OPV in terms of 'climate-dependent energy harvesting' through TENG power generation.

SESSION SB06.15: Processing of Photovoltaic and Optoelectronic Devices

Session Chairs: Beatrice Fraboni and Tse Nga Ng

Thursday Morning, December 1, 2022

Hynes, Level 3, Room 312

8:30 AM *SB06.15.01

Strategies to Improve the Efficiency of Organic Photovoltaics Thomas D. Anthopoulos; King Abdullah University of Science and Technology, Saudi Arabia

The power conversion efficiency (PCE) of organic photovoltaics (OPVs) has been increasing steadily over the past decade with reported PCE values now exceeding 19% and 20%, for single and tandem cell configurations, respectively. Despite the breath-taking progress, however, further improvements are anticipated via i) the use of new materials, and ii) by minimising performance losses associated with incumbent cell architectures and materials. In this talk, I will discuss recent work in my group in the field of OPVs with focus on practical strategies for boosting the cell performance. In particular, I will discuss the development and use of electronic additives, such as molecular dopants, and the implementation of self-assembling monolayers (SAMs) as charge extracting interlayer technologies for OPVs. I will show how addition of dopants can improve the PCE of state-of-the-art OPVs while the use of SAMs can dramatically increase the material utilization and circularity of the ensuing cells without compromising their performance.

9:00 AM SB06.15.02

Non-Halogenated and Low Synthetic Complexity Active Layer for Efficient Outdoor and Indoor Organic Photovoltaics Sergi Riera-Galindo¹, Xabier Rodríguez-Martínez², Marta Sanz², Laura López-Mir³, Olle Inganäs² and Mariano Campoy-Quiles¹; ¹Institut de Ciència de Materials de Barcelona, Spain; ²Linköping University, Sweden; ³Eurecat Technology Centre, Spain

Organic photovoltaics (OPV) requires the use of non-halogenated solvents and low synthetic complexity (SC) materials, without compromising power conversion efficiency (PCE), for large-scale processing as a low-cost and sustainable energy harvesting technology. First, we present a non-halogenated and low SC ink formulation for the active layer of organic solar cells, comprising PTQ10 and PCBM as donor and acceptor materials, respectively, showing a record PCE of 7.5% in blade coated devices under 1 sun, and 19.9% under indoor LED conditions. We have achieved these high performances analysing by combinatorial screening the compatibility of the active layer with 5 different electron transport layers (ETLs) in inverted architecture. On the other hand, we report the impact of the molecular weight of the donor polymer PTQ10 with benchmark non fullerene acceptors (Y6, Y12, IDIC) on the organic solar cell performance. In all cases, we have characterized the performance of the solar cells as a function of the thickness of the active layer. The PCE improves from values around 2% up to more than 10% with the optimized active layer thickness under 1 sun conditions. Further, we characterized the system by using a plethora of techniques such as recombination processes from light intensity-dependent measurements, field effect mobility, photoluminescence as well as grazing incidence wide angle X-ray scattering. Regarding the stability, semi-transparent devices based on fullerene and manufactured entirely in air *via* lamination show indoor PCEs exceeding 10% while retaining more than 80% of the initial performance after 400 and 350 hours of thermal and light stress, respectively. In the case of NFAs based devices, we report the thermal stability dependence with the molecular weight of the donor polymer PTQ10. As a result, we show promising materials to bridge the gap between research and industry, for indoor and outdoor low-cost OPV applications.

9:15 AM SB06.15.03

Performance and Long-Term Stability of Industrially Manufactured Non-Fullerene Based Organic Photovoltaics (OPV) Ngoc-Le Maria Lena Nguyen^{1,2}, Sebastian Meier¹, Morten Madsen² and Tamara Nunes Domschke¹; ¹ASCA GmbH, Germany; ²Mads Clausen Institute (MCI), Denmark

In the past years, organic photovoltaics (OPV) has experienced noticeable progress in material developments, device optimization, and industrial implementation towards commercialization. From lightweight, flexibility and the ability of solution-processing and large-area production at low-cost, organic solar cells have attracted increasing interests from academic and industrial entities. Initially, conjugated polymers were used as donor and fullerene as acceptor materials. However, the limitations in terms of synthetic flexibility, weak intrinsic absorption capability in the visible and near infrared region and poor coordination of energy levels restrained their further application. The evolution of non-fullerene electron acceptors (NFA) has mainly overcome these drawbacks. Hence, NFAs have been identified as promising materials for future OPV applications, and maximum power conversion efficiencies

(PCEs) of over 19% have been reported already. However, such high PCE numbers have so far only been achieved for small-area devices (few mm²), usually fabricated using non-scalable materials (evaporated MoO₃), processing techniques (e. g. spin-coating) and conditions (inert environment), which together with the use of rigid substrates is far away from meeting industrial requirements.

This work focuses on large-scale solution-based manufacturing of NFA devices by means of roll-to-roll processing, taking into consideration industrial standards. Using a commercially available NFA-based material system and optimizing the device architecture, the active layer morphology and the coating process, PCEs of over 10% on cell level and close to 7% on module level were achieved so far, with potential for further improvements. In parallel, the stability of the fabricated devices was carefully investigated and optimized as well with a focus on thermally and photo-induced changes. The NFA-based devices feature very good photostability, with more than 80% of the initial PCE maintained after 2000 h of continuous illumination and under open-circuit conditions. Based on previous experience, even better results are expected at operating conditions, i.e. when holding the devices at the maximum power point. Thermal stability limiting factors, were studied by means of GIWAXS as well as UV-Vis-NIR, PL and impedance spectroscopy and steps were taken to stabilize the device performance under high continuous heat. The results presented in this work confirm the potential of NFAs for the next generation of high performing OPV solar cells and show promise for their commercialization.

9:30 AM SB06.15.04

Optimized Vertical Phase Separation via Systematic Y6 Inner Side-Chain Modulation for Non-Halogen Solvent Processed Inverted Organic Solar Cells Seung Un Ryu and Taiho Park; Pohang University of Science and Technology (POSTECH), Korea (the Republic of)

Organic solar cells (OSCs) have entered a new phase of development with the advent of a high-performance non-fullerene acceptor known as Y6. Considering that the molecular curvature shape of Y6 allows for dense intermolecular packing with a grid-like packing structure, the modification of branched alkyl chains located on the pyrrole motif of Y6 is expected to have a significant impact on morphological properties, such as molecular packing/orientation behavior and vertical phase separation. In this work, we fine-tune the branched alkyl chain attached to nitrogen atoms of the Y6 main backbone and systematically investigate the relationship between the morphological features and photovoltaic performance of OSCs with a PM6 donor polymer. The systematic alkyl chain engineering effectively reduces the aggregation of Y6-analogs and substantially improves solubility, thereby providing solution processability in a non-halogenated solvent. Additional in-depth analyses reveal that the modification of branched alkyl chains allows the formation of an optimized bulk heterojunction morphology, which is advantageous for an inverted device architecture. In particular, the PM6:Y6-HU-based inverted OSC utilizing *o*-xylene as a processing solvent achieves a power conversion efficiency of 17.4% with a fill factor of 77.9% under the binary blend system and single non-halogen solvent processing.

9:45 AM SB06.15.05

High-Performance Organic Photodetectors Processed from Green Solvent Hoang Luong¹, Zhifang Du¹, Sina Sabury², Austin Jones², Ziyue Zhu¹, Patchareepond Panoy¹, Sangmin Chae¹, Ahra Yi¹, Hyo Jung Kim³, Steven Xiao⁴, Viktor Brus⁵, Manjunatha Reddy⁶, John Reynolds² and Thuc-Quyen Nguyen¹; ¹University of California, Santa Barbara, United States; ²Georgia Institute of Technology, United States; ³Pusan National University, Korea (the Republic of); ⁴1-Material Inc, Canada; ⁵Nazarbayev University, Kazakhstan; ⁶University of Lille, France

Organic photodetectors (OPDs) have emerged as a promising platform for a photosensing and optical communications in the last decades for their lightweight, flexibility, and great industry potential for high throughput solution processing. However, traditional solvents used for OPDs processing conditions are commonly highly toxic halogenated organic solvents like chlorobenzene (CB), *o*-dichlorobenzene, and chloroform, which are not only harmful to human health upon exposure but can also cause long-term effects on the ecosystem. Herein, we showcase a high-performance OPD based on a newly designed bulk heterojunction (BHJ) comprised of a PM7-D5 donor polymer and the Y12 non-fullerene acceptor processed from a green solvent, 2-methyltetrahydrofuran (2-MeTHF). The PM7-D5:Y12 OPDs simultaneously exhibits a remarkably high detectivity (with shot-noise-limited specific detectivity of above 10¹⁴ Jones) and surpasses the performances of OPDs processed from traditional chlorinated solvents. The relationship between processing solvents, active layer morphology, and photo-sensing performance of PM7-D5:Y12 devices were elucidated by combining several thin-film solid-state characterizations (atomic force microscopy (AFM), grazing-incidence wide-angle X-ray scattering (GIWAXS), transmission electron microscopy (TEM), and solid-state nuclear magnetic resonance (ssNMR) spectroscopy). The results suggest that the donor-acceptor molecules are well phase-separated with minimal disruption to the PM7-D5 and Y12 backbone packing, while smaller domain sizes due to changes to the sidechain conformations of acceptor molecules are observed in 2-MeTHF cast film in comparison to films processing from CB or *o*-xylene, which facilitates the charge generation and collection process in the device. In addition, the PM7-D5:Y12 OPDs are employed as wearable flexible devices to monitor heart rate and blood oxygen saturation, which suggests the potential for practical applications.

10:00 AM BREAK

SESSION SB06.16: Bioelectronics
Session Chairs: Olivier Bardagot and Gitti Frey
Thursday Morning, December 1, 2022
Hynes, Level 3, Room 312

10:30 AM *SB06.16.01

The Impact of Channel Hydration on the Performance of Electrolyte Gated Transistors Sahika Inal; King Abdullah University of Science and Technology, Saudi Arabia

Organic mixed (ionic and electronic) charge conductors and electrochemical phenomena at the solid-liquid interface have garnered significant attention for applications in bioelectronics, electrochromics, energy storage/generation, neuromorphic computing, and thermoelectrics. These devices operate in electrolytes that render ions mobile in the film, making the coupling between electronic and ionic charges crucial. A prime example of such devices is the organic electrochemical transistor (OECT), a high gain transducer used commonly to monitor bioelectronic signals. In this talk, I will introduce the emerging class of conjugated polymers that have been synthesized for use in OECT channels. Having developed in operando techniques, we found that the ions enter the semiconducting polymer channel hydrated, and the excess swelling of the polymeric channel had a significant effect on OECT performance, which can be traced back to changes in the overall structural order. I will introduce two postprocessing approaches that limit the water uptake of the film during device operation. These approaches enhance the mixed conductivity of polymers while preventing degradation and lead to OECTs with longer shelf life and operational stability.

11:00 AM SB06.16.02

Elucidating Strength of Ionic Interactions in Conductive Polymers Spencer Yeager, Linze Du Hill, Jonthan K. Harris, Songyan Yu and Erin L. Ratcliff; The University of Arizona, United States

Pi-conjugated polymers (CP) have been utilized in a number of opto-electronic and (photo)electrochemical applications, including photovoltaics, organic electrochemical transistors (OECTs), organic field effect transistors (OFETs), electrochromic devices and biosensors. These soft materials can be easily and reversibly doped using electrochemistry, where the solvent and supporting electrolyte (anions and cations) can intercalate into the relaxed film to support long-lived carriers to do electrochemical work. The resulting enhancement of electronic properties such as conductivity are known. However, quantification of the strength of intermolecular interactions within the system, namely Coulombic attraction between anions and polarons, is less understood. Herein we postulate that the dielectric of the solvent system can impact the relative strength of interaction and depends strongly on the fraction of supporting counterion cation present. As a prototype system, we start from poly(3-hexylthiophene) (P3HT) and an ionic liquid 1-ethyl-3-methylimidazolium bis(trifluoromethylsulfonyl)imide ([EMIM][TFSI]). We consider different local environments including vacuum deposited ionic liquid on the polymer, interfacing the polymer with ion gels, and a moderate dielectric acetonitrile with complementary supporting electrolyte. Electrochemical and spectroscopic techniques are combined to probe in situ doping fractions using a prototypical OECT. Chemical shifts in the core level S 2p, F 1s, N 1s, and C 1s electrons corresponding to the [TFSI] and P3HT were observed as a function of the percentage of doped P3HT and give direct insight into the extent of electron density exchange between the system components. Insights gained are then used to lower the operating voltages of OECTs, towards all-printable configurations. Collectively, these studies help provide a better understanding of the effects that anions have on the polymer, allowing for improved design guidelines when implementing these systems for device-relevant applications.

11:15 AM SB06.16.03

Electrochemical Doping Mechanisms in the Ordered and Disordered Domains of P3HT Priscila Cavassin, Isabelle Holzer, Demetra Tsokkou, Olivier Bardagot, Julien Rehaut and Natalie Banerji; University of Bern, Switzerland

Organic mixed ionic-electronic conductors (OMIECs) are a class of organic materials that efficiently support both ionic and electronic transport. Due to this remarkable property, a broad range of emerging technologies, from energy storage to bioelectronics, rely on OMIECs. [1] A key property of these materials is their ability to be electrochemically doped, which is an efficient and reversible method to increase the materials electric conductivity. This process relies on the injection of carriers into the organic film, while the counterions from an electrolyte infiltrate the film and maintain charge neutrality. The electrochemical doping relies on a complex interplay between multiple factors, from electrolyte choice to molecule design and film morphology, and due to the increasing number of applications that rely on this process, there has been great interest in further understanding its properties and fundamental mechanisms. [2]

In this work, we explore the impact of the polymer film morphology on the electrochemical doping. We use time-resolved visible-near infrared (Vis-NIR) and in-situ Raman spectroscopy combined with electrochemical measurements to show that the ordered and disordered domains of poly(3-hexylthiophene) (P3HT) are doped through different mechanisms and kinetics. We demonstrate that for intermediate doping levels, polarons and bipolarons (singly and doubly charged species) coexist exclusively in the disordered domains. In the ordered domains, only polarons are observed until there are no more ordered undoped chains, and only at this point bipolarons start to be formed at these domains. We propose a kinetic model that described the reactions that take place and show that the ordered phase is doped faster than the disordered for all doping levels.

To confirm our propositions, we used in-situ electrochemical Raman spectroscopy, a technique very sensitive to local conformation. We obtained good agreement with the trends observed with Vis-NIR spectroscopy. Additionally, we compared the doping of P3HT films with different degrees of morphology. We use regiorandom P3HT to investigate the doping in purely disordered films, and the results strongly correlate with our proposed kinetic model. Finally, by measuring the THz conductivity of our films, we investigate how the polarons and bipolarons impact electronic conductivity.

[1] J. Chung, A. Khot, B. M. Savoie, B. W. Boudouris, ACS Macro Letters, **2020**, 9, 646-655.

[2] E. M. Thomas, M. A. Brady, H. Nakayama, B. C. Popere, R. A. Segalman, M. L. Chabiny, Advanced Functional Materials, **2018**, 28, 1803687.

11:30 AM SB06.16.04

Hierarchical Self-Assembly of PEDOT:PSS to Enable Intrinsically Water Stable Conductors Laine Taussig¹, Masoud Ghasemi², Tatiana Proksch¹, Albert Kwansa¹, Sanggil Han³, Ruipeng Li⁴, George G. Malliaras³, Yaroslava G. Yingling¹ and Aram Amassian¹; ¹North Carolina State University, United States; ²The Pennsylvania State University, United States; ³University of Cambridge, United Kingdom; ⁴Brookhaven National Laboratory, United States

Owing to the vastly tunable material properties, PEDOT:PSS has been regarded as one of the most promising material platforms for organic bioelectronics, neuromorphic computing, and transparent conducting electrodes in a wide array of optoelectronic and photovoltaic applications. As PEDOT:PSS is an electrostatically stabilized colloidal suspension, it is no surprise that the addition of ionic additives of late have shown some of the most remarkable control over the properties of PEDOT:PSS, including formation of conducting gels. Here, we report in-depth multi-modal experimental (in situ/ex situ GIWAXS, TEM, conductivity, rheology) and computational (MD) investigations of the effects of ionic additives on PEDOT:PSS from solution to solid state. Findings reveal new insights into solution-phase self-assembly of this material that explain its solid-state thin film properties such as high electronic conductivity, remarkable water insolubility, and crystalline structure. We demonstrate water-stable printing of PEDOT:PSS interconnects and devices, including OECT devices, without the need of crosslinking agents. This work offers new insights into the mechanisms responsible for the highly attractive properties of PEDOT:PSS for applications including wearable and implantable bioelectronic devices and neuromorphic computing.

SESSION SB06.17: Structure, Degradation in Organic and Hybrid Photovoltaics

Session Chairs: Matthew Bidwell and Antonio Facchetti

Thursday Afternoon, December 1, 2022

Hynes, Level 3, Room 312

2:00 PM *SB06.17.01

Excited State Photodegradation of Organic Photovoltaic Materials Mihirsinh Chauhan, Ambika Pathak, Jacob Mauthe, Samuel Shepard, Somayeh Kashani, Xingao Zhang, Benjamin Hines, Felix Castellano, Harald Ade and Aram Amassian; North Carolina State University, United States

Stability or lack thereof is currently the Achilles heel of organic photovoltaics, which is otherwise close to reaching a power conversion efficiency of 20% and can already be processed using scalable manufacturing approaches using green and sustainable materials. Photodegradation is only empirically studied,

is not well understood, and there continue to be widely held misconceptions about the effectiveness of encapsulation whereby it is thought that effective blocking of O₂, H₂O and UV can address photodegradation. Unfortunately, modern donor and acceptor materials photodegrade in inert atmosphere under visible light illumination simply by being in the excited state, pointing to inherent photostability issues associated to the excitonic nature of conjugated materials that must be understood at a fundamental level and then mitigated either through material design or through engineering of the photophysics and photochemistry within the BHJ layer. In this talk, we will present our understanding of excited state photodegradation of conjugated materials in inert atmosphere and how this is directly associated to excited state lifetime in materials. We will demonstrate how photodegradation is dependent on the chemical resilience of various molecular classes and ways to mitigate photodegradation in inert atmosphere through judicious design of quenching approaches, including in bulk heterojunction films.

2:30 PM SB06.17.02

Visualizing Degradation at the Nanoscale from Morphological and Energetic Perspectives in Organic Photovoltaics Gaurab J. Thapa, Mihirsinh Chauhan, Daniel Dougherty and Aram Amassian; North Carolina State University, United States

Organic photovoltaics (OPVs) have received tremendous interest in recent decades due to their flexibility, ease of processing and cost effectiveness [1-3]. With the advent of non-fullerene acceptors (NFA), the efficiency of these solar cells has broken previous records and has currently achieved power conversion efficiency (PCE) > 18% [4]. OPVs is now confronting the next bottleneck which is its instability. Multiple pathways for degradation of organic solar cells have been reported [5], the most common route for the active layer being photodegradation and morphological degradation. The stability of NFA-based OPVs is contingent on the morphology and its evolution throughout the lifetime of the device. Since interfacial/mixed phase energetics are crucial for charge generation [6], it is imperative to maintain the energetics of Donor (D), Acceptor (A) rich region and mixed region in the blends during device aging and operation. Moreover, changes in the energetics caused by the morphological evolution due to de-mixing of D and A materials in the mixed region can have a vital role on degradation of device performance. A definitive morphological picture of the BHJ during degradation studies, down to a length scale of a few molecules, is therefore urgently needed, as this can shed light on the energetic landscape and its evolution within the BHJ. In this work, we take a deeper dive into the morphological aspect of degradation utilizing scanning tunneling microscopy/spectroscopy (STM/S), a unique and quite effective tool for characterizing morphology and associated energetics. We study the morphology of stable and unstable systems and the evolution of their domain and mixed phase energetics. We focus on PM6-based blends with ITIC-4F, Y6 and PC₇₁BM. Along with investigating the properties of the neat materials, we visualize and identify D and A-rich phases within the various BHJs and compare energetics within BHJ to neat D and A materials to correlate with its miscibility properties. In addition, we compare the histogram of Local Densities of States (LDOS) of the PM6 and A-rich phases in their neat and blend forms to gain insight into the energetic disorder as these materials are mixed in the blends. Finally, we visualize morphological degradation of PM6:Y6 and evaluate changes of LDOS within PM6, Y6 and mixed domains within the BHJ due to thermal annealing which is in correlation with changes observed in device performance parameters.

Reference:

1. B.E. Logan, M. Elimelech, Nat. Commun. 488 (2012) 313–319.
2. Y. Zhang, J. Wang, X. Wang, Renew. Sustain. Energy Rev. 32 (2014) 255–270.
3. H. Fu, C. Li, P. Bi, X. Hao, F. Liu, Y. Li, Z. Wang, Y. Sun, Adv. Funct. Mater. (2019), 29, 1807006.
4. Q. Liu, Y. Jiang, K. Jin, J. Qin, J. Xu, W. Li, J. Xiong, J. Liu, Z. Xiao, K. Sun, S. Yang, X. Zhang, L. Ding, Chinese Science Bulletin (2020), 65, 272-275.
5. M. Jørgensen, K. Norrman, S. A. Gevorgyan, T. Tromholt, B. Andreasen and F. C. Krebs, Adv. Mater., 2012, 24, 580–612.
6. H. Xin *et al.*, Polymer Nanowire/Fullerene Bulk Heterojunction Solar Cells: How Nanostructure Determines Photovoltaic Properties. ACS Nano, 4, 1861-1872 (2010).

2:45 PM BREAK

SESSION SB06.18: Materials and Devices, Flexible Optoelectronics
Session Chairs: Scott Keene and Anna Köhler
Thursday Afternoon, December 1, 2022
Hynes, Level 3, Room 312

3:15 PM *SB06.18.01

Mechanically Flexible Organic and Hybrid Semiconductor Devices—Role of Composition and Film Morphology Antonio Facchetti; Northwestern University/Flexterra Inc, United States

In this presentation we report the realization of new semiconductor films and devices with considerable mechanical flexibility and stretchability. Thus, organic films with great mechanical stress tolerance were realized for NDI and DPP-based polymers by creating porous honeycomb morphologies via a breath figure method. These films can be stretched by a strain larger than 100% and can retain excellent semiconducting properties. Furthermore, we were able to fabricate metal oxide films with considerable flexibility by incorporating organic polymers, or using organic polymers, to achieve desirable compositions or fibrotic film morphologies. The resulting devices, eg, TFTs, circuits and sensors, exhibit excellent response and good performance also upon considerable mechanical deformations.

3:45 PM SB06.18.02

Climbing “Up” the Near-Infrared Window of Dye-Sensitized Upconversion for Photovoltaics Kristin Becker¹, Maxim S. Pshenichnikov¹, Andries Meijerink² and J. C. Kees Hummelen¹; ¹University of Groningen, Netherlands; ²Utrecht University, Netherlands

One of the most promising and frequently talked about solutions to the current energy crisis and environmental pollution are *solar cells*. Classical silicon solar cells have a fundamental limit of power conversion of 32% and are nowadays very close to reaching that limit. This limit can be exceeded either by better adapting the solar cell to the solar spectrum or by changing the solar spectrum to one that a classical, cheap solar cell can use. The latter can be done by the process of photon upconversion, a non-linear process where two (or more) photons of longer wavelength (lower energy) are sequentially absorbed, followed by the emission of light at shorter wavelength (higher energy) than the excitation one. All the photons with energy lower than the bandgap of silicon (1.12 eV) go through the silicon layer without being absorbed. By incorporating an upconversion layer below the silicon layer in the device, such low energy photons can be absorbed in the upconverter layer, upconverted to higher energy photons, which can be reflected back and initiate exciton formation in the silicon layer. These two layers can be electrically isolated, which gives us the opportunity to optimize them separately in order to gain

optimum efficiency of the solar cell. In theory, the use of an ideal upconverter (2 bandgaps) with a photovoltaic active layer (with a bandgap of 2 eV) can increase the power conversion efficiency up to 50.7%.¹

This research aims to study the process of dye-sensitized upconversion in the (so far) unexplored near-infrared (NIR-II) window ($\lambda = 1000 - 1700$ nm) for use in hybrid silicon/organic photovoltaics. Sensitization in the proposed window is challenging but using energy transfer from a luminescent species on a surface layer to lanthanide ions in the core of nanoparticle (NP) provides opportunities that cannot be realized in bulk materials.²

To achieve the upconversion in this range, we propose a hybrid organic/inorganic system consisting of an organic dye serving as an “antenna” and a lanthanide-based NP that will act as an upconverter. A newly synthesized cyanine dye that absorbs and emits in the NIR ($\lambda_{\text{max}} = 1380$ nm) will be attached (via a carboxylate linker group) to the NP, enhancing the upconverted luminescence due to a high molar absorption coefficient of the dye. The excitation energy transfers to the upconverting NP consisting of lanthanide ions, erbium and ytterbium (Er^{3+} & Yb^{3+}). The upconverted emission that follows, achieved by the Er^{3+} ions in the carefully designed NP, is 980 nm. The wavelength of the upconverted photons falls into the absorption window of silicon, opening avenues to modify existing silicon solar cells with new hybrid materials that could go beyond the Shockley-Queisser limit.

[1] T. Trupke, M.A. Green, P. Würfel Improving solar cell efficiencies by up-conversion of sub-band-gap light *J Appl Phys*, **2002**, 92, 4117-4122.

[2] Zou, W., Visser, C., Maduro, J., Pchenitnikov, M. S., Hummelen, J.C., Broadband dye-sensitized upconversion of near-infrared light. *Nature Photon*, **2012**, 6, 560–564.

SESSION SB06.19: Structure, Morphology and Organic Solar Cells

Session Chairs: Marina Leite and Olivier Margeat

Friday Morning, December 2, 2022

Hynes, Level 3, Room 312

9:00 AM SB06.19.02

Effects of Molecular Encapsulation on the Photophysical and Charge Transport Properties of a Naphthalene Diimide Bithiophene Copolymer.

Stefano Pecorario^{1,2}, Jeroen Royakkers³, Hugo Bronstein⁴ and Mario Caironi¹: ¹Istituto Italiano di Tecnologia, Italy; ²Politecnico di Milano, Italy;

³Maastricht University, Netherlands; ⁴University of Cambridge, United Kingdom

Molecular encapsulation is a powerful synthetic concept that can be used to study polymer chains (or molecules) in isolation by shielding the conjugated backbone with protective macrocycles, and preventing electronic cross communication between the π -systems. Here, we present a molecularly encapsulated form of the naphthalene diimide bithiophene copolymer PNDIT2, one of the most widely used semiconducting polymers with high charge mobility for n-type field-effect transistors and non-fullerene acceptors in organic photovoltaic blends. We introduced enclosing macrocycles covalently bonded to the bithiophene units, while the naphthalene diimide moieties are left open for intermolecular interactions. We found that the encapsulated equivalent shows more backbone planarity when compared to PNDIT2. Furthermore, molecular encapsulation prevents the polymer chains from pre-aggregating in common organic solvents, while allowing π -stacking in the solid state and fostering thin film crystallinity through an intermolecular-lock mechanism. As a result, field-effect transistors still exhibit n-type semiconducting behavior, despite charge mobility being lower than in PNDIT2 as a result of the lack of the fibrillar microstructure that results from pre-aggregation in solution. Thus, molecular encapsulation appears as an effective method to adjust the nanomorphology of cast films while preserving the electrical structure of the core polymer and the thin film charge transport properties.

References:

(1) Pecorario, S.; Royakkers, J.; Scaccabarozzi, A. D.; Pallini, F.; Beverina, L.; Bronstein, H.; Caironi, M. Effects of Molecular Encapsulation on the Photophysical and Charge Transport Properties of a Naphthalene Diimide Bithiophene Copolymer. *Chem. Mater.* 2022.

<https://doi.org/10.1021/acs.chemmater.2c01894>.

(2) Royakkers, J.; Bronstein, H. Macrocylic Encapsulated Conjugated Polymers. *Macromolecules* 2021. <https://doi.org/10.1021/acs.macromol.0c01916>.

9:15 AM SB06.19.03

Unraveling the Correlation Between Structure and Performance by Optical Techniques on Organic Solar Cells

Carmen M. Ruiz Herrero¹, Yatzil Avalos², Anil K. Bharwal¹, David Duché¹, Jean-Jacques Simon¹, Christine Vidélot-Ackermann² and Jörg Ackermann²: ¹Aix Marseille Univ., Univ. de Toulon, UMR CNRS 7334, IM2NP, France; ²Centre Interdisciplinaire de Nanoscience de Marseille (CINaM, UMR CNRS 7325), France

Organic based photovoltaics present nowadays a bright future, due to its suitability for the integration on systems related with the IoT, its compatibility with lightweight and flexible substrate and the possibility of being deposited by easily scale-up techniques such as ink-jet printing. Furthermore, the development of Non-Fullerene Acceptors (NFA) has led to a jump on performances, approaching the 20% milestone. Nevertheless, there is still a lack of knowledge on fundamental properties of the devices that can compromise the successful transition of this technology into the industrial step.

In particular, there is still not a clear understanding of how the materials arrange themselves in the active layer and which impact it has on its optical and electrical transport properties and thus on the final performance of the functioning devices. In order to investigate the structural arrangement long time-consuming techniques such as synchrotron X-ray diffraction or Transmission Electron Microscopy (TEM) must be used. This, compound with the fact that samples have to be prepared on special conditions suitable for the measurement set-up limits the amount of information we can actually extract that will apply to the functioning device. In this work, we propose to use optical nondestructive techniques to explore the structural properties of the active layer on an actual device and compare with the electrical transport properties and performances.

For this, we analyze solar cells made by liquid deposition techniques with active layers composed by different NFA/polymers at different post-annealing temperatures. These devices have been studied with raman spectroscopy to determine the structural organization of the active layer, revealing the importance of NFA and polymer compatibility for enhancing a better microstructural arrangement of both materials. Photoluminescence measurements have also been carried both on separate materials and on solar cells to quantify the effective charge separation and its correlation with the active layer structure. Finally, Photovoltage Decay measurements allow us to have an estimation of the recombination states on these devices.

9:30 AM BREAK

SESSION SB06.20: Optoelectronic Processes in Organic Solar Cells and Diodes

Session Chairs: Aram Amassian and Ellen Moons

10:00 AM *SB06.20.01

Radiative and Non-Radiative Recombination in Organic Photovoltaics [Koen Vandewal](#); Hasselt University, Belgium

The currently best organic solar cells suffer from relatively large voltage losses due to non-radiative recombination as compared to inorganic or perovskite solar cells. Further enhancement of the power conversion efficiency to values over 20% will require a reduction of these losses, inevitably corresponding to an increase in the electroluminescence quantum efficiency of the devices.^[1] For a large number of donor-acceptor combinations, we have observed that non-radiative voltage losses decrease with increasing charge-transfer-state energies, consistent with non-radiative decay being facilitated by a common high frequency molecular vibrational mode.^[2] We further identify small molecule donor-acceptor blends with an optical gap in the visible spectral range, with strongly reduced non-radiative losses as compared to systems with a gap in the near infrared (NIR).^[3] This highlights the possibility of a simultaneous occurrence of a high photovoltaic quantum efficiency as well as a high electroluminescence quantum efficiency, occurring in a single organic donor-acceptor blend. For photovoltaic blends with strong absorption in the NIR, we show that the lowest non-radiative decay rates correspond to systems with the narrowest emission linewidths and steepest absorption tails.^[4]

[1] Vandewal et al, Nature Materials 8, 904 (2009)

[2] Benduhn et al, Nature Energy 2, 17053 (2017)

[3] Ullbrich et al, Nature Mater. 18, 459 (2019)

[4] Liu et al, Joule 5, 2365 (2021)

10:30 AM SB06.20.02

The Role of Dipole Interactions on Intermolecular Charge Transfer in Y6 Non-Fullerene Acceptor Studied by Electroabsorption Spectroscopy [Sudhi Mahadevan](#)¹, [Taili Liu](#)² and [Sai Wing Tsang](#)¹; ¹City University of Hong Kong, China; ²Yunnan Normal University, China

Organic photovoltaic cells (OPVs) with Y6 as electron acceptor have recently been reported with record high efficiency and negligible photovoltage loss. It is generally believed that intermolecular electrostatic interactions between Y6 molecules lead to strong charge transfer (CT) characteristics which results in efficient exciton dissociation and reduced non-radiative recombination. However, it is still unclear about the contribution of intermolecular dipoles and its effect on different dimer formations and enhanced CT characteristics. Here, we investigate the contribution of anisotropic dipoles to excimer formation and its impact on CT properties using electroabsorption (EA) spectroscopy. The EA spectra of Y6 are strongly dependent on the molecular packing as we observe strong second derivative characteristics around the S0 to S1 excitation while increasing the loading ratio of Y6 in the polymer matrix. We also observe dipole orientation in packed Y6 film while increasing the molecular concentration by quantitative analysis of the first harmonic EA spectra of pristine Y6. These preferred oriented dipoles are found responsible for the distinctive molecular packing of Y6 which leads to strong intermolecular charge transfer. Quantitatively, fitting the EA spectrum highlights the significance of polarizability (p) between ground and excited states in electron delocalization and intermolecular charge transfer property of Y6. The extracted Δu values of monomer and dimer configurations show excellent consistency with theoretical values from quantum calculation results. Our work mainly highlights the application of electroabsorption spectroscopy as a powerful technique to probe charge transfer characteristics, intermolecular interactions, binding energy, and delocalization of excitons etc. in pristine Y6. This research work provides insight into better molecular design of novel photovoltaic materials by tuning the intermolecular electrostatic interactions and delocalization of electron wavefunctions.

10:45 AM SB06.20.03

Exciton Transport in Nonfullerene Acceptors and Semiconducting Polymers Boosted by Transient Quantum Delocalization [Samuele Giannini](#)¹, [Jochen Blumberger](#)² and [David Beljonne](#)¹; ¹University of Mons, Belgium; ²University College London, United Kingdom

The transport of excitons in molecular systems is essential to the function of flexible optoelectronic devices (including organic solar cells) and biological light-harvestings. It is remarkable, however, that the nature of excitons and related transport mechanism in these soft materials have puzzled the community for so many years. Even for apparently simple systems such as organic single crystals: some experiments would better fit a localized particle picture, while others a coherent wave-like interpretation.

Our non-adiabatic molecular dynamics simulations show that energy carriers in OSs are neither waves nor particles, as previously assumed. By solving the coupled nuclear-electronic motion, we observe that in molecular OSs and non-fullerene acceptors (NFAs), including Y6, exhibiting some of the highest measured (singlet) exciton diffusion length to date [1], excitons undergo a transient quantum delocalization/localization mechanism that underpins the larger spatial displacements and diffusivity of the excitonic wavefunction in these materials [1] (in agreement with what found experimentally). This mechanistic scenario, by which the excitons can thermally access delocalized states within the excitonic band giving rise to long-range exciton transport, is similar to what we found for charge carrier transport in high charge carrier mobility OSs [3,4]. Similarities and differences will be discussed. Remarkably, we also found that an analog transient delocalization mechanism takes place when simulating (singlet) exciton diffusion in highly ordered conjugated polymer nanofiber of P3HT [5,6]. Importantly, in the latter case, the mechanism is highly sensitive to the interplay between delocalization along the polymer chains and long-range interactions along the stacks [6]. Surprisingly, the diffusion coefficient is predicted to rocket by 3 orders of magnitude when going beyond nearest-neighbour intermolecular interactions in fibers of extended (30-mer) polymer chains (in line with transient absorption microscopy measurements [5]) and to be resilient to interchain energetic and positional disorders.

On the basis of our simulations we discuss a path for improving the exciton diffusion constant in organic semiconductors.

[1] Firdaus, Y. et al. Long-range exciton diffusion in molecular non-fullerene acceptors. *Nat. Commun.* 11, 5220 (2020)

<!--StartFragment-->[2] Giannini, S. et al. Exciton transport in molecular organic semiconductors boosted by transient quantum delocalization. *Nat. Commun.* 13, 2755 (2022).<!--EndFragment-->

[3] Giannini, S. et al. Quantum localization and delocalization of charge carriers in organic semiconducting crystals. *Nat. Commun.* 10, 3843 (2019).

[4] Giannini, S., et al. Flickering Polarons Extending over Ten Nanometres Mediate Charge Transport in High-Mobility Organic Crystals. *Adv. Theory Simul.* 3, 2070021 (2020).

[5] Sneyd, A. J. et al. Efficient energy transport in an organic semiconductor mediated by transient exciton delocalization. *Sci. Adv.* 7, eabh4232 (2021).

[6] Proshan, S., Giannini, S., Wang, L. and Beljonne, D. Long-Range Interactions Boost Singlet Exciton Diffusion in Nanofibers of π -Extended Polymer Chains. *J. Phys. Chem. Lett.* 12, 8188–8193 (2021).

8:00 AM *SB06.21.01

Investigating Dopant Intercalation into Semiconducting Polymer Crystals by TEM, Rutherford Backscattering and Polarized UV-vis-NIR Spectroscopy [Martin Brinkmann](#)¹, Yuhan Zhong^{1,2}, Shubhradip Guchait¹, Dominique Müller², Viktoriia Untilova¹, Laurent Herrmann¹ and Thomas Heiser²; ¹Institut Charles Sadron CNRS, France; ²ICUBE, France

Doping of polymer semiconductors is a central topic in plastic electronics and especially in the design of new better performing thermoelectric materials. Sequential doping of highly ordered polymer semiconductors is widely used to tune the charge carrier density that determines the thermoelectric properties. Various studies have demonstrated that dopant molecules intercalate into the layers of side chains in the crystals of polymer semiconductors.(1-3) It is therefore essential to clarify the way dopants are incorporated into the crystal lattice of the pristine polymer and how this is related to the dopant size and electron affinity. A combination of electron diffraction and polarized UV-vis-NIR spectroscopy on highly oriented P3HT and PBTTT thin films allows to quantify the amount of intercalated dopant molecules as well as the molecular orientation of dopants such as F4TCNQ, F6TCNNQ with respect to the polymer chains. A mapping of the orientational distribution of dopant molecules in the polymer crystal can thus be obtained. In the case of P3HT/F6TCNNQ, modeling of the diffraction patterns of doped crystals identifies the stoichiometry of the doped polymer phase and confirms the dopant orientation obtained from spectroscopy measurements as well as the lattice parameter variation induced by intercalation. In the case of Magic blue, Rutherford Backscattering is used to quantify the dopant amount in the films, Polarized UV-vis-NIR helps determine the diffusion coefficients of the dopant into the P3HT matrix whereas TEM demonstrates preferential location of MB in the amorphous phase of P3HT. It is demonstrated that the highest charge conductivities (up to 3000 S/cm) are observed in oriented P3HT films when the amorphous phase of P3HT is selectively doped with MB.

References.

- (1) Untilova, V.; Biskup, T.; Biniek, L.; Vijayakumar, V.; Brinkmann, M. Control of Chain Alignment and Crystallization Helps Enhance Charge Conductivities and Thermoelectric Power Factors in Sequentially Doped P3HT:F4TCNQ Films. *Macromolecules* 2020, 53 (7), 2441–2453.
- (2) V. Untilova, H. Zeng, P. Durand, P. Allgayer, L. Herrmann, N. Leclerc and M.Brinkmann. Intercalation and ordering of F6TCNNQ and F4TCNQ dopants in regioregular poly(3-hexylthiophene) crystals: impact on anisotropic thermoelectric properties of oriented thin films *Macromolecules* 2021, 54, 13, 6073-6084.
- (3) Vijayakumar, V.; Zhong, Y.; Untilova, V.; Bahri, M.; Herrmann, L.; Biniek, L.; Leclerc, N.; Brinkmann, M. Bringing Conducting Polymers to High Order: Toward Conductivities beyond 105 S cm⁻¹ and Thermoelectric Power Factors of 2 mW m⁻¹ K⁻². *Advanced Energy Materials* 2019, 9, 1900266.

8:30 AM SB06.21.02

Organic Light-Emitting Devices Using Common Uneven Aluminum-Foil as the Electrode [Satoru Ohisa](#), Taku Oono, Masashi Miyakawa, Takahisa Shimizu and Toshimitsu Tsuzuki; Japan Broadcasting Corporation (NHK), Japan

Here, we report the fabrication of organic light-emitting devices (OLEDs) using common uneven aluminum-foil as the electrode substrates, which show surface roughness of several hundred nanometers. In general, the use of such uneven electrodes causes serious electric leakage due to the application of ununiform electric field, resulting in improper operation of OLEDs. In this work, extraordinary thick phosphotungstic acid (H₃PW₁₂O₄₀) (PWA) buffer layer of several hundred nanometers was used for the mitigation of the ununiform electric field. PWA showed the property of negative differential resistance (NDR), and the property contributed to the realization of both of the low driving voltage and the suppression of the leakage currents. The origin of the NDR was also investigated by various analytical methods. We applied PWA to the OLEDs using aluminum-foil electrode substrates, and obtained leak-free OLEDs with uniform luminance images. Large area OLEDs with a light-emitting area of 64 cm² were fabricated. Even in crumpled and torn states, they emitted steady luminescence.

8:35 AM SB06.21.03

Laser Oscillation of Organic Distributed-Feedback Lasers at the Edge of a Mini Stopband [Hidekazu Shimotani](#)¹, Taiki Miura¹, Thangavel Kanagasekaran² and Katsumi Tanigaki³; ¹Tohoku University, Japan; ²Indian Institute of Science Education and Research Tirupati, India; ³Beijing Academy of Quantum Information Sciences, China

Organic semiconductor lasers have continued to attract attention because of their broad spectrum and diversity of materials, covering all wavelengths from UV to near IR.[1] In recent years, laser oscillation by current pumping, which does not require an external pumping source, has been actively studied. As a resonator structure for this purpose, DFB (Distributed Feedback) resonators with a single longitudinal mode and low threshold are often used.[2, 3] Although most of the laser oscillation wavelengths can be explained by the Bragg condition, several experimental results have been reported for polymer DFB lasers doped with organic semiconductors that do not match the Bragg condition in any mode.[4] Here, we report the conditions that determine the oscillation wavelength of organic DFB lasers using 5,5'-bis(biphenyl-4-yl)-2,2':5',2''-terthiophene (BP3T) single crystals, a promising material for injection lasers,[5-9] with various thicknesses as an active layer. Analysis using experimentally obtained refractive indexes revealed that the oscillation wavelengths of some BP3T DFB lasers are at the edge of a stopband, while the others are at an edge of the mini stopband,[10] which satisfies the phase-matching condition between different transverse modes and has not been considered in DFB lasers so far. Finite-element optical-waveguide simulations of the BP3T DFB laser verified the coupling of different transverse modes.

[1] H. Shang et al., "Comparative Study of Single and Dual Gain-Narrowed Emission in Thiophene/Furan/Phenylene Co-Oligomer Single Crystals", *J. Phys. Chem. C* 121, 2364 (2017).

[2] T. Kanagasekaran et al., "Towards electrically driven organic semiconductor laser with field-effective transistor structure", arXiv:1903.08869 [physics.optics] (2019).

[3] A. S. D. Sandanayaka et al., "Indication of current-injection lasing from an organic semiconductor" *Appl. Phys. Express* 12, 061010 (2019).

[4] V. Navarro-Fuster et al., "Film thickness and grating depth variation in organic second-order distributed feedback lasers", *J. Appl. Phys.* 112, 043104 (2012).

[5] S. Z. Bisri et al., "High Mobility and Luminescent Efficiency in Organic Single-Crystal Light-Emitting Transistors", *Adv. Funct. Mater.* 19, 1728 (2009).

[6] K. Oniwa et al., "Single crystal biphenyl end-capped furan-incorporated oligomers: influence of unusual packing structure on carrier mobility and luminescence", *J. Mater. Chem. C* 1, 4163 (2013).

[7] H. Tamura et al., "Theoretical Analysis on the Optoelectronic Properties of Single Crystals of Thiophene-furan-phenylene Co-Oligomers: Efficient Photoluminescence due to Molecular Bending", *J. Phys. Chem. C* 117, 8072 (2013).

[8] T. Kanagasekaran et al., "Equivalent ambipolar carrier injection of electrons and holes with Au electrodes in air-stable field effect transistors", *Appl.*

Phys. Lett. 107, 043304 (2015).

[9] T. Kanagasekaran et al., "A new electrode design for ambipolar injection in organic semiconductors", *Nature Commun.* 8, 999 (2017).

[10] T. Miura et al., "Laser oscillation of an organic distributed-feedback laser at the edge of a mini stopband", *Appl. Phys. Express* 14, 052007 (2021)

8:40 AM SB06.21.07

Sticky Thermoelectric Materials to Fabricate Flexible Peltier Sheets Norifusa Satoh, Masaji Otsuka and Jin Kawakita; National Institute for Materials Science, Japan

Flexible Peltier sheets benefit to fit complex objects like human bodies and deliver cold energy efficiently because the amount of heat transfer increases with the contact area. To make a solid Peltier plate into a flexible sheet, however, we need a new material with a high Seebeck coefficient like inorganic materials and a low thermal conductivity like organic materials to generate and maintain the temperature difference between the top and bottom sides of the sheet. Herein, we employ Bi₂Te₃-based sticky thermoelectric (TE) materials due to the following two features: First, sticky TE materials have been inversely designed to mass-produce flexible TE generation sheets through lamination or roll-to-roll processes without using electric conductive adhesives. Second, sticky TE materials have been demonstrated as an inorganic/organic hybrid material of TE particles and low-volatilizable organic solvents to show Seebeck coefficients based on the TE particles and low thermal conductivities based on the organic solvents. In this presentation, we discuss the relation between Peltier performance and electric resistance.

8:45 AM SB06.21.07

Organic-Photoconductive-Film-Stacked Image Sensor with Thin-Film-Transistor-Based Active Pixel Sensor Readout Circuits Koki Imamura¹, Toshikatsu Sakai¹, Hidenori Yakushiji², Yuta Hashimoto², Tatsuya Aotake², Yuichi Sadamitsu², Hiroto Sato¹ and Satoshi Aihara¹; ¹Japan Broadcasting Corporation, Japan; ²Nippon Kayaku Co., Ltd., Japan

Organic photoconductive films (OPFs) are attractive optoelectronic materials because they possess high absorption coefficients surpassing those of conventional silicon photodiodes and are thus promising candidates for use in photoconductive parts of flexible, large-area imaging devices. In such applications, thin-film transistor (TFT)-based signal readout circuits with amorphous oxide semiconductors (AOSs) such as indium–gallium–zinc-oxide (IGZO) are useful owing to the high field-effect mobilities of AOSs (>10 cm²/Vs), because image sensor applications require high response speeds and high-pixel-density integration. For example, IGZO-TFT-based flat-panel imagers have been proposed for the detection of X-rays [1]. On the other hand, our group has developed a three-layer-stacked image sensor for realizing compact cameras with high light utilization efficiency using two indium–tin–zinc-oxide (ITZO)-TFT-based readout circuits with blue/green-selective OPFs stacked on a complementary metal oxide semiconductor image sensor (for detecting transmitted red light) with a quarter video graphics array (QVGA) resolution (320 × 240) [2]. Most studies to date, however, have used the passive pixel sensor architecture, which contains one TFT in each pixel for readout of accumulated signals as a small current; thus, images reproduced from the TFT-based sensor were susceptible to external noise. To overcome this obstacle, introducing an active pixel sensor (APS) architecture is necessary, which has three TFTs in each pixel and can perform in-pixel signal amplification [3]. In this study, we describe an excellent performance of our blue-light-sensitive OPF including a dark current low enough to be used as a photoconversion unit of an APS [4], and we demonstrate imaging operation of the OPF-stacked TFT-based APS with a pixel number of 128 × 96 and a pixel pitch of 50 μm.

The TFTs used in this study had a bottom-gate staggered structure, and their channel width and length were 10 μm and 2 μm, respectively. The TFT-based readout circuit was fabricated on a glass substrate by sequentially forming gate electrodes (molybdenum (Mo) alloy, 50 nm), a gate insulator (silicon oxide, 200 nm), pixel electrodes (indium-tin-oxide, 50 nm), an active semiconductive layer (ITZO, 30 nm), via holes in the gate insulator, source/drain electrodes (Mo alloy, 70 nm), signal lines (Mo alloy/aluminum (Al)/Mo alloy, 75 nm), and a passivation layer (organic insulator, 600 nm). After fabrication of the TFT circuits, the OPF was formed on the pixel area by thermally evaporating in the order of an electron-blocking layer (2,7-bis(carbazol-9-yl)-9,9-spirobifluorene, 30 nm), a blue-light-sensitive active layer (2,9-diphenyl-dinaphtho-[2,3-*b*:2',3'-*f*]thieno[3,2-*b*]thiophene, 200 nm), a hole-blocking layer (4,6-bis(3,5-di(pyridin-4-yl)phenyl)-2-methylpyrimidine, 50 nm), and a counter electrode (Al, 30 nm).

TFT and OPF performances were then measured. The on-off ratio and the extracted field-effect mobility of the TFTs were >10⁸ and 24 cm²/Vs, respectively. The OPF exhibited the blue-light sensitivity with a peak external quantum efficiency of ~59%, and the dark current density of the OPF was 88 pA/cm². Finally, an imaging experiment was conducted with an image sensor test system. Images from test charts with a blue light-emitting diode backlight were projected onto a camera lens and focused on the sensor. By applying operation voltages of a QVGA array at 60 frames per second, we successfully obtained an image output from the fabricated sensor with 128 × 96 pixels. The results obtained here are potentially applicable to not only three-layer-stacked image sensors with enhanced image quality, but also flexible, large-area TFT-based APSs.

[1] R. A. Lujan et al., *IEEE Electron Device Lett.* 33, 688 (2012).

[2] T. Sakai et al., *ACS Appl. Electron. Mater.* 3, 3085 (2021).

[3] K. Imamura et al., *Jpn. J. Appl. Phys.* 60, 064002 (2021).

[4] K. Imamura et al., *Jpn. J. Appl. Phys.*, in press (2022).

8:50 AM SB06.21.11

Data Science Guided Experiments Identify Conjugated Polymer Solution Concentration as a Key Parameter in Organic Field-Effect Transistor Device Performance Rahul Venkatesh¹, Yulong Zheng¹, Campbell Viersen¹, Aaron Liu¹, Carlos Silva¹, Martha Grover¹ and Elsa Reichmanis²; ¹Georgia Institute of Technology, United States; ²Lchigh University, United States

Organic semiconducting polymers have demonstrated potential in the production of large-area, low-cost, flexible electronic devices. Recently discovered push–pull copolymers (donor–acceptor (D–A) polymers), with a polymer backbone consisting of alternating electron-deficient (acceptor) and electron-rich (donor) units, have exhibited significant improvement in electronic performance compared to semicrystalline homopolymers. The high charge carrier mobility observed in D–A polymers has been attributed to the rigid, planar backbone conformation with minimal steric hindrance between the donor and acceptor units. However, the vast and complex device processing space combined with a lack of standardized reporting makes reproducibility within the field difficult and impedes the development of these materials. Curating and analyzing centralized datasets is a promising approach to resolve the issue of reproducibility, gain new insights, and guide future experiments. Here, a data set was constructed containing processing and performance information of 115 published organic field-effect transistor (OFET) devices, fabricated using the commercially available D–A polymer, DPP-DTT. A customized classification algorithm was applied to the data set, which interestingly identified polymer solution concentration as a key processing parameter in OFET device performance. The algorithm recommended a reduced experimental design range for polymer solution concentration that would potentially result in higher OFET hole mobilities as compared to devices fabricated outside this design range. Experiments performed to confirm the insights from the data curation and analysis exercise revealed a strong influence of solution concentration on the polymer chain interactions and electronic performance. Based on the recommendations by the classification algorithm and insights from supporting experiments, it was identified that OFET devices fabricated at the critical polymer chain overlap concentration, resulted in enhanced hole mobility. It is hypothesized that the polymer chain overlap in the solution state contributes to improved charge transport in the solid-state. The results highlight the advantage of integrating materials informatics approaches into the existing polymer electronics methodologies.

9:05 AM SB06.21.12

PRESENTED ON-DEMAND ONLY: Multipurpose Organic-Inorganic Hybrid Dielectrics with Photothermal Crosslinking of Zirconium-Oxo Clusters Gahye Kim and Myung-Gil Kim; Sungkyunkwan University, Korea (the Republic of)

A hybrid structure of organic and inorganic building blocks enables us to design and tailor new materials with desired features and functions. Metal-oxo cluster molecules is one of the organic-inorganic hybrid materials. Metal-oxo cluster molecules having functional capping ligands offer remarkable promise in terms of thin film applications. Although there are a lot of metal-oxo cluster molecules reported so far, harnessing their potential is largely limited by lack of material processing strategy. We adopt a photothermally activated, cross-linked, and stable metal-oxo cluster molecular assembly based on hexanuclear zirconium-oxo cluster ($Zr_6O_4OH_4(OMc)_{12}$) (OMc: methacrylate) which can be a suitable for a new dielectric material in terms of electronic device applications since the zirconium-oxo core enhances the dielectric functionality and together the organic ligand (methacrylate) imparts a polymerizable functionality. Overall study not only proves that zirconium-oxo cluster activated by soft photothermal processing can be a new dielectric material candidate, but also other metal-oxo cluster thin film system may be further investigated by similar approach. The hexanuclear zirconium-oxo cluster is synthesized, and its thin film is prepared by a solution process and then photothermally treated with various conditions. The effect of DUV irradiation on zirconium-oxo cluster thin film is characterized by a leakage current profile and dielectric constant measurements. Very interestingly, the photothermal activation strategy used in this work enables a direct patterning of the thin film like photolithography. We find that both a cluster spacing and degree of polymerization in the zirconium-oxo cluster molecular assembly can be well modulated by photothermal processing conditions. We demonstrate that the photothermally activated zirconium-oxo cluster thin film can be successfully applied to a gate dielectric material for thin-film field-effect transistors with different active layers. We believe that the photothermal activation strategy in this work allows a variety of metal-oxo cluster materials to be a promising dielectric material system for soft electronic applications, which could be generalized to other material systems.

9:10 AM SB06.21.13

PRESENTED ON-DEMAND ONLY: Orientation of Exciton-Polarons and Strain-Enhanced Photoluminescence in Soluble Phthalocyanine Thin Films Libin Liang^{1,2}, KimNgan Burrill^{3,1} and Madalina Furis^{4,1}; ¹University of Vermont, United States; ²Intel Corporation (CA), United States; ³Intel Corporation (NM), United States; ⁴The University of Oklahoma, United States

Organic molecules, such as pentacene, rubrene and phthalocyanine are at the forefront of materials research, due to their desired electric and mechanical properties. They represent the feasible alternative to traditional silicon-based semiconductor applications when flexible electronics platforms are required, where materials will experience complex strain environment. Octabutoxy phthalocyanine (H_2 -OBPc) is a soluble derivative of the Phthalocyanine (Pc). They have π -conjugated systems and large directional intermolecular interactions, which allow the formation of molecular crystal with well-defined structure of J-aggregate, where molecules are in a head-to-tail fashion. In the expanded theory of molecular exciton, the Frenkel exciton can couple between lattice and intramolecular vibration to form exciton-polaron state, and consequently exciton-polarons can delocalize along the coherent J-aggregates. In this case, the short-ranged excitonic exchange depends on the relative orientation of the HOMO (Highest Occupied Molecular Orbital) and LUMO (Lowest Unoccupied Molecular Orbital) from NN molecules in the crystal, while the long-ranged excitonic exchange depends on lattice vibration. The formation of these one-dimensional delocalized exciton states grants H_2 -OBPc the potential for efficient excitation energy transport in the coherent exciton regime.

In this work, H_2 -OBPc polycrystalline thin films were prepared using a solution-based deposition technique. These ordered thin films with macroscopic grain size (millimeter scale) uniquely offer the opportunity to spatially explore optical and excitonic properties within a single crystalline grain, free from the influence of grain boundaries or static disorder. Temperature-dependent absorption and photoluminescence (PL) experiment show when temperature $T < 175$ K, additional bulk bandgap transition state presents at 900 nm and 930 nm, respectively. Incident light k-vector dependent absorption experiment indicates this bandgap transition is linearly polarized within substrate plane that obeys the Davydov selection rules. [1] The PL studies further reveal the temperature-dependent polarization of these excitons, implying the formation of exciton-polaron due to the coupling between exciton and lattice vibrations in the J-aggregates. Strain-dependent absorption and PL studies imply that external tensile strain can soften the lattice vibration mode and tune the above exciton-phonon coupling. Remarkably, an 80% enhancement in PL intensity is observed with a tensile strain of 4.9%, which is equivalent to a temperature reduction approximately by 100 K below room temperature. [2] Our study demonstrates strain-engineering of coherent delocalized exciton states in flexible organic electronics.

Reference

[1] *J. Phys. Chem. C* **2021**, 125, (51), 27966-27974. <https://doi.org/10.1021/acs.jpcc.1c08253>

[2] *J. Phys. Chem. C* **2022**. <https://doi.org/10.1021/acs.jpcc.2c01382>

9:15 AM SB06.21.14

PRESENTED ON-DEMAND ONLY: Solution-Processable POSS-Fluorene-Core Based Blue Lumophores with Lower Synthesis Costs and Process Complexity Parvez Akhtar, Rina Mahato, Anzalna Hamrah, Chinmoy K. Hazra and Madhusudan Singh; IIT Delhi, India

Polyhedral oligomeric silsesquioxanes (POSS) have previously been proposed as versatile chemical platforms for potential applications in displays and solid-state lighting [1,2], based on favorable charge transport, light absorption, and emission, resulting in high-efficiency OLEDs[3], including pyrene-based organic-inorganic hybrid materials[4,5]. However, synthetic processes for this class of lumophores require multiple stages and expensive process chemicals for purification. It is thus technologically relevant to synthesize cost-effective and efficient methods for synthesizing highly hindered novel chromophore compounds. We report on synthesis of a novel fluorene-based core emitter and its incorporation with the POSS platform or application in solution-processable OLEDs. A fluorene core was first methylated and alkylated using 1-chlorohexane. A Suzuki-Miyura cross-coupling reaction was used to link the pyrene moiety to the fluorene core. The Si-H terminal bond of the POSS cage was functionalized using hydrosilylation (Karstedt's catalyst) with this MFPy blue emitter to produce the final compound (MFPy-POSS). The synthesized materials were confirmed by proton NMR 400MHz (JEOLJNM-ECA Series (Delta V4.3)-400 MHz-FT-NMR). UV-Vis spectrometry (Perkin-Elmer) was used to infer a band gap of 2.94 ± 0.04 eV. Photoluminescence spectra (Ocean optics HR4000, 405 nm source) exhibit a prominent peak at 437nm (FWHM ~86 nm). For organic LED fabrication, indium tin oxide (ITO) coated glass substrates were cleaned in a standard cleaning process prior to spin-coating poly(3,4-ethylene dioxythiophene) polystyrene sulfonate (PEDOT:PSS, Sigma-Aldrich), dehydration bake in the air (120°C), followed by spin-coating of the active material consisting of the lumophore and standard electron and hole conducting materials, under nitrogen, and a dehydration anneal at 110°C. Samples were transferred under nitrogen for thermal evaporation at a base pressure of $\sim 6.5 \times 10^{-6}$ Torr (Angstrom Engineering) of bathocuproine (BCP, 300 Å), LiF (8 Å), and Al (1000 Å) to complete the devices with a shadow-masked top contact of area 0.3×0.3 cm². Current-voltage (J-V) and light-intensity-voltage (L-V) characteristics were acquired using a Keithley 2450 SMU and a Newport 918-UV photodiode. Initial device data: a turn-on voltage (6V) with a deep blue EL emission color at 437.4 nm (FWHM ~83 nm) and CIE coordinates of (0.163, 0.134). The luminance of the device is 1761 cdm⁻², at a current efficiency is 0.33 cd/A. Work is ongoing on the device design, active material ink composition, and material chemistry to improve these figures of merit.

- [1] Froehlich et al., A. Chem. Mater. 2007, 19, 4991–4997.
[2] Singh et al., Soft Matter 5.16 (2009), p.3002.
[3] Yang et al., Chem. Mater. 2010, 22, 4776–4782
[4] Kotchpradist et al., Journal of Materials Chemistry C 1.32 (2013), pp. 4916–4924.
[5] Cheng et al., Journal of Materials Chemistry C 4.27(2016), pp.6461–6465.

9:20 AM SB06.21.15

FET Mobility Versus Iodine Doping of P3HT Latonya Waller, Makhes Behera, Sam Sun and Messaoud Bahoura; Norfolk State University, United States

Polymers as the active layer for organic field effect transistors (OFETs) are inherently flexible, lightweight, cost-effective, biocompatible, and processing can be very versatile. Doping can drastically change and modulate the electronic properties of semiconductors and enable tunable FET devices. In this work, the charge mobility in a p-type conjugated polymer Poly-3-hexyl-thiophene (P3HT) doped by iodine are being evaluated. Preliminary results shows that the FET charge mobility initially increases at low doping concentrations but decreases at high doping concentrations. Mechanisms of such trend are being evaluated.

9:25 AM SB06.21.16

Design and Synthesis of New Two-Dimensional Non-Fullerene Acceptors for Indoor Light Harvesting Jianping Lu, Yinghui He, Salima Alem, Stephen Lang and Ye Tao; National Research Council of Canada, Canada

In recent years, organic photovoltaic (OPV) cells have attracted much interest for applications in indoor light harvesting to efficiently convert indoor light into electricity. As a matter of fact, OPV cells already outperform polycrystalline silicon photovoltaic devices in term of power conversion efficiency (PCE) under various indoor light sources largely due to the development of high-performance non-fullerene acceptors to replace previous widely used fullerene derivatives, such as PC₆₁BM and PC₇₁BM. On the other hand, modern inorganic semiconductors based miniaturized electronic devices and sensors are highly efficient and some of them only require a few tens of microwatts of energy to operate. This makes it quite appealing to power them with OPV cells because of the unique features associated with OPVs, such as low cost, light weight, mechanical flexibility, customized shapes and form factors, high throughput production using solution processes, and facile integration with sensors. Recently, our group has designed and synthesized a new series of two-dimensional non-fullerene acceptors based on a rigid electron-deficient benzo[4,5]imidazo[2,1-a]isoindole central core. When blended with a p-type polymer (PM6), one of our non-fullerene acceptors demonstrated a promising PCE of 19.4% and a high V_{oc} of 0.75 V under an indoor LED illumination of 1300 lux in the PV cells with an active area of 1 cm². For comparison, the well-studied PM6:Y6 bulk heterojunction blend fabricated in our lab gave a V_{oc} of 0.66 V and a PCE of 17.5% under the same illumination condition. With rational design of side chains and substituents to finely tune the solubility, intermolecular packing, and energy levels of our new non-fullerene acceptors, we believe that their PV performance under indoor light can be further improved, which makes them promising materials for indoor light harvesting to power miniaturized electronic devices and sensors for applications in internet of things (IoT) and smart homes.

9:30 AM DISCUSSION TIME

SYMPOSIUM SB07

Magnetic Materials for Soft Robotics and Nanorobotics
November 29 - December 6, 2022

Symposium Organizers

Jiyun Kim, Ulsan National Institute of Science and Technology
Lamar Mair, Weinberg Medical Physics, Inc.
Salvador Pane i Vidal, ETH Zurich
Joseph Tracy, North Carolina State University

* Invited Paper
+ Distinguished Invited

SESSION SB07.01: Processing and Engineering Properties I
Session Chairs: Denys Makarov and Josep Puigmartí-Luis
Tuesday Morning, November 29, 2022
Hynes, Level 3, Room 308

8:00 AM *SB07.01.01

Multifunctional Magnetic Origami Robots Ruike Renee Zhao; Stanford University, United States

Millimeter/centimeter-scale origami robots have recently been explored for biomedical applications due to their inherent shape-morphing capability.

However, they mainly rely on passive or/and irreversible deformation that significantly hinders the clinic functions in an on-demand manner. Here, we report magnetically actuated crawling and swimming origami robots for effective locomotion and targeted drug delivery in severely confined spaces and aqueous environments. We design our robots based on the Kresling origami, whose thin shell structure 1) provides an internal cavity for drug storage, 2) permits torsion-induced contraction as the mechanism for crawling and controllable drug release, 3) serves as propellers that spin for propulsion to swim, 4) offers anisotropic stiffness to overcome the large resistance from the severely confined spaces in biomedical environments. These magnetic origami robots can potentially serve as minimally invasive devices for biomedical diagnoses and treatments.

Biometric soft robotic crawlers have attracted extensive attention in various engineering fields, owing to their inherent adaptivity to different terrains. Earthworm-like crawlers realize locomotion through in-plane contraction, while inchworm-like crawlers exhibit out-of-plane bending-based motions. The in-plane contractive crawling mechanism surpasses the bending-based one in confined spaces where out-of-plane motion is either constrained or unfeasible. Although in-plane contraction crawlers are more effective in confined spaces, miniaturization is challenging due to the limitations of actuation methods and complex structures. To address those challenges, we report a magnetically actuated small-scale origami crawler with in-plane contraction. The contraction mechanism is achieved through a four-unit Kresling origami assembly consisting of two Kresling dipoles with two-level symmetry designed for purely translational crawling motion. Magnetic actuation is utilized to provide appropriate torque distribution on the crawler, enabling a small-scale and untethered robot with both crawling and steering capabilities. Because the Kresling crawler exhibits anisotropic and magnetically tunable structure stiffness, it can overcome the large resistance from severely confined spaces during crawling. Finally, the multifunctionality of the crawler is explored by utilizing the internal cavity in the Kresling origami for drug storage and release. The magnetic origami crawler has the potential to serve as a minimally invasive device for biomedical diagnoses and treatments.

8:30 AM SB07.01.02

Magnetically Tunable Bistable Structures [Aniket Pal](#)¹ and [Metin Sitti](#)^{1,2,3}, ¹Max Planck Institute for Intelligent Systems, Germany; ²ETH Zürich, Switzerland; ³Koç University, Turkey

Bistable structures have become a common strategy in compliant mechanisms and soft robotics to overcome the intrinsic limitations of soft materials (e.g., high dissipation, low speeds and forces) as well as to create new functionalities (e.g., energy absorption, motion, deployable structures). The responses of bistable structures are determined by their geometric design and the mechanical properties of their constituent material. Here we introduce a strategy to dynamically program the responses of bistable structures by tuning their elastic energy landscape with external magnetic fields. We demonstrate that the stable states of a slender beam, fabricated with a magnetoactive elastomer, can be dynamically controlled to switch between a monostable and bistable response and the more energetically favorable state of a bistable element can be specified. We then harness the tunable responses of such bistable beams to control the propagation of solitary transition waves in an array of such beams, connected by linear spring elements. Specifically, we demonstrate the external magnetic-field-based control of the direction, speed, shape, and length of propagation of transition waves; without the need to change any of the physical components (beams and linear springs) of the array. We also show reconfigurable functional devices, such as logical gates, where a single physical system can be controlled to act as different gates with an external magnetic field.

8:45 AM SB07.01.03

Tailoring the Multistability of Origami-Inspired, Buckled Magnetic Structures via Compression and Creasing [Yi Li](#); University of Connecticut, United States

Origami-inspired multistable structures are gaining increasing interest because of their potential applications in fields ranging from deployable structures to reconfigurable microelectronics. The multistability of such structures is critical for their applications but is challenging to manipulate due to the highly nonlinear deformations and complex configurations of the structures. In this talk, I will present a comprehensive experimental and computational study to tailor the multistable states of origami-inspired, buckled ferromagnetic structures and their reconfiguration paths. Using ribbon structures as an example, a design phase diagram is constructed as a function of the crease number and compressive strain. As the crease number increases from 0 to 7, the number of distinct stable states first increases and then decreases. The multistability is also shown to be actively tuned by varying the strain from 0% to 40%. Furthermore, analyzing energy barriers for reconfiguration among the stable states reveals dynamic changes in reconfiguration paths with increasing strain. Guided by studies above, diverse examples are designed and demonstrated, from programmable structure arrays to a soft robot. These studies lay out the foundation for the rational design of functional, multistable structures.

9:00 AM *SB07.01.04

Magneto-active Metamaterials for Controlling Sound and Vibrations [Abigail Juhl](#)¹, [Vincent Chen](#)^{1,2}, [Carson Willey](#)^{1,2}, [Phil Buskohl](#)¹, [Kathryn H. Matlack](#)³, [Connor D. Pierce](#)³, [Stephan Rudykh](#)⁴, [Nitesh Arora](#)⁴ and [Artemii Goshkoderia](#)⁵; ¹AFRL, United States; ²UES, Inc., United States; ³UIUC, United States; ⁴University of Wisconsin–Madison, United States; ⁵Technion–Israel Institute of Technology, Israel

Phononic metamaterials are subwavelength materials designed to control the propagation of elastic or acoustic waves for use in applications such as sound and vibration mitigation. The geometry, periodicity, and material properties that make up the metamaterial define the scattering behavior and resulting dispersion from the structure. The metamaterial's dispersion properties are typically set at the time of manufacture, making it difficult to alter the frequencies that are permitted/prohibited to propagate without fabricating a new sample. However, if external stimuli can be used to dynamically vary the mechanical properties or the shape of the metamaterial, the dispersion properties can be tuned without remanufacture. In this work, magnetorheological elastomers (MREs) will be investigated as a means to adaptively tune the band gap properties of phononic metamaterials. The MREs in this work are composed of isotropically dispersed 3-10 micron iron particles within a PDMS matrix. Three demonstrations of magnetic field induced tuning will be presented for different metamaterial architectures. In the first demonstration, remote application of a magnetic field was applied to a 3D printed MRE elastic metamaterial to induce a stiffening of the MRE modulus to shift the frequency of vibration control to a higher frequency band. In the second demonstration, neodymium magnets are placed on a MRE-based acoustic plate by magnetic attraction and it is shown that that the absorption, transmission loss, and effective density of the acoustic metamaterial can be tailored through their reconfigurable spatial placement. And in the final example, we take advantage of the magneto-mechanical coupling within the MRE to promote an instability induced pattern change in a MRE/neat elastomer composite architecture. By understanding the magnetomechanical behavior, it may be possible to program the instability pattern formation for use in dynamic band gap control.

9:30 AM BREAK

10:00 AM SB07.01.05

Protein-Based Magnetic Composites for Self-Healing and Reconfigurable Actuators [Zenghao Zhang](#) and [Abdon Pena-Francesch](#); University of Michigan–Ann Arbor, United States

Soft microrobots can achieve controlled motion and shape changing upon actuation, and thus are capable of performing non-invasive surgery in the human

body. Among soft actuation systems, magnetic actuation is advantageous for healthcare applications since magnetic fields can penetrate tissue, and can generate both pulling forces and torques remotely. One current challenge is that magnetic microrobots typically have limited actuation modes, which are determined mainly by the internal magnetization profile of the robot. In this study, we developed a magnetic soft composite based on squid-derived proteins and rare-earth magnetic particles with discrete magnetization profiles, and used self-healing to reconfigure their magnetization and actuation modes. The self-healing properties of the squid-derived protein matrix enable the rearrangement of modular components with different magnetic properties. By tailoring the composition, the anisotropy of the thermo-mechanical properties, the geometrical robot design, and the actuation magnetic field, we demonstrate control over complex robot deformations, and reversible reconfiguration of actuation modes. This work opens up the design space of magnetic soft robots and their reconfigurable actuation modes via the discrete programming of the magnetization directions and intensities throughout the microrobot body. This freedom in design can provide key advantages in soft and small-scale actuation to perform specific tasks in confined environments, with application in healthcare and industrial micromanipulation.

10:15 AM SB07.01.06

Design of Organic Soft Magnets for Applications in Small-Scale Robotics [Abdon Pena-Francesch](#); University of Michigan, United States

Traditional magnetic materials consist of heavy metals and rare-earth elements that typically entail corrosion, toxicity, and sustainability concerns. On the other hand, organic magnetic materials present a metal-free opportunity to develop lightweight non-toxic magnets. Although magnetic molecules based on stable free radicals have been used as monolayers and dopants in spintronics and as imaging contrast agents, shortcomings in stability, limited processing, and loss of properties have hindered their expansion into other fields such as small-scale soft robotics. To address these issues, we have developed intrinsically magnetic polymer gels with stable nitroxide radicals in their backbone structure. Using TEMPO precursors, we can design the polymer network to tailor the bulk mechanical and magnetic properties. Although weaker than purely metallic magnets, these organic magnets exhibit lightweight, non-toxic, compliant, and bulk paramagnetic properties suitable for small-scale robotics applications, such as remote manipulation and navigation through confined spaces.

10:30 AM *SB07.01.07

Magnetic Programming of Soft-Bodied Wireless Miniature Medical Robots [Metin Sitti](#); Max Planck Institute for Intelligent Systems, Germany

Wireless miniature medical robots have the unique capability of navigating, operating and staying inside risky and currently hard- or impossible-to-reach small spaces inside the human body. On the other hand, soft-bodied robots have the unique capabilities of shape programming, physical adaptation, safe physical interaction, and multifunctional diverse behaviors. Combining the strengths of both systems, this presentation reports on our recent soft-bodied wireless miniature medical robots with magneto-elastic active materials, actuated and controlled by external magnetic fields and gradients. Magnetizing hard magnetic microparticles, embedded inside the elastomeric body of soft robots, in programmed orientations and magnitudes enable diverse, dynamic and programmable shape deformations on these soft robots. We can even reprogram such magnetization properties to drastically change the shape modes of the robots. Using various magnetic (re)programming methodologies, first, we propose a magneto-elastic sheet-shaped soft robot, called Wormmate. Wormmate is inspired by soft-bodied organisms, such as spermatozooids, caterpillars, jellyfishes, and bacteria. It has over nine locomotion modalities at the same time to be able to navigate in diverse confined environments inside the human body. Next, a baby jellyfish-inspired magneto-elastic milliwimmer is shown to realize multiple functionalities by producing diverse controlled fluidic flows around its body. Then, an array of cilia-inspired magneto-elastic cilia is developed to generate metachronal waves for efficient biological fluid pumping and fluidic object manipulation. Moreover, we propose a jig-assisted 3D assembly method to create the most advanced soft miniature robots with heterogeneous diverse materials and complex magnetic programming for medical device and other applications. Finally, it is possible to scale down such soft-bodied magnetic robots down to microscale by merging two-photon 3D microprinting and magnetic assembly techniques. As example wireless soft medical devices, a soft peristaltic pump, a tubular surface-anchoring metamaterial-based shape-programmable soft device, a stent-like soft robot, and an on-demand drug-releasing soft capsule are demonstrated. Such soft devices are guided under ultrasound and x-ray imaging to achieve various local active medical functions, such as drug delivery, liquid biopsy, stem-cell treatment, embolization, clot opening, and hyperthermia.

11:00 AM SB07.01.08

3D-printed Magnetic Elastomers: Identifying Key Structure & Processing Parameters for Enhanced Magnetoactive Performance [Brittany Nelson-Cheeseman](#), James M. Ennis, Jimmy Lu, Sarah Ziemann, Nathan A. Fischer, Thomas M. Calascione and Thomas Höft; University of St. Thomas, United States

Magnetic elastomers are of interest for soft robotic applications where remote contactless activation is desired. These composite smart materials are made of magnetic particulate embedded in an elastomeric matrix and respond to applied magnetic fields with mechanical deformation, termed magnetoaction. It's been shown that anisotropic structures and properties within these materials leads to increased magnetoactive performance. Magnetic annealing is the main processing technique that has been used to increase magnetoactive performance through the introduction of local anisotropy. For further enhancements to magnetoaction, the 3D-printing technique, Fused Deposition Modeling (FDM), can be used to create additional anisotropy in the structures and properties of magnetic elastomers. FDM creates anisotropic sub-structures within a part by extruding 1D lines of the molten material (termed "infill") in 2D patterns that build up to a 3D part. This infill pattern is entirely customizable with respect to orientation and percentage filling allowing for one to readily tune the properties of the resulting part. While it's been clearly shown that these parameters significantly influence the resulting mechanical and magnetic properties of FDM-printed parts, their influence on magnetoaction (the confluence of mechanical and magnetic responses) has yet to be reported. Here, we investigate how a variety of parameters on multiple length-scales influence magnetoaction in FDM-printed magnetic elastomers. In particular, we study how FDM *infill percentage* and *infill orientation* relative to applied magnetic field influences magnetoaction of the printed part. We also report on additional filament and extrudate studies, where filament is the stock material used for FDM printing and extrudate is what exits the FDM nozzle before it builds up to larger printed structures. These studies involve *magnetic annealing* and a variety of *soft vs. hard magnetic particulates* in order to understand how these parameters (before the 3D printed structure has been introduced) can additionally influence magnetoaction of these materials. These parameters are then explored in the 3D printed structures to understand how they interact with the 3D printed structural features. A custom setup is used to measure magnetoaction, whereby the sample is suspended vertically from a fixed point and a transverse DC magnetic field is applied up to 0.4 T along the horizontal axis. The degree of magnetoaction is quantified as the angle of deflection of the sample relative to vertical for a given applied field. The data is captured visually in digital images that are then digitally processed in order to determine the quantitative deflection angle for a given applied field. Supporting magnetic, mechanical and structure (SEM) studies are utilized to investigate the origins of the differences in magnetoaction. We find that for the FDM architectures studied that the greatest magnetoaction is found for a combination of low infill percentages and infill oriented perpendicular to the applied magnetic field. These effects arise from both maximizing anisotropy and limiting infill crosslinking within the structure. We also find that magnetic annealing of the stock filament increases magnetoaction in the filament, and that this increase is maintained in the extrudate after extrusion through the FDM nozzle. This surprisingly and exciting result allows for more accessibility to FDM-printing of high performance magnetic elastomers. Finally, we find that the soft magnetic particulates (Fe and Fe₃O₄) give both the greatest magnetoaction and magnetoaction at lower fields when magnetically annealed, while the hard magnetic particulate (SrFerrite) gives the greatest difference in magnetoaction when magnetic annealing is applied. All of these results together highlight a number of key structure and processing parameters that lead to enhanced magnetoactive performance in 3D-printed magnetic

elastomers.

11:15 AM SB07.01.09

Magnetoactive Properties of 3D Printed Magnetic Elastomer Structures—Effects of Infill Orientation and Infill Percentage James M. Ennis¹, Hannah G. Thatcher¹, Thomas M. Calascione^{2,1}, Jimmy Lu¹, Nathan A. Fischer¹, Sarah Ziemann¹, Thomas Höft¹ and Brittany Nelson-Cheeseman¹; ¹The University of St. Thomas, United States; ²University of Colorado Boulder, United States

Magnetic elastomers are flexible smart materials that can be manipulated by magnetic fields to achieve reversible mechanical deformation. These highly configurable materials are instrumental in transforming biomedical applications in soft robotics enabling the manipulation of artificial muscles and other bio-actuators. Magnetic elastomer structures must be customizable to satisfy these complex applications leading to the use of fused filament fabrication (FFF) in creating them. FFF is a 3D printing process where material is extruded in 1D lines (infill) to build 2D planes layer-by-layer, resulting in a 3D structure. Structures can be created with different levels of anisotropy and complicated interior geometries enabling control of both the magnetic and mechanical properties. The meso structure or infill of a 3D printed part is critical in fine-tuning its properties since it defines the internal structure. Both infill percentage and infill orientation affect mechanical and magnetic properties of 3D printed magnetic elastomer parts. This research used magnetoactive testing to investigate how varying the internal meso structure affected the mechanical response of the structures within an applied magnetic field. Different infill percentages (40%, 60%, and 100%) were tested to account for different mechanical stiffnesses, and different linear infill orientations (0, 45, and 90 degrees) were tested to account for different internal geometries. The macro structure was a rectangular beam with dimensions of 60x5x5 mm³. The elastomers were made with a microstructure of 40wt% magnetite (Fe₃O₄) with a thermoplastic polyurethane (TPU) matrix. To account for any magnetoactive effects due to the print layering or infill orientation, each sample was magnetoactively tested with three different transverse magnetic field orientations (Front, Back and Top) by rotating the sample around the longitudinal axis by 90-degree increments. The samples were placed between two electromagnets emitting up to a 0.4 Tesla field, and the angle of deflection was recorded as a function of applied field by using MATLAB to overlay pictures taken at each field strength with the sample at 0 Tesla. The samples that showed magnetoaction provided clear infill design goals for increased magnetoactive performance. These design goals enabled some samples to reach the maximum angle of deflection for the testing setup. *Infill Percentage:* Lower infill percentages translated to less material in the cross-section of the sample and thus lower bending stiffness, allowing for more magnetoaction. *Infill Orientation:* 0-degree (along long axis of sample) created much less crosslinking between infill lines which led to more flexibility within the sample, and more magnetoaction. *Print Layering Orientation:* Transverse fields applied parallel to the print plane (Front/Back sample orientations) demonstrated the most magnetoaction due to less crosslinking from adjacent layers. This layer crosslinking heavily constrained the bending stiffness in certain sample orientations (Top) similar to the infill orientation effects. The anisotropy of the meso structure likely also contributed to the large response from the 0-degree 40% and 60% samples. The long, isolated lines of the 0-degree meso structure had the greatest magnetic shape anisotropy causing the greatest rearrangement of the structure to align with the applied magnetic field. The sample would thus deflect to be as parallel as possible with the transverse field. It was concluded that for this fixed base material, it is more important to 3D print structures with lower stiffnesses (40% infill) than more net magnetic particulate (100% infill) in achieving the most magnetoaction. According to this data, meticulously designed 3D printed magnetite-TPU structures seem to be well suited for creating components easily stimulated by a magnetic field unlocking many possibilities for the creation of useful technologies in the biomedical field.

11:30 AM *SB07.01.10

Analytical Approaches to Modeling Thin-Film Magnetic Actuators Benjamin A. Evans¹, Jessica A. Liu², Minjeong Ha³, Eduardo Sergio Oliveros Mata³, Gilbert S. Cañón Bermúdez³, Denys Makarov³ and Joseph B. Tracy²; ¹Elon University, United States; ²North Carolina State University, United States; ³Helmholtz-Zentrum Dresden-Rossendorf, Germany

Flexible thin-film magnetic actuators are canonical constructs that underpin many magnetic soft-robotic devices. Understanding their behavior is therefore essential to the successful design and implementation of a broad range of magnetic actuators. In most cases, thin-film magnetic actuators may be effectively modeled with closed-form analytical expressions employing simple fundamental physical principles. Such closed-form solutions capture essential behavior of the devices across an expansive multidimensional parameter space, providing a powerful analytical platform for rapid design and optimization. This framework is easily accessible to outside users and translates readily to a wide variety of specific applications. In addition, analytical modeling provides ready insight into the physical mechanisms of device behavior, aiding in conceptual understanding and design.

In this work we explore simple analytical models that describe the performance of flexible magnetic films under the influence of actuating fields. We distinguish the effects of magnetic torques induced by uniform fields from magnetic forces mediated by applied field gradients and provide a framework for evaluating their relative impact. Considering films with both hard- and soft-magnetic fillers, we develop predictive expressions for range of motion, available actuating force, and work done by the device on its environment [1]. These models are then applied to special cases of thermoplastic shape-memory polymers and ‘snapping’ devices with stored elastic energy, and figures of merit are developed to characterize performance [2].

Throughout, predictions are shown to be in good agreement with experimental results derived from both soft- and hard-magnetic thin-film actuators comprised of both elastic [3] and thermoplastic matrices [2], thus validating a powerfully predictive modeling framework. This framework provides opportunities for rapid design and optimization of devices for specific tasks and aids in the identification and realization of unexpected behaviors.

[1] GS Cañón Bermúdez, M Navarro López, BA Evans, KV Yershov, D Makarov, OV Pylypovskiy, ‘Shapeable magnetism from macro- to nanoscale’ in *Curvilinear Micromagnetism: From Fundamentals to Applications*, eds. D. Makarov, D. Sheka, (Springer, 2022).

[2] JA-C Liu, JH Gillen, SR Mishra, BA Evans, JB Tracy, “Photothermal and Magnetically Controlled Reconfiguration of Polymer Composites for Soft Robotics,” *Science Advances*, 5 (8), 2019.

[3] M Ha, GS Cañón Bermúdez, JA-C Liu, ES Oliveros Mata, BA Evans, JB Tracy, D Makarov, “Reconfigurable Magnetic Origami Actuators with On-Board Sensing for Guided Assembly,” *Advanced Materials*, 33 (25), 2021.

SESSION SB07.02: Processing and Engineering Properties II

Session Chairs: Abigail Juhl and Joseph Tracy

Tuesday Afternoon, November 29, 2022

Hynes, Level 3, Room 308

1:30 PM *SB07.02.01

Magnetic Composites—From Printed Magnetoelctronics to Smart Magnetic Soft Robots Denys Makarov; Helmholtz-Zentrum Dresden-Rossendorf

e.V., Germany

Composites consisting of magnetic fillers in polymers and elastomers enable new types of applications in soft robotics, reconfigurable actuation and sensorics. In particular, soft-bodied robots emerge as the closest synthetic system analogous to living organisms mimicking their mechanical behavior and going beyond in performance. We will introduce lightweight, durable, untethered and ultrafast soft-bodied robots performing large amplitude of deformations at high frequencies of up to 100 Hz and exhibit high specific energy density of 10.8 kJ/m³/mT [1]. Our soft-bodied robots can walk, swim, levitate, and transport cargo being driven using external magnetic fields. This inspires new classes of soft robots that impact biosensorics [2], biological tissue engineering, confined and high-speed mechanical (tissue) manipulation, and serve as working models to study fast biomechanical processes like hydro- and aero- dynamics of fast-moving organisms.

These mechanically active structures are typically designed to work in a specific prior defined parameter range and can malfunction when the conditions are changed. Specifically for magnetic soft robots, the change of the intrinsic magnetic properties due to temperature activations or time relaxation can lead to modifications in the actuation pattern. We present ultrathin and reconfigurable magnetic origami actuators based on a composite consisting of shape memory polymers and magnetic microparticles [3]. Self-sensing is achieved by laminating ultrathin magnetosensitive e-skins [4] on soft origami actuators. The sensor assesses the magnetic state of the actuator (magnetized vs. non-magnetized) and decides on its actuation pattern even before the actual actuation is done experimentally. Furthermore, the sensor enables communication of the actuator with external devices (rotation stage, electromagnets) for self-guided assembly of an initially flat layout and provides the possibility to control the sequentiality and quality of the folding process.

Magnetic composites can be readily used to realise not only actuators but also magnetic field sensors. We demonstrate that printed magnetoelectronics can be stretchable, skin-conformal, capable of detection in low magnetic fields and withstand extreme mechanical deformations [5,6]. We feature the potential of our skin-conformal printable sensors in augmented reality settings, where a sensor-functionalized finger conducts remote and touchless control of virtual objects manageable for scrolling electronic documents and zooming maps under tiny permanent magnet.

Furthermore, we will present high performance dispenser printed magnetic field sensors based on non-magnetic half-metallic bismuth powder [7]. Printed Bi sensors reveal non-saturating large magnetoresistance (LMR) effect, reaching up to 146% resistance change at room temperature at 5 T (>3900% at 20 K at 7 T). The LMR is a fingerprint of topological properties of the band structure of Bi. In this respect, this work constitutes the very first use of topological material properties in printing technologies. Due to their thermal and mechanical stability, the sensors printed on thermoplastic foils can be reformed in a stable three-dimensionally shaped object enabling applications of our technology for in-mold electronics. We demonstrate magnetically controlled interactive devices based on a printed array of sensors, to be used for interactive advertisement, smart wallpapers, and security input panels.

[1] X. Wang et al., *Communications Materials* 1, 67 (2020).

[2] J. Mystkowska et al., *Sensors* 21, 7122 (2021).

[3] M. Ha et al., *Adv. Mater.* 33, 2008751 (2021).

[4] G. S. Canon Bermudez et al., *Adv. Funct. Mater.* 31, 2007788 (2021).

[5] M. Ha et al., *Adv. Mater.* 33, 2005521 (2021).

[6] E. S. Oliveros Mata et al., *Applied Physics A* 127, 280 (2021).

[7] E. S. Oliveros Mata et al., *Adv. Mater. Technol.* 2200227 (2022).

2:00 PM SB07.02.02

On Fracture Toughness of Isotropic and Anisotropic Magnetoactive Elastomer Under an External Magnetic Field [Nusrat Jahan Salim](#), Ignacio Arretche, Connor D. Pierce and Kathryn H. Matlack; University of Illinois at Urbana Champaign, United States

The emerging studies in the field of soft robotics include design, modeling, and manufacturing of soft active materials that can control soft bodies. Magneto-mechanical coupling has been recently explored as a mechanism for soft robotic control, for example in elastomeric materials that incorporate magnetic particles, typically known as magnetoactive elastomers (MAEs). Magneto-mechanical properties of MAEs such as tunable damping, vibration control, and soft structure deformation under magnetic fields have been extensively studied. Further, the magneto-mechanical coupling can be amplified by curing the MAEs in a magnetic field, producing a highly anisotropic chain-like microstructure. However, fracture toughness mechanisms in MAEs, and their dependence on anisotropy and an applied magnetic field, have not yet been explored. Cracks or any kind of damage can lead to impaired function and control of soft robotic materials. While the dependence of volume fraction and orientation of reinforcing particles on the damage response of soft materials has been studied, the fracture behavior of MAEs, which contain micron-sized reinforcing particles, is currently unknown. In this work, we experimentally study the fracture toughness and toughening mechanisms of MAEs and their dependence on particle volume fraction and chain anisotropy. To fabricate the MAEs, micron-sized carbonyl iron particles (CIPs) were suspended, and then cured, in a polydimethylsiloxane (PDMS - Sylgard 184) matrix. Magnetic fields were applied in different directions while curing to introduce anisotropy in the particle chains. We quantified the effect of particle volume fraction and chain orientation on fracture toughness through a unified experimental method with and without magnetic fields. Various volume fractions and chain orientations of CIPs were used to explore the dependence of the damage mechanisms on CIP volume fraction and chain orientation without a magnetic field. The results show that increasing particle volume fraction increases the fracture toughness. Further, fracture toughness is enhanced when particles are aligned with the direction of loading. To elucidate the dependence of fracture toughness on the magneto-mechanical coupling, similar experiments were repeated under an applied magnetic field. Finally, SEM micrographs were used to explain the micromechanics behind the variations in fracture toughness. This revealed that the mechanism is driven by inducing and controlling crack pinning, crack deflection, and interface debonding of particles. These experiments can provide a basis to understand fracture of MAEs that could enable improved damage mechanisms in soft robots controlled by magneto-mechanical coupling.

2:15 PM SB07.02.03

Digitally Controlled Self-Assembly of Magnetic Materials by Micro Atmospheric Pressure Plasma Jet [Luke J. Tinsley](#), Prakash Karipoth and Russell A. Harris; University of Leeds, United Kingdom

Introducing a magnetic response to soft materials is of growing interest to a number of fields, with the ability to fabricate soft structures featuring spatially varied anisotropic magnetic properties being key to enabling many applications. Magnetically actuated soft robots are an example of this, demonstrating remarkable feats throughout healthcare and micro-robotic applications owing to their untethered operation and inherent dimensional scalability. In particular for medical applications, it is desirable to be able to tune the design of the soft robot to the specificities of the patient. Digitally driven fabrication approaches, such as 3D printing, provide the flexibility to do this, but come with limitations linked to processing speed, resolution, and compatible materials. Here we present a novel approach to the patterning of magnetic materials whereby they self-assemble into a programmable shape, overcoming these limitations. This is accomplished by exposing a silicone elastomer film to a highly localised source of plasma, produced by a bespoke computer-controlled micro atmospheric pressure plasma jet (μ APPJ), to selectively create patterns of plasma treatment across its surface. The plasma induces a chemical change on the surface of the film, which corresponds to a large increase in the polar component of free surface energy. Consequently, polar fluid dispersions containing customised magnetic nanoparticles, which have undergone chemical functionalisation to enable stable suspension in the fluid, align with the treated regions autonomously. Subsequent evaporation of the polar fluid then leaves solely the magnetic material. We show that through variation of the voltage and frequency used to generate plasma in the μ APPJ the resolution of the treatment can be varied between 50 μ m and 1200 μ m. Furthermore,

a maximum processing rate of $3.6\text{mm}^2\text{s}^{-1}$ is orders of magnitude quicker than comparable 3D printing techniques and due to the dynamically controllable resolution, large patterns with fine details can be processed efficiently. We demonstrate the process through the fabrication of stretchable, soft and magnetically responsive thin films.

2:30 PM SB07.02.04

Reprogrammable Hard-Magnetic Cilia Matthew R. Clary¹, Joseph B. Tracy¹, Saraah N. Cantu¹, Benjamin A. Evans² and Jessica A. Liu¹; ¹North Carolina State University, United States; ²Elon University, United States

Artificial magnetic cilia are hair-like structures that are actuated with magnetic fields. Most prior research on magnetic cilia has involved soft magnetic materials, in which the absence of magnetic hysteresis limits the ability to program their magnetization state. In contrast, use of hard magnetic materials in magnetic cilia makes possible programming and reprogramming of the magnetization state and corresponding actuation behaviors. In this work, hard-magnetic cilia are fabricated through self-assembly by solvent casting of a slurry of NdFeB microparticles dispersed in a solution of a thermoplastic polyurethane elastomer. These hard-magnetic cilia are capable of attractive and repulsive responses to magnetic fields, which are determined by the remanent magnetization of the NdFeB microparticles. An array of cilia can be magnetically reprogrammed by immobilizing the cilia in ice, applying a damped alternating magnetic field first to reduce the remanent magnetization, and then remagnetizing the cilia with a large external field. Through this approach, different responses to magnetic fields can be programmed, including spatially non-uniform behaviors. Reprogrammed hard-magnetic cilia exhibit unique behaviors in a rotating magnetic field. When the magnetization direction is reprogrammed along the width of the cilia, rotation and torsion cause the cilia to slowly coil and then quickly uncoil in a snapping behavior. A theoretical model explains the observed effects and provides a comparison between hard-magnetic and soft-magnetic cilia.

2:45 PM BREAK

SESSION SB07.03: Multifunctional Magnetic Soft, Micro- and Nanorobots

Session Chairs: Brittany Nelson-Cheeseman and Metin Sitti

Tuesday Afternoon, November 29, 2022

Hynes, Level 3, Room 308

3:15 PM *SB07.03.01

Magnetic 3D Micro-Machines and Functional Soft Composites Meng Li; MPI for Intelligent Systems, Stuttgart, Germany

Summary: 3D mechanical structures integrated with functional magnetic components enable complex motions at the sub-millimeter scale. Magnetic composites that respond synergistically to optical and magnetic stimuli enable self-sustained motions by forming physical negative feedback loops.

3:45 PM SB07.03.02

Capacitor Integrated Magnetic Actuator Hajun Lee¹, Yeonwoo Jang¹, Junghyo Kim¹, Heejae Won¹, Kwon-Hyung Lee¹, Sang-Young Lee² and Jiyun Kim¹; ¹Ulsan National Institute of Science and Technology, Korea (the Republic of); ²Yonsei University, Korea (the Republic of)

In robotics, especially in soft robotics with electronic devices such as motors, light emitting diodes (LEDs) and sensors, a stable power supply is one of the major concerns to operate their components properly. For the remote control and simple body structure without tethering to outer signal/power line, integration of the power source such as battery or capacitor is an unavoidable option. Although there are several types of substitutes such as thermal-, optical-, and hygro-energy based systems, it is obvious that electric energy is still used as major power source.

Most of electronic systems rely on batteries for their power supply and many of electronic energy harvesting systems require batteries for stable energy storage and supply. Accordingly, researches on materials and manufacturing methods related to power sources have been actively conducted, and they led remarkable improvement of the energy efficiency and electrochemical properties related to safety and stability. Conventional-shaped power sources, however, is limitation in design of electronic devices because they have to secure specific space and geometry for the deployment of power sources. For the reason, developing advanced power sources with various form factor has been encouraged for scalability, design diversity, shape compatibility, and so on. There were several approaches to promise form factor-free power sources in printable power sources or smart materials combined power sources. Although they showed high flexibility and responsibility to external stimuli compared to previous rigid counterparts, it was still a challenge to integrate them into complex surface or 3D structure, and an additional actuator was required to be fabricated and attached for actuation. To address this limitation, we fabricated a capacitor-integrated magnetic actuator having monolithic structure by combining flexible capacitor as a power source and soft magnetic actuator as driving parts. We used neodymium-based magnetic particle to compose an active material of capacitor to assign magnetically responsibility. Mask-based printing technique makes it possible to fabricate several capacitors having seamless pattern on a single substrate at once. The pattern of the capacitors is created from linear shape to origami pattern for 3D structure, and it is designed for series connection, parallel connection, or hybrid connection between each capacitor. Furthermore, not only by pre-patterning of capacitor, but also by magnetic actuation on the designed electronic circuit, we can control the state of connection of the capacitors to certain circuit as a switch, for example, on and off control and changing connection state from series to parallel.

Finally, we built a firefly-shaped robot to demonstrate a LED lighting control using magnetic actuation. We installed a LED for lighting in the tail of the 3D printed firefly-shaped body and, on the shoulder, origami patterned capacitor-integrated magnetic actuator which was designed as a pair of wings.

Wings were connected parallelly and each of them composed of serially connected 3 capacitors. According to on and off of the external magnetic field, origami patterned wings were folded and stretched. When the wing was folded by applied magnetic field, the tab from the electrode of the capacitor connected to the electric circuit, and then a LED is turned on. Conversely, the LED is turned off when the wing is stretched.

Here, we suggest a new approach to fabricate power supplyable actuator having monolithic structure. We demonstrated several capacitor-integrated magnetic actuators by leveraging power source with magnetic functionality. Our fabrication methods provide the way to design power source having different energy level related to series/parallel connection as well as shape-morphing properties.

4:00 PM *SB07.03.03

MOFBOTS—Metal—Organic Framework-Based Biomedical Magnetic Microrobots Josep Puigmartí-Luis; Universitat de Barcelona, Spain

In the field of small-scale robotics there is a growing interest on providing locomotion to soft materials, as these materials mimic more closely the physicochemical properties of biological tissues. Hydrogels, for example, can efficiently lead to biocompatible and biodegradable advanced small-scale robots that can find application in the biomedical field, e.g. in diagnostics and/or targeted drug delivery. However, even though hydrogels are an excellent

platform to accomplish a new generation of functional small-scale robots, other materials that could allow highly integrated robotic platforms are yet highly demanded. In this context, metal-organic frameworks (MOFs), a class of soft material with high porosity and tunable physicochemical properties, could be a key component for developing future highly integrated small-scale robotic platforms. While some initial efforts have been made to produce mobile MOF-based small-scale machines, the locomotion features of most of these systems are not at the level of sophistication of current state-of-the-art micro- and nanoswimmers.

In this presentation, I will present our recent contributions to the field where three-dimensional MOF-based soft micromachines have been designed, fabricated and characterized. I will show how these structures can swim and follow complex trajectories by means of weak rotating magnetic fields. The proposed systems can achieve, for example, single cell targeting in a cell culture media and/or a controlled delivery of cargo payloads inside a complex microfluidic channel network. We believe that this new approach towards the fabrication of highly integrated multifunctional systems will undoubtedly open new avenues in soft robotics beyond current applications.

4:30 PM SB07.03.04

Magnetic Alignment for Plasmonic Control of Gold Nanorods Coated with Iron Oxide Nanoparticles Mehedi Hasan Rizvi¹, Ruosong Wang², Jonas Schubert², William D. Crumpler¹, Christian Rossner^{2,3}, Amy L. Oldenburg⁴, Andreas Fery^{2,5} and Joseph B. Tracy¹; ¹North Carolina State University, United States; ²Leibniz-Institut für Polymerforschung Dresden e.V, Germany; ³Dresden Center for Intelligent Materials (DCIM), Germany; ⁴University of North Carolina at Chapel Hill, United States; ⁵Technische Universität Dresden, Germany

Plasmonic nanoparticles that can be manipulated with magnetic fields are of interest for advanced optical applications, diagnostics, imaging, and therapy. Alignment of gold nanorods yields strong polarization-dependent extinction, and use of magnetic fields is appealing because they act through space and can be quickly switched. In this work, cationic polyethyleneimine-functionalized superparamagnetic Fe₃O₄ nanoparticles (NPs) are deposited on the surface of anionic gold nanorods coated with bovine serum albumin. The magnetic gold nanorods (MagGNRs) obtained through mixing maintain the distinct optical properties of plasmonic gold nanorods that are minimally perturbed by the magnetic overcoating. Magnetic alignment of MagGNRs arising from magnetic dipolar interactions on the anisotropic gold nanorod core is comprehensively characterized, including structural characterization and enhancement (suppression) of the longitudinal surface plasmon resonance and suppression (enhancement) of the transverse surface plasmon resonance for light polarized parallel (orthogonal) to the magnetic field. MagGNRs can also be driven in rotating magnetic fields to rotate at frequencies of at least 17 Hz. For suitably large gold nanorods (148 nm long) and Fe₃O₄ NPs (13.4 nm diameter), significant alignment is possible even in modest (<500 Oe) magnetic fields. An analytical model provides a unified understanding of the magnetic alignment of MagGNRs.

4:45 PM SB07.03.05

Magnetic Actuation of Magneto-Photonic Particles for Targeted Light Delivery Seung Yeol Lee and Ognjen Ilic; University of Minnesota Twin Cities, United States

The capability to deliver light of desired properties (wavelength, intensity, polarization, etc.) to any target spot in a medium has broad relevance for applications across biology and biomedicine to nano-chemistry and radiation therapy. Key challenges for such delivery are that (i) it exhibits high directionality and significant selectivity for desired light properties, that (ii) it be adaptively controlled with a non-invasive mechanism, and that (iii) it does not require direct line-of-sight access to the target spot. However, existing platforms for light delivery, such as nanoscale scatterers or photonic surfaces with subwavelength patterns, have their limitations on actively orienting the direction of light scattering.

Here, we discuss a concept of a magneto-photonic particle with an optically active surface for targeted light delivery where the particle can be remotely actuated with a magnetic field. The photonic surface that provides sophisticated control of direction of scattering properties is patterned onto the particle using nanoimprint lithography, which enables the production of complex features at nanoscale resolution, while being highly scalable. Once the orientation of the pattern of a photonic surface and direction of magnetization are synchronized, the position of the target spot of light delivery can be controlled with an external magnetic field. We believe our approach can be used to realize a platform that enables targeted delivery of light within relevant biological windows, with possible applications in opto-genetics, neural stimulation, and localized heating.

SESSION SB07.04: Poster Session

Session Chairs: Lamar Mair, Salvador Pane i Vidal and Joseph Tracy

Tuesday Afternoon, November 29, 2022

8:00 PM - 10:00 PM

Hynes, Level 1, Hall A

SB07.04.01

Impact of 3D Printing Extrusion on Magnetically Annealed High Performance Hard/Soft Magnetic Elastomers Jimmy Lu, Nathan A. Fischer, Sarah Ziemann, James M. Ennis, Thomas Höft and Brittany Nelson-Cheeseman; University of St. Thomas, United States

Magnetic elastomers are flexible materials that can mechanically deform under the application of a magnetic field. This magnetoactive motion is highly desirable for developing biocompatible soft robots. The magnetic particulate within the polymer matrix gives magnetic elastomers unique magnetoactive properties depending on whether it is magnetically hard or soft. Hard magnetic elastomers can perform more complex movements, but soft magnetic elastomers have a greater magnetoactive response to the field. The unique properties of both hard and soft magnets can be transferred into magnetic elastomers by combining hard and soft magnetic particulate into one elastomer. 3D printing, such as Fused Deposition Modeling (FDM), can also enhance the magnetoactive properties of magnetic elastomers by creating anisotropy within the part. It allows users to create complex-shaped components easily and makes magnetic elastomers more accessible. Since 3D printing allows for accurate and rapid prototyping of flexible designs, the printability of magnetic elastomers allows for exciting applications in soft robotics. Typically, 3D printing filaments are the stock material for FDM. Recent work has shown that magnetic annealing of magnetic elastomer filaments during extrusion creates greater magnetoaction in the filaments; however, it is unclear whether this enhanced performance is maintained once they are subsequently extruded through the FDM printing nozzle. This research investigates whether the enhanced performance of magnetically annealed magnetic elastomer filaments remains after they are extruded through a 3D printer nozzle. The following three types of composite samples were made from a thermoplastic polyurethane matrix and varying amounts of soft and hard magnetic particulate (carbonyl iron (Fe) and strontium ferrite (SrF)): 5vol%Fe + 10vol%SrF, 10vol%Fe + 5vol%SrF, and 0vol%Fe + 15vol%SrF. The composites were extruded into 1.75 mm diameter filaments. Magnetically annealed filaments traveled through a uniform axial magnetic field. Final samples were then extruded through a 0.8 mm FDM printer nozzle into 220 mm long extrudate samples. The magnetoactive properties were measured by a custom setup, whereby short extrudate samples were hung freely and vertically between two electromagnets. Images of samples' behaviors were captured at incremental

transverse magnetic field strengths from 0-0.4T. Then, an image processing program was developed to overlay images so that the angle of deflection at a given applied field could be analyzed. The mechanical properties were obtained by tensile testing. The magnetic properties were captured via hysteresis loops. The enhanced magnetoactive performance seen from magnetic annealing of the filaments was still present in the final extrudate samples, indicating that the magnetic annealing effects were preserved after printer nozzle extrusion. These higher performance magnetic annealing effects were (1) magnetoaction at lower applied fields for the Fe-containing samples and (2) non-zero magnetoaction in the highest SrF samples (control samples showed no magnetoaction). Quantitatively, the least magnetoactive deflection was seen in the highest SrF samples. The mechanical data showed that as the percentage of SrF increased, the mechanical stiffness of the composite variant increased simultaneously. Therefore, the high stiffness could be a contributing factor to the low magnetoaction of the high SrF samples. Magnetically, the samples with more SrF content had lower saturation magnetization (M_s) and higher coercive field (H_c), which would also contribute to the limited magnetoactive response. Since the enhanced magnetoactive properties of the filaments from magnetic annealing hold after the FDM extrusion process, this unconventional approach to magnetic annealing of magnetic elastomers shows promising potential 3D print the accurate and complex components that high-performance soft robotic applications require.

SB07.04.02

Reproducible and Long-Ranged Magnetic Organization of Micropillar Arrays [Jeong Eun Park](#)¹, Sei Jin Park², Augustine Urbas³, Zahun Ku³ and Jeong Jae Wie¹; ¹Inha University, Korea (the Republic of); ²Lawrence Livermore National Laboratory, United States; ³Air Force Research Laboratory, United States

The magnetically responsive organization has been explored mostly in the form of spherical magnetic particles coated with a polymer. This process is beneficial for remotely triggering chain-like organization of magnetic composites by highly penetrable magnetic fields. However, magnetic interactions often prevent the uniform and reversible organization of multiple magnetic objects. Instead, for reproducible magnetic organization, periodically arranged micropillar arrays are adopted as a geometric form of magnetic polymer composites. While the pillar base consists of magnetically inert and soft neat polydimethylsiloxane (PDMS), the pillar top is made of PDMS and highly concentrated magnetic particles. Here, the pillar base acts as the soft hinge for the reversible organization of micropillars, and the pillar top serves as a highly magnetized micro-magnet under an external magnetic field. As the magnetic field increases, adjacent two dipolar micropillars are paired by quadrupolar attractive forces. By further increasing the magnetic field, two paired micropillars are quad-assembled, and finally connectively assembled. In this presentation, we would discuss the critical magnetic field threshold for the stepwise organizations as well as parameters affecting the magnetic organization including the cross-sectional geometry of micropillars and angles of the magnetic field with respect to the micropillars.

SB07.04.03

Magneto-Responsive Shape Fixable Vitrimer Micropillar Arrays [Jae Gyeong Lee](#), Hojun Moon, Woongbi Cho, Jisoo Jeon, Jeong Eun Park and Jeong Jae Wie; Inha University, Korea (the Republic of)

Magneto-responsive materials have been emerged owing to the contactless actuation with untethered system at the room temperature. However, temporary magneto-induced structure disappears after removing external magnetic fields and recovers its original configuration. In this study, we manufactured micropillar arrays with vitrimer matrix embedding magnetic particles to retain magneto-induced temporary shape. We introduced epoxy vitrimer to facilitate dynamic covalent bond via transesterification. We also discuss trade-off relationships between mechanical stiffness and magnetization depending on the concentration of magnetic particles through the investigation of structure-property relationship. The maximum magneto-mechanical bending is obtained with an optimum magnetic particle concentration. Furthermore, we will discuss shape fixation of vitrimer micropillar arrays by magnetically driven thermomechanical stimuli.

SB07.04.04

Nanowire Motion Control by Magnetic Field [Roman Kolisnyk](#), Allison Harpel, Pang-Hsiao Liu, Yicong Chen and Bethanie J. Stadler; University of Minnesota, United States

The development of next generation nanomachines—such as drug delivery vehicles, on-board nano-agitation devices, self-assembled structures and nanocomposites—requires efficient manipulation of nanoparticle motion. Magnetic field manipulation provides a contactless, sensitive, easy and cost-effective solution to the problem. Moreover, this method could be a good indicator of viscoelastic properties of fluids. Here, magnetic nanowires (MNWs) of various lengths and radii were fabricated via electrochemical deposition into nanoporous templates, using a Cu film sputtered on one side of the template as a working electrode. To create suspensions, the nanowires were removed from the template by first etching away the Cu film and then dissolving the template in NaOH. The nanowires were then collected with a permanent magnet placed against the wall of the flask containing them, rinsed several times with water, and then redispersed using ultrasonic agitation and placed into the liquid to be studied. The small dimensions of nanoscale entities result in an extremely low Reynolds number, which means the fluid is viscous and the drag force dominates the inertia force. A rotating external magnetic field can apply a magnetic torque to balance the drag torque and rotate the MNWs in sync with the field. Magnetic torque arises when the magnetic field is not parallel to the nanowires. As the viscosity of the fluid increases, the time required to align the nanowire in the direction of the field increases. In addition, nanowire size has a large effect on their rotation speed - a longer MNW will experience slower acceleration and larger drag, while a MNW with larger diameter rotates faster because the drag force is a weak function of r but the magnetic driving force and rotational inertia are proportional to r^2 . If the density of MNWs is high, a local field effect may occur where the field experienced by each particle is the sum of the applied external field and the local field induced by neighboring particles. The consequence of the local field is that the dipoles may not align in the direction of the applied field. At low-frequency rotations of the magnetic field, the nanowires rotate synchronously with the applied field. The nanowires phase lag increases with rising of the rotating field frequency and when the critical frequency is reached that is proportional to the square of the field strength asynchronous regime of the nanowires motion arises. In addition, when the frictional torque exceeds the magnetic torque, the MNW no longer synchronizes with the rotating external field. In the asynchronous regime, the phase lag angle of a rotating MNW increases periodically with time as the MNW rotates more slowly than the external magnetic field. When increasing the viscosity of fluid the frequency of synchronous and asynchronous regimes decreases. When the driving field frequency is very high the nanowire will keep oscillating around its position. By exploring MNW diameters from 20-200nm and lengths from 1-5 μ m and rotation frequencies from 60-200rpm in liquids from aqueous to viscous (including cryopreservation agents for the new field of nanowarming organs and tissues), a phase diagram of MNW control has been created.

SB07.04.05

Understanding Magnetocapillary Particle Dynamics Through Bayesian Parameter Estimation, Model Selection and Experiment Design [Dimitri Livitz](#), Kiran Dhatt-Gauthier and Kyle J. Bishop; Columbia University, United States

The field-induced motion of magnetic microparticles at curved liquid interfaces can be used to drive mixing and transport of emulsion droplets. Accurate models of these magnetocapillary motions are useful in designing time-varying fields to achieve targeted functions (e.g., droplet propulsion). Existing models reproduce many of the qualitative behaviors observed in experiments but fail to accurately predict particle trajectories along the interface of a

spherical droplet. Here, we apply methods of Bayesian data analysis to investigate and compare a series of improved models incorporating additional physics that aim to improve model accuracy and enable predictive design. We develop strategies for batching data from multiple experiments that helps to accelerate parameter estimation and model selection. We show how experimental design can be used to accelerate these processes further to enable accurate predictions using data from few carefully selected experiments. The improved model identified by this procedure highlights the significance of gravitational forces and particle orientation in predicting magnetocapillary dynamics. More generally, the analysis methods developed herein should prove useful in other contexts involving large datasets and ODE-based models.

SB07.04.06

Vortex-Induced Cargo Transportation by Programmable Collective Behavior of Polymer Nanocomposite Robots [Sukyoung Won](#)¹, Hee Eun Lee¹, Young Shik Cho², Kijun Yang¹, Jeong Eun Park¹, Seung Jae Yang¹ and Jeong Jae Wie¹; ¹Inha University, Korea (the Republic of); ²Seoul National University, Korea (the Republic of)

Cooperation of multiple robots is essential to enhance actuation efficiency for time-consuming missions and complete complicated tasks that are unable from a single robot. Herein, we present agile (~180 body lengths per second) and collective above-water swimming of multiple polymer nanocomposite robots, which can transport thousands of microplastics via the water vortex control. To achieve agile above-water swimmability and resultant vortex generation, a musculoskeletal system-mimetic design is adopted to prepare stiff yet lightweight hierarchical nanocomposite robots. By simply varying magnetic frequencies of a pulsed electromagnetic field, swimming modes of the nanocomposite robots are selectively programmed on-demand between rectilinear translational swimming and rotational swimming, allowing the robots to block, deliver, confine, or release thousands of floating microbeads in a divided space rapidly and simultaneously. Moreover, through the collective behavior, the multiple nanocomposite robots generate vortex and demonstrate a collection of > 4,000 floating microplastics in an open space. We further discuss the vortex-induced transportation capability of semi-submerged and underwater millimeter-scale cargos with rolling resistance or sliding resistance.

SB07.04.07

Magnetically Controlled Micro-Deformation of 3D Cell Culture Environments for Long-Term Mechanobiological Studies *In Situ* [Daphne Asgeirsson](#)¹, Avni Mehta¹, Nicolas Hesse¹, Michael G. Christiansen¹, Anna Scheeder², Andrea De Micheli³ and Simone Schuerle¹; ¹ETH Zürich, Switzerland; ²University of Cambridge, United Kingdom; ³University Children's Hospital of Zürich, Switzerland

In living tissues, mechanical forces are key regulators of cell fate and behavior. In addition to chemical signals, physical parameters such as material stiffness or shear stress provide cues that are pivotal during developmental processes and the maintenance of physiological function.¹ At the same time, alterations in tissue mechanical properties have been shown to both indicate and drive the progression of pathological states such as tumor growth and malignant transformation.^{2,3} These physical forces are increasingly considered and integrated in the design of biomimetic *in vitro* systems for basic research, drug development and personalized medicine. Approaches targeting stiffness of cell environments, perfusion of *in vitro* systems or (cyclic) stretch and compression of tissue constructs have been implemented to measure and control forces within a model of interest.⁴

To study the mechanics of 3D tissue models *in vitro* from the perspective of individual tissue-residing cells, we used rod-shaped magnetic microparticles (μ Rods) to probe and manipulate sample volumes on the microscale. The combination of an eight-coil electromagnetic field generator and high-resolution optical microscopy enabled us to study the heterogenous mechanical landscape within Collagen I (Col I) hydrogel networks in 3D. Further, analysis of fluorescently labelled Col I network deformation during magnetically controlled deflection of embedded μ Rods indicated that displacement of the Col I fibers propagated across a distance that exceeded multiple times the length of a single μ Rod.⁵

Using a motor-driven Halbach-cylinder to create a uniform rotating magnetic field, we performed long-term magnetic actuation of μ Rod-enriched 3D tissue samples within a cell culture incubator. With this tool, we sought to examine how cyclic microscale deformation of 3D ECM models influences the invasive behavior of metastatic cancer models as a function of the applied actuation pattern. High-resolution fluorescence imaging of cell-free ECM samples monitored the collagen integrity during actuation. Supplemented with cells, our studies provided insight about the progress of cell invasion to the surrounding matrix over several days of culture. The presented method aims to complement current approaches to analyze patterns of mechano-sensitivity within biomimetic *in vitro* models that could, for instance, accelerate the development of drugs targeting mechanical signaling pathways.

References

1. Engler, A. J., Sen, S., Sweeney, H. L. & Discher, D. E. Matrix elasticity directs stem cell lineage specification. *Cell* 126, 677–689 (2006).
2. Plodinec, M. et al. The nanomechanical signature of breast cancer. *Nat. Nanotechnol.* 7, 757–765 (2012).
3. Riehl, B. D., et al. The Role of Microenvironmental Cues and Mechanical Loading Milieus in Breast Cancer Cell Progression and Metastasis. *Front. Bioeng. Biotechnol.* 8, 2296–4185 (2021).
4. Ondeck, M. G. et al. Dynamically stiffened matrix promotes malignant transformation of mammary epithelial cells via collective mechanical signaling. *Proc. Natl. Acad. Sci. U. S. A.* 116, 3502–3507 (2019).
5. Asgeirsson, D. O. et al. 3D magnetically controlled spatiotemporal probing and actuation of collagen networks from a single cell perspective. *Lab Chip* 21, 3850–3862 (2021).

SB07.04.08

Local Stiffness Tailoring of Magneto-Active Composites Produced by Laser Powder Bed Fusion [Kilian Schäfer](#)¹, Matthias Lutzi¹, Dariusz Laniewski¹, Sebastian Bruns² and Oliver Gutfleisch¹; ¹Functional Materials, Germany; ²Physical Metallurgy, Germany

Mechanically soft sensors and actuators are beneficial when compliant and safe interaction with the human body is needed [1]. Magnetic actuation mechanisms allow fast response, wireless operation and the possibility to operate in enclosed confined spaces. With additive manufacturing, the production of magneto-active composites in complex and bioinspired shapes is possible. However, to completely transfer the functional properties of biologic systems to technology, the fabrication of composites with locally different mechanical properties is needed, since natural materials often have gradients in their mechanical properties [2]. In addition, in a soft robotics system like a locomotion assistance system the mechanical soft functional materials are often connected to rigid components, which results in the stiffness mismatch at the interface, which can lead to mechanical failure [3].

In this work, we present a method to locally tailor the stiffness of a magneto-active compound, consisting of hard magnetic Nd₂Fe₁₄B particles in a thermoplastic polyurethane (TPU) matrix with laser powder bed fusion. In this process, a laser beam selectively fuses powder layer by layer. By utilizing different laser parameters at different locations during the process, the mechanical properties of the composite are modified locally. For the process, the digital file of the parts must be divided into regions which should have different properties in the end. Hereby, the minimum layer height of these regions must be an integer multiplier of the layer height if the laser parameters are changed in the z-direction. If a gradient in x-y direction is needed, these regions should be the same size as the hatch distance.

The range in which the mechanical properties can be tailored is investigated with compression and tensile tests of the composite produced with different laser parameters. The stiffness can be increased tenfold when the laser power is increased from low to high values. The stiffness gradient within one sample is verified by line scans of Vickers indentations with a nanoindentation system.

After magnetisation of the composites, the actuation performance is tested within an electromagnet. We present a shape that contracts when a magnetic field is applied. The shape consists of two platforms with beams in between the platforms to provide flexibility. The two platforms can then connect to other parts of a soft robotics system. With the presented method, the platforms can be produced with high stiffness and gradually reduced stiffness towards the centre of the shape, where more flexibility is needed for the actuation. A larger deformation can be reached when a magnetic field is applied to the gradient composite in comparison to a non-gradient counterpart. We show that the production of shapes with locally tailored stiffnesses with a single process is possible with laser powder bed fusion, which can be applied in bioinspired magneto active composites and help to integrate the soft functional components into robotic systems.

[1] Kim, Y., Parada, G. A., Liu, S., & Zhao, X. (2019). Ferromagnetic soft continuum robots. *Science Robotics*, 4(33).

[2] Liu, Zengqian, et al. "Functional gradients and heterogeneities in biological materials: Design principles, functions, and bioinspired applications." *Progress in Materials Science* 88 (2017): 467-498.

[3] Rothmund, Philipp, et al. "Shaping the future of robotics through materials innovation." *Nature Materials* 20.12 (2021): 1582-1587.

This work was financially supported by the Deutsche Forschungsgemeinschaft (DFG, German Research Foundation), Project ID No. 405553726, TRR 270 and the RTG 2761 LokoAssist (Grant no. 450821862).

SESSION SB07.05: Magnetic Micro- and Nanorobots
Session Chairs: Hongsoo Choi and Simone Schuerle
Wednesday Morning, November 30, 2022
Hynes, Level 3, Room 308

8:15 AM *SB07.05.01

Ultraflexible, Reconfigurable and Self-Propelling Particle Structures Assembled and Driven by Magnetic Fields [Orlin D. Velev](#); North Carolina State University, United States

We will present strategies for the magnetic field driven assembly, manipulation, and propulsion of a rich variety of colloidal particle structures. We will first present responsive structures made of filaments from lipid-coated magnetic nanoparticles suspended in water. The nanocapillary liquid binding results in ultra-high filament flexibility and responsivity. Alternatively, the nanoparticle chains can be embedded inside silicone microbeads, resulting in a few types of soft macromagnets and microvoxels. These soft magnets can be incorporated into homocomposite thixotropic silicone pastes and can be directly shaped on a 3D printer to enable multiple classes of active magnetically reconfigurable structures. In the second part of the talk, we will discuss the principles of using magnetic assembly and actuation of dynamically reconfigurable active particle structures. We will show how assemblies of Janus polymer-metal microcubes can store energy through magnetic polarization of the metallic facets and release it on-demand by microscale reconfiguration. The reconfiguration pattern of folding and shape changes of the assemblies is encoded in the sequence of the cube orientation. Such structures can be directionally moved, steered, and maneuvered by external magnetic fields, acting as prototypes of microbots, micromixers and other active microstructures. These reconfigurable clusters can also be designed to be self-motile in media with non-Newtonian rheology. Such active assemblies can serve as microtools for interfacial studies in liquid crystal and biological systems.

8:45 AM SB07.05.02

Nature-Inspired Soft Robotics—On Magnetically-Actuated Artificial Cilia and Magnetic Micro-Swimmers [Patrick Onck](#); Univ of Groningen, Netherlands

Nature has developed astonishing concepts to manipulate fluids at small length scales and to enable micro-organisms to efficiently navigate through fluids at low Reynolds numbers. Motile biological cilia for instance can produce net fluid flows at low Reynolds numbers because of their asymmetric motion and emerging metachrony of collective beating. Mimicking this with magnetic artificial cilia can find application in microfluidic devices for fluid transport, mixing and directional particle transport. In addition to magnetic artificial cilia, also soft robotic magnetic micro-swimmers can be applied for future wireless medical robots for operation inside the human body. In this presentation I will discuss recent work we carried out [1-4] on the computational modelling of magnetically-actuated artificial cilia and soft-robotic magnetic micro-swimmers performed in close collaboration with experimental groups.

To generate fluid transport we studied the metachronal beating of magnetically-actuated artificial cilia whose individual non-reciprocal motion and collective metachronal beating patterns can be independently controlled [1,2]. We have developed a computational framework that is able to account for the magnetic actuation forces, the ciliary deformation, the coupled interaction with the surrounding fluid and the resulting fluid flow. We study arrays of magnetic cilia subject to a full range of metachronal driving patterns, including antiplectic, symplectic, lacoplectic and diaplectic waves. We analyse the induced primary flow, secondary flow and mixing rate as a function of the phase lag between the cilia and explore the underlying physical mechanism.

In addition, we developed a versatile particle transportation platform consisting of arrays of magnetic artificial cilia actuated by a rotating magnet [3]. By performing a tilted conical motion, the artificial cilia are capable of transporting particles on their tips, along designated directions that can be fully controlled by the externally applied magnetic field, at high resolution (particle precision), with varying speeds and for a range of particle sizes. The results show that the adhesion and friction between the particle and the cilia are essential ingredients of the mechanism underlying the multi-directional transportation. This work offers an advanced solution to controllable transport particles along designated paths in any direction over a surface, which has potential applications in diverse fields including lab-on-a-chip devices, in-vitro biomedical sciences, self-cleaning and antifouling.

In addition to magnetic artificial cilia, we also studied soft robotic magnetic micro-swimmers for future wireless medical robots operating inside channels, vessels, tubes and cavities of the human body, filled with flowing or stagnant biological fluids [4]. Driven by different external magnetic fields, the swimmer's motion can be changed between undulation crawling, undulation swimming, and helical crawling. By using computational modelling, we analyze the transport mechanisms of the soft robots and study the effect of different parameters to provide guidelines for the design of the robots in specific applications. Our design method provide unprecedented opportunities for studying ciliary biomechanics and creating cilia-inspired object manipulation, lab- and organ-on-a-chip devices, mobile microrobots wireless microfluidic pumping and bioengineering systems.

1. Dong, X. et al. *Science Advances*, 6(45), p.eabc9323 (2020).

2. Zhang, R. et al. *Soft Matter*, 18, 3902 (2022).

3. Zhang, S., et al. ACS Nano, 14(8), pp.10313-10323 (2020).

4. Ren, Z. et al., Science Advances, 7(27): eabh2022 (2021).

9:00 AM *SB07.05.03

Magnetic Nanorobotics—Fabrication, Materials and Forces Peer Fischer^{1,2}; ¹Max Planck Institute for Medical Research, Germany; ²Heidelberg University, Germany

Micro-/nano-robotics holds great potential for biomedical applications. Structures that are smaller than the macromolecular mesh size in gel-like media and tissues may be propelled relatively more easily compared to larger structures, even though the strength of the magnetic moment reduces with size. We have shown that magnetic nanopropellers can penetrate real biological tissues. If functionalized with enzymes they can soften mucine so that they can be propelled with weak magnetic fields. If coated with an anti-adhesion layer, they can propel over cm distances through the vitreous of the eye and steered to a small region at the optic disc of the retina. Our work indicates that transport into and inside tissues requires careful design, but is possible such that micro and nanopropellers can overcome biological barriers. This is an important first step to realize targeted delivery in dense tissues. An important aspect is the choice of magnetic material that is used to penetrate tissues and/or for the delivery of genetic material into cells. Magnetic nanopropellers and nanorobotic systems benefit from hard magnets. Fully biocompatible magnetic nanocarriers, that are not cytotoxic and that ideally also degradable over time, are promising tools for biomedical applications, but call for careful material choices. In this talk, we discuss the material selection, fabrication, and the resultant forces that are necessary for magnetic actuation and penetration of tissues.

9:30 AM BREAK

10:00 AM SB07.05.04

Elucidating Mechanotransduction in Magnetomechanical Neuromodulation Amanda Gomez, Rohini Guntur and Gabriela Romero; The University of Texas at San Antonio, United States

Neuromodulation techniques have shown great potential for the treatment of neurological disorders. Specifically, the use of novel magnetic nanotechnologies have allowed for non-invasive and targeted approaches that can stimulate deep structures. Magnetic nanodiscs (MNDs) are suitable for evoking neural activity because they are transducers of low-frequency and low-amplitude alternating magnetic fields (AMFs). When targeted to the cell membrane MNDs AMFs-triggered mechanoactuation enhances or inhibits cell membrane receptors for the modulation of biological signaling. However, there remains largely unknown information about the underlying cellular and molecular mechanisms of magnetomechanical neuromodulation. It is known that cortical neurons express different mechanosensitive ion channels such as TRPV1, TRPV2, TRPV4, Piezo1, TRPC1 and indirectly actuated G-protein coupled receptors. This project aims to investigate magnetomechanical neuromodulation using 685 nm MNDs targeted to the cell membrane of primary rat cortical neurons and unveil the key ion channels involved during mechanotransduction.

10:15 AM SB07.05.05

Micro-Scale Aerosol Jet Printing of Magnetic Materials for Soft Robotics Silvia Taccola¹, Samuel C. Moorcroft^{1,1}, James McDonald¹, Hadi Bakhshi², Wolfdiétrich Meyer² and Russell A. Harris¹; ¹University of Leeds, United Kingdom; ²Fraunhofer Institute for Applied Polymer Research, Germany

Small-scale magnetic soft structures that respond to an externally applied magnetic field have attracted wide research interest because of their unique capabilities and promising potential in a variety of fields, especially for applications in soft robotics. Current attempts for their micro-fabrication are largely based on adapted conventional template-driven fabrication processes, e.g. photolithography, template-based electro-deposition, and soft lithography, which require multiple processing steps and complex instrumentation, making them expensive and time-consuming, and do not effectively support mass customisation. Alternatively, digital fabrication technologies such as 3D printing facilitate the manufacturing of soft robots but are often limited by material selection and offer limited printing resolution. Within this framework, aerosol jet printing (AJP) is an emerging digitally driven, non-contact and mask-less printing process that has distinguished advantages over other technologies as it offers direct-write, high-resolution, versatile deposition of a wide range of materials onto a variety of substrates. Although AJP has primarily been used for surface patterning, researchers are beginning to explore its potential for producing 3D microstructures with complex architectures. Moreover, dual-material aerosol jet printing has been successfully demonstrated for the printing of composite structures with variable composition. Such capabilities illustrate the possible value of AJP in this field as an enabling manufacturing process which could introduce new possibilities of producing unique soft magnetic structures at the micro- and meso-scale by harnessing the unique capabilities of the process.

In this work, two different approaches are presented: 1) single material aerosol jet deposition of magnetic nanoparticles (MNPs) on soft/flexible substrates; 2) dual-material aerosol jet deposition of polymer/MNPs free-standing nanocomposite structures. Using the first approach, micro-patterns of MNPs in the region of 20 µm wide were successfully printed onto soft and flexible materials commonly used in soft robotics and biomedical engineering applications, such as polydimethylsiloxane (PDMS) films and poly-L-lactic acid (PLLA) nanofilms. The second approach allows the fabrication of magnetic nanocomposite with tailorable and controllable composition. An MNPs ink and a polymer ink are separately atomized in different atomizers and the resulting aerosols are mixed uniformly and *in situ* during the AJP process prior to deposition. The mix ratio of the two aerosols determines the MNPs loading in the nanocomposite, which can be used to locally control the magnetic properties of the printed structures, a significant feature that can't be achieved in traditional multi-materials printing using liquid/liquid or liquid/solid phases. The entire manufacturing process is digitally driven, thereby providing the capability to rapidly alternate and produce different designs, and to do so within time and cost boundaries that would be unachievable by template-based manufacturing approaches.

We believe that the use of this scalable, accurate, and versatile digitally-driven processing technology could enable a route for the development of novel magnetic microstructures.

SESSION SB07.06: Applications of Magnetic Micro- and Nanorobots I

Session Chairs: David Cappelleri and Salvador Pane i Vidal

Wednesday Morning, November 30, 2022

Hynes, Level 3, Room 308

11:00 AM *SB07.06.01

Engineering Magnetic Micro-and Nanorobots for Biomedicine Simone Schuerle; ETH Zürich, Switzerland

Engineering robots at the cellular scale could allow us to gain new insights into disease development and provide more targeted means for diagnostic and

therapeutic interventions. Magnetic fields have proven to serve as safe strategy to wirelessly power magnetic microrobots for remote control in physiological environments. In this talk I will give an overview of three distinct examples of magnetic micro- and nanorobots for biomedical applications and describe their respective design and control schemes.

First, I will present a method for 3D spatiotemporal probing of tissue models from a single cell perspective using microrobots. We fabricated rod-shaped magnetic microrods and leveraged 3D magnetic field generation, physical modeling, and image analysis to reveal local shear moduli and remotely apply mechanical stimuli [1]. The heterogenous mechanical landscape of a tumor's extracellular matrix (ECM) is in part a result of increased local release of enzymes, in particular certain proteases, which degrades the ECM and is associated with tumor invasion. In a next example, I will describe nanorobots that are either activated or detected via magnetic fields and designed to report a tumor's proteolytic activity as novel diagnostic [2].

Last, I will show how an individual, synthetic and swarms of living magnetic microrobots can help to locally enhance transport of nanoparticles (NPs) mimicking drug carriers in a tissue model [3]. We employed two distinct micropropeller designs powered by rotating magnetic fields to increase diffusion-limited transport of NPs by enhancing local fluid convection. In the first approach, we use a single synthetic magnetic microrobot called an artificial bacterial flagellum, and in the second approach, we control swarms of magnetotactic bacteria to create a directable "living ferrofluid" by exploiting ferrohydrodynamics. With both strategies, we demonstrated the ability to locally and wirelessly drive convective transport in tissue models. The latter strategy has also shown to outperform synthetic ferrofluids in terms of ferrohydrodynamic coupling to drive NP transport (Fig.1) [4]. Lastly, I will share insights into how these living magnetic microrobots can be further engineered to function as therapeutic vectors themselves that can be magnetically controlled [5].

References

- [1] Asgeirsson et al., *Lab Chip*, **21**, 3850-3862, 2021
- [2] Schuerle et al. *Nano Lett.*, **16**, 10, 6303-6310, 2016
- [3] Schuerle et al., *Sci. Adv.*, vol. **5**, no. 4, eaav4803, 2019
- [4] Mirkhani, et al., *Adv. Funct. Mater.*, 2003912, 2020
- [5] Gwisai et al, bioRxiv, doi.org/10.1101/2022.01.03.473989, 2022

11:30 AM SB07.06.02

Targeted Magnetic Vortex Disc Delivery Enables Magneto-Mechanical Control of Mouse Behavior Florian Koehler¹, Katherine Lei¹, Belinda Hetzler², Ye Ji Kim¹, Rebecca Gillette¹, Dirk Trauner² and Polina Anikeeva¹; ¹Massachusetts Institute of Technology, United States; ²New York University, United States

Low frequency magnetic fields pass through the body without attenuation, enabling the delivery of magnetic stimuli to deep tissue structures. We and others have previously demonstrated that magnetic nanodiscs (MNDs) composed of iron oxide can exert force on mechanoreceptors and control Ca²⁺ influx into sensory neurons in dorsal root ganglia and human embryonic kidney cells (HEK293) engineered to express the putative mechanoreceptor TRPV4¹. These prior studies have, however, relied on electrostatic targeting of the MNDs to cell membranes, and consequently magnetomechanical modulation lacked specificity to a particular cell type.

Here, we demonstrate the functionalization of MNDs with Benzylguanine (BG), a moiety that specifically binds to the genetically expressed SNAP tag to enable targeted delivery of MNDs to mechanosensitized cells. We employ a slowly varying alternating magnetic field to deliver the stimuli to the MNDs. Using Ca²⁺-imaging, we confirm the targeted stimulation of HEK293 cells and primary hippocampal neurons engineered to express mechanoreceptors. We further investigate the effects of the magnetomechanical stimulation on the cell membrane potential using the patch clamp electrophysiology.

Finally, we explore the possibility of magnetomechanical stimulation as a means to control neuronal activity and behavior in untethered freely-moving rodents. We anticipate that magnetomechanical stimulation will complement an existing array of tools aimed at connecting molecular and circuit function in the context of behavior.

1. Gregurec et al, ACS Nano 2020.

11:45 AM SB07.06.03

Magnetically Actuable 3D Liquid Multi-Electrode Arrays for Electrophysiological Monitoring of Brain Organoids Enji Kim^{1,2}, Young-Geun Park¹, Inhea Jeong¹, Junghoon Kim^{1,2}, Eunseon Jeong^{1,2}, Seung-Woo Cho^{1,2} and Jang-ung Park^{1,2}; ¹Yonsei University, Korea (the Republic of); ²Institute for Basic Science (IBS), Korea (the Republic of)

Brain organoids have emerged as a miniaturized substitute for the human brain to investigate the electrophysiological developments and mechanisms in three-dimensional (3D) neural network circuits. To fully apprehend the volumetric neural connectivity, monitoring of signals arising inside the organoid, intra-organoid signal, is imperative. However, existing devices require either the section of organoids or the insertion of rigid electrodes to grasp intra-organoid signals, which destruct the 3D cellular organization of the organoids and cause inflammatory responses. Also, a restricted number of electrodes in fixed positions is inadequate for the examination of complex neural activity throughout the organoid. These limitations have disturbed the chronic electrophysiological analysis in the 3D spatial scope of the organoids.

Herein, we present a magnetically actuable 3D liquid multi-electrode array (MEA) by high-resolution 3D printing of biocompatible metals for electrophysiological monitoring of brain organoids. Adaptable spatial distribution and soft mechanical properties of 3D liquidous microelectrodes enable long-term recording of intra-organoid signals from entire spatial points throughout the organoid. Furthermore, the flexibility of these 3D liquidous electrodes facilitates magnetic control in the tip position of the electrodes. Targeted recording from desired locations guided by magnetic actuation multiplies the density of recording sites inside the organoid with the identical number of electrodes. High-resolution 3D mapping of recorded signals through a multi-spot detectable electrode array is a promising method to clarify the origins of neurodevelopmental diseases by understanding the electrophysiological volumetric network of brain organoids.

1:30 PM *SB07.07.01

MANiACs to Micro-Force Sensing Microrobots—Magnetic Soft Microrobots for Biomedical Applications David Cappelleri; Purdue University, United States

Small soft robotic systems are being explored for myriad applications in medicine. Specifically, magnetically actuated microrobots capable of remote manipulation hold significant potential for *in vivo* applications such as targeted delivery of therapeutics and biologicals as well as for *in vitro* applications such as micromanipulation and biological material characterization. In this talk I will present families of wireless soft mobile microrobots driven by external magnetic fields that we have developed over the years for biomedical applications. These include the micro-scale tumbling microrobots (μ TUM), magnetically aligned nanorods in alginate capsules microrobots (MANiACs), and the micro-force sensing mobile microrobots (μ FSMM), and recent work in the area of adaptive soft microrobotics for advanced functionality.

2:00 PM SB07.07.02

Scalable Magnetic Torque Based Actuation Enhances Tumor Infiltration of Bacterial Drug Delivery Vehicles Tinotenda Gwisai¹, Nima Mirkhani¹, Michael G. Christiansen¹, Thuy Trinh Nguyen¹, Vincent Ling² and Simone Schuerle¹; ¹ETH Zurich, Switzerland; ²Takeda Pharmaceuticals, United States

Bacterial microrobots combining self-propulsion and preferential tumor accumulation have been recognized as promising drug delivery vehicles for targeted cancer therapy. Tumor-targeting bacteria are appealing because of their capacity to autonomously navigate through the body, transport a wide range of payloads, and modulate intratumoral inflammatory responses. Nevertheless, translation of this approach has been hindered by incomplete clinical responses, in part due to insufficient tumor colonization. Developing control strategies to enhance accumulation of bacteria within tumors is essential for facilitating robust colonization while concurrently lowering the required dose of bacteria, thus increasing therapeutic efficacy and safety.

Recently, innately magnetic strains of bacteria acting as steerable therapeutic agents have been manipulated with external magnetic fields. *In vivo*, strains of magnetotactic bacteria (MTB) carrying payloads have been shown to preferentially proliferate in deoxygenated regions of tumors following magnetic guidance. Magnetic control strategies for these living bacterial microrobots have thus far utilized directing magnetic fields, limited by propulsive forces of the bacterial flagella motor, or poorly scalable magnetic field gradients.

We established a hybrid control strategy that harnesses magnetic torque-driven motion followed by autonomous taxis-based locomotion to enhance the infiltration of *Magnetospirillum magneticum* AMB-1 as a carrier for covalently-coupled liposomes (MTB-LP). Unlike some forms of magnetic stimulus, uniform rotating magnetic fields (RMF) can be generated at clinically relevant scales for deep sites within the body. We demonstrated the suitability of RMF for simultaneous actuation and inductive detection, which could be exploited for closed-loop operation and real-time monitoring. We also assessed extravasation with computational models and *in vitro*, and found that the main mechanism driving the enhancement of translocation is increased surface exploration resulting from torque-driven translational motion at the cell interface. In a 3D tumor model, fluorescently labeled MTB-LP achieved stable colonization of the core regions of spheroids, with up to 21-fold higher signal in samples exposed to RMF. Finally, we demonstrated, for the first time to our knowledge, enhanced MTB tumor accumulation under RMF *in vivo*. Our findings illustrate that the MTB-LP platform combined with an RMF actuation scheme is a versatile biohybrid system that could improve targeting and colonization of therapeutic bacteria in tumors.

2:15 PM SB07.07.03

Scalable Scheme for Spatially Selective Actuation of Living Microrobots, Demonstrated by Colonization of Tumor Spheroids Nima Mirkhani, Tinotenda Gwisai, Michael G. Christiansen and Simone Schuerle; ETH Zürich, Switzerland

The ability to minimize off-target effects is a desirable feature for drug delivery platforms. This is often realized by either localizing the accumulation of active compounds to the target site or by selectively activating the portion that arrives in the targeted tissue. In the context of bacterial therapeutics, it is rational to ensure localized delivery since any off-target accumulation may result in complications associated with their toxicity. Simultaneously, due to their tumor tropism, local amplification at the tumor site can act as a form of selective activation. However, targeted accumulation of bacteria equipped with onboard sensing is contingent on the ability of their innate propulsive forces to overcome biological barriers. As a result, strategies for targeted introduction of external energy can potentially offer a much-needed element for enhanced selectivity of these living therapeutics. Magnetotactic bacteria (MTB) that biomineralize iron-rich nanocrystals provides this opportunity owing to their intrinsic responsiveness to magnetic fields.

We report on a spatially selective actuation scheme for the remote manipulation of MTB as a model system for magnetically responsive delivery vehicles. This actuation strategy is realized by superimposing a magnetostatic selection field onto a rotating magnetic field (RMF). The spatially controlled bacterial accumulation in tumor spheroids as a physiologically relevant model of cancer is studied. Human breast cancer cells, MCF-7, are used to form spheroids of roughly 400 μ m in diameter. Spheroids are then placed inside separate wells containing MTB suspension within a 1.5cm \times 1.5cm workspace. Since spheroid colonization relies on penetration of bacteria into these 3D cancer models, we first verify spatial selectivity of the actuation of MTB in response to the selection field by measuring their translational velocity inside the wells. Results under 12 mT RMF at 14 Hz superimposed by the gating field from small magnets demonstrate the suppression of torque-driven motion of MTB. The same experiment with the stronger magnetostatic field improves the level of off target suppression but also reduces the extent of actuation within the target well.

While the main resistance force and torque arise primarily from viscous drags for actuation in suspension, the spheroid presents an additional barrier for successful penetration. To account for the added resistance, prepared samples with spheroids are exposed to RMF of 20 mT and 14 Hz for 1 hour. Small NdFeB block magnets are responsible for the gating field in all the spatially selective actuations. Following magnetic actuation, the tumor spheroids are washed thoroughly in culture media and then incubated for 24 hours. Staining bacteria with a proliferative dye allows tracking of daughter cells within the course of the experiment.

Quantification of the stained bacteria demonstrates significantly higher accumulation (2.3 fold) when exposed to the RMF compared to control. Most importantly, MTB colonization of the target spheroids is shown to not experience any drop under application of the selection field, resulting in an approximately 3-fold increase compared to the control. However, at off-target sites, a significantly lower accumulation is observed in the presence of a superimposed gating field. The trade-off between the overall suppression and selectivity is caused by the field gradients present in the miniaturized system. While stronger static fields lead to complete suppression of the off-target transport, the associated field gradients cause forces that act against the transport to the target. However, scaled-up setups with larger targeting areas feature lower field gradients which makes this undesired effect less physiologically relevant. Owing to the scalability and selectivity of the proposed control strategy, the progress towards the clinical translation of magnetically based delivery strategies can be facilitated.

2:30 PM BREAK

3:30 PM *SB07.07.05

Selective Artificial Neural Network and Stimulation by Targeted Delivery of Neuronal Cells Using Magnetically Controlled Cell-Based Cellbots

Hongsoo Choi; Daegu-Gyeongbuk Institute of Science and Technology, Korea (the Republic of)

Several *in vitro* neural network models have been developed to mimic neural networks' reconstruction and interconnection to study brain function and related diseases. Traditional manufacturing methods, including two-photon polymerization, have been chosen to build sophisticated microrobots for neuronal cell delivery, but the manufacturing time to make a single microrobot has limited its practical use. Here we report various magnetically actuated cell-based microrobots (cellbots) for selective neurite alignment, neuronal connections, and/or selective stimulation. A biodegradable spherical gelatin methacrylate (GelMA) microrobot was fabricated in a flow-focusing droplet generator by shearing a mixture of GelMA, photoinitiator, and superparamagnetic iron oxide nanoparticles (SPIONs) with a mixture of oil and surfactant. Human turinate stem cells (hNTSCs) were loaded onto the GelMA microrobot, and the hNTSC-loaded microrobot exhibited a precise rolling motion in response to an external rotating magnetic field. The microrobot was enzymatically degraded by collagenase and released hNTSCs proliferated and differentiated into neuronal cells. A stamping magnetoelectric microrobot (SMM) composed of neuron-like cell spheroids loaded with magnetoelectric nanoparticles will be also presented. The SMM allows for effective targeted delivery of cells to multiple target areas (via minimally invasive stamping with magnetic actuation) to facilitate selective neuronal differentiation through magnetoelectric (ME) stimulation. The SMMs were made using SH-SY5Y cells, and magnetoelectric nanoparticles for ME stimulation reacted to an alternating magnetic field, ensuring targeted cell differentiation. The proposed cellbots show the potential for *in vitro* cell delivery and neural experiments to understand how neurons communicate in the neural network by actively connecting neural clusters.

4:00 PM SB07.07.06

Inductively Detectable Nanorobots for Detecting Protease Activity Michael G. Christiansen, Ines Oberhuber, Matej Vizovišek, Lucien Stöcklin, Manuel Strahm and Simone Schuerle; ETH Zürich, Switzerland

Proteases, a class of enzymes that cleave peptide bonds, are centrally involved in healthy processes throughout the human body. Many chronic ailments, including cancer, arthritis, and nonhealing wounds exhibit altered patterns of extracellular protease activity, making proteases a powerful diagnostic target for stratifying patients, monitoring treatment, or informing therapeutic decision making. For measurement of proteolytic activity to become commonplace in the clinic, new technologies are needed to lower the barrier to detection at the point-of-care.

Here, we explore a concept for the inductive detection of protease activity based on magnetic nanorobots. These nanorobots consist of a self-assembled monolayer of iron oxide magnetic nanoparticles (25 nm) on a larger silica core (600 nm), covalently bound via selectively cleavable peptide linkers. Cleavage of these linkers then triggers the magnetic nanoparticles to dissociate from the core particle, altering their magnetization response to applied magnetic fields. To detect their disassembly, a prototype pulsed field magnetometer has been designed, which makes use of capacitive discharge to produce a driving field with a variable timescale of 100s of μ s and adjustable magnitude of 10s of mT. Compared to inductive detection based on alternating magnetic fields, the pulsed field approach offers the possibility for a smaller form factor and full integration into mass producible printed circuit boards, considerations that suggest greater suitability for point-of-care detection devices.

4:15 PM SB07.07.07

Magnetic Soft Robotic Platform Enables the Decoupling and Reprogramming Complex Gaits Generated by Invertebrates Neng Xia¹, Bowen Jin², Dongdong Jin¹, Zhengxin Yang¹, Chengfeng Pan¹, Qianqian Wang¹, Fengtong Ji¹, Veronica Iacovacci^{1,3}, Carmel Majidi⁴, Yang Ding² and Li Zhang^{1,1,1}; ¹The Chinese University of Hong Kong, China; ²Beijing Computational Science Research Center, China; ³Scuola Superiore Sant'Anna, Italy; ⁴Carnegie Mellon University, United States

The complex and highly multimodal locomotion behavior of natural organisms allows them to dynamically adapt to complex environments and achieve energy-efficient or fast propulsion. These biological behaviors at different scales generally involve the coupling of basic motion primitives. Emulating and investigating their coupling locomotion are of great significance for understanding their fundamental mechanisms and developing high-performance robots. Despite advances in developing new simulation models and bio-mimetic testbeds, it generally remains challenging to analyse the complex coupling effect of locomotion gaits adopted by invertebrates. Herein, we develop a magnetic-responsive robotic platform to understand and analyse the coupling effect of swimming gaits adopted by midge larva. Studies are performed with a magnetic soft robot – named LarvaBot – that is operated using magnetic field inputs to decouple and reconstruct the complex wiggling motion of midge larvae. Diverse new coupled gaits can be generated and tuned with a phase shift by the LarvaBot, including the key swimming gaits adopted by natural larvae, which consist of side-to-side flexures and body rotation. Our studies reveal that the optimal rotation amplitude and the synchronization of curling and rotation can significantly enhance the propulsion performance. The magnetic LarvaBot exhibits multimodal locomotion and upstream capability at the moderate Reynolds number (Re) regime. The robotic platform offers new insight into the design and operation of new soft-bodied swimmers with coupled swimming gaits that may outperform their natural counterparts.

The research work was financially supported by the Hong Kong Research Grants Council with Project No. JLFS/E-402/18 and E-CUHK401/20, the ITF project with Project No. MRP/036/18X funded by the HKSAR Innovation and Technology Commission (ITC), the Croucher Foundation Grant with Ref. No. CAS20403, the CUHK internal grants, and National Science Foundation of China (NSFC-NSAF Grant No. U1930402). The authors thank the support from Multi-scale Medical Robotics Centre (MRC), InnoHK, at the Hong Kong Science Park, and the SIAT-CUHK Joint Laboratory of Robotics and Intelligent Systems. V.I. acknowledges funding from the European Union's Horizon 2020 research and innovation programme under the Marie Skłodowska-Curie Grant Agreement No. 894425.

SESSION SB07.08: Virtual Session I: Magnetic Materials for Soft Robotics and Nanorobotics

Session Chairs: Jiyun Kim and Joseph Tracy

Tuesday Morning, December 6, 2022

SB07-virtual

9:15 AM SB07.08.02

Magnetically Enhanced Marangoni Convection for Efficient Mass and Heat Transfer Like a Self-Driving Liquid Conveyor Belt Feng Lin¹, Hang Zhang², Tian Tong³, Runjia Li³, Jiming Bao³ and Zhiming Wang²; ¹Yunnan University, China; ²University of Electronic Science and Technology of China, China; ³University of Houston, United States

Temperature gradient-induced Marangoni convection has attracted much attention for basic research and applications since it provides an effective means for mass and heat transfer through a liquid surface flow. Here we first propose a general principle to enhance such surface flow by hindering its transition to recirculation flow using an external field. We subsequently identify ferrofluid and use it to validate the principle since its reduced magnetic susceptibility at higher temperatures will make the heated surface liquid stay on the surface by a thermomagnetic body force. Using a laser beam to create a heated local

surface and a magnet beneath the ferrofluid to provide a vertical field, a high speed and long-range Marangoni flow is confirmed experimentally and further supported by computational fluid dynamics simulations. To demonstrate possible applications, we show a self-driving pipeless liquid conveyor belt that can efficiently transfer heat from a source to sink without external power. The demonstration of enhanced Marangoni convection opens new avenue to explore interfacial fluid dynamics and its wide applications.

9:30 AM *SB07.08.03

Self-Assembled Nanoscale Ciliary Actuators Hoon E. Jeong, Minsu Kang, Minho Seong and Donghyuk Lee; Ulsan National Institute of Science and Technology (UNIST), Korea (the Republic of)

Self-assembly of nanoparticles (NPs) is a powerful route to constructing higher-order structures. However, the programmed self-assembly of NPs into non-close-packed, 3D, shape-morphing nanocilia arrays remains elusive, whereas dynamically actuated nanometer cilia are universal in living systems. Here, a programmable self-assembly strategy is presented that can direct magnetic NPs into a highly ordered responsive artificial nanocilia actuator with exquisite nanometer 3D structural arrangements. The self-assembled artificial NP cilia can maintain their structural integrity through the interplay of interparticle interactions. Interestingly, the nanocilia can exhibit a field-responsive actuation motion through “rolling and sliding” between assembled NPs rather than bending the entire ciliary beam. It is demonstrated that oleic acid coated over the NPs acts as a lubricating bearing and enables the rolling/sliding-based actuation of the cilia.

Acknowledgements:

This work was supported by the National Research Foundation (NRF) of Korea grant (2021R1A2C3006297 and 2019M3C1B7025092).

10:00 AM DISCUSSION TIME

SESSION SB07.09: Virtual Session II: Magnetic Materials for Soft Robotics and Nanorobotics

Session Chairs: Lamar Mair and Salvador Pane i Vidal

Tuesday Morning, December 6, 2022

SB07-virtual

10:30 AM *SB07.09.01

Magnetic Origami for Soft Robotics and Microrobotics Oliver G. Schmidt; Research Center MAIN, Germany

On-chip micro-origami is used to generate highly integrated 3D magnetic microsensor arrays driven by active matrix electronics for soft magnetic e-skin applications [1]. The 3D magnetic sensors respond to the displacement of magnetically rooted hair creating directional perception in the vicinity of the artificial skin surface. Similar technology is used to manufacture highly integrated microelectronic catheters with drug delivery and magnetic sensing capabilities [2] as well as autonomously and remotely controlled microelectronic microbots [3].

[1] C. Becker, B. Bao, D. D. Karnaushenko, V. K. Kumar, B. Rivkin, Z. Li, M. Faghih, D. Karnaushenko, O. G. Schmidt, Nature Comm. 13, 2121 (2022)

[2] B. Rivkin, C. Becker, B. Singh, A. Aziz, F. Akbar, A. Egunov, D. D. Karnaushenko, R. Naumann, R. Schäfer, M. Medina-Sanchez, D. Karnaushenko, O. G. Schmidt, Sci. Adv. 7, acb15408 (2021)

[3] V. K. Kumar, Y. Nan, D. Karnaushenko, Y. Hong, B. Sun, F. Striggow, D. D. Karnaushenko, C. Becker, M. Faghih, M. Medina-Sanchez, F. Zhu, O. G. Schmidt, Nature Electron. 3, 172 (2020)

11:00 AM *SB07.09.02

Flexible Magnetic Sensorics Jürgen Kosel; Silicon Austria Labs, Austria

Current trends for digitalization and green tech require materials that can enable sensor systems with new features and functionalities, while considering the availability of resources and sustainability in general. In these regards, magnetic materials are particularly attractive, as they offer unique capabilities like remote interaction, and they can be environmentally benign. One such material are iron-based magnetic nanowires, which feature both a large remanent magnetization and biocompatibility. Their fabrication via electrochemical deposition is efficient and provides a high control over the structural and magnetic properties. By using them as fillers in polymer composite materials, a flexible magnetic sensor skin is created, which can be remotely interrogation, is biocompatible and conformable. It combines mechanical flexibility with magnetic functionality. Through the concentration of the filler particles, the magnetic and mechanical properties of the composite materials can be widely modulated and tailored for the specific needs of an application. Examples will be shown, in which the magnetic composites are employed for the localization of subcutaneous medical devices or as tactile skins, for flow measurements or braille reading. As ultra-flexible magnetic skins, they can be worn like tattoos or camouflaged with the color of the skin tone and enable gesture-controlled wireless operations. This is demonstrated by controlling a wheelchair with facial gestures. Modern fabrication processes combined with the advantages of magnetic sensor systems are a strong combination, which can lead to new sensor solutions. Examples are flexible magnetic tunnel junction sensors, which offer a high magnetic field sensitivity. They are employed for 3-axes orientation monitoring on biomedical instruments. On the other end of the spectrum are laser-induced graphene Hall effect sensors with less sensitivity but high temperature and corrosion resistance. Coated with a magnetic composite material, a robust tactile sensing platform is realized.

11:30 AM *SB07.09.03

Moving with Magnets—Taking a Look at Microswimmers with Random Shapes Damien Faivre; CEA Cadarache, France

Microswimmers are smart devices with potential applications in biotechnology and in particular medicine. Helicoidal magnetic micropropellers with their remote control via rotating magnetic fields have emerged as the standard devices with a linear velocity-frequency dependence propulsion mechanism. My group has gone an alternative path, synthesizing and studying magnetic micro- and nanoswimmers with random shapes.

Besides devices exhibiting the standard velocity-frequency dependence propulsion, we found more complex, non-linear velocity-frequency dependences, which offered new possibilities for the actuation control. We particularly emphasized a behavior we called frequency-induced reversal of swimming direction (FIRSD) where the propeller swims in two opposing directions for two different field frequencies of the external actuating magnetic field, while no other parameter is changed. We tested if recent 3D-printing techniques enabled the reproduction of these devices in large quantities. However, the identically shaped swimmers do not only displayed the FIRSD but also exhibited a variety of additional behaviors that arose from differences in their magnetic moment orientations. This underlined not only the role of shape in microswimmer behavior but also the importance of determining magnetic properties of future micropropellers that act as intelligent devices, as single-shape templates with different magnetic moments can be utilized for different

operation modes.

12:00 PM DISCUSSION TIME

SESSION SB07.10: Virtual Session III: Magnetic Materials for Soft Robotics and Nanorobotics
Session Chairs: Lamar Mair and Joseph Tracy
Tuesday Afternoon, December 6, 2022
SB07-virtual

1:00 PM *SB07.10.02

Plasmonic and Magnetic Hybrid Nanostructures for Smart Materials [Yadong Yin](#); University of California, Riverside, United States

Smart materials hold great promises for many intriguing applications in soft robotics as they exhibit chemical and physical responses to the applied external stimuli. This presentation will focus on the synthesis and assembly of plasmonic and magnetic hybrid nanostructures for enabling optical and mechanical responses for robotic applications. In particular, we will discuss a novel space-confined synthesis method for the production of magnetic/plasmonic hybrid nanostructures. The shape-dependent plasmonic and magnetic properties can be integrated into anisotropic hybrid nanostructures such as nanorods and nanodisks to not only control their nanoscale connectivity but also enable collective orientational alignment, allowing the design of smart materials with colorimetric and mechanical responses.

1:30 PM SB07.10.03

Soft Driving Coils for Conformal Electromagnetic Actuators [Cindy K. Harnett](#); University of Louisville, United States

New developments in magnetically driven soft actuators typically focus on the magnetic materials' orientation, microstructure and reconfigurability. Meanwhile the driving apparatus is usually a rigid circuit at some distance from the magnet. These setups enable researchers to control the magnetic field strength and direction in free space, controlling untethered magnetic materials. However, in soft robotic skins, soft active surfaces, and in wearable applications such as haptics for augmented reality, the driving circuit and magnetically actuated material are usually integrated into the same surface. In these systems, there are fewer requirements for magnetic actuation at a distance, and more requirements for the system to be conformal, thin, and lightweight. This presentation describes a textile-based method for designing thin electromagnetic driving coils with surface actuation in mind. It covers methods for modeling the magnetic forces specifically from thin wire coils, describes coil fabrication methods, and evaluates the produced coils' blocking forces, thermal performance, and bandwidth.

For haptic systems that generate pressure sensations, devices are usually designed to produce vertical forces by inflation or by solenoid-type actuation. While the thin driving coils discussed in this work can produce vertical forces, their lateral force production is stronger over longer distances because lateral operation keeps the magnetic material close to the coils where the field and its gradient are strongest. These lateral motions produce lesser-explored haptic brushing sensations in the 5-mN "pleasant touch" range.

Toward actuators that produce such lateral forces, a new rotary actuator is demonstrated on a 250-micron thick driving surface consisting of embroidered magnet wire in a nonwoven porous textile. Its thermal characteristics are measured in the 0- to 1 Ampere driving current range. A flexible and breathable 3D woven spacer fabric provides both thermal and mechanical isolation for the actuator coils and a moving magnet. Methods will be discussed for using stationary magnetic materials to provide restoring torque and latching forces for position holding. In addition, textile and thin sheet cutting methods can translate rotary magnetic motion into vertical motion of curved thin-film or thin-fabric beams by twisting the attachment points. This alternative to direct vertical magnetic motion is able to lift thin beams >5 centimeters above the surface for light-touch haptic actuators, soft robotic skins that can change their surface texture, and other applications requiring soft active surfaces. High-speed automated assembly methods will also be discussed for placing magnetic materials on top of coils using textile machinery.

2:15 PM DISCUSSION TIME

SYMPOSIUM SB08

Bioinspired and Biological Polymers—From Living Organisms to Sustainable Functional Materials in Photonics, Electronics and
Biology
November 28 - December 6, 2022

Symposium Organizers

Gianluca Maria Farinola, Università degli Studi di Bari Aldo Moro
Chiara Ghezzi, University of Massachusetts Lowell
Fiorenzo Omenetto, Tufts University
Silvia Vignolini, University of Cambridge

Symposium Support

Gold
Science Advances | AAAS

* Invited Paper
+ Distinguished Invited

SESSION SB08.01: Biopolymers
Session Chairs: Gianluca Maria Farinola and Fiorenzo Omenetto
Monday Morning, November 28, 2022
Hynes, Level 3, Room 313

10:30 AM *SB08.01.01

Molecular Design and Biosynthesis of Polypeptides Inspired by Spider Silk Spinning [Keiji Numata](#)^{1,2}; ¹RIKEN Inst, Japan; ²Kyoto University, Japan

Structural protein is one of the key factors to realize the unique properties and functions of natural tissues and organisms. However, use of structural proteins as structural materials in human life is still challenging. One of the major drawbacks of protein/polypeptide-based materials is their limited synthesis/process method. My research group has successfully synthesized various polypeptides, such as spider silk protein-like and elastin-like multiblock polypeptides, even with unnatural amino acids or nylon units, via chemoenzymatic polymerization. Those artificial polypeptides containing unnatural units achieve several properties that cannot be done by natural polypeptides. These synthetic polypeptides with nylon units are highly biodegradable and less environmentally toxic. Thus, this enzyme-mediated polymerization of amino acid monomers provides a new insight for material design of polypeptide. My research group also reported the new finding in spider silk spinning, which is essential to clear the hierarchical structure of spider silk. The scalable and sustainable synthesis method along the clarified structure-function relationship of natural proteins provides a new insight for structural and functional material design of amino acids-based polymers.

11:00 AM SB08.01.02

Reverse Engineering Spider Silk by Disassembly and Assembly Dinidu Perera, Linxuan Li and [Hannes C. Schniepp](#); College of William & Mary, United States

Spider silk combines outstanding strength and toughness with biocompatibility and light weight, thus outperforming some of the best synthetic materials. Despite extensive research, fully comprehensive experimental evidence of the formation and morphology of the internal structure of spider silk is still limited and controversially discussed. We used mechanical exfoliation to completely exfoliate spider silk, which showed that the silk of the golden orb-weaver is entirely composed of parallel, 10 nm-diameter nanofibrils featuring a particular morphology. This process allowed us to mass-produce spider silk nanofibrils for the first time. Furthermore, we show that the silk protein possesses an intrinsic mechanism to form nanofibrils of the same morphology via shear-induced molecular self-assembly, which can be easily triggered *in vitro*. By altering the physical and chemical environment of this process, we were able to study the conditions of formation of spider silk and to reveal both physical and chemical triggers for assembly at molecular scales. This knowledge will help understand the fundamentals of this exceptional material, paving the way for the realization of silk-inspired high-performance materials.

11:15 AM SB08.01.03

Protein Secondary Structure in Spider Silk Nanofibrils Qijue Wang and [Hannes C. Schniepp](#); College of William & Mary, United States

Nanofibrils play a pivotal role in spider silk and are responsible for many of the impressive properties of this outstanding natural material. However, little is known about the internal structure of these protein fibrils. We carried out polarized Raman and polarized Fourier-transform infrared spectroscopies on native spider silk nanofibrils for the first time and determined the concentrations of six distinct protein secondary structures, including β -sheets, and two types of helical structures, for which we also determined orientation distributions. Our advancements in peak assignments are in full agreement with the published silk vibrational spectroscopy literature. We further corroborated our findings with X-ray diffraction and magic-angle spinning nuclear magnetic resonance experiments. Based on the latter and on polypeptide Raman spectra, we assessed the role of key amino acids in different secondary structures. For the recluse spider we developed a structural model with unprecedented detail, featuring seven levels of structural hierarchy. The approaches we developed are directly applicable to other proteinaceous materials.

11:30 AM SB08.01.04

BioMIPs Biocompatible Biomimetics—Molecular Imprinting Ties the Knot with Natural Polymers. Synthesis, Properties and Future Perspectives of Silk Molecularly Imprinted Nanoparticles. [Alessandra Maria Bossi](#)¹ and Devid Maniglio²; ¹University of Verona, Italy; ²University of Trento, Italy

The process of molecular imprinting allows to produce biomimetics of nanometric dimensions (nanoMIPs) by means of a template assisted synthesis [1]. NanoMIPs are gaining momentum for their outstanding recognition properties *in vitro* and *in vivo*, proving effective in cell imaging, tumor-cell targeting, drug delivery [2-5]. The expectations for nanoMIPs in medicine stake high. Yet, nanoMIPs are currently prepared starting from synthetic monomers (e.g. acrylamides), while focal point for their translation into clinical applications should be biocompatibility.

In this framework, we imagined a possible breakthrough development, based on the original idea to synthesize fully biocompatible nanoMIPs starting from the natural polymer silk fibroin, that is characterized by non-toxicity and high biocompatibility. Given the natural origin, we named the silk imprinted nanoparticles bioMIPs.

We investigated and optimized the synthesis of the bioMIPs by a three parameters (quantity of silk fibroin, pH, photoinitiator) response surface method (RSM) that enabled to model the landscape of the possible synthetic conditions. In set conditions, uniform (polydispersity index < 0.25) nanometer sized populations of bioMIPs, with $Z_{average} \sim 50$ nm or $Z_{average} \sim 100$ nm, were obtained.

The possibility to imprint recognition cavities on the bioMIP and the ability of these bioMIPs to trap a defined target molecule was also studied. Target molecules of different sizes (i.e. a peptide and a protein) were chosen as templates, so to consider the effects of the template size on the imprinting process [6,7]. Both isothermal titration nanocalorimetry and fluorescence spectroscopy proved the molecular recognition abilities of the formed bioMIPs. The estimated dissociation constants of the bioMIPs for the targets were in the nanomolar range, moreover the bioMIPs had selectivity and specificity for the target and a quasi-single binding site per nanoparticle. Additionally, the bioMIPs proved to be nontoxic for cultured mouse embryonic fibroblasts even at significantly high concentrations (2 mg/mL). Finally, we produced functional biomaterials with tailored recognition by coupling the bioMIPs to silk micro- and nano-fibers. Such bioMIP-silk specialized functional fibers proved to selectively trap the targeted molecule [6].

Hence, the unprecedented combination of silk fibroin building blocks to molecular imprinting appears as a compelling strategy to entail cognitive-functions to bio-nanoparticles. BioMIPs open for a new class of biomimetics that conjugate natural polymers to the custom design of molecular recognition

abilities, with foreseen impact in precision medicine and instructive biomaterials.

References

1. Y. Hoshino, T. Kodama, Y. Okahata, K.J. Shea *J. Am. Chem. Soc.* 2008, 130, 15242.
2. S. Piletsky, F. Canfarotta, A. Poma, A.M. Bossi, S. Piletsky, *Trends Biotechnol.* 2020, 38, 368.
3. A.M. Bossi, *Nat. Chem.*, 2020, 12, 111.
4. K. Haupt, P.X. Medina Rangel, B.T.S. Bui, *Chem. Rev.* 2021, 120, 9554.
5. Y. Dong, W. Li, Z. Gu, R. Xing, Y. Ma, Q. Zhang, Z. Liu, *Angew. Chem. Int. Ed.* 2019, 58, 10621.
6. A.M. Bossi, A. Bucciarelli, D. Maniglio, *ACS Appl. Mater. Interfaces*, 2021, 13, 312431.
7. A.M. Bossi, D. Maniglio, *Microchem. Acta*, 2022, 189, 66.

11:45 AM SB08.01.05

Artificial Enzymes and Electrochemically Molecularly Imprinted Polymers Rigoberto C. Advincula^{1,2,3}; ¹Case Western Reserve University, United States; ²The University of Tennessee, Knoxville, United States; ³Oak Ridge National Laboratory, United States

Molecular complexes that are inspired from biological enzyme-substrate interactions can be mimicked with the lock-and-key templating process. The use of functional monomers that can be electrochemically polymerized enables the formation of cross-linked polymer films with cavities that enable high binding assays of analytes: chemical and biological. There are a number of methods to improve sensitivity and selectivity in sensors but usually, this requires more elaborate instrumentation methods. In this talk, we will show the effective and bio-inspired artificial enzymes for the detection of chemical and biological analytes. We will focus on the demonstration of electropolymerized molecularly imprinted polymer (E-MIP) sensor elements and their ability to utilize transduction methods such as surface plasmon resonance (SPR) spectroscopy or quartz crystal microbalance (QCM) to enable high sensitivity and selectivity. The monomer and molecular design for optimized analyte interaction enable effective templating protocols in a conducting polymer matrix with tunable oxidative states to enable a high volume of analyte-cavity sites. Optimized electropolymerization methods are important for film deposition and surface characterization.

SESSION SB08.02: Designing and Understanding Biomaterials

Session Chairs: Fiorenzo Omenetto and Massimo Trotta

Monday Afternoon, November 28, 2022

Hynes, Level 3, Room 313

1:30 PM *SB08.02.01

Biomaterial Innovation Through Deep Time—How Spiders Have Evolved Spectacular Silks and Inspire Biomimetics Jessica E. Garb; University of Massachusetts Lowell, United States

Spiders are unrivalled in the diversity of high-performance silk types they produce. Biomaterial studies of spider silk primarily focus on orb-weavers, renowned for their seven functionally distinct silk types, including the well-studied dragline due to its ease of collection and high tensile strength. However, orb-weavers are just one of many spider lineages that have further diversified silk into materials with unusual structures and properties, modified for wide-ranging mechanical demands. In this talk I provide an overview of the rich diversity of spider silks and highlight how recent advances in genomics are revealing the greater complexity of these materials, as well as recipes to mimic or re-imagine them. In addition to reviewing the silk types investigated to date and their underlying genetics, I will highlight unexplored species and silk types that could yield roadmaps to novel biomaterials and describe the challenges to closing our knowledge gaps.

2:00 PM SB08.02.02

Phase Front Assembly for Mesostructured Design of Biopolymer Microneedles Doyoon Kim, Yunteng Cao, Zheng Li, Federica Rigoldi, Hui Sun, Rajeev Ram and Benedetto Marelli; Massachusetts Institute of Technology, United States

Many biological processes, including biomineralization, are modulated via condensation phenomena at the interface between biopolymer matrices and inorganic ions. Despite their enormous inspiration for high-performing materials design, little is known about simultaneous behaviors of inorganic ion crystallization and biopolymers assembly. In this study, we present the control of co-occurring silk fibroin assembly and inorganic nucleation at their phase front to drive the formation of microneedles with designed nano-porous and hollow microstructures. This phase front assembly approach, for the first time, enabled the one-pot manufacturing of mesostructured microneedles with hollow and nanoporous tips: different internal microneedle structures develop in one type of mold via the interaction of silk fibroins and ionic salts. These mesostructured microneedles will serve as new connecting tools between biotic-abiotic worlds. For the agricultural application, we demonstrate the transport of biomolecules and detection of early-stage bioaccumulation of environmental contaminants (e.g., cadmium and arsenic) in tomato plants.

2:15 PM SB08.02.03

Efficient Deployment of Gibberellic Acid in Plants with Minimal Wounding Using Silk-Based Microneedles Yunteng Cao¹, Sally Koh^{2,3}, Yangyang Han⁴, Javier Tan², Doyoon Kim¹, Nam-Hai Chua^{4,2}, Daisuke Urano^{2,3,4} and Benedetto Marelli^{1,4}; ¹Massachusetts Institute of Technology, United States; ²Temasek Life Sciences Laboratory, Singapore; ³National University of Singapore, Singapore; ⁴Singapore-MIT Alliance for Research and Technology, Singapore

New systems capable of precise and efficient agrochemical delivery in plants will foster precise agricultural practices and provide new tools to study plants and design crop traits, as conventional delivery practices such as standard spray suffer from a significant loss, severe environmental side effects, and limited access to remote plant tissues. We previously demonstrated that silk-based microneedles could circumvent these limitations, capable of delivering a variety of payloads ranging from small molecules to large proteins into specific loci of various plant tissues. However, the plant responses to microneedle injection and microneedles' efficacy in deploying physiologically relevant biomolecules are unknown. Here, we show that gene expression associated with *Arabidopsis thaliana* wounding responses decreases within 24-hours post microneedles' application. Microneedles-mediated gibberellic acid (GA₃) injection in *A. thaliana* mutant *fi-10* is more effective and efficient than spray in activating GA₃ pathways and accelerating bolting. Microneedles' efficacy in delivering GA₃ is also observed in several crop species, i.e., tomato (*Solanum lycopersicum*), romaine lettuce (*Lactuca sativa*), and carmel spinach (*Spinacia oleracea*), underpinning the use of this new tool in plant science and agriculture.

2:30 PM SB08.02.04

An Engineered Standard Amino Acid for Unconventional Silk Fibroin with Unique Water-Responsivity Woojin Choi, Milae Lee, Kyungtae Park, Moonhyun Choi, Sungwon Jung and Jinkee Hong; Yonsei University, Korea (the Republic of)

In nature, water diffusion is the principal driving force of all organisms for performing the homeostatic motions, so-called hydration-adaptive actuation. For instance, animals reshape their feather through the hydration-adaptive buckling, and plant seeds exhibit a twisted opening response to osmotic stimulation. The structural biopolymer, such as silk fibroin, and keratin, spontaneously demonstrate the hydration-adaptive crystallization, *i.e.*, phase transition into β -sheet crystals. This crystallization enhances structural stability. Meanwhile, the crystallized biopolymers become inert and hardly interact with the surroundings. Hence, the inevitable biopolymeric crystallization exerts significant leverages in biomedical fields, for instance, pros in human-robot interfaces or cons in tissue adhesives. However, the underpinning chemical and physical aspects of hydration-adaptive crystallization have rarely been investigated up to date.

We have developed an unconventional silk fibroin by regulating hydration-adaptive crystallization, the mechanism of water responsivity in nature. Technically, the crystallization rate is modulated by activating a standard amino acid (Serine; Ser). Inspired by the natural activation of polar amino acid of an insect and shellfish *via* chelation of Ca^{2+} , the silk fibroins with different activities of Ser (7.90-10.8%) are prepared through divalent cation-mediated protein modification. In detail, Ser morphs into the exposed activated status according to the interaction between the divalent cation and the hydroxyl group of Ser.

A rheological model of case II diffusion through silk fibroin is demonstrated to deeply understand the hydration-adaptive crystallization. Case II diffusion is relevant to the hydration-adaptive crystallization as it regards the water-biopolymer interaction as a decisive parameter in entire diffusion kinetics.

According to the proposed model, activated Ser enables downregulating the rate of silk fibroin crystallization. Moreover, the crystallization of protein secondary structures is monitored *in situ* by Raman spectroscopy. Both model and empirical results exhibit the inverse relationship between Ser activity and the crystallization rate, proving the active Ser-dependent crystallization kinetics. Particularly, a 30% increased activity of Ser results in an approximately 55% decreased rate of hydration-adaptive crystallization from 0.206 to 0.0936.

The mechanism of amino acid-based regulation of hydration-adaptive crystallization is figured out based on the thermodynamic water stability. In the hydrated biopolymer, the less-stable water molecules bridge the frame amino acids and cause crystallization. The hydroxyl group of Ser is more favorable in water stabilization than the carboxyl group of Gly and Ala. Hence, the crystallization-triggering water molecules spontaneously construct the stable lattice network in the silk fibroin with highly-activated Ser. The measured results (*i.e.*, number of hydrogen bonding of water molecule and exothermic enthalpy) indicate that the water stability is enhanced by approximately 2.5 folds by a 20% increased activity of Ser. In summary, the active Ser stabilizes the water molecules and delays the hydration-adaptive crystallization.

Finally, the active Ser-dependent crystallization regulation realizes the unconventional silk fibroin, irrelevant to the crystallization-induced inevitable loss of adhesive force. The silk fibroin with less-activated Ser losses 82% of initial adhesive force after 120 s hydration, suggesting the limited biomedical potential. Meanwhile, the silk fibroin with highly-activated Ser maintains a strong adhesiveness of 160 kJ m^{-3} , enabling stable adhesion on *ex vivo* porcine mandible tissue. In conclusion, the amino acid-based regulation technology imparts the unique mechanochemical response to the silk fibroin itself.

2:45 PM BREAK

3:15 PM *SB08.02.05

Building Biomaterials with Bioinspired Elastic Molecules Anthony Weiss; University of Sydney, Australia

There is an unmet demand for ways to restore functional tissues following damage. Elastic tissues do not typically regenerate in adults because they rely on an exogenous supply of elastin's primary building block, tropoelastin. We have developed ways to make and use tropoelastin to build a range of elastic repair materials. To our surprise, tropoelastin also promotes broader tissue repair. Powerfully, the use of tropoelastin promotes healing following surgery, including the recovery of full thickness wounds.

An emerging model for tropoelastin is that it delivers this potency by emulating extracellular matrix interactions including those needed in development and repair. This paradigm for enhanced tissue repair encompasses a novel, pure, synthetic material that promotes the repair and fixation of soft tissues. These biomimetic and bioinspired materials leverage an innate ability to promote new blood vessel formation and cell recruiting properties to accelerate healing. Utilizing our accumulated knowledge of their assembly and interactions has led to the realization of a diverse range of powerful biomaterials with tunable mechanical and self-assembly properties.

3:45 PM DISCUSSION TIME

4:00 PM SB08.02.07

***In Situ* Mineralization for the Mechanical Reinforcement of Metal-Coordinate Polymer Hydrogels** Jake Song, Sungjin Kim, Crystal Owens, Gareth H. McKinley and Niels Holten-Andersen; Massachusetts Institute of Technology, United States

Metal-coordination interactions are promising chemical motifs for the design of bioinspired polymeric materials that mimic the mechanical performance of biogenic materials such as the arthropod fangs and mussel byssal threads. Building upon the use of such motifs for the design of associative polymer gels, we demonstrate a bioinspired strategy to introduce additional mechanical reinforcement and novel functionalities into metal-coordinate hydrogels, by using the strongly metal-coordinating ligands as templates for the mineralization of metallic nanoparticles in the hydrogels *in situ*. We demonstrate ability to induce significant mineralization of iron oxide nanoparticles in a catechol-based polymer network, which results in significant stiffening (surpassing that arising from metal-ion coordination alone) as well as magneto-responsivity in the hydrogel. These findings further advance our utilization of metal-coordination interactions in bioinspired soft materials, and offer promise for their use in technological areas such as soft robotics, energy harvesting, and medicine.

4:15 PM DISCUSSION TIME

4:30 PM SB08.02.09

Studying the Effect of Dextran Conjugation on Thermosensitive Bottlebrush Polymer Conformations Through Coarse Grained Molecular Dynamics and Deep Learning Soumil Y. Joshi, Parisa Farzeen and Sanket A. Deshmukh; Virginia Tech, United States

Dextran, a neutral bacterial exopolysaccharide made up of repeating 1-6 linked glucose subunits, has been widely recognized for its water solubility, inherent inertness and biodegradable nature. Owing to these properties and its ability to conjugate with different polymers, dextran has shown promise in several biomedical applications. Copolymers between dextran and poly(N-isopropylacrylamide)(PNIPAM) - a thermosensitive polymer with a lower critical solution temperature (LCST) of 305 K - and their star-like architectures have shown potential for creating targeted drug delivery systems. This has led to significant research in studying other soft-material architectures consisting of dextran-PNIPAM copolymers, with bottlebrush polymers (BBPs),

being a particularly interesting example. BBPs, traditionally seen as worm-like cylindrical molecules, can be designed in various shapes by adjusting structural parameters such as the grafting density as well as side chain length and arrangement. Furthermore, temperature-sensitive BBPs (TS-BBPs) of PNIPAM, have shown that the shapes of these architectures significantly impact their overall conformations, leading to different properties and applications. In the present work, we perform coarse-grained (CG) molecular dynamics (MD) simulations of BBPs of dextran-PNIPAM copolymers, broadly belonging to three shapes - (i) cake-like, (ii) dumbbell-like and (iii) plus-like. We study in comparison to non-dextran conjugated BBPs, the effect of BBP shape and temperature (below and above LCST of PNIPAM) on the conformations of overall BBPs, their backbones and side chains as well as the structure of solvent around these architectures. We also investigate the effect of dextran chain length and conjugation density on these architectures by grafting dextran 10-mers and 30-mers onto the TS-BBP in different arrangements. Through conventional analyses like free volume, contact maps, asphericity, etc., we show that the lengths of conjugated dextran chains around the backbone and their immediate environments influence the compactness of overall structures while also affecting PNIPAM conformations in the core of these architectures to varying degrees. Finally, we use a recently developed convolutional neural network (CNN)-based analysis protocol to quantify the similarities and differences between conjugated and non-conjugated TS-BBPs by capturing molecular-level features that may go unnoticed using conventional analysis. Through this analysis, we attempt to unravel the relationship between the degree of dextran conjugation and its effect on PNIPAM side chains in the TS-BBP, to further provide guidance in designing novel BBPs of dextran-PNIPAM conjugates.

This work was supported by GlycoMIP, a National Science Foundation Materials Innovation Platform funded through Cooperative Agreement DMR-1933525.

4:45 PM SB08.02.10

Innovating and Characterizing Bioinspired Soft Materials with Multiscale Models and Machine-Learned Metamodels [Jingjie Yeo](#); Cornell University, United States

Globally, rapidly aging human populations are significantly accelerating the occurrence of non-communicable diseases. Understanding the fundamental mechanisms of tissue damage due to aging can provide predictive capabilities that will inform medical treatments. Coupled with this understanding, nature-inspired dynamically responsive biomedical devices and implants can address this major health crisis due to their excellent environmental adaptability and biocompatibility. We apply multiscale molecular modelling and machine-learned metamodels to characterize aging-related diseases and engineer various candidate materials in two aspects: (1) dynamically-responsive silk and silk-elastin-like materials, and (2) customized molecular and material designs for ligands and polymers. Through this approach, we unveil the myriad material properties of chemically and physically processed silk-based materials, such as ionic conductivity. We also rapidly and efficiently determine the material parameters of constitutive models governing the time-dependent behavior of soft polymers. We further design customized ligands that potentially bind better to integrins than existing ligands for neural implants.

SESSION SB08.03: Poster Session
Session Chairs: Gianluca Maria Farinola and Chiara Ghezzi
Monday Afternoon, November 28, 2022
8:00 PM - 10:00 PM
Hynes, Level 1, Hall A

SB08.03.01

An Autopilot Single Polymer Jet Self-Constructing Organ-Scale-Mimicking 3D Electrospun Scaffolds for Tissue Engineering Applications
[Balchandar Navaneethan](#)^{1,2,1} and [Chia-Fu Chou](#)^{1,1}; ¹Academia Sinica, Taiwan; ²National Tsing Hua University, Taiwan

Genetics and exogenous factors, such as aging, diseases and injury, affecting the human body highly demand clinical repairs to restore the functions and morphologies of the damaged tissues or organs. Tissue engineering is an emerging multidisciplinary field involving biology, medicine, and engineering to modernize the ways which can improve the health and quality of life of affected people by restoring, maintaining or enhancing tissue and organ functions. A successful scaffold construction requires mimicking the native tissue both physiologically and anatomically.

Electro(static) spinning is one of the most established techniques for constructing ECM mimicking fibrous scaffolds from various biodegradable polymers/biomaterials with diverse morphologies. However, smaller pores from the inter-fiber gaps than the human cells and poor jet path controllability due to complex jet-field interactions produce cell-impermeable sheet-like 2D scaffolds. We report here a “novel autopilot polymer single jet (AJ) electrospinning” capable of self-switching between cantilever-like armed jet motion (M1) and whipping motion (M2) due to charge-retention and dissipation of pre-deposited fibers. This new operation mechanism empowers successful fabrication of cell permeable porous scaffolds with buckled fibers that exhibited gradient porosity and mechanical strength thus satisfying physiological requirements from simple, homemade electrospinning setup in one shot. In this study, we also show the AJ-electrospinning is reproducible, robust and tunable which brings consistency to electrospinning produced scaffolds for the first time.

Further, we also demonstrated the self-searched writing of AJ on various 3D templates in the attempt of fabricating 3D scaffolds mimicking human organs anatomically, in which the AJ took various 3D bending paths which follows dynamically the self-modulated optimal field lines to deposit fibers on different sides of a 3D collector. Novel writing strategies were adopted thus avoided the competitive field lines to templates having complex 3D geometries. The AJ displayed high target recognition/specificity and resolution with pattern features as small as 100 μm to 10's cm and capable of direct writing challenging 2D and 3D scaffolds, including human-organ-scale 3D face, female breast & nipple and vascular graft, by achieving conformal fiber deposition thus produced exact 3D replicas. The physical and biological characteristics revealed as-spun scaffolds were spongy and showed exceptional shape memory through M1/M2 switching of AJ-electrospinning with multi-directional 3T3 cells attachment and proliferation. To our knowledge, this is the first study to introduce reproducibility and direct-writing 3D scaffolds with excellent shape memory to the century-old electrospinning thus pave the path of adding this technique as a new 3D scaffold fabrication method.

SB08.03.03

Tyrosinase-Mediated Redox System for Tissue Engineering [Su-Hwan Kim](#); Dong-A University, Korea (the Republic of)

Hydrogel system based on enzyme-mediated mild crosslinking reaction has been a promising approach in tissue engineering. Inspired by skin melanin synthesis and marine mussel adhesion, tyrosinase-mediated hydrogel crosslinking has been exploited as cell-friendly reactions and explicit reaction mechanisms. Hydrogel prepared by tyrosinase exhibits appealing properties as a dynamic scaffold for cell delivery and as a bioink for 3D bioprinting. Recapitulating the structure of the native extracellular matrix (ECM), innovative tyrosinase-mediated hydrogel crosslinking has now shifted to the field of translational medicine. Biomimetic hydrogel with in situ tyrosinase crosslinking can be efficiently and easily applicable to the disease model for therapeutic

purposes. We demonstrate that the novel enzyme-based crosslinking hydrogel has a robust potential in tissue engineering and regenerative medicine.

SB08.03.05

Exploring the Diverse Morphology of Porous Poly(lactic Acid) Fibers for Developing Long-Term Controlled Antibiotic Delivery Systems JR Kim; Korea Institute of Industrial Technology, Korea (the Republic of)

E. coli and *S. aureus*, along with many other bacteria can cause pathogenic effects. One of the most common bacteria species commonly presenting on human skin is *S. epidermidis*: about two-thirds of human infections and a serious threat to human life. *E. coli*, the gram-negative strain, is commonly found in the large intestine of humans and other warm-blooded animals that can cause various types of extraintestinal infections. Nanofibers have recently been used in fibrous materials for a wide range of applications in medicine and hygiene, including health care and coatings, medical devices, water purification systems, and air filters. Consequently, the use of antimicrobial fibers has become an attractive idea because microorganism activity in textiles are detrimental to both the user and textile itself.

Poly(lactic acid) (PLA) is a natural biodegradable thermoplastic aliphatic polyester that can be replaced synthetic polymers in terms of environmental aspects as well as their biodegradable nature, high safety, mechanical strength, fabricability, and biocompatibility properties. Electrospinning is one of the most widely used techniques to fabricate PLA nanofiber mats in hygiene, medical, and industrial filter applications. In particular, functional PLA fibers such as core-sheath, or porous morphology have been studied to carry and control the release of antimicrobial agents. In this study, porous functional PLA fibers obtained through electrospinning techniques with the different ratios of solvents in a high-humidity environment. In this study, a variety of porous surfaces were developed using polymer-solvent systems to enhance surface physical properties with the average size and the depth of pores of PLA fibers from various electrospinning conditions and solvents formulations. These porous PLA fibers have high surface to volume ratio, small fiber average diameter, and high nanoscale porosity. These high surface to volume ratio and nanoscale porosity result in controlled release of antimicrobial agents.

The aim of this study was to fabricate various morphology of porous PLA fibers and control the release of antibacterial agents, such as chitosan, trimethyl chitosan (TMC), gentamicin, kanamycin, and amikacin. Antimicrobial agents-loaded to porous PLA fibers were evaluated antibacterial activities using three types of antibacterial assays (inhibition zone tests, live/dead bacterial cell assays and antibacterial kinetic growth assays) against *E. coli* and *S. epidermidis*. Among the samples, gentamicin-loaded PLA fibers had the most bactericidal activity, with the widest inhibition zone and the highest visible dead bacteria on the fiber. In order to analyze quantitatively antibacterial activities, chitosan and chitosan derivatives-loaded PLA fibers, growth kinetic curves were analyzed using OD₆₀₀ against *E. coli* and *S. epidermidis*. For the results, we found that antibacterial performance was as follows gentamicin > amikacin > kanamycin > TMC > chitosan and more efficient on *S. epidermidis* than *E. coli*. This is mainly attributed to the different peptidoglycan layer structures in the cell wall of *E. coli* and *S. epidermidis*. *S. epidermidis* has a thicker peptidoglycan layer with a higher cross-linking degree in the cell wall compared with that of *E. coli*. It has been found that nonporous PLA fibers exhibits the initial-burst release profile whereas porous PLA fibers with highly porosity or deep-depth pores indicate a steady release. This study offers how to develop various morphology of PLA fibers to carry antibacterial agents efficiently and how long to control the release of antimicrobial agents depending on the type of PLA fibers to protect humans from biohazards in many applications. This investigation will provide a better and comprehensive understanding of porous microfiber formation during electrospinning and the fiber morphology-antibacterial property relationship.

SB08.03.06

Radiopacified and Hyaluronan Enhanced Polyethylene for Use as Artificial Heart Valve Leaflets Justin Gangwish, Cara Leone, Julianne Kindsfater, Harvinder Singh Virk and Susan P. James; Colorado State University, United States

Over 80,000 heart valve replacements were performed in the United States in 2014 and the global need is expected to exceed 850,000 by 2050. Currently available replacements fall into two categories, mechanical valves and bioprosthetic valves. While both types of valves improve patient's lives, they also pose significant risks to patient health. Mechanical valves are durable but require patients to take vitamin K antagonists for life-long anticoagulation therapy. Vitamin K antagonists have significant risks including but not limited to risk of death from minor trauma, significant fetal loss for pregnant women, and major dietary restrictions. Bioprosthetic valves have significant reoperation rates ranging up to 20% within 10 years of implantation when they are implanted via open heart surgery. However, when implanted via catheter, failure rates for bioprosthetic valves are even higher. 50% of these valves have structural deterioration within 7 years of implantation. A paradigm shift is needed to address the growing need for artificial heart valves. An ideal valve would operate in a non-thrombogenic manner preventing the need for anticoagulants, provide longevity seen from mechanical valves, could be placed via catheter preventing the surgical risks associated with open heart procedures, and would be made from low-cost materials. Furthermore, designing a radiopacified valve that could be monitored in-vivo using computed tomography could help prevent irregular deployment, monitor for leaflet deterioration, and prevent poor placement leading to coronary artery overlap. Finally current valves are evaluated using echocardiograms which identifies issues only once valve function has been reduced. Direct imaging with CT scans has the potential to shift the paradigm from waiting on a reduction in function to active monitoring of valve behavior.

In this work we describe a method to incorporate radiopaque materials (tungsten and bismuth trioxide) into linear low-density polyethylene (LLDPE) so that the material can be imaged via x-ray. The radiopacified LLDPE is then treated with hyaluronic acid to form an interpenetrating polymer network that has been previously shown to increase blood compatibility. This final material is structurally complex consisting of radiopaque filler embedded in LLDPE with an interpenetrating polymer network between the LLDPE and hyaluronic acid. The material is demonstrated to be radiopaque when imaged using an EPX-F2800 x ray source and a Universal Imaging MyRad digital radiography machine. Next the material was evaluated for the presence of hyaluronic acid using captive bubble contact angle goniometry and toluidine blue O staining. The captive bubble contact angle goniometry shows a significant increase in hydrophilicity (a hallmark of hyaluronic acid), while the toluidine blue O stains carboxyl groups found in HA. Control samples were not hydrophilic, nor did they stain with toluidine blue O. Uniaxial tensile testing demonstrated the radiopaque materials had no significant reduction in yield strength or yield strain compared to control materials and only slight reductions in toughness, elongation at break, and ultimate tensile strength. Finally, the material was demonstrated to be non-cytotoxic when cultured with red blood cells. This work demonstrates significant progress toward developing a structurally complex heart valve leaflet material that addresses the major shortcomings of currently available replacements while providing an additional diagnostic tool for physicians and patients to evaluate the health of the replacement valve.

SB08.03.08

Functions of Prolyl Hydroxylation in Elastin Chengeng Yang and Anna Tarakanova; University of Connecticut, United States

Connective tissues and organs of high tensile strength, like lung, heart and skin, extensively express elastin. Elastin is a key extracellular matrix protein responsible for elasticity, resilience, and mechanical strength in these tissues; on this basis, elastin-based materials have been widely applied in various fields such as tissue regeneration and drug delivery. During elastogenesis, the hierarchical elastic fiber assembly process, elastin is subject to a less-studied post-translational modification, prolyl hydroxylation, where, mediated by prolyl-4-hydroxylase, a hydroxyl group replaces one of the hydrogen atoms at the C-gamma position in proline residues. The structural stability of other connective tissue proteins, such as collagen, is thought to be mediated in part through hydroxylation of proline residues. This calls into question the role of prolyl hydroxylation in elastin. According to recent experimental studies, elastin-like peptides with hydroxyproline modifications are more resistant to enzymatic digestion, and subject to an abnormal behavior in elastogenesis. We hypothesize that hydroxylation alters elastin's biological behavior via protein-solvent interactions. To substantiate our hypothesis, we used existing mass

spectrometry data of elastin samples obtained from humans to build representative molecular models and perform extensive molecular dynamics simulations. As a starting point, we employ our recently developed fully atomistic model of elastin's precursor, tropoelastin. Our findings suggest that in comparison to prolines, hydroxyprolines exhibit an increase in hydrogen bonding with water and a rise in surrounding hydrophilic hydration. Such enhanced protein-solvent interactions rearrange the residue's local configurations, reducing elastin's global dynamics required for essential biological process, thereby preventing it from targeted degradation and hierarchical assembly. Overall, our investigation provides insights into functions of prolyl hydroxylation in elastin at a nanoscopic scale. We propose that strategically-placed hydroxyproline residues may be useful for tuning the sustainability of engineered elastin-based materials.

SB08.03.09

Crocodile Skin-Inspired Stretchable Piezoresistive Pressure Sensor [Seung Goo Lee](#)¹, Giwon Lee² and Kilwon Cho²; ¹University of Ulsan, Korea (the Republic of); ²Pohang University of Science and Technology, Korea (the Republic of)

Stretchable pressure sensors are important components of multimodal electronic skin needed for potentializing numerous Internet of Things applications. In particular, to use pressure sensors in various wearable/skin-attachable electronics, both high deformability and strain-independent sensitivity must be realized. However, previously reported stretchable pressure sensors cannot meet these standards because they exhibit limited stretchability and nonuniform sensitivity under deformation. Herein, inspired by the unique sensory organ of a crocodile, we developed an omnidirectionally stretchable piezoresistive pressure sensor made of polydimethylsiloxane (PDMS)/silver nanowires (AgNWs) composites with microdomes and wrinkled surfaces. Our stretchable pressure sensor exhibits high sensitivity that changes negligibly even under uniaxial and biaxial tensile strains of 100% and 50%, respectively. This behavior is attributed to the microdomes responsible for detecting applied pressures being weakly affected by tensile strains while the isotropic wrinkles between the microdomes deform to effectively reduce the external stress. In addition, because our device comprises all-PDMS-based structures, it exhibits outstanding robustness under repeated mechanical stimuli. Our device shows strong potential as a wearable pressure sensor and an artificial crocodile sensing organ, successfully detecting applied pressures in various scenarios. Therefore, our pressure sensor is expected to find applications in electronic skin for prosthetics and human-machine interface systems.

SB08.03.10

Machine Learning Enabled Biofabrication [Ruishan Liu](#), Sebastian Timmler, Yang Cao, Yifei Pan and Yan Yan Shery Huang; University of Cambridge, United Kingdom

The versatility and consistency of tissue engineering scaffolds could be vastly enhanced by converging different 3D printing, biofabrication, and data-driven techniques into a single process flow. Here, we report additive manufacturing of three-dimensional fibrous devices via integrating fused filament deposition and low-voltage electrospinning patterning. Polylactic acid scaffolds and gelatin fibres (with 3-5 μm diameter and 150 μm inter-fibre pitch) were printed automatically without manual stacking. Fibroblast cell line and brain cancer cell line were seeded onto the three-dimensional fibres. Cell attachment and proliferation experiments demonstrated good biocompatibility of the culture devices manufactured. We subsequently applied a machine learning model to find the correlations between operating parameters and fibre device quality. Future work involving multi-functional fibres deposition is proposed to accelerate the application of fibrous devices in tissue engineering and drug discovery applications.

SB08.03.11

Universal Coating for Spheroid Culturing on Arbitrary Materials [Jingxian Wu](#) and Haeshin Lee; Korea Advanced Institute of Science and Technology, Korea (the Republic of)

Three-dimensional culture of cells, allowing cells to interact with their surroundings in all dimensions, provides a more *in vivo* like microenvironment than traditional two dimensional cell culture. Organoids and artificial tissues or organs made by three dimensional cell culture are promising in both *in vivo* transplantation and *in vitro* experiments such as disease modeling and drug screening. However, existing three dimensional culture methods are always dependent on specific substrates or equipment, such as round-bottom culture plate, cell spinner and cell rotator. In addition, cell spheroids with uniform and controlled size are still difficult to make while are highly required in various applications to ensure the reliable and reproducible results. In this study, we developed a universal coating for three dimensional cell culture. The coating was made with chitosan-gallol (CHI-G), and both somatic cells and stem cells automatically self-assemble into spheroids on it. CHI-G coating could be universally coated onto any materials in any shapes simply by immersing and shaking in the CHI-G solution for 48 hours. As a result, any materials coated with CHI-G coating could be substrates for spheroid culturing. We coated CHI-G onto the surface of regular two-dimensional cell culture platform (eg. cell culture plate with flat bottom and glassware for confocal) and inner-surface of three dimensional materials (eg. porous scaffolds and silicon tubes), and cell spheroids were cultured inside. Interestingly, cell spheroids cultured on substrates with different shapes could be applied in different scenarios. Porous scaffolds with spheroids cultured and imbedded inside is promising to be used as tissue engineering scaffolds. Silicon tubes with CHI-G coated on the inner-surface could be used as the device for continuous generation of spheroids. With the continuous injection of cell suspension solution and cell culture medium into the CHI-G coated silicon tube, spheroids could be generated and collected at the another end of the long silicon tube. The size of cell spheroids generated in silicon tubes is much more uniform than those generated on the two dimensional culture plate, which is mainly because of the restriction of round shape in tube. Furthermore, by changing the cell density of the cell suspension solution injected, spheroids with controlled size ranging from 60 μm - 300 μm could be generated, thus realizing fabricating spheroids with controlled size in a continuous and high-throughput way.

SB08.03.12

Tuning the Elastic Modulus of Ionically Crosslinked Alginate Hydrogels [Elaine Nagahara](#), Yi Zuo and Luo Gu; Johns Hopkins University, United States

Introduction: Alginate hydrogels have unique mechanical properties that can be used to control biological responses in tissue engineering applications. Stiffness, for instance, has been shown to influence cell adhesion, differentiation, morphology, etc. in both 2D and 3D culture. The advancement of designing tissue-specific biomaterials therefore depends on our ability to chemically or physically tune these mechanical properties. In this study, we characterized how changes in calcium concentration influence the initial elastic modulus of ionically crosslinked alginate hydrogels independent of their varying stress relaxation rates. In addition, we observed that overmixing resulted in a reduced elastic modulus.

Materials and Methods: Alginate hydrogels (15 mm diameter, 2 mm thick) were formed by ionically crosslinking LF20/40 alginate with CaSO_4 . Alginate polymers of four different molecular weights were used to make hydrogels with four different rates of stress relaxation; lower molecular weight results in faster stress relaxation. The crosslinker concentration was adjusted (13.4 mM-54.9 mM) to tune the elastic moduli of the hydrogels to achieve the same modulus (7 kPa) independent of the various stress relaxation rates. After incubating the gels in medium for 2-3 days, compression testing was used to measure their elastic moduli.

The effect the amount of mixing has on the elastic modulus was evaluated on the fastest stress relaxing hydrogels. They were mixed five, seven, and eleven times before their moduli were characterized.

Results and Discussion: From the slowest to the fastest stress relaxing hydrogels, crosslinker concentrations of 13.4 mM, 26.8 mM, 37.8 mM, and 47.6

mM, respectively, were initially used. The two fastest relaxing hydrogels were much softer than 7 kPa; the fastest relaxing gels had an average elastic modulus of 2.1 kPa, and the second fastest relaxing gels had an average elastic modulus of 4.4 kPa, so the calcium concentration was increased for those two conditions. From slowest to fastest stress relaxation rates, the hydrogels had final average elastic moduli of 8.5 kPa, 7.2 kPa, 7.8 kPa, and 6.2 kPa with crosslinker concentrations of 13.4 mM, 26.8 mM, 42.7 mM, and 54.9 mM, respectively. While all four conditions had average moduli near 7 kPa, the target value, the second slowest relaxing hydrogels had the closest average elastic modulus to 7 kPa. The second fastest relaxing hydrogel had the lowest variability followed by the second slowest relaxing condition. This result may be explained by the fact that these two conditions had alginate solutions with intermediate viscosity (due to their intermediate molecular weights) and intermediate calcium concentrations compared to the slowest and fastest relaxing conditions. The slowest relaxing gels are made with alginate solution that is highly viscous, so it is difficult to combine the alginate solution with the crosslinking solution quickly enough to evenly mix the two, resulting in considerable variability. The fastest relaxing hydrogels are made with a high crosslinker concentration, which causes the alginate solution to crosslink quickly, again making it difficult to achieve more homogeneous mixing. The effects of the amount of mixing of the alginate and crosslinker solutions were studied using the fastest stress relaxing hydrogels. They had average elastic moduli of 10.3 kPa, 6.2 kPa, and 5.8 kPa when mixed five, seven, and eleven times, respectively. There was a significant difference between the hydrogels that were mixed five times and seven times as well as the hydrogels that were mixed five times and eleven times. These preliminary results suggest that increased mixing results in lower elastic moduli. While enough mixing is desired to evenly distribute the crosslinks, overmixing can result in damaging the gel after crosslinks have formed, causing some to rearrange. Such rearrangement can give rise to an inhomogeneous gel with reduced elastic modulus.

SB08.03.13

Fabricating Stretchable Paper-Based Substrates with a Core-Sheath Structure for Papertronics Joab Dorsainvil; Binghamton University, The State University of New York, United States

Introduction: Paper-based bioelectronics, papertronics is an emerging technology for next-generation sensing and energy storage due to its significant material properties; including high surface-to-volume ratio, porous structure, biocompatibility, biodegradability, low-cost availability, foldability, and lightweight composition^[1]. However, due to the intrinsic mechanical properties of cellulose, these stiff mechanics create undesirable substrates for stretchable bioelectronics. As a result, papertronics demonstrate limited conformability to the complex microarchitecture of skin and fail to exhibit deformation mechanics required to address the mechanical mismatch between rigid electronics and skin. To bridge the gap between papertronics and electronics skin (e-skin), herein we studied engineering strategies to exploit the material, chemical, and physical properties of paper (cellulose acetate or cellulose) amalgamated with the soft mechanics of a silicone elastomer (e.g., Dupont Liveo Soft Skin Adhesives) through coaxial electrospinning. The core-sheath silicone elastomer-cellulose acetate fibers mimic the extracellular matrix of human skin while maintaining the chemical surface properties of paper, enabling the integration of electronic components with existing manufacturing and printing techniques.

Materials and Methods: Cellulose acetate (CA) (MW = 30,000) and organic solvents (e.g., THF, DMF, Acetone) were purchased from Sigma Aldrich. The 7-9700 soft skin silicone adhesive (SSA) was gifted from DuPont. We used a coaxial needle with an electrospinning unit (MSK-NFES-3; MTI Corporation, CA) to create the fibrous mats while systematically testing operational parameters (e.g., feed rate, applied voltage, polymer concentration, etc.). Scanning electron microscopy (SEM) and confocal microscopy was used to analyze fiber alignment and core-sheath structure. Fiber diameter was measured with the utilization of ImageJ. Mechanical properties of the engineered fiber mat were evaluated by tensile testing with a 5 N load cell at a 5.10 mm sec⁻¹ strain rate. Fourier transform infrared (FTIR) spectroscopy and Electron Dispersive Spectroscopy (EDS) determined the chemical and elemental characteristics of the fabricated stretchable papers.

Results and Discussion: SEM confirmed a fibrous structure of the fiber mat with an average fiber diameter of $1.38 \pm 0.37 \mu\text{m}$ (n=250). Confocal microscopy revealed the core-sheath structure of the SSA core (blue) and CA sheath (red) via coaxial electrospinning. Energy dispersive spectroscopy (EDS) identified elemental peaks that reflect a core-sheath structure of an individual SSA-CA fiber. Using this stretchable paper, we were able to develop a microbial fuel cell by stacking three stretchable papers as an anode, membrane, and cathode material, which generated a max power output of 10.5 μW in PBS.

Conclusions: The coaxial structure of cellulose acetate and soft skin adhesive improves the stretchability of paper substrates up to 45% strain which is greater than the stretchability of conventional paper substrates (<2%). Fabricating an MFC device using our stretchable paper demonstrates fabrication processing compatibility of these materials and thus shows the potential for future application in various ranges of papertronics while also sharing characteristics from soft bioelectronics.

Acknowledgments: This research is supported by the National Science Foundation (NSF; ECCS#2020486). We thank DuPont for donating the SSA elastomer.

Reference: [1] Martinez, A, W et al. *Angewandte Chemie* (2007) 46 (8), 1318-20.

SB08.03.14

A Technology for Rare Earth Elements Recovery by Genetically Engineered Elastin-Like Polypeptide Zohaib Hussain and Inchan Kwon; Gwangju Institute of Science and Technology (GIST), Korea (the Republic of)

Rare earth elements (REEs) are described as the vitamins of modern industry owing to their use in high-tech and clean-energy industries. Growing concerns of the unpredictable supply, possible health risks, and unsustainable extraction practices demand the development of green technologies for the selective extraction and recovery of REEs. Protein based polymers called elastin-like polypeptides (ELP) were genetically engineered for the selective and repeated recovery of REEs. ELP exhibits a fully reversible thermal coacervation behavior over multiple cycles of cooling and heating and was exploited to enable easy recovery of the bound REEs for repeated use. A lanmodulin protein which exhibits an unusually high affinity and selectivity for REEs was fused to the ELP to provide the highly selective nature to the biopolymers in the presence of higher concentrations of competing non-REEs. Selective binding of REEs was demonstrated at an expected ratio of 2 REE/biopolymer, and minimal binding of competing heavy metals (magnesium and zinc), even at a 300-fold excess, was observed. The REEs were extracted and recovered easily, enabling continuous reuse of the biopolymers. Utility of the biopolymers for REEs recovery from real world samples such as steel slag leachate (≈ 0.13 mol% REEs) was demonstrated with no decrease in recovery efficiency, the recovery efficiencies of non-REEs were minimal. Results establish the potential of engineered thermoresponsive protein-based polymeric materials as biotechnological tools for environmentally friendly extraction and recovery of REEs with a minimum carbon footprint, which is essential for the sustainability of metal life cycles, from mining to end-of-life to recycling.

SB08.03.15

Bio-Inspired Surface for Real-Time Coronavirus Detection Andrea Barbaglia, Andrea Valsesia and Pascal Colpo; European Commission Joint Research Centre, Italy

The COVID-19 global crisis shows that preparedness plans need to be developed, including methodologies enabling the early stage detection and identification of potential health threats, in order to contrast effectively future pandemics [1]. In particular, new technologies enabling the identification of the "latency period", in which the virus is circulating among small communities but it is not yet recognized, are sought. Despite many efforts, current technologies for virus detection based on PCR or immuno-recognition show significant limitations. In particular, PCR cannot resolve the latency period, as

it requires typically 24 to 48 hours to analyse the samples. On the other hand, immune assays show much lower sensitivity, giving rise to a significant amount of false negatives.

In this project, we developed a new bio-inspired surface allowing highly sensitive, real-time virus detection in air samples. This system is a label-free virus detection platform, with single viral particle sensitivity. Its concept, inspired by biology, could give rise to a new generation of lab-on-chip devices for studying many different viral infections, not only related to the respiratory system.

[1] Cevik, M. et al. Severe Acute Respiratory Syndrome Coronavirus 2 (SARS-CoV-2) Transmission Dynamics Should Inform Policy, *Clinical Infectious Diseases* 73(S2), S170–6 (2021).

SB08.03.16

The Molecular Structure and Mechanics of Beta Keratin (corneous Beta Protein) and Beta Fibril Chiang H. Lin, He Y. Kang, Chien Y. Pan and Chia-Ching Chou; National Taiwan University, Taiwan

In reptiles and birds, the claws, scales, feathers, and beaks are composed of beta keratin with exceptional material properties and outstanding performance. The beta keratin protein is a hierarchical structure, and a four-antiparallel-beta-sheet of 34 amino acids forms a monomer, the basic unit of materials. We focus on a bottom-up atomistic model of the beta keratin to study the molecular structure and the mechanics of the different hierarchical assemblies, including monomer, dimer, and fibril. For the monomer and dimer systems, the unfolding force in the dimer is larger than the monomer. Moreover, beta strands unfold at the monomer's pulling end for the dimer when the dimeric-sandwich structure remains intact in the peak force regime. For the fibril model, the unfolding peak force in shear loading is larger than in tensile loading. In shear and tensile loading, the initial unfolding of the fibril occurs in the interface of the interdimer, and the dimer structure remains when the fibril fails, suggesting that the dimer serves as a more stable building block of the beta keratin. We further compare our results with the mechanical properties of other proteins with similar beta-sheet structures and discuss how the hydrogen bond formation affects the mechanics between the materials. Our study provides insight into the quantitative comparison to the hierarchical structure of beta keratin at the atomistic level. The results could be further applied to designing bioinspired materials for the specific functions from a bottom-up perspective.

SB08.03.17

One Pot Synthesis of Reinforced Hydrogels with Bioinspired Complex Microstructures Using Magnetic Assisted Slip Casting Slocha Sapasakulvanit, Xin Ying Chan and Hortense Le Ferrand; Nanyang Technological University, Singapore

Composite materials with bioinspired microstructures are of high interest in numerous engineering applications. Indeed, thanks to their unique microstructure where inorganic particles are distributed in hierarchical patterns, unusual combinations of properties can be achieved, such as strength and toughness in nacre-like composites. However, contrary to many synthetic composites, nature produces its materials in a 'one pot' fashion where inorganic and organic components are assembled simultaneously. Also, water plays a great role in natural composites and is often absent in synthetic materials. Although examples of nacre-like hydrogels exist, they often contain a low concentration of reinforcing inorganic particles and more complex microstructures have not been realized. To address this issue, we developed a one pot synthesis approach where complex microstructures are built while the concentration of inorganic particles is getting concentrated. We study the capabilities and limits of the method and carry out mechanical testing to illustrate how the microstructure and presence of water can be leveraged to increase strength and toughness. To do so, we used an established method called magnetically assisted slip-casting (MASC) and adapted it to interpenetrated hydrogel matrices. MASC uses an external magnetic field that controls the orientation of magnetically responsive anisotropic particles in a water-based suspension, which is being removed through a porous mold. MASC therefore offers the capability of building complex bioinspired microstructures. Here, we used MASC to assemble Al_2O_3 microplatelets while polymerizing an interpenetrating network hydrogel made of poly-acrylamide (PAM) and poly(N-isopropylacrylamide) (PNIPAM). The resulting composites, containing around 40 vol% of Al_2O_3 , show tunable alignment of microplatelets with polymer strands in-between when observed under SEM. From compression tests, aligned samples containing the hydrogel show higher strength and toughness than aligned samples without the hydrogel and randomly aligned samples, which were 6.5 MPa and 1000 kJ/m³, respectively. Interestingly, thanks to the presence of hydrogel inside, the dried samples absorb moisture from air and show small recovery under compression. These results highlight the potential of MASC as a processing method to create reinforced hydrogels for development of novel materials.

SB08.03.18

Euglena gracilis-Derived Extracellular Vesicles as Skin-Regenerative Wound Healing Agents Hwira Baek¹, Yuri Go¹, Seungpyo Hong² and Jin Woong Kim¹; ¹Sungkyunkwan University, Korea (the Republic of); ²University of Wisconsin-Madison, United States

Extracellular vesicles are known as an important mediator for signaling in cell-cell communication and cellular processes including immune response and antigen presentation. Since extracellular vesicles contain therapeutic proteins, a variety of cell therapeutic strategies are developing while avoiding side effects such as low survival rate and immune rejection response associated with direct use of cells as a therapeutic agent. Most of the exosome studies conducted so far are based on animal-originated cells. Recently, there are challenging attempts to extract extracellular vesicles from other types of raw materials such as plant cells and microalgae. The approach to obtain extracellular vesicles from microalgae is of special interest because they have abundant biomolecules such as proteins, vitamins, minerals, and amino acids. This study proposes using microalgae containing carbohydrate bioactives, an *Euglena gracilis*-derived extracellular microvesicle (EMV_{EG}) system, for enhanced skin regeneration. The critical deformation ratio, 1.67, during cell extrusion enables us to tune the particle size of the EMV_{EG} at approximately 1 μm, thus satisfying the encapsulation yield of b-1,3-glucan and the cellular delivery performance. In vitro 5-bromo-2'-deoxyuridine and cell scratch assays revealed that the EMV_{EG} promoted the proliferation and migration of skin cells, thereby increasing both collagen synthesis and the expressions of proliferation-associated proteins. An ex vivo wound healing test using both artificial and porcine skin revealed that similar to that seen using b-1,3-glucan, the EMV_{EG} could substantially increase the cell population, expressing the proliferation-related protein, termed proliferating cell nuclear antigen. These results demonstrate that our EMV_{EG} system shows considerable potential in the field of skin regeneration. This technique is expected to design new types of extracellular vesicles that are applicable for skin regeneration in the pharmaceutical and cosmetic industries.

SB08.03.19

Investigation of the Self-Assembly and Nanomechanical Properties of Synthetic Amyloid Peptides Hannah G. Abernathy¹, Jhinuk Saha², Vijay Rangachari², Tristan D. Clemons¹ and Sarah E. Morgan¹; ¹University of Southern Mississippi, United States; ²The University of Southern Mississippi, United States

Amyloids are highly ordered, self-assembled protein aggregates most commonly associated with neurological diseases such as Alzheimer's and Parkinson's. However, their structural self-assembly into highly stable aggregates or fibrils has been shown to enhance cellular functions such as cell growth, bio-adhesion, and mechanical strength in various organisms. Synthetic biomaterial films or gels (inspired by natural amyloids) with tunable properties can be designed through peptide sequence changes that promote specific intermolecular interactions to form fibrils and strongly adhere to a

variety of surfaces. Although synthetic amyloid-based materials have shown promise, there is still a lack of understanding of the influence peptide structure has on adhesive and mechanical properties. For this work, a library of amyloid peptides was synthesized and their self-assembly was investigated under varying environmental conditions. The structural and nano-mechanical properties were characterized using circular dichroism (CD) spectroscopy and atomic force microscopy (AFM) in quantitative nanomechanical mapping (QNM) mode.

SB08.03.20

Development Biomimetic Functionally Graded Materials That Mimic Insect Self-Cleaning Organs Masanori Yoshida¹, Rikima Kuwada¹, Ito Shuto², Mikihiro Hayashi¹ and Daisuke Ishii¹; ¹Nagoya Institute of Technology, Japan; ²Nikkou Kasei Co. LTD., Japan

Functionally graded materials (FGMs) are the materials with varying composition and structure gradually over volume, resulting in corresponding changes in the properties of the materials. Unlike traditional composites of homogeneous materials, FGMs can compromise between the desirable properties of the component materials in the desirable places in the materials. The exoskeleton of insects is a notable example of FGMs in nature. Cuticle, the constituent material of insect exoskeleton, is characterized by a wide range of elastic moduli, which can be as high as metals and as low as rubbers, are integrated without boundaries to achieve high strength, lightweight, and multifunctions.

The purpose of this study is to analyze the correlation between the composition and functionality of exoskeletons developed through evolution and to apply the insights to the engineering of novel biomimetic FGMs.

Honeybee (*Apis mellifera*) was selected as a model organism in this study. The antennae of honeybees have many sensors like the five human senses, and when the antennae become contaminated, dirt accumulates on the surface sensors and interferes with the sensing function. Therefore, in order to maintain their sensing function, honeybees clean their antennae using antenna cleaners on their forelegs. We focused on antennae and its specific body parts, antenna cleaners, to investigate the correlation of its material composition and functionality.

A confocal laser scanning microscope (CLSM) was used to analyze the morphology and composition of antennae and antenna cleaners. The CLSM images showed that both antennae and antenna cleaners were not homogeneous in composition, but had a combination of soft and hard parts. The antenna cleaner was also found to have a sandwich structure with soft parts sandwiched between hard parts by observation at high magnification.

We analyzed the correlation between composition and functionality by quantitatively analyzing the efficiency of the antenna cleaners in removing contaminants from the antennae. The results showed that most of the contaminants were removed in a single cleaning and that contaminants were more easily removed closer to the tip than at the base of the antennae. Based on these results, we thought that the high removal rate of antenna cleaners can be attributed to the sandwich structure, and will try to fabricate biomimetic FGMs based on these structures. In this study, we attempted to develop the FGMs with a sandwich structure having a soft and a hard layer by using vitrimers which are a special type of cross-linked material with associative dynamic covalent bonded cross-links. Vitrimers can enhance interfacial adhesion and help fabricate FGMs because the bond exchanges are occurred by heat treatment. At last, we evaluated the interfacial adhesion of the fabricated materials by atomic force microscope (AFM) and the cleaning efficiency of the fabricated materials by independent test.

SB08.03.21

Evaluation of Fluid Resistance Reduction and Antifouling Function of Scale-Mimicking Surfaces Honoka Sugiyama and Daisuke Ishii; Nagoya Institute of Technology, Japan

In recent years, many studies have been conducted to improve the antifouling properties of surfaces in water and to reduce the fluid resistance, and it needs to elucidate the essence of the structural shape and surface composition that provide optimal properties. For example, fish scales are hydrophilic surfaces with riblet structures, and it is known that these structures produce a water layer in water flows to prevent adhesion of dirt and exhibit excellent self-cleaning ability. It is also believed that the microstructures of the scale surface are responsible for further improvement of antifouling properties and reduction of fluid resistance.

The purpose of this study is to evaluate the properties of shark mimetic surfaces that could lead to the elucidation of the unexplained mechanism of shark fluid resistance reduction. Measurement method of dynamic wetting in a liquid atmosphere that established in our laboratory was used to evaluate the antifouling properties and reduction of fluid resistance ability of microstructured surfaces in a water atmosphere.

In the past, surface properties under a water atmosphere were mostly evaluated only from static contact angles. However, surface properties under an air atmosphere are evaluated by combining static and dynamic wettabilities. The reason is dynamic wettability shows functional behavior that cannot be predicted from static wettability. Therefore, we have created a new experimental method to measure the dynamic wettability under a water atmosphere.

The dynamic contact angles of air bubbles and oil droplets on the surface with tilting were measured in a water atmosphere.

Experimental substrates were a commodity polymer resin with a riblet structure mimicking shark scales. Hydrophilicity and hydrophobicity of the polymer surfaces were changed by fabricating a self-assembled monolayer after gold-ion sputtering. 10mL of ethanol solutions including hydrophilic and hydrophobic molecules with thiol groups were prepared and the gold-coated polymer substrates were immersed in each ethanol solutions for 3 hours. After immersion, the substrate was washed thoroughly with ethanol and dried naturally. 5 kinds of surface-modified substrates having various ratio of hydrophilic and hydrophobic molecules in outermost surfaces were fabricated and measured by the dynamic wettability analyze system in air or water atmospheres. In an air atmosphere, 15 μ L of water or 6 μ L of n-hexadecane was attached and the substrate was tilted. In a water atmosphere, 11 μ L of an air bubble or 20 μ L of n-hexadecane was attached and tilted.

As a result, the value of the contact angle when air bubbles were attached in a water atmosphere was larger than that expected from the contact angle when water was attached in an air atmosphere. In addition, the tilt angle required for the bubbles to leave the substrate was smaller. This is thought to be because of product of a water layer on the substrate surface by the shark's microstructure. This result suggests that the shark's scale surface prevents bubbles from attaching to the substrate and reduces fluid resistance by not creating surface irregularities.

Next, the contact angle value when n-hexadecane was attached in a water atmosphere was significantly larger than the value expected from the contact angle when hexadecane was attached in an air atmosphere. However, the tilt angle required for the n-hexadecane to leave the substrate was also large. This is thought to be because of the difference in the height of the microstructure on the shark-mimetic surface. This is thought to this difference in height cause a petal effect, which prevents the oil droplets from leaving the substrate surface even when the substrate is tilted up to 90°. These results strongly emphasize the necessity of measuring dynamic wetting behavior in water atmosphere and indicate the possibility of creating new functional surfaces through further clarification of the functions of organisms existing in water.

SB08.03.22

Evaluation of Metal Surfaces with Microscopic Mimetic Structures and New Forming Methods for Metal Substrates Sumire Isachi and Daisuke Ishii; Nagoya Institute of Technology, Japan

Despite being gill-breathing organisms, *Ligia exotica* are unable to swim. They breathe to use transported water without external energy caused by using capillary action of microscopic protrusion structures on the surface of their legs. Energy-less liquid-control surfaces not to require the external energy will be possible to create in mimicking of the structure of legs. In previous studies, it has been found that fabrication of microscopic protrusion structures on the polymer surface enables spontaneous liquid transport. However, while polymers are easy to form, there is a fear of deformation and softening above the glass transition temperature. Therefore, the goal of this research is to replace the material of the mimic substrate from polymer to metal. For this purpose,

we fabricated a metal film on the surface of a polymer substrate with a mimic structure and checked shapes of droplets on the surface to verify whether the substrate material could be replaced from polymer to metal. Next, a new metallization method was examined, in which a metal substrate is formed by thick plating on a porous polymer mold.

Polymer substrates with mimic structures were fabricated by pouring polydimethylsiloxane (PDMS) into polyethylene (PE) molds. Conical and triangular pyramidal protrusions were fabricated and arranged evenly spaced grid. We also examined whether the behavior of the droplets differed depending on the kinds of metal, such as gold and nickel, and the method of the metal coatings, such as gold vapor deposition and electroless plating. A 1.5 μL drop of water was dropped onto each prepared substrate and spreading of the droplet was observed. As a result, the spaces between the protrusions functioned as flow paths, and the droplets spread vertically and horizontally. Further, the droplet shape on the metal surface was like that on the polymer surface, with the droplet shape being nearly square on each substrate with conical structures, and nearly rectangular on each substrate with triangular pyramids. The aspect ratio was calculated from the wetting shapes of droplet at the point when wetting stopped. The aspect ratio was about 1.0 for cones and about 1.5 for triangular cones. The difference in wetting shape is closely related to the capillary pressure caused by the structure shape. In the case of conical protrusions, the distance between adjacent protrusions is equal from vertical to horizontal, and the strength of capillary pressure does not vary from vertical to horizontal. On the other hand, in the case of triangular pyramidal protrusions, the distance between adjacent protrusions is not constant, which causes a difference in the strength of capillary pressure. Even if the surface is coated with metal, the projection shape without any change, so the capillary pressure gradient is the same as on the polymer surface and the droplets have the same shape.

From the above, it was confirmed that the structure inspired by the legs of *ligia exotica* can be applied to metal surfaces. As the next step, we tried to fabricate a metal substrate with the mimic structure by the thick plating method. A thin metal film was fabricated on the surface of the mold, and electrolytic plating was utilized to obtain the metal substrate. To facilitate detachment of the mold after molding the metal substrate, the mold was made of flexible PDMS, but PDMS substrates have a very weak durability of the metal thin film fabricated on their surface. Therefore, the PDMS molds were immersed in a polydopamine solution to form a hydrophilic dopamine film on the surface of the molds, and metal films were fabricated on the dopamine film. As a result, the durability of the metal film against peeling increased and electrolytic plating became possible for thicker plating.

SB08.03.23

A Systematic Study of Polydopamine (PDA) Building Blocks [Jiwon Lim](#), Shuo Zhang and Jinsang Kim; University of Michigan–Ann Arbor, United States

Since mussel-inspired polydopamine (PDA) was introduced in 2007, dopamine chemistry has attracted huge attention due to the surface-independent coating capability in mild alkaline conditions. Based on the unique binding property, PDA and its related analogues (i.e. phenolic polymers) have been adopted in various fields such as cell culture, composites, microfluidics, drug delivery membrane, and others. However, a comprehensive understanding of PDA is still limited owing to the abundant reactive sites of dopamine monomer. Due to the polymerization in multiple regions, PDA has various building blocks, which are composed of 5,6-dihydroxyindole (DHI) and dopamine units in various oxidation states. This complex structure restricts the systematic analysis of PDA.

Here, we rationally designed the series of PDA derivatives (DA1, DA2, DA3, DA4, DA5, DA6, and DA7) and synthesized its corresponding polymers to investigate the role of each building block as well as bonding mechanisms on different substrates. The chemical structures of each polymer are logically controlled by blocking or removing reactive sites that enable the successful isolation of building blocks of PDA. Therefore, a series of polymers is characterized to disclose a secret of PDA. First, molecular structures are confirmed by Nuclear Magnetic Resonance (NMR), Mass spectrometry, Fourier-transform infrared spectroscopy (FTIR), and X-ray Photoelectron Spectroscopy (XPS). Then we focused on the adhesion and cohesion mechanism of PDA derivatives that determine various coating modes on metal, silicon, polymers, etc. Based on the comparison among DA1, DA2, and DA4, we found both catechol and amine play a pivotal role in surface-independent adhesion regardless of the presence of DHI unit. In contrast, DA5, a catechol-only polymer, exhibits limited adhesion. Meanwhile, film and particle morphologies were examined by Scanning Electron Microscopy (SEM) and Atomic Force Microscopy (AFM) to reveal the aggregation mechanism that determines the surface roughness and the coating thickness. Finally, the optical properties of PDA are analyzed by UV-vis spectroscopy. We successfully figured out the origin of the dark brown color of PDA that is attributed to the combination of various oxidized modes of catechol quinone and DHI units.

SB08.03.25

NIR-Sensitive Polymer for Living Cell Photostimulation [Vito Vurro](#)¹, Ilaria Venturino^{1,2} and Guglielmo Lanzani^{1,2}; ¹Istituto Italiano di Tecnologia, Italy; ²Politecnico di Milano, Italy

Optical methods represent a powerful and non-invasive tool to stimulate and probe biological matter. In particular, conjugated molecules and macromolecules have been demonstrated a great platform to interface with cells and living organisms.^{1,2} This interaction has been promoted by materials high optical absorption/emission cross sections, versatility in chemical synthesis and low toxicity. Even though the efficiency of this approach has been demonstrated in neurosciences and cardiology,^{3–5} the visible light absorption and the relative low penetration inside human body is still a critical point.

In this work, we evaluate the use of a novel NIR-absorbing organic bulk heterojunction (composed by a conjugated polymer and a small molecule) for living cells photostimulation. We initially developed a fabrication method to produce a diffuse interface shaping the material in the form of nanoparticles. Furthermore, we evaluate biocompatibility and photostimulation ability of the proposed blend.

References

1. Di Maria, F., Lodola, F., Zucchetti, E., Benfenati, F. & Lanzani, G. The evolution of artificial light actuators in living systems: from planar to nanostructured interfaces. *Chem. Soc. Rev.* **47**, 4757–4780 (2018).
2. Hopkins, J. *et al.* Photoactive Organic Substrates for Cell Stimulation: Progress and Perspectives. *Adv. Mater. Technol.* **4**, 1800744 (2019).
3. Maya-Vetencourt, J. F. *et al.* A fully organic retinal prosthesis restores vision in a rat model of degenerative blindness. *Nat. Mater.* **16**, 681–689 (2017).
4. Lodola, F., Vurro, V., Crasto, S., Di Pasquale, E. & Lanzani, G. Optical Pacing of Human Induced Pluripotent Stem Cell Derived Cardiomyocytes Mediated by a Conjugated Polymer Interface. *Adv. Healthc. Mater.* **8**, 1900198 (2019).
5. Vurro, V. *et al.* A Polymer Blend Substrate for Skeletal Muscle Cells Alignment and Photostimulation. *Adv. Photonics Res.* **2**, 2000103 (2021).

SB08.03.26

Ideal Diffuse Reflector with Layered Structure Inspired by Animal Eyes [Junyong Ahn](#), Seohan Yun, Taehyun Ryu and Junyong Park; Kumoh National Institute of Technology, Korea (the Republic of)

Many wild animals that are active at night have evolved to have layered eye structures that include thin reflectors to improve night vision. Light incident on the eyes of these wild animals is primarily absorbed by the retina, but some transmission loss is unavoidable. A naturally occurring biological reflector located behind the retina provides an opportunity for the retina to absorb residual light. In this presentation, we introduce a new type of diffuse reflector

with excellent scattering properties by applying the optical amplification mechanism resulting from the layered structure to the scattering behavior. The newly developed diffuse reflector has a biologically inspired layered structure of an ordered nanoporous medium serving as a scattering layer and a metallic thin film serving as a reflective layer. The secondary scattering caused by the reflector enables an exceptionally homogeneous diffuse reflection close to the Lambertian distribution, which is predicted through optical simulations (FDTD or FEM) and verified experimentally. Finally, we present several advanced optics, including smart contact lenses, by utilizing miniaturized diffuse reflectors through photopatterning.

SB08.03.27

A Highly Conductive, Dry Adhesive Patch with a Layered Structure for Independent Control of Adhesion and Conductivity [Seohan Yun](#), Junyong Ahn and Junyong Park; Kumoh National Institute of Technology, Korea (the Republic of)

Since the 2000s, various types of dry adhesives have been proposed that mimic the hierarchical ciliary structure of gecko lizard's paws. Recently, deviating from the research paradigm of simply mimicking the adhesive function, conductive dry adhesives made of nanocomposites in which conductive nanomaterials (e.g., CNTs and AgNWs) are dispersed in an elastomeric matrix have been developed. Attempts have been made to acquire various bio-signals by using them as skin-mountable dry electrodes, but their sensitivity is still limited due to the inherent trade-off relationship between electrical conductivity and adhesion in typical nanocomposites. Here, we propose a functionally layered, highly conductive, dry adhesive patch through rational design of spray coating and molding processes. Lateral collapse of the high aspect ratio ciliary structures, which frequently occur during spray coating of conductive dispersions, can be avoided through optimization of the process sequence. The dry adhesion and electrical conductivity of the patch are independently controlled by the aspect ratio of the ciliary structure and the amount of spray-coated AgNWs. We have finally succeeded in realizing a large-area (4 in²), defect-free dry adhesive patch that exhibits high electrical conductivity (< 100 ohms) and favorable normal adhesion (> 1.3 N/cm²) to human skin. Several proof-of-concepts utilizing the developed highly conductive dry adhesive patch will be presented.

SB08.03.28

Self-Assembly of Glucose Containing “Janus-Type” Linear Dendritic Block Copolymers for Biomedical Applications [Kevin Green](#)¹, Mahesh L. Yaddehige², Davita L. Watkins^{3,2}, Lisa K. Kemp¹ and Sarah E. Morgan¹; ¹The University of Southern Mississippi, United States; ²The University of Mississippi, United States; ³The Ohio State University, United States

The self-assembly of highly branched Janus dendrimers (JD) into Janus dendrimersomes (JDS) comprised of a hydrophilic/hydrophobic bilayer has shown promise for drug encapsulation and delivery. However, at higher concentrations and degrees of generation, the hydrophilic portions of traditional JDs have proved to be cytotoxic. To improve biocompatibility, JDs have been decorated with saccharide groups which assisted in the self-assembly of non-toxic Janus glyco-dendrimersomes (JGDS). It has been seen that, due to distinct peptide/polymer hydrogen bonding interactions, saccharide stereochemistry plays an important role in carbohydrate functions such as biological recognition, protein binding, and peptide aggregation pathways. This work explores using synthetic glycopolymers as the hydrophilic layer to amplify the structures' hydrogen bonding ability, potentially enhancing the self-assembly of JGDS. The stereospecific arrangements of the pendant saccharide groups may be used for cell targeting, lectin specific binding in the body, and to mimic the biological glyco-clustering effect. Linear glycopolymers were synthesized through reversible addition fragmentation chain transfer (RAFT) at different target molecular weights and coupled to polylactic acid (PLA) branched dendrons. While maintaining a constant molecular weight of the hydrophobic dendron and altering the hydrophilic segment, a multitude of nanostructures may be seen. Coupled conjugates and nanostructures were characterized through nuclear magnetic resonance (NMR), gel permeation chromatography (GPC), dynamic light scattering (DLS), transmission electron microscopy (TEM), and atomic force microscopy (AFM).

SB08.03.29

Chloroplast Encapsulation in Pectin Hydrogel via Thiol-ene Photo-Click Reaction [Jaeho Choi](#), Jonghyun Shin, Youngwoo Han, Changhee Woo, Woojin Jeong, Jinho Hyun, Seon-Yeong Kwak and Chang Seok Ki; Seoul National University, Korea (the Republic of)

Bioengineered chloroplast has great potentials in carbon sequestration as well as production of biological molecules. Although plants are preferred in chloroplast engineering, isolated chloroplasts provide benefits in terms of environmental friendliness, abundant resource in nature, and cost effectiveness. For example, the isolated chloroplasts are more efficient than plant in carbon dioxide absorption, because they did not discharge carbon dioxide unlike plants. However, isolated chloroplasts lose their photosynthetic activity quickly. It requires a novel platform for chloroplast incubation as maintaining intactness of chloroplast. Chloroplast encapsulation in biopolymers or synthetic materials has been proposed to prolong the photosynthetic activity. Nevertheless, sufficient photosynthetic activity of encapsulated was not achieved in these attempts. In this study, we fabricated pectin hydrogels as a novel matrix, which mimicked plant cytosol for preservation chloroplast photosynthetic activity. Chloroplast-laden pectin hydrogels were formed via thiol-ene photo-crosslinking with pectin-norbornene and dithiothreitol. As a result of modulus measurement, the network integrity was maintained in incubation medium for 14 days. In pectin hydrogel, the encapsulated chloroplasts showed photosynthetic activity for 7 days, while the depletion of the photosynthetic activity of the chloroplasts suspended in the medium was relatively quick. The use of antioxidant even improved the photosynthetic activity in pectin hydrogel. Importantly, caffeic acid was most effective in preventing chloroplast damage by reactive oxygen species during photosynthesis. In conclusion, photo-crosslinked pectin hydrogel provided a suitable microenvironment for encapsulated chloroplasts, resulting in extended photosynthetic activity.

SB08.03.30

Vertically Aligned Peptide Nanotube Arrays as a Substrate for Neural Cell Differentiation [Jordan Pagliuca](#), Alecsander Da Silva, Prathyushakrishna Macha and Milana C. Vasudev; University of Massachusetts Dartmouth, United States

There is an increasing need for biocompatible neuronal cell proliferation and regeneration scaffolds as regeneration of the neurite structures is slow and complex, which results in permanent nerve cell damage. Non-invasive electrical stimulation could potentially enhance neural cell proliferation and differentiation. Interfacing cells with biocompatible materials with electrical properties could be harnessed to introduce potential gradients across the cell membrane for neurological activation and repairs. The ability to stimulate individual neurons can impact the development of neural networks, and enhanced motor rehabilitation. The influence of voltage stimulation on human neural progenitor cells will be studied in-vitro using a high-density array of peptide-based nanotubes deposited via plasma-enhanced chemical vapor deposition (PECVD). Peptide-based building blocks containing aromatic amino acids that can self-assemble to form highly organized nanoscale structures with key functional properties such as biocompatibility, high aspect ratios, semi-conductivity, and stiffness will be used as the scaffold in this study. Tryptophan and tyrosine are aromatic amino acids known for their redox properties and roles in neurotransmitter synthesis. These structures have the ability to “carry” cells, which should result in functional modifications and an alteration in protein behavior, which can lead to highly polarized cells. Following the analysis of physicochemical properties of these peptide nanostructures, we studied the biological interactions and influence these scaffolds on human bone marrow neuroblasts and neural progenitor cells and subjected to an electrical stimulation. Prior studies have used carbon nanotubes scaffolds for subsequent electrical stimulation protocols, but their cytotoxicity makes their use in many biological systems undesirable. Electrical stimulation can induce the depolarization of the plasma membrane, as well as affect the function of membrane proteins, including enzyme activity and ion-transporting channels. These processes are most likely generated via the increased presence of reactive oxygen species (ROS), which are highly reactive molecules that have also been found to potentially act as an intermediate signal transducer

between neural cells for the purpose of cell differentiation. To test the same, MTT (3-(4,5-dimethylthiazol-2-yl)-2,5-diphenyltetrazolium bromide) cytotoxicity studies, morphological cellular interaction imaging through SEM and confocal imaging, dopamine-enzyme linked immunosorbent assay, immunostaining for neuronal markers, and real-time polymerase chain reaction (q-PCR) for gene expression were carried out on the neuronal cells cultured on the synthesized peptide bioscaffolds.

SB08.03.32

Molecular Dynamics Simulations for RNA—Benchmark and Folding-Stretching Experiments Arpenik K. Kroyan and Sondre K. Schnell; Norwegian University of Science and Technology, Norway

The ability to accurately model RNA in computer simulations is important as potential applications are increasing with the mRNA vaccine platform. Various length and shape of RNA chains as well as their interactions with the environment, play an important role in medicine, origin of life and homochirality studies. The extensive experimental research on short RNA strings provide an excellent opportunity to utilize those structures as benchmarks for nucleic acids force-fields[1], and increase our understanding of structural and dynamic properties RNA strings. In recent years, *all-atom* molecular dynamics was used to show accurate RNA folding[2], dynamic protein-RNA binding[3] and plasticity of dsRNA duplexes[4] among others. We have studied a series of RNA dinucleotides, tetranucleotides and hairpin loops, GAGA (IZIG) and UUCG (2KOC), with respect to structural stability in vacuum, and in presence of implicit- and explicit water, for AMBER-OL3, OPLS-AA/M, and CHARMM-36. The results of J3 coefficients from dihedral angles were compared with experimental NMR data. For these models, AMBER recreated the structures with best agreement with experimental data, compared to OPLS and CHARMM. Based on results stretching-folding experiments were conducted on selected nucleotides in AMBER-OL3/bsc0 force field with explicit water and vacuum. The dynamic and mechanical properties of RNA chains were shown as a function of chain length and investigated further for size effects.

[1] J. Zhao et al. “Nuclear Magnetic Resonance of Single-Stranded RNAs and DNAs of CAAU and UCAAUC as Benchmarks for Molecular Dynamics Simulations”. In: *J. Chem. Theory Comput.* 16.3 (2020), pp. 1968–1984. doi:10.1021/acs.jctc.9b00912.

[2] A. M. Yu et al. “Computationally reconstructing co-transcriptional RNA folding from experimental data reveals rearrangement of non-native folding intermediates”. In: *Nat. Comput. Sci.* 81.4 (2021), pp. 870–883. doi:10.1016/j.molcel.2020.12.017.

[3] M. Krepl et al. “MD simulations reveal the basis for dynamic assembly of Hfq RNA complexes”. In: *J. Biol. Chem.* 296.100656 (2021), pp. 1–15. doi:10.1016/j.jbc.2021.100656.

[4] W. He et al. “The structural plasticity of nucleic acid duplexes revealed by WAXS and MD”. In: *Sci. Adv.* 7.17 (2021), pp. 1–15. doi:10.1126/sciadv.abf6106.

SB08.03.33

Glycopolyelectrolyte Nucleic Acid Transfection Agents to Address Tick-Borne Diseases Sarah E. Morgan, Kelli Stockmal, Latoyia P. Downs, Lisa K. Kemp and Shahid Karim; University of Southern Mississippi, United States

Black-legged ticks (*I. scapularis*) are vectors for a number of pathogenic bacteria, parasites, and viruses that affect both humans and livestock. Reducing the expression of key tick proteins, such as Selenoprotein K (SelK), through RNA interference is a promising approach to reduce pathogen transmission, but efficient delivery of nucleic acids to arthropods has proven challenging. Cationic glycopolymers have shown great promise with human cells as non-viral gene delivery vehicles to protect RNA and enhance delivery while also mitigating polymer cytotoxicity. Previous work established that glucose- and galactose-based glycopolymers exhibited variations in hydrogen bonding patterns in solution and resulted in different polymer-protein aggregation behavior. In this study, statistical acrylamide-based cationic glycopolymers with glucose or galactose pendent groups were synthesized by RAFT polymerization and the effects of saccharide pendent group and cationic monomer loading on polymer cytotoxicity, RNA complexation, and SelK gene knockdown in ISE6 cells were evaluated. All polymers exhibited low cytotoxicity, yet RNA/copolymer complex cell uptake and gene knockdown were highly dependent on saccharide structure and N:P (amino to phosphate groups) ratio.

SB08.03.34

The Role of Water Hydration States in a Bacteria Derived Biopolymer (EPS) /Nanoclay Hydrogel Ziyi R. Qian¹, Yi Yang², Yiwei Fang³, Miriam Rafailovich³, Kuan-Che Feng³, Allen Bethancourt³ and Steven Larson⁴; ¹Wayzata High School/Garcia Institute, United States; ²Amador Valley High School/Garcia Institute, United States; ³Stony Brook University, The State University of New York, United States; ⁴U.S. Army Corps of Engineers, United States

With the onset of climate change, there is increasing concern about its effects on soil erosion. Microorganisms produce extracellular polymeric substances (EPS) that have shown potential in lessening the impact of environmental stressors. Specifically, a *Rhizobium tropici* (*R. tropici*) derived biopolymer has been reported to effectively strengthen the soil and mitigate soil erosion. Another study suggests that this biopolymer enhances the plant growth, proliferates leaf production and develops a compact root structure. To probe the mechanism behind EPS and its role in compacting soil and stimulating plant growth, we studied water retention and water-biopolymer, soil-biopolymer interactions.

EPS produced from *Rhizobium tropici* bacteria were ethanol precipitated into EPM(ethanol precipitated materials). 5%, 10%, 20% EPM biopolymers rehydrated with different kaolinite (EPK) concentrations were prepared. For each concentration of biopolymer and water mixture, four samples were made, containing clay that are 0%, 5%, 10%, and 20% by mass. The hydrated water molecules in polymer can be divided into three classes: free water, intermediate water (weakly bonded), and non-freezing water (tightly bonded). Differential Scanning Calorimetry (DSC) was carried out on EPS/EPK hydrated samples by a cooling scan from 25°C to -50°C followed by a heating scan to 25°C at 10 °C/min rate. The proportion of the freezable water (free water), non-freezable water was calculated based on the enthalpy of the melting peaks. The calculated non-freezable water in rehydrated EPS increased from 5% to 21% with higher EPS concentrations. This indicates a possible formation of a more compact structure when EPS is at high concentration. In the EPS/EPK system, the presence of a secondary melting peak at -8°C which is not observed in EPK/water mixture indicates that kaolinite in EPS induces a weakly bounded water layer. On the other hand, the percentage of non-freezable decreases as more EPK is introduced in EPS. A possible explanation of this is that the surface of kaolinite contact water diminishes the surface where water is enclosed by entangled biopolymer EPS. A model of nacre-like structure of EPS-EPK-EPS is supported by cryo-SEM images, and postulated to be the mechanism of EPS stabilizing the soil.

Next, the water retention behavior of EPS was investigated by two means. A low concentration of 1% rehydrated EPS water solution droplet ~ 5 µL was dropped on untreated silicon wafer. Subsequently, the droplet width and height versus time were measured at 3-minute intervals using the goniometer. Using water contact angle analysis, the rate of evaporation was determined for each sample at pH 5, 6, 7, 8, and 9 to simulate performance in real environmental soil conditions. Lastly, the water retention ability of biopolymer EPS was also assessed by taking one droplet~10 mg on a mass balance to record the rate of evaporation by mass over time.

Calorimetry data indicated that higher concentrations of biopolymer and percent of non-freezable water were positively correlated. Also, the addition of kaolinite changes the surface chemistry of EPS biopolymer. Droplet analysis of all three solutions revealed that the biopolymer evaporated height-wise, while water evaporated equally in height and width. Biopolymer solutions from varying pH all evaporated height-wise, with greater height change in solutions further from the original 7 pH solution. The formation of a complex from the EPS/EPK may explain its soil strengthening ability. These suggest

possible applications such as maintaining crop-soil moisture and aiding soil compaction during freeze-thaw cycles. Future goals are to solidify our understanding of the interaction between EPS and nanoclay with field tests, and properties that promote soil health, paving the way to an environmentally friendly future.

Work supported by the ERDC (W912HZ-20-2-0054) and the Morin Charitable Trust.

SB08.03.35

The Role Played by the Extra-Fibrillar Volume in the Structural and Mechanical Properties of Bones Amadeus Alcantara^{1,1,2}, Levi C. Felix^{1,1}, Douglas S. Galvao^{1,1}, Paulo Sollero^{1,1} and Munir Skaf^{1,1}; ¹University of Campinas, Brazil; ²Massachusetts Institute of Technology, United States

Due to their complex network of distinct physical structures at different length scales, bones are responsible for body support, structure, motion, and several other functions for many different life forms. At the nanoscale scale, bones can be characterized as a fiber composite, i.e., a bundle of mineralized collagen fibrils surrounded by a matrix of water and calcium minerals. Different fractions of these constituents lead to different bone mechanical properties, making each bone unique, thus patient-specific.

It is well established in the literature that a higher concentration of mineral content leads to superior mechanical properties, i.e., stiffer bones. Moreover, most of the mineral content in bones, about 80%, is found in the matrix surrounding the fibrils, also labeled the extra-fibrillar volume (EFV). However, the literature presents models that include minerals in the intra-fibrillar volume (IFV) only, models that resemble mineralized collagen fibrils.

In this study, we investigate the structural and mechanical properties of all-atom bone molecular models constituted of type-I collagen, hydroxyapatite, and water through molecular dynamics (MD) simulations. Our models resemble fibers in bones, they encompass an EFV, explore different degrees of mineralization, and consider mineral content in both the EFV and the IFV, consistent with experimental observations presented in the literature. An analysis of the radial distribution function reveals that the local tetrahedral order of water is lost in similar ways in the EFV and IFV regions for all mineralized models, as calcium and phosphate ions are strongly coordinated with water molecules. By performing MD simulations using LAMMPS, we subject our models to uniaxial tensile loads and analyze their mechanical response. An analysis of the spatial stress distribution shows that the EFV plays a crucial role in the mechanical response of bone fibers. Both mineral and water content concentrate higher stresses when located in the EFV. Our results also corroborate the well-established finding that high mineral content makes bone stiffer. Our study reveals the EFV, which has been only recently contemplated in all-atom models, as an essential region to be considered when studying the mechanical properties of bones at the nanoscale. The mechanical properties of bones at such small scales can directly affect the properties at higher length scales, making bone more or less prone to fracture. Further development and studies on such elaborate all-atom models can give us additional insight into deformation and failure processes in bone, leading to a better understanding of bone diseases like osteoporosis.

SB08.03.36

Deposition of DNA onto Polymethacrylate (PMMA) Thin Film Gratings in Preparation for the Tagmentation of DNA with Tn5 Transposase Rachel Y. Na^{1,2}, Deryn O'Leary^{3,2}, Hannah Saks^{4,2} and Jonathan Sokolov²; ¹Friends Academy, United States; ²Stony Brook University, The State University of New York, United States; ³Our Lady of Mercy Academy, United States; ⁴Walt Whitman High School, United States

In recent years, next-generation sequencing (NGS) has significantly advanced high-throughput sequencing. However, the NGS library preparation process can result in the loss of information regarding spatial organization, making reassembly difficult [1]. This study examines the application of depositing DNA onto flat polydimethylsiloxane (PDMS) samples that are then contact-printed onto PMMA-coated thin film gratings to suspend the DNA (bridging) and provide steric clearance for the Tn 5 transposase to simultaneously cut and label the DNA strands, a process termed tagmentation.

Samples of PDMS were dipped into solutions of λ DNA (NEB) in either DNase I reaction buffer (NEB) or Tris-EDTA (TE) buffer with sodium chloride to promote DNA adsorption to PDMS. Glycerol was also added to some solutions at a 1% (v/v) concentration to encourage the DNA to transfer from the PDMS to the Si grating. The samples were then imaged with a LEICA fluorescence microscope at 10x and 63x magnification. Samples with linearly stretched DNA were stamped onto a PMMA-coated Si wafer for various lengths of time up to 180 seconds using various weights up to 70 g. Results indicated that PDMS cured in a 60°C oven for 48 hours increased the adhesion of DNA onto the PDMS. However, this made it too difficult for the DNA to be stamped and transferred onto the Si wafer. PDMS that was cured for less time (4 hours) resulted in improved separation of adsorbed strands. Additionally, the NaCl made it difficult to transfer the DNA, causing the DNA to tear and not bridge. To address this problem, glycerol was added instead of salt to aid transfer. Furthermore, it was found that finer gratings were preferable because the DNA did not need to stretch as far to bridge. A solution with a concentration of 2.5 ng λ DNA per μ L of DNase I reaction buffer with 1% (v/v) added glycerol deposited on PDMS and stamped across an 8.6 μ m linear grating for 15 seconds and no weight yielded the best results thus far. Further development of this method will allow NGS to be analyzed with minimal risk of losing important genome information.

We acknowledge the Morin Charitable Trust for funding.

[1] Cho, NaHyun & Goodwin, Sara & Budassi, Julia & Zhu, Ke & McCombie, W. & Sokolov, Jonathan. (2017). Fragmentation of Surface Adsorbed and Aligned DNA Molecules using Soft Lithography for Next-Generation Sequencing. *Journal of Biosensors & Bioelectronics*. 08. 10.4172/2155-6210.1000247.

SB08.03.37

Lubricant Skin on Diverse Biomaterials with Complex Shapes via Polydopamine-Mediated Surface Functionalization for Biomedical Applications Kijun Park and Jungmok Seo; Yonsei University, Korea (the Republic of)

Implantable biomedical devices require an anti-biofouling, mechanically robust, low friction surface for a prolonged lifespan and improved performance. However, there exist no methods that could provide uniform and effective coatings for medical devices with complex shapes and materials to prevent immune-related side effects and thrombosis when they encounter biological tissues. Herein, we developed a facile method to fabricate a robust lubricant-infused surface for biomedical devices which can be applied to any materials regardless of their size, shape, and composition. The application of the robust lubricant-infused surface to the materials was facilitated by a bio-inspired adhesive polymer, polydopamine (PDA) that activates the substrate surface to form stable covalent bonds with an engineered fluorinated polymer. The bio-inspired adhesive layer makes the application of the fluorinated polymer suitable for any type of surface with different material compositions and shapes. The resultant fluorinated polymer forms a very thin layer with a controllable thickness which exhibits swelling behavior in fluorinated lubricant forming lubricant-infused skin (L-skin). This allows the surface to maintain an adequate amount of lubricant even without the hierarchical structures of conventional liquid-infused surfaces. The smooth surface of L-skin provides superior anti-biofouling properties against viscoelastic fluids (blood, saliva, bacterial suspension) and solids (feces, biological tissues) which make L-skin suitable for biomedical applications. Unlike conventional self-assembled monolayer (SAM) based lubricant-infused surfaces, L-skin is both mechanically and chemically robust that maintains its functionality following swabbing, scratching, and sterilizations. To further investigate the wide adaptability of the

L-skin, various applications in which complex structure requires anti-biofouling properties were demonstrated in small diameter bioprinting needle (Inner diameter = 53 μm), microfluidic channels (Channel height 150 μm), and long narrow silicone tubing (2 meters long).

SB08.03.38

Biopolymers from a Bacterial Extracellular Matrix Affect the Morphology and Structure of Calcium Carbonate and Calcium Oxalate Crystals David N. Azulay, Malachi Fraenkel, Ilanit Ben Simhon, Razan Abbasi, Sergei Remennik, Amarendar Reddy and Liraz Chai; The Hebrew University of Jerusalem, Israel

Biomineralization is a mineral precipitation process occurring in the presence of organic molecules and used by various organisms to serve a structural and/or a functional role. Many biomineralization processes occur in the presence of extracellular matrices that are composed of proteins and polysaccharides.

There is growing evidence that bacterial biofilms induce calcium carbonate mineralization, giving the system enhanced mechanical properties and that this process may be related with their extracellular matrix (ECM). In addition, recently, it has been suggested that bacteria and biofilms may play a role in calcium oxalate kidney stones genesis and development. Therefore, we explored, *in vitro*, the effect of the ECM components, the exopolysaccharide EPS, and the protein TasA on calcium carbonate and calcium oxalate crystallization. Moreover, the protein TapA was also tested on calcium carbonate. By characterizing the crystals using SEM, micro-Raman spectroscopy, FTIR, XRD, FIB-SEM and SAED we showed that: In both the calcium carbonate and calcium oxalate, the biopolymers had an effect on the morphology of the crystals by the interaction of the polymers with specific planes. In the presence of the proteins the calcium carbonate crystals were composed of single crystalline domains that assemble together into spherulites (in the presence of TapA) or dumbbell-like shapes (in the presence of TasA). The TasA produced rounded microstructure crystals of calcium oxalate. The EPS, in addition, affected the structure of the crystals, producing less thermodynamically stable crystals, vaterite and calcium oxalate dihydrate.

Our results suggest the EPS affects the nucleation of calcium minerals unlike the proteins that seem to affect only the crystal growth. Biomineralization processes induced by bacterial ECM macromolecules make biofilms more robust and difficult to remove when they form, for example, on pipes and filters in water desalination systems or on ship hulls. Understanding the formation conditions and mechanism of formation of calcium carbonate and calcium oxalate in the presence of bacterial biopolymers may lead to the design of suitable mineralization inhibitors as well as better approaches for kidney stones treatments.

SB08.03.39

Photoinduced Polymerization of Small Molecules for the Formation of Organic Electronic Devices Marios Savvakis¹, Xenofon Strakosas¹, Tobias Abrahamsson¹, Maciej Gryszel¹, Katriann Arja¹, Mathieu Linares¹, Ioannis Petsagkourakis², Eva Miglbauer¹, Marc-Antoine Stoeckel¹, Benjamin Granroth¹, Jennifer Gerasimov¹, Magnus Berggren¹ and Daniel Simon¹; ¹Linköping University, Sweden; ²RISE, Research Institute of Sweden, Sweden

The application of small self-organized molecular systems for the formation of soft and in situ electrodes with combined electrical and biochemical signals leads to new means of bridging the biology-technology gap. Such systems have seen increased attention over the past few years with their promise of entirely novel pathways for monitoring and augmenting biological function. In parallel, organic electrochemical transistors (OECTs) have become a standard tool in the field of organic bioelectronics as they can take full advantage of ion (biomolecule) injection from an electrolyte (or physiological system) to modulate the volumetric conductivity of an organic semiconductor channel. In addition, overall biocompatibility and synthetic tunability of the organic conductive polymers make OECTs ideal for interfacing with biological systems. In this work we have combined the burgeoning field of in situ formed organic electronic materials into an OECT platform by using light-assisted photocatalysis. Specifically, we used direct light excitation, as well as excitation of porphyrins, for the in situ photoinduced polymerization of conjugated oligomers. The conjugated oligomers, bis[3,4-ethylenedioxythiophene]3thiophene sulfonic acid (ETE-S, *i.e.*, an EDOT-thiophene-EDOT trimer with a sulfonate ligand) and a variety of derivatives (ETE-CooNa and EEE-CooNa) were implemented, and the photoinduced polymer films were assessed by cyclic voltammetry as well as transistor output and transfer characteristics. The resulting OECTs exhibited excellent figures of merit (Transconductance, on/off ratio) with performance approaching PEDOT:PSS but with several advantages. We believe that these results pave the way for expanded in situ bioelectronics and even OECTs and similar component fully formed/fabricated in vivo.

SB08.03.40

Determining the Efficiency of Using Transposase (Tn5) to Cut DNA on PMMA Surfaces Tanya Shukla¹, Yuhang Wu² and Jonathan Sokolov³; ¹Ardley High School, United States; ²Worcester Academy, United States; ³Stony Brook University, The State University of New York, United States

DNA sequencing technology has been evolving throughout the past century, however, in the past 10 years, new approaches to sequencing technology, namely Next Generation Sequencing (NGS), have been emerging to make this process more streamlined. With current technology, sequencing reads are limited to the order of 10,000 base pairs or less. Therefore, cutting the DNA into sequenceable portions is vital [2]. After cutting, the spatial ordering of the DNA fragments is usually lost, requiring a complex computational method for reassembly. One novel solution to this problem is using soft lithography and hydrophobic surfaces instead of solution-based cutting [1]. This allows for preservation of DNA order.

In our experiment, Transposase (Tn5), an enzyme that cuts and moves DNA strands, was tested at its ability to fragment surface-immobilized DNA on a PMMA surface. Tn5 solution was made by mixing transposase solution, Tagmantase buffer, and water of varying concentrations. Silicon wafers were cut into 6 mm wide and 15 mm long samples to be spun cast with 70 nm thick films of PMMA. The wafers were dipped into DNA solution and later in Tn5 solution for the DNA-cutting reaction. Using a Leica Fluorescent microscope, images of the SyBr Gold labeled DNA strands were taken and then used for data analysis. To test the efficacy of using SDS and Proteinase K as a Tn5 removal agent, this experimental procedure was repeated with different concentrations of Tn5 solutions (0.0008 mg Tn5/mL, 0.0016 mg Tn5/mL, and 0.0032 mg Tn5/mL) for both SDS and Proteinase K reactions. Additionally, Proteinase K reactions were repeated at both room temperature as well as 55 degrees C.

The results indicate that after Proteinase K removed Tn5, DNA strands were cut into linear segments with ordering preserved; while with SDS, the DNA strands were curled up and in disorder. The trials with Proteinase K were analyzed using ImageJ. It was found that DNA strands were fragmented after the Tn5 reaction. At 0.0016 mg Tn5/mL, room temperature and heated, the strand length averaged 1.87 μm and 0.91 μm respectively after the Tn5 reaction. Before the Tn5 reaction, the strand lengths averaged 16.20 μm and 16.29 μm respectively. At 0.0032 mg Tn5/mL, room temperature and heated, the strand length averaged 0.71 μm and 1.05 μm respectively after the Tn5 reaction. Before the Tn5 reaction, the strand lengths averaged 17.91 μm and 12.28 μm respectively. This indicates that Tn5 can effectively fragment DNA on surfaces when the transposase is pre-loaded onto the DNA in solution before surface adsorption.

We would like to acknowledge the Morin Charitable Trust for funding.

[1] Cho, N. H., Goodwin, S., Budassi, J., Zhu, K., McCombie, W. R., & Sokolov, J. (2017). Fragmentation of surface adsorbed and aligned DNA molecules using soft lithography for next-generation sequencing. *Journal of Biosensors & Bioelectronics*, 08(04). <https://doi.org/10.4172/2155-6210.1000247>

[2] Goodwin, S., McPherson, J. D., & McCombie, W. R. (2016). Coming of age: Ten Years of next-generation Sequencing Technologies. *Nature Reviews*

SB08.03.41

Self-Polymerized Plant Polyphenols as Antibacterial Agents Zhen Tian and Young Jo Kim; University of New Hampshire, United States

Polyphenols are a class of biologically active compounds that are derived from plant-based natural products such as fruits, vegetables, coffee, and tea. Polydopamine, dopamelanin, gallic acid, pyrogallol, and tannic acid contain the representative chemical features of polyphenols which can form coordination bonding with protons, ions, or electrons via redox reaction. Due to their physical, chemical, and electrochemical properties, polyphenols have attracted significant interest in various research areas, including charge storage, heavy metal ions removal, or drug delivery. Recent studies have shown that phenol-based polymeric particles can inhibit bacterial growth and prevent biofilm formation by releasing the reactive oxygen species in aqueous environment. However, the surface disruption of polymers in complex surroundings and the poor efficiency due to the low surface area to volume ratio of the coating remain the potential challenges that shorten the long-term stability.

Herein we report the facile synthesis of a free-standing poly(pyrogallol) (1,2,3-trihydroxybenzene, PPG) polymer that can be used as an environmental friendly and efficient antibacterial agent. PPG consists of homogeneous nanofibrous microstructure containing the chemical moieties that allow the reversible redox reaction via catechol or gallol groups. Fourier transform infrared spectroscopy and X-ray photoelectron spectroscopy corroborated the formation of the ether functional groups that are induced by the polymerization between the hydroxyl group and the carbons of the benzene. The antibacterial activity of PPG was examined using the gram-negative *Escherichia coli*. The antibacterial activity was quantitatively evaluated by a colony count method after incubating the *E. coli* with the concentration of 1.5×10^5 CFU mL⁻¹. The survival rates were compared with the natural melanins extracted from *Sepia Officinalis* that contains the catechol groups. PPG achieved 63.1% and 99.9% *E. coli* inhibition within 30 min and 4 h of incubation, which is approximately 50% higher than the catechol-containing melanins. This is mainly due to the higher density of phenolic compounds available in PPG to produce ROS in the aqueous environment. The results herein suggest that PPG exhibits potential to be utilized as functional antibacterial agents for a variety of applications in biomedical and environmental engineering.

SB08.03.42

Determining the Extent to Which Sodium Dodecyl Sulfate Could Desorb DNA from Flat Surfaces Derek Days¹, Ohm P. Patel² and Jonathan Sokolov³; ¹Noble and Greenough School, United States; ²Patchogue-Medford High School, United States; ³Stony Brook University, The State University of New York, United States

The use of Tn5 transposases is essential to Next Generation Sequencing (NGS) as it is required to cut DNA into shorter and more manageable lengths while also labeling the shortened strands to be later rearranged into the original sequence[1]. However, Tn5 transposases have to wrap around DNA in order to cut, posing an issue for surface-adsorbed DNA samples[2]. In recent transposon experiments, evidence suggests that sodium dodecyl sulfate (SDS), which is already used to remove the Tn5 transposases from DNA molecules after cutting is complete, could desorb the DNA from a flat surface, specifically polymethyl methacrylate (PMMA) spun-cast on silicon. Finding a method of desorbing DNA from a flat surface remains important because it provides an opportunity to increase the efficiency and decrease the cost of NGS in fields such as medical diagnoses and forensic science. Although there are already existing methods of desorbing DNA, they are cumbersome and time-consuming. In this study, we aimed to investigate whether or not SDS could desorb surface-adsorbed DNA. To do this, 0.286% DNA in DNase buffer dyed with SYBR Gold was prepared and machine-dipped onto PMMA spun-cast onto silicon. After doing so, the DNA sample was imaged under a fluorescence microscope under 63x magnification to determine the quality of the sample. Once the quality was confirmed, the sample was placed into a well containing 350 μ L of varying concentrations of SDS in water. This way, half of the wafer would have been treated with SDS while the other side would serve as a control. The wafer, still in the well, was then placed into a column heater and heated at 55°C for 20 minutes. Once finished, the wafer was once again placed under the microscope for analysis. Initially, it was thought that the SDS did in fact desorb the DNA from the surface as no DNA could be seen on the SDS-treated side. Microscope images showed a distinct border between the SDS-treated side, where no DNA was visible, and the non-SDS side, where DNA was clearly visible. However, after re-dyeing the SDS-treated side in SYBR Gold, DNA was once again shown on the surface. This implied that SDS could not desorb surface-adsorbed DNA but could remove SYBR Gold dye from DNA. Although SDS likely cannot desorb surface-adsorbed DNA, future experiments will be done on Triton X-100 instead in an effort to find an easier method of desorbing DNA from flat surfaces.

[1] Feng, Kuan. "Comprehensive Sequencing with Surface Tagmentation Based Technology." (2018). https://digitalrepository.unm.edu/biom_etds/188

[2] Cho N, Goodwin S, Budassi J, Zhu K, McCombie WR, et al. (2017) Fragmentation of Surface Adsorbed and Aligned DNA Molecules using Soft Lithography for Next-Generation Sequencing. *J Biosens Bioelectron* 8: 247. doi: 10.4172/2155-6210.1000247

We thank the Morin Charitable Trust for funding.

SB08.03.43

Rheological and Toxicological Properties of the Extracellular Polymeric Material (EPM) Produced by *Rhizobium Tropicum* ATCC 49672 Eliana Samuels¹, Maytal Chelst¹, Gabriel Rothman², Marcia Simon³, Miriam Rafailovich³, Kuan-Che Feng³, Yiwei Fang³, Stephen Walker³ and Steven Larson⁴; ¹Yeshiva University High School for Girls, United States; ²The Frisch School, United States; ³Stony Brook University, The State University of New York, United States; ⁴ERDC, United States

Soil erosion is a significant issue costing the U.S. economy forty-four billion dollars per year and increasing water pollution (Sulaeman & Westhoff, 2020). Typical erosion treatments use toxic, non-biodegradable petrochemicals that pose threats to surrounding ecosystems and agricultural efforts. An alternative may come from symbiotic *Rhizobium tropicum* bacteria which secrete gel-like biopolymers known as EPS that can then be ethanol precipitated into EPM (non-dialyzed EPS) (Maróti & Kondorosi, 2014). EPS soil treatments have been tested by the ERDC and results indicate that the soil was strengthened substantially, reducing erosion. REF Analysis of the vegetation showed that plant root systems were larger, which was postulated to be a contributing factor to the soil stability increase. The role of bacterial infection and nitrogen sequestration in root development has been extensively studied, but less is known about the role of bacterial EPS in strengthening the soil via gelation or other interactions with the soil particles. In order to study the possible mechanisms through which the EPS can strengthen soil, we performed a series of experiments where the biopolymer was precipitated in alcohol and subsequently rehydrated. In this manner no bacteria was present and only the material properties of the EPS are probed.

The rehydrated EPM's rheology behavior with various concentrations was tested on DHR-2 rheometer oscillation-amplitude and oscillation-frequency mode. The results show that upon rehydration the polymer formed a gel at concentrations of 2% with a modulus $G' = 20$ Pa. The modulus increases approx. linearly with concentration to a value of $G' = 300$ Pa at a concentration of 20%. In each case a distinct yield point was observed, at 20-170 Pa between the lowest and highest concentrations measured, where G' approached zero. The systems were rested for 30 min without an applied force and the amplitude scan was repeated. The gels completely recovered in each case after at least three cycles, indicating that in each case physical gels were formed and then reformed when the forces were removed. Measurement of the gels in the frequency mode indicated shear thinning behavior in all cases at room temperature. The chemical structure of the gels was investigated using Raman spectroscopy and TGA. RAMAN spectroscopy indicated that the EPM was

composed of polysaccharides with a high content of potassium dihydrogen phosphate. TGA showed that ~50% of the gel was removed at T<100C, and another 10% was removed at T<257C. This is consistent of a gel with large water content, while the additional 20% indicated strongly adsorbed water and a high degree of water retention. A surprisingly high fraction, ~30% of the gel was stable to temperatures of at least 800C. This temperature is higher than organic polymers, and was attributed to the dihydrogen phosphate salts. RAMAN spectroscopy of this residue confirmed this where one large and narrow peak was observed consistent with a crystalline compound formation. Auxiliary testing for the antibacterial, antiviral, and cytotoxic effects of the EPM were performed to determine the safety of EPM application into soil. Results indicated that EPM is neither antiviral nor antibacterial. Application of EPM into human fibroblast cultures indicated no adverse effects on the doubling time nor any other function of the tissue.

Work supported by the ERDC (W912HZ-20-2-0054) and the Morin Charitable Trust.

E. M. G. K. (2014, June). Nitrogen-fixing rhizobium-legume symbiosis: Are polyploidy and host peptide-governed symbiont differentiation general principles of endosymbiosis? *Frontiers in Microbiology*.

Larson, S., Nijak Jr, G., Corcoran, M., Lord, E., & Nestler, C. (2016, June). Evaluation of Rhizobium tropici-derived Biopolymer for Erosion Control of Protective Berms. US ERDC.

Sulaeman, D., & Westhoff, T. (2020, Feb.). The causes and effects of soil erosion, and how to prevent it. World Resources Institute.

SB08.03.44

Extraction and Characterization of *Stichopus cf. horrens* Collagen with Potential Stimuli-Responsive Properties as Collagen-Based Films Kim Marie D. Sisican, Vicenzo Paolo M. Torreno, Eizadora T. Yu and Marlon T. Conato; University of the Philippines, Philippines

The mutable collagenous tissue (MCT) of echinoderms has been extensively studied because of its mechanism that allows rapid change in its stiffness and extensibility. Collagen is also the most abundant protein in the extracellular matrix and provides its main structural component. Thus, research on its physicochemical and mechanical properties will be useful for identifying its potential for cosmeceutical and biomedical applications. Moreover, the unique properties of MCTs can also be an inspiration for the design of new smart functional biomaterials. Sea cucumbers, like other echinoderms, also have MCTs that respond according to different environmental stress conditions. There are many sea cucumber species found in the Philippines, but only a few are studied well. Among the less studied ones is the *Stichopus cf. horrens*, which is also commonly found in other Southeast Asian countries. In this study, we have extracted the collagen from *S. horrens* and characterized its physicochemical properties. Pepsin-solubilized collagen (PSC) was prepared, and using SDS-PAGE we observed the presence of the β , $\alpha 1$, $\alpha 2$, and $\alpha(1)3$ chains at 75 to 250 kDa, typical for Type I collagen. Protein identification and sequence analysis were also performed. Protein blast search showed the presence of sequences commonly found in Type VII and XII collagen. This suggests that *S. horrens* collagen is heterotypic, consistent with related proteomic studies of collagen from other species. The maximum absorbance of PSC was also measured at 212 nm using UV-Visible spectrometry, attributed to the presence of multiple peptide chains of collagen. The susceptibility of collagen to heat is another way of determining its potential application. We identified a higher maximum transition temperature ($T_m = 56^\circ\text{C}$) for the PSC extracted from *S. horrens* using differential scanning calorimetry (DSC) as compared to other sea cucumber species. The T_m of collagen correlates to its stability and durability, suggesting that *S. horrens* PSC has higher thermal stability—uncharacteristic of marine-derived collagen. After the physicochemical characterization, the extracted collagen was used for the facile preparation of collagen-based films through the solvent casting method using phosphate-buffered saline at pH 7.4 as the solvent. The FTIR spectra of the films showed the characteristic peaks of collagen—Amide A (3341 cm^{-1}), I (1657 cm^{-1}), II (1553 cm^{-1}), and III (1241 cm^{-1}). AFM imaging also showed that the collagen fibers making up the films have a diameter of $145 \pm 31\text{ nm}$. Due to the high thermal stability of *S. horrens* PSC based on the DSC findings, the thermal response of the films was also analyzed using thermomechanical analysis (TMA) at a constant applied force of 0.1 N. Here, we observed that thermal degradation only starts at a temperature of $>190^\circ\text{C}$. Meanwhile, at lower temperatures of 100 and 150°C , the films changed from translucent and soft into an opaque and brittle physical state due to the removal of moisture. Subsequent AFM images showed that the collagen fibers are still present and intact after TMA. Upon exposure to ambient temperature (25°C) for 10 min, the collagen-based films returned to their original translucent and soft state due to the reabsorption of moisture. TMA analysis at lower temperatures was repeated at least three times before the films started degrading based on apparent discoloration. This study shows that *Stichopus cf. horrens* is a potential source of collagen that can be prepared into useful smart biomaterials, such as collagen-based films stable at higher temperatures, for food and biomedical applications.

SB08.03.45

Bio-Inspired Macromolecular Ordering in Elastomer Composites to Achieve Enhanced Contact Electrification Andris Šutka, Linards Lapčinskis, Osvalds Verners, Liva Germane and Juris Blums; Riga Technical University, Latvia

Polymer contact electrification (a.k.a. triboelectrification) is crucial for mechanical energy harvesting in triboelectric nanogenerators (TENG), droplet generators, and ferroelectrets [1]. Polymer triboelectrification can be enhanced in several ways, including surface functionalization, adjustment of the electronic and physicochemical properties or by increasing the specific contact area via nanostructuring.

Contact electrification can be observed also in nature. Spider ballooning is one of the most exciting natural phenomena. Using electrified strands of silk, spiders can travel in the airstream for distances of hundreds of kilometers [2]. Spider silk is electrified due to contact and friction with airborne particles or during the spinning process. A strong surface charge is required to ensure the electrostatic flight, holding the weight of a spider even in the absence of any air stream.

This work presents triboelectric polymer composites with structure inspired by the macromolecule ordering in spider-silk leading to strongly enhanced contact electrification. The ordering in polyether block amide (PEBA) is induced by the addition of inorganic goethite ($\alpha\text{-FeOOH}$) nanowires that form hydrogen bonds with the elastomeric matrix. The addition of as little as 0.1 vol% of $\alpha\text{-FeOOH}$ into PEBA increases the surface charge by more than order of magnitude. Hydrogen bonds between $\alpha\text{-FeOOH}$ and PEBA promote the formation of inclusions with higher degree of macromolecular ordering, analogous to the structure of spider silk. The formation of these inclusions is proven *via* nanoindentation hardness measurements, and correlated with H-bond induced changes in structure shown by fourier transform infra-red spectroscopy, and direct scanning calorimetry. Theoretical studies reveal that the irregularity in hardness provides stress accumulation on the polymer surface during contact-separation. Subsequent molecular dynamic studies demonstrate that stress accumulation promotes the mass-transfer during contact electrification. The proposed macromolecular structure design provides a new paradigm for developing materials for applications in mechanical energy harvesting.

References

[1] B. -Y. Lee, D. H. Kim, J. Park, K. -I. Park, K. J. Lee, C. K. Jeong, *Sci. Technol. Adv. Mater.* **2019**, *20*, 758.

[2] E. L. Morley, P. W. Gorham, *Phys. Rev. E* **2020**, *102*, 012403.

SB08.03.46

Investigating Virus-Induced Thrombogenicity at the Molecular Level Ekam Singh¹, LeAnn Tai², Keonhyoung Kim³, Matthew Lu⁴, Miriam Rafailovich⁵, Kuan-Che Feng⁵, Adam Hansen⁵ and Kao Li⁵; ¹Washington High School, United States; ²Arnold O. Beckman High School, United States; ³Jefferson Forest High School, United States; ⁴Chapel Hill High School, United States; ⁵Stony Brook University, The State University of New York, United States

Fibrinogen is a plasma-soluble glycoprotein that is responsible for thrombogenesis, the formation of blood clots. While thrombogenesis is an important process, excessive blood coagulation can cause serious health conditions such as strokes, heart attacks, and embolisms. Viruses such as SARS-CoV-2 and H1N1 can cause thrombosis in host vascular systems, despite endothelial cells lacking the necessary receptors for SARS-CoV-2. Epithelial cells surrounding blood vessels are susceptible to viral infection, and once infected, produce lipids in and around cells. When blood vessels are damaged, infected cells and conditioned media enter the bloodstream, and provide ample hydrophobic surfaces for fibrinogen to polymerize onto and for thrombosis to occur. Here a model is proposed to explain the correlation between virus-induced lipid secretion and fibrinogen fiber formation.

To study the formation of fibrinogen fibers on hydrophobic surfaces, solutions of polybutadiene, polystyrene, and polylactic acid were spincast onto silicon wafers for their thrombogenic and biocompatible nature. Fibrinogen was added to the films, imaged through AFM, and analyzed for morphological properties. To test lipid production, Madin-Darby canine kidney (MDCK-2) cells and human umbilical vein endothelial cells (HUVEC) were plated and infected with the H1N1 virus. Human gingival keratinocytes as models of epithelial cells were also infected with H1N1 through direct infection and conditioned media taken from previous MDCK-2 cultures. After fixing, cultures were stained for actin, lipids, and DNA, and imaged using EVOS microscopy. The images showed multiple lipid droplets concentrated within the MDCK-2 and the gingival keratinocyte cells following infection. Conditioned media and infection in MDCK-2 and HUVEC cultures yielded increases in lipid droplets of 35.13% and 15.02%, respectively. On the HUVEC cultures no brightly stained droplets were visible following direct infection. Only large diffuse regions of green stain were visible following exposure to the conditioned media. Some of these large domains were also found in the epithelial cell cultures following infection, and were likely formed when the lipid droplets were released into the media following the disintegration of infected cells. These diffuse lipid rich regions were then carried from the conditioned media onto the surface of the endothelial tissue after exposure to the conditioned media, demonstrating that the hydrophobic secretions of an infected culture spreads to nearby tissue at the systemic scale.

Polyvinylpyrrolidone (PVP), a hydrophilic surface, will be treated with conditioned media taken from control and H1N1-infected MDCK-2 cultures. According to the model, the non-infected sample should remain relatively hydrophilic, while the infected sample should become more hydrophobic, as measured through contact angle analysis. It is hypothesized that fibrinogen fibers will form on the infected hydrophobic polymer surface and not form on non-infected hydrophilic surfaces. This project reveals that fibrinogen fibers after viral infection are due to the lipid showers in epithelial tissue that make the environment suitable for blood coagulation, which provides insights into the treatment of COVID.

Acknowledgements:

The authors gratefully acknowledge and thank the Morin Charitable Trust for support, as well as Dr. Miriam Rafailovich for mentorship and technical guidance.

SB08.03.47

An On-Demand Bioresorbable, Ultrasound-Mediated Triboelectric Nanogenerator as an Energy Solution of Electronic Medicine System Dong-Min Lee and Sang-Woo Kim; Sungkyunkwan University, Korea (the Republic of)

Over twenty million people in the United States have so far benefitted from implantable medical devices (IMDs) intended for different purposes; therapeutic, diagnostic and rehabilitation. Efforts to improve IMDs have seen the development and use of transient materials, which dissolve in the body after a programmed lifetime, therefore, eliminating the need for secondary surgery to remove the IMD. However, the conventional lithium-ion batteries are non-transient, therefore limiting the use of transient IMDs. Recent advances in energy harvesting technologies have provided transient materials based options with great potential to power transient IMDs. Photovoltaic and thermoelectric in vivo energy harvesters were introduced as sources of power for transient electronics, but their use is limited by lack of light sources, and constant body temperature, respectively. On the other hand, the biodegradability of piezoelectric catalysts is unverified limiting the use piezoelectric nanogenerators in transient electronics. Triboelectric nanogenerators (TENGs) are an emerging technology with great potential for powering transient IMDs, offering a number of advantages including wide material selection and minimizable system scale. Conventional transient TENGs exploit passive operation, referring the circumstances in which their transience starts when implanted and deployed inside the body. Due to the long timescale from the loss of energy generation to the complete transience, undesirable burdens and potential hazards can be induced to the patients.

Here, we demonstrate a new protocol by establishing a remotely stimulated transience mechanism using biologically certified ultrasound sources. To demonstrate the feasibility of ultrasound-triggered TENGs, we developed a fully biodegradable and implantable TENG (FBI-TENG) consisting of a magnesium (Mg) electrode layer, poly(3-hydroxybutyrate-co-3-hydroxyvalerate) (PHBV) membranes, and a poly(ethylene glycol)-based polymeric composite (PHBV/PEG) layer. We aimed to determine the efficiency of the FBI-TENG by solely altering the degree of ultrasound intensity. The ultrasound-triggered transient process which originated from high ultrasound intensity, was initiated by the microporous structure of the PHBV encapsulation layer developed using finite element method (FEM) simulation that facilitates the distribution of intensified acoustic pressure inside the micropores. When the FBI-TENG was inserted into a porcine tissue, we observed a significant reduction in electrical output 20 minutes after applying high ultrasound intensity. Our findings support that ultrasound, a verified non-invasive and reliable power source, can be used for powering IMDs and for provoking device dissolution after a programmed lifetime.

SESSION SB08.04: Functional Biomaterials I
Session Chairs: Jessica Garb and Benedetto Marelli
Tuesday Morning, November 29, 2022
Hynes, Level 3, Room 313

8:30 AM SB08.04.01

Self-Assembled Peptides Form a Highly Catalytic Interface on Graphite Wei Luo¹, Hironaga Noguchi¹, Chen Chen¹, Yoshiki Nakamura¹, Chishu Homma¹, Oleksii Zozulia², Ivan Korendovych² and Yuhei Hayamizu¹; ¹Tokyo Institute of Technology, Japan; ²Syracuse University, United States

De novo-designed peptides emerged to form nano-fibrils in solution and exhibited chemical reactions with activities comparable to natural enzymes.¹ These materials are often referred to as catalytic amyloids.² Their versatility in productive accommodation of various cofactors,³ highly designable sequences, and simple molecular structures that can be produced in large amounts at low cost offers an exciting possibility for creating highly efficient hybrid materials for different electrochemical applications. Although all the currently reported applications of these catalytic peptide amyloids were demonstrated in solution, there are no attempts to incorporate these into complex assembled structures on solid surfaces for electrochemical applications. We hypothesized that assembling catalytic peptides on a graphitic surface would fully harness the catalytic potential of peptide assemblies in an electrochemical manner and create a highly functional interface capable of efficiently catalyzing practical chemical reactions. There have been multiple reports demonstrating peptide self-assembly on graphite surfaces.^{4,5} These catalytic amyloids may have the ability to form self-assembled structures on the surface. In a proof-of-concept study, we focused on peroxidation reactions due to their potential applications in various processes ranging from cancer

therapy, and wastewater purification, to polymer production. Especially, the enhanced capability of accelerating the reduction of H₂O₂ is essential for constructing the electrocatalysts of various peroxidation applications due to its role as an electron acceptor in most peroxidase reactions. Furthermore, peroxidase activity in natural enzymatic and model systems has been extensively studied, providing important activity and stability benchmarks. To test our hypothesis, we employed several peptides found to self-assemble in the presence of hemin into catalytic amyloids with high peroxidation activities in solution. Among them, we selected highly active (LMLHLFL, LILHLFL) and moderately active (LHLHLFL, VHVHVYV) peptides in this work.⁶ First, we investigated their ability to form highly ordered nanostructures on graphite surfaces. Atomic force microscope images revealed that all peptides could form monomolecular-thick peptide self-assembled thin film on graphite surfaces. Hemin molecules were successfully immobilized on the peptide thin film on the graphite surfaces. The immobilized hemins on peptides exhibited their catalytic activities under electrochemical measurements over H₂O₂.

Additionally, we introduced 3,3',5,5'-tetramethylbenzidine (TMB) to demonstrate the model of peroxidase reactions for multiple substrates and analyze the efficiency during the electron transfer process. In both catalytic reactions, the highly ordered nanostructures of peptides with hemins promoted peroxidation with kinetic parameters approaching the natural enzymes in the same reaction at a fraction of the cost. The robust structure, ease of production, and high peroxidation activities of our hybrid system make them notable interfaces for electrocatalysis.

References

1. C. M. Rufo, Y. S. Moroz, O. V. Moroz, J. Stohr, T. A. Smith, X. Hu, W. F. DeGrado and I. V. Korendovych, *Nat Chem*, 2014, 6, 303–309.
2. O. V. Makhlynets, P. M. Gosavi and I. V. Korendovych, *Angew Chem Int Ed Engl*, 2016, 55, 9017–9020.
3. O. Zozulia and I. V. Korendovych, *Angew Chem Int Ed Engl*, 2020, 59, 8108–8112.
4. Y. Hayamizu, C. R. So, S. Dag, T. R. Page, D. Starkebaum and M. Sarikaya, *Sci. Rep.*, 2016, 6, 33778.
5. P. Li, K. Sakuma, S. Tsuchiya, L. Sun and Y. Hayamizu, *ACS Appl. Mater. Interfaces*, 2019, 11, 20670 – 20677.
6. W. Luo, H. Noguchi, C. Chen, Y. Nakamura, C. Homma, O. Zozulia, I. Korendovych, and Y. Hayamizu, *Nanoscale*, 2022, 14, 8326–8331.

8:45 AM SB08.04.02

Squid-Inspired Polypeptides as Dynamic Self-Healing Materials [Abdon Pena-Francesch](#); University of Michigan, United States

Squids have developed predatory teathed structures in their suction cups that are composed of structural proteins. Unlike other hard tissue in cephalopods, these biological materials are stabilized by β -sheet nanocrystalline structures that give rise to high-strength materials without mineralization. Here, we introduce cephalopod-inspired polypeptides with a repetitive diblock design (alanine-rich and glycine-rich blocks) that self-assemble into β -sheet nanocrystalline structures. These β -sheet nanocrystals act as physical and reversible hydrogen-bonded crosslinks in supramolecular protein networks, where β -sheet size and network topology regulate the physical properties. We demonstrate the dynamic properties of squid-inspired polypeptides in self-healing networks with healing strength and kinetics (~25 MPa strength after 1 second of healing) surpassing those typically found in other natural and synthetic soft polymers. This family of proteins and their biosynthetic derivatives open new opportunities in bioinspired design for adaptive functional materials, and we demonstrate their potential in actuator prototypes for applications in soft robotics and wearable technology.

9:00 AM SB08.04.03

Surfaces with Instant, Persistent and Broad-Spectrum Antimicrobial Efficacy [Taylor Repetto](#), Abhishek Dhyani, Dylan Bartikofsky, Carmen Mirabelli, Zhihe Gao, Sarah Snyder, Geeta Mehta, Christiane E. Wobus, J. Scott VanEpps and Anish Tuteja; University of Michigan, United States

Surfaces contaminated with infectious bacteria and viruses contribute to transmission and pose a significant threat to global public health. Common liquid spray disinfectants kill microbes in seconds to minutes, yet they require reapplication often. Surfaces that rely on heavy metals or metallic nanoparticles for antimicrobial efficacy remain antimicrobial over a long period of time but take hours to kill pathogens leaving time for disease transmission. There is currently no surface that can provide instant and persistent antimicrobial efficacy against a broad spectrum of bacteria and viruses. Inspired by the naturally antimicrobial secondary metabolites secreted by plants, we created a new class of highly durable polyurethane surfaces capable of rapid disinfection (>4-log reduction in minutes) of various pathogens, including *Escherichia coli*, *Pseudomonas aeruginosa*, methicillin-resistant *Staphylococcus aureus*, and SARS-CoV-2. These surfaces maintain this efficacy over several months and under significant environmental duress due to the chemical stabilization of the natural antimicrobial components within the polyurethane. Additionally, we show that the surfaces can be applied to surfaces using various commercial techniques such as spray-, flow-, or brush-coating allowing for a wide range of potential applications.

9:15 AM SB08.04.04

Cephalopod-Inspired Material Design for Potential Food Applications [Bianca C. Datta](#)^{1,2}; ¹Massachusetts Institute of Technology, United States; ²New Harvest, United States

As the global population rises alongside a worsening climate outlook, alternative proteins such as plant and cell-based meat provide exciting avenues for meeting the increasing demand for meat sourced from animals and have implications for planetary and human health. While food science is a well-established field with a rich history, inclusion of methods and research paradigms from the materials community can accelerate the development of promising food technologies. In this work, we review the complex and interesting structure and functionality of cephalopods, the landscape of existing materials advances towards replicating these creatures, and extensions towards food and edible materials. In doing so, we bridge the rich culinary traditions around cuttlefish, octopus, and squid¹ with advancements in tissue engineering and bio-inspired design.

Few creatures generate as much wonder and curiosity as cephalopods. Renowned for their protective and communicative capabilities (camouflage, texture and shape change), they also demonstrate fascinating behavioral and cognitive abilities². Researchers have looked to cephalopods for inspiration in designing systems as varied as displays³, programmable coloration⁴, self-healing coatings⁵, mechanochromic windows⁶, and bioelectronics⁷. Here, we look to their unique structure and properties to inspire a new domain of compelling alternative food materials.

References:

1. Mouritsen, Ole G., and Klavs Styrbaek. "Cephalopod gastronomy—a promise for the future." *Frontiers in Communication* 3 (2018): 38.
2. Schnell, Alexandra K., and Nicola S. Clayton. "Cephalopod cognition." *Current Biology* 29.15 (2019): R726-R732.
3. Wilson, Daniel J., and Leila F. Deravi. "Artificial cephalopod organs for bio-inspired display: progress in emulating nature." *Matter* 4.8 (2021): 2639-2642.
4. Wang, Yu, et al. "Generation of Complex Tunable Multispectral Signatures with Reconfigurable Protein-Based, Plasmonic-Photonic Crystal Hybrid Nanostructures." *Small* (2022): 2201036.
5. Manabe, Kengo, Emiko Koyama, and Yasuo Norikane. "Cephalopods-Inspired Rapid Self-Healing Nanoclay Composite Coatings with Oxygen Barrier and Super-Bubble-Phobic Properties." *ACS Applied Materials & Interfaces* 13.30 (2021): 36341-36349.
6. Ke, Yujie, et al. "Cephalopod-inspired versatile design based on plasmonic VO₂ nanoparticle for energy-efficient mechano-thermochromic windows." *Nano Energy* 73 (2020): 104785.

7. Kautz, R.; Gorodetsky, A. A. Revisiting A Classic Inspiration Source: Cephalopod-Derived Materials for Bioelectronics In Roadmap on Semiconductor-Cell Biointerfaces. *Phys. Biol.* 2018, 15, 031002.

9:30 AM BREAK

10:00 AM SB08.04.05

Design of Lightweight and High-Strength Functionally Graded Materials Inspired by the Hard Shells of Plants [Rikima Kuwada](#) and Daisuke Ishii; Nagoya Institute of Technology, Japan

Functionally graded materials (FGMs) are novel composite materials with gradual variations in their structures and chemical compositions throughout their bodies, so that FGMs possess locally tailored properties. Since FGMs consist of continuous structures without borders of physical property changes, conflicting physical properties within a material can be maintained not to break in their bodies. In contrast to isotropic bulk materials, the structures and chemical compositions of FGMs can be accurately designed to create tailored multifunctional properties. Noted to the natural world, there are many kinds of FGMs such as bones, teeth, bamboos, shells, and crustacean shells. They continuously change their microstructures and chemical compositions, with corresponding smooth changes in mechanical properties such as hardness, stiffness, and toughness. These natural materials mentioned above are composed of elements lighter than iron, such as carbon, silicon, and calcium. They are both lightweight and strong with limited resources by placing these elements in the necessary quantities and in the necessary places. In recent years, much research has been conducted to mimic these natural materials to reduce the weight and increase the strength of materials. In this study, we focused on the grass species, Job's tears (*Coix lacryma-jobi*). The seeds of Job's tears are covered with the involucre, a thin, lightweight, hard shell containing a high amount of silica. This shell is only about 740 μm thick, but is strong enough to withstand a load of about 280 N. We analyzed the spatial distribution of porosity, chemical composition, and hardness of these shells to investigate the factors that contribute to their lightweight and high-strength. Then, FGMs mimicking the shells of Job's tears were fabricated based on the analysis results. We used scanning electron microscopy (SEM) to observe the cross-sectional microstructures of the shell of Job's tears and energy dispersive X-ray spectroscopy (EDX) to analyze their chemical compositions. The inner layer of the shell was composed of tubular plant cells with a diameter of approximately 2 μm . The plant cells became smaller and more isotropic toward the outer layer and were densely distributed. The outermost layer of the shell was deposited with fine particles less than 100 nm in diameter. Therefore, the porosity of the shell decreased toward the outer layer. EDX analysis showed that the shells contained more silica toward the outer layers.

We measured the change in hardness from outer to inner layer in the cross-section of the shell by Vickers hardness test and nanoindentation test. The Vickers hardness test revealed that the outer layer of the shell was about four times harder than the inner layer, and the nanoindentation test showed a gradual decrease in elastic modulus from the outer to the inner layer of the shell. In addition, we analyzed the stiffness characteristics of the shells by performing three-point bending tests in different loading directions. The shells withstood three times more strain and twice as much load when bent from the outer layer of the shell compared to when bent from the inner layer.

These results indicate that the outer layer of the shell is harder and the inner layer softer due to spatial gradients in both shell porosity and chemical composition. This material property would allow the shell to withstand loads from outside the shell.

Based on our analyses, we fabricated FGMs mimicking the shells of Job's tears. We printed porous materials with a spatial gradient of porosity using fused deposition modeling 3D printer and polyurethane filaments whose extent of foaming and hardness changes with heating temperature. By impregnating the porous materials with glass or silicone resin, we expressed the spatial gradient in chemical compositions and hardness. This study may provide design guidelines for lightweight, high-strength organic/inorganic hybrid FGMs.

10:15 AM SB08.04.06

Peptidomimetic Wet-Adhesive PEGtides with Synergistic and Multimodal Hydrogen Bonding [Minseong Kim](#) and Byeong-Su Kim; Yonsei University, Korea (the Republic of)

The remarkable underwater adhesion of mussel foot proteins has long been an inspiration in the design of peptidomimetic materials. Although the synergistic wet adhesion of catechol and lysine has been recently highlighted, the critical role of the polymeric backbone has remained largely underexplored. Here, we present a peptidomimetic approach using poly(ethylene glycol) (PEG) as a platform to evaluate the synergistic compositional relation between the key amino acid residues (i.e., DOPA and lysine), as well as the role of the polyether backbone in interfacial adhesive interactions. A series of PEG-based peptides (PEGtides) were synthesized using functional epoxide monomers corresponding to catechol and lysine via anionic ring-opening polymerization. Using a surface force apparatus, highly synergistic surface interactions among these PEGtides with respect to the relative compositional ratio were revealed. Furthermore, the critical role of the catechol-amine synergy and diverse hydrogen bonding within the PEGtides in the superior adhesive interactions was verified by molecular dynamics simulations. Our study sheds light on the design of peptidomimetic polymers with reduced complexity within the framework of a polyether backbone.

10:30 AM SB08.04.07

Sea-Mussel Inspired Bioadhesives for Surgical Applications [Aishwarya V. Menon](#), Jonathan J. Wilker and Julie C. Liu; Purdue University, United States

Current methods of surgical joinery look as though they were devised in a medieval torture chamber. Sutures concentrate mechanical stresses, punch holes into healthy tissue, and create sites for infection. Patient outcomes will improve when we can devise alternate means of connecting tissues. Adhesives are appealing here. However, we do not yet have any materials that are simultaneously able to set in a wet environment, create strong bonds between tissues, and exhibit no toxicity. Further properties that are desirable include cure times compatible with surgeries, an ability to degrade, and having moduli (i.e., flexibility or stiffness) matched to the surrounding substrates. Our research team has developed sea-mussel inspired synthetic adhesives by taking cues from the way they attach themselves strongly onto surfaces in the ocean and synthesizing glues that mimic their chemistry. We have recently shifted our focus from synthetic to natural materials and developed inexpensive, bio-derived and non-toxic bioadhesives from corn protein (Zein) and Tannic acid (TA). Zein being a by-product of ethanol production from corn has been used as a wood adhesive. Tannic acid is a plant-based polyphenol and also one of the cheapest sources to impart sea-mussel inspired chemistry to any adhesive. We studied the *in vitro* burst pressures of these bioadhesives on several tissue substrates including sausage casings, porcine skin, heart, liver, lungs, aorta, dura and stomach. Our studies found these natural bioadhesives really promising with the ability to withstand pressures greater than the normal physiological pressures experienced in most of these organs. Moreover, we successfully conducted *ex vivo* studies on multiple tissue substrates to demonstrate the ability of our bioadhesives to plug body fluid leakages. We envision the potential application of our bioadhesives to seal surgical incisions and wounds under wet conditions.

10:45 AM SB08.04.10

Highly Nanoporous Multi-Functional Wood Aerogels [Yuan Yuan Li](#); KTH Royal Institute of Technology, Sweden

Aerogels, featuring low density ($< 0.5 \text{ g/cm}^3$), high porosity ($> 90\%$), and high specific surface area (SSA) ($> 100 \text{ m}^2/\text{g}$), show vital roles in various areas such as super thermal insulation, separation, catalyst, etc. Cellulose stands out ascribing to the abundant and fossil-free resources and the favorable

mechanical properties. The mainstream fabrications of cellulose aerogels are from a bottom-up approach, the energy consumption and hierarchical porous structure reconstruction are challenging for cost-effective and scalable production. A top-down approach directly from wood was reported recently through delignification and sometimes followed by hemicellulose extraction. However, the SSA is low and meso/micro pores are limited. Here, we propose an approach to fabricate hierarchical wood aerogel through cell wall partial dissolution and regeneration in the lumen space. The aerogel combines high SSA (up to 250 m²/g) with good mechanical strength (1.2 MPa) and abundant of meso/micro pores. The aerogel could be further modified for advanced applications such as thermal insulation, energy harvesting, etc.

11:00 AM SB08.04.11

The Impact of Mycelium Inoculation on 3D Printed Structural Composites [Sabrina Shen](#), Nicolas A. Lee and Markus J. Buehler; Massachusetts Institute of Technology, United States

The creation of living materials has received increased attention for its potential to provide sustainable, functional materials with novel properties. Mycelium-based materials have been of particular interest due to their relatively rapid growth rate and filamentous hyphae, which can act as fibrous reinforcement in packaging, structural, and other material applications. Characterization of mycelium composites in the materials science and architecture fields has typically been limited in scope, often focusing on bulk mechanical properties in sheets or molded bricks with single-material feedstocks. Here, we introduce a library of living-hybrid composites for additive manufacturing with resolution as high as 1 mm, and specifically characterize the impact of various inoculation methods, printing methods, and time-resolved growth on mechanical and chemical properties. We further explore interesting phenomena such as self-healing behavior and potential applications for these bio-hybrid composites.

11:15 AM SB08.04.12

All Bio-Phosphors for Highly Performing Low-Energy Biohybrid Light Emitting Diodes [Sara Ferrara](#) and Rubén D. Costa; Technical University of Munich, Germany

Bio-phosphors have emerged as an alternative to rare-earth color down-converting filters in light-emitting diodes (LEDs). They are mainly produced with biogenic emitters, like Fluorescent Proteins (FPs), embedded in polymer matrices.¹⁻³ The first biohybrid LED (Bio-HLED) with FP-phosphors featured a loss <10% of the emission intensity after 100 h.¹ This performance was recently enhanced using zero-thermal quenching PMMA-FP phosphors, reaching >150 days and 5 min of stability at low and high powers.⁴ However, the ideal combination of highly efficient and stable fully biogenic phosphors is still in its infancy.⁵ Here, we disclose the optimization of a bio-derived biodegradable polymer hosting and stabilizing a natural red FP – *mCherry*, as red-emitting phosphor in Bio-HLEDs. The photoluminescent properties of the bio-phosphors - PLQY > 20% with $\lambda_{em} = 630$ nm - led to Bio-HLEDs with excellent photostabilities > 2000 h operating, representing 2 orders of magnitude enhancement. We are strongly convinced that our work represents a crucial breakthrough in the development of red emitting bio-phosphors and in the stabilization of further natural FPs.

1. Weber, M. D. *et al.* Bioinspired Hybrid White Light-Emitting Diodes. *Adv. Mater.* **27**, 5493–5498 (2015).

2. Fernández Luna, V. *et al.* Deciphering Limitations to Meet Highly Stable Biohybrid Light Emitting Diodes. *Adv. Funct. Mater.* **29**, 1904356 (2019).

3. Aguino, C. F. *et al.* Single-Component Biohybrid Light-Emitting Diodes Using a White-Emitting Fused Protein. *ACS Omega* **3**, 15829–15836 (2018).

4. Espasa, A. *et al.* Long-living and Highly Efficient Biohybrid Light Emitting Diodes with Zero-thermal-Quenching Biophosphors. *Nat. Commun.* **11**, 1–10 (2020).

5. Fernández-Luna, V. *et al.* Biogenic Fluorescent Protein-silk Fibroin Phosphors for High Performing Light Emitting Diodes. *Mater. Horizons* **7**, 1790–1800 (2020).

SESSION SB08.05: Functional Biomaterials II
Session Chairs: Paul Meredith and Giuseppe Paternò
Tuesday Afternoon, November 29, 2022
Hynes, Level 3, Room 313

1:30 PM *SB08.05.01

Biomaterials for Boosting Food Security [Benedetto Marelli](#); Massachusetts Institute of Technology, United States

Applications of robotics and sensing technologies, big data analysis and biotechnology in farming, plant and food science are highly sought to guarantee global food security while mitigating the environmental impact of agriculture. In this scenario, the potential benefit of applying biomaterials science and drug delivery principles to enhance food security remains underexplored when compared to material- based research efforts in biomedicine, energy and optoelectronics. In this seminar, we highlight recent development in the nanomanufacturing of structural proteins to engineer a new generation of advanced materials that can be interfaced with food and plants. We will present newly developed techniques to direct the assembly of structural proteins into nanostructured, hierarchical materials that can serve as: edible coatings to prolong the shelf-life of perishable food, microenvironments to boost seed germination in marginal land and injectors to precisely deliver payloads in plant vasculature. These examples will provide an opportunity to discuss how the establishment of a successful interface between biomaterials and plants tissues requires the development of a basic scientific knowledge on: mechanics of disorder to order transitions in proteinaceous materials during condensation phenomena, fluid mechanics and transport phenomena in plants vasculature, and swelling of porous materials exposed to plant fluids.

2:00 PM SB08.05.02

Adaptive Recombinant Nanoworms from Genetically Encodable Star Amphiphiles [Davoud Mozhdchi](#); Syracuse University, United States

Recombinant nanoworms are promising candidates for materials and biomedical applications ranging from templated synthesis of nanomaterials to multivalent display of bioactive peptides and targeted delivery of theranostic agents. However, the molecular design principles to synthesize these assemblies (which are thermodynamically favorable only in a narrow region of the phase diagram) remains unclear. To advance the identification of design principles for programmable assembly of proteins into well-defined nanoworms and to broaden their stability regimes, we were inspired by well-documented findings of topological engineering for accessing rare mesophases formed by synthetic macromolecules. To test this design principle in biomacromolecular assemblies, we used posttranslational modifications (PTMs) to generate lipidated proteins with precise topological and compositional asymmetry. Using an integrated experimental and computational approach, we show that the material properties (thermoreponse and nanoscale assembly) of these hybrid amphiphiles are modulated by their amphiphilic architecture. Importantly, we demonstrate that the judicious choice of amphiphilic architecture can be used to program the assembly of proteins into adaptive nanoworms, that undergo a morphological transition (sphere-to-nanoworms) in response to temperature stimuli. Due to their amphiphilicity, these nanoworms can easily solubilize hydrophobic chemotherapeutics without resorting to

complex, inefficient, and time-consuming conjugation/purification protocols. The recombinant nature of this system enables the fusion of genetically encoded bioactive or targeting peptides, which can be used to optimize the delivery and efficacy of these nanoplateforms. We anticipate that these methods will be generalizable to other classes of proteins and PTMs. Thus, this work advances the study and design other hybrid systems, such as proteins modified with other classes of lipids or charged PTMs such as phosphorylation.

2:15 PM BREAK

2:45 PM SB08.05.04

Robust Spines of Biopolymer Microspheres for Enhanced Adhesion [Muchun Liu](#), Yunteng Cao, Zheng Li, Rajeev Ram and Benedetto Marelli; Massachusetts Institute of Technology, United States

Polymeric microparticles are widely used in agriculture, food processing, biomedical and electronic industries. Their structures and surface patterns are critical in specific applications. However, assembling intricate polymeric microstructures in a simple, repeatable, and at-scale manner is challenging compared with inorganic counterparts. To address this issue, we will describe a universal, template-free approach to fabricating spiny biopolymer microspheres. Silk fibroin – a natural protein with outstanding mechanical properties, biodegradability, and biocompatibility – is selected as an example here. Silk fibroin spiny microspheres are prepared with different sizes, spine numbers, and payloads. The mechanically robust spines are analyzed and tested. The enhanced adhesion performance in agriculture and micro-robotic applications will be demonstrated.

3:00 PM DISCUSSION TIME

3:15 PM SB08.05.06

Cellulose Nanocrystals Orientation Order Control via Tuning Nanocrystals Coulombic Interactions [Daria Bukharina](#), Minkyu Kim, Moon Jong Han and Vladimir Tsukruk; Georgia Institute of Technology, United States

Here we present how the ionic strength and effective charge density affect the final structural organization of cellulose nanocrystals (CNCs) after drying suspensions with different ionic strengths in terms of quantitative characteristics of the orientation order. We demonstrated that electrolyte's introduction into CNCs dispersion results in dramatic changes in electrical double layer thickness and subsequently, the effective charge density, measured experimentally, as well as the interparticle interaction energy calculated from the DLVO theory. The question of whether electrostatic interactions by themselves can control the nanocrystals' chiral organization is frequently debatable. We showed with high-resolution AFM that the reduction of the Debye charge screening length below a critical value of 3 nm results in the loss of the long-range helicoidal order and the transition to a disordered morphology with random packing of nanocrystals within thin films' layers. Subsequently, very high local orientation ordering with the 2D orientation factor, S , obtained by applying image analysis software that was within 0.8–0.9, gradually decreased to a random order with the final value $S = 0.1–0.2$. The effect of Coulombic interaction on CNCs chiral assembly is clearly supported by the measured shrinking of the helical pitch length and shifting the photonic band gap from 400 to 250 nm, and increase in helical twisting power from 4 to 6 μm^{-1} and doubling of the twisting angle between neighboring monolayers from 5.5 to 9°. Thus, we conducted quantitative characterization of the CNCs molecular organization down to the level of individual nanocrystals and their orientational organization at nanoscale and microscale levels. Simultaneously with these comprehensive molecular characteristics, we measured optical appearance, chiral activity, and evaluated their charged state, offering unique comprehensive and quantitative characterization of the molecular orientational order of the CNCs.

3:30 PM SB08.05.07

Laser Processing of Aligned Poly(lactic Acid) Nanofibers—Process, Structure and Function [Matthew Flamini](#), Mohamad Keblawi and Vince Beachley; Rowan, United States

Problem:

Electrospun nanofibers should have higher strength than their larger scale counterparts, however, due to the difficulty in drawing the fibers, a critical processing step that creates high molecular alignment in the fiber, their promise of high strength remains unkept. Individual nanofibers have been drawn using a parallel based track collection and drawing system, but this has only been done at ambient temperatures. The proper application of heat will allow for the fibers to be drawn to much higher draw ratios, and allow for the release of chain entanglements and imperfect crystal structures so that the resultant fibers can have optimal chain alignment and straight chain crystals.

Solution:

We aim to apply the technique of laser zone drawing to track electrospun nanofibers. Laser zone drawing heats up just a small portion of the fiber at a time, allowing for precise thermal control over the fiber, both spatially and temporally. This technique has been applied to larger fibers with incredible results but has yet to be applied to nanofibers. We believe that by combining the techniques of track electrospinning and laser zone drawing, we can create nanofibers with near ideal macromolecular properties, which may result in polymer nanofibers with the highest tensile strength to date. Additionally, this method is scalable and flexible, and should be applicable to any thermoplastic polymer that can be spun into nanofibers.

Methods:

Track electrospinning and Laser Processing: Poly(lactic acid) (PLA) nanofibers are electrospun onto a parallel track collection system, which allows to the collection of aligned nanofibers. The fibers are then transferred onto a robotic stage which passes the fibers through a 9.3 micron wavelength laser beam.

Raman Spectroscopy:

Single fiber Raman spectroscopy is used to measure changes in the molecular alignment and crystallinity of the fibers.

Scanning Electron Microscopy (SEM):

SEM is used to evaluate the diameters and morphology of the fibers.

Mechanical Properties:

Dynamic Mechanical Analysis is used to determine the modulus of fiber mats, because individual fibers do not produce a large enough load.

Results:

We have demonstrated that PLA fibers of different diameters can be predictably thinned to diameters of less than 20% of the original diameter with low variability simply by increasing the power density of the processing laser. This allows for the nanofibers' diameters to be precisely controlled after the spinning process. We have also established that this effect is not dependent on the duration of laser exposure, indicating that the fibers reach thermal equilibrium during the process, despite being exposed to very high laser power densities. This is explained by their enormous surface area to volume ratio, which only increases as they thin, which keeps them from melting even under extreme laser exposure. We have also demonstrated that the fibers can be thinned in a single step, as there was no difference in diameter compared to fibers that were treated multiple times at incrementally increasing powers. By comparing the power density of the laser to the diameter, using Newton's law of cooling, and assuming thermal equilibrium, we can calculate the convective heat transfer coefficient of the nanofibers. Knowing this will allow us to predictably raise the fibers' temperature using the laser, which will aid in the zone drawing process, by allowing us to heat just above T_g , which has been shown to be the optimal temperature for zone-drawing.

3:45 PM SB08.05.08

Modelling and Simulation of DNA-Based Nanomaterials [Torsten John](#)¹, Jeffrey Gorman¹, Hyungmin Jun^{1,2}, Xiao Wang¹ and Mark Bathe¹;
¹Massachusetts Institute of Technology (MIT), United States; ²Jeonbuk National University, Korea (the Republic of)

In nature, simple molecular building blocks self-assemble into complex structures to achieve outstanding functionality. For example, proteins are made up of amino acids and DNA (deoxyribonucleic acid) is made up of nucleotides. Proteins and DNA are involved in most processes in life, from genetic encoding of information to enzyme catalysis. The large sequence space and the variation of the physicochemical properties of biomolecules leads to their functional diversity. Inspired by the superior properties of such self-assembled systems, materials with unique properties can be designed. The base pair complementarity of DNA and the origami method laid the foundation for the field of DNA nanotechnology and synthesis of 2D and 3D nanostructures of desired geometry. Bioconjugate chemistry enables the modification of DNA strands with functional molecules that can be designed with optimized spacings and orientations within the DNA backbone, leading to applications in energy transfer, vaccine development, or enzyme catalysis.

In this work, we present the design of DNA origami for the development of functional nanostructures. Modeling and simulation have been used to better understand the molecular structure of functional DNA structures and to guide new designs. The 2D and 3D DNA structures were first generated using the ATHENA software package, followed by coarse-grained oxDNA simulations to investigate the structural integrity of the DNA nanostructures. As an example, hybrids of DNA wireframe structures decorated with fluorescent molecules have been tailored to achieve the desired spectroscopic properties. The goal was to mimic and engineer the outstanding efficiency of fluorophores in large protein complexes such as the light-harvesting antenna complex. Fully atomistic molecular dynamics (MD) simulations provided further insights. This approach enables the design of hybrid systems with functional properties for applications where molecules need to be arranged on the nanometer scale.

References

X. Wang[#], S. Li[#], H. Jun[#], [T. John](#), K. Zhang, H. Fowler, J.P.K. Doye, W. Chiu*, M. Bathe*, Planar 2D Wireframe DNA Origami, *Sci. Adv.* 8 (2022) eabn0039.

H. Jun, X. Wang, M.F. Parsons, W.P. Bricker, [T. John](#), S. Li, S. Jackson, W. Chiu, M. Bathe*, Rapid prototyping of arbitrary 2D and 3D wireframe DNA origami, *Nucleic Acids Res.* 49 (2021) 10265–10274.

4:00 PM SB08.05.09

Computational Reverse-Engineering Analysis for Scattering Experiments (CREASE) on Biomacromolecular Assemblies [Zijie Wu](#) and Arthi Jayaraman; University of Delaware, United States

Many biomacromolecules are known to undergo thermoresponsive assembly into various morphologies, making them promising candidates for temperature-modulated applications such as drug delivery and tissue engineering. As two examples, methylcellulose (MC) chains self-assemble to form fibrillar structure in aqueous solutions at elevated temperature [Schmidt et al. *Macromolecules*, 2018, 51, 7767-7775]; elastin-like peptide-collagen-like peptide (ELP-CLP) conjugates self-assemble to form vesicles at physiological temperatures [Luo and Kiick, *J. Am. Chem. Soc.* 2015, 137, 15362-15365]. Understanding the assembled macromolecular structure - domain shapes and dimensions - is key to precise control of the behaviors of such biomacromolecular materials in commercial applications. Small-angle scattering (SAS) is a useful experimental technique to characterize the structure of polymer assembly in solutions. However, interpretation of the SAS output - a scattering profile of averaged intensity $I(q)$ at various wave factors (q) - often relies on analytical models only available for several conventional structures. Interpretation of $I(q)$ vs. q plots for unconventional/non-equilibrium assembled structures with simple/complex polymer conformations remains challenging as relevant analytical models are not always available for such cases. In this talk, we present our recently developed computational method, CREASE, to analyze SAS results obtained from structures with high dispersity in dimensions formed upon assembly of complex polymer chemistries. Using genetic algorithm (GA) as the optimizer, CREASE takes as input $I(q)$ vs. q plot and a general category of assembly morphology (e.g., “semiflexible fibril” or “bilayer vesicle”) and provides as output the relevant dimensions of the structure and dispersity in the dimensions whose computed scattering profile most closely matches input scattering profile. We test the performance of CREASE on both scattering profiles of methylcellulose fibrils and ELP-CLP vesicles and compare the predicted dimensions with those obtained from fitting analytical models. We also show how CREASE can be accelerated by incorporating neural network (NN) models. This talk will demonstrate CREASE’s potential to extract useful information about microscopic structure from SAS outputs without being limited by off-the-shelf scattering models and greatly improve the interpretability of small-angle scattering as a method to characterize polymer structures.

4:15 PM SB08.05.10

Enzyme-Free Biorecognition with Tailored PEDOT Derivatives [Christina J. Kousseff](#)¹, Achilleas Savva², Zixuan Lu², Shofarul Wustoni³, Roisin Owens², Sahika Inal³ and Christian Nielsen¹; ¹Queen Mary University of London, United Kingdom; ²University of Cambridge, United Kingdom; ³King Abdullah University of Science and Technology, Saudi Arabia

The structure-based tuneability of the electronic and optical properties of conjugated polymers has enabled their application across a range of fields, including energy harvesting and optoelectronics. However, in the context of biological sensing, the use of conjugated polymers has thus far incorporated little specificity in terms of covalent modification.¹ Previously, we demonstrated a crown ether-functionalised PEDOT which displayed improved adhesion and electrochromic behaviors compared to unmodified PEDOT.² Now, we move towards an expanded landscape of materials investigating copolymers, deposition parameters, and alternative functional groups which enable the precise fine-tuning of material characteristics and functionalities.

Developing robust, highly selective, biologically compatible sensing platforms is of critical importance because the measurement of analyte concentrations in biological samples is crucial for the management or detection of many diseases.³ Currently, many devices which function for this purpose are complex, multi-component systems. However, directed synthetic strategy with conjugated polymers enables the fine-tuning of analyte specificity, electroactive or optical functionality, and physical and morphological properties, within a single multi-purpose material. In addition, these entirely organic systems offer affordability, biocompatibility, and simple design and fabrication.

Here, we present a novel covalently modified EDOT monomer featuring pendant analyte-binding groups which, when electropolymerised in the presence of a glucose template, forms a porous molecularly imprinted matrix which is shown to be electrochemically responsive to glucose. Supported by in-depth topographical, electrochemical, QCM, and OECT analysis, we will discuss how this new design platform can be used to introduce sensing capability in an enzyme-free, single polymeric material, for next-generation device fabrication.

1. J. Borges-González, C. J. Kousseff, C. B. Nielsen, *J. Mater. Chem. C.*, **2019**, 7, 1111-1130
2. C. J. Kousseff, F. E. Taifakou, W. G. Neal, M. Palma, C. B. Nielsen, *J. Polym. Sci.*, **2022**, 60, 504-516
3. S. Wustoni, A. Savva, R. Sun, E. Bihari, S. Inal, *Adv. Mater. Interfaces*, **2019**, 6, 1800928

4:30 PM SB08.05.11

Multi-Valued Logic Structures for Optical Biocomputing—Photonically Triggered Bio-Organic Field-Effect Transistors Moon Jong Han, Minkyu Kim and Vladimir Tsukruk; Georgia Institute of Technology, United States

Here, a photonic bio-organic multiphase structure is proposed for thin-film electronic nets integrated with multilevel logic elements for multilevel computing via reconfigurable photonic band gaps in chiral biomaterials. Inspired by an artificial intelligence system having efficient information integration and computing capabilities, the photon active dielectric layer of the chiral nematic cellulose nanocrystal is coupled to a printed p-type and n-type organic semiconductor as a bifunctional logic element. These adaptive logic elements can trigger customized quantized electrical output signals under light having different photon energies and with different photonic band gaps in active dielectric layers. A bifunctional structure enables complex memory operations due to repeated changes in photonic band gaps controlled by expansion and contraction of chiral nematic pitches and photon energy controlled by light absorption of complementary organic semiconductor layers. This conceptual demonstration of a multivalued logic structure facilitates an optical calculation system for low-power optical information processing integrated into an interface between a human and a machine.

SESSION SB08.06: Materials from Photosynthetic Organisms

Session Chairs: Jessica Garb and Anthony Weiss

Wednesday Morning, November 30, 2022

Hynes, Level 3, Room 313

8:30 AM *SB08.06.01

Plant Based Biohybrid Systems for Energy Applications Eleni Stavrinidou; Linköping University, Sweden

Plant processes such as photosynthesis, production of biomaterials and environmental sensing and adaptation, can be used in technology via integration of functional materials and devices. We demonstrated that plants can be functionalized with electronic materials by leveraging their biocatalytic machinery. Specifically, conjugated oligomers based on thiophene and EDOT polymerize in-vivo forming conductors within the plant structure. We showed that the polymerization is enzymatically catalyzed by endogenous peroxidases that are present in the plant cell walls, resulting in conducting polymers integrated within the plant cell wall structure. The plant is not only catalyzing the polymerization but also templates the polymer in a favorable manner. Recently we demonstrated intact plants with electronic roots that continue to grow and develop enabling plant-biohybrid systems that maintain fully their biological processes. The electronic roots were used to build supercapacitors that outperformed previous plant biohybrid charge storage demonstrations. Here I will also present our latest results on developing plant based biohybrid circuits for enhanced energy storage in plants and a demonstration in powering an electrochromic display. Furthermore, extending the concept to trees I will present our results on functionalizing wood in-vivo prior to harvest.

9:00 AM SB08.06.02

Polydopamine Polymerization in Anoxygenic Photosynthetic Organisms Rossella Labarile^{1,2}, Danilo Vona², Maria Varsalona^{1,2}, Matteo Grattieri^{2,1}, Paolo Stufano¹, Roberta Ragni², Stefania R. Cicco¹, Gianluca Maria Farinola² and Massimo Trotta¹; ¹Consiglio Nazionale delle Ricerche, Italy; ²Università degli Studi di Bari Aldo Moro, Italy

Photosynthetic microorganisms represent attractive tools for the harvesting and the conversion of solar light in bioelectronic devices [1, 2]. The optimization of the interfaces of poorly conductive bacteria with electronic components can be achieved *via* biocompatible polymers that encapsulate the bacterial cells and allow the intimate contact between the outer cell membrane and the electron acceptor surface, required for an efficient electron transfer in biohybrid systems.

The outer membrane of the metabolically active photosynthetic purple non sulfur bacterium *Rhodobacter (R.) sphaeroides* was coated with polydopamine (PDA), a bioinspired polymer produced by the self-polymerization of dopamine. Although the presence of oxygen is an essential requirement for dopamine polymerization [3], the PDA coating formation around the cell membrane occurred also in anaerobic condition.

Laccases, enzymes belonging to multi-copper oxidases family, have been reported to oxidize a wide range of phenolic compounds and aromatic amines, including dopamine. Using laccase, the polymerization rate of the dopamine monomer was greatly increased, and the polymer film resulted more uniform compared to traditional self-polymerization and uncontrolled mechanism [4].

Laccases have a wide taxonomic distribution in Nature but with few or little evidence of their presence in anaerobes, since these enzymes use oxygen as an electron acceptor [5]. Here we investigate the process of anaerobic polymerization of dopamine in the growth medium of *R. sphaeroides*.

Similarly, laccase from *T. versicolor* was also used to improve dopamine polymerization around the photosynthetic organisms belonging to diatom microalgae, with the goal of wastewater treatment and their bioremediation.

[1] F. Milano, A. Punzi, R. Ragni, M. Trotta, G. M. Farinola, *Adv. Funct. Mater.*, 29, 1805521, (2019)

[2] a. M. Di Lauro, S. la Gatta, C. A. Bortolotti, V. Beni, V. Parkula, S. Drakopoulou, M. Giordani, M. Berto, F. Milano, T. Cramer, M. Murgia, A. Agostiano, G. M. Farinola, M. Trotta, F. Biscarini, *Adv. Electron. Mater.*, 6, 1900888, (2020)

b. M. Di Lauro, G. Buscemi, M. Bianchi, et al., *MRS Advances* 5, 985–990 (2020)

[3] H. Lee, S.M. Dellatore, W.M. Miller, P.B. Messersmith, *Science* 318(5849):426-30 (2007)

[4] Q. Zhou, W. Wu, T. Xing, *RSC Adv.*, 12, 3763-3773 (2022)

[5] F. Berini, M. Verce, L. Auscè, et al., *Appl Microbiol Biotechnol* 102, 2425–2439 (2018)

9:15 AM SB08.06.03

Algae-Based Biohybrid Microrobots for Biomedical and Environmental Applications Fangyu Zhang, Liangfang Zhang and Joseph Wang; University of California, San Diego, United States

Bioinspired microrobots capable of actively moving in versatile biological fluids and environmental surroundings have attracted considerable attention for biomedical and environmental applications because of their unique dynamic features that are otherwise difficult to achieve by their static counterparts. Herein, algae-based biohybrid microrobots are fabricated via click chemistry to functionalize algae with different agents from small molecules to nanoparticles (eg. angiotensin-converting enzyme 2 (ACE2) receptor and antibiotics-loaded cell membrane-coated nanoparticles). The resulting biohybrid microrobot displays fast (>100 μm/s) and long-lasting self-propulsion in diverse simulated biofluid and aquatic media, obviating the need for external fuels. In a mouse model of acute pneumonia, the resulting antibiotics-loaded biohybrid algae-based microrobots achieve significant therapeutic efficacy in reducing the bacterial burden and effective treatment of bacterial infection, while showing negligible *in vivo* toxicity. In another example, the ACE2-

modified algae microrobots display effective “on-the-fly” removal of SARS-CoV-2 pseudovirus in many contaminated water matrices.

9:30 AM SB08.06.04

Polyethylenimine Based Nanoparticles for Enhancing Photosynthesis in Plants [Cyril Routier](#)¹, Lorenzo Vallan², Yohann Daguerre³, Marta Juvany³, Emin Istif², Cyril Brochon², Georges Hadziioannou², Torgny Hasholm³, Eric Cloutet², Eleni Pavlopoulou² and Eleni Stavrinidou¹; ¹Laboratory of Organic Electronics, Department of Science and Technology, Linköping University, SE-60174, Norrköping, Sweden., Sweden; ²Laboratoire de Chimie des Polymères Organiques (LCPO-UMR 5629), Université de Bordeaux, Bordeaux INP, CNRS, F-33607 Pessac, France, France; ³Umeå Plant Science Centre, Department of Forest Genetics and Plant Physiology, Swedish University of Agricultural Sciences, SE-90183 Umeå, Sweden., Sweden

During photosynthesis, plants use light energy to transform carbon dioxide and water into carbohydrates for their own growth. The photosynthetic process comprises many steps that can in principle be optimized to have higher efficiency. RuBisCO (Ribulose 1,5-bisphosphate carboxylase/oxygenase) catalyzes the carboxylation reaction that is the initial reaction for carbon fixation and conversion of CO₂ to sugars. The reaction occurs in organelles called chloroplasts present in leaf cells. However, RuBisCO has naturally a poor affinity for CO₂ and the transfer of the atmospheric CO₂ to the RuBisCO enzyme is highly limited by the diffusion of CO₂ through the stomata and the intercellular space which ultimately considerably reduces the photosynthesis rate. Polyamines have been shown *in-vitro* to be able to transfer carbon dioxide to RuBisCO for the carboxylation reaction. In this work, we present biocompatible fluorescent polyethylenimine nanoparticles for enhancing the CO₂ transfer to the RuBisCO enzyme. With *in vitro* and *in vivo* studies, we evaluated the nanoparticles uptake of atmospheric CO₂ and transfer kinetics to RuBisCO for the carboxylation reaction. Then, we introduced the nanoparticles into the plant apoplast via localized infiltration. First, we studied the toxicity of the nanoparticles and results showed no evidence of a direct harmful impact. We then investigated their distribution within the plant leaf with confocal microscopy and showed that the nanoparticles not only are present in the intercellular space but also in the direct centers of photosynthetic activity: the chloroplasts, which indicate the possibility of a pathway to increase the diffusion of CO₂ in the plant tissue.

9:45 AM BREAK

10:15 AM *SB08.06.05

The Soft Power of Bacterial Photosynthesis—Harnessing Light for Exploiting Electrons [Massimo Trotta](#)^{1,2}, Rossella Labarile^{1,2}, Maria Varsalona^{2,1}, Gabriella Buscemi^{2,1}, Danilo Vona², Matteo Grattieri^{2,1} and Gianluca Maria Farinola²; ¹Consiglio Nazionale delle Ricerche, Italy; ²Università degli Studi di Bari Aldo Moro, Italy

Bacterial photosynthesis has huge applicative potential when it comes to have small, metabolic active and versatile living catalysts. The use of photosynthetic bacteria in non-conventional or in polluted environments to catalyze light transduction is very promising in bioelectronics. The strategy to connect these light converting bacteria to external, non-biological wiring will be presented, along with some recent results that will illustrate the advancements of the interfacing between electrodes and living microorganisms.

Photosynthetic bacteria in self-assembled biocompatible coatings for the transduction. Phosbury. (Fonds Nationale Suisse, CRSII5_205925)

10:45 AM SB08.06.06

Pectin Hydrogel as Isolated Chloroplast Niche for *In Vitro* Photosynthesis [Jonghyun Shin](#), Jaeho Choi, Youngwoo Han, Woojin Jeong, Chang Seok Ki and Seon-Yeong Kwak; Seoul national university, Korea (the Republic of)

Chloroplasts absorb atmospheric carbon dioxide in the plants, which play an important role in converting global carbon into a chemical energy source by light. Since isolated chloroplasts quickly lose their photosynthetic activities once isolated from plants, extending their viability is essential in engineering chloroplasts for sustainable carbon sequestration. Here, we suggest a plant cytosol-mimicking matrix to extend the photosynthetic activities of isolated chloroplasts. Encapsulation of chloroplasts within photo-clickable pectin hydrogels enabled uniform distribution of chloroplasts within the hydrogel and securely entrapped chloroplasts to maintain the mechanical properties. Antioxidants were introduced to protect chloroplasts from photooxidative damage. We evaluated the comprehensive *in vitro* photosynthetic activities by monitoring chlorophyll concentration, O₂ evolution, electron transfer rate, ATP synthesis, and glucose export. As a result, we found that antioxidants alone prolonged the isolated chloroplasts' lifespan by 48 hours, and encapsulation within the pectin hydrogel extended their lifespan by 168 hours. In 96 hours of incubation, the chloroplast-laden pectin hydrogel with antioxidants showed a 3-fold O₂ concentration and 8-fold electron transfer rate compared to encapsulated chloroplasts without antioxidants. In addition, the ATP synthesis and glucose export were increased by 1.6-fold and 1.2-fold, respectively. These results will provide the potential perspective on the generation of carbon-fixing materials, the manipulation of biological functions, and the production of therapeutics using chloroplast culture in designing environmentally sustainable materials.

11:00 AM SB08.06.07

A Fruit Salad Recipe for Vision Restoration—Use of Natural Dyes for Photosensitive Organic Semiconductor Devices Toward Retinal Implants [Aimee R. Sweeney](#), Leslie Askew, Cedric Vallée, Daniel Whelligan and Maxim Shkunov; University of Surrey, United Kingdom

Vision loss due to the degeneration of photoreceptor cells in the retina occurs in millions of people every year worldwide through diseases such as retinitis pigmentosa and age-related macular degeneration. The development of a photosensitive organic semiconductor device that can function in a way to replace lost or damaged photoreceptor cells may be a possible treatment for those suffering with these diseases. We demonstrate that natural dyes extracted from various berries and vegetables are excellent chromophore candidates for colour-specific organic devices with similar absorption spectra to those produced by human rod and cone cells. Using fabrication methods resembling those used in the development of dye-sensitised solar cells, bio-derived chromophores have been investigated and the production of active devices interfaced with electrolyte, phosphate buffered silane, have been demonstrated. Devices produce photo-current and photo-voltage spectra in the spectral regions corresponding to the activity of cones and rods. Our results show the chromophores can respond to pulsed light in a similar way to photoreceptor cells and produce a rising photovoltage. In summary, we discuss if natural dyes can lead us to devices capable of stimulating neuronal circuitry in human eye.

11:15 AM SB08.06.08

Three-in-One Woody Zinc-Air Battery Engraved by Laser [Hiroya Abe](#); Tohoku University, Japan

For the realization of sustainable development goals, regional ecosystems must develop and use universal sustainable technologies, and the widespread use of renewable energy is essential for this purpose. Thus, there is an urgent need to develop renewable energy production and storage devices. A wood-derived carbon is a promising electrode as an energy device because its high porosity improves the carbon's surface area. Recently, we have reported a highly active wood-derived electrochemical catalyst for oxygen reduction reaction which occurs on the cathode of metal-air batteries and fuel cells (1). The pyrolyzed wood performed high porosity and high catalytic activity. Pyrolysis is required to control the atmosphere at high temperatures and under inert

gas, resulting in being expensive and cumbersome. Herein, we report the direct laser-pyrolysis of wood chips for an anode and cathode with a commercial blue laser and establish a three-in-one zinc-air battery.

Paulownia was used as a wood carbon source. Wood chips were pyrolyzed with the blue laser under the ambient atmosphere. The irradiated area became black and metallic. The obtained carbon had macro-scale pores confirmed by an optical microscope and showed the graphitic peaks confirmed by Raman spectra. The electric resistance was improved by increasing the intensity of the blue laser, and the obtained carbon performed highly active electrocatalytic activity by adding metal sources as catalysts.

We confirmed the electrocatalytic activity of the cathode for the oxygen reduction reaction. In this study, the $\text{Fe}(\text{NO}_3)_3$ was used as a metal source and added to the wood before the pyrolysis (wood-Fe). In addition, iron phthalocyanine was modified on the obtained carbon material using the organic solvent as a molecular catalyst (wood-FePc). The molecular catalysts are promising materials since they show superior oxygen reduction activity without any pyrolysis processes (2). The oxygen reduction properties were evaluated in 0.1 M KOH, and the catalytic activity was found to increase in the order of wood, wood-Fe, and wood-FePc. From these results, the wood-derived laser-induced graphene for the electrocatalysts of the oxygen reduction reaction was successfully obtained from wood using the blue laser under the ambient atmosphere.

Finally, we established the three-in-one zinc-air battery. The wood chips have porous structures, resulting in the solvent and electrolyte can be absorbed into their structure. We irradiated the laser at double sides on the wood chip to form the cathode and anode without a connection between each electrode. The FePc and zinc powder loaded onto the cathode and anode, respectively. The open-circuit potential was observed by adding the electrolyte (0.1 M KOH) into the wood chip. The woody battery showed over 10 mA/cm² and 5 mW/cm². The wood chip irradiated with the laser at double sides acted as the three-in-one zinc-air battery consisting of the cathode, anode, and separator without an assembly process.

References: 1) Y. Goto, Y. Nakayasu, H. Abe, Yuto Katsuyama, T. Itoh and M. Watanabe, *Phil. Trans. R. Soc. A* (2021) 379: 20200348. 2) H. Abe et al., *NPG Asia Materials* 11, Article number: 57 (2019)

11:30 AM SB08.06.09

Tunable Energy Absorption in Bioinspired Materials Designed for Additive Manufacturing [Ludovico Musenich](#), Lorenzo Strozzi, Alessandro Stagni and Flavia Libonati; University of Genoa, Italy

Diatoms are the most widespread organisms in our planet's aquatic environments and among the most ecologically important. Indeed, the tens of thousands of existing species of these microalgae produce about half of the oxygen we breathe and are an extraordinary example of how Nature is capable of cyclically adapting biological systems to the natural environment by playing with the universality-diversity dualism. In diatoms, in particular, this binomial is determined by the multiscale architecture of their biosiliceous exoskeleton known as the "frustule". This biological material, in addition to being a marvelous and sophisticated physical barrier against predators, through its hierarchical porous structure allows diatoms to acquire nutrients through filtration, exploit buoyancy phenomena for photosynthesis processes, and thermally regulate the organism. Given the amazing multifunctionality of the frustule, diatoms are still widely studied for applications in filtration, drug delivery, biosensing, energy harvesting, and scaffolding. Yet, little is known regarding their mechanical properties. To extend the knowledge of the present relationship between the morphology of diatom frustules and their structural performance, in this work we focused on the mechanical analysis of the frustule of the diatom *Coscinodiscus* sp. Starting from the analysis of the multilayer structure that characterizes the microscale, we built biomimetic models on a macroscopic scale using CAD tools and studied their deformational behavior, both through numerical finite element simulations and through experimental tests performed on samples fabricated through additive manufacturing. In particular, we focused on the effect produced by variation in the morphological details that distinguish the natural sandwich-like structure of the frustule on its energy absorption properties. Through predictive techniques, we then researched the optimal topology and analyzed the potential benefits of using bioinspired design for the architected materials. Nature's design principles used to make biological materials and, in particular, the use of functional gradients and structural heterogeneity are a formidable source of ideas for increasing the efficiency and performance of man-made materials, and this research is evidence of that. To reinforce this, as a possible application, we propose in addition a new bioinspired prototype protective helmet designed for micromobility and outdoor activities that combines lightweight and the energy-absorbing capacity from impacts with breathability, waterproofing, and aesthetics.

SESSION SB08.07: Biopolymer and Biomaterials for Advanced Technologies

Session Chairs: Gianluca Maria Farinola and Massimo Trotta

Wednesday Afternoon, November 30, 2022

Hynes, Level 3, Room 313

1:45 PM SB08.07.01

Alginate Hydrogel Formation by Microdroplet Reactions on the Open-Channel Microfluidics [Hiroyuki Kai](#); Tokyo University of Science, Japan

The alginate hydrogel is a natural polysaccharide that has high biocompatibility and is used for drug delivery, dressing for wound healing, scaffold for 3D bioprinting, etc. It can be readily prepared by mixing sodium alginate with divalent cations such as Ca^{2+} in solution to crosslink the alginate polymer chains. The most common method to facilitate the crosslinking of sodium alginate is to add a small amount of solution of sodium alginate into a bulk solution of CaCl_2 slowly or in a dropwise manner. CaCl_2 permeates into a blob of the alginate solution to immediately crosslink the alginate and form a hydrogel. Morphologies of the alginate solution being added (droplet or a stream of liquid, droplet size, etc.) affect the morphologies and properties of the resulting hydrogel, which are important for different applications. Since CaCl_2 solution is normally of a bulk volume, if this reaction was conducted in a setting where both reactants are in microdroplets, it may lead to unique characteristics. However, it is difficult to facilitate efficient reactions between microdroplets by conventional techniques.

In this study, crosslinking reactions between sodium alginate and CaCl_2 were conducted by spraying them on the substrate surface with wettability patterning that collects and mixes microdroplets on the surface. We fabricated highly-branched "open microfluidic channels" [1,2,3] by patterning different wetting properties such as hydrophilic and hydrophobic ones. When aqueous microdroplets are sprayed on the open microfluidic channels, they are captured and transported along a hydrophilic channel surrounded by a hydrophobic surface, driven by capillary action. Superhydrophobic coating of TiO_2 and Capstone (R) ST-100 turns to be superhydrophilic upon irradiation with UV light, which makes complex patterning possible by simple photolithography. This photo-patternable surface was used to fabricate a highly branched tree-like microfluidic channels to collect microdroplets and facilitate mixing of solution at a large number of branching points that exists throughout the surface.

On the fabricated microfluidic surface, aqueous solution of 20 g/L sodium alginate (500-600 cP at 10g/L, 20 °C) and that of 20 g/L CaCl_2 were prepared. Droplets of different aqueous solutions were sprayed onto the unused channels using a spray nozzle with a controlled rate: (1) sodium alginate solution, (2) CaCl_2 solution, (3) both using two spray bottles containing each of them. The positions of liquid blobs after spraying were recorded by a digital camera.

When droplets of CaCl₂ solution, which has low viscosity, were sprayed on the channels, they were transported through the channels to form a large liquid blob at the focal point (the root of the tree structure) within 1 s. When droplets of sodium alginate solution were sprayed on the unused channels, they were also transported to the focal point despite their high viscosity (estimated viscosity is 1×10^3 cP). On the other hand, when the two kinds of droplets were simultaneously sprayed on the channels, the transport of droplets to the focal point was apparently hindered. This hindered transport can be attributed to crosslinking of alginate by Ca²⁺ upon merging of fine droplets of sodium alginate and those of CaCl₂ at the branching points, which turned the fluid droplet to a non-fluid hydrogel.

In conclusion, we demonstrated mixing and reactions of microdroplets of sodium alginate and CaCl₂ to form hydrogel on the microfluidic surface. More detailed investigation of the reaction dynamics between droplets as well as properties of the resulting alginate hydrogel is in progress.

[1] H. Kai, R. Toyosato, M. Nishizawa, *RSC Adv.*, 8, 15985-15990, 2018.

[2] H. Kai, *μ TAS 2020*.

[3] H. Kai, *2021 MRS Fall Meeting & Exhibit*.

2:00 PM SB08.07.02

Controlled Assembly of Sequence-Defined Peptoids into Hierarchical Materials Chun-Long Chen; Pacific Northwest National Laboratory, United States

Peptoid (N-substituted glycines), as one of the unique sequence-defined synthetic “foldamers that mimic proteins and peptides for functions, - have recently received increasing attention for the design and synthesis of biomimetic nanomaterials with hierarchical structures.¹ Due to the unique proteinase-resistance, chemical and thermal stabilities of peptoids, peptoid-based nanomaterials are promising candidates for applications in photonics,^{2,3} flexible electronics,⁴ and biological systems.^{2,3,5} Recently, by designing amphiphilic peptoids that contain aromatic hydrophobic domains, our group recently reported their self-assembly into highly crystalline membrane-mimetic 2D nanosheets^{2,6} and 1D nanotubes,⁷ we demonstrated that these peptoid-based nanomaterials are highly stable and a wide range of functional groups can be precisely placed within these materials to achieve programmable functions. To gain a better understanding of their formation mechanisms of these biomimetic materials, herein, I will report my group’s recent discovery of designing short peptoid oligomers, including tetramers, for controlled assembly into twisted nanoribbons, helices, along with nanosheets and nanotubes. Mechanistic studies using X-ray diffraction, AFM, TEM combined with computational simulations indicate the asymmetric packing of amphiphilic peptoids is the main driving force that leads to the formation of twisted nanoribbons and nanohelices. Tuning hydrophilic side chain chemistry and the number of hydrophobic side chains can significantly influence the peptoid assembly pathways and dynamics for the formation of hierarchical materials with designed morphologies.

References:

(1) Li et al., *Chem. Rev.* **2021**, 14031. Cai et al., *Acc. Chem. Res.* **2021**, 81. Yang et al., *Chem. Mater.* **2021**, 3047.

(2) Song et al., *ACS Mater. Lett.* **2021**, 420.

(3) Wang et al., *ACS Applied Bio Materials* **2020**, 6039.

(4) Li et al., *Macromol. Rapid Commun.* **2022**, 2100639.

(5) Cai et al., *Research* **2021**, 9861384. Song et al., *Small* **2018**, 1803544.

(6) Jin et al., *Nat. Commun.* **2016**, 12252.

(7) Jian et al., *Nat. Commun.* **2022**, 3025. Jin et al., *Nat. Commun.* **2018**, 270.

2:15 PM SB08.07.03

Biodegradable, All-Organic Transistors Printed on a Bioderived Polymer Fabrizio A. Viola and Mario Caironi; Italian Institute of Technology, Italy

The growing demand of disposable electronics raises serious concerns for the corresponding increase in the amount of electronic waste (e-waste), with severe environmental impact. Organic electronics has been proposed long ago as a sustainable and energy efficient technological platform. Yet, such technology is inevitably leading to a drastic increase of plastic waste if common approaches for flexible substrates are followed. In this scenario, **biodegradable electronics** is an incipient need in order to mitigate the above mentioned issues. Flexibility, solution processability, low capital expenditure and energy-efficient processes, which are distinctive features of organic electronics, have to be complemented by a sustainable end-of-life of materials employed. This requirement calls for solutions where materials, especially substrates that represent the largest volume, can be biodegraded in the environment with no harm, yet assuring that no precious resources are dispersed. In this work, we successfully employed a bioderived and biodegradable biopolymer as a substrate for an **all-organic field effect transistor** (OFET) based on an inkjet printed polymer semiconductor. The **OFETs showed good reproducibility**, a proper current modulation and **extremely low leakage**, which remained almost unaltered **also after intensive mechanical stresses as bending and rolling**. Such mechanical stability and flexibility, together with the biodegradability and bioderivation, make this approach an appealing candidate for the development of sustainable printed electronics, with widespread future applications in the biomedical and food packaging sector.

2:30 PM BREAK

SESSION SB08.08: Photonics and Optics with Biomaterials

Session Chairs: Christopher Bettinger and Keiji Numata

Wednesday Afternoon, November 30, 2022

Hynes, Level 3, Room 313

3:30 PM *SB08.08.01

The Impact of Bacteria Exposure on the Plasmonic Response of Nanosilver and Hybrid Photonic Crystals Giuseppe M. Paterno^{1,2}, Francesco Scotognella^{1,2} and Guglielmo Lanzani^{2,1}; ¹Politecnico di Milano, Department of Physics, Italy; ²Istituto Italiano di Tecnologia, Italy

Silver, in the form of nanostructures, is widely employed as an antimicrobial agent. Despite the large body of work addressing the effects of silver on the antibacterial mechanism and on the (bio)physical chemistry pathways that drive bacterial eradication, little effort has been devoted to the investigation of nanostructured silver plasmon response upon interaction with bacteria. We investigate the bacteria-induced changes of the plasmonic response of silver nanoplates after exposure to the bacterial model *Escherichia coli* (*E. coli*). Ultrafast pump-probe measurements indicate that the dramatic changes on particle size/shape and crystallinity, likely stemming from a bacteria-induced oxidative dissolution process, translate into a clear modification of the

plasmonic response.¹ Finally, we exploit such an effect to build up photonic crystals embedding silver nanostructures, which have the potential to reveal colorimetrically the presence of bacteria.²⁻⁵ This study opens innovative avenues in the bio-physics of bio-responsive materials.

References

1. Paternò, G. M. *et al.* The impact of bacteria exposure on the plasmonic response of silver nanostructured surfaces. *Chem. Phys. Rev.* **2**, 021401 (2021).
2. Paternò, G. M. *et al.* Hybrid One-Dimensional Plasmonic-Photonic Crystals for Optical Detection of Bacterial Contaminants. *J. Phys. Chem. Lett.* **10**, 4980–4986 (2019).
3. Paternò, G. M. *et al.* Integration of bio-responsive silver in 1D photonic crystals: towards the colorimetric detection of bacteria. *Faraday Discuss.* **223**, 125–135 (2020).
4. Normani *et al.*, Design of 1D photonic crystals for colorimetric and ratiometric refractive index sensing. *Opt. Mater.* **X 8**, 100058 (2020).
5. Paternò *et al.*, Distributed Bragg reflectors for the colorimetric detection of bacterial contaminants and pollutants for food quality control. *APL Photonics* **5**, 080901 (2020).

4:00 PM SB08.08.02

Nature's Strategy to Color "Blue"—Cases for Avian Feathers Jong-Souk Yeo, Deok-Jin Jeon, Jihun Kang and Seunghwan Moon; Yonsei University, Korea (the Republic of)

Colors of avian feathers can be produced by pigmentation and/or structural coloration. Interestingly, avian plumage colors, where optical nanostructures are present, only produce the color "blue". The reason why nature uses structural coloration instead of pigmentation to produce blue in the short wavelength regions of the visible spectrum is poorly understood, despite its fundamental significance to physiology and potential to spark advances in biomimetic applications. We may postulate that natural blue pigments are chemically less stable than red pigments due to their molecular complexity so that evolutionary process has led birds to use structural ways to produce diverse array of blue colors. Here, we discuss nature's strategy to produce color "blue" with structural ways by elucidating various cases of avian feathers using optical measurement, electron microscopy, numerical modeling, and biomimicry. We show that how birds produce and enhance appearance from photonic crystal or photonic glass nanostructures by addressing ingenious biological designs. To understand the various color-showing mechanisms in avian feathers, the correlations between the avian nanostructures and colorations were analyzed quantitatively, and the avian structural colors were mimicked with synthetic pathways to verify our understanding. For the case of common pheasant, we find that the photonic crystal nanostructures in their feathers can further modulate color in combination with the surrounding thin-film-like cortex layer to produce brilliant colors from blue to green. For Eurasian jay displaying periodic array of blue and white colors in their feathers, our analysis indicates that they vary colors by controlling only the thickness of color-producing optical nanostructures using multiple scattering effects. On the other hand, Kingfisher modulates plumage colors from blue to cyan by changing channel width of optical nanostructures. All these findings suggest that birds have various efficient way to produce blue colors with structural coloration. Inspired by nature's strategy to color "blue", we also demonstrate biomimetic "green" fabrication methods to display brilliant blue colors using synthetic nanoparticles and controlling the conditions similar to the cases in avian optical nanostructures.

This study was funded by the National Institute of Ecology through the grant number (NIE-C-2021-18) and Human Frontier Science Program through the grant number (RFP0047/2019).

4:15 PM SB08.08.03

Bio-Pigment Xanthommatin and Cephalopod Skin Photonics Richard M. Osgood¹, Akshay Nagar^{1,2}, Sean Dinneen¹, Valerie Adams³, Jin Ho Kim¹, Leila Deravi⁴ and Randy Hughes⁵; ¹DEVCOM SC, United States; ²Brown University, United States; ³Army Public Health Center, United States; ⁴Northeastern University, United States; ⁵U.S. Army Research Laboratory, United States

Biomaterials and biopolymer materials such as biopigments (melanin, xanthommatin, etc.) have fascinating optical properties, such as bright and structural color and advanced camouflage. These material properties are explored in basic research to learn about how the skin of cephalopods (e.g., squid, octopus) functions optically, based on pigment, texture, and photon-scattering granules (~50-500 nm in size). Natural pigment molecules and bio-polymers are attractive for photonics applications: displays, adaptive lenses, underwater optical communications, etc.

Small-molecule biopigments readily dissolve in polymer hosts, resist ultraviolet light, are toxicologically benign, and can be fabricated using large-scale chemical methods. Over 500 mg was synthesized and dried in our laboratory for toxicological analysis. Because of their small-molecule nature, their ability to combine with polymers such as polyvinyl alcohol (PVA), their manufacturability (biological and chemical synthesis), their high refractive index (RI), and their sustainability (they're eaten by animals), the bio-pigments and associated bio-polymers are useful for photonically functional thin films, anti-reflective coatings, photonic scattering for color, etc. Large-scale environmentally friendly synthesis may enable new designs of lightweight optical systems that can adapt and change shape, have a high numerical aperture, and aid in underwater detection or imaging.

The chromatophores in squid skin change from an expanded, pancake-like shape to a punctate, spherical shape and back again to influence photonic scattering and color; they are colored yellow, red, and brown, and are responsible for the bulk color changes. Underneath the chromatophore lie less-obvious iridocyte cells - multilayered Bragg reflectors that reflect color iridescently. The chromatophore cell, in its expanded state, contains multiple layer of sub-monolayers of photon-scattering granules.

Our group discovered that the cephalopod's Xa pigment has a high RI ($n > 1.55$), at 589 nm and at 532 nm. For the latter experiment, n may have been artificially low. Recently, we have carried out more comprehensive broadband (300 nm – 3200 nm) ellipsometric spectroscopy to determine the optical indices (n and absorption coefficient k) of Xa, extracting natural Xa pigment from the squid's chromatophores and forming smooth, high-quality films with concentrations of Xa as much as 90% in polyvinyl alcohol (PVA). Many samples containing natural Xa, and some with artificial Xa, show the same trends, providing a more complete description of Xa's optical properties (n , k) across the entire wavelength range of interest. We have observed an unreported infrared absorption peak and associated reduction in n , and explain possible origins.

Armed with ellipsometric data, we model optical properties (e.g., reflectivity) using a four-flux model (forward and backwards-propagating specular and diffuse light), to gain a more complete and quantitative understanding of squid skin optics, improving on an analytical model of light scattering and absorption developed in 2008 that made important breakthroughs, but lacked separate experimental data on fundamentals for the Xa, and did not comprehensively treat the full optical problem. Here, we update this model analytically, taking better account of the optical coupling between chromatophore and underlying iridocyte. Our 4-flux optical model of the chromatophore will not ignore the background reflectivity and scattering. The to-be-reported physics modeling and theory, with experimental characterization, will enable new bio-pigment and bio-polymer materials and applications. By understanding how the color of the chromatophores changes, another important step can be taken to harnessing artificial and novel material platforms for more efficient control of light at the nanoscale. We discuss possible new functional nanophotonic systems, based on the bio-pigments, and possible applications.

4:30 PM SB08.08.04

Controlled Afterglow Luminescent Particles for Photochemical Tissue Bonding Seong-Jong Kim and Sei Kwang Hahn; Pohang University of Science and Technology, Korea (the Republic of)

Upconversion materials (UCMs) have been developed to convert tissue-penetrating near-infrared (NIR) light into visible light. However, the low energy

conversion efficiency of UCs have limited their further biophotonic applications. Here, we developed controlled afterglow luminescent particles (ALPs) of ZnS:Ag,Co with strong and persistent green luminescence for photochemical tissue bonding (PTB). The co-doping of Ag⁺ and Co²⁺ ions into ZnS:Ag,Co particles with the proper vacancy formation of host ions resulted in high luminescence intensity and long-term afterglow. In addition, the ALPs of ZnS:Ag,Co could be recharged rapidly under short ultraviolet (UV) irradiation, which effectively activated rose bengal (RB) in hyaluronate – RB (HA-RB) conjugates for the crosslinking of dissected collagen layers without additional light irradiation. The remarkable PTB of ZnS:Ag,Co particles with HA-RB conjugates was confirmed by *in vitro* collagen fibrillogenesis assay, *in vivo* animal wound closure rate analysis, and *in vivo* tensile strength evaluation of incised skin tissues. Taken together, we could confirm the feasibility of controlled ALPs for various biophotonic applications.

SESSION SB08.09: Bioelectronics
Session Chairs: Eleni Stavrinidou and Massimo Trotta
Thursday Morning, December 1, 2022
Hynes, Level 3, Room 313

8:30 AM *SB08.09.01

Gelatin-Based Bioelectronics for Electrophysical Monitoring [Christopher J. Bettinger](#); Carnegie Mellon University, United States

This talk will describe recent advances in the use of gelatin-based bioelectronics to interrogate the structure and function of organs. Materials processing and device fabrication strategies will be presented. Device demonstrations to interrogate gastro-enterological and cardiac organ systems will be presented.

9:00 AM DISCUSSION TIME

9:15 AM BREAK

9:45 AM *SB08.09.04

Learning from Nature and a Century-Old Nobel Laureate to Make Mechanochromic Materials at Scale [Mathias Kolle](#) and Benjamin Miller; Massachusetts Institute of Technology, United States

Dynamic optical appearance plays a critical role for many animals that rely on adaptive camouflage or bright and varying color displays for their survival. The materials employed by these organisms have inspired scientific and engineering efforts to emulate their dynamic optical behavior in synthetic material analogues, such as mechanochromic photonic materials, which change their optical properties in response to mechanical forces. Mechanochromic materials provide a versatile platform for colorimetric force sensing in a variety of different research and technology fields, including healthcare, robotics, and human-computer interaction. We have developed a roll-to-roll manufacturing technique based on combining Lippmann photography with holographic recording materials, providing a fast, scalable, low-cost method of producing mechanochromic photonic sheets. The benefits of this technique include high-resolution spatial patterning across the entire RGB color space, printing in the near-infrared region to create hidden patterns that appear when stretched, control of the angular distribution of reflected light, and tuning of the mechanical properties of the material to map color variations to different force ranges.

10:15 AM SB08.09.05

Measuring Charge Transport Properties in Single and Double-Stranded RNA Oligonucleotides at the Nanoscale [Subrata Chandra](#), Keshani G. Pattiya Arachchillage and Juan M. Artes Vivancos; University of Massachusetts Lowell, United States

RNA oligonucleotides and their biophysics are an essential part of therapeutics, sensing, and forensics applications. They have gained importance in the research focus in recent years for several reasons. Not only do several pathogens (e.g., SARS-CoV2) have RNA genomes, but many therapeutic¹, biotechnological², and modern molecular technologies (e.g., Gene editing³, gene silencing⁴) use RNA oligonucleotides at their core. Single-molecule electrical techniques have allowed studying the charge transfer process in biomolecules with unprecedented resolution in the last decade⁵. In the biomolecular electronics discipline, the electronic and charge-transport (CT) properties of short oligonucleotides (dsDNA & DNA: RNA hybrid) have been reported extensively⁶. But despite its biophysical and biological importance, the single-molecule electronic properties of double-stranded(ds)RNA and single-stranded (ss) RNA have not been studied to that extent.

Biomolecular electronics, the discipline studying the charge transfer process in biomolecules, has the potential to describe the interaction between electronic materials and biological systems (RNAs) at molecular interfaces. We use the Scanning tunneling microscope-assisted break junction method (STM-BJ)⁷ to study charge transport in short oligonucleotides by reproducible conductance histograms related to their biomolecular structure and conformations. Each biomolecule will be confined within a nanometric gap at a well-defined molecular orientation to measure its electrical properties. Herein, we measured, for the first time, the conductance of individual dsRNA molecules and compared it with the conductance of DNA: RNA hybrids⁸. The average conductance values are similar for both biomolecules, but the distribution of conductance values shows an order of magnitude higher variability for dsRNA, indicating higher molecular flexibility of dsRNA. In our next study, we have demonstrated base-mediated charge transport in specific single-stranded 5 and 10 base pairs(bp) RNA oligonucleotide sequences. We found base stacking is the main factor for getting a probable conductance value for those spontaneously formed RNA oligonucleotide junctions. By comparing with their DNA counterpart, we have found that single-stranded DNA for both 5 and 10 bp sequences are less conductive than RNA due to a lack of base stacking in them.

These results pave the way for measuring various biomolecular interactions at a single-molecule level. In the future, we will measure the conductance of a protein (Argonaute)- RNA complex. This can give us a better understanding of the formation of the RISC(RNA-induced silencing complex) complex and allow the study of the thermodynamics and kinetics of gene expression at the individual complex level. Lastly, we can use these fundamental results for designing next-generation smart biomaterials and biosensors that may address improved biological performances and advanced health monitoring.

References:

1. C. F. Bennett and E. E. Swayze, *Annu. Rev. Pharmacol. Toxicol.*, 2010, 50, 259–293.
2. J. A. Doudna and E. Charpentier, *Science*, 2014, 346, 6213.
3. D. B. T. Cox, R. J. Platt, and F. Zhang, *Nat. Med.*, 2015, 21, 121–131.
4. Zhang, Y., W. Dubitzky, et al., RNA-induced Silencing Complex (RISC), in *Encyclopedia of Systems Biology*, Editors. 2013, Springer New York: New York, NY, p.1876-1876.
5. K. G. G. P. Arachchillage, S. Chandra, A. Piso, T. Qattan and J. M. A. Vivancos, *J. Mater. Chem. B*, 2021, 9(35), 6994–7006
6. Li, Yuanhui, et al. "Comparing charge transport in oligonucleotides: RNA: DNA hybrids and DNA duplexes." *The journal of physical chemistry letters*

7.10 (2016); 1888-1894.

7. B. Xu and N. J. Tao, Science, 2003, 301, 1221–1223.

8. Chandra, Subrata, et al. "Single-molecule conductance of double-stranded RNA oligonucleotides." *Nanoscale* 14.7 (2022): 2572-2577.

10:30 AM SB08.09.06

Towards Functionalized PEDOT:PSS for OECT-Based Sensing of Cytokine Bernhard Burtcher, Chiara Diacci and Daniel Simon; Linköping University, Sweden

Poly(3,4-ethylenedioxythiophene) doped with polystyrene sulfonate (PEDOT:PSS) is the most common organic semiconductor in OECTs. The comparably high transconductance compared to OFETs, combined with easy circuit integration, makes them good candidates for biosensors. While metabolites and neurotransmitters have been successfully sensed with OECTs, reports on other inflammatory proteins and especially cytokines are few.¹⁻³

Here, we demonstrate a modification strategy using a small linker molecule to attach to the sulfonates on PSS, which then allows EDC/NHS coupling to bind a recognition element. In this study, we choose aptamers as the recognition elements to demonstrate the concept. Aptamers are synthetic oligonucleotides that exhibit high specificity, low production costs, good shelf-life, and can be modified for various immobilization strategies,⁴ making this a versatile, cheap, up-scalable approach. While first investigations focus on cytokine sensing with aptamers, the approach is easily adaptable to bind other elements of interest (e.g., antibodies, enzymes, ...).

1. Kergoat, L. et al. Detection of glutamate and acetylcholine with organic electrochemical transistors based on conducting polymer/platinum nanoparticle composites. *Adv. Mater.* 26, 5658–5664 (2014).

2. Tang, H., Lin, P., Chan, H. L. W. & Yan, F. Highly sensitive dopamine biosensors based on organic electrochemical transistors. *Biosens. Bioelectron.* 26, 4559–4563 (2011).

3. Burtcher, B. et al. Sensing Inflammation Biomarkers with Electrolyte-Gated Organic Electronic Transistors. *Adv. Healthc. Mater.* 10, 2100955 (2021).

4. Machashi, K. et al. Label-Free Protein Biosensor Based on Aptamer-Modified Carbon Nanotube Field-Effect Transistors. *Anal. Chem.* 79, (2007).

10:45 AM SB08.09.07

Phenylalanine Assisted Conductivity Enhancement in PEDOT:PSS Films Divyansh Chamria and Ramesh Adhikari; Colgate University, United States

Biological materials such as amino acids are attractive due to their smaller environmental footprint, ease of functionalization, and potential for creating biocompatible surfaces for devices. Here, we report facile self-assembly and characterization of highly conductive films of composites of phenylalanine, an aromatic amino acid, and PEDOT:PSS, a commonly used conducting polymer, which has been shown to have increased conductivity when doped with polar organic compounds. However, the behavior observed with Phenylalanine is significant because it is non-polar in nature and is biologically derived. We have observed that the composite films formed by introducing aromatic amino acid phenylalanine in PEDOT:PSS can improve the conductivity of the film to about 594 S/cm, a 400% increment compared to the conductivity of a pristine PEDOT:PSS film of about 1.5 S/cm. In addition, the conductivity remains high even with a 10 vol% PEDOT:PSS solution. These conductive properties show a clear trend with changed proportions and the composites appear physically distinct. Using DC and AC measurement techniques, we have determined that the conduction in the highly conductive composites is purely due to efficient electron transport compared to pure PEDOT:PSS films. As observed from SEM and AFM, this is likely due to the phase separation of PSS chains from PEDOT:PSS globules which has previously been shown to increase conductivity since PSS regions impede charge transport. Fabricating composites of bioderived simple amino acids with conducting polymers using facile techniques such as the one we report here opens up opportunities for the development of low-cost biocompatible and biodegradable electronic materials with desired electronic properties.

11:00 AM SB08.09.08

Electrochemically Driven Polymerization of pH Sensitive Polymers on High Density Microelectrode Arrays for Neural Patterning *In Vitro* Jens Duru¹, Nako Nakatsuka¹, Josephine Löhle¹, Marcello Pozzi¹, Benedikt Maurer¹, Benjamin Simona², Csaba Forró³ and János Vörös¹; ¹ETH Zürich, Switzerland; ²Ectica Technologies, Switzerland; ³Stanford University, United States

In-vitro neuroscience makes use of dissociated neural networks of iPSC derived or animal origin, grown on the surface of microelectrode arrays (MEA) for electrical access. Upon exposure of neurons to a MEA surface, neurons adhere and connect to each other at random, creating highly complex systems. The complexity of neural networks can be reduced by various surface patterning methods, which render part of the surface cell adhesive and other parts cell repellent [1]. Alternatively, the use of biocompatible microstructures is a popular method to confine the neural adhesion and guide the growth of their axons. In the past, polydimethylsiloxane-based microstructures were used with great success to pattern precise neural networks *in vitro* on low-density glass MEAs with an electrode pitch of 500 μm [2,3] and more recently on high density complementary metal-oxide-semiconductor (CMOS) MEAs [4], that offer up to 26'400 electrodes at a pitch of 17.5 μm .

Here, we demonstrate an alternative patterning method that aims to establish neural guidance structures directly on the surface of the CMOS MEA with a spatial resolution only limited by the electrode pitch of the MEA. By inducing hydrolysis locally on user-defined electrode sets, the pH can be selectively altered in the vicinity of the selected electrodes. This mechanism allows for the local formation of polymers that show a pH-dependent formation, such as transglutaminase crosslinked hydrogel which assembles close to neutral pH [5] or the nature-inspired biopolymer polydopamine that forms in slightly basic (pH > 8) environments [6]. We demonstrate that we can alter the pH with single-electrode precision and can quantify the induced pH change optically using the pH reporter 5-(and-6)-carboxy SNARF-1. Using CMOS MEAs with platinum black coated microelectrodes, we are able to inject large enough currents to shift the local pH of the precursor solutions precisely from 6.6 to 8.4 for dopamine polymerization and 5.8 to 7.5 to form hydrogel. We observe constant pH elevations without precision loss for up to 35 min, which is enough time for local polymer formation. Finally, we provide preliminary results that show that the formed hydrogel guides the growth of primary rat cortical neurons and that the observed effects are dependent on the polymerization time of the hydrogel.

[1] Aebersold et al. "Brains on a chip": Towards engineered neural networks. *Trends in Analytical Chemistry* (2016)

[2] Ihle et al. An experimental paradigm to investigate stimulation dependent activity in topologically constrained neuronal networks. *Biosensors and Bioelectronics* (2022)

[3] Girardin et al. Topologically controlled circuits of human iPSC-derived neurons for electrophysiology recordings. *Lab on a Chip* (2022)

[4] Duru et al. Engineered Biological Neural Networks on High Density CMOS Microelectrode Arrays. *Frontiers in Neuroscience* (2022)

[5] Milleret et al. Electrochemical Control of the Enzymatic Polymerization of PEG Hydrogels: Formation of Spatially Controlled Biological Microenvironments. *Advanced Healthcare Materials* (2013)

[6] Lee et al. Mussel-Inspired Surface Chemistry for Multifunctional Coatings, *Science* (2007)

11:15 AM SB08.09.09

Sustainable Biopolymer Binders for Conformable Multifunctional Electrically Conductive Coatings Pietro Cataldi^{1,2}, Vicente Orts Mercadillo², Giovanni Perotto¹, Mark A. Bissett², Ian Kinloch², Mario Caironi¹ and Athanassia Athanassiou¹; ¹Italian Institute of Technology, Italy; ²The University of Manchester, United Kingdom

There is a growing demand for transitioning electronic circuitry and components from stiff and rigid substrates to compliant and flexible platforms, such as thin plastics, textiles, and foams. In parallel, the push for replacing expensive metals-based inks with cost-effective conductive inks has led to the development of formulations with novel nanomaterials and binders.[1,2] Among the nanomaterials, 2D materials, and in particular graphene-related materials (GRMs), have drawn attention due to their increasingly facile and scalable production, high electrical conductivity, and compatibility with industrial manufacturing methods.[3] The resulting conformable electronic materials are poised to unlock thrilling applications in the wearable, healthcare, and Internet of Things sectors. Nevertheless, the substrates, the binders, and the solvents employed are so far often selected without considering the outcome in terms of material sustainability.

We developed electrically conductive composite coatings based on GRMs and biobased and/or biodegradable binders.[2,4] The fabrication is simple and exploits green solvents such as alcohol and/or water. Sustainable binders, ranging from biopolymers and natural waxes such as polyvinyl alcohol and beeswax to proteins from the waste stream such as keratin extracted from wool/feather wastes, were preferred depending on the selected sustainable substrates (i.e., cellulose-/biopolymer-based). The as-obtained materials display a low sheet resistance of about 10 Ohm/sq and excellent stability to tens of folding events, hundreds of abrasions, and thousands of bending cycles. Thus, they can be applied as deformable conductors or strain sensors, depending on the material formulation (i.e., 2D-1D nanofiller hybridization and binder:nanofiller ratio) and the consequent electrical percolation preservation/disruption after mechanical stress. These materials are multifunctional since they exhibit enhanced thermal conductivities. As such, they can be applied simultaneously for thermal dissipation and electromagnetic interference shielding. Due to their flexibility, multifunctionality, and reduced footprint, such versatile electrically conductive coatings have the potential to enable applications in the wearables and conformable electronics field, reducing the environmental impact of the conductive materials for electronics simultaneously.

References:

- [1] Ergoktas M. S. et al., **2020**, Nano Letters, DOI:10.1021/acs.nanolett.0c01694.
- [2] Cataldi P. et al., **2020**, Advanced Functional Materials, DOI:10.1002/adfm.201907301.
- [3] a) Kovtun A., **2019**, 2D Materials, DOI:10.1088/2053-1583/aafc6e; b) Cataldi et al., **2018**, Applied Sciences, DOI:10.3390/app8091438.
- [4] a) Wu et al., **2020**, Advanced Electronics Materials, DOI: 10.1002/aelm.202000232; b) Cataldi et al., **2019**, ACS Sustainable Chemistry and Engineering, DOI: accsuschemeng.9b02415.

11:30 AM SB08.09.10

Hydrogel Protector for Stabilizing Water Splitting Photoelectrodes Byungjun Kang, Jeiwan Tan, Kyungmin Kim, Donyoung Kang, Hyungsoo Lee, Sunihl Ma, Gyumin Jang, Jooho Moon and Hyungsuk Lee; Yonsei University, Korea (the Republic of)

Human beings are facing severe problems related with the global climate change. There have been international efforts to replace carbon-based energy system with carbon-free/hydrogen-based energy one. Solar hydrogen conversion techniques gains attention as they can produce hydrogen using sunlight and water without emission of greenhouse gas. Photoelectrochemical (PEC) water splitting is considered as one of the promising solar hydrogel conversion techniques because it can be realized using low-cost thin-film materials. However, current low-cost thin-film based PEC devices have a relatively short lifespan due to its low structural stability. Light-absorbing semiconductor of the PEC device severely suffer from photocorrosion by electrolyte. Although amorphous TiO₂ is deposited via atomic layer deposition on the device to provide physical separation between the semiconductor and electrolyte, photoelectrons accumulated near the device surface induce the reduction and dissolution of the TiO₂ layer. In addition, platinum (Pt), which is the best hydrogen evolution reaction (HER) catalyst, can be easily agglomerated and detached from the PEC device.

Although various strategies including insertion of functional layer under the catalyst have been introduced, still there is a need to develop a versatile protection strategy which can prevent both co-catalyst detachment and photocorrosion for practical operation of PEC devices. We hypothesize that device-on-top protector made of nanoporous polymeric network may prevent the dissociation of components of the PEC device. A protector with a high transparency and water content can be preferred in order not to disturb light transmission and electrolyte transfer to the device. We are inspired by ocean plants where algae cells are covered by 'hydrogel' which has a transparent and nanoporous polymer network structure having high water content. In this study, we demonstrate that the hydrogel protector on the PEC device enhances the structural stability of the PEC devices. As a hydrogel protector, we selected low cost polyacrylamide which has high chemical inertness in electrolyte solution. The hydrogel was coated on a reference Pt/TiO₂/Sb₂Se₃ photocathode via a mold casting method. Dynamics of hydrogen bubbles in the hydrogel and their escape can depend on the mechanical and structural properties of the hydrogel. We demonstrate that trapped bubbles cause the fracture of the protector in the case of high concentration of hydrogel. When the hydrogel protector is relatively thick, hydrogen bubbles are trapped inside the protector leading to reduction in photocurrent. With the protector having the optimal properties, bubbles can effectively escape from the protector through micro gas tunnels which are formed in the hydrogel at the initial stage of the PEC operation. The hydrogel protector coated on the PEC device can prevent detachment of Pt catalyst and dissolution of TiO₂ layer. Compared to without protector, the lifetime of the Pt/TiO₂/Sb₂Se₃ photocathode covered by the hydrogel protector was increased by 100 folds. Furthermore, we showed the hydrogel protection strategy can be applied to various types of PEC devices including SnS photocathode and BiVO₄ photoanode. We expect that further engineering of the hydrogel in terms of microstructure, poroelastic property, and chemical property can help to develop a semi-permanent hydrogen production system.

SESSION SB08.10: Biomedical Applications I
Session Chairs: Brendan Harley and Eleni Stavrinidou
Thursday Afternoon, December 1, 2022
Hynes, Level 3, Room 313

1:30 PM *SB08.10.01

Biopolymeric Materials for Organoid Bioprinting Sarah C. Heilshorn; Stanford University, United States

Organoids are three-dimensional, multi-cellular constructs with emergent structural properties that mimic organizational features found in natural tissue. Individual organoids can fuse together to form tissue-like structures, termed "assembloids," that can serve as *in vitro* models of human development and disease. A key requirement for assembloid fabrication is the spatial positioning of individual organoids, which is currently performed manually. To automate and scale-up this biofabrication process, we have developed a family of biopolymers that work together with a custom-built electromagnetic

bioprinter. Here, we demonstrate the capacity for an iron-oxide nanoparticle-laden hydrogel to mediate the spatial patterning and subsequent fusion of human induced pluripotent stem cell (iPSC) derived neural organoids within a support hydrogel. The support material is shear-thinning and self-healing to accommodate the motion of the electromagnetic printer, promote organoid hydration, and achieve stable placement within three-dimensional space while organoid fusion occurs. Unlike aspiration-mediated biofabrication approaches that can lead to irreversible plastic deformation of cellular aggregates, magnetic lifting was well tolerated by the organoids. We leveraged this system to create precisely arranged neural assembloids with excellent viability and maintenance of the internal cytoarchitecture of individual organoids. In summary, this platform represents a significant advance in the emulation of large, compositionally diverse neural tissues to enable high-throughput studies of neural development and disease.

2:00 PM SB08.10.02

DNA Aptamers and Self-Assembled DNA Materials as Bioinspired Modulators of Calcium Mineralization [Aren E. Gerdon](#); Emmanuel College, United States

Synthetic DNA, as small functional molecules or in large self-assembled structures, provides exquisite addressability, functionality, and fidelity. As a polyelectrolyte with repeating negative charge DNA mimics poly-anionic proteins found in enamel, bone, and marine organisms. DNA aptamers have been selected to influence calcium phosphate mineral formation using a novel precipitation SELEX method. These aptamers have been demonstrated to slow mineralization kinetics while altering materials morphology depending on pH and the presence of G-quadruplex secondary structures. Current research efforts have been in applying DNA aptamers to calcium phosphate mineralization of collagen and to calcium carbonate mineralization. Using DNA aptamers in coordination with DNA self-assembled materials, such as DNA origami, is currently being explored as a means for building and mimicking hierarchical structures.

2:15 PM SB08.10.03

Dynamic Hydrogels as Models of Liver Fibrosis Progression [Yueming Liu](#), Aidan Gilchrist, Yuan Guan, Gary Peltz and Sarah C. Heilshorn; Stanford University, United States

Hydrogels have emerged as a promising platform for three-dimensional (3D) *in vitro* models of disease progression. However, widely utilized animal-derived matrices (e.g. Matrigel/Cultrex) are highly variable and do not allow for tuning of biophysical and biochemical cues. Additionally, such matrices do not capture the dynamic features of the *in vivo* extracellular matrix (ECM), which is remodeled during disease progression and causes further dysregulation of cell behavior. Here, we present an engineered matrix crosslinked by dynamic covalent bonds that enable on-demand tuning of material mechanics to model the stiffening of the liver during fibrosis.

During disease progression of fibrosis, there is an associated increase in the deposition of elastin, fibronectin (FN), and hyaluronan (HA), resulting in an increase in stiffness. We have established a liver-mimetic environment by incorporating HA modified with benzaldehyde functional groups and a recombinant elastin-like protein (ELP) modified with hydrazine functional groups to create a HA-ELP (HELP) matrix. The engineered elastin-like protein (ELP) contains a cell-adhesion motif from fibronectin and a peptide sequence derived from elastin. When mixed, the benzaldehyde and hydrazine functional groups form dynamic hydrazone bonds, which can break and reform at physiological conditions, creating a dynamic microenvironment. By altering the wt% of HA and ELP, we have assembled a suite of HELP gels whose stiffnesses (0.5 – 6 kPa) reflect that of normal liver through those with advanced stages of fibrosis. To regulate HELP stiffness during culture, we have introduced a small molecule competitor that competes for crosslinking sites, which can decrease the crosslink density and stiffness of HELP. Over time these competitors diffuse out of the hydrogel, which leads to an increase in crosslink density that mimics the stiffening environment that occurs during the progression of fibrosis.

Using a library of competitors, we demonstrate that HELP stiffness can be reduced by an order of magnitude in a dose-dependent manner. By altering the chemical functionality of the competitor, we can tune the time-scale of modulus recovery, ranging from < 1 day to over three weeks. This enables us to examine the effect of acute stiffening and the effect of gradual stiffening occurring over a >2 week period. Using this chemically defined, adaptable hydrogel platform, we developed a model of liver fibrosis progression using human hepatic organoids (HO). We combine HELP with laminin-111 to promote the formation and culture of HO, and demonstrate long-term growth of HO across a variety of stiffnesses. Finally, we demonstrate that incorporation of competitors does not impact HO growth and morphology. Human HO grown in HELP matrices are viable, proliferative, and metabolically active, and they continue to express markers of differentiated hepatic tissue and accumulate lipids in a stiffness-dependent manner. We are currently evaluating the altered metabolic profile and lipid accumulation in these gradually stiffening materials.

Overall, we have developed a dynamic HELP hydrogel with on-demand control of mechanical properties using crosslinking competitors. We demonstrated formation and growth of HO in dynamic HELP with liver-mimetic stiffnesses to model liver fibrosis progression.

2:30 PM BREAK

3:00 PM SB08.10.04

3D-Bioprinted Phantom with Human Skin Phototypes for Biomedical Optics [Wonjun Yim](#), Jiajing Zhou, Lekshmi Sasi and Jesse V. Jokerst; University of California San Diego, United States

We report 3D-bioprinted skin-mimicking phantoms with skin colors ranging across the Fitzpatrick scale. These tools can help understand the impact of skin phototypes on biomedical optics. Synthetic melanin nanoparticles of different sizes (70–500 nm) and clusters were fabricated to mimic the optical behavior of melanosome. The absorption coefficient and reduced scattering coefficient of the phantoms are comparable to real human skin. We further validated the melanin content and distribution in the phantoms versus real human skins *via* photoacoustic (PA) imaging. The PA signal of the phantom could be improved by (i) increasing melanin size (>1,000-fold), (ii) increasing clustering (2–10.5-fold), and (iii) increasing concentration (1.3–8-fold). We then used multiple biomedical optics tools (e.g., PA, fluorescence imaging and photothermal therapy) to understand the impact of skin tone on these modalities. These well-defined 3D-bioprinted phantoms may have value in translating biomedical optics and reducing racial bias.

3:15 PM SB08.10.05

Thermal Transport in Neuron-Inspired Polymer-Gold Nanoparticle Tree Networks [Xingfei Wei](#) and Rigoberto Hernandez; Johns Hopkins University, United States

Complex networks of polymer linked nanoparticles have potential applications in chemical separation, biomedicine and nanophononics. Inspired by Cajal's picture of a single neuron [Gomez-Marín, *Science*, 2022, vol 375, issue 6586, p 1237], the tree-like single neuron structure could be the key to developing new brain-like computing materials. In this work, we have designed computational models of binary tree networks using polymers and gold nanoparticles (AuNP) to mimic a neuron structure. The tree structure and thermal transport properties in polymer-AuNP networks are uncovered using all-atom molecular dynamics simulations. We vary the height of the binary tree structure from 1 to 5 levels corresponding to a total number of 2 to 32 leaves. The

heat flux in both directions, from leaves to the root and from the root to leaves, are reported. Two polymer types of similar branch chain length with different backbone stiffness are compared, *viz.* polyethylene (PE) and poly(*p*-phenylene) (PPP). We also compared tree networks with different branch chain length using 12 and 50 carbon length PE. The results from our simulations provide useful guidance for developing new bioinspired materials and devices.

3:30 PM SB08.10.06

Wireless Localized Electrical Stimulation of Neurons Using Biomimetic Synthesized EDOT-Pyrrole Nanoparticles Nicolas Muzzio¹, Manuel E. Martinez-Cartagena², Rohini Thevi Guntunur¹, Vanessa Fisher¹ and Gabriela Romero¹; ¹University of Texas at San Antonio, United States; ²Research Center in Applied Chemistry, Mexico

Non-invasive manipulation of cell signaling is critical in basic neuroscience research and in developing therapies for neurological disorders and new tissue engineering and regenerative medicine approaches. Current techniques for drug-free, selective, and deep stimulation of the nervous system present major drawbacks such as low spatial resolution, limited target depth or the requirement of highly invasive neurosurgical procedures. To overcome these limitations, nanotechnology approaches are being developed to allow for wireless and cell-type specific neuronal stimulation. Though it is known that electric fields modulate several biological processes and that neurons are electrogenic cells, electrical stimulation and conductive cues have been disregarded in tissue engineering and regenerative medicine approaches until recently. In this work, biomimetically synthesized conductive copolymer 3,4-ethylenedioxythiophene (EDOT)-Pyrrole nanoparticles (RB02 NPs) were used for enhancing neuronal differentiation and for wireless and localized neurostimulation.

Biomimetic synthesis of EDOT-Pyrrole copolymers doped with PSS was carried out using hematin as catalyst. The obtained RB02 NPs were characterized by means of Raman spectroscopy, Fourier transform infrared spectroscopy, electron microscopy and dynamic light scattering. The electrochemical properties were characterized by galvanostatic charge discharge, voltammetry, and electrochemical impedance spectroscopy. For electrical stimulation of neurons, NPs were charged by applying 3V using platinum electrodes, obtaining C-RB02 NPs. NPs effect on ND7/23 neuron hybrid cell line viability was assessed by live/dead staining using flow cytometry. ND7/23 differentiation was evaluated by cell cytoskeleton staining and quantification of morphological parameters such as dendrite number and length. Primary cortex neuronal stimulation was studied by calcium influx detectable through the dynamic fluorescence changes of Fluo-4.

The NPs presented a pseudocapacitive behavior and large specific capacitance, allowing their use as nanocapacitors by charging them through electrical current exposure, obtaining C-RB02 NPs. The live/dead assay showed that RB02 NPs presented no toxicity towards ND7/23 cells. Furthermore, charged NPs enhanced cell differentiation at short times after addition (<6 hours), evidenced in cells with more and longer dendrites. Charged RB02 NPs largely increased cortex neuronal activity assessed by intracellular calcium dynamics.

In conclusion, biomimetic synthesized conductive RB02 NPs were used for the localized stimulation of neurons. Biomimetic synthesis was utilized to avoid cytotoxicity of the nanomaterials associated with traditional wet chemistry protocols. RB02 NPs displayed similar charge-transfer velocity and larger specific capacitance than PEDOT:PSS, benchmark in electroconductive material for bioengineering. Electroconductive RB02 NPs were shown to enhance ND7/23 differentiation within 3 hours of co-culturing. The differentiation effect was more pronounced when charged nanoparticles were employed. Charged RB02 NPs largely increased neuronal activity in primary rat cortical networks assessed by calcium imaging. Overall, biocompatible RB02 NPs fabricated here have a great potential for the remote control of biological signaling, which is anticipated to contribute to the progress of basic neuroscience research and for developing neurological therapies.

3:45 PM SB08.10.07

Yield-Stress and Creep Control Depot Formation and Persistence of Injectable Hydrogels Following Subcutaneous Administration Carolyn K. Jons and Eric A. Appel; Stanford University, United States

Hydrogels that can be injected into the body using standard needles or catheters enable a minimally invasive strategy to prolong local delivery of therapeutic drug and cellular cargo. In particular, physically crosslinked hydrogels exhibit shear-thinning and self-healing behaviors enabling facile injectability and depot formation upon administration. While prior efforts to characterize these systems have focused on injectability and cargo release behaviors, prediction of cargo release in the body often assumes the materials form a depot rather than spreading out upon administration. Here, we evaluate how hydrogel rheology correlates with depot formation and persistence following subcutaneous administration in mice with two physiochemically-distinct, physically crosslinked hydrogel systems. We evaluate calcium-alginate and polymer-nanoparticle hydrogel systems exhibiting variable mechanical behaviors across several rheological properties (stiffness, viscoelasticity, yield stress, and creep). By relating measured rheological properties to depot formation and persistence time following subcutaneous administration, for these two gel systems we identify that yield stress is predictive of initial depot formation while creep is predictive of depot persistence. Indeed, only materials with yield stresses greater than 25 Pa form robust depots, and reduced creep correlates with longer depot persistence. These findings provide predictive insights into design considerations for hydrogel technologies capable of extended controlled release of therapeutic cargo.

4:00 PM SB08.10.08

Hyaluronic Acid Hydrogel with Gradient Mechanical Properties for Tissue Engineering Mina Kwon, Hye Eun Choi and Ki Su Kim; Pusan National University, Korea (the Republic of)

For cell physiology, the microenvironment can play an important role, and hydrogels can provide a three-dimensional microenvironment to allow native cell growth in vitro. Hydrogels, a crosslinked hydrophilic polymer that does not dissolve in water, have been widely studied as an artificial extracellular matrix (ECM) that can mimic the ECM of various tissues due to its high water retention capacity, permeability to cellular nutrients and metabolites, excellent mechanical properties and biocompatibility. The mechanical properties of the extracellular matrix (ECM) contribute to the regulation of various cellular behaviors, and controlling the mechanical properties of hydrogels is of key importance in enabling various cell-hydrogel interactions. However conventional hydrogels have a homogeneous environment with an isotropic distribution limiting complete mimicking of the complex architectures of native tissues and pathological gradients found in tumors, scars, and wounds. In this work, we report hydrogel with gradient mechanical properties using hyaluronic acid which is a natural polymer and an excellent candidate for use in tissue engineering due to its excellent biocompatibility and bio-functions. Hyaluronic acid was conjugated with methacrylate and ¹H NMR spectrum confirmed the successful synthesis of methacrylated hyaluronic acid. We successfully prepared the gradient hydrogel via photocrosslinking method, and the studies were performed with syringe pumps for gradient generation and a fluidic mixer for homogenous mixing of hydrogel precursors with different crosslinker concentrations. The gradient hydrogel was characterized and assessed the feasibility of tissue engineering application. The successful formation of the gradient in crosslinking density is confirmed by NMR spectrum and the viscoelastic properties of the hydrogels were tested on a rheometric fluid spectrometer. Scanning electron microscopy confirmed the different cross-sectional morphology and the pore size in our hydrogel system. For in vitro test, L929 fibroblasts were encapsulated in gradient hydrogel and stiffness-dependent cellular behaviors are monitored using a confocal microscope. In all samples, cells are highly active and spread well along the hydrogel

substrate, and enhanced cell spreading was confirmed as the degree of crosslinking decreases. We further investigated the hydrogels' cell differentiation ability by culturing human adipose tissue-derived mesenchymal stem cells (hAD-MSCs) and stiffness-dependent hAD-MSCs morphology, migration, and differentiation were studied. In vitro drug release analysis was conducted to evaluate the drug release profile of gradient hydrogel and a gradual release of the model drug was observed. Taken together, this gradient hydrogel will be exploited in a tissue engineering platform to mimic variable mechanical gradient tissues.

4:15 PM SB08.10.09

Functional Contact Lens for Colorimetric Visualization of Glucose Level Jeongin Seo¹, Jumi Kang¹ and Kyueui Lee^{1,2}; ¹Kyungpook National University, Korea (the Republic of); ²Kyungpook National University Hospital, Korea (the Republic of)

A non-invasive glucose monitoring system is ideal for measuring glucose levels. However, most diabetic patients still rely on the traditional invasive finger-prick measurements due to the cost issue. We developed a disposable contact lens-based colorimetric glucose sensing platform. A plant-derived polyphenolic polymer called poly(tannic acid) having substantial molecular adhesion was used as a functional coating layer for conjugating a nucleophilic molecule, 4-mercaptophenylboronic acid. The boronic acid-functionalized contact lenses showed a strong and reversible binding affinity for glucose depending on pH conditions. The bound glucose can be released by immersing the contact lens in an acidic enzymatic cocktail, resulting in an immediate color change. This allows a facile colorimetric determination of glucose levels. The glucose concentration dependent color change was quantified by UV-vis studies. The successive chemical modifications of the contact lens surface were characterized by XPS analysis and contact angle measurements. An in-vitro cytotoxicity test (i.e., CCK-8 assay) confirmed the biocompatibility of the system. Taken together, our glucose-sensing contact lens is expected to successfully replace the conventional glucose measurement methods; this will be especially beneficial for low-income people.

4:30 PM SB08.10.10

Mechanistic Study of Block Copolymer Interaction with Cell Membranes and Model Lipid Bilayers Mihee Kim¹, Timothy Lodge², Joseph Metzger², Benjamin Hackel² and Frank Bates²; ¹Los Alamos National Laboratory, United States; ²University of Minnesota Twin Cities, United States

Disruption of cell plasma membranes, a crucial component of cells, is fatal for cellular functions. Poloxamer 188 (P188), a poly(ethylene oxide)-*b*-poly(propylene oxide)-*b*-poly(ethylene oxide) (PEO-PPO-PEO) triblock copolymer, is known to protect cell membranes against various external stresses and injuries, demonstrating its potential to treat diseases such as Duchenne muscular dystrophy or ischemia-reperfusion injury. However, the mechanism by which the polymer protects the cell membrane is poorly understood. Here, I present several systematic approaches to exploring how amphiphilic block copolymers interact with cell membranes and model lipid bilayers. First, we probed how block copolymer architecture affects cell membrane protection using a cellular membrane integrity assay and precisely synthesized PEO-PPO diblock copolymers. To gain a more quantitative assessment of the interactions at the molecular level, we employed supported lipid bilayers as model cell membranes. Binding kinetics and surface coverage of similar molecular weight P188 and a PEO homopolymer were examined using surface plasmon resonance spectroscopy. Distribution of P188 and PEO within the bilayer was studied using neutron reflectivity and atomic force microscopy. We discovered that P188 and PEO both adhere to the lipid bilayer with slow binding kinetics, and surprisingly, both penetrate into the inner lipid leaflet, suggesting that PEO plays a significant role in driving the block copolymer interactions with cell plasma membranes. Study with fluorescent dye-labeled polymers translates these findings to living tissue. Collectively, these results provide important clues regarding how block copolymers protect cell membranes.

4:45 PM SB08.10.11

Fabrication of Drug Loaded PLGA Microparticles Using a Microfluidic Flow-Focusing Device for Sustained Release Formulations Nelia D. Viza; Merck, United States

Long acting injectables aim to improve the current standard of care for various infectious diseases and neurological disorders, by eliminating the oral dose. As a result, decreasing dosing frequency with highly active, well-tolerated medications offers an avenue by which the challenges of pill/treatment fatigue, and desire for anonymity can be addressed, while also improving outcomes. To further simplify the dosing schedule and improve adherence, we aim to develop a pulsatile release formulation that enables long-acting delivery of API through either a subcutaneous or intramuscular administration.

A microfluidic approach is proposed to fabricate biodegradable, biocompatible PLGA drug loaded microparticles to enable high drug loading, sustained-release formulations. A glass focus-flow microfluidic design was used to form single oil-in-water emulsions and fabricate PLGA drug loaded microparticles. The dispersion, or oil phase, consists of the drug, organic solvents, and polymer. The continuous, or water phase, consists of a water miscible surfactant. The drug loaded (API_A), single emulsions formed droplets ranging from 150 um to 300 um. The size of the diameter has been shown to be tunable to a desired value based on the capillary number and the relative fluid velocities ratio.

A solvent evaporation step is incorporated to remove two organic solvents. As a result, a 73% reduction in drug loaded (API_A) microparticle size is observed after a timeframe of two days. Gas chromatography confirmed there to be no residual organic solvents detected in washing steps or in dissolved drug loaded (API_A) microparticles. SEM images showed a spherical shape maintained after mixing and washing steps. However, some large pores were captured on the microparticles based on the SEM images, perhaps due to one of the organic solvents, which is also miscible in water, leaving the PLGA polymer upon droplet formation.

A lyophilization step was incorporated after the washing step of the microparticles, to improve drug loading efficiency assessment using UV spectrometry. Furthermore, drug loading efficiency increased, from 3% to 10%, by increasing the polymer to API_A ratio. Due to one of the organic solvents forming a stream upon droplet formation on a chip, as the possible root cause to our low drug loading efficiency, a different API (API_B) was assessed. Furthermore, prodrugs of API_A, are also currently being investigated to improve its hydrophobicity and therefore increase its drug loading efficiency.

API_B, with its lower solubility in water, was also investigated and showed significant improvement to drug loading efficiency, in comparison to API_A, and eliminated the need of one of the organic solvents. The control release functionality of API_B, using a USP-4 apparatus is currently being investigated. An exploratory PK/PD study will also be conducted to test the microfluidic technology.

SESSION SB08.11: Biomedical Applications II
Session Chairs: Gianluca Maria Farinola and Chiara Ghezzi
Friday Morning, December 2, 2022
Hynes, Level 3, Room 313

8:30 AM SB08.11.01

Motor Mobility Determines Actin-Myosin Network Contraction Characteristics Donyoung Kang and Hyungsuk Lee; Yonsei University, Korea (the Republic of)

Dynamic behaviours driven by intracellular cytoskeleton such as migration, division and endocytosis are mainly regulated by the contraction of cytoskeleton network consisting of cytoskeleton and motor proteins. Depending on the functional demand in each cell function, various structures and contraction characteristics of cytoskeleton networks are observed. For example, in the early phase of cytokinesis, chromosome segregation is progressed by the radial-directional contraction of the linear assembly of microtubules and motor protein dynein. During cleavage furrow ingression, the ring-shaped actin-myosin structure attached to the inner surface of cellular membrane shrinks at a constant speed by the circumferential-directional contraction of the ring.

Many have studied how the contractile behaviours of cytoskeleton-motor protein networks depend on protein concentrations, chemical environments and geometric boundaries. In vitro experiments found that concentrations of motor protein and network crosslinkers play a crucial role in modulating contraction speed of the cytoskeleton-motor network. KCl concentration is critical for the global and synchronized contraction of actin-myosin network. The speed and length scale of the network contraction were significantly affected by the network shape such as square and circle. Nonetheless, it remains unclear how the mechanical boundary condition of the motor protein determines the dynamics characteristics of cytoskeleton-motor protein network contraction.

Here, we analysed the contractile behaviours of actin-myosin network in two different mechanical boundary conditions of motor protein, myosin. We prepared "immobilized motor" (IMM) condition by firmly attaching myosin thick filaments to a glass surface. In "mobile motor" (MM) condition, actin network cross-linked with actin binding proteins (ABPs) were prepared on a glass surface coated with cellular lipid membrane allowing movement of motor proteins. Contraction of actin-myosin network in IMM and MM conditions were visualized using fluorescence-conjugated actin. We found that the relative concentration of actin and ABP which defines a network connectivity determines the contraction shape and speed. While contracting actin-myosin networks exhibited radial patterns in IMM condition, a global and isotropic contraction was observed in MM condition. Contraction speed increased with the network connectivity in MM but decreased with it in IMM condition.

To elucidate the mechanism of the actin contraction depending on the boundary condition of motor protein, we developed a computational model tracking each component of network such as actin, ABP and myosin during contraction. The radial contractile pattern of actin network was exhibited in IMM condition similar to the experimental results. The computational simulation found that local actin-myosin clusters gathered into a larger one leading to a global contraction in MM condition.

In summary, we showed how the characteristics of actin-myosin network contraction depend on the mechanical boundary condition of myosin motor protein. Changes of contraction behaviours in terms of contraction pattern and speed by the network connectivity depends on the mobility condition of motor protein. While the contraction speed increased proportional to network connectivity in MM, it decreased in IMM condition. Our study provides an intuition into not only the mechanism of cell dynamics but also the design of biomimetic systems. By modulating the mechanical boundary condition of motor protein, a dynamic molecular system transporting substances to a target destination can be designed.

8:45 AM SB08.11.02

Influence of Ca/P in Modified-Simulated Body Fluid Solution on Intrafibrillar Mineralization of Collagen with Polydopamine to Generate Collagen-PDA-HAP Scaffolds Urasawadee Amornkitbamrung, Yongjae In and Hyunjung Shin; Sunkyunkwan University, Korea (the Republic of)

Large bone defects have attracted attention as a remain major challenge in bone tissue engineering. In bone tissue, the mineralized collagen fibril is an important basic building block which collagen molecules are hierarchically assembled into fibrils and mineralized with the formation of hydroxyapatite (HAP) nanocrystals. Due to the uniformly distribution HAP in collagen fibrils and together built up hierarchically from nano to macrostructures in bone tissue, mineralized collagen fibril is regards as the important level for the mechanical properties. Collagen based scaffolds have been increasing used in tissue engineering due to its excellent biocompatibility. However, the insufficient mechanical strength and structural support limit it wider in bone regeneration application. Many attempts have been devoted to improve collagen-HAP based scaffolds' properties by understanding the process of bone mineralization to fabricate bone mimicking scaffolds. The mineralization pathway of HAP has been suggested as non-classical crystallization as reported, but the physical and chemical mechanism is still poorly understood with a difficult challenge, especially in collagen fibril's structure. In this work, with the presence of polydopamine (PDA) to promote the biomineralization process, the structure of intrafibrillar mineralized collagen-PDA fibrils in modified-simulated body fluid (m-SBF) solution was studied at the nano scale by STEM-EDS techniques to investigate a detail hydroxyapatite intrafibrillar mineralization pathway. Collagen-amorphous calcium phosphate (ACP) fibrils was obtained by assembling Collagen-PDA fibrils in SBF solution with the present of Mg^{2+} and polyaspartic acid as a precursor stabilizer. Then later the phase transformation of ACP to HAP was determined by tuning the phosphate concentrations in m-SBF. It was found, in this work, that the phase transformation of ACP to HAP in Collagen fibrils can be accelerated even in 12 hr-mineralization with the m-SBF solution of calcium and phosphate ratio of 1:10, higher phosphate ratio produces a monodentate Ca-P geometry and evolved directly to HAP, while the lower 1:5 would affect in slower phase transformation kinetic, and for 1:1 the crystallization of HAP cannot be initiated even up to 7 days of mineralization. The finding suggests that an elevated concentration of phosphate is crucial for initiate phase transformation of ACP to HAP. From these studies and strategy, we adopted to fabricate mechanically self-sustained Collagen-PDA-HAP hydrogels. By controlling the mineralization, it is beneficial for collagen-based scaffolds' fabrication design. A synergistic effect was also investigated and observed in the Collagen-PDA-ACP and Collagen-PDA-HAP for both in vitro osteogenic differentiation of bone marrow mesenchymal stem cells (BMSCs). Thus, the results presented in this work could serve a better understanding the mechanism of the HAP mineralization in collagen fibrils, which may provide approaches to effective, and materials design for efficient osteogenesis bone tissue engineering.

9:00 AM SB08.11.05

Hyaluronate-Black Phosphorus-Upconversion Nanoparticles Complex for Non-Invasive Theranosis of Skin Cancer Gibum Lee, Jung Ho Lee and Sei Kwang Hahn; Pohang University of Science and Technology, Korea (the Republic of)

Black phosphorus (BP) has been widely investigated for various biomedical applications with the unique characteristics of 2D nanomaterials including its high photothermal conversion efficiency, biocompatibility, biodegradability and ultraviolet (UV)-mediated reactive oxygen species (ROS) generation. However, the finite depth of light penetration has limited further development of BP-based photomedicines. Here, we developed hyaluronate-BP-upconversion nanoparticle (HA-BP-UCNP) complex for near-infrared (NIR) light mediated multimodal theranosis of skin cancer with photoacoustic (PA) bioimaging, photodynamic therapy (PDT), and photothermal therapy (PTT). In contrast to the conventional BP-based skin cancer theranosis systems, HA-BP-UCNP complex could be non-invasively delivered into the tumor site to induce the cancer cell apoptosis upon NIR light irradiation. HA in the complex facilitated the transdermal delivery of BP into the tumor tissue under the skin. Upon 980 nm NIR light irradiation, UCNP converted the light to UV-blue light to generate ROS by sensitizing BP in the HA-BP-UCNP complex for PDT. Remarkably, 808 nm NIR triggered PTT for the apoptosis of tumor cells. The photoacoustic imaging of BP successfully visualized the non-invasive transdermal delivery of HA-BP-UCNP complex into the mice skin. The cell viability test revealed the low cytotoxicity of HA-BP-UCNP complex in fibroblast cells. On the other hand, the complex showed high cytotoxicity to tumor cells under NIR light irradiation by PDT and PTT. The combination therapy of PDT and PTT by 980 + 808 nm NIR light irradiation drastically reduced tumor growth compared to only single NIR light irradiation for up to 7 days in skin cancer model mice. The antitumor effect of HA-BP-UCNP complex with NIR light irradiation was also confirmed by immunohistochemical TUNEL assay. Taken together, we could demonstrate the feasibility of HA-BP-UCNP complex as a non-invasive theranostic nanoplatform for skin cancer.

9:15 AM BREAK

9:45 AM SB08.11.06

Calcifications Can Trigger or Suppress Breast Precancer Malignancy Potential as a Function of Mineral Type in a 3D Tumor Model Netta Vidavsky; Ben-Gurion University of the Negev, Israel

The breast precancer stage will not necessarily develop into invasive breast cancer and theoretically does not always require treatment. However, it is impossible to predict whether precancers will become invasive cancer. More than 90% of breast precancer cases contain pathological minerals called microcalcifications. Most microcalcifications are calcium phosphate in the form of apatite, and their composition and crystal properties correlate with malignancy in clinical samples and may have a prognostic value. In clinical samples, apatite crystals with high and low carbonate content are associated with benign and malignant lesions, respectively, and calcium oxalate dihydrate (COD) is always found in benign lesions. Recent *in vitro* and *in vivo* studies show that specific changes in the properties of apatite crystals can trigger precancer progression.

Here, we developed a breast tumor *in vitro* model consisting of synthetic microcalcification analogs embedded in precancer multicellular spheroids that mimic the 3D microenvironment of mammary ducts. As microcalcification analogs, we use various synthetic mineral types that are physiologically relevant: apatite with high and low carbonate content and COD. Our methodology includes micro-CT for 3D imaging of mineral particles within soft tissues and scanning electron microscopy and vibrational spectroscopy for mineral characterization.

We show that cell proliferation and the expression of proteins associated with cancer change with the properties of the embedded mineral in our *in vitro* model. Low carbonate apatite promotes precancer malignancy compared to other types of minerals or conditions of no added mineral. Surprisingly, COD suppresses precancer malignancy compared to apatite or conditions of no added mineral. This finding suggests that microcalcifications can affect precancer cells by either triggering them to proliferate or inhibiting their proliferation, even compared to conditions of no minerals. Possibly, the presence of COD crystals only in benign clinical tissues is not random but is a result of its tumor-suppressing qualities. Insights from this study may suggest in the future ways of affecting disease progression by manipulating the crystal properties of breast microcalcifications *in situ*.

10:00 AM SB08.11.07

PhoCoil—An Injectable and Photodegradable Single-Component Recombinant Protein Hydrogel for Localized Therapeutic Delivery Nicole Gregorio and Cole A. DeForest; University of Washington, United States

Hydrogels have found widespread utility in many research areas including controlled therapeutic delivery and tissue engineering. Many gel systems have been developed that mimic properties of the extracellular matrix (ECM), providing biocompatibility and enabling 3D cell culture. Traditionally, hydrogels have been formed from polymeric precursors that are either naturally occurring or synthetic. Natural gels are derived from naturally occurring biomolecules, often extracted from tissues. As such, many of these hydrogels mimic the ECM at a chemical and/or structural level, making them a top choice for biomedical applications, but lack in their tunability, providing researchers with few options to control these systems in a defined manner. They also frequently suffer from batch-to-batch variation, creating technical challenges in their implementation. In contrast, hydrogels formed from synthetic polymers retain batch-to-batch similarity and provide significantly more tunability through incorporation of diverse chemistries during synthesis or crosslinking. However, many of these materials are dissimilar to the chemical and/or structural makeup of the ECM. On top of this, both synthetic and natural hydrogels are intrinsically polydisperse. This results in networks with an ill-defined inter-crosslink distance, impacting material elasticity and contributing to overall heterogeneity in these ideally homogenous systems. To unite the advantages of synthetic and natural hydrogels, there has been growing interest in engineering materials from recombinant proteins. These efforts remain nascent but promise perfectly monodisperse, customizable gel networks, with molecular tunability achieved through engineering at the amino acid and fusion protein levels, while also mimicking the proteinaceous nature of the ECM and conferring high biocompatibility. Our work is focused on further enabling external tunability of recombinant hydrogels by installing stimuli-responsivity, which has often been limited to synthetic polymers.

We have developed and characterized a novel, stimuli-responsive recombinant gel platform named PhoCoil. This material is injectable, photodegradable, and formed from a single protein. PhoCoil is crosslinked through homopentameric, physical coiled-coil interactions, resulting in a reversible gel-sol transition in response to applied shear force. Coil domain pairs are connected by an intrinsically disordered protein, originally engineered for high expression and low immunogenicity, providing intra-protein mobility and enabling intermolecular interactions without steric restriction. At the center of the protein is PhoCl, a photolabile green-fluorescent protein which undergoes irreversible cleavage of the polypeptide backbone in response to visible light. The resultant PhoCoil protein hydrogel is shear thinning and self-healing due to its physical crosslinking, enabling easy injection, as well as degradable on-demand in response to cytocompatible light. PhoCoil degradation can be spatiotemporally triggered through conventional mask-based and laser-scanning photolithography. Controlled hydrogel softening can also be achieved by modulating the light dosage, or through co-formulation with a non-light-responsive coiled-coil protein network. PhoCoil is the first fully recombinant protein hydrogel to utilize PhoCl as a cleavable linker and is differentiated from other previously developed photoresponsive recombinant hydrogels by its stability in ambient light and its simple single-component formulation, which does not require any small molecule or metal additives. PhoCoil hydrogels have applications in *in vitro* cell culture, as they show high cytocompatibility and enable bioorthogonal post-encapsulation release for single-cell analysis. Of particular interest is the use of PhoCoil for controlled, localized drug or cell delivery via post-injection photodegradation, which has been demonstrated in proof-of-concept *ex vivo* studies.

10:15 AM SB08.11.08

Development of a 3D *In Vitro* Model of the Neurovascular Unit (NVU) Using a Conducting Polymer Device for Real-Time Monitoring Chiara Barberio, Aimee Whithers, Chrysanthi-Maria Moysidou, Rachana Acharya, Shani Kirma Elias and Roisin Owens; University of Cambridge, United Kingdom

The neurovascular unit (NVU) is an essential component of the central nervous system with a vital role in maintaining brain homeostasis. The early onset of several neurological disorders has been associated with alterations in the blood-brain barrier (BBB), a component of the NVU that protects the brain microenvironment from potentially harmful substances circulating in the bloodstream (e.g., small molecule drugs, bacteria).¹ Despite recent advances in the study of neuro-pathologies, at present there are very limited effective treatments against neurological disorders and amongst others, the lack of appropriate research tools is a major limitation. *In vivo* animal models have high costs, are time-consuming, and carry uncertainties in the translation to human biology. Therefore, there is a compelling need to explore technologies capable of better resembling the human brain *milieu* in health and disease. 3D *in vitro* models, such as 3D gels and scaffolds integrating human cells are excellent inert supports prompting *in vivo-like* tissue generation.² Here, we used a composite electroactive scaffold integrating biomolecules of the human brain extracellular matrix (ECM) as a biomimetic substrate for hosting vascular endothelial and neural cells representative of the NVU. We reconstructed the neural tissue microenvironment using a tri-culture cell model, whose barrier formation, integrity, and neural-glia compartment were characterized via Confocal and Two-Photon Microscopy, showing the development of a multicellular neurovascular unit-like structure. Electrochemical Impedance Spectroscopy (EIS) was also used as a sensitive tool to provide a continuous and non-invasive readout of cell properties and tissue generation real-time. This NVU model has great potential as test bed for screening neurological drugs and disease modelling.

References

- [1] Bhalerao, A. *et al.* In vitro modeling of the neurovascular unit: advances in the field. *Fluids and barriers of the CNS* **17**, 22 (2020).
- [2] Moysidou, C. M., Barberio, C. & Owens, R. M. Advances in Engineering Human Tissue Models. *Front. Bioeng. Biotechnol.* **8**, 620962 (2021).

SESSION SB08.12: Virtual Session
Session Chairs: Gianluca Maria Farinola and Chiara Ghezzi
Tuesday Morning, December 6, 2022
SB08-virtual

8:00 AM *SB08.12.01

The Avenue to “Green” in Organic Bioelectronics Mihai Irimia-Vladu; Johannes Kepler Universität Linz, Austria

Through its appealing avenues of processing the component devices at room temperature and from low-cost precursor materials, organic electronics has a tremendous potential for the development of products able to achieve the goals of production sustainability as well as environmental and human friendliness for electronics.

In an effort to stave off the e-waste growth, the presenter and his research group went further down the path opened by organic electronics research and investigated a large number of biomaterials as substrates, dielectrics, semiconductors and smoothening layers for the fabrication of organic field effect transistors, integrated circuits and organic solar cells. The presentation will focus on the highlights of our recent research, especially with respect to materials investigated, devices fabricated and the immense potential for follow up research:

- Flexible natural and biodegradable substrates
- Natural dielectrics
- Bioorigin, H-bonded semiconductors in the families of indigos, anthraquinones and acridones
- Biodegradation protocols for organic semiconductors

These highlights will be placed in the context of the mountain that one has to climb in order to reach the coveted “green” connotation for electronics, sensors and integrated circuits:

- Biocompatibility issue
- Biodegradability issue
- Compostability issue
- Cost of production / energy expanded in production issue
- Materials choice issue (carbon footprint)
- Toxicity and the environmental impact of the synthetic avenue for component materials

The potential of follow-up research in the green electronics field is immense, with large area electronics fabrication, biomedical implants, bio-sensing and smart labeling, representing only the tip of the iceberg of many more immediate possibilities of high interest for our group. Natural and nature-inspired materials have the unrivalled capability to create “safe-first” electronic markets for human and environment, with minimal or even neutral carbon footprint.

8:30 AM SB08.12.02

Bio-Inspired Skin Wearable Hydrophobic Voice Recognition Acoustic Sensor Based On *f*-MWCNTs-BaTiO₃@PDMS Composite Conductive Network Sasikumar Ragu and Byungki Kim; Korea University of Technology and Education, Korea (the Republic of)

Skin wearable piezoelectric nanogenerators (WPENGs) have recently drawn significant attention owing to their unique properties, like flexibility, sensitivity, and self-powered nature. Barium Titanate (BaTiO₃) is one of the eco-friendly piezoelectric ceramics. In recent days, BaTiO₃-based piezo-fillers use in WPENGs has attracted broad concern. Herein, bio-inspired microcracks, skin wearable, cost-effective, highly sensitive, and flexible PENGs were developed using functionalized multi-walled carbon nanotubes (*f*-MWCNTs) doped barium titanate (BaTiO₃)/poly(dimethylsiloxane) (PDMS) film. *f*-MWCNTs/BaTiO₃@PDMS was prepared by mixing of *f*-MWCNTs/BaTiO₃ and PDMS polymer solution by the overnight vacuum drying process. The sensor film was prepared by sandwiching *f*-MWCNTs/BaTiO₃@PDMS film between two PDMS films, followed by making electrical connections with two copper wires to form the WPENG. The as-prepared composite and PENG film were characterized by powder X-ray diffraction (PXR), Fourier transform infrared spectroscopy (FT-IR), field emission scanning electron microscopy (FE-SEM), transmission electron microscopy (TEM), energy-dispersive X-ray analysis (EDX), Raman spectroscopy, and X-ray photoelectron spectroscopy (XPS). The composite PXR data revealed the degree of crystallinity is 63%. FE-SEM and TEM results clearly showed that BaTiO₃ in-situ coupled with *f*-MWCNTs with the addition of BaTiO₃ with *f*-MWCNTs. The real-time application of the developed sensor was carried out by attaching the sensor to the throat to detect the minute oscillations produced during speaking. Monosyllabic, disyllabic, and polysyllabic words were spoken by the reader and their corresponding waveforms are recorded to show the ability of the sensor to clearly differentiate between these words. The sensor is also equally sensitive to male and female voices. A disyllabic word was spoken by a male and a female, and the recorded waveforms have a similar trend with different amplitudes. These results indicate the potential of the fabricated sensor to detect the human vocal cord vibrations efficiently, and paving a path to design a system for a wider range of applications in the next generation of noise detection and skin wearable sensors.

8:45 AM SB08.12.03

Designing Macroscopic Photonic Surfaces with Controlled Assembly of Polyhedral Emulsion Drops Jong Bin Kim, Seong Kyeong Nam, Sanghyuk Park and Shin-Hyun Kim; KAIST, Korea (the Republic of)

Colloidal arrays create structural colors originating from the constructive interference by the periodicity of the nanostructures. They are highly bright and angle-dependent when the colloids are periodically stacked. There have been several strategies to crystallize colloids in a film format; dip-coating, doctor-blading, infiltration, and roll-to-roll process. However, these methods cannot induce regioselective crystallization in the first place, but rather require additional processes for the patterning. Recently, many researchers exploit the secondary assembly of photonic spheres to construct a photonic surface. However, the spherical compartments have low reflectivity because of the lack of a planar region for backward reflection. Furthermore, several layers of spheres are needed because their monolayer inevitably leaves vacancy due to the interstices between roundish morphologies.

Here, we induce polyhedral deformation of photonic emulsions with built-in crystalline colloidal arrays to create planar surfaces with no voids even with a monolayer of emulsions. We use a microfluidic device to create monodisperse emulsions in fluorocarbon oil of which fast evaporation deforms emulsions

with the surfactant-stabilized interface even in the air. Inside the emulsions are silica particles dispersed in acrylate polymer and crystallized by interparticle repulsion, where the crystallization is enhanced by a shear force from the interface. The emulsions are extruded using a nozzle, assembled into a monolayer, and deformed to polyhedrons. As a result, the iridescent rainbow colors are developed on the particles, which are enhanced by thermal energy before curing. The surface is perfectly flat and it is UV-crosslinked to create fixed structural colors, leading to a more reflective photonic surface than a monolayer of photonic spheres.

The colloidal arrays are rearranged during the deformation of emulsions from spheres to polyhedrons and they follow the shear force that is larger on the polyhedron side than top or bottom because of larger curvature change and larger relocation of the fluid inside the emulsions. A large portion of colloids are crystallized from the side wall of the polyhedrons, but there are polycrystalline arrays inside the compartment because not all the regions are rearranged from a sideward shear force. (10-11) planes of hcp lattice are dominant at the center of the polyhedron, while (111) planes of fcc lattice are at the edge. (10-11) planes of hcp lattice stem from the combination of two shear forces from the top and side of polyhedrons, the latter of which is stronger so that they outnumber (111) planes of fcc lattice even at the center; the center part is close to top/bottom, but far from side. In contrast, the occurrence of (10-11) planes of hcp lattice is exceeded by that of (200) planes of fcc lattice which is slanted more compared to (111) planes of fcc lattice growing from the top. As the colloidal arrangement is polycrystalline with two dominant planes, the structural colors from the film assembled by emulsions are both iridescent and less angle-dependent. The accurate control of crystallization is not needed during the film formation because the colloidal arrays are crystallized in emulsions in advance; hand-assisted placement of emulsions in a mold rapidly forms a photonic surface. Most importantly, emulsions can be assembled and fixed on a three-dimensional surface which forms structurally-colored 3D objects such as a beetle and turtle. The advantage of this strategy is that the as-formed film can be diversely colored by deforming differently colored emulsions together or stacking the different groups layer by layer. It proposes a new way of regioselective manual formation of structural-color films and patterns both on 2D and 3D objects, of which the printed results have highly uniform color and height. Also, it unveils a new mechanism of colloidal crystal formation in polyhedral photonic compartments.

9:00 AM SB08.12.04

Bio-Inspired Porous Anodic Alumina/Aluminum Flake Powder for Multi-Band Compatible Low Detectability [Siqu Fu](#); Shanghai Jiaotong University, China

Continuous development and advancement in modern detection technologies have increased demand for multi-band (e.g. visual, infrared) compatible camouflage. However, challenges exist in the requirements of incompatible structure resulting from the adaptation to different camouflage effects. This study is inspired by the light absorption structure of butterfly wing scales and demonstrates porous anodic alumina/ aluminum flake powder material, prepared by microscopic powder anodic oxidation technique for visual and infrared camouflage. The fabricated structures manipulate compromise condition for visual camouflage by low reflectance ($R(400\sim 800\text{ nm})=0.32$) and dual-band infrared camouflage by low emission ($\epsilon(3\sim 5\ \mu\text{m})=0.081$ and $\epsilon(8\sim 14\ \mu\text{m})=0.085$). Further, the characteristic of short-range disorder in these bio-inspired structure allows maintenance of the camouflage performance under omni-directional detection ($0\sim 60^\circ$). This study provides new insight and feasible method for coordinated manipulation of electromagnetic waves via bio-inspired structural design and improved fabrication.

9:15 AM SB08.12.05

Polysaccharide-Based Multi-Functionalization for Intravascular Catheters—Biocompatible Method to Enhance Antimicrobial and Antithrombotic Performances [Se Kye Park](#)^{1,2}, [Jae Hak Shin](#)³, [Jae Hee Jung](#)³, [Dong Uk Lee](#)¹, [Dong Yun Lee](#)², [Seung Hwa Yoo](#)⁴ and [Dong Yun Choi](#)¹; ¹Korea Institute of Industrial Technology, Korea (the Republic of); ²Kyungpook National University, Korea (the Republic of); ³Sejong University, Korea (the Republic of); ⁴Jeonbuk National University, Korea (the Republic of)

Intravascular catheters (IC) are indispensable medical devices that allow diagnostics of heart conditions, drainage or injection of drug fluids and delivery of other surgical devices. However, IC has the potential to cause serious complications that put the patient at risk of death. The major critical issues with insertion of ICs are blood stream infections, thrombosis and damage of blood vessel[1, 2, 3].

Therefore, Antimicrobial, antithrombotic activity and low-friction functions are essential for the surface of intravascular catheters (ICs). One of the strategy for the multi-functionalization of ICs includes coating with hydrogel embedding antimicrobial and antithrombotic agents. Although catheters with hydrogel coating that contain antimicrobial agents contently prevent these issues, undesired side effects of cytotoxicity and tolerance can be caused. Moreover, hydrogel coated ICs showed unsatisfactory performance because of progressive loss of these functions owing to the leaching of functional agents from the coating layer[4].

O-carboxymethyl chitosan (CMC), could be a particularly promising material for functionalization of ICs owing to its outstanding functions including non-toxicity, biodegradability, biocompatibility, antimicrobial and antithrombosis properties. Although CMC has a sufficient hemocompatibility, the antithrombotic activity is questionable due to its incomplete performance of thrombosis reduction and lack of clinical use cases[5]. Furthermore, there are only a few studies related to the multi-functionalization of IC by introducing chitosan derivatives such as CMC. Therefore, verification of such multi-functional performance, including antithrombotic activity, is still an unresolved challenge in the introduction of chitosan derivatives such as CMC to ICs. Here, we introduce a novel strategy for biocompatible and eco-friendly surface multi-functionalization of the ICs with CMC. In order to improve the intrinsic performance of CMC, we fabricated the surface of coating layer to be rough. Nanoscale porous CMC (pCMC) coating layer of pre-treated IC was simply fabricated through a selective leaching of the water-soluble polyethylene glycol (PEG) from heterogeneous CMC-PEG composite. The pCMC layer surface exhibited superhydrophilicity due to the increase in roughness. Especially, the antifouling effect by superhydrophilicity showed excellent anti-adhesion of *Escherichia coli* and platelets, and it gave a synergistic effect along with the intrinsic functions of CMC. Meanwhile, despite the rough surface of the pCMC layer, it showed adequate low frictions property under continuous wet friction conditions. Furthermore, we demonstrated that the practical pCMC coated IC tube provides superior trackability in a curved artificial blood vessel. The potential of the proposed coating strategy can be offered not only ICs, but also wide range of polymer-based vascular devices such as vascular filters, grafts, pacemakers and soft robots.

References

- [1] L. Liu, et. al., *Biomater. Sci.* **2020**, *8*, 4074.
- [2] I. H. Jaffer, et. al., *J. Thromb. Haemost.* **2015**, *13*, S72.
- [3] R. I. Mehta, et. al., *Am. J. Med.* **2017**, *130*, e287.
- [4] D. C. Leslie, et. al., *Nat. Biotechnol.* **2014**, *32*, 1134.
- [5] S. K. Park, et. al., *Chem. Eng. J.* **2022**, *433*, 134565.

Acknowledgements

This work was supported by the Korea Medical Device Development Fund grant funded by the Korea government (the Ministry of Science and ICT, the Ministry of Trade, Industry and Energy, the Ministry of Health & Welfare, the Ministry of Food and Drug Safety) (Project Number: KMDF_PR_20200901_0081, 1711138107)

Corresponding author

Dong Yun Choi, E-mail: dychoi311@kitech.re.kr

9:20 AM SB08.12.06

Deployable 3D Bioprinting for Modelling Cancer with Simulated Tumor Microenvironment Yaqi Sheng, Corrado Mazzaglia and Yan Yan Shery Huang; The University of Cambridge, United Kingdom

Three-dimensional (3D) bioprinting has emerged as a promising tool for constructing *in vitro* cancer models with tumor microenvironments (TME) in a rapid and reproducible manner. To realize the translational impacts of 3D bioprinting in a wider cancer research community, innovations in bioprinting workflows still required to integrate affordability, user-friendliness, and biological relevance. Here, we developed 'Bioarm', a simple, yet highly effective extrusion bioprinting platform, which can be folded into a carry-on pack, and rapidly deployed between facilities. Bioarm enabled TME reconstruction by printing 3D core-shell tumoroids with cancer-associated fibroblasts (CAFs) deposited as the shell. The population of CAFs showed heterogeneity in tumoroids and produced de novo synthesized extracellular matrices, demonstrating more *in vivo*-like characteristics compared to traditional 2D co-culture models. Embedding the 3D printed tumoroids in an immune cell laden collagen matrix permitted tracking of the cancer-immune interactions, and subsequent immune perturbation under immunotherapy treatments. Our deployable extrusion bioprinting workflow could significantly widen the accessibility of 3D bioprinting for replicating TME with complex multi-compartmental architectures, and for developing personalized cancer drug screening strategies.

9:25 AM DISCUSSION TIME

SESSION SB08.13: Virtual Session II
Session Chairs: Chiara Ghezzi and Giuseppe Paternò
Tuesday Morning, December 6, 2022
SB08-virtual

10:30 AM *SB08.13.01

Chemical Decoration of Living Microalgae for Bioremediation Daniilo Vona¹, Cesar Vicente-Garcia¹, Pietro Cotugno¹, Emiliano Altamura¹, Stefania R. Cicco², Roberta Ragni¹ and Gianluca Maria Farinola¹; ¹Università degli Studi di Bari Aldo Moro, Italy; ²CNR-ICCOM, Italy

Many microorganisms produce specific protection structures, known as spores or cysts, exploited to increase their resistance to adverse environmental conditions. Scientists started to produce biomimetic materials inspired by these natural membranes, especially for industrial and biomedical applications.[1] Diatoms, for instance, are marine organisms able to uptake inorganic silicates from the ocean in order to build highly porous biosilica shells, called frustules, at mild environmental conditions. Diatoms shells, exploited for years for producing biohybrid materials for applications in photonics, optoelectronics and biomaterial science, can be chemically decorated via the common surface silanization reactions or the *in vivo* incorporation of functional organic molecules.[2] Our group has managed to obtain, via green processing, phosphorescent nanoparticles and fluorescent biosilica with specific optical features starting from simple feeding of diatoms with new synthesis fluorescent dyes [3-5]. We also produced 2D diatoms-based scaffolds for tissue engineering applications, after *in vivo* functionalization of living algae with pharmacological molecules like bisphosphonates, active towards osteogenic promotion and against osteo-resorption and bone degradation. [6-7] In this abstract we present biological data on the biocompatibility of a polydopamine-based artificial coating with diatom cells. Here living *Thalassiosira weissflogii* [8] cells were individually encapsulated with soft, artificial and easily functionalizable polydopamine layers with adhesive properties similar to feet proteins found in mussels. Polydopamine did not strongly interfere with diatom cells growth kinetics, and it can be exploited for entrapping detoxifying agents, like natural enzymes, and magnetic nanoparticles useful for living cells recovery after the decontamination process. These outcomes pave the way to the use of living diatom cells in the area of biomedicine, cell-based sensors and natural, and living devices for bioremediation. Polydopamine does not only confer certain sorption properties towards pollutants to surfaces [9], but it can encapsulate degrading functions, like catalytically active nanoparticles or enzymes, which bio-transform pollutants into small non toxic organic molecules.

Acknowledgements: D.V. acknowledges the financial support from Fondo Sociale Europeo "Research for Innovation (REFIN)"; project n°87429C9C - Alghe vive per la bonifica dell'ambiente marino (AlgAmbiente).

References

- [1] Lo Presti, M., Vona, D., Ragni, R., Cicco, S.R., Farinola, G.M. MRS Comm. 11, 213–225 (2021).
- [2] Ragni, R., Cicco, S.R., Vona, D. and Farinola, G.M. Adv. Mater. 1704289,1-23 (2017).
- [3] Leone, G., De la Cruz Valbuena, G., Cicco, S. R., Vona, D., Altamura, E., Ragni, R., Molotokaite, E., Cecchin, M., Cazzaniga, S., Ballottari, M., D'Andrea, C., Lanzani, G. Sci. Rep. 11 (1), 5209 (2021).
- [4] Ragni, R., Scotognella, F., Vona, D., Moretti, L., Altamura, E., Ceccone, G., Mehn, D., Cicco, S.R., Palumbo, F., Lanzani, G., Farinola, G.M. Adv. Funct. Mater., 28 (24), 1706214 (2018).
- [5] Della Rosa, G., Vona, D., Aloisi, A., Ragni, R., Di Corato, R., Lo Presti, M., Cicco, S. R., Altamura, E., Taurino, A., Catalano, M. and Farinola, G. M. ACS Sustain Chem Eng, 7, 2, 2207–2215 (2018).
- [6] Cicco, S.R., Vona, D., De Giglio, E., Cometa, S., Mattioli Belmonte, M., Palumbo, F., Ragni, R. and Farinola, G.M., Chem Plus Chem, 80, 1104–1112 (2015).
- [7] Cicco, S.R., Vona, D., Leone, G., De Giglio, E., Bonifacio M., Cometa, S, Fiore, S. Palumbo, F, Ragni, R., Farinola, G.M., Materials Science & Engineering C 104 109897 (2019).
- [8] Vona, D., Cicco, S.R., Ragni, R., Vicente-Garcia, C., Leone, G., Giangregorio, M.M., Palumbo, F., Altamura, E., Farinola, G.M. Photochem. Photobiol. Sci. 21, 949–958 (2022).
- [9] Aresta, A., Cicco, S.R., Vona, D., Farinola, G.M., Zambonin, C. Separations, 9(8), 194 (2022).

11:00 AM SB08.13.02

CatchGel—A Molecular to Macroscale Investigation of Catch Bond-Crosslinked Polysaccharide Hydrogels Zarah Walsh-Korb^{1,2} and Michael A. Nash^{1,2}; ¹University of Basel, Switzerland; ²ETH Zürich, Switzerland

Nature's exquisite designs are a constant source of inspiration for materials scientists, yet our ability to replicate biological interactions on the macroscale in engineered systems is often severely limited. Biological systems exist in perfectly balanced environmental conditions that regulate the functionality of

the processes within the system. Thus, a major obstacle in exploiting biological interactions in macroscale materials is a lack of understanding of how the changing chemical environment - from the molecular to the macroscale - affects the intrinsic molecular functionality of the biological unit, ultimately impacting macroscale behaviour.

From a material design standpoint bacterial adhesins are particularly interesting proteins. These proteins are expressed on bacterial cell surfaces to allow them to bind to, and colonise, a host. Many of these bacterial adhesins exhibit so-called 'catch bond' behaviour. Essentially, the adhesive force of these receptor-ligand complexes increases when subjected to high shear, in contrast to traditional 'slip' bonds, which decrease/rupture under high shear. On reaching a maximum applied force, the catch bond then reverts to slip bond behaviour resulting in a catch-and-roll type action that bacterial cells use to move in a targeted fashion along a surface. This behaviour also allows pathogens to continue to colonise host organisms despite aggressive actions from the host to remove colonies.

Transplanting catch bond-forming protein receptors and ligands onto polysaccharide chains opens up the possibility of creating bio-based hydrogel networks with unique tensile properties. Specifically, networks that display both shear-thinning and shear-thickening properties depending on the applied force, which also have the potential to self-heal as complexes rupture and reform. However, the complexity of intermolecular interactions in both catch-bond forming adhesin complexes and bio-based polymers mean the road to macroscale materials is less than straightforward.

Focusing on adhesins isolated from *Staphylococcus epidermidis* (serine-aspartate repeat protein G (sdrG)) and *Staphylococcus aureus* (serine-aspartate repeat protein E (sdrE), clumping factor A (clfA) and clumping factor B (clfB)), we use single molecule force spectroscopy to probe the fundamental interactions between these adhesins and their specific ligands to understand the impact of orientation, substrate, mutations and environmental composition on the stability of the catch bond behaviour. Expressing adhesins on yeast cells and probing substrate interactions with spinning disk microscopy, a deeper understanding of cooperative interactions as a function of environmental complexity is gained. Finally, functionalisation of polymer chains with adhesins and their corresponding ligands creates the building blocks for the catch bond cross-linked hydrogel networks, whose macroscale mechanical properties are probed using rheological measurements, completing the molecular to macroscale transition.

This multi-length scale approach to the design of catch bond cross-linked materials provides fundamental understanding of the impact of protein orientation, mutations and environment as we transition from the cell to a synthetically designed macroscale matrix. Examining how protein behaviour and macroscale materials properties change as a function of protein composition and environmental complexity allows more accurate development and manipulation of adhesin-derived responsive biomimetic materials. Thus, leading to a greater understanding of the nano-macroscale relationships in complex multiphase systems and enhanced strategies for the translation of biological interactions into macroscale materials.

11:15 AM SB08.13.03

Facile Preparation of Starch Biopolymer-Based Hydrogels for Flexible Electronics—Strain-Sensitive Batteries and Self-Powered Sensors [David F. Xie](#)¹, [Cong Ma](#)² and [Peng Liu](#)²; ¹Newcastle University, United Kingdom; ²Guangzhou University, China

As a renewable biopolymer, high-amylose starch due to its higher content of linearly structured chains is more interesting to realise enhanced material properties and new functionality. However, the full dissolution of the compact granule structure of high-amylose starch is challenging under moderate conditions, which limits its applications. In this work, we have revealed that high-amylose maize starch (HAMS) granules can be easily destructed by certain concentrations of ZnCl₂, MgCl₂ and CaCl₂ solutions (43 wt%, 34 wt% and 31 wt%, respectively) at a moderate temperature (under 50 °C) without chemical derivatization. In particular, the ZnCl₂ and CaCl₂ solutions resulted in complete dissolution of HAS granules and the regenerated starch from the CaCl₂ solution was completely amorphous.

We found by simple mixing of the HAMS with a CaCl₂ solution followed by heating the mixture at 80 °C for 5 min, a flexible and ionically conductive starch-based hydrogel can be obtained. By varying the starch/CaCl₂ dry mass ratio, the materials exhibited tuneable mechanical strength (500–1300 kPa), elongation at break (15–32%), Young's modulus (4–9 MPa) and toughness (0.05–0.26 MJ/m³), suitable electrical resistivity (3.7–9.2 Ω m), and strain-responsiveness. With plasticisation, a more flexible starch-based hydrogel was obtained, which can be easily reprocessed and has self-healing ability. The hydrogel was then developed into a galvanic cell-type battery, with an output voltage of 0.81 V, and a self-powered (SP) wearable sensor, which had high sensitivity (1.5371 kPa⁻¹) even under weak compression stress. This SP sensor can be used to detect human activities involving small strain such as wrist pulse and throat vibration. Considering the easy processability, cost-effectiveness, high strain-sensitivity, robustness, and greenness of the starch-based hydrogel and electronics, their brilliant application prospect is foreseen.

11:30 AM SB08.13.06

Spider's Pad Inspired Viscoelastic Hydrogel Damper for Nearly Dynamic Noise-Free Bioelectronics [Byeonghak Park](#)^{1,2} and [Tae-il Kim](#)¹; ¹Sungkyunkwan University, Korea (the Republic of); ²Stanford University, United States

Bioelectronics needs to continuously monitor mechanical and electrophysiological signals for patients. However, the signals always include artifacts by patients' unexpected movement (e.g. walking and respiration under ~30 Hz). The current method to remove them is a signal process using a bandpass filter which may cause signal loss. We present an unconventional bandpass filter material, viscoelastic gelatin/chitosan hydrogel damper inspired by the viscoelastic cuticular pad in a spider to remove dynamic mechanical noise artifacts selectively [1]. The hydrogel exhibits frequency-dependent phase transition that results in a rubbery state that damps low-frequency noise and a glassy state that transmits the desired high-frequency signals. It serves as an adaptable passfilter that enables to the acquisition of high-quality signals from patients even with minimizing signal process for advanced bioelectronics.

[1] B. Park et al. "Cuticular pad-inspired selective frequency damper for nearly dynamic noise-free bioelectronics." *Science* 376, 624-629 (2022).

11:45 AM DISCUSSION TIME

SYMPOSIUM SB09

Hydrogel Technologies for Humans and Machines
November 28 - December 7, 2022

[Symposium Organizers](#)

Yuhang Hu, Georgia Institute of Technology
Daniel King, Hokkaido University
Mark Tibbitt, ETH Zürich
Xuanhe Zhao, Massachusetts Institute of Technology

Symposium Support

Bronze

Journal of Materials Chemistry B
Soft Matter | Royal Society of Chemistry

* Invited Paper
+ Distinguished Invited

SESSION SB09.01: Hydrogel Adhesives I—Honoring the Memory of Dr. Daniel King
Session Chairs: Jue Deng and Xuanhe Zhao
Monday Morning, November 28, 2022
Hynes, Level 3, Room 310

10:30 AM *SB09.01.01

Development of Adhesive, Non-Swelling, Electroconductive and Viscoelastic Hydrogels for Bioelectronics Younsoo Kim, Pohang University of Science and Technology, Korea (the Republic of)

As a new class of materials, implantable flexible electrical conductors have recently been developed and applied to bioelectronics. An ideal electrical conductor requires high conductivity, tissue-like mechanical properties, low toxicity, reliable adhesion to biological tissues, and the ability to maintain its shape in wet physiological environments. Despite significant advances, electrical conductors that satisfy all these requirements are insufficient. Herein, a facile method for manufacturing a new conductive hydrogel through the simultaneous exfoliation of graphite and polymerization of zwitterionic monomers triggered by microwave irradiation is introduced. The mechanical properties of the obtained conductive hydrogel are similar to those of living tissue, which is ideal as a bionic adhesive for minimizing contact damage due to mechanical mismatches between hard electronics and soft tissues. Furthermore, it exhibits excellent adhesion performance, electrical conductivity, non-swelling, and high conformability in water. Excellent biocompatibility of the hydrogel is confirmed through a cytotoxicity test using C2C12 cells, a biocompatibility test on rat tissues, and their histological analysis. The hydrogel is then implanted into the sciatic nerve of a rat, and neuromodulation is demonstrated through low-current electrical stimulation. This hydrogel has been shown tissue-like extraneuronal electrodes, which improve the tissue-electronic interfaces, promising next-generation bioelectronics applications.

11:00 AM SB09.01.02

Tissue-Interfacing Actuating Adhesive Prevents Muscle Atrophy Through Mechanical Stimulation Sungmin Nam, Bo Ri Seo, Alexander Najibi, Stephanie McNamara and David Mooney; Harvard University, United States

Introduction Hydrogel tissue adhesives serve as an attractive tool kit for surgical interventions, as they can provide mechanical support and hemostatic capacity while sealing the wound site and preventing leakage. While most existing strategies have focused on the biochemical properties of tissue adhesives, much less effort has been devoted to engineering their mechanical functions. One promising function of adhesives is the ability to provide mechanical stimulation to the tissue to promote tissue healing and rehabilitation. It is known that externally imposed mechanical stimuli and physical cues can regulate various biological processes, including cell proliferation, migration, and differentiation, through a process termed mechanotransduction, which converts mechanical signals into changes in cell function. Thus, hydrogel adhesives capable of generating active mechanical stimulation, in addition to the adhesive function, are expected to further promote wound closure, tissue healing and rehabilitation. The objective of this study is to develop a hydrogel adhesive system with a soft actuation mechanism to provide mechanical stimulation directly and locally on the target tissue in a precisely controlled manner. We hypothesized that the active hydrogel adhesive could activate disuse muscles and prevent the development of muscle atrophy.

Materials & Methods Active hydrogel adhesive was developed by combining a soft robotic actuator based on a shape memory alloy (SMA) spring and an elastomer that ensheathes the SMA, and a tough adhesive that efficiently transmits actuation to the underlying tissue. The actuation of SMA was achieved by applying a voltage (5V). The actuator and tough adhesive were assembled using benzophenone chemistry. The adhesive was then applied to tissue with chitosan and coupling reagents, 1-ethyl-3-(3-dimethylaminopropyl) carbodiimide (EDC) and sulfated N-hydroxy-succinimide (NHS). To induce disuse muscle atrophy, hindlimb immobilization was performed for 2 weeks in female C57BL/6J mice with 14-18 weeks of age. One hindlimb was maintained in a knee joint extension and ankle plantar flexion position, and fixed by wrapping the hindlimb with a non-elastic surgical bandage to the foot. Mechanical stimulation was performed every day for 5 minutes at ~20 % of tissue strain and 0.1 Hz.

Results & Discussion The active hydrogel adhesive successfully achieved robust adhesion to muscle tissue ($>500 \text{ J/m}^2$), maintained *in vivo* stability for 2 weeks, and was able to create tissue strain of up to 20%. Real-time high frequency ultrasound imaging revealed that the skeletal muscle underlying the adhesive was substantially deformed along the actuation axis during actuation, demonstrating mechanical stimulation *in vivo*. Next, the therapeutic effects on disuse muscle atrophy were evaluated. Mice treated with mechanical stimulation while undergoing disuse atrophy had muscle fibers with much larger cross-sectional area compared to untreated mice. The gross size and weight of muscles was also significantly greater in the stimulated mice. Muscle function analysis showed that the muscles of the treated mice generated substantially higher tetanic forces than those of untreated mice, with force levels similar to those of muscles in healthy, active mice. These results indicate that the active adhesive could prevent, or at least delay, the occurrence of disuse muscle atrophy due to immobilization.

Conclusions This work reports a hydrogel adhesive system with mechanically active elements, which not only forms robust tissue adhesion, but also generates stimulation on the target tissue for mechanotherapy. Mechanical stimulation was found to attenuate the onset of muscle atrophy, preventing the loss of muscle mass and maintaining muscle force generation. This work demonstrates the therapeutic potential of mechanical stimulation in the context of muscle atrophy and paves the way for the implementation of these stimulations in hydrogel adhesives.

11:15 AM SB09.01.04

A 3D Printable Tissue Adhesive [Sarah Wu](#), Jingjing Wu, Hyunwoo Yuk, Heejung Roh and Xuanhe Zhao; Massachusetts Institute of Technology, United States

Tissue adhesive materials are promising alternatives to sutures and staples for joining tissues, sealing defects, and immobilizing implantable devices. However, existing adhesive glues and patches typically offer little tunability over their shapes and physical properties, limiting their ability to be used for diverse applications. Here, we introduce a new strategy for fabricating customized adhesive patches and implantable devices using a 3D printable tissue adhesive ink based on a poly(acrylic acid)-grafted polyurethane brush-like polymer. The material confers high adhesion performance by integrating toughness, flexibility, and stretchability of the polyurethane backbone with tissue bond-forming moieties in the poly(acrylic acid) chains. As a result, the printed tissue adhesive patches exhibit fast, conformable, strong, and stable adhesion with defect specificity. Coupled with multi-material 3D printing, the tissue adhesive can also be used to manufacture various implantable devices, such as bioelectronic and drug delivery patches. Through in vivo rat and ex vivo pig models, we demonstrate the biocompatibility and potential versatility of the 3D printable tissue adhesive platform.

11:30 AM SB09.01.05

One-Pot Synthesis of Dual Functionalised Hyaluronic Acid for Tuneable and Adhesive Double Crosslinked Hydrogel Networks [Cameron Milne](#), Wenxin Wang and Sigen A; University College Dublin, Ireland

Routine techniques to close wounds such as sutures and staples have significant drawbacks which can negatively impact wound recovery. Whilst sutures and staples have high tensile strength, they are time consuming to administer, require high surgical skill, create additional damage to the wound environment, can allow for bacterial infiltration and do not completely prevent fluid ingress and egress. Tissue adhesives have been studied for many decades as potential replacements of sutures but poor adhesion, mechanical properties, and biocompatibility precludes many systems' translation to clinic. Although there are commercially available products e.g. Evicel, BioGlue, and ReSure, most have critical compromises that limit their efficacy. In this work, an aldehyde and methacrylate functionalised Hyaluronic acid (HA) biopolymer (HA-MA-CHO) has been synthesised for use in a novel, adhesive, biocompatible and biodegradable double crosslinked hydrogel network (DCN) for the effective closure and sealing of wounds. Aldehyde (CHO) groups are able to bond with native proteins on the tissue surface and act as a crosslinking site by reacting with the disulphide containing crosslinker 3,3'-dithiobis(propanoic hydrazide) (DTPH), forming a single crosslinked soft hydrogel network (SCN) with shear-thinning and self-healing properties. The gel can then be further cured and strengthened with rapid UV-photopolymerization of the methacrylate groups to create a DCN. This two stage gelation and administration process of the hydrogel allows for easy in-situ application of UV crosslink-able pre-hydrogel solutions. This DCN hydrogel shows remarkable versatility as the storage modulus (G') has shown to be highly tuneable ($10^3 - 10^5$ Pa) by varying polymer concentrations, degrees of methacrylate substitutions and HA-MA-CHO:DTPH molar ratios to allow for application to many different wound environments. The hydrogel prepared showed high adhesion to porcine skin surpassing a burst pressure result for the commercially available tissue adhesive BioGlue by 52%. Along with these properties the DCN hydrogels also showed excellent cell viability.

SESSION SB09.02: Hydrogel Adhesives II
Session Chairs: Jue Deng and Xuanhe Zhao
Monday Afternoon, November 28, 2022
Hynes, Level 3, Room 310

1:30 PM SB09.02.01

Controlled Tough Bioadhesion with Ultrasound [Zhenwei Ma](#)¹, Claire Bourquard², Zu-hua Gao³, Outi Supponen² and Jianyu Li¹; ¹McGill University, Canada; ²ETH Zürich, Switzerland; ³The University of British Columbia, Canada

Tough adhesion of hydrogels and biological tissues has significant implications in engineering and medicine, but remains challenging to form and control. Here, we report an ultrasound (US)-mediated bioadhesion technology to achieve tough bioadhesion with controllability and fatigue resistance. Without chemical reactions, our strategy amplifies the adhesion energy and interfacial fatigue threshold between hydrogels and porcine or rat skin by up to 100 and 10 times. Combined experiments and theoretical modeling identify the key mechanism to be US-induced cavitation, which propels and anchors primers into tissues with mitigated barrier effects. The US effects are potent yet localized to enable spatial patterning of tough bioadhesion, on-demand detachment, and transdermal drug delivery. This work expands the material repertoire for tough bioadhesion and enables bioadhesive technologies with high-level controllability.

The US-mediated bioadhesion is achieved in two steps. We first apply the US to a primer solution/suspension of anchoring agents spread on tissue substrates with an ultrasonic transducer for a short period of time. Sequentially, we cover the treated area with a hydrogel patch with gentle compression. As a model system, we deploy a chitosan (Chi) solution and a polyacrylamide-alginate (PAAm-*alg*) hydrogel as the primer and the hydrogel patch, respectively. Our results show an adhesion energy of 1500 J m^{-2} obtained on porcine skin with the US treatment, more than 15 times higher than that of the no-US control. Our strategy is demonstrated with a large repertoire of materials. We confirm the adhesion enhancement by US with other hydrogels, including another double-network poly(N-isopropylacrylamide)-alginate (PNIPAm-*alg*) hydrogel and a single-network PAAm hydrogel. The same efficacy is observed with other anchoring primers such as proteins (gelatin) and nanoparticles (chitosan nanocrystals, aldehyde-functionalized cellulose nanocrystals). Besides skin, our strategy is applicable to various biological tissues, including buccal mucosa and aorta.

We then delve into the mechanism underlying US-mediated bioadhesion, where we combine experiments and theoretical modeling to substantiate the link between the US-mediated cavitation and bioadhesion. The US substantially enhances both the peak intensity of cavitation microbubble and bioadhesion. Fatigue fracture tests reveal a significantly enhanced interfacial fatigue threshold Γ_0 from $\sim 5 \text{ J m}^{-2}$ (no-US) to $\sim 65 \text{ J m}^{-2}$. The results substantiate the existence of strong interfacial bonding, which typically only observed with covalent bonds, in contrast to often weak physical interactions such as entanglement resulted from interdiffusion. US also serves as a regulator for tough bioadhesion. As the US effects scale with the distance between the transducer and the tissue (d), simply maneuvering the US transducer could control the bioadhesion in magnitude and space. To understand and predict the spatially controlled bioadhesion, we conduct theoretical modeling on the acoustic field produced by the US transducer between the horn and the substrate. We extract the area on the substrate where the absolute pressure drops below the vapor pressure in every acoustic cycle, thereby enabling the formation of cavitation bubbles. At various d , we obtain drastically different pressure profiles on the tissue substrate, from which the regions impacted by cavitation are estimated. The simulation results agree with the experimental measurements. Besides the spatial control, we demonstrate that US can enable temporal control over bioadhesion by using a thermo-gelling gelation as anchoring primer and the heating effect of US.

Together, we report US-mediated bioadhesion to precisely control hydrogel bioadhesion in space and time. The universal applicability of our strategy promises impacts in broad areas ranging from human-machine interface and precision medicine.

1:45 PM SB09.02.02

New Adhesive Hydrogel Splint to Correct Malacic Trachea (Tracheomalacia) Vijay Kumar Rana¹, Ece Uslu¹, Sokratis Anagnostopoulos¹, Peyman Karami¹, Francois Gorostidi², Kishore Sandu², Nikolaos Stergiopoulos¹ and Dominique P. Pioletti¹; ¹École Polytechnique Fédérale de Lausanne, Switzerland; ²Le Center hospitalier universitaire vaudois (CHUV), Switzerland

Tracheomalacia (TM) is an illness in which the tracheal cartilage is too soft to ensure the mechanical support of the airways.¹ This results in an excessive and potentially lethal collapse and narrowing of the airways. Current treatment techniques including, tracheal reconstruction, tracheoplasty, endoluminal, and extraluminal stents, however, come with certain limitations.²⁻⁴

We will present a new and simple approach to correct TM where a (malacic) Trachea can be supported extraluminally by the adhesive hydrogel splint (patch). To this end, a new hydrogel formulation has been synthesized. We found that these hydrogel patches provide profound wet adhesion on the tracheal surface, thanks to a two-step photo-polymerization approach that help to anchor the surface much better than previously known adhesive hydrogels. A finite element model of a rabbit trachea was also developed to investigate the deformation and stress responses under maximum negative pressure with and without wrapping an adhesive hydrogel patch to it.

The numerical studies revealed that the hydrogel patch has the potential to preserve a more physiological shape of the trachea by constraining the membrane folding. Therefore, to validate the numerical model, and examine the potential use of the adhesive hydrogel, μ -CT and *ex vivo* experiments were also executed, respectively. To this end, few cartilage rings were removed from a healthy trachea to mimic the TM condition before executing these experiments in absence and presence of a hydrogel patch. At last, we could prove the hypothesis that airway collapse can be restrained by fixing the adhesive hydrogel splints superficially to a malacic trachea.

Interestingly, hydrogels developed herein also displayed outstanding wet adhesion on the surface of other soft tissues (skin, liver, heart, kidney, and lung), and inorganic surfaces (glass, wood, plastic, and ceramic *etc.*).

References:

- A. Kamran, R. W. Jennings, *Front. Pediatr.* **7**, 1–9 (2019).
J. S. Choi, J. Seok, M. R. Eom, E. Jung, S. A. Park, S. M. Joo, Y. J. Jun, K. W. Son, S. K. Kwon, *Clin. Exp. Otorhinolaryngol.* **14**, 328–337 (2021).
C. Serrano-Casorran, S. Lopez-Minguez, S. Rodriguez-Zapater, C. Bonastre, J. A. Guirola, M. A. De Gregorio. *Pediatr. Pulmonol.* **55**, 1757–1764 (2020).
F. Gorostidi, C. Courbon, M. Burki, A. Reinhard, K. Sandu, *Laryngoscope.* **128**, E53–E58 (2018).

2:00 PM SB09.02.03

Stimuli-Detachable Adhesion of Hydrogels on Elastomer Substrate and Sequential Structural Change of the Soft Hybrids In Cho, Eunseok Heo, Hye Been Koo and Jae-Byung Chang; Korea Advanced Institute of Science and Technology, Korea (the Republic of)

Fabrication of soft hybrid incorporating hydrogel and elastomers have huge potential in various research fields such as soft electronics and robotics, microfluidics, and tissue engineering. Recently, robust adhesion of hydrogel on diverse elastomer surfaces has been achieved by activating surface-adsorbed hydrophobic initiators to graft hydrogel polymer chains from the elastomer substrate. In addition, a recently established adhesion approach permits the separation of the adhesion between elastomers and hydrogels when exposed to light. However, chemical stimuli-detachable strong adhesion between hydrogels and elastomers has not yet been demonstrated. In this study, we present a novel method for adhering hydrogels to elastomer surfaces. To enable chemically-detachable adhesion, various hydrogels are immersed, dipped or brushed with hydrogel-precursor solution containing reversible chemical linkers. Topological adhesion of hydrogels and elastomers are then obtained with the assist of hydrophobic initiator contained in elastomer substrate. The proposed method allows the separation of attached elastomers and hydrogel, upon different chemical stimulation. We first demonstrate that this technology is applicable to a wide variety of hydrogels and elastomers. We then demonstrate the sequential folding and on-demand structural change of such soft hybrids by utilizing the detachable adhesion of various stimuli-responsive hydrogels to elastomer surfaces.

2:15 PM SB09.02.04

Design and One-Step Fabrication of an *In Situ* Formed Hyaluronic Acid-Based Tough Hydrogel with a Long-Short Chain Network Structure Rujian Song, Sigen A and Wenxin Wang; University College Dublin, Ireland

As the dominant component form of cells, extracellular matrix, tissues, and organs, hydrogels have been used in various biological and biomedical application areas, including wound dressings, drug delivery vehicles, tissue engineering scaffolds, soft robotics, and contact lenses. However, the high-water content of traditional hydrogels results in low mechanical properties, especially low toughness, making them unsuitable for most physiological load-bearing situations. Recently, intensive efforts have been devoted to improving the toughness property of hydrogels, such as constructing more homogeneous hydrogel networks, introducing reversible or irreversible bonds in the original hydrogel framework, and introducing structures in the hydrogel with folding, sliding, or high cross-linkage points. However, the above-mentioned tough hydrogels not only inevitably use bio-toxic monomers, crosslinkers or initiators, but also require a complicated preparation process. Hence, a new tough hydrogel with a simple preparation process and good biocompatibility has a high potential for bio-application. In this work, we hypothesized that the introduction of a single network with distinct chain lengths is able to improve the toughness of the hydrogel. Specifically, two structural features of tough long and short-chain (LSC) hydrogels were proposed in particular: (i) the skeleton of rigid hydrogel networks formed by short chains is relatively homogeneous, and (ii) some flexible long chains are connected with the rigid network skeleton. Here we report a universal example of LSC-hydrogels composed of biocompatible materials including thiolated hyaluronic acid (HA-SH), acrylated hyaluronic acid (HA-A), polyethylene glycol dithiol (PEG-DSH), and polyethylene glycol diacrylate (PEG-DA). In detail, PEG-DSH and PEG-DA act as long chains in the hydrogel network, while the HA-A and HA-SH act as short chains. Remarkably, the combination of long and short chains results in a multi-fold increase in the limit stress and toughness of the hydrogel, while retaining the advantage of extremely simple and safe *in situ* gel formation. Most importantly, this simple and effective criterion for LSC-hydrogels can be extended to numerous classical single network (SN) - hydrogel systems and provide new directions for the design and preparation of tough SN-hydrogels.

2:30 PM SB09.02.05

Granule-Enhanced Viscoelastic Materials for Dynamic Biological Interfaces Jiuyun Shi, Yiliang Lin, Jiping Yue and Bozhi Tian; The University of Chicago, United States

The formation of the intimate interface between materials and dynamic biological systems serves as the basis for revolutionary disease diagnosis and treatment. However, the complexity of anisotropic structure, viscoelastic mechanics, and dynamic responsiveness of the native tissue pose significant challenges to creating adequate-contact and long-lasting interfaces for therapeutic delivery or biological signaling transduction. Here, we introduced a

viscoelastic dynamic granular hydrogel system which forms the dynamic biointerface with the biological tissues. Through the dynamic mechanical analysis, we revealed that the dynamic granular hydrogel system has viscoelastic behavior and environmental responsiveness. Furthermore, we demonstrated that the dynamic granular composite system has enhanced biological affinity and retention ability with the biological tissue after surface modification. Our results suggest that dynamic granular hydrogels are effective in treating ulcerative colitis and repairing skin wounds as regenerative medicine. Additionally, we proved that the dynamic granular hydrogels have the potential to be interfacial material for bioelectronic devices.

2:45 PM BREAK

SESSION SB09.03: Hydrogels for Biomedical Applications I
Session Chairs: Jingjing Wu and Xuanhe Zhao
Monday Afternoon, November 28, 2022
Hynes, Level 3, Room 310

3:15 PM SB09.03.01

3D Ionic Microgel Printing of Degradable Ionic Junctions Ran Huo and Jianyu Li; McGill University, Canada

Ionotronics exhibit intrinsic deformability and ionic conductance that better match the human body mechanically and electrically compared to electronics. Ionic junctions are a unique and critical ionotronic component that possesses current rectification behavior analogous to electrical p-n junctions. Existing ionotronics and ionic junctions, however, are limited in electrical and mechanical performances and are difficult to process, optimize, and degrade. Herein, we report the design, fabrication, and characterization of degradable ionic junctions fabricated via 3D ionic microgel printing. Combining ionic microgels and a degradable secondary network, the ionic junctions feature high mechanical toughness ($>1000 \text{ Jm}^{-2}$), high interfacial toughness, excellent electrical performance (current rectification ratio >100), and rapid degradation. Taking advantage of the intrinsic printability of jammed microgels, the ionic junctions can be 3D-printed into various shapes in high resolution with high fidelity. We further demonstrate the applications of ionic junctions in the form of a diode, a transistor, and a full-wave rectifier. By merging ionotronics, 3D printing, and degradable hydrogels, this work highlights high-performance sustainable ionotronics, which would impact broad areas ranging from wearables to human-machine interfaces.

3:30 PM SB09.03.02

Liquid-Infused Microstructured Bioadhesives Halt Non-Compressible Hemorrhage Guangyu Bao¹, Luc Mongeau¹, Christian Kastrup² and Jianyu Li¹; ¹McGill University, Canada; ²Versiti Blood Research Institute, United States

Uncontrolled hemorrhage accounts for more than 30% of trauma deaths. Despite tremendous research efforts, critical challenges remain in treating non-compressible and deep-narrow hemorrhages. Common strategies reliant on hemostatic agents alone to promote blood clotting are limited by slow clotting rate and coagulopathies. Alternative strategies are bioadhesive sealants that block the bleeding site physically. Removal of interfacial fluids is critical for adhesion formation and sealing performance of the bioadhesives. However, existing bioadhesives are slow and ineffective to remove the rapid pressurized blood at the interface due to their non- and nano-porous structures.

Inspired by the microstructured adhesives that adhere to bio-fouled surfaces in nature, here we propose new sealants based on *liquid-infused microstructured bioadhesives* (LIMBs) to halt non-compressible hemorrhage. Such bioadhesives can rapidly absorb and clot whole blood while forming strong bioadhesion, without the need for compression, to resist blood pressure and seal bleeding sites. We demonstrate a significantly improved hemostatic efficacy and biocompatibility of LIMB in rats and pigs compared to clinically used counterparts.

The optimized LIMB is porous, soft, tough, and stretchable. It contains macropores of $\sim 200 \mu\text{m}$ that exceed the dimensions of blood components, such as red blood cells. Despite the porous structure, LIMB exhibits high fracture energy ($>1500 \text{ J m}^{-2}$) and large deformability (stretch limit >6). These properties exceed soft tissues/organs such as cartilage and blood vessels. We partially fill the pores with adhesive functional liquid and leave some open. When being attached to the tissues, the capillary suction from the dry pores removes the barrier fluids from the interface, thereby enabling instant adhesion. The adhesive functional liquid stored within LIMB is then automatically transported to the interface to form strong, tough, and universal adhesion without the need for compression. Benefited by the dry matrix, LIMB can concentrate blood components and accelerate clotting, as evidenced by the blood clotting index used by many prior studies.

Drawing upon the excellent pressure-free adhesion and clotting ability, LIMB provides excellent efficacy in halting non-compressible and deep-incision hemorrhages. When being used as an implantable hemostat in a rat liver volume defect model (4 mm in diameter and 3 mm in depth), LIMB shows low blood loss (99.8 mg) and quick time to hemostasis (31.5 s), in contrast to the 517.1 mg and 165.8 s from SURGIFOAM, a commercial hemostatic gelatin sponge. LIMB also demonstrates very mild foreign body reactions, minimal inflammation, and allergy responses after being implanted in rats after 2 weeks. In a rat liver incision model (7 mm in length and 3 mm in depth), LIMB significantly reduced blood loss compared to non-structure bioadhesives, standard gauze, and Combat Gauze. In a pig liver incision model (15 mm in length and 10 mm in depth), the average blood loss for gauze and LIMB are 69.5 and 17.1 mL, respectively. 4 out of 6 pig injuries treated with LIMB stop bleeding within 10 min, but only 2 of 7 injuries treated with plain gauze succeed.

In conclusion, our new design leverages bioinspired architecture, tough adhesives, and liquid infiltration. The resulting microstructured bioadhesives can form instant and strong adhesion with bio-fouled surfaces without the need for compression. The bioadhesives are biodegradable, easy to implement, and stable for long-term storage. They show excellent biocompatibility and hemostatic efficacy compared to several existing hemostatic agents and bioadhesives, as demonstrated by the decreased blood loss in non-compressible and deep-and-narrow hemorrhages in small and large animal models. We anticipate that the reported design principle and the material system will galvanize the development and translation of bioadhesives and hemostatic materials to manage hemorrhage.

3:45 PM SB09.03.03

Optimizing a Minimally Invasive Reverse Thermo-Responsive Liquid Embolic Agent Polymer Treatment for Brain Aneurysms Evelyn Shue¹, Noah Fensterheim², Shaheer Khan³, Dohyun Kim⁴, Briana Poon⁵, Lorenzo Verona⁶, Elaina Heghes⁷, Megha Gopal⁸, Nakisa Dashti⁸, Aaron Sloutski^{8,9}, Robert Wong⁸, Daniel Cohn⁹, Chandramouli Sadasivan⁸ and Miriam Rafailovich⁸; ¹Richard Montgomery High School, United States; ²Ida Crown Jewish Academy, United States; ³Half Hollow Hills High School East, United States; ⁴Seoul Foreign School, Korea (the Republic of); ⁵Arlington High School, United States; ⁶American School of Milan, Italy; ⁷South Side High School, United States; ⁸Stony Brook University, The State University of New York,

United States; ⁹The Hebrew University of Jerusalem, Israel

Brain aneurysms are sac-like pathological dilations of intracranial blood vessels. Left untreated, they can rupture and cause fatal brain hemorrhages or ischemic strokes. Current treatments, like metallic implants, remain relatively ineffective, with unfavorable outcomes in 20-30% of cases or more [1]. This project seeks to develop an injectable, reverse-thermoresponsive (RTR), radiopaque, shape-conforming, crosslinkable, biodegradable liquid embolic agent (LEA). Made of pluronic polymer F88-DMA, contrast agent iohexol, and a crosslinker solution of ammonium persulfate (APS) and tetramethylethylenediamine (TEMED), the LEA easily injects through a catheter at room temperature, forms micelles at body temperature, leading to physical gelation, and chemically crosslinks via free-radical polymerization. The LEA should remain stable in the aneurysm to prevent further enlargement and allow wound healing. External stress should also not deform it. Before crosslinking, the F88-DMA polymer had a modulus of 28.13 kPa that increased to 142.10 kPa after crosslinking. Carotid arteries have an average wall shear stress of 0.85 ± 0.2 Pa, within the viscoelastic region of F88-DMA [2].

Various concentrations of TEMED and other additives were mixed with F88-DMA and tested *in vitro* to determine the optimal injectability and time for the polymer gel to solidify physically and crosslink chemically. The polymer gel must change phases at the optimal time so as to not solidify prematurely in the catheter or remain liquid too long in the aneurysm and get washed away by the bloodstream. Just as optimizing gel injectability is key, so too is optimizing the volume of the gel injected. Iohexol, an iodine-rich radiopaque contrast agent, was thus added into the LEA for visibility in angiography during the injection process.

Once injected and crosslinked, the gel is exposed to osmotic forces that promote swelling, potentially inducing aneurysm rupture. To prevent this, we added low concentrations of a four-armed polymer with crosslinkable methacrylate endgroups, known as tetramers. Placed in a static saline solution, we found that adding tetramer reduced gel swelling by ~50%.

Due to concerns over LEA-induced thrombogenesis, blood was drawn from a rabbit and mixed immediately with the APS/TEMED crosslinker. There was no thrombus formation even after an hour and APS/TEMED was thus found to be not thrombogenic. In further *in vivo* experiments, the LEA was successfully injected through a patient-sized microcatheter into a ligated rabbit carotid artery. The gel crosslinked and occluded the vessel for three weeks before explant, where the gel was recovered. Histology will be represented.

The LEA is biodegradable as a function of the patient-specific wound healing process such that the blood vessel returns completely to its original healthy state. An enzymatically degradable crosslinker, made of a peptide with a Gly-Leu motif in the center, was incorporated into the gel to bond with F88-DMA. When Matrix Metalloproteases (MMPs) were added, they cleaved the crosslinker's Gly-Leu motif, breaking it and triggering the liquefaction and disappearance of the LEA from the aneurysm. The peptide crosslinker could not induce chemical crosslinking absent APS/TEMED, but disturbance of this peptide alone proved sufficient to degrade the crosslinked gel.

Current results on radiopacity, injectability, stability, thrombogenicity, and biodegradability establish pluronic polymers and various additives as promising agents in the pursuit of a novel LEA brain aneurysm treatment. Future experimentation will test the effect of additives on the LEA's cytotoxicity and cell-adhesive properties.

Thanks to Morin Charitable Trust

[1] Taschner, et al. "Second-Generation Hydrogel Coils for the Endovascular Treatment of Intracranial Aneurysms." *Stroke*.

[2] Sui, B., et al. "Assessment of Wall Shear Stress in the Common Carotid Artery of Healthy Subjects Using 3.0-Tesla Magnetic Resonance." *Acta Radiologica*.

4:00 PM SB09.03.04

Silk Embolic Material for Transcatheter-Directed Drug Delivery [Jingjie Hu](#); North Carolina State University, United States

Transcatheter embolization is a minimally invasive procedure that uses embolic agents to intentionally block diseased or injured blood vessels for therapeutic purposes. Embolic agents in clinical practice are limited by recanalization, risk of non-target embolization, failure in coagulopathic patients, high cost, and toxicity. In this study, a silk-based embolic material (SEM) was developed and optimized to provide tandem integration of both embolization and the delivery of therapeutics. Natural silk was processed into fibroin proteins of varying lengths and was combined with charged nanosilicate disks to allow optimized mechanical property and injectability using clinical catheters. SEMs loaded with fluorochrome labeled albumin and Nivolumab, a widely used immunotherapy drug, showed a sustained release profile over 28 days *in vitro*. In a porcine renal survival model, drug loaded SEMs successfully embolized porcine arteries without recanalization and delivered both albumin and Nivolumab into the interstitial space of the renal cortex. Mechanistically, the delivery of therapeutics has been found to be optimal when the internal elastic membrane of the embolized artery was disrupted. Our results suggested that SEMs has the potential to be a next-generation biofunctional embolic agent to treat a wide range of vascular diseases.

4:15 PM SB09.03.05

Delivery of CAR-T Cells in a Transient Injectable Stimulatory Hydrogel Niche Improves Treatment of Solid Tumors [Abigail Grosskopf](#), Louai L. Labanieh, Crystal M. Mackall and Eric A. Appel; Stanford University, United States

Adoptive cell therapy (ACT) has proven to be very effective in treating blood cancers, but traditional approaches to ACT are poorly effective in treating solid tumors observed clinically. Novel delivery methods for therapeutic cells have shown promise for treatment of solid tumors when compared with standard intravenous administration methods, but the few reported approaches leverage biomaterials that are complex to manufacture and have primarily demonstrated applicability following tumor resection or in immune-privileged tissues. In this talk, I will describe simple-to-implement supramolecular hydrogels for the controlled co-delivery of CAR-T cells and stimulatory cytokines that improve treatment of solid tumors. We develop Polymer-Nanoparticle hydrogels based on modified cellulose polymers and core-shell nanoparticles that interact to form an injectable hydrogel. The unique architecture of this material both simultaneously inhibits passive diffusion of entrapped cytokines, and permits active motility of entrapped cells to enable long-term retention, viability, and activation of CAR-T cells. We develop the formulation through novel *in vitro* studies and demonstrate its efficacy with cancer models in mice. The generation of a transient inflammatory niche following administration affords sustained exposure of CAR-T cells, induces a tumor-reactive CAR-T phenotype, and improves efficacy of treatment.

4:30 PM SB09.03.06

Optimization of Hydrogel Compositions to Enable the Ultra-Fast Immunostaining and Super-Resolution Imaging of Thick Tissue Slices [Woonggi Lee](#), Junyoung Seo, Eunseok Heo and Jae-Byum Chang; Korea Advanced Institute of Science and Technology, Korea (the Republic of)

Hydrogel is a soft, transparent, biocompatible material that is frequently employed in biological applications such as bioimaging and bioimplantable

devices. Hydrogels serve as scaffolds for protecting biological reactivity and storing position information of biomolecules, particularly in bioimaging. Expansion microscopy (ExM) is one of several imaging techniques that uses an electrolyte hydrogel to anchor all the proteins within biological specimens to polymer backbones and expand the entire specimens homogeneously to improve resolution. Another imaging technology, termed ELAST, employs hydrogels with long-chain polymers and entangles them with proteins, allowing for the elastic stretching of biological specimens without the formation of cracks in order to increase immunostaining speed. Recently, a hydrogel that permits the expansion and stretching of tissue has been reported. In this study, the composition of hydrogels is optimized to achieve a greater expansion factor, a more uniform expansion, and more stretchability. Using the optimized hydrogel, we demonstrate the staining of a 500-um thick specimen within a single day and the volumetric imaging of axon, myelin sheath, and neuronal marker (NF-L, MBP, MAP2) with a lateral resolution of 60 nm.

SESSION SB09.04: Poster Session: Hydrogels for Humans and Machines
Session Chairs: Yuhang Hu and Xuanhe Zhao
Monday Afternoon, November 28, 2022
8:00 PM - 10:00 PM
Hynes, Level 1, Hall A

SB09.04.01

Multifunctional Injectable Hydrogel for *In Vivo* Diagnostic and Therapeutic Applications Wanghee Lee and Dae-Hyeong Kim; Seoul National University, Korea (the Republic of)

Injectable hydrogels show high potential for *in vivo* biomedical applications owing to their distinctive mode of administration into the human body. In this study, we propose a material design strategy for developing a multifunctional injectable hydrogel with good adhesiveness, stretchability, and bioresorbability. Its multifunctionality, whereupon multiple reactions occur simultaneously during its injection into the body without requiring energy stimuli and/or additives, was realized through meticulous engineering of bioresorbable precursors based on hydrogel chemistry. The multifunctional injectable hydrogel can be administered through a minimally invasive procedure, form a conformal adhesive interface with the target tissue, dynamically stretch along with the organ motions with minimal mechanical constraints, and be resorbed *in vivo* after a specific period. Further, the incorporation of functional nanomaterials into the hydrogel allows for various *in vivo* diagnostic and therapeutic applications, without compromising the original multifunctionality of the hydrogel. These features are verified through theranostic case studies on representative organs, including the skin, liver, heart, and bladder.

SB09.04.02

User-Demand Fast-Curable Ocular Glues Enforced by Multilength Tunable Networks Hyeon Lee¹, Ajeesh Chandrasekharan¹, Keum-Yong Seong¹, Yeon Ji Jo², Samdae Park³, Seonyeong An¹, Seungsoo Lee³, Hyeji Kim⁴, Hyungju Ahn⁴, Sungbaek Seo¹, Jong Soo Lee² and Seung Yun Yang¹; ¹Pusan National University, Korea (the Republic of); ²Pusan National University Hospital, Korea (the Republic of); ³SNvia, Korea (the Republic of); ⁴Pohang Accelerator Laboratory, Korea (the Republic of)

Achieving fast and secure wound closure without ocular foreign body sensation is highly desired in ophthalmologic surgery. Sutureless approaches using tissue adhesives are gaining popularity, but their practical use is limited by the difficulty in controlling adhesion time and satisfying safety standards without compromising adhesive performance. Herein, we report user-demand hydrogel-forming ocular glues based on multilength photo-crosslinkable hyaluronic acid (HA), achieving firm tissue adhesion under wet and dynamic conditions and possessing cornea-like optical transparency. The HA-based photocurable glue (HA photoglu) quickly seals wounds upon nontoxic low-energy light exposure (320-500 nm, < 5s, < 1 Jcm⁻²), and its mechanical and adhesive properties are improved by introducing short and long crosslinkable moieties into HA through one-step synthesis, forming multilength networks. Furthermore, the HA photoglu provides stable sealing in wet environments like ocular mucous surface, a clear vision with a light transmittance of more than 95% over the entire visible range, and a lubricating surface with minimal ocular sensation (generating less than 10% frictional force than suture groups). In a rabbit corneal incision model, the HA photoglu showed improved wound healing efficacy based on histological evaluation compared to control groups.

SB09.04.03

Hydrolysis-Driven Viscoelastic Transition in Triblock Copolyether Hydrogels with Acetal Pendants Jinsu Baek¹, Seyoung Kim², Byeong-Su Kim¹ and Soo-Hyung Choi²; ¹Yonsei University, Korea (the Republic of); ²Hongik University, Korea (the Republic of)

While the hydrolytic cleavage of ester groups is widely exploited in degradable hydrogels, the scission at the midst of chain backbones can bring dramatic changes in the mechanical properties of the hydrogels. However, the predictive design of the mechanical profile of the hydrogels is a complex task, mainly due to the randomness of the location of chain scission. To overcome this challenge, we herein present degradable ABA triblock poly(ethylene oxide)-based hydrogels containing an A-block bearing acetal pendant, which provides systematically tunable mechano-temporal properties of the hydrogels. In particular, hydrophobic endocyclic tetrahydropyranyl or exocyclic 1-(cyclohexyloxy)ethyl acetal pendants are gradually cleaved by acidic hydrolysis, leading to the gel-to-sol transition at room temperature. Most importantly, a series of dynamic mechanical analyses coupled with *ex situ* NMR spectroscopy revealed that the hydrolysis rate can be orthogonally and precisely tuned by changing the chemical structure and hydrophobicity of acetal pendants. This study provides a new platform for the development of versatile degradable hydrogels in a highly controllable manner.

SB09.04.04

Rheo-SAXS Observation of Structural Change in Shear Thickening Polymer Gel Keishi Akada¹, Soichiro Okubo², Kazuya Tokuda², Koji Yamaguchi², Takamasa Onoki², Tatsuya Yamada³, Syogo Tejima³ and Jun-ichi Fujita¹; ¹University of Tsukuba, Japan; ²Sumitomo Electric Industries, Ltd., Japan; ³Research Organization for Information Science & Technology, Japan

Background:

Shear thickening fluid (STF), often termed as a dilatant fluid, is a non-Newtonian fluid characterized by significant increase in viscosity when the applied shear rate above a critical value. It shows wide application prospects in shock absorption, body protection, and damper systems. However, these viscosity changes occur in a dynamic process, in which shear stress is applied, and the viscosity returns to its original state when the shear stress is removed. This reversible phase change makes it difficult to measure the dynamic microstructural changes that lead to the shear thickening phenomena. In this study, we performed a rheo-SAXS, which is simultaneous measurements of viscosity with small-angle X-ray scattering (SAXS) or ultra-small-angle X-ray scattering (USAXS) using an X-ray transmission solution cell. This real-time observation of the structural changes in colloidal silica solution showed the aggregation

process of polymers and compressing colloidal particles responsible for the ST.

Experiment:

The silica colloid sample was prepared by dispersing a silica sol (Snowtex ST-S, Nissan Chemical) with a particle size of 9 nm and PEG solution [1]. The viscosity and SAXS/USAXS were measured simultaneously using a rheometer (ONRH-1, Ohna Tech Inc.) in combination with a polycarbonate X-ray transmission Couette cell. The obtained spectra were resolved in the XY direction to elucidate anisotropic changes with respect to shear flow, and were plotted against the scattering vector Q. The experiments were performed at the Sumitomo Electric Beamline BL16 at the Kyushu Synchrotron Light Source Center and BL40XU, BL19B2 at SPring-8.

Results:

A viscosity measurement of the silica colloidal sample showed sharp increase of viscosity at a critical shear rate of 10 [1/s], indicating phase change of ST. SAXS spectra were acquired while rotating at several constant shear rate before and after ST transition, compared obtained spectral intensity. At shear above the critical shear rate, the spectral intensity centered at 0.01 1/nm increases in USAXS, indicating the formation of a floc of about 600 nm. SAXS spectra also showed similar anisotropy, with the 50 nm spacing intensity decreasing only in the velocity direction. The results suggest that the polymer network was restructured, forming larger flocs, and the silica clusters were compressed in the flow.

Acknowledgments:

This work was supported by Innovative Science and Technology Initiative for Security Grant Number JPJ004596, ATLA, and AKENHI Grant Number JP25107002, JSPS, Japan.

[1] Kamibayashi, M., Ogura, H. & Otsubo, Y. *J. Colloid Interface Sci.* **321**, 294–301 (2008).

SB09.04.05

Conductive Hydrogels Embedding Three Dimensionally Connected Graphene Networks for Biomedical Applications Junggeon Park, Seungjun Lee and Jae Young Lee; GIST, Korea (the Republic of)

Conductive hydrogels afford efficient electrical communication with biological systems while providing soft and hydrated interfaces, which have garnered great attention for various biomedical applications, such as tissue engineering scaffolds and prosthetics. However, several issues, including high electrical properties with minimal incorporation of conductive components and simple fabrication of various shapes, remain a challenge. In this study, we developed novel conductive hydrogel system composed of three-dimensionally connected reduced graphene networks using graphene-coated agarose microbeads and thermal annealing. Differently charged graphene-coated agarose microbeads self-assembled to form granulate hydrogels, which can be easily handled and processed to produce various shapes of constructs. Subsequent mild heating allowed for the production of the conductive hydrogels (named thermally annealed graphene-channeled agarose hydrogel (TAGAH)) containing a three-dimensionally connected rGO network, which was formed via graphene rearrangement, thermal reduction, and agarose syneresis. TAGAH showed high electrical conductivity ($\sim 20 \text{ mS cm}^{-1}$) with a very small amount of graphene ($\sim 1.5 \text{ mg mL}^{-1}$), substantially low impedance (> 10 -fold lower than that of controls), and tissue-like softness ($\sim 150 \text{ kPa}$ Young's modulus). Various conductive constructs system could be easily fabricated by molding and 3D printing. *In vitro* cytocompatibility and *in vivo* tissue compatibility of these conductive hydrogels were confirmed by cell culture studies and subcutaneous implantation for 8 weeks. Moreover, potential biomedical applications of TAGAH-based materials as soft bioelectrodes, pressure sensors, strain sensors, and conductive tissue scaffolds were successfully demonstrated.

SB09.04.06

Reprogramming Factor-Based Injectable Hydrogels Containing Human Stem Cells for Cartilage Tissue Engineering Promotes 3D Cartilage Differentiation and Cartilage Regeneration Sumi Choi; Dong-A University, Korea (the Republic of)

Cartilage bears the load distributed in the joint and plays a pivotal role in stabilizing the joint through lubrication and shock absorption. Damage to the articular cartilage can accelerate joint degeneration and cause other joint diseases. Due to the nature of cartilage insufficient vascularization and lack of nerves and lymphatic vessels, the self-renewal process of articular cartilage rarely occurs after injury. Because non-human vertebrates have the potential to regenerate tissues such as bone, cartilage, muscle, nerve, and blood vessels, their signaling pathways and reprogramming factors have been investigated to induce chondrocyte differentiation from human stem cells. In this study, we specified chondrogenic factors in lizards capable of regenerating amputated tails. We identified the target molecule endoplasmic protein (ENPL, heat shock protein 90 kDa beta member 1) as a chondrogenic factor in 2D human tonsil-derived mesenchymal stem cells (hTMSC). Additionally, we designed a cartilage-mimetic hydrogel composed of hyaluronic acid and chondroitin sulfate for delivering ENPL and hTMSCs to damaged cartilage tissue. ECM-based 3D hydrogels can provide a mechanical and biochemical tissue microenvironment suitable for cartilage growth. The hTMSCs in the 3D hydrogel structure were successfully differentiated into chondrogenic cells. Additionally, a mouse osteoarthritis model confirmed the synergistic effect of cartilage regeneration of ENPL protein and bioactive hydrogels. This study demonstrates that ECM-based ENPL-equipped hydrogels can provide a therapeutic option for cartilage tissue engineering.

In this study, we present options for cartilage therapy of bioactive hydrogel-based scaffolds that induce *in situ* implantation, systems capable of forming cross-links, and stem cell chondrogenesis. Injectable hydrogels can provide a system for repairing and repairing damaged cartilage by delivering cells with minimal invasiveness to target sites of damaged tissues, including delivery of irregularly shaped areas. Here, we introduce an enzyme-mediated cross-linking method to fabricate injectable hydrogels. These enzyme-based reactions are suitable under cell-friendly physiological conditions. Natural proteins and tissues are rich in primary amines and imidazole groups and thiol groups that can bind phenolic moieties. Oxidation of phenol to ortho-quinone is the main function of tyrosinase (Ty). Because ortho-quinone is highly electrophilic, it can participate in various reactions such as Schiff-base reaction, Michael addition, and coupling reactions. In this regard, we designed a Ty-cross-linkable hydrogel by modifying hyaluronic acid (HA) and chondroitin sulfate (CS) with tyramine (TA). HA and CS are the components of the extracellular matrix (ECM), commonly used in tissue engineering, and can provide a biological and chemical environment for cartilage tissue. TA was conjugated to HA and CS using EDC/NHS chemistry for hydrogel crosslinking of HA and CS. Here, HA-TA and CS-TA generated by conjugating TA are advantageous for Ty-mediated crosslinking. Ty oxidizes the phenolic group of TA to form a quinone group. These reactive groups readily form covalent bonds with other chemical moieties such as amines, thiols, and imidazole groups. In this study, we show that TA-based hydrogels composed of ECM can provide cells and tissues with biocompatibility, cell compatibility, and a biomimetic environment. In addition, we targeted HSP90b1, which is related to the survival and proliferation of chondrocytes, by paying attention to the mechanism of lizard tail regeneration in which cartilage is regenerated instead of bone to induce cartilage differentiation. We demonstrate that Ty-based hydrogels incorporating the target protein ENPL can serve as strong candidates for cartilage regeneration with the added benefit of the biochemical response of ECM.

SB09.04.07

Injectable Fibrogel for Tissue Engineering Application Yanting Shen; The University of Hong Kong, Hong Kong

Hydrogels are valuable tools in tissue engineering and regenerative medicine due to their 3D structure, good permeability, and drug-releasing properties. In

particular, the injectable hydrogel has attracted considerable attention on account of its injectability with minimal invasiveness and usability for irregularly shaped sites. However, the scalable formation, together with the matching physicochemical properties and the controllable drug release rates for precise control over biophysical and biomedical cues to direct endogenous cells remain challenges. Here, we show that these shortcomings can be circumvented through an oil-free, biocompatible, biomimetic, and fully scalable fibrogel. *In vitro*, this fibrogel shows favorable biocompatibility and considerable vascularization abilities. The potential use of the fibrogel for advancing tissue regeneration is explored by a mice excision skin model showing that the fibrogel promotes wound healing with a rapid rate of new tissue regeneration and the appearance of *de novo* regenerated healthy tissue. The combination of injectability and tailorable properties of this fibrogel can be a promising approach in biomedical fields such as therapeutic delivery, medical dressing, and 3D tissue scaffolds for tissue engineering.

SB09.04.08

A Biomimetic 3D Glioblastoma Triculture Model Carolynn M. Brooks, Sawnaz Shaidani and David L. Kaplan; Tufts University, United States

Glioblastoma multiforme, or GBM, is an aggressive form of brain cancer that is hallmarked by highly immunosuppressive properties and therapeutic resistance. Recent studies have experimented with creating *in vitro* culture models of GBM tumors but are unable to adequately recapitulate the immunogenicity of the tumor microenvironment (TME). This may be due to a lack of multiple cell types, which are crucial to the heterogeneity of the microenvironment and GBM tumor characteristics. Expanding further upon the 3D bioengineered brain model established by Sood et. al, we proposed culturing glioblastoma cells, microglia, and astrocytes together to create a novel triculture model, first in 2D and then in a 3D porous silk scaffold supplemented with an ECM hydrogel. We have cultured the three lines at three different ratios to determine the optimal combination for harmonious proliferation in 2D. Quantitative viability and cytotoxicity assays (LDH, WST-1) were implemented to confirm survival and health of the cultures whereas qualitative immunostaining and fluorescent imaging were performed to observe cellular migration and proliferation. Once this optimal ratio was determined, the three cell types were seeded at four different total densities into porous 3D silk scaffolds infused with ECM hydrogels to observe spatiotemporal distribution of the cells over time (1 week and 4 weeks). Similar methods of analysis have been performed with the addition of two assays (CSPG ELISA, MMP assay) to quantify proteins associated with 3D culture characteristics. Further optimization of the GBM model will be determined through a drug screening implementing temozolomide, vincristine, and clomipramine to characterize the model's immunosuppressive response against different therapeutic agents. The successful establishment of this 2D and 3D triculture model will provide researchers with a comprehensive GBM model for potential investigation into other properties of the tumor microenvironment and future development of therapeutics to treat this deadly disease.

SB09.04.09

Tissue-Like Skin-Device Interface for Wearable Bioelectronics by Using Ultrasoft, Mass-Permeable and Low-Impedance Hydrogels Yoonsoo Shin^{1,2} and Dae-Hyeong Kim^{1,2}; ¹Seoul National University, Korea (the Republic of); ²IBS (Institute for Basic Science), Korea (the Republic of)

Hydrogels consist of a cross-linked porous polymer network and water molecules occupying the interspace between the polymer chains. Therefore, hydrogels are soft and moisturized, with mechanical structures and physical properties similar to those of human tissue. Such hydrogels have a potential to turn the microscale gap between wearable devices and human skin into a tissue-like space. Here, we present material and device strategies to form a tissue-like, quasi-solid interface between wearable bioelectronics and human skin. The key material is an ultrathin type of functionalized hydrogel that shows unusual features of high mass-permeability and low impedance. The functionalized hydrogel acted as a liquid electrolyte on the skin and formed an extremely conformal and low-impedance interface for wearable electrochemical biosensors and electrical stimulators. Furthermore, its porous structure and ultrathin thickness facilitated the efficient transport of target molecules through the interface. Therefore, this functionalized hydrogel can maximize the performance of various wearable bioelectronics.

SB09.04.10

Fabrication of Skeletal Muscle Fibers Within Hollow Silk Matrices Madison Fletcher¹, Sophia Theodossiou^{1,2} and David L. Kaplan¹; ¹Tufts University, United States; ²Boise State University, United States

The controlled flow and flexibility of coaxial needles allows multi-layered gels in the form of gel fiber scaffolds to be formed, with important utility in the field of tissue engineering. Coaxial needles can generate outer and inner layered hollow structures, allowing for the fabrication of macroscale crosslinked hydrogel fibers that are promising as scaffolds for muscle growth. To develop *in vitro* muscle fiber formation, the inner layer of the hydrogels support 3D growth and cell spreading of encapsulated myogenic cells. Silk fibroin (SF) from the *Bombyx mori* silkworm functions as a scaffold that allows cells to distribute throughout the core of the hydrogel. Our objective was to develop a core-shell muscle cell hydrogel system using SF as the shell and the inner channel as the cell-supporting component, to generate environments for the 3D growth and maturation of mouse skeletal muscle myoblasts (C2C12). We hypothesized that the addition of SF and extracellular matrix (ECM) materials would promote the long-term growth and survival of the cells for muscle-related outcomes.

Our methods first include culturing C2C12 cells in standard growth media. While passing confluent cells, two syringes were placed in a syringe pump and then attached to the inner (core) and outer (shell) ports of a coaxial needle using medical tubing. The core solution syringe was filled with the C2C12 cell suspension, collagen type I (Col1), SF, horseradish peroxidase (HRP) and hydrogen peroxide (H₂O₂), all suspended in standard growth media. The shell solution syringe was filled with sodium alginate (Na-Alg). A calcium chloride (CaCl₂) bath was used to crosslink the Na-Alg in order to form fiber-shaped gels. Fibers of desired length were cultured for up to 21 days in standard growth media. Fibers without SF/ECM components served as controls. Live-dead staining and light microscopy were used to assess cell viability following encapsulation.

The coaxial needle system generated mechanically stable core-shell fibers with distinct inner and outer layers with control over the contents of the layers and the length of the fibers. Na-Alg formed the outer shell (1.5mm diameter), while the inner conduit (0.8mm diameter) was filled with the C2C12 cell suspension. Rapid crosslinking due to the enzymatic reaction generated a structure that encompassed the core materials upon extrusion and held shape for 21 days with minimal leakage. The cross linked hydrogel fibers were sufficiently stable to generate 3 meter-long structures. Over time, the integrity of the outer layer's crosslinked hydrogel slowly decreased, but the addition of CaCl₂ in the growth media ameliorated this effect. At the same time, the cells suspended in SF rather than in just growth media resisted calcium toxicity under the processing conditions used. One day after extrusion, fluorescence images showed viable C2C12s that were distributed evenly throughout the core of the hydrogel fibers. The C2C12s proliferated over the 21-day period, measured through microscopy, with culture media changed every 4 days. After 5 days in culture, microscopy images showed cell alignment and developing matrix material, when compared to fibers without SF that showed more disordered cells.

This method of fiber preparation supports the survival and alignment of skeletal muscle cells in developing core-shell hydrogel myofibers for muscle tissue engineering applications. Future improvements of the method include better approximating the mechanical stimuli cells experience during *in vivo* growth.

SB09.04.11

TissueFab[®] Ready-to-Use Bioinks for the Fabrication of Tissue Constructs Kevin T. Dicker, Vinson Chu, Emma Hainstock, Megan Muroski and Gangadhar Panambur; MilliporeSigma, United States

3D bioprinting is a powerful enabling tool for regenerative medicine and drug discovery. Despite promising advancements in 3D bioprinting technology, a need still remains for high quality commercially available ready-to-use bioinks to empower these studies. In response, we have developed a platform of bioinks, *TissueFab*[®], that are compatible with diverse widely studied cell types and bioprinting platforms. *TissueFab*[®] is a family of ready-to-use bioinks based on natural proteins and polysaccharides and synthetic polymers with high batch-to-batch consistency. These bioinks are designed for optimal printability and mechanical properties for micro-extrusion based bioprinting which we verified on the most popular commercial bioprinters thus demonstrating the printer agnostic characteristic of the bioinks. The bioinks were designed to photochemically crosslink with a wide range of compatible wavelengths of light. Separately, moving past photo-crosslinking, we have developed a class of ionically crosslinkable bioinks, Facile Curable, which avoid the use of light and photoinitiators to form a stable construct while maintaining high cell viability. *TissueFab*[®] bioinks were validated for high cell viability, proliferation and metabolic activity using C2C12 mouse myoblast cells, human mesenchymal stem cells (hMSCs) or human adult dermal fibroblasts (HDFa). For bone tissue engineering applications, we have shown that hMSCs bioprinted in *TissueFab*[®] - *Bone bioinks* show an increase in osteogenic differentiation. Additionally, *TissueFab*[®] - *Conductive bioinks* exhibit enhanced conductivity making them attractive for bioprinting electroactive tissues such as neural or muscular tissue. *TissueFab*[®] bioinks provide a robust tissue-mimetic platform for 3D bioprinting applications with both high printability and cytocompatibility to aide in addressing drug testing and tissue engineering challenges.

SB09.04.13

Investigating the Freezing-Thawing Process for PVA Hydrogels and Facile Screening of Effects of Additives Through Turbidity Measurement Boonjae Jang, Jennie Paik and L. Jay Guo; University of Michigan, United States

Poly(vinyl alcohol) hydrogels are being investigated for wide applications in soft robotics, tissue engineering, wearable electronics, etc. due to their tunable mechanical properties. The freezing-thawing process is most widely used to obtain physically crosslinked PVA hydrogels by the formation of crystalline domains in the hydrogels. However, the freezing-thawing process is the most time-consuming process, and research on the process optimization of the preparation of PVA hydrogels is lacking. In this study, we show that it is possible to optimize the processing time of the hydrogel by controlling the freezing temperature, freezing time, thawing temperature, and thawing time, among various factors that affect gel characteristics during the freeze-thaw process. In addition, the gelation effects on the addition of various polyols or salts were compared and analyzed. We used the turbidity of the hydrogels by PVA crystals as a measure of the density and size of the crosslinked crystals, which can be correlated to the UV-Vis extinction spectra. Freezing temperatures by the reduction of freezing point were measured for various PVA solutions containing polyols or salts. Thawing at a temperature about 2 degrees lower than the freezing point for each PVA solution showed the highest turbidity. Moreover, the turbidity of the PVA hydrogel frozen for 30 minutes reached the maximum after 1-hour thawing and interestingly it showed similar turbidity with the PVA hydrogel frozen for 24 hours and thawed for 30 minutes. Thus, the processing time could be reduced significantly with optimized freezing-thawing conditions. Also, the turbidity of the PVA hydrogels containing various salts followed the order of the Hofmeister series due to the different interactions between ions and PVA chains. Additive polyols affected the turbidity of the PVA hydrogels followed such order: diethylene glycol > glycerol > 1,4-butanediol. The molecular size and hydrophobicity of the polyols might influence the interactions between polyols and PVA chains. This study facilitates the preparation of freeze-thawed PVA hydrogels and provides an effective screening method for the effect of various additives to obtain desired physical properties.

SB09.04.14

A Low Impedance, High Current, High Charge Density, Scalable and Soft Energy Converter Liu Hongzhen and Lizhi Xu; The University of Hong Kong, Hong Kong

Flexible energy conversion devices, especially those based on low-frequency mechanical energy, are crucial for developing flexible electronics. Here, we report a flexible power generation device that utilizes ionic streaming potential to generate electrical output. Taking advantage of the Li-ion anchoring ability of the oxygen-containing functional groups on the activated carbon cloth and the PVA hydrogel backbone, exploiting the difference in ion concentration caused by deformation, our device can generate an electrical output with the short-circuit current being up to 4 mA, and the power density reaching 425 mW per square meter. At the same time, the internal resistance is only 122 ohms. After 7500 cycles, the device can still maintain 97.38% of the peak current output. The working parameters, such as electrolyte concentration, frequency and speed of the mechanical driving force, and carbon cloth oxidation time, were systematically studied and optimized. When used to harvest mechanical energy, the device demonstrated outstanding charging capability, charging a 2F capacitor from 0.34 mV to 30.1 mV in 371 s at 80 kPa pressure. The device can power in vitro wearable devices and medical applications such as electronically controlled drug release.

SB09.04.17

Designing and Shaping Microfluidic Flow Profiles in Stokes Flow Regime with Deep Learning Zhenyu Yang¹, Zhongning Jiang² and Ho Cheung Shum¹; ¹The University of Hong Kong, Hong Kong; ²City University of Hong Kong, Hong Kong

The ability to shape flow profiles is critical for microfluidic fabrication of hydrogel fibers and particles with customizable structures and multiscale features. The flow profiles, referring to the lateral cross-sectional shape of the flow fields, can be transformed into diverse and complex shapes, depending on the flow and boundary conditions. The recently proposed inertialess flow profile engineering method deploys sequential steps in the channel to transform the flow profiles in Stokes flow regime, facilitating flow profile engineering. The steps with complex geometries are vital for diverse profile shapes; however, investigating the flow profiles and their transformations around such steps relies on iterative and time-consuming simulations or experiments. As a result, designing a flow profile with fully customized features remains computationally challenging.

Here we develop two deep neural networks for solving this forward design problem. The first model, based on variational autoencoder (VAE) architecture, takes the images of the step shapes as input and outputs the image of the transformed flow profiles. The model accuracy is metricized by the percentage of matched pixel values between the images of the predicted profiles and simulated profiles, and the test accuracy reaches 98.06%. Only minor differences can be visually identified between the predicted and observed profiles. Moreover, the model can predict the output flow profile of steps with unseen types of geometries, such as parallel steps or concave steps, with high accuracy, indicating the model have, to some extent, captured the underlying physical relationships between the step geometries and the output flow profiles.

The second model uses U-Net architecture to predict the profile transformations around a step. Before the training, the streamline data are compressed into transformation matrices, which only include the mapping of fluid element positions between the inlet and outlet profiles. The accuracy is evaluated as the percentage of matched elements in the transformation matrices between the predictions and the ground truth, and reaches 83% after 150 epochs of training. Plotting the predicted transformation matrices as the vector fields shows that the predictions can capture both the significant large-scale secondary flows as well as the small vortices. Moreover, the net transformation matrix of a step sequence can be computed by superposing the transformation matrices of the individual steps, enabling prediction of the output flow profiles of arbitrary step sequences and inlet flow profiles. With the current model accuracy, the flow profiles remain comparable to the simulation and experimental results after transformation by a sequence of 4 steps.

In conclusion, the VAE-based model can predict the flow profiles accurately, and can be generalized to unseen step topologies, while the inlet profiles and the number of steps are fixed. The U-Net-based model can be used to predict the flow profiles of multiple steps, with potential to further improve the

accuracy. We anticipate the model will allow predicting the flow profiles transformed by a large number of sequenced steps, thus significantly accelerating the design cycle of complicated flow profiles.

SB09.04.18

Electrothermal Soft Manipulator Enabling Safe Transport and Handling of “Living” Cell Sheets and Bioelectronic Devices Byoung Soo Kim^{1,2}, Min Ku Kim³, Jonghwi Lee⁴, Chi Hwan Lee⁵ and Hyunjoon Kong²; ¹Korea Institute of Ceramic Engineering and Technology, Korea (the Republic of); ²University of Illinois at Urbana-Champaign, United States; ³Hanyang University, Korea (the Republic of); ⁴Chung-Ang University, Korea (the Republic of); ⁵Purdue University, United States

Ultrathin materials made with “living” cells and microelectronic chips have emerged as significant technologies that improve the performance of tissue reconstruction, therapeutics, and healthcare monitoring. However, handling these thin and delicate materials remains a grand challenge because the external force applied for gripping and releasing can easily deform or damage the materials. This study presents a soft manipulator that can handle thin and fragile materials, such as “living” cell/tissue sheets and ultrathin electronic devices, without causing damage. The soft manipulator consists of a thermo-responsive, micro-channeled hydrogel, and a thin micro electric heater connected to an electrical power unit. Turning the power to the soft manipulator on and off makes the individual microchannels of the gel shrink and expand within 10 seconds and, in turn, lift or detach an object like a cephalopod’s suction cup controlled by a bioelectric signal. This quick adhesion/detachment process is achieved by a pressure change through the anisotropically aligned microchannels of the gel with tissue-like softness. In particular, the soft manipulator enables the transportation of ultrathin and fragile cell sheets and thin film devices in both wet and dry conditions. This soft manipulator would be useful for handling a broad array of cell/tissue sheets and ultrathin electronic materials.

SB09.04.19

Digital Light Processing (DLP) Printing of MOF-Embedded Multi-Layered Hydrogel for the Localized Controlled Release of Anti-Cancer Agents Justin P. Edaugh^{1,1,2}, Erick L. Ribeiro^{1,1,2} and Rigoberto C. Advincula^{1,1,2}; ¹The University of Tennessee, Knoxville, United States; ²Oak Ridge National Laboratory, United States

According to the World Health Organization (WHO), cancer is currently the leading cause of global mortality, accounting for approximately 10 million deaths across the world in 2020. As a result, the research and development of novel oncologic treatment strategies have become a central topic of modern medicine. Despite the continuous effort, current clinical cancer treatment approaches still face several issues. Non-specificity associated with most current chemotherapy, for instance, along with their inability to deliver anti-cancer agents *via* a precise spatial-temporal controlled mechanism, often result in low therapeutic indices, as well as adverse side effects on healthy tissues. Metal-Organic Frameworks (MOFs) have become popular for applications in anti-cancer treatments, owing to their low cytotoxicity, high biodegradability, high biocompatibility as well as excellent chemical and physical stability. Moreover, the extensive variety of chemical and structural configurations arising from a library consisting of approximately 90,000 existing MOF compositions enable unlimited possibilities for their utilization in the rational design of hybrid systems with selective functionalities. Additive manufacturing, also known as three-dimensional (3D) printing, has revolutionized the biomedical industry, due to its ability to rapidly prototype complex 3D objects. Herein, we present the manufacturing of a scaffold-like multi-layered architecture composed of a graphene-based substrate interfaced with a Digital Light Processing (DLP)-printed hydrogel phase containing pH-responsive nanocarriers as a model system for cancer treatment *via* localized controlled release of chemotherapeutic agents. More specifically, the selected drug model, curcumin, was encapsulated within Zeolitic Imidazolate Frameworks (ZIF-8) structures (CCM-ZIF-8) and subsequently dispersed into a photopolymerizable poly(ethylene glycol) diacrylate (PEGDA)-based hydrogel. Finally, DLP was applied to yield a multi-layered CCM-ZIF-8/Hydrogel phase, which was interfaced with a graphene-based substrate to produce the pH-responsive drug release system. The delivery mechanism of chemotherapeutic agent is initiated upon contact of the CCM-ZIF-8/Hydrogel with the targeted area: the lower pH arising from cancer cells induces the decomposition of ZIF-8 phase, which proceeds layer-by-layer, resulting in the controlled release of the chemotherapeutic agents. In addition, the graphene-based substrate imposes a unidirectional diffusion of the drug toward the target area, while serving as a support for the layered printed CCM-ZIF-8/Hydrogel phase. Various structural and thermomechanical characterizations, such as Fourier Transform Infrared Spectroscopy (FTIR), Tensile Tests, Compression Tests, and Thermogravimetric Analysis (TGA), of the hydrogels, revealed the effects of curcumin-encapsulated ZIF-8 (CCM-ZIF-8) addition. Furthermore, *in vitro* drug release tests were performed, confirming the pH-responsiveness of the ZIF-8 MOFs.

SESSION SB09.05: Hydrogels for Biomedical Application II
Session Chairs: Yuhang Hu and Jingjing Wu
Tuesday Morning, November 29, 2022
Hynes, Level 3, Room 310

8:30 AM *SB09.05.01

Creation of a Hydrogel-Based Implant for Resurfacing of Articular Cartilage Benjamin Wiley; Duke University, United States

Replacement of damaged cartilage and subchondral bone with an equivalent synthetic construct would alleviate pain and improve mobility for millions of people. Key hurdles for this unmet need are the development of a hydrogel with a strength that exceeds that of cartilage and fixation of this hydrogel onto the surface of an articulating joint. This presentation will describe the first hydrogel with a tensile strength and compressive strength (50.5 MPa and 98.1 MPa) that exceeds that of cartilage (40 MPa and 59 MPa), and the first attachment of a hydrogel to a metal backing (which can integrate with bone) with a shear strength (1.98 MPa) that exceeds that of cartilage on bone (1.16 MPa). The high strength was achieved through reinforcement of crystallized polyvinyl alcohol with bacterial cellulose. To achieve an attachment strength 70% greater than that of cartilage on bone, freeze-dried bacterial cellulose was secured to a metal backing with an adhesive and a shape memory alloy clamp prior to infiltration and crystallization of the polyvinyl alcohol. The bacterial cellulose-reinforced polyvinyl alcohol was 3 times more wear-resistant than cartilage over 1 million cycles and exhibited the same coefficient of friction, whereas the coefficient of friction for annealed PVA increased to be 6.75 times greater than cartilage after 1 million cycles of wear. This work shows that BC-PVA hydrogel is a strong, wear-resistant material that will not damage opposing cartilage, and it can be secured to a metal base for integration with bone.

9:00 AM SB09.05.02

Low Voltage-Controlled Hydrogels for Drug Delivery Applications Illaria Abdel Aziz¹, Johannes Gladisch¹, Sophie Griggs², Maximilian Moser², Magnus Berggren¹, Iain McCulloch² and Eleni Stavrinidou¹; ¹Linköping University, Sweden; ²University of Oxford, United Kingdom

Hydrogels emerged as promising actuators for a variety of applications, as tissue engineering, contact lenses and drug delivery, among others. In the latter, they represent a valuable alternative to standard pharmaceutical cues, as they can be placed in the proximity of the delivery region and exogenously or endogenously actuated. Indeed, interesting results showed controlled drug release triggered by pH, temperature, light and chemical changes. However, the physiological environment is highly dynamic, and changes in pH or temperature can be correlated to other reasons than the target of the drug delivery, thus the selectivity of these type of hydrogels is limited.

Electrically responsive hydrogels (E-hydrogels) represent a valuable alternative since the drug can be delivered on demand by an exogenous electrical stimulus. Some E-hydrogels have been proposed and characterized. Generally based on polyelectrolytes exposing fixed charges, the loading is driven by electrostatic interactions upon soaking the hydrogel in a solution containing the drug, and upon voltage addressing, the drug is then released. The materials proposed so far, as poly(2-(acrylamido)-2-methylpropanesulfonic acid), poly(acrylic acid), poly(acrylamide), chitosan and poly(2-hydroxyethyl methacrylate) (PHEMA) among others, showed promising results, though limited by high voltage and poor mechanical properties. We propose here a class of semiconducting organic polymers, based on polythiophene backbone and ethylene glycol (EG) side chains as a valuable alternative for E-hydrogels. When in contact with an electrolyte, upon electrochemical doping, ions from the electrolyte will enter the polymer matrix to compensate for the injected charges in the backbone. Upon reverse potential, the ions leave the polymer. This doping/de-doping mechanism is accompanied by a huge volumetric increase, up to 300% with respect to the initial values, due to ion intercalation and water intake, and we hypothesize that this volumetric increase could be used as a method for delivering big molecules or proteins. We show that the polymer exhibits excellent control ranging from 800-1000 Da, with release/leaking ratios up to 200%, and good control for bigger proteins in the range 5000-30000 Da with release/leaking ratios up to 30%, in the voltage window (-0.2, 0.5) V. The release fitting shows that the process is mostly driven by matrix swelling, thus confirming the deterministic delivery mediated by the voltage. Moreover, we show that pulsatile release is also possible, and a drug dose curve can be obtained by applying different potentials. The proposed EG-side chain polythiophenes are a valuable alternative in the field of E-hydrogels, since they show excellent control over a large range of proteins, and they can be actuated within a low potential window (*i.e.* -0.2, 0.5 V).

9:15 AM SB09.05.03

Bioinspired Fabrication of Small-Diameter Blood Vessels Richard Y. Cheng^{1,2,3}, David Miranda-Nieves^{1,2,3}, Shashi Malladi⁴, Yuming Zhang⁴, Carolyn Haller^{1,2}, Torsten Meissner^{1,2}, Axel Guenther⁴ and Elliot Chaikof^{1,2,3}, ¹Beth Israel Deaconess Medical Center, United States; ²Harvard Medical School, United States; ³Wyss Institute, United States; ⁴University of Toronto, Canada

Coronary artery bypass grafting is the most commonly performed cardiac surgery worldwide, but the standard of care remains the engraftment of patient-obtained veins that leads to stenosis or occlusion in nearly half of all cases after one year. This high failure rate has resulted in a demand for alternative strategies like tissue engineering which enable the formation of vessel-mimetic conduits with precise control over biomaterial composition and cell distribution. However, balancing vascular cell activity, biomaterial organization, and mechanical strength in these blood vessel mimetic conduits while maintaining long-term patency post-engraftment *in vivo* remains a significant challenge.

In response, the Chaikof lab and collaborators have developed a large-scale biofabrication process to quickly synthesize mechanically robust, free-standing, ultrathin biomaterial sheets as scaffold building blocks for vascular tissue engineering. Microfluidic extrusion, hydrodynamic focusing, and strain-induced pulling is applied to a naturally occurring type-I collagen protein solution, forming highly aligned sheets with physical dimensions of 1.9 μm thickness, 2.4 mm width, and >230 mm length. These sheets are then seeded with vascular smooth muscle cells, assembled into a tubular conduit with an inner diameter of 1.5mm via an automated rolling process, and subsequently endothelialized. Macroscopic brightfield imaging shows an open-lumen vessel with homogenous wall thickness conducive for unobstructed flow, and preliminary data obtained from multiphoton z-stack imaging reveals circumferential alignment of vascular smooth muscles with uniform distribution of endothelial cells in the lumen surface shortly after fabrication. Furthermore, incorporation of cell-viable biomaterial crosslinkers in the fabrication process improves the conduit mechanical properties of suture retention, burst pressure, and compliance to levels comparable to physiological arterial vessels.

Taken together, we report here a novel tissue engineering platform that enables the rapid and scalable production of “off-the-shelf” living engineered blood vessels incorporating primary vascular wall cells for prospective surgical engraftment. Current efforts are focused on investigating alternative cell sources compatible with the bioengineered vessel conduit, including genome-edited iPSC-derived vascular cells designed to evade the host immune system post-engraftment.

9:30 AM SB09.05.04

A Fast Gelation, Self-Healing Dynamic Hyaluronic Acid-Based Hydrogel for 3D Cell Encapsulation Melissa Johnson, Sigen A and Wenxin Wang; University College Dublin, Ireland

Dynamic hydrogels for three-dimensional (3D) cell encapsulation that better mimic the dynamic nature of the extracellular matrix have been developed as a result of advances in dynamic chemistry. Dynamic covalent hydrogels have emerged as the most promising biomaterials to overcome the constraints of current conventional hydrogel systems, such as static mechanical properties, irreversible linkages, difficulty in delivery and limited control over biophysical properties (*i.e.* porosity, degradation and strength). To address these limitations, a dynamic covalent hydrogel system based on aldehyde functionalised hyaluronic acid (HA-CHO) and thiolated hyaluronic acid (HA-SH) has been developed with tunable properties. The dynamic covalent chemistry of the thiol-aldehyde addition provides the hydrogel system with highly desirable rapid gelation and self-healing properties. Here we demonstrate that the molar ratio of the two functional groups (thiol and aldehyde) in the hydrogel system has a direct effect on whether a double crosslinked network or a single network forms. In order to improve the hydrogel mechanical properties, a higher thiol functional group ratio was used to increase the crosslinking density as thiol-aldehyde and disulfide crosslinking mechanisms produce a double crosslinked dynamic network. Moreover, the *in vitro* cell viability assessments of both functionalised materials (HA-CHO and HA-SH) show good biocompatibility. Overall, this work introduces the straightforward preparation of a new dynamic hydrogel system that has the potential to be an ideal 3D scaffold for culturing cells due to its excellent biocompatibility, self-healing, and fast gelation properties.

9:45 AM DISCUSSION TIME

9:45 AM BREAK

10:15 AM *SB09.05.06

User-Programmable Hydrogel Biomaterials to Probe and Direct 4D Stem Cell Fate Cole A. DeForest; Univ of Washington, United States

The extracellular matrix directs stem cell function through a complex choreography of biomacromolecular interactions in a tissue-dependent manner. Far from static, this hierarchical milieu of biochemical and biophysical cues presented within the native cellular niche is both spatially complex and ever changing. As these pericellular reconfigurations are vital for tissue morphogenesis, disease regulation, and healing, *in vitro* culture platforms that recapitulate such dynamic environmental phenomena would be invaluable for fundamental studies in stem cell biology, as well as in the eventual

engineering of functional human tissue. In this talk, I will discuss some of our group's recent successes in reversibly modifying both the chemical and physical aspects of synthetic hydrogel-based cell culture platforms with user-defined spatiotemporal control through a collection of bioorthogonal photochemistries. Results will highlight our ability to modulate intricate cellular behavior including stem cell differentiation, protein secretion, and cell-cell interactions in 4D.

10:45 AM SB09.05.07

Bioresorbable Origami Actuators for Intestinal-Retentive Drug Delivery Spencer Matonis, Bozhong Zhuang, Zeynep Temel and Christopher J. Bettinger; Carnegie Mellon University, United States

Introduction: The gastrointestinal (GI) tract provides a convenient, non-invasive access point for medical therapeutics and diagnostics. Ingestible devices have traditionally been limited to transient operation and rigid, inorganic structures, largely due to a lack of robust, biodegradable materials. As shown in this work, genipin-crosslinked gelatin (Gelapin) biopolymers offer a high degree of mechanical tunability and can be fabricated into a diverse range of functional geometries. Leveraging auxetic origami design and laser processing techniques, we demonstrate the potential for edible, self-deployable Gelapin actuators. Such structures can be fabricated into intestinal-retentive interfaces capable of packing up to $\sim 10\text{cm}^2$ of surface area into a standard "000" pill for future bioelectronic and drug-delivery platforms.

Methods: All raw materials were acquired from Millipore-Sigma (Milwaukee, WI, USA) and used as-received unless otherwise noted. For this study, genipin dissolved in ethanol and water was used to crosslink 300-Bloom, Type A porcine gelatin. Approximate crosslinking percentages were calculated based on the occupation of free amine sites using a ninhydrin assay. Varying amounts of glycerol plasticizer were incorporated into solution and the resulting biogels were dehydrated for 24 hours at 70°C . Auxetic origami designs were etched using a Rabbit CO_2 laser (Middletown, Ohio) to create hill and valley crease lines. For initiating the origami folds, a 3D-printed polymer mold was used to compress the etched substrates by 10% from their initial height. Mechanical and viscoelastic properties of biogel and bioplastic samples were evaluated using a tabletop RSA-G2 Solids Analyzer and Discovery HR 20 Rheometer by TA Instruments (New Castle, DE) along with a Instron Universal Testing System (Norwood, MA).

Results: In order to survey the mechanical tunability of gelapin as a function of crosslinking density, a variety of mechanical tests were done both in the gel and plastic state. Storage modulus of the hydrated biogel was measured in the linear viscoelastic region at a frequency of 1Hz as the sample crosslinked in-situ between parallel plates. After 36 hours, the un-crosslinked sample exhibited a storage modulus of 1.95kPa, while the fully crosslinked sample measured at 11.09kPa, an increase of 469%. A similar degree of mechanical tunability was demonstrated via uniaxial tensile tests of Gelapin bioplastic dog bones. These samples were prepared using glycerol as a plasticizer at constant loading (35% mass relative to gelatin) and laser-cut for testing. The resulting stress-strain plots show Young's modulus increasing from 32MPa to 417MPa and strain at failure decreasing from 963% to 108% between 0% and 100% crosslinking, respectively. This baseline mechanical data for Gelapin can be used to describe deployment due to elastic strain energy from a confined pill volume. Similarly, swelling kinetics can be used to identify deployment forces resulting from osmotic actuation in GI fluid. Gelapin biogels showed a nearly exponential decay in swelling capacity as a function of crosslinking with equilibrium mass changes shifting from +55% all the way to -4% (syneresis) over an extended 60hr period.

Conclusion: Here we have described thorough mapping of the Gelapin system's mechanical, rheological and swelling properties. Additionally, Gelapin bioplastics are demonstrated to be compatible with a highly scalable CO_2 etching process for the production of detailed, expandable origami structures. In future research, we aim to leverage this material knowledge in order to construct and evaluate a semi-empirical model for the bimodal deployment of gelapin origami actuators. This model will be applied to optimize geometric and material design parameters of an auxetic origami tube capable of dilating to a diameter of 25mm, while exerting sufficient radial pressure to be retained in the small intestine for prolonged periods of time (>8hrs).

11:00 AM SB09.05.08

Dynamic and Tunable Hydrogel for Extended Co-Delivery of Subunit Influenza Vaccine Olivia Saouaf and Eric A. Appel; Stanford University, United States

The robust material properties of a dynamic, self-healing, and injectable hydrogel make this drug delivery platform ideal for sustained release of subunit vaccine components to enhance the body's immune response to difficult vaccine candidates. Cargo spatial and temporal exposure in the body and immune cell interaction can be coordinated by tuning hydrogel dynamic and structural characteristics. We have designed a supramolecular polymer-nanoparticle (PNP) hydrogel whose composition can be altered to tune slow release of vaccine cargos into the body, enabling a more potent, durable, and high-quality immune response. The PNP hydrogel is formed by dynamic noncovalent interactions between PEG-b-PLA nanoparticles and dodecyl-modified hydroxypropyl methylcellulose polymers. Adjusting hydrogel formulation affects the diffusion and dynamic mesh size of the polymer network, affording precise control over the encapsulation and release of molecular cargo. In this presentation we will discuss the development of PNP materials, the dependence of cargo diffusivity on hydrogel composition, and the influence of cargo release on vaccine efficacy. We will describe the use of PNP hydrogels for sustained delivery of a subunit influenza vaccine comprising components of varying molecular weight and chemical composition. Characterization of cargo diffusivity in PNP networks lends an understanding of the release profiles of vaccine cargoes and a deeper knowledge of the dynamics of polymer-particle interactions in a supramolecular network. We will demonstrate the ability to modulate the material properties of our unique supramolecular hydrogel to produce an effective *in vivo* drug delivery platform.

11:15 AM SB09.05.09

Macroporous Hydrogels for *In Situ* Immune Cell Homing and Modulation Hua Wang; University of Illinois at Urbana Champaign, United States

The past decade has witnessed significant progress in the development of cancer immunotherapy, especially with the success of checkpoint blockades and T cell therapies. However, the low patient response of checkpoint blockades, poor efficacy of T cell therapies against solid tumors, and severe side effects in both have limited their wide application. These issues motivate the development of new immunotherapies with persistent tumor-specific humoral and T cell responses and reduced side effects, which lies in the ability to precisely modulate immune cells, especially dendritic cells (DCs) and T cells. In this presentation, I will introduce the use of immune cell-homing macroporous hydrogels for *in situ* recruitment and modulation of immune cells, and further development of potent immunotherapies.

In the first part, I will talk about DC-homing macroporous hydrogels for immunomodulation. We show that macroporous alginate hydrogels loaded with chemokines (e.g., GM-CSF) and azido-sugar nanoparticles can recruit and metabolically label DCs with azido groups *in situ*, which allows for their subsequent tracking and targeted modulation over time. Azido-labeled DCs were detected in lymph nodes for weeks, and could covalently capture dibenzocyclooctyne (DBCO)-bearing antigens and adjuvants via efficient click chemistry for improved antigen-specific CD8^+ T cell responses and antitumor efficacy against lymphoma and melanoma. We also show that azido-labeling of DCs allowed for *in vitro* and *in vivo* conjugation of DBCO-modified cytokines, including DBCO-IL-15/IL-15R α , to improve priming of antigen-specific CD8^+ T cells. The cytokine conjugation approach enables continuous modulation of T cells during the T cell priming process and thus can improve the antigen-specific CD8^+ T cell response, which could bring therapeutic benefits for treating cancer, autoimmune disorders, and other immune-related diseases.

In the second part, I will introduce an injectable T cell-responsive macroporous hydrogel that enables *in situ* activation and expansion of T cells. The

macroporous gel is composed of a crosslinked polymeric network with macropores (~150 μm) that are large enough to home T cells. In the presence of T cells that can gradually disrupt the gel network surrounding the macropores, activation cues trapped in the network can be released for *in situ* activation and expansion of T cells. This T cell-responsive macroporous gel enables the expansion of functional T cells *in vitro* and *in vivo*, is stable over weeks upon subcutaneous injection, and can result in enhanced CD8⁺ T cell response and antitumor efficacy. We further showed that the T cell-responsive macroporous gel enables *in situ* homing and expansion of adoptively transferred T cells, for improving the antitumor efficacy of conventional T cell therapies. This injectable, T cell-responsive macroporous gel provides an unprecedented platform for *in vivo* expansion of engineered T cells in a precisely controlled manner, for timely and more effective treatment of diseases.

11:30 AM SB09.05.10

Double Layer of Fibronectin-collagen Coating of poly(acrylamide-co-acrylic acid) Hydrogel Particles to Modulate Cell Migration Alfonso Pepe, Duy T. Nguyen, Diego I. Pedro, Griffin Golde and W. Gregory Sawyer; University of Florida, United States

The use of biomolecules as biomaterial coatings is recognized as a promising approach to modulate the biological response of different cells. Collagen (COL) and fibronectin (FIB) are the two most common extracellular matrix proteins (ECM) that have been widely used for the studies of cell adhesion and migration. However, the mechanistic difference between each protein or their synergy on cell migration is poorly understood. In this work, we investigated migratory behaviors of cancer spheroid models in 3-dimension (3D) as a function of extracellular matrix composition, cell adhesion, and mechanical properties of the medium.

In this work, an ensemble of liquid-like solid (LLS) conjugated with collagen type-I and fibronectin was developed. In brief, acrylamide monomer (AAM) 4 %w/v, bis-acrylamide (BIS) 0.3 %w/v and acrylic acid (AA) 1 %w/v hydrogel was prepared via free radical polymerization in pH 5.5 MES buffer (0.7 M). The polymerized hydrogel was mechanically disaggregated using a series of stainless-steel meshes of a selected size to create microgel particles. The microgel particle suspension was sorted and characterized with a mean of 80 μm and a standard deviation of 20 μm . The particles were activated in a solution of EDC and NHS. The activated microgel particles were conjugated with collagen I and fibronectin solutions in PBS, subsequently quenched with ethanolamine. The collagen modified microgels were co-conjugated with fibronectin by incubation with a fibronectin-PBS solution. The LLS was equilibrated with cell culture media for 1 h prior to the cell experiments.

Collagen and fibronectin were successfully detected on the LLS surface by immunofluorescence microscopy. The signal intensity profile shows strong correlation with protein concentration and cell adhesion. The results revealed that the intermolecular forces between the fibronectin and the collagen are sufficient to keep the fibronectin onto the collagen-coated particles. Furthermore, we reported a remarkable difference in invasive phenotype of breast cancer spheroids in 3D between the COL-LLS, FIB-LLS, and their respective compositions. The collagen-fibronectin (COL-FIB) complex, upon conjugated on to the LLS particles, facilitated stronger cell adhesion and spreading as measured with a bio-tribometer. A 3D invasion assay also demonstrated faster and more active migrators at the peripheral region of the tumor spheroids when cultured in COB-FIB-LLS. The cancer cells with invasive phenotype rapidly migrate deep into the 3D LLS matrix exhibiting stark contrast with COL-LLS or FIB-LLS alone where cells spread more gradually. The experiment also revealed a relationship between cell adhesion and migration velocity. It has been reported that mature adhesion complexes lead to reduced velocity. In our study, we demonstrated that the effect is abrogated by tuning the mechanical properties of the LLS microgels and protein concentrations. The results of this study revealed an underlying mechanism of COL-FIB complex that could enable more sufficient cell attachment and migration. An understanding on cell migratory behaviors in 3D within a well-designed and controlled ECM composition would enable much valuable insights in basic research.

SESSION SB09.06: Shape Morphing Hydrogels
Session Chairs: Ryan Hayward and Yuhang Hu
Tuesday Afternoon, November 29, 2022
Hynes, Level 3, Room 310

1:30 PM *SB09.06.01

Photochemically-Driven Shaping of Thin Hydrogel Sheets Containing Light-Sensitive Supramolecular Complexes Ryan C. Hayward; University of Colorado Boulder, United States

The ability to precisely define the shape or motion of responsive polymers has wide ranging applications from soft robotics to biomaterials. Among the available stimuli to select from, light represents a simple, remote method of prescribing shape change with a high degree of spatial and temporal control. Our group, and others, have previously leveraged photothermal effects in temperature-sensitive hydrogels to drive shape change, self-assembly, and collective motion. However, photothermally addressable materials require constant illumination to maintain a shape change and suffer from decreased resolution due to thermal broadening. These limitations have stimulated work by numerous groups on photochemically-responsive hydrogels. While azobenzene and related photoswitches offer attractive properties including highly tunable lifetimes and excellent photostability, historically their modest change in polarity upon photoswitching has limited the light-induced response that can be achieved. To enhance this effect, our group has studied photochemically driven shape changes in thin hydrogel disks using host-guest interactions between azobenzene and cyclodextrin. Patterned illumination of the disks with ultraviolet light results in localized deswelling, giving rise to shapes with either positive or negative Gaussian curvature. The reversibility of the host-guest complexation allowed for the shapes to be erased with visible light and repatterned an arbitrary number of times. In addition, we demonstrate azobenzene derivatives that enable both swelling and deswelling of hydrogels entirely with visible light, allowing for increased penetration depth and improving compatibility with materials for cell and tissue culture.

2:00 PM *SB09.06.02

On-Chip Formation of Deformable Hydrogel 3D Architectures via Swelling-Driven Buckling Riku Takahashi¹, Hiroki Miyazako², Aya Tanaka¹ and Masumi Yamaguchi¹; ¹NTT Basic Research Laboratories and Bio-Medical Informatics Research Center, Japan; ²The University of Tokyo, Japan

Technology to reproduce the microstructure (channels, folds, etc.) and stimulating environment (mechanical stimuli, chemical stimuli, etc.) of living organisms *in vitro* is crucial for the fabrication of an organ-on-a-chip capable of advanced cell culture. In particular, if such a biological environment can be constructed on a solid substrate, including a sensor substrate, it can be developed as an organ-on-a-chip platform with potential applications in disease modeling and drug discovery through various types of data acquisition. Hydrogel is the best candidate as a base material because of its excellent permeability, biocompatibility, and ability to mimic the biological environment at the material level. On the other hand, the unique feature of gels, swelling, causes a volume mismatch between them and solid substrates, making it difficult to fabricate hybrid devices due to delamination or fracture. In this talk, we introduce "buckle delamination", a method to fabricate three-dimensional (3D) architectures of hydrogel films on a chip by using swelling

as a driving force. This phenomenon is a type of instability induced by the mismatch between the volume expansion ratio of the thin film and the supporting substrate. This mismatch generates compressive stress, which causes part of the thin film to delaminate and buckle from the substrate, forming a hollow 3D architecture. First, we applied this phenomenon to hydrogel films and proposed a method to precisely control the architecture and position through microfabrication techniques. Using polyacrylamide gel and glass substrates as model materials, we have shown that by chemically controlling the adhesion pattern between the two materials, buckle delamination can be induced at arbitrary locations and continuous channel-like structures can be fabricated. Furthermore, by tuning the physical parameters of the hydrogel, the shape of the 3D architecture can be controlled based on patterns of instability. We then demonstrated that the channel-like architectures can work as a fluidic device. The device is based on a soft and flexible hydrogel film, which can passively expand and contract in the radial direction, like a blood vessel, in response to fluid flow. We have also demonstrated that the permeability and biocompatibility of this device allows for long-term culture of cells and the formation of vascular-like tissue in the channel. Finally, we will show that the architecture formation by "buckle delamination" is a processing method based on a universal physical phenomenon and that it can be applied to various types of swellable hydrogel. Notably, by using a stimulus-responsive gel film, the channel architecture formed on a solid substrate can be deformed quickly, largely, and bio-mimetically like an organ (e.g., peristalsis in the intestinal tract) in response to stimulus patterns. We believe that these results will be useful for designing devices that reproduce the dynamic in vivo environment on solid substrates, and may also contribute to the creation of organ-on-a-chip platforms and soft biomimetic robots.

2:30 PM SB09.06.03

Programmable Auxeticity in Hydrogel Metamaterials via Shape-Morphing Unit Cells [Oliver Skarsetz](#)¹, [Viacheslav Slesarenko](#)² and [Andreas Walther](#)^{1,2}; ¹Johannes Gutenberg University of Mainz, Germany; ²University of Freiburg, Germany

Mechanical metamaterials recruit unique mechanical behavior that is unavailable in bulk materials from a periodic unit cell structure with a specific geometry. However, such metamaterials can typically not be reconfigured once manufactured. Herein, we introduce shape morphing of a hydrogel metamaterial via spatio-selective integration of responsive actuating elements to reconfigure the mesoscale unit cell geometry to reach programmable auxeticity on the macroscale. Via thermal control, the unit cell angle of a honeycomb structure can be precisely programmed from 68° to 107°. This results in negative, zero or positive Poisson's ratio under applied tensile strain. This concept of shape-morphing hydrogel metamaterials via the addition of actuating struts into otherwise passive architectures offers a new strategy for reconfigurable metamaterials and extends applications of hydrogels in general. It can be readily extended to other architectures and may find applications in mechanical computing as well as soft robotics.

2:45 PM SB09.06.04

Preliminary Reconfigurable Nerve-Artery Microphysiological System for 3D Cell Culture and Immunostaining [Selina Banerjee](#), [Bryan Schellberg](#), [Dylan Miller](#) and [Ryan Koppes](#); Northeastern University, United States

Tissue engineered microphysiological systems (MPS), also known as organs-on-chips, have recently emerged as a more patient-relevant and cost-effective alternative for disease modeling and drug discovery compared to traditional cell culture and animal models. Despite their increased functional relevance, most current MPS lack capabilities for analysis of individual components or layers through biological assays. Furthermore, current MPS rarely use 3D cell cultures to accurately mimic biological structures.

Here, we present a preliminary nerve-artery MPS. This novel MPS includes three removable layers: a three-chamber glass-bottom 3D cell culture layer which allows the contact of different cell types with GelPins (previously published by our lab) [1], with the middle 3D chamber in contact with a 2D cell culture layer through a semi-permeable membrane, and a removable media reservoir at the top of the assembly. The MPS also includes separate pipetting access ports to each chamber, which allows the specific addition and removal of cell culture medium, treatments, or reagents. This design allows specific endpoint analyses for each chamber, including immunostaining for the 3D hydrogel layer, and western blotting, flow cytometry, PCR, and immunostaining for the 2D layer. Furthermore, the glass bottom of the 3D hydrogel layer allows for high-resolution light and fluorescent microscopy of both the 2D and 3D layers, with the layers assembled or separated.

The manufacturing and assembly of the MPS include the use of stereolithography (SLA) 3D printing, laser cutting, and layer-by-layer assembly (as previously published by our lab) [2]. First, an SLA-printed clear resin piece is attached to a glass coverslip to form the bottom of the assembly. To form the three-chamber hydrogel cell culture layer, a Viton rubber gasket and modified GelPin [1] made of polyethylene terephthalate (PET) are laser cut and assembled with 3M 966 tape, and attached to the glass coverslip. Above the 3D cell culture layer is the 2D cell culture layer, which includes a laser-cut semi-permeable PET membrane. Above this 2D layer is the removable media reservoir layer, which includes a laser-cut Viton rubber gasket attached to a laser-cut polymethyl methacrylate (PMMA) piece. The 3D layer, 2D layer, and media reservoir are held together using flat head screws and nuts. Together, the three layers form a biomimetic structure to simultaneously model a nerve and artery: neurons can be cultured in the outer 3D hydrogel chambers to form the nerve component, and smooth muscle cells and endothelial cells can be cultured in the middle hydrogel chamber and the single-chamber 2D layer, respectively, to form the arterial component. To our knowledge, this design is the only nerve-artery model that includes 3D cell culture or an MPS.

As a proof of concept, F11 (mouse neuroblastoma - rat dorsal root ganglion) cells were encapsulated in 5% gelatin methacrylate (GelMA) hydrogel and seeded in the outer hydrogel chambers in the 3D layer of the MPS. The encapsulated cells were cultured in differentiation media for 2 weeks, fixed, immunostained for NeuN and actin, and imaged with an inverted fluorescent microscope. This study demonstrates that the MPS can be successfully used for longer-term 3D cell culture, immunostaining, and imaging experiments. Furthermore, the simple fabrication methods used to assemble the MPS can rapidly be modified to model other tissues or include other endpoint analyses, flow channels, or probes. Overall, this novel MPS has shown promising results for use as a nerve-artery model, and its applications and uses can be expanded with further research and development.

[1] Soucy et al., 2020. *Advanced Biosystems*. <https://doi.org/10.1002/adbi.202000133>

[2] Holic et al., 2020. *ACS Biomaterials Science & Engineering*. <https://doi.org/10.1021/acsbomaterials.0c00190>

3:00 PM BREAK

3:30 PM *SB09.07.01

Hydrogels of Arrested Phase Separation Zhigang Suo; Harvard University, United States

We have developed a process that self-assembles a nanocomposite using a hydrogel-forming polymer and a glass-forming polymer. The process separates the polymers into a hydrogel phase and a glass phase. The two phases arrest at the nanoscale and are bicontinuous. Submerged in water, the nanocomposite maintains the structure and resists further swelling. We demonstrate the process using commercial polymers, achieving high water content, as well as load-bearing capacity comparable to that of polyethylene. During the process, a rubbery stage exists, enabling us to fabricate objects of complex shapes and fine features. We conduct further experiments to discuss likely molecular origins of arrested phase separation, swell resistance, and ductility. Potential applications of the nanocomposites include artificial tissues, high-pressure filters, low-friction coatings, and solid electrolytes. This talk is prepared on the basis of a paper co-authored with G. Zhang, J. Kim, and S. Hassan.

4:00 PM *SB09.07.02

Cavitating Hydrogels—From Molecular Connections to Buried Interfaces Alfred J. Crosby; Univ of Massachusetts, United States

Failure, or fracture, remains one of the most important, yet most challenging, topics in materials science. This challenge is especially true for soft materials, such as hydrogels and biological tissues. Understanding failure in these systems is critical for developing important technologies, from robust prosthetic materials to protective gear for mitigating debilitating injuries. However, the ultra-soft nature of these materials makes quantifying failure processes difficult. Here, we present two recent advances: 1) understanding how cavitation-based deformations lead to either reversible or irreversible damage in hydrogel materials, and 2) new cavitation-based methods for measuring materials properties of buried interfaces between ultra-soft hydrogel materials. For the first topic, we describe the results of a multi-university, multi-disciplinary study that combined the use of precisely-defined polymer networks, molecular dynamic simulations, and classical and new characterization methods to develop and validate of theoretical relationships between molecular network architecture and macroscale cavitation and fracture processes. For the second topic, we are motivated by the critical role that interfacial properties play in determining the failure of biological tissues, as well as ultra-soft materials that are designed to interface with these tissues. We introduce methods that provide straightforward, quantitative measurements of the elasto-adhesion length scale for ultra-soft hydrogel interfaces. These methods provide new means for characterizing interfacial properties within living systems, and they have added benefits of offering pathways for high-throughput characterization of hydrogel adhesion properties, in general. Collectively, the results and discussion presented here are important for enhancing our fundamental understanding of ultra-soft hydrogel materials and the mechanisms that control their failure across a range of size scales.

4:30 PM DISCUSSION TIME

4:45 PM SB09.07.04

Molecular Dynamics (MD) Simulations of Soil-Strengthening Nanocomposite-Polyelectrolyte Hydrogels Jerry Zhang¹, Vincent Wang², Anthony Zhu³, Arkajyoti Sinha⁴, Shoumik Saha⁵, Dilip Gersappe³ and Miriam Rafailovich⁵; ¹Minnetonka Senior High School, United States; ²Irvington High School, United States; ³Barrington High School, United States; ⁴Lexington High School, United States; ⁵Stony Brook University, The State University of New York, United States

Nanocomposite-polyelectrolyte hydrogels are gels formed from a mixture of charged polymer chains and nanofillers. They can absorb large amounts of water, mimic biological fluids/tissues, and more recently, they can potentially serve as a sustainable alternative to concrete for soil strengthening purposes. Despite the large number of studies on polyelectrolytes and their adsorption onto oppositely charged particles, little is known about the mechanism of network formation and structure of such charged hydrogels. Thus, we use molecular dynamics (MD) simulations to investigate the effect of charge on the gelation of our system and related properties including viscosity, network formation, cluster geometry, and polymer adsorption onto filler particles.

We use a coarse-grained approach, where nanofillers are modeled as rigid bodies of disk-like shapes. Polyelectrolyte chains are modeled as beads connected by finitely extensible nonlinear elastic (FENE) springs. All pairwise interactions are defined by the truncated and shifted 12-6 Lennard-Jones (LJ) potential. Systems also included uncharged solvent particles and free-floating univalent counterions for both nanofillers and polymer chains to ensure electroneutrality.

We vary the charge of both the filler particles and the polyelectrolyte beads independently. Upon reaching equilibrium, we use the Green-Kubo relation to calculate viscosity by integrating the stress-autocorrelation function (SAF), the step-strain test (SST) to determine the mechanical stability, the radial distribution function (RDF) of the polymers with respect to the fillers in order to measure adsorption, and finally, a network clustering algorithm (NCA) to test for cluster formation. If clustering occurs, we quantify cluster geometry by calculating the gyration tensor, allowing us to determine asphericity, acylindricity, and relative shape anisotropy.

Our initial results for systems with charge magnitudes of $q=1$ for both the polymer and filler beads show both the SAF and SST decaying to zero, implying gelation was not induced, while the RDF and NCA suggested that adsorption and clustering, respectively, also did not occur. We did observe increasing viscosity with charge magnitude, suggesting that larger charge magnitudes could induce gelation. Results also show that the cluster geometry of nanofillers is an important determinant of the final properties of the hydrogel where the assembly is mediated by polymer and nanofiller net charges. Our work will be able to determine structural information and conditions for hydrogel design. They will also enable experimental teams to manufacture and test nanocomposite hydrogels with the specific charge properties that our models predicted would exhibit enhanced behaviors.

We would like to thank the Morin Charitable Trust for funding this project as well as Prof. Miriam Rafailovich and the Garcia Research Program for making this work possible. We would also like to acknowledge the mentorship of Shoumik Saha and Prof. Dilip Gersappe for their guidance and support. All simulations were run on the Stony Brook University SeaWulf supercomputer.

SESSION SB09.08: Mechanics and Physics of Hydrogels II

Session Chairs: Yuhang Hu and Sarah Wu

Wednesday Morning, November 30, 2022

Hynes, Level 3, Room 310

8:45 AM SB09.08.01

Mucin Networks—A Mechanical Fuse that Protects Epithelial Cell Surfaces During Shear Diego I. Pedro, Alfonso Pepe, Duy T. Nguyen and W.

Gregory Sawyer; University of Florida, United States

Mucin dysfunction is implicated in many infectious and inflammatory diseases of the respiratory tract, the digestive tract, the reproductive tract, cancer, and the ocular surfaces. All moist epithelial surfaces are protected by a secreted layer of mucus, which is a low yield strength, high-water content, network of mucin glycoproteins. As a part of the innate immune system, these mucin networks provide hydration, protection, and help to exclude pathogens providing a reservoir for antimicrobial molecules. Although widely described as a “slippery” barrier on epithelial surfaces, the mechanics and self-healing properties of mucin network dynamics and their role in epithelial cell friction and shear are poorly understood. Experiments on self-mated epithelial cell surfaces at physiological contact pressures reveal shear stress limits of a mucin network, made of purified MUC2 and membrane mucins including MUC1 and MUC4¹. Micro-rheological measurements using magnetic tweezers provide insights into the network rheology, and molecular biology techniques reveal thresholds for the production of proinflammatory cytokines and apoptosis.

In this work, hemi-spherical polyacrylamide hydrogel probes with a 2 mm radius of curvature and a shell thickness of 250 μm were used to maintain constant contact pressures ~ 1 kPa across the epithelial cell interfaces. The poly-acrylamide gels (water content $\sim 87.5\%$) were equilibrated in Keratinocyte Growth Media (KGM-Gold™). Bioconjugation of polyacrylamide with collagen type-I (0.4 mg/ml) was performed using 1mM Sulfo-SANPAH². Glass-bottomed culture-dishes were coated with fibronectin for cell adhesion. Human Corneal Epithelial Cells (hTCEpi) were cultured for ~ 2 days to form a monolayer with $>90\%$ confluency on both the probes and the culture dishes. In situ biotribology experiments were performed at 37 ± 0.2 °C, 5% CO₂, and $\sim 100\%$ relative humidity. A normal load of 400 μN was applied between the two surfaces. Friction force measurements were recorded on a custom fabricated biotribometer³ with a 3 mm stroke length, and a sliding speed of 1 mm/s. Contact pressure was calculated by from the measured contact area and applied force. All microscopy was performed in situ on a Nikon A1R confocal microscope. Purified MUC2 at 5 wt% in KGM-Gold™ was continuously flowed to the sample to induce transport conditions reducing inflammation and cell death. The magnetic tweezers were used for micro-rheology following the design of Lammerding⁴ with 6 μm superparamagnetic fluorescent bead.

Experiments with the reciprocal sliding of two hTCEpi epithelial surfaces revealed the upregulation and production of proinflammatory cytokines at shear stresses ≥ 40 Pa, and almost complete apoptosis and cell removal at 100 Pa. Experiments on self-mated epithelial cells showed friction coefficients that monotonically increased to $\mu > 0.2$ over 300 cycles without the addition of soluble MUC2. A 5 %w addition of MUC2 maintained low shear stress (~ 40 Pa) for over 300 cycles, and enhanced mucin protection. When transport conditions were induced, damage rate was significantly reduced, suggesting faster mucin-gel-self-healing phenomenon under this condition emphasizing the role of the self-healing time for appropriate mucin protection under shear. Magnetic-tweezers with microbeads revealed a definitive yield-stress and elasticity of the mucin network consistent with the measured shear stresses during sliding.

In this model, the fragile mucin network reduced shear stress, friction, and friction-induced damage, and it was found to self-heal faster under transport conditions.

¹Pedro DI, et al. *Tribol Lett* 69, 155 (2021) ²Wang YL and Pelham RJ Jr. (1998). *Methods Enzymol.* 298:489-496 ³Uruña JM, et al. *Tribol Lett* 66, 141 (2018) ⁴Rich JP, et al. (2011). *Soft Matter* 7:9933-9943

9:00 AM DISCUSSION TIME

9:15 AM SB09.08.03

Dynamic Covalent Crosslinking Strategies for Tunable Hydrogel Networks Rebekah Tan, Joey H. Wong, Xian Jun Loh and Kun Xue; Institute of Materials Research and Engineering, Singapore

Dynamic covalent systems are interesting as they are composed of bonds which show covalent character, but become reversible under environmental stimuli such as temperature or pH [1,2]. Boronic acids in particular can bind with cis-1,2 or cis-1,3 diols to form into boronate esters, and this is affected by pH and other diols [3,4]. As a building block in supramolecular engineering, boronate crosslinks can be used to dynamically crosslink onto polymers to generate hydrogel networks with tunable states and properties.

Hydrogel printing has the contrasting needs of a highly processable and printable hydrogel, and a higher mechanical strength post deposition [5]. To expand the repertoire of materials suitable for hydrogel patterning, we report versatile polymer networks comprising of polyvinyl alcohol crosslinked with PEG-diboronates crosslinkers at low ratios [6]. These pre-gel networks are highly processable and extendable: they can be pulled up into thin strands and used for patterning of thin lines, and show shear thickening at higher shear rates. The pre-gels can be easily converted into a hydrogel state by pH adjustment and show clear antibacterial effects. Valuably, the pre-gels can be integrated into a 3D printing setup to print programmable lines and shapes and subsequently converted into patterned hydrogels. This study demonstrates that dynamic boronate networks can switch between a processable state and a mechanically stronger state and could offer alternate strategies and possibilities for hydrogel patterning applications.

Due to its relative stability and reprocessability, dynamic covalent crosslinking of supramolecular units onto polymer chains is an alternative way to fabricate supramolecularly crosslinked polymers. We functionalised the PVA polymer backbone with the carboxylate functionality through boronate crosslinking. This enabled the formation of a suprapolymeric conjugate with dynamically attached carboxylate moieties, which could subsequently form into supramolecular crosslinked hydrogels via ionic and electrostatic crosslinks. When crosslinked by calcium, a stronger hydrogel was formed which could not self-heal. When the polyelectrolyte branched polyethylenimine (PEI) was added, a stable hydrogel was formed with antibacterial properties.

In summary, we have shown that dynamic covalent boronate crosslinking can generate pH-switchable hydrogel states for printing applications or can be used to construct a suprapolymeric conjugate in combination with secondary supramolecular interactions. Dynamic covalent crosslinks can act as building blocks for the fabrication of functional yet responsive hydrogel materials.

References

1. Chakma, P.; Konkolewicz, D., *Dynamic Covalent Bonds in Polymeric Materials*. *Angewandte Chemie International Edition* 2019, 58 (29), 9682-9695.
2. Xue, K., Liow, S. S., ..., & Loh, X. J. (2018). A Recent Perspective on Noncovalently Formed Polymeric Hydrogels. *The Chemical Record*, 18(10), 1517-1529. doi:<https://doi.org/10.1002/tcr.201800015>
3. Dong, Y., Wang, W., Veisheh, O., Appel, E. A., Xue, K., ... Anderson, D. G. (2016). Injectable and Glucose-Responsive Hydrogels Based on Boronic Acid-Glucose Complexation. *Langmuir*, 32(34), 8743-8747. doi:10.1021/acs.langmuir.5b04755
4. Brooks, W. L. A., & Sumerlin, B. S. (2016). Synthesis and Applications of Boronic Acid-Containing Polymers: From Materials to Medicine. *Chemical Reviews*, 116(3), 1375-1397. doi:10.1021/acs.chemrev.5b00300
5. Lee, S. C., et al. (2020). "Physical and Chemical Factors Influencing the Printability of Hydrogel-based Extrusion Bioinks." *Chemical Reviews* 120(19): 10834-10886.
6. Tan, R., ..., Xue, K. * (accepted). "Versatile and extendable boronate-based tunable hydrogel networks for patterning applications." DOI: <https://doi.org/10.1021/acsspm.2c00614>. *- corresponding author

9:30 AM SB09.08.04

Degradation Controls Spreading and Interfacial Coverage of Nanogels at Soft Interfaces—Insights from Mesoscale Modeling Vaibhav A. Palkar¹, Devanshu Thakar² and Olga Kuksenok¹; ¹Clemson University, United States; ²Indian Institute of Technology Gandhinagar, India

Adsorption of nanogel and microgel particles onto liquid-liquid interfaces finds several potential applications. These particles are known to spread over the interface adopting shapes depending on the original size, shape, and crosslink density of the particles. In this work, we study controlled degradation of nanogels upon application of an external stimulus to dynamically control the topography of soft nanostructured interfaces. We use the Dissipative Particle Dynamics (DPD) simulation approach, along with an adapted form of the modified Segmental Repulsive Potential (mSRP) to characterize degradation and spreading of nanogels over the interface. To establish a baseline, we first simulate degradation of individual nanogel particles suspended in a solvent and track the evolution of particle size and shape via the gyration tensor up to the reverse gel point, where nanogel particles completely dissolve in the solvent. We show that the nature of the polymer-solvent interaction significantly affects the evolution of shape during degradation. Further, we simulate the adsorption and spreading of these nanogels onto the interface between two liquids and observe that this process is affected significantly by the strength of the repulsion between the two liquids. We compare the size and shape evolution of nanogels degrading at the interface with those degrading in the bulk and measure an extent of spreading during degradation. Our results indicate that controlled degradation of the nanogels results in an enhanced extent of interfacial spreading and provides a way to control interface topography at the nanoscale.

9:45 AM BREAK

SESSION SB09.09: Hydorgel Actuator, Sensor and Machines I
Session Chairs: Yuhang Hu and Sarah Wu
Wednesday Morning, November 30, 2022
Hynes, Level 3, Room 310

10:15 AM SB09.09.01

Three-Dimensional Stiffness Control of Double-Network Hydrogels by Bi-Ag Redox Reaction Ethan Frey¹, SooiK Im¹, Sam Cheeseman², Jinwoo Ma¹, Jan Genzer¹, Michael Dickey¹ and Vi Khanh Truong^{2,3}; ¹North Carolina State University, United States; ²Royal Melbourne Institute of Technology, Australia; ³Flinders University, Australia

Connecting soft and rigid materials is crucial for numerous applications, including synthetic tendons and stretchable electronics. However, large gradients in stiffness can delaminate interfaces under strain. Gradual stiffness gradients allow stress to be distributed evenly to maintain adhesion. Previous work on stiffness gradients has been limited to stiffness control in only one dimension and often lacked precision. This work utilizes redox reactions in double network hydrogels to modulate the stiffness in three dimensions and form gradual stiffness gradients. Polyacrylamide-alginate hydrogels containing bismuth particles were reacted with silver nitrate to form silver particles and bismuth ions, which crosslinked the carboxylic groups of the alginate. Stiffness gradients were created by changing the exposure time to silver nitrate solution. This gradient in dynamic modulus was mapped by cutting the hydrogels into pieces and measuring each individually with a rheometer. Digital image correlation (DIC) analysis was used to create a 2-D map of strain level, confirming the gradient in stiffness and revealing that stiffness only increased at the locations of the bismuth particles. Therefore, stiffness gradients were additionally created by changing the particle distribution. This was done by altering the viscosity of the precursor solution and curing time to allow the particles to partially settle during curing. The resulting hydrogels actuated during the redox reaction due to localized stress on one side of the hydrogel. Lastly, the hydrogels exhibited excellent antibacterial properties due to the presence of bismuth and silver, both potent antibacterial agents in their nanoparticle and ionic form. Zone of inhibition testing and a colony-forming unit evaluation was performed to analyze these properties. In summary, this system allows for stiffness to be controlled in three dimensions, down to the size of individual bismuth particles. Therefore, these Bi-Ag double network hydrogels offer a solution for the fluid integration of rigid and soft materials, and their antibacterial properties could be helpful in many biomedical applications.

10:30 AM SB09.09.02

Autonomous Soft Robotics Using Chemical Fuels Giorgio Fusi¹, Daniele Del Giudice², Stefano Di Stefano² and Andreas Walther^{1,3}; ¹Johannes Gutenberg-Universität Mainz, Germany; ²Università degli studi di Roma "La Sapienza", Italy; ³Cluster of Excellence livMatS @ FIT - Freiburg Center for Interactive Materials and Bioinspired Technologies, University of Freiburg, Germany

Hydrogel actuators generate mechanical motion through volume changes in response to stimuli as varied as pH, heat, light or magnetic fields. Methods of controlling pH have primarily focused on sequential addition of reagents to alternately raise and lower pH, use of photoacids, or multi-component enzymatic reaction networks. We demonstrate the coupling of a one-molecule dissipative reaction network to a pH-responsive hydrogel actuator, leading to transient motion. Exploiting the rapid proton release upon addition of fuel, followed by spontaneous decarboxylation and proton consumption by the resulting intermediate species, transient pH drops in the timescale of minutes to days can be achieved. Matching reaction cycle timescale to the rate of gel (de)swelling results in an autonomous system where fully reversible contraction of gel actuators and bending of bilayer devices is obtained. Our results illustrate the use of a tunable chemical reaction network to control centimeter-scale hydrogel actuators and exploit their motion to generate mechanical force. Due to its simplicity and cyclability derived from its resistance to waste accumulation, this method of control is likely to prove attractive for a wide variety of pH-responsive hydrogel systems, and can be readily integrated into larger reaction systems and more complex device architectures displaying chemomechanical feedback.

10:45 AM SB09.09.03

Stimuli-Responsive Ion-Diffusive Ultrasoft Hydrogel for Zero-Powered Bioelectronics Sungwon Jung¹, Sangmin Lee² and Jinkee Hong¹; ¹Yonsei University, Korea (the Republic of); ²Chung-ang University, Korea (the Republic of)

Bioelectronics are emerging devices applied for human that are a promising solution for self-care and smart healthcare. Among them, non-invasive bioelectronics such as electrical stimulation patches are considered as the realistic and feasible medical applications for minimizing anxiety in patients with low immune responses or toxicity problems. Accordingly, multifunctional soft materials, for instances, skin-adhesive, conductive hydrogel for application to non-invasive bioelectronics are essential. Moreover, the number of self-powered system without using extra power source for bioelectronics also has been reported, however, there are still have limitations that require specific movement or environment.

Here in, we introduce a 1) stimuli-responsive ion-diffusive hydrogel (IDH) with optimized softness, skin-adhesive for bioelectronics and 2) a system capable of tissue vitalization by accumulating energy generated and lost spontaneously from humans contact with in daily life using. The IDH was synthesized by using polyacrylamide (PAAM), oxidized hyaluronic acid (OHA) and PEDOT:PSS with schiff-base and hydrogen bonding-based triple

network. By tuning the oxidation rate of OHA, optimized the mechanical property of IDH which has similar elastic modulus with human skin (~ 19.24 kPa) and shear adhesion strength (~ 57 J/m²) which is optimized mechanical properties for patients comfortability. Furthermore, the IDH has electrical stimuli-responsive ion loading/releasing properties because of reduction/oxidation of PEDOT:PSS which is capable for iontophoretic drug releasing bioelectronics. The IDH shows higher ion loading efficiency inside to IDH when DC electric field is applied, and also shows higher ion releasing and penetration to porcine skin when the opposite DC electric field is applied.

The zero-powered system, called body-mediated energy loss conversion (BELC), is structurally designed system of stacked conductors and insulators. The BELC can convert energy loss from electronic devices and physical activity to usable energy via transfer through the human body as a medium. By applying IDH and the BELC system, body-mediated bioelectronics (BMB) patch was designed and fabricated. The BMB patch can internally concentrate electric field and various outputs during human activity (walking, running, typing on laptop, etc.) was measured (14.3 mV/mm of electric field output during running). Furthermore, iontophoretic ion-penetration through porcine skin during human activity was also investigated. The proposed multifunctional IDH is believed to be widely used for non-invasive bioelectronics and also BMB is expected to overcome the drawbacks of conventional bioelectronics and can pave the path to zero-powered bioelectronics with permanent operation.

11:00 AM SB09.09.04

Strong and Fast Hydrogel-Based Actuators by Electroosmotic Turgor Pressure Hyeonuk Na¹, Yong-Woo Kang¹, [Chang Seo Park](#)¹, Sohyun Jung², Ho-Young Kim³ and Jeong-Yun Sun^{4,5}; ¹Multi-Functional Soft Materials Laboratory Department of Materials Science and Engineering, Korea (the Republic of); ²SOFT FOUNDRY, Seoul National University, Korea (the Republic of); ³Department of Mechanical Engineering, Seoul National University, Korea (the Republic of); ⁴Department of Material Science and Engineering, Seoul National University, Korea (the Republic of); ⁵Research Institute of Advanced Materials (RIAM), Seoul National University, Korea (the Republic of)

Hydrogels are promising as materials for soft actuators because of qualities such as softness, transparency, and responsiveness to stimuli. However, weak and slow actuations remain challenging as a result of low modulus and osmosis-driven slow water diffusion, respectively. We used turgor pressure and electroosmosis to realize a strong and fast hydrogel-based actuator. A turgor actuator fabricated with a gel confined by a selectively permeable membrane can retain a high osmotic pressure that drives gel swelling; thus, our actuator exerts large stress (0.73 megapascals (MPa) in 96 minutes (min)) with a 1.16 cubic centimeters of hydrogel. With the accelerated water transport caused by electroosmosis, the gel swells rapidly, enhancing the actuation speed (0.79 MPa in 9 min). Our strategies enable a soft hydrogel to break a brick and construct underwater structures within a few minutes.

11:15 AM SB09.09.05

Strain Sensor with Self-Healing Ability Using a Dry-Resistant Hydrogel-Based Conductive Composite [Jungyoon Seo](#), Taehoon Hwang and Hwasung Lee; Hanyang University, Korea (the Republic of)

Self-healing and conductive hydrogels had attracted great attention for applications as electronic skin and flexible strain sensors due to their excellent flexibility and strain-sensitivity. In particular, Poly(vinyl alcohol)(PVA)-based hydrogels were widely used for devices that require self-healing ability. However, traditional PVA-based hydrogels had limited long-term use because it is difficult to retain water in cold or hot environments. Here, We increased anti-freezing and anti-drying performance by introducing glycerol, BTCA(1,2,3,4-Butanetetracarboxylic acid), and SPA(sodium polyacrylate), thereby improving the safety of long-term use. Then, carbon nanotubes(CNTs) were introduced into the hydrogel, which assign conductivity to the hydrogel. The conductive hydrogel reliable recovery performance and superior self-healing ability without deterioration in electrical performance. The hydrogels were simply made of strain sensors and detected some real skin epidermis movements such as finger bending, wrist bending, facial movements changes. This work had the potential to be used to fabricate conductive, anti-drying/freezing, stretchable and strain-sensitive device applications.

SESSION SB09.10: Hydrogel Actuator, Sensor and Machines II

Session Chairs: Giovanni Bovone and Mark Tibbitt

Wednesday Afternoon, November 30, 2022

Hynes, Level 3, Room 310

1:45 PM SB09.10.02

Mechanoreceptor Inspired Iontronic Pressure Sensing for Humans and Machines Yuta Dobashi¹, Jerry C. Ku^{1,1}, Joel Ramjst², Victor X. Yang^{1,2} and [John D. Madden](#)³; ¹University of Toronto, Canada; ²Toronto Metropolitan University, Canada; ³University of British Columbia, Canada

The human somatosensory network relies on ionic currents to sense, transmit, and process tactile information. We investigate hydrogels that similarly transduce pressure into ionic currents, forming a piezoionic skin. As in rapid- and slow-adapting mechanoreceptors, piezoionic currents can vary widely in duration, from milliseconds to hundreds of seconds. These currents are shown to elicit direct neuromodulation and muscle excitation, suggesting a path toward bionic sensory interfaces. The signal magnitude and duration depend on cationic and anionic mobility differences. Patterned hydrogel films with gradients of fixed charge provide voltage offsets akin to cell potentials. The combined effects enable the creation of self-powered and ultrasoft piezoionic mechanoreceptors that generate a charge density four to six orders of magnitude higher than those of triboelectric and piezoelectric devices. We explore the applications of these iontronic mechanotransduction effect in the context of both humans and machines - from implantable pressure-sensing hydrogels to bionic skins.

2:30 PM BREAK

SESSION SB09.11: 3D/4D Printing of Hydrogels

Session Chairs: Giovanni Bovone and Mark Tibbitt

Wednesday Afternoon, November 30, 2022

Hynes, Level 3, Room 310

3:30 PM SB09.11.01

Dynamic Photomask Printer for Fabrication of Organs-on-Chip (OoC) [Shu-Yung Nina Chang](#)¹, Terry T. Ching^{1,1,2} and Michinao Hashimoto^{1,1}; ¹Singapore University of Technology and Design, Singapore; ²National University of Singapore, Singapore

In this work, we developed a system to fabricate organs-on-a-chips (OoCs) using a prefatory fluidic chip and a do-it-yourself (DIY) photomask printer. The photomask printer allows direct photopolymerization of bioinks to create microfluidic channels in the prefatory chip, and the patterns of microchannels can be digitally and dynamically controlled. Existing OoCs are predominantly fabricated using soft lithography, whereby microfluidic chips were fabricated with a fixed channel design. Unlike the conventional OoC fabrication method, our system confers the flexibility to fabricate the desired microfluidic chip design *in situ* and use cell-laden hydrogel patterns as a part of the channel architecture of the OoCs.

In our DIY photomask printer, a high-resolution liquid crystal display (LCD) screen (with a pixel size of $32\ \mu\text{m} \times 32\ \mu\text{m}$) was used to project photomasks to create intricate microchannels smaller than $80\ \mu\text{m}$ in horizontal dimensions in the OoCs. With sequential photopolymerization of hydrogels laden with different cell types *in situ*, we successfully patterned multiple cell types at precise locations on the multicellular OoCs (multi-OoC) to mimic the spatial organization of cells *in vivo*. As a demonstration, we fabricated multi-OoC to model vascularized tissues, where primary-cells-laden hydrogels and cancer cells-laden hydrogels were endothelialized with a layer of endothelial cells surrounding their exterior to form a barrier against the perfusing microfluidic channel. After culturing for 7 days, we observed the formation of tight junctions between the endothelial cells in our multi-OoCs. Disruption of these tight junctions was also triggered upon cytokine stimulation, resulting in the migration of metastatic cancer cells to the microfluidic channel. Secondly, the dynamic nature of our photomask printer enabled the designing of OoC *in situ* such that live images could be used to create a photomask accordingly. Using a live photomask, confinement of biological tissues in suspension culture, such as pre-formed cancer spheroids, was achieved in our system for perfusion culture. Such confinement would allow for easier visual monitoring compared to the conventional spinning culture of cell spheroids and organoids. Lastly, we demonstrated that the height of OoCs fabricated in our system was readily varied by changing the height of the spacer consisting of adhesive tapes. Such flexibility in our system allowed us to create OoC to mimic the hierarchical structure in blood vessels by varying the cross-sectional heights throughout the prefatory chip. In this design of OoCs, we achieved branching endothelial cells-laden fluidic channels with gradually decreasing heights, from $600\ \mu\text{m}$ to $200\ \mu\text{m}$.

These demonstrations showed the potential of our system to create biomimetic structures by recapitulating the spatial organization of different cell types and the three-dimensional (3D) geometry of biological tissues on OoCs. The flexible and rapid OoC fabrication enabled by our system will contribute to increasing the efficiency of high throughput drug screening using biomimetic structures.

3:45 PM SB09.11.02

Stretchable and Shrinkable Hydrogel-Based Replication Using a Single 3D-Printed Structure via an Iterative Shrinking Process Eunseok Heo, Jun Chang Yang, In Cho, Hyun-Hee Lee, Yong-Jin Yoon, Steve Park and Jae-Byum Chang; Korea Institute of Science and Technology, Korea (the Republic of)

Recently, 3D printing has attracted significant attention in various fields as it can easily generate arbitrary 3D structures directly from a computer-aided design (CAD) model without any molds or templates. As a low-cost method for 3D fabrication, 3D printing has been widely employed in applications requiring sophisticated 3D structures, such as lab-on-a-chip in the diagnostic industry or patient-customized products in the biomedical field. However, low printing throughput has hindered the broader usage of this technology. To synthesize identical structures of different sizes or materials, each must be separately printed, increasing time and expense. Replication of 3D-printed structures via a molding process with size-tunable molds can be used to solve this issue, but it is limited to tapered or vertical profiles, such as microneedles or simple cylindrical shapes. Here, we demonstrate the generation of replicas of diverse sizes and materials, starting from a single 3D-printed template of complex shape. To achieve this, we use molds composed of stretchable hydrogel, which shrinks isotropically. Using the stretchability of the hydrogel, the 3D-printed structure is separated from the embedding hydrogel without crack formation. Then, polycaprolactone (PCL) fragments are introduced to fill the cavities of the hydrogel mold. The PCL-filled hydrogel structure is heated to $60\ ^\circ\text{C}$, a temperature at which the hydrogel mold shrinks as it dries, while at the same time, PCL melt and fills the cavities. This process can be repeated; diverse replicas with varying sizes and materials can be generated from a single 3D-printed template. Finally, we demonstrate the size reduction of the 3D-printed template with complex interconnecting geometries, which are not available with conventional molding methods.

4:00 PM SB09.11.03

Programming Differentiation of Neural Stem Cells with 4D Printed Multilayer Smart Scaffolds Yi Yang, Omar A. Khater, Nathan D. Gallant and Ying Zhong; University of South Florida, United States

Spinal cord injury (SCI) could permanently disconnect the central nervous system (CNS) and the body below it. It would cause different paralysis depending on the damaged segments of the spinal cord. The therapeutical method for SCI remains challenging due to the difficulties of neuron regeneration. Stem cells are promising to realize neuron regeneration due to their excellent differentiation potential. However, conventional ways for stem cell differentiation cannot control or guide the direction of the neural cells, making it difficult to be used in SCI therapy, as the spinal cord requires aligned neural bundles. Here, porous multilayer scaffolds that composites polydimethylsiloxane (PDMS) and poly(N-isopropylacrylamide) (PNIPAAm) layers were 4D printed. It imitates the extracellular matrix of neural stem cells in terms of strain and elasticity stimulation to enhance and guide PC-12 stem cell differentiation. Different printing parameters and surface treatment procedures were evaluated for the purpose of enhancing the polymer-cell adhesion. Various layer thicknesses and designs were investigated to understand the thermal-related reversible bending behaviors of the scaffolds. It was confirmed that by changing the temperature within the survival range of the cells, the 4D printed smart scaffolds can bend and recover reversibly, providing controllable strain on the cells at the desired frequency to program the differentiation behavior of neural stem cells.

Key word: 4D printing; PDMS; PNIPAAm; Neural stem cell; Cell culturing; Differentiation.

4:15 PM SB09.11.04

Hydrogel Based 3D/4D Printing Systems and Their Applications in Soft Robotics MD Nahin Islam Shiblee and Hidemitsu Furukawa; Yamagata University, Japan

Hydrogel actuators with soft-robotic capabilities, as well as biomimetic advanced materials with simple and programmable fabrication processes, are currently in high demand. In this work, we will demonstrate 4D printing phenomena using different hydrogel-based systems to create bilayer actuator systems. A variety of hydrogels, such as shape memory hydrogels, inter-crosslinking hydrogels, etc., have been developed and their physical properties have been characterized to understand their response behaviors under methodical application of water absorption and temperature. While shape memory-based hydrogel systems require two different compositions to create an actuating prototype, we have also successfully achieved 4D printed systems based on single inter-crosslinking hydrogels where single materials enable variable swelling degree resulting from printing conditioning. The deformation mechanism of the 4D printed structures has been studied by tuning of printing parameters, e.g. scan number, total UV light irradiation time, etc., and also by optimizing initiator concentration for the stereolithography printing process. These 4D-printed systems are designed to imitate living organisms that exhibit multi-directional actuation.

8:45 AM SB09.12.01

Bioinspired Structural Composite Hydrogel with a Combination of Mechanical and Thermal Properties Donghwan Ji and Jaeyun Kim; Sungkyunkwan University, Korea (the Republic of)

Hydrogels are water-filled three-dimensionally crosslinked polymer networks with completely different characteristics compared to typical materials like liquids, metals, ceramics, and plastics. Hydrogels have been utilized as soft robot components, flexible backbones of bioelectronics, conductive membranes, and artificial biological tissues. For these applications, developing hydrogels with a desirable combination of stiffness and toughness is a critical issue.

Since the development of soft yet tough double-network hydrogel, many studies have exhibited synthetic hydrogels applicable for soft tissues whose elastic moduli range from a few pascals to several kilopascals. Despite that, creating much strong, stiff, and tough hydrogels similar to load-bearing tissues, such as tendons and cartilages with elastic moduli in the MPa-to-GPa range, still remains challenging.

To achieve such mechanical property, in this study, we apply a bioinspired structure and fracture mechanisms into a double-network hydrogel and develop structural composite hydrogels. A natural structural composite, nacre, which consists of ductile polymeric matrices and stiff inorganic microplatelets (microsized tablets) in a layered structure, has mechanisms of an effective load transfer from the matrix to the platelet and fracture resistance through platelet pull-out. That leads to the combination of stiffness and toughness. Indeed, we had previously developed composite materials (a kind of plastic) and demonstrated the reinforcing effect and mechanism of layered inorganic microplatelets in polymer matrices of the material.

We expand this approach to a wet hydrogel system and present a bioinspired structural composite hydrogel composed of tough double-network polymer matrices and stiff alumina microplatelets assembled in a layered structure. To fabricate such hydrogel, we suggest a straightforward method, which is a reconstruction process comprising “drying-induced unidirectional shrinkage of a pre-gel” and “additional crosslinking with rehydration in an ionic solution”. During unidirectional drying/shrinkage, the pre-gel of the random compound becomes a thin film of layer-by-layer assembled microplatelets within highly densified polymer matrices; and then, subsequent crosslinking/rehydration fastens the densified layered structure with fully crosslinked polymer networks. During the process, the polymer–platelet interactions are also enhanced.

As a result, the structural composite hydrogel exhibited highly enhanced mechanical performance, withstanding more load and dissipating more energy along with a crack deflection and platelet pull-out. The resulting tensile strengths, elastic moduli (on the order of several MPa), and high fracture energies (up to 2 kJ m⁻²) are comparable to those of the stiff load-bearing tissues such as the ligament and tendon. Such mechanically robust hydrogel with the densified polymer matrix and strong polymer–platelet interactions also exhibited high ionic conductivity. The conductive hydrogel containing cations, such as Li⁺ and Zn²⁺, was utilizable as a stable gel electrolyte almost without compromising mechanical performance. Further, the layered alumina platelets allowed the hydrogel to possess outstanding in-plane thermal diffusivity. When the hydrogel is introduced to serve as a gel electrolyte membrane, the hydrogel is expected to prevent rigid electronic components (electrodes) from inducing heat localization and thermal damage as well as to avoid a mechanical mismatch.

9:00 AM SB09.12.02

Nanoparticles Influence on Rheological Behavior of Poloxamer-Casein Hydrogels Louise L. Tundisi¹, Jéssica H. Fonsêca¹, Janaina Artem Ataide¹, Marcos A. D'Ávila¹, Daniel Kohane² and Priscila G. Mazzola¹; ¹UNICAMP, Brazil; ²Harvard Medical School, United States

Poloxamer 407 (P407)–Casein hydrogel was chosen to terbinafine-loaded polycaprolactone nanoparticles (PCL-TBH-NP). In this study, terbinafine hydrochloride (TBH) was encapsulated into polycaprolactone (PCL) nanoparticles, which were further incorporated into poloxamer-casein hydrogel in different addition order, to evaluate the effect of gel formation. Nanoparticles were prepared by nanoprecipitation technique and characterized by evaluating its physicochemical characteristics and morphology. The nanoparticles had a mean diameter of 196.7 ± 0.7 nm, PDI of 0.07, negative ζ potential (-0.7138mV), and high encapsulation efficiency (>98%). PCL-NP modulated terbinafine release in artificial sweat. Rheological properties were analyzed by temperature sweep tests at different addition orders of nanoparticles into hydrogel formation. Rheological behavior of hydrogels were evaluated, considering different concentrations of nanoparticles, and different addition orders. When nanoparticles were added to the final P407-Casein hydrogel (M1), a decrease in gelation temperature from 28°C to 26°C (p<0.05) and below were observed. Above 0.4 mg/mL of nanoparticles, strong gels with modulus almost temperature-independent were observed, and 0.4 mg/mL showed the highest storage modulus. In the second preparation method, where nanoparticles were firstly added to casein solution, followed by addition of P407 (M2), the gelation temperature also decreased: at 0.8 mg/mL of nanoparticles shifted from 28°C to 20°C (p<0.05) the gelation temperature and had an increase in the storage module from 9.42 to 29.7kPa (p<0.05). The nanoparticle's addition to the hydrogel significantly influenced gelation temperature, the viscoelastic properties and provided stable gels at the two preparation methods. Moreover, the nanoparticle addition order leads to different rheological behavior for the same nanoparticle concentration; thus, a suitable nanoparticle concentration to improve hydrogel mechanical properties can be addition order dependent.

9:15 AM SB09.12.03

CARS Microscopy as an *In Situ* Characterization Technique for Living Composites Christopher Long, Patrik Johansson, Michelle Huang, Renato Navarro, Michael Haney, Christy Munson, Tony Wyss-Coray, Sarah C. Heilshorn and Annika Enejder; Stanford University, United States

Tissue mimicking materials provide a physiologically relevant 3D environment for cell growth and tissue morphogenesis, shaped in a dynamic reciprocal interaction between the cells and host material. Hence, the matrix must be characterized together with the living cellular component as an integrated system. Traditional cell characterization techniques such as immunofluorescence microscopy are insufficient here, as they probe cell responses without correlating them to the characteristics of the matrix environment. Furthermore, the limited penetration depth of the UV/visible light probe beams and artifacts introduced by fluorophores make it difficult to characterize 3D cell-matrix organizations and interaction mechanisms. Instead, multi-parametric techniques are required, which can characterize the host material simultaneously with the cells in 3D without physical sectioning. For this purpose, we have developed a robust imaging platform that incorporates spectral coherent anti-Stokes Raman scattering (CARS) microscopy on a standard confocal microscope. CARS microscopy is a label-free method that maps lipids and proteins in cells and the surrounding matrix by probing their inherent molecular vibrations. Through analysis of a broad range of vibrational signatures, resulting in spatially resolved spectral images, we simultaneously characterize the matrix meso-structure and the phenotypes of the resident cells. We have used this technique to study a unique class of recombinant biopolymer hydrogels, termed HELP gels, composed of a recombinant polysaccharide (hyaluronic acid) and a recombinant elastin-like protein (ELP) crosslinked via dynamic covalent chemistry. HELP gels can encapsulate a variety of embedded cells, which alter their morphology and phenotype in response to matrix stiffness. Through CARS analysis of the polymer phase-separation within these hydrogels, we gained a mechanistic understanding of how to alter polymer hydrophilicity to fine-tune hydrogel structure and produce gels with specific mechanical stiffnesses. The mechanical tunability of these hydrogels makes them an attractive platform for developing *in vitro* models of human tissues and their diseased states.

Ongoing work is exploring these tunable HELP gels as brain mimetic matrices, leveraging CARS to simultaneously probe the dynamic meso-structure of the host gel and the phenotypes of the encapsulated cells based on their lipid profiles. HELP gels were formulated to match the stiffness of brain tissue and used to encapsulate human induced pluripotent stem cell-derived microglia-like cells (iMGs). Microglia are the resident immune cells of the brain, the activation of which is associated with a shift in metabolism and the accumulation of lipid stores. Cell genotypes characterized by metabolic dysfunction have been correlated with the progression of Alzheimer's disease (AD). By studying the lipid metabolism in HELP-encapsulated iMGs derived from AD-risk patients, detailed insights into the underlying mechanisms will be gained. We show that iMGs are viable in HELP gels and—in the manner of native brain microglia—accumulate lipid droplets, which are detected *in situ* using CARS microscopy given the unique vibrational signature of lipids. Furthermore, by encapsulating neurons and astrocytes in addition to microglia, we may evaluate lipid transport and metabolism between these cell types. To validate this *in vitro* model, samples of human brain tissue from healthy donors and AD patients were characterized by CARS microscopy and traditional immunofluorescence microscopy. Consistent with reports from others, we quantified a significant increase in lipid accumulation within the microglia of AD patients ($p = 0.05$). Taken together, these data demonstrate the usefulness of CARS microscopy to assist in the design, validation, and experimentation of tissue mimics as models of human disease progression.

9:30 AM SB09.12.04

Supramolecular Reinforcement of Polymer–Nanoparticle Hydrogels for Modular Materials Design Giovanni Bovone, Elia A. Guzzi, Stéphane Bernhard, Tim Weber, Dalia Dranseikiene and Mark W. Tibbitt; ETH Zürich, Switzerland

Moldable hydrogels can flow under applied stress (shear-thin) and reform a stable network (self-heal) when the stress is removed. An emerging class of moldable biomaterials are polymer–nanoparticle (PNP) hydrogels, which are formed from reversible intermolecular interactions between polymer chains and nanoparticles.¹ PNP hydrogels are used as injectable or extrudable materials in biomedical and industrial applications, however, the mechanical properties of PNP hydrogels are limited and network formation is restricted to interactions between specific combinations of polymer chains and nanoparticles.^{2–4}

In this study, we developed a simple strategy to reinforce PNP hydrogels and expand the application spectrum of this class of materials.⁵ We included α -cyclodextrin (α CD) in the hydrogel formulation as a supramolecular motif enabling mechanical reinforcement and modular design. Rheological measurements demonstrated that the addition of α CD improved the mechanical stability of PNP (CD–PNP) hydrogels in a concentration-dependent manner, achieving storage moduli up to $G' \approx 10$ kPa ($\omega = 1$ rad s^{-1}). The tested formulations retained the ability to shear-thin and self-heal. Our hypothesis is that mechanical reinforcement was caused by threading of α CD onto PEGylated nanoparticles and polypseudorotaxane formation, which enhanced nanoparticle–nanoparticle interactions.^{6,7} We further leveraged these interactions to decouple mechanical properties from material functionality. We exchanged the structural polymers (hydroxypropylmethylcellulose, collagen, alginate, and methacrylated hyaluronic acid), and nanoparticles (block copolymer nanoparticles, gold nanoparticles, and iron nanoparticles), forming stable hydrogel networks ($\tan \delta < 1$, $\omega = 1$ rad s^{-1}) that were not possible to be fabricated without CD-reinforcement. CD–PNP formulations showed improved properties and tunability for 3D bioprinting and drug delivery applications and the application spectrum of this class of materials was broadened to electroconductive and magnetic applications.

Overall, supramolecular reinforcement improved PNP hydrogel mechanical properties and broadened the application spectrum without the need to re-engineer the network interactions. Reinforced CD–PNP hydrogels are a useful platform for applications where moldability, mechanical strength, and functionality are needed.

References:

- [1] Appel, E. A., Tibbitt, M. W. et al. *Nat. Commun.* 6, 6295, (2015)
- [2] Fenton, O. S. et al. *Biomacromolecules* 20, 4430–4436, (2019)
- [3] Stapleton, L. M. et al. *Nat. Biomed. Eng.* 3, 611–620, (2019)
- [4] Guzzi, E. A. et al. *Small* 15, 1905421, (2019)
- [5] Bovone, G., Guzzi, E. A., Bernhard, S. et al. *Adv. Mater.* 34, 2106941, (2021)
- [6] Harada, A. et al. *Nature* 370, 126–128, (1994)
- [7] Liu, K. L. et al. *Soft Matter* 7, 11290–11297, (2011)

9:45 AM SB09.12.05

Hygroscopic Hydrogel Composites with Enhanced Sorption Kinetics Gustav Graeber, Leon C. Gaugler, Carlos D. Diaz, Xinyue Liu, Bachir El Fil, Xiangyu Li and Evelyn N. Wang; MIT, United States

Hydrogels are polymeric networks that can store large quantities of water. Their synthesis is scalable and economical, while their material properties are easily tunable. These qualities make hydrogels attractive materials for numerous applications related to energy and water. Recently, hydrogels that capture water vapor are receiving increased research interest. Such hygroscopic hydrogels can be used in sorption-based thermal energy storage, atmospheric water harvesting, dehumidification and passive cooling. For these applications, the specific water uptake of the material as a function of temperature as well as the sorption kinetics are important, since they translate into e.g., higher energy and power density, or increased water production. Sorption kinetics describe the rate at which the material can adsorb and desorb water vapor. While recent research on sorbents is mostly focused on optimizing the water uptake, sorption kinetics and material integration into devices are considered less. Here, we experimentally study various methods to enhance the sorption kinetics of hygroscopic hydrogels and their integration into practical devices. Combining confocal microscopy of the wet state and scanning electron microscopy of the dry state with dynamic vapor sorption studies, we correlate hydrogel synthesis parameters with material properties and sorption kinetics. Specifically, we investigate the fundamental effects of freeze-drying and molding, as well as the fabrication of hydrogel composite structures with enhanced heat transfer and mechanical stability. To this end, we integrate hydrogels (e.g., polyacrylamide or poly(*N*-isopropylacrylamide)) with hygroscopic salts (e.g., lithium chloride) and fin and foam structures (e.g., aluminum and copper). It is expected that these insights will allow hydrogels to realize their full potential in practical devices that address important challenges related to energy and water.

10:00 AM BREAK

SESSION SB09.13: Tough Hydrogels
Session Chairs: Jue Deng and Jingjing Wu
Thursday Morning, December 1, 2022
Hynes, Level 3, Room 310

10:30 AM SB09.13.01**Tough Ionogels by Tuning Interactions Between Solvent and Polymer Networks** Meixiang Wang; North Carolina State University, United States

Ionogels are compelling materials for technological devices due to their excellent ionic conductivity, thermal and electrochemical stability, and non-volatility. However, most existing ionogels suffer from low strength and toughness. Here, we report simple one-step methods to achieve ultra-tough and stretchable ionogels by tuning solvents (*i.e.*, ionic liquids)-polymer chains dipole-dipole interactions. In poor solvents, the polymer chains in the network can form phase separation that act as sacrificial bonds to toughen the ionogel. By contrast, in good solvents, the polymer chains are highly solvated and can form strong interactions (noncovalent crosslinks) with the solvent. These noncovalent interactions can be broken to dissipate energy and thus toughen the ionogels. The ionogels achieved by these strategies showed extremely high fracture strength (10-80 MPa), fracture energy ($\sim 24 \text{ kJ m}^{-2}$) and Young's modulus (50-1,000 MPa), while being highly stretchable (400-800% strain) and having self-healing and shape-memory properties. Importantly, these strategies are proved to be generalized, which offer a promising way to tough ionogel and may help to expand their applications.

10:45 AM SB09.13.02**Nonlinear Mechanics of Biopolymer and Tissue-Mimetic Hydrogels** Jake Song, Serra Yesilata, Marcelo Garcia and Gareth H. McKinley; Massachusetts Institute of Technology, United States

While biopolymer gels made of rigid polymers such as fibrin and actin filaments have been reported to exhibit softening under compression and stiffening under extension, tissues (commonly consisting of cells embedded in a biopolymer network) have been reported to behave in an opposite manner and exhibit stiffening under compression and softening under extension. These findings naturally raise the question of whether such asymmetric nonlinear elastic properties of biopolymer gels and tissues might result in significant differences in how these materials fail under extensional and compressive loading conditions. We investigate this problem by performing extension-based and compression-based fracture tests on model gel systems that exhibit different asymmetry in their nonlinear elastic properties. We share early lessons learned from our investigation, which sheds light on the fracture properties in biological materials and engineering principles for designing such properties in synthetic soft materials.

11:00 AM SB09.13.03**Spatially-Targeted Reinforcement of Hydrogel Microstructure by Cross-Linking of Double Network Hydrogels Using Femtosecond Laser** Kaneto Tsunemitsu¹, Akira Watanabe², Hiroaki Onoe¹ and Mitsuhiro Terakawa¹; ¹Keio University, Japan; ²Tohoku University, Japan

Controlling elastic modulus as well as breaking stress is crucial for fabricating soft devices. Double network hydrogels (DN gels) have been reported to show high mechanical strength due to their unique network structure formed by two types of polymer networks. However, in the previously reported fabrication methods, DN gels were fabricated by cross-linking two different hydrogel polymers over the entire hydrogel. To the best of our knowledge, spatially selective formation of DN gel structures inside a hydrogel on a micrometer scale and the associated enhancement of local mechanical strength have yet to be demonstrated. In this study, we applied multi-photon polymerization (MPP) using a femtosecond laser to the cross-linking method of hydrogels and attempted spatially-selective formation of DN gels inside a hydrogel block. Hydrogels were prepared by the following two methods for comparison and evaluation. The first method was cross-linking of the 1st gel by UV irradiation followed by cross-linking of the 2nd gel by MPP using a femtosecond laser. By cross-linking the 2nd gel in a limited zone in the 1st gel, DN gel was formed in a spatially-selective manner. The second method was fabricating DN gels using MPP induced by femtosecond laser pulse irradiation for cross-linking of both the 1st and 2nd gels. This method was used to investigate spatially-selective changes in mechanical properties. As result, the stiffness changed in the DN gel where the 2nd gel was spatially-selectively cross-linked. The elastic modulus of the DN gel was higher than that of the single network gel. These results show that the mechanical properties have changed in the zone where the DN gel was locally formed. To demonstrate the potential of the method for soft robotics, we attempted to impart arbitrary mechanical strength in targeted locations and investigated the grasping property of a micro-object. We fabricated U-shaped gel tweezers and a glass bead with a diameter of 100 μm was grasped with the tweezers. The glass bead was slipped through the gel structure due to the significant deformation of the gel when only the single network gel was used because the structure was too flexible to transmit external force to the contact area with the bead. On the other hand, the glass bead was successfully grasped by the U-shaped structure with DN gel microstructures near the contact area with the glass bead, demonstrating the potential of the method for hydrogel-based soft devices.

11:15 AM SB09.13.04**Orthogonally Crosslinked Hydrogels to Improve Mechanical Strength and Broaden Applications of Thermo-Responsive Hydrogels** Joey H. Wong, Valerie Ow, Jun Jie Chang, Xian Jun Loh and Kun Xue; Institute of Materials Research and Engineering, Singapore

Injectable hydrogels are highly attractive due to their minimally invasive administration to the body. Our group has previously used polyurethane thermogels as well as its component micelles in tissue engineering and drug delivery applications [1-3]. However, conventional injectable hydrogels normally possess poor mechanical properties, and deform and break under repeated loading [4,5]. To improve the mechanical strength and broaden the application of the polyurethane thermogels, we have utilized two different strategies leveraging upon orthogonal crosslinks. Firstly, we prepared thermogelling polyurethane diacrylate (EPC-DA) hydrogels which are injectable and can be orthogonally photocrosslinked into fatigue-resistant implants. The thermogelation process occurs due to hierarchical physical self-assembly from micelles into hydrogels, and hence thermogels can serve as a dynamic source of polymeric micelles for further photocrosslinking [6]. The hybrid-crosslinked poly(PEG/PPG/PCL urethane) diacrylate (EPC-DA) hydrogel has a dissipative micellar network and a secondary covalent network typical to strong hydrogels. The mechanical properties can be tuned by changing photocrosslinking conditions, and the hybrid-crosslinked EPC-DA hydrogels exhibited high stability and sustained release properties. In contrast to common injectable hydrogels, EPC-DA hydrogels exhibited excellent anti-fatigue properties with >90% recovery during cyclic compression tests, and showed shape stability after application of force and immersion in aqueous buffer for 21 days. The EPC-DA hydrogel formed a shape stable hydrogel depot in an *ex vivo* porcine skin model, with establishment of a temporary soft gel before *in situ* fixing by UV crosslinking. Secondly, we covalently conjugated sodium alginate onto thermoresponsive polyurethanes, leveraging upon the ability of alginate to gelate with cations. We prepared hybrid polymers (EPC-Alg) that are responsive to both temperature and Ca^{2+} , and can form orthogonally crosslinked hydrogels which are non-toxic to cells. Higher alginate fractions increased the hydrophilicity and Ca^{2+} response of the EPC-Alg hydrogel, enabling tunable modulation of the gel stiffness and gelation temperature. The hydrogels could also encapsulate cell spheroids with high cell viability, demonstrating its feasibility towards 3D cell encapsulation in cell-based biomedical applications such as cell encapsulation and cell therapy. In summary, we have demonstrated two differing strategies to strengthen thermo-responsive hydrogels for application as an anti-fatigue implant and for cell encapsulation.

References

1. Zhao, X.; Seah, I.; Xue, K.; Wong, W.; Tan, Q. S. W.; ...; Su, X.; Loh, X. J., Antiangiogenic Nanomicelles for the Topical Delivery of Aflibercept to Treat Retinal Neovascular Disease. *Advanced Materials* 2021, n/a (n/a), 2108360.

2. Xue, K.; Liu, Z.; Jiang, L.; Kai, D.; Li, Z.; Su, X.; Loh, X. J., A new highly transparent injectable PHA-based thermogelling vitreous substitute. *Biomaterials Science* 2020, 8 (3), 926-936.
3. B.H. Parikh, Z. Liu, P. Blakeley, Q. Lin, M. Singh, J.Y. Ong, K.H. Ho, J.W. Lai, H. Bogireddi, K.C. Tran, J.Y.C. Lim, K. Xue, A. Al-Mubaarak, ..., X.J. Loh, X. Su, A bio-functional polymer that prevents retinal scarring through modulation of NRF2 signalling pathway, *Nature Communications* 13(1) (2022) 2796.
4. Zhang Yu, S.; Khademhosseini, A., *Advances in engineering hydrogels*. Science 2017, 356 (6337), eaaf3627.
5. Xue, K.; Wang, X.; Yong, P. W.; Young, D. J.; Wu, Y.-L.; Li, Z.; Loh, X. J., Hydrogels as Emerging Materials for Translational Biomedicine. *Advanced Therapeutics* 2019, 2 (1), 1800088.
6. Zhang, K., K. Xue*, and X.J. Loh, Thermo-Responsive Hydrogels: From Recent Progress to Biomedical Applications. *Gels*, 2021. 7(3): p. 77. *- co-corresponding

11:30 AM SB09.13.05

Small Biomolecular Detection Based on Small-Signal Transconductance of Suspended Double-Network Hydrogels as Organic Electrochemical Transistors Alex C. Tseng and Toshiya Sakata; The University of Tokyo, Japan

Semiconducting double-network (DN) hydrogels are a promising materials platform for development of bioelectronics and biosensors, as the composite structure offers means for readily tailoring electrical, electrochemical, and importantly, mechanical properties to design device functions and improve biocompatibility. Previously, we demonstrated that DN hydrogels prepared by radical polymerization of acrylamide monomers in suspension with commercially sourced PEDOT:PSS (poly(3,4-ethylenedioxythiophene) complexed with poly(styrenesulfonate)) solutions are able to maintain the good electrical transport properties of PEDOT despite compositions of ~70% water by volume [1]. By incorporating phenylboronic acid (PBA) moieties in the polyacrylamide network, selective binding sites for biomolecules bearing vicinal diols (e.g., glucose or dopamine) were prepared. To obtain an electrochemical and non-enzymatic response to biomolecule concentration, we couple the PBA binding equilibrium with an electrocatalyzed peroxo pathway for O₂ reduction (ORR) on cathodically polarized PEDOT [2]. As the response signal does not require the target to be consumed, this detection scheme avoids the oxidizing conditions which may give rise to confounding signals from common interferents in biological assays (e.g. antioxidant species).

Simultaneously, increasing channel thickness and reduced volumetric capacitance in composite hydrogels motivates a shift towards application as a transducer with built-in amplification rather than as a typical ionic amplifier of Faradaic currents flowing from a sensitized gate electrode. By leveraging the mechanical strength of hydrogels, we fabricate organic electrochemical transistors (OECTs) with suspended channels on flexible polyimide substrates that enable 3D access for mass transport of analyte biomolecules and ions drifted by applied potentials. Accordingly, this configuration improves the OECT bandwidth by about two-fold thanks to a reduction in effective thickness. In conjunction with the use of a traditional reference/counter electrode pair, this enables the poising of small-signal (AC) transconductance measurements (via DC gate potential, AC amplitude and frequency) to directly probe at the rate of ORR with changes in PBA equilibrium. That is, the current of electrons supplied at the OECT drain for the regeneration of PEDOT catalyst is directly measured at a characteristic frequency for ORR. The resulting signal achieves sub-millimolar sensitivity for glucose in phosphate buffer, which is promising for non-invasive monitoring application.

[1] A. C. Tseng *et al.*, *ACS Appl. Mater. Interfaces*, vol. 14, no. 21, pp. 24729–24740, Jun. 2022.

[2] E. Mitra *et al.*, *Advanced Sustainable Systems*, vol. 3, no. 2, p. 1800110, Feb. 2019.

SESSION SB09.14: Hydrogels in Health and Environment Applications

Session Chairs: Jue Deng and Jingjing Wu

Thursday Afternoon, December 1, 2022

Hynes, Level 3, Room 310

1:30 PM SB09.14.01

Large-Scale Production of Amphiphilic Magnetic Janus Particle with 3D-Printed Parallelized and Multiplexed Microfluidic Device for Oil Remediation Seonghun Shin¹, Seongsu Cho¹, Ryungeun Song², Hyejeong Kim³ and Jinkee Lee^{1,3}; ¹Sungkyunkwan University, Korea (the Republic of); ²Princeton University, United States; ³Korea University, Korea (the Republic of)

Oil pollution in water is fatal to the ecosystem and threatens our health. To reduce the oil pollution, remediation materials have been used. However, the conventional remediation materials, such as chemical dispersants and oil absorbents, have limitations and other disadvantages. For instance, chemical dispersants are known to cause toxicity, and their performance relies on oil conditions, and water environments. Moreover, the use of oil absorbents results in a large amount of waste and secondary contamination. To overcome these problems, safer and more effective solid particle-based remediation materials have been developed to replace conventional remediation materials. However, these materials have not been used for industrial applications due to the problems such as labor-intensive device fabrication, complex processes for particle production and functionalization, and slow production rate. In this study, we presented Amphiphilic Magnetic Janus Particles (AMJPs) as remediation material to resolve these problems. AMJPs are dumbbell-shaped and consist of bio-inert materials: PEGDA hydrogel part and PPGDA polymer part embedded with oleic acid coated Fe₂O₃ nanoparticles. AMJPs were produced in a single step with a 3D-printed microfluidic device and had amphiphilicity and magnetism without any functionalization step. To increase the production rate of AMJPs, we fabricated a parallelized droplet generator consisting of 10 droplet generation junctions connected via flow distributors. This device could produce particles 10 times faster than a single device while maintaining the same level of particle size dispersity. In addition, the device has modular connectors and can be multiplexed. This allowed us to multiplex 4 parallelized devices and boost the production rate by 40 times when compared with a single device while maintaining the single peak particle size distribution. We experimentally verified that AMJPs adsorbed to the oil-water interface for lowering surface energy and made the oil film into stable Pickering emulsions. We conducted experiments to quantify oil removal performance and confirm the versatility of AMJPs. We found that the volume of the remaining film of kerosene and mineral oil decreased by more than 96% at dosage of 750 mg/ml. Also, AMJPs could form o/w Pickering emulsion regardless of oil type, viscosity, water pH, and ion concentration. Especially for the oil, AMJPs could cover a very wide range of viscosity (1~10⁵ cP). Further, we confirmed that AMJPs are recyclable and can capture and separate super heavy non-traditional crude oil in sea water. For industrial and practical applications, large-scale production of AMJPs would be an effective and versatile remediation material for oil adsorption and recovery.

Acknowledgment

This research was supported by Basic Science Research Program through the National Research Foundation of Korea (NRF) funded by the Ministry of Education (2021R1A6A1A03039696), the Ministry of Science, ICT & Future Planning (2020R1A2C3010568) and the Korea government (MIST)

(2020R1A5A1019649).

1:45 PM DISCUSSION TIME

2:00 PM SB09.14.03

Hierarchical Composite Self-Sorted Gel Noodles [Libby J. Marshall](#)¹, Matthew Wallace², Najet Mahmoudi³, Giuseppe Ciccone¹, Massimo Vassalli¹ and Dave Adams¹; ¹University of Glasgow, United States; ²University of East Anglia, United Kingdom; ³ISIS Pulsed Neutron and Muon Source, United Kingdom

Multicomponent systems provide extra control over supramolecular systems and are an easy method for introducing functionality. For example, bioactive peptides can be incorporated into the gel network to improve cell culture viability. Here we discuss multicomponent systems composed of two structurally similar functionalised dipeptides: 2NapLG and 2NapFF. 2NapFF self-assembles into long 1D structures (worm-like micelles) at high pH (pH 10.5) and forms viscous solutions. The small-angle neutron scattering (SANS) data from 2NapFF is best fit to a hollow cylinder model at concentrations of 5 mg/mL and greater. 2NapLG forms spherical micelles in solution at high pH, giving non-viscous solutions. SANS data from 2NapLG are of low intensity and best fit to a power law only. Mixing these two components results in greatly increased viscosity compared to the individual components alone at the same concentrations. We have used a variety of techniques, including circular dichroism, SANS and NMR spectroscopy to investigate how these two components interact during self-assembly at high pH.

According to SANS data, the multicomponent systems form hollow cylinders with different radii and thickness to those formed by 2NapFF alone. We have used numerous NMR experiments to further investigate the interactions between 2NapLG and 2NapFF in solution at high pH. The integrals corresponding to protons on 2NapFF measured during ¹H NMR spectroscopy show decreased intensity in the presence of 2NapLG, suggesting that more 2NapFF molecules are in the assembled state in the multicomponent system. We were able to confirm that 2NapLG forms physical interactions with the structures formed by 2NapFF using nuclear Overhauser effect (NOE) NMR experiments. In samples of 2NapLG alone, we observed a positive NOE difference. This confirms that 2NapLG behaves like a small molecule in solution at high pH, i.e. does not form persistent structures. However, in the presence of 2NapFF, a negative NOE difference was observed. This shows that 2NapLG does interact with the large structures formed by 2NapFF. What is perhaps most interesting is that a negative NOE difference was also detected on the aromatic protons. This was completely unexpected as the methyl and aromatic protons are very far apart on the molecule. This implies exchange with the micelles that is not observed in 2NapLG alone and within these structures, the methyl group is close enough in space to interact with the aromatic protons. For 2NapFF, the aromatic signal (most likely from the aromatic rings on the phenylalanine residues) was selectively inverted. We observed NOE to other aromatic protons and to the CH₂ groups. The NOE difference is negative, as we would expect from the formation of worm-like micelles. No NOE was observed to protons on 2NapLG. This implies that the assembly between 2NapFF and 2NapLG is orthogonal, i.e. the two molecules are not intimately mixed within the structures.

2NapFF can be used to form supramolecular noodles. We expected that the 2NapFF/2NapLG multicomponent system would form mechanically superior noodles to 2NapFF alone according to data from viscosity and small-angle scattering experiments. This hypothesis was confirmed using nanoindentation. While 2NapFF forms supramolecular hydrogels on a reduction in pH, 2NapLG forms crystals under the same conditions. By exploiting this behaviour, we have formed crystals within supramolecular noodles the first reporting, to our knowledge, of such behaviour.

2:15 PM SB09.14.04

Bridge-Rich and Loop-Less Hydrogel Networks Through Suppressed Micellization of Multiblock Polyelectrolytes [Jihoon Han](#)¹, Saeed Najafi², Joan-Emma Shea² and Younsoo Kim¹; ¹Pohang University of Science and Technology (POSTECH), Korea (the Republic of); ²University of California at Santa Barbara, United States

Most ABA triblock polyelectrolytes-based physical hydrogels wherein the middle and end blocks are hydrophilic and charged blocks, form three-dimensional networks through micellar packing and generation of non-interlocked loops, resulting in decreased elasticity. This effect can be mitigated by maximizing the fraction of elastically effective bridges in the hydrogel network. Previous observations have shown that the ratio of bridges increases with increasing the relative length of the middle block and the concentration of ABA triblock polyelectrolytes [1]. However, despite the numerous efforts, there was a limit to maximizing the fraction of bridges based on the micelle structure [2]. Therefore, we aim to molecularly design block polyelectrolytes that can hinder the formation of neutral loops that are not involved in hydrogel elasticity and instead promote the formation of the mechanical links during the self-assembly process, which can result in hydrogels with higher elastic modulus. Herein, we report polyelectrolytes complex (PEC) hydrogels with network constructed by designing BABAB pentablock and BABABABAB nonablock polyelectrolytes with a structure that maximizes the entropy penalty of micellization. These polyelectrolytes directly self-assemble into branched and bridge-rich network units (netmers) instead of forming self-entangled independent micelles. As a result, netmers are hierarchically stacked to create a bridge-rich network, increasing hydrogel elasticity. Note that the synthesized BABABABAB nonablock polyelectrolytes had a larger number of blocks present in the BABAB pentablock polyelectrolytes; therefore, the gelation efficiency was maximized due to the larger degree of freedom and higher number of coacervate nodes. The more charge pattern of BABABABAB nonablock polyelectrolytes can promote the formation of crosslinks, and due to the structural advantages of the network, the mechanical properties of the hydrogel networks containing BABABABAB nonablock polyelectrolytes were greater than those of the conventional ABA triblock polyelectrolytes-based hydrogels. Furthermore, the shear modulus of the hydrogel significantly exceeds the theoretical value based on the phantom network theory of rubber elasticity, indicating that the topological constraints of netmer can promote the formation of entangled bridges, which play roles as physical crosslinks.

References

- [1] Watanabe, H., Sato, T., Osaki, K. *Macromolecules*, 33, 2545 (2000).
- [2] Jones, R. L., Kane, L., Spontak, R. J. *Chem. Eng. Sci.*, 51, 1365 (1996).

SESSION SB09.15: Virtual Session I
Session Chairs: Yuhang Hu, Daniel King and Xuanhe Zhao
Wednesday Morning, December 7, 2022
SB09-virtual

8:30 AM *SB09.15.02

Energy-Autonomous Seawater Desalination by Thermo-Responsive Hydrogels [Sebastian Seiffert](#); Johannes Gutenberg University Mainz, Germany

Water scarcity is one of the most serious global challenges of our time. One of the main solutions to address this challenge is water desalination. In this respect, forward osmosis (FO) has gained significant attention. For this purpose, thermo-responsive hydrogels containing ionic groups are a class of materials that can be potentially utilized as draw agent. The ionic groups induce the water flow in the process, and they also serve to block and thereby separate salt. By increase of temperature above the volume phase transition temperature (VPTT) of the hydrogels, the hydrogels shrink, whereby the absorbed, purified water is recovered. Considering this effect, the idea of a membrane-free FO desalination process by ionic hydrogels has been introduced, in which hydrogels serve as both separation and draw agents. However, the use of thermo-responsive hydrogels in that approach is faced with different challenges such as (i) the significant detrimental effect of charged groups on the water recovery efficiency of hydrogels, and (ii) the need for designing FO agents with high salt rejection and water flow performance as well as with low fouling effect. Considering these challenges, we study the influence of the chemical composition, morphology, microstructure, and molecular architecture of charged, thermo-responsive hydrogels based on N-isopropyl acrylamide (NIPAAm) and sodium acrylate (SA) on the efficiency of FO seawater desalination in terms of salt rejection and water recovery. Based on these achievements, we aim to design a simple, efficient, and relatively non-expensive desalination process with a production capacity targeted to serve the demands of small villages via FO process.

9:00 AM *SB09.15.03

PRESENTED ON-DEMAND ONLY: Cooperative Task Achievement by a Swarm of Active Matters [Akira Kakugo](#); Hokkaido University, Japan

Cooperation is a strategy that has been adopted by groups of organisms to execute complex tasks more efficiently than single entities. Cooperation increases the robustness and flexibility of the working groups and permits sharing of the workload among individuals. Here, we demonstrate molecular transportation through the cooperative action of a large number of artificial molecular machines i.e. active matters, photoresponsive DNA-conjugated microtubules driven by kinesin motor proteins. Mechanical communication via conjugated photoresponsive DNA enables these microtubules to organize into groups upon photoirradiation. The groups of transporters load and transport cargo, and cargo unloading is achieved by dissociating the groups into single microtubules. The group formation permits the loading and transport of cargoes with larger sizes and in larger numbers over long distances compared with single transporters. We also demonstrate that cargo can be collected at user-determined locations defined by ultraviolet light exposure.

9:30 AM SB09.15.04

Giant Strain-Induced Crystallization in Ideal-Network Elastomers [Chase Hartquist](#), Shaoting Lin and Xuanhe Zhao; Massachusetts Institute of Technology, United States

Aligned crystalline domains can form in the amorphous network of elastomers when subject to large elongations. The increased crystallinity can effectively pin and blunt cracks, giving enhanced mechanical strength and fracture toughness. Strain-induced crystallization is reversible since ordered chains can disassemble during bulk retraction. However, the effect of strain-induced crystallization is limited in conventional elastomers by polydispersity, random network architecture, and dense chain entanglements. This work demonstrates that strain-induced crystallization in ideal-network elastomers can reach up to 50%, more than twice the effect of strain-induced crystallization reported in existing elastomers (e.g., 20% for natural rubber). Our experiments show that an ideal-network elastomer with a low polydispersity, high degree of homogeneity, and low chain entanglement density attains an amplified extent to which reversible hydrogen bonds form during stretching. This giant strain-induced crystallization simultaneously gives the ideal-network elastomer high fracture toughness and low mechanical hysteresis. We also show that the limiting stretch of ideal-network elastomers follows an abnormal scaling since giant strain-induced crystallization enables the material to stretch near its elastic limit. Polymer chains in the network display shorter initial end-to-end lengths, producing a higher elongation ratio when they straighten and break. We found that the ultimate stretch of an ideal-network elastomer follows the abnormal scaling, exceeding the established theoretical stretch limit, which is the square root of the number of monomers per chain. Ideal-network elastomers provide a foundation for the design of the next frontier of enhanced rubbery materials whose properties approach fundamental mechanical limits.

9:45 AM DISCUSSION TIME

SESSION SB09.16: Virtual Session II
Session Chairs: Yuhang Hu, Daniel King and Xuanhe Zhao
Wednesday Morning, December 7, 2022
SB09-virtual

10:30 AM SB09.16.01

Finite Element Modeling of Coupled Swelling and Deformation of Biopolymer Thin Film [Sanghamitra Debta](#), Pijush Ghosh and Ratna K. Annabattula; Indian Institute of Technology Madras, India

Polymeric gels are a three-dimensional network of physically or chemically cross-linked polymer networks that can absorb a considerable amount of water (sometimes 600 times their volume) without disintegrating. They are known for their broad applicability in the biomedical field. One of the unique characteristics of these polymeric gels is their responsive behaviour when exposed to external stimuli. The polymer film in this study actuates in the presence of water vapour. When the polymeric gels are made into thin films ranging from 100-200 μm in thickness and exposed to water vapour, they show reversible shape change. The reason for this is the diffusion of water vapour into the polymeric network, which leads to the deformation of the film. This reversible shape change has many potential applications in soft robotics.

In this work, a coupled swelling-induced deformation model is discussed based on the Flory-Huggins theory [1]. It considers the change in free energy due to the mixing of the water molecule with the polymeric network. Here, the change in material properties is incorporated by considering Young's modulus to be dependent on the concentration of the water vapour in the film [2]. Owing to the similarities between the diffusion and heat transfer equations, the inbuilt ABAQUS coupled temperature-displacement elements present in the ABAQUS material library is used to simulate the swelling-induced deformation of polymer thin film [3]. The finite element (FE) model results are corroborated with the experiments obtained for the stimuli-responsive cross-linked chitosan-water vapour system by comparing the folding path and curvature. The developed model can predict the behaviour and shape change of thin films in response to vapour and aid in developing and designing new material models for specific applications.

References

1. Flory, P., 1942. Thermodynamics of high polymer solutions. *J. Chem. Phys.* 10, 51–61. Flory, P.J., Rehner, J., 1943. Statistical mechanics of cross-linked polymer networks II. Swelling.

2. Rath, A., Mathesan, S., Ghosh, P., 2016a. Folding behaviour and molecular mechanism of cross-linked biopolymer film in response to water. *Soft Matter* 12 (45), 9210–9222.
3. Toh, W., Liu, S., Ng, T.Y., Hong, W., 2013. Inhomogeneous large deformation kinetics of polymeric gels. *Int. J. Appl. Mech.* 5, 1350001.

10:45 AM SB09.16.02

Stereolithography 3D Printing of Functional Hydrogel Nanocomposites Afra S. Alketbi, Aikifa Raza and TieJun Zhang; Khalifa University, United Arab Emirates

Hydrogels are recognized as one of the most promising functional materials, as they are dynamic, tunable, biocompatible, biodegradable, and capable of encapsulating large water content. On this basis, hydrogels and their composites are gaining tremendous popularity in various fields such as biomedical, food packaging and agriculture, water purification, sensing, and soft robotics, etc. However, hydrogels utilization is limited by the traditional processing methods, mainly molding for 3D geometries, which is a huge drawback for rapid product development. Moreover, molding techniques suffer from materials limitation as it allows only for a single material utilization. The limitation of conventional fabrication can be overcome by the recent advances in additive manufacturing, which enable the fabrication of complex three-dimensional and hybrid structures with enhanced functionality. Herein, we utilize stereolithography 3D printing to fabricate hydrogel nanocomposite through a novel approach. The direct 3D printing of composite inks, particles in ink, show limitations such as inhomogeneous particle distribution, agglomeration, and scattering of curing light, thus compromising the printed object quality and resolution. To avoid this, a new strategy is devised to introduce nanoparticles into the 3D printed hydrogels post the printing process. Metal salts as precursors of nanoparticles are added into the printing ink to develop different types of nanoparticles, including Fe_3O_4 , NiO, and CuO, post the printing. The proposed method allows for the development of hybrid 3D structures in one device without compromising the printing resolution. The versatility of the proposed approach to fabricate 3D hydrogel composites using wide range of nanoparticles offers huge potential to practically utilize hydrogels for water, food and energy nexus.

11:00 AM SB09.16.03

Mechanically Reinforced Conductive Hydrogel Microfibers Prepared by Microfluidic Devices Gea Fitria, Arti Singh and Jinhwan Yoon; Pusan National University, Korea (the Republic of)

Fiber shape soft conducting materials have demonstrated their potential applications to be used in soft electronic systems. In this work, long hydrogel microfiber is prepared based on the coagulation of chitosan in cold water and simultaneous photopolymerization and photocrosslinking of acrylate. After further reinforcement of the chitosan chain in crosslinking agents, medium of the hydrogel microfiber was exchanged with the aqueous electrolyte solution. The resulting ionic hydrogel exhibits high stretchability and conductivity as well as dry-free properties. Owing to its mechanical robustness and ionic conductivity, we envision a highly stretchable soft electrode with the prepared ionic hydrogel microfiber, showing its potential for applications in soft electronics and wearable devices.

11:15 AM SB09.16.04

Wirelessly Operated Flexible Wound Infection Sensing Tag Based on Bioresponsive Hydrogel Ze Xiong and John S. Ho; National University of Singapore, Singapore

Wearable biosensors linked with smartphones provide an opportunity to detect pathophysiological events in real-time to notify patients and their caregivers. Such technology has the potential to transform the diagnosis, prevention, and management of chronic medical conditions by enabling continuous monitoring outside of traditional clinical settings. Chronic wounds represent one such condition where management is a major healthcare challenge, consuming over 5% of the healthcare budget. A key factor contributing to the inability of chronic wounds to heal is the presence of pathogenic bacteria, which secrete virulent enzymes that destroy host tissues and disrupt wound recovery. Prompt detection of wound infection is thus critical for clinical intervention to improve patient outcomes. However, current methods for detection either rely on subjective clinical assessments or time-consuming culture-based laboratory tests, leading to delays in the timely administration of proper treatment. Here, we propose and demonstrate a sensing technology, termed Wireless INfection Detection On Wounds (WINDOW), that detects bacteria virulence using a flexible, wireless, and battery-free sensing tag. This sensing tag is based on a custom DNA hydrogel (DNAgel) that provides a radio-frequency detectable response to deoxyribonuclease (DNase), an enzyme secreted by opportunistic pathogens. When exposed to extracellular DNase, the DNAgel is degraded via non-specific cleavage of DNA strands, resulting in the dissolution of the hydrogel. This changes the dielectric permittivity of the region above an interdigitated electrode and therefore modulates its capacitance. By connecting the electrode to an embedded system, this electronic signal can be read out in a wireless and battery-free manner at 13.56 MHz using near-field communication (NFC), a connectivity technology found on most modern smartphones for short-range communication and wireless power transfer. WINDOW has a thin and flexible form factor that enables it to be conformally embedded into wound dressings to wirelessly track virulence factor activity on demand. We demonstrate the potential of WINDOW for real-time detection of clinically-relevant amounts of *S. aureus* both *in vitro* and in a mouse wound model before the visible manifestation of infection. This technology may facilitate timely detection of wound infections for improved management of surgical or chronic wounds.

Reference: A wireless and battery-free wound infection sensor based on DNA hydrogel. *Sci. Adv.*, 2021, 7, eabj1617.

11:30 AM SB09.16.05

Developed Multi-Functional Hydrogel for Metal Ion Removal Pansilu E. Alwis and Thilini Gunasekara; University Of Sri Jayewardenepura, Sri Lanka

High rates of metal and chemical consumption in industrial processes have resulted in a significant amount of waste, containing high levels of hazardous heavy metals in water resources. Because of their bio-accumulative, and toxicity, heavy metals cause massive environmental pollution. Heavy metals are toxic to almost all living species and are able to accumulate in the food chain, whereas excessive concentrations of other metals, such as magnesium and calcium, also have an influence on toxicity in humans and other animals. Therefore, such toxic metals must be removed by water purification. On that note, adsorption is an excellent approach to get rid of metals and metal ions. Hydrogel is an attractive adsorbent that can be used to eliminate contaminants from water bodies.

Water purification multi-functional hydrogel was synthesized from poly(acrylic acid) polyacrylamide copolymer and modified with urea to improve the adsorption efficiency of the hydrogel by increasing the active metal ion binding sites. Synthesized hydrogel (PAA-co-PAAm-modified with Urea) was characterized using FTIR, XRD, and TGA.

FTIR study confirmed polymerization, and urea modification in the hydrogel. The peak acquired due to the stretching vibration of the N—C—N bond was verified by the modification of the hydrogel with urea. The hydrogel's amorphous nature was confirmed by XRD analysis, which was revealed by broad peaks. On the TGA thermogram, there were five distinct stages of thermal decompositions related to weight losses of physically bound water, chemically bonded water, or lattice water, loss of $-\text{NH}_2$ as ammonia, release of H_2O , CO_2 , and acrylic acid due to the breakdown of the C-C backbone and subsequent degradation of organic groups,

The developed hydrogel had the absorption capacities for the metal ions Cd(II), Co(II), Cu(II), Fe(III), Mn(II), Zn(II), and Mg(II) ions of 67.54 mg/g, 69.81

mg/g, 50.98 mg/g, 97.28 mg/g, 45.37 mg/g, 60.74 mg/g, 25.41 mg/g, and 67.09 mg/g respectively. Adsorption isotherm models and kinetic models of adsorption were also explored in the synthesized hydrogel. In kinetic determination, pseudo-first order, pseudo-second order, and particle diffusion kinetics models were investigated. In the pseudo-second-order kinetic model, adsorption of Cd(II), Co(II), Cu(II), Fe(III), Mn(II), and Mg(II) ions were well behaved. This suggests the adsorption was chemisorption, but the adsorption of Zn(II) ion was fitted to pseudo-first-order kinetics, indicating physisorption.

Freundlich and Langmuir isotherm models were investigated in the isotherm inquiry. The Freundlich isotherm model was used to fit the adsorption of Cd(II), Co(II), Cu(II), Fe(III), Mn(II), and Mg(II) ions, confirming that multilayer adsorption occurred. Nevertheless, the adsorption of Zn(II) ion followed monolayer adsorption and was fitted to the Langmuir isotherm model.

High amount of N functional groups of the hydrogel has increased the metal ion binding capacity and thus has yielded an excellent hydrogel for metal ion removal endeavors.

11:45 AM SB09.16.06

A Biomimetic Joint Model with Heterogenous Oxygen Environments Louis Ong, Indira Prasadam and Yi-Chin Toh; Queensland University of Technology, Australia

Crosstalk between subchondral osteoblasts and chondrocytes played significant role in OA pathogenesis. However, physiological coculture of osteoblasts and chondrocytes is limited by *in vitro* generation of differential oxygen concentrations across the cartilage-bone tissue interface. Chondrocytes in the cartilage require a low (1%) oxygen environment while osteoblasts in bone tissues require normoxic (>9%) oxygen environment to maintain their tissue-specific functions. Current approaches to control oxygen gradients in microfluidic devices rely on diffusion gradients generated across a porous matrix using active gas networks, which is limited to monocultures and cannot mimic tissue interfaces with distinct oxygen tensions. Jammed packed microgels (JPMs) are a novel class of hydrogels that are formed by swelling aqueous solution in microgels which interact with each other via weak physical forces, resulting in their shear-yielding properties. However, the use of this class of hydrogels in tissue culture remains limited.

In this work, we demonstrated the use of polyacrylate JPMs to tune and mimic a heterogenous oxygen environment that mimics the tissue interface of the articular joint. We demonstrated the oxygen content tunability of the JPMs by functionalising the JPMs with two reducing agents: Oxyrase (oxygen reducing enzyme) and sodium sulphite, two common reducing agents used in anaerobic cultures. By optimizing the concentrations of reducing agents, we found that 0.1U Oxyrase (commonly used in anaerobic microbial cultures) could maintain a low oxygen level of 1.35% for up to 48 hrs. The biocompatibilities of the JPMs for primary chondrocytes cultured in both normoxic and hypoxic JPMs demonstrated the JPMs, along with their functionalised reducing agents can support the viabilities of cell cultures. By controlling the type and concentration of the reducing agents, we demonstrated a host of JPMs with different oxygen contents, suitable for mimicking different physiological oxygen tensions. We further established patterning of JPMs with different oxygen content in a microfluidic device, mimicking a bone-cartilage oxygen tension. In situ oxygen sensing within the microfluidic device showed that we can establish and maintain physiological heterogenous oxygen level of cartilage (2% oxygen) and bone (10% oxygen) for 2 days within a cell incubator. On-chip hypoxic culture of primary human chondrocytes exhibited hypoxic response by upregulating hypoxic inducing factor alpha (HIF α), indicative of the hypoxic environment on-chip. Finally, we established co-cultures of allogenic pairs of patient-derived chondrocytes with osteoblasts under the heterogeneous oxygen environments. We showed that co-cultures under heterogenous oxygen physicochemical environment significantly enhanced chondrogenic phenotypes (i.e. increased aggrecan and decreased type I collagen expressions) as compared to coculture maintained under homogeneous oxygen levels without affecting the phenotypes of the osteoblasts within the co-cultures.

This work demonstrated the first instance of osteoblast-chondrocyte microfluidic co-cultures with patterned oxygen levels for up to 4 days. Chondrocytes cocultured under low oxygen environment with osteoblast exhibited enhanced chondrogenic expression compared to monocultures and co-cultures without oxygen control. This platform can potentially be utilized for further osteoarthritis (OA) drug screening applications.

12:00 PM SB09.16.07

Shape-Memory Ideal Polymer Networks with Giant Tunable Thermal Conductivity Chase Hartquist, Shaoting Lin, Buxuan Li, James Zhang, Gang Chen and Xuanhe Zhao; Massachusetts Institute of Technology, United States

Since polymer networks are conventionally known as thermal insulators, strategies to enhance their thermal conductivity offer promising solutions to complicated thermal management problems. Thermally conductive polymer fibers and films have been processed by thermal drawing to achieve heightened measured thermal conductivities that match those of metals. However, dramatic thermal transport enhancement has only been shown using irreversible processing. Here we report ideal polymer networks that achieve giant tunable thermal conductivity. The thermal conductivity enhances by over four times its initial value in the stretched direction, from 0.3 Wm⁻¹K⁻¹ to 1.5 Wm⁻¹K⁻¹. This thermal conductivity change is reversible and can be tuned over many cycles. Crosslinks enable the material to quickly stretch and retract above the glass transition temperature, and the ideal-network architecture promotes chain alignment and stretchability. This shape-memory material retains the structure of the deformed configuration and becomes semicrystalline when cooled to room temperature. Structural characterization and molecular simulation indicate that stretching facilitates alignment of crystalline domains that contributes to bulk heat transport. These findings provide important steps towards realizing tunable, polymeric thermal switches for advanced applications of building materials, electronics, flexible devices, and heat exchangers.

12:15 PM DISCUSSION TIME

SYMPOSIUM SB10

New E-Textile Materials and Devices for Wearable Electronics
November 28 - December 8, 2022

Symposium Organizers

Tricia Carmichael, Univ of Windsor
Jesse Jur, North Carolina State University
Christian Müller, Chalmers University of Technology

Symposium Support

Bronze

IOP Publishing

Journal of Materials Chemistry C

* Invited Paper

+ Distinguished Invited

SESSION SB10.01: Manufacturing

Session Chairs: Trisha Andrew, Tricia Carmichael and Esma Ismailova

Monday Morning, November 28, 2022

Hynes, Level 3, Room 311

10:30 AM SB10.01.01

America's Evolving Strategy in Advanced Functional Fabrics Michelle G. Farrington; AFFOA, United States

For E-textiles to truly make the shift from generating small volume products for highly specialized markets to a widely adopted toolkit of technologies used to enable products across a diverse set of applications, the industry must mature in a number of ways that go beyond the demonstration of new capabilities. Industry infrastructure development must be undertaken in order to support lower product development costs and faster time to market for e-textile products. These infrastructure elements include simulation environments, digital threads, and addressing standards gaps to name a few. Through collaborative R&D work enabled by a public-private partnership, AFFOA is resolving manufacturing technology gaps through investment in broad industry infrastructure development. Example projects combining government needs with industry driven technology roadmaps will illustrate the current methods our Institute uses to address technology and infrastructure gaps.

10:45 AM *SB10.01.02

Phase Segregated and Highly Conductive PEDOT-PSS for Textile Electronics—Wiring, WiFi, Radar, Electrochromic Color Change, Power Generation, Resistive Heating, ECG, EMG, EDA and Loudspeakers/Microphones Gregory A. Sotzing; University of Connecticut, United States

Polyethylenedioxythiophene-polystyrene sulfonate (PEDOT-PSS) has been shown to phase segregate at polyethylene terephthalate and nylon fabric surfaces in the presence of delustering agent such as silica, titania, and alumina. This chemistry involves the formation of silicate, titanate and aluminate sulfonate esters with the polystyrene sulfonic acid to instill phase segregation leading to an enrichment of PEDOT sulfur at the air interface as observed by looking at the PEDOT (Sulfur):PSS (Sulfur) ratio using X-ray Photoelectron Spectroscopy (XPS). PEDOT-PSS sheet resistances were measured both in the DC, and even better in the AC. Electron microscopy of the fabrics show a continuous coating of PEDOT-PSS on each individual fiber of the textile, and current carrying aspects of the material could be analogized to Litz wire. Indeed, less PEDOT-PSS screen printed onto the fabric resulted in higher impedance at low frequencies while maintaining the impedance at higher frequencies. For DC application, we have explored the use of PEDOT-PSS fabrics for resistive heating, copper replacement in circuit to light a 60W incandescent bulb, circuit wires and resistors, and electrochromic (electronic color change) fabric prepared by an open-air method. For AC applications, work will be presented on wearable fabric WiFi, radar, power generation, electrocardiography (ECG), electromyography (EMG), electrodermal activity (EDA), and loudspeakers. As to fabric choice, these applications have been demonstrated on nonwovens such as polyester and nylon synthetic leathers as well as spandex (4-way and 2-way). With the many applications that PEDOT-PSS can provide, one can envision integrated fabric electronics where power can be generated, stored and then utilized by the fabric wearable sensory system and information transmitted via WiFi.

11:15 AM *SB10.01.03

PEDOT:PSS Fibers—Fabrication, Properties, Applications and Challenges Ruben Sarabia, Paula Alarcon Espejo and Matthew Weisenberger; University of Kentucky, United States

PEDOT:PSS is one of the most used conductive polymers in the field of electronic textiles due to its commercial availability, water-based formulation, high electrical conductivity, between others. Different fabrication techniques have been used to process PEDOT:PSS into fibers. The resultant fibers' properties are highly dependent on the process parameters. For example, the conductivity can vary from 0.1 S/cm to more than 4000 S/cm. In this talk, we will discuss the current state of the art of electrically conductive PEDOT:PSS fibers and our work in this field. We will also talk about some of the potential applications of the fibers. Finally, current challenges such as scalability, stability or electrical contacts will be discussed.

11:45 AM SB10.01.04

Reel-to-Reel Fabrication of Smart Sensing Threads Ege Ozgul, Wenxin Zeng and Sameer R. Sonkusale; Tufts University, United States

There has been an emergence of thread based wearable and implantable devices due to their superior flexibility and ability to provide intimate tissue/organ interfaces [1][2]. In prior works, smart threads have been realized for sensing biomarkers of wound healing [1], sensing electrolyte levels in sweat[2][3], monitoring physical activity, and for sensing volatile gasses[2]. Even transistors have been realized on threads[2]. Sensing threads are realized through coating of functional inks using a manual dip-and-dry approach. However this results in non-uniform threads and uneven responses. This abstract addresses a key technological need to enable precise controlled coating of threads for any ink types. This is achieved using a custom built reel-to-reel dip-coating and drying apparatus, which is the focus of this presentation. For a specific case study, we propose the realization of stretchable strain sensing thread with remarkable uniformity (<4% error) over a meter long reel. Strain sensing threads are promising sensors for a wide range of wearable electronics applications. As their resistance depends on the tension, these threads can be used for measuring tension, pressure, and vibrations.

A benchtop reel-to-reel coating system has been designed for uniform coating of any functional inks on any thread type. The platform transfers the thread from one spool to another using two stepper motors driven by microcontroller at user-defined rate. During the transfer, ink is applied using a custom-built 3D printed cartridge. Ink formulation eventually dictates the functionality of smart thread. For proof of principle, we use a carbon ink to realize strain sensing threads. The ink-coated thread is then heated and dried in a temperature-controlled heating chamber. During the fabrication process, the tension of

the thread is measured simultaneously, and a feedback loop is used to adjust the speed of the motor, so that the tension of the thread remains constant. This way, the thread is coated with consistent electrical properties along its length. Once the carbon layer dries, the carbon particles allow electrons to pass through and make the thread conductive.

To analyze the threads, multiple threads were coated with carbon ink under different tensions. Baseline resistance variation is less than 4% over meter long length. Then the electrical conductivity and strain sensitivity of each thread is measured, which ranges from 0.62 to 2.53 M Ω , a 277% resistance change when stretched and unstretched from 4 to 6 cm. We report multiple utilities for strain sensing threads thus realized, such as monitoring of physical activity, posture, arm/leg/finger movements and pressure. By changing the ink and the cartridge, one can coat other functional inks on threads such as chemoresponsive dyes to realize gas sensors, or semiconducting inks to realize transistors.

References:

- [1] Mostafalu, P., Akbari, M., Alberti, K.A. et al., (2016). *Microsystems & Nanoengineering*, 2:1-10.
- [2] Xia, J., Khaliliazar, S., Hamed, M.M. et al. (2021). *MRS Bulletin* 46, 502–511
- [3] Terse-Thakoor, T., Punjija, M., Matharu, Z. et al., (2020). *npj Flexible Electronics*. ;4:18.

SESSION SB10.02: Health Monitoring
Session Chairs: Jesse Jur, Ruben Sarabia and Gregory Sotzing
Monday Afternoon, November 28, 2022
Hynes, Level 3, Room 311

1:30 PM *SB10.02.01

Health Monitoring with Electronic Textiles from Solution Processable Conducting Polymers [Esma Ismailova](#); Mines St Etienne /BEL, France

In the last decade, there has been an increased use of organic electronics for biomedical applications. Bioelectronic devices made of conducting polymers show unique properties to interface with the human body and provide an efficient physiological monitoring. The development of state-of-the-art organic electronic devices on textiles to promote their wearability and allow the democratization of health monitoring systems is rapidly becoming possible. Novel approaches are needed to evolve traditional microfabrication techniques to produce organic electronic textiles. The solution processability of conducting polymers offers excellent performances in devices fabrication on textiles preserving their stretchability, breathability and yielding ubiquitous systems. Examples of a “non-traditional” micropatterning technique for cutaneous electrodes development on knitted textiles and traditional inkjet printing to directly design functional sensors on woven and non-woven fabrics will be showcased. These devices are designed to allow multimodal health data collection, which is essential in advancing technologies towards next generation of personalized diagnostics and therapies.

2:00 PM SB10.02.02

Sensing Floss—Saliva Diagnostics on a Thread [Atul Sharma](#) and Sameer R. Sonkusale; Tufts University, United States

Stress significantly impacts a patient's overall health; when stressed, the adrenal gland produces corticosteroids (such as cortisol) and adrenaline into the bloodstream. Cortisol negatively affects the regulation of various physiological processes such as carbohydrate metabolism and blood glucose levels. Long-term stress can disrupt homeostasis in the cardiovascular, renal, skeletal, and endocrine systems, leading to the development of chronic diseases. Moreover cortisol levels vary throughout the day. Because of its central role, continuous monitoring of cortisol levels in the human body is critical for health and wellness. Cortisol levels are often measured using immunochemical and analytical methods in blood, plasma, serum, oral fluid, sweat, and hair samples. Of these methods, saliva provides the most abundant, non-invasive source of cortisol biomarker. Towards the goal of routine stress-level examination, we engineer a thread-based electrochemical sensor for quantifying cortisol directly in saliva. The thread platform resembles a floss, which we define here as “sensing floss”. Threads offer the most flexible option for tissue-embedded sensing, microfluidics, and bioelectronics compared to other flexible platforms. This work demonstrates the design of thread-based sensing floss both as a saliva sampler and for the realization of ultrasensitive and label-free electrochemical detection of cortisol in saliva using differential pulse voltammetry (DPV). To fabricate the cortisol sensing floss, a commercial gold-coated thread was used as a conductive base electrode surface to capture and strengthen the signal. The gold-coated thread was initially cleaned with isopropyl alcohol (sonication, 15 minutes) and plasma treatment (5 minutes), resulting in a smoother and cleaner surface for immobilization of the recognition element. The gold thread surface was then treated with dithiobis(succinimidyl propionate) (DSP, 4 mM in DMSO), formed a self-assembled monolayer, and rinsed with DMSO and phosphate buffer. Later, it was incubated with a designated concentration of cortisol-specific monoclonal antibody, mAb-cortisol (10 ng mL⁻¹) at 4°C for 4 hrs under a humid environment, and further incubated with bovine serum albumin (BSA) to incorporate an antifouling layer, and finally washed with buffer. The detection of the target analyte (cortisol) is based on the binding event between the cortisol molecule and the covalently immobilized mAb-Cortisol on the gold electrode surface, where an adopted conformation of the antigen-antibody complex alters the electron transfer rate at the electrode, resulting in a drop in measured current level. The surface topology and electrochemical properties of a cortisol-biosensor were studied using Fourier transform infrared spectroscopy, scanning electron microscopy, cyclic voltammetry, and electrochemical impedance spectroscopy. Under optimum experimental circumstances, the devised cortisol-biosensor demonstrated a dynamic range from 1.0 pg mL⁻¹ to 1.03 ng mL⁻¹ with a linear range of 1.0 pg mL⁻¹ to 0.52 ng mL⁻¹ and a limit of detection (LOD) of 1.0 pg mL⁻¹ (S/N = 3) in cortisol spiked saliva samples. DPV measurements are carried out in the presence of a redox probe containing 1.0 mM Ferri/Ferro cyanide in PBS (0.10 M, pH 7.2, 0.10M KCl). Our results show that the sensing floss is capable of detecting cortisol in both spiked buffer media and saliva samples. The analytical figures of merit of the cortisol-sensing platform confirm that the designed sensing floss could be particularly successful for low-level detection and continuous monitoring of salivary cortisol. The sensing floss can be extended to detection of other biomarkers in saliva for variety of health indicators and disease conditions.

2:15 PM SB10.02.03

All PEDOT:PSS Fully-Textile Wearable Chemical Sensors [Erika Scavetta](#), Beatrice Fraboni, Isacco Gualandi, Francesco Decataldo, Federica Mariani, Domenica Tonelli, Danilo Arcangeli and Marta Tassarolo; University of Bologna, Italy

Organic ElectroChemical Transistors (OECTs) are promising electronic platforms to realize chemical sensors since they can provide intrinsic signal amplification without the need of a freestanding reference electrode, they can operate at low power (< 100 μ W) and can be easily miniaturized and adapted to non-flat, flexible and textile substrates. In addition, providing high sensitivity together with biocompatibility and low-cost, they could be proposed as analytical tools for the reliable detection of a wide range of low concentration analytes even in biological fluids such as sweat and wound exudate.

All poly(3,4-ethylenedioxythiophene):poly(styrene-sulfonate) (PEDOT:PSS) OECTs can be used as chemical sensors for the detection of redox analytes that are oxidized at PEDOT:PSS, such as ascorbic acid, dopamine, adrenaline or uric acid [1].

On the other hand, the selectivity issue must be addressed to allow the widespread use in real-life applications, through a proper functionalization of the gate electrode with molecules able to selectively interact with the target analyte [2, 3]. In this regard, pH or chloride sensors have been described by our

research group, entrapping iridium oxide or silver/silver chloride nanoparticles on the PEDOT polymer, thus developing two terminal sensors able to work without an external gate electrode.

One of the most appealing features of OECT chemical sensors is the possibility of realizing the whole device in a fully-textile form using easy scalable procedures thus allowing the development of a compact, lightweight, cost-effective, and easy to wear platform for monitoring healthcare and sport activities in real-time.

This contribution describes two examples of fully-textile wearable chemical sensors based on PEDOT:PSS OECTs. The first one is a multi-thread biosensing platform that can detect chloride ions (Cl^-) concentration and pH level simultaneously without interference. The textile sensors are simple threads, based on natural and synthetic fibers that show excellent sensitivity, reproducibility, selectivity, long term stability and the ability to work with small volumes of solution. The performance of the developed textile devices is demonstrated in artificial human perspiration to perform on-demand and point-of-care epidermal fluids analysis.

The second example of application is a fully-textile smart bandage for pH [4] and uric acid detection, to be applied for hard-to-heal wounds (i.e. severe and/or chronic) monitoring, where it is critical to constantly evaluate the healing stages and the overall wound condition.

The use of special medical-grade textile materials provides a passive sampling system, which enables the continuous, real-time and non-invasive analysis of wound fluid.

REFERENCES

[1] I. Gualandi, M. Marzocchi, E. Scavetta, M. Calienni, A. Bonfiglio, B. Fraboni, *J. Mater. Chem. B* **2015**, *3*, 6753.

[2] I. Gualandi, M. Tessarolo, F. Mariani, D. Arcangeli, L. Possanzini, D. Tonelli, B. Fraboni, E. Scavetta, *Sensors* **2020**, *20*, 1.

[3] I. Gualandi, M. Tessarolo, F. Mariani, T. Cramer, D. Tonelli, E. Scavetta, B. Fraboni, *Sens. Actuators B* **2018**, *273*, 834.

[4] F. Mariani, M. Serafini, I. Gualandi, D. Arcangeli, F. Decataldo, L. Possanzini, M. Tessarolo, D. Tonelli, B. Fraboni, E. Scavetta, *ACS Sens.* **2021**, *6*, 2366.

2:30 PM BREAK

3:00 PM *SB10.02.04

Garment Integrated Sensor Systems for Longitudinal Sleep Tracking Trisha L. Andrew; University of Massachusetts Amherst, United States

Chemical vapor deposition is a single-step processing method for forming functional polymer films on unconventional substrates, such as commodity textiles, and allows fabrication of rugged and sensitive fabric-based sensors for wearable electronics and smart farms. I will detail the materials science and engineering advances made by my team during the process of assembling various garment-integrated sensor systems and plant-based sensors for longitudinal health monitoring in native environments. In particular, I will highlight our recent work in developing garments for portable brain activity monitoring and activity tracking, and systems for in-home sleep monitoring.

3:30 PM SB10.02.05

Stretchable, Breathable and Washable Textile Sensor for Human Motion Monitoring Lina Sanchez Botero, Anjali Agrawala and Rebecca Kramer-Bottiglio; Yale University, United States

Advancing the accuracy and ubiquity of in-situ human motion monitoring requires the development of soft wearable sensors that maximize wearer's comfort. To translate wearable sensing technologies beyond laboratory settings and into real-world applications, it is important to develop light-weight, breathable sensors that can be seamlessly integrated into commercial clothing and interface directly with human skin without losing signal fidelity. Here, we report the fabrication of a soft textile capacitive sensor capable of describing everyday human motions due to its high conformability and mechanical flexibility. Unlike established capacitive strain sensors, which usually rely on stretchable elastomers, our sensor is constructed out of thin films of breathable adhesive and fabrics. Our soft sensor exhibits good stretchability (>90%), excellent durability (repeating cyclic deformation > 5000 cycles), and high water-vapor transmission rate (~ 50g/h.m²) which allows sweat evaporation, an important parameter of comfort. Additionally, we verified that our sensor can function under analogous conditions to human body temperature and sweat (89% relative humidity and 35 °C) and function after washing. The sensor also shows highly stable capacitance over a high range of excitation frequencies (up to 1 MHz), facilitating its implementation with commercial circuitry. Furthermore, the manufacturing process of these sensors can be scalable and customizable at low cost, paving the way for the next generation of flexible and comfortable wearable sensors.

3:45 PM SB10.02.06

On Textiles Microfluidic Organic Biosensing via Additive Manufacturing Marina Galliani¹, Pooya Azizian² and Esma Ismailova¹; ¹EMSE, France; ²Leitat technological Center, Spain

Recent advances in personalized healthcare show a tendency to use biochemical sensing platforms built on wearable substrates to continuously monitor the presence and concentration of key metabolites in sweat. The seamless integration of sensors with microfluidic components defines the scope for the manufacture of future wearable point-of-care devices. The adjustable wicking properties of textiles and their fibril structure naturally allow for the absorption, diffusion, and storage of sweat. We present a scalable additive technique for a textile-based skin-mounted microfluidics development on clothes. Our new method allows the patterning of hydrophobic regions in non-woven fabrics, creating boundaries of hydrophilic micro-channels. Along these channels, a capillary flow allows a directed collection of sweat from the skin to the sensing receptor using only the wicking properties of the fabric. Digital printing techniques provide a direct method for high resolution and reproducible deposition of flexible materials. On this basis, we have fabricated microfluidic modules with different architectures for the collection, storage, and analysis of sweat. Directly printing an organic bioelectronic sensor onto microfluidics allows a unique integration strategy for a low-cost fabric-based sweat detection platform. The method presented here demonstrates a new approach for the monolithic integration of bioelectronic devices with sweat collection and analysis capability in textile garments.

4:00 PM SB10.02.07

Novel 3D Electrodes Embedded In Smart Garments for ECG Sensing Applications Vimanyu Beedasy^{1,2}, Patrick Smith¹ and Mark Catchpole²; ¹The University of Sheffield, United Kingdom; ²Conductive Transfers Ltd., United Kingdom

Smart garments are becoming increasingly popular due to a rising demand for a wider range of functionality promised by the Internet of Things (IoT). Smart garments consist of embedded electronic components such as sensors that can be used for sensing applications to enable healthcare benefits where information such as heart rate, body temperature, levels of sweat, and even body pressure exerted over a particular area can be monitored. However, the integration of the sensor within the garment remains a key challenge to date, particularly for electrocardiogram (ECG) sensing applications as traditional electrodes must be fitted by a clinician in order to obtain an accurate ECG signal. These particular electrodes are often used in combination with a hydrogel to ensure contact with the skin, especially in regions of the body that are more susceptible to body hair, which can cause skin irritation and discomfort in the long term. In terms of functionality, the electrodes must maintain contact with the skin (even through hair follicles and around various body

morphologies) in order to ensure ECG signal fidelity. Additionally, the use of multiple disposable electrodes per patient raises the issue of sustainability in the long-term.

In this paper, we discuss a patent pending design of a smart garment consisting of 3D dry electrodes that are embedded for healthcare monitoring applications, bringing the advantage of reduced skin irritation. This garment was successfully prototyped using a combination of techniques, based on the screen printing process. Multiple layers of various functional materials were sequentially added to form a thin film circuit, about 100 μm thick, consisting of a stretchable conductive silver flake-based electrode surrounded by an equally stretchable ink encapsulant, and an adhesive layer which was used to embed the circuit into the garment under heat and pressure. During the heat transfer process, the encapsulation layer prevented ink dissipation into the synthetic fibres of the garment which could degrade the electrical performance of the electrodes.

The next process employed embossing to produce 3D electrodes consisting of “macropillars”. First, an iterative computational finite element analysis of the embossing process was done to identify high stress concentrations around the macropillars. The 3D features of the electrodes can be up to 4 mm in height; the use of stretchable inks and a stretchable fabric prevents failure due to stress and shear concentrations, and also due to inter-layer delamination. The embossing process was then performed under heat and pressure to permanently form the macropillars, resulting in the formation of 3D conductive electrodes.

The skin contact to the patient is also facilitated by using a compression garment combined with the 3D electrodes. Moreover, the placement of the 3D electrodes within the compression garment can be done according to the requirements of the patient given the bespoke nature of the 3D electrodes. For example, different electrode configurations such as EASI formation (5 leads), Fontaine formation (5 leads) or Lewis formation (5 leads) can be employed without being influenced by the natural body indentations and hair follicles as the combined usage of 3D electrodes and compression ensures contact with the skin. Further tests were performed according to ASTM standards to evaluate the influence of stretch on the electrical performance of the electrodes, and it was found that electrical resistance was stable up to 20 % strain, thereby ensuring a reliable signal and high signal-to-noise ratio.

One key application of this smart garment with 3D electrodes is for healthcare at home using IoT, especially since hospital at home offers significant cost savings over treatment in hospitals, particularly during post-operation recovery.

4:15 PM SB10.02.08

Wearable MXene-Bioelectronics for Diagnostics and Personalized Rehabilitation Raghav Garg^{1,1,2}, Nicolette Driscoll^{1,1,2}, Sneha Shankar^{1,1,2}, Todd Hullfish¹, Josh Baxter¹ and Flavia Vitale^{1,1,2}; ¹University of Pennsylvania, United States; ²Corporal Michael J. Crescenz Veterans Affairs Medical Center, United States

Real-time diagnosis of neural and neuromuscular diseases requires reliable and continuous monitoring. Wearable bioelectronics enable the necessary non-invasive electrophysiology sensing to study, diagnose, and treat neural and neuromuscular disorders. Multi-disciplinary advancements in materials, electronics, and biomedical engineering are enabling newer soft and flexible technologies for wearable electrophysiology sensing. However, current devices are limited by fabrication approaches that are expensive and do not scale, hindering immediate clinical translation. Here we leverage safe and scalable liquid-phase processing of two-dimensional (2D) $\text{Ti}_3\text{C}_2\text{T}_x$ MXenes and infuse the nanomaterial into laser-patterned cellulose-polyester fabrics, to fabricate high-resolution bioelectronic interfaces (MXtrodes) for wearable electrophysiology sensing. Our fabrication paradigm allows the MXtrodes arrays to be highly versatile since their morphology, scale, and spatial distribution can be easily customized to be subject and application specific, giving them a major advantage over commercially available systems. Furthermore, MXtrodes exhibit low skin impedances without the need for any conductive gels, thereby increasing user compatibility and electrode stability. We demonstrate the clinical applicability of the MXtrode arrays by recording high-density surface electromyography (HDsEMG) patterns in the calf muscles during different tasks, from walking to controlled contractions. The high-density, high-sensitivity, and low-noise of the MXtrodes even during dynamic motions results in electrophysiology recordings with signal quality comparable with state-of-the-art commercial sensors, but with much higher accuracy and resolution. Our results underscore the application of MXene-based wearable bioelectronics in studying neuromuscular function and disease pathologies, as well as clinical rehabilitation paradigms.

4:30 PM SB10.02.09

Reusable Surface-Enhanced Raman Spectroscopy Membranes and Textiles via Template-Assisted Self-Assembly and Micro-/Nano-Imprinting Aditya Garg, Wonil Nam and Wei Zhou; Virginia Tech, United States

The development of wearable sensors for continuous real-time monitoring of human physiological status has attracted extensive research efforts. While significant commercial success has been made in wearable physical sensors for monitoring physiological parameters like heart rate and body temperature, wearable chemical sensors are still under intense research and development for applications in personal health management, including body biofluids analysis, wound monitoring, and human-centered environmental sensing of hazardous chemicals. Surface-enhanced Raman spectroscopy (SERS) has emerged as a powerful tool for ultrasensitive fingerprint recognition of molecules with considerable potential in wearable biochemical sensing. However, previous efforts to fabricate wearable SERS devices by directly treating fabrics with plasmonic nanoparticles have generated a nonuniform assembly of nanoparticles, weakly adsorbed on fabrics via van der Waals forces. Here, we report the creation of washing reusable SERS membranes and textiles via template-assisted self-assembly and micro-/nano-imprinting approaches. Uniquely, we employ a capillary force-driven self-assembly process to generate micropatch arrays of Au nanoparticle (NP) aggregates within hydrophobic microstructured templates, which are then robustly bonded onto semipermeable transparent membranes and stretchable textiles using a UV-resist based micro/nanoimprinting technique. Compared to previously developed wearable SERS devices, our fabrication technique offers several advantages: (1) good uniformity control of the spatial distribution and intensity of SERS hotspots, (2) good manufacturing compatibility with many types of delicate membrane/fabric materials due to the mild UV micro/nanoimprinting process at room temperature, and (3) strong mechanical bonding between Au NPs and the wearable substrates via a UV-cured resist. Due to the good mechanical robustness of the UV-resist immobilized Au NP aggregates, we could regenerate contaminated SERS hotspots using user-friendly detergent-water washing processes over multiple cleaning cycles without degrading the sensing performance. Moreover, we demonstrate that substituting conventional UV-resists with carbon nanotube-polymer composite resists can generate conductive wearable SERS devices, enabling electrochemical SERS for improved sensitivity and selectivity of detection in multi-analyte systems. Therefore, we envision that the template-assisted self-assembly and micro-/nano-imprinting approaches can help create wearable washing reusable SERS fabrics/membranes with advanced materials properties via polymer nanocomposites for specific needs in different biochemical sensing applications.

8:30 AM SB10.03.01

Silkworms as a Factory of Functional Wearable Energy Storage Fabrics [Nageh K. Allam](#); American University in Cairo, Egypt

Feeding *Bombyx mori* larvae with chemically-modified diets affects the structure and properties of the resulted silk. Herein, we provide a road map for the use of silkworms as a factory to produce semiconducting/metallic natural silk that can be used in many technological applications such as supercapacitor electrodes. The silkworms were fed with four different types of chemicals; carbon material (graphite), sulfide (MoS₂), oxide (TiO₂ nanotubes), and a mixture of reactive chemicals (KMnO₄/MnCl₂). All the fed materials were successfully integrated into the resulted silk. The capacitive performance of the resulted silk was evaluated as self-standing fabric electrodes as well as on glassy carbon substrates. The self-standing silk and the silk@glassy carbon substrate showed a great enhancement in the capacitive performance over that of the unmodified counterparts. The specific capacitance of the self-standing blank silk negative and positive electrodes was enhanced 4 and 5 folds, respectively upon the modification with KMnO₄/MnCl₂ compared to that of the plain silk electrodes.

8:45 AM SB10.03.03

Washable Virus Blocking Textile for SARS-CoV-2 Powered by Human Body Triboelectric Energy Harvesting [Minki Kang](#)¹, Byung-Ok Choi^{2,3,4}, Nam-Hyuk Cho^{5,5,6} and Sang-Woo Kim^{1,4}; ¹Sungkyunkwan University, Korea (the Republic of); ²Samsung Medical Center, Sungkyunkwan University School of Medicine, Korea (the Republic of); ³Samsung Medical Center, Korea (the Republic of); ⁴Sungkyunkwan University (SKKU), Korea (the Republic of); ⁵Seoul National University College of Medicine, Korea (the Republic of); ⁶Seoul National University Medical Research Center and Bundang Hospital, Korea (the Republic of)

Effective mitigation technology to prevent the spread of severe acute respiratory syndrome coronavirus 2 (SARS-CoV-2) is required before achieving population immunity through vaccines. Here we demonstrate a virus blocking textile (VBT) which repulses SARS-CoV-2 by applying repulsive Coulomb force to respiratory particles, powered by human body triboelectric energy harvesting. We found that SARS-CoV-2 has negative charges and a human body generates high output current of which peak-to-peak value reaches to 259.6 μ A at most, based on triboelectric effect. Thereby, the human body can sustainably power a VBT to have negative electrical potential and the VBT highly blocks SARS-CoV-2 by repulsing them. In acrylic chamber study, we found that the VBT blocks SARS-CoV-2 by 99.95 % and SARS-CoV-2 in the VBT is 13-times reduced. Our work provides the first technology that prevents the spread of virus based on repulsive Coulomb force and triboelectric energy harvesting.

9:00 AM SB10.03.04

Triboelectrification Induced Self-Powered Microbial Blocking by Harvesting Kinetic Energy from Human Motion [Young Jun Kim](#) and Sang-Woo Kim; Sungkyunkwan University, Korea (the Republic of)

Conventional air-transmitted pathogen protection methods such as face masks typically involve obvious pressure drops and uncomfortable long-term wearing. Alternative methods, such as antimicrobial textiles can utilize the nanomaterial-modified functional fabrics for effective microbial prevention, whereas suffering from limited treatment throughput, high cost, and potential toxicity from nanomaterial release. Herein, we develop a novel microbial blocking textile using fabrics with opposite triboelectrification properties as the outer and inner layer that induces triboelectric charges by harvesting kinetic energy from human motion. The induced triboelectric negative charges at the outer layer on the microbial blocking textile achieve efficient air-transmitted pathogens blocking based on the electrostatic repulsion between the fabric and microbes. This self-powered triboelectrification-induced microbial blocking system with optimized material (PTFE and nylon) and structure (rib-knitted) achieves highly efficient microbial blocking (>95%) under a very high airflow of 2.0 m/s. Further, the pressure drop for the microbial blocking by this novel process is extremely low (<30 Pa). Our results demonstrate a promising method for rapid and self-powered air-transmitted pathogen blocking by involving triboelectric charges from human motion to meet vital needs to protect public health.

9:15 AM SB10.03.05

Investigation and Optimization of Direct-Write Printed Metasurfaces on Fabric [Adria Kajenski](#)¹, Guinevere Strack¹, Shahriar Khushrushahi² and Alkim Akyurtlu¹; ¹University of Massachusetts Lowell, United States; ²Notch Inc, United States

Wearable electronics covers a wide range of devices of varying complexity in a multitude of applications. Fabrication methods include weaving, embroidery, or direct-write printing. Printing has the advantage of coating individual fibers for seamless printed designs. Several printing processes can be used to fabricate wearable devices; however, direct-write printing is cost and time effective, producing consistent line widths using a variety of inks and substrates.

The RF metasurface is a passive device and is an example of a simple, wearable technology that can be produced via additive manufacturing. RF metasurfaces can be tailored by adjusting element shape or dimensions, providing reflection, transmission, or absorption within a frequency regime of choice. Here, a stop-band filter is designed at 5.8 GHz using an array of square loops. Textile substrate-based metasurfaces are versatile and have been used in various applications including anti-jamming and EMF shielding. [1]

The fabric-based printed metasurfaces are fabricated by direct-write printing two silver nanoparticle inks on single-sided polyurethane coated nylon substrates with thread masses of 70D and 200D, using a Nordson PRO4 dispensing system. The quality of the print heavily relies on a reasonable window of textile fiber thread mass and ink viscosity. Low viscosity inks printed on heavy thread mass fibers are more likely to introduce cracks and demonstrate fragility in tests. High viscosity inks are more forgiving and fully coat fibers, providing continuity regardless of thread mass. The textiles are subjected to wash and dry cycles, and mechanical testing of twisting, compression, and abrasion is performed. It is imperative to use a highly flexible ink resistant against mechanical distortion and resistance to wash and dry cycles. Lifetime of the textile metasurface is monitored over several months, demonstrating excellent longevity. Even when subjected to damage, the material may still perform depending on the number of defects and their location. RF performance and conductivity are used to assess the integrity of the wearable metasurface, and analysis of the failure mechanisms are conducted using SEM imaging. Quality and durability of the printed metasurface is dependent on the substrate type, thickness, and presence of a protective polyurethane coating. The protective coating on the reverse, non-printed side provides reinforcement, preventing ink from penetrating the fabric. This opens the possibility of printing on both sides, which can be used for introducing a second resonance, or in antenna applications for improving gain and bandwidth.

As part of this presentation, the performance and stability of the different inks on the different substrate thicknesses will be shown, and details of the ink and substrate interaction along with the mechanisms of failure will be presented. Details of the performance and durability of the metasurface samples will be demonstrated, and optimization of printing and testing processes will be reported.

[1] Printed Metasurfaces for Wearables A. Kajenski, S. Khushrushahi, G. Strack, and A. Akyurtlu; 2020 IEEE International Symposium on Antennas and Propagation and USNC-URSI Radio Science Meeting, Denver, CO 2022

9:30 AM BREAK

10:00 AM SB10.03.06

Thermally Drawn Multi-Material Fibers for Electronic Textiles Fabien Sorin¹, Andreas Leber¹, Chaoqun Dong², Hritwick Banerjee¹, Stella Laperroussaz¹, William Esposito¹ and Inès Richard¹; ¹Ecole Polytechnique Federale de Lausanne, Switzerland, Switzerland; ²University of Cambridge, United Kingdom

Advanced functionalities integrated within fibers and fabrics are at the heart of the technological developments for electronic textiles. While functionalities are often added to the fibers or textiles via different deposition strategies, an emerging alternative approach relies in integrating materials and devices within the individual fibers. The thermal drawing process in particular, the technique used to fabricate telecommunication optical fibers, have experienced a series of materials and processing breakthroughs that have significantly expand the kind of materials and architectures that can be integrated into fibers. Flexible and even stretchable polymer fibers have been demonstrated to integrate metallic electrode arrays, electrically addressed semiconducting and piezoelectric domains, micro-channels, or textured surfaces with nanometer feature sizes. This provides fibers with novel advanced optical but also electronic and optoelectronic functionalities, with intriguing opportunities in energy harvesting and storage, fiber probes and optprobes, sensing, bioengineering and advanced e-textiles. In this presentation, we would like to introduce the vibrant field of multi-material fibers and highlight the several opportunities for the electronic textiles community. We will in particular present the fabrication approach, materials and achievable architectures offered by this process leading to novel electronic fibers and textiles (Adv. Materials 31, 1802348 (2019) (review paper from our group)). We will then discuss several recent results from our group starting with a first design that allows for the detection and localization of pressure along the fiber axis (J. Phys. D: Appl. Phys. 50, 144001 (2017)). We will then move to new designs based on the thermal drawing of thermoplastic elastomers, that enables to realize soft and deformable fibers (Adv. Mat. 30, 1707251 (2018)). We will show in particular electronic fibers and e-textiles that integrate conducting nano-composites (Adv. Funct. Mat. 30, 1904274 (2019)), and an innovative design where several liquid metal electrodes are co-drawn within an elastomeric cladding, forming distributed sensors based on transmission line principles (Nature Electronics 3, 316 (2020)). The achieved combination of pressure points localization and textile stretching enabled with only two contact points at a fiber end is unprecedented. We will also demonstrate similar soft fiber architectures and textile adapted for self-powered sensors and energy harvesters relying on the triboelectric effects (Nature Communications. 11, 3537 (2020)). We will conclude with the recent demonstration of the drawing of metallic glasses we could achieve, with feature sizes down to a few nanometers within a flexible fibers (Nature Nanotechnology 15, 875 (2020)), paving the way towards novel opportunities for fibers and textiles in bioengineering, sensing, electrochemistry (ACS Appl. Mat. and Int. 13, 43356 (2021)), and fabrics for the composite industry (Adv. Mat. Technologies 6, 2000957 (2021)).

10:15 AM SB10.03.08

3D Architecturing Strategy on a State-of-the-Art Liquid Crystal Spun Carbon Nanotube Fiber for Fiber-Shaped Supercapacitor with Ultra-High Electrochemical Performance Jeong-Gil Kim^{1,2}, Hayoung Yu^{1,3}, Jae Young Jung¹, Min Ji Kim^{1,3}, Hyeon Su Jeong¹ and Nam Dong Kim¹; ¹Korea Institute of Science and Technology, Korea (the Republic of); ²Korea Advanced Institute of Science and Technology, Korea (the Republic of); ³Gwangju Institute of Science and Technology, Korea (the Republic of)

Fiber-shaped supercapacitors (FSSCs) are the most cutting-edge power sources for wearable electronics, however the essentially limited cylindrical space of fibers hinders high electrochemical performance, which should be overcome by the precise and systematic architectural process. Here, we suggest a simple but effective 3D architecture technique for fabricating FSSCs with high flexibility and electrochemical performance. Utmost liquid crystal spun carbon nanotube fiber (CNTF) is an ideal 1D core component that can achieve desirable properties demanded in FSSCs such as high conductivity and superior mechanical flexibility. GO is vertically composited to the surface of CNTF (VG@CNTF) by electrophoretic deposition process to fabricate a stereoscopic hybrid 3D structure. At this time, immediately depositing pseudo-capacitive active materials after the deposition of GO is a key process for maintaining the 3D structure of VG. Notably, the asymmetric FSSCs exhibit not only remarkable electrochemical performance of 65 Wh kg⁻¹ at 100 kW kg⁻¹ but also extraordinary flexibility and stability (capacitance retention of 98.60% at bending angles of 90° and 93.1% after 5,000 bending cycles). Moreover, the FSSC device integrated with common cotton yarn exhibits reliable performance even under harsh mechanically deformed environments. This study could lead to a breakthrough into the development of high-performance FSSCs for wearable applications.

10:30 AM SB10.03.09

MXene-Polymer Nanocomposite Fiber-Based Triboelectric Nanogenerator Md Mehdi Hasan¹, Md Sazid Bin Sadeque¹, Hilal Pecenek², Ilgin Albasar^{1,3}, Fatma Kilic Dokan⁴, M. Serdar Onses^{1,2,2} and Mustafa Ordu¹; ¹Bilkent University, Turkey; ²Erciyes University, Turkey; ³TOBB University of Economics and Technology, Turkey; ⁴Kayseri University, Turkey

Triboelectric nanogenerators (TENG) utilizes the universal triboelectrification effect to harvest ambient mechanical energy by coupling contact electrification with electrostatic induction. Ferroelectric polyvinylidene fluoride (PVDF) polymer improves triboelectric charge density by utilizing spontaneous polarization making this an excellent candidate for flexible TENG. 2D nanomaterials like MXenes improve triboelectric performance, thanks to abundant electronegative surface terminating groups and high surface area. Furthermore, MXenes significantly improve the output power of PVDF and its copolymer-based TENG by dielectric modulation through microcapacitor formation and microscopic dipole generation through interfacial polarization. Here, we present Ti₃C₂T_x MXene-PVDF nanocomposite triboelectric fibers as energy-generating textiles by the scalable thermal fiber drawing. In this work, we will demonstrate three key outcomes: (1) rheological attributes for the successful drawing of nanocomposite fibers, (2) the effect of MXene addition and thermal drawing on the electroactive phase transition in fibers, and finally (3) the effect of MXene on the performance of TENG. The preliminary results of our fiber shows 2% increase in open-circuit voltage (upto 11.8 V), and 17% increase in short circuit current (upto 0.11 μA) upon 2.5 wt% of nanomaterials loading. The insights gained from this study will significantly contribute to our understanding of two-dimensional nanomaterials integrated fibers towards scalable fabrication of high-performance textiles.

10:45 AM SB10.03.10

Self-Powered E-Textile Based on Dynamic Schottky DC Generator Jun Liu¹, Yanbin Wang², Ruizhe Yang¹ and Tian Li²; ¹University at Buffalo, The State University of New York, United States; ²Purdue University, United States

The growing demand for sustained power is one of the main challenges for wearable electronics, implantable devices, distributed sensors, etc., which are the critical elements for future Internet of Things (IoT) and Point of Care (POC). With recent advances in fabric materials and weaving techniques, low-power consumption sensor, wireless data transmission and cloud processing, the new era of Smart textile has come of age. However, the problem of powering smart textile system in the field at low cost, efficiently and for extended periods has remained unsolved. The Schottky DC generator is capable of generating a 3-4 orders' higher DC current density (10-100 A/m²) compared to transient alternating current (AC) generation in conventional piezoelectric

or triboelectric nanogenerators, thus overcoming the power output limitation and frequency restriction in biomechanical energy harvesting. Moreover, the Schottky DC generation concept provide a new sensing mechanism for human activity monitoring with high electromechanical responsivity and multidirectional sensitivity. The flexible Schottky DC generator concept has recently been demonstrated and integrated with E-textile with conducting polymer system. In this talk, the original concept, recent progress, and future perspectives will be discussed.

11:00 AM SB10.03.11

Printed Photovoltaic Modules on Solution-Coatable Ultra-Thin Substrates for Mechanically Imperceptible Energy-Harvesting in E-Textiles Mayuran Saravanapavanantham, Jeremiah Mwaura and Vladimir Bulovic; Massachusetts Institute of Technology, United States

Owing to the ultra-thin functional film thicknesses and intrinsically amorphous nature of emerging organic photovoltaics (OPV), they are well suited for integration into flexible/stretchable form-factors necessary to enable power-harvesting capabilities in e-textiles. To date, large scale demonstrations of such devices have primarily been on rigid glass or thick plastic substrates (>100 μm), thereby limiting their conformal integration onto surfaces, a feature critical for their adoption into e-textiles. Recent reports of devices fabricated on ultra-thin (<5 μm) substrates make use of intrinsically hard-to-scale chemical vapor deposition (CVD) or solution-coating methods employing high-temperature (>250C) imidization processes requiring a nitrogen-ambient environment. Herein, we report on a novel approach to prepare ultra-thin releasable polyester (PET) substrates in air-ambient conditions through a roll-to-roll compatible solution-coating process. Subsequently we demonstrate fabrication of fully-printed OPV modules on the substrates and their integration onto a high-strength (5kN/m tensile strength), light-weight (<15 g/m^2) composite fabric. Access to such coatable and ultra-thin substrates amenable to subsequent integration into e-textiles enables a platform not only suitable for energy-harvesting but any thin-film technology including displays, sensors, transceivers and compute elements.

11:15 AM SB10.03.12

Intrinsically Stretchable and Printable Lithium-Ion Battery for Free-Form Configuration Jeong Gon Son^{1,2}; ¹Korea Institute of Science and Technology, Korea (the Republic of); ²Korea University, Korea (the Republic of)

For next-generation wearable and implantable devices, energy storage devices should be soft and mechanically deformable, and easily printable on any substrate or active devices. Herein, we introduce a fully stretchable lithium-ion battery system for free-form configurations in which all components, including electrodes, current collectors, separators, and encapsulants, are intrinsically stretchable and printable. The stretchable electrode acquires intrinsic stretchability and improved interfacial adhesion with the active materials via functionalized physically crosslinked organogel as a stretchable binder and separator. Intrinsically stretchable current collectors are fabricated in the form of nanocomposites consisting of a matrix with excellent barrier properties without swelling in organic electrolytes, and nanostructure-controlled multimodal conductive fillers. Due to structural and materials freedoms, we successfully fabricate the several types of stretchable lithium-ion battery that reliably operates under various stretch deformations with capacity and rate capability comparable with non-stretchable battery over 2.5 mWh cm^{-2} at 0.5 C even under high mass loading conditions over 10 mg cm^{-2} , including stacked configuration, direct integration on both sides of a stretch fabric and application of various electrode materials and electrolytes. Especially, our stretchable battery printed on the stretch fabric also exhibits high performance and stretch/long-term stabilities in the air even when wearing and pulling.

11:30 AM SB10.03.13

Towards Green, Mass Customization of Electronic Fabrics Wenyu Wang, HaoTian Harvey Shi, Yan Yan Shery Huang and Ruishan Liu; University of Cambridge, United Kingdom

Traditional textile production has established fabrication processes of pre-treatment, dyeing, and finishing to obtain desired textile appearances and functionalities. Even though electronic textiles exhibit substantially enhanced functionalities than traditional textiles, their processing methods remain largely like those of traditional textiles, which include dip-coating, spraying, electrodeposition, or the use of coagulation bath. However, these processes often consume vast amount of water and energy, while producing significant amounts of chemical wastes. Here, we propose the integration of fibre spinning and 3D printing, which allows electrical functionalities to be embedded into/onto the microfibre structures on-demand. Tuning the spinning and print path of microfibres could generate customized patterns of e-fabrics. Such an on-demand, scalable method is foreseen to significantly reduce the chemical and material usage for e-fabric creation, as well as minimizing resultant waste generation.

SESSION SB10.04: Functional Materials and Devices I

Session Chairs: Jesse Jur and Christian Müller

Tuesday Afternoon, November 29, 2022

Hynes, Level 3, Room 311

1:30 PM *SB10.04.01

Emerging Technologies and Research in Electronic Textiles Tushar Ghosh; North Carolina State University, United States

The continued interest and growth in wearable and soft electronics devices have synergistically ushered in an entirely new area of innovative research and commercialization of e-textile products. Systems/devices in this category include multifunctional fibers and textiles with electronic capabilities having potential applications ranging from weapon systems to everyday textiles. The underlying science and technology of e-textiles are intertwined with many new and emerging fields such as nanotechnology, biomimetics, molecular electronics, etc. In this presentation, the general area of e-textiles will be introduced with an overview of the current state of the art and the challenges. More importantly, the presentation will focus on the complex challenges posed by the need for collaborative research in e-textiles involving multiple disciplines. The subsequent discussion will focus on the continuing effort at the SMARTextiles laboratory at N.C. State University to seamlessly integrate electronic functionalities directly into fibers and textiles to develop electrical devices such as sensors and actuators. In one of our ongoing research, tricomponent melt extrusion is being used to produce sensory fibers [1,2]. Once woven into a fabric, the fibers can be used as a sensor array to detect pressure, moisture, etc. In another research, an easy-to-manufacture, tunable, fully-textile sensor system that can detect pressure, humidity, or wetness is being studied [3,4]. Here capacitive pressure sensors are formed via a traditional sewing process with commercially available conductive sewing yarns. In both cases, the simple sensor design using conventional fabrication techniques resulted in practical and scalable methods of producing textile-based sensory arrays. The relationship between the sensor's physical, mechanical, and electromechanical properties, including hysteresis and sensory response, will be discussed. In addition to sensors, actuators are also essential for many e-textile applications. Therefore, we are exploring the movement and morphing in biological systems to develop advanced flexible structures [5]. For example, the nastic motion of plants in response to environmental stimuli, e.g., the rapid closure of the Venus flytrap's leaves, utilizes snap-through instabilities originating from the anisotropic deformation of plant tissues. In contrast, ballistic tongue projection of chameleon is attributed to direct

mechanical energy transformation by stretching elastic tissues in advance of rapid projection to achieve higher speed and power output. We have developed a bistable all-polymer laminate containing dielectric elastomers, which double as both structural and active materials. The electrical actuation of bistable structures obviates the need for continuous application of electric field to sustain their transformed state. The experimental results are qualitatively consistent with our theoretical analyses of prestrain-dependent shape and bistability. We are currently exploring similar fiber-based structures for textile applications.

2:00 PM SB10.04.02

A Heat-Based Self-Decontaminating Textile Material for Wearables Marquise D. Bell, Te Faye Yap, Kai Ye, Anoop Rajappan, Colter J. Decker, Yizhi J. Tao and Daniel J. Preston; Rice University, United States

The ongoing COVID-19 pandemic has caused severe shortages of personal protective equipment (PPE) and strained medical supply chains due to the disposable nature of PPE, which creates a need for constant replenishment to cope with high-volume usage [1]. To address this increase in demand, and to reduce the amount of waste generated by disposable PPE, we developed a reusable textile-based composite material that relies on dry heat decontamination [2], enacted through Joule heating of a conductive textile, to inactivate pathogens.

This wearable material is composed of four layers adhered to each other through a stacked lamination fabrication process which has been implemented in prior work to fabricate similar layered textile-based wearable devices [3]. The four layers that comprise this material are: (i) a plain-woven substrate textile infused with thermoplastic polyurethane on one side, (ii) a serpentine-patterned electrically conductive textile that enables Joule heating, (iii) an electrically insulating dielectric surface layer of thermoplastic polyurethane to prevent electrical contact with the wearer, and (iv) a thermally insulating base textile layer that interfaces with the wearer's skin to allow safe contact during the dry heat decontamination process. Through this facile and scalable fabrication approach, we created a wearable material capable of achieving the high surface temperatures ($> 100\text{ }^{\circ}\text{C}$) required for viral inactivation within short time frames ($< 5\text{ s}$) while maintaining a comfortable temperature at the point of contact with the skin ($< 30\text{ }^{\circ}\text{C}$).

The geometrical parameters of this material dictate its thermal performance for the inactivation of viral contaminants and can be predetermined, prior to fabrication, based on a desired level of virus inactivation. We quantified the inactivation efficacy of our composite material through experiments supported by analytical modeling predictions using a time-varying temperature profile [4], illustrating the effectiveness and practicality of our approach. We demonstrate how this material can be easily integrated into regular clothing (shown using gloves in this work) and can perform rapid dry heat decontamination, especially in untethered, on-the-go applications. This work provides a simple design and fabrication process for a composite textile material that enables quick and repeatable in situ dry heat decontamination with the ability to reduce waste created by disposable PPE and mitigate the risk of disruptions in supply chains.

[1] N. J. Rowan and J. G. Laffey, "Unlocking the surge in demand for personal and protective equipment (PPE) and improvised face coverings arising from coronavirus disease (COVID-19) pandemic – Implications for efficacy, re-use and sustainable waste management," *Science of The Total Environment*, vol. 752, p. 142259, Jan. 2021, doi: 10.1016/j.scitotenv.2020.142259.

[2] T. F. Yap, Z. Liu, R. A. Shveda, and D. J. Preston, "A predictive model of the temperature-dependent inactivation of coronaviruses," *Applied Physics Letters*, vol. 117, no. 6, p. 060601, Aug. 2020, doi: 10.1063/5.0020782.

[3] V. Sanchez *et al.*, "Smart thermally actuating textiles," *Advanced Materials Technologies*, vol. 5, no. 8, p. 2000383, Jul. 2020, doi: <https://doi.org/10.1002/admt.202000383>.

[4] T. F. Yap, C. J. Decker, and D. J. Preston, "Effect of daily temperature fluctuations on virus lifetime," *Science of The Total Environment*, vol. 789, p. 148004, Oct. 2021, doi: 10.1016/j.scitotenv.2021.148004.

2:15 PM *SB10.04.03

Development of Test Methods for Heating Textiles Patricia I. Dolez¹, Justine Decaens², Ikra Shuvo¹ and Shakil Mahmud¹; ¹University of Alberta, Canada; ²CTT Group, Canada

The integration of electronic and data processing functions within textile products has given rise to e-textiles. They can sense variations in the environment, either external or from the wearer, react by performing an action, and even adapt their properties. E-textiles offer major opportunities in healthcare, protection, and sportswear among others. However, in order to further develop this thriving E-textile industry sector, standardized testing and quality control methods are crucial for safeguarding product quality, regulating performance consistency, and ensuring consumer safety.

In the specific case of Joule heating textiles, several products have already reached the market. However, issues have been reported in terms of efficiency, durability and safety. The lack of efficiency may be associated with a higher response time, heterogeneous heat distribution, and/or irregular heating levels during repeated applications. In addition, different factors associated with daily life use can lead to a premature decrease in performance and ultimately reduce the lifespan of heating textile. Such factors can be mechanical (abrasion and repeated stretching and bending), related to textile care processes (laundering, ironing) and environmental (e.g. corrosion due to perspiration). Heating textiles may also create safety issues to the wearer due to short circuits, overheating, and fire incidents.

A test protocol has been developed to quantitatively assess the heating efficiency of heating textiles in a repeatable way. It uses thermocouples to measure the change in temperature at the surface of the heating textile during the heating and cooling phases. Various boundary conditions were applied with different fabrics/flexible materials simulating realistic use scenarios of heating textiles. The robustness of the test protocol was assessed with different heating textile structures: a conductive nonwoven fabric combining silver-coated nylon and polyester fibers; the same nonwoven fabric encapsulated with a polyurethane film; a heating fabric with an embroidered carbon fibre yarn; and a silicone rubber heating pad incorporating copper wires. Mathematical models were also developed to describe quantitatively the heating and cooling effectiveness of the heating textiles.

In terms of durability, the work focuses on five damaging conditions that are relevant to heating textile use in consumer products: abrasion, laundering, exposure to perspiration, repeated stretching, and repeated bending. The effect of these damaging conditions on the heating textile performance is studied using different types of Joule heating textiles – knitted, woven, nonwoven, embroidered/stitched/inserted, coated, and laminated. The conditions of the damaging treatment are selected to simulate realistic product use situations, e.g. in terms of the frequency and number of cycles of the bending and stretching motion and number of laundering cycles applied. The durability of the heating textile is assessed by comparing its heating performance after exposure to the damaging treatment with its initial efficiency. For the safety assessment, the test protocols characterize the propensity of the heating textile products to short circuits, ignition, and overheating.

The test and quality control protocols developed as part of this research aim to be reliable and robust as well as applicable to a wide range of Joule heating textiles with different structures. They are intended for Standards Development Organizations such as ASTM International and the International Electrotechnical Commission (IEC). We hope that they will contribute to lifting some of the barriers that currently limit the growth of the e-textile industry.

2:45 PM BREAK

3:15 PM *SB10.04.04

Protecting Firefighters and Donor Hearts by Smart Uses of Textiles [Hyun-Joong Chung](#); University of Alberta, Canada

Textiles are extreme engineering materials that have been optimized mostly for clothing uses for thousands of years. The properties of the wonder materials are tunable by varying their fabric patterns, fiber/yarn composition, and constituting materials. In this talk, I will present two examples of utilizing textiles to protective human lives: (i) a wearable sensor that predicts the end-of-life of firefighter's personal protective garment and (ii) a textile-enforced elastomeric tube that facilitates blood circulation in an ex-vivo heart perfusion (EVHP) device for heart transplant surgery.

ANECDOTE 1: Firefighters' lives rely much on the performance of fire-resistant garments. While the garment is composed of textiles that perform exceptionally well in terms of maintaining mechanical robustness such as tear resistance, the performance of these textiles degrade slowly by aging. The major acceleration factors for the aging include high temperature, moisture, and ultraviolet (UV) light. The most serious problem of the aging behavior is that it is virtually undetectable; detectable consequences of the aging is the colour change of the textile, but tensile strength of the aged textile at the moment of detection is merely at the 20~30% of that of as-made ones. Whereas the performance limit of the protective textile is at ~50% of performance retention, the aging is a life-threatening problem for firefighters. In order to address the problem, our team is currently developing an end-of-life sensor of protective textiles. The wearable sensor is attached on the firefighter's protective garment, and undergoes the same life-experiences of the garment including high temperature, UV and water exposure, and laundering cycles. In the presentation, the design concept of the end-of-life sensor, which includes graphene-based conductive tracks and a sacrificial polymer layer, will be discussed. Understanding and quantifying the degradation of the sacrificial polymer is important. Here, we studied thermally- and hydrothermally-induced aging behavior of high performance polymers by quantifying the gradual loss of tensile strength and elongation at break. Time-temperature superposition principle was used as a framework to quantify the activation energy of degradation. Chemical degradation mechanism was studied by FT-IR with hypothesis-driven and machine-learning assisted methods to elucidate the vulnerable chemical bonding for degradation.

ANECDOTE 2: EVHP is an innovative technology in which a donor heart is kept alive and beating outside of the human body. During EVHP, the organ is kept near body temperature (37 °C) and perfusate (enriched blood) flows through the heart chambers, simulating physiological conditions. Currently, overly stiff tubing used in EVHP devices causes premature pressure wave reflection during heartbeat, which can increase risk of donor organ rejection. Use of aorta-inspired compliant tubing for EVHP devices, namely, RTV silicone elastomer tubes 'jacketed' by a sleeve of knitted fabric, was hypothesized to potentially mitigate this problem. We used a custom-built flow loop to pump fluid into sections of compliant tubing at known pressures and measured the response; our main finding was that the tubes deform rapidly as pressure initially increases, but eventually display 'self-regulation' behavior where their continued distension is tempered by the stiffening of fibres in the fabric. The experimental findings were supported by our 3-dimensional finite element simulations in ABAQUS using material coefficients obtained from uniaxial tensile tests of the tubing materials. Finally, we will showcase the efficacy of the fabric-jacketed tube in facilitating blood circulation in EVHP devices.

3:45 PM SB10.04.05

Smart Textiles in Extreme Environments [Braden M. Li](#)^{1,2}, [Robin Dietrich](#)², [Alex E. Flynn](#)², [Alex Parkison](#)², [Deanna Sessions](#)², [Wilson Kong](#)², [Zachary Farrell](#)², [Rahel Rudd](#)¹ and [Christopher E. Tabor](#)²; ¹Air Force Life Cycle Management Center, United States; ²Air Force Research Laboratory, United States

The ability to impart "smart" functionality (i.e. stimuli responsiveness & sensing) coupled with the innate flexibility and comfort of textiles make smart textiles well suited to address the key challenges associated with developing the next generation clothing solutions to support emergency personnel (first responders, military, medics). It is not uncommon for these critical personnel to operate within extreme environmental conditions, ranging from dry arctic regions (-55°C) to hot / humid conditions. In this presentation, key material challenges and solutions will be shared that are being addressed within the US Air Force to enable next generation smart textiles in extreme conditions to better enable personnel to perform their duties by providing both physiological state awareness and mitigating detrimental states such as hypothermia and cognitive fatigue. Herein we discuss our efforts exploring the use of polymers with enhanced thermal properties coupled with printable liquid metal (EGaIn) inks to create conformable, flexible, and robust functional textile laminates suitable for applications such as active heating, electrophysiological sensing, and on-body data / power routing. These innovative material sets present new opportunities for additional textile-based wearable sensing, haptics, and augmented/virtual reality (AR/VR) applications that were previously unrealized due to intrinsic material limitations.

4:00 PM SB10.04.06

Ultra-Low Energy Adaptive Personal Thermoregulation—A Kirigami-Enabled Electrochromic Wearable Variable Emittance (WeaVE) Device [Ting-Hsuan Chen](#)¹, [Yaoye Hong](#)², [Ching-Tai Fu](#)^{1,3}, [Ankita Nandi](#)^{1,4}, [Wanrong Xie](#)¹, [Jie Yin](#)² and [Po-Chun Hsu](#)¹; ¹Duke University, United States; ²North Carolina State University, United States; ³University of Southern California, United States; ⁴California Institute of Technology, United States

Personal thermoregulation is of key importance for human skin temperature stabilization and personalized thermal comfort. However, a long-standing trade-off exists between tunable functionality, energy consumption, and wearability. Inspired by the mid-infrared electrochromic conductive polymers, we developed the first **ultra-efficient wearable variable-emittance device (WeaVE)**, enabling the tunable radiative heat transfer coefficient to fill the missing gap between thermoregulation energy efficiency and controllability.

WeaVE is an electrically driven, kirigami-enabled electrochromic thin-film device that can effectively tune the thermal radiation heat loss of the human body. The device can also maintain its cooling/heating state without energy input, thereby stabilizing the human body heat dissipation in response to varying ambient temperature with orders of magnitude less energy input compared to active devices or heating, ventilation, and air-conditioning (HVAC) systems. We also show that the kirigami design can achieve stretchability and conformal deformation under various modes of deformation and exhibits excellent mechanical stability after 1000 cycles. The integration of sensors and electronic control also enable programmable personalized thermoregulation. Our results show that **with less than 5.58 mJ/cm² energy input per switching, WeaVE provides 4.9 °C (8.8 °F) expansion of the thermal comfort zone, which is equivalent to a continuous power input of 33.9 W/m²**. This is more than 1,000 times switching for a 1m² WeaVE with a typical smartphone battery, corresponding to months of usage. WeaVE provides an entirely new scheme to breaking the dilemma between conventional personal thermoregulation devices' functionality and energy consumption and maintaining the wearability requirement simultaneously.

4:15 PM SB10.04.07

Laser-Induced-Graphene Formation on the Kevlar Textiles for Wearable Electronic Devices [Dongwook Yang](#), [Han Ku Nam](#), [Truong-Son D. Le](#), [Youngeun Lee](#), [Young-Ryeul Kim](#), [Seung-Woo Kim](#) and [Young-Jin Kim](#); Korea Advanced Institute of Science and Technology, Korea (the Republic of)

Wearable electronic devices are being widely employed in various situations, including firefighting, the military, fitness/well-being, and healthcare. One of the promising technology candidates for realizing wearable electronics is constructing conductive electrodes directly onto textiles or fibers. Direct laser writing can support the direct conversion of textiles into electrically conductive Laser-Induced-Graphene (LIG) by irradiating the intense laser beam for

converting specified precursor materials into LIG via photothermal reactions; this offers the more flexible design changes with faster manufacturing process. The introduction of ultrafast femtosecond lasers with shorter pulse durations could improve the patterning resolution while minimizing the unexpected material ablation. Kevlar is one of the fabrics having a high melting temperature so fits well for the successful synthesis of LIG using the ultrashort femtosecond laser pulses. We examined the electrical sheet resistance, surface morphology with an SEM, and chemical composition with a micro-optic Raman spectrum. After the characterization, we applied this patterning strategy to realize various wearable electronic sensors (e.g. strain sensors, temperature sensors, bending sensors) and energy storage devices on Kevlar. Textiles are made up of woven, nonwoven, and knit structures, each with its own set of physical properties.

A Yb-doped fiber femtosecond laser, power/polarization control optics, a Galvano scanner, beam-delivery mirrors, and a central control unit make up our direct-laser-writing system. At a 200-kHz repetition rate, the laser generates a repeated pulse train with a 1030-nm wavelength and a 350-fs pulse duration. For patterning of fabric strain sensors and energy storage devices, the laser's average power varied from 0.5 to 3 W while the beam-scanning speed varied from 10 to 30 mm/s. A Galvano scanner angularly scanned the laser beam, which was then focused on target fabrics with an f-theta lens. On-demand, the entire system was concurrently commanded to produce arbitrary patterns. For validating the physical and chemical characterization of LIG, sheet resistance, SEM, XRD, FT-IR, and Raman spectroscopy were conducted. Kevlar to LIG conversion in ambient air was achieved using femtosecond laser direct writing, which may be used in a variety of wearable devices. The resulting LIG is used to construct wearable strain sensors, bending sensors, temperature sensors, and supercapacitors based on the physical characteristics of different fabrics due to its features. The bending sensor is effectively realized for woven cloth. The TCR of the nonwoven temperature sensor is employed for monitoring body temperature, and the capacitance of the nonwoven supercapacitor is 12 mF/cm². The knit strain sensor is well established, and finger movements and human heartbeats were all detected. As a result of the direct conversion of Kevlar to LIG, LIG-based wearable sensors might be used in the military, firefighting, and sports sectors, among other things. Furthermore, we will investigate the possibilities of LIG production with ordinary fabrics, as well as the cleaning challenges associated with textile LIG devices.

4:30 PM SB10.04.08

Length Scale and Composition Dependent Large Deformation Mechanical Behavior of Hydrogen-Bonded Polymer Nanofibers Adwait Gaikwad and Pavan V. Kolluru; Texas A&M University, United States

There usually exists a trade-off between making a material ductile so that it can support large deformation and making it strong so that it can withstand large forces. Biological soft materials such as spider silk or collagen have inspired the use of a network of dynamic bonds (hydrogen bonding or metal coordination), which dissipate energy through rupture and reformation during the deformation, to simultaneously improve strength and toughness. Similarly, fabricating small nanoscale structures has also been reported to help overcome the strength-toughness trade-off. In this study, we systematically study the combined effect of structural length scale and hydrogen bond (H-bond) concentration on the mechanical behavior of polyvinylpyrrolidone (PVP) and tannic acid (TA) nanofibers. Using a unique submicron scale uniaxial mechanical testing with microelectromechanical system (MEMS), the elastoplastic mechanical response of individual PVP-TA fibers was studied as a function of their fiber diameter and molar concentration of TA (i.e., effect of H-bond density). Our studies reveal a complex interdependence of nanofiber mechanical response on the fiber diameter and TA concentration. It was observed that elastic and plastic properties of PVP-TA nanofibers are very differently dependent on the fiber diameter and TA concentration, with the thinnest fibers being stiffer and more resilient, at lower TA concentrations, while thicker fibers show better elastic response at large TA concentrations. In contrast, the plastic deformation response of PVP-TA nanofibers was found to display a more complex, non-monotonic dependence of on fiber diameter and TA concentration. This presentation will outline these trends and infer the underlying role of the H-bonded network in controlling submicron scale mechanical behavior. The results of this study will effectively help develop novel hydrogen-bonded polymers with effective mechanical and functional responses.

4:45 PM SB10.04.09

Liquid-Metal-Superlyophilic and Conductivity-Strain-Enhancing Scaffold for Permeable Superelastic Conductors Qiuna Zhuang and Zijian Zheng; Hongkong Polytechnic University, China

Stretchable electronics find widespread uses in a variety of applications such as wearable electronics, on-skin electronics, soft robotics, and bioelectronics. Stretchable electronic devices conventionally built with elastomeric thin films show a lack of permeability, which not only impedes wearing comfort and creates skin inflammation over long-term wearing but also limits the design form factors of device integration. Liquid metal (LM) has recently been used as an advanced stretchable material for constructing stretchable and wearable electronics. However, due to the poor wettability of LM and the large dimensional change during stretching, it remains very challenging to obtain a high conductivity with minimum resistance increase over large tensile strains while maintaining adequate permeability.

To address the challenge, an LM-superlyophilic and stretchable fibrous thin-film scaffold is reported, on which LM can be readily coated or printed to form permeable superelastic conductors. In contrast to conventional LM-based conductors where LM particles are filled into an elastic matrix or printed on the surface of an elastic thin film, the LM can quickly infuse into the LM-superlyophilic scaffold (within seconds) and form bi-continuous phases. The LM-superlyophilic scaffold shows unprecedented advantages of an extremely high uptake of the LM and a conductivity-enhancement characteristic when stretched. As a result, the LM-based conductor displays and ultrahigh conductivity of 155,900 S cm⁻¹ and a marginal resistance change by only 2.5 fold at 2,500% strain. The conductor also possesses a remarkable durability over a period of 220,000 cycles of stretching tests. The printing of LM onto the LM-superlyophilic scaffold for the fabrication of various permeable and wearable electronic devices is demonstrated.

SESSION SB10.05: Poster Session

Session Chairs: Tricia Carmichael, Jesse Jur, Christian Müller and Myung-Han Yoon

Tuesday Afternoon, November 29, 2022

8:00 PM - 10:00 PM

Hynes, Level 1, Hall A

SB10.05.01

Soft And Flexible Enzyme Fibers for Powering Wearable Devices from Body Fluids Shiqi Wu, Yi Ding, Wenyao Lei, Daniella Marie B. Gatus and Takeo Miyake; Waseda University, Japan

Wearable devices with biocompatible mechanical behavior have garnered much attention in field of power harvesting, biomedical sensing and others. Functionalized fibers could be used in wearable devices as several elements of display, sensor, medical therapy, and batteries. Here, we demonstrated a soft and flexible enzyme fibers for a biobattery in wearable devices.

The proposed fibers consist of an enzyme/Poly(1-vinylimidazole)-Osmium/carbon nanotube(CNT)/fiber for biofuel oxidation, and enzyme/multi-layered CNT/fiber for oxygen reduction. These fibers applied to the skin applications on cloth, bracelet, and semi-implantation of needle insertion.

[1] Biosensors and Bioelectronics, 179, 113107, 2021. "Fiber-crafted biofuel cell bracelet for wearable electronics"

[2] Biosensors and Bioelectronics, 165, 112287, 2020. "A needle-type biofuel cell using enzyme/mediator/carbon nanotube composite fibers for wearable electronics"

[3] Biosensors and Bioelectronics, 141, 111471, 2019. "Wearable high-powered biofuel cells using enzyme/carbon nanotube composite fibers on textile cloth"

SB10.05.02

High-Performance Textile Supercapacitors Based on Laser-Induced Graphene Composite Electrodes Soongeun Kwon, [Hak-Jong Choi](#), Junhyoung Ahn, Hyungjun Lim, Geehong Kim, Kee-Bong Choi and JaeJong Lee; Korea Institute of Machinery and Materials, Korea (the Republic of)

Electronic textiles (E-textiles) have garnered extensive attention due to their extended usage in various applications such as sensors, actuators, and energy harvesting, and storage devices, and even displays. While individual functions of each E-textile have been separately researched, the energy storage device to power E-textiles should be integrated in the form of textile for practical applications. Supercapacitors (SCs), thin-film energy storage devices, have received a great deal of attention as power sources for wearable, textile or stretchable electronic devices due to their fast charging capability, long life cycle, and good safety. Various ink printing techniques (screen printing, inkjet printing, 3D printing) have been employed to fabricate electrode patterns of textile SCs. Even though these ink printing techniques are considered to be compatible with large-scale production, the preparation of inks based on high performance nanomaterials requires a costly, time-consuming and complicated process including high temperature synthesis or dispersion in an organic solvent. A cost-effective and facile textile SC fabrication process without ink materials is thus required.

Laser-induced graphene (LIG), obtained by the direct laser writing of various types of carbon precursors, have widely researched as electrode materials of flexible supercapacitors with the advantages of 3D porous electrodes with high crystallinity, hierarchical porosity, and high surface area. However, these superior properties of LIG electrode were not applied in textile energy storage devices yet.

In this work, LIG-based textile SCs (LIG-SCs) were fabricated by thermal transfer printing. A LIG directly laser-written on a PI film was transferred onto the adhesive film area of textile substrates during thermal transfer printing. The electrochemical performances of the as-fabricated textile LIG-SCs were investigated. Especially, LIG-SCs based on LIG-metal composite electrodes exhibit fast ion transport for high-rate performance with capacitive rectangular shapes at high scan rates of up to 20V/s, suggesting outstanding rate capability among graphene-based textile SCs. Moreover, LIG-SCs demonstrated the possibility of practical usage as textile energy storage devices such as cyclic stability, a waterproof property, and control of the working voltage or capacitance by series or parallel connection.

SB10.05.03

Carbon Nanotube Textile Skin Electrodes for ECG Sensing Md Milon Hossain^{1,2}, Braden M. Li¹, [Busra Sennik](#)¹, Jesse S. Jur¹ and Philip Bradford¹; ¹NC State University, United States; ²Khulna University of Engineering & Technology, Bangladesh

Advanced carbon materials, metallic nanoparticles and conductive polymers are widely used for fabricating textile electrodes. Among the carbon materials, carbon nanotubes (CNT) demonstrate high aspect ratio, excellent mechanical properties, ultralight weight, good thermal and electrical properties. However, most of the electrodes fabricated using CNTs are composite film and lack breathability and comfort. Here we report the fabrication of CNTs wrapped textile yarns which are strong and flexible for different textile processing. We developed a textile processable yarn by wrapping CNTs over cotton and spandex yarn in a core-shell structure. The spandex core renders the yarn with high stretchability and ultra-conformability to the skin providing high reliability against mechanical deformation and motion artifacts. No adhesive and tethering required for our developed electrode to measure ECG and could be worn and washed as a regular textile. We demonstrated that the systematic design of the electrode will record comparable ECG signals of Ag/AgCl electrode in different body movement conditions.

SB10.05.04

OEET Based Lactate for Real Time Diabetic Wound Monitoring Yuchen Shao, Manisha Gupta, Jiaxin Fan and [Paul Lavryshyn](#); University of Alberta, Canada

Diabetic patients have an increasing risk of developing the diabetic foot ulcer (DFU). If left untreated these wounds can lead to foot amputations. Clinical research has shown that real time monitoring of the lactate concentration helps guide therapy and improve patient outcome [1]. Blood tests for measuring lactate levels can provide only the systemic levels. We are developing a non-invasive and low-cost lactate biosensor which can provide the localized wound lactate levels and can provide continuous measurements to monitor the wound health.

In this research, we developed a 3D-printed lactate sensor on top of the flexible Kapton substrate. Organic electrochemical transistors (OEETs) are chosen for the biosensor because of its good performance for the ion-to-electron transduction and signal amplification. Sensors are fabricated using Optomec Aerosol Jet 5X printer with Au as the source and drain electrode, Pt as the gate, poly(3,4-ethylenedioxythiophene) doped with polystyrene sulfonate (PEDOT:PSS) as the channel and polyimide as the insulator layer. The printed gate was first dropped casted with mixed chitosan and LoX. Functionalized sensors were stored under 4 degrees for 24hrs until they were fully dried and then washed with DI water and PBS solution. The device was measured in simulated wound fluid and has the response range from 500uM up to 5mM with a sensitivity of 117 uA/mM. Later, the layer-by-layer strategy was attempted according to the sequence nafion, chitosan and LoX, which exhibited a better range up to 10mM. Modifications to the functionalization method, such as carboxy-functionalized multi-walled carbon nanotubes (MWCNT) mixed with Tetrathiafulvalene (TTF), nafion, L-Lactate oxidase (LoX) and chitosan in acetic acid were dropped casted one after the other will be tried for further improvement. In addition, pH and extra reactions are also taken into consideration to help further correction for the lactate sensor. The results from the developed lactate sensor will be presented.

[1] Jia W, Bandothkar AJ, Valdés-Ramírez G, et al. *Electrochemical tattoo biosensors for real-time noninvasive lactate monitoring in human perspiration*. *Analytical Chemistry*. 85(14):6553-6560. doi:10.1021/ac401573r

SB10.05.05

Electrospun Fiber Laminate Triboelectric Nanogenerator for Acoustic Energy Harvesting Artis Linarts, Kaspars Malnieks and Linards Lapčinskis; Riga Technical University, Latvia

Triboelectric nanogenerators (TENG) are intriguing energy harvesting devices that convert mechanical energy into electricity and could power small portable devices or charge batteries [1]. Here we report acoustic triboelectric nanogenerator (A-TENG) consisting of polymer nanofibers made with electrospinning technique. A-TENG consist of up to 30 layers of polymer fibre mats with total thickness of 200µm. Two polymers with opposed properties were chosen and with a custom made electrospinning device the fibres were collected on a rotating drum collector covered with a flexible electrode. Different triboelectric surface properties of laminate creates multiple triboelectric interfaces with dipole alignment across the volume of laminate; therefore this design allows electrical power generation in very low vibrations environments (40dB sound pressure).

The reported laminates in this study hold a great potential in the field of flexible triboelectric nanogenerator.

[1] Z.L. Wang "Triboelectric Nanogenerators as New Energy Technology for Self-Powered Systems and as Active Mechanical and Chemical Sensors", ACS Nano 7 (2013) 9533-9557.

This work has been supported by the European Regional Development Fund within the Activity 1.1.1.2 "Post-doctoral Research Aid" of the Specific Aid Objective 1.1.1 "To increase the research and innovative capacity of scientific institutions of Latvia and the ability to attract external financing, investing in human resources and infrastructure" of the Operational Programme "Growth and Employment" (No.1.1.1.2/VIAA/3/19/416).

SB10.05.06

Smart Sensing Sutures for Real-Time Glucose Monitoring Mossab K. Alsaedi, Junfei Xia, Atul Sharma, Rachel Riccio, Rachel E. Owyung, L. M. Romero and Sameer R. Sonkusale; Tufts University, United States

Real-time monitoring of glucose levels in living organisms is a key indicator of various biological processes. Specifically, monitoring glucose and other biomarkers in avian species (e.g. house sparrows) is a key indicator of the animal's stress level. Current stress level monitoring methods are invasive and require multiple interactions with the animal (collecting blood samples at different time points). Therefore, a less invasive and continuous monitoring method is preferred.

Flexible bioelectronics have emerged in the fields of precision health and medicine as they offer seamless electronic-tissue interface in terms of physical contact and mechanical properties (comparable elastic moduli). Threads have previously been utilized in biomedical applications to realize thread-based transistors, biosensors, and even drug-delivery platforms. Threads' one-dimensional, flexible characteristics ensure seamless integration with underlying tissues and organs better than two-dimensional, planar platforms and ensure intimate contact with tissue/organ surfaces, as exemplified by sutures. The fibers they are comprised of can be specifically chosen from biocompatible sources, such as silk and poly(lactic-co-glycolic acid) (PLGA), to tailor their use more towards biomedical applications. Further, thread-based biosensors are small and light enough not to interfere with flight movement during continuous real-time monitoring.

In this study, we realize sensing sutures for glucose monitoring using electrochemical principles. We use a three-electrode system: the working and counter electrodes are made of medical-grade sutures while the reference electrode is a commercial Ag/AgCl (1 M KCl) electrode. The conductive layer on the working and counter electrodes is gold via solution-based electroless deposition and plating. This produces a more uniform and connected coating layer of gold on the thread's rough, uneven surface. Compared to other conductive coatings, such as carbon which requires multiple coatings for adequate conductivity, electroless deposition of gold produces a more flexible conductive suture. Gold nanoparticles were synthesized, characterized, and deposited on the sutures. In addition to the conductive layer, an electron-mediating layer (Prussian blue) is electrically deposited and enzyme-chitosan bilayers are coated. Glucose oxidase, which is the enzyme immobilized in the enzyme-chitosan matrix, catalyzes the electron-producing reaction that glucose undergoes in the presence of oxygen and, as a result, alters the current in the system. At all steps, FTIR and SEM are utilized to confirm the presence and quality of each coated layers.

We demonstrate functionality of sensors by obtaining calibration curves and test data for real-time glucose monitoring, sensor stability, sensor repeatability, and analyte interference. The sensing sutures had a sensitivity value of 0.933 ± 0.115 nA/mM within a range from 0 mM to 54.9 mM glucose with an LOD value of 0.62 mM. They demonstrated successful real-time monitoring of change in glucose concentration over an operating period of 40 minutes and sensor stability of at least five days. In addition, the sensing sutures showed selectivity towards glucose even with the presence of other molecules, such as lactate. Tests and measurements were performed in 1X phosphate-buffered saline (PBS). Furthermore, future tests will be done using ex-vivo tissue models and in-vivo animal models. While glucose sensing has been reported, sensing sutures can be expanded to other analytes, such as lactate, electrolytes, chemokines, and metabolites.

SB10.05.07

Aptamer Functionalisation of Semiconducting Polymer Thin Films for Applications in Biosensing Organic Field-Effect Transistors William Neal, Matteo Palma and Christian Nielsen; Queen Mary University of London, United Kingdom

Point-of-care devices are a promising area of technology, with applications in personalised healthcare. Such devices aim at improving secondary preventative medical strategies, by detecting a disease before symptoms start to develop. Multipurpose, portable and easy-to-use sensing devices will increase the accessibility of diagnostics, resulting in earlier detection and treatment of disease. Integration into wearable technology would enable constant health monitoring, effectively minimising diagnostic times.

Developing upon initial work published within our group, we propose to incorporate favourable solution processable organic semiconducting polymers into a biosensing field-effect transistor. Functionalising a field-effect transistor with receptors, would allow for selective and amplified detection of analytes. Biomarker specific aptamers would endow the device with highly selective and chemically resistant sensing properties. However, receptor functionalisation of semiconducting polymers is challenging, as high-performance materials lack chemical groups exploitable for covalent attachment.

We will present foundational work carried out towards fabricating a biosensing platform. By blending a high-performance polymer (DPP-DTT), with a cross-linking agent (glutaraldehyde), the resulting polymer thin-films can be successfully functionalised with receptors. Primary amine terminated aptamers, in solution, react with glutaraldehyde, via a condensation reaction, covalently attaching the receptor to the surface. Successful thin-film functionalisation is observed in several characterisation techniques. Atomic force microscopy, X-ray photoelectron spectroscopy, fluorescent microscopy and water contact angle measurements are presented, as supporting evidence of the functionalisation of the receptor to the surface of the thin-film. Covalent attachment of the aptamer to the polymer was confirmed, as well as the accessibility of the aptamer binding to the target biomarker. Preliminary device architecture and polymer thin-film functionalisation strategies are presented, and once further optimised, combined to fabricate a sensor for detection of target biomarkers.

SB10.05.09

Fully Stretchable Sandwich Structured Textile-Based Triboelectric Nanogenerator with a Crepe Paper-Induced Surface Microstructure Kim Da Eun and Youn Tae Kim; Chosun University, Korea (the Republic of)

As various wearable devices are released, self-powered wearable energy harvesting technology is in the spotlight as a next-generation technology. Among them, research on triboelectric nanogenerator (TENG), which efficiently converts mechanical energy into electrical energy, is being actively conducted. In particular, the textile-based TENG is one of the most promising energy harvesters for realizing wearable devices and self-powered smart clothing. However, most of the existing textile-based TENGs generate energy only in the intentional vertical-contact mode, and have poor durability against twisting or bending deformation using metal materials.

This study, we propose a sandwich structured textile-based TENG (STENG) with a stretchability and fully flexibility for wearable energy harvesting. One side of stretchable textile is coated with micropatterned EcoFlex and used as a negative triboelectric material. The performance of power generation was improved by patterning the EcoFlex surface based on the microstructure of the crepe paper surface. The other side, acetate cloth tape is attached to the stretchable textile as a serpentine structure, and is used as a positive triboelectric material. Since this is a serpentine structure, it is possible to expand and

contract up to 50% in the lateral direction. The top of the acetate cloth is sewn with yarn to generate an air gap, which can generate energy even in stretching mode. That is, through friction between micropatterned EcoFlex and acetate, STENG harvests mechanical energy in the contact-separate, stretching, and rubbing modes. In addition, since all flexible materials are used, the structure is free from deformation. The output of 361.3 V and 58.2 μA in the contact-separate mode, the output of 166.1 V and 23 μA in the stretching mode, and the output voltages and currents of 119.5 V and 17 μA in the rubbing mode were observed. This is the result of 250% improvement in output performance compared to the flat EcoFlex-based STENG without nanopatterns. Finally, we successfully demonstrated the operation of the 135 LEDs using STENG's output without external power source. These findings could provide a textile-based power source with practical application in future e-textile and self-powered electronics.

SB10.05.11

A Coupled Electrochemical-Mechanical Analysis of Textile Battery Using Multi-Scale Modeling [Dongwon Jang](#) and [Woong-Ryeol Yu](#); Seoul National University, Korea (the Republic of)

Textile battery is a novel fiber-shaped energy storage device that has the capability of flexibility fabricated by numerous yarn assemblies (i.e., woven fabric). Carbon fiber and polymer electrolyte are used for textile battery, each of which contributes to acting as an electrochemical electrode and transporting Li-ion with superior mechanical properties. It is difficult to predict effective electrochemical and mechanical behaviors of yarn-based whole textile battery due to complexity. Herein, we developed a simplified yarn model of textile battery comparing electrochemical and mechanical similarities between yarn scale and filament scale. First, electrochemical and mechanical homogenization methods were applied to the yarn model and visual modeling of carbon fiber and polymer electrolyte was implemented in the filament model. Comparison between homogenized yarn model and filament model was quantitatively carried out using 3D shape descriptors (compactness and cubeness) and a volume-averaged method, demonstrating high accuracy and efficient computational time of the homogenized yarn model. Next, a damage model under flexible condition (i.e., bending) was incorporated into the homogenized yarn model to consider external load effect on the electrochemical performance of textile battery. The effect of different bending conditions on the voltage profile and capacity of textile battery was investigated. Using the developed homogenized yarn model including damage, the electrochemical and mechanical performances of textile battery can be simulated, and detailed results will be presented at the conference.

SB10.05.12

Investigation of Reliability of a Flexible Pressure Sensor Based on a Polyethylene Carbon Composite - Velostat [Anis Fatema](#) and [Aftab M. Hussain](#); International Institute of Information Technology Hyderabad, India

Nanoparticle-based polymer composite materials are receiving attention for the development of sensors for various flexible and wearable electronic applications. However, it is important to test a material's reliability to validate the quality of the product and to ensure that the results obtained are accurate and repeatable. Flexible pressure sensors utilized in wearable and textile devices are subjected to continuous force and stress that may affect the sensor's response in the long run. Hence, reliability assessment is an essential factor to consider when designing any sensor. In this work, we have tested the reliability of a carbon-impregnated polymer composite named velostat, over repeated usage and bending cycles during the course of a year. It is an opaque conductive film of polyethylene impregnated with carbon particles, making it an electrically conducting composite material. It has been extensively explored because it is low-cost, thin, flexible, lightweight, and easy to fabricate. It works on the principle of piezoresistivity; the higher the pressure applied to the velostat, the higher the conductivity and the lower the resistance.

We evaluated the reliability of velostat by implementing this material into the design of a flexible pressure sensor array. The reliability assessment was performed on the pressure sensor array for one year. The sensor array was designed and fabricated as a multi-layer matrix structure. The top and bottom layers were the protective layers made of PVC sheets on which the conductive layers were pasted. The protective layers were transparent, thin, soft, and inexpensive. The thickness of the protective layers was $135 \pm 1 \mu\text{m}$ each. The conductive layers were conductive adhesive copper tapes. The copper electrodes were pasted in a crossbar architecture format and had a rectangular cross-section. The ends of the copper tapes were soldered with wires connected to the microcontroller. The thickness of copper tape with an adhesive layer was measured to be $60 \pm 1 \mu\text{m}$. The middle layer was the piezoresistive material, velostat. Four copper electrodes were pasted on each protective layer. The size of each sensor pixel was $10 \text{ mm} \times 10 \text{ mm}$, and they were separated by a distance of 50 mm. Hence, it was a 4×4 sensor matrix with 16 individual pressure sensors and a total thickness of $434 \mu\text{m}$ (as measured by a Mitutoyo micrometer).

To analyze the reliability of the velostat-based pressure sensor, we conducted experiments for twelve months. In the first experiment, we tested the sensor's response every fortnight by applying a load of 1 kg to all sixteen sensors. We observed that with time, there is a change in the sensor response due to the non-homogeneous characteristics of the velostat. The sensor's response changed with an average standard deviation of 0.09 V. We also tested the sensor response to the application of higher loads by applying weights ranging from 1 kg to 12 kg every fortnight. We observed that there is less gradation in the resistance during the starting three months. As the molecules in the velostat start settling, the resistance shows more gradation on applying pressure and is closer to the ideal graph. We also evaluated the decay rate of the sensor. The decay rate is calculated by taking the sensor's response voltage ratio for all the weights. We observed that in the initial three months, there was a deviation in the decay rate by 0.11, which was reduced to 0.02 in the last six months' analysis.

The results obtained from the experimental tests for reliability show a practical possibility of implementing velostat-based pressure sensors in wearable and healthcare devices. The sensor mat is highly scalable and can be used in various applications like foot pressure monitoring, gait analysis, sitting posture recognition and correction, body pressure measurement, detection of bed sores, and many more.

SB10.05.13

Flexible Triboelectric Laminates—Energy Harvesters for Wearable Electronics [Kaspars Malnieks](#), [Andris Šutka](#), [Linards Lapčinskis](#) and [Artis Linarts](#); Riga Technical University, Latvia

Triboelectric nanogenerator (TENG) devices have attracted considerable interest in the field of mechanical energy harvesting due to their low weight and mechanical softness. There are many innovative TENG devices from low-cost materials presented in the literature for mechanical energy harvesting from human motion, vibrations, wind, water flow, and waves[1].

Herein we report a new paradigm of triboelectric polymers – the triboelectric laminate – a volumetric material with electromechanical response comparable to the benchmark soft piezoelectric material polyvinylidene difluoride. The electromechanical response in the triboelectric laminate arises from aligned dipoles, generated from orientation of contact electrification in the laminates bulk volume. The triboelectric laminates where the polymer bilayers with different triboelectric properties are stacked to form laminates, together with the separator between each bilayer and for an electrodes we use flexible polyisoprene conductive carbon black composite. The dipoles are forming between sequential bilayers consisting of two different polymer fibres of different diameter. The loose interface between fibre bilayers ensures friction and triboelectric charging between two polymers. The electric output from the electrospon triboelectric laminate increases with increasing the density of bilayers. Triboelectric laminate generates Volumetric energy density of $21.13 \mu\text{J cm}^{-3}$ and a peak average power density of $46.19 \mu\text{W cm}^{-3}$ are observed from six layer laminate. Our material concept has clear benefits over the other flexible devices for mechanical energy harvesting. It does not require any poling procedures and electromechanical response is stable over 24 hours of continuous operation. Moreover, the electromechanically responsive material can be made from all types of polymers, thus providing ample of room for further improvements or functionalities such as stretchability, biodegradability, or biocompatibility. The concept of a triboelectric laminate can be

introduced into existing triboelectric nanogenerator form factors, to dramatically increase charge harvesting of a variety of devices.

This work has been supported by the European Regional Development Fund within the Activity 1.1.1.2 "Post-doctoral Research Aid" of the Specific Aid Objective 1.1.1 "To increase the research and innovative capacity of scientific institutions of Latvia and the ability to attract external financing, investing in human resources and infrastructure" of the Operational Programme "Growth and Employment" (No.1.1.1.2/VIAA/3/19/404)

1. Wang, S., Lin, L. & Wang, Z.L., "Triboelectric nanogenerators as self-powered active sensors", *Nano Energy*, (2015)vol. 11, pp. 436-462.

SB10.05.14

Conductive Polymer Based Pressure Sensors for Optimization of String Instruments Practice Noemy Gagnon-Lafrenais, Pierre Kateb, Xin Zhou and Fabio Ciccoira; Polytechnique Montréal, Canada

Repetitive movements in string instrument performance can lead to injuries such as tendonitis and muscular fatigue. It is believed that the pressure applied on a bow can influence the quality and magnitude of sound produced by the instrument. We are interested in exploring the correlation between the applied force at the hand and bow interface and the vibrations recorded on the stick of the bow.

Poly(3,4-ethylenedioxythiophene)polystyrene sulfonate (PEDOT:PSS)-based[FC1] materials have been widely explored as potential candidates for precise pressure sensor¹. Some recent applications, such as PEDOT:PSS polyurethane foam have been successfully demonstrated for a foot pressure sensor².

In this project, we demonstrate a pressure sensor made of a PEDOT:PSS-based soft Organohydrogel which can be applied on the right hand at critical contact points whilst using a violin bow. The pressure sensor consists of an organohydrogel disk encapsulated in a transparent film. An interdigitated silver (Ag) electrode is printed on one of the substrates with an inkjet printer. The gel is a mixture of poly(3,4-ethylenedioxythiophene), ethylene glycol and tannic acid (PEDOT:PSS/EG/TA), which It has been demonstrated by our group that this material has a high conductivity of approximately 15 S/cm.

Cyclic compression tests have been realized on the organohydrogel. It has shown a response in resistivity for up to 7.5% strain for a 4 mm thick sample. The gel also showed moderate stability for up to 40 cycles. Moreover, we have been able to show that the designed pressure sensor has a response in resistivity to very subtle variations of pressure, while playing a two-octaves scales on the violin.

Future objectives are to study in more detail how the variation of applied force affects the resistance of the material. Furthermore, we wish to compare the effect of pressure on sound production by attaching a contact microphone to the bow. With these two sets of data, we will be able to build a model that will provide visual support when solving issues linked with string instrument practices. It will be a helpful tool in the optimization of sound production and the resolution of exceeding pressure that can link to injuries such as tennis and golfer's elbow.

SESSION SB10.06: Functional Materials and Devices II
Session Chairs: Edwin Jager, Jesse Jur and Darren Lipomi
Wednesday Morning, November 30, 2022
Hynes, Level 3, Room 311

8:30 AM SB10.06.01

Chip on a Fiber Toward the E-Textile Computing Platform Tae-Wook Kim; Jeonbuk National University, Korea (the Republic of)

Fiber electronics are of considerable interest for wearable applications and smart textiles, and they can facilitate communication and the interaction between humans and surroundings. As a basic element of functional textiles, the one-dimensional (1D) form of thread-like fibers offers high flexibility, isotropic deformations, breathability, and light weight in fabric structures. The 1D functional fibers can be further processed into two-dimensional (2D) textile and three-dimensional (3D) yarn configurations through traditional textile engineering techniques, such as twisting, weaving, sewing, knitting, knotting, and interlacing. Owing to such intrinsic merits, in recent years, fiber-based device components that perform optoelectronic functions, such as health/environmental monitoring, displays, sensing, energy harvesting, energy storage, electromagnetic shielding, and information processing, have been integrated directly into fabrics to demonstrate futuristic clothes. The existing electronic fiber platforms are generally composed of only one type of electronic component with a single function on a fiber substrate that is attributed to all around wrapping of an active layer on the entire fiber without patterning at the desired area on the surface of the fiber during the manufacturing process. Moreover, a precise connecting process between each electronic fiber is essential to configure the desired electronic circuits or systems into the 2D textile while minimizing the degradation of the device performance. Although assembly of those functional fibers can be used for recording, detecting, and readout data sequentially, similar to conventional integrated circuits and multifunctional devices on 2D wafers, both limitations on scaling down and difficulty in the configuration of the electronic circuit remain major obstacles for the implementation of practical electronic fiber systems. To impart multiple functions to the textile, the methods of inserting small electronic components into a fiber strand or yarn have been considered emerging candidates, enabling the implementation of a thermally drawn digital fiber and e-yarn. However, a limitation to the thermal drawing approach and the mounting of small components on the top surface of a filament is the low device density. A new strategy to fabricate a high-density electronic microfiber possessing multiple electronic components and circuits as well as maintaining excellent electrical performance has not yet been reported. In this work, we present a new electronic fiber platform that enables LSI of electronic device components on the surface of a 1D fiber, defined as a monofilament with a diameter of 150 μm. By using high-resolution maskless photolithography with a capillary tube-assisted coating method, multiple miniaturized device units are integrated onto a very narrow and thin fiber surface. As a proof-of-concept demonstration, basic electronic devices (field-effect transistors, inverters, and ring oscillators) and sensors (photodetectors, signal transducer, and distributed temperature sensors consisting of thermocouples) are fabricated onto the two different sides of the rectangular fiber. The chip on a fiber exhibits various electronic functions (UV detection and switching electrical signals in a single transistor, symmetric input/output behaviour in the n-type inverter, oscillation characteristics of 5-stage ring oscillator) and thermal sensing performance. We believe that our approach is one of the big steps to implement a high-density electronic fiber platform for integrated electronic textiles.

8:45 AM *SB10.06.02

Continuous Wet-Spinning of Two-Dimensional Colloid Nanoplates into Fibers for Wearable Energy and Sensor Applications Tae Hee Han; Hanyang University, Korea (the Republic of)

The miniaturized fiber-based wearable devices are considered promising alternatives compared to conventional heavy three-dimensional (3D) and two-dimensional (2D) devices. Large-scale, straightforward wet-spinning of two-dimensional (2D) materials has emerged as a promising direction for processability to develop meter-long dimensional fibers. For example, graphene fibers (GFs) have great potential in future portable wearable electronics, which have gained considerable attention owing to high electrical conductivity, lightweight, tiny volume, outstanding mechanical flexibility, excellent

deformability, low cost, and the ability to be woven into smart textile fabrics. Herein this work, I introduce that GFs are derived from wet-spinning of graphene oxide (GO) dispersions which are demonstrated as safe electrodes for wearable energy and sensor applications. The Ni/NiO/GF sensors exhibit a 16-fold higher response to NO₂ gas and effective recovery characteristics. Furthermore, the Ni/NiO/GF with excellent mechanical flexibility and deformability were integrated into the commercial cotton fabric, thus demonstrating the feasibility of using the hybrid graphene fibers in wearable gas sensors. Additionally, hybrid metal oxide/GF all-solid-state supercapacitors exhibited an enhanced volumetric capacitance compared to pristine GF electrodes. The excellent performance and simple large-scale wet-spinning process pave the way for portable wearable electronics devices. Finally, I will introduce this wet-spinning strategy can be applied to another type of 2D nanosheets, such as MXene. By taking advantage of strong molecular interactions between MXene sheets, mechanically strong fibers can be fabricated by drawing the MXene gel. Because Ti₃C₂T_x MXene fiber has dense lamella and a highly aligned multiscale structure, MXene fibers exhibit outstanding electrical conductivity and a high mechanical modulus compared with other MXene-based assemblies.

9:15 AM SB10.06.03

High Mobility Organic Electrochemical Transistors for Electronic Textiles Paula Alarcon Espejo^{1,2}, Ruben Sarabia^{1,2}, Maryam Shahi^{1,2}, Matthew Weisenberger^{1,2} and Alexandra Paterson^{1,2}; ¹University of Kentucky, United States; ²Center for Applied Energy Research, United States

To date, PEDOT:PSS fibers demonstrate high electrical and thermal conductivity as well as exceptional mechanical properties making them promising candidates for use as fundamental building blocks of next-generation smart electronic textiles. Organic electrochemical transistors (OECTs) play an essential role in many bioelectronic applications. PEDOT:PSS is one of the most widely used channel materials in biocompatible OECTs due to its ability to facilitate mixed ionic and electronic conduction. Recently, the integration of PEDOT:PSS fibers in transistors has been a topic of interest due to its light weight, flexibility, and ability to integrate electronic functions in textiles. PEDOT:PSS fibers have potential to be used to obtain mechanical, electrical, chemical and thermal data for various environmental stimuli. One of the main challenges in OECTs device engineering is related to the contact interface between the semiconductor and the source-drain. Contact resistance affects charge transfer, lowering the performance in device operation and can lead to failure. In this work, we demonstrate the application of PEDOT:PSS fibers in OECTs and the performance of these devices based on the channel morphology and contact resistance.

9:30 AM BREAK

10:00 AM SB10.06.04

Influence of Textile Architecture on the Electrical Resistivity of Inkjet Printed Ag Nanoparticle Inks Zixin Wang and Brian Derby; University of Manchester, United Kingdom

Textile substrates provide promising platforms for wearable technology that can provide both strength and flexibility making them potentially more comfortable to wear than rigid wearable alternatives. They can be made stretchable, breathable, and washable and are easily integrated into clothing. Inkjet printing is widely used to fabricate printed electronic devices and is also a common tool for patterning textiles. However, it is well known that the rough and porous textile surface makes it difficult to reliably print electrically conductive structures onto textile substrates. Here we report the use of X-Ray computed tomography (CT) to reveal the distribution of Ag ink after ink jet printing onto polyester textile substrates. CT images clearly show that the penetration of ink into the textiles is strongly influenced by the fibrous architecture of the fabric with capillarity confining the ink within the yarn tows running in the warp and weft directions of the weave. We have used image segmentation methods to identify connectivity of the silver objects after heat treatment and this demonstrates that connectivity, and hence electrical conductance, is less likely between tows running in each direction. This information shows that the electrical conductivity of a printed patch of Ag ink can be represented by a number of electrically independent Ag networks running in parallel and that the conductivity scales approximately with the size of the largest Ag network present.

Here we use CT imaging to analyse the distribution of Ag after printing and sintering in 6 different woven fabrics each made from the same polyester fibre with fibre diameter either 10 µm or 16 µm. Each fabric is a plain weave but with different yarn and fibre densities giving fabric weights in the range 80 – 450 g.cm⁻². We used a Fujifilm Dimatix 2800 to print 10 pL drops of a Ag nanoparticle ink at 10 µm drop spacing, with 5 layers of overprinting, to print identical patterns on each textile. After sintering at 150 °C the electrical properties of individual yarn tows in the fabric were measured using a 4-point probe. The printed fabric conductance values span three orders of magnitude, confirming the strong influence of fibre architecture on electrical properties. Image segmentation of the CT results from each fabric conclusively shows that the highest electrical conductance correlates with the presence of largest volume amongst the interconnected Ag objects. Three of the fibre architectures that show the highest electrical performance have equivalent conductivity values that are over an order of magnitude lower than that of bulk Ag and are also considerably lower than that achievable by inkjet printing Ag inks onto polymer film substrates. This work confirms that textile substrates can be used as substrates for printed conducting structures and that the fibre architecture controls the distribution of ink, the likely precision and resolution of deposition, as well as the conductivity of the printed structure.

10:15 AM SB10.06.05

Triboresistive Touch Position Sensors Younghoon Lee^{1,2}, Sungsoo Lim¹ and Jeong-Yun Sun¹; ¹Seoul National University, Korea (the Republic of); ²MIT, United States

Recent growing pursuit of skin-mountable devices has been impeded by the complicated structures of most sensing systems, containing electrode grids, stacked multilayers, and even external power sources. Here, a type of touch sensing, termed “triboresistive touch sensing”, is introduced for gridless touch recognition based on monolayered ionic power generators [1]. A homogeneous monolayer, i.e., ionic poly(dimethylsiloxane) (PDMS), generates electricity based on the electric field generated by touch. Voltages generated at each corner of the ionic PDMS rely on resistance between touch points and each corner, ensuring recognition of the touch positions without the need for electrode grid layers and external power sources. With notable advantages of high transparency (96.5%), stretchability (539.1%), and resilience (99.0%) of the ionic PDMS, epidermal triboresistive sensing is demonstrated to express touch position and readily play a musical instrument. A gridless system of triboresistive sensing allows rearrangement of the touch sections according to a given situation without any physical modification, and thus easily completes consecutive missions of controlling position, orientation, and gripping functions of a robot.

Reference

[1] Lee, Younghoon, et al. "Triboresistive Touch Sensing: Grid Free Touch Point Recognition Based on Monolayered Ionic Power Generators." *Advanced Materials* (2022): 2108586.

10:30 AM SB10.06.06

Lightweight and Flexible Flat-Knit Metasurfaces, Reflectarrays and Array Antennas Michael Carter¹, Leah Resneck², Younes Ra'di³ and Nanfang Yu¹; ¹Columbia University, United States; ²North Carolina State University, United States; ³The City University of New York, United States

Phased arrays and more generally metasurfaces are a ubiquitous class of optical devices that operate based on the local control of the phase response, and sometimes amplitude response, of individual antenna elements in an overall array ordered such that the collective phase response satisfies some required profile needed to shape an outgoing reflected or transmitted wavefront in a desired manner [1-3]. Lightweight, low-cost phased arrays and metasurfaces that are easily stowable and deployable are desirable for a number of terrestrial and space-based communications and sensing applications [4-5]. Textiles represent an appealing platform for lightweight, low-cost and flexible antennas and considerable research attention in the past few decades has been dedicated towards developing simple fabric-based wearable antennas for communications and on-body sensing applications [6-9]. Considerably less research effort has been dedicated towards fabric-based antenna arrays and more complex types of antennas, such as Yagi-Uda antennas, reflectarrays and other types of functional textile-based devices such as frequency-selective surfaces and integrated waveguides [10-12].

In this work we demonstrate a novel type of lightweight, flexible textile metasurfaces and array antennas made via flat-knitting; these include a metasurface lens, a metasurface vortex beam generator, and a Yagi-Uda antenna. The textile devices were fabricated using a Shima Seiki SRY123LP flat-knitting machine at the Zeis Textile Extension – Knitting Laboratory, NCSU. Two meta-unit archetypes based on different colorwork knitting techniques were used: a simple patch antenna archetype utilizing intarsia colorwork for the Yagi-Uda antenna and a more complex float-jacquard antenna archetype for the metasurface lens and vortex beam generator. Characterization of the device performance in the mm-wave frequency range was carried out at the Advanced Science Research Center, CUNY, and all three devices exhibit desired wavefront shaping capabilities. We compare the tradeoffs between intarsia and float-jacquard flat-knit metasurfaces and compare our flat-knit devices to traditional planar rigid metasurfaces and reflectarrays. Finally, we comment on extensions of this work towards quasi-3D and conformal flat-knit array antennas.

- [1] Yu, Nanfang, et al. *Sci.* 334, 333-337 (2011).
- [2] Berry, D., R. Malech, and W. Kennedy. *IEEE Trans. Antennas and Propag.* 11, 645-651 (1963).
- [3] Pozar, David M., Stephen D. Targonski, and H. D. Syrigos. *IEEE Trans. Antennas and Propag.* 45, 287-296 (1997).
- [4] Hodges, Richard E., et al. *IEEE Trans. Antennas Propag. Mag.* 59, 39-49 (2017).
- [5] Arya, Manan, et al. *AIAA Scitech 2019 Forum.* 2019.
- [6] Locher, Ivo, et al. *IEEE Trans. on Adv. Packag.* 29.4 (2006): 777-788.
- [7] Klemm, Maciej, and Gerhard Troester. *IEEE Trans. on Antennas and Propag.* 54.11 (2006): 3192-3197.
- [8] Lilja, Juha, et al. " *IEEE Trans. on Antennas and Propag.* 60.9 (2012): 4130-4140.
- [9] Mao, Chun Xu, et al. *IEEE Trans. on Antennas and Propag.* 68.9 (2020): 6527-6537.
- [10] Tahseen, Muhammad M., and Ahmed A. Kishk. *IEEE Antennas Propag. Lett.* 17, 46-49 (2017).
- [11] Alonso-González, Leticia, et al. *IEEE Trans. on Antennas and Propag.* 66.10 (2018): 5291-5299.
- [12] Alonso-González, Leticia, et al. *IEEE Trans. on Microw. Theory and Tech.* 66.2 (2017): 751-761.

10:45 AM SB10.06.07

A Washable and Reusable Sensor System for Moisture Detection Ji-Tzuoh Lin and Cindy Harnett; University of Louisville, United States

This presentation investigates the integrity and repeatability of a washable system for moisture detection that integrates a polymer optical fiber (POF) with a consumer optical time-of-flight (ToF) sensor at the edge of an absorbent textile. Throughout the COVID-19 pandemic, disposable paper products have been in short supply, including diapers, paper towels, respirators, tampons, and incontinence supplies. Interest in washable and reusable products has soared. At the same time, there is a growing product roster of disposable electronic sensors for healthcare, such as moisture sensors in disposable diapers. These devices typically interface with a computer using resistive electronic traces and are not intended to be reused. Non-noble metal thin films, including the silver plating used in many e-textiles, corrode over time with exposure to water, losing their conductivity. All-polymer optical fiber based sensing methods promise a better washability outcome, as long as the materials can detect the signal of interest and can handle the mechanical stress of the wash-and-dry cycle. Better printable electronic materials, alloys, and soft composites are being developed, but soft optical sensors also have two key advantages versus electronic sensors: lower temperature sensitivity, and immunity to electromagnetic interference. The materials are deformable and often intrinsically stretchable, with similar mechanical properties to wearable stretch fabrics and soft robotic systems.

In the work reported here, a moisture sensor created from a plastic optical fiber (POF) is embedded in an absorbent bedding system that connects to a detachable optoelectronic readout module. This solution addresses the supply-chain challenge through reusability. The most popular type of plastic optical fiber (POF), polymethyl methacrylate (PMMA), is more suitable than glass fiber because of its flexibility and ability to recover from few-percent strains. However, PMMA is mildly hygroscopic. Fibers that absorb water can become brittle during the machine wash cycle, which soaks, rinses, and tumbles the fibers, resulting in fatigue on the fibers and ultimately breakage. Our approaches include three upgrades to commercial PMMA fibers. First, a waterproof coating is developed to mitigate damage to PMMA optical fiber caused by water absorption during the washing cycle. Second, a commercial embroidery machine is used to attach the fibers along paths in a nonwoven stabilizer layer with closely-spaced stitches, for well-distributed mechanical stress along the fiber. Third, PMMA is compared to alternative urethane-based fibers that have lower optical clarity but better stretchability for mechanical resilience.

A magnetic housing was also developed for quickly and uniformly assembling connectors onto the ends of soft waveguides, increasing the optical transmission of soft materials by improving their alignment with the optical source and detector. The connector provides a quick and repeatable reconnection to the sensor pad after the wash.

In the tests to be presented, PMMA fibers and other POFs are integrated into fabric pads, connected to junctions whose optical transmission changes in the presence of moisture, and the optical transmission in wet and dry conditions is tested with the magnetically-coupled optical source/sensor pair both before and after wash cycles. The integrity of the fiber is validated by comparing the wet/dry contrast intensity of the fibers before and after the wash cycle.

11:00 AM SB10.06.08

Direct Handwriting of All-Solution-Processed and Intrinsically Flexible Multicolor Perovskite Light-Emitting Diodes and Photodetectors on Textiles and Papers Junyi Zhao¹, Li-Wei Lo¹, Zhibin Yu² and Chuan Wang¹; ¹Washington University in St. Louis, United States; ²Florida State University, United States

Textiles and papers, made of percolation yarn- and fiber- networks, are commonly used in our daily life and they hold great potential to be platforms for next-generation flexible and wearable electronics. In this work, we report a versatile and ultra-fast mask-free fabrication strategy that enables direct handwriting of all-solution-processed halide perovskite optoelectronic devices onto papers, textiles (cotton, polyester, and nylon), and other unconventional

substrates including metal foil, plastic film, rubber balloon, vinyl glove, and even 3-dimensional surfaces such as glass vial or spheres. More specifically, we have developed and formulated universal electronic inks that could either be used in printing/coating machines or loaded into ballpoint pens for direct handwriting on target substrates. These electronic inks include poly(3,4-ethylenedioxythiophene) polystyrene sulfonate (PEDOT:PSS) and poly(ethylene oxide) (PEO) composite ink for transparent anodes, perovskite and polystyrene (PS)/ poly(methyl methacrylate (PMMA) composite ink for the photoactive layer, polyethylenimine (PEI) ink for the electron transporting layer, and silver nanowires ink for semi-transparent cathodes. The PEO component blended in the PEDOT:PSS conducting ink not only helped planarize the rough percolating yarn/fiber substrates, but also improved the conductivity and conformability of conducting film, thus leading to improved device performance and stability. By directly writing the above functional inks onto the substrate layer by layer, we have demonstrated high-performance multicolor light-emitting diodes (LEDs) with emissions covering the entire visible spectrum and photodetectors (PDs) in both a vertical photodiode configuration and a planar photoconductor configuration. The direct-drawn LEDs exhibited a brightness as high as 15,225 cd m⁻² with a turn-on voltage of 2.4 V; and the PDs exhibited an on-off ratio over 10⁴, a responsivity up to 132 mA/W, and a response time of less than 15 ms. Compared with existing microfabrication and printing processes, the direct handwriting approach allows high-performance optoelectronics being easily fabricated by untrained individuals in a time-efficient and cost-effective manner. The formulated inks buffered with handwriting technique are especially meaningful for early-stage demonstration and ideally suited for low-cost and large-area application scenarios such as E-Textiles, E-Packaging, and E-Papers with less stringent requirements on resolution. Additionally, the handwritten LEDs showed extraordinary robustness which could be bent to a 1 mm extreme curvature radius for over 5000 cycles without decay in performance. Overall, such low-cost and eco-friendly textile/paper-based LEDs and PDs could pave way for the integration of optoelectronics with wearable and human-machine interface applications.

11:15 AM SB10.06.09

Ultra-Lightweight and Ultra-Flexible PDMS/MWCNT Open-Cell Foam Nanocomposite BioSensors for Pressure Mapping Pardis Ghahramani, Kamran Behdinan, Hani E. Naguib and Zinan Cen; University of Toronto, Canada

Biomedical pressure-detecting sensors have attracted great interest in a wide spectrum of healthcare monitoring applications including injury prevention and motion analysis. However, current technologies in the market possess some drawbacks including low working pressure ranges, high hysteresis effects, and low recoverability in conditions where limited air ventilation exists such as shoe insoles, which adversely affect the performance of these sensors. To overcome these challenges, in this study a novel ultralightweight piezoresistive open-cell foam nanocomposite sensor which operates based on resistivity change in the material while an external force is applied to it, is designed and fabricated. Polydimethylsiloxane (PDMS)/multi-walled carbon nanotube (MWCNT) foam nanocomposite with two governing factors of porosity and conductive filler content was fabricated by a manufacturing approach that integrated solution casting and particulate leaching method. Mechanical properties of PDMS/MWCNT open-cell foam nanocomposite were characterized by the compression tests and its elastic and plastic behaviour were investigated. Experimental results indicated that samples with 60% porosity had higher energy absorption and mechanical strength than the samples with 70% and 80% porosities. Moreover, foam nanocomposites at the same porosities showed larger energy absorption and mechanical strength when they contained higher MWCNTs in their structure. PDMS/MWCNT foam nanocomposite demonstrated high flexibility, high compressibility up to 90%, and high recoverability in addition to limited mechanical hysteresis (less than 3%) without experiencing noticeable macroscopic damage which provides a great advantage over the similar piezoresistive sensors in the literature.

11:30 AM SB10.06.10

Self-Assembly in Supercritical Fluids—High Resolution Patterning on Curved and Flexible Surfaces Loren G. Kaake; Simon Fraser University, Canada

Organic electronic devices, especially those based on polymeric materials, offer the promise of highly flexible and stretchable circuitry and wearable electronics. However, manufacturing techniques for these promising devices has lagged behind materials development. Contrast this with small molecule devices on rigid substrates, where physical vapor deposition has already brought organic light emitting diodes into widespread use. Key advantages of this technique include thin film deposition without the need for complex in-situ chemical transformations as well as fine and highly reproducible patterning. We have developed a method of thin film formation that has all of the advantages of physical vapor deposition, while working with polymeric materials and enabling deposition on curved and flexible substrates. This technique leverages the unique properties of supercritical, near-critical, and/or subcritical fluids.¹ Counter to typical solutions, the saturation solubility of a solid solute first increases, and then decreases with increasing temperature near its critical point. We have leveraged this non-monotonic solubility behavior to deposit films onto a heated substrates. The decreasing solubility at the substrate surface simply precipitates the polymer from solution. Because the substrates are heated resistively, we can control the local heating by patterning resistive heating elements on the substrate. This we accomplished by performing photolithography on a substrate coated with indium tin oxide. When the lines were resistively heated, material deposited directly and selectively onto them. The technique also works when a thin polymer layer is inserted between the electrode array and the supercritical fluid, allowing the photolithographically patterned electrode array to serve as a patterning master for additive manufacturing onto thin and flexible materials. Moreover, the technique does not rely on line of sight mass transfer or cumbersome printing heads. We leveraged this advantage to deposit materials on to the curved interior of an elastomeric hemisphere approximately 3 mm in diameter.¹ The process will be shown to work with an aliphatic polymer and two types of organic semiconducting polymers.^{2,3} We postulate that this is a generalizable and scalable manufacturing technique that will become vital in the development of high resolution polymer circuitry.

1. Yousefi, N.; Maala, J. J.; Louie, M.; Storback, J.; Kaake, L. G., Physical Supercritical Fluid Deposition: Patterning Solution Processable Materials on Curved and Flexible Surfaces. *ACS Appl Mater. Interfaces* **2020**, *12*, 17949-17956.
2. Yousefi, N.; Saeedi Saghez, B.; Pettipas, R. D.; Kelly, T. L.; Kaake, L. G., Physical supercritical fluid deposition of polymer films: controlling the crystallinity with pressure. *Mater. Chem. Front.* **2021**, *5*, 1428-1437.
3. Yousefi, N.; Saeedi Saghez, B.; Pettipas, R. D.; Kelly, T. L.; Kaake, L. G., The role of solvent additive in polymer crystallinity during physical supercritical fluid deposition. *New J. Chem.* **2021**, *45*, 11786-11796.

SESSION SB10.07: Functional Materials and Devices III
Session Chairs: Tricia Carmichael and Tae Hee Han
Wednesday Afternoon, November 30, 2022
Hynes, Level 3, Room 311

1:30 PM *SB10.07.01

Haptic Biomaterials for Two-Way Communication with Human Physiology Darren J. Lipomi; University of California, San Diego, United States

Human culture is replete with artifacts that interact with the senses of sight, hearing, taste, and smell. Material objects whose purpose is to produce a thoughtful or emotional response through the sense of touch, however, are rare. In this talk, I present my group's recent work on the intersection between the science of soft materials and the science of touch. This field, which we have named "organic haptics," combines active polymers, contact mechanics, and psychophysics. We are beginning to understand the ways in which stick slip friction, adhesion, and capillary forces between planar surfaces and human skin affect the ways materials produce tactile objects in consciousness as mediated by the sense of touch. This work, which combines human subject experiments, laboratory mockups of human skin, and analytical models accounting for friction, has led to several important observations. In particular, we have elucidated the mechanism by which humans can differentiate hydrophilic from hydrophobic surfaces when bulk parameters such as hardness, roughness, and thermal conductivity are held constant. We examined the role of relief structures in the skin—i.e., fingerprints—in determining the human ability to differentiate between surfaces. We have taken the insights from these psychophysical experiments to design new electroactive and ionically conductive materials to produce "actuator skins" whose goal is to produce realistic sensations for applications in tactile therapy, instrumented prostheses, education and training, and virtual and augmented reality.

2:00 PM SB10.07.02

Electromechanical Simulation for Predictive Design of Textile Electronic Systems [Caitlin Knowles](#), Beomjun Ju, Kun Luan, Marissa Noon and Jesse S. Jur; North Carolina State University, United States

The electronic textile (e-textile) substrate has a substantial impact on the electrical performance, yet this impact is rarely evaluated in literature as fabrics have non-linear, anisotropic physical properties that are difficult to predict. The surrounding textile platform is therefore largely unexplored in its ability to enhance or degrade the electromechanical performance of the system. Cloth simulations generally require complex geometrical models and high computational expenditure. However, the recent emergence of particle-based 3D garment simulation in the apparel industry has allowed for rapid and increasingly accurate simulations. This work describes a methodology of predictive design and modeling of screen-printed interconnects using a particle-based 3D garment simulation tool. Specifically, the impact of various polyester-spandex substrates on the electromechanical performance was investigated and a simulation technique to predict the electrical resistance change with elongation was evaluated. A system-first testing method was developed to reliably assess the substrate impact on the system's electromechanical performance. The experimental set-up was then simulated using both particle-based and finite element simulation techniques. The relative resistance change ($\Delta R/R_0$) at 25% strain ranged from 8.2%-60.3% depending on the fabric substrate, with positive correlations between the electrical performance and the stiffness in the stretching direction. The same correlations were observed in the simulated stress and strain in the interconnect, providing evidence that the 3D simulation program can be used as a predictive platform for prototyping. The proposed method demonstrates the potential of particle-based, 3D garment simulation programs for a rapid, scalable, and accessible performance-predictive design of e-textile products.

2:15 PM SB10.07.03

Piezoelectric Fibers Endow Textiles with Acoustic Functionalities [Grace H. Noel](#)¹, Henry Cheung¹, Wei Yan² and Yoel Fink¹; ¹Massachusetts Institute of Technology, United States; ²Nanyang Technological University, Singapore

As hierarchical structures that contain multiple interfaces that serve as scattering points, textiles are traditionally thought of as structures that damp vibrations and sound. Harnessing the sensitivity of a piezoelectric composite in a fiber form factor, however, we introduce new ways for textiles to interact with sound by incorporating the "acoustic fiber" into fabrics. First, we weave an acoustic fiber into traditional fabrics to develop fabric microphones to capture sound. The acoustic fibers are created using a thermal drawing technique in which viscoelastic materials flow in a laminar regime, maintaining the cross-sectional geometry of the preform. In the fiber device, the piezoelectric domain of P(VDF-TrFE) with 20 wt% barium titanate nanoparticles is sandwiched between two carbon-loaded polycarbonate electrodes, each containing two copper wires that are fed in during the draw. The active layer and electrodes are encapsulated by a soft SEBS elastomer cladding. The measured d_{31} piezoelectric coefficient of the active domain of the fiber is 46 pC/N, which is more than double the values reported previously in literature (~20 pC/N). Coupling the acoustic characterization with laser vibrometry measurements, we deduce that the modulus of the fabric influences the curvature of the fiber, which is key to its electrical output. Through an axial bending mechanism, the fiber couples to the fabric to detect nanometer-scale vibrations in the fabric that result from the incoming acoustic pressure. In addition to fabric microphones, the acoustic fiber lends itself to many diverse applications. An array of fibers can be used to determine the direction of incident sound, and the fiber woven into a shirt can detect heartbeat and breathing rate. Additionally, rather than damping sound, textiles can be used as speakers, creating sound by applying a voltage to an acoustic fiber on fabric. Recent advances in these particular applications will be discussed.

2:30 PM BREAK

3:30 PM *SB10.07.04

Electroactive Textile Actuators for Soft Exoskeletons and Wearable Haptics [Edwin Jager](#); Linköping University, Sweden

Conducting polymers like polypyrrole can be electrochemically oxidised and reduced. These redox reactions are accompanied by a flow of counter ions and solvents from the electrolyte into or out of the polymer matrix to maintain charge balance and osmotic pressure resulting in a volume change of the conjugated polymer. This volume change can be exploited to fabricate electrochemically driven actuators in various formats from bending bilayer microactuators to macroscopic textile actuators. Yarn and textile actuators are fabricated by coating commercially yarns and fabrics with such conjugated polymers. First a thin layer of PEDOT (poly(3,4-ethylenedioxythiophene)) is applied to make the yarns or fabrics electrically conductive. Next, the yarns/fabrics are coated with the electromechanically active polypyrrole using electro-synthesis. Finally, the yarn/textile actuators are actuated by applying the appropriate redox potentials. To achieve in-air actuation, the yarns/fabrics are coated with ionogels, that function as the ion source/sink to drive the electrochemical reactions. Two ionogel coated yarns are assembled forming the anode/cathode pair of the electrochemical circuit enabling fully integrated, in-air actuation. Using advanced textile processing such yarn actuators are integrated into fabrics using weaving or knitting. These textile actuators can be integrated in garments such as soft exoskeletons and wearable haptic devices. The latest results of our textile actuators will be presented.

4:00 PM SB10.07.05

Inkjet-Printed Controllable Textile Strain Sensors for Human Motion Detection [Beomjun Ju](#), Caitlin Knowles and Jesse S. Jur; North Carolina State University, United States

Flexible strain sensors have been attractive recently to detect and monitor human motion detection for an entertaining purpose like VR or AR, and medical purpose like rehabilitation. However, current strain sensors are not feasible to integrate with wearable platforms due to the complicated manufacturing and embedding issues. Electronic textiles (e-textiles) can be an attractive alternative to conventional rigid and bulky sensors because of intrinsic textile properties such as flexibility, stretchability, breathability, washability, and high durability under extreme deformations. This work presents a novel technique for developing textile strain sensors by only inkjet-printing of metal-organic decomposition silver ink on knit fabrics along with different directions (warp, weft, bias).

For material selection, we printed a 5×20 mm conductive pattern along with bias direction on knit fabrics having different tightness. The gauge factor increased from 0.16 to 19.7 according to the increase of the tightness factor of the fabrics from 2.35 to 3.46. This is related to the ink penetration depth depending on the tightness factor. Also, yarn-level structural changes while stretching showed direction-dependent behavior. This affected the relative resistance change and gauge factor because the number of contact points between conductive paths on the yarns changed during deformation. Stretching along with weft direction showed the lowest gauge factor for all fabrics, and there was a drastic resistance increase or instant off-state along with warp direction. Stretching along with bias direction combining both warp and weft direction showed a reasonable gauge factor. Also, the gauge factor of the strain sensors can be controlled by printing paths. The increase in the number of printing paths made the ink more penetrated and showed a lower gauge factor. This means that the printed pattern can work as a strain sensor or interconnect by arranging pattern directions and printing paths. Also, the knit-based textile strain sensors have a wide range of sensing performance up to 60 % due to high flexibility as knit fabric's own property.

For a use-case scenario in wearable technologies, we fabricated a full arm sleeve with two parts of printed conductive paths, including the strain sensor along with bias direction and interconnect along with weft direction, then connected to a readout circuit and Bluetooth data transmission system. The strain sensor-embedded armband showed the resistance change that can be translated to the strain by elbow motion. This allows for a full range of elbow motion to monitor the movement without having bulky equipment attached to the arm and should remain comfortable and breathable without hindering the effectiveness of the fabric. Also, we simulated the armband prototype using CLO 3D, which is commercial particle-based 3D garment simulation software, to predict the sensing performance of the developed sensors. Due to the facile process of directly inkjet-printing on fabrics, the developed textile strain sensors can be easily integrated with wearable devices for human motion detection. Thus, they have huge potential in practical and manufacturable applications.

4:15 PM SB10.07.06

Perfusable Knits—Knitted Silicone Tube for Wearable Device Atsushi Takano and Michinao Hashimoto; Singapore University of Technology and Design, Singapore

Background. Wearable devices with embedded fluidic channels have demonstrated reconfigurable applications as fluid-based sensors and actuators (e.g., conductive ink, liquid metal and compressed air). Methods for fabricating flexible constructs with fluidic channels are essential for the development of wearable devices with advanced functions. Currently available fabrication methods are primarily based on soft lithography and three-dimensional (3D) printing, however, which are yet suboptimal in terms of fabricating embedded fluidic channels in large surface areas with complex 3D structures.

Contribution. We present an alternative route to fabricate channel-embedded, flexible constructs by knitting silicone tubes and structural yarns, which we termed perfusable knit (PK). Silicone tubes serve as both the structural components (i.e., the part constituting the textile and garments) and the functional components (i.e., the part where functional fluids are infused or perfused).

Technical achievement. PK was fabricated with a manual knitting machine using commercially available silicone tubes with 2-mm outer diameter (OD) and 1-mm inner diameter (ID). Fabrication of two-dimensional (2D) textile and three-dimensional (3D) wearable devices was readily achieved by this approach. We identified knitting gauges and patterns of knitting (e.g., jersey, rib and garter) suitable for the fabrication of 3D knitted structures. Inlay knitting with an automated knitting machine was also demonstrated to integrate silicone tubes with the textile, which served as another platform to handle liquid embedded in the textile. Tensile tests confirmed that the elongation of the textile knitted with silicone tubes was anisotropic in terms of stretchability. The textile made of the silicone tube filled with conductive ink exhibited deformation-specific electrical responses that can be used for motion sensing. Crucially, the mechanical anisotropy affected the electrical responses exhibited by embedded conductive inks. As a demonstration, a wearable force sensor in the form of a mitten consisting of silicone tube, acrylic yarn, and conductive fluids were developed for motion sensing of the finger using electrical resistance.

Significance. Overall, we developed a unique fabrication method for flexible and wearable devices by directly knitting perfusable silicone tubes. We envisage that PK will provide alternative routes for the design and fabrication of 3D wearable devices containing functional fluids, allowing for the sensing of electrical and chemical signals using sensors integrated into garments.

SESSION SB10.08: Virtual Session I: New E-Textile Materials and Devices for Wearable Electronics I
Session Chairs: Tricia Carmichael and Christian Müller
Tuesday Morning, December 6, 2022
SB10-virtual

8:00 AM *SB10.08.02

E-Textiles Power Modules—Removing the Reliance on Conventional Batteries S.P. Beeby¹, Sheng Yong¹, Nick Hillier¹, Junjie Shi¹ and Mahmoud Wagih²; ¹University of Southampton, United Kingdom; ²University of Glasgow, United Kingdom

Whilst research into electronic textiles (e-textiles) has led to ever-increasing levels of functionality and integration, the supply of power is typically limited to the use of conventional rigid batteries. Improved integration enables electronic systems to be hidden within a textile and become invisible to the user but the supply of power has not kept pace with these developments and the reliance on batteries compromises the concealed nature of the system as a whole. Removing the reliance on traditional batteries requires alternative energy supplies and/or textile-based energy storage devices (supercapacitors or batteries).

Power can be supplied by a variety of energy harvesting technologies that can convert ambient sources of energy into electrical power. Sources of power include the kinetic energy associated with the physical displacement of, or strains within, a textile. Thermal energy can be captured from temperature gradients across a fabric and solar energy in the form of light incident on the surface of the fabric can also be harvested. In addition, wireless power transfer (WPT) offers the potential to capture electromagnetic energy. These energy sources could be used to power e-textile systems directly or, more likely, to recharge textile-based energy storage devices.

This talk presents an overview of energy harvesting, WPT and energy storage devices explored at the University of Southampton. Kinetic energy has been harvested from textiles using piezoelectric, ferroelectric and triboelectric transduction mechanisms. Thermal energy harvesting has previously been demonstrated using printed thermoelectric generators. Thin film organic and dye sensitised photovoltaic cells have also been realised on textiles. WPT research includes flexible textile antennas developed to capture radio frequency electromagnetic waves and textile-based coils used to transfer energy using resonant inductive power transfer. Examples of textile-based supercapacitors and batteries will also be presented. Finally, textile power modules that

combine mechanical and RF energy harvesting power sources with the textile-based energy storage will be demonstrated. The talk will highlight the challenges and constraints that arise when working with textiles and discuss the future work required remove the reliance on conventional batteries.

8:30 AM *SB10.08.03

Textile Devices with Integrated Electronic and Microfluidics Towards Wearable μ TAS [Mahiar M. Hamedi](#); KTH, Sweden

We show methods to make next-generation textiles that embed microfluidic, and bioelectronic sensors at the fiber and architectural level for new wearable devices.

9:00 AM SB10.08.04

Battery-Free, Tuning Circuit Inspired Wireless Sensor Systems for Detection of Multiple Biomarkers in Bodily Fluids [Jinghua Li](#); Ohio State University, United States

Tracking concentration of biomarkers in biofluids can provide crucial information about health status. However, the complexity and non-ideal form factors of conventional digital wireless schemes impose challenges in realizing bio-integrated, lightweight, and miniaturized sensors. Inspired by the working principle of tuning circuits in radio frequency electronics, our recent study reports a class of battery-free wireless biochemical sensors: in a resonance circuit, the coupling between a sensing interface and an inductor-capacitor oscillator through a pair of varactor diodes converts a change in electric potential into a modulation in capacitance, resulting in a quantifiable shift of the resonance circuit. Proper design of sensing interfaces with bio-recognition elements enables the detection of various biomarkers, including ions, neurotransmitters, and metabolites. Demonstrations of “smart accessories” and miniaturized probes suggest the broad utility of this circuit model. The design concepts and sensing strategies provide a realistic pathway to building bio-integrated electronics for wireless biochemical sensing.

9:15 AM *SB10.08.05

Two-Dimensional Field-Effect Heterostructures for Wearable and Textile Electronics [Felice Torrissi](#); Imperial College London, United Kingdom

Solution processing of graphite and other layered materials provides low-cost stretchable inks enabling electronic textile devices [1]. However, the limited quality of the two-dimensional (2d) material inks, the complexity of the layered arrangement, and the lack of a suitable dielectric 2d material ink [2] has impeded the fabrication of active field effect devices on fabric based on fully-printed 2d heterostructures. In this talk I will demonstrate fully inkjet printed 2d material active heterostructures with graphene, MoS₂ and hexagonal-boron nitride (h-BN) links (Fig 1a), and use them to fabricate all inkjet printed flexible and washable ambipolar, n- and p-type field effect transistors (FETs) on textile, reaching a field effect mobility of $\mu \sim 105 \pm 29 \text{ cm}^2 \text{ V}^{-1} \text{ s}^{-1}$ on polyester fabric, at low operating voltages ($< 5 \text{ V}$) (Fig. 1b). The devices maintained their performance even under $\sim 4\%$ tensile strain and showed stable operation for periods up to 2 years, indicating the two-fold role of the h-BN layer as a flexible dielectric and encapsulant. Finally, I will show how hybrid inkjet-printing of 2D and organic semiconducting inks enables all-printed complementary logic circuits [4] on rigid and flexible substrates. The viability of our process for printed and textile electronics is demonstrated by fully inkjet printed electronic circuits, such as reprogrammable volatile memory cells, complementary inverters, and OR logic gates with graphene/h-BN FETs.

References

[1] Torrissi, F. & Carey, T. Nano Today 23, 73 – 96 (2018).

[2] Torrissi, F. & Carey, T.; Samori P. and Palermo, V. Eds., Wiley, Weinheim (2018).

[3] Carey et al. Nature Commun, 8 1202, (2017).

[4] Carey et al. Adv. Electron. Mater. (2021)

10:15 AM DISCUSSION TIME

SESSION SB10.09: Virtual Session II: New E-Textile Materials and Devices for Wearable Electronics II

Session Chairs: Jesse Jur and Myung-Han Yoon

Wednesday Afternoon, December 7, 2022

SB10-virtual

9:00 PM *SB10.09.01

Semiconductor Fibers for Smart Clothing [Gang Wang](#); State Key Laboratory for Modification of Chemical Fibers and Polymer Materials, Donghua University, China

Semiconductor devices in the form of fibers and fabrics have important applications in the fields of information and communication, medical care, human-machine interface etc. How to obtain good flexibility and weavability while maintaining excellent semiconductor performance and then integrate industrial weaving technology is the key to realize its application in the field of wearable smart fabrics. And the introduction of fiber structure through shear processing is an effective way to achieve this. In the field of semiconductor hybrid fiber and integrated fabric electronics, our work is mainly carried out in the following three aspects. First, design high-performance semiconductor printing ink. By regulating the aggregation and rheological properties of semiconductor polymer molecular chains, we obtained the printing ink with excellent printing and semiconductor performances. Second, prepare large-area and high-oriented flexible thin film transistor devices by microfluidic printing. Based on the idea of multi-dimensional hybrid design, we built the high-precision microfluidic printing equipment. Through shearing and manifold design, we realized the printing preparation of nanofiber-based flexible transistor arrays. Thirdly, construct single-fiber logic devices. The micro-nano structure regulation idea that make fibers by microfluidic shear and proton exchange was proposed to realize the continuous preparation of semiconductor hybrid fiber at the kilometer level, obtaining signal amplification, logic operation and other functions, and also exploring the application in smart clothing.

9:30 PM SB10.09.02

Electromechanical Properties of Wearable and Flexible Pressure Sensing Fabrics Enabled by Integrating Yarn Sensor into Textile Structure for Compression Textiles [Yiyi Yang](#), [Xiao Tian](#), [Ben Niu](#) and [Tao Hua](#); The Hong Kong Polytechnic University, China

Compression textiles are functional textiles that can apply pressure to specific areas of the human body for a variety of purposes, which are commonly made by using extensible and elastic woven and knitted fabrics. When the extended fabric is worn, such as on a cylindrical shaped limb, internal stress will be generated in the fabric, and thus the resultant interfacial pressure will be exerted onto the body. In this regard, an elastic strain sensing fabric can be used

to measure the resultant pressure. However, there is very limited literatures on the study on such strain/pressure sensing fabrics as well as the dependence on the influencing parameters. In this study, a pressure exerting and sensing fabric was firstly developed by integrating yarn based polydopamine-enhanced strain sensor into elastic woven fabric substrates via advanced weaving technologies. Herein the fabrication and characterization of the strain/pressure sensing fabrics were demonstrated, and the effects of woven fabric structure and parameters upon sensing outcomes were investigated. To find out the most appropriate parameters for fabric substrates, the fabrics in three different structures with varied densities were developed. Fabrics which perform the best in the elastic and recovery test were chosen as the substrates, in which the yarn-based sensors were integrated into for fabricating strain/pressure sensing fabrics. The mechanical and electromechanical properties of the strain/pressure sensing fabrics under both unidirectional tension and a curved form were evaluated by using a newly setup of a test protocol. Consequently, the pressure-displacement and electrical resistance-displacement curves as well as the resultant electrical resistance-pressure were obtained to characterize the fabric sensor developed in terms of electromechanical properties. The experiment results show that the fabric pressure increases with the increase of press depth, and thus the increase of the electrical resistance of extended sensing fabrics, presenting good sensing performance including sensitivity, hysteresis as well as repeatability. Moreover, the results have further revealed the effects of fabric substrate parameters on the sensing properties, including fabric density and applied fabric pretension. The sensing fabrics also show very good stability under 2000 press-release cycles, indicating the ability to enable a continuous monitoring on the applied pressure. In addition, the fabrication of these sensing fabrics was relatively convenient. Therefore, it is expected to be compatible with industrial manufacturing for fabricating flexible and large-area fabric-based sensors for various applications in a foreseeable future.

Acknowledgement

The authors are very grateful for the financial support from the Research Grant Council of Hong Kong with the Project of 15209420.

References

1. Xiong, Y., and Tao, X. M., Compression garments for medical therapy and sports, *Polymers*, 2018, 10, 663.
2. Niu, B., Yang, S., Tian, X. and Hua, T., Highly sensitive and stretchable fiber strain sensors empowered by synergetic conductive network of silver nanoparticles and carbon nanotubes, *Applied Materials Today*, 2021, 25, 101221.
3. Maqsooda, M., Nawaba, Y., Umarb, J., Umaira, M. and Shakera, K., Comparison of compression properties of stretchable knitted fabrics and bi-stretch woven fabrics for compression garments, *The Journal of The Textile Institute*, 2017, 108, 522–527.
4. Wang, Y. Y., Hua, T., Zhu, B., Li, Q., Yi, W. J. and Tao, X. M., Novel fabric pressure sensors: design, fabrication, and characterization, *Smart Materials and Structures*, 2011, 20(6), 065015.

9:35 PM *SB10.09.03

Fibrous Supercapacitor and Hydroelectric Nano-Energy Generator Using Silk-Based Conductive Textile Byungil Hwang: Chung-Ang University, Korea (the Republic of)

With the acceleration of technological advances in flexible and wearable electronics, there are needs for a highly reliable wearable energy storage and harvesting system. Fibrous supercapacitor and hydroelectric nano-energy generator are promising candidates for the power sources of wearable electronics due to their flexibility and seamlessness to human body. To fabricate the fibrous energy storage and harvesting system, the development of reliable fibers that can supply electrical power even under harsh external damages. In this study, highly conductive and reliable silk yarns are developed utilizing an Ag nanowire, multi walled carbon nanotubes (MWCNT, 3 – 7 walls), and poly(3,4-ethylenedioxythiophene):poly(styrenesulfonate) (PEDOT:PSS) composite coating. The conductive silk yarn electrodes are fabricated via a sequential dip-coating process of silver nanowires, multi walled carbon nanotubes (MWCNT, 3 – 7 walls), and poly(3,4-ethylenedioxythiophene):poly(styrenesulfonate) (PEDOT:PSS). The composite-coated silk yarn electrodes are stable under cyclic bending as well as under washing in water. Due to the synergetic effect of the three conducting materials, an excellent electrochemical performance is obtained resulting in high volumetric energy and power densities of 8-13 mWh cm⁻³ and 8-19 W cm⁻³, respectively. A yarn-type supercapacitor is demonstrated by integrating composite-coated silk yarn electrodes with a hydrogel electrolyte, showing a promising stability as evidenced by the retention of over 94% and 93% of the specific capacitance after 90 degree bending and stretching. In addition, the conductive fibers are applied to hydroelectric nano-energy generator. Transpiration driven ion conduction through the conductive fibers generates electrical current more than 4,000s by dropping water. The potential of the fibrous hydroelectric nano-energy generator to operate a small wearable device is demonstrated. The developed fibrous supercapacitor and nano-energy generator with the excellent mechanical and electrochemical stabilities will be a promising candidate for a sub-energy storage/harvesting system of the next generation wearable electronic devices.

10:05 PM SB10.09.04

Effects of Super-Elastic Dielectric Yarn in Multi-Yarn Knits for a Highly Stretchable Strain Sensor, Resistor and Interconnect in a Single Knit Hong Yee Low^{1,1,1}, Ujjaval Gupta^{1,1}, Pei Zhi Chia^{1,1}, Ying Yi Tan^{1,1}, Jun Liang Lau² and Gim Song Soh^{1,1,1}, ¹Singapore University of Technology and Design, Singapore; ²Rehabilitation Research Institute of Singapore, Singapore

Multi-yarn knitting is a promising approach to achieve electrically functional textile. Through computer numerical control (CNC) knitting, multiple yarn types can be knitted in a single knitting process hence the properties of the knitted fabric are the results of complex interplay between the intrinsic properties of the yarns (or combination of yarns) used and the knit structures (loop length and stitch patterns). Much research in CNC knitting has focused on the development of functional yarns, particularly electrically conductive yarns. Such yarn has been incorporated in the form of electrically conductive knit pattern and have been demonstrated as strain/stretch sensors, piezoelectric and capacitive sensors for wearable and non-wearable applications. Current approaches have focused on improving the sensitivity and repeatability through specially formulated yarn as a single conductive component in the knit, however, are generally limited in the form of simple geometry such as stripe and patch.

In this work, we report the design and fabrication of strain sensor, electrical interconnects and resistor distributed within a single piece of the knitted soft wearable in a single knit job. The strain dependent electrical resistance pattern for the sensor, interconnect and resistor are greatly contrasting. In a strain sensor, it is desirable to produce a large change in resistance for enhanced sensitivity. On the other hand, an interconnect or a resistor should produce negligible change in resistance when stretched, with further requirements for interconnect to have low electrical resistance while resistor to have high electrical resistance. The vastly different electrical characteristics of the knit was achieved through the mechanical coupling between electrically conductive and dielectric yarns.

In multi-yarn knitting, the type of mechanical coupling between yarns of dissimilar properties depends on the intrinsic properties of the yarn and the stitch pattern. The stitch patterns are a unit cell of knitting instructions that repeat periodically to form a knitted fabric. It has been determined that a high ratio of the Young's modulus of the conductive yarn (E_c) to that of the dielectric yarn (E_d), $>10^3$ is an important enabling factor. In a knitted textile, the super-elastic dielectric yarn functions to control the electrical contact points in the conductive yarn (negligible stretchability) in the following manner: enables periodic contact points formation and breaking in the conductive yarn during stretching of the textile (strain sensor). The dielectric yarn also preserves the original contact points in the conductive yarn during stretching of the textile (interconnect and resistor) and prevents the formation of contact points (resistor) in the conductive yarn during stretching of the textile. Through the above design approach, a highly stretchable all knitted electrical components of sensors and a network of interconnects in the form of a knee brace has been achieved. As a soft wearable, the knitted sensorised knee brace is in close contact with the skin, allowing the customization of the sensor placement based on skin strain measurements. Through user tests, knee joint motions

obtained from the knee brace with knitted electrical components have been validated with image capture motion sensing data (VICON).

10:20 PM SB10.09.05

Uni-Active Material Comprised Triboelectric Nanogenerator for High-Performance Wearable Electronics Anand Babu and Dipankar Mandal; Institute of Nano Science and Technology, India

The demand for energy and portable electronics is in full swing with the rapidly increasing population of the world. Self-powered devices and sensors are working like the panacea to fill this gap. Owing to its low cost, broad choice of materials, and easy fabrication techniques, triboelectric nanogenerator (TENG) is a promisingly viable technology for fabricating self-powered devices/sensors. Fundamentally, the working principle of the TENG is based on the combined effect of contact electrification and electrostatic induction. Surface area, roughness, and charge density of the contacting surfaces are the key player in determining the overall performance of TENG. Conventionally, two dielectric materials with different triboelectric natures are used to fabricate the TENG. However, the choice of a combination of different materials based on their charge density is one of the prime challenging tasks. Here, we have proposed an effective way to fabricate a TENG with a single (unit) material only (abbreviated as U-TENG), comprised of electrospun nylon-11 nanofibers with different triboelectric natures. The triboelectric nature of the nylon-11 nanofibers is tuned by changing the voltage polarity in the electrospinning setup. Technically, there is a change in the surface potential by using the alternate voltage polarity (positive and negative polarity), which leads to generating different charge density, and subsequently gives rise to a change in work function, a critical factor in defining the triboelectric nature, this is a key factor in designing U-TENG. The tuning of surface potential or, say, the tuning of triboelectric nature of the materials by using alternate voltage polarity also shows promising results for other polymers as well. Owing to its high sensitivity, U-TENG has immense capability to be successfully implemented as a self-powered wearable sensor, which is demonstrated as an ultrahigh sensitive acoustic sensor with a very high mechanoacoustic. Owing to its high sensitivity in the low-to-middle decibel (60–70 dB) sounds, U-TENG is plausibly capable of distinguishing different voice signals depending on the condition of the vocal cord. The effective voice recognition ability of U-TENG indicates that it has a high potential to open an alternative pathway for medical professionals to detect several diseases such as neurological voice disorder, muscle tension dysphonia, and vocal cord paralysis related to the voice without using any chemical/invasive technique.

References

- (1) A Babu, P Malik, N Das, D Mandal, D. Surface Potential Tuned Single Active Material Comprised Triboelectric Nanogenerator for High Performance Voice Recognition Sensor. *Small*. 2022, 2201331.
- (2) C Wu, A. C. Wang, W. Ding, H. Guo, Z. L. Wang, Z. L. Wang. Triboelectric Nanogenerator: A Foundation of the Energy for the New Era. *Adv. Energy Mater.* 2019, 9, 1–25.
- (3) H Guo, X Pu, J Chen, Y Meng, M. H. Yeh, G. Liu, Q. Tang, B Chen, D. Liu, S. Qi, C. Wu, C Hu, J Wang, Z L Wang, A Highly Sensitive, Self-Powered Triboelectric Auditory Sensor for Social Robotics and Hearing AIDS. *Sci. Robot.* 2018, 3, 1–10.

10:35 PM DISCUSSION TIME

SESSION SB10.10: On-Demand Presentation
Thursday Morning, December 8, 2022
SB10-virtual

7:00 AM SB10.10.01

Electrically Conductive nylon/poly(pyrrole) Nanotubes-Based Composite Fibers Prepared by Wet-Spinning Kiran Rana; Indian Institute of Technology Delhi, India

Wearable electronic textiles and camouflaged textiles are technologically important materials that are critical for the future growth of technical textiles. For these applications, flexible polymer-based conducting fibers are absolutely necessary. Towards this, various materials like intrinsically conducting polymers (ICPs), MXenes, and metallic and CNT/graphene-based materials have been used as electrically conductive fillers in the polymer matrix. Among these, ICPs are promising materials as they are lightweight, dispersible, and easy to synthesize. However, the blend of the conjugated polymers with spinnable polymers has usually yielded poor electrical properties in the past.

In this study, it was hypothesized that the anisotropic nanostructure of ICPs may provide a better connecting network and may yield improved electrical properties of the blends. In order to investigate this, we have synthesized anisotropic nanostructures of poly(pyrrole), viz. poly(pyrrole) nanotubes (PPyNT), and blended them with nylon-6 to obtain solution spun composite fibers. The composite fibers, thus obtained, showed good DC electrical conductivity of up to 10 S/m at a low percolation threshold. This study further investigated the effect of loading of PPyNTs on the mechanical and electrical properties of the conductive composite fibers.

SYMPOSIUM SB11

Engineering Biomaterials with Synthetic Biology
November 28 - December 8, 2022

Symposium Organizers

Tom Ellis, Imperial College London
Neha Kamat, Northwestern University

Ben (Keith) Keitz, The University of Texas at Austin
Seunghyun Sim, University of California, Irvine

* Invited Paper
+ Distinguished Invited

SESSION SB11.01: Biologically Programming Materials I
Session Chairs: Neha Kamat and Ben (Keith) Keitz
Monday Morning, November 28, 2022
Hynes, Level 3, Room 305

10:30 AM *SB11.01.01

Control of Enzymatic Membranes [Monica Olvera de la Cruz](#), Curt Waltmann and Jeremy Wang; Northwestern University, United States

Aggregates of proteins in cells mediate cell interactions and organize the local environment to promote specific cellular functions including synthesizing molecules. I will discuss advances in designing aggregates that mimic cellular protein aggregates by modifying protein interactions and/or by using synthetic molecules to organize enzymatic proteins in non-biological environments. The assembled membranes are capable of making useful chemicals and breaking down toxins.

11:00 AM SB11.01.02

Developing Controllable Synthetic Cells [Michael Booth](#); University College London, United Kingdom

Synthetic cells, lipid membrane-bound compartments that mimic living cells, are a promising technology for studying living systems and as drug delivery vehicles. However, real-world application of synthetic cells requires methods of controlling their function for spatiotemporal activation and to reduce off-target effects. My group are developing methods to externally control these soft biomaterials with multiple stimuli, including light, temperature, and chemical signals. We are using our 'remote-controlled' synthetic cells to mimic living processes and form controllable interfaces between living and non-living materials. Current advances include the development of a dual light-activated cell-free AND gate and the light-activated communication between synthetic cells and bacteria.

11:15 AM SB11.01.03

Greasing Protein Wheels—Harnessing Post-Translational Lipidation for Bioinspired Materials Science and Engineering [Davoud Mozhdaji](#); Syracuse University, United States

Advances in recombinant DNA technology have expanded our ability to design and produce protein-based materials with superior control over the biomacromolecule's length, sequence, and structure. Despite these positive attributes, proteins still lack the chemical diversity of their synthetic analogues due to the limited repertoire of canonical amino acids. This limitation restricts the available chemical design space (and thus the function) of protein-based biomaterials. In our quest to overcome this evolutionary constraint, we are inspired by a solution offered by Nature: leveraging specific chemical transformations to modify proteins with non-proteinogenic building blocks, a process called post-translational modification (PTM), which expands the chemical diversity of the proteome by more than two orders of magnitude.

Our focus is to reprogram PTMs to synthesize *de novo* designed hybrid biopolymers with programmable self-assembly. In this talk, I will discuss our recent work on leveraging post-translational lipidation to create genetically encoded amphiphiles with temperature-programmable assembly. Though the chemical biology of lipidation is under intense investigation, protein lipidation remains a major, untapped resource in our synthetic, biomaterials, and therapeutic toolkit. Facile, scalable, and inexpensive lipidation of proteins is currently an unmet synthetic capability. Lipidated proteins cannot be produced by genetic code expansion methods due to the stringent preference of ribosomes for amino acid-derived motifs. Alternatively, their multi-step convergent semi-synthesis is laborious and technically challenging. To address these challenges, we have developed operationally simple, high yield biosynthetic routes for the production of lipidated proteins that facilitates their production to study their materials properties.

I will demonstrate that the effect of lipidation on the assembly, nano-morphology, and material properties of lipidated proteins diverges significantly from experimental results and theoretical predictions of structurally related materials such as amphiphilic polymers and peptide-amphiphiles. Our working hypothesis is that the molecular syntax of lipidated proteins encodes for interactions that are absent in synthetic polymers and short peptides. Specifically, the large molecular surface of lipids enables them to contact multiple segments of peptide chains, and these nonnative interactions synergize/interfere with the ability of proteins to fold, resulting in distinctive functional consequences. Revealing this "*molecular syntax*" will enable the development of the next generation of biomaterials and therapeutics that rival the exquisite hierarchy and capabilities of biological systems.

11:30 AM SB11.01.04

Membrane-Based Artificial Neurons for Brain-Like Signal Processing at the Edge of Biology [Michelle Makhoul-Mansour](#), Joshua Maraj and Stephen A. Sarles; the University of Tennessee, United States

Bottom-up synthetic biology has transformed the design and modification of custom biomolecules and living cells. It also provides paths for developing functional biomolecular materials for use in applications such as targeted drug delivery, tissue regeneration and even smart, wearable bioelectronics. In contrast to traditional electronic components that are heavy, non-biocompatible, and power hungry, synthetic biomolecular materials are soft, biocompatible, and leverage similar structures and transport properties of biological cells. These are needed to improve sensing and signal processing functions at the biotic/abiotic interface: the *edge of biology*. Specifically, synthetic biomolecular materials would benefit from the adaptive properties of memristors and neuromorphic devices that enable brain-like signal processing, in-memory computing capabilities, and activity-dependent plasticity. Recent research directions in this field intend to bridge the gap between modern day computing and biological tissues by carefully engineering new neuromorphic devices inspired by how the brain processes and stores information.

A new type of two-terminal, neuromorphic device—a *biomolecular memristor*—has been introduced by Sarles *et al.* Biomolecular memristors are

assembled at the interfacial bilayer of lipid-coated aqueous droplets dispersed in oil using the droplet interface bilayer (DIB) technique. DIB membrane-based devices are highly modular and scalable, can be functionalized to various types of stimuli, and offer tunable memristance and activity-dependent plasticity. Herein, we examine new functionality of biomolecular memristors doped with voltage-activated ion channels: spontaneous voltage spiking (self-regenerative pulses akin to action potentials in nerve cells) upon injection of a DC current. We hypothesize that spontaneous spiking voltages can be generated in response to injected DC currents due to the combined effects of membrane capacitance and voltage-dependent ion channel gating that show negative differential resistance (NDR). Preliminary results show that NDR can be achieved in DIBs using alamethicin peptides and protamine introduced on one side of the membrane. Spiking behaviors are examined by injecting DC currents and measuring the resulting changes in membrane voltage. The addition of NDR, a property of “active” devices, to DIB memristive elements can improve the storage density and reduce power consumption through local amplification in neuromorphic circuits. Our goal is to build a scalable material system of biomolecular *neuristors* that emulate the “leaky integrate and fire” and nonlinear dynamic functions of neurons. This brings us a step closer to enabling spiking neural networks (SNNs) functionality for real-time spatio-temporal data processing at the edge of biology using soft, compatible bioelectronic materials.

11:45 AM SB11.01.05

Poster Spotlight: Membrane Fusion—How Cubic Lipid-siRNA Constructs Escape the Endosome Lining Zheng and Cecilia Leal; University of Illinois at Urbana-Champaign, United States

Small interfering RNA (siRNA) silences gene expression and has shown great potential in medical applications. However, intracellular delivery of siRNA remains a great challenge. Lipid nanoparticles have been one of the most successful siRNA carriers to date, but their delivery efficiency is limited due to low endosomal release. We have shown that cubic structured lipid nanoparticles (cubosomes) loaded with siRNA - cuboplexes, show greater siRNA knockdown compared to traditional lamellar structured liposomes. In this work, we aim to elucidate the reason behind this difference in delivery efficiency. We will show confocal microscopy (CF), flow cytometry and live cell imaging data demonstrating higher cellular uptake of cubosomes compared to liposomes. CF, fluorescent based fusion assays, cryogenic transmission electron microscopy and dynamic light scattering measurements indicate that compared to liposomes, cubosomes are more prone to fuse and form aggregates with endosomes, which implies a stronger pore forming capability that leads to siRNA escape. These results support our suggestion that cubosomes can lower the free energy required to promote endosome pore formation and establish a topologically active delivery mechanism.

*This work is supported by the NIH (1DP2EB024377-01).

11:50 AM SB11.01.06

Poster Spotlight: Controlling Material Properties via Transcriptional Regulation of Extracellular Electron Transfer (EET) from *S. oneidensis* Gina Partipilo¹, Austin J. Graham² and Ben (Keith) Keitz¹; ¹University of Texas at Austin, United States; ²University of California, San Francisco, United States

Extracellular electron transfer (EET) is an anaerobic respiration process in bacteria that couples carbon oxidation to the reduction of extracellular metal species. Though performed by a wide variety of microbes, the model organism *Shewanella oneidensis* directs EET through a well-defined protein pathway, the Mtr-pathway. EET from the gram-negative, genetically tractable bacteria can serve as a link between the biotic and abiotic by directing the reduction of a suitable metal catalyst. Through engineering the proteins in the Mtr-pathway, we can exert metabolic and genetic control over a variety of synthetic transformations, not limited to atom-transfer radical polymerization (ATRP) and Cu(I)-catalyzed alkyne-azide cycloaddition (CuAAC). As a result, EET and the Mtr-pathway can serve as tunable handles for materials formed via these chemistries. Simple buffer gates controlling the transcription of Mtr-pathway genes allows for material formation to “turn-on” the reaction with an inducer molecule. A buffer-NOT gate allows for induction to “turn off” the reaction. Utilizing higher complexity genetic circuits, a series of two-input logic gates can be employed to control material stiffness and conversion. The PEG-hydrogels stiffness can be predictably controlled with the two-input gates utilizing both CuAAC and ATRP. Furthermore, the material stiffness appears to closely mimic the synthetic biology rules traditionally measured with fluorescence. This indicates that more existing synthetic biological circuits can be employed to control material properties. Our results investigate the applications of biocatalytic EET for use in engineered living-materials with a higher degree of computation. Furthermore, controlling material properties through a bacterial interface allows for a high degree of control in complex environments. Utilizing a small molecule system, EET-catalyzed CuAAC fluorescently labelled live mammalian cell membranes without harming cell viability. These results indicate that there may be an opportunity for applying these computational hydrogels as scaffolding for wound repair or cell differentiation, as changes in the environment can allow *S. oneidensis* to actuate changes to material properties.

11:55 AM SB11.01.07

Poster Spotlight: Engineering the Extracellular Matrix with DNA-Based Devices for Modulation and Force Sensing Applications Peter E. Beshay, Melika Shakhosseini, Carlos Castro and Jonathan W. Song; The Ohio State University, United States

It is well appreciated that reciprocal communication between cells and the surrounding extracellular matrix (ECM) can modulate the properties and the behavior of both the ECM and cells to influence both form and function. For example, modulation of the mechanical properties of the ECM by cells is believed to significantly influence the progression of certain diseased tissue such as fibrosis, healing wounds, or the stroma of tumors, all of which are known to exhibit ECM remodeling through the cross-linking of fibrillar collagen and/or deposition of non-collagenous ECM. In addition, interstitial flow through the ECM plays a major role in modulating cancer metastasis by redistributing chemokines, leading to chemotaxis, or through the activation of cell-surface mechanosensors, such as focal adhesion proteins, that promote cell motility. Current advances in Atomic Force Microscopy (AFM), and Magnetic Resonance Imaging (MRI) provided significant insights on the effect biophysical forces on disease progression. However, those techniques do not provide insights into effect of remodeling the same tissue sample nor provide a direct way of measuring the forces exerted by interstitial flow in the ECM. Here, we present a hybrid system that utilizes microfluidic devices and DNA-based nanoscale devices that will enable manipulating properties and measuring biophysical forces in the ECM at a sub-cellular level.

DNA-based molecular sensors have been of particular interest for studying cell interactions due to their high tunability, sensitivity and easy integrability into various biological systems. However, measuring cell-ECM interactions due to fluid flow using these sensors has yet to be achieved. Here, we present a DNA origami-based force probe that is capable of measuring fluid flow forces in the ECM. The probe, which is about 100 nm in size, consists of two barrels of DNA connected by six flexible linkers; allowing the device to fluctuate between open and closed states. Probe fluctuations is then reported using single molecule Förster resonance energy transfer (smFRET). The dynamics of the probe and its force sensitivity can be tailored by changing the interaction strength between its linkers. To enable the measurement of fluid flow forces in the ECM, we demonstrate our ability to anchor our probe to the fibers of collagen I-based hydrogels. We also present a three-channel microfluidic device comprising an “interstitial space” channel sandwiched between two “vessel” channels as a mean for applying physiologically relevant fluid flows. This microfluidic device can hence mimic interstitial fluid flow on the ECM by applying different pressure gradients on its channels. The integration of the DNA-engineered ECM with this microfluidic system will enable the spatiotemporal measurement of interstitial flow forces in the ECM, allowing for studying the effect of these forces on cancer cell motility and metastasis.

1:30 PM *SB11.02.01

Self-Healing of Biomineralized Engineered Living Building Materials Elizabeth Delesky, Rollin Jones, Sherri Cook, Jeffrey Cameron, Mija Hubler and Wil V. Sruibar III; University of Colorado Boulder, United States

Living building materials (LBMs) are an emergent class of structural materials that leverage the biomineralization capability of microorganisms within sand-hydrogel scaffolds to produce living, load-bearing structures. In this study, we produced LBMs using a physically crosslinkable hydrogel-sand scaffold and two microorganisms with different biomineralization pathways—*Synechococcus sp.* PCC 7002 (photosynthetic) and *S. pasteurii* (ureolytic)—and investigated their self-healing capacity. Our results reveal that both *Synechococcus sp.* PCC 7002 and *S. pasteurii* demonstrated exceptional viability within all LBMs for more than 20 days. LBM prisms were pre-loaded to 40% of their structural capacity in compression or flexure. Damaged LBMs containing *Synechococcus sp.* PCC 7002 exhibited a full rebound of their original compressive and flexural strengths, respectively, after three days of healing at 50% relative humidity (RH) (*i.e.*, ambient conditions). In contrast, LBMs containing *S. pasteurii* exhibited marginal recovery of their original compressive and flexural strengths, respectively, after three days of healing at 50% RH. The compressive and flexural strengths of all LBMs fully rebounded after seven days of healing at 50% RH. Results substantiate that the self-healing ability of the hydrogel alone plays a critical role in facilitating healing of LBMs, as evidenced by high rebounds in compressive and flexural strengths by the hydrogel-sand scaffold after three or seven days of healing 50% RH.

2:00 PM SB11.02.02

Surface-Adhered Biomembrane Networks Formed on High Energy Surfaces of SiC and Al₂O₃ Ruslan Ryskulov¹, Esteban Pedrueza Villalmanzo^{1,2}, Aldo Jesorka¹, Lin Xue³, Elif Köksal³, Karolina Spustova³ and Irep Gözen³; ¹Chalmers University of Technology, Sweden; ²University of Gothenburg, Sweden; ³University of Oslo, Norway

Reservoirs of lipid molecules, specifically onion shell vesicles, spread on high energy surfaces, e.g. Al₂O₃, to form a stack of molecular films (double bilayer). Eventually, the spreading lipid exhausts the reservoir, and rising tension ruptures of the films [1]. Gözen and later Köksal *et al.* discovered that this disruptive process generates a network of nanotubes, which redistributes lipid material in order to alleviate local tension (Marangoni flow), and vesicles grow from the tubes [2,3]. We have shown that local heating accelerates the growth and transformation of containers, and initiates their fusion. Similar processes might have occurred in warm environments on the Early Earth. Our current work aims to utilize this system and **control** soft matter **transformations with IR light** to design and construct reconfigurable chemical reaction networks (CRNs) on engineered surfaces.

In the context of the origin of life, the formation of the earliest primitive compartments and their transformation to biological cells is not known in detail, and is a subject of intensive research. Köksal *et al.* suggested the involvement of solid high energy surfaces as source of energy for autonomous shape transformations of lipid assemblies, protocell and nanotube network formation, and encapsulation of solutes therein. Such surface-supported networks of vesicles and soft nano-conduits might have functioned as primitive CRNs in the prebiotic world. Their simplicity and ease of formation inspired further development as a soft matter reactor nanotechnology. We combined an inverted laser induced fluorescence microscope with a focused 1470 nm IR-B laser and a spatial light modulator (SLM) for generating designed irradiation patterns (digital holography) in order to elevate the temperature locally at the surface and simultaneously observe lipid film transformations.

Membrane compartment formation, growth, and merging was accelerated by local heating with an IR fibre. We developed an *in situ* temperature measurement setup and confirmed consistency with conditions in warm natural environments, such as the “Lost City” hydrothermal vents (~70°C) [4]. Thermocouple absorption of IR energy was taken into account. The actual temperature in the proximity of the fibre ending (distance to the protocell) was determined by linear approximation. We further employ thermally evaporated SiC surfaces for improved adhesion control, which allows for efficient MLV spreading into double bilayer structures and rapid growing of protocells colonies [5], even without additional fusogenic agents, such as Ca⁺⁺ ions. Further research aims to implement chemical/enzymatic reactions within such networks in order to gain new insights into possible protocell development scenarios in the context of the origins of life.

References

- [1] I. Gözen, P. Dommersnes, I. Czolkos, A. Jesorka, T. Lobovkina, and O. Orwar, "Fractal avalanche ruptures in biological membranes," *Nature Materials*, vol. 9, pp. 908-912, 2010/11/01 2010.
- [2] I. Gozen, M. Shaali, A. Ainal, B. Ortmen, I. Poldsalu, K. Kustanovich, et al., "Thermal migration of molecular lipid films as a contactless fabrication strategy for lipid nanotube networks," *Lab on a Chip*, vol. 13, pp. 3822-3826, 2013 2013.
- [3] E. S. Köksal, S. Liese, L. Xue, R. Ryskulov, L. Viitala, A. Carlson, et al., "Rapid growth and fusion of protocells in surface-adhered membrane networks," *bioRxiv*, p. 2020.03.10.980417, 2020.
- [4] I. Gözen, E. S. Köksal, I. Pöldsalu, L. Xue, K. Spustova, E. Pedrueza-Villalmanzo, *et al.*, "Protocells: Milestones and Recent Advances," *Small*, vol. n/a, p. 2106624, 2022/03/23 2022.
- [5] K. Spustova, C. Katke, E. Pedrueza Villalmanzo, R. Ryskulov, C. N. Kaplan, and I. Gözen, "Colony-like Protocell Superstructures," *bioRxiv*, p. 2021.09.16.460583, 2021.

2:15 PM SB11.02.03

Hierarchical Coatings of Biological Building Blocks via Self-Limiting Electrospray Deposition Sarah Park¹, Lin Lei¹, Kelly Kyker-Snowman¹, Darrel Dsouza¹, Robert Zipkin², Emran Lallow¹, Joel Maslow³, Hao Lin¹ and Jonathan Singer¹; ¹Rutgers University, United States; ²MedChem 101, United States; ³GeneOne Life Science, United States

Electrospray deposition (ESD) is a spray coating process that utilizes a high voltage to atomize a flowing solution into charged microdroplets. These self-repulsive droplets evaporate as they travel to a target grounded substrate, depositing the solution solids as thin films. These thin films can be utilized in biomedical applications including drug and therapeutics delivery in addition to the fabrication of medical implants and biosensors. Our lab has categorized various modes of ESD, including self-limiting electrospray deposition (SLED). In SLED, the material arrives onto a target as a dried spray, carrying a charge that eventually begins to repel itself over time. The charged spray is redirected to regions that are uncoated such that manipulation of the electrostatic repulsion, hydrodynamic forces, and evaporation kinetics can be employed to conformally cover 3D architectures with micro-coatings. The generated coatings are hierarchical, possessing either nano-shell, nanoparticle, or nanowire microstructure, which can be smoothed through further post processing. We envision SLED as being a replacement for dip or conventional-spray coating, where its greatest advantage would be the potential for much higher materials utilization. While many studies have presumed high efficiency in ESD, this is rarely quantified. Here, we show how architecting the local charge landscape can lead to SLED coatings approaching 100% deposition efficiency on microneedle arrays and other complex substrates of relevant

therapeutics with the building blocks and signals for synthetic biology, including DNA vaccines, proteins, amino acids, bioactive small molecules, and biocompatible conductors.

2:30 PM SB11.02.04

Screening Methods for Hydrophobins and Peptides as Potential Promoters of Polymer Adhesion Mark T. Kozlowski, Jose A. Wippold and Joshua A. Orlicki; U.S. Army Research Laboratory, United States

Bacterial cell surface display libraries have been adapted to identify potentially promising proteins and peptides with adhesive characteristics against an array of diverse substrates. The peptide display libraries were screened using methods previously developed by the Army Research Laboratory to find promising peptide sequences that interacted strongly with substrates such as gold or ITO nanoparticles. The current work combines peptide display with microfluidic approaches to screen material substrates (e.g. polymers, metals) that may exhibit weaker interactions than those probed previously. In addition to the display of a peptide library, a class of natural surfactants known as hydrophobins have been expressed on the bacteria surface. Hydrophobins are used by fungi to breach air-water interfaces when colonizing new environments, and have already been shown to adhere to highly non-polar surfaces, such as Teflon or polystyrene.

Progress towards identifying proteins and peptides that promote bacterial adhesion to diverse polymer substrates and demonstration of microfluidic-based methods for obtaining semi-quantitative data on binding affinity with reasonable throughput will be discussed. This work will ultimately merge the screening tools of synthetic biology approaches to address long-standing challenges in materials science, providing new insights for probing adhesion.

2:45 PM BREAK

3:15 PM *SB11.02.05

Programming Microorganisms to Assemble Macroscopic Living Materials Sara Molinari, Robert F. Tesoriero, Esther Jimenez and Caroline Ajo-Franklin; Rice University, United States

Challenged by a changing climate, dwindling natural resources, and a growing global population, we need advanced, renewable materials that meld the sustainability of biological materials with the functionality of conventional materials. To help address this need, my research group creates sustainable and environmentally-responsive living materials by seamlessly integrating conventional materials with living systems. One major effort in our group is to engineer microorganisms to grow into multifunctional, hierarchically ordered macroscopic materials by introducing non-natural extracellular matrices. Living materials synthesized by organisms, such as bones and shells, exhibit remarkable mechanical properties due to their hierarchical assembly of hard and soft components across the nanometer to the micron scales. While engineering macroscopic analogs to these materials would open new frontiers, there is currently no bottom-up route to do so that enables control of the composition, hierarchical structure, and properties of living materials. In this talk, I will describe our approach to constructing such hierarchically ordered materials by programming bacteria. We report growth of macroscopic materials from freshwater bacteria that display and secrete an engineered self-interacting protein. This protein formed an extracellular de novo matrix and assembled cells into hierarchically-ordered, centimeter-scale materials. We showed that the mechanical, catalytic, and morphological properties of these materials can be tuned through genetic modification of the self-interacting protein. Our work identifies novel genetic tools, design and assembly rules for growing macroscopic materials with both wide-ranging mechanical properties and customizable functions. We anticipate the modularity of this approach will permit the incorporation of different protein polymers in the de novo matrix, thus allowing to generate materials with a variety of desired compositions, structures, and properties. We envision specific matrix properties that can be combined synergistically with existing cellular functions to greatly expand the opportunities for biological materials in human health, energy, and the environment.

3:45 PM SB11.02.06

Secretion-Catalyzed Assembly of Protein Biomaterials on a Bacterial Membrane Surface Qi Xie and Stephen D. Fried; Johns Hopkins University, United States

Protein-based biomaterials have historically played a key role in tissue engineering, and additional exciting applications as self-healing materials and sustainable polymers are emerging. Their fibrous forms are often the most applicable. Over the past few decades, recombinant expression and production of various fibrous proteins from microbes have been demonstrated; however, the resulting proteins typically must then be purified and processed by humans to form usable fibers and materials. Here, we show that the Gram-positive bacterium *Bacillus subtilis* can be programmed to secrete silk through its translocon. Surprisingly, we discover that this translocation mechanism drives the silk proteins to assemble into fibers spontaneously on the cell surface, in a process we call secretion-catalyzed assembly (SCA). Furthermore, these fibers form self-healing hydrogels with minimal processing. This work provides a blueprint to achieve autonomous assembly of protein biomaterials in useful morphologies directly from microbial factories.

4:00 PM SB11.02.07

Advancing New Living Materials by Understanding Assembly Principles Robert F. Tesoriero^{1,1}, Sara Molinari¹, Dong Li², Kathleen Ryan³, Paul Ashby² and Caroline Ajo-Franklin¹; ¹Rice University, United States; ²Lawrence Berkeley National Laboratory, United States; ³University of California, Berkeley, United States

Like natural materials such as wood and bone, engineered living materials (ELMs) require specific conditions to facilitate proper assembly. By elucidating these assembly parameters in relation to the mechanism of material formation, we become able to better understand a material's potential application space. Our research group has recently developed the first example of a *macroscopic bottom-up de novo* engineered living materials (BUD-ELMs) in the bacterium *Caulobacter crescentus*¹. To understand and optimize the conditions that promote proper material assembly, we grew BUD-ELM cultures under various shaking conditions. We have found that this material not only requires shaking to assemble from planktonic culture, but also that the assembly process is sensitive to specific shaking conditions. To describe these conditions under a single parameter, we developed the modified volumetric power input ($P_{v,a}$), which takes into account both the shear forces experienced by the culture and the size of the air-water interface onto which the material forms. By analyzing the resulting size of material samples grown under different $P_{v,a}$ values, we were able to determine an optimal $P_{v,a}$ range for maximum material formation. Additionally, we used this model to predict the optimal shaking conditions for larger flask sizes, demonstrating the potential to scale up cultures for increased material production. By interpreting this data in conjunction with Western blot analysis and atomic force microscopy, we propose that during BUD-ELM assembly, *Caulobacter* cells adhere to a secreted BUD-protein matrix that forms at the air-water interface. Based on this mechanism, we hypothesized that this sequential assembly process would allow for integration of non-engineered bacterial species into the material's structure. To explore this concept, we developed a co-culturing approach for BUD-ELM-forming *C. crescentus* and the model cyanobacterium *Synechocystis* sp. PCC 6803. We observed the stochastic incorporation of live *Synechocystis* cells within the material by fluorescence microscopy. This result not only provides further support to our proposed assembly mechanism, but also enables a novel platform for photosynthetic, co-cultured ELMs. By further engineering *Synechocystis* cells, we hope to expand this platform to provide a novel class of ELMs with reduced nutrient requirements, increased lifespan, and user-defined functionality.

4:15 PM *SB11.02.09

Transforming Natural Microbial Biofilms into Functional Materials Sarah M. Glaven¹, Lina Bird¹, Brian Eddie¹, Isabel Baker¹ and Meghna Thakur²;
¹U.S. Naval Research Laboratory, United States; ²George Mason University, United States

Autotrophic bacteria form biofilms and use inorganic energy sources (e.g. gases, minerals, and electrodes) to fix carbon dioxide (CO₂). Such living materials could be developed as catalysts for biosynthesis, where CO₂ is captured and transformed into useful biomolecules. The problem is that autotrophic bacteria are difficult to grow under laboratory conditions and often rely on syntrophic partners whose contribution to growth cannot be reproduced in pure culture, rendering them genetically intractable. In order to develop autotrophic marine bacteria for technological use, tools to genetically manipulate them directly, without the need for standard laboratory isolation and cultivation, are required. In this talk, I will describe my team's work toward *in situ* genome editing of autotrophic bacteria in an electrode biofilm. I will present recent results demonstrating a CRISPR-based genome editing tool called INTEGRATE in two different biofilm-forming marine bacteria, *Marinobacter atlanticus* and "*Candidatus* Tenderia electrophaga". *M. atlanticus* is a heterotrophic testbed strain that forms biofilms on electrodes and is being used to optimize INTEGRATE for marine bacteria. "*Ca. Tenderia electrophaga*" is an electroautotroph, growing only from CO₂ fixation and electron uptake from an electrode, that exists in a consortia of ca. 20 other species, including *M. atlanticus*. Insertion of a fluorescent marker protein into *M. atlanticus* biofilm cells was tracked in real-time using confocal microscopy, yielding approximate transformation efficiency in mature biofilms. Biofilm transformation protocols developed with *M. atlanticus* were applied to "*Ca. Tenderia electrophaga*" to show, for the first time, successful genome integration of a fluorescent marker protein in an uncultivated electroautotroph. Genetically modified "*Ca. Tenderia electrophaga*" was stable after further enrichment, however, further editing was required to provide a selective advantage over the natural strain. This work represents the first step towards *in situ* genome editing of microbial communities that form electroactive biofilms as an approach towards developing living catalytic materials for CO₂ fixation.

SESSION SB11.03: Poster Session
Session Chairs: Neha Kamat and Ben (Keith) Keitz
Monday Afternoon, November 28, 2022
8:00 PM - 10:00 PM
Hynes, Level 1, Hall A

SB11.03.02

Interfacial Assembly of Bacterial Microcompartment Shell Proteins in All Aqueous Emulsions Dharani Abeyasinghe¹, Eric J. Young^{2,3}, Andrew T. Rowland¹, Cheryl A. Kerfeld^{2,3} and Christine D. Keating¹; ¹The Pennsylvania State University, United States; ²Michigan State University, United States; ³Lawrence Berkeley National Laboratory, United States

Compartmentalization is one of the most rudimentary hallmarks of living systems as it is essential to localize chemical species and functional components and to maintain biochemical gradients. Artificially designed 'protocells' (*i.e.*, elementary compartments from which living cells could have evolved from) are used to gain better insights into the role of compartmentalization. All aqueous emulsions formed through liquid-liquid phase separation (LLPS) have emerged as a compartmentalization strategy through which to assemble protocells. Examples include complex coacervates and aqueous two-phase systems. Furthermore, researchers have combined LLPS with lipid self-assembly to create lipid-based membrane-bound protocells. Similarly, self-assembling proteins could offer an alternative approach for making synthetic cell membranes, as evidenced by the existence of natural protein-based organelles and vesicles such as bacterial microcompartments (BMCs). Exploiting the interactions between such protein assemblies and LLPS provides new avenues to make responsive membrane-bound protocells with customizable properties. BMCs are 40 to ~600 nm protein containers formed by a semi-permeable protein shell surrounding an enzymatic core which allows bacteria to compartmentalize key metabolic pathways. The shell facets are composed of hexamer-shaped protein building blocks that associate laterally by shape complementation and weak electrostatic forces. Because of their self-assembly properties, BMC shell proteins are promising building blocks that can be repurposed to design novel nano to micron-scale higher-order protein architectures. In this study, we examined the assembly and positioning of BMC shell proteins when they are combined with a polylysine/polyaspartate coacervate system. Confocal fluorescence imaging showed that BMC shell proteins adsorb at the interface between the coacervate droplets and the dilute continuous phase. Our findings highlight the importance of electrostatic interactions between BMC shell proteins and polycations which can be tuned by varying the polycation/polyanion charge ratio. Functional properties of these protein bound compartments (*e.g.*, permeability, compartmentalization of enzymatic reactions) were also investigated. This study provides insights in establishing a prototype for a new class of proteinaceous protocell chassis for compartmentalizing functionality.

SB11.03.03

Poster Spotlight: Controlling Material Properties via Transcriptional Regulation of Extracellular Electron Transfer (EET) from *S. oneidensis* Gina Partipilo¹, Austin J. Graham² and Ben (Keith) Keitz¹; ¹University of Texas at Austin, United States; ²University of California, San Francisco, United States

Extracellular electron transfer (EET) is an anaerobic respiration process in bacteria that couples carbon oxidation to the reduction of extracellular metal species. Though performed by a wide variety of microbes, the model organism *Shewanella oneidensis* directs EET through a well-defined protein pathway, the Mtr-pathway. EET from the gram-negative, genetically tractable bacteria can serve as a link between the biotic and abiotic by directing the reduction of a suitable metal catalyst. Through engineering the proteins in the Mtr-pathway, we can exert metabolic and genetic control over a variety of synthetic transformations, not limited to atom-transfer radical polymerization (ATRP) and Cu(I)-catalyzed alkyne-azide cycloaddition (CuAAC). As a result, EET and the Mtr-pathway can serve as tunable handles for materials formed via these chemistries. Simple buffer gates controlling the transcription of Mtr-pathway genes allows for material formation to "turn-on" the reaction with an inducer molecule. A buffer-NOT gate allows for induction to "turn off" the reaction. Utilizing higher complexity genetic circuits, a series of two-input logic gates can be employed to control material stiffness and conversion. The PEG-hydrogels stiffness can be predictably controlled with the two-input gates utilizing both CuAAC and ATRP. Furthermore, the material stiffness appears to closely mimic the synthetic biology rules traditionally measured with fluorescence. This indicates that more existing synthetic biological circuits can be employed to control material properties. Our results investigate the applications of biocatalytic EET for use in engineered living-materials with a higher degree of computation. Furthermore, controlling material properties through a bacterial interface allows for a high degree of control in complex environments. Utilizing a small molecule system, EET-catalyzed CuAAC fluorescently labelled live mammalian cell membranes without harming cell viability. These results indicate that there may be an opportunity for applying these computational hydrogels as scaffolding for wound repair or cell differentiation, as changes in the environment can allow *S. oneidensis* to actuate changes to material properties.

SB11.03.04

Nucleic Acid-Templated Growth of Iron Oxide Nanoparticles for Colorimetric Cell Detection Yoonbin Ji; University of Seoul, Korea (the Republic of)

With the recent development of nucleic acid nanotechnology, DNA-based materials have been considered for biosensing probe materials with their stability and programmability. Moreover, the hybridization of DNA materials with inorganic materials such as gold, silver, or iron oxide was also drawn attention for exploiting their exceptional functionality. However, the conjugation of biomolecules with inorganic molecules was expensive and laborious. Here we introduce the novel method for fabricating DNA/iron oxide nanoparticle (IONP) hybridized structures by using charge interaction between nucleic acid and metallic cations for co-precipitation reaction. DNA microstructure fabricated via the well-known rolling circle amplification (RCA) method was highly porous and negatively charged and could act as active sites for IONP growth reaction. Synthesized DNA/IONP hybrid showed core-shell structure with homogeneously covered iron oxide particles on a single DNA microparticle. Rationally designed DNA template with aptamer sequence, aptamer-DNA/IONP exhibited specific cancer cell targeting ability and was easily observed by colorimetric assay via Prussian blue staining.

SB11.03.05

The Regulation of RNA Polymerization and the Synthesis of Sponge-Like RNA Particles by Viscosity Moon S. Hyun and Jong Bum Lee; University of Seoul, Korea (the Republic of)

By utilizing a wide range of biological activities of RNA, RNA nanotechnology has advanced significantly for its prospective medicinal applications. However, the heterogeneity between individual patients and disease still calls for personally optimized nanoparticle design to enhance clinical outcomes. Therefore, RNA nanostructures manufactured via rolling circle transcription (RCT)-based enzymatic RNA self-assembly have gotten much interest as a possible way to control the nanoparticle design and improve the therapeutic RNA loading capacity. Here, we used viscosity to modulate enzymatic RNA polymerization and investigated how viscosity influences the synthesis of sponge-like RNA particles by modifying enzyme activity and molecular interactions between reaction components. The increase in viscosity under reaction circumstances resulted in a slower rate of RNA polymerization, indicating that viscosity regulates polymerase activity. Furthermore, when the solution viscosity increased, the inorganic crystallization of magnesium pyrophosphate, which serves as a structural foundation for sponge-like RNA particles, was reduced. As a result, the size of the sponge-like RNA particles decreased as the solution viscosity increased. In addition, in excessively viscous circumstances, the sponge-like structures vanished. Finally, the size of the sponge-like RNA particles was fine-tuned by modulating the template DNA to monomer rNTP ratio utilizing another previously described size reduction approach. Depending on each patient and disease, the needed size of the sponge-like RNA particles will be varied. As a result, we proposed novel ways to precisely manipulate the size of sponge-like RNA particles to meet various personalized demands.

SB11.03.06

Poster Spotlight: Engineering the Extracellular Matrix with DNA-Based Devices for Modulation and Force Sensing Applications Peter E. Beshay, Melika Shahhosseini, Carlos Castro and Jonathan W. Song; The Ohio State University, United States

It is well appreciated that reciprocal communication between cells and the surrounding extracellular matrix (ECM) can modulate the properties and the behavior of both the ECM and cells to influence both form and function. For example, modulation of the mechanical properties of the ECM by cells is believed to significantly influence the progression of certain diseased tissue such as fibrosis, healing wounds, or the stroma of tumors, all of which are known to exhibit ECM remodeling through the cross-linking of fibrillar collagen and/or deposition of non-collagenous ECM. In addition, interstitial flow through the ECM plays a major role in modulating cancer metastasis by redistributing chemokines, leading to chemotaxis, or through the activation of cell-surface mechanosensors, such as focal adhesion proteins, that promote cell motility. Current advances in Atomic Force Microscopy (AFM), and Magnetic Resonance Imaging (MRI) provided significant insights on the effect biophysical forces on disease progression. However, those techniques do not provide insights into effect of remodeling the same tissue sample nor provide a direct way of measuring the forces exerted by interstitial flow in the ECM. Here, we present a hybrid system that utilizes microfluidic devices and DNA-based nanoscale devices that will enable manipulating properties and measuring biophysical forces in the ECM at a sub-cellular level.

DNA-based molecular sensors have been of particular interest for studying cell interactions due to their high tunability, sensitivity and easy integrability into various biological systems. However, measuring cell-ECM interactions due to fluid flow using these sensors has yet to be achieved. Here, we present a DNA origami-based force probe that is capable of measuring fluid flow forces in the ECM. The probe, which is about 100 nm in size, consists of two barrels of DNA connected by six flexible linkers; allowing the device to fluctuate between open and closed states. Probe fluctuations is then reported using single molecule Förster resonance energy transfer (smFRET). The dynamics of the probe and its force sensitivity can be tailored by changing the interaction strength between its linkers. To enable the measurement of fluid flow forces in the ECM, we demonstrate our ability to anchor our probe to the fibers of collagen I-based hydrogels. We also present a three-channel microfluidic device comprising an “interstitial space” channel sandwiched between two “vessel” channels as a mean for applying physiologically relevant fluid flows. This microfluidic device can hence mimic interstitial fluid flow on the ECM by applying different pressure gradients on its channels. The integration of the DNA-engineered ECM with this microfluidic system will enable the spatiotemporal measurement of interstitial flow forces in the ECM, allowing for studying the effect of these forces on cancer cell motility and metastasis.

SB11.03.08

Anisotropic Nanofiber-Laden Hydrogel as Guidance to 3D Cell Orientation Cholong Choi, Suntae Kim and Chaenyung Cha; UNIST, Korea (the Republic of)

Along with continuous research in biotechnology, there is a growing demand for cell culture platforms that can provide a more biological microenvironment to induce complex cell behavior. The extracellular matrix (ECM) controls chemical signals and stores cytokines and nutrients beyond the structural support of tissue. It also serves to control the physical signals mediated by the integrins and has structural diversity. On the other hand, in conventional plastic substrates such as flasks and well plates, cells are attached to the surface and cultured so the behavior of cells can be explored only by the response to chemical signals such as growth factors. To mimic various biological tissues, an extracellular matrix environment suitable for each cell activity must be served.

The three-dimensional hydrogel culture system can control mechanical properties within a physiological range by controlling crosslinking density of polymer. Hydrogel can also provide a microenvironment that mimics natural surroundings for cell growth. However, overall hydrogel structures were difficult to control the fine physical properties of the cell niche. The limitation of controlling the local environment around cells can be studied by introducing other nanomaterials within hydrogels.

Electrospun nanofibers are widely used as scaffolds in tissue engineering that they are easy to fabricate and can simulate the structure of natural proteins derived from ECM. The other advantage of introducing nanofibers is that the porosity of the hydrogel can be maintained and the stiffness of the local area is controlled by the fiber density. Moreover, nanofibers can recreate the topographical heterogeneity of ECM architectures.

In particular, aligned structures of connective tissue can be easily found across soft tissue, skeletal muscle, heart tissue, and cancer tumor. From a microscopic point of view, the aligned structure affects angiogenesis, ECM reconstruction, and, electrical signal propagation in neurons. From a macroscopic point of view, it supports tendon loading, transmits muscle force, and is used to determine the malignant prognosis of tumors.

However, the traditional strategy to control the direction of cell migration is to give a chemical or physical cell adhesion gradient that would change cellular fates. Moreover, mimicking anisotropy in a three-dimensional structure still has been a challenge. Hence, this research demonstrates to regulate the orientation of cells along gelatin nanofibers aligned under an external magnetic field. This work establishes a new multifunctional scaffold strategy that mimics the aligned three-dimensional fiber structure of various nature tissues with independent control of physical and chemical properties.

SB11.03.09

Programmable Nanofibers as a Platform for Engineered Living Materials [Hoda Hammad](#) and Anna Duraj-Thatte; Virginia Tech University, United States

Innovation in material sciences has been the primary driver of significant changes in human history. Over the course of evolution, living cells -unicellular or multi-cellular- have tailored their pathways to synthesize complex materials responding to different environmental stimuli. Autonomous growth, self-organization, self-repair, responsiveness, and other characteristics of these living systems opened a different paradigm at the interface between material science and biological engineering. Inspired by nature and living systems, synthetic biology aims at using biological systems to perform user-defined functions. Through genetic engineering, synthetic biology extended its impact into material science. Living cells have been utilized as bio-factories producing programmable materials tailored to biotechnological applications ranging from biomedical to agriculture fields. Incorporation of the engineered living cells into materials enabled novel functionalities such as self-healing, autonomous assembly, adaptivity, and self-regeneration that synthetic materials lack. Therefore, synthetic biology paved the way for active, dynamic, and functional biomaterials. Our advanced understanding of bacterial systems highlighted them as an ideal chassis for pioneering the living materials field. The majority of the bacteria, inherently, exist as biofilms endorsed in an extracellular matrix composed of polysaccharides, proteins, nucleic acids, and other biomolecules. The ability of bacterial biofilms to self-assemble into higher-order structures has made them an attractive programmable platform for engineered living materials (ELMs). The current knowledge of genetic tools on model organisms such as *E. coli* made it an ideal organism for genetic prototyping in the field of ELMs. We will discuss different engineering techniques and synthetic biology tools that leveraged the power of the native curl system, the primary structural protein component of the *E. coli* biofilm, as a protein scaffold in different ELMs applications.

SB11.03.10

Poster Spotlight: Membrane Fusion—How Cubic Lipid-siRNA Constructs Escape the Endosome [Lining Zheng](#) and Cecilia Leal; University of Illinois at Urbana-Champaign, United States

Small interfering RNA (siRNA) silences gene expression and has shown great potential in medical applications. However, intracellular delivery of siRNA remains a great challenge. Lipid nanoparticles have been one of the most successful siRNA carriers to date, but their delivery efficiency is limited due to low endosomal release. We have shown that cubic structured lipid nanoparticles (cubosomes) loaded with siRNA - cuboplexes, show greater siRNA knockdown compared to traditional lamellar structured liposomes. In this work, we aim to elucidate the reason behind this difference in delivery efficiency. We will show confocal microscopy (CF), flow cytometry and live cell imaging data demonstrating higher cellular uptake of cubosomes compared to liposomes. CF, fluorescent based fusion assays, cryogenic transmission electron microscopy and dynamic light scattering measurements indicate that compared to liposomes, cubosomes are more prone to fuse and form aggregates with endosomes, which implies a stronger pore forming capability that leads to siRNA escape. These results support our suggestion that cubosomes can lower the free energy required to promote endosome pore formation and establish a topologically active delivery mechanism.

*This work is supported by the NIH (1DP2EB024377-01).

SESSION SB11.04: Designing and Printing Living Materials I
Session Chairs: Ben (Keith) Keitz and Seunghyun Sim
Tuesday Morning, November 29, 2022
Hynes, Level 3, Room 305

8:45 AM *SB11.04.01

Shape-Morphing Living Composites [Taylor H. Ware](#); Texas A&M University, United States

Stimuli-responsive polymers respond to their environment without requiring motors, sensors, or power supplies. Notably, the stimulus-response of many synthetic smart materials is derived wholly from physical properties, and as a result, these materials require powerful stimuli, such as heat, to induce shape change. By comparison, the stimulus-response of living organisms can be triggered by weak physical stimuli or specific biochemicals. We will discuss fabricating living yeast-hydrogel and bacteria-hydrogel composites capable of undergoing programmed shape change. As the cells are higher in modulus (~100×) than the gel, cell proliferation results in a macroscopic shape change of the composite. Importantly, genetic manipulation of the cells enables the stimulus that induces shape change to be controlled. For example, we will discuss composites where volume change on exposure to a single biochemical (L-histidine) is 14× higher than volume change when exposed to highly similar biochemicals (D-histidine and other amino acids). The use of this shape-changing material for future applications in drug delivery and sustainable manufacturing will be discussed.

9:15 AM SB11.04.02

Bacterial Patterning of Soft Materials [Ismar E. Miniél Mahfoud](#) and Ben (Keith) Keitz; The University of Texas at Austin, United States

Extracellular electron transfer (EET) is an anaerobic respiration mechanism through which electroactive microbes interact with and influence their environment. Using membrane-bound cytochromes, these organisms deposit electrons onto external electron acceptors such as metals and metal oxides. By controlling the expression and activity of EET proteomic elements, it is possible to use electroactive microbes as actuators that confer biological control over abiotic material properties. For example, we have shown that electrons produced by EET-capable organisms can activate exogenous metal catalysts, resulting in radical crosslinking of hydrogel precursors. Additionally, we have also created genetic logic circuits that predictably regulate EET pathway genes and EET flux in *Shewanella oneidensis* in response to one or more chemical inducers. With the development of these fundamental logic gates, we envision more complex architectures that would allow for spatiotemporal control of hydrogel crosslinking.

Communities of bacterial cells communicate by secreting chemical signals that act on others in the population in a concentration-dependent manner, usually leading to transcription of specific genes. By engineering strains to utilize these systems, gene expression can be tuned in a spatiotemporally dependent manner. These patterning circuits can spatially control transcription of EET-relevant genes and can be used to pattern crosslinkable materials,

such as hydrogels.

To the end of developing this technology, we have engineered *Shewanella oneidensis* “sender” cells that, under control of an inducible gene circuit, secrete a diffusible signal. We have also engineered “receiver” cells that express GFP in the presence of the signal. In petri-dish based assays, when fully induced sender cells are placed on top of a lawn of receiver cells and allowed to incubate, a circular “halo” of fluorescence is observed within the signal diffusion gradient produced by the sender cell population. We have found that we can modulate the size and intensity of the fluorescence pattern by varying the induction level of the sender cells. Using image analysis, we were able to quantify the intensity, size, symmetry, and consistency of the pattern.

The experiment was then repeated with receiver cells that express a key EET pathway protein instead of GFP. A colorimetric reporter of Iron(II) allowed visualization of a “halo” of EET-driven Iron(III) reduction that was very similar in size and shape as the fluorescence experiment, indicating not only spatiotemporal control of EET gene expression, but visual and genetic predictability of EET patterns using the fluorescence system. Future experiments will involve more complex genetic logic within receiver cells to create more intricate patterns as well expanding the reduction substrate scope to dyes and crosslinkable material precursors.

This technology will lay the groundwork for the engineering of living materials that can react to and interact with complex environments in applications such as chronic wound healing, tissue engineering, device fabrication, and the modeling of developmental signaling systems. Finally, this work will more broadly contribute to the development of EET as a universal interface that allows bacteria to confer genetic control over a large range of material properties.

9:30 AM SB11.04.03

Programmable Microbial Foundry for Functional Living Materials [Avinash Manjula-Basavanna](#); Northeastern University, United States

Living cells have the unparalleled ability to produce materials under ambient conditions from abundantly available benign components. This remarkable manufacturing capability of living cell is harnessed in the emerging field of Engineered Living Materials for various functional applications. In this talk, I will present our recent efforts to program the microbial foundry to produce the AquaPlastic [1] and the Microbial Ink [2].

AquaPlastic is a novel bioplastic produced from engineered microbial biofilms and it biodegrades to ~90% in just 45 days. AquaPlastic is resistant to organic solvents, strong acid, and base, which can be further utilized to form the protective coatings on various 1D and 2D substrates. AquaPlastic can also be molded, healed, and welded by using water. This work on AquaPlastic paves the way for packaging and coating applications, and to build a sustainable world.

Microbial Ink is a new class of bioink produced entirely from the genetically engineered microbes by a bottom-up approach. The shear-thinning property of the Microbial Ink coupled with its high viscosity, high yield-stress and shape fidelity facilitated the extrusion-based 3D printing into multi-layered architectures. The Microbial Ink was further programmed by using rationally designed genetic circuits in microbial cells to produce; A) Therapeutic Living Material – On demand secretion of an anticancer drug, B) Sequestration Living Material – Selective removal of toxic moieties and C) Regulatable Living Material – To control the number of cells by inducing (on demand) cell death. This work enables unprecedented avenues to manufacture macroscopic Functional Living Architectures and showcases advanced capabilities of Engineered Living Materials.

[1] Nature Chemical Biology, 2021, 17, 732

[2] Nature Communications, 2021, 12, 6600

9:45 AM BREAK

10:15 AM *SB11.04.04

Freeform Printing of Complex Living Materials Using a Low-Cost DIY 3D Bioprinter [Anne S. Meyer](#); University of Rochester, United States

3D printing of engineered bacteria is an evolving field that employs the tools of synthetic biology to express desired proteins and peptides while maintaining control over the shape and spatial organization of the resultant biomaterials. Previous bacterial 3D printers have been limited to producing low aspect ratio prints that become unstable and collapse under their own weight at greater heights. By leveraging open-source hardware and software, we have designed and modified a low-cost, commercial 3D printer into a bacterial bioprinter that can print complex, free-standing structures with high aspect ratios. To print complex structures with sharply defined edges, a novel syringe mount was designed with retraction functionality that pauses bio-ink extrusion during non-printing periods. Our new printer deposits bio-ink within gel slurries with viscoplastic properties, allowing delivery of bio-ink gellification agents immediately upon printing. This technique allows us to print stable, high aspect ratio (15:1), free-standing structures with sharper resolutions and internal cavities. A challenge to bioprinting is providing a supply of fresh nutrients and exchanging waste byproducts to support the health of the embedded microbes without damaging the printed structures. To address this, we developed a method to incubate the bioprints within a stable agarose-based gel slurry that permits diffusion of nutrients. Bioprints of engineered *Escherichia coli* strains incubated within a nutrient-infused slurry for seven days demonstrated 100-times higher colony-forming units compared to bioprints incubated without added nutrients, suggesting that nutrients diffuse through the slurry to increase viability of bacteria within bioprints. Printing complex structures by combining a low-cost 3D printer with a nutrient delivery method will enable the printing of complex biomaterials with extended functional lifespans and novel applications, including enzymatic degradation, multifunctional sensors, biofilm applications, and more.

10:45 AM SB11.04.05

Printing and Characterizing RNA Gradient Generators [Moshe Rubanov](#), [Pepijn Moerman](#) and [Rebecca Schulman](#); Johns Hopkins University, United States

Living organisms detect and produce gradients for a variety of different tasks, including morphogenesis^{1,2}, chemotaxis^{3,4}, and distributed computation⁵. Synthetic gradient generators have been developed to recreate the spatially heterogeneous chemical environments seen in biological systems. Some previously developed methods for gradient generation include using droplet mixers, hydrogel secretion, membrane channels, and pipette injectors⁶. However, these methods generally create gradients that are difficult to reproduce, are transient (lasting no more than 2 hours), introduce convection, or are difficult to model. Stable gradient generators have been reliably produced using microfluidic convection-based microchannels⁷ which produce gradients using a replenishing reservoir of a source and sink. However, convection-based microchannel gradients are difficult to integrate into multiple independently produced gradients capable of interacting with each other within the same chamber. Additionally, the gradient generator developed produces RNA, which can be coupled to fluorescent reporters and to control downstream dynamic processes^{8,9}. To build a tunable RNA gradient generator, we anchor transcription templates within hydrogel posts photopatterned within a microfluidic flow cell. These posts act as a chemical source, constantly producing RNA. The RNA diffuses out of the hydrogel posts where it is degraded in solution. We use T7 RNAP and RNase A/T1 to drive local RNA transcription

and global degradation, respectively. Tuning the location and size of the hydrogel posts, along with T7 RNAP and RNase A/T1 concentrations, enables the building of a tunable set of RNA gradients. To measure these gradients, we use hydrogels with attached “reporter” complexes that react with the RNA and produce a fluorescent signal. Multiple photopatterned source hydrogels could also be used to form more complex additive gradients, more closely recreating environments in cell populations². This platform makes it possible to direct local self-assembly of nucleic acid responsive nanostructures and nanoparticles, and for the study of complex microenvironments in cell cultures.

Bibliography

1. Ellison, D. *et al.* Cell–cell communication enhances the capacity of cell ensembles to sense shallow gradients during morphogenesis. *PNAS* **113**, E679–E688 (2016).
2. Grant, P. K. *et al.* Interpretation of morphogen gradients by a synthetic bistable circuit. *Nat Commun* **11**, 5545 (2020).
3. Alon, U., Surette, M. G., Barkai, N. & Leibler, S. Robustness in bacterial chemotaxis. *Nature* **397**, 168–171 (1999).
4. Sourjik, V. & Wingreen, N. S. Responding to chemical gradients: bacterial chemotaxis. *Current Opinion in Cell Biology* **24**, 262–268 (2012).
5. Alberghini, S. *et al.* Consequences of relative cellular positioning on quorum sensing and bacterial cell-to-cell communication. *FEMS Microbiology Letters* **292**, 149–161 (2009).
6. Somaweera, H., Ibragimov, A. & Pappas, D. A review of chemical gradient systems for cell analysis. *Analytica Chimica Acta* **907**, 7–17 (2016).
7. Hosokawa, M. *et al.* Microfluidic Device with Chemical Gradient for Single-Cell Cytotoxicity Assays. *Anal. Chem.* **83**, 3648–3654 (2011).
8. Matsuura, S. *et al.* Synthetic RNA-based logic computation in mammalian cells. *Nat Commun* **9**, 4847 (2018).
9. English, M. A. *et al.* Programmable CRISPR-responsive smart materials. *Science* **365**, 780–785 (2019).

11:00 AM SB11.04.06

Yeast Biomaterial for Environmental Remediation [Christos E. Athanasiou](#); Georgia Institute of Technology, United States

Traces of heavy metals found in water resources, due to mining activities and e-waste discharge, pose a global threat. Conventional treatment processes fail to remove toxic heavy metals, such as lead, from drinking water in a resource-efficient manner when their initial concentrations are low.

In this talk, we will present how by using a yeast biomaterial we can effectively remove trace lead from water via a rapid mass transfer process, achieving an uptake of up to 12 mg lead per gram of biomass in solutions with initial lead concentrations below 1 part per million. Furthermore, we will discuss our efforts on using advanced experimental and computational characterization techniques to investigate the lead adsorption mechanisms, and present our discovery that lead adsorption is linked to a significant increase in yeast cell wall stiffness. These findings open new opportunities for using environmentally friendly and abundant biomaterials for advanced water treatment targeting emerging contaminants.

SESSION SB11.05: Designing and Printing Living Materials II

Session Chairs: Ben (Keith) Keitz and Seunghyun Sim

Tuesday Afternoon, November 29, 2022

Hynes, Level 3, Room 305

1:30 PM *SB11.05.01

Genomically Recoded Organisms—Living Foundries for Producing Programmable Biomaterials [Farren J. Isaacs](#); Yale University, United States

Materials produced from synthetic chemical processes provide access to a broad range of chemical structures yet are constrained by the lack of sequence-defined polymerization methods. In contrast, biological systems employ sequence-controlled processes to synthesize biomolecules, in which the molecular information encoded by nucleic acids is converted into sequence-controlled protein polymers. However, nature is constrained to a small set of organic monomeric building blocks, the 20 canonical amino acids, thereby limiting the chemical diversity of polymeric biomaterials. Advances in synthetic biology permit the genetic encoding of synthetic chemistries at monomeric precision, enabling the synthesis of programmable proteins with tunable properties. Here, I describe the design and construction of genomically recoded organisms (GROs) possessing open coding challenges. These open codons, together with engineered translation machinery, enable site-specific and multi-site nsAA incorporation in proteins at high yields and purity where multiple identical nsAAs provide the dominant chemical and biophysical properties to proteins or biopolymers. Finally, I will describe the production of sequence-defined biomaterials with applications in highly-conductive protein nanowires and functionalized biotherapeutics. The use of GROs to produce multifunctional, structurally complex materials can be expanded toward the development of a programmable new class of genetically encoded biomaterials with diverse chemistries and broad applications for new classes of enzymes, materials, and therapeutics.

2:00 PM SB11.05.02

Dynamic Optical Systems Inspired by Cephalopods [Georgii Bogdanov](#), Nikhil Kaimal, Atrouli Chatterjee, Alon Gorodetsky and Aleeza Farrukh; University of California, Irvine, United States

Cephalopods (e.g., squids, octopuses, and cuttlefish) have captivated the imagination of both the general public and scientists alike due to their sophisticated nervous systems, complex behavioral patterns, and visually stunning coloration changes. By drawing inspiration from the structures and functionalities of tunable cephalopod skin cells, we have designed and engineered human cells that contain reconfigurable protein-based photonic architectures and, as a result, possess tunable transparency-changing and light scattering capabilities (1). In turn, we have visualized the refractive index distributions of analogous engineered cells with three-dimensional label-free holotomographic microscopy techniques, and as a consequence, we have developed a detailed understanding of the relationship between their global optical characteristics and subcellular ultrastructures (2). We have moreover extended these efforts to the predictive engineering of the refractive indices and light-scattering properties of multiple self-assembled protein-based platforms, both *in vitro* and *in vivo* (2,3). Finally, we have developed improved chemical and genetic strategies for manipulating the sizes, numbers, and refractive indices of our subcellular structures (4). Our combined findings may facilitate an improved understanding of cephalopod camouflage mechanisms and lead to the development of unique tools for applications in biophotonics and bioengineering.

Chatterjee A., *et al.*, *Nat Commun.* **11**, 2708 (2020).

Chatterjee A., *et al.*, *In Revision*.

Umerani M.J., *et al.*, *PNAS*, **117**, 32891-32901 (2020).

Bogdanov G., *et al.*, *Submitted*.

2:15 PM SB11.05.03

The Influence of *Rhizobium tropici* Produced EPM Biopolymer on Green Bush Bean Root and Plant Growth [Shirley X. Yu](#)¹, Huiting Luo², Youyou Zheng³, Zihan Wang⁴, Melany Fernandez⁵, Miriam Rafailovich², Marcia Simon², Stephen Walker², Jay Gao² and Steven Larson⁶; ¹Collingwood School, Canada; ²Stony Brook University, United States; ³Asheville School, United States; ⁴Mulgrave School, Canada; ⁵Suffolk County Community College, United States; ⁶Army Engineer Research and Development Center, United States

With the increase in severe weather events due to climate change, plant development both aboveground (providing vegetation cover) and belowground (enhancing root systems) is crucial in limiting soil erosion. Traditional chemical fertilizers do allow for these developments but have environmental consequences from polluting waterways to disturbing the natural biodome. Hence, much effort is currently being invested in finding alternative means to enhance plant growth and mitigate soil erosion through the application of environmentally sustainable materials. A *Rhizobium tropici* (R. tropici) derived biopolymer has been reported as an effective, biodegradable additive to reduce soil erosion. We, therefore, chose to study its effectiveness for root and stem/leaf growth of plants in the early stages of development, starting from the germination of the seeds through the initial growth of leaves and shoots. The plants used were green bush beans due to their relatively short germination time of 7-12 days which allowed us to see the effects of the fertilizers within a short period of time.

Two biopolymer fertilizers, both ethanol precipitable materials (EPM) derived from R. tropici bacteria ATCC strain under the same cultivation environment and procedure but grown in two laboratories, were tested. Green bush beans were divided into five groups: control (tap water) and four EPM treatments. The EPM treatments consisted of the combinations of 50 mg/L EPM1 (from the first lab), 50 mg/L EPM2 (from the second lab), 100 mg/L EPM1, and 100 mg/L EPM2. The beans underwent 10 days of germination and then were transplanted into soil for 3 weeks of further watering with tap water or EPM solutions daily. Mass measurements were used to investigate whether the EPM biopolymer influenced the growth of the roots versus the stems and leaves differently. As such, the green bush bean plants were removed from the soil for roots and plant analysis after 3 weeks of transplantation. The soil was washed off and the plants were dried completely to ensure that the mass was only of the intended roots and stems/leaves. The effects of each treatment were recorded by measuring the masses and lengths of the roots and stems/leaves individually. Mass measurements were used to investigate whether the EPM biopolymer influenced the growth of the roots versus the stems and leaves differently.

Watering bush bean seeds with EPM concentrations as low as 50 mg/L and 100 mg/L produced a small increase in the germination rate: from 87% to 93% for seeds grown for 10 days in a moist environment. The root mass of the plants treated with the EPM solutions increased compared to the control by 29% to 71% (for EPM1) and by approximately 14% (for EPM2). The plants treated with either of the EPM solutions have a mass of stems and leaves that is higher than the control by 45% and 58% for EPM1 and EPM2, respectively. Furthermore, the result shows that there was a 21% to 43% increase in plant height for plants treated with EPM solution. EPM1 and EPM2 solution treated plants showed enhancement in both root and stem/leaf mass compared to the control, but the EPM1 solution was better for root development and EPM2 solution was better for stems and leaves development—consistent with plants typically preferring either root or leaf production. These results suggest that the EPM biopolymer stimulates bush bean plants to develop a denser root structure and a larger leaf and shoot system, which enhances plant survival. Taken together, these results may explain the reported increase in resistance to soil erosion when biopolymer was used to irrigate different berm slope sites.

We would like to thank the US Army Corps of Engineers (ERDC) for their support (W912HZ-20-2-0054) in this research, Dr. Michael Sadowsky for providing the *Rhizobium tropici* CIAT 899 (UMR 1899) strain, and the Morin Charitable Trust for the funding.

2:30 PM DISCUSSION TIME

2:45 PM BREAK

SESSION SB11.06: Biologically Programming Materials II
Session Chairs: Neha Kamat, Ben (Keith) Keitz and Seunghyun Sim
Tuesday Afternoon, November 29, 2022
Hynes, Level 3, Room 305

3:15 PM SB11.06.01

Living Material Systems with Multilayered Genetic Circuits for Biomedical Nanomaterials [Urtu Seker](#); Bilkent University, Turkey

We have developed self-actuating genetic circuits for nanomaterial synthesis using a protein based scaffolding. The self-actuated living material systems can sense the environmental signal, process the signal using the sensor gene circuits, process the gene circuits and create an output which the final nanomaterial scaffolding biofilm protein.¹ In the follow-up study we have focused on nanomagnet synthesizing and tumor colonizing living material systems. The high cancer incidence grows the demand for efficient cancer diagnostic tools with minimized side effects nowadays. Developments in this aspect bring magnetic nanoparticles (MNPs) for biomedical applications due to their stability, biocompatibility, and magnetism properties. In nature, magnetic nanocrystals are synthesized in certain organisms, including many bacteria, which help their spatial orientation and survival by sensing the earth's geomagnetic field. This work aims to convert *Escherichia coli* to accumulate magnetite, which can further be coupled with drug delivery modules. For that, we designed bacterial machines in a way to accumulate magnetite using genetic circuitries hiring Mms6 with iron-binding activity and essential in magnetite crystal formation. Our work demonstrates that the combinatorial effect of Mms6 with ferroxidase, iron transporter protein, and material binding peptide enhances the paramagnetic behavior of the cells in magnetic resonance imaging (MRI) measurements. Alternatively, cellular machines are also engineered to display Mms6 peptide on the cell surface via an autotransporter protein² providing easy synthesis conditions that showed augmented MRI performance. Our findings are promising for endowing a probiotic bacterium, able to accumulate magnetite intracellularly or extracellularly, serving as theranostics agent for cancer diagnostics via MRI scanning, drug delivery, and hyperthermia treatment.³ The study was supported TUBITAK 115M108

3:30 PM SB11.06.02

Programmable Living Materials with Engineered Spore-Forming Bacteria and Synthetic Macromolecules [Seunghyun Sim](#); University of California, Irvine, United States

In this talk, I will present the Sim lab's recent efforts in developing programmable living materials with engineered spore-forming bacteria, *Bacillus subtilis*, and synthetic macromolecules. Programmable aspects of these living materials, both in terms of genetic engineering of *B. subtilis* and molecular-level control in synthetic polymers, will be discussed. I will also highlight unique properties and characteristics of these living materials.

3:45 PM SB11.06.03

Genetic Logic Gates Enable Patterning of Amyloid Nanofibers Recep E. Ahan, Cemile E. Ozcelik, Ebuzer Kalyoncu and [Urtu Seker](#); Bilkent

University, Turkey

Many biological structures contain spatially organized materials produced by cells. Appearance of organized materials in distinct kingdoms indicates that organized materials provide advantages against natural selection. There are many examples of biological process which harvest the power of unique feature of spatially organized structures. Here, we developed recombinase enabled logic gates to synthesize organized materials in *E. coli*. The gates can utilize to record exposure of environmental signals and adjust to synthesize certain types of CsgA based fibrillous biofilm materials. Composition of fibrillous/cell biofilm material can be regulated by user-defined signals. We envision that recombinase based genetic circuits provide available route to the control composition and spatial organization of living materials.

The study was supported by TUBITAK Grant Numbers 114M163 and 216M127. U.O.S.S. thanks the TUBA-GEBIP Award. E.K. thanks TUBITAK BIDEB Graduate Fellowship.

SESSION SB11.07: Virtual Session I
Session Chair: Seunghyun Sim
Wednesday Morning, December 7, 2022
SB11-virtual

9:00 AM SB11.07.01

Chemically Modified *Bifidobacterium bifidum* for Cancer Immunotheranostics Using Photothermal Therapy [Sheethal Reghu](#) and Eijiro Miyako; Japan Advanced Institute of Science and Technology (JAIST), Japan

Conventional cancer therapies face a myriad of shortcomings which has hampered their widespread application. Bacteria-driven cancer therapy has emerged as a very promising therapeutic strategy, offering numerous advantages such as high selectivity, specificity, and high-targeting efficiency. They possess numerous unique mechanisms for treating cancer that are unachievable with standard methods.^[1] In this project, we report the modification of an anaerobic bacteria, *Bifidobacterium bifidum*, which exhibits an innate anticancer efficiency.^[2] The bacteria were modified by incorporating a photothermal agent, indocyanine green with cremophor EL, by incubation process.^[3] Cremophor EL, an FDA-approved polyoxyethylene castor oil derivative, commonly used in poorly water-soluble drugs was added to indocyanine green molecules for encapsulation thereby forming indocyanine green with cremophor EL nanoparticles. After overnight incubation with *Bifidobacterium bifidum*, indocyanine green with cremophor EL molecules penetrated the bacterial membrane forming the modified bacteria, thereby changing their color from white to green. These modified bacteria were capable of absorbing light in the near-infrared (NIR) region thereby making them provide an excellent photothermal conversion efficiency. Characterization of these chemically modified bacteria was carried out using UV spectroscopy, transmission electron microscopy, fluorescence spectroscopy, and confocal microscopy to determine their absorption range, structural and morphological changes, and to elucidate their mechanism resulting in their modification. Furthermore, they exhibited low toxicity and high temperature elevation in *in-vitro* studies with and without laser irradiation. *In vivo* studies were conducted in syngenic tumor mice models to study the tumor targeting efficiency using colon26 cancers. The modified anaerobic bacteria were intratumorally injected and their accumulation was observed solely in the hypoxic environment inside the tumor leaving other organs, and their distribution was determined using an NIR fluorescent imaging system. Additionally, the treatment of these colon cancers was carried out by photothermal therapy, by irradiating the tumors at 0.7W using an 808nm NIR laser after 24 hours of intratumoral injection. The application of photothermal therapy was observed by the temperature elevation caused by the NIR laser on the tumor surface resulted in excellent anticancer efficiency causing the disappearance of the tumor after a few days. The blood test results in tumor mice models also revealed that the modified bacteria were completely non-toxic and biocompatible in mice. Various tissue staining techniques were also carried out to explain the mechanism of tumor suppression. In summary, this study demonstrates a very simple mechanism of nanoengineering the bacteria without any complicated genetic manipulation, rather a much simpler process to modify bacteria to increase their efficiency at the same time maintaining their morphology, function, and structure. This study demonstrates the potential for bacteria therapy in cancer theranostics as they can provide a paradigm-shifting knowledge for the development of next-generation anticancer agents by nanoengineering the bacteria.

References

1. Forbes, N. S. Nat. Rev. Cancer, 2010,10, 785–794.
2. Abdolalipour, E. et. al., Microbial Pathogenesis, 2020, 145, 104207.
3. Reghu, S. and Miyako E. Nano Letters, 2022, 22, 1880-1888.

9:15 AM *SB11.07.03

Biochemical Networks for Controlling the Growth and Metamorphosis of Soft Materials [Rebecca Schulman](#); Johns Hopkins University, United States

Complex cellular behaviors such as motion and division are directed by far-from-equilibrium chemical networks that regulate the assembly and reconfiguration of a cell's architecture at the molecular scale. The ability to program the evolution of synthetic materials using designed chemical networks in fashions similar to the way biological networks regulate a cell and tissue architecture could be a route to building radically new materials that could grow into specific shapes, heal, or adapt to their environments. Building and improving these systems might also provide new perspectives on the structural organization of cells and tissues and on the genetic and signal transduction networks that regulate these cell and tissues' structures and therefore, functions. We have been developing synthetic components that dynamically assemble and change the shapes of biomolecular materials, specifically hydrogels and semiflexible polymer networks, and corresponding synthetic chemical networks that can regulate these materials' dynamic assembly. I will describe how different biomolecular signals can induce different dynamic polymerization and depolymerization processes in these materials and how chemical networks can be coupled to these materials to induce dynamic material behavior. To understand what new behaviors can arise in these systems when their chemical networks become large and complex, we have recently developed integrated synthetic *in vitro* genetic regulatory networks consisting of oligonucleotide templates, T7 RNA polymerase and an RNase. These networks can consist of tens of different interconnected network elements and could be used to build synthetic regulatory networks of complexities comparable to those of simple viruses or those that construct macromolecular complexes inside cells.

9:45 AM DISCUSSION TIME

7:00 AM SB11.08.01

Diblock Polypeptide Hydrogels as Bioinks for 3D Printing in Tissue Engineering Muireann Cosgrave; Royal College of Surgeons Ireland, Ireland

The use of 3D printing in tissue engineering (bio-printing) has rapidly increased throughout recent times, namely due to its ability to construct more complex, cell-viable 3D structures.¹ Hydrogels are a prominent choice for bio-ink formulations as they can be engineered to simulate the native extracellular matrix (ECM).² Furthermore, their mechanical properties can be altered to optimize printability and cytocompatibility properties. For particular applications, the choice of hydrogel used in bio-printing processes encompasses several important considerations, particularly that its strength is stable and suitable for the printing process, whilst also being comparable in strength to that of the native tissue it is replacing.²

Here we present a range of amphiphilic star-shaped diblock co-polypeptides consisting of methacrylamide functionalized poly(L-glutamate)-b-(L-leucine) with different star architectures. The hydrophobic side chains of the L-leucine blocks drive the self-assembly of the polypeptides in water, spontaneously forming stable hydrogels. The mechanical properties of these materials are readily tuned by varying the star architecture and the monomer feed used. They also possess shear-thinning and self-recovery properties, indicating their suitability for extrusion based 3D printing. Complex 3D printed structures can be readily generated and then photo-crosslinked using visible light (405 nm) in the presence of comonomers. Printed hydrogels show good biocompatibility and represent viable bio-ink material platforms for tissue engineering.

References

(1) Li, J.; Wu, C.; Chu, P. K.; Gelinsky, M. 3D Printing of Hydrogels: Rational Design Strategies and Emerging Biomedical Applications. *Mater. Sci. Eng. R Rep.* **2020**, *140*, 100543. <https://doi.org/10.1016/j.mser.2020.100543>.

(2) Ramiah, P.; du Toit, L. C.; Choonara, Y. E.; Kondiah, P. P. D.; Pillay, V. Hydrogel-Based Bioinks for 3D Bioprinting in Tissue Regeneration. *Front. Mater.* **2020**, *7*, 76. <https://doi.org/10.3389/fmats.2020.00076>.

SYMPOSIUM SB12

Novel Soft Materials and Systems for Artificial Skin and Soft Robotics and Haptics
November 28 - December 7, 2022

Symposium Organizers

Lucia Beccai, Istituto Italiano di Tecnologia
Piero Cosseddu, University of Cagliari
Ingrid Graz, Johannes Kepler University
Darren Lipomi, University of California, San Diego

Symposium Support

Bronze
Materials Horizons

* Invited Paper

+ Distinguished Invited

SESSION SB12.01: Applications I

Session Chairs: Lucia Beccai, Piero Cosseddu, Ingrid Graz and Darren Lipomi
Monday Morning, November 28, 2022
Hynes, Level 3, Room 309

10:30 AM SB12.01.01

Skin-Actuator Interactions for Vibrotactile Haptic Applications Jin-Tae Kim, James E. Colgate and John A. Rogers; Northwestern University, United States

Recent advances in skin-integrated vibrotactile haptic devices offer the capability of realizing a sense of touch, not only at the fingertips but across all regions of the body in virtual settings. However, many challenges lie ahead for creating realistic tactile interactions, owing to the complexity and lack of understanding of our somatosensory system and associated skin-actuator interactions. Here, we experimentally explored nearly all types of off-the-shelf vibrotactile sensors including an eccentric rotating mass (ERM), linear resonant actuator (LRA), tactor, and piezoelectric actuator interfacing directly to the skin surface and skin-like materials. Non-intrusive optical methods, including 3D Digital Image Correlation (DIC), Particle Tracking Velocimetry (PTV) and Eulerian Video Magnification (EVM), were implemented to decipher important continuum mechanic properties relevant to mechanoreception, including strain and acceleration at different depths in a skin phantom. Additional parameters, such as contact area, power input, frequency, and viscoelasticity, as well as customized perception tests, are considered to further correlate skin-actuator interactions and tactile perception. These findings will provide reference data for model validations and optimal strategies for developing next generation haptic devices.

10:45 AM SB12.01.02

Bioinspired Robotic Cutaneous Sensor System for Softness Detection Haotian Chen, Ivan Furfaro and [Stephanie P. Lacour](#); Ecole Polytechnique Federale de Lausanne, Switzerland

Softness perception is a unique feature of the human skin, which is very useful during object manipulation tasks. However, this distinctive function relies on the skin deformation under pressure, and is hard to mimic in traditional robotic technology.

Although some research groups have developed several compliance sensing modules based on flexible or stretchable electronic technologies, the interaction between a soft artificial device and a target object, in terms of Young's modulus, is rarely considered. Specifically, when the target material is stiffer than the sensor, a large deformation occurs in the device while there is negligible deformation on the contacted object. Conversely, a softer object may deform more than the soft sensing module itself. As a result, even under the same external pressure, the deformation of the sensor depends on the difference in Young's moduli of the materials forming the target object and the sensor. Such variation could cause significant errors in the measurement and thus, hinder the correct characterization of the compliance.

Inspired from the human tactile system, we report on liquid metal-based soft sensor modules for softness detection. Each sensing unit comprises a strain sensor and a pressure sensor to measure deformation and pressure simultaneously. We propose an analytical mechanical model to describe the interaction between the soft sensor and the soft target, and simulate the system using finite element modeling. Following a calibration, we successfully distinguished engineering materials such as rubber and hydrogel and some biological tissues including chicken chest and heart. Next we prepared a 4x4 sensor matrix and successfully quantified the compliance and spatial distribution of several objects. This softness sensing technology may be implemented in applications such as robotic palpation or precise teleoperation.

11:00 AM SB12.01.03

A Nanomesh Pressure Sensor for Monitoring Finger Manipulation While Avoiding Interference with Human Sensations [Sunghoon Lee](#), Tomoyuki Yokota and Takao Someya; The University of Tokyo, Japan

An ultimate goal of biological information measurement is to monitor states of a living body in a non-invasive, continuous and accurate manner without disturbing the natural functions or activities of the living body. Because sensors in direct contact with biological tissues are inevitably exposed to physical disturbances caused by physical contact, considerable efforts have been made to minimize the effects of sensors. In temperature measurement, for example, it is necessary to reduce heat capacity or thermal conductance of sensors in order to suppress the effect of heat transfer from the object to the sensor. In addition, because our living body is soft and has a three-dimensional structure, it is required to use soft and/or flexible sensors to reduce the effects from modulus differences, and to achieve the stable contact to the curved objects. Recent development of soft and flexible pressure sensors has enabled to detect biological information such as human pulse or intraocular pressure, and human motions.

To continuously monitor biological information over a long period of time, sensors are required to exhibit a high mechanical durability. Soft and flexible pressure sensors allow an operation in bent or twisted states. The use of ultra-thin substrates and CNT/graphene nanofibers reduces a mechanical stress to sensors in the bent state, and results in an accurate detection of pressure with a bending radius of 80 μm . Recently, pressure sensors using porous PDMS or microstructured PDMS with Ag-NW coating have maintained a high pressure sensitivity (20 kPa^{-1}) without a damage under large pressure loads in MPa range. Furthermore, the use of rubber or textile gloves to protect the sensors significantly improves the durability of sensors, because such thick and durable materials prevent the sensors from causing mechanical damage to external forces.

However, there still remain challenges to achieve practical durability of sensors while maintaining a natural skin sensation. When the thickness of the material applied to the skin is reduced, the skin can sense external changes more easily. However, thin materials are vulnerable, because the force required to penetrate and/or break the material, is proportional to the thickness of the material. Furthermore, thin materials are easily scraped off against surface frictions. In order to improve the frictional durability while maintaining the overall thickness thin, it is necessary to reduce a friction coefficient of the surface materials to reduce scraping, or to introduce rigid protective materials to minimize a plastic/rubber deformation of the surface materials. However, such approaches cause a difference with the surface of a normal finger and an influence on the sensation due to a difference in mechanical properties with the skin.

Here, we present extremely durable nanomesh pressure sensors that can be attached on human skin without affecting human senses. The nanomesh sensors are ultra-thin (10 μm) and lightweight, and all layers are composed of nanoporous structures. The sensors exhibit a high mechanical durability against lateral pressures such as shearing or friction, as well as vertical pressing. The performance of sensors can be maintained without a significant degradation or breaking, although the surface of sensor was directly rubbed while pressing with a high pressure of more than few hundreds kPa.

11:15 AM *SB12.01.04

Fibers and Meshes Designed as Artificial Muscles [Andreas Lendlein](#); University of Potsdam, Germany

Fibers from shape-memory polymers (SMP) can be programmed to shrink, twist, bend or even knot themselves upon exposure to heat. Their integration in textiles can enable complex macroscopic motions or lead to changes in haptics or diffusivity of water vapor. Here (sub)micron fibers and meshes are presented, which were prepared by electrospinning. Fiber meshes from crosslinked semi-crystalline polymers exhibited a thermally-controlled actuation capability, which could be used to reversibly adjust pore diameters in polymer filters [1]. The fiber diameter has been identified as effective design parameter with regard to actuator performance. A high degree of molecular orientation could be obtained by processing for small diameter fibers. The angles between stacked layers, in which fibers are aligned in parallel, and the covalent interlinking at fiber contact areas are relevant design parameters for the fabrication of fiber meshes with anisotropic actuation capabilities [3]. Finally, electrospun meshes from degradable shape-memory polymers [4] have been explored as epicardial patch system, which can guide postinfarct myocardial remodeling processes [5].

References

- [1] Sauter T., et al., *Mater. & Design* 202, 109546, 2021
- [2] Zhang Q., et al., *Smart Mater. Struc.* 28, 055037, 2019
- [3] Sauter T., *Appl. Mater. Today* 29, 101562, 2022
- [4] Lendlein A., Langer R. S., *Science* 296, 1673, 2002
- [5] Tung W. T., et al., *Adv. Funct. Mater.* 2110179, 2022

Monday Afternoon, November 28, 2022
Hynes, Level 3, Room 309

2:00 PM *SB12.02.01

Ultra-Soft Transducers with Organic Electronics for Skin-Sensor Systems [Takao Someya](#)^{1,2}, Tomoyuki Yokota¹, Sunghoon Lee¹ and Kenjiro Fukuda²;
¹The University of Tokyo, Japan; ²RIKEN, Japan

Extremely soft and lightweight electronic devices can acquire biological signals such as pressures [1,2], blood pressure [2], electrocardiogram [3] on the skin, cell sheets, and textiles with minimized uncomfortableness when attached and without sensory interference. Combining such ultra-soft sensory systems with an ultra-lightweight or wireless power supply makes it possible to realize self-powered transducers [5,6]. We will report recent progress of the ultra-flexible organic photonic system and the nanomesh based skin sensors. To realize the air-stable organic photonic system, we developed the ultra-flexible organic light emitting diode with inverted structure. The lifetime of the OLED is longer than 1 week. In addition, we realized the self-adhesive nano sheet which was reinforced by polymer nanofiber. We succeed to monitor the ECG signal for a one week by attaching the nano-sheet electrode. [1] S. Lee et al., Science, 370, 966-970, (2020). [2] J. Zhong et al., Adv. Mater. 34, 2107758 (2022). [3] T. Yokota et al., Adv. Mater. Technol. Doi: 10.1002/admt.202200454 [4] S. Lee et al., Nat. Nanotechnol. 14, 156-1160 (2019). [5] S. Park et al., Nature 561, 516-521 (2018). [6] H. Jinno et al., Nat. Commun. 12, 2234 (2021).

2:30 PM SB12.02.03

High-Resolution Piezo-Resistive Film Based on Aligned Nickel Particle Network for Mimicking Receptor Systems of Human Skin [Hanul Kim](#), Seongdae Choi, Jiseok Seo and Yongtaek Hong; Seoul National University, Korea (the Republic of)

Electronic skin (E-skin), which is electronics that mimic the properties of human skin, has recently received increasing attention owing to its various applications, such as the human-machine interface and health monitoring devices. For the E-skin to interact with its surroundings in the same way as real human skin does, it is necessary to develop skin-like flexible sensors capable of detecting most of the physical contacts and physiological activities of the human body. Hence, a flexible pressure sensor for E-skin applications is required to detect external pressure at various levels to cover the entire pressure range in our daily life. In addition, as tactile receptors are distributed all over human skin in high density, a pressure sensor array for mapping high-resolution pressure distribution is also needed. To date, many studies focused on the pressure performances of a single sensor, attaining high sensitivity through additional microstructures. However, their pressure response quickly reached the saturation region at the level of simple touch and showed limitations in achieving high-resolution arrays due to crosstalk effects from the adjacent pixels. Organic field-effect transistor (OFET) based structures also have been adopted to overcome the crosstalk effect, but they used high cost and time-consuming processes such as photolithography or evaporation process.

In this work, we demonstrate a facile fabrication of flexible piezoresistive film based on anisotropically aligned micro-sized Nickel (Ni) particles embedded in polydimethylsiloxane (PDMS) composite. First, we prepare an uncured mixture of Ni/PDMS and place between the two strong magnets. Using the ferromagnetic property of Ni particles, whole particles in the film are aligned in the direction of a vertical magnetic field. After the curing process, filamentous conduction paths of Ni particles are formed, enhancing the pressure sensitivity and minimizing crosstalk effects compared to the film with randomly distributed Ni particles. To obtain the pressure sensor array, electrodes are deposited on the top and bottom sides of the film by spray-coating silver nanowire (AgNWs) ink. As the sensing pixels are defined at the intersection of top and bottom electrodes, the resolution of the sensor array can be adjusted by the pitch of the deposited electrode array up to 100dpi, which far exceeds the receptor density of human skin. This system is advantageous in imitating the receptor systems of human skin that have different densities for each body part. Using a resolution-varying read-out circuit that includes top and bottom electrode arrays with multiple pitches ranging from 0.25 mm to 1 mm, we can present an identical pressure distribution at various spatial resolutions using a single piezo-resistive sheet, detecting the same way as the human hand which has 4-fold difference in receptor density. The sensor can also detect a broad pressure range of up to 373kPa in high sensitivity, covering the entire pressure stimuli associated with human activities. This work was supported by the Industry technology R&D program(20006400) funded By the Ministry of Trade, Industry & Energy(MOTIE, Korea).

2:45 PM SB12.02.04

High-Efficiency Stretchable Light-Emitting Polymers from Thermally Activated Delayed Fluorescence [Wei Liu](#)^{1,2}, Cheng Zhang¹, Juan J. de Pablo^{1,2} and Sihong Wang^{1,2}; ¹The University of Chicago, United States; ²Argonne National Laboratory, United States

Stretchable electroluminescent (EL) polymers are the key components for realizing skin-like displays and optical bio-stimulations, which can offer unique functionality for information visualization, wirelessly signal/power transmission, and medical therapies. However, in contrast to other types of stretchable devices, such as sensors and transistors, stretchable EL devices have lagged behind in terms of combining high stretchability with high EL efficiency. All stretchable emitters reported to date have been based on “first-generation” EL polymers that can only harness the singlet excitons with a theoretical quantum yield of 25%. In this work, we present a material design concept for imparting the stretchability onto “third-generation” EL polymers that can harness all the excitons through thermally activated delayed fluorescence (TADF), thereby with a theoretical near-unity quantum yield. Our novel design concept for such stretchable light-emitting polymers is the backbone insertion of flexible, linear units between TADF units, which, as shown both experimentally and theoretically, provides very effective strain dissipation for stretchability without causing any sacrifice to the EL performance. Therefore, enabled by the highly efficient TADF processes and extraordinary stretchability, record-high external quantum efficiency (EQE) is achieved even at 100% strain. Besides, the concept is generalizable to achieve blue-green-red full-color stretchable light-emitting polymers. Demonstrated by the fully stretchable organic light-emitting diodes (OLEDs), the stretchable TADF polymers provide an unparalleled path towards achieving all the desired EL and mechanical characteristics, including high efficiency, brightness, switching speed, stretchability, and low driving voltage.

3:00 PM BREAK

3:30 PM SB12.02.05

3D-Stacked Thin-Film Transistors for Simultaneous Detection of Pressure and Temperature [Youngmin Jo](#) and Sungjune Jung; Pohang University of Science and Technology, Korea (the Republic of)

Deformable sensors can be conformally attached to a curvilinear surface, so they can detect stimuli successfully. They have been widely investigated in electronic-skin applications such as soft robots and prostheses. Due to emerging nanotechnology and materials science, various deformable sensors have recently been developed. Fabrication of sensors using thin-film transistors (TFTs) is one of the primary development trends. The sensors have shown some advantages such as improvement in sensitivity and minimal crosstalk. However, the TFTs are affected by temperature T , which causes a T -responsiveness of the sensor which is intended to detect some stimulus, not T . To detect an accurate stimulus regardless of T , the T influence must be calibrated. Although a multi-functional sensor with T calibration was proposed, their calibration methods required T sensors that used poly(vinylidene fluoride-co-trifluoroethylene). To utilize the calibration method widely, a more-general T sensor must be used for the calibration method. In this study, we demonstrate

a multi-functional sensor that can detect pressure P and T synchronously. The multi-functional sensor is composed of a T sensor and a P sensor. A T sensor is fabricated using organic thin-film transistors (OTFTs). On the T sensor, a P sensor is fabricated using OTFTs and a piezo-resistive sheet. The T sensor is influenced by only a change of T , whereas the P sensor is influenced by a change of both P and T . To produce accurate P information regardless of T , the current value of the P sensor is calibrated using the T value produced from the T sensor. Finally, the multi-functional sensor is attached to a robotic gripper and the gripper with the sensor successfully holds and lifts a hot cup.

3:45 PM SB12.02.06

Controllable Degradation Conductors for Soft Robotic Tactile Skin [Pietro Cataldi](#), Lorenzo Natale and Athanassia Athanassiou; Italian Institute of Technology, Italy

Materials employed in tactile sensors for robotics are typically an engineered version of current rigid, bulky, and long-lasting materials for electronics.[1] Thus, they are not suitable for flexible and motile parts of robots and do not mimic the human or animal skin that is soft, flexible, and biodegradable.[2,3] As a result, the development of tactile sensors that are conformable, lightweight, and produced with degradable and readily available materials is crucial.[3]

Among various technologies, capacitive sensors have been successfully employed to build sensorized skins for robots. The main challenge in adopting this technology is the need for conductors and dielectrics materials with appropriate properties. While biobased and biodegradable dielectrics such as biopolymers and natural polymers, like proteins, are abundant, conductors that degrade after performing a specific function are unavailable.[4]

We propose electrical conductors with a controllable degradation, finely controlled through the material formulation. We show that the degradation can be tuned from minutes to months, depending on the composition. This unique technology is suitable for applications where long-term stability is crucial, such as robotic skin and those requiring environmentally controlled degradation, such as bioresorbable transient electronics. The conductors display Ohmic I-V curves and sheet resistance in the order of 10 Ohm/sq. They can be applied as a coating to various flexible dielectric substrates. We assembled such conformable electrical conductors with degradable dielectrics to build soft capacitive tactile sensors that exhibit tunable degradation. Such soft haptics sensors can be designed ad hoc to sensitize various parts of the robots, from the fingers to the feet. Indeed, depending on the Young modulus of the dielectric used to build the capacitors, different degrees of deformation can be achieved at a specific load applied (from grams to kilograms). This artificial skin is assembled as human mimicking robotic skin for the iCub humanoid robot, the flagship open-source robot developed by the Italian Institute of Technology.[1]

References:

- [1] *iCub: The not-yet-finished story of building a robot child*, Natale L. et al., **2017**, Science Robotics, DOI: 10.1126/scirobotics.aaq1026.
- [2] *Carbon nanofiber versus graphene-based stretchable capacitive touch sensors for artificial electronic skin*, Cataldi P. et al., **2018**, Advanced Science, DOI: 10.1002/advs.201700587.
- [3] *Becoming Sustainable. The New Frontier in Soft Robotics*, Hartman F. et al., **2020**, Advanced Materials, DOI: 10.1002/adma.202004413.
- [4] a) *Biodegradable Polymeric Materials in Degradable Electronic Devices*, Feig V.R. et al., **2018**, ACS Central Science, DOI: 10.1021/acscentsci.7b00595; b) *Stretchable and Fully Degradable Semiconductors for Transient Electronics*, Tran H. et al., **2019**, ACS Central Science, DOI: 10.1021/acscentsci.9b00850.

4:00 PM *SB12.02.07

Tactile Sensitivity to Molecular Scale Phenomenon—New Routes for Fine Touch [Charles Dhong](#); University of Delaware, United States

For the sense of sight or hearing, displays and speakers can recreate a wide variety of scenes and sounds. For touch, however, haptic devices cannot recreate the variety of sensations from our everyday experiences. The ability to recreate rich and accurate tactile sensations could have broad implications in human machine interfaces, soft robotics, and disability rehabilitation. While most haptic devices rely on reconfigurable bumps or electrical stimulation, we explore how tactile sensations can be created through materials chemistry.

A challenge to rationally controlling touch is that fine touch is a complex mechanical event where the finger, a deformable and heterogeneous interface, slides across an object, generating friction. These mechanical vibrations from friction are the source of mechanical stimuli which ultimately lead to a tactile percept. In this talk, we describe our efforts to modulate friction through surface chemistry to generate tactile sensations. Through mechanical testing and novel analysis, we can predict whether or not humans can discriminate between two coatings, which allows us to rapidly screen through materials prior to human testing. Using this platform, we show that humans can perceive molecular level differences—even when supported on relatively smooth silicon wafers. These molecular level phenomena range from single atom substitutions in silane-derived monolayers, to the degree of crystallinity in polystyrene films. Our materials chemistry-based routes are complementary to many existing haptic actuators and could broaden the variety of tactile sensations generated in haptic devices.

4:30 PM SB12.02.08

Flexible High Sensitivity Tactile Sensors for Electronic Skin Applications [Antonello Mascia](#), Andrea Spanu, Annalisa Bonfiglio and Piero Cosseddu; University of Cagliari, Italy

Nowadays, in an increasingly interconnected world, where the daily monitoring of various bio/physical parameters is growing rapidly, electronic devices and sensors are permeating everyday life. In this context, flexible and conformal materials and systems have allowed a dramatic growing of bio-integrated electronic systems for monitoring different parameters and, particularly, epidermal electronic is a new field of application in which electronic devices can be transferred directly onto the skin.

To fulfill this aim, device architectures that can match the mechanical properties of the human skin have to be developed. Moreover, it is necessary to develop a procedure that allows to transfer onto the skin such devices in a reliable way, while preserving their performances.

In this work we report a tattoo-like electronic systems, that can be easily fabricated on sub-micrometer thick plastic substrates and employed for the detection of several parameters. The proposed system has been fabricated on a plastic carrier, coated with a water-soluble material acting as sacrificial layer. At the top of such structure, an ultrathin film of Parylene C is deposited through a large area deposition process. This procedure is compatible with the fabrication of several kinds of electronic devices, such as sensors or electrodes for the monitoring of electro-physiological parameters.

We have used such approach for the fabrication of high sensitivity transistor-based tactile sensors, employing a Sub-micrometer Channel Organic Charge Modulated Field Effect Transistor (SC-OCMFET). This architecture represents a versatile tool for the realization of a wide range of sensing applications, from bio/chemical to force/pressure sensing. The proposed device is based on a floating gate organic transistor, capable to be operated at low voltages thanks to an ultra-thin, hybrid dielectric. In order to achieve sensitivity to pressure, a piezoelectric thin film, namely PVDF, is coupled with the sensing area of the device. In this way, when a pressure is applied on the PVDF, the charges induced in the piezoelectric film led to a variation of transistor threshold voltage and a current variation can be detected as a result of the applied pressure. The signal of the piezoelectric material is thus locally amplified by the short-channel transistor. As the device sensitivity depends on the ratio between the sensing area and the channel area of the transistor, a reduction of the

channel length can lead to a significant increase in the sensor sensitivity. We herein propose an easy and reproducible approach for the fabrication of sub-micrometer SC-OCMFTs that does not require expansive and time consuming high resolution techniques, and that allowed us to achieve very high sensitivity, if compared to the previously reported planar devices. Moreover, this approach, allows at the same time to dramatically reduce the area occupied by the amplifying transistors, which is very important when dealing with the fabrication of arrays and matrices of tactile sensors. The fabricated devices are capable to detect very small stimuli, with an impressive sensitivity, and can detect forces within a range from 0.01 up to 1 N and pressures below 100 Pa. Moreover, since the PVDF is also a pyroelectric material, temperature variations ranging from 10° up to 45 °C could be also detected. Interestingly, since the responses of the device to the two different physical stimuli are characterized by marked differences in sensitivity and response time, it is possible to employ the same device for the fabrication of multimodal tactile sensing systems. The highly flexibility of the developed structure, and the easiness of the employed process, make this solution very interesting for the fabrication of multimodal, highly compliant artificial skin.

4:45 PM SB12.02.09

A Conformable Thermo-Actuated Tactile Display Arianna Mazzotta^{1,2}, Silvia Taccola³, Ilaria Cesini¹, Russell A. Harris³ and Virgilio Mattoli¹; ¹Istituto Italiano di Tecnologia, Italy; ²Scuola Superiore Sant'Anna, Italy; ³University of Leeds, United Kingdom

Conformable electronic devices have the capability to adhere to non-flat surfaces without changing their properties and performances. They are therefore able to easily comply with the multiple deformations of the human skin allowing imperceptibility, high comfort level, and continuous use for the user. In addition to several other sensorized devices, conformable electronics could be used to provide stimuli to the human body, for example through the development of tactile displays for visually impaired people or for human-machine interfaces.

In this work, we propose a conformable and disposable thin haptic display capable of providing vibro-tactile sensations. The device consists of a matrix of unit cells that can be selectively activated in order to reproduce Braille characters and/or complex dynamic information. This new device exploits the low thermal capacity of thin conductive films that allow the generation of fast, controlled, and localized heat flow. Each unit cell is characterized by a printed micro serpentine-shaped resistor that can heat up due to the Joule Effect.

Each resistor is inside a small chamber containing air. In particular, the upper wall of this chamber consists of a deformable PDMS membrane that swells - following the applied pulsed voltage - thanks to the thermal expansion of the air. The soft display can be attached to human skin using double-sided medical tape so that this movement elicits a vibro-tactile sensation on the skin.

Finite Element Simulations were first conducted in order to verify that the chosen geometry permitted localized heating with consequent swelling of the membrane. A process of Aerosol Jet Printing technique allowed the fabrication of the very small serpentine-shaped resistors by directly printing silver nanoparticle ink on a 25 µm Kapton substrate. The printing parameters identified were used to achieve a good trade-off between a high resolution of the designs (70 µm line-width) and a suitable level of conductivity. The next steps of the fabrication allowed us to create closed volumes of "trapped" air at the level of the resistors by techniques including plasma treatment and spin coating. After the assessment and optimization of the fabrication process, the device was assessed by functional tests that revealed a fast activation time of each cell (in the order of tens of ms), low working voltages (< 10 V), and an output force above the perception threshold at that working frequency.

This conformable soft display has multiple benefits. Firstly, the printing techniques offer great versatility and fast prototyping for the design of specific applications. Secondly, owing to its low thickness, the display conforms to the skin, increasing the level of perception of tactile sensation. Moreover, the presented working principle allows the fabrication of a light, flexible, and low-voltage device, paving the way for the development of a fully-portable haptic device in the future.

SESSION SB12.03: Materials I

Session Chairs: Lucia Beccai and Emanuela Del Dottore

Tuesday Morning, November 29, 2022

Hynes, Level 3, Room 309

8:00 AM SB12.03.01

Graphene-Based Intrinsically Stretchable Two-Dimensional-Contact Electrodes for Highly Efficient Organic Light-Emitting Diodes HuanYu Zhou¹, Shin Jung Han¹, Amit Kumar Harit², Dong hyun Kim², Dae Yoon Kim³, Yong Seok Choi³, Hyeokjun Kwon¹, Kwan-Nyeong Kim¹, Gyeong-Tak Go¹, Hyung Joong Yun⁴, Byung Hee Hong³, Min Chul Suh³, Seung Yoon Ryu², Han Y. Woo² and Tae-Woo Lee¹; ¹Seoul National University, Korea (the Republic of); ²Korea University, Korea (the Republic of); ³Graphene Square, Korea (the Republic of); ⁴Korea Basic Science Institute, Korea (the Republic of); ⁵Kyung Hee University, Korea (the Republic of)

Intrinsically stretchable organic light-emitting diodes (ISOLEDs) are becoming essential components of wearable electronics. However, the efficiencies of the ISOLEDs have been highly inferior to their rigid counterparts, which is due to the lack of ideal stretchable electrode materials that can overcome the poor charge injection at one-dimensional metallic nanowire/organic interfaces. We demonstrate highly-efficient ISOLEDs that use two-dimensional-contact stretchable electrodes (TCSEs) that incorporate a graphene layer on top of embedded metallic nanowires. The graphene layer modifies the work function, promotes charge spreading, and impedes inward diffusion of oxygen and moisture. The work function (WF) of 3.63 eV is achieved by forming a strong interfacial dipole after deposition of a newly-designed conjugated polyelectrolyte with crown ether and anionic sulfonate groups on TCSE; this is the lowest value ever reported among ISOLEDs, which overcomes the existing problem of very poor electron injection in ISOLEDs. Subsequent pressure-controlled lamination yielded a highly efficient fluorescent ISOLED with an unprecedentedly high current efficiency of 20.3 cd/A, which even exceeds that of an otherwise-identical rigid counterpart. Lastly, a three-inch five-by-five passive matrix ISOLED was demonstrated using convex stretching. This work can provide a rational protocol for designing intrinsically stretchable high-efficiency optoelectronic devices with favorable interfacial electronic structures.

Reference

Adv. Mater. Accepted Author Manuscript 2203040. <https://doi.org/10.1002/adma.202203040>

8:15 AM SB12.03.02

Good and Bad Elastomers for Stretchable Gold Nanowire Composites Samuel Lienemann¹, Ulrika Linderhed^{2,1}, Ioannis Petsagkourakis^{2,1}, Nara Kim¹, Valerio Beni² and Klas Tybrandt¹; ¹Linköping University, Sweden; ²RISE, Sweden

Soft and stretchable electronic materials for wearables and implants can have a demanding set of requirements, including biocompatibility, specific mechanical and electromechanical properties, long-term stability, and good electrode performance. To meet these requirements, we have over the years developed stretchable gold nanowire-based conductors for a variety of applications, such as implantable electrode arrays, organic thermoelectric generators, and organic supercapacitors and batteries. Different types of elastomers can be advantageous for certain applications based on their properties

and processing. However, when using different elastomers together with gold nanowires we have noticed huge differences in electromechanical performance of the composites, despite similarities in Young's modulus of the elastomers. Here I present our investigation into the causes of these major variations by comparing the performance, properties, and behavior of 5 different elastomer systems of similar modulus in combination with gold nanowires. The findings have implications when choosing elastomers for stretchable electronic composites and provide support for the interpretation of variations in electromechanical performance.
<http://www.liu.se/soft-electronics>

8:30 AM *SB12.03.03

Sustainable Materials and Design Approaches for Soft Electronics and Robotics [Martin Kaltenbrunner](#); Johannes Kepler University, Austria

Modern societies rely on a wide range of electronic and robotic systems, with emerging stretchable and soft form factors enabling an ever more intimate integration of the digital and biological spheres. These advances however often take their toll on our ecosystem, with high demands on energy, contributions to greenhouse gas emissions and severe environmental pollution. Mitigating these adverse effects is amongst the grand challenges of our society and at the forefront of materials research. The currently emerging forms of soft, biologically inspired electronics and robotics have the unique potential of becoming not only like their natural antitypes in performance and capabilities, but also in terms of their ecological footprint. This talk introduces materials and methods or soft systems that facilitate a broad range of applications, from sustainably powered, transient electronic skins to metabolizable soft robots. Based on highly stretchable biogels and degradable elastomers, our forms of soft electronics and robots are designed for prolonged operation in ambient conditions without fatigue, but fully degrade after use through biological triggers. Electronic skins provide sensory feedback such as pressure maps, strain, temperature and humidity sensing. Recent advances in 3D printing of biodegradable hydrogels enables omnidirectional soft robots with multifaceted optical sensing abilities. Tackling the challenge of autonomous operation, soft, stretchable and biodegradable batteries are introduced that power wearable sweat sensors. Pushing the boundaries further, design concepts that exploit mechanical instabilities for fast actuation in soft robotics systems to environmentally friendly cooling systems based on the giant elastocaloric crystallization effect are demonstrated.

9:00 AM SB12.03.04

Material and Device Designs in Biomimetic Polymer Electronics [Sihong Wang](#); The University of Chicago, United States

The vast amount of biological mysteries and biomedical challenges faced by humans provide a prominent drive for seamlessly merging electronics with biological living systems (e.g. human bodies) to achieve long-term stable functions. Towards this trend, one of the key requirements for electronics is to possess biomimetic form-factors in various aspects for achieving long-term biocompatibility. To enable such paradigm-shifting requirements, polymer-based electronics are uniquely promising for combining advanced electronic functionalities with biomimetic properties. In this talk, I will introduce our new molecular design, chemical synthesis, and physical-processing concepts for polymer semiconductors, which enabled the incorporation of multiple biomimetic properties with advanced electronic functionalities. Fundamental understandings that have been obtained about the structure-property relationship in these unprecedented material designs are serving as the foundation for opening up this new research direction for polymer semiconductors. Furthermore, enabled by these new materials, we have also created new device designs and fabrication processes for building unprecedented functional devices (i.e., sensors, LEDs, transistors) that are intrinsically stretchable with unperturbed performance when operating conformably on human bodies. Collectively, our research is opening up a new generation of electronics that fundamentally changes the way that humans interact with electronics.

9:15 AM SB12.03.05

Molecular-Scale Design of Piezoelectric Core-Shell Nanofibers for Wearable Electronic Devices Application [Guangshuai Han](#), Yining Feng and Na Lu; Purdue University, United States

Wearable electronics as a viable mean to realize human-machine interaction have been developed and evolved over the centuries. Polymer-based piezoelectric materials, which can conformably convert human motions to electrical signals, exhibit excellent potential in the application of wearable electronics. However, the discovery and design of functional composites with high piezoelectricity and long-term stability is a significant challenge. Limited study has focused on theoretical modeling approaches to design high-performance polymer-based piezoelectric materials. Herein, we adopt the molecular dynamic approach to design a core-shell structure polyvinylidene fluoride (PVDF) based composite with enhanced crystallinity and electroactivity. Based on the results from the molecular dynamic simulation, the strong intermolecular interaction among the hydrogen bonding is an effective strategy to enhance the crystalline phase of the PVDF. In addition, we synthesized the nano-fibrous composites using the sol-gel method with a piezoelectric shell structure and conductive core structure. The optimized core-shell structure and enhanced crystallinity were confirmed by the experimental characterization results. The as-fabricated flexible piezoelectric devices exhibit significantly enhanced piezoelectricity with a 4 times increase in signal intensity. This unique core-shell structure of piezoelectric nanofibers opens up broader applications such as the Internet of Things and the human-machine interface. Moreover, this work could provoke a new approach for accelerating the design and discovery of functional materials for wearable electronics by using molecular dynamics simulation.

9:30 AM SB12.03.06

Chip-Less Wireless Electronic Skins by Remote Epitaxial Freestanding Compound Semiconductors [Yeongin Kim](#)^{1,2}, Jun Min Suh¹, Jiho Shin¹, Yunpeng Liu¹, Hanwool Yeon^{1,3}, Kuan Qiao¹, Hyunseong Kum^{1,4}, Chansoo Kim¹, Han Eol Lee^{1,5}, Chanyeol Choi¹, Hyunseok Kim¹, Doyoon Lee¹, Jaeyong Lee¹, Jihoon Kang¹, Sungsu Kang⁶, Jihoon Kim⁶, Sungkyu Kim⁷, Joshua Perozek¹, Keja Wang¹, Yongmo Park¹, Kumar Kishen¹, Lingping Kong¹, Tomas Palacios¹, Jungwon Park⁸, Min-Chul Park⁸, Hyung-jun Kim⁸, Yun Seog Lee⁹, Kyusang Lee⁹, Jiyeon Han¹⁰ and Jechwan Kim¹;
¹Massachusetts Institute of Technology, United States; ²University of Cincinnati, United States; ³Gwangju Institute of Science and Technology, Korea (the Republic of); ⁴Yonsei University, Korea (the Republic of); ⁵Jeonbuk National University, Korea (the Republic of); ⁶Seoul National University, Korea (the Republic of); ⁷Sejong University, Korea (the Republic of); ⁸Korea Institute of Science and Technology, Korea (the Republic of); ⁹University of Virginia, United States; ¹⁰Amorepacific R&D Center, Korea (the Republic of)

Health monitoring platforms based on electronic skins have included flexible/stretchable sensors, electronic circuits, and skin-compatible adhesive patches. They have applications in biophysical tracking of fitness and wellness, and clinical management. The broader use of e-skins in our daily lives can be boosted by the capability to communicate data wirelessly. A major shortcoming of conventional wireless e-skins is rigid integrated circuit (IC) chips, such as near-field communication (NFC) and radio frequency identification (RFID) chips. Those IC chips compromise overall flexibility. Also, the data accuracy of analog-to-digital converters (ADCs) in IC chips are dependent on power consumption. The power constraint in wireless e-skin systems often leads to reduced sensitivity of sensing data converted by ADCs. Thousands of transistors in IC chips generate a lot of heat and consume significant power, leading to reduced wireless distance. Chip-less wireless e-skin sensors based on inductor-capacitor (LC) resonators have been reported, but their applications are limited to pressure and strain sensing with relatively low sensitivity because of the limitations of capacitive sensor designs.

We report a chip-less wireless e-skin technology based on surface acoustic wave (SAW) sensors. Our wireless SAW e-skin shows high strain sensitivity (the minimum detectable strain of 0.048 %); low energy consumption (3.7 nJ/measurement); versatility as a sensing platform for strain, UV, and ion

concentrations in sweat; and long-term wearability of one week. The excellent piezoelectricity and single-crystallinity of our ultrathin freestanding membrane of gallium nitride (GaN) on soft patch enable wireless communication without IC chips. The ultrathin GaN epitaxial layers are grown on graphene-coated GaN substrates by remote homoepitaxy and are easily released from the weak graphene-GaN interface by 2D material-based layer transfer (2DLT) process. These results present routes to cheap, low-power, high-sensitivity, and versatile platforms for wireless health monitoring devices.

9:45 AM BREAK

10:15 AM SB12.03.07

Characterization of Elastomers and Elastomer-Based Sensors in Extreme Environments [Elze Porte](#)^{1,2}, Sophia Eristoff¹, Anjali Agrawala¹ and Rebecca Kramer-Bottiglio¹; ¹Yale University, United States; ²University College London, United Kingdom

Soft devices for assistive action or health monitoring can improve wearer comfort compared to their more rigid counterparts. These devices may be used in extreme temperature and humidity conditions around the world or in extraterrestrial settings. Extreme low humidity and temperature conditions can be experienced towards the poles and extreme high humidity and temperature in hot climates towards the equator. Robots in these extreme environments are exposed to very different conditions than to the lab environments in which they are developed and tested. However, limited data is available on the material characteristics of commonly used elastomers in soft robots at different temperature and humidity conditions. This lack of knowledge can lead to unexpected behavior of the system and ultimately failure.

In this study, we characterize four commonly used elastomers in soft robotics (Ecoflex, Dragon Skin, Smooth-Sil, and Sylgard) in a temperature range of -40°C to 80°C and humidity range of 5% to 95% RH. We performed pull-to-failure, stiffness, and stress-relaxation tests, using image tracking techniques to determine the true stress and strain of the soft materials. We manufactured capacitive sensors with Dragon Skin and Smooth-Sil as base materials and carried out electromechanical characterization, measuring the capacitance response to tensile strain in the different environmental conditions.

We found that both the mechanical behavior of the elastomers and the electromechanical behavior of the sensors depend on the environmental conditions of operation. All elastomers show temperature dependent behavior, with typical stiffening of the material and a lower strain at failure with increasing temperature. The stress-relaxation behavior was most sensitive to sub-zero temperatures, with both reduced and increased relaxation observed. No clear trends were observed between the mechanical behavior of the elastomers and humidity conditions. The capacitive sensors exhibited changes in performance that related to both humidity and temperature conditions. A nonlinear relationship was found between the capacitance of the sensors and the temperature conditions. The capacitance was found to be decreasing with temperature between 0°C and 80°C and to be increasing with temperature between -40°C and 0°C. The humidity response of the sensors resulted in a slightly lower capacitance at low humidity and a slightly higher capacitance at high humidity.

The results from this study show that the environmental conditions of operation need to be considered in the design of a robotic system. The potential change in stiffness, failure point, and relaxation of the materials can affect design choices such as the used materials, range of motion, and power requirements. The temperature and humidity dependent sensor performance means that sensor output can only be accurately read with knowledge of the environmental conditions in which they operate. In conclusion, this study provides essential insights into elastomer behavior for the design and successful operation of soft robotic systems for wearable applications outside of a lab setting.

10:30 AM *SB12.03.08

Laser Induced Graphene for Soft Electronics, Sensors and Functional Surfaces [Francesco Greco](#)^{1,2}; ¹Scuola Superiore Sant'Anna, Italy; ²Graz University of Technology, Austria

Laser Induced Graphene (LIG) is a porous conductive carbon material produced by laser-induced pyrolysis of various polymer precursors. LIG fabrication on polyimide was first described in 2014 and ever since the research on this material has attracted much attention, especially for its technological applications. An infrared or other (UV, vis) laser sources are used to this purpose. The photothermal pyrolysis process allows for fast and maskless scribing of circuits onto insulating precursors in ambient condition, thus enabling new developments in flexible/stretchable/wearable electronics, electrochemical sensors, energy harvesting and storage, soft robotics, among others.¹⁻⁴

Here, we present some results of our group on: 1) fundamental Investigation of LIG, its structure and properties; 2) technological applications in soft electronics, sensors, functional surfaces.

The LIG morphology and properties (especially conductivity) can be tuned by varying the laser fluence and adjusting the rastering parameters. This results in various LIG types: a flat porous LIG, a dense forest of long carbon nanofibres bundles or a "sponge" structure. A corresponding variation in crystal structure, defects, and surface area is observed. The adoption of a UV laser source with a galvo scanner head enables the reduction in size of scribed features down to 5-10 mm width, with an overall improvement of LIG homogeneity. Also, by locally changing the oxygen content of the atmosphere at the scribing beam spot, a dramatic change of surface wettability is obtained. Tunable wettability over the full range of water contact angle is achieved from superhydrophilic (0°) to superhydrophobic (>150°). Patterns with high wettability contrast can be created, opening the way to various applications in self guiding of fluids over surfaces and biomimetic fog harvesting. Applications in soft, wearable sensors and supercapacitors are obtained by embedding of LIG in thin stretchable elastomers (PDMS, medical grade Polyurethane). These include: stretchable connectors, skin contact electrodes for electrophysiology, sensors for temperature and strain/pressure monitoring, wearable electrochemical sensors for monitoring of urea, tyrosine, pH in sweat.^{4,5} Also, we coupled LIG/PDMS with stimuli responsive polymer hydrogels deposited by initiated chemical vapour deposition (iCVD). These were investigated as soft actuating structures with thermal- and moisture-triggered response.⁶ Most recent advancements include the investigation of sustainable approaches to green electronics and sustainable soft robotics. Several bioderived polymers and raw natural materials (e.g. agricultural and food industry waste, shells, etc) are studied as suitable precursors for LIG and LIG based sensors.

References

- (1) Lin, J. et al. *Nat. Commun.* **2014**, *5*, 5714.
- (2) Ye, R. et al. *Adv. Mater.* **2019**, *31*, 1803621.
- (3) Vivaldi, F. M. et al. *ACS Appl. Mater. Interfaces* **2021**, *13*, 30245–30260.
- (4) Dallinger, A. et al. *ACS Appl. Mater. Interfaces* **2020**, *12*, 19855.
- (5) Keller, K. et al. *Front. Mater.* **2021**, *8*, 290.
- (6) Dallinger, A. et al. *ACS Appl. Polym. Mater.* **2021**, *3*, 1809.

11:00 AM SB12.03.09

Selective Transformation of PEDOT:PSS into Highly Conductive Hydrogels by Laser-Induced Phase Separation [Daeyeon Won](#), Deog-Gyu Seo, Seung Hwan Ko and Junhyuk Bang; Seoul National University, Korea (the Republic of)

Engineering conductive hydrogels with high electrical conductivity and mechanical stability in aqueous environments are important in research fields such as bioelectronics, e-skin, and energy devices. Especially, bioelectronics has actively adopted conductive hydrogels as bio-interfacing electronic material owing to similar natures to biological tissues. The softness and high water contents of hydrogels can minimize mechanical mismatch with biological tissues that can potentially realize long-term medical diagnosis or treatment such as neural signal recording and nerve stimulation.

The most commercialized conducting polymer, Poly(3,4-ethylenedioxythiophene):poly(styrene sulfonate) (PEDOT:PSS) is a promising candidate for the fabrication of conductive hydrogels based on its electrical conductivity and electrochemical properties. However, fabricating PEDOT:PSS hydrogels still has critical issues in aqueous instability and poor electrical conductivity. "Phase separation method" that redesigns the arrangement and crystallinity of PEDOT:PSS binary system has been rapidly studied to achieve high conductivity with aqueous stability. Ironically, most of the phase separation additives are cytotoxic and require a long detoxification process. Moreover, high-resolution patterning techniques of PEDOT:PSS hydrogels are required for bioelectronics, but conventional processes are limited by low resolution or process complexity such as inkjet printing and photolithography.

We introduce a novel biocompatible manufacturing process that overcomes such limitations explained above. Through the laser-induced phase separation of PEDOT:PSS, the phase distribution of binary PEDOT and PSS was dramatically reconstructed. The micro-patterned PEDOT:PSS hydrogels achieved high electrical conductivity and aqueous stability with 6- μm spatial resolution. We further demonstrated stable neural signal recording and stimulation with PEDOT:PSS hydrogels electrodes fabricated by laser.

11:15 AM SB12.03.10

Laser-Induced Liquid Metal-Graphene Composite for Stretchable Electronics Sooik Im, Ethan Frey, Adam Bachmann, Jan Genzer and Michael Dickey; North Carolina State University, United States

Gallium-based liquid metals have been extensively studied in the soft-matter community due to their intrinsically soft and stretchable properties with excellent electrical and thermal conductivity. Liquid metal particles are especially of interest because their electrical properties can be tuned using external stimuli to rupture their 3 nm-thick oxide layers. In one of these methods, a focused laser beam provides photothermal energy to sinter liquid metal particles, making conductive paths. However, this process requires high laser power to achieve high electrical conductivity because liquid metal has low absorption of infrared (IR), the wavelength at which the laser is operated.

Here, we increased the IR absorption of liquid metal particles by coating them with poly(amic acid). After the coating, the power required to sinter the liquid metal particles dropped by half. During the laser process, the poly(amic acid) was converted to graphene flakes, known as laser-induced graphene. As a result, liquid metal-graphene bilayers formed. We were then able to pattern the bilayers on hard substrates as well as transfer them to soft substrates. The transferred layers are stretchable, maintaining electrical conductivity.

11:30 AM SB12.03.11

Omnidirectionally Stretchable Electronics Substrate Film Having Negative Poisson's Ratio Using Auxetic-Structured Glass-Fabric Reinforcement Yung Lee, Junho Jang, Hyunhwan Lee and Byeong-Soo Bae; Korea Advanced Institute of Science and Technology, Korea (the Republic of)

Nowadays, as the application of electronic devices is broadening into portable, deformable, and wearable forms, non-rigid material-based electronics with free form factors are required. To realize the wearable and stretchable devices, stretchable substrate is an essential component. Elastomers are widely used as the substrate of stretchable electronics due to their high stretchability and resilience. However, the elastomeric substrates suffer from severe distortion during stretching because of their high Poisson's ratio (PR), which is a demerit for its usage such as a display substrate. In addition, there has been limitation to wearable devices because of the different behavior with human skin that expands along multiple direction with 1-degree of freedom bending of joint. To overcome these, meta-structures having negative PR (NPR), namely the auxetics, has been proposed. Though, general auxetic materials exhibit NPR characteristic by transversal expansion of empty spaces upon elongation, which hinders its usage as a substrate because of the structural discontinuity and a limited practical area.

Here, we propose an omnidirectionally stretchable substrate film without any discontinuity and empty spaces on the surface using an auxetic-structured selective reinforcement with glass-fabric into elastomeric matrix. The film is composed of two domains: i) auxetic-structured glass-fabric reinforced domain that induces NPR characteristic and ii) pristine elastomer domain that induces resilience and surface continuity. To achieve an ideal NPR characteristic (i.e. theoretical maximum value of unfilled auxetic structure) while maintaining a continuous surface, the two domains should have a substantially different elastic modulus. To investigate the effect of modulus difference between two domains and geometrical parameters of auxetic structure such as thickness, shape, and dimension, an experimental study is performed using digital image correlation (DIC) analysis. By modifying the mechanical properties of component materials and auxetic structure, a controllable PR between -1 to 0.5 is achieved. The optimized glass-fabric reinforced substrate exhibits NPR characteristics with maximum NPR value of -0.95, stretchability of 20% with 10,000 cycles of repetition. The proposed substrate also exhibits high thermal stability (>350°C), dimensional stability (<50 ppm/°C), and low surface roughness ($R_a < 100\text{nm}$), showing its capability to high temperature and solution processes. We demonstrate the omnidirectionally stretchable substrate as a wearable biosensor platform such as ECG sensor, providing stable conformal contact to human joint. Having NPR, the substrate expands omnidirectionally under uniaxial extension like a human skin. We also fabricate a distortion-free stretchable light-emitting devices using the omnidirectionally stretchable glass-fabric reinforced substrate.

SESSION SB12.04: Applications II
Session Chairs: Piero Cosseddu and Ingrid Graz
Tuesday Afternoon, November 29, 2022
Hynes, Level 3, Room 309

1:30 PM *SB12.04.01

Soft Neuromorphic E-Skin Zhenan Bao; Stanford University, United States

In this talk, I will discuss our approach toward a monolithically integrated soft e-skin.

2:00 PM SB12.04.02

Innate Self-Sensing Capability for Fiber-Reinforced Soft Actuator with Only Essential Components Hwajoon Kim¹, Seungbeom Noh¹, Jinho Kim¹, Seonggyu Lee¹, Gyowook Shin², Chankyu Lee³, Yonglae Park² and Jaehong Lee¹; ¹Daegu Gyeongbuk Institute of Science and Technology, Korea (the Republic of); ²Seoul National University, Korea (the Republic of); ³University of California, United States

Soft robots are emerging as next-generation robotics due to their high mechanical compliance, large deformation resulting from excellent stretchability and flexibility, and outstanding adaptability to various shapes and surface morphology. To effectively control such soft robots and actuators in practical applications, a sensing system that can monitor their movements and deformation in real-time is fundamentally essential. Nevertheless, most of previously reported soft actuators do not provide real-time physical feedback signals or provide only limited physical feedback signals, due to the lack of a sensing

system. Consequently, it is difficult to maintain accurate and consistent actuation under unintended external loads in practical applications. In this regard, research on the feedback control system of soft actuators using additional sensing components such as soft strain, bending, and pressure sensors has been intensively studied. However, such additional sensing components can interrupt the operation of soft actuators due to mechanical and structural mismatching between the sensor components and soft actuators. Moreover, the additional sensing components make the entire actuating system highly complicated. Therefore, soft actuators with self-sensing capability that can sense their movements themselves without additional sensing components are required.

Here, we present pneumatic fiber-reinforced soft actuators with self-sensing capability by using only their essential components: an elastomeric chamber, axial strain-limiting fiber, and two radial expansion-limiting fibers. The self-sensing fiber-reinforced soft actuator is designed to monitor their deformation itself by winding two inextensible conductive fibers around the elastomeric chamber in a double-helical structure. The wound conductive fibers simultaneously perform two roles: radial expansion-limiting fibers for the actuator and fiber-based capacitive bending sensor. Based on the capacitive bending sensor inherently embedded in the soft actuator, we demonstrated that the bending deformation of the soft actuators was successfully measured during the operation of the actuator. An analytical prediction and a FEM simulation model were developed to explain the correlation between the mechanical and electrical behavior of the soft actuators. Moreover, negligible hysteresis and outstanding stability were observed against repeated pressurizing-releasing cycles (10,000 cycles). Based on the self-sensing capability, we verified the closed-loop feedback control of the fiber-reinforced soft actuator, which provides a stable and accurate actuation independent of unintended external loading. Finally, stable picking of various objects under external loading was demonstrated by designing the gripper system. To the best of our knowledge, this is the first demonstration of a self-sensing soft actuator that leverages an essential component of the actuator also as a sensor, eliminating any mismatch between the actuator and sensor.

2:15 PM SB12.04.03

Human Hand-Inspired Stiffness-Tunable Soft Gripper Formed by the Split-Brushing Adhesion of Diverse Hydrogels Hye Been Koo, Eunseok Heo and Jae-Byum Chang; Korea Institute of Science and Technology, Korea (the Republic of)

Humans, animals, and even insects interact with the environment via their grippers having various morphologies and functions. In contrast to other grippers found in nature, the functions of human hands are unique. Even when heavy objects are placed on them, their high stiffness prevents deformation. In addition, they are flexible, allowing the fingers of hands to bend easily to grab various objects. Various attempts have been undertaken in recent years to mimic the morphologies and functions of human hands using hydrogels. However, the majority of present hydrogel grippers are limited since they are readily deformed but their stiffness is insufficient for lifting heavy objects or supporting huge loads. These two features, high stiffness and ease of bending, are challenging to obtain with a single hydrogel system, as finger stiffness must be low for bending to be possible. In this paper, we demonstrate a hydrogel gripper whose stiffness can be easily adjusted by temperature from a few to hundreds of megapascals. This gripper is comprised of various hydrogels with distinct functionalities, including a hydrogel with high stiffness, a hydrogel with temperature-dependent stiffness change, and a hydrogel with temperature-dependent volume change. In order to build this hydrogel gripper by integrating these three hydrogels, we present a unique hydrogel adhesion approach, which we refer to as split-brushing adhesion, which enables strong adherence between various hydrogels. The only trigger that can activate this hydrogel gripper is temperature. We demonstrate that the bending of the fingers of this gripper can be regulated by temperature and that the bent fingers are stiff, allowing them to grasp heavy things.

2:30 PM BREAK

3:00 PM *SB12.04.04

Electronic Skins for Healthcare and Virtual Reality Stephanie P. Lacour; EPFL, Switzerland

Skin-interfaced electronics are becoming powerful tools for applications in human-machine interaction and digital capture of human movement and physiology, which offer promising perspectives in e-health applications. We report on microfabricated electronic skins prepared with silicone and liquid metal conductors. Based on a combination of soft lithography, directional patterning, thermal evaporation or spray coating of gallium, the soft technology enables a range of designs and geometries that can be used to form liquid metal-based stretchable electronic conductors. The versatility of the technology enables a palette of sensor designs that can offer transparency ($T > 89\%$), large metallization density ($2/5 \mu\text{m line/gap}$), and high electromechanical performance (strain $> 10\%$, $> 100\text{k cycles}$). We will illustrate the technology capability demonstrating soft sensors for minimally invasive hand tracking, closed-loop soft actuation control and softness sensing.

3:30 PM SB12.04.05

Soft Skin-Attachable Full-Spectrum Tactile Stimulator Based on Laterally Multilayered Dielectric Elastomer Actuators Siyoung Lee^{1,2}, Jonghyun Son¹, Geun Yeol Bae³, Giwon Lee¹, Mihai Duduta² and Kilwon Cho¹; ¹Pohang University of Science and Technology, Korea (the Republic of); ²University of Toronto, Canada; ³Kumoh National Institute of Technology, Korea (the Republic of)

Haptic (e.g., skin-stimulation) technology has been applied based on garments such as gloves, vests, and suits for virtual reality and augmented reality (VR/AR) to provide users with the most natural and realistic feeling. To provide more comfortable wearability and immersive experience, conventional electromagnetic actuators, are relatively heavy, bulky, and stiff, should be replaced with thin, soft, light and skin-attachable skin-stimulating devices. Dielectric elastomer actuators (DEAs) are the suitable candidates for soft haptics, because they are composed of soft dielectric polymer and can rapidly respond over a wide frequency range. However, they have still significant challenges to the realization and commercialization of skin-attachable stimulators. First, the operating voltage for actuation should be lowered from typical operating voltages of several to tens of kilovolts for DEAs. Secondly, at low operating voltages, DEAs should exhibit significant and variable displacements exceeding the thresholds for activation of the mechanoreceptors in the skin dermis. Thirdly, DEAs should also realize diverse actuations with various frequencies and temporal patterns to provide a realistic experience for users to distinguish the textures by feeling dynamic vibration.

Here, we report a low-voltage-driven and skin-attachable DEA-based stimulator that covers the full perception range of all mechanoreceptors on human skin and that can be worn comfortably and reliably on a human finger. We realized the low-voltage operation ($\sim 200 \text{ V}$) of DEAs by exploiting the novel design of multilayer DEAs in which hundreds (~ 900 layers) of elastomer layers with thin dielectric distance ($10 \mu\text{m}$) and compliant electrodes are laterally aligned. The laterally multilayered DEA (LMDEA) can be fabricated in a single process including sophisticated photolithography and secondary sputtering, which is much simpler than the complicated and time-consuming stacking process for previous multilayer DEAs. Further, to enhance the actuation performance, we harnessed the low young's modulus and high permittivity of ionic liquids into the dielectric elastomer layer. The fabricated LMDEA showed significant contractive displacement (i.e., $160 \mu\text{m}$ as static and $55 \mu\text{m}$ as 200 Hz dynamic displacements) in the frequency range up to 800 Hz at the operating voltage of 200 V which is much lower than those of previous DEAs. Moreover, the structural/material design enables LMDEAs to have a high actuation force of more than 200 mN at the same operating voltage and to show high operation stability with no electric breakdown but high electrode conductivity based on stable impedance values during a duration test (> 0.7 million cycles).

The finger band skin-stimulator consisting of two LMDEAs and a needle was skin-attachable on the finger due to the thinness ($35 \mu\text{m}$) of the LMDEAs. The needle connecting to the contracting LMDEAs generated mechanical stimulation (up to 30 times) greater than the threshold displacement of human skin for various frequencies ($1 \sim 200 \text{ Hz}$) at an operating voltage within 200 V . Also, we demonstrated that the skin-stimulator can apply various

vibrational stimuli to the human skin by varying the magnitude, frequency, and even pattern of the applied voltage. Therefore, LMDEAs show the significant potential for use in haptic communication, human machine interfaces for VR/AR, touch therapy, and beyond.

3:45 PM SB12.04.06

Stretchable Strain Sensor Enabled Smart Clothing for Motion Capturing Applications [Zinan Cen](#), Fraser Robinson, Goldie Nejat and Hani E. Naguib; University of Toronto, Canada

Motion capturing technologies provide insightful information of the human body and has a wide range of applications including in virtual reality, sport analysis, physical rehabilitation, and socially assistive robotics. Conventional motion capture methods using camera systems fall victim to varying light conditions and occlusion, therefore usually requires studio settings. Such limitations motivated research in obtaining motion data through on-user sensors such as inertial measurement units (IMU). However, IMUs are rigid, have high power consumption, and suffer from signal drift, all of which restrict the capability of IMUs for long term usage. With recent development in nanomaterial, highly sensitive strain sensors with large working strain range have been fabricated. Their low power consumption, lightweight, and ability to conform to curved surfaces show great potential as an alternative for motion capturing applications. In this paper, we designed a stretchable strain sensor enabled smart clothing that is capable of monitoring upper limb movements of the users. Each strain sensor is composed of a highly stretchable elastomer layer and a conductive layer. The elastomer layer is made from a thermoplastic polyurethane (TPU) fibrous mat fabricated via electrospinning. Carbon nanotube (CNT) ink is dispensed onto the elastomer layer and air dried to form the conductive layer. As the sensor is stretched, discontinued phase of CNT is formed across the conductive layer reducing the density of conductive pathways, which increases the resistance of the sensor proportional to the strain experienced. Smart clothing was developed by attaching multiple stretchable strain sensors at various locations that maximize strain during motion. A convolution neural network (CNN) model was developed to estimate the joint angles of shoulders and elbows using strain signals from the smart clothing. To address the non-linear and hysteretic behavior of the sensors, signals in past time steps were included in the input to the CNN model. The functionality of the smart clothing was demonstrated through the integration with a socially assistive robot (SAR) to provide dressing assistance. Namely, smart clothing on the user is used for joint angle mapping, which are then classified into different dressing steps. The completion status of each dressing steps allows the SAR to provide appropriate instructions to the users. Experiments validated the performance of the joint angle mapping model, and dressing action classifier.

4:00 PM SB12.04.07

Encoding of Tactile Information in Hand via Skin-Integrated Wireless Haptic Interface [Kuanming Yao](#), Jingkun Zhou, Lidai Wang and Xinge Yu; City University of Hong Kong, Hong Kong

Vivid haptic feedback is still a remaining challenge in truly immersive virtual/augmented reality (VR/AR). Since the tactile sensitivity among different individuals and different parts of hand within a person varies widely, a universal method to encode tactile information into faithful feedback in hands according to the sensitivity features is urgently needed. In addition, existing haptic interfaces worn on the hand are usually bulky, rigid, and tethered by cables, which is a hurdle for accurately and naturally providing haptic feedback.

Here we report a soft, ultrathin, miniaturized and wireless electrohaptic system (WeTac) that delivers finely controlled current pulses through the hand to induce tactile sensations as the skin-integrated haptic interface. It's featured with a compact driver unit that can be wirelessly controlled by a mobile device via Bluetooth, and the battery is wirelessly rechargeable, which gets the driver unit rid of any tethering cables or cords, and allows the user to do activities without any bounding feelings. The WeTac could be worn on hands to provide programmable spatio-temporal electrohaptic feedback patterns through a thin, soft hydrogel-based hand patch, which has 32 stimulation pixels over the palmar side, with a high spatial resolution of 1.8 pixel/inch² in average and 4.5 pixel/inch² in densest area. Compared to other electrohaptic device with denser array, WeTac has a wider coverage range (whole hand) than simply on the fingertip.

To make it more universally fit to general public users, we investigated the thresholds features among different groups of people. It's found that although the general distribution patterns are similar (the fingers are much more sensitive than the palm, especially the fingertips), people's threshold levels are closely related to gender, age, job and personal experiences. Thus it's necessary to customize stimulation strength according to specific user's threshold. By detailed investigation of an individual's threshold maps at different electrical parameters, suitable stimulation parameter combinations are acquired for personalized feedback tuning in VR/AR or human-robotic interaction scenarios. Pressure distributions for actions like grasping a tennis ball and a virtual mouse running across the palm can be correctly projected with high spatiotemporal resolution by specified algorithm. It can also help to feel the pressure of a robotic hand when the user controls it to touch an object. This illustrates the potential of our device in realizing faithful and vivid virtual touching in various applications for boosting a more immersive experience in virtual world (i.e. Metaverse). We believe that skin-integrated wireless haptic interface could also assist the development of other fields in the future, like remote control of robotics, sensory feedback from prosthetics, catastrophe alerting, skill training, education, etc.

(Research article was accepted in principle by *Nature Machine Intelligence*)

SESSION SB12.05: Poster Session I
Session Chairs: Lucia Beccai, Piero Cosseddu and Darren Lipomi
Tuesday Afternoon, November 29, 2022
8:00 PM - 10:00 PM
Hynes, Level 1, Hall A

SB12.05.01

Materials-Enabled Stretchable, Flexible and Wearable Electronics and Their Biomedical Applications [Nadecem Qaiser](#) and Vincent Tung; King Abdullah University of Science and Technology, Saudi Arabia

The pursuit of state-of-the-art stretchable, flexible and wearable electronics has changed our daily-life activities. To achieve the desired stretchability designs that can stretch due to topology and intrinsically stretchable materials significantly impact the efficacy of IoT and IoE applications [1,2]. As the mechanics of these devices dictate the overall response of the devices, the geometrical topology of interconnects such as serpentine and lateral spiral play a decisive role. Likewise, various materials, including copper and carbon nanotubes, have proved their great performance for identical devices while encapsulating in flexible polymers. Therefore, these stretchable designs and materials play an important role in bio-related flexible devices. Currently, wearable and flexible electronics analyze sweat, glucose, blood pressure, and other skin conditions. However, localized jaw-bone swelling called parotid swelling caused by some viruses has never been tracked before. This work reports carbon nanotubes (CNTs)-based piezoresistive sensing patch encapsulated in a highly flexible polymer and can record muscle deformations in real-time. The developed patch offers an excellent gauge factor (~16) for

in-plane stretching and spatial expansion with low hysteresis. We fabricated the pneumatic actuator that experienced volumetric expansion and thus redefined the gauge factor to calibrate the volumetric muscle expansion. Moreover, we employ a Bluetooth-low-energy system that can send information about muscle activity in real-time to a smartphone app. We utilized COMSOL calculations to reveal the mechanical robustness of the patch. The experiments showed the sensing patch's greater cyclability, making it a great choice for personal healthcare, i.e., monitoring the real-time POC of human muscle swelling. Likewise, another application of copper-based stretchable interconnect is in thermal therapy. Thermal therapy is widely used to treat arthritis- the stiffness or pain of human muscle/bone. This work reveals the copper-based stretchable thermal patch that can digitally control the temperature of the patch, making it an excellent device for thermal therapy. We have used a CMOS-compatible nano/microfabrication scheme to make the thermal patch encapsulated in polyimide, making it flexible. The developed thermal patch gives a safe range of heating, can be stretched to fit any part of the body, and be wirelessly controlled. Our results have shown the exciting applications of copper and CNT-based smart patches, opening doors to various futuristic bio-medical applications.

References

- 1- N. Qaiser, A. N. Damdam, S. M. Khan, S. Bunaiyan, M. M. Hussain, *Adv. Funct. Mater.* 2007445 (2020).
- 2- N. Qaiser, A. N. Damdam, S. M. Khan, S. F. Shaikh, M. M. Hussain, *Appl. Phys. Lett.*, 115, 181904 (2019).

SB12.05.02

Triboresistive Touch Sensing—Grid-Free Touch Point Recognition Based on Monolayered Ionic Power Generators Younghoon Lee¹, [Sungsoo Lim](#)¹ and Jeong-Yun Sun^{1,2}; ¹Seoul National University, Korea (the Republic of); ²Research of Institute Advanced Materials, Korea (the Republic of)

Recent growing pursuit of skin-mountable devices has been impeded by complicated structures of most sensing systems, containing electrode grids, stacked multi-layers, and even external power sources. Here, we introduce a type of touch sensing, termed triboresistive touch sensing, for gridless touch recognition based on monolayered ionic power generators in Fig. 1. A homogeneous monolayer, i.e. ionic PDMS, generates electricity based on the electric field generated by touch. Voltages generated at each corner of ionic PDMS relied on resistance between touch points and each corner, ensuring recognition of the touch positions without need for electrode grid layers and external power sources. With notable advantages of high transparency (96.5%), stretchability (539.1%), and resilience (99.0%) of the ionic PDMS, epidermal triboresistive sensing was demonstrated to express touch position and readily play a musical instrument. Gridless system of triboresistive sensing allowed to rearrange touch sections according to a given situation without any physical modification, and thus easily completed consecutive missions of controlling position, orientation, and gripping functions of a robot.

SB12.05.03

A Strategy Reducing Interfacial Stress by Placing Pores Around Serpentine Electrodes for Highly Durable Stretchable Electronics [Seungkyu Lee](#), Jun Chang Yang and Steve Park; Korea Advanced Institute of Science and Technology, Korea (the Republic of)

The development of stretchable electronic devices has brought great attention to next-generation wearable devices such as electronic skins (E-skins) and electrical tattoos.^[1] In the field of wearable technology, there is a growing demand for soft electronics in health monitoring and various types of applications such as the Internet of Things and soft actuators, VR/AR.^[2-3] The stretchable functional electronics has been adopted for increasing durability under stretching by using intrinsically stretchable materials and structural dynamics designs. Especially, many research about gaining stretchability through structural designs such as serpentine interconnects and kirigami structure have been reported.^[4-6] Among the various structural designs of stretchable electronics, the "island-leg" design represents a widely used strategy, and bridge-modified interconnects in the middle area (i.e., trenches) between non-stretchable elements such as islands provide stretchability and flexibility. However, these devices are susceptible to mechanical failure such as fatigue breakdown of ductile materials and brittle material destruction, and peeling of adhesive interfaces. A delamination occurs due to mechanical mismatch (i.e., modulus, stretchability) between the serpentine and the elastomer substrate. Therefore, device stretchability is reduced because the material can reach the limit locally in smaller macro variants. Here, pores near the serpentine electrode can be proposed to effectively improve stretchability and durability of stretchable electronic system. The system configuration includes a serpentine and a pore with a convex oval design around it. The serpentine electrode made of the designed polyimide reduces the von mises stress between the interface and the electrode. The T-shaped pores in the substrate absorb the stress concentration near the serpentine electrode, which is prone to microcracking. The pores presented in this study have an effect of reducing stress by about four times compared to electrodes without pores. Experimental measurements and finite element analysis (FEA) on island bridge designs using interconnects between serpentine electrode and substrates confirm the validity of substrate pore strategies. Furthermore, the various applications such as heater, display, and e-skin are demonstrated.

1. N. Qaiser, A. N. Damdam, S. M. Khan, S. Bunaiyan, M. M. Hussain, Design criteria for horseshoe and spiral-based interconnects for highly stretchable electronic devices. *Adv. Funct. Mater.* 31, 2007445 (2021).
2. S. Y. Hong, M. S. Kim, H. Park, S. W. Jin, Y. R. Jeong, J. W. Kim, Y. H. Lee, L. Sun, G. Zi, J. S. Ha, High-sensitivity, skin-attachable, and stretchable array of thermo-responsive suspended gate field-effect transistors with thermochromic display. *Adv. Funct. Mater.* 29, 1807679 (2018).
3. J. O. Kim, J. S. Hur, D. Kim, B. Lee, J. M. Jung, H. A. Kim, U. J. Chung, S. H. Nam, Y. Hong, K. S. Park, J. K. Jeong, Network structure modification-enabled hybrid polymer dielectric film with zirconia for the stretchable transistor applications. *Adv. Funct. Mater.* 30, 1906647 (2020).
4. C. A. Silva, J. lv, L. Yin, I. Jeerapan, G. Innocenzi, F. Soto, Y. G. Ha, J. Wang, Liquid metal based island-bridge architectures for all printed stretchable electrochemical devices. *Adv. Funct. Mater.* 30, 2002041 (2020).
5. R. Xu, Y. Zhang, K. Komvopoulos, Mechanical designs employing buckling physics for reversible and omnidirectional stretchability in microsupercapacitor arrays. *Mater. Res. Lett.* 7, 110–116 (2019).
6. A. J. Bandodkar, J.-M. You, N.-H. Kim, Y. Gu, R. Kumar, A. M. V. Mohan, J. Kurniawan, S. Imani, T. Nakagawa, B. Parish, M. Parthasarathy, P. P. Mercier, S. Xu, J. Wang, Soft, stretchable, high power density electronic skin-based biofuel cells for scavenging energy from human sweat. *Energy Environ. Sci.* 10, 1581–1589 (2017).

SB12.05.04

High-Power Photonic Skin for Wearable Photodynamic Therapeutics of Skin Cancer [Yongmin Jeon](#)¹, Eou-Sik Cho¹, Sang Jik Kwon¹, Ye Ji Shin¹, So Yeong Jeong² and Yongjin Park²; ¹Gachon University, Korea (the Republic of); ²Korea Advanced Institute of Science and Technology, Korea (the Republic of)

Conformal and soft bioelectronic devices with various form-factors based on soft functional materials such as 2D materials and organic materials recently have been receiving considerable attention and research is actively being conducted. Among various soft bioelectronic devices, extremely thin and ultraflexible photonic skin type opto-bioelectronic devices have the advantage of superior wearable and bio-compatible characteristics. On this basis, they are being utilized in wearable biosignal diagnosis applications including skin-type pulse oximetry and wearable treatment devices such as skin-type phototherapeutics. However, the previous 2D material, thin film organic material-based photonic skin, has disadvantages of high operational voltage (>10 volts) and low output power, and problems such as high heat generation and long treatment time of several hours or more in applications such as photodynamic therapeutics have occurred.

In this talk, I will show a high-power photonic skin of 100mW/cm² or more under 8V through structural and optical design of an OLED in the form of parallel vertical stacking. This high-power photonic skin has a folding reliability of 350um, which is the level of skin wrinkles, based on ultra-thin properties of 10 micrometers, and also has reliability properties allowing it to be washed with water. In parallel stacked OLED based photonic skin, the shape of the wavelength, the output, and the luminous efficiency could be optimized by adjusting the thickness of each stacked OLED layer. In order to confirm the possibility of photodynamic therapeutics application using this low-voltage, high-output photonic skin, singlet oxygen generation efficiency was confirmed by measuring the singlet oxygen generation ratio, which was improved roughly four-fold compared to a previously reported OLED. In addition, the therapeutic effect of reducing cancer cell viability in melanoma cancer cells was confirmed even after a short irradiation of only 30 minutes. In conclusion, the possibility of application of photodynamic therapeutics to various skin cancers and bacteria using high-power photonic skin was confirmed.

- [1] Y. Jeon, I. Noh, Y. Seo, J.H. Han, Y. Park, E. H. Cho, K.C. Choi, ACS Nano, 2020
- [2] Y. Jeon, H. Choi, J. H. Kwon, S. Choi, K. Park, K.C. Choi, Light: Science & Applications, 2019
- [3] Y. Jeon, H. Choi, K. Park, K.C. Choi, Journal of the Society for Information Display, 2020

Acknowledgement : This research was supported by a grant of the Korea Health Technology R&D Project through the Korea Health Industry Development Institute (KHIDI), funded by the Ministry of Health & Welfare, Republic of Korea (grant number: HI22C0290). Also, this work was supported by the National Research Foundation of Korea (NRF) grant funded by the Korea government (MSIT) (No. 2022R1F1A1065534).

SB12.05.05

A Wearable System for Detecting Hand Motion Using Strain Sensors Sangmin Lee¹, Dongbin Jo^{1,2} and Wanjun Park¹; ¹Hanyang University, Korea (the Republic of); ²Samsung Electronics Co., Ltd., Korea (the Republic of)

A wearable system for detecting hand motion is presented using strain sensors with carbon-based nanomaterials. The system can detect hand gestures with data obtained from ten sensors, and sign language gestures can be converted to English alphabet letters through a mapping process. Most of the conventional motion detecting methods are image-based methods, however these approaches have limitations with large and burdensome peripheral devices, and due the influence of surrounding environment such as light and shadow. Therefore, there is a need for a detecting system which can operate without influence of environmental factors and which could be worn on the body, in order to take advantages such as accurate motion detection and portability. Our carbon-elastomer composites sensor applied to this system shows excellent stretchability characteristics providing no discomfort while moving when attached to the human body, and has excellent durability without deterioration in performance even after long cycles. Finally, a wearable system was demonstrated, so that the 26 English alphabet sign gestures could be translated into letters real time.

SB12.05.06

Development of Kirigami-Based Stretchable Electronics for Wearable Electronic Devices Bongkyun Jang¹, Sejeong Won², Hyeon-Don Kim¹, Jachwa Lee², Jaegu Kim¹, Hak-Joo Lee² and Jae-Hyun Kim¹; ¹Korea Institute of Machinery and Metals, Korea (the Republic of); ²Center for Advanced Meta-Materials, Korea (the Republic of)

Stretchable electronic devices are electronic circuits fabricated onto stretchable substrates. So far, many researchers have applied elastic materials such as silicones or polyurethanes to stretchable substrates. A design of kirigami patterns based on mechanical metamaterials can provide the substrates with high stretchability. These mechanical metamaterials are artificial mechanical structures that exhibit unconventional mechanical properties that originated from their structures rather than their compositions. Especially, auxetic metamaterials show a negative Poisson's ratio that enables a lot of applications in soft robotics, medical devices, and stretchable electronics. Nano and microscale fabrication technology can contribute to the fabrication of kirigami-based mechanical metamaterials since nano and microscale structures can realize the appropriate properties of metamaterials that are suitable for the specific application. In this study, we developed the fabrication process of stretchable electronic devices using kirigami patterning of polymeric substrates. We designed and fabricated the distortion-free micro-LED (Light Emitting Devices) display using flexible electronic circuits and kirigami technology. In addition, we demonstrated the wearable and skin-attachable biomedical devices of stretchable micro-LED for phototherapy and beauty. These fabrication technologies can contribute to the manufacturing of stretchable electronics for free design form factors.

SB12.05.08

Broadband Mechanoresponsive Liquid Metal Sensors Md Saifur Rahman, Julia Huddy, Andrew B. Hamlin and William J. Scheideler; Dartmouth College, United States

Stretchable electronics have the fundamental advantage of matching the complex geometries of the human body, providing novel opportunities for real-time biomechanical sensing. We report a new method for high frequency AC-enhanced resistive mechanical sensing that leverages the deformability of liquid metals to enhance low-power detection of mechanical stimuli in wearable electronics. The fundamental mechanism for this enhancement is the geometrical modulation of the AC skin effect, which induces current crowding at the surface of a liquid metal trace. We apply 1-50 MHz excitation in combination with DC sensing to quantitatively pinpoint mechanical modes of deformation such as stretching in-plane and compression out-of-plane that are otherwise impossible to distinguish by traditional methods. This novel sensing method, which we explore by FEA simulations, is experimentally employed in a glove to simultaneously detect various hand gestures and tactile forces as well as a respiratory sensor band to monitor breathing rate. In addition to this multifunctionality, we show how this AC sensing modality can enable high SNR readout at 100X lower power consumption compared with DC, enabling a new generation of efficient wearable radio-frequency (RF) systems for haptics and biomedical sensing.

SB12.05.09

Tissue-Adaptive Biongel Based on Piezo-Driven Ion Confinement for Mechanical Biosignal Acquisition System Jihong Kim, Joo S. Kim, Hanbin Choi, Dong J. Kim, Bokyoung Kim and Do Hwan Kim; Hanyang University, Korea (the Republic of)

As advancements in management remain insufficient for chronic patients, death per cardiovascular disease has perpetually increased, becoming a global encumbrance today. For the effective approach towards the challenges of healthcare technologies in this field, the use of implantable bioelectronics shows optimistic potential to precisely monitor the mechanical biosignals (blood pressure, respiratory rate) in real-time. However, since conventional bioelectronics commonly use rigid metal and inorganic materials, a mechanical mismatch occurs between the bioelectronics and soft tissues, resulting in

low sensitivity and signal-to-noise ratio (SNR). To overcome these concerns, the tissue-level modulus of soft materials (e.g., hydrogel and ionogel) is critical for the development of implantable bioelectronics. Despite the fact that the soft hydrogel can firmly adhere to tissues, the impaired long-term stability caused by dehydration of solvent, and ion exchange between biological ions and synthetic ions leads to erroneous monitoring of biosignals.

In this talk, we propose a novel design of biocompatible ionogel (Bionogel) exploiting a piezo-driven ion confinement structure that prevents ion exchange and enables precise mechanical biosignal readout. To introduce mechanosensitive characteristics to the proposed design of the ion confinement structure, we develop soft Bionogel composed of hydrogen-bonded choline-based ion pairs on the surface of functionalized gold particles (AuNPs) embedded into chitosan biopolymer matrix. Unlike the phenomenon of the ion transfer at the interface between hydrogel and tissues, our Bionogel is capable of minimizing ion exchange by capturing ions. Such confined ion pairs can be dissociated under mechanical stimuli, resulting in reversible ion pumping. Notably, our Bionogel-based mechanotransducer exhibits exceptional mechanosensitivity ($S = 14.60\text{-}10.18 \text{ kPa}^{-1}$) over a wide range of pressures (0 – 100 kPa). Furthermore, cell (Human Dermal Fibroblast) viability and cytotoxicity tests performed on Bionogel signify the enhanced biocompatibility compared to the conventional ionogel and conducting polymer. As a result, we believe that the successful integration of the Bionogel-based mechanotransducer into the implantable bioelectronics capable of perceiving subtle signals from the human body can serve as a blueprint for the development of the next-generation health monitoring system.

SB12.05.12

Long-Term *In Vivo* Operation of Implanted Cardiac Nanogenerators in Swine [Jun Li](#); University of Wisconsin--Madison, United States

Implantable nanogenerators (i-NG) provide power to cardiovascular implantable electronic devices (CIEDs) by harvesting biomechanical energy locally eliminating the need for batteries. However, its long-term operation and biological influences on the heart have not been tested. Here, we evaluate a soft and flexible i-NG system engineered for long-term *in vivo* cardiac implantation. It consisted of i-NG, leads, and receivers, and was implanted on the epicardium of swine hearts for 2 months. The i-NG system generated electric current throughout the testing period. Biocompatibility and biosafety were established based on normal blood and serum test results and no tissue reactions. Heart function was unchanged over the testing period as validated by normal electrocardiogram (ECG), transthoracic ultrasound, and invasive cardiac functional measures. This research demonstrates the safety, long term operation and therefore the feasibility of using i-NGs to power the next generation CIEDs.

Reference:

[1] Long-term *in vivo* operation of implanted cardiac nanogenerators in swine, *Nano Energy*, 2021, 90, 106507.

SB12.05.13

An Intrinsically Stretchable Multi-Biochemical Sensor for Sweat Analysis Using a Photo-Patternable Silicone Elastomer [Seungwan Kim](#)^{1,1}, Joohyuk Kang², Injun Lee^{1,1}, Wonryung Lee² and Byeong-Soo Bae^{1,1}; ¹Korea Advanced Institute of Science and Technology, Korea (the Republic of); ²Korea Institute of Science and Technology, Korea (the Republic of)

Patterning of stretchable materials such as PDMS, Ecoflex, which is widely used in stretchable electronics, is a necessity in methods to fabricate multi-layer of stretchable integrated circuits. Nevertheless, previous patterning methods for stretchable materials, such as soft lithography and laser lithography, can leave residues or damage on the underlying layer. Fabrication of sophisticated and multi-functional stretchable biosensors requires development of an intrinsically stretchable material that can be directly patterned without any effect on the primary layer.

Here, we developed Photo-patternable Ecoflex (PPE) to directly integrate intrinsically-stretchable nanocomposite. We used benzophenone as a photo-inhibitor to hinder cross-linking of Ecoflex by the radical reaction, so that Ecoflex could be patterned using photolithography. PPE was then combined with the stretchable silver (Ag) composite as an encapsulation layer by using a direct patterning process. The homogeneous interface between encapsulation and conductor contributes to efficient strain energy dissipation, so at 250% strain, stretchable electrodes with PPE encapsulation showed 50% higher electrical conductance than stretchable electrodes without PPE encapsulation. Using this PPE integrated stretchable conductor, we fabricated an intrinsically stretchable and multi-chemical sensor that can monitor the levels of pH, glucose and lactate in sweat. All sensors showed durability (i.e., $\leq 10\%$ change at 50% strain and $\leq 15\%$ change over 1000 cycles at 20% strain). Finally, the intrinsically stretchable device was demonstrated to continuously monitor the glucose and lactate levels in human sweat. The measured glucose level was quantified as 70 mg/dL in the fasting state and 100 mg/dL after food intake. The measured lactate level was from 5 mM to 16 mM during exercise. Both measurements were consistent with those from commercial assay kits.

SB12.05.15

Electrolyte-Gated Synaptic Transistor for Artificial Electronic Skin Through Bioinspired Skin-Healing Snail Secretion [Kyungho Park](#), Dong Hyun Choi, Jusung Chung, Kyungmoon Kwak, Jong Bin An, Jae Seong Han and Hyun Jae Kim; Yonsei University, Korea (the Republic of)

The sense of touch is an important way the human body interacts with the environment, enabling to accurately perceive, grasp, and manipulate a variety of objects. However, most studies for tactile sensing lack learning and memory functions, making active and direct interaction with the environment difficult. Recently, by inserting a neuromorphic computing system that mimics the functions and information processing of the biological nervous system into the conventional electronic skin (E-skin), many researchers have attempted to implement a future E-skin that can simultaneously perform cognition, learning, and memory. For the realization of artificial synapses required for neuromorphic computing systems, electrolyte-gated synaptic transistors (EGSTs) have been studied due to various advantages such as low power consumption, printability, and the opportunity to fabricate novel device architectures. However, biocompatibility must be considered for application to artificial E-skin.

Herein, we propose EGSTs using snail secretion as the electrolyte, which is a biocompatible and skin-healing material suitable for natural skin for artificial E-skin. To fabricate snail secretion EGSTs, we deposited indium gallium zinc oxide (IGZO) channel by radiofrequency (RF) magnetron sputtering on a heavily boron-doped silicon wafer with a thermally oxidized 120 nm thick silicon dioxide film, as the substrate. Thereafter, indium tin oxide (ITO) electrodes as the source and drain were also deposited by RF magnetron sputtering process via shadow mask consisting of a width/length ratio of 1000/150 μm . For activation of IGZO and ITO film, they were annealed at 300°C in the air for 1 h. Finally, snail secretion was dripped on the top of the IGZO channel.

Snail secretion including glycolic acid, allantoin, and mucin, which were skin-healing functional materials, contains a large number of hydroxyl groups, which can promote the transfer of protons (i.e., hydrogen ions) through temporary hydrogen bond formation. Therefore, it is suitable for the implementation of biological synapses. To verify the biological synapses, we confirmed the anticlockwise hysteresis characteristic of snail secretion EGSTs under the gate voltage (V_G) sweep $\pm 3.0 \text{ V}$. A negative threshold voltage (V_{th}) shift from -0.32 to -0.66 V was observed. The negative V_{th} shift could be caused by protons trapped at the interface between the IGZO and snail secretion. It could be predicted by the synaptic weight of biological synapses. Therefore, to investigate the synaptic weights, we measured the paired-pulse facilitation (PPF) characteristics of snail secretion EGSTs. PPF means that a larger second excitatory postsynaptic current (EPSC) is triggered when the second pre-synaptic spike pulse is applied before the first EPSC is recovered to the initial value. When paired pre-synaptic spikes with a pulse width of 10 ms apply with a time interval (TI) of 10 ms, the PPF index, defined as the amplitude ratio between the second EPSC (A_2) and the first EPSC (A_1), was 168.8%. And, to confirm the learning-forgetting (L-F) characteristics of our devices, we conducted consecutive 100 positive pulses (V_G of 1 V, TI of 10 ms) and followed by 50 negative pulses (V_G of -0.75 V , TI of 10 ms). As a

result, it was confirmed that our device has precise control for L-F by observing its linear characteristics. Finally, we measured the spike rate dependent plasticity characteristics of our devices, which can be judged on the ability of the artificial E-skin to be subjected to a stimulus applied to a certain abnormality. When 800 nA was set as the threshold, the 30 pulses applied at 10, 20, and 25 Hz did not exceed the threshold, but the threshold was exceeded at 50 Hz. These results could be recognized as pain by repeated and strong stimulation in the artificial E-skin. Therefore, we believe that snail secretion EGSTs will contribute to the development of improved artificial E-skin.

SB12.05.16

Bioactive and Antimicrobial Patterned Nanofibers Scaffold for Skin Regeneration and Wound Healing Shrouk M. Abdo and Nageh K. Allam; American University in Cairo, Egypt

Chronic wounds have created a global burden on the patient and health care systems as severe non-healed wound complications may lead to limb amputation and quality of life. Current research on Wound care and skin regeneration has been focused on developing practical therapeutic approaches for chronic wound management. Specifically, there is a need to create a wound dressing material that can promote cells growth, migration, and distribution across the wound area and provide protection. Moreover, they should be able to deliver drugs and bioactive molecules, which promote wound healing and tissue regeneration. Electrospun nanofibers (NFs) have shown great potential as functional wound dressing material. Aligned, crossed, and fine diameter fibers are advantageous for wound healing. In this regard, the present study used poly(glycerol-sebacate) (PGS) and polycaprolactone (PCL) mixture with benign solvents to form PGS/PCL electrospun nanofibers (NFs) on ground collector and mesh-like collector. This process produced randomly aligned PGS/PCL NFs and organized crossed PGS/PCL NFS, which resemble the basket-mesh pattern of collagen fibrils in the skin tissue. Under the scanning electron microscope, the fibers collected on the mesh collector showed organized crossed fibers with smaller diameter distribution than the randomly aligned fibers collected on the ground collector. Uniaxial mechanical testing indicated that the patterned fibers have significantly improved mechanical properties. Further elements were added to the structure to promote wound healing through Hyaluronic acid (HA) coating. To provide antimicrobial property, zinc oxide (ZnO) nanopowders have been added to the polymers mixture. HA coating was realized through scaffold surface activation by sodium hydroxide (NaOH) to improve the surface polarity and allow hydrogen bonding with HA. The ZnO nanopowder was fabricated via the microwave-assisted

5

method. Fourier-transform infrared spectroscopy (FTIR) and Energy-dispersive X-ray spectroscopy (EDX) have been used to confirm the successful addition of HA and ZnO to the structure. Water contact angle showed that HA-coating had improved the hydrophilic property of the scaffold as well as water-up take capacity. In vitro biocompatibility test using fibroblast cell line L929 indicated that 2% (w/w) ZnO has no cytotoxicity on the cells, and HA-coating promotes cells viability. In-vitro wound healing assay showed that the scaffold could improve cells migration to the scratch area, and HA-coating made it more significant. Colony-forming unit assay (CFU) showed a significant antimicrobial activity of the nanofibers loaded with ZnO after 12 hours against gram-negative E. coli. Synergistically, the crossed scaffold loaded with ZnO and coated with HA was proven to have an antimicrobial property and improves cells viability and migration, which are required for wound healing and skin regeneration.

SB12.05.17

Autonomous Self-Healable Ionoconductor for User-Customized Electronics Yong Min Kim; University of Seoul, Korea (the Republic of)

Implementing self-healing capabilities in a deformable platform is one of the critical challenges for achieving future wearable electronics with high durability and reliability. Conventional systems are mostly based on polymeric materials, so their self-healing usually proceeds at elevated temperatures to promote chain flexibility and reduce healing time. Here, we propose a new ionic cluster (IC)-driven self-healable ionoconductor composed of rationally designed copolymers and ionic liquids. After complete cleavage, the ionoconductor can be repaired with high efficiency (~90.3%) within 1 min even at 25 °C, which is mainly attributed to the dynamic formation of ICs between the charged moieties in copolymers and ionic liquids. By taking advantage of the superior self-healing performance, stretchability (~1130%), non-volatility (over 6 months), and ability to be easily shaped as desired through cutting and re-assembly protocol, reconfigurable, deformable light-emitting electroluminescent displays are successfully demonstrated as promising electronic platforms for future applications.

SB12.05.18

Stretchable Li-Ion Battery Using Origami Scale Structure for Untethered Soft Robots Myoung-Ho Kim^{1,2}, Minsub Oh¹, Hoo-Jeong Lee² and Seungmin Hyun^{1,3}; ¹Korea Institute of Machinery and Metals, Korea (the Republic of); ²Sungkyunkwan University, Korea (the Republic of); ³University of Science and Technology, Korea (the Republic of)

In recent years, technology of soft robotics has emerged as an important issue for the robot industry. Compared to conventional industrial metallic robots in controlled environments, soft robots are highly expandable in responding to non-standardized environments. Due to these characteristics, it is expected to be used not only in daily life, but also in specific applications such as treatment of disease and disaster relief. The development of a structure that is free to deformation with energy source is also essential to improve the technology. The integration of flexible structure and energy supply is very important to reduce the waste of space and weight of soft robots for versatility and portability. However, there are many difficulties due to the absence of batteries with high reliability under deformation. In this study, we propose a novel geometric structure for stretchable devices, created by folding well-defined two-dimensional patterns with cutouts to produce an extremely stretchable structure with superior reliability and bi-axial deformability. The structure is designed to mimic the hinge of a snakeskin so that its unit cells do not interfere with each mutual movement enabling stable deformations without mechanical damage. In addition, to maximize areal density and stretchability, the optimal shape of unit is determined. The unit-based geometric structure is applied to a stretchable Li-ion battery and constructed of hexagonal pouch cells and parallelogram interconnections. In situ electrochemical characterization confirms that the performance of the battery is maintained under dynamic deformation with a stretching ratio of 90% and a 10-mm-radius bending curvature, guaranteeing a long-lasting cycle life. Finally, the geometrically designed structure-based battery is applied to movable robots, crawling and

slithering, with dynamic bi-axial deformations and can be pivotal role in the development of flexible electronics including human-friendly wearable electronics and soft robots.

SB12.05.19

UV-curable Acryl-Polyurethane for Human-Compatible Flexural 3D Printing Structures Won Bin Lim, Ji-Hong Bae, Jin-Gyu Min, Ju-Hong Lee, Min-Ji Seo and PilHo Huh; Pusan National University, Korea (the Republic of)

An acryl-functionalized urethane prepolymer series with various compositions were synthesized using polyethylene glycol (PEG) and hexamethylene diisocyanate (HDI). Optimizing blending formulation for human-compatible 3D printing structures was based on MTT assays for cytotoxicity. The MTT assay was used to determine the biocompatibility of acryl-urethane (AU) resin for mammalian HaCaT cells. In the case of polyol, the most important component of the resin, treatment with poly(tetramethylene ether) glycol (PTMG) and polycaprolactone diol (PCL) induced concentration-dependent cytotoxicity, whereas PEG showed no cytotoxic effect. AU resin was designed by the addition of 2-hydroxyethyl methacrylate (2-HEMA) as a suitable material for digital light processing (DLP) 3D printing. The optimizing photo-initiator and additive were selected by UV-spectroscopy. The formulation containing the UV-curable AU resin and photo-curable additives was exposed to 405 μm UV radiation to produce the 3D structures. The effects of the photo-initiator/multifunctional acrylate value and UV absorptive power on the 3D printing performance were evaluated in terms of the mechanical properties and dimensional resolution. The surface properties of the 3D structures were tuned by controlling the photo-initiator type and composition in the AU resin. The resolution quality of the 3D printed wearable bands showed distinct differences by UV curing time, viscosity, and exposure amount. Overall, this UV-curable AU resin can be a promising prepolymer for the DLP printing of flexible photo-resin for biocompatible and photo-curable applications.

SB12.05.20

Passive 3D Printed Fully Elastic Pill for Sampling of Gut Microbiome Ruben Del Rio Ruiz, Rachel E. Owyung and Sameer R. Sonkusale; Tufts University, United States

Technologies capable of noninvasively sampling the luminal content of the GI tract have the potential to improve our understanding of the role of microbiome in health and various medical conditions. Microbial conditions in the gut are typically inferred from the analysis of fecal DNA and fecal metabolites [1]. This approach is inadequate for characterizing the microbiome upstream of the distal colon [2, 3]. To gain new insights into the many beneficial functions of the gut microbiota, it is essential to sample in different locations in the gut, particularly organs located upstream of the colon. Orally ingestible medical devices for gut engineering have been reported for sensing and diagnosis [4]. Most devices are rigid, and some require complex fabrication and assembly techniques. Our prior work on ingestible pills for sampling the gut microbiome [3] relied on a passive osmotic pump and was validated in animal models. However, the design suffered from leakage and post-sampling contamination due to the lack of a closing valve. Here, we describe the development and testing of an ingestible, fully elastic, lightweight, biocompatible, battery-less, 3D-printed, micro-engineered pill for sampling the gut microbiome. The pill is locked with an automatic closing valve which utilizes highly hydrophilic sodium polyacrylate beads, both as an absorbent for passive suction, and for locking the intake when the beads are swollen, and sampling is completed. Results from in-vitro experiments show that the flexible elastic pill is capable of sampling reliably with negligible leakage and contamination.

Stereo-lithography (SLA)-based 3D printing was used to fabricate the ingestible device using a bio-compatible/photo-curable elastic resin (50A) using a Form 2 printer. The pill was designed and fabricated in two sections: The bottom case has two-sided elliptical inlets and two internal microvalves for closing of the inlets autonomously. The top case is utilized as a shield for the pill once the beads are inserted. Three sodium polyacrylate beads are inserted in the pill. Upon exposure to fluid, the beads swell and mechanically push on the microvalves to close the inlets. The pill is then placed inside a pH-sensitive enteric coating to delay sampling until it enters the small intestine, where the coating dissolves in the higher pH environment. Natural peristaltic motion ensures mobility to the pill through the GI tract without any active motion.

The pill's sampling performance was tested by measuring the time required to acquire sample from the same buffer solution. Results show that within 20 minutes beads were fully swollen and microvalves locked both inlets, preventing additional sample acquisition. Finally, rigorous contamination tests were performed by submerging post-sampled pills in Rhodamine B dyed DI water for 30 minutes and 16 hours. Dye uptake by the pill was measured using UV-Vis spectroscopy. Results show no measurable contamination, indicating that the automatic closing valve worked as expected.

In summary, this abstract describes a flexible battery-less ingestible device for sampling intestinal microbiome from the small intestine with a self-closing mechanism to prevent contamination and leakage. Future research will focus on adjusting the composition of the enteric coating to control the location of sampling in the GI tract.

[1] J. Qin, et al. A human gut microbial gene catalogue established by metagenomic sequencing. *Nature*, 2010.

[2] D. Kumral, et al. Gut movements: A review of the physiology of gastrointestinal transit. *Digestive Diseases and Sciences*, 2018.

[3] H. Nejad, et al. Ingestible osmotic pill for in vivo sampling of gut microbiomes. *Advanced Intelligent Systems*, 2019.

[4] N. Mandsberg, et al. Orally ingestible medical devices for gut engineering. *Advanced Drug Delivery Reviews*, 2020.

SB12.05.21

All-Solution Processed Conformable Strain Sensor for Precise Muscle Movement Detection On Skin Surface Hayun Kim, Cheayoung Lee, Hyunjun Yoo and Yongtaek Hong; Seoul National University, Korea (the Republic of)

With the development of more precisely controlled artificial skin, soft robotics and human-machine interfaces, highly sensitive sensors to detect skin surface deformation has gained tremendous significance for their wide range of use in various fields such as device operation control, motion tracking and advanced interface. To keep pace with these trends, many studies have been introduced to suggest the next generation sensor for precise mapping of skin surface deformation. Over the past few years, major research has been conducted to measure and interpret bioelectric signals such as electrocardiography (ECG) and electromyography (EMG). These studies succeeded in obtaining accurate data by analyzing the signals generated by the human body, but when the size of the target muscles becomes smaller or the number and size of sensor electrodes become smaller, the accuracy of data decreases rapidly, making it difficult to obtain valid information. Also, for the EMG signal with a small signal-to-noise ratio (SNR), it was almost impossible to specify the exact point of signal occurrence, which is critical in real-time signal monitoring. Therefore, a reliable sensor capable of measuring the real-time movement of the skin without interfering with the fine movement of the muscles is highly desirable for next-generation electronics requiring immediate and close measurement of small and minor input signals.

In this work, we propose an all-solution processed skin-conformable strain sensor that is highly reliable for low-strain skin deformation sensing. Our strain sensor is facile and large-area compatible based on the spray coating method, maintaining high cycle stability and moderate resistance by taking advantage of both silver nanowire (AgNW) and carbon black (CB) blended as a sensing material. A mixture of AgNW and CB dispersed in ethanol is spray-coated on the polyimide film. After vaporizing the solvents, polydimethylsiloxane (PDMS) is poured onto the sensor film, and the entire substrate is spin coated.

After annealing, sensor film is embedded into PDMS and easily detached from the polyimide (PI) film. The fabricated sensor shows high cycle stability of over 6,000 cycles under repeated 5% strain with excellent linearity and gauge factor over 20. At the same time, the thickness of the sensor is under 300 μm , assuring high conformability and precise detection of skin deformation. To further demonstrate the feasibility of our sensor toward precise muscle movement deformation, data obtained from our sensor attached to the human muscle was compared to the actual skin deformation rate measured with a 3D

digital image correlation (3D-DIC) device. Our sensor has succeeded in precisely tracking deformation at a given location without interfering with muscle movement. This study provides a new pathway to map skin deformation especially in the single muscle movement with a low deformation rate under 5%, which is clearly distinguished from other sensors applied to large strains such as joint flexure. Furthermore, our sensor can be applied to any type of deformable substrate with potential applications such as wearable devices, soft robotics and advanced user interface. The detailed methods and results will be discussed later.

This work was supported by the Technology Innovation Program (No.20008801, Development of muscular function management solution based on electronic skin with EMG IMU and Strain sensor) funded By the Ministry of Trade, Industry & Energy(MOTIE, Korea).

SESSION SB12.06: Devices and Systems II
Session Chairs: Francesco Greco and Ignazio Roppolo
Wednesday Morning, November 30, 2022
Hynes, Level 3, Room 309

8:00 AM SB12.06.01

Stretchable and Biodegradable Batteries with High Energy and Power Density [Doris Danninger](#) and Martin Kaltenbrunner; Johannes Kepler University Linz, Austria

Realizing a sustainable, technologically advanced future will necessitate solving the electronic waste problem.^[1] Biodegradable forms of electronics offer a viable path through their environmental benignity. With both the sheer number of devices produced every day as well as their areas of application ever increasing, new concepts of degradable batteries able to sustain the high power demands of modern electronics must be developed. Simultaneously, integration of electronics in close interaction with its user or powering soft robotic devices necessitates high degrees of compliance, rendering stretchable batteries indispensable. With the first stretchable battery demonstrated by our group in 2010, we since advance such concepts towards environmentally benign materials.^[2] We demonstrate a concept for merging intrinsically stretchable materials with engineered stretchability by kirigami-patterning on a component level. With this method, we achieve high-power biodegradable batteries with reversible elasticity up to 35% when stretched uniaxially and 20% for biaxial extension. Using a combination of molybdenum metal foils, a molybdenum trioxide paste and magnesium metal foils as electrode materials, a peak power output of $196 \mu\text{W cm}^{-2}$ and an energy density of 1.72 mWh cm^{-2} is realized. The biodegradable batteries are used to power an on-skin biomedical sensor patch, enabling monitoring of sodium concentration in sweat. We designed a flexible circuit board in a small form factor allowing the collection of sensor data, while solely being powered by our biodegradable battery. The whole device is non-obtrusive and comfortable to the wearer. This concept provides a versatile route for high-power biodegradable batteries, enabling untethered soft electronic devices in a sustainable future.

[1] Hartmann, F., Baumgartner, M., Kaltenbrunner, M., "Becoming Sustainable, The New Frontier in Soft Robotics". *Adv. Mater.* 2021, 33, 2004413

[2] S. Bauer, S. Bauer-Gogonea, I. Graz, M. Kaltenbrunner, C. Keplinger, R. Schwödiauer, "25th anniversary article: a soft future: from robots and sensor skin to energy harvesters", *Advanced Materials* 26(1), 149-162, 2014

8:15 AM SB12.06.02

A Highly Flexible, Non-Flammable Li-Ion Battery via Co-Optimization of Electrode Cohesive and Adhesive Strength [Guangqi Ouyang](#); University of California, Los Angeles, United States

With the development of flexible and wearable electronics, the thickness of current wearable devices can scale down to hundreds of microns and the flexibility of the devices can be less than 1 mm bending radius [1]. Therefore, to match the progress of wearables, the design of flexible batteries needs to consider form factor, flexibility. However, traditional batteries (i.e. Coin cell, pouch cell, cylindrical cell) have not scaled down in a similar manner as their device counterparts, which makes the final size of the integrated system is limited. In addition, regarding flexibility, traditional battery structures fail to match the flexibility of devices they power, compromising the advantage of wearable devices. In past few decades, researchers have developed various types of flexible batteries for powering wearable biomedical devices, including fibrous batteries, and rubbery batteries. However, they are still limited in flexibility, stability, and output performance.

According to research [2,3], a battery fails during flexing in two modes: cohesive failure and adhesive failure. As for the cohesive mode, stress concentration and propagation happen within electrode layers due to its complex particle-network structures, which causes non-uniform Li intercalation and deintercalation processes. As for the adhesive failure mode, electrode layers delaminate from current collector layers, thus significantly increasing their contact resistance. Both modes strongly hurt battery stability and electrochemical performance.

Based on our previous work[4], we demonstrate a "land-bridge" electrode design to reduce cohesive stress concentration within electrode layers and a "Site-pinning" approach to increase adhesive strength between electrodes and current collectors. The coupled optimization of these two methods gives the battery achieve > 1000 times bending under 5 mm bending radius, 1 mAh/cm^2 capacity density, < 300 um total thickness.

First, as for "land-bridge" design, a 8x8 electrode matrixes are casted on a 600 nm current collectors in PDMS singulation walls. By taking the advantage of low Young's Modulus of PDMS and the "land-bridge" design, the bending stress within electrode layer is significantly reduced. In addition, we also develop a 5 um flexible SU8 layer between electrodes and current collectors to improve the adhesive strength. We prove that the hydrogen bond between SU8 layer and electrode forms hydrogen bonding enhances the electrode adhesive strength to flat current collector. Finally, to address the safety concerns of the Li-ion battery for wearables, an ionic liquid electrolyte (1M Lithium bis(fluorosulfonyl)imide (LiFSI) in 1-Butyl-1-methylpyrrolidinium bis(trifluoromethylsulfonyl)imide (Py₁₄TFSI)) is used in this work to provide non-flammability.

[1] Hanna, A. et al. Extremely Flexible (1mm Bending Radius) Biocompatible Heterogeneous Fan-Out Wafer-Level Platform with the Lowest Reported Die-Shift (<6 μm) and Reliable Flexible Cu-Based Interconnects. in 2018 IEEE 68th Electronic Components and Technology Conference (ECTC) 1505–1511 (IEEE, 2018). doi:10.1109/ECTC.2018.00229.

[2]Chang, J., Huang, Q., Gao, Y. & Zheng, Z. Pathways of Developing High-Energy-Density Flexible Lithium Batteries. *Advanced Materials* 33, 2004419 (2021).

[3] Liang, G., Zhu, J., Chen, A., Yang, Q. & Zhi, C. Adhesive and cohesive force matters in deformable batteries. *npj Flex Electron* 5, 1–4 (2021).

[4]Ouyang, G., Whang, G., MacInnis, E. & Iyer, S. S. Fabrication of Flexible Ionic-Liquid Thin Film Battery Matrix on FlexTrate™ for Powering Wearable Devices. in 2021 IEEE 71st Electronic Components and Technology Conference (ECTC) 1620–1626 (2021)

8:30 AM *SB12.06.03

Artificial Mechanoreceptors from Hydrogels—Capacitive, Triboelectric and Piezoionic Sensors for Ionic Skin and as Interfaces with the Nervous System John D. Madden and Yuta Dobashi; Univ of British Columbia, Canada

Millivolt potentials and nanoampere ionic currents are the signals at the heart of our sensory system, and our nervous system in general. Can we make use of ionic signals in artificial sensors and neural interfaces? Here we discuss three versions of artificial ionic sensors.

In the first, the hydrogels are used as ionic conductors in capacitive or piezoresistive sensors. These are low power, soft sensors that build on the ionic skin concept developed almost a decade ago - combining mechanical toughness, transparency and compliance. Here there is no need for hard electronics or wires, except to deliver and record electronic signals. The interface between the ionic and electronic, and the wet nature of the hydrogels, are challenges - but there are solutions. The scalability of these approaches to create skins containing arrays of sensors is discussed, and compared with implementations using conductive elastomers.

In the second approach, change in surface contact between a hydrogel and a conductor or other charged interface, can lead to the generation of significant voltages. Hydrogel toughness and deformability, combined with mobile salt content, provide advantages for creating compliant sensors or even generators. Potentials at the level of volts or higher can be generated, making detection simple. Charge density and electromechanical coupling are relatively small, so generators will need to operate at high frequencies to run electronics. They rely on an electronically conductive interface, but can be self-powered (i.e. no input electrical energy is needed - the energy from the mechanical work done is sufficient).

A third sensing approach uses motion of ions induced by pressure gradients. This can include streaming, in which ions of one polarity are carried by moving solvent, producing currents and charging. In general, what can be called a piezoionic effect is involved - where there is an effect of pressure on the motion of ions. This is akin to piezoelectrics, except that it relies on a gradient, and charges are mobile rather than bound into a crystal. In hydrogels with both mobile anions and cations, such as Na⁺ and Cl⁻, the net current produced may be simply a result of anions being effectively larger than cations, experiencing more drag as they move through the hydrogel, and leading to a net current as the cations flow more freely. Voltages are small - typically millivolts. But charge can be large. And responses can be surprisingly fast - in the same range as our mechanoreceptors. The net effect can stimulate a nerve and lead to muscle contraction, fully self-powered. This transduction and transmission should be possible without the use of any metallic conductors, though this has yet to be shown, and our demonstration uses fine wires. Wires allow the signals to be transferred over larger distances, due to the much lower resistivity of metals than ionic conductors. As with any interface between electronics and tissue, there are electrical and mechanical impedance mismatches. These can be managed using conducting polymer coatings that absorb enormous concentrations of ions, or, perhaps, by avoiding the use of electronics completely. To expand the possibilities of ion only sensors, an active ionic system like that provided by our sodium/potassium ion pumps, is likely needed.

9:00 AM SB12.06.04

Rubbery Complementary Thermoelectric Generator Fabricated from Intrinsic Stretchable N-Type Semiconductor Yongcao Zhang, Diego Rosas Villalva and Derya Baran; King Abdullah University of Science and Technology, Saudi Arabia

Stretchable thermoelectric generators (TEGs) have proven to be promising candidates for wearable electronics and can harvest electrical energy from body heat. However, high-performance stretchable n-type TEGs lag the development of the organic thermoelectric (OTE). Here, we developed a novel n-type semiconducting nanofiber and an intrinsically stretchable n-type TEGs fabricated from percolated nanofiber network in the elastomeric materials. Taking advantage of nanofiber structure, extraordinary thermoelectric properties have been achieved by sequential doping. With increasing dopant concentration, a transition of the Seebeck coefficient from n-type to p-type was observed. Owing to the percolation network of n-type semiconducting nanofiber, the fabricated intrinsic stretchable TEGs retain their conductivity under high strains. The incorporation of stretchable p-type TEG material also allows to achieve the stretchable complementary TEG and harvest energy from different arbitrary surfaces. The demonstrated intrinsic stretchable n-type semiconductor will provide more insight toward complementary circuits and sensors

9:15 AM SB12.06.05

Hydrogels Based Triboelectric Nanogenerators (TENGs) for Energy Harvesting and Self-Powered Tactile Sensors Giuseppina Pace^{1,2} and Marino Lavorgna¹; ¹Consiglio Nazionale delle Ricerche, Italy; ²Italian Institute of Technology, Italy

New low power technologies, as the one largely developed for the internet of Things (IoT), wearable and portable electronics, require only few tens of microwatts up to few mW of power supply to operate. This makes it possible their sustainable integration with energy harvesters that can scavenge the environmental wasted energy. In addition to provide the required electrical power to low power electronics, mechanical and thermal energy harvester can also be designed as self-powered sensors. This aspect hugely widens their potential impact in a variety of application fields including soft-robotics, artificial skin, and haptics.

Between mechanical energy harvesters, triboelectric nanogenerators (TENGs) have gained increasing attention as novel low-cost energy solution. Furthermore, they can be fabricated with low environmental impact materials and scalable printing processing. Recent developments in TENGs technology show that they can be used in different applications going from wearable and self-powered sensors to wind and sea wave energy harvesting (blue energy).

[1] Differently from other mechanical energy harvesters, as piezoelectric and electromagnetic generators, TENGs can be fabricated from non-toxic, biodegradable and recyclable materials and can efficiently operate also in the low frequency range. [2]

TENGs energy conversion mechanism relies on the charge transfer which occur between two materials placed under friction forces and that own different electron affinities. Strategies to increase the charging of triboelectric materials (tribomaterials) through chemical modification or surface patterning have been proposed. We recently demonstrated that the electrode work function as well as electrode capacitance must be considered to improve TENGs power output, a main aspect which has been often disregarded in previous work. [3,4]

Here, we highlight the fundamental role played by the interface between the tribomaterial and the electrode in contributing to the increase of energy harvesting and tactile sensing of novel TENGs based on hydrogels. The specific role of composition, structure and electrolytic capacitance of hydrogel based on polyvinyl alcohol derivatives, will be highlighted, and clarified. This work intends to provide useful guidelines for the future design of new materials and device structure design leading to improved TENGs performances, fostering their sooner integration into novel low power electronics.

References:

- C. Wu, A. C. Wang, W. Ding, H. Guo and Z. L. Wang, *Adv. Energy Mater.*, 2019, **9**, 1–25.
- Y. Zi, H. Guo, Z. Wen, M. H. Yeh, C. Hu and Z. L. Wang, *ACS Nano*, 2016, **10**, 4797–4805.
- G. *Pace, F. Bonaccorso, *Nano Energy*, 2020, **76**, 104989.
- G. *Pace, F. Bonaccorso *Nano Energy*, 2021, **87**, 106173.

9:30 AM SB12.06.06

Stretchable Redox-Active Semiconducting Polymers for High-Performance Organic Electrochemical Transistors Yahao Dai, Shilei Dai and Sihong

Wang; University of Chicago, United States

Wearable health monitoring technologies that can be integrated intimately with human bodies are of rapidly increasing interest in daily healthcare and self-diagnosis. Organic electrochemical transistor (OECT) is an emerging device platform for next-generation human-integrated bioelectronics owing to its high amplification and sensitivity to biological signals, and non-volatile signal retention for memory and computing applications. However, owing to the lack of stretchable redox-active semiconducting polymers, skin-like softness and stretchability have not yet been realized in high-performance OECTs for achieving seamless tissue-electronics interfaces. Here, we report two stretchable polymer semiconductors for OECT devices, namely poly(2-(3,3'-bis(2-(2-(2-methoxyethoxy)ethoxy)ethoxy)-[2,2'-bithiophen]-5)yl thiophene) (p(g2T-T)) and poly-[3,3'-bis(2-(2-(2-methoxyethoxy)ethoxy)ethoxy)-2,2'-bithiophene] (p(gT2)), which give exceptional stretchability over 200% strain. In particular, the p(g2T-T) also shows great mechanical robustness for being able to sustain charge carrier mobility over 5000 stretching cycles, together with the OECT performance on par with the state of the art. Validated by the systematic structural characterization, sufficient chain alignment during stretching for stress dissipation is determined as the key enabler of high stretchability. By comparing the mechanical and electrical performance of different polymer semiconductors, the key design features for enabling the combination of high stretchability and high OECT performance are determined as non-linear backbone architecture, moderate side-chain density, and sufficiently high molecular weight. Using those highly stretchable polymer semiconductors, we fabricated an intrinsically stretchable OECT with the high normalized transconductance ($\sim 223 \text{ S cm}^{-1}$) and biaxial stretchability up to 100% strain. Furthermore, we demonstrated on-skin electrocardiogram (ECG) recording based on our stretchable OECT, and fabricated an intrinsically stretchable neuromorphic device with over 800 distinct memory states and good state retention capability ($> 10^4 \text{ s}$) with the high stretchability of up to 100% strain over 100 repeated cycles.

9:45 AM BREAK

10:15 AM SB12.06.07

Motion Artifact-Resilient Embedded Sensors by Mechanically Rendered Stable Zone [Chanho Jeong](#)^{1,2} and Tae-il Kim²; ¹Carnegie Mellon University, United States; ²Sungkyunkwan University, Korea (the Republic of)

Recently, miniaturized and lightweight sensors have changed the conventional hard and bulk medical equipment to flexible form, allowing users to engage in daily activities while having sensors equipped or implanted. This simple change has provided continuous data acquisition of human conditions for the high yield of diagnosis. However, the continuously measured physiological/electrophysiological signals from a body-interfaced device are inevitably embedded into physical noise from body movement. This is because the body always moves by the skeletal system, which is controlled by muscle contraction and relaxation. Therefore, human-interactive devices that are closely placed to the body are also affected by skin and muscle movement. Consider that, in many cases, the transducer of the sensors is supposed to be deformed by the amount of the targeted physical quantity. However, unintended deformation of the sensor induces unexpected tensional or compressive force, generating errors. For these reasons, dynamic motion always diminishes the quality of the data, and reduces the signal-to-noise ratio. As an example, a tactile sensor aims to recognize touch. However, dynamic movement is also a factor that generates signal change without touch, and results in the user recognizing a virtual touch that does not really exist. The canceling of dynamic noises and extraction of the target signal are essential issues in body-interfaced devices.

The most common method is signal processing for noise canceling. However, this requires additional data processing, which potentially incurs signal loss of the original data. Alternatively, unconventional signal filtering using structures, materials, or designs of electrodes has been suggested. Representative examples are bending-insensitive devices using neutral planes, unidirectional sensors with precisely aligned patterns to have rather high sensitivity in one direction, and stretching insensitive sensors using wavy or origami forms that enable the sensors to change along with the deformation, while maintaining their performance. However, these methods concentrated on a single dynamic effect, and they also faced other problems. To resist dynamic movement, the sensor should be resilient to various deformations, like stretching, compression, and bending. The neutral plane method has high effectiveness for bending insensitivity, but no resistivity to stretching and compression. Unidirectional sensors are difficult to expand to various sensors, because they need to accompany processes that are of complicated structure, or difficult. In the case of origami and wavy 3D structures, some operating space over the whole device is required to properly work, and it is barely used for implantable devices.

Notably, motion-induced noise operates through the body surface direction, and the film shape sensor has varying sensitivity according to the orientation of the device. To eliminate dynamic motion artifacts more efficiently and universally, in this research, the film sensor is placed in a position where motion noises apply to a relatively insensitive direction, while letting the target stimuli apply to the sensitive area. The principles of the unidirectional sensors mentioned above are expanded from 2D body surface to 3D space, and the study is conducted on motion artifact-minimized sensors that do not require specifically aligned patterning to take a strict process and limit the variety of fabrication. The study aims to show sensors that focus on human-interactive devices while showing insensitivity to 75 % stretching, 25 % compression, and 5 mm radius of curvature bending, while maintaining the sensing ability of the sensor. As an demonstration, the pulse signal on a wrist is well measured while the hand is rotating, and artificial skin implanted on rat can distinguish external pressure from the effect of movement noise.

10:30 AM *SB12.06.08

Interfacing Imperceptible Electronics with the Human Body—New Solutions and Approaches [Andrea Spanu](#); University of Cagliari, Italy

The advent of epidermal electronics, which can be traced back to the beginning of the 2010 decade, radically changed the idea of electronics/human body interfacing, blurring the boundaries between the system to be analyzed (the human body) and the tools that are necessary to effectively transduce its multifaceted biosignals. In particular, the newborn possibility of a seamless integration of electronic devices and the human skin quickly led to the rise of new perspectives and outlooks that ultimately lead to imperceptible electronics, a concept that literally break the obsolete dichotomy between the “soft” human body on one side and the “rigid” recording device on the other side.

Nowadays, two of the most interesting fields of applications of epidermal electronics are undoubtedly the development of sensing systems for robotic skin, and the engineering of bioelectrodes for the monitoring of biopotential, such as electrocardiography (ECG), electromyography (EMG) and electroencephalography (EEG) signals from the surface of the skin. Regarding the first application, we show here an approach based on Parylene C sub-micrometric substrates and the piezo(and piro) electric polymer PVDF coupled to an organic transistor called Organic Charge Modulated FET (OCMFET) for the development of tactile sensors for robotic skin applications. Thanks to the versatility of the OCMFET structure, the low-cost materials and the low-resolution fabrication processes, this method allows to easily obtain ultrasensitive temperature and force sensors on ultra-conformable substrates that can be easily transferred onto a target surface (including a robotic end effector or the human skin) without losing their characteristics. As pertains to the second application (which represents one of the most appealing example of the possible integration between this novel branch of electronics and the human body), despite the numerous different approaches that have been proposed so far, some of the intrinsic weaknesses of using ultrathin electrodes within the biomedical domain are still yet to be solved. The first issue is related to the breathability of these epidermal patches, an important aspect when on-body measurements are taken into consideration. With the intent of overcoming this issue and thus improving the comfort of the subject during the measurement, we developed a simple yet effective solution for the development of tattoo electrodes for biopotential recordings, which relies on biocompatible materials and low-resolution fabrication techniques. In particular, Parylene C-based submicrometer-thick electrodes have been rendered breathable through a large area, oxygen plasma-based perforation technique, surpassing the breathability of common textiles like jeans and approaching that of knitted clothing, thus making these electrodes suitable for long-term biopotential recordings. The second important aspect that we recently tackled is related to the methods of

connection of such imperceptible films to the external electronics, a problem that effectively voids some of the main advantages of having an ultra-thin and conformable device. The adopted solution relies on free-standing, ultra-thin PEDOT:PSS based functional films with conductive and ferrimagnetic properties, thanks to the integration of inexpensive ferrite powder layers within the film itself. The obtained electrodes can be transferred on the skin as temporary tattoos and directly contacted using magnetic connectors without compromising their conformability. The proposed approaches, being at the edge between the fervent fields of epidermal and organic electronics, represent interesting examples of how it is possible to obtain high-performing and conformable tactile sensors, while at the same time overcoming some of the more important issues and limitations that stem from interfacing electronics and the human body.

11:00 AM SB12.06.09

Design of a Fully-Resorbable Soft Electronic Device for Neural Stimulation and Monitoring [Simon Regal](#)^{1,1}, Maxime Leprince^{1,2}, Pascal Mailley¹, Napoleon Torres-Martinez¹, Jenny Molet¹, Fabien Sauter-Starace¹, Isabelle Texier-Nogues¹ and Rachel Auzely-Velty²; ¹University Grenoble Alpes, CEA, Leti, France; ²University Grenoble Alpes, CNRS, France

Currently, clinical electrocorticography (EcoG) electrode matrices are embedded in inelastic silicone rubber. For subchronic studies, neural implants need to be removed during a second surgery in order to limit immune system reactions or infectious risks. However, any surgery involves risks for the patients and can lead to complications. The development of transient electronic devices opens the way to new medical possibilities for mid-term post-surgical follow-up, such as electrophysiological monitoring, on-demand and controlled drug delivery, or electrical stimulation in tissue regeneration. Implants able to degrade harmlessly inside the body eliminate the need of removal surgery with associated risks. Compared to non-degradable devices, they potentially reduce inflammation responses and chronic adverse conditions that could decrease device functionality.

A bioelectronic device consisting of poly(lactic-co-glycolic acid) (PLGA) films as insulating substrates, sputtered molybdenum (Mo) as conductive tracks, and conductive polymer electrodes for tissue interface, has been fabricated using microfabrication techniques. With their mixed ionic/electronic conductivity and tunable mechanical, electrical, electrochemical, and biological properties, conductive polymers are materials of choice for the design of the conductive electrodes of such transient devices. Herein, resorbable materials based on sulfated hyaluronan modified with phenylboronic moieties (HAS-PBA) as dopants of poly(3,4-ethylenedioxy)thiophene (PEDOT) were specifically developed for this application.

The thickness of the entire device is 40 μm thick with Mo tracks of only 500 nm, whereas the length and width are respectively 9 mm and 4 mm. Electrical impedance spectroscopy showed that the PEDOT:HAS-PBA layer reduced the electrode impedance (580 Ω at 1 kHz), providing a better interface than Mo metal alone (3400 Ω at 1 kHz). The charge storage capacity of electrode material showed an increase from 5 mC/cm^2 to 26 mC/cm^2 for Mo and PEDOT:HAS-PBA, respectively. The device was developed for a working period between 1 and 2 months, and a complete resorption around 3 months. In vitro characterization of device stability for electrophysiological monitoring followed by device degradation was carried out over a 3-month period. The next step will be to implant the device subdurally in contact with rat brain cortex for electrical stimulation and recording, and to explore its bioresorbability properties *in vivo*.

In summary, we describe the development of a thin and flexible device that is suitable for different applications such as pre-surgical localization of epileptogenic foci or post-surgical monitoring of brain activity. The lifetime of our device is perfectly adapted to these applications.

11:15 AM SB12.06.10

Air-Stable Ultra-Flexible Organic Photonic System for Cardiovascular Monitoring [Tomoyuki Yokota](#), Iwao Shirayama and Takao Someya; The University of Tokyo, Japan

Optical bioimaging techniques, such as imaging using fluorescent probes, photoacoustic imaging, and near-infrared spectroscopy, are noninvasive methods that is widely used in medical devices for measuring biological information from outside. In recent years, with the development of semiconductor technology, miniaturization of these imaging devices has become possible. In particular, organic optical devices have such features as high efficiency, flexibility, and low weight; hence, they are being increasingly applied to healthcare through integration into wearable devices. For example, a flexible device that integrates an organic light-emitting diode (OLED) and an organic photodetector (OPD) can be attached to a finger, and the pulse wave can be calculated by measuring the light reflected from the body. Measuring the blood oxygen ratio using two-color light sources, such as red and green, or red and near-infrared light-emitting diodes, is also possible. Other biometric data, such as veins and fingerprint images, can also be obtained using high-resolution imaging sensors. Improving the conformability of the device to the body is important to perform such *in vivo* imaging with high accuracy.

Soft optical devices should be developed to improve the conformability of devices to the skin. Previously, extremely soft organic optical devices have been realized by ensuring the elasticity of the substrate and required materials. Owing to the development of new materials and processes, soft organic optical devices can achieve the same electrical properties as devices fabricated on glass or thick plastic film substrates. Furthermore, the thickness of the film substrate can be reduced to realize ultrathin organic optical devices with improved skin conformability. An OLED that is formed on a 1.5 μm -thick plastic substrate and can be attached to the skin has been reported.

However, the integration of multiple types of organic optical device, such as OLEDs and OPDs, on the same thin substrate of less than 50 μm without using the lamination process has not been reported. This is because organic optical devices fabricated on a flexible substrate are not stable and require an encapsulating layer with high barrier properties, and making the film thinner while maintaining the barrier properties is difficult. Furthermore, to integrate different optical devices, it is necessary to fabricate the devices using a vacuum process, which results in insufficient characteristics of the organic photodiodes or organic photovoltaics. Therefore, it is necessary to form OPDs using a solution process and improve the stability of the organic optical devices to integrate high-performance organic optical devices on the same ultrathin substrates.

In this study, we developed an ultra-flexible optical sensor system wherein OLEDs and organic photodiodes are integrated on the same substrate by improving the air stability of ultra-flexible OLEDs and photodiodes. By applying an inverted structure, the ultra-flexible OLEDs were operated for more than 10 days, even without a high-barrier passivation layer. The ultra-flexible OLEDs exhibited high air stability, wherein the current density was maintained at more than 50% of the initial state. The organic photodiodes also demonstrated high air stability, with less than 1% change in photocurrent and less than 10 nA/cm^2 dark current after 10 days. The sensor system integrating these air-stable optical devices is extremely thin, with a total thickness of 5 μm . Therefore, it can be directly attached to the skin, and the pulse wave can be measured easily. Furthermore, we succeeded in measuring the pulse wave propagation time by combining an optical system with an electrocardiogram. When the blood pressure value was calculated from the measured pulse wave propagation time, a high correlation coefficient of 0.89 was achieved. This value was measured using a conventionally used cuff-type blood pressure-monitoring system.

11:30 AM SB12.06.11

Honeycomb Film Morphologies for High-Performance Stretchable Electrochemical Transistors [Antonio Facchetti](#); Northwestern University/Flexterra Inc, United States

The realization of fully stretchable electronic materials is central to advancing new types of mechanically agile and skin-integrable optoelectronic device technologies. Here we demonstrate a materials design concept combining a porous organic semiconductor honeycomb film morphology with a biaxially pre-stretched platform that enables high-performance organic electrochemical transistors (OECTs) with charge transport stability up to 30-140% tensile strain, limited only by metal contact fatigue. The pre-stretched honeycomb channel semiconductor, donor-acceptor polymer DPP-g2T

(DPP=diketopyrrolopyrrole, 2T=dithiophene), exhibits high ion uptake with ultra-stable electrochemical and mechanical properties, > 1500 redox cycles with 10000 stretching cycles under 30% strain. Highly reliable electrocardiogram recording cycles and synapse responses under varying strains, along with mechanical finite element analysis, underscore that the present stretchable OECT design strategy is suitable for diverse applications requiring stable signal output under deformation with low power dissipation and robustness to mechanical deformation.

SESSION SB12.07: Applications III
Session Chairs: Ingrid Graz and Darren Lipomi
Wednesday Afternoon, November 30, 2022
Hynes, Level 3, Room 309

1:30 PM *SB12.07.01

Soft Adaptive Robots Inspired by Nature Barbara Mazzolai and Emanuela Del Dottore; Istituto Italiano di Tecnologia, Italy

Natural organisms are adaptive, constantly learning and evolving. Since the dawn of life on Earth 3.8 billion years ago, natural species have evolved behaviors with characteristics suited to survive in their environment and to sustain life for generations. Perfection is not nature's goal. Nature focuses on evolution. Therefore, nature experiments, re-combines the existing and adapts according to results. Thus, why are roboticists looking at natural organisms for the robot revolution? By looking at natural organisms' life and evolution strategies, nature can provide engineers with the rules to design and develop functional embodiments and energy-efficient behaviors, which are the keys for artificial machines to better deal with unstructured and challenging environments.

With this vision, our approach is to take inspiration from plants and soft animals in order to design robots with high morphological adaptability, distributed sensory systems, as well as energy-saving mechanisms.

More specifically, in this talk, I will explain how soft animals and plants offer new insights to generate new multi-functional materials for morphological adaptation and computation, mechanisms for moving-by-growing, strategies for climbing and adhesion, multi-sensory information processing and distributed architecture of functionalities, as well as new forms of energy. Examples will include recent advances in artificial self-growing robots, technologies and mechanisms for adaptive anchoring, soft manipulators for adaptive grasping, and biodegradable robots. These eco-robots will find applications for environmental exploration, monitoring, precision agriculture, and for improving basic knowledge on natural phenomena.

2:00 PM SB12.07.02

Soft Actuators Made of Discrete Grains Sophia T. Eristoff¹, Sang Yup Kim^{1,2}, Lina Sanchez Botero¹, Trevor Buckner¹, Osman Dogan Yirmibesoglu¹ and Rebecca Kramer-Bottiglio¹; ¹Yale University, United States; ²Sogang University, Korea (the Republic of)

Soft actuators grant soft robots meaningful mechanical force while maintaining inherent compliance. Stimuli-responsive soft actuators respond to changes in the environment to initiate actuation, allowing for remote actuation and further enhancing the adaptability of soft robots. Recent advances have shown thermo-responsive phase-change actuators can produce high forces with significant volumetric expansions. These phase-change actuators rely on the thermally-driven liquid-to-gas phase-change of encapsulated low boiling point solvent within a soft bulk elastomer. Simultaneously, granular media has the opportunity to shift between critical states via jamming, exhibits bulk reconfigurability via different particle packings, and can provide viscosity enhancement to enable 3D printing of a variety of materials. In this work, we present soft granular actuators, where each grain consists of a hyperelastic silicone shell and multiple low boiling point solvent cores. When subject to temperatures past the boiling point of the encapsulated solvent, each individual grain undergoes rapid volumetric expansion of approximately 700%. The actuation force of a single grain is large enough to lift a mass 2000x its own weight in less than 2 milliseconds. Additionally, individual grains can be arranged in a soft silicone pouch and when subject to a change in ambient pressure, the grains collectively undergo jamming behavior and a stark increase in stiffness is observed. When grains are embedded in an uncured resin, they induce thixotropic behavior of the carrier resin, enabling 3D printing of freeform soft actuators with high shape retention. Furthermore, the granular composite can be printed onto a variety of inanimate objects to impart motion. In sum, distinct soft granular actuators enable scalable actuation from micro-scale individual grains to meso- or macro-scale granular agglomerates. When embedded in resin, grains enable freeform 3D printing of actuators with high resolution and large volumetric expansions. Combining the advantageous properties of phase-change soft actuation and granular media, this work presents the opportunity to realize soft actuators with tunable bulk properties, compatibility with self-assembly techniques, and on-demand reconfigurability.

2:15 PM BREAK

3:15 PM *SB12.07.04

Vine Growing Robots for Medical Applications—Design and Miniaturization Tania Morimoto; University of California, San Diego, United States

Soft growing robots, also known as vine robots or tip-everting robots, have recently emerged as a promising class of soft robot. They consist of an inflatable, thin-walled, hollow tube that is inverted inside itself. The inverted material everts, or extends, from the tip of the robot as it is pressurized with air or fluid, in a manner similar to how plants grow. This method of movement is fundamentally different from that of traditional soft, flexible robots and manual surgical tools, since they are not pushed from the base and therefore result in no relative movement between the robot body and the environment. These robots therefore have significant potential for improved safety and navigability through highly constrained and sensitive areas deep inside the human body. However, current vine robot designs are fundamentally limited in how small they can be scaled, therefore limiting their applicability in realistic clinical scenarios. This talk will focus on our approach to addressing this challenge of vine robot miniaturization. First, we analyze the impact of the vine robot design parameters on their miniaturization. Second, we propose several new vine robot architectures that overcome the current scaling limitations. Critically, there are several material dependent design parameters that significantly affect the scaling capabilities of a given robot architecture. Third, we investigate several approaches to integrating actuators that can enable steering of the vine robots, even at small scales. Finally, we highlight the potential impact of the proposed robot architectures and associated models through experimental validation of a robot designed for endovascular surgery.

3:45 PM SB12.07.05

Transparent and Highly Voltage-controllable Electro-tactile Actuator Kyeonghee Lim, Sumin Kim and Jang-ung Park; Yonsei University, Korea (the Republic of)

Tactile sensation plays key roles in the realization of senses of prosthetics, virtual reality (VR), augmented reality (AR), and display touch panels. In recent years, vibro-tactile technology was dominant in this field of research. However, until now, most vibro-tactile devices have critical limitations to provide a variety of sensations and stimulation in close intervals due to their bulky forms. Therefore, electro-tactile device is a promising candidate for a tactile

stimulation system. Herein, we demonstrate a transparent, voltage-controllable electro-tactile actuator capable of presenting a variety of senses and high-resolution tactile information of 2 mm. This electro-tactile actuator is advantageous to control the frequency, amplitude, and pulse width of applied electrical pulses to different mechanoreceptors. We exhibited the effectiveness of this actuator through cognitive experiments on human subjects and neuronal signals from the fingertips to the brain. Through the cognitive experiments, 10 subjects detected stimulation at a low voltage on the fingertip electro-tactile device (<10 V), and it was possible to cause a large range of senses such as vibration, tapping, hardness, and pain by varying stimulation frequency (10-300 Hz). Pulse signals transmitted into the skin through an actuator were also measured as neuronal signals. This electro-tactile actuator is expected to work in many fields, including transparent mobile displays, artificial prosthetics, or even VR and AR tactile displays due to its accuracy in local stimulation, and high transparency.

4:00 PM SB12.07.06

A Method to Measure and Optimize Full Cycle Efficiency of Soft Electrostatic Actuators [Steven L. Zhang](#)¹, Soo Jin Adrian Koh¹, Philipp Rothmund¹, Toshihiko Fukushima¹, Sophie Kirkman¹ and Christoph Keplinger^{1,2,2}; ¹Max Planck Institute for Intelligent Systems, Germany; ²University of Colorado Boulder, United States

Energy efficiency of actuators is a critically important metric for untethered and mobile robotic systems. The field of soft electrostatic actuators is missing an universal, easy to use tool and a standard that allow measurement and analysis of actuator's intrinsic electrostatic-mechanical efficiency. Thus, in this work, a method to measure and optimize the efficiency of soft electrostatic actuators is developed, where the four work conjugate parameters: voltage, charge, force, and displacement, can be monitored in real time. The full cycle efficiency of electrostatic actuators can be calculated by dividing the area enclosed in the force-displacement plane and the area enclosed in the charge-voltage plane. We demonstrate our method using HASEL actuators as a model system, and the intrinsic electrical and mechanical losses were studied, and efficiency was calculated at different driving voltages and loads. It was found that there is an optimal load resulting in an efficiency of 58% for HASEL actuators. The method can be further used to study the impact of various parameters such as frequency, and the use of new materials systems and geometries on the efficiency.

4:15 PM SB12.07.07

Millimeter-Scale Soft Electrohydraulic Actuators for Locomotion in Aquatic Environments [Florian Hartmann](#) and Herbert R. Shea; École Polytechnique Fédérale de Lausanne, Switzerland

Undulating fin and tail propulsion—used by marine animals across many size scales—represents an efficient locomotion method, both on and under water. It is silent and enables a variety of maneuvers. Robotic swimmers can achieve such life-like locomotion using soft actuators but typically measure several tens of centimeters, preventing applications that benefit from smaller scales. Here we present the design, material approaches, and fabrication processes of soft mm-scale electrohydraulic actuators. Our actuators use zipping of metalized polymers films to displace a dielectric fluid, which generates bending of fins, creating a periodic undulation. We developed a fabrication strategy based on multilayer lamination to enable actuators which operate reliably when submerged in water at voltages from 500 V to 2 kV. The actuators are fast, capable of operation up to 20 Hz, and provide suitable amplitudes for swimming, with bending angles up to 15 degrees. With these actuators, we demonstrate flatworm-inspired robots, only a few tens of millimeters long, that locomote both on or under water.

4:30 PM SB12.07.08

Soft and Highly Integrated Electronic Fibers [Fabien Sorin](#)¹, Andreas Leber¹, Chaoqun Dong², Hritwick Banerjee¹ and Stella Laperroussaz¹; ¹Ecole Polytechnique Federale de Lausanne, Switzerland, Switzerland; ²University of Cambridge, United Kingdom

Stretchable optical and electronic fibers constitute increasingly important building blocks for a myriad of emerging applications, such as in robotics, sensing, medical implants or e-textiles. They are particularly suitable for wearables and smart textiles as seamlessly integrated devices that can bring high added values for monitoring, energy harvesting, haptic and even actuation functionalities. Yet, it remains challenging to fabricate efficient and advanced soft fiber-base devices that can undergo significant mechanical deformation in a simple and scalable way. The preform-to-fiber thermal drawing technique is a powerful platform to fabricate multi-material fibers with complex architectures and functionalities. Until recently, this fabrication approach has been restricted to rigid thermoplastic or glass fibers, preventing their use for mechanical sensing or actuation, and rendering difficult their use in wearable approaches or within textiles.

In this contribution we will show how we could revisit the selection criteria for cladding materials compatible with the thermal drawing process, and fabricate super-elastic fibers with advanced electronic functionalities. We will demonstrate how, thanks to a deeper rheological characterization, we could identify thermoplastic elastomers that could be drawn from a solid preform at high viscosity (Advanced Materials, 2018, 201707251). Subsequently, we will demonstrate that thermoplastics, liquid metals, and conductive polymer composites could be co-drawn with prescribed architectures within thermoplastic elastomer cladding. This allowed us to successfully fabricate stretchable optical but also electronic fibers that are used as precise and robust pressure, strain or more generally deformation and haptic sensors. We will in particular show examples of electronic fibers for strain or pressure sensing, that can be integrated into textiles and fabrics for large area pressure mapping (Adv. Funct. Mat. 30, 1904274 (2019)), and for polymer composite part monitoring (Adv. Mat. Technologies 6, 2000957 (2021)). We will also introduce an original strategy based on fibers that integrate tens of liquid metal electrodes that can act as a soft transmission line for sensing multiple mechanical deformation events along the entire fiber length (Nature Electronics 3, 316 (2020)). Based on the same combination of micro-structured thermoplastic elastomers and liquid metal electrodes, we will present self-powered strategies via soft triboelectric fibers (Nature Communications. 11, 3537 (2020)). These examples of fibers enable to realize, with a few connections at fiber ends, robust large area sensing fabrics, paving the way towards novel opportunities for advanced yet scalable soft electronics, soft prosthesis, wearable devices and electronic textiles. We will conclude with a hint on recent developments (currently under review) of steerable multi-material soft fibers to realize highly integrated thin catheters with micro-channels, optical waveguides and electrodes, paving the way towards novel opportunities in soft robotics.

SESSION SB12.08: Poster Session II
Session Chairs: Piero Cosseddu and Ingrid Graz
Wednesday Afternoon, November 30, 2022
8:00 PM - 10:00 PM
Hynes, Level 1, Hall A

SB12.08.01

Soft Actuators Based on Liquid Crystal Elastomer and Laser Induced Graphene [Stella Drewes](#)¹, [Alexander Dallinger](#)¹ and [Francesco Greco](#)^{1,2}; ¹Graz

University of Technology, Austria; ²Scuola Superiore Sant'Anna, Italy

Thermoresponsive Liquid Crystal Elastomers (LCEs) are widely studied for their use as soft actuators as they feature excellent actuation properties including large actuation strains and reversible actuation processes. To overcome the prevalent limitations of rigid heating elements hindering the actuation performance of soft actuators, composites of LCEs and a soft heating structure promise a great enhancement of the actuation behaviour. As compliant heating elements conductive tracks of Laser Induced Graphene (LIG) are used which are obtained from laser scribing with an IR CO₂ laser on a polymeric precursor substrate. The precursor is converted into a conductive porous carbon thanks to a photothermal pyrolysis process. By embedding these conductive LIG tracks in a thermoresponsive LCE matrix a temperature sensitive soft actuator was built in which the LIG served as a Joule heating element to resistively heat the LCE and trigger an actuation. The actuation performance of the LCE and the LCE/LIG composite were investigated regarding actuation strain and stress and a demonstrator was produced.

SB12.08.02

Development of High-Resolution Elastomeric Electrodes Using Gold Nanosheets and Its Applications [Seongsik Jeong](#), Jiyun Lee, Hyeseon Jo, Seojun Heo and Haejin Kim; Gyeongsang National University, Korea (the Republic of)

Soft electronics necessitate the electronic devices that can communicate with various parts of the human body and acquire bio-signals with a sufficient quality, resolution, and stability. In that sense, the elastomeric electrodes with an appropriate form factor, the similar mechanical properties with a human-skin or an organic tissue, and a sufficient mechanical stretchability without compromising the electrical performances (e.g., electrical conductivity and interfacial resistance) need to be fulfilled. Also, elastomeric electrodes with high-resolution patterns need to be acquired to develop device applications with high integration density and improved performances. In addition to the successful demonstration of the gold nanosheets (AuNSs) based elastomeric electrodes with high mechanical durability and reliability, the development of high-resolution and elastomeric electrodes has been a big challenge due to lack of understandings in the fabrication parameters. In this work, the correlation between the AuNS structure and the patterning resolution were explored to carry out the elastomeric electrodes with a high-resolution pattern with several tens of micrometers. The optimized manufacturing process enabled the development of the AuNSs elastomeric electrodes with high-resolution, mechanical stretchability up to 100% and mechanical durability simultaneously. The developed AuNSs elastomeric electrodes showed the sheet resistance less than 10 Ω /sq under the 100% mechanical strain. In addition, the mechanical integrity of the AuNSs based elastomeric electrodes could be confirmed by examining the electrical performances even after 30% reciprocating 100,000 stretch-release cycles, which showed a marginal conductivity degradation after the tests. Based on the successful implementation of the elastomeric electrodes, elastomeric transistors were fabricated by using poly(3-hexylthiophene-2,5-diyl) (P3HT), poly(styrene-block-butadiene styrene) (SBS) nanocomposite semiconductors and 1-Ethyl-3-methylimidazolium bis(trifluoromethyl-sulfonyl)imide (EMIM-TFSI) based ion-gel dielectric. It is noted that the elastomeric transistor almost maintained their initial performances under 100% mechanical strain. Furthermore, the elastomeric inverter and logic circuits developed by connecting the number transistors with a proper design showed outstanding performances regardless of various mechanical strain. The overall experimental results are expected to contribute to the fast advancement of related industries such as wearable smart health monitoring devices, displays with different form-factors, and sensors by developing high-resolution elastomeric electrodes high mechanical durability.

Acknowledgement

We would like to acknowledge the financial support from the National Research Foundation of Korea (NRF) grant funded by the Korean government (NRF-2022R1C1C1011130).

SB12.08.03

Ion-Dipole-Mediated, Mechanosensitive Iontronic Skin with Ultrafast Self-Healing Both in Air and Underwater [Zhengyang Kong](#)¹, Joo S. Kim¹, Hanbin Choi¹, Elvis K. Boahen¹, Dong J. Kim¹, Wu B. Ying² and Do Hwan Kim¹; ¹Hanyang University, Korea (the Republic of); ²Ningbo Institute of Materials Technology and Engineering, Chinese Academy of Sciences, China

The properties of the human skin such as self-healing and mechano-sensation even in aquatic environments has inspired the design of various underwater self-healing based iontronic sensors that respond to strain, stress, and pressure. Stretchable iontronic sensors that emulate these functionalities as well as high sensitivity can be utilized in wide range of applications including water-resistant human-machine interface, and wearable sensors in high humidity environment (water, sweat, etc.). However, it is usually challenging to design iontronic sensors with stretchability, high sensitivity, and self-healable ability both in-air and underwater simultaneously. Conventionally, normal self-healing is attained via dynamic bonds, but these bonds will be saturated or coordinated with water molecules in high humidity conditions causing breakdown of the reversible process and subsequent loss of self-healing properties. Moreover, the sensitivity to water molecules can defunctionalize the electrical properties and mechanical property of the sensor limiting its sensing ability in aquatic environment. Hence, it is necessary to design and develop materials with underwater self-healing ability and outstanding waterproof properties for highly sensitive iontronic to ensure stability in humid conditions as well as prolong the lifespan of the device. Here, we describe a highly deformable iontronic sensor from a novel designed polymer matrix with excellent waterproof property, high sensitivity and can autonomously self-heal in both dry and humid conditions. Our design strategy is the combination of fluorinated groups, glyceryl benzenediborate (GB) and hydroxyl-terminated polybutadiene (HTPB) in the design of a novel polyurethane (PU) structure together with compatible ionic species to create an iontronic sensor. First, the self-healing ability of the sensor originates from the dynamically reversible boronate bonds in the GB, which can undergo both bond exchange reaction in air and reversible hydrolysis underwater. The superb waterproof property was obtained due to the fluorinated groups within the hydrophobic soft segment of the PU that have stronger hydrophobic properties, which can ensure the stability of all performance in water. We also can maximize the underwater self-healing ability by adjusting the hydrophobicity to control the water intake. Moreover, the highly electronegative fluorine atoms interact with the cation of the ionic liquid via ion-dipole interaction establishing ion confinement effect. The ions are therefore trapped by the carbon-fluorine bonds generating ultra-low initial capacitance value. Under external stimuli such as stress or strain, the ion-dipole interactions are broken creating a high increase in capacitance change generating high sensitivity. As a result, the novel iontronic sensor can achieve excellent sensing performance and self-healing properties both in dry and wet conditions for the development of next-generation wearable sensors.

SB12.08.04

Development of High-Resolution Stretchable Electrodes and Its Applications Using Gold Nanosheets (AuNSs) [Hyeseon Jo](#), Seongsik Jeong, Jiyun Lee, Seojun Heo and Haejin Kim; Gyeongsang National University, Korea (the Republic of)

With an increase of the interest in wearable devices and healthcare monitoring systems, research on the development of stretchable electrodes has been conducted to develop wearable applications with sufficient reliability and lifetime. To develop the stretchable devices with superior reliability, it is essential to acquire highly durable and high-performance stretchable electrodes that can sustain the mechanical strain without any electrical performance degradation. Furthermore, the stretchable electrodes necessitate high-resolution patterning capability to achieve a high degree of integration when designing the stretchable circuits or sensors. In this work, gold nanosheets (AuNSs) stretchable electrodes with high-resolution patterns were carried out by adjusting the structure of the AuNSs through the parameter analysis during the synthesizing process. Specifically, a polydimethylsiloxane (PDMS) elastomer was used as a matrix to embed the AuNSs and develop the stretchable electrodes in a nanocomposite format that can exhibit a high mechanical

durability and excellent electrical performances. Application of hot-pressing to the AuNSs facilitated a firm contact between the AuNSs and hence they remained intact when stretched. With optimized hot-pressing conditions, superior properties of the AuNSs stretchable electrodes, including lower surface roughness, high mechanical durability, excellent electrical conductivity, and high stretchability, can be achieved. Based on the manufactured stretchable electrodes, the electrical performances with respect to the mechanical strain of a high-resolution stretchable electrodes were examined by measuring the electrical conductivity of the electrodes under different levels of the mechanical strain up to 100%. The resulted AuNSs stretchable electrodes showed the sheet resistance lower than 10 Ω /sq. Regardless of the mechanical strain. Also, the stretchable electrodes maintained their electrical performances without any further degradation even after 100,000 of stretch-release cycles. In addition, the dynamic electrical performance of the elastomeric transistor was investigated by determining the drain current ($-I_D$) in real-time corresponding to various types of mechanical stimuli, such as stretching, twisting, and poking. When continuous and sequential mechanical stimulation was received, the ON and OFF currents of the transistor measured for 60 seconds were confirmed. The overall experimental results is expected to contribute to accelerating the growth of wearable applications including displays with various form-factors, healthcare monitoring sensors, and soft robots.

Acknowledgements

We would like to acknowledge the financial support from the National Research Foundation of Korea (NRF) grant funded by the Korean government (NRF-2022R1C1C1011130).

SB12.08.05

High-Resolution Au Stretchable Electrodes toward Soft Integrated Circuits and Sensors Seojun Heo, Jiyun Lee, Seongsik Jeong, Hyeseon Jo and Haejin Kim; GyeongSang National University, Korea (the Republic of)

As interest in wearable devices has increased in recent decades, a considerable effort has been devoted to develop mechanically elastomeric devices including sensors, transistors, logic circuits, and integrated circuits. For an accomplishment of the true realization and commercialization of the wearable device applications necessitate the development of the elastomeric electrodes with high conductivity, environmental stability, low contact resistance, stable performance against various mechanical stimuli, and high integration, it is still difficult to achieve simultaneously. Development of gold based elastomeric electrodes by using 1D/2D gold particles have been proposed to meet the requirements as addressed above. As such, 2D gold nanosheets (AuNSs) were considered to be one of the great candidates in developing the elastomeric electrodes with high mechanical integrity, high electrical conductivity, low contact resistance. Nevertheless conventional AuNSs based elastomeric electrodes which were fabricated by using mechanical stamping or lift-off processes, limited in providing the high-resolution patterns.

In this work, we developed a stretchable device that meets all the aforementioned requirements using AuNSs on which a 2-D percolation network is formed. Specifically we investigated the effect of the AuNS structure on the resolution of the electrode pattern during the wet etching process. Through the wet etching process, the integration of AuNSs electrode patterns could be enhanced to achieve the resolution in tens of micrometers. Also, the ligand on the surface of the gold nanosheets was effectively removed by using the hot-pressing process with aim to lower the contact resistance between the AuNSs and to improve the electrode conductivity. Furthermore low resistance changes under 30% 1-million stretch-release cycle tests were conducted to ensure the durability of the elastomeric electrodes. The elastomeric transistors maintaining their performances regardless of the mechanical strain was manufactured by using an organic semiconductor nanocomposites and ion-gel. Finally, stretchable devices including inverters, logic gates and oscillators were developed to broaden the application scope in the soft electronics. Development of high-resolution AuNS stretchable electrodes is expected to aid in the rapid advancements the application scope in soft electronics.

ACKNOWLEDGEMENT

We would like to acknowledge the financial support from the National Research Foundation of Korea (NRF) grant funded by the Korean government (NRF-2022R1C1C1011130).

SB12.08.06

Bio-Inspired Electronic Eyes for Artificial Vision System Min Su Kim and Dae-Hyeong Kim; Seoul National University, Korea (the Republic of)

Recent technological developments in mobile electronics and machine vision have required advanced imaging recognition systems. However, conventional imaging devices using a flat sensor array have several limitations such as complex lens optics, optical aberration and large module size. To solve this problem, bio-inspired image sensors mimicking the structural and functional advantages of the of nature eye have been extensively studied. A curved image sensor that mimics hemispherical structure of the animal retina can effectively overcome the limitations of conventional imaging systems. It has a simple configuration and miniaturized module size while maintaining high optical performance such as wide field of view (FoV) and low optical aberration.

In addition, curved image sensors applying unique properties of organisms that evolved to survive in specific environments have also been reported. For example, artificial imaging systems that mimic the compound eyes found in insects have infinite depth of field (DoF) and a wide FoV. Imaging systems that mimic telescopic vision of avian eye and the visual system of xenops peckii for recognizing image depth have been demonstrated. By using various optical filters, artificial vision inspired by mantis shrimp can enhance the color sensitivity.

Recently, our group mimics the unique vision of feline eye. Feline-eye-inspired vision system mimics the variable pupil and biological reflector. Blurring the background to distinguish the prey from the complex environment is essential for targeting the prey. In the dim environment, the feline pupil fully dilates to make narrow DoFs in the both vertical and horizontal direction. In the bright environment, the feline pupil contracts to become a vertically elongated shape, resulting in a narrow vertical DoF and a deep horizontal DoF. In both cases, the focus is made on the overlapped region of the DoFs, and the background environment is blurred. Therefore, felines can target the prey at both night and day. Tapetum lucidum is a multi-layered tissue located between the retina and choroid. It consists of periodically repetitive cells including arrays of parallel crystal rods. Each array of rods ($n = 1.83$) and each intervening layer ($n = 1.33$) are approximated as alternating layers with a high and low refractive index. The transmitted light is reflected back to the photoreceptor via tapetum lucidum, which enhances the sensitive scotopic vision.

The device, inspired by the unique vision of the feline, consists of a hemispherical silicon photodiode array integrated with an artificial tapetum lucidum and a variable aperture. The artificial tapetum lucidum made of a patterned inverse opal structure is located behind the ultrathin silicon photodiode. It enhances the photo-absorption by reflecting the light back to the photodiode, which increases the sensitivity under a low light condition. The variable aperture mimics the feline's pupillary movement, whose shape changes between the vertically-elongated slit-like shape and the fully-dilated circular shape. This variable aperture enables the targeted imaging with asymmetric depth-of-fields as well as the facile control of the incident light amount.

SB12.08.09

Reconfigurable and Reusable Soft Modular Blocks Assembly for Soft Robotic Skin Yoon Jaeyoung, Hayun Kim and Yongtaek Hong; Seoul National

University, Korea (the Republic of)

Soft electronics have been widely researched due to their applicability to arbitrarily curved surfaces where conventional electronic devices cannot be applied. Furthermore, the mechanical mismatch at the devices-soft body interfaces can be minimized due to their softness. Among the methods for imparting softness to electronics and devices, the most adopted technology is stretchable hybrid electronics (SHE); SHE is a methodology of manufacturing soft electronics or devices by electrically connecting rigid or soft circuits or sensors (islands) via stretchable interconnects (bridges). The soft devices based on this island-bridge structure can be attached to curvilinear surfaces. It is also applied to human skins or soft robotics and can perform its original function without significant degradation, even under deformations. Recently, body attachable soft devices attached to human skin to collect and transmit data such as vital signals and body movements have been manufactured. In addition, research to apply soft electronics to soft robotics is increasingly being studied. For soft robotics applications, soft circuits or electronics are required to retain their functionality even under dynamic deformation (e.g., bending, twisting, or inflating) of soft robotics. Furthermore, because soft robotics can be used in various environments, their body size and actuation motion can be programmed in multiple ways. Accordingly, a new manufacturing method is required to complete soft circuits for the robotic skin.

In this work, we demonstrate reconfigurable and reusable soft modular blocks assembly based on SHE for soft robotic skin. Our soft modular block assembly technology enables immediate electrical circuit creation when soft modular blocks are assembled; This can be achieved by a sticky and highly conductive contact pad. These contact pads are fabricated on the electrodes of the FPCB, and soft modular blocks with these contact pads are assembled onto curvilinear and deformable soft bodies. Finally, the assembled blocks are physically and electrically connected through stretchable interconnect blocks. Silver nanowires (AgNWs)-embedded PDMS are chosen for the interconnect block because AgNWs network has the advantage that conduction path is maintained even under stretching deformation of PDMS. The vertically-aligned Ni particles are introduced into the PEIE (Polyethylenimine ethoxylate) and PDMS (polydimethylsiloxane) matrix for the high conductivity of the pad. An electrical conduction path is formed between Ni particles exposed on the surface of the contact pad and the AgNWs on the surface of the interconnect blocks. Furthermore, we demonstrated the assembly of soft modular LED blocks on a soft body. The LEDs on the blocks are immediately turned on when the LED blocks and interconnect blocks are assembled. In addition, the soft modular LED blocks can be disassembled to complete the other device with a new configuration. This immediate soft device creation and soft blocks reconfiguration of our technology can be utilized as soft robotic skin. We demonstrated the applicability of our technology as soft robotic skins through integration with soft modular blocks assembly and soft robots.

This research was supported by the Display Center of Samsung Display and Seoul National University.

SB12.08.10

Development of Elastic Synaptic Devices based on Mechanically Durable and Stretchable Electrodes Jiyun Lee, Seojun Heo, Seongsik Jeong, Hyesoon Jo and Haejin Kim; Gyeongsang National University, Korea (the Republic of)

The human brain is a complex neural network with more than 100 billion neurons and 100 trillion synapses, which act as bridges to connect the neurons for signal communications. Moreover, it is a biocomputing system that covers advanced computation and cognitive processes while using only 20W of power. The development of neuromorphic devices to mimic the functions of such an efficient information processing and storage capability is emerging as a key technology in digital environments, which necessitate complicated information processing and high-density information storage functions. In particular, there has been a surge in related research on neuromorphic systems that mimic the electronic synapses with the operation of transmitting and computing the information signals. The electrical properties (e.g., electrical post-synaptic current (EPSC), paired-pulse facilitation (PPF)) of the developed synapse are characterized when the synapses connecting neurons exchange spike signals to process the information. The early stage of the research on developing synaptic devices was mainly based on a CMOS-based integrated circuit that requires numerous transistors to realize synapse characteristics, resulting in a limitation in the system complexity and reduced integration. Memristors were first proposed to overcome the limits however, high-power consumption per unit device was considered to be one of the disadvantages compared to the bio-synapse. Recently, the three-terminal synaptic transistors mimicking the human brain function were considered to be one of the outstanding candidates that fulfill various requirements to mimic the bio-synaptic systems. Also, synaptic devices with mechanical stretchability were developed to meet the increasing demand and interest in wearable device applications. In this work, elastomeric synaptic transistors were developed to perform various synaptic behaviors, including EPSC, PPF, long-term memory (LTM), and STM under various mechanical stimuli. Specifically, the elastomeric electrodes were manufactured by using the gold nanosheets (AuNSs) embedded within the elastomer polydimethylsiloxane (PDMS). Also, an organic semiconductor Poly(3-hexylthiophene-2,5-diyl) (P3HT) nanocomposites and ion-gel were utilized as elastomeric semiconductor and dielectric, respectively. Transfer characteristics of the devices were derived by applying a pulse-type voltage to the gate electrodes. Other synaptic characteristics, including EPSC, and PPF values were carried out under various levels of the mechanical strain, which resulted in stable performances regardless of the various level of the mechanical strain. Also, LTM was achieved by repeatedly learning for a short time while continually administering a pulse-type spike at 0.15s intervals. In addition, it was confirmed that the synapse characteristics were well maintained under the mechanical stimuli up to 100%. Overall, the developed elastomeric synaptic devices with advanced signal transmission and cognition functions while consuming less energy are expected to contribute to the advancement of soft robot engineering and the development of next-generation intelligent wearable devices.

SB12.08.12

3D Printing of Liquid Metal Embedded Elastomers for Soft Thermal and Electrical Materials Phillip Won¹, Conor S. Valentine¹, Mason Zadan¹, Chengfeng Pan², Michael Vinciguerra¹, Dinesh K. Patel¹, Seung Hwan Ko³, Lynn S. Walker¹ and Carmel Majidi¹; ¹Carnegie Mellon University, United States; ²The Hong Kong University of Science and Technology, Hong Kong; ³Seoul National University, Korea (the Republic of)

Liquid metal embedded elastomers (LMEEs) are composed of a soft polymer matrix embedded with droplets of metal alloys that are liquid at room temperature. These soft matter composites exhibit exceptional combinations of elastic, electrical, and thermal properties that make them uniquely suited for applications in flexible electronics, soft robotics, and thermal management. However, the fabrication of LMEE structures have primarily relied on rudimentary techniques that limit patterning to simple planar geometries. Here, we introduce an approach for direct ink write (DIW) printing of a printable LMEE ink to create three-dimensional shapes with various designs. We use eutectic gallium-indium (EGaIn) as the liquid metal, which reacts with oxygen to form an electrically insulating oxide skin that acts as a surfactant and stabilizes the droplets for 3D printing. To rupture the oxide skin and achieve electrical conductivity, we encase the LMEE in a viscoelastic polymer and apply acoustic shock. For printed composites with a 80% LM vol. fraction, this activation method allows for a volumetric electrical conductivity of $5 \times 10^4 \text{ S cm}^{-1}$ (80 % LM vol.) – significantly higher than what had been previously reported with mechanically sintered EGaIn-silicone composites. Moreover, we demonstrate the ability to print 3D LMEE interfaces that provide enhanced charge transfer for a triboelectric nanogenerator (TENG) and improved thermal conductivity within a thermoelectric device (TED). The 3D printed LMEE can be integrated with a highly soft TED that is wearable and capable of providing cooling/heating to the skin through electrical stimulation.

SB12.08.13

A Generalizable, Multimodal Wireless Chemical Sensing Scheme for Bio-Integrated Electronics Tzu-Li Liu and Jinghua Li; Ohio State University, United States

Monitor biomolecule in bodily fluid plays an important role of reflecting health status and medical treatment. However conventional approaches rely on in-lab equipment or complex wireless electronics, which typically need battery source or complex circuits, and limit the use of real-time monitoring and bio-integrated applications. We aimed to bridge the gap between biochemical sensing and wireless electronics.

We have developed a class of inductor-capacitor (LC) chemical sensors inspired by radio frequency (RF) tuning circuits. The wireless flexible circuit can seamlessly integrate with bio tissue/ personal accessories due to its flexible, concise, and battery-free circuit. Compared to the conventional LC circuit, in which the biochemical sensing interface needs to be within the transmitter, our design can modulate into two function parts: an antenna coupler, that separately encapsulates, and an extended biochemical sensing interface, that can be direct contact with the targeted region.

We have demonstrated its universal sensing capability by using common bio-sensitive elements (e.g., ion-selective membranes, aptamers, and enzymes) on the sensing interface. We also demonstrate its multifunctionality as a sensor metric, which allows the detection of multiple biomarkers simultaneously. The demonstration as “smart accessories” and “miniaturized probe” based on this methodology suggests its broad capability in advanced wireless scenarios.

SB12.08.14

Wearable Soft Robotics Gripper for Increased Access to Soft Robotics Education [Abigail R. Lockhart-Calpito](#)¹, Jonathan Chinana^{2,1}, Harrison Young¹, Lucas Gerez¹, Holly M. Golecki^{3,1} and Conor J. Walsh¹; ¹Harvard University, United States; ²Navajo Technical University, United States; ³University of Illinois at Urbana-Champaign, United States

In recent years, the field of soft robotics has gained a significant amount of attention due to its various applications and increase in research, such as wearable robots, assembly line machines, surgical robots and search and rescue devices. A Soft Robotics Toolkit (SRT) project was developed as an open access resource to support the effort to educate and expose users from K-12 to the field of soft robotics. The SRT aims to overcome the challenge of disseminating robotic-hardware resources and to spread soft robotics educational content, which is less prevalent than that of traditional robotics. The Soft Robotic Gripper (SRG) kit was developed to encourage users to explore design, fabrication, and application of soft robotic technologies. Our motivation is to develop a soft robotics kit which can help fill this gap in academics. The initial SRG kit allowed users to assemble a hand held gripper with two silicone fingers, controlled by a center hub of electronics to grip and release objects. The silicone fingers are cast with a user-assembled mold constructed from cardboard and glue provided in the kit. Channels through the mold are made with toothpicks in order to provide clearance for the tendon actuator. The gripper could be configured to be operated manually and automatically, with an ultrasonic sensor and motor. The previous SRG was evaluated and well received by K-12 students in the USA and India.

We converted the previous kit into a wearable device which could be attached to the user's forearm and hand to better highlight the potential applications of soft robotics in assistive wearable devices. The electronics and hardware are fixed to a size-customizable sleeve which is attached to the user's forearm. The SRG extends from the wrist and is tendon driven. These modifications bolster the educational potential of the device by creating more avenues for exploration and encouragement in creative thinking in the field of assistive devices. We simplified the previous electronic design, allowing all electronics to be added to a breadboard. This will allow user interaction and engage with assembling a circuit.

Our secondary goal was to reduce the production cost of the device, increasing the accessibility of the kit. Manufacturing advantages include a reduced reliance on custom injection molded components and PCBs, which both increased production cost and limited creative freedom of users. A control has also been implemented in the wearable SRG in which the plantar flexion of one of the users fingers can be used to open and close the fingers. We replaced the custom electronics and hardware components with simpler, off the shelf alternatives. This allows users to gain an understanding of common electronics, allowing for translation of their learned skills to other future projects and existing K-12 curricula. These changes allowed for the only custom piece in the kit to be a wearable garment.

The effectiveness of the kit was decided by user testing and cost analysis. The revised SRG toolkit contains soft robotic components that are simple to assemble into the wearable SRG, in addition to a straightforward and educational guide on how to build your own wearable robot. The contents of the kit is sufficient for the baseline robot, but alterations can be made depending on the user's desires. The previous electronics were successfully simplified on the current design of the wearable, tendon-actuated SRG. The improved SRG kits were beta tested with middle and high school students at an outreach event hosted by researchers. With this data, the researchers uncovered the successes and challenges resulting from the building process in order to inform design iterations. This project has increased access to soft robotics education. Furthermore, the transition from a hand held device to a wearable device will motivate students to learn about prosthetic and assistive devices inspiring future innovators in soft wearable robotics.

SB12.08.15

Development and Evaluation of an Accessible Soft Aquatic Robot [Jaylynn Kim](#)^{1,2}, Baran Mensah^{3,2}, Harrison Young², Lucas Gerez², Holly M. Golecki^{1,2} and Conor J. Walsh²; ¹University of Illinois at Urbana-Champaign, United States; ²Harvard University, United States; ³Massachusetts Institute of Technology, United States

The field of soft robotics has garnered attention as a medium for education due to its hands-on fabrication methods, accessible materials, and applications in a wide range of STEM fields. With the potential for a more diverse set of disciplines and applications, a soft aquatic robot was developed for educational purposes as a project inspired by marine biologists' use of underwater robots that mimic fish to explore underwater habitats. The soft aquatic robot is simple, easy to build, and functional, making it an ideal candidate for use as a manufacturable educational tool for K-12 students. The aquatic robot is composed of a hybrid rigid body and a soft tail that uses the Fin Ray® Effect, a model of fish fin deformation during swimming, and is oscillated by two electromagnets located in the watertight body. The robot uses an open-loop control system to simplify the system's electronics. The use of an off the shelf microcontroller and motor driver to alternate the polarity of the electromagnets allows students to learn widely used tools to control robotic platforms, including Arduino microcontrollers. The electronics are also designed to be simplistic and compact, allowing ease of setup and minimization of the robot's size. The soft tail was designed to be compatible with a single open-faced mold, facilitating the replication and manufacturing of the soft structure. The ease of replication allows for students to gain hands-on experience with the fabrication of soft robotics materials in a classroom setting. Functionality of the soft robotic swimmer was measured by measuring the thrust generated by the tail and the robot's top speed in body lengths per second. The replicability was measured as a percentage of successful replications of the tail through user testing from the targeted demographic, K-12 school students, in an outreach program. The soft aquatic robot was tested with a group of students to validate an increase in familiarity and interest in engineering fields. The development of this low cost and accessible kit will allow young students to be exposed to new materials, robotics, and the field of engineering, which are less accessible due to high cost and equipment.

SB12.08.17

3D-Printed Triboelectric Nanogenerator Sensors for Soft Haptic Interfaces [Hyeonseo Song](#), Jin Pyo Lee, Yeonwoo Jang and Jiyun Kim; UNIST, Korea (the Republic of)

Haptic interfaces allow us to interact with the virtual environment by sensing our realistic tactile information and delivering them to the computer system. However, rigid and cumbersome form factors of haptic interfaces limit the comfortable interfaces and various applications. Here we report triboelectric-based 3D-printed soft haptic interfaces with free-form factor. An elastic material 3D printing enables us to fabricate soft haptic interfaces with 3D sensors

as we desire. After printing some components of the 3D flexible sensors, we use the active materials to achieve surface modification of printed components and assemble those functionalized components into a single structure. When we apply the external force to the sensor structure with multiple components, those components are contacted or separated from each other. Due to their different surface electron affinities the triboelectric effect occurs, which derives the electron transfer and generates the electrical signal. This electrical signal is transmitted as realistic tactile information to the computer system for interacting with the virtual environmental system. We expect these soft haptic interfaces will contribute to expand the haptic technologies for various applications.

SB12.08.18

Biostable Neuromorphic Devices Enabled by Plasma Polymerized PTFE for Long-term Wearable Bioelectronics [Dong Hyun Choi](#), Kyungho Park, Kyungmoon Kwak, Hyung Tae Kim, Jusung Chung and Hyun Jae Kim; Yonsei University, Korea (the Republic of)

As the coronavirus disease 2019 pandemic has been prolonged, the limitation of the face-to-face medical system that mankind has built previously have been highlighted. This is because the bed occupancy rate increases as the number of newly confirmed cases and severe cases occurring around the elderly increases, which causes a shortage of beds and medical personnel. Accordingly, telehealth medical systems such as home treatment and telemedicine have attracted attention. Therefore, a new paradigm that can stably respond to changes in living biosignals anytime and anywhere is required to realize a telehealth medical system.

Long-term wearable bioelectronics has the potential to break the existing face-to-face medical system. By attaching a medical device onto the body, living biosignals can be continuously collected and processed anytime, anywhere. Furthermore, it can be spontaneously transmitted to the medical staff through medical applications. However, for long-term wearable bioelectronics, conventional electronic materials could not be applied due to their brittle nature and poor biostability. In addition, long-term wearable bioelectronics requires superior reliability and uniformity under the device level so that temporal and inter-device electrical characteristics are consistent.

In this research, we propose a plasma polymerized polytetrafluoroethylene (PTFE) as the active layer for flexible and biostable neuromorphic devices satisfying the strict requirements of long-term wearable bioelectronics. The neuromorphic computing system is inspired by the human brain, such that it can emulate biological synapses to concurrently perform cognition, learning, and memory. Therefore, it has advantages realizing a telehealth medical system that stably responds to changes in living biosignals anytime and anywhere. Also, PTFE is flexible and biostable material to be mainly used as a non-stick or chemical stable coating for cookware and scientific tools. Since its outstanding thermal stability, it has the advantage that plasma polymerization is enabled through the sputtering process, unlike other polymers or organic materials. With deposition by the sputtering process, PTFE could have superior film quality and large area uniformity than the conventional solution process, and secure superior reliability at the device level and inter-device uniformity.

To emulate this biological synapse, we fabricated an artificial synapse with a metal-insulator-metal structured neuromorphic device. To fabricate the PTFE-based neuromorphic device, the PTFE for the active layer was deposited by radio frequency magnetron sputtering on an indium-tin oxide coated polyethylene terephthalate substrate. After the deposition, the sample was annealed at 100°C for 1 h in ambient air. Then, Al top electrode was deposited by an electron beam evaporator via a shadow mask. To measure the current-voltage characteristics of the PTFE-based neuromorphic device, the positive and negative voltage sweeps applied to the top electrode. The set and reset voltages were 2.7 V and -2.1 V, respectively. And the device showed a stable resistive switching window over 10^3 at a 0.1 V of reading voltage for 100 consecutive cycles. For the excitatory post-synaptic current (EPSC) variation depending on the pulse width, the EPSC increased drastically and immediately returned to its initial value, but it took more time to return to its initial value as the spike pulse width increased. The potentiation-depression characteristics according to 10 repetitions of consecutive 10 positive pulses, followed by 10 negative pulses were measured. The EPSC of the PTFE-based neuromorphic device can be precisely controlled by multiple cyclical positive and negative spike pulses. Based on these results, PTFE-based neuromorphic devices may considerably contribute to the development of neuromorphic computing platforms and long-term wearable bioelectronics.

SB12.08.19

Development of an Accessible and Affordable Rehabilitation Glove David R. Medina^{1,2} and [Ayoub Ellouzi](#)³; ¹University of Illinois Urbana Champaign, United States; ²University of Illinois at Urbana-Champaign, United States; ³Bunker Hill Community College, United States

Each year, approximately 12,500 individuals survive spinal cord injuries (SCI). As of 2016, the population with SCI was estimated to be 276,000. As a result, many are left with a drastic reduction of upper extremity function, specifically in the hands. This can impact the quality of life and independence of a person. While the recovery of the hand is function highly desired, limited treatments are available to aid in recovery, let alone affordable treatments. Along with SCIs, strokes can also lead to a reduction in extremity function. The limb that is most prone to paralysis is the hand, as a stroke causes loss of sensation and inability to move the hand. One of the most effective methods of restoring hand activity is physical therapy (PT). Physical therapists rely on repetitive hand exercises to slowly regain the function of the limbs of the patients. Oftentimes, this process can take years of constant physical therapy with the aid of a therapist. A rehabilitation device that can help the patient perform these exercises from home would help patients to perform regular exercises at home and in some cases save the patient from traveling and also reduce the cost of recovery. Several emerging technologies address hand rehabilitation. A glove termed the Soft Rehabilitation Device is a pneumatic glove that assists patients with grip control and makes grasping motions easier. Attached with a waist pack that controls the pneumatics and can program with exercises the patient can control. The "Music Glove" by Flint Rehab works by motivating users to perform hundreds of therapeutic hand and finger exercises while playing an engaging musical game, NEOFECT's RAPAE Smart Glove is a biofeedback system to help patients with neurological and musculoskeletal injuries regain their hand mobility. Based on this research, all the currently available rehabilitation gloves sit at a price range above the thousands when factoring in the subscription-based training software some brands lude. A more affordable and open-source solution is needed. In this project, we used accessible soft-robotics building techniques available on the Soft Robotics Toolkit and a 3D printer to build the mold or finger shape using silicon material. After determining the shape of the glove and choosing the appropriate type of fabric using design heuristics, the elements of the glove were identified. The final prototype includes flex sensors and accelerometers, off-the-shelf microcontrollers, and a fluidic control board. Using this prototype, two types of movement were successfully achieved which are flexion and extension motions. We aim to provide instructions for an open-source design of a rehabilitation glove to create an affordable and easy-to-implement device on the Soft-Robotics Toolkit. Creating an open-source device will lead to further developments and innovation with patients as end users and designers.

Primary authors: Ayoub Ellouzi, David Medina

Co-authors: Jesse Grupper, Harvard University, MA, Alex Beaudette, Harvard University, MA, Erik Siggelkoe, Bunker Hill Community College, MA, Holly Golecki, University of Illinois at Urbana-Champaign, IL, Conor Walsh, Harvard University, MA.

Funder Acknowledgement(s): NSF EFRI REM (Award #1830896)

Faculty Advisor/Mentor: Prof. Erik Siggelkoe, ersiggel@bhcc.edu, Dr. Holly Golecki, golecki@illinois.edu.

8:00 AM SB12.09.01

A 3D Printed Liquid Metal Emulsion for Low-Stress-Activated Stretchable Electronics [Ramon E. Sanchez](#), Stephanie F. Zopf and John W. Boley; Boston University, United States

Integrating liquid metal (LM) into 3D stretchable devices remains a manufacturing challenge due to its intrinsically low viscosity and high surface tension. Current manufacturing methods require the use of complicated lithography and molding techniques which increase fabrication complexity and limit widespread adoption. Modifying the LM rheology by creating LM emulsions dispersed in a carrier liquid can create a stable 3D printed emulsion, which can be integrated with other printed materials in a single fabrication process, reducing manufacturing complexity. This work presents a 3D printable strain-induced electrically conductive liquid metal emulsion for the programmable assembly of soft conductive composites. This liquid metal emulsion exhibits shear yielding and shear thinning rheology that is compatible with direct ink writing (DIW). Examples of complex self-supported 3D printed structures with spanning features are presented to demonstrate the 3D printability of this emulsion. Stretchable liquid metal composites are fabricated by integrating this emulsion into a multi-material printing process along with a 3D printable elastomer, combined with manual pick and place of off-the-shelf electronics. The as-printed composites exhibit a low electrical conductivity but can be transformed into highly conductive composites by a single axial strain at stresses that are an order of magnitude smaller than previous stress-activated emulsions. The effects of axial strain and cyclic loading on the electrical conductivities and sensitivities of these composites are characterized. The electrical conductivity increases with activation strain, with a maximum observed conductivity of $2.32 \times 10^5 \text{ Sm}^{-1}$ at strains greater than or equal to 200%. The electrical conductivity of these composites reaches a steady state for each strain after one cycle and remains stable with low variation ($< 7\%$) over 1,000 cycles. The strain sensitivities of these composites are constant and significantly lower than that of a bulk conductor, making them suitable as stretchable conductors. The utility of these composites is shown by employing them as wiring into a single fabrication process for a stretchable array of LEDs.

8:15 AM SB12.09.02

Facile Synthesis and 3D Printing of Soft Materials and Their Applications in Sensors [Kumkum Ahmed](#); Shibaura Institute of Technology, Japan

Ion conductive polymers and elastomers have drawn worldwide attention for their multifunctional applicability in batteries, electroactive soft robotics, and sensors. In this work, facile synthesis of network polymers via thiol-ene reaction has been focused on to create 3D printable flexible and soft sensing materials. A variety of materials such as ionic gels, ionic porous polymers, elastomers, and composites have been synthesized and characterized. To develop ionic liquid-based gels and porous polymers, ionic liquid has been incorporated into the thiol-ene network of thiol-based multifunctional monomers and acrylate crosslinkers. By carefully selecting the polymerizing conditions and solvents, developing gel and/or porous polymers are designed. In addition to ionic liquid-based gels and porous polymers, PDMS-based polymers, gels, and elastomers are also synthesized using multi-functional vinyl sulfones and dual functional thiol containing PDMS crosslinkers initiated via thiol-ene reaction mechanism. The developed gels and elastomeric materials showed 3D printability with good resolution with tunable conductivity (ionic gels and porous polymers), mechanical flexibility, and high thermal stability and showed piezo-capacitive sensing characteristics. These 3D-printable, designable materials can find prospective scope in the fields of MEMS, microfluidics, and sensors.

8:30 AM *SB12.09.03

Responsive Soft Polymers Fabricated via Light-Induced 3D Printing [Ignazio Roppolo](#); Politecnico di Torino, Italy

In the last decade light-induced 3D printing experienced an explosion of interest, especially from the materials point of view. In fact, while in the past most of the attention was devoted just to obtain fast and precise printing, in the latest years the focus of academic and industrial research is moving toward the synthesis of materials with improved mechanical properties or with new functionalities.

This 3D printing technology is of particular interest for soft polymers. In fact, those materials have complex tooling and often are fabricated via casting, which requires multiple steps and involves many limitations. On the other hand, light-induced 3D printing can offer the possibility to build object with almost arbitrary shape with also high precision without tooling.

However, be limited to “material properties” + “design of the structure” archetype doesn’t allow to understand the full potentialities of 3D printing. In this talk, it will be showed how responsive soft polymers can be developed by an engineered study of the photocurable formulations, of the local properties of the materials and of the devices’ design.

Increasing step by step the level of complexity, different functional soft polymers will be showed: (i) PDMS-like 3D printable monomers, which can be used to replace standard silicone for complex structures(1); (ii) self-healing 3D printable hydrogels, which can be shaped almost arbitrarily and have the properties of self-recovery from damages(2) and (iii) 4D printable structures with programmed microstructure in which controlled movements or shapeshifting are induced by an external magnetic field(3-5).

[1] G. Gonzalez, A. Chiappone, K. Dietliker, C.F. Pirri, I. Roppolo (2020) *Advanced Materials Technologies*, 5(9), 2000374

[2] M. Caprioli, I. Roppolo, A. Chiappone, L. Larush, C.F. Pirri, S. Magdassi (2021) *Nature Communication*, 12, 2461.

[3] S. Lantean, G. Barrera, C.F. Pirri, P. Tiberto, M. Sangermano, I. Roppolo, G. Rizza (2019) *Advanced Materials Technologies*, 4(11), 1900505

[4] S. Lantean, I. Roppolo, M. Sangermano, M. Hayoun, H. Dammak, G. Rizza (2021) *Additive Manufacturing*, 47, 102343.

[5] S. Lantean, I. Roppolo, M. Sangermano, M. Hayoun, H. Dammak, G. Barrera, P. Tiberto, C. F. Pirri, L. Bodelot, G. Rizza (2022) *Advanced Materials Technologies*, accepted.

9:00 AM SB12.09.04

Stretchable 3D Printed Thermoelectric Generators for Liquid Crystal Elastomer Actuation, Control and Energy Recovery [Mason Zadan](#), Dinesh K. Patel and Carmel Majidi; Carnegie Mellon University, United States

Liquid crystal elastomers (LCE) are a class of shape memory polymers that exhibit muscle like work energy densities and contraction strains. By transitioning between a liquid and crystalline phase the mesogens, induced by thermal stimuli, reorient themselves inducing macroscopic contractions and expansions upwards of 40%. By precisely controlling heating and cooling, LCE responses can be tailored for actuation and locomotion in soft systems. Recently, this material architecture has been explored for soft robotic actuators and systems. The main limitations of LCE actuators are their slow response times, stemming from high transition temperatures and passive convective cooling. LCEs also suffer from poor energy efficiencies with energy partially lost through convective heat transfer. As a potential solution, in this talk, I focus on recent work in bendable and stretchable thermoelectric devices (TED) that convert temperature differentials across oppositely doped semiconductors into a potential difference through the Seebeck effect along with acting as

active heaters and coolers through the Peltier effect. Through the Seebeck effect, TEDs are introduced to address energy efficiency issues by introducing passive environmental energy harvesting along with internal regenerative energy recovery in soft robotic systems. Through the Peltier effect, TEDs are introduced to actively heat and cool LCE layers for actuation. This is enabled by developing 3D printed high density TEDs with semiconductors wired together with Eutectic Gallium Indium (EGaIn) liquid metal (LM) interconnects to actively heat and cool and recover energy from LCEs while staying mechanically compliant. These LCE-TED transducers, allow for single input multidirectional actuation enabling integration into a PI-controller with <0.5 degree error. As energy harvesters these LCE-TEDs are integrated into a robotic walker recycling environmental waste heat along with recovering small amounts of energy through regenerative energy harvesting. Energy harvesting and actuation characterization is given highlighting device power densities, deflection, blocking force, and robust mechanical characterization.

9:15 AM SB12.09.05

All-Printed Stretchable Integrated Electrochemical Sensing System with Digitized Electrochromic Display Lu Yin, Mengzhu Cao, Kyeong Nam Kim, Sheng Xu and Joseph Wang; University of California, San Diego, United States

The rapidly developing flexible wearable sensing systems commonly rely on wireless communication or colorimetric assays for data interfacing, which cannot operate independently and requires external electronics to obtain exact numerical data. In this work, we present a wearable sensing epidermal patch with dedicated batteries as the energy supply and an electrochromic display for data visualization, all integrated into a highly compact, stretchable form factor. The patch can operate with multiple types of sensing mechanisms for electrolyte and metabolite monitoring, rapidly displaying the sensing result within a second. Fabricated via layer-by-layer screen-printing of customized elastomeric composite inks, the device demonstrates high flexibility and stretchability enduring thousands of stretching deformation cycles without affecting its performance. Merging low-power consumption, autonomous operation, and superior mechanical performance, the device is of high practicality and convenience for various applications in professional sports, personalized wellness management, and beyond.

9:30 AM SB12.09.06

Directly-Printed Soft Three-Dimensional Electrodes for High-Density Electromyography Recording for Long Term Monitoring of Ischemia and Volumetric Muscle Loss in Murine Models Moohyun Kim, Sumin Kim and Jang-ung Park; Yonsei University, Korea (the Republic of)

In modern electromyography (EMG) recording, conventional surface electrodes are commonly used. These electrodes tend to be rigid and do not conformally attach with skin surfaces. Modern research focuses developing electrodes on flexible substrate that have good surface adhesion with biological interfaces. These devices are still limited as the sensing electrodes as they do not conformally contact with the body. Also, the flexible substrates tend to be bulky in size which limits seamless in-situ electrode deployment. The recording signal obtained by surface electrodes are weaker than needle-based electrode that penetrates the epidermis layer of the skin, removing signal resistance. That said, these needle-based electrodes are highly intrusive and cause inflammations when used for a prolonged duration. For long-term EMG monitoring of patients with muscular disability, clinical approach favors using surface electrodes which are skin-compatible but lacks signal quality. Herein, we present a substrate-less device that is made of biocompatible soft electrodes for high-density EMG recording. These electrodes are directly printed to form three-dimensional (3D) structure on water-soluble thin film. These electrodes are injected into the skin to remove signal interfaces from epidermis layer, producing high-quality EMG signals that modern surface electrodes fail to capture. Furthermore, the simple and easily manipulatable printing technique allows printing of array of 3D soft electrodes for high-density EMG recording to monitor complex musculoskeletal movement. Furthermore, the soft electrodes have self-repairing property that provides mechanical durability for more advanced and intense movements. Due to its non-invasive property, we are able to detect and monitor the rehabilitative effect of muscle extracellular drugs in murine models of ischemia and volumetric muscle loss. The long-term recording of EMG signal shows the extensiveness of muscle-rehabilitative drugs to treat muscle trauma, providing new possibility for drug screening. The seamless method of device implementation and the significant quality of EMG signals provides interesting prospect for advanced clinical study or human-robot interfaces.

9:45 AM BREAK

10:15 AM SB12.09.07

Multimaterial Printing of Artificial SA-II Mechanoreceptors Using Engineered Composites with Negative Piezoresistance Mina Lee, Michael Sotzing and Alex Chortos; Purdue University, United States

The peripheral nervous system collects and efficiently transmits large amounts of sensory information using parallel signaling. Afferent nerves encode tactile stimuli recognized by cutaneous mechanoreceptors into action potentials and transmit them from the periphery to the central nervous system. Creating an artificial peripheral nervous system could enable important applications in medical devices and robotics. Therefore, interest in neuromorphic systems has been increasing. Recently, there has been a proliferation of research into mimicking slowly adapting type 1 (SA-I) afferent nerve that measures pressure on the skin. Biological skin includes a multitude of receptors for different stimuli. Therefore, to mimic the capabilities of the biological somatosensory system, it is necessary to develop artificial afferent nerves that are sensitive to a range of stimuli such as stretching and vibration. We developed a flexible artificial afferent nerve that emulates a slowly adapting type 2 (SA-II) mechanoreceptor that detects skin stretching. The artificial afferent nerve consists of a piezoresistive composite mimicking Ruffini endings and a ring oscillator that converts the strain information into a frequency-domain signal that mimics action potentials. The coupling between the sensor and oscillator requires two unique sensor properties: (1) the sensor resistance must decrease while being stretched to achieve increasing frequency output, and (2) the resistance must change by several orders of magnitude to match bio-inspired frequency ranges. To meet these requirements, we implemented a composite material exhibiting negative piezoresistance over several orders of magnitude. The piezoresistor consists of nickel particles as the conductor and a continuous phase consisting of elastomers and oil. Varying the ratios of these components allows for tuning the material's properties, including the elastic modulus, dynamic range, and range of resistance change. As the oil content increased, the range and rate of resistance variation increased. This wide range of tunability suggests that our artificial neurons could potentially be adapted to different applications. Our artificial SA2 receptors are fabricated using a single multi-material print that includes pick-and-placing of an integrated circuit chip, printing a stretchable conductor as interconnects, and printing the negative piezoresistive material as a sensing component. Our printed artificial afferent nerves will aid in advances in neural prosthetics, soft robotics, and wearable electronics.

10:30 AM *SB12.09.08

Printed Electronic Skin allowing Robots to Feel, Learn and Mimick the Mechanical and Thermal Pain Reflexes Joao Neto, Radu Chirila, Abhishek Singh Dahiya, Fengyuan Liu and Ravinder Dahiya; University of Glasgow, United Kingdom

Biological skin comprises thousands of distributed receptors (mechanoreceptors, nociceptors etc.) which allow us to detect a wide range of mechanical and thermal stimuli and react accordingly. This work presents a printed electronic-skin (e-Skin) with pressure and temperature sensors connected with a peripheral nervous system-like localised learning scheme, allowing robots to mimick the mechanical and thermal pain related reflexes. The "bio-like" learning with pressure sensors is achieved using printed array (12x14) of synaptic transistor-based neural system on flexible substrate. Likewise, the thermal pain reflexes were obtained with a nanowire based soft thermoreceptive e-Skin having miniaturized (~700µm²) artificial thermoreceptors. Both

mechanical and thermal e-Skin prototypes were integrated on the fingertip of a robotic hand and biological system like reflexes are demonstrated in response to pernicious mechanical and temperature stimuli via localized learning at the hardware level. The localised learning could substantially reduce the data latency and decrease the cognitive load on the robotic platform.

11:00 AM SB12.09.09

Crawl, Climb, Perch and Fly—Origami, Kirigami and 3D Printing of Soft Robots for Versatile Locomotions Terry T. Ching^{1,2}, Joseph Zhi Wei Lee¹, Shane Kyi Hla Win¹, Luke Soe Thura Win¹, Danial Sufiyan¹, Charlotte Pei Xuan Lim¹, Nidhi Nagaraju¹, Yi-Chin Toh³, Shaohui Foong¹ and Michinao Hashimoto¹; ¹Singapore University of Technology and Design, Singapore; ²National University of Singapore, Singapore; ³Queensland University of Technology, Australia

Background. Untethering soft robotics from electrical or pneumatic power is one of the major challenges facing the field. Maintaining a sufficiently high power-to-weight ratio is the key problem of untethered operations. Untethered operations necessitate that the robot has sufficient mechanical power to carry its structural weight as well as additional payloads such as power sources (i.e. batteries), actuators (i.e. pneumatic pumps, valves), and microcontrollers. Existing demonstrations of untethered soft robots typically involve weighty slabs of pneumatic network actuators (PneuNets) made from silicone rubber, which further decreases the power-to-weight ratio. In addition, the fabrication of these PneuNets actuators heavily relies on replica molding, which renders them unsuitable for rapid prototyping.

Contribution. Combining 3D printing and kirigami-based thin-film polymers allowed the development of a novel method for the fabrication of pneumatically-driven actuators. Our technique effectively decreased the overall weight of the actuating units (20 g), which can be combined with lightweight pneumatic pumps and a control board. The developed actuating units are modular, allowing for rapid prototyping of soft actuators that are customizable and capable of complex locomotions (i.e., crawl, climb, perch and fly).

Technical achievement. To realize the lightweight soft robots, the weight of the structure was reduced using PVC sheets (0.18-mm thick) with predesigned incisions by a cutting plotter. A single sheet of material is prone to twisting and bending. However, a rolled sheet with a curved surface gains anisotropic structural rigidity without adding extra weight. Selectively rolling sections of the PVC sheet aided in the reinforcement of the overall rigidity of the structure. The reduction of the overall weight of the actuators was further achieved by making lightweight pneumatic balloons. Direct ink writing (DIW) of silicone adhesive on silicone sheets (0.8-mm thick) allowed fabricating silicone balloons that served as standardized actuation modules for all the demonstrated locomotions. Next, to convert the expansion of the silicone balloons to bending motion, we took advantage of the mechanical properties of the curved surfaces; analogous to the cross-sectional curvature found in the blade of a tape measure (i.e., spring return pocket tape measures). The slight cross-sectional curvature keeps the blade rigid when extended. Crucially, the cross-sectional curvature permitted anisotropic motions of the film actuator. By sandwiching a silicone balloon between two sheets of PVC in this curved configuration, we reproducibly demonstrated bending motion when the balloon was pneumatically expanded. Harnessing the bending motion and using the kirigami-patterned structural frame, we prototyped soft robots mimicking the locomotion of (1) crawling turtle, (2) climbing inchworm, (3) perching bat, and (4) flying and foldable wing of a ladybug. Importantly, the overall weight of the structure (kirigami of PVC sheets using a cutting plotter) and silicone balloons in both instances weighed < 20 g but could carry a payload of > 100 g, which is a substantial weight reduction compared to the existing soft robots system. As such, the soft robot was capable of carrying additional payloads (e.g., pneumatic pump (8 g), valves (5 g each), battery (~15 g), and microcontroller (~7 g)) to achieve untethered operation.

Significance. Overall, we designed a method of fabricating lightweight, untethered soft robots capable of mimicking locomotion such as crawling, climbing, perching and flying. Advantageously, our approach allows designing locomotions and prototyping new structures only using the PVC sheets and repositioning the modular actuators. Ultimately, we envisage potential applications of the developed actuators in rehabilitation, disaster relief, and space exploration.

11:15 AM SB12.09.10

High Precision Embedded 3D Printing of Soft Materials via the Solvent Exchange Method Wonsik Eom, Tanver Hossain, Vidush Parasramka, Randy H. Ewoldt and Sameh Tawfik; University of Illinois at Urbana-Champaign, United States

Embedded 3D printing enables the direct ink writing of ultrasoft materials which, due to gravity, cannot support their own weight in the air such as large aspect ratio 3D objects, thin closed shells, and hierarchically branched vessel networks. The support gel surrounding the extruded filaments prevents their sag or collapse. Gel-embedded printing resolution is currently on the order of 50 micrometers, limited by the interfacial tension ratios of the printing materials and support gel, the viscosity and the yield stress of the two materials, and the time required to post-cure by heat or UV light. Herein, we have significantly extended the library of printable materials and the achievable resolution and feature size by developing an embedded ink write exploiting the solvent exchange method. The printed material is initially dissolved in a solvent, which as soon as the filament is extruded from the nozzle solidifies due to the miscibility of the solvent in the gel. Hence, no post-curing is required, and the resolution is only limited by the nozzle size down to 3.2 micrometers. We applied this method to print intricate thread spools mimicking the skeins found in the hagfish slime, hair arrays, and complex fiber architecture similar to those found in biological tissue.

11:30 AM SB12.09.11

Ultrasensitive 3D Printed Self-Healing Ionic Hydrogels for Wearable Multifunctional Sensing Giorgio Mogli¹, Annalisa Chiappone², Ignazio Roppolo¹ and Stefano Stassi¹; ¹Politecnico di Torino, Italy; ²Università di Cagliari, Italy

The demand to connect the human and technology worlds has increased dramatically in recent years. Softness, multi-sensing capability, self-healing ability, and adaptability are all characteristics of living tissues. Robots and machines, on the other hand, are generally stiff and unable to self-repair. As a result, devices with intermediate qualities are required to connect the two worlds. Tactile or smart sensors, which are devices that can feel external stimuli such as deformations, temperature, wetness, and light, and are inspired by the human skin, which is the greatest sensor tissue of living humans, could be an ideal option. The key difference between standard sensors and these ones is that they are made of flexible materials to be more adaptable to the uneven surfaces of soft tissues and robots. Tactile sensors can be used in a variety of disciplines, including wearables [1], e-skin [2], prosthetics [3], and soft robotics [4], because to this capability. As a result of these advancements, the global market for soft tactile sensors has seen incredible growth in recent years. In particular, despite its relevance in biomedicine, reproducing haptic sensation remains a task that has yet to deliver consolidated results: flexible strain sensors are great candidates to overcome this difficulty.

Because of their softness and water-rich environment, hydrogels are attractive options for the production of sensing-active materials, as they may be able to overcome mechanical incompatibilities between humans and electronics. Hydrogels are water-based materials that can be easily manufactured and have great transparency and stretchability without losing conductivity.

Herein, an extremely flexible strain sensor based on a 3D printable self-healing hydrogel is presented. The photocurable ink was prepared by mixing an aqueous solution of Poly (vinyl alcohol) (PVA) with acrylic acid (AAc), Poly (ethylene glycol) diacrylate (PEGDA), a water-compatible photoinitiator and sodium chloride (NaCl) to endow ionic conductivity. The device were then printed with a commercial Digital Light Processing printer. The sensor, exploitable both as piezoresistor or piezocapacitor, presents high sensitivity to external stimuli, together with an extreme stretchability. The sensors show self-healing ability at room temperature without any stimuli and are able to restore both mechanical properties and strain sensitivity after the self-healing procedure and also after a drying and water restoring process. The very high strain sensitivity and the 3D printing capability enables the hydrogel to be

implemented into complex shape wearable strain sensors to monitor various human motion and physiological data, making it a viable solution for the creation of easily manufactured and conformable devices.

[1] Huang F, Wei W, Fan Q, Li L, Zhao M, Zhou Z. Super-stretchable and adhesive cellulose Nanofiber-reinforced conductive nanocomposite hydrogel for wearable Motion-monitoring sensor. *J Colloid Interface Sci.* 2022;615:215-226.

[2] Lei Z, Wang Q, Sun S, Zhu W, Wu P. A Bioinspired Mineral Hydrogel as a Self-Healable, Mechanically Adaptable Ionic Skin for Highly Sensitive Pressure Sensing. *Adv Mater.* 2017;29(22):1-6.

[3] Kim J, Lee M, Shim HJ, et al. Stretchable silicon nanoribbon electronics for skin prosthesis. *Nat Commun.* 2014;5.

[4] Pang Y, Xu X, Chen S, et al. Skin-inspired textile-based tactile sensors enable multifunctional sensing of wearables and soft robots. *Nano Energy.* 2022;96(January).

11:45 AM SB12.09.12

Stretchable Printed Circuit Board and Organic Circuit for Ultra-Flexible Biosignal Sensor Rei Kawabata^{1,2}, Teppei Araki^{1,2}, Mihoko Akiyama¹, Tianxu Wu¹, Yusuke Okabe³, Hiroataka Koga¹, Takafumi Uemura¹, Masaya Nogi¹, Katsuaki Suganuma¹ and Tsuyoshi Sekitani^{1,2}; ¹SANKEN (The Institute of Scientific and Industrial Research), Japan; ²Department of Applied Physics, Graduate School of Engineering, Osaka University, Japan; ³Cemedine Co., Ltd., Japan

Printable and stretchable electrodes are attracting considerable attention in the development of wearable devices for long-term health care monitoring. In this study, we developed stretchable electrodes using silver microparticles (AgP) and a small amount of silver nanowires (AgNWs). The developed electrodes enabled low-temperature curing at 100 °C with cyclic durability over 50% strain. An amplification device using a stretchable printed circuit board was fabricated using our stretchable electrode that successfully amplified pseudo biosignals and maintained its amplification factor over 50% strain. Electrodes in wearable devices can continuously probe bioelectrical signals and realize high signal-to-noise ratio with signal amplification at the probe [1, 2]. However, typical rigid electrodes are difficult to mechanically conform to the skin. Hence, composites of silver particles and polymer are a promising solution for the development of stretchable and printable electrodes [3, 4]; conventional Ag-based stretchable electrodes require complex chemical treatment and high-temperature annealing for the enhancement of their conductivity and durability. Improvement of the electrical properties of stretchable electrodes based on a simple, low-temperature printing process therefore remains challenging.

Our stretchable electrode contains AgP with a small amount of AgNWs, enabling it to maintain conductivity of over 5×10^3 S cm⁻¹ and lower its fabrication temperature from 150 °C to 100 °C. Further, the durability strain of the stretchable electrode increased 7.5 times upon the addition of 1 wt% AgNWs. A stretchable printed circuit board based on our stretchable electrode was developed and implemented to fabricate an ECG amplification device. In this device, the organic thin film transistor and other components with mechanical properties different from those of a stretchable electrode were integrated to amplify the pseudo-ECG with an amplification factor of over 10 under strain. The stretchable printed circuit board is expected to promote the development of wearable devices with enhanced biocompatibility and contribute to the realization of long-term biosignal measurement, enabling the early detection of diseases.

[1] W. Gao, et al., *Nature* **529** 509–14 (2016)

[2] M. Sugiyama, et al., *Nat. Electron.* **2** 351–60 (2019)

[3] N. Matsuhisa, et al., *Nat. Mater.* **16** 834–40 (2017)

[4] J. Liang, et al., *Adv. Mater.* **28** 5986–96 (2016)

SESSION SB12.10: Materials II

Session Chairs: Ravinder Dahiya and Andrea Spanu

Thursday Afternoon, December 1, 2022

Hynes, Level 3, Room 309

1:30 PM *SB12.10.01

Towards Robust and Sustainable Soft Robots through Self-Healing Polymers Julie Legrand, Seppe Terryn, Ellen Roels, Seyedreza Kashf Tabrizian, Pasquale Ferrentino, Zhanwei Wang, Fatemeh Sahraeeazartamar, Joost Brancart and Bram Vanderborght; Vrije Universiteit Brussel, Belgium

Soft robots are flexible machines with numerous advantages. They provide safe human-machine interaction and are able to achieve complex motions with regard to their rigid counterparts. However, the softness of this type of robot makes them susceptible to cuts, shears, and punctures due to sharp objects. Moreover, those robots are often made of non-recyclable plastics, which forces the user to throw the robot away and replace it completely when damaged. The Brubotics and FYSC groups of the Vrije Universiteit Brussel work on an alternative to make soft robots more robust and sustainable. To do so we use Diels-Alder (DA) polymers, resulting from reactions between a diene (furan) and a dienophile (maleimide). Those reactions form thermoreversible cross-links in the polymer network. The reversible covalent bonds of this polymer allow recovering from macroscopic damage, like cuts and punctures, upon a heat-cool cycle (90°). Therefore, the polymer can be cut and healed back together to reform a single part with full recovery of the initial material properties [1]. By varying the network properties of the polymer, different mechanical properties, ranging from hyperelastic (100 kPa) to hard thermosets (10 GPa) can be obtained leading to multi-material parts with strong multi-material interfaces [1]. This material has been used to build complex, multi-material, soft actuators, grippers and prosthetics, but also modular and reconfigurable robots [1,2]. As the DA bonds are completely reversible, a soft robot can be robustly assembled, then disassembled, using its pieces for reassembling another robot. Sensing capabilities can be added to those robots by making the DA polymers conductive. To do so, (hybrid) carbon black and nanoclay fillers are added, creating a conductive DA polymer that can be molded or 3D printed. A conductivity ranging from 10 μ to 100 S/m can be obtained depending on the proportion of carbon black and fillers added [3]. Using this technique, soft strain and capacitive self-healing sensors can be built and integrated in our soft, self-healing robots to provide feedback information to control them. Using the same sensors, damage detection of the self-healing robot can be performed by detecting reduced or absence of conductivity. In case of damage, the robot can be warmed up at $\pm 90^\circ$ for approximately 1h, which increases the mobility of the DA bounds, and then cooled down, let to heal, for 24h [1]. This healing process can either be performed by the operator or by the robot itself, by integrating either a heater [4] or shape memory alloy wires inside the robot's body. Shape memory alloy wires can be driven by an electrical current. The wire therefore heats up and shrinks, which allows to simultaneously close the wound and heat the damaged area up to heal it. Although the control of soft robots is challenging, relatively accurate results can be obtained by using finite element methods based on an experimental characterization of the materials to build the inverse kinematic controller [5]. Combining those above-mentioned techniques allows to create and control robust, sustainable soft robots for industrial and medical applications.

[1] Terryn, S., et al. (2017). Self-healing soft pneumatic robots. *Science Robotics*, 2(9).

- [2] Roels, E., et al. (2019). A multi-material self-healing soft gripper. In 2019 2nd IEEE International Conference on Soft Robotics (RoboSoft).
 [3] Roels, E., et al. (2022). Self-healing sensorized soft robots. *Materials Today Electronics*. (Accepted)
 [4] Tabrizian, S. K., et al. (2022). A Healable Resistive Heater as a Stimuli-Providing System in Self-Healing Soft Robots. *IEEE Robotics and Automation Letters*, 7(2).
 [5] Ferrentino, P. et al. (2021). FEA-Based Inverse Kinematic Control: Hyperelastic Material Characterization of Self-Healing Soft Robots. *IEEE Robotics & Automation Magazine*.

2:00 PM SB12.10.02

Self-Healing and Stretchable Ionically Conductive Materials for Electronics and Soft Robotics Yu Jun Tan; National University of Singapore, Singapore

Living matter self-heals when suffering from injuries. For instance, human skin heals from wounds of various degrees. On the contrary, synthetic materials degrade over time due to fatigue, corrosion, or damage. Meanwhile, living matter conducts electricity using ions, such as the neurons in the human body; in contrast, synthetic electronics conduct electricity using electrons. Therefore, inspired by the remarkable capability of nature, smart and self-healing ionotronics and soft robotics are being intensively researched to mimic natural systems. A stretchable ionogel consists of ionic component(s) confined within a solid polymer network. Self-healing ionogels were developed based on (i) ions immobilized in self-healing polymers; and/or (ii) dynamic interactions between the ionic components with the polymer. A self-healing ionotronic device functions by using both the mobile ions and electrons, whilst they can self-repair damages inflicted on them. We developed self-healing and stretchable double network ionogels by integrating a covalently cross-linked acrylic acid network and a dynamic ionically cross-linked coordination between the acrylic acid chains and metal ions [1]. We also developed a self-healing ionogel composed of a fluorocarbon elastomer and a fluorine-rich ionic liquid, which offers fast and repeatable electro-mechanical self-healing in wet, acidic and alkali environments due to the ion-dipole interactions [2]. These self-healing ionogels can be 3D printed using extrusion-based methods. The inks exhibited thixotropic behavior that is favorable for extrusion-based 3D printing. We demonstrated that these materials can be used in pressure and strain sensing applications and serve as transparent electrodes in optoelectronics for soft robotics [3].

References:

- [1] Li H, Zheng H, Tan YJ, Tor SB, Zhou K. Development of an Ultrastretchable Double-Network Hydrogel for Flexible Strain Sensors. *ACS Appl. Mater. Interfaces* 2021. [2] Cao Y†, Tan YJ†, Li S, Lee WW, Guo H, Wang C, Benjamin Tee CK. Self-healing electronic skins for aquatic environments. *Nat. Electron.* 2019;2: 75-82. [3] Tan YJ, Godaba H, Chen G, Tan MST, Li G, Lee PM, Cai Y, Li S, Shepherd RF, Ho JS, Benjamin Tee CK. A Transparent, Self-healing and High-κ Dielectric for Low-field-emission Stretchable Optoelectronics. *Nat. Mater.* 2020; 19: 182–188

2:15 PM SB12.10.03

Self-Healing Effects of Small Molecule Acids on a Ultra-Conformable Stretchable Mixed Conducting Polymer Complex Colton Duprey¹, Hadi Rouhi¹, Katherine Webb² and Evan K. Wujeik¹; ¹The University of Alabama, United States; ²Vanderbilt University, United States

Polymeric piezoresistive sensors show great promise in movement monitoring, biosensing, and soft robotics. Their polymer composition provides flexibility and stretchability allowing for unique applications where traditional metallic materials are too brittle and rigid. A templated polymer complex composed of poly(2-acrylamido-2-methyl-1-propanesulfonic acid), polyaniline, and a small molecule dopant. The impacts the various dopants have on the material's conductivity, stretchability, mechanical and self-healing properties, and piezoresistive sensitivity are studied. Generally, small molecule dopants that increase conductivity decrease stretchability and mechanical stability, which stems from more acidic dopants being able to protonate and facilitate ion transport throughout the sensor. Conversely, functional groups with increased hydrogen bonding tend to increase mechanical and self-healing properties. By increasing our understanding of the impact these various dopants have on the properties of the polymer complex, the material can be tailored to specific applications, allowing for increased sensitivity when needed or increased stretchability when required. This will allow for the development of novel materials as we seek to manufacture better stretchable electronics.

2:30 PM BREAK

3:00 PM SB12.10.04

Towards Self-Healing Electronics—Hydrogen Bonded Conjugated Polymers via Ureidopyrimidinone Megan M. Westwood and Bob Schroeder; University College London, United Kingdom

As electronic devices become increasingly integrated in our lives, the progression from portable to wearable devices is inevitable and offers the possibility of advanced healthcare diagnostics for future generations.¹ Aiming to mimic human skin, these new materials must be stretchable and have the ability to heal in response to stress. Organic semiconductors, specifically conjugated polymers, are a promising candidate for realising electronic skin as they are intrinsically flexible and can be modified *via* chemical design to achieve both high performance and that allow energy dissipation under stress through introduction of supramolecular motifs.

Prior research has shown that incorporating pendant hydrogen bonding groups into a conjugated polymer can result in recovery of the mechanical properties after deformation.^{2,3} However, the induced structural disorder reduces electronic performance which has to date only partially been recovered and the direct effect of non-covalent groups is not fully understood. Maximising the strength of dynamic bonds through use of a quadruple hydrogen bonded system, such as ureidopyrimidinone (UPy), offers a design pathway to more efficient healing semiconductors.⁴

We have synthesised a series of fluorene based polymers bearing UPy groups to investigate their directing effects within a conjugated polymer matrix. Here, the purpose was to decouple competitive interactions between hydrogen bonding within sidechains and the polymer backbone. Spectroscopic, thermal and mechanical analysis showed dramatic changes within the polymer structure upon installation of only 10% UPy with respect to other solubilising side chains. In this presentation we will discuss the structure-property relationships exhibited in these materials and the effect on self-healing efficiency in optical devices, offering a design paradigm for future biomimetic materials.

References

- [1] J. Y. Oh & Z. Bao, *Adv. Sci.*, 2019, 6, 1900186.
 [2] J. Y. Oh *et al.*, *Nature*, 2016, 539, 411-415
 [3] A. Gasperini *et al.*, *Macromolecules*, 2019, 52, 6, 2476-2486.
 [4] R. P. Sijbesma *et al.*, *Science*, 1997, 278, 1601-1604.

3:15 PM SB12.10.05

Water-Accelerated Autonomous Self-Healing Elastomer for Underwater Wearable Electronics. Fang-Cheng Liang and Chi-Ching Kuo; Institute of Organic and Polymeric Materials, Research and Development Center of Smart Textile Technology, National Taipei University of Technology, Taiwan

The conventional self-healing mechanism is a highly energy-consuming temperature-dependent inducing spontaneous repairation and thus impedes further integration in electronic (e-) skin. Herein, we present an innovative concept of a water-assisted room-temperature autonomous self-healing mechanism based on synergistically dynamic covalent Schiff-based imine bonds with weak hydrogen bonds. Significantly, the supramolecular water-assisted self-healing polymeric (WASHP) films possess rapid self-healing kinetic and high stretchability behavior through the reversible dissociation/association process. In comparison with the pristine room-temperature SHP, our WASHP demonstrates the remarkably mechanical performance for self-healing elastomers at room temperature so far, alongside accelerated the self-healing time up to 1hr and exhibits superior performance including tensile strain increased up to 9050%, self-healing efficiency up to 95%, and toughness up to 144.2 MJ/M³, respectively. As a proof-of-concept, we designed a versatile WASHP-based light-emitting touch-responsive device (WASHP-LETD) and perovskite quantum-dots-based (PeQDs) white LED backlight. The WASHP-LETD possesses remarkable mechanical deformation performance (pressure, bending, and strain), whereas WASHP-PeQDs exhibit outstanding long-term stability even under water environment beyond 1 year, highlighting its potential utilized in white LED with highly pure white color rendering. This work provides a mechanically robust approach for producing eco-friendly, economical, and waterproof e-skin device components.

3:30 PM SB12.10.06

Ultra-Stretchable Self-Healing Mixed Conductive Polymer Composite with Silver Nanowires Showing Increased Mechanical Performance Colton Duprey¹, Hadi Rouhi¹, Yang Lu² and Evan K. Wujcik¹; ¹The University of Alabama, United States; ²Georgia Institute of Technology, United States

Effective wearable sensors, stretchable electronics, and soft robotics materials must have a sufficiently high balance of conductivity, stretchability, and robustness. Intrinsically conductive polymers offer a critical step toward improving wearable sensor materials due to their tunable conductivity, soft/compliant nature, and ability to complex with other synergistic molecules (e.g., polyacids, small molecule dopants). The addition of nanofillers offers the potential to improve the properties of these polymer composite for soft robotics and wearable applications. While nanofillers typically increase conductivity at the expense of mechanical properties, here we show an increase in mechanical properties, which the interface between the polymer matrix and the AgNW is hypothesized to be integral for the formation of an active network. These form a polymer nanocomposite with high electronic sensitivity, unprecedented mechanical properties (a maximum strain of 4693% at ambient humidity; ~52 RH%), and repeatable, autonomous self-healing efficiencies of greater than 98%. To illustrate the remarkable sensitivity, the material was employed as a biomedical sensor (pulse, voice recognition, motion), topographical sensor, and high sensitivity sensor.

3:45 PM SB12.10.07

Fabrication of a Flexible Electroadhesive Component by Additive Manufacturing for Wall-Climbing Robots Taekyu An, Sukeun Yoon and Jihoon Kim; Kongju National University, Korea (the Republic of)

Existing robots that are capable of climbing walls mostly rely on rigid actuators such as electric motors, but soft wall climbing robots based on electroadhesion (EA) have not yet been widely achieved. EA electrically generates an electrostatic force to activate the adhesion force. EA as compared to other adhesion solutions can possibly adhere without damage to the target surface with a relatively simple system, low weight, and low electric consumption. EA consists of two interdigitated electrodes, a dielectric layer, and an insulating layer. The dielectric layer must have high dielectric constant and high insulation resistance to increase its adhesion force. However, high insulation resistance and dielectric constant are conflicting parameters, and it is important to find a trade-off point. In this study, to implement EA through additive manufacturing, flexible-EA(F-EA) pad was manufactured by forming electrode patterns on flexible copper clad laminate (FCCL) using digital light processing (DLP). The photocurable resin patterned on FCCL by DLP was used as an etchant resistor. Portions of the Cu layer without the photocured resin was removed during wet chemical etching, leaving the electrode patterns on FCCL. To enhance electroadhesive force, ceramic composite layer was printed over the patterned FCCL. The electroadhesive force was simulated by a finite element method (COMSOL) according to various electrode patterns and compared to the experiments. The climbing robot was operated by rotating the track with wheels while having the F-EA embedded in the track. The size of the track was designed considering the adhesion force of the embedded F-EA and the weight of the climbing robot. Experimental results revealed that climbing robot has excellent climbing performance on a wide variety of surface.

4:00 PM DISCUSSION TIME

4:15 PM SB12.10.09

Soft Robotics for Reactive Skins, Haptics, and Biosensors in Smart Minimally Invasive Surgical Tools. Arinchevan Gerald and Sheila Russo; Boston University, United States

Robotic Minimally Invasive Surgery (R-MIS) provides significant advantages to both the surgeon and the patient, such as improved accuracy, automated surgical tasks, faster patient recovery times, and reduced patient trauma. However, many current R-MIS systems do not possess haptic feedback, relying instead on sensory substitution in the form of visual cues to the surgeon. The lack of direct tactile feedback can result in excessive application of forces onto the patient's tissue. This is particularly problematic in the case of flexible surgical instruments such as endoscopes, wherein frictional forces affect force transmission along the length of the device. Excessive forces in colonoscopy can lead to severe adverse events (SAEs) such as bleeding, perforation, and splenic injury. This highlights the necessity of a comprehensive haptic feedback system that can sense forces exerted by the colonoscope onto the tissue and directly relay haptic feedback to the surgeon.

In prior work, we developed a soft robotic reactive skin that can be mounted onto a colonoscope to detect incident force on colon tissue. In our current work, we augment the sensing capabilities of the soft robotic skin with a wearable pneumatic glove that provides haptic feedback to the surgeon. Incident force on the soft robotic skin triggers the pneumatic actuators on the glove, causing them to inflate and provide haptic feedback to the user's fingers. The glove consists of a main fabric piece and modular actuators that wrap around the base of the fingers. The glove is designed to be minimally intrusive and possesses a low vertical profile (1 mm), allowing the endoscopist to maintain finger dexterity and grasp the colonoscope. The actuators are controlled by enabling proportional inflation based on the magnitude of the incident forces on the sensors. The glove was validated using a series of experiments. First, the duty cycle of the glove control system was varied to assess the ability of the actuators to hold pressure at discrete values to enable the surgeon to distinguish between different magnitudes of force. The actuators inflate once the incident force crosses a predefined threshold value of 1 N and reaches max pressure at a force value of 2.2 N. The threshold value can be tuned depending on the nature of the procedure as forces experienced in colonoscopies are highly variable (i.e., up to 40 N). This test was further expanded to ascertain the force mapping capabilities of the haptic glove, i.e., to determine the output force of the actuators in response to the incident forces on the soft robotic skin. The force exerted by the actuators increased directly in proportion to the incident force with a max value of 20 N, which was 9 times larger than the incident force. The haptic feedback system was then subject to an in-vitro surgical evaluation. The haptic glove was worn by an endoscopist whilst performing a mock colonoscopy using an artificial colon. The soft robotic skin was mounted on the colonoscope to provide force sensing that was relayed as haptic feedback to the endoscopist via the wearable device. The endoscopist performed the procedure with and without haptic feedback and evaluated each case using a NASA task load index. The colonoscopy trial with haptic feedback had improved sub-scores compared to the case without haptic feedback, signifying an easier, less demanding workload for the endoscopist.

This soft robotic haptic feedback system can be expanded to mimic varied physical sensations encountered during MIS such as tissue palpation or bending of the flexible surgical tool. It can also be used to alert the surgeon to SAEs, such as bleeding when integrated with biosensors. The versatility and modular nature of the glove also makes it suitable to be adapted to other MIS procedures where haptic feedback is beneficial, such as bronchoscopy or neurosurgery.

4:30 PM SB12.10.10

Tunable Tissue-Like Conductive Hydrogel Scaffolds for Neural Cell Differentiation [Christina M. Tringides](#), Marjolaine Boulingre and David Mooney; Harvard University, United States

Multielectrode arrays would benefit from intimate engagement with neural cells, but typical arrays do not present a physical environment that mimics that of neural tissues. We hypothesized that a porous, conductive hydrogel scaffold with appropriate mechanical and conductive properties could support neural cells in 3D, while tunable electrical and mechanical properties could modulate the growth and differentiation of the cellular networks. By incorporating carbon nanomaterials into an alginate hydrogel matrix, and then freeze-drying the formulations, scaffolds which mimic neural tissue properties were formed. Neural progenitor cells (NPCs) incorporated in the scaffolds formed neurite networks which spanned the material in 3D, and differentiated into astrocytes and myelinating oligodendrocytes. Viscoelastic and more conductive scaffolds produced more dense neurite networks, with an increased percentage of astrocytes and higher myelination. Application of exogenous electrical stimulation to the scaffolds increased the percentage of astrocytes and the supporting cells localized differently with the surrounding neurons. The tunable biomaterial scaffolds can support neural co-cultures for over 12 weeks, and enable a physiologically-mimicking *in vitro* platform to study the formation of neuronal networks. As these materials have sufficient electrical properties to be used as electrodes in implantable arrays, they may allow for the creation of biohybrid neural interfaces and living electrodes.

4:45 PM SB12.10.11

Silicone Materials with Tunable MRI Contrast for Applications in Soft Robotic Medical Phantoms [Yasmine Osmani](#), Ben Dickie, James O'Connor, Brian Derby and Steve Edmondson; The University of Manchester, United Kingdom

The availability of soft robotic phantoms, with realistic motion, would be a significant advance in developing cancer treatments by magnetic resonance imaging (MRI) guided radiotherapy; but is currently limited by available silicone materials. A successful soft phantom must display the appropriate balance of mechanical properties, MRI contrast and manufacturability. Here, we present material development for 3D printable silicone materials that work towards overcoming this challenge.

Robotic phantoms must present MRI relaxation times that simulate biological tissues, typically assessed using time constants T_1 and T_2 for longitudinal and transverse relaxation. Human tissue relaxation times can range from 600 – 3000 ms for T_1 and 35-110 ms for T_2 , although the precise range depends on the magnetic field strength used during a particular scan. Therefore, appropriate phantom materials should allow for significant T_1 and T_2 tunability. For soft robot fabrication the challenge is to develop compositions that achieve the desired relaxation values, have optimum pre-cure viscoelasticity for printability, while also maintaining post-cure mechanical properties comparable to those human tissues; which typically range from <100 kPa – 1 MPa. This work aims to present material formulations to 3D print MRI compatible soft robots with tunable and values.

We have developed printable silicone blend composed of high viscosity and low viscosity PDMS materials, which was then blended with silicone oils of varying lengths, to allow for relaxation rate tuning. This simple approach has extended the T_1 relaxation range, of typical unmodified silicones, from 1159 - 1229 ms to 1140 – 2313 ms and the T_2 relaxation range from 14 – 23 ms to 13 - 34 ms. Ink printability has been assessed using rheological characterisation. At an angular frequency, ω , of 10 s^{-1} , the addition of 30% silicone oil decreased the storage modulus G' from 9.0 kPa to 7.4 kPa and the yield stress from 8.6 kPa to 1.3 kPa, confirming that the ink remained printable. Simplified brain phantoms were then produced via extrusion 3D printing. These were imaged in a clinical grade MRI scanner, and showed appropriate contrast under T_1 weighted imaging.

Our preliminary data on printable silicone formulations has demonstrated that it is possible to fabricate soft robotic structures via additive manufacturing with appropriate T_1 weighted imaging contrast. Further work is needed to access materials with appropriate T_2 contrast and optimise the post curing mechanical properties to be consistent with that of human tissue. This material blend presents a promising option not only for MRI applications but also surgical training phantoms, substrate and scaffold structures, soft facial prosthetics and electronic skin.

SESSION SB12.11: Materials III
Session Chairs: Francesco Greco and Andrea Spanu
Friday Morning, December 2, 2022
Hynes, Level 3, Room 309

9:15 AM SB12.11.02

Understanding the Mechanics of 3D Knitting for Additive Manufacturing of Textile-Based Soft Robots [Vanessa Sanchez](#)^{1,2}, Kausalya Mahadevan¹, Gabrielle Ohlson¹, Moritz A. Graule¹, Michelle C. Yuen¹, Clark B. Teeple¹, James C. Weaver¹, James McCann³, Katia Bertoldi¹ and Robert J. Wood¹; ¹Harvard University, United States; ²Stanford University, United States; ³Carnegie Mellon University, United States

Soft robots allow gentle, safe interactions between devices and people and can even account for a level of environmental and task-specific uncertainty due to their inherent material compliance. Challenges remain, however, in creating affordable, accessible, durable, and customized devices for where light weight, comfort against skin, and low-form factor are paramount, including personalized healthcare, thermoregulation, and assistive technology. The ability to additively manufacture textile-based soft robots on-demand would address these limitations, with V-bed weft knitting representing a promising approach due to its highly multi-dimensional design space. Specifically, knitting has the ability to tune material properties across four distinct length scales, from yarn-scale material incorporation, to local stitch geometries, to self-assembled architectures from collections of stitches, and finally at the scale of engineered global shaping. Yet as a consequence of the broad frontier in this emerging field, there is a lack of understanding of how these parameters (1) tune mechanical properties such as anisotropic stress-strain behavior and (2) affect system-level manufacturability, both of which must be established through physics-based guidelines in order for integrated devices to be created effectively.

In this work, we take a step toward establishing these guidelines by developing a library of knit structures and studying how local stitch geometry, self-folding structures, and constituent material properties tune the anisotropic stress-strain behavior of knits. We relate this knowledge to global shaping

strategies used in knitting to create monolithically 3D-knit soft robots. Resulting devices can perform a variety of application-specific tasks using complex and multi-degree-of-freedom motions. Furthermore, we highlight the ability to pair knit actuation with direct integration of deformation sensing.

9:30 AM BREAK

10:00 AM SB12.11.06

Stretchable and Lightweight Soft Conductive Composites Embedded with Liquid Metal Microfiber Networks Jiexian Ma, Pu Zhang and Zihan Liu; SUNY Binghamton, United States

Soft conductive composites are essential components of stretchable electronics, soft robotics, soft sensors and actuators. Liquid metals are ideal fillers of soft conductive composites because of their high conductivity and supreme compliance. Existing liquid metal composites usually require a relatively high filling ratio of liquid metals, which inevitably make the composites heavy and expensive. In this presentation, We report the design and fabrication of a new paradigm of liquid metal composites by embedding liquid metal microfiber networks into soft elastomers. Experimental results indicate that this new composite is highly conductive, lightweight, super-stretchable, and low cost. The mechanical and electrical properties of this new liquid metal composite are characterized. In addition, we will demonstrate a few potential applications in stretchable electronics and sensing.

10:15 AM SB12.11.07

Solvent-Assisted Filling and Selective Dewetting of Liquid Metal for Layer-Structured 3D Interconnect and VIA for Stretchable Electronics Woojin Jung and Tae-il Kim; Sungkyunkwan University, Korea (the Republic of)

As research on stretchable electronics is developing rapidly and becoming complex, the requirement for novel fabrication method for 3D interconnects owing to stable vertical interconnect access (VIA) for complex printed circuit boards (PCBs) is emerging. However, there are only a few attempts to resolve this issue. This is because the electrically conductive material filling VIAs must be intrinsically stretchable. Due to this, many researchers adopted Gallium-based liquid metal to fabricate VIAs. Its liquid nature allows it to adapt its shape to extreme mechanical stimulation, such as stretching or torsion. Using this advantage, researchers manually inject the liquid metal into VIAs, which is unsuitable for fine interconnects below the mm scale. Here, we demonstrate solvent-assisted liquid metal filling into various interconnect shapes, including VIAs and selective dewetting of liquid metal exposing PCB board. This process is spontaneous. Therefore, it takes advantage to fabricate small patterns, even sub-micrometer circuits. We provide the theoretical background of liquid solvent-assisted liquid metal filling and selective dewetting. Also, We suggest the design criteria for the geometry and dimension of liquid metal interconnects to obtain structural stability without dewetting based on theoretical and computational background. The experimental evidence agrees with the design criteria. We demonstrate a simple stretchable NFC device with this novel fabrication method and design criteria. We successfully transferred micrometer-size light-emitting diodes (LEDs) with only 230 micrometers to the stretchable liquid metal PCB without any soldering process. This is because the liquid metal makes conformal contact with the electrodes of LEDs and adheres firmly. The device operates stably under repetitive stretching and releasing due to the stable connection of VIA between the upper and lower layer.

10:30 AM SB12.11.08

Tracking High Voltage Capacitance Evolution as Indicator for Electrode Degradation in Dielectric Elastomer Actuators Haleh Shahsa, Jiahao Gu, Ang Li, Siyoung Lee and Mihai Duduta; University of Toronto, Canada

Dielectric elastomer actuators (DEAs) are soft, electrically driven devices that convert electrical energy to mechanical deformation. Despite their advantages, the widespread adoption of DEAs is limited by limited understanding of failure modes. Here we report a method to continuously monitor high voltage capacitance during DEA actuation as an indicator of device degradation. Our approach can track energy conversion efficiency, but also show changes in the device's properties in real-time. This unprecedented insight enables a novel way to study DEAs, evaluate degradation mechanisms, and correlate material structure to device performance.

Carbon nanotube (CNT)-based electrodes are a promising option for making DEAs as they are highly conductive and compliant. The long-term performance of CNT-based DEAs, however, is limited because of their structure degradation. The CNT concentration affects the performance of the DEA and the breakdown field. The high concentration will cause an early breakdown, while the low concentration will lead to poor electromechanical performance. With our high voltage capacitance tracking method, we optimize a specific set of carbon nanotube electrodes to demonstrate a DEA capable of withstanding 5 kV DC actuation ($>100 \text{ V}/\mu\text{m}$) for over 3 hours continuously, with peak specific strain energy of $>90 \text{ J/kg}$ and peak electro-mechanical energy conversion rate of 7%.

Metal nanowires, such as Silver and Copper, provide high conductivity and are widely being used for transparent stretchable electronics. Moreover, they are significantly larger than CNTs, and maintain a high aspect ratio across scales. Mixing the CNTs with metal nanowires at different mixing ratios changes the decay rate of DEAs as compared to pure CNT electrodes. This work is a necessary step towards developing ultra-resilient DEAs and enabling a wide range of applications, from wearable devices to soft machines across different scales.

SESSION SB12.12: Applications IV
Session Chairs: Piero Cosseddu and Darren Lipomi
Friday Afternoon, December 2, 2022
Hynes, Level 3, Room 309

1:30 PM SB12.12.01

Light Driven Bio Hybrid Actuators Illaria Venturino^{1,2}, Vito Vurro¹, Matteo Moschetta¹, Silvio Bonfadini¹, Valentina Sesti^{1,2}, Chiara Bertarelli^{1,2}, Luigino Criante¹ and Guglielmo Lanzani^{1,2}; ¹Istituto Italiano di Tecnologia, Italy; ²Politecnico di Milano, Italy

Bio hybrid actuation is a novel trend in soft robotics combining soft polymeric scaffold and biological active component (i.e. flagella, bacteria). A promising class of bio hybrid actuators are those based on muscle cells.¹ Muscular tissues are characterized by outstanding performance (i.e. high efficient energy storage, high power/weight ratio, self-repair capability)² that are very promising in actuation field especially if compared with other type of actuators. These features can be reproduced *in vitro* mimicking the native muscle structure and organization and leading to the already mentioned bio hybrid actuators. Typically, these devices are controlled by an electrical pulses, applied by electrodes to the tissue.

An interesting alternative to the electrical stimulation can be given by the use of light. Photostimulation can be a competitive alternative to the classic one

due to its low damaging level and high spatial and temporal resolution³. Since muscle cells are not sensible to light several strategies have been found (i.e. optogenetics, IR stimulation, photo sensitive materials).^{4,5} In this work we present the skeletal muscle cells photopacing mediate by a photochromic molecules, named Ziapin2.⁶ This molecule is an azobenzene compound that is able to isomerize due to light interaction. This approach was tested on single skeletal muscle cells and on muscle tissue realized exploiting the same cell line and a micro-patterned Polydimethylsiloxane (PDMS) thin film.

Bibliography

¹ S. Kim, C. Laschi, and B. Trimmer, *Trends in Biotechnology* 31, 287 (2013).

² L. Ricotti and A. Menciassi, *Biomed Microdevices* 14, 987 (2012).

³ V. Vurro, I. Venturino, and G. Lanzani, *Appl. Phys. Lett.* 120, 080502 (2022).

⁴ R. Parameswaran, K. Koehler, M.Y. Rotenberg, M.J. Burke, J. Kim, K.-Y. Jeong, B. Hissa, M.D. Paul, K. Moreno, N. Sarma, T. Hayes, E. Sudzilovsky, H.-G. Park, and B. Tian, *Proc Natl Acad Sci USA* 116, 413 (2019).

⁵ S.-J. Park, M. Gazzola, K.S. Park, S. Park, V. Di Santo, E.L. Blevins, J.U. Lind, P.H. Campbell, S. Dauth, A.K. Capulli, F.S. Pasqualini, S. Ahn, A. Cho, H. Yuan, B.M. Maoz, R. Vijaykumar, J.-W. Choi, K. Deisseroth, G.V. Lauder, L. Mahadevan, and K.K. Parker, *Science* 353, 158 (2016).

⁶ G.M. Paternò, E. Colombo, V. Vurro, F. Lodola, S. Cimò, V. Sesti, E. Molotokaite, M. Bramini, L. Ganzer, D. Fazzi, C. D'Andrea, F. Benfenati, C. Bertarelli, and G. Lanzani, *Adv. Sci.* 7, 1903241 (2020).

1:45 PM SB12.12.02

Stacked Rigid and Compliant Dielectric Structures for Increasing Force Range in Soft Capacitive Sensors Kieran Morton¹, Ryusuke Ishizaki², Bertille Dupont¹, Austin Weir¹, Victor Mitchell¹, Han C. Nguyen¹ and John D. Madden¹; ¹The University of British Columbia, Canada; ²Honda R&D Co. Ltd., Japan

Soft force sensors have a myriad of applications including soft robotics, medical devices, and industrial environments. Compared to mechanoreceptors in the skin, emerging technologies are still poor in the combination of sensitivity, directional distinction, and dynamic range. In this work a capacitive sensing approach is presented that employs a mechanically structured dielectric to enable a combination of high sensitivity at low forces that correspond to light touch, and an ability to operate at high forces needed for tight gripping. The sensor uses the change in capacitance resulting from the movement of four electrodes on the top surface of the dielectric relative to a bottom electrode to determine normal and shear displacements, and corresponding forces. A soft silicone elastomer (Shore Hardness 00-30) is used to form the body and conductive elements of the sensor. Initial work using a dielectric with a pillar structure showed high sensitivity at pressures of up to 76 kPa, but signal saturation occurred at higher loading as pillars are flattened and contact one another at large strains. To increase force range while maintaining sensitivity, a two-stage dielectric architecture is used to create a structure which is highly compliant to normal and shear forces at small forces, while maintaining reasonable sensitivity at high normal forces. Several shapes are explored for the purposes of enhancing low-force response, combining a softer upper architecture such as pyramids with stiffer lower pillars. A molding and bonding process is used to fabricate these stacked sensors. Four primary designs are presented in this work with different combinations of pyramid and square structures. The selection of structures is informed by literature on pyramidal sensors, empirical design, and simulations. COMSOL is used to predict sensor response. These sensors are characterized in a three-axis characterization setup for low-force, and a single-axis characterization setup for high-force. The combination of inverted pyramids in the high sensitivity layer and square pillars in the high force layer achieves a balance of high sensitivity while maintaining a wide dynamic range and a relatively flat, skin-like upper surface. This sensor functions in a normal force range of 0.05 N - 50 N. At lower forces (0-20 N) shear displacements are measured, with a sensitivity of 265 fF/N (1.35 fF/Pa), enabling detection of a displacement of 23 mm, corresponding to a force of 60 mN, and a shear stress of 89 Pa. The normal force sensitivity is 54 fF/N (0.28 fF/kPa), down to a normal force of 13 mN. This resolution is similar to that of human mechanoreceptors at frequencies of less than 20 Hz. At large loads (25 N - 50 N), there is some hysteresis and loss of sensitivity, but a change of 15 fF/N (0.08 fF/kPa) enabling force discrimination. Multi-stage dielectric structures consisting of two different pillar shapes allow for capacitive sensors to have a large force range, and yet high sensitivity to light touch, by combining shapes of varying compliance in series. Force range and sensitivity have potential to adapt to higher levels by using stiffer elastomers. Lateral spatial resolution in these sensors is several millimeters – significantly lower than in skin – but is resolvable by making the sensing skin thinner to increase resolution.

2:00 PM SB12.12.03

A Soft Tensile Valve for Analog and Self-Sensing Control of Soft Actuators Junsoo Kim, Jun Kyu Choe, Hyeonsoo Song, Jiyun Kim and Joonbum Bae; Ulsan National Institute of Science and Technology, Korea (the Republic of)

Utilizing inflation of flexible materials, pneumatic soft robots have expanded unexplored fields previously inaccessible to hard robots. Soft robots are especially specialized for adaptation to complex environments and safe interaction with humans, via harnessing intrinsic compliance. However, pneumatic soft actuators have been generally controlled by hard electronics such as controllers and solenoid valves. When these hard electronics are located externally, the robot must be tethered by tubes and electrical cables, and when they are integrated within the robot, its entire softness is sacrificed. To realize autonomous control of soft robots without electronic components while achieving untethered and fully softness, soft valves capable of controlling pressure using on/off switching mechanisms have been developed (octobot, soft check valve, soft bistable valve, buckling-sheet ring oscillator, etc.). However, these soft valves are challenging to be utilized in proportional applications where continuous and precise control is required because they only discontinuously control the pressure based on the on/off switching mechanisms. Additionally, they require additional sensors for analog sensing of human motion in human-robot interaction, making the system more complex and demanding the use of sensors and electronic controllers. In this work, we developed a STV (soft tensile valve) for analog and self-sensing control of pneumatic soft actuators without any electronic devices. The developed STV continuously adjusts the pressure according to stretching deformation, making it easy to self-sense simple human movements due to its linear and stretchable form, like a soft stretching sensor.

The main part of the STV consists of concentric inner and outer tubes, and yarns, helically wrapping the inner tube with a constant pitch, with two channels: 1) An inlet channel is a cavity between the inner and outer tubes 2) An outlet channel is a cavity inside the inner tube. Constant supply pressure is supplied to the inlet channel, while the outlet channel is exhausted to the atmosphere via the in/out connector on one end of the STV. A chamber connector at the other end of the STV has a chamber port that supplies pressure to the actuator, which is located in the middle of the inlet and outlet channels. Stretching the STV causes helical yarns to deform the shape of the inner tube, resulting in continuous change of chamber pressure due to the change of pneumatic resistance of the inlet and outlet channels. To accommodate task-dependent customizations, the profile of chamber pressure can be programmed by adjusting design parameters such as the number of helical yarns, pitch length, and in/out directions, etc.

By mechanically embedding abilities of self-sensing and continuous pressure control, STV can replace sensors, controllers, and solenoid valves in simple human-robot interaction. As applications, we demonstrate an untethered and electronic-free soft gripper with continuously adjustable gripping force and a soft exosuit that adaptively changes the elbow assist torque according to the elbow angle. We expect STV to pave the way for electronic free and fully soft robots in human-robot interaction.

2:15 PM SB12.12.04

Soft Artificial Electrorceptors for Noncontact Spatial Perception Won Jun Song, Younghoon Lee, Yeonsu Jung, Ho-Young Kim and Jeong-Yun Sun;

Seoul National University, Korea (the Republic of)

Elasmobranch fishes, such as sharks, skates and rays, use a network of electroreceptors distributed on their skin to locate adjacent prey. The receptors can detect the electric field generated by the biomechanical activity of the prey. By comparing the intensity of the electric fields sensed by each receptor in the network, the animals can perceive the relative positions of the prey without making physical contact. Inspired by this capacity for prey localization, we developed a soft artificial electroreceptor that can detect the relative positions of nearby objects in a noncontact manner by sensing the electric fields that originate from the objects. By wearing the artificial receptor, one can immediately receive spatial information of a nearby object via auditory signals. The soft artificial electroreceptor is expected to expand the ways we can perceive space by providing a new sensory modality that did not evolve naturally in human beings.

2:30 PM SB12.12.05

Evaluation of Mechanical Properties of Polycaprolactone (PCL) Staple Electrospun Nanoyarns Using Novel Fabrication Technique [Mohamad Keblawi](#) and Vince Beachley; Rowan University, United States

Biotextiles are biomaterials with textile structure designed for biomedical applications. Depending on their structural properties, biocompatibility, and biostability, biotextiles can be used for various tissue engineering applications such as scaffolds and implants. Electrospun nanofibers have been widely used in many biomedical applications ranging from tissue engineering to drug delivery. Electrospun nanoyarns are biotextiles fabricated using electrospun nanofibers. Currently, electrospun nanoyarns are produced using continuous fiber filaments. As opposed to continuous filament yarns, staple yarns are produced by spinning discrete fiber segments. Due to the difficulty in adapting textile manufacturing processes, staple nanoyarn production is yet to be explored. This study aims to introduce and create a high throughput device capable of collecting and fabricating staple nanoyarns of different materials utilizing the electrospinning technique. The device consists of a roving belt that is used to continuously collect discrete nanofiber segment, which are then spun to create the yarn. The purpose of the project is to fabricate nanoyarns that utilize the advantages of electrospun nanofibers such as high surface-to-volume ratio, and ease of surface functionalization while controlling nanofibers parameters such as fiber length and density, feed rate etc, which current methods do not allow. This will facilitate the systematic investigation of the properties of nanoyarns. Polycaprolactone (PCL) is one of the most widely used polymers for biomedical applications due to its biocompatibility and desirable biodegradation profile. PCL electrospun nanoyarns of various parameters will be fabricated using the proposed device, and their mechanical properties will be explored and compared.

SESSION SB12.13: Virtual Session
Session Chairs: Piero Cosseddu and Darren Lipomi
Wednesday Morning, December 7, 2022
SB12-virtual

8:00 AM *SB12.13.01

Ion-Based Dynamic Tactility for Healthcare and Robotics [Unyong Jeong](#) and Taeyeong Kim; Pohang University of Science and Technology, Korea (the Republic of)

Human skin has different types of tactile receptors that allow distinguishing of mechanical stimuli and temperature. The receptors are composed of ion conductors and their operation is based on the dynamics of the ions. A large number of thermoreceptors and mechanoreceptors are spatially distributed in the dermis, hence the spatial profiles of strain and temperature on the skin can be perceived distinctively. The viscoelastic deformability of the ionic receptors maintains stable electrical signals under large shear strains. This talk presents artificial ionic receptor designs that can simultaneously detect thermal and mechanical information. Two variables are derived from the analysis of the ion relaxation dynamics; the charge relaxation time as a strain-insensitive intrinsic variable to measure absolute temperature, and the normalized capacitance as a temperature-insensitive extrinsic variable to measure the strain. In the fast transient somatosensory processing, the ensemble of the first spikes in the spike trains encodes the dynamic tactile information. This talk proposes artificial dynamic sensory systems based on a new concept, position-encoded spike spectrum (PESS).

8:30 AM *SB12.13.02

Wearable Sensors and Actuators for Mediated Social Touch [Heather Culbertson](#); University of Southern California, United States

Social touch is a complex but crucial component of our daily interactions. Touch has been shown to be able to both convey and elicit emotions, even in the absence of other contextual cues. However, the sense of touch is almost universally removed from all digital interpersonal communication. We are limited in our attempts to express emotions to lines of text on a screen or simple emojis. Our lab is developing a method to allow individuals to send digital touch messages to their friends and partners through wearable haptic devices with the goal of conveying emotions.

Our work seeks to create a wearable haptic device that uses combinations of common social touch gestures (strokes, pats, pokes, squeezes, and massage) to convey emotions to a user through mediated social touch. This talk will discuss a set of wearable haptic sensors and actuators that have been designed to sense and display social touch to the user. These wearable systems use a variety of haptic modalities, including pressure, skin slip, vibration, and electrotactile to convey these social touch gestures with varying realism. I will also discuss our results on conveying emotion through mediated social touch and how the perceived emotion (valence and arousal) can be controlled using the touch's speed.

9:00 AM SB12.13.03

3D Electrically Conductive, *In Situ* Assembled VOC Sensor Incorporating Ti₃C₂T_x MXene and Graphene Nanoribbon (GnR) [Sara Mohseni Taromsari](#), Chul Park and Hani E. Naguib; University of Toronto, Canada

Detection of exhaled volatile organic compounds (VOCs) have long been critical in breathalyzing as a non-invasive diagnosis method. In this regard, development of wearable electrochemical sensors that can accurately monitor exhaled VOCs with various concentrations is essentially important for therapeutic applications. In this study, a novel flexible, highly sensitive, fast responding VOC sensors have been designed and fabricated that can be incorporated into breath analysis devices. Firstly, Ti₃C₂T_x MXene was chosen and synthesized to utilize its high electrical conductivity (5000 S/m) and abundant -O, -OH and -F terminal groups inherently grafted on its surface area. Next, MXene was hybridized with graphene oxide nanoribbon (GONR), synthesized by chemical unzipping of multi-walled carbon nanotubes (MWCNT). The hybridized compounds were then thermally annealed in an Ar atmosphere at 700 °C, to reduce the GONR to graphene nanoribbon (GnR) in presence of MXene and benefitting from its large aspect ratio (500), bridging effect and facile orientation. The redox reaction during the annealing process, transferred the oxygen groups from GONR to MXene, further significantly

increasing MXene's reactive epoxy groups. Secondly, a novel fabrication technique was developed by combining coaxial electrospinning of styrene-butadiene-styrene (SBS)@cetyltrimethylammoniumbromide (CTAB) core@shell membranes and simultaneous electrospinning of MXene and GNR hybrids. The formation of electropositive CTAB shell of SBS membranes electrostatically attracted the electronegative nanohybrids, which enabled in-situ formation of a 3-D electroactive network. The manipulation of MXene's terminal groups and significant increase in the more active oxygen groups, resulted in up to 10-fold enhanced ammonia, acetone, ethanol and methanol response compared to the neat MXene and GNR sensors. The in-situ selective deposition of the fibers led to a 3-D active and conductive structure with enhanced specific surface area of 148% and 125% compared to the neat SBS and conventionally coated SBS and XYZ directions conductivity of 12.21 S/m, 11.75 S/m, 10 S/m, respectively. Thanks to these enhancements, the sensors demonstrated expanded working range of 40 ppb-6000 ppm attributed. The sensors also exhibited mechanical stability for up to 600 deformation cycles which is required for integration into wearable devices and environmental stability when exposed to 80% relative humidity (RH).

9:15 AM SB12.13.04

A Bio-Inspired Interactive Soft Machine Integrated with Embodied Highly Stretchable, Multifunctional Electronic Circuit Feiyang Yuan, Zhixin Xie, Jiaqi Liu, Lufeng Tian, Bohan Chen, Zhongqiang Fu, Sizhe Mao and Li Wen; Beihang University, China

The octopus's tentacles have unique sensing and locally computing capabilities, contributing to their extraordinary manipulation in complex environments. In this study, we imitate this unique feature of octopus tentacles and implement a bio-inspired soft tentacle robot that integrates highly deformable sensors and control circuits. In particular, we integrate IC chips, electronic components, and flexible sensing (suction, bending, and temperature sensing) through printing and transferring liquid metal circuits onto stretchable silicone substrate. Electronic intelligence was embedded into the tentacle. As a result, the tentacle can perceive and processes information, thus endow grasping decision and altering control parameters. Then, we realize the interactive control of the prototype with one human finger. We designed a liquid metal sensing circuit and embedded three vacuum suction cups for haptic feedback. The results show that the tentacle prototype with an integrated sensing-control circuit can reconstruct its bending curve. The robot system can complete the tasks of identifying and avoiding obstacles, detecting and closed-loop grasping objects in an unstructured environment. Through the suction haptic feedback, one can operate the bio-inspired prototype to search, grasp and fetch the target object without visual information. This paper provides a new method for soft robots that operate in unstructured environments and interact safely with humans.

9:30 AM SB12.13.05

Delivering Multi-Sensory and Multi-Scale Haptic Cues through Wearables Marcia K. O'Malley; William Marsh Rice University, United States

Vibrotactile haptic feedback is ubiquitous for notifications and alerts in portable devices such as phones, smart watches, and fitness trackers, but the set of possible notifications is limited by the nature of the eccentric motors so often used to deliver such cues. Wearable haptics refers to systems worn on the body or integrated into clothing that can provide haptic feedback to the wearer in a wide range of forms, such as vibrotactile, cutaneous, skin stretch, pressure, and kinesthetic feedback. The potential for wearable haptics is supported by technological advancements in sensing and actuation that allow for the design and deployment of flexible materials, fabrics, and small-footprint actuators that can augment and enhance human performance. While rigid and grounded haptic feedback devices have been explored as a means to train new motor skills, rehabilitate movement coordination after neurological injury, and even augment human force output capabilities in tasks such as lifting or running, the application space is limited due to the weight and scale of such devices. Wearable haptic devices seek to overcome the limitations of rigid and grounded haptic devices.

In recent years, my group has been designing novel wearable haptic systems that provide multiple haptic modalities of feedback to the user, including vibration, skin stretch, pressure, and kinesthetic feedback, all packaged in bands that can be worn on the arm. We are also exploring how to encode high-fidelity haptic cues that can be actively explored by the fingers within low-fidelity haptic cues that are displayed on the arm. We are particularly interested in applications where the provision of such feedback has a measurable impact on human performance. In this talk, I will present some of our wearable haptic systems, describe our target applications, and highlight the distinguishing features our hardware while identifying opportunities for improvement.

9:45 AM SB12.13.06

PRESENTED ON-DEMAND ONLY: Functional Polymer Gels Based on Oligomer Fluids Zhenwu Wang; Karlsruhe Institute of Technology, Germany

Polymer gels, such as hydrogels, have been widely used in biomedical applications, flexible electronics, and soft machines. Polymer network design and its contribution to the performance of gels have been extensively studied. In this study, the critical influence of the solvent nature on the mechanical properties and performance of soft polymer gels is demonstrated. A polymer gel platform based on poly(ethylene glycol) (PEG) as solvent is presented. Compared to the corresponding gels based on water and ethylene glycol, the PEGgel with physically cross-linked poly(hydroxyethyl methacrylate-co-acrylic acid) demonstrates high stretchability and toughness, rapid self-healing, and long-term stability. Depending on the molecular weight and fraction of PEG, the tensile strength of the PEGgels varies from 0.22 to 41.3 MPa, fracture strain from 12% to 4336%, modulus from 0.08 to 352 MPa, and toughness from 2.89 to 56.23 MJ m⁻³. Finally, rapid self-healing of the PEGgel is demonstrated and a self-healing pneumatic actuator is fabricated by 3D printing. The enhanced mechanical properties of the PEGgel system may be extended to other polymer networks (both chemically and physically cross-linked). Such a simple 3D-printable, self-healing, and tough soft material hold promise for broad applications in wearable electronics, soft actuators, and robotics.

10:00 AM SB12.13.07

PRESENTED ON-DEMAND ONLY: Understanding Continues Force/Energy-Displacement Path of Multistable Metamaterials to Program Their Functionalities Hossein Mofatteh, Benyamin Shahryari, Armin Mirabolghasemi and Hamid Akbarzadeh; McGill, Canada

Mechanical metamaterials are designed to show properties that do not exist in conventional materials. Bistability and multistability as unconventional properties have recently been realized in alternative architectures, such as an inclined beam, curved beam, shallow shells, Origami, and shellulars. Using multistable mechanical metamaterials to develop deployable structures, electrical devices, and mechanical memories raises two unanswered questions. First, can mechanical instability be programmed to design sensors and memory devices? Second, how can we tune mechanical properties at the post-fabrication stage via loading/unloading? Answering these questions requires a thorough understanding of the snapping sequences and variations of the elastic energy in multistable metamaterials. Herein, we model multistable metamaterials as a chain to be transformed into the desired shape by applying deformation on one point. We develop an algorithm based on the snapping sequences for modeling a chain composed of bistable cells. Its solution provides a continuous path with all possible configurations and snap-back released energy. Furthermore, by investigating a 1D chain, we found instability forces are deriving factors of snapping sequence. It has been shown that the order of instability forces determines how many configurations are achievable. We comprehensively unveil the mechanics of deformation sequences and continuous force/energy-displacement curves. This method offers an insight into the programmability of multistable chains, which is exploited here to fabricate a mechanical sensor/memory with sampling and data reconstruction functionalities.

10:15 AM DISCUSSION TIME

SESSION SB12.14: Virtual Session II
Session Chairs: Lucia Beccai and Piero Cosseddu
Wednesday Afternoon, December 7, 2022
SB12-virtual

1:00 PM *SB12.14.01

Toward the Design of High-Realism Texture Displays James E. Colgate; Northwestern University, United States

An unsolved problem in haptics is the realistic display of texture. In other words, it is generally not possible to measure a real-world texture such as a wooden surface, and then based on that measurement, display a virtual texture that, when explored by the bare fingertip, feels convincingly like the original. In this talk, I'll discuss recent experiments that have shed light on the requirements for texture display, as well as progress in developing effective displays.

In a first set of experiments, the skin vibrations caused by sliding over a texture were recorded and then precisely replayed as subjects' index fingers moved over an electroadhesion-based variable friction device. Although an excellent match was achieved in the vibrations, the subjective experience of the replay was little like that of the original texture. Replays were much weaker and qualitatively different. We speculated that the difference was due to the nature of the variable friction technology, which produces stimuli that are synchronous across the contact area of the fingerpad. Physical textures, in contrast, produce distributed stimuli reflecting the spatial inhomogeneity of both the texture and the skin.

In a second set of experiments, we explored the role of asynchronous, inhomogeneous stimuli by using a 14 pin, high-bandwidth pin array to create various vibratory indentation patterns on the index finger. We found that inhomogeneity did, in fact, play a significant role in the subjective experience: greater inhomogeneity led to greater subjective intensity. Surprisingly, it proved difficult to explain these results based on a standard elastic half-space model of skin mechanics, but easy to explain them based on a simple model of surface strain.

Taken together, these studies underscore the importance of distributed actuation, but fall short of providing a prescription for displays capable of high realism. The necessary spatial density and temporal bandwidth are not fully known, and significantly, the relative importance of normal versus lateral surface tractions is not well-understood. We explored this latter topic in a third set of experiments performed with a soft, wearable array of ferromagnetic "pucks". Subjects wore this array on their index fingers while exploring surfaces with various shapes and configurations of magnets hidden underneath. The array provided principally lateral tractions, yet proved quite capable of revealing spatial details such as the locations of edges and vertices. In ongoing work, the ferromagnetic pucks are being replaced by individually addressable electroadhesive pucks (still in a soft, wearable device) so that dynamic, texture-like stimuli may be created. Progress in achieving realism will be discussed.

1:30 PM SB12.14.02

Silver Nanowire Based Transparent and Flexible Force Sensors Nagasarvari Garikapati, Sreekeerthi Pamula and Parasuraman Swaminathan; Indian Institute of Technology Madras, India

Flexible electronics has permeated diverse fields owing to its ease of fabrication, robustness, lightweight, and cost-effectiveness. Touch sensors are used in various areas such as biometric authentication and display devices. Among the plethora of touch sensing techniques adopted, capacitive sensing is popular owing to its high sensitivity, simple structure, thermal stability, and low power consumption [1].

Silver nanowires (AgNWs) have excellent electrical, optical, and mechanical properties and can withstand small bending radii and high strain without affecting the optoelectronic properties. They are thus a viable candidate for transparent, flexible, and foldable devices [1]. Herein, we report flexible force sensors based on capacitive touch sensing, printed using AgNW ink on polyethylene terephthalate (PET) and polydimethylsiloxane (PDMS) substrates, which are both transparent and flexible. The patterns were printed using a custom-built extrusion-based direct writer. PDMS is used to encapsulate the device to provide it with mechanical stability as well as environmental protection. It also acts as the sensing dielectric. PDMS has a low surface energy and is well known for its flexibility, thermal stability, biocompatibility, transparency in the visible region, hydrophobicity, and chemical resistance [2, 3]. Moreover, PDMS can be spin-coated directly on the device and cured below 150 °C, which is compatible with many flexible substrates. The capacitance of the printed network varies with the thickness of the PDMS layer, which can be adjusted using the spin coating parameters.

When metal oxide nanoparticles such as zinc oxide (ZnO) are added to the PDMS matrix, porosity in the polymer matrix tends to reduce and the barrier protection is increased. Moreover, ZnO possesses high hardness, low refractive index, and hydrophobicity [4]. Therefore, PDMS-ZnO is also used as an encapsulant cum dielectric in this work and the force response of the sensors with PDMS and PDMS-ZnO coatings is compared. The change in intrinsic capacitance on touch is sensed by an LCR meter and the applied force is measured as a function of the change in capacitance to calibrate the touch sensor as a force sensor.

Experimentally obtained results have been validated computationally by designing and modelling these capacitance-based planar force sensors using COMSOL simulation software. To incorporate the property of flexibility, the capacitive behaviour of these devices in both flat and bent configurations is compared. The direction of bending and the force applied play a crucial role in the net change in capacitance.

References

- [1] N. M. Nair, K. Daniel, S. C. Vadali, D. Ray, and P. Swaminathan, Flexible and Printed Electronics, 045001 (2019)
- [2] J.M. Han, J.W. Han, J.Y. Chun, C.H. Ok, and D.S. Seo, Japanese Journal of Applied Physics, 47, 8986-8988 (2008)
- [3] X. Cui, G. Zhu, Y. Pan, Q. Shao, C. (xinxin) Zhao, M. Dong, Y. Zhang, Z. Guo, Polymer, 138, 203-210 (2018)
- [4] Sh. Ammar, K. Ramesh, B. Vengadaesvaran, S. Ramesh, A.K. Arof, Progress in Organic Coatings, 92, 54-65 (2016)

1:45 PM SB12.14.03

Multistimuli Responsive Sensors at High Resolution Anna Maria Coclite; Graz University of Technology, Austria

Embedding sensors in smart architectures that record the response from the environment and transform it in a measurable signal is the objective of artificial skins. In this talk, an artificial skin based on a hybrid multi-stimuli responsive material, combining force, temperature and humidity sensing will be presented. The new sensor concept is realized by combining a hydrogel and a piezoelectric material in an array of core-shell structures. This architecture is achieved thanks to the use of vapor-based technologies for material processing, i.e. initiated chemical vapor deposition, atomic layer deposition and nanoimprint lithography. We demonstrate that the skin can detect the stimuli with lateral resolution below the one of human skin. Possible applications

stem from robotics to smart prostheses.

I. T. Abu Ali, P. Schäffner, M. Beleggratis, G. Schider, B. Stadlober, A. M. Coclite, (2022) Smart Core-Shell Nanostructures for Force, Humidity and Temperature Multi-Stimuli Responsiveness, *Adv. Mater. Technol.*, DOI: 10.1002/admt.202200246.

2:00 PM SB12.14.04

Ultraflexible Ferroelectric Transducers and Organic Circuits for Energy-Efficient Wireless Health Patches [Andreas Petritz](#)^{1,2}, Esther Karner-Petritz^{1,2}, Takafumi Uemura², Philipp Schäffner¹, Teppei Araki², Barbara Stadlober¹ and Tsuyoshi Sekitani²; ¹Joanneum Research Forschungsgesellschaft mbH, Austria; ²Osaka University, Japan

Health is a very precious commodity, as we experience every day and especially in these times shaken by a pandemic. Continuous recording of health status through diagnostic techniques that combine high wearing comfort with high reliability, accuracy and cost-effectiveness is therefore very desirable. In this context, we present an ultraflexible solution for the power supply of wireless medical patches for monitoring of heart rate and blood pressure. The ultraflexibility is due to the very low overall thickness (only 2.5 μm in total) of the ferroelectric polymer transducers, organic rectifiers and capacitor components manufactured on a substrate only 1 μm thick, and it guarantees high sensitivity (15 nC N⁻¹), superior component reliability (over 6000 cyclic loading) and a very high peak power density (1 mW cm⁻³ at 2 Hz excitation). Our health patch solution not only includes this radically reduced layer thickness, but also new material combinations (ferroelectric polymers on parylene), novel device concepts (organic thin-film transistor-based diodes) and new integration principles (multi-stack transducers on 3D curved surfaces).¹

¹Petritz, A., Karner-Petritz, E., Uemura, T. et al. Imperceptible energy harvesting device and biomedical sensor based on ultraflexible ferroelectric transducers and organic diodes. *Nat Commun* 12, 2399 (2021). <https://doi.org/10.1038/s41467-021-22663-6>

2:15 PM SB12.14.05

PRESENTED ON-DEMAND ONLY Skin-Conformable Stretchable Sensor for Highly Anisotropic Piezoelectric Signals to Detect Convoluted Multi-axial Motions [Asad Nauman](#), Jun-Chan Choi, Jae-Won Lee, Dong Yeol Hyeon, Kwi-Il park and Hak-Rin Kim; Kyungpook National University, Korea (the Republic of)

Stretchable and multidimensional strain sensors are of great interest for their applications in, health monitoring, soft robots, and detection of human joint motion. Human joints involving ranges of complex motion and joint forces, need to be monitored in real-time with high precision and conformability of wearable strain sensors. For various complex motions, involving different strain ranges, require specific sensitivity for each motion to be introduced, due to the trade-off between sensor sensitivity and stretchability. Traditional stretchable and flexible strain sensors fabricated based on uniform sensing substrate, lack the tunability and anisotropic sensitivity. Many of the existing monitoring systems to continuously monitor the complex joint motion of the human body, that is, wrist, finger, neck, and shoulder, suffer from severe limitations due to their rigid structures and lack of complex motion detection. These sensors fail to give multidirectional deformation information and are sufficiently inadequate for data processing.

In the recent era, stretchable sensors have given new dimensions of research to facilitate the applications of wearable healthcare sensors in monitoring human motions and vital signs. Stretchable piezoelectric sensors due to their quick response to mechanical deformation and adequate sensitivity are one of the suitable candidates for human body motion monitoring. However, the lack of multifunctional ability and adequate stretchability simultaneously in a single unit, makes it difficult for these sensors to detect the complex joint motion of human joints with large strains and multi-axial motions. To achieve the desired anisotropic sensitivity and stretchability, besides the adaptation of intrinsic material stretchability, structural engineering is of high importance. Here, we proposed a mechanically architected heterogeneous structure with intrinsically stretchable active piezoelectric and passive elastomer gratings to tune the sensor's sensitivity depending on the deformation direction. Strain redistribution over the heterogeneous structure is optimized by the mechanical and structural parameter optimization to realize the tunable sensitivity. The local vertical stress distribution over the active piezoelectric material is enhanced when the deformation strain is applied parallel to the alignment direction of gratings, which results in higher sensitivity of output voltage while lower stretchability. The finite element analysis shows an interestingly high concentration of localized stresses inside the piezoelectric layer compared to the passive layer which gives the proof of higher output signals in parallel deformation. The stress distribution and as a result the sensitivity is tuned to the minimum value as the deformation strain angle is perpendicular. The fabricated sensor can monitor and distinguish complex joints motion such as stretching ratio, bending direction, radius, and motion mode simultaneously within one sensor unit. The final device is highly stretchable, lead-free, and skin conformable due to the PDMS matrix and soft Ecoflex. Further, we have used a single electrode piezoelectric configuration for the first time as a sensing unit to increase conformability and portability. A successful demonstration of each motion mode and direction detection and monitoring has been performed experimentally and validated through simulations.

This work was supported by the National Research Foundation of Korea (NRF) grant funded by the Korean government (MSIT) (No 2019R1A2C1005531).

2:20 PM DISCUSSION TIME

SYMPOSIUM SF01

Smart Functions of Stimuli-Responsive Materials
November 28 - December 7, 2022

Symposium Organizers

Jonathan Barnes, Washington University
Po-Yen Chen, University of Maryland
Noemie-Manuelle Dorval Courchesne, McGill University
Siowling Soh, National University of Singapore

Symposium Support
Bronze
ChemComm
Washington University in St. Louis, Department of Chemistry

* Invited Paper
+ Distinguished Invited

SESSION SF01.01: Smart Functions of Stimuli-Responsive Materials I
Session Chairs: Po-Yen Chen and Siowling Soh
Monday Morning, November 28, 2022
Sheraton, 5th Floor, The Fens

10:30 AM *SF01.01.01

Shape Memory in Self-Adapting Colloidal Crystals Chad A. Mirkin; Northwestern University, United States

Reconfigurable, mechanically responsive crystalline materials are central components in many sensing, soft robotic, and energy conversion and storage devices. Crystalline materials can readily deform under various stimuli, and the extent of recoverable deformation is highly dependent upon bond type. Indeed, for structures held together via simple electrostatic interactions, minimal deformations are tolerated. In contrast, structures held together by molecular bonds, in principle, can sustain much larger deformations and more easily recover their original configurations. Herein, we study the deformation properties of well-faceted colloidal crystals engineered with DNA. These crystals are large in size ($> 100 \mu\text{m}$) and have a body-centered cubic (BCC) structure with a high viscoelastic volume fraction ($> 97\%$). Therefore, they can be compressed into irregular shapes with wrinkles and creases, and remarkably, these deformed crystals, upon rehydration, assume their initial well-formed crystalline morphology and internal nanoscale order within seconds. For most crystals, such compression and deformation would lead to permanent, irreversible damage. The significant structural changes to the colloidal crystals are accompanied by dramatic and reversible optical property changes. For example, while the original and structurally recovered crystals exhibit near-perfect ($> 98\%$) broadband absorption in the UV-vis region, the deformed crystals exhibit significantly increased reflection (up to 50% of incident light at certain wavelengths), mainly due to increases in their refractive index and inhomogeneity. This work shows that preparing crystals held together with macromolecular bonds are a viable strategy for creating shape memory materials that can be deliberately engineered to exhibit a wide range of reversible structural and property changes simply not accessible with conventional crystalline architectures held together by other types of bonds.

11:00 AM *SF01.01.02

Encoding Assembly, Transformations and Functions of Nanoscale Architectures Oleg Gang; Columbia University/Brookhaven National Laboratory, United States

The ability to organize diverse types of functional nanocomponents into the targeted architectures promises to enable a broad range of nanotechnological applications, from new classes of engineered biomaterials to photonic devices and materials for energy applications. However, current methods are limited in their ability to create 3D nanostructures with prescribed architecture and integration of different types of nanocomponents. The talk will present our progress in establishing a self-assembly platform for the encoded fabrication of designed large-scale and finite-size nano-architectures from diverse inorganic and biomolecular nanocomponents through the DNA-programmable assembly. The recent advances in creating periodic and hierarchical organizations from inorganic nanoparticles and proteins will be presented. The formed nanostructures can be further transformed into fully inorganic 3D replica via nano-templating. The use of the developed assembly approaches for generating functional nanomaterials with nano-optical, mechanical, and biochemical functions will be demonstrated. Finally, the progress in creating nanomaterials with switchable states will be discussed.

11:30 AM *SF01.01.03

Reactions, Materials and Assemblies Under Rotation Bartosz A. Grzybowski^{1,2}; ¹Ulsan National Institute of Science and Technology, Korea (the Republic of); ²Polish Academy of Sciences, Poland

The uses of rotary systems, e.g., centrifuges or evaporators, are commonplace in separations, but much less explored as the means of controlling the outcomes of chemical reactions or molecular-scale self-assembly or separation processes. Nevertheless, the idea of setting a reaction vessel on spinning is appealing because rotation can generate centripetal and shear forces that could be hard to maintain in a stationary frame of reference. In my talk, I will discuss how this concept can be used to couple macroscopic rotation to events taking place at much smaller scales, down to the molecular. I will illustrate how rotation can mediate self-organization of complex fluidic reactors (driving multistep reaction sequences), affect molecular conformations and enhance crystallization processes, help purify complex mixtures, or set up microgravity conditions for levitating reaction units.

RELEVANT RECENT LITERATURE: *Nature* **586**, 57-63, 2020; *Nature* **579**, 73-79, 2020, *Nat. Rev. Mat.* **7**, 338–354, 2022.

SESSION SF01.02: Smart Functions of Stimuli-Responsive Materials II
Session Chairs: Jonathan Barnes and Emanuele Marino
Monday Afternoon, November 28, 2022
Sheraton, 5th Floor, The Fens

1:30 PM *SF01.02.00

Logical Breakdown: Encoding Boolean-based Responsiveness into Hydrogel Biomaterials Cole A. DeForest; Univ of Washington, United States

The successful transport of drug- and cell-based therapeutics to diseased sites represents a major barrier in the development of clinical therapies. Targeted delivery can be mediated through degradable biomaterial vehicles that utilize disease biomarkers to trigger payload release. Here, we report a modular chemical framework for imparting hydrogels with precise degradative responsiveness by using multiple environmental cues to trigger reactions that operate

user-programmable Boolean logic. By specifying the molecular architecture and connectivity of orthogonal stimuli-labile moieties within material crosslinkers, we show selective control over gel dissolution and therapeutic delivery. To illustrate the versatility of this methodology, we synthesized seventeen distinct stimuli-responsive materials that collectively yielded all possible YES/OR/AND logical outputs from input combinations involving enzyme, reductant, and light. Using these hydrogels we demonstrate the first sequential and environmentally stimulated release of multiple cell lines in well-defined combinations from a material. We expect these platforms will find utility in several diverse fields including drug delivery, diagnostics, and regenerative medicine.

2:00 PM *SF01.02.01

Artificial Molecular Machines That Work at All Scales [Nicolas Giuseppone](#); University of Strasbourg, France

Making molecular machines that can be useful in our macroscopic world is a challenging long-term goal of nanoscience. Inspired by the protein machinery found in biological systems, and based on the theoretical understanding of the physics of motion at the nanoscale, organic chemists have developed a number of molecules that can produce work when triggered by various external chemical or physical stimuli. In particular, basic molecular switches that commute between (meta)stable states, and more advanced molecular motors that produce unidirectional cyclic motions out-of-equilibrium when fueled with external energy, have been reported. However, the integration of individual molecular motors in a continuous mechanical process that can have measurable effects at various length scales and up to the macroscale remains an important objective. We will discuss advances developed by our group on artificial molecular machines, which involve their mechanical coupling with polymer systems. We will show how it becomes possible to integrate them and to make use of their mechanical work going from individual molecular devices to macroscopic materials.

2:30 PM *SF01.02.02

Reversibly Photocontrolled Polymer Networks Through Photoswitchable Dynamic Covalent Bonds [Julia Kalow](#); Northwestern University, United States

In polymer networks based on dynamic covalent bonds, changes in reactivity can be translated into macroscopic responses. Light offers precise, tunable, and noninvasive spatiotemporal control over molecular reactivity. The Kalow lab has designed crosslinks that allow us to tune the thermodynamics and kinetics of dynamic covalent bonds with light, including visible light, based on the conformation of an adjacent photoswitch. When incorporated into polymer networks, the stability or lifetime of these dynamic covalent bonds can be tuned with light. I will discuss the molecular mechanisms underlying these macroscopic changes, as well as rational optimization of photoswitches to enable applications in 3D cell culture.

3:00 PM BREAK

3:30 PM SF01.02.05

Photoswitchable Polymers for Gated Protonic Conductivity [Rachael Hannah](#)¹, Ryan C. Chiechi² and Ben L. Feringa¹; ¹University of Groningen, Netherlands; ²North Carolina State University, United States

Biological systems rely on ionic gradients to function, therefore materials that can conduct protons or larger ions have the potential to interface with living organisms, and have useful applications in medical technology. Incorporating photoswitches into these materials could enable gating of ionic conductivity, given a particular stimulus. Photoswitches are a class of molecular machines wherein the molecule undergoes a conformational change in response to light stimulation. Photoswitches have already been incorporated into a variety of polymers, either into the backbone or as pendant groups, to provide novel functional materials. Spiropyran is a type of photoswitch that undergoes a ring-opening reaction upon irradiation with ultraviolet light to form a highly conjugated, zwitterionic merocyanine form. Incorporation of spiropyrans into various hard and soft materials is a well-studied field, and they have been shown to be able to switch protonic conductivity on and off in metal organic frameworks (MOFs). We have synthesised styrene-based polymers with spiropyran pendant groups anchored through methacrylate moieties (SP-MA) via RAFT polymerisation methods, to be able to control the ionic conductivity of the material with ultraviolet light. The synthesised polymers exhibit photoswitching behaviour in solution and in thin films with high on/off ratio and good fatigue resistance. We then investigated the protonic conductivity of the polymers, by first swelling with ethanol and doping the polymers with sulphuric acid. Acid doping induces the ring-opening reaction, giving the protonated merocyanine, and trapping the proton. Irradiation with visible light induces the ring-closing reaction, giving a free proton, which can then move through the material. The polymer's ability to gate protonic conductivity in thin film devices was measured with impedance spectroscopy.

3:45 PM SF01.02.06

Nanocrystal Superparticles with Whispering-Gallery Modes Tunable Through Chemical and Optical Triggers [Emanuele Marino](#), Harshit Bharti, Jun Xu, Cherie R. Kagan and Christopher B. Murray; University of Pennsylvania, United States

Whispering-gallery microresonators have the potential to become the building blocks for optical circuits. However, encoding information in an optical signal requires on-demand tuning of optical resonances. Tuning is achieved by modifying the cavity length or the refractive index of the microresonator. Due to their solid, nondeformable structure, conventional microresonators based on bulk materials are inherently difficult to tune. In this work, we fabricate irreversibly tunable optical microresonators by using semiconductor nanocrystals. These nanocrystals are first assembled into colloidal spherical superparticles featuring whispering-gallery modes. Exposing the superparticles to shorter ligands changes the nanocrystal surface chemistry, decreasing the cavity length of the microresonator by 20% and increasing the refractive index by 8.2%. Illuminating the superparticles with ultraviolet light initiates nanocrystal photo-oxidation, providing an orthogonal channel to decrease the refractive index of the microresonator in a continuous fashion. Through these approaches, we demonstrate optical microresonators tunable by several times their free spectral range.

Reference: E. Marino et al., Nano Letters, In press, 2022. DOI: 10.1021/acs.nanolett.2c01011.

4:00 PM SF01.02.07

Design and Application of Dynamic Polypyrrole Core-Shell Particles [Weize Yuan](#) and Timothy Swager; Massachusetts Institute of Technology, United States

Conducting polymer fabricated oil-in-water (o/w) colloidal particles had been developed via a single step of in situ interfacial polymerization of an emulsion phase. A unique core-shell structure of these particles was exhibited where the shell was governed by a thin layer of polypyrrole (pPy) film at the o/w interface. These core-shell particles demonstrated unique actuation configurations when pPy is chemically oxidized into the charged state or alternatively reduced into the non-charged state. Notably, these particles showed their ability to expand up to 400% in dimension while retaining their structure and were able to shrink back to their original sizes when reduced. The forces generated from their particles' interface during expansion can be calculated by measuring the size of the triggered inflation of pPy particles inside the different polyethylene glycol (PEG) gels. In addition, post functionalization of pPy particles via a thiol-Michael reaction was able to modify the hydrophobicity of pPy particles' interface. The particles hence showed remarkable conformal coating behavior onto hydrophilic membranes with the attached carboxylates functional groups on the particle surfaces. The

capability of post-functionalize pPy core-shell particles' surface provides the chance for them to be further bio-conjugated as well. Organic dyes compatible with the core-shell particles could be trapped within the interior of the core structure, indicating the prospects of pPy particle as a platform for loading small molecules. The dynamic structures and unique properties of these pPy particles have been demonstrated to be applicable in actuation, coating, and biosensing.

4:15 PM SF01.02.08

Optimal Design Methodology for Maximum Electro-Momentum Coupling in Piezoelectric Metamaterial Scatterers Jcong-Ho Lee, Zhizhou Zhang and Grace Gu; University of California, Berkeley, United States

As an elastodynamic bianisotropy, Willis coupling has been widely employed for acoustic metamaterials in which the linear momentum is additionally coupled to strain at the macroscale while it is coupled only to velocity by mass density at the microscale. Recently, a novel coupling, called electro-momentum coupling, is discovered for piezoelectric materials responding to electric fields such that the macroscopic momentum can also be coupled with electric stimuli. This electromechanical bianisotropy implies the possibility of programmable functionality in piezoelectric metamaterial devices as electro-momentum coupling can be smartly controlled by modulation of external stimuli, *i.e.*, active wave manipulation by stimulus modulation. However, the theory of how the electro-momentum coupling coefficient depends on external stimuli has not been developed in the previous literature. At the same time, how to rationally design microstructures with consideration for their sensitivity to the coupling coefficient has not been widely studied for two-dimensional cases. In this work, we aim to propose a general, optimal design methodology to design microstructures of piezoelectric metamaterials with external stimuli that can reach the theoretical maximum bianisotropic performance of scattering proposed in our previous work for piezoelectric metamaterial scatterers. Additionally, machine learning algorithms will be used to efficiently complement computational approaches in the design framework as well as to overcome the intrinsic nonlinearities of coupling.

4:30 PM SF01.02.09

Multifunctional Photoresponsive Organic Molecule for Electric Field Sensing and Modulation Patrick J. Saris, Shakthi Srinivasan and Andrea M. Armani; University of Southern California, United States

Bioelectricity is crucial to the normal function of organisms. It is also likely to be an indicator of damage or disease and can drive wound healing. We have engineered a molecular tool to study nanoscale electrical environments that can both “read” and “write” the surrounding bioelectric field. The “read” module is a voltage sensitive fluorescent dye which exhibits aggregation induced emission and two photon absorption. The “write” module consists of a pair of photoconductive organic molecules inspired by xerography, which can be activated with ultraviolet light to modify the local electric field. The rational and computational design of each module, as well as the reduction in crosstalk between the modules, will be discussed. Our all-optically-controlled molecular device is compatible with imaging techniques already widely used by researchers in the field, while adding co-localized multifunctional control.

SESSION SF01.03: Smart Functions of Stimuli-Responsive Materials III

Session Chairs: Po-Yen Chen and Siowling Soh

Tuesday Morning, November 29, 2022

Sheraton, 5th Floor, The Fens

8:30 AM *SF01.03.01

Responsive Soft Matter via Multi-Material 3D Printing Jennifer A. Lewis; Harvard University, United States

Soft responsive materials are of great interest for applications ranging from soft robotics to frequency shifting antennae. By combining inverse design and multi-material 3D printing, we have created soft materials that actuate in response to external stimuli. We have developed multiple printable inks composed of different elastomeric matrices, whose mechanical properties and shape-morphing behavior are programmed on demand. Several examples will be highlighted, including planar and 3D architectures with controlled local composition and structure.

9:00 AM *SF01.03.02

Soft Medical Robots Xuanhe Zhao; Massachusetts Institute of Technology, United States

This talk will discuss the smart materials, fabrication, and clinical translations of soft medical robots. We will use a magnetically-steerable soft guidewire robot capable of teleoperated robotic neurointervention as an example. We will first discuss the theory of magnetically-responsive soft materials that enables predictive models for the large deformation and actuation of the soft robot. Then we will discuss how to use the massive simulation data of the models to guide the design, 3D printing, and control of the soft robot. Thereafter, we will demonstrate the soft guidewire robots' applications in remotely treating hemorrhagic and ischemic strokes by robotic aneurysm coiling and clot retrieval, respectively. We will validate the safety and efficacy of the soft guidewire robot in both phantom models and live pig models, and compare its performances with experienced neurointerventionalists carrying out manual operations. I will conclude the talk with a vision for the future development and impacts of soft medical robots – aided by and synergized with technologies such as mechanics-based AI, VR, and precision medicine.

9:30 AM *SF01.03.03

Programmable Shape-Change and Crawling Gels David H. Gracias; Johns Hopkins University, United States

The living world is composed of materials with a large water content and understanding how to create smart hydrogel materials and structures is critical to enable human-collaborative robots, biomedical and adaptive devices. In this talk, I will describe results on temperature and DNA stimuli responsive gels that illustrate the use of molecular design, micro/mesoscale patterning, and segmentation and swelling/deswelling to drive complex shape change, programmability, and even unidirectional locomotion. Importantly, these functions are driven by temperature or chemical signals without the need for any wires, tethers, or external power sources. They illustrate the ability to control and manipulate shape, curvature, and displacement by environmental cues offering the potential for smart materials and devices with a wide range of applicability in engineering and medicine.

10:00 AM BREAK

10:30 AM *SF01.03.04

Stimuli-Responsive Polymer-Ligated Nanoparticles and Nanorods—From Self-Assembly to Tailored Optical and Catalytic Properties Zhiqun Lin;

National University of Singapore, Singapore

In this talk, I will discuss a unique amphiphilic-nonlinear-block-copolymer-nanoreactor strategy for crafting stable hairy nanocrystals (nanoparticles (NPs) and nanorods (NRs)) with light- as well as thermal-promoted reversible and reliable self-assembly and tunable optical and catalytic properties. The size and shape of hairy nanocrystals can be precisely tailored by modulating the length of inner hydrophilic block of nonlinear block copolymers. The permanent anchoring of stimuli-responsive polymers on the nanocrystal surface renders the attractive feature of self-assembly and disassembly of nanocrystals on demand using stimuli of different wavelengths of light or temperature. In the first study, photo-responsive polymer-ligated noble metal NPs and NRs display tunable surface-plasmon resonance absorption and the reversible transformation of NPs and NRs between their dispersed and aggregated states. In the second study, thermo-responsive polymer-ligated noble metal NPs manifest controllable catalytic activity in nonmonotonic (i.e., non-Arrhenius-type dependence on temperature) or on/off (i.e., effectively switched “on” and “off” catalysis over temperature) manner over a broad region of temperature. By extension, this strategy enables the crafting of a family of stable stimuli-responsive nanocrystals and their assemblies for fundamental research in self-assembly and crystallization kinetics of nanocrystals as well as potential applications in optics, optoelectronics, magnetic technologies, sensory materials and devices, catalysis, nanotechnology, and biotechnology.

11:00 AM *SF01.03.05

Electrostatic Self-Assembly of Nanoparticles into Static and Out-of-Equilibrium Materials [Rafal Klajn](#); Weizmann Institute of Science, Israel

Self-assembly of inorganic nanoparticles into ordered structures (superlattices) has led to a wide range of nanomaterials with unique optical, magnetic, electronic, and catalytic properties. Various interactions have been employed to direct the crystallization of NPs, including van der Waals forces, hydrogen bonding, as well as electric and magnetic dipolar interactions. Among them, Coulombic interactions have remained largely underexplored, owing to the rapid charge exchange between nanoparticles bearing high densities of opposite charges (superionic nanoparticles). In this talk, I will describe a new method to assemble superionic nanoparticles under conditions (room temperature, concentrated salt solutions) that preserves their native surface charge density. Under these conditions, the Coulombic interactions between superionic nanoparticles are reminiscent of short-range intermolecular interactions. Our methodology was used to assemble oppositely charged NPs into high-quality superlattices exhibiting Catalan shapes. This methodology can be applied to a wide range of charged nanoparticles of various sizes, shapes, and compositions. I will also discuss how electrostatic interactions can be used to assemble nanoparticles into transient assemblies, whose lifetime depends on and can be controlled by the availability of a small-molecule ionic “fuel”.

11:30 AM *SF01.03.06

Active Matter Swarms for Cargo Capture, Transport, and Delivery [Ayusman Sen](#); The Pennsylvania State University, United States

Autonomous nano/microparticles are of great current interest due to their potential applications in cargo delivery, nanoscale assembly, robotics, fluidics, and chemical/biochemical sensing. Light provides a particularly useful means of manipulating motility since the stimulus can be applied remotely, patterned with a photomask, and readily translated to irradiate specified locations. A single particle generates a relatively small propulsive force and cannot be employed to transport a large payload. As with social insects, such as ants, the solution lies in designing swarms of particles that can act cooperatively. Accordingly, the three outstanding challenges in the expanding field of autonomous nano/microparticle systems are: 1) to design fuel-free systems in which directed motion of nano/microparticle swarms can be powered solely by light, 2) to demonstrate function that can only be carried out by swarms, rather than by individual particles, and 3) to repeatedly pickup, transport, and deliver multiple cargo types. We will simultaneously showcase all three capabilities using titanium dioxide microparticle swarms. The swarms can be moved directionally using light. The swarms can collect and release a variety of inert cargo particles on demand. Moreover, the cargo particles of different sizes can be sorted and released sequentially.

SESSION SF01.04: Smart Functions of Stimuli-Responsive Materials IV
Session Chairs: Noemie-Manuelle Dorval Courchesne and Olga Kuksenok
Tuesday Afternoon, November 29, 2022
Sheraton, 5th Floor, The Fens

1:30 PM *SF01.04.01

Actuation of 3D Printed Nanocolloidal Hydrogel with Structural Anisotropy [Eugenia Kumacheva](#); Univ of Toronto, Canada

Polymer hydrogels exhibit actuation properties that result in stimulus responsive reversible shape transformations and have promising applications in soft robotics, drug delivery systems, sensors, and microfluidic devices. Actuation occurs due to differential hydrogel swelling and is achieved by modulating site-specific composition of hydrogel sheets, either laterally (in-plane), or via a bilayer approach. We proposed a different strategy for hydrogel actuation that originates solely from its structural anisotropy. For 3D-printed single-layer hydrogels formed by cellulose nanocrystals (CNCs) and gelatin methacryloyl we showed that shear-induced orientation of CNCs results in anisotropic mechanical and swelling properties of the hydrogel. Upon swelling in water, planar hydrogels acquired multiple complex 3D shapes that are achieved by (i) varying CNC orientation with respect to the shape on the hydrogel sheet and (ii) patterning the hydrogel with the regions of shear-mediated and random CNC orientation. This study shows the capability to generate multiple shapes from the same hydrogel actuator based on the degree of its structural anisotropy. Furthermore, it introduces a biocompatible nanocolloidal ink with shear-thinning and self-healing properties for additive manufacturing of hydrogel actuators.

2:00 PM *SF01.04.02

3D Fabrication of Biohybrid Networks Using Protein Mechanophores [Alshakim Nelson](#); University of Washington, United States

Bio-sourced and biodegradable polymers for additive manufacturing could enable the rapid fabrication of parts for a broad spectrum of applications ranging from healthcare to aerospace. However, a limited number of these materials are suitable for vat photopolymerization processes. Herein, we report a process to fabricate protein-based constructs using commercially available vat photopolymerization printers. Bovine serum albumin (BSA) is a single-chain nanoparticle that can be chemically derivatized with acrylate and methacrylate functionalities. Aqueous resins were formulated from these materials to produce complex 3D geometrical constructs with a resolution comparable to commercial resins. While BSA is often used in cell culture protocols and diagnostic assays, we demonstrate that BSA can serve as junctions within polymer networks to afford stiff hydrogels and bioplastics with unique physical properties. Protein-based shape-memory objects that utilize BSA as mechanophores will be highlighted as opportunities for future applications.

2:30 PM *SF01.04.03

Self-Healing Hydrogels—From Soft Robots to Self-Repairing Biomaterials [Shyni Varghese](#); Duke University, United States

Polymer networks are widely used in biomedical and environmental applications. Hydrogels with “living” functions such as self-healing and stimuli-responsiveness are particularly attractive because of their ability to repair structural damages and adapt to the environmental changes. Furthermore, self-healing hydrogels with shear-thinning properties can be potentially used to deliver biomolecules or as building blocks towards in situ curing scaffolds. Herein, I will briefly discuss our efforts in creating self-healing hydrogels and harnessing their properties for applications in soft robotics and tissue repair.

3:00 PM BREAK

3:30 PM SF01.04.04

Modeling Hydrogels with Host-Guest Interactions—Focus on Pattern Formation and Restructuring [Olga Kuksenok](#) and Yao Xiong; Clemson University, United States

Pattern formation and reconstruction under external stresses plays an important role in defining functionality of a broad range of soft confined systems. Herein we focus on dynamic control of pattern formation and restructuring in hydrogels with host-guest interactions. We extend the three-dimensional gel Lattice Spring Model (gLSM) to capture the dynamics of the PNIPAAm hydrogels with pendant azobenzene moieties immersed into alpha-cyclodextrins (alpha-CD) solutions under the UV and visual light. While planar *trans*-azobenzene moieties can be recognized and efficiently accommodated by the alpha-CD cavities to form inclusion complexes, an exposure to UV irradiation drives the *trans*-to-*cis* photoisomerization and dissociation of the complexes. We first demonstrate that the proposed model accurately reproduces volume phase transitions in azobenzene-functionalized hydrogels with host-guest interactions reported in recent experiments. We then use spatiotemporal variations in UV irradiation to control pattern formation in thin hydrogel films under the rigid and soft confinements and to control hysteresis loops. The soft confinement is introduced via illuminating the ridges of the thin hydrogel samples with UV light and thereby introducing localized regions with higher rigidity. We show that controllable feedback mechanisms can be introduced into the networks with host-guest interactions via well-defined illumination patterns.

3:45 PM SF01.04.06

Biotemplating of Functional Nanomaterials into Magnetically Driven Microrobots for Biomedical Applications [Carlos Franco Pujante](#)¹, Salvador Pane i Vidal¹ and Josep Puigmarti-Luis²; ¹ETH Zurich, Switzerland; ²Universitat de Barcelona, Spain

In micro and nanorobotics research, while a significant body of small-scale device investigation has been dedicated to building artificial versions of nature, other studies have exploited biological structures as templates or scaffolds to engineer robotic devices or machinery. This approach, known as Biotemplating, offers a robust methodology for manufacturing small-scale devices (i.e., micro and nanorobots) with potential applications in different fields like biomedicine.

Herein, we present a universal biotemplating approach that uses naturally occurring helical architectures to obtain controlled 3D assemblies of nanocrystalline of various functional materials like metal-organic frameworks (MOFs), piezoelectric nanoparticles, and 2D materials. Our process exploits *Spirulina platensis*, filamentous cyanobacteria with a helical body, which provides the shape of the final composite microstructure. Next, we create a magnetic helical chassis on top of the *Spirulina platensis*, which is subsequently coated with various functional nanocrystals. The resulting composite helical structure is a highly integrated, magnetically driven functional material-based microrobot.

In particular, taking advantage of these highly tunable materials, we demonstrated outstanding localizing drug delivery when biocompatible porous materials like Mil-100 nanoparticles are integrated with our magnetic biotemplates. Additionally, the inclusion of piezoelectric nanoparticles like Barium Titanate (BTO) allows us to fabricate magnetically driven microrobots with the capacity to degrade fibril proteins, such as A β -42 amyloid aggregates, involved in Alzheimer's disease. Our studies demonstrated that, under low-power ultrasound stimulation, the piezoelectric microrobots generate reactive oxygen species (ROS) that can disintegrate the protein aggregates into smaller amyloids in less than one hour. Finally, the unique physicochemical properties of 2D-Materials like Molybdenum Disulfide (MoS₂) grants the microrobots with the ability to locally increase the temperature. Our microrobots offer exceptional capabilities for photothermal ablation, inducing cancer cell killing with similar efficiency as state-of-the-art chemotherapeutic drugs. Moreover, the chemistry of the MoS₂ can be easily modified in order to achieve additional functionalities. For example, we show that the microrobots can also serve as on-the-fly biorecognition platforms by decorating their surface with streptavidin-functionalized gold nanoparticles, which can selectively capture and transport biotin-coated microbeads.

In summary, we have created a universal biotemplating-based methodology to fabricate 3D helical assemblies with functional nanocrystals. Taking advantage of the specific chemistry associated with each kind of functional material, we are able to tune the microrobots to the application of interest. The countless possibilities of our newly introduced biotemplated methodology are only matched by the amount of different functional systems and their specific properties, opening the door to a vast number of application in micro and nanorobotics.

4:00 PM SF01.04.07

One-Step, Rapid 3D Printing of Multi-Stimuli-Responsive Bilayer Structures for Microscale Actuators and Sensors [Xiao Huan](#) and Ji Tae Kim; The University of Hong Kong, China

Microscale stimuli-responsive structures play an important role in micromechanical systems as they can serve as sensors or actuators¹⁻⁵. However, the development of simple and rapid methods for their fabrication remains an unsolved challenge⁶⁻⁸. Here, we present a one-step, bi-material 3D printing method for fabricating multi-stimuli-responsive microactuators⁹. A two-phase femtoliter meniscus formed on a theta micropipette is used to print a freestanding bilayer microstructure with programmed shape and composition, which undergoes an asymmetric volume change upon the adsorption or desorption of water. The printed bilayer structures exhibit reversible, preprogrammed actuation under time-varying humidity and infrared (IR) light stimuli. Furthermore, the method provides unprecedented process simplicity in multi-segmented structuring, configuring useful microscale moves such as gripping micro-objects. In this talk, I will also discuss the potential of our method to afford a diverse class of smart-bilayer devices such as actuators, sensors, and energy harvesters, by diversifying printing materials.

1. M. Li, A. Pal, A. Aghakhani, A. Pena-Francesch and M. Sitti: Soft actuators for real-world applications. *Nature Reviews Materials* **7**, 235 (2022).
2. C.S.X. Ng, M.W.M. Tan, C. Xu, Z. Yang, P.S. Lee and G.Z. Lum: Locomotion of Miniature Soft Robots. *Advanced Materials* **33**, 2003558 (2021).
3. D. Melling, J.G. Martinez and E.W.H. Jager: Conjugated Polymer Actuators and Devices: Progress and Opportunities. *Advanced Materials* **31**, 1808210 (2019).
4. S. Palagi and P. Fischer: Bioinspired microrobots. *Nature Reviews Materials* **3**, 113 (2018).
5. X.-Q. Wang and G.W. Ho: Design of untethered soft material micromachine for life-like locomotion. *Materials Today* **53**, 197 (2022).

6. X. Le, W. Lu, J. Zhang and T. Chen: Recent Progress in Biomimetic Anisotropic Hydrogel Actuators. *Advanced Science* **6**, 1801584 (2019).
7. L. Hu, Y. Wan, Q. Zhang and M.J. Serpe: Harnessing the Power of Stimuli-Responsive Polymers for Actuation. *Advanced Functional Materials* **30**, 1903471 (2020).
8. M. Ilami, H. Bagheri, R. Ahmed, E.O. Skowronek and H. Marvi: Materials, Actuators, and Sensors for Soft Bioinspired Robots. *Advanced Materials* **33**, 2003139 (2021).
9. X. Huan, S. Lee, H. Lee, Z. Xu, J. Yang, M. Chen, Y. Liu and J.T. Kim: One-Step, Continuous Three-Dimensional Printing of Multi-Stimuli-Responsive Bilayer Microactuators via a Double-Barreled Theta Pipette. *ACS Applied Materials & Interfaces* **13**, 43396 (2021).

4:15 PM SF01.04.08

IR-Responsive Plasmonic Indium Tin Oxide/Polyketone Nanocomposites with Fast Self-Healing Features [Andrea Pucci](#)¹, Alessio Gabbani¹, Francesco Pineider¹, Virgilio Mattoli², Valentina Cappello², Mauro Gemmi², Arianna Mazzotta², Esteban Araya Hermosilla², Marina Ruggeri¹, Francesco Picchioni³, Ranjita Bose³ and Felipe Orozco³; ¹University of Pisa, Italy; ²Istituto Italiano di Tecnologia, Italy; ³University of Groningen, Netherlands

Materials endowed with (very) fast self-healing are highly demanded to get rid of polymer pollution and enhance the materials service life. On this account, in this contribution, nanocomposites with rapid self-healing thermo-responsive characteristics were proposed and based on the homogeneously dispersed indium tin oxide (ITO) nanocrystals (NCs). ITO NCs were used as an infrared photothermal source due to their remarkable near-infrared (NIR) plasmonic properties and visible transparency. A furan grafted polyketone (PKFU) was utilized as supporting polymer matrix and obtained by the Paal-knorr functionalization of PK and crosslinked via the Diels-Alder (DA) reaction of an aromatic bismaleimide. Nanocomposites containing the 0.4–1.5 wt% of ITO NCs showed strong NIR absorption and, once exposed to IR irradiation, displayed fast heating (30 seconds) up to temperatures higher than 160 °C and superior to 60 °C gathered by the bare PKFU. The addition of ITO NCs did not affect the thermal behaviour of the matrix with the retro-Diels-Alder onset at 95 °C and the softening point at 50 °C that triggered the healing process. It was worth noting that the nanocomposite containing the 0.9 wt% of ITO NCs displayed the fastest healing rate that occurred after 1 second of IR irradiation, i.e. significantly faster than 50 seconds required for the bare crosslinked PKFU.

SESSION SF01.05: Smart Functions of Stimuli-Responsive Materials V
 Session Chairs: Po-Yen Chen and Siowling Soh
 Wednesday Morning, November 30, 2022
 Sheraton, 5th Floor, The Fens

8:15 AM *SF01.05.01

Stimuli Responsive Covalent Nanogels—A Chemically Versatile Drug Delivery Platform [Nazila Kamaly](#); Imperial College London, United Kingdom

Nanogels are hydrogels within the nanometer range consisting of crosslinked porous polymer networks with the ability to retain high volumes of water or biological fluids whilst maintaining their structure. They have a wide range of chemical flexibility in their design, allowing their characteristics such as size, charge, degree of porosity and degradability to be easily tuned by the choice of monomeric building blocks. Since nanogels can retain a high volume of water, they are extremely biocompatible. This excellent and unique property makes them an ideal nanoplatform for the delivery of biological drugs such as enzymes and proteins. Nanogels are prepared via polymerization of monomers or precursors by chemical crosslinking or via physical crosslinking of preformed polymers via amphiphilic or electrostatic interactions. In particular, covalently crosslinked and co-polymerized nanogels (Figure 1) have superior properties as they offer: 1) encapsulation stability for biologically sensitive payloads, 2) they have low immunogenicity and toxicity, and can be designed to be fully biodegradable, 3) multiple biological payloads can be delivered in a single nanogel, facilitating combination therapies, 4) their synthesis can be aqueous based and easily scaled, and 5) they are soft nanoparticles that can easily squeeze through restricted sites under hemodynamic shear flow. In this manner, nanogels are the ideal delivery platform for biological drugs especially since biological therapeutics can be encapsulated into nanogels using mild aqueous reaction conditions. In this talk I will present some of our work on stimuli-responsive nanogels.

8:45 AM *SF01.05.02

Multiresponsive Hydrogels as Smart Materials for Actuator and Sensor Functions in Microfluidic Application [Brigitte Voit](#)^{1,2}; ¹Leibniz Institute of Polymer Research Dresden, Germany; ²Technische Universität Dresden, Germany

Responsive polymeric materials are becoming a highly studied field especially with regard to their use in technical applications, e.g. as sensors and actuators in microsystems and microfluidic applications, since they are able as volume gels to carry out mechanical work reacting on e.g. chemical stimuli. In addition, compartmentalization becomes an issue for being able to localize specific actions and reactions e.g. by patterning specific hydrogel compartments. We will report on the preparation and integration of responsive and biocompatible hydrogel dots and hydrogel dot arrays of high flow and shear stability in microfluidic channel and chamber reactors. For that, multiresponsive hydrogels are developed making use of interpenetrating network approach and the concept of graft copolymer networks for retaining responsiveness for up to four different stimuli in one hydrogel.¹ The hydrogels have been adapted for integration into microfluidic devices as volume-changing gels, adjusting degree of swelling as well as mechanical stability and allowing their use as effective sensors and actuators as needed for a chemical valve function. First examples of their use as chemical transistors and the development of logical modules for achieving basic logic gate functions through a microfluidic setup are shown.² Further optimization has been achieved by combining in double-crosslinked systems permanent and dynamic and reversible crosslinking points introducing redox functions and host-guest interactions.^{3,4,5} The dynamic responsive behavior could be translated into micrometer hydrogel dots in microsystems combining actuator function with specific bioresponse. First results are presented to use reversible redox bonding in hydrogels for triggered peptides capturing.⁶

¹Gräfe, D.; Erdmann, T.; Richter, A.; Appelhans D.; Voit, B. *ACS Appl. Mater. Interfaces*, 2017, 9, 7565. ²Frank, P.; Gräfe, D.; Probst, C.; Häfner, S.; Elstner, M.; Appelhans, D.; Kohlheyer, D.; Voit, B.; Richter, A., *Adv. Funct. Mater.* 2017, 1700430.

³Che, Y.; Zschoche, Z.; Appelhans, D.; Obst, F.; Voit, B.; *J. Polymer Science: Polym. Chem A*, 2019, 57, 2590.

⁴Che, Y.; Liubimtsev, N.; Zschoche, S.; Gaitzsch, J.; Bauer, T.; Appelhans, D.; Voit, B. *Soft Matter*, 2020, 16, 6733.

⁵Liubimtsev, N.; Kösterke, T.; Che, Y.; Appelhans, D.; Gaitzsch J., Voit, B. *Polym. Chem.*, **2022**, 13, 427

⁶Jiao, C.; Obst, F.; Geisler, M.; Che, Y.; Richter, A.; Appelhans, A.; Gaitzsch, J.; Voit, B. *Polymers (MDPI)*, 2022, 14, 267.

9:15 AM *SF01.05.03

Rational Molecular Design of Stimuli-Responsive Conjugated Functional Materials for Optical Biosensors [Jinsang Kim](#); Univ of Michigan, United States

Conjugated polymers (CPs) and organic molecules have become emerging materials for many modern technologies due to their readily tunable properties by variation of chemical structure and easy fabrication. Particularly the stimuli-responsive properties have gained much interest in sensor application of conjugated organic and polymeric materials. Our self-signaling optical sensors are designed to achieve high sensitivity by means of the external stress-responsive optical property of conjugated polymers. Receptors are rationally designed to provide specificity toward a target analyte to realize high selectivity. DNA aptamer design, specific chemical reaction, secondary bonding, lipid molecule, and antibody-antigen interaction have been utilized in the receptor design. The concept, design principles, and applications of polydiacetylene-based optical sensory systems for the detection of DNA, proteins, metal ions, influenza virus, antibiotics, prostate specific antigen, nerve agents, platelet activation, and melamine will be discussed. Novel sensory systems based on emissive super-cooled liquids and metal-free purely organic phosphors (POPs) will also be briefly presented. In our recent development of highly emissive and metal-free purely organic phosphorescence materials for the last decade, directed intermolecular heavy atom effects were rationally implemented in aromatic carbonyl molecules to promote spin-orbit coupling and suppress vibrational dissipation. Due to rather slow electron spin flipping of POPs, the slow phosphorescence feature renders highly sensitive oxygen quenching via energy transfer from POP's triplet state to surrounding oxygen molecules in the ground state. This unique phenomenon has been utilized in a newly devised lipid-polymer hybrid POP turn-on nanoprobe for chorioretinal hypoxia detection *in vivo* using rabbit retinal vein occlusion and choroidal vascular occlusion models.

9:45 AM BREAK

10:15 AM *SF01.05.04

Non-Viral Nanocarriers for the Delivery of Nucleic Acids and Genome Editors [Sarah Gong](#); University of Wisconsin–Madison, United States

The CRISPR/Cas9 system is a revolutionary and versatile genome editing technique with wide-ranging utility. It can target and edit disease-causing mutations in a sequence-dependent manner, resulting in a permanent genetic change and thus offering the promise to cure genetic diseases. *In vivo* somatic genome editing using CRISPR/Cas9 is anticipated to be the next wave of therapeutics for many major health threats. However, one major hurdle to clinical translation of the CRISPR-based gene therapy is the lack of safe and efficient delivery systems for the CRISPR genome editors. We sought to develop customizable, safe and efficient nanoplatforms to deliver a wide range of biologics *in vitro* and *in vivo*. Our design criteria include (1) good biocompatibility, (2) high loading content and loading efficiency, (3) excellent stability before reaching the target cell, (4) high specificity to target tissue/cell, (5) high cellular uptake, (6) efficient endosomal escape capability, (7) rapid release of the cargo inside the cytosol via a stimuli-responsive release mechanism, (8) efficient transport to the nucleus, and (9) ease of production, storage, and transport.

Following this set of design criteria, we have engineered several types of multifunctional nanocarriers for safe and efficient delivery of biologics during the past few years, including polymeric Cas9/sgRNA ribonucleoprotein (RNP) nanocapsules¹, GSH-responsive silica nanocapsules², and self-assembled polymeric RNP or RNP-ssODN nanoparticles³. Our judiciously designed nanocarriers can encapsulate various types of payloads (i.e., DNA, mRNA, Cas9/sgRNA RNP, Cas9 mRNA/sgRNA, base editor, etc.) with high loading contents and high loading efficiencies. The versatile surface chemistry allows for surface PEGylation and/or targeting ligand conjugation that improves the pharmacokinetics and cell/tissue-specific delivery efficiency. These nanocarriers can induce high transfection efficiency/genome editing efficiencies *in vitro* and *in vivo* in different cells/tissues without apparent toxicity. Specifically, through local or systemic administrations, our nanocarriers were proved to be effective in transfection or genome editing in neurons and astrocytes in the brain (via both local and systemic delivery), retinal pigment epithelium (RPE) cells in the retina (via subretinal injection), myofibers and satellite cells in the muscle (via intramuscular injection), epithelial cells in the lung (via intratracheal administration), and hepatocytes in the liver (via intravenous injection). Moreover, the *in vivo* biocompatibility and immunogenicity of these nanocarriers after systemic or local administrations were demonstrated by systematic investigation of the blood biochemical parameters, inflammatory cytokines and organ/tissue histology. Thus, we anticipate that these multifunctional nanocarriers can be further tailored to enable gene therapy for many different types of diseases including Alzheimer's disease, Duchenne muscular dystrophy, and cystic fibrosis.

Acknowledgment: Many researchers in the Gong lab including Dr. Yuyuan Wang, Dr. Ruosen Xie, Dr. Guojun Chen, Dr. Xiuxiu Wang and in our collaborators' labs including Dr. Bikash Pattnaik, Dr. Pawan K. Shahi, Dr. Krishanu Saha, Dr. Amr A. Abdeen, Dr. David M. Gamm, Dr. Marina Emborg, Dr. Jeanette M. Metzger, Dr. Jon Levine, Dr. Masatoshi Suzuki, Dr. Kathy Snow, and Dr. Steve Murray contributed to these projects.

References:

- 1 Chen, G. *et al.* A biodegradable nanocapsule delivers a Cas9 ribonucleoprotein complex for *in vivo* genome editing. *Nature nanotechnology* 14, 974-980 (2019).
- 2 Wang, Y. *et al.* *In vivo* targeted delivery of nucleic acids and CRISPR genome editors enabled by GSH-responsive silica nanoparticles. *Journal of Controlled Release*, 336:296-309 (2021).
- 3 Xie, R. *et al.* pH-Responsive Polymer Nanoparticles for Efficient Delivery of Cas9 Ribonucleoprotein With or Without Donor DNA. *Advanced Materials*, 2110618 (2022).

10:45 AM SF01.05.06

Active Molecular Junctions with Sub-Nanometer Tunability for Reconfigurable Nanosystems [Farnaz Niroui](#); Massachusetts Institute of Technology, United States

Controlled and reversible mechanical reconfiguration is core to embedding intelligent and adaptive performance within devices. Achieving such tunability at the nanoscale is a fundamental challenge. As dimensions are reduced to the few nanometers, surface adhesive forces become dominant causing instability and irreversible collapse in mechanically mobile structures. We present a platform in which mechanically reconfigurable molecular layers with engineered mechanical properties are used as tunable interconnects between neighboring surfaces. In this design, molecular layers serve as nanoscale springs to balance out the surface adhesive forces, enabling a controlled and reversible reconfiguration. Utilizing this hybrid organic-inorganic platform, which can be stimulated electrostatically or thermally, we demonstrate sub-10 nm active structures with < 1 nm precision in tuning. With these tunable building blocks, we achieve active modulation of optical and electrical responses which we further use to demonstrate applications in reconfigurable nanoscale devices and active surfaces.

11:00 AM SF01.05.09

Morphing and Color-Changing Liquid Crystal Elastomer Structures for Soft Robotics [Xueju Wang](#) and Yi Li; University of Connecticut, United States

The large, reversible shape-changing behaviors of liquid crystal elastomers (LCEs), resulting from liquid crystal-polymer network couplings, are promising for many applications. Despite intensive studies, harnessing molecular-material-structure interactions of LCEs for the design of locally controlled shape-morphing structures remains a challenge. In this talk, I will present our recent effort on a facile and versatile strategy to tailor the stiffness and the morphing behavior of reconfigurable LCE structures via locally controlled mesogen alignment and crosslinking densities. Selective photopolymerization of

spatially aligned LCE structures yields well-controlled lightly and highly crosslinked domains of distinct stiffness and selective permanent mesogen programming, which enables various previously inaccessible stiffness-heterogeneous geometries, as demonstrated in diverse morphing LCE structures via integrated experimental and finite element analysis. Furthermore, reprogramming of the non-photopolymerized regions allows for reshaping, as shown in a sequentially shape-morphing LCE rod and “face”. The heterogenous morphing LCE structures have the potential for many applications including in artificial muscles, soft robotics, and many others. In addition, I will introduce a simple strategy for creating 3D thermochromic LCE structures with synchronous shape-morphing and color-changing capabilities for biomimetic robotics.

SESSION SF01.06: Smart Functions of Stimuli-Responsive Materials VI
Session Chairs: Noemie-Manuelle Dorval Courchesne and Wilson Kong
Wednesday Afternoon, November 30, 2022
Sheraton, 5th Floor, The Fens

1:30 PM SF01.06.02

Programming Responsive Living Materials Seunghyun Sim; University of California, Irvine, United States

In this talk, I will present the Sim lab's recent efforts in programming materials comprising engineered living functionalities and synthetic macromolecules. Interplay between these two elements and the resulting living materials' dynamic nature will be discussed.

1:45 PM SF01.06.03

Mesoscale Photomechanical Coupling in Photoactive Liquid Crystal Elastomers Ruobing Bai and Zhengxuan Wei; Northeastern University, United States

Some molecules can absorb light of a certain wavelength and change their shape, dissociate, or combine to form new molecules. Embedding these molecules into a rubbery liquid crystalline polymer network enables photoactive liquid crystal elastomers (LCEs) that generate large deformation and decent amount of mechanical work upon light illumination. Photomechanical actuation of photoactive LCEs has attracted increasing attention in recent years due to its wireless and fast energy transmission, rich tunability, capability of micromachines, and delivery of high energy density. New applications include photo-responsive robots, metamaterials, motors, optical waveguides, fibers, and other light-modulated devices. However, compared to an individual photoactive molecule, most existing macroscopic photoactive LCEs perform much poorer in their actuation performance (e.g., work output, thermodynamic efficiency, deformation) by orders of magnitude, severely limiting their application in real working scenarios. This contrast highlights an urgent research need for mechanistic understanding of photomechanics in these materials at the mesoscale (e.g., micrometer) that bridges a nanoscale molecule and a macroscale material. This talk will present our recent progress in such fundamental understanding of mesoscale photomechanical coupling. Incorporating the single molecule photoreaction and the long-range directional molecular interaction into a continuum theoretical framework, we investigate multiple interesting phenomena including tunable molecular alignment, photomechanical phase transformation and material instability, formation of microstructure, temperature-modulated photo-actuation, and their consequences in macroscopic applications.

3:00 PM SF01.06.05

Stimuli-Responsive Liposomal Drug Delivery Platforms for Controlled Release Jinchao Lou and Michael D. Best; University of Tennessee-Knoxville, United States

Liposomes are effective drug delivery nanocarriers due to their unique bilayer structure and versatile nature in encapsulating both hydrophilic and hydrophobic drugs within the hydrophobic bilayer and aqueous core, respectively. To control the time and location of cargo release, different triggered release strategies have been developed to minimize off-target effect as well as increase the drug potency. Commonly explored stimuli include internal stimuli (i.e. pH) or external stimuli (i.e. light). To expand the toolbox, here, we present novel strategies for targeting a variety of stimuli, all of which are proven to be upregulated in certain diseased cells and are closely related to numerous pathological conditions. To do so, lipids are designed to undergo chemical or conformational changes upon coming in contact with target stimuli. Such structural changes are expected to disrupt the membrane integrity and cause the release of encapsulated cargo when these lipids are incorporated within the membrane bilayer. For each case, the design and synthesis of the desired responsive lipids will be discussed. Fluorescence-based release assays to evaluate release properties utilizing both hydrophilic and hydrophobic dyes, as well as dynamic light scattering (DLS) analysis and scanning transition electron microscopy (STEM) techniques to probe the membrane property change before and after triggered release will also be presented.

2:15 PM BREAK

3:15 PM SF01.06.07

Metamaterial Sensing and Memory via Multistability and Viscoelastic Effects Katherine Riley and Andres F. Arrieta; Purdue University, United States

The concept of intelligence in materials is gaining increasing attention as a means to enhance the inherent responsiveness and adaptability of engineered systems. Basic changes in material properties, such as stiffness or density, or even larger scale reactions, such as shape memory, are well-established material responses to environmental stimuli, including shifts in temperature, pH, or humidity. Engineered metamaterials may incorporate these fundamental material responses in combination with multiscale structural architectures and carefully designed unit cells to achieve advanced functionalities, including programmable morphing, sensing, and memory.

In this research, we examine a polymer metamaterial composed of dome-shaped unit cells connected by a base membrane. The spatially distributed domes have varying geometries and corresponding stability properties. These metamaterials are cast or 3D printed using viscoelastic, polymeric materials, with embedded piezoelectric sensing strips composed of a polymer-based filament with conductive additives. The interaction of the material viscoelasticity with the structural mono, meta, or bistability of the unit cells allows for the metamaterial to have unique, time-dependent behaviors which may be used for distributed mechanical sensing and memory. These include the critical mechanosensing capabilities of nonlinear signal amplification and filtering and thresholding. Inspired by mechanosensors found in nature, the metamaterial amplifies mechanical signals above a predetermined threshold, corresponding to the minimum snap-through force of the domes, while filtering out those below this threshold. This amplification is due to the highly nonlinear strains experienced by the unit cell during snap-through. Furthermore, the viscoelastic behaviors of stress relaxation, creep, and creep recovery may be used to sense the time elapsed in a local stable state or since a snap-through event triggered by an environmental stimulus, such as a mechanical load or change in temperature. The phenomenon of pseudo-bistability, in which a unit cell structure exhibits bistability for only a limited amount of time due to viscoelastic

material relaxation, is particularly interesting as it allows the metamaterial to sense, react, and self-reset after a programmed delay. The pseudo-bistability may be further manipulated by exploiting thermal properties of the polymer material. These combined material and structural capabilities ultimately enable the metamaterial to sense and remember spatiotemporal patterns that convey information about the metamaterial's environmental history. This class of intelligent metamaterials that can sense and respond to distributed external stimuli over large areas have potential applications in a wide range of industries, including soft robotics, advanced packaging, and smart buildings.

3:30 PM SF01.06.09

Shell-Mediated Deformation and Fracture Behavior of Liquid Metal Particles for Mechanoresponsive Electronics Wilson Kong¹, Nicholas Morris^{2,3}, Zachary Farrell^{2,1} and Christopher E. Tabor¹; ¹Air Force Research Laboratory, United States; ²UES, Inc., United States; ³Nextflex, United States

Responsive materials utilizing room-temperature liquid metals (LM) are gaining strong interest in flexible electronics, 3D printing, and biomedical therapeutics. The facile production of LM core-shell particles is enabled through the rapid formation of a passivating surface oxide that prevent LM droplets from coalescing. Rupturing these oxides can facilitate mechanically-responsive switching from electrically insulating to conducting states. While the relative ease of gallium oxide deformation is attractive for intrinsically stretchable electronics, the oxide shell dominates much of the LM mechanical behavior. Previous works show that this oxide matures over time under ambient conditions, which can increase the stiffness of the LM particles.¹ Chemical functionalization of LM particles have demonstrated ways to disrupt the oxide formation or hinder its growth.² However, the lack of complete control over the LM oxidation may introduce mechanical hysteresis into these materials systems. Furthermore, environmental conditions and dynamics of particle strain also play a large role in influencing this hysteresis. Therefore, having an improved understanding on the influencing factors towards LM particle rupture can potentially improve efforts in controlling its mechanical response. In this work, we demonstrate the deformation and fracture behavior for single-particles of eutectic Ga-In (eGaIn) alloy under variable conditions. Through in situ compression testing, this investigation focuses on the effects of 1) oxygen content, 2) compression rate, and 3) particle coatings that influences the eGaIn mechanical behavior. By coating eGaIn with materials having well-known mechanical properties (i.e., silica), we can supersede the properties of the gallium oxide and develop LM particles with predictable and tunable mechanical behavior under ambient conditions. Compared to oxide-coated eGaIn, SiO₂-eGaIn particles fracture in an abrupt and brittle manner. The silica shell thickness can be modified to change the mechanical properties of eGaIn particles as desired. With controllable stiffness and fracture behavior that is not dependent on the environmental conditions, these modified eGaIn particles can be explored for a variety of mechanoresponsive applications including pressure-sensitive solders or sensing devices.

Farrell, Zachary J., and Christopher Tabor. "Control of gallium oxide growth on liquid metal eutectic gallium/indium nanoparticles via thiolation." *Langmuir* 34.1 (2018): 234-240.

Morris, Nicholas J., Zachary J. Farrell, and Christopher E. Tabor. "Chemically modifying the mechanical properties of core-shell liquid metal nanoparticles." *Nanoscale* 11.37 (2019): 17308-17318.

SESSION SF01.07: Poster Session

Session Chairs: Noemie-Manuelle Dorval Courchesne and Patrick Saris

Wednesday Afternoon, November 30, 2022

8:00 PM - 10:00 PM

Hynes, Level 1, Hall A

SF01.07.01

Sensitive Determination of SARS-COV-2 and the Anti-Hepatitis C Virus Agent Velpatasvir Enabled by Novel Metal-Organic Frameworks Nageh K. Allam; American University in Cairo, Egypt

Herein, we report on the electrochemical determination of velpatasvir (VLP) as the main constituent of Eplclusa, a SARS-COV-2 and anti-hepatitis C virus (HCV) agent, using a novel metal-organic framework (MOF). The NH₂-MIL-53(Al) MOF was successfully modified with 5-bromo-salicylaldehyde to synthesize 5-BSA=N-MIL-53(Al) MOF. The synthesized MOF has been characterized using Fourier transform infrared spectroscopy, X-ray powder diffraction, scanning electron microscopy, cyclic voltammetry, square wave voltammetry, and electrochemical impedance spectroscopy. The modified MOF showed higher electrochemical activity and response than the bare NH₂-MIL-53(Al) MOF. Compared to the bare carbon paste electrode (CPE), the 5-BSA=N-MIL-53(Al)/CPE platform was shown to enhance the electrochemical oxidation and detection of the anti-SARS-COV-2 and anti-HCV agent. Under optimized conditions, the 5-BSA=N-MIL-53(Al)/CPE platform showed a linear range of 1.11×10^{-6} to 1.11×10^{-7} and 1.11×10^{-7} to 25.97×10^{-6} M Britton-Robinson buffer (pH 7) with a detection limit and limit of quantification of 8.776×10^{-9} and 2.924×10^{-8} M, respectively. Repeatability, storage stability, and reproducibility in addition to selectivity studies and interference studies were conducted to illustrate the superiority of the electrode material. The study also included a highly accurate platform for the determination of VLP concentrations in both urine and plasma samples with reasonable recovery.

SF01.07.02

Probing Macromolecular Complexes with a Reconfigurable Nanoscale DNA Force Spectrometer Yuchen Wang, Michael Darcy, Ralf Bundschuh, Michael Poirier and Carlos Castro; The Ohio State University, United States

Single molecule force spectroscopy is a powerful approach to studying the structure of biological materials and their kinetic properties. Nevertheless, the probes limit integration into complex systems, and the cost and complexity of the equipment and assays limit broader use. DNA-based nanodevices are a promising alternative that allows for probing the force response of biomolecules such as nucleosome. Here, we build on these prior works to develop a nanoscale DNA force spectrometer (nDFS). Specifically, the nDFS allow for enhanced control over forces and especially the application of compression forces. Moreover, the readout from electron microscopy can provide the unique chance to observe the detailed sample structure conformation under force instead of end-to-end distance.

The hinge structure nDFS is fabricated by scaffold DNA origami, and it consists of two arms connected by several single-stranded DNA scaffold linkers. The device behaves like a torsional spring where the arms are stiff, and the mechanical properties are determined by the design of the hinge vertex. We demonstrated the ability to control both the equilibrium angle and stiffness by modifying the detailed vertex architecture. Specifically, the mean angle can be tuned over a range of 35 deg to 87 deg, which provides a passive approach to modulating forces applied by the nDFS. We also developed an active approach to the nDFS open or closed by forming or disrupting a DNA duplex strut between the arms, controlled via strand displacement. The toggling strategy is used to 1) apply compressive forces to a 249 bp double-stranded DNA (dsDNA) 2) and apply tensile forces to mon-nucleosome or tetra-nucleosome array, as proved experimentally. For future work, we seek to expand the applicability of nDFS to a broader experimental environment by enhancing the structural stability in low ionic conditions and increasing the force measurement range.

SF01.07.03

Soft-Robotic Actuations of Collectively Assembled Soft-Electronics Based on MXene/Liquid Crystal Elastomer Bilayer Woongbi Cho¹ and Jeong Jae Wic^{2,1}; ¹Inha university, Korea (the Republic of); ²Inha University, Korea (the Republic of)

To achieve remotely controlled shape-reconfiguration in miniaturized soft-electronics, liquid crystalline polymer with alignment programming is a great candidate to replace the passive deformation of stretchable electronics under mechanical tension. In this presentation, we introduce programmable and shape-reconfigurable and locomotive soft-electronics by preparing the MXene/liquid crystalline elastomer bilayer (MLB) with a concept of collective assembly. The high light-to-heat conversion efficiency and high electrical conductivity ($\sim 5,100 \text{ S cm}^{-1}$) of MXene layer enables MLB to perform photo-/electro-thermally driven reversible in-plane bending and torsional twisting according to offset angle of molecular alignment by near-infrared (NIR) light irradiation and voltage application. Importantly, the introduction of collective assembly enhances the diversity and functionality in shape-reconfiguration of MLB via attaching the ends of MLBs by utilizing the conductive paste. To demonstrate applicability as a soft-robotic system, we engineer the both geometries and alignment nature of applied MLBs blocks for assembly to achieve various remotely controllable dynamic motions including crawling, continuous rotation, as well as jumping and slingshot inspired actions via snap-through buckling.

SF01.07.04

Covalent Adaptable-Conjugated Polymer Network for Self-healing Electronics Laine Taussig¹, Cedric Plesse², Fabrice Goubard² and Aram Amassian¹; ¹North Carolina State University, United States; ²CY Cergy Paris Universite, France

Covalent adaptable networks (CAN's) have emerged as an innovative class of materials as they possess advantageous properties of both thermoplastics and thermosets enabling dimensional stability and dynamic response to external stimuli. With the addition of conducting nanoparticles, CAN's have been used to successfully fabricate electronically conducting composites that are mechanically and chemically robust and can self-repair, therefore extending the lifetime and application of soft electronics. In this work, an electronically conducting CAN is demonstrated by employing vinylous urethane vitrimer and conjugated polymer poly(3,4-ethylenedioxythiophene) polystyrene sulfonate (PEDOT:PSS). To our knowledge, this system is the first fully organic electronically conducting vitrimer. Due to the nature of the covalent network, the material is chemically resistant to solvents, as it maintains a constant crosslink density, and is soft and bendable at room temperature. At elevated temperatures, the transamination exchange reaction is activated and accelerated in the presence of acidic PSS, therefore exhibiting fast reorganization and stress relaxation. We demonstrate temperature activated self-healing and shape memory functions of this material while maintaining conductivity above 100 S/cm. The findings shown here have promising potential for use in self-healing organic electronics such as sensors and wearable devices.

SF01.07.05

One-Step Droplet Fluidic Production of Multi-Component Conjugated Polymer Janus Microspheres with Integrated Photonic, Magnetic and Catalytic Microswimmer Functionality Chenxi Hao, Liam Jowett and Gareth Redmond; University College Dublin, Ireland

Conjugated polymers have been extensively investigated with respect to potential applications in diverse areas ranging from opto-electronics to energy conversion to life sciences. Technological embodiments usually involve thin polymer films or, for applications in aqueous or biological media, the covalent modification of polymer molecules by incorporation of polar or ionic functionalities. In this study, we explored simple conjugated polymer microspheres where manipulation of microsphere morphology, composition, surface functionality, and sphere-environment interactions, respectively, permit investigation and demonstration of stimulus-responsive behaviors.

Specifically, we applied digital droplet fluidics to the production of size monodisperse conjugated polymer-based microspheres. To this end, using real-time *in situ* (on-chip) optical imaging methods, we developed a T-junction microfluidic droplet generation technology for the production of aqueous suspensions of surfactant-stabilised micro-droplets that contain fluorescent conjugated polymer and associated organic solvent. Collection of droplets followed by gradual solvent extraction results in the formation of 'hardened' spherical polymer micro-particles whose morphological, compositional and optical properties can be studied using appropriate methods. We selected poly[2-methoxy-5-(2'-ethylhexyloxy)-1,4-phenylene vinylene] (MEH-PPV) as a reference conjugated polymer as the ethyl-hexyl side chains provide for good solubility in many common organic solvents. We studied MEH-PPV/CHCl₃ droplet formation in surfactant/water flows and systematically varied parameters, such as, relative flow rates of the phases, surfactant concentration, polymer concentration, and polymer molecular weight to identify effects on MEH-PPV microsphere morphological and spectroscopic properties. In addition, a range of other solvents and co-solvents, e.g., toluene, DCM, EtOAc, MeCN, porogens, e.g., 2-methyl-pentane, and surfactants, e.g., oleic acid, were also screened. Imaging studies were extensively employed for morphology characterisation and data were combined with spectroscopy data to build a comprehensive process-property map for this system. In addition, real-time *in situ* optical imaging of the progress of solvent extraction permitted elucidation of the mechanism of surface 'dimpling' during the formation of morphologically textured emissive MEH-PPV microspheres.

By including additional components in the organic phase, the microfluidic approach was extended to the single-step formation of biphasic 'Janus' or 'snowman' microparticles composed of emissive MEH-PPV and biocompatible, biodegradable poly(D,L-lactide-co-glycolide) (PLGA) as well as triphasic, 'multi-lobed' PLGA-MEH-PPV-PLGA micro-particles characterised by correlative confocal fluorescence-SEM. Further incorporation of superparamagnetic oleic-acid stabilised Fe₃O₄ nanoparticles permitted the formation of magnetic field-responsive fluorescent MEH-PPV-PLGA Janus particles that behaved as a type of active matter that exhibited magnetic field-induced liquid-solid extraction and other dynamic phenomena, such as, field-assisted single-particle lateral translocation and dipole-mediated multi-particle chaining both of which were monitored during real-time *in situ* imaging studies. In addition, these particles exhibited a well-defined fluorescence quenching response in the presence of electron deficient model organic compounds that permitted demonstration of low threshold detection of volatile nitroaromatics. Finally, asymmetric photoinduced deposition of Pt islands on Janus microparticles of PCB/MEH-PPV-PLGA with embedded oleic-acid stabilised Fe₃O₄ nanoparticles permitted the fabrication and demonstration of novel magnetic field responsive catalytic microswimmers.

SF01.07.06

Enzyme Responsive Rigid-Rod Aromatics Target "Undruggable" Phosphatases to Kill Cancer Cells in Mimetic Bone Microenvironment Meihui Yi¹, Fengbin Wang², Weiyi Tan¹, Jer-Tsong Hsieh³, Edward H. Egelman² and Bing Xu¹; ¹Brandeis University, United States; ²University of Virginia, United States; ³University of Texas, United States

Bone metastasis remains a challenge in cancer treatment. Here we show that enzymatic responsive rigid-rod aromatics, acting as the substrates of "undruggable" phosphatases, to kill cancer cells in mimetic bone microenvironment. By phosphorylating the hydroxyl and conjugating nitrobenzoxadiazole (NBD) to the carboxylate of hydroxybiphenylcarboxylate (BP), we obtained pBP-NBD (**1P**) as a substrate of both acid and alkaline phosphatases. **1P** effectively kill both metastatic castration-resistant prostate cancer cells (mCRPCs) (e.g., VCaP or PC3) and osteoblast mimic cells (Saos2) in their co-culture. Fluorescent imaging reveals that **1P** enter Saos2 almost instantly to target the endoplasmic reticulum (ER) of the cells and that co-culturing with Saos2 cells boosts the cellular uptake of **1P** by mCRPCs. Using cryo-EM, we determined the nanotube structures of both enzyme substrate **1P** (2.4 Å

resolution, pH 5.6) and enzymatic processed compound **1** (2.2 Å resolution, pH 7.4). The helical packing of both nanotubes is identical, held together by strong pi-stacking interactions. Besides reporting the atomistic structure of nanotubes formed by the assembly of rigid-rod aromatics, this work expands the pool of molecules for designing EISA substrates that selectively target TME.

SF01.07.07

Fast and Large Motion of Self-Oscillating Gels Based on High Diffusivity Induced by Phase-Separated Structures Jaewon Choi¹, Taehun Chung¹, Ryo Yoshida² and Younsoo Kim¹; ¹Pohang University of Science and Technology (POSTECH), Korea (the Republic of); ²The University of Tokyo, Japan

Unlike conventional stimuli-responsive gels, self-oscillating gels can spontaneously repeat swelling/de-swelling without on-off switching of external stimuli such as temperature, pH, etc. This mechanical oscillation is achieved by inducing the Belousov-Zhabotinsky (BZ) reaction. [1] Due to these characteristics, they have been attracting attention, as they can be utilized as biomimetic and living materials showing heartbeat-like motions. However, the degree of swelling/de-swelling change that causes mechanical oscillation of the gel was usually small and slow. In addition, for the overall mechanical oscillation of the gel, the size of the gel must be smaller than a chemical wave of several hundred micrometers, so the entire swelling/de-swelling oscillation has not yet been shown in the bulk-scale gel of centimeters or more. Furthermore, the BZ reaction required strong acidic conditions, and the duration of this reaction was short. These problems could be overcome by using specific hydrated protic ionic liquids (PILs) as an alternative medium for the BZ reaction. [2] However, no oscillation was observed in conventional self-oscillating gels because of the low diffusivity of the BZ substrates into the gels in the highly viscous solution, such as hydrated PILs. [3]

Herein, we designed novel self-oscillating gels showing fast and large deformation by tuning the internal structure of the gels. Using the collapsed form of poly(*N*-isopropylacrylamide) in a salt solution, it is possible to synthesize the phase-separated structures showing fast and large shrinkage of the gels. [4] We prepared the poly(NIPAAm-*co*-Ru(bpy)₃) gel with the phase-separated structures, and it was immersed in a catalyst-free BZ solution containing the substrates (malonic acid, sodium bromate, and nitric acid or hydrated PILs). Interestingly, our phase-separated gels can oscillate even in a highly viscous solution owing to its high diffusivity. Furthermore, our gel exhibited a fast propagation rate and long wavelength of the chemical wave. As a result, even in centimeter-scale bulk gels, overall swelling/de-swelling oscillations could be exhibited, an unprecedented oscillation that significantly improved the dimension of oscillations. This presentation will discuss the synthetic strategy of self-oscillating gels and their improved performance on oscillation period, amplitude, and diffusivity.

References

- [1] R. Yoshida, *et al.*, *J. Am. Chem. Soc.*, **118**, 5134 (1996).
- [2] T. Ueki, *et al.*, *Angew. Chem. Int. Ed.*, **51**, 11991 (2012).
- [3] T. Masuda, *et al.*, *Angew. Chem.*, **130**, 16935 (2018).
- [4] T. Chung, *et al.*, *Gels*, **7**(1), 18 (2021).

SF01.07.08

Tuning Chiro-Optoelectrical Signals Enabled Precise Patterning for Encryption Application Moon Jong Han, Minkyu Kim and Vladimir Tsukruk; Georgia Institute of Technology, United States

Multifunctional biomolecules for organic field-effect transistors (OFETs) based on chiral photonics have received much attention for next-generation optoelectronics including quantum information and encryption as well as integrated logic circuits. Despite recent advances, OFETs for encryption applications responding to both humidity and light, exhibiting reconfigurable and multivalued logic systems, are not reported. Herein, a simple and promising approach for highly secure optoelectronic encryption by facilitating humidity-sensitive chiral pitch of cellulose nanocrystals (CNCs) dielectric layer is suggested. By the addition of salt into the photonically-active chiral nematic CNCs network, the remarkable photonic band gap is shifted, converting into distinguishable and quantized electric signals directly depending on repetitive change and humidity, and incident wavelength of light. The interdisciplinary convergence between CNC nanotechnology and the multivalued logic system can provide optoelectronic counterfeiting, imaging, and information processing with logic nodes triggered by the polarization of light, humidity, and salt concentration. As a proof-of-concept, the integrated circuits sensing circularly polarized light and humidity are demonstrated as a physically unclonable functional device.

SF01.07.09

Accelerated DNA Hydrogel Self-Assembly via Single Base-Pair Mismatch for Enzyme-Free Picomolar MicroRNA Detection Hyebin Na, Jae Chul Park and Yoon Sung Nam; Korea Advanced Institute of Science and Technology, Korea (the Republic of)

Over decades the demand for point-of-care testing (POCT) has increased due to the outbreak of global pandemics caused by infectious diseases. There are substantial developments in the POCT systems targeting microRNAs (miRNA) which regulate the expression of various target genes. To make POCT possible, the enzymatic amplification should be replaced because of the difficulties rising from enzyme storage and handling. We use a target-catalyzed toehold-mediated strand displacement (TMSD) cascade with three hairpin DNAs for the enzyme-free isothermal amplification technique. Furthermore, we assembled Y-shaped DNA products formed by TMSD cascade reaction into a hydrogel using biotin-streptavidin interaction, following a closely-packed three-dimensional network of Förster resonance energy transfer (FRET) donor and acceptor. The signal amplification was 4.8 times higher than that without hydrogel assembly. However, the hydrogel-based miRNA detection system shows a limit of detection (LOD) of 1.5 nM, which is similar to that of the system without amplification. The low sensitivity is caused by the low TMSD reaction affinity between RNA and DNA, which has around 35 times lower reaction rate constant than that of DNA and DNA. Herein, we present a new system using a single mismatch to the stem of the hairpin DNA. The mismatch lowers the local stability of hairpin DNA and accelerates the cascade TMSD reaction. For empirical verification, we introduced a mismatch in each of the three hairpin DNAs for the TMSD cascade system. The mismatch-induced accelerating only works with the first hairpin DNA, which supports our theory that the RNA-DNA TMSD is the rate-limiting reaction, not the DNA-DNA TMSD. We also investigated the effect of the mismatch position by comparing the first hairpin DNAs with a mismatch at the 5 th, 9 th, and 13 th nt from the toehold. The system with 5 th nt mismatch was the one with the most rapid and efficient reaction. The results suggest that the mismatch near the toehold efficiently facilitates the opening of the hairpin DNA by miRNA. The mismatch-induced thermodynamic driving method dramatically improves the LOD sensitivity from 1.5 nM to 60 pM. This work was supported by the National Research Foundation of Korea (NRF) grant funded by the Korea government (MSIT) (2020R1A2C2004168).

[1] Cheol Am Hong, Jae Chul Park, Hyebin Na, Huiju Jeon, and Yoon Sung Nam, *Biosensors and Bioelectronics* (2021) 182, 113110

[2] Jae Chul Park, Se Yeon Choi, Moon Young Yang, Lin Nan, Hyebin Na, Ha Neul Lee, Hyun Jung Chung, Cheol Am Hong, and Yoon Sung Nam, *ACS Applied Materials & Interfaces* (2019) 11, 37, 33525-33534

SF01.07.10

Electro-Mechanical Leak Detection System Utilizing Conductive Fluids Morgan A. Payne, J Taylor Quinn, Eric Balle and Allyson Causey; Texas A&M University, United States

Due to the chemical recovery process employed within Black Liquor Recovery Boilers, the Pulp and Paper industry experiences a unique problem when a leak or fault occurs in a bottom floor composite tube. Water leaking from these tubes into a surrounding smelt bed poses the potential for catastrophic losses as it reacts violently and instantaneously with the smelt bed's high sodium and sulfur content. The acoustic sensing techniques and methodologies currently utilized for the detection of leaks within these systems, despite being universally accepted, are unreliable and erroneous. The acoustic detection system relies on the propagation of minute vibrations along these boiler tubes and throughout the smelt bed. The dampening effect of the smelt bed on these vibrations presents a significant problem for this system, often resulting in undetected leaks. An electro-mechanical leak detection system, utilizing conductive fluid coating, was designed, and operated to enhance detection response time, based on the necessity for the improvement of the current leak detection systems employed within Black Liquor Recovery Boilers. This detection system provided continuous identification via live resistance measurements of a conductive fluid layer applied to the surface of the boiler tubes. When a leak or fault occurred, the disruption of the coating's surface area resulted in a detectable resistance change. To demonstrate the system's improved accuracy and real time performance in the recognition of leaks and faults compared to the current acoustic detection, the system was implemented and evaluated with various scenarios. The results proved this prototype system can alert an operator to a leak in 20 seconds. This research into the utilization of conductive coatings, specifically within an electric leak detection system for Black Liquor Recovery Boilers, provides a starting point for continued research on the industrial applications of conductive fluids.

SF01.07.11

***Diphylleia grayi*-Inspired Hydrochromic Adhesive PDMS Film Using Nano Sphere Lithography** [SeungJe Lee¹](#), Minji Ko¹, Gang Yeol Yoo², Keyong Nam Lee¹, Yun Jae Eo¹ and Young Rag Do¹; ¹Kookmin University, Korea (the Republic of); ²KOREA ELECTRONICS TECHNOLOGY INSTITUTE, Korea (the Republic of)

Many living things in nature have the ability to change their colors, and this has inspired the development of bio mimetic technology, such as flexible information display devices, color control applications, and energy-free applications. Inspired by the ability of *Diphylleia grayi* to become transparent on rainy days, we developed a hypochromic adhesive PDMS film. We produced a *Diphylleia grayi*-inspired PDMS film by forming a nanocavity structure on the surface of a PDMS (Polydimethylsiloxane) film based on Mie theory. The formation of nanocavities on the PDMS surface induced scattering, reducing the surface transmittance, and leading to transparency in wet state. Nanocavity structures were fabricated using polystyrene (PS)-based nanosphere lithography (NSL) and PDMS transfer methods. Nanosphere lithography using polystyrene beads is suitable for forming various cavities because the process makes it easy to adjust the diameter via reactive-ion etching (RIE). Scattering-induced PDMS films were optimized using polystyrene beads of various sizes (0.2, 0.4, 0.6, 1.0, and 2.0 μm). The greatest contrast between wet and dry states was shown in the 1.0 μm cavity structured PDMS film (44.93% (ΔT) $T = 59.11$ -14.18%) and 54.88% ($\Delta\text{H} = 69.42$ -14.54%). The optimized film with 1.0 μm nano-pores suggests the possibility of application to various water-changing applications that require color change, such as smart windows, camouflage, and transparent umbrellas for rainy weather. To improve the wettability of the PDMS surface, polyvinyl alcohol (PVA) was used to modify the surface. The PDMS film surface was measured with a scanning electron microscope (SEM). The scattering effect of the nano-cavity structure was measured by UV-visible spectroscopy, and the haze value was measured using a hazemeter.

SF01.07.12

Fabrication of Graphene-Incorporated Thermoresponsive Nanocomposite Hydrogels with Precision Control of Programmable Actuation Jisu Hong, Jiseok Han and [Chaenyung Cha](#); Ulsan National Institute of Science and Technology, Korea (the Republic of)

Hydrogels capable of stimuli-responsive deformation are widely explored as intelligent actuators for diverse applications. It is still a significant challenge, however, to "program" these hydrogels to undergo highly specific and extensive shape changes with precision, because the mechanical properties and deformation mechanism of the hydrogels are inherently coupled. Herein, two engineering strategies are simultaneously employed to develop thermoresponsive poly(N-isopropyl acrylamide) (PNIPAm)-based hydrogels capable of programmable actuation. First, PNIPAm is copolymerized with poly(ethylene glycol) diacrylate (PEGDA) with varying molecular weights and concentrations. In addition, graphene oxide (GO) or reduced graphene oxide (rGO) is incorporated to generate nanocomposite hydrogels. These strategies combine to allow the refined control of mechanical and diffusional properties of hydrogels over a broad range, which also directly influences variable thermoresponsive actuation. It is expected that this comprehensive design principle can be applied to a wide range of hydrogels for programmable actuation.

SF01.07.13

A Reconfigurable Pixelated Metamaterial with Rich Mechanical and Shape-Shifting Reconfigurability [Jun Kyu Choe](#), Jiyeon Lee, Hajun Lee, Yeonwoo Jang, Hyeonseong Song and Jiyun Kim; Ulsan National Institute of Science and Technology, Korea (the Republic of)

Mechanical metamaterials refer to collectively structured forms of unique micro-architectures that can exhibit previously unattainable properties, such as negative Poisson's ratio, programmable shape transformation, negative or tunable coefficients of thermal expansion, and high stiffness-to-weight ratio structures. Traditional mechanical metamaterials were fabricated with simple designs using rigid bodies connected with mechanical hinges, but recent efforts to exploit soft materials with instabilities and stimuli-responsive materials have opened the avenues for mechanical metamaterials which can demonstrate dramatic shape and mechanical reconfigurability. These reconfigurable soft architectures that respond to their environment have various potential applications, such as soft robotics, flexible electronics, and human-machine interfaces (HMI). However, most shape-shifting mechanical metamaterials presented to date focused on increasingly complex structures with predetermined mechanical properties that cannot be altered post-fabrication, while stimuli-responsive metamaterials produced only simple, homogeneous changes in mechanical properties. We introduce a real-time reprogrammable shape- and rigidity-morphing metamaterial, where the stiffness of each unit micro-architecture of a pixelated structure is independently controlled on-demand, producing rich shape reconfigurability and tailoring capability of local or global mechanical properties. This concept is realized through harnessing solid-liquid phase transition of low-melting-point-alloy (LMPA) layers, discretely embedded inside each unit cell of an elastomeric endoskeleton, originally designed to show buckling-induced auxetic behavior. The selective stiffness control of each pixel releases a tremendous number of hidden states driven by different deformation mechanisms and patterns. The morphed shape can be further permanently maintained without requiring external stimuli or energy inputs for the load-bearing applications especially when the materials need to actively transform to adjust to circumstances. Finally, we show that local stiffness tuning can be leveraged for the global mechanical characteristics, enabling multi-state analog control of the stress-strain characteristics and Poisson's ratio of the material between two extreme states.

SF01.07.14

Transparent Liquid-Solid Interface Triboelectric Nanogenerators with Silver Nanowires [Onuralp Cakir¹](#), [Doga Doganay¹](#), [Melih O. Cicek¹](#), [Sahin Coskun²](#) and [Husnu E. Unalan¹](#); ¹Middle East Technical University, Turkey; ²Eskisehir Osmangazi University, Turkey

Triboelectric nanogenerators (TENGs) have been of great interest since they were proposed. Power is generated by static electricity caused by the contact of two separate surfaces. Therefore, any place where there is motion can be an effective work place for smart TENGs to be used as both self-powered sensors and energy harvesting units. In this study, the use of optimized Ag NW network in a liquid-solid interface triboelectric nanogenerator system as the current collector layer is explored. A thin PDMS layer is spin coated onto the Ag NW network to fabricate transparent TENG electrodes. The triboelectric

response between the water droplets and the PDMS layer is investigated. The TENG device is found to produce up to 1.8 V and 40 nA per water droplet. The resulting transparent self-powered sensor with optimized Ag NW network is suitable for many sensing applications such as chemical concentration measurement and heater activation under rainy weather.

This work was supported by The Scientific and Technological Research Council of Turkey (TUBITAK) under Grants No: 121N708 and 119N413.

SF01.07.15

Floating Buoy as a Triboelectric Nanogenerator for Blue Energy Harvesting Onur Demircioglu, Melih O. Cicek, Doga Doganay, Gunay Gazaloglu, Ahmet C. Yalciner, Simge Cinar and Husnu E. Unalan; Middle East Technical University, Turkey

Triboelectric nanogenerators (TENGs) can be used as both self-powered sensors and energy harvesting units anywhere there are stimuli from both the environment and human activities. Given situations like these, water waves are one of the best sources of environmental stimuli for TENGs to harness waste energy. In this study, a low-cost adaptation of a TENG was made by modifying a commercial buoy used by sailors and marine workers. A pendulum mechanism was used for the fabrication of the TENGs. While the inside of the buoy was coated with polyurethane (PU) foam, the counter triboelectric layer was prepared by coating an aluminum ball with poly (dimethyl siloxane) connected to a spring inside the buoy. As a result of contact-separation caused by wave stimulus on the buoy, triboelectrification was provided even in low frequency regime. An open-circuit voltage (V_{oc}) of 141 V and a short-circuit current (I_{sc}) of 8.89 μA were obtained from measurements made in a coastal port laboratory to simulate the actual state of sea waves. In addition, a power of 1.07 W/m² was obtained at an impedance match of 300 M Ω under a wave frequency of 1 Hz and a wave height of 11.8 cm, which is characteristic of Turkey's typical coastal waves. This study demonstrates that blue energy harvesting by TENGs can be an effective solution for low power electronics in the marine environment.

SF01.07.16

Elastic Photonic Microbeads Containing Non-Close-Packed Colloidal Crystals for Photonic Inks Jong Hyun Kim, Jong Bin Kim, Yehun Choi, Sanghyuk Park and Shin-Hyun Kim; Korea Advanced Institute of Science and Technology, Korea (the Republic of)

Crystalline colloidal arrays exhibit vivid structural colors through wavelength-selective diffraction, which shows high color purity and brightness. The resonant wavelength of structural color is easily tuned by adjusting the lattice constant between crystal planes or refractive index. Moreover, the structural colors are non-fading and non-toxic, unlike chemical pigments. These novel properties of colloidal crystals have the potential to be applied to coloration fields such as displays, aesthetics, and color pigments. In particular, the colloidal arrays can be formed in microbeads format using emulsion droplets, which can be used as a new material of photonic inks for cosmetics, printings, and paintings, as an alternative to chemical pigments. For example, the colloidal particles can be self-assembled in the droplets by solvent evaporation, which enables the structural coloration by forming close-packed colloidal arrays. However, the evaporation-induced assembly method requires a long time for the crystallization of colloidal particles. Moreover, the microbeads with close-packed arrays have low mechanical stability as the colloidal particles are simply in contact with each other without a medium. To overcome the time-consuming process and ameliorate the mechanical property, the colloidal particles form non-close-packed arrays in the photocurable medium due to the interparticle repulsion, which is emulsified in water to form oil-in-water (O/W) emulsion droplets. The repulsive interparticle interaction induces the spontaneous crystallization of colloidal particles without the evaporation process, which can enable the production of the microbead with high mechanical stability by photopolymerizing resin of emulsion droplets. Nevertheless, the low color saturation and brightness of photonic microbeads due to the low colloidal crystallinity and incoherent scattering is still a problem for the practical application of photonic inks.

Here, we suggest a novel strategy to produce elastic photonic microbeads with enhanced color brightness and saturation through oil-in-oil (O/O) emulsion templates. The elastic microbeads are produced by emulsifying a photocurable dispersion in the mineral oil using a microfluidic device. As the photocurable dispersion, the silica particles are dispersed in poly(ethylene glycol) phenyl ether acrylate (PEGPEA). The silica particles form non-close-packed colloidal arrays due to the interparticle repulsion by the solvation layer. The emulsion droplets of silica-PEGPEA dispersions are collected and irradiated by ultraviolet to photopolymerize of PEGPEA and form photonic microbeads. The photonic microbeads show brilliant structural color with color bright enhancement because the crystallinity of colloidal arrays is higher than those prepared by the O/W emulsion template. The high crystallinity is attributed to the reduced influence on the repulsive interparticle interaction by the continuous phase. When the continuous phase of water or oil diffuses into the emulsion droplets, water molecules disturb the interparticle repulsion of silica particles by hydrogen bonding with silica particles whereas oil molecules do not interact with silica particles, which can enhance the crystallinity of silica particles. Moreover, the color saturation of microbeads can be further enhanced by transferring the microbeads into the mixture of the mineral oil and silicone oil. When the microbeads are suspended in the oil mixture where the refractive index between microbeads and oil mixture is matched, the incoherent scattering can be suppressed at the surface of microbeads, which can enhance the color performance. Furthermore, the microbeads with enhanced color brightness and saturation are highly deformable, which can improve the fluidity of the oil mixture. Therefore, the elastic photonic microbeads can be used as colorants in photonic inks for printings of structural colors.

SF01.07.17

Multifunctional Highly Porous PolyHIPE Materials for Sorption, Filtration and Wound Dressing Applications Matthew D. Thum, Nickolaus weise, Maryssa Beasley, Grant Daniels, Spencer Giles, Kenan Fears, Chris So and Jeffrey Lundin; US Naval Research Laboratory, United States

Multifunctional porous polymers can serve as the basis for numerous applications and using high internal phase emulsion (HIPE) templating has proven a facile method of producing a tunable porous polymer scaffold. In this study, novel therapeutics were incorporated into an absorbent, mechanically robust, and hemostatic high surface area polymer foam through HIPE synthesis. Specifically, we demonstrate the use of HIPEs composed of hydrophilic acrylates, and polyethylene glycol (PEG) monomers as the basis for a multifunctional microporous polymer scaffolds and show compatibility with either enzymatic peptide decontaminants, or quaternary ammonium salts for added functionality. Furthermore, we discuss using 3D printing as a means to control the spatial loading of additives and fabricate structures with individually specific morphologies. The robustness of HIPE templating and 3D printing is examined by evaluating the effect of additive incorporation, and polymerization technique, on the activity of the dopant. Materials characterization included ATR-IR, gel fraction, DSC, TGA, and SEM analysis to evaluate effects of therapeutic loading on polymerization and the micro-structure of the polymer foams. Chemical decontamination capabilities were determined via simulant (2-CEES, and Demeton-S) challenges monitored via GCMS and antimicrobial assays were performed against *S. Aureus*. We demonstrate HIPE templating as a highly versatile approach to the design of porous polymer materials for sorption, filtration, and wound dressing applications. The relatively inexpensive fabrication and simple detoxification chemistry paired with the porous foam form factor presents an interesting approach to the development of a broad spectrum self-decontaminating material.

SF01.07.18

Microscale Photothermal Actuation Examined in Stiff/Soft Composites Jorge Jimenez¹, Georgia Kaufman², Michael Gallegos², Emily Huntley², Holly M. Golecki¹ and Bryan Kaehr^{2,3}; ¹University of Illinois at Urbana-Champaign, United States; ²Sandia National Laboratories, United States; ³Center for Integrated Nanotechnologies, United States

The development of micro-scale tools employing smart, autonomous materials can enable widespread applications—from microsurgery and diagnostics, to the assembly of complex microdevices. With continuing development of smart and environmentally responsive materials compatible with 3D printing, cue-

driven tools such as micro-grippers with high spatial and temporal precision can give rise to biocompatible devices. In this work, we investigate additive manufacturing of microgrippers based on bioinspired heuristic designs coupled with environmentally actuated hydrogels to form hybrid microsurgical tools. The aim of this work is to develop robust micro-grippers integrated into imaging/optogenetic devices at the scale of single fiber optics and individual biological cells to enable single cell extraction or localized drug delivery. Using multiphoton lithography, we fabricate resin grippers and scissors that incorporate inert skeletal components. Hydrogels that respond to changes in temperature, pH and light are used to control device movements, and are fabricated in situ from the light output of the tip of the fiber. We evaluate the response time, accuracy and cyclability of grippers. By leveraging gripper geometry, surface treatments, and hydrogel chemistry, we iterate on designs to optimize for response time. Following this optimization, we designed microgrippers that incorporate a photothermal transducer within a thermally responsive gel actuator fabricated on the tip of a 200-micron diameter core fiber and demonstrate capture and release of microscale objects. Overall, this work provides a foundation to integrate stimuli responsive mechanical functions with micro-scale optical devices.

SF01.07.20

Unsupervised Machine Learning for Accelerated Density-Dependent Liquid Crystal Simulations [Haritosh Patel](#), Baptiste Lemaire and Haichao Wu; Harvard University, United States

Material science, including rational design and discovery, has been motivated by the needs of today and tomorrow. Within the Aizenberg lab, a class of materials known as adaptive materials are currently being developed for their applications in soft robotics, energy harvesting, and more. Adaptive materials are classified by their ability to show a spectrum of complex behaviours under various stimuli. For example, the use of molecules that exhibit crystal-like properties in a liquid state, referred to as liquid crystals (LCs), have been used to recreate polymeric skins with capabilities of real-time drug delivery. These materials can be polymerized into liquid crystal elastomers (LCEs); they are able to produce anisotropic soft actuation with elastic behaviour. As the materials being designed become increasingly complex, complete understanding of their behaviour is difficult from just experimental and theoretical approaches. Hence, the use of accurate and fast simulation methods can play a critical role in providing material behavioural insight and ultimately into rational material design.

Conventional simulation methods that model the behaviour of individual molecules and groups of atoms are molecular dynamic (MD) and Monte Carlo (MC) methods. The methods, although differing in approach, both take an all-atom approach. MD simulations slowly evolve a system of molecules based on their position and trajectories determined by Newtonian physics, whereas MC simulations holistically perturb the system with small random steps, only accepting the changes that lower the energy of the system. As both approaches require calculating the force or energy exerted on or by each atom, the time required to complete one simulation can take hours if not days on dedicated research clusters. This provides motivation for designing a new approach to simulation that can provide similar accuracy while drastically reducing execution times. This research consists in using neural networks to slash computation times while maintaining a high level of accuracy. The conventional approach and paradigm that simulations are segmented in time and dimensional scales can be broken by use of machine learning to investigate properties to high degree of precision even at large scales.

In this research, we developed a neural network that can be used for predicting phase transitions of monomeric LCs, referred to as mesogens. Efforts were made to optimize neural network architecture, cost functions, and learning hyperparameters. In this work we prove the hypothesis that the fundamental method in which neural networks learn is in part synonymous to MC methods. MC iterations are accepted or declined based on a probabilistic distribution of the overall system to minimize free energy. Every iteration of the system is provided a small perturbed state. This state is accepted in general if the energy of the system is reduced and declined otherwise. Similarly, to this, each learning iteration of the neural network, instead tunes its neuron weights and biases in such a manner that the cost function is minimized. We take inspiration from the Onsager model as the free energy analog for the form of the cost function. In contrast to MC methods, the learning of a neural network system was accomplished within few hundred iterations (a small fraction compared to MC methods). Additionally, once a network has reached convergence, it can provide insight of various systems of similar environmental parameters without the need of re-learning, whereas MC methods must iterate through a simulation for every unique initial condition. Hence by leveraging the energy minimization aspect from MC methods, but implementing the ideology behind neural networks, we can maintain high accuracy while reducing simulation time. The proposed research outline indicates exploration of an innovative method for understanding material properties which has the potential of accelerating rational material design.

SF01.07.21

Light-Induced High Frequency Oscillation of Aligned Azobenzene Liquid Crystalline Polymers [Kyung Min Lee](#), Ecklin Crenshaw and Nicholas P. Godman; Air Force Research Laboratory, United States

Photoactuators are attractive systems in which light energy is converted into motion. Previously, we reported the oscillatory behavior of cantilevers composed of glassy, azobenzene-functionalized liquid crystalline polymer networks (azo-LCNs). The azo-LCN cantilever containing 20% azobenzene oscillates at high frequencies (50-120 Hz) and large amplitudes when exposed to light from a 442 nm coherent wave (CW) laser. The frequency of photoinduced oscillations was strongly affected by the aspect ratio of the cantilever, whereas the amplitude of the oscillation was affected by temperature. An azobenzene functionalized LC elastomer (azo-LCE) was prepared and the photoresponsive behavior is compared with the glassy azo-LCN. The glass transition temperature of azo-LCE is lower than room temperature. The fundamental photoresponses of these glassy and elastomeric azobenzene liquid crystal polymers (azo-LCN and azo-LCE) are further compared by examining the cantilever aspect ratio, laser intensity, and temperature. This photoinduced large bending and oscillation response of azo-LC polymers can be used for soft robotics and flow control.

SF01.07.22

Enhanced Stability and Solubility of Photoacids in Binary Solvent Mixtures for Light-Driven Reversible CO₂ Capture-Release [Anna de Vries](#)¹, Manuel Reiter¹, Kateryna Goloviznina², Evgeniya Vorobyeva¹, Yayuan Liu³, T. Alan Hatton⁴, Mathieu Salanne² and Maria Lukatskaya¹; ¹ETH Zurich, Switzerland; ²Sorbonne Université, France; ³Johns Hopkins University, United States; ⁴Massachusetts Institute of Technology, United States

Rapid rise of atmospheric CO₂ levels urgently requires more affordable carbon capture technologies with innovations beyond present-day energy intensive regeneration processes such as temperature or pressure swing [1]. Recently, pH-swing was proposed as a promising low energy alternative approach for CO₂ release. A pH-swing - i.e. cycling between CO₂ absorption at high pH, forming HCO₃⁻, and CO₂ desorption at low pH - omits the need to increase temperature or decrease pressure during desorption for sorbent regeneration [2]. Controlled and reversible acidification of a solution can be achieved by the excitation of photoacids. Metastable photoacids are organic molecules that can reversibly lower pH of a solution under UV-visible light. Merocyanine-type photoacids can decrease the pH by up to 3.5 units in less than 30 seconds (pH-jump), and then reverse to the original pH in darkness within 15 minutes through thermal relaxation [3, 4]. The non-invasive nature of these light switchable proton emitters renders highly relevant applications in functionalized surfaces, such as membranes [5] and sensors [6], or pH-driven reactions such as hydrogel formation [7] or CO₂ absorption/release [8]. Merocyanine-type photoacids are generally limited by their low chemical stability due to hydrolysis (half-life is 16 hours) and low solubility in water (0.19 mM) [5]. In aprotic organic solvents such as dimethyl sulfoxide (DMSO), photoacids display higher chemical stability and solubility, however pH-jump in such solvents is not reversible [3].

Herein we propose to dissolve photoacids in water-DMSO solvent mixtures to achieve the ‘best of both worlds’: high reversibility of pH-jump as well as high chemical stability and solubility. By combining pH-jump, solubility and stability studies, we demonstrate that solubility can be enhanced by 2 orders of magnitude, and half-life increased by 1 order of magnitude in DMSO-water mixtures. UV-Vis absorption, Nuclear Magnetic Resonance spectroscopy, Small-Angle X-ray Scattering and Polarizable Molecular Dynamics simulations were used to reveal the role of H-bonding networks and modified solvent structure to enable these enhancements. Besides optimizing for specific properties, binary solvent mixtures provide an additional degree of freedom to tune photoacid properties such as pK_a and relaxation kinetics that can also be applied to other types of photoacids. Finally, the photoacid in an optimal solvent mixture of 15% DMSO in water enables a highly reversible, stable and controlled CO₂ capture-release system. With higher stability and solubility, photoinduced pH-swing has the potential to drastically reduce energy demand, material degradation and infrastructure of mature carbon capture technologies by ambient CO₂ desorption that is controlled by visible light.

- [1] S. E. Renfrew, D. E. Starr, P. Strasser, *ACS Catal.* 10, 21, 13058–13074 (2020) <https://doi.org/10.1021/acscatal.0c03639>
- [2] S. Jin, M. Wu, Y. Jing, R. G. Gordon, M. J. Aziz, *Nat Commun* 13, 2140 (2022) <https://doi.org/10.1038/s41467-022-29791-7>
- [3] C. Berton, D. Maria Busiello, S. Zamuner, E. Solari, R. Scopelliti, F. Fadaei-Tirani, K. S. C. Pezzato, *Chem. Sci.*, 11, 8457-8468 (2020) <https://doi.org/10.1039/D0SC03152F>
- [3] L. Wimberger, J. Andréasson, J. Beves, *Chem. Commun.* 58, 5610-5613 (2022) <https://doi.org/10.26434/chemrxiv-2022-wnts7>
- [4] W. White, C. D. Sanborn, D. M. Fabian, S. Ardo, *Joule*, 2(1), 94-109 (2018) <https://doi.org/10.1016/j.joule.2017.10.015>
- [5] T. Khalil, A. Alharbi, C. Baum, Y. Liao, *Macromolecular Rapid Commun* 39(15), 1800319 (2018) <https://doi.org/10.1002/marc.201800319>
- [6] A. Meeks, M. M. Lerch, T. B. H. Schroeder, A. Shastri, J. Aizenberg, *J. Am. Chem. Soc.* 144, 219-227 (2022) <https://doi.org/10.1021/jacs.1c08778>
- [7] R. Bennett, S. Clifford, K. Anderson, G. Puxty, *Energy Procedia* 114, 1-6 (2017) <https://doi.org/10.1016/j.egypro.2017.03.1139>
- [8] N. Abeyrathna, Y. Liao, *J. Phys. Org. Chem.* 30.8, e3664 (2017) <https://doi.org/10.1002/poc.3664>

SF01.07.23

Microfluidics-Assisted Production of Dual Responsive Microcapsule for Urolithiasis Therapy Byung Kwon K. Kang and Dong-Pyo k. Kim; Pohang University of Science and Technology, Korea (the Republic of)

Stimuli-responsive drug delivery systems are receiving great attention in drug delivery research because they have promising potential as a controlled drug delivery method. Recently, various drug delivery systems have been developed that can respond to extrinsic (ultrasound, light, temperature, magnetic and electric fields) and intrinsic stimuli (pH, enzymes, and oxidation). Among these stimuli, the ultrasonically stimulated drug delivery system has been shown to be applicable as a practical drug delivery system due to its non-invasiveness and deep permeability.

Urolithiasis is a hard crystal stone of accumulated minerals and salts in the ureter, ureteropelvic junction, and kidney due to dietary habits and genetic calcium metabolism. Kidney stones can cause kidney pain, obstruction of urinary flow, and urinary tract infections. Surgical treatment methods (ureteroscopy, percutaneous nephrolithiasis, and extracorporeal shock wave lithotripsy) were required to treat the kidney stone. However, traditional surgery treatments lead to secondary diseases such as infections and bleeding during the treatment process. This work disclosed a chelator encapsulated microcapsule with ultrasound/magnetic responsive systems for urolithiasis treatment application. PLGA-based microcapsules loaded with chelating solutions and magnetic nanoparticles were produced in a microfluidics double-droplet generator with a uniform size ($393 \pm 14 \mu\text{m}$). The microcapsules (MNP-HMP/PLGA) exhibited magnetic mobility by the external magnetic field and controlled release by ultrasound. In addition, the therapeutic microcapsules were proven to have excellent chelator delivery efficacy, cell viability, and superior urolithiasis removal efficacy than conventional oral administration (citrate ingestion) in the kidney mimic chip. To the best of our knowledge, ultrasound/magnetic responsive microcapsule for urolithiasis therapy has not been reported. Finally, this novel drug delivery system with non-invasive/targeted/externally-stimulated drug release properties overcomes the limitations of traditional stone treatment methods and suggests a new approach to stone treatment.

SF01.07.24

Wireless Stimuli-Responsive Trimodal Display Enabled by Direct Capacitive Coupling Jihye Jang, Jin Woo Oh, Hyeokjung Lee, Hyowon Han and Cheolmin Park; Yonsei University, Korea (the Republic of)

With recent advances in stimuli-interactive displays, the development of a stand-alone stimuli-interactive display with no electrical interconnection is of great interest. Here, we present a stimuli-responsive polymer-based wireless display powered by direct capacitive coupling. A wireless stimuli-responsive display (WiSD), which is capable of sensing and visualizing various stimuli such as pressure, temperature, and humidity, consists of three layers: 1) two in-plane metal electrodes with a separated gap, 2) a ferroelectric polymer composite layer for field-induced electroluminescence (EL) and inverse piezoelectric sound, and 3) a stimuli-responsive polymer-based layer, respectively from bottom to top. Alternative current (AC) power supplied between the two in-plane electrodes of a power unit separated from the WiSD is wirelessly transferred to the WiSD via capacitive coupling. The stimulus applied on the stimuli-responsive layer is displayed by AC field-induced EL and inverse piezoelectric sound, which are dependent on the impedance of the stimuli-responsive layer. The AC-to-AC direct capacitive coupling, which does not require resonant frequency matching or current rectification, allows for efficient sensing and visualizing of a variety of stimuli with a broad range of AC frequency, including built-in house power (220 V/60 Hz). Furthermore, our WiSD does not require electrical interconnection, making it suitable for the wireless dynamic monitoring of the delivery of diverse medical fluids to patients in a timely and accurate manner. Moreover, a haptic wireless trimodal interactive display mounted on a human finger broadens the applicability of the WiSD, whereby finger touch is displayed through various outputs of AC EL, inverse piezoelectric sound, and tactile vibration, allowing for developing a wireless three-mode braille smart display.

SF01.07.25

Visible-Light Active Flexible and Durable Photocatalytic Antibacterial Ethylene-co-vinyl Acetate—Ag/AgCl/ α -Fe₂O₃ Composite Coating Svetlana Vihodceva¹, Andris Šutka¹, Anna Kahru², Maarja Otsus² and Kaja Kasemets²; ¹Riga Technical University, Latvia; ²National Institute of Chemical Physics and Biophysics, Estonia

When particles are mixed in polymer, particle surfaces become passivated by polymer matrix, leading to significantly reduced photocatalytic and, thus, also reduced antibacterial activity, as the catalytic particles become isolated from the outer environment and microorganisms reaching the surface. Herein, we demonstrate a facile and rapid approach for coating preparation at room temperature, yielding good adhesion of particles in combination with the particles' interface location. Flexible ethylene-co-vinyl acetate Ag/AgCl/ α -Fe₂O₃ composite coatings were prepared by the spin-coating method. The synthesized photocatalytically active coating surface exhibited a distinct and rapid inhibition of bacterial growth, with at least a 7-log reduction of gram-positive bacteria *Staphylococcus aureus* viability after 30 min of visible-light illumination. We also analyzed the shedding of the Ag-ions and reactive oxygen species production from the composite coating and showed that reactive oxygen species played the main role in the photocatalytic bacterial inactivation, destroying the bacteria cell as proven by the Confocal Laser Scanning Microscopy.

SF01.07.27

Dynamic, Multi-Stimuli-Responsive, Core Cross-Linked Polymeric Nanocarriers Synthesized by PhotoATRP-Induced Self-Assembly Shayesteh Tafazoli and James F. Reuther; Umass Lowell, United States

Smart, multi-stimuli-responsive polymers that possess dynamic covalent bonds exhibit reversibility under equilibrium conditions. These are covalent bonds capable of exchanging or switching between several molecules in different environments. They have innumerable applications in areas including sensors, actuators, switchable wettability, and biomedical and environmental applications. In this project by utilizing one-pot, photo-controlled atom transfer radical polymerization induced self-assembly (PhotoATR-PISA) mediated by UV light ($\lambda = 365$ nm) using parts per million (ppm) levels (ca. <20 ppm) of a copper catalyst, varied polymeric nanostructures morphologies, ranging from nanospheres to worm-like micelles, were obtained at ambient temperature. Polymeric nanocarriers cross-linked efficiently via a clean, efficient, and controllable coumarin photodimerization improving the stability of nanocarriers for targeted delivery. At the same time, cross-linking of nanocarriers with N,N-cystamine bismethacrylamide (CBMA) could be cleaved via the responsiveness of the disulfide cross-link when exposed to the redox environment. In addition, kinetics of release could be tailored by the pH of the surrounding medium. Thus, the system also showed pH-responsive, redox-responsive, and photo-responsive controlled release behavior with a full release of cargo only observed in the right sequence of stimuli. The multi-stimuli-responsive nature of polymeric nanocarrier was used successfully for the controlled encapsulation and on-demand release of the hydrophobic molecule (Nile Red) as a drug simulant.

SESSION SF01.08: Smart Functions of Stimuli-Responsive Materials VII

Session Chairs: Yunteng Cao and Torsten John

Thursday Morning, December 1, 2022

Sheraton, 5th Floor, The Fens

8:45 AM SF01.08.02

Soft On-Demand—Electrochemical Modulation of Polythiophene Mechanical Properties for Smart Actuators Ilaria Abdel Aziz¹, Johannes Gladisch¹, Sophie Griggs², Maximilian Moser², Magnus Berggren¹, Iain McCulloch² and Eleni Stavrinidou¹; ¹Linköping University, Sweden; ²University of Oxford, United Kingdom

Interfacing electronics and biology opens the need for materials having suitable electrical and mechanical properties, as mixed ionic/electronic conductivity and softness. Among all materials, polythiophene conjugates emerged for their high biocompatibility, ionic as well as electronic conduction, and optical properties in the visible range. Remarkable results have been obtained interfacing polythiophenes-based transistors and actuators with mammalian cells, as well as plants, to a lower extent. However, the phenomena occurring at the interface between the material and the aqueous environment, as water intercalation and oxygen reduction reactions, are raising interest for their impact on the device performances and stability. In particular, volumetric changes driven by water intake during electrochemical doping/de-doping emerged as a limitation for transistor performances, since the irreversible water intake results in lamellar order disruption and consequently reduced hole mobility.

While this volumetric change represents a limitation for transistor devices, it opens to a new class of electrically addressable actuators, where both mechanical stimulation and mixed conduction play together. Since the electrochemical doping/de-doping is accompanied by water intake in the thin film structure, we expect the mechanical properties to change accordingly. Here, we investigate the volumetric changes and their correlation with the mechanical properties of a new group of polythiophene based materials, conjugated to ethylene glycol (EG) side chain of different lengths. The EG-side chains account for a better stabilization of the water. According to previous publications, our findings show that the electrochemical doping drives volumetric changes in aqueous environment up to 250% vs initial volume. Additionally, we demonstrate that the amount of volume change depends on the ionic strength of the solvent and the side chain length. Moreover, the water intake determines changes in the mechanical properties, in particular softening the material upon volumetric expansion.

Our findings deterministically correlate the mechanical properties, the volume changes and the doping state of the material, laying the basis for the development of low-voltage electrically addressable devices. This class of material and devices has a great potential interest for bioelectronic applications, as it accounts for ionic/electronic conduction and on-demand modification of stiffness, emerging as a smart platform for mammalian and plant cell stimulation and monitoring.

9:00 AM SF01.08.03

Helical-Shaped Self-Oscillating Gels Showing Autonomous and Magnified Mechanical Oscillation Taehun Chung¹, Hyein Kim¹, Young-Ki Kim¹, Ryo Yoshida² and Younsoo Kim¹; ¹Pohang University of Science and Technology, Korea (the Republic of); ²The University of Tokyo, Japan

Helical structures exist across multiple length scales, from DNA, collagen fibrils, and bacterial flagella to plant tendrils. They are important in living organisms in a biological context because of their unique properties, such as traveling and sensing. From an engineering point of view, these helical structures can be used in microscale soft robots.

"Self-oscillating" gels have become a distinguished class of smart soft materials because they undergo spontaneous and cyclic swelling-deswelling changes without on-off switching of external stimuli.[1] However, the practical applications of self-oscillating gel are still limited due to a small change in the degree of swelling (deswelling) and non-directional actuation by isotropic deformation.

Herein, to improve the degree of deformation of gels, we report an unprecedented method to convert an isotropic deformation into anisotropic and unidirectional deformation of gel. As a result of introducing a three-dimensional periodic gradient structure by photopolymerization into the gel network, a helical-shaped gel could be synthesized. The helical-shaped gels exhibited amplified uniaxial winding and unwinding during the Belousov-Zhabotinsky (BZ) reaction. In addition, the helical-shaped gels showed a significant change in length according to self-oscillation compared to the conventional rod-shaped gel. When one end of the gel is fixed, the helical-shaped gel repeatedly performs winding and unwinding movements without fatigue with a large amplitude (~14%), even at a constant temperature and without applying external stimuli. When the gel is floated on the water surface, and a BZ reaction occurs spontaneously inside the gel, it reciprocates at a constant speed. This presentation will discuss synthetic strategy, structure analysis, and improved self-oscillation of helical-shaped gels.

Reference

[1] R. Yoshida *et al.*, *J. Am. Chem. Soc.*, **118**, 5134 (1996).

9:15 AM SF01.08.04

Light-Controlled Neurotransmitter Delivery in Solid State Nanopores for Retinal Prosthetics Angela F. De Fazio¹, Pascal Welzen², Jan Van Hest², Elisabetta Colombo^{1,3}, Fabio Benfenati^{1,3}, Francesco De Angelis¹ and Marzia Iarossi⁴; ¹Istituto Italiano di Tecnologia, Italy; ²Eindhoven University of Technology, Netherlands; ³IRCCS Ospedale Policlinico San Martino, Italy; ⁴Italian Institute of Technology, Italy

Achieving precise control on the regulation of a flow is of utmost importance to obtain a reliable valve for the selective delivery of material from one side

to the other of the valve itself, in the attempt to mimic the selectivity and properties of cell membranes. In the literature numerous efforts of externally controlled gating have been reported; however, many of these strategies lack of scalability, fast responsiveness of the gating, efficient external control. In this work, we aim to achieve controllable delivery of a neurotransmitter, glutamate, using light-gated solid-state channels. The channels were obtained by milling conical nanopores in a 500 nm thick Si₃N₄ membrane; then they were functionalized with an azobenzene-based polymer. The presence of numerous azobenzene molecules generates a polymeric structure able to switch between an expanded *trans* structure and a collapsed *cis* configuration. This conformational switch results into a gating behaviour inside the channels, between a closed (*trans* isomer) and an open (*cis* isomer) configuration. The polymer functionalisation was examined by AFM, while the amount of loaded polymer was quantified using a quartz microbalance. The *cis-trans* isomerisation within the channels was monitored by ellipsometry.

To test the light responsiveness and the gating efficiency, the nanopatterned membrane was encased in a home-made microfluidic device consisting of a chamber on top of the membrane and a bottom reservoir, located underneath the membrane. This was used to flow glutamate molecules through the channels. The gating capability was monitored by Current-Voltage (IV) measurements, while the amount of translocated neurotransmitter was quantified by fluorescence spectroscopy.

This light-gated microfluidic device may represent a viable option for any application requiring precise and controlled delivery of specific molecules in specific locations. For example, we envision the use of this technology in the field of retinal prosthetics, where it could be employed to restore the light-evoked glutamate outflow on the denervated inner retinal neurons upon photoreceptors degeneration.

9:30 AM SF01.08.05

3D Printed Hydrogels as Photothermal Actuators [Melanie M. Ghelardini](#)¹, Martin Geisler², Niclas Weigel², Jameson P. Hankwitz¹, Nicolas Hauck², Jonas Schubert², Andreas Fery^{2,3}, Joseph B. Tracy¹ and Julian Thiele^{2,4}; ¹North Carolina State University, United States; ²Leibniz Institute for Polymer Research, Germany; ³Institute of Physical Chemistry and Polymer Physics, Technische Universität Dresden, Germany; ⁴Dresden Center for Intelligent Materials, Technische Universität Dresden, Germany

Thermoresponsive hydrogels are 3D printed with embedded gold nanorods (GNRs) with average dimensions of 81 × 23 nm, which enable shape change through photothermal heating. GNRs are chosen for their tunable and intense extinction, which results in high photothermal heating efficiencies. The GNRs are functionalized with bovine serum albumin (BSA) and mixed with a photoinitiator and poly(*N*-isopropylacrylamide) (PNIPAAm) macromer to form an ink for 3D printing by direct ink writing. Use of a PNIPAAm macromer increases the homogeneity and optical transparency of the resulting gel in its swollen state in comparison with free-radical polymerization. The ink is printed into a gelatinous support structure to provide mechanical stability during printing and concurrent photo-crosslinking, preventing the spreading of the deposited ink prior to complete crosslinking. Use of a support structure is vital for maintaining the integrity of the print, as it compensates for the low viscosity of PNIPAAm, which restricts its use in extrusion-based printing. After crosslinking, the support structure is removed through heating in a water bath at 28 °C, which allows completion of 3D printing well below the transition temperature of the PNIPAAm. The 3D-printed composite exhibits a lower critical solution temperature of ~34 °C, whereupon it transitions from a transparent, swollen state to a shrunken, phase-separated state. Upon exposure to a near-infrared LED, the GNRs transduce light into heat, thus raising the temperature and driving the phase transition and shrinkage of the hydrogel-GNR composite. Reversible shrinkage is observed over multiple cycles of photothermal heating, demonstrating the promise of 3D-printed, photoresponsive structures as hydrogel actuators.

9:45 AM SF01.08.06

A Flexible Shape Memory Polymer Adhesive with Dual Adaptations [ChangHee Son](#)¹, Placid Ferreira¹ and Seok Kim^{2,1,3}; ¹University of Illinois, United States; ²Pohang University of Science and Technology, Korea (the Republic of); ³Yonsei University, Korea (the Republic of)

A shape memory polymer (SMP) makes conformal and hermetic contact with a target surface at its soft, rubbery state, while it produces a high-strength dry adhesion at the rigid, glassy state. Recent SMP adhesive investigations demonstrate that SMP can stick to a variety of rough surfaces as well as rigid surfaces underwater. However, it is somehow challenging to achieve and maintain a strong adhesion on a flexible adherends such as common fabrics due to a modulus mismatch where the flexible adherends would easily be peeled off from SMP adhesives which are too rigid to adapt to the target surface flexing. Here, we present the dual adaptation of an SMP adhesive consisting of a thin SMP layer and a backing fabric, which involves the shape adaptation to produce a strong adhesive contact and the flexure adaptation to tolerate a flexing target surface. In order to determine the criteria for optimizing both shape and flexure adaptations, we present a theoretical justification and computational and experimental research. On the basis of these results, we demonstrate a dry and underwater adhesion performance of a thin SMP adhesive on common clothing to highlight its potential applications.

10:00 AM BREAK

10:30 AM SF01.08.07

Actively-Triggerable Metals via Liquid Metal Embrittlement for Biomedical Applications [Vivian R. Feig](#)^{1,2}, Eva Remlova², Robert Langer¹ and Giovanni Traverso^{1,2}; ¹Massachusetts Institute of Technology, United States; ²Brigham and Women's Hospital, United States

Actively-triggerable materials, which break down upon introduction of an exogenous bio-orthogonal stimulus, enable precise control over the lifetime of biomedical technologies as well as adaptation to unforeseen circumstances, such as changes to an established treatment plan. Yet most actively-triggerable materials are low-strength polymers and hydrogels with limited long-term durability. By contrast, metals possess advantageous functional properties, including high mechanical strength and conductivity, that are desirable across several applications within biomedicine. To realize actively-triggerable metals, we leveraged a mechanism called liquid metal embrittlement, in which certain liquid metals penetrate the grain boundaries of certain solid metals and cause them to dramatically weaken or dissolve. In this work, we demonstrate that eutectic gallium indium (EGaIn), a biocompatible alloy of gallium, can be formulated to reproducibly trigger the breakdown of aluminum within different physiologically-relevant environments. The breakdown behavior of aluminum after triggering can further be readily controlled by manipulating its grain structure. Finally, we demonstrate three possible use cases of biomedical devices constructed from actively-triggerable metals.

10:45 AM SF01.08.08

Self-Healing Elastomers for Information Storage and UV-Sensing [Tiwa Yimyai](#)^{1,1,2}, Daniel Crespy¹ and Abdon Pena-Francesch²; ¹Vidyasirimedhi Institute of Science and Technology (VISTEC), Thailand; ²University of Michigan–Ann Arbor, United States

Most electronic devices are composed of rigid and brittle components, which are typically not compliant and limit their applications. In contrast, flexible electronic devices are developed using compliant polymers to overcome the fracture problems of rigid devices, as well as to adapt to multiple conformations in a wide range of applications such as electronic skins, flexible displays, and tactile sensors. However, soft electronic polymer materials are typically vulnerable to mechanical damage caused by repeated use and accidental puncture with sharp objects, leading to functional failure. Therefore, self-healing materials provide an opportunity for repairing the damage and extending life-time. Herein, a self-healing polyurethane elastomer that is flexible, stretchable, and transparent was prepared. The self-healing elastomer relies on dynamic exchange reactions of disulfide bonds in its molecular structure upon activation with temperature. Inspired by the process of tattooing on human skin, a soft stretchable platform for reversible and irreversible information

encryption was developed by microstructuring the polymer matrix with a functional dye solution. Upon the healing of the polymer, the dye was embedded in the polymer matrix, protected from abrasion and extraction with solvents. By storing a UV-sensing dye in the polymer matrix, we successfully produced a photochromic self-healing polymer elastomer, which exhibited a great potential for wearable technologies in harsh environments that require resiliency, protection, and in-situ repair.

11:00 AM SF01.08.09

The Use of Phase Change Materials to Create Variable Stiffness Linkage-Fabrics Christian Partik, Elze Porte, Martyna Michalska and Mark Miodownik; University College London, United Kingdom

Animate materials that can respond to the input from their environment and dynamically change shape have seen increasing applications in recent years in the fields of soft robotics and assistive technology [1,2]. Their ability to morph from a flexible to a rigid state is one of their key attributes. However, current shape-changing structures that utilise actuators often require a constant energy supply to retain their rigid shape, while they return to the original structure when the energy is removed [3,4]. This limits the utility of the materials for applications such as assistive technology and deployable structures where energy use needs to be minimised to meet design requirements. This research aims to address this problem by developing a stiffness-changing structure that does not require constant energy input to maintain either the low or high stiffness state.

Phase change materials (PCMs) have traditionally been used as energy storage materials due to their high latent heat [5], but little attention has been paid to their potential for mechanical applications using the cyclic liquid to solid phase change of these materials. Phase change materials can be cooled below their solidification temperature and stay in their supercooled liquid phase for an indefinite period. Solidification can be triggered through the introduction of nucleation sites such as crystals by using electrical or mechanical triggers. By heating the material above its solidification temperature the phase change can be reversed.

In this work, we show that the mechanical properties of linkage-fabric structures can be controlled by the use of a phase change material incorporated into the fabric. We use sodium acetate trihydrate ($\text{CH}_3\text{COONa} \times 3\text{H}_2\text{O}$) as the phase change material with the nucleation from the liquid to the solid-state controlled by an electric impulse [6]. The linkage-fabric structures were designed using CAD software to create a flexible interlocking structure that when actuated modulates the stiffness of the fabric. The structures were 3D printed in nylon using Selective Laser Sintering (SLS). For each sample, supercooled sodium acetate and the conducting paths for the electrical signals were manually incorporated. The phase change response of the sodium acetate was triggered by silver electrodes with microcrystals embedded onto their surface, through which a DC voltage has been supplied. We present data on the effect of sodium acetate solution composition on the mechanical stiffness of the actuated fabrics, the reversibility of this change and the impact of fabric design on its property. The work shows that phase change materials can be used for the construction of linkage-fabrics with variable stiffness without requiring constant energy input. The work opens up myriad opportunities to exploit these structures in applications for deployable structures and assistive technology.

Refs:

1. Animate Materials, Royal Society Perspective, Feb 2021, ISBN: 978-1-78252-515-8. <https://royalsociety.org/-/media/policy/projects/animate-materials/animate-materials-report.pdf>
2. Ball, P. Animate Materials, MRS Bulletin volume 46, pages 553–559 (2021)
3. M. Ransley, P. Smitham, and M. Miodownik, Active Chainmail fabrics for soft robotic applications, Smart Mater. Struct., 26, 08LT02 (2017).
4. Ploszajski, A. R., Jackson, R., Ransley, M., & Miodownik, M. (2019). 4D Printing of Magnetically Functionalized Chainmail for Exoskeletal Biomedical Applications. MRS Advances, 4 (23), 1361-1366. doi:10.1557/adv.2019.154
5. Lane, G. A., & Ph, D. (1983). Lane, G. A - Solar Heat Storage - Latent Heat Materials vol II Technology-CRC Press (1983).
6. Dong, C., Qi, R., Yu, H., & Zhang, L. (2022). Electrically-controlled crystallization of supercooled sodium acetate trihydrate solution. Energy and Buildings, 260, 111948. <https://doi.org/10.1016/j.enbuild.2022.111948>

11:15 AM SF01.08.10

4D Printing of Dicyclopentadiene/BaTiO₃ Polymer Composites Hyoseop Kang and Woong-Ryeol Yu; Seoul National University, Korea (the Republic of)

Dicyclopentadiene (DCPD) is a thermosetting polymer capable of spontaneous frontal ring-opening metathesis polymerization (FROMP) by the thermal initiation of local sites. As such, DCPD can be printed into a free-standing structure without supports, which is not possible with a conventional fused deposition moulding printer. In addition, cyclooctane can be incorporated into DCPD during FROMP to develop new smart materials with shape memory performance. In the meantime, BaTiO₃ is one of piezoelectric ceramics with excellent dielectric and piezoelectric properties, being a promising material for piezoceramic devices. Due to its poor formability and brittleness, BaTiO₃ is used as a filler for polymer composites. In this research, a piezoceramic composite was prepared using DCPD and BaTiO₃ and printed into a free-standing structure without supports. For this, BaTiO₃ nanoparticles were dispersed uniformly in DCPD solution, which was confirmed using SEM and EDS analysis. Then, optimal 3D printing condition of the composite solution was explored. Lastly, the shape memory performance and the dielectric constant of the printed composite were measured to investigate the possibility of a piezoelectric ceramic device.

11:30 AM SF01.08.11

Stimuli Responsive Molecular-Conductor Composites Raphael Pfattner^{1,2}, Elena Laukhina², Marta Mas-Torrent^{1,2}, Vladimir Laukhin¹, Jaume Veciana^{1,2} and Sergi Riera-Galindo¹; ¹Materials Science Institute of Barcelona (ICMAB-CSIC), Spain; ²Networking Research Center on Bioengineering, Biomaterials and Nanomedicine (CIBER-BBN), Spain

Developing smart materials that can respond to an external stimulus is of major interest in artificial sensing devices able to read information about the physical, chemical and/or biological changes produced in our environment. Additionally, if these materials can be deposited or integrated on flexible, transparent substrates, their appeal is greatly increased. The BEDT-TTF=bis(ethylenedithio)-tetrathiafulvalene based quasi-two-dimensional organic superconductor β -(BEDT-TTF)₂I₃ was first reported back in 1984.^[1] Soon it became clear that ion radical salts derived from BEDT-TTF exhibit tunable electronic band structures. Therefore, such molecules are excellent building blocks for engineering a rich and diverse family of organic crystalline metals and semiconductors. When processed in composites, the high electrical performance of single crystals can be combined with the processing properties of polymers where at the percolation threshold, fascinating novel optoelectronic properties emerge.^[2] Such systems can be further tuned by choosing the nature of the conductor enabling high sensitivity towards strain, pressure, temperature, humidity or even contactless radiation sensing *i.e.* bolometers.^[3-5] This rich class of materials ranges from metals to semi-metals and semiconductors and is highly sensitive to a variety of external stimuli. Mechanisms of responses are discussed and correlated with fundamental properties of charge transport in these systems. Such materials allow for selective sensing enabled due to molecular design and structural control of the active components. These findings are highly promising for multidimensional selective sensing made possible by tuning molecular composition to maximize and, importantly, to decouple responses to strain, pressure, temperature, radiation, and recently also

humidity as an external stimulus. An attractive field of application in this context is human health care targeting environmental conditions relevant for human physiology.

References:

- E. B. Yagubskii, I. F. Shchegolev, V. N. Laukhin, et.al., JETP Lett., (1984), 39, 12.
R. Pfattner, E. Laukhina, J. Li, et.al, ACS Appl. Electron. Mater. (2022), 4, 2432.
E. Laukhina, R. Pfattner, L. R. Ferreras, et. al., Adv. Mater., (2009), 21, 1-5.
R. Pfattner, V. Lebedev, E. Laukhina, et.al., Adv. Electr. Mater., (2015), 1, 1500090.
R. Pfattner, E. Laukhina, L. Ferlauto, et.al, ACS Appl. Electr. Mater., (2019), 1, 1781.

11:45 AM SF01.08.12

Bioprinting Osmotically Actuated Tissue-Like Materials McKayla L. Torbett¹, Aida Fica², Manish Kumar², Berkin Dortdivanlioglu² and Stephen A. Sarles¹; ¹The University of Tennessee, Knoxville, United States; ²The University of Texas at Austin, United States

Hierarchical biomimetic materials that operate at the same, or greater, level of sophistication as biological tissues are yet to be fully realized, in part, because artificial materials fail to recreate the intricate network of compartmentalized cells as found in natural tissues. Compartmentalization is key in recreating the inherent physicochemical phenomena responsible for maintaining homeostasis in living organisms, such as tunable mechanical properties, selective permeability, stimuli responsiveness, and cellular communication. The Droplet Interface Bilayer (DIB) is a phospholipid model membrane consisting of a lipid bilayer formed at the interface of two monolayer-coated aqueous droplets in oil and is promising for realizing soft intelligent materials, as each droplet naturally forms a cellular compartment and can join with others to form a tissue-level hierarchy with customizable cells. This study aims to construct and characterize the collective and stimuli-responsive behaviors of multilayered, tissue-like compartmentalized materials built from lipid-stabilized aqueous compartments. To demonstrate the benefit of compartmentalized materials and to yield prototypes that will help us better understand their emergent properties, we chose to design an osmotically actuated material. Utilizing a commercially available, pneumatic bioprinter, nanoliter-sized aqueous volumes suspended in oil have been successfully printed in 2D and 3D arrangements to form networks of sophisticated, compartmentalized constructs. A change in conformation is induced as programmed osmolarity gradients, present within the printed structure, drive water towards cells of a higher solute concentration, thereby swelling or shrinking adjoining droplets accordingly. Permeability measurements obtained for single lipid bilayers, coupled with discrete printing parameters allow for the prediction and fine-tuned control of osmotic actuation and stimuli-responsiveness. Ongoing efforts seek to incorporate integral membrane proteins and pore-forming channels into the intercompartment membranes to accelerate water transport and, thus, osmotic actuation. Overall, the involuntary folding of printed networks results in a synthetic tissue-like material more closely resembling the collective functionalities and sophisticated behavior of biological tissues and unlocks many other stimuli-responsive functions capable through the use of biomolecules.

SESSION SF01.09: Smart Functions of Stimuli-Responsive Materials VIII

Session Chairs: Torsten John and Muchun Liu

Thursday Afternoon, December 1, 2022

Sheraton, 5th Floor, The Fens

1:30 PM SF01.09.01

Rapid and Reversible Shape Memory Effect in Colloidal Crystals Engineered with DNA Heather Calcaterra¹, Seungkyu Lee¹, Sangmin Lee², Wisnu Hadibrata¹, Byeongdu Lee³, EunBi Oh¹, Koray Aydin¹, Sharon Glotzer² and Chad Mirkin¹; ¹Northwestern University, United States; ²University of Michigan—Ann Arbor, United States; ³Argonne National Laboratory, United States

Mechanically responsive crystals, which exhibit reversible, rapid, and complex dynamics, are essential to the development of flexible electronics, artificial muscles, and various dynamic components in soft robotics. However, due to the limited flexibility of atomic bonds, only a small number of reversible deformation modes have been realized for these materials. Colloidal crystals engineered with DNA represent an ideal platform for the development of mechanically responsive crystals, owing to the stimuli-responsiveness and high fidelity of the DNA bonds that define the crystal. Herein, we report the reversible mechanical responsiveness of colloidal crystals engineered with DNA to deformations typically considered irrecoverable in conventional molecular and atomic crystals. These advances were obtained through the synthesis of large (>100 μm) single crystals, which enable previously unrealizable characterization techniques including in-situ optical microscopy and single-crystal x-ray diffraction. These techniques shed light into both the unprecedented nature of the macroscale deformation and recovery as well as the resilient and flexible internal structure of the single crystals. Since single crystals are the basis for many optical and electronic device components, the synthetic methods and crystal deformation capabilities described in this work lay the foundation for the realization of advanced structural materials for applications such as optics, chemical sensing, and many others which require the properties of both soft and crystalline materials.

1:45 PM SF01.09.02

Enhanced Atmospheric Water Uptake of Hydrogels at Elevated Temperatures Xinyue Liu, Lenan Zhang, Shaoting Lin and Evelyn N. Wang; Massachusetts Institute of Technology, United States

To prevent the dehydration of living organisms, it is crucial to obtain and retain water, especially in hot weather. However, most materials, including plants, biological tissues, and inorganic sorbents, can lose more water at a high temperature and capture more water at a low temperature, because of the exothermic water vapor adsorption. Here, we discover a class of hydrogels that exhibit enhanced atmospheric water uptake when the temperature is elevated. For example, the adsorbed water in hydrogels is doubled when we increase the temperature from 25°C to 75°C and maintain 20% relative humidity. This abnormal temperature dependence of water vapor adsorption can be attributed to the first-order phase transition of polymer networks. We also developed a thermodynamic theory to analyze and predict the equilibrium water vapor adsorption at different temperatures and relative humidity. Our finding has profound implications for thermal energy management and atmospheric water harvesting.

2:00 PM SF01.09.03

Bio-Inspired and Stimuli-Responsive Adhesive Hydrogel Structure Fabricated by Single-Exposure Photolithography Jinsik Yoon and Wook Park; Kyung Hee University, Korea (the Republic of)

[Introduction] Since adhesive structures that can be attached by specific morphology do not require special chemical properties, diverse materials can be

adopted, and numerous researchers have applied bio-inspired frames in nature. Mainly, the mimicked adhesive structures consist of complex three-dimensional (3D) shapes rather than simple 2D shapes, and, in order to fabricate these structures, a series of rather complex processes are involved. Herein, we present the 3D bio-inspired (male diving beetle foot) adhesive structure fabrication utilizing a simple single-exposure photolithography system. The adhesive structure made of photocurable hydrogel cannot be attached in a contracted environment such as dried and ethanol, but the structures will be deformed into a concave adhesive shape by local expansion in an underwater environment. In addition, it is confirmed that adhesion can be controlled by stimuli according to changes in the surrounding environment.

[Materials and Methods] A photolithography system, based on a mercury-xenon lamp ultraviolet (UV) light source (365 nm, Hamamatsu) with a fiber-based light guide to solidify photocurable polymers, a digital micromirror device (DMD, Texas Instruments) to reflect desired UV light patterns, and objective lens (Olympus) to adjust the pattern size, was utilized in order to create 3D adhesive hydrogel structures. The photocurable hydrogel material was prepared by mixing Poly(ethylene glycol) diacrylate (Mn 700, Sigma-Aldrich) and Irgacure 1173 (photoinitiator, BASF) by a vortex mixer (Scientific Industries).

[Results and Discussion] The 3D hydrogel structure fabricated through the single-exposure photolithography process was expected to maintain different polymeric network densities locally, and through Raman spectroscopy analysis, the local carbon double bonding (1635 cm^{-1}) intensity was demonstrated to be different. The hydrogel structures exposed to dry or ethanol solution were not able to adhere due to the convex surface based on shrinkage. But, the hydrogels soaked in water environment were transformed into a concave shape due to local expansion based on difference of polymeric densities, enabling adhesion. The expanded and adhesive hydrogel structure immersed in water was saturated with pull-off force under the pre-loading condition of about 70 kPa, and the force was about 130 mN. Additionally, the change of hydrogel structures according to temperature change was analyzed. The hydrogel structures could not be adhered due to shrinkage on the basis of water temperature increase around 50 degrees Celsius. Contrary to the previous case, the hydrogel structures could be adhered in accordance with expansion based on ethanol temperature increase nearly 40 degrees Celsius.

[Conclusion] We have shown bio-inspired and stimuli-responsive adhesive hydrogel structures fabricated by utilizing a single-exposure photolithography process. The created hydrogel structures are transformed into an adhesive form by local expansion in water, and in addition, the frame is transformed according to the change of the surrounding thermal environment. Thus, the adhesion states can be controlled. We believe that the manufactured adhesive hydrogel structure will contribute to soft actuation and robotics fields.

2:15 PM SF01.09.04

Physically Crosslinked Thermoresponsive Polymer Hydrogels for Cooling-Triggered Drug Release Romario Lobban and Leon Bellan; Vanderbilt University, United States

Physically crosslinked thermoresponsive polymer hydrogels undergo a well-known gel-to-sol transition upon being cooled below their LCST. Accompanying this transition is a massive increase in the release rate of sequestered payloads. We explore the possibility of using such a system for cooling-triggered, local release of pain relief therapeutics. Currently, opioid addiction and abuse result in over 115 deaths per day in the US alone. A safer, non-systemic, local mechanism for relief from acute (e.g. perioperative pain) and chronic pain is therefore needed. Ideally, patients and caregivers should be able to trigger this mechanism, non-invasively and on demand, via an external stimulus. As icepacks are already widely applied to temporarily ease local pain, introducing a drug delivery mechanism switched "ON" by cooling would enable long duration, enhanced pain relief triggered by a method with which patients are already familiar. Herein, we describe how cooling-triggered drug release can be achieved using a drug-loaded physically crosslinked thermoresponsive polymer hydrogel encapsulated in a rate-limiting nanoporous membrane.

We formulated a Soluplus (a polyvinyl caprolactam copolymer from BASF) solution (10%-30% w/v, with 3% CaCl_2) and loaded 0.5%-1%w/w_{gel} Nile Red (NR, as a model molecule for bupivacaine, a common anesthetic) into it. We then heated this solution above its LCST within a mold to form 0.2 ml hydrogel pellets. Finally, we dipped these pellets in an alginate bath for 4 minutes to encapsulate them in ~500-micron-thick, calcium-crosslinked alginate shells. We placed these pellets in a 40°C PBS well for 3 hours to account for any initial burst release. Next, we alternated each pellet between warm (40°C) and cool (~23°C) separate wells, allowing the pellets to spend 24 hours at each temperature. The amount of NR released into the wells at the different temperatures was then determined using a plate reader. Additionally, to ensure that the NR is released in a form accessible to cells, we exposed HUVEC cells to solution drawn from the wells containing the pellets and observed their fluorescence (NR fluoresces minimally in water but becomes very fluorescent in nonpolar environments such as lipid membranes).

We observed that pellets released ~100 times more NR into the surrounding PBS when kept at ~23°C compared to when kept at 40°C. As the LCST of our Soluplus formulation is ~30°C, this indicates that its gel-to-sol transition results in a huge increase in the rate of release of NR. When HUVEC cells were exposed to the PBS into which a hydrogel device had released NR, they showed clear signs of NR uptake, indicating availability to cells. NR release from the pellets described above can therefore be switched ON by cooling below the LCST of the constituent hydrogel and OFF again by heating above said LCST. The payload released is shown to be available to cells. These results demonstrate that physically crosslinked thermoresponsive polymer hydrogels can be used for cooling-activated drug release, a promising new approach for patient triggered, on-demand delivery of therapeutics.

2:30 PM SF01.09.05

Tricolor Visible Wavelength-Selective Hydrogels for Cell Encapsulation and Release Teresa Rapp and Cole A. DeForest; University of Washington, United States

Over the past decade, photoresponsive biomaterials have birthed a surge of innovation in targeted drug delivery and 4D cell culture. Compared to other material-modifying stimuli (e.g., pH, enzymes, heat etc.), light is a particularly powerful stimulus for targeted drug delivery, uniquely affording spatiotemporal control in an orthogonally specified manner with different wavelengths. Despite its established promise in laboratory settings, significant challenges remain in pushing these technologies to the clinic. Current photosensitive materials are constrained by their reliance on high-energy UV light which is poorly penetrant through human tissue, limiting the depths to which they may be used for *in vivo* treatment. Additionally, photoresponsive materials developed thus far most typically respond to one or potentially two distinct wavelengths, thereby missing significant opportunities for reaction multiplexing by taking advantage of the entire spectrum of visible and IR light. In this work, I will discuss our recent results in designing and synthesizing a series of visible light-responsive cytocompatible polymer crosslinkers for next-generation hydrogel photodegradation. Translating well-established photochemistries of ruthenium polypyridyl complexes and *ortho*-nitrobenzyl moieties into the biomaterials space, we have created a series of crosslinkers that selectively respond to either red, green, or blue light. When incorporated within step-growth polymeric hydrogel networks, stable gels are formed that are highly sensitive to low-intensity visible light irradiation, reversing gelation within seconds through up to 2 cm of tissue. Reaction cytocompatibility ensures that cells in gels exhibit excellent viability throughout encapsulation, long-term culture, and photorecovery for downstream single-cell analysis. Permitting for the first time sequential photodegradation events deep within living tissue, we anticipate that these user-programmable biomaterial systems will pave a new and sustainable route to clinical drug delivery.

1:00 PM *SF01.10.01

Self-regulated Mixing Leads to Hierarchical Composites with Design Flexibility Ting Xu¹, Le Ma¹, Hejing Huang² and Alfredo Alexander-Katz²;
¹University of California, Berkeley, United States; ²Massachusetts Institute of Technology, United States

The modernization toward nanocomposites has been stalled due to the inability to modulate their structures over all length scales albeit of surging developments in colloidal synthesis and self-assembly. Realization of large scale assemblies requires long-range diffusivity, a fundamental challenge in nanoscopically ordered systems. This is due to the competition between the enthalpic forces to form assemblies and the kinetic barriers to diffuse through ordered domains. We hypothesize that forming nanostructures in dilute, miscible solution will overcome these fundamental challenges and experimentally realized this by leveraging entropy-driven phase behavior upon increasing composition diversity, akin to that seen in high entropy alloys. The complex blends, composed of nanoparticles/block copolymers/small molecules, self-regulate the spatial distribution of each component to enhance miscibility and, thus, minimize the enthalpic effects. The resultant entropy-driven phase behavior enables NP ordering unachievable before, even in dilute solutions, with unparalleled design flexibility. This makes it kinetically feasible to realize nanoscopic ordering-induced macrophase separation with tunable microstructures. In addition to opening all-new pathways to modulate nanocomposites, these energetic insights may be applicable to understand behavior in other complex blends such as liquid-liquid phase separation.

1:30 PM SF01.10.02

Fluorescent Polymer Particles of Nanometer and Micrometer Lengthscales Towards Labeling Applications—Synthesis and Properties Nikunj Kumar Visaveiyia; The City College of New York, United States

Various types of fluorescent organic dyes of diverse characteristics are routinely utilized for labeling purposes due to their easy use, low cost, and availability of full emission wavelength range. However, organic dyes are very sensitive to their surrounding in which they rapidly degrade either via chemical degradation or photodegradation. To avoid the concern of degradability, inorganic nanoparticles, in particular, quantum dots are highly versatile and photostable. However, quantum dots are relatively toxic to biological systems, and hence their widespread and safe uses are a concern. Alternatively, dye-doped polymer particles are promising for labeling and imaging due to their properties that overcome limitations of photodegradation as well as toxicity. Fluorescent polymer particles can be prepared simply by incorporating fluorescent dyes in the polymer nanoparticle matrix. In this work, various experimental strategies for the nanoscale fluorescent polymer particles have been developed to bind the fluorophores inside the matrix covalently or non-covalently, as well as at the surface through direct adsorption or based on bio-conjugation. Besides, Hydrophilic and hydrophobic microscale fluorescent polymer particles were prepared via photopolymerization by droplet microfluidics. Highly controlled color compositions were inserted inside the fluorescent polymer microparticles, and a color combination library of the multi-colored fluorescent polymer microparticles was synthesized. Furthermore, soft and bright particulate assemblies were enabled through interfacial interactions at the intermediate scale between the nanometer and micrometer length scale. Overall in this work, various techniques for the synthesis of nanoscale fluorescent polymer particles, as well as microscale fluorescent polymer particles with hydrophobic and hydrophilic characteristics, and assembly of the fluorescent polymer particles at the multiscale level are presented.

1:45 PM SF01.10.03

Self-Orienting and Self-Actuating Materials Based on Anomalous Ultrasonic Scattering Matthew Stein, Sam Keller, Yujie Luo and Ognjen Ilic; University of Minnesota, United States

Contactless manipulation by waves is broadly applicable in systems ranging from assembly and imaging to holography and haptics. However, conventional laws of wave scattering intrinsically limit the actuation force based on the shape and the size of the object: for example, common manipulation mechanisms work for objects with a dimension smaller than the wavelength or a shape that is highly symmetric and often rely on complex feedback control and object tracking. Here, we introduce the concept of a stimuli-responsive acoustic material whereby the dynamics and motion become controllable by a deliberately engineered metamaterial surface.

We present theory, simulations, and experiments to show how the embedding of momentum-shaping surface scatterers can steer and bend ultrasonic waves and lead to programmable self-actuation. To demonstrate the versatility of this concept, we present several examples of advanced actuation functionalities, including autonomous path following and contactless tractor beaming, that are uniquely enabled by anomalous ultrasonic scattering and are beyond the limits of traditional wave-matter interactions. Our work shows how deliberate patterning of a material surface can open new frontiers in contactless actuation and enable unprecedented control of self-actuating dynamics with subwavelength resolution.

2:00 PM SF01.10.04

Polybutadiene Elastomers with Degradation Profiles Programmed by Microencapsulation and Controlled Release of Metathesis Catalysts Brad H. Jones, Samuel C. Leguizamón, Hannah Narcross and Koushik Ghosh; Sandia National Laboratories, United States

The principles of microencapsulation and controlled, *in situ* release of functional compounds have been exploited extensively in the development of stimuli-responsive materials, such as self-healing composites and coatings with sensing capabilities. In contrast, there are comparatively few examples by which the same principles have been utilized for stimuli-responsive polymer degradation, despite recent evidence that *in situ* transformations may present new and improved opportunities for remediation of plastic waste. With this context in mind, we illustrate that microencapsulation of alkene metathesis catalysts provides a powerful method to create polybutadiene (PB) elastomers with programmable degradation profiles. Such catalysts, highly active towards depolymerization of PB via ring-closing metathesis, are rendered effectively latent by microencapsulation within a glassy polymer. The micron-sized polymer/catalyst particles are easily compounded into PB resin which is subsequently crosslinked by radical chemistry, yielding particle-loaded elastomers with similar mechanical properties to particle-free controls. Relying on judicious selection and design of the encapsulant or encapsulating system, the catalyst can be released *in situ* through temperature, time, or light exposure, among other phenomena, thereby initiating rapid depolymerization of the elastomer to soluble products. We anticipate that this approach can be expanded to deliver existing and emerging functional compounds for chemical transformation of polymers with reduced resource requirements, as well as precise control over the conditions under which such transformations are effected.

2:15 PM SF01.10.05

Data-Driven Pathway to Predict Stimuli-Responses of Hollow Polymers Kazi Zihan Hossain and M. Rashed Khan; University of Nevada, Reno, United States

Melt-extruded hollow thermoplastic polymers are a new class of materials for stimuli-responsive applications, i.e., shape reconfigurable robotic clothes, ultra-stretchable touch and twist sensors, and programmable knitted textiles. Under large deformation (stimuli), such materials exhibit hyperelasticity. However, the stimuli-responsive functional behavior of such materials remains a crucial knowledge gap that persists in literature due to time and strain of energy-dependent property variations. This talk will introduce a data-driven pathway harnessing integrated computational materials engineering (ICME) to study, predict, and optimize hyperelastic hollow polymer fibers' behavior. To do so, we calibrated properties utilizing a constitutive materials model, extracted the parametric values using TN (three networks) model, and emulated experimental stress-strain behavior in a finite-element-based multiphysics environment with 99.99% confidence. We also tested and verified our model's accuracy for different compositions of thermoplastics and fabrics. Optimizing the stimuli-responsive functional behavior from hollow thermoplastic fibers requires numerous cost-incurring melt-extrusion runs to characterize strain-dependent behavior. However, from our proposed finite element analysis, we can not only predict strain-dependent behavior but also change shape and geometries for new understandings without running additional melt-extrusions or experiments. Additionally, our ICME approach can be extended to other stimuli (e.g., temperature, humidity, and chemical exposure) for the next generation of pre-programmed functional device fabrication from hyperelastic hollow fibers that may not even exist to date (i.e., body-worn programmable digital clothes).

2:30 PM SF01.06.08

Aptamer-Actuated Two-Dimensional Photonic Crystal Hydrogel Sensors [James Westbay](#), Kyeongwoo Jang and Sanford Asher; University of Pittsburgh, United States

We previously pioneered photonic crystal (PC) hydrogel materials for sensing applications. Here we report novel stimuli-responsive, two-dimensional PC hydrogels that utilize DNA aptamers as molecular recognition agents. The PC hydrogel consists of a PC array embedded into a DNA-functionalized hydrogel. Hybridized strands of DNA attached to the hydrogel polymer network form reversible hydrogel crosslinks. One of the strands contains an aptamer sequence that sensitively and specifically binds a chemical target. On addition of the aptamer's binding target, competitive aptamer-target binding breaks hydrogel crosslinks, actuating swelling. This in turn increases the lattice spacing of the embedded PC array, shifting PC Bragg diffraction. Thus, the concentration of the chemical target can be monitored through PC Bragg diffraction shifts. As proof-of-concept, we fabricated aptamer-actuated PC hydrogels using a well-studied adenosine-binding aptamer. Our PC hydrogels specifically respond to adenosine in both pure-buffer and serum solutions with <30 μ M limits of detection. We are currently investigating the generalizability of these materials by fabricating PC hydrogels that respond to proteins.

2:45 PM DISCUSSION TIME

SESSION SF01.11: Virtual Session II: Smart Functions of Stimuli-Responsive Materials X
Session Chairs: Baptiste Blanc and Ritu Raman
Wednesday Morning, December 7, 2022
SF01-virtual

8:00 AM *SF01.11.01

Autonomous and Life-Like "Self-Oscillating" Polymer Gels as Novel Functional Softmaterials [Ryo Yoshida](#); The University of Tokyo, Japan

Several types of stimuli-responsive polymer gels that reversibly swell and deswell in response to environmental changes have been developed by many researchers. By using these gels as "intelligent" or "smart" gels, many applications in soft actuators as artificial muscles, drug delivery systems, cell culture systems in tissue engineering, purification or separation systems, biosensors, shape memory materials, and molecular recognition systems, etc. have been explored.

On the other hand, in 1996, the author reported "self-oscillating" polymer gels that spontaneously repeat swelling-deswelling changes in a closed solution without any on-off switching by external stimuli, such as heart muscle. They have attracted considerable attention as a new type of gel with an autonomous function that is clearly different from conventional stimuli-responsive gels. The autonomy in the gel is provided by the design, which creates a dissipative structure in the material. The gel has an energy-conversion system involving an oscillatory chemical reaction (called the Belousov-Zhabotinsky (BZ) reaction) which allows periodic mechanical motion of the polymer chain. Since the first report, the author has systematically developed self-oscillating polymer gels from fundamental behavior to construction and demonstration of material systems for potential applications in biomimetic materials, such as autonomous soft actuators, automatic transport systems, and functional fluids exhibiting autonomous sol-gel oscillations similar to those of the amoeba. Recently, BZ gels with similar properties have sometimes been called "Yoshida gels". In this presentation, the research developments and recent progress on self-oscillating polymer gels from the author's group are summarized.

8:30 AM SF01.11.03

Exercise-Mediated Biochemical Secretion Guides Maturation and Repair of Neuromuscular Actuators [Ritu Raman](#), Naomi Lynch and Angel Bu; Massachusetts Institute of Technology, United States

Introduction: Stimuli-responsive actuators that match the flexibility and adaptability of skeletal muscle are of significant interest in powering the next-generation of responsive machines. However, abiotic actuators have yet to match muscle's energy efficiency or its ability to dynamically adapt to gain-of-function cues, such as exercise, and loss-of-function cues, such as damage. We have engineered bioactuators, powered by skeletal muscle and controlled by motor neurons, and deployed them as functional actuators in soft robots. Deeper understanding of the stimuli-responsive nature of these bioactuators requires studying how damage that disrupts intercellular signaling between motor neurons and skeletal muscle can impact mobility.

Measuring and modulating intercellular signaling requires tools for longitudinal tracking of biochemicals exchanged between cells within tissues. We leveraged a custom-built micro-invasive interstitial fluid sampling tool to measure biochemical signaling in space and time within our bioactuators. We used this tool to identify muscle-secreted cytokines that are upregulated in response to exercise, driving hierarchical tissue assembly. Moreover, we show that exercise-mediated biochemical secretion enhances repair after injury and accelerates functional integration of bioactuators implanted in animals. We anticipate that this will advance understanding of how to design bioactuators that are robustly responsive to injury when deployed in real-world applications.

Methods: We use our established protocols to engineer neuromuscular bioactuators using mouse and human skeletal muscle and motor neuron lines. Briefly, bioactuators are formed by embedding optogenetic skeletal muscle myoblasts and motor neurons within separate layers of a fibrin/Matrigel hydrogel and growing them around a flexible skeleton. Neuromuscular junctions are formed within 3 days and muscle contraction can be controlled via light stimulation of the muscle or upstream chemical stimulation of the neurons. We have developed a tool, composed of a nanofluidic pump coupled to a micro-scale probe, that enables minimally-invasive sampling of interstitial fluid from tissues. We use mass spectrometry to quantify secretion of hundreds

of peptides and proteins in parallel.

Results & Discussion: Our bioactuator and sampling tool enabled investigating the impact of exercise-mediated biochemical secretion on tissue maturation and response to injury. Sampling interstitial fluid in engineered tissues showed significant proteomic differences between control and exercised groups. Specifically, light-stimulated exercise of optogenetic muscle upregulates the secretion of cytokines that enhance nerve growth including axon guidance pathways mediated by netrin and nicotinic acetylcholine receptor signaling pathways. When bioactuators were implanted in a volumetric muscle loss model *in vivo*, targeted exercise upregulated secretion of cytokines that promoted innervation and angiogenesis, enhanced functional recovery after injury. These results indicate: 1) our sampling tool can be used to monitor intercellular signaling in stimuli-responsive living materials; 2) exercise-mediated cytokine secretion can be used to guide assembly of such materials; 3) stimuli-responsive living materials can modulate intercellular signaling *in vivo* and enhance integration of implanted tissues.

Conclusion: There is a critical need to develop bioactuators for functional applications, and to monitor and modulate intercellular communication within such stimuli-responsive living materials. We have developed a bioactuator and sampling tool that enables monitoring intercellular signaling, and established how exercise-mediated biochemical secretion guides tissue maturation. This platform is being used to advance mechanistic understanding of neuromuscular tissues and develop stimuli-responsive bioactuators for engineered living machines.

8:45 AM SF01.11.04

Enhanced Mechanoluminescence Intensity of PDMS-ZnS—Cu by Varying ZnS Particle Volumetric Content and Kirigami Structure Incorporation [Michael A. Listyawan](#)¹, Geon-Tae Hwang² and Jungho Ryu¹; ¹Yeungnam University, Korea (the Republic of); ²Pukyong National University, Korea (the Republic of)

Mechanoluminescence (ML) material has an innate characteristic to exert luminescence as a response to mechanical stimuli such as tensile, compression, friction, etc. Its unique characteristic of exerting light without any electrical energy is enabling this material for a wide range of applications such as wind-driven displays, stress sensors, strain sensors, etc. One of which is a ubiquitous lighting device, where commonly lighting applications require electricity that involves components to support the circuitry. Bypassing the need for electricity will not only improve efficiency but even reduce cost substantially and improve the durability of the device since numerous components might fail and break at any given time. However, the ML material faces many challenges to be adopted as a practical and functional application which mainly is the intensity. With this study, we can enhance the luminescence intensity from the elastomer composite of PDMS-ZnS: Cu significantly by increasing the powder volumetric content up to 30% without any significant decrease in stretchability. Nevertheless, with higher than 30% volumetric content, has a lesser luminescence output but it has higher intensity if applied with lower displacement. Additional finite elements analysis (FEA) simulation is also done to observe the mechanisms. We also detect a lower load-luminescence activation when incorporated with kirigami structures. The luminescence intensity of different kirigami shapes is compared, and the stress-strain relation is mapped using FEA simulation. Overall, the kirigami shape incorporation improves the overall stretchability range and has a better sensitivity according to the simulation. However, each shape has a different stretching range, and some shapes are more sensitive to load as the edges act as a stress concentrator. The T-shaped kirigami cuts possess the widest range out of all compared kirigami shapes.

9:00 AM SF01.11.05

PRESENTED ON-DEMAND ONLY: Supramolecular Hybrid Hydrogels as Rapidly On-Demand Dissoluble, Self-Healing and Biocompatible Burn Dressings [Aslihan Gokaltun](#)¹, Letao Fan¹, Luca Mazzaferro², Delaney Bryne¹, Martin L. Yarmush¹, Tianhong Dai¹, Ayse Asatekin² and Berk Usta¹; ¹Harvard Medical School, United States; ²Tufts University, United States

Supramolecular hydrogels (SHs), a novel class of PCHs, are held together by non-covalent crosslinks such as host-guest chemistry, electrostatic interactions, and hydrogen bonding. These hydrogels can respond to environmental stimuli such as light, pH, and electric field. Unlike most synthetic hydrogels with permanent chemical crosslinks, SHs can undergo dissolution in response to various environmental stimuli and self-heal when damaged. Despite decades of efforts, state-of-the-art synthetic burn dressings to treat partial-thickness burns are still far from ideal. Current dressings adhere to the wound and necessitate debridement. This work describes the first “supramolecular hybrid hydrogel (SHH)” burn dressing that is biocompatible, self-healable, and stimuli-responsive (on-demand dissoluble) for easy and trauma-free removal, prepared by a simple, fast, and scalable method. These SHHs leverage the interactions of a custom-designed cationic copolymer via host-guest chemistry with cucurbit[7]uril and electrostatic interactions with clay nanosheets coated with an anionic polymer to achieve enhanced mechanical properties and fast, on-demand dissolution. The SHHs show high mechanical strength (> 50 kPa), self-heal rapidly in ~1 min, and dissolve quickly (4-6 min) using amantadine hydrochloride (AH) solution that breaks the supramolecular interactions in the SHHs. Neither the SHHs nor the AH solution have any adverse effects on human dermal fibroblasts or epidermal keratinocytes *in vitro*. The SHHs also do not elicit any significant immune response *in vitro*. Furthermore, *in vivo* murine experiments show no immune or inflammatory cell infiltration in the subcutaneous tissue and no change in circulatory cytokines compared to sham controls. Thus, these SHHs present excellent burn dressing candidates to drastically decrease pain and time associated with dressing changes.

Due to the ease of their fabrication, which only involves two steps of mixing, we expect these novel SHHs will enable large-scale yet low-cost fabrication, addressing a critical bottleneck for translation to clinical applications. Further, due to this ease and the speed (15 seconds) of SHH formation, we envision that the dressings could even be formed at the bedside and on-field synthesis of the patients with customizations as necessary. Such novel and on-demand dissoluble SHHs have great potential as second-degree burn dressings. They will i) provide easy burn care, ii) eliminate mechanical and surgical debridement, iii) promote wound healing and enhance the healing process to treat second-degree burns. To this end, we will follow up this study with investigations on the *in vivo* efficacy of SHHs in burn wound healing progress. We expect our invention to remove the challenges and shortcomings associated with current burn dressings and bear pain-free (or reduced pain), easy to apply, and removable burn dressings.

9:15 AM SF01.11.06

Collective Behavior Triggers Chemomechanical Oscillations in Active Hydrogels [Baptiste Blanc](#)^{1,2}, Johnson Agyapong^{3,2}, Ian Hunter², Ali Aghvami² and Seth Fraden²; ¹Massachusetts Institute of Technology, United States; ²Brandeis University, United States; ³Syracuse University, United States

Quorum sensing refers to the ability of yeast and other unicellular organisms to switch behavior in response to increasing numbers or density, inducing responses such as oscillating production of chemicals and biofilm formation. There has been much interest in obtaining a quorum sensing behavior in synthetic analogues, employing, for example the enzyme urease or the Belousov Zhabotinsky (BZ) reaction, for novel bioinspired smart material. In this work, we demonstrate that the quorum sensing response of an assembly of soft small BZ hydrogels (smaller than their critical size to oscillate on their own) can trigger their chemomechanical oscillations. We first report that a single spherical BZ gel smaller than a critical size of 350 micrometers in diameter does not chemically oscillate when left alone. In contrast, a 2D layer made of the same spherical BZ gels present chemical oscillations that last for days. To understand the physicochemical cause of this critical size, we experimentally engineer the coupling of single BZ gels to their environment by imposing a flow of reactants around them. By comparing the oscillation patterns obtained in a convective flow set up with those obtained when only diffusion takes place, we establish experimentally that the passive transport of the inhibitor outside the bead produced by the BZ reaction solely controls the pattern of oscillations. We finally discuss why this discovery paves the way to the design of optimized BZ chemomechanical machines.

9:30 AM SF01.11.07

Tunable Rigidochromism of Copper-Pyrazolate Complexes Yuichiro Watanabe¹, Benjamin Washer², Matthias Zeller², Sergei Savikhin², Lyudmila V. Slipchenko² and Alexander Wei²; ¹Kyoto University, Japan; ²Purdue University, United States

Copper(I) ions and pyrazoles can self-assemble into macrocyclic clusters with intense solid-state phosphorescence at ambient temperatures. We are investigating a series of tetranuclear Cu-pyrazolate (Cu_4pz_4) complexes whose luminescence relies on a cluster-centered triplet state (^3CC), and whose energies are influenced by substituents far from the Cu_4 core. These remote substituent effects are steric in nature and support a tunable rigidochromism with emissions ranging from yellow to deep blue, confirmed by TD-DFT calculations. As pyrazole ligands increase in structural complexity, polymorphs with different luminescent wavelengths emerge that allow rigidochromic behavior to be tuned by extrinsic physical and chemical stimuli (i.e. heat, and hydrocarbon vapor treatment).

9:45 AM SF01.11.08

Thermo-Responsive Modulus Tuning of 3D Printed Hydrogels Kusuma Betha Cahaya Imani and Jinhwan Yoon; Pusan National University, Korea (the Republic of)

Materials with a controllable mechanical property are highly studied in recent years, because of their many possible applications. One of the popular materials to be studied is hydrogel, because of its ability to contain a high amount of water, allowing for mechanical properties control through external stimuli. In this study, a combination of micelles, ionic bonding, and hydrophobic association was used to prepare hydrogel. A fine mechanical tuning by temperature control was achieved through the hydrophobic association. In addition, there is a sharp stiffness change from rubbery to glassy material, induced by phase separation at high temperature. This ability is attractive for the development of biomimetic materials, and safety equipment which requires both elastic and stiff property at room and high temperature.

9:50 AM SF01.09.06

PRESENTED ON-DEMAND ONLY: Tuning Multiferroic $\text{La}_x\text{Sr}_{1-x}\text{Fe}_{12}\text{O}_{19}$ from Ferroelectrics to Antiferroelectrics Guolong Tan; Wuhan University of Technology, China

The appearance of antiferroelectrics (AFE) in ferromagnetism (FM) system would give birth to a new type of multiferroic candidate, which is significant to the development of novel devices for energy storage. Here we demonstrate the realization of full antiferroelectrics in magnetic $\text{La}_{0.5}\text{Sr}_{0.5}\text{Fe}_{12}\text{O}_{19}$ system (AFE+FM), which also presents strong magnetodielectric response (MD) and giant magnetoresistance (GMR) effect. The combination of antiferroelectricity and ferromagnetism in one structure would create new types of multiferroic candidates. Here we propose a novel type of multiferroic candidate $\text{La}_x\text{Sr}_{1-x}\text{Fe}_{12}\text{O}_{19}$, whose room temperature state could be tuned from ferroelectrics to antiferroelectrics by changing x from 0 to 0.5. The antiferroelectric phase was achieved at room temperature by replacing 0.5Sr^{2+} ions with 0.5La^{2+} ions in $\text{SrFe}_{12}\text{O}_{19}$, whose phase transition temperature of ferroelectrics (FE) to antiferroelectrics was brought down from 174°C to -141°C , while the temperature of antiferroelectrics converting to paraelectrics (PE) shifts from 490°C to 234°C after the substitution, generating a wide space between -141°C ~ 234°C to accommodate the antiferroelectric state in $\text{La}_{0.5}\text{Sr}_{0.5}\text{Fe}_{12}\text{O}_{19}$ system. The fully separated double P-E hysteresis loops reveal the antiferroelectrics in $\text{La}_{0.5}\text{Sr}_{0.5}\text{Fe}_{12}\text{O}_{19}$ ceramics. $\text{La}_{0.2}\text{Sr}_{0.7}\text{Fe}_{12}\text{O}_{19}$, however, exhibits a hybrid ferroelectric/antiferroelectric state. Both compounds exhibit strong ferrimagnetism. In addition, the $\text{La}_{0.5}\text{Sr}_{0.5}\text{Fe}_{12}\text{O}_{19}$ ceramic demonstrates strong magnetoelectric coupling and giant magnetoresistance effect. A 1.1T magnetic field generates electronic polarization of $0.95\text{mC}/\text{cm}^2$, reduces the resistance by 117% (GMR), enhances dielectric constants by 540% and right shifts the maximum dielectric loss peak by 208 kHz, showing giant magnetodielectric effect (GMD). The combined functional responses provide an opportunity to develop novel multiferroic memories and energy storage devices.

10:05 AM DISCUSSION TIME

SYMPOSIUM SF02

Materials for Extreme Conditions
November 28 - December 7, 2022

Symposium Organizers

Alexander Goncharov, Carnegie Institution of Washington
Ke Han, Florida State Univ
Florence Lecouturier-Dupouy, CNRS-LNCMI
Wenge Yang, Center for High Pressure Science & Technology Advanced Research

* Invited Paper
+ Distinguished Invited

SESSION SF02.01: Low Temperature on Materials
Session Chairs: Alexander Goncharov and Nathan Mara
Monday Morning, November 28, 2022
Sheraton, 3rd Floor, Commonwealth

10:45 AM SF02.01.04

Analysis of Multichannel GaN/AlGa_N Superlattice Device Conduction at Cryogenic Temperatures [Annaliese Drechsler](#)^{1,2}, Patrick Shea², Robert Howell² and Aristos Christou¹; ¹University of Maryland, United States; ²Northrop Grumman Corporation, United States

GaN/AlGa_N and related heterostructures are key device structures to create the next generation of high electron mobility transistors, high power switches, and high frequency FETs. Typically, these devices are operated at room temperature or above, and high temperature operation, physics, and degradation have been widely studied. Recently, new applications have emerged for these materials including integration with superconductors for amplifier loads, photon detection, superconducting magnets, or other energy storage applications. To ensure that selected GaN/AlGa_N devices are compatible with cryogenic operation, their behavior must be studied down to 4K. In this work, we investigate the parametric changes associated with cryogenic operation for the Superlattice Castellated Field Effect Transistor (SLCFET) and demonstrate operation of a SLCFET switch with exceptionally high performance at 4K.

Typical GaN/AlGa_N devices are fabricated into HEMTs where charge is conducted by the interfacial piezoelectric strain between the GaN and AlGa_N. This device structure maintains conductivity at low temperatures since the charge originates from strain instead of dopants. The SLCFET device similarly utilizes GaN and AlGa_N, but to form a multichannel superlattice. The topmost channel is undoped, generating charge carriers like the GaN HEMT, but the lower channels don't experience this strain and require dopants to conduct charge, which may demonstrate freeze out due to insufficient carrier activation energy at low temperatures. Due to the combined nature of the structure, the cryogenic performance of the device was unknown.

To characterize this performance, a 4-point Van der Pauw structure for epitaxial resistance was measured using a non-magnetic Quantum Design PPMS system cooled from 300K to 3.5K. The resistivity decreased from the typical 300K value of 70 Ω/sq to 26 Ω/sq. This result is critical as it provides the first indication that the SLCFET device is not experiencing dopant freeze-out, despite having doped channels. If this was occurring, the resistance would decrease initially due to reduced scattering and then increase sharply once the thermal energy is insufficient to overcome the charge carrier formation activation energy barrier. Instead, the resistance shows a linear decrease from 300 to 150K and then begins to plateau. This suggests that the observed initial decrease is due to carrier mobility increase, likely from reduced electron-phonon scattering, which is then limited by defect scattering once the resistance starts to plateau.

To further understand this behavior, Hall Effect structures were tested using a 14T Quantum Design PPMS System. The samples were cooled to 4K and the magnetic field was swept from -4 to 4T. From the Hall coefficient, the average carrier density across the tested samples was calculated to be 5.69×10^{17} carriers/cm³, within the typical range reported from room temperature characterization. This similarly indicates that the resistance decrease is not a result of increased charge carrier density. The resistance decrease then must be attributed to an increasing mobility, which has been calculated to increase from a typical average of 1500 cm²/Vs to an exceptionally high 4151.5 cm²/Vs. SLCFET switch was then analyzed using gate voltage-drain current characterization in a liquid-He Dewar. The on-state current shows a ~3x increase from the reduced resistance, while off-state leakage is reduced. Interestingly, the pinch-off voltage is nearly constant. The parametric changes can similarly be attributed to the mobility increase from reduced phonon scattering enabled by cryogenic conditions.

In conclusion, we studied the behavior of the multichannel SLCFET GaN/AlGa_N device at cryogenic conditions. The epitaxial structure was observed to decrease in resistance which is attributed to a mobility increase due to reduced phonon scattering. The SLCFET switch structure was demonstrated with improved performance at 4K.

11:00 AM SF02.01.05

Architectural Cellular Structure via Freeze-Drying Method for High Strength and High Resilience [Jongbeom Kim](#) and Seung Min J. Han; Korea Advanced Institute of Science and Technology, Korea (the Republic of)

3D architectural cellular structures that are fabricated via additive manufacturing methods are currently receiving much interest due to the tunable properties that can be realized by simply tuning the architecture of structures. However, the most of additive manufacturing methods do not meet the resolution to the nanoscale. Multiphoton lithography raises its resolution to the nanoscale, but there is a scalability issue that takes over several days to weeks to fabricate a centimeter-sized structure, making it difficult to use in bulk material applications. In this study, the freeze-drying method was used as a 3D structure manufacturing method. In the freeze-drying method, the solution is sublimed after frozen, leaving a solute in the inverse structure of the ice crystal inside to form a 3D structure. Due to this fabrication method, a 3D structure can be fabricated in a one-step process regardless of the material, and a centimeter-scale bulk structure can be easily produced depending on the size of the frozen template. As materials constituting a 3D structure, silver nanowire was added to a polymer solution containing cellulose nanofiber (CNF) or polyvinylalcohol (PVA) to fabricate a structure that has a high strength-to-mass ratio. In addition, controlling the cooling direction, the directionality of the ice crystals generated can be aligned to the same direction, so that the pores of the 3D structure grow in a frozen direction. This is called the directional freeze-drying method. Using the directional freeze-drying method, the structure with high strength as well as excellent resilience according to the directionality of the structures was fabricated. Structures were fabricated using various materials as well as polymers by freeze-drying. A 3D structure was fabricated using pollen, which can be commonly collected in the environment, and showed the possibility of using a pollen 3D structure for oil absorption.

SESSION SF02.02: Materials for Space and Insulation
Session Chairs: Alexander Goncharov and Nathan Mara
Monday Afternoon, November 28, 2022
Sheraton, 3rd Floor, Commonwealth

1:30 PM SF02.02.01

Carbon Nanotube Arrays as Adhesives Under Harsh Conditions as in Space Technology Christian Lutz and [Hendrik Hoelscher](#); Karlsruhe Institute of Technology, Germany

For their potential use as dry adhesives under harsh conditions, we discuss the potential use of carbon nanotube (CNT) and nanofiber (CNF) arrays. The basic idea is to mimic the fine fibril structure of gecko toes by CNTs and CNFs. For that, we investigated the temperature dependence of the adhesion of carbon nanotube arrays by atomic force microscopy (AFM) in a temperature range from -20 °C to +240 °C. In order to mimic the specific conditions for space application as close as possible, we glued tiny meteoritic particles to AFM cantilevers as probes. The measurements revealed that the adhesion forces are practically constant in the investigated temperature range. Long-term measurements confirm the expected durability of carbonic arrays. The overall properties did not change after exposing the sample to simulated space condition. Additionally, we measured the adhesion between ice and carbon nanotubes at -20 °C and obtained similar results. For these measurements, we used a bundle of CNTs as probe and grow a closed ice layer as sample

surface.

Lutz et al., Analysis of Carbon Nanotube Arrays for Their Potential Use as Adhesives Under Harsh Conditions as in Space Technology, Trib. Lett. 67, 10 (2019)

1:45 PM SF02.02.02

Improvement of Calcium–Magnesium–Alumino-Silicate (CMAS) and Hot Corrosion Resistance of Functionally Graded Al₂O₃/CYSZ Thermal Barrier Coatings (TBCs) Fatih Kirbiyik¹, Mustafa G. Gok², Dermot Brabazon³ and Gultekin Goller¹; ¹Istanbul Technical University, Turkey; ²Gaziantep University, Turkey; ³Dublin City University, Ireland

CMAS dusts and hot corrosion salts are one of the most serious threats to gas turbine blades. Both of these, at high temperatures, penetrate into the thermal barrier coating (TBC) on the turbine blade surface and/or degrade the chemical structure of the coating. Therefore, it usually causes stress-induced damage. In this study, a laser surface modification process was performed to increase the CMAS and hot corrosion resistance of functionally graded alumina/ceria-ytria stabilized zirconia (Al₂O₃/CYSZ) TBCs. Single layered CYSZ was chosen as the comparison to the developed and tested TBC material because it has high corrosion stability. Thermal cycling and thermal gradient tests were performed to understand the simultaneous effect of CMAS and hot corrosion, on CYSZ TBC and the laser surface modified Al₂O₃/CYSZ TBC. For thermal cycling and thermal gradient tests, TBCs with a mixture of CMAS powder and hot corrosion salt on their surfaces were heated to 1200°C by using a laser beam. The thermal cycle test was performed as heating from the surface of the TBC and then followed by air cooling, while the thermal gradient test was performed as heating from the surface of TBC and simultaneous water cooling from the back surface of the substrate. Damages in both coatings and their mechanisms were characterized using detailed macroscopic, microscopic (SEM) and phase (XRD) analyses.

2:00 PM SF02.02.03

Broadband Highly Reflective Materials as Multilayer Insulation Shields Xuanjie Wang, Chieloka D. Ibekwe and Shankar Narayan; Rensselaer Polytechnic Institute, United States

Critical for the functioning of many cryogenic systems, multilayer insulation (MLI) systems are used when lower heat leakage rates are required, including storage, transfer, thermal protection, and low-temperature processor. Three major modes of heat transfer in MLI are radiation, solid conduction and gas conduction. Among them, the radiation heat from the outer space is decisive, which strikes on the first reflective layer and heats up the inner layers. In order to shield from the harsh environment of space and harmful radiation from sun and earth, MLI systems have to provide several attributes, including being lightweight, highly reflective, thermally insulating, mechanically robust and electrically conductive. In our study, a broadband high reflection is achieved through geometry control of nanostructure by cost-effective manufacture method. Specifically, the hierarchical nanostructure with more than 90% reflectance shows excellent insulation ability under the illuminance of one sun, achieving 40% less heat gain compared to the conventional aluminum reflector in the calorimetric measurement. The optical simulation guides the geometry control in the fabrication process with tuned structures. The reflector is stable under long time UV exposure environment. The simple manufacturing techniques presented in this study to generate nanoengineered surfaces can lead to further advancements in solar reflectors with well-controlled optical properties for different conditions.

2:15 PM SF02.02.04

Developing Spacecraft Reliability for Lunar Missions—Radiation Shielding Ronald H. Freeman; Journal of Space Operations & Communicator, United States

Radiation exposure from SPEs presents a significant hazardous concern for exploration missions outside the protection of the Earth's magnetic field, which could impair their performance and result in possible mission failure. The impracticability of Earth-Moon transits for repairs, replacements affords a need for greater self-reliability of lunar spacecraft. Radiation environment consists mainly of solar wind (including electrons and protons) to cosmic protons and ions as primary space environment. And, radiation secondary space environment of electrons and neutrons influences spacecraft as well as spacecraft electronic devices; results in spacecraft single event effect; causes displacement damage dose. The objective is to show distinct radiation-mitigating strategies and how they may be designed into different hierarchical levels of a system with the greater functional reliability as well as quicker resilient-like post-fault recoverability. The following radiation-mitigating strategies will be discussed and compared.

1. The satellite structure is the first radiation shield layer. A novel material known as boron nitride nanotubes (BNNTs) per their mechanical properties, suggest replacement of aluminum alloys as structural components for spacecraft, while also providing radiation shielding. More enhanced BNNT performance may be achieved when loaded with hydrogen. A comparison may be made with another shielding material under review, polyethylene composites. Moreover, technologies under review enable greater hydrogen storing capacity in BNNTs.
2. Radiation flux to dose conversions from OLTARIS and HZETRN afford efficacy comparative analyses for different novel radiation-mitigating strategies.
3. Electronic equipment used in the satellite missions is another layer of vulnerability with ionizing particle encounters, causing problems in normal operations. So, the combination of high-density shielding materials such as tantalum and tungsten and low-density ones such as polyethylene can be considered as an ideal strategy.
4. Space computers suffer from the unwanted effects of cosmic energy. A single-event upset (SEU) occurs when high-energy particles or heavy ions strike a complementary metal oxide semiconductor (CMOS) device and cause unintended, logic-level transition.
5. In partial reconfiguration (PR), a partial bitstream is loaded into a select section of configuration memory to drive a change in logic. When a fault occurs in either the foreground circuitry of the FPGA or in the configuration memory region corresponding to the foreground circuitry, PR will restore that region to its original state. Detection and repair of SEU-induced faults are accomplished through a comprehensive strategy including partial reconfiguration (PR) of impacted cores, error correction codes (ECC) for memory that cannot be partially reconfigured, and soft error mitigation monitoring for the configuration memory of the FPGA.
6. As radiation-based faults are a great concern to spaceflight hardware, the concept of shielding, in which some sort of material serves as a boundary between cosmic radiation and the hardware at risk. Alternatively, radiation-hardened semiconductor manufacturing modifications are another method of mitigating radiation-induced faults in system hardware and have shown effectiveness. Radiation hardened by design (RHBD) methods will be discussed and comparatively analyzed.
7. Other approaches include fault-mitigation strategies based on a Redundant Multiprocessor System implemented within the FPGA fabric; improved characterizations of the radiation environments to which RadPC would be exposed, and a numerical modeling tool known as the Cosmic Ray Effects on MicroElectronics (CREME96) would be used to model the radiation environment. RadPC contributes to the field of space computing by providing a cost-effective, radiation-tolerant design using a commercial-off-the-shelf FPGA to actively respond to radiation-induced faults in the device.

2:30 PM BREAK

SESSION SF02.03: High Temperature on Materials
Session Chairs: Alexander Goncharov and Nathan Mara
Monday Afternoon, November 28, 2022
Sheraton, 3rd Floor, Commonwealth

3:00 PM *SF02.03.01

Elevated Temperature Thermomechanical Stability of Metallic Interfaces Containing 3D Character Nathan Mara¹, Justin Cheng¹, Zezhou Li¹, Shuozhi Xu², Youxing Chen³, Mauricio De Leo¹, Jonathan Poplawsky⁴, Nan Li⁵, John K. Baldwin⁵ and Irene J. Beyerlein²; ¹University of Minnesota, United States; ²University of California, Santa Barbara, United States; ³University of North Carolina at Charlotte, United States; ⁴Oak Ridge National Laboratory, United States; ⁵Los Alamos National Laboratory, United States

2-dimensional (2-D) sharp interfaces with distinct boundaries demarcating an abrupt discontinuity in material properties in nanolayered composites have been studied for almost twenty years and are responsible for enhanced behaviors such as strength, radiation damage tolerance, and deformability. However, 2-D interfaces have their limitations with respect to deformability and toughness. 3-D interfaces are defined as heterophase interfaces that extend out of plane into the two crystals on either side and are chemically, crystallographically, and/or topologically divergent, in three dimensions, from both crystals they join. Here, we focus on the thermal stability (up to 500° C) and mechanical behavior of nanolayered Cu/Nb containing interfaces with 3-D character. By co-sputtering the bimaterial interfaces between the constituent pure phases, the resulting compositional gradient gives rise to new interphase boundary structures, which have been analyzed and quantified via S/TEM and Atom Probe Tomography. Micropillar compression results show that the strength of Cu/Nb nanocomposites containing 3-D interfaces is significantly greater than those containing 2-D interfaces. Mechanical anisotropy, as well as shear banding is observed during pillar compression with retention of continuous layers across the shear band. We will present our recent results on deformation of such 3-D interfaces and structures, and describe their structural evolution mechanistically through the use of atomistic and Phase Field Dislocation Dynamics simulations.

3:30 PM SF02.03.02

Design of a Multiscale Porous High-temperature Ceramic Heat Exchanger Xiangyu Li^{1,2}, Chad Wilson¹, Lenan Zhang¹ and Evelyn N. Wang¹; ¹Massachusetts Institute of Technology, United States; ²The University of Tennessee, Knoxville, United States

The efficiency of a heat engine can be significantly improved by operating in a high-temperature and high-pressure environment. However, such extreme operating condition poses a severe challenge to the heat exchanger design. Although recently developed super alloys and ceramics can survive high temperatures and high-pressure loads, using these materials in a traditional heat exchanger design requires high cost and yields low power density. In this work, we propose a high power density ceramic heat exchanger for high-temperature applications enabled by a multiscale porous design. By optimizing the design of centimeter-scale macrochannels and micrometer-scale microchannels, significant improvement to both the heat transfer and structural strength are predicted, with a negligible pressure drop penalty, compared to current state-of-the-art solutions. An optimized design is expected to achieve high power density, light weight, low cost along with less than 4% pressure drop penalty. Furthermore, the heat exchanger design is customizable for different applications in hybrid and electric aerospace applications, as well as terrestrial power generation such as nuclear power generation and concentrated solar power generation, promising more than 2.5x thermal performance compared to state-of-the-art solutions utilizing commercially available superalloy and ceramic materials, while providing the benefits of low cost, scalable fabrication, low pressure drop and high structural strength.

3:45 PM SF02.03.03

Morphological Instabilities of Nanorods at Elevated Temperature. Omar Hussein¹, Keith Coffman², Khalid Hattar³, Eric Lang³, Shen Dillon⁴ and Fadi Abdeljawad¹; ¹Clemson University, United States; ²University of Illinois Urbana-Champaign, United States; ³Sandia National Laboratories, United States; ⁴University of California, Irvine, United States

Recent advances in high-precision manufacturing and self-assembly techniques have enabled the fabrication of materials architectures with intricate nanoscale features. Notable examples include nanolattices, nanoscale rods, nanoporous materials, and stochastic nanostructures. Integrating complex designs with nanoscale induced materials properties enables a myriad of applications, including electronics, energy and microfluidic devices, structural, and photonics. While such materials enable enticing combinations of properties, the microstructural stability of nanoscale morphologies under high-temperature environments remains poorly understood. Owing to the increased interfacial contribution to the total free energy in nanoscale geometries, these structures are at highly non-equilibrium states and evolve by a wide range of mechanisms. Recent experiments demonstrate a morphological instability in which a polycrystalline micro- or nanoscale rod breaks up into single-crystal domains, a phenomenon reminiscent of the Plateau-Rayleigh instability in liquid jets. Our high temperature in situ annealing studies of a model alumina rod with a bamboo grain structure demonstrated the pinch-off instability initiated at a GB. Here, we develop a theoretical model to investigate the impact of grain boundaries (GBs) on the morphological instabilities of polycrystalline nanoscale rods. A neutral stability surface is obtained, which demarcates stable and unstable perturbations with respect to the breakup. Our analysis shows that GBs play a destabilizing role in which the critical wavelength for the instability decreases with increasing the GB energy. Further, it is shown that perturbation amplitudes introduced through grain size differences influence the magnitude of the critical wavelength for the instability. We complement our thermodynamic treatment with phase-field simulations that capture the kinetics of morphological instability. The study reveals that increasing the GB energy leads to accelerated pinch-off kinetics. Moreover, it is shown that variations in grain size could provide a pathway for the morphological instability, in which GB migration and shrinkage of small grains result in the development of free surface perturbations whose wavelengths exceed the critical value for the instability. In broad terms, our approach provides avenues to investigate the microstructural stability of nanolattices and nanoporous materials.

4:00 PM SF02.03.04

Refractory Alloys with Ru-Based B2 Precipitation-Strengthened Microstructures Sebastian A. Kube^{1,2}, Carolina Frey¹, Kaitlyn Mullin¹, Chiyo McMullin¹ and Tresa M. Pollock¹; ¹University of California, Santa Barbara, United States; ²Yale University, United States

To strengthen Refractory Multi Principal Element Alloys at 1200°C and beyond, one strategy aims to design stable microstructures of B2 precipitates embedded within a BCC matrix, which emulates the γ - γ' structure found in Superalloys. Here, we focus on Ru-based B2 intermetallics as one promising group of precipitates with a high thermal stability. We comprehensively explore the resulting space of alloy systems. We arc-melt a wide range of compositions and determine phase stability and mechanical performance under various thermal processing conditions.

4:15 PM SF02.03.05

Impact of Grain Boundary Pinning Using Silicon Refractory Inclusions in Screen Printed Silver Flake Inks for High Temperature Printed Electronics Applications Arjun Wadhwa¹, Jaime Benavides Guerrero¹, Mohammad Saadati¹, Martin Bolduc^{2,1} and Sylvain G. Cloutier¹; ¹Ecole

Technology Superiure, Canada; ²Université du Québec à Trois-Rivières, Canada

The world of printed electronics is a fast-growing dynamic field employing the process of printing a functional material onto a low-cost substrate to form a device. Screen printing is one of the premier methods used to fabricate high-volume, low-cost devices typically with silver conductive pastes. These materials are limited to relatively low operational temperatures up to approximately 150 °C¹. In this work, we demonstrate the ability to improve the thermal stability of commercially available silver screen printable ink² to fabricate a temperature sensing printed device capable to operate at high temperatures up to 700 °C. This is achieved by impregnating the silver ink with controlled quantities of silicon micro particles. First, we present the modification procedure of the ink and the mechanism employed to achieve enhanced thermal stability and its advantages compared to the traditional unadulterated silver ink^{3,4}. Next, we outline the characterization procedure to quantify the grain growth and electrical conductivity of the modified ink processed at incremental temperature ranges over time. Further, we benchmark the enhanced stability of the modified ink versus the virgin ink and the state of the art⁵ illustrating how the modification potentially allows low-cost silver inks to be utilized in high temperature environments in aerospace, chemical production, automotive industries. Finally, we validate the performance of the modified ink under elevated temperature conditions as a all silver resistance temperature detector (RTD).

1. Kim, M. et al. Effect of Curing Temperature on Nano-Silver Paste Ink for Organic Thin-Film Transistors. *J. nanosci. nanotech.* 12, 3272–3275 (2012).
2. Metalon HPS FG32 Technical Data Sheet.
3. Akbarpour, M. R., Farvizi, M. & Kim, H. S. Microstructural and kinetic investigation on the suppression of grain growth in nanocrystalline copper by the dispersion of silicon carbide nanoparticles. *Materials & Design* 119, 311–318 (2017).
4. Hu, J., Wang, X., Zhang, J., Luo, J. & Zhang, Z. A general mechanism of grain growth -I. Theory. *Journal of Materiomics* 1007–1013 (2021).
5. Alan, S., Kim, S. B., Bailey, C., Ma, A. W. K. & Dardona, S. Direct Write Fabrication of Platinum-Based Thick-Film Resistive Temperature Detectors. *IEEE Sensors Journal* 18, (2018).

4:30 PM SF02.03.06

***In Situ* Explorations of Serrated Plastic Flow in a CoCrFeNiW-C Alloy at Elevated Temperatures** Shaolou Wei and Cem Tasan; Massachusetts Institute of Technology, United States

Multi-component Co-alloys are a class of promising metallic materials for high-temperature applications. Provided the appreciable screening of their yield strength preservation trends depending on different alloy design strategies, systematic understandings of their plastic deformation response are still in lack. The present work is focused on the plastic deformation mechanisms of a CoCrFeNiW-C alloy in the 650-750 °C temperature range, with emphases on dislocation slip intermittency and the resultant serrated plastic flow. By integrating high-temperature *in situ* SEM-based tests, statistical analyses, and theoretical calculations, the following mechanistic insights will be discussed: (1) What causes the serrated plastic flow response and thereby the transition in its module? (2) What are the latent dynamic features amongst the serration incidents? (3) What kinds of deformation substructures are associated with the serrated plastic flow? Quantitative analysis of the dislocation slip mechanisms as well as their impacts on damage initiation will also be revealed in greater depth.

4:45 PM SF02.03.07

LPBF of SiC-Reinforced In718 and CoCrFeNi for Improved High-Temperature Strength Alexander D. O'Brien, Emre Tekoglu and Ju Li; MIT, United States

With the ongoing development of advanced nuclear energy systems, there is an ever increasing need to design materials capable of achieving long lifetimes in high-temperature, high-irradiation, corrosive environments. Among those materials currently under consideration for the next generation of reactors, nickel superalloys are considered to be a staple due to their excellent high-temperature creep and oxidation resistances, and high entropy alloys are seen as promising candidates due to their considerable high-temperature strength and radiation resistances. Either category of material could be considered an excellent starting point for the development of critical components for new reactor systems. However, the upper ceiling on the capabilities of both could still be expected to be limiting factors in reactor operating conditions, making further improvement in their high-temperature capabilities highly desirable. We report on the fabrication of two new high-temperature metal matrix composites based on an Inconel 718 nickel superalloy and a CoCrFeNi high entropy alloy reinforced with SiC nanowires for improved strength. Composite powders of each material were prepared by high-speed blender declustering of as-received nanowires and the base alloy powders, followed by mechanical alloying via ball mill to produce a homogenous distribution of SiC on the surfaces of the metal particles. Additive manufacturing of composite powders was performed via laser powder bed fusion, which would provide a scalable method of producing these especially difficult to manufacture materials in any number of complex geometries. Analysis of the as-printed specimens revealed dissolution of the nanowires during laser melting, which was found to result primarily in the in-situ formation of Nb and Ti-based silicide and carbide nanoparticles in the Inconel composite, while silicon oxide nanoparticles were observed in the CoCrFeNi matrix. In both cases, the nanowire dissolution process and resulting nanoparticles appear to contribute to the formation of more desirable microstructures during printing, reducing the formation of cracks and pores and decreasing the average grain sizes compared to unreinforced samples prepared under the same conditions. Mechanical characterizations also revealed notable increases in hardness and tensile strengths of both composites, confirming the benefits of reinforcement. We believe that this work presents a simple and effective method for improving the strength and usability of high temperature materials prepared by additive manufacturing that may prove important in the face of ever-harshening environments in the energy sector.

SESSION SF02.04: Poster Session I: Materials for Extreme Conditions

Session Chairs: Florence Lecouturier-Dupouy and Nathan Mara

Monday Afternoon, November 28, 2022

8:00 PM - 10:00 PM

Hynes, Level 1, Hall A

SF02.04.01

Facile Li⁺ Transport in NMC811||Graphite Lithium-Ion Batteries at Low Temperatures Enabled by Using Low-Polarity Solvents Bo Nan¹, Long Chen¹, Nuwanthi D. Rodrigo², Oleg Borodin³ and Nan Piao¹; ¹University of Maryland, College Park, United States; ²University of Rhode Island, United States; ³US Army Research Laboratory, United States

Li-ion batteries (LIBs) using graphite anode and high voltage nickel-rich cathodes (LiNi_xCo_yMn_zO₂ (x+y+z=1)) are the most promising energy storage technology in the foreseeable future. However, charging these LIBs at low temperatures (≤ -20 °C) remains challenging because the excessive resistances

encountered by lithium-ion in and across the bulk electrolytes and the interphases induce lithium plating on graphite anodes and electrolytes decomposition on the cathodes, which accelerate the capacity decay of the batteries. In particular, the significant increase of the charge-transfer resistance is the most problematic one and has barely been studied and well-regulated. Herein, we introduce a strategy of using low-polarity-solvents electrolytes that can reduce the resistance and activation energy in the charge transfer process effectively, allowing facile lithium-ion transport at subzero temperatures. The exemplary electrolyte enables the $\text{LiNi}_{0.8}\text{Mn}_{0.1}\text{Co}_{0.1}\text{O}_2$ ||graphite (NMC811||Gr) LIBs to deliver 81% of its room-temperature capacity at 1/3C at -20 °C and keep 84% and 78% of its room-temperature capacity at -30 °C and -40 °C, respectively, while maintaining decent energy density, fast-charging capability, and stability at room temperature and high temperature of 50 °C. The effective electrolyte engineering approach demonstrated in this work together with molecular simulations provides new insight and a general guideline for designing practical low-temperature electrolytes for LIBs.

SF02.04.02

Nanofibrous Polymeric Coatings as High-Performing Broadband Reflectors—Application in Multilayer Insulation Systems for Extreme Environments Chieloka D. Ibekwe, Xuanjie Wang, Brandon Bolzani and Shankar Narayan; Rensselaer Polytechnic Institute, United States

Multilayer insulation (MLI), also referred to as superinsulation, are thermal insulation materials used to prevent heat loss by radiation in spacecraft and cryogenic systems. They usually consist of multiple layers of reflectors (metallic reflectors or thin polymer films with vapor-deposited aluminum on one or both sides of each film), and spacers arranged hierarchically. These stacked layers have a cumulative effect of reflecting nearly all incident radiation. With an improved reflectance of each individual layer of reflector material, the overall performance of the MLI system goes up.

In this work, composite polymeric nanofibrous coatings of desired thicknesses were deposited on aluminum foil substrate by a controlled electrospinning nanofiber production method. Ultra-high broadband optical reflectance was achieved in the UV-NIR wavelength range of the solar spectrum, which is an improvement on the reflectance of the bare aluminum foil substrate. The coatings were exposed to UV radiation to investigate the UV resistance and durability. The thermal insulation performance of the electrospun coating was then quantified by calorimetric tests under vacuum conditions. Our results show the feasibility of using electrospun nanofibrous coatings with tailored properties as high performing broadband reflectors in multilayer insulation systems for space applications.

SF02.04.04

Thermal Imaging to Characterize Performance of Space Grade Ablative Silicones Daria Monaenkova¹, Cody Schoener¹, Christopher Windiate¹ and Curt Johnson²; ¹Dow, United States; ²Alloy Construction Company, United States

For decades Dow Silicones has been developing silicone solutions for aerospace, defense, and avionics. Silicone ablative coatings are a part of DOWSIL™ materials family and have been designed to prevent direct flame contact with underlying surfaces and protect rocket launch infrastructure and deployment devices, as well as aircraft engines, from extreme temperatures and oxygen attack. During launch, the rocket exterior is subjected to extreme temperatures over 1500 °C in seconds, chemical exposure to fuel and intense vibration during takeoff. Silicone ablatives are easy to apply and offer superior performance under high shear, high heat flux environments, toughness, low thermal conductivity, and extended operation temperature range. The ablative coatings dissipate heat through thermochemical degradation. Slow release of pyrolysis gases creates a cooling effect within the material. The goal of this work was to demonstrate the performance of these formulations at close-to-reality thermal conditions. A custom imaging solution was designed to record heating and cooling behavior of a subset of application-tailored ablative coatings. In the experiments the coatings were applied to ceramic tiles and subjected to extreme temperatures for up to 30 seconds. The heating and cooling events were recorded with a high-resolution scientific long-wave infrared camera coupled with a machine vision camera. The details of the experimental set up, time-temperature profiles of the coated substrates, and thermal and digital images of the ablatives will be reported.

SF02.04.05

Coupling Characterization Techniques to Uncover New Understanding of Electrical Treeing Mechanisms and Physiochemical Properties Kerry L. Davis, Mohamadreza Arab Baferani, Yang Cao, Bryan D. Huey, Yara Suleiman and Sina Shahbazmohamadi; University of Connecticut, United States

Electrical treeing is a precursor to electrical breakdown in insulation systems. Unfortunately, every insulation system is prone to this defect-driven aging and degradation process, with profound implications for power systems, electronics, manufacturing, and lately the rapid rise in vehicle electrification. Prior characterization studies were mostly limited to visible light microscopy, during and after testing. Some researchers have used SEM, TEM, NMR, FTIR, laser, and ultrasound as well, but none of these techniques have gained popularity since not much additional data can be extracted compared to what is already available from visible light microscopy. Here, we implement much less commonly employed approaches in order to further investigate the underlying mechanisms in electrical treeing. This includes X-Ray Computed Tomography (xCT), which can uniquely resolve full tree structures in 3-dimensions including measuring tree channel diameters. Additionally, few researchers have taken advantage of Atomic Force Microscopy (AFM), especially Conductive Atomic Force Microscopy (C-AFM) or the recently developed Tomographic AFM which can map conductivity networks in 3D. This work thus couples visible light microscopy, xCT, C-AFM, AFM milling, and SEM, revealing not only the complex morphology of the electrical treeing, but also the physiochemical properties of its microstructures. While the first electrical treeing was already discovered on the surface of an “electrophore” by G C Lichtenburg in 1777, modern materials characterization of electrical tree features during and post-test are insightful for all stages of the treeing phenomenon: pre-treeing, tree initiation, tree growth, and runaway breakdown. Increased electrification in society can help to mitigate global warming, underlining the importance of optimizing future materials microstructures, device designs, and manufacturing approaches for power systems.

SF02.04.06

In-Situ Mechanics of Steel, Superalloys and Bond Coating at -130°C to 1000°C Sanjit Bhowmick and Eric Hintsala; Bruker, United States

High-strength structural materials such as Steel, Ni-based superalloys and diffusion bond coats are widely used in challenging environments with exposure to mechanical fatigue, particle impact, and erosion at elevated temperatures. Diffusion aluminide bond coats are an example of compositionally and microstructurally graded coatings with significant variation in engineered mechanical properties across the cross-section. Nanoindentation, pillar compression and cantilever bending, particularly *in situ*, can be considered as a well-suited technique for measuring the properties of such complex microstructural materials as the deformation volume can be carefully controlled to probe different precipitates and microstructural zones. In this study, an SEM nanomechanical instrument with integrated high-temperature and cryogenic stages was used to conduct pillar compression and cantilever bending experiments at -130°C and up to 1000°C.

Tuesday Morning, November 29, 2022
Sheraton, 3rd Floor, Commonwealth

8:30 AM *SF02.05.01

Pressure-Induced Phase Transformation, Optical Coupling and Coalescence of Nanoparticle [Hongyou Fan](#); Sandia National Laboratories, United States

Naturally occurring system responses such as folding and unfolding in self-assembled DNA bundles show that natural designs are hierarchical, with structures and property on multiple scales arising through interactions of subunits or building blocks. Mimicking these designs in the fabrication of active materials requires a clear picture of the energy landscape that governs local interactions such as hydrogen bonding, van der Waals interactions, dipole-dipole interactions, and capillary forces, which will provide correct thermodynamic end points as well as facile kinetics for precise control of hierarchical structure leading to responsive functions. To date, fabrication of active and responsive nanostructures has been conducted at ambient pressure and largely relied on these specific chemical or physical interactions. Using pressure-induced assembly (PIA) that we recently demonstrated as an artificial actuator, we can emulate the natural folding and unfolding processes to: explore the energy landscapes that govern local interactions; design new classes of active materials with structures and functions that are not attainable for current nanomaterials; and investigate new properties resulting from folding and unfolding processes. We show that under a hydrostatic pressure field, the unit cell dimension of ordered 3D nanoparticle arrays can be manipulated to reversibly shrink and swell during compression and release of pressure. This allows for precise tuning of interparticle symmetry and spacing - ideal for controlled investigation of distance-dependent energy couplings and collective chemical and physical properties such as surface plasmon resonances. Moreover, beyond a threshold pressure, nanoparticles are forced into contact and sinter, forming new classes of chemically and mechanically stable 1-3D nanostructures that cannot be manufactured by current top-down or bottom-up methods. Depending on the orientation of the initial nanoparticle arrays, 1-3D ordered nanostructures (Au, Ag, CdSe, etc.) including nanorods, nanowires, nanosheets, and nanoporous networks can be fabricated. The PIA method mimics embossing and imprinting manufacturing processes and opens exciting new avenues for the study of responsive behaviors of active materials during compression (folding) and pressure release (unfolding). Stress-dependent control over the structure of nanoparticle or building block arrays provides a unique and robust system for the understanding of collective chemical and physical characteristics of nanocrystal superlattices.

Sandia National Laboratories is a multimission laboratory managed and operated by National Technology and Engineering Solutions of Sandia, LLC., a wholly owned subsidiary of Honeywell International, Inc., for the U.S. Department of Energy's National Nuclear Security Administration under contract DE-NA0003525.

9:00 AM *SF02.05.02

High Pressure Study of UTe_2 in Pulsed Magnetic Field [Daniel Braithwaite](#); Univ Grenobles Alpes, Grenoble INP, CEA, IRIG/PHELIQS, France

The unconventional superconductivity in the heavy-fermion paramagnet UTe_2 has recently attracted a lot of attention [1], particularly due to the reinforcement of superconductivity with magnetic field [2], and the probable spin-triplet and possibly topological nature of the superconducting order parameter. Pressure is a powerful tuning parameter in this system inducing multiple superconducting phases, changes of the magnetic anisotropy, and long range magnetic order [3]. A challenge is now to characterize the effects of combined pressure and magnetic fields applied along variable directions in this strongly anisotropic paramagnet. Several studies under pressure in high static magnetic field have been published, but a full investigation of this system requires magnetic field higher than the maximum available static magnetic fields. Here, we present an investigation of the electrical resistivity of UTe_2 under pressure up to 3 GPa and pulsed magnetic fields up to 58T applied along the hard magnetic directions b and c. We show that, near the critical pressure, a field-enhancement of superconductivity coincides with a boost of the effective mass related to the collapse of metamagnetic and critical fields[4]. These new elements improve our understanding of the interplay between magnetism and superconductivity, and the nature of these phases.

References

- [1] S. Ran *et al.*, Science **365**, 684 (2019)
- [2] G. Knebel *et al.*, Journal of the Physical Society of Japan **88**, 063707 (2019).
- [3] D. Braithwaite *et al.*, Communications Physics **2**, 147 (2019).
- [4] M. Valiska *et al.* Phys Rev **B104**, 214507 (2021)

9:30 AM BREAK

10:00 AM *SF02.05.04

Geomimicry—Synthetic Diamond Inclusion as a Functional Materials Device That Retains Extremely Favorable High-Pressure Properties [Hokwang Mao](#)¹, [Zhidan Zeng](#)¹, [Qiaoshi Zeng](#)¹, [Qingyang Hu](#)¹ and [Wendy L. Mao](#)²; ¹Center for High Pressure Science & Technology Advanced Research, China; ²Stanford University, United States

High pressures induce changes of properties and structures that could greatly impact materials science if such changes were preserved for ambient applications. Mimicking the geological process of diamond formation that the pressures and high-pressure phases in diamond inclusions can be preserved by the strong diamond envelope, we demonstrate that such process opens a great potential for creation of functional materials with extremely favorable properties.

10:30 AM *SF02.05.05

Melts and Disordered Structures Under Extreme Conditions [Toshimori Sekine](#)^{1,2}; ¹Center for High Pressure Science and Technology Advanced Research, China; ²Osaka University, Japan

Extreme conditions provide creation of new chemical bonding in materials. Pressure densifies materials and temperature enhances reactivity. Although we are exploring new fields using various techniques of static and dynamic compressions, recent progress in dynamic compression is challenging to provide high-resolution measurements temporally and spatially in a limited volume. Shock compression is a unique technique to generate multi extreme conditions in materials for a short time (nanoseconds to microseconds) because shock wave propagates as fast as tens micrometers per nanosecond and because pressures exceeding the material strength can be generated. The shock compressed state is determined through the Rankine-Hugoniot relations when we measure two parameters such as shock velocity and particle velocity. Strain rate at the shock front is 10^6 s⁻¹ to 10^9 s⁻¹, depending upon how we generate shock waves. Temperature induced by shock compression depends upon the pressure and compressibility of material. Thanks to the recent laser technology development, application of high power laser becomes popular to reach unique high-pressure region of TPa (1000 GPa) high pressures in small volumes by the inertia.

I will present recent experimental results on silicate and carbonate and discuss the melts and disordered structures at extreme conditions. The state is called warm dense matter where the density is a few times of the solid and temperature is typically around and above 10000 K.

Partial support by NSFC No. 41974099 is acknowledged.

11:00 AM SF02.05.06

Nitrogen-Hydrogen, Carbon Monoxide, Phosphorus and iron Extended Solids Under Pressure—Beyond Pentazole, Chain and Molecular Structures Iskander G. Batyrev; DEVCOM U.S. Army Research Laboratory, United States

Structures of extended solids H-N, CO-N, P-N, and Fe-N under pressure are predicted using evolutionary algorithms based on DFT calculations. The found structures complement results of the previous, never ultimate because of evolutionary nature structure searches. We focus on the structures with three dimensional covalent bonds. The HN4 structure found at 50 GPa has P4m symmetry group. Lowering the pressure down to 10 GPa changes the symmetry to Pmc21. Both structures are found to be metallic according to hybrid functional calculations. The structure of CON2 crystal at 40 GPa is made of eight-membered rings of singly bonded CON2 molecules in a three-dimensional framework structure in the space group of P43. It has high mass density comparable with that of cubic gauche nitrogen and high content of nitrogen atoms forming a spiral perpendicular to the eight member rings. PN4 has the highest concentration of nitrogen out of all known structures of P-N solids. The predicted structure of PN4 at 50 GPa has a P2/m symmetry group, and the crystal is metallic according to hybrid functional DFT calculations. The structure of the found iron-nitrogen compound FeN4 with symmetry group P21/c has high mass density and contains layers of Fe-N pentagons plane network and nitrogen dimers connecting the planes. Calculated phonon dispersions indicate dynamical stability of the systems, calculated Raman active frequencies of the compounds are compared with available experiments.

11:15 AM SF02.05.07

Pressure-Dependent Behavior and Low and High Temperature Photoluminescence (PL) of Isotope Free Boron Arsenide Mahendra Subedi^{1,2}, Jose Perez¹, Bibhudutta Rout¹, Pawan Koirala², Tengting Lyu¹, Hao Yan¹, Evan Hathaway¹ and Jingbiao Cui¹; ¹University of North Texas, United States; ²The University of Texas at Dallas, United States

We report high-pressure and low and high temperature photoluminescence (PL) and Raman measurements of isotope free boron arsenide (BAs). The Raman spectrum at ambient pressure shows two peaks at 715 cm⁻¹ and 696.5 cm⁻¹ that corresponds to the vibrational modes of ¹⁰B and ¹¹B isotopes respectively. We observed that ¹⁰B and ¹¹B peaks blueshift with increase in pressure that is due to phonon hardening. We also observed LO/TO phonon splitting with the increase in pressure from 10 GPa to 20 GPa, that occurs due to different rates of phonon hardening between two phonons (LO/TO) in both ¹⁰B and ¹¹B isotope samples. High-pressure Raman spectra also suggest that as pressure increases, the conduction band minimum corresponding to the donor level decreases affecting the discharge of free carriers from defect states (1). The PL measurements reveal an indirect bandgap of about 1.72 eV. BAs is investigated as a power electronic device because of its ultrahigh thermal conductivity greater than 1300 W m⁻¹ K⁻¹, second to diamond, as predicted by First-principles calculations and reported experimentally (2). In heat management, BAs opens a whole new potential as a novel optoelectrical material due to its predicted high electron (~1400 cm²V⁻¹s⁻¹) and hole mobilities (~2100 cm²V⁻¹s⁻¹) (3). BAs has a comparable lattice constant and thermal expansion coefficient to Si, making it feasible to integrate in electronic devices (4,5). Our work establishes a foundation for strain engineering to regulate strain in the transistor channel that enhances transport properties of BAs which ultimately improves device performance.

References:

1. Meng X, Singh A, Juneja R, Zhang Y, Tian F, Ren Z, et al. Pressure-Dependent Behavior of Defect-Modulated Band Structure in Boron Arsenide. *Advanced Materials*. 2020 Nov 1;32(45).
2. Tian F, Ren Z. High Thermal Conductivity in Boron Arsenide: From Prediction to Reality. *Angewandte Chemie*. 2019 Apr 23;131(18):5882–9.
3. Liu TH, Song B, Meroueh L, Ding Z, Song Q, Zhou J, et al. Simultaneously high electron and hole mobilities in cubic boron-V compounds: BP, BAs, and BSb. *Physical Review B*. 2018 Aug 27;98(8).
4. Broido DA, Lindsay L, Reinecke TL. Ab initio study of the unusual thermal transport properties of boron arsenide and related materials. *Physical Review B - Condensed Matter and Materials Physics*. 2013 Dec 11;88(21).
5. Tian F, Luo K, Xie C, Liu B, Liang X, Wang L, et al. Mechanical properties of boron arsenide single crystal. *Applied Physics Letters*. 2019 Apr 1;114(13).

11:30 AM SF02.05.08

Thermal Conductivity of Perovskites Under Pressure Songrui Hou, Richard Wilson and Chen Li; University of California, Riverside, United States

SrTiO₃ has soft optic phonons whose frequencies decrease upon cooling. The soft phonon mode at the *R* point is known to be related to the cubic-tetragonal phase transition in SrTiO₃ at ~105 K. This soft mode related phase transition introduces extra phonon scattering and results in a weak temperature dependence of the thermal conductivity of SrTiO₃ at high temperature, i.e., weaker than the typical 1/*T* dependence. Previous research reveals that pressure can also drive the soft mode related phase transition in SrTiO₃. In this work we aim to study the pressure dependence of the thermal conductivity of SrTiO₃ under pressure, $\Lambda(P)$. We measure the pressure dependent Raman spectrum of SrTiO₃ to confirm there is a phase transition around 9 GPa. We carry out time-domain thermoreflectance measurements in diamond anvil cells to obtain the thermal conductivity of SrTiO₃ up to 30 GPa. The results are compared with the control sample KTaO₃. The Raman spectrum of KTaO₃ suggests KTaO₃ does not experience phase transition up to 20 GPa. The second-order Raman peak shifts of SrTiO₃ and KTaO₃ display similar pressure dependence. We find SrTiO₃ has a much weaker pressure dependence in $\Lambda(P)$ than KTaO₃. We simulate our $\Lambda(P)$ data of SrTiO₃ and KTaO₃ by Leibfried-Schlömann equation. The equation fits the $\Lambda(P)$ of KTaO₃ well but overestimate the pressure dependence of SrTiO₃. We attribute the suppression on $\Lambda(P)$ of SrTiO₃ to extra phonon scattering introduced by soft mode related phase transition.

11:45 AM SF02.05.09

Evidence for Pressure Induced Unconventional Quantum Criticality in the Coupled Spin Ladder Antiferromagnet C₉H₁₈N₂CuBr₄ Tao Hong; Oak Ridge National Laboratory, United States

Quantum spin-1/2 ladders with two legs have been serving as a model low-dimensional spin system for discovery and understanding new phenomena. Here we present a comprehensive study of the effect of hydrostatic pressure on the magnetic structure and spin dynamics in a spin-1/2 coupled ladder antiferromagnet C₉H₁₈N₂CuBr₄ (DLCB for short). In DLCB, the inter-ladder coupling is sufficiently strong to drive the system to the long-range antiferromagnetic ordering phase below *T*_N=2.0 K. Analysis of the spin Hamiltonian suggests that DLCB is close to the quantum critical point in two dimensions at ambient pressure and zero field [1, 2]. The single-crystal heat capacity and neutron diffraction measurements suggest that the magnetic order breaks down above a critical pressure *P*_c ~1.0 GPa [3]. Estimates of the critical exponents suggest that this transition may fall outside the traditional Landau paradigm. By contrasting with quantum Monte Carlo calculations of the dynamic structure factor, the follow-up inelastic neutron scattering at 1.3 GPa further indicates an exotic quantum-disordered phase above *P*_c[3], characterized by two well-separated gapped modes, including one continuum-like and another resolution-limited excitation in distinct scattering channels.

References:

- [1] T. Hong *et al.*, Phys. Rev. B **89**, 174432 (2014).
[2] T. Hong *et al.*, Nat. Phys. **13**, 638 (2017).
[3] T. Hong *et al.*, Nat. Commun. **13**, 3073 (2022).

Acknowledgements:

This research used resources at High Flux Isotope Reactor and Spallation Neutron Source, a DOE Office of Science User Facility operated by the Oak Ridge National Laboratory (ORNL).

SESSION SF02.06: High Pressure II
Session Chairs: Alexander Goncharov and Wenge Yang
Tuesday Afternoon, November 29, 2022
Sheraton, 3rd Floor, Commonwealth

2:30 PM SF02.06.02

Ultrastable Amorphous Sb₂Se₃ and Its Density-Driven Superconductivity Wenge Yang; Center for High Pressure Science & Technology Advanced Research, China

Chalcogenide glasses have been considered as a promising semiconductor in photovoltaic applications. The metastable nature limits its application condition, thus searching for ultrastable glass formation condition has attracted much effort. Here we report an enhancement in thermal stability by 17K comparing to ordinary formation condition in Sb₂Se₃ by optimizing the substrate temperature during the thermal evaporation process. Ultrastable amorphous Sb₂Se₃ showed the smallest surface roughness and highest refractive index. By in situ high temperature-high energy synchrotron X-ray diffraction, the difference in structure relaxation between ordinary and ultrastable amorphous Sb₂Se₃ was manifested by local structure evolution. Upon compression, amorphous Sb₂Se₃ undergoes a LDA to HAD transition at 24 GPa, defined as the amorphous density surpassing the crystal counterpart, and the superconductivity emerges. The superconducting critical temperature is enhanced when pressure induced crystallization at 51 GPa. HDA phase, featured by multivalent bonding, plays a pivotal role in the delocalization of electrons and the occurrence of superconductivity in the amorphous state. The results presented here provide a structural basis for the incipient structure of pressure-induced superconductivity in amorphous solids.

2:45 PM SF02.06.04

Investigating Ferroelastic and Multiferroic Behavior of Rutile-Like Frameworks Muzi Chen and Andrew Cairns; Imperial College London, United Kingdom

The prototypical rutile structure (TiO₂, TeO₂, etc.) has been shown to undergo a ferroelastic transformation from a tetragonal structure to the orthorhombic structure on compression or cooling. Following the ferroelastic transition, the structure shows negative linear compressibility (NLC) in one of the orthogonal directions. Negative linear compression (NLC) is the property of a material that refers to the phenomenon that when a system is uniformly compressed, it expands in at least one linear direction.¹ Material with negative compression properties has many promising applications in engineering, such as sensitive pressure sensing, actuators, and the development of artificial muscle—critically depends on the intrinsic NLC response. Therefore, we are interested in investigating whether this phenomenon occurs in its structural analogues.

In our work, we investigated the structural analogues to rutile, which are transition metal dicyanamide and tricyanomethanide systems, abbreviated as M(dca)₂ and M(tcm)₂ (M = Mn, Cu, Fe, Co, Ni, and Zn). Both variable-temperature diffraction and high-pressure diffraction were employed. Our results show significant negative thermal expansion (NTE) and negative linear compressibility (NLC) in a series of M(dca)₂ and M(tcm)₂ materials. The magnitude of thermal and pressure-induced structural changes in each case was proved to be affected by the transition metal size and Jahn Teller distortions.

Reference:

- [1] Andrew B. Cairns and Andrew L. Goodwin. Negative linear compressibility. Phys. Chem. Chem. Phys., 17:20449–20465, 2015.

3:00 PM BREAK

SESSION SF02.07: Other Extreme Environments I
Session Chairs: Alexander Goncharov and Wenge Yang
Tuesday Afternoon, November 29, 2022
Sheraton, 3rd Floor, Commonwealth

3:30 PM SF02.07.01

Oxygen-Tailored Grain Growth Mechanism on Pt Films Thermistors—Deposition, Annealing and Application on Carbon Nanotubes-Based Microbolometers Erica Freire Antunes, Atasi Dan, Christopher Yung, Nathan A. Tomlim, John H. Lehman and Michelle S. Stephens; National Institute of Standards and Technology, United States

Uncooled microbolometers with vertically aligned carbon nanotubes (VACNTs) as an absorber and electrical substitution calibration have been developed by the NIST for broadband sensing of Earth outgoing radiation [1,2]. The current fabrication challenge is coupling a thin film thermistor to the devices. The key requirement for the thin film thermistor, besides a high temperature coefficient of resistance (TCR) [3] and low 1/f noise, is surviving to the harsh carbon nanotube growth environment [4]. In the present work, Pt thin film thermistors were microfabricated on Si wafers coated by SiO₂/SiN_x/AlO_x films, similar to a microbolometer membrane. The Pt film were deposited by DC magnetron sputtering, and the deposition parameters, such as power, pressure, Ar/O₂ ratio, and film thickness were investigated. The samples were also submitted to a post-annealing to maximize their electrical conductivity and, consequently, the TCR [5]. Microstructural and morphological analysis of Pt film suggest that the TCR values can be tailored by the grain growth type mechanism defined during annealing step. The control of the grain size distribution through a normal grain growth with a preferential orientation Pt (111) has been achieved for samples with deposition environment free-of-oxygen [5]. Adding O₂ at the Pt sputtering atmosphere can lead to a Pt film with O₂ trapped on the Pt face-centered cubic crystalline structure, a misorientation of the grains, an oxide formation, and even an amorphization [6]. As platinum

oxides are not stable in high temperatures, the loss of oxygen can induce different grain growth mechanisms during annealing. Abnormal growth with bimodal distribution of grains can occur in high annealing temperatures for Pt films. Depending on the O₂/Ar ratio at the deposition, the distribution of grain sizes after annealing can become unimodal as in normal growth, but with grains much larger than the Pt film thickness. It implies that an anisotropic grain boundary mobility leads to giant grain growth [7-9]. Finally, Pt thermistors were submitted to the VACNT growth environment to assess any change in the TCR values, resulting from their exposure to the hydrogen/hydrocarbon plasma at high temperatures.

Funding for this work was supplied by NIST, the NASA Instrument Incubator Program (IIP), and the NASA Earth Venture Continuity Program (EV-C).

References:

- [1] N. A. Tomlin et al., "Overview of microfabricated bolometers with vertically aligned carbon nanotube absorbers", *AIP Advances* **10**, 055010 (2020)
- [2] C. S. Yung et al., "BABAR: Black Array of Broadband Absolute Radiometers for far infrared sensing" *SPIE Proceeding 109800F* (2019)
- [3] A. Yamashita et al., "Development of High TCR Platinum Thin Films", *IEEE Transactions on Sensors and Micromachines* **124**, 242–247 (2004)
- [4] J. Lehman et al., "Carbon nanotube-based black coatings", *Applied Physics Reviews* **5**, 011103 (2018)
- [5] Atasi et al., "Optimization and annealing of the temperature coefficient of resistance of Pt thin-film thermistors". Intern. Conf. on Metallurgical Coatings and Thin Films (ICMCTF). San Diego/CA-USA (2022).
- [6] M. Hecq, et al., Sputtering deposition, XPS and X-ray diffraction characterization of oxygen-platinum compounds, *Journal of the Less Common Metals* **64**, 25-37 (1979)
- [7] D.-S. Lee et al., "Preferred Orientation Controlled Giant Grain Growth of Platinum Thin Films on SiO₂/Si Substrates", *Jpn. J. Appl. Phys.* **40** L1 (2001)
- [8] A. J. Birnbaum et al. "Oxygen-induced giant grain growth in Ag films." *Appl. Phys. Lett.* **111**, 163107 (2017).
- [9] A. M. Gusak et al. "Modeling of abnormal grain growth in (111) oriented and nanotwinned copper". *Sci Rep* **11**, 20449 (2021).

3:45 PM SF02.07.02

Molecular Dynamics Estimations of Transport Properties of Pure Water and Methane Hydrate Systems at Pre-Nucleation Conditions Andre Guerra, Samuel Mathews, Alejandro Rey, Milan Maric and Phillip Servio; McGill University, Canada

Gas hydrates are inclusion compounds, in which gas molecules are trapped inside the solid phase of water. In the transition from liquid to the solid phase, water molecules form a lattice structure that arises from hydrogen bonds between adjacent molecules. If the phase transition occurs at severe enough pressures and in the presence of dissolved gas species in liquid water, the gas molecules can become trapped in "cages" as the solid lattice structure forms. Gas hydrates have been an active research topic due to their occurrence in the oil and gas industry. As a result, much of the body of knowledge focuses on water-in-oil emulsion gas hydrate systems. Recently, however, new green technologies that utilize gas hydrate formation phenomena in non-oil systems such as pre- and post-combustion carbon capture from flue gas, natural gas transport, and storage, or the desalination of seawater have been proposed. Most of these technologies require continuous or semi-continuous flow systems maintained near and at hydrate nucleation conditions. These technologies would benefit from improved prediction capabilities of transport properties at pre-nucleation conditions in their process design and control.

This work intended to extend the current understanding of water and gas hydrate systems by developing improved molecular simulations to estimate the viscosity, diffusivity, and thermal conductivity of pure water and methane hydrate systems at various conditions. LAMMPS molecular dynamics package was used to explore the performance of the TIP4P/2005 and TIP4P-ice water force fields in the context of transport property estimations of subcooled water systems. Various estimation methods were tested including the Green-Kubo and Einstein formulations for viscosity, diffusivity, and thermal conductivity. A new Stokes-Einstein formulation for viscosity was also tested in this work. This work implemented systems consisting of approximately 7,600 atoms that were methodically equilibrated with the primary intent to develop stable and physically representative systems adequate for the estimation of bulk phase transport properties via the methods above. Finally, the data generated in this study were compared to experimental data to validate their accuracy. This includes experimental viscosity measurements of methane hydrates systems collected by our research group in previous experimental work. The present study showed that the TIP4P-ice force field for water resulted in improved estimation of viscosity for pure water systems when compared to the TIP4P/2005 force field results. However, discrepancies in the estimations for the viscosity of methane hydrate systems indicate the necessity for re-parametrization of the TIP4P-ice force field taking new viscosity experimental data into consideration for gas hydrate applications.

4:00 PM SF02.07.03

Tunable Magnetic Structure and Topological Electronic States in Square-Net Materials Ratnadwip Singha¹, Tyger H. Salters¹, Samuel M. Teicher² and Leslie Schoop¹; ¹Princeton University, United States; ²University of California Santa Barbara, United States

Though numerous topological semimetals have been discovered in recent years, their band structures are rarely ideal. The linear band crossings are often obscured by trivial parabolic bands near the Fermi energy. Materials with square-net motif in their crystal structure proved to be an exception as they host clean Dirac cones over large energy range in the band structure [1-3]. *LnSbTe* (*Ln*=lanthanides) family of materials with antimony square-net is one such example which also introduces magnetism in topological electronic states [4-6]. We show that in this group of compounds, a high degree of tunability can be achieved by changing the electron count at the square-net. Increased electron filling results in structural distortion and formation of charge density waves (CDWs). Moreover, the CDW modulation vector can be tuned continuously. These structural changes also lead to rich magnetic phase diagrams. As a specific example, we discuss CeSbTe, where a complex "devil's staircase" magnetic structure is observed within a certain electron filling [7]. We also show that the CDW creates idealized non-symmorphic Dirac semimetal, where all the trivial bands are gapped out near Fermi energy. Thus, we present a unique template material, where the topological band structure can be controlled by electron filling (tuning chemical potential), CDWs (gapping out non-essential band crossings), or magnetic field (changing the magnetic ordering).

References

1. L. M. Schoop, *et al.* *Nat. Comm.* **7**, 11696 (2016).
2. R. Singha, *Proc. Natl. Acad. Sci. USA* **114**, 2468 (2017).
3. S. Klemenz, *et al.* *Annu. Rev. Mater. Res.* **49**, 185 (2019).
4. L. M. Schoop, *et al.* *Sci. Adv.* **4**, eaar2317 (2018).
5. M. M. Hosen, *et al.* *Sci. Rep.* **8**, 13283 (2018).
6. S. Yue, *et al.* *Phys. Rev. B* **102**, 155109 (2020).
7. R. Singha, *et al.* *Adv. Mater.* **33**, 2103476 (2021).

4:15 PM DISCUSSION TIME

4:30 PM SF02.07.06

A Novel Design of a High-Efficient Adsorption-Based Atmospheric Water Extractor for Extreme Conditions Bachir El Fil, Xiangyu Li, Gustav Graeber, Emily Lin, Chad Wilson, Chenyang Li, Yang Zhong and Evelyn N. Wang; Massachusetts Institute of Technology, United States

Portable water supply has always been a critical part of any expeditionary tasks, especially in situations where portable or even ground water is scarce. Atmospheric water extraction is a system that is capable to obtain portable water, providing more mobile, flexible and self-sufficient operations. Unfortunately, state-of-the-art fog-harvesting and dew systems are limited to high humidity. For extreme conditions where portable water is scarce, adsorption-based atmospheric water extractor promises to supply drinking water regardless of the weather conditions. In this work, we leverage the adsorption properties of adsorbents including MOFs (e.g., MIL-101, UiO-66) and silicas to design a biomass-driven high performance atmospheric water extractor that is capable of producing abundant amount of water at extreme dry conditions (< 15% relative humidity). We first model and experimentally demonstrate the performance under a wide range of operating conditions. The innovative design of compact, mobile, and highly efficient atmospheric water extractor can provide a guideline for future water extractors.

SESSION SF02.08: Poster Session II: Materials for Extreme Conditions

Session Chairs: Alexander Goncharov and Wenge Yang

Tuesday Afternoon, November 29, 2022

8:00 PM - 10:00 PM

Hynes, Level 1, Hall A

SF02.08.01

Design and Modeling of Hydrogel-Based Adsorbent Bed for Energy Storage [Liliosa Eyang Cole](#), Bachir El Fil, Xiangyu Li, Xinyue Liu, Carlos D. Diaz, Gustav Graeber, Leon C. Gaugler and Evelyn N. Wang; Massachusetts Institute of Technology, United States

Waste heat generation is ubiquitous in power systems operating in residential and industrial settings. While reuse of waste heat is common practice in industrial systems, an increase in the energy density of a waste heat collector is crucial for the improvement of system efficiency and feasibility. The hydrophilic nature of hydrogels creates a compelling prospect for thermal energy storage (TES), in the form of a chemical potential. In this work, we take advantage of the sorption capabilities of hydrogels, combined with waste heat collection from existing power systems such as HVAC, to design and engineer a hydrogel/salt composite. This composite is to be integrated into a compact TES device, to deliver an energy density greater than 200 kWh/m³/day.

The hydrogel/salt synthesis requires paramount characterization and testing of polymer/salt combinations, to yield an effective, durable, and mechanically robust, high water uptake material, that will enable the required high-energy capacity. The composite's kinetics and low-temperature desorption capabilities play a critical role in surpassing the device design requirements. A novel technique is used to adhere the hydrogel onto the device, while maintaining good mechanical and thermal stability. This novel technique allows for an effective thermal conductivity greater than 1 W/m K. We developed a numerical model to simulate and predict the heat and mass transfer of the hydrogel within the device. The critical component where the hydrogel is mounted is a tube-fin heat exchange. The thickness and kinetics of the hydrogel composite layer is optimized to maximize the energy density of the TES. We characterize the hydrogel experimentally to validate the developed numerical models.

SF02.08.02

Core-Shell Structured Ultrahyperbranched Polymer Based Hydraulic Fracturing Fluid Crosslinker [Wengang Li](#)¹, Harbi Harbi¹, Majad Khan² and Muhammad Tahir²; ¹Saudi Aramco, Saudi Arabia; ²King Fahd University of Petroleum and Minerals, Saudi Arabia

Hydraulic fracturing operation has been widely used in oil and gas industry production applications. Fracturing fluid plays a key role in transiting pressure, transporting proppant and minimizing possible leaking during the job, with thickeners and crosslinkers together to enhance fluid viscosity. Commercial crosslinkers are mostly borates or inorganic salts. Some polymeric crosslinker have also been used for guar gum and polyacrylamide (PAM) thickeners. When compared with linear and branched polymers, hyperbranched polymers have attracted significant attention due to their extraordinary properties, such as a lower viscosity, higher solubility, smaller size and higher surface functional group concentrations. Such properties make hyperbranched polymers potential candidates for downhole applications with low formation damage.

This paper demonstrated the A to Z for a novel core-shell structured ultrahyperbranched polymer (UHP) for applications of hydraulic fracturing fluid crosslinker. The UHP was designed and synthesized by growing a hyperbranched polymer shell structure from the surface of a pre-existing hyperbranched polymer core that acts as a macroinitiator. Characterizations for UHPs have been performed, such as FT-IR, NMR and GC-MS. Gelation properties with fracturing fluids were tested with rheometer following ISO 13503-1 method. Multiple functional groups were tested for different conditions. The synthesized UHPs have been approved potential crosslinkers for polymer based fracturing fluids.

The UHP crosslinkers will be further investigated for compatibility with current fracturing fluid package and tested in the field for future fracturing operations.

SF02.08.03

Development of Ion-Selective Electrodes for Detection of Nitrogen-Based Ions Among Soil Nutrients [Seonghyun Hong](#), Seongjun Hong and Yang-Rae Kim; Kwangwoon University, Korea (the Republic of)

Recently, analyzing soil nutrients has been vastly emphasized in developing next-generation agriculture based on smart-farm. Remarkably, there is much attention to the on-site and real-time analysis of nutrients inside the soil. As a result, some attempts have been made to achieve this purpose. If it is realized, it enables minimal use of fertilizers and finally reduces overall analysis cost.

Conventional methods for analyzing soil nutrients include colorimetry, spectrophotometry, flame photometry, and atomic spectrometry. However, some of them require pre-processing steps and expensive equipment. Some methods are also challenging because of selectivity, on-site detection, and multiple analysis.

Ion-selective electrode (ISE)-based potentiometry has several advantages compared to the conventional methods. First, it allows minimal pre-treatment steps, especially for the soil sample. Second, it enables cost-effective analysis because it does not require expensive equipment. Third, it has superior selectivity compared to other methods. Fourth, on-site, real-time, and multiple monitoring of soil nutrients effectively works through miniaturization of the measurement part.

Nitrogen (N), phosphorus (P), and potassium (K) are estimated to be essential elements among several soil nutrients. In particular, nitrogen-based ions (ammonium, nitrate, and nitrite) are critical for efficient crop growth. Therefore, developing sensors for accurate and fast analysis of nitrogen-based nutrients is necessary. In this study, several ISEs have been prepared to detect nitrogen-based ions. The membranes of ISEs were optimized by changing the components (matrix, ionophore, plasticizer, and lipophilic additive) and their amounts. The experiments were carried out in a buffer solution, similar to the soil environment. The sensitivity and selectivity of ISEs were intensively investigated and compared with commercial ISEs. Finally, preliminary

experiments were performed inside the soil to monitor nitrogen-based ions directly and simultaneously. This work was carried out with the support of Cooperative Research Program for Agriculture Science and Technology Development (Project No. PJ015725032021) Rural Development Administration, Republic of Korea.

SF02.08.04

Super Hydrophobic Polymeric Film for CMP Conditioner by Initiated Chemical Vapor Deposition (iCVD) Taeyoon Kim, Chulwoo Bae and Taesung Kim; Sungkyunkwan University, Korea (the Republic of)

Chemical mechanical polishing (CMP) has been widely used in semiconductor manufacturing. The CMP process is essential for the planarization of semiconductor wafers and highly integrated devices, which is a process that mechanically removes the chemical reaction layer created on the wafer surface. At the same time, the slurry liquid is supplied onto the polishing pad with asperity. For this purpose, a slurry solution containing abrasive particles and chemical compounds to perform a polishing role, a polishing pad providing adequate pressure and asperity with the surface of a wafer, and a diamond conditioner for maintaining the surface roughness of the polishing pad are required.

In the CMP process, shot asperity and glazing pores are produced due to friction and load applied between the CMP wafer and the CMP pad. In addition, the pores of the CMP pad are clogged by the slurry, thereby reducing the efficiency of the CMP process. In order to prevent this phenomenon, a diamond conditioner has been used to regenerate the pad surface and remove the slurry particles from the surface of the CMP Pad. The CMP pad conditioner has a stainless body with diamond edges fixed on Ni metal and an alloy coating. The diamond is shaken by physical force during the CMP process, which causes a crack. As acid or base solution penetrates this gap and corrodes the metal, diamonds fall out, or metal contamination occurs, damaging the wafer. The PTFE spray coating method has been applied to the CMP conditioner to prevent corrosive solutions such as acid and base. However, due to the poor bonding strength between PTFE and metal, the PTFE coating was easily peeled off from the load received during the CMP process, and it was not easy to coat uniformly.

In this study, hydrophobic polymer coating through ICVD method on the CMP conditioner and their hydrophobicity improvement were evaluated to prevent acid or base solution penetration. First, the surface of the CMP conditioner was modified using plasma and a silane coupling agent to increase the bonding force between the polymer coating and the metal. 1,3,5,7-tetravinyl-1,3,5,7-tetramethylcyclotetrasiloxane was coated through the iCVD method, a technology that directly forms a polymer coating on the surface in the vapor phase. 1H,1H,2H,2H-Perfluorodecyl acrylate, which plays a role in hydrophobicity, was coated thereon. Characteristics of the surface of the CMP pad conditioner coated with the hydrophobic polymer were analyzed. FT-IR and XPS confirmed that organic materials were successfully formed on the surface, and the hydrophobicity of the surface was observed by the water droplet formed a high contact angle. In addition, the chemical stability of these CMP pad conditioners against corrosion from strong acid and the degree of peeling was tested in the CMP conditioning process.

SESSION SF02.09: Corrosion

Session Chairs: Nathan Mara and Dierk Raabe

Wednesday Morning, November 30, 2022

Sheraton, 3rd Floor, Commonwealth

8:30 AM *SF02.09.01

Phase Transformations Under Redox Conditions: Example of Hydrogen-Based Direction Reduction of Iron Oxide Dierk R. Raabe, Yan Ma and Isnaldi Souza Filho; Max Planck Institute for Iron Research, Germany

The lecture presents recent progress in understanding the nucleation, transport and redox mechanisms of the phase transformations occurring during hydrogen-based direct reduction of iron oxides. The kinetics of the transformation and reactions strongly depend on mass transport kinetics, nucleation during the multiple phase transformations, the oxide's chemistry, microstructure, and on damage and fracture associated with the phase transformation and mass transport phenomena occurring during reduction. Understanding these effects is key to make hydrogen-based reduction of iron ores commercially viable, enabling massive CO₂ reductions in the metallurgical sector.

9:00 AM SF02.09.03

Structure-Modified Fluorescent Carbon-Dots with Improved Colloidal Stability in Porous Media at High Salinity and Temperature for Reservoir Tracer Application Weij Wang, Haofeng Song and Ayrat Gizzatov; Aramco Americas: Aramco Research Center-Boston, United States

Tracer technology has been increasingly used in inter-well tests to investigate reservoir performance, reservoir connectivity and residual oil saturation for providing useful information to improve decision making in reservoir management. Stable nanoparticle tracers with high-sensitive real-time detectability are highly desired, and as one of the nanoparticles tracers, carbon dots (C-dots) have been studied and tested as nano-agent tracer in field trial for reservoir monitoring in. In this research, we report a modified method to synthesize fluorescent C-dots with enhanced colloidal stability at ultra-high salinity and lowered retention in reservoir rocks for tracer application.

With a modified synthesis procedure, fluorinated and sulfonated functional groups were incorporated into the C-dots. The synthesis reaction occurs at hydrothermal condition with inexpensive starting materials and is readily to scale up for industrial application. Optical properties of the synthesized colloidal C-dots were studied by UV-visible and fluorescence spectroscopies. Retention and transport the C-dots in carbonate rocks were evaluated by core flooding experiments. The synthesized C-dots were readily dispersible in brines with extremely high salinity (TSD >120,000ppm) at high temperature (95°C), and still exhibit high quantum yield for fluorescence, enabling sensitive detectability by optical spectroscopic or imaging techniques. Coreflooding experiments revealed neglectable adsorption of the C-dots on reservoir rocks.

The synthesized C-dots exhibit improved stability at simulated oil reservoir conditions and lowered retention in reservoir rocks, while remained high fluorescence property, enabling their use as optically detectable nano-agent tracer in oil field application.

9:15 AM BREAK

9:45 AM SF02.09.06

Soft, Pressure-Tolerant, Flexible Electronic Sensors for Sensing Under Harsh Environments Xueju Wang and Yi Li; University of Connecticut, United States

Energy-efficient, miniaturized electronic ocean sensors for monitoring and recording various environmental parameters remain a challenge because conventional ocean sensors require high-pressure chambers and seals to survive the large hydrostatic pressure and harsh ocean environment, which usually entail a high-power supply and large size of the sensor system. In this talk, I will introduce soft, pressure-tolerant, flexible electronic sensors that can operate under large hydrostatic pressure and salinity environments, thereby eliminating the need for pressure chambers and reducing the power consumption and sensor size. By using resistive temperature and conductivity (salinity) sensors as an example for demonstration, the soft sensors are made of lithographically patterned metal thin films (100 nm) encapsulated with soft oil-infused elastomers and tested in a customized pressure vessel with well-controlled pressure and temperature conditions. The resistance of the temperature and pressure sensors increases linearly with a temperature range of 5 °C–38 °C and salinity levels of 30–40 Practical Salinity Unit (PSU), respectively, relevant for this application. Pressure (up to 15 MPa) has shown a negligible effect on the performance of the temperature and salinity sensors, demonstrating their large pressure-tolerance capability. In addition, both temperature and salinity sensors have exhibited excellent cyclic loading behaviors with negligible hysteresis. Encapsulated with our developed soft oil-infused rough polydimethylsiloxane (PDMS), the sensor has shown excellent performance under 35 PSU salinity water environment for more than 7 months. The soft, pressure-tolerant, and non-invasive electronic sensors reported here are suitable for integration with many platforms including animal tags, profiling floats, diving equipment, and physiological monitoring.

10:00 AM SF02.09.07

Studying the Effect of Silicon and Oxygen on the Structure and Performance of Titanium Nitride Coatings [Gilad Zorn](#), Patrick Shower, Anteneh Kebede, Scott Weaver, Rachel Rose, Jae-Hyuk Her and Josh Salisbury; General Electric Research Center, United States

Titanium nitride (TiN) coatings have a wide range of applications due to their practical properties such as high hardness, good corrosion resistance, heat resistance and excellent wear resistance. They have been widely used in various industries including decorative coatings, diffusion barriers and hard coatings. The properties of TiN can be greatly enhanced by addition of other elements, such as Si [1–3]. Incorporation of Si in the TiN cubic structure leads to formation of TiSiN coatings characterized by high hardness and high oxidation resistance up to 800 °C. This enables synthesizing coatings and designing materials with a broad range of applications, especially as materials that should perform under harsh environments. The ternary TiSiN system is formed due to the total miscibility of Si, which creates a solid solution while preserving the crystalline structure B1 of TiN. Si is also believed to create nanocomposite structure of TiSiN coatings consisting of nanocrystalline TiN grains encapsulated by an amorphous silicon nitride (Si₃N₄) matrix. To achieve high hardness TiN films, significant bonding strength between Ti and N must be achieved. If the bonding is too weak, the surface of the coating can oxidize, forming titanium oxynitride and eventually TiO₂ even at room temperature conditions [4]. The oxynitride and oxide forms are known to exhibit a lower hardness than TiN and experience oxidation propagation.

This study is focused on the effect of Si and oxygen level on the TiN film's characteristics. X-ray Photoelectron Spectroscopy (XPS) was used to study the compositions and high resolution XPS was used to determine the surface oxide to nitride ratios. Mechanical tests were performed with nano indenter to determine the hardness of these coatings. The study shows the correlation between the hardness of the films and the percentage of the XPS titanium oxide component. X-ray diffraction confirmed the formation of titanium nitride cubic phase and different crystallographic orientations were observed depending on the composition of each film. The results of this study show that adding Si and reducing the oxygen level improved the performance of the TiN films as hard coatings.

1. Akhte, Rumana; Zhou, Zhifeng; Xie, Zonghan, Munroe, Paul *Surface and coating technology* 425 (2021) 127687.
2. Akhte, Rumana; Zhou, Zhifeng; Xie, Zonghan, Munroe, Paul *Applied surface Science* 563 (2021) 150356.
3. Greczynski, G.; Bakhit, B.; Hultman, L.; Odén, M. *Surface and coating technology* 398 (2020) 126087.
4. Logothetidis, S.; Meletis, E.I.; Stergioudis, G.; Adjaottor, A.A. *Thin Solid films* 338 (1999) 304.

This material is based upon work supported by the U.S. Department of Energy, Office of Fossil Energy and Carbon Management under Award Number FE0031911.

10:15 AM SF02.09.08

Kinetics of High-Temperature Corrosion in Austenitic Steel Alloys from First Principles [Seaton Ullberg](#)¹, Iman Abdallah², Xueyang Wu¹, Adrien Couet², John H. Perepezko², Michael R. Tonks¹ and Simon Phillpot¹; ¹University of Florida, United States; ²University of Wisconsin–Madison, United States

Manufacturers of internal combustion engines seeking to optimize performance and efficiency design their components to operate at temperatures upwards of 700 °C. Under these extreme conditions, corrosive gases resulting from incomplete combustion reactions can drive the formation of a multilayered oxide film atop austenitic steel alloys which would be resistant at lower operating temperatures. In this work, we use density functional theory (DFT) calculations to evaluate the migration energy barrier of point defects in each phase of the oxide film to understand the atomistic mechanisms by which the corrosion process progresses. Particular attention is directed towards the MnCr₂O₄ spinel layer which has been observed experimentally to form rapidly and in direct contact with the alloy - mediating the flow of cations and oxidizing agents between the alloy and oxide film. These DFT results are extended to conditions representative of the application environment through the use of an ab-initio thermodynamics framework which translates the effects of finite temperature and pressure into adjustments of chemical potential.

This work was supported by the US Department of Energy Office of Energy Efficiency and Renewable Energy Project Number 1919-1744.

10:30 AM SF02.09.09

On the Enhanced Corrosion Resistance of PVDF-HFP/Nylon Composite Coatings [Karen Y. Patino Jaimés](#)^{1,2,3}, Eugene Caldoni^{1,4,3}, Ellis Kim^{1,2,3}, Evelyn Winn^{2,3}, James Lambert^{2,3}, Erick L. Ribeiro^{1,2,3} and Rigoberto C. Advincula^{2,3,5}; ¹University of Tennessee Knoxville, United States; ²The University of Tennessee, Knoxville, United States; ³Oak Ridge National Laboratory, United States; ⁴North Dakota State University, United States; ⁵Case Western Reserve University, United States

Organic polymeric coatings are widely employed for minimizing the effects of corrosion on metallic surfaces owing to their intrinsic ability to provide interfacial passivation while exhibiting outstanding mechanical integrity, thermal stability, and chemical resistance. Polymers with strongly-bonded electronegative atoms on their backbones are ideal coating matrices as they typically exhibit exceptional corrosion resistance. The inclusion of micro- and nanostructured additives, which can further delay the diffusion of aggressive electrolyte species through the coating layer, yields polymer composites with improved barrier properties and corrosion protection. Herein, we used Nylon 12 particles as fillers for poly(vinylidene fluoride-co-hexafluoropropylene) (PVDF-HFP) matrix, a highly thermally stable semi-fluorinated copolymer with low surface energy, and investigated the ability of the resulting composite coatings to protect mild steel substrates from corrosion. Results from electrochemical measurements indicate that small amounts of Nylon 12 (less than 2 wt.%) are needed to optimize the overall protection performance of the PVDF-HFP composite coatings. The corrosion resistance is mainly evaluated by Impedance analysis and Potentiodynamic chemistry in a 3.5 wt% NaCl test solution, supported by microscopy, spectroscopy, contact angle tests, and dielectric measurements.

SESSION SF02.10: Infrared and Laser Beam
Session Chairs: Alexander Goncharov and Nathan Mara
Wednesday Afternoon, November 30, 2022
Sheraton, 3rd Floor, Commonwealth

1:30 PM SF02.10.01

Selective Infrared Phonon Stimulation to Tune Thermal Transport [Gaurav Kumar](#)¹ and Peter W. Chung²; ¹Purdue University, United States; ²University of Maryland, United States

The recent developments in high power optical sources at far-to-mid infrared (IR) frequencies (0.1 to 100 THz) have provided the means to investigate and control material properties in solid-state and condensed matter systems under nonequilibrium conditions¹. In particular, in energetic materials where phonons are the primary carriers of heat, optical heating, and ultrafast spectroscopy have enabled the investigation of shock-induced chemistry², and ignition modulation³. In this work⁴, we determine the degree to which material properties such as thermal diffusivity and conductivity can be modulated via a selective nonequilibrium infrared stimulation of phonons. Using the molecular crystal RDX, we use detailed momentum-dependent coupling information across the entire Brillouin zone and the phonon gas model to show that selective stimulation of certain low and mid frequency phonons can have a substantial positive/negative effect on the overall thermal transport properties. Specifically in the case of RDX, stimulating modes at $\sim 22.74 \text{ cm}^{-1}$ over a linewidth of 1 cm^{-1} can lead to enhanced scattering rates that reduce the overall thermal diffusivity and conductivity by 15.58% and 12.46%, respectively, from their equilibrium values. In contrast, stimulating the modes near $\sim 1140.67 \text{ cm}^{-1}$ over a similar bandwidth can produce an increase in the thermal diffusivity and conductivity by 55.73% and 144.07%, respectively. The large changes suggest a mechanism to evoke substantially modulated thermal transport properties through light matter interaction.

(1) Nicoletti, D.; Cavalleri, A. *Advances in Optics and Photonics* **2016**, *8*, 401.

(2) Powell, M. S.; Sakano, M. N.; Cawkwell, M. J.; Bown, P. R.; Brown, K. E.; Bolme, C. A.; Moore, D. S.; Son, S. F.; Strachan, A.; McGrane, S. D. *Journal of Physical Chemistry A* **2020**, *124*, 7031–7046.

(3) Alibay, Z.; Olsen, D.; Biswas, P.; England, C.; Xu, F.; Ghildiyal, P.; Zhou, M.; Zachariah, M. R. *ACS Applied Nano Materials* **2022**, acsanm.1c04157.

(4) Kumar, G.; Chung, P. W. *ACS Omega* **2022**, *7*, 12787–12794.

1:45 PM SF02.10.02

Laser Damage to Liquid Crystal Alignment Materials in Ordinary and Extraordinary Modes Zoey Davidson¹, Jason Wallace^{2,3}, Yasaman Sargolzaeiaval¹, Nathaniel Urban², Stavros G. Demos², Kenneth L. Marshall² and [Selim Elhadji](#)¹; ¹Seurat Technologies, United States; ²University of Rochester, United States; ³D'Youville College, United States

We report on the laser-damage threshold of common liquid crystal alignment materials, including rubbed polyimides, rubbed nylon, and a photoaligned azobenzene. The photoaligned azobenzene is, in principle, more laser-damage resistant because of the no-touch processing in the clear aperture¹ with the added benefit of ease of scaling and processing. We further compare the polarization dependence of the damage threshold with respect to the alignment direction in ordinary and extraordinary modes at a near-infrared wavelength. Studies on polarization dependence on laser damage of liquid crystals with alignment layers have been very limited,² and none include photoalignment. Laser-damage thresholds depend substantially on the presence of aligned liquid crystal materials. We also compare laser-damage-threshold dependence on the electrical actuation state of the nematic liquid crystal material. These data inform design of high-power beam-shaping devices for applications in fusion, 3-D printing, and defense systems.

This material is based upon work supported by the Department of Energy National Nuclear Security Administration under Award Number DE-NA0003856, the University of Rochester, and the New York State Energy Research and Development Authority.

1. K. L. Marshall *et al.*, Proc. SPIE **8828**, 88280N (2013).

2. K. L. Marshall, K. R. P. Kafka, N. D. Urban, J. U. Wallace, and S. G. Demos, "Multiparameter Laser Performance Characterization of Liquid Crystals for Polarization Control Devices in the Nanosecond Regime," accepted at Nature: Scientific Reports.

2:00 PM SF02.10.03

Optimized Liquid Crystals for High-Power Laser Beam Manipulation—An Evaluation and Feasibility Study [Yasaman Sargolzaeiaval](#)¹, Jason Wallace^{2,3}, Zoey Davidson¹, Nathaniel Urban², Stavros G. Demos², Kenneth L. Marshall² and [Selim Elhadji](#)¹; ¹Seurat Technologies, Inc, United States; ²University of Rochester Laboratory for Laser Energetics (LLE), United States; ³D'Youville College, United States

Nematic liquid crystals (LC's), ubiquitous in high resolution displays, are typically composed of rod-shaped molecules that exhibit large dielectric anisotropy, high birefringence and excellent transparency in many regions of the electromagnetic spectrum. These properties make them well suited for use in various lasers and optical components, as well as in hybridized metamaterials as alternatives to existing semiconductor and phase change materials. Recently, the single shot laser damage threshold of both saturated and unsaturated nematic LC's revealed an intrinsic relationship between the degree of chemical bond saturation within LC molecules and laser damage¹. These results suggest that rational molecular design routes exist for improving both the laser damage threshold and operational threshold of electrically switchable LC's. In this study we investigated one such optimized LC and characterized its laser damage threshold and switching behavior in the near-IR region. We also studied the lifetime of LC's upon exposure to a train of 1053 nm laser pulses with an average power density in the kW/cm² regime and pulse repetition rates of 10 to 40 Hz. The thermal accumulation and spatial temperature profile during high power laser exposure was modeled using 3D simulations to estimate the LC lifetime and operation.

1. Kosc, T. Z., et al. "Investigation of parameters governing damage resistance of nematic liquid crystals for high-power or peak-intensity laser applications." Scientific Reports 9.1 (2019): 1-10.

2:15 PM SF02.10.04

Surface Fatigue Behavior of Laser Peened Single Crystalline Turbine Blades—A Multicycle Nanoindentation Study [Noah Holtham](#) and Keivan Davami; University of Alabama, United States

Turbine blades are one of the most critical components in a modern gas turbine engine as they convert high energy combustion products into mechanical

work and drive the main turbine shaft. Although they are remarkably resilient, the blades are prone to damage initiated at the surface from mechanisms such as stress corrosion cracking, fatigue, and foreign object damage. Additionally, the growing need for higher-efficiency combustion engines requires higher operating temperatures which only accelerates the kinetics of crack growth and other deleterious effects. Fortunately, methods of fortifying the surface through localized cold working techniques show promise at significantly delaying crack growth, creep rate, and corrosion; thereby enabling longer service lives. In this work, one such method known as laser peening (LP) was applied to single crystal Nickel-based superalloy turbine blades. Sections of the turbine blades were cut into flat plates and LPed on a face approximately parallel to the [001] plane. The peening was conducted over 4 consecutive layers with an irradiance of 7 GW/cm² to maximize the depth of plastic deformation without causing reverse plastic straining and consequently degrading the mechanical properties. Following LP, one set of samples was placed in a furnace at 700 °C for 300 hours to gauge the retention of LP-induced microstructural modifications under thermal exposures similar to those experienced in gas turbine engines. Cyclic nanoindentation fatigue tests were then conducted to provide insight into the surface-level energy absorption of CMSX-4 and how that behavior changes after LP and thermal exposure. Indentation tests were performed with a load of 500 mN at 300 cycles using a Berkovich tip within dendrite core regions of each sample to reduce error associated with anisotropic mechanical properties. The LPed specimen showed a dramatic reduction in indentation depth in comparison to baseline sample which is likely due to the compressive residual stresses and work hardened microstructure impeding dislocation motion and limiting the depth to which the indenter can induce plastic deformation. Interestingly, the thermally-exposed samples presented an increase in indentation depth compared to the LPed specimen but did not regress all the way to the baseline depth, which is a testament to the thermal stability of LP-induced dislocation structures under high-temperature loads. Additionally, optical profilometry was used in tandem with indentation data to gauge the indent topography following the fatigue test. It was observed that significant pile-up occurred on the LPed samples following thermal exposure which could stem from the reconfiguration of dislocation into subgrains and a consequently change in dislocation mobility to promote pile-up, though this mechanism is not well understood. Overall, the surface fatigue tests performed in this work show the promise of LP as a post-processing treatment for the extension of single crystal Ni-based superalloy turbine blades lives which can be of great use in the creation more sustainable air travel and power generation.

2:30 PM BREAK

SESSION SF02.11: Additive Manufacture for Extreme Environments
Session Chairs: Nathan Mara and Rongmei Niu
Wednesday Afternoon, November 30, 2022
Sheraton, 3rd Floor, Commonwealth

3:30 PM SF02.11.01

Additive Manufacturing of Superhydrophobic/Superoleophilic Fluoropolymer Composite Membranes for Oil/Water Separation and Anti-Icing Applications Eugene Caldonia^{1,2,3}, Lucas Kilpatrick^{2,3}, Xiang Cheng^{4,3}, Li-Han Rong^{4,3}, Erick L. Ribeiro^{2,3}, David Dabkowski^{2,3,2} and Rigoberto C. Advincula^{2,3,4}; ¹North Dakota State University, United States; ²The University of Tennessee, Knoxville, United States; ³Oak Ridge National Laboratory, United States; ⁴Case Western Reserve University, United States

Superhydrophobic materials repel water by combining the effects of low surface energy and hierarchical surface roughness. Although membranes made of such materials find applications in high-efficiency oil and water separation and deicing, traditional manufacturing techniques and materials limit the size and geometry of such membrane constructions. This study focuses on the design and fabrication of porous superhydrophobic membranes for oil/water separation applications. The membranes, composed of poly(vinylidene fluoride-co-hexafluoropropylene) (PVDF-HFP) matrix with varying amounts of silica particles, were 3D printed via direct ink writing. The printed PVDF-HFP membrane with 30 wt% silica displayed the best anti-wettability with a contact angle of ~161°, anti-icing with capability to delay frost formation, and superoleophilicity, allowing oil to pass, but rejecting water, through its openings. Such surface characteristics are mainly attributed to the synergistic effect of surface roughness brought by the presence of silica particles and low surface energy due to PVDF-HFP. Spectroscopic, microscopic, thermal, dynamic mechanical, and dielectric analyses are employed to characterize the printed membranes. Combined with mechanical robustness and high thermal stability, the silica-filled fluoropolymer membrane is practically useful in solving industrial problems concerning water contamination, oil spill, and ice formation.

3:45 PM SF02.11.02

Hydrogel Infusion Additive Manufacturing of High Entropy Alloys Max Saccone¹, Seneca Velling¹, Rebecca A. Gallivan¹, Kai Narita¹, Daryl W. Yee² and Julia R. Greer¹; ¹California Institute of Technology, United States; ²Massachusetts Institute of Technology, United States

Additive manufacturing (AM) of metal components has emerged as a uniquely powerful tool for creating parts with complex geometries, with applications from the aerospace to the biomedical industries. High entropy alloys (HEAs), which are alloys composed of four or more principal components, are known to be strong, heat-resistant, and corrosion-resistant. However, the compositional space occupied by HEAs is immense, so AM pathfinding requires high-throughput fabrication methods.

We developed a vat photopolymerization AM technique called hydrogel infusion additive manufacturing (HIAM), which enables fabrication of a wide variety of metals and alloys with complex shapes, microscale resolution, and overall cm-scale dimensions. HIAM makes use of a single resin composition and a single set of processing conditions during the vat photopolymerization process, followed by infusion of appropriate metal precursors into a 3D hydrogel structure. Heat treatment in oxidizing followed by reducing atmospheres converts the polymer/precursor matrix into the target metal. Unlike previous vat photopolymerization strategies which have target materials or precursors incorporated into the resin during the printing process, HIAM does not require re-optimization of resins and resin curing parameters when the target material is changed; relevant process control parameters are shifted to the hydrogel infusion and heat treatment steps.

We have previously demonstrated the fabrication of Cu metal and CuNi alloys with nanoindentation hardness ~50% greater than predicted by the Hall-Petch relationship. We have also used HIAM to fabricate octet microlattice architectures with beam diameters on the order of 50 μm from several materials including copper, nickel, silver, cobalt, cupronickel alloys, and tungsten. Here, we expand the scope of the HIAM technique by demonstrating the fabrication of CuNiCoFe microlattices with ~50 μm beam diameters.

We use x-ray diffraction, thermogravimetric analysis, and differential calorimetry to characterize the microstructural evolution of CuNiCoFe from hydrogel to oxide to alloy and show that despite thermodynamic predictions of a single face-centered cubic phase, certain processing conditions lead to non-equilibrium two-phase behavior. We further investigate the binding affinity of each metal precursor for the gel network via isothermal titration calorimetry experiments, and construct and validate a model to predict the partitioning of precursors in the infusion solution and in the hydrogel structure.

The ability to create high entropy alloys with arbitrary composition via a facile polymer-based AM process will enable researchers to further development of specialty HEAs for extreme conditions. This work sheds light on the non-equilibrium characteristics of high entropy alloys, which can and paves the path to fabricating arbitrarily complex alloys via the streamlined HIAM process.

4:00 PM SF02.11.03

3D-Printed PDMS-Based Membranes for CO₂ Separation Applications Dianne Gutierrez^{1,2}, Eugene Caldon^{3,2,4}, Zhenzhen Yang^{2,4}, Xian Suo^{2,4}, Xiang Cheng^{5,4}, Sheng Dai^{2,4}, Richard Espiritu¹ and Rigoberto C. Advincula^{2,4,5}; ¹University of the Philippines, Philippines; ²The University of Tennessee, Knoxville, United States; ³North Dakota State University, United States; ⁴Oak Ridge National Laboratory, United States; ⁵Case Western Reserve University, United States

In this study, polydimethylsiloxane (PDMS)-based membranes containing silica for CO₂/N₂ gas separation were developed and fabricated via direct ink writing. Silica particles, with an optimum loading of 10 wt%, were used as fillers and thixotropic agent to enable 3D-printability of the PDMS ink. The printability of the inks was assessed by rheology, while the membranes were characterized by spectroscopy, microscopy, thermal analyses, and mechanical measurements to evaluate their suitability and practicality for carbon capture applications. Results showed that the printed membranes were nonporous, with thermal stability up to 400 °C, stretchability up to 163% of its initial length, and possessing an elastic modulus of 2.95 MPa. In terms of gas separation performance, the PDMS-based membranes showed high permeability for CO₂ gas, but with slightly low selectivity for CO₂/N₂ gas pair. The inclusion of silica particles resulted in an increased gas permeability without significant effect on the membrane selectivity. The performance and properties of the PDMS-silica membrane demonstrated the potential of 3D printing as an economical and sustainable fabrication method in developing materials for carbon capture applications.

4:15 PM SF02.11.04

Additive Manufacturing Beyond the Gaussian Beam—Insights from Microstructure-Based Modelling Robert D. Moore¹, Theron Rodgers², Sergio Turteltaub³, Daniel Moser², Heather Murdoch⁴ and Fadi Abdeljawad^{1,1}; ¹Clemson University, United States; ²Sandia National Laboratories, United States; ³Delft University of Technology, Netherlands; ⁴DEVCOM U.S. Army Research Laboratory, United States

Laser-powder-bed-fusion (LPBF) additive manufacturing (AM) has redefined design and manufacturing due to its ability to produce complex geometries with lower processing times and reduction in overhead costs. In traditional LPBF, a Gaussian laser beam is used as the energy input source. Existing experimental and computational studies mainly focus on establishing design maps relating Gaussian beam LPBF process parameters to resultant microstructures. Recent experimental findings revealed that the use of laser beams with complex profiles, such as Bessel or ring beams, opens a new design space by which AM microstructures can be tailored. However, an understanding of the thermal fields produced by these alternative laser beams and their impact on resultant microstructures remains poorly understood. Using a recently developed mesoscale model coupling thermal transport and microstructural evolution during metal AM, we explore the development of temperature fields and grain microstructures during LPBF using Ring and Bessel-like beams. Parametric studies are performed to reveal the influence of beam parameters and to quantify their effects by establishing solidification and temperature gradient spatial maps. Comparisons between the different beam profiles have shown that under specific beam parameters, both Bessel-like and Ring beams elicit a more equiaxed microstructure than a Gaussian beam of equivalent power, affecting the resultant mechanical properties of the printed components. Herein, we discuss expanding the AM parameter space to include laser beam profiles, while connections to multiscale modeling will be used to establish structure-property linkages with a primary focus on the mechanical properties of AM materials.

4:30 PM SF02.11.05

Shape-Dependence on the Deformation Mechanism of Small Platinum Nanoparticles at High Temperature Ingrid M. Padilla Espinosa¹, Tevis D. Jacobs² and Ashlie Martini¹; ¹University of California Merced, United States; ²University of Pittsburgh, United States

In addition to traditional displace plasticity mechanisms where the atoms move in a collective fashion, deformation in small nanoparticles can also occur via surface diffusion. At the macroscale, diffusion often occurs at high temperatures and can be correlated to the melting point. For nanoparticles, the contribution of diffusive plasticity also depends strongly on particle size, resulting in nanoscale creep. As the nanoparticle size reduces, there are more atoms at the surface compared to the bulk which have fewer neighboring atoms, thus reducing the diffusion activation energy and reducing the melting point. While the effects of temperature, size, and strain rate on nanoparticle deformation have been previously investigated, the role of particle shape remains largely undefined.

We used molecular dynamics models to study the effects of surface energy and shape on the deformation mechanism of platinum nanoparticles under compression at temperatures ranging between 300 K and 800 K for three different shapes and three different sizes. A transition from displace to diffusive deformation mechanism was observed for all nanoparticles with the increase in temperature. The results also demonstrate significant differences in deformation mechanisms between differently shaped particles, even for the same diameter, temperature, and strain rate. These differences are linked to the surface energy and diffusivity of the different facets and edges. Our findings provide a new understanding of the previously unexplored role of surface energy in the deformation of small metal nanoparticles, enabling the calculation of size-, shape-, and temperature-dependent nanoparticle properties and deformation mechanisms. Such understanding is crucial for designing nanoparticle-based systems where changes in properties occur from nanoparticle structural changes due to plastic deformation.

SESSION SF02.12: Poster Session III: Materials for Extreme Conditions

Session Chairs: Nathan Mara and Rongmei Niu

Wednesday Afternoon, November 30, 2022

8:00 PM - 10:00 PM

Hynes, Level 1, Hall A

SF02.12.01

3D Printing via Direct Ink Writing (DIW) of Self-Healing Elastomers Erick L. Ribeiro^{1,2,3}, Emily Buckner^{1,2,3}, Eugene Caldon^{2,2,3} and Rigoberto C. Advincula^{2,2,3}; ¹The University of Tennessee, Knoxville, United States; ²The University of Tennessee, Knoxville, United States; ³Oak Ridge National Laboratory, United States

Autonomous self-healing elastomers have attracted much attention owing to their capacity to enhance the lifespan, stability, and safety of products. The ability to utilize such materials to manufacture complex structures via three-dimensional (3D) printing techniques is highly desired and has the potential to

impact several fields, ranging from medicine to aerospace, and the electronics industry. Nonetheless, the complexity arising from the self-healing elastomers intrinsic polymeric structure and rheological properties have restricted their 3D printing applications to manufacturing only at lab-scale operation. Herein, we present our findings on the addition of poly(BCOE), a well-known autonomous self-healing polymer (SHP), to a commercially available silicone rubber (Dow DOWSIL™ 795). More specifically, we investigated the dispersion of poly(BCOE) in the commercial adhesive matrix in different mass ratios (0, 10, 30, and 50 wt%), and their corresponding effects during the production of tensile bars via Direct Ink Writing (DIW). FTIR spectra of SHP samples confirm the presence of urethane group hydrogen bonds, which are associated with its autonomous self-healing properties. DSC reveals that the crystallization temperatures of Dow795 and 10 wt%-SHP/Dow795 are both -45 °C. In addition to that, TGA curves demonstrate the thermal degradation temperature range, where an increase in the mass ratio of the SHP with respect to the adhesive matrix resulted in a lower degradation temperature. Such findings confirm the successful dispersion of poly(BCOE) in the Dow795 matrix. Incomplete degradation indicates that constituent materials within Dow795 undergo thermal degradation at higher temperatures. These findings indicate the successful dispersion and the resulting interaction between poly(BCOE) and the adhesive matrix, which can be tailored to further tune the properties of the Dow795.

SF02.12.02

Additively Manufactured Epoxy/Silica Composite Coatings with Controlled Electrolyte Diffusion at the Coating/Metal Interface [Karen Y. Patino Jaimes](#)^{1,2}, [Taegyung Park](#)^{1,2}, [Eugene Caldona](#)^{1,3,2}, [Anna Kho](#)^{1,1}, [Zane J. Smith](#)^{1,1,2}, [Demiana Barsoum](#)^{1,2}, [Erick L. Ribeiro](#)^{1,2} and [Rigoberto C. Advincula](#)^{1,2,4},
¹The University of Tennessee, Knoxville, United States; ²Oak Ridge National Laboratory, United States; ³North Dakota State University, United States; ⁴Case Western Reserve University, United States

Coating application techniques such as dipping, spraying, spin casting, and doctor blading have been widely employed, but the use of 3D printing in coating preparation has not been fully explored. Compared to conventional coating approaches, 3D printing of coatings offers finer parameter tuning with higher accuracy, precision, reproducibility, coating uniformity, and durability, all of which promote decreased porosity and defects, and controlled electrolyte diffusion. In this work, epoxy/silica composite coatings are 3D printed via direct ink writing on mild steel surface and electrochemical impedance spectroscopy (EIS) is employed to evaluate the resulting protection performance. For comparison, the same epoxy/silica coatings are prepared by spin, dip, spray coating, and doctor blade technique. Epoxy resin is chosen as the coating matrix due to its excellent mechanical, thermal, and dielectric performance at relatively low cost. Silica particles, on the other hand, are used as fillers to enhance, not only the coating's mechanical and corrosion resistance but also its thixotropy, making it amenable to be 3D printed. Results indicate that the 3D printed coating sample with 100% infill density was able to maintain a very high impedance modulus of $10^9 \Omega \text{ cm}^2$ even after 35 days of continuous immersion in 3.5 wt% NaCl test solution. Different resistance behaviors, as evidenced by impedance measurements, were also observed for spin, dip, spray coated, and doctor bladed samples, as well as 3D printed coatings with 50% and 75% infill densities. 3D printing could be a promising coating preparation technique as it, not only affords automation, digital design, and conformability but is also an excellent approach to solving important coating failures and investigating the transport of electrolytes through thin films.

SF02.12.04

Molecular Modeling of Interfacial Structure, Kinetics and Processes of sII Gas Hydrate Systems for Engineering Applications [Samuel Mathews](#), [Andre Guerra](#), [Phillip Servio](#) and [Alejandro Rey](#); McGill University, Canada

Gas hydrates are crystalline compounds composed of a hydrogen bonded backbone of water molecules enclosing guest molecules in cages stabilized by Van der Waals forces. Initially, large scale gas hydrate research was centered around flow assurance problems in hydrocarbon extraction, transportation, and processing. Interest then grew in the usage of hydrates to store hydrocarbons and hydrogen, for desalination processes, and for carbon capture and storage. Their potential use in carbon capture and storage and for energy exploitation makes gas hydrates an excellent candidate for further research. Characterizing the material properties of a crystal that requires extreme formation conditions and sublimates rapidly in standard atmosphere is experimentally challenging. While the equilibrium formation conditions lie in the megapascal range for gas hydrates, experimental conditions of formation and engineering environment involve extreme pressures in the gigapascal range. Controlling sample purity and system homogeneity is often difficult in devices designed to measure interfacial properties because they are not designed for extreme conditions and stresses. Finally, testing different guest molecules, external pressures, surface effects, and extracting fundamental information about molecular interfacial behaviors is nearly impossible without critical disruption of the structure stability. This project circumvents these issues by using molecular dynamics (MD) simulations with high experimental fidelity to study gas hydrates and provide methods to prototype new systems for implementation of efficient green technology in extreme formation environments, where the high-pressure driving force ensures the crystal formation. It is essential to understand the fundamental physical and chemical mechanisms at the molecular level and the nanoscopic behaviors leading to macroscopic properties to clarify phenomena that govern potential applications of these structures. This work uses MD as implemented in the Large-scale Atomic/Molecular Massively Parallel Simulator to characterize the temperature and pressure effects on the interfacial tension, energy of interfaces, and growth rate of natural gas hydrates to overcome the complexity of experimentally understanding their performance in extreme environments and prove that theoretical modeling, prediction, and advanced characterization techniques can explain the structural and transport properties under extreme environments. Our work has shown that there is excellent agreement between sI methane hydrates and experimental values, with the interfacial energy decreasing with temperature. Preliminary results show that the sII natural gas hydrates show the same behavior. Our work has shown that hydrates nucleate preferentially with film-shaped nucleation, then cap-shaped, lens-shaped, and homogeneous nucleation. We have confirmed the presence of a novel pre-melting layer at the interface between the structures. We have been able to produce temperature and pressure correlations of surface tension for engineering applications. The excess entropy, adsorption, radial pair distribution function, and charge distribution at the interface were calculated to confirm our findings. This information yields data to determine which conditions favor or hinder hydrate formation in applications of interest. This project studies molecular origins of macroscale, real world behavior of important energy-related materials. The impact of surface coverings is crucial in pipeline and natural gas infrastructure, and in storage technologies, but its molecular behavior is not sufficiently characterized. Using MD, statistical mechanics, and machine learning to develop an efficient workflow, interfacial behavior can be studied rapidly, effectively evaluating new green energy solutions. This provides guidance for future material development in extreme subsea environments, engineering applications, and harsh nucleation conditions.

SF02.12.05

A Beneficial Use of Basalt Fibers [Douglas X. Shattuck](#)^{1,2}, [Vernon Robertson](#)³, [Markus J. Buehler](#)¹ and [Haley Talbot](#)⁴; ¹Massachusetts Institute of Technology, United States; ²St Joseph School, United States; ³JEOL USA, United States; ⁴Malden Catholic High School, United States

Basalt fibers are easy to produce here on earth. Basalt, a common earth material, is plentiful and has been widely characterized since the 1920s. It has been processed into fiber and used in a variety of commercial products. Basalt regolith is also an abundant resource on the lunar surface and several simulants have been compounded from spectrographic data provided by NASA and the ESA.

Our goal was to investigate the physical and functional properties of basalt fibers made from simulated lunar regolith to see if it might be suitable for constructing lunar habitats. We did multiple tests on the fibers and plan to do many more in future research. Our current study includes electron microscope data and EDS analyses provided by JEOL USA. Our regolith simulants were provided by Exolith Labs and fibers were prepared by the Fiber Lab at RWTH

Aachen University.

The properties of our simulants and fibers are consistent with properties of terrestrial basalt products and to the degree that they match what is on the moon, are likely to be able to be processed on the moon in the same way they are on earth. We also believe current technology can be adapted and transported to the moon to provide competent building and insulating material as well as a host of other useful products.

SESSION SF02.13: Materials and Field
Session Chairs: Doan Nguyen and Sergei Zherlitsyn
Thursday Morning, December 1, 2022
Sheraton, 3rd Floor, Commonwealth

8:30 AM *SF02.13.01

Hot Hydride Superconductivity Above 500 K Stanley Tozer¹ and Audrey Grockowiak²; ¹National High Magnetic Field Laboratory, United States; ²Brazilian Center for Research in Energy and Materials (CNPEM), Brazil

Neil Ashcroft's [1] theoretical predictions that indicated alloying dense hydrogen with metals could produce conventional superconductivity at very high temperatures and pressures and recent structural search methods identifying candidates and pressure-temperature conditions for synthesis have accelerated the race to room temperature superconductivity. This led to the synthesis of binary hydrides at 1.7 Mbar with critical superconducting transition temperatures of 260 K in LaH₁₀ [2,3]. Our serendipitous synthesis of a metallic La-based superhydride from La metal and ammonia borane with an initial T_c onset of 294 K is inhomogeneous as to be expected given the growth conditions, but in line with other reported work [3,4]. Thermal excursions to higher temperatures promoted a chemical reaction to a higher order system that irreversibly drove the transition onset temperature to 556 K. X-Ray structural data validate the pressure measured via Raman some six months prior and speak to the inhomogeneous growth and pressure gradient that led to the non-zero resistance whilst confirming the formation of a higher order hydride [5].

Portions of this work were performed at HPCAT (Sector 16), Advanced Photon Source (APS), Argonne National Laboratory. HPCAT operations are supported by DOE NNSA's Office of Experimental Sciences. The Advanced Photon Source is a U.S. Department of Energy (DOE) Office of Science User Facility operated for the DOE Office of Science by Argonne National Laboratory under Contract No. DEAC02-06CH11357. Part of this work was performed at the National High Magnetic Field Laboratory, which is supported by NSF Cooperative Agreement No. DMR-1157490/1644779 and by the State of Florida. M.A., R.K. and R.H. acknowledge funding from the U.S. National Science Foundation (DMR-1933622). A portion of this work was performed at the European Synchrotron Radiation Facility (ESRF) and DESY PETRA III, beamline P02.2(Hamburg, Germany), a member of the Helmholtz Association HGF. U.S. National Science Foundation (DMR-1933622) and the DOE-NNSA (DE-NA0003975, CDAC) funded a portion of this effort. We acknowledge the support of the HLD at HZDR, member of the European Magnetic Field Laboratory (EMFL) and (MPI Dresden) for putting their FIB and cleanroom equipment at our disposal.

¹Ashcroft, N. W. *Phys. Rev. Lett.* **92**, 187002 (2004).

²Somayazulu, M. et al. *Phys. Rev. Lett.* **122**, 027001 (2019).

³Drozdov, A. P. et al. *Nature* **569**, 528–531 (2019).

⁴Osmond, I. et al. *Phys Rev B* **105**, L220502 (2022).

⁵Grockowiak, A. D. et al. *Front. Electron. Mater* (2022). <https://doi.org/10.3389/femat.2022.837651>

9:00 AM SF02.13.02

Electron Beam Assisted Plastic Deformation of Single Crystalline Sapphire Jeongin Paeng¹, Sung-Gyu Kang², Young-Kyun Kwon³ and In-Suk Choi¹; ¹Seoul National University, Korea (the Republic of); ²Max-Planck-Institut für Eisenforschung GmbH, Germany; ³Kyung Hee University, Korea (the Republic of)

Oxide materials with covalent bonds are brittle and show low plasticity at room temperature. Interestingly, it has been reported that electron-beam irradiation alters the interatomic bond nature and promotes the ductile plastic deformation of amorphous silicon oxide. However, the question remains about the e-beam effect on the deformation of crystalline oxides. In this study, we observed that electron-beam irradiation affects the deformation behavior of crystalline oxide material. In-situ mechanical tests of single-crystalline aluminum oxide (sapphire) show that electron beam irradiation reduces the critical resolved shear stress required for dislocation activation. Furthermore, the corresponding atomic-scale simulation (density functional theory) demonstrates that excess electrons generated by incident electron-matter interaction are concentrated in the defect state and reduce the Al-Al repulsion during deformation, reducing the general stacking fault energy.

9:15 AM BREAK

SESSION SF02.14: Materials and Magnetic Fields I
Session Chairs: Doan Nguyen and Sergei Zherlitsyn
Thursday Morning, December 1, 2022
Sheraton, 3rd Floor, Commonwealth

10:00 AM *SF02.14.01

Material Requirements and Choices for Non-Destructive Pulsed Magnets Sergei Zherlitsyn; Helmholtz-Zentrum Dresden-Rossendorf, Germany

The Dresden High Magnetic Field Laboratory (HLD) is a pulsed-field user facility, which provides external and in-house researchers with the possibility to perform a broad range of experiments in pulsed magnetic fields [1]. Being a member of the European Magnetic Field Laboratory (EMFL), HLD provides access and supports more than 100 scientific projects annually. The HLD develops, manufactures, and operates the non-destructive pulsed magnets for the field range up to 95 T and beyond. The choice of materials in magnet design plays a crucial role.

Here I will discuss various issues of material requirements and the choice of materials for pulsed magnet designs. Most of the pulsed magnets are stress

limited due to the strong Lorentz forces with a stress level of the materials very close to the ultimate tensile strength (UTS). Specifically, the conductors should possess a number of contradicting properties, such as high electrical conductivity, high UTS, high ductility, high specific heat, low fatigue, and low magnetoresistance. A very popular approach in the magnet design is a distributed internal reinforcement, which sustains the mechanical stresses inside the coil winding. Here the choice and combination of materials are very important as well. I will report on our long-standing experience with various materials for the pulsed-magnet designs. Obviously, we need novel high-strength materials to generate magnetic fields beyond 100 T with the non-destructive pulsed magnets.

I acknowledge the support of the HLD at HZDR, a member of the European Magnetic Field Laboratory (EMFL).

[1] <http://www.hzdr.de/hld>

10:30 AM *SF02.14.03

Requirement and Development of Advanced Conductors for Ultra-High Field Pulsed Magnets Doan Nguyen, John Carpenter, Daniel Blaschke, Cody Miller and Abigail Hunter; Los Alamos National Lab, United States

High magnetic fields have been critically important research tools for condensed matter physicists. The National High Magnetic Field Laboratory's Pulsed Field Facility at Los Alamos National Laboratory is one of few research centers in the world that can create and use ultra-high pulsed magnetic fields up to 100 tesla for scientific research. Present research frontiers in quantum matter, including topological matter and superconductivity, require magnetic fields beyond 100 tesla and several high field facilities around the world are actively working toward that ambitious goal. The power and stored energy required to generate a magnetic field increase exponentially with the field amplitude. Therefore the better conductors with higher mechanical strength and electrical conductivity are required to nondestructively generate magnetic fields above 100 tesla with acceptable risk and cost. The first part of this talk will present the simulation results to understand the requirements of advanced conductors for pulsed magnets to practically achieve magnetic fields beyond 100 tesla. The second part of the talk will present our integrated experimental-modeling effort on the pathway to produce the novel conductor with tensile strength and electrical conductivity required to enable the goal of 120 T.

11:00 AM *SF02.14.04

Silver-Copper Composite Wires Prepared by Spark Plasma Sintering and Wire Drawing for Non-Destructive Pulsed High Magnetic Fields—Influence of Alloying on Electrical Resistivity and the Tensile Strength Simon Tardieu¹, David Mesguich², Antoine Lonjon², Florence Lecouturier-Dupouy¹, Nelson Ferreira¹, Geoffroy Chevallier^{2,3}, Arnaud Proietti⁴, Claude Estournès^{2,3} and Christophe Laurent²; ¹CNRS - Laboratoire National des Champs Magnétiques Intenses, France; ²CIRIMAT, France; ³Plateforme Nationale CNRS de Frittage Flash, France; ⁴Centre de microcaractérisation Raimond Castaing, France

LNCMI-Toulouse produces some of the most intense non-destructive pulsed magnetic fields in the world with a European record of 98.8 T and aims at reaching more than 100 T. The generation of high pulsed magnetic requires the use of coils wound of wires with exceptional properties. To limit the heating, wires need to show a high conductivity and they also must have a high strength to be able to resist the Lorentz forces. Classical methods for strengthening copper wires involve the preparation of composite wires, such as copper-stainless steel (Cu-SS) and copper-niobium (Cu-Nb) or alloyed wires such as copper/silver (Cu/Ag). The Cu/Ag microstructure presents Cu-rich and Ag-rich solid solutions. These Cu/Ag wires exhibit a UTS value higher than 1 GPa but also a high electrical resistivity.

For several years, LNCMI and CIRIMAT have been working on the preparation of Ag-Cu composite wires by powder metallurgy, spark plasma sintering (SPS) and wire drawing with the aim of obtaining Ag-Cu wires with a low electrical resistivity. We have already shown that Ag-Cu (0.5 - 10 vol. % Ag) composite wires present an UTS similar to that of Cu/Ag alloy wires containing about 20 times more Ag, and interestingly also show an electrical resistivity about 1.5 times lower.

In the present work, we prepare and study 1 vol. % Ag-Cu composite wires and Cu/Ag alloy wires. The samples were prepared using the same silver and copper powders, mixing and wire drawing processes but the cylinders (wire precursors 8 mm in diameter and 33 mm long) were sintered by SPS at different temperature.

Ag nanowires (diameter 0.2 μm , length 30 μm) were synthesized in-house and mixed with a micrometric Cu powder. One cylinder is sintered at 400 $^{\circ}\text{C}$, where the solubility of Ag in Cu is below 0.1 vol. %, in order to obtain a composite microstructure, i.e. pure Ag nanowires dispersed in a pure Cu matrix. The second sample is sintered at 600 $^{\circ}\text{C}$, where the solubility of Ag in Cu is equal to about 2.4 vol. %, which allows the Ag to dissolve into the Cu to form Cu/Ag alloy nanowires.

The diameter of the cylinders is reduced by wire drawing at room temperature, in several passes, thus producing progressively finer wires (diameter 1 - 0.2 mm). Wires with ultrafine elongated (200-700 nm) Cu grains oriented along the drawing axis are thus prepared. The pure Ag nanowires or the Cu/Ag alloy nanowires are dispersed along the grain boundaries of the Cu matrix.

The 1 vol. %Ag composite wires and alloy wires show similar UTS (1100 MPa at 77 K), reflecting an equivalent strengthening effect for pure Ag and Cu/Ag alloy nanowires. However, it is shown that the formation of a Cu/Ag alloy, despite it is highly localized, results in a significantly higher electrical resistivity compared to un-alloyed wires (0.56 vs 0.49 $\mu\Omega\cdot\text{cm}$, at 77 K).

This study confirms the importance of preparing composite wires in order to obtain the most suitable properties for high magnetic fields.

SESSION SF02.15: Materials and Magnetic Fields II/Panel Discussion
Session Chairs: Florence Lecouturier-Dupouy and Sergei Zherlitsyn
Thursday Afternoon, December 1, 2022
Sheraton, 3rd Floor, Commonwealth

1:30 PM *SF02.15.01

Spark Plasma Sintering of Copper-Matrix Composites as Cylinders with Micrometric Grain Size towards the Preparation of High-Strength Conducting Wires for Resistive Magnets Christophe Laurent¹, Simon Tardieu^{1,2}, David Mesguich¹, Antoine Lonjon¹, Nelson Ferreira², Geoffroy

Chevallier^{1,3}, Arnaud Proietti⁴, Claude Estournès^{1,3} and Florence Lecouturier-Dupouy²; ¹CIRIMAT, Université Toulouse 3 Paul Sabatier, CNRS-INP-UT3, France; ²Univ Toulouse 3, France; ³Université Toulouse 3, France; ⁴Centre de Microcaractérisation Raimond Castaing, UMS 3623, France

Spark plasma sintering (SPS) resembles hot-pressing because a uniaxial pressure is applied to the sample, but a key difference is that heating is performed by the application of a dc pulsed current to the pressing die and powder compact. Therefore, SPS allows higher heating and cooling rates than hot-pressing, allowing for lower sintering temperatures and shorter holding times. It is thus possible to avoid grain growth and prepare samples with a very fine microstructure. Moreover, a key limitation compared to pressureless sintering was lifted when the possibility to sinter complex-shape samples was demonstrated. The basics of SPS will be presented.

We will in particular present the case of cylinders that serve as precursors for the preparation of wires of pure copper, carbon nanotube - copper composites and silver nanowire - copper composites. Such wires may find some applications when ultra-high strength must be combined to a high electrical conductivity, as required for high-field magnets, or when lightweight materials are needed such as for aerospace power and engineering.

SPS allows one to prepared copper cylinders with micrometer-sized grains, typically ten times lower than conventional copper cylinders prepared by routes involving melting-solidification, and therefore a relatively high temperature, either for alloying or for the preparation of the pure copper sample to be used in a composite. SPS cylinders with only about 90% of their full density were found suitable for the rest of the study, because a too high density hampers the deformability of the cylinder during wire-drawing, resulting in sample breaking.

The microstructure of the powders, cylinders (8 or 24 mm in diameter) and wires will be presented as well as the mechanical properties and electrical resistivity of the wires measured at 293 K and 77 K.

2:00 PM DISCUSSION TIME

2:30 PM BREAK

3:00 PM SF02.15.03

Study of Fluctuation Induced Conductivity and Pseudogap State in Single Grain GdBa₂Cu₃O_{7-δ} Superconductor in Presence of External Magnetic Field Subhasis Shit¹, Devendra K. Namburi², Sitikantha D. Das¹ and Tapan K. Nath¹; ¹Indian Institute of Technology, Kharagpur, India; ²University of Cambridge, United Kingdom

In high-temperature superconductors (HTSCs), the appearance of superconducting fluctuations beyond the critical temperature (T_c) gives rise to the precursor effect of the occurrence of phase coherence even in the normal state, sometimes far from T_c . It is believed that the presence of Cooper pairs above T_c and their interactions with the normal state electrons are the primary cause of appearance of fluctuations in the sample. In earlier studies, it has been found that due to fluctuations present in HTSCs, heat capacity, conductivity, and diamagnetic susceptibility eventually enhance in the vicinity of T_c because of their high temperature, short coherence length, low density of carriers and anisotropic structures. Among various HTSCs, YBa₂Cu₃O_{7-δ} (YBCO) is the most studied and promising system both in scientific and technological aspects because of its high superconducting transition ($T_c=92$ K) with a high upper critical field ($H_{c2}\approx 150$ T at 0 K) as well as high critical current density ($J_c\approx 0.33\times 10^6$ A-cm⁻² at 77 K). In our study, we have chosen magnetically ordered rare earth element Gd³⁺ having moment, $\mu_{eff}=7.97 \mu_B$ in place of Y³⁺. Though Gd has antiferromagnetic ordering at low temperature ($T_N=2.24$ K), still superconductivity arises in GdBa₂Cu₃O_{7-δ} (GdBCO) sample above the boiling point of liquid nitrogen. But, it is believed that magnetic ions have a negative impact on superconductivity. The contribution of localized magnetic moments of Gd³⁺ ion also produces tilted magnetic hysteresis loop which eventually affects the critical current density. Despite of its exceptional nature, no analysis of fluctuation conductivity and pseudogap behavior of GdBCO have been studied in the framework of existing theories. Based on the theory proposed by Aslamazov and Larkin, we have studied the fluctuation phenomenon in single grain GdBCO superconductor close to the superconducting mean field transition temperature (T_c^{mf}) in the presence of external magnetic field. It is observed that the fluctuations in GdBCO, near T_c^{mf} (in the critical field region), are beyond 3D-XY-E scaling for both zero and finite fields, indicating weakly first-order transition from normal to superconducting state. Local pairs model suggests that at $T=T>T_c^{mf}$ (T' is the temperature below which the metallic slope in the resistivity deviates), strongly coupled bosons (SCBs) obeying Bose-Einstein Condensation (BEC) theory, are first formed in the sample. However, as the temperature approaches towards T_c^{mf} , they will evolve into the fluctuating Cooper pairs (FCPs) obeying BCS theory. So, in the temperature limit $T_c^{mf}<T<T'$ there is a transformation from BEC to BCS phase. In GdBCO superconductor, we have investigated the complete evolution process of BEC to BCS phase meticulously in the presence of external magnetic field. From the temperature dependent study of the pseudogap parameter, it is found that the transformation from BEC to BCS phase is not abrupt in the sample. Initially at $T=T'$, the SCBs are formed and remain in the sample upto $T=T_{pair}$. Here, T_{pair} is the temperature where pseudogap parameter is maximized. Thereafter, in the range $T_{2D-SW}<T<T_{pair}$ (T_{2D-SW} is the intersecting temperature between 2D fluctuation and Short-Wave region), the SCBs still exist but the number decreases rapidly because some of them initiate to pair up. Further decreasing the temperature at $T<T_{2D-SW}$, all the SCBs completely transform into weakly bounded and tightly overlapped FCPs and start to follow the classical fluctuation theories. The values of T_{pair} obtained from temperature dependent study of pseudogap parameter decrease when the magnetic field increases from zero to 4 T. Superconducting gap ($\Delta(0)$) for all magnetic fields calculated from the local pairs model are within the BCS limit, but the magnitudes reduce as the field escalates.

3:15 PM SF02.15.04

Investigating the Role of Interactions on the Stability of Magnetic Anisotropy in L1₀ Magnetic Materials Nica Jane Ferrer¹, Gursagar Singh¹, Cy Elliott¹, Benjamin J. Wieder^{2,1,3} and Gregory A. Fiete^{1,2}; ¹Northeastern University, United States; ²Massachusetts Institute of Technology, United States; ³Princeton University, United States

Recent studies have revealed the superior magnetic properties of L1₀ magnetic materials which lead to a vast number of applications ranging from magnetic recording to medical imaging. While there is a wealth of experimental studies and numerical simulations aimed at finding ways to tune the magnetic properties of these L1₀ magnetic materials, there is inadequate attention given to understanding the underlying mechanisms that govern the magnetic properties of these materials, such as their magnetic anisotropy. Hence, this study aims to elucidate how fundamental interactions such as the electron-electron interaction combined with crystal symmetry affect the magnetic anisotropy of L1₀ magnetic materials. To achieve this, the material is modeled by a tight-binding Hamiltonian with electron-electron interactions accounted for using a Hartree-Fock mean-field approximation. This approach allows us to calculate the magnetic anisotropy as a function of the interaction strength and work through crystal symmetry-related trends in the anisotropy. These trends can be directly compared against material-specific *ab initio* calculations.

3:30 PM *SF02.15.05

Precipitation in CuCrZr Composites Rongmei Niu and Ke Han; National High Magnetic Field Laboratory, United States

Subjecting conductors to cold-deformation usually increases their hardness but decreases their conductivity. When we deformed solution-treated samples of Cu_{0.66at.%}Cr_{0.05at.%}Zr wires, however, we were able to increase hardness by ~100% while also increasing conductivity by 24%. We attribute this simultaneous enhancement of hardness and conductivity to the formation of disc-shaped, semi-coherent precipitates, less than a nanometer in thickness, during cold deformation. The driving force for this deformation-induced coherent precipitation was the presence in the matrix of 78% of total alloying

elements in supersaturated solid solution. (During solution-treatment, the remaining 22% formed irregular micron-scale particles, mostly scattered distributed, that contributed only marginally to hardness.) The post- deformation aging of our samples further increased their hardness by 27%~38% and their conductivity by as much as 80%, despite the fact that the total Cr content in aging-induced coherent precipitates was only ~0.33 at.% (0.24 wt.%). These precipitates were only a couple of nanometers in thickness, but their Cr content (1.2-8.4 at.%) was relatively greater than that of deformation-induced precipitates

4:00 PM SF02.15.06

Advanced REBCO Conductors Customized for Ultra-High Magnetic Field Applications Venkat Selvamannickam; University of Houston, United States

High current (10-100 kA) cables are needed for magnets operating at 20 T and above for fusion, particle accelerators and other ultra-high magnetic field applications. The number of tape stands required for these cables can be greatly reduced using high critical current REBCO tapes – this is important given the high cost and limited production volume of REBCO. We have demonstrated REBCO tapes with critical currents as high as 1,836 A/4 mm at 4.2 K, 20 T using Advanced Metal Organic Chemical Vapor Deposition (A-MOCVD), which is more than 3x and 5x the critical current of the best and typical industry REBCO tapes respectively. We have recently scaled up our A-MOCVD technology to 50-meter lengths to repeatedly produce uniform and high J_c tapes. Our high-current tapes have been utilized to make round REBCO STAR® wires that exhibit engineering current density of ~ 600 A/mm² at 4.2 K, 30 T. At the extreme conditions of ultra-high magnetic fields, the high-current REBCO conductors experience immense mechanical forces which generally limit the maximum operating fields of the magnets. Higher strength architectures are being developed to utilize the high-current capabilities of our advanced REBCO conductors in magnetic fields of 20 T and above.

This work was supported by awards from the U.S. Department of Energy Office of Science, U.S. Department of Energy Advanced Manufacturing Office, Advanced Research Projects Agency-Energy and SBIR awards from the U.S. Department of Energy and Naval and Sea Systems Command (NAVSEA).

4:15 PM SF02.15.07

Planar Defects in High-Strength Materials for High Field Magnets Ke Han¹, Yan D. Xin¹, Bailing An² and Vince Toplosky³; ¹Florida State Univ, United States; ²Northeastern University, China; ³Florida State University, United States

High field magnets use certain materials with planar defects that strengthen the materials. These defects can be introduced by cold deformation that produces high densities of both dislocations and planar defects or by phase transformation that mainly helps to form planar defects and strengthening particles. These defects in crystals act as obstacles to resist dislocation motions. The increased density of these obstacles increases the mechanical strength. Under tensile loading, such as the loading condition in high field magnets or in fabrication, the materials may soften or harden depending on the interaction of the obstacles with the dislocations evolved during the loading. Studying the behaviors of such defects in such environments helps researchers to predict the maximum strength achievable of these materials, to make efficient use of them in magnets, and to manufacture materials to meet the requirements of the magnets, particularly when the magnetic stress reaches the strength of certain components in high field magnets. The goal of this research is to understand the strengthening effect of planar defect on selected materials for high field magnets. We will discuss the role of planar defects on deformation and on phase transformation.

Acknowledgements

This was performed at the National High Magnetic Field Laboratory, USA, which is supported by National Science Foundation Cooperative Agreement [Grant No. NSF DMR-1644779] and the State of Florida, USA.

4:30 PM PANEL DISCUSSION

SESSION SF02.16: Other Extreme Environments II

Session Chairs: Bachir El Fil and Christopher Schuh

Friday Morning, December 2, 2022

Hynes, Level 3, Room 310

8:00 AM SF02.16.01

Zn-Doped P-Type Gallium Nitride Through Nuclear Transmutation Doping Processes Jeongwoo Kim¹, Andrei S. Patapenka², Sergey D. Chemerisov² and Jae Kwon³; ¹University of Missouri-Columbia, United States; ²Argonne National Laboratory, United States; ³Infinity Power, United States

For the last decades, Zinc (Zn) has been studied as a p-type dopant for gallium nitride (GaN) as an alternative to magnesium although high-quality doping was unachievable. Here, we introduce ways to produce p-type GaN with uniformly doped Zn using nuclear transmutation doping processes.

First, we found that photonuclear transmutation doping (PNTD) is one of the promising ways for high-quality Zn doping. In collaboration with Argonne National Laboratory (ANL), GaN with a large number of Zn was obtained by controlling the beam energy for the PNTD process and we found p-type properties from the Zn-doped GaN. The uniform Zn distribution in the crystal was confirmed by using secondary-ion mass spectrometry (SIMS) measurements. In addition, the transmutation doping concentration of Zn was modeled by gamma-ray spectroscopy, Monte Carlo-based simulation program, and a nuclear data library. The concentration of Zn produced by the PNTD turns out to be $2.25 \times 10^{17}/\text{cm}^3$. Hall-effect measurement indicated that the hole carrier concentration was $8.802 \times 10^{16}/\text{cm}^3$ and I-V characteristics of diodes fabricated from Zn-doped GaN support the p-type characteristics.

Second, proton transmutation doping (PTD) is also considered to be another nuclear transmutation doping process for Zn-doped p-type GaN. Zn production through the PTD process was simulated and we found that Zn production is maximally dominating when the proton energy is around 46 MeV. Unlike PNTD, however, the PTD process will leave the radioactivity concerns due to ⁶⁸Ge ($T_{1/2} = 270.95$ days).

8:15 AM SF02.16.02

Thermodynamic Modeling of High-Performance Adsorption-Based Atmospheric Water Harvesting (AWH) in Arid Conditions Chenyang Li, Lenan Zhang, Yang Zhong, Xiangyu Li, Bachir El Fil and Evelyn N. Wang; Massachusetts Institute of Technology, United States

Global access to safe drinking water is a great challenge today and projected to remain so in the next decades. Atmospheric water harvesting (AWH) technologies have the potential to enable decentralized water supply in remote regions where infrastructure is lacking. Adsorption-based AWH,

specifically, could further expand water accessibility in arid climates by leveraging advances in novel sorbents materials such as Metal-organic frameworks (MOFs), which operate at low relative humidity conditions. To guide materials design towards high-performance AWH in extremely environments, a generalized thermodynamic framework that predicts the theoretical efficiency limits, based on fundamental material properties and device operating conditions, is highly valuable. In this work, we first introduce the fundamental phenomenon of adsorption isotherm shifting with temperature observed in MOF-303 and MOF-801 from both theoretical and experimental perspectives. Adsorption isotherm is the most important adsorbent property and key to modeling the energetic behavior of adsorption systems. Next, we propose a high-fidelity thermodynamic framework that incorporates this isotherm-shift effect and more accurately predicts AWH efficiency than previous models. The new predictions overall show significant improvements from literature results. Most interestingly, the upper bounds of adsorption-based AWH efficiency could exceed previous limits, and the optimization of key parameters, including desorption temperature and adsorbent adsorption enthalpy, tend to follow highly nonlinear trends that challenge popular conceptions. This work bridges the important knowledge gap between adsorbent materials development and device design, providing insights towards high-performance adsorption-based AWH technologies.

8:30 AM SF02.16.03

Proppant Reinforcement by Surface Polymerization—A Systematic Laboratory Investigation [Wengang Li](#)¹, [Edreese Alsharrah](#)², [Mohanraj Krishnan](#)² and [Abdullah Garni](#)¹; ¹Saudi Aramco, Saudi Arabia; ²Alfaisal University, Saudi Arabia

Frac proppants, usually silica sand or ceramic spheres, have been widely applied in both conventional and unconventional oil gas production operations, with an essential function of supporting the created fractures by hydraulic pressure to keep the hydrocarbon flowing. To stand for high stress, enhancement of proppants has been performed by coating methods. Commercial resin coated proppant are mainly fabricated with novolac or epoxy resin, where the hardness and pressure resistance of product are limited by resin properties, and the pressure/temperature resistance are determined by the natural properties of commercial resins.

This paper demonstrated a novel method to fabricate coated proppants for HTHP applications by surface polymerization methods and dual coating protocol. The sand particles were firstly coated with polystyrene-poly(methyl methacrylate) copolymer (PS-PMMA) composite with commercial graphene (CG) (first composite layer) and subsequently coated with epoxy-CG composite (second composite layer). Chemical, mechanical, thermal and morphological characterizations for the composite layers and dual-coated sand proppants were investigated in detail by Fourier transform-infrared spectroscopy (FT-IR), nano-indentation, thermogravimetric (TGA), optical, and scanning electron microscopic (SEM) techniques.

The fabricated silica sand based proppant can hold 12-14k psi pressure and the thermal stability of the dual coating has reached as high as 368 °C. The elasticity (E), hardness (H), and the fracture toughness (K_{IC}) of the dual coating (PS-PMMA/DVB)-(Epoxy-CG) have been investigated with a maximum of 7.78 GPa, 0.34 GPa, and 3.22 MPa m^{1/2} respectively. A 3-D morphology effect has also been observed to further enhance proppant mechanical property, fulfilled by poly(styrene-methyl methacrylate)/divinyl benzene (PS-PMMA/DVB) plus epoxy resin dual coating.

This surface polymerization coating method has been established on silica sand with wide range of size, 20/40 mesh to 100 mesh and nano-sand. The mechanically and thermally reinforced dual-coated sand particles with very high-stress resistance will be successful proppants for hydraulic fracture operations.

8:45 AM SF02.16.04

Topological Protected Mismatch of Mechanical Metamaterials [Haning Xiu](#)¹, [Harry Liu](#)², [Xiaoming Mao](#)², [Zi Chen](#)¹ and [Jiabao Nie](#)³; ¹Brigham and Women's Hospital, United States; ²University of Michigan—Ann Arbor, United States; ³Northeastern University, United States

Recent advances in mechanical metamaterials and topological phases have given rise to topological mechanical metamaterials (TMMs) that exhibit exotic topological properties, thus enabling promising applications such as energy absorption, impact mitigation devices, and stress-avoiding implants. Maxwell lattices, a representative class of TMMs, exhibit attractive mechanical properties at the surfaces/interfaces and distinct properties between different surfaces when they are topologically polarized. Understanding the motions and deformations of the topological Maxwell lattices is critical for designing impact resistant metamaterials for mechanical and biomedical applications. However, most studies on dynamics of TMMs focus on the linear regime and rarely take the topological effects into account. To address this knowledge gap, molecular dynamics simulations using the spring-mass system are employed to study the dynamics of the Maxwell lattices. Importantly, auxiliary springs are added on the Maxwell lattices to achieve local bistability, and to improve the impact mitigation effects of the lattices. Energy dissipation due to friction is also simulated through introducing a damping term. Various impact loadings and boundary conditions of the lattice (with/without bistable units) are studied to compare the reaction forces transmitted from the impact surface to the opposite edge and kinematic characteristics. The theoretical analysis is employed to identify how the topological polarization causes different impact resistance at different surfaces. The new findings can improve the design of topological Maxwell lattice that can exhibit high-performance impact mitigation and energy absorption properties and can enable the applications of TMMs in architected scaffolds for cell and tissue engineering, engineered bioimplants, and meta-implants for minimally invasive delivery.

9:00 AM SF02.16.05

A Machine-Learned Spin-Lattice Interatomic Potential for Dynamic Simulations of Defective Magnetic Iron [Jacob Chapman](#) and [Pui-Wai Ma](#); UKAEA, United Kingdom

Critical components in many technologies for power generation, sensing, computation and communications exploit magnetic materials. Their viability in extreme environments, efficacy and performance depend upon magnetic phenomena and rely heavily on materials development for continued improvement. Theoretical understanding of how magnetic properties relate to the underlying microstructure provides valuable insight for tuning characteristic properties and determining the viability and fatigue of aged materials. Iron based alloys are particularly important industrial materials which may obtain a wide variety of complex magnetic states which significantly affect the materials mechanical properties. Nonetheless, studies often explicitly neglect magnetic degrees of freedom. The development of a general-purpose spin-lattice interatomic potential has proven to be a challenge [1,2].

We successfully develop a first of its kind machine-learned spin-lattice potential (MSLP) that can perform dynamic simulations of magnetic materials that includes explicit non-collinear magnetic and lattice degrees of freedom as well as changes in the length of the magnetic moments [3]. The physics-informed MSLP was achieved by supplementing a spin-lattice Hamiltonian with a neural network term [4]. The neural network was trained to a large database of configurations represented using a proper mix of local configurational and magnetic descriptors to provide data-driven corrections to unknown physics in the conventional spin-lattice Hamiltonian. It reproduces the energies of various magnetic states of BCC and FCC phases at different volumes as well as the complex magnetic configurations in the vicinity of a vacancy and self-interstitial atoms. This includes the reversal and quenching of magnetic moments at the defect core. The MSLP results are all in quantitative agreement with density functional theory calculations.

The Curie temperature is calculated using spin-lattice dynamics [5] and is in good agreement with experiments. The new machine-learned potential can perform scalable dynamic simulation with good stability at high temperature. We then apply the potential to study the magnetic structure near different mesoscopic scale dislocation loops in iron at finite temperatures. Such an investigation has not previously been possible with current state of the art theoretical or experimental methods. The effect of radiation induced defects on the interaction of magnetic fluctuations and lattice vibrations is examined.

The MSLP developed in this work transcends current treatments using DFT and molecular dynamics, in addition to other spin-lattice potentials which only treat near-perfect crystal cases, enabling simultaneous evaluation of mechanical deformations, magnetic fluctuations and defect properties at mesoscopic scales for the first time.

- [1] Nikolov et al npj Comput. Mater. 7, 153 (2021)
- [2] Novikov et al npj Comput. Mater. 8, 13 (2022)
- [3] J. Chapman & P.-W. Ma, <https://arxiv.org/abs/2205.04732>
- [4] Behler, J. & Parrinello, M. Phys. Rev. Lett. 98 (2007), 146401; Behler, J. J. Chem. Phys. 134 (2011), 074106
- [5] Ma, P.-W. & Dudarev, S. L. Phys. Rev. B 83 (2011), 134418; Ma, P.-W. & Dudarev, S. L. Phys. Rev. B 86 (2012), 054416; Ma, P.-W., Dudarev, S. L. & Woo, C. H. Comput. Phys. Commun. 207 (2016), 350.

This work has been carried out within the framework of the EUROfusion Consortium, funded by the European Union via the Euratom Research and Training Programme (Grant Agreement No 101052200 — EUROfusion). The views and opinions expressed herein do not necessarily reflect those of the European Commission. This work also received funding from the Euratom research and training programme 2019-2020 under grant agreement No. 755039. We acknowledge funding by the RCUK Energy Programme (Grant No. EP/W006839/1), and EUROfusion for providing access to Marconi-Fusion HPC facility in the generation of data used in this manuscript.

9:15 AM SF02.16.06

A Data-driven Discovery Pipeline for Flue Gas Separation Homopolymer Membranes Hsianghan Hsu¹, Matteo Manica², Ronaldo Giro³, Binquan Luan⁴, Akihiro Kishimoto¹, Lisa Hamada¹, Mathias Steiner³ and Seiji Takeda¹; ¹IBM Research-Tokyo, Japan; ²IBM Research-Zurich, Switzerland; ³IBM Research-Brazil, Brazil; ⁴IBM T.J. Watson Research Center, United States

Introduction:

Flue gas generated by human activities is one of the most significant causes of global warming because a large portion of CO₂ is emitted to the earth's atmosphere yearly. To reduce the emission, separation of CO₂ is a near-term goal where polymer membranes represent a cheap and environmentally friendly approach from their fabrication to their in-situ application. Furthermore, recent advancements in machine learning (ML) enable in-silico membrane design targeted toward finding more energy-efficient and robust in-situ performance candidates. Here, we present a discovery pipeline for data-driven polymer membrane design covering several phases: data preparation, ML model training, ML model sampling, generated candidates filtering and analysis.

Data preparation:

Although an ever growing collection of datasets for small molecules are easing the process of building ML models for material design, the data coverage for polymers remains low, essentially because it's challenging to collect high-quality data. In this work, we consider a benchmark polymer database (PI1M) with ~ 1M p-SMILES (polymer-SMILES) [1] generated in-silico starting from the PolyInfo [2] database. For generating properties associated to the p-SMILES, we adopted a Quantitative Structure-Property Relationships approach implemented in our Polymer Property Prediction engine [3]. By capturing the structural information such as topological variables, connectivity indices, and group contribution, we have been able to associate to the structures physical properties accurately in a high-throughput fashion.

Generative modeling:

To generate alternative polymers, following the lead of Gómez-Bombarelli et al. [4], we jointly trained a VAE (based on RNN cells) and an MLP on its latent space using p-SMILES representations of polymers and focusing on the following target properties: T_g, half-decomposition temp. (T_{dh}), and solubility. The learning process converged after 100 epochs (learning rate=1e-3 and batch size=64), and using gaussian processes it was possible to sample polymers with a solubility distribution matching the one observed for PI1M samples. The training experiments as well as the inference pipelines have been implemented using GT4SD [5].

Filtering and validation

In terms of generating innovative monomer candidates, physical validation times (from newly generated p-SMILES to CO₂ permeability) are unfeasible. To overcome this limitation, we explored the chemical space of the generated p-SMILES using TMAP [6], since it allows to analyze candidates according to their local and global neighborhood in terms of structural similarity. A few candidates have been selected with their high T_g, T_{dh}, and a solubility value that falls into a range of interest. It is straightforward to validate the candidates using molecular dynamics simulations with software packages such as LAMMPS [7] or GROMACS [8]. Such a discovery pipeline can be easily automated and its results leveraged to establish a feedback loop to further fine-tune the model on different building blocks.

Conclusion:

Herein, we demonstrated how enriching PI1M data using simulations we can design a data-driven discovery pipeline relying on conditional generative models for homopolymer membranes. Given the generality of the components implemented the approach can be easily extended to co-polymer membrane discovery.

References:

- [1] <https://github.com/RUIMINMA1996/PI1M>
- [2] <https://polymer.nims.go.jp/en/>
- [3] https://github.com/IBM/polymer_property_prediction
- [4] Gómez-Bombarelli R. et al., ACS Central Science **2018** 4 (2), 268-276. <https://doi.org/10.1021/acscentsci.7b00572>
- [5] <https://github.com/GT4SD/gt4sd-core>
- [6] Probst, D., Reymond, J.L. Visualization of very large high-dimensional data sets as minimum spanning trees. *J Cheminform* **12**, 12 (2020). <https://doi.org/10.1186/s13321-020-0416-x>
- [7] <https://www.lammps.org/>
- [8] <https://www.gromacs.org/>

9:30 AM BREAK

10:00 AM SF02.17.01

Modeling Fretting Wear Resistance of Surfaces Exposed to Extreme Conditions in Nuclear Reactors Ting Yang¹, T. A. Venkatesh² and Ming Dao¹;
¹Massachusetts Institute of Technology, United States; ²Stony Brook University, United States

The materials used in several parts of a nuclear reactor experience a combination of extreme conditions, i.e., mechanical stresses, radiative conditions and corrosive environments. For example, pressurized water nuclear reactors typically contain a large number of fuel rods (about 50,000). These fuel rods are cylindrical in shape, contain radioactive material in their cores and are surrounded by a cladding layer. These fuel rods are kept in place with spacer grids such that there is space between the fuel rods for water to flow through and absorb the heat from the fuel rods, which can then be used to produce power. At the regions where the spacers are in contact with the exterior of the fuel rods (i.e., the surface of the cladding that surrounds the radioactive fuel rod core), vibrational loads caused by turbulence in the water induce fretting damage, which can lead to cracking and deterioration of the cladding layer, resulting in serious radioactive leak issues. It has been reported that, of all the causes of such leaks, grid-to-rod contact fatigue damage is the most prominent, accounting for more than 70% of the problems.

In such nuclear fuel rod applications where high cyclic loads are involved [1], surfaces with high yield strength and wear resistance are required. As surfaces with homogeneous or graded nanostructures have been shown experimentally to significantly increase the yield strength and enhance surface wear resistance [2-5], in this work, we systematically investigate the potential for such novel nanomaterials for nuclear fuel-rod applications. In particular, we examine the fretting behavior of graded nanomaterials and compare them with homogeneous structures through a comprehensive computational study coupled with dimensional analysis. Using dimensional analysis, a set of dimensionless functions that takes the loading condition, the mechanical properties of the constituent materials, and geometric parameters into account are constructed to characterize surface damage on the structure with the graded nanostructured surface upon frictional sliding. Analytical expressions are proposed to explain experimental and computational observations to provide more insights into surface damage mechanisms, including shakedown behavior for nanostructured surface layers upon fretting wear. For numerical modeling, fretting sliding simulations are performed by finite element method (FEM).

A comprehensive theoretical/computational framework is established for identifying the influence of mechanical properties of the constituent materials and geometric parameters such as material hardening, friction coefficient, and gradient function vs. depth on the surface deformation and damage for structures with graded nanostructured surfaces upon fretting frictional sliding. Using this framework, the plastic shakedown behavior vs. strain hardening, friction and the plastic gradient is quantified. It is also demonstrated that graded nanomaterials exhibit enhanced resistance to frictional sliding wear with a smaller plastic deformation zone. Optimization of such nanomaterials and potential for their applications in nuclear fuel rods are discussed.

References:

- [1] Blau PJ. *Wear* 2014; 313(1):89-96.
- [2] Singh A, Dao M, Lu L, Suresh S. *Acta Materialia* 2011; 59(19):7311-7324.
- [3] Cao SC, Liu J, Zhu L, Li L, Dao M, Lu J, Ritchie RO. *Scientific Reports* 2018; 8(1):5088.
- [4] Bernoulli D, Cao SC, Lu J, Dao M. *Surface and Coatings Technology* 2018; 339:14-19.
- [5] Long J, Pan Q, Tao N, Dao M, Suresh S, Lu L. *Acta Materialia* 2019; 166:56-66.

10:15 AM SF02.17.02

Materials Genomics Search for Possible Helium-Absorbing Nano-Phases in Fusion Structural Materials Haowei Xu¹, So Yeon Kim¹, Di Chen², Jean-Philippe Monchoux³, Thomas Voisin⁴, Cheng Sun⁵ and Ju Li¹; ¹Massachusetts Institute of Technology, United States; ²University of Houston, United States; ³French National Centre for Scientific Research, France; ⁴Lawrence Livermore National Laboratory, United States; ⁵Idaho National Laboratory, United States

Civilian fusion demands structural materials that can withstand the harsh environments in fusion plasma reactors. The structural materials often transmute under 14.1 MeV fast neutrons, producing helium (He), which embrittles the grain boundary (GB) network. Adding load-bearing second-phase nanoparticles (0D) or nanowires (1D) with atomic-scale free volume and low He-embedding energy E_{emb} as volumetric He sinks may shield the 2D GBs from He segregation and combat He embrittlement; however, the ability to disperse low- E_{emb} nano-phases to screen GB from Helium embrittlement has not been fully unlocked yet due to the lack of material selection guidelines. Here we show that neutron-friendly and mechanically strong nano-phases with atomic-scale free volume can have low E_{emb} and >10 at% He-absorbing capacity, and could thus be exceptionally advantageous for soaking up He on top of resisting radiation damage and creep, provided they have thermodynamic compatibility and wettability with the matrix as well as high enough melting point. Our preliminary experimental demonstration proves that He-embedding energy is a good *ab initio* predictor of He shielding tendencies in hetero-phase materials, and can be used for computational screening. In this context, we present a list of compounds expected to be good He-absorbing nano-phases, taking into account E_{emb} , the neutron absorption, and activation cross-sections, the melting temperature, the thermodynamic compatibility, and the wetting angle of the nano-phases with the Fe matrix as an example.

10:30 AM SF02.17.03

Polychromatic Multiplexing Stress-Strain Diffractometer Sean Fayfar¹, Jay Theodore Cremer² and Boris Khaykovich¹; ¹Massachusetts Institute of Technology, United States; ²Adelphi Technology, United States

The development of new materials for extreme conditions such as high pressure or radiation requires improvements in characterization techniques, especially with in-situ measurements during synthesis. Neutron scattering techniques have been gaining popularity with the development of new smaller neutron sources and new beamline developments at national facilities. Current engineering beamlines with stress-strain diffractometers at national facilities require long measurement times due to the small gauge volumes of samples. We present our development of a stress-strain diffractometer intended to be optimized for improved efficiency compared with current designs at national facilities and to also be suitable for small research reactors such as the MIT Reactor and laboratory-based neutron generators. The diffractometer will utilize a polychromatic neutron beam to illuminate all the lattice planes within the sample simultaneously allowing for a series of bent perfect crystals to be placed after the sample; these crystals will be used as analyzers rather than monochromators. The silicon crystal analyzers are transparent to neutrons, which has the benefit of multiplexing capabilities with analyzers placed in subsequent order with each measuring the strain of a different lattice plane. Multiplexing is also accomplished by placing analyzers at $2\theta \approx \pm 90^\circ$, which allows the strain to be measured in two directions simultaneously. We will present results from both experimental testing and ray-tracing simulations for this instrument configuration and report on the current state of the construction of the prototype instrument at the MIT Reactor.

We acknowledge useful discussions with A. Stoica. This work is supported by the U.S. Department of Energy (DOE), Office of Science, under a Small Business Technology Transfer (STTR) Grant, Grant No. DE-SC0020555.

10:45 AM SF02.17.04

Interaction of Neutrons with Strain-Engineered Fibrous Boron-Doped Polyethylene Materials [Duo Xu](#)¹, Volodymyr Korolovych¹, Cody A. Paige¹, Lembit Sihver² and Svetlana V. Boriskina^{1,1}; ¹Massachusetts Institute of Technology, United States; ²Chalmers University of Technology, Sweden

Studies of materials interactions with neutron beams are important for developing a fundamental understanding of material properties, studying materials degradation in extreme environments, and for the development of new radiation shielding materials for terrestrial and space applications. When ionizing particles, such as energetic electrons, protons, and gamma-rays interact with materials or tissue, they produce secondary particles, including thermal neutrons. As a result, neutrons are dominant near planetary surfaces and in atmospheres, induce high biological damage and present a risk factor for space exploration. The development of new lightweight multifunctional materials with simultaneous flexibility in mechanical properties, radiation shielding capability, and form factors is of high interest for aerospace, healthcare, and nuclear industries as well as for military applications.

Hydrogen is the ideal particle for stopping broad-spectrum primary radiation while also providing protection against secondary neutrons. Hydrogen is highly concentrated in polyethylene (PE) and all-hydrocarbon olefin block co-polymers, making PE a popular choice of material for radiation shielding composites [1]. It is well known that doping hydrogenated polymers with Boron-rich nanomaterials can further improve their performance for shielding both primary and secondary ionizing radiation [2]. However, the role of nanomaterial size, form-factor, and orientation as well as the effects of the melt-spinning-induced crystallinity, alignment, and phase separations within blended polymer matrices are poorly understood as most modeling approaches often do not capture this information. Multiple and inelastic scattering of neutrons by the internal structure of fibrous composite materials can affect their radiation shielding performance and material degradation pathways.

Through a combination of computer modeling, additive manufacturing via Fused Deposition Modeling (FDM) 3D-printing, weaving, and knitting, we engineer composite fibrous materials composed of PE-based blended resins as well as of PE-based polymer matrix doped by Boron-rich nano- and micro-particles. These materials are then characterized with neutron spectroscopy. We aim to develop a fundamental understanding of the role of nano-dopants as well as material- and fabrication-process-induced crystallinity and phase separations in composite PE-based fibrous materials on their wavelength-dependent multiple scattering and inelastic scattering of neutrons.

FDM printing and fiber spinning enable control over the polymer strength, stiffness by shear and strain deformations during the melt-extrusion process, resulting in aligned polymer chains and control over the material crystallinity, allowing studies of a wide range of composite materials of identical chemical composition but different internal structure. Most intriguing, such composite 3D printed materials and textiles can be recycled and reused in different form factors at the end of the product lifecycle. The developed fundamental understanding of neutron-matter interactions can be useful for engineering new composite radiation shielding materials like those developed by the Cosmic Shielding Corporation (CSC) [3] as well as PE-based textiles for terrestrial applications [4].

DX and VK contributed equally. Correspondence should be addressed to LS and SVB. This research is funded by the Cosmic Shielding Corporation (CSC), Atlanta, GA (for the Boron-doped 3D printed PE materials development). We also thank the ORNL for awarding us beam time for neutron scattering measurements (Proposal IPTS-28797.1 for NScD 2022-A) and William Heller for his help in running the experiment.

[1] S.V. Boriskina, MRS Energy & Sustainability 6, E14, 2019.

[2] M. Cai, et al, AAAS Space: Science & Technology, 9754387, 2022.

[3] R.K. Kaul, et al, United States Patent (10) Patent No.: US 7,855,157 B1, Dec. 21, 2010.

[4] M. Alberghini, et al. Nature Sustainability 4,715–724, 2021.

11:00 AM SF02.17.06

Predictions of Novel Features in X-Ray Scattering Spectra for Thermometry [Alina Kononov](#)¹, Thomas Hentschel², Stephanie Hansen¹ and Andrew Baczewski¹; ¹Sandia National Laboratories, United States; ²Cornell University, United States

Design and interpretation of inertial confinement fusion experiments rely on accurate models of material properties far from ambient temperatures and densities. Validation of these models with data from focused experiments is in turn limited by uncertainties in measured sample conditions. In particular, electronic temperatures in the warm dense matter regime are typically inferred from detailed balance of plasmon features in x-ray Thomson scattering spectra, but this approach loses sensitivity for thermal energies above the plasmon energy. Using real-time time-dependent density functional theory, we predict that spectral features arising from scattering into thermally depleted core orbitals can be used as alternative diagnostics at higher temperatures. Our first-principles calculations for aluminum and iron heated to 1 eV and 20 eV validate a simpler average-atom model modified to capture behavior near solid densities. Furthermore, we uncover subtle signatures of atomic order at comparable energy transfers, offering opportunities for simultaneous inference of ionic and electronic temperatures which may be out of equilibrium during e.g., laser heating. This work advances characterization techniques critical for understanding the performance of materials in extreme environments.

SNL is managed and operated by NTESS under DOE NNSA contract DE-NA0003525.

11:15 AM SF02.17.07

Computational Modeling of Scattering Processes in Warm Dense Beryllium [Brian Robinson](#)¹, Alina Kononov², Andre Schleife¹, Andrew Baczewski² and Stephanie Hansen²; ¹University of Illinois at Urbana-Champaign, United States; ²Sandia National Laboratories, United States

Accurate predictions of electrical and thermal conductivities play an important role in the design of inertial confinement fusion (ICF) targets, where they can affect compression, instability growth, and energy losses. The warm dense matter (WDM) regime, with near-solid densities and temperatures above ~ 1 eV (10 kK), is particularly difficult to model due to the confluence of degeneracy, thermal, and strong coupling effects. Here, we study electron-electron (el-el) and electron-phonon (el-ph) scattering processes in beryllium, a common ICF material, in the WDM regime from first principles. Specifically, we find el-el lifetimes by fitting the imaginary part of the self-energy from many-body perturbation theory GW calculations to the Landau theory of the Fermi liquid. From this data, we predict el-el lifetimes on the order of hundreds of fs near the Fermi energy and tens of fs under excitations of 1 eV. We also simulate time-dependent el-ph relaxation dynamics by solving the Boltzmann transport equation, helping us to disentangle the relative importance of both processes. Revelations from this work will improve collision frequencies and scattering cross sections entering conductivity models used for ICF target design.

1:45 PM SF02.18.01

Design and Preparation of Halogenated Polynorbornenes via Systematic Structural Variation for Energy Storage up to 200°C Stuti Shukla¹, Chao Wu¹, Ankit Mishra², Gregory Sotzing¹, Yang Cao¹ and Priya Vashishta²; ¹University of Connecticut, United States; ²University of Southern California, United States

High temperature flexible dielectric polymers are critical for rapid high-power needs under extreme electric fields and temperature. This work relates to the design and systematic study of halogenated polynorbornenes and the relationship that the dielectric properties have on changing the halogen from fluorine to chlorine to bromine. Further, in addition to changing the halogen systematically, the position of the halogen has been varied as well in going from the ortho to para position on a pendant phenyl derivatized imide. Variation of halogen position results in a change in energy required for a phenyl group rotation. The correlation between size, free volume, energy of rotation and position of halogen addition on the structural, thermal, and dielectric properties of the polymer will be reported. In this work, changing the pendant halogens (F, Cl, Br) at para and ortho position on the benzene increases the glass transition temperature from ~220 to 245°C, discharge energy density changes from 5 to 6.2J/cm³, dielectric constant range ~ 2.8-3.0 @100Hz frequency and charging-discharging electric field ~625-700MV/m @200°C. The energy of rotation, free volume and loss also increase in going from fluorine to bromine at the para position. As a result, electrical breakdown and loss phenomena are better understood for designing novel high temperature polymer dielectrics with high energy density and low loss at elevated temperature.

2:00 PM SF02.18.02

Optimizing Performance of Low-Quality Graphite for High-Temperature Thermal Storage Shomik Verma, Colin Kelsall, Kyle Buznitsky, Alina LaPotin and Asegun Henry; Massachusetts Institute of Technology, United States

Energy storage is a critical component of achieving the clean energy transition, due to the intermittency of common renewable generation technologies like wind and solar. Thermal energy storage (TES) is one cost-competitive option for large-scale, long-duration energy storage. TES stores energy in the form of heat, allowing use of a wider variety of cheaper storage materials than traditional electrochemical batteries.

The specific TES technology considered in this work is called thermal energy grid storage with thermophotovoltaics (TEGS-TPV). In the charge cycle, resistance heating is used to heat liquid tin to high temperatures (~2400°C), which is then flowed through graphite blocks to heat them. As the thermal storage medium, the graphite retains this heat for several (>10) hours. During discharge, colder tin (~1900°C) is flowed through the graphite, and the heated tin at the outlet is flowed past TPV cells which convert the light emitted by the tin pipes at these high temperatures to electricity. Technoeconomic analysis indicates the cost per energy of TEGS-TPV is <\$20/kWh-e and the cost per power is <0.40/W-e.

These promising technoeconomics are enabled by cheap (<\$0.50/kg) graphite as the storage material. However, this graphite is often low quality, formed by molding machining scraps or recycling used graphite. It is therefore porous, has poor mechanical strength, and may contain impurities. Understanding the high-temperature thermal properties of low-quality graphite is critical to evaluating its performance as a thermal storage material.

The first part of this study measures graphite's high-temperature thermal properties including density, specific heat, and thermal conductivity, following ASTM standards. We use machines that measure properties up to 1500°C, and we extrapolate the measurements to the temperature region of interest with physics-based correlations. Using these properties, we can calculate the thermal diffusivity of the graphite, which directly correlates with thermal performance. Based on the measurements taken, we find low-quality graphite has low thermal conductivity (~10 W/mK) at room temperature, and worsening qualities with increasing temperature. In comparison, high-quality graphite has room temperature thermal conductivity around 100 W/mK.

The second part of the study investigates how best to operate the charge and discharge cycles given the less ideal properties of low-quality graphite. A transient 3D multiphysics simulation is set up coupling the liquid tin fluid flow to the conductive heat transfer within the graphite. Several flow configurations were tested, including varying the spacing and diameter of tin tubes within the graphite, considering flowing tin through several graphite blocks in series, or changing the flowrate as a function of time. An optimal design was determined to ensure near-constant power output through the storage duration.

Finally, the third part of the study develops a lumped capacitance model to accelerate computation of transient liquid metal and graphite temperatures. The developed model splits each block into 5 pieces and considers each as isothermal. This results in errors of less than 1% through the transient storage duration when compared to the 3D multiphysics model, with 3 orders of magnitude faster computation time. This allows rapid calculation of transient graphite and tin temperatures for varying charge/discharge profiles, for example based on daily generation and demand curves.

In conclusion, this study investigates the high-temperature properties of low-quality graphite to optimize its performance as a thermal storage material. By combining measurements with modeling, we determine ideal charge and discharge geometries, and develop a lumped capacitance model for accelerated transient calculations. Overall, our study helps to enable cheap long-duration storage to ease the transition to a clean energy future.

2:15 PM SF02.18.03

High Energy Density Hygroscopic Hydrogel Thermo-Adsorptive Storage Bachir El Fil, Xiangyu Li, Xinyue Liu, Carlos D. Diaz, Gustav Graeber, Lilosia Eyang Cole, Leon C. Gaugler and Evelyn N. Wang; Massachusetts Institute of Technology, United States

Despite significant interest in thermal storage devices, state-of-the-art phase change material (PCM) systems lack the high energy densities, while the low temperature of the building waste heat cannot charge thermos-chemical material (TCM) systems. Here, we transform thermal energy storage (TES) by proposing a new approach with the adsorption of hydrogel/salt composites. Hydrogel adsorbents are hydrophilic dry polymer networks with hierarchical pore structures. Through swelling, it enables a much higher water uptake and significantly lower cost compared to traditional adsorbents including the commercial zeolites and MOFs, at high water vapor pressure. Salts, on the other hand, adsorb water vapor efficiently at low vapor pressure, but after deliquescence, the salt solutions are strongly corrosive. Here we incorporate hygroscopic salts into a hydrogel matrix to prevent the hydrated salts from deliquescence while greatly enhancing the hydrogel's adsorption capacity at low relative pressure levels. As a result, a water uptake of about 1.0 g/g at the operating relative pressure level (~ 30%) with high cyclability can be achieved by a unique hydrogel/salt combination. To achieve superior kinetics, several methods were considered to tune the porosity of the hydrogel such as freeze drying and ice templating. Additionally, we fine-tune the low critical solution temperature (LSCT) of the hydrogel in such a way to minimize its regeneration temperature significantly. Finally, we leverage the high-water uptake,

superior kinetics, and low desorption temperature of the hydrogel to design and demonstrate a high energy density thermal storage system. Due to the favorable properties of the hydrogel adsorbent, not only does our proposed TES unit have more than 3 higher energy density compared to state-of-the-art PCM solutions, but it is also cost-effective.

2:30 PM BREAK

SESSION SF02.19: Strain Rate on Materials
Session Chairs: Dierk Raabe and Christopher Schuh
Friday Afternoon, December 2, 2022
Hynes, Level 3, Room 310

3:00 PM *SF02.19.01

Towards Quantitative Understanding of Melting and Erosion Caused by Hypervelocity Impacts Jasper Lienhard, Keith A. Nelson and Christopher A. Schuh; Massachusetts Institute of Technology, United States

If a material experiences a high-rate impact with enough kinetic energy, the resulting plasticity and adiabatic heat generation can lead to local melting. Such melting is a source of erosive wear, because liquid is easily ejected from the impact site, and can also facilitate the removal of solid matter. Our recent works have aimed at understanding the melt-induced erosion process during hypervelocity impacts of microparticles. With impactors including hard particles as well as soft metals, we explore the heating, melting, and ejection of matter for microparticles launched and imaged with a laser system. In-situ videography provides insight on the development of ejecta during the impact event, as well as the kinetic energy associated with plasticity. Ex-situ quantitative measurements of impact sites provide accurate assessment of the volume of ejected matter. By combining in- and ex-situ quantitative measurements, we are able to conclude that only a small amount of liquid formation is needed to achieve remarkable phenomenological changes in erosion behavior.

3:30 PM SF02.19.02

Comparing High Strain Rate Shear Response and Resistance to Adiabatic Shear Bands in 3D Printed and Wrought Inconel 718 Russell Rowe¹, Anthony Palazotto² and Keivan Davami¹; ¹The University of Alabama, United States; ²Air Force Institute of Technology, United States

With the increased demand for additively manufactured components in the aerospace industry, the necessity for characterization of 3D printed materials under nominal and off-nominal loading conditions grows rapidly. In this research, the resistance to adiabatic shear band (ASB) formation in 3D printed and wrought Inconel 718 will be compared. Reliable turbine fan-blade containment systems, which are required on many aircrafts for safe operation of gas turbine engines, are commonly made from high-strength titanium or nickel-based superalloys. When engine fan blades fail, the fragments impact the containment systems walls at high velocities and either cause global plastic deformation, which is preferred, or localized plastic deformation, in the form of shear plugging. During plugging, intense plastic shear strains may cause ASBs, which is the localization of shear strain into a very narrow band of material, which can cause premature catastrophic failure. In a region of intense shear strain, both work hardening and thermal softening occur causing a thermo-mechanical instability. At a critical value of shear strain, thermal softening effects dominate and any increased hardness from work hardening effects is completely mitigated, thus forming an ASB. Dynamic shear tests were carried out using a split Hopkinson pressure bar to compress “top-hat geometry” shear samples and high strength steels stopper rings were attached to the samples to limit their deformation. After mechanical testing, each sample was sectioned and prepared for microscopy to characterize the ASB formation based on the strain in the sample. A shear strain value of 3.23 was observed to result in ASB formation across the entirety of the shear region. The samples that experienced a higher strain clearly showed cracks that traveled partially along the ASB. One sample was tested without the shear stopper ring, and this allowed the crack to travel along the ASB across the entire shear region breaking the sample into two pieces. The ASBs observed in the printed samples were approximately 4-microns wide which are markedly narrower than the 7-micron wide bands in the wrought material. Microhardness tests conducted on the material surrounding the ASB revealed that the material hardness increases around the ASB with a peak in microhardness at the center of the ASB. This hardness peak in the ASB center is often attributed to nanoscale grains that formed by dynamic recrystallization occurring when ASB forms. Determining at what shear strain an ASB may form will help future fan-blade containment system designs ensure the safety for future aircraft.

3:45 PM SF02.19.03

Permanent Bandgap Engineering in Quasi-2D Tellurium Synthesized via Hot-Pressing Naveed Hussain¹, Ahmed Shehzad² and Maxim Shcherbakov¹; ¹University of California, Irvine, United States; ²Shenzhen University, China

Two-dimensional (2D) tellurium (Te) is an emerging 2D semiconductor [1] with attractive characteristics, such as high carrier mobility, large electro-optic activity, superior air-stability, and strong spin-orbit coupling, etc. [2-3] The application of quasi-2D Te in optics and optoelectronics has been restricted due to its narrow indirect band gap of ~ 0.35 eV. Quasi-2D Te has been theoretically predicted to undergo dramatic indirect-direct bandgap transition [4] (0.35 eV to 1.92 eV) through strategies such as confinement effect [5] and external strain, [6] making it promising for nano-optoelectronics. [7] Another study predicts enabling of a colossal bandgap opening, resulting in strong absorption of UV to UV-blue visible lights upon induction of a biaxial compressive strain in quasi-2D tellurium. [8] However, experimentally achieving such massive yet irreversible bandgap modulation has remained a daunting task. Bandgap modulation through mechanical straining in ultrathin 2D materials has long remained an exciting avenue to achieve desired functionalities at nanoscale. [3] However, most of these demonstrations have reported volatile or short-lived strains, causing a reversible narrow bandgap modulation and temporary tailoring of their properties. By maintaining a high-pressure enforced non-slipping condition and exploiting the coefficient of thermal expansion (CTE) mismatch between tellurium and the growth substrates at elevated temperatures, we report a strategy that yields non-volatile strain induction in ultrathin 2D nanoflakes of tellurium, achieving an optimal irreversible biaxial compressive strain as high as -4.7 % on a sapphire substrate. Consequently, UV-Vis absorption and photoluminescence (PL) spectroscopy studies reveal a permanent indirect-direct bandgap modulation from 0.35 eV (bulk) to 3.18±0.1 eV (2D) at a modulation rate of 691 meV/%, which is ~400% larger than that of highest ever reported value is achieved in strained tellurium nanoflakes. [9] Our micro-Raman, micro-PL and high-resolution transmission electron microscopy studies further confirm the long-lived retention of modulated bandgap, resulting in superior absorbance and ultrabright photoemission in UV spectral region. Strained 2D tellurium exhibits robust band-to-band radiative excitonic recombination and high intrinsic quantum efficiency of c.a. 79.5±0.5%, calculated by using the following formula: [10]

PL Quantum Yield (%) = $\tau_r / \tau_{nr} = 79.5 \pm 0.5\%$

Where τ_r and τ_{nr} are radiative and non-radiative recombination lifetimes.

Our findings indicate the superior performance of strained 2D tellurium for optoelectronic applications and its possible utilization for UV sources in the classical and quantum optical regimes. The strategy suggests that controlled and non-volatile bandgap engineering can be generalized to other 2D

semiconductors for on-demand applications in nano(opto)-electronics.

Bibliography

- [1] Y. Wang, G. Qiu, R. Wang, S. Huang, Q. Wang, Y. Du, W. A. Goddard, M. J. Kim, X. Xu, *Nature Electronics* **2018**, *1*, 228-236.
- [2] G. Qiu, C. Niu, Y. Wang, M. Si, Z. Zhang, W. Wu, P. D. Ye, *Nature Nanotechnology* **2020**, *15*, 585-591.
- [3] Y. Wang, S. Yao, P. Liao, S. Jin, M. J. Kim, G. J. Cheng, W. Wu, *Advanced Materials* **2020**, *32*, 2002342.
- [4] B. Wu, X. Liu, J. Yin, H. Lee, *Materials Research Express* **2017**, *4*, 095902.
- [5] X. Huang, J. Guan, Z. Lin, B. Liu, S. Xing, W. Wang, J. Guo, *Nano Lett* **2017**, *17*, 4619-4623.
- [6] Zhili Zhu, Xiaolin Cai, Chunyao Niu, Chongze Wang, Qiang Sun, Xiaoyu, Z. G. Han, and Yu Jia, *cond-mat*. **2016**.
- [7] M. Amani, C. Tan, G. Zhang, C. Zhao, J. Bullock, X. Song, V. R. Shrestha, Y. Gao, K. B. Crozier, M. Scott, A. Javey, *ACS Nano* **2018**.
- [8] H. Ma, W. Hu, J. J. N. Yang, **2019**.
- [9] Y. L. Huang, Y. Chen, W. Zhang, S. Y. Quek, C.-H. Chen, L.-J. Li, W.-T. Hsu, W.-H. Chang, Y. J. Zheng, W. Chen, *Nature communications* **2015**, *6*, 1-8.
- [10] H. Zhang, L. V. Besteiro, J. Liu, C. Wang, G. S. Selopal, Z. Chen, D. Barba, Z. M. Wang, H. Zhao, G. P. Lopinski, *Nano Energy* **2021**, *79*, 105416.

4:00 PM SF02.19.04

A New High-Resolution Launch Pad for Laser-Induced Particle Impact Testing [Alain S. Reiser](#) and Christopher A. Schuh; Massachusetts Institute of Technology, United States

Laser-induced particle impact testing (LIPIT) has unveiled the behavior of a wide range of materials at high strain rates and small scales since its introduction ten years ago. In this first decade of high-velocity microparticle impact research, hardly any modification of the original experimental setup has been necessary. However, future avenues for the field require advancements of the experimental method to expand its breadth. Here we introduce a new design concept for the launch pad that offers a number of improvements. First, it enables precision of the impact location better than typical particle diameters. Second it paves the way to patterning of advanced impactors to be used for LIPIT. Third, it unlocks experiments at higher temperatures than previously possible. This talk will review these new capabilities and others more generally enabled by evolution of the LIPIT launch structure.

4:15 PM SF02.19.05

Exploring the Deformation Mechanism of Metals at Ultra-High Strain Rate Nanoindentation Testing [Yuwei Zhang](#), Benjamin Hackett and George Pharr; Texas A&M University, United States

In this study, we performed nanoindentation on single crystal aluminum at various indentation depth through impact (strain rate $> 10^3$ 1/s) and quasistatic (strain rate = 10^{-2} 1/s) nanoindentation. With the help of FIB lift out and STEM detector in SEM, we found distinct microstructure under the indents at two extreme strain rate. The subgrain structures under the indents from impact test extends deeper than the indents deformed at low strain rate. Informed by Orowan equation, we think the large strain rate ($\sim 10^3$ 1/s) from impact test is largely accommodated by the increase of mobile dislocation density. This work highlights the importance of scrutinizing the microstructural evolution in understanding the plastic deformation of materials at extreme conditions.

4:30 PM SF02.19.06

Architected Materials under Extreme Impact Conditions Thomas Butruille and [Carlos M. Portela](#); Massachusetts Institute of Technology, United States

Ultralight mechanical metamaterials enabled by advanced manufacturing processes have previously achieved density-normalized strength and stiffness properties that are inaccessible to bulk materials, but the majority of this work has focused on static loading while the mechanical properties of these metamaterials under dynamic loading conditions have remained largely unexplored. Properties such as energy absorption of these metamaterials are of high interest for protective applications and recent works on their dynamic response have demonstrated the benefit of architecture for impact mitigation.

Here, we systematically study the response of metamaterials under microprojectile impact using two-photon lithography as a rapid prototyping technique for microscopic polymeric microlattices. We fabricate suspended thin-plate lattice architectures of varying thicknesses and morphologies to characterize their response to microparticle impact. We employ the laser-induced particle impact test method to accelerate ~ 30 μm -diameter microparticles to velocities of up to 800 m/s, and use ultra high-speed imaging of the impact process to measure impact energetics. To isolate the effect of architecture, we maintain a constant relative density across prototypes and probe them with a range of impact energies. Additionally, we analyze our experiments in a dimensionless framework to provide a first-order estimate of impact response across materials and length scales. Lastly, we study the impact response using an explicit dynamics finite-element representation to provide insight on the impact mechanisms. This investigation provides a framework for the rapid design and characterization of future metamaterials for a variety of energy absorption applications.

4:45 PM SF02.19.07

Understanding Dynamic Recrystallization-to-plasticity Linkages in Cold Spray via Nanomechanical Property Mapping and Profilometry-Based Indentation Plastometry [Bryer C. Sousa](#) and Danielle L. Cote; Worcester Polytechnic Institute, United States

The high-strain rate impact phenomena underpinning solid-state metallurgical cold gas dynamic spray processing introduces severe plastic deformation states, which results in the formation of heterogeneous strain gradients throughout the consolidated microstructure. In addition, particle-particle interfacial dynamic recrystallization has been observed in various cold sprayed material systems. However, the degree of dynamic recrystallization achieved as a function of the impact velocity and the applied stress upon particle impact has yet to be linked to the plasticity of resultant consolidations. In turn, the present work utilizes various gas-atomized Al alloy feedstock powders, coupled with a range of particle impact velocities tuned through changes in carrier gas pressure and temperature to generate an array of fully dense consolidations with various degrees of interfacial dynamic recrystallization achieved. Consolidations will be studied through profilometry-based indentation plastometry testing and analysis and nanomechanical property mapping and clustering analysis methods. Consequently, a clear linkage between recrystallization and resultant uniform plastic stress-strain behavior will emerge through coupling mechanical property evaluation with dynamic recrystallization during cold spray processing.

8:00 AM *SF02.20.01

Pressure-induced Dramatic Changes in Optoelectronic Metal Halides Xujie Lü; Center for High Pressure Science and Technology Advanced Research, China

Perovskite-related metal halides exhibit unique structures and outstanding optoelectronic properties that have enabled a wide range of technological applications including solar cells, light-emitting diodes, lasers, and radiation detectors. Two main focuses include understating the structure-property relationships and exploring advanced new materials with enhanced and/or emergent functionalities. In this talk, I will present our recent efforts in investigating metal halides using high pressure, an alternative approach to exploring novel materials with desirable properties that also permit a deeper understanding of a wide range of phenomena. Using the state-of-the-art high-pressure techniques coupled with *in situ* synchrotron-based and in-laboratory property measurements, we characterized the changes in the lattice, electronic, optical, and optoelectronic properties of various metal halides with different dimensionalities including 3D, 2D, and 1D, and further revealed their structure-property relationships. High-pressure research opens a new way to understand the fundamental mechanisms of optoelectronic metal halides and explore novel materials with superior properties.

8:30 AM *SF02.20.02

Emergent Magnetic Phase in Pressure-Tuned Antiferromagnetic Topological Insulator Mingliang Tian^{1,2}, Xuliang Chen² and Zhaorong Yang²; ¹Anhui University, China; ²Hefei Institutes of Physical Science, CAS, China

Zintl material EuCd₂As₂ attracts much recent research interest as it can manifest various ideal topological quantum states under certain conditions just within the same host. While the ground state of this material is expected to be an antiferromagnetic (AFM) topological insulator or axion insulator as outlined by the Zintl concept and theoretical band calculations, yet all samples from previous works experimentally show an AFM semimetal state. Based on successful synthesis of single crystals of EuCd₂As₂ having an AFM insulating state and a negative colossal magnetoresistance (CMR, ~10,000%) effect, here we present a comprehensive high-pressure study of this unique material. We found that the AFM transition temperature is raised linearly from ~9.5 K at ambient pressure to ~55.0 K at 24.0 GPa; meanwhile, the CMR persists whereas its maximum magnitude first increases, reaching ~40,000% at 12.6 GPa, and then decreases significantly. Beginning at ~24.0 GPa, a ferromagnetic metallic phase with an ordinary negative MR shows up, which is accompanied by a trigonal P3m1 to monoclinic C2/m structural transition. The emergent phase dominates over the pristine AFM insulating one upon completion of the structural transition beyond ~40 GPa. Our results demonstrate the tunability of quantum states by pressure and may offer crucial insights into understanding of the interplay of magnetism and transports in EuCd₂As₂ and its derivatives.

9:00 AM SF02.20.03

Characterization and Performance Evaluation of Geocomposite Materials Under Extreme Environmental Conditions S A K V Miyuradarshi Piyathilake and Christopher Bareither; Colorado State University, United States

Waste containment infrastructure is essential to protect human health and the environment. This infrastructure should consist of robust barrier systems that can isolate municipal, industrial, medical and hazardous waste to avoid contaminant leakage and pollution under extreme environmental conditions. Thus, it is essential these barrier systems withstand high temperatures, pressures and strain deformations that can impact their long-term resilience. Recently, geocomposite materials that consist of geomembranes (GMX) and geosynthetic clay liners (GCL) have emerged as a promising barrier system due to their durability and low cost. GMX is usually made of High-Density Polyethylene or Low-Density Polyethylene while GCL consist of a layer of bentonite clay encapsulated between two polypropylene geotextiles. The promising combination of GCL and GMX gives rise to a durable, cost-effective barrier system under extreme environments.

This research focus on the degradation of GCL and GMX polymers in real-world applications. We simulated harsh, real-world conditions and studied oxidation, free radical formation, crystallinity and tensile properties to understand the material performance. Geocomposites were exposed to Cu (pH=2), Bauxite (pH=12) based mineral process solutions and DI water for 1, 6 and 10 months while applying a 20 kPa normal stress. Next, they were subjected to 2 GPa normal stress to mimic the strain these materials experience under high load in the field. This was followed by imaging, spectroscopy and mechanical characterization to analyze material stability.

SEM images show that GCL exists as bundles of fibers with an average diameter of 40 μm while GMX is a textured film with a thickness of 1.6 mm. Thermal studies via DSC revealed that GMX is composed of antioxidants while GCL does not contain antioxidants. We also quantified the heat of fusion and extracted polymer crystallinity. Both materials showed an increase in crystallinity (9.5% for GCL and 6% for GMX after 10-month immersion) following chemical and stress treatments. This increase in crystallinity was directly proportional to immersion time and solution strength. Higher crystallinity suggests higher degradation since free radicals formed during oxidation create crystalline regions/clusters that makes it more brittle.

FTIR results showed that Carbonyl Indices for both the Carbonyl compounds band (1650-1850 cm⁻¹) and Hydroperoxide/Alcohol band (3200-3550 cm⁻¹) increase for GMX and GCL with solution immersion and stress. This suggests that hydroperoxides, alcohol, and carboxyl groups form as a result of oxidation. XRD was performed to extract the crystallinity of the polymers. For GMX, we see a crystallinity increase of 10.5% and 5.5% in Cu and Bauxite solutions respectively, and for GCL it is 10.7% and 18.7%. We notice the impact is higher for GCL due to the lack of antioxidants. XPS confirmed the above results and revealed that C-C bonding has reduced in percentage after exposure, where alcohols (-OH), ketones (-C=O) and carboxyl groups (O-C=O) have increased in percentage, which is a clear indication of oxidation after treatment.

The mechanical properties were also consistent with spectroscopic and thermal results. Young's modulus gradually increased for 1-, 6-, and 10-month samples. This is severe for 10-month samples: 23-27% for GMX and 37-41% for GCL. Yield strength and tensile strength also showed a similar trend. This proves that harsh chemicals and stress can deteriorate overall mechanical performance. Our research sheds light on micro-level chemical reactions and correlates that to macro-level catastrophic failure in barrier systems. We envision to extend our fundamental understanding and develop a universal model that can predict the life-time of geocomposites for harsh environmental conditions. The impact of this research is significant; it can reduce pollution and protect the environment from toxic, hazardous waste materials under extreme conditions.

9:15 AM SF02.20.04

Structure and Dynamics of Supercritical Water Determined Using Quantum Molecular Dynamics Nitish Baradwaj, Aravind Krishnamoorthy, Ken-ichi Nomura, Aiichiro Nakano, Rajiv Kalia and Priya Vashishta; University of Southern California, United States

Water subjected to very high temperatures and pressures inside the Earth's Mantle exists in its supercritical form. It exhibits extraordinary properties such as having a low dielectric constant, which stems from the breakdown of hydrogen bonds at supercritical temperatures. This makes supercritical water a non-polar solvent and the basis for many innovative technologies. In this study we investigate the hydrogen bonds, its lifetime in supercritical water (0.1

gr/cc to 1.0 gr/cc) at 1000K, along with structure and various dynamical correlations studied through the velocity autocorrelation function, current-current correlation function, and their Fourier transforms from position and velocity trajectories calculates using SCAN Exchange-Correlation functional within DFT.

This work was supported as part of the Computational Materials Sciences Program funded by the U.S. Department of Energy, Office of Science, Basic Energy Sciences, under Award Number DE-SC0014607.

9:30 AM *SF02.20.05

Microstructure Characterization of Oxide-Particle-Dispersion Strengthened Copper Matrix Composite Glidcop® [Yan D. Xin](#), Jun Lu and Ke Han; Florida State Univ, United States

Glidcop® is an oxide-particle-dispersion strengthened copper composite that has a combination of high mechanical strength and high electrical conductivity. It has been used as a conductor for 60 T and 100 T ultrahigh field pulsed magnets by the National High Magnetic Field Laboratory, USA. In the quest for even higher magnetic field, material development is crucial. Since the mechanical properties of a material are often determined by its microstructure, comprehensive characterization of the microstructure of the material is necessary. In this work, we studied the microstructure of Glidcop® AL-60, AL-25 and AL-15, using both scanning electron microscopy (SEM) and transmission electron microscopy (TEM).

We identified crystal phases of the alumina in these composites and investigated their size and density distribution. We confirmed that Orowan strengthening where dislocations bowing around alumina particles is the main strengthening mechanism. In addition, we carried out studies of samples after plastic deformation to investigate the origin of wire breakage during wire drawing.

10:00 AM DISCUSSION TIME

SESSION SF02.21: Virtual Session II: Materials for Extreme Conditions II

Session Chair: Wenge Yang

Tuesday Morning, December 6, 2022

SF02-virtual

10:30 AM *SF02.21.01

Superconductivity in Superhydrides—New Experimental Developments [Mikhail Erements](#)¹, Vasily Minkov¹, Vadim Ksenofontov¹ and Sergey Bud'ko^{2,3}; ¹Max Planck Institute for Chemistry, Germany; ²Ames Laboratory, U.S. Department of Energy, Iowa State University, United States; ³Iowa State University, United States

Since the discovery of superconductivity at ~200 K in H₃S [1], similar or higher transition temperatures, T_c s, have been reported for various hydrogen-rich compounds under ultra-high pressures [2]. Superconductivity was experimentally proved by different methods, including electrical resistance, magnetic susceptibility, optical infrared, and nuclear resonant scattering measurements. The crystal structures of superconducting phases were determined by X-ray diffraction. Numerous electrical transport measurements demonstrate the typical behavior of a conventional phonon-mediated superconductor: zero resistance below T_c , the shift of T_c to lower temperatures under external magnetic fields, and pronounced isotope effect. Remarkably, the results agree with the theoretical predictions, which describe superconductivity in hydrides within the framework of the conventional BCS theory.

Magnetic properties, one of the most important characteristics of a superconductor, have not been satisfactorily defined. Recently, we developed SQUID magnetometry under extreme high-pressure conditions [3] and report characteristic superconducting parameters for H₃S and LaH₁₀—the representative members of two families of high-temperature superconducting hydrides. In particular, we determine a London penetration depth λ_L of ~20 nm in H₃S and ~30 nm in LaH₁₀. These compounds have the values of the Ginzburg-Landau parameter $\kappa \sim 12$ –20 and belong to the group of “moderate” type II superconductors. We further develop magnetic measurements with the trapped magnetic flux. This technique provides a strong magnetic response and, what is more important, eliminates the huge background of a bulky diamond anvil cell.

A large part of the report will be a discussion of possibilities of further increasing T_c to room temperature and above, with emphasis on experimental aspects.

1. Drozdov, A.P., et al., *Conventional superconductivity at 203 K at high pressures*. Nature 2015. **525**: p. 73.

2. Flores-Livas, J.A., et al., *A perspective on conventional high-temperature superconductors at high pressure: Methods and materials*. Phys. Rep., 2020. **856**: p. 1-78.

3. Minkov, V.S., et al., *Magnetic field screening in hydrogen-rich high-temperature superconductors*. Nature Communications, 2022.

11:00 AM SF02.21.02

Development of a Novel Insulating Coating Formulation [Rashmi R. Wijayarathna](#) and Madhubhashini Maddumaarachchi; University of Sri Jayewardenepura, Sri Lanka

Large buildings consume plenty of energy and cost for cooling purposes per year. For this, a variety of thermal insulation strategies would be appealing solutions. This study provides new insights into thermal insulating coatings. This research demonstrates the development of a thermal insulating coating containing a porous membrane created by poly(methyl methacrylate) binder. Ammonium bicarbonate (NH₄HCO₃) was used as the readily available, inorganic pore-forming agent which was incorporated into the organic binder using a water-in-oil (W/O) emulsion. A series of 0%, 1%, 5%, and 10% (w/v) concentrations of ammonium bicarbonate incorporated paint films were prepared. Decomposition of NH₄HCO₃ produces ammonia and carbon dioxide gas bubbles which developed porous structures within the binder during the solvent evaporation process. Air is trapped inside the pores and makes an air layer that can act as the thermal barrier layer in the paint film. Optical microscopic images and SEM images were taken to confirm the formation of W/O emulsion and the formation of porous structures inside the paint, respectively. When the concentration of pore-forming agents increases, more interconnected porous structures in the paint film have resulted. It can be suggested that 5% of NH₄HCO₃ was the optimal value. The insulation property of these paint films was tested using a self-developed thermal insulating property measurement device having four DHT 11 temperature sensors. The data were collected and reported using Arduino UNO software and Processing 3 software, respectively. Results demonstrated that there is no gradual increase of the insulation property while increasing the NH₄HCO₃ content. Nevertheless, 1% and 10% of NH₄HCO₃ incorporated paint films showed a 2°C to 4°C of absolute temperature difference, indicating a good thermal insulating property of the paint film. This research work provides insights into a good cost-

effective solution for thermal insulation enhancement in the conventional paint formulation.

11:15 AM SF02.21.03

Novel High-Strength Bioinspired Coatings for Hypervelocity Debris Mitigation Chad A. McCoy, Guangping Xu, Hongyou Fan, Jens Schwarz and Jenny Xiong; Sandia National Laboratories, United States

Materials designed for use in extreme environments must have strong mechanical and/or thermal resistance to withstand the insults experienced for their desired application. Some of the most stressing environments, which require both mechanical and thermal resistance, are use in pulsed power facilities, magnetic fusion reactors, and space debris and radiation protection. Ideal materials for these applications must combine high strength and thermal resistance with low weight high x-ray transmission. Materials which meet these needs and do not cause significant hazards to personnel and the environment are not presently available.

Novel layered nanocomposite coatings have been fabricated from silica and sugar-derived carbon biomimic natural seashell structures. These coatings have been demonstrated to have high x-ray transmission, which enables their use as diagnostic windows for pulsed power facilities and magnetic fusion reactors. The coatings are stable to temperatures exceeding 800 °C, which outperforms other high-strength, low-weight materials. The materials are environmentally friendly and do not pose any health risks to personnel, which enables them to be used for diagnostics in extreme environments.

Testing of their functionality as debris shields for pulsed power facilities, magnetic confinement fusion reactors, and micrometeoroid impact is ongoing. Variable thickness of coatings on silicon substrates were exposed to debris generated on the Z Pulsed Power Facility at Sandia National Laboratories and the deformation to a witness plate shielded by the coatings was measured. Deformation of the witness plate behind a 50 μm thick substrate coated with 35 μm of this material was less than that of a 100 μm thick bare substrate. Coating of 40 μm of material on a 100 μm thick substrate resulted in no measurable deformation to the witness plate. The results demonstrate that this coating is viable for use as debris shields in extreme environments.

Sandia National Laboratories is a multimission laboratory managed and operated by National Technology & Engineering Solutions of Sandia, LLC, a wholly owned subsidiary of Honeywell International Inc., for the U.S. Department of Energy's National Nuclear Security Administration under contract DE-NA0003525.

11:30 AM SF02.21.04

Morphology Dependent Microstructural Deformation and Structure-Property Relationship Studies on Styrenic Thermoplastic Elastomer Films Khadar B. Shaik, Abul Huq, Alamgir Karim and Anil Bhowmick; University of Houston, United States

Thermoplastic elastomers (TPEs) containing polystyrene (PS) hold a special class of molecular chain arrangements of the hard and soft segments giving rise to many well-defined nanostructures. The orientation and ordering of these nanodomains affect the mechanical properties of TPEs to a very large extent. Accordingly in this work, we investigated this behavior and characterized the impact of different morphologies on the uniaxial tensile properties as well as the deformation of PS domains within the rubbery matrix. Various phase-separated morphologies have been obtained by solution casting bulk films of different thicknesses using four different solvents. The extent to which PS domains order and orient have been varied from 70 - 92 nm in grain sizes and parallel to vertical orientations. The domain periodicities also range from 22 nm to 26 nm. This has been correlated to the interactions of polymers and solvents and the solvent volatilities. Further, the elastic modulus decreased for laterally oriented domains compared to vertical ones and their tensile strength also reduced. Deformation resulting in anisotropic Small Angle X-ray Scattering (SAXS) has been evaluated along equatorial and meridional axes for strains until 500%. The degree of deformation (inter-domain spacing, domain distortion) swifts linearly for small strains (less than 50%) as the polystyrene domains deform in a non-affine manner throughout the extension. The study of such property dependencies play an important role in designing materials needed to withstand the requirements of specific applications.

11:45 AM SF02.21.05

Recent Progress in the Potential of Ionic Liquids as High Temperature Electrolytes for Energy Storage Systems Kallidanthiyil Chellappan Lethesh, Ahmed Bahaa, Musbaudeen O. Bamgbopa and Rahmat Agung Susantyoko; Dubai Electricity & Water Authority, United Arab Emirates

Ionic liquids are low-temperature molten salts with unique properties such as low volatility, extensive liquid range, high thermal stability, and high solubility of organic, inorganic, and polymeric materials. Ionic liquids find applications both in industry and academia because of the flexibility to tune their properties according to the requirements. Ionic liquids are promising electrolytes for energy storage systems because they can address the safety concerns associated with using organic electrolytes. Because of the growing interest in ionic liquids-based electrolytes, many ionic liquids are available on the market. The electrochemical properties of ionic liquids are susceptible to their purity, and there is no systematic study on the electrochemical properties of commercially available ionic liquids.

In this MRS submission, we are going to present the recent progress of research and development of ionic liquids as high temperature electrolytes for energy storage. The progress will be based on the literature from other's works as well as from our research group's works. We have published an important milestone where the electrochemical stability of 22 commercially available and commonly used ionic liquids were studied using cyclic voltammetry in the temperature range 288.15 K to 358.15 K. Ionic liquids based on imidazolium, pyrrolidinium, piperidinium, and tetraalkylammonium cations combined with bis(fluorosulfonyl) imide and bis(trifluoromethanesulfonyl) imide were selected because of their hydrophobic nature. The temperature sensitivity of the anodic and cathodic potential limits was evaluated by combining the cyclic voltammetry experiments and a linear regression model. The ionic liquids under investigation displayed an electrochemical stability window of 4.1 V to 6.1 V. This study revealed that temperature had a mixed effect on the electrochemical stability of the ionic liquids. Despite the structural similarity of anions used in the study, bis(trifluoromethanesulfonyl) imide anion-based ionic liquids showed better electrochemical stability than the bis(fluorosulfonyl) imide anion analog due to the presence of more fluorine atoms. The increase in the alkyl chain length on the cation increased the electrochemical stability of the ionic liquids due to their ability to transfer electrons to the hetero atom on the cation. It was speculated that the presence of ether functionality could increase the electrochemical window of the ionic liquids because of the interaction between the oxygen atom on the ether group and the positively charged nitrogen atom on the cation. On the contrary, introducing the ether group to the cationic core reduced the electrochemical stability window. The inability of the ether functionality to donate electrons to the positively charged nitrogen atom and decrease in the electron density on the positively charged hetero atom due to its interaction with the ether group was responsible for the lower electrochemical stability of ether-containing ionic liquids. A similar effect was observed with the functionalization of the cation with aromatic groups. Pyrrolidinium and piperidinium-based ionic liquids showed higher electrochemical stability windows among the different cations studied. This might be because of the difference in their electrochemical degradation mechanism compared to imidazolium and tetraalkylammonium cations.

12:00 PM *SF02.21.06

New Compounds Predicted from Crystal Structure Searching Jian Sun; Nanjing University, China

In this talk, I will introduce the methods developed in my group, especially the machine learning and graph theory aided crystal structure prediction method (Magus) [1]. In addition, I will show some of our recent progress in the applications of these methods to predict new compounds, including planetary

minerals [2-5] and polymeric nitrogen compounds [6-7], etc.

REFERENCE

1. Kang Xia et al., "A novel superhard tungsten nitride predicted by machine-learning accelerated crystal structure search", *Sci. Bull.* 63, 817 (2018).
2. Cong Liu et al., "Mixed coordination silica at megabar pressure", *Phys. Rev. Lett.* 126, 035701 (2021).
3. Hao Gao et al., "Superionic Silica-Water and Silica-Hydrogen Compounds in the Deep Interiors of Uranus and Neptune", *Phys. Rev. Lett.* 128, 035702 (2022).
4. Cong Liu et al., "Multiple superionic states in helium-water compounds", *Nature Physics* 15, 1065 (2019).
5. Cong Liu et al., "Plastic and Superionic Helium Ammonia Compounds under High Pressure and High Temperature", *Phys. Rev. X* 10, 021007 (2020).
6. Nilesh P. Salke et al., "Tungsten hexanitride with single-bonded armchair-like hexazine structure at high pressure", *Phys. Rev. Lett.* 126, 065702 (2021).
7. Chi Ding et al., "High Energy Density Polymeric Nitrogen Nanotubes inside Carbon Nanotubes", *Chin. Phys. Lett.* 39, 036101 (2022) (Express Letter).

12:30 PM SF02.21.07

Measurement of Powder Thermal Diffusivity by Laser Flash Method Ummay Habiba and Rainer Hebert; University of Connecticut, United States

In laser powder bed fusion (LPBF) additive manufacturing, the thermal diffusivity of the powder bed is a very important factor. The thermal characteristics of the powder bed have a significant impact on the mechanical characteristics of the products created by LPBF. This work uses a laser flash three-layered analysis in the DLF1600 instrument, which has a special powder cell to enclose the powdered sample, to assess the thermal diffusivity of metallic powder, nickel-based super alloy Inconel718 (IN718). Measurements were performed at different temperatures. Test data were also analyzed in the R software for further verification.

12:45 PM DISCUSSION TIME

SESSION SF02.22: Virtual Session III: Materials for Extreme Conditions III
Session Chairs: Ke Han and Florence Lecouturier-Dupouy
Wednesday Morning, December 7, 2022
SF02-virtual

8:00 AM *SF02.22.01

New Findings on Cu-Ag Wire for the Pulsed High Field Magnet Koichi Kindo¹, Kazuki Matsui¹, Yoshikazu Sakai¹ and Akihiro Kikuchi²; ¹Univ of Tokyo, Japan; ²National Institute for Materials Science, Japan

Non-destructive pulsed magnet is the most important tool for a precise measurement under very high magnetic field. Generating high magnetic field, however, has been hard task because the magnet is destroyed due to considerable Maxwell stress. The stress reaches about 2 GPa in the field of 70 Tesla(T). The simplest solution for generating high field non-destructively is making a coil by use of the wire having higher strength. The Cu-Ag wire has been one of the best candidate for the coil-wire because the wire has the tensile strength of about 1.1 GPa and the conductivity of about 80% of pure copper. By using the wire, we succeeded in generating a field of 85.8 T in 2011 by mono coil system. The coil-wire of the same bobbin generated the 85 T-class field many times, but the wire of another bobbin could not reach to the same class field. The best wire could not be reproduced although we continued to produce wires with similar physical properties. There were many wires having the same strength and conductivity as to the best wire but nothing could generate the field exceeding 80 T. This would be a mystery because the maximum field mainly depends on the tensile strength of the wire. Our efforts to reproduce the best wire were in vain. 10 years have passed since it became mystery.

To solve the mystery, we firstly classified the wires into good ones and bad ones. This classification indicated clearly that the quality of the wire depends on the manufacturing process, especially drawing one. In November 2021, we tested a wire regarded as an ideal combination of manufacturing process. The result was satisfactory. We succeeded in generating a magnetic field of 85.97 T completely non-destructively, breaking the previous record in 2011. The mystery of Cu-Ag wire was solved. The key for solving the mystery lays in the manufacturing process, especially drawing one. Based on these results, we are producing wires that have undergone the ideal manufacturing process to generate the 85 T-class magnetic fields stably. After reproducing the best wire, we have succeeded in making the 85 T-class fields repeatedly. Our progress in the wire production will be presented.

8:30 AM SF02.22.02

Effect of Heat Treatment on Laser-PBF Ti-6Al-4V Microstructure Sayaka Maruta; Mitsubishi Heavy Industries, Ltd., Japan

Ti-6Al-4V is widely used in the aerospace industry because of its high specific strength, excellent heat resistance and corrosion resistance. On the other hand, the manufacturing cost is higher than other alloys due to its high cutting and material cost. AM (Additive Manufacturing), which can provide them with enhanced functionality through high flexibility of design and improvement of material yield by near-net shape, is expected to be a solution to the above problem. In particular, the Laser-PBF (Powder Bed Fusion) method enables high-precision building of complex shapes, so this method is being applied to products.

However, since process of AM is a new technology, there are many unclear points regarding the relationship between manufacturing conditions, quality, and mechanical properties, and it is important to clarify the fundamental phenomena in order to obtain stable material properties. The purpose of this study is to control the material properties by optimizing the microstructure. The effect of different process parameters (power, scan speed, hatch spacing, layer thickness) and heat treatment conditions on the microstructure was evaluated experimentally. The test specimens were built by L-PBF method under several conditions of process parameters. After observing the as-built microstructure, heat treatment was carried out under several conditions (with reference to the β transformation temperature). Microstructures after building and heat treatment were compared to evaluate the effect of different building conditions on the microstructure after heat treatment. Also, the heat treatment condition in which the improvement in the fatigue property was expected from the microstructure after the heat treatment was shown.

As a result of the above tests, it was suggested that the influence of process parameters on the as-built microstructure was small compared with the change of heat treatment conditions, but the as-built microstructure may have a slight influence on the microstructure after heat treatment. In addition, it was clarified that the selection of the heat treatment condition at the temperature in which the α colony formation by the coarsening of the α lath did not occur was an effective means for the fatigue property improvement.

8:45 AM *SF02.22.05**Copper Alloys Requirements for High Field Resitive Magnets** Francois Debray; French High Magnetic Field Facility (LNCMI), France

To go beyond the State of the Art of superconducting electromagnets, high field magnets made with optimized copper alloy coils are available in a restricted number of facilities worldwide.

In Europe, 4 large scale facilities are members of the European Magnetic Field Laboratory.

There are located in Dresden and Toulouse for pulsed magnetic field and Nijmegen and Grenoble for continuous magnetic fields.

We will present the state of the Art of the material used today in these facilities and an overview of the ongoing developments.

9:15 AM DISCUSSION TIME

SESSION SF02.23: Virtual Session IV: Materials for Extreme Conditions IV

Session Chairs: Alexander Goncharov and Wenge Yang

Wednesday Morning, December 7, 2022

SF02-virtual

10:30 AM SF02.23.02**Defect Evolution Under High-Velocity Impact in the Metal Cold Spray Process** Damodara Reddy, Zhi-Qian Zhang and Sridhar Narayanaswamy; IHPC, Singapore

In this talk, we present defect-mediated microstructural evolution for high-velocity impact, as is applicable for the metal Cold Spray process. With molecular dynamics simulations, we simulate the complex bonding mechanisms under extreme conditions of large localized plastic deformation, localized melting, and extremely high strain rate. We show that for copper/copper system, impact induced local melting leads to adhesive bonding at the interface. More importantly, we probed the bonding over a range of impact velocities and find the grain boundary-like amorphous phase interlocking and metallurgical bonding are dominant at low and medium impact velocities, while metallurgical bonding and mechanical interlocking are dominant at high impact velocities.

We also present an experimentally validated computational model for microstructural evolution with the characteristics determined using a dislocation density-based model implemented in a Eulerian finite element framework. A comparison of the numerical and experimental results from Scanning Electron Microscope (SEM), Electron Backscatter Diffraction (EBSD) and Kernel Average Mis-orientation (KAM) analyses, reveal the evolution of cell size and mis-orientation resulting in grain refinement at the particle-substrate and particle-particle interfaces. Although there is a large plastic deformation due to high speed impact, the dislocation density in the particle decreases with distance from the impacting interface and this feature is observed in both the simulation results and the experimental characterization data. The validated model can be effectively leveraged to predict microstructural evolution under different process conditions including spray angle, pre-heat temperature, and impact velocity.

10:45 AM SF02.23.03**Multi-Scale Piezo-Elasticity of sI Methane Gas Hydrates—From Bonds to Cages to Lattices** Xiaodan Zhu, Alejandro Rey and Phillip Servio; McGill University, Canada

Research and exploration of new green energy have become critical to addressing the current focus on energy sustainability and scarcity. Gas hydrates, found in deep ocean or permafrost areas under high pressures and low temperatures, are a competitive alternative. This is because it has approximately twice the amount of energy stored in fossil fuels and oils and provides a significant storage capacity due to its unique guest-host structure. Because of hydrates' high energy content and excellent storage capacity, they are a strong candidate for supplying energy while mitigating the effects of global warming. However, these extreme environmental factors create a solid barrier to studying the properties of hydrates in the laboratory and for commercial explorations. As a result, We use multi-scale theory-modelling simulation to explore the piezo-effect of sI methane gas hydrates and investigate the stability limits at 0 Kelvin.

This work uses density functional theory (DFT) in conjunction with homogenization methods and the theory of mixtures to investigate the structure, thermodynamics, and elasticity of sI methane hydrates subjected to pressure loads at three scales, atoms, cages, and lattice at 0 Kelvin. In the hydrate system, the distribution functions of bond parameters are characterized, providing a novel understanding of the spread of values at the smallest scale. The roles of various cages at the mesoscale, such as continuous phase and disperse inclusion, have been identified. Different deformation mechanisms (affine and non-affine) are observed at the continuum scale, corresponding to different fracture mechanisms (brittle and ductile) under tensile and compressive pressures.

Taken together, the systematic atomic-cage-lattice multi-scale characterization proves fruitful in linking processes that connect mechanical properties, cage geometry, and hydrogen bonding. The multi-scale methodology can be generalized to other gas hydrates or water-based systems to improve the fundamental understanding and obtain engineering correlations.

11:00 AM SF02.23.04**Magnetotransport Measurements for Infinite-Layer Nickelate Superconductors—Rare Earth Dependence** Lin Er Chow¹, King yau Yip², Mathieu Pierre³, Shengwei Zeng¹, Zhaoting Zhang¹, Tobias Heil⁴, Julia Deuschle⁴, Proloy Nandi¹, Sujith Kunniniyil Sudheesh¹, Zhi Shih Lim¹, Zhaoyang Luo¹, Marc Nardone³, A. Zitouni³, Peter A. Van Aken⁴, Michel Goiran³, Swee Kuan Goh², Walter Escoffier³ and Ariando Ariando¹; ¹National University of Singapore, Singapore; ²The Chinese University of Hong Kong, Hong Kong; ³Université de Toulouse, France; ⁴Max Planck Institute for Solid State Research, Germany

Standing beside copper in the periodic table, Ni¹⁺ state in infinite-layer phase hosts 3d⁹ electronic structure with lifted orbital degeneracy that resembles Cu²⁺ state in the high-*T_c* cuprate superconductors [1,2]. Realizing and studying superconductivity in nickelate has been one of the most strategic paths to a closer step toward the secret makeup of high-temperature superconductivity. Despite more than two decades of theoretical predictions, superconducting infinite-layer nickelate was only successfully synthesized in 2019 in the thin-film form [3]. Obstructed by challenging material synthesis and various structural defects, many critical parameters such as the upper critical fields and superconducting anisotropies for this newfound quasi-two-dimensional layered superconductor remain poorly understood. In continuation of our efforts in optimizing the stabilization of the superconducting infinite-layer phase, we successfully fabricate high crystallinity samples with virtually a monocrystalline infinite-layer phase with thickness > 10 nm, more than twice the previously achieved thickness. We perform a series of magnetotransport measurements using magnetic fields up to 55 T at a temperature down to 30 mK.

In contrast to the expected trend from cuprates, we observed a strong dependence of the upper critical fields on the rare earth ion [4]. The intrinsic angular dependence of the superconducting observables will also be discussed.

- [1] T. M. Rice, *Phys. Rev. B - Condens. Matter Mater. Phys.* **59** (1999) 7901-7906
- [2] K. W. Lee, W. E. Pickett, *Phys. Rev. B - Condens. Matter Mater. Phys.* **70** (2004) 1-7
- [3] D. Li *et al.*, *Nature* **572** (2019) 624-627
- [4] L. E. Chow *et al.*, *arXiv:2204.12606* (2022)

Acknowledgment:

This research is supported by the Ministry of Education (MOE), Singapore, under its Tier-2 Academic Research Fund (AcRF), Grant No. MOET2EP50121-0018, and Research Grants Council of the Hong Kong SAR, Grant No. A-CUHK 402/19. We acknowledge the support of LNCMI-CNRS, a member of the European Magnetic Field Laboratory (EMFL) under the proposal numbers TMS10-219 and TMS10-221 and the funding support from the European Union's Horizon 2020 research and innovation programme under grant agreement No 823717 - ESTEEM3.

11:15 AM SF02.23.05

Dimensionally and Environmentally Ultra-Stable Polymer Composites Reinforced with Carbon Fibres for Extreme Conditions [Michal Delkowski](#)^{1,2}, Christopher T. Smith¹, Jose Anguita¹ and S. Ravi P. Silva¹; ¹University of Surrey, Advanced Technology Institute, United Kingdom; ²Airbus Defence and Space, Germany

Highly stable composite and polymeric materials are essential in advanced applications. For many space missions, carbon-fibre reinforced polymers (CFRPs), which feature high strength to weight ratio are important, easing mass budget requirements for heavier payloads. Satellites use CFRP for various components including support structures, optical benches, telescope tubes and parabolic reflectors. However, it is important that these materials withstand the harsh space environment such as thermal cycling in vacuum (from cryogenic to hot), UV radiation and mechanical loads, while simultaneously maintaining their structural integrity and material dimensionality.

While today's ultra-high performance composites are able to exhibit a near-zero (even negative) coefficient of thermal expansion, the dimensional instabilities that result from moisture ingress and release, remain the fundamental vulnerability of composite materials. This restricts many applications particularly for spacecraft constructions. Here we address this challenge by developing a space-qualifiable physical superlattice nano-barrier structure, which is deposited via a custom-built deposition system and without vacuum interruption. The structure blends within the mechanical properties of the composite, thus becoming part of the composite itself. The resulting enhanced composite features mechanical integrity and a strength that is superior to the underlying composite, while remaining impervious to distortions caused by moisture, outgassing and other environmental effects. We demonstrate production capability for a model-sized component for the Sentinel-5 mission and demonstrate such capability for future European Space Agency (ESA) and National Aeronautics and Space Administration (NASA) programmes such as Copernicus Extension, Earth Explorer and Science Cosmic Visions.

References

- [1] Anguita, J. V.; Smith, C. T. G.; Stute, T.; Funke, M.; Delkowski M.; Silva, S. R. P. Dimensionally and Environmentally Ultra-Stable Polymer Composites Reinforced with Carbon Fibres. *Nature Materials*, 2020, 19, 474.
- [2] Delkowski M.; Smith, C. T. G.; Anguita, J. V.; Silva, S. R. P. Increasing the robustness and crack resistivity of high-performance carbon fiber composites for space applications. *iScience-Cell Press*, V 24, Issue 6, 102629, June 25, 2021.
- [3] Smith, C. T. G.; Delkowski M.; Anguita, J. V.; Cox C.D.; Haas C.; Silva, S. R. P. Complete Atomic Oxygen and UV Protection for Polymer and Composite Materials in a Low Earth Orbit. *ACS Appl. Mater. Interfaces* 2021, 13, 6670–6677.

11:30 AM SF02.23.06

Oxidation Resistance of Atomically Flat Cu(111) Surface—A First Principles Study [Bipin Lamichhane](#) and Seong-Gon Kim; Mississippi State University, United States

Copper is one of the important materials used in modern technology and industries, but oxidation of copper deteriorates its application in nanotechnology. Our recent first principles total-energy calculations based on density functional theory is used to investigate the oxidation resistance of atomically flat Cu(111) surface. The exchange-correlation energy is described by the generalized gradient approximation (GGA) of Perdew–Burke–Ernzerhof (PBE) and projected augmented wave (PAW) method is employed. Our results show that atomically flat Cu(111) without multi-atomic steps is oxidation resistant. The energy barrier for oxygen penetrating flat surface and mono-atomic step is very high in comparison to multi-atomic steps. Also, incremental oxygen adsorption energy for the fcc site of the flat surface becomes positive and oxygen resistant above the oxygen coverage of 50%. These calculated results are consistent with the recent experimental finding.

11:45 AM SF02.23.07

Surfboards Under Extreme Conditions—Why Do They Fail? Brett Connellan and [Marc In het Panhuis](#); University of Wollongong, Australia

Surfing waves with boards either for sport, culture or religious purposes was first practiced by the Polynesians. Surfing with surfboards consisting of balsa wood started to spread from Hawaii to mainland USA and Austral. Modern surfboards with a foam core were introduced at the end of the 1950's.

It is convenient to think of surfboards as composite materials, for example, a PU surfboard consists of a foam-wood core encased in fibre glass and sealed with resin. In addition, surfboards are also fitted out with up to five fin boxes and a leash plug. The former is used to fit surfboards fins, while the latter is used to connect the surfer to the board using a so-called leash.

The mechanical characteristics of surfboards most valued by surfers is mechanical stiffness and is generally referred to as flex. During characteristic surfing manoeuvres (bottom turns) a surfboard will bend either due to the shape of wave or the force exerted on the board by the surfer or a combination of both effects.

Surfers routinely put their surfboards under extreme wave conditions which results in mechanical failure of surfboards (generally referred to as “snapping”).

In this presentation we discuss the mechanical characteristics of surfboards in terms of damping, flex, recovery and modal analysis. We present a detailed analysis of the mechanical recovery behaviour and mechanical failure mechanisms of surfboards under extreme wave conditions.

11:50 AM SF02.23.08

Influence of Environment on Self-Propagating Reactions in Al/Ni Multilayer Foils Deepshikha Shekhawat; Technical University of Ilmenau, Germany

Influence of Environment on Self-Propagating Reactions in Al/Ni Multilayer Foils

Deepshikha Shekhawat^{1*}, Mostafa Baloochi¹, Vishal Amarbhai Raheja¹, Joachim Döll², Sebastian Matthes³, Marcus Glaser⁴, Jörg Pezoldt^{1*}

¹ FG Nanotechnologie, Institut für Mikro- und Nanoelektronik and Institut für Mikro- und Nanotechnologien MacroNano^a and Institut für Werkstofftechnik, TU Ilmenau, Postfach 100565, 98684 Ilmenau, Germany; mostafa.baloochi@tu-ilmenau.de (M.B.); vishal-amarbhai.raheja@tu-ilmenau.de (V.A.B.)

² Zentrum für Mikro- und Nanotechnologien, TU Ilmenau, Gustav-Kirchhoff-Straße 7, 98693 Ilmenau, Germany; joachim.doell@tu-ilmenau.de (J.D.)

³ FG Werkstoffe der Elektrotechnik, Institut für Werkstofftechnik, Institut für Mikro- und Nanotechnologien MacroNano®, TU Ilmenau, Gustav-Kirchhoff-Strasse 5, 98693 Ilmenau, Germany; sebastian.matthes@tu-ilmenau.de (S.M.)

⁴ FG Fertigungstechnik, Institut für Mikro- und Nanotechnologien MacroNano®, TU Ilmenau, Postfach 100565, 98684 Ilmenau, Germany; marcus.glaser@tu-ilmenau.de (M.G.)

* Correspondence: deepshikha.shekhawat@tu-ilmenau.de (D.S.); joerg.pezoldt@tu-ilmenau.de (J.P.)

Abstract: Reactive multilayer systems signify as an energetic materials potentially for extremely short thermal treatment compared to standard reactive techniques. As there are several factors leading the reaction front velocity, released energy, microstructural and morphological changes are of great interest. In the current investigation, alternative Al and Ni layers deposited by magnetron sputtering technique where Al is starting layer with a 1:1 atomic ratio of Al and Ni onto different substrate. In order to elucidate the influence of different environmental condition, a two-dimensional numerical model was developed to study convective heat loss and thermal properties on the self-propagating reaction in Al/Ni multilayer foils. Reaction heat of the fabricated foils were determined by Differential Scanning Calorimetry (DSC). Self-propagating reaction was introduced on the surface of the foils by an electrical spark. The reaction front velocity was noted with a high speed camera. Activation energy is set with these velocity data to modify the numerical model. Temperature of reaction front of the self-propagating reaction was calculated and compared with the obtained temperature by time-resolved pyrometer measurements. X-ray diffraction investigation of reacted multilayers confirmed that all reactants reacted and formed AlNi phase as a finale phase. Finally, it is predicted that (1) increasing thermal conductivity of the surroundings can increase the transfer of the reaction front; (2) effect of heat convection losses on reaction properties are insignificant, e.g., the foils can maintain their properties in liquid environment.

Keywords: reactive multilayers; self-sustained reaction; nickel; aluminum; propagation velocity; phase transformation; magnetron sputtering

12:05 PM DISCUSSION TIME

SYMPOSIUM SF03

Plasma Technologies for Emerging Materials Science and Applications
November 29 - December 8, 2022

Symposium Organizers

Carla Berrospe-Rodríguez, University of California, Riverside
Wei-Hung Chiang, National Taiwan University of Science and Technology
Fiorenza Fanelli, National Research Council (CNR)
Tsuoyohito Ito, The University of Tokyo

* Invited Paper

+ Distinguished Invited

SESSION SF03.01: Plasma-Surface Interaction
Session Chairs: Wei-Hung Chiang and Chi-Chin Wu
Tuesday Morning, November 29, 2022
Sheraton, 3rd Floor, Hampton

10:15 AM SF03.01.02

Atomic Layer Control of MoS₂ by RIE with Mixed (Ar+O₂+CF₄) Plasma and Its Etching Mechanism with Numerical Analysis Changmin Kim¹, Muyoung Kim², Donghyun Cho², In-Young Park², Sungkwon Jo², Daewoong Kim², Woo Seok Kang², Taesung Kim¹ and Hyeong-U Kim²;

¹Sungkyunkwan University, Korea (the Republic of); ²Korea Institute of Machinery and Materials, Korea (the Republic of)

The two-dimensional transition metal dichalcogenides (2D TMDs) has been researched actively because their unique characteristic which is tunable band gap and uniform band edge through a number of layers can be used to make optoelectronics, photonics, sensing, and nanoelectronics. To control the number of layers of 2D material, the various method of plasma synthesis and etching technologies are being studied. Especially, the MoS₂ has high electron mobility and high current. Also, the band gap depends on the number of layers of MoS₂. The band gap is changed from bulk layers (1.2eV) to monolayer (1.8 eV) of MoS₂. Among the various method of plasma synthesis and etching, plasma-enhanced chemical vapor deposition (PECVD) and reactive ion etching (RIE) is one of the effective techniques for synthesis and control of the layer of 2D material. The PECVD is the instrument in which thin films of

various materials can be synthesized on the substrates at low temperatures than chemical vapor deposition (CVD). The low deposition temperature, high purity of material, good step coverage, and easy control of reaction parameters are the advantage of PECVD. The RIE is one of the popular etching methods. The etching rate and selectivity are higher than normal physical and chemical etching. Especially, RIE is the anisotropic etching which is a technique of microfabrication. The advantage of anisotropic etching is possible to fabricate a fine pattern. In this study, we tried to find an optimized condition for controlling the layer-by-layer of MoS₂ by using the PECVD and RIE systems.

The density functional theory (DFT) which is a computational quantum mechanical modeling method is used to determine the suitable reactive gas for plasma etching of MoS₂. First the post-analysis, the MoS₂ was measured to confirm the number of layers of MoS₂ by Raman spectroscopy. In addition, the chemical structure of MoS₂ was confirmed by X-ray photoelectron spectroscopy (XPS). Also, the layers of MoS₂ are directly confirmed by Transmission electron microscope (TEM) and atomic force microscope (AFM). Second in-situ analysis, the Optical emission spectroscopy (OES) was conducted to check the element of gas that is affected to plasma status during the process of plasma etching. The numerical simulation was used to figure out the plasma etching mechanism of MoS₂. The effect of each element of MoS₂ and reactive gases are analyzed by the numerical simulation.

10:30 AM SF03.01.03

Plasma-Enhanced Spatial ALD of SiO₂ Investigated by Gas-Phase Infrared and Optical Emission Spectroscopy Maria Mione¹, Vincent Vandalon¹, Alfredo Mameli², Fred Roozeboom^{1,2} and Erwin Kessels¹; ¹Eindhoven Univ of Technology, Netherlands; ²TNO/Holst, Netherlands

Atomic layer deposition (ALD) has become a true enabling nanotechnology with many applications in the semiconductor industry. Often the process is plasma-enhanced (i.e., plasma-enhanced ALD) as this allows for the deposition of more materials (such as SiO₂) and also at lower substrate temperatures. In this presentation a spatial ALD process for SiO₂ will be reported which enables a higher productivity. Nanoscale SiO₂ films have many applications in self-aligned patterning, trench filling, encapsulation and passivation etc. in both nanoscale semiconductor devices but also in large-area electronics, displays, and photovoltaics.

The spatial ALD process was developed in a rotary spatial ALD reactor using bisdiethylaminosilane (BDEAS, SiH₂[N(C₂H₅)₂]₂) and an atmospheric O₂ plasma [1]. Within the substrate temperature range of 100-250 °C, the process demonstrates self-limiting growth with a growth-per-cycle between 0.12 and 0.14 nm and SiO₂ films exhibiting material properties *on par* with those reported for low-pressure plasma-enhanced ALD [2].

Gas-phase infrared spectroscopy on the reactant exhaust gases and optical emission spectroscopy on the plasma region are used to identify the species that are generated in the ALD process. Based on the identified species and a calibration procedure, we propose a reaction mechanism where BDEAS molecules adsorb on -OH surface sites through the exchange of one of the amine-ligands upon desorption of diethylamine (DEA, HN(C₂H₅)₂). The remaining amine ligand is removed through combustion reactions activated by the O₂ plasma species leading to the release of H₂O, CO₂, CO in addition to products such as N₂O, NO₂, and CH-containing species. These volatile species can undergo further gas-phase reactions in the plasma as indicated by the observation of OH*, CN* and NH* excited fragments in emission. Furthermore, the infrared analysis of the precursor exhaust gas indicated the release of CO₂ during precursor adsorption. Moreover, this analysis has allowed the quantification of the precursor depletion yielding values between 10 % and 50 % depending on the processing parameters. On the basis of these results, the overall surface chemistry of the spatial ALD process of SiO₂ will be discussed.

[1] M. Mione, V. Vandalon, A. Mameli, W.M.M. Kessels, and F. Roozeboom, J. Phys. Chem. C 125, 24945 (2021)

[2] G. Dingemans, C.A.A. van Helvoirt, D. Pierreux, W. Keuning, W.M.M. Kessels, J. Electrochem. Soc. 159, H277 (2012)

10:45 AM SF03.01.04

Controlling Surface Oxidation States for Precise Nanoscale Patterning of Etch-Resistant Materials Taylor Smith¹, Ethan Crumlin^{2,2} and Jane P. Chang¹; ¹University of California, Los Angeles, United States; ²Lawrence Berkeley National Laboratory, United States

Copper is the primary material used for the interconnects of an integrated circuit (IC). The dual damascene process was initially developed to deposit and pattern copper due to the difficulties of using traditional dry etching techniques, but the dual damascene process is reaching its practical limits. Atomic layer etching (ALE) is emerging as a process that could help replace the dual damascene process. In this work, we examine an ALE process that uses directional ions from reactive plasmas (oxygen or nitrogen) coupled with formic acid vapor exposure to precisely etch copper films. During the modification step, oxidation or nitridation changes the oxidation state of copper, thereby changing the free electron characteristics of metallic copper into localized chemical bonds that facilitate the subsequent reaction with the organic vapor. Plasma oxidation or nitridation of copper has been accomplished using an ICP plasma source, and the resulting copper oxide and nitride film has been characterized by X-ray photoelectron spectroscopy (XPS) to quantify the composition. Angle-resolved XPS (AR-XPS) is used to determine a depth profile of the oxidized and nitridized copper surface. The FA vapor exposure is carried out using a custom-built reactor, with scanning electron microscopy (SEM) used to determine total thickness removal and XPS used to confirm the chemical removal of copper nitride. In addition, ambient pressure X-ray photoelectron spectroscopy (AP-XPS) was used to examine the FA vapor exposure step in particular detail. These in operando measurements aided in proposing the surface reaction mechanism of the modified copper surface during the vapor phase removal.

11:00 AM SF03.01.05

Plasma Synthesis of High Entropy Boride via Thermal Reduction of Metal Oxides Bria C. Storr¹, Carolina Amezcaga² and Shane A. Catledge¹; ¹University of Alabama at Birmingham, United States; ²Auburn University, United States

Metal oxide thermal reduction enabled by microwave-induced plasma was used to synthesize high entropy borides. This approach capitalized on the ability of microwaves to efficiently transfer thermal energy to enhance reactions in the presence of low-temperature plasma. The precursors, metal oxides and reducing agents, were blended by a high-energy ball mill and annealed via microwave plasma. A single-phase hexagonal AlB₂-type structure characteristic of high-entropy borides was produced by utilizing either boro/carbothermal reduction or borothermal reduction. The microstructural and mechanical properties were compared using the different thermal reduction approaches with and without carbon as a reducing agent. The plasma annealed HEB with configuration (Hf_{0.2}, Zr_{0.2}, Ti_{0.2}, Ta_{0.2}, Mo_{0.2})B₂ yielded a higher measured hardness from boro/carbothermal reduction compared to that from borothermal reduction (38 ± 4 GPa vs. 28 ± 3 GPa, respectively). To further examine the effect of the plasma on the homogeneity of HEB transformation, several sample cross-sections of the annealed HEB pellets were analyzed. The cross-section of the sample that is most exposed to the plasma is less porous than the least exposed portion of the sample.

11:15 AM SF03.01.06

Vertically Extended Channel Thin-Film Transistors Using Dry Etched Tungsten Gate for Ultra-High-Resolution Display Sein Lee, Se-Yeon Jung, Jeong-Min Park and Jang-Yeon Kwon; Yonsei University, Korea (the Republic of)

The significance of backplane devices for ultra-high-resolution (UHR) displays has increased with the recent development of augmented reality (AR) and virtual reality (VR) devices. Since the human visual resolution can distinguish up to 60 pixels per degree (PPD), the AR/VR device panel needs at least

3000 pixels per inch (PPI) to exceed the human retina resolution limit for a clear display without screen effect. As a result, the unit pixel pitch of thin film transistor (TFT) for UHR display should not be only smaller than a few micrometers ($\sim 3 \mu\text{m}$), but TFT channel length should also be sub-micrometers level. In active-matrix organic light emitting diode (AMOLED) display type, self-aligned top gate (SATG) TFT has been widely used as a planar backplane device structure because of its low parasitic capacitance and tolerance of illumination degradation caused by the light from emitting layer [1-2]. However, SATG TFT has fundamental disadvantages for device miniaturization due to its essentially required area of metallization region for reducing contact resistance and scaling limit of channel induced by carrier diffusion shrinking effective channel length. For this reason, we suggested a size-tunable oxide channel VTFT structure that can achieve a high pixel density on account of structural benefit on device footprint.

In this work, we fabricated scalable amorphous indium gallium zinc oxide (a-IGZO) based VTFT with a dry etched gate layer. In the previously published VTFT structure, the channel length is determined by the thickness of the spacer between the source and drain electrodes [3]. Owing to the spacer etching process, uneven backchannel roughness and high off current have become well-known issues of VTFT. On the contrary, the proposed vertically extended channel (VEC) TFT structure has controllability of an effective channel aspect ratio because the source and drain electrodes could be patterned by a photolithography process. Also, VEC TFT has a small device footprint ($4.5 F^2$), so it is suitable for high-density applications. Furthermore, since the sidewall profile of the dry-etched tungsten gate was optimized by several etchants such as fluorine-based and chlorine-based gases, the electrical performance of the vertical channel could be improved by the anisotropically etched gate metal.

To sum up, we not only realized the oxide channel VTFT that meets high performance for AR/VR display, but opened new application possibilities to UHR electronic devices platform.

[1]. Kang, Dong Han, et al. "Self-aligned coplanar a-IGZO TFTs and application to high-speed circuits." *IEEE electron device letters* 32.10 (2011): 1385-1387.

[2]. Wang, Guoying, et al. "8.3: High Stability Against Light and Heat Based on the Top Gate Self-Aligned a-IGZO TFTs under OLED Display." *SID Symposium Digest of Technical Papers*. Vol. 49. 2018.

[3]. Petti, Luisa, et al. "Flexible quasi-vertical In-Ga-Zn-O thin-film transistor with 300-nm channel length." *IEEE Electron Device Letters* 36.5 (2015): 475-477.

SESSION SF03.02: Plasmas for Energy Related Nanostructures
Session Chairs: Jane Chang and Wei-Hung Chiang
Tuesday Afternoon, November 29, 2022
Sheraton, 3rd Floor, Hampton

1:30 PM *SF03.02.01

Design of Composite Nanoparticles by Plasma Spraying for Solid-State Lithium-Ion Batteries with High Densities and High Cyclabilities Makoto Kambara^{1,2}, Ryoshi Ohta^{1,2}, Takeo Hiraoka², Toshimi Tanaka³ and Masashi Dougakiuchi⁴; ¹Osaka University, Japan; ²The University of Tokyo, Japan; ³Takeuchi Electric Co, Japan; ⁴Shimane Institute for Industrial Technology, Japan

Silicon is the strongest candidate for the anode of high density lithium ion batteries (LiB) owing to its high theoretical capacities and have been extensively investigated from the "nanostructure" material design perspectives to cope with fracturing during long recharging cycles and to attain both high capacity and high cycle stability. Such nanomaterials are also expected to be the potential anode of the next generation all solid state LiB with the so-called "bulk cell" structure which carries higher unit capacities. In particular, since unstable formation of solid electrolyte interphase (SEI) that is a detrimental issue for long life operation of the cell with the liquid electrolyte could be no longer the problem for solid state LiB, electrode design to maximize the capacity and cycle stability maintaining high ionic conductivities becomes the major target of the recent research. Even so, the ideal structure of silicon active materials for solid state LiB is not yet identified. Furthermore, to respond to the demands from ever-growing EV markets, the affordable processing of such structured nanomaterials at large quantity has become the practical and essential issues. With these issues in mind, we have successfully produced silicon nanoparticles from low-cost powder feedstock by plasma spraying at throughputs as high as 1.5 kg/h. Furthermore, with particular attention to oxidation of nanoparticles during collection from the reaction reactors, the size and the oxygen content of these nanoparticles are independently controlled. As a result, the important effect of the size and the oxygen content of nanoparticles on the battery properties of the all solid state LiB are separately identified. These characteristics of the nanoparticle structures on the battery performance and the possible ideal nanocomposite particle design will be discussed during presentation.

2:00 PM SF03.02.02

Carbon Nano Onions by Plasma Enhanced Nanoparticle Jet Deposition—Synthesis and Application as High Current Density Electrodes for Redox Flow Batteries Fabio Di Fonzo¹, Simone Fiorini Granieri^{1,2}, Gerardo M. Pagano^{1,2} and Matteo Zago²; ¹Italian Institute of Technology, Italy; ²Politecnico di Milano, Italy

Carbon Nano-Onions (CNO) are carbon nanoparticles with an inner structure constituted of curved graphene sheets, arranged in a concentric arrangement resembling an onion. CNO has shown remarkable characteristics in many fields and electrochemistry in particular. Despite this, CNOs are still produced mainly by annealing at temperature higher than 1500°C nanodiamonds in high vacuum condition [Kuznetsov, V.L. et al. *Carbon* 32, (1994)].

In this work we describe a new production method for CNOs, called plasma enhanced nanoparticle jet deposition, NanoJeD, which allows high throughput and tunability of both CNO structure and of their self-assembly in mesostructures useful for electrochemical energy storage.

The NanoJeD system was invented [US2013017342] about 10 years ago and it has been used so far for the deposition of functional mesoporous films of TiO₂ [I. Biganzoli, *J. Modern Phys.*, 2012], Si [G. Nava et al., *J. Mater. Chem. C.*, 2017] and SiO_x [Nava et al., *Nanotechnology*, 2018]. Simply speaking, the NanoJeD source is a two-stage nanoparticle source comprising a high-pressure reaction chamber and a low-pressure deposition chamber, separated by a rectangular slit nozzle. The pressure ratio between the two chambers is kept above 3 to ensure a supersonic expansion across the slit. In the high pressure chamber the process gas, an Ar-C₂H₂ mixture, is injected perpendicularly to a capacitively coupled, radiofrequency (RF) low pressure plasma operating in dusty mode. Acetylene decomposes within the plasma region and hydrogenated carbon clusters nucleate and grow. The size of the H:C clusters can be controlled by varying the residence time within the plasma region and C₂H₂ partial pressure. The clusters are quenched, focused and accelerated in the supersonic expansion across the slit. The size distribution follows the typical lognormal distribution of a plasma induced chemical reaction, even if the distribution of sizes is quite narrow around 20 nm. The inertial deposition onto the substrate is defined by the Stokes number of each nanoparticle.

Moreover, the pressure ratio among the two chambers defines the impaction kinetic energy of the clusters upon a substrate placed perpendicularly to the slit nozzle. As previously reported with other materials, high pressure ratios lead to dense mesoporous films, whilst low pressure ratios establish the growth of arrays of hierarchical nanostructures [Nava et al., *Nanotechnology*, 2018]. The resulting functional thin film is then thermally treated in vacuum in order to optimize the graphitization degree and defect density. The geometrical constrain of the NP, allow only the formation of curved graphitic planes, in a so

called turbostratic CNO structure. For $800\text{ }^{\circ}\text{C} < T < 1100\text{ }^{\circ}\text{C}$ this process grants a high level defectiveness on the graphitic planes, while preserving high electronic conductivity and specific surface areas in excess of 400 square meter per gram. The above-described process has been characterized by RAMAN, TGA, FTIR, in situ TEM, BET, XPS.

We demonstrate the use of optimized CNO functionalized gas diffusion electrodes for redox flow batteries (RFB). In particular, the mesostructured CNO electrode showed remarkable performances in vanadium RFB applications. The forementioned film, deposited over a carbon paper, has been thoroughly characterized by cyclic voltammetry, symmetric cell and finally in full cell. From charge/discharge curves of full cell test, the system efficiencies have been calculated and a nominal current density as high as 600 mA/cm^2 with 70.8% energy efficiency was obtained, with a stability over 1000 cycles. This result is the best performance reported in the literature for an electrode of pure C and demonstrate the high potential impact of the plasma based NanoJeD technology in the field of energy storage.

2:15 PM SF03.02.04

Low-Pressure Plasma Induced A-Site Exsolution of Ag Nanoparticles from Perovskite Oxide Platform Hessian Khalid, Attaul Haq, Paul Maguire and Davide Mariotti; Ulster University, United Kingdom

Nowadays research on the synthesis and application of nanostructured perovskite oxide has drawn great attention. Among them, exsolution of nanoparticles (NPs) from oxide platform is considered as an effective method for various energy conversion/storage, and catalytic applications. Exsolution offers great controllability on the NPs size and distribution along with displaying good anchorage with the oxide support. Conventional exsolution routes often require extreme processing conditions i.e., elevated temperature and lengthy processing times. Recently, our group has demonstrated a new pathway to exsolution of Ni NPs, within minutes rather than hours, from perovskites ($\text{La}_{0.43}\text{Ca}_{0.37}\text{Ti}_{0.94}\text{Ni}_{0.06}\text{O}_{2.955}$) using plasmas operating at room temperature.¹ Herein, we have demonstrated the exsolution of silver (Ag) NPs from perovskite oxide scaffold through low pressure plasma. Perovskite oxide (POx) having a composition of $\text{La}_{(1-x)}\text{Ag}_x\text{FeO}_3$ (LAFO) with varying Ag doping (0.01 - 0.05 %) was synthesized to understand the maximum solubility of Ag in the perovskite matrix. LAFO was then treated in low-pressure plasma for 15 min resulting in the exsolution of Ag NPs from LAFO matrix at room temperature. The average size of Ag NPs lies within the range of 10-20 nm with a uniform exsolution over the entire exposed surface. The nature of exsolved NPs were found to be metallic as supported by XPS analysis. The strong socketing nature of such NPs were observed in high-resolution TEM. Plasma exsolution of Ag will open new dimension of research in the field of exsolution and provides future solutions in electrocatalysis and in many plasmonic based applications.

References

1. Khalid, H., Haq, A.U., Savaniu, C., Irvine, J.T. and Mariotti, D., 2020, May. Plasma Gas-Phase Electrochemistry to Induce Nanoparticles Exsolution from Non-Stoichiometric Perovskite Oxides. In *237th ECS Meeting with the 18th International Meeting on Chemical Sensors (IMCS 2020)(May 10-14, 2020)*. ECS.

2:30 PM BREAK

SESSION SF03.03: Plasma Catalysis
Session Chairs: Nicolas Boscher and Erwin Kessels
Tuesday Afternoon, November 29, 2022
Sheraton, 3rd Floor, Hampton

3:15 PM *SF03.03.01

Plasma Synthesis of Nanostructure-Supported Metal Nanoparticles for Energy Storage and Conversion: PLA-PECVD Approach and Outlook for Enhanced Sustainability Sylvain Coulombe; McGill University, Canada

The plasma medium enables the direct coupling of renewable (possibly intermittent) electricity sources with chemical reactors providing processing conditions not achievable with traditional approaches. The full gamut of gas phase chemistry, from nonequilibrium to equilibrium is achievable through an almost unlimited number of combinations of reactor and power supply designs, volume and surface interactions, reactants and energy delivery schemes, and materials combinations. Multiphase and multi-stage reactors add even more options. In the context of the energy transition, processing plasmas play multiple roles, from the direct conversion and synthesis of gases (e.g., CO_2 methanation, CH_4 pyrolysis, NH_3 synthesis from and cracking to H_2) and liquids to the synthesis of advanced materials acting as catalysts, selective (ab)adsorbers, energy storage and transport vectors, to name a few applications. Of particular interest is the synthesis and functionalization of nanomaterials and nanostructures with optimal performances and minimal uses of resources. We developed a dual-plasma source approach for the synthesis, deposition and functionalization of fine nanoparticles (NPs) onto nanostructured substrates with minimal use of resources. Pulsed laser ablation (PLA) of a metal target under an inert low-pressure environment leads to the formation of fine (3-5 nm) nanoparticles from the metal vapor plasma plume expansion and supersaturation. Surface charging by the plasma electrons ensures electrostatic repulsion of the as-produced nanoparticles and uniform dispersion over the collecting substrate. The background pressure and ablation time are varied to adjust the granularity and open porosity of the coatings. An alternating system of two pure metal targets allows the synthesis, deposition and formation of triple-interface nanomaterials (Metal A + Metal B) NPs@substrate for optimal adsorption (immobilization) of dissimilar gaseous molecules and catalytic activity. Pre- or post-PLA radiofrequency (RF) plasma-enhanced chemical vapor deposition (PECVD) of the substrate enables surface activation, tuning of the adsorption properties and compatibility with host materials. Simultaneous PLA and RF plasma in reactive gas atmospheres enables the formation of compound nanoparticles (metal oxide, nitride) and thermodynamically unfavorable phases. Several examples of successful nanoparticle decoration (low NP loading) and granular coating formation (high NP loading) will be presented, including platinum nanoparticles on multiwalled carbon nanotubes (Pt NP@MWCNT) as electrocatalysts, ruthenium oxynitride on MWCNT (Ru NP@MWCNT) as supercapacitor electrodes, and cobalt-molybdenum and ruthenium-iron on boron nitride nanotubes as gas conversion catalysts (CoMo NP@BNNT and RuFe NP@BNNT). Preliminary results on the deposition of dual function materials for optimal gas adsorption and catalytic activity will be presented.

Though the PLA-PECVD approach enables the synthesis of nanostructures with extraordinary performances and with high energy and material efficiencies, the sustainability of the process and produced nanomaterials are questionable. Looking ahead, truly sustainable plasma-enabled technologies and materials will need to be circular. Material structure upgradability or at the very least, recyclability, needs to be added as a hard-coded process and material design constraint. Life cycle and circularity assessments shall become as important as the performance and economics in the decision-making processes. This requires a paradigm shift in our usual linear way of thinking which will undoubtedly lead to innovation in plasma processing and material selection and assembly.

3:45 PM SF03.03.02

Plasma-Bioresource-Derived Multifunctional Porous NGQD/AuNP Nanocomposites for Water Monitoring and Purification Darwin Kurniawan¹,

Michael Ryan Rahardja¹, Kostya (. Ostrikov² and Wei-Hung Chiang¹; ¹National Taiwan University of Science and Technology, Taiwan; ²Queensland University of Technology, Australia

Metal-organic composites with controlled structures and properties are actively pursued for diverse applications such as optoelectronics, sensing, imaging, drug delivery, cancer therapy, energy generation and storage, environmental monitoring and purification, and many others. Among those applications, stable 3D architectural multifunctional metal-organic composites with high efficacy in water treatment are highly desired for next-generation clean and sustainable technologies. Current synthesis methods of metal-organic composites face major problems including long preparation time, laborious step, toxic chemicals, harsh solvent, high temperature, uncontrolled structures and properties.

Here we report rapid and environment-friendly plasma engineering of lightweight and porous 3D NGQD/AuNP composites from chitosan using non-thermal microplasmas at ambient conditions without toxic chemicals and high temperature treatment. The highly reactive species generated by the plasma are used to simultaneously synthesize both NGQDs and AuNPs from chitosan containing gold salt. Moreover, synergistic effect of the NGQDs and AuNPs as the nanocross-linkers can accelerate the cross-linking of chitosan to form a 3D porous composite without the need of toxic chemicals and high-temperature treatment. The engineered composites exhibit multifunctional properties including stable solid-state PL emission, tunable surface functionalities, catalytic ability, high porosity, and mechanical robustness, having potential for water treatment including selective PL detection of Hg²⁺, remarkable adsorption of remazol brilliant blue R (RBBR), and catalytic reduction of 4-nitrophenol (4-NP). Furthermore, our method can also yield colloidal NGQDs used for Cr(VI) detection in solution, ranging from 1 to 100 μM with a 61 nM limit of detection (LoD). Our work provides not only a general method to engineer organic-metal composites with defined structures and properties, but also a new insight into their rational design for emerging applications.

4:00 PM SF03.03.03

Oxygen Plasma Induced Heterostructure of 1T-WS₂/a-WO₃ with Hydrogen Spillover Effect as an Advanced HER Electrocatalyst Jinill Cho¹, Hyunho Seok² and Taesung Kim^{1,2}; ¹SungKyunKwan University, Korea (the Republic of); ²Sungkyunkwan University, Korea (the Republic of)

The usage of tungsten disulfide (WS₂) as a hydrogen evolution reaction (HER) electrocatalyst provides several ways to outperform its intrinsic catalytic activity. This study introduces a nanodomain tungsten oxide (WO₃) interface with 1T-WS₂ to improve HER performance by facilitating the transport of protons to the active site. H₂S plasma sulfurization on W layer fabricated 1T-WS₂ and subsequent O₂ plasma was treated to form amorphous WO₃ (a-WO₃), resulting in heterointerface of patchwork structure of 1T-WS₂/a-WO₃. The introduction of a-WO₃ in 1T-WS₂ promotes the hydrogen spillover effect, which indicates the transfer of absorbed protons from a-WO₃ to 1T-WS₂. As a result, 1T-WS₂/a-WO₃-1.2 (ratio of 1T-WS₂ to a-WO₃) exhibits remarkable HER performance in that 1T-WS₂ consumes more protons supplied from a-WO₃ with an overpotential of 212 mV at 10 mA/cm². From density functional theory calculation (DFT), it can be concluded that the WO₃ region shows a higher binding energy for intermediate hydrogen compared to 1T-WS₂. This means a-WO₃ with strong hydrogen affinity plays an important role in hydrogen spillover effect. This approach paves a new way to induce efficient proton transport for high catalytic activity and energy storage.

4:15 PM SF03.03.04

Decoupling Mass Transport and Catalytic Effects in the Plasma-Driven Reduction of CO₂ to CO on Heterogeneous Catalysts Formed by Atomic Layer Deposition Samuel K. Conlin, David Parette and Robert H. Coridan; University of Arkansas, United States

Plasma catalysis has been traditionally used for processes such as the removal of volatile organic compounds (VoC's) from industrial waste streams and the production of ozone. Recently, significant work has studied the use of heterogeneous plasma catalysis for CO₂ conversion. This process can be used to generate chemical fuels from CO₂, such as CO, CH₄ and alcohols. The role of the heterogeneous catalyst to CO₂ reduction in a plasma system is typically the convolution of a number of simultaneous effects. In considering the performance of a catalyst, the effects of surface catalysis, mass transport due to multiscale structure, and local electric field enhancements can each contribute to the overall chemical transformation. The complex nature of these reactors makes it difficult to determine the true reason for differences in performance. Atomic layer deposition (ALD) is a technique capable of depositing layers of catalyst materials with nearly atomic precision in the layer composition. By controlling the composition of nanometer-scale thin films of catalyst onto high surface area scaffolds, we decouple the effects of mass transport and catalysis while having atomically precise control over their composition. Here we intend to develop an experimental scheme for comparing the catalytic effects of plasma CO₂ reduction catalysts without the introduction of significant structural variability. We will describe recent work to use ALD-derived plasma CO₂ reduction catalysts onto high surface area scaffolds. We show how to decouple the mass transport and catalytic effects in these catalyst-scaffold systems using gas chromatography and optical emission spectroscopy. Finally, we compare this approach to more traditional synthesis and coating methods such as sol-gel and wet impregnation methods. As a result, we can unambiguously identify the role that heterogeneous catalysis in plasma-driven transformations of CO₂.

4:30 PM *SF03.03.05

Plasma Catalysis—An Emerging Technology for Power-to-X Xin Tu; University of Liverpool, United Kingdom

The activation of small, inert molecules with strong chemical bonds (e.g., CO₂, CH₄, and N₂) for the production of higher-value fuels and chemicals has attracted significant interest. However, the activation of these molecules remains a great challenge as they are thermodynamically stable and require a significant amount of energy for activation. Non-thermal plasmas (NTPs) offer an emerging and attractive alternative for the activation of strong chemical bonds under ambient conditions. The combination of NTP with heterogeneous catalysis has great potential to generate a synergistic effect from the interactions between the plasma and catalysts, which can activate catalysts at low temperatures and improve the activity and stability of the catalysts, resulting in the remarkable enhancement of conversion, selectivity, and yield of end-products, as well as the energy efficiency of the process. Moreover, plasma processes can be turned on and off instantly, providing great flexibility for decentralised chemical production and energy storage via Power-to-X using renewable energy, particularly intermittent renewable energy. In this presentation, we will show the potential of plasma-catalytic Power-to-X technologies for the synthesis of fuels and chemicals, including CH₄ activation, CO₂ conversion, and ammonia synthesis.

SESSION SF03.04: Poster Session
Session Chairs: Fiorenza Fanelli and Tsuyohito Ito
Tuesday Afternoon, November 29, 2022
8:00 PM - 10:00 PM
Hynes, Level 1, Hall A

SF03.04.01

Fabrication and Performance Evaluation of Lithium Cobalt Oxide (LiCoO₂) Thin-Film Electrodes by PE-PLD Method Yuva Sumiyoshi, Kenzo Ibano, Yuki Yamada, Yasuyuki Kondo, Heun T. Lee and Yoshio Ueda; Osaka University, Japan

Lithium Cobalt Oxide (LiCoO₂) thin films are widely used as cathode materials in lithium-ion and all-solid-state batteries due to their high operating voltage, excellent capacity, and superior cycle characteristics. Pulsed laser deposition (PLD) is one method for synthesizing such thin film electrodes. Many process parameters exist for PLD, including oxygen gas pressure, laser power, target/substrate position, deposition time, and post-annealing temperature. However, wider flexibilities are needed to further control the crystallinity and composition of the functional electrodes. Here, another extension of PLD technology is plasma enhanced pulsed laser deposition (PE-PLD). In this method, PLD is performed in a plasma environment to control film stoichiometry and optimize crystal structure growth. In particular, the use of reactive oxygen plasma results in interaction with both substrate and PLD ablation plume. In PE-PLD, the oxygen plasma is not only a source of oxygen atoms needed for thin film growth, but also a source of thermal energy to the substrate (including surface activation) to assist in the growth of the oxide thin film without additional substrate heating [2]. To date, thin films deposited by PE-PLD using pure transition metal targets have shown favorable properties such as lower resistivity, fewer cracks, and improved crystallinity with increasing oxygen pressure [3]. However, the use of Lithium Cobalt Oxide targets and their effects on thin film electrochemical performance has not yet been reported. In this study, we report on the effect of using LiCoO₂ targets on the deposited thin film crystal structure properties (e.g. lattice constant, texture) and its effect on the electrochemical performance.

[1] Qiuying Xia, Mingzhu Ni, Minghua Chen, Hui Xia. Low-temperature synthesized self-supported single-crystalline LiCoO₂ nanoflake arrays as advanced 3D cathodes for flexible lithium-ion batteries. *The Royal Society of Chemistry* 2019,7,6187-6196

[2] S. Rajendiran, D. Meehan, E. Wagenaars. Plasma-enhanced pulsed laser deposition of copper oxide and zinc oxide thin films. *AIP Advances* 10,065323(2020)

[3] Chia-Man Chou, Chih-Chang Lai, Chih-Wei Chang. Radio-frequency oxygen-plasma-enhanced pulsed laser deposition of IGZO films. *AIP Advances* 7,075309(2017)

SF03.04.02

Deposition Kinetics in the Magnetron Sputter Deposition of Aluminum Doped Zinc Oxide Thin Films Yifei Sun¹, Nadia Foo Kune², Michael Klysinger² and James R. Doyle²; ¹Cornell University, United States; ²Maclester College, United States

We study the growth mechanism of aluminum-doped zinc oxide films deposited using magnetron sputtering by examining the effects of precursor gas phase scattering and substrate temperature on the film properties. The best quality films, deposited at a substrate temperature of 240° C and an argon pressure substrate distance product of 80 mTorr-cm, have a resistivity of 5.4×10^{-4} Ohm-cm and an average transparency in the visible-near IR spectrum (400-1100 nm) of 90%. In general the properties of films deposited on unheated substrates were much more sensitive to working gas pressure than films deposited on heated substrates. The unheated substrate films exhibit a pronounced maximum in carrier concentration and mobility at a pressure-target distance product of 50-80 mTorr-cm, but surprisingly x-ray diffraction and optical transmission results imply that this maximum corresponds to a minimum in film structural quality. This result is consistent with modulation of Zn concentration in the films and electron transport limited by grain boundary scattering. We propose that the strong dependence of film properties with working gas pressure on unheated substrates is due to changes in the properties of the precursor flux due to the differential scattering with the working gas. The unheated films retain a strong memory of the properties of the incident flux, whereas the films deposited at high temperatures are less sensitive to the incident flux due to temperature activated surface reactions. We will present preliminary gas transport and film growth simulation results to support this proposal.

SF03.04.03

Electric Field Measurements in High-Pressure Hydrogen and Nitrogen Environments by Detecting Visible Lights Induced in Coherent Anti-Stokes Raman Scattering Scheme Takeru Koike, Hitoshi Muneoka, Kazuo Terashima and Tsuyohito Ito; The University of Tokyo, Japan

Electric field is one of the most important parameters for controlling plasma materials processing. It accelerates charged particles and the energetic particles are taking various important roles. For example, they are colliding with background species to create reactive species and/or with solid materials to proceed sputtering and/or implantations. Therefore, knowing electric field is essential for advance control of plasma processing. Since various plasma processing in high-pressure environments have been developed, further development of electric field measurements in high-pressure environments are desired.

In this study, we are demonstrating electric field measurements by using coherent anti-Stokes Raman scattering with visible light detections. With irradiations of an infrared laser whose energy is matching to the Raman transition energy of probe molecules and a laser at 532 nm, a light whose energy is sum of ones of two irradiated lasers is induced with electric field with the electric-field-dependent intensity. It has been demonstrated that this method is suitable for high-pressure environments and highly sensitive measurements, e.g. 0.5 V/mm detection, have been realized with an atmospheric-pressure hydrogen environment [1]. It has been also confirmed that the measurement scheme works also in nitrogen-containing environments [2]. Further details will be presented in the symposium.

[1] T. Koike, H. Muneoka, K. Terashima, T. Ito, "Electric-field-induced coherent anti-Stokes Raman scattering of hydrogen molecules in visible region for sensitive field measurement," *Phys. Rev. Lett.* in press.

[2] T. Koike, H. Muneoka, K. Terashima, T. Ito, "Generation of electric-field-induced anti-Stokes Raman scattering in visible region from nitrogen in air," submitted.

SF03.04.04

Hierarchical Wrinkling on Elastomer with Plasma-Polymer Fluorocarbon Thin Film for High-Performance and Transparent Triboelectric Nanogenerator Eunmi Cho^{1,2}, Jin-Seong Park² and Sang-Jin Lee¹; ¹Korea Research Institute of Chemical Technology (KRICT), Korea (the Republic of); ²Hanyang University, Korea (the Republic of)

Triboelectric nanogenerators (TENGs) have recently received extensive attention as a new technology of energy harvesting to serve the increasing demand of energy in the internet of things (IoT) era. Polytetrafluoroethylene (PTFE) is a representative triboelectrification material because of F atom makes it the most attractive to electrons. In addition, properties of PTFE, which are chemical resistance, thermal resistance, low coefficient of friction or good lubricity, and biocompatibility also provide a variety of applications in TENG device. However, PTFE has limited applications in various devices the low flexibility due to its thickness, difficulty in adhering to a substrate due to its low surface energy, and low transparency due to haze. In this study, a plasma polymer fluorocarbon (PPFC) thin film is suggested as a high-performance triboelectrification material for TENG. The PPFC thin film fabricated by sputtering using a carbon nanotubes (CNT)-PTFE composite target exhibits properties similar to those of PTFE, such as hydrophobicity, high surface charge potential and chemical resistance. Additionally, the PPFC thin film shows ultrathin thickness and transparency. Not only that, when a PPFC thin film is coated on a stretchable and biocompatible styrene-ethylene-butylene-styrene (SEBS) substrate, wrinkles are simultaneously generated on the surface, which increases the surface contact area and hydrophobicity. The surface contact area is regarded as a crucial factor that influences TENG performance by increasing

surface charge density upon electrification event. We fabricated a PPFC coated hierarchical wrinkled architecture (HWA) TENG with dual-wavelength wrinkles through additional plasma surface treatment. HWA-TENG shows a high output performance of 200V and 30 μ A due to the combination of increased surface area effect of HWA and high surface charge potential characteristics of PPFC thin film. It has been demonstrated that HWA-TENG can be successfully applied to a transparent triboelectric rain drops energy harvester and a conformal artificial triboelectric skin. HWA-TENG, which has eco-friendly, simple fabrication process and high output performance, is expected to be applied to various devices such as conformal human body sensors.

SF03.04.05

Gas Sensing Properties of Tungsten Oxide with Helium-Induced Nanostructure Hayato Hikota, Kenzo Imano, Heun T. Lee and Yoshio Ueda; Osaka University, Japan

Ethylene is a known plant hormone that is produced in fruits and vegetables at 10-100 ppm levels. It promotes ripening of fruits and vegetables, but its excessive presence can lead to progressive spoilage.

Monitoring ethylene production is important to properly control the quality of fruits and vegetables.

There are many types of gas sensors, including semiconductor, catalytic combustion, and thermal conduction types. Among them, semiconductor gas sensors using metal oxides are advantageous for low-concentration gas detection, and their sensitivity increases with larger surface area and more complex structure.

It has been confirmed that characteristic nanostructures are formed when tungsten is irradiated with helium plasma under certain conditions. The nanostructures are called "Fuzz" and show changes in physical properties such as significant increase in surface area and blackening of the surface. Semiconductor sensors using the nanostructures have been extensively researched and developed, and in fact, nanostructures formed by helium plasma have been confirmed to respond as sensors. Furthermore, the addition of metal nanoparticles to the sensor increases the change in resistance when gas is introduced due to chemical sensitization. This technique has been studied as a method for improving gas sensor performance, and gold, palladium, and platinum were employed as catalyst metals in this experiment.

Based on the above background, this study was conducted to verify the ethylene sensing performance of a sensor using helium-induced nanostructures and to study the reaction rate change when a metal catalyst is added to the sensor.

The gas sensor used in this study was manufactured through a five-step process.

1. a thin film of W was deposited on a glass substrate by magnetron sputtering to a thickness of about 1 μ m.
2. the deposited metal surface was irradiated with He plasma to induce fine nanostructures on the surface.
3. oxidation of the metallic thin film with fuzz structures was performed.
4. Au electrodes were placed at both ends of the sample by electron beam deposition.
5. catalytic metals (Au, Pd, Pt) were added by PLD method.

The fabricated gas sensor samples were placed in a quartz furnace and air containing the sensing gas and dry air were introduced alternately every 10 minutes, and the change in resistance was measured to evaluate the sensing characteristics.

SF03.04.06

Plasma Discharge in Solution for the Synthesis of Highly Dispersed Graphene-Supported Palladium Catalysts for the Fuel Cell Applications SangYul Lee¹, Jung-Wan Kim² and Sungmin Kim³; ¹Korea Aerospace University, Korea (the Republic of); ²Incheon National University, Korea (the Republic of); ³KITECH, Korea (the Republic of)

The direct formic acid fuel cell (DFAFC) has attracted considerable attention due to their high energy efficiency, low operating temperature, and low pollutant emission. Platinum (Pt) is the most commonly used anode catalyst in DFAFC. However, the high cost of Pt based catalysts has been one of the major barriers to limit the commercial application of DFAFC. Palladium (Pd) catalysts were supposed to be promising alternative catalysts in formic acid oxidation reaction due to their lower cost, superior activity and greater resistance to CO compared with Pt-based catalysts. The main interests in preparing Pd catalysts for DFAFC have focused on using graphene sheets as a carbon based supporter of Pd catalysts because of their good dispersibility and high conductivity. Recently, a method for the synthesis of the nanocrystals by means of plasma discharge in liquid phase, so-called solution plasma process (SPP) is introduced and SPP is an attractive method for the synthesis of nanoparticles because it is faster (microseconds), simpler (one-step method) and more cost-effective (only requiring an ion source) than traditional colloid methods. In this study, graphene supported Pd catalysts (Pd/G) were synthesized via a facile one-step SPP process. Palladium(II) chloride (PdCl₂) were used as precursor for the plasma discharge in graphene dispersed D.I. water and the effects of various discharge conditions on the dispersibility of Pd nanoparticles (Pd NPs) on the surface of graphene were investigated. The crystalline structures and morphologies of synthesized catalysts were characterized using X-ray diffraction (XRD) and high resolution transmission electron microscopy (HR-TEM). XRD result shows that Pd/G was successfully synthesized without any impurities and oxides. The peak of graphene (002) was detected near 25° with typical XRD pattern of Pd NPs. In the HR-TEM images, Pd NPs was well dispersed on the surface of graphene, which could be possible via the mono-layer structure of graphene. The dispersibility of Pd NPs increased as applied voltage increased from 1.6 to 3.2 kV and also strongly affected by the discharge time, as well. The high dispersibility at high voltage and increased discharge time could be attributed to the repulsive force caused by the high electric charge on the Pd NPs. Detailed experimental results will be presented.

ACKNOWLEDGEMENT

THIS WORK WAS SUPPORTED BY 2020 KOREA AEROSPACE UNIVERSITY FACULTY RESEARCH GRANT.

SF03.04.07

Biological Functions of Oligo-alginate and Its Derivative Nanoceria Biocomposite Synthesized Using Solution Plasma Jung-Wan Kim^{1,2,3}, Ji Min Kim³, Su-Jin Kang², Davoodbasha MubarakAli⁴ and SangYul Lee⁵; ¹Incheon National University, Korea (the Republic of); ²Graduate School of Incheon National University, Korea (the Republic of); ³Research Center for Bio Materials & Process Development, Incheon National University, Korea (the Republic of); ⁴B.S.Abdur Rahman Crescent Institute of Science and Technology, India; ⁵Korea Aerospace University, Korea (the Republic of)

Solution plasma process (SPP) is an efficient and safe method for the development of functional biomaterials via synthesis of various nanometal particles, depolymerization of bio macromolecules such as alginate and chitosan, or synthesis of various nanometal-macromolecule biocomposites. Alginate is an acidic hetero-polysaccharide with potentials in biomedicine and foods due to non-toxicity and biocompatibility. However, its application as biomaterials is limited due to low solubility and high viscosity. SPP had been employed to depolymerize alginate to oligoalginate (OA) without adding any hazardous chemicals to solve the problems. In previous studies, OA enhanced the growth of lettuce and HEK293 human cells. In this study, alginate solution (0.75%) was discharged by plasma at 800 V, 35 kHz for 15-90 min. The resulting OAs were excellent antioxidants as DPPH and superoxide radical scavengers. OA prepared by discharging plasma for 60 min promoted growth of *Bacillus licheniformis* greatly. The bacterium grew to OD₆₀₀ of 11.8 in tryptic soy broth (TSB) and to OD₆₀₀ of 20.6 in TSB supplemented with 2.0% OA in 72 hr of cultivation. Sporulation rate was greatly enhanced by 2.0% OA (162 folds) in

24 hr of cultivation. Transcriptome analysis revealed that 904 genes out of 4,350 genes were expressed more than two-folds by OA. The most affected genes were those for metabolic process (270 genes) and the genes related to biotin synthesis were expressed 139.5 folds higher. In the meanwhile, expression of *N*-acetylmuramoyl-L-alanine amidase, one of autolysins, decreased by 19.5 folds. Most of the sporulative genes (55/58) were expressed by more than two folds, supporting the stimulation of sporulation by OA. *Nanoceria* (nCe) has potential in biomedical applications due to their distinctive low redox potential of the Ce⁴⁺/Ce³⁺ redox couple. Synthesis of OA-nCe biocomposites was attempted using SPP to enhance antioxidant activities of each component. Plasma was discharged in the OA solutions (0.6-0.8%) containing 1-5 mM CeNO₃ at 800 V, 30 kHz for 15 min. UV-Vis spectroscopy showed two peaks at ~330 nm and ~360 nm with absorbance of 2.1-5.3 and 2.8-4.4, respectively. Among the biocomposites synthesized, 0.8% OA/5 mM nCe showed the highest peaks. FT-IR analysis indicated that chemical bonds of OAs were not affected by plasma discharge. Prevalence of nCe as Ce³⁺ and Ce⁴⁺ was detected in the 0.8% OA/5 mM nCe biocomposite by the XPS analysis, and cubical nCes well-dispersed in the OA matrix were observed by SEM/EDS and TEM. The average size of nCes in the biocomposite was 6.4±2.9 nm with the zeta-potential of -45.1±1.3 mV. DPPH, hydroxyl, super oxide, and H₂O₂ radical scavenging activity of 0.8% OA/5 mM nCe was 75.1%, 100%, 79.1%, and 100%, respectively. The biocomposite inhibited biofilm formation of *Vibrio vulnificus* by 95.9%. Therefore, more effective antioxidant and antibacterial biocomposite was obtained by using OA and nCe via SPP that can be utilized as a ROS quencher and a biofilm inhibitor.

SF03.04.08

Low-Temperature Plasma Synthesis of Plastics-Derived Graphene Quantum Dots Ren-Jie Weng, Darwin Kurniawan, Yu-Yuan Cheng, Yi-Ju Chang, Rong-Chen Jhang and Wei-Hung Chiang; National Taiwan University of Science and Technology, Taiwan

Plastic waste(PW) recycling is an important factor for environmental protection and zero carbon-emission society. However, about 80% PW is not properly-recycled, causing serious environment issue. Traditional recycling methods such as methanolysis, glycolysis, hydrolysis, ammonolysis, aminolysis, and hydrogenation are usually low efficiency, and the products are low economic value added. Graphene quantum dots (GQDs) have obtained a tremendous research interest owing to their unique material properties including tunable bandgaps, biocompatibility, chemical and photo-stability, making them promising candidate for next generation optoelectronics, biomedical-based sensing and imaging, energy conversion and storage, and nanocatalysis. However the current synthesis methods are usually time-consuming, complicated and not environmental-friendly. Here we demonstrate a simple, scalable and generic low-temperature plasma synthesis of PW-derived GQD (PWGQD) using microplasma-assisted electrochemical process. Recently microplasma-based technologies have attracted a lot of attentions due to the advantages for nanomaterials synthesis and processing. Detailed absorbance, photoluminescence (PL), Raman spectroscopy and transmission electron microscopy (TEM) studies suggest the PWGQDs can synthesized from various PW including polyethylene terephthalate (PET), high density polyethylene (HDPE), polyvinyl chloride (PVC), low density polyethylene (LDPE), polypropylene (PP), polystyrene (PS), polylactic acid (PLA), poly carbonate (PC). The morphologies, surface functionalities, defect densities, and optical properties can be controlled by the plasma condition and precursor types. *In situ* optical emission spectroscopy (OES) and *ex situ* mass spectrometry study reveals that plasma-generated reactive species play a role and can interact with the precursors for GQD synthesis in a cascaded chemical reaction.

SF03.04.09

Microplasma Engineering of Bioresource-Derived Surface-Functionalized Graphene Quantum Dots as Ultrahigh Sensitive Optical Nanosensors Neha Sharma, Darwin Kurniawan and Wei-Hung Chiang; National Taiwan University of Science and Technology, Taiwan

Recently, graphene quantum dots (GQDs) caught attention due to their a vast range of application in different fields of science and technology. It is a new type of graphene-based nanomaterials with lateral size less than 10 nm. GQDs have attracted many researchers because of its tunable fluorescence, chemical and photo stability, low toxicity and biocompatibility. Synthesizing GQDs using bioresource-containing precursors is an environment friendly and green route. Graphene quantum dots show high conductivity, larger surface area and long life. Therefore, GQDs can be used as catalysts, fuel cells, drug delivery as well as fluorescence based sensor for sensing of different pollutants, Metal ions, dyes which are very toxic to environment as well as human being as it pollute mainly water sources can cause health issues. It is very harmful to life of plants, animals and also human being. Detection of these metal ion using GQDs can help preventing diseases in human and harmful impact on environments.

There is a number of techniques for the synthesis of GQDs using biomass precursors. However most of them are time consuming, costly, harsh reaction condition and includes use of toxic chemicals. Here we approached microplasma method for synthesis of GQDs from different biomass precursors, which is one of the most promising approaches for nanomaterial synthesis due to its simple approaching and stable and low cost. High electron density in microplasma provides non-thermal dissociation of molecular gases to form reactive species such as OH radical, O radical, O₂ radical. These reactive species in precursor solution interact with chemical species and form GQDs.

Here we report an effective synthesis of tunable GQDs under ambient condition by using microplasma. Here we used different biomass precursor for the synthesis of GQDs, including chitosan, fructose, lignin, citric acid and starch. Tunable fluorescence can be explored by controlling the chemistry of reactions during the synthesis. This method leads to highly crystalline particles with tunable properties and high reproducibility from simple biomass. GQDs synthesized from different biomass shown selectivity to different metal ions due to their surface functional functionalities. This work shows a promising method to synthesis of GQDs with different functionality and not only for metal ion detection but also for many other future applications such as drug delivery, nanomedicines, disease detection and therapy.

SF03.04.11

Tunable 3D Cone or Corn Seed Shape Nanostructure on Polydimethylsiloxane Surface with Oxygen Plasma Treatment Mina Shanbedi and Alamgir Karim; University of Houston, United States

We report on a plasma-based method to fabricate a repeatable three-dimensional structure on polydimethylsiloxane (PDMS) surfaces. The pattern shape and its radius and height are controllable, and the shape can vary between rounded head corn seed shape and cone shape. The PDMS film has a periodic channeling pattern as the base pattern, and then the plasma treatment creates the cone shape with a specific method to impose the film to air plasma. By controlling the time and plasma power and also controlling the physical position of the film to plasma, a 3D shape pattern with a high surface area is shaped on the PDMS surface. This plasma-based procedure provides a simple, fast, and inexpensive method for creating patterned chemical functionalities on 2D and 3D PDMS surfaces for directed assembly and the development of micro-scale sensors and bio-chip devices. The film wrinkling bilayer is characterized by morphology and topography characterizing methods such as atomic force microscopy imaging and scanning electron microscopy. The roughness and the size of the film pattern have been related to the time and power of the plasma device and encountering position. The wrinkling amplitude and the phase grating were also mathematically modeled by considering the wrinkling of the oxidized layer and glassy behavior.

SF03.04.12

Patch Repair of Composites Using Electric Field Plasma Induced Heating and Curing Anubhav Sarmah, Smita Dasari and Micah Green; Texas A&M University, United States

Here, we demonstrate a novel methodology of repairing cracks or damages in carbon fiber reinforced composites (CFRCs) using Dielectric Barrier

Discharge (DBD) induced heating and curing. This study involves the use of a epoxy-impregnated carbon fiber patch or prepreg, which is laid upon the cracked or affected area of a composite in order to eventually mitigate the damage. The DBD applicator generates an electric field plasma; conductive carbon fibers heat up when exposed to this plasma, and the heat is transferred to the surrounding epoxy, thus curing the patch. This cured patch acts as a structural additive to the damaged part, significantly improving its mechanical properties and rendering it fit for further use. Differential Scanning Calorimetry (DSC) experiments show that the glass transition temperature and degree of cure of the exposed patch can be controlled by adjusting the target temperature and residence time of the DBD-induced heating process; patches of varying initial degrees of cure allow for repairs in damaged composites with varying curvatures. Furthermore, the mechanical properties of damaged and repaired samples were compared using tensile testing; a ~78% increase in ultimate tensile strength of the DBD-repaired sample was observed compared to the damaged sample. This study establishes Dielectric Barrier Discharge generated plasma as an energy efficient, out-of-oven alternative for damage repair in carbon fiber composites.

SF03.04.13

Vacancy-Rich Palladium Hydride Synthesis Using Tandem Electrochemical Loading and DC Plasma Metal Sputtering [Oliver Horner](#) and [Curtis Berlinguette](#); The University of British Columbia, Canada

Metal hydrides with lattice vacancies, such as palladium hydride, can exhibit superconductivity with a high transition temperature. The study of these metal hydrides, however, has been limited as their synthesis requires experimentally inaccessible high pressure and temperature conditions. Vacancy formation in metal hydrides can be promoted by two methods: high hydrogen contents within the metal hydride, and sputter-depositing metal in a hydrogen rich atmosphere.

Here, I report the development of a bespoke platform for rapid fabrication of vacancy-rich metal hydrides leveraging metal sputtering and high hydrogen concentration. A pulsed DC argon plasma will sputter deposit metal onto a hydrogen-permeable Pd target that is simultaneously electrochemically-loaded with hydrogen from the opposite face by water electrolysis. This provides a hydrogen-rich atmosphere during sputter deposition and promotes high hydrogen loading.

SF03.04.14

Atmospheric Pressure Plasma Surface Processing of Metals for Water Condensation Antonella Uricchio¹, Teresa Lasalandra¹ and [Fiorenza Fanelli](#)²; ¹University of Bari "Aldo Moro"- Department of Chemistry, Italy; ²National Research Council (CNR), Institute of Nanotechnology (NANOTEC), Italy

Water vapor condensation on solid surfaces is a well-known phase-change phenomenon essential in a wide range of applications such as in thermal power plants, chemical industries, water harvesting, refrigeration, electronics cooling, and seawater desalination [1]. In the last decades, several processes have been optimized to modify metal surfaces in terms of chemical composition, morphology and wettability, in order to modulate their water condensation performances [2].

In this contribution we propose the use of low-temperature atmospheric pressure plasma (APP) for fine tuning the surface properties of aluminum (Al) samples with the aim of developing novel materials for enhanced water condensation. In particular, various APP deposition processes, including plasma-enhanced chemical vapor deposition (PECVD) and aerosol-assisted plasma deposition (AAPD), were used to coat Al samples with both smooth hydrophobic polymer thin films (i.e., hydrocarbon and fluorocarbon films) and superhydrophobic organic-inorganic nanocomposite coatings [3,4]. The chemical composition, morphology and wettability of the different samples was studied by various techniques, such as Fourier-transform infrared spectroscopy, X-ray photoelectron spectroscopy, scanning electron microscopy, white-light vertical scanning interferometry and water contact angle goniometry. The condensation mode, the droplet growth kinetics and the condensate removal mechanism were investigated performing experiments in a purposely designed condensation chamber under controlled conditions (e.g., relative air humidity and subcooling temperature).

Preliminary results revealed that water vapor condensation on hydrophilic pristine samples occurs via filmwise mechanism. In contrast, on hydrophobic plasma-coated samples a stable dropwise condensation mode is obtained. On the other hand, flooding condensation is observed on the superhydrophobic samples coated with nanocomposite films. Here, large pinned droplets form due to condensation within the film micro/nanostructures, leading to surface flooding. Interestingly, by depositing on the nanocomposite coating a thin fluorocarbon layer, coalescence-induced jumping-droplet condensation is achieved. In this case small droplets merge and undergo a self-propelled out-of-plane jumping induced by the surface energy release upon droplet coalescence. Overall, these findings provide novel insights into the use of plasma-assisted deposition processes for the tuning of the water condensation performances of metal surfaces towards industrially relevant applications.

Acknowledgements:

This research was supported by the Italian Ministry for University and Research (MUR) under grant ARS01_00849.

References:

- [1] B. El Fil et al., International Journal of Heat and Mass Transfer 160, 120172 (2020)
- [2] A. Goswami et al., Surface and Interfaces 25, 101143 (2021)
- [3] A. Uricchio et al., Applied Surface Science 561, 150014 (2021)
- [4] A. Uricchio, F. Fanelli, Processes 9, 2069 (2021)

SF03.04.15

3D-Printed Plasma-Treated Super-Amphiphilic Surface for Fog Harvesting Van-Tuan Nguyen, Sayed Sajid Hussain, Eunhee Park, Ngoc-Anh Nguyen, Oleksii Omelianovych and [Ho Suk Choi](#); Chungnam National University, Korea (the Republic of)

The development of super lyophilic surfaces has received tremendous attention due to its wide application in industry and engineering. However, there are still difficulties in preparing super-amphiphilic surfaces, especially those with microstructures. This study reports the fabrication of versatile super-amphiphilic microgroove surfaces (SAMS) through physical and chemical modification. The microgroove structure is achieved through the Fused Deposition Modeling 3D printing method using layer-by-layer (XZ direction) printing, and the surface chemical composition is adjusted through vacuum argon plasma treatment. It also controls the surface roughness coefficient and hydroxyl content through the printed layer height/nozzle diameter ratio and plasma treatment time to optimize the capillary force between the grooves to obtain the most appropriate SAMS. The achieved SAMS demonstrates versatility to absorb common solvents of various polarities, including carbon tetrachloride, ethylene glycol, and water. SAMS showed high fog collection performance of 678 g m⁻² h⁻¹ due to its super amphiphilic properties and microgroove structure, and improved the collection rate by 51.30% and 16.41%, respectively, compared to planar and microgroove surfaces.

SF03.04.16

Plasma-Ionic Liquid Reduction for Synthesizing High-Entropy Alloy Nanoparticles Gilhwan Lee, Enkhjin Chuluunbat, Eunhee Park, Ngoc-Anh Nguyen and [Ho Suk Choi](#); Chungnam National University, Korea (the Republic of)

We report a novel cost-effective and scaling process for syntheses of the quinary IrPdPtRhRu HEA-NPs. The process is based on the plasma ionic liquid

reduction strategy. The combination of PXRD, HRTEM, XPS, and EDX analyses confirms that the application of the developed wet plasma reduction method yields the IrPdPtRhRu HEA-NPs. HEA-NPs with the size of ≈ 5 nm were synthesized under mild temperature, and atmospheric pressure, and without support assistance. All elements constituting the as-prepared IrPdPtRhRu HEA-NPs are uniformly distributed in the FCC single-phase nanostructure. The valence band emission suggests the hybridization of the metal orbitals in the IrPdPtRhRu HEA-NPs. The work function (WF) of 4.63 eV for the HEA is determined by UPS. WF value is lower than the WFs of the metals from which the HEA consists, suggesting higher catalytic activity. The IrPdPtRhRu/C electrocatalyst shows excellent catalytic performance toward hydrogen evolution reaction (HER) with the overpotential of 60 mV at a current density of 10 mA cm⁻². Tafel slope of 40 mV dec⁻¹ was recorded in the alkaline electrolyte. HEA electrocatalyst exhibits long-term stability for 6 h without significant decay under a high constant current density of 100 mA cm⁻². The findings in this study contribute to the basic scientific understanding of catalysts and provide a platform for further development of HEA-NPs electrocatalysts for large-scale applications.

SF03.04.17

Synthesis of Nano-Size Glass Frit Powder by DC Thermal Plasma for Cu Termination in MLCC Kyu-Hang Lee¹, Tae-Wook Kim¹, Ye-Jin Jin¹, Soo-Min Lee¹, Gye-Young Jo¹, Kyu-Hoon Lee¹, Young-Hwan Jeon², Weon-Chae Seo³ and Byung-Koo Son¹; ¹Cheorwon Plasma Research Institute, Korea (the Republic of); ²AMOGREENTECH, Korea (the Republic of); ³AMOTECH, Korea (the Republic of)

With the miniaturization and multifunctionalization of electronic devices, MLCC (Multilayer Ceramic Capacitor), which is used as a passive element, is also required to be miniaturized and high-capacity. For this reason, thinning technology of Cu termination is becoming important. In this study, we synthesized nano glass frit powders of 150 nm or less to apply to MLCC 1005 size products and used these nano glass frit powders to manufacture paste. The characteristics of the manufactured paste were evaluated after the Cu termination was applied. Nano-size glass frit powders have been synthesized by DC (Direct Current) thermal plasma. A micro-sized glass frit powder was fed in the DC thermal plasma. In the high temperature of DC thermal plasma that is of higher than 6,000 K, the glass frit powder was vaporized. The size of produced glass frit particle can be controlled by the working power, the flow of working gas and quenching gas, the process pressure in a reactor and the feeding ration of raw materials. In this study, the conditions for producing nano glass frit powder with a size of 150 nm or less were set to 60 kW for DC power, 80, 100, 120 lpm for working gas flow, 50, 100 lpm for quenching gas flow, 300 torr for process pressure, and 300 g/hr for feeding rate. The produced nano glass powder was produced in paste using high pressure homogenizer and 3-roll-milling equipment. The manufactured paste was dipping and blotting simultaneously through dipping equipment to manufacture Cu termination. Nano glass frit powders that were less than 150 nm in diameter were observed morphology and the paste and Cu termination were observed by morphology, melting temperature and density.

Acknowledgement

This work was supported by the Technology development Program(S3176611) funded by the Ministry of SMEs and Startups(MSS, Korea)

SF03.04.18

Introducing Durable and Uniform Surface Coatings on Garments with Complex Contours Using Low Pressure Plasma Enhanced Chemical Vapor Deposition (PECVD) Dilru R. Ratnaweera, Ranitha Fernando, Samith Amarasena, Malindu Ariyasinghe and Rajitha Botheju; Twinery, Innovations by MAS, Sri Lanka

Textile industry is responsible for about 20% of the global clean water pollution due to the traditional dyeing and finishing processes. After many years of research and development, water free and effluent free surface functionalization of garments is now possible with our patented low pressure PECVD technology. This specific PECVD system consists of a 2000-liter vacuum chamber, which accommodates about 100 medium size t-shirts at once, a chemical dosing system, two parallel radio frequency (RF) electrodes and a dynamic vacuum system. The chemical inlets, chemical guiding system and dynamic vacuum outlets were placed in a manner to assure uniform distribution of activated chemicals within the plasma chamber to functionalize inner and outer surfaces of garments with complex and nonuniform contours. Two main energy sources were used to bring the selected chemistries into the plasma form. First chemicals were introduced into the plasma chamber via a preheating chamber to boost the kinetic energy. Then RF waves were used to bring the preheated chemicals to the plasma stage. Surface functionalizing chemicals were continuously pumped into the change with the flowrates of 0.1 to 1 g/min while maintaining the pressure of the chamber in between 0.1 to 1 mbar. Garments were hanged within the chamber while keeping at least 2 cm gaps among each other.

Surface functionalization was done at two stages. At first, substrates (garments) were activated with Argon plasma for about 5 to 10 minutes. Then the surface functionalization was done for about 20 to 30 minutes with selected chemistries. Surface functionalizing chemicals were carefully selected, where each molecule has two regions, a region that easily activates with the RF source to create plasmas and a region that provides the required end functionality to the fabric surface. The selected chemistries were anchoring to the substrates with covalent bonds while making crosslinked network with adjacent chemisorbed molecules. Different functionalities such as super hydrophobic, oleophobic, hydrophilic, bacteriostatic were introduced on to inner and outer surfaces of the garments in uniform and substrate agnostic manner with the above PECVD system. Process parameters were tuned to assure the performance and wash durability of the surface functionalized garments while maintaining aesthetic intact.

SESSION SF03.05: Plasma-Enhanced Chemical Vapor Deposition

Session Chairs: Fiorenza Fanelli and Davide Mariotti

Wednesday Morning, November 30, 2022

Sheraton, 3rd Floor, Hampton

8:30 AM *SF03.05.01

Environmentally-Friendly Plasma-Enhanced Chemical Vapor Deposition (PECVD) Processes for Industrial Applications Daphne Pappas¹, Dhia B. Salem², Ryan Robinson¹, Andrew Sy¹, Vitalij Hieronymus-Schmidt² and Bjorn Kolbe²; ¹Plasmatreat USA, United States; ²Plasmatreat GmbH, Germany

Industrial emissions of hazardous air pollutants have attracted the attention of environmental protection agencies in most countries around the world. Efforts focus on the enforcement of tight regulations related to the operation of wet chemical stations, paint and coating applications, gaseous manufacturing, photolithography, and electronics packaging processes.

Plasma-Enhanced Chemical Vapor Deposition (PECVD) has been the preferred method for the deposition of thin coatings of well-controlled properties for several decades. It is considered a dry chemistry method as the coatings produced by this technology do not require drying or curing. Also, as nanoscale materials are being produced, they require minimal volumes of precursor chemicals. The low energy requirements and minimal consumption of chemicals classify PECVD processes as environmental-friendly. Additionally, plasma-based processes are used as surface preparation methods for several different types of materials and can replace solvent cleaning which is typically used to improve the wettability and bonding to adhesives, paints, and various

coatings.

Depending on the treated material and the type of adhesives used, plasma surface activation or cleaning are not always sufficient to provide stable long-time adhesion, especially under various environmental conditions, where the variation of temperature and humidity can be detrimental. To overcome this challenge, recent research work has focused on the combination of specialized precursor chemistries and plasma reactive species to generate nanocoatings of tunable properties and functionality.

In this work, the results from a study focusing on adhesion-promoting PECVD coatings on metal surfaces will be presented. Stainless steel and 6061 aluminum alloy substrates were treated with atmospheric-pressure plasma processes utilizing siloxane-based precursor chemistries for the development of nanocoatings. Following the plasma treatment, a polyurethane-based adhesive (Sikaforce-840) was applied on the metal coupons for lap shear testing. Results from the mechanical testing showed an increase of the adhesive strength of steel from 3 MPa to 12MPa, while the aluminum coupons exhibited a 10x increase compared to the untreated materials. Examples from the testing of various organosilicon coating chemistries on a 2-part epoxy adhesive will also be presented. An overview of the fundamental plasma-surface interactions will be discussed to provide a better understanding of the adhesion mechanism.

9:00 AM SF03.05.02

Corona Discharge-Enabled Electrostatic Printing for Ultra-Fast Patterning Zijian Weng¹, Marcelo Farfan¹, Parinitha Giridharan¹, Evan Williams¹, David Murphy¹, Long Wang² and Ying Zhong¹; ¹University of South Florida, United States; ²California Polytechnic State University, Pomona, United States

Substrate pattern printing techniques have been widely studied among the flexible electronics field due to their contributions to vast multifunctional applications. A vast amount of printing techniques has been developed to create complex 2D patterns to achieve different functionalities. However, some current printing techniques require study on the formulation of ink, compatibility of the printing nozzles, and the cleaning process of direct contact method, which are time consuming. In this paper, a novel Corona discharge-enabled electrostatic printing (CEP) ultrafast non-contact method is introduced to print a sub 100 microns resolution pattern within 1 second with the help of "sandstorm" and "net" effects. A detail mechanism study of these effects is shown in this paper to demonstrate the printing principle of CEP by using equation derivation, COMSOL simulations and high-speed camera capturing studies. The Roll-to-Roll-Compatible and binder-free features of CEP enable an ultrafast, simple and pure printing process, patterning high quality flexible electronics with temperature, strain and humidity multifunctional sensing abilities.

9:15 AM SF03.05.03

Flowable Chemical Vapor Deposition of Lightly Porous Low k SiCOH Dielectrics—Remote Plasma Deposition Processing, Film Analysis and Gap-Fill Application in Nano Device Fabrication Son V. Nguyen¹, Thomas J Haigh¹, Matthew T. Shoudy¹, Yiping Yao¹, Huai Huang¹, Hosadurga Shobha¹, Michael Rizzolo¹, Donald Canaperi¹, Jean Wynne¹, Steve Bedell², Kevin Wynne³ and William Lanford³; ¹IBM Research-Albany Nanotech, United States; ²IBM T.J. Watson Research Center, United States; ³University at Albany, State University of New York, United States

Low k and porous low k SiCOH dielectrics have been implemented in Cu Low k metallization of integrated circuits for high-performance nanoelectronic CMOS devices for more than two decades (1). For the last several years, the low k SiCOH dielectric plasma deposition process normally involves the deposition of blanket planar film for using copper damascene interconnects fabrication. Due to the low conformality of plasma deposited in SiCOH film, the dielectric deposition process is normally limited to blanket planar film deposition. For the new generation of 3-D nano device fabrication in which both logic and memory are integrated into a single chip, there is a need to develop an advanced low-temperature low k SiCOH film that enables advanced high aspect ratio gap fill properties. In recent a study, we briefly described an advanced development of the Fully Aligned Via (FAV) process using flowable chemical vapor deposition (FCVD) low k SiCOH and laser/nitrogen implanted FCVD SiCOH film capable of filling recess gaps with self-planarization (2,3) with decent device performance. This inventive FAV approach enables the advanced fabrication of robust 5 nm node device structure fabrication. The advanced remote plasma porous low k p-SiCOH with post UV treatment dielectric, robust reliability, and fabrication integration robustness is needed for the critical and top requirements in the device's reliability and performance.

This paper presents the comprehensive deposition processes, post-deposition UV cure, and film analysis by advanced nuclear reaction analysis, FTIR, RBS, and MIS electrical measurement to optimize the film's stability and composition. The flowable film was engineered for advanced gap-fill application of low k porous SiCOH that can achieve high aspect ratio gap-fill (>10:1 aspect ratio) with low dielectric constant ($k \leq 2.75$) while still maintaining about the same excellent electrical, mechanical, fabrication integration robustness and reliability of conventional plasma CVD SiCOH film. The optimal FCVD process was developed for manufacturing worthy 300 mm CVD system to deposit SiCOH using organosilicon precursors with remote O₂ plasma at low deposition temperature (80-100C) and the UV cure at higher temperature (385-400C).

This FCVD SiCOH film with varying compositions was engineered to create a good low k dielectric capable of excellent high aspect ratio nanostructure gap fill performance but with a lower dielectric constant with good mechanical properties, interface adhesion, and excellent electrical properties.

REFERENCES

- 1) Al Grill, Steve Gate, Son Nguyen, E.T. Ryan, D. Priyadarshini; Appl. Phys. Rev. 1, 011306 (2014); <http://dx.doi.org/10.1063/1.4861876>.
- 2) Benjamin D. Briggs, C. B. Peethala, D. L. Rath, J. Lee, S. Nguyen, N. V. LiCaus, P. S. McLaughlin, H. You, D. Sil, N. A. Lanzillo, H. Huang, R. Patlolla, T. Haigh Jr, Y. Xu, C. Park, P. Kerber, H. K. Shobha, Y. Kim, J. Demarest, J. Li, G. Lian, M. Ali, C. t Le, E. T. Ryan, L. A. Clevenger, D. F. Canaperi, T. E. Standaert, G. Bonilla, and E. Huang, International Electron Device Meeting 2017, Proceeding Volume Paper 14.2.1, pp. 338-341, San Francisco, California.
- 3) "Ion Implantation and Laser Annealing for Toughening Low-k Dielectric in Scaled-down Interconnects". D. Sil, O. Gluschenkov, Y. Sulehria, D. Durrant, H. Huang, N. Lanzillo, H. Shobha, N. O'Haller, Y. Yao, M. Sunder, C. R. Thomas, J. Lee, M. Shoudy, S. Nguyen, T. Nogami, C. B. Peethala, B. Haran, J. Liu, S. Halty, and F. Mazzamuto, International Interconnect Technology Conference, June 2-5, 2019, Paper 6.4, Proceeding IITC, Brussel, Belgium

9:30 AM *SF03.05.04

Plasma Initiated Chemical Vapour Deposition—From the Growth Mechanisms to Ultrathin Low-k Polymer Insulating Nicolas Boscher, Dominique Abessolo Ondo and François Loyer; Luxembourg Institute of Science and Technology, Luxembourg

Plasma processes are highly versatile methods that enable the formation of a vast variety of materials directly in thin films form. Nevertheless, the many reactive species composing plasmas are responsible for a non-negligible number of side reactions, yielding altered chemistries compared to conventional polymerization processes. In this work, we demonstrate how the combination of ultrashort nanosecond plasma discharge ($t_{ON} \approx 100$ ns) and long plasma off-time ($t_{OFF} = 0.1 - 100$ ms) promotes plasma-induced polymerisation over plasma-state polymerisation. During the plasma on-time, a defined number of radical and neutral fragments, which can play both the roles of polymerization initiation or termination groups, are produced. When using vinylic monomers, the conventional polymerization pathway is strongly favoured during the off-time, yielding linear polymer core and unprecedented molecular weights for an atmospheric-pressure plasma processes. In addition to the significance of the monomer structure, the saturation ratio, i.e. the monomer partial pressure over its saturated vapour pressure (P_M/P_{sat}), is demonstrated as a key parameter of the thin film's growth. While low P_M/P_{sat} values result in the prevalence of gas phase reactions, excessively high P_M/P_{sat} values lead to the formation of poorly cured polymer layers, when operating at low plasma

pulse frequency. Taking advantage on the understanding gained on the nanosecond pulsed plasma deposition of polymer layers, ultrathin (*ca.* 10 nm) and conformal polymer layers with low leakage current densities (*ca.* 10^{-9} A/cm² at 20 V) are prepared. The careful selection of the monomer structure enables to decrease the dielectric constant from 4.2 to 2.8.

10:00 AM BREAK

SESSION SF03.06: Plasmas in High-Density Environments I
Session Chairs: Tsuyohito Ito and Uwe Kortshagen
Wednesday Morning, November 30, 2022
Sheraton, 3rd Floor, Hampton

10:30 AM SF03.06.02

Rapid Plasma Synthesis of Blackened Oxygen-Deficient Zinc Oxide Ruairi McGlynn¹, Paul Brunet¹, Praveen Kumar², Quentin Ramasse³, Miryam Arredondo-Arechavala² and Davide Mariotti¹; ¹Ulster University, United Kingdom; ²Queen's University Belfast, United Kingdom; ³SuperSTEM, United Kingdom

Zinc oxide (ZnO) has long attracted attention in a range of fields such as electronics, solar cells, photocatalysis and biological applications.¹ It has a characteristic large bandgap of 3.1–3.4 eV giving rise to absorption of light in the UV range below 400 nm. However, for applications which favour absorption over a wider energy range such as photocatalysis, solar thermal harvesting this restriction to UV is a limitation to application. Therefore, increasing the range of absorption represents a necessity to drive these technologies further. More recently it is emerging that modifying the number of defects in the Zinc material can give rise to enhanced photocatalytic activities and even absorption in the visible range. Several groups have utilised chemical methods to formulate hydrogenated ZnO and other forms of defect-rich ZnO by chemical methods.^{2–4} These materials do not display the characteristic white colouration, appearing visibly black, further demonstrated by a reduction from 94% to sub-45% reflection in the visible light range.² These materials demonstrated enhanced photocatalytic properties when compared to traditional ZnO with test cases of methylene blue² or methyl orange degradation³ and hydrogen evolution.⁵ Thus far the theories presented in literature have highlighted the key role of defects in the crystal lattice, in particular oxygen deficiencies or vacancies in the colour change from the typical ZnO white to black.^{2,6} In this work we report a new method to produce Zn-rich ZnO complex produced using atmospheric-pressure plasma. The addition of a 2% H₂/Ar mixture at 0.1 litres per minute into the standard 1 litre per minute flow of helium gas is critical to the formation of the darkened powder. We have characterized the synthesised material, utilising transmission electron microscopy, alongside X-ray diffraction and X-ray photoelectron spectroscopy to characterise the structural information including defects and surface chemistry respectively. The material we produce is determined to contain two long-ordered and well-defined structures, a shell of Wurtzite ZnO and a core that is comprised of either O-deficient Zn or Zn in a hexagonal lattice. There is a clear and sharp change in atomic plane between these regimes. In addition, the stability of the material in several typical solvents or under thermal annealing at several hundred degrees Celsius is explored, before we test the material for several different applications, such as solar thermal and biological applications.

References

- (1) Qi, K.; Cheng, B.; Yu, J.; Ho, W. *J. Alloys Compd.* **2017**, *727*, 792–820. <https://doi.org/10.1016/j.jallcom.2017.08.142>.
- (2) Xia, T.; Wallenmeyer, P.; Anderson, A.; Murowchick, J.; Liu, L.; Chen, X. *RSC Adv.* **2014**, *40* (78), 41654–41658. <https://doi.org/10.1039/c4ra04826a>.
- (3) Yan, C.; Yan, G.; Cheng, W.; Qiu, Y.; Wang, L. *Mater. Lett.* **2020**, *265*, 127442. <https://doi.org/10.1016/j.matlet.2020.127442>.
- (4) Badreldin, A.; Abdel-Wahab, A.; Balbuena, P. B. *ACS Appl. Energy Mater.* **2020**, *3* (11), 10590–10599. <https://doi.org/10.1021/acsam.0c01642>.
- (5) Zhang, N.; Shan, C. X.; Tan, H. Q.; Zhao, Q.; Wang, S. P.; Sun, Z. C.; Xia, Y. De; Shen, D. Z. *Nanotechnology* **2016**, *27* (22), 1–7. <https://doi.org/10.1088/0957-4484/27/22/22LT01>.
- (6) Sharma Kanakillam, S.; Krishnan, B.; Sepulveda Guzman, S.; Amilcar Aguilar Martinez, J.; Avellaneda Avellaneda, D.; Shaji, S. *Appl. Surf. Sci.* **2021**, *567* (April), 150858. <https://doi.org/10.1016/j.apsusc.2021.150858>.

10:45 AM SF03.06.03

Opportunities for Metal Oxide Synthesis with Atmospheric Pressure Microplasmas Davide Mariotti; Ulster University, United Kingdom

Metal oxides are an extraordinary class of materials that have found wide applicability for a number of century-defining technologies (e.g. flat-panel display, capacitors and energy storage) mainly due to their dielectric properties and chemical inertness. Doping, defect engineering, quantum confinement and extending to clusters, ternary or high entropy oxides can create disruptive materials with new or improved properties. Atmospheric pressure microplasmas represent a viable synthesis platform to achieve exceptional tuning capability therefore achieving an exquisite control of the size, composition and defects of metal oxide nanoparticles. In this contribution we will report on the synthesis and properties of metal oxide nanoparticles spanning a wide range of chemical compositions including oxides from Ca, Co, Cu, Mn, Mo, Ni, Sn, and Zn. We will report on the technological and application opportunities as well as on the fundamental aspects that relate to the synthesis methodologies and material structural properties. Future prospects involving complex oxides will also be presented and discussed.

References

- [1] Ni C *et al.* *Green Chemistry* **20** (2018) 2101
- [2] Wagner A J *et al.* *Physical Review E* **80** (2009) 065401R
- [3] McGlynn R *et al.* *Solar Energy* **203** (2020) 37
- [4] Velusamy T *et al.* *Plasma Processes & Polymers* **14** (2017) 1600224
- [5] Nolan H *et al.* *Plasma Processes & Polymers* **14** (2018) 1800112
- [6] Liu Y *et al.* *Scientific Reports* **5** (2015) 15765
- [7] Haq AH *et al.* *Nature Communications* **10** (2019) 817

SESSION SF03.07: Plasmas in High-Density Environments II
Session Chairs: Tsuyohito Ito and Makoto Kambara
Wednesday Afternoon, November 30, 2022
Sheraton, 3rd Floor, Hampton

1:30 PM SF03.07.01

High-Strength Composites Fabricated Using Graphene Synthesized in Atmospheric Plasmas Arpita Bhutani, Jonathan Griffin, Sidney Chenevert, David Miller and Albert Dato; Harvey Mudd College, United States

Graphene created using atmospheric-pressure microwave-generated plasmas can enhance the strength of acrylonitrile butadiene styrene (ABS), which is a thermoplastic polymer that is widely used in automotive components, electronic devices, and 3D printing. Here we present new knowledge on the relationships between the processing, structure, and properties of ABS reinforced with gas-phase-synthesized graphene (GSG). The process of dispersing GSG into ABS and the injection molding of ABS-GSG composites will be discussed. Additionally, transmission electron microscopy images of the filler-matrix interfaces in ABS-GSG specimens will be shown. We reveal that loading ABS with a relatively small amount of GSG (0.1 wt%) results in a remarkable 19.4% increase in tensile strength. The results suggest that unique strengthening mechanisms exist in ABS reinforced with graphene obtained using microwave plasma technology. This presentation highlights how substrate-free plasma-based techniques produce graphene that can greatly contribute to the development of high-strength composites.

1:45 PM SF03.07.02

Influence of the Surface Roughness on the Adhesion of Thermal Plasma Spray Al_2O_3 Coatings Tony Krüger¹, Holger Testrich¹, Rüdiger Foest¹, Thorben Kewitz¹ and Franz Faupel²; ¹Leibniz-Institute for Plasma Science and Technology, Germany; ²Christian-Albrechts-University of Kiel, Germany

Atmospheric thermal plasma spraying is an innovative coating process, widely used in aerospace, medicine, and other industries to enhance the characteristic work piece surface properties, e.g. wear resistance, corrosion resistance, thermal insulation, etc. For surface customization, masks are used to protect areas of the workpiece from unwanted coatings. However, due to the nature of plasma spraying, a gradual accumulation of spray material on masks can lead to a change in the flow dynamics near the edges causing a loss of contour accuracy and thickness homogeneity of the actual coating. Additionally, accumulated particles can fall off the masking and get embedded in the coating. This poses a problem, e.g. for conductive coatings, as these particles represent impurities that can lead to a change in the conductivity or resistance.

To tackle this problem, research is done on generating masks' surface conditions that affect film adhesion and promote swift delamination, while optimum plasma spraying conditions are maintained. Samples were spray coated with Al_2O_3 (2kg/h) using atmospheric pressure plasma spraying. As device served an Oerlicon Metco F4MB-XL Spray Gun (DC, I=600A, U=32V, gases: Ar, H₂). In thermal spray processes, adhesion between the coating material and the substrate surface is of complex character. However, besides of physical (van der Waals) and chemical interactions, and metallurgical processing, adhesion of coatings to a substrate surface is mainly established by mechanical anchoring [1, 2].

In order to improve the understanding of relevant coating mechanisms, the influence of the surface roughness on coating adhesion is studied on a methodical basis. For this reason, prior to applying the spray coating, the surface roughness R_a of stainless steel (Type: 1.4301) was enhanced by using corundum blasting to provide a defined reference value. Subsequently, R_a was systematically reduced by means of Plasma Electrolytic Polishing (PEP), in order to provide a sample series with a defined range of surface roughness. PEP is an environmentally friendly hybrid process, assumed to combine classical electrolysis and atmospheric plasma processes. It is used to efficiently smooth out surfaces, clean off surface residues, and deburr edges, by using an electrolyte that is harmless during disposal and therefore relatively environmentally friendly, compared to classical electrolysis.

Tactile profilometry was carried out to measure the surface roughness obtained in PEP treatment (measured with KLA+ Alpha-Step® D-600). Moreover, the effects of additional interface layers (SiO_x, TiN) and substrate materials (quartz glass) on film adhesion were investigated. During PEP, with increasing polishing time the surface roughness could be reduced to a minimum of $R_a \approx 0.05 \mu\text{m}$. Further reduction was not achieved, presumably, because the (selective) material removal during PEP of steel stimulates both processes; surface smoothing and roughening.

Whereas the sandblasted specimens provide sufficient coating adhesion, the formation of adhering coatings is efficiently suppressed at smaller R_a . Below a critical roughness, swift and complete delamination is observed for Al_2O_3 coatings with a typical thickness above 100 μm . Additionally, it was observed that Al_2O_3 coatings exhibit low adhesion on smooth quartz glass, whereas solid coatings on corundum blasted glass surfaces could be attained.

(Funded by the European Union and the State of Mecklenburg-Western Pomerania, TBIV-1-321).

[1] Ruzbarský, J. & Panda, A., Plasma and Thermal Spraying, Springer International Publishing, 2017, DOI: 10.1007/978-3-319-46273-8

[2] Kewitz, T. et al., Atmosphärendruck-Plasmaspritzen in der Hochspannungstechnik - thermische und elektrische Isolierschichten aus Al_2O_3 , Jena, MEOX Projektmanagement GbR, 2019, 59-68, ISBN: 978-3-00-063646-2

2:00 PM *SF03.07.03

Laser-Assisted Mass Spectrometry in Open Air Yong-Feng Lu; Univ of Nebraska, United States

Laser-assisted mass spectrometry (LAMS), based on laser ablation of solid samples, has been one of the most powerful analytical techniques for atomic and molecular analyses. However, conventional mass spectrometry (MS) needs to be carried out in a vacuum, which largely limits the analysis efficiency. To extend the applications of LAMS and make it fit for open-air and in situ applications, we investigated open-air operated LAMS (OA-LAMS) for simple and fast analyses. However, OA-LAMS brings challenges. The ambient gases, such as O₂ and H₂O, react with the ions and atoms produced by laser ablation during the plasma cooling process which leads to the formation of compound ions and complicates the spectra and analyses. The lifetimes of the ions and atoms are also reduced due to the fast recombination in the open-air environment, resulting in low sensitivity. The signals detected in OA-LAMS also show nonlinear trends which complicates the subsequent analyses.

Analyzing signatures of an isotope, used for deciphering nuclear events, controlling radioactive wastes, etc., is one of the most powerful abilities of MS. Therefore, open-air interference on isotope analyses in OA-LAMS needs to be addressed. The primary cations, such as Pb^+ and UO_2^+ , demonstrate obvious light-isotope enrichments. On the other hand, the secondary cations, such as PbOH^+ and UO_2OH^+ , yield isotope signatures close to the bulky samples. Isotope signatures were also investigated under different conditions, such as humidity, laser power, and sampling distance. The results demonstrate a potential methodology for characterizing isotope signatures in OA-LAMS.

Three approaches were investigated to improve the OA-LAMS sensitivity using magnetic field, resonant excitation, and external ion source.

In magnetic-field-enhanced OA-LAMS, a magnetic field is used to confine the laser-induced plasma (LIP). The increased collision in plasma enhances the ionization rate of the analytes. In addition, the nonuniform nature of the magnetic field generates a force to drive the positive ions toward the weaker field, which is the direction of the MS inlet orifice. Obviously improved signature-to-noise ratios (SNRs) are observed for Al, Si, and Pb. With the magnetic field, the limit of detections (LODs) at a low ppm level have been achieved.

In resonant-excitation-enhanced OA-LAMS, a wavelength-tunable pulsed laser is used to match the specific atomic and molecular excitation states of the analytes. Through resonant excitation, the analytes in the LIP are more likely to form detectable ions. Different atomic excitation and molecular excitation states of U were investigated. The results indicate that molecular excitation of uranium dioxide (UO_2) at 314.09 nm can reach the best LOD for U (10 ppb).

In ion-enhanced OA-LAMS, an external DART ion source is incorporated. Analytes are vaporized from the solid phase through laser desorption. They are ionized by the external DART ions (protonated water) through penning ionization and charge transfer. In addition, the DART ions are also activated by laser irradiation since the wavelength of the laser is in the range of the OH bending vibrations. Rhodamine 6G, urea, and testosterone were investigated. The results show obvious sensitivity enhancements for all analytes. The enhancement factors for R6G, urea, and testosterone were 31, 11, and 4, respectively.

2:30 PM BREAK

3:30 PM SF03.07.04

Graphene Synthesized in Atmospheric Plasmas is Inherently Superhydrophobic [Albert Dato](#), M. Weston Miller and Makenna Parkinson; Harvey Mudd College, United States

Graphene produced in the gas phase using atmospheric-pressure microwave plasma technology exhibits a remarkable lotus-like water repellency. The ability of lotus leaves to repel water is desired in a wide range of applications, such as self-cleaning surfaces, waterproof textiles, anti-icing coatings, and biomedical devices. Creating artificial materials that exhibit the nonwettability of natural lotus leaves has been challenging. Superhydrophobic surfaces have been fabricated by mimicking the structure and chemistry of lotus leaves. Additionally, water-repellent coatings have been created by modifying graphene obtained through the exfoliation of graphite or substrate-based processes. However, the large-scale manufacturing of a broad range of nonwettability applications through biomimicry or modified graphene is neither sustainable nor practical. In this presentation, we reveal that gas-phase-synthesized graphene (GSG) is inherently superhydrophobic. The comparable static contact angles and roll-off angles of water droplets in direct contact with lotus leaves and as-synthesized GSG will be shown. Fascinating high-speed camera videos of water droplets impacting and rebounding from lotus leaves and GSG will be discussed. Furthermore, we demonstrate that hydrophilic materials instantly become superhydrophobic when coated with GSG. These results indicate that graphene sheets created through substrate-free plasma-based techniques have unique water-repelling mechanisms. This presentation highlights how plasmas can greatly contribute to the development of highly water-repellent surfaces.

3:45 PM *SF03.07.06

Pulsed Plasmas in Liquids for Materials Applications [Achim von Keudell](#); Ruhr University Bochum, Germany

Plasmas inside and in contact with liquids are a promising field for material synthesis and electrolysis. The understanding of the physics of the plasma ignition and sustainment is, however, still in its infancy due to the complexity of the phenomenon. For example, in the case of nanosecond high voltage pulses applied to a sharp tungsten electrode, electrostriction is very large so that rupture of the liquid occurs at a negative pressure of at least 24 MPa. Cavitation voids are formed and ignition inside these voids may occur. However, also field effects inside the liquid or at the tungsten liquid interface may cause ignition. Ignition converts the liquid spontaneously in the plasma state, which then expands this initial void to form a bubble. This creates a pressure pulse of the order of 10s of GPa depending on the HV voltage and the emission of acoustic waves that can be observed via shadowgraphy. The plasmas are observed with emission spectroscopy using a temporal resolution of 2 ns. This reveals a broad continuum consisting of black body radiation and line radiation of the hydrogen Balmer series. The hydrogen emission lines are significantly broadened from Stark broadening and affected by self absorption. It is shown that the plasma behave very similar for positive and negative polarity applied to the tungsten electrode. The temporal evolution of the electron density does not significantly depend on the polarity. This indicates that plasma generation follows similar mechanisms for both polarities. It is proposed that field ionization of water molecules or field emission at the internal surfaces of nanopores drives ionization and plasma propagation. Examples for the use of such plasma for electrolysis are given.

SESSION SF03.08: Plasmas for Functional Materials

Session Chairs: Carla Berrospe-Rodríguez and Achim von Keudell

Thursday Morning, December 1, 2022

Sheraton, 3rd Floor, Hampton

8:45 AM *SF03.08.01

Low-Temperature Plasmas for Materials Discovery—InGaN Nanoparticles with Tunable Properties [Rebecca J. Anthony](#); Michigan State University, United States

Nanomaterials continue to offer exciting opportunities to explore materials properties that could enable a vision of sustainable energy production, personalized health care, and new technologies for enhancing the success and well-being of global populations. Further, as devices and applications enabled by nanomaterials mature, there is a need to use scalable and efficient manufacturing strategies for production, which is where plasma reactors enter the picture. Research teams across the world have demonstrated the vast range of nanomaterials that are accessible using plasmas, including some nanoparticles that are difficult or impossible to synthesize using colloidal approaches, and with precision in size, surface properties, and functionality that are prohibited by other vapor-phase methods. One emerging area is in the tunable synthesis of alloyed nanoparticles, which can exhibit complex process-property-function relationships. Here, we present on alloys of indium and gallium nitride nanoparticles made using a flow-through nonthermal plasma reactor.

GaN is a wide-bandgap semiconductor, making it important as a UV source for lighting and communications, and for power transistor applications, as well as potential use as a photocatalyst and in other energy technologies. By contrast, indium nitride (InN) has a bandgap in the infrared, and is an effective optical absorber and can be used in solar photovoltaics and high-speed electronics. Alloyed indium gallium nitride (InGaN) has a tunable bandgap between these extremes, spanning the visible spectrum based on composition. This bandgap tunability has been used in light emission technologies for epitaxially grown layers and fabricated quantum well structures. Previously we have reported on gallium nitride (GaN) nanoparticle synthesis using plasmas, demonstrating size control via adjusting the residence time of the nanoparticles in the plasma. More recently we have synthesized InN nanoparticles in a similar reaction pathway, and we present our results exploring InGaN nanoparticle synthesis including demonstrating bandgap tunability. However, the competing influences of quantum confinement-based bandgap widening, composition-based bandgap adjustment, and internal strain and surface effects introduce a large degree of uncertainty in predicting the bandgap of these materials. This brings about an important opportunity to use the versatility of plasma reactors to uncover the physical, chemical, and mechanical contributions to property and function for InGaN nanoparticles, towards predictable nanomanufacturing. In this presentation, we share our findings on controlling composition, size, and surface of plasma-produced InGaN nanoparticles using a nonthermal plasma reactor, with perspectives on the potential for materials discovery using plasmas.

9:15 AM SF03.08.02

New Plasma-Enabled Synthesis of Designer Nanoporous Metallic Films [Peer Fischer](#)^{1,2}, Hyunah Kwon¹, Hannah N. Barad^{3,1}, Alex R. Silva Olaya⁴, Mariana Alárcon-Correa^{1,2} and Gunther Wittstock⁴; ¹Max Planck Institute for Intelligent Systems, Germany; ²Heidelberg University, Germany; ³Bar-Ilan University, Israel; ⁴Carl von Ossietzky University of Oldenburg, Germany

Nanoporous metal films (NPMFs) are metallic layers of nanometric thickness containing voids, similar to pores in three-dimensional materials. This structure allows the presence of a high number of low coordinated atoms that determine the physicochemical properties of the films. NPMFs are used in transparent electrodes, plasmonically active materials with very high surface-to-volume ratios, and as active electrode materials for energy conversion and sensing. Generally, NPMFs are obtained by wet chemical dealloying, which involves the selective chemical etching of the less-noble metals from the alloy, which cannot be completely removed for thermodynamic reasons. The remainder of the less noble element (usually dopant levels) is difficult to precisely control and affects the characteristics of the resulting NPMFs. Additionally, the requirement of an alloy restricts the minimum thickness that can be manufactured with the desired porous structure/interconnected solid phase.

Here, we report a novel dry synthesis method based on the plasma treatment of metal nanoparticles formed by physical vapor deposition that produces ultra-thin NPMFs with highly curved and adjustable pore structures, and thicknesses in the order of the diameter of the original nanoparticles. Our approach is general, requires no solution-processing or harsh chemicals, and can be applied to many metals including non-noble ones (e.g. Au, Pt, Ni, and Fe) and their combinations. Nanopore and ligament sizes can be easily tuned by control of plasma conditions (type of gas, pressure, etc.). The resulting NPMFs are impurity-free, remarkably stable, and highly active for electrocatalysis. We demonstrate various NPMFs using different metals and their combinations, including several that have thus far not been shown to form NPMFs. We also present their remarkable performance, including their optical and electrical properties, as well as their exemplary electrocatalytic performance. We expect that these novel nanomaterials, synthesized by the plasma-based dry method we developed, will allow for their incorporation into many new applications and extensively advance the NPM field.

9:30 AM OPEN DISCUSSION

10:00 AM BREAK

SESSION SF03.09: Plasmas for Green and Bio Applications
Session Chairs: Carla Berrospe-Rodríguez and Achim von Keudell
Thursday Morning, December 1, 2022
Sheraton, 3rd Floor, Hampton

10:30 AM SF03.09.01

Hydrogen Plasma Reduction of Iron Ore for “Green Steel” Production Zichang Xiong, [Sachin Kumar](#), Julian Held, Peter Bruggeman and Uwe R. Kortshagen; University of Minnesota-Twin Cities, United States

In 2020, steel production accounted for 7-9% of anthropogenic CO₂ emissions. Decarbonizing steel production is a priority for both governments and industry. Before this background, the direct reduction of iron ore with “green hydrogen”, produced via electrolysis of water with renewable energy, could make important contributions towards green steelmaking. In this presentation, we present results of the reduction of iron oxide, both hematite and magnetite, with hydrogen microwave plasma. The plasma is maintained by coupling microwave power in the kW range into an argon:hydrogen gas mixture. Micrometer-sized iron oxide particles are entrained in this gas stream and pass through the plasma on timescales of hundreds of milliseconds. We demonstrate more than 90% reduction of both hematite and magnetite under optimal conditions. The proposed plasma technology is fully electric and does not rely on carbon-based fuels for heat or reduction. It also eliminates the energy required and emissions related to pelletization of iron ore concentrates. As such, it may provide a pathway towards carbon-free steel production with “green hydrogen.”

Acknowledgment:

This work was supported by the University of Minnesota under the Ronald L. and Janet A. Christenson Chair in Renewable Energy.

10:45 AM SF03.09.02

Green Steel Making Through Hydrogen Plasma Reduction of Iron Oxides [Dierk R. Raabe](#), Isnaldi S. Filho, Yan Ma and Hauke Springer; Max Planck Institute for Iron Research, Germany

We present a study about the reduction of iron oxide (hematite) using a hydrogen-based plasma, produced in an electric arc furnace. The evolution of chemical composition and phase transformations was investigated in several intermediate states. The balance between the initial input mass and the arc power determines hematite reduction kinetics. Within 15 minutes of exposure to hydrogen plasma, full reduction is achieved. The wüstite reduction is the rate-limiting stage towards complete reduction. The reduction reaction is exothermic, and the total conversion rates (i.e. iron production) are equivalent to hydrogen-based direct reduction. Micro- and nanoscale chemistry and microstructure probing as well as energy dispersive spectroscopy and atom probe tomography show that the gangue elements partition to the remaining oxide regions. Si-enrichment was observed in the interdendritic fayalite domains, at the wüstite/iron hetero-interfaces and in the oxide particles inside iron. With proceeding reduction, however, such elements are gradually removed from the samples so that the final iron product is nearly free of gangue-related impurities. Our findings provide microstructural and atomic-scale insights into the composition and phase transformations occurring during iron ore reduction by hydrogen plasma, propelling better understanding of the underlying thermodynamics and kinetic barriers of this essential process (1).

(1) Souza Filho, I. R.; Ma, Y.; Kulse, M.; Ponge, D.; Gault, B.; Springer, H.; Raabe, D. Sustainable Steel through Hydrogen Plasma Reduction of Iron Ore: Process, Kinetics, Microstructure, Chemistry. *Acta Mater.* 2021, 213, 116971.

11:00 AM SF03.09.03

Challenges in Plasma-Based Low-Temperature Synthesis of MAX-Phase Protective Coatings for Metallic Bipolar Plates [Martin Rohloff](#)¹, Uwe Lindemann¹, Antje Quade¹, Anja Albrecht¹, Manoj Prabhakar², Chun-Hung Wu², Julian Kapp³, Verena Lukassek³, Michael Rohwerder² and Angela Kruth¹; ¹Leibniz Institute for Plasma Science and Technology, Germany; ²Max Planck Institute for Iron Research, Germany; ³Zentrum für BrennstoffzellenTechnik, Germany

For the transition from a fossil-based to a sustainable energy economy, humanity urgently needs a clean energy supply. In this context, hydrogen plays a

key role as it serves as chemical energy carrier which solely produces water as reaction product in cold combustion processes in fuel cells. A maximum voltage of 1.23 V can be harnessed from such a fuel cell in theory. To increase gained power from fuel cells, the number of single fuel cells needs to be multiplied and combined to a fuel cell stack.

Bipolar plates are considered as crucial components in fuel cell stacks as they establish electric connection between the single cells. Moreover, bipolar plates also need to supply reaction gases and distribute them all over the whole electrode areas, have to take care for gas separation between the single cells, serve for cooling of the cells, and need to provide fluid and gas tight sealing of the system. For this purpose, bipolar plates made of metals and alloys are most promising alternatives for conventional graphite-compound-based bipolar plates. However, the biggest drawback of a metallic bipolar plate is its insufficient resistance to the harsh chemical conditions in fuel cell stacks under operation conditions. In consequence, corrosion resistant coatings need to be applied onto the surface of metallic bipolar plates. Recently, research on novel materials and materials processing routes for corrosion protection of metallic bipolar plates is intensified. In this context, MAX-phases are of emerging interest.

By discovery of the novel complex carbide Ti_3SiC_2 by Jeitschko and Novotny [1] and subsequent intensive research by Barsoum et al. [2-5] it was shown that a class of ternary materials comprised of an early transition metal ("M"), an A-group element (mostly group IIIA and group IVA, "A"), and C and/or N ("X") according to the general formula $M_{n+1}AX_n$ ($n = 1-3$) exhibits remarkable properties. Due to weak metallic bonds between M and A as well as due to covalent bonds between M and X, these materials exhibit tremendous combination of ceramic and metallic properties like corrosion resistance, hardness and high electric conductivity. The unique combination of electric conductivity and chemical inertness enables MAX-phase compounds to be applied as corrosion resistant coatings for electrical components working under harsh chemical conditions, e.g. as thin corrosion resistant coatings for metallic bipolar plates.

However, biggest challenge in application of dense MAX-phase coatings on metallic substrates are high temperatures of usually about 750 °C required for crystallization of amorphous precursors – temperatures which cause unfavorable changes in the metallic substrates, e.g. recrystallization processes in steel. Hence, development of a low-temperature synthesis route for MAX-phase-based coatings is crucially required to enable their application as protective coating and to draw benefit from their unique set of properties.

In this work, we will elucidate our low-temperature plasma-process-based approaches to deposit MAX-phase coatings by means of high power impulse magnetron sputtering in combination with plasma immersion ion implantation. Biggest challenges will be derived by in-depth characterization (XRD, XPS, SEM/EDX, TEM/EDX/SAED) of obtained coatings in correlation with locally and compositionally resolved electrochemical corrosion testing.

[1] W. Jeitschko, H. Nowotny, Monatshefte für Chemie 98, 329 (1967).

[2] M.W. Barsoum, T. El-Raghy, J. Am. Ceram. Soc. 79, 1953 (1996).

[3] A.T. Procopio, T. El-Raghy, and M.W. Barsoum, Met. Mat. Trans. 31A, 333 (2000).

[4] M.W. Barsoum, M. Ali, T. El-Raghy, Characterization of Ti_4AlN_3 , Met. Mat. Trans. 31A, 1857 (2000).

[5] A.T. Procopio, T. El-Raghy, and M.W. Barsoum, Met. Mat. Trans. 31A, 373 (2000)

11:15 AM SF03.09.04

Influence of a Remote Plasma on the Chemical Vapour Deposition of ZrO_2 Based Layers Philipp A. Maaß, Vitali Bedarev, Sebastian M. Beer, Marina Prenzel, Marc Böke, Anjana Devi and Achim von Keudell; Ruhr-University Bochum, Germany

Chemical vapour deposition (CVD) is a widely applied technique used for thin film deposition. The combination with a plasma source (PECVD) enables the fine-tuning of parameters, opening new possibilities for the fabrication of functional coatings, such as thin thermal barrier coatings.

An evaporated metalorganic precursor is transported into the reaction chamber by a nitrogen-flow of 50 sccm at pressures of about 100 Pa. A ZrO_2 layer is deposited onto a heated substrate in the centre of the chamber with a growth rate of several 100 nm/h.

To influence and improve the reaction chemistry, a microwave plasma source is mounted opposite the substrate surface. The discharge interacts with the incoming precursor molecules, with the aim to reduce the reaction temperature and change the deposition properties.

During this process, the growth rate and substrate temperature are monitored by in-situ ellipsometry to obtain insights into chemical kinetics and mass transport phenomena. The deposited layers are characterised in stoichiometry and crystallinity, using X-ray photoelectron spectroscopy (XPS) and X-ray diffraction (XRD).

Depositions are carried out with and without the use of the plasma source. This enables the investigation of the plasma's influence on the precursor, the layer growth and the layer characteristics. It is shown that the growth species in the PECVD case are more reactive than in the CVD case leading to more efficient carbon removal from the film and to the growth of higher energy facets.

11:30 AM SF03.09.05

Biocide Nano Copper-Silver Layer Active Against Surrogate Virus and Bacteria Lorena Reyes-Cardona¹, Omar Sepulveda-Robles², [Argelia Almaguer-Flores¹](#) and Sandra E. Rodil¹; ¹Universidad Nacional Autonoma Mexico, Mexico; ²Centro Medico Nacional Siglo XXI, Mexico

Bacteria and respiratory viral transmission by expelled saliva microdroplets and aerosols are essential concerns for health care workers, situation has been exacerbated by the SARS-CoV-2 pandemic. The development of nanomaterials with antimicrobial activity to use it as nanolayers in personal protection equipment (PPE), such as facemasks, respirators, protective clothing, or helmets, could be an option against the transmission of these pathogens. For this purpose, a silver and copper nanolayer named SakCu® was deposited on one side of a 70 gsm spun-bond polypropylene using the magnetron sputtering technique. Here, we evaluate the antibacterial and antiviral activity of SakCu® against drops (emulating sneeze or coughing secretions) falling on the material or aerosols passing through it. Virus viability assays were used to study the survival of PaMx54, PaMx60, and PaMx61 (ssRNA, *Leviviridae*) and PhiX174 (ssDNA, *Microviridae*) as surrogates for non-enveloped viruses. Colony forming unit determination was used to evaluate the survival of aerobic (*Escherichia coli*, *Pseudomonas aeruginosa*, *Staphylococcus aureus*, *Staphylococcus epidermidis*) and anaerobic (*Porphyromonas gingivalis*, *Aggregatibacter actinomycetemcomitans* serotype b, *Streptococcus mutans*, *Actinomyces israelii*) bacteria. Since the aerosols and microdroplets can be filtrated by the polypropylene, it was essential to determine the effect of the SakCu® nanolayer on its filtration efficiency. Therefore, measurements of the filtration efficiency using assorted sizes of NaCl particles (0.3, 0.5 and 1.0 mm) were done.

Viral viability assays with phages PaMx54, PaMx60, PaMx61, and PhiX174 showed a total reduction of viral viability between 2 - 4 h contact incubation with the silver and copper nanolayer; viral replication of both viruses was inhibited between 42% and 64% after pass through the SakCu® using a simulated viral filtration system. Bacteria growth inhibition by contact with nanomaterial and through-pass varied according to the specie, showing a range reduction between 70% to 92% for aerobic bacteria and >90% for anaerobic strains. Similar percentages of bacterial inhibition were obtained after 24 h of bacteria-contact incubation with the coated polypropylene. The results of the filtration efficiencies indicate that no significant differences were observed between the uncoated and coated polypropylene for the three measured sizes. The filtration efficiencies were 12.7 % for 0.3 microns, 32.5 % for 0.5 microns, and 55.7 % for 1.0 microns, indicating that despite a significant fraction of the viral and bacterial aerosol could go through the polypropylene textiles with or without the nanocoating, the antimicrobial efficiency was caused by the presence of the SakCu® nanolayer. In conclusion, our results showed a high bactericidal and antiviral activity of SakCu® by either contact or aerosol pathogens. Therefore, the Ag-Cu nanolayer (SakCu®) could be adapted for different PPEs to reduce and prevent the transmission of aerosol-borne pathogenic bacteria and respiratory viruses, including SARS-CoV-2.

11:45 AM SF03.09.06

Rapid Fabrication of NiO Nanoparticle Film as Hole Transport Layer Using Gas Phase Microplasma [Dilli Babu Padmanaban](#)¹, Subha Sadhu¹, Warda Mushtaq², Zachary Holman² and Davide Mariotti¹; ¹Ulster University, United Kingdom; ²Arizona State University, United States

There is always a challenge in direct application of nanomaterials. Many nanoparticle synthesis techniques are intrinsically accompanied with post and pre-processes that are costlier and time consuming. In the light of this, atmospheric pressure microplasmas-based techniques are simple and could provide rapid, time efficient solutions for a wide range of applications. Microplasmas are special kind of sub-millimetre plasmas that have achieved attractive performance in nanomaterial processing.^{1,2} This technique has been used for synthesis of several nanomaterials such as metals and transition metal oxides.³ In this talk, we want to show the synthesis of nickel oxide (NiO) nanoparticle using gas phase microplasmas and demonstrating its application as a hole transport layer for perovskite solar cell. NiO is a well-known p-type semiconductor used widely as electrode materials for solar cells, batteries, and supercapacitors.^{4,5,6} Although NiO nanoparticles and films were synthesised by other physical and chemical based techniques, these often present drawbacks such as precursor toxicity and post-synthesis steps.⁷ Here we show the one-step preparation of NiO nanoparticles with a solid metallic Ni wire as main precursor and He/O₂ gas mixture. The nanoparticles were characterised and found to have a particle size distribution around ~5 nm and consists of mostly NiO cubic 'Bunsenite' crystal phase for various inlet oxygen gas fraction. When directly deposited, nanoparticle films show a planar or columnar features depending on process duration and O₂ gas concentration. Further, we will also present the preliminary results on the application of NiO nanoparticle film as a transport layer for solar cell.

Reference

- (1) Chiang, W.; Mariotti, D.; Sankaran, R. M.; Eden, J. G.; Ostrikov, K. (Ken). Microplasmas for Advanced Materials and Devices. *Adv. Mater.* **2020**, *32* (18), 1905508. <https://doi.org/10.1002/adma.201905508>.
- (2) Mariotti, D.; Belmonte, T.; Benedikt, J.; Velusamy, T.; Jain, G.; Švrček, V. Low-Temperature Atmospheric Pressure Plasma Processes for "Green" Third Generation Photovoltaics. *Plasma Process. Polym.* **2016**, *13* (1), 70–90. <https://doi.org/10.1002/ppap.201500187>.
- (3) Mariotti, D.; Sankaran, R. M. Microplasmas for Nanomaterials Synthesis. *J. Phys. D. Appl. Phys.* **2010**, *43* (32), 323001. <https://doi.org/10.1088/0022-3727/43/32/323001>.
- (4) Yin, X.; Guo, Y.; Xie, H.; Que, W.; Kong, L. B. Nickel Oxide as Efficient Hole Transport Materials for Perovskite Solar Cells. *Sol. RRL* **2019**, *3* (5), 1900001. <https://doi.org/10.1002/solr.201900001>.
- (5) Li, W.; Erickson, E. M.; Manthiram, A. High-Nickel Layered Oxide Cathodes for Lithium-Based Automotive Batteries. *Nat. Energy* **2020**, *5* (1), 26–34. <https://doi.org/10.1038/s41560-019-0513-0>.
- (6) Luo, Z.; Liu, L.; Yang, X.; Luo, X.; Bi, P.; Fu, Z.; Pang, A.; Li, W.; Yi, Y. Revealing the Charge Storage Mechanism of Nickel Oxide Electrochromic Supercapacitors. *ACS Appl. Mater. Interfaces* **2020**, *12* (35), 39098–39107. <https://doi.org/10.1021/acsami.0c09606>.
- (7) Narender, S. S.; Varma, V. V. S.; Srikar, C. S.; Ruchitha, J.; Varma, P. A.; Praveen, B. V. S. Nickel Oxide Nanoparticles: A Brief Review of Their Synthesis, Characterization, and Applications. *Chem. Eng. Technol.* **2022**, *45* (3), 397–409. <https://doi.org/10.1002/ceat.202100442>.

SESSION SF03.10: Virtual Session I: Plasma-Surface Interactions and Processing of Materials

Session Chairs: Wei-Hung Chiang and Fiorenza Fanelli

Tuesday Morning, December 6, 2022

SF03-virtual

10:30 AM *SF03.10.01

Unraveling Surface Chemistry in Plasma Catalysis by Microscopic Modeling [Erik Neyts](#); Univ of Antwerp, Belgium

Plasma catalysis is a promising technique for - in particular - conversion of harmful or useless gases into value-added compounds. Typical examples include conversion of CO₂ and CH₄ into CO, formaldehyde or CH₃OH, and nitrogen fixation, i.e., conversion of N₂ into NH₃ or NO_x compounds. The overall bottlenecks of these processes, i.e., to make the plasma catalytic processes competitive with existing technologies, are often the conversion yield and the energy conversion. These are determined by a large variety of variables - which are ultimately determined by the underpinning microscopic mechanisms.

Microscopic modeling may provide a means to investigate these mechanisms. In particular, molecular dynamics and derived techniques offer a unique insight into these mechanisms. This talk will highlight various techniques that address the unique plasma/surface interactions that form the foundation of the microscopic surface process mechanisms.

11:00 AM *SF03.10.02

Synthesis of Nanocomposite Thin Films in an Atmospheric Pressure Plasma [Francoise Massines](#)^{1,2}, [Alexandre Perdrau](#)^{1,2}, [Beatrice Plujat](#)^{2,3} and [Noemi Barros](#)^{2,1}; ¹CNRS, France; ²UPVD, France; ³CNRS PROMES, France

Atmospheric pressure PECVD (AP-PECVD) combines the advantages of PECVD: low temperature process and low temperature, and AP: no pumps and in-line coating. A configuration like that of industrial corona treatment, useful for in-line coating of large surface, appears as the best one. It is based on a linear dielectric barrier discharge directly interacting with the substrate and typically working in a range of frequency of several tens of kHz. As example, in a Penning gas mixture like Ar with some tens of ppm of NH₃, by adding SiH₄, it leads to high quality SiN_x:H thin films for photovoltaic cells.

Another advantage of being at atmospheric pressure is that liquid or colloidal solution are easily injected in the plasma using an aerosol. To produce a nanocomposite, two different precursors should be used, one to synthesize the matrix and the other for the nanoparticles (NPs) that are embedded in the matrix. At first a colloidal suspension of pre-synthesized NPs in a solvent was tried. The study of the coatings made from an aerosol of TiO₂ NPs in isopropanol showed that all the NPs contained in a droplet aggregate, leading to porous thin films. However, this study also showed that the matrix growth and the NPs transport onto the substrate can be controlled by the alternation of two plasma frequencies: a high one to polymerize the matrix and a low one to control the NPs transport. This was confirmed using SiO₂ NPs in ethyl lactate as precursors.

Then, to try to avoid NPs aggregation, the possibility of forming NPs directly in the plasma is explored. A great advantage of this solution is to be safe by design as NPs are not at all manipulated. Thus, an aerosol of a solution of metallic salt in a solvent able to form a polymer thin film is used. The first results made with a gold salt in isopropanol will be presented. They show that plasmonic layers are easily obtained. The frequency alternation is also useful to transport NPs on to the surface and have enough power to reduce the salt and induces the growth of the matrix. Gold NPs are formed in the plasma, their aggregation is avoided and plasmonic resonance peaks range from 540 nm to 750 nm depending on the process parameters. Thus the coupling of a dielectric barrier discharge in a configuration useful for in-line treatment and an aerosol of metallic salt in a polymerizable liquid appears as promising solution to synthesize dense nanocomposite thin film in safe by design and ecofriendly manner at atmospheric pressure.

11:30 AM *SF03.10.03

Active Machine Learning to Guide Discovery of Non-Equilibrium Plasma Interactions with Complex Interfaces [Ali Mesbah](#); University of California Berkeley, United States

Active learning (AL) is the branch of machine learning concerned with systematically querying samples from an experimental system (or a computational model) to train a data-driven model that maps (experimental) design parameters to process performance measures. AL has emerged as a useful tool for guiding high-throughput experiments and expensive computations in a variety of science and engineering fields. In this talk, we will discuss the promise of constrained and multi-objective Bayesian optimization methods for AL-guided exploration of the multivariable and highly nonlinear parameter space of non-equilibrium plasmas (NEPs) in a systematic and resource-efficient manner. We will demonstrate how AL approaches can pave the way for automated and “optimal” exploration of the parameter space of NEPs, towards establishing insights into the complex behavior of the plasma when interacting with interfaces.

12:00 PM SF03.10.04

Breakthrough Science on Transformation of Fungal Mycelium into Nanostructured Ultrananocrystalline Diamond Material via Microwave Plasma Pyrolysis Benjamin Stein, [Orlando Auciello](#) and Maria J. Arellano-Jimenez; The University of Texas at Dallas, United States

Fungal mycelium has been recently promoted as an environmentally sustainable natural material to potentially replace a wide range of materials commonly used today in various technologies, including nano-porous scaffolds for biological cell cultivation, wound dressings, electrical circuit boards, biosensors, substitute leather, building materials and medical bandages. The feasibility of transforming mycelium into carbon-based materials for various nanotechnologies has been previously demonstrated using a Microwave Assisted Pyrolysis (MAP) process, involving microwave (MW) energy to heat polar water molecules contained in biomass, in controlled environments, either directly or via the addition of microwave absorbers such as activated carbon, whereby the natural chitin in the mycelium is carbonized to produce carbon allotropes like biochar or activated carbon in solid or powder form. This abstract describes breakthrough materials science that relates to Nanomaterials, Soft Materials and Biomaterials, and Structural and Functional Materials topics at the MRS Fall meeting 2022. The materials science to be presented relates to research performed by our group developing a transformation of mycelium into a unique nanoscale carbon-based material via a new fast and low-cost pyrolysis process produced in a plasma-reactor integrated into a commonly available kitchen microwave oven. In the novel microwave plasma pyrolysis (MPP) process described in this abstract, the microwave energy is directed to a low pressure (<10 Torr) gaseous environment of Ar gas, flown into a sealed circular quartz tube inside the microwave oven, containing residual atmospheric N₂ and O₂. At the low 10 Torr pressure, the MW power, directed at the flowing gas, induces the formation of a plasma containing Ar⁺, N⁺, O⁺ ions, and Ar⁰, N⁰, O⁰ neutral atoms, and free electrons, all acting on the mycelium biomass, inducing physical / chemical transformations. The data to be presented reveals that the MPP process transform the mycelium into a “myco-diamond” matrix with a unique ultrananocrystalline diamond (UNCD) nanostructure (3-5 nm grains) inserted into macro, micro, and nanoscale structures. The UNCD structure produced by the MPP process is identical to a transformational UNCD coating (3-5 nm grains), previously developed by Auciello’s group using patented MPCVD and HFCVD growth processes. Verification of the MPP-induced transformation of mycelium into UNCD was performed via complementary materials analysis techniques including Raman spectroscopy, for chemical analysis, Scanning Electron Microscopy (SEM), to determine the myco-diamond surface morphology, High Resolution Transmission Electron Microscopy (HRTEM), to confirm UNCD nanostructure, and X-Ray Diffraction (XRD) to confirm diamond structure. All analysis techniques confirmed the formation of UNCD, identical to UNCD coatings previously grown by MPCVD and HFCVD processes¹. The MPP process represents a scalable and low-cost method of producing UNCD nanomaterials derived from renewable biological sources. O. Auciello, J. J. Alcantar-Peña, E. de Obaldía, Ch. 1-Book, “Ultrananocrystalline Diamond Coatings for New Generation High-Tech and Medical Devices”, O. Auciello (Ed.), Cambridge, July 2022.

12:15 PM SF03.10.05

Non-Stoichiometry of Indium Oxide Thin Films—The Role of the Pulsed Deposition Method [Magdalena Nistor](#); NILPRP - National Institute for Laser, Plasma and Radiation Physics, Romania

Pulsed electron beam deposition (PED) is now a well-established method to grow oxide thin films, superlattices or heterostructures on rigid or flexible substrates for applications in energy, optoelectronics and photovoltaics [1]. PED has features in common with the pulsed laser deposition but uses a pulsed electron beam instead of a laser beam for ablating a material and formation a plasma plume that mediates the growth of thin films. Apart from this classic aspect, PED, when operated at low oxygen pressure controls oxygen incorporation and hence the stoichiometry of oxide films, leading to the growth of oxygen-deficient metastable phases that cannot be obtained in bulk form [2]. We report on the non-stoichiometry (cation-anion ratio) of indium oxide thin films in relation to structure, optoelectronic properties and plasma parameters. The effect of ablation plasma on the film properties was investigated by ion probes. In the indium oxide films with a high level of non-stoichiometry the phase separation occurs with the formation of metal clusters embedded in a stoichiometric crystalline oxide matrix. The metal clusters induce very specific transport properties; otherwise the films are still non-degenerate or degenerate semiconductors. By controlling the growth and plasma parameters, the properties of nanocomposite oxide films could be tailored from transparent and insulating films to absorbing and metallic films for energy applications, nonvolatile data storage devices and nonlinear optical devices. [1] M. Nistor et al., Appl. Surf. Sci. **563**, 150287 (2021); [2] M Nistor, et al., Appl. Surf. Sci. **307**, 455 (2014)

12:45 PM DISCUSSION TIME

SESSION SF03.11: Virtual Session II: Plasmas for Green and Bio Applications

Session Chairs: Wei-Hung Chiang and Fiorenza Fanelli

Tuesday Afternoon, December 6, 2022

SF03-virtual

6:30 PM *SF03.11.04

Plasma Technologies for the Creation of Tailorable Biosignalling Interfaces for Cell Culture Materials, Porous 3D Scaffolds and Micro/Nanoparticles [Marcela Bilek](#), Clara T. Tran, Aaron Gilmour, Behnam Akhavan, Laura Haidar, Rashi Walia, Kanako Sato, Xuege A. Feng, Shelley Wickham, Anna Waterhouse, Giselle Yeo and Stuart Fraser; Univ of Sydney, Australia

Modern biomedical research and clinical practice rely on a wide range of materials formed into complex structures to provide suitable environments for cells and tissues. These materials range from metals and glasses to plastics and hydrogels. Constraints on mechanical and optical properties required for particular in-vivo and in-vitro applications are usually not compatible with providing the optimum biological microenvironments for the interfacing cell

types.

Here we describe rapid, wet-chemistry-free, plasma-based approaches that utilize environmentally-friendly ionized gases to activate a range of materials and structures for spontaneous, reagent-free, covalent functionalization with bioactive molecules. Molecules that can be immobilized whilst retaining their functions include but are not limited to oligonucleotides, enzymes, peptides, aptamers, cytokines, antibodies, cell-adhesion extra-cellular matrix molecules and histological dyes. Their immobilization occurs via surface-embedded radicals that are created by energetic ions from the ionized gas bombarding the materials' surfaces prior to contact with the biomolecules [1]. Typical time scales of cell cultures necessitate covalent tethering because physical bonding would be susceptible to exchange with biomolecules from the culture media and robust spatial patterning of the molecules is required to replicate physiologically relevant structures.

This presentation will examine the fundamental science and process adaptations that enable such surface modifications to be applied to the internal surfaces of multi-well plates, complex, porous materials and micro/nanostructures whilst retaining favorable optical properties. Strategies to pattern immobilized molecules on the surfaces will be examined. Applications enabling biological studies of the response of individual cells to proteins on a sub-cellular scale [3], and the preparation of multi-functionalizable nanoparticles [4] will be discussed. The surface embedded radicals are shown to enable polymerization of hydrogels from thus activated surfaces [5] and control of the density and orientation of surface-immobilized bioactive peptides through pH variations and/or the application of external electric fields during the immobilization [6].

[1] *PNAS* **108**:14405-14410 (2011);

[2] *ACS Appl. Mater. and Interfaces* (2018);

[3] *ACS Appl. Nano Materials* (2018);

[4] *Adv. Funct. Materials* (2020);

[5] *Nat. Comm.* 9:357 (2018)

7:00 PM *SF03.11.01

Carbon Decarbonase—Plasma-Electrified Nanocarbon Processes for Zero-Carbon World Kostya (. Ostrikov¹, Wei-Hung Chiang², Zheng Bo³, Holger Kersten⁴, Igor Denysenko⁵, Volker Bruesser⁶ and Liming Dai⁷; ¹QUT, Australia; ²National Taiwan University of Science and Technology, Taiwan; ³Zhejiang University, China; ⁴University of Kiel, Germany; ⁵Kharkiv Karazin National University, Ukraine; ⁶INP Greifswald, Germany; ⁷University of New South Wales, Australia

This presentation focuses on the applications of plasma nanoscience and nanotechnology to produce functional solid nanocarbon materials, liquid fuels and chemicals, and value-added gaseous products through the plasma-enabled conversion of carbon-rich precursors. These plasma-enabled processes are pursued for the development of clean energy and sustainable green chemistry solutions to achieve zero-carbon-emissions industrial processes and help decarbonize the way we live more broadly. Using the analogy with natural enzymes where naming conventions include their function, and also the "-ase" ending, here we introduce a concept of "carbon decarbonase". This concept implies the production of value-added carbon products typically from carbon-rich waste (in solid, liquid or gaseous forms). These waste-derived carbon products in turn present interesting advanced functional properties which help achieve the global goals of decarbonizing the world, set by the recent UN sustainability programs and climate-change meetings. These carbon-based functional "decarbonases" include water desalination and purification membranes, advanced structures for energy conversion in its various forms, electrocatalytic and photocatalytic processes for energy and environmental applications, electrode materials for next-generation energy storage materials and several others. These applications are ultimately aimed for decarbonising the main greenhouse gas emissions generating industries. Radically new approaches are needed to achieve these challenging goals, and one of the viable solutions is based on electrification of the production of materials, chemicals, and fuels. Selected case studies will discuss the utilization of the *re-carbon – de-carbon – up-carbon* sustainable cycle in the production of advanced carbon nanomaterials which can perform as "decarbonases". To this end, we apply the innovative P2X (Power-to-X) approach, where X denotes the many products that can be fabricated using clean and renewable power P, including plasma-electrified power. We discuss several possibilities to utilize the plasma-power (plasma-P in P2X equation), paying particular attention to highly-efficient processes and technologies based on low-temperature plasmas, including low-pressure and atmospheric-pressure plasma discharges. Applications of plasmas to produce selected health, biomedical, and hygiene products using the highlighted approaches are discussed as well. Support from the Alexander von Humboldt Foundation through the Humboldt Award Program, the Australian Research Council, Centre for Materials Science, Centre for Clean Energy Technologies and Practices, and Centre for Waste-free-World is kindly appreciated.

7:30 PM *SF03.11.02

Nonthermal Plasma-Sustained CO₂ Methanation Over Ru-Based Multi-Metallic Catalysts Chunyuan Zhan¹, Shuya Xu¹, Hyun-Ha Kim² and Tomohiro Nozaki¹; ¹Tokyo Institute of Technology, Japan; ²National Institute of Advanced Industrial Science and Technology (AIST), Japan

As a future low-carbon technology with minimum CO₂ emission, synthetic methane formation from CO₂, known as methanation or Sabatier reaction, is being highlighted ($\text{CO}_2 + 4\text{H}_2 = \text{CH}_4 + 2\text{H}_2\text{O}$; $\Delta H = -165 \text{ kJ/mol}$). Methanation is an exothermic reaction and the low-temperature condition is favored thermodynamically to achieve high CH₄ selectivity. Meantime, room temperature operation is obviously impossible kinetically: Catalyst temperature needs to increase up to 300-400 °C so that methanation reaction occurs at a high reaction rate while maintaining high selectivity. If catalyst activity is excellent, catalyst temperature reaches up to 500 C, creating a detrimental hotspot at the reactor inlet: high-performance catalyst would conflict with the low-temperature operation and high CH₄ selectivity and yield may not be realized. In order to optimize reaction conditions, high CH₄ selectivity, and yield, nonthermal plasma (NTP) was applied to heterogeneous catalytic reactions. NTP activates CO₂ and H₂ which promotes methanation at 100 C, while heat generation by methanation cooperatively promotes radical-enhance methanation at an elevated temperature of around 300 C. As a result, CH₄ yield achieved 100 % without an external heating source. NTP-catalyst interfacial reaction is the primary key to the reaction enhancement, while unique heat and mass transfer play a unique role in the methanation reaction at high yield.

This study focuses on the nonthermal plasma effect on CO₂ methanation over Ru-based multi-metallic catalyst using dielectric barrier discharge (DBD). To this end, CO₂ conversion behaviors in a packed-bed DBD reactor at 30 kPa with catalyst temperature between 150 °C and 400 °C were investigated. Two types of catalysts were studied: First, La(3wt%)-Ni(11wt%)/Al₂O₃ catalyst was studied as a control catalyst. Second, this catalyst was modified by adding Ru(1wt%) in order to promote hydrogen spillover which is the key step for CH₄ synthesis at high yield [1]. The total flow rate was 1200 cm³/min (at STP*) and dielectric barrier discharge (DBD) was applied at 30 W which corresponds to the specific energy input of 0.38 eV/molecule. H₂/CO₂ ratio was varied from 2 to 10.

Ru-modified catalyst yielded CH₄ selectivity and CO₂ conversion of 100%, respectively at 300 °C: CH₄ yield reached the thermodynamic equilibrium. In contrast, without Ru modification, CH₄ yield was 30% with 60% CH₄ selectivity at 350 °C. Moreover, there is no reaction promotion by DBD without Ru at all [2]. Obviously, Ru promotes hydrogen spillover that promotes CO₂ conversion and CH₄ selectivity simultaneously. More importantly, the catalytic performance of Ru-modified catalyst is further improved by superposing DBD.

The tentative reaction pathway is as follows. CO₂ and H₂ are dissociated on Ru and Ni respectively, while Ru also provides H adsorption sites that spill over hydrogen to nearby Ni sites. CO₂ is directly reduced to CO, followed by C or CH_xO formation and then hydrogenated to form CH₄. Additionally, CO

is obtained from formate (HCOO) through prior generation of bicarbonate (HCO_3) while the Ru-support interface and Lanthanum (La) make contributions to this. Our previous study showed that La provides reactive sites which form carbonate species when CO_2 is activated by DBD [3]. Carbonate further reacts with surface hydrogen when Ru is co-exist nearby La and Ni. HAADF-STEM analysis support such mechanism because Ru, Ni, and La are well dispersed and overlapped on Al_2O_3 support. We are performing *in situ* infrared absorption spectroscopy which reveals a transient behavior of surface species under the presence of DBD. More detailed mechanistic insight is presented in the symposium.

* STP: Standard Temperature and Pressure (25 °C and 101 kPa).

This work has been supported by JST CREST (JPMJCR19R3).

[1] S Saeidi et al, *Prog Energ Combust*, **85** (2021) 100905.

[2] X Chen et al, *J CO₂ Util*, **54** (2021) 101771.

[3] Z Sheng et al, *Phys Chem Chem Phys*, **22**(34) (2020) 19349.

8:00 PM DISCUSSION TIME

SESSION SF03.12: Virtual Session III: Plasma Synthesis and Processing of Materials

Session Chairs: Darwin Kurniawan and Tomohiro Nozaki

Tuesday Afternoon, December 6, 2022

SF03-virtual

9:00 PM SF03.12.03

Surface Morphology Refinement and Laves Phase Control of Inconel 718 During Plasma Arc Additive Manufacturing by Alternating Magnetic Field Yi Zheng; Shanghai Key Laboratory of Materials Laser Processing and Modification, School of Materials Science and Engineering, Shanghai Jiao Tong University, China

Improving formability and mechanical properties has always been one of the challenges in the field of additive manufacturing (AM) of nickel-based superalloys. In this work, the effect of a coaxially coupled alternating magnetic field (AMF) on surface morphology and mechanical properties of plasma arc additive manufactured Inconel 718 deposit were investigated. The exploratory experiments involve two aspects: (i) the effect of different AMF parameter on the morphology and grain structure of the single-pass bead was explored and (ii) an appropriate AMF (30Hz, 12mt) parameter was selected for the fabrication of a 20-layer Inconel 718 thin-walled deposit. Results show that the electromagnetic stirring promoted grain refinement of the single-pass bead, and the finest grains were achieved with AMF of 12mt and 30Hz. The Lorentz force induced by AMF strongly changes the flow behavior of the plasma jet and the molten pool, suppressing the tendency of the liquid metal in the molten pool to flow down on the two side face of deposit, which in turn remarkably improved the surface accuracy of the thin-walled deposit. Furthermore, the electromagnetic stirring induced by AMF can effectively enhance the convection between the dendrites, which could not only contribute to the formation of finer dendrites but also alleviates the enrichment of the elements (i.e., Nb and Mo) at solid-liquid interface and inhibits the precipitation of Laves phase. The smallest primary dendritic arm spacing (~13 μm) and lowest Laves phases area fraction (3.12%) were witnessed in the bottom region of the AMF-assisted deposit. The mechanical test confirmed that the microhardness of the deposit was moderately improved and the tensile properties were slightly enhanced compared with the counterpart without AMF. This paper provides guidelines for tailoring the microstructure and the mechanical properties of Inconel 718 via AMF, indicating the significant application potential of AMF for the arc-based AM process.

9:15 PM SF03.12.04

Electrical Explosion as a Methodology for One-Step Preparation of Nano-Materials with Particular Structure and Composition Chen Li¹, Ruoyu Han¹, Yuchen Cao¹, Qifan Li² and Ming Gao³; ¹Beijing Institute of Technology, China; ²University of Electronic Science and Technology of China, China; ³Shenzhen Institute of Advanced Technology, Chinese Academy of Sciences, China

Electrical explosion, characterized by ultrafast heating ($dT/dt \sim 10^{11}$ K/s) and quenching (10^{10} K/s) rates of the sample, is a powerful tool for synthesizing nanomaterials, including pure metal, alloy and metallic compounds and composites. This method is highly productive (200 g/h or more) and provides high-quality powders with particle size less than 100 nm; moreover, $\mu\text{m}/\text{mm}$ -thick coating or film can be synthesized within a short period ($\mu\text{s}/\text{ms}$ timescale). Benefitted from the simple and inexpensive device as well as the great efficient, it provides desirable possibility for industrial production. Micromorphology, microstructure and functionality should be most concerned in nanomaterials filed. Researches including our works show that the produced products characteristics is prominently influenced by the explosive behaviors and dynamic process of wires. For example, the thermal instability (e.g. stratification) in discharge process who causes the discrepant parameters of density and temperature will leads to the inhomogeneous nanoparticle size. Sufficient plasma process maintains the exploded products at a high temperature and promotes the growth process after nucleation, as a result, average particle size increases. Different breakdown modes, like surficial or internal, lead to distinctive energy deposition mechanism (Joule heating for surface breakdown and heat transport/radiation for internal) and result in relatively dispersive nanoparticles or agglomerated particle-clusters, respectively. Except nanoparticles produced by exploding wire itself, the accompanied effect, like strong shockwaves and high-speed expanded metallic products (~ km/s), is valuable in layered materials exfoliation and surface decoration. Exploding a copper wire in a graphite powder-contained tube (polymethyl methacrylate-PMMA), the strong impact of pressure and thermal metal turbulence effectively exfoliate graphite into thin nanosheets, and copper vapor quenches and nucleates on the surface of the nanosheets forming homogeneous nanoparticles (<100 nm). A novel structure of metallic elements decorated-thin nanosheets based composite is synthesized. Moreover, other layered materials (e.g., black phosphorus and bismuth selenide) can also be exfoliated and decorated by this method. To sum up, whatever use exploding wire as the source for nanomaterials production or as a tool for materials treatment due to its high-pressure and temperature attributions, explosive behaviors and dynamic process are the most substantial influenced elements. Further investigating on the physical mechanisms can give a significative guidance on practical application.

SESSION SF03.13: On-Demand Presentation

Thursday Morning, December 8, 2022

SF03-virtual

7:00 AM SF03.13.01

Plasma Assisted *In Situ* Synthesis of Nanodiamonds for Functional Textiles [Karan Chandrakar](#); Indian Institute of Technology Delhi, India

Carbonaceous material is abundant in nature, and its nanostructures have drawn interest due to their unique features. The conventional synthesis of these nanostructures is a time-consuming procedure that necessitates the utilization of high temperature and pressure. In this study, the utilization of atmospheric pressure low-temperature plasma for *in-situ* production of carbon nanostructures on polyester fabric surface was investigated.

The nanostructures formed due to the *in-situ* plasma synthesis from carbon precursor (alcohol) were characterized by HRTEM-Saed patterns and Raman spectra which confirmed the formation of crystals of nanodiamonds. The surface modification was found to significantly enhance the functional properties, such as wettability and flame retardancy, of the polyester fabric, which were also wash durable. FTIR and Raman spectroscopies indicated the existence of interactive forces between the *in-situ* formed nanodiamonds and the polyester surface. This research presents a revolutionary method for *in-situ* functionalization of textiles by carbon nanodiamonds that does not compromise the intrinsic qualities of the material used for various functional applications.

Key words : Carbon nanostructures, Nanodiamond, Polyester

SYMPOSIUM SF04

Integrated Experimental and Modeling Approaches for Understanding Interfacial Effects at Different Physical Scales in Crystalline Materials

November 29 - December 7, 2022

Symposium Organizers

Thomas Bieler, Michigan State University
Abigail Hunter, Los Alamos National Laboratory
Garritt Tucker, Colorado School of Mines
Mohammed Zikry, North Carolina State University

* Invited Paper

+ Distinguished Invited

SESSION SF04.01: Grain Boundaries and Interfaces I

Session Chairs: Edward Kober and Garritt Tucker

Tuesday Morning, November 29, 2022

Sheraton, 3rd Floor, Berkeley

8:45 AM *SF04.01.01

Dislocation, Disconnection, Disclination, Step and Facet Associated with Twinning in Metals and Minerals [Jian Wang](#); University of Nebraska--Lincoln, United States

Due to the small shear vector associated with twinning, deformation twinning is often activated in crystalline materials, especially for metals with low symmetry or low stack fault energy and minerals with large lattice constant. Nucleation, propagation and thickening of deformation twins are accomplished through gliding of twinning dislocations associated with atomic shuffles. Twinning dislocation has both dislocation character and step character. It is generally observed that twinning dislocations pile up to form coherency gliding disclination, step and even facet during twinning. The topological model demonstrates that such terraced interfaces, with coherency strains accommodated by arrays of dislocations and disconnections, can migrate without long-range diffusion. In this lecture, our objective is to concentrate on defects relevant to interface motion, and these exhibit dislocation, disclination, or step character, or some combination thereof. We take twinning in hcp metals as many defect examples. The definition of shuffles within the topological model is presented. The concept of anisotropic kinetics for twinning disconnections has recently been elucidated.

9:15 AM SF04.01.03

Analysis of Grain Boundary (GB) Structure and Dislocation-GB Interactions Using Unsupervised Machine Learning Nithin Mathew, [Avanish Mishra](#), Sumit Suresh, Khanh Dang, Saryu Fensin and Edward Kober; Los Alamos National Laboratory, United States

Dislocation-Grain Boundary (GB) interactions play an important role in determining the mechanical response of structural materials. This interaction is strongly influenced by GB structure, especially in the presence of GB dislocations. Many methods have been proposed for characterization of GB structure using structural/polyhedral units, which have been applied to both minimum energy and metastable structures. We will present a method to characterize GB structure using a complete and symmetry-adapted set of atomic environment descriptors, namely the Strain functional descriptors (SFD), in conjunction with unsupervised machine learning methods such as Gaussian Mixture Models (GMM), Principal Component Analysis (PCA) and t-distributed Stochastic Neighbor Embedding (t-SNE). Structural units are identified for GBs, reducing thousands (~5000) of metastable states to six different classes. The physical insights derived from SFDs are used to isolate the distribution of deformed/undeformed atomic environments from these six classes at GB. The variation in the atomic arrangement at GB is further examined by developing a similarity metric to delineate GB regions into 'most similar' or 'most dissimilar' with respect to the undeformed lattice. Dislocation-GB interactions are analyzed using these classes and the similarity metric. Dislocation-GB interaction sites

with higher similarity (to undeformed lattice) results in transmission across the GB, whereas the lower similarity region leads to dislocation pinning/absorption due to local reconstructions. In addition, identified classes and the similarity metric are shown to be good descriptors for developing supervised machine learning models of GB properties.

9:30 AM SF04.01.04

Towards Quantum-Accurate Modeling of Polycrystalline Grain Boundary Environments [Malik Wagih](#) and Christopher A. Schuh; Massachusetts Institute of Technology, United States

The properties of grain boundaries (e.g., diffusion, mobility, and solute segregation) are strongly dependent on the array of the local atomic environments present at the boundary. Therefore, to fully understand the structure-property relationships for grain boundaries, it is essential to study grain boundaries with atomic resolution. However, the most important general low-symmetry grain boundaries are inaccessible to quantum mechanical simulation methods. As a result, researchers tend to focus on high-symmetry coincident site lattice (CSL) grain boundaries in bicrystals, which are accessible to quantum methods, as opposed to the more complex polycrystalline grain boundaries. In this talk, using solute segregation for illustration, we will discuss the shortcomings of using CSL grain boundaries as a general model for grain boundary environments. In addition, we will discuss our recently developed algorithmic framework that can be used to study grain boundary local atomic environments in polycrystals with quantum accuracy. Using this framework, we are able to directly compute from quantum methods the full spectrum of solute segregation energies in polycrystals, and to build a comprehensive segregation database across the alloy space.

9:45 AM BREAK

SESSION SF04.02: Grain Boundaries and Interfaces II
Session Chairs: Irene Beyerlein and Nan Li
Tuesday Morning, November 29, 2022
Sheraton, 3rd Floor, Berkeley

10:30 AM *SF04.02.01

Grain Boundary-Dislocation Interaction Simulations Designed to Allow Transmission David E. Page¹, David T. Fullwood¹, Robert Wagoner² and [Eric R. Homer](#)¹; ¹Brigham Young Univ, United States; ²The Ohio State University, United States

The advance of experimental and simulation tools have advanced our ability to examine grain boundary (GB)-dislocation interactions in greater numbers and detail. These interactions underpin the well-known Hall-Petch relationship, which still lacks understanding of just how each individual GB-dislocation interaction contributes to the overall material response. Predicting the types of GB-dislocation interactions that can occur remains a challenge because the conditions for each can be so complex and unique. We designed a specific set of simulations to address these challenges and account for the variability that is inherent in these types of interactions. The simulations are limited to [112] tilt boundaries in FCC Ni, such that slip plane and slip direction alignment are maximized for transmission. Additionally, it is well-known that GBs can assume different atomic configurations, so we examined 3 different atomic structures for each GB. We present the results of these simulations and the corresponding GB-dislocation interactions. Interestingly, despite the attempts to maximize transmission in these simulations, only 4 of the 27 simulations show direct transmission. Another 5 simulations have dislocation nucleation at another site, somewhat removed from the site of impact. The remaining simulations demonstrate absorption of the dislocation with no indications of transmission or nucleation of any kind. These results are discussed in the context of the literature and the impact it could have on how we may wish to consider GB-dislocation interactions in general.

11:00 AM *SF04.02.02

Grain Boundary Dislocation Interaction Using Atomistic Modeling [Saryu Fensin](#), Sumit Suresh, Khanh Dang, Nithin Mathew and Avnish Mishra; Los Alamos National Laboratory, United States

A material's ability to accommodate stress induced through mechanical loads is dependent on the ease with which dislocations (line defects) can move through the microstructure to relieve accumulated stress. Grain boundaries (GBs) are the largest impediment to this motion – this is true to some extent regardless of the grain size. The GB structure defines whether a dislocation can transmit across a GB, be partially absorbed at the GB, or glide along the GB and re-emit, altering the GB structure. Our recent MD results suggest that Dislocation grain Boundary interactions (DiGBi) are sensitive to GB structure as characterized by structural units that make up the GB. This work shows that altering the GB structure by changing the GB plane, causes changes in the structural units which alters GB interactions with dislocation loops. However, outstanding questions remain about DiGBi as a function of changes in the local atomic arrangements of GBs. This talk will show examples highlighting the affect of altering grain boundary structure on interaction with dislocations.

11:30 AM SF04.02.03

Calculations of Grain Boundaries with a Parametrized Embedded Atom Method Interatomic Potential [Yasir Mahmood](#)¹, Murray Daw¹, Michael Chandross² and [Fadi Abdeljawad](#)¹; ¹Clemson University, United States; ²Sandia National Laboratories, United States

Atomic simulations based on inter-atomic potentials offer a powerful tool for a fundamental understanding of materials processes and properties. The conventional approach for devising an interatomic potential is fitting a set of functions to basic properties obtained from experiments or density functional theory calculations, or both, and using this fit to explore more complex properties. Recently, Daw & Chandross [1] have introduced a comparatively simple parametric functional form based on the Embedded Atom Method for FCC metals. This model takes an inside-out approach, allowing us to generically explore the dependencies of complex properties on the function parameters, and then determining the parameter space that corresponds to a real element. Due to the generic nature of this approach, the model is referred to as EAM-X. In this work, we explore FCC grain boundary (GB) properties in this EAM-X parameter space. We use a representative set of [001] and [110] symmetric tilt, [111] symmetric twist, and [001] asymmetric tilt boundaries. We find that the GB energy can be factored neatly into two parts: one that depends on the boundary parameters evaluated at a chosen reference point in the parameter space, the other being a smooth function of the EAM-X parameters. Generally, the second factor correlates very well with the shear moduli, confirming earlier observations by Holm, Olmsted and Foiles [2], and Foiles [3]. On the whole, our approach provides future avenues to rapidly explore trends in GB properties for a wide range of FCC metals.

[1] M. S. Daw & M. Chandross, "Simple Parameterization of Embedded Atom Method Potentials for FCC Metals" (submitted).

[2] Holm, E. A., Olmsted, D. L., & Foiles, S. M. (2010). Comparing grain boundary energies in face-centered cubic metals: Al, Au, Cu and Ni. *Scripta Materialia*, 63(9), 905-908.

[3] Foiles, S. M. (2010). Temperature dependence of grain boundary free energy and elastic constants. *Scripta Materialia*, 62(5), 231-234.

11:45 AM SF04.02.04

Development of Strain Functionals for Physics Informed Machine Learning of Grain Boundary Structures Edward M. Kober¹, Avanish Mishra¹, Colin M. Adams² and Nithin Mathew¹; ¹Los Alamos National Laboratory, United States; ²Arete, United States

The analysis of molecular dynamics simulations of the deformation of metals and the validation of potential functions used in these simulations compared require a robust set of descriptors that can identify a wide variety of crystal and defect structures. The use of strain functionals descriptors for characterizing such arbitrarily ordered atomistic structures is demonstrated here for use in conjunction with machine learning applications. This approach is derived using a Taylor series expansion of the geometry of the local atomic neighborhood, ensuring both numerical convergence and a direct relationship to physical properties. They are reduced to a minimal non-redundant set using closure relationships from angular momentum / spherical tensor properties. The resulting functionals naturally describe the deformations in terms of simple physical concepts: measuring how tetrahedral or cubic a geometry is, how much shear or trigonal deformation is present. This formulation cleanly maps onto other entities that are described by tensor formulations: strain, stress, elasticity, and other physical properties. Using these as a basis facilitates the development of physically-informed models from machine-learning applications. Here, the method is extended out to sixth order, which is necessary to fully distinguish all possible crystallographic symmetries. The approach has been extended to the analysis of vector (velocities, forces) and tensor (stress, strain) fields as well. Applications of the method to the characterization of grain boundaries will be shown.

SESSION SF04.03: Grain Boundaries and Interfaces III

Session Chairs: Saryu Fensin and Nithin Mathew

Tuesday Afternoon, November 29, 2022

Sheraton, 3rd Floor, Berkeley

1:30 PM *SF04.03.01

On the Effect of 3D Grain Boundary Orientation on Slip Transfer and Fracture in Ti Eugenia Nieto^{1,2}, Eshan Ganju³, Nikhilesh Chawla³ and Javier Llorca^{2,1}; ¹IMDEA Materials Institute, Spain; ²Technical University of Madrid, Spain; ³Purdue University, United States

Grain boundaries play a crucial role during plastic deformation of polycrystals, acting as physical barriers that hinder dislocation motion and potential sites for damage nucleation and fracture. Their influence is more severe in metals with hexagonal closed-packed lattice because of the limited number of available slip systems as well as the large differences in the critical resolved shear stresses to active dislocation slip, which difficult the accommodation of plastic deformation in the microstructure. Thus, it is important to develop robust geometrical criteria to assess whether slip transfer/blocking will occur at a given grain boundary and what is the influence of grain boundary orientation on the nucleation of cracks. Most of the experimental information available to this end has been obtained by means of slip trace analysis and high-resolution digital image correlation (HR-DIC) on the surface of deformed specimens in which the grain orientation was determined by electron backscatter diffraction (EBSD). However, these results lack information about the grain boundary orientation perpendicular to the surface, which is known to play a significant role to control slip transfer/blocking as well as damage nucleation at grain boundaries.

In this talk, the mechanisms of slip transfer and blocking are analyzed in commercially pure Ti thin foils subjected to uniaxial tensile loading. The microstructure of the polycrystal was characterized by means of laboratory diffraction contrast tomography (LabDCT) to obtain information about the crystallographic orientation of the grains as well as about the grain boundary geometry on the specimen surface and through the thickness. The samples presented a strong basal texture typical of cold rolled thin foils, with a bimodal distribution of grain boundary misorientation angles with either very little or highly disoriented grains. After tensile deformation, a thorough slip transfer/blocking analysis was performed in more than 300 grain boundaries via slip trace analysis coupled with HR-DIC in selected areas. The strain concentrations around grain boundary areas captured by HRDIC allowed to uniquely identify slip blocking/transfer events while the slip traces observed on the surface of the sample were correlated with the crystal orientation of the grains to determine the active slip system. In addition, intergranular cracks were identified at grain boundaries and triple junctions as well as transgranular cracks parallel to the active slip systems.

The information on the deformation and damage nucleation mechanisms was combined with the full 3D information of the microstructure provided by LabDCT to assess the influence of the 3D grain boundary orientation slip transfer and damage at grain boundaries. Different metrics based on geometrical factors (grain boundary misorientation, Luster-Morris parameter, residual Burgers vector, LRB factor) and/or driving forces (critical resolved shear stresses for slip and/or twinning) were employed to assess the likelihood of slip transfer/blocking and fracture across grain boundaries. These results provide novel information to understand the effect of grain boundaries in polycrystal deformation and to simulate their influence on the mechanical behavior.

2:00 PM *SF04.03.02

Slip Transmission Across Three-Dimensional Crystalline Interfaces Irene J. Beyerlein¹, Shuozhi Xu¹, Justin Cheng² and Nathan Mara²; ¹University of California, Santa Barbara, United States; ²University of Minnesota, United States

Even after their introduction some decades ago, metallic nanostructured, multi-phase composites have continued to draw world-wide interest due to their exceptionally high strength and hardness and outstanding tolerance to extreme conditions, such as elevated temperatures, irradiation, and high-rate impact. The combination makes them an exciting class of materials for meeting the demands of future applications, such as nuclear power reactors, propulsion systems, and microelectromechanical devices. At present, however, they are not suitable for long-time service due to insufficient toughness and a greater tendency to develop shear localizations than their more coarsely structured counterparts. A unique and important feature of these materials is the physical dominance of biphasic interfaces, the atomically thick boundary between the dissimilar phases in the composite. The deformation response of the biphasic interface and interactions with moving dislocations can have a profound effect on overall material behavior, suggesting the appealing potential to control its localization tendencies via design of the interface itself. In this talk, we will focus on the behavior of nanolayered nanocomposites made with extraordinarily "thick" interfaces under mechanical deformation. We will discuss efforts to characterize and design the morphology, size, and chemistry of the interface, especially in its third dimension (normal to the interface plane). Results from a model developed to simulate the dynamic interactions of

individual dislocations and these 3D interfaces under applied stress will be presented. The talk will share our findings to date, which indicate that both the macroscopic and microscopic responses are sensitive to interface thickness and through-thickness chemical gradients. We will conclude with a discussion on the intriguing possibility to design 3D thick interfaces to attenuate shear concentrations and postpone instabilities without sacrificing strength.

2:30 PM SF04.03.03

Extracting Relative Grain Boundary Energies from Triple Junction Geometry in Nanocrystalline Thin Films—Effect of Film Geometry on Interfacial Equilibrium Matthew J. Patrick¹, Gregory S. Rohrer², Ooraphan Chirayutthanasak³, Sutatch Ratanaphan³, Eric R. Homer⁴, Gus L. Hart⁴, Yekaterina Epshteyn⁵ and Katayun Barmak¹; ¹Columbia University, United States; ²Carnegie Mellon University, United States; ³King Mongkut's University of Technology, Thailand; ⁴Brigham Young University, United States; ⁵The University of Utah, United States

Grain boundary character distributions (GBCD) and relative grain boundary energy distributions (GBED) are routinely calculated from 3D serial-section electron backscatter diffraction (EBSD) data from microcrystalline bulk samples, and are consistently found to be inversely correlated. The GBEDs are calculated based on triple junction geometry and the assumption of force balance via the Herring condition. For nanocrystalline thin films, precession electron diffraction (PED) has proven an effective method to measure the GBCD, but the GBED has not been reconstructed. In the work reported here, we adapt the established energy reconstruction method to PED data from films with columnar grain structures, where serial sectioning is not required to determine boundary inclination. For a 40 nm-thick, sputter-deposited, nanocrystalline tungsten film, the relative GBED obtained by this method does not correlate to grain boundary energies which are interpolated with Read-Shockley-Wolf (RSW) functions from molecular dynamics calculations. Furthermore, while the boundary populations in this data-set have been previously demonstrated to show both an inverse log-linear correlation with the RSW-calculated energies and a clear correlation to the GBCD of comparable microcrystalline bcc materials, the populations of boundaries show no inverse relationship to the relative energies obtained here. This failure indicated that the assumed Herring condition does not successfully relate triple junction geometry and boundary energy in this system, and thus cannot be used to extract relative boundary energies. This film had not experienced grain growth, however, and so its structure may reflect a metastable state. To address this, a set of aluminum samples were also examined: a film in its as-deposited state and after 30 and 150 minutes at 400°C. Here, the film experiences significant grain growth, with equivalent circle diameter of mean area increasing by more than 40% after 150 minutes of annealing. Still, when the relative energies are reconstructed from the data-set the inverse relationship with population is not recovered, even when accounting for certain boundaries (i.e. coherent twins) which are not likely perpendicular to the plane of the film. When compared to aluminum grain boundary energies recently calculated with molecular dynamics, the populations show an obvious inverse trend with energy, in line with the previously reported correlation of the nanocrystalline GBCD to the bulk microcrystalline results. The failure of the energy reconstruction model to reproduce the expected trends likely implies that the assumed conventional Herring condition of force balance is not an appropriate avenue for energy extraction in thin films, indicating that the Herring equation does not fully specify the geometry at triple junctions in these systems. While boundary character follows well established thermodynamic expectations, this result points to other factors, including those related to thin film geometry, which must play a significant role in determining triple junction geometry in these spatially constrained systems.

2:45 PM BREAK

SESSION SF04.04: Grain Boundaries and Interfaces IV
Session Chairs: Avinash Dongare and Jian Wang
Tuesday Afternoon, November 29, 2022
Sheraton, 3rd Floor, Berkeley

3:30 PM *SF04.04.01

Hydrogen Trapping at Grain Boundaries and Embrittlement in High-Strength Al-Alloys Dierk R. Raabe, Huan Zhao and Baptiste Gault; Max Planck Institute for Iron Research, Germany

High-strength Al-alloys help reduce the weight of automobiles, but they are susceptible to environmental degradation. Hydrogen (H) embrittlement is often pointed as the main culprit, however, the mechanisms underpinning failure are elusive: atomic-scale analysis of H inside an alloy remains a challenge, and this prevents deploying alloy design strategies to enhance the materials' durability. Here we successfully performed near-atomic scale analysis of H trapped in second-phase particles and at grain boundaries in a high-strength 7xxx Al-alloy. We used these observations to guide atomistic *ab-initio* calculations which show that the co-segregation of alloying elements and H favours grain boundary decohesion, while the strong partitioning of H into the second-phases removes solute H from the matrix, hence preventing H-embrittlement. Our insights further advance the mechanistic understanding of H-assisted embrittlement in Al-alloys, emphasizing the role of H-traps in retarding cracking and guiding new alloy design (1).

(1) Zhao, H., Chakraborty, P., Ponge, D. *et al.* Hydrogen trapping and embrittlement in high-strength Al alloys. *Nature* **602**, 437–441 (2022)

4:00 PM DISCUSSION TIME

4:15 PM *SF04.04.03

Tracking Grain Boundary Microstates via Microscopy and Deep Learning Emily Hopkins¹, Ryan Jacobs², Priyam Patki³, Kevin Field³, Dane Morgan², Jaime Marian⁴, David Srolovitz^{5,6} and Mitra L. Taheri¹; ¹Johns Hopkins University, United States; ²University of Wisconsin–Madison, United States; ³University of Michigan–Ann Arbor, United States; ⁴University of California, Los Angeles, United States; ⁵The Hong Kong University, Hong Kong; ⁶University of Pennsylvania, United States

Achieving radiation tolerance in crystalline materials will require a thorough understanding of defect evolution and corresponding material responses to ion bombardment. Tailoring grain boundaries to behave as enhanced defect sinks poses a potential solution toward the development of more radiation tolerant materials; however, critical nuances illustrating the microstructural response of grain boundaries under irradiation have yet to be explained. In particular, the relationship between GB structural states and their effect on the rate of defect absorption is unclear. In this study, we utilize automated object detection models of in situ TEM experiments to offer new insight into transient GB states and analyze cyclic absorption behavior. By providing an indicator of changes in GB absorption mechanisms and recognizing GB absorption responses in real time, we move closer to explaining GB metastability with the onset of radiation damage.

8:30 AM *SF04.05.01

Plasticity Mechanisms in Laser Processed Al-Si Alloys with Heterogeneous Microstructures [Amit Misra](#)¹ and Jian Wang²; ¹University of Michigan–Ann Arbor, United States; ²University of Nebraska–Lincoln, United States

A range of heterogeneous Al-Si microstructures, comprising of nanoscale Al-Si eutectic domains with nanotwinned Si fibers and sub-micron-scale primary Al, with or without Si nano-precipitates, were fabricated by processing as-cast Al-20wt.%Si alloy using laser rapid solidification. *In situ* tensile testing in a scanning electron microscope demonstrated high tensile strength, ≈ 600 MPa, and ductility, $\approx 10\%$, and high strain hardening rate, ≈ 7 GPa. Microstructural characterization revealed the plastic co-deformation mechanisms between soft Al grains and the surrounding relatively harder nanoscale Al-Si eutectic. The progression of plasticity in nanoscale Al-Si eutectic with increasing applied strain is accommodated by dislocation plasticity in the nano-Al channels and cracking in Si nanofibers. The propagation of nano-cracks is suppressed by surrounding Al, retaining good ductility of the sample. Cross-sectional scanning/transmission electron microscopy of nanoindentations revealed a transition in morphology from high aspect ratio nano-fibrous Si to short nano-fibrous Si, preferentially located along triple junctions of the dynamically recovered sub-grains in Al. Molecular dynamics simulations of the interaction of glide dislocations in Al with the flat Si/Al interfaces revealed climb and cross-slip mechanisms but no direct slip transmission into Si. The role of the heterogeneous Al-Si microstructure in enhancing strain hardening rate and resulting in plasticity in micro-tensile sample even after fracture of nanoscale Si fibers is discussed by integrating experimental characterization with atomistic simulations and dislocation theory. This research is supported by DOE, Office of Science, Office of Basic Energy Sciences.

9:00 AM SF04.05.02

Interfaces Induced Extra Strain Hardening in Additive Manufactured Laminated Steels [Zhi Li](#)¹ and Huajian Gao^{2,1}; ¹Agency for Science, Technology and Research, Singapore; ²Nanyang Technological University, Singapore

Metallic alloys with heterogeneous microstructure have demonstrated superior mechanical properties, including high strength, extra work hardening and high ductility. By manipulating the thermal stability and inducing site-specific recrystallization in metal additive manufacturing, laminated 316L steels have been recently printed with various lamella structures and phase compositions, demonstrating extra strain hardening and high ultimate strength under tensile loading. We present a theoretical and numerical study on the flow behavior of the laminated structure by considering the strengthening effects of the interface affected zone. It is shown collectively from the experiments and simulations that extra back stress is developed in the interface affected zone during the deformation process, and the magnitude of this extra back stress changes with the lamella structure. Our work provides new understandings of the deformation mechanism in the heterogeneous alloys and demonstrates the potential of engineering the interfaces for enhanced mechanical properties.

9:15 AM SF04.05.03

Kinetically-Driven Microstructure and Mechanical Properties of 3D Micro-Architected Metal Alloys Formed via Hydrogel Infusion Additive Manufacturing (HIAM) [Thomas Tran](#), Rebecca Gallivan and Julia R. Greer; California Institute of Technology, United States

Hydrogel infusion-based additive manufacturing (HIAM) to create 3D micro-architected metals is unique in its absence of melt pool solidification. By nucleating and growing parent oxide phases and subsequently reducing them, HIAM provides a kinetically-driven pathway for forming boundaries in polycrystalline metal microarchitectures. Using EBSD and TEM analysis, we characterize these boundaries, defects, and other microstructural features within Cu, Ni, and Cu-Ni alloys produced by this technique over a span of thermal treatment conditions. These metals and alloys exhibit anomalous nanoindentation hardnesses, exceeding predictions of the classical Hall-Petch relation by at least 30%, which we postulate to be due to the present networks of high-angle grain boundaries, annealing twin boundaries, and higher-order coincident site lattice (CSL) boundaries. We explore the role of formed boundaries by conducting site-specific compression experiments on nano- and micropillars carved from individual grains -- as well as spanning specific boundaries --, isolating the contribution of each type of boundary to plasticity in HIAM-produced metals. We present a phenomenological framework that accounts for the contribution of special boundaries to global mechanical properties, which helps inform HIAM as a novel means to create 3D-architected metals and alloys with non-equilibrium microstructures and compositions.

9:30 AM SF04.05.04

Phase-Field Modeling of Grain Growth in Thin Films on Planar and Non-Planar Substrates [Ahmad Nadeem](#), Hwanwook Lee, Muhammad H. Ali, Kiran Raj and Kwon Yongwoo; Hongik University, Seoul, Korea (the Republic of)

The phase-field technique is the most effective for modeling and simulating microstructure evolution, such as grain formation in a polysilicon channel of V-NAND flash memory. It estimates the development of grain boundaries in areas with excessive free energy. The material system should evolve in such a way that the total free energy, which is the driving factor for grain growth, is minimized, resulting in a smaller grain boundary. Process engineers put a lot of emphasis on grain size since it is strongly connected to effective material properties. We adopt phase-field method to simulate the microstructure evolution during the post-annealing to crystallize as-deposited amorphous films in the semiconductor processing. This process is called solid-phase crystallization. Initially, nucleation occurs and then grain growth follows. Our main interest is studying how the final grain size is determined. The dependence on nucleation density, nucleation site location, film thickness, and annealing temperature is primarily investigated. The sheet resistance and conductivity of the polycrystalline films derived from phase-field modeling are also calculated. Nonplanar films are also being studied because the designs of cutting-edge nanodevices, such as multi-bridge channel field effect transistor (MBC-FET) in sub 3nm nodes, 3D-NAND flash memory, and so on, are becoming more three-dimensional. Accordingly, the grain formation in geometrically confined structures is becoming of great interest. In this work, we demonstrate our phase-field simulation on thin films for which we developed our in-house C++ code and present our simulation results.

9:45 AM SF04.05.05

Regularized Anisotropic Motion-By-Curvature in Phase-Field Theory [Thomas Philippe](#); Condensed Matter Physics Group, Ecole polytechnique, France

The kinetic equation for anisotropic motion-by-curvature, largely used to model the dynamics of grain boundaries and interfaces, is ill-posed when the surface energy is strongly anisotropic. In this case, corners or edges are present on the Wulff shape, which span a range of missing orientations. In the sharp-interface problem the surface energy is augmented with a curvature-dependent term that rounds the corners and regularizes the dynamic equations. This introduces a new length scale in the problem, the corner size. In phase-field theory, an approximation of the Willmore energy is often added to regularize the model. We discuss the convergence of the Allen-Cahn version of the regularized phase-field model toward the sharp-interface theory for

strongly anisotropic motion-by-curvature, in two and three dimensions, for large corner size with respect to interface thickness. We also study the opposite limit, for corner size smaller than the interface width, and show that the shape of corners differs from the sharp-interface picture. However, we find that the phase transition at the interface is preserved and presents the same properties than the classical problem. This demonstrates that regularization also operates in the intermediate regime, i.e. for corner size and interface width of same order, that is numerically more attractive and allows for simulations in three-dimensions. As an illustration, we investigate the dynamics of the faceting instability, when initially unstable surfaces decompose into stable facets. Finally, we study nucleation of crystal surfaces in a two-phase system.

10:00 AM BREAK

SESSION SF04.06: Interface Roles in Microstructural Evolution II
Session Chairs: Donald Brenner and Amit Misra
Wednesday Morning, November 30, 2022
Sheraton, 3rd Floor, Berkeley

10:30 AM *SF04.06.01

Predicting Variants During Phase Transformation and Twinning in BCC Microstructures During Deformation and Unloading [Avinash M. Dongare](#) and [Avinash Mishra](#); University of Connecticut, United States

The deformation behavior of BCC metal microstructures at high pressures has contributions from dislocation slip, deformation twinning, and phase transformation. While deformation twinning is a common mode of deformation in BCC metals at high pressures, Fe-based microstructures also demonstrate a BCC \rightarrow HCP phase transformation when deformed above a threshold pressure of ~ 13 GPa. Recent studies have demonstrated the BCC \rightarrow HCP \rightarrow BCC phase transformation can result in a distribution of twins in the bcc microstructure. This distribution of twins is attributed to the selection of HCP phase variants during compression and their stability and reverse transformations during unloading. Understanding and predicting the role of microstructure and stress-states on these variant selections during deformation and their stability and reverse transformation behavior during unloading is important. The current efforts to investigate variant selections in BCC metals are largely limited to real-time *in situ* x-ray diffraction (XRD) and for single-crystal (sc) systems. In addition, the interpretations of the plasticity contributions from diffractograms are non-trivial, especially when multiple modes of deformation may be operating. Molecular dynamics (MD) simulations can successfully capture various deformation modes in metals and complement experiments using simulated diffractograms at various stages of evolution. This talk will discuss the use of virtual XRD to characterize the variant selections and their plasticity contributions during plastic deformation. The simulations investigate the role of BCC microstructure and loading stress-states on variant selections during phase transformation and twinning in BCC Fe microstructures as predicted using MD simulations. In addition, the simulations investigate the stability and the reverse transformation behavior of the variants during unloading. The simulations are able to unravel the role of variant selection and transformation that renders a distribution of twin boundaries in unloaded microstructures. The characterization of the phase/twin variants is based on a newly developed virtual texture analysis (VirTex) algorithm that enables the creation of EBSD maps of the simulated microstructures to compare with experimental EBSD maps. In addition, the capabilities and limitations of virtual x-ray diffraction (XRD) on the simulated microstructures to characterize the phase/twin variants will be presented.

11:00 AM *SF04.06.02

Solute Partitioning Behavior within Nanocrystalline Grain Boundaries [Gregory B. Thompson](#)¹, [Xuyang Zhou](#)^{1,2}, [Reza Kamachali](#)³, [Jonathan Priedeman](#)¹, [Dierk R. Raabe](#)², [Brad L. Boyce](#)⁴ and [Blythe G. Clark](#)⁴; ¹University of Alabama, United States; ²MPIE, Germany; ³Federal Institute for Materials Research and Testing (BAM), Germany; ⁴Sandia National Laboratories, United States

Spinodal decomposition is often described as a 'barrier-free' transformation. Unlike nucleation and growth, where defects play a dominant role in the nucleation of the secondary phase, such defects are largely considered inconsequential to this continuous phase transformation. At the nanoscale, where a high density of planar defects exists, their presence can have a profound influence on the temporal evolution of this phase transformation. In this presentation, the phase separation of a Pt(Au) nanocrystalline alloy is characterized using a correlative method of electron diffraction and atom probe. A competition between interfacial segregation to the grain boundaries and spinodal decomposition is observed. A density-based phase field model for the grain boundary character's influence on the Gibbsian free energy is used to elucidate this evolution. Finally, how the Au solute within the grain boundary regulates faceting is discussed.

11:30 AM SF04.06.03

Phase-Field Modeling of Solid-State Metathesis Reactions [Guanglong Huang](#)¹, [David Montiel](#)¹, [Rebecca D. McAuliffe](#)², [Gabriel M. Veith](#)² and [Katsuyo Thornton](#)¹; ¹University of Michigan, United States; ²Oak Ridge National Laboratory, United States

To fully understand the process of phase transformation, it is important to follow the evolution of the system in detail, including those occurring at interfaces. This is particularly true in solid-state metathesis (SSM) reactions, where multiple chemical species with different charge states interact in a complex manner. However, temporal and spatial resolutions available in experiments are often limited, posing a challenge to construct a full picture of the process. In this presentation, we will discuss an integrated experimental-modeling effort to address this issue. We propose a phase-field model to simulate the evolution of ionic concentrations (in terms of mole fractions) and phase fractions in SSM reactions. The evolution of ionic concentrations is obtained via the reduction of a free energy, including a free energy landscape that has local minima located at the compositions of products. We utilize two Lagrange multipliers to impose constraints on the sum of mole fractions and of electroneutrality. Using this model, we study the effect of different reaction pathways (e.g., bulk diffusion, grain boundary diffusion and surface diffusion), as well as the effect of the mobility of each ion on the reaction dynamics. We then demonstrate the capability of the model by applying it to simulate a thin-film reaction for the synthesis of FeS₂. The values of the thickness and roughness of the interface between two precursors are determined based on X-ray reflectivity measurements. We set the mobilities of ions based on the diffusivities suggested by the experiment. The simulated diffusion behavior is in qualitative agreement with the experiment. In addition, the simulation predicts a nonplanar evolution of phases, which was not initially expected.

11:45 AM SF04.06.04

Coupling Reversion and Partial Recrystallization for Hetero-Structured Metastable Microstructural Design [Shaolou Wei](#) and [Cem Tasan](#); Massachusetts Institute of Technology, United States

Achieving a desirable strength-ductility synergy in metallic alloys indispensably relies on the understanding and control of crystalline defects and the

interplay involved therein. An effective pathway to approach this is to activate plastic strain-induced martensitic transformation because of the salient strain hardenability resulting from massive dislocation-phase boundary interactions. Provided the appreciable attempts to maximize the mechanical benefits of such a displacive transformation, microstructural design concepts based on its complementary part, *i.e.* martensite reversion via thermal annealing appear rather scant. Here we present a microstructural design strategy by combining plastic strain-induced epsilon-martensite reversion and partial recrystallization. We will show that by exploiting the displacive nature of epsilon-martensite reversion to promote strength, and by activating partial recrystallization to balance ductility, a feasible pathway to overcome the rule-of-mixture bound can be paved. Through *in situ* tensile tests under synchrotron X-ray diffraction and post-mortem electron channeling contrast imaging (ECCI) characterization, we underpin the dominant role of mechanical faulting throughout the entire strain hardening process. Assessments of individual strengthening mechanisms will also be presented to shed a bit more quantitative light on the heterogeneous microstructures by design.

SESSION SF04.07: Interface Roles in Microstructural Evolution III

Session Chairs: Abigail Hunter and Mohammed Zikry

Wednesday Afternoon, November 30, 2022

Sheraton, 3rd Floor, Berkeley

1:30 PM *SF04.07.01

The Austenite/Martensite Interface Structure, Kinetics, Resulting Transformation Strain—Theory and Experiment William A. Curtin¹, F. Maresca², E. Polatidis³, M. Smid³ and H. Van Swygenhoven³; ¹Ecole Polytechnique Federale de Lausanne, Switzerland; ²U. Groningen, Netherlands; ³Paul Scherrer Institute, Switzerland

In next-generation high-strength/high-toughness steels, the austenite/martensite (fcc/bcc) interface is the dominant microstructural feature controlling important properties. In spite of decades of research, the fundamental structure, mechanism of motion, and transformation strain due to this interface have remained uncertain. Here, an atomistic fcc-bcc iron interface is constructed that completely matches experimental observations and reveals a defect structure differing from longstanding theory assumptions while also violating conditions believed essential for a glissile interface. Based on this interface, we develop a new crystallographic double-shear theory of lath martensites that provides predictions in near-perfect agreement with both simulations and experiments. In a classic Fe-Ni-Mn alloy, we then use *in-situ* high resolution digital image correlation to measure the transformation strain and confirm the parameter-free theory [1]. The theory predicts increasing the fcc/bcc lattice parameter ratio increases the transformation strain, which is validated with literature data and then provides a new path for developing tougher high-strength steels.

[1] F. Maresca et al., *Acta Materialia* 200, 246-255 (2020)

2:30 PM BREAK

SESSION SF04.08: High Entropy Materials and Superalloys

Session Chairs: Ashley Bucsek and William Curtin

Wednesday Afternoon, November 30, 2022

Sheraton, 3rd Floor, Berkeley

3:30 PM *SF04.08.01

Multiscale Simulations of Interfacial Effects in High Entropy Alloys Diana Farkas; Virginia Tech, United States

This presentation will address the multiplicity of possible interfacial structures in compositionally complex alloys and the possible effects on the material mechanical response. Atomistic simulation techniques with model empirical potentials are used to study the effects of compositional complexity on grain boundary structures and dislocation behavior under applied strain. A multiscale technique is utilized to study the fracture response of these alloys.

4:00 PM *SF04.08.02

Computational Studies of Interfaces in High Entropy Ceramics: Chemical Ordering, Structure and Stability Donald Brenner¹, Sam Diagle¹, Belicia Castillo¹, Simon Divilov², Hagen Eckert², Stefano Curtarolo², Jon-Paul Maria³, Douglas Wolfe³, Eva Zurek⁴, Cormac Toher⁵ and William Fahrenholtz⁶; ¹North Carolina State University, United States; ²Duke University, United States; ³The Pennsylvania State University, United States; ⁴University at Buffalo, The State University of New York, United States; ⁵The University of Texas at Dallas, United States; ⁶Missouri University of Science and Technology, United States

It is well established in conventional alloys that stresses at grain boundaries, free surfaces, dislocations and related defects can attract solute atoms and in some cases induce ordering. In high-entropy ceramics, configurational entropy makes a relatively large contribution to the free energy (and hence stability) compared to ceramics with fewer components. Using first principles calculations and analytic modeling, we have been exploring whether interfaces and defects in high-entropy carbides induce similar chemical ordering, and if this ordering changes the interfacial stability and mechanical properties. Of particular interest are energies to form twins, whether ordering around dislocations increases (or decreases) the barrier for motion, and the effects of ordering on grain boundary energy, decohesion, and inter- versus trans-granular fracture.

4:30 PM SF04.08.04

Slip Behavior at Grain Boundaries Assessed with Nanoindentation Hardness TaNbTiV Refractory High Entropy Alloy Thomas R. Bieler and Eugenia Nieto; Michigan State University, United States

Preparation of refractory high entropy alloys by melt solidification led to dendritic segregation, which provides different compositions that can be used to assess the mechanical properties as a function of composition using nanoindentation arrays. EBSD orientation maps combined with backscattered electron images show that each grain consists of its own dendrite, and grain boundaries are usually along inter-dendritic zones. Hardness values track with local composition, with softer values in Ta dendrite cores and harder values in the interdendritic regions, but hardness also depended on grain orientation and grain boundaries. Relatively few indents exhibited obvious shear bands, which were usually correlated with {112} slip planes, and more often observed in the softer high-Ta dendrite cores. AFM characterization of selected indents on grain boundaries suggests uniform deformation on both sides of the

boundary such that quantifying effects related to slip transfer is difficult.

SESSION SF04.09: Poster Session
Session Chairs: Abigail Hunter and Nithin Mathew
Wednesday Afternoon, November 30, 2022
8:00 PM - 10:00 PM
Hynes, Level 1, Hall A

SF04.09.02

Effect of Elemental Segregation on Resistance of Grain Boundary Migration in High-Entropy Alloys Kohei Shiotani, Tomoaki Niiyama and Tomotsugu Shimokawa; Kanazawa University, Japan

High-entropy alloys (HEAs), which are solid solution materials obtained by mixing five or more than five elements with near equimolar fractions, have attracted significant attention because of their unique mechanical properties. Grain boundary (GB) migration velocity of some HEAs has been reported to be slower than that of conventional alloys; however, the origin of the slow GB migration is not yet fully understood. For dilute alloys, conventional theory and recent atomistic simulations have shown that dynamic GB segregation increases the driving force required for the GB migration; therefore, it is important to elucidate conditions under which dynamic GB segregation occurs in HEAs and its mechanism. In this study, we systematically investigate the dynamic GB segregation phenomena in HEAs by performing molecular dynamics simulations of GB migration under various deformation conditions for equimolar and non-equimolar HEA models.

As model alloys, we use $(\text{FeNiCrCo})_{1-x}\text{Cu}_x$, where the concentration of Cu is changed in the range of $x = 0-1$ and the other four elements are kept equimolar fractions each other. In this HEA model, Cu tends to segregate to GBs. The analysis models are bicrystal with a $\Sigma 17$ tilt-GB. At the initial atomic configuration, five kinds of elements are randomly distributed on the bicrystal lattice sites. By applying shear deformation at various constant strain rates and 80 % of the melting temperature, we investigate the strain rate dependence of the resistance of GB migration caused by the dynamic GB segregation. The velocity of GB migration is proportional to the shear strain rate based on the shear-coupling theory.

First, through the analyses with the equimolar HEA ($x = 0.2$), it is found that the resistance of GB migration reaches the maximum at the GB migration velocity of 1 m/s. At velocities slower than 1 m/s, GB segregation by Cu can be observed, but at velocities faster than 1 m/s, the GB segregation is hardly observed. Calculation of the diffusion coefficient for Cu within the GBs shows that Cu can follow the moving GBs by GB diffusion. These suggest that the dynamic GB segregation increases the resistance of the GB migration and the drag capacity of Cu determines the GB migration velocity at the maximum driving force. Next, through the analyses with the non-equimolar HEAs, the resistance reaches the maximum at the Cu concentration of $x = 0.6$, where the difference in Cu concentration in the matrix and GB during the GB migration shows almost the maximum value. This indicates that different Cu concentrations in the matrix and the GB increases the resistance of GB migration. The results suggest that designing for diffusion capacity and tendency of GB segregation can produce HEAs that exhibit better mechanical properties.

SESSION SF04.10: Solutes and Segregation
Session Chairs: Samuel Hemery and Abigail Hunter
Thursday Morning, December 1, 2022
Sheraton, 3rd Floor, Berkeley

8:30 AM *SF04.10.01

Tuning Nanocrystals and Nanocomposites by Doping and Interface Modification Daniel Kiener, Michael Wurmshuber, Michael Burtscher, Klemens Schmuck and Markus Alfreider; Montanuniversität Leoben, Austria

In order to accomplish a resource conserving future for our planet, it is inevitable to increase material performance. This requires on the one hand to design ever stronger materials to increase the load bearing capability of the materials employed in increasingly harsher environments. On the other hand, safety considerations also necessitate a certain ductility and fracture toughness in order to prevent fatal overload failure upon critical operation events. Furthermore, reuse and circular material use concepts also suggest to advance from overly complex alloying strategies back to lean alloying or even just minor doping additions.

To respond to these demands, we designed nanocrystalline W-based materials and nanocomposite based on the thermodynamically insoluble pairing of W with Cu. Starting from powders as initial input materials before refining to the bulk nanostructured material using severe plastic deformation, it remains a trivial task to vary the fraction of strong vs. ductile phase or to add minor amounts of doping elements, such as C, B, Hf or Re, to modify the material or interface conditions. The selection of these doping elements was guided by thermodynamic considerations and ab initio computations of interface properties.

Based on a comprehensive microstructural examination and micromechanical experiments, we will discuss how interface segregation engineering and microstructural design allow to adjust strength, ductility and fracture toughness of nanostructured and nanocomposite materials.

9:00 AM SF04.10.02

Spectrum of Grain Boundary Segregation Vibrational Entropy in Dilute Ni(Pd) Polycrystals Nutth Tuchinda and Christopher A. Schuh; Massachusetts Institute of Technology, United States

Understanding vibrational entropy of grain boundary segregation is important to understand the equilibrium state at finite temperatures. While the recent works have shown the importance of treating the grain boundary network as a collective of sites with varying atomic environments, progress in quantifying the distributions of segregation vibrational entropy is still limited to only a few systems for small coincident site lattice (CSL) boundaries. Here we apply a variant of the harmonic approximation to quantify the spectrum of vibrational entropy of grain boundary segregation in a Ni(Pd) polycrystalline system. The results show a strong correlation between 0-K segregation energy and vibrational entropy in agreement with previously reported results from small CSL boundaries using Monte Carlo simulations. The spectrum can be used with the established spectral thermodynamic framework to predict equilibrium solute content at finite temperatures, enabling a pathway to model interfacial segregation in polycrystalline materials at finite temperatures.

9:15 AM SF04.10.03

Grain-Boundary Solute Segregation and Associated Shear Localization Mechanisms in Random FCC Ag, BCC Nb and HCP Zr Polycrystals
Frederic Sansoz, Tara Nenninger and Eve-Audrey Picard; The University of Vermont, United States

Different segregation types in nanocrystalline alloys have been described in the literature as being either homogeneous or heterogeneous, which differently impacts their mechanical properties. In heterogeneous segregation, solute atoms are clustered along some grain boundaries (GBs), while other GB regions remain solute-free, as evidenced with Ni segregation in nanocrystalline Ag. This talk presents our recent efforts to better understand solute segregation and interaction within random GB networks, with particular focus on heterogeneous Ni segregation in different FCC, BCC and HCP alloys, and their roles on plastic deformation mechanisms such as shear localization. Using hybrid MC/MD, we simulated and analyzed solute segregation in random Ag, Al, Nb and Zr polycrystals, each with same solute content of 4 at.% Ni. A spectrum of segregation configurations from fully heterogeneous to fully homogeneous is revealed. Second, a fast algorithm based on atomic-scale GB segregation energy spectra was developed and applied to quantify the alloy tendency for GB solute clustering in both symmetric GBs and random GBs of polycrystals. This presentation will underscore the importance of solute interactions in profoundly altering segregation and mechanical behavior in stable nanocrystalline alloys.

9:30 AM SF04.10.04

An Accelerated Approach to Learn the Solute-Solute Interaction Spectra in Grain Boundaries Thomas Matson and Christopher A. Schuh; Massachusetts Institute of Technology, United States

Recent progress in understanding the thermodynamic stabilization of nanocrystalline alloys via grain boundary solute segregation has revealed the need for spectral information which captures the full distribution of grain boundary environments. Our recently developed accelerated framework, which predicts segregation energy spectra from the local atomic environments at the grain boundary, has made spectral information accessible even with ab-initio methods. However, this framework has only been applied in the dilute limit, and does not yet account for the spectral nature of solute-solute interactions. In this talk, we review our recent development of an atomistic, physically motivated method to measure the full spectrum of grain boundary solute interactions, and discuss a case study on the results of this method for a general polycrystal of Al(Mg). Additionally, we present a modified version of our accelerated framework, which uses the Smooth Overlap of Atomic Positions (SOAP) to construct descriptors for specific nearest neighbor pairs, and demonstrate its use for multiple binary alloys, including Al(Mg), Pt(Au), and Ag(Cu), using existing interatomic potentials.

9:45 AM SF04.10.05

The Grain Boundary Solute Drag Hypersurface—Insights from Theoretical and Machine Learning Studies Malek Alkayyali and Fadi Abdeljawad; Clemson University, United States

Nearly all functional and structural materials are polycrystalline systems, they are composed of crystalline grains that are separated by grain boundaries (GBs). It is well established that GBs play a critical role in a wide range of phenomena during materials processing or under service conditions. Of particular interest is GB migration and associated grain growth, as these processes control many crystal-size-dependent properties. Recent experimental studies have demonstrated stagnant grain coarsening due to GB solute segregation. However, most studies are focused on the thermodynamic aspect of solute segregation, and the role of GB solute drag remains poorly understood. The interaction of migrating GBs with elemental species influences GB dynamics, where the GB solute atmosphere exerts a drag, resisting GB migration. Herein, we present a solute drag model in concentrated alloys that accounts for solute-solute interactions in both the bulk and GBs and captures experimentally observed effects such as asymmetrical and multi-layer segregation. Our analysis suggests a self-similar behavior for the solute drag-GB velocity curves. Further, it is shown that the magnitude of GB solute drag is a function of bulk and interface alloy thermodynamics parameters, solute transport coefficients, and driving force; the GB solute drag is a hypersurface. Simulation data obtained using our mathematical model are used to train an artificial neural network (ANN) model to predict the solute drag hypersurface. Our results are used to explain experimental observations of sluggish grain growth in a wide range of metallic alloys. Moreover, the trained ANN shows the role of the recently observed asymmetric GB solute segregation in solute drag. In broad terms, our model provides avenues to explore the role of solute drag in GB dynamical processes.

10:00 AM BREAK

SESSION SF04.11: Fracture, Fatigue and Strain Inhomogeneity at Interfaces
Session Chairs: Thomas Bieler and Abigail Hunter
Thursday Morning, December 1, 2022
Sheraton, 3rd Floor, Berkeley

10:30 AM *SF04.11.01

From Slip Localization to Crack Formation at (0001) Twist Grain Boundaries in Ti Alloys Subjected to Dwell-Fatigue and Fatigue Loadings Cyril Lavogiez¹, Patrick Villechaise¹, Jean-Charles Stinville², Fulin Wang³, Marie-Agathe Charpagne², Meghan G. Emigh³, Tresa M. Pollock³, Valery Valle¹ and Samuel Hemery¹; ¹Institut Pprime, France; ²University of Illinois at Urbana-Champaign, United States; ³University of California Santa Barbara, United States

Titanium components employed in the aerospace industry generally experience fatigue loadings during in-service operation. Intense research efforts were put into the understanding of crack formation mechanisms to enable accurate prediction of the fatigue performance as well as microstructure optimization. However, literature review reveals an intricate situation owing to the competition between different mechanisms. In this presentation, a brief overview of microstructural features found at crack initiation sites in a variety of alloys with different microstructures and loading conditions will be reported first. Based on collected data, the occurrence of a single crack nucleation mechanism involving (0001) twist grain boundaries will be discussed and a criterion to identify candidates for crack initiation will be proposed. Details of the mechanism governing crack nucleation will then be described. Characteristics of these critical grain boundaries, including potential composition heterogeneities, were studied using TEM. In addition, their role in the early slip activity was investigated with a statistical significance using a combination of in situ tensile testing with high resolution DIC, EBSD and TEM. The transition from localized plasticity to crack formation at (0001) twist grain boundaries will finally be discussed in light of these results.

11:00 AM *SF04.11.02

In Situ Nanomechanical Testing to Understand the Role of Grain Boundary Structure in Materials Nan Li¹, Dongyue Xie¹, Saryu Fensin¹, Abigail Hunter¹, Darby Luscher¹, Muh-Jang Chen² and Mohammed A. Zikry²; ¹Los Alamos National Laboratory, United States; ²North Carolina State University, United States

Grain boundary is one of the most important planar defects in materials. Correlated mechanical response under loading leads to localized strain accumulation and structural changes in the vicinity of the boundary. This can determine whether dislocations can nucleate, transmit, or just be blocked at the boundary. In order to understand this process, we have performed *in situ* pillar compression in a scanning electron microscope coupled with electron backscatter diffraction scanning. The bicrystalline pillars, with the chosen boundary in the middle, are prepared in a shape of rectangular cuboid. During the uniaxial compression, the indentation has been paused at different strains to perform the electron backscatter diffraction scanning. Depending on the boundary structure, various interactions with dislocations at the boundary are captured. Correlated with the electron backscatter diffraction mapping at different strain states, we are able to quantify the lattice rotation and local strain tensor along the loading axial. Such information has helped us to better understand the mechanical role of grain boundaries and provided a unique validation for the modeling at both atomic and mesoscales.

11:30 AM SF04.11.03

Plastic Strain Inhomogeneity in ($\alpha+\beta$) Titanium Alloys—A Focused *In Situ* Exploration of Transformed β -Colonies Shaolou Wei¹, John Foltz², Luis Ruiz-Aparicio² and Cem Tasan¹; ¹Massachusetts Institute of Technology, United States; ²ATI Specialty Materials, United States

($\alpha+\beta$) titanium alloys demonstrate diverse microstructural combinations that enable fruitful pathways to engineer the macroscopic load-bearing performances. The microscopic deformation mechanisms leading to plastic strain inhomogeneity are, on the other hand, rather complex and deemed detailed considerations. Transformed β -colonies are one such example. Exhibiting a Burgers orientation relationship (BOR) between the BCC-structured retained β -phase (β_r) and the HCP-structured transformed β -phase (β_t), the transformed β -colonies have triggered appreciable interest in correlating slip activation and its crystallographic properties that can be relevant in microstructural design. By studying a Ti-Al-V-Fe-Sn alloy via integrated *in situ* SEM-based DIC, *in situ* synchrotron X-ray diffraction, and crystallographic theory, this presentation aims to address three fundamental aspects of the transformed β -colonies: (1) What is the critical factor that dominates plastic strain accommodation in different β_t variants? (2) What are the characteristics of plastic strain partitioning between β_r and β_t phases? (3) How does the BOR contribute to slip transferability across the β_r/β_t boundaries? Broader implications for cooperative and heterogeneous plastic deformation and their roles in damage initiation will also be discussed.

11:45 AM SF04.11.04

Microstructural Inelastic Deformation and Fracture Modes in Crystalline Materials Muh-Jang Chen¹, Dongyue Xie², Saryu Fensin², Nan Li² and Mohammed A. Zikry¹; ¹North Carolina State University, United States; ²Los Alamos National Laboratory, United States

Interrelated aspects of thermo-mechanical behavior with a specific focus on microstructural characteristics, such as partial and total dislocations densities and grain-boundary (GB) that span the nano to the micro, and how these characteristics affect failure modes, such as fracture nucleation in crystalline materials, will be presented. Recently developed methodologies have been used for a detailed analysis of fracture nucleation and the accurate characterization of intergranular and transgranular crack growth. Criteria for dislocation-density mechanisms and immobilization are directly related to interactions with GB ledges and propagating cracks in polycrystalline aggregates. The effects of interfaces, such as GB blockage, dislocation-density motion, and pileups on fracture nucleation will be discussed. The predictions are validated with micropillar compression experiments and provide further understanding of how defects, such as partial and total dislocation-densities, affect failure nucleation and intergranular and transgranular fracture.

SESSION SF04.12: Virtual Session: Grain Boundaries and Interfaces I
Session Chairs: Abigail Hunter and Garritt Tucker
Tuesday Afternoon, December 6, 2022
SF04-virtual

9:00 PM *SF04.12.01

Predicting Slip Transfer from Atomistic to Microscale—Methodology, Mechanisms and Applications Liming Xiong; Iowa State University, United States

Engineering alloys are usually heterogeneous and contain a high density of interfaces such as stacking faults, grain boundaries (GBs), and phase boundaries (PBs). When subjected to plastic deformation, the overall performance of these materials is largely dictated by the interaction between the dislocation-mediated slip and those interfaces. Due to the length-scale limitation, a fully atomistic model usually can only accommodate a few dislocations without considering much material microstructure complexities. In contrast, our concurrent atomistic-continuum (CAC) approach unifies the atomistic and continuum description of materials. It can accommodate the long-range dislocation slip and the atomically structured interfaces all within one model. Here we will present our recent development of an adaptive CAC for predicting slip transfer in plastically deformed polycrystalline alloys with its grain size spanning from nanometers to micrometers. The slip-interface reaction-induced complex internal stress as well as its contributions to the subsequent structure changes, such as lattice rotation, twinning (nucleation, growth, variant selection), and phase transformation, will be all characterized from the bottom up. The obtained results will be then informed into a local stress- or couple stress-based slip transfer metrics. An implementation of such metrics in higher length scale models, such as crystal plasticity finite element, dislocation dynamics, or phase field models, will significantly improve their predictive capability. This in turn, will lead to an atomistic-to-microscale computational platform that can be used for predicting the microstructure evolutions in a variety of engineering materials exposed to extreme stress, corrosive, irradiations, and even a combination of them.

9:30 PM *SF04.12.02

Investigation of Near Grain Boundary Gradient Zones Using HRDIC and HREBSD David T. Fullwood¹, Tristan Russell^{2,1}, Ryan Sperry¹, Landon Hansen^{3,1}, Guowei Zhou⁴, Ehsan Taghipour⁵ and Robert Wagoner⁵; ¹Brigham Young University, United States; ²Los Alamos National Laboratory, United States; ³Kitty Hawk Technologies, United States; ⁴Shanghai Jiao Tong University, China; ⁵The Ohio State University, United States

It is well known that deformation behavior in polycrystalline materials is modified significantly in the region of grain boundaries (GBs), in comparison to the response at the center of grains. This study observes various aspects of deformation response in FCC nickel and BCC tantalum using high-resolution digital image correlation (HRDIC) and high-resolution electron backscatter diffraction (HREBSD). Contrasting behavior is observed in terms of slip band nucleation and propagation, modification to active slip systems near GBs, strain and orientation gradients and geometrically necessary dislocation (GND) distributions, and transmission across GBs. Correlations between local microstructural features and deformation response in the near-boundary gradient zones are analyzed. The insights are used to assess the performance of crystal plasticity type models and inform the next generation of simulation approaches.

10:00 PM SF04.12.03

Development of a Systematic and Efficient Method for Searching for the Most Stable Grain Boundary Structures—A Method Based on Non-Identical Termination Combination Yuki Hata¹, Yaoshu Xie², Kiyou Shibata^{1,2} and Teruyasu Mizoguchi^{1,2}; ¹Grad. Sch. of Eng., the Univ of Tokyo, Japan; ²IIS, the Univ. of Tokyo, Japan

The rich diversity of grain boundaries (GBs) can affect macroscopic properties of entire material in various situations. Determining GB structures as systematically and as rapidly as possible is the first step toward understanding the properties of materials with GBs. Currently, a common method for determining the GB structure is a sequential grid search of rigid body translation (RBT), which is computationally expensive. Therefore, there is a need to develop a systematic and efficient method to search for the most stable GB structures.

The GBs are generally considered to be complex and have random structures, but it is known that characteristic structures (structural unit) appear on some GBs [1][2]. In this study, we have found that the structural units of the most stable GBs are naturally reproduced in a comprehensive combination set of GB plane terminations without considering the variation in RBT. Since the number of GB plane terminations is limited systematically by the crystal geometry, it may be possible to reduce the number of candidates for searching the most stable GB structures by focusing only on non-identical GB plane terminations. Based on this assumption, here we propose a new method for searching the most stable GB structures based on the non-identical GB plane terminations.

We chose symmetric tilt GBs with three rotational axes of [100], [110], and [111] in fcc Cu and bcc Mo as our research targets. Based on coincident site lattice theory, 170 GBs with Σ less than 100 were selected. First, relaxation calculations have been performed based on conventional brute-force RBT grid searching method. Then, in the same way, the relaxation calculations have been performed only on structures with non-identical end-face (termination) combinations among them. The most stable GB's energies and computational cost obtained by these two methods were compared. In addition, we have taken one GB with $\Sigma > 100$ ($\Sigma 157[001](-11\ 6\ 0)$), which generally requires a large amount of computational cost to determine the most stable GB structure, as an example and evaluated utility of our new method. The relaxation calculations were performed with the LAMMPS code [3] and GB model were made by Interface Master [4].

For almost all of the 170 GBs, the most stable GB structures obtained from the structures screened by focusing on the combination of non-identical GB plane terminations have shown agreement with those obtained from the conventional brute-force calculations with high accuracy.

We have also found that the number of the screened structures, with which is necessary to obtain the most stable GB, decreases down to several times value of Σ . For example, our method can find the most stable structure of $\Sigma 157[001](-11\ 6\ 0)\Sigma$ GB with only 1/120th the number of candidate structures of the conventional brute-force calculations. This result indicates that the selection of the candidate structures based on the GB plane termination is closely related to the conditions for the most stable GB structures and can be applied to the fast determination of GB structures. This result indicates that the generated structures by changing the GB plane termination are sufficient enough to determine the most stable GB structures.

These results suggest that the GB plane termination plays an important role in determining whether GB structures of single-element crystals become the most stable or not. To determine the most stable structure of GBs systematically and efficiently, it would be effective to focus on the combination of non-identical terminations. We are now applying this method to other GBs such as twist GBs and GBs in oxides.

[reference]

- [1] A. P. Sutton *et al*, Philos. Trans. R. Soc. Lond. A 309, 1–36 (1983).
- [2] K. Inoue *et al*, Mater. Trans. 56, 281–287 (2015).
- [3] A. P. Thompson *et al*. Comput. Phys. Commun. 271, 108171 (2022).
- [4] Y. S. Xie, K. Shibata, and T. Mizoguchi *et al.*, submitted.

10:15 PM SF04.12.04

Integration of Experimentation and Modeling in Heterogeneous Microstructures by Precision Nanocrystallization Mark Atwater and Joby M. Anthony III; Liberty University, United States

Heterogeneous microstructures offer a complementary approach to balance strength and ductility. In their various forms, regions of nanoscale grains provide strengthening to regions of coarser grains in which dislocation mediated plasticity is maintained. These interfaces result in hetero-deformation induced (HDI) hardening, which causes a back stress in the coarse-grained regions and forward stress in the nanoscale regions. These unique microstructures require multi-scale modeling to fully capture the interactions, and they are often challenging to control experimentally. We have developed methods to precisely induce local deformation hardening in materials, such that modeling can be accurately validated. Characterizing the behavior and interaction of grain boundaries and dislocations is vital to predict mechanical properties and performance of the selected material. Many historical and novel material behavior modeling techniques validate the application of some algorithm or implemented codes against physical experiments, but uncertainty in predicting material behavior increases if the modeling technique does not well capture many features of mechanical performance that may arise from complex microstructures. Integrated Computational Materials Engineering (ICME) is a physics-based modeling paradigm to characterize a material's properties to predict its performance for some boundary conditions which may vary drastically with time. At the electronic and atomistic length scales, ICME relies on Density Functional Theory (DFT) to characterize the quantum mechanics interactions between electrons and Modified Embedded Atom Method (MEAM) interatomic potentials to characterize how a unit cell of material interacts with its neighbors given so much strain. The change in microstructure can then be examined by Dislocation Dynamics (DD), which relies on the formulated MEAM potential and dislocation velocity quantified at the lower length scales. Again, the ability of DD to characterize interactions between dislocations and grain boundaries is only as good as the techniques at the lower length scales. DD simulations and later Finite Element Analysis (FEA), is also only as confident as the data is for the MEAM potentials and dislocation velocity. These multiscale factors in the development of a computational framework and the real-world performance of heterogeneous microstructures created through precision nanocrystallization will be discussed.

SESSION SF04.13: Virtual Session: Grain Boundaries and Interfaces II

Session Chair: Abigail Hunter

Wednesday Afternoon, December 7, 2022

SF04-virtual

9:00 PM *SF04.13.01

Study of Pseudomorphically Transformed bcc Mg in Mg/Nb Multilayer Nanocomposites Under Extreme Conditions Sid Pathak¹, Manish Jain², Nathan Mara³, Irene J. Beyerlein⁴, Marko Knezevic⁵ and Johann Michler⁶; ¹Iowa State University of Science and Technology, United States; ²University of

Nevada, Reno, United States; ³University of Minnesota Twin Cities, United States; ⁴University of California at Santa Barbara, United States; ⁵University of New Hampshire, United States; ⁶Empa–Swiss Federal Laboratories for Materials Science and Technology, Switzerland

In recent years two-phase nanolayered composites with individual layer thicknesses varying from 200-300nm down to 1-2 nm have been the subject of intensive study because of their unusual physical, chemical and mechanical properties. For example, with decreasing layer thicknesses (down to nanometer length scales) the mechanical response of these nanocomposites becomes increasingly interface dominated, and they exhibit ultrahigh strengths approaching the theoretical limit for ideal crystals. Moreover if the constituent phases present large differences in strength, elastic modulus and ductility, these multilayers give rise to new possibilities for the deformation mechanisms and properties of the composite as a whole. In this work we explore the possibility of synthesizing multilayered composites where one constituent phase has a low ductility, with a final goal of enhancing both the strength and ductility of the system.

Using physical vapor deposition (PVD) techniques we synthesized a hexagonal close-packed (HCP) – body-centered cubic (BCC) Mg-Nb system (where twinning in Mg leads to its lack of ductility), over a range of layer thicknesses ranging from 5 nm to 200 nm. We investigated the structure of the hitherto-unknown bcc Mg phase in the Mg/Nb multilayer nanocomposite under high pressures in a diamond anvil cell experiment using synchrotron radiation x-ray diffraction (XRD). We utilize a suite of small scale testing techniques to evaluate the deformation mechanisms in these nanocomposites that involve both compressive loading scenarios such as (a) high throughput nanoindentation testing, to more-specialized FIB-fabricated (b) micro-pillar compression, and (c) micro-tensile tests. The mechanical data obtained from these tests are correlated with the structure information at complementary length scales using techniques such as XRD, SEM, and TEM. The use of such diverse testing technologies allows a detailed characterization of the structure-property correlations at each length scale of interest; ranging from the response of each individual interface within the laminate to properties of the ensemble.

The specialized testing techniques such as FIB-fabricated micro-pillar compression and micro-tensile experiments are used to characterize the anisotropic response of the nanolayered composite, with interfaces oriented either normal, parallel and oblique (45°) to the compression axis. Each of these configurations generate unique mechanical information: thus while compressions and tensions normal and parallel to the interface are important for a complete understanding of the anisotropy of properties and size-related effects, the tests with the interfaces loaded obliquely provide a measure of interfacial shear strength. Ductility and fracture toughness at the micrometer level are investigated using *in-situ* observations inside an SEM coupled with a micro-tensile geometry. Tests repeated as a function of layer thickness and interface orientations provide us with valuable information regarding the Mg-X interface character.

We have also extended our techniques to measuring the strain rate sensitivity (SRS) of the Mg-X nanocomposites using *in situ* strain rate jump experiments conducted under both indentation and micro-compression/micro-tensile loading scenarios. Elevated temperature measurements are especially important, since the SRS for nano-(bcc)Mg is expected to differ from its nano-(hcp)Mg counterpart as a function of temperature from which activation energies/volumes for deformation mechanisms can be extracted. Results from these tests were analyzed in terms of the measured activation energies and activation volumes from sub-micrometer sized Mg/Nb multilayer nanocomposites. These findings reveal an alternative solution to obtaining lightweight metals critical needed for future energy efficiency and fuel savings.

9:30 PM DISCUSSION TIME

SYMPOSIUM SF05

Harnessing Functional Defects for Energy and Electronic Frontiers
November 28 - December 7, 2022

Symposium Organizers

Carmela Aruta, National Research Council
Panchapakesan Ganesh, Oak Ridge National Laboratory
Yuanyuan Zhou, Hong Kong Baptist University
Hua Zhou, Argonne National Laboratory

* Invited Paper
+ Distinguished Invited

SESSION SF05.01: Harvesting Functional Defects in Halide Perovskites I
Session Chairs: Hua Zhou and Yuanyuan Zhou
Monday Morning, November 28, 2022
Sheraton, 3rd Floor, Gardner A/B

10:30 AM *SF05.01.01

Intrinsic Defects and Charge-Carrier Localisation in Metal Halide Semiconductors [Laura Herz](#); University of Oxford, United Kingdom

Metal halide semiconductors have emerged as attractive materials for solar cells with power-conversion efficiencies now exceeding 25%. However,

challenges and opportunities remain relating to material microstructure, defect formation, ionic migration and toxicity.

We show that FAPbI₃ perovskite, which has recently been implemented in highly efficient solar cells, can exhibit a peculiar structural defect that leads to intrinsic quantum confinement of charge carriers, apparent through surprising oscillatory features in the absorption spectrum.^[1] By determining the threshold film thickness at which the amplitude of the peaks is appreciably decreased, and through ab initio simulations of the absorption features, we have estimated the length scale of confinement to be 10–20 nm. Such domains may result from δ_{H} -phase barriers or ferroelectric effects and, depending on application, may be either detrimental (e.g. to charge extraction in solar cells) or advantageous (e.g. to light emitting devices). We further show^[2] that such nanoscale electronic effects can be controlled through partial replacement of the FA cation with Cs. We find that Cs-cation exchange causes a weakening of quantum confinement in the perovskite, arising from changes in the bandstructure, the length scale of confinement, or the presence of δ_{H} -phase electronic barriers. We further observe photon emission from quantum-confined regions, highlighting their potential usefulness to light-emitting devices and single-photon sources.^[2] Overall, these structural defects present a new and intriguing quantum electronic phenomenon in a nominally bulk semiconductor, offering intrinsic nanoscale optoelectronic properties without necessitating cumbersome additional processing steps.

We further report on ultrafast charge-carrier self-trapping in lead-free silver-bismuth semiconductors^[3-5] which promise lower toxicity and potentially higher barriers against ion migration than their more prominent lead-halide counterparts. We examined the evolution of photoexcited charge carriers in the double perovskite Cs₂AgBiBr₆ using a combination of temperature-dependent photoluminescence, absorption and optical pump–terahertz probe spectroscopy.^[3] We observe rapid decays in terahertz photoconductivity transients that reveal an ultrafast, barrier-free localization of free carriers on the time scale of 1.0 ps to an intrinsic self-trapped small polaronic state. We further demonstrate the novel lead-free semiconductor Cu₂AgBiI₆ which exhibits several advantages over Cs₂AgBiBr₆, namely a low exciton binding energy of ~29 meV and a lower and direct band gap near 2.1 eV,^[4,5] making it a significantly more attractive lead-free material for photovoltaic applications. However, charge carriers in Cu₂AgBiI₆ are found to exhibit similarly strong charge-lattice interactions^[5] to those in Cs₂AgBiBr₆, suggesting a link with the presence of AgBi. The presence of such self-trapping therefore emerges as a serious challenge for this class of materials.

[1] A. D. Wright, G. Volonakis, J. Borchert, C. L. Davies, F. Giustino, M. B. Johnston, and L. M. Herz, *Nature Materials* **19**, 1201 (2020).

[2] K. A. Elmostekawy, A. D. Wright, K. B. Lohmann, J. Borchert, M. B. Johnston, and L. M. Herz, *ACS Nano* **16** (2022) 10.1021/acsnano.2c02970.

[3] A. D. Wright, L. R. V. Buizza, K. J. Savill, G. Longo, H. J. Snaith, M. B. Johnston, and L. M. Herz, *J. Phys. Chem. Lett.*, **12** (2021), 3352–3360.

[4] H. C. Sansom, G. Longo, A. D. Wright, L. R. V. Buizza, S. Mahesh, B. Wenger, M. Zanella, M. Abdi-Jalebi, M. J. Pitcher, M. S. Dyer, T. D. Manning, R. H. Friend, L. M. Herz, H. J. Snaith, J. B. Claridge, and M. J. Rosseinsky, *JACS*, **143** (2021), 3983–3992.

[5] L. R. V. Buizza, A. D. Wright, G. Longo, H. C. Sansom, C. Q. Xia, M. J. Rosseinsky, M. B. Johnston, H. J. Snaith, and L. M. Herz, *ACS Energy Letters*, **6** (2021), 1729–1739.

11:00 AM *SF05.01.02

Visualising and Mitigating Problematic Defects in Halide Perovskite Photovoltaic Absorbers [Samuel D. Stranks](#); University of Cambridge, United Kingdom

Halide perovskites are exciting materials showing high performance in photovoltaic devices, among other device platforms. This performance is in part due to the fact that many of the defects in halide perovskites appear to be electronically benign. However, there are still deep traps in halide perovskites that limit performance and need addressing.

Here, I will outline work where we have characterised deep trap states in halide perovskite absorber materials. We find that there are small nanoscale clusters of impurity phases including hexagonal polytypes that have high defect densities leading to deep trap states. Furthermore, these defective sites are where photo-instability pathways are seeded, realising a fundamental link between carrier traps and device stability. I will outline how managing these particularly problematic defects – through passivation and material composition control – will be key to further pushing device performance and stability.

11:30 AM *SF05.01.03

Tailored Interfaces in Metal Halide Perovskites for Efficient Carrier Transfer [Juan Pablo Correa Baena](#); Georgia Institute of Technology, United States

Perovskite solar cells promise to yield efficiencies beyond 30% by further improving the quality of the materials and devices. Electronic defect passivation and suppression of detrimental charge-carrier recombination at the different device interfaces has been used as a strategy to achieve high performance perovskite solar cells. However, the mechanisms that allow for carriers to be transferred across these interfaces are still unknown. In this presentation, I will discuss the role of crystal surface structural defects on optoelectronic properties of lead halide perovskites through synchrotron-based techniques. The importance of interfaces and their contribution to detrimental recombination will also be discussed.

SESSION SF05.02: Harvesting Defects in Multifunctional Oxides

Session Chairs: Hyeon Han and Hua Zhou

Monday Afternoon, November 28, 2022

Sheraton, 3rd Floor, Gardner A/B

1:30 PM *SF05.02.01

Structure and Properties of Low Dimensional Epitaxial Oxides; Interfaces and Superlattices [Gertjan Koster](#); University of Twente, Netherlands

In complex oxide materials the occurrence of ferroelectric, ferromagnetic or other properties are for the most part determined by the detailed oxygen coordination of metal cations. More specifically, in the case of perovskite-type materials ABO₃, where A and B are metal cations, by the BO₆ octahedral orientations and rotations. At interfaces in epitaxial oxide hetero structures, for example magnetic junctions or capacitive structures, this oxygen sub-lattice is found to be different from its bulk counterpart.

I will briefly introduce the current status of the often used technique to fabricate epitaxial layers, ‘atomically controlled PLD’, as well as give a few examples of oxygen sub-lattice and interface engineering achieved by controlled thin film parameters such as, composition, digital thickness variation, polar discontinuous interfaces or the insertion of oxide buffer layers that influence the perovskite-type BO₆ sub-lattice or related structures. I will further elaborate on the effects of such thin film parameters on the structure and properties of various model systems that have been subsequently studied by *in situ*

characterization techniques, high resolution scanning transmission electron microscopy or other spectroscopic techniques (XAS, RIXS, PNR etc.). More practically, often-encountered problems due to dead-layer effects, which normally hamper many functional devices, could be identified.

2:00 PM *SF05.02.02

Growth of Oxide Thin Films on Different Natures of Substrates for Various Electronic and Medical Applications Wilfrid Prellier; CRISMAT Laboratory, France

Transition metal oxides often having a perovskite structure form a wide and technologically important class of compounds. In these systems, ferroelectric, ferromagnetic, ferroelastic, or even orbital and charge orderings can develop and eventually coexist. These orderings can be tuned by external electric, magnetic, or stress field, and the cross-couplings between them enable important multifunctional properties, such as piezoelectricity, or magneto-elasticity. In spite of the large number of observations and promise of epitaxial oxide thin films, most of the investigations have been focused on films on low-index commercially-available single-crystal substrates, which have limited the scope of the study, and the applications. Here, we will present how oxide thin films can be grown on different types of substrates including polycrystalline substrates, and glass templates. Examples will be given to show different applications that can be utilized for medical or electronics.

2:30 PM SF05.02.03

Atomic Scale Structure and Electronic Structure of Defects at Misfit Dislocations in CeO₂/MgO Heterostructure Pratik P. Dholabhai; Rochester Institute of Technology, United States

Among the numerous functionalities of mismatched oxide heterostructures and thin films, one of their most promising energy applications is in solid oxide fuel cell (SOFC) electrolytes. Epitaxial growth of oxide thin films on substrates above critical thickness result in the formation of misfit dislocations. These functional extended defects influence key material properties of thin film SOFC electrolytes. Nevertheless, fundamental understanding of the atomic scale structure and electronic structure of misfit dislocations and their intricate interaction with mobile oxygen vacancies at functional oxide interfaces is lacking. In this work, first principles density functional theory was used to elucidate the atomic scale structure and electronic structure of misfit dislocations for experimentally observed epitaxy in CeO₂/MgO heterostructure. Rotation of CeO₂ thin film is uncovered as one potential mechanism eliminating the surface dipole, which results in experimentally observed epitaxy. In Gd-doped CeO₂ thin film, thermodynamic stability and electronic structure of oxygen vacancies in the neighborhood of misfit dislocations will be contrasted against their behavior in the bulk and at surfaces. Changes in the electronic density of states and interface electronic charge transfer due to defect formation in the vicinity of misfit dislocations and their impact on ionic transport will be discussed. Present results are instrumental in understanding the intricate interplay between misfit dislocations, dopants, and oxygen vacancies and their ultimate impact on ionic transport in thin film SOFC electrolytes.

We acknowledge support from NSF CAREER Award DMR-2042311.

2:45 PM SF05.02.04

Oxygen Vacancies in High Entropy Perovskite Oxides—A Computational Study about Local Ordering, Distortion and Redox Activity Boyuan Xu¹, Stephan Lany², Jiyun Park¹, Dawei Zhang³, Xingbo Liu⁴, Jian Luo³ and Yue Qi¹; ¹Brown University, United States; ²National Renewable Energy Laboratory, United States; ³University of California, San Diego, United States; ⁴West Virginia University, United States

High entropy perovskite oxides (HEPOs), typically consist of four or more elements fully mixed at {A} or/and {B} sites in ABO₃ perovskite lattices. Mixing multiple cations can reach a significant configurational entropy that offers a wide, unexplored new compositional space with vast tunability to meet challenging requirements of real applications. One of applications is the two-step solar thermochemical hydrogen generation (STCH) techniques, in which HEPOs are believed to provide higher redox capacities, longer durability and lower reduction temperature.

Multiple cation mixing introduces new computational challenges, such as composition design rule for higher hydrogen yield, strategy to sample and analyze possible configurations, and nonstoichiometry prediction for HEPO system with spread oxygen vacancy formation energies. In this research, density functional theory (DFT) is combined with Metropolis Monte Carlo method (DFT-MC) to efficiently sample the possible cation configurations and discover the role of each {B} site elements on oxygen vacancy formation. (La_{0.8}Sr_{0.2}){MnFeCoAl}O₃ (LS_MFCA) was simulated first as one of the materials that shows good STCH performance. Cation positions or magnetic moment exchanged configurations were used in the DFT-MC simulations at 1600 K (reduction temperature in STCH process), and more than 2600 bulk, 3000 vacancy configurations that gave rise stable energies in MC simulations were saved for further analysis.

The neutral oxygen vacancy formation energy in LS_MFCA is sensitive to {B} site element type, charge state, local ordering and structural distortion. The oxidation state determined by magnetic moments shows that the charge states on {MnFeCoAl} are Mn⁴⁺, Fe³⁺, Co³⁺, and Al³⁺ and Co³⁺ is the predominant redox active element, which agrees with the in-situ X-ray photoelectron spectroscopy (XPS) observations. Cation mixing causes local lattice distortion. Cation Bond Valence Sum (BVS) descriptor analysis shows that Co-O bonds in bulk LS_MFCA structures are much more stretched (weakened) than Mn-O and Al-O bonds, while Fe-O bonds are slightly compressed (strengthened). Since the oxygen vacancy formation causes volume expansion in many oxides, the stretched bonds will lower the vacancy formation energy near Co. Among the saved structures, the configurations of the two B-cations connected to the oxygen (or vacancy) were analyzed for possible {B} site preference or local ordering. The elemental combination of the {B} pairs connecting to oxygen in the bulk LS_MFCA is close to random, but more than 80% of the {B} pairs connecting to oxygen vacancy contains Co. This means the local excess space due to Co³⁺-O bond stretching outpaced the tendency to generate vacancies near Mn⁴⁺, leading to the oxygen vacancy generation favoring Co site.

3:00 PM BREAK

3:30 PM *SF05.02.05

Ferroelastic Domain Walls in BiFeO₃ as Memristive Networks J. Rieck^{1,2}, D. Cipollini^{2,1}, M. Salverda¹, C.P. Quinteros^{1,3}, L.R.B. Schomaker^{2,1} and Beatriz Noheda^{1,2}; ¹University of Groningen, Netherlands; ²Cognigron - Groningen Cognitive Systems and Materials Center, Netherlands; ³ECYT-UNSAM, CONICET, Argentina

Domain walls of ferroic oxides have been extensively investigated as functional defects. In particular, ferroelastic domain walls of ferroelectric oxide perovskites have shown enhanced conductivity with respect to the insulating domains. Memristive behaviour has also been demonstrated in these nanoscale objects. However, until now, these properties have been measured on individual domain walls with current flowing between electrodes located at the bottom and top of the thin film samples. Here we show that lateral current flow from wall to wall is also possible in these materials, therefore allowing information transfer through the domain wall network and making these systems promising for brain-inspired applications.

4:00 PM SF05.02.06

Spatially Resolved Electrical Analysis of Epitaxial Defect-Stabilized Hafnium Oxide Thin Films [Niclas Schmidt](#)¹, Silvia Karthäuser¹, Nico Kaiser², Tobias Vogel², Eszter Piroos², Lambert Alff², Regina Dittmann¹ and Rainer Waser¹; ¹Forschungszentrum Jülich GmbH, Peter-Grünberg-Institut 7 (PGI-7), Germany; ²Advanced Thin Film Technology Division, Institute of Materials Science, TU Darmstadt, Germany

Hafnium oxide (HfO₂) is a transition metal oxide which receives great research interest due to its compatibility with complementary metal-oxide-semiconductor (CMOS) technology, as well as its ferroelectric and memristive properties. One key to improve the performance of hafnium oxide based non-volatile resistive random access memory (ReRAM) devices is specifically tuning the electronic properties. Here, the precise engineering of defects, such as doping with other transition metals or the variation of the oxygen content, plays a major role. The objective is to improve the formation and disruption of a conductive filament by diffusion of oxygen vacancies in valence change mechanism (VCM) type of ReRAM devices. Scanning probe techniques, such as conductive atomic force microscopy (c-AFM), are powerful tools to investigate the switching behavior and electronic properties at the surface of transition metal oxides with highest local precision.[1]

The purpose of this study is to identify filament locations on the nanoscale and to examine their minimal size with respect to the sample stoichiometry of hafnium oxide thin films. The hafnium oxide samples with varying oxygen content were grown by molecular beam epitaxy (MBE) on c-cut sapphire substrates with an intermediate TiN layer acting as bottom electrode. The oxygen flow during evaporation was varied to grow a series of samples, starting from stoichiometric, monoclinic HfO₂ and going to substoichiometric, highly oxygen deficient HfO_{2-x}, where a low-temperature cubic phase could be identified.[2] Subsequently, the samples were analyzed without breaking the vacuum by c-AFM and scanning tunneling microscopy/spectroscopy (STM/S). The RMS surface roughness of the hafnium oxide films, which have a thickness of 10nm, is about 1nm or less, measured by c-AFM. By performing a series of conductivity maps, a gradual increase in conductivity of the hafnium oxide layer with decreasing oxygen content and increasing amount of the substoichiometric cubic phase can be determined. The onset behavior of the conductivity for each case of the different oxygen deficiencies has a similar appearance. In particular, while the first conductive pathways are identified along grain boundaries and expand with increasing bias voltage, distinct grains show a gradual onset behavior in a voltage range of about 1V. Analogous to the onset of the general conductivity, the forming behavior of grains is likewise dependent on the mean oxygen vacancy content defined by the growth process. Moreover, the switching behavior for the different stoichiometries is analyzed with one focus on the smallest switchable structure. For a more profound perception of the electronic properties around the Fermi level, the most conductive samples are investigated by STS. Thereby, the target is the identification of possible in-gap states caused by introduced defects.[3]

References:

- [1] R. Dittmann *et al.*, Proc. IEEE 2012, **100**(6), 1979-1990
- [2] N. Kaiser *et al.*, ACS Appl. Mater. Interfaces 2022, **14**, 1290-1303
- [3] N. Schmidt *et al.*, ACS Appl. Nano Mater., *submitted*

4:15 PM SF05.02.07

Growth of High-Crystalline α -Ga₂O₃ Thin Films on Sapphire Substrates Using Template Engineering for High Voltage α -Ga₂O₃ Power Devices [Byoungsoo Kim](#), Duyoung Yang, Yongjo Park and Ho Won Jang; Seoul National University, Korea (the Republic of)

With the rapid expansion of the industry, the demand for high-efficiency and durable power semiconductors in harsh conditions such as high temperature and high voltage has increased. Gallium oxide (Ga₂O₃) is a potential material for next-generation power devices, with a bandgap energy of 4.8-5.3 eV, which is higher than Si, SiC, and GaN. Ga₂O₃, especially corundum structured α -Ga₂O₃, has gotten a lot of interest among Ga₂O₃ phases, owing to its special characteristics such as epitaxial growth on a cheap sapphire substrate and the presence of p-type materials with the same crystal structure. However, the mismatch of the lattice and thermal expansion coefficients between α -Ga₂O₃ and sapphire, however, causes a high density of threading dislocations (TDs) and cracks in films. High-density TDs act as leakage current paths within the device, reducing efficiency and limiting lifetime. Solving these problems is essential for the development of high-performance devices based on α -Ga₂O₃. Herein, we proposed the template engineering for the high-quality and strain-free α -Ga₂O₃ films by adopting the compositionally graded α -(Al_xGa_{1-x})₂O₃ layers and a thin sapphire nano-membrane.

In the first chapter, compositionally graded α -(Al_xGa_{1-x})₂O₃ layers are adopted to reduce threading dislocations for high-quality epitaxial α -Ga₂O₃ films. The evolution of strain relaxation and the inclination of threading dislocations in graded α -(Al_xGa_{1-x})₂O₃ layers are confirmed by reciprocal space mapping (RSM) and transmission electron microscopy (TEM). Through RSM and TEM studies, we confirmed that compressive strain enhances the inclination of dislocations, and therefore, the dislocations merge and annihilate in the graded α -(Al_xGa_{1-x})₂O₃ layers. The calculated density of threading dislocations in α -Ga₂O₃ films with a graded α -(Al_xGa_{1-x})₂O₃ buffer layer is reduced by 64.9% compared with that of α -Ga₂O₃ films deposited directly grown on a bare sapphire substrate. Furthermore, a fabricated lateral-structure Schottky diode reveals enhanced breakdown voltages and forward current density due to the improved crystalline quality by using the graded α -(Al_xGa_{1-x})₂O₃ buffer layer.

In the second chapter, the properties of the α -Ga₂O₃ thin films selectively grown on the thin substrates, stripe patterned sapphire nanomembrane, were investigated. First, the microstructure of α -Ga₂O₃ was investigated about the pattern direction, leading to the conclusion that it is preferable to construct the pattern in the [100] direction for device development. The thin substrate absorbed the stress applied to the thin film due to the strain partitioning effect, resulting in a 13.6% drop in misfit edge dislocation density of α -Ga₂O₃ and an 18.7% decrease in the 104 FWHM value of the XRD ω -rocking curve. The thin film's stress was analyzed using reciprocal space mapping, and it was proven that the thin substrate was responsible for the highest stress reduction of 51.6%, due to the strain partitioning effect.

This work will pave the way for high-quality α -Ga₂O₃ growth and its related application development, with follow-up research predicted to lead to the advancement of high-performance power devices.

4:30 PM SF05.02.08

Fabrication and Characterization of IrO_x Nanosheets for Methane Sensors [Tatsuki Umeda](#), Takahisa Tanaka and Ken Uchida; The University of Tokyo, Japan

Introduction

CH₄ is a greenhouse gas that throughs the second largest impact on global warming after CO₂, and it is essential to develop a technology to continuously monitor CH₄ emissions [1]. Recently, it has been reported that C-H bond of CH₄ can be cleaved at the IrO₂(110) surface in an ultrahigh vacuum [2]. However, the reaction has only been verified in ultrahigh vacuum, and it has not yet been clarified whether the C-H cleavage reaction by IrO₂ occurs in the standard atmosphere or whether this reaction can be applied to CH₄ resistive sensors.

In this study, IrO_x nanosheets with IrO₂(110) were fabricated using reactive sputtering system and examined their resistive response to CH₄ in dry air. The impacts of film deposition conditions on the sensor response were also investigated.

Experimental Method

To fabricate IrO_x-based CH₄ sensors, reactive sputtering system (Target: Iridium, Base pressure: 5×10⁻³ Pa, RF power: 80 W, Substrate temperature: as-is)

was used. IrO_x nanosheets of approximately 30 nm and 5 nm in thickness were deposited on 1- μ m-thick thermal oxide (SiO₂) films on Si substrates. The chamber pressure during the deposition process was 0.67 Pa, and the flow ratio of O₂ against the total flow of 20 sccm was set to 10, 20, or 40%. After IrO_x deposition, the films were annealed process at 500°C for 30 min in an O₂ atmosphere. X-ray diffraction (XRD) and X-ray reflectivity (XRR) measurements were performed to 30-nm-thick IrO_x nanosheets. On the 5-nm-thick IrO_x nanosheets, 50-nm-thick Au electrodes were deposited, and the electrode pattern was formed by a metal shadow mask. The fabricated sensors were initialized by exposing to dry air for 5 minutes at 200°C. The sensing evaluation sequence is as follows. The sensors are 1) exposed to dry air with 50-ppm CH₄ for 1 minute, and then 2) exposed to dry air without CH₄ for 3 minutes. The sensor characteristics were evaluated at 200°C by repeating 1) and 2) twice. The sensor responses ($\Delta R/R_0$) were evaluated as the ratio of resistance change ($\Delta R = R - R_0$) due to the target gas (CH₄) with respect to the initial resistance (R_0), where R_0 is the initial sensor resistance.

Results and Discussion

In XRD 2θ - θ measurements of IrO_x nanosheets after O₂ annealing, the peak from IrO₂ (110) was observed, regardless of the O₂ flow ratio. The broadening of the IrO₂(110) peak width indicates that the size of the IrO₂ microcrystals decreased with an increase in the O₂ flow ratio. XRR measurements of the nanosheets showed that the density of IrO_x nanosheets decreased as the O₂ flow ratio increased, implying that the nanosheets became sparser. Nanosheets made with a 10% O₂ flow ratio showed no sensor response at 200°C, whereas the sensor was responded to CH₄ at 200°C for the nanosheets made with 20 and 40% O₂ flow ratio, where the size of IrO₂ grains and density of IrO_x films were smaller than the 10% counterpart. This suggests that the size of IrO₂ crystals and/or the voids in the IrO_x nanosheets affected the sensor response to CH₄. In the previous study, it has been reported that CH₄ is oxidized by the bridging O atoms (O_{br}) on coordinatively unsaturated IrO₂ (110) surface and is desorbed as CO or CO₂ [3]. Thus, we consider that the oxidation reaction and resultant desorption of CH₄ and O_{br} led to the increase in resistance because the hopping transfer of electrons between the microcrystals was more difficult due to increased gaps between microcrystals. Therefore, it is expected that the sensor response to CH₄ can be increased by fabricating IrO_x nanosheets with narrower gaps between the microcrystals.

Acknowledgements

This work was partly supported by JSPS KAKENHI Grant Number 18H05243, 19H00756 and JST CREST Grant Number JPMJCR1912.

References

- [1] T. Hong *et al.*, *Trends Analyt. Chem.*, **125**, 115820 (2020).
- [2] Z. Liang *et al.*, *Science*, **356**, 299 (2017).
- [3] C. J. Lee *et al.*, *J. Phys.: Condens. Matter*, **34**, 284002 (2022).

4:45 PM SF05.02.09

Functional Silicon Oxide Nanolayers for Temperature Sensing on 4H-SiC Gernot Fleckl; TU Wien, Austria

Silicon Carbide's (SiC) physical properties make it an excellent candidate for high performance applications in harsh environments. Especially its large bandgap of ~3.25 eV, high electric breakdown field of 3 MV/cm and a high thermal conductivity represent outstanding material properties which qualify SiC for power electronics and high operating temperatures. The materials oxidizability to silicon oxide (SiO₂) is a major advantage in comparison to other large bandgap materials, like GaN. SiO₂ is favored as it is a well-known material in both, electrical properties and fabrication. Still, there are major drawbacks of device stability and charge carrier mobility due to insufficient oxidation at the interface between SiO₂ and SiC. Furthermore, the growth rates of thermal SiO₂ on SiC are rather low in comparison to silicon (Si), even at high temperatures of 1000°C and above. Therefore, the dry thermal oxidation of SiC is an ineffective method and not suited for device fabrication in semiconductor foundries.

The aim of the work was to find new approaches to overcome these drawbacks. Therefore, an implantation dominated oxidation method was introduced, able to fabricate SiO₂-nanolayers. Unlike originally expected, an unprecedented property of the fabricated SiO₂-layers occurred: the materials polarization characteristic is strongly dependent on its temperature. The effect is fully reversible after cooling down to room temperature with minor hysteresis effects. The materials new property appears to be related with a defect induction into the SiO₂-layer, caused by the novel, implantation dominated fabrication method. The materials behavior is highly functional with many possible applications but its most obvious in temperature sensing. The devices were calibrated by an allocation of extracted permittivities to temperatures in range between 300 K to 575 K. To gain information about the sensing accuracy, 30 randomly chosen temperatures within the calibration range were approached and capacity-over-frequency spectra recorded. By an interpolation of the calibration curve, each from capacity-over frequency spectra extracted permittivity can be dedicated to a certain temperature.

The sensor concept is based on a simple MOS capacitor, incorporating the functional SiO₂-layer as dielectric material. The bulk materials high thermal conductivity of 280 Wm⁻¹K⁻¹ makes 4H-SiC an excellent candidate as a carrier for a functional material for temperature sensing. Any change in temperature on its surface is quickly conducted to the functional SiO₂-layer, changing its polarization immediately. By this work not only a novel and simple temperature sensor concept is introduced but a functional SiO₂-based dielectric material.

SESSION SF05.03: Harvesting Functional Defects in Halide Perovskites II

Session Chairs: Mahshid Ahmadi and Andrej Singer

Tuesday Morning, November 29, 2022

Sheraton, 3rd Floor, Gardner A/B

8:30 AM *SF05.03.01

High Photoluminescence Quantum Yield Downconversion in Ytterbium-Doped Metal Halide Perovskites Minh N. Tran, Iver J. Cleveland, Joseph R. Geniesse, Yukun Liu, Seda Sarp and Eray S. Aydil; New York University (NYU) Tandon School of Engineering, United States

Redshifting the solar spectrum received by a solar cell with an overlayer that creates two near-infrared (NIR) photons from each ultraviolet (UV) and blue photon via quantum cutting can increase their power conversion efficiencies while reducing their degradation by UV light and heating. Yb-doped CsPb(Cl_{1-x}Br_x)₃ (x<0.65) has emerged as a potential quantum cutting material for this application because the Yb³⁺ emission via ²F_{5/2} → ²F_{7/2} electronic transition at 1.24 eV is close to the bandgap of silicon (~1.1 eV) and photoluminescence quantum yields (PLQY) approaching 200% (2 NIR photons per UV photon) has been demonstrated in colloidal dispersions, and thin films synthesized using solution-based approaches.¹ These films, however, exhibit significant sub-bandgap absorption. We are using physical vapor deposition (PVD), specifically evaporation, as an alternative for depositing films with high PLQY and low sub-bandgap absorption. We explore the PVD of thin Yb-doped CsPb(Cl_{1-x}Br_x)₃ (x<0.65) and Yb-doped lead-free double perovskite films (e.g., Cs₂AgBiX₆ with B = Bi, In, Sb and X=Cl, Br) via co-deposition from metal halide precursors. Yb is doped into the host halide perovskite, which absorbs in the UV and visible regions of the electromagnetic spectrum and then transfers energy to two Yb³⁺, exciting them from the ²F_{7/2} ground state to the ²F_{5/2} state. The excited Yb³⁺ emits NIR photons at ~1.24 eV upon relaxation. In this scenario, the two Yb³⁺ that receive the energy must be close to each other and likely also to a defect that captures the exciton. A likely candidate is a charge-compensated defect complex involving three corner-connected PbX₆

octahedra where one octahedron has a Pb vacancy (V_{Pb}), and two neighboring octahedra have Yb^{3+} ions that substitute in Pb^{2+} lattice sites (Yb_{Pb}).² PLQY from PVD $CsPb(Cl_{1-x}Br_x)_3$ depends strongly on the annealing environment implicating surfaces and their importance in achieving quantum cutting and PLQY. To replace Pb and contrast $CsPb(Cl_{1-x}Br_x)_3$ with a material where Pb is heterosubstituted to form a double perovskite, we deposited Yb-doped $Cs_2AgBiBr_6$ films using PVD. Yb^{3+} ions substitute into the double perovskite structure of $Cs_2AgBiBr_6$, specifically the $AgBr_6^{5-}$ and/or $BiBr_6^{3-}$ octahedra. Robust, reproducible, and stable PLQY as high as 95% are achieved with $Cs_2AgBiBr_6$ films doped with 8% Yb. This high PLQY indicates facile and efficient energy transfer from the perovskite host, $Cs_2AgBiBr_6$, to Yb, making $Cs_2AgBiBr_6$ the most promising lead-free down-conversion material.³ However, downconversion is achieved even when the excitation energy is less than ~ 2.5 eV, indicating that the mechanism is not via quantum cutting. It is interesting to note that Yb^{3+} substitution into neither Ag^+ nor Bi^{3+} lattice positions has the potential to form a defect like $Yb_{Pb} - V_{Pb} - Yb_{Pb}$ in $CsPb(Cl_{1-x}Br_x)_3$. PLQY of Yb-doped $Cs_2AgBiBr_6$ thin films synthesized via physical vapor deposition depends strongly on how the substrate temperature changes during the deposition because it determines the amount of Bi incorporated into the film. Yb-doped $Cs_2AgBiBr_6$ films with PLQY as high as 95% are obtained only with excess $BiBr_3$ and by ramping substrate temperature during the deposition. Ramping the substrate temperature reduces $BiBr_3$ loss from the film by promoting reactions that form $Cs_2AgBiBr_6$.

1. D. M. Kroupa, J. Y. Roh, T. J. Milstein, S. E. Creutz and D. R. Gamelin, *ACS Energy Lett.*, 2018, **3**, 2390-2395.
2. T. J. Milstein, D. M. Kroupa and D. R. Gamelin, *Nano Lett.*, 2018, **18**, 3792-3799.
3. M. N. Tran, I. J. Cleveland, J. R. Geniesse and E. S. Aydil, *Materials Horizons* (2022). <https://dx.doi.org/10.1039/D2MH00483F>

9:00 AM *SF05.03.02

Defect Management Through Additive Engineering and Light Soaking in Sn-Based Perovskite Solar Cells and LEDs Ivan Mora-Sero; Universitat Jaume I, Spain

Halide perovskite solar cells have revolutionized the photovoltaic field in the last decade. In a decade of intensive research it has been a huge improvement in the performance of these devices, however, the two main drawbacks of this system, the use of hazardous Pb and the long term stability, still to be open questions that have not been fully addressed. The photoconversion performance of perovskite solar cells containing alternative metals to Pb is significantly lower than the reported for devices containing Pb, where Sn-based perovskite solar cells is the alternative reporting higher photovoltaic performance close to 14%. Nevertheless, Sn-based perovskite solar cells exhibit a long term stability lower than their Pb containing counterparts, making stability their main problem. In this talk, we highlight how the use of proper additives and light soaking for defect engineering can increase significantly the stability of formamidinium tin iodide (FASnI₃) solar cells, and discuss about the different mechanism affecting this stability, beyond the oxidation of Sn²⁺, and how they can be countered. Effect in Sn-based perovskite LEDs will be also analyzed.

9:30 AM SF05.03.03

Physical Vapor Deposition of Yb-doped Double Perovskite Halide $Cs_2AgIn(Br, Cl)_6$ Yukun Liu, Iver J. Cleveland, Minh N. Tran and Eray S. Aydil; Tandon School of Engineering, New York University, United States

Inorganic double perovskite halides $A_2B^+B^{3+}X_6$ ($A = Cs, Rb, B^+ = Ag, Na, B^{3+} = In, Sb, \text{etc.}$ and $X = Br, Cl$) have been receiving attention as an alternative to the extensively studied $APbX_3$ because of their potential to eliminate Pb while preserving some of their attractive optical and electronic properties. For instance, downconversion and nearly perfect quantum cutting with photoluminescence quantum yields (PLQY) approaching 200% have been achieved with Yb-doped $CsPb(Cl, Br)_3$,¹ but the search for an as efficient perovskite without Pb continues. Quantum cutting down conversion phosphors are receiving increasing attention, as overlayers for solar cells, owing to their capacity of red-shifting photons from sunlight to those of lower energies and enhancing the efficiencies of solar cells by reducing charge recombination and energy losses as hot carriers relax to band edges. Yb^{3+} stands out among rare earth metals as an ideal downconverter because it can emit at ~ 1.25 eV, just above the bandgap of 1.1 eV of crystalline silicon, and can potentially quantum cut one incoming photon in the UV range to two NIR photons when embedded in a host with bandgap > 2.5 eV. We have been exploring double all inorganic halide perovskites as a host for Yb^{3+} . $A_2B^+B^{3+}X_6$ structure has been reported to be stable to heat, moisture, and exposure to light.² Specifically, we use physical vapor deposition (PVD) as a solvent-free, ligand-free technique with precise control over parameters such as film thicknesses and composition and as a synthesis technique that can overcome limitations such as poor precursor solubilities in solvents. This talk will cover the physical vapor deposition of undoped and Yb-doped $Cs_2AgSbBr_6$ and $Cs_2AgInCl_6$ thin films as well as undoped $Cs_2AgInBr_6$. The latter, $Cs_2AgInBr_6$, has been difficult to synthesize using other methods. We show that while cubic $Cs_2AgInBr_6$ can be formed at high temperatures, it appears to be unstable at room temperature, ultimately decomposing into more stable products such as $Cs_3In_2Br_9$, Cs_2AgBr_3 , $CsAgBr_2$, $InBr_3$ and $AgBr$, likely depending on local composition. Specifically, co-deposited precursors $CsBr$, $AgBr$, and $InBr_3$ react at and above ~ 100 °C to form cubic $Cs_2AgInBr_6$. This structure remains stable long enough to be studied when cooled down to room temperature. However, it ultimately decomposes. In contrast, $Cs_2AgInCl_6$ can be formed via codeposition of the precursors easily and is stable. XRD confirmed the formation of $Cs_2AgInCl_6$, which can be doped with Yb up to 12% without impurity phases. So far, NIR PLQY values of 28.1% have been achieved when doped with 4% of Yb. The major obstacle in depositing $Cs_2AgSbBr_6$ lay in the volatility of the Sb precursor, $SbBr_3$. PLQY values could be improved to $\sim 14\%$ either by increasing the amount of $SbBr_3$ flux or adopting a sandwich deposition structure where $SbBr_3$ is placed between two layers of $CsBr$ and co-deposited $CsBr$, $AgBr$ and $YbBr_3$. In contrast, $Cs_2AgInCl_6$ could be deposited and formed easily owing to the higher evaporation temperature of $InCl_3$. These films could be doped with Yb by coevaporating $YbCl_3$ with the other precursors. Achieving high PLQY requires annealing at 300 °C for 1 hour. .

1. Crane, M. J. *et al.* Single-Source Vapor Deposition of Quantum-Cutting $Yb^{3+}:CsPb(Cl_{1-x}Br_x)_3$ and Other Complex Metal-Halide Perovskites. *ACS Appl. Energy Mater.* **2**, 4560–4565 (2019).
2. Tang, H. *et al.* Lead-Free Halide Double Perovskite Nanocrystals for Light-Emitting Applications: Strategies for Boosting Efficiency and Stability. *Adv. Sci.* **8**, 2004118 (2021).

9:45 AM BREAK

SESSION SF05.04: Understanding Functional Defects by Theoretical, Modelling and Computational Methods
 Session Chairs: Panchapakesan Ganesh and Paul Kent
 Tuesday Morning, November 29, 2022
 Sheraton, 3rd Floor, Gardner A/B

10:15 AM *SF05.04.01

Understanding Defect Driven Phase Transitions in Correlated Quantum Materials with Quantum Monte Carlo Paul R. Kent, Jaron T. Krogel and Panchapakesan Ganesh; Oak Ridge National Laboratory, United States

One of the most promising routes for manipulating the properties of correlated solids for technological applications is through control of defects, doping, and stoichiometry. However, the mechanisms that drive the electronic and magnetic transitions in these materials and the specific role of defects not fully understood. For example, the perovskite SrCoO₃ is a ferromagnetic metal, while the oxygen-deficient (n-doped) brownmillerite SrCoO_{2.5} is an antiferromagnetic insulator. The challenge in predicting and understanding these behaviors from the intricate couplings of charge, spin, orbital, and lattice degrees of freedom. These challenge standard modeling approaches, requiring either significant empiricism or adoption of new methodologies to make progress. Here we outline our use of the highly accurate ab initio quantum Monte Carlo (QMC) approach to address these challenges. To control computational costs, we have developed a protocol of using QMC results to validate more scalable approaches via magnetic moments, charge densities, and thermodynamic properties. We present results for bulk and heterostructures of VO₂[1,2], our model for how doping controls the metal-insulator transition in the correlated-perovskites[3], and the role of defects in the MnBi₂Te₄ system following this protocol.

This work was supported by the U.S. Department of Energy, Office of Science, Basic Energy Sciences, Materials Sciences and Engineering Division, as part of the Computational Materials Sciences Program and Center for Predictive Simulation of Functional Materials.

1. P. Ganesh et al., Physical Review B 101 155129 (2020).
2. Q. Lu et al., Scientific Reports 10 1 (2020).
3. M. Bennett et al., Physical Review Research 4 L022005 (2022).

10:45 AM SF05.04.02

Multicrystalline Informatics—A Methodology to Realize High-Performance Multicrystalline Materials Noritaka Usami¹, Yutaka Ohno², Hiroaki Kudo¹, Kentaro Kutsukake³, Takuto Kojima¹ and Tatsuya Yokoi¹; ¹Nagoya University, Japan; ²Tohoku University, Japan; ³RIKEN, Japan

We introduce our methodology, “multicrystalline informatics”, which integrates experiments, theory, computation, and machine learning to establish a universal guideline to maximize the macroscopic performance of multicrystalline materials by controlling microstructures and reducing crystal defects. We employ silicon as a model material and prepare various helpful machine learning tools for efficient materials development.

A realistic three-dimensional multicrystalline model of a silicon ingot for solar cells grown by directional solidification was obtained by integrating grain segmentation and orientation prediction by a machine learning model using multidimensional optical images of silicon wafers. The region of the interest was selected to contain the generation point of dislocation clusters as evidenced by photoluminescence images to reveal the spatial distribution of crystal defects. Finite element stress analysis was performed on the three-dimensional model by referring to the temperature distribution during crystal growth obtained from the simulation. The analysis results indicated that dislocations were generated along the main slip system where the greatest shear stress was applied. As for the experimental approach, multiscale structural analysis including transmission electron microscopy clarified that dislocations were generated from a curved Σ3 grain boundary with stepped microscopic {111} facets. It seems that high shear stress at the step edge would be responsible for the generation of dislocations.

As an alternative approach to access the underlying mechanism of the generation of dislocations, we attempt to apply image translation methods such as generative adversarial networks to obtain the likelihood distribution of dislocations generation from optical images or other processed images. By considering various models employing different images as a pseudo color input image, combining a grain boundary image and two optical images with different illumination angles showed a realistic output image. This indicates that a grain boundary network and crystal orientations play an essential role in the generation of dislocations. A further study to apply explainable artificial intelligence may help clarify the physics behind the phenomena.

11:00 AM SF05.04.04

High-Throughput Search for Defect-Based Qubits for Quantum Information Science Applications Yihuang Xiong¹, Diana Dahliah², Céline Bourgeois^{2,1}, Sinead M. Griffin^{3,3}, Alp Sipahigil⁴ and Geoffroy Hautier^{1,2}; ¹Dartmouth College, United States; ²Université Catholique de Louvain, Belgium; ³Lawrence Berkeley National Laboratory, United States; ⁴University of California, Berkeley, United States

Silicon is an attractive platform for implementing solid-state qubits due to the mature process technology and commercial compatibility. The color centers in silicon have seen a resurgence of interest in quantum information science, including the T-center and Se⁻. [1,2] Using first-principles methods, we performed a high-throughput search for charged defects in silicon for qubit applications. By evaluating the thermodynamic, electronic, and optical properties, we suggest possible candidates that are promising for quantum defects and shed light on their electronic structures and potential excitation mechanism compared to the other well-known systems (e.g., NV⁻ center in diamond).

[1] Bergeron, L., Chartrand, C., Kurkjian, A. T. K., Morse, K. J., Riemann, H., Abrosimov, N. V., Becker, P., Pohl, H.-J., Thewalt, M. L. W. & Simmons, S., "Silicon-Integrated Telecommunications Photon-Spin Interface," *PRX Quantum* **1**, 20301 (2020). DOI: 10.1103/PRXQuantum.1.020301

[2] Morse, K.J., Abraham, R.J., DeAbreu, A., Bowness, C., Richards, T.S., Riemann, H., Abrosimov, N.V., Becker, P., Pohl, H.J., Thewalt, M.L. & Simmons, S., "A photonic Platform for Donor Spin Qubits in Silicon," *Science advances*, **3**(7), p.e1700930 (2017). DOI: 10.1126/sciadv.1700930

11:15 AM SF05.04.05

sp³-Doped (6,5) Single-Walled Carbon Nanotubes as a New Class of Materials for Spin Qubit Technology Kasidet Jing Trerayapiwat¹, Jia-Shiang Chen², Xuedan Ma^{2,3} and Sahar Sharifzadeh^{1,1}; ¹Boston University, United States; ²Argonne National Laboratory, United States; ³The University of Chicago, United States

Single-walled carbon nanotubes (SWCNTs) doped with sp³ defects are a promising class of optoelectronic materials with bright tunable photoluminescence and localized spin density. We study a series of sp³ defects within (6,5) SWCNT that result in one single unpaired spin within the bandgap of the tube and show, using experimental and computational techniques, that this spin has a decoherence time competitive with molecular spin qubits. Density functional theory (DFT) studies indicate that an unpaired spin localizes around the defect site. We simulate dephasing of the localized spin by considering spin-nuclear spin bath interactions as the main source of decoherence at low temperature. We apply the cluster correlation expansion method with a pure-dephasing spin Hamiltonian to doped SWCNT in presence of solvent molecules at near 0 K and estimate the magnitude of the intrinsic dephasing time (T₂). Combined with other decoherence mechanisms based on empirical parameters, we calculate a real dephasing time in good agreement with measured Hahn spin echo T₂ and suggest a way to further improve dephasing time.

The authors acknowledge financial support from NSF DMR-19005990.

11:30 AM SF05.04.06

First-Principles Study of the Stark Effect of the NV Center Louis Alaerts and Geoffroy Hautier; Dartmouth College, United States

The NV center is a defect found in diamond and consists of a nitrogen substitution and a adjacent vacancy. It is arguably the most studied defect thanks to its particular electronic structure which leads to several important quantum technology applications such as solid-state qubit or in quantum sensing. In particular, the spin-conserving optical transition from the 3A_2 state to the 3E state at 1.945eV plays an important role in all the aforementioned applications. This optical transition is accompanied with a change of dipole moment. Applying an electric field will therefore change the energy difference between the two levels, a phenomenon well-known and called the Stark effect. The Stark shift is detrimental for quantum emitters as fluctuation of the local field will cause spectral diffusion. It is therefore important to quantify this effect with precision.

In this poster, we present the results of our density functional theory calculation on the NV center. We use several methods to compute the dipole moment of the 3A_2 ground-state and the 3E excited-state such as the modern theory of polarization or electric field calculation. We then compare the different methods used with experimental results.

SESSION SF05.05: Harvesting Functional Defects in Energy Materials I

Session Chairs: Panchapakesan Ganesh and Yiyang Li

Tuesday Afternoon, November 29, 2022

Sheraton, 3rd Floor, Gardner A/B

1:30 PM *SF05.05.01

Defects and Design in Energy Materials [Matthew Rosseinsky](#); University of Liverpool, United Kingdom

The presence of defects is essential for many functional properties of materials. For example, segregation of substitutional defects to domain boundaries in nanostructured self-assembled composites can be harnessed to control the stability and performance of solid oxide and proton conducting fuel cell cathodes (*Advanced Materials Interfaces* 9, 2102131, 2022; *J. Mater. Chem. A*, 2022, 10, 2559). However, materials design approaches have predominantly focussed on perfectly ordered average structures, because of the challenges associated with disorder. Focussing on low thermal conductivity (*Science* 373, 1017-1022, 2021), we show how average structure prediction coupled with machine learning affords outperforming materials with defect elimination through formation of aperiodic structural motifs (*Angewandte Chemie-International Edition*, 2021, 60, 2–11). This emphasises the future scope to build in functional defects by design.

2:00 PM SF05.05.02

Tuning Surface Acidity—Novel Strategy for Recovery of Degraded Oxygen Exchange Kinetics in Mixed Conducting Oxides [Han Gil Seo](#), Anna F. Staerz, Dennis Kim, James LeBeau and Harry Tuller; Massachusetts Institute of Technology, United States

The performance and viability of applications ranging from energy conversion and storage devices (solid oxide fuel/electrolyser cells (SOFCs/SOECs), permeation membranes, batteries), and sensors are presently limited by performance degradation due to impurity poisoning, for example in SOFCs, due to chromia and silica impurities coming from metal interconnects and furnace refractories respectively. We recently showed that the oxygen surface exchange kinetic (k_{chem}) values of the mixed conducting oxide, $Pr_{0.1}Ce_{0.9}O_{2-x}$ (PCO), can be systematically varied by over 6 orders of magnitude by infiltrating the surface with binary oxides ranging from strongly acidic to strongly basic. Basic lithia increased k_{chem} by nearly 1,000 times over that of pristine PCO, while acidic silica depressed k_{chem} by nearly the same factor with variations in k_{chem} attributed to the induced relative accumulation or depletion of surface electrons. With this insight, we hypothesized that surface acidity could be used not only to predict the effect of a single additive on oxygen exchange, but also to recover the oxygen exchange degraded by acidic additives.

Here, we demonstrate that a drastic depression in the oxygen exchange kinetics of PCO induced by infiltration of acidic binary additives (*e.g.* chromia and silica in this work), can be fully recovered by subsequent infiltration of basic additives (*e.g.* lithia and calcia). Electrical conductivity relaxation measurements on porous PCO specimens were used to examine the impact of serial infiltration of basic additives on the degraded exchange rate of oxygen. In parallel, the electrochemical performance of screen-printed PCO symmetric cells (cathode|electrolyte|cathode) with serial infiltration of basic additives were further assessed by electrochemical impedance spectroscopy in terms of area-specific resistance with similar trends observed. Surface microstructures of the respective infiltrated specimens were examined by scanning transmission electron microscopy with electron energy loss spectroscopy to characterize the chemical nature and distribution of the additives.

2:15 PM SF05.05.03

Structural Contribution of Fe-Enhanced Oxygen Evolution Electrocatalysis in Nickel Oxides [Tae Gyu Yun](#), Jumi Bak and Sung-Yoon Chung; Korea Institute of Science and Technology, Korea (the Republic of)

Controlling electronic states is crucial in electrocatalysis because it controls charge transfer behavior, which is crucial for improving catalytic reaction efficiency. While many complex oxides have been subjected to a variety of chemical changes to cause a change in electronic states at catalytically active sites, there have been few studies to investigate the impact of local crystal structures on electronic states under the same composition. Here we compare the electrocatalysis of the oxygen evolution reaction (OER) between amorphous and crystalline perovskite nickelates in a thin film when Fe is added as an active site. The enhancement of OER activity by Fe in amorphous films with a random atom configuration is found to be insensitive to the Fe doping method. In crystalline films, on the other hand, an order of magnitude change in OER activity is induced, which is substantially influenced by the resultant structure variation during doping. For extremely high activity, theoretical studies consistently show a significant rise in the density of Fe 3d states beneath the Fermi level. Our findings show that the atomic-scale structure of crystalline oxide catalysts is an important factor to consider when trying to understand how to improve OER catalysis.

2:30 PM BREAK

3:00 PM *SF05.05.04

Interaction and Transformation of Defects in Energy Materials [Andrej Singer](#); Cornell University, United States

Non-equilibrium defects often dictate macroscopic functional properties of materials. In energy materials, dislocations and planar defects significantly modify reversibility and kinetics. Nevertheless, transient imperfections briefly appearing during ionic transport have been challenging to capture, limiting understanding of their life cycle and impact. I will present our recent operando x-ray nanoimaging results, where we track the dynamics of metastable defects within alkaline ion intercalation hosts and proton conducting ceramics. In intercalation oxides, three-dimensional coherent X-ray imaging reveals

the transformation and self-healing of a metastable domain boundary, glissile dislocation loop, and stacking faults. In proton conducting ceramics, an abundant defect activity is observed, culminating in the cracking of individual grains. The presence of high dimensional defects in energy materials observed with operando nanoimaging suggest their abundance and highlights the importance of defect engineering for developing next-generation energy solutions.

3:30 PM SF05.05.05

Shifting and Breaking Scaling Relations at Transition Metal Telluride Edges for Selective Electrochemical CO₂ Reduction Courtney Brea and Guoxiang Hu; Queens College, CUNY, United States

The electrochemical reduction of CO₂ (CO₂RR) to hydrocarbons and alcohols provides a means to solve problems pertaining to fossil energy shortages and environmental pollution. However, developing electrode catalysts that can perform this transformation with a low overpotential and a high product selectivity remains a challenge. Two-dimensional (2D) transition metal dichalcogenides (TMDCs) have emerged as promising catalysts for the CO₂RR, where primarily the edges are responsible for the catalytic activity. Herein by using first-principles density functional theory (DFT), we study 48 TMDC edges with six different chemical compositions (MX₂, M = Mo, W; X = S, Se, Te). By plotting their phase diagrams, we provide guidelines on the synthesis conditions for the edges. Furthermore, by computing the binding energies of key reaction intermediates, we find that the linear scaling relations can be broken by the edge reconstruction and shifted by the chemical composition. Specifically, compared with sulfide and selenide edges, more telluride edges show similar affinity to Cu towards the reaction intermediates. The computed free-energy diagrams show that certain reconstructed telluride edges exhibit high catalytic activity and selectivity for CO₂ reduction to CH₃OH and CH₄. These insights help pave the way for efficient and selective electrochemical CO₂RR on transition metal tellurides.

3:45 PM SF05.05.06

Charge Density Manipulation by Transition Metal Heteroatoms on Tungsten Trioxide for Photocatalytic CO₂ Reduction Chih-Yang Huang^{1,2,1}, Ying-Ren Lai¹, Kuei-Hsien Chen² and Li-Chyong Chen¹; ¹National Taiwan University, Taiwan; ²Academia Sinica, Taiwan

In the past decades, the greenhouse gases and renewable energy topics have attracted attention because of the expeditious climate change. Photocatalytic (PC) CO₂ reduction into value-added molecules can be a potential method to address the abovementioned problems. However, PC CO₂ reduction suffers from the low production rate, which contributed to low surface electron density. That is electron-rich surface is essential for superior catalytic activity. Engineering the surface defects such as point defects is an effective way to manipulate the local electronic structure and activate the inert surface. Point defect can be introduced by doping heteroatoms and the generation of vacancies. In the field of catalysis, heteroatom doping or single-atom catalysts (SACs) is a rapidly developing approach due to its unique electronic properties to boost catalytic performances. Although most studies on the SACs have used highly active noble metals, their high cost limits their utilization for industry applications. So, we choose transition metals with the 3d electronic configuration (i.e., Cr, Fe, and Ni atoms) as the candidate heteroatoms. However, the influences of transition metal heteroatom doping on charge density distribution haven't been clearly studied yet. Herein, we theoretically predict and experimentally confirm the heteroatom-assisted charge density redistribution on the surface of tungsten trioxide (WO₃). Density functional theory (DFT) calculations show that the anchored transition metals play a role as electron contributors to the neighbor atoms. Synchrotron-based x-ray absorption near-edge structure (XANES) and Fourier transform extended x ray absorption fine structure (FT EXAFS) are performed to prove the presence of single atoms thereon the WO₃ surface. Further, the x-ray photoelectron spectroscopy (XPS) technique is used to find the direction and amount of transferred charge. Finally, the PC CO₂ reduction yields also unveil that the production rate is proportional to the amount of transferred (donated) electron. This study provides insights into the correlation between CO₂ conversion and the surface charge distribution, implying the significance of the surface charge density in the field of catalysis.

4:00 PM SF05.05.07

Metallurgical Alloying Enables Supersaturated Cu Solid Solution for Efficient CO₂-to-ethanol Electroconversion Ji Yong Kim¹, Heh Sang Ahn¹, Dae-Hyun Nam², Eun Soo Park¹ and Young-Chang Joo¹; ¹Seoul National University, Korea (the Republic of); ²Daegu Gyeongbuk Institute of Science and Technology, Korea (the Republic of)

Converting CO₂ into value-added chemicals through electrocatalysis not only utilizes the CO₂ to achieve net negative carbon emission, but also enables long-term storage of intermittent renewable electricity. There has been a great interest in electrochemical CO₂ reduction reaction (CO₂RR) to produce liquid fuels which has high energy density. In light of the progress, energy efficiency and reaction rate for C₂₊ products have been largely improved, especially for ethylene (C₂H₄) production. However, the development of electrocatalysts that efficiently produce ethanol (C₂H₅OH), another C₂ product which is one of the most essential organic chemical, has been retarded. To enhance C₂H₅OH productivity, heteroatom alloying and defective sites have been known to be effective by promoting preferential binding with reaction intermediates and lower an energy barrier of rate-determining step. Herein, we developed alloy catalysts in which Cu sites were evenly dispersed in Ag lattice over a thermodynamic immiscibility for efficient C₂H₅OH production. For precise microstructural control, alloying and chemical de-alloying strategies were adopted which were scalable for porous electrode. Removing sacrificial metal through the de-alloying formed defect sites such as vacancy in the catalysts which were effective to enhance the affinity to the reaction intermediate. Microstructural optimization was judiciously carried out based on metallurgical considerations in the perspective of composition and undercooling. Cu catalysts from eutectic composition and rapid quenching acquired high porosity and the undercoordinated sites after the de-alloying, enabling robust CO₂-to-C₂₊ products electroconversion at the Faradaic efficiency (FE) of 80.1±1.6% and partial current density of -127.7±30.3 mA/cm² using membrane electrode assembly (MEA) reactor in a neutral electrolyte. Main products of the de-alloyed Cu was C₂H₄. Thereafter, introduction of the heteroatom (Ag) to the Cu catalysts was conducted to steer the catalysis toward C₂H₅OH production. Elemental distribution of Ag conformed to the immiscibility at initial addition of heteroatoms. However, it was noteworthy that non-equilibrium alloying exploiting large undercooling enabled dissolution of Cu in Ag₂Al phase overcoming the immiscibility. After removing Al, supersaturated solid solution of Ag-Cu alloy was fabricated. Well-defined crystal structure and even distribution of Cu sites significantly facilitated C₂H₅OH formation rather than C₂H₄, achieving the maximum selectivity of 40.4±2.4% and full cell energy efficiency of 14.4%. The relative productivity of C₂H₅OH to C₂H₄ was widely controlled within the range of 0.1 to 1.9. Our metallurgical alloying strategy not only extended the range of alloy catalysts beyond thermodynamic immiscibility, but also highlighted the modifications of microstructure and atomic configuration for efficient production of liquid chemicals from CO₂.

4:15 PM SF05.05.08

Designing a Highly Active and Selective Defect-Rich g-C₃N₄ Photocatalyst for CO₂RR: Experimental and Theoretical Insights Mahmoud K. Hussien^{1,2}, Amr Sabbah¹, M. Karen Qorbani³, Heng-Liang Wu³, Ming-Chang Lin², Li-Chyong Chen³ and Kuei-Hsien Chen^{1,3}; ¹Academia Sinica, Taiwan; ²National Yang Ming Chiao Tung University, Taiwan; ³National Taiwan University, Taiwan

Photocatalytic CO₂ reduction into valuable chemicals and fuels is a promising approach to alleviate the global energy and environmental crises. Recently, achieving high catalytic activity and selectivity using single-material photocatalyst in the absence of any sacrificial electron donor, photosensitizer, or cocatalyst has become a major challenge in the photocatalysis research field. It is far more challenging to produce outstanding catalytic performance from a naturally abundant, metal-free photocatalyst using an environmentally benign approach. Recently, graphitic carbon nitride (g-C₃N₄) has attracted great

attention as a metal-free photocatalyst due to its medium band gap, low cost, and high chemical stability. Unfortunately, the low specific surface area, poor visible light-harvesting ability, slow charge interjection rate, and fast charge carrier recombination limit the practical application of pristine g-C₃N₄ in photocatalytic applications. Among the variety of modification strategies, defect engineering has been demonstrated as a viable strategy for modifying the optical, structural, and electronic features of g-C₃N₄ for improved photocatalytic performance. Prior research has mostly focused on the modification of g-C₃N₄ with a single specific defect. Unfortunately, a single defect can not simultaneously solve all the shortcomings of g-C₃N₄. Herein, a novel green method is developed to prepare a functionalized nanoporous nonmetal-doped g-C₃N₄. The newly designed defect-rich g-C₃N₄ has excellent photocatalytic performance in the gas-phase CO₂ reduction reaction (CO₂RR) with nearly 100% selectivity towards carbon monoxide (CO) production. In-depth mechanistic and theoretical studies were performed to provide a detailed mechanism of CO₂RR. Besides, temperature-dependent and intensity-dependent photoluminescence (PL) measurements were investigated to understand the exciton dissociation mechanism. DFT calculations supported by synchrotron-based X-ray absorption near-edge spectroscopy (XANES) analysis were utilized to determine the active site towards CO₂RR. The results show that the numerous-defect modification technique prolongs the visible light absorption, increases the surface area, improves the adsorption capacity, decreases the charge recombination rate, and promotes the exciton dissociation of the modified g-C₃N₄. This study provides a new energy-efficient route for the engineering of graphitic carbon nitride for photocatalytic applications. Besides, it presents a deeper understanding of the role of each type of the defect in the outstanding photocatalytic performance of the modified g-C₃N₄.

SESSION SF05.06: Poster Session: Harvesting Functional Defects
Session Chairs: Hua Zhou and Yuanyuan Zhou
Tuesday Afternoon, November 29, 2022
8:00 PM - 10:00 PM
Hynes, Level 1, Hall A

SF05.06.01

Effects of Fe Species on the Surface of TiO₂ Nanostructures and Their Influence on Photocatalytic CO₂ Reduction Waldir J. Avansi¹, Paulo Henrique Eleuterio Falsetti¹, Gelson Thiago dos Santos Tavares da Silva² and Caue Ribeiro²; ¹University de Sao Carlos, Brazil; ²Embrapa, Brazil

In the last decades, global energy demand for fossil fuels has resulted in increased CO₂ emission in the atmosphere, leading to several negative impacts on the environment¹⁻³. Among the various methods studied to overcome this problem, the photocatalytic conversion of CO₂ into solar fuels (CH₄, HCO₂H, CH₂O and CH₃OH) using semiconductors has been considered a promising technology¹⁻³. Titanium dioxide (TiO₂), which has several advantages when applied in heterogeneous photocatalysis, have been extensively studied for the photocatalytic conversion of CO₂¹⁻⁴. As a matter of fact, different modification techniques have been employed to improve the efficiency of TiO₂ in this process, such as surface modifications, doping of metals and non-metals, and so on¹⁻⁴. Thus, the aim of this work is to evaluate the effects of Fe on the photocatalytic CO₂ reduction of different TiO₂ morphologies. The different TiO₂ morphologies were obtained by the synthesis route proposed by Mendonça et al. through a hydrothermal reaction by changing the pH of the reaction medium⁵. TiO₂ decoration was performed using an impregnation method adapted from Xie et al.⁴ Different proportions of Fe were evaluated (0.2, 0.8 and 1.6 % of mass). For comparison purposes, the same process was performed using commercial TiO₂ anatase. XRD measurements revealed that all samples exhibited TiO₂ anatase crystalline phase, while EDS results confirmed the presence of Fe and the absence of contaminants in the samples. DRS UV-Vis showed a tendency of band gap energy (Eg) decrease related to the increase in the amount of Fe in all studied samples. Electron microscopy revealed that the as-synthesized samples had a faceted - TiO₂ morphology regardless of the presence of Fe. XPS results confirmed the presence of different Fe species (FeOOH and Fe₂O₃) in the samples, with a strong interaction between Ti and loaded Fe. The photocatalytic CO₂ conversion results showed that the studied samples successfully converted CO₂ into CO and CH₄. The higher amount of Fe (1.6 % of Fe) on TiO₂ nanocrystals led to a better performance in the production of CH₄. The improved photocatalytic performance can be attributed to faceted TiO₂ nanocrystals and the efficient electron transfer due to the presence of Fe species on their surface.

References:

- 1 - Xiong, Z.; Lei, Z.; Youzi, L.; Liangchen, D.; Zhao, Y.; Junying, Z. A review on modification of facet-engineered TiO₂ for photocatalytic CO₂ reduction. *Journal of Photochemistry and Photobiology C: Photochemistry Reviews* 36, 24–47, 2018
- 2 - Low, J.; Cheng, B.; Yu, J. Surface modification and enhanced photocatalytic CO₂ reduction performance of TiO₂: a review. *Applied Surface Science*, 392, 658–686, 2017.
- 3 - Shehzad, N.; Muhammad, T.; Johari, K.; Murugesan, T.; Hussain, M. A critical review on TiO₂ based photocatalytic CO₂ reduction system: Strategies to improve efficiency. *Journal of CO₂ Utilization*, 26, 98-122, 2018.
- 4 - Xie, Jijia et al. Highly selective oxidation of methane to methanol at ambient conditions by titanium dioxide-supported iron species. *Nature Catalysis*, 1(11), 889–896, 2018.
- 5 - De Mendonça, V. R.; Ribeiro, C. Influence of TiO₂ morphological parameters in dye photodegradation: a comparative study in peroxo-based synthesis. *Applied Catalysis B: Environmental*, 105(3–4), 298–305, 2011.

SF05.06.02

Sn/Sb Segregation Effect at Polycrystalline Hematite Interfaces Flavio L. De Souza^{1,2}; ¹Brazilian Nanotechnology National Laboratory, Brazil; ²University Federal-ABC, Brazil

The effect of atomic structure modification in hematite has become a key factor for the rational design of the highly efficient system. Herein, this study describes the segregation effects of Sn and Sb-dopants on both solid-solid (grain boundaries) and solid-liquid interfaces (surfaces) of polycrystalline hematite. From an experimental point of view, the proper sintering process allows freezing of a state of electronic defects, in which the electrical properties of hematite are controlled by the grain boundary and Sn or Sb segregation. Impedance spectroscopy and dc conductivity measurements show that current flows through preferential pathways associated with Sn or Sb segregation that occurs at the grain boundary, leading to a decrease in grain-boundary resistance. By employing the ab initio approach, the potential barrier reduction was observed on polycrystalline interfaces due to the dopant, which causes an increase in the inter-grain electron transport. Concomitantly, the dopants' segregation on hematite surfaces results in a decrease in the oxygen vacancy formation energy. Such vacancies lead to the experimentally observed rise of the flat band potential. The comprehension of the electronic effects of dopants on both types of interfaces has important implications to explain the experimental results, also enabling the control and design of interfaces for different higher-efficiency applications.

The authors acknowledge financial support from FAPESP (Project Nos. CEPID-13/07296-2 and 17/02317-2). F.L.S. acknowledges the support from the FAPESP (Grant No. 17/11986-5) and Shell and the strategic importance of the support given by ANP (Brazil's National Oil, Natural Gas, and Biofuels Agency) through the R&D levy regulation. The authors also acknowledge the Laboratório Nacional de Computação Científica (Project No. SCAFMat2) for

computer time.

SF05.06.03

Construction of Long-Range EAM-Type Interatomic Interaction Model for Dynamical Analyses on Long-Periodic Polytypism [Shinya Ogane](#)¹, Kazumasa Tsutsui² and Koji Moriguchi¹; ¹Tohoku University, Japan; ²Nippon Steel, Japan

Many crystalline compounds are composed of one or more structural units. When these units can be stacked in different ways to form stable or metastable phases, the resulting phases are known as polytypes [1]. Among these polytypes, the crystalline systems composed of close-packed (CP) layers have especially attracted attention on their fundamental and technological properties for many years. The material engineering demand for polytype phase control is diverse [2-4]. However, the scientific control of the polytype phase is still incomplete in the field of practical materials engineering and predicting polytype phase stability for a material has also been a long-standing issue in condensed matter physics and/or materials science. This is because the polytype control technology has many uncertainties since the polytype formation mechanism has yet been physically unsolved.

To provide a useful theoretical tool in this situation, we have constructed EAM-type potentials that can be applied to atomic-level dynamical analyses on long-period polytypism. In this study, the metallic lanthanum (La) system has been selected as a prototype system analyzing the dynamical processes of polytype formations for the following reasons; (i) the ground state for pure La is the 4H structure which is the simplest long-periodic polytype, (ii) La has the phase stability in both 4H and 3C phases below 583K [6], and (iii) it is, therefore, expected that the phase transition phenomena including 4H and/or 3C polytype structures can be investigated by the molecular dynamical (MD) studies such as crystal growth kinetic simulations.

We have recently presented a theoretical consideration on the CP polytype total energetics using the geometrical analysis on the correlation between interlayer interactions and interatomic ones [7]. These results suggest that short-range interactions are not enough to describe the CP polytype energetics and provide significant insights for creating interatomic models successfully showing the polytypes other than 3C and 2H structures as a ground state. We have succeeded in constructing an EAM-type potential that mimics the energetics of metallic La based on the first-principles calculations [8]. The following three procedures are found to be essentially important for deriving an interatomic interaction model with the 4H structure as the ground state; (i) The cutoff radius should be set to have a relatively longer distance (three or more interlayer distances in the 4H stacking). (ii) The equations of state for the energetics of 2H, 3C, and 4H structures need to be reproduced as accurately as possible. (iii) The adiabatic potential along important transition paths among crystal structures such as the Bain path for the bcc-fcc transition must be exactly considered [9,10].

We have calculated the Generalized stacking fault energy (GSFE) surface for some CP structures using the present potential constructed. Both unstable stacking fault and stable fault energies for La are much lower than ones for Al calculated by another EAM-type potential [11]. Therefore, La has low energy barrier required for forming stacking defects, and polytype formations can easily appear. The presentation of the day will also discuss other basic properties, the transferability for the potential constructed, and some of the dynamical phenomena by the MD analyses.

- [1] A. L. Ortiz, et al., *J. Appl. Cryst.* 46, 242 (2013).
- [2] E. M. T. Fadaly et al., *Nature*. 580, 205 (2020).
- [3] Z. Fan et al., *Nat. Commun.* 6, 7684 (2015).
- [4] E. Abe et al. *Philos. Mag. Lett.* 91, 690 (2011).
- [5] Murray S. Daw and M. I. Baskes, *Phys. Rev. B* 29, 6443 (1984).
- [6] A. B. Lysenko et al., *Crystallogr. Rep.* 50, S10 (2005).
- [7] S. Ogane and K. Moriguchi, *MRS Advances* 6, 170 (2021).
- [8] K. Moriguchi et al., *MRS Advances* 6, 163 (2021).
- [9] K. Moriguchi and M. Igarashi, *Phys. Rev. B* 74, 024111 (2006).
- [10] G. Grimvall et al., *Rev. Mod. Phys.* 84, 945 (2012).
- [11] Y. Mishin *et al.*, *Phys. Rev. B* 59, 3393(1999).

SF05.06.04

Effect of Embedding Cavities into Reduced Graphene Oxide-coated Micropillar on Boiling Heat Transfer Enhancement [Maroosol Yun](#)¹, Gechong Choi², Donghwi Lee³, Beom Seok Kim⁴ and Hyung Hee Cho¹; ¹Yonsei University, Korea (the Republic of); ²Hyundai Steel Co. Ltd, Korea (the Republic of); ³Jeonbuk National University, Korea (the Republic of); ⁴Seoul National University of Science and Technology, Korea (the Republic of)

As cooling capacity demands for systems of high heat flux, i.e. data storage center, nuclear fusion reactor, and computer chip cooling, continuously grows, boiling heat transfer with phase change could be a favorable method since it utilizes latent heat, which allows smaller superheat of system. Critical heat flux (CHF), which indicates the maximum cooling capacity can be obtained by fully developed nucleate boiling, is determined by vapor film formation on the heated surface. If the vapor film covers the entire heated surface, an abrupt increase in wall temperature is observed as the thermal conductivity of the vapor film is a few orders of magnitude smaller than that of liquid-phase working fluid. To delay the formation of vapor film, bubble coalescence should be prevented to supply sufficient, fresh working fluid. The merging of adjacent bubbles can be suppressed by controlling bubble characteristics. Nanoparticle coating with graphene/graphene-oxide could generate smaller bubbles compared to the plain surface, by offering a myriad of micro-sized cavities which promote bubble nucleation. However, bubble coalescence still occurs with high heat flux conditions. To ensure liquid paths with high thermal load, the location of bubbles should be considered. Here, we propose reduced graphene oxide (rGO)-coated patterned surfaces with micropillar array and microcavities to pattern nucleation sites, thus, to suppress bubble coalescence observed in our previous work, rGO coated micropillar. The rGO-coated nucleation pattern surfaces were prepared by stepwise methods of deep reactive ion etching (DRIE) and nanofluid boiling with 0.0005 wt% rGO solution. Micropillars are made to be 20 μm in height, 4 μm in diameter, and 20 μm in pitch, respectively, and square cavities' width is 200 μm , and 1 mm in pitch, respectively. Fabricated surfaces of micropillar only, cavity embedded surface were evaluated by deionized (DI) water pool boiling experiment. The experimental conditions are the saturated temperature of DI water at atmospheric pressure. Experimental surfaces of Plain, rGO-coated micropillar, rGO-coated cavity embedded surface recorded 89 W/cm², 224 W/cm², and 261 W/cm² in CHF and 20.4 kW/m²K, 74.3 kW/m²K, and 85.8 kW/m²K in maximum heat transfer coefficient, respectively. CHF and HTC records confirm that the nucleation pattern surface exhibits superior heat transfer performance to the rGO-coated micropillar surface. Bubble visualization results show that rGO-coated nucleation pattern surfaces have separated bubble departure with the presence of cavities, while bubbles merge laterally with the high heat flux on the rGO-coated micropillar surface. Thus, the CHF and HTC are heightened for the cavity-embedded case owing to the suppressed bubble merger on the heated surface. Bubble images which are taken at 50 W/cm² heat flux show liquid paths between the cavity pattern on the cavity embedded surface. This means the working fluid could imbibe through the microstructures; thus, bubble coalescence can be effectively suppressed, delaying the CHF. The notable improvement on CHF and HTC in the rGO-coated nucleation pattern surfaces indicates cavity embedment for bubble merger resistance can be a powerful design for nanoparticle-coated surfaces, allowing 320% increased HTC compared to the plain surfaces. This study will be helpful for designing nanoparticle-coated surfaces for enhanced boiling heat transfer on cooling systems for high heat flux devices like heat exchangers and fusion reactors.

SF05.06.05

Defect Dominated Hierarchical Ti-Metal-Organic Frameworks via a Linker Competitive Coordination Strategy for Toluene Removal [Jin Jie](#) and

Jong Hyeok Park; Yonsei University, Korea (the Republic of)

As relatively new porous materials, metal-organic frameworks (MOFs) have become attractive materials for many applications, especially for gas adsorption and photocatalysis, due to their high function tunability, porosity, and crystallinity. Recently, impressive improvements and achievements have been reported thanks to the numerous effort on improving the performance of MOFs in those two aspects. Representatively, the construction of the hierarchical pore in microporous MOFs can overcome the micropore blockage to improve the diffusion of the large molecules and the accessibility of their active sites. However, most of the methods to control the formation of hierarchically porous MOF have focused on the crystal growth steps, topology structure design, or post-treatment, few approaches regarding the nucleation process have been adapted due to its random fluctuation and difficulty to predict.

Herein, we proposed a novel linker competitive coordination strategy based on the electronegativity difference of two kinds of organic linkers (H2BDC and NH2-H2BDC) to tailor the pore size of the Ti-MOF (MIL-125). The different electronegativity can determine the nucleation rate of those linkers. By simply controlling the feed ratio of these two organic linkers, a series of Ti-MOFs with continuously tunable hierarchical porosity is directly obtained as evidenced by the DFT pore size distribution and N₂ sorption isotherms. Besides, we also demonstrated that the missing-linker defect is created during this process and plays dominated role in the construction of the hierarchical pore.

The demonstration of toluene removal shows that the competitive coordination strategy not only contributes to wide pore size distribution to enhance the adsorption performance of toluene but also endows good charge separation ability to facilitate photocatalytic performance. Finally, the toluene removal efficiency of optimal Ti-MOF with mixed organic linkers of a 1:1 molar ratio is 2.14 times and 1.88 times of the pristine MIL-125 and MIL-125(NH₂), respectively.

In conclusion, we constructed a hierarchically porous MIL-125 with tailored pore size via a simple linker competitive coordination strategy and verified the superiority of the hierarchical pore structure by evaluating the adsorption and photocatalytic performance of as-obtained Ti-MOFs for toluene mineralization. Given that this approach is a one-pot method and shows some merits, such as low cost, controllable pore size distribution, without impurity, and avoiding additional post-treatment processes, it can be a new prospect to optimize the porosity of Ti-MOF for various heterogeneous catalysis applications.

SF05.06.06

Enhancing BH_{max} Through Control of Functional Defects in Ferromagnetic τ Mn-Al Using Equal Channel Angular Extrusion and Ti Addition Thomas Keller, Ian Baker and Geoffroy Hautier; Dartmouth College, United States

Manganese-Aluminum permanent magnet alloys are a promising alternative to rare-earth permanent magnets (REPMs), due to their advantages of lower raw material cost, more robust global supply chains, and higher corrosion resistance. The ferromagnetic Mn-Al τ phase is a metastable ordered L10 structure that is of particular interest to applications such as electric car motors and direct drive wind turbine generators. The maximum energy product (BH_{max}) of the τ phase is strongly dependent on the microstructure of the permanent magnet. Twins and antiphase boundaries (APBs) have been shown to lower BH_{max}, while dislocations and refined grain size have been shown to improve coercivity (H_c) and BH_{max}. Equal channel angular extrusion (ECAE) is a technique for imparting high strain into a material without changing its cross-sectional area. The high amount of strain is demonstrated to introduce high defect density into the bulk. In this study, we employ ECAE for the purpose of improving the coercivity of Mn₅₄Al₄₆ bulk ingots, using crystalline defects as pinning sites to inhibit magnetic domain motion. Using ECAE, coercivity is shown to increase from 95 kA/m to over 183 kA/m, without any loss to the saturation magnetization (M_s). This results in a BH_{max} improvement from 8.6 kJ/m³ to 20.9 kJ/m³. We investigate the microstructure to understand which defects affect the increase in H_c and why they do not diminish M_s of the ordered τ structure. Furthermore, we substitute Ti for Al to improve BH_{max}, as Ti is anticipated to energetically favor APBs to the bulk τ phase. In this way, we demonstrate how the addition of 1 at.% Ti for Al in a Mn₅₄Al₄₅Ti₁ alloy improves τ phase BH_{max} to 11.5 kJ/m³ when annealed without ECAE. We investigate the microstructure to confirm if Ti suppresses APB formation and the effect of Ti addition on other defects.

SF05.06.07

Synthesis of PtSe₂ Nanoparticles and the Se Vacancy Defect Formation (PtSe_x) Towards Hydrogen Evolution Reaction Victor S. Lemos¹, Carolina P. Torres¹, Isabela J. Vieira^{1,2}, Edson R. Leite^{1,3}, Adalberto Fazzio¹ and João B. Souza Junior^{1,2}; ¹Brazilian Center for Research in Energy and Materials (CNPEM), Brazil; ²Universidade Estadual de Campinas (Unicamp), Brazil; ³Universidade Federal de São Carlos (UFSCar), Brazil

The hydrogen evolution reaction (HER) has been a topic of interest. Like other gas evolution reactions, the HER needs an overpotential, and catalyst engineering aims to maximize the process's effectiveness. The best catalysts for the HER are the Pt catalysts, but due to their high cost and rarity are not viable candidates.¹ New studies show a lot of promising catalysts for the HER, among them are the transition metal dichalcogenides (TMDCs), which can be obtained as a 2D nanostructure, and a lot of effort is being made to improve these materials. The PtSe₂ is a TMDC that shows high potential due to its high catalytic and conductivity properties.² Many paths exist to induce defects on the surface of materials.³ Our focus is on a new method of synthesis of PtSe₂ nanoparticles through the selenization of previously synthesized Pt nanoparticles. The selenization process was performed in a closed alumina reactor with an excess of Se in the presence of Pt nanoparticles. At higher temperatures, Se becomes liquid and the selenization reaction occurs. The excess of Se was removed by solubilization in trioctylphosphine (TOP) and centrifugation. First, Pt nanoparticles were synthesized using 90 mg of Pt(acac)₂, 10 mL of oleylamine, and 1 mL of oleic acid in a three-neck round bottom flask with a condenser attached to a Schlenk line. The system is heated to 80 °C under vacuum and constant stirring for complete precursor solubilization. Then, under N₂ atmosphere, the temperature was raised to 250 °C for 60 min for precursor decomposition, particle nucleation, and growth. The products are isolated by centrifugation, washed with acetone, and dispersed in hexane. Excess Se is added to the mixture of Pt nanoparticles and heated to 400 °C for 120 min. To remove the Se byproduct, TOP was added to the final reaction product, kept under stirring for 2 hours, and washed with hexane several times followed by centrifugation. To induce defects into PtSe₂ nanoparticles, the PtSe₂ was dispersed in 1 mL of hexane and 1.6 mL of butyl-lithium hexane solution was added under magnetic stirring, followed by 10 min in ultrasonic bath. The dispersion was washed with hexane. To see the changes in the structure of the PtSe₂ the material was characterized by High-Resolution Transmission Electron Microscopy (HRTEM) and EDS chemical analysis. The images of the PtSe₂ revealed few-layered ordered flakes (~5.1 Å between layers) with high crystallinity. After the lithium treatment, the defects were visible in the flakes that look like broken structures with small regions of atomic ordering. Energy Dispersive X-ray Spectroscopy (EDS) showed that the Pt/Se ratio decreased from 2 for ordered PtSe₂ to 1.5 after intercalation. EDS indicated that Se vacancies are induced in the structure (PtSe_x), which was corroborated by X-ray Photoelectron Spectroscopy (XPS) results. The new PtSe_x structure presented huge shifts in Raman Spectroscopy of 40 cm⁻¹, and E_g/A_{1g} peak intensity inversion and a new peak appeared at a lower energy of spectrum due to the defects. After confirming the defects, we made preliminary catalytic tests, resulting in an overpotential of 145 mV (measured at 10 mA cm⁻²) for the PtSe_x nanoparticles. We hope that future improvement in PtSe_x defect engineering and catalyst optimization in the electrode could lead to an even better HER performance.

The authors would like to acknowledge FAPESP (Grants 2018/05159-1, 2021/03321-9) and CNPq (409787/2021-3).

1. Eftekhari, A. *et al.* Int. J. Hydrog. Energy. 2017, 42, 16, 1053-11077.
2. Ghorai, A. *et al.* Dalton Trans. 2016, 45, 14979-14987.
3. Ping, X. *et al.* Nano Lett. 2021, 21, 9, 3857-3863

SF05.06.08

First-Principles Study of Photocatalytic Activity of Amorphous TiO₂ Surface [Motoyasu Kato](#), Tomoyuki Tamura and Mitsuhiro Honda; Nagoya Institute of Technology, Japan

TiO₂ is a typical photocatalytic material that is relatively inexpensive and highly safe, and has been actively studied to improve its performance for wider range of applications. One of our group reported that the formation of an amorphous structure on TiO₂ surface increased the reaction rate by about 13 times compared to the anatase surfaces. However, its high catalytic activity was reduced when the amorphous surface was scraped by etching. Therefore, it is considered that the control of the amorphous surface is the key of improving the catalytic activity.

STEM-EELS has been widely used in recent years to observe nanoscale atomic-arrangements and electronic structures with high spatial resolution. In particular, ELNES (electron energy-loss near-edge structures) is able to provide sensitive information on chemical bonding, valence states and coordination. We observed amorphous surfaces of TiO₂ samples with high photocatalytic activity using the atomic-resolution electron microscope (JEOL ARM-200F @Nitech), and found that spectra for the surface region were significantly different from those for bulk region. In this study, we identify amorphous surface structures that contribute to improve the catalytic activity using first-principles calculations, combining with electron-microscopy observations.

Amorphous surface models were generated by quenching from the melt using classical MD method and subsequent relaxation using first-principles method with VASP code [1]. Ti *L*-edge ELNES were simulated for those models with QMAS code [2]. We found that Ti *L*-edge ELNES for 4-coordinated Ti in the amorphous surface region are in good agreement with experimental results. In addition, in order to clarify the origin of the high photocatalytic activity of the amorphous surface, we investigated the chemical reaction between 4-coordinated Ti and adsorbed molecules. Our results suggest that oxygen defects in the amorphous surface contribute to the improvement of photocatalytic activity.

References : [1] G. Kresse et al, Phys. Rev. B 54, 11169-11186 (1996), Phys. Rev. B 59, 1758-1775 (1999). [2] T. Tamura et al., Phys. Rev. B 85, 205210 (2012).

SESSION SF05.07: Harvesting Functional Defects for Iontronics and Neuromorphic Computing

Session Chairs: Peijun Guo and Linn Leppert

Wednesday Morning, November 30, 2022

Sheraton, 3rd Floor, Gardner A/B

9:00 AM *SF05.07.04

Ionic Control of Emergent Physical Phenomena in Epitaxial Oxide Thin Films [Hyeon Han](#) and Stuart S. Parkin; Max Planck Institute, Germany

Iontronics is an emerging science and technology that shows fascinating physical phenomena, particularly in oxide thin films controlled by ionic motion and arrangement. The most significant impact of iontronics is that iontronic devices enable us to control exotic physical properties, such as insulator-metal transitions, emergent superconductivity, and tunable magnetism, which are extremely difficult or even impossible with conventional field-effect-transistors. Here, we show how the oxygen vacancy channels (OVCs) in brownmillerite SrCoO_{2.5} thin films can be manipulated via ionic gating (IG). In addition, we demonstrate the epitaxial growth of single-domain *T*-Nb₂O₅ thin films, for the first time, critically with the ion channels oriented perpendicular to the film's surface. We show that the insertion of just a small amount of Li via IG results in a colossal insulator to metal transition with almost eleven orders of magnitude decrease in resistivity. In situ experiments, in conjunction with theoretical calculations, reveal a series of transitions between distinct crystal and electronic structures as the Li content is systematically increased. These include hidden phases that have not previously been identified. Furthermore, by replacing the conventional Au gate electrode with Li-containing gate electrodes, tunable and low voltage operation via Li-chemical potential control is demonstrated. Finally, we present a new concept to tailor octahedral distortion, magnetism, and anomalous Hall effect in ferromagnetic SrRuO₃ thin films via hydrogenation. These findings open a new path towards the exploration of hidden phases and the development of novel electrochemically controlled electronic devices.

9:30 AM SF05.07.02

Influence of Humidity Level on Synaptic Behaviour of Redox Transistors with Proton Defects Enhanced Electrochemical Reaction [Lingli Liu](#), Putu Andhita Dananjaya and Wen Siang Lew; Nanyang Technological University, Singapore

Biologically-inspired neuromorphic computing systems are attractive for next-generation computing technologies. This non-conventional computing approach offers processing parallelism, cognitive capability and boasts high energy efficiency. In recent years, the redox transistor has emerged as a potential candidate for artificial synaptic devices that can concurrently execute signal transmission and memory operations. In this work, a complementary metal-oxide semiconductor-compatible redox transistor with a highly linear weight update is presented. The synaptic weight represented by the channel conductance is modulated under an electrochemical reaction followed by electric field-driven ion migrations in and out of the channel. This electrochemical reaction involved in such device operation is known to correlate strongly with humidity. However, available studies which specifically address this humidity aspect are still limited. We investigate the humidity-sensitive pre-oxidation process of the pristine W channel required to initiate the switching operation, which can be attributed to the proton defects-enhanced electrochemical process. Under the bipolar pulse scheme, the gradual oxidation of W derived from the progressive activation of the proton transport channels is observed. Performances of the redox transistor under different moisture levels are presented, i.e., pre-oxidation and potentiation/depression. Excellent endurance performance with more than 256 k synaptic weight updates can be obtained. Furthermore, a handwritten digit recognition accuracy of more than 90% is achieved in a 4-layer neural network simulation. Overall, it is concluded that the as-presented redox transistor is a promising candidate for realizing hardware implementation of the artificial neural network.

9:45 AM SF05.07.03

Tunable Ion Hopping in Tantalum Oxide Resistive Switching Memory by Zirconium Doping [Young-Woong Song](#) and Jang-Yeon Kwon; Yonsei University, Korea (the Republic of)

Artificial intelligence (AI) has received great attention for powerful performance over broad areas. However, conventional devices are unsuitable for multiply-accumulate operation (MAC), which is essential for the artificial neural network. This due to limitations in the architecture and device physics. In this context, in-memory computing technology is emerging. There have been numerous reports on establishing neural network with next generation memory devices, [1] but only few are fully hardware implemented due to imperfections of the devices. [2] Although resistive switching memory (RRAM) based on binary oxides is a promising candidate, it suffers from critical drawbacks: Stochastic switching process, sudden formation or rupture of conducting path. Inconsistent ionic motion in the switching medium is assumed to be related with the unreliable performance of the devices. Metal cation

doping of binary oxides can facilitate or regulate the resistive switching process, by forming additional bonds with oxygen. We adopted doping as a method for tuning analog switching properties of RRAMs and studying the switching principles towards further understanding.

We found that zirconium (Zr) doping effectively suppress sudden changes of cell conductance, which can be highly related with ionic hopping modulation. RRAM based on mixture of tantalum oxide (TaO_x) and Zr as a metal cation dopant was fabricated. We specified switching type of our devices to be filamentary, as local conducting paths with nanometer scale dimension were observed by conductive atomic force spectroscopy. The thickness of the switching medium is ~ 40 nm, confirmed by AFM. TaO_x RRAM exhibited gradual current hysteresis along voltage sweep of $0 \sim 5 \sim 0$ V, resistance modulated from high resistance state (HRS) of 10 pA to low resistance state (LRS) of 5 nA, determined at 0.3 V read voltage. When voltage sweep of $0 \sim 5 \sim 0$ V is applied, the devices return to HRS, showing bipolar resistive switching behavior.

Doping concentrations of Zr in TaO_x is observed to be from 3.79 \sim 7.25 at %, determined by X-ray photoelectron spectroscopy. TaO_x RRAMs with 0, 3.57, 5.35 at % Zr doping concentrations exhibited similar HRS of 10 \sim 16 pA, whereas LRS significantly decreased (0 % : 5.78 nA, 3.57 % : 907 pA, 5.35 % : 283 pA). It is expected that Zr doping does not influence the intrinsic resistance of the cell, but takes role in the resistive switching process, regulating ionic hopping and formation of conducting filament. Incorporation of Zr in the TaO_x lead to multiple bonding with oxygen, where oxygen vacancies are the constituent of the conducting path.

For artificial neural network applications, analog resistive switching properties of the devices were investigated by voltage pulse scheme. Zr doped TaO_x RRAMs exhibit gradual potentiation and depression of 200 conductance levels switching window within 0.1 \sim 1.4 nA. Gradual conductance modulation for 200 states is hardly achieved in previously reported RRAMs. [3] The devices exhibit low power consumption of micro-Watts, which is comparable to previously reported RRAMs.

In conclusion, we realized in-memory computing unit with Zr doped TaO_x RRAM that meets two criteria, superior analog switching properties and simple cell structure. Metal cation doping of resistive switching memory opened a new method to study switching phenomena and proved the higher potential towards hardware implementation of neural network and AI.

< References >

- [1] F. Cai *et al.*, "A fully integrated reprogrammable memristor-CMOS system for efficient multiply-accumulate operations," *Nat. Electron.* 2, 290 (2019)
- [2] P. Yao *et al.*, "Fully hardware-implemented memristor convolutional neural network," *Nature*, 577, 641 (2020)
- [3] T. Shi *et al.*, "A Review of Resistive Switching Devices: Performance Improvement, Characterization, and Applications," *Small Struct.*, 2, 2000109 (2021)

10:00 AM BREAK

10:30 AM SF05.07.05

Defining Properties via Material Microstructure—Defect and Strain Engineering Approaches for Developing Ferroelectric AlScN John Wellington-Johnson, Jialin / James Wang, Azadeh Ansari, Lauren M. Garten and [Nazek El-Atab](#); Georgia Institute of Technology, United States

AlN has long been used as a low loss piezoelectric material but only recently has it emerged that with the addition of scandium $\text{Al}_x\text{Sc}_{1-x}\text{N}$ also becomes ferroelectric [2] AlScN has a high electromechanical coupling coefficient (k^2), low loss tangent, and high piezoelectric coefficient (d_{33} AlScN ~ 44 pC/N), along with a large polarization [3]. Unfortunately, the electric fields needed to reorient the polarization, the coercive field, of AlScN is near the breakdown strength of the material, reducing the reliability and viability for memory or electronics applications [3]. Strain engineering approaches can be used to lower the *coercive field* (E_c), reducing the energy needed to switch the ferroelectric dipole, because strain favors the layered hexagonal structure. Furthermore, defect engineering can enhance piezoelectric properties and manifest ferroelectric properties.

This talk details the development the impact of strain, defects, and doping on the ferroelectric and piezoelectric response of AlScN thin films. $\text{Al}_x\text{Sc}_{1-x}\text{N}$ thin films are fabricated on a range of different substrates using DC and RF sputtering techniques with varying $\text{N}_2:\text{Ar}$ gas ratios, from 350 - 400 degrees C. X-ray photoelectron spectroscopy (XPS) studies show changes in Sc target power influence not only the concentration of Sc in the microstructure but also the crystalline quality. The impact of Sc on the lattice is further corroborated through X-Ray Diffraction (XRD) studies which show a structural shift towards as a function of increased Sc, up to $\text{Sc}_{0.4}$. Phase formation beginning at 350 degrees C, but enhanced crystalline orientation begins above 400 degrees C. Ferroelectric, piezoelectric, and dielectric measurements are used to track the impact of microstructure and composition on the ferroelectric and dielectric response. Polarization-electric field loops with defining hysteretic ferroelectric shapes and observations of coercive field shifts up to 30V away from the breakdown voltage are presented. The impact of defects on breakdown strength will be discussed. Piezoresponse force microscopy and First-Order Reversal Curve (FORC) measurements demonstrate the domain kinetics across microstructures; CV and PUND measurements illustrate film quality, and further characterize the contributing and shifting electrical responses. Overall, this work provides insight into the impact of film microstructure on the ferroelectric response as a function of doping, strain, and defect concentration.

References

- [1] Esteves, Giovanni, et al. "AlN/SiC MEMS for high-temperature applications." *Journal of Microelectromechanical Systems* 28.5 (2019): 859-864
- [2] Fichtner, Simon, et al. "AlScN: A III-V semiconductor based ferroelectric." *Journal of Applied Physics* 125.11 (2019): 114103.
- [3] Lu, Yuan. Development and characterization of piezoelectric AlScN-based alloys for electroacoustic applications. Diss. Albert-Ludwigs-Universität Freiburg im Breisgau, 2019.

10:45 AM SF05.07.06

Low-Current and High Temperature Nonvolatile Analog Memory Through the Electrochemical Control of Point Defects Yiyang Li and [Thomas Defferriere](#); University of Michigan, United States

Modern machine learning and artificial intelligence workflows consume vast amounts of energy due to the need to move massive quantities of data between memory and processor. Analog, in-memory computing can be much more energy efficient by simultaneously acting as both memory and processor. In-memory computing has been limited by the lack of an analog nonvolatile memory with reliable switching and low-current and voltage operations.

In this work, we show how electrochemical random access memory (ECRAM) can fulfill this needed. Inspired from a battery, ECRAM electrochemically shuttles oxygen vacancy point defects between two transition metal oxides with a solid electrolyte sandwich. The oxygen vacancy concentration is able to deterministically control the analog resistance states, just as how the state of charge of a battery is a reproducible analog value. Whereas earlier ECRAM devices based on lithium ions and protons would rapidly lose state (self-discharge) when scaled to nanosized dimensions, our solid-state, oxygen-based ECRAM is not only nonvolatile at room temperature, but can also switch and retain state at 200C, well above the operating temperature of any solid-state memory. ECRAM's ability to electrochemically move point defects within solids provide new approaches for both analog and high-temperature memory.

11:00 AM SF05.07.07

Visible Light Induced Negative Photo Conduction in Wide Bandgap Oxides Based Memristor for Nonvolatile Opto-Electronic Memory and Photo Sensing Dayanand Kumar, Lana Joharji and Nazek El-Atab; King Abdullah University of Science and Technology, Saudi Arabia

The photo sensor based on wide bandgap oxides relies on the phenomenon of defect generated negative photoconductivity in memristors. Wide bandgap oxides naturally are unresponsive to low energy light, particularly in the visible regime and higher wavelengths owing to their large bandgap energies. Due to the bandgap energy being larger than the energy of the photons in the visible range, they are transparent to visible light and the visible photons are incapable of causing photocarrier generation within the oxide and are therefore naturally photo unresponsive. This has restricted the use of oxide based photosensors to rely on other lower bandgap materials for a photo response or to be restricted strictly to the higher energy ultraviolet band. However, in the phenomenon studied in this work, through electrically generated defect states within the oxide, it is possible to sensitize wide bandgap oxides to respond to visible light regimes. This is accomplished due to the defect generation creating sub-bandgap states in the forbidden gap which can respond to visible energy photons. The mechanism has been theorized to work as follows; when the oxide system is electrically stressed beyond the breakdown field, the lattice oxygen bonds are severed. If this is done in a constrained manner by means of a current compliance to prevent catastrophic breakdown, the effect is reversible and results in a change in the resistive state of the device and is termed soft breakdown. Such a phenomenon is widely used in memristive devices. During this breakdown, the lattice bonds are broken, and the oxygen is displaced as ions into the interstitial spaces as a metastable vacancy-ion equilibrium. The ions do not naturally recombine with the vacancy and restore the lattice of the oxide as there is an energy barrier that prevents this. However, such an energy may be supplied by means of optical illumination which can cause the vacancy-ion pairs to recombine and return the pristine state of the oxide consequently resulting in a resistance increase in the system. When optical energy greater than the bandgap of the defect state to the conduction band is provided to such a system, a vacancy trap state electron may be excited to the conduction band, resulting in a positive charging of the vacancy state. This creates an electrostatic force between the positively charged vacancy and the negatively charged interstitial ion resulting in a recombination of the two and reformation of the oxide.

In this work, we present a novel bilayer ITO/SiO₂/HfO_x/Pt memristor for optoelectronic nonvolatile memory storage and photo sensing. The device demonstrates good photo sensing characteristics in terms of highly stable endurance at least 200 (electrical SET/optical RESET) cycles for blue light (intensity: 10 mW/cm², wavelength: 405 nm) and excellent retention (10⁵ s) without any disruption. These features of the memristive device would allow us to produce either an optoelectronic nonvolatile memory for data storage or photo sensing in single memristive cell.

11:15 AM SF05.07.08

Electrochemical Control of Resistance States in Metal Oxide Bilayer Stack Thomas Defferriere¹, Baoming Wang¹, John Rozen², Takashi Ando², Frances M. Ross¹ and Harry Tuller¹; ¹Massachusetts Institute of Technology, United States; ²IBM T.J. Watson Research Center, United States

Electrochemical control of metal oxide based devices has emerged recently as an attractive approach to achieving reprogrammable microelectronic devices that move beyond simple semiconductor device physics principles. The operational concept of such devices relies on the shuttling of ionic species from an ionic conducting oxide towards either an active interface or active oxide layer where a chemical reaction or exchange of ionic species occurs, changing the functional properties of that layer. Devices exhibiting electronic/magnetic/optical and thermal switching have been demonstrated to offer unique advantages over their more traditional electronic counterparts. For example, electronic switching devices, either in two-terminal device configurations typical of memristive devices or three-terminal configurations akin to a transistor device, have the ability to directly emulate neuronal behavior potentially leading to more efficient neuromorphic computational hardware. Beyond purely electronic applications, the advantages of using ionic species to modulate the functional properties of metal oxides (mechanical, ferroelectric, magnetic, optical, and thermal) offer unique perspectives to redesign traditional applications considering the ubiquitous use of these metal oxide materials for their functional properties.

While electrochemically gated microelectronic devices have been demonstrated in many materials systems, open questions still remain about how to best optimize their device performance. While ionic mobility within and interfacial ion transfer between the two solid layers are key device parameters, little reliable information exists regarding these key parameters given the predominantly electronic character of metal oxide material near room temperature. Such knowledge is vital for mastering overall device performance such as speed, retention, and predictability. To address these challenges, we have investigated the reversible exchange of ions between two adjacent solid oxide layers.

Specifically, we have measured the reversible ionic transport and interfacial transfer kinetics in a thin film bilayer oxide system based on a Pr_xCe_{1-x}O₂/La_{2-x}Ce_xCuO₄ stack that uses model materials for which the defect chemical and transport properties have already been carefully characterized. These materials offer high ionic mobilities and can accommodate large levels of non-stoichiometry. By studying the characteristics of our devices with a combination of electrochemical impedance spectroscopy and potentiostatic measurements, we demonstrate the ability to reversibly modulate the bilayer device resistance near room temperature and isolate the resistance contributions of both layers as a function of the total device resistive state. We show that these changes can be directly correlated with the respective materials' defect chemistries, typically investigated at elevated temperatures under varying gas atmospheres. Dynamic current-voltage studies enable us to separate the rate-limiting kinetics related to the defect mobilities and the interfacial exchange kinetics of the system. The findings in this work can be expected to aid in developing material selection and design criteria for similar bilayer systems, and be used to achieve faster resistance switching speeds, larger resistance switching ranges, and longer device retentions.

SESSION SF05.08: Harvesting Functional Defects in Energy Materials II

Session Chairs: Hui Xiong and Hua Zhou

Wednesday Afternoon, November 30, 2022

Sheraton, 3rd Floor, Gardner A/B

1:30 PM *SF05.08.01

Electrochemically-induced Amorphous to Crystalline Transformation in Niobium Oxide Electrodes for Lithium-Ion Batteries Pete Barnes^{1,2}, Yuxing Zuo³, Kiev Dixon¹, Dwen Hou¹, Sungsik Lee⁴, Justin Connell⁴, Hua Zhou⁴, Yuzi Liu⁴, Paul H. Davis², Olivia Maryon¹, Shyue Ping Ong³ and Hui Xiong¹; ¹Boise State University, United States; ²Idaho National Laboratory, United States; ³University of California, San Diego, United States; ⁴Argonne National Laboratory, United States

Intercalation-type metal oxide electrodes are promising negative electrode materials for safe and stable operation of rechargeable lithium-ion batteries due to the reduced risk of Li plating at low voltages. Nevertheless, lower energy and power density along with cycling instability remain a bottleneck for their implementation, especially for desirable fast charging applications. Recent studies have shown enhanced electrochemical charge storage in metal oxide electrodes that contain intentional structural defects (e.g., vacancies and interstitials). In this talk, we will discuss an electrochemically driven amorphous-to-crystalline (a-to-c) transformation in a nanoporous Nb₂O₅ material for Li-ion storage. Through integrated experimental and computational study, we

elucidated the mechanism of multi-electron transfer reaction in the a-to-c Nb2O5 electrode as well as its enhanced kinetics for Li-ion batteries.

2:00 PM SF05.08.02

Dynamics of Defects in 2-D MnO2 During Charge-Discharge Cycling Scott T. Misture; Alfred University, United States

MnO₂ in its many forms has attractive properties for a wide range of applications from catalysis to charge storage. 2-D MnO₂ nanosheets demonstrate an interesting response to reduction of Mn⁴⁺ to Mn³⁺, where Jahn-Teller distorted Mn³⁺ is displaced out of the plane of the nanosheet forming a “surface Frenkel” defect. We find that introducing this unusual defect results in dramatic improvements in the electrochemical charge storage capacity as well as the catalytic activity for many reactions. Specimens were prepared via exfoliation of nominally defect-free KxMnO₂ crystals and by electrodeposition to enable studies of a range of Mn³⁺ defect content. The talk centers on the application of advanced materials characterization tools for study of complex nanoscale 2-D oxides. In-situ and in-operando studies using high energy X-ray diffraction, X-ray pair distribution functions, EXAFS/XANES and Raman spectroscopy will be discussed. We show that linking electrochemical measurements to local structure characterization results enables us to understand the mechanisms by which charging occurs in supercapacitor electrodes. It is clear that the Mn³⁺ defects are not altered during electrochemical cycling but that they dramatically alter the electronic band structure, yielding large improvements in charge transfer resistance. Further detailed PDF and Raman studies show that partial nanoscale conversion to tunnel-form MnO₂ is a primary degradation mechanism that lowers capacitance compared to the layered MnO₂.

2:15 PM SF05.08.03

Resisting Dendrites in Lithium Batteries, One Pinhole at a Time Solomon Oyakhire, Wenbo Zhang, Yi Cui and Stacey F. Bent; Stanford University, United States

For humanity to successfully transition from fossil fuels, the mismatch in the demand and supply of renewable energy must be addressed by reliable, high energy storage systems. One promising energy storage system is the lithium metal battery (LMB), owing to the high gravimetric capacity of lithium (3860 mAh/g). The potential gain in volumetric and gravimetric energy density offered by LMBs could usurp today's lithium-ion battery technology and revolutionize energy storage. However, the lifetime of LMBs is hindered by morphological instabilities experienced during the electrodeposition of lithium.

Modifications of the solid electrolyte interphase (SEI) and electrolyte are the most common strategies for improving lithium metal morphology. However, electrolyte and SEI engineering are often tedious, based on trial and error, and insufficient for enhancing lithium electrodeposition. Here, we demonstrate a new, alternative strategy for controlling lithium metal morphology and improving electrochemical performance that is independent of the electrolyte and SEI. By modifying the current collector with atomic layer deposited (ALD) thin films of ZnO, SnO₂, and Al₂O₃, we show that lithium deposits atop, rather than beneath, the thin films, resulting in changes in lithium morphology and battery performance that are strongly dependent on the electrical resistance of the ALD films. The results show that low resistance copper modification films like SnO₂ and ZnO provide numerous sites for lithium nucleation and promote the formation of high surface area (fast electrolyte consuming) lithium deposits, while the highly resistive Al₂O₃-modified copper reduces the available sites for lithium nucleation and promotes the formation of low surface area (slow electrolyte consuming) clusters of lithium deposits.

We propose and demonstrate the first recorded mechanism for the connection between electrical resistance and lithium growth - we propose that, in resistive substrates, lithium metal nucleates atop only pinhole or defect sites, then grows laterally by the radial diffusion of lithium ions from the electrolyte. We prove this mechanism analytically, using diffusion controlled current equations, and experimentally by introducing patterned pinholes into a resistive, pinhole-free substrate. We generalize the concept of resistance-controlled morphology and demonstrate high battery performance in three distinct classes of electrolytes, culminating in anode-free pouch cells that retain 60% of their initial discharge capacity after 100 cycles. This work presents a new approach for understanding the electrodeposition of lithium and tuning the performance of lithium metal batteries.

2:30 PM BREAK

3:30 PM SF05.08.04

Ionic Transport in Natural Phyllosilicates Giyeok Lee¹, Gunyoung Heo¹, Mirella S. Santos² and Aloysius Soon¹; ¹Yonsei University, Korea (the Republic of); ²École normale supérieure (ENS) de Lyon, France

Electrochemical ion-insertion in anisotropic solids is conventionally important for high-performance energy harvesting systems and understanding the underlying coupled ion-electron transfer mechanism, transportation of guest ions, and the redox of these anisotropic solids are of utmost importance for the engineering of these energy harvesting systems [1]. Natural clay minerals (e.g., in the class of phyllosilicates) show great promise as anisotropic host solids for these applications but are still poorly understood and a clear atomistic picture of the underlying mechanisms is still missing. Especially, the direct relationship between the efficiency of energy conversion (e.g., from the salinity gradient between the sea water and saline water) and the layer charge of clay minerals is insufficient to design the clay-based energy materials, which can play a critical role in maximizing efficiency. In this work, using vermiculite as an archetypical but promising layered host material [2], we construct different supercell models with varying 3+/4+ ion ratios in the tetrahedral layers and examine the role of interlayer surface charges on ionic transport via first-principles derived machine-learning potential enabled molecular dynamics simulations [3]. Through this study, we will provide a first-step understanding of the underlying atomistic design rules in natural clay materials for energy applications, which has the potential to establish itself as design rules for efficient vermiculite-based energy material.

[1] S. Kim, S. J. Choi, K. Zhao, H. Yang, G. Gobbi, S. Zhang, and J. Li, *Nat. Commun.* **7**, 10146 (2016)

[2] L. Cao, H. Wu, C. Fan, Z. Zhang, B. Shi, P. Yang, M. Qiu, N. A. Kahn, and Z. Jiang, *J. Mater. Chem. A* **9**, 14576 (2021)

[3] A. P. Bartók, M. C. Payne, R. Kondor, and G. Csányi, *Phys. Rev. Lett.* **104**, 136403 (2010)

3:45 PM SF05.08.05

New Fast Oxygen Ion Conductor Perrierite-Type Oxide La₄Mn₅Si₄O_{22+δ} Discovered by Harnessing the Materials Project and High-Throughput Computation Jun Meng, Md Sariful Sheikh, Ryan Jacobs and Dane Morgan; University of Wisconsin–Madison, United States

Oxygen-ion conducting materials are important for a variety of applications such as solid-oxide fuel cells, gas sensors, catalysts, and oxygen separation membranes. Applications typically utilize oxygen-active materials operating at high temperatures (e.g. ~800 °C for fuel cells). The key issue that limited industrial applicability is the high operating temperature which results in high system cost, materials degradation, and slow start-up and shutdown cycles. Development of alternative electrolyte/electrodes materials with good oxygen ionic conductivity at low temperature (room temperature-400 °C) is of great interest. However, fast oxygen conductor materials are concentrated in only a handful of materials structure families such as perovskite, fluorite, manganite, melilite, scheelite, and apatite. Hence, it is critical to find new materials which transport oxygen ion efficiently at low temperatures. In this work, we developed a high-throughput computational screening of the 33,975 oxide materials from the Materials Project database and discovered the new structure family of interstitial oxygen diffuser based on perrierite-type oxide La₄Mn₅Si₄O₂₂ (LMSO). We used a hierarchy of screening criteria including the geometric free space, thermodynamic stability, synthesizability, redox-active elements, diffusion pathways, ab initio calculated defect

formation energy and diffusion barrier. Our screening has yielded several material families to date, among which LMSO was selected for investigation with higher-level DFT hybrid functional calculations and experimental ionic conductivity measurements. Interstitial oxygen formation energy and migration energy were studied by Density Function Theory (DFT) calculations with SCAN functional. The formation energy of interstitial oxygen is -0.11 eV at a concentration of 2.3% under air condition, indicating that LMSO is oxygen hyperstoichiometric with an expected composition of $\text{La}_4\text{Mn}_5\text{Si}_4\text{O}_{22+0.5}$ in air. Oxygen ion diffusion pathways and energetics were studied by ab initio Molecular Dynamic (AIMD) simulation, showing migration pathways along the connected sorosilicate Si_2O_7 groups through an interstitial mechanism. The migration barrier is predicted as 0.45 eV and 0.69 eV based on AIMD simulation and the Climbing Image-Nudged Elastic Band (CI-NEB) calculation, respectively. The diffusivity of oxygen ion is calculated to be 10^{-5} cm^2/s and the ionic conductivity is 0.1 S/cm at 800 °C. The above computational predictions have been verified by experimental investigations. The existence of interstitial oxygen ($\delta \sim +0.5$) is validated by the Electron Probe Micro-analyzer (EPMA) and iodometric titration method, and the ionic conductivity is measured as 0.11 S/cm at 800 °C, consistent with the computational results. Experimental studies show that LMSO has mixed electronic and oxygen ionic conduction, indicating that LMSO is a very promising oxygen active material for numerous applications.

4:00 PM SF05.08.06

Surface-Based Post-Synthesis Manipulation of Defects in Metal Oxides using Liquid Water Heonjae Jeong, Nabeel Abuyazid, Elif Ertekin and Edmund Seebauer; Univ of Illinois, United States

Lowered chemical coordination at metal oxide surfaces facilitates the creation of interstitial atoms that would not otherwise form in the bulk. For example, clean surfaces of ZnO and TiO_2 create interstitials of oxygen (O_i)^{1,2} from adsorbed O atoms with energy barriers near or below roughly 1 eV. The atomic configurations for interstitial injection resemble those for site hopping in the bulk, with barriers only slightly higher. The modest hopping barriers of O_i in oxides, coupled with those for injection, make clean surfaces likely pathways for populating the nearby bulk with O_i near room temperature, thereby accessing a regime wherein kinetic rather than thermodynamic effects dominate defect behavior and opening new possibilities for functional defect manipulation. Post-synthesis regulation of defects such as vacancies becomes possible near room temperature, together with formation of new types of complexes. Here we show by isotopic self-diffusion measurements combined with first-principles calculations by density functional theory (DFT) that poison-free oxide surfaces inject O_i when contacted with liquid water near room temperature. For single-crystal oxides of zinc, titanium and gallium, O_i penetrates to depths ranging between 20 nm and 2 μm . This O_i almost certainly eliminates oxygen vacancies within the penetration depth, and probably forms stable complexes with hydrogen interstitials that neutralize their action as adventitious donors. The results point the way toward uses in photocatalysis, photoelectrochemistry, renewable energy production and storage, and advanced electronics that could benefit from such manipulation.

References

1. Jeong, H., Ertekin, E. & Seebauer, E. G. Kinetic Control of Oxygen Interstitial Interaction with $\text{TiO}_2(110)$ via the Surface Fermi Energy. *Langmuir* **36**, 12632–12648 (2020).
2. Jeong, H., Li, M., Kuang, J., Ertekin, E. & Seebauer, E. G. Mechanism of Creation and Destruction of Oxygen Interstitial Atoms by Nonpolar Zinc Oxide(10-10) Surfaces. *Phys. Chem. Chem. Phys.* **23**, 16423–16435 (2021).

4:15 PM SF05.08.08

Fundamental Understanding of a Defect Density and Catalytic Activity for Methane Combustion Using Colloidally Engineered Pd Nanoparticles Jinwon Oh and Matteo Cargnello; Stanford University, United States

Recently, defect engineering has been widely used in catalysis study to enhance catalytic activity. Defect sites in nanomaterials have a high energy state due to their unsaturated coordination or strain effects. Therefore, these sites have different absorption/desorption energy of reactant/intermediate molecules than those without defects, and the difference potentially affects the activity of catalysts. Among various types of defects, planar defects such as stacking fault, grain boundary, and twin boundary have been highly studied in the field of catalysis due to their stability during a reaction. There are various ways to introduce defects in catalysts, but those methods often inevitably introduce changes in the size or shape of nanoparticles which also have the potential to affect the catalytic activity. However, to address the direct correlation between the defect density and intrinsic activity of catalyst materials, it is required to control and exclude the change in other variables than defect densities, including the size and shape of nanoparticles. Therefore, the method to control defect density in nanoparticles while minimizing the change of other variables is highly required.

Here we chose a Pd nanoparticle catalyst for methane combustion reaction as a model system. We vary the amount of phosphorous in Pd nanoparticles using wet chemical synthesis to modify defect density in nanoparticles without changing other factors such as shape and size. Firstly, we synthesize well-defined colloidal Pd nanoparticles and expose them to phosphorous sources to introduce a phosphorous into a Pd crystal structure. Next, nanoparticles are exposed to an oxygen environment to extract phosphorous. Structural rearrangement is expected to occur at this step due to the diffusion of phosphorous atoms, resulting in defects forming. Using this method, we successfully synthesize Pd nanoparticles with different defect densities and compare their intrinsic activity for the methane combustion reaction. Finally, we confirm that Pd nanoparticles with a high density of defects show higher intrinsic activity for this reaction. This study provides a way to introduce defects in nanoparticles and fundamental insights for the correlation between a defect density and activity.

SESSION SF05.09: Functional Defects in Light Harvesting

Session Chairs: Nuria Bagues and Bryan Huey

Thursday Morning, December 1, 2022

Sheraton, 3rd Floor, Gardner A/B

8:30 AM *SF05.09.01

Spatially Resolved Defect Formations in Metal Halide Perovskites Jonghee Yang¹, Diana K. LaFollette², Benjamin Lawrie³, Anton V. Ievlev³, Juan Pablo Correa Baena² and Mahshid Ahmadi¹; ¹University of Tennessee, Knoxville, United States; ²Georgia Institute of Technology, United States; ³Oak Ridge National Laboratory, United States

Metal halide perovskites (MHPs) are currently leading materials towards high-performance optoelectronics. Despite today's scientific renaissance of the MHPs, a key constraint hesitating one-step towards their realization is stability. There are several challenges which must be overcome to improve the stability of MHP devices. One of these challenges is the understanding and control of their defect chemistry. Conventional spectroscopy faces serious obstacles to investigate defects in MHPs. In this talk, I will discuss a combination of spatially-resolved chemical and spectroscopic analysis, including time-of-flight secondary-ion mass spectroscopy (ToF-SIMS), cathodoluminescence (CL) spectroscopy and conductive atomic force microscopy (c-AFM) to systematically explore the fate of defects in MHP systems [1-3]. Our observations provide key features that must be considered towards development of

MHP optoelectronics, which guarantees excellent performances and longevities.

D. Kim, Y. Liu, A. V. Ievlev, K. Higgins, O. S. Ovchinnikova, J. S. Yun, J. Seidel, S. V. Kalinin, M. Ahmadi, Unraveling the Hysteretic Behavior at Double Cations-Double Halides Perovskite - Electrode Interfaces, *Nano Energy* (2021) 89, 106428.

D. Kim, K. Higgins, M. Ahmadi, Navigating Grain Boundaries in Perovskite Solar Cells, *Matter* (2021) 4, 5, 1442.

J. Yang, D. LaFollette, B. Lawrie, A. Ievlev, S. Kalinin, J.-P. Correa-Baena, M. Ahmadi, Spatially Resolved Defect Formations in Metal Halide Perovskites, under review (2022)

9:00 AM SF05.09.03

Selective Amorphization of Oxide Surface by Introducing Hydrogen Impurity Seohan Kim¹ and Joonho Bang²; ¹Uppsala University, Sweden;

²Gyeongsang National University, Korea (the Republic of)

The oxide semiconductors have been widely used in various electronic devices such as flat panel displays and solar cells. Especially, crystalline oxide semiconductors are attracting industrial interest due to their high electron mobility that arises from the well-aligned periodic array of the constituent elements. However, the rough surface morphology resulting from the grain growth triggers severe drawbacks in their thin-film applications. In this study, we demonstrate a surface amorphization of the oxide semiconductor thin film by introducing hydrogen gas during the deposition process. The surface of the crystalline In-Sn-O thin film is selectively amorphized, allowing for smooth surface morphology without any degradation of the electrical properties. In addition, the progressive surface amorphization offers the tunability of the work function, leading to the improved power conversion efficiency of the thin-film solar cell. The present study provides a tractable way to achieve the smooth surface of the crystalline thin films.

9:15 AM BREAK

9:45 AM *SF05.09.04

Electronic Properties and Migration Dynamics of (Functional) Defects in Heterogeneous Metal-Halide Perovskites from First Principles Linn Leppert; University of Twente, Netherlands

Halide double perovskites are an emerging class of photoactive materials with considerable structural and electronic diversity [1,2, 3] and reliable stability towards heat and moisture under ambient conditions. However, in contrast to ABX₃ perovskites like CH₃NH₃PbI₃, most halide double perovskites have comparably large band gaps and exhibit signatures of strongly bound and self-trapped excitons [4, 5]. In the first part of this talk, I will show how the band gap of Cs₂AgBiBr₆ can be dramatically altered by dilute alloying with symmetry-matched impurities leading to significantly reduced band gaps while preserving long carrier lifetimes [6]. I will also discuss the challenges that first principles numerical modelling techniques face for accurately describing defects in this chemically and electronically diverse family of materials [7].

In the second part of my talk, I will focus on the migration dynamics of halide vacancies in CsPbBr₃. Migration of halide vacancies is one of the primary sources of phase segregation and material degradation in lead-halide perovskites. We use first principles density functional theory to compare migration energy barriers and paths of bromine vacancies in the bulk and at a surface of CsPbBr₃. We find that surfaces facilitate bromine vacancy migration due to their soft structure that allows for bond length variations larger than in the bulk. Our calculations also demonstrate that this effect can be mitigated by lattice-matched passivation with alkali halide salts [9].

[1] F. Giustino, H. Snaith, ACS Energy Lett. 1, 1233 (2016).

[2] M. Filip, F. Giustino, Proc. Nat. Acad. Sci. 115, 5397 (2018).

[3] M. Wolf, B. Connor, A. Slavney, H. Karunadasa, Ang. Chem. Int. Ed. 60, 16264 (2021).

[4] R. I. Biega, M. Filip, L. Leppert, J. B. Neaton, J. Phys. Chem. Lett. 12, 2057 (2021).

[5] L. R. V. Buizza, H. C. Sansom, A. D. Wright, A. M. Ulatowski, M. B. Johnston, H. J. Snaith, L. M. Herz, Adv. Funct. Mater. 32, 2108392 (2022).

[6] A. H. Slavney, L. Leppert, D. Bartesaghi, A. Gold-Parker, M. F. Toney, T. J. Savenije, J. B. Neaton, H. I. Karunadasa, J. Am. Chem. Soc., 139, 5015 (2017).

[7] L. Leppert, T. Rangel, J. B. Neaton, Phys. Rev. Materials 3, 103803 (2019).

[8] R.-I. Biega, L. Leppert, J. Phys. Energy 3, 034017 (2021).

10:15 AM *SF05.09.05

Ion-Gated Transistors Based on Metal Oxides—From Electronics to Iontronics and Li-Iontronics Clara Santato; Ecole Polytechnique de Montreal, Canada

Ion-gated transistors (IGTs) employ ionic gating media (e.g. ionic liquids, polymer electrolytes, aqueous saline solutions) to modulate the density of the charge carriers in the transistor channel. The high capacitance featured by IGTs permits, among others, to use them in the study of insulator-to-metal transitions. Considering IGT-based technologies, not only IGTs operate at voltages as low as 0.1-1 V but they can also feature mechanical flexibility, printability and easy integration with chemo- and bio-sensing platforms.

Metal oxides are transistor channel materials interesting for their processability in air, at low temperature. They also constitute the basis for battery cathode materials in lithium-ion batteries.

In this contribution, we will discuss the opportunity IGTs offer to be employed as in situ diagnosis tools to evaluate the state of health of Li-ion batteries from the point of view of the evolution of the electronic properties of the battery cathodes (e.g. charge carrier density, electronic charge carrier mobility) as a function of the electrode (lithiation and de-lithiation) cycling conditions.

10:45 AM SF05.09.06

Giant & Controllable Photoplasticity and Photoelasticity in Compound Semiconductors Jiahao Dong¹, Yifei Li¹, Yuying Zhou², Alan Schwartzman¹, Haowei Xu¹, Bilal Azhar³, Joseph W. Bennett⁴, Ju Li^{1,1} and Rafael Jaramillo¹; ¹Massachusetts Institute of Technology, United States; ²Chinese Academy of Sciences, China; ³Cornell University, United States; ⁴University of Maryland Baltimore County, United States

We show that the wide-band gap compound semiconductors ZnO, CdS, and ZnS feature large photo-plastic and photo-elastic effects that are mediated by point defects. We measure the mechanical properties of single crystals (ZnO and CdS) and ceramics (ZnS) using nanoindentation, and we find that elasticity and plasticity vary strongly with moderate illumination. For instance, the elastic stiffness of CdS can increase by 20% due to blue illumination of intensity 1.4 mW/cm². Above-band-gap illumination (e.g. UV light) has the strongest effect, and the relative effect of sub-band gap illumination varies between samples – a clear sign of defect-mediated processes. We show giant optomechanical effects can be tuned by materials processing and varying point defect concentration. The photo-plastic effect can be understood by a long-established theory of charged dislocation motion. The photo-elastic effect requires a new theoretical framework. Using density functional theory (DFT), we find that the point defect ionization is accompanied by large lattice

distortions and large changes in elastic constants in both CdS and ZnS. DFT predicts a large photoelastic effect, on the order of 5% for realistic point defect concentration. Our results update the longstanding but lesser-studied field of semiconductor optomechanics, and suggest interesting applications.

11:00 AM SF05.09.07

Hot Electron Enhanced Defect Diffusion in Semiconductors Under Laser Irradiation Yifan Yao and Andre Schleife; University of Illinois, Urbana Champaign, United States

Precise manipulation of defect diffusion is important for cutting-edge applications in the semiconductor industry and quantum computing. Thermal annealing is the major technique to increase defect mobility, which becomes challenging in manufacturing at atomic-scale precision as the entire sample is elevated to a high temperature. Recently, our group predicts that under proton irradiation, hot electrons localized near oxygen vacancies in MgO reduce the migration barrier, providing an alternative route to increase defect mobility. Similarly, such hot electron distributions are expected to be achieved under laser irradiation but require a detailed understanding of coupled laser-electron-ion interactions. In this work, we employ a combination of first-principles methods to quantitatively describe multi-temporal dynamics triggered by external laser irradiation. We first use the time-dependent density functional theory to investigate the excited electron dynamics. By tuning the laser parameters, we achieve a hot electron distribution that is similar to the one predicted to reduce the migration barrier of oxygen vacancies by 0.94 eV under proton irradiation. Then, to quantify the number of excited oxygen vacancies, we examine the hot electron lifetime accounting for the electron-electron and electron-phonon scattering. Finally, we reveal that the oxygen vacancy diffusion mediated by laser-induced hot electrons can be increased by 10^5 at 900 K for the largest experimentally available oxygen vacancy concentration of 10^{18} cm^{-3} . Such enhancement at this defect concentration is 2 orders of magnitude greater compared to proton irradiation due to the high vacancy excitation rate under laser irradiation. Also, while laser and ion irradiation differ in their beam precision of the affected sample region, both enable higher accuracy of defect manipulation than annealing the entire sample. Moreover, we expect this mechanism is applicable to intrinsic or extrinsic defects in other wide bandgap semiconductors with defect-related states located within the bandgap. Therefore, we explore the enhanced gallium vacancy diffusion in GaN and the debonding of carbon divacancy in diamonds for their vital importance in semiconductor electronics and quantum computing. We acknowledge financial support from the Office of Naval Research under Grant No. ONR N00014-18-1-2605.

SESSION SF05.10: Understanding Functional Defects by Advanced Characterizations and Manipulations

Session Chairs: Rama Vasudevan and Yuanyuan Zhou

Thursday Afternoon, December 1, 2022

Sheraton, 3rd Floor, Gardner A/B

1:30 PM *SF05.10.01

Nanoscale Volumetric Mapping of Functional Properties at Microstructural Interfaces and Defects Luis Ortiz¹, Karla Del Cid-Ledeza¹, Jackson Kaszas¹, Ramamoorthy Ramesh², Yuanyuan Zhou³ and Bryan D. Huey¹; ¹University of Connecticut, United States; ²University of California, Berkeley, United States; ³Hong Kong Baptist University, Hong Kong

Real world capacitors, transistors, solar cells, and other devices are increasingly 3 dimensional in response to persistent demands for smaller footprints and improved energy efficiency. Microstructural features such as epitaxial interfaces, grain boundaries, composition gradients, and strain fields—whether engineered, or unavoidably resulting from fabrication constraints—are correspondingly increasingly important. In order to elucidate the influence of such traditional defects on local and even emergent properties, Tomographic Atomic Force Microscopy (TAFM) has been developed and applied for through-thickness nanoscale property mapping. Examples of normal and lateral strain effects for monolithic films, 2d heterostructures, and 3d nanocomposites are demonstrated for ferroelectrics, dielectrics, and multiferroics. Differential photoconduction at grains and grain boundaries in halide perovskite solar cells is also identified, including incorporating carrier selective architectures to directly identify any charge-dependent preferential networks. Such novel volumetric mapping of nanoscale properties is crucial for optimizing future devices.

2:00 PM *SF05.10.02

In Situ Investigation of Point Defects in Functional Materials Using Advanced Electron Probes Alejandra Guedeja-Marron¹, Francisco Fernandez-Canizares¹, Gabriel Sanchez-Santolino¹, Juan I. Beltran¹, Paolo Perna², Lucas Perez¹ and Maria Varela¹; ¹Universidad Complutense de Madrid, Spain; ²IMDEA Nanociencia, Spain

Harnessing relevant behaviors in multifunctional materials relies, now more than ever, on understanding and controlling the properties and responses of relevant point defects. The success of aberration correction in the electron microscope, in fact, has allowed electron probes to bear on this task with atomic resolution in real space and with single atom sensitivity both in imaging and spectroscopy. Recent years have also witnessed the development of specimen holders that allow modifying samples in-situ. The effects of external stimuli, such as temperature or bias, can be now explored at the flick of a switch. We are now perfectly poised to explore the presence and responses of point defects to externally applied driving forces that mimic operando conditions of future devices in detail. This talk will review examples of in-situ investigations of point defects in the scanning transmission electron microscope (STEM) in materials of interest for fields as diverse as spintronics or energy. An example can be found in the study of single Bi dopants in Cu nanowires with very low doping levels. These are very interesting systems due to the spin Hall effect associated with the presence of Bi. However, the dopant size and the presence of defects such as grain boundaries may promote Bi segregation when the temperature is raised or electric polarization is applied, which may affect the electrical performance of future devices based on these wires. Density-functional theory calculations show that for Bi doping levels below 1% the most stable dopant configuration is sitting within a Cu lattice site. Larger doping levels result in a distribution of different types of defects, being the substitutional ones the less prone to react to temperatures of a few hundred degrees C. Other point defects of interest in functional materials are vacancies. We will again combine theory, experiment and simulation to quantify and detect small concentrations of O vacancies in complex oxides. Simulations show that virtual detector optimization in 4D-STEM techniques can, in fact, lead to vacancy detection for vacancy compositions below 0.7%. Experiments including in-situ reduction processes will also be discussed. Acknowledgements: Financial support from Spanish MICINN/FEDER RTI2018-097895-B-C43 and RTI2018-099054-J-I00 is acknowledged.

2:30 PM SF05.10.03

Dephasing Dynamics of Local Vibrational Modes in Diamond Defects Detected Using Perturbed Free Induction Decay Terng Junn Keat, Daniel J. Coxon, Michael Staniforth, Vasilios G. Stavros, Mark E. Newton and James Lloyd-Hughes; University of Warwick, United Kingdom

Infrared pump-probe spectroscopy is a powerful technique used to measure the population lifetime time T_1 and the total dephasing time T_2 of vibrational energy state transitions in many functional defects. Measuring T_2 provides valuable insight into interactions between the defect of interest and its local

lattice environment. However, the standard method of extracting T_2 from equilibrium spectra uses a Voigt function fit that is often unreliable due to a large number of fit parameters and sensitivity to data quality. Perturbed free induction decay (PFID) appears in some pump-probe measurements and counter-intuitively appears at negative time delays [1]. While often ignored in vibrational energy state transition measurements, the PFID can provide useful information about the system under study. Here we present the use of PFID as a method to 1) reliably measure the dephasing times T_2 across different defect environments and for different vibrational modes and 2) predict higher energy state transitions that cannot be observed using equilibrium measurements such as Fourier Transform Infrared (FTIR) Spectroscopy.

We carry out infrared pump-probe measurements on the N_3VH diamond defect, which exhibits both stretch mode (S) and bend mode (B) vibrational energy transitions. This was done on a set of diamonds with different origins, all containing the N_3VH to explore its dephasing dynamics across different diamond lattice environments. The B mode transitions all gave $T_2 = 2.8 \pm 0.1$ ps, whereas the S mode transitions gave a faster $T_2 < 1.7$ ps and were also sample dependent. The faster dephasing given by S mode vibrations suggests that it provides a stronger coupling to crystal lattice phonons compared to the B mode vibrations. We find that S mode vibrations are also sensitive to strain in the local lattice through measuring defect concentrations in each sample. We then present a numerical model of the PFID signal, building on previous work by Yan et al. [2]. Simulating the PFID signal based on our energy level model of the N_3VH defect and the extracted T_2 shows excellent agreement with experimental data. This demonstrates the feasibility of using PFID to directly measure dephasing lifetimes.

We further carry out an infrared pump-probe measurement on the 3237 cm^{-1} absorption feature which originates from an unknown diamond defect to uncover any possible coupling between this vibrational mode and the N_3VH defect. While no transient absorption change was observed at positive time delays, a PFID signal was detected at negative delays. Analysis of this PFID signal suggested a transition involving a higher energy state, which was then found at 3030 cm^{-1} . This opens up the possibility of using PFID signals in infrared pump-probe spectroscopy to predict higher-lying energy state transitions in previously unknown defects.

[1] P. Hamm, Coherent effects in femtosecond infrared spectroscopy, *Chem. Phys.* 200, 415 (1995).

[2] S. Yan, M. T. Seidel, and H.-S. Tan, Perturbed free induction decay in ultrafast mid-IR pump-probe spectroscopy, *Chem. Phys. Lett.* 517, 36 (2011).

2:45 PM BREAK

3:15 PM *SF05.10.04

Structural Defects in Thin Films of Complex Oxide Materials Investigated by AC-STEM Nuria Bagues^{1,1}, Louise Colfer², Elahe Farghadany³, Michael Schmidt², Robert E. Williams¹, Alp Schirlioglu³, Lynette Keeney² and David McComb^{1,1}; ¹The Ohio State University, United States; ²University College Cork, Ireland; ³Case Western Reserve University, United States

Correlating defect structure and functionality through direct observation using aberration corrected electron microscopy offers a unique opportunity for functionalized, thin-film deposited nanostructures; specifically, in the case of defects originating during thin film grown processes and relaxation mechanisms. An example of such defects are misfit dislocations or twins that affect local physical properties in epitaxial thin films of complex oxides [1, 2]. Characterizing these structural defects is critical to understanding their effect on functionality, and often requires the use of complex and complementary methods. Aberration corrected scanning transmission electron microscopy (AC-STEM) provides an unparalleled method to observe and identify the crystallographic and compositional variations on the atomistic scale occurring from non-ideal deposition parameters and resulting in defects that could compromise the local physical properties. Indeed, characterizing and describing functional defect provides a potent tool for optimizing properties and predicting materials for future energy and electronic applications.

For this talk, we combine AC-STEM imaging and spectroscopy techniques to investigate structural defects and interfaces in thin films of complex oxides. Two systems of complex oxides with structural defects will be presented: (1) a multiferroic, the Aurivillius phase, $Bi_6Ti_xFe_yMn_zO_{18}$ (B6TFMO), which exhibits desired properties at room-temperature, and (2) an ionic conductor (Nd,Li) TiO_3 (NLTO). Various AC-STEM methods, such as high-angle annular dark-field (HAADF)-STEM and integrated differential phase contrast (iDPC)-STEM imaging, as well as electron energy loss spectroscopy (EELS) - spectrum imaging (SI) are used to characterize the defect structures in these systems. Combining the imaging and spectroscopy analysis, the influence of interfaces and defects on the local chemistry and physical behavior will be discussed, shedding light on the possibilities and limitations of these defects on functionality.

References:

[1] Sandiumenge *et al.* Misfit Dislocation Guided Topographic and Conduction Patterning in Complex Oxide Epitaxial Thin Films. *Advanced Materials Interfaces* 3 (14, 1600106) (2016).

[2] Balcells *et al.* Enhanced conduction and ferromagnetic order at (100)-type twin walls in $La_{0.7}Sr_{0.3}MnO_3$ thin films, *Physical Review B* 92, (7, 075111) (2015).

3:45 PM *SF05.10.05

Characterizing and Exploiting Topological and Point Defects in Ferroelectric Thin Films—Optimizing Electromechanical Response and Investigating Energy Landscapes with Automated Experiments Kyle P. Kelley¹, A. Borisevich¹, A.N. Morozvska², V. Sharma³, J.C. Yang⁴, Panchapakesan Ganesh¹, Stephen Jesse¹, Sergei V. Kalinin³ and Rama K. Vasudevan¹; ¹Oak Ridge National Laboratory, United States; ²National Academy of Sciences of Ukraine, Ukraine; ³The University of Tennessee, Knoxville, United States; ⁴National Cheng Kung University, Taiwan

The static and dynamic properties of ferroelectric thin films are heavily impacted by the presence and distribution of both point- and topological defects. Harnessing and controlling these factors has been critical to improving the dielectric and electromechanical properties of ferroelectric thin films [1,2]. However, many of the mechanisms that associate functional properties with changes to material properties are still difficult to pinpoint, and their effects at the nanoscale are still poorly understood in many cases [3].

In this talk, we will discuss our work on studying and characterizing both point- and topological defects in ferroelectric thin films. First, we explore the ability to dynamically modify the electromechanical response of defective $BaTiO_3$ thin films [4], via injection of vacancies in ultra-high vacuum environments by the scanning probe tip. Multiple lines of evidence from detailed piezoresponse force spectroscopy and atomic resolution imaging via scanning transmission electron microscopy are used to measure the local structure and functionality of these films. A strong environmental dependence on the local dynamics is found on the piezoresponse as a function of field cycling. These measurements are corroborated by thermodynamic, first-principles and reactive force field calculations, which point towards a mechanism of increased electromechanical response engendered by dynamic injection of vacancies in the scanning probe volume.

At the same time, topological defects such as domain walls and vortices can also be critical to understanding and modifying the dielectric and piezoelectric properties of thin films [5]. We discuss a newly developed automated experiment framework that explores the interplay between grain boundaries, domain switching, and domain wall de-pinning, to attempt to quantitatively measure the impact of local domain structure and longer-range elastic fields on the dynamics of topological defects in a model $PbTiO_3$ thin film grain boundary. Preliminary reinforcement learning methodologies to optimize the domain

wall geometries will be discussed. This work was supported by the Center for Nanophase Materials Sciences (CNMS), which is a US Department of Energy, office of Science User Facility at Oak Ridge National Laboratory.

References

- [1] N. Setter, et al. *Journal of applied physics* 100.5 (2006): 051606.
- [2] A. J. Bell, P. M. Shepley and Y. Li. *Acta Materialia* 195 (2020): 292-303.
- [3] R. K. Vasudevan et al. *Advanced Functional Materials* 23.1 (2013): 81-90.
- [4] K. P. Kelley et al. *Advanced Materials* 34.2 (2022): 2106426.
- [5] G. F. Nataf et al *Nature Reviews Physics* 2.11 (2020): 634-648.

4:15 PM SF05.10.06

Operando Investigation of the Gas Sensing Mechanisms in SnO₂, Sn₃O₄ and SnO Nanomaterials [Pedro H. Suman](#)^{1,2}, Benjamin Junker², Udo Weimar², Nicolae Barsan² and Marcelo Orlandi¹; ¹São Paulo State University (UNESP), Brazil; ²University of Tübingen, Germany

Semiconducting metal oxides (SMOx) have been the most used sensing materials for detecting multiple gaseous compounds over the last decades. However, fundamental questions concerning the surface reactions responsible for their performance still need further comprehension. In this context, operando techniques can provide insights into surface chemistry and electronic properties of chemoresistive gas sensors in working conditions. Here, a phenomenological study of the sensing mechanism of single-crystalline SnO₂, Sn₃O₄, and SnO nanobelts is presented by using operando Diffuse Reflectance Infrared Fourier Transform (DRIFT) spectroscopy. DRIFT spectra and DC resistance measurements were recorded simultaneously in the presence of multiple target gases, including H₂, CO, NO₂, ethanol, and acetone, at 200°C and 300°C. The influence of water vapor adsorption in the background atmosphere was also analyzed. This study allowed the real-time monitoring and identification of the adsorbed species on the surface of the sensing layer and their impact on the output electrical signals in each experimental condition. Based on the results, detection mechanisms were proposed for these tin oxide nanostructures with different oxygen stoichiometries. The results are particularly interesting for Sn₃O₄ and SnO materials, which are less studied than SnO₂.

Acknowledgement: This work is supported by the São Paulo Research Foundation (FAPESP), grant #2016/20808-0, grant #2019/26333-2, and grant #2013/07296-2.

- [1] P.H. Suman, A.A. Felix, H.L. Tuller, J.A. Varela, M.O. Orlandi, *Sens. Actuators B Chem.* 208, 122 (2015).
- [2] S. Wicker, M. Guiltat, U. Weimar, A. Hemeryck, and N. Barsan, *J. Phys. Chem. C* 121, 25064 (2017).
- [3] D. Degler, B. Junker, F. Allmendinger, U. Weimar, and Nicolae Barsan, *ACS Sens.* 5, 3207 (2020).

SESSION SF05.11: Virtual Session I: Harvesting Defect in Halide Perovskites
Session Chairs: Hua Zhou and Yuanyuan Zhou
Tuesday Morning, December 6, 2022
SF05-virtual

8:00 AM *SF05.11.01

Smart Additive and Interface Engineering to Achieve Perovskite Solar Cells with High Efficiency and Stability, and Efficient Capturing of Degraded Pb-Containing By-Products [Alex K. Jen](#)^{1,2}; ¹City University of Hong Kong, Hong Kong; ²University of Washington, United States

Minimizing energy loss and improving stability are the key aspects to transcend the current limitations on the performance of perovskite photovoltaics (PVSC). Our recent study combining additive and interface engineering to dramatically improve the efficiency and long-term operational stability of the PVSCs. By introducing a non-volatile additive functioning both as crystallization modulator and defects passivator, high power conversion efficiency and stability can be achieved simultaneously. In addition, innovative methods have also been developed to efficiently trap decomposed Pb-containing by-products for solving the very challenging environmental issue in PVSCs for facilitating their commercialization.

This talk is divided into two parts: (1) Progress of achieving the highest efficiency (24.8%) in inverted planar junction perovskite solar cells (PVSCs) through smart interface engineering using 0D, 1D, and 2D perovskites; (2) Demonstration of simultaneously achieving high PCE, excellent operational stability, and the ability to capture degraded Pb-containing by-products using efficient and very low cost cation exchange resins and sulphonated graphene aerogels for PVSC encapsulation

8:30 AM *SF05.11.02

Inactive Secondary Phase Stabilizes Perovskite for Efficient Solar Cells [Jingbi You](#); Chinese Academy of Sciences, China

In halide perovskite solar cells, the formation of a secondary phase of excess lead iodide has little effect on power conversion efficiencies (PCEs), but can be detrimental to device stability and lead to large hysteresis effects in voltage sweeps. We converted lead iodide into inactive secondary phase, which effectively stabilizes the perovskite. We obtained a certified PCE of 25.6% for FAPbI₃ perovskite solar cells based on this strategy. Devices retained 96% of their original PCE values after 1000 hours shelf storage and 80% after 500 hours of thermal stability testing at 85 Celsius .

9:00 AM *SF05.11.03

High Efficiency Tin Perovskite Solar Cells [Zhijun Ning](#); ShanghaiTech University, China

The development of high performance lead free perovskite solar cells (PSCs) is important to address the environmental concern of heavy metal lead. In recent years, tin perovskite solar cell (TPSCs) is developing quickly and emerging as a promising candidate for high efficiency lead free PSCs. Meanwhile, the narrow bandgap of tin perovskite solar cells enables it potential to be used for the fabrication of tandem solar cells. In this presentation, I will summarize recent work of our group about tin perovskite solar cells, including the introduction of low-dimensional structure, crystal growth kinetic control to manipulate its nanostructure and orientation, as well as device structural engineering to reduce interface carriers recombination. Based on these efforts, the highest efficiency of tin perovskite solar cells is up to 14.6% that is certified in an independent agency. In addition, the fabrication of low dimensional inorganic tin perovskite solar cells will be introduced, as well as the construction of bilayer structure on film surface to reduce carriers recombination.

9:30 AM SF05.11.04

X-Ray Ptychographic Tomography of Morphological Defects in Metal Halide Perovskites [Yalan Zhang](#)¹, Mingwei Hao¹, Hua Zhou², Junjing Deng² and Yuanyuan Zhou¹; ¹Hong Kong Baptist University, Hong Kong; ²Argonne National Laboratory, United States

Perovskite-based solar cells (PSCs) are considered a disruptive photovoltaic technology with their power conversion efficiency rapidly climbing to certified 25.7%. To exploit its maximum potential, the microstructure and morphological defects of metal halide perovskites (MHPs) must be fully characterized, understood, and then tailored. Recently, X-ray ptychography has emerged as a new imaging technique that can combine advantages of coherent X-ray diffractive imaging and conventional scanning transmission X-ray microscopy techniques. With the latest development, it can achieve 3D tomography of materials structures with a high resolution of sub-10 nm while it may cause little damage on soft material samples compared to another characterization tool. Here I will present our recent achievement leveraging X-ray ptychographic imaging to characterize MHPs, revealing various 3D structural defects fully or partially buried underneath the surface. We demonstrate X-ray ptychography as a new, powerful, non-intrusive characterization method for illuminating the complete microstructure of perovskites for energy applications.

References

[1] Y. Zhang, M. Hao, H. Zhou, J. Deng, Y. Zhou, J. Energy Chem. *in press*.

9:45 AM SF05.11.05

Spin Dynamics of Low Sodium Type-II Silicon Clathrates [Joseph Briggs](#)¹, Yanan Liu¹, Ahmad A. A. Majid¹, Justin Johnson², P. Craig Taylor¹, Meenakshi Singh¹, Reuben T. Collins¹ and Carolyn A. Koh¹; ¹Colorado School of Mines, United States; ²National Renewable Energy Laboratory, United States

In this work we examine the relaxation and coherence times of Na in silicon clathrate thin films for potential use in quantum applications. Diamond silicon (d-Si) is under active investigation as a quantum material motivated to a large extent by the depth of knowledge surrounding this material and its dominant position in microelectronics. Type II silicon clathrate represents an interesting alternative Si crystal structure. This cage-like inclusionary compound is made up of a silicon lattice with interstitial “guests” such as sodium situated inside the cages. The Na atoms, which are decoupled from the lattice, act as shallow donor atoms and are potential qubits. In addition, unlike d-Si, type II Si clathrate has a direct or quasi-direct bandgap which may allow easier optical access to Na electronic states which makes it of interest as a potential material for microelectronics, LEDs, and solar cell applications. Most reported studies of silicon clathrate have utilized powders. Powders, however, are not the preferred form factor for optoelectronic studies or transport measurements and the measurements reported here use low Na content, type II Si clathrate films. To synthesize these materials, a two-step procedure adapted from powder synthesis has been developed. First, sodium is evaporated from a crucible and diffused into a silicon wafer under an inert gas atmosphere to form NaSi. The wafer is then annealed under vacuum to thermally decompose the film into clathrate. The clathrate films are then characterized through a variety of techniques including x-ray diffraction, Raman spectroscopy, scanning electron microscopy, photoluminescence, and, of particular importance to this study, continuous wave and pulsed electron paramagnetic resonance (EPR). EPR gives insight into the electronic properties of the Na donors and their placement and interactions within the silicon cages. The naturally occurring Na isotope, ²³Na, has nuclear spin 3/2 with the EPR spectrum exhibiting four hyperfine lines associated with the interaction of the electronic and nuclear spins. Hyperfine features associated with Na atoms in neighboring cages and clustered Na are also observed as well as a dangling bond signature indicative of a minority phase of disordered Si. Pulsed-EPR spectra clearly exhibit spin echo signals with T1 times in the microsecond regime at temperatures near 10K. By probing the spin echo’s of specific Na hyperfine interactions, we have gained insight into the relaxation and coherence times of electron spins bound to the Na of low Na doped type-II silicon clathrates. The effects of various parameters (i.e. temperature, pulse duration, magnetic field center) on the relaxation and coherence times are also explored. Results of this work provide new understanding of the spin properties of Na in Si clathrates and provides useful insights into the potential use of Na in Si clathrate as a qubit material. This work was supported by National Science Foundation award #2114569.

9:50 AM DISCUSSION TIME

SESSION SF05.12: Virtual Session II: Harvesting Defect in Functional Perovskites
Session Chairs: Zhijun Ning and Yuanyuan Zhou
Tuesday Morning, December 6, 2022
SF05-virtual

10:30 AM *SF05.12.00

Exploiting Functional Defects in Epitaxial Oxide Thin Films for Giant Piezoelectricity and Synaptic Electronics [Huajun Liu](#); Institute of Materials Research and Engineering, A*STAR, Singapore, Singapore

Transition metal oxide thin films exhibit many interesting properties, including superconductivity, ferroelectricity, piezoelectricity and electrochemical activities for energy applications. Defects, such as oxygen vacancies, have long been known to be detrimental to certain functional properties of oxide thin films. However, by properly designing and controlled synthesis, the defects can be beneficial and even greatly improve the functional properties. In this talk, I will discuss our recent work on the giant piezoelectricity and memristive behaviour induced by antisite defects in NaNbO₃ (NNO) epitaxial thin films. Through precise control of Na deficiency, Nb atoms occupy vacant Na positions and form the Nb_{Nb} antisite defects in NNO films. These antisite defects self-assembled to form vertical nanopillar structures. Such nanopillar regions with local structural and polar heterogeneity give rise to giant piezoelectric coefficients while maintain a high Curie temperature (Science, 369, 292, 2020). The antisite defects also induce resistive switching behaviour and tunable resistance states by electric field. The NNO film based devices exhibit synaptic plasticity under applied electrical pulses, promising for the application in neuromorphic computing.

11:00 AM *SF05.12.01

Controlling Defect-Assisted Nonradiative Recombination in Halide Perovskites [Chris G. Van de Walle](#); University of California, Santa Barbara, United States

Halide perovskites offer impressively high solar conversion efficiencies and are being considered for applications as light emitters. These materials are often called “defect tolerant”, but we show that the impact of point defects on device efficiency has not been properly assessed to date. We have performed comprehensive studies for the prototypical hybrid perovskite MAPbI₃ [MA=(CH₃NH₂)], as well as for other halide perovskites. To achieve accurate and reliable results, our first-principles calculations are based on hybrid density functional theory with spin-orbit coupling included [1]. Rigorous calculations of nonradiative recombination coefficients show the limitations of the widely adopted rule that only defects with charge-state transition levels deep in the

band gap can be efficient nonradiative recombination centers. We demonstrate that the position of the level does not directly determine the capture rates, due to strong lattice coupling and anharmonicity in the halide perovskites [2]. Our results clearly show that (1) point defects can indeed be present in relevant concentrations in the halide perovskites and (2) some of these point defects lead to nonradiative recombination rates that are just as high as in conventional semiconductors. We therefore conclude it is incorrect to call the halide perovskites “defect tolerant”. A more relevant distinction, compared to conventional semiconductors, is that halide perovskites with modest defect densities can be grown using low-cost deposition techniques. For MAPbI₃ the results indicate that iodine interstitials are most harmful, and hence iodine-rich synthesis conditions should be avoided. Experimental reports have indicated, however, that iodine-poor conditions are also detrimental. We explain this puzzle by demonstrating that iodine-poor conditions lead to formation of hydrogen vacancies on the MA molecule, which act as very efficient nonradiative recombination centers [3]. By contrast, hydrogen vacancies are not a problem in FAPbI₃ [FA=CH(NH₂)₂], rationalizing why FA is essential for realizing high efficiency in hybrid perovskites. Our findings also indicate the advantages of avoiding the organic cation altogether [4]. We show that the common belief that the organic cation suppresses defect-assisted nonradiative recombination is unfounded. Our study suggests that all-inorganic halide perovskites hold great promise for high-efficiency optoelectronic applications.

Work performed in collaboration with X. Zhang, M. Turiansky, and J.-X. Shen, and supported by DOE.

[1] X. Zhang, M. E. Turiansky, J.-X. Shen, and C. G. Van de Walle, *Phys. Rev. B* **101**, 140101 (2020).

[2] X. Zhang, M. E. Turiansky, and C. G. Van de Walle, *J. Phys. Chem. C* **124**, 6022 (2020).

[3] X. Zhang, J.-X. Shen, M. E. Turiansky, and C. G. Van de Walle, *Nat. Mater.* **20**, 971 (2021).

[4] X. Zhang, M. E. Turiansky, and C. G. Van de Walle, *Cell Rep. Phys. Sci.* **2**, 100604 (2021).

11:30 AM SF05.12.02

High Throughput Optical Measurements and Machine Learning Analysis of Hybrid Perovskites [Abigail Hering](#), Meghna Srivastava and Marina S. Leite; University of California, Davis, United States

Hybrid organic-inorganic perovskites are an emerging class of materials for energy-efficient devices. Intriguingly, their high density of defects has not prevented this material from presenting nearly optimal optical properties for light-absorbing and -emitting application. A primary challenge to commercialize optoelectronics based on hybrid perovskites lies on the lack of material stability. To advance the understanding of the role of environmental stressors in the optical behavior of perovskites, we implement high-throughput steady-state environmental photoluminescence (PL) while exposing the samples to distinct levels of temperature and relative humidity. Then, we use these measurements to compare the performance of linear regression, Echo State Network (ESN), and Auto-Regressive Integrated Moving Average with eXogenous regressors (ARIMAX) machine learning algorithms when predicting the PL response of perovskites with variable chemical composition. While linear regression is not adequate to forecast PL (with average normalized root mean square error, NRMSE, >20%), both ESN and ARIMAX enable reliable predictions, with NRMSE < 16% and 8%, respectively. Overall, our results indicate the promise of machine learning to accelerate the development of stable perovskites. Further, the paradigm presented here can be extended to other perovskites families.

11:45 AM SF05.12.03

Halide Perovskite Mem-Emitter for Analog Salience Processing [Si En T. Ng](#); Nanyang Technological University, Singapore

To sense is the ability to extract critical information from the environment. However, in a realistic scenario, we are often exposed to a myriad of stimuli at the same time. To effectively scan across them, the objects in the image can be processed based on their saliences and a set of regulatory equations. Since these differential equations are dependent on inputs from the near history, processing them sequentially with digital computers (physically separated memory and processing units) would be very inefficient. Analog computing in modern applications is revisited for its efficient use of resources (power and footprint). To emulate the neuronal processes in analog fashion, the three device functionalities required are the interconnectivity, distinct wavelengths and the temporal dependencies of the transmission. In contrast to electrical physical wiring, higher levels of interconnectivity can be achieved by emitter-based systems processing information with light as the transmission medium. Here, we fabricated a mem-emitter (memory emitter) device comprising of an organic emitter and a perovskite emitter. The mem-emitter device has dual distinct emission wavelengths. Initially, the red organic emitter is first activated due to the small recombination zone spatially located at the organic emitter layer. However, with repeated electrical pulsing, ionic drift in the halide perovskite layer results in the widening of the recombination zone, enabling the green perovskite layer to emit. As a result, the emission spectra from the device not only depends on the present input but also the operational history of the device as well. We first studied the widening of the recombination zone; both the electroluminescence and photoluminescence spectra of the bilayer stack are compared. Interestingly, the photoluminescence spectra did not exhibit any emission from the red organic emitter. This highly suggests that the color change is not due to reabsorption but a spatial shift in recombination zone. Furthermore, we have optimized the pulse operation conditions for the mem-emitter device, achieving a dynamic gain of 470% in the green emission. Finally, we showcase two use cases of our mem-emitter device in analog temporal processing. Firstly, the temporally dependent green emission represents the self-inhibitory process in a salience processing network. For the first time, with a physical circuit comprising of mem-emitters and photodiodes, we managed to emulate inhibition of return - a key adaptive functionality in salience processing. Secondly, we utilize an array of mem-emitter devices as a physical salience heatmap display for the first time. With optimized pulse schemes, our mem-emitter array is capable of encoding analog salience values into distinct emissive colors – red, orange and green. With its dynamic temporal memory, the proposed dual wavelength mem-emitter device offers significant advantages in efficient salience processing with fewer components and smaller energy consumption.

12:00 PM SF05.12.05

Atomistic Solution to the Doping Bottleneck in Compound Semiconductors [Olivier C. Gagné](#); Carnegie Institution for Science, United States

Activation and tuning of the useful properties of semiconductors intended for photovoltaic, electronic, electrochemical and other applications hinges on their successful release of charge carriers, a process typically achieved in appreciable quantity via substitutional incorporation of foreign ions into the host crystal structure. As it stands, the rate-limiting step in designing efficient semiconductors is the identification of the most viable dopant ions to achieve n- and/or p-type conductivity – a process severely clouded by our incomplete understanding of chemical bonding behavior in solids. Today, doping studies rely exclusively on resource-intensive first-principles calculations, with little chemical guidance available to computationalists on where to focus their resources. An atomistic understanding of the factors underlying ion substitutions in solids would provide such guidance, and would further enable rapid calculations to be made for host/dopant combinations prior to their synthesis in lieu of expanding costly resources in low-return compositional spaces.

Three major factors underlie doping difficulties in semiconductors: [1] dopant insolubility, [2] dopant un-ionizability, and [3] dopant compensation. Factor [3] is terminal whereby formation of compensated defects is caused by the charge carrier itself, and not the identity of the dopant. However, difficulties associated with factors [1] and [2] may be circumvented via appropriate dopant selection, whose ease of substitution in the host crystal structure dictates dopant level depth in the band structure. Factors known to influence dopant level depth include similarities in atomic orbital energies, size of the

substituting ions, and local bonding geometry – all of which amenable to guidance via an adequate, systematized understanding of crystal-chemical behavior.

By and large, the primary reason underlying our inability to model ion substitution in solids (and therefore semiconductor doping) has been our collective failure to systematically describe, rationalize and quantify pairwise chemical bonding behavior across the periodic table of elements. We recently remediated to this problem via wide-scale analysis of chemical bonding in solids in the form of bond-length dispersion analyses. Results were reported for cations bonded to O²⁻ and N³⁻,^[1] covering 177,446 reliable bond lengths hand-picked from 9210 crystal-structure refinements for oxides, and 6,770 bond lengths from 720 crystal-structure refinements for nitrides; equivalent analysis for cations bonded to S²⁻, Se²⁻ and Te²⁻ is underway. These data were subsequently used to identify and quantify structural, electronic and/or bond-topological mechanisms underlying anomalous bonding behavior across the periodic table.

Having quantified the most elusive of crystal-chemical variables for the very first time, i.e. chemical bonding behavior, we successfully developed an atomistic model of ion substitution which instantaneously and quantitatively predicts solubility limits between ion configurations at ambient conditions. Our model quantitatively reproduces doping profiles for all popular compound semiconductors (e.g. III-V, II-VI semiconductors), and can further make instantaneous predictions for the doping of ternary, quaternary and higher-dimensional systems. Thus, our model resolves the doping bottleneck in compound semiconductors while enabling the pursuit of complex, bespoke semiconductor design with bulk properties adapted to end-user needs.

References:

[1] Gagné, O. C. & Hawthorne, F. C. (2016). *Acta Cryst.* B72, 602-625; Gagné, O. C. (2018). *Acta Cryst.* B74, 49-62; Gagné, O. C. & Hawthorne, F. C. (2018a). *Acta Cryst.* B74, 63-78; Gagné, O. C. & Hawthorne, F. C. (2018b). *Acta Cryst.* B74, 79-96; Gagné, O. C. & Hawthorne, F. C. (2020). *IUCrJ* 7, 581-629; Gagné, O. C. (2021). *Chem. Sci.* 12, 4599-4622.

12:15 PM DISCUSSION TIME

SESSION SF05.13: Virtual Session II: Harvesting Defect in Functional Oxides
Session Chairs: Panchapakesan Ganesh and Hua Zhou
Wednesday Morning, December 7, 2022
SF05-virtual

8:00 AM *SF05.13.01

Atomic Site HAADF-STEM and EELS of Complex Oxides Thin Films—The Role of Oxygen Vacancies Regina Ciancio; CNR-IOM, Italy

Complex oxides are fascinating systems which host a vast array of unique phenomena, such as high temperature (and unconventional) superconductivity, ‘colossal’ magnetoresistance, all forms of magnetism and ferroelectricity, as well as (quantum) phase transitions and couplings between these states. The recent years have witnessed considerable achievements in the ability to grow thin film heterostructures of these materials with atomic precision. With this level of control, the electrostatic boundary conditions at oxide surfaces and interfaces can be used to form new electronic phases or novel low-dimensional states at the interfaces inaccessible in bulk oxides. Oxygen vacancies play crucial roles in determining the physical properties of metal oxides and controlling and manipulating the defect structure provides a degree of freedom for harvesting and tailoring the functional properties of oxides. This is the case of anatase titanium dioxide TiO₂, where the formation of oxygen vacancies has been proved to effectively tune the amount of Ti³⁺ ions [1-2] and to extend the photoresponse of TiO₂ from the UV towards the visible-light region [3].

The correlation between the functional and atomic scale properties requires a detailed analysis by local probe techniques with advanced capabilities, allowing the accurate determination of the atomic positions, the chemical composition and the electronic state with atomic resolution. In this regard, aberration-corrected STEM and the possibility to couple STEM imaging (in Z-contrast or Annular Bright Field) and EELS spectroscopy enables to determine the chemistry, crystal and electronic structure of new materials locally, with atomic resolution, and often in a quantitative way by the smart combination of imaging and spectroscopy.

This lecture will review the tremendous impact of having access to atomic resolution HAADF-STEM, complemented by spectroscopic analysis, atomistic calculations and multislice simulation of atomic resolution STEM in oxide thin films. The case of anatase TiO₂ thin films will be described, where oxygen vacancies are observed to form arrays of ordered superstructures with varying oxygen content which reflect into a Ti^{3+/Ti⁴⁺} mixed population [4]. The combination of atomically resolved STEM-EELS along with extensive atomistic and multislice simulations lead to the validation of a new model for the defect structures in anatase that excludes the typical shear-plane structures, like the Ti_nO_{2n-x} Magnéli phases, which are commonly claimed to occur in titanium dioxide. The relevant case of La_{0.7}Sr_{0.3}MnO₃ thin films will also be discussed where the evidence of a structural shift of Mn ions correlated with the reduction of Mn valence state is found to be correlated with the preferential formation of oxygen vacancies at the interface with the substrate [5]. In both the cases, the identification of secondary structures as well as the determination of the intrinsic structure of oxygen defects is a crucial step to improve the functionalities of such material systems and to open up new options to engineer devices with targeted properties.

References

[1] Role of Oxygen Deposition Pressure in the Formation of Ti Defect States in TiO₂(001) Anatase Thin Films, *ACS Appl. Mater. Interfaces* 2017, 9, 23099–23106
[2] Distinct behavior of localized and delocalized carriers in anatase TiO₂ (001) during reaction with O₂, *Phys. Rev. Mater.* 4, 025801 (2020)
[3] Tuning the Optical Absorption of Anatase Thin Films Across the Visible-To-Near-Infrared Spectral Region, *Phys. Rev. Appl.* 2020, 13, 044011
[4] Unveiling Oxygen Vacancy Superstructures in Reduced Anatase Thin Films, *Nano Lett.* 2020, 20, 6444–6451
[5] Evidence of Mn-Ion Structural Displacements Correlated with Oxygen Vacancies in La_{0.7}Sr_{0.3}MnO₃ Interfacial Dead Layers, *ACS Appl. Mater. Interfaces* 2021, 13, 46, 55666–55675

8:30 AM *SF05.13.03

Effect of Polaron Formation on Optical and Carrier Transport Properties of Transition Metal Oxides as Photoelectrodes from First-Principles Calculations Yuan Ping; University of California Santa Cruz, United States

Transition metal oxides are promising photoelectrode materials for solar-to-fuel conversion applications. However, their performance is limited by the low carrier mobility due to the formation of small polarons. Recent experimental studies have shown improved carrier mobility and conductivity by atomic doping; however the underlying mechanism is not understood. A fundamental atomistic-level understanding of the effects on small polaron transport is

critical to future material design with high conductivity. In this talk, we will discuss the effect of small polaron formation on optical and carrier transport properties of transition metal oxides from first-principles calculations. First, we resolve the conflicting findings that have been reported on the optical gap of a well-known catalysis Co_3O_4 as an example [1]. We confirm that the formation of small hole polarons significantly influences the optical absorption spectra and introduces extra spectroscopic signature below the intrinsic band gap, leading to a 0.8 eV transition that is often misinterpreted as the band edge that defines the fundamental gap.

Then we discuss the formation of small polarons' effect on carrier concentration, by resolving the controversy of nature of "shallow" or "deep" impurities of intrinsic oxygen vacancies in BiVO_4 as an example [2], i.e. how to unify different experiments with the correct definition of ionization energy in polaronic oxides. We further discuss why certain dopants can have very low optimal concentrations (or very early doping bottleneck) in polaronic oxides such as Fe_2O_3 , through a novel "electric-multipole" clustering between dopants and polarons [3]. These multipoles can be very stable at room temperature and are difficult to fully ionize compared to separate dopants, and thus they are detrimental to carrier concentration improvement. This allows us to uncover mysteries of the doping bottleneck in hematite and provide guidance for optimizing doping and carrier conductivity in polaronic oxides toward highly efficient energy conversion applications. In addition, we show the importance of synthesis condition such as synthesis temperature and oxygen partial pressure on dopant and polaron concentrations, and how to optimize the synthesis condition based on theoretical predictions [4].

At the end, we show different theoretical models for polaron mobility calculations from a macroscopic dielectric continuum picture with an example of spin polarons in CuO [5] and a microscopic polaron hopping picture by combining generalized Landau-Zener theory and kinetic Monte-Carlo samplings for doped oxides [6]. Our first-principles calculations provide important insights and suggest design principles for optimal optical and transport properties of polaronic oxides.

References:

- [1] "Optical Absorption Induced by Small Polaron Formation in Transition Metal Oxides – The Case of Co_3O_4 ", T. Smart, T. Pham, Y. Ping*, and T. Ogitsu*, *Physical Review Materials (Rapid Communications)*, **3**, 102401(R), (2019).
- [2] "The Role of Point Defects in Enhancing the Conductivity of BiVO_4 ", H. Seo, Y. Ping and G. Galli*, *Chemistry of Materials*, **30**, 7793, (2018).
- [3] "Doping Bottleneck in Hematite: Multipole Clustering by Small Polarons", T. Smart, V. Baltazar, M. Chen, B. Yao, K. Mayford, F. Bridges, Y. Li, and Y. Ping*, *Chemistry of Materials*, **33**, 4390, (2021).
- [4] "The Critical Role of Synthesis Conditions on Small Polaron Carrier Concentrations in Hematite- A First-Principles Study", Tyler Smart, Mingpeng Chen, Valentin Urena Baltazar, Frank Bridges, Yat Li, Yuan Ping*, *Journal of Applied Physics*, **130**, 245705, (2021).
- [5] "Mechanistic Insights of Enhanced Spin Polaron Conduction in CuO through Atomic Doping", T. Smart, A. Cardiel, F. Wu, K. Choi and Y. Ping*, *npj Computational Materials*, **4**, 61, (2018).
- [6] "Combining Landau-Zener Theory and Kinetic Monte Carlo Sampling for Small Polaron Mobility of Doped BiVO_4 from First-principles", F. Wu and Y. Ping*, *Journal of Materials Chemistry A*, **6**, 20025, (2018).

9:00 AM DISCUSSION TIME

SYMPOSIUM SF06

Defect and Disorder-Driven Material Transport Properties and Functionalities
November 28 - December 6, 2022

Symposium Organizers

Cody Dennett, Massachusetts Institute of Technology
Marat Khafizov, The Ohio State University
Lucas Lindsay, Oak Ridge National Laboratory
Zhiting Tian, Cornell University

* Invited Paper
+ Distinguished Invited

SESSION SF06.01: Nitrides
Session Chairs: Cody Dennett and Navaneetha Krishnan Ravichandran
Monday Morning, November 28, 2022
Sheraton, 3rd Floor, Fairfax A/B

10:30 AM *SF06.01.01

Understanding Extrinsic and Intrinsic Anisotropic Heat Transport in Crystalline Materials Yee Kan Koh; National University of Singapore, Singapore

Although thermal transport in cubic crystals is isotropic, thermal transport could be highly anisotropic, depending on crystallographic orientations. The anisotropy in thermal transport could originate from either intrinsic (e.g., crystal structures) and extrinsic (e.g., defects) factors. In this talk, I will present

our recent works that advance the fundamental understanding of intrinsic and extrinsic anisotropy in thermal transport in crystalline materials. I will first discuss the anisotropy thermal transport in single-crystal InN films induced by dislocations. I will report strong thermal transport anisotropy governed by highly oriented threading dislocation arrays along the cross-plane direction in micron-thick, single-crystal indium nitride (InN) films. We find that the cross-plane thermal conductivity is more than tenfold higher than the in-plane thermal conductivity at 80 K when the dislocation density is on the order of $\sim 3 \times 10^{10} \text{ cm}^{-2}$. This large anisotropy is not predicted by the conventional models. With enhanced understanding of dislocation-phonon interactions, our results open new regimes for tailoring anisotropic thermal transport with line defects, and will facilitate novel methods for directed heat dissipation in thermal management of diverse device applications. Then, I will discuss the intrinsic thermal transport anisotropy in layered, two-dimensional (2D) crystals such as black phosphorus (BP) and MoTe_2 . We find that the anisotropy in the cross-plane direction behaves differently from the anisotropy in the in-plane directions. We find that, contradictory to common beliefs, anisotropy in the heat capacity and relaxation times also contribute significantly to the overall anisotropy in thermal transport. We will discuss the origin of the anisotropy in more details in the talk.

11:00 AM SF06.01.02

Chemical States and Bandgap Energy of Thin and Ultra-Thin Titanium Nitride Thin Films [Manosi Roy](#)¹, Kaushik Sarkar¹, Jacob Som¹, Abiodun Odusanya¹, Mark A. Pfeifer², Darrah Dare², Valentin Craciun³ and Dhananjay Kumar¹; ¹North Carolina A & T State University, United States; ²Cornell University, United States; ³National Institution for Laser, Plasma and Radiation Physics, Romania

Singly crystalline titanium nitride (TiN) and partially oxidized titanium nitride (TiNO_x) thin films have been grown in a rock-salt structure on sapphire substrates using high vacuum conditions during pulsed laser deposition (PLD). The film thickness was varied in the length scale from a few unit cells to several unit cells. X-ray photoelectron spectroscopy (XPS) analysis has shown that oxygen content of the TiNO_x films increases with film thickness (or deposition time), which in turn, affects the exposure time of the ablated materials to the residual oxygen in the deposition chamber (the source of TiN oxidation). The lattice constant of the TiNO_x films, measured using XRD, is found to increase with the oxygen content in the film that is validated by the density functional theory (DFT) calculations. The lattice constant increase is explained using enhanced electrostatic repulsion between O^{2-} orbitals in the absence of vacant Ti^{3+} sites; in order to maintain charge neutrality within the lattice, one Ti^{3+} cation vacancy is created for every three substitutions of N^{3-} ions by O^{2-} ions. We have observed an asymmetric 'V' shape variation in the optical bandgap as a function of film thickness. The bandgap values decreased from 3.89 eV to 3.30 eV as the film thickness increased from 1.5 nm to 4 nm and then increased from the minimum of 3.30 eV to 3.87 eV as the film thickness increased from 4 nm to 30 nm. The bandgap variation following the left arm of the V-curve is attributed to the quantum confinement effect, while the variation of the bandgap following the right arm of the V-curve is believed to be associated with the increased defects density of the Ti^{3+} cations that is caused by the charge imbalance in the TiNO_x lattice due to partial substitution of N^{3-} by O^{2-} ions.

11:15 AM *SF06.01.03

Thermal Characterisation of Nanoscale Wide Bandgap Transistors Martin Kuball and [James W Pomeroy](#); University of Bristol, United Kingdom

Wide bandgap RF and power electronic devices are needed to meet future efficiency and performance requirements, providing ultra-high areal power densities. "Conventional" wide bandgap transistors, with 100's nm sized channel hot spots, are already thermal limited, driving the development of new thermal management solutions such as GaN-on-diamond. However, the thermal dissipation problem is now being amplified by the development of scaled devices, such as finFETs, SLCFETs, nanowire transistors, etc., where channel sizes and layer thicknesses are less than the bulk phonon mean free path, which suppresses thermal conductivity, increasing thermal resistance. Bulk thermal properties can no longer be assumed for <100's nm-sized structures, making thermal simulation results more uncertain; this is also true for thin films and superlattices. We examine two case studies: SLCFETs (RF switches) and thin-GaN HEMTs, which deliver improved electrical performance, but have thermal dissipation trade-offs. We use a combination of Raman nanoparticle thermometry, thermoreflectance and thermal simulation to illustrate how feature sizes influence thermal dissipation and how structures can be thermally optimised. We discuss how peak temperatures in highly scaled devices cannot be measured directly with existing optical thermography techniques and the critical need for nanoscale thermal imaging, motivating the development of super-resolution quantum-dot thermal imaging (QTI), to beat the diffraction limit.

11:45 AM SF06.01.04

Quantifying the Effects of Disorder on Mobility of Nitride Semiconductors [Robert Makin](#), Krystal R. York, Andrew S. Messecar and Steven Durbin; Western Michigan University, United States

Measuring the degree of disorder within crystalline samples began in the early 1930s with Bragg and Williams, who developed the order parameter S —which ranges from 0 (disordered) to 1 (ordered)—to quantify the degree of disorder in binary metal alloys. Recently, we have extended their x-ray diffraction based methodology to measure S from Raman spectra, reflection high-energy electron diffraction patterns (RHEED) and electron microscopy images. Quantifying the degree of disorder in samples allows for relationships to be uncovered between the order parameter and property of materials. In fact, for system-level properties that are dominated by pair-wise interactions, it can be shown using cluster expansion theory in combination with spin modeling that these properties have a linear dependence on S^2 . Recently, we have experimentally verified this relationship holds for band gaps of semiconductors ranging from 2D to heterovalent ternary materials. Here, we demonstrate that the mobility of electrons in nitride semiconductors also exhibits a linear relationship with S^2 .

Samples of undoped GaN, Mg-doped InN and Zn-doped InN were grown by plasma-assisted molecular beam epitaxy, and their degree of ordering was measured using both RHEED patterns and SEM images. For GaN, samples were grown in compositions ranging from Ga-rich to N-rich; all of these samples were determined to be n-type from Hall effect measurements. The electron mobility of the samples was observed to increase linearly with decreasing value of S . The largest range of order parameters and mobilities was obtained for nominally stoichiometric samples, where mobilities varied linearly from $138 \text{ cm}^2/(\text{Vs})$ to $5 \text{ cm}^2/(\text{Vs})$ for S^2 values between 0.113 and 0.332, respectively. For Mg-doped InN, samples were grown with Mg concentrations ranging from 1×10^{16} to $1 \times 10^{20} \text{ cm}^{-3}$ and all samples were confirmed to be n-type by variable magnetic field Hall effect measurements. Similar to undoped GaN, these samples all exhibited a linear increase in the electron mobility with decreasing S of the sample. The largest range of order parameters was obtained for doping concentrations on the order of $1 \times 10^{17} \text{ cm}^{-3}$, where measured electron mobilities ranged from $295 \text{ cm}^2/(\text{Vs})$ to $16 \text{ cm}^2/(\text{Vs})$ for S^2 values between 0.064 and 0.221, respectively. For Zn-doped InN, samples were grown with Zn concentrations ranging from 1×10^{15} to $1 \times 10^{16} \text{ cm}^{-3}$ and all samples were determined to be n-type. Like the GaN and Mg-doped InN samples, the Zn-doped InN samples all showed an increase in electron mobility with decreasing S value. The largest range of order parameters was obtained for doping concentrations on the order of $1 \times 10^{15} \text{ cm}^{-3}$, where measured electron mobilities varied linearly between $700 \text{ cm}^2/(\text{Vs})$ and $48 \text{ cm}^2/(\text{Vs})$ for S^2 values between 0.008 and 0.202, respectively.

These experimentally-verified linear relationships between disorder and electron mobilities for each material, as well as the trends observed among these materials, can be physically understood through the lens of structural motifs (nearest neighbor bonding environments of the atoms in the lattice) and the dependence of the different motif types on the degree of disorder within the lattice. Importantly, these results present a possible pathway to increase the mobility of nitride semiconductors through the control of the degree of disorder in the materials, and present a framework for investigating similar relationships between disorder and mobility in other semiconductor systems.

This work was supported in part by the National Science Foundation under Grant DMR-2003581, and the MacDiarmid Institute for Advanced Materials (New Zealand).

SESSION SF06.02: Alloys and Amorphous Materials
Session Chairs: Valentino Cooper and Lucas Lindsay
Monday Afternoon, November 28, 2022
Sheraton, 3rd Floor, Fairfax A/B

1:30 PM *SF06.02.01

Nanoscale Phase Transitions in Amorphous Materials Under Swift Heavy Ion Irradiation Flyura Djurabekova¹, Aleksii A. Leino¹, Henrique Vazquez¹ and Patrick Kluth²; ¹University of Helsinki, Finland; ²The Australian National University, Australia

Analyzing the behaviour of amorphous materials under swift heavy ion irradiation by means of molecular dynamics simulations, we have discovered unexpectedly fast phase transition processes that take place on a nanoscale in the regions affected by the passing ion. The behavior is characteristic to a specific combination of pressure and temperature that may appear in the wake of a swift heavy ion passing through the material. We relate this behavior to the strong tetrahedral network in Si-based materials that also explains rich polymorphism in these materials. We determine that the fine structure of the track is composed of two distinct amorphous phases that result from the different pressure levels in the core and in the shell during solidification. The mechanism involving ultrafast nanoscale phase transitions sheds the light on the origin of the core-shell fine structure observed in a-SiO₂ and a-Si₃N₄, as well as the dense core in a-Si.

On the other hand, in amorphous Ge fast phase transitions under swift heavy ion irradiation lead to nanoporosity that displays a peculiar self-organization process. Low-density solid to high-density liquid transitions lead to formation of initially almost randomly distributed pores which grow with ion fluence and eventually self-organize in well-separated layers parallel to the sample surface. This self-organization mechanism depends on the ion energy, thickness of the amorphous Ge layer and the angle of ion incidence and is potentially caused by the fragmentation of ion tracks into segments of characteristic length. Using molecular dynamics simulations we investigate the process of pore formation and the mechanisms leading to self-organization of the pores in a layered structure.

2:00 PM SF06.02.02

Enhancement of Critical Current Density and Strong Vortex Pinning in High Entropy Alloy Superconductor Ta_{1/6}Nb_{2/6}Hf_{1/6}Zr_{1/6}Ti_{1/6} Synthesized by Spark Plasma Sintering Jin Hee Kim¹, Rahmatul Hidayati¹, Soon-Gil Jung², Yusuff A. Salawu³, Heon-Jung Kim³, Jae Hyun Yun¹ and Jong-Soo Rhyee¹; ¹Kyung Hee University, Korea (the Republic of); ²Sungkyunkwan University, Korea (the Republic of); ³Daegu University, Korea (the Republic of)

We synthesized the high entropy alloy (HEA) Ta_{1/6}Nb_{2/6}Hf_{1/6}Zr_{1/6}Ti_{1/6} compound by planetary ball milling and the spark plasma sintering (SPS) method. The sintered HEA sample had a BCC crystal structure with small amount of secondary phases. The superconducting phase transition is observed in the electrical resistivity ($T_c \sim 7.8$ K) and magnetic susceptibility ($T_c \sim 7.6$ K) measurements, and the T_c was similar to that of an arc-melted sample. The zero-temperature limit of the upper critical magnetic fields $H_{c2}(0) = 10.5$ T and coherence length $\xi = 5.66$ nm were slightly decreased or comparable to the arc-melted HEA sample ($H_{c2}(0) = 12.05$ T and $\xi = 5.23$ nm). The field-dependent isothermal magnetization hysteresis $M(H)$ exhibited the typical type-2 superconducting behavior with magnetic flux avalanches in the low magnetic field region. The calculated critical current densities were significantly increased by 286 % ($J_c = 32,606$ A cm⁻² at 2 K) \sim 687 % ($J_c = 73,200$ A cm⁻² at 4 K) compared to the arc-melted HEA sample ($J_c = 11,401$ A cm⁻² at $T = 2$ K). The enhanced J_c of the sintered HEA sample is caused by enhancement of the pinning force due to point pinning as well as surface pinning effects. The vortex relaxation measurements showed stable remanent magnetization for over 10,000 s after magnetic fields were turned off, which is unlike conventional superconducting vortex relaxation behavior. The strong pinning force in the SPS sintered Ta_{1/6}Nb_{2/6}Hf_{1/6}Zr_{1/6}Ti_{1/6} compound is beneficial for practical applications because of the significantly enhanced critical current density J_c with stable remanent magnetization $M_{rem}(t)$.

2:15 PM SF06.02.03

Designing Electronic and Magnetic Order with Compositional Disorder T. Zac Ward¹, Elbio Dagotto^{1,2} and Alessandro R. Mazza^{1,2}; ¹Oak Ridge National Laboratory, United States; ²The University of Tennessee, Knoxville, United States

In this talk, we will discuss developments in entropy-assisted synthesis that are allowing never before possible levels of parameter disorder to be hosted on positionally ordered single crystal lattices. We will present recent results on single crystal high entropy correlated oxides showing how compositional complexity can be used to drive novel tunability of charge and spin orderings.

Substitutional doping is a cornerstone of experimental approaches used to explore mechanistic responses to changes in the charge, orbital, lattice, and spin contributions of strongly correlated and quantum materials. The energy scales of these parameters can have near degeneracies, which means that minute extrinsic shifts to untargeted values, as with ion size variance, must also be considered. However, even well diluted disordering from doping can play an important or even dominating role in the emergence of macroscopic behaviors, such as, high T_c superconductivity, magnetic texture, scalable non-fermi liquid responses, and metal-insulator transitions. Synthesis of crystalline systems that host broad parameter disorder is exceptionally challenging, since traditional substitutional doping routes are dominated by formation enthalpy. This means that increasing substitution on a single sublattice-site beyond a few percent often results in the formation of unintended secondary phase formations or compensating vacancy creation. Thus, while substitutional doping may give a direct route to accessing fundamental parameter tunability in computational approaches, enthalpic effects during synthesis drive element clustering which limits mixing and reduces the number of desired composite microstates that exist in well-mixed regions.

2:30 PM SF06.02.04

Predicting Short-Range Ordering/Clustering Kinetics in Binary FCC Solid Solution Alloys Using a Mean-Field Method Anas Abu-Odeh¹, Blas Uberuaga² and Mark Asta^{1,3}; ¹UC Berkeley, United States; ²Los Alamos National Laboratory, United States; ³Lawrence Berkeley National Laboratory, United States

At equilibrium, disordered solid solution alloys will have some level of short-range ordering (SRO) or clustering (SRC). SRO/SRC has been experimentally shown to affect the mechanical properties of concentrated FCC and HCP solid solution alloys through the rise of planar slip, and atomistic simulations have shown an effect on dislocation behavior for FCC, HCP, and BCC solid solution alloys due to the presence of a diffuse anti-phase boundary. While the presence of SRO/SRC in solid solutions is thermodynamically expected, it is unclear how long of an annealing time is required to reach the equilibrium SRO/SRC state of an alloy. Previous experimental resistivity and diffuse intensity measurements of binary alloys undergoing

isothermal annealing have shown that the SRO/SRC relaxation times of these alloys span many orders of magnitude and depend on the material system, alloy composition, and temperature. The ability to predict these relaxation times can facilitate designing experiments dependent on SRO/SRC. Kinetic Monte Carlo (kMC) simulations provide an avenue for these predictions but are dependent on parameterizing vacancy transition state energies sampled from a sufficient variety of chemical environments. In the absence of a reliable interatomic potential, this would require many expensive density-functional theory (DFT) calculations. A quicker alternative method that circumvents these calculations would be desirable. Using interactions parameterized by embedded atom method descriptions of Cu-Au and Cu-Ni, which exhibit SRO and SRC, respectively, we compare relaxation kinetics modeled through kMC as well as a mean-field method (MFM). This method estimates the decay rate of concentration waves in a stable solid solution and requires two simple inputs: a mobility factor related to interdiffusion, and a reciprocal space dependent SRO/SRC diffuse intensity. This latter input is readily obtained from canonical Monte Carlo (cMC) simulations at equilibrium. We find that the relaxation times of real space SRO/SRC and regions of enhanced SRO/SRC diffuse intensity obtained from the MFM agree to within an order of magnitude to those obtained from kMC. It is also able to capture the unique transient behavior of SRC present in Cu-Ni. These results suggest that the MFM allows for order of magnitude estimates for experimental design of SRO/SRC and can also be connected to current theories of SRO/SRC strengthening. While the mobility parameter in this study was obtained from kMC, for a general binary alloy, this parameter can be obtained from mobility databases fit to experiments. Obtaining diffuse intensity information would require cMC simulations parameterized by an interatomic potential or DFT but would not require vacancy transition state calculations. The success of the MFM for these binary systems suggests that extensions of this method to SRO/SRC kinetics in multicomponent systems may also be a satisfactory alternative to kMC.

2:45 PM SF06.02.05

Computational Study on Atomic Arrangements of CuZn Alloy Determining Ethylene and Ethanol Selectivity [Deokgi Hong](#)¹, [Yeji Baek](#)², [Hakhyeon Song](#)², [Sungwoo Lee](#)¹, [Young-Chang Joo](#)¹, [Jihun Oh](#)² and [Gun-Do Lee](#)¹; ¹Seoul National University, Korea (the Republic of); ²Korea Advanced Institute of Science and Technology, Korea (the Republic of)

Electrochemical CO₂ reduction reaction (CO₂RR) is a promising route to alleviate the problems of global warming and realize the carbon neutral cycle. Selectivity control in CO₂RR over Cu-based catalyst is an important issue for multicarbon product generation. Especially, C₂ products like ethylene and ethanol has high economic efficiency and energy density. Among various approaches to enhance the C₂ product selectivity of Cu-based catalyst, alloying is promising method. The alloy atoms added to the Cu lattice modify the reaction mechanism by diversifying the structure of the active site and changing the electronic structure. However, the complex atomic structure of the active sites on the Cu-based alloy surface impedes our understanding on the origin of enhanced C₂ product selectivity. Therefore, it is necessary to understand the effect of atomic arrangement on C₂ product selectivity of Cu-based alloys. Our group synthesized CuZn alloys with different Zn compositions and conducted electrochemical measurements to investigate the effect of atomic arrangement on the C₂ product selectivity of CuZn alloys. [1] We controlled the phase of the CuZn alloys to exclude other factors affecting the C₂ product selectivity, except for the atomic arrangement. All alloy samples exhibited random solid solution properties. It was observed that the ratio of ethanol production to ethylene production increased as the atomic composition of Zn increased from 10% to 33%. DFT calculations were performed to understand the change in C₂ product selectivity according to Zn composition and the effect of atomic arrangement on C₂ product selectivity. We classified the atomic arrangement on the CuZn alloy surface into three types of Cu-rich, Zn-rich and Cu-Zn interfacial sites and calculated the free energy change of CO₂RR on the three types of sites. Then we compared the energy changes at the step where the reaction pathways for ethanol production and ethylene production branched. As a result, it was confirmed that ethanol production was more dominant at Cu-Zn interface sites and ethylene production was more dominant at Cu-rich sites. Therefore, as the Zn content increased, the ratio of Cu-Zn interfacial sites increased, and accordingly, the ratio of ethanol production to ethylene production increased.

This study contributes to understanding the effect of local atomic arrangement in CuZn alloys on C₂ product selectivity and provides insight into the prediction of catalytic performance of disordered metal lattices.

[1] Y. Baek, H. Song, D. Hong, S. Wang, S. Lee, Y.-C. Joo, G.-D. Lee and J. Oh, *J. Mater. Chem. A*, 2022, 10, 9393–9401.

3:00 PM BREAK

3:30 PM *SF06.02.06

Disorder Driven Relaxor Ferroelectrics—A Computational Design Strategy [Valentino R. Cooper](#); Oak Ridge National Laboratory, United States

High entropy, multi-component metal alloys, have superior mechanical properties and high radiation tolerances; which are, in part, driven by configurational entropy. Recently, an oxide analogue comprised of MgO, CoO, NiO, CuO and ZnO was synthesized; exhibiting a truly entropy-stabilized, reversible phase transition from a multiphase material to a single rock salt-ordered phase above 850-900°C. This entropy-driven stabilization may engender many unique properties, such as high melting temperatures, radiation resistance and other anomalous responses. Here, we discuss a design strategy for the prediction of synthesizable disordered oxides. Our effort employs first principles studies of 2-component oxides to develop design rules based on the relationship between pairwise enthalpies of formation, ΔH , and configurational entropy of the disordered material. A similar chemical identity-to- ΔH map was previously explored using the class of high entropy alloys, where the stability of multicomponent metal alloys was correlated to the enthalpy of mixing of binary and ternary compounds. Here, the focus will be on the exploration and discovery of synthesizable entropy-stabilized Ba-based perovskites that rely on configurational disorder to foster relaxor ferroelectric behavior.

This work was supported by the U.S. D.O.E., Office of Science, BES, MSED using resources at NERSC and OLCF.

4:00 PM SF06.02.07

Effect of Elemental Segregation in High-Entropy Alloys on Materials Transport Properties [Kai H. Nordlund](#), [Jesper Byggmästar](#), [Flyura Djurabekova](#), [Fredric Granberg](#) and [Filip Tuomisto](#); University of Helsinki, Finland

High-entropy alloys are considered to exhibit so called sluggish diffusion, which may at least partly explain many of their unusual macroscopic properties. However, the origins of this effect remain unclear, in part because the atom-level modelling of dynamic processes in an alloy with 5 or more elements is very challenging. To improve on this, we have recently developed a machine-learning interatomic potential for the 5-element refractory metal high-entropy alloy VNbTaMoW [1]. Using such potentials, it is possible to use molecular dynamics and Metropolis Monte Carlo simulations to examine elemental segregation effects of defects and dislocations in a true high entropy alloy. The simulation results and associated positron annihilation experiments [2] show major elemental segregation effects in the intermediate atomic environment around both vacancy- and interstitial-like defects in high entropy alloys. The defect migration is then strongly affected by this segregation. This implies that the point defect migration cannot be treated in the traditional manner of a certain defect type having a well-defined migration energy.

[1] J. Byggmästar, K. Nordlund, and F. Djurabekova, *Phys. Rev. B* 104, 104101 (2021)

[2] F. Tuomisto, I. Makkonen, J. Heikinheimo, F. Granberg, F. Djurabekova, K. Nordlund, G. Velisa, H. Bei, H. Xue, W. J. Weber, and Y. Zhang, *Acta Materialia* 196, 44 (2020),

4:15 PM SF06.02.08

Atomistic Modeling of Surface Segregation Driven by Defect Transport in Binary Alloy Guofeng Wang and Siming Zhang; University of Pittsburgh, United States

Surface segregation process in binary alloys results in the surface layers with their own set of composition and structure different from the bulk ones, which serves as an important model system to advance understanding of interface dynamics in nanoscale systems for future materials design. Moreover, surface segregation affects greatly the catalytic, friction, and anti-corrosion properties of binary alloys. In this study, we applied the first-principles density functional theory computational method to predict the surface segregation profiles as related the transport of different vacancies in binary alloy nanostructures.

(1) For Cu₂₀Au₈₀ random solid solution alloy, our computation reveals that structural defect, i.e., surface steps, could induce compositional and structural evolution in the subsurface of a Cu(Au) solid solution and lead to a stacked sequence of Cu-Au ordered phases in the subsurface. The presence of a monatomic step at the surface induces the formation of an antiphase boundary that extends from the surface step to deeper layers by maintaining the same composition profile associated with each terrace.

(2) For ordered Cu₃Au (100) surface, we modelled an adatom process underlying transient surface segregation dynamics through the temperature-change-driven creation and annihilation of thermal vacancies in the bulk and the resulting bulk-surface mass exchanges. Our computational results indicate that the lower vacancy formation energy for Cu than Au in Cu₃Au results in more bulk thermal vacancies of Cu with the increase in temperature, for which the excess Cu atoms are expelled onto the surface as adatoms that aggregate as Cu-rich clusters. Decreasing temperature drives more Cu adatoms than Au adatoms back to the bulk, thereby making the adatoms Au rich.

(3) Using the example of Pt₈₅Fe₁₅ alloy nanoparticles (NPs), we modelled the composition-dependent ordering processes on the single-particle level. Our results reveal that ordering transformations are controlled by the vacancy-assisted diffusion of Pt and Fe atoms in the nanoparticles. In Pt₈₅Fe₁₅ nanoparticles, Fe is predicted to be the fast-migrating species; the inward diffusion of surface Fe and outward diffusion of core Fe atoms lead to this particular structure of the Pt₈₅Fe₁₅ NPs of an outermost Pt shell, a Pt₃Fe L₁₂ ordered phase underneath, and an inner Pt-enriched core.

4:30 PM SF06.02.09

Title: Role of Sn Concentration in the Amorphous-to-Crystalline Transition of the Mixed Oxide SnO₂/TiO₂ Pritha Biswas, Tamara Koledin, Melissa K. Santala and Janet Tate; Oregon State University, United States

Although rutile titania is the thermodynamically stable phase at a high temperature in the bulk, stabilization of this polymorph at a lower temperature with a high surface-to-volume ratio remains an elusive target in the field of catalysis and low-temperature gas sensing. Stabilization of rutile TiO₂ by isostructural alloying with the isovalent dopant Sn is one of the most established methods^{1,2} among the variety of doping routes. We describe the deposition of metal Sn between two amorphous TiO₂ layers and show that rutile TiO₂ results upon annealing at 500 °C once the Sn:Ti ratio exceeds a critical value. Below that value, anatase TiO₂ is formed. Phase identification and corresponding morphologies of the different phases of the SnO_x/TiO_y system with different percentages of Sn have been characterized by x-ray diffraction (XRD), transmission electron microscopy (TEM), scanning electron microscopy (SEM), and Raman spectroscopy. Initial ex-situ XRD and Raman measurements at different stages of oxide formation indicate that the rutile phase forms directly from the amorphous precursor and that the transformation is not a polymorphic anatase-to-rutile transition. Based upon the layered geometry of the SnO₂/TiO₂ mixture, we propose that the incorporation of Sn between two amorphous TiO₂ layers changes the *amorphous precursor* of TiO₂ by scavenging oxygen from the TiO₆ octahedra that then form an oxygen-deficient environment with short-range order, which ultimately stabilizes the rutile polymorph of TiO₂.³

1. F. Wang, J. H. Ho, Y. Jiang, R. Amal, ACS Appl. Mater. Interfaces 2015, 7, 23941–23948.

2. L. Trotochaud, S. W. Boettcher, Chem. Mater. 2011, 23, 4920–4930.

3. J. S. Mangum, L. M. Garten, D. S. Ginley, B. P. Gorman, J. Amer. Ceram. Soc. 2020, 103, 2899–2907.

4:45 PM SF06.02.10

Zeta Potentials and NMR—Probing Ion-Surface Interactions in an Inhomogeneous Solid-Liquid Media Using Nuclear Magnetic Resonance Ruth Zlanscu Tan^{1,2}, Vincent Sarou-Kanian¹ and Michael Deschamps^{2,1}; ¹CNRS, France; ²University of Orleans, France

The accurate description of interface phenomena in solid-liquid heterogeneous media is a common issue in many scientific fields^{1,2,3}. Whatever the domain, the main question remains : how much do we know about the interaction between the surface of a solid and the molecules and ions of the liquid phase ?

In this work, we are specifically interested in individual ion-surface interactions and we managed to probe them using Nuclear Magnetic Resonance (NMR). NMR is a well-known characterisation method for probing local structure around spin bearing atoms, as well as their dynamics at the nanometer scale through relaxation at high fields. These features make it a suitable tool to differentiate ions according to their location (interface or bulk?) and dynamics in such media (slow or fast motion?), in solid-liquid mixtures with relatively low amounts of liquids.

Oxides powders (TiO₂ and Al₂O₃) were mixed with aqueous electrolytes containing several types of ions (NO₃⁻, NH₄⁺, Br⁻, Na⁺, Li⁺, Rb⁺, Cs⁺), with quadrupolar spins that are observable in NMR, in the 0.1 M - 2 M concentration range. NMR longitudinal relaxation times (T₁) and signal areas measurements allowed us to indirectly characterize the quadrupolar interactions at the solid-liquid interface and to observe pH sensitive ion-surface interactions, which can be correlated with zeta-potential measurements. Moreover, competitions between ions can be characterized *in situ* by NMR and we showed that a complex picture emerges when solutions with two cations are in contact with the solid surface.

[1] A. Bede et al., Cement and Concrete Research, 89, (2016), 56–62

[2] P.G. Rouxhet et al. : Matériaux & Techniques, 93, (2005), 13-26

[3] M. Fleury and F. Deflandre, Magnetic Resonance Imaging, 21, (2003), 385–387

8:30 AM *SF06.03.01

Thermal Transport in Micro-to-Nanoscale Systems Affected by Volumetric and Surface Disorder—A First-Principles Study [Navaneetha Krishnan Ravichandran](#); Indian Institute of Science, India

In nanoscale crystalline semiconductor films and wires, where the surface area-to-volume ratio is large, phonon scattering at surface disorder affects heat transport, particularly at low temperatures. In a previous study, we experimentally extracted the phonon specularity parameter, which quantifies the relative extent of specular-to-diffuse scattering of phonons at a rough surface, using transient grating measurements of lengthscale-dependent thermal conductivities in sub-micron thick silicon films [1]. We showed that, in our silicon films, phonons with wavelengths shorter than 8 nm undergo partial specular reflection at the boundaries, resulting in significant reduction in the thermal conductivity of these films compared to bulk silicon. In the first part of this talk, I will describe our recent computational effort to describe this additional thermal resistance due to phonon-boundary scattering in nanoscale wires and films made from III-V compounds and other low-dimensional materials, informed by the aforementioned experimentally extracted phonon specularity parameter.

In chemically grown bulk crystals, volumetric disorder such as substitutional defects and vacancies are often present in significant concentrations. Phonon scattering with defects in these crystals cause additional resistance to heat flow, apart from the anharmonicity-driven intrinsic phonon-phonon scattering. In the second part of this talk, I will describe our group's ongoing effort to study the relative importance of phonon-phonon and phonon-defect scattering in modulating the thermal conductivity of compound semiconductors at different defect concentrations and temperatures, using our in-house unified first-principles computational framework [2].

This work is supported by a Core Research Grant from the Science and Engineering Research Board, India (Grant no: CRG/2020/006166) and a Young Investigator Award from the Infosys Foundation.

[1] Navaneetha K. Ravichandran, Hang Zhang & Austin Minnich, *Physical Review X* 8 (4), 041004, 2018

[2] Navaneetha K. Ravichandran & David Broido, *Physical Review B* 98 (8), 085205, 2018

9:00 AM SF06.03.02

Utilizing Order-Disorder Phase Transitions for Solid-State Cooling: From Thermodynamics to Devices [Adam H. Slavney](#), Jinyoung Seo, Vidhya M. Dev and Jarad A. Mason; Harvard University, United States

Vapor-compression air conditioning is a technology which is essential to modern life. However, the established hydrofluorocarbon refrigerants central to this technology are potent greenhouse gases—one to five thousand times more effective than CO₂. The unintentional release of these refrigerants to the atmosphere during air conditioner installation, maintenance, and disposal is currently responsible for ca. 4% of planetwide global warming and is expected to rise to 10% of all warming by 2050. To eliminate this source of atmospheric emissions, we are developing solid-state barocaloric materials which can serve as direct replacements for hydrofluorocarbons in air conditioners and other heat-pump applications. We have recently discovered a promising new family of barocalorics: layered halide perovskites with long alkyl ammonium tails. These materials undergo solid-solid, order-disorder transitions within the alkyl sublattice which are analogous to the melting of simple *n*-alkanes, albeit confined to two dimensions by the layered perovskite structure. Layered perovskite transitions occur near ambient temperature and with high transition entropies making them able to adsorb and release significant amounts of heat in the temperature range relevant for indoor cooling. Additionally, these phase transitions show low hysteresis, and the transition temperatures are highly sensitive to pressure. This combination of properties enables layered perovskites to realize efficient barocaloric cooling with a pressure swing of 200 bar or less—a range achievable with standard hydraulic systems—whereas prior barocaloric systems require pressures above 1000 bar to realize measurable cooling. To demonstrate this in practice, we have designed and constructed a custom barocaloric prototype device and achieved efficient barocaloric cooling at pressures at and below 200 bar for the first time. I will discuss our current progress, ongoing challenges, and future directions of this work.

9:15 AM SF06.03.03

Water/Zirconia Interfacial Behavior—Water Adsorption and H⁺ Subsurface Diffusion [Saul Perez Beltran](#)¹, Pablo Gargano^{2,3}, Mariano Forti², Gustavo Emilio Ramirez Caballero⁴, Gerardo H Rubiolo^{2,5}, Perla B. Balbuena¹ and Paula R. Alonso²; ¹Texas A&M, United States; ²Comisión Nacional de Energía Atómica, Argentina; ³Universidad Nacional de San Martín, Argentina; ⁴Universidad Industrial de Santander, Colombia; ⁵Consejo Nacional de Investigaciones Científicas y Técnicas (CONICET), Argentina

We evaluated the interfacial behavior between water and zirconia using a computational approach based on density functional theory (DFT), ab-initio molecular dynamics (AIMD) and constrained molecular dynamics (c-AIMD). ZrO₂ crystallites improve corrosion resistance in Zr-Nb alloys by hindering H⁺ diffusion, which is essential to ensuring the safe operation of heavy water reactors.¹ Among the different ZrO₂ polymorphs, monoclinic ZrO₂ (m-ZrO₂) is the most naturally occurring form at low pressure². Meanwhile, the high-pressure cubic ZrO₂ (c-ZrO₂) grows from Zr(OH)₄ decomposition and in radiated Ce-doped tetragonal ZrO₂ materials;^{3,4} its occurrence has been reported via transmission electron microscopy (TEM) in Zr-based alloyed fuel clads for light-water reactors and Zr surfaces.^{5,9}

We studied dissociative water adsorption on pristine and defective c-ZrO₂(111) and m-ZrO₂([endf]-->11) surfaces using the DFT engine Vienna ab-initio simulation package (VASP, version 5.4.0).¹⁰ The surface defects studied included an oxygen vacancy, interstitial oxygen, and substitutional Ta and Nb.^{2,11-13} The first step involved the surfaces' optimization via DFT in a vacuum. Then, we added water molecules into the simulation cell and ran AIMD simulations for about ten ps intervals at 300, 900 and 1500K. These calculations showed dissociative water adsorption even at 300 K, with the adsorption of H⁺ and OH⁻ groups in surface oxygen and Zr atoms. The presence of defects led to a surface reconstruction in some cases and favored the water dissociation. Moreover, an interfacial oxygen exchange occurred at 1500 K.

For the second part of this work, we studied the H⁺ subsurface diffusion via c-AIMD calculations. The outermost surface layers showed the highest energy barrier, with some exceptions due to defects. However, the inner layers showed a lower energy barrier for the H⁺ diffusion, which was most evident between the second and third layers; the more buried the layer, the lower the energy change. The presence of defects showed a lowered energy barrier in some cases, which led us to believe that surface defects trigger material failure. We elucidated the H⁺ diffusion mechanism in each case.

References

1. Cox, B.; Garzarolli, F.; Rudling, P., *Advanced Nuclear Technology International* **2004**.
2. Luo, H.; Tian, D.; Zeng, C.; Fu, Y.; Wang, H., *Computational Condensed Matter* **2017**, *11*, 1-10.
3. Nazir, M. A.; Mahmood, T.; Zafar, A. A.; Akhtar, N.; Hussain, T.; Saeed, M. A.; Aleem, F.-e.; Saeed, A.; Raza, J.; Cao, C., *Phys. Rev. B: Condens. Matter*, **2021**, *604*, 412462.
4. Katz, J., *Am. Ceram. Soc.* **1971**, *54*, 531.
5. Lu, Z.; Chernatynskiy, A.; Noordhoek, M. J.; Sinnott, S. B.; Phillpot, S. R., *J. Nucl. Mater.*, **2017**, *486*, 250-266.
6. Ploc, R. A., *J. Nucl. Mater.*, **1983**, *113* (1), 75-80.
7. Ploc, R. A., *J. Nucl. Mater.*, **1983**, *115* (1), 110-117.

8. Ploc, R. A., *J. Nucl. Mater.*, **1982**, *110* (1), 59-64.
9. Noordhoek, M. J.; Liang, T.; Chiang, T.-W.; Sinnott, S. B.; Phillpot, S. R., *J. Nucl. Mater.*, **2014**, *452* (1), 285-295.
10. Kresse, G.; Furthmüller, J., *Phys. Rev. B* **1996**, *54* (16), 11169-11186.
11. Lackner, P.; Hulva, J.; Köck, E.-M.; Mayr-Schmölzer, W.; Choi, J. I. J.; Penner, S.; Diebold, U.; Mittendorfer, F.; Redinger, J.; Klötzer, B.; Parkinson, G. S.; Schmid, M., *J. Mater. Chem. A* **2018**, *6* (36), 17587-17601.
12. Hinuma, Y.; Toyao, T.; Kamachi, T.; Maeno, Z.; Takakusagi, S.; Furukawa, S.; Takigawa, I.; Shimizu, K.-i., *J. Phys. Chem. C*, **2018**, *122* (51), 29435-29444.
13. Tolba, S. A.; Allam, N. K., *Sci. Rep.* **2019**, *9* (1), 10159.

9:30 AM SF06.03.04

Effect of Positional and Energetic Disorder on Charge Transport in Nanocrystal Quantum Dot Thin Films Yunhua Xing, Nuri A. Yazdani, Weyde Lin, Maksym Yarema, Raphael Zahn, Vanessa Wood and Simon Wintersteller; IfE, D-ITET, ETHZ, Switzerland

Understanding and controlling mobility disorders in self-assembled nanocrystal (NC) solids is crucial for accelerating development for NC solids-based electronics [1]. Especially, compared to energetic disorder, the impact of positional disorder on charge carrier transport is less studied due to the challenges of experimentally controlling the films has not yet been clarified due to its diversity and complexity. We present in this work, we seek to fill the knowledge gap by demonstrating an approach to systematically investigate different types of disorder and their impact on charge transport in NC solids [2]. We computationally construct and quantify the artificial NC thin films containing different types of realistic disorders. By applying density functional theory (DFT) parameterized Kinetic Monte Carlo (KMC) simulations, we extract statistics to quantify the probe effective carrier mobility and origins of the understand charge transport behavior at an “artificial atomic (NC)” level. We demonstrate that the impact of positional disorder on charge transport depends on the type of disorder and how it affects the spacing between neighboring NCs. We found that certain disorders that shorten inter-NC distances can enhance the carrier transport, while random packing of NCs and energetic disorder due to a distribution of NC sizes decreases mobility 2- to 4-fold. We further demonstrate how electric field impacts the charge transport in disordered NC thin films. Finally, we address the detrimental impact of deep electronic trap states on carrier mobility, particularly at low electric field and when the films are otherwise highly ordered. Overall, we show that our approach can be a power tool to investigate charge transport in NC-solid-based devices. And based on our results, we suggest what to prioritize in terms of synthesis and thin film fabrication in the future development of NC devices.

[1] Liu, M.; Yazdani, N.; Yarema, M.; Jansen, M.; Wood, V.; Sargent, E. H. Colloidal quantum dot electronics. *Nat. Electron.* **2021**, *4*, 548–558.

[2] Xing, Y.; Yazdani, N.; Lin, W.; Yarema, M.; Zahn, R.; Wood, V. Effect of Positional Disorders on Charge Transport in Nanocrystal Quantum Dot Thin Films. *ACS Applied Electronic Materials* **2022** *4* (2), 631-642.

9:45 AM BREAK

10:15 AM *SF06.03.05

Interfacial and Bulk Defect Resolution Using Machine-Learning Augmented Ultrafast Diffraction Mingda Li; Massachusetts Institute of Technology, United States

Materials defects are ubiquitous and play a key role in materials’ functional properties. However, there has been a lack of non-contact, non-destructive defect quantification tools to resolve complex defect profiles when multiple types of defects are present. Here we introduce an alternative approach for defect quantification, using the fact the phonons – major heat carriers in insulators and semiconductors – are sensitive to defect scattering: phonon-frequency-resolved relaxation time and transmittance are known to contain direct and quantitative knowledge of materials’ bulk and interfacial defect structures. However, frequency-resolve phonon relaxation and transmittance are long considered not measurable. We design an integrate theoretical-experimental-machine-learning framework to extract such quantities by using machine-learning to analyze time-resolved diffraction patterns: ultrafast diffraction offers high-dimensional data in time-momentum space where phonon thermal transport is reflected on the atomic vibrations and thereby diffraction intensities, and scientific machine learning is used to solve an inverse thermal transport problem and extract those frequency-resolved phonon transport with significantly increased reliability¹. We anticipate the work representing an alternative pathway for non-contact, quantitative defect resolution.

¹ <https://arxiv.org/abs/2202.06199>

10:45 AM SF06.03.07

Tuning the Properties of Thin Metal Films via Disorder Alessandro Troglia¹ and Roland Bliem^{1,2}; ¹Advanced Research Center for Nanolithography, Netherlands; ²University of Amsterdam, Netherlands

Crystalline order is typically considered a prerequisite for an ideal material. Disorder is thus commonly perceived as detrimental, even though it is a key advantage in important classes of materials. Structural disorder in amorphous alloys, for example, benefits various macroscopic properties, such as hardness or corrosion resistance, leading to an excellent performance as coatings, barrier layers, catalysts, or in advanced electronics [1]. So rather than distracting and detracting from perfection, structural disorder can serve as an ideal design parameter for new corrosion-resistant, hard, and selectively reactive alloys.

Typically, crystallinity and amorphicity in alloys are connected to specific stoichiometries, making the effects of structure and composition difficult to disentangle. In the present work we make use of pulsed laser deposition (PLD) to prepare crystalline and amorphous alloy layers of identical composition by growing thin films under two very different types of conditions, close to and far from equilibrium. We study the structural, mechanical, and electronic properties as well as the surface chemistry of polycrystalline and amorphous films for two selected alloys: CuZr and HfMoNbTiZr. CuZr is a model system for metallic glasses with composition-dependent glass-forming ability [2], whereas the high-entropy alloy (HEA) HfMoNbTiZr has exclusively been observed in its crystalline form [3].

In contrast to literature results, HfMoNbTiZr films grown with PLD at room temperature show no sign of crystallinity in grazing-incidence X-ray diffraction (GI-XRD) and transmission electron microscopy (TEM). Even an increase of the deposition temperature to 700°C is insufficient to induce crystallization, which starts at 900°C. The liquid-like diffraction features of the amorphous films shift to higher diffraction angles and decrease in width with increasing deposition temperature. This indicates that a lower-energy glassy structure is formed for high-temperature growth. It further suggests that the packing density in amorphous HEA thin films is tuneable, which could be of interest for their applications as energy storage medium [4]. The remarkable thermal stability of the amorphous phase and its facile formation highlight the potential of complex alloys for high-temperature applications requiring structural stability.

For CuZr, on the other hand, smaller variations in temperature are sufficient to induce crystallization. Room-temperature PLD leads to amorphous layers according to GI-XRD, while films of the same composition are polycrystalline when deposited at 500°C. Raman spectroscopy measurements show no discernible features for the amorphous layers while broad but distinct modes related to Cu and Zr oxides are observed for polycrystalline films. The effect

of disorder on the surface chemical properties of CuZr was measured using X-ray photoelectron spectroscopy (XPS) by comparing as-grown and air-exposed CuZr films. The XPS results show a remarkable preference in the surface oxidation of the Cu species. Cu is fully metallic for the amorphous film whereas both oxide and hydroxide components are observed for the crystalline layer.

Our results demonstrate that the level of structural disorder in thin alloy films can be tuned from polycrystalline to fully amorphous using PLD. This structural disorder significantly influences the surface reactivity and oxidation resistance of the model compound CuZr.

[1] A. Inoue, A. Takeuchi. *Acta Mater.* 59, 2243 (2011).

[2] Z. Altounian, T. Guo-hua, and J. O. Strom-Olsen. *J. Appl. Phys.* 53 4755 (1982).

[3] N.N. Guo, L. Wang, L.S. Luo, X.Z. Li, Y.Q. Su, J.J. Guo, H.Z. Fu. *Materials & Design* 81, 87 (2015).

[4] H. Shen, J. Zhang, J. Hu, J. Zhang, Y. Mao, H. Xiao, X. Zhou, X. Zu. *Nanomaterials* 9, 248 (2019).

11:00 AM SF06.03.08

Correlation of Oxygen Nonstoichiometry on Chemical Expansion in LCCO Thin Films [Hendrik Wulfmeier](#)^{1,2}, [Dhyan Kohlmann](#)¹, [Thomas Defferriere](#)², [Harry Tuller](#)² and [Holger Fritze](#)¹; ¹Clausthal University of Technology, Germany; ²Massachusetts Institute of Technology, United States

Mixed electronic/ionic conductors (MIECs) are of great technological interest with applications, for example, in solid oxide fuel cells (SOFCs). Reduction of operation temperatures is needed both for extended life and reduced costs, but this increases the demand for more electrocatalytically active electrodes. The MIEC layer compound lanthanum cerium cuprate ($\text{La}_{1-x}\text{Ce}_x\text{CuO}_{4+\delta}$, LCCO) shows promise in this regard given relatively high electronic conductivities at reduced temperatures [1], as well as the ability to accommodate both oxygen excess and deficiency, the latter making it an attractive candidate for both the SOFC cathode and anode [2], and thus a promising material for reversible SOFCs. In this work, oxygen nonstoichiometry in LCCO thin films is characterized in the temperature range of 500 to 700 °C. The determination of the oxygen nonstoichiometry in thin films is a challenging task, especially at elevated temperatures. Piezoelectric nanobalances, based on catangasite (CTGS, $\text{Ca}_3\text{TaGa}_3\text{Si}_2\text{O}_{14}$) single crystals, were applied to monitor changes in δ in these thin oxide films [3] reaching values of up to $\delta = -0.118$ at e.g. 600 °C and $\log(p_{\text{O}_2}) = -13$.

Changing oxygen content in LCCO films, for positive or negative values of δ , results in chemical expansion that can lead to stresses resulting in cracks and malfunction. In the case of thin films this chemical expansion occurs mainly perpendicular to the substrate. In lateral direction of the substrate, mechanical stress is generated leading to substrate bending. The surface near film expansion is characterized by X-ray diffraction under temperature and p_{O_2} variation. We characterize the overall thin-film expansion of LCCO films deposited on single crystalline yttria stabilized zirconia (YSZ) substrates acting as oxygen pumping cells by high-temperature laser-Doppler vibrometry (LDV) [4]. An applied voltage results in an oxygen activity which corresponds to an effective oxygen partial pressure and can be calculated via the Nernst relation. When a sinusoidal excitation voltage is applied to the cell, the reversible *breathing* of the LCCO film can be detected via LDV. If the excitation frequency is low enough, a quasi-stationary state is reached. At 500 °C and an excitation frequency of 100 μHz , positive and negative voltages of ± 0.5 V correspond to oxygen activities of $\log(a_{\text{O}_2}) = -10$ and $+10$, respectively. In both cases thin-film expansion of only a few nm, results in total displacements (i.e. thin-film expansion plus substrate bending) of 64 nm and 239 nm respectively.

[1] C.S. Kim, H.L. Tuller: *Sol. State Ion.*, 320, 233-238 (2018) DOI: 10.1016/j.ssi.2018.03.015

[2] Q. Liu et al.: *Int. J. Hydrogen Energy*, 46, 9818-9825 (2021) DOI: 10.1016/j.ijhydene.2020.06.063

[3] S. Schröder et al.: *Appl. Phys. Lett.*, 112, 213502 (2018) DOI: 10.1063/1.5025389

[4] H. Wulfmeier et al.: *Z. Phys. Chem.*, 236, 1013–1053 (2022) DOI: 10.1515/zpch-2021-3125

11:15 AM SF06.03.09

Understanding the Structure-Dielectric Property Relationships of $(\text{Ba}_{0.8}\text{Ca}_{0.2})\text{TiO}_3\text{-Bi}(\text{Mg}_{0.5}\text{Ti}_{0.5})\text{O}_3$ Perovskites [Colin Freeman](#) and [Derek Sinclair](#); University of Sheffield, United Kingdom

There is a constant search for new functional ceramics particularly in the improvement of their dielectric properties such as higher temperature operating ranges. In the last two decades a particularly exciting set of materials have been identified based around a mix of a BaTiO_3 with an Bi perovskite such as BiScO_3 , $\text{Bi}(\text{Mg}_{0.5}\text{Ti}_{0.5})\text{O}_3$ and $\text{Bi}(\text{Zn}_{0.5}\text{Ti}_{0.5})\text{O}_3$ [1-4]. These materials produce a relatively flat permittivity-temperature profile at high temperatures. Structurally, these materials appear pseudo-cubic but detailed investigations have highlighted structural variation over the length-scale viewed [5]. This couples with localised atomic relaxations [6-7] and potential chemical inhomogeneity [8]. Collectively this makes a highly disordered material that demonstrates complex mixing behaviour and properties. Understanding the structure-property relationships present are vital to understand for designing future materials in this area.

We present a set of atomic-level simulations to examine the structure, thermodynamics, and dielectric properties of $(\text{Ba}_{0.8}\text{Ca}_{0.2})\text{TiO}_3\text{-Bi}(\text{Mg}_{0.5}\text{Ti}_{0.5})\text{O}_3$ perovskites. By examining thousands of atomic configurations we are able to comment on the mixing properties and demonstrate that the solid-solution is non-ideal and only specific configurations can form at higher $\text{Bi}(\text{Mg}_{0.5}\text{Ti}_{0.5})\text{O}_3$ content. We identify the main structural relaxations that take place in the structure connect this to the dielectric properties of the materials by examining the polarisation of the system. Our analysis allows us to link the material disorder with disrupting ferroelectric domains linking to the flat permittivity profiles reported.

[1] C.-C. Huang and D. P. Cann, *JOURNAL OF APPLIED PHYSICS*, 2008, 104

[2] B. Xiong, H. Hao, S. Zhang, H. Liu and M. Cao, *JOURNAL OF THE AMERICAN CERAMIC SOCIETY*, 2011, 94, 3412–3417.

[3] Q. Zhang, Z. Li, F. Li and Z. Xu, *JOURNAL OF THE AMERICAN CERAMIC SOCIETY*, 2011, 94, 4335–4339.

[4] A. Zeb and S. J. Milne, *JOURNAL OF THE AMERICAN CERAMIC SOCIETY*, 2013, 96, 2887–2892

[5] M. A. Beuerlein, N. Kumar, T.-M. Usher, H. J. Brown-Shaklee, N. Raengthon, I. M. Reaney, D. P. Cann, J. L. Jones and G. L. Brennecke, *JOURNAL OF THE AMERICAN CERAMIC SOCIETY*, 2016, 99, 2849–2870.

[6] V. Krayzman, I. Levin, J. C. Woicik and F. Bridges, *APPLIED PHYSICS LETTERS*, 2015, 107, year.

[7] A. Pramanick, S. Nayak, T. Egami, W. Dmowski, A. S. Budisuharto, F. Marlton, M. R. Jorgensen, V. S. Venkateshwarlu and K. A. Beyer, *PHYSICAL REVIEW B*, 2021, 103, 214105.

[8] T. Roncal-Herrero, J. Harrington, A. Zeb, S. J. Milne and A. P. Brown, *ACTA MATERIALIA*, 2018, 158, 422–429.

1:30 PM SF06.04.01

Exploring Phonons Across the Order-Disorder Barocaloric Phase Transition in Adamantane Bernet Meijer¹, Richard Dixey¹, Robin Perry², Anthony Phillips¹ and Helen C. Walker³; ¹Queen Mary University London, United Kingdom; ²University College London, United Kingdom; ³Rutherford Appleton Laboratory, United Kingdom

For years the scientific community has widely followed the maxim that structure dictates functionality and disorder is something to be avoided as far as possible. Those using inelastic neutron scattering (INS) to study phonons have therefore restricted themselves to near perfect crystalline material, sweeping any evidence of disorder under the carpet, using the argument that it is too difficult to analyse data from disordered systems and that simulations are beyond the scope of current computational power. However, it is now quite clear that computational physics has made more than enough progress to build both random and correlated disorder into phonon simulations [1,2]. It is therefore time for INS experimentalists to exploit these developments and finally explore the phonon spectrum of “real” functional materials with inherent disorder in order to determine their thermal properties.

Adamantane is a molecular crystal built up from near spherical molecules that undergoes an order-disorder transition between a low temperature ordered phase and a dynamically disordered phase at room temperature. This disorder between two possible orientations arises from the centroid of each molecule being a crystallographic centre of symmetry, even though the molecules themselves are not centrosymmetric, and neutron total scattering has revealed that there is no correlation between these orientations [3]. Our current interest in adamantane stems from the phase transition being associated with a large change in entropy, and a large change in volume, such that the phase transition can be driven by the application of pressure. This makes adamantane an example of a barocaloric, materials offering technological application potential for environmentally friendly refrigeration.

We have measured the phonon spectrum in both phases of single crystal adamantane as a function of temperature and hydrostatic pressure on the LET direct geometry neutron spectrometer at ISIS. The spectra in the low temperature phase are well reproduced by combining the output from GULP with Euphonic, a python package which calculates phonon bandstructures, density of states and INS intensities from force constants [4]. In the high temperature phase, the INS data show a significant broadening of the phonon branches. We will compare this with the results of simulations based on a supercell lattice dynamical approach [2] to treat the rotational disorder explicitly.

[1] Seyf, H.R., Yates, L., Bougher, T.L., ... & Henry, A. Rethinking phonons: The issue of disorder. *Npj Comput Mater* 3, 49 (2017) <https://doi.org/10.1038/s41524-017-0052-9>

[2] Overy, A.R., Simonov, A., Chater, P.A., Tucker, M.G., & Goodwin, A.L. Phonon broadening from supercell lattice dynamics: Random and correlated disorder. *Phys. Status Solidi B* 254, 1770221 (2017) <https://doi.org/10.1002/pssb.201770221>

[3] Beake, E.O.R., Tucker, M.G., Dove, M.T., & Phillips, A.E. Orientational disorder in adamantane and adamantanecarboxylic acid. *Chem. Phys. Chem. Commun.* 18, 459 (2017) <https://doi.org/10.1002/cphc.201601219>

[4] <https://github.com/pace-neutrons/Euphonic>

1:45 PM *SF06.04.02

Exploring the Potential Energy Surface to Describe Phonon-Defect Scattering Georg Madsen; TU Wien, Austria

Defects play an important role in engineering the electronic properties of semiconductor materials. At the same time they can strongly influence the phonon scattering processes and thereby the thermal conductivity. In the talk, I will highlight both the need for a global exploration of the potential energy surface (PES) governing the competing defect structures and how the details of the regions surrounding the defect atoms can change the scattering strength by orders of magnitude. I will discuss approaching this juxtaposition by a combination of an evolutionary strategy and machine learned force fields. The approach is based on modifying the covariance matrix adaption evolution strategy (CMA-ES) to suit the specific problem of point defects. I will furthermore introduce a fully differentiable neural network force field that can be trained both on energies and forces and it can accelerate both the PES exploration and the calculation of force constants.

[1] A. Kundu, F. Otte, J. Carrete, P. Erhart, W. Li, N. Mingo, G. K. H. Madsen, *Phys. Rev. Mater.* 3 (2019) p094602

[2] M. Arrigoni, G. K. H. Madsen, *npj Computational Materials* 7 (2021) p71

[3] H. Montes-Campos, J. Carrete, S. Bichelmaier, L. M. Varela, G. K. H. Madsen *J. Chem. Inf. Model* 62 (2022) p88

2:15 PM SF06.04.03

Unravelling the Impact of Disorder on the Electronic Properties Of Mixed-Metal Chalcogenides Adair Nicolson¹, Kazuki Morita², Seán R. Kavanagh^{1,2}, Aron Walsh² and David O. Scanlon¹; ¹University College London, United Kingdom; ²Imperial College London, United Kingdom

Mixed-metal mixed-anion systems have seen a significant rise in interest as ‘perovskite-inspired materials’ as are expected to combine the excellent stability seen in metal chalcogenide solar cells with the well-known performance of hybrid halide perovskite solar cells.^[1]

$\text{Sn}_2\text{SbS}_2\text{I}_3$ is a promising solution-processed photovoltaic absorber having achieved efficiency above 4% in initial devices.^[2] Theoretical work predicts that the material family of $\text{A}_2\text{BCh}_2\text{X}_3$ mixed-metal chalcogenides could also be ferroelectric, with $\text{Sn}_2\text{SbS}_2\text{I}_3$ having strong lattice polarization and large dielectric constants.^[3]

However, this family has not been rigorously explored resulting in confusion in the literature regarding the structure of these materials, with some works observing disorder in room temperature crystals.^[4] Without a proper description of the structure, prediction of the electronic properties cannot be accurately performed. Understanding the extent of the disorder in these systems is of key importance due to its tendency to quench favourable properties such as macroscopic polarisation.

Using Density Functional Theory, Cluster expansion and Monte Carlo techniques, we have systematically examined the cation disorder in $\text{Sn}_2\text{SbS}_2\text{I}_3$ for the first time and will discuss its likely impact on the potential for this material family to produce ferroelectric and photovoltaic devices.^[5]

References

[1] Nie, R.; Sumukam, R. R.; Reddy, S. H.; Banavoth, M.; Seok, S. I. Lead-Free Perovskite Solar Cells Enabled by Hetero-Valent Substitutes. *Energy Environ. Sci.* **2020**, *13* (8), 2363–2385.

[2] Nie, R.; Lee, K. S.; Hu, M.; Paik, M. J.; Seok, S. I. Heteroleptic Tin-Antimony Sulfoiodide for Stable and Lead-Free Solar Cells. *Matter* **2020**, *3* (5), 1701–1713.

[3] Kavanagh, S. R.; Savory, C. N.; Scanlon, D. O.; Walsh, A. Hidden Spontaneous Polarisation in the Chalcogenide Photovoltaic $\text{Sn}_2\text{SbS}_2\text{I}_3$. *Materials Horizons* **2021**

[4] Doussier, C.; Moëlo, Y.; Léone, P.; Meerschaut, A.; Evain, M. Crystal Structure of $\text{Pb}_2\text{SbS}_2\text{I}_3$, and Re-Examination of the Crystal Chemistry within the Group of (Pb/Sn/Sb) Chalcogeno-Iodides. *Solid State Sciences* **2007**, *9* (9), 792–803.

[5] Nicolson, A. T. J.; Morita, K.; Kavanagh, S. R.; Walsh, A.; Scanlon, D. O. Submitted (2022)

2:30 PM BREAK

3:00 PM *SF06.04.04

Influence of Defects on Thermal and Electrical Transport G. J. Snyder; Northwestern University, United States

Defects, such as point defects (impurity, vacancies or interstitial atoms) are well known to impede thermal and electrical transport in materials by scattering electrons and phonons. This is perhaps best documented in the study of thermoelectric materials where it is important to reduce phonon thermal conductivity without disrupting the electrical conductivity.

In semiconductors (such as thermoelectrics) or insulators, the electrical transport is determined by the defects. To make a n-type or p-type semiconductor we typically use point defects to introduce a slight valence imbalance that leads to excess electrons or holes. Often intrinsic defects such as vacancies, interstitials or antisite defects, provide the necessary carriers to make the semiconductor conducting. Most materials, however, require extrinsic dopants to be a good conductor and intrinsic defects often only make it more difficult. Sometimes intrinsic defects are so prevalent they are *killer defects* that prevent any dopant from making the material n-type or p-type. By understanding that atomic chemical potentials influence defect energy and also define regions in phase diagrams we can use *phase boundary mapping* to explore all the possible thermodynamic defect states of a material to avoid killer defects. The most dramatic demonstration of this is the discovery of high performance thermoelectric Mg_3Sb_2 which only occurs in Mg-rich Mg_3Sb_2 where Mg-vacancies are suppressed.

Point defects are also well known to reduce thermal conductivity in solid solution alloys. Although the random distribution of atoms is essential to scatter phonons, the simple analytic theory explains why thermal conductivity is not simply correlated to entropy in high entropy alloys. For a full spectrum engineering of phonon scattering from lower dimension defects, such as line defects (dislocations) and planar defects (grain boundaries) must also be used and better understood. The phonon scattering of dislocations is much less studied. However, from simple dimensionality arguments it can be shown that the T^2 temperature dependence observed in polycrystalline materials probably arises from periodic dislocation arrays. This mechanism provides a simple replacement for the commonly used diffuse mismatch model that is more physical as it predicts that low energy, low angle grain boundaries scatter phonons less than high energy, high angle grain boundaries.

3:30 PM SF06.04.05

Ab Initio Models of Orientational Order and Phase Transitions in Hybrid Piezoelectric Materials Kasper Tolborg and Aron Walsh; Imperial College London, United Kingdom

Piezoelectric materials interconverting electrical and mechanical energy find applications in diverse areas as sensors, actuators, and high precision motors. Current state-of-the-art piezoelectric materials are made from lead-based ceramics, which pose significant environmental issues and precludes design of biocompatible devices. Recent progress in molecular and hybrid organic-inorganic piezoelectric materials have led to discovery of new materials with properties rivaling the lead-based ceramics, and with the additional prospects of being solution processable, flexible, and potentially biocompatible [1,2]. However, conventional computational methods fail to predict their large piezoelectric response [3], and pertinent phase transitions to disordered, centrosymmetric phases appear near or above room temperature, which may hamper their practical applications. Thus, proper computational modelling of this materials class must include nanoscale effects for response properties, and entropic effects to phase stability [4].

Here, we present the development of ab initio models for the ordering of dipolar molecules in hybrid piezoelectric materials. Based on model Hamiltonians fitted to density functional theory (DFT) data and Monte Carlo simulations, we predict and rationalise the order-disorder phase transitions in these materials. We show that a model Hamiltonian based on internal energies calculated from DFT fails to quantitatively reproduce phase transition temperatures, whereas inclusion of vibrational free energy effects improves the agreement with experiment significantly. This highlights the importance of vibrational entropy in describing phase stability for a materials class seemingly driven by configurational entropy.

Besides prediction of phase stability, our model Hamiltonian also provide insights into the strong piezoelectric response, which has been reported to be influenced by metastable phases [3].

[1] Y.-M. You, W.-Q. Liao, D. Zhao et al., *Science*, 2017, **357**, 306-309

[2] W.-Q. Liao, D. Zhao, Y.-Y. Tang et al., *Science*, 2019, **363**, 1206–1210.

[3] P. S. Ghosh, S. Lisenkov, I. Ponomareva, *Phys. Rev. Lett.*, 2020, **125**, 207601

[4] K. Tolborg, J. Klarbring, A. Ganose, A. Walsh, *ChemRxiv*, 2022, 10.26434/chemrxiv-2022-vw0dg

3:45 PM SF06.04.06

Accelerated Densification in Nanocrystalline Ni Challenges Organic Burn-Off Yannick Naunheim and Christopher A. Schuh; MIT, United States

Nanocrystalline metals are high defect-density materials due to the numerous grain boundaries and interfaces that provide rapid-diffusion kinetics as compared to their polycrystalline counterparts. In this talk, we present a set of Ni-base powders and alloys that are produced via sintering of high-energy ball milled powders. Due to the large plastic deformation, the powders are nanocrystalline and the consolidation is accelerated by structural refinement. Some alloys are further out of chemical equilibrium through mechanical alloying and supersaturation with an immiscible solute. These highly-driven powders evolve during a sintering cycle and undergo a kinetically accelerated phase-evolution leading to low-temperature onset of densification. In some of the sintered powders, the fast consolidation can compete with organic burn-off, which is a new challenge to additive manufacturing, such as for binder jetting. We will discuss strategies to address the competition between rapid consolidation and organic volatilization.

4:00 PM DISCUSSION TIME

4:15 PM SF06.04.08

Optimized Lithography-Free Fabrication of Sub-100 nm Nb_2O_5 Nanotube Films as Negative Supercapacitor Electrodes—Tuned Oxygen Vacancies and Cationic Intercalation Nageh K. Allam, Doha M. Sayed and Kholoud E. Abousalem; American University in Cairo, Egypt

The direct growth of sub-100 nm thin-film metal oxides has witnessed a sustained interest as a superlative approach for the fabrication of smart energy storage platforms. Herein, sub-100 nm Zr-doped orthorhombic Nb_2O_5 nanotube films are synthesized directly on the Nb-Zr substrate and tested as negative supercapacitor electrode materials. To boost the pseudocapacitive performance of the fabricated films, supplement Nb^{4+} active sites (defects) are subtly induced into the metal oxide lattice, resulting in a 13% improvement in the diffusion current at 100 m V/s over that of the defect-free counterpart. The defective sub-100 nm film (H-NbZr) exhibits areal and volumetric capacitances of 6.8 mF/cm² and 758.3 F/cm³, respectively. The presence of oxygen-deficient states enhances the intrinsic conductivity of the thin film, resulting in a reduction in the band gap energy from 3.25 to 2.5 eV. The assembled supercapacitor device made of nitrogen-doped activated carbon (N-AC) and H-NbZr (N-AC//H-NbZr) is able to retain 93, 83, 78, and 66% of its first cycle capacitance after 1000, 2000, 3000, and 4500 successive charge/discharge cycles, respectively. An eminent energy record of approximately 0.77 $\mu W h/cm^2$

at a power of 0.9 mW/cm² is achieved at 1 mA/cm² with superb capability.

SESSION SF06.05: Poster Session
Session Chairs: Cody Dennett and Lucas Lindsay
Tuesday Afternoon, November 29, 2022
8:00 PM - 10:00 PM
Hynes, Level 1, Hall A

SF06.05.01

Computational and Characterization Methods to Quantify Chemical Ordering in Compositionally Complex Alloys Anne Barnett¹, Daniel Foley¹, Elaf Anber¹, Yevgeny Shlafstein^{1,2}, Peng Yi¹, Michael L. Falk¹ and Mitra L. Taheri¹; ¹Johns Hopkins University, United States; ²Columbia University, United States

Non-uniform, chemically complex alloy landscapes are challenging to fully characterize. Difficulty arises in confirming the ordering mechanisms, in quantitatively describing order, and in rigorously relating such order to experimental measurement of reciprocal space lattices patterns. Precession Electron Diffraction (PED) can extract quantitative ordering information in metallic systems, including slight changes in ordering that occur at high spatial resolution, but there remains a need for more evidence of local behavior. Focusing on binary and ternary alloys, hybrid Monte-Carlo/Molecular Dynamics simulations were performed to generate experimentally comparable models to compliment conclusions about the ordering signatures previously found using PED. To assign a value to systems with varied degrees of disorder, the Warren-Cowley parameter was used to quantify chemical short-range order by considering pairwise bonding tendencies in these systems. This parameter is well-defined mathematically but does not directly provide any physical interpretation. We use the Warren-Cowley parameter to benchmark the chemical state of systems generated both experimentally and computationally. Modeling results, experimental PED patterns, and SRO parameters illustrate the benefits of a combined methodology to facilitate quantification of systems with intermediate levels of disorder. This analysis also provides important information about the local nature of chemical ordering in highly complex, metallic systems.

SF06.05.02

Enhanced Photocatalytic Performance of Transition Metal-Doped CeO₂ Nanoparticles Jeong-Woo Nam¹, Jeong Min Ha¹, Youngsoo Kim¹, Hangil Lee² and Young-Sang Yoon¹; ¹Yeongnam University, Korea (the Republic of); ²Sookmyung Women's University, Korea (the Republic of)

Since CeO₂ nanoparticle is widely used as photocatalyst, many researchers have tried to improve the photocatalytic activity of CeO₂ nanoparticles by transition metal ion doping. It is well known that photocatalytic activity is related to oxygen vacancies on nanoparticles. In this study, CeO₂ nanoparticles doped with Cr (Cr@CeO_x) or Fe (Fe@CeO_x) were prepared to check the enhanced photocatalytic activity by increasing oxygen vacancies compared to CeO₂ nanoparticles.

The change in the crystal structure for all the samples was identified by the X-Ray diffraction (XRD), in which all the XRD patterns correspond to typical cubic-structure of CeO₂. In Raman spectra, a prominent band at ~467 cm⁻¹ by the F_{2g} Raman active mode in cubic-structure of CeO₂ and a D band at around 250 and 600 cm⁻¹ appearing as its oxygen vacancies are observed. In particular, the F_{2g} peak of Cr@CeO_x and Fe@CeO_x is shifted to a slightly lower wavenumber, resulting from the increase in oxygen vacancies due to CeO₂ lattice distortion by dopants. Therefore, for all the CeO₂ nanoparticles, the characteristic cubic-structure is reserved with the change in the amount of oxygen vacancies.

In addition, the local electronic structures in the unoccupied state regions of the transition metal-doped CeO₂ nanoparticles were compared with the those of CeO₂ nanoparticles using X-Ray absorption spectroscopy (XAS). Based on the ratio of the 4f and 5d-e_g peaks related to oxygen vacancies in the O K-edge spectra, we verified that oxygen vacancies increase by transition metal ion doping.

Finally, we examined the photocatalytic degradation(PCD) rates of 5-hydroxymethylfurfural in the presence of each CeO₂ samples. With PCD results, we confirmed that the transition metal-doped CeO₂ show the excellent PCD efficiency compared to CeO₂.

SF06.05.03

Physical Unclonable Function from Disordered Silane-Based Self-Assembled Monolayers Subin Lee, Juhyung Seo and Hocheon Yoo; Gachon University, Korea (the Republic of)

As the quantity of the information increases, it is crucial to implement low-power operation devices. Here, we present physical unclonable function devices using two self-assembled monolayer (SAM) materials, octadecyl trichlorosilane (ODTS) and 1H,1H,2H,2H-Perfluorooctyltriethoxysilane (PFOTES), which have different chain lengths, terminal functional groups, and dipoles. The surface was treated by UV-ozone before the SAM coating process to make it hydrophilic on a p-doped Si substrate. The current value at zero voltage bias was evaluated to utilize the electrical characteristics of the electrical characteristics of the different SAMs on the p-doped Si substrate without an external electric field. The current values of the device-to-device were dispersed based on a specific current. We performed atomic force microscope (AFM), Kelvin probe force microscopy (KPFM), Raman spectroscopy, X-ray photoelectron spectroscopy, contact angle, and ultraviolet-visible spectroscopy to analyze the mixed SAM structure and its electrical properties. We verified the current dispersion caused by dipole affection, not the physical accumulation of SAM materials through the AFM and KPFM patterns of Z-phase and potential on the device surface. Compared to the median value each security key, higher value is defined as the state '1' whereas lower value is defined as the state '0'. The uniqueness and security were evaluated by the 50-66 % of uniformity and 41.1-52.9 % of inter-HD.

SF06.05.06

Synthesis of Self-Modified Black BaTiO_{3-x} Nanoparticles and Effect of Oxygen Vacancy for the Expansion of Piezocatalytic Application Myeongjun Ji, Jeong Hyun Kim, Cheol-hui Ryu and Young-In Lee; Seoul National University of Science and Technology, United States

Piezocatalysis has been considered a promising green and sustainable technology because of its ability to promote the passive conversion of natural mechanical energy into electrochemical energy. Among various piezoelectric materials, barium titanate (BaTiO₃) nanoparticles have been actively studied as a piezocatalyst due to their non-toxicity, physicochemical stability, and high piezoelectric potential. However, the low carrier concentration of BaTiO₃ is a significant drawback that limits their applicability as piezocatalyst only in ultrasonic systems, which can thermally excite BaTiO₃ via cavitation.

Although the ultrasonic system can simultaneously supply thermal energy for the generation of carriers and high pressure as the driving force for chemical reactions, this system requires bulky, and expensive facilities that result in space constraints. Therefore, a novel strategy that can overcome the limitation of material is still necessary for the development of a high-performance piezocatalyst that convert the various natural low mechanical energy.

Self-modification is a useful technique to modulate the electrochemical properties of oxide materials via the introduction of atomic defects such as oxygen

vacancies and/or low valence metal ions. However, only a few reports on the synthesis of self-modified black BaTiO_{3-x} are available, and investigations on the piezocatalyst performance of black BaTiO_{3-x} nanoparticles have not yet been reported. Moreover, the conventional synthesis methods of black metal oxides depend on the post-treatment methods to form the atomic vacancies. Since these methods require complicated and prolonged processes that are inappropriate for practical application, it is still necessary to develop facile and versatile synthesis methods for the synthesis of black metal oxide. In this study, the self-modified black BaTiO_{3-x} nanoparticles were successfully synthesized by a simple solid-state reaction using defective raw materials in a reducing atmosphere. From these results, the initial atomic defects in raw material were demonstrated as the critical factor to determine the size and defect concentration of final products. Therefore, the synthesis mechanism of black BaTiO_{3-x} was systematically investigated in terms of the initial defect concentration of raw material. In order to study the effect of atomic defects on piezocatalytic performance, the piezocatalytic performance of self-modified BaTiO_{3-x} nanoparticles was evaluated under an ultrasonic system and stirring system compared with commercial white BaTiO₃ nanoparticles. The piezocatalytic performance of self-modified BaTiO_{3-x} nanoparticles showed a higher degradation efficiency of about 4.28 times than white BaTiO₃ under the stirring system, and the effect of self-modification was clearly identified. This study demonstrated a pioneering strategy that can promote the practical applications of BaTiO₃ as a piezocatalyst in an environment that requires low energy harvesting.

SF06.05.07

Implications of Water Intercalation in Graphene-Based Biomedical Devices Long Term Performance [Elena del Corro](#)¹, Marta D. Fernández¹, Anton Guimera², Xavier Illa³ and Jose A. Garrido¹; ¹ICN2, Spain; ²CNM, Spain; ³CIBER, Spain

Due to its aspect ratio, i.e. large surface exposure for a minimal thickness, events occurring at the graphene interface are of crucial interest, especially for its application in sensing devices, where differently supported graphene is in direct contact with the atmosphere or even with aqueous electrolyte containing ions and molecules of different nature. Among the existing variety of interfacial events associated to graphene, water intercalation between graphene and the supporting material, its mechanism and implications, needs to be fully understood. Water intercalation in graphene causes decoupling from the substrate, which may derive in desirable effects such as doping or strain release. However, such decoupling can also, compromise the stability and, thus, the lifetime of the graphene electronic devices.

Me and my group develop new technologies based on graphene for neuro-medical applications, where the durability of the neural probes is a required aspect, especially for chronic implants. In this work we aim to address water intercalation phenomena in our graphene technology, by combining simultaneous electrical characterization with *in-operando* Raman spectroscopy and Kelvin Probe Force microscopy.

Besides possible water residual confined between graphene and the substrate at the moment of the transfer (wet), we aim to evaluate the entrance of water during the device characterization in aqueous electrolyte. To this end, two possible routes for the water to enter are evaluated: graphene point defects and graphene edges. Graphene based solution field effect transistors (gSGFETs) have been fabricated on Si/SiO₂ substrates with different width to length ratios and the graphene channel has been passivated (SU8 and polyimide) using different configurations, protecting all or some of the graphene edges. Additionally, UVO treatment is used to generate vacancies in the graphene honeycomb that could act as additional routes for the water penetration.

Electrical and electrochemical characterization of the devices will be combined with Raman spectroscopy that accounts for graphene-substrate decoupling through the energy of the 2D phonon, and KPFM to obtain the graphene work function which is substrate dependent (water versus silicon, in this case). Aging agents such as high temperature will be used to mimic chronic operando conditions and study the effect of water intercalation .

This work aims to provide valuable information that will help in the development of new fabrication protocols designed for minimizing water intercalation events, thus extending the lifetime of our technology in its operational environment.

SF06.05.08

Computational Investigation of Short-Range Order Suppression in High-Entropy Disordered Rocksalt Cathode Materials [Alexander Squires](#)^{1,2} and David O. Scanlon^{2,3}; ¹University College London, United Kingdom; ²Faraday Institution, United Kingdom; ³Thomas Young Centre, United Kingdom

Disordered rock salt cathode materials are perceived as excellent candidates for application as future lithium-ion cathode materials enabling chemistries beyond commercial Ni-Mn-Cotechnologies [1]. Suppressing short-range order (SRO) in disordered rocksalt cathode materials is crucial to maximizing their performance. Disordered rocksalt cathodes can possess long-range “0-TM” percolation networks, which allow for fast and facile lithium diffusion, ensuring a good rate capability and high capacity [2]. SRO is typically associated with reduced connectivity of these 0-TM networks [3]. Alloying many transition metals together across the cation sublattice in a rocksalt structure, creating so-called high entropy rocksalts, has been proposed as a method for minimizing SRO [4, 5]. This approach is expected to improve Li transport through the bulk by suppressing the formation of a single dominant SRO type by increasing competition between a larger number of transition metal species [6]. While the high-entropy cathode concept has been shown to have initial promise, typically studies on these materials have not gone far beyond “proof of concept” stages, identifying optimal compositions remains an open question. When designing new energy materials which contain many component elements, working within sustainability and cost constraints becomes even more important. Many transition metals with favorable electrochemical properties are subject to high and volatile prices, with supply chain issues, precluding their use of truly sustainable cost-effective energy storage technologies [7]. Taken together, this poses an exciting design challenge in identifying low-cost, high-entropy rocksalt compositions which can remain insensitive to market fluctuations and supply chain issues, while retaining excellent electrochemical performance. In this work, we use cluster-expansion parameterized Monte Carlo simulations to examine the connectivity of the Lipercolation network when varying the number and concentration of different transition metals. We then assess the electrochemical properties and stability of these systems using first-principles approaches. Also included in our cathode design is an analysis of time-series data for the cost and availability of the component elements to ensure that not only are any proposed compositions excellent candidate cathode materials but also should represent cost-effective potential future cathodes.

1. Clément, R. J. et al. 2020. “Cation-Disordered Rocksalt Transition Metal Oxides and Oxyfluorides for High Energy Lithium-Ion Cathodes.” *Energy & Environmental Science* 13 (2): 345–73.

2. Lee, Jinhyuk et al. 2014. “Unlocking the Potential of Cation-Disordered Oxides for rechargeable Lithium Batteries.” *Science* 343 (6170): 519–22.

3. Ji, Huiwen, et al. 2019. “Hidden Structural and Chemical Order Controls Lithium Transport in Cation-Disordered Oxides for Rechargeable Batteries.” *Nature Communications* 10 (1): 592.

4. Wang, Qingsong, et al. 2019. “Multi-Anionic and-Cationic Compounds: New High Entropy Materials for Advanced Li-Ion Batteries.” *Energy & Environmental Science* 12 (8): 2433–42.

5. Sarkar, Abhishek, et al. 2018. “High Entropy Oxides for Reversible Energy Storage.” *Nature Communications* 9 (1): 3400.

6. Lun, Zhengyan, et al. 2021. “Cation-Disordered Rocksalt-Type High-Entropy Cathodes for Li-Ion Batteries.” *Nature Materials* 20 (2): 214–21.

7. Murdock, Beth E., et al. 2021. “A Perspective on the Sustainability of Cathode Materials Used in Lithium-ion Batteries.” *Advanced Energy Materials*, September, 2102028

SF06.05.10

Tailoring Resistive Switching in Cerium Oxide Films by Grain Boundary Engineering [Hongyi Dou](#)¹, Markus Hellenbrand², Ming Xiao², Zedong Hu¹, Aiping Chen³, Judith L. MacManus-Driscoll², Quanxi Jia⁴ and Haiyan Wang¹; ¹Purdue University, United States; ²University of Cambridge, United Kingdom; ³Los Alamos National Laboratory, United States; ⁴University at Buffalo, The State University of New York, United States

Resistive random-access memory, in particular valence change memory made of transition metal oxides, has great potential for applications in next-generation memories and neuromorphic computing. In valence change memory, the different resistance states are realized by the drift and migration of oxygen vacancies under different electrical fields. Defect engineering methods utilizing defect-defect interaction in tuning the concentration and transport of the oxygen vacancies have been studied extensively. Despite the efforts on investigating the impact of single extended defects, such as dislocations and grain boundaries, studies of the collective contribution of grain boundaries in different grain morphologies are still missing. Here, three different grain morphologies: “network”, “scaffold”, and “island” are realized in CeO₂ by simply tuning the growth temperature to investigate the impact of grain morphologies on resistive switching performance. Under the same oxidizing environment during growth, the devices with the three grain morphologies demonstrated vastly different resistive switching behaviors. The experimental results show the best overall resistive switching performance in the “scaffold” structure, where the vertical grain boundaries extended through the film helps with proper oxygen vacancy concentration as well as oxygen vacancy migration under external bias. The coexistence of both interfacial and filamentary switching modes found only in the devices with the “scaffold” structure further confirms its contribution. In contrast, the “network” (“island”) structure results in excessive (insufficient) oxygen vacancy concentration and oxygen vacancy migration paths. The research provides guidance for grain boundary engineering of the oxide switching material to tune the resistive switching performances for memory and neuromorphic computing applications.

SF06.05.11

Investigation of Thermal Stress Effects During Annealing of HfO₂ Thin Film Using Molecular Dynamics Simulations [Kiran Raj](#) and Kwon Yongwoo; Hongik University, Korea (the Republic of)

Hafnia is the major high-k dielectric material in mainstream semiconductor devices in logic and memory. Recent three-dimensional device structures require a few nanometers-thick conformal films on nonplanar substrates. Representative examples are gate oxide in multi-bridge channel field effect transistor (MBC-FET) for next-generation complementary metal-oxide-semiconductor (CMOS) technology and blocking oxide in vertical-NAND flash memory. Such thin high-k dielectric film is vulnerable to thermal stress generated by Joule heating during the switching operations. Also, the thermal stress may result in defect formation at the nanoscale, which may further give rise to leakage current issues. Moreover, the presence of intrinsic residual stress resulting from the fabrication process has been found to cause the failure of thin films by cracking or delamination. We employ molecular dynamics simulations using LAMMPS to investigate the effect of the thermal stress during the annealing of amorphous hafnia and silica-made thin films. The amorphous structures are modeled using the Charge-Optimized Many-Body (COMB) potential that facilitates variable charge by allowing charge exchange between the constituent atoms. In this study, we report the deformation/fracture behavior of the thin films at various annealing temperatures. Our study may provide insights into the thermal issues prevalent in thin films owing to the high-temperature gradient during the operation or fabrication and also address the ways to alleviate such undesirable deformation behavior.

SESSION SF06.06: Novel Structural and Functional Behaviors
Session Chairs: Lucas Lindsay and Lilia Woods
Wednesday Morning, November 30, 2022
Sheraton, 3rd Floor, Fairfax A/B

8:45 AM *SF06.06.01

Multinary Chalcogenides: a Fruitful Playground for Property Tuning via Cation Substitution [Lilia Woods](#); University of South Florida, United States

Multinary chalcogenides offer a vast selection of materials with diverse properties due to flexibility of structure, morphology, composition, doping, and other factors. By employing a hierarchical strategy based on cross-cation substitution we can build complex ternary and quaternary systems starting with simpler II-VI binary materials. Within this fruitful approach, I₂-II-IV-VI₄, I-II₂-III-VI₄, and I-III-IV-VI₄ classes of materials can be obtained. While I₂-II-IV-VI₄ has been extensively explored in the past, I-II₂-III-VI₄ and I-III-IV-VI₄ systems are much less studied. In this presentation, we present first principles simulations to examine the structural diversity of these newer classes of materials. Several metastable phases that are also dynamically stable, are found for I-II₂-III-VI₄. Compositions from the I-III-IV-VI₄ class are also studied showing highly defective chalcopyrite-like structures among others. Simulations for the electronic and phonon properties are also conducted, which help us find common features and mechanisms that limit the transport in these materials. Given the inherently low thermal conductivity, electronic property tuning possibilities, and earth-abundant constituents in many compositions, these materials are examined in the context of thermoelectricity as potential candidates for environmentally friendly energy conversion devices.

Support from the US National Science Foundation under Grant No. DMR-1748188 is acknowledged.

9:15 AM SF06.06.02

Quantifying Long- and Short-Range Cationic Disorder in (Ag,Cu_{1-x})₂ZnSnSe₄-Based Kesterite Lattice [Shaham Quadir](#)¹, Mohammad Qorbani¹, Amr Sabbah², Kuei-Hsien Chen² and Li-Chyong Chen¹; ¹National Taiwan University, Taiwan; ²Academia Sinica, Taiwan

Research on earth-abundant and non-toxic kesterite-based Cu₂ZnSn(S,Se)₄ (CZTS/Se) solar cells has recently drawn significant attention in the photovoltaic sector. However, the large open-circuit voltage deficit ($V_{OC,def}$) issue in CZTS/Se solar cell remains unsolved even after a decade of research and prospects. This study focuses on investigating the fundamental limitations of CZTSe solar cells, in particular the large V_{OC} deficit. One of the reasons that substantially impairs the photovoltaic (PV) performance of CZTSe is the occurrence of intrinsic point/cluster defects. Understanding the nature of and controlling cation disorder remains a crucial challenge for improving the PV performances. Herein, a cation substitution technique has been introduced to control and passivate the defect states in the bandgap of CZTSe by incorporating Ag. Different x values of (Ag_xCu_{1-x})₂ZnSnSe₄ (ACZTSe) materials were synthesized to provide a comprehensive understanding of defect states for ACZTSe. To determine the relationships among cation disorder, defect concentration, overall long-range crystallographic order, and local atomic-scale structure for (Ag_xCu_{1-x})₂ZnSnSe₄ (ACZTSe) material, the combination of neutron diffraction and synchrotron-based x-ray absorption techniques are implemented. The joint Rietveld refinement technique is used to quantify the concentration of defects in Ag-alloyed stoichiometric and non-stoichiometric Cu₂ZnSnSe₄ (CZTSe) powder samples. As the main outcome, the cation distribution was determined to quantify the intrinsic point defects. This directly shows that Ag effectively inhibits the high concentration of the deep Cu_{Zn}

antisite and promotes shallower defects such as Cu-vacancy (V_{Cu}), which is important for improved photovoltaic performance. Moreover, we studied the atomic-scale structure of ACZTSe as a function of composition using x-ray absorption spectroscopy (XAS). X-ray absorption near-edge structure (XANES) and extended X-ray fine structure (EXAFS) analyses of the nearest neighbor shell have been performed by the simultaneous fitting of all K-edges to determine oxidation states, charge transfer mechanism (reflecting the occupancy of electronic states at/near the probed element) and structural parameters, respectively. Temperature-dependent photoluminescence has been performed to understand the defect states inside the bandgap. Finally, the combination of these techniques provided new structural insight, useful for controlling disorder in kesterite-based materials. This information can be applied in diverse energy-related applications such as solar cells, photoelectrochemical water splitting, thermoelectrics, optoelectronics, and advanced Li-ion batteries.

9:30 AM SF06.06.04

Structural Dynamics of Solid Ionic Conductors Roman Korobko, Rituraj Sharma, Thomas M. Brenner and Omer Yaffe; Weizmann Inst of Science, Israel

Solid ionic conductors are commonly crystalline compounds in which electric current is carried by charged atoms. Since the current requires a mass transfer of the conducting ions, the rest of the atoms presumably remain in place to maintain a crystallographic structure. In this presentation, I will show how the structural dynamics influence the properties of selected solid ionic conductors, change local structure and symmetry, and thus contribute to the ionic conductivity.

Our research group uses a state-of-art custom-built Raman spectroscopy system to study structural dynamics and anharmonic effects. By applying modern experimental and computational techniques, we can detect relaxational and anharmonic motions of the ions, which were previously considered immobile. These discoveries contribute to a deeper understanding of the basic ionic conductivity mechanism of some important materials in the field of solid-state electrochemistry.

9:45 AM SF06.06.05

Polaronic States and Their Impact on Charge Carrier Mobility in Lithium Titanium Oxide Battery Electrodes Matthias Kick¹, Cristina Grosu¹, Christoph Scheurer² and Harald Oberhofer³; ¹Massachusetts Institute of Technology, United States; ²FHI Berlin, Germany; ³University Bayreuth, Germany

Lithium-ion batteries are without a doubt a key technology in the coming energy revolution. It is thus surprising that one of the more prevalent Li battery anode materials, reduced lithium titanium oxide (LTO, $Li_4Ti_5O_{12}$), is still poorly understood on a microscopic level. While recent theoretical and experimental evidence suggests that a polaron hopping mechanism is responsible for the increased electronic conductivity of reduced LTO (compared to pristine LTO), no such explanation exists for the concurrent improvements to the ionic mobility. In this computational study, we show that the presence of polaronic Ti^{3+} centers leads to a significant lowering of Li hopping barriers in both bulk and surface reduced LTO. In agreement with experimental observations our results also suggests that polaron formation upon lithiation of LTO leads to a similar reduction of barrier heights. Further, to gauge polaronic charge mobility, we compute the relative stabilities of different localization patterns and estimate polaron hopping barrier heights. Altogether, our analysis hints at a correlated movement of Li ions and polarons, highlighting LTO's potential for rational defect engineering.

10:00 AM BREAK

10:30 AM SF06.06.07

Liquid-Like Mass Transport, Without Melting, In Solid Metallic Films via Ultrafast Laser Enhancement of Point Defect Diffusion Abdul R. Ansari, Ben Torralva and Steven M. Yalisove; University of Michigan, United States

Ultrashort laser pulses (150 fs) at fluences below that needed to melt a material excite electrons into unoccupied states for brief moments of time significantly weakening bonding for possibly as long as 10 nanoseconds. The ions drift with their room-temperature velocity and create transient lattice disorder. Approximately 1-2% of the atoms in the high velocity tail of the Boltzmann distribution will have sufficient energy to create a Frenkel pair. Repeated irradiation leads to an accumulation of point defects and vastly increases (12 to 20 orders of magnitude) mass transport via an ultrafast laser enhanced diffusion mechanism.

Our previous work with semiconductors has demonstrated that repeated exposures of a gallium arsenide (GaAs) surface to ultrashort laser pulses leads to the generation followed by enhanced diffusion of point defects. The defects diffuse to the surface and their accumulation leads to morphological changes that are observed as Laser Induced Periodic Surface Structures (LIPSS). We have shown that high spatial frequency LIPSS (HSFL) are formed while irradiating GaAs with 1000 pulses. The diffusion process is electronically driven and occurs on timescales shorter than 10 ns, the time it takes for a majority of the excited carriers to equilibrate after irradiation. This suggests that the ultrafast laser enhanced diffusion coefficient is increased by up to 20 orders of magnitude over the room temperature value. This is the same order of magnitude value as diffusion in a melt. Hence we observe liquid-like mass transport while remaining in the solid phase.

This talk will show that a similar process can also work in metals, leading to atomic scale mixing from defect- and disorder-driven departures from a perfect lattice. We set out to study this mixing with ultrashort laser irradiation using fluences below that needed to melt a material in a single exposure. We chose a well studied system (Ni/W) that offers the promise of thermally stable nanostructured materials previously grown with electrochemical methods [1].

Alternating film stacks of Ni and W were deposited onto a glass substrate by magnetron sputter deposition. A working gas pressure of 2 mTorr and 3 mTorr was used for growing the Ni and W, respectively. A 100 nm Ni film was first deposited on the glass substrate as a heat sink. 12 alternating layers of Ni and W were then deposited on the heat sink such that a layer of W was present on the surface. The Ni layers were 2.5 nm and the W layers were 1.5 nm thick so that the layers are an average of 27 at% W. Multiple pulses from a Ti:Sapphire laser with $\lambda = 780$ nm and pulse duration $t = 150$ fs were used to irradiate the surface of the stack, on the W layer.

We will present scanning electron micrographs showing that irradiating the alternating film stack with 1,000 pulses leads to the formation of HSFL on the surface of the films. Using transmission electron microscopy, we will show that the HSFL is composed of the top 6 layers, meaning that the laser affected the material to a depth of only ~12 nm below the surface. Furthermore, we will show with x-ray dispersive spectroscopy that the layers are mixed. This solid-state mass transport enhancement process will be discussed in the context of ultrashort lattice disordering, bond softening, diffusion and defect generation mechanisms.

[1] A. J. Detor, M. K. Miller, and C. A. Schuh, "Solute distribution in nanocrystalline Ni-W alloys examined through atom probe tomography," *Philos. Mag.*, vol. 86, no. 28, pp. 4459-4475, Oct. 2006, doi: 10.1080/14786430600726749.

10:45 AM SF06.06.08

Defect-driven Biocidal Enhancement of Cuprous Oxide Brian Lejeune, Xiaoyu Zhang, Su Sun, Julia Hines, Ashlyn Reilly, Heather Clark and Laura Lewis; Northeastern Univ, United States

Non-stoichiometric metal-oxides are known for their enabling roles in energy conversion and storage devices, sensors and catalysts, among other

applications. Indeed, the compound Cu_2O (cuprous oxide or cuprite), which is copper-deficient in its native state, has been documented as a contact-kill antimicrobial material; however the origins of its biocidal effectiveness are not well understood. To this end, it is of interest to investigate how cuprite's antipathogenic character scales with the density of copper vacancies; these defects are hypothesized to donate highly elevated local electrical potential that disrupts cell membranes and/or virus protein shells. In this work, commercial cuprous oxide powder (99.99%) was processed using high-energy cryomechanical milling to amplify lattice disorder and was subsequently incorporated into coatings. Coatings made from these processed powders demonstrate a self-sterilizing response to *E. coli* bacteria that is 4x (400%) faster than coatings made from unprocessed powder. No viable bacteria (> 99.999% (5-log10) reduction) are detected in bioassays performed after two hours of exposure of *E. coli* to coatings of processed cuprous oxide, while a greater than 99% bacterial reduction is achieved within 30 minutes of exposure. Further, these coatings are hydrophobic and need no external energy input to activate their contact-kill capability. The upregulated antibacterial response of the processed powders is positively correlated with extensive induced crystallographic disorder and microstrain in the Cu_2O lattice, and is accompanied by color changes that are consistent with an increased semiconducting bandgap energy. Electron microscopy reveals that cryomilled powder consists of well-crystallized nanoscale regions enmeshed within a highly lattice-defective particle matrix. These results highlight avenues for further enhancement of the antipathogenic capability of this abundant, inexpensive, robust and easily handled metal-oxide powder for wider deployment in contact-kill surfaces.

Funding Acknowledgement: This work was conducted at Northeastern University under the auspices of NSF DMR Grant #2029194 (for determination of fundamental materials aspects) and DEVCOM Soldier Center Contract Agreement W911QY-19-9-0011 (for experiments related to preparation of coatings).

11:00 AM SF06.06.09

Ionic Peltier Effect in Liquid Electrolytes [Zhe Cheng](#), Arghya Patra, Beniamin Zahiri, Paul Braun and David Cahill; University of Illinois at Urbana-Champaign, United States

The Seebeck effect in ionic thermoelectric (i-TE) materials has been extensively studied recently because Seebeck coefficients in i-TE materials are found to be orders of magnitude higher than their counterparts in electronic thermoelectric materials. However, the reverse phenomenon of the Seebeck effect, namely the Peltier effect, remains unexplored in i-TE materials partly due to the experimental difficulty in thermal measurements. Here, we report the first experimental observation of the ionic Peltier effect at the lithium metal-liquid electrolyte interfaces (LiPF_6 and LiTFSI) by developing an ultra-sensitive differential temperature metrology (10 uK temperature resolution). By sandwiching liquid electrolytes between two lithium metal plates to form a coin cell, we can measure the Peltier heat generated in the ionic systems quantitatively by measuring the temperature difference of the two sides of the coin cell with an applied electrical current. To make the effect of the parasitic Joule-heating negligible in the measurements, small electrical currents (mA-scale) are applied because Peltier heat is proportional to current while Joule-heating is proportional to the square of current. The results show that the observed Peltier heat strongly depends on the types and concentrations of electrolytes dissolved in the supporting solvents. Our work sheds light on the thermoelectric effects with ions as the energy carriers, and will impact energy conversion and storage applications such as ionic thermoelectric materials and batteries.

11:15 AM SF06.06.10

Obtaining the Charge Carrier Diffusion Length in Disordered Semiconductors from Photoconductivity Transients [Hannes Hempel](#), Markus Schleunig, Moritz Kölbach, Fatwa F. Abdi, Roel van de Krol, Klaus Schwarzbarg, Rainer Eichberger and Dennis Friedrich; Helmholtz Zentrum Berlin, Germany

Long diffusion lengths of photo-excited charge carriers are crucial for high power conversion efficiencies of photoelectrochemical and photovoltaic devices. In ordered materials, the diffusion length is usually determined from the product of charge carrier lifetime and mobility, which both can be measured by time-resolved photoconductance measurements. However, in disordered or defect-rich materials effects such as (multiple-)trapping, carrier localization and polaron formation can lead to time-varying mobilities and lifetimes that are not accounted for in the conventional analysis. Therefore, here, a generalized analysis is presented that is valid for time-dependent mobilities and time-dependent lifetimes. It determines the diffusion length directly from the integral of a photoconductivity transient, regardless of the nature of carrier relaxation. This approach is presented on amorphous silicon, a prototype of disordered materials, and BiVO_4 , one of the most studied photoanode materials for solar water splitting. To this end, photoconductivity transients are measured from 100 fs to 100 μs by the combination of time-resolved terahertz (TRTS) and microwave spectroscopy (TRMC). Our generalized analysis allows monitoring the temporal evolution of the charge carrier displacement, which converges for both materials after ~ 100 ns to a diffusion length of a few tens of nanometers. For BiVO_4 , the obtained diffusion length is significantly shorter than the typical thin film thickness, which rationalizes the photocurrent loss in the corresponding photoelectrochemical device. Our novel analysis significantly simplifies the determination of the diffusion length and will allow a robust comparison between material classes subject to different relaxation processes.

11:30 AM SF06.06.11

Mechanism Elucidation of Resistance Relaxation Phenomenon in Pt/Nb-doped SrTiO_3 Junctions for AI Applications [Hayato Nakamura](#), Hiromasa Aoki, Hiroyuki Kai and Kentaro Kinoshita; Tokyo University of Science, Japan

Resistive switching (RS) devices of a Schottky junctions consisting of a doped wide bandgap oxide such as SrTiO_3 (STO) and a high work function metal such as Pt have been the subject of considerable interest in terms of both non-volatile and volatile resistance relaxation nature. When used as general non-volatile memory, the continuously tunable write/erase characteristics are advantageous for multibit application [1]. In this sense, resistance state retention characteristics are important and improving resistance volatility is crucial. On the other hand, when used in new computational paradigm for the breakthrough of von Neumann-type computing, controllability of resistance relaxation phenomenon is critically important. It has been reported that the resistance relaxation phenomenon after RS in Pt/Nb(0.5 wt%)-doped STO can be used to mimic synaptic plasticity for AI applications [2]. The development of nanoscale devices with this neuromorphic functionality is the basis for hardware implementation of artificial neural networks. For practical application, details of the resistive relaxation phenomenon is required to be understood. Schottky parameters (SPs) such as barrier height (SBH) and depletion width (W_D) can be determined by combining current-voltage (I - V) and capacitance-voltage (C - V) measurements. To date, this has been conducted only for two extreme states, high-resistance states (HRS) and low-resistance states (LRS) [3]. Changes in SPs with subsequent resistance relaxation have not been reported.

In this study, sequential I - V and C - V measurements of a Pt/Nb:STO junction were performed on the same junction to extract time evolution of SPs during the relaxation. This is the first report on the time dependence of SPs as a function of resistance during the relaxation. I - V and C - V measurements were performed by the 2-terminal method using a semiconductor parameter analyzer and impedance analyzer, respectively. Since the resistance value changes logarithmically after RS, the switching unit was used to instantly switch to the circuit for C - V measurements after setting the junction to HRS or LRS using the circuit for I - V measurements.

The relaxation phenomenon until 1000 s after RS was sequentially captured. All SPs such as SBH and W_D linearly depend on the logarithm of time as the change in resistance during the relaxation was. After setting to LRS, SBH was estimated to be changed from 0.57 to 0.63 eV and from 0.81 to 0.87 eV by

the I - V and C - V measurement, respectively, showing an increase of 0.06 eV independently of measurement methods. Furthermore, the ideal factor n of the Schottky barrier was also decreased from 3.2 to 2.9 with increasing SBH. Considering the time dependence of n , the donor concentration (N_D) decreased from $7.5 \times 10^{19} \text{ cm}^{-3}$ to $6.5 \times 10^{19} \text{ cm}^{-3}$ and W_D increased from 19.0 nm to 20.8 nm after LRS. This change is considered to be caused by the trapping of electrons in the defects, which were once de-trapped by the application of forward bias to set the device to LRS. The revealed continuous change in the SPs suggests that resistance relaxation is brought about by electron trapping/de-trapping to/from oxygen defects rather than oxygen vacancy diffusion that likely gives discontinuity. This is consistent with the result of impedance spectroscopy measurement that no peak was observed in imaginary part of the dielectric constant for the frequency range of 10 Hz-5 MHz.

The present study showed that time dependent SPs of metal/oxide junctions undergoing relaxation can be obtained by the simple method. We are now investigating the time dependence of SPs on doping concentration, electrode type, etc., to establish a method to control the relaxation characteristics of Pt/Nb:STO junction for AI applications.

[1] E. Mikheev, *Nat. Commun.* 5, 3990 (2015).

[2] T. F. Tiotto *et al.*, *Fron. Neurosci.* 14, 627276 (2021).

[3] C. Park *et al.*, *J. Appl. Phys.* 103, 054106 (2008).

SESSION SF06.07: Novel Methods
Session Chairs: Cody Dennett and Jonathan Malen
Wednesday Afternoon, November 30, 2022
Sheraton, 3rd Floor, Fairfax A/B

1:30 PM *SF06.07.01

Phonon Quasiparticle Breakdown and Novel Excitations in Strongly Disordered Solids [Olivier Delaire](#); Duke University, United States

A deeper understanding atomic motions in solids is needed to refine microscopic theories of transport and thermodynamics, in order to design improved materials. In particular, the behavior of phonons in crystalline materials is key to rationalize numerous functional properties, ranging from thermoelectrics for cooling or waste-heat harvesting to multiferroics and phase-change materials for information processing, or superionics for solid batteries. Yet, textbook models of lattice dynamics fall short in crystalline systems featuring disorder, which disrupts translational periodicity and conventional phonon band structures. For instance, alloying may result in resonance modes that lack the propagation of conventional phonons [1,2], and spontaneous nanostructures associated with structural instabilities and sublattice disordering can lead to strong phonon scattering and glassy thermal transport [3,4]. In addition, weak bonding and strong anharmonicity can yield large vibrational amplitudes [5] and even thermally driven ionic delocalization that can lead to atomic dynamics intermediate between those of crystalline solids and those of liquids [6,7]. I will describe our combined use of state-of-the-art neutron and x-ray scattering techniques together with first-principles and machine-learning augmented simulations to probe the complex atomic structure and dynamics of disordered materials. Deviations from long-range crystalline order are probed through diffuse scattering measurements while inelastic neutron/x-ray scattering reveals both the spatial and temporal correlations of atomic motions. We rationalize our experimental data using our large-scale simulations based on surrogate neural-net force-fields trained against ab-initio data with machine learning. This integrated approach provides insights into the effect of disorder on phonons and points to descriptors that could enable future materials design.

[1] O. Delaire, I. I. Al-Qasir, A. F. May, C. W. Li, B. C. Sales, J. L. Niedziela, J. Ma, M. Matsuda, D. L. Abernathy, T. Berlijn, “Heavy-impurity resonance, hybridization, and phonon spectral functions in $\text{Fe}_{1-x}\text{M}_x\text{Si}$, $\text{M}=\text{Ir,Os}$ ”, *Phys. Rev. B* 91, 094307 (2015).

[2] O. Delaire, T. Swan-Wood, and B. Fultz, “Negative entropy of mixing for solutions of vanadium-platinum”, *Physical Review Letters* 93, 185704 (2004).

[3] J. L. Niedziela, D. Bansal, J. Ding, T. Lanigan-Atkins, C. Li, A. F. May, H. Wang, J. Y. Y. Lin, D. L. Abernathy, G. Ehlers, A. Huq, D. Parshall, J. W. Lynn, and O. Delaire, “Controlling phonon lifetimes via sublattice disordering in AgBiSe_2 ”, *Phys. Rev. Materials* 4, 105402 (2020).

[4] J. Ma*, O. Delaire*, A. F. May, C. E. Carlton, M. A. McGuire, L. H. VanBebber, D. L. Abernathy, G. Ehlers, Tao Hong, A. Huq, Wei Tian, V. M. Keppens, Y. Shao-Horn, and B. C. Sales, “Glass-like phonon scattering from spontaneous nanostructure in AgSbTe_2 ”, *Nature Nanotechnology* 8, 445–451 (2013).

[5] T. Lanigan-Atkins*, X. He*, M. J. Krogstad, D. M. Pajeroski, D. L. Abernathy, Guangyong NMN Xu, Zhijun Xu, D.-Y. Chung, M. G. Kanatzidis, S. Rosenkranz, R. Osborn, and O. Delaire, “Two-dimensional overdamped fluctuations of soft perovskite lattice in CsPbBr_3 ”, *Nature Materials* 20, 977–983 (2021).

[6] J. L. Niedziela, D. Bansal, A. F. May, J. Ding, T. Lanigan-Atkins, G. Ehlers, D. L. Abernathy, A. Said & O. Delaire, “Selective Breakdown of Phonon Quasiparticles across Superionic Transition in CuCrSe_2 ”, *Nature Physics*, 15, 73–78 (2019).

[7] Jingxuan Ding, Jennifer L. Niedziela, Dipanshu Bansal, Jiuling Wang, Xing He, Andrew F. May, Georg Ehlers, Douglas L. Abernathy, Ayman Said, Ahmet Alatas, Yang Ren, Gaurav Arya, and Olivier Delaire, “Anharmonic lattice dynamics and superionic transition in AgCrSe_2 ”, *PNAS* 117 (8) 3930–3937 (2020).

2:00 PM *SF06.07.02

Energy Transport at Organic-Inorganic Interfaces of Nanocrystals Suspended in Solvents or Assembled into Solid Superlattices [Jonathan A. Malen](#)¹, Alexander Christodoulides¹, Yuxing Liang¹, Zhongyong Wang², Benjamin Diroll³, Richard Schaller³ and Robert Wang⁴; ¹Carnegie Mellon University, United States; ²University of Michigan–Ann Arbor, United States; ³Argonne National Laboratory, United States; ⁴Arizona State University, United States

Nanocrystals in solution or assembled into solids have numerous potential applications in electronics, optoelectronics, and biomedical engineering. Hard/soft interfaces at the core/ligand, ligand/ligand, and ligand/solvent create a complex and uncharted vibrational landscape for thermal energy transport that will influence their technological feasibility. Here we show that core/ligand bonding sites and ligand/ligand interdigitation can significantly impact energy transport at these interfaces. In the case of nanocrystal suspensions we use infrared pump, electronic probe spectroscopy to probe energy transport from CdSe nanocrystals into the surrounding solvent. The IR pump pulse excites vibrations of one or few ligands per nanocrystal and the energy moves into the nanocrystal and solvent in parallel, allowing this method to uniquely isolate thermal conductances at the core/ligand and ligand/solvent interface. Preliminary analyses suggest that core/ligand conductances are 5-10 times higher than ligand/solvent conductances and are insensitive to grafting density, perhaps because a sparse set of strong binding sites dominates thermal conductance. In the case of nanocrystal assemblies we report thermal transport and mechanical measurements on single-domain colloidal PbS nanocrystal superlattices that have long-range order as well as measurements on nanocrystal films that are comparatively disordered. Over a nanocrystal diameter range of 3.0–6.1 nm, we observe that the superlattices have thermal conductivities

and Young's moduli that are up to ~3 times higher than those of the corresponding films. Our measurements and computational modeling indicate that stronger ligand–ligand interactions due to enhanced ligand interdigitation and alignment in nanocrystal superlattices account for the improved thermal transport and mechanical properties.

2:30 PM BREAK

SESSION SF06.08: Nuclear Materials
Session Chairs: Cody Dennett and Michael Manley
Wednesday Afternoon, November 30, 2022
Sheraton, 3rd Floor, Fairfax A/B

3:30 PM SF06.08.01

Nanoscale Mechanisms for Reducing Thermal Boundary Resistance via Ion Bombardment Thomas W. Pfeifer¹, Henry Aller², Eric Hoglund¹, Ethan A. Scott³, John A. Tomko¹, Habib Ahmad⁴, Ashutosh Giri⁵, Alan Doolittle⁴, Khalid Hattar³, Alan McGaughey² and Patrick E. Hopkins¹; ¹University of Virginia, United States; ²Carnegie Mellon University, United States; ³Sandia National Laboratories, United States; ⁴Georgia Institute of Technology, United States; ⁵University of Rhode Island, United States

Given the role of interfaces as the limiting thermal resistance within devices, methods for the reduction of thermal boundary resistance (TBR) are desired. Similarly, with ion bombardment as a prominent method for the doping of semiconductors, the influence of the defects resulting from ion irradiation must be explored.

We present an experimental and computational study wherein we investigate the TBR across defected / pristine crystalline-crystalline interfaces.

Experimentally, we use Time Domain Thermoreflectance to measure the TBR across an aluminum / gallium nitride (GaN) interface, where the GaN has been bombarded with various doses of carbon, nitrogen, and gallium ions.

Computationally, we explore a Silicon / Heavy Silicon toy system in which we introduce void / interstitial defect pairs.

We observe a decrease in TBR through the introduction of these defects, both experimentally and in our simulations. We theorize that this TBR reduction is due to enhanced scattering within the defected material, which serves to assist the transfer of energy between different vibrational populations. This enhancement occurs between bulk and interfacial modes in addition to across the interface, suggesting that the TBR can be engineered by manipulating just a single material involved. We also note the presence of slight deformation of the lattice between defects, amplifying the effects from relatively-sparse ion-induced defects.

3:45 PM SF06.08.02

Atypical Phonon Scattering by the Fission Products in Thorium Dioxide Linu Malakkal¹, Ankita Katre², Shuxiang Zhou¹, Chao Jiang¹, David Hurley¹, Chris Marianetti³ and Marat Khafizov⁴; ¹Idaho National Laboratory, United States; ²SP Pune University, India; ³Columbia University, United States; ⁴The Ohio State University, United States

This work presents the first principles calculations of the lattice thermal conductivity degradation due to point defects in thorium dioxide using an iterative solution of the Pierels-Boltzmann transport equation. We have used the advanced non-perturbative Green's function methodology to compute the phonon-point defect scattering rates that consider the local distortion around the point defect, including the mass difference changes, interatomic force constants, and structural relaxation near the point defects. The point defects considered in this work include a single vacancy of thorium and oxygen, single substitutions of xenon krypton, zirconium, and iodine in the thorium site, and the three bound configurations of the Schottky defects. The results of the phonon-defect scattering rate reveal that among all the considered intrinsic defects, the thorium vacancy scatters the phonon most due to the substantial changes in force constant and structural distortions. But the scattering of phonons due to the substitutional defects unveils that the zirconium atom scatters phonon less effectively, like the generally observed trend. Contrary to the general trend that the substitutional atoms scatter phonon less effectively than vacancies the xenon, krypton, and iodine in thorium sites have an effect comparable to the vacancy defects. This striking difference in the phonon scattering of the substituted atoms is due to the local chemical environment changes. Xenon and krypton are noble gases, and iodine is an electronegative element, making it difficult to form bonds with the neighboring oxygen atoms. Finally, these results can serve as the benchmark for the analytical models and help the engineering scale modeling effort for nuclear design.

4:00 PM SF06.08.04

Intragranular Thermal Conductivity of Pristine and Proton-Irradiated alpha-U and delta-UZr₂ Zilong Hua¹, Hao Ma², Tiankai Yao¹, Shuxiang Zhou¹, Cody A. Dennett³, Amey Khanolkar¹, Lingfeng He¹, Michael E. Manley² and David Hurley¹; ¹Idaho National Laboratory, United States; ²Oak Ridge National Laboratory, United States; ³Massachusetts Institute of Technology, United States

U-Zr system is a promising metallic fuel candidate for the next generation of fast reactors. Its structure-induced thermal anisotropy has been expected, but related experimental investigation is incomplete. Here we present recent measurement results of thermal conductivity in alpha-U and delta UZr₂ before and after proton irradiated. Thermoreflectance measurements were conducted inside single grains with the grain size of approximately 100 micrometer.

Experimental data in a wide temperature range are compared with simulation, and with the use of advanced characterization, the transport mechanisms are investigated. These new insights are expected to aid in fuel performance modeling and fuel design.

SESSION SF06.09: Material Properties Mediated by Atomic Scale Defects
Session Chairs: Yongjie Hu and Marat Khafizov
Thursday Morning, December 1, 2022
Sheraton, 3rd Floor, Fairfax A/B

8:30 AM *SF06.09.01

Defect-Scattering Mediated Lattice and Thermal Transport Yongjie Hu; University of California, Los Angeles, United States

Defect- and disorder-scattering plays an important role in the lattice and thermal transport of crystalline materials, while sometimes leads to complex behaviors and poses challenge to fundamental understanding. In this talk, we will discuss in situ experimental characterizations and first-principles calculations for understanding and controlling such defect-interactions. Our measurements show disorder-driven behaviors in thermal performance under controlled chemical disorders. Our computational results predict the thermal and lattice transport of disordered crystals, in good agreement with experiments. The study provides understanding of the effects of defect scattering beyond quantum perturbation theory and enables rational engineering routes to design novel functions.

9:00 AM SF06.09.02

Enthalpy-Entropy Compensation of Point Defects Diffusion in Crystalline Materials [Simon Gelin](#); The Pennsylvania State University, United States

Experimental data accumulated over more than 120 years show not only that diffusion coefficients of impurities ordinarily obey the Arrhenius law in crystalline solids, but also that diffusion pre-exponential factors measured in a same solid increase exponentially with activation energies. This so-called compensation effect has been argued to result from a universal positive linear relationship between entropic contributions and energy barriers to diffusion. However, no physical model of entropy has ever been successfully tested against experimental compensation data. In this presentation, I will demonstrate that atomistically computed harmonic vibrational entropic contributions account for most of compensation effects in silicon and aluminum. I will then show that, on average, variations of atomic interactions along diffusion reaction paths simultaneously soften low frequency phonons and stiffen high frequency ones. This behavior explains the origin of compensation: because relative frequency variations are larger in the lower region of the spectrum, softening generally prevails over stiffening and entropy ubiquitously increases with energy.

9:15 AM SF06.09.03

Imaging and Manipulating Surface Electronic Landscapes under Ambient Conditions [Saima A. Sumaiya](#)¹, Jun Liu² and Mehmet Z. Baykara¹;

¹University of California, Merced, United States; ²University at Buffalo, The State University of New York, United States

Electronic properties of material surfaces play a central role in their functionality for a large number of emerging applications, ranging from chemical sensors to ultrafast electronics. However, methods typically employed to measure such properties require pristine vacuum conditions, limiting the relevance of obtained results to realistic applications operating in ambient conditions. We show here that the method of conductive atomic force microscopy (C-AFM) can measure the electronic landscape of a variety of material surfaces with atomic resolution under ambient conditions, including features such as single atomic defects. In particular, we describe (i) the first observation of room-temperature charge ordering on a transition metal carbide (i.e. an MXene) thin crystal, α -Mo₂C, with signatures of rotational symmetry breaking with respect to the underlying lattice, and (ii) the capability to “switch” the charge state of defects on molybdenum disulfide (MoS₂) *in situ* by way of current vs. voltage spectroscopy. Finally, we find that the mechanism behind the atomic-resolution characterization capabilities of C-AFM involves the presence of a confined, electrically conductive pathway at the tip-sample contact, under high-speed scanning.

9:30 AM SF06.09.04

Influence of Local Charge and Magnetic Ordering on Point Defect Properties in Magnetite (Fe₃O₄) [Shivani Srivastava](#)¹, Blas Uberuaga² and Mark Asta^{1,3}; ¹University of California, Berkeley, United States; ²Los Alamos National Laboratory, United States; ³Lawrence Berkeley National Laboratory, United States

Magnetite (Fe₃O₄) is found as a constituent phase in oxide scales formed on iron under a variety of corrosion conditions. When exposed to an oxidizing corrosion environment, the point defects and their transport play an important role in determining the rates of corrosion.

The work presented here employs first-principles calculations using PBE+U functional to investigate the role of local ordering of Fe²⁺/Fe³⁺ cations in magnetite on the point defect properties occurring under equilibrium conditions. The bulk structure of magnetite, featuring coupled charge, spin and orbital order, undergoes a bulk order-disorder phase transition at around 120 K. Even above this transition, there is evidence of strong local order, consistent with results from calculations presented here. We study the effect of this local order on the energetics underlying defect formation and migration. Owing to the strong coupled charge, spin and orbital order, magnetite(Fe₃O₄) exhibits a strong dependence of defect properties on local charge order and underlying magnetic order.

We focus on sampling multiple local environments and their associated effects on the underlying defect properties. Our results show that different local environments, generated due to ordering of Fe²⁺/Fe³⁺ cations, stabilize different charge states of point defects such as oxygen and iron vacancies, depending on charge redistribution around the defect. We also find that iron-oxygen divacancies are stable in this system and have high binding energy under reducing conditions. The relatively high stabilization of defects in certain local chemical environments can lead to formation of percolation networks modifying the ionic transport in these systems. As shown in previous studies^[1], the interplay of defect formation and energetics of disordering plays an important role in determining radiation tolerance of complex oxides. The implications of our results for the effects of irradiation on magnetite formation during oxidation/corrosion of iron will be discussed.

[1] Kreller, C. R.; Uberuaga, B. P. The Role of Cation Ordering and Disorder on Mass Transport in Complex Oxides. *Current Opinion in Solid State and Materials Science* 2021, 25 (2), 100899. <https://doi.org/10.1016/j.cossms.2021.100899>.

9:45 AM SF06.09.05

Symmetry-Breaking and Reconstruction at Point Defects in Solids [Seán R. Kavanagh](#)¹, Irea Mosquera-Lois², Aron Walsh² and David O. Scanlon³;

¹University College London & Imperial College London, United Kingdom; ²Imperial College London, United Kingdom; ³University College London, United Kingdom

Point defects are a universal feature of crystalline materials. Their identification is often addressed by combining experimental measurements with theoretical models. The standard approach of simulating defects is, however, prone to miss the ground state atomic configurations associated with energy-lowering reconstructions from the idealised crystallographic environment.¹⁻⁵ Missed ground states compromise the accuracy of calculated properties.

To address this issue, we report an approach to efficiently navigate the defect configurational landscape using targeted bond distortions and rattling.⁶ Application of our workflow to a range of materials (CdTe, GaAs, Sb₂S₃, Sb₂Se₃, CeO₂) reveals symmetry breaking in each host crystal that is not found via conventional local minimization techniques. The point defect distortions are classified by the associated physico-chemical factors. We demonstrate the impact of these defect distortions on derived properties, including formation energies, concentrations and charge transition levels. Our work presents a step forward for quantitative modelling of imperfect solids.

1. Arrigoni, M. & Madsen, G. K. H. Evolutionary computing and machine learning for discovering of low-energy defect configurations. *npj Comput Mater* 7, 1–13 (2021).

2. Mosquera-Lois, I. & Kavanagh, S. R. In search of hidden defects. *Matter* **4**, 2602–2605 (2021).
3. Lany, S. & Zunger, A. Metal-Dimer Atomic Reconstruction Leading to Deep Donor States of the Anion Vacancy in II-VI and Chalcopyrite Semiconductors. *Phys. Rev. Lett.* **93**, 156404 (2004).
4. Kavanagh, S. R., Walsh, A. & Scanlon, D. O. Rapid Recombination by Cadmium Vacancies in CdTe. *ACS Energy Lett.* **6**, 1392–1398 (2021).
5. Kavanagh, S. R., Scanlon, D. O., Walsh, A. & Freysoldt, C. Impact of metastable defect structures on carrier recombination in solar cells. *Faraday Discuss.* (2022) doi:10.1039/D2FD00043A.
6. Mosquera-Lois, I., Kavanagh, S. R., Walsh, A., Scanlon, D. O. Symmetry-breaking and reconstruction at point defects in solids. *npj Computational Materials* (In submission)

10:00 AM BREAK

10:30 AM *SF06.09.06

Electronic Structure and Coherence Properties of Spin Defects in Semiconductors from First Principles [Giulia Galli](#); University of Chicago, United States

We discuss recent progress in investigating the electronic structure and coherence properties of spin defects in three- and two-dimensional materials using first principles electronic structure calculations (DFT and many body perturbation theory), and spin Hamiltonians. In particular, we will present results for defects in diamond and SiC using newly developed quantum embedding theories.

11:00 AM SF06.09.08

High-Valence Doping in Lithium-Excess Disordered Rock Salt Cathode Materials [Bonan Zhu](#)^{1,2} and David O. Scanlon^{1,2}; ¹University College London, United Kingdom; ²The Faraday Institution, United Kingdom

Lithium-excess manganese-based disordered rock salts offer great opportunities for further increasing the capacities of lithium-ion batteries (> 300 mAh⁻¹). However, the existing materials are known to exhibit undesirable capacity fading and hysteresis^{1,2}. Doping with high-valence transition metals offers the opportunity for tuning the short-range order of the disordered lattice as well as lowering the valence state of Mn, thereby mitigate the capacity fading through cationic redox. In this study, we construct cluster expansion models to investigate the effect of incorporating W dopants. The short-range orderings are extracted from Monte-Carlo simulations. While the inclusion of W raises the cationic redox capacity of Mn, the preferential configuration of W-Li cation nearest neighbour reduces the concentration of zero-transition-metal channels that allow Li conduction. Quantitative analysis shows a moderate reduction of active Li content, but the existence of Li-percolating networks remains affected. On the other hand, analysis of the charge densities shows that the oxidation state of W dopants can be different from the assumed 6+ state as in WO₃, highlighting the delicate coupling between ionic and electronic structures in defective disordered materials. Effects of doping with other high-valence dopants, such as Sb, as well as co-anion doping will also be discussed.

(1) Lun, Z.; Ouyang, B.; Cai, Z.; Clément, R. J.; Kwon, D.-H.; Huang, J.; Papp, J. K.; Balasubramanian, M.; Tian, Y.; McCloskey, B. D.; Ji, H.; Kim, H.; Kitchaev, D. A.; Ceder, G. Design Principles for High-Capacity Mn-Based Cation-Disordered Rocksalt Cathodes. *Chem* **2020**, *6* (1), 153–168. <https://doi.org/10.1016/j.chempr.2019.10.001>.

(2) Clément, R. J.; Lun, Z.; Ceder, G. Cation-Disordered Rocksalt Transition Metal Oxides and Oxyfluorides for High Energy Lithium-Ion Cathodes. *Energy Environ. Sci.* **2020**, *13* (2), 345–373. <https://doi.org/10.1039/C9EE02803J>.

11:15 AM SF06.09.09

The Influence of Atomic-Scale Defects on Thermal Transport in MoS₂ [Pingping Chen](#)¹, Aroop K. Behera¹, Ethan A. Scott², Christopher M. Smyth², Tzu-Ming Lu², Suprem R. Das¹ and C. Thomas Harris²; ¹Kansas State University, United States; ²Sandia National Laboratories, United States

Transition-metal dichalcogenides, such as molybdenum disulfide (MoS₂), have attracted considerable attention as tunable band-gap semiconductors that may be fabricated in a monolayer format and that give rise to unique electrical and thermal properties. These physical properties are directly linked to the layer structure, which is sensitive to defects and impurities. While several computational studies have investigated the thermal conductivity of supported and encapsulated MoS₂, the impact of lattice defects on the thermal conductivity of MoS₂ and the thermal boundary conductance between MoS₂ and its support substrate has not been studied experimentally as a function of both defect density and layer number. In this work, we use frequency domain thermal reflectance to study the thermal transport properties of mechanically exfoliated MoS₂ flakes with controlled defect densities and a known number of layers, which are supported on sapphire substrates. The sulfur defect density is controlled via hydrogen-based plasma, and x-ray photoelectron spectroscopy is used to characterize the density of these sulfur vacancy defects. In combination with our materials characterization, we provide an effective thermal conductance analysis to explain the reduction in thermal transport due to carrier scattering by vacancies. The results from this study serve to further enhance our understanding of the fundamental physics of phonon transport in the presence of defects and provide a pathway for studying thermal transport in nanoscale electronic devices based upon 2D materials.

SESSION SF06.10: Virtual Session I
 Session Chairs: Cody Dennett and Lucas Lindsay
 Tuesday Morning, December 6, 2022
 SF06-virtual

10:30 AM SF06.10.01

Ce Defect Diffusion in Ceria Using Defects Chemical Calculation and Density Functional Theory [Hyun-Kyu Kim](#)¹, Seol Hee Oh², Jong-Ho Lee² and Yeong-Cheol Kim¹; ¹KoreaTech, Korea (the Republic of); ²Korea Institute of Science and Technology, Korea (the Republic of)

CeO₂ shows high oxygen storage/release capacity (OSC) due to its aliovalency between +3 and +4 as functions of temperature and oxygen partial pressure. Addition of Zr in CeO₂ enhances the OSC further, and recently Ce_{0.75}Zr_{0.25}O₂ (CZO) has been studied for anode support of solid oxide fuel cell. However, Zr and Ce in CZO have been reported to be separated under reduction.

Since the phase separation occurs through the constituents' diffusion, we studied Ce defects diffusion to understand the main defect for the phase separation. Ce defects are the main focus, as a rate-limiting element, because oxygen is a well-known fast diffusion element. Several defect concentrations in CeO₂ are calculated for diffusion coefficient by using defects chemical calculation. Migration enthalpy of Ce vacancy and interstitial is calculated by

using NEB method with consideration of oxygen vacancy clustering effect. Ce interstitial with an oxygen vacancy is found to be the main diffusion element under oxidation and reduction, contradicting a recent article [1].

[1] Stefan Beschmitt et al., J. Physical Chemistry, 27307 (2015).

10:35 AM SF06.10.03

Origin of Giant Magnetocapacitance Effect in $K_{0.5}Na_{0.5}NbO_3/La_{0.67}Sr_{0.33}MnO_3$ Superlattices Soumen Pradhan¹, Oleg I. Lebedev², Martando Rath², Fabien Veillon², Wilfrid Prellier² and M. S. Ramachandra Rao¹; ¹Indian Institute of Technology (IIT) Madras, India; ²Laboratoire CRISMAT, Normandie Université, France

In recent years, multiferroic systems have been the subject of enormous interest due to their wide range of applications in spintronics, sensors, actuators, multistate memory devices etc. Artificial superlattices (SLs) have gained much attention in current research because of their potential to realize new functionalities like ferroelectricity, multiferroicity and superconductivity. Here, we have explored magneto-capacitance (MC) performance in SLs of pure ferroelectric and ferromagnetic sublayers for multiferroic applications. $K_{0.5}Na_{0.5}NbO_3$ (KNN)/ $La_{0.67}Sr_{0.33}MnO_3$ (LSMO) SLs with LSMO sublayer thicknesses of 5, 7, 9 and 11 unit cell (u.c.) keeping KNN thickness fixed at 6 u.c. were deposited on (001)-oriented $SrTiO_3$ substrates alternately for 15 times using pulsed laser deposition (PLD) technique. The crystallinity and layer-by-layer growth of both the constituents were confirmed from X-ray diffraction as well as transmission electron microscopy. SLs with LSMO layer of 9 and 11 u.c. show coherent growth on the substrates. The Curie temperature (T_C) of ~ 206 K even in the SL with thicker LSMO sublayer indicates the presence of defects in the SLs. Also, spin-glass behavior in the SLs was observed below 50 K as confirmed from magnetic measurements. The insulating nature in the SLs with 7 and 9 u.c. and insulator to metal transition for 11 u.c. were observed in the transport study. However, defects induced large negative magneto-resistance (MR) of $\sim 98\%$ was realized at 100 K in the SLs with 9 and 11 u.c. The capacitance as well as magneto-capacitance show high value at low frequency and reduce monotonically upon increase in the frequency. This can be well explained by MR coupled Maxwell-Wagner relaxation model. Finally, the giant MC of $\sim 766\%$ at standard frequency of 1 kHz with 9 T magnetic field at 100 K for SL with optimum LSMO sublayer thickness of 9 u.c. can be used for multistate memory applications.

10:50 AM SF06.10.04

Viscoelastic Damping in Defect-Engineered CoNiCrFeMn High Entropy Alloy by Molecular Dynamics Simulations Akash A. Deshmukh and Raghavan Ranganathan; Indian Institute of Technology Gandhinagar, India

High-frequency mechanical vibrations and sound propagation in materials are governed by their viscoelastic behavior. Efficient viscoelastic damping is necessary to enhance the stability, safety, and service life of dynamic systems such as brake discs, shielding devices, high-frequency resonators, etc. Therefore, there is an increasing demand for the design and development of materials with high damping capability. Recently, viscoelastic studies in alloys have attracted a lot of attention as these materials possess simultaneously high stiffness and high loss tangent, thereby resulting in a high loss modulus. The inadequacy of the traditional alloys such as the low working temperature of Cu-based damping alloys, and anti-corrosion treatment of the Fe-based damping alloys have limited their applications. High Entropy Alloys (HEAs) exhibit simple solid solutions and excellent mechanical properties such as high hardness, high strength, good corrosion, and wear resistance and are good candidates for high-frequency damping applications. Moreover, defects such as stacking faults, twin boundaries, interstitials, and vacancies are intrinsic to crystals and have the ability to further enhance damping. In the present work, three defects namely stacking fault, edge dislocation, and vacancies were introduced in the FCC single-phase solid solution CoNiCrFeMn HEA to investigate its viscoelastic response. A Modified Embedded Atom Method (MEAM) potential was used to describe the interatomic interactions. Non-equilibrium molecular dynamics simulations via oscillatory shear deformation were performed to understand the viscoelastic behavior under a frequency range spanning 3 decades, from GHz to THz. It was noted that each defect exhibited a significant enhancement in damping over the defect-free alloy, while considered individually. However, the coexistence of all three defects dramatically improved the damping performance of the alloy up to 172% more compared to the defect-free structure. Below the peak damping frequency, the loss modulus was fitted successfully by power-law scaling. The enhancement in loss moduli for various defected structures was observed to result from the anharmonic coupling of phonon modes as verified by the mode-dependent Gruneisen parameters. The inclusion of defects also shifted the peak damping frequency to larger values. This work thus demonstrates that HEAs with carefully engineered defects have promising applications in damping high-frequency vibrations.

11:05 AM SF06.10.05

Improving the Quality of Rigid PU Foam Sandwich Insulation Panels Gulab Malunjar¹, Hieu McElroy², Adebola Ogunniyi² and Mirella Coroneo³; ¹Dow Chemical International Pvt. Ltd, India; ²The Dow Chemical Company, United States; ³Dow Italia S.R.L., Italy

Metal-faced sandwich panels with a rigid polyurethane (PUR) or polyisocyanurate (PIR) core are used in construction as insulating panels. The discontinuous process for their production consists of injecting a reacting polyurethane (PU) mixture in a mold, usually in a single point, where the liquid flows up to 12 m in length and reacts, growing in volume and filling the cavity. The injection is well known to be a source of defects and of non-uniform foam properties, which are potentially critical factors for the final performance of the panel. The ability of a foam formulation to flow and fill the cavity of a sandwich panel can have a significant impact on the orientation of the foam cells, affecting insulation and structural properties of the foam, and affecting the tendency of a foam panel to blister when installed in the field. Developing a better way to distribute foam in a panel could, therefore, enable the reduction of defects in panels during production.

A Finite Element Method (FEM) was used to predict the filling of a mold cavity with PU foam, using different distribution devices. An advanced numerical model was used to simulate the foam injection and expansion processes in a single step. Foam flow simulation solvers were coupled with an advanced global stabilization algorithm and a multi-criteria adaptive meshing technology. These new technologies enabled a realistic prediction of foam flow and foam expansion. The finite element model was validated for an accurate foam molding solution. PU foams were then characterized independently to generate the modeling parameters for the simulation. The foam filling simulation shows realistic flow pattern inside the mold and used to predict optimal filling conditions (i.e. temperatures, gating and venting). The simulation accounts for the pressure effect inside and outside of the mold. It also predicts the density distribution in foam. With this approach, we can now perform *in silico* optimization of the foam manufacturing process to achieve defect-free foam panels.

11:20 AM SF06.10.06

Thermal Resistance Across Si-Ge Interface from Non-Equilibrium Phonons Jinchun Han, Xun Li and Sangyeop Lee; University of Pittsburgh, United States

As nanostructured devices become prevalent, interfaces often introduce large thermal resistance imposing challenges for thermal management and opening opportunities for developing ultralow-thermal conductivity materials. However, the interfacial thermal transport remains poorly understood due to complex physics and limited methodologies. Although past studies have focused on the atomistic scale phenomena at the interface, the phenomena on a larger scale, for example, the complex interplay between the interfacial scattering and intrinsic phonon-phonon scattering, have not been comprehensively studied.

Widely used methods in the past include the Landauer's formalism which ignores the intrinsic scattering of phonons and molecular dynamics simulation which has a much smaller length scale than the typical mean free paths of phonons.

To explore the role of intrinsic scattering of phonons on the interfacial thermal resistance at micro- and meso-scales, we solve the Peierls-Boltzmann transport equation in both reciprocal and real spaces using a Monte Carlo method with *ab initio* inputs. Our hypothesis is that the interfacial scattering largely distorts the phonon distribution near the interface, and intrinsic phonon scattering attempts to relax the distorted (non-equilibrium) distribution to a local equilibrium distribution. During this process, a large amount of entropy is generated according to the Boltzmann's *H*-theorem. Indeed, our solution for a Si-Ge interface shows a large degree of non-equilibrium in phonon distribution, particularly at Ge side, which makes a significant contribution to thermal resistance. Our study provides a new tool to bridge the gap for *ab initio* simulation between atomistic scale and less studied microscale. Also, it brings a new insight into the significant role of phonon-phonon scattering on interfacial thermal resistance.

11:35 AM SF06.10.07

Thermal Transport in Solid Materials with Defects and Dislocations Based on a Machine Learning Method Zc Yang and Fan Yang; Stevens Institute of Technology, United States

Thermal transport properties are essential for sustainable energy and thermal management. It is also important to incorporate the effect of defects, which widely exist in materials in real world, when calculating thermal transport properties. The prevailing methods for the calculation of thermal transport properties would be either not accurate, using the molecular dynamic (MD) simulation, or time consuming, when applying first-principles calculations. Recently, people applied a reliable method to calculate the transport properties with the combination of the advantages of MD and first-principles through machine learning. In this work, we used a machine learning method based on gaussian regression, called Gaussian Approximation Potential¹ (GAP) method, to achieve a fast and accurate prediction of thermal conductivity of unknown solid materials. We built interatomic potentials using data from density functional theory (DFT) calculation through the training of GAP and applied the potential to calculate the thermal conductivity of cubic boron nitride (cBN), which is a material with ultra-high thermal conductivity². Our simulation results were compared with first-principles calculation and experimental results and showed great agreement. This method was then extended to explore the change of thermal conductivity with the effect of defects and dislocations. Instead of compensating relaxation time with dislocation models³, our method incorporates the effect of dislocations to interatomic potentials. And our results showed good agreement with the reference.

1. Bartók, A. P., *et al.*, Physical Review Letters (2010) 104 (13), 136403
2. Chen, K., *et al.*, Science (2020) 367 (6477), 555
3. Klemens, P. G., Proceedings of the Physical Society. Section A (1955) 68 (12), 1113

11:50 AM DISCUSSION TIME

SESSION SF06.11: Virtual Session II
Session Chairs: Giorgia Fugallo and Lucas Lindsay
Tuesday Afternoon, December 6, 2022
SF06-virtual

1:00 PM *SF06.11.01

Impact of Defects on Phonon Transport in ThO₂ Miaomiao Jin¹, Marat Khafizov², Beihan Chen¹, Cody A. Dennett³ and David Hurley⁴; ¹Penn State University, United States; ²The Ohio State University, United States; ³Massachusetts Institute of Technology, United States; ⁴Idaho National Laboratory, United States

Defects in ThO₂ can significantly degrade the thermal conductivity of ThO₂ due to enhanced phonon-defect scattering. In this talk, the impact of point defects, dislocation loops, and grain boundaries are evaluated based on results from non-equilibrium and equilibrium molecular dynamics simulations. Specifically, for point defects, the defect concentration-dependent thermal conductivities are calculated, and these results enable the extraction of phonon-defect scattering cross-section for each type of point defect. Regarding dislocation loops, the impact of two types of experimentally observed dislocation loops (perfect and faulted) is examined considering various loop sizes and orientations. The scattering parameters are deduced based on Klemens' formalism after the simulation cell size effect is considered. In the case of grain boundaries (GBs), symmetrically tilt GBs are created over a wide range of tilt angles. The interfacial (Kapitza) resistance is found to correlate well with GB energy. In addition, the spectral/modal analysis of phonon contribution to the total resistance/conductance reveals the dominating phonon modes for thermal transport across GBs.

1:30 PM *SF06.11.02

The role of Extrinsic Disorder in the Phononic and Thermal Response of Multilayered Materials Giorgia Fugallo^{1,2}; ¹CNRS, France; ²Ecole Polytechnique, France

In multilayered materials, while strong covalent bonding provides the stability of the sub-nanometric elementary units, the whole assembly is held together by weak van der Waals interactions. The individual building blocks hence maintain most of their intrinsic characteristics also when arranged together to form a crystalline solid. In principle, novel material properties can be thus tailored by controlling those of the elementary units. If it is true that this bottom-up strategy in the synthesis of new materials has been intensively followed since the '80s, it is also true that more recently a growing interest has been put on the comprehension of the role that extrinsic disorder can play in the performance of these materials, with applications that goes from quantum technologies to thermoelectricity. In this talk I will present different examples of how it is possible to tune the phononic and thermal properties of multilayered materials by including structural/chemical disorder.

2:00 PM SF06.11.03

Synthesis and Characterization of a High-Entropy Spinel Oxide Single Crystal Evan Krysko¹, Lujin Min¹, Yu Wang¹, Na Zhang¹, Fankang Li², Kaleb Burrage², Masaaki Matsuda², Mauricio Terrones¹ and Zhiqiang Mao¹; ¹The Pennsylvania State University, United States; ²Oak Ridge National Laboratory, United States

High-entropy materials generally refer to compounds which involve mixing five or more elements in nearly equimolar concentrations at an equivalent atomic site. These compounds are stabilized into a single phase by the high configurational entropy caused by the varying sizes and masses of their constituent elements. Prior work has shown competing magnetic interactions enabled by high entropy generate novel magnetic phases. Given that oxides

with the spinel structure contain a variety of magnetic ordering, high-entropy spinel oxides, if successfully made, would provide a platform for the further study of high-entropy tuning of magnetism. This research aimed to synthesize a novel high-entropy oxide with the spinel structure and to determine the effects of its lattice distortions on its magnetization. In this work, an (Mg, Mn, Fe, Ni, Co)Al₂O₄ single crystal was synthesized for the first time using the optical floating zone growth technique. The sample was confirmed to be a phase pure high-entropy oxide (HEO) using X-ray diffraction (XRD) and energy-dispersive spectroscopy (EDS). Through magnetization measurements, we found (Mg, Mn, Fe, Ni, Co)Al₂O₄ exhibits a spin-glass state though the parent phases show either antiferromagnetic or ferrimagnetic ordering or spin glass. Furthermore, we also found that (Mg, Mn, Fe, Ni, Co)Al₂O₄ has much greater thermal expansion than its parent compounds from neutron scattering measurements.

We would like to acknowledge the funding from the Materials Research Science and Engineering Centers (MRSEC). The neutron scattering measurements were collected at the High Flux Isotope Reactor (HFIR) at the Department of Energy's Oak Ridge National Laboratory.

2:05 PM DISCUSSION TIME

SYMPOSIUM SF07

Frontiers of Intermetallics Science for Structural and Functional Materials Design
November 28 - December 6, 2022

Symposium Organizers

Yoshisato Kimura, Tokyo Institute of Technology
Manja Krueger, Otto-von-Guericke University
Akane Suzuki, GE Research
Matthew Willard, Case Western Reserve University

Symposium Support

Silver
GE Research

* Invited Paper
+ Distinguished Invited

SESSION SF07.01: Structural Intermetallics I
Session Chairs: Florian Pyczak and Masao Takeyama
Monday Morning, November 28, 2022
Sheraton, 5th Floor, Riverway

10:30 AM *SF07.01.01

Recent Progress in the Development of Intermetallic γ -TiAl Based Alloys Enabled by *In Situ* Synchrotron X-Ray Diffraction and Scattering Petra Spoerk-Erdely¹, Gloria Graf¹, Michael Musi¹, Peter Staron², Andreas Stark², Emad Maawad² and Helmut Clemens¹; ¹Montanuniversität Leoben, Austria; ²Helmholtz-Zentrum Hereon, Germany

Intermetallic titanium aluminide alloys based on the ordered γ -TiAl phase are innovative materials for lightweight high-temperature applications. In addition to their low density of roughly 4 g/cm³, their high specific Young's modulus and strength even at elevated temperatures, and their good oxidation and burn resistance, especially their excellent creep properties make these alloys a material of choice for challenging structural applications. Following intensive research and development activities, γ -TiAl based alloys have recently entered service in the automotive and aircraft engine industries, e.g. as low-pressure turbine blades in environment-friendly jet engines, as engine valves in sports and racing cars, or as turbocharger turbine wheels. In the course of the past decades, the development of these complex multi-phase alloys has benefited greatly from the application of (*in situ*) synchrotron X-ray techniques. Diffraction and scattering techniques, in particular, have offered access to the atomic structure of the material and provided insights into a variety of microstructural parameters. Advanced experimental setups, which are steadily refined, have even allowed the exploration of elaborate manufacturing processes and yielded insights that have so far been inaccessible by means of conventional methods. Here, a practical introduction and overview of recent progress in this field of research are provided. Current prospects at modern synchrotron radiation sources will be illustrated by means of selected recent case studies pertaining to different stages in the development of modern γ -TiAl based alloys (*i.e.*, fundamental research, manufacturing, and fine-tuning of properties for application). In this context, available setups for *in situ* high-energy X-ray diffraction and small-angle X-ray scattering experiments will be discussed in terms of their advantages as well as their limitations. This talk reaches out not only to the TiAl scientific community, though. By addressing the key question as to how to actually simulate real-life conditions such as applied loads and high temperatures in a laboratory environment, researchers with a general background in materials science may also find in it a collection of ideas that are indeed applicable to many different materials systems.

11:00 AM SF07.01.02

Plasticity and Brittleness of the Ordered β_0 Phase in a TNM-TiAl Alloy Guy Molénat¹, Jean-Philippe Monchoux¹, Michael Musi², Petra Spoerk-Erdely², Helmut Clemens² and Alain Couret¹; ¹CEMES/CNRS, France; ²Montanuniversität Leoben, Austria

The aim of this work is to study the deformation mechanisms in the ordered β_0 phase containing some ω_0 precipitates of a TNM-TiAl alloy ($\text{Ti}_{51.05}\text{Al}_{43.9}\text{Nb}_4\text{Mo}_{0.95}\text{B}_{0.1}$ in at.%) and to look for the origin of the low ductility at room temperature of this alloy.

The alloy produced by Spark Plasma Sintering exhibits a near lamellar microstructure made of lamellar γ/a_2 colonies surrounded by γ and β_0 grains. Tensile tests were performed at room temperature to determine the mechanical properties and the ductility of the alloy. The rupture surface of the deformed material were investigated by scanning electron microscopy.

Two types of TEM (Transmission Electron Microscopy) experiments were used to explore the behaviour of these dislocations and to study the deformation mechanisms. The first one lies in investigating the deformation microstructure in thin foils extracted from bulk samples previously deformed in tension at room temperature, while the second type consists in performing *in situ* tensile tests inside a TEM that allows the direct observation of the dislocation dynamics under stress and in real time.

At room temperature, the material exhibits a limited ductility with cleavage surfaces along the lamellae interfaces of the colonies. The β_0 grains contain nano-precipitates of the ω_0 phase and deform plastically by both $\langle 111 \rangle$ superdislocations and $\langle 001 \rangle$ dislocations. The $\langle 111 \rangle$ superdislocations are dissociated into two superpartial dislocations separated by an antiphase boundary. They glide in $\{011\}$ planes and have the tendency to be localized into pile-ups, an effect demonstrated as the result of the ω_0 precipitation that harden the β_0 grains and favour deformation concentration. The $\langle 001 \rangle$ dislocations are found to be split into two identical superpartial dislocations separated by a stacking fault. They are elongated along their screw orientation and also anchored at these small nano-precipitates of ω_0 phase. *In situ* straining experiments performed at room temperature show that they move by jumps between these elongated configurations.

These results are discussed to explain the low ductility of this alloy. The stress concentration due to the pile-up formation on grain boundaries is assumed to induce fracture along lamellae interfaces in neighbouring lamellar colonies.

11:15 AM SF07.01.03

***In Situ* Fracture Behaviour of Tailored TNM Alloys** Michael Burtscher¹, Markus Alfreider¹, Helmut Clemens¹, Christoph Gammer² and Daniel Kiener¹; ¹Montanuniversität Leoben, Austria; ²Austrian Academy of Sciences, Austria

Titanium aluminium alloys are constantly evolving as tremendous efforts have been set to improve their mechanical properties at elevated temperatures. Thus, new alloys were developed and tailored via heat treatments to fulfil the demanding requirements of aviation and automotive applications. However, these optimizations notoriously have led to decreased room temperature ductility and reduced fracture toughness. Within this study, two advanced TNM alloys have been investigated by in-situ micromechanical notched cantilever tests and sophisticated transmission electron microscopy techniques. Using these methods, the mechanical properties of distinct interfaces regarding the fracture toughness, *J*-integral and fracture stress could be evaluated at any point during the experiment. Furthermore, the crack propagation could be tracked in-situ and sudden fracture events were linked to the failure of distinct microstructural components. The presented method allowed to identify strengthening mechanisms such as e.g. particles along common α_2/γ interfaces or bridging. To further deepen the understanding of the fracture mechanisms along this interface type, strain maps of the fully lamellar microstructure were conducted edge-on for both alloys. To do so, 4D scanning transmission electron microscopy including scanning nanobeam electron diffraction was performed. From these experiments, strain accumulations caused by misfit dislocations or silicide particles were identified and linked to fracture events. Furthermore, these results were discussed in the light of existing literature.

Based on these results, further alloy design and tailored microstructures will be adapted to enable a higher room temperature ductility and fracture toughness of these alloys.

11:30 AM SF07.01.04

Development of TiAl Alloys for High Temperature Applications Seong-Woong Kim, Min-Sik Kim, Ji-Sung Park and Seung Eon Kim; Korea Institute of Materials Science, Korea (the Republic of)

Research on developing new TiAl alloys for high temperature applications is introduced. At KIMS, we have developed new TiAl alloys which have excellent room temperature and high temperature properties. Especially, the new alloy showed excellent oxidation resistance in the temperature range from 900 to 1000°C by forming stable Al_2O_3 oxidation layer. Process development of casting, forging as well as 3d printing on the newly developed KIMS alloys was introduced. Especially, small size turbine wheel and blade were manufactured by centrifugal casting process. The results from the testing and validation of TiAl blade were shown that KIMS alloy can be used as a turbine blade above 900°C. In addition, we proposed some underlying mechanism of high temperature strength of KIMS alloy from TEM and SEM observations. Finally, the operation test of micro gas turbine is now under examination to confirm the possibility of the application of the new alloy in the gas turbine engine.

11:45 AM SF07.01.05

Additively Manufactured β -Ti5553 with Laser Powder Bed Fusion—Microstructures and Mechanical Properties of Bulk and Lattice Parts Margaret Wu¹, Marissa Linne¹, Jean-Baptiste Forien¹, Nathan Barton¹, Jianchao Ye¹, Kavan Hazeli², Morris Wang³ and Thomas Voisin¹; ¹LLNL, United States; ²The University of Arizona, United States; ³UCLA, United States

Ti5553 (Ti-5Al-5Mo-5V-3Cr wt.%) is a titanium alloy with promising applications in safety-critical structures due to its high strength-to-weight ratio and near- β microstructure which opens pathways for tailoring mechanical performance based on annealing conditions. In order to utilize its advantageous properties, efficient manufacturing must be possible. Laser powder bed fusion (L-PBF) involves the layer-by-layer fabrication of complex geometries such as lattices which help reduce component weight. Moreover, L-PBF expedites part deployment since components can be built on-demand without multi-step assembly. Thus, the successful realization of L-PBF Ti5553 relies on a fundamental understanding of the alloy's additively manufactured microstructure and mechanical behavior. In support of production efforts at Lawrence Livermore National Lab and Kansas City National Security Campus, the present work investigates the hierarchical microstructures and mechanical properties of L-PBF Ti5553 bulk and lattice parts. The characterization techniques include room-temperature tensile tests, nanoindentation, scanning electron microscopy (SEM), electron backscatter diffraction (EBSD), and transmission electron microscopy (TEM). The presence of second-phase (ω) nanoprecipitates in the lattice material distinguishes its microstructure from that of the bulk and moreover, indicates the challenges in predicting bulk mechanical response based on lattice properties. The present results provide a starting framework for the successful printing of Ti5553 bulk and lattice parts by comprehensively examining the processing-structure-property-paradigm of the deposited material system.

1:30 PM *SF07.02.01

Control of Crystallographic Texture in Powder Bed Fusion Additive Manufacturing of Intermetallics and the Related Superalloys Takayoshi Nakano; Osaka Univ, Japan

Additive manufacturing (AM) enables the production of complex, net-shape geometries. Additionally, in AM of intermetallic compounds and the related superalloys, which has received less attention, the microstructure and crystallographic texture of the product can be arbitrarily controlled by selecting appropriate process parameters, thereby enabling unprecedented superior properties. This paper discusses recent progress pertaining to texture evolution mechanisms and control methods, with an emphasis on laser-beam and/or electron beam powder bed fusion (PBF). One of the unique characteristics of PBF is that the crystallographic texture can be varied as a function of position within the product by controlling the scan strategy. The transient behavior of the texture and the factor used to control it via the scan strategy are discussed. In addition, the texture evolution behavior of highly symmetrical Ni-base superalloys as well as relatively low symmetrical TiAl intermetallic compound and disilicide is discussed. The importance of the crystallographic, multiplicity, of the preferential crystal growth direction is described to understand the evolution behavior of the texture in such heat-resistance materials.

This study was supported by Grants-in-Aid for Scientific Research (JP18H05254) from the Japan Society for the Promotion of Science (JSPS). This study was also partly supported by Council for Science, Technology and Innovation (CSTI), Cross-ministerial Strategic Innovation Promotion Program (SIP), Materials integration, for revolutionary design system of structural materials, from the Japan Science and Technology Agency (JST).

2:00 PM SF07.02.02

Direct Insight into Additive Manufacturing of TiAl with Diffraction Methods Adriana De Andrade, Florian Pyczak, Marcus W. Rackel, Jan Rosigkeit, Andreas Stark and Peter Staron; Helmholtz-Zentrum Hereon, Germany

Additive manufacturing (AM) provides inherent advantages for the processing of intermetallics. Most often intermetallics are high performance materials more expensive than competing conventional alloys. Thus, the near net shape processing capability of AM causing no material loss is advantageous. In addition, the properties of most intermetallics are very sensitive to variations of the chemical composition making the good chemical homogeneity of the powder based AM methods beneficial. Accordingly, TiAl low-pressure turbine blades for the current GE9X engine are produced by Electron Beam Melting. However, AM processes pose also many problems for intermetallics. Many intermetallic materials including TiAl are brittle compared to conventional alloys and the high heating and cooling rates experienced during AM can cause cracking and damage. The complex phase diagram of many intermetallics exacerbates this problem. TiAl for example shows a number of phase transformations and two-phase regions or in advanced alloys also three-phase and even more-phase regions between melting point and room temperature. If those phase transformations are associated with volume change or if too large volume misfits between phases exist internal stresses will occur. At lower temperatures, TiAl parts are too brittle to withstand those stresses and will fail during AM. This is one reason to use Electron Beam Melting instead of Laser Beam Melting for AM of TiAl despite the latter being less costly. Heating of the powder bed and the already processed section of the part is easier in Electron Beam Melting. With TiAl being less brittle at higher temperatures, this enables crack free processing.

In this contribution, the results of the characterization by high-energy X-ray diffraction of TiAl alloys during AM are presented. Directly after solidification, the phase constitution of TiAl is far away from the situation in the finished part. It resembles very closely the phase constitution directly at the melting point. The assumption of the final microstructure and phase constitution takes place in the layers below the surface. These experience a cyclic heat treatment due to the melting and solidification of the on top powder layer. The maximum temperature of this thermal cycle decreases with increasing distance from the melting and solidifying top layer. From the development of lattice constants and phase fractions, it is possible to reconstruct the internal processes in the material during this complex heat treatment scheme. The phase diagram is no good guide to understand the situation because the phase constitution and microstructures are away from equilibrium. Only by direct measurement one can acquire information about the microstructure formation in the TiAl part necessary to optimize the process or adapt the material to the process.

2:15 PM SF07.02.03

Revolutionary Approach to Develop Novel TiAl Alloys for Powder Processed LPT Blades in Jet Engines Masao Takeyama, Hirotoyo Nakashima, Ryoosuke Yamagata and Yotaro Okada; Tokyo Institute of Technology, Japan

An integrated inverse design approach to accelerate the development of novel titanium aluminides for LPT blades in jet engines, specifically focusing on powder processing, such as MIM (Metal Injection Molding) and AM (Additive Manufacturing), has been undertaken, in collaboration with industries and universities, under the project of “Materials Integration for Revolutionary Design System of Structural Materials” in Cross-ministerial Strategic Innovation Promotion Program (SIP) in Japan. We have successfully developed a novel TiAl alloy with mechanical properties superior to the currently existing alloys and fabricated into 200 mm LPT blade by both MIM and AM processes. Our integrated computational materials design system is composed of three modules: “Mechanical-property Prediction Modules (MPM)”, “Microstructure Design Module (MDM)” and “Process Design Module (PDM)”. For example, the system works as follows: specific values of the properties required by industries, say, tensile strength and fracture toughness, are at first input into the MPM, and the MPM calculates and outputs the volume fraction of the most important microstructure constituent to meet the required properties, based on our mechanical property database (DB). Then, the volume fraction value is input into the MDM, and the MDM optimizes alloy composition and heat treatment condition to have the microstructure, based on our multi-component phase diagram DB. The proposed alloy with the composition is then cast into bar ingots and powdered by EIGA by industries. All of the powders are used for MIM (<45 μ m) and for AM-EBM (>45 μ m) without any waste and fabricated into LPT through each PDM. Tokyo Tech is in charge of the integrated system of MPM and MDM, so that this talk focuses on some points to integrate the modules to the system. For MPM, the key is the digitalization of β/γ cellular microstructure because the bcc β -Ti phase introduced by the cellular transformation ($\alpha_2+\gamma \rightarrow \beta+\gamma$) significantly affects the mechanical properties. For MDM, the most critical point is the reliable knowledge on the phase diagram with oxygen. We found that oxygen tremendously affects the phase equilibria among β -Ti, α -Ti (α_2 -Ti₃Al) and γ -TiAl phases and eventually changes the transformation pathways to control the microstructures. Without this information, thus it is impossible to build up the system since a large amount of oxygen is picked up in MIM process in comparison with AM process. The details of MPM and MDM including the calculation methods will be independently presented by our co-authors in this symposium.

A part of this study has been carried under the research of SIP II in JST (Japan Science and Technology Agency).

2:30 PM SF07.02.04

Microstructure Design Module for the Development of Powder Processed LPT Blade in TiAl Alloys Hirotoyo Nakashima, Yoshihiro Gohda and Masao Takeyama; Tokyo Institute of Technology, Japan

In order to reduce the cost and time required to develop the TiAl low-pressure turbine blade for jet engines, we have built an inverse problem approach using two modules: one is the mechanical properties prediction module (MPM) to predict the microstructures that satisfy the required properties, and the other is the microstructure design module (MDM) to specify the composition range and heat treatment conditions for tailoring the microstructures. In this

presentation, the MDM is highlighted. In this module, the two-step heat treatment of the lamellar formation and subsequent aging is assumed. The temperature and composition dependence of the volume fraction of each phase, as well as the supersaturation for the discontinuous precipitation of α_2 -Ti₃Al + γ -TiAl \rightarrow β -Ti + γ , are calculated in the framework of CALPHAD method. Furthermore, the effects of oxygen on the phase equilibria and kinetics are considered aiming at its application to powder processes such as metal injection molding. Therefore, the key is to understand the effects of oxygen experimentally and to construct a thermodynamic database that accurately reproduces them. Two series of quaternary Ti-Al-M-O alloys (M: transient metal elements) with various oxygen levels were studied at the temperature range between 1573 K and 1273 K using the combination of wavelength dispersive spectroscopy and soft X-ray emission spectroscopy. Then, thermodynamic parameters for two quaternary systems as well as the constituent sub-systems were assessed. Selected important interaction parameters and their composition dependence were optimized based on the *ab-initio* calculation using KKR-CPA method. The newly assessed database reproduces phase boundaries in multi-component systems with an accuracy of 1% for metal elements and 0.2% for oxygen concentrations. In the presentation, we will demonstrate an alloy design based on this module.

2:45 PM BREAK

3:15 PM SF07.02.05

Mechanical-Properties Prediction Module for the Development of Powder Processed LPT Blade in TiAl Alloys Ryoosuke Yamagata, Yotaro Okada, Hirotoyo Nakashima and Masao Takeyama; Tokyo Institute of Technology, Japan

In order to accelerate the development of TiAl LPT blade in jet engines and reduce the extensive experimental efforts, some computational approaches to predict the required mechanical properties, in addition to the module to specialize the alloy composition to be able to control microstructure, are needed. We built up the sophisticated materials integration system for the inverse problem consisting of two modules of mechanical-properties prediction (MPM) and microstructure design (MDM). In the presentation, then, focus is placed on the MPM how the ultimate tensile strength (UTS) can be predicted. Note that the output of this module is a concrete value of the microstructural constituent governing the property. Therefore, the quantitative analysis by digitalizing the microstructural constituents is needed as one of the databases (DB) of the module. Another important DB to predict the UTS is the work hardening rate of the microstructural constituents. There are two important microstructural constituents in the alloys: one is the lamellar microstructure consisting of α_2 -Ti₃Al and γ -TiAl phases and the other the cellular microstructure consisting of β -Ti and γ phases, since we revealed the introduction of the cellular microstructure is effective in increasing the mechanical properties. Then, volume fraction of this β/γ cellular microstructure (V_c) was quantitatively analyzed from back-scattered electron images taken from a scanning electron microscope by an image analysis software. The work hardening rate of each microstructural constituent was evaluated by two ways, one is calculating by an analysis of forward problem that dividing the differential between experimentally measured UTS and 0.2% proof strength (σ_0) by elongation (ϵ), the other is directly measurement by digital image correlation technique with in-situ tensile test. The UTS of alloys were able to be predicted by simple linear compound law using the UTS of α_2/γ lamellar microstructure and β/γ cellular microstructure, and V_c . And these UTS of each microstructural constituent could also be predicted using their σ_0 , ϵ and work hardening rate. The calculated UTS could reproduce the experimentally measured UTS well, it has a margin of error of only $\pm 5\%$. By using this method, the volume fraction of the microstructure constituent to meet the required properties that contribute to an input value into the MDM can be output. This work was supported by Council for Science, Technology and Innovation (CSTI), Cross-ministerial Strategic Innovation Promotion Program (SIP), "Material Integration" for revolutionary design system of structural materials.

3:30 PM SF07.02.06

Oxygen Diffusion and Hardening in γ -TiAl Camille Thenot^{1,2}, Damien Connétable³, Daniel Monceau³, Pierre Sallot⁴, François Jomard⁵ and Jean-Philippe Monchoux^{1,2}; ¹CEMES-CRNS UPR 8011, France; ²Université de Toulouse, France; ³CIRIMAT-ENSIACET, France; ⁴Safran Tech, France; ⁵Université de Versailles Saint-Quentin-en-Yvelines, France

TiAl alloys are sensitive to loss of ductility by exposure in air at temperatures around 700°C and for durations as low as one hour. Though this effect is detrimental for the development of the TiAl alloys as materials for hot parts in automotive and aeronautical engines, it remains poorly understood. Thus, we address here the questions of the penetration kinetics of oxygen in a Ti-48Al-2Cr-2Nb alloy of near γ microstructure, and of the impact of this penetration on the tensile properties of this material at room temperature. For this purpose, tensile specimens have been exposed in a 20% O₂ + 80% Ar atmosphere, for temperatures ranging from 400°C to 700°C, and for exposure durations of one hour. The tensile tests show that, in addition to the known effect of loss in ductility, the yield stress increases significantly. Therefore, the origin of this effect has been looked for through investigations of the microscopic deformation mechanisms by transmission electron microscopy. In particular, the dislocation morphologies have been determined in samples of different oxygen concentrations. To quantitatively determine the oxygen penetration kinetics, the diffusion coefficient of oxygen in the γ phase has been determined theoretically by DFT calculations. In parallel, experimental values have been obtained for the first time, using ¹⁸O isotope and SIMS concentration profile analyzes, in the following conditions: temperature from 500°C to 700°C, exposure durations from 1 h to 48 h. Surprisingly, the experimental diffusion kinetics were significantly lower than those theoretically predicted. This discrepancy is discussed in terms of potential effects of the Nb and Cr substitutional solutes on the interstitial diffusion mechanisms of oxygen. The main result of these studies is that oxygen dissolution and diffusion in the γ phase is probably not at the origin of the increase in yield stress.

3:45 PM SF07.02.07

Detailed Study of the Effect of Zirconium in Intermetallic γ -TiAl Based Alloys Michael Musi¹, Stefan Kardos¹, Lukas Hatzenbichler¹, David Holec¹, Andreas Stark², Melissa Allen³, Volker Güther³, Helmut Clemens¹ and Petra Spoerk-Erdelyi¹; ¹Montanuniversität Leoben, Austria; ²Helmholtz-Zentrum Hereon, Germany; ³GfE Metalle und Materialien GmbH, Germany

The outstanding material-specific properties of intermetallic γ -TiAl based alloys make them excellent candidates for high-temperature structural applications in the aerospace and automotive industry. In order to seize new application areas, an increased service temperature and improved mechanical properties are necessary. Considering that modern engineering γ -TiAl based alloys consist mainly of γ -TiAl phase with some amounts of α_2 -Ti₃Al phase and β_0 -TiAl phase, depending on the amount of Al and additional alloying elements, strengthening of the γ phase is a key point to further advance this class of materials. A promising alloying element meeting the requirements to be an effective solid solution strengthener for the γ phase is Zr. While its beneficial effect on the mechanical properties is already known in the scientific community, a detailed study of its influence on the phase transformations in the Al range of engineering γ -TiAl based alloys is still missing. Consequently, the present work investigates six model alloys based on the Ti-(42-46)Al-(2-4)Zr (at.%) system regarding the influence of Zr on the microstructure and phase transitions. Microstructural characterization reveals a stabilization of the γ phase due to Zr, leading to an increase of the γ fraction at expense of α_2 in the microstructure, which consists predominately of lamellar α_2/γ colonies and a minor amount of globular γ phase after hot-isostatic pressing. The material's hardness is increased due to both solid solution strengthening and lamellar refinement of the α_2/γ colonies by Zr. The phase transformation behaviour and the related impact of Zr were investigated by differential scanning calorimetry (DSC) as well as high-energy X-ray diffraction (HEXRD) utilizing synchrotron radiation. Especially, two different types of in-situ HEXRD heating experiments were conducted in order to investigate, on the one hand, the solid-state transformations below the material's solidus temperature, and, on the other hand, by employing a newly developed experimental setup, the liquid-solid transformations at higher temperatures. Both DSC and HEXRD experiments clearly show that the Zr additions increase the temperature stability range of the γ phase, which ultimately transforms into α -Ti(Al) phase upon

heating. However, phase transformations above the γ phase dissolution temperature, especially, involving the liquid phase, are drastically shifted towards lower temperatures when alloying with Zr, thus effectively narrowing the α single-phase field region. Complementarily, heat treatments above the solidus temperature reveal microstructural features associated with these phase transformations, e.g. formation of liquid phase between the α and β grains in the three-phase $\alpha+\beta+L$ phase field region. Subsequent water-quenching results in the transformation of the liquid phase into γ phase and of the β phase into α_2 laths, respectively, while in the alloy variants rich in Al, a portion of the high-temperature α phase transforms into massive γ phase. Furthermore, the combination of X-ray diffraction and ab-initio calculations based on density functional theory (DFT) grants valuable insights into the effect of Zr and Al on the lattice parameters of the γ phase. More precisely, Zr causes a strong reduction of the tetragonality of this phase due to an asymmetric influence on the lattice parameters, i.e. a significant elongation of the shorter crystal axis, while the longer axis remains mostly unaffected.

4:00 PM *SF07.02.08

Local Phase Transformations—A New Creep Strengthening Mechanism in Ni-Base Superalloys [Michael J. Mills](#)¹, Ashton Egan¹, Semanti Mukhopadhyay¹, Longsheng Feng², Fei Xue³, Emmanuelle Marquis³, Maryam Ghazisaeidi¹, Steven Niezgod¹ and Yunzhi Wang¹; ¹The Ohio State University, United States; ²Lawrence Livermore National Laboratory, United States; ³University of Michigan, United States

Polycrystalline Ni-based superalloys are vital materials for disks in the hot section of aerospace and land-based turbine engines due to their exceptional microstructural stability and strength at high temperatures. In the drive to increase operating temperatures and hold times in these engines, hence increasing engine efficiency and reduction of carbon emissions, creep properties of these alloys becomes increasingly important. At these higher temperatures, new deformation modes become active. Several alloy compositions and microstructure variants of commercial disk alloys are being explored, including γ' strengthened alloys as well as compositions promoting γ' and γ'' co-precipitation. Microtwinning and stacking fault shearing are important operative mechanisms in the critical 600-800°C temperature range. Advanced electron-microscopy-based techniques have been used to gain new insights into these mechanisms and the rate-limiting processes during high temperature deformation. Atomic-scale chemical and structural changes associated with stacking fault and microtwin interfaces within γ' precipitates have been identified and indicate that local phase transformations (LPT) occur commonly during creep of superalloys. Furthermore, the important deformation modes can be modulated by LPT formation, enabling a new path for improving high temperature properties. In another phenomenon related to LPT, some superalloys exhibit preferential precipitation along annealing twin boundaries (ATBs). It is surprising that ATBs act as heterogeneous nucleation sites since they are low energy boundaries. However, in superalloys that exhibit this behavior, LTP appears to occur at these ATBs and aid in nucleation of γ' (and γ'') precipitates. The implications of this effect with respect to localization of slip is being characterized using in situ deformation experiments in the SEM. This work is part of a GOALI-DMREF program funded by the National Science Foundation in which collaborators are exploring the thermodynamic driving force for LPT formation using DFT modeling, and phase field dislocation dynamics modeling is being used to explore the interaction of dislocations with γ' microstructures under the cooperative shearing and local compositional changes associated with the LPT mechanism.

SESSION SF07.03: Functional Intermetallics I
Session Chairs: Hideki Hosoda and Yoko Yamabe-Mitarai
Tuesday Morning, November 29, 2022
Sheraton, 5th Floor, Riverway

8:30 AM *SF07.03.01

Recent Progress of NiMnGa Ferromagnetic Shape Memory Alloy/Polymer Composites [Hideki Hosoda](#)¹, Wan-Ting Chiu¹, Pimpet Sratong-on², Masaki Tahara¹ and Volodymyr Chernenko^{3,4,1}; ¹Tokyo Institute of Technology, Japan; ²Thai-Nichi Institute of Technology, Thailand; ³BCMaterials and University of Basque Country, Spain; ⁴Ikerbasque, Basque Foundation for Science, Spain

Heusler type NiMnGa is a prototype ferromagnetic shape memory alloy (FSMA) which can be driven not only by temperature change but also by magnetic field. In conventional shape memory alloys (SMAs), shape change occurs by martensite variants reorientation (MVR), and the shape recovery occurs during heating through reverse martensitic transformation (MT) into parent (austenite) phase. Thus, the motion frequency is very limited by the heating/cooling speed. On the other hand, FSMA can be driven isothermally by magnetic field, since the actuation is caused by the reversible twin boundary motion (twinning and detwinning) of martensite variants under equivalent magnetostress. Then, FSMA is considered as a new actuator material with fast response and large stroke. The maximum actuation strain of NiMnGa is around 5.8% in 5M martensitic state and 9.6% in 7M martensitic state. A drawback of NiMnGa is that the large magnetoactuation can appear in the single crystal state only. This is because in polycrystalline state the constraint force from the neighbor grains is larger than the magnetostress and thus suppresses MVR by magnetic field. In order to overcome this problem, we have innovated polymer-matrix-based composite materials containing single-crystalline NiMnGa grain particles. By using Bi microalloying we have developed a technique which allows easy disintegration of polycrystalline NiMnGa into single grains which are magnetostrain active. At present, the value of magnetostrain of the silicone composites containing 20vol% 5M- and 7M- martensitic NiMnGa particles (Chiu et al., Scripta Mater., 2022) or 30vol.% 5M-martensitic NiMnGa particles (Sratong-on et al., Sci. Rep., 2019) is 4.0% under 0.7 T. In this presentation, we summarize recent progress of the NiMnGa FSMA / silicone polymer composites. This research is partially supported JSPS by Kakenhi 20K20544, 22H00256 and 22K14491, the Research Center for Biomedical Engineering, and World Research Hub Program of International Research Frontiers Initiative, Tokyo Institute of Technology.

9:00 AM SF07.03.02

Novel Co-Al-Si Shape Memory Alloys with B2-Structured Parent Phase [Shunya Mochimaru](#), Tatsuya Ito, Sheng Xu, Xiao Xu, Toshihiro Omori and Ryoosuke Kainuma; Tohoku University, Japan

Shape memory alloys, such as Ti-Ni-based (Ti-Ni, Ti-Ni-Cu), Cu-based (Cu-Al-Ni, Cu-Zn-Al), and Fe-based (Fe-Ni-Co-Al-Ta-B, Fe-Mn-Al-Ni) alloys, display shape memory effect and pseudoelasticity due to thermoelastic martensitic transformation. They have offered many technology advantages for various applications such as eyeglass frames, coupling devices, medical devices, and seismic dampers. In recent years, some Co-based shape memory alloys such as Co-Ni-Ga have been reported and they have attracted much attention because of their ability to be used at high temperatures above 373 K. In this study, we present the results of novel Co-Al-Si shape memory alloys showing the thermoelastic martensitic transformation from a B2-structured parent phase. The crystal structures of parent and martensite phases were determined by transmission electron microscopy (TEM), and the transformation temperatures were investigated by measuring the temperature dependence of electric resistivity. Furthermore, it was found that some alloys show excellent pseudoelasticity at temperatures from 298 K to 453 K. Thus, the new Co-based shape memory alloys show great promise for applications requiring high-temperature pseudoelastic properties.

9:15 AM SF07.03.03

Multi-Stage Superelasticity in SrNi₂P₂ Intermetallic Compound via Lattice Collapse and Expansion and the Influence of Cryogenic Temperature Shuyang Xiao¹, Vladislav Borisov², Adrian Valadan², Guilherme Gorgen-Lesseux³, Roser Valenti², Paul Canfield³ and Seok-Woo Lee¹; ¹University of Connecticut, United States; ²Goethe University, Germany; ³Iowa State University, United States

Superelastic crystalline solids are able to recover their original shape even after the large amount of deformation is applied. The shape recovery of most superelastic crystalline solids usually occurs through a reversible phase transition between martensitic and austenitic phase. Although this shear process provides up to ~10% of elastic strain, there are several issues that limit their elastic performance. Usually, this shear process requires high activation temperature to reverse the phase transition. So, it is difficult to exhibit superelasticity at cryogenic temperature. Also, the shear process often drives dislocations to move and causes large accumulation of dislocations, which eventually prevent the reversal of phase transition. Therefore, it is desirable to seek out a new class of superelastic material that can overcome these issues through a completely different superelasticity mechanism. In this presentation, we report our first discovery of the giant superelasticity in a novel intermetallic compound SrNi₂P₂ via a unique phase transition process, lattice collapse-expansion and the influence of cryogenic temperature.

SrNi₂P₂ single crystals were grown using solution-growth technique, and *in-situ* uniaxial compression and tension tests on [001]-oriented SrNi₂P₂ micropillars, which were fabricated using focused-ion-beam milling, were conducted at room temperature, 200K, and 100K. Room temperature mechanical testing revealed the giant superelasticity with a remarkably huge elastic strain limit near 20% if both compression and tension are considered. Up to our knowledge, this giant elastic strain corresponds to one of the highest elastic strain limits ever reported for crystalline solids. This excellent superelastic performance is achieved through multiple-stage lattice collapse and expansion under compression and tension by forming and breaking P-P bonds in two co-existing different crystal structures in SrNi₂P₂. Based on Density Function Theory (DFT) calculation and High-Resolution Transmission Electron Microscope (HRTEM), P-P bonds are formed or broken partially depending on the stress state, leading to the multi-stage lattice collapse and expansion. Fraction of P-P bonds seems to be controlled primarily by entropy under a given stress, so the total number of P-P bonds is determined by thermodynamics under a give stress and temperature. Unlike shear process of martensite-austenite transition, no dislocation is involved in the superelasticity process of SrNi₂P₂. Simple making and breaking bond process seems to guarantee ultrahigh fatigue life with presumably nearly infinite number of cycles. Our state-of-the-art *in-situ* cryogenic nanomechanical testing revealed that forming and breaking P-P bonds is strongly sensitive to cryogenic temperature. At lower temperature, phase transition becomes easier under compression but more difficult under tension. This difference can be explained by thermal contraction. Due to the thermal contraction at lower temperature, which reduces P-P distance, making P-P bonds becomes easier, but breaking P-P bonds becomes more difficult. One noticeable result is that even under cryogenic environment (~100K), SrNi₂P₂ still exhibit superelasticity, implying that SrNi₂P₂ is capable of shape recovery at very low temperature unlike conventional superelastic crystalline solids such as Ni-Ti intermetallic compounds. Our experimental and computational results provide a fundamental insight into understanding the superelasticity mechanisms of SrNi₂P₂. Furthermore, our work suggests its strong potential as a cryogenic superelastic material that could be useful to develop an impact resistance material for aerospace engineering under cryogenic environment.

9:30 AM SF07.03.04

High-Quality Intermetallic Nanoparticles from Amalgams Maksym Yarema and Jasper Clarysse; ETH Zurich, Switzerland

Amalgamation is the alloying of two metals, one of which is in liquid form. While broadly applied in metallurgy or dentistry, amalgamation process is yet majorly disregarded for nanotechnology. Recently, we developed the nanoscale amalgamation reaction for the synthesis of intermetallic and alloyed nanoparticles. [1] Starting from monometallic seeds, we carry out a thermal decomposition of metal-amides to dispatch low-melting metals to the surface of nanoparticles and thus trigger a time-efficient and homogeneous alloying to bimetallic compositions. Our new synthesis is convenient and reproducible universal method for high-quality intermetallic nanoparticles, providing uniform compositions and phase purity already after a few minutes of reaction (whereas short reaction time is the key for excellent size distributions). Finally, nanoscale amalgamation gives access to unique bimetallic nanoparticles of very dissimilar metals (for example easily reducible Au, Pd or Pt with much more active Ga or Zn), which is impossible via traditional co-precipitation methods. Combining metals at the nanoscale is a powerful strategy for many applications: large surface area for efficient catalysis, size-dependent properties for ultralow-power phase-change memory and high-Q factor plasmonic applications, small diameter for effective nanomedicine or ultrafine-grain thermoelectrics and additive manufacturing are just to name a few. Our synthesis supplies high-quality intermetallic nanoparticles for this wide range of emerging applications.

[1] J. Clarysse, A. Moser, O. Yarema, V. Wood, and M. Yarema, Science Advances, 2021, 7, eabg1934.

9:45 AM SF07.03.05

Observation of Non-Hookean Huge Elastic Deformation in a Bulk Heusler-Type Cu–Al–Mn Alloy Sheng Xu, Xiao Xu, Toshihiro Omori and Ryosuke Kainuma; Tohoku University, Japan

The familiar metals and alloys in our daily lives are mostly crystalline materials, and they elastically deform because of temporary stretching or contracting of bonds between atoms. The ideal elastic strain for a crystalline metal is the strain at which the lattice itself disintegrates and hence set a firm upper bound of the elastic strain of the material. Theoretically, this strain value can be in the order of 10% for most crystalline metals with absolutely no defects. However, a macroscopic block of conventional crystalline metals practically suffers a very limited elastic deformation of <0.5% with a linear stress-strain relationship obeying Hooke's law. In this presentation, we present our recent results on the experimental observation of a large tensile elastic deformation with an elastic strain of >4.3% in a Cu–Al–Mn single-crystalline alloy with an L2₁-ordered structure at its bulk scale at room temperature. The large macroscopic elastic strain that originates from the reversible lattice strain of a single phase is demonstrated by *in-situ* microstructure and neutron diffraction observations. Furthermore, the tensile elastic reversible deformation, which is nonhysteretic and quasilinear, is associated with a pronounced elastic softening phenomenon. The increase in the stress gives rise to a reduced Young's modulus, unlike the traditional Hooke's law behavior. This non-Hookean huge tensile elastic deformation behavior is discussed in terms of the strong lattice anharmonicity in the present bulk Heusler-type Cu–Al–Mn crystalline alloy. The experimental discovery of a non-Hookean huge elastic deformation offers the potential for the development of bulk crystalline metals as high-performance mechanical spring materials for use as metallic seals and connectors, or for new applications via "elastic strain engineering."

10:00 AM BREAK

10:30 AM *SF07.03.06

Potential of Multi-Element Alloys as High-Temperature Shape Memory Alloys Yoko Yamabe-Mitarai; The University of Tokyo, Japan

Shape recovery in shape memory alloys (SMAs) occurs by reverse martensitic transformation from martensite to austenite phases. SMAs are used in wide applications such as medical devices, actuators, and household electric applications etc. If SMAs can be used at high temperatures, their application will expand, for example, in aerospace field. TiNi intermetallic compounds is the most used SMAs. The crystal structures of the martensite and austenite phases in TiNi are B2 and B19' in Strukturbericht expression, respectively. However, the martensitic transformation temperature (MTT) of TiNi is lower than 100 °C. To use SMAs at high temperatures, MTT should be increased. Various attempts have been made to increase the MTT of SMAs, such as addition of

alloying elements to TiNi or selection of other intermetallic compounds with high MTT. We have focused on TiPt and TiPd as high-temperature SMAs (HT-SMAs) due to their high MTT above 500 °C. Martensitic transformation, microstructure, and shape recovery of TiPt or TiPd alloys have been investigated. The addition of alloying elements was a certain effect on strength improvement of austenite, but not sufficient. It also had the disadvantage of lowering the MTT in many cases. Recently, multi-component alloys, in particularly medium- or high-entropy alloys, have been attracted as new structural materials because their severe lattice distortion and sluggish diffusion are expected to improve the high-temperature strength of SMAs. In this presentation, phase transformation, microstructure and shape recovery of multi-component SMAs together with TiPt or TiPd base SMAs will be introduced.

11:00 AM SF07.03.07

Actinide Nitride Thin Films—Outlook and Future Directions [Kevin D. Vallejo](#)¹, [Brelon J. May](#)¹, [Cody A. Dennett](#)², [Paul Simmonds](#)³ and [David Hurley](#)¹; ¹Idaho National Laboratory, United States; ²Massachusetts Institute of Technology, United States; ³Boise State University, United States

Actinide-based materials possess unique physics due to the presence of *5f* electrons. Owing to their importance as critical nuclear energy materials, their study has mainly focused on these applications, leaving plenty of fundamental physics aspects open for investigation. Examples include the three magnetic phases of Th, which are directly correlated to its impurity density, and the charge density wave anomaly present in α -U at low temperatures. The effective examination of unique quantum phenomena in these materials requires high purity monocrystalline samples. However, the formation of large area single-crystalline actinide compounds is particularly underexplored relative to other material systems because of limited source availability and safety regulations. High quality actinide containing samples will help provide more accurate experimental values for physical properties used by atomistic computer modelling approaches. In turn, this will enable more accurate models of compounds with strongly correlated electron systems. However, current thin-film synthesis techniques for actinide-based materials make use of alloys or functionalized compounds which leave behind impurities and affect crystal quality. Molecular beam epitaxy (MBE) presents an attractive avenue for the study of actinide heterostructures because of the high degree of control over purity, dimensionality, strain, and interfaces between monolithically grown materials. MBE also uses high purity elemental sources and is known for producing highly crystalline material. Thus, by using this technique for synthesis of these complex materials, we can reduce the presence of elemental impurities and defects and simplify the characterization and interpretation of the physical properties. Idaho National Laboratory has recently installed an MBE chamber equipped with electron beam sources, several high temperature cells, and a nitrogen plasma source to facilitate the deposition of low vapor-pressure elements. This work looks to establish the foundational knowledge for the synthesis and characterization of actinide-nitrides with complex oxidation states; wherein, initial studies will employ transition metals as early-stage surrogates for actinide-based nitride materials. We aim to synthesize single crystal, epitaxial (UN) and thorium nitride (Th₃N₄), both of which are promising nuclear fuel candidates for upcoming reactor architectures. The properties of these crystal phases has been an active research field and the synthesis and characterization efforts will be greatly benefited from MBE grown samples. Experimental validation of computational models will result in faster nuclear fuel validation and implementation of nuclear reactors for clean energy solutions.

11:15 AM SF07.03.08

Molecular Beam Epitaxy of Novel Nitrides [Brelon J. May](#), [Kevin D. Vallejo](#), [David Hurley](#) and [Krzysztof Gofryk](#); Idaho National Laboratory, United States

Nitride materials have a diverse set of applications, but the system is significantly underexplored compared to oxides. Several recent papers have revealed that there are numerous stable nitride compounds which have yet to be created. Vacuum deposition is an ideal method for the discovery and study of novel materials as it allows for stabilization of materials outside of thermodynamic limits through engineering of the growth kinetics. It also allows for delicate stoichiometry control, enabling careful tuning of composition-dependent physical properties, and materials with high crystallinity and purity. The preparation of monocrystalline samples from ultra-pure atomic sources will allow for examination of the physical properties of these materials without the added complications of grain boundaries or impurities, and to elucidate any directional dependence of these properties which may be present in low-symmetry crystals. This work aims to synthesize single crystalline thin films in this relatively uncharted material space using molecular beam epitaxy (MBE). Growth windows, the vacuum deposition equivalent to commonly employed thermodynamically limited phase diagrams, will be established for a variety of materials. These outline the parameters required to achieve specific phases and include substrate temperature, flux ratios, growth rate, and strain. The focus for the work here is initially given to the exploration of transition metal nitrides containing Cr, Zr, Mn, Nb, Ti, and Ni. The factors which control the formation of different crystalline phases and stoichiometries will be investigated for binary and ternary compounds. While various new ternary phases involving these elements have been predicted to be stable, the physical properties have not been predicted. However, the properties of the binary constituents and the select few known ternary compounds are of interest to various facets of research including: magnetism, semiconductors, superconductors, plasmonics, thermoelectrics, high hardness, stability in extreme environments, and anti-corrosive coatings, these novel ternary compounds will likely have similar properties. Additionally, developing the growth windows for compounds containing elements with complex oxidation states will provide a platform for additional studies involving heavier elements with *5d*, *4f*, and eventually *5f*-electrons. Utilizing these elements in carefully engineered crystal structures is particularly interesting because of their high sensitivity to temperature, strain, increased spin-orbit interactions, as well as magnetic and electric fields. MBE is known for the precise deposition of thin films with sharp interfaces. This will allow for the synthesis of multilayer heterostructures of different materials with compatible crystal symmetry, enabling the combination of multiple properties, study of interface effects, and comparison to random alloys with the same overall composition. Select elements can also be combined with the well-studied Group-III Nitride material system, laying the foundation for future integration of these novel materials with existing semiconductor optoelectronics.

11:30 AM SF07.03.09

Effect of Elastic Strains on the Catalytic Activity of Intermetallic Compounds for the Hydrogen Economy [Carmen Martínez](#)^{1,2}, [José Manuel Guevara](#)¹ and [Javier Llorca](#)^{1,3}; ¹IMDEA Materials Institute, Spain; ²Universidad Complutense de Madrid, Madrid, Spain; ³Universidad Politécnica de Madrid, Spain

The hydrogen economy strongly depends on two critical reactions for the production of hydrogen and the generation of green energy, namely the hydrogen evolution reaction (HER) and the oxygen reduction reaction (ORR). Pt is the best catalyst in both cases (HER and ORR) and allows high reaction rates to be reached in an acidic environment with very small overpotentials. Nevertheless, Pt cost and scarcity limit the widespread application of this strategy to use hydrogen as a clean energy source. Thus, there is a significant interest in discovering cheaper and more abundant catalysts to replace Pt.

In this investigation, a high-throughput simulation strategy based on first principles simulations has been implemented to discover intermetallic compounds with high catalytic activity for the HER and ORR through the application of elastic strains. The methodology was initially validated for 13 late transition metals. To this end, the adsorption energy of the intermediate species (H*, O*, and OH*) in the catalytic process was determined by density functional theory calculations on surface slabs with different orientations (fcc(111), hcp(0001), and bcc(101)) subjected to different strain states (uniaxial, biaxial, shear, and a combination of them) up to the mechanical stability limits, as indicated by phonon calculations. This information was used to calculate the catalytic activity of each transition metal for both HER and ORR, and the theoretical results were in agreement with the experimental data in the literature [1,2].

Afterward, this methodology was used to explore the catalytic activity for the HER and the ORR of intermetallic compounds with stoichiometries AB and

A3B and fcc, hcp, and bcc lattices. To this end, the potential intermetallic candidates were screened from the Materials Project database, and those that were toxic, radioactive, or unstable were discarded, leading to a sample of approximately 300 compounds. Those with oxygen adsorption energies lower than -2.5 eV were also discarded due to the formation of oxides under working conditions and the adsorption energies of the intermediate species (H*, O*, and OH*) were calculated for the most stable surfaces of each material using density functional theory calculations. This information was used to determine the catalytic activity and further calculations for the intermetallic compounds with the best performance introducing the effect of elastic strains. The results show that the scaling relations (that limit the catalytic performance of transition metals) are not maintained in the case of intermetallic compounds due to the variation in the most favorable adsorption site for the different adsorbates. Moreover, elastic strains can be used to improve the catalytic performance of intermetallic compounds by changing the free energy barrier associated with the rate-limiting reaction or even the rate-limiting reaction. The present investigation provides a general framework to assess the effect of elastic strains on the catalytic activity of intermetallic compounds and the design of new catalysts with improved performance and/or selectivity of the intermediate species.

References

- [1] C. Martínez-Alonso, J. M. Guevara-Vela, J. LLorca, *Phys. Chem. Chem. Phys.* **2022**, 24, 4832-4842.
- [2] C. Martínez-Alonso, J. M. Guevara-Vela, J. LLorca, *Phys. Chem. Chem. Phys.* **2021**, 23, 21295-21306.

11:45 AM SF07.03.10

Microwave Heating of Nanocrystals for Rapid, Low-Aggregation Intermetallic Phase Transformations Daniel J. Rosen¹, Alexandre Foucher^{1,2}, Emanuele Marino¹, Shengsong Yang¹, Eric A. Stach¹ and Christopher B. Murray¹; ¹University of Pennsylvania, United States; ²Massachusetts Institute of Technology, United States

The use of intermetallic Pt-Co nanocrystals (NCs) for the electrocatalytic oxygen reduction reaction is quickly gaining interest thanks to the higher electrochemical stability of the intermetallic L1₀ phase compared to a random alloy Al phase. However, the thermal treatment that enables the intermetallic phase transformation also causes considerable NC aggregation, resulting in a significant loss of electrochemically active surface area. Herein, we report the use of microwave radiation to induce the intermetallic phase transformation in Cu-doped Pt-Co NCs. We demonstrate that microwave radiation reduces NC aggregation while allowing for a complete phase transformation in only 30 s. These microwave-treated NCs demonstrate higher mass activity for the oxygen reduction reaction while maintaining electrochemical stability similar to the thermally annealed samples.

SESSION SF07.04: Functional Intermetallics II
Session Chairs: Matthew Kramer and Hossein Sepehri Amin
Tuesday Afternoon, November 29, 2022
Sheraton, 5th Floor, Riverway

1:30 PM *SF07.04.01

Eliminating Heavy Rare-Earth Elements in Permanent Magnets Through Grain Boundary Engineering Wei Tang¹, Gaoyuan Ouyang¹, Iver E. Anderson^{1,2}, Jun Cui^{1,2} and Matthew J. Kramer^{1,2}; ¹Ames Laboratory, United States; ²Iowa State University, United States

High performance electric motors for electric vehicles, efficient wind generators and a variety of commercial and industrial motors all require high-performance permanent magnets (PM) which can maintain their energy product at temperatures up to 200°C. For the Nd₂Fe₁₄B based PMs, this has been achieved primarily by replacing the Nd with heavy rare-earth elements (Tb, Dy and Ho). Of the rare-earth elements (REE), these are truly rare, with the cost of Dy typically about 10x that of Pr and Nd. The heavy REEs increase the temperature range by enhancing anisotropy field and lowering its temperature dependence. They also lower the remanence of the alloy relative to the light REE. While applying the Dy only to the surfaces of the magnetic reduces the overall amount needed, it does increase the processing steps needed for the final product. An alternative approach to enhancing the temperature range is to reduce the grain size (dia. < 2 μm), so that grain sizes are closer to those of the magnetic domain size, hence improving the resistance to demagnetization. However, reducing the grain size in sintered magnets is fraught with several challenges. Not only does the grain size need to be reduced, but the distribution of grain sizes also needs to be top-size limited since a small number of large grains can have a disproportionately large effect on decreasing coercivity. Finer grained samples are more susceptible to oxidation, harder to fully magnetically align and, most importantly, need to be sintered to full density without excessive grain growth. We will present results from various methods for reducing grain size, passivating the grains, and using sintering aids to minimize grain growth.

2:00 PM SF07.04.02

FeCoMnAl Soft Magnetic Alloys Ian Baker¹, Youxiong Ye¹, Scott Lish¹, Liubin Xu², Si Chen³, Yang Ren³, Aparna Saksena⁴, Baptiste Gault⁵, Markus Wittman¹ and Haixuan Xu²; ¹Dartmouth College, United States; ²The University of Tennessee, Knoxville, United States; ³Argonne National Laboratory, United States; ⁴Max Planck Strabe 1, Germany; ⁵Imperial College London, United Kingdom

Soft magnets play a vital role in the efficient energy conversion in a variety of important industries including wide-bandgap semiconductors, electric vehicles, aeronautics and aerospace, particularly at high temperatures. Improving the efficiency of modern power electronics and electrical machines via advanced soft magnets has the potential to significantly contribute to global energy savings, thereby leading to a reduction of the associated carbon footprint. Here, we present microstructural characterization and property measurements on two novel FeCoMnAl alloys, one single-phase B2 and one nanostructured B2 + b.c.c., which have good soft magnetic properties up to ~873 K. Both alloys exhibit a high saturation magnetizations, high Curie temperatures, low coercivities, and high electrical resistivities. TEM-based ALCHEMI analysis showed that in the B2 phase the Al atoms preferentially occupy one sublattice site whereas the other elements tend to partition between both sublattice sites. DFT calculations predict magnetic properties consistent with the experimental results and indicate that Fe, Co, and Mn elements predominately contribute to the ferromagnetism.

2:15 PM SF07.04.03

Rapid Multi-Property Assessment of Additively Manufactured Co-Fe-Ni Alloys Varun Chaudhary¹, Wei H. Teh², Shilin Chen², Shakti P. Padhy¹, Cheng C. Tan² and Raju V. Ramanujan¹; ¹Nanyang Technological University, Singapore; ²Institute of Materials Research and Engineering, Singapore

New materials exhibiting an attractive combination of magnetic, mechanical and electrical properties can play a vital role in improving the performance of next generation rotating electrical machines. However, developing such a material using conventional approaches is expensive, time consuming and misses goofs of possible compositions and processing parameters. On the other hand, the accelerated discovery approach relies on high throughput synthesis, characterization, property evaluation, predictive machine learning (ML) and modelling to rapidly screen a huge number of compositions. The assessment of the structure as well as the magnetic, mechanical, and electrical properties of compositionally graded Co-Fe-Ni alloy samples processed by laser additive

manufacturing (AM) was rapidly carried out. The AM process facilitated the rapid synthesis of a compositionally graded material library and the subsequent assessment of several properties. A large change in these properties was observed as a function of composition. Saturation magnetization varied from 60 to 230 emu/g, coercivity from 0.5 to 66.4 Oe, resistivity from 9.4 to 72.6 $\mu\Omega$ cm, microhardness from 90 to 400 Hv, ultimate tensile strength from 465 to 1167 MPa etc. Novel compositions, e.g., $\text{Co}_{30}\text{Fe}_{60}\text{Ni}_{10}$, $\text{Co}_{10}\text{Fe}_{80}\text{Ni}_{10}$, etc., with an optimum magnetic-mechanical-electrical property set have been identified by our approach. This work is supported by the AME Programmatic Fund by the Agency for Science, Technology and Research, Singapore under Grant No. A1898b0043.

2:30 PM BREAK

3:00 PM *SF07.04.04

Development of Magnetic Refrigeration Materials for Cryogenic Applications Hossein Sepehri Amin, Xin Tang, Jiawei Lai, Anton Bolyachkin, Tadakatsu Ohkubo and Kazuhiro Hono; NIMS, Japan

Hydrogen will play a major role in the establishment of a renewable-energy-based society and realization of carbon neutrality. However, one of the major challenges is the storage and transportation of hydrogen: the H_2 gas has large volume and its liquefaction is necessary. The current available technology for hydrogen liquefaction is conventional gas compression systems based on the Joule-Thomson effect, which is costly and inefficient at low temperatures. Cryogenic magnetic refrigeration (CMR) is a prospective environmentally friendly technology for temperature below 120 K, and it can theoretically exhibit a higher efficiency as compared to those of conventional gas compression systems. In the CMR, the gaseous hydrogen is pre-cooled down to ~ 77 K by using liquid nitrogen, and, at the second stage, the magnetic liquefier provides a further decrease in temperature down to 20 K (H_2 liquefaction temperature). However, the lack of magnetic refrigerant materials with high magnetic entropy change in a wide temperature range of 77-20 K required for the hydrogen liquefaction is a bottle-neck for practical applications of MR cooling systems

In this talk, we will first demonstrate how data science can be used to develop magnetocaloric materials with giant and reversible magnetocaloric effect at the cryogenic temperatures. We conducted machine learning on a dataset extracted from literature on Fe_2P based alloys to predict optimum alloy composition which results in a decrease of transition temperature below 100 K. Combination of machine learning and experimental validations resulted in realization of rare-earth free $(\text{Mn},\text{Fe},\text{Co})_2(\text{P},\text{Si})$ based compounds which exhibit a large magnetocaloric performance in isothermal magnetic entropy change (ΔS_m) of 7.5–11.5 J/kgK at the temperatures below 100 K [1]. This study demonstrates that data-driven development of magnetocaloric materials can efficiently boost the optimization of their properties, thus aiding the practical applicability of magnetic refrigeration technology. In the second part of the talk, we will show a series of materials with a giant magnetocaloric effect (MCE) in magnetic entropy change ($-\Delta S_m > 0.2 \text{ Jcm}^{-3}\text{K}^{-1}$) in the $\text{Er}(\text{Ho})\text{Co}_2$ -based compounds, suitable for operation in the full temperature range required for hydrogen liquefaction (20-77 K) [2]. We found that the giant MCE becomes reversible, enabling sustainable use of the MR materials, by eliminating the magneto-structural phase transition revealed by detailed cryogenic and in-situ microstructure characterizations. We will discuss how this discovery can lead to the application of $\text{Er}(\text{Ho})\text{Co}_2$ -based alloys for hydrogen liquefaction using MR cooling technology for the future green fuel society.

[1] J. Lai et al. "Machine learning assisted development of Fe_2P -type magnetocaloric compounds for cryogenic applications" *Acta Mater.* 232 (2022) 117942.

[2] Xin Tang, et al. "Magnetic refrigeration material operating at a full temperature range required for hydrogen liquefaction" *Nature Comm.* 13 (2022) 1.

3:30 PM SF07.04.05

High-Resolution Magnetic Domain Wall Imaging by DPC STEM Yoshiki O. Murakami¹, Takehito Seki^{1,2}, Yuichi Ikuhara^{1,3} and Naoya Shibata^{1,3}; ¹University of Tokyo, Japan; ²JST Presto, Japan; ³Japan Fine Ceramics Center, Japan

Permanent magnets are utilized in many applications such as the main power motor in electric vehicles. It is known that the coercivity, the resistance to changes in magnetization, of magnets can be significantly improved by suppressing the formation of magnetization reversal nuclei and preventing the growth of the reversal nuclei [1]. Micromagnetic simulations predicted that the local change in magnetic properties such as magnetocrystalline anisotropy is crucial to prevent the growth of the reversal nuclei [2]. Thus, the coercivity may be improved by optimizing microstructures consisting of the phases with different magnetic properties. The existence of various phases in microstructures has been reported in high coercive Nd-Fe-B permanent magnets [3], but the key microstructural features to improve the coercivity are still not well understood. It is thus essential to identify one-by-one relationship between microstructural features and their magnetic properties. One of the methods to directly measure the local magnetic properties is to measure the magnetic domain wall (DW) width. DW width varies with the change in the ratio of exchange stiffness and magnetocrystalline anisotropy where the DW is located. The larger DW width indicates larger exchange stiffness or smaller magnetocrystalline anisotropy. However, direct and precise measurement of DW width requires high spatial resolution, since DW is a nanometer-sized magnetic structure.

Differential phase contrast scanning transmission electron microscopy (DPC STEM) [4] is an imaging technique of local electromagnetic fields inside specimens. Combined with recently developed magnetic-field-free atomic resolution STEM [5], DPC STEM now enables visualization of nanoscale magnetic structures in magnetic free environment. Furthermore, one can obtain structural information in the same field of view through other STEM techniques such as high-angle annular dark field images and electron energy loss spectroscopy (EELS).

In this study, we directly measured DW width in La-substituted Nd-Fe-B magnets by DPC STEM. In this magnet, Nd is non-uniformly substituted by La, and the magnetocrystalline anisotropy is expected to locally fluctuate with Nd concentration. To confirm the correlation of DW width and Nd concentration, we measured DW width by DPC and analyzed Nd composition by EELS at the same area. The results show the DW width increases with the decrease in Nd concentration. Details will be reported in the presentation.

1) O. Gutfleisch, *J. Phys. D: Appl. Phys.* 33 (2000).

2) G. Hrkac, et al. *Appl. Phys. Lett.* 23 (2010).

3) T. G. Woodcock, et al. *Acta Mater.* 77 (2014).

4) N. Shibata *et al.*, *Acc. Chem. Res.* 50 (2017).

5) N. Shibata *et al.*, *Nat. Commun.* 10 (2019).

3:45 PM SF07.04.07

Thermomechanical Nanomolding in 2D Mehrdad Kiani¹, Quynh Sam¹, Hyeuk Jin Han¹, Yeon Sik Jung² and Judy Cha¹; ¹Cornell University, United States; ²Korea Advanced Institute of Science and Technology, Korea (the Republic of)

Fabrication of intermetallic nanostructures over wafer-scale distances is critical for applications such as catalysis, energy storage, and microelectronics. Current top-down and bottom-up fabrication approaches, such as CVD or colloidal synthesis, are limited to simple material compositions, have poor morphology and size variance, and lack control of crystallinity. Recently, thermomechanical nanomolding, whereby a polycrystalline feedstock is pressed through a mold with 1D pores at an elevated temperature ($\sim 0.5T_m$), has been shown by Jan Schroers' group at Yale University to form periodic arrays of single crystal, defect free nanowires. Since composition is determined by the feedstock material, this technique can be easily used to form nanowires of a wide range of intermetallic compounds.

Building upon this work, we investigated thermomechanical nanomolding for fabrication of 2D nanostructures. Using 2D Si trenches with a SiO_2 liner as a

mold, we successfully nanomold both single element and intermetallic compounds over ~1 cm distances. SEM, EBSD, and S/TEM imaging confirm that 2D linear trenches can be formed with no apparent gaps; however, the final structures are not always single crystal, in contrast to 1D nanomolding. While 1D nanowire growth is driven by interfacial diffusion, the lower surface to volume ratio and post-mold structures indicate that other growth mechanisms, such as deformation twinning and grain reorientation, play an important role during nanomolding.

4:00 PM SF07.04.08

Controlling Devitrification in FeSiB Amorphous System for Advanced Soft Ferromagnets Xiaoyu Zhang¹, Wentao Liang¹, Rafael Perez del Real², Manuel Vazquez² and Laura Lewis^{1,1}; ¹Northeastern University, United States; ²Instituto de Ciencia de Materiales de Madrid, Spain

The performance of advanced soft ferromagnets relies on the formation of an optimized nanocrystalline structure through controlled devitrification from amorphous precursors. This structure is conventionally achieved via small additions of early/late transition metal elements (Nb, Cu, *etc.*) that allow for tuning of devitrification kinetics but also degrade saturation magnetization. Here, building from an in-depth study of as-quenched amorphous nanostructures produced by different rapid solidification conditions, we identify that specifics of small quenched-in crystallites strongly determine devitrification kinetics in FeSiB system free of transition metal additions.

Samples of composition Fe₇₉Si₁₁B₁₀ were fabricated into two forms: 1) melt-spun ribbons of ~25 μm in thickness and 2) water-quenched microwires of ~150 μm in diameter. While identical chemical composition and overall X-ray amorphous structure of both as-quenched forms are confirmed, nanoscale differences are revealed by high-resolution transmission electron microscopy. In specific, the water-quenched microwires feature small (~30 nm in diameter) Fe(Si) crystallites dispersed throughout their volume, in contrast to the melt-spun ribbons that exhibit amorphous structure with Fe(Si) nanocrystalline islands (~2 nm in thickness, ~50 nm in diameter) confined to the surfaces. Analysis of calorimetric data reveals that the microwires devitrify via nucleation from pre-existing nuclei, resulting in reduced activation energy, followed by diffusion-controlled grain growth. On the other hand, the ribbons exhibit continuous nucleation followed by interface-controlled growth. It is contemplated that the different devitrification behavior exhibited by the two sample types is attributed to their unique nanostructural state, which is subtly affected by the rapid solidification conditions. These results provide insights into the control of devitrification to achieve high-moment, high-performance nanocrystalline soft ferromagnets without alloying additions.

Acknowledgments: IEEE Magnetics Society Educational Seed Funding, Northeastern University, and ICMM/CSIC, Spain

4:15 PM SF07.04.09

Thermomechanical Nanomolding of Topological Materials Quynh Sam¹, Mehrdad Kiani¹, Hyeuk Jin Han² and Judy Cha¹; ¹Cornell University, United States; ²Yale University, United States

Topological intermetallic nanomaterials have novel symmetry-protected electronic states that are advantageous for applications such as catalysis¹, electronics², and quantum computing³. Fabrication of intermetallic nanomaterials is hindered by the lack of high throughput synthesis methods that allow for tight control of phase, morphology, and stoichiometry. Here, we present the use of thermomechanical nanomolding (TMNM) to fabricate nanowires of topological intermetallic materials. Developed by Jan Schroers' group at Yale University, TMNM is a scalable fabrication process where a bulk feedstock is pressed through a mold with nanosized pores at elevated temperatures and pressures. Starting with a polycrystalline feedstock, TMNM forms defect-free, single crystalline nanowires with consistent growth orientation and composition.⁴ TMNM is materials agnostic and has been successfully used to create nanowires of several different topological materials.⁵ Furthermore, high pressures and temperatures used in the molding process can be exploited to study phase stability with the possibility of producing metastable phases through nanoscale confinement effects.

We used TMNM to fabricate nanowires of several different topological intermetallic materials. Due to the presence of symmetry-protected surface states, these topological materials have enhanced electronic properties that make them attractive candidates for next-generation interconnect materials. High-resolution S/TEM analysis reveals formation of high-quality, single-crystalline nanowires with consistent composition. Surprisingly, we observe that high levels of vacancies can be tolerated in these single-crystalline molded nanowires without forming any extended defects, such as nanoscale voids or phase separation. The molded nanowires show promising electrical properties where their resistivity values do not increase with decreasing dimensions of the nanowires, in contrast to the increasing resistivity of Cu interconnects at the nanoscale. Thus, we present TMNM as a high throughput fabrication method to form nanowires of topological intermetallic materials with controlled structure and electrical properties with promising applications in energy-efficient computing technologies.

References

1. D. Wang, Q. Peng, Y. Li, Nano Res. **3**, 574-580 (2010).
2. H.J. Han, D. Hynek, Z. Wu, L. Wang, P. Liu, J. V. Pondick, S. Yazdani, J.M. Woods, M. Yarali, Y. Xie, H. Wang, and J.J. Cha, APL Mater. **8**, 011103 (2020).
3. S.M. Frolov, M.J. Manfra, and J.D. Sau, Nat. Phys. 2020 167 **16**, 718 (2020).
4. N. Liu, Y. Xie, G. Liu, S. Sohn, A. Raj, G. Han, B. Wu, J.J. Cha, Z. Liu, and J. Schroers, Phys. Rev. Lett. **124**, 036102 (2020).
5. Z. Liu, N. Liu, and J. Schroers, Prog. Mater. Sci. **125**, 100891 (2022).

4:30 PM SF07.04.10

Topological Metal Nanowires for Interconnect Gangtae Jin^{1,2}, Hyeuk Jin Han², James L. Hart¹, Quynh Sam¹, Mehrdad Kiani² and Judy Cha^{1,2}; ¹Cornell University, United States; ²Yale University, United States

Topological semimetals (TSMs) possess topologically protected surface states near the Fermi level with high carrier densities and high mobilities, holding distinct potential for low-dissipation on-chip interconnects that may outperform current copper interconnects for continued dimensional scaling of CMOS technologies. To explore the feasibility of nanoscale interconnects using TSMs, synthesis of TSMs with controlled dimensions, structural characterization, and transport properties at the nanoscale are essential. Here, we report synthesis of various TSM nanowires (MoP₂, CoSi, FeGe) with controlled dimensions and crystallinity by chemical vapor deposition and nanomolding. The demonstration of nanostructured TSM nanowires provides opportunities for careful investigations of design rules for TSMs-based nanoscale interconnects.

SESSION SF07.05: Poster Session: Frontiers of Intermetallics Science for Structural and Functional Materials Design

Session Chairs: Yoshisato Kimura, Manja Krueger, Akane Suzuki and Matthew Willard

Tuesday Afternoon, November 29, 2022

8:00 PM - 10:00 PM

Hynes, Level 1, Hall A

SF07.05.02

Microstructure Characterization of Spark-Plasma Sintered Compacts of MoSiBTiC Powder Produced by Gas Atomization Shuntaro Ida, Hayato Arai, Kohei Umeda, Xi Nan, Nobuaki Sekido and Kyosuke Yoshimi; Tohoku University, Japan

The creep strength of the first-generation MoSiBTiC alloy (Mo-5Si-10B-10Ti-10C, at%) is superior to that of SiC/SiC composites, and the specific strength of this alloy is comparable to that of ceramics matrix composite at 1250°C. On the other hand, its high strength properties make hot forging and processing into complex shapes difficult. Therefore, the processing of the MoSiBTiC alloy by powder metallurgy has been investigated. In this study, the powder and sintered compact of the first-generation MoSiBTiC alloy were prepared by electrode induction gas atomization (EIGA) and spark-plasma-sintering (SPSed compact).

The spherical powder of the first-generation MoSiBTiC alloy was produced by the EIGA method. The microstructure of the powder was much more refined than that of the alloy produced by the arc-melting method (Cast sample). Interestingly, some solidification steps in the Cast sample disappeared in the powder. These differences are attributed to the rapid cooling effect of the EIGA method. Dense and sound powder compacts were successfully obtained by the SPS process. The composition of the SPS compacts was close to the nominal composition of the first-generation MoSiBTiC alloy. Therefore, it was found that there were no significant compositional changes during the powder process. The microstructure of the SPSed compact was considerably (almost one order) finer than that of the Cast sample, with random crystallographic orientation distribution and less anisotropic morphology along the solidification direction observed in the Cast sample.

SF07.05.03

Oxide Scale Analysis of Cr and Nb-added MoSiBZrC Alloy Xinyu Yan, Xi Nan, Shuntaro Ida, Nobuaki Sekido and Kyosuke Yoshimi; Tohoku University, Japan

Mo-Si-B alloys with the addition of ZrC, so-called MoSiBZrC alloys, combine moderate room-temperature fracture toughness and superior high-temperature strength. This is because of the synergistic effect of toughening and high-temperature strengthening by the ZrC phase. However, MoSiBZrC alloys, as well as MoSiBTiC, suffer from catastrophic oxidation at and above 700 °C, caused by the rapid volatilization of MoO₃. For this reason, many efforts have been made to improve oxidation performance. For instance, our previous studies revealed that Cr addition can remarkably improve the oxidation resistance of the MoSiBTiC alloy. Also, it was reported that Nb addition to Ti alloys decelerates the diffusion of oxygen ions in the oxide scale and contributes to the formation of compact oxide layers. Therefore, in the present study, the effect of Cr and Nb additions on the oxide scale formation of MoSiBZrC alloy was analyzed.

Alloy ingots with selected compositions were prepared by conventional arc-melting in an Ar atmosphere. The oxidation tests were carried out at 800 °C. Compared with the base MoSiBZrC alloy, the alloys with Cr and/or Nb additions exhibited considerably reduced weight losses during oxidation. The Cr addition increased the oxidation resistance of the MoSiBZrC alloy because the high amount of Cr dissolved in the Mo solid solution phase and formed as protective Cr₂(MoO₄)₃. The Nb addition decreased the thickness of the oxide layer. In the alloys with Cr and Nb addition, the CrNbO₄ layer formed beneath the Cr₂(MoO₄)₃, which further decelerated the diffusion of O²⁻ ions. Moreover, in the Cr-added alloys, a substantial amount of cracks were observed in the substrate near the oxide-substrate interface, but the crack density decreased by the Nb addition. It is considered that the Nb addition might effectively work to suppress the spallation of the oxide scale.

SF07.05.04

On the Possibility of the Yield Stress Anomalous Increase in L1₂-Fe₃Ge Zhenghao Chen and Haruyuki Inui; Kyoto University, Japan

The L1₂-ordered structure is one of the most wide-known structures in the field of high-temperature structural materials owing to its superior high-temperature strength. This is believed to be attributed to the anomalous increase of yield stress with increasing temperature (referred to as yield stress anomaly, YSA), which is caused by a thermally activated (111)-(010) cross slip of Anti-phase boundary (APB) coupled $b=1/2[101]$ superpartial dislocations. However, not all L1₂-compounds are necessary to exhibit the YSA phenomenon. The L1₂-Fe₃Ge was considered one of those for a long time. This was related to the fact that slip on the (010) plane is exclusively activated in L1₂-Fe₃Ge with their polycrystal specimens that either the (111) slip or the YSA was believed not to occur. Besides, unfortunately, the preparation of single-crystal specimens in bulk size is extremely difficult. For that reason, almost nothing is known at present about the deformation behavior of the L1₂-Fe₃Ge in detail.

In the present study, we investigate the compressive deformation behavior of L1₂-Fe₃Ge in their micropillar single-crystal specimens at room temperature. Emphasis is placed on the deformation microstructures of the L1₂-Fe₃Ge through detailed transmission electron microscopy (TEM) investigation, paying special attention to whether or not the YSA occurs in this L1₂-compound.

For the compression orientation near [001], the (111) slip in L1₂-Fe₃Ge is successfully observed. This is the first time to experimentally observe the (111) slip in L1₂-Fe₃Ge. The critical resolved shear stress (CRSS) for (111) slip is estimated as ~240MPa, which is resulted to be approximately 8 times higher than that for (010) slip (~35MPa). The extremely huge gap in the CRSS between the (111) slip and the (010) slip is considered responsible for the absence of the (111) slip in polycrystal deformations. Typical dislocation structures corresponding to the Kear-Wilford lock are observed after deformation on (111) slip, suggesting a possibility of the occurrence of YSA in L1₂-Fe₃Ge, even at room temperature. This exciting discovery brings L1₂-Fe₃Ge an opportunity to serve as the γ' strengthening phase in γ/γ' two-phase superalloys and hence opens a new category in the field of high-temperature structural materials, the Fe-based superalloy strengthened by L1₂-Fe₃Ge variants.

SF07.05.05

Controlling Mg₂Si Intermetallic Phase in Al-Si-Mg Alloy by Laser Additive Manufacturing Process and Post Heat Treatments Keito Saki¹, Yuki Otani¹, Naoki Takata¹, Asuka Suzuki¹, Makoto Kobashi¹ and Masaki Kato²; ¹Nagoya university, Japan; ²Aichi Center for Industry and Science Technology, Japan

Laser powder bed fusion (L-PBF) process is one of the metal additive manufacturing techniques capable of producing complex geometrical forms. The AlSi10Mg alloy with a nominal composition of Al-10Si-0.3Mg (mass%) is one of the representative Al alloys used for the L-PBF process. The L-PBF manufactured AlSi10Mg alloy exhibits a fine cellular microstructure consisting of the α -Al matrix with supersaturated Si solid solution and surrounding Al/Si eutectic network. The characteristic microstructure is considered to contribute to a superior strength of the L-PBF processed Al-Si alloys compared to the conventional cast alloys. In general, Al-Si-Mg alloys are artificially aged to achieve high strength by promoting the fine precipitation of Si and the β -Mg₂Si phase (including the metastable phase) in the α -Al matrix. It has been reported that nanoscale precipitates of the Mg₂Si phase introduced by aging treatments contributed to the further hardening of the L-PBF manufactured AlSi10Mg alloy. The insight can open an opportunity for further strengthening of L-PBF manufactured Al-Si-Mg alloys by controlling a combination of the Mg₂Si phase with the Si phase. In this study, we designed an alloy composition of Al-10Si-4.5Mg (mass%) based on the calculated phase diagram of the Al-Si-Mg ternary system. Thermodynamic calculations assessed relatively high fractions (approximately 8% in equilibrium) of the Mg₂Si phase in the designed alloy composition. We made an attempt at the L-PBF processing using an Al-10Si-4.5Mg alloy powder. The microstructural characteristics were clarified for the L-PBF processed samples and then the age-

hardening behavior associated with the precipitation of the Mg₂Si phase will be investigated.

The gas atomized Al-10Si-4.5Mg alloy powder with a mean particle size of approximately 20 μm was applied for the L-PBF manufacturing using a ProX DMP 200 machine (3D Systems). The applied process parameters were as follows: scan speed (v) = 0.6~1.8 m/s, laser power (P) = 51~140 W, laser spot size ~100 μm, powder layer thickness = 30 μm, and hatch distance = 100 μm. The relative density was measured by the Archimedes method. The Al-10Si-4.5Mg alloy samples with an approximate dimension of 15 mm × 15 mm × 10 mm were manufactured under the conditions of v = 1.0~1.8 m/s and P = 77~128 W. The samples manufactured under v = 1.0 m/s and P = 128 W exhibited a highest relative density of 92%. Microscopic cracks perpendicular to the building direction were often observed in all of the manufactured samples. Such crack propagation would be a dominant contributor to the reduced relative densities of the Al-10Si-4.5Mg alloy samples. The manufactured samples exhibited melt-pool structures composed of many elongated α -Al phases (primary solidified) surrounded by numerous granular Mg₂Si phases and fine Si phases (formed in eutectic reactions). The microstructural morphology was in good agreement with the calculated Scheil solidification sequence of liquid (L)+ α → L+ α +Mg₂Si → L+ α +Mg₂Si+Si in the alloy composition. On the other hand, a relatively coarse equiaxed cellular microstructure decollated with granular Mg₂Si phase was observed at the melt-pool boundaries. The relatively coarse and brittle Mg₂Si phase localized at melt-pool boundaries may contribute to the crack propagation perpendicular to the building direction. The hardness of the as-manufactured sample was over 180 HV, which was much higher than that of the AlSi10Mg alloy (~130HV). This superior hardness would be attributed to the granular Mg₂Si phase. Si and Mg solute contents inside the α -Al matrix were approximately 2.2 and 1.0 mass%, respectively. The high solute contents indicate the possibility of further precipitation strengthening by the post heat treatments. The age-hardening behavior and its associated precipitation of the Mg₂Si phase (together with Si phase) will be presented.

SF07.05.06

Controlling α /Al₆Fe Two-Phase Eutectic Structure in Cast Al-Fe Alloys by Addition of Mn and Cu Elements Naoki Okano, Naoki Takata, Asuka Suzuki and Makoto Kobashi; Nagoya University, Japan

Aluminum (Al) alloys are widely used in transportation equipment and aerospace because of their lightweight and high specific strength. Al-Fe alloys have been investigated as candidate materials for high-temperature applications, but the coarsened θ -Al₁₃Fe₄ phase ($mC102$) has a detrimental effect on the mechanical performance of the cast Al-Fe alloys. In rapidly solidified alloys, the refined Al₆Fe metastable phase ($oC28$) would increase strength without compromising ductility. The refined Al₆Fe metastable phase would transform into the coarsened θ stable phase at elevated temperatures, resulting in the reduction of high-temperature strength in thermal exposure. The stabilization of the Al₆Fe phase by the addition of a third element (Mn or Cu) would be effective to improve the microstructural stability at elevated temperatures. In the present study, Mn and Cu were selected as the added third elements in terms of the crystal structure of Al₆Fe phase. The added Mn is expected to replace the Fe sublattice of the Al₆Fe phase ($oC28$) and form a stable Al₆(Fe, Mn) phase in the Al-Fe-Mn ternary system. In the Al-Fe-Cu ternary system, α phase is in equilibrium with the Al₂₃CuFe₄ phase with the same orthorhombic crystal structure ($oC28$), suggesting that the Al₆Fe phase would be stabilized by Cu addition. Herein, for understanding the effects of Mn and/or Cu additions on the formation of Al₆M (M: Fe, Mn, Cu) phase in the solidification microstructures of Al-Fe alloys, we fabricated Al-Fe-Mn, Al-Fe-Cu ternary alloys, and Al-Fe-Cu-Mn quaternary alloys solidified at different cooling rates. The solidification microstructures and high-temperature strength were systematically investigated.

Various Al-Fe alloys with compositions of Al-1%Fe, Al-1%Fe-1%Mn, Al-1%Fe-1%Cu, and Al-1%Fe-1%Cu-1%Mn (mol%) were prepared by solidification at different cooling rates. The raw materials were melted in an induction furnace in the temperature range of 800-900°C for 1800 s in an Ar atmosphere. The molten materials were prepared at two different cooling rates. Some were cooled by switching off the power source to the furnace (cooling rate: 0.3 °C×s⁻¹). The others were cast into an iron mold to form rod-shaped ingots at a higher cooling rate (145 °C×s⁻¹).

In the furnace-cooled Al-1%Fe alloy, the coarsened θ -Al₁₃Fe₄ stable phase was formed in the α (fcc) matrix. The cast Al-1%Fe alloy exhibited several elongated α phases surrounded by refined α /Al₆Fe eutectic structure. In the Al-1%Fe-1%Mn alloy, the Al₆(Fe, Mn) phase appeared regardless of the cooling rate. The refined α /Al₆(Fe, Mn) two-phase eutectic microstructure occupied almost the entire area in the cast sample. In the furnace-cooled Al-1%Fe-1%Cu alloy, the Al₂₃CuFe₄ phase was formed in the final solidification zone. The cast Al-1%Fe-1%Cu alloy showed the same microstructural morphology as the cast Al-1%Fe binary alloy, and the Cu tended to distribute into the Al₆Fe phase. The fine eutectic microstructure was observed in the cast Al-1%Fe-1%Cu-1%Mn alloy as well as in the cast Al-1%Fe-1%Mn alloy. The added Cu and Mn elements were enriched in the intermetallic phase, which may contribute to the stabilization of the Al₆M phase.

The 0.2% proof stress of the cast Al-1%Fe alloy was about 90 MPa at room temperature and decreased with increasing temperature. The 0.2% proof stress at 300°C was about 50 MPa. With the addition of 1 mol% Mn and Cu, the 0.2% proof stress at room temperature increased to 120~130 MPa. The combined addition of Mn and Cu increased the 0.2% proof stress to about 150 MPa, and the reduction in strength level by increasing test temperature appeared less pronounced for the Al-1%Fe-1%Mn-1%Cu quaternary alloys. The moderate reduction in strength could be due to the fine eutectic structure containing the Al₆M phase stabilized by Mn and Cu elements.

SF07.05.07

Expansion of Pettifor Structural Map to Search for High-Concentrated Solid Solution-Based Multi-Phase Alloys Syuki Yamanaka, Ken-ichi Ikeda and Seiji Miura; Hokkaido University, Japan

Recently, novel alloy design methods using high-concentrated solid solutions, such as high-entropy alloys, are attracting attention. By introducing the strengthening phase to a high-concentrated solid solution with excellent mechanical properties, it is expected to produce high-performance materials. Because the number of combinations of multiple elements is too large, a guideline for selecting constituent elements for searching for new high-concentrated solid solution-based multi-phase alloys is needed. Our goal is to develop a rapid screening scheme for multi-component material development.

The Pettifor maps are useful maps for binary compounds A_xB_y with various x/y ratios in an easy-to-understand notion in terms of the Mendeleev number [1]. Given that it can describe a wide range of binary compounds, the order of the Mendeleev number is related to factors governing the binary interaction energy, such as electron concentration. Therefore, this idea is expected to be effective in describing the stability of not only binary compounds but also binary solid solutions. By creating the map for solid solutions and combining it with the conventional Pettifor map for binary compounds, both combinations that form a stable solid solution and the compound that may equilibrate each other can be found in a short time survey without checking a huge number of phase diagrams one by one. For a typical example, in the case of a ternary alloy with Co and Al additions to pure Ni, these maps will tell us Co forms an fcc continuous solid solution with Ni, together with the candidates of Al-containing compounds such as Ni₃Al-L1₂, NiAl-B2 and CoAl-B2. For the relationship between the binary system and multi-component system, our previous works revealed that many multi-component compounds are derived by substituting a specific site of a binary compound for other elements, e.g., (Ni, Co)₃(Al, Ta, W) derived from L1₂-Ni₃Al [2,3]. This knowledge leads us to expect that, information such as the crystal structure of binary solid solutions is helpful to evaluate the stability of multi-component solid solutions. The main aims of the present work are to investigate the stability of multi-component solid solutions thermodynamically, create the map for binary primary solid solutions and confirm our idea is effective in selecting the constituent elements in multi-component systems.

Under such considerations, the map proposed in this study includes detailed information about each binary solid solution such as its crystal structure, its maximum solubility and the presence of its competing phases within the 1,411 binary phase diagrams in a single map. This map clearly shows which solutes dissolve largely in which solvents, allowing an immediate evaluation of the potential for multi-component high-concentrated solid solution formation. Then, by comparing this map with the Pettifor maps, the compound to be selected as a stable phase in a multi-component system can be

estimated. For example, considering the Ti addition to CoCrFeMnNi alloy, the stabilization of the solid solution by combining Co, Cr, Fe, Mn and Ni can be confirmed in the map of this study. Also, in the conventional Pettifor maps, as the candidate compounds composed of the constituent element with Ti, there are only the Laves phases (TiCo_2 , TiCr_2 , TiFe_2 and TiMn_2) in the AB_2 map and the B2 compounds (CoTi, FeTi and MnTi) in the AB map. In previous experiments [3], it was confirmed that the high-concentrated fcc phase equilibrates with AB_2 Laves compound in Ti-added CoCrFeMnNi alloy. Thus, our scheme can easily estimate the combination of a stable high-concentrated solid solution and the candidate compounds. This study will enable the rapid development of high-performance multi-component materials.

[1] D. G. Pettifor, *J. Phys. C, Solid. State.*, 19, 285 (1986)

[2] S. Yamanaka, K. Ikeda and S. Miura, *MRS advances*, 4(25-26), 1497 (2019)

[3] S. Yamanaka, K. Ikeda and S. Miura, *J. Mater. Res.*, 36, 2056 (2021)

SF07.05.08

Plastic Deformation Behavior of Single Crystalline Pearlitic Steel Investigated by Micropillar Compression Method Mutsumi Morisaki, Nobuyuki Kadota, Kyosuke Kishida and Haruyuki Inui; Kyoto University, Japan

Pearlitic steel has been used in a wide variety of practical applications, such as rails, bridge cables and high-strength wires because of their ultra-high strength, which is closely related to their lamellar structure composed of alternating ferrite (α) and cementite (θ -Fe₃C) layers. The strength of pearlitic steel wires has known to be improved further by cold drawing, which results in the refinement and alignment of the lamellar structure. However, the detailed mechanism of the microstructure evolution during cold drawing process has not been fully clarified yet. This is mainly because of the lack of information on plastic deformation behavior of cementite. Recently, we have systematically investigated room temperature deformation behavior of cementite single crystals as a function of the loading axis orientation by utilizing micropillar compression method and have successfully identified five different slip systems operative at room temperature and their critical resolved shear stress (CRSS). In the present study, we have applied the micropillar compression method to investigate plastic deformation behavior of individual pearlite lamellar grains, whose loading axis orientations are (nearly) parallel to the lamellar boundary planes with the Bagaryatsky orientation relationship ($(112)_\alpha // (010)_\theta$, $[-110]_\alpha // [001]_\theta$). Operative slip systems in each lamella and their transfer behavior through lamellar interfaces were investigated experimentally through the trace analysis of slip traces appeared on side surfaces of micropillar specimens. When the loading axis was nearly parallel to $[-110]_\alpha$ and $[001]_\theta$, both α -Fe and θ -Fe₃C lamellar were confirmed to plastically deform by the activation of their primary slip systems with their slip traces propagating continuously through many alpha-theta interfaces. In contrast, when the loading axis was about 15 degrees away from $[-110]_\alpha$ and $[001]_\theta$, non-primary slip systems were activated in both phases, while the continuation of slip traces was maintained. Possible factors that control the operative slip systems in both phases were discussed based on the information on the operative deformation modes in θ -Fe₃C obtained by our previous micropillar experiments, geometrical relationship between slip systems in alpha and theta phases, and strain compatibility at alpha-theta interfaces.

SF07.05.10

Bi-Doping Strategy for Achieving Single Crystal Particles of Ni-Mn-Ga and Investigations of Ni-Mn-Ga/Polymer Composites Towards Smart Materials Wan-Ting Chiu¹, Pimpet Sratong-on², Masaki Tahara¹, Volodymyr Chernenko^{3,4,1} and Hideki Hosoda¹; ¹Tokyo Institute of Technology, Japan; ²Thai-Nichi Institute of Technology, Thailand; ³UPV/EHU Science Park, Spain; ⁴Basque Foundation for Science, Spain

The shape change of the ferromagnetic shape memory alloy (FSMA) is manipulatable via applying an external magnetic field [1]. The NiMnGa-based alloys are considered promising FSMA for applications as magnetic field-driven devices; however, their high brittleness inhibits their practicability. Therefore, in this work, a grain separator, Bi element, was intentionally introduced into the polycrystalline NiMnGa alloys to separate the grains and make NiMnGa alloys even brittle. The introduced concentration of the Bi element was varying from 0.00 at.% to 0.05 at.% to optimize the doping amount and the properties of the bulk NiMnGa specimens. The Bi-doped polycrystalline NiMnGa alloys were then mechanically disintegrated into single-crystalline particles by a well-controlled crushing system. The NiMnGa single crystal particles were utilized for the fabrications of the composites with the volume fraction (vol.%) of the single-crystal particles at 20% by an integration of the single-crystal particles with a silicone polymer matrix. The single crystal NiMnGa particles/silicone polymer composite materials were successfully fabricated for realizing the applications of the high-speed actuator. The Bi doping studies were performed using concentrations of 0.00, 0.01, 0.03, and 0.05 at.%. Elemental mapping (i.e., Ni, Mn, Ga, and Bi) of each alloy was conducted to reveal the distribution details of each element. It is found that with the addition of the Bi separator to the NiMnGa polycrystalline bulk materials, the grains were successfully separated. In addition, it was shown that the higher concentration of the Bi doping, the more grain boundaries could be observed. This effect was already saturated at 0.03 at.%. The average grain size, analyzed by using ImageJ software, was around 210 μm for NiMnGa polycrystalline bulk alloys doped by 0.03 and 0.05 at.% Bi. A co-existence of the 5M- and the 7M-martensite phases was found in the single crystal NiMnGa particles at 27 °C, whereas at 39 °C only a single 5M-martensite phase, and at 51 °C only the parent austenite phase (A), were observed. Hence, the following sequence of phase transformations was observed 7M/5M \rightarrow 5M \rightarrow A [2].

The micro-strains of particles in composites with volume fraction of particles of 20 vol.% (co-existence of 5M- and 7M-martensite phases), Composite A (CA), and 30 at. % (5M-martensite phase), Composite B (CB), were measured by a micro-CT and analyzed by a polar decomposition method [3]. The composites were compressed from 0% to 50% of the total deformation strain. It was found that the particle composed of 7M-martensite performed the largest micro-strain among all the tested particles. On the other hand, the 5M-martensite particles in CA and CB composites exhibit similar micro-strain. It is worth noting that the loading-unloading hysteresis of CA was reduced greatly owing to the released spatial interference among the particles.

References

[1] H.E. Karaca, I. Karaman, B. Basaran, Y.I. Chumlyakov, H.J. Maier, *Acta Mater.* 54(1) (2006) 233-245.

[2] C. Segui, V.A. Chernenko, J. Pons, E. Cesari, V. Khovailo, T. Takagi, *Acta Mater.* 53(1) (2005) 111-120.

[3] P. Sratong-on, V.A. Chernenko, J. Feuchtwanger, H. Hosoda, *Sci. Rep.* 9 (2019) 3443.

[4] W.-T. Chiu, P. Sratong-on, M. Tahara, V.A. Chernenko, H. Hosoda, *Scr. Mater.* 207 (2022) 114265.

SF07.05.11

A Study on the Relationship Between the Size and Magnetic Properties of Nd₂Fe₁₄B Through the Fabrication of Fine-Grained Magnets Using Submicron Fe Jeong Hyun Kim¹, Myeongjun Ji¹, Cheol-hui Ryu¹ and Young-In Lee^{1,2}; ¹Seoul National University of Science and Technology, Korea (the Republic of); ²The Institute of Powder Technology, Korea (the Republic of)

With the demand for high efficiency in green technology fields such as energy conversion systems, wind turbines, and electric vehicles, Nd₂Fe₁₄B sintered magnets have to store high energy density and be stable for devices in various operating temperatures. For high coercivity in accordance with this requirement, several attempts are being investigated to develop heavy rare-earth element (HRE)-lean or free Nd-Fe-B magnets. A promising approach to achieve coercivity enhancement while avoiding scarcity of resources and the expense of remanence due to antiferromagnetic coupling between HRE and Fe is to control the microstructure, such as grain size. The size-dependent coercivity tends to maximize when the magnetic dimension reaches a critical diameter (about 260nm for Nd₂Fe₁₄B) where only a single domain is supported. Furthermore, the fine grains suppress domain reversal at high temperatures, improving the thermal stability of the coercivity and its suitability to the motor operating environment.

As an attempt at grain refinement, conventional metallurgy techniques mainly controlled the milling parameters to reduce the size of feedstock particles but

had limitations in size reduction. Accordingly, bottom-up synthesis accompanied by a reduction-diffusion (R-D) process, which overcomes the limitations of top-down methods and has advantages such as low energy consumption, low raw material cost, and uniform morphology, has emerged as an attractive way to control the particle size. Motivated by the advantages of chemical-based synthesis, the size control of Nd₂Fe₁₄B particles has been conducted in a few studies through concentration of the solution and R-D conditions as variables, but magnetic properties predominantly depended on crystallinity and composition rather than size. In addition, there is an inherent limitation that it is difficult to even sinter due to low productivity, imperfection, and oxidation of nanoparticles, as a result, research to confirm the size effect on magnetic properties of Nd₂Fe₁₄B by a chemical-based method has not yet been reported. Therefore, it remains a major assignment to develop the magnetic properties of a sintered magnet by forming submicron grains using chemically synthesized particles of an appropriate size.

In this study, we adopted an effective approach using submicron Fe powder to synthesize Nd₂Fe₁₄B by applying the size dependence of final magnetic particles on transition metal precursors. Chemical-based methods including ultrasonic spray pyrolysis (USP) and hydrogen reduction process for the synthesis of submicron seed powder were proposed and performed. And then in order to fabricate a fine-grained Nd-Fe-B sintered magnet with high magnetic properties, the R-D process and sintering conditions were optimized using the synthesized submicron iron. Finally, the interaction between oxygen content and physical and magnetic properties according to the size of Nd₂Fe₁₄B was systematically investigated and the effect of size on magnetic properties was elucidated by controlling the particle size of Nd₂Fe₁₄B using Fe seed particles with a size varying from nano to microscale.

SF07.05.12

Controlling Chemical Ordering in Permanent Magnet Compounds Xiaoyu Zhang, Brian Lejeune and Laura Lewis; Northeastern University, United States

Next-generation advanced permanent magnets require high magnetocrystalline anisotropy that is donated by chemical ordering. While it remains highly challenging to control chemical order in the “holy grail” FeNi permanent magnet system (*aka* tetrataenite), the analogous proxy system of MnAl provides a good platform for investigating and understanding the chemical ordering in ferromagnets. To this end, the disorder (hcp ϵ -phase) – order (L1₀ τ -phase) phase transformation in Mn₅₅Al₄₅ compound is investigated here. Structural, magnetic, and calorimetric data confirmed the attainment of L1₀ ordered τ -MnAl upon heating two different quenched forms of metastable, disordered ϵ -MnAl: melt-spun ribbon solidified from a molten precursor and water-quenched one from the already solidified ribbon. While both quenched Mn₅₅Al₄₅ samples exhibit nominally phase-pure (~99 wt.%) ϵ -MnAl phase, the ordering transformation of the melt-spun ribbon occurs ~40 degrees lower than that of the water-quenched one. Kinetic analysis reveals that the ordered τ -phase in the melt-spun ribbon develops from pre-existing nuclei, in contrast to that in the water-quenched alloy that exhibits a constant nucleation rate with fewer quenched-in nuclei. It is contemplated that specifics of as-quenched microstructure that originate from quenching conditions tailor the chemical order in the MnAl system. The results of this work provide insights into controlling phase stabilities and chemical ordering kinetics in other relevant ferromagnetic systems of applied interest as permanent magnets.

Acknowledgments: This work was supported by the U.S. Department of Energy, Office of Basic Energy Sciences under Award Number DE SC0022168 and performed at Northeastern University.

SF07.05.13

En Route to High Coercivity in Rare-Earth-Lean Permanent Magnet Materials Henri J. Baldino¹, Kevin W. Jinn¹, Chaoya Han², Alexander Gabay², Brian Lejeune¹, Chaoying Ni², George Hadjipanayis^{1,2} and Laura Lewis^{1,1}; ¹Northeastern University, United States; ²University of Delaware, United States

Permanent magnets enable clean energy technologies such as wind turbine generators and hybrid vehicle regenerative motors. The expanding importance of these materials married with unpredictable supply restrictions underscores the importance of developing high-performance magnet substitutes of lower critical element content. To this end, the rare-earth-lean (Sm,Zr)(Fe,Co,Ti)₁₂ (“1-12”) compound has theoretical high-temperature performance that can surpass that of the NdFeB supermagnets, if only sufficient magnetocrystalline anisotropy energy could be converted into high coercivity to resist demagnetization. Advancing this objective, novel synthesis approaches have recently produced 1-12 powder containing single, defect-free crystallites of extremely high coercivity. In this work we correlate magnetic data with structural data to hone in on the characteristics of these high-coercivity crystallites, with the goal understand the impact of synthesis conditions on the intrinsic and technical magnetic properties of this compound.

Magnetic and particle size data were collected from 1-12 ferromagnetic powders made by a tailored synthesis process that combined mechanical activation with high-temperature calciothermic reduction. The data were analyzed to correlate processing conditions, including thermal treatment temperature and acetic acid concentration (utilized to remove unreacted calcium metal) from the powders. While all powder crystallites possess nominally the same composition, magnetic hysteresis loops indicate the presence of multiple hard magnetic phases, with a maximum of 15% of the powder exhibiting a record 2.2 T coercivity at room temperature. The underlying structural characteristics of the powder crystallites, including the evolution of particle transformations to form the desired 1-12 compound, are investigated to elucidate the origins of magnetic performance and provide guidance for its amplification.

This material is based upon work supported by the U.S. Department of Energy, Office of Science, Office of Basic Energy Sciences under Award Number DE SC0022168.

SF07.05.14

The Hydrogenated Intermetallic Compound Pd₇₀Ag₃₀ Both Amorphous and Crystalline—Their Electronic Properties Oscar A. Ibañez Martínez¹, Renela M. Valladares¹, Isaías Rodríguez², David Hinojosa², Salvador Villarreal² and Ariel A. Valladares²; ¹Facultad de Ciencias, UNAM, Mexico; ²Instituto de Investigaciones en Materiales, UNAM, Mexico

Metal-Hydrogen alloys have been studied due to their widespread applications; in particular, the palladium-hydrogen system manifests superconductivity [1]. Palladium, alloyed with noble metals (Ag, Au, Cu) also shows superconductivity when hydrogenated with a ratio of 80% hydrogen; in this case, the superconducting transition temperature is maximum, T_C=15.6 K [2] for a concentration of Pd₇₀Ag₃₀. In this work we computationally generated and studied an amorphous structure of the intermetallic palladium-silver alloy Pd_{100-x}Ag_x, x=30 at% and compared it with the crystalline counterpart. The amorphization process follows the *undermelt-quench* approach [3] on a 216-atom supercell of the PdAg alloy using *ab initio* molecular dynamics. Hydrogen was interstitially inserted for a ratio H/(Pd+Ag) = 0.8 in the supercells. The obtained structures were characterized with the Pair Distribution Function (PDF). In order to compare crystalline and amorphous hydrogenation, the topology and the electronic structures were obtained. In this work they will be contrasted, analyzed and discussed.

[1] Skoskiewicz, T. (2022). *Superconductivity in the Palladium-Hydrogen and Palladium-Nickel-Hydrogen Systems*. In Görlich (Ed.), Volume 11, Number 2 June 16 (pp. 825-828). Berlin, Boston: De Gruyter. <https://doi.org/10.1515>.

[2] Stritzker, B. *High superconducting transition temperatures in the palladium-noble metal-hydrogen system*. Z. Physik 268, 261–264 (1974). <https://doi.org/10.1007/BF01669889>.

[3] A. A. Valladares. in *Glass Research Progress*, edited by: Jonas C. Wolf and Luka Lange, Nova Science Publishers, Inc., 2008. Pp. 61-123.

SF07.05.15

Structural and Electronic Properties of the α and β Phases of the Intermetallic Compound PdBi₂ Both Amorphous and Crystalline Gerardo Antonio Martínez, Renela M. Valladares, David Hinojosa, Isaías Rodríguez and Ariel A. Valladares; UNAM, Mexico

The study of superconducting alloys has shown that the intermetallic compounds are an attractive family of materials. Those that contain bismuth may exhibit superconductivity [1, 2, 3]. Within these alloys we find the intermetallic crystalline phases α -PdBi₂ and β -PdBi₂ with $T_c = 1.73$ K and 4.25 K respectively [4]. In this work we report the study of the topology and electronic structure of both the amorphous and crystalline phases of the above-mentioned intermetallic compounds. The amorphization was accomplished by using the process called the *undermelt-quench* approach [5]. This process is based on *ab initio* molecular dynamics and consists in heating the supercells to temperatures just below the liquidus temperature and then cooling it down to close to absolute zero. This process was applied to the α and β phases of the material, using supercells with a total of 216 atoms for the binary system. In order to compare the crystalline and the amorphous systems, the topology and electronic structure were obtained and these results will be presented and discussed.

[1] N. N. Zhuravlev and G. S. Zhdanov, Zh. Eksp. i Teoret. Fiz. 25, 485 (1953).

[2] N. E. Alekseevskii, N. N. Zhuravlev, and I. I. Lifanov, Zh. Eksp. i Teoret. Fiz. 27, 125 (1954).

[3] N. N. Zhuravlev, Soviet Phys.—JETP 5, 1064 (1957).

[4] B. T. Matthias, T. H. Geballe, and V. B. Compton; Rev. Mod. Phys. 35 (1963) 1.

[5] A. A. Valladares. in *Glass Research Progress*, edited by: Jonas C. Wolf and Luka Lange, Nova Science Publishers, Inc., 2008. Pp. 61-123

SF07.05.16

A Lightweight Ti-Al-Based Shape Memory Alloy with B2-Ordered Structure Yuxin Song, Sheng Xu, Xiao Xu, Toshihiro Omori and Ryosuke Kainuma; Tohoku University, Japan

The β -type Ti-based alloys have recently attracted much attention due to their exceptional properties such as low Young's modulus, shape memory effect and gum-metal-like behavior. Among them, β -type Ti-based shape memory alloys such as Ti-Nb-Ta-Zr and Ti-Mo-Al, which undergo thermoelastic martensitic transformation from a β (body-centered cubic) parent phase to an α'' (orthorhombic) martensite phase, show great promise for applications in medical devices due to their superelasticity and biocompatibility. However, the transformation strain by superelasticity is usually small to be less than 3% in these conventional β -type Ti-based shape memory alloys. In this talk, we report a novel B2-structured Ti-Al-Cr shape memory alloy with a greater superelastic strain. The crystal structure and lattice parameters of both parent phase and martensite phase were determined using the X-ray and neutron diffraction methods. The mechanical properties of the alloy were evaluated by uniaxial tensile or compressive tests on single-crystal samples at room temperature. It was found that the alloy exhibits excellent superelastic behavior with a recoverable strain over 7%. The experimentally observed transformation strain is consistent with the calculated one using the lattice parameters on the base of lattice deformation theory. This newly-developed Ti-Al-Cr shape memory alloy is a promising candidate for medical applications. This alloy is also characterized by its lower density than that of the conventional β -type Ti-based alloys containing high-density Nb or Mo, having potential as a lightweight shape memory alloy.

SF07.05.17

Crystallographic Characterization of Zirconium-Based Samples Containing Tin, Niobium and Iron elements—*In Situ* High-Temperature X-Ray Diffraction Results Jeong Min Ha, Tae Hyun Kwon, Jeong-Woo Nam, Youngsoo Kim and Young-Sang Youn; Yeungnam University, Korea (the Republic of)

In situ high-temperature X-ray diffraction (HT-XRD) is a useful technique that can provide very valuable information on *in situ* crystallographic properties such as lattice parameter and phase transformation at a certain temperature. Through *In situ* HT-XRD, we have studied the crystallographic characterization of zirconium-based samples containing minor alloying elements of tin, niobium, and iron at a temperature range of 30–870 °C with intervals of 40 °C. The *a*- and *c*-axes lattice parameters of the hexagonal Zr crystal structure were calculated from the *in situ* HT-XRD spectra using the Pawley refinement. We confirmed that the *a*-axis lattice parameters of the hexagonal Zr crystal structure for the zirconium-based samples with tin element are decreased compared to those for a pure zirconium sample, in contrast to the zirconium-based samples with other minor alloying elements (i.e., niobium and iron). This effect is the greatest when 3 wt% tin was added in zirconium. On the other hand, the *c*-axis lattice constants for all the zirconium-based samples are not declined by the minor alloying elements as compared to the pure zirconium.

SF07.05.18

Computational Approaches for Studying the Nucleation of Voids at the Nanoscale Vicente Munizaga, Peng Yi and Michael L. Falk; Johns Hopkins, United States

Solid state precipitation and growth of different phases inside solid solutions is an important part of the design and manufacturing of metallic alloys. Intermetallic precipitates are one of the most effective methods to strengthen metals because such precipitates often resist dislocation motion.

One optimal microstructure for improving the strength of metals is a high density of small precipitates. It has recently been demonstrated that in Mg alloys this microstructure can result from the defects generated by the mechanical deformation [1]. Vacancies and voids are commonly found among these defects.

The agglomeration of vacancies has been in the center of our attention because these structures may play a crucial role in the nucleation of intermetallic precipitates that remains poorly characterized. It is known that voids can change the composition in their vicinity by attracting or repelling solute [2]. This could promote or suppress the nucleation of precipitates.

Furthermore, the formation of voids from agglomeration of vacancies is itself a nucleation process that is not fully understood. Current models assume that voids nucleate from a uniform concentration of vacancies [3]. However, in direct molecular dynamics simulations we have observed that agglomerations of vacancies could remain locally stable before creating a well-defined internal surface. This could suggest that the nucleation of a void with a defined internal surface could involve a two-step process.

Nucleation is known to be a “rare event”, which means extracting kinetic information from computational simulations is challenging. By means of Replica Exchange Transition Interface Sampling (RETIS) we can quantify aspects of the void nucleation process through the sampling of independent phase-space paths. The resulting data is useful for elucidating the kinetics of void nucleation. Using this data, we aim to validate or improve existing void nucleation models.

[1] S.E. Prameela, P. Yi, Y. Hollenweger, B. Liu, J. Chen, L. Kecskes, D. Kochmann, M.L. Falk, T.P. Weihs, "Strengthening magnesium alloys with nanoscale precipitates and solute clusters," *Mechanics of Materials*, 2022, in press.

[2] X. Wang, C. Hatzoglou, B. Sneed, Z. Fan, W. Guo, K. Jin, D. Chen, H. Bei, Y. Wang, W. J. Weber, Y. Zhang, B. Gault, K. L. More, F. Vurpillot and J. D. Poplawsky. "Interpreting nanovoids in atom probe tomography data for accurate local compositional measurements", *Nat. Communications* (2020) 11:1022

[3] K. F. Kelton, A. L. Greer. "Nucleation in Condensed Matter: Applications in Materials and Biology" (Elsevier, Netherlands, 2016)

SF07.05.19

Corrosion Prediction of Advanced High-Strength Steel Using *In Situ* Electrochemical Atomic Force Microscopy with Deep Learning [ChangHyo Sun](#)¹, Panthan Sriboriboon¹, Junghun Han², Sang-Jin Ko¹, Jung-Gu Kim¹, Sejung Yang² and Yunseok Kim^{1,3}; ¹Sungkyunkwan University, Korea (the Republic of); ²Yonsei University, Korea (the Republic of); ³KIST-SKKU Carbon-Neutral Research Center, Korea (the Republic of)

Observing the physical properties of each microstructure is the key to understanding the various properties of metals. For instance, corrosion, such as oxidation and reduction, can be influenced by microstructures. Recently, as corrosion begins at the nanometer or micrometer scale, local corrosion studies related to microstructures using microscopic techniques are being conducted. However, to understand the corrosion mechanism, it is not sufficient to observe morphological change by ex-situ experiments. Furthermore, understanding the overall corrosion mechanism requires observing microstructures in real time and even predicting surface changes. In this presentation, various physical properties such as height, surface potential, and capacitance gradient according to microstructure in advanced high-strength steel, which is applied automotive, were investigated by atomic force microscopy (AFM). Furthermore, we performed the prediction of morphological change through a combination of in-situ electrochemical AFM (EC-AFM) images and deep learning techniques for understanding the corrosion mechanism. We show that the combination of deep learning to in-situ EC-AFM images can show not only identification of microstructures, but also insight into the corrosion mechanism. Consequently, this approach can be easily applied to other intermetallic-based alloys.

SESSION SF07.06: Structural Intermetallics III
Session Chairs: Martin Heilmair and Alexander Knowles
Wednesday Morning, November 30, 2022
Sheraton, 5th Floor, Riverway

8:30 AM *SF07.06.01

Bcc-Super alloys—bcc Refractory Metals Reinforced By Ordered-bcc Intermetallic Precipitates [Alexander J. Knowles](#); University of Birmingham, United Kingdom

The microstructure template of a disordered matrix reinforced by ordered-intermetallic precipitates offers a potent design strategy for high temperature materials, enabling strength alongside damage tolerance, which has been central to the success of fcc Ni-superalloys. Such a strategy is equally applicable to bcc-based systems, which offer advantages of increased melting point, lower cost, and/or lower density. However, whilst bcc-superalloys based upon a refractory metal, Ti, Cr or Fe matrix, strengthened by ordered-bcc intermetallic precipitates are possible, further research and development is need for them to become a commercial reality.

In this talk, opportunities for bcc-superalloys systems will be discussed, from binaries to ternaries and more complex alloys, including Refractory High Entropy Superalloys. It will then discuss our latest developments in tungsten-based bcc-superalloys, beta-Ti superalloys and chromium superalloys. Prospectives will be given for the onward development of the bcc-superalloy concept for application in nuclear fusion, Gen-IV fission, gas turbines and concentrated solar power.

9:00 AM SF07.06.02

Phase and Microstructure Stability of BCC-V/MAX Two-Phase Alloys With Quaternary Additives [Seiji Miura](#)¹, Hiroto Kudo¹, Shiho Takebe¹, Nobuaki Sekido² and Ken-ichi Ikeda¹; ¹Hokkaido University, Japan; ²Tohoku University, Japan

Max phases have attracted attentions because of its high strength, high melting point and low density [1]. The present authors conducted a broad research for establishing the BCC-V based materials with Max phase V₂AlC as a dispersoid for strengthening. It was found that BCC-V matrix alleviates the delamination tendency of MAX phase during plastic deformation even at relatively lower temperature, however, the microstructure stability of V-Al-C ternary alloys is not enough. In this study effect of various quaternary elements on the microstructure stabilization is investigated. Based on the V-Al-C ternary phase diagram [2], we prepared alloy ingots with and without quaternary additives such as Cr, Ti, Mo and W. An Ar-arc melting machine was used to melt the sample several times, and a part of ingot sealed in a evacuated silica tube was subjected to a heat-treatment at 1473 K for 1 week. Microstructure observation using FE-SEM and WDS analysis for determining the composition of each phase is conducted, and the EBSD analysis was also conducted to understand the crystallographic orientation relationship between BCC-V and MAX phase. It was confirmed that the alloys with and without the heat-treatment have two-phase microstructure, however, plate-like V₂AlC-MAX phase in as-cast alloys with Ti spheroidized during the heat-treatment. On the other hand, the MAX phase in alloys with Cr, Mo or W keep its plate-like structure even after the heat-treatment. It was confirmed that V has large solubility of Cr, Mo and W, while Ti tends to be in MAX phase because Ti forms MAX phase (Ti₂AlC). In our previous study it was found that the BCC-V and MAX phase has a certain crystallographic orientation relationship. The lattice mismatch between BCC-V and MAX in ternary alloys are evaluated to be about 9%, and the value increases in alloys with Ti because Ti increases the lattice constant of MAX by replacing smaller V atom. On the other hand either Mo and W increase the lattice constant of BCC-V solid solution, resulting in decreasing the lattice mismatch between BCC-V phase and MAX phase. Smaller inter-phase boundary energy between BCC-V and MAX phase caused by smaller lattice mismatch might be a reason why Mo and W stabilize the microstructure of alloys. In the presentation a part of the mechanical testing will be presented.

Acknowledgement

This work was supported by a grant from JSPS KAKENHI for Scientific Research on Innovative Areas "MFS Materials Science (Grant Numbers JP18H05482)".

References

[1] M. W. Barsoum and T. El-Raghy: *Am. Sci.*, 2001, 89, 334-343.

[2] B.Hallstedt, *CALPHAD: Computer Coupling of Phase Diagrams and Thermochemistry*, 2013, 41, 156-159.

9:15 AM SF07.06.03

New Proximate Structures for {110}(111)-Type Antiphase Boundaries in BCC-Derived Ordered Intermetallics Justin Mayer, K. V. Vamsi, Ram Seshadri and Tresa M. Pollock; University of California, Santa Barbara, United States

A new model, known as the diffuse multi-layer fault model (DMLF), has provided an accurate high-throughput method for evaluating the energetics of planar faults within alloys of complex composition. Specifically, the DMLF, which approximates a planar fault through a series of proximate structures that capture the local bonding environment within the vicinity of the fault, has been used recently to assess the energetics of planar faults within FCC alloys [1] as well as the $\{111\}a/2(110)$ antiphase boundary observed within FCC-derived L_{12} ordered intermetallics. [2] Within this work, we report on the successful extension of this model to the antiphase boundaries present on $\{110\}$ planes within the BCC-derived B2 and L_{21} ordered intermetallics. Through coupling the DMLF to a large database of symmetrically distinct atomic configurations on a host BCC lattice, proximate structures have been identified for the $\{110\}a/2(111)$ antiphase boundary within the B2 and L_{21} intermetallic and the $\{110\}a/4(111)$ antiphase boundary observed in the L_{21} intermetallic. Density functional theory calculations are employed to validate the accuracy of the formation energies of these newly identified proximate structures relative to those calculated via the more conventional, and computationally costly, supercell method. The use of the B2 and L_{21} proximate structures to predict the thermodynamic stability of planar faults in BCC-derived ordered intermetallics with a complex composition will also be discussed.

[1] K. V. Vamsi, M. A. Charpagne, and T. M. Pollock, "High-throughput approach for estimation of intrinsic barriers in FCC structures for alloy design," *Scr. Mater.*, 204, 114126.

[2] K. V. Vamsi and T. M. Pollock, "A new proximate structure for the APB (111) in L_{12} compounds," *Scr. Mater.*, 182, 38-42.

9:30 AM DISCUSSION TIME**9:45 AM BREAK****10:15 AM *SF07.06.05**

B2 Precipitation-Strengthened Refractory Compositionally Complex Ta-Mo-Ti-Cr-Al alloys Martin Heilmaier¹, Alexander Kauffmann¹, Stephan Laube¹, Aditya Tirunilai¹, Daniel Schliephake¹, Bronislava Gorr¹, Steven Schellert² and Hans-Juergen Christ²; ¹Karlsruhe Institute of Technology, Germany; ²University Siegen, Germany

Refractory compositionally complex alloys (RCCA) are promising candidates for high-temperature structural applications [1]. Many of the reported alloys consist of A2 or B2 phases with additional intermetallic phases often located at grain boundaries. However, to achieve good mechanical performance at elevated temperatures as well as sufficient ductility at room temperature, the proper formation of a strengthening phase is crucial. Recently, Senkov and co-workers [2] reported a microstructure with coherent cuboidal precipitates and promising high-temperature strength in the Al-Mo-Nb-Ta-Ti-Zr system. However, the alloy lacks ductility at room temperature, which could be attributed to an ordered B2 matrix phase with disordered A2 precipitates.

Following along above conceptual path we report here on the current status of our investigations within the Ta-Mo-Ti-Cr-Al system which exhibits a promising combination of strength and oxidation resistance at elevated temperatures [3]. The objective is to attain a suitable multi-phase microstructure of A2 matrix and B2 precipitates. Thermodynamic calculations were employed with an in-house database to predict specific transformation sequences of ordering and diffusion-controlled phase separation within this system. As already observed in the Ta-free subsystem MoTiCrAl, Al has a significant effect on the ordering transition of A2 towards B2 [4]. However, in the case of the MoTiCrAl system, no multi-phase phase field has been predicted and confirmed after the homogenization. This changes by the addition of Ta, as a multi-phase field is predicted [5]. To minimize the formation of inherently brittle Laves phase, the Cr concentration was adjusted accordingly [6]. The microstructure of two compositions (high and low in Al, respectively) were investigated experimentally by scanning and transmission electron microscopy, while the phase transitions were determined by means of differential scanning calorimetry. The microstructure of the alloy with high Al concentration exhibited a B2 matrix with A2 precipitates; in contrast, an A2 matrix with B2 precipitates was determined in the Al-lean alloy. The necessary reaction sequences are discussed in detail and provide information about the phase diagram structure necessary to reproducibly obtain the desired two-phase microstructures. Microstructural peculiarities, such as segregation at planar defects as well as their implications on the mechanical properties will be discussed.

References:

[1] D. B. Miracle, M.-H. Tsai, O. N. Senkov, V. Soni and R. Banerjee, Refractory high entropy superalloys (RSAs), *Scripta Materialia*, vol. 187, pp. 445-452, 2020

[2] O. N. Senkov, C. Woodward and D. B. Miracle, Microstructure and Properties of Aluminum-Containing Refractory High-Entropy Alloys, *JOM*, vol. 66, pp. 2030-2042, 2014

[3] B. Gorr, F. Müller, S. Schellert, H.-J. Christ, H. Chen, A. Kauffmann and M. Heilmaier, A new strategy to intrinsically protect refractory metal based alloys at ultra high temperatures, *Corrosion Science*, vol. 166, p. 108475, 2020

[4] S. Laube, H. Chen, A. Kauffmann, F. Müller, B. Gorr, J. Müller, B. Butz, H.-J. Christ and M. Heilmaier, Controlling crystallographic ordering in Mo-Cr-Ti-Al high entropy alloys to enhance ductility, *Journal of Alloys and Compounds*, vol. 823, p. 153805, 2020

[5] S. Laube, S. Schellert, A. Tirunilai, D. Schliephake, B. Gorr, H.-J. Christ, A. Kauffmann and M. Heilmaier, Microstructure tailoring of Al-containing compositionally complex alloys by controlling the sequence of precipitation and ordering, *Acta Materialia*, vol. 218, p. 117217, 2021

[6] F. Müller, B. Gorr, H.-J. Christ, H. Chen, A. Kauffmann, S. Laube und M. Heilmaier, Formation of complex intermetallic phases in novel refractory high-entropy alloys NbMoCrTiAl and TaMoCrTiAl: Thermodynamic assessment and experimental validation, *Journal of Alloys and Compounds*, vol. 842, p. 155726, 2020

10:45 AM SF07.06.06

Evolution of a Novel Ta-Nb-Ti Multi-Component Alloy for Potential Biomedical Applications Maximilian Regenber¹, Janett Schmelzer¹, Georg Hasemann¹, Jessica Bertrand² and Manja Krueger¹; ¹Otto-Von-Guericke Universität Magdeburg, Institute of Materials and Joining Technology, Germany; ²Universitätsklinikum Magdeburg, Germany

The modern material class of equiatomic multi-component alloys, especially high-entropy alloys (HEAs) gained tremendous attention in the scientific community over recent years. This can be attributed to two main reasons: Firstly, the new concept of combining several elements (at least 5 principal elements with concentrations between 5 and 35 at. % [1]) in contrast to conventional alloys, mostly containing only two or three elements in addition to the main alloy constituent. This results in a broad variety of possible combinations thus leading to completely novel materials. Secondly, recently developed refractory metal based high-entropy alloys (RHEAs) have shown properties that are superior to the ones of current state-of-the-art alloys, which are based on several unique thermodynamic effects [2-5]. However, besides the outstanding mechanical properties, abrasion resistance and thermal resistance, a vast variety of chemical elements used in RHEAs also belong to the category of biocompatible elements, hence leading to potentially new biomedical materials.

In consideration of this background and due to the excellent biocompatibility of the constituents [6], an equiatomic composition of Ta, Nb and Ti as multi-component base alloy was chosen for investigations.

The alloy examined was produced using an arc melting furnace under Ar atmosphere, metallographically prepared and investigated respectively. Scanning electron microscopy (SEM) analysis revealed the presence of a dendritic microstructure, with an enrichment of high-melting elements in the dendrites, as well as Ti in the interdendritic regions (verified by means of EDS mappings). Microstructure analysis by means of X-ray diffraction (XRD) showed, that there are two types of body-centered cubic (bcc) crystal structures (Im-3m I: $a = 3.287 \text{ \AA}$; Im-3m: $a = 3.291 \text{ \AA}$) present in the as-cast state. To get a better understanding of the microstructure evolution, heat-treatment experiments regarding different temperatures and times were performed. Moreover, the biocompatibility of the novel alloy Ta-Nb-Ti was evaluated by means of cell (f.e. osteoblasts) attachment, as well as monocyte inflammatory response analysis and compared to samples of elemental Ta, Nb, alloy Co-28Cr-6Mo and alloy Ti-6Al-4V. First results indicate competitive osteoblast attachment, as well as comparable expressions of fibrosis markers in comparison to the conventionally used biomedical materials. In addition, the Ta-Nb-Ti alloy showed reduced inflammatory capacity, indicating a high potential for use as prospective biomedical material.

References

1. Yeh, J.W.; Chen, S.K.; Lin, S.J.; Gan, J.Y.; Chin, T.S.; Shun, T.T.; Tsau, C.H.; Chang, S.Y. Nanostructured high-entropy alloys with multiple principal elements: Novel alloy design concepts and outcomes. *Adv. Eng. Mater.* **2004**, *6*, 299-303+274.
2. Regenber, M.; Hasemann, G.; Wilke, M.; Halle, T.; Krüger, M. Microstructure Evolution and Mechanical Properties of Refractory Mo-Nb-V-W-Ti High-Entropy Alloys. *Metals (Basel)*. **2020**, *10*, 1530.
3. George, E.P.; Curtin, W.A.; Tسان, C.C. High entropy alloys: A focused review of mechanical properties and deformation mechanisms. *Acta Mater.* **2020**, *188*, 435–474.
4. Xiao, Y.; Zou, Y.; Sologubenko, A.S.; Spolenak, R.; Wheeler, J.M. Size-dependent strengthening in multi-principal element, face-centered cubic alloys. *Mater. Des.* **2020**, *193*, 108786.
5. Shittu, J.; Pole, M.; Cockerill, I.; Sadeghilaridjani, M.; Reddy, L.V.K.; Manivasagam, G.; Singh, H.; Grewal, H.S.; Arora, H.S.; Mukherjee, S. Biocompatible High Entropy Alloys with Excellent Degradation Resistance in a Simulated Physiological Environment. *ACS Appl. Bio Mater.* **2020**, *3*, 8890–8900.
6. Andersen, P.J. 1.1 Metals for Use in Medicine. In *Comprehensive Biomaterials II*; Elsevier, 2017; Vol. 1, pp. 1–18 ISBN 9780081006924.

11:00 AM SF07.06.08

Nanostructured NiAl-(Cr,Mo) In-Situ Composites Processed by Selective Electron Beam Melting Jan Vollhüter, Andreas Förner, Abdullah Jamjoom, Zongwen Fu, Steffen Neumeier, Carolin Körner and Mathias Göken; Friedrich-Alexander-Universität Erlangen-Nürnberg, Germany

The intermetallic B2 phase NiAl possesses promising properties as a high-temperature material with a very high melting point, low density, good thermal conductivity, and excellent oxidation resistance. However, the high-temperature strength and the room temperature fracture toughness show poor performances which disqualify the usage of single-phase NiAl for structural applications as a high-temperature material. However, the addition of 28 at. % Cr and 6 at. % Mo to NiAl leads to an eutectic alloy, which forms a two-phase rod-like or lamellar eutectic microstructure during directional solidification. These in-situ composites show superior mechanical properties over single-phase NiAl. New additive manufacturing methods, such as selective electron beam melting (SEBM) provides very high cooling rates which produces nanostructured composites with very small lamellar spacings between the B2-NiAl and the bcc Cr solid solution. The room temperature fracture toughness of NiAl-(Cr,Mo) composites benefits from a smaller lamellar spacing and the creep strength can be superior to the creep strength of TiAl-alloys.

In this study, dense and crack-free specimens of eutectic NiAl-(Cr,Mo) in-situ composites have been processed via selective electron beam melting using an Arcam A2 machine. In dependence on the processing parameters, a lamellar network-like microstructure can be obtained. For alloys with a lower Mo content, also rod-like structures introduced by discontinuous precipitation can be found in the additively manufactured composites. These discontinuous precipitations are triggered by an in-situ heat treatment in the building chamber or an ex-situ heat treatment. The different types of microstructures are investigated by their mechanical properties, microstructure, and chemical composition. APT investigations are used to further analyze and understand the formation of the nanostructured phases. The high-temperature properties are analyzed by compression and creep experiments, whereby the post-creep defect structure is further investigated by TEM to understand the deformation mechanisms. Furthermore, the room temperature fracture toughness of the different morphologies is studied by testing FIB-milled micro bending cantilevers. The best creep results and high-temperature flow stress are shown by the network-like composites, while the lamellar composites show superior fracture toughness. Consequently, the correlation between microstructure and mechanical properties requires a trade-off between room temperature- and high-temperature properties.

11:15 AM SF07.06.09

Fabrication of AlCoCrFeNi High Entropy Alloy via Binder Jetting and Direct Energy Deposition: Characterization, Microstructural Modification, and Analysis Jide E. Overinde, Justin Almeida, Ioannis Mastorakos, Philip Yuya and Ajit Achuthan; Clarkson University, United States

Additively manufactured high entropy alloys are in the early stage. More studies are required on how their compositions, processing routes, and microstructural evolutions intertwine to influence their (mechanical) properties for various fields of applications. In this study, the equiatomic AlCoCrFeNi high entropy alloy was fabricated via two additive manufacturing routes: binder jetting (3DBJ) and direct energy deposition (DED). The response of the samples to isothermal heat treatment was investigated and compared with the as-printed samples. The microstructural evolution was studied using backscattered electrons images from scanning electron microscopy (SEM). Energy dispersive spectroscopy (EDS) was used to probe the constituent's composition/distribution. The different phases present in the microstructure were investigated using X-ray diffractometer (XRD) and electron-backscattered diffraction (EBSD) techniques. Moreover, the mechanical properties data captured via nanoindentation were evaluated and mapped to show a representation of how they vary through the bulk alloy. Interplays of these essential parameters are responsible for the various mechanical properties exhibited by the alloy. The isothermal heat treatments significantly modified the microstructures of the alloy. However, the 3DBJ and DED samples respond differently, as diffusion mechanisms like grain boundary precipitation, precipitate-free zones (PFZ), and Widmanstätten structure were more observable in the 3DBJ samples. The 3DBJ samples exhibit higher values of mechanical properties than the DED samples. The higher mechanical properties in 3DBJ samples are also linked to intermetallics such as sigma phase and ordered BCC (B2). Consequently, the effects of these phenomena are summarized by the difference between the properties of the as-printed samples (2 - 13 GPa hardness, 130 - 240 GPa reduced modulus) and those of the heat-treated samples (4 - 8 GPa hardness, 160 - 200 GPa reduced modulus). The ongoing exploits provide significant insight into how to exploit the immense opportunities AlCoCrFeNi high entropy alloy has for fields of applications such as the tools, automobile, structures, and aerospace industries.

1:30 PM *SF07.07.01

Heat-Resistant Cr-Si Alloys Strengthened by Intermetallics—Microstructure, Oxidation and Creep Uwe Glatzel¹, Petra Pfizenmaier¹, Mathias Galetz² and Anke S. Ulrich¹; ¹University of Bayreuth, Germany; ²DEHEMA Forschungsinstitut (DFI), Germany

A two phase alloy of Cr, bcc, solid solution matrix strengthened by a Cr₃Si, A15 ordered, intermetallic phase was investigated with the goal of achieving an alloy with properties "Beyond Nickel-Based Superalloys". In comparison to the commonly used Ni-base superalloys, these Cr-Si alloys may enable higher working temperatures and lower densities slightly above 7 g cm⁻³. In addition, Cr is the only refractory metal which intrinsically builds an oxide scale suitable for protecting the alloy from oxidation. Si improves the oxide scale formation even further as well as a high temperature strength by precipitation of an intermetallic phase Cr₃Si. We observed that the addition of further alloying elements such as Mo, Ge, and Pt leads to an improvement in creep properties (Mo), oxidation resistance (Ge), and nitridation resistance (Pt) by maintaining the two-phase microstructure. Creep tests were conducted at temperatures at 980°C and higher and reveal promising results. The microstructures, scales, and reaction products were investigated by XRD, SEM, EPMA and Image Analysis.

2:00 PM SF07.07.02

Printability of V-Si-B Alloys: Mechanical Properties and Oxidation Performance Janett Schmelzer¹, Silja-Katharina Rittinghaus² and Manja Krueger¹; ¹Otto-von-Guericke-University Magdeburg, Germany; ²University of Wuppertal, Germany

There nearly is no other industry placing such high demands on materials as aircraft construction. Due to the mature design of the aircraft engines, further competition will take place with innovative materials and manufacturing processes. In the vicinity of the combustor, where engine parts are burden with temperatures higher than 500 °C, Ni-based superalloys have been state-of-the-art for many years. However, Ni-based superalloys come along with a high density (~ 8.5 g/cm³). Weight reduction is an important issue to achieve the target of increased thermodynamic efficiency including less fuel consumption and a reduced amount of exhaust emissions. To this end, research activities focus on new light-weight materials with good high-temperature properties to increase the thrust-to-weight ratio in aircraft engines by replacing Ni-based superalloys. Vanadium points out as an interesting candidate, since it offers the lowest density ($\rho = 6.11 \text{ g/cm}^3$) in comparison to other high-melting metals. Moreover, alloyed with Si and B, a multi-phase microstructure consisting of a vanadium solid solution (V_{ss}) phase next to the intermetallic phases V₃Si and V₅SiB₂ [1,2] forms, which offers a low ductile-brittle-transition as well as enhanced high temperature strength and creep resistance next to an improved oxidation resistance [1]. However, conventional ingot metallurgical processing of V-Si-B material and subsequent machining is energy- and time-consuming due to the different behavior of the ductile solid solution phase and the brittle silicides. This work presents the first study on additive manufacturing of a high melting point near-eutectic V-based alloy via additive manufacturing (AM) process. The feasibility of printing pre-alloyed V-Si-B powder material was demonstrated. V-Si-B powder was manufactured via gas atomization (GA) process out of solid raw materials meeting the requirements for AM regarding flowability and particle size. After developing suitable process parameters for the generation of crack-free samples, the microstructure of the materials was analyzed in detail using SEM/EDS and EBSD analyses. An overview about the ambient and high temperature material properties of a V-9Si-5B alloy is given. In terms of high-temperature mechanical properties, the brittle-to-ductile transformation temperature (BDTT) and the creep rate at a potential application temperature were determined as well as first investigations on the oxidation resistance.

[1] M. Krüger, Scripta Mater. **2019**, 121, 75–78.

[2] G. Hasemann, M. Krüger, M. Palm, F. Stein, Mater Sci Forum. **2018**, 941, 827-832.

2:15 PM SF07.07.03

Microstructure and Mechanical Properties of Ternary Eutectic V-Si-B Alloys Georg Hasemann¹, Weiguang Yang², Ruth Schwaiger² and Manja Krueger¹; ¹Otto von Guericke Universität Magdeburg, Germany; ²Forschungszentrum Jülich GmbH, Germany

The V-Si-B system has gained scientific interest as a new low-density, refractory metal-based structural intermetallic alloy system. The alloy design is strongly influenced and driven by the developments in the field of Mo-Si-B alloys and shares some interesting structural and microstructural features. Very recently, the formations of ternary eutectic V_{ss} -V₃Si-V₅SiB₂ microstructure has been reported [1] which contains the same isomorphous phases as the ternary eutectic in the well-studied Mo-Si-B system: a refractory metal-based solid-solution phase (Mo_{ss} or V_{ss}) and the two intermetallic phases with either an A15 (Mo_3Si and V_3Si) or a D8₁ (Mo_5SiB_2 and V_5SiB_2) structure. In contrast to the Mo-based system, where the intermetallic Mo_3Si represents the major phase within the ternary eutectic microstructure, the V_{ss} -V₃Si-V₅SiB₂ eutectic features the ductile solid-solution phase as the major component. This fact makes the V-Si-B ternary eutectic very interesting in terms of its mechanical properties.

The present work is focused on the compressive stress-strain behavior of different near-eutectic V-Si-B alloy. Compression tests were performed using an electro-mechanical universal testing machine and a constant crosshead speed corresponding to an initial (engineering) strain rate of 10^{-3} s^{-1} . The yield stresses were determined by the 0.2% offset method. The temperature dependence of its yield stress between room temperature and 1000 °C was investigated in the as-cast and annealed state (1400 °C for 100 hrs) of the fully eutectic alloy V-9Si-6.5B and were compared to literature values of different V-based alloys [2–4].

References

[1] W.G. Yang, G. Hasemann, M. Yazlak, B. Gorr, R. Schwaiger, M. Krüger, J. Alloys Compd. **902** (2022) 163722.

[2] H. Bei, E.P. George, E.A. Kenik, G.M. Pharr, Z. Met. **95** (2004) 505–512.

[3] S. Xie, E.P. George, MRS Proc. **980** (2007) 0980-II08-05.

[4] M. Krüger, Scr. Mater. **121** (2016) 75–78.

2:30 PM BREAK

3:30 PM *SF07.07.04

Microstructure Designs and Processing for Mo-Si-B Alloys John H. Perepezko¹, Dan J. Thoma¹, Longfei Liu¹, Phalgun Nelaturu¹, Ankur K. Agrawal¹, Fan Zhang² and Laurence Marks³; ¹University of Wisconsin--Madison, United States; ²Computherm LLC, United States; ³Northwestern University, United States

Recently, considerable effort has been devoted to the development of ultra-high temperature structural materials as alternatives to Ni-based superalloys to improve the energy efficiency of gas turbine systems. Among the several potential candidates, Mo-Si-B alloys have received much attention due to their high melting point and high temperature strength, but also have some remaining challenges to improve ductility, lower density and enhance environmental

resistance. In the Mo-Si-B system microstructures with a Mo solid solution (Mo_{ss}) Mo_3Si and Mo_5SiB_2 (T_2) phases have been the focus of attention. However, the Si solubility in the Mo_{ss} phase diminishes the ductility and toughness. In order to address this issue, a new series of Mo-Si-B alloys in the $Mo_{ss}+T_2+Mo_2B$ three phase region has been designed to examine the effect of the lower Si solubility limit in the Mo_{ss} phase on the microstructure, hardness and oxidation behavior. The results showed that the Mo-Si-B alloys in the $Mo_{ss}+T_2+Mo_2B$ three phase region have higher fracture toughness and the same level oxidation resistance as alloys in the $Mo_{ss}+T_2+Mo_3Si$ three phase region. Selected additions of Al and Ti enable a density reduction to below 9 gm/cm^3 . In order to examine the Al addition effect on the $Mo_{ss}+T_2+Mo_2B$ three phase region the microstructures and oxidation of Mo-Si-B alloys at different Al addition level was examined at 800, 1100, 1200, and 1300°C for both isothermal oxidation and cyclic oxidation exposure along with an analysis of the oxidation kinetics and oxide layer morphologies.

While refractory metal intermetallic alloys (RMIA) offer an attractive option to extend operational capability beyond what is currently available with Ni-base superalloys the processing of the RMIA to manufacture dimensionally controlled shapes in a commercially cost-effective way is challenging. For RMIA the directional solidification approach used for Ni base superalloys has serious difficulties. For example, there are very limited choices for suitable mold materials that are nonreactive with the alloy melt. The solidification path for large ingots in RMIA involving intermetallic silicide and boride phases usually yields product phases that are not part of the equilibrium phase microstructure. Due to the high-temperature stability and sluggish diffusion in refractory metals, homogenization requires very high temperatures ($>1500^\circ\text{C}$) and long annealing times ($>1\text{ day}$) that are not commercially cost effective. A conventional powder metallurgy processing approach for RMIA involves several steps including the hot pressing of RMIA powders, high-temperature sintering, and then usually a hot isostatic press (HIP) treatment to achieve full density. Even with these multiple processing steps, it is difficult to produce complex shapes with accurate geometric control. To circumvent these challenges, an additive manufacturing (AM) route offers a new, rapid and effective strategy. With AM methods such as directed energy deposition (DED) and liquid powder bed fusion (LPBF), alloying is accomplished by the melting and reactive synthesis of component powder mixtures to full density so that the size scale of any nonequilibrium solidification products is limited that facilitates post-alloying homogenization. This approach has been demonstrated to yield the fabrication of homogeneous alloys with well-defined shapes. Besides the successful use of AM, the guidance from computational thermodynamics to identify compositions that meet density, strength and ductility goals and the use of dimensionless numbers to guide the AM process has been essential to achieve fully dense component with the desired microstructures.

4:00 PM SF07.07.05

Environmental Protection Coating System for Refractory Metal Alloys in Extreme Environments [Ranran Su](#) and John H. Perepezko; University of Wisconsin-Madison, United States

The refractory multi-principal elements alloys (RMPEAs) are promising structural materials to help increase power efficiency in high-temperature oxidation environments, while the intrinsic poor oxidation resistance of the refractory elements limits their application. The oxidation behavior of a refractory high entropy alloy WMoTaNbV is investigated at 1300°C . By using an innovative two-step coating strategy with Mo-precoat followed by Si-B pack cementation, a multilayer Mo-Si-B coating with strong oxidation resistance and compatibility as well as a diffusion barrier is developed. The coating can protect the substrate at 1300°C for more than 750 h of thermal cycles. An RMPEA boride phase develops at the alloy/coating interface after longtime service and acts as an additional diffusion barrier to maintain the coating integrity. The oxidation test results demonstrated that this two-step coating system provides robust oxidation protection at high temperatures and can be widely applied in RMPEAs.

4:15 PM SF07.07.06

Pesting Resistance in High Mo Containing Alloys [Alexander Kauffmann](#), Daniel Schliephake, Susanne Obert, Aditya Tirunilai, Frauke Hinrichs, Bronislava Gorr and Martin Heilmaier; KIT, Germany

Refractory metal based alloys exhibit intrinsically high creep resistance at anticipated application temperatures beyond 1100°C due to high solidus temperatures. However, apart from ductility issues at low temperatures, oxidation resistance at elevated temperatures is often observed a fundamental problem for the further development of this group of alloys.

Among others, Mo-based alloys have attracted particular research interest [1]. However, the disordered, body centered cubic solid solution, rich in Mo and required to obtain reasonable toughness and low brittle-to-ductile transition temperatures, usually forms volatile MoO_3 already at temperatures below 1000°C . The progress of oxidation occurs rather fast and typically leads to a complete disintegration of the part within short periods of time. Thus, this so-called pesting behavior is a catastrophic type of oxidation.

In the present study, we provide recent results on the development of pesting-resistant high Mo containing alloys specifically addressing this fundamental problem when oxidation resistance is considered [2-6]. The alloys with this surprising and not expected property are Ti-rich, two-phase or three-phase alloys from the Mo-Si-Ti system. All of the identified alloys feature: (i) Fine-scale microstructures of the solid solution and one or two silicides originating from eutectic reactions, solid state transformations or combination thereof. (ii) Surprisingly adherent and passivating TiO_2/SiO_2 duplex and/or TiO_2 top layers after oxidation in laboratory air that limit the oxidation progress and the contribution of evaporation at temperatures of 800 up to 1200°C . (iii) Low densities in conjunction with reasonable creep resistance. A holistic overview is provided about the nature of the TiO_2 which is typically not considered a passivating oxide and the microstructural and chemical requirements of pesting resistance.

Apart from Mo-Si-Ti, further alloys were developed also featuring fine-scaled microstructures of Mo-rich solid solution and silicide phases. Indeed, another alloy from the Mo-Si-Cr system exhibiting pesting resistance was identified but significantly differentiating in the mechanism to suppress MoO_3 formation at 800°C [7]. The common and differentiating features of the two developments are highlighted to provide further insights into research opportunities.

[1] J.H. Perepezko, M. Krüger, M. Heilmaier, Mo-Silicide Alloys for High-Temperature Structural Applications, *Materials Performance and Characterization*, 10, 22-145, 2021.

[2] D. Schliephake, A. Kauffmann, X. Cong, C. Gombola, M. Azim, B. Gorr, H.-J. Christ, M. Heilmaier, Constitution, oxidation and creep of eutectic and eutectoid Mo-Si-Ti alloys, *Intermetallics*, 104, 133-142, 2019.

[3] S. Obert, A. Kauffmann, M. Heilmaier, Characterisation of the oxidation and creep behaviour of novel Mo-Si-Ti alloys, *Acta Materialia*, 184, 132-142, 2020.

[4] S. Obert, A. Kauffmann, S. Seils, S. Schellert, M. Weber, B. Gorr, H.-J. Christ, M. Heilmaier, On the chemical and microstructural requirements for the pesting-resistance of Mo-Si-Ti alloys, *Journal of Materials Research and Technology*, 9, 8556-8567, 2020.

[5] M. Weber, B. Gorr, H.-J. Christ, S. Obert, A. Kauffmann, M. Heilmaier, Effect of Water Vapor on the Oxidation Behavior of the Eutectic High-Temperature Alloy Mo-20Si-52.8Ti, *Advanced Engineering Materials*, 22, 2000219, 2020.

[6] S. Obert, A. Kauffmann, S. Seils, T. Boll, S. Kauffmann-Weiss, H. Chen, R. Anton, M. Heilmaier, Microstructural and Chemical Constitution of the Oxide Scale formed on a Pesting-Resistant Mo-Si-Ti Alloy, *Corrosion Science*, 178, 109081, 2021.

[7] F. Hinrichs, A. Kauffmann, A.S. Tirunilai, D. Schliephake, B. Beichert, G. Winkens, K. Beck, A. Ulrich, M. Galetz, Z. Long, H. Thota, Y. Eggeler, A. Pundt, M. Heilmaier, A novel nitridation- and pesting-resistant Cr-Si-Mo alloy, *Corrosion Science*, submitted, 2022.

4:30 PM SF07.07.07

Oxidation Behavior of Spark Plasma Sintered Compacts of MoSiBTiC Powder Produced by Gas Atomization Xi Nan, Hayato Arai, Kohei Umeda, Shuntaro Ida, Nobuaki Sekido and Kyosuke Yoshimi; Tohoku University, Japan

The first generation MoSiBTiC alloy with the nominal composition of 65Mo–5Si–10B–10Ti–10C in at% exhibits excellent high temperature creep resistance and specific strength for application at the temperature up to at least 1300°C. But the oxidation behavior should also be paid attention to since it is a big issue for such Mo-based alloys and could be well affected by the microstructure at the material surface. In this study, gas atomized MoSiBTiC powder was used to produce the compact by spark plasma sintering (SPS) method, and a relative density of almost 100% was achieved. Compared to the conventional arc-melted MoSiBTiC alloy, also prepared in this work, SPS compact showed greatly refined microstructure and a small compositional change during the process. By the microstructure refinement, the oxidation performance of the SPS compact slightly deteriorated at 800°C but improved at 1100 °C. Moreover, the effect of microstructure refinement on the oxidation behavior at a higher temperature such as 1500 °C is not remarkable. This distinction at the three temperatures is considered to be attributed to different reasons. Surface modification using the pack cementation method was also applied to the SPS compact to further improve the high-temperature oxidation resistance. With the development of an approximately 100 μm thick silicide layer on the top surface, the sample exhibited remarkably enhanced oxidation resistance at the temperature up to at least 1300 °C.

SESSION SF07.08: Structural Intermetallics V
Session Chairs: Jennifer Carter and Steffen Neumeier
Thursday Morning, December 1, 2022
Sheraton, 5th Floor, Riverway

8:30 AM *SF07.08.01

Data-Driven Researches Under the Concept of Materials Integration Masahiko Demura; National Institute for Materials Science, Japan

The concept of Materials Integration is to computationally link among processing, structure, property, and performance for accelerating materials research and development [1,2] and is comparable to that of Integrated Computational Materials Engineering. To embody the Materials Integration, we have developed a system named MInt (Materials Integration by Network Technology) [3]. In MInt, one can implement any types of prediction models based on computational simulations, theoretical or empirical formulas, and machine learning algorithms as a module. Furthermore, one can connect several modules to design a workflow that comprehensively predicts from processing through microstructure to property and/or performance. MInt executes a workflow by delivering the output data from a module to the input port of the next module and stores all the computational results in order. MInt is a platform to accumulate the materials scientists' knowledge digitalized as modules and workflows, which are stored not in isolation but in the form of graph network. At this moment, the modules and workflows implemented in MInt are mainly for conventional structural alloys such as steels, aluminum, and Ni-based superalloys, but one can expand its application fields by adding new modules and workflows.

Data-driven approach plays an important role in Materials Integration. Firstly, it is useful to make the prediction modules more accurate; for example, data assimilation technique can adjust model parameters included in the computational simulation or the theoretical or empirical formula to improve predictability. Secondary, it helps to build a comprehensive workflow even if all the mechanisms are not fully understood. For a missing link, machine learning provides a non-linear regression model based on experimental data without physical background. On top of that, certain data-driven methods, such as sparse modeling and feature importance analysis, contribute to finding the physical picture. Lastly, it provides a realistic means of solving the inverse problem, i.e., finding the optimal material and processing that meets the desired performance. Since MInt provides an application programming interface to execute the workflow and extract the computed results, one can apply any types of optimization algorithms including Bayesian optimization, Monte-Carlo tress search and so on. In this talk, I would like to share some examples of where the data-driven approach has worked.

[1] Demura M, Koseki T. Mater Japan. 2019;58(9):489-493. doi:10.2320/materia.58.489 [2] Demura M. Mater Trans. 2021;62(11):1669-1672. doi:10.2320/matertrans.MT-M2021135 [3] Minamoto S, Kadohira T, Ito K, Watanabe M. Mater Trans. 2020;61(11):2067-2071. doi:10.2320/matertrans.MT-MA2020002

9:00 AM *SF07.08.02

Multi-Variate Process Models for Predicting Site-Specific Microstructure and Properties of Inconel 706 Forgings Jennifer L. Carter¹, Nishan Senanayake¹ and Tiffany Dux²; ¹Case Western Reserve University, United States; ²Howmet Forging, United States

The performance of superalloy forgings hinges on the careful design of the thermomechanical history to promote distributions of oft-dependent microstructural features. Establishing predictive process-structure-property (PSP) models to tailor manufacturing routes requires immense cost due to the time-consuming tasks of quantifying statistically significant observations of different predictors and performance metrics across multiple lengthscales [1]. Power analysis indicates that for a simple multivariate linear model of one performance metric, P, dependent on six input process predictors (k = 6) (i.e., $P = f(k_1, k_2, \dots, k_6)$) with 80% predictive power would require over 120 observations; to predict n performance metrics (P_1, P_2, \dots, P_n), a statistical study protocol would require 120n observations (ANOVA would require 175n). Measuring a statistical number of observations of predictors and metrics is challenging at both ends of the lengthscales spectra. Nanoscale precipitates, like the distribution of the γ' and γ'' precipitates in Inconel 706 have required transmission electron microscopy which does not readily lend itself to transition from qualitative analysis to statistical measures [3]. While conventional mechanical testing, on the other hand, requires relatively large volumes of material for a single observation. In both cases, these predictors and metrics are observed destructively resulting in development efforts that take many years to establish the database necessary for PSP models. Since PSP models benefit from an iterative design paradigm, this motivates the development of high-throughput measurements, both experimental approaches [4, 5] and physics-based predictions [6] if the dramatic design paradigm shift predicted by the Materials Genome Initiative. In this paper, high-throughput measures of the precipitation distributions in Inconel 706 from experimental observations and physics-based simulations are used to reduce the necessary "physical" observation space necessary to predict PSP models. Heritage data from five years of development work conducted by Howmet Aerospace Forgings were used to demonstrate the method. DEFORM simulations of thermal history were used to supply time-temperature boundary conditions to CALPHAD simulations in ThermoCalc/PRISMA of the resulting γ' and γ'' precipitate distributions at discrete locations within thermomechanically processed Inconel 706. Computer vision algorithms were developed to observe features in scanning electron micrographs. These features were used to tailor the CALPHAD interfacial energy and predict features from other processing conditions. In this manner, the number of physical observations of γ' the γ'' distributions is reduced by 25x (100's to 4); and it relies on more readily available experimental and computational approaches allowing for industrial use with limited available technical resources. When combined within the heritage data frame, gradient

boost machine learning PSP models were trained following a 4:1 train-split procedure. The predictive power of many models was 80% or higher, estimated by R^2 value on the test data.

1. Li S, Kattner UR, Campbell CE (2017) Integrating Mater Manuf Innov 6:229–248. <https://doi.org/10.1007/s40192-017-0101-8>
2. Jones SR, Carley S, Harrison M (2003) Emerg Med J 20:453. <https://doi.org/10.1136/emj.20.5.453>
3. Zhang S, Zeng L, Zhao D, et al (2022) Mater Sci Eng A 839:142836. <https://doi.org/10.1016/j.msea.2022.142836>
4. Senanayake NM, Carter JLW (2020) Integrating Mater Manuf Innov 9:446–458. <https://doi.org/10.1007/s40192-020-00195-z>
5. Senanayake N, Mukhopadhyay, S, Carter JLW (2020) Superalloys 2020. Seven Springs, PA, p 10
6. Kuehmann CJ, Olson GB (2009) Mater Sci Technol 25:472–478. <https://doi.org/10.1179/174328408X371967>

9:30 AM SF07.08.03

Modeling Antiphase Boundary Energies of Ni₃Al-Based Alloys Using Automated Density Functional Theory and Machine Learning [Enze Chen](#)^{1,2}, Artur Tamm³, Tao Wang⁴, Mario E. Epler⁴, Mark Asta^{1,2} and Timofey Frolov⁵; ¹University of California, Berkeley, United States; ²Lawrence Berkeley National Laboratory, United States; ³University of Tartu, Estonia; ⁴Carpenter Technology Corporation, United States; ⁵Lawrence Livermore National Laboratory, United States

Ni-based superalloys are a superior class of structural materials used in aircraft turbines and power plants due to their excellent high-temperature strength, creep resistance, and corrosion resistance. Antiphase boundaries (APBs) are planar defects within the Ni₃Al precipitates that contribute to the strengthening of these superalloys, which motivates a better understanding for how chemical heterogeneity affects the APB energy. The APB energy varies with not only solute chemistry and concentration, but also sublattice site preference in the ordered (L1₂ structure) Ni₃Al precipitates. In order to systematically study these effects and optimize the APB energy in Ni₃Al intermetallics, we leverage high-throughput calculations to generate a large dataset of APB energies and we analyze what these data reveal about influential properties in superalloy design [1].

First, we use a thermodynamic model implemented in PyDII [2] combined with density functional theory (DFT) calculations to predict the site preference of alloying additions to Ni₃Al. We employ more high-throughput DFT calculations to calculate the APB energy for over 100 ternary Ni₃Al-based alloys and we generate a set of physically-motivated descriptors to build machine learning (ML) models for the APB energy from these data. The ML models not only give accurate predictions of the APB energy, but they also provide insight into the correlations between different descriptors and the APB energy, thus demonstrating how our automated, data-driven approach recovers known physics [1]. We discuss how this methodology allows us to intelligently screen for promising superalloy chemistries through validation with commercial superalloys that are far more compositionally complex than our training set.

[1] Enze Chen, et al. “Modeling antiphase boundary energies of Ni₃Al-based alloys using automated density functional theory and machine learning,” *npj Comput. Mater.* 8, 80 (2022).

[2] Hong Ding, et al. “PyDII: A python framework for computing equilibrium intrinsic point defect concentrations and extrinsic solute site preferences in intermetallic compounds,” *Comput. Phys. Commun.* 193 (2015).

9:45 AM SF07.08.04

The Effect of Antiphase Boundary Tubes on the Strengthening of FeAl and Ni₃Al [Rachel D. Osmundsen](#) and Ian Baker; Thayer School of Engineering at Dartmouth College, United States

Intermetallic alloys show a dramatic increase in their work hardening rate (WHR) when ordered. For example, L1₂-ordered Ni₃Fe has a ~50% greater WHR than f.c.c. disordered Ni₃Fe. Starting in 1962, antiphase boundary (APB) tubes, which are a defect unique to deformed ordered alloys, were theorized to explain this phenomenon. APB tubes have since been identified via transmission electron microscopy (TEM). Theories abound as to how APB tubes increase the strengthening of intermetallics, but there is little experimental evidence in favor or against these theories. Understanding the structure-property relationship between APB tubes and strengthening is important as ordered alloys are common strengthening components in structural superalloys, e.g. Ni₃Al-type precipitates in Ni-based superalloys.

In this work, experiments performed on B2-ordered FeAl and L1₂-ordered Ni₃Al show that APB tubes do not impact the WHR of ordered intermetallics. Single crystals of B2-ordered FeAl were deformed and the microhardness was measured with APB tubes present and then after the APB tubes were annihilated (with no additional changes in the deformation microstructure). The hardness did not change, showing that APB tubes do not affect the strengthening of FeAl. In L1₂-ordered Ni₃Al, the exact annihilation temperature of APB tubes was not already known. So, single crystals of L1₂-ordered Ni₃Al were lightly deformed and observed in the TEM. *In-situ* TEM heating was performed to determine the APB tube annihilation temperature. The annihilation temperature was then compared to the existing literature on the mechanical properties of Ni₃Al and it was determined that APB tubes do not affect the strengthening of Ni₃Al. APB tubes may be more accurately viewed as evidence of the motion of the complex superdislocation interactions that are the source of the high WHR in intermetallics, rather than the source of the strengthening themselves.

10:00 AM BREAK

10:30 AM SF07.08.06

Improving the High-Temperature Strength of L1₂-Co₃(Al,W) by Ni and Ta Additions [Zhenghao Chen](#), Kyosuke Kishida and Haruyuki Inui; Kyoto University, Japan

Microstructures of the ternary Co-Al-W system consist of two phases, an ordered Co₃(Al,W) phase (L1₂ crystal structure, usually designated as the γ' phase) and a face centered (fcc) Co-rich solid solution. There has been a significant research activity in the development of Co-based superalloys where Co₃(Al,W) is the strengthening phase with an initial expectation that high-temperature mechanical properties of Co-based superalloys would outperform those of Ni-based alloy. This was related to the fact that precipitation of the γ' phase in the γ matrix occurs coherently and forms cuboidal precipitates like in Ni-based superalloys with the advantage that both the melting temperature and the elastic stiffness are higher for Co than for Ni. However, in spite of the expectation, the high-temperature creep strength of Co-based superalloys which were so far developed are modest, only comparable to those of Ni-based superalloys of the first generation. A lower phase stability of γ' phase, which causes a low high-temperature strength was suggested to be responsible for this disappointing find. In fact, the addition of elements that increase the γ' phase stability (L1₂-stabilizer) is reported to improve the creep properties of the Co-based alloys. The γ' high-temperature strength is also expected to be improved in these alloys but nothing is known at present about how a higher high-temperature strength of the γ' phase is achieved by L1₂-stabilizer additions.

In the present study, we investigate the compression behavior of L1₂-compounds Co₃(Al,W) with Ni and Ni+Ta additions, which are known as L1₂-stabilizers, in a temperature range from room temperature to 1000°C, in order to elucidate the effects of stability of the L1₂ phase on the mechanical properties. Emphasis is placed on the deformation microstructures of these L1₂ compounds through detailed transmission electron microscopy (TEM) investigations, paying special attention to how the anomalous increase in yield stress (often referred to as ‘yield stress anomaly’ in L1₂ compound research)

occurs in these L₁₂ compounds.

The result shows that the addition of Ni and Ta increases the high-temperature strength of the γ' phase. The strength increase is shown to be more significant as the amount of additions of these elements and thereby the stability of the L₁₂ phase increases. The reduction of the onset temperature of yield stress anomaly (YSA-onset) due to the increased complex stacking fault (CSF) energy and the increased anti-phase boundary (APB) energy is considered to account for the strength increase at high temperatures. The increased strength of the L₁₂ phase due to a higher phase stability thus partly accounts for the improved creep strength of Co-based superalloys upon alloying with Ni and Ta.

10:45 AM SF07.08.07

On the Origin of the Superior Mechanical Properties of the Equiatomic Cr-Co-Ni Medium-Entropy Alloy LeLi¹, Zhenghao Chen¹, Hisanori Tanimoto², Haruyuki Inui¹ and Kyosuke Kishida¹; ¹Kyoto University, Japan; ²University of Tsukuba, Japan

High- and medium-entropy alloys (HEAs/MEAs) have attracted extensive interest for their extraordinary and promising mechanical performance, such as excellent combination of strength and ductility that increase at cryogenic temperatures and exceptional fracture toughness. Systematic work has revealed that the equiatomic Cr-Co-Ni MEA exhibits remarkably higher strength and ductility than the Cr-Mn-Fe-Co-Ni and other subsets. The improved strengths have motivated intensive detailed research to explore their micro-scale origins via experimental approaches and theoretical calculations. These results have implied that the type and bonding of atoms, instead of number of elements, are more important for solid solution hardening in HEAs. The high strength is believed to be related to the severe and ubiquitous crystal lattice distortion, such as the mean-square atomic distortion (MSAD) model. The excellent tensile ductility of the Cr-Co-Ni MEA is generally attributed to the high propensity of deformation twinning resulting from its low stacking fault energy. Thin layers of the hexagonal close packed (HCP) structure are formed in association with deformation twins in the Cr-Co-Ni MEA. This indicates that not only TWIP (twinning induced plasticity) but also TRIP (transformation induced plasticity) are responsible for the excellent tensile ductility of the Cr-Co-Ni MEA as in the case of high-Mn steels. On the other hand, the local chemical inhomogeneity derived from preferred bonding between specific atoms, usually termed short-range ordering (SRO), is widely believed to be another reason for its peculiar properties. The effect of SRO on the atomic-scale structures have been investigated extensively in theoretical calculations. In experimental work, a few studies have indicated that the formation of SRO can act as additional obstacle to dislocation motion, while no measurable effect of SRO on strength are claimed in other studies. However, it is well known that in polycrystals grain size and boundaries induce scattered results of mechanical response. Therefore, single crystals are of prime important to investigate the critical resolved shear stress (CRSS), stacking fault energy (SFE) and twinning shear stress as well as the possible effects of SRO on these parameters. In the present study, we investigate the plastic deformation behavior of bulk single crystals of the equiatomic Cr-Co-Ni after various heat treatment, in order to experimentally deduce materials parameters (such as CRSS for slip, twinning shear stress as well as SFE) and the contribution of SRO in Cr-Co-Ni MEA. Single crystals of Cr-Co-Ni were grown from a polycrystalline rod with an optical floating-zone furnace. The single crystals were annealed at 1473 K for 168 hours as the beginning materials. Then, the specimens were further annealed at 573-1373 K for various duration to introduce SRO. Tensile and Compressive tests were conducted at room and liquid nitrogen temperatures. A careful tilting observation along various zones were conducted to get the diffraction information by transmission electron microscopy, and the results were compared with those obtained by theoretical simulation for atomic structures with various degrees of SRO. Synchrotron X-ray diffraction was also applied to characterize the atomic-scale structures.

11:00 AM SF07.08.08

Strain Rate Dependence of Flow Stress in Single-Crystal Micropillars of bcc FeCrNi Solid Solutions Tianqi Zhu¹, Naoki Takata¹, Makoto Kobashi¹ and Masataka Yoshino²; ¹Nagoya University, Japan; ²JFE Steel Corporation, Japan

Multi-component alloys with a single-phase microstructure (generally known as medium/high entropy alloys) have recently emerged as a new class of alloys. In particular, body-centered cubic (bcc) solid solution alloys exhibit superior strength retention up to high temperatures but low toughness at ambient temperature. This issue is closely related to the ductility control of conventional ferritic stainless steels with FeCrNi solid solutions at various temperatures. To fundamentally understand the roles of solute elements in plastic deformation of multi-component bcc FeCrNi alloys, we investigated the strain rate dependence of flow stress in single-crystals of bcc Fe-Cr-Ni alloys with different solute Cr and Ni contents by micropillar compression tests in terms of thermal activation of dislocation motion.

Fe-Cr binary alloys (with 18% and 40% Cr) and Fe-18%Cr-Ni ternary alloys (with 1% or 2% Ni) were used in the present study. These alloy ingots were hot-rolled to approximately 4 mm thickness and solution-treated at 1300 °C for 1800 s, followed by water quenching. The solution-treated alloy samples exhibited fully recrystallized microstructures with the bcc single-phase. High-index orientations for the favorable activation of a single slip system were selected for the compression directions (corresponding to the crystallographic directions normal to the sample surface). We used a Focused Ion Beam (FIB) to fabricate cylindrical micropillar specimens with different diameters (d) of approximately 2 and 5 μm on the sample surface of the solution-treated alloys. We performed the micropillar compression tests at a wide range of initial strain rates ($\sim 10^{-5}\text{s}^{-1}$ to $\sim 10^{-2}\text{s}^{-1}$) using a load-controlled mode at ambient temperature. The measured values of flow curves were used to calculate the strain rate sensitivity (m). Afterward, the slip traces of the compressed micropillars were observed to identify the activated slip system. Transmission electron microscope (TEM) to evaluate the dislocation morphologies before and after the micropillar compression test.

In the Fe-18%Cr binary alloy, single-crystal micropillars with $d = 2 \mu\text{m}$ exhibited a relatively high strain-rate sensitivity ($m = 0.12$) of stress required for the slip initiation. The m value became lower (0.04) in the large-sized micropillars with $d = 5 \mu\text{m}$. The m value was equivalent to one of pure iron. The added solute Ni element in bcc solid solutions reduced the m value in both specimen sizes. The Fe-18%Cr-2%Ni ternary alloy exhibited low m values below 0.01. All compressed micropillars showed the predominant activation of the [111] (12-3) single slip system. These results suggested the sluggish kinetics of kink-pair nucleation and motion of screw dislocations interacted with solute Ni atoms. The Fe-40%Cr binary alloy showed higher yield strength and much lower m values than the Fe-18%Cr alloy, regardless of the specimen size. The compressed micropillars of the Fe-40%Cr alloy micropillars exhibited the slip activation on multi-planes (from (110) to (11-2)). These results suggest the interaction of dislocations on multi-planes might be enhanced by high-concentrated Cr solute element in bcc solid solutions. The roles of solute Ni and Cr elements in the thermal activation process of dislocation motion will be discussed in terms of the activation volume of plastic deformation.

11:15 AM SF07.08.09

Microstructure, Mechanical Properties and Long-Term Stability of FeMnNiAlCr High Entropy Alloys for Concentrated Solar Power Systems Edwin S. Jiang and Ian Baker; Dartmouth College, United States

As one of the major approaches in harvesting and converting solar energy, concentrated solar power (CSP) offers advantages in cost-effective energy storage and the capability to provide electricity when the sun is absent. Following Carnot's theorem, the CSP systems prefer higher operation temperature for higher conversion efficiency. However, currently-employed tubing materials cannot work at temperatures exceeding 873 K due to mechanical, corrosion, and oxidation limitations. To solve this challenge, high entropy alloys (HEAs) are being considered due to their novel mechanical properties especially at high temperatures. In this study, we present microstructural characterization, tensile strength, and creep resistance of FeMnNiAlCr high entropy alloys, with different Mn content ($x = 32.9 - 42 \text{ at. } \%$) at temperatures of 873-1023 K. The effect of recrystallization, which is achieved by cold-rolling and annealing, on the microstructures and mechanical properties were also studied. Both as-cast and recrystallized alloys exhibit high strength, good creep resistance, and long-term stability at high temperature. *In-situ* deformation experiments were conducted in the transmission electron microscope to

examine the deformation mechanisms. The results suggest the potential of FeMnNiAlCr HEAs as a cost-effective candidate for CSP systems.

SESSION SF07.09: Structural Intermetallics VI
Session Chairs: Masahiko Demura and Scott McCall
Thursday Afternoon, December 1, 2022
Sheraton, 5th Floor, Riverway

1:30 PM *SF07.09.01

Design and Behavior of High Intermetallic Content Al-Ce Alloys Scott McCall¹, Hunter Henderson¹, Seungjin Nam², Ryan Ott² and Orlando Rios³; ¹Lawrence Livermore National Lab, United States; ²Ames Laboratory, United States; ³The University of Tennessee, Knoxville, United States

The thermodynamic and kinetic features of the Al-Ce alloy system enable the intermetallic volume fraction of intermetallic particles to be increased significantly, while remaining processable by conventional and advanced manufacturing processes. Here, we present recent work to establish Al-Ce alloys for casting, wrought, and additively manufactured alloys that leverage high intermetallic fraction for enhanced properties. Thermodynamic features are combined with thermophysical and structural properties to fashion alloys with property sets tailored to intended applications. Furthermore additional alloying elements can induce complex changes in phase distribution and strength, both of which are also a function of solidification rate. Promising Al-Ce-X-Y and sometimes -Z candidates for particular applications will also be discussed.

This research was sponsored by the Critical Materials Institute, an Energy Innovation Hub funded by the U.S. Department of Energy (DOE), Office of Energy Efficiency and Renewable Energy and Advanced Manufacturing Office. Work performed at LLNL under contract DE-AC52-07NA27344

2:00 PM SF07.09.02

Phase Stability of A₂B-Type GCP Compound in Ni-Cr-Mo System Alloys at Elevated Temperatures Ryota Nagashima, Hirotoyo Nakashima and Masao Takeyama; Tokyo Institute of Technology, Japan

Most of the geometrically close-packed (GCP) compounds are A₃B type, whereas a very few A₂B type GCP compound exists. The Ni₂Cr (*oP6*) is one of them. According to the Ni-Cr phase diagram, this phase is a Kurnakov-type compound and is stable up to 867 K. Recently, our systematic phase diagram study on Ni-Cr-Mo ternary system experimentally reveals that a single-phase region of Ni₂(Cr, Mo) with *oP6* crystal structure exists as an island with compositions around Ni-15Cr-15Mo (at.%), up to about 1073 K, approximately 200 K higher than the binary Ni₂Cr compound. The reason why Mo in solution in Ni₂Cr phase stabilizes the phase is bonding energy between Cr and Mo in Cr site should be negative, because thermodynamical calculation shows that modifying ternary-interaction parameter $L_{Cr,Mo;Ni}$ to negative is the most strongly contributes to reproduce the experimental phase diagram in other thermodynamical parameters, e.g. end-members and interaction parameters among binary and ternary elements. This result is very attractive from both fundamental and engineering viewpoints. The Ni₂Cr phase could be an alternative strengthener to Ni₃Al- γ' phase in Ni-based alloys, if we can further increase the phase stability. In this study, then, in order to verify the mechanism of the increase in phase stability of Ni₂Cr compound by Mo addition, effect of 5th and 6th group elements on the phase equilibria at elevated temperatures were systematically examined. Thermodynamic calculations to evaluate the phase stability of this phase is also conducted, by taking the interaction parameters among the three elements into account. Two series of alloys were prepared: series I with nominal compositions of Ni-15Cr-15(Mo, M) (at.%) by replacing Mo with M by every 5 at.% and series II with those of Ni-15Cr-15Mo-5M by addition of 5at.%M to Ni-15Cr-15Mo. These alloys were prepared by arc melting in argon atmosphere with non-consumable tungsten electrode as 35 g button ingots. These ingots were firstly cold rolled by 40% in height, and solution treated at 1473 K for 24 h, followed by a water quench, in order to eliminate the micro segregation. Then, they were equilibrated at 1173-973 K for up to 1000 h. It was found that, in any alloys containing M, the observed Ni₂(Cr, Mo) single phase region in the ternary system was reduced, even in the case of V where Ni₂V is also the A₂B type GCP compound with the *oP6* structures. Instead, the stable A₃B-type GCP phases of Ni₃V- γ' (D0₂₂), Ni₃Nb- δ (D0_a) and Ni₃Ta- δ (D0_a) appears in the quaternary systems, indicating that the M elements apparently destabilize the *oP6* phase with respect to the A₃B-type GCP phases. The A₂B type GCP phase has B-B bonding unlike A₃B type, so the total bonding energy should always be smaller for A₂B than A₃B ($\Omega_{A-B} < 0$). The thermodynamically stable existence of the Ni₂(Cr, Mo) phase, despite the thermodynamic existence of the Ni₃Mo- δ phase in the binary system, must be caused by not only the interaction among ternary elements but also size effects. Based on these results, together with the thermodynamic calculations on the observed A₂B and A₃B type GCP phases, elements which do not form A₃B type GCP phase would possibly be effective in increasing the stability of Ni₂Cr. The size effect as well as atomic scale considerations on the difference in phase stability between A₃B and A₂B type GCP phases will also be touched in detail. A part of this research was supported by JST-Mirai Program Grant Number JPMJMI21E7, Japan.

2:15 PM SF07.09.03

Direct Observation of Zonal Dislocations in σ -FeCr by Atomic-Resolution Scanning Transmission Electron Microscopy Kyosuke Kishida, Masaomi Okutani, Hirotaka Suzuki and Haruyuki Inui; Kyoto University, Japan

Dislocations are the lattice defects that are mainly responsible for plastic deformation of crystalline materials through their glide motion. The glide motion of dislocations on a slip system generally takes place on a crystallographic plane between two adjacent atomic layers in the case of most metallic materials with relatively simple crystal structures such as face-centered cubic (FCC) and body-centered cubic (BCC) metals. However, the dislocation glide process in materials with complex crystal structures has not been fully clarified yet, because it can be very complicated often involving multiple atomic planes during dislocation glide. One of the dislocation glide models predicted to operate in complex materials is the zonal dislocation model, in which non-uniform atom shuffling is predicted to occur in multiple atomic planes called shear zone. The zonal dislocation model was introduced by M.L. Kronberg to describe possible glide motion of dislocations of the $\{110\}<001>$ slip in β -U with the tetragonal Ab structure (identical to D_{8h} structure of σ -FeCr). However, it has never been experimentally verified to occur. This is because β -U is one of the typical radioisotopes, which prevents from further detailed experimental study of its dislocations. Another reason is that the brittleness of the sigma-phase arising from the complex crystal structure has made impossible for plastic flow to occur by dislocation glide. Recently, we have systematically investigated fundamental deformation behavior of hard and brittle materials by utilizing micropillar compression method and have successfully identified the activation of $\{110\}<001>$ slip in σ -FeCr at room temperature. In the present study, we investigated dislocation core structures of $\{110\}<001>$ slip in σ -FeCr by atomic-resolution scanning transmission electron microscopy and confirmed that $<001>$ dislocations glide on $\{110\}$ are of the zonal-type but the thickness of the shear zone was different from that predicted by Kronberg. New atomic shuffling model in the shear zone was proposed based on the experimentally observed dislocation core structure.

2:30 PM SF07.09.04

Strengthening by Controlled Al_kFe Intermetallic Phase in Al-Fe Based Alloys Additive-Manufactured by Laser Powder Bed Fusion Naoki Takata¹, Wenyuan Wang¹, Takanobu Miyawaki¹, Yue Cheng¹, Asuka Suzuki¹, Makoto Kobashi¹ and Masaki Kato²; ¹Nagoya University, Japan; ²Aichi Center for

In recent, laser powder bed fusion (L-PBF) has emerged as one of the most representative metal additive manufacturing techniques capable of producing metallic components by using a scanning laser beam to selectively melt consecutive bedded-powder layers. The L-PBF process enables not only the manufacturing of complex geometrical forms but also the fabrication of Al alloys with superior mechanical properties. The L-PBF manufactured Al-2.5Fe (mass%) binary alloy exhibits a high tensile strength of approximately 300 MPa due to the fine morphology of Al₆Fe metastable phase (orthorhombic, *oC24*). The strength level slightly decreases after long-term exposure at elevated temperatures, indicating the feasibility of employing lightweight heat-resistant materials. However, increasing Fe alloy content significantly reduces L-PBF processability due to the formation of coarsened Al₁₃Fe₄ stable phase. It is therefore required to stabilize the fine Al₆Fe phase by third alloy elements for further strengthening without a loss of L-PBF processability for Al-Fe alloys. The present study was undertaken to investigate the effect of selected third elements (Mn or Cu) on the microstructure and mechanical properties of the Al-Fe binary alloy additive manufactured by the L-PBF process.

In this study, attempts of L-PBF processing using the gas-atomized Al-2.5Fe-2Mn or Al-2.5Fe-2Cu (mass%) ternary alloy powder with an average particle size of about 20 μm were made. Rectangular alloy samples were fabricated using a metal AM ProX DMP 200 machine (3D Systems, USA) under a wide range of laser scan speed (0.6 ~ 1.4 m/s) and laser power (102 ~ 204 W). The applied laser-scanning hatch distance, powder-bed thickness, and beam focus size were 0.1 mm, 0.03 mm, and ~0.1 mm, respectively. The results of measuring the sample density provided the optimum laser parameter sets for the manufacturing of both alloy samples with high relative densities above 99 %, indicating high L-PBF processability for the Mn or Cu added Al-Fe alloy powders. The L-PBF manufactured samples exhibited microstructure consisting of a number of melt pools in which regions locally melted and rapidly solidified due to scanning laser irradiation. The added Mn element was partitioned into the refined Al₆Fe phase, resulting in the formation of Al₆(Fe, Mn) phase with an orthorhombic structure (*oC24*). A certain amount of solute Mn (approximately 0.8 mass%) was detected in the α-Al matrix. Numerous nanoscale particles of Al₆(Fe, Mn) phase were homogeneously dispersed in the α-Al matrix, whereas relatively coarsened Al₆(Fe, Mn) phases with a cellular morphology appeared localized along melt-pool boundaries. Similar microstructures containing the Al₁₃CuFe₄ phase (orthorhombic, *oC24*) were observed in the L-PBF processed Al-2.5Fe-2Cu alloy samples. These results indicate the added third element could stabilize the refined Al₆Fe phase formed in rapid solidification by the L-PBF process. The L-PBF processed Al-2.5Fe-2Mn and Al-2.5Fe-2Cu alloys exhibited higher strength of approximately 360 MPa than the Al-2.5Fe binary alloy and an adequate tensile ductility of approximately 10 % in total elongation at ambient temperature. The high-temperature strength of the L-PBF manufactured ternary alloys will be presented.

SESSION SF07.10: Virtual Session I
Session Chairs: Yoshisato Kimura and Hiroyuki Yasuda
Tuesday Morning, December 6, 2022
SF07-virtual

8:00 AM SF07.10.01

Effect of Product Shape on Microstructure and Mechanical Properties of Ti-48Al-2Cr-2Nb Alloys Fabricated by Additive Manufacturing Hiroyuki Y. Yasuda¹, Ken Cho¹, Hajime Kawabata¹, Masao Takeyama² and Takayoshi Nakano¹; ¹Osaka University, Japan; ²Tokyo Institute of Technology, Japan

Additive manufacturing is one of highly efficient processes to fabricate TiAl low pressure turbine blade. In the present study, large triangular prisms and small cylindrical rods of Ti-48Al-2Cr-2Nb alloys were prepared by electron beam powder bed fusion (EB-PBF) to examine the effect of product shape on the microstructure and mechanical properties. The microstructure after EB-PBF depends on the process parameter such as beam current and scanning speed. Under an optimum condition, peculiar banded structure composed of duplex-like structure and equiaxed γ grains (γ band). Such microstructure is homogeneously formed in cylindrical rods 10 mm in diameter. On the other hand, in the case of the triangular prisms, the microstructure vary from area to area. In the thick area, the banded structure is formed, while typical lamellar structure composed of the α_2 and γ phases can be seen in the thin area. It is also noted that hardness distribution was also inhomogeneous depending on the microstructure. In EB-PBF process, an electron beam moves showing a snake pattern. In the thin area, the beam moves forth and back quickly, resulting in an increase in temperature. This leads to the formation of the lamellar structure. In order to get homogeneous microstructure throughout the triangular prisms, the process parameter is changed from area to area. As a result, homogeneous microstructure consisting of the banded structure was formed and the hardness distribution of the triangular prisms also became homogeneous.

8:15 AM SF07.10.02

Relationship Between Microstructure and Mechanical Properties of β -Containing TiAl Alloys Fabricated By Additive Manufacturing Ken Cho¹, Hirota Odo¹, Hiroyuki Y. Yasuda¹, Hirotoyo Nakashima², Masao Takeyama² and Takayoshi Nakano¹; ¹Osaka University, Japan; ²Tokyo Institute of Technology, Japan

In recent years, TiAl alloys containing the β phase are expected to expand the application scope of the alloys due to their superior mechanical properties at high temperatures. Electron beam powder bed fusion (EB-PBF) that is one of the additive manufacturing processes for metallic materials has attracted much attention as a fabrication process of TiAl alloy parts for aerospace applications with complex geometries. Furthermore, it is possible to obtain unique microstructures by repeated and rapid fusion and solidification during the EB-PBF process, resulting in excellent mechanical properties. In the present study, relationships between microstructure and mechanical properties of β -containing TiAl alloys prepared by the EB-PBF process were investigated focusing on the influence of the input energy density. Specimens fabricated at low energy densities contain ultrafine lamellar structure composed of the α_2 and γ phases, together with the β/γ cells discontinuously precipitated at the lamellar grain boundary. The ultrafine lamellar grains and the β/γ cells are effective in increasing strength and ductility of the alloys, respectively. In addition, we developed new heat treatment processes to control the morphology of the microstructure. The alloys subjected to optimum heat treatments exhibit higher strength and larger ductility at 1023 K, compared with the cast alloys.

This work was supported by Council for Science, Technology and Innovation (CSTI), Cross-ministerial Strategic Innovation Promotion Program (SIP), "Materials integration" for revolutionary design system of structural materials" (Funding agency: JST).

8:30 AM SF07.10.03

Modeling Titanium Aluminide Based Alloys from Atomic to Lamellar Scales Sridhar Narayanaswamy, Mark Jhon, Jerry Quek, Balaji Selvarajou, Guo Tianfu and Wang Zhao; IHPC, Singapore

Titanium aluminide-based alloys have found use in the aerospace industry in applications such as low pressure turbine blades due to their light weight and

high temperature properties. It is necessary to develop a deep understanding of the structure-property correlations of these materials in order to understand how to engineer their mechanical properties. To this end, we have used models at multiple length scales to explore the relationship between temperature, microstructure, and mechanical properties. At the atomic scale, we performed a critical evaluation of existing empirical potentials and found that potentials based on the Embedded Atom Method and the Modified Embedded Atom method were capable of replicating most (but not all) mechanical properties as compared to DFT and experiment. For example, all existing models tend to overestimate the thermal expansion coefficients in the α 2-Ti3Al structure. At the lamellar structure, we developed a crystal plasticity model that explicitly accounts for the alternating lamellae of γ -TiAl and α 2-Ti3Al. By phenomenologically including experimentally observed trends such as the temperature-dependent yield stress anomaly and deviations from Hall-Petch behavior, we were able to establish relationships between orientation dependent deformation, structural length scales such as lamellae thickness, and stress state.

8:45 AM SF07.10.05

Kink-Band formation in Various Mille-Feuille Structured Mg- and Al-Based Materials [Koji Hagihara](#), Toko Tokunaga and Shuhei Ohsawa; Nagoya Institute of Technology, Japan

Mg-based LPSO phase is known to contribute to increase in both of strength and ductility of Mg alloys. As a deformation mode in it, kink-band formation is recently focused. A kink band is a deformation band formed by the explosive generation of dislocations in a localized region and their subsequent alignment along a direction normal to the slip plane. However, details of its formation criteria have not yet been clarified. According to the study on the LPSO phase, its unique crystal structure which is constructed by the alternative stacking of soft and hard layers, called mille-feuille structure, are supposed as plausible factors to govern the formation of deformation kink bands.

To confirm these assumptions, we have examined the deformation behavior of several directionally solidified Mg-based and Al-based two-phase eutectic alloys with lamellar microstructure as a model material, such as Mg/Mg₁₇Al₁₂, Mg/Mg₂Yb and Al/Al₂Cu. Consequently, the formation of kink-bands was confirmed in all the alloys, as expected. The details of the deformation microstructure and accompanying deformation behavior will be discussed in the presentation.

9:00 AM SF07.10.06

Precipitation from Microscopic Segregation in Ni-Based Superalloy Additively Manufactured by Powder Bed Fusion—A Phase-Field Study [Yuichiro Koizumi](#), Masayuki Okugawa, Makoto Wakabayashi, Kazufumi Nose and Sei Hirooka; Osaka University, Japan

Powder bed fusion (PBF) is a category of additive manufacturing (AM) applied to the fabrication of metal parts with various materials, including superalloys. Solidification by PBF is characterized by a high cooling rate of around 1 million K/s. Recent studies have revealed the very fine submicron-sized celluller structures associated with solute segregations between the cells in Ni-based superalloys fabricated by the PBF process. Such segregation is expected to affect the precipitation of the γ' -phase. In this study, we utilized phase-field simulation to investigate the precipitation of γ' -phase from the solute segregation formed by rapid solidification in PBF. The multiphase-field method was applied to the simulation of microstructural evolution in directional solidification under various solidification conditions focusing on solute segregation. A composition consisting of five major elements of Inconel738LC alloy was selected as the model. Initially, cellular structure with intercellular micro-segregation was generated by simulating directional solidification under a condition with a cooling rate of 10⁶ K/s, solidification rate of 10⁻¹ m/s, and temperature gradient of 10⁷ K/m, which is a typical solidification condition in PBF process. γ' forming elements, (i.e. Al and Ti) segregated at the intercellular region. The growth of γ' precipitates and the relaxation of the segregation occurred simultaneously, and there was no significant influence of the segregation on the precipitates in the subsequent aging at relatively high temperature. In contrast, the precipitation occurred preferentially at the intercellular segregation in the case of aging at relatively low temperature. This work was supported by Council for Science, Technology and Innovation, Cross-ministerial Strategic Innovation Promotion Program, “Materials Integration for revolutionary design system of structural materials” (Funding agency: JST).

9:15 AM SF07.10.07

Transitions Among Stress-Induced Martensitic Phases in Ti-10V-2Fe-3Al During Continuous Deformation [Abhishek Rastogi](#) and Suresh Neelakantan; Indian Institute of Technology Delhi, India

Revealing the possibility of transition among stress-induced martensitic phase during continuous cold deformation in metastable β titanium alloy, Ti-10V-2Fe-3Al (Ti-1023) is the main objective of this study. In general, martensitic transformations induced either by quenching or load application have a significant influence on the mechanical properties of metastable β -Ti alloys. It is known that martensitic transformation in metastable β -Ti is highly dependent on the alloy content and deformation. With the increase in β stabilizing elements, HCP- α' martensite transforms to orthorhombic- α'' martensite upon quenching from a single β phase. However, deformation-dependent martensitic transformation involves the role of lattice strain and atomic shuffle. β to α'' and β to α' transformation differ in terms of atomic shuffle displacement, wherein the former requires less displacement than the latter [4]. Therefore, β to α'' transformation can be considered crystallographically incomplete as compared to β to α' transformation. At sufficiently high strain, it can be assumed that the formation of the α'' is exhausted, and other stress-induced deformation mechanism may also activate, resulting in the possibility of α'' to α' transformation. In the present investigation, Ti-1023 alloy was solution treated in the single β phase-field followed by water quenched. Solution-treated samples were unidirectionally cold rolled to 5%, 15%, 25%, 35% and 43% thickness reduction levels. The resulting microstructures are extensively analyzed by XRD and TEM analysis. XRD and TEM confirm the transformation of β to α'' to α' . Lattice parameters ratios, as well as volumetric strain (%) calculations, provide indications about the transitions of α'' to α' . Furthermore, the TEM results confirm the dominant presence of α'' martensites at low cold rolling percentage compared to α' martensites observed at high cold rolling percentage. It has been observed that the driving force for martensitic transformation is the combined effect of lattice strain induced by cold rolling and the different alloying elements influencing the atomic shuffle displacements. A correlation of the lattice strain and alloying elements with atomic shuffle displacements on the transformation of β to α'' to α' in Ti-1023 has been established.

9:35 AM DISCUSSION TIME

SESSION SF07.11: Virtual Session II
Session Chairs: Yoshisato Kimura and Hiroyuki Yasuda
Tuesday Morning, December 6, 2022
SF07-virtual

10:30 AM SF07.11.01

Phase-Field Simulation of Antiphase Domain Growth for $D0_3$ Ordered Fe_3Al Alloy Yuheng Liu, Madoka Watanabe, Masayuki Okugawa, Tsubasa Sato and Yuichiro Koizumi; Osaka University, Japan

[Introduction] The mechanical or magnetic properties of the ordered phases are closely related to the antiphase domain (APD) structures, such as the APD size and the characteristics of antiphase domain boundaries (APBs). For example, it has been reported that pseudoelasticity is caused in Fe_3Al by the interaction between APBs and dislocations ^[1]. Phase-field (PF) simulation has been proved to be an effective way of studying the formation and time-evolution of APD for ordered phases. Koizumi et al. ^[2] studied the ordering mobility in nearly stoichiometric Fe_3Al at constant temperatures by the PF method. The objective of this study is to develop PF simulations applicable to temperature variations for the APD growth in $D0_3$ ordered Fe_3Al alloy, aiming at the optimization of aging conditions for ordering in the future.

[Methods] PF simulations of ordering in Fe-28at.%Al alloy were performed for the cases of constant cooling rate and isothermal aging. The dimension of the simulation domain area was a cube with a size of 30 nm. Thermodynamic equilibrium at 873 K was assumed as the initial state for all simulations. The evolution of $D0_3$ APD during cooling to 673 K at rates of 0.1–1000 K/s and that during aging at constant temperatures of 673 K, 723 K, and 773 K for 1 h after cooling at 100 K/s were examined and compared with experimental results.

[Results] The simulation results for the case of constant cooling rate showed that the growth of the $D0_3$ APD takes place before the detectable long-range order (LRO) appears. Moreover, slower cooling rates resulted in larger APD sizes. On the other hand, although the ultimate LRO obtained by isothermal aging at a lower temperature is higher than that at a higher temperature, $D0_3$ -LRO exhibited a significant increase earlier in aging at higher temperatures. Besides, the growth of $D0_3$ APD also begins earlier when aging at higher temperatures, which is due to the larger ordering mobility at the higher temperature. In conclusion, isothermal aging at higher temperatures after cooling at a higher rate is considered suitable for the fast growth of $D0_3$ APD in the Fe_3Al .

[References]

[1] H. Yasuda et al.: "Effect of ordering process on giant pseudoelasticity in Fe_3Al single crystals", *Acta Mater.* **51** (2003) 5101–5112.

[2] Y. Koizumi et al.: "Solute and vacancy segregation to $a/4\langle 111 \rangle$ and $a/2\langle 100 \rangle$ antiphase domain boundaries in Fe_3Al ", *Acta Mater.* **56** (2008) 5861–5874.

10:45 AM SF07.11.02

Observation of Multiple Weyl Points in $SrAlGe$ Compound Parul Jain^{1,2}; ¹Indian Institute of Technology Delhi, India; ²G C Faridabad, India

Topological semimetals with multiple topological phases have gained renewed interest from the materials research community as new materials started to appear with tunable or concurrent quasiparticle excitations of different types.

Here, in this work, using Density Functional Theory (DFT) we studied a new topological semimetal $SrAlGe$, which has similar lattice structure to $LaPtSi$, a newly identified candidate [1] with multiple topological phases. The magnetic properties emerging from the $4f$ electrons of Samarium in $SrAlGe$ grant further scope to tune the topological states magnetically. First, we find that the material $SrAlGe$ is thermodynamically more stable in the antiferromagnetic phase. All the further calculations are done on this ground state antiferromagnetic phase. Second, we analyse and report the splitting of $4f$ -orbital in the 12-fold coordination of Sm in presence of spin-orbit coupling. Finally, we study the topological properties of the material. Band-structure shown in the figure 1(b) reveals multiple Lorentz symmetry violating (Type-II) Weyl nodes very close to the Fermi energy. Further, we studied the exotic surface states using a Wannier-based tight-binding Hamiltonian.

[1] Shi, Xianbiao, et al. "Topological states in the noncentrosymmetric superconductors $LaPtSi$ and $LaPtGe$." *Physical Review B* 104.24 (2021): 245129.

11:20 AM DISCUSSION TIME

SYMPOSIUM SF08

Advanced Ceramics and Glasses—From Advanced Manufacturing to Data-Driven Methods for Synthesis and Mechanical Characterization

November 28 - December 8, 2022

Symposium Organizers

Christos Athanasiou, Brown University
Florian Bouville, Imperial College London
Hortense Le Ferrand, Nanyang Technological University
Izabela Szlufarska, University of Wisconsin

* Invited Paper

+ Distinguished Invited

SESSION SF08.01: Advanced Ceramics and Glasses I

Session Chairs: Christos Athanasiou, Florian Bouville and Hortense Le Ferrand

Monday Morning, November 28, 2022

Sheraton, 5th Floor, Public Garden

10:30 AM *SF08.01.01

Resilience in Lightweight Ceramic Architected Materials Enabled by Curvature and Geometry [Carlos M. Portela](#) and Somayajulu Dhulipala; Massachusetts Institute of Technology, United States

The field of architected materials has enabled engineered materials with mechanical properties that were previously thought unattainable. For instance, hollow truss-based lattices demonstrate high stiffness- and strength-to-weight ratios but these structures suffer from a bending-dominated response and stress concentrations at the sharp joints, the latter of which result in failure. Such stress concentrations become particularly challenging when working with nominally brittle materials, such as ceramics. As an alternative, aperiodic and asymmetric morphologies attained through spinodal decomposition (spinodal metamaterials) may provide a route to combat these stress concentrations due to their finite (low) curvature and bicontinuous morphologies. Such morphologies could provide a pathway to engineer ceramic materials with unique combinations of properties such as low density, high stiffness, and extreme mechanical resilience.

In this study, we explore the effect of curvature and geometric anisotropy on the stiffness, strength and toughness of spinodal metamaterials. The spinodal morphologies are generated using a computational spinodal decomposition framework where tunable anisotropy is introduced by energetically penalizing preferential directions for interface formation, resulting in a mean-curvature and Gaussian-curvature distribution that is dependent on the direction of the surface normal. Using a two-photon lithography process, we fabricate prototypes of these anisotropic spinodal morphologies possessing nanoscale ceramic coatings and spatially varying curvature distributions and perform in-situ nanomechanical uniaxial compression experiments to determine their curvature-dependent stiffness, strength, and toughness. Complemented by analytical and finite element models of the as-fabricated morphologies, we demonstrate a relation between curvature distributions, the stress distribution, and the mechanical properties of these metamaterials. Our findings present the potential of architected spinodal metamaterials as a route to create new ceramic-based materials with widely tunable properties.

11:00 AM *SF08.01.02

Exploring Process-Microstructure-Property Relationships in Inorganic Materials—From Advanced Manufacturing to Mechanical Characterizations [Jun Lou](#); Rice University, United States

Fabricating inorganic materials with designed three-dimensional nanostructures is an exciting yet challenging area of research and industrial application. We recently developed an approach to 3D print high quality nanostructures of silica with sub-200 nm resolution and with flexible capability of rare earth element doping [1]. The printed SiO₂ can be either amorphous glass or polycrystalline cristobalite controlled by the sintering process. The 3D printed nanostructures demonstrate attractive optical properties. For instance, the fabricated microtoroid optical resonators can reach quality factors (Q) over 10⁴. Moreover, importantly for optical applications, doping and co-doping of rare earth salts such as Er³⁺, Tm³⁺, Yb³⁺, Eu³⁺ and Nd³⁺ can be directly implemented in the printed SiO₂ structures, showing strong photoluminescence at the desired wavelengths. Additionally, mechanical properties of the 3D printed silica and its composite nanostructures have been carefully studied.

On the other hand, nanomaterials such as carbon nanotubes, hexagonal boron nitride (h-BN) and graphene platelets, are promising candidates for reinforcing ceramic matrix composites. To quantitatively study the toughening behavior in two-dimensional (2D) material reinforced ceramics, pull-out experiments were conducted to investigate the properties of the interface between multi-layer h-BN nanosheet and polymer-derived ceramic (PDC) using nanoindentation-assisted micro-mechanical devices integrated with scanning electron microscopy (SEM) [2]. The failure process was monitored *in situ* with precise quantitative measurements of the relative displacements across the interface that were obtained with digital image correlation (DIC). A micromechanical analysis shows that the interfacial failure in these materials is governed by the interfacial strength at small length scales, rather than the interfacial fracture energy.

[1] X. Wen, B. Zhang, W. Wang, F. Ye, S. Yue, H. Guo, G. Gao, Y. Zhao, Q. Fang, C. Nguyen, X. Zhang, J. Bao, J.T. Robinson, P.M. Ajayan, J. Lou, *3D-printed silica with nanoscale resolution*, Nature Materials, Vol. 20, 1506-1511, 2021.

[2] B. Zhang, X. Liu, H. Guo, K. Yang, G. Gao, B.W. Sheldon, H. Gao, J. Lou, *Quantitative In-situ Study of Strength-governed Interfacial Failure Between h-BN and Polymer-derived Ceramic*, Acta Materialia, Vol. 210, 116832, 2021.

11:30 AM *SF08.01.03

Multiscale Mechanics of Bioinspired Material Intelligence [Markus J. Buehler](#); Massachusetts Institute of Technology, United States

Digital biomaterials are designed through an integrated approach of large-scale computational modeling, material informatics, and artificial intelligence/machine learning to optimize and leverage novel smart material manufacturing for advanced mechanical properties. In this talk we show how we use mechanics to fabricate innovative materials from the molecular scale upwards, with tailored mechanical properties, while sourced from sustainable resources, and breaking the barriers between living and non-living systems. Applied specifically to protein-based materials, this integrated materiomimetic approach is revolutionizing the way we design and use materials, and has the potential to impact many industries, as we harness data-driven modeling and manufacturing across domains and applications. The talk will cover several case studies focused on the discovery of unifying mechanical principles covering distinct scales and modalities, from spider webs and silk, to collagen, to biomineralized materials, as well as applications to food and agriculture, showing we mechanics can be applied to uncover universal scaling laws that govern mechanical behavior. We further discuss manufacturing methods that enable us to synthesize computationally designed architectures with high precision, spanning multiple scales from the nano to the macro level.

SESSION SF08.02: Advanced Ceramics and Glasses II
Session Chairs: Christos Athanasiou and Florian Bouville
Monday Afternoon, November 28, 2022
Sheraton, 5th Floor, Public Garden

1:30 PM *SF08.02.01

Embedded Printing in Ceramics [Eduardo Saiz](#)¹, Shitong Zhou¹, Iuliia Elizarova¹, Florian Bouville¹, Philip Withers² and Xun Zhang²; ¹Imperial College London, United Kingdom; ²The University of Manchester, United Kingdom

Ceramics exhibit a range of unique properties that make them the ideal candidates for many applications, particularly those involving demanding environments. However, these same properties, such as the high hardness, that make ceramics so interesting also make their shaping challenging. In addition, many high-end applications demand the integration of ceramics in multicomponent composites and devices with a sophisticated degree of structural control. Additive manufacturing is opening new opportunities to address these needs but presents its own set of challenges. In this presentation we introduce embedded printing as an alternative to introduce structures in dense ceramic bodies. This is achieved by printing in a self-healing ceramic gel

that enables the printing in its interior followed by subsequent healing to form a dense, defect-free ceramic that encapsulates the printed structure. We will discuss the necessary matching of the properties of the viscoelastic response of gel and ink in order to print structures inside the ceramic that retain their shape and illustrate the technique with a couple of case studies. One is the printing of sacrificial structures to introduce complex microchannel arrangements in a ceramic body. The other is to embed metallic structures designed to enhance fracture resistance by orders of magnitude.

2:00 PM SF08.02.02

Addressing Nanoscale Heterogeneity in Compositionally Complex Ceramic Oxides [Katharine Page](#)^{1,2}; ¹The University of Tennessee, Knoxville, United States; ²Oak Ridge National Laboratory, United States

The recent emergence of multicomponent, high-entropy oxides (HEOs) has sparked research into novel ceramics with significant compositional and structural diversity. The wide range of achievable materials presents promising research opportunities, as they may be custom-designed to enhance performance in any of a number of important applications, such as thermal barrier coatings and solid oxide fuel cells. In these arenas and in many others, the extent to which high entropic lattice disorder versus specific chemical short-range order, nanoscale phase segregation, and intrinsic defect/disorder states are achievable remains an open research question. We present detailed investigation of the defects, local atomic order, microstructure, and thermomechanical properties achieved in a family of rare-earth and transition metal-based pyrochlore and fluorite HEOs prepared through compositional tuning and variation in synthesis/processing conditions. A combination of local to long-range electron, X-ray and neutron scattering probes are employed to investigate the complex configurational diversity and associated structure-property trends in the series. Experimentally derived models are supported by Density Functional Theory calculations and Metropolis Monte Carlo simulations. We demonstrate that nanostructured oxides produced through polymeric steric entrapment and other low temperature reaction routes are promising precursors for the synthesis of compositionally complex pyrochlore/fluorite ceramics with specific nanoscale ordering motifs. We also discuss the exquisite level of experimental characterization and theoretical modeling that may be required to understand the phase stability, atomic structure, and respective properties of emerging HEO materials classes, highlighting some remaining challenges.

2:15 PM SF08.02.03

3D Printed Silica with Nanoscale Resolution [Boyu Zhang](#)¹, Xiewen Wen¹, Weipeng Wang¹, Hua Guo¹, Guanhuai Gao¹, Qiyi Fang¹, Christine Nguyen¹, Xiang Zhang¹, Jiming Bao², Jacob T. Robinson¹, Pulickel Ajayan¹ and Jun Lou¹; ¹Rice University, United States; ²University of Houston, United States

SiO₂ (silica) is one of the most widely used inorganic materials that demands fabrication methods with nanoscale resolution. Fabricating silica with designed three-dimensional nanostructures is an exciting yet challenging area of research and industrial application. The emerging technology of additive manufacturing (AM) can create fine structures through layer-by-layer deposition to generate complex architectures and simplify fabrication processes. AM of fused silica glass was realized via stereolithography with the resolution of tens of microns. However, the relatively low spatial resolution limits their applications in micro-electronics, MEMS, and micro-photonics. To address the limitation, we propose an approach to 3D print silica nanostructures with sub-200 nm resolution via two-photon polymerization. The technique involves 2PP enabled AM of functionalized colloidal silica nanocomposite ink, followed by pyrolysis and sintering, where the post-processing procedure determines the crystallinity of the structures produced, which can be either amorphous glass or polycrystalline cristobalite. In this technique, making a suitable "ink" containing silica nanoparticles (NPs) and two-photon polymerizable precursor is the dominating factor. The nanocomposite ink has low viscosity, high transparency, and high heat conductivity. The 3D printed nanostructures demonstrate attractive optical properties. The fabricated microtoroid optical resonators can reach quality factors (Q) over 10⁴. Moreover, doping and co-doping of rare earth salts such as Er³⁺, Tm³⁺, Yb³⁺, Eu³⁺ and Nd³⁺ can be directly implemented in the printed SiO₂ structures, showing strong photoluminescence at the desired wavelengths. Especially for Er³⁺, the final printed structures exhibit photoluminescence around 1.55 μm, making the proposed technology a powerful tool for optical telecommunication applications. It is also envisioned that arbitrary 3D structure of crystalline silicon can be fabricated by magnesium reduction of printed crystalline silica, making the dream of 3D printing silicon chips a reality.

2:30 PM BREAK

3:00 PM *SF08.02.04

Using a Convolutional Neural Network to Identify the Microstructural Features that Lead to Anisomorphic Grain Growth [Amanda Krause](#); Carnegie Mellon University, United States

Grain growth, a common mechanism in ceramic processing, is difficult to predict because it is influenced by many factors, including porosity, raw powder size and shape, impurities and sintering conditions. To parse out these effects, grain growth studies commonly rely on qualitative comparisons of micrographs because of inadequate physical descriptors of grain size and shape. However, new data techniques can extract high order parameters that better describe microstructural features. In this study, we establish whether a convolutional neural network (CNN) can distinguish two initial microstructures of calcia-doped alumina, which appear similar by traditional grain growth metrics but then evolve differently during grain growth. If a unique signature can be extracted, it can provide mechanistic-insight into grain boundary motion for improved grain growth predictions.

The goal here is to collect a signature that distinguishes two alumina microstructures prepared with the same raw materials, slip casting process, and sintering conditions. However, one sample is slip cast in a magnetic field, which causes the equiaxed particles to rotate and preferentially align the c-axis of their unit cell, resulting in a bulk crystallographic texture. Recent studies show that the textured microstructure evolves differently from the untextured sample, resulting in a larger grain size and unique grain morphology. Here, we will evaluate the developed CNN used to identify these microstructures. Briefly, the CNN is trained from at least five micrographs with ~200 grains each from each timestep. The CNN consists of two convolutional layers with an increasing number of filters to learn increasingly abstract features.

The convolutional layers are followed by three fully connected layers with a decreasing number of nodes. The signature is extracted as a scalar quantity from the penultimate layer in the network. We will discuss the accuracy of the CNN to predict the microstructure's processing path and its implications regarding how crystallographic orientation influences grain growth. Furthermore, we will demonstrate the need for a new higher order physical descriptor of microstructures.

3:30 PM SF08.02.06

Machine-Learned Quantification of Local Structure and Its Effects in Fracture of Silica Glass and Deformation of Metallic Glass [Thomas J. Hardin](#) and Mark Wilson; Sandia National Laboratories, United States

The variety of local atomic environments found in a glass far exceeds that found in a crystalline material. This makes the task of linking physically important phenomena (e.g. crack nucleation or shear transformation) to local structural risk factors particularly challenging in glassy materials. We present case studies in two simulated materials (silica glass and a binary metallic glass) using unsupervised machine learning techniques (the Gaussian Integral Inner Product Distance with agglomerative clustering and diffusion maps) to extract local structural features, and supervised machine learning to link those features to mechanical behavior. We pinpoint preexisting defects in the as-quenched state as risk factors leading to fracture nucleation in silica, and show how detailed quantification of structural evolution in a metallic glass shear band points the way to improved stateful plastic models. We also consider the

comparative merits of human-designed versus machine-learned structural descriptors for glass and look forward to ways to use them synergistically. SNL is managed and operated by NTESS under DOE NNSA contract DE-NA0003525 (SAND2022-8095 A).

3:45 PM SF08.02.07

Machine Learning Approaches for the Automatic Design of Micro-Architected Triply Periodic Minimal Surface Scaffolds for Bone Tissue Engineering Pasquale Vena¹, Luca D'Andrea¹, Silvia Ibrahim¹ and Massimo W. Rivolta²; ¹Politecnico di Milano, Italy; ²Università degli Studi di Milano, Italy

Due to their peculiar architecture, Triply Periodic Minimal Surfaces (TPMS) find applications in many engineering domains. The increasing capability of additive manufacturing (AM) technologies allows the printing of microstructured materials with unparalleled spatial resolution and repeatability. This makes the design of TPMS-based material systems and device a feasible approach. Application of TPMS structure in Bone Tissue Engineering scaffolds design is particularly attractive. Indeed, scaffolds made with bioactive materials like glass ceramics and Hydroxyapatite and with specific morphological (such as porosity, pore interconnectivity, micro-feature characteristic size) and mechanical properties can be designed by taking advantage of the TPMS features.

The design of biomechanically reliable BTE scaffolds, possibly following a patient-specific approach, is still a complex task that is based on multidisciplinary input such as biomechanics, transport properties and mechanobiology. Classical optimization approaches may be unsuitable for such a complex approach in which multiple objectives need to be met simultaneously. For this purpose, the use of Machine Learning methodologies can be a suitable approach to support the selection of a design with prescribed multi-disciplinary properties.

In this study, we assessed whether a ML model may support the identification of TPMS architectures by leveraging biomechanical and morphological parameters as design inputs. The ML model was composed by three components. The first and second ones predict the geometrical parameters whereas the third one identifies the architecture type (i.e. diamond, gyroid and IWP). To do so, two regression and one classification problems were designed. Here, we considered three different TPMS architectures fully parametrized by two geometrical parameters. A dataset of TPMS architectures was created by solving the direct problem, i.e. imposing the geometrical parameters and the architecture type. Elastic and strength properties have been obtained through finite element modeling; while post-processing of the simulated micro-CT images of the TPMS structure was used to assess morphological parameters (the main ones are: wall thickness, wall spacing, volume fractions and geometrical anisotropy). Fluid transport properties were estimated by assessing the effective pore connectivity index. A total amount of 38 features were extracted from each of the 1258 designs (352, 476, 430 designs for diamond, gyroid and IWP, respectively).

The pseudo-experimental dataset was partitioned into a training set (60%), a validation set (20%) and a test set (20%). A ML greedy feed-forward feature selection algorithm was used with the aim of selecting the most informative descriptors. Once the selection of the most relevant features was identified the optimal design was obtained by defining the optimal values of the features.

The effectiveness of the predictive capability of the proposed approach was quantified by comparing the optimal structure obtained through the regressions and the actual values of the features for geometry extracted from the validation sets.

The results obtained through this approach have proven the suitability of the proposed ML algorithm to design suitable TPMS scaffold architectures, allowing for patient specificity which prescribes specific biomechanical (stiffness and strength) and transport properties (mainly related to the morphological parameters).

SESSION SF08.03: Poster Session: Advanced Ceramics and Glasses

Session Chairs: Christos Athanasiou and Florian Bouville

Monday Afternoon, November 28, 2022

8:00 PM - 10:00 PM

Hynes, Level 1, Hall A

SF08.03.01

Vitrification Range and Plasma Resistance of Bismuth Aluminosilicate Glass Young Min Byun^{1,2}, JaeHo Choi^{1,2}, YoonSung Jung^{1,2}, Kyung Won Min^{1,2}, Won Bin Im¹ and Hyeong-Jun Kim²; ¹Hanyang University, Korea (the Republic of); ²Korea Institute of Ceramic Engineering and Technology (KICET), Korea (the Republic of)

Reducing contaminant particles in the semiconductor etching process has been an important issue for improving the yields of semiconductor production. Recently, the plasma resistance glass (PRG) proposed as a new material to replace the plasma resistant material made of crystalline ceramics. Etching rate of PRG was lower than that of quartz glass, alumina, and sapphire. There is almost no change in the microstructure even after etching, so it is expected to be a suitable material for reducing particulate contaminants. Components to be aware of in the semiconductor process include alkali metals, heavy metals, etc. It can cause a defect of internal voltage on the oxide film, reduced lifetime, and crystal defects. Research has shown that the etching rate was an index of plasma resistance. It depends on the boiling temperature of the fluoride compound formed by a chemical reaction of plasma fluorine radicals. Bismuth was the component remaining after excluding the components to be avoided in the semiconductor process, and at the same time, the boiling temperature of BiF₃ is 900°C. It was expected to contribute to the reduction of the etch rate. However, since bismuth aluminosilicate glass was not well known, information about the clear vitrification range and properties of glasses were lacking. In this study was to investigate the vitrification range of Bi-Al-Si-O, which has not been studied, and to evaluate the plasma resistance. So we intend to investigate the vitrification range, thermal, physical properties, and plasma resistance of the ternary phase diagram.

SF08.03.02

Reliability of Chemical Strengthened Soda-Lime Glass Containers Kyung Won Min^{1,2}, Jae Ho Choi^{1,2}, YoonSung Jung^{1,2}, Young Min Byun^{1,2}, Won Bin Im² and Hyeong-Jun Kim²; ¹Hanyang University, Korea (the Republic of); ²Korea Institute of Ceramic Engineering and Technology, Korea (the Republic of)

Soda-lime glass has been used for a long time as a glass container because of its ease of melting, the abundance of raw materials, and cheapness. However, the glass container is damaged due to contact and collision between the containers, in the process of washing, filling, and capping, so the strength of the container is reduced to one-thousandths. HEC (Hot End Coating) and CEC (Cold End Coating) are applied to compensate for the decrease in the strength of glass containers. It is known that the mechanical properties of soda-lime glass can be improved using chemical strengthening. Therefore, in this study, the chemical strengthening was applied under annealing conditions to increase the strength of the container. For chemical strengthening, melted KNO₃ was spray-coated on a glass container. The strengthening temperature was performed at T_g±50°C. for 1 hour and then the cooling rate was 5°C/min until 100°C. After washing the strengthened glass container, mechanical properties and surface changes were confirmed. After that, reliability evaluation was conducted

through surface roughness change according to the presence or absence of HEC and chemical strengthening. Reliability was confirmed by measuring the impact strength value.

SF08.03.03

Processing Brittle Ultrahard Material and Glass with Polycrystalline Tools Using Electro-Discharge and Mechanical Machining System Eun-Ji Gwak, Jongkeun Sim, Chungmo Kang, Jae Hyeon Ahn, Jun Sae Han, Tae-Jin Je and Doo-Sun Choi; Korea Institute of Machinery & Materials(KIMM), Korea (the Republic of)

Ultra-hard and brittle materials have drawn enormous attention as a master mold or itself in manufacturing flexible displays, IT-electronics-semiconductor devices and bio-diagnostic kits when they have holes, channels or other free forms whose dimensions are in micro- and nano-scale. Especially, in machining those hard and brittle ceramic into ultra-fine feature size under 100 μm , errors in size or shape can be occurred by run-out during tool-setting. In this research, we introduce a newly developed ultra-precision machining system with both electro-discharge and mechanical machining modules for brittle ceramic materials using PCD(polycrystalline diamond) and PCBN(polycrystalline boron nitride) tools and suggest optimized machining conditions using a machining signal analyzing system. Force and acoustic emission data were obtained and correlated with resulting morphologies on material surfaces.

Acknowledgement : This work was supported by the Technology Innovation Program (20010984, Development of multiple machining system technology integrated electro discharge and mechanical working for ultrahigh hard material and application machining technology using micro tool having size of 20 μm) funded By the Ministry of Trade, Industry & Energy(MOTIE, Korea) and by the Korea Institute of Machinery and Materials (NK238E).

SF08.03.04

Study of Transparent Layer by Type of SiO₂ Raw Material of Quartz Glass Crucible YoonSung Jung^{1,2}, Jae Ho Choi^{1,2}, Kyung Won Min^{1,2}, Young Min Byun^{1,2}, Won Bin Im¹, Seung-Min Kang³ and Hyeong-Jun Kim²; ¹Hanyang University, Korea (the Republic of); ²Korea institute of Ceramic Engineering and Technology, Korea (the Republic of); ³Hanseu University, Korea (the Republic of)

Quartz crucible for manufacturing silicon ingots has a two-layer structure with inner and outer layer. The inner layer, which is in direct contact with the molten silicon, should minimize silicon contamination due to incorporation of impurities and crucible fragments. Therefore, a high-pure SiO₂ synthetic powder had been used. In this study, crucibles were prepared using the three types of high-pure SiO₂ synthetic powder; (1) powder produced by crushing and heat-treating the gel manufactured by the sol-gel method (2) powder manufactured by sol-gel method, crushed and heat-treated (3) powder produced by water glass ion exchange method, crushed and heat-treated. Both the synthetic powder had a purity of 6 N and a particle size of D₅₀ 70 to 160 μm , and the microstructure of the powder showed a difference depending on the production method. Therefore, there was a difference in the distribution of bubbles generated in the transparent layer of the crucible. We also confirmed the possible effect on ingot quality as the number of bubbles in the transparent layer increases.

SF08.03.05

Visualization of Crystalline Phase in Glass by Atom-Decomposed XRD Simulation Yuji Inoue¹, Tomoyuki Tamura¹, Ryo Kobayashi¹, Ayaka Kidani¹ and Reo Katayama²; ¹Nagoya Institute of Technology, Japan; ²Nagoya University, Japan

Recently, the development of functional glasses with the phase separation has been extensively researched, and the phase separation process is required to be clarified. However, for glasses without periodic structures, the diffraction patterns generally show broad peaks, and it is difficult to analyze the local structures only by XRD experiments.

In this study, we have developed a tool to analyze local structures by atom-by-atom decomposition of the XRD patterns for atomic configurations obtained by molecular dynamics simulations. We can visualize local structures that contribute significantly to a XRD peak of interest using atom-decomposed XRD patterns. Furthermore, we can analyze the effects of local structures such as coordination number on XRD patterns.

SF08.03.06

Graph Theory-Based Structural Analysis on Density Anomaly of Silica Glass Aik Rui Tan¹, Shingo Urata², Masatsugu Yamada² and Rafael Gomez-Bombarelli¹; ¹Massachusetts Institute of Technology, United States; ²AGC Inc., Japan

Understanding the structure of glassy materials is a tremendous challenge both experimentally and computationally. Despite decades of scientific research, for instance, the structural origin of the density anomaly in silica glasses is still not well understood. Atomistic simulations based on molecular dynamics (MD) produce atomically resolved structures, but extracting insights about the role of disorder in the density anomaly is challenging. Here, we quantify the topological differences between structural arrangements from MD trajectories using a graph-theoretical approach. Structural differences in silica glasses exhibiting density anomalies are captured using a graph similarity metric. To balance the accuracy and speed of the MD simulations, we utilized force matching potentials to generate the silica glass structures. This approach involves casting all-atom glass configurations as networks, and subsequently applying a graph-similarity metric (D-measure). Calculated D-measure values are then taken as the topological distances between two configurations. By measuring the topological distances of silica glass configurations across a range of temperatures, distinct structural features could be observed at temperatures higher than the fictive temperature. In addition, we compared topological distances between local atomic environments in the glass and crystalline silica phases. This approach suggests that more coesite-like and quartz-like local structures, emerge in silica glasses when the density is at a minimum during the heating process.

SF08.03.07

Understanding the Mixing and Properties of High Entropy Perovskites Ali Nasrallah, Ge Wang, Derek Sinclair and Colin Freeman; The University of Sheffield, United Kingdom

High-Entropy Oxides (HEOs) have gathered a lot of attention over the past few years particularly around their formation and properties¹⁻⁴. The perovskite lattice (ABO₃) is a particularly exciting opportunity as mixing can be carried out on both the A or B site presenting a wealth of enthalpic and entropic possibilities to achieve a single-phase solid solution with a favourable Gibbs free energy⁴.

Using a combination of computational modelling and experimental studies, we have examined several 3-, 4-, and 5-B element oxides with combinations of (Ga, Y, In), Nb, (Ti, Zr, Sn). We have studied the influence of a range of factors including the ionic size of the sites, the tolerance factor and the ionic size variation which we can then link to the formation of single-phase materials.

Our experiments on Ba-based perovskites demonstrate that single phases can be formed in a range of 4 and 5-B element perovskites with mixed valence charges (e.g. 3+, 4+ and 5+) but mixing was far more challenging with only 3-B element systems. By adjusting the A-site using Sr and Ca we were able to reduce the ionic size penalties and form further 3-B site single phase systems indicating that the size of the A cation also has an effect on the mixing process.

We have coupled the experimental work with a mixture of classical and ab initio simulation work examining the enthalpy of mixing and comparing to the

phase formation from experiment. Our DFT simulations have identified the different mixing and hybridisation characteristics of the ions which affects their ability to mix and can run counter to expected ion size behaviour. Our classical simulations have optimised and examined hundreds of different structures which allows us to comment on the ideality of the solid solutions formed and the competition between entropy and enthalpy in the stability of a phase. We are also able to examine different secondary structures and how their enthalpic stability compares. From our results, we offer thoughts on the differing rules governing the mixing processes in these perovskite phases.

References

- (1) Sarkar, A.; Wang, Q.; Schiele, A.; Chellali, M. R.; Bhattacharya, S. S.; Wang, D.; Brezesinski, T.; Hahn, H.; Velasco, L.; Breitung, B. High-Entropy Oxides: Fundamental Aspects and Electrochemical Properties. *Adv. Mater.* **2019**, *31* (26), 1806236. <https://doi.org/10.1002/ADMA.201806236>.
- (2) Sarkar, A.; Velasco, L.; Wang, D.; Wang, Q.; Talasila, G.; de Biasi, L.; Kübel, C.; Brezesinski, T.; Bhattacharya, S. S.; Hahn, H.; Breitung, B. High Entropy Oxides for Reversible Energy Storage. *Nat. Commun.* **2018**, *9* (1). <https://doi.org/10.1038/S41467-018-05774-5>.
- (3) Rost, C. M.; Sacht, E.; Borman, T.; Moballegh, A.; Dickey, E. C.; Hou, D.; Jones, J. L.; Curtarolo, S.; Maria, J. P. Entropy-Stabilized Oxides. *Nat. Commun.* **2015**, *6* (1), 1–8. <https://doi.org/10.1038/ncomms9485>.
- (4) Banerjee, R.; Chatterjee, S.; Ranjan, M.; Bhattacharya, T.; Mukherjee, S.; Sourav Jana, S.; Dwivedi, A.; Maiti, T. High-Entropy Perovskites: An Emergent Class of Oxide Thermoelectrics with Ultralow Thermal Conductivity. **2022**, *8*, 10. <https://doi.org/10.1021/acssuschemeng.0c03849>.

SF08.03.08

Effect of TiO₂ Nanoparticle Coating on the Mechanical Properties of Glass Fibers Md Kawsar Ahmed¹, Ali Bagheri Behboud¹, Arda Kurucu¹, Gökseven Kurt Çömlekçi² and Mustafa Ordu¹; ¹Bilkent University, Turkey; ²Sisecam Science Technology and Design Center, Turkey

Glass fibers are extensively employed as the reinforcing material in composites in a variety of fields such as renewable energy and aerospace. Bare E-glass fibers were coated with different concentrations of rutile TiO₂ nanoparticles to improve mechanical strength of fibers. Microscopic and spectroscopic analyses were performed on the fibers to investigate the presence of nanoparticles over the surface of individual filaments. Tensile tests were performed on the coated and uncoated fibers by following standardized preparation and characterization techniques. Results show that nanoparticle-coated fibers are less likely to fail at a given strength compared to uncoated fibers. Moreover, the tensile strength of the fibers has increased between 7.31% and 11.71%, depending on the concentration of TiO₂ nanoparticles in the solutions.

SF08.03.10

First-Principles Local-Stress Calculations for Oxide Glass Materials Takumu Ito¹, Tomoyuki Tamura¹ and Shingo Tanaka²; ¹Nagoya Institute of Technology, Japan; ²National Institute of Advanced Industrial Science and Technology (AIST), Japan

In glass materials, local physical properties vary due to distributions of coordination numbers, interatomic distances and bond angles. Therefore, it is essential to understand local atomic configurations in glass materials. Classical molecular-dynamics simulations have been widely performed. Recently, first-principles simulations based on density functional theory (DFT) have also been applied to glass models. However, by plane-wave based DFT methods, a total energy and a stress tensor can be obtained as quantities integrated or averaged in an entire supercell. To understand on the nature of local structures in glass materials, the analysis of local distribution of energy and stress is important. In this study, we analyzed atomic stresses in oxide glass materials using first-principles local-stress calculations [1] developed by one of our groups.

Generally, in oxide materials, cations show tensile stresses and anions show compressive stresses. For a SiO₂ glass model [2], atomic stresses of four-coordinated Si and two-coordinated O have a wide distribution due to the deviation in local atomic environments, but average values are close to those of the quartz-type SiO₂ crystal. We found that formation energies of oxygen vacancies depend on sites and have strong correlations with atomic stresses. In a P-Si-Na-O glass model [3], the coordination number of Si is distributed from 4 to 6, and oxygen atoms can be classified into bridging oxygens (BO) and non-bridging oxygens (NBO). Tensile stresses of six-coordinated Si are higher than those of 4-coordinated Si and are close to those of the stishovite SiO₂ crystal. We found that compressive stresses of NBO are smaller than those of BO and has a strong correlation with adsorption energies of protons. From these results, the analysis of atomic stresses is effective in predicting defect formation processes.

References: [1] M. Kohyama et al., *Mater. Trans.* **62**, 1 (2021). [2] T. Tamura et al., *Phys. Rev. B* **69**, 195204 (2004). [3] K. Takada et al., *Phys. Chem. Chem. Phys.* **23**, 14580 (2021).

SF08.03.11

Advanced Manufacturing of Chalcogenide Glass Through Femtosecond Laser Processing—From Waveguides to 3D Dimensional Micro-Structures Fabrication Gözden Torun¹, Kathleen Richardson² and Yves Bellouard¹; ¹Galatea Lab., Ecole Polytechnique Federale de Lausanne, Switzerland; ²CREOL and College of Optics and Photonics, United States

The advanced 3D micro- and nano- structuring of mid-IR material, such as chalcogenide glass, is of high-interest for the fabrication of photonic devices in general, and for spectroscopy applications in particular. Yet, the processing of these materials at microscales remains challenging and limited.

Here, we investigate the use of femtosecond laser for producing arbitrary three-dimensional patterns with varying physical properties in four ternary chalcogenide glass compositions: Ge₂₃Sb₇S₇₀, Ge₂₃As₇S₇₀, Ge₂₃Sb₇Se₇₀, and Ge₂₃As₇Se₇₀.

Interestingly, under specific laser exposure conditions, we observe the occurrence of both, densification and self-organization patterns formation, for which we explore the response to chemical etching. Furthermore, in an attempt to unravel generic laser-induced transformation mechanisms common to the four glass compositions investigated here, we systematically correlate pulse-to-pulse structural changes with material's inner structures evolution, using both, elemental and micro-Raman observations.

These observations emphasize the potential of ultrafast lasers not only for introducing waveguiding properties in chalcogenide glass, but also, for patterning them at the micro-scale.

SESSION SF08.04: Advanced Ceramics and Glasses III
Session Chairs: Christos Athanasiou and Eduardo Saiz
Tuesday Morning, November 29, 2022
Sheraton, 5th Floor, Public Garden

8:45 AM SF08.04.02

Phase-Dependent Mechanical Stability of 3D Zirconia Microstructures Jędrzej P. Winczewski¹, Stefan Gabel², Stefan Zeiler², Manuel Herrera³, Arturo

Susarrey Arce¹, Han Gardeniers¹ and Benoit Merle²; ¹University of Twente, Netherlands; ²Friedrich-Alexander-Universität Erlangen-Nürnberg (FAU), Germany; ³Centro de Nanociencias y Nanotecnología, Universidad Nacional Autónoma de México, Mexico

In the past decade, significant progress has been made in the three-dimensional (3D) structuring of different classes of materials on the microscale. Direct laser writing (DLW) permits unprecedented shape control and resolution among the additive manufacturing approaches. One of the viable routes focuses on the surface functionalization of the 3D structures, e.g., via electroplating^[1] or atomic layer deposition^[2], which can be combined with other processes for the removal of the polymeric core to obtain hollow architectures. Alternatively, solid-beam structures can be formed via tailor-made solutions enabling the fabrication of solid-beam structures composed of materials other than solely organic polymers have been extensively studied. The recent endeavors resulted in several tailor-made solutions extending the range of materials that can be 3D-printed to metals (e.g., Ni^[3]), ceramics (e.g., ZnO^[4] TiO₂^[5]), and composites (Au nanoparticle-laden polymer^[6]). From the perspective of mechanical stability, such materials often exhibit excellent chemical, mechanical and physicochemical stability when compared with polymeric materials.

In this study, we investigate the additive manufacturing of microscale 3D zirconia structures and the dependence of their mechanical stability on the crystallographic phase. We are using our previously-established method,^[7] we first pattern pre-ceramic structures, which transform into the self-miniaturized ceramic replicas upon the annealing in the air. We then modify the photoresin composition to improve the material performance under extreme stresses. The *in situ* nanomechanical material performance is assessed in a nanoindentation study for different 3D architectures and crystallographic phases of zirconia. Focused ion beam tomography is conducted better to understand the inner structure of the 3D materials. Besides, the additional focus is dedicated to precisely determining the crystallographic phase (X-ray powder diffraction, Raman Spectroscopy), chemical composition (X-Ray photoelectron spectroscopy), and defects of the materials (Cathodoluminescence) to better understand the opportunities and current limitations of the presented methodology.

The capability of our additive manufacturing methodology is presented with various 3D lattice structures of micro-to-nano feature sizes. Besides the sole focus on improving the material and structure performance under high strains, our methodology can be utilized to fabricate phosphors,^[7] which can in the future find applications in, e.g., 3D light-emitting devices.

Keywords: additive manufacturing, zirconia, direct laser writing, nanoindentation.

References:

- [1] G. Williams, M. Hunt, B. Boehm, A. May, M. Taverne, D. Ho, S. Giblin, D. Read, J. Rarity, R. Allenspach, S. Ladak, *Nano Res.* **2018**, *11*, 845.
- [2] D. Jang, L. R. Meza, F. Greer, J. R. Greer, *Nat. Mater.* **2013**, *12*, 893.
- [3] A. Vyatskikh, S. Delalande, A. Kudo, X. Zhang, C. M. Portela, J. R. Greer, *Nat. Commun.* **2018**, *9*, 593.
- [4] D. W. Yee, M. L. Lifson, B. W. Edwards, J. R. Greer, *Adv. Mater.* **2019**, *31*, 1901345.
- [5] A. Vyatskikh, R. C. Ng, B. Edwards, R. M. Briggs, J. R. Greer, *Nano Lett.* **2020**, *20*, 3513.
- [6] Q. Hu, X. Z. Sun, C. D. J. Parmenter, M. W. Fay, E. F. Smith, G. A. Rance, Y. He, F. Zhang, Y. Liu, D. Irvine, C. Tuck, R. Hague, R. Wildman, *Sci. Rep.* **2017**, *7*, 17150.
- [7] J. Winczewski, M. Herrera, C. Cabriel, I. Izeddin, S. Gabel, B. Merle, A. Susarrey Arce, H. Gardeniers, *Adv. Opt. Mater.* **2022**, DOI 10.1002/adom.202102758.

9:00 AM SF08.04.03

High Hydrogen Impurity—A hidden Role Aggravating PECVD Amorphous SiN_x Coating Cracking Yutao Dong, Xin Yin and Xudong Wang; University of Wisconsin-Madison, United States

Silicon nitride (SiN_x) film has been widely utilized in passivation coating and dielectric devices due to its chemical stability and excellent insulating properties. Films developed by the plasma-enhance chemical vapor deposition (PECVD) approach exhibit superiority with good uniformity and high deposition rate. However, under a normal PECVD process, residual stress usually builds up along with increasing SiN_x thickness^[1]. High film stress will lead to SiN_x film cracking to restrict the practical applications. Though there are studies about SiN_x film stress aiming to improve film toughness, limited information has been dug out to build up the relationships between chemical composition, atomic arrangement, and film stress. In this work, we uncovered the hidden role of high H impurity in PECVD amorphous SiN_x films at the initial growth due to low deposition temperature in normal deposition conditions. Thin and thick SiN_x films grown on silicon (Si) wafers were selected to compare H impurity and bond configuration at different deposition stages. Both X-ray photoelectron spectroscopy (XPS) and Fourier-transfer infrared spectrum (FT-IR) spectrums indicated higher H impurity at the incipient growth as N-H bonds which were much shorter than the Si-N bonds as backbone of SiN_x matrix. Those shorter N-H bonds resulted in a shrinking tendency to induce extra tensile strain at the SiN_x/Si interface. Therefore, at critical thickness, the original SiN_x film exhibited severe cracking initiated from the SiN_x/Si interface and propagated vertically through whole SiN_x film. To avoid high H impurity concentration near SiN_x/Si interface, Si wafer was soaked in reaction chamber with sufficient time to make sure it was under stable deposition temperature. Correspondingly, SiN_x films were more homogenous with consistent atomic spacing. As a result, these long-soaking grown SiN_x films could tolerate stress with 42% fewer cracks film compared to original SiN_x films. In addition, crack length statistical analysis indicated that only ~14% of crack length was longer than 4 cm in long-soaking SiN_x compared to ~52% of crack length above 4 cm in original SiN_x film. This work provides a long-soaking strategy to regulate interfacial tensile strain attributed to unreacted N-H bonds and alleviate cracks in thick SiN_x PECVD coating.

References:

- [1] X. Xu*, Q. He, T. Fan, Y. Jiang, L. Huang, T. Ao, C. Ma, *Applied Surface Science*, 2013, 264, 823-831.

9:15 AM SF08.04.04

Study of the Effect of Chromium Doping on the Grain Boundary Character of WC-Co Max Emmanuel¹, Oriol Gavalda-Diaz^{1,2}, Ben Britton^{1,3}, Katharina Marquardt¹ and Finn Giuliani¹; ¹Imperial College London, United Kingdom; ²The University of Nottingham, United Kingdom; ³The University of British Columbia, Canada

Cemented carbides (WC-Co) are a class of composites that combine the hardness of a metallic carbide (WC) with the toughness of a metallic binder (Co). Applications of WC-Co include metal cutting, mining, construction, and wood and plastic working. The main reason for their consumption in a wide array of applications is their unique combination of high hardness and toughness relative to other hard materials such as ceramics (e.g. aluminium oxide and silicon carbide) and diamond. Cemented carbide remains a growing market with an increase in annual world consumption from 10 t in 1930 to 50000 t in 2008. With the growth in demand for WC-Co, it is beneficial to understand WC-Co more thoroughly.

Fracture and wear affect the performance and lifetimes of tools composed of WC-Co. Cracks in WC-Co has been found to predominantly propagate along WC/WC and WC/Co interfaces at low cobalt contents as is the case in typical commercial grades [1]. Hence, it is useful to gain an understanding of WC boundaries given that the material toughness is related to energy dissipation, which in turn corresponds to crack path. This knowledge can be employed for

grain boundary engineering (GBE) of WC-Co tools with superior performance and lifetimes.

In this work an evaluation of the WC grain boundary character distributions (GBCD) for the most abundant boundary type ($\Sigma 2$) has been analysed for a standard (WC-10wt%Co) and a chromium doped (WC-10wt%Co-1wt%Cr%) WC-Co sample. This evaluation is based on Rohrer et al.'s five parameter GBCD analysis [2]. Statistically, relative boundary populations are determined from GBCD analysis. Since boundary populations are inversely correlated with boundary energies, GBCD analysis will give an indication of relative grain boundary energies. Fracture energies of these boundaries were measured via double cantilever beam (DCB) tests. Relative populations of $\Sigma 2$ boundaries on each sample was then compared with their respective measured fracture energies.

It was found that the area fraction of $\Sigma 2$ boundaries increased threefold with chromium doping. Furthermore, it was found that the length fraction of $\Sigma 2$ boundaries were greater within WC/WC boundaries compared to all possible WC interfaces in the WC-Co microstructure regardless of doping. Fracture energies of $3.57 \pm 0.28 \text{ Jm}^{-2}$ were measured for $\Sigma 2$ boundaries on the standard sample. In contrast a successful (stable crack growth) DCB test could not be performed on the chromium doped variant. It was hypothesised that the chromium doping altered the boundary chemistry of the $\Sigma 2$ boundaries as observed from the increased fraction of $\Sigma 2$ boundaries in the doped sample. This in turn likely increased the $\Sigma 2$ boundary fracture toughness and hence the reason for the failed DCB tests on the doped sample.

References

- [1] K. P. Mingard, H. G. Jones, M. G. Gee, B. Roebuck and J. W. Nunn, *International Journal of Refractory Metals and Hard Materials*, 36, 136 (2013). Available from: doi: 10.1016/j.ijrmhm.2012.08.006.
[2] G. S. Rohrer, D. M. Saylor, B. E. Dasher, B. L. Adams, A. D. Rollett and P. Wynblatt, *Zeitschrift für Metallkunde*, 95, 197 (2004). Available from: doi: 10.3139/ijmr-2004-0043.

9:30 AM BREAK

10:00 AM *SF08.04.05

Hybrid Multiscale Ceramics—Enhanced Mechanical Behavior and Energy Applications [Diletta Giuntini](#)^{1,2}; ¹Eindhoven University of Technology, Netherlands; ²Technische Universität Hamburg-Harburg, Germany

Nano/micro-structured ceramics combine the unique features of ultrasmall building blocks and their organization into tailored architectures to foster emergent properties up to the macroscale. Many functional applications open up, such as in catalysis, energy and optoelectronics. One of the current main challenges in materials science and engineering is the fabrication of such multiscale materials, and more specifically bridging scales in materials manufacturing. To obtain finely tuned macroscale properties, building blocks assembly and optimization of both material constituents and interfaces are key. This talk will tackle these aspects for some promising examples or nano- and micro architected ceramic-based materials. Insights will be shown on how to tailor macro-mechanical behavior and functional properties via fundamental investigations and a strategic combination of different material processing technologies.

10:30 AM SF08.04.06

Bioinspired Glass Composites with Damage-Sensing Functionalities [Tommaso Magrini](#)¹, [Florian Bouville](#)², [Alessandro Lauria](#)³, [André R. Studart](#)³ and [Chiara Daraio](#)¹; ¹California Institute of Technology, United States; ²Imperial College London, United Kingdom; ³ETH Zürich, Switzerland

Lightweight composites have become key structural materials for aircrafts and future energy-efficient transportation systems. Nevertheless, the design of composites featuring high strength and high fracture toughness remains an open challenge due to the usual trade-off between these sets of properties in most manmade materials. Taking inspiration from the strong and tough hierarchical architecture of mollusk shells, I designed and fabricated fracture-resistant glass-reinforced composites by combining soft polymer layers with alternating, nacre-like layers that are infiltrated with the same polymer.¹ In my talk, I will highlight the fracture behavior and the toughening mechanisms that govern the high crack growth resistance of these hierarchical glass composites. In particular, I will focus on the effects of plastic deformation and bridging by the polymer phase on the early- and late stages of the fracture process. These effects have been elucidated by using a mechanochromic organic phase, capable of pre-emptively detecting and reporting the evolution of damage through a simple optical readout. The composites signal the presence of damage via a fluorescence color change that arises from the force-activation of mechanophore molecules embedded in the organic matrix.² By optical imaging mechanically loaded composites it is possible to localize damage prior to fracture and to elucidate the key role of plasticity during rupture of the hierarchical composites. Although several examples have shown that polymers can be made damage-reporting using mechanophores, just a handful of examples have targeted the reinforcing phase for the same purpose. To fill this gap, I will also highlight progresses on how high-aspect-ratio glass-reinforcing particles, directly gathered from the upcycling of glass industry residuals, can be engineered to provide optical warnings before and during extended fracture events. With this research, I aim at displaying how multifunctional bioinspired glass composites, capable of combining high strength, high toughness and damage-sensing properties can be fabricated and characterized. I will provide new insights into the interplay of multiscale toughening mechanisms in hierarchical bioinspired architectures and I will offer guidelines for the design of novel multifunctional bioinspired composites.

References

- T Magrini, A Senol, R Style, F Bouville, AR Studart, *Journal of the Mechanics and Physics of Solids* (2022) 159, 104750
T Magrini, D Kiebal, D Grimm, A Nelson, S Schrettl, F Bouville, C Weder, AR Studart, *ACS Applied Materials & Interfaces* (2021) 13 (23), 27481-27490

10:45 AM SF08.04.08

Ultrafast High-Temperature Sintering of Dense Alumina with Bioinspired Microstructures [Rohit P. Behera](#), [Matthew J. Reavley](#), [Zehui Du](#), [Gan Chee Lip](#) and [Hortense Le Ferrand](#); Nanyang Technological University, Singapore

Bioinspired microstructures in ceramics have the potential to fulfil combined unusual properties such as local anisotropy with high hardness, stiffness and toughness, but their current fabrication methods remain challenging due to the time-consuming, energy-extensive sintering method. Here, we report a strategy to sinter dense ceramics with bioinspired heterogeneous microstructures that have tunable stiffness and toughness within seconds. This strategy combines a colloidal directed assembly i.e., magnetic assisted slip casting (MASC) with templated grain growth (TGG) using ultrafast high-temperature sintering (UHS). The hierarchical microstructural designs result from the local orientation of alumina microplatelets coated with Fe_3O_4 nanoparticles dispersed in a matrix of alumina nanoparticles. After UHS, the presence of Fe_3O_4 led to ceramics with about 98% density and a toughness (K_{I0}) of $5.89 \text{ MPa.m}^{0.5}$ in nacre-like orientations. We further explored periodically oriented and multi-layered microstructured ceramics using different compositions to attain an overall toughness (K_{I0}) of about $5.73 \text{ MPa.m}^{0.5}$ combined with enhanced energy dissipation rates of $\sim 200 \text{ J. m}^{-2}$ that can exhibit high local stiffness and toughness across multiple directions. Our proof-of-concept specimens demonstrate that MASC and UHS can fabricate dense, tough and

preferentially textured ceramic in time-saving, cost-effective and energy-efficient ways, opening the design space for achieving ceramic parts with local structural properties.

11:00 AM SF08.04.09

Understanding Fracture Mechanisms in Tough Ceramic Composites Inspired from Nacre [Victoria Vilchez](#) and Florian Bouville; Imperial College London, United Kingdom

Compared to metals and polymers, ceramics are great candidates for applications involving extreme environments like high temperatures, radiations, humidity or corrosion. The ionic-covalent nature of their bonds make them very strong and stiff materials, although intrinsically brittle. This poor resistance to damage propagation greatly limits the use of ceramics in high-performance domains that cannot tolerate catastrophic failure, such as aeronautics or biomedical applications. For this reason, improving toughness has been a major axis of research in ceramic engineering over the past decades. To this day, the key mechanisms highlighted to improve ceramics' resistance to crack growth mostly reside in a fine control of the microstructure. This includes reinforcing the bulk matrix with fibers and fillers to bridge the crack behind its tip or adding features that resist progression ahead of the crack tip such as residual compressive stresses and transformation toughening. More recently, other microstructures inspired from biological materials have been investigated, specifically ceramic-based materials such as bone, dentin, or nacre. Indeed, millions of years of evolution have gifted these materials with sophisticated hierarchical structures that enable them to resist fracture propagation despite being primarily composed of brittle ceramics. Among these materials, nacre stands out as having one of the simplest microstructures yet exhibiting many toughening mechanisms. Nacre is one of the main components of many seashells and is composed of 95 vol% calcium carbonate platelets stacked in a brick-and-mortar fashion. This microstructure provides nacre with intricate toughening mechanisms such as deflection, branching, interlocking, shearing, viscoelastic dissipation, all acting at different length scales. Taking inspiration from nacre, many processes and compositions have been developed to produce tough ceramic-based composites. Using the current standards of fracture mechanics, it has been proven that nacre-like composites exhibit higher values of fracture toughness and improved crack-resistance curves compared to bulk ceramics. However, characterizing fracture in such materials that exhibit high degrees of deflection and branching remains a challenge, and all the mechanisms that account for improved damage resistance in nacre-like composites have not been characterized or explained. We have worked on characterizing fracture propagation in ceramic-based nacre-like composites, with the aim of determining the role of microstructure and composition on the mechanical response. To this end, we have developed analytical tools validated by finite element analysis to measure crack resistance curves of highly deflected and branched cracks. We have used it to study and reveal the influence of specific parameters related either to the composition, such as the interphase and addition of residual stresses, or to the microstructure, with the presence of short- and long-range order, on the crack propagation behavior in brick-and-mortar structures.

SESSION SF08.05: Advanced Ceramics and Glasses IV
Session Chairs: Florian Bouville and Tommaso Magrini
Tuesday Afternoon, November 29, 2022
Sheraton, 5th Floor, Public Garden

1:30 PM SF08.05.01

Direct 3D Printing of Biomimetic Bioceramic Scaffolds by Cement Routes [Caner Durucan](#) and Hüseyin Engin Sever; METU, Turkey

Bioceramic-based 3-dimensionally constructed structures and scaffolds are widely used for hard tissue engineering applications and as hard tissue analogs. Robocasting, where a bioceramic powder-binder combination in paste form is used as feed material can be used to develop 3D preforms. The hardening and shape preservation of the printed structures is usually achieved by subsequent polymerization of the organic component. In this study, a novel hybrid printing paste mainly composed of calcium phosphate cement (CaPC) has been developed to achieve *in situ* hardening during printing process. The cement component is α -tricalcium phosphate ($\text{Ca}_3(\text{PO}_4)_2$), which readily converts to hardened hydroxyapatite ($\text{Ca}_{10}(\text{PO}_4)_6(\text{OH})_2$ or HAp) upon hydration. The hydration product in a calcium-deficient HAp, in that sense it offers higher bioactivity and osteoconductive property as it is resembling chemistry of natural bone mineral better than any other CaP. Parametric printing studies has been performed to determine optimal formulation of the printing paste. Meanwhile, validation of the processing approach, i.e. cement-conversion kinetics, HAp formation efficiency/extent, shape preservation for 3D-printed structures, mechanical properties has been examined. In addition, a microstructural modification approach to control and alter microporosity adaptable to 3D-printing process by incorporation of an inorganic pore generator has been demonstrated. .

1:45 PM SF08.05.02

Pyrolyzed Ultra-Sharp Glassy Carbon Microneedles [Chaoqun Zhou](#), Aykut Aksit, Betsy Szeto, Richard L. Li, Anil K. Lalwani and Jeffrey W. Kysar; Columbia University, United States

We report glassy carbon ultra-sharp microneedles pyrolyzed from a polymeric precursor structure fabricated via Two-Photon Polymerization lithography (2PP). The glassy carbon microneedles have tip radius of curvature of 1 μm , diameters ranging from 22 μm to 26 μm , and lengths ranging from 106 μm to 126 μm . They are capable of safely penetrating the 1.5 mm wide and 35 μm thick round window membrane in a guinea pig model that serves as a barrier between the middle and inner ear spaces. The precursor needle has a tip diameter of 7.5 μm , a base diameter of 100 μm and a length of 600 μm . To maintain structural integrity during pyrolysis, we show that the exposed surface area to volume ratio of the polymeric precursor needs to be within a certain range. Upon designing the polymeric precursor structure under these constraints, the structures can shrink by up to 81% during pyrolysis while maintaining structural integrity. The pyrolyzed glassy carbon is elastic with a brittle failure mechanism with a Young's modulus of 9.0 GPa and characteristic strength of 710 MPa. Furthermore, glassy carbon is known to be biocompatible. We show that the pyrolyzed ultra-sharp glassy carbon microneedles perforate the round window membrane safely and can serve to enable safe direct delivery of therapeutics into the inner ear delivery. In addition to glassy carbon microneedles, this pyrolysis process can be adapted to fabricate many other biomedical devices.

2:00 PM SF08.05.03

Thermoplastic Extrusion of Piezoelectric Lead-Free Ceramics for Biological Membrane Applications. [Simone Santucci](#), Astri Bjørnetun Haugen and Bhaskar Reddy Sudireddy; Technical University of Denmark, Denmark

The inclusion of piezoelectric ceramics has been in recent years a fast increasing hot topic. Piezoelectric lead-free materials such as BaTiO₃ or K_{0.5}Na_{0.5}NbO₃ (KNN) have been studied in a wide range of applications such as neural and bone tissue repair, or bacterial/planktonic membranes^{1,2}. For many of these applications, porous systems are necessary in order to increase the active surfaces and maximize the interaction with the biological matter. A promising manufacturing method for porous ceramics is thermoplastic extrusion. This method produces robust cylindrical membranes, also in presence

of pores former, and it is also scalable up to industrial levels³.

In the case of planktonic/bacteria membranes, the device requires high piezoelectricity (depending on the application can be > 100 pC/N), suitable pores size and distribution (1-10 μm), and strong support. However, pores decrease the magnitude of piezoelectric effect both locally and in the overall device. Here we manufactured tubular porous piezoelectric membranes by thermoplastic extrusion, using graphite and/or polymethyl methacrylate (PMMA) as pore formers and lead-free ceramics as support material. The influence of pore formers on the microstructure, mechanical properties and piezoelectric effect is studied, as well as the sintering temperature and extrusion parameters. The overall device is suitable for biological applications, in particular planktonic/bacteria membrane. Finally, the manufacturing process is scalable and easily integrable in an industrial environment.

(1) Xu, Q. et al., *Adv. Mater.* **2021**, 2008452, 2008452. <https://doi.org/10.1002/adma.202008452>.

(2) Kumar, S. et al., *J. Ind. Eng. Chem.* **2021**, 97, 95–110. <https://doi.org/10.1016/j.jiec.2021.02.016>.

(3) Haugen, A. B. et al., *J. Eur. Ceram. Soc.* **2017**, 37 (3), 1039–1047. <https://doi.org/10.1016/j.jeurceramsoc.2016.10.001>.

2:15 PM SF08.05.04

Characterizing the Local Yield Surface in Simulated Glasses Spencer Fajardo¹, Bin Xu¹, Dihui Ruan¹, Rahul Meena¹, Michael Shields¹, Thomas Hardin², Michael Chandross² and Michael L. Falk¹; ¹Johns Hopkins University, United States; ²Los Alamos National Laboratory, United States

Amorphous materials, unlike their crystalline counterparts, have no obvious defects that help facilitate plastic instability, and so methods that predict the locations of plastic events are highly sought after. Two-dimensional model glasses have been used extensively to study amorphous materials and to develop a theoretical basis for determining the location of plastic events. One method that has resulted from such investigations is the Local Yield Stress (LYS) method in which nanoscale regions of the material are probed to quantify the incremental stress necessary to induce plastic rearrangement. The resultant local yield stress depends on the sense of the mechanical load applied on a local region. Higher accuracy predictions can be obtained by sampling many disparate mechanical loads. Doing so allows one to develop a more accurate picture of the “local yield surface,” the limiting stresses that the material can withstand before yielding along all possible mechanical loadings. In three dimensions, the number of distinct mechanical tests needed to accurately sample the local yield surface increases. The resulting dataset is computationally expensive to produce. We seek to use this data to compactly characterize this high-dimensional “surface” and to enable extrapolation along deformations that were not explicitly tested in the original dataset. This can, in principle, be accomplished by describing the local yield surface in terms of a discrete number of Shear Transformation Zones (STZs). By characterizing the number of STZs in a local region we will be able to predict areas of high plasticity more accurately in amorphous materials, eventually leading to the accurate modeling of plastic response and the design of materials with mechanical properties catered to specific needs.

SNL is managed and operated by NTESS under DOE NNSA contract DE-NA0003525.

2:30 PM BREAK

3:00 PM SF08.05.06

Validating a Facile Approach to Measuring Fracture Toughness by Instrumented Indentation Without Imaging Crack-Lengths Jacob L. Hempel, Andrew Meyer, Ryan C. Hill and Yang-Tse Cheng; University of Kentucky, United States

Probing the fracture toughness of brittle materials by measuring the crack-length generated from indentation experiments is often practiced in many areas of materials research. However, when the cracks are too small to be measured accurately, an energy-based approach has recently been proposed by several researchers. In the work presented here, this approach is compared with the well-known crack-length method on six different materials. We found that the energy-based method and crack-length method yield significantly different results for all materials but converge if the energy method is modified with a correction factor using a calibration sample.

3:15 PM SF08.05.07

Visualization of the Final Stage of Sintering in Nanoceramics with Atomic Resolution Tanna E. Fiuza, Marlon Muniz da Silva, Jefferson Bettini and Edson R. Leite; Brazilian Center for Research in Energy and Materials, Brazil

Sintering is a thermally active process, in which densification (or pore elimination) and grain growth can occur. In general, the driving force for densification is lowering the surface free energy by replacing solid-gas interfaces, leading to a new solid-solid interface with a lower system's free energy [1-6]. The optimization of the ceramic's densification process lies in a better comprehension of the sintering steps and related mechanisms. Many models satisfactorily describe the sintering at a micrometric scale, however, nanometric effects make the direct extrapolation of these models to the nanoscale more complicated [7-9]. By high-resolution transmission electron microscopy, particularly real-time measurements, we followed the pore elimination process in a self-standing ZrO₂ thin film produced by monoclinic ZrO₂ nanoparticles. The absence of carbon membrane and the surface cleaning by removing the capping ligands produced an ideal scenario to perform the experiments. We found a high anisotropic pore elimination, with a gradual and linear decrease in pore area as a function of time. The pore shrinkage occurs with atoms from a rough surface being redistributed on the solid-gas interface, while atoms are attached to a faceted surface. In the final stage, the pore becomes rounded and shrinks until complete elimination. Also, the pore acts as a pin, reducing GB mobility. In summary, these results can contribute to a better understanding of the sintering process in nanoceramics, and to the improvement of kinetic models that better describe the densification process at the nanoscale.

[1] Bordia, R. K.; Kang, S. L.; Olevsky, E. A. *J. Am. Ceram. Soc.* **2017**, 100 (6), 2314–2352

[2] Gong, Z.; Zhao, W.; Guan, K.; Rao, P.; Zeng, Q.; Liu, J.; Feng, Z. *J. Am. Ceram. Soc.* **2020**, 103 (10), 5900–5913

[3] Wollmershauser, J. A.; Feigelson, B. N.; Gorzkowski, E. P.; Ellis, C. T.; Goswami, R.; Qadri, S. B.; Tischler, J. G.; Kub, F. J.; Everett, R. K. *Acta Mater.* **2014**, 69, 9–16

[4] Mitchell, S.; Qin, R.; Zheng, N.; Pérez-Ramírez, J. *Nat. Nanotechnol.* **2021**, 16 (2), 129–139

[5] Cao, A.; Lu, R.; Veser, G. *Phys. Chem. Chem. Phys.* **2010**, 12 (41), 13499

[6] Rahaman, M. N. *Sintering of Ceramics*; CRC Press, 2007

[7] Castro, R. H. R.; Gouvêa, D. *J. Am. Ceram. Soc.* **2016**, 99 (4), 1105–1121

[8] Chen, I.-W.; Wang, X. *Sintering of Nanograin Ceramics*. In *Ceramics Science and Technology*, Riedel, R.; Chen, I., Eds.; Wiley-VCH Verlag GmbH & Co. KGaA, 2012; pp 441–455

[9] Kang, S.-J. L. *Grain Boundary Energy and Sintering*. In *Sintering: Densification, Grain Growth and Microstructure*, Kang, S.-J. L., Ed.; Elsevier Butterworth-Heinemann, Oxford, 2004; pp 139–143.

3:30 PM SF08.05.08

Experimental Mechanical Characterization of 3D-Printed Hydroxyapatite and Finite Element Model Implementation of High Porous Scaffold for Bone Tissue Engineering Luca D'Andrea¹, Francesco Bainsi², Enrica Vernè², Martin Schwentenwein³, Dario Gastaldi¹ and Pasquale Vena¹; ¹Politecnico di

Milano, Italy; ²Politecnico di Torino, Italy; ³Lithoz GmbH, Austria

Bone is a self-healing tissue, but some pathologies, aging, non-physiologic conditions and trauma may cause a critical size bone defect that cannot heal spontaneously. The implant of bioceramic scaffolds is a promising approach for the treatment of these pathologic conditions. Among bioceramics, hydroxyapatite (HAP) is a good candidate for its chemical affinity with the native bone's mineral component, thus ensuring biocompatibility and promoting osteo-integration. As HAP mechanical property is heavily influenced by its brittle nature, a robust experimental characterization of the bulk material is required for the design of mechanically reliable scaffolds.

Furthermore, recent developments in 3D printing technologies allow for a wide variety of micro-structured devices meeting patient-specific needs. In this work, we deal with HAP material obtained through DLP-stereolithography which is a printing technology allowing for very fine spatial resolution and high printing fidelity. However, as the technological process includes a sintering phase at high temperature, the properties of the obtained material are strongly affected by the intrinsic defects which characterize the final product. For this reason, in this study, the mechanical characterization of the material samples having a simple geometrical shape and obtained through the same process as that used for the scaffold production and having the same characteristic size of the microstructural features of the scaffolds is proposed.

For this purpose, we 3D-printed three different kinds of beams (i.e. simple beams, notched beams and cantilevers) in small scale (approximate size of beams 1mmx0.4mmx10mm). The samples have been subjected to confocal laser imaging, micro-Computed Tomography scanning and mechanical tests. The confocal laser scanning provided the size of the samples having the purpose to complement mechanical tests and to assess printing fidelity; the micro-CT analyses had the purpose to quantify the intrinsic porosity of the material resulting from the sintering process. The mechanical tests were micro-bending test and Berkovich nanoindentation.

The micro-bending tests were used to assess the flexural stiffness and strength, while the nano-indentation tests have been used to verify whether elastic property exhibits a scale effect, expected in case micro-defects occur in the material.

Using the same material and 3D-printing technology, high porous scaffolds were manufactured through DLP stereolithography. Micro-Computed Tomography scans were performed on the scaffolds to obtain the real geometry of the scaffolds. After a proper binarization process, a finite element model was implemented using the real geometry and the mechanical parameters found in the above-described experiments. Micro-CT based finite element analyses on the 3D-printed scaffolds were performed with the aim to determine the macroscopic elastic and strength properties of the scaffolds. The obtained macroscopic properties are validated through comparison with macroscopic experimental data already available.

The experimental and numerical framework presented in this work has shown the capability of in-silico models of 3D-printed scaffolds to predict biomechanically relevant properties, provided that intrinsic properties of the materials are available with specific reference to the manufacturing process parameters and geometrical size of the micro-architecture.

SESSION SF08.06: Virtual Session
Session Chair: Hortense Le Ferrand
Wednesday Morning, December 7, 2022
SF08-virtual

8:00 AM *SF08.06.01

Processing and Mechanical Behavior of 3D Printed Ceramic Lattices and Their Derived Interpenetrating Phase Composites Zehui Du¹, Yida Zhao¹ and Pengcheng Ye²; ¹Nanyang Technological University, Singapore; ²Creatz3D Pte Ltd., Singapore

Ceramics and their derived composites which are lightweight and with high strength and high toughness have been long sought after for various engineering applications. In this work, various alumina ceramic based microlattices, including Simple Cubic, Octet Truss and Kelvin Cell have been fabricated using computer-aided design tool and stereolithography 3D printing process. Subsequently, interpenetrating phase composites (IPCs), with the ceramic lattices as backbone and infiltrated with a second phase (e.g., epoxy or aluminum alloy), have been further developed. The mechanical behavior of the ceramic lattices and the IPCs under quasi-static compression tests has been systematically studied by experiments and simulation. Results show that Simple Cubic lattices generally initiate the fractures at the struts in the outermost lattice planes, while the Octet Truss and Kelvin Cell lattices fracture at the (110) diagonal plane. With a second phase infiltrated into the lattices, the resultant composites inherit similar fracture behavior as their corresponding lattices, but in a more gradual manner. The stiffness and compressive strength of the lattices follow the order of Simple Cubic > Octet Truss > Kelvin Cells. The compressive strength of IPCs is generally higher than that of the ceramic lattices. Composites with 50 vol% alumina simple cubic lattices and filled with epoxy exhibit a high compressive strength of 440 MPa and energy absorption of 12 J/g (at 16% strain). The energy absorption is almost 100% higher than that of epoxy and much better than that of the ceramic lattices. The factors controlling the mechanical properties of the lattices and IPCs, including relative density, topology, matrix materials and lattice defects arising from 3D printing, will be discussed and the perspectives on the application of the lattices and IPCs will be given in the presentation.

8:30 AM SF08.06.04

Ceramic Fibres with Controlled Micro- and Macrostructures by Sol-Gel Electrospinning Shiling Dong¹, Barbara Maciejewska¹, Maria Lissner¹, Daniel Thomson¹, David Townsend¹, Robert Millar², Nik Petrinic¹ and Nicole Grobert^{1,2}; ¹University of Oxford, United Kingdom; ²Williams Advanced Engineering Limited, United Kingdom

Electrospinning is a well-developed technique for fabricating one-dimensional (1D) fibres in the form of two-dimensional (2D) nonwoven mats. In junction with sol-gel synthesis, single and multiphase ceramic fibres made of oxides and nitrides have been produced. Such ceramic fibre mats, with a unique combination of large surface area, high porosity, flexibility, show great premises for advanced applications such as flexible electronics and sensors. However, the ability to tune the morphology, porosity and the macroscopic shape of fibre product is still limited. For example, it is challenging to produce highly porous three-dimensional (3D) fibre architectures which are desired in tissue engineering, air filtration, absorbent, etc. Thus, developing strategies to control the micro- and macrostructures of ceramic fibres is the key to facilitate their practical implementation and broaden potential usages.

Here, we report several solution modification strategies to effectively tune the structure of electrospun fibres, allowing customised fibre porosity and surface area. At the microscopic level, inducing liquid-liquid phase separation in spinning solution leads to core-shell fibre structures without the need of employing a complex spinneret. The pores size and shape can be controlled by varying the ratio of alkoxides, solvent, and polymer component. Also, electrospin the solutions with homogeneously dispersed submicron-sized polymer powders gives hybrid fibres. Such powders act as pore-forming templates to render mesopores and macropores inside fibre after calcination. At the macroscopic level, modifying the electrical conductivity of the spinning solution triggers different electrodynamic behaviour of electrified solution jet. The as-spun fibres spontaneously assemble into sponge-like macrostructure with centimetre-scale height, which is in sharp contrast to the conventional electrospun thin nonwovens. After calcination, the resultant ceramic fibre

sponges show extremely high porosity (about 99.9%), high specific surface area (up to 128 m²/g), excellent flexibility and elasticity. Overall, we introduce novel solution modification strategies towards a new class of electrospun ceramic fibres with unprecedentedly controlled micro- and macrostructures.

8:45 AM SF08.06.06

Phase Formation of Cubic Silicon Carbide from Reactive Silicon-Carbon Multilayers Dwarakesh Sudhahar, [Deepshikha Shekhawat](#), Joachim Döll and Jörg Pezoldt; TU Ilmenau, Germany

Phase Formation of Cubic Silicon Carbide from Reactive Silicon-Carbon Multilayers
Dwarakesh Sudhahar ¹, Deepshikha Shekhawat ^{1*}, Joachim Döll ², Jörg Pezoldt ^{1*}

¹ FG Nanotechnologie, Institut für Mikro- und Nanoelektronik and Institut für Mikro- und Nanotechnologien MacroNano^a and Institut für Werkstofftechnik, TU Ilmenau, Postfach 100565, 98684 Ilmenau, Germany; dwarakesh.sudhahar@tu-ilmenau.de (D.S.)

² Zentrum für Mikro- und Nanotechnologien, TU Ilmenau, Gustav-Kirchhoff-Straße 7, 98693 Ilmenau, Germany; joachim.doell@tu-ilmenau.de (J.D.)

* Correspondence: deepshikha.shekhawat@tu-ilmenau.de (D.S.); joerg.pezoldt@tu-ilmenau.de (J.P.)

Abstract: The scope of this paper is to produce efficient and low-cost silicon carbide multilayers. The method is formed on self-propagating high-temperature synthesis of binary silicon-carbon based reactive multilayers. In order to do so the silicon carbide is fabricated by means of the magnetron sputtering method. The silicon and carbon bilayers were fabricated with two different bilayer thicknesses. The silicon and carbon are deposited in an alternative layer with a total thickness of 1 µm. The entire system is annealed by rapid thermal analysis at different temperatures starting from 500 C to 1100 C and heating uprate. In order to find the phase formation, morphology, and reaction enthalpy the samples were investigated with XRD, SEM and FTIR. From XRD analysis we could find that the formation of the silicon-carbide phase was initiated from 700 C with increasing bilayer thickness the silicon carbide phase formation was partially suppressed by the silicon recrystallization due to resulting lower carbon diffusion into silicon. The transformation process proceeds in a four-step process. From this, it was noted that when compared to low bilayer thickness samples, the formation of the SiC phase is delayed with increasing bilayer thickness and needs a high temperature. The grain size and morphology of the samples were well studied with SEM analysis and the measured average thickness of the Si and the C layers are 53 and 48 nm, respectively.

Keywords: phase transition, reactive materials, reaction enthalpy, X-ray diffraction, differential scanning calorimetry

8:50 AM DISCUSSION TIME

SESSION SF08.07: On-Demand Presentation
Thursday Morning, December 8, 2022
SF07-virtual

7:00 AM SF08.07.01

Crystallization Kinetics of Ordered Mesoporous Alumina Under Transient Joule Heating [Leyan Wang](#) and Kwan Wee Tan; Nanyang Technological University, Singapore

Well-ordered mesoporous alumina materials derived from block copolymer self-assembly are desirable for many applications such as environmental separation and carbon sequestration. We have developed an improved synthesis protocol mixing block copolymers with stable alumina sol precursors to access various ordered morphologies, including 2D hexagonal cylinders and 3D cubic lattices, as well as 2D lamellar and multiscale hierarchically ordered mesoporous architectures, to our knowledge for the first time. Coupling block copolymer self-assembly with Joule heating provide further enhancements yielding highly crystalline ordered alumina and alumina/carbon structure within second timeframes. Here we will describe the Joule heating-induced crystallization kinetics studies of block copolymer-directed mesoporous alumina and other oxide systems. The X-ray scattering data fits well with established models providing a clearer understanding of crystal growth under such nonequilibrium transient high-temperature conditions.